
REVIEW OF PARTICLE PHYSICS*

Particle Data Group

Abstract

The *Review* summarizes much of particle physics and cosmology. Using data from previous editions, plus 2,717 new measurements from 869 papers, we list, evaluate, and average measured properties of gauge bosons and the recently discovered Higgs boson, leptons, quarks, mesons, and baryons. We summarize searches for hypothetical particles such as supersymmetric particles, heavy bosons, axions, dark photons, etc. Particle properties and search limits are listed in Summary Tables. We give numerous tables, figures, formulae, and reviews of topics such as Higgs Boson Physics, Supersymmetry, Grand Unified Theories, Neutrino Mixing, Dark Energy, Dark Matter, Cosmology, Particle Detectors, Colliders, Probability and Statistics. Most of the 120 reviews are updated, including many that are heavily revised.

The *Review* is divided into two volumes. Volume 1 includes the Summary Tables and 97 review articles. Volume 2 consists of the Particle Listings and contains also 23 reviews that address specific aspects of the data presented in the Listings.

The complete *Review* (both volumes) is published online on the website of the Particle Data Group (pdg.lbl.gov) and in a journal. Volume 1 is available in print as the *PDG Book*. A *Particle Physics Booklet* with the Summary Tables and essential tables, figures, and equations from selected review articles is available in print, as a web version optimized for use on phones, and as an Android app.

The 2024 edition of the *Review of Particle Physics* should be cited as:
S. Navas *et al.* (Particle Data Group), *Phys. Rev. D* **110**, 030001 (2024)

DOI: 10.1103/PhysRevD.110.030001

For the online version see pdg.lbl.gov:



© 2024

Except where otherwise noted, content of this work (the *Review of Particle Physics*) is licensed under a Creative Commons Attribution 4.0 International (CC BY 4.0) license.

*The publication of the *Review of Particle Physics* is supported by the Director, Office of Science, Office of High Energy Physics of the U.S. Department of Energy under Contract No. DE-AC02-05CH11231; by an implementing arrangement between the governments of Japan (MEXT: Ministry of Education, Culture, Sports, Science and Technology) and the United States (DOE) on cooperative research and development; by the Italian National Institute of Nuclear Physics (INFN); and by the European Laboratory for Particle Physics (CERN). Individual collaborators receive support for their PDG activities from their respective institutes or funding agencies.

Particle Data Group

S. Navas¹, C. Amsler², T. Gutsche³, C. Hanhart⁴, J.J. Hernández-Rey⁵, C. Lourenço⁶, A. Masoni⁷, M. Mikhasenko⁸, R.E. Mitchell⁹, C. Patrignani¹⁰, C. Schwanda¹¹, S. Spanier¹², G. Venanzoni^{13,14}, C. Z. Yuan¹⁵, K. Agashe¹⁶, G. Aielli¹⁷, B.C. Allanach¹⁸, J. Alvarez-Muñiz¹⁹, M. Antonelli²⁰, E.C. Aschenauer²¹, D.M. Asner²¹, K. Assamagan²¹, H. Baer²², Sw. Banerjee²³, R.M. Barnett²⁴, L. Baudis²⁵, C.W. Bauer²⁴, J.J. Beatty²⁶, J. Beringer²⁴, A. Bettini[†], O. Biebel²⁸, K.M. Black²⁹, E. Blucher³⁰, R. Bonventre²⁴, R.A. Briere³¹, A. Buckley³², V.D. Burkert³³, M.A. Bychkov³⁴, R.N. Cahn²⁴, Z. Cao¹⁵, M. Carena^{35,30,36}, G. Casarosa^{37,14}, A. Ceccucci⁶, A. Cerri^{38,14,39}, R.S. Chivukula⁴⁰, G. Cowan⁴¹, K. Cranmer²⁹, V. Crede⁴², O. Cremonesi⁴³, G. D'Ambrosio⁴⁴, T. Damour⁴⁵, D. de Florian⁴⁶, A. de Gouvêa⁴⁷, T. DeGrand⁴⁸, S. Demers⁴⁹, Z. Demiragli⁵⁰, B.A. Dobrescu³⁵, M. D'Onofrio¹³, M. Doser⁶, H.K. Dreiner⁵¹, P. Eerola⁵², U. Egede⁵³, S. Eidelman[‡], A.X. El-Khadra⁵⁵, J. Ellis^{56,6}, S.C. Eno¹⁶, J. Erler⁵⁷, V.V. Ezhela⁵⁴, A. Fava³⁵, W. Fetscher⁵⁸, B.D. Fields^{59,55}, A. Freitas⁶⁰, H. Gallagher⁶¹, T. Gershon⁶², Y. Gershtein⁶³, T. Gherghetta⁶⁴, M.C. Gonzalez-Garcia^{65,66,67}, M. Goodman⁶⁸, C. Grab⁵⁸, A.V. Gritsan⁶⁹, C. Grojean^{70,71}, D.E. Groom²⁴, M. Grünewald⁷², A. Gurtu^{6,73}, H.E. Haber⁷⁴, M. Hamel⁷⁵, S. Hashimoto⁷⁶, Y. Hayato^{77,78}, A. Hebecker⁷⁹, S. Heinemeyer⁸⁰, K. Hikasa^{81,82,83}, J. Hisano^{84,85}, A. Höcker⁶, J. Holder^{86,87}, L. Hsu³⁵, J. Huston⁸⁸, T. Hyodo⁸⁹, Al. Ianni⁹⁰, M. Kado⁹¹, M. Karliner⁹², U.F. Katz⁹³, M. Kenzie⁹⁴, V.A. Khoze⁹⁵, S.R. Klein^{96,97}, F. Krauss⁹⁵, M. Kreps⁶², P. Krizan^{98,99}, B. Krusche[‡], Y. Kwon¹⁰¹, O. Lahav¹⁰², L.P. Lellouch¹⁰³, J. Lesgourgues¹⁰⁴, A.R. Liddle¹⁰⁵, Z. Ligeti²⁴, C.-J. Lin²⁴, C. Lippmann¹⁰⁶, T.M. Liss¹⁰⁷, A. Lister¹⁰⁸, L. Littenberg²¹, K.S. Lugovsky²⁴, S.B. Lugovsky⁵⁴, A. Lusiani^{109,14}, Y. Makida⁷⁶, F. Maltoni^{110,111}, A.V. Manohar⁴⁰, W.J. Marciano²¹, J. Matthews¹¹², U.-G. Meißner^{113,4}, I.-A. Melzer-Pellmann⁷⁰, P. Mertsch¹⁰⁴, D.J. Miller³², D. Milstead¹¹⁴, K. Mönig¹¹⁵, P. Molaro^{116,117}, F. Moortgat^{6,118}, M. Moskvic⁶, N. Nagata¹¹⁹, K. Nakamura^{76,78}, M. Narain[‡], P. Nason^{43,121}, A. Nelles^{115,93}, M. Neubert¹²², Y. Nir¹²³, H.B. O'Connell³⁵, C.A.J. O'Hare¹²⁴, K.A. Olive⁶⁴, J.A. Peacock¹²⁵, E. Pianori²⁴, A. Pich⁵, A. Piepke¹²⁶, F. Pietropaolo^{6,127}, A. Pomarol^{128,129}, S. Pordes³⁵, S. Profumo⁷⁴, A. Quadt¹³⁰, K. Rabbertz¹³¹, J. Rademacker¹³², G. Raffelt⁹¹, M. Ramsey-Musolf^{133,134,135}, P. Richardson⁹⁵, A. Ringwald⁷⁰, D.J. Robinson²⁴, S. Roesler⁶, S. Rolli¹³⁶, A. Romaniouk^{137,54}, L.J. Rosenberg¹³⁸, J.L. Rosner³⁰, G. Rybka¹³⁸, M.G. Ryskin⁵⁴, R.A. Ryutin⁵⁴, B. Safdi⁹⁷, Y. Sakai⁷⁶, S. Sarkar¹³⁹, F. Sauli[§], O. Schneider¹⁴⁰, S. Schönert¹⁴¹, K. Scholberg¹⁴², A.J. Schwartz¹⁴³, J. Schwiening¹⁰⁶, D. Scott¹⁰⁸, F. Sefkow⁷⁰, U. Seljak^{97,24}, V. Sharma⁴⁰, S.R. Sharpe¹³⁸, V. Shiltsev[¶], G. Signorelli^{37,14}, M. Silari⁶, F. Simon¹³¹, T. Sjöstrand¹⁴⁴, P. Skands⁵³, T. Skwarnicki¹⁴⁵, G.F. Smoot^{146,97,24,147,148}, A. Soffer⁹², M.S. Sozzi³⁷, C. Spiering¹¹⁵, A. Stahl¹⁴⁹, Y. Sumino⁸³, F. Takahashi⁸³, M. Tanabashi^{84,85}, J. Tanaka¹⁵⁰, M. Taševský¹⁵¹, K. Terao^{152,153}, K. Terashi¹⁵⁰, J. Terning¹⁵⁴, U. Thoma¹¹³, R.S. Thorne¹⁰², L. Tiator⁵⁷, M. Titov¹⁵⁵, D.R. Tovey¹⁵⁶, K. Trabelsi¹⁵⁷, P. Urquijo¹⁵⁸, G. Valencia⁵³, R. Van de Water³⁵, N. Varelas¹⁵⁹, L. Verde^{67,66}, I. Vivarelli¹¹¹, P. Vogel¹⁶⁰, W. Vogelsang³, V. Vorobyev⁵⁴, S.P. Wakely^{30,36}, W. Walkowiak¹⁶¹, C.W. Walter¹⁴², D. Wands¹⁶², D.H. Weinberg¹⁶³, E.J. Weinberg¹⁶⁴, N. Wermes⁵¹, M. White^{97,24}, L.R. Wiencke¹⁶⁵, S. Willocq¹³⁵, C.L. Woody²¹, R.L. Workman¹⁶⁶, W.-M. Yao²⁴, M. Yokoyama^{119,78}, R. Yoshida⁶⁸, G. Zanderighi^{91,167}, G.P. Zeller³⁵, R.-Y. Zhu¹⁶⁸, S.-L. Zhu¹⁶⁹, F. Zimmermann⁶, P.A. Zyla²⁴

Technical Associates: J. Anderson²⁴, M. Kramer²⁴, P. Schaffner²⁴, W. Zheng¹⁵

1. *Universidad de Granada, Dpto. de Física Teórica y del Cosmos & C.A.F.P.E., Granada, Spain*
2. *Stefan Meyer Institute for Subatomic Physics, Austrian Academy of Sciences, Vienna, Austria*
3. *Universität Tübingen, Institut für Theoretische Physik, Tübingen, Germany*
4. *Forschungszentrum Jülich, Institute for Advanced Simulation, Jülich, Germany*
5. *IFIC — Instituto de Física Corpuscular, Universitat de València — C.S.I.C., Valencia, Spain*
6. *CERN, European Organization for Nuclear Research, Genève, Switzerland*
7. *INFN Sezione di Cagliari, Monserrato, Italy*
8. *Institut für Experimentalphysik 1, Ruhr-Universität Bochum, Bochum, Germany*
9. *Indiana University, Department of Physics, Bloomington, IN, USA*
10. *Università di Bologna and INFN, Dip. Scienze per la Qualità della Vita, Rimini, Italy*
11. *HEPHY, Vienna, Austria*
12. *University of Tennessee, Department of Physics and Astronomy, Knoxville, TN, USA*
13. *University of Liverpool, Department of Physics, Liverpool, UK*

*Support from Projects PID2021-124591NB-C41 and -C43, funded by MICIU/AEI/10.13039/501100011033 and FEDER, UE

†Coordination activities supported directly by INFN.

‡Deceased.

§Retired.

¶Supported by Fermi Research Alliance, LLC under Contract No. DE-AC02-07CH11359 with DOE.

14. *INFN Sezione di Pisa, Pisa, Italy*
15. *Institute of High Energy Physics, Chinese Academy of Sciences, Beijing, China*
16. *University of Maryland, Department of Physics, College Park, MD, USA*
17. *Università degli Studi di Roma "Tor Vergata", Rome, Italy*
18. *Department of Applied Mathematics and Theoretical Physics, University of Cambridge, Cambridge, UK*
19. *Instituto Galego de Física de Altas Enerxías (IGFAE) & Dept. Física de Partículas, Universidade de Santiago de Compostela, Santiago de Compostela, Spain*
20. *Lab. Nazionali di Frascati dell'INFN, Frascati, Italy*
21. *Brookhaven National Laboratory, Nuclear and Particle Physics Directorate, Upton, NY, USA*
22. *University of Oklahoma, Department of Physics and Astronomy, Norman, OK, USA*
23. *University of Louisville, Louisville, KY, USA*
24. *Physics Division, Lawrence Berkeley National Laboratory, Berkeley, CA, USA*
25. *Universität Zürich, Physik-Institut, Zürich, Switzerland*
26. *Ohio State University, Department of Physics, Columbus, OH, USA*
27. *INFN and Dipartimento di Fisica e Astronomia, Università di Padova, Padova, Italy*
28. *Ludwig-Maximilians-Universität, Fakultät für Physik, München, Germany*
29. *University of Wisconsin, Department of Physics, Madison, WI, USA*
30. *University of Chicago, Enrico Fermi Institute and Department of Physics, Chicago, IL, USA*
31. *Department of Physics, Carnegie Mellon University, Pittsburgh, PA, USA*
32. *University of Glasgow, School of Physics and Astronomy, Glasgow, UK*
33. *Jefferson Lab, Newport News, VA, USA*
34. *University of Virginia, Department of Physics, Charlottesville, VA, USA*
35. *Fermi National Accelerator Laboratory, Batavia, IL, USA*
36. *University of Chicago, Kavli Institute for Cosmological Physics, Chicago, IL, USA*
37. *University of Pisa, Pisa, Italy*
38. *Dipartimento Scienze fisiche, della Terra e dell'ambiente, Università degli Studi di Siena, Siena, Italy*
39. *Department of Physics and Astronomy, University of Sussex, Brighton, UK*
40. *Department of Physics, University of California at San Diego, La Jolla, CA, USA*
41. *Department of Physics, Royal Holloway, University of London, London, UK*
42. *Florida State University, Department of Physics, Tallahassee, FL, USA*
43. *INFN Sezione di Milano-Bicocca, Piazza della Scienza, Milano, Italy*
44. *INFN Sezione di Napoli, Napoli, Italy*
45. *Institut des Hautes Etudes Scientifiques, Bures-sur-Yvette, France*
46. *UNSAM - Universidad Nacional de San Martín, International Center for Advanced Studies (ICAS) and Instituto de Ciencias Físicas (ICIFI), Buenos Aires, Argentina*
47. *Northwestern University, Department of Physics and Astronomy, Evanston, IL, USA*
48. *University of Colorado at Boulder, Department of Physics, Boulder, CO, USA*
49. *Yale University, New Haven, CT, USA*
50. *Boston University, Department of Physics, Boston, MA, USA*
51. *Universität Bonn, Physikalisches Institut, Bonn, Germany*
52. *Research Council of Finland, Helsinki, Finland*
53. *Monash University, School of Physics and Astronomy, Melbourne, Australia*
54. *Affiliation provided upon request*
55. *University of Illinois, Department of Physics, Urbana, IL, USA*
56. *King's College London, Department of Physics, London, UK*
57. *Institut für Kernphysik, Johannes Gutenberg University, Mainz, Germany*
58. *ETH Zurich, Institute for Particle Physics and Astrophysics, Zurich, Switzerland*
59. *University of Illinois, Department of Astronomy, Urbana, IL, USA*
60. *University of Pittsburgh, Department of Physics and Astronomy, Pittsburgh, PA, USA*
61. *Tufts University, Department of Physics and Astronomy, Medford, MA, USA*
62. *University of Warwick, Department of Physics, Coventry, UK*
63. *Department of Physics and Astronomy, Rutgers University, NJ, USA*
64. *University of Minnesota, School of Physics and Astronomy, Minneapolis, MN, USA*
65. *CN Yang Institute for Theoretical Physics, Stony Brook University, Stony Brook, NY, USA*
66. *Institució Catalana de Recerca i Estudis Avancats, Barcelona, Spain*

67. *Instituto de ciencias del Cosmos (ICC), University of Barcelona, Barcelona, Spain*
68. *Argonne National Laboratory, Argonne, IL, USA*
69. *Johns Hopkins University, Baltimore, MD, USA*
70. *Deutsches Elektronen-Synchrotron DESY, Hamburg, Germany*
71. *Institut für Physik, Humboldt-Universität zu Berlin, Berlin, Germany*
72. *University College Dublin, School of Physics, Dublin, Ireland*
73. *TIFR, Mumbai, India*
74. *Santa Cruz Institute for Particle Physics, University of California, Santa Cruz, CA, USA*
75. *Université Paris-Saclay, CEA, LIST, F-91120 Palaiseau, France*
76. *KEK, High Energy Accelerator Research Organization, Tsukuba, Japan*
77. *Kamioka Observatory, ICRR, The University of Tokyo, Tokyo, Japan*
78. *The University of Tokyo, Kavli IPMU (WPI), The University of Tokyo Institutes for Advanced Study, Kashiwa, Japan*
79. *Heidelberg University, Institute for Theoretical Physics, Heidelberg, Germany*
80. *Instituto de Física Teórica (UAM/CSIC), Universidad Autónoma de Madrid, Madrid, Spain*
81. *Division for Interdisciplinary Advanced Research and Education, Tohoku University, Sendai, Japan*
82. *Institute of Liberal Arts and Sciences, Tohoku University, Sendai, Japan*
83. *Tohoku University, Department of Physics, Sendai, Japan*
84. *Department of Physics, Nagoya University, Nagoya, Japan*
85. *Nagoya University, Kobayashi-Maskawa Institute, Nagoya, Japan*
86. *University of Delaware, Department of Physics and Astronomy, Newark, DE, USA*
87. *University of Delaware, Bartol Research Institute, Newark, DE, USA*
88. *Michigan State University, Dept. of Physics and Astronomy, East Lansing, MI, USA*
89. *Department of Physics, Tokyo Metropolitan University, Tokyo, Japan*
90. *INFN - Laboratori Nazionali del Gran Sasso, Assergi, Italy*
91. *Max-Planck-Institut für Physik (Werner-Heisenberg-Institut), Garching, Germany*
92. *Department of Particle Physics, Tel-Aviv University, Tel Aviv, Israel*
93. *Friedrich-Alexander-Universität Erlangen-Nürnberg, Erlangen Centre for Astroparticle Physics, Erlangen, Germany*
94. *University of Cambridge, Cambridge, UK*
95. *University of Durham, Institute for Particle Physics Phenomenology, Department of Physics, Durham, UK*
96. *Nuclear Science Division, Lawrence Berkeley National Laboratory, Berkeley, CA, USA*
97. *University of California, Department of Physics, Berkeley, CA, USA*
98. *Faculty of Mathematics and Physics, University of Ljubljana, Jadranska, Slovenia*
99. *Jozef Stefan Institute, Ljubljana, Slovenia*
100. *University of Basel, Institute of Physics, Basel, Switzerland*
101. *Yonsei University, Department of Physics, Seoul, Republic of Korea*
102. *University College London, Department of Physics and Astronomy, London, UK*
103. *Aix-Marseille Univ, Université de Toulon, CNRS, CPT, Marseille, France*
104. *Institute for Theoretical Particle Physics and Cosmology (TTK), RWTH, Aachen, Germany*
105. *Instituto de Astrofísica e Ciências do Espaço, Universidade de Lisboa, Lisbon, Portugal*
106. *GSI, Helmholtzzentrum für Schwerionenforschung, Darmstadt, Germany*
107. *The City College of New York, New York, NY, USA*
108. *University of British Columbia, Department of Physics and Astronomy, Vancouver, BC, Canada*
109. *Scuola Normale Superiore, Pisa, Italy*
110. *Université catholique de Louvain, Centre for Cosmology, Particle Physics and Phenomenology (CP³), Louvain-la-Neuve, Belgium*
111. *Università di Bologna and INFN, Dipartimento di Fisica e Astronomia, Bologna, Italy*
112. *Louisiana State University, Department of Physics and Astronomy, Baton Rouge, LA, USA*
113. *Universität Bonn, Helmholtz-Institut für Strahlen- und Kernphysik, Bonn, Germany*
114. *Stockholms Universitet, AlbaNova University Centre, Fysikum, Stockholm, Sweden*
115. *Deutsches Elektronen-Synchrotron DESY, Zeuthen, Germany*
116. *INAF-OATS, Trieste, Italy*
117. *Institute for Fundamental Physics of the Universe, Trieste, Italy*
118. *University of Ghent, Dept. of Physics and Astronomy, Ghent, Belgium*
119. *The University of Tokyo, Department of Physics, Tokyo, Japan*

120. *Brown University, Department of Physics, Providence, RI, USA*
121. *Dip. di Fisica "G. Occhialini", Università di Milano-Bicocca, Milano, Italy*
122. *Johannes Gutenberg University, PRISMA Cluster of Excellence and Mainz Institute for Theoretical Physics, Mainz, Germany*
123. *Department of Particle Physics and Astrophysics, Weizmann Institute of Science, Rehovot, Israel*
124. *University of Sydney, Sydney, Australia*
125. *University of Edinburgh, Royal Observatory, Institute for Astronomy, Edinburgh, UK*
126. *University of Alabama, Department of Physics and Astronomy, Tuscaloosa, AL, USA*
127. *INFN Sezione di Padova, Padua, Italy*
128. *Universitat Autònoma de Barcelona, Departament de Física, Barcelona, Spain*
129. *IFAE, Universitat Autònoma de Barcelona, Barcelona, Spain*
130. *Georg-August-Universität Göttingen, II. Physikalisches Institut, Göttingen, Germany*
131. *Karlsruhe Institute of Technology, Karlsruhe, Germany*
132. *University of Bristol, HH Wills Physics Laboratory, Bristol, UK*
133. *Tsung-Dao Lee Institute, Shanghai Jiao Tong University, Shanghai, China*
134. *Shanghai Jiao Tong University, Shanghai, China*
135. *University of Massachusetts, Department of Physics, Amherst, MA, USA*
136. *DOE, Washington, DC, USA*
137. *Universität Innsbruck, Department of Astro and Particle Physics, Innsbruck, Austria*
138. *University of Washington, Department of Physics, Seattle, WA, USA*
139. *University of Oxford, Rudolf Peierls Centre for Theoretical Physics, Oxford, UK*
140. *Institute of Physics, Ecole Polytechnique Fédérale de Lausanne (EPFL), Lausanne, Switzerland*
141. *Department of Physics, Technical University Munich, Munich, Germany*
142. *Duke University, Physics Department, Durham, NC, USA*
143. *University of Cincinnati, Department of Physics, Cincinnati, OH, USA*
144. *Lund University, Department of Astronomy and Theoretical Physics, Lund, Sweden*
145. *Syracuse University, Department of Physics, Syracuse, NY, USA*
146. *The Hong Kong University of Science and Technology, Kowloon, Hong Kong*
147. *Donostia International Physics Center (DIPC), Donostia-San Sebastián, Spain*
148. *Paris Centre for Cosmological Physics, APC (CNRS), Université de Paris, Paris, France*
149. *III. Physikalisches Institut, Physikzentrum, RWTH Aachen University, Aachen, Germany*
150. *International Center for Elementary Particle Physics (ICEPP), The University of Tokyo, Tokyo, Japan*
151. *Institute of Physics, Czech Academy of Sciences, Prague, Czech Republic*
152. *SLAC National Accelerator Laboratory, Menlo Park, CA, USA*
153. *Stanford University, Stanford, CA, USA*
154. *Department of Physics, University of California, Davis, CA, USA*
155. *IRFU, CEA, Université Paris-Saclay, F-91191 Gif-sur-Yvette, France*
156. *University of Sheffield, Department of Physics and Astronomy, Sheffield, UK*
157. *IJCLab, CNRS/IN2P3, Université Paris-Saclay, Orsay, France*
158. *University of Melbourne, School of Physics, Victoria, Australia*
159. *University of Illinois at Chicago, Chicago, IL, USA*
160. *California Institute of Technology, Kellogg Radiation Laboratory, Pasadena, CA, USA*
161. *Universität Siegen, Department für Physik, Siegen, Germany*
162. *University of Portsmouth, Institute of Cosmology and Gravitation, Portsmouth, UK*
163. *Ohio State University, Department of Astronomy and CCAPP, Columbus, OH, USA*
164. *Columbia University, Department of Physics, New York, NY, USA*
165. *Dept. of Physics, Colorado School of Mines, Golden, CO, USA*
166. *George Washington University, Department of Physics, Washington, D.C., USA*
167. *Technische Universität München, München, Germany*
168. *California Institute of Technology, High Energy Physics, Pasadena, CA, USA*
169. *School of Physics, Peking University, Beijing, China*

HIGHLIGHTS OF THE 2024 EDITION OF THE REVIEW OF PARTICLE PHYSICS

All PDG data and review articles are available online at pdg.lbl.gov.

869 new papers with 2,717 new measurements

120 reviews (most are revised)

- 320 new measurements from *LHC* experiments (ATLAS, CMS and LHCb).
- Extensive *Higgs boson* coverage from 231 new papers and 557 measurements with latest results on mass, couplings, decay width and branching ratios, plus searches for other neutral and charged Higgs bosons.
- *Supersymmetry*: 36 new papers with 148 measurements with major exclusions.
- *Top quark*: 35 new papers provide latest results on mass, coupling, and the discovery of four top quark production at LHC.
- *W mass*: CDF published a new measurement of the *W* mass. It is more precise than the world average at the time, but the two results disagree. See comments in Particle Listings and our *W* mass review referencing the extensive studies done by the *LHC* TeV M_W working group.
- *c-, b-hadron physics*: 161 papers and 597 measurements provide world-best data on lifetimes, mixing, CP violation, CKM angles, and constraints on new physics.
- *Neutrino Physics*: 10 new papers with measurements on neutrino mass, mixing, and CP-violation.
- *Meson resonances*: Substantial improvements, including new cross particle fits involving $J/\psi(1S)$, $\psi(2S)$ and $\eta_c(1S)$, merging of $\pi_1(1400)$ and $\pi_1(1600)$ with non- $q\bar{q}$ quantum numbers into same node, listing of complex pole positions when available, and inclusion of recently observed states. Several mesons now considered established added to Summary Tables.
- New *naming scheme* for the many recently discovered mesons and baryons with *c* or *b* quarks that are not compatible with conventional $q\bar{q}$ or qqq structures. Listed in “Other mesons” and “Exotic baryons” sections.
- Major revision of *Higgs Physics* review summarizes latest LHC results and constraints on new physics.
- Major revision of *Cosmic rays* review, now covering all components of cosmic rays including neutrinos (which were previously discussed in Neutrino Telescopes in Particle Detectors for Non-Accelerator Physics).
- Major revision of *Large time-projection chambers for rare event detection* in Particle Detectors for Non-Accelerator Physics.
- Major revision of *Top Quark* review summarizes latest LHC results and constraints on new physics from top quark.
- Major revision of *Heavy Non- $q\bar{q}$ Mesons* review follows new naming scheme for states not compatible with $q\bar{q}$ or qqq structures.
- *Semiconductor detectors* section of Particle Detectors at Accelerators review includes recent developments.
- New section on goodness-of-fit tests and expanded discussion of statistical tests in *Statistics* review.
- Updated EWK fit in *Electroweak Model and Constraints on New Physics* review.
- *Semileptonic B Hadron Decays, Determination of V_{cb} and V_{ub}* includes latest results and discusses long-standing issues with inclusive and exclusive measurements.
- Updated cross section results in the *Neutrino Cross Section Measurements* review.
- Updated τ decay parameters and branching ratio (BR) fits, including new treatment of $BR(a_1(1260) \rightarrow \pi\gamma)$.

VOLUME 1: SUMMARY TABLES AND REVIEWS

Highlights	6	Experimental Methods and Colliders	
Introduction	11	31. Accelerator physics of colliders (rev.)	559
History plots	19	32. High-energy collider parameters (rev.)	569
Online particle physics information (rev.)	20	33. Neutrino beam lines at high-energy proton synchrotrons (rev.)	574
SUMMARY TABLES		34. Passage of particles through matter (rev.)	575
Gauge and Higgs bosons	25	35. Particle detectors at accelerators (rev.)	591
Leptons	28	36. Particle detectors for non-accelerator phys. (rev.)	649
Quarks	32	37. Radioactivity and radiation protection (rev.)	679
Mesons	33	38. Commonly used radioactive sources (rev.)	685
Meson quick reference table	91	Mathematical Tools	
Baryon quick reference table	92	39. Probability	689
Baryons	93	40. Statistics (rev.)	694
Searches not in Other Sections	112	41. Machine Learning	711
Tests of conservation laws	114	42. Monte Carlo techniques	748
REVIEWS, TABLES, AND PLOTS		43. Monte Carlo event generators (rev.)	752
Constants, Units, Atomic and Nuclear Properties		44. Monte Carlo neutrino event generators	764
1. Physical constants (rev.)	137	45. Monte Carlo particle numbering scheme (rev.)	768
2. Astrophysical constants and parameters (rev.)	138	46. Clebsch-Gordan coefficients, spherical harmonics, and d functions	772
3. International system of units (SI)	140	47. SU(3) isoscalar factors and representation matrices	773
4. Periodic table of the elements (rev.)	141	48. SU(n) multiplets and Young diagrams	774
5. Electronic structure of the elements (rev.)	142	Kinematics, Cross-Section Formulae, and Plots	
6. Atomic and nuclear properties of materials (rev.)	144	49. Kinematics	777
7. Electromagnetic relations	146	50. Resonances (rev.)	781
8. Naming scheme for hadrons (rev.)	148	51. Cross-section formulae for specific processes	792
Standard Model and Related Topics		52. Neutrino cross section measurements (rev.)	801
9. Quantum chromodynamics (rev.)	153	53. Plots of cross sections and related quantities (rev.)	807
10. Electroweak model and constraints on new physics (rev.)	185	Particle Properties	
11. Higgs boson physics, status of (rev.)	211	<u>Gauge Bosons</u>	
12. CKM quark-mixing matrix (rev.)	270	54. Mass and width of the W boson (rev.)	815
13. CP violation in the quark sector (rev.)	280	55. Z boson	817
14. Neutrino masses, mixing, and oscillations (rev.)	295	<u>Charged Leptons</u>	
15. Quark model (rev.)	322	56. Muon anomalous magnetic moment (rev.)	822
16. Heavy-quark & soft-collinear effective theory (rev.)	341	57. Muon decay parameters (rev.)	826
17. Lattice quantum chromodynamics (rev.)	350	58. τ branching fractions (rev.)	829
18. Structure functions (rev.)	367	59. τ -lepton decay parameters (rev.)	832
19. Fragmentation functions in e^+e^- , ep and pp collisions (rev.)	389	<u>Quarks</u>	
20. High Energy Soft QCD and Diffraction (rev.)	406	60. Quark masses (rev.)	834
Astrophysics and Cosmology		61. Top quark (rev.)	844
21. Experimental tests of gravitational theory (rev.)	431		
22. Big-Bang cosmology (rev.)	444		
23. Inflation (rev.)	457		
24. Big-Bang nucleosynthesis (rev.)	474		
25. Cosmological parameters (rev.)	482		
26. Neutrinos in cosmology (rev.)	491		
27. Dark matter (rev.)	499		
28. Dark energy (rev.)	515		
29. Cosmic microwave background (rev.)	524		
30. Cosmic rays (rev.)	535		

(Continued on next page.)

<u>Mesons</u>	
62. Form factors for semileptonic kaon ($K_{\ell 3}$), radiative pion ($\pi_{\ell 2\gamma}$) & kaon ($K_{\ell 2\gamma}$) decays (rev.)	871
63. Spectroscopy of light meson resonances (rev.)	874
64. Scalar mesons below 1 GeV (rev.)	888
65. Rare kaon decays (rev.)	896
66. CPT invariance tests in neutral kaon decay (rev.)	902
67. V_{ud} , V_{us} , Cabibbo angle, and CKM unitarity (rev.)	904
68. CP -violation in K_L decays (rev.)	908
69. Review of multibody charm analyses (rev.)	911
70. D^0 - \bar{D}^0 mixing (rev.)	917
71. D_s^+ branching fractions	927
72. Leptonic decays of charged pseudoscalar mesons (rev.)	929
73. Production and decay of b -flavored hadrons (rev.)	940
74. Polarization in B decays (rev.)	951
75. B^0 - \bar{B}^0 mixing (rev.)	955
76. Semileptonic B -hadron decays, V_{cb} and V_{ub} (rev.)	962
77. CKM angles from B hadrons, determination of (rev.)	980
78. Spectroscopy of mesons containing two heavy quarks (rev.)	985
79. Heavy non- $q\bar{q}$ mesons (rev.)	994
<u>Baryons</u>	
80. Baryon decay parameters	1001
81. N and Δ resonances	1002
82. Λ and Σ resonances	1007
83. Pole structure of the $\Lambda(1405)$ region	1010
84. Pentaquarks (rev.)	1012
Hypothetical Particles and Concepts	
85. Extra dimensions (rev.)	1021
86. W' -boson searches (rev.)	1029
87. Z' -boson searches (rev.)	1033
88. Supersymmetry: theory (rev.)	1038
89. Supersymmetry: experiment (rev.)	1058
90. Axions and other similar particles (rev.)	1079
91. Quark and lepton compositeness, searches for (rev.)	1098
92. Dynamical electroweak symmetry breaking: implications of the H^0 (rev.)	1104
93. Grand unified theories (rev.)	1119
94. Leptoquarks (rev.)	1134
95. Magnetic monopoles (rev.)	1138
INDEX (Volumes 1 and 2 combined)	1145

VOLUME 2: PARTICLE LISTINGS (available online only)

Illustrative key and abbreviations

Illustrative key	1171
Abbreviations	1172

Gauge and Higgs bosons

(γ , gluon, graviton, W , Z , Higgs, Axions)	1185
--	------

Leptons

(e , μ , τ , Heavy-charged lepton searches, Neutrino properties, Number of neutrino types, Double- β decay, Neutrino mixing, Heavy-neutral lepton searches)	1297
---	------

Quarks

(u , d , s , c , b , t , b' , t' (4^{th} gen.), Free quarks)	1371
--	------

Mesons

Light unflavored (π , ρ , a , b) (η , ω , f , ϕ , h)	1411
Strange (K , K^*)	1538
Charmed (D , D^*)	1592
Charmed, strange (D_s , D_s^* , D_{sJ})	1657
Bottom (B , V_{cb}/V_{ub} , B^* , B_J^*)	1681
Bottom, strange (B_s , B_s^* , B_{sJ}^*)	1865
Bottom, charmed (B_c)	1893
$c\bar{c}$ (η_c , $J/\psi(1S)$, χ_c , h_c , ψ)	1898
$b\bar{b}$ (η_b , Υ , χ_b , h_b)	2023
Other mesons (T_c , T_b tetraquarks)	2062

Baryons

N	2081
Δ	2137
Λ	2161
Σ	2187
Ξ	2218
Ω	2231
Charmed (Λ_c , Σ_c , Ξ_c , Ω_c)	2234
Doubly charmed (Ξ_{cc})	2262
Bottom (Λ_b , Σ_b , Ξ_b , Ω_b , b -baryon admixture)	2263
Exotic baryons (P_c pentaquarks)	2285

Searches not in Other Sections

Magnetic monopole searches	2289
Supersymmetric particle searches	2292
Technicolor	2347
Searches for quark and lepton compositeness	2348
Extra dimensions	2352
WIMP and dark matter searches	2359
Other particle searches	2374

INTRODUCTION

1. Overview	11
2. Particle Listings responsibilities	11
3. Consultants	12
4. Naming scheme for hadrons	15
5. Procedures	15
5.1 Selection and treatment of data	15
5.2 Averages and fits	15
5.2.1 Treatment of errors	15
5.2.2 Unconstrained averaging	16
5.2.3 Constrained fits	16
5.3 Rounding	17
5.4 Discussion	17
History plots	19

ONLINE PARTICLE PHYSICS INFORMATION

1. Introduction	20
2. Particle Data Group (PDG) resources	20
3. Particle physics information platform	20
4. Literature databases	20
5. Journals	21
6. Conference and seminars databases	21
7. Research institutions	21
8. People	21
9. Experiments	21
10. Jobs	21
11. Software packages and repositories	22
12. Data repositories and preservation	22
13. Particle physics education and outreach	22
14. Regional HEP efforts	22



Introduction

1 Overview

The *Review of Particle Physics* is a comprehensive review of the field of Particle Physics and of related areas in Cosmology. It is divided into two volumes. Volume 1 includes the “Summary Tables” and “Reviews, Tables, and Plots”. Volume 2 consists of the “Particle Listings”.

The *Review* is updated each year and made available on the PDG website (pdg.lbl.gov). In even-numbered years, the *Review* is also published in a journal and printed as the *PDG Book* together with an abridged *Particle Physics Booklet* containing Summary Tables and essential tables, figures, and equations from selected review articles. This edition is an updating through January 2024.

The Summary Tables give our best values and limits for particle properties such as masses, widths or lifetimes, and branching fractions, as well as an extensive summary of searches for hypothetical particles and a summary of experimental tests of conservation laws.

The 95 review articles in Reviews, Tables and Plots cover a wide variety of theoretical and experimental topics. Together with the Summary Tables they provide an exhaustive reference for the practicing particle physicist. Two more review articles, Online Particle Physics Information and Tests of Conservation Laws, can be found in the introduction and Summary Tables, respectively.

The Particle Listings are a compilation/evaluation of data on particle properties. They contain all the data used to get the values given in the Summary Tables. They also give information on unconfirmed particles and particle searches. In this edition, the Particle Listings include 2,717 new measurements from 869 papers, in addition to the 46,838 measurements from 12,909 papers that first appeared in previous editions [1]. 23 review articles are part of the Particle Listings and address specific aspects of the data presented in the Listings. Because of the large quantity of data, the Particle Listings are not an archive of all published data on particle properties. We refer interested readers to earlier editions for data now considered to be obsolete.

We organize the particles into six categories:

- Gauge and Higgs bosons
- Leptons
- Quarks
- Mesons
- Baryons
- Searches not in other sections

The last category only includes searches for particles that do not belong to the previous groups. For example, it includes searches for supersymmetric particles, compositeness and extra dimensions, while searches for heavy charged leptons are with the leptons.

In Sec. 2 of this Introduction, we list the main areas of responsibility of the authors of the Particle Listings. Our many consultants, without whom we would not have been able to produce this *Review*, are acknowledged in Sec. 3. In Sec. 4, we mention briefly the naming scheme for hadrons, and in Sec. 5, we discuss our procedures for choosing among measurements of particle properties and for obtaining best values of the properties from the measurements.

The accuracy and usefulness of this *Review* depend in large part on interaction between its users and the authors. We appreciate comments, criticisms, and suggestions for improvements of any kind. Please send them to pdg@lbl.gov from where they will be forwarded to the appropriate author according to the list of responsibilities in Sec. 2 below.

In addition to the online publication at pdg.lbl.gov, the *Review* is available in different formats:

- The printed *PDG Book* includes volume 1 only, *i.e.* it contains the Summary Tables and most review articles. Since the 2016 edition [2] the detailed tables from the Particle Listings are no longer printed.
- The *Particle Physics Booklet* includes the Summary Tables plus essential tables, figures, and equations from selected re-

view articles. Starting with the Booklets of the 2018 edition, we have excluded most text and explanations in order to revert back to a more pocket-sized format. The Booklet is available in print, as a web version optimized for use on phones, and as an Android app (see pdg.lbl.gov/booklet).

- *pdgLive* (pdgLive.lbl.gov) is a web application giving more interactive access to PDG data than the static web pages and PDF files that are also available.
- Files that can be downloaded from the PDG website include a table of masses, widths, and PDG Monte Carlo particle ID numbers; PDF files of volume 1 (PDG Book), volume 2 (Particle Listings) and Booklet; individual review articles; all figures; and an archive file containing the complete PDG website (except for pdgLive).
- Starting with the 2024 edition, the data published in the *Review of Particle Physics* is available in machine-readable format through a new PDG API (Application Programming Interface). See pdg.lbl.gov/api for details.

Copies of the *PDG Book* or the *Particle Physics Booklet* can be ordered from our website or directly at pdg.lbl.gov/order. For special requests only, please email pdg@lbl.gov in North and South America, Australia, and the Far East, and pdg-products@cern.ch in all other areas.

This *Review* is considered to be a single comprehensive review of particle physics and related areas. Therefore we prefer that it be cited as a whole, rather than citing *e.g.* an individual review article that is part of this *Review*. For the 2024 edition, the proper citation is:

S. Navas *et al.* (Particle Data Group), Phys. Rev. D **110**, 030001 (2024).

If you wish to refer to a specific part of the *Review*, for example to the Higgs boson review article, the following form should be used:

Status of Higgs Boson Physics in S. Navas *et al.* (Particle Data Group), Phys. Rev. D **110**, 030001 (2024).

2 Particle Listings responsibilities

* Asterisk indicates the people to contact with questions or comments about Particle Listings sections. Please contact them by e-mail to pdg@lbl.gov.

• Gauge and Higgs bosons

γ	A. Bettini, D.E. Groom*
Gluons	R.M. Barnett,* A.V. Manohar
Graviton	A. Bettini,* D.E. Groom
W, Z	M. Grünewald,* A. Gurtu*
Higgs bosons	S. Heinemeyer,* K. Hikasa, J. Tanaka
Heavy bosons	R. Bonventre,* K.A. Olive, M. Tanabashi
Axions	C. O’Hare, K.A. Olive, G. Raffelt,* F. Takahashi

• Leptons

Neutrinos	M. Goodman, C.-J. Lin,* K. Nakamura, K.A. Olive, A. Piepke
Double- β decay	A. Bettini*, A. Piepke
e, μ	A. Bettini,* C. Grab
τ	A. Lusiani, K. Mönig*

• Quarks

Quarks	R.M. Barnett,* A.V. Manohar
Top quark	Y. Sumino, W.-M. Yao*
b', t'	Y. Sumino, W.-M. Yao*
Free quark	A. Bettini,* C.-J. Lin

• Mesons

π, η	A. Bettini,* C. Grab
K (stable)	G. D’Ambrosio, C.-J. Lin*
D (stable)	G. Casarosa, J. Rademacker, D. Robinson*
B (stable)	A. Cerri,* P. Eerola, M. Kreps, Y. Kwon, W.-M. Yao*

- | | |
|---|--|
| <ul style="list-style-type: none"> Unstable mesons C. Amsler,* T. Gutsche, C. Hanhart, J.J. Hernández-Rey, C. Lourenco, A. Masoni, M. Mikhasenko, R.E. Mitchell, S. Navas, C. Patrignani, C. Schwanda, S. Spanier, G. Venanzoni, C.Z. Yuan • <u>Baryons</u> <ul style="list-style-type: none"> Stable baryons C. Grab, D. Robinson* Unstable baryons V. Burkert, V. Crede, U. Thoma, L. Tiator, R.L. Workman* Charmed baryons G. Casarosa, J. Rademacker, D. Robinson* Bottom baryons A. Cerri,* P. Eerola, M. Kreps, Y. Kwon, W.-M. Yao* • <u>Miscellaneous searches</u> <ul style="list-style-type: none"> Monopole A. Bettini,* D. Milstead Supersymmetry H.K. Dreiner,* A. de Gouvêa, I.-A. Melzer-Pellmann, K.A. Olive, I. Vivarelli Technicolor K. Agashe,* K.A. Olive, M. Tanabashi Compositeness M. Tanabashi, J. Terning* Extra Dimensions T. Gherghetta, K.A. Olive, D. Robinson* WIMP, DM, Other H. Baer, A. Bettini,* W.-M. Yao* | <ul style="list-style-type: none"> • P. Blasi (GSSI) • M. Bona (QMUL) • C. Bonifazi (ICAS and ICIFI, UNSAM) • D. Bose (Indian Inst. Tech., Kharagpur) • E. Brost (BNL) • R. Bruce (CERN) • D.A. Bryman (TRIUMF) • C. Buck (MPIK) • M. Cadeddu (INFN, Cagliari) • X. Calmet (Sussex U.) • M. Calvi (INFN, Milano-Bicocca) • J. Cao (IHEP Beijing) • F. Capozzi (L'Aquila U.) • L. Capriotti (INFN, Ferrara) • T. Carli (CERN) • B. Carlo (INFN, LNGS) • N. Cartiglia (INFN, Torino) • G. Cavoto (Rome U.; INFN, Rome) • S. Cebrian Guajardo (U. de Zaragoza) • F. Cerutti (LBNL) • R. Cervantes (FNAL) • M. Chan (EdUHK, Hong Kong) • M. Charles (CNRS) • C. Chen (CPPM Marseille) • K. Chen (Taiwan National U. Physics Dep.) • M. Chen (Queen's U.) • Y. Chen (Taiwan National U. Physics Dep.) • Y. Chenghui (IHEP Beijing) • M. Chianese (INFN, Napoli; UNINA) • Y. Chinone (KEK) • V. Chobanova (CERN) • J. Chou (Rutgers U.) • C. Clement (Stockholm U.) • G. Colangelo (Bern U.) • P. Coloma (UAM/CSIC, U. Autónoma de Madrid) • R. Contino (Rome U. Sapienza) • A. Cortes Gonzalez (Physik, Humboldt U.) • N. Crescini (Neel U.) • M. Cruz (Honduras U.) • A. Cukierman (Stanford U.; SLAC) • C. Da Via (Manchester U.) • C. Davies (Glasgow U.) • F. de Almeida Dias (NIKHEF) • A. De Angelis (INFN, Padova) • J. De Blas (Granada U.) • R. Della Monica (Salamanca U.) • D. d'Enterria (CERN) • A. Derbin (NRC Kurchatov Inst. PNPI) • J. de Vries (CERN) • A. de Wit (Zurich U.) • A. Di Domenico (INFN, Rome) • E. Di Marco (CERN) • L. Dong (IHEP Beijing) • G. Drexlin (KIT) • J.J. Dudek (IReS) • K. Dundas (Columbia U.) • B. Dutta (TAMU) • V. Dutta (UC Santa Barbara) • A. Egorov (LPI Moscow) • S.R. Elliott (LANL) • R. Engel (KIT) |
|---|--|

3 Consultants

The Particle Data Group benefits greatly from the assistance of hundreds of physicists who are asked to referee review articles and verify every piece of data entered into this *Review*. Of special value is the advice of the PDG Advisory Committee, which meets biennially and thoroughly reviews all aspects of our operation. The members of the 2022 committee are:

- S. Demers (Yale)
- D. d'Enterria (CERN)
- J. Frieman (FNAL)
- S. Gori (UCSC)
- T. Nakada (EPFL)
- M. Yokoyama (Tokyo)

We have especially relied on the expertise of the following people for advice on particular topics:

- I. Abt (MPP, Garching)
- R. Acciarri (FNAL)
- M. Albaladejo (IFIC, Valencia)
- S. Alderweireldt (Edinburgh U.)
- S. Alioli (INFN, Milano-Bicocca)
- A. Antognini (ETH Zurich)
- E. Aprile (Columbia U.)
- E. Armengaud (CEA Saclay, DSM/IRFU/SPP)
- M. Artuso (Syracuse U.)
- N. Asbah (CERN)
- P. Athron (Nanjing U.)
- G. Azuelos (U. de Montreal)
- P. Azzurri (INFN, Pisa)
- R. Battiston (Trento U.)
- R.A. Battye (Manchester U.)
- O. Behnke (DESY, Hamburg)
- G. Bell (Siegen U.)
- J. Bellido Caceres (Adelaide U.)
- V. Belyaev (ITEP)
- N.P. Berger (LAPP)
- F. Betti (Edinburgh U.)
- T. Biekotter (KIT)

- A. Esposito (Rome U. Sapienza)
- T. Evans (Oxford U.)
- S. Fang (IHEP Beijing)
- Y. Farzan (IPM, Tehran)
- K. Ferguson (UC Los Angeles)
- A. Ferrari (CERN)
- A. Ferrari (Uppsala U.)
- C. Finley (Stockholm U.)
- W. Fischer (BNL)
- M. Flores (Wits U.; Philippines U., Quezon City)
- J. Flynn (Southampton U.)
- P. Fonte (LIP)
- J. Formaggio (MIT)
- D. Franco (Paris U.)
- K. Freese (Michigan U.; Nordita, Stockholm)
- T. Fujii (OMU Osaka)
- T. Fujita (Ochanomizu U.)
- R. Garisto (APS)
- C. Gatti (INFN, LNF)
- V. Gavrin (INR, Moscow)
- B. Geoffrey (Wits U.)
- A. Gilbert (Northwestern U.)
- V. Gligorov (CNRS)
- S.N. Gninenko (Russian Academy of Sciences)
- A. Godinho (CERN)
- J. Gomez Cadenas (DIPC)
- M. Goodsell (LPTHE, Paris)
- S. Gori (UC Santa Cruz)
- S.A. Gottlieb (Indiana U.)
- E. Goudzovski (Birmingham U.)
- L. Gouskos (CERN)
- P. Grabmayr (Tübingen U.)
- A. Greljo (Basel U.)
- A. Grohsjean (DESY, Hamburg)
- Y. Guo (Fudan U. Shanghai)
- P. Guzowski (Manchester U.)
- C. Ha (Northwestern U.)
- F. Halzen (Wisconsin U.)
- K. Harigaya (Chicago U.)
- F.A. Harris (Hawaii U.)
- F. Hartmann (KIT)
- A. Heijboen (NIKHEF)
- J. Heitger (WWU)
- S. Higashino (Kobe U.)
- A. Himmel (FNAL)
- A. Hinzmann (Hamburg U.)
- A. Hoang (HEPHY, Vienna)
- Y. Hochberg (Racah Inst. Hebrew U.)
- S. Hoof (INFN, Padua)
- X. Huang (PMO, Nanjing; USTC China)
- T. Huege (KIT)
- N. Huesken (JGU, Mainz)
- T. Humair (DESY, Hamburg)
- N. Huntemann (PTB, Braunschweig)
- N. Ilic (Toronto U.)
- K. Inoue (Osaka U.)
- K. Inoue (Tohoku U.)
- D. Jackson-Kimball (CSU Hayward)
- L. Jacob (LPSC, IN2P3)
- C. James (CIRA)
- P. Janot (CERN)
- B. Jayatilaka (FNAL)
- M. Jewell (Yale U.)
- C. Joram (CERN)
- A. Kalweit (CERN)
- M. Kamionkowski (Johns Hopkins U.)
- T. Kaneko (KEK)
- D. Kar (Wits U.)
- S. Karanth (UJ, Krakow)
- B. Ke (IHEP Beijing)
- E.T. Kearns (Boston U.)
- O. Kepka (CERN)
- J. Kieseler (Karlsruhe U.)
- Y. Kim (IBS, Daejeon)
- K. Kirch (ETH Zurich)
- E. Klempt (Bonn U.)
- J. Knolle (Ghent U.)
- A. Knue (Freiburg U.)
- B. Ko (IBS, Daejeon)
- K. Kohri (KEK; SOKENDAI; Kavli IPMU, UTIAS)
- E. Kou (LAL Orsay)
- D. Kovalskyi (MIT)
- G. Kramberger (Jozef Stefan Inst.)
- A. Kramida (NIST)
- S. Kraml (LPSC, Grenoble)
- G. Krintiras (CERN)
- W. Kuehn (Giessen U.)
- Y. L (IHEP Beijing)
- A. Lague (Toronto U.)
- H. Lee (IBS, Daejeon)
- A. Lenz (Siegen U.)
- O. Leroy (CPPM Marseille)
- J.D. Lewis (FNAL)
- H. Li (IHEP Beijing)
- P. Li (CERN)
- S. Li (IHEP Beijing)
- Z. Li (IHEP Beijing)
- Y. Liang (Guangxi U.)
- L. Liao (IHEP Beijing)
- J. Libby (Indian Inst. Tech., Madras)
- P. Lichard (Silesian U., Opava)
- Z. Ligeti (LBNL)
- C. Lin (Chicago U.)
- T. Linden (Stockholm U.)
- M. Lisanti (Princeton U.)
- E. Lisi (INFN, Bari)
- C. Liu (USTC China)
- G. Lucente (INFN, Bari)
- H. Ma (IHEP Beijing)
- Y. Ma (KwaZulu-Natal U.)
- F. Mahmoudi (IP2I, Lyon)
- S. Malde (Oxford U.)
- M. Maltoni (UAM/CSIC, U. Autónoma de Madrid)
- L. Manenti (NYU, Abu Dabi)
- C. Manzari (LBNL; UC Berkeley)
- R. Manzoni (ETH Zurich)
- M. Margoni (INFN, Padova)
- L. Mariscano (INFN, Genova)
- M. Martin (DESY, Hamburg)
- M. Masciovecchio (CERN)
- T. Masubuchi (UTokyo)
- M. Masuzawa (KEK)

- A. Mathad (ETH Zurich)
- S. Meinel (Arizona U.)
- C. Milardi (INFN, LNF)
- D. Mitzel (Heidelberg U.)
- R.N. Mohapatra (U. Maryland)
- P. Monni (CERN)
- J. Montejo (CERN)
- S. Moriyama (ICRR)
- H. Mu (CERN)
- S. Narison (Montpellier U.)
- K. Ni (UC San Diego)
- A. Nicholson (North Carolina U.)
- S. Nishida (KEK)
- A. Notari (ICC, U. of Barcelona)
- P.E. Onyisi (Texas U. Austin)
- L. Pagnanini (GSSI)
- T. Pajero (Phys. Dep. Oxford U.)
- N. Palanque-Delabrouille (LBNL)
- B. Pant (IIT, Jodhpur)
- I. Papaphilippou (CERN)
- J.R. Pelaez (UCM, Madrid)
- C. Pena (FNAL)
- S. Perazzini (CERN)
- D. Pereima (CERN)
- A. Pereiro (Santiago de Compostela U.)
- F. Petricca (MPP, Garching)
- F. Piccini (INFN, Pavia)
- P. Piminov (Budker Inst., Novosibirsk)
- J. Pinfeld (Alberta U.)
- D. Pinna (Wisconsin U.)
- T. Poddar (TIFR Mumbai)
- S. Polikarpov (MEPhI Moscow)
- A. Pompili (INFN, Bari)
- N. Porayako (MPIK)
- W. Porod (Würzburg U.)
- R. Puthumanaillam (CERN)
- W. Qian (IHEP Beijing)
- R. Quagliani (CERN)
- M. Rama (CERN)
- A. Read (Oslo U.)
- F. Redi (CERN)
- A. Reimers (DESY, Hamburg)
- L. Reina (Florida State U.)
- F. Resnati (ETH Zurich)
- J. Richard (IP2I, Lyon)
- S. Rodrigues Sandner (IFIC, Valencia)
- D. Roenchen (FZ Jülich)
- K. Rogers (Toronto U.)
- C. Rovelli (INFN, Rome)
- G. Ruggiero (Lancaster U.)
- T. Saab (Florida State U.)
- W. Saenz-Arevalo (LPNHE Paris)
- R. Salerno (CNRS)
- J. Santiago (Granada U.)
- N. Saoulidou (Athens U.)
- P. Schmidt-Wellenburg (PSI)
- I. Schulthess (DESY, Hamburg)
- B. Schwingenheur (MPIK)
- S. Scorza (LPSC, Grenoble)
- Y.K. Semertzidis (IBS, Daejeon; KAIST)
- S. Seo (FNAL)
- S. Serednyakov (Budker Inst., Novosibirsk)
- A.G. Shamov (Budker Inst., Novosibirsk)
- D. Shemyakin (Novosibirsk U.)
- D. Sheng (USTC China)
- M. Shiozawa (ICRR)
- D. Shwartz (Budker Inst., Novosibirsk)
- C. Smarra (SISSA/INFN, Trieste)
- L. Soffi (INFN, Rome)
- P. Sommer (CERN)
- A.L. Spadafora (LBNL)
- E. Spadaro (INFN, Milano-Bicocca)
- S. Srinivasan (Manchester U.)
- J. Steggemann (ETH Zurich)
- I.W. Stewart (MIT)
- A. Suzuki (LBNL)
- O. Tajima (Kyoto U.)
- J. Terol Calvo (IAC)
- R. Tesarek (FNAL)
- M. Tobar (UWA, Perth)
- D. Tonelli (Trieste U.)
- E. Torrence (Oregon U.)
- N. Tran (FNAL)
- A. Tricoli (BNL)
- S.M. Turchikhin (CERN)
- Y. Unno (KEK)
- P.L. Vahle (William and Mary Coll.)
- K. Valerius (KIT)
- R.G. Van De Water (LANL)
- C. van Eldik (Erlangen U.)
- R. Van Kooten (Indiana U.)
- K. Van Tilburg (NYU, New York)
- T. Vazquez Schroeder (McGill U.)
- M. Viel (SISSA/INFN, Trieste)
- E. Vitagliano (Padova U.)
- M. Volpe (APC, Paris)
- K. von Sturm (INFN, Padova)
- K. Vos (Maastricht U.)
- M. Vos (IFIC, Valencia)
- A.P. Walker-Loud (LBNL)
- L. Wan (Boston U.)
- M. Wang (INFN, Milano-Bicocca)
- X. Wang (Adelaide U.)
- Z. Wang (NYU, New York)
- N. Wardle (Imperial Coll. Physics Dep.)
- A. Watson (Leeds U.)
- G. Watt (Durham U.)
- M. Weber (Bern U.)
- J. Wei (PMO, Nanjing)
- R. Wendell (Kyoto U.)
- L. Winslow (MIT)
- P. Winter (ANL)
- S. Witte (Phys. Dep. Oxford U.)
- C. Wittweg (Zurich U.)
- B. Yang (Seoul National U.)
- Y. Yang (MIT)
- J. Ye (Columbia U.)
- H. Yin (CERN)
- P. Yin (IHEP Beijing)
- J. Yoo (Seoul National U.)
- Z. You (Sun Yat-sen U.)
- Q. Yue (Tsinghua U.)

- D. Zerwas (LAL Orsay)
- X. Zhang (JGU, Mainz)
- Y. Zhang (Zhengzhou U.)
- M. Zhao (NKU)
- R. Zhao (UCAS, Beijing)
- L. Zhiqing (Shandong U.)
- G. Zsigmond (PSI)

4 Naming scheme for hadrons

We introduced in the 1986 edition [3] a new naming scheme for the hadrons. Changes from older terminology affected mainly the heavier mesons made of u , d , and s quarks. Otherwise, the only important change to known hadrons was that the F^\pm became the D_s^\pm . None of the lightest pseudoscalar or vector mesons changed names, nor did the $c\bar{c}$ or $b\bar{b}$ mesons (we do, however, now use χ_c for the $c\bar{c}$ χ states), nor did any of the established baryons. The Summary Tables give both the new and old names whenever a change has occurred.

In the 2018 edition [4], the naming scheme was extended to address the naming of charmonium and bottomonium states that were commonly referred to as X , Y , or Z states in the literature. The further discovery of various exotic hadron states — including in particular tetraquarks and pentaquarks containing $qq\bar{q}\bar{q}$ and $qqqq$ minimal quark content, respectively — has rendered the 2018 extension insufficient. In this edition, the naming scheme is revised and extended to cover all experimentally-known states. The current scheme is described in “Naming Scheme for Hadrons” (p. 1) of this *Review*. A table details the correspondence between the names newly adopted by the PDG and those that have previously appeared in the literature.

We give here our conventions on typesetting style. Particle symbols are italic (or slanted) characters: e^- , p , Λ , π^0 , K_L , D_s^+ , b . Charge is indicated by a superscript: B^- , Δ^{++} . Charge is not normally indicated for p , n , or the quarks, and is optional for neutral isosinglets: η or η^0 . Antiparticles and particles are distinguished by charge for charged leptons and mesons: τ^+ , K^- . Otherwise, distinct antiparticles are indicated by a bar (overline): $\bar{\nu}_\mu$, \bar{l} , \bar{p} , \bar{K}^0 , and $\bar{\Sigma}^+$ (the antiparticle of the Σ^-).

5 Procedures

5.1 Selection and treatment of data

The Particle Listings contain all relevant data known to us that are published in journals. With very few exceptions, we do not include results from preprints or conference reports. Nor do we include data that are of historical importance only (the Listings are not an archival record). We search every volume of 30 journals through our cutoff date for relevant data. We also include later published papers that are sent to us by the authors (or others).

In the Particle Listings, we clearly separate measurements that are used to calculate or estimate values given in the Summary Tables from measurements that are not used. We give explanatory comments in many such cases. Among the reasons a measurement might be excluded are the following:

- It is superseded by or included in later results.
- No error is given.
- It involves assumptions we question.
- It has a poor signal-to-noise ratio, low statistical significance, or is otherwise of poorer quality than other data available.
- It is clearly inconsistent with other results that appear to be more reliable. Usually we then state the criterion, which sometimes is quite subjective, for selecting “more reliable” data for averaging. See Sec. 5.4.
- It is not independent of other results.
- It is not the best limit (see below).
- It is quoted from a preprint or a conference report.

In some cases, *none* of the measurements is entirely reliable and no average is calculated. For example, the masses of many of the baryon resonances, obtained from partial-wave analyses, are quoted as estimated ranges thought to probably include the true

values, rather than as averages with errors. This is discussed in the Baryon Particle Listings.

For upper limits, we normally quote in the Summary Tables the strongest limit. We do not average or combine upper limits except in a very few cases where they may be re-expressed as measured numbers with Gaussian errors.

As is customary, we assume that particle and antiparticle share the same spin, mass, and mean life. The Tests of Conservation Laws table, following the Summary Tables, lists tests of CPT as well as other conservation laws.

We use the following indicators in the Particle Listings to tell how we get values from the tabulated measurements:

- OUR AVERAGE —From a weighted average of selected data.
- OUR FIT —From a constrained or overdetermined multiparameter fit of selected data.
- OUR EVALUATION —Not from a direct measurement, but evaluated from measurements of related quantities.
- OUR ESTIMATE —Based on the observed range of the data. Not from a formal statistical procedure.
- OUR LIMIT —For special cases where the limit is evaluated by us from measured ratios or other data. Not from a direct measurement.

An experimentalist who sees indications of new a particle will of course want to know what has been seen in that region in the past. Hence, we include in the Particle Listings all reported states that, in our opinion, have sufficient statistical merit and that have not been disproved by more reliable data. However, we promote to the Summary Tables only those states that we feel are well-established. This judgment is, of course, somewhat subjective and no precise criteria can be given. For more detailed discussions, see the reviews section on Particle Properties.

5.2 Averages and fits

We divide this discussion on obtaining averages and errors into three sections: (1) treatment of errors; (2) unconstrained averaging; (3) constrained fits.

5.2.1 Treatment of errors

In what follows, the “error” δx means that the range $x \pm \delta x$ is intended to be a 68.3% confidence interval about the central value x . We treat this error as if it were Gaussian. Thus, when the error is Gaussian, δx is the usual one standard deviation (1σ). Many experimenters now give statistical and systematic errors separately, in which case we usually quote both errors, with the statistical error first. For averages and fits, we then add the two errors in quadrature and use this combined error for δx .

When experimenters quote asymmetric errors $(\delta x)^+$ and $(\delta x)^-$ for a measurement x , the error that we use for that measurement in making an average or a fit with other measurements is a continuous function of these three quantities. When the resultant average or fit \bar{x} is less than $x - (\delta x)^-$, we use $(\delta x)^-$; when it is greater than $x + (\delta x)^+$, we use $(\delta x)^+$. In between, the error we use is a linear function of x . Since the errors we use are functions of the result, we iterate to get the final result. Asymmetric output errors are determined from the input errors assuming a linear relation between the input and output quantities.

In fitting or averaging, we usually do not include correlations between different measurements, but we try to select data in such a way as to reduce correlations. Correlated errors are, however, treated explicitly when there are a number of results of the form $A_i \pm \sigma_i \pm \Delta$ that have identical systematic errors Δ . In this case, one can first average the $A_i \pm \sigma_i$ and then combine the resulting statistical error with Δ . One obtains, however, the same result by averaging $A_i \pm (\sigma_i^2 + \Delta_i^2)^{1/2}$, where $\Delta_i = \sigma_i \Delta [\sum (1/\sigma_j^2)]^{1/2}$. This procedure has the advantage that, with the modified systematic errors Δ_i , each measurement may be treated as independent and averaged in the usual way with other data. Therefore, when appropriate, we adopt this procedure. We tabulate Δ and invoke an automated procedure that computes Δ_i before averaging, and we include a note saying that there are common systematic errors.

Another common case of correlated errors occurs when experimenters measure two quantities and then quote the two and their

difference, e.g., m_1 , m_2 , and $\Delta = m_2 - m_1$. We cannot enter all of m_1 , m_2 and Δ into a constrained fit because they are not independent. In some cases, it is a good approximation to ignore the quantity with the largest error and put the other two into the fit. However, in some cases correlations are such that the errors on m_1 , m_2 and Δ are comparable and none of the three values can be ignored. In this case, we put all three values into the fit and invoke an automated procedure to increase the errors prior to fitting such that the three quantities can be treated as independent measurements in the constrained fit. We include a note saying that this has been done.

5.2.2 Unconstrained averaging

To average data, we use a standard weighted least-squares procedure and in some cases, discussed below, increase the errors with a “scale factor.” We begin by assuming that measurements of a given quantity are uncorrelated, and calculate a weighted average and error as

$$\bar{x} \pm \delta\bar{x} = \frac{\sum_i w_i x_i}{\sum_i w_i} \pm \left(\sum_i w_i \right)^{-1/2}, \quad (1)$$

where

$$w_i = 1/(\delta x_i)^2.$$

Here x_i and δx_i are the value and error reported by the i th experiment, and the sums run over the N experiments. We then calculate $\chi^2 = \sum w_i (\bar{x} - x_i)^2$ and compare it with $N - 1$, which is the expectation value of χ^2 if the measurements are from a Gaussian distribution.

If $\chi^2/(N - 1)$ is less than or equal to 1, and there are no known problems with the data, we accept the results.

If $\chi^2/(N - 1)$ is very large, we may choose not to use the average at all. Alternatively, we may quote the calculated average, but then make an educated guess of the error, a conservative estimate designed to take into account known problems with the data.

Finally, if $\chi^2/(N - 1)$ is greater than 1, but not greatly so, we still average the data, but then also do the following:

(a) We increase our quoted error, $\delta\bar{x}$ in Eq. (1), by a scale factor S defined as

$$S = [\chi^2/(N - 1)]^{1/2}. \quad (2)$$

Our reasoning is as follows. The large value of the χ^2 is likely to be due to underestimation of errors in at least one of the experiments. Not knowing which of the errors are underestimated, we assume they are all underestimated by the same factor S . If we scale up all the input errors by this factor, the χ^2 becomes $N - 1$, and of course the output error $\delta\bar{x}$ scales up by the same factor. See Ref. [5].

When combining data with widely varying errors, we modify this procedure slightly. We evaluate S using only the experiments with smaller errors. Our cutoff or ceiling on δx_i is arbitrarily chosen to be

$$\delta_0 = 3N^{1/2} \delta\bar{x},$$

where $\delta\bar{x}$ is the unscaled error of the mean of all the experiments. Our reasoning is that although the low-precision experiments have little influence on the values \bar{x} and $\delta\bar{x}$, they can make significant contributions to the χ^2 , and the contribution of the high-precision experiments thus tends to be obscured. Note that if each experiment has the same error δx_i , then $\delta\bar{x}$ is $\delta x_i/N^{1/2}$, so each δx_i is well below the cutoff. (More often, however, we simply exclude measurements with relatively large errors from averages and fits: new, precise data chase out old, imprecise data.)

Our scaling procedure has the property that if there are two values with comparable errors separated by much more than their stated errors (with or without a number of other values of lower accuracy), the scaled-up error $\delta\bar{x}$ is approximately half the interval between the two discrepant values.

We emphasize that our scaling procedure for errors in no way affects central values. And if you wish to recover the unscaled error $\delta\bar{x}$, simply divide the quoted error by S .

(b) If the number M of experiments with an error smaller than δ_0 is at least three, and if $\chi^2/(M - 1)$ is greater than 1.25,

we show in the Particle Listings an ideogram of the data. Figure 1 is an example. Sometimes one or two data points lie apart from the main body; other times the data split into two or more groups. We extract no numbers from these ideograms; they are simply visual aids, which the reader may use as he or she sees fit.

Each measurement in an ideogram is represented by a Gaussian with a central value x_i , error δx_i , and area proportional to $1/\delta x_i$. The choice of $1/\delta x_i$ for the area is somewhat arbitrary. With this choice, the center of gravity of the ideogram corresponds to an average that uses weights $1/\delta x_i$ rather than the $(1/\delta x_i)^2$ actually used in the averages. This may be appropriate when some of the experiments have seriously underestimated systematic errors. However, since for this choice of area the height of the Gaussian for each measurement is proportional to $(1/\delta x_i)^2$, the peak position of the ideogram will often favor the high-precision measurements at least as much as does the least-squares average. See our 1986 edition [3] for a detailed discussion of the use of ideograms.

5.2.3 Constrained fits

In some cases, such as branching ratios or masses and mass differences, a constrained fit may be needed to obtain the best values of a set of parameters. For example, most branching ratios and rate measurements are analyzed by making a simultaneous least-squares fit to all the data and extracting the partial decay fractions P_i , the partial widths Γ_i , the full width Γ (or mean life), and the associated error matrix.

Assume, for example, that a state has m partial decay fractions P_i , where $\sum P_i = 1$. These have been measured in N_r different ratios R_r , where, e.g., $R_1 = P_1/P_2$, $R_2 = P_1/P_3$, etc. [We can handle any ratio R of the form $\sum \alpha_i P_i / \sum \beta_i P_i$, where α_i and β_i are constants, usually 1 or 0. The forms $R = P_i P_j$ and $R = (P_i P_j)^{1/2}$ are also allowed.] Further, assume that each ratio R has been measured by N_k experiments (we designate each experiment with a subscript k , e.g., R_{1k}). We then find the best values of the fractions P_i by minimizing the χ^2 as a function of the $m - 1$ independent parameters:

$$\chi^2 = \sum_{r=1}^{N_r} \sum_{k=1}^{N_k} \left(\frac{R_{rk} - R_r}{\delta R_{rk}} \right)^2, \quad (3)$$

where the R_{rk} are the measured values and R_r are the fitted values of the branching ratios.

In addition to the fitted values \bar{P}_i , we calculate an error matrix $\langle \delta \bar{P}_i \delta \bar{P}_j \rangle$. We tabulate the diagonal elements of $\delta \bar{P}_i = \langle \delta \bar{P}_i \delta \bar{P}_i \rangle^{1/2}$ (except that some errors are scaled as discussed below). In the Particle Listings, we give the complete correlation matrix; we also calculate the fitted value of each ratio, for comparison with the input data, and list it above the relevant input, along with a simple unconstrained average of the same input.

Three comments on the example above:

(1) There was no connection assumed between measurements of the full width and the branching ratios. But often we also have information on partial widths Γ_i as well as the total width Γ . In this case we must introduce Γ as a parameter in the fit, along with the P_i , and we give correlation matrices for the widths in the Particle Listings.

(2) We try to pick those ratios and widths that are as independent and as close to the original data as possible. When one experiment measures all the branching fractions and constrains their sum to be one, we leave one of them (usually the least well-determined one) out of the fit to make the set of input data more nearly independent. We now do allow for correlations between input data.

(3) We calculate scale factors for both the R_r and P_i when the measurements for any R give a larger-than-expected contribution to the χ^2 . According to Eq. (3), the double sum for χ^2 is first summed over experiments $k = 1$ to N_k , leaving a single sum over ratios $\chi^2 = \sum R_r^2$. One is tempted to define a scale factor for the ratio r as $S_r^2 = \chi_r^2 / \langle \chi_r^2 \rangle$. However, since $\langle \chi_r^2 \rangle$ is not a fixed quantity (it is somewhere between N_k and N_{k-1}), we do not know

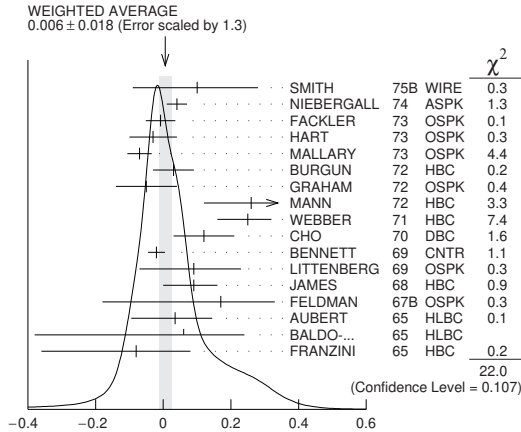


Figure 1: A typical ideogram. The arrow at the top shows the position of the weighted average, while the width of the shaded pattern shows the error in the average after scaling by the factor S . The column on the right gives the χ^2 contribution of each of the experiments. Note that the next-to-last experiment, denoted by the incomplete error flag (\perp), is not used in the calculation of S (see the text).

how to evaluate this expression. Instead, we define

$$S_r^2 = \frac{1}{N_k} \sum_{k=1}^{N_k} \frac{(R_{rk} - \bar{R}_r)^2}{\langle (R_{rk} - \bar{R}_r)^2 \rangle}. \quad (4)$$

With this definition the expected value of S_r^2 is one. We can show that

$$\langle (R_{rk} - \bar{R}_r)^2 \rangle = \langle (\delta R_{rk})^2 \rangle - (\delta \bar{R}_r)^2, \quad (5)$$

where $\delta \bar{R}_r$ is the fitted error for ratio r .

The fit is redone using errors for the branching ratios that are scaled by the larger of S_r and unity, from which new and often larger errors $\delta \bar{P}'_i$ are obtained. The scale factors we finally list in such cases are defined by $S_i = \delta \bar{P}'_i / \delta \bar{P}_i$. However, in line with our policy of not letting S affect the central values, we give the values of \bar{P}_i obtained from the original (unscaled) fit.

There is one special case in which the errors that are obtained by the preceding procedure may be changed. When a fitted branching ratio (or rate) \bar{P}_i turns out to be less than three standard deviations ($\delta \bar{P}'_i$) from zero, a new smaller error ($\delta \bar{P}''_i$)⁻ is calculated on the low side by requiring the area under the Gaussian between $\bar{P}_i - (\delta \bar{P}''_i)$ ⁻ and \bar{P}_i to be 68.3% of the area between zero and \bar{P}_i . A similar correction is made for branching fractions that are within three standard deviations of one. This keeps the quoted errors from overlapping the boundary of the physical region.

5.3 Rounding

While the results shown in the Particle Listings are usually exactly those published by the experiments, the numbers that appear in the Summary Tables (means, averages and limits) are subject to a set of rounding rules.

The basic rule states that if the three highest order digits of the error lie between 100 and 354, we round to two significant digits. If they lie between 355 and 949, we round to one significant digit. Finally, if they lie between 950 and 999, we round up to 1000 and keep two significant digits. In all cases, the central value is given with a precision that matches that of the error. So, for example, the result (coming from an average) 0.827 ± 0.119 would appear as 0.83 ± 0.12 , while 0.827 ± 0.367 would turn into 0.8 ± 0.4 .

In cases where there are asymmetric errors, if these errors differ by less than 10 percent of the average of the two errors, the average is instead used as a symmetric error in the displayed result and the rounding is determined by this average. Otherwise, the narrower of the two asymmetric errors is used to determine the rounding on both.

Rounding of this form is also performed on the value of limits that come from calculations (but not on limits that are directly taken from a single source).

Finally, we should point out that in several instances, when a group of results come from a single fit to a set of data, we have chosen to keep two significant digits for all the results. This happens, for instance, for several properties of the W and Z bosons and the τ lepton.

5.4 Discussion

The problem of averaging data containing discrepant values is nicely discussed by Taylor in Ref. [6]. He considers a number of algorithms that attempt to incorporate inconsistent data into a meaningful average. However, it is difficult to develop a procedure that handles simultaneously in a reasonable way two basic types of situations: (a) data that lie apart from the main body of the data are incorrect (contain unreported errors); and (b) the opposite—it is the main body of data that is incorrect. Unfortunately, as Taylor shows, case (b) is not infrequent. He concludes that the choice of procedure is less significant than the initial choice of data to include or exclude.

We place much emphasis on this choice of data. Often we solicit the help of outside experts (consultants). Sometimes, however, it is simply impossible to determine which of a set of discrepant measurements are correct. Our scale-factor technique is an attempt to address this ignorance by increasing the error. In effect, we are saying that present experiments do not allow a precise determination of this quantity because of unresolvable discrepancies, and one must await further measurements. The reader is warned of this situation by the size of the scale factor, and if he or she desires can go back to the literature (via the Particle Listings) and redo the average with a different choice of data.

Our situation is less severe than most of the cases Taylor considers, such as estimates of the fundamental constants like \hbar , *etc.* Most of the errors in his case are dominated by systematic effects. For our data, statistical errors are often at least as large as systematic errors, and statistical errors are usually easier to estimate. A notable exception occurs in partial-wave analyses, where different techniques applied to the same data yield different results. In this case, as stated earlier, we often do not make an average but just quote a range of values.

A brief history of early Particle Data Group averages is given in Ref. [5]. Our History Plots show the time evolution of some of our values of a few particle properties. Sometimes large changes occur. These usually reflect the introduction of significant new data or the discarding of older data. Older data are discarded in favor of newer data when it is felt that the newer data have smaller systematic errors, or have more checks on systematic errors, or have made corrections unknown at the time of the older experiments, or simply have much smaller errors. Sometimes, the scale factor becomes large near the time at which a large jump takes place, reflecting the uncertainty introduced by the new and inconsistent data. By and large, however, a full scan of our history plots shows a dull progression toward greater precision at central values quite consistent with the first data points shown.

We conclude that the reliability of the combination of experimental data and our averaging procedures is usually good, but it is important to be aware that fluctuations outside of the quoted errors can and do occur.

ACKNOWLEDGMENTS

The publication of the *Review of Particle Physics* is supported by the Director, Office of Science, Office of High Energy Physics of the U.S. Department of Energy under Contract No. DE-AC02-05CH11231; by an implementing arrangement between the governments of Japan (MEXT: Ministry of Education, Culture, Sports, Science and Technology) and the United States (DOE) on cooperative research and development; by the Italian National Institute of Nuclear Physics (INFN); and by the European Laboratory for Particle Physics (CERN). Individual collaborators receive support for their PDG activities from their respective institutes or funding agencies.

We thank all those who have assisted in the many phases of preparing this *Review*. We particularly thank the many who have

responded to our requests for verification of data entered in the Listings, and those who have made suggestions or pointed out errors.

We are grateful to the staff at CERN, DESY, IHEP Beijing, KEK, LBNL, and NISER who take care of the mailing and distribution of our products.

This work used resources of the National Energy Research Scientific Computing Center, a DOE Office of Science User Facility supported by the Office of Science of the U.S. Department of Energy under Contract No. DE-AC02-05CH11231.

References

- [1] The previous edition was: R.L. Workman *et al.* (Particle Data Group), *Prog. Theor. Exp. Phys.* **2022**, 083C01 (2022).
- [2] C. Patrignani *et al.* (Particle Data Group), *Chin. Phys.* **C40**, 10, 100001 (2016).
- [3] M. Aguilar-Benitez *et al.* (Particle Data Group), *Phys. Lett.* **170B**, 1 (1986).
- [4] M. Tanabashi *et al.* (Particle Data Group), *Phys. Rev. D* **98**, 3, 030001 (2018).
- [5] A. H. Rosenfeld, *Ann. Rev. Nucl. Part. Sci.* **25**, 555 (1975).
- [6] B.N. Taylor, “Numerical Comparisons of Several Algorithms for Treating Inconsistent Data in a Least-Squares Adjustment of the Fundamental Constants,” U.S. National Bureau of Standards NBSIR 81-2426 (1982).

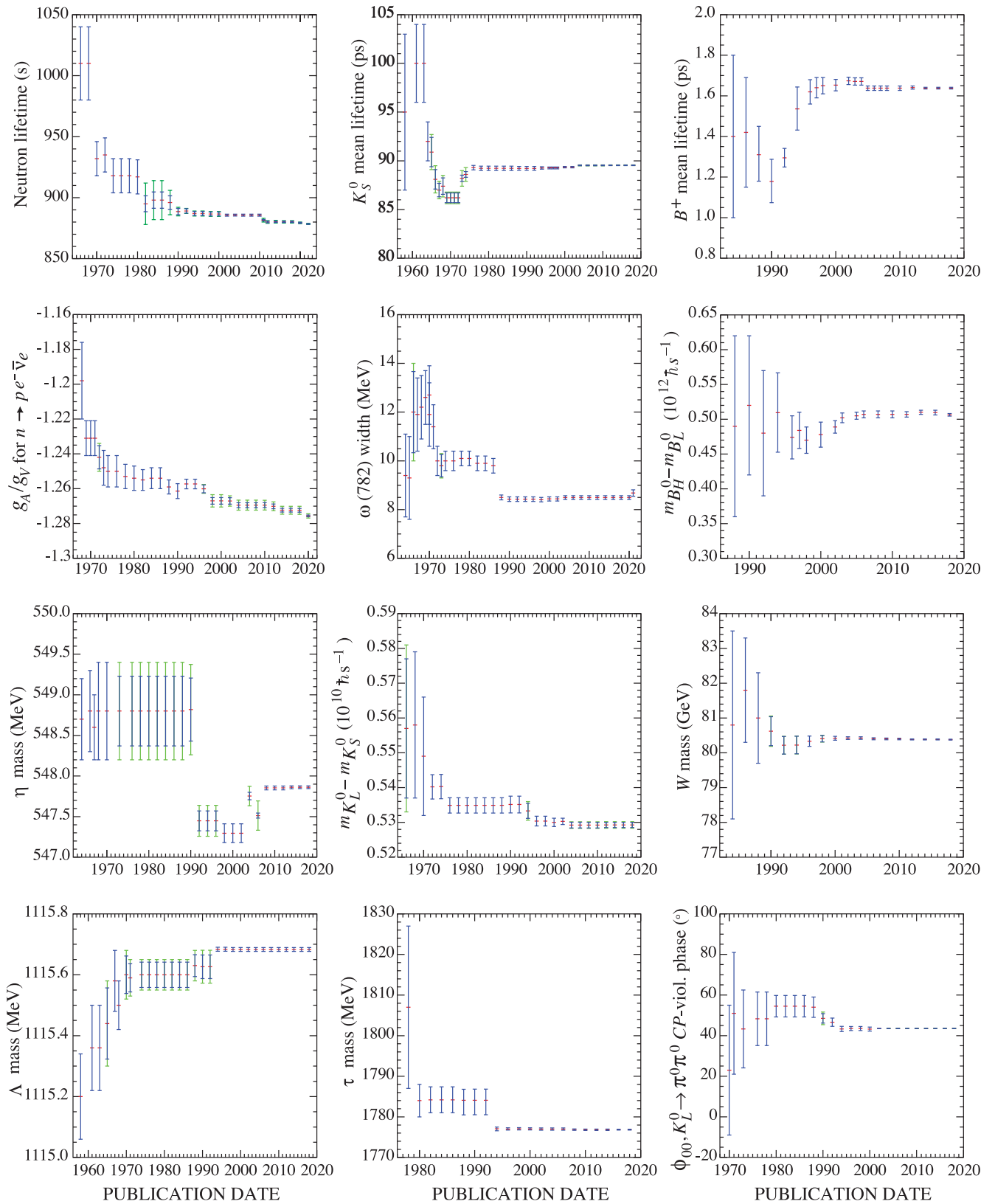


Figure 1: A historical perspective of values of a few particle properties tabulated in this *Review* as a function of date of publication of the *Review*. A full error bar indicates the quoted error; a thick-lined portion indicates the same but without the “scale factor.”

Online Particle Physics Information

Revised August 2023 by K. Assamagan (BNL) and H.B. O'Connell (FNAL).

1	Introduction	20
2	Particle Data Group (PDG) resources	20
3	Particle physics information platform	20
4	Literature databases	20
5	Journals	21
6	Conference and seminars databases	21
7	Research institutions	21
8	People	21
9	Experiments	21
10	Jobs	21
11	Software packages and repositories	22
12	Data repositories and preservation	22
13	Particle physics education and outreach	22
14	Regional HEP efforts	22

1 Introduction

Online resources are used in a diverse and expanding set of ways in particle physics. Many of these resources have become central to our collective work. We provide a brief curated selection of the major resources here. An expanded and regularly updated online repository is referred to below and can be found at

<https://github.com/particledatagroup/hep-resources>

By contrast, it is meant to be inclusive and catalog all useful resources related to particle physics. The community is warmly invited to contribute in order to ensure a broad and up to date coverage of relevant resources. Practical details are available online.

2 Particle Data Group (PDG) resources

- **Review of Particle Physics (RPP):** A comprehensive report on the fields of particle physics and related areas of cosmology and astrophysics, including both review articles and a compilation/evaluation of data on particle properties. The review section includes articles, tables and plots on a wide variety of theoretical and experimental topics of interest to particle physicists and astrophysicists. The particle properties section provides tables of published measurements as well as the Particle Data Group's best values and limits for particle properties such as masses, widths, lifetimes, and branching fractions, as well as an extensive summary of searches for hypothetical particles. RPP is published as a large book every two years, with partial updates made available once each year on the web.

All the contents of the book version of RPP are available online:

<https://pdg.lbl.gov>

The printed book can be ordered:

<https://pdg.lbl.gov/order>

Of historical interest is the complete RPP collection which can be found online:

<https://pdg.lbl.gov/publications>

- **Particle Physics booklet:** An abridged version of the Review of Particle Physics, available as a pocket-sized 250-page booklet. It is one of the most useful summaries of physics data. The booklet contains an abbreviated set of reviews and the summary tables from the most recent edition of the Review of Particle Physics.

The PDF file of the booklet can be downloaded:

<https://pdg.lbl.gov/current/booklet.pdf>

The printed booklet can be ordered:

<https://pdg.lbl.gov/order>

A mobile version of the booklet is also available:

<https://pdg.lbl.gov/booklet>

- **PDGLive:** A web application for browsing the contents of the PDG database that contains the information published in the Review of Particle Physics. It allows one to navigate to a particle of interest, see a summary of the information available, and then proceed to the detailed information published

in the Review of Particle Physics. Data entries are directly linked to the corresponding bibliographic information in INSPIRE.

<https://pdglive.lbl.gov>

- **Computer-readable files:** Data files that can be downloaded from the PDG include tables of particle masses and widths, PDG Monte Carlo particle numbers, and cross-section data. The files are updated with each new edition of the Review of Particle Physics.

<https://pdg.lbl.gov/files>

- **PDG API:** In addition to the fixed-format data files that have been available for many years, PDG is developing new tools to access PDG data in machine-readable format (currently available as beta versions).

<https://pdg.lbl.gov/api>

3 Particle physics information platform

INSPIRE: INSPIRE serves as a one-stop information platform for the particle physics community, comprising interlinked databases on literature, authors, jobs, seminars, conferences, institutions and experiments (each described in more detail below). Run in collaboration by CERN (which hosts INSPIRE), DESY, Fermilab, IHEP, IN2P3 and SLAC, it has been serving the scientific community for almost 50 years. Previously hosted at SLAC and known as SPIRES, it was the first website outside Europe and the first database on the web. Close interaction with the user community and with arXiv, ADS, HEPData, ORCID, PDG and publishers is the backbone of INSPIRE's evolution. Since 2020, it is running on a modernized platform that is continuously being improved.

<https://inspirehep.net/>

4 Literature databases

Most research articles in the field of high-energy physics are first made available on the arXiv eprint server, where researchers can learn about the latest developments by browsing through the new announcements five days a week. They are indexed, together with all other publications in high-energy physics and related fields, in the INSPIRE literature collection. For neighboring fields such as astrophysics or mathematics, other databases are more exhaustive.

- **ADS:** The SAO/NASA Astrophysics Data System is a Digital Library portal offering access to 15 million bibliographic records in Astronomy and Physics. The ADS search engine also indexes the full-text for many publications in this collection and tracks citations. The system also provides access and links to a wealth of external resources, including electronic articles hosted by publishers and arXiv, data catalogs and a variety of data products hosted by the astronomy archives worldwide. The ADS can be accessed at:

<http://ads.harvard.edu/>

- **arXiv.org:** A repository of full-text articles in physics, astronomy, mathematics, computer science, statistics, nonlinear sciences, quantitative finance, quantitative biology, electrical engineering and systems science, and economics. Papers are submitted by registered authors to arXiv, often as preprints in advance of submission to a journal for publication; includes postprints, working papers, and other relevant material. Established in 1991, the repository is interlinked with ADS and INSPIRE, among others. Readers can browse subject categories or search by author, title, abstract, date, and other fields. Receive daily update alerts for subfields by email or RSS.

<https://arxiv.org>

- **INSPIRE Literature:** The literature collection, the flagship of the INSPIRE suite, serves more than 1.5 million bibliographic records with a growing number of full-text articles attached and metadata including author affiliations, abstracts, references, experiments, keywords as well as links to arXiv, ADS, PDG, HEPData, publisher platforms and other servers. It provides fast metadata searches that can be eas-

ily refined using facets, plots extracted from full text, author disambiguation, author profile pages and citation analysis.

<https://inspirehep.net/literature>

- **MathSciNet:** This database of almost 4 million items provides reviews, abstracts and bibliographic information for much of the mathematical sciences literature. Over 125,000 new items, most of them classified according to the Mathematics Subject Classification, and more than 90,000 reviews of the current published literature are added each year. Author identification allows users to search for publications by author and citation data allows users to track the history and influence of research publications.

<https://www.ams.org/mathscinet>

OSTI.GOV: A portal to free, publicly available DOE-sponsored R&D results including technical reports, bibliographic citations, journal articles, conference papers, books, multimedia and data information. It consolidates OSTI's home page and the now-retired primary search tool SciTech Connect. It contains over 3 million records, including citations to 1.5 million journal articles, 1 million of which have digital object identifiers (DOIs) linking to full-text articles on publishers' websites.

<https://www.osti.gov/>

5 Journals

- **CERN Journal List:** This list of journals and conference series publishing particle physics content provides information on Open Access, copyright policies and terms of use for CERN authors.

<https://scientific-info.cern/submit-and-publish/publish-open-access>

- **INSPIRE Journals:** A database of almost 4,000 journals relevant to HEP and related fields. Each entry displays the papers published in the journal that are included in the INSPIRE Literature database.

<https://inspirehep.net/journals>

- **SCOAP³ Journals:** A list of journals currently financed by the SCOAP³ consortium. All HEP publications in those journals are made freely available under Open Access conditions at no cost for the authors.

<https://www.scoap3.org/phase3-journals/>

6 Conference and seminars databases

- **INSPIRE Conferences:** The database of more than 26,000 past, present, and future conferences, schools, and meetings relevant to high-energy physics and related fields is searchable by title, acronym, series, date and location. Included are information about published proceedings, links to conference contributions in the INSPIRE HEP database, and links to the conference website when available. New conferences can be submitted from the entry page.

<https://inspirehep.net/conferences>

- **INSPIRE Seminars:** Created to support the surge of online seminars during the COVID-19 pandemic, this database already contains more than 2,700 seminars in high-energy physics and related fields. Seminars can be filtered by date, series and subject and exported to a calendar. Direct links to join the online seminar and external resources are included. All seminars are community-maintained and can be submitted from the entry page.

<https://inspirehep.net/seminars>

- **researchseminars.org:** A list of research seminars and conferences, organized by topic and seminars series or conference.

<https://researchseminars.org/>

7 Research institutions

- **INSPIRE Institutions:** INSPIRE Institutions contains over 11,500 institutes, laboratories, and universities, where research on particle physics and astrophysics is led. Every record includes, whenever possible, as detailed information, such as address, web links, experiments, and links to INSPIRE papers authored by people affiliated to that institu-

tion. One can search for a particular institution by name, acronym, and location.

<https://inspirehep.net/institutions>

- **Research Organization Registry (ROR):** The Research Organization Registry (ROR) is a global, community-led registry of open persistent identifiers for research organizations. It includes IDs and metadata for more than 100,000 organizations and counting. Registry updates are curated through a community process and released on a rolling basis.

<https://ror.org/>

8 People

- **INSPIRE Authors:** Searchable worldwide database of more than a hundred thousand active, departed, retired, and deceased people associated with particle physics and related fields. The affiliation history of these researchers, their e-mail addresses, ORCIDs, web pages, experiments they participated in, PhD advisor, information on their graduate students and links to their papers and seminars are provided, as well as a user interface to update this information.

<https://inspirehep.net/authors>

- **ORCID:** Registry providing persistent digital identifiers allowing to unambiguously identify researchers. Through integration in key research workflows such as manuscript and grant submission, it supports automated linkages between scientists and their professional activities ensuring that their work is recognized.

<https://orcid.org>

9 Experiments

- **INSPIRE Experiments:** Contains more than 3,700 past, present, and future experiments in particle physics. It lists and classifies both accelerator and non-accelerator experiments as well as theory collaborations. Includes official experiment name and number, location, and collaboration lists. Simple searches by participant, title, experiment number, institution, date approved, accelerator, or detector, return a description of the experiment, including a complete list of authors, title, overview of the experiment's goals and methods, and a link to the experiment's web page if available. Recently, it has expanded its scope to include particle accelerators besides experiments and to link them together.

<https://inspirehep.net/experiments>

- **Cosmic ray/Gamma ray/Neutrino and similar experiments:** This extensive collection of experiment websites is organized by focus of study and by location. Additional sections link to educational materials, organizations, and other useful resources. The site is maintained at the Max Planck Institute for Nuclear Physics, Heidelberg.

<https://www.mpi-hd.mpg.de/hfm/CosmicRay/CosmicRaySites.html>

- **Wikipedia particle experiments:** A list of particle experiments with Wikipedia pages.

https://en.wikipedia.org/wiki/Category:Particle_experiments

10 Jobs

- **AAS Job Register:** The American Astronomical Society publishes once a month graduate, postgraduate, faculty and other positions mainly in astronomy and astrophysics.

<https://jobregister.aas.org/>

- **Academic Jobs Online:** A full-service online recruiting site for academic institutions worldwide in all disciplines and areas.

<https://academicjobsonline.org/>

- **APS Careers:** A gateway for physicists, students, and physics enthusiasts to information about physics jobs and careers. It contains Physics job listings, career advice, upcoming workshops and meetings, and career and job-related resources provided by the American Physical Society.

<https://www.aps.org/careers/employment/>

- **INSPIRE Jobs:** Lists academic and research jobs in high energy physics, nuclear physics, accelerator physics and astrophysics with the option to post a job or to receive email notices of new job listings. Several hundreds of jobs are listed all year round, with more activity during the application season.

<https://inspirehep.net/jobs>

- **IOP Careers:** Career information and resources primarily aimed at university students are provided by the UK Institute of Physics.

<https://www.iop.org/careers-physics/your-future-with-physics>

- **Physics Today Jobs:** Online recruitment advertising website for Physics Today magazine, published by the American Institute of Physics. Physics Today Jobs is the managing partner of the AIP Career Network, an online job board network for the physical science, engineering, and computing disciplines. Over 6,000 resumes are currently available, and nearly 5,000 jobs were posted in 2018.

<https://jobs.physicstoday.org/>

- **Physicsworld Jobs:** A recruitment service run by IOP Publishing that connects employers from different industry sectors with jobseekers who have a background in physics and engineering.

<https://www.physicsworldjobs.com/>

11 Software packages and repositories

A vast number of software tools are used for various aspects of high-energy physics research. Due to their number, their often specialized purpose and the quickly-changing nature of software, no attempt has been made to present them in this chapter. The accompanying online version contains an extensive categorized list

of software.

12 Data repositories and preservation

Initiatives to preserve and disseminate data produced during different stages of research, from Monte Carlo events to machine-readable versions of tables in papers, have grown in recent years. Unfortunately, there currently exists no central resource aggregating all these data as is the case for the more established means of scholarly communication. Instead, there are a number of repositories targeting different types of data and research subjects. They are listed in the online version.

13 Particle physics education and outreach

Particle physics public engagement efforts are widespread, with laboratories, experiments, universities and individual researchers engaged in a range of efforts. The online version of this chapter provides links to resources for particle physicists wanting to become engaged in public education as well as resources that physicists can provide directly to students, teachers or lay people. There are classroom activities, interactive websites, films, and direct links to education offices at institutions and experiments. Many researchers also engage the public via a variety of social media platforms. Additionally, a selection of news sites relevant for experts and for the general public are provided.

14 Regional HEP efforts

The online version of this chapter provides links to summaries of regional HEP activities across Europe, Japan, the US, Africa, Latin America, and other regions that may be classified as developing or emerging. This list of summaries is not exhaustive and is based on the expert knowledge of the authors at the time of information gathering; the narrative was developed in July 2023 and will require periodic updates as the HEP landscape changes.

SUMMARY TABLES OF PARTICLE PHYSICS

Gauge and Higgs bosons	25
Leptons	28
Quarks	32
Mesons	33
Baryons	93
Searches not in Other Sections*	112
Tests of conservation laws	114
Meson Quick Reference Table	91
Baryon Quick Reference Table	92

* There are also search limits in the Summary Tables for the Gauge and Higgs Bosons, the Leptons, the Quarks, and the Mesons.



SUMMARY TABLES OF PARTICLE PROPERTIES

Extracted from the Particle Listings of the
Review of Particle Physics

S. Navas *et al.* (Particle Data Group),
Phys. Rev. D. **110**, 030001 (2024)

Available at <https://pdg.lbl.gov>

Particle Data Group

S. Navas, C. Amsler, T. Gutsche, C. Hanhart, J.J. Hernández-Rey,
C. Lourenço, A. Masoni, M. Mikhasenko, R.E. Mitchell, C. Patrignani,
C. Schwanda, S. Spanier, G. Venanzoni, C.Z. Yuan, K. Agashe, G. Aielli,
B.C. Allanach, J. Alvarez-Muñiz, M. Antonelli, E.C. Aschenauer,
D.M. Asner, K. Assamagan, H. Baer, Sw. Banerjee, R.M. Barnett,
L. Baudis, C.W. Bauer, J.J. Beatty, J. Beringer, A. Bettini, O. Biebel,
K.M. Black, E. Blucher, R. Bonventre, R.A. Briere, A. Buckley,
V.D. Burkert, M.A. Bychkov, R.N. Cahn, Z. Cao, M. Carena, G. Casarosa,
A. Ceccucci, A. Cerri, R.S. Chivukula, G. Cowan, K. Cranmer, V. Crede,
O. Cremonesi, G. D'Ambrosio, T. Damour, D. de Florian, A. de Gouvêa,
T. DeGrand, S. Demers, Z. Demiragli, B.A. Dobrescu, M. D'Onofrio,
M. Doser, H.K. Dreiner, P. Eerola, U. Egede, S. Eidelman, A.X. El-Khadra,
J. Ellis, S. C. Eno, J. Erler, V.V. Ezhela, A. Fava, W. Fetscher, B.D. Fields,
A. Freitas, H. Gallagher, T. Gershon, Y. Gershtein, T. Gherghetta,
M.C. Gonzalez-Garcia, M. Goodman, C. Grab, A.V. Gritsan, C. Grojean,
D.E. Groom, M. Grünewald, A. Gurtu, H.E. Haber, M. Hamel,
S. Hashimoto, Y. Hayato, A. Hebecker, S. Heinemeyer, K. Hikasa,
J. Hisano, A. Höcker, J. Holder, L. Hsu, J. Huston, T. Hyodo, Al. Ianni,
M. Kado, M. Karliner, U.F. Katz, M. Kenzie, V.A. Khoze, S.R. Klein,
F. Krauss, M. Kreps, P. Krizan, B. Krusche, Y. Kwon, O. Lahav,
L.P. Lellouch, J. Lesgourgues, A.R. Liddle, Z. Ligeti, C.-J. Lin,
C. Lippmann, T.M. Liss, A. Lister, L. Littenberg, K.S. Lugovsky,
S.B. Lugovsky, A. Lusiani, Y. Makida, F. Maltoni, A.V. Manohar,
W.J. Marciano, J. Matthews, U.-G. Meißner, I.-A. Melzer-Pellmann,
P. Mertsch, D.J. Miller, D. Milstead, K. Mönig, P. Molaro, F. Moortgat,
M. Moskvic, N. Nagata, K. Nakamura, M. Narain, P. Nason, A. Nelles,
M. Neubert, Y. Nir, H.B. O'Connell, C.A.J. O'Hare, K.A. Olive,
J.A. Peacock, E. Pianori, A. Pich, A. Piepke, F. Pietropaolo, A. Pomarol,
S. Pordes, S. Profumo, A. Quadt, K. Rabbertz, J. Rademacker, G. Raffelt,
M. Ramsey-Musolf, P. Richardson, A. Ringwald, D.J. Robinson, S. Roesler,
S. Rolli, A. Romaniouk, L.J. Rosenberg, J.L. Rosner, G. Rybka,
M.G. Ryskin, R.A. Ryutin, B. Safdi, Y. Sakai, S. Sarkar, F. Sauli,
O. Schneider, S. Schönert, K. Scholberg, A.J. Schwartz, J. Schwiening,
D. Scott, F. Sefkow, U. Seljak, V. Sharma, S.R. Sharpe, V. Shiltsev,
G. Signorelli, M. Silari, F. Simon, T. Sjöstrand, P. Skands, T. Skwarnicki,
G.F. Smoot, A. Soffer, M.S. Sozzi, C. Spiering, A. Stahl, Y. Sumino,
F. Takahashi, M. Tanabashi, J. Tanaka, M. Taševský, K. Terao, K. Terashi,
J. Terning, U. Thoma, R.S. Thorne, L. Tiator, M. Titov, D.R. Tovey,
K. Trabelsi, P. Urquijo, G. Valencia, R. Van de Water, N. Varelas,
L. Verde, I. Vivarelli, P. Vogel, W. Vogelsang, V. Vorobyev, S.P. Wakely,
W. Walkowiak, C.W. Walter, D. Wands, D.H. Weinberg, E.J. Weinberg,
N. Vermes, M. White, L.R. Wiencke, S. Willocq, C.L. Woody,
R.L. Workman, W.-M. Yao, M. Yokoyama, R. Yoshida, G. Zanderighi,
G.P. Zeller, R.-Y. Zhu, S.-L. Zhu, F. Zimmermann, P.A. Zyla

Technical Associates:

J. Anderson, M. Kramer, P. Schaffner, W. Zheng

©2024

(Approximate closing date for data: January 15, 2024)

GAUGE AND HIGGS BOSONS

 γ (photon)

$$I(J^{PC}) = 0,1(1^{--})$$

$$\text{Mass } m < 1 \times 10^{-18} \text{ eV}$$

$$\text{Charge } q < 1 \times 10^{-46} e \quad (\text{mixed charge})$$

$$\text{Charge } q < 1 \times 10^{-35} e \quad (\text{single charge})$$

$$\text{Mean life } \tau = \text{Stable}$$

 g (gluon)

$$I(J^P) = 0(1^-)$$

$$\text{Mass } m = 0 \text{ [a]}$$

$$\text{SU}(3) \text{ color octet}$$

graviton

$$J = 2$$

$$\text{Mass } m < 1.76 \times 10^{-23} \text{ eV}$$

 W

$$J = 1$$

$$\text{Charge} = \pm 1 e$$

$$\text{Mass } m = 80.3692 \pm 0.0133 \text{ GeV [b]}$$

$$W/Z \text{ mass ratio} = 0.88136 \pm 0.00015$$

$$m_Z - m_W = 10.818 \pm 0.013 \text{ GeV}$$

$$m_{W^+} - m_{W^-} = -0.029 \pm 0.028 \text{ GeV}$$

$$\text{Full width } \Gamma = 2.085 \pm 0.042 \text{ GeV}$$

$$\langle N_{\pi^\pm} \rangle = 15.70 \pm 0.35$$

$$\langle N_{K^\pm} \rangle = 2.20 \pm 0.19$$

$$\langle N_p \rangle = 0.92 \pm 0.14$$

$$\langle N_{\text{charged}} \rangle = 19.39 \pm 0.08$$

W^- modes are charge conjugates of the modes below.

W^+ DECAY MODES	Fraction (Γ_i/Γ)	Confidence level	$\frac{p}{(\text{MeV}/c)}$
$\ell^+ \nu$	[c] (10.86 ± 0.09) %		—
$e^+ \nu$	(10.71 ± 0.16) %		40185
$\mu^+ \nu$	(10.63 ± 0.15) %		40185
$\tau^+ \nu$	(11.38 ± 0.21) %		40165
hadrons	(67.41 ± 0.27) %		—
$\pi^+ \gamma$	< 7 × 10 ⁻⁶	95%	40184
$D_s^+ \gamma$	< 6 × 10 ⁻⁴	95%	40160
cX	(33.3 ± 2.6) %		—
$c\bar{c}$	(31 ⁺¹³ ₋₁₁) %		—
invisible	[d] (1.4 ± 2.9) %		—
$\pi^+ \pi^+ \pi^-$	< 1.01 × 10 ⁻⁶	95%	40184

 Z

$$J = 1$$

$$\text{Charge} = 0$$

$$\text{Mass } m = 91.1880 \pm 0.0020 \text{ GeV [e]}$$

$$\text{Full width } \Gamma = 2.4955 \pm 0.0023 \text{ GeV}$$

$$\Gamma(\ell^+ \ell^-) = 83.984 \pm 0.086 \text{ MeV [d]}$$

$$\Gamma(\text{invisible}) = 499.2 \pm 1.5 \text{ MeV [f]}$$

$$\Gamma(\text{hadrons}) = 1744.4 \pm 2.0 \text{ MeV}$$

$$\Gamma(\mu^+ \mu^-)/\Gamma(e^+ e^-) = 1.0001 \pm 0.0024$$

$$\Gamma(\tau^+ \tau^-)/\Gamma(e^+ e^-) = 1.0020 \pm 0.0032 \text{ [g]}$$

Average charged multiplicity

$$\langle N_{\text{charged}} \rangle = 20.76 \pm 0.16 \quad (S = 2.1)$$

Couplings to quarks and leptons

$$g_V^\ell = -0.03783 \pm 0.00041$$

$$g_V^u = 0.266 \pm 0.034$$

$$g_V^d = -0.38^{+0.04}_{-0.05}$$

$$g_A^\ell = -0.50123 \pm 0.00026$$

$$g_A^u = 0.519^{+0.028}_{-0.033}$$

$$g_A^d = -0.527^{+0.040}_{-0.028}$$

$$g^{V\ell} = 0.5008 \pm 0.0008$$

$$g^{Ve} = 0.53 \pm 0.09$$

$$g^{V\mu} = 0.502 \pm 0.017$$

Gauge & Higgs Boson Summary Table

Asymmetry parameters ^[h]

$A_e = 0.1515 \pm 0.0019$
$A_\mu = 0.142 \pm 0.015$
$A_\tau = 0.143 \pm 0.004$
$A_s = 0.90 \pm 0.09$
$A_c = 0.670 \pm 0.027$
$A_b = 0.923 \pm 0.020$

Charge asymmetry (%) at Z pole

$A_{FB}^{(0\ell)} = 1.71 \pm 0.10$
$A_{FB}^{(0u)} = 4 \pm 7$
$A_{FB}^{(0s)} = 9.8 \pm 1.1$
$A_{FB}^{(0c)} = 7.07 \pm 0.35$
$A_{FB}^{(0b)} = 9.92 \pm 0.16$

Z DECAY MODES	Fraction (Γ_i/Γ)	Scale factor/ Confidence level	p (MeV/c)
e^+e^-	(3.3632±0.0042) %		45594
$\mu^+\mu^-$	(3.3662±0.0066) %		45594
$\tau^+\tau^-$	(3.3696±0.0083) %		45559
$\ell^+\ell^-$	[c] (3.3658±0.0023) %		—
$\ell^+\ell^-\ell^+\ell^-$	[f] (4.55 ±0.17) × 10 ⁻⁶		45594
invisible	(20.000 ±0.055) %		—
hadrons	(69.911 ±0.056) %		—
$(u\bar{u}+c\bar{c})/2$	(11.6 ±0.6) %		—
$(d\bar{d}+s\bar{s}+b\bar{b})/3$	(15.6 ±0.4) %		—
$c\bar{c}$	(12.03 ±0.21) %		—
$b\bar{b}$	(15.12 ±0.05) %		—
$b\bar{b}b\bar{b}$	(3.6 ±1.3) × 10 ⁻⁴		—
ggg	< 1.1 %	CL=95%	—
$\pi^0\gamma$	< 2.01 × 10 ⁻⁵	CL=95%	45594
$\eta\gamma$	< 5.1 × 10 ⁻⁵	CL=95%	45592
$\rho^0\gamma$	< 4.0 × 10 ⁻⁶	CL=95%	45591
$\omega\gamma$	< 3.9 × 10 ⁻⁶	CL=95%	45591
$\eta'(958)\gamma$	< 4.2 × 10 ⁻⁵	CL=95%	45589
$\phi\gamma$	< 7 × 10 ⁻⁷	CL=95%	45588
$\gamma\gamma$	< 1.46 × 10 ⁻⁵	CL=95%	45594
$\pi^0\pi^0$	< 1.52 × 10 ⁻⁵	CL=95%	45594
$\gamma\gamma\gamma$	< 2.2 × 10 ⁻⁶	CL=95%	45594
$\pi^\pm W^\mp$	[j] < 7 × 10 ⁻⁵	CL=95%	10176
$\rho^\pm W^\mp$	[j] < 8.3 × 10 ⁻⁵	CL=95%	10151
$J/\psi(1S)X$	(3.51 ^{+0.23} _{-0.25}) × 10 ⁻³	S=1.1	—
$J/\psi(1S)\gamma$	< 1.2 × 10 ⁻⁶	CL=95%	45541
$\psi(2S)X$	(1.60 ±0.29) × 10 ⁻³		—
$\psi(2S)\gamma$	< 2.4 × 10 ⁻⁶	CL=95%	45519
$J/\psi(1S)J/\psi(1S)$	< 2.2 × 10 ⁻⁶	CL=95%	45489
$\chi_{c1}(1P)X$	(2.9 ±0.7) × 10 ⁻³		—
$\chi_{c2}(1P)X$	< 3.2 × 10 ⁻³	CL=90%	—
$\Upsilon(1S)X + \Upsilon(2S)X$ + $\Upsilon(3S)X$	(1.0 ±0.5) × 10 ⁻⁴		—
$\Upsilon(1S)X$	< 4.4 × 10 ⁻⁵	CL=95%	—
$\Upsilon(1S)\gamma$	< 1.1 × 10 ⁻⁶	CL=95%	45103
$\Upsilon(2S)X$	< 1.39 × 10 ⁻⁴	CL=95%	—
$\Upsilon(2S)\gamma$	< 1.3 × 10 ⁻⁶	CL=95%	45043
$\Upsilon(3S)X$	< 9.4 × 10 ⁻⁵	CL=95%	—
$\Upsilon(3S)\gamma$	< 2.4 × 10 ⁻⁶	CL=95%	45006
$\Upsilon(1, 2, 3S)\Upsilon(1, 2, 3S)$	< 1.5 × 10 ⁻⁶	CL=95%	—
$D^0\gamma$	< 2.2 × 10 ⁻³	CL=95%	45575
$(D^0/\bar{D}^0)X$	(20.7 ±2.0) %		—
$D^\pm X$	(12.2 ±1.7) %		—
$D^*(2010)^\pm X$	[j] (11.4 ±1.3) %		—
$D_{s1}(2536)^\pm X$	(3.6 ±0.8) × 10 ⁻³		—
$D_{sJ}(2573)^\pm X$	(5.8 ±2.2) × 10 ⁻³		—
$D^*(2629)^\pm X$	searched for		—
B^+X	[k] (6.08 ±0.13) %		—
$B_s^0 X$	[k] (1.59 ±0.13) %		—
$B_c^+ X$	searched for		—
$\Lambda_c^+ X$	(1.54 ±0.33) %		—
$\Xi_c^0 X$	seen		—
$\Xi_b X$	seen		—
b -baryon X	[k] (1.38 ±0.22) %		—
anomalous γ + hadrons	[l] < 3.2 × 10 ⁻³	CL=95%	—
$e^+e^-\gamma$	[l] < 5.2 × 10 ⁻⁴	CL=95%	45594

$\mu^+\mu^-\gamma$	[l] < 5.6	× 10 ⁻⁴	CL=95%	45594
$\tau^+\tau^-\gamma$	[l] < 7.3	× 10 ⁻⁴	CL=95%	45559
$\ell^+\ell^-\gamma\gamma$	[n] < 6.8	× 10 ⁻⁶	CL=95%	—
$q\bar{q}\gamma\gamma$	[n] < 5.5	× 10 ⁻⁶	CL=95%	—
$\nu\bar{\nu}\gamma\gamma$	[n] < 3.1	× 10 ⁻⁶	CL=95%	45594
$e^\pm\mu^\mp$	LF [j] < 2.62	× 10 ⁻⁷	CL=95%	45594
$e^\pm\tau^\mp$	LF [j] < 5.0	× 10 ⁻⁶	CL=95%	45577
$\mu^\pm\tau^\mp$	LF [j] < 6.5	× 10 ⁻⁶	CL=95%	45577
$p e$	L,B < 1.8	× 10 ⁻⁶	CL=95%	45589
$p\mu$	L,B < 1.8	× 10 ⁻⁶	CL=95%	45589

H
was H^0

$J = 0$

Mass $m = 125.20 \pm 0.11$ GeV (S = 1.4)
Full width $\Gamma = 3.7^{+1.9}_{-1.4}$ MeV (assumes equal
on-shell and off-shell effective couplings)

H Signal Strengths in Different Channels

Combined Final States = 1.03 ± 0.04

$WW^* = 1.00 \pm 0.08$

$ZZ^* = 1.02 \pm 0.08$

$\gamma\gamma = 1.10 \pm 0.06$

$c\bar{c}$ Final State < 14, CL = 95%

$b\bar{b} = 0.99 \pm 0.12$

$\mu^+\mu^- = 1.21 \pm 0.35$

$\tau^+\tau^- = 0.91 \pm 0.09$

$Z\gamma = 2.2 \pm 0.7$

$\gamma^*\gamma$ Final State = 1.5 ± 0.5

Fermion coupling (κ_F) = 0.94 ± 0.05

Gauge boson coupling (κ_V) = 1.023 ± 0.026

$t\bar{t}H$ Production = 1.10 ± 0.18

HH Production Cross Section in pp Collisions < 2.4, CL = 95%

tH production = 6 ± 4

H Production Cross Section in pp Collisions at $\sqrt{s} = 13$ TeV =
 56.8 ± 3.4 pb

H DECAY MODES	Fraction (Γ_i/Γ)	Confidence level	p (MeV/c)
WW^*	(25.7 ±2.5) %		—
ZZ^*	(2.80±0.30) %		—
$\gamma\gamma$	(2.50±0.20) × 10 ⁻³		62600
$b\bar{b}$	(53 ±8) %		—
e^+e^-	< 3.0 × 10 ⁻⁴	95%	62600
$\mu^+\mu^-$	(2.6 ±1.3) × 10 ⁻⁴		62600
$\tau^+\tau^-$	(6.0 ^{+0.8} _{-0.7}) %		62575
$Z\gamma$	(3.4 ±1.1) × 10 ⁻³		29392
$Z\rho(770)$	< 1.21 %	95%	29384
$Z\phi(1020)$	< 3.6 × 10 ⁻³	95%	29378
ZJ/ψ	< 1.9 × 10 ⁻³	95%	29267
$Z\psi(2S)$	< 6.6 × 10 ⁻³	95%	29214
$J/\psi\gamma$	< 2.0 × 10 ⁻⁴	95%	62561
$J/\psi J/\psi$	< 3.8 × 10 ⁻⁴	95%	62523
$\psi(2S)\gamma$	< 1.05 × 10 ⁻³	95%	62546
$\psi(2S)J/\psi$	< 2.1 × 10 ⁻³	95%	62507
$\psi(2S)\psi(2S)$	< 3.0 × 10 ⁻³	95%	62491
$\Upsilon(1S)\gamma$	< 2.5 × 10 ⁻⁴	95%	62242
$\Upsilon(1S)\Upsilon(1S)$	< 1.7 × 10 ⁻³	95%	61881
$\Upsilon(2S)\gamma$	< 4.2 × 10 ⁻⁴	95%	62199
$\Upsilon(3S)\gamma$	< 3.4 × 10 ⁻⁴	95%	62172
$\Upsilon(nS)\Upsilon(mS)$	< 3.5 × 10 ⁻⁴	95%	—
$\rho(770)\gamma$	< 1.04 × 10 ⁻³	95%	62597
$\omega(782)\gamma$	< 5.5 × 10 ⁻⁴	95%	62597
$K^*(892)\gamma$	< 2.2 × 10 ⁻⁴	95%	62597
$\phi(1020)\gamma$	< 5 × 10 ⁻⁴	95%	62596
$e\mu$	LF < 4.4 × 10 ⁻⁵	95%	62600
$e\tau$	LF < 2.0 × 10 ⁻³	95%	62587
$\mu\tau$	LF < 1.5 × 10 ⁻³	95%	62587
invisible	< 10.7 %	95%	—
γ invisible	< 2.9 %	95%	—

Gauge & Higgs Boson Summary Table

Neutral Higgs Bosons, Searches for**Mass limits for heavy neutral Higgs bosons (H_2^0, A^0) in the MSSM**

$m > 1121$ GeV, CL = 95%	($\tan\beta = 10$)
$m > 1475$ GeV, CL = 95%	($\tan\beta = 20$)
$m > 1677$ GeV, CL = 95%	($\tan\beta = 30$)
$m > 1826$ GeV, CL = 95%	($\tan\beta = 40$)
$m > 1950$ GeV, CL = 95%	($\tan\beta = 50$)
$m > 2062$ GeV, CL = 95%	($\tan\beta = 60$)

Charged Higgs Bosons (H^\pm and $H^{\pm\pm}$), Searches for**Mass limits for $m_{H^\pm} < m(\text{top})$ in the MSSM**

$m > 155$ GeV, CL = 95%

Mass limits for $m_{H^\pm} > m(\text{top})$ in the MSSM

$m > 181$ GeV, CL = 95%	($\tan\beta = 10$)
$m > 249$ GeV, CL = 95%	($\tan\beta = 20$)
$m > 390$ GeV, CL = 95%	($\tan\beta = 30$)
$m > 894$ GeV, CL = 95%	($\tan\beta = 40$)
$m > 1017$ GeV, CL = 95%	($\tan\beta = 50$)
$m > 1103$ GeV, CL = 95%	($\tan\beta = 60$)

New Heavy Bosons ($W', Z', \text{leptoquarks, etc.}$), Searches for**Additional W Bosons**

W' with standard couplings	
Mass $m > 6000$ GeV, CL = 95%	(pp direct search)
W_R (Right-handed W Boson)	
Mass $m > 715$ GeV, CL = 90%	(electroweak fit)

Additional Z Bosons

Z'_{SM} with standard couplings	
Mass $m > 5150$ GeV, CL = 95%	(pp direct search)
Z'_{LR} of $SU(2)_L \times SU(2)_R \times U(1)$ (with $g_L = g_R$)	
Mass $m > 630$ GeV, CL = 95%	($p\bar{p}$ direct search)
Mass $m > 1162$ GeV, CL = 95%	(electroweak fit)
Z'_χ of $SO(10) \rightarrow SU(5) \times U(1)_\chi$ (with $g_\chi = e/\cos\theta_W$)	
Mass $m > 4800$ GeV, CL = 95%	(pp direct search)
Z'_ψ of $E_6 \rightarrow SO(10) \times U(1)_\psi$ (with $g_\psi = e/\cos\theta_W$)	
Mass $m > 4560$ GeV, CL = 95%	(pp direct search)
Z'_η of $E_6 \rightarrow SU(3) \times SU(2) \times U(1) \times U(1)_\eta$ (with $g_\eta = e/\cos\theta_W$)	
Mass $m > 3.900 \times 10^3$ GeV, CL = 95%	(pp direct search)

Scalar Leptoquarks

$m > 1800$ GeV, CL = 95%	(1st gen., pair prod., $B(eq)=1$)
$m > 1755$ GeV, CL = 95%	(1st gen., single prod., $B(eq)=1$)
$m > 1700$ GeV, CL = 95%	(2nd gen., pair prod., $B(\mu q)=1$)
$m > 660$ GeV, CL = 95%	(2nd gen., single prod., $B(\mu q)=1$)
$m > 1460$ GeV, CL = 95%	(3rd gen., pair prod., $B(\tau b)=1$)
$m > 1280$ GeV, CL = 95%	(3rd gen., single prod., $B(\tau b)=1$)

(See the Particle Listings for assumptions on leptoquark quantum numbers and branching fractions.)

Diquarks

Mass $m > 7200$ GeV, CL = 95%	(E_6 diquark)
-------------------------------	------------------

Axiglun

Mass $m > 6600$ GeV, CL = 95%

Axions (A^0) and Other Very Light Bosons, Searches for

See the review on "Axions and other similar particles."

The best limit for the half-life of neutrinoless double beta decay with Majoron emission is $> 7.2 \times 10^{24}$ years (CL = 90%).

NOTES

In this Summary Table:

When a quantity has "($S = \dots$)" to its right, the error on the quantity has been enlarged by the "scale factor" S , defined as $S = \sqrt{\chi^2/(N-1)}$, where N is the number of measurements used in calculating the quantity. We do this when $S > 1$, which often indicates that the measurements are inconsistent. When $S > 1.25$, we also show in the Particle Listings an ideogram of the measurements. For more about S , see the Introduction.

A decay momentum p is given for each decay mode. For a 2-body decay, p is the momentum of each decay product in the rest frame of the decaying particle. For a 3-or-more-body decay, p is the largest momentum any of the products can have in this frame.

- [a] Theoretical value. A mass as large as a few MeV may not be precluded.
- [b] This value does not include the AALTONEN 22 measurement by CDF. See the W mass section in the listings for details.
- [c] ℓ indicates each type of lepton (e, μ , and τ), not sum over them.
- [d] This represents the width for the decay of the W boson into a charged particle with momentum below detectability, $p < 200$ MeV.
- [e] The Z -boson mass listed here corresponds to a Breit-Wigner resonance parameter. It lies approximately 34 MeV above the real part of the position of the pole (in the energy-squared plane) in the Z -boson propagator.
- [f] This partial width takes into account Z decays into $\nu\bar{\nu}$ and any other possible undetected modes.
- [g] This ratio has not been corrected for the τ mass.
- [h] Here $A \equiv 2g_V g_A / (g_V^2 + g_A^2)$.
- [i] Here ℓ indicates e or μ .
- [j] The value is for the sum of the charge states or particle/antiparticle states indicated.
- [k] This value is updated using the product of (i) the $Z \rightarrow b\bar{b}$ fraction from this listing and (ii) the b -hadron fraction in an unbiased sample of weakly decaying b -hadrons produced in Z -decays provided by the Heavy Flavor Averaging Group (HFLAV, http://www.slac.stanford.edu/xorg/hflav/osc/PDG_2009/#FRACZ).
- [l] See the Z Particle Listings for the γ energy range used in this measurement.
- [n] For $m_{\gamma\gamma} = (60 \pm 5)$ GeV.

Lepton Summary Table

LEPTONS

e	$J = \frac{1}{2}$
Mass $m = (548.579909065 \pm 0.000000016) \times 10^{-6}$ u	
Mass $m = 0.51099895000 \pm 0.0000000015$ MeV	
$ m_{e^+} - m_{e^-} /m < 8 \times 10^{-9}$, CL = 90%	
$ q_{e^+} + q_{e^-} /e < 4 \times 10^{-8}$	
Magnetic moment anomaly	
$(g-2)/2 = (1159.65218062 \pm 0.00000012) \times 10^{-6}$	
$(g_{e^+} - g_{e^-}) / g_{\text{average}} = (-0.5 \pm 2.1) \times 10^{-12}$	
Electric dipole moment $d < 0.041 \times 10^{-28}$ ecm, CL = 90%	
Mean life $\tau > 6.6 \times 10^{28}$ yr, CL = 90% [a]	

μ	$J = \frac{1}{2}$
Mass $m = 0.1134289259 \pm 0.0000000025$ u	
Mass $m = 105.6583755 \pm 0.0000023$ MeV	
Mean life $\tau = (2.1969811 \pm 0.0000022) \times 10^{-6}$ s	
$\tau_{\mu^+} / \tau_{\mu^-} = 1.00002 \pm 0.00008$	
$c\tau = 658.6384$ m	
Magnetic moment anomaly $(g-2)/2 = (11659205.9 \pm 2.2) \times 10^{-10}$	
$(g_{\mu^+} - g_{\mu^-}) / g_{\text{average}} = (-0.11 \pm 0.12) \times 10^{-8}$	
Electric dipole moment $ d < 1.8 \times 10^{-19}$ ecm, CL = 95%	

Decay parameters [b]

$\rho = 0.74979 \pm 0.00026$
$\eta = 0.057 \pm 0.034$
$\delta = 0.75047 \pm 0.00034$
$\xi P_{\mu} = 1.0009 \pm 0.0016$ [c]
$\xi P_{\mu} \delta / \rho = 1.0018 \pm 0.0016$ [c]
$\xi' = 1.00 \pm 0.04$
$\xi'' = 0.98 \pm 0.04$
$\alpha/A = (0 \pm 4) \times 10^{-3}$
$\alpha'/A = (-10 \pm 20) \times 10^{-3}$
$\beta/A = (4 \pm 6) \times 10^{-3}$
$\beta'/A = (2 \pm 7) \times 10^{-3}$
$\overline{\eta} = 0.02 \pm 0.08$

μ^{\pm} modes are charge conjugates of the modes below.

μ^- DECAY MODES	Fraction (Γ_i/Γ)	Confidence level	ρ (MeV/c)
$e^- \overline{\nu}_e \nu_{\mu}$	$\approx 100\%$		53
$e^- \overline{\nu}_e \nu_{\mu} \gamma$	[d] $(6.0 \pm 0.5) \times 10^{-8}$		53
$e^- \overline{\nu}_e \nu_{\mu} e^+ e^-$	[e] $(3.4 \pm 0.4) \times 10^{-5}$		53
Lepton Family number (LF) violating modes			
$e^- \nu_e \overline{\nu}_{\mu}$	LF [f] < 1.2	%	90%
$e^- \gamma$	LF < 4.2	$\times 10^{-13}$	90%
$e^- e^+ e^-$	LF < 1.0	$\times 10^{-12}$	90%
$e^- 2\gamma$	LF < 7.2	$\times 10^{-11}$	90%

τ	$J = \frac{1}{2}$
Mass $m = 1776.93 \pm 0.09$ MeV	
$(m_{\tau^+} - m_{\tau^-})/m_{\text{average}} < 2.8 \times 10^{-4}$, CL = 90%	
Mean life $\tau = (290.3 \pm 0.5) \times 10^{-15}$ s	
$c\tau = 87.03$ μm	
Magnetic moment anomaly = -0.057 to 0.024 , CL = 95%	
$\text{Re}(d_{\tau}) = -0.185$ to 0.061×10^{-16} ecm, CL = 95%	
$\text{Im}(d_{\tau}) = -0.103$ to 0.0230×10^{-16} ecm, CL = 95%	

Weak dipole moment

$\text{Re}(d_{\tau}^W) < 0.50 \times 10^{-17}$ ecm, CL = 95%
$\text{Im}(d_{\tau}^W) < 1.1 \times 10^{-17}$ ecm, CL = 95%

Weak anomalous magnetic dipole moment

$\text{Re}(\alpha_{\tau}^W) < 1.1 \times 10^{-3}$, CL = 95%
$\text{Im}(\alpha_{\tau}^W) < 2.7 \times 10^{-3}$, CL = 95%
$\tau^{\pm} \rightarrow \pi^{\pm} K_S^0 \nu_{\tau}$ (RATE DIFFERENCE) / (RATE SUM) = $(-0.36 \pm 0.25)\%$

Decay parameters

See the τ Particle Listings for a note concerning τ -decay parameters.

$\rho(e \text{ or } \mu) = 0.745 \pm 0.008$
$\rho(e) = 0.747 \pm 0.010$
$\rho(\mu) = 0.763 \pm 0.020$
$\xi(e \text{ or } \mu) = 0.985 \pm 0.030$
$\xi(e) = 0.994 \pm 0.040$
$\xi(\mu) = 1.030 \pm 0.059$
$\eta(e \text{ or } \mu) = 0.013 \pm 0.020$
$\eta(\mu) = 0.094 \pm 0.073$
$(\delta\xi)(e \text{ or } \mu) = 0.746 \pm 0.021$
$(\delta\xi)(e) = 0.734 \pm 0.028$
$(\delta\xi)(\mu) = 0.778 \pm 0.037$
$\xi(\pi) = 0.993 \pm 0.022$
$\xi(\rho) = 0.994 \pm 0.008$
$\xi(a_1) = 1.001 \pm 0.027$
$\xi(\text{all hadronic modes}) = 0.995 \pm 0.007$
$\xi'(\mu) = 0.2 \pm 1.0$
$\overline{\eta}(\mu) = -1.3 \pm 1.7$
$(\xi\kappa)(e \text{ or } \mu) = 0.5 \pm 0.4$
$(\xi\kappa)(e) = -0.4 \pm 1.2$
$(\xi\kappa)(\mu) = 0.8 \pm 0.6$

τ^{\pm} modes are charge conjugates of the modes below. " h^{\pm} " stands for π^{\pm} or K^{\pm} . " e' " stands for e or μ . "Neutrals" stands for γ 's and/or π^0 's.

τ^- DECAY MODES	Fraction (Γ_i/Γ)	Scale factor / Confidence level	ρ (MeV/c)
Modes with one charged particle			
particle $^- \geq 0$ neutrals $\geq 0 K^0 \nu_{\tau}$	$(85.24 \pm 0.06) \%$		—
("1-prong")			
particle $^- \geq 0$ neutrals $\geq 0 K_L^0 \nu_{\tau}$	$(84.58 \pm 0.06) \%$		—
$\mu^- \overline{\nu}_{\mu} \nu_{\tau}$	[g] $(17.39 \pm 0.04) \%$		885
$\mu^- \overline{\nu}_{\mu} \nu_{\tau} \gamma$	[e] $(3.67 \pm 0.08) \times 10^{-3}$		885
$e^- \overline{\nu}_e \nu_{\tau}$	[g] $(17.82 \pm 0.04) \%$		888
$e^- \overline{\nu}_e \nu_{\tau} \gamma$	[e] $(1.83 \pm 0.05) \%$		888
$h^- \geq 0 K_L^0 \nu_{\tau}$	$(12.03 \pm 0.05) \%$		883
$h^- \nu_{\tau}$	$(11.51 \pm 0.05) \%$		883
$\pi^- \nu_{\tau}$	[g] $(10.82 \pm 0.05) \%$		883
$K^- \nu_{\tau}$	[g] $(6.96 \pm 0.10) \times 10^{-3}$		820
$h^- \geq 1$ neutrals ν_{τ}	$(37.00 \pm 0.09) \%$		—
$h^- \geq 1 \pi^0 \nu_{\tau}$ (ex. K^0)	$(36.50 \pm 0.09) \%$		—
$h^- \pi^0 \nu_{\tau}$	$(25.93 \pm 0.09) \%$		878
$\pi^- \pi^0 \nu_{\tau}$	[g] $(25.49 \pm 0.09) \%$		878
$\pi^- \pi^0$ non- $\rho(770) \nu_{\tau}$	$(3.0 \pm 3.2) \times 10^{-3}$		878
$K^- \pi^0 \nu_{\tau}$	[g] $(4.33 \pm 0.15) \times 10^{-3}$		814
$h^- \geq 2 \pi^0 \nu_{\tau}$	$(10.81 \pm 0.09) \%$		—
$h^- 2 \pi^0 \nu_{\tau}$	$(9.48 \pm 0.10) \%$		862
$h^- 2 \pi^0 \nu_{\tau}$ (ex. K^0)	$(9.32 \pm 0.10) \%$		862
$\pi^- 2 \pi^0 \nu_{\tau}$ (ex. K^0)	[g] $(9.26 \pm 0.10) \%$		862
$\pi^- 2 \pi^0 \nu_{\tau}$ (ex. K^0), scalar	< 9	$\times 10^{-3}$ CL=95%	862
$\pi^- 2 \pi^0 \nu_{\tau}$ (ex. K^0), vector	< 7	$\times 10^{-3}$ CL=95%	862
$K^- 2 \pi^0 \nu_{\tau}$ (ex. K^0)	[g] $(6.5 \pm 2.2) \times 10^{-4}$		796
$h^- \geq 3 \pi^0 \nu_{\tau}$	$(1.34 \pm 0.07) \%$		—
$h^- \geq 3 \pi^0 \nu_{\tau}$ (ex. K^0)	$(1.25 \pm 0.07) \%$		—
$h^- 3 \pi^0 \nu_{\tau}$	$(1.18 \pm 0.07) \%$		836
$\pi^- 3 \pi^0 \nu_{\tau}$ (ex. K^0)	[g] $(1.04 \pm 0.07) \%$		836
$K^- 3 \pi^0 \nu_{\tau}$ (ex. K^0)	[g] $(4.8 \pm 2.1) \times 10^{-4}$		766
η			
$h^- 4 \pi^0 \nu_{\tau}$ (ex. K^0)	$(1.6 \pm 0.4) \times 10^{-3}$		800
$h^- 4 \pi^0 \nu_{\tau}$ (ex. K^0, η)	[g] $(1.1 \pm 0.4) \times 10^{-3}$		800
$a_1(1260) \nu_{\tau} \rightarrow \pi^- \gamma \nu_{\tau}$	$(4.0 \pm 1.5) \times 10^{-4}$		—
$K^- \geq 0 \pi^0 \geq 0 K^0 \geq 0 \gamma \nu_{\tau}$	$(1.552 \pm 0.029) \%$		820
$K^- \geq 1 (\pi^0 \text{ or } K^0 \text{ or } \gamma) \nu_{\tau}$	$(8.59 \pm 0.28) \times 10^{-3}$		—
Modes with K^0's			
K_S^0 (particles) $^- \nu_{\tau}$	$(9.43 \pm 0.28) \times 10^{-3}$		—
$h^- \overline{K}^0 \nu_{\tau}$	$(9.87 \pm 0.14) \times 10^{-3}$		812
$\pi^- \overline{K}^0 \nu_{\tau}$	[g] $(8.38 \pm 0.14) \times 10^{-3}$		812
$\pi^- \overline{K}^0$	$(5.4 \pm 2.1) \times 10^{-4}$		812
(non- $K^*(892)^- \nu_{\tau}$)			
$K^- K^0 \nu_{\tau}$	[g] $(1.486 \pm 0.034) \times 10^{-3}$		737
$K^- K^0 \geq 0 \pi^0 \nu_{\tau}$	$(2.99 \pm 0.07) \times 10^{-3}$		737
$h^- \overline{K}^0 \pi^0 \nu_{\tau}$	$(5.32 \pm 0.13) \times 10^{-3}$		794

Lepton Summary Table

$f_1(1285)\pi^-\nu_\tau \rightarrow$ $3\pi^-2\pi^+\nu_\tau$	[g] (5.2 ± 0.4) × 10 ⁻⁵	-
$\pi(1300)^-\nu_\tau \rightarrow$ $(\rho\pi)^-\nu_\tau$	< 1.0 × 10 ⁻⁴ CL=90%	-
$(3\pi)^-\nu_\tau$	< 1.9 × 10 ⁻⁴ CL=90%	-
$\pi(1300)^-\nu_\tau \rightarrow$ $((\pi\pi)_{S\text{-wave}}\pi)^-\nu_\tau$ $(3\pi)^-\nu_\tau$	< 1.9 × 10 ⁻⁴ CL=90%	-
$h^-\omega \geq 0$ neutrals ν_τ	(2.40 ± 0.08) %	708
$h^-\omega\nu_\tau$	(1.99 ± 0.06) %	708
$\pi^-\omega\nu_\tau$	[g] (1.95 ± 0.06) %	708
$K^-\omega\nu_\tau$	[g] (4.1 ± 0.9) × 10 ⁻⁴	610
$h^-\omega\pi^0\nu_\tau$	[g] (4.1 ± 0.4) × 10 ⁻³	684
$h^-\omega2\pi^0\nu_\tau$	(1.4 ± 0.5) × 10 ⁻⁴	644
$\pi^-\omega2\pi^0\nu_\tau$	[g] (7.2 ± 1.6) × 10 ⁻⁵	644
$h^-2\omega\nu_\tau$	< 5.4 × 10 ⁻⁷ CL=90%	250
$2h^-h^+\omega\nu_\tau$	(1.20 ± 0.22) × 10 ⁻⁴	641
$2\pi^-\pi^+\omega\nu_\tau$ (ex. K^0)	[g] (8.4 ± 0.6) × 10 ⁻⁵	641

Lepton Family number (LF), Lepton number (L),
or Baryon number (B) violating modes

L means lepton number violation (e.g. $\tau^- \rightarrow e^+\pi^-\pi^-$). Following common usage, LF means lepton family violation and not lepton number violation (e.g. $\tau^- \rightarrow e^-\pi^+\pi^-$). B means baryon number violation.

$e^-\gamma$	LF	< 3.3 × 10 ⁻⁸ CL=90%	888
$e^-\gamma\gamma$	LF	< 2.5 × 10 ⁻⁴ CL=90%	888
$\mu^-\gamma$	LF	< 4.2 × 10 ⁻⁸ CL=90%	885
$\mu^-\gamma\gamma$	LF	< 5.8 × 10 ⁻⁴ CL=90%	885
$e^-\pi^0$	LF	< 8.0 × 10 ⁻⁸ CL=90%	883
$\mu^-\pi^0$	LF	< 1.1 × 10 ⁻⁷ CL=90%	880
$e^-K_S^0$	LF	< 2.6 × 10 ⁻⁸ CL=90%	819
$\mu^-K_S^0$	LF	< 2.3 × 10 ⁻⁸ CL=90%	815
$e^-\eta$	LF	< 9.2 × 10 ⁻⁸ CL=90%	804
$\mu^-\eta$	LF	< 6.5 × 10 ⁻⁸ CL=90%	800
$e^-\rho^0$	LF	< 2.2 × 10 ⁻⁸ CL=90%	719
$\mu^-\rho^0$	LF	< 1.7 × 10 ⁻⁸ CL=90%	715
$e^-\omega$	LF	< 2.4 × 10 ⁻⁸ CL=90%	716
$\mu^-\omega$	LF	< 3.9 × 10 ⁻⁸ CL=90%	711
$e^-K^*(892)^0$	LF	< 1.9 × 10 ⁻⁸ CL=90%	665
$\mu^-K^*(892)^0$	LF	< 2.9 × 10 ⁻⁸ CL=90%	659
$e^-K^*(892)^0$	LF	< 1.7 × 10 ⁻⁸ CL=90%	665
$\mu^-K^*(892)^0$	LF	< 4.3 × 10 ⁻⁸ CL=90%	659
$e^-\eta'(958)$	LF	< 1.6 × 10 ⁻⁷ CL=90%	630
$\mu^-\eta'(958)$	LF	< 1.3 × 10 ⁻⁷ CL=90%	625
$e^-f_0(980) \rightarrow e^-\pi^+\pi^-$	LF	< 3.2 × 10 ⁻⁸ CL=90%	-
$\mu^-f_0(980) \rightarrow \mu^-\pi^+\pi^-$	LF	< 3.4 × 10 ⁻⁸ CL=90%	-
$e^-\phi$	LF	< 2.0 × 10 ⁻⁸ CL=90%	596
$\mu^-\phi$	LF	< 2.3 × 10 ⁻⁸ CL=90%	590
$e^-e^+e^-$	LF	< 2.7 × 10 ⁻⁸ CL=90%	888
$e^-\mu^+\mu^-$	LF	< 2.7 × 10 ⁻⁸ CL=90%	882
$e^+\mu^-\mu^-$	LF	< 1.7 × 10 ⁻⁸ CL=90%	882
$\mu^-e^+e^-$	LF	< 1.8 × 10 ⁻⁸ CL=90%	885
$\mu^+e^-e^-$	LF	< 1.5 × 10 ⁻⁸ CL=90%	885
$\mu^-\mu^+\mu^-$	LF	< 2.1 × 10 ⁻⁸ CL=90%	873
$e^-\pi^+\pi^-$	LF	< 2.3 × 10 ⁻⁸ CL=90%	877
$e^+\pi^-\pi^-$	L	< 2.0 × 10 ⁻⁸ CL=90%	877
$\mu^-\pi^+\pi^-$	LF	< 2.1 × 10 ⁻⁸ CL=90%	866
$\mu^+\pi^-\pi^-$	L	< 3.9 × 10 ⁻⁸ CL=90%	866
$e^-\pi^+K^-$	LF	< 3.7 × 10 ⁻⁸ CL=90%	813
$e^-\pi^-K^+$	LF	< 3.1 × 10 ⁻⁸ CL=90%	813
$e^+\pi^-K^-$	L	< 3.2 × 10 ⁻⁸ CL=90%	813
$e^-K_S^0K_S^0$	LF	< 7.1 × 10 ⁻⁸ CL=90%	736
$e^-K^+K^-$	LF	< 3.4 × 10 ⁻⁸ CL=90%	739
$e^+K^-K^-$	L	< 3.3 × 10 ⁻⁸ CL=90%	739
$\mu^-\pi^+K^-$	LF	< 8.6 × 10 ⁻⁸ CL=90%	800
$\mu^-\pi^-K^+$	LF	< 4.5 × 10 ⁻⁸ CL=90%	800
$\mu^+\pi^-K^-$	L	< 4.8 × 10 ⁻⁸ CL=90%	800
$\mu^-K_S^0K_S^0$	LF	< 8.0 × 10 ⁻⁸ CL=90%	696
$\mu^-K^+K^-$	LF	< 4.4 × 10 ⁻⁸ CL=90%	699
$\mu^+K^-K^-$	L	< 4.7 × 10 ⁻⁸ CL=90%	699
$e^-\pi^0\pi^0$	LF	< 6.5 × 10 ⁻⁶ CL=90%	878
$\mu^-\pi^0\pi^0$	LF	< 1.4 × 10 ⁻⁵ CL=90%	867
$e^-\eta\eta$	LF	< 3.5 × 10 ⁻⁵ CL=90%	699
$\mu^-\eta\eta$	LF	< 6.0 × 10 ⁻⁵ CL=90%	653
$e^-\pi^0\eta$	LF	< 2.4 × 10 ⁻⁵ CL=90%	798
$\mu^-\pi^0\eta$	LF	< 2.2 × 10 ⁻⁵ CL=90%	784
$p e^- e^-$	L, B	< 3.0 × 10 ⁻⁸ CL=90%	641
$\bar{p} e^+ e^-$	L, B	< 3.0 × 10 ⁻⁸ CL=90%	641

$\bar{p} e^+ \mu^-$	L, B	< 2.0 × 10 ⁻⁸ CL=90%	635
$\bar{p} e^- \mu^+$	L, B	< 1.8 × 10 ⁻⁸ CL=90%	635
$p \mu^- \mu^-$	L, B	< 4.0 × 10 ⁻⁸ CL=90%	618
$\bar{p} \mu^+ \mu^-$	L, B	< 1.8 × 10 ⁻⁸ CL=90%	618
$\bar{p} \gamma$	L, B	< 3.5 × 10 ⁻⁶ CL=90%	641
$\bar{p} \pi^0$	L, B	< 1.5 × 10 ⁻⁵ CL=90%	632
$\bar{p} 2\pi^0$	L, B	< 3.3 × 10 ⁻⁵ CL=90%	604
$\bar{p} \eta$	L, B	< 8.9 × 10 ⁻⁶ CL=90%	475
$\bar{p} \pi^0 \eta$	L, B	< 2.7 × 10 ⁻⁵ CL=90%	360
$\Lambda \pi^-$	L, B	< 7.2 × 10 ⁻⁸ CL=90%	525
$\bar{\Lambda} \pi^-$	L, B	< 1.4 × 10 ⁻⁷ CL=90%	525
e^- light boson	LF	< 9 × 10 ⁻⁴ CL=95%	-
μ^- light boson	LF	< 6 × 10 ⁻⁴ CL=95%	-

Heavy Charged Lepton Searches

 L^\pm – charged lepton

Mass $m > 100.8$ GeV, CL = 95% ^[h] Decay to νW .

 L^\pm – stable charged heavy lepton

Mass $m > 102.6$ GeV, CL = 95%

Neutrino Properties

See the note on “Neutrino properties listings” in the Particle Listings.

Mass $m < 0.8$ eV, CL = 90% (tritium decay)

Mean life/mass, $\tau/m > 300$ s/eV, CL = 90% (reactor)

Mean life/mass, $\tau/m > 7 \times 10^9$ s/eV (solar)

Mean life/mass, $\tau/m > 15.4$ s/eV, CL = 90% (accelerator)

Magnetic moment $\mu < 0.064 \times 10^{-10} \mu_B$, CL = 90% (solar + radiochemical)

Number of Neutrino Types

Number $N = 2.996 \pm 0.007$ (Standard Model fits to LEP-SLC data)

Number $N = 2.92 \pm 0.05$ (S = 1.2) (Direct measurement of invisible Z width)

Neutrino Mixing

The following values are obtained through data analyses based on the 3-neutrino mixing scheme described in the review “Neutrino Masses, Mixing, and Oscillations.”

$$\sin^2(\theta_{12}) = 0.307 \pm 0.013$$

$$\Delta m_{21}^2 = (7.53 \pm 0.18) \times 10^{-5} \text{ eV}^2$$

$$\sin^2(\theta_{23}) = 0.553 \pm_{-0.024}^{+0.016} \text{ (S = 1.1) (Inverted order)}$$

$$\sin^2(\theta_{23}) = 0.558 \pm_{-0.021}^{+0.015} \text{ (Normal order)}$$

$$\Delta m_{32}^2 = (-2.529 \pm 0.029) \times 10^{-3} \text{ eV}^2 \text{ (Inverted order)}$$

$$\Delta m_{32}^2 = (2.455 \pm 0.028) \times 10^{-3} \text{ eV}^2 \text{ (Normal order)}$$

$$\sin^2(\theta_{13}) = (2.19 \pm 0.07) \times 10^{-2} \text{ (S = 1.2)}$$

$$\delta, \text{ CP violating phase} = 1.19 \pm 0.22 \text{ } \pi \text{ rad (S = 1.2)}$$

$$\langle \Delta m_{21}^2 - \Delta \bar{m}_{21}^2 \rangle < 1.1 \times 10^{-4} \text{ eV}^2, \text{ CL} = 99.7\%$$

$$\langle \Delta m_{32}^2 - \Delta \bar{m}_{32}^2 \rangle = (-0.12 \pm 0.25) \times 10^{-3} \text{ eV}^2$$

NOTES

In this Summary Table:

When a quantity has “(S = ...)” to its right, the error on the quantity has been enlarged by the “scale factor” S, defined as $S = \sqrt{\chi^2/(N-1)}$, where N is the number of measurements used in calculating the quantity. We do this when $S > 1$, which often indicates that the measurements are inconsistent. When $S > 1.25$, we also show in the Particle Listings an ideogram of the measurements. For more about S, see the Introduction.

A decay momentum p is given for each decay mode. For a 2-body decay, p is the momentum of each decay product in the rest frame of the decaying particle. For a 3-or-more-body decay, p is the largest momentum any of the products can have in this frame.

[a] This is the best limit for the mode $e^- \rightarrow \nu \gamma$.

Lepton Summary Table

-
- [b] See the review on “Muon Decay Parameters” for definitions and details.
- [c] P_μ is the longitudinal polarization of the muon from pion decay. For $V-A$ coupling, $P_\mu = 1$ and $\rho = \delta = 3/4$.
- [d] This only includes events with energy of $e > 45$ MeV and energy of $\gamma > 40$ MeV. Since the $e^- \bar{\nu}_e \nu_\mu$ and $e^- \bar{\nu}_e \nu_\mu \gamma$ modes cannot be clearly separated, we regard the latter mode as a subset of the former.

- [e] See the relevant Particle Listings for the energy limits used in this measurement.
- [f] A test of additive vs. multiplicative lepton family number conservation.
- [g] Basis mode for the τ .
- [h] L^\pm mass limit depends on decay assumptions; see the Full Listings.

Quark Summary Table

QUARKS

The u -, d -, and s -quark masses are the \overline{MS} masses at the scale $\mu = 2$ GeV. The c - and b -quark masses are the \overline{MS} masses renormalized at the \overline{MS} mass, i.e. $\overline{m} = \overline{m}(\mu = \overline{m})$. The t -quark mass is extracted from event kinematics (see the review "The Top Quark").

u	$I(J^P) = \frac{1}{2}(\frac{1}{2}^+)$
$m_u = 2.16 \pm 0.07$ MeV, CL = 90% Charge = $\frac{2}{3} e$ $I_z = +\frac{1}{2}$ $m_u/m_d = 0.462 \pm 0.020$, CL = 90%	
d	$I(J^P) = \frac{1}{2}(\frac{1}{2}^+)$
$m_d = 4.70 \pm 0.07$ MeV, CL = 90% Charge = $-\frac{1}{3} e$ $I_z = -\frac{1}{2}$ $m_s/m_d = 17-22$ $\overline{m} = (m_u + m_d)/2 = 3.49 \pm 0.07$ MeV, CL = 90%	
s	$I(J^P) = 0(\frac{1}{2}^+)$
$m_s = 93.5 \pm 0.8$ MeV, CL = 90% Charge = $-\frac{1}{3} e$ Strangeness = -1 $m_s / ((m_u + m_d)/2) = 27.33_{-0.14}^{+0.18}$, CL = 90%	
c	$I(J^P) = 0(\frac{1}{2}^+)$
$m_c = 1.2730 \pm 0.0046$ GeV, CL = 90% Charge = $\frac{2}{3} e$ Charm = $+1$ $m_b - m_c = 3.45 \pm 0.05$ GeV	
b	$I(J^P) = 0(\frac{1}{2}^+)$
$m_b = 4.183 \pm 0.007$ GeV, CL = 90% Charge = $-\frac{1}{3} e$ Bottom = -1	
t	$I(J^P) = 0(\frac{1}{2}^+)$
Charge = $\frac{2}{3} e$ Top = $+1$	

Mass (direct measurements) $m = 172.57 \pm 0.29$ GeV [a,b] (S = 1.5)
 Mass (from cross-section measurements) $m = 162.5_{-1.5}^{+2.1}$ GeV [a]
 Mass (Pole from cross-section measurements) $m = 172.4 \pm 0.7$ GeV
 $m_t - m_{\bar{t}} = -0.15 \pm 0.20$ GeV (S = 1.1)
 Full width $\Gamma = 1.42_{-0.15}^{+0.19}$ GeV (S = 1.4)
 $\Gamma(Wb)/\Gamma(Wq(q = b, s, d)) = 0.957 \pm 0.034$ (S = 1.5)

t-quark EW Couplings

$F_0 = 0.693 \pm 0.013$
 $F_- = 0.315 \pm 0.010$
 $F_+ = -0.005 \pm 0.007$
 $F_{V+A} < 0.29$, CL = 95%

DECAY MODES	Fraction (Γ_i/Γ)	Confidence level	P (MeV/c)
$Wq(q = b, s, d)$			—
Wb			—
$e\nu_e b$	(11.10 ± 0.30) %		—
$\mu\nu_\mu b$	(11.40 ± 0.20) %		—
$\tau\nu_\tau b$	(10.7 ± 0.5) %		—
$q\bar{q}b$	(66.5 ± 1.4) %		—
$\gamma q(q = u, c)$	[c] < 4.5	$\times 10^{-5}$	95%
$\Delta T = 1$ weak neutral current (TI) modes			
$Zq(q = u, c)$	TI	[d] < 1.2	$\times 10^{-4}$ 95%
Hu	TI	< 1.9	$\times 10^{-4}$ 95%
Hc	TI	< 4.3	$\times 10^{-4}$ 95%
$\ell^+ \bar{q} q' (q = d, s, b; q' = u, c)$	TI	< 1.6	$\times 10^{-3}$ 95%
Lepton Family number (LF) violating modes			
$e^\pm \mu^\mp c$	LF	< 8.9	$\times 10^{-7}$ —
$e^\pm \mu^\mp u$	LF	< 7	$\times 10^{-8}$ —

b' (4th Generation) Quark, Searches for

Mass $m > 190$ GeV, CL = 95% ($\rho\bar{\rho}$, quasi-stable b')
 Mass $m > 1390$ GeV, CL = 95% ($B(b' \rightarrow Zb) = 1$)
 Mass $m > 1350$ GeV, CL = 95% ($B(b' \rightarrow Wt) = 1$)
 Mass $m > 1570$ GeV, CL = 95% ($B(b' \rightarrow Hb) = 1$)
 Mass $m > 46.0$ GeV, CL = 95% ($e^+ e^-$, all decays)

t' (4th Generation) Quark, Searches for

$m(t'(2/3)) > 1280$ GeV, CL = 95% ($B(t' \rightarrow Zt) = 1$)
 $m(t'(2/3)) > 1295$ GeV, CL = 95% ($B(t' \rightarrow Wb) = 1$)
 $m(t'(2/3)) > 1310$ GeV, CL = 95% (singlet t')
 $m(t'(2/3)) > 1350$ GeV, CL = 95% (t' in a weak isospin doublet (t', b'))
 $m(t'(5/3)) > 1.460 \times 10^3$ GeV, CL = 95% ($t'(5/3) \rightarrow tW^+$)

Free Quark Searches

All searches since 1977 have had negative results.

NOTES

- [a] A discussion of the definition of the top quark mass in these measurements can be found in the review "The Top Quark."
 [b] Based on published top mass measurements using data from Tevatron Run-I and Run-II and LHC at $\sqrt{s} = 7$ TeV. Including the most recent unpublished results from Tevatron Run-II, the Tevatron Electroweak Working Group reports a top mass of 173.2 ± 0.9 GeV. See the note "The Top Quark" in the Quark Particle Listings of this Review.
 [c] This limit is for $\Gamma(t \rightarrow \gamma q)/\Gamma(t \rightarrow Wb)$.
 [d] This limit is for $\Gamma(t \rightarrow Zq)/\Gamma(t \rightarrow Wb)$.

Meson Summary Table

LIGHT UNFLAVORED MESONS ($S = C = B = 0$)

For $I = 1$ (π, b, ρ, a): $u\bar{d}, (u\bar{u}-d\bar{d})/\sqrt{2}, d\bar{u}$;
for $I = 0$ ($\eta, \eta', h, h', \omega, \phi, f, f'$): $c_1(u\bar{u} + d\bar{d}) + c_2(s\bar{s})$

 π^\pm

$$J^G(J^PC) = 1^-(0^-)$$

Mass $m = 139.57039 \pm 0.00018$ MeV ($S = 1.8$)
Mean life $\tau = (2.6033 \pm 0.0005) \times 10^{-8}$ s ($S = 1.2$)
 $c\tau = 7.8045$ m

$\pi^\pm \rightarrow \ell^\pm \nu \gamma$ form factors [a]

$F_V = 0.0254 \pm 0.0017$
 $F_A = 0.0119 \pm 0.0001$
 F_V slope parameter $a = 0.10 \pm 0.06$
 $R = 0.059^{+0.009}_{-0.008}$

π^- modes are charge conjugates of the modes below.

For decay limits to particles which are not established, see the section on Searches for Axions and Other Very Light Bosons.

π^\pm DECAY MODES	Fraction (Γ_i/Γ)	Confidence level	Scale factor/ Confidence level	p (MeV/c)
$\mu^+ \nu_\mu$	[b] (99.98770 \pm 0.00004) %			30
$\mu^+ \nu_\mu \gamma$	[c] (2.00 \pm 0.25) $\times 10^{-4}$			30
$e^+ \nu_e$	[b] (1.230 \pm 0.004) $\times 10^{-4}$			70
$e^+ \nu_e \gamma$	[c] (7.39 \pm 0.05) $\times 10^{-7}$			70
$e^+ \nu_e \pi^0$	(1.036 \pm 0.006) $\times 10^{-8}$			4
$e^+ \nu_e e^+ e^-$	(3.2 \pm 0.5) $\times 10^{-9}$			70
$\mu^+ \nu_\mu \nu \bar{\nu}$	< 9 $\times 10^{-6}$	90%		30
$e^+ \nu_e \nu \bar{\nu}$	< 1.6 $\times 10^{-7}$	90%		70
Lepton Family number (LF) or Lepton number (L) violating modes				
$\mu^+ \bar{\nu}_e$	L [d] < 1.5 $\times 10^{-3}$	90%		30
$\mu^+ \nu_e$	LF [d] < 8.0 $\times 10^{-3}$	90%		30
$\mu^- e^+ e^+ \nu$	LF < 1.6 $\times 10^{-6}$	90%		30

 π^0

$$J^G(J^PC) = 1^-(0^{+-})$$

Mass $m = 134.9768 \pm 0.0005$ MeV ($S = 1.1$)
 $m_{\pi^\pm} - m_{\pi^0} = 4.5936 \pm 0.0005$ MeV
Mean life $\tau = (8.43 \pm 0.13) \times 10^{-17}$ s ($S = 1.2$)
 $c\tau = 25.3$ nm

For decay limits to particles which are not established, see the appropriate Search sections (A^0 (axion) and Other Light Boson (X^0) Searches, etc.).

π^0 DECAY MODES	Fraction (Γ_i/Γ)	Confidence level	Scale factor/ Confidence level	p (MeV/c)
2γ	(98.823 \pm 0.034) %		S=1.5	67
$e^+ e^- \gamma$	(1.174 \pm 0.035) %		S=1.5	67
γ positronium	(1.82 \pm 0.29) $\times 10^{-9}$			67
$e^+ e^+ e^- e^-$	(3.34 \pm 0.16) $\times 10^{-5}$			67
$e^+ e^-$	(6.46 \pm 0.33) $\times 10^{-8}$			67
4γ	< 2 $\times 10^{-8}$	CL=90%		67
invisible	< 4.4 $\times 10^{-9}$	CL=90%		-
$\nu_e \bar{\nu}_e$	< 1.7 $\times 10^{-6}$	CL=90%		67
$\nu_\mu \bar{\nu}_\mu$	< 1.6 $\times 10^{-6}$	CL=90%		67
$\nu_\tau \bar{\nu}_\tau$	< 2.1 $\times 10^{-6}$	CL=90%		67
$\gamma \nu \bar{\nu}$	< 1.9 $\times 10^{-7}$	CL=90%		67
Charge conjugation (C) or Lepton Family number (LF) violating modes				
3γ	C < 3.1 $\times 10^{-8}$	CL=90%		67
$\mu^+ e^-$	LF < 3.8 $\times 10^{-10}$	CL=90%		26
$\mu^- e^+$	LF < 3.2 $\times 10^{-10}$	CL=90%		26
$\mu^+ e^- + \mu^- e^+$	LF < 3.6 $\times 10^{-10}$	CL=90%		26

 η

$$J^G(J^PC) = 0^+(0^{+-})$$

Mass $m = 547.862 \pm 0.017$ MeV
Full width $\Gamma = 1.31 \pm 0.05$ keV

C-nonconserving decay parameters

$\pi^+ \pi^- \pi^0$ left-right asymmetry = $(0.09 \pm 0.11) \times 10^{-2}$
 $\pi^+ \pi^- \pi^0$ sextant asymmetry = $(0.12 \pm 0.10) \times 10^{-2}$
 $\pi^+ \pi^- \pi^0$ quadrant asymmetry = $(-0.09 \pm 0.09) \times 10^{-2}$
 $\pi^+ \pi^- \gamma$ left-right asymmetry = $(0.9 \pm 0.4) \times 10^{-2}$
 $\pi^+ \pi^- \gamma$ β (D-wave) = -0.02 ± 0.07 ($S = 1.3$)

CP-nonconserving decay parameters

$\pi^+ \pi^- e^+ e^-$ decay-plane asymmetry $A_\phi = (-0.6 \pm 3.1) \times 10^{-2}$

Other decay parameters

$\pi^0 \pi^0 \pi^0$ Dalitz plot $\alpha = -0.0296 \pm 0.0016$ ($S = 1.7$)
Parameter Λ in $\eta \rightarrow \ell^+ \ell^- \gamma$ decay = 0.716 ± 0.011 GeV/c²

 η DECAY MODES

	Fraction (Γ_i/Γ)	Confidence level	Scale factor/ Confidence level	p (MeV/c)
Neutral modes				
neutral modes	(71.96 \pm 0.30) %		S=1.3	-
2γ	(39.36 \pm 0.18) %		S=1.1	274
$3\pi^0$	(32.57 \pm 0.21) %		S=1.2	179
$\pi^0 2\gamma$	(2.55 \pm 0.22) $\times 10^{-4}$			257
$2\pi^0 2\gamma$	< 1.2 $\times 10^{-3}$	CL=90%		238
4γ	< 2.8 $\times 10^{-4}$	CL=90%		274
invisible	< 1.0 $\times 10^{-4}$	CL=90%		-
Charged modes				
charged modes	(28.04 \pm 0.30) %		S=1.3	-
$\pi^+ \pi^- \pi^0$	(23.02 \pm 0.25) %		S=1.2	174
$\pi^+ \pi^- \gamma$	(4.28 \pm 0.07) %		S=1.1	236
$e^+ e^- \gamma$	(6.9 \pm 0.4) $\times 10^{-3}$		S=1.2	274
$\mu^+ \mu^- \gamma$	(3.1 \pm 0.4) $\times 10^{-4}$			253
$e^+ e^-$	< 7 $\times 10^{-7}$	CL=90%		274
$\mu^+ \mu^-$	(5.8 \pm 0.8) $\times 10^{-6}$			253
$2e^+ 2e^-$	(2.40 \pm 0.22) $\times 10^{-5}$			274
$\pi^+ \pi^- e^+ e^- (\gamma)$	(2.68 \pm 0.11) $\times 10^{-4}$			235
$e^+ e^- \mu^+ \mu^-$	< 1.6 $\times 10^{-4}$	CL=90%		253
$2\mu^+ 2\mu^-$	(5.0 \pm 1.3) $\times 10^{-9}$			161
$\mu^+ \mu^- \pi^+ \pi^-$	< 3.6 $\times 10^{-4}$	CL=90%		113
$\pi^+ e^- \bar{\nu}_e + c.c.$	< 1.7 $\times 10^{-4}$	CL=90%		256
$\pi^+ \pi^- 2\gamma$	< 2.1 $\times 10^{-3}$			236
$\pi^+ \pi^- \pi^0 \gamma$	< 6 $\times 10^{-4}$	CL=90%		174
$\pi^0 \mu^+ \mu^- \gamma$	< 3 $\times 10^{-6}$	CL=90%		210

**Charge conjugation (C), Parity (P),
Charge conjugation \times Parity (CP), or
Lepton Family number (LF) violating modes**

$\pi^0 \gamma$	C [e] < 9 $\times 10^{-5}$	CL=90%	257
$\pi^+ \pi^-$	P, CP < 4.4 $\times 10^{-6}$	CL=90%	236
$2\pi^0$	P, CP < 3.5 $\times 10^{-4}$	CL=90%	238
$2\pi^0 \gamma$	C < 5 $\times 10^{-4}$	CL=90%	238
$3\pi^0 \gamma$	C < 6 $\times 10^{-5}$	CL=90%	179
3γ	C < 1.6 $\times 10^{-5}$	CL=90%	274
$4\pi^0$	P, CP < 6.9 $\times 10^{-7}$	CL=90%	40
$\pi^0 e^+ e^-$	C [f] < 8 $\times 10^{-6}$	CL=90%	257
$\pi^0 \mu^+ \mu^-$	C [f] < 5 $\times 10^{-6}$	CL=90%	210
$\mu^+ e^- + \mu^- e^+$	LF < 6 $\times 10^{-6}$	CL=90%	264

 $f_0(500)$

$$J^G(J^PC) = 0^+(0^{++})$$

also known as σ ; was $f_0(600)$, $f_0(400-1200)$

See the review on "Scalar Mesons below 1 GeV."

Mass (T-Matrix Pole \sqrt{s}) = $(400-550) - i(200-350)$ MeV

Mass (Breit-Wigner) = 400 to 800 MeV

Full width (Breit-Wigner) = 100 to 800 MeV

 $f_0(500)$ DECAY MODES

	Fraction (Γ_i/Γ)	Confidence level	p (MeV/c)
$\pi\pi$	seen		-
$\gamma\gamma$	seen		-

 $\rho(770)$

$$J^G(J^PC) = 1^+(1^{--})$$

See the review on "Spectroscopy of Light Meson Resonances."

T-Matrix Pole $\sqrt{s} = (761-765) - i(71-74)$ MeV

ρ^0 mass (Breit-Wigner) = 775.26 ± 0.23 MeV [g]

ρ^0 full width (Breit-Wigner) = 147.4 ± 0.8 MeV [g] ($S = 2.0$)

 $\rho(770)$ DECAY MODES

	Fraction (Γ_i/Γ)	Confidence level	Scale factor/ Confidence level	p (MeV/c)
$\pi\pi$	~ 100 %			363
$\rho(770)^\pm$ decays				
$\pi^\pm \gamma$	(4.5 \pm 0.5) $\times 10^{-4}$		S=2.2	375
$\pi^\pm \eta$	< 6 $\times 10^{-3}$	CL=84%		152
$\pi^\pm \pi^+ \pi^- \pi^0$	< 2.0 $\times 10^{-3}$	CL=84%		254

Meson Summary Table

$\rho(770)^0$ decays			
$\pi^+\pi^-\gamma$	(9.9 ± 1.6) × 10 ⁻³		362
$\pi^0\gamma$	(4.7 ± 0.8) × 10 ⁻⁴	S=1.7	376
$\eta\gamma$	(3.00 ± 0.21) × 10 ⁻⁴		194
$\pi^0\pi^0\gamma$	(4.5 ± 0.8) × 10 ⁻⁵		363
$\mu^+\mu^-$	[h] (4.55 ± 0.28) × 10 ⁻⁵		373
e^+e^-	[h] (4.72 ± 0.05) × 10 ⁻⁵		388
$\pi^+\pi^-\pi^0$	(1.01 ± 0.54 -0.36 ± 0.34) × 10 ⁻⁴		323
$\pi^+\pi^-\pi^+\pi^-$	(1.8 ± 0.9) × 10 ⁻⁵		251
$\pi^+\pi^-\pi^0\pi^0$	(1.6 ± 0.8) × 10 ⁻⁵		257
$\pi^0e^+e^-$	< 1.2 × 10 ⁻⁵	CL=90%	376

 $\omega(782)$

$$I^G(J^{PC}) = 0^-(1^--)$$

Mass $m = 782.66 \pm 0.13$ MeV (S = 2.0)Full width $\Gamma = 8.68 \pm 0.13$ MeV

$\omega(782)$ DECAY MODES	Fraction (Γ_i/Γ)	Scale factor/ Confidence level	ρ (MeV/c)
$\pi^+\pi^-\pi^0$	(89.2 ± 0.7) %		327
$\pi^0\gamma$	(8.35 ± 0.27) %	S=2.2	380
$\pi^+\pi^-$	(1.53 ± 0.12) %	S=1.2	366
neutrals (excluding $\pi^0\gamma$)	(7 ± 8) × 10 ⁻³	S=1.1	-
$\eta\gamma$	(4.5 ± 0.4) × 10 ⁻⁴	S=1.1	200
$\pi^0e^+e^-$	(7.7 ± 0.6) × 10 ⁻⁴		380
$\pi^0\mu^+\mu^-$	(1.34 ± 0.18) × 10 ⁻⁴	S=1.5	349
e^+e^-	(7.38 ± 0.22) × 10 ⁻⁵	S=1.9	391
$\pi^+\pi^-\pi^0\pi^0$	< 2 × 10 ⁻⁴	CL=90%	262
$\pi^+\pi^-\gamma$	< 3.6 × 10 ⁻³	CL=95%	366
$\pi^+\pi^-\pi^+\pi^-$	< 1 × 10 ⁻³	CL=90%	256
$\pi^0\pi^0\gamma$	(6.7 ± 1.1) × 10 ⁻⁵		367
$\eta\pi^0\gamma$	< 3.3 × 10 ⁻⁵	CL=90%	162
$\mu^+\mu^-$	(7.4 ± 1.8) × 10 ⁻⁵		377
3γ	< 1.9 × 10 ⁻⁴	CL=95%	391

Charge conjugation (C) violating modes

$\eta\pi^0$	C < 2.1 × 10 ⁻⁴	CL=90%	162
$2\pi^0$	C < 2.2 × 10 ⁻⁴	CL=90%	367
$3\pi^0$	C < 2.3 × 10 ⁻⁴	CL=90%	330
invisible	< 7 × 10 ⁻⁵	CL=90%	-

 $\eta'(958)$

$$I^G(J^{PC}) = 0^+(0^{+-})$$

Mass $m = 957.78 \pm 0.06$ MeVFull width $\Gamma = 0.188 \pm 0.006$ MeV

$\eta'(958)$ DECAY MODES	Fraction (Γ_i/Γ)	Confidence level	ρ (MeV/c)
$\pi^+\pi^-\eta$	(42.5 ± 0.5) %		232
$\rho^0\gamma$ (including non-resonant)	(29.5 ± 0.4) %		165
$\pi^+\pi^-\pi^-\gamma$			
$\pi^0\pi^0\eta$	(22.4 ± 0.5) %		239
$\omega\gamma$	(2.52 ± 0.07) %		159
ωe^+e^-	(2.0 ± 0.4) × 10 ⁻⁴		159
$\gamma\gamma$	(2.307 ± 0.033) %		479
$3\pi^0$	(2.50 ± 0.17) × 10 ⁻³		430
$\mu^+\mu^-\gamma$	(1.13 ± 0.28) × 10 ⁻⁴		467
$\pi^+\pi^-\mu^+\mu^-$	(1.9 ± 0.4) × 10 ⁻⁵		401
$\pi^+\pi^-\pi^0$	(3.61 ± 0.17) × 10 ⁻³		428
($\pi^+\pi^-\pi^0$) S-wave	(3.8 ± 0.5) × 10 ⁻³		428
$\pi^\mp\rho^\pm$	(7.4 ± 2.3) × 10 ⁻⁴		106
$2(\pi^+\pi^-)$	(8.3 ± 0.9) × 10 ⁻⁵		372
$\pi^+\pi^-2\pi^0$	(1.8 ± 0.4) × 10 ⁻⁴		376
$2(\pi^+\pi^-)$ neutrals	< 1 %	95%	-
$2(\pi^+\pi^-)\pi^0$	< 1.8 × 10 ⁻³	90%	298
$2(\pi^+\pi^-)2\pi^0$	< 1 %	95%	197
$3(\pi^+\pi^-)$	< 3.1 × 10 ⁻⁵	90%	189
$K^\pm\pi^\mp$	< 4 × 10 ⁻⁵	90%	334
$\pi^+\pi^-e^+e^-$	(2.42 ± 0.10) × 10 ⁻³		458
$\pi^+e^-\nu_e + c.c.$	< 2.1 × 10 ⁻⁴	90%	469
γe^+e^-	(4.91 ± 0.27) × 10 ⁻⁴		479
$\pi^0\gamma\gamma$	(3.20 ± 0.24) × 10 ⁻³		469
$\pi^0\gamma\gamma$ (non resonant)	(6.2 ± 0.9) × 10 ⁻⁴		-
$\eta\gamma\gamma$	< 1.33 × 10 ⁻⁴	90%	322
$4\pi^0$	< 4.94 × 10 ⁻⁵	90%	380

e^+e^-	< 5.6 × 10 ⁻⁹	90%	479
$e^+e^-\pi^+\pi^-$	(4.5 ± 1.1) × 10 ⁻⁶		479
invisible	< 6 × 10 ⁻⁴	90%	-

Charge conjugation (C), Parity (P),
Lepton family number (LF) violating modes

$\pi^+\pi^-$	P,CP < 1.8 × 10 ⁻⁵	90%	458
$\pi^0\pi^0$	P,CP < 4 × 10 ⁻⁴	90%	459
$\pi^0e^+e^-$	C [f] < 1.4 × 10 ⁻³	90%	469
$\pi^0\rho^0$	C < 4 %	90%	111
ηe^+e^-	C [f] < 2.4 × 10 ⁻³	90%	322
3γ	C < 1.0 × 10 ⁻⁴	90%	479
$\mu^+\mu^-\pi^0$	C [f] < 6.0 × 10 ⁻⁵	90%	445
$\mu^+\mu^-\eta$	C [f] < 1.5 × 10 ⁻⁵	90%	273
$e\mu$	LF < 4.7 × 10 ⁻⁴	90%	473

 $f_0(980)$

$$I^G(J^{PC}) = 0^+(0^{++})$$

See the review on "Scalar Mesons below 1 GeV."

T-matrix pole $\sqrt{s} = (980-1010) - i(20-35)$ MeV [1]

Mass (Breit-Wigner) = 990 ± 20 MeV [1]

Full width (Breit-Wigner) = 10 to 100 MeV [1]

$f_0(980)$ DECAY MODES	Fraction (Γ_i/Γ)	ρ (MeV/c)
$\pi\pi$	seen	476
$K\bar{K}$	seen	36
$\gamma\gamma$	seen	495

 $a_0(980)$

$$I^G(J^{PC}) = 1^-(0^{++})$$

See the review on "Scalar Mesons below 1 GeV."

T-matrix pole $\sqrt{s} = (970-1020) - i(30-70)$ MeV [1]Mass $m = 980 \pm 20$ MeV [1]Full width $\Gamma = 50$ to 100 MeV [1]

$a_0(980)$ DECAY MODES	Fraction (Γ_i/Γ)	ρ (MeV/c)
$\eta\pi$	seen	319
$K\bar{K}$	seen	†
$\eta'\pi$	seen	†
$\rho\pi$	not seen	137
$\gamma\gamma$	seen	490

 $\phi(1020)$

$$I^G(J^{PC}) = 0^-(1^{--})$$

Mass $m = 1019.461 \pm 0.016$ MeVFull width $\Gamma = 4.249 \pm 0.013$ MeV (S = 1.1)

$\phi(1020)$ DECAY MODES	Fraction (Γ_i/Γ)	Scale factor/ Confidence level	ρ (MeV/c)
K^+K^-	(49.1 ± 0.5) %	S=1.3	127
$K_L^0K_S^0$	(33.9 ± 0.4) %	S=1.2	110
$\rho\pi + \pi^+\pi^-\pi^0$	(15.4 ± 0.4) %	S=1.2	-
$\eta\gamma$	(1.301 ± 0.024) %	S=1.2	363
$\pi^0\gamma$	(1.32 ± 0.05) × 10 ⁻³		501
$\ell^+\ell^-$	-		510
e^+e^-	(2.979 ± 0.033) × 10 ⁻⁴	S=1.2	510
$\mu^+\mu^-$	(2.85 ± 0.22) × 10 ⁻⁴	S=1.2	499
ηe^+e^-	(1.08 ± 0.04) × 10 ⁻⁴		363
$\pi^+\pi^-$	(7.3 ± 1.3) × 10 ⁻⁵		490
$\omega\pi^0$	(4.7 ± 0.5) × 10 ⁻⁵		171
$\omega\gamma$	< 5 %	CL=84%	209
$\rho\gamma$	< 1.2 × 10 ⁻⁵	CL=90%	215
$\pi^+\pi^-\gamma$	(4.1 ± 1.3) × 10 ⁻⁵		490
$f_0(980)\gamma$	(3.22 ± 0.19) × 10 ⁻⁴	S=1.1	29
$\pi^0\pi^0\gamma$	(1.12 ± 0.06) × 10 ⁻⁴		492
$\pi^+\pi^-\pi^+\pi^-$	(3.9 ± 2.8) × 10 ⁻⁶		410
$\pi^+\pi^+\pi^-\pi^-\pi^0$	< 4.6 × 10 ⁻⁶	CL=90%	342
$\pi^0e^+e^-$	(1.33 ± 0.07) × 10 ⁻⁵		501
$\pi^0\eta\gamma$	(7.27 ± 0.30) × 10 ⁻⁵	S=1.5	346
$a_0(980)\gamma$	(7.6 ± 0.6) × 10 ⁻⁵		39
$K^0\bar{K}^0\gamma$	< 1.9 × 10 ⁻⁸	CL=90%	110
$\eta'(958)\gamma$	(6.21 ± 0.20) × 10 ⁻⁵		60

Meson Summary Table

$\eta\pi^0\pi^0\gamma$	< 2	$\times 10^{-5}$	CL=90%	293
$\mu^+\mu^-\gamma$	(1.4 ± 0.5)	$\times 10^{-5}$		499
$\rho\gamma\gamma$	< 1.2	$\times 10^{-4}$	CL=90%	215
$\eta\pi^+\pi^-$	< 1.8	$\times 10^{-5}$	CL=90%	288
$\eta\mu^+\mu^-$	< 9.4	$\times 10^{-6}$	CL=90%	321
$\eta U \rightarrow \eta e^+ e^-$	< 1	$\times 10^{-6}$	CL=90%	-
invisible	< 1.7	$\times 10^{-4}$	CL=90%	-

Lepton Family number (LF) violating modes

$e^\pm\mu^\mp$	LF	< 2	$\times 10^{-6}$	CL=90%	504
----------------	----	-----	------------------	--------	-----

 $h_1(1170)$

$$I^G(J^{PC}) = 0^-(1^+ -)$$

Mass $m = 1166 \pm 6$ MeV
Full width $\Gamma = 375 \pm 35$ MeV

$h_1(1170)$ DECAY MODES	Fraction (Γ_i/Γ)	ρ (MeV/c)
$\rho\pi$	seen	305

 $b_1(1235)$

$$I^G(J^{PC}) = 1^+(1^+ -)$$

Mass $m = 1229.5 \pm 3.2$ MeV ($S = 1.6$)
Full width $\Gamma = 142 \pm 9$ MeV ($S = 1.2$)

$b_1(1235)$ DECAY MODES	Fraction (Γ_i/Γ)	Confidence level	ρ (MeV/c)
$\omega\pi$	seen		348
$[D/S \text{ amplitude ratio} = 0.277 \pm 0.027]$			
$\pi^\pm\gamma$	(1.6 ± 0.4) $\times 10^{-3}$		607
$\eta\rho$	seen		†
$\pi^+\pi^+\pi^-\pi^0$	< 50 %	84%	535
$K^*(892)^\pm K^\mp$	seen		†
$(K\bar{K})^\pm\pi^0$	< 8 %	90%	248
$K_S^0 K_L^0 \pi^\pm$	< 6 %	90%	235
$K_S^0 K_S^0 \pi^\pm$	< 2 %	90%	235
$\phi\pi$	< 1.5 %	84%	147

 $a_1(1260)$ [1]

$$I^G(J^{PC}) = 1^-(1^+ +)$$

T-Matrix Pole $\sqrt{s} = (1209^{+13}_{-10}) - i(288^{+45}_{-12})$ MeV
Mass (Breit-Wigner) = 1230 ± 40 MeV [1]
Full width (Breit-Wigner) = 250 to 600 MeV [1]

$a_1(1260)$ DECAY MODES	Fraction (Γ_i/Γ)	ρ (MeV/c)
3π	seen	577
$(\rho\pi)_{S\text{-wave}}, \rho \rightarrow \pi\pi$	seen	353
$(\rho\pi)_{D\text{-wave}}, \rho \rightarrow \pi\pi$	seen	353
$(\rho(1450)\pi)_{S\text{-wave}}, \rho \rightarrow \pi\pi$	seen	†
$(\rho(1450)\pi)_{D\text{-wave}}, \rho \rightarrow \pi\pi$	seen	†
$f_0(500)\pi, f_0 \rightarrow \pi\pi$	seen	-
$f_0(980)\pi, f_0 \rightarrow \pi\pi$	seen	179
$f_0(1370)\pi, f_0 \rightarrow \pi\pi$	seen	†
$f_2(1270)\pi, f_2 \rightarrow \pi\pi$	seen	†
$\pi^+\pi^-\pi^0$	seen	576
$\pi^0\pi^0\pi^0$	not seen	577
$K K \pi$	seen	250
$K^*(892)K$	seen	†
$\pi\gamma$	seen	608

 $f_2(1270)$

$$I^G(J^{PC}) = 0^+(2^+ +)$$

T-Matrix Pole $\sqrt{s} = (1260-1283) - i(90-110)$ MeV
Mass (Breit-Wigner) = 1275.4 ± 0.8 MeV ($S = 1.1$)
Full width (Breit-Wigner) = $186.6^{+2.8}_{-2.2}$ MeV ($S = 1.5$)

$f_2(1270)$ DECAY MODES	Fraction (Γ_i/Γ)	Scale factor/ Confidence level	ρ (MeV/c)
$\pi\pi$	(84.3 ± 2.8) %	S=1.2	623
$\pi^+\pi^-2\pi^0$	(7.7 ± 1.2) %	S=1.2	563
$K\bar{K}$	(4.6 ± 0.4) %	S=2.7	404
$2\pi^+2\pi^-$	(2.8 ± 0.4) %	S=1.2	559

$\eta\eta$	(4.0 ± 0.8) $\times 10^{-3}$	S=2.1	326
$4\pi^0$	(3.0 ± 1.0) $\times 10^{-3}$		565
$\gamma\gamma$	(1.42 ± 0.24) $\times 10^{-5}$	S=1.4	638
$\eta\pi\pi$	< 8 $\times 10^{-3}$	CL=95%	478
$K^0 K^- \pi^+ + \text{c.c.}$	< 3.4 $\times 10^{-3}$	CL=95%	293
e^+e^-	< 6 $\times 10^{-10}$	CL=90%	638

 $f_1(1285)$

$$I^G(J^{PC}) = 0^+(1^+ +)$$

Mass $m = 1281.8 \pm 0.5$ MeV ($S = 1.7$)
Full width $\Gamma = 23.0 \pm 1.1$ MeV ($S = 1.6$)

 $f_1(1285)$ DECAY MODES

$f_1(1285)$ DECAY MODES	Fraction (Γ_i/Γ)	Scale factor/ Confidence level	ρ (MeV/c)
4π	(32.7 ± 1.8) %	S=1.2	568
$\pi^0\pi^0\pi^+\pi^-$	(21.8 ± 1.2) %	S=1.2	566
$2\pi^+2\pi^-$	(10.9 ± 0.6) %	S=1.2	563
$\rho^0\pi^+\pi^-$	(10.9 ± 0.6) %	S=1.2	336
$\rho^0\rho^0$	seen		†
$4\pi^0$	< 7 $\times 10^{-4}$	CL=90%	568
$\eta\pi^+\pi^-$	(35 ± 15) %		479
$\eta\pi\pi$	(52.2 ± 1.9) %	S=1.2	482
$a_0(980)\pi$ [ignoring $a_0(980) \rightarrow K\bar{K}$]	(38 ± 4) %		238
$\eta\pi\pi$ [excluding $a_0(980)\pi$]	(14 ± 4) %		482
$K\bar{K}\pi$	(9.0 ± 0.4) %	S=1.1	308
$K\bar{K}^*(892)$	not seen		†
$\pi^+\pi^-\pi^0$	(3.0 ± 0.9) $\times 10^{-3}$		603
$\rho^\pm\pi^\mp$	< 3.1 $\times 10^{-3}$	CL=95%	390
$\gamma\rho^0$	(6.1 ± 1.0) %	S=1.7	406
$\phi\gamma$	(7.4 ± 2.6) $\times 10^{-4}$		235
e^+e^-	< 9.4 $\times 10^{-9}$	CL=90%	641

 $\eta(1295)$

$$I^G(J^{PC}) = 0^+(0^- +)$$

See the review on "Spectroscopy of Light Meson Resonances."

Mass $m = 1294 \pm 4$ MeV ($S = 1.6$)
Full width $\Gamma = 55 \pm 5$ MeV

 $\eta(1295)$ DECAY MODES

$\eta(1295)$ DECAY MODES	Fraction (Γ_i/Γ)	ρ (MeV/c)
$\eta\pi^+\pi^-$	seen	487
$a_0(980)\pi$	seen	248
$\eta\pi^0\pi^0$	seen	490
$\eta(\pi\pi)_{S\text{-wave}}$	seen	-
$\sigma\eta$	seen	-
$K\bar{K}\pi$	seen	320

 $\pi(1300)$

$$I^G(J^{PC}) = 1^-(0^- +)$$

Mass $m = 1300 \pm 100$ MeV [1]
Full width $\Gamma = 200$ to 600 MeV [1]

 $\pi(1300)$ DECAY MODES

$\pi(1300)$ DECAY MODES	Fraction (Γ_i/Γ)	ρ (MeV/c)
$\rho\pi$	seen	404
$\pi(\pi\pi)_{S\text{-wave}}$	seen	-

 $a_2(1320)$

$$I^G(J^{PC}) = 1^-(2^+ +)$$

T-Matrix Pole $\sqrt{s} = (1305-1321) - i(52-58)$ MeV
Mass (Breit-Wigner) = 1318.2 ± 0.6 MeV ($S = 1.2$)
Full width $\Gamma = 107 \pm 5$ MeV

 $a_2(1320)$ DECAY MODES

$a_2(1320)$ DECAY MODES	Fraction (Γ_i/Γ)	Scale factor/ Confidence level	ρ (MeV/c)
3π	(70.1 ± 2.7) %	S=1.2	624
$\eta\pi\pi$	(14.5 ± 1.2) %		535
$\omega\pi\pi$	(10.6 ± 3.2) %	S=1.3	366
$K\bar{K}$	(4.9 ± 0.8) %		437
$\eta'(958)\pi$	(5.5 ± 0.9) $\times 10^{-3}$		288
$\pi^\pm\gamma$	(2.91 ± 0.27) $\times 10^{-3}$		652
$\gamma\gamma$	(9.4 ± 0.7) $\times 10^{-6}$		659
e^+e^-	< 5 $\times 10^{-9}$	CL=90%	659

Meson Summary Table

 $f_0(1370)$

$$I^G(J^{PC}) = 0^+(0^{++})$$

See the review on "Spectroscopy of Light Meson Resonances."

T-Matrix Pole $\sqrt{s} = (1250-1440) - i(60-300)$ MeV

Mass (Breit-Wigner) = 1200 to 1500 MeV

Full width (Breit-Wigner) = 200 to 500 MeV

$f_0(1370)$ DECAY MODES	Fraction (Γ_i/Γ)	ρ (MeV/c)
$\pi\pi$	seen	672
4π	seen	617
$4\pi^0$	seen	617
$2\pi^+2\pi^-$	seen	612
$\pi^+\pi^-2\pi^0$	seen	615
$\rho\rho$	seen	†
$2(\pi\pi)$ s-wave	seen	–
$\pi(1300)\pi$	seen	†
$a_1(1260)\pi$	seen	35
$\eta\eta$	seen	411
$K\bar{K}$	seen	475
$K\bar{K}\eta\pi$	not seen	†
6π	not seen	508
$\omega\omega$	not seen	†
$\gamma\gamma$	seen	685
e^+e^-	not seen	685

 $\eta(1405)$

$$I^G(J^{PC}) = 0^+(0^{-+})$$

See the review on "Spectroscopy of Light Meson Resonances." See also $\eta(1475)$.Mass $m = 1408.7^{+2.0}_{-1.2}$ MeV ($S = 2.2$)Full width $\Gamma = 50.3 \pm 2.5$ MeV ($S = 1.6$)

$\eta(1405)$ DECAY MODES	Fraction (Γ_i/Γ)	Confidence level	ρ (MeV/c)
$K\bar{K}\pi$	seen		424
$\eta\pi\pi$	seen		562
$a_0(980)\pi$	seen		344
$\eta(\pi\pi)$ s-wave	seen		–
$f_0(980)\pi^0 \rightarrow \pi^+\pi^-\pi^0$	not seen		–
$f_0(980)\eta$	seen		†
4π	seen		638
$\rho\rho$	<58 %	99.85%	†
$\rho^0\gamma$	seen		491
$K^*(892)K$	seen		122

 $h_1(1415)$

$$I^G(J^{PC}) = 0^-(1^{+-})$$

Mass $m = 1409^{+9}_{-8}$ MeV ($S = 1.9$)Full width $\Gamma = 78 \pm 11$ MeV **$f_1(1420)$**

$$I^G(J^{PC}) = 0^+(1^{++})$$

See the review on "Spectroscopy of Light Meson Resonances."

Mass $m = 1428.4^{+1.5}_{-1.3}$ MeV ($S = 1.8$)Full width $\Gamma = 56.7 \pm 3.3$ MeV ($S = 1.3$)

$f_1(1420)$ DECAY MODES	Fraction (Γ_i/Γ)	ρ (MeV/c)
$K\bar{K}\pi$	seen	440
$K\bar{K}^*(892) + c.c.$	seen	167
$\eta\pi\pi$	possibly seen	574
$\phi\gamma$	seen	350

 $\omega(1420)$ [k]

$$I^G(J^{PC}) = 0^-(1^{--})$$

Mass $m = 1410 \pm 60$ MeV [i]Full width $\Gamma = 290 \pm 190$ MeV [i]

$\omega(1420)$ DECAY MODES	Fraction (Γ_i/Γ)	ρ (MeV/c)
$\rho\pi$	seen	480
$\omega\pi\pi$	seen	437

 $b_1(1235)\pi$
 e^+e^- seen
seen112
705 **$a_0(1450)$**

$$I^G(J^{PC}) = 1^-(0^{++})$$

See the review on "Spectroscopy of Light Meson Resonances."

T-Matrix Pole $\sqrt{s} = (1290-1500) - i(30-140)$ MeVMass (Breit-Wigner) = 1439 ± 34 MeV ($S = 1.8$)Full width (Breit-Wigner) = 258 ± 14 MeVBranching fractions are given relative to the one **DEFINED AS 1**.

$a_0(1450)$ DECAY MODES	Fraction (Γ_i/Γ)	ρ (MeV/c)
$\pi\eta$	0.093 ± 0.020	607
$\pi\eta'(958)$	0.033 ± 0.017	384
$K\bar{K}$	0.082 ± 0.028	523
$\omega\pi\pi$	DEFINED AS 1	458
$a_0(980)\pi\pi$	seen	310
$\gamma\gamma$	seen	719

 $\rho(1450)$

$$I^G(J^{PC}) = 1^+(1^{--})$$

See the review on "Spectroscopy of Light Meson Resonances."

Mass $m = 1465 \pm 25$ MeV [i]Full width $\Gamma = 400 \pm 60$ MeV [i]

$\rho(1450)$ DECAY MODES	Fraction (Γ_i/Γ)	ρ (MeV/c)
$\pi\pi$	seen	720
$\pi^+\pi^-$	seen	719
4π	seen	669
e^+e^-	seen	732
$\eta\rho$	seen	311
$a_2(1320)\pi$	not seen	55
$K\bar{K}$	seen	541
K^+K^-	seen	541
$K\bar{K}^*(892) + c.c.$	possibly seen	229
$\pi^0\gamma$	seen	726
$\eta\gamma$	seen	630
$f_0(500)\gamma$	not seen	–
$f_0(980)\gamma$	not seen	398
$f_0(1370)\gamma$	not seen	92
$f_2(1270)\gamma$	not seen	177

 $\eta(1475)$

$$I^G(J^{PC}) = 0^+(0^{-+})$$

See the review on "Spectroscopy of Light Meson Resonances." See also $\eta(1405)$.Mass $m = 1476 \pm 4$ MeV ($S = 1.4$)Full width $\Gamma = 96 \pm 9$ MeV ($S = 1.7$)

$\eta(1475)$ DECAY MODES	Fraction (Γ_i/Γ)	ρ (MeV/c)
$K\bar{K}\pi$	seen	477
$K\bar{K}^*(892) + c.c.$	seen	245
$a_0(980)\pi$	seen	396
$\gamma\gamma$	seen	738
$K_S^0 K_S^0 \eta$	possibly seen	†
$\gamma\phi(1020)$	possibly seen	386

 $f_0(1500)$

$$I^G(J^{PC}) = 0^+(0^{++})$$

See the review on "Spectroscopy of Light Meson Resonances."

T-Matrix Pole $\sqrt{s} = (1430-1530) - i(40-90)$ MeVMass (Breit-Wigner) = 1522 ± 25 MeVFull width (Breit-Wigner) = 108 ± 33 MeV

$f_0(1500)$ DECAY MODES	Fraction (Γ_i/Γ)	Scale factor	ρ (MeV/c)
$\pi\pi$	$(34.5 \pm 2.2) \%$	1.2	749
$\pi^+\pi^-$	seen		748
$2\pi^0$	seen		749
4π	$(48.9 \pm 3.3) \%$	1.2	700
$4\pi^0$	seen		700

Meson Summary Table

$2\pi^+ 2\pi^-$	seen	696
$2(\pi\pi)$ s-wave	seen	—
$\rho\rho$	seen	†
$\pi(1300)\pi$	seen	163
$a_1(1260)\pi$	seen	234
$\eta\eta$	(6.0±0.9) %	1.1 528
$\eta\eta'(958)$	(2.2±0.8) %	1.4 107
$K\bar{K}$	(8.5±1.0) %	1.1 579
$\gamma\gamma$	not seen	761

$$f_2'(1525) \quad I^G(J^{PC}) = 0^+(2^{++})$$

Mass $m = 1517.3 \pm 2.4$ MeV (S = 2.8)
Full width $\Gamma = 72_{-6}^{+7}$ MeV

$f_2'(1525)$ DECAY MODES	Fraction (Γ_i/Γ)	ρ (MeV/c)
$K\bar{K}$	(88.8 ± 2.2) %	576
$\eta\eta$	(10.3 ± 2.2) %	525
$\pi\pi$	(8.2 ± 1.5) × 10 ⁻³	747
$\gamma\gamma$	(1.12±0.15) × 10 ⁻⁶	759

$$f_2(1565) \quad I^G(J^{PC}) = 0^+(2^{++})$$

See the review on "Spectroscopy of Light Meson Resonances."

T-Matrix Pole $\sqrt{s} = (1495-1560) - i(40-110)$ MeV
Mass (Breit-Wigner) = 1571 ± 13 MeV
Full width (Breit-Wigner) = 132 ± 23 MeV (S = 1.1)

$f_2(1565)$ DECAY MODES	Fraction (Γ_i/Γ)	ρ (MeV/c)
$\pi\pi$	seen	774
$\pi^+ \pi^-$	seen	773
$\pi^0 \pi^0$	seen	774
$\rho^0 \rho^0$	seen	125
$2\pi^+ 2\pi^-$	seen	722
$\eta\eta$	seen	563
$\omega\omega$	seen	64
$K\bar{K}$	seen	611
$\gamma\gamma$	seen	785

$$\pi_1(1600) \quad I^G(J^{PC}) = 1^-(1^{-+})$$

See the review on "Spectroscopy of Light Meson Resonances."

Mass (T-Matrix Pole \sqrt{s}) = (1480-1680) - $i(150-300)$ MeV
Mass (Breit-Wigner, $\eta\pi$ mode) = 1354 ± 25 MeV (S = 1.8)
Mass (Breit-Wigner, non- $\eta\pi$ mode) = 1645 $_{-17}^{+40}$ MeV (S = 1.3)
Full width (Breit-Wigner, $\eta\pi$ mode) = 330 ± 35 MeV
Full width (Breit-Wigner, non- $\eta\pi$ mode) = 370 $_{-80}^{+50}$ MeV

$\pi_1(1600)$ DECAY MODES	Fraction (Γ_i/Γ)	ρ (MeV/c)
$\pi\pi\pi$	seen	795
$\rho^0 \pi^-$	seen	631
$f_2(1270)\pi^-$	not seen	304
$b_1(1235)\pi$	seen	343
$\eta'(958)\pi^-$	seen	532
$\eta\pi$	seen	725
$f_1(1285)\pi$	seen	300

$$a_1(1640) \quad I^G(J^{PC}) = 1^-(1^{++})$$

Mass $m = 1655 \pm 16$ MeV (S = 1.2)
Full width $\Gamma = 250 \pm 40$ MeV (S = 1.8)

$a_1(1640)$ DECAY MODES	Fraction (Γ_i/Γ)	ρ (MeV/c)
$\pi\pi\pi$	seen	800
$f_2(1270)\pi$	seen	314
$\sigma\pi$	seen	—
$\rho\pi$ S-wave	seen	638

$\rho\pi$ D-wave	seen	638
$\omega\pi\pi$	seen	607
$f_1(1285)\pi$	seen	309
$a_1(1260)\eta$	not seen	†

$$\eta_2(1645) \quad I^G(J^{PC}) = 0^+(2^{-+})$$

Mass $m = 1617 \pm 5$ MeV
Full width $\Gamma = 181 \pm 11$ MeV

$\eta_2(1645)$ DECAY MODES	Fraction (Γ_i/Γ)	ρ (MeV/c)
$a_2(1320)\pi$	seen	242
$K\bar{K}\pi$	seen	580
$K^* \bar{K}$	seen	404
$\eta\pi^+ \pi^-$	seen	685
$a_0(980)\pi$	seen	499
$f_2(1270)\eta$	not seen	†

$$\omega(1650) [1] \quad I^G(J^{PC}) = 0^-(1^{--})$$

Mass $m = 1670 \pm 30$ MeV [1]
Full width $\Gamma = 315 \pm 35$ MeV [1]

$\omega(1650)$ DECAY MODES	Fraction (Γ_i/Γ)	ρ (MeV/c)
$\rho\pi$	seen	647
$\rho(1450)\pi$	seen	145
$\omega\pi\pi$	seen	617
$\omega\eta$	seen	500
$e^+ e^-$	seen	835
$\pi^0 \gamma$	not seen	830

$$\omega_3(1670) \quad I^G(J^{PC}) = 0^-(3^{--})$$

Mass $m = 1667 \pm 4$ MeV
Full width $\Gamma = 168 \pm 10$ MeV

$\omega_3(1670)$ DECAY MODES	Fraction (Γ_i/Γ)	ρ (MeV/c)
$\rho\pi$	seen	645
$\omega\pi\pi$	seen	615
$b_1(1235)\pi$	possibly seen	361

$$\pi_2(1670) \quad I^G(J^{PC}) = 1^-(2^{-+})$$

Mass $m = 1670.6_{-1.2}^{+2.9}$ MeV (S = 1.3)
Full width $\Gamma = 258_{-9}^{+8}$ MeV (S = 1.2)

$\pi_2(1670)$ DECAY MODES	Fraction (Γ_i/Γ)	Confidence level	ρ (MeV/c)
3π	(95.8±1.4) %		808
$f_2(1270)\pi$	(56.3±3.2) %		327
$\rho\pi$	(31 ± 4) %		647
$\sigma\pi$	(10 ± 4) %		—
$\pi(\pi\pi)$ S-wave	(8.7±3.4) %		—
$\pi^\pm \pi^+ \pi^-$	(53 ± 4) %		806
$K\bar{K}^*(892) + c.c.$	(4.2±1.4) %		453
$\omega\rho$	(2.7±1.1) %		302
$\pi^\pm \gamma$	(7.0±1.2) × 10 ⁻⁴		829
$\gamma\gamma$	< 2.8 × 10 ⁻⁷	90%	835
$\eta\pi$	< 5 %		739
$\pi^\pm 2\pi^+ 2\pi^-$	< 5 %		735
$\rho(1450)\pi$	< 3.6 × 10 ⁻³	97.7%	145
$b_1(1235)\pi$	< 1.9 × 10 ⁻³	97.7%	364
$f_1(1285)\pi$	possibly seen		322
$a_2(1320)\pi$	not seen		291

$$\phi(1680) \quad I^G(J^{PC}) = 0^-(1^{--})$$

Mass $m = 1680 \pm 20$ MeV [1]
Full width $\Gamma = 150 \pm 50$ MeV [1]

Meson Summary Table

$\phi(1680)$ DECAY MODES	Fraction (Γ_i/Γ)	ρ (MeV/c)
$K\bar{K}^*(892) + \text{c.c.}$	seen	462
$K_S^0 K \pi$	seen	621
$K\bar{K}$	seen	680
$e^+ e^-$	seen	840
$\omega \pi \pi$	not seen	623
$K^+ K^- \pi^+ \pi^-$	seen	544
$\eta \phi$	seen	290
$\eta \gamma$	seen	751
$f_2'(1525) \gamma$	not seen	155

$$\rho_3(1690) \quad I^G(J^{PC}) = 1^+(3^{--})$$

Mass $m = 1688.8 \pm 2.1$ MeV
Full width $\Gamma = 161 \pm 10$ MeV ($S = 1.5$)

$\rho_3(1690)$ DECAY MODES	Fraction (Γ_i/Γ)	Scale factor	ρ (MeV/c)
4π	$(71.1 \pm 1.9) \%$		790
$\pi^\pm \pi^+ \pi^- \pi^0$	$(67 \pm 22) \%$		787
$\omega \pi$	$(16 \pm 6) \%$		655
$\pi \pi \pi$	$(23.6 \pm 1.3) \%$		834
$K\bar{K} \pi$	$(3.8 \pm 1.2) \%$		629
$K\bar{K}$	$(1.58 \pm 0.26) \%$	1.2	685
$\eta \pi^+ \pi^-$	seen		727
$\rho(770) \eta$	seen		520
$\pi \pi \rho$	seen		633
$a_2(1320) \pi$	seen		307
$\rho \rho$	seen		335

$$\rho(1700) \quad I^G(J^{PC}) = 1^+(1^{--})$$

See the review on "Spectroscopy of Light Meson Resonances."
Mass $m = 1720 \pm 20$ MeV [1] ($\eta \rho^0$ and $\pi^+ \pi^-$ modes)
Full width $\Gamma = 250 \pm 100$ MeV [1] ($\eta \rho^0$ and $\pi^+ \pi^-$ modes)

$\rho(1700)$ DECAY MODES	Fraction (Γ_i/Γ)	ρ (MeV/c)
$2(\pi^+ \pi^-)$	seen	803
$\rho \pi \pi$	seen	653
$\rho^0 \pi^+ \pi^-$	seen	651
$\rho^\pm \pi^\mp \pi^0$	seen	652
$a_1(1260) \pi$	seen	404
$h_1(1170) \pi$	seen	450
$\pi(1300) \pi$	seen	349
$\rho \rho$	seen	372
$\pi^+ \pi^-$	seen	849
$\pi \pi$	seen	849
$K\bar{K}^*(892) + \text{c.c.}$	seen	496
$\eta \rho$	seen	545
$a_2(1320) \pi$	not seen	334
$K\bar{K}$	seen	704
$e^+ e^-$	seen	860
$\pi^0 \omega$	seen	674
$\pi^0 \gamma$	not seen	855
$f_0(1500) \gamma$	not seen	187

$$a_2(1700) \quad I^G(J^{PC}) = 1^-(2^{++})$$

T-Matrix Pole $\sqrt{s} = (1630-1780) - i(60-250)$ MeV
Mass $m = 1706 \pm 14$ MeV ($S = 1.2$)
Full width $\Gamma = 380_{-50}^{+60}$ MeV ($S = 3.9$)

$a_2(1700)$ DECAY MODES	Fraction (Γ_i/Γ)	ρ (MeV/c)
$\eta \pi$	$(2.5 \pm 0.6) \%$	758
$\eta' \pi$	seen	574
$\gamma \gamma$	$(7.9 \pm 1.7) \times 10^{-7}$	853
$\rho \pi$	seen	669
$f_2(1270) \pi$	seen	357
$K\bar{K}$	$(1.3 \pm 0.8) \%$	695
$\omega \pi^- \pi^0$	seen	639
$\omega \rho$	seen	347

$$f_0(1710) \quad I^G(J^{PC}) = 0^+(0^{++})$$

See the review on "Spectroscopy of Light Meson Resonances."
T-matrix pole $\sqrt{s} = (1680-1820) - i(50-180)$ MeV
Mass (Breit-Wigner) = 1733_{-7}^{+8} MeV ($S = 1.5$)
Full width (Breit-Wigner) = 150_{-10}^{+12} MeV ($S = 1.3$)

$f_0(1710)$ DECAY MODES	Fraction (Γ_i/Γ)	ρ (MeV/c)
$K\bar{K}$	seen	712
$\eta \eta$	seen	671
$\eta \eta'$	not seen	417
$\pi \pi$	seen	856
$\gamma \gamma$	seen	866
$\omega \omega$	seen	372

$$\pi(1800) \quad I^G(J^{PC}) = 1^-(0^{-+})$$

See the review on "Spectroscopy of Light Meson Resonances."
Mass $m = 1810_{-11}^{+9}$ MeV ($S = 2.2$)
Full width $\Gamma = 215_{-8}^{+7}$ MeV

$\pi(1800)$ DECAY MODES	Fraction (Γ_i/Γ)	ρ (MeV/c)
$\pi^+ \pi^- \pi^-$	seen	878
$f_0(500) \pi^-$	seen	-
$f_0(980) \pi^-$	seen	624
$f_0(1370) \pi^-$	seen	366
$f_0(1500) \pi^-$	not seen	232
$\rho \pi^-$	not seen	731
$\eta \eta \pi^-$	seen	660
$a_0(980) \eta$	seen	471
$a_2(1320) \eta$	not seen	†
$f_2(1270) \pi$	not seen	441
$f_0(1370) \pi^-$	not seen	366
$f_0(1500) \pi^-$	seen	232
$\eta \eta'(958) \pi^-$	seen	373
$K_0^*(1430) K^-$	seen	†
$K^*(892) K^-$	not seen	568

$$\phi_3(1850) \quad I^G(J^{PC}) = 0^-(3^{--})$$

Mass $m = 1854 \pm 7$ MeV
Full width $\Gamma = 87_{-23}^{+28}$ MeV ($S = 1.2$)

$\phi_3(1850)$ DECAY MODES	Fraction (Γ_i/Γ)	ρ (MeV/c)
$K\bar{K}$	seen	785
$K\bar{K}^*(892) + \text{c.c.}$	seen	602

$$\eta_2(1870) \quad I^G(J^{PC}) = 0^+(2^{-+})$$

Mass $m = 1842 \pm 8$ MeV
Full width $\Gamma = 225 \pm 14$ MeV

$\eta_2(1870)$ DECAY MODES	Fraction (Γ_i/Γ)	ρ (MeV/c)
$\eta \pi \pi$	seen	816
$a_2(1320) \pi$	seen	434
$f_2(1270) \eta$	seen	119
$a_0(980) \pi$	seen	651
$\gamma \gamma$	seen	921

$$\pi_2(1880) \quad I^G(J^{PC}) = 1^-(2^{-+})$$

Mass $m = 1874_{-5}^{+26}$ MeV ($S = 1.6$)
Full width $\Gamma = 237_{-30}^{+33}$ MeV ($S = 1.2$)

$\pi_2(1880)$ DECAY MODES	Fraction (Γ_i/Γ)	ρ (MeV/c)
$\eta \eta \pi^-$	seen	702
$a_0(980) \eta$	seen	528
$a_2(1320) \eta$	seen	76
$f_0(1500) \pi$	seen	294
$f_1(1285) \pi$	seen	485
$\omega \pi^- \pi^0$	seen	744

Meson Summary Table

 $f_2(1950)$

$$I^G(J^{PC}) = 0^+(2^{++})$$

T-Matrix Pole $\sqrt{s} = (1830-2020) - i(110-220)$ MeV
 Mass (Breit-Wigner) = 1936 ± 12 MeV ($S = 1.3$)
 Full width (Breit-Wigner) = 464 ± 24 MeV

$f_2(1950)$ DECAY MODES	Fraction (Γ_i/Γ)	ρ (MeV/c)
$K^*(892)\bar{K}^*(892)$	seen	377
$\pi^+\pi^-\pi^0$	seen	958
$\pi^0\pi^0$	seen	959
4π	seen	921
$\eta\eta$	seen	798
$K\bar{K}$	seen	833
$\gamma\gamma$	seen	968
$\rho\bar{\rho}$	seen	238

 $a_4(1970)$

$$I^G(J^{PC}) = 1^-(4^{++})$$

Mass $m = 1967 \pm 16$ MeV ($S = 2.1$)
 Full width $\Gamma = 324^{+15}_{-18}$ MeV

$a_4(1970)$ DECAY MODES	Fraction (Γ_i/Γ)	ρ (MeV/c)
$K\bar{K}$	seen	851
$\pi^+\pi^-\pi^0$	seen	959
$\rho\pi$	seen	825
$f_2(1270)\pi$	seen	559
$\omega\pi^-\pi^0$	seen	801
$\omega\rho$	seen	601
$\eta\pi$	seen	902
$\eta'(958)\pi$	seen	743

 $f_2(2010)$

$$I^G(J^{PC}) = 0^+(2^{++})$$

Mass $m = 2010^{+60}_{-80}$ MeV
 Full width $\Gamma = 200 \pm 60$ MeV

$f_2(2010)$ DECAY MODES	Fraction (Γ_i/Γ)	ρ (MeV/c)
$\phi\phi$	seen	†
$K\bar{K}$	seen	876

 $f_0(2020)$

$$I^G(J^{PC}) = 0^+(0^{++})$$

T-Matrix Pole $\sqrt{s} = (1870-2080) - i(120-240)$ MeV
 Mass (Breit-Wigner) = $1982^{+54.1}_{-3.0}$ MeV
 Full width (Breit-Wigner) = 440 ± 50 MeV

$f_0(2020)$ DECAY MODES	Fraction (Γ_i/Γ)	ρ (MeV/c)
$\rho\pi\pi$	seen	814
$\pi^0\pi^0$	seen	982
$\rho\rho$	seen	617
$\omega\omega$	seen	608
$\eta\eta$	seen	826
$\eta'\eta'$	seen	254

 $f_4(2050)$

$$I^G(J^{PC}) = 0^+(4^{++})$$

Mass $m = 2018 \pm 11$ MeV ($S = 2.1$)
 Full width $\Gamma = 237 \pm 18$ MeV ($S = 1.9$)

$f_4(2050)$ DECAY MODES	Fraction (Γ_i/Γ)	ρ (MeV/c)
$\omega\omega$	seen	637
$\pi\pi$	$(17.0 \pm 1.5)\%$	1000
$K\bar{K}$	$(6.8^{+3.4}_{-1.8}) \times 10^{-3}$	880
$\eta\eta$	$(2.1 \pm 0.8) \times 10^{-3}$	848
$4\pi^0$	$< 1.2\%$	964
$\gamma\gamma$	seen	1009
$a_2(1320)\pi$	seen	567

 $\phi(2170)$

$$I^G(J^{PC}) = 0^-(1^{--})$$

Mass $m = 2164 \pm 6$ MeV
 Full width $\Gamma = 106^{+24}_{-18}$ MeV ($S = 2.0$)

$\phi(2170)$ DECAY MODES	Fraction (Γ_i/Γ)	ρ (MeV/c)
e^+e^-	seen	1082
$\phi\eta$	seen	728
$\omega\eta$	seen	848
$\phi\eta'$	seen	440
$\phi\pi\pi$	seen	815
$\phi f_0(980)$	seen	402
$K^+K^-f_0(980) \rightarrow$ $K^+K^-\pi^+\pi^-$	seen	-
$K^+K^-f_0(980) \rightarrow K^+K^-\pi^0\pi^0$	seen	-
$K^{*0}K^\pm\pi^\mp$	not seen	762
$K^*(892)^0\bar{K}^*(892)^0$	not seen	613

 $f_2(2300)$

$$I^G(J^{PC}) = 0^+(2^{++})$$

Mass $m = 2297 \pm 28$ MeV
 Full width $\Gamma = 150 \pm 40$ MeV

$f_2(2300)$ DECAY MODES	Fraction (Γ_i/Γ)	ρ (MeV/c)
$\phi\phi$	seen	529
$K\bar{K}$	seen	1037
$\gamma\gamma$	seen	1149
$\Lambda\bar{\Lambda}$	seen	273

 $f_2(2340)$

$$I^G(J^{PC}) = 0^+(2^{++})$$

Mass $m = 2346^{+21}_{-10}$ MeV
 Full width $\Gamma = 331^{+27}_{-18}$ MeV

$f_2(2340)$ DECAY MODES	Fraction (Γ_i/Γ)	ρ (MeV/c)
$\phi\phi$	seen	580
$\eta\eta$	seen	1037
$\eta'\eta'$	seen	677

STRANGE MESONS ($S = \pm 1, C = B = 0$)

$$K^+ = u\bar{s}, K^0 = d\bar{s}, \bar{K}^0 = \bar{d}s, K^- = \bar{u}s, \text{ similarly for } K^{*s}$$

 K^\pm

$$I(J^P) = \frac{1}{2}(0^-)$$

Mass $m = 493.677 \pm 0.015$ MeV [n] ($S = 2.8$)
 Mean life $\tau = (1.2380 \pm 0.0020) \times 10^{-8}$ s ($S = 1.8$)
 $c\tau = 3.711$ m

CPT violation parameters ($\Delta = \text{rate difference/sum}$)

$$\Delta(K^\pm \rightarrow \mu^\pm \nu_\mu) = (-0.27 \pm 0.21)\%$$

$$\Delta(K^\pm \rightarrow \pi^\pm \pi^0) = (0.4 \pm 0.6)\% [o]$$

CP violation parameters ($\Delta = \text{rate difference/sum}$)

$$\Delta(K^\pm \rightarrow \pi^\pm e^+ e^-) = (-2.2 \pm 1.6) \times 10^{-2}$$

$$\Delta(K^\pm \rightarrow \pi^\pm \mu^+ \mu^-) = 0.010 \pm 0.023$$

$$\Delta(K^\pm \rightarrow \pi^\pm \pi^0 \gamma) = (0.0 \pm 1.2) \times 10^{-3}$$

$$\Delta(K^\pm \rightarrow \pi^\pm \pi^+ \pi^-) = (0.04 \pm 0.06)\%$$

$$\Delta(K^\pm \rightarrow \pi^\pm \pi^0 \pi^0) = (-0.02 \pm 0.28)\%$$

T violation parameters

$$K^+ \rightarrow \pi^0 \mu^+ \nu_\mu \quad P_T = (-1.7 \pm 2.5) \times 10^{-3}$$

$$K^+ \rightarrow \mu^+ \nu_\mu \gamma \quad P_T = (-0.6 \pm 1.9) \times 10^{-2}$$

$$K^+ \rightarrow \pi^0 \mu^+ \nu_\mu \quad \text{Im}(\xi) = -0.006 \pm 0.008$$

Slope parameter g [ρ]

(See Particle Listings for quadratic coefficients and alternative parametrization related to $\pi\pi$ scattering)

$$K^\pm \rightarrow \pi^\pm \pi^+ \pi^- \quad g = -0.21134 \pm 0.00017$$

$$K^\pm \rightarrow \pi^\pm \pi^0 \pi^0 \quad g = 0.626 \pm 0.007$$

$$(g_+ - g_-) / (g_+ + g_-) = (-1.5 \pm 2.2) \times 10^{-4}$$

$$(g_+ - g_-) / (g_+ + g_-) = (1.8 \pm 1.8) \times 10^{-4}$$

Meson Summary Table

 K^\pm decay form factors [a,q]Assuming μ - e universality

$$\lambda_+(K_{\mu 3}^\pm) = \lambda_+(K_{e 3}^\pm) = (2.959 \pm 0.025) \times 10^{-2}$$

$$\lambda_0(K_{\mu 3}^\pm) = (1.76 \pm 0.25) \times 10^{-2} \quad (S = 2.7)$$

Not assuming μ - e universality

$$\lambda_+(K_{e 3}^\pm) = (2.956 \pm 0.025) \times 10^{-2}$$

$$\lambda_+(K_{\mu 3}^\pm) = (3.09 \pm 0.25) \times 10^{-2} \quad (S = 1.5)$$

$$\lambda_0(K_{\mu 3}^\pm) = (1.73 \pm 0.27) \times 10^{-2} \quad (S = 2.6)$$

 $K_{e 3}$ form factor quadratic fit

$$\lambda'_+(K_{e 3}^\pm) \text{ linear coeff.} = (2.59 \pm 0.04) \times 10^{-2}$$

$$\lambda''_+(K_{e 3}^\pm) \text{ quadratic coeff.} = (0.186 \pm 0.021) \times 10^{-2}$$

$$\lambda'_+(K_{\mu 3}^\pm) \text{ (LINEAR } K_{\mu 3}^\pm \text{ FORM FACTOR FROM QUADRATIC FIT)} \\ = (24 \pm 4) \times 10^{-3}$$

$$\lambda''_+(K_{\mu 3}^\pm) \text{ (QUADRATIC } K_{\mu 3}^\pm \text{ FORM FACTOR)} = (1.8 \pm 1.5) \times 10^{-3}$$

$$M_V \text{ (VECTOR POLE MASS FOR } K_{e 3}^\pm \text{ DECAY)} = 890.3 \pm 2.8 \text{ MeV}$$

$$M_V \text{ (VECTOR POLE MASS FOR } K_{\mu 3}^\pm \text{ DECAY)} = 878 \pm 12 \text{ MeV}$$

$$M_S \text{ (SCALAR POLE MASS FOR } K_{\mu 3}^\pm \text{ DECAY)} = 1210 \pm 50 \text{ MeV}$$

$$\Lambda_+ \text{ (DISPERSIVE VECTOR FORM FACTOR IN } K_{e 3}^\pm \text{ DECAY)} = \\ (2.460 \pm 0.017) \times 10^{-2}$$

$$\Lambda_+ \text{ (DISPERSIVE VECTOR FORM FACTOR IN } K_{\mu 3}^\pm \text{ DECAY)} \\ = (25.4 \pm 0.9) \times 10^{-3}$$

$$\ln(C) \text{ (DISPERSIVE SCALAR FORM FACTOR IN } K_{\mu 3}^\pm \text{ decays)} \\ = (182 \pm 16) \times 10^{-3}$$

$$K_{e 3}^+ |f_S/f_+| = (-0.08_{-0.40}^{+0.34}) \times 10^{-2}$$

$$K_{e 3}^+ |f_T/f_+| = (-1.2_{-1.1}^{+1.3}) \times 10^{-2}$$

$$K_{\mu 3}^+ |f_S/f_+| = (0.2 \pm 0.6) \times 10^{-2}$$

$$K_{\mu 3}^+ |f_T/f_+| = (-0.1 \pm 0.7) \times 10^{-2}$$

$$K^+ \rightarrow e^+ \nu_e \gamma |F_A + F_V| = 0.133 \pm 0.008 \quad (S = 1.3)$$

$$K^+ \rightarrow \mu^+ \nu_\mu \gamma |F_A + F_V| = 0.165 \pm 0.013$$

$$K^+ \rightarrow e^+ \nu_e \gamma |F_A - F_V| < 0.49, \text{ CL} = 90\%$$

$$K^+ \rightarrow \mu^+ \nu_\mu \gamma |F_A - F_V| = -0.153 \pm 0.033 \quad (S = 1.1)$$

Charge radius

$$\langle r \rangle = 0.560 \pm 0.031 \text{ fm}$$

Forward-backward asymmetry

$$A_{FB}(K_{\pi\mu\mu}^\pm) = \frac{\Gamma(\cos(\theta_{K\mu}) > 0) - \Gamma(\cos(\theta_{K\mu}) < 0)}{\Gamma(\cos(\theta_{K\mu}) > 0) + \Gamma(\cos(\theta_{K\mu}) < 0)} < 0.9 \times 10^{-2}, \text{ CL} \\ = 90\%$$

 K^- modes are charge conjugates of the modes below.

K^+ DECAY MODES	Fraction (Γ_i/Γ)	Scale factor/ Confidence level (MeV/c)	p
Leptonic and semileptonic modes			
$e^+ \nu_e$	$(1.582 \pm 0.007) \times 10^{-5}$		247
$\mu^+ \nu_\mu$	$(63.56 \pm 0.11) \%$	S=1.2	236
$\pi^0 e^+ \nu_e$	$(5.07 \pm 0.04) \%$	S=2.1	228
Called $K_{e 3}^+$.			
$\pi^0 \mu^+ \nu_\mu$	$(3.352 \pm 0.034) \%$	S=1.9	215
Called $K_{\mu 3}^+$.			
$\pi^0 \pi^0 e^+ \nu_e$	$(2.55 \pm 0.04) \times 10^{-5}$	S=1.1	206
$\pi^+ \pi^- e^+ \nu_e$	$(4.247 \pm 0.024) \times 10^{-5}$		203
$\pi^+ \pi^- \mu^+ \nu_\mu$	$(1.4 \pm 0.9) \times 10^{-5}$		151
$\pi^0 \pi^0 \pi^0 e^+ \nu_e$	$< 3.5 \times 10^{-6}$	CL=90%	135
Hadronic modes			
$\pi^+ \pi^0$	$(20.67 \pm 0.08) \%$	S=1.2	205
$\pi^+ \pi^0 \pi^0$	$(1.760 \pm 0.023) \%$	S=1.1	133
$\pi^+ \pi^+ \pi^-$	$(5.583 \pm 0.024) \%$		125
Leptonic and semileptonic modes with photons			
$\mu^+ \nu_\mu \gamma$	[r,s] $(6.2 \pm 0.8) \times 10^{-3}$		236
$\mu^+ \nu_\mu \gamma$ (SD ⁺)	[a,t] $(1.33 \pm 0.22) \times 10^{-5}$		-
$\mu^+ \nu_\mu \gamma$ (SD ⁺ INT)	[a,t] $< 2.7 \times 10^{-5}$	CL=90%	-
$\mu^+ \nu_\mu \gamma$ (SD ⁻ + SD ⁻ INT)	[a,t] $< 2.6 \times 10^{-4}$	CL=90%	-

$e^+ \nu_e \gamma$	$(1.03 \pm 0.14) \times 10^{-5}$		247
$\pi^0 e^+ \nu_e \gamma$	[r,s] $(2.698 \pm 0.033) \times 10^{-4}$		228
$\pi^0 e^+ \nu_e \gamma$ (SD)	[a,t] $< 5.3 \times 10^{-5}$	CL=90%	228
$\pi^0 \mu^+ \nu_\mu \gamma$	[r,s] $(1.25 \pm 0.25) \times 10^{-5}$		215
$\pi^0 \pi^0 e^+ \nu_e \gamma$	$< 5 \times 10^{-6}$	CL=90%	206

Hadronic modes with photons or $\ell\bar{\ell}$ pairs

$\pi^+ \pi^0 \gamma$ (INT)	$(-4.2 \pm 0.9) \times 10^{-6}$		-
$\pi^+ \pi^0 \gamma$ (DE)	[r,s] $(6.0 \pm 0.4) \times 10^{-6}$		205
$\pi^+ \pi^0 e^+ e^-$	$(4.24 \pm 0.14) \times 10^{-6}$		205
$\pi^+ \pi^0 \pi^0 \gamma$	[r,s] $(7.6 \pm 6.0_{-3.0}) \times 10^{-6}$		133
$\pi^+ \pi^+ \pi^- \gamma$	[r,s] $(7.1 \pm 0.5) \times 10^{-6}$		125
$\pi^+ \gamma \gamma$	[r] $(1.01 \pm 0.06) \times 10^{-6}$		227
$\pi^+ 3\gamma$	[r] $< 1.0 \times 10^{-4}$	CL=90%	227
$\pi^+ e^+ e^- \gamma$	$(1.19 \pm 0.13) \times 10^{-8}$		227

Leptonic modes with $\ell\bar{\ell}$ pairs

$e^+ \nu_e \nu\bar{\nu}$	$< 6 \times 10^{-5}$	CL=90%	247
$\mu^+ \nu_\mu \nu\bar{\nu}$	$< 1.0 \times 10^{-6}$	CL=90%	236
$e^+ \nu_e e^+ e^-$	$(2.48 \pm 0.20) \times 10^{-8}$		247
$\mu^+ \nu_\mu e^+ e^-$	$(7.06 \pm 0.31) \times 10^{-8}$		236
$e^+ \nu_e \mu^+ \mu^-$	$(1.7 \pm 0.5) \times 10^{-8}$		223
$\mu^+ \nu_\mu \mu^+ \mu^-$	$< 4.1 \times 10^{-7}$	CL=90%	185

Lepton family number (LF), Lepton number (L), $\Delta S = \Delta Q$ (SQ) violating modes, or $\Delta S = 1$ weak neutral current (S1) modes

$\pi^+ \pi^+ e^- \bar{\nu}_e$	SQ	$< 1.3 \times 10^{-8}$	CL=90%	203
$\pi^+ \pi^+ \mu^- \bar{\nu}_\mu$	SQ	$< 3.0 \times 10^{-6}$	CL=95%	151
$\pi^+ e^+ e^-$	S1	$(3.00 \pm 0.09) \times 10^{-7}$		227
$\pi^+ \mu^+ \mu^-$	S1	$(9.17 \pm 0.14) \times 10^{-8}$	S=1.8	172
$\pi^+ e^+ e^- e^+ e^-$		$< 1.4 \times 10^{-8}$	CL=90%	227
$\pi^+ \nu\bar{\nu}$	S1	$(1.14 \pm 0.40_{-0.33}) \times 10^{-10}$		227
$\pi^+ \pi^0 \nu\bar{\nu}$	S1	$< 4.3 \times 10^{-5}$	CL=90%	205
$\mu^- \nu e^+ e^+$	LF	$< 8.1 \times 10^{-11}$	CL=90%	236
$\mu^+ \nu_e$	LF	[d] $< 4 \times 10^{-3}$	CL=90%	236
$\pi^+ \mu^+ e^-$	LF	$< 1.3 \times 10^{-11}$	CL=90%	214
$\pi^+ \mu^- e^+$	LF	$< 6.6 \times 10^{-11}$	CL=90%	214
$\pi^- \mu^+ e^+$	L	$< 4.2 \times 10^{-11}$	CL=90%	214
$\pi^- e^+ e^+$	L	$< 5.3 \times 10^{-11}$	CL=90%	227
$\pi^- \mu^+ \mu^+$	L	$< 4.2 \times 10^{-11}$	CL=90%	172
$\pi^- \pi^0 e^+ e^+$	L	$< 8.5 \times 10^{-10}$	CL=90%	205
$\mu^+ \bar{\nu}_e$	L	[d] $< 3.3 \times 10^{-3}$	CL=90%	236
$\pi^0 e^+ \bar{\nu}_e$	L	$< 3 \times 10^{-3}$	CL=90%	228
$\pi^+ \gamma$	[v]	$< 2.3 \times 10^{-9}$	CL=90%	227

 K^0

$$I(J^P) = \frac{1}{2}(0^-)$$

50% K_S , 50% K_L

$$\text{Mass } m = 497.611 \pm 0.013 \text{ MeV} \quad (S = 1.2)$$

$$m_{K^0} - m_{K^\pm} = 3.934 \pm 0.020 \text{ MeV} \quad (S = 1.6)$$

Mean square charge radius

$$\langle r^2 \rangle = -0.077 \pm 0.010 \text{ fm}^2$$

T-violation parameters in K^0 - \bar{K}^0 mixing [q]

$$\text{Asymmetry } A_T \text{ in } K^0\text{-}\bar{K}^0 \text{ mixing} = (6.6 \pm 1.6) \times 10^{-3}$$

CP-violation parameters

$$\text{Re}(\epsilon) = (1.596 \pm 0.013) \times 10^{-3}$$

CPT-violation parameters [q]

$$\text{Re } \delta = (2.5 \pm 2.3) \times 10^{-4}$$

$$\text{Im } \delta = (-1.5 \pm 1.6) \times 10^{-5}$$

$$\text{Re}(y), K_{e 3} \text{ parameter} = (0.4 \pm 2.5) \times 10^{-3}$$

$$\text{Re}(x_-), K_{e 3} \text{ parameter} = (-2.9 \pm 2.0) \times 10^{-3}$$

$$|m_{K^0} - m_{\bar{K}^0}| / m_{\text{average}} < 6 \times 10^{-19}, \text{ CL} = 90\% [x]$$

$$(\Gamma_{K^0} - \Gamma_{\bar{K}^0}) / m_{\text{average}} = (8 \pm 8) \times 10^{-18}$$

Tests of $\Delta S = \Delta Q$

$$\text{Re}(x_+), K_{e 3} \text{ parameter} = (-0.9 \pm 3.0) \times 10^{-3}$$

 K_S^0

$$I(J^P) = \frac{1}{2}(0^-)$$

Mean life $\tau = (0.8954 \pm 0.0004) \times 10^{-10} \text{ s}$ (S = 1.1) Assuming CPTMean life $\tau = (0.89564 \pm 0.00033) \times 10^{-10} \text{ s}$ Not assuming CPT

$$c\tau = 2.6844 \text{ cm} \quad \text{Assuming CPT}$$

CP-violation parameters [v]

$$\begin{aligned} \text{Im}(\eta_{+-0}) &= -0.002 \pm 0.009 \\ \text{Im}(\eta_{000}) &= -0.001 \pm 0.016 \\ |\eta_{000}| &= |A(K_S^0 \rightarrow 3\pi^0)/A(K_L^0 \rightarrow 3\pi^0)| < 0.0088, \text{CL} = \\ &90\% \\ \text{CP asymmetry } A &\text{ in } \pi^+ \pi^- e^+ e^- = (-0.4 \pm 0.8)\% \end{aligned}$$

K_S^0 DECAY MODES	Fraction (Γ_i/Γ)	Scale factor/ Confidence level	p (MeV/c)
Hadronic modes			
$\pi^0 \pi^0$	(30.69 ± 0.05) %		209
$\pi^+ \pi^-$	(69.20 ± 0.05) %		206
$\pi^+ \pi^- \pi^0$	(3.5 $\pm_{-0.9}^{+1.1}$) × 10 ⁻⁷		133
Modes with photons or $\ell\bar{\ell}$ pairs			
$\pi^+ \pi^- \gamma$	[s,z] (1.79 ± 0.05) × 10 ⁻³		206
$\pi^+ \pi^- e^+ e^-$	(4.79 ± 0.15) × 10 ⁻⁵		206
$\pi^0 \gamma \gamma$	[z] (4.9 ± 1.8) × 10 ⁻⁸		230
$\gamma \gamma$	(2.63 ± 0.17) × 10 ⁻⁶	S=3.1	249
$\mu^+ \mu^- \mu^+ \mu^-$	< 5.1 × 10 ⁻¹²	CL=90%	119
Semileptonic modes			
$\pi^\pm e^\mp \nu_e$	[aa] (7.14 ± 0.06) × 10 ⁻⁴		229
CP violating (CP) and $\Delta S = 1$ weak neutral current (S1) modes			
$3\pi^0$	CP < 2.6 × 10 ⁻⁸	CL=90%	139
$\mu^+ \mu^-$	S1 < 2.1 × 10 ⁻¹⁰	CL=90%	225
$e^+ e^-$	S1 < 9 × 10 ⁻⁹	CL=90%	249
$\pi^0 e^+ e^-$	S1 [z] (3.0 $\pm_{-1.2}^{+1.5}$) × 10 ⁻⁹		230
$\pi^0 \mu^+ \mu^-$	S1 (2.9 $\pm_{-1.2}^{+1.5}$) × 10 ⁻⁹		177

 K_L^0

$$I(J^P) = \frac{1}{2}(0^-)$$

$$\begin{aligned} m_{K_L} - m_{K_S} &= (0.5293 \pm 0.0009) \times 10^{10} \text{ h s}^{-1} \quad (S = 1.3) \quad \text{Assuming } CPT \\ &= (3.484 \pm 0.006) \times 10^{-12} \text{ MeV} \quad \text{Assuming } CPT \\ &= (0.5289 \pm 0.0010) \times 10^{10} \text{ h s}^{-1} \quad \text{Not assuming } CPT \\ \text{Mean life } \tau &= (5.116 \pm 0.021) \times 10^{-8} \text{ s} \quad (S = 1.1) \\ c\tau &= 15.34 \text{ m} \end{aligned}$$

Slope parameters [p]

(See Particle Listings for other linear and quadratic coefficients)

$$\begin{aligned} K_L^0 \rightarrow \pi^+ \pi^- \pi^0: g &= 0.678 \pm 0.008 \quad (S = 1.5) \\ K_L^0 \rightarrow \pi^+ \pi^- \pi^0: h &= 0.076 \pm 0.006 \\ K_L^0 \rightarrow \pi^+ \pi^- \pi^0: k &= 0.0099 \pm 0.0015 \\ K_L^0 \rightarrow \pi^0 \pi^0 \pi^0: h &= (0.6 \pm 1.2) \times 10^{-3} \end{aligned}$$

 K_L decay form factors [q]

Linear parametrization assuming μ - e universality

$$\begin{aligned} \lambda_+(K_{\mu 3}^0) &= \lambda_+(K_{e 3}^0) = (2.82 \pm 0.04) \times 10^{-2} \quad (S = 1.1) \\ \lambda_0(K_{\mu 3}^0) &= (1.38 \pm 0.18) \times 10^{-2} \quad (S = 2.2) \end{aligned}$$

Quadratic parametrization assuming μ - e universality

$$\begin{aligned} \lambda'_+(K_{\mu 3}^0) &= \lambda'_+(K_{e 3}^0) = (2.40 \pm 0.12) \times 10^{-2} \quad (S = 1.2) \\ \lambda''_+(K_{\mu 3}^0) &= \lambda''_+(K_{e 3}^0) = (0.20 \pm 0.05) \times 10^{-2} \quad (S = 1.2) \\ \lambda_0(K_{\mu 3}^0) &= (1.16 \pm 0.09) \times 10^{-2} \quad (S = 1.2) \end{aligned}$$

Pole parametrization assuming μ - e universality

$$\begin{aligned} M_V^\mu(K_{\mu 3}^0) &= M_V^e(K_{e 3}^0) = 878 \pm 6 \text{ MeV} \quad (S = 1.1) \\ M_S^\mu(K_{\mu 3}^0) &= 1252 \pm 90 \text{ MeV} \quad (S = 2.6) \end{aligned}$$

Dispersive parametrization assuming μ - e universality

$$\begin{aligned} \Lambda_+ &= (2.51 \pm 0.06) \times 10^{-2} \quad (S = 1.5) \\ \ln(C) &= (1.75 \pm 0.18) \times 10^{-1} \quad (S = 2.0) \\ K_{e 3}^0 |f_S/f_+| &= (1.5 \pm_{-1.6}^{+1.4}) \times 10^{-2} \\ K_{e 3}^0 |f_T/f_+| &= (5 \pm_{-5}^{+4}) \times 10^{-2} \\ K_{\mu 3}^0 |f_T/f_+| &= (12 \pm 12) \times 10^{-2} \\ K_L \rightarrow \ell^+ \ell^- \gamma, K_L \rightarrow \ell^+ \ell^- \ell'^+ \ell'^-: \alpha_{K^*} &= -0.205 \pm \\ &0.022 \quad (S = 1.8) \\ K_L^0 \rightarrow \ell^+ \ell^- \gamma, K_L^0 \rightarrow \ell^+ \ell^- \ell'^+ \ell'^-: \alpha_{DIP} &= -1.69 \pm \\ &0.08 \quad (S = 1.7) \\ K_L \rightarrow \pi^+ \pi^- e^+ e^-: a_1/a_2 &= -0.737 \pm 0.014 \text{ GeV}^2 \\ K_L \rightarrow \pi^0 2\gamma: a_V &= -0.43 \pm 0.06 \quad (S = 1.5) \end{aligned}$$

CP-violation parameters [v]

$$\begin{aligned} A_L &= (0.332 \pm 0.006)\% \\ |\eta_{00}| &= (2.220 \pm 0.011) \times 10^{-3} \quad (S = 1.8) \\ |\eta_{+-}| &= (2.232 \pm 0.011) \times 10^{-3} \quad (S = 1.8) \\ |\epsilon| &= (2.228 \pm 0.011) \times 10^{-3} \quad (S = 1.8) \\ |\eta_{00}/\eta_{+-}| &= 0.9950 \pm 0.0007^{[bb]} \quad (S = 1.6) \\ \text{Re}(\epsilon'/\epsilon) &= (1.66 \pm 0.23) \times 10^{-3}^{[bb]} \quad (S = 1.6) \end{aligned}$$

Assuming CPT

$$\phi_{+-} = (43.51 \pm 0.05)^\circ \quad (S = 1.2)$$

$$\phi_{00} = (43.52 \pm 0.05)^\circ \quad (S = 1.2)$$

$$\phi_\epsilon = \phi_{SW} = (43.52 \pm 0.04)^\circ \quad (S = 1.2)$$

$$\text{Im}(\epsilon'/\epsilon) = -(\phi_{00} - \phi_{+-})/3 = (-0.002 \pm 0.005)^\circ \quad (S = 1.7)$$

Not assuming CPT

$$\phi_{+-} = (43.4 \pm 0.5)^\circ \quad (S = 1.2)$$

$$\phi_{00} = (43.7 \pm 0.6)^\circ \quad (S = 1.2)$$

$$\phi_\epsilon = (43.5 \pm 0.5)^\circ \quad (S = 1.3)$$

CP asymmetry A in $K_L^0 \rightarrow \pi^+ \pi^- e^+ e^- = (13.7 \pm 1.5)\%$

$$\beta_{CP} \text{ from } K_L^0 \rightarrow e^+ e^- e^+ e^- = -0.19 \pm 0.07$$

$$\gamma_{CP} \text{ from } K_L^0 \rightarrow e^+ e^- e^+ e^- = 0.01 \pm 0.11 \quad (S = 1.6)$$

$$j \text{ for } K_L^0 \rightarrow \pi^+ \pi^- \pi^0 = 0.0012 \pm 0.0008$$

$$f \text{ for } K_L^0 \rightarrow \pi^+ \pi^- \pi^0 = 0.004 \pm 0.006$$

$$|\eta_{+-\gamma}| = (2.35 \pm 0.07) \times 10^{-3}$$

$$\phi_{+-\gamma} = (44 \pm 4)^\circ$$

$$|\epsilon'_{+-\gamma}|/\epsilon < 0.3, \text{CL} = 90\%$$

$$|\bar{g}_{E1}| \text{ for } K_L^0 \rightarrow \pi^+ \pi^- \gamma < 0.21, \text{CL} = 90\%$$

T-violation parameters

$$\text{Im}(\xi) \text{ in } K_{\mu 3}^0 = -0.007 \pm 0.026$$

CPT invariance tests

$$\phi_{00} - \phi_{+-} = (0.34 \pm 0.32)^\circ$$

$$\text{Re}(\frac{2}{3}\eta_{+-} + \frac{1}{3}\eta_{00}) - \frac{A_j}{2} = (-3 \pm 35) \times 10^{-6}$$

 $\Delta S = -\Delta Q$ in $K_{\mu 3}^0$ decay

$$\text{Re } x = -0.002 \pm 0.006$$

$$\text{Im } x = 0.0012 \pm 0.0021$$

K_L^0 DECAY MODES	Fraction (Γ_i/Γ)	Scale factor/ Confidence level (MeV/c)	p
Semileptonic modes			
$\pi^\pm e^\mp \nu_e$	[aa] (40.55 ± 0.11) %	S=1.7	229
Called $K_{e 3}^0$.			
$\pi^\pm \mu^\mp \nu_\mu$	[aa] (27.04 ± 0.07) %	S=1.1	216
Called $K_{\mu 3}^0$.			
(π atom) ν	(1.05 ± 0.11) × 10 ⁻⁷		188
$\pi^0 \pi^\pm e^\mp \nu$	[aa] (5.20 ± 0.11) × 10 ⁻⁵		207
$\pi^\pm e^\mp \nu e^+ e^-$	[aa] (1.26 ± 0.04) × 10 ⁻⁵		229
Hadronic modes, including Charge conjugation × Parity Violating (CPV) modes			
$3\pi^0$	(19.52 ± 0.12) %	S=1.6	139
$\pi^+ \pi^- \pi^0$	(12.54 ± 0.05) %		133
$\pi^+ \pi^-$	CPV [cc] (1.967 ± 0.010) × 10 ⁻³	S=1.5	206
$\pi^0 \pi^0$	CPV (8.64 ± 0.06) × 10 ⁻⁴	S=1.8	209
Semileptonic modes with photons			
$\pi^\pm e^\mp \nu_e \gamma$	[s,aa,dd] (3.79 ± 0.06) × 10 ⁻³		229
$\pi^\pm \mu^\mp \nu_\mu \gamma$	(5.65 ± 0.23) × 10 ⁻⁴		216
Hadronic modes with photons or $\ell\bar{\ell}$ pairs			
$\pi^0 \pi^0 \gamma$	< 2.43 × 10 ⁻⁷	CL=90%	209
$\pi^+ \pi^- \gamma$	[s,dd] (4.15 ± 0.15) × 10 ⁻⁵	S=2.8	206
$\pi^+ \pi^- \gamma$ (DE)	(2.84 ± 0.11) × 10 ⁻⁵	S=2.0	206
$\pi^0 2\gamma$	[dd] (1.273 ± 0.033) × 10 ⁻⁶		230
$\pi^0 \gamma e^+ e^-$	(1.62 ± 0.17) × 10 ⁻⁸		230
Other modes with photons or $\ell\bar{\ell}$ pairs			
2γ	(5.47 ± 0.04) × 10 ⁻⁴	S=1.1	249
3γ	< 7.4 × 10 ⁻⁸	CL=90%	249
$e^+ e^- \gamma$	(9.4 ± 0.4) × 10 ⁻⁶	S=2.0	249

Meson Summary Table

$\mu^+ \mu^- \gamma$	$(3.59 \pm 0.11) \times 10^{-7}$	S=1.3	225
$\mu^+ \mu^- \mu^+ \mu^-$	$< 2.3 \times 10^{-9}$	CL=90%	119
$e^+ e^- \gamma \gamma$	[<i>dd</i>] $(5.95 \pm 0.33) \times 10^{-7}$		249
$\mu^+ \mu^- \gamma \gamma$	[<i>dd</i>] $(1.0 \pm_{-0.6}^{+0.8}) \times 10^{-8}$		225

Charge conjugation \times Parity (CP) or Lepton Family number (LF) violating modes, or $\Delta S = 1$ weak neutral current (SI) modes

$\mu^+ \mu^-$	SI	$(6.84 \pm 0.11) \times 10^{-9}$		225
$e^+ e^-$	SI	$(9 \pm_{-4}^{+6}) \times 10^{-12}$		249
$\pi^+ \pi^- e^+ e^-$	SI	[<i>dd</i>] $(3.11 \pm 0.19) \times 10^{-7}$		206
$\pi^0 \pi^0 e^+ e^-$	SI	$< 6.6 \times 10^{-9}$	CL=90%	209
$\pi^0 \pi^0 \mu^+ \mu^-$	SI	$< 9.2 \times 10^{-11}$	CL=90%	57
$\mu^+ \mu^- e^+ e^-$	SI	$(2.69 \pm 0.27) \times 10^{-9}$		225
$e^+ e^- e^+ e^-$	SI	$(3.56 \pm 0.21) \times 10^{-8}$		249
$\pi^0 \mu^+ \mu^-$	CP,SI [ee]	$< 3.8 \times 10^{-10}$	CL=90%	177
$\pi^0 e^+ e^-$	CP,SI [ee]	$< 2.8 \times 10^{-10}$	CL=90%	230
$\pi^0 \nu \bar{\nu}$	CP,SI [<i>ff</i>]	$< 3.0 \times 10^{-9}$	CL=90%	230
$\pi^0 \pi^0 \nu \bar{\nu}$	SI	$< 8.1 \times 10^{-7}$	CL=90%	209
$e^\pm \mu^\mp$	LF [aa]	$< 4.7 \times 10^{-12}$	CL=90%	238
$e^\pm e^\pm \mu^\mp \mu^\mp$	LF [aa]	$< 4.12 \times 10^{-11}$	CL=90%	225
$\pi^0 \mu^\pm e^\mp$	LF [aa]	$< 7.6 \times 10^{-11}$	CL=90%	217
$\pi^0 \pi^0 \mu^\pm e^\mp$	LF	$< 1.7 \times 10^{-10}$	CL=90%	159

Lorentz invariance violating modes

$\pi^0 \gamma$	$< 1.7 \times 10^{-7}$	CL=90%	230
----------------	------------------------	--------	-----

$K_0^*(700)$ $I(J^P) = \frac{1}{2}(0^+)$

also known as κ ; was $K_0^*(800)$

See the review on "Scalar Mesons below 1 GeV."

Mass (T-Matrix Pole \sqrt{s}) = $(630-730) - i(260-340)$ MeV

Mass (Breit-Wigner) = 845 ± 17 MeV

Full width (Breit-Wigner) = 468 ± 30 MeV

$K_0^*(700)$ DECAY MODES	Fraction (Γ_i/Γ)	ρ (MeV/c)
$K \pi$	100 %	256

$K^*(892)$ $I(J^P) = \frac{1}{2}(1^-)$

Mass (T-Matrix Pole \sqrt{s}) = $(890 \pm 14) - i(26 \pm 6)$ MeV

$K^*(892)^\pm$ hadroproduced mass $m = 891.67 \pm 0.26$ MeV

$K^*(892)^\pm$ in τ decays mass $m = 895.5 \pm 0.8$ MeV

$K^*(892)^0$ mass $m = 895.55 \pm 0.20$ MeV (S = 1.7)

$K^*(892)^\pm$ hadroproduced full width $\Gamma = 51.4 \pm 0.8$ MeV

$K^*(892)^\pm$ in τ decays full width $\Gamma = 46.2 \pm 1.3$ MeV

$K^*(892)^0$ full width $\Gamma = 47.3 \pm 0.5$ MeV (S = 2.0)

$K^*(892)$ DECAY MODES	Fraction (Γ_i/Γ)	Confidence level	ρ (MeV/c)
$K \pi$	~ 100 %		289
$K^0 \gamma$	$(2.46 \pm 0.21) \times 10^{-3}$		307
$K^\pm \gamma$	$(9.8 \pm 0.9) \times 10^{-4}$		309
$K \pi \pi$	$< 7 \times 10^{-4}$	95%	223

$K_1(1270)$ $I(J^P) = \frac{1}{2}(1^+)$

Mass $m = 1253 \pm 7$ MeV (S = 2.2)

Full width $\Gamma = 90 \pm 20$ MeV [¹]

$K_1(1270)$ DECAY MODES	Fraction (Γ_i/Γ)	Scale factor	ρ (MeV/c)
$K \rho$	(38 ± 13) %	2.2	†
$K_0^*(1430) \pi$	(28 ± 4) %		†
$K^*(892) \pi$	(21 ± 10) %	2.2	286
$K \omega$	(11.0 ± 2.0) %		†
$K f_0(1370)$	(3.0 ± 2.0) %		†
γK^0	seen		528

$K_1(1400)$ $I(J^P) = \frac{1}{2}(1^+)$

Mass $m = 1403 \pm 7$ MeV

Full width $\Gamma = 174 \pm 13$ MeV (S = 1.6)

$K_1(1400)$ DECAY MODES	Fraction (Γ_i/Γ)	ρ (MeV/c)
$K^*(892) \pi$	(94 ± 6) %	402
$K \rho$	(3.0 ± 3.0) %	293
$K f_0(1370)$	(2.0 ± 2.0) %	†
$K \omega$	(1.0 ± 1.0) %	284
$K_0^*(1430) \pi$	not seen	†
γK^0	seen	613
$K \phi$	seen	†

$K^*(1410)$ $I(J^P) = \frac{1}{2}(1^-)$

T-matrix pole $\sqrt{s} = (1368 \pm 38) - i(106 \pm_{-59}^{+48})$ MeV

Mass $m = 1414 \pm 15$ MeV (S = 1.3)

Full width $\Gamma = 232 \pm 21$ MeV (S = 1.1)

$K^*(1410)$ DECAY MODES	Fraction (Γ_i/Γ)	Confidence level	ρ (MeV/c)
$K^*(892) \pi$	> 40 %	95%	410
$K \pi$	(6.6 ± 1.3) %		612
$K \rho$	< 7 %	95%	305
γK^0	$< 2.3 \times 10^{-4}$	90%	619
$K \phi$	seen		†

$K_0^*(1430)$ $I(J^P) = \frac{1}{2}(0^+)$

T-matrix pole $\sqrt{s} = (1431 \pm 6) - i(110 \pm 19)$ MeV

Mass $m = 1425 \pm 50$ MeV [¹]

Full width $\Gamma = 270 \pm 80$ MeV [¹]

$K_0^*(1430)$ DECAY MODES	Fraction (Γ_i/Γ)	ρ (MeV/c)
$K \pi$	(93 ± 10) %	619
$K \eta$	$(8.6 \pm_{-3.4}^{+2.7})$ %	486
$K \eta'(958)$	seen	†

$K_2^*(1430)$ $I(J^P) = \frac{1}{2}(2^+)$

T-matrix pole $\sqrt{s} = (1424 \pm 4) - i(66 \pm 2)$ MeV

$K_2^*(1430)^\pm$ mass $m = 1427.3 \pm 1.5$ MeV (S = 1.3)

$K_2^*(1430)^0$ mass $m = 1432.4 \pm 1.3$ MeV

$K_2^*(1430)^\pm$ full width $\Gamma = 100.0 \pm 2.2$ MeV (S = 1.1)

$K_2^*(1430)^0$ full width $\Gamma = 109 \pm 5$ MeV (S = 1.9)

$K_2^*(1430)$ DECAY MODES	Fraction (Γ_i/Γ)	Scale factor / Confidence level	ρ (MeV/c)
$K \pi$	(49.9 ± 1.2) %		620
$K^*(892) \pi$	(24.7 ± 1.5) %		420
$K^*(892) \pi \pi$	(13.4 ± 2.2) %		373
$K \rho$	(8.7 ± 0.8) %	S=1.2	320
$K \omega$	(2.9 ± 0.8) %		313
$K^+ \gamma$	$(2.4 \pm 0.5) \times 10^{-3}$	S=1.1	628
$K \eta$	$(1.5 \pm_{-1.0}^{+3.4}) \times 10^{-3}$	S=1.3	488
$K \omega \pi$	$< 7.2 \times 10^{-4}$	CL=95%	106
$K^0 \gamma$	$< 9 \times 10^{-4}$	CL=90%	627

$K(1460)$ $I(J^P) = \frac{1}{2}(0^-)$

$K(1460)$ DECAY MODES	Fraction (Γ_i/Γ)	ρ (MeV/c)
$K^*(892) \pi$	seen	-
$K \rho$	seen	-
$K_0^*(1430) \pi$	seen	-
$K \phi$	seen	-

$K_1(1650)$ $I(J^P) = \frac{1}{2}(1^+)$

Mass $m = 1650 \pm 50$ MeV

Full width $\Gamma = 150 \pm 50$ MeV

Meson Summary Table

K*(1680)

$$I(J^P) = \frac{1}{2}(1^-)$$

Mass $m = 1718 \pm 18$ MeVFull width $\Gamma = 320 \pm 110$ MeV ($S = 4.2$)

K*(1680) DECAY MODES	Fraction (Γ_i/Γ)	ρ (MeV/c)
$K\pi$	(38.7±2.5) %	782
$K\rho$	(31.4 $^{+5.0}_{-2.1}$) %	571
$K^*(892)\pi$	(29.9 $^{+2.2}_{-5.0}$) %	618
$K\phi$	seen	387
$K\eta$	(1.4 $^{+1.0}_{-0.8}$) %	683

K₂(1770) [gg]

$$I(J^P) = \frac{1}{2}(2^-)$$

Mass $m = 1773 \pm 8$ MeVFull width $\Gamma = 186 \pm 14$ MeV

K₂(1770) DECAY MODES	Fraction (Γ_i/Γ)	ρ (MeV/c)
$K\pi\pi$		794
$K_2^*(1430)\pi$	seen	287
$K^*(892)\pi$	seen	654
$Kf_2(1270)$	seen	53
$Kf_0(980)$	possibly seen	466
$K\phi$	seen	441
$K\omega$	seen	607

K₃*(1780)

$$I(J^P) = \frac{1}{2}(3^-)$$

T-matrix pole $\sqrt{s} = (1754 \pm 13) - i(119 \pm 14)$ MeVMass $m = 1779 \pm 8$ MeV ($S = 1.2$)Full width $\Gamma = 161 \pm 17$ MeV ($S = 1.1$)

K₃*(1780) DECAY MODES	Fraction (Γ_i/Γ)	Confidence level	ρ (MeV/c)
$K\rho$	(31 ± 9) %		616
$K^*(892)\pi$	(20 ± 5) %		657
$K\pi$	(18.8 ± 1.0) %		815
$K\eta$	(30 ± 13) %		721
$K_2^*(1430)\pi$	< 16 %	95%	292

K₂(1820) [gg]

$$I(J^P) = \frac{1}{2}(2^-)$$

Mass $m = 1819 \pm 12$ MeVFull width $\Gamma = 264 \pm 34$ MeV

K₂(1820) DECAY MODES	Fraction (Γ_i/Γ)	ρ (MeV/c)
$K\pi\pi$	seen	819
$K_2^*(1430)\pi$	seen	328
$K^*(892)\pi$	seen	683
$Kf_2(1270)$	seen	191
$K\omega$	seen	640
$K\phi$	seen	483

K₀*(1950)

$$I(J^P) = \frac{1}{2}(0^+)$$

Mass $m = 1957 \pm 14$ MeVFull width $\Gamma = 170 \pm 50$ MeV ($S = 2.2$)

K₀*(1950) DECAY MODES	Fraction (Γ_i/Γ)	ρ (MeV/c)
$K^-\pi^+$	(52±14) %	911

K₂*(1980)

$$I(J^P) = \frac{1}{2}(2^+)$$

Mass $m = 1990^{+60}_{-50}$ MeV ($S = 2.8$)Full width $\Gamma = 348^{+50}_{-30}$ MeV ($S = 1.3$)**K₂*(1980) DECAY MODES**Fraction (Γ_i/Γ) ρ (MeV/c)

$K^*(892)\pi$	possibly seen	791
$K\rho$	possibly seen	762
$Kf_2(1270)$	possibly seen	424
$K\phi$	seen	627
$K\eta$	seen	850

K₄*(2045)

$$I(J^P) = \frac{1}{2}(4^+)$$

Mass $m = 2048^{+8}_{-9}$ MeV ($S = 1.1$)Full width $\Gamma = 199^{+27}_{-19}$ MeV**K₄*(2045) DECAY MODES**Fraction (Γ_i/Γ) ρ (MeV/c)

$K\pi$	(9.9±1.2) %	960
$K^*(892)\pi\pi$	(9 ± 5) %	804
$K^*(892)\pi\pi\pi$	(7 ± 5) %	770
$\rho K\pi$	(5.7±3.2) %	744
$\omega K\pi$	(5.0±3.0) %	740
$\phi K\pi$	(2.8±1.4) %	597
$\phi K^*(892)$	(1.4±0.7) %	368

**CHARMED MESONS
(C = ±1)** $D^+ = c\bar{d}, D^0 = c\bar{u}, \bar{D}^0 = \bar{c}u, D^- = \bar{c}d$, similarly for D^* 's**D[±]**

$$I(J^P) = \frac{1}{2}(0^-)$$

Mass $m = 1869.66 \pm 0.05$ MeVMean life $\tau = (1033 \pm 5) \times 10^{-15}$ s $c\tau = 309.8$ μm **c-quark decays** $\Gamma(c \rightarrow \ell^+ \text{ anything})/\Gamma(c \rightarrow \text{ anything}) = 0.096 \pm 0.004$ [hh] $\Gamma(c \rightarrow D^*(2010)^+ \text{ anything})/\Gamma(c \rightarrow \text{ anything}) = 0.255 \pm 0.017$ **CP-violation decay-rate asymmetries** $A_{CP}(\mu^\pm \nu) = (8 \pm 8)\%$ $A_{CP}(K^0 e^\pm \nu) = (-0.6 \pm 1.6)\%$ $A_{CP}(K_S^0 \pi^\pm) = (-0.41 \pm 0.09)\%$ $A_{CP}(K_L^0 K^\pm) \text{ in } D^\pm \rightarrow K_L^0 K^\pm = (-4.2 \pm 3.4) \times 10^{-2}$ $A_{CP}(K^\pm 2\pi^\pm) = (-0.18 \pm 0.16)\%$ $A_{CP}(K^\mp \pi^\pm \pi^\pm \pi^0) = (-0.3 \pm 0.7)\%$ $A_{CP}(K_S^0 \pi^\pm \pi^0) = (-0.1 \pm 0.7)\%$ $A_{CP}(K_S^0 \pi^\pm \eta) \text{ in } D^\pm \rightarrow K_S^0 \pi^\pm \eta = (-0.9 \pm 3.1) \times 10^{-2}$ $A_{CP}(K_S^0 \pi^\pm \pi^+ \pi^-) = (0.0 \pm 1.2)\%$ $A_{CP}(K^\pm \pi^+ \pi^- \pi^0) \text{ in } D^\pm \rightarrow K^\pm \pi^+ \pi^- \pi^0 = -0.04 \pm 0.06$ $A_{CP}(\pi^\pm \pi^0) = (0.4 \pm 1.3)\%$ ($S = 1.7$) $A_{CP}(\pi^\pm \eta) = (0.3 \pm 0.5)\%$ $A_{CP}(\pi^\pm \pi^0 \eta) \text{ in } D^\pm \rightarrow \pi^\pm \pi^0 \eta = (-6 \pm 7) \times 10^{-2}$ $A_{CP}(\pi^\pm \eta \eta) \text{ in } D^\pm \rightarrow \pi^\pm \eta \eta = (8 \pm 9) \times 10^{-2}$ $A_{CP}(\pi^\pm \eta' (958)) = (0.41 \pm 0.23)\%$ ($S = 1.2$) $A_{CP}(\bar{K}^0 / K^0 K^\pm) = (0.11 \pm 0.17)\%$ $A_{CP}(K_S^0 K^\pm) = (-0.01 \pm 0.07)\%$ $A_{CP}(K_S^0 K^\pm \pi^0) \text{ in } D^\pm \rightarrow K_S^0 K^\pm \pi^0 = (1 \pm 4) \times 10^{-2}$ $A_{CP}(K_L^0 K^\pm \pi^0) \text{ in } D^\pm \rightarrow K_L^0 K^\pm \pi^0 = (-1 \pm 4) \times 10^{-2}$ $A_{CP}(K^\pm K^\mp \pi^\pm) = (0.37 \pm 0.29)\%$ $A_{CP}(K^\pm K^*0) = (-0.3 \pm 0.4)\%$ $A_{CP}(\phi \pi^\pm) = (0.01 \pm 0.09)\%$ ($S = 1.8$) $A_{CP}(K^\pm K_0^*(1430)^0) = (8^{+7}_{-6})\%$ $A_{CP}(K^\pm K_2^*(1430)^0) = (43^{+20}_{-16})\%$ $A_{CP}(K^\pm K_0^*(700)) = (-12^{+18}_{-13})\%$ $A_{CP}(a_0(1450)^0 \pi^\pm) = (-19^{+14}_{-16})\%$ $A_{CP}(\phi(1680) \pi^\pm) = (-9 \pm 26)\%$ $A_{CP}(\pi^\pm 2\pi^0) \text{ in } D^\pm \rightarrow \pi^\pm 2\pi^0 = (5.6 \pm 2.7)\%$ $A_{CP}(\pi^+ \pi^- \pi^\pm) = (0.5 \pm 2.0)\%$ $A_{CP}(2\pi^\pm \pi^\mp \pi^0) \text{ in } D^\pm \rightarrow 2\pi^\pm \pi^\mp \pi^0 = (0.3 \pm 2.0)\%$ $A_{CP}(2\pi^\pm \pi^\mp 2\pi^0) \text{ in } D^\pm \rightarrow 2\pi^\pm \pi^\mp 2\pi^0 = (-4 \pm 4)\%$ $A_{CP}(\pi^+ \pi^- \pi^\pm \eta) \text{ in } D^\pm \rightarrow \pi^+ \pi^- \pi^\pm \eta = (3 \pm 5) \times 10^{-2}$ $A_{CP}(K_S^0 K^\pm \pi^+ \pi^-) = (-4 \pm 7)\%$ $A_{CP}(K^\pm \pi^0) = (-3 \pm 5)\%$ $A_{CP}(K^\pm \eta) \text{ in } D^\pm \rightarrow K^\pm \eta = (-6 \pm 11) \times 10^{-2}$

Meson Summary Table

 χ^2 tests of CP-violation (CPV)

- Local CPV in $D^\pm \rightarrow \pi^+ \pi^- \pi^\pm = 78.1\%$
 Local CPV in $D^\pm \rightarrow K^+ K^- \pi^\pm = 31\%$
 Local CPV in $D^\pm \rightarrow K^+ K^- K^\pm = 31.6\%$

CP violating asymmetries of P-odd (T-odd) moments

- $A_T(K_S^0 K^\pm \pi^\mp) = (-3 \pm 8) \times 10^{-3}$ [ii] (S = 1.1)
 $A_{Tviol}(K^+ K^- K_S^0 \pi^\pm)$ in $D^\pm \rightarrow K^+ K^- K_S^0 \pi^\pm = (-3.3 \pm 2.7)\%$

 D^+ form factors

- $f_+(0)|V_{cs}|$ in $\bar{K}^0 \ell^+ \nu_\ell = 0.719 \pm 0.011$ (S = 1.6)
 $r_1 \equiv a_1/a_0$ in $\bar{K}^0 \ell^+ \nu_\ell = -2.13 \pm 0.14$
 $r_2 \equiv a_2/a_0$ in $\bar{K}^0 \ell^+ \nu_\ell = -3 \pm 12$ (S = 1.5)
 $f_+(0)|V_{cd}|$ in $\pi^0 \ell^+ \nu_\ell = 0.1407 \pm 0.0025$
 $r_1 \equiv a_1/a_0$ in $\pi^0 \ell^+ \nu_\ell = -2.00 \pm 0.13$
 $r_2 \equiv a_2/a_0$ in $\pi^0 \ell^+ \nu_\ell = -4 \pm 5$
 $f_+(0)|V_{cd}|$ in $D^+ \rightarrow \eta \ell^+ \nu_\ell$ ($\ell = e$ or ν) = $(8.4 \pm 0.4) \times 10^{-2}$
 $r_1 \equiv a_1/a_0$ in $D^+ \rightarrow \eta e^+ \nu_e = -5.3 \pm 2.7$ (S = 1.9)
 $r_V \equiv V(0)/A_1(0)$ in $D^+ \rightarrow \omega e^+ \nu_e = 1.24 \pm 0.11$
 $r_2 \equiv A_2(0)/A_1(0)$ in $D^+ \rightarrow \omega e^+ \nu_e = 1.06 \pm 0.16$
 $r_V \equiv V(0)/A_1(0)$ in $D^+, D^0 \rightarrow \rho e^+ \nu_e = 1.64 \pm 0.10$ (S = 1.2)
 $r_2 \equiv A_2(0)/A_1(0)$ in $D^+, D^0 \rightarrow \rho e^+ \nu_e = 0.84 \pm 0.06$
 $r_V \equiv V(0)/A_1(0)$ in $\bar{K}^*(892)^0 \ell^+ \nu_\ell = 1.49 \pm 0.05$ (S = 2.1)
 $r_2 \equiv A_2(0)/A_1(0)$ in $\bar{K}^*(892)^0 \ell^+ \nu_\ell = 0.802 \pm 0.021$
 $r_3 \equiv A_3(0)/A_1(0)$ in $\bar{K}^*(892)^0 \ell^+ \nu_\ell = 0.0 \pm 0.4$
 Γ_L/Γ_T in $\bar{K}^*(892)^0 \ell^+ \nu_\ell = 1.13 \pm 0.08$
 Γ_+/ Γ_- in $\bar{K}^*(892)^0 \ell^+ \nu_\ell = 0.22 \pm 0.06$ (S = 1.6)

Most decay modes (other than the semileptonic modes) that involve a neutral K meson are now given as K_S^0 modes, not as \bar{K}^0 modes. Nearly always it is a K_S^0 that is measured, and interference between Cabibbo-allowed and doubly Cabibbo-suppressed modes can invalidate the assumption that $2\Gamma(K_S^0) = \Gamma(\bar{K}^0)$.

D^+ DECAY MODES	Fraction (Γ_i/Γ)	Scale factor/ Confidence level	p (MeV/c)
Inclusive modes			
e^+ semileptonic	(16.07 \pm 0.30) %	–	–
μ^+ anything	(17.6 \pm 3.2) %	–	–
K^- anything	(25.7 \pm 1.4) %	–	–
K_S^0 anything	(33.1 \pm 0.4) %	–	–
K^+ anything	(5.9 \pm 0.8) %	–	–
$K^*(892)^-$ anything	(6 \pm 5) %	–	–
$\bar{K}^*(892)^0$ anything	(23 \pm 5) %	–	–
$K^*(892)^0$ anything	< 6.6 %	CL=90%	–
η anything	(6.3 \pm 0.7) %	–	–
η' anything	(1.04 \pm 0.18) %	–	–
ϕ anything	(1.12 \pm 0.04) %	–	–
$\pi^+ \pi^+ \pi^-$ anything	(15.25 \pm 0.20) %	–	–
Leptonic and semileptonic modes			
$e^+ \nu_e$	< 8.8 $\times 10^{-6}$ CL=90%	935	–
$\gamma e^+ \nu_e$	< 3.0 $\times 10^{-5}$ CL=90%	935	–
$\mu^+ \nu_\mu$	(3.74 \pm 0.17) $\times 10^{-4}$	932	–
$\tau^+ \nu_\tau$	(1.20 \pm 0.27) $\times 10^{-3}$	90	–
$\bar{K}^0 e^+ \nu_e$	(8.72 \pm 0.09) %	869	–
$\bar{K}^0 \mu^+ \nu_\mu$	(8.76 \pm 0.19) %	865	–
$K^- \pi^+ e^+ \nu_e$	(4.02 \pm 0.18) %	S=3.2	864
$\bar{K}^*(892)^0 e^+ \nu_e, \bar{K}^*(892)^0 \rightarrow K^- \pi^+$	(3.77 \pm 0.17) %	–	722
$(K^- \pi^+)$ [0.8–1.0] GeV $e^+ \nu_e$	(3.39 \pm 0.09) %	–	864
$(K^- \pi^+)$ S -wave $e^+ \nu_e$	(2.28 \pm 0.11) $\times 10^{-3}$	–	–
$\bar{K}^*(1410)^0 e^+ \nu_e, \bar{K}^*(1410)^0 \rightarrow K^- \pi^+$	< 6 $\times 10^{-3}$ CL=90%	–	–
$\bar{K}_2^*(1430)^0 e^+ \nu_e, \bar{K}_2^*(1430)^0 \rightarrow K^- \pi^+$	< 5 $\times 10^{-4}$ CL=90%	–	–
$K^- \pi^+ e^+ \nu_e$ nonresonant	< 7 $\times 10^{-3}$ CL=90%	864	–
$\bar{K}^*(892)^0 e^+ \nu_e$	(5.40 \pm 0.10) %	S=1.1	722
$K^- \pi^+ \mu^+ \nu_\mu$	(3.65 \pm 0.34) %	–	851
$\bar{K}^*(892)^0 \mu^+ \nu_\mu, \bar{K}^*(892)^0 \rightarrow K^- \pi^+$	(3.52 \pm 0.10) %	–	717
$K^- \pi^+ \mu^+ \nu_\mu$ nonresonant	(1.9 \pm 0.5) $\times 10^{-3}$	–	851
$\bar{K}^*(892)^0 \mu^+ \nu_\mu$	(5.27 \pm 0.15) %	–	717

$K^- \pi^+ \pi^0 \mu^+ \nu_\mu$	< 1.5 $\times 10^{-3}$ CL=90%	825
$\bar{K}_1^0(1270)^0 e^+ \nu_e, \bar{K}_1^0 \rightarrow K^- \pi^+ \pi^0$	(1.06 \pm 0.15) $\times 10^{-3}$	–
$\bar{K}_0^*(1430)^0 \mu^+ \nu_\mu$	< 2.3 $\times 10^{-4}$ CL=90%	380
$\bar{K}^*(1680)^0 \mu^+ \nu_\mu$	< 1.5 $\times 10^{-3}$ CL=90%	105
$\pi^0 e^+ \nu_e$	(3.72 \pm 0.17) $\times 10^{-3}$	S=2.0
$\pi^0 \mu^+ \nu_\mu$	(3.50 \pm 0.15) $\times 10^{-3}$	927
$\eta e^+ \nu_e$	(1.11 \pm 0.07) $\times 10^{-3}$	855
$\eta \mu^+ \nu_\mu$	(1.04 \pm 0.11) $\times 10^{-3}$	851
$\pi^- \pi^+ e^+ \nu_e$	(2.49 \pm 0.11) $\times 10^{-3}$	S=1.2
$f_0(500)^0 e^+ \nu_e, f_0(500)^0 \rightarrow \pi^+ \pi^-$	(6.4 \pm 0.6) $\times 10^{-4}$	–
$\rho^0 e^+ \nu_e$	(1.90 \pm 0.10) $\times 10^{-3}$	S=1.2
$\rho^0 \mu^+ \nu_\mu$	(2.4 \pm 0.4) $\times 10^{-3}$	770
$\omega e^+ \nu_e$	(1.69 \pm 0.11) $\times 10^{-3}$	771
$\omega \mu^+ \nu_\mu$	(1.77 \pm 0.21) $\times 10^{-3}$	767
$\eta'(958) e^+ \nu_e$	(2.0 \pm 0.4) $\times 10^{-4}$	690
$a(980)^0 e^+ \nu_e, a(980)^0 \rightarrow \eta \pi^0$	(1.7 \pm 0.8 / 0.7) $\times 10^{-4}$	–
$b_1(1235)^0 e^+ \nu_e, b_1^0 \rightarrow \omega \pi^0$	< 1.75 $\times 10^{-4}$ CL=90%	–
$\phi e^+ \nu_e$	< 1.3 $\times 10^{-5}$ CL=90%	657
$D^0 e^+ \nu_e$	< 1.0 $\times 10^{-4}$ CL=90%	5

Hadronic modes with a \bar{K} or $\bar{K}K\bar{K}$

$K_S^0 \pi^+$	(1.562 \pm 0.031) %	S=1.7	863
$K_L^0 \pi^+$	(1.46 \pm 0.05) %	–	863
$K^- 2\pi^+$	[jj] (9.38 \pm 0.16) %	S=1.6	846
$(K^- \pi^+)$ S -wave π^+	(7.52 \pm 0.17) %	–	846
$\bar{K}_0^*(1430)^0 \pi^+, \bar{K}_0^*(1430)^0 \rightarrow K^- \pi^+$	[kk] (1.25 \pm 0.06) %	–	382
$\bar{K}^*(892)^0 \pi^+, \bar{K}^*(892)^0 \rightarrow K^- \pi^+$	(1.04 \pm 0.12) %	–	714
$\bar{K}^*(1410)^0 \pi^+, \bar{K}^*(1410)^0 \rightarrow K^- \pi^+$	not seen	–	381
$K^- \pi^+ \pi^0$	[kk] (2.3 \pm 0.7) $\times 10^{-4}$	–	371
$\bar{K}_2^*(1430)^0 \pi^+, \bar{K}_2^*(1430)^0 \rightarrow K^- \pi^+$	[kk] (2.2 \pm 1.1) $\times 10^{-4}$	–	58
$\bar{K}^*(1680)^0 \pi^+, \bar{K}^*(1680)^0 \rightarrow K^- \pi^+$	(1.45 \pm 0.26) %	–	–
$K_S^0 \pi^+ \pi^0$	[jj] (7.36 \pm 0.20) %	–	845
$K_S^0 \rho^+$	(6.14 \pm 0.35) %	–	677
$K_S^0 \rho(1450)^+, \rho^+ \rightarrow \pi^+ \pi^0$	(1.5 \pm 1.2 / 1.4) $\times 10^{-3}$	–	–
$\bar{K}^*(892)^0 \pi^+, \bar{K}^*(892)^0 \rightarrow K_S^0 \pi^0$	(2.64 \pm 0.32) $\times 10^{-3}$	–	714
$\bar{K}_0^*(1430)^0 \pi^+, \bar{K}_0^*(1430)^0 \rightarrow K_S^0 \pi^0$	(2.7 \pm 0.9) $\times 10^{-3}$	–	–
$\bar{K}_0^*(1680)^0 \pi^+, \bar{K}_0^*(1680)^0 \rightarrow K_S^0 \pi^0$	(10 \pm 7 / 10) $\times 10^{-4}$	–	–
$\bar{\pi}^0 \pi^+, \bar{\pi}^0 \rightarrow K_S^0 \pi^0$	(6 \pm 5 / 4) $\times 10^{-3}$	–	–
$K_S^0 \pi^+ \pi^0$ nonresonant	(3 \pm 4) $\times 10^{-3}$	–	845
$K_S^0 \pi^+ \pi^0$ nonresonant and $\bar{\pi}^0 \pi^+$	(1.37 \pm 0.21 / 0.40) %	–	–
$(K_S^0 \pi^0)$ S -wave π^+	(1.27 \pm 0.27 / 0.33) %	–	845
$K_S^0 \pi^+ \omega$	(7.1 \pm 0.5) $\times 10^{-3}$	–	606
$K_S^0 \pi^+ \eta$	(1.31 \pm 0.05) %	–	722
$K_S^0 \pi^+ \eta'(958)$	(1.90 \pm 0.21) $\times 10^{-3}$	–	481
$K^- 2\pi^+ \pi^0$	[ll] (6.25 \pm 0.18) %	–	817
$K_S^0 2\pi^+ \pi^-$	[ll] (3.10 \pm 0.09) %	–	814
$K_S^0 \pi^+ 2\pi^0$	(2.89 \pm 0.09) %	–	817
$K_S^0 a_1(1260)^+, a_1^+ \rightarrow \rho(770)^+ \pi^0$	(8.7 \pm 1.6) $\times 10^{-3}$	–	–
$K_S^0 a_1(1260)^+, a_1^+ \rightarrow f_0(500) \pi^+, f_0 \rightarrow \pi^0 \pi^0$	(1.0 \pm 0.6) $\times 10^{-3}$	–	–
$\bar{K}_1^0(1400)^0 \pi^+, \bar{K}_1^0 \rightarrow \bar{K}^*(892)^0 \pi^0, \bar{K}^*(892)^0 \rightarrow K_S^0 \pi^0$	(2.3 \pm 0.4) $\times 10^{-3}$	–	–
$\bar{K}^*(892)^0 \rho^+, \bar{K}^*(892)^0 \rightarrow K_S^0 \pi^0$	(9.7 \pm 0.9) $\times 10^{-3}$	–	–
$\bar{K}^*(892)^0 \pi^+ \pi^0$ non-resonant, $\bar{K}^*(892)^0 \rightarrow K_S^0 \pi^0$	(2.6 \pm 0.7) $\times 10^{-3}$	–	–
$K_S^0 \rho^+ \pi^0$ non-resonant	(4.8 \pm 0.5) $\times 10^{-3}$	–	–
$K^- 2\pi^+ \eta$	(1.35 \pm 0.12) $\times 10^{-3}$	–	657

Meson Summary Table

D^0

$$I(J^P) = \frac{1}{2}(0^-)$$

Mass $m = 1864.84 \pm 0.05$ MeV

$m_{D^{\pm}} - m_{D^0} = 4.822 \pm 0.015$ MeV

Mean life $\tau = (410.3 \pm 1.0) \times 10^{-15}$ s

$c\tau = 123.01$ μm

Mixing and related parameters

$$|m_{D_1^0} - m_{D_2^0}| = (0.997 \pm 0.116) \times 10^{10} \hbar \text{ s}^{-1}$$

$$(\Gamma_{D_1^0} - \Gamma_{D_2^0})/\Gamma = 2\gamma = (1.394 \pm 0.056) \times 10^{-2}$$

$$|q/p| = 0.995 \pm 0.016$$

$$A_{\Gamma} = (0.089 \pm 0.113) \times 10^{-3}$$

$$\phi_{K_S^0 \pi \pi} = 0.02_{-0.05}^{+0.04}$$

$K^+ \pi^-$ relative strong phase: $\cos \delta = 0.990 \pm 0.025$

$K^- \pi^+ \pi^0$ coherence factor $R_{K \pi \pi^0} = 0.792 \pm 0.033$

$K^- \pi^+ \pi^0$ average relative strong phase $\delta^{K \pi \pi^0} = (198 \pm 10)^\circ$

$K^- \pi^- 2\pi^+$ coherence factor $R_{K 3\pi} = 0.52_{-0.09}^{+0.10}$

$K^- \pi^- 2\pi^+$ average relative strong phase $\delta^{K 3\pi} = (149_{-16}^{+26})^\circ$ ($S = 1.4$)

$$D^0 \rightarrow K^- \pi^- 2\pi^+, R_{K 3\pi} (\gamma \cos \delta^{K 3\pi} - x \sin \delta^{K 3\pi}) = (-3.0 \pm 0.7) \times 10^{-3} \text{ TeV}^{-1}$$

$K_S^0 K^+ \pi^-$ coherence factor $R_{K_S^0 K \pi} = 0.70 \pm 0.08$

$K_S^0 K^+ \pi^-$ average relative strong phase $\delta^{K_S^0 K \pi} = (0 \pm 16)^\circ$

$K^* K$ coherence factor $R_{K^* K} = 0.94 \pm 0.12$

$K^* K$ average relative strong phase $\delta^{K^* K} = (-17 \pm 18)^\circ$

CP-even fractions (labeled by the D^0 decay)

CP-even fraction in $D^0 \rightarrow K_S^0 \pi^+ \pi^- \pi^0$ decays = $(23.6 \pm 0.9)\%$

CP-even fraction in $D^0 \rightarrow \pi^+ \pi^- \pi^0$ decays = $(97.3 \pm 1.7)\%$

CP-even fraction in $D^0 \rightarrow \pi^+ \pi^- \pi^+ \pi^-$ decays = $(74.6 \pm 1.6)\%$ ($S = 1.2$)

CP-even fraction in $D^0 \rightarrow \pi^+ \pi^- 2\pi^0$ decays = 0.68 ± 0.08

CP-even fraction in $D^0 \rightarrow 2\pi^+ 2\pi^- \pi^0$ decays = 0.44 ± 0.10

CP-even fraction in $D^0 \rightarrow \pi^+ \pi^- 3\pi^0$ decays = $0.52_{-0.27}^{+0.34}$

CP-even fraction in $D^0 \rightarrow 2\pi^+ 2\pi^- 2\pi^0$ decays = 0.79 ± 0.26

CP-even fraction in $D^0 \rightarrow K^+ K^- \pi^0$ decays = $(73 \pm 6)\%$

CP-even fraction in $D^0 \rightarrow K^+ K^- \pi^+ \pi^-$ decays = $(74.1 \pm 3.0)\%$

CP-violation decay-rate asymmetries (labeled by the D^0 decay)

$$A_{CP}(K^+ K^-) = (4 \pm 5) \times 10^{-4}$$

$$A_{CP}(2K_S^0) = (-1.9 \pm 1.1)\% \quad (S = 1.1)$$

$$A_{CP}(\pi^+ \pi^-) = (0.13 \pm 0.14)\%$$

$$A_{CP}(\pi^0 \pi^0) = (0.0 \pm 0.6)\%$$

$$A_{CP}(\rho \gamma) = (6 \pm 15) \times 10^{-2}$$

$$A_{CP}(\phi \gamma) = (-9 \pm 7) \times 10^{-2}$$

$$A_{CP}(K^*(892)^0 \gamma) = (-0.3 \pm 2.0) \times 10^{-2}$$

$$A_{CP}(\pi^+ \pi^- \pi^0) = (0.4 \pm 0.4)\%$$

$$A_{CP}(\eta \pi^+ \pi^-) \text{ in } D^0, \bar{D}^0 \rightarrow \eta \pi^+ \pi^- = (0.9 \pm 1.3) \times 10^{-2}$$

$$A_{CP}(\rho(770)^+ \pi^- \rightarrow \pi^+ \pi^- \pi^0) = (1.2 \pm 0.9)\% \text{ [qq]}$$

$$A_{CP}(\rho(770)^0 \pi^0 \rightarrow \pi^+ \pi^- \pi^0) = (-3.1 \pm 3.0)\% \text{ [qq]}$$

$$A_{CP}(\rho(770)^- \pi^+ \rightarrow \pi^+ \pi^- \pi^0) = (-1.0 \pm 1.7)\% \text{ [qq]}$$

$$A_{CP}(\rho(1450)^+ \pi^- \rightarrow \pi^+ \pi^- \pi^0) = (0 \pm 70)\% \text{ [qq]}$$

$$A_{CP}(\rho(1450)^0 \pi^0 \rightarrow \pi^+ \pi^- \pi^0) = (-20 \pm 40)\% \text{ [qq]}$$

$$A_{CP}(\rho(1450)^- \pi^+ \rightarrow \pi^+ \pi^- \pi^0) = (6 \pm 9)\% \text{ [qq]}$$

$$A_{CP}(\rho(1700)^+ \pi^- \rightarrow \pi^+ \pi^- \pi^0) = (-5 \pm 14)\% \text{ [qq]}$$

$$A_{CP}(\rho(1700)^0 \pi^0 \rightarrow \pi^+ \pi^- \pi^0) = (13 \pm 9)\% \text{ [qq]}$$

$$A_{CP}(\rho(1700)^- \pi^+ \rightarrow \pi^+ \pi^- \pi^0) = (8 \pm 11)\% \text{ [qq]}$$

$$A_{CP}(f_0(980) \pi^0 \rightarrow \pi^+ \pi^- \pi^0) = (0 \pm 35)\% \text{ [qq]}$$

$$A_{CP}(f_0(1370) \pi^0 \rightarrow \pi^+ \pi^- \pi^0) = (25 \pm 18)\% \text{ [qq]}$$

$$A_{CP}(f_0(1500) \pi^0 \rightarrow \pi^+ \pi^- \pi^0) = (0 \pm 18)\% \text{ [qq]}$$

$$A_{CP}(f_0(1710) \pi^0 \rightarrow \pi^+ \pi^- \pi^0) = (0 \pm 24)\% \text{ [qq]}$$

$$A_{CP}(f_2(1270) \pi^0 \rightarrow \pi^+ \pi^- \pi^0) = (-4 \pm 6)\% \text{ [qq]}$$

$$A_{CP}(\sigma(400) \pi^0 \rightarrow \pi^+ \pi^- \pi^0) = (6 \pm 8)\% \text{ [qq]}$$

$$A_{CP}(\text{nonresonant } \pi^+ \pi^- \pi^0) = (-13 \pm 23)\% \text{ [qq]}$$

$$A_{CP}(\pi^+ \pi^- 2\pi^0) \text{ in } D^0, \bar{D}^0 \rightarrow \pi^+ \pi^- 2\pi^0 = (-2.5 \pm 2.0)\%$$

$$A_{CP}(a_1(1260)^+ \pi^- \rightarrow 2\pi^+ 2\pi^-) = (5 \pm 6)\%$$

$$A_{CP}(a_1(1260)^- \pi^+ \rightarrow 2\pi^+ 2\pi^-) = (14 \pm 18)\%$$

$$A_{CP}(\pi(1300)^+ \pi^- \rightarrow 2\pi^+ 2\pi^-) = (-2 \pm 15)\%$$

$$A_{CP}(\pi(1300)^- \pi^+ \rightarrow 2\pi^+ 2\pi^-) = (-6 \pm 30)\%$$

$$A_{CP}(a_1(1640)^+ \pi^- \rightarrow 2\pi^+ 2\pi^-) = (9 \pm 26)\%$$

$$A_{CP}(\pi_2(1670)^+ \pi^- \rightarrow 2\pi^+ 2\pi^-) = (7 \pm 18)\%$$

$$A_{CP}(\sigma f_0(1370) \rightarrow 2\pi^+ 2\pi^-) = (-15 \pm 19)\%$$

$$A_{CP}(\sigma \rho(770)^0 \rightarrow 2\pi^+ 2\pi^-) = (3 \pm 27)\%$$

$$A_{CP}(2\rho(770)^0 \rightarrow 2\pi^+ 2\pi^-) = (-6 \pm 6)\%$$

$$A_{CP}(2f_2(1270) \rightarrow 2\pi^+ 2\pi^-) = (-28 \pm 24)\%$$

$$A_{CP}(\pi^+ \pi^- \pi^0 \eta) \text{ in } D^0, \bar{D}^0 \rightarrow \pi^+ \pi^- \pi^0 \eta = (-6 \pm 6) \times 10^{-2}$$

$$A_{CP}(K^+ K^- \pi^0) = (-1.0 \pm 1.7)\%$$

$$A_{CP}(K^*(892)^+ K^- \rightarrow K^+ K^- \pi^0) = (-0.9 \pm 1.3)\% \text{ [qq]}$$

$$A_{CP}(K^*(1410)^+ K^- \rightarrow K^+ K^- \pi^0) = (-21 \pm 24)\% \text{ [qq]}$$

$$A_{CP}((K^+ \pi^0)_{S\text{-wave}} K^- \rightarrow K^+ K^- \pi^0) = (7 \pm 15)\% \text{ [qq]}$$

$$A_{CP}(\phi(1020) \pi^0 \rightarrow K^+ K^- \pi^0) = (1.1 \pm 2.2)\% \text{ [qq]}$$

$$A_{CP}(f_0(980) \pi^0 \rightarrow K^+ K^- \pi^0) = (-3 \pm 19)\% \text{ [qq]}$$

$$A_{CP}(a_0(980) \pi^0 \rightarrow K^+ K^- \pi^0) = (-5 \pm 16)\% \text{ [qq]}$$

$$A_{CP}(f_2'(1525) \pi^0 \rightarrow K^+ K^- \pi^0) = (0 \pm 160)\% \text{ [qq]}$$

$$A_{CP}(K^*(892)^- K^+ \rightarrow K^+ K^- \pi^0) = (-5 \pm 4)\% \text{ [qq]}$$

$$A_{CP}(K^*(1410)^- K^+ \rightarrow K^+ K^- \pi^0) = (-17 \pm 29)\% \text{ [qq]}$$

$$A_{CP}((K^- \pi^0)_{S\text{-wave}} K^+ \rightarrow K^+ K^- \pi^0) = (-10 \pm 40)\% \text{ [qq]}$$

$$A_{CP}(K^+ K^- \eta) \text{ in } D^0, \bar{D}^0 \rightarrow K^+ K^- \eta = (-1.4 \pm 3.5) \times 10^{-2}$$

$$A_{CP}(f_2(1020) \eta \rightarrow K^+ K^- \eta) \text{ in } D^0, \bar{D}^0 \rightarrow \phi(1020) \eta = (-2 \pm 4) \times 10^{-2}$$

$$A_{CP}(K_S^0 \pi^0) = (-0.20 \pm 0.17)\%$$

$$A_{CP}(K_S^0 \eta) = (0.5 \pm 0.5)\%$$

$$A_{CP}(K_S^0 \eta') = (1.0 \pm 0.7)\%$$

$$A_{CP}(K_S^0 \phi) = (-3 \pm 9)\%$$

$$A_{CP}(K^- \pi^+) = (0.2 \pm 0.5)\%$$

$$A_{CP}(K^+ \pi^-) = (-0.9 \pm 1.4)\%$$

$$A_{CP}(D_{CP \pm 1}) \rightarrow K^{\mp} \pi^{\pm} = (13.1 \pm 1.0)\%$$

$$A_{CP}(K^- \pi^+ \pi^0) = (0.1 \pm 0.5)\%$$

$$A_{CP}(K^+ \pi^- \pi^0) = (0 \pm 5)\%$$

$$A_{CP}(K_S^0 \pi^+ \pi^-) = (-0.1 \pm 0.8)\%$$

$$A_{CP}(K^{\mp} \pi^{\pm} \eta) \text{ in } D^0, \bar{D}^0 \rightarrow K^{\mp} \pi^{\pm} \eta = (-1.9 \pm 1.6) \times 10^{-2}$$

$$A_{CP}(K_S^0 \pi^0 \eta) \text{ in } D^0, \bar{D}^0 \rightarrow K_S^0 \pi^0 \eta = (-3.9 \pm 3.3) \times 10^{-2}$$

$$A_{CP}(K^{\mp} \pi^{\pm} \pi^0 \eta) \text{ in } D^0, \bar{D}^0 \rightarrow K^{\mp} \pi^{\pm} \pi^0 \eta = (-8 \pm 5) \times 10^{-2}$$

$$A_{CP}(K^*(892)^- \pi^+ \rightarrow K_S^0 \pi^+ \pi^-) = (0.4 \pm 0.5)\%$$

$$A_{CP}(K^*(892)^+ \pi^- \rightarrow K_S^0 \pi^+ \pi^-) = (1 \pm 6)\%$$

$$A_{CP}(\bar{K}^0 \rho^0 \rightarrow K_S^0 \pi^+ \pi^-) = (-0.1 \pm 0.5)\%$$

$$A_{CP}(\bar{K}^0 \omega \rightarrow K_S^0 \pi^+ \pi^-) = (-13 \pm 7)\%$$

$$A_{CP}(\bar{K}^0 f_0(980) \rightarrow K_S^0 \pi^+ \pi^-) = (-0.4 \pm 2.7)\%$$

$$A_{CP}(\bar{K}^0 f_2(1270) \rightarrow K_S^0 \pi^+ \pi^-) = (-4 \pm 5)\%$$

$$A_{CP}(\bar{K}^0 f_0(1370) \rightarrow K_S^0 \pi^+ \pi^-) = (-1 \pm 9)\%$$

$$A_{CP}(\bar{K}^0 \rho^0(1450) \rightarrow K_S^0 \pi^+ \pi^-) = (-4 \pm 10)\%$$

$$A_{CP}(\bar{K}^0 f_0(600) \rightarrow K_S^0 \pi^+ \pi^-) = (-3 \pm 5)\%$$

$$A_{CP}(K^*(1410)^- \pi^+ \rightarrow K_S^0 \pi^+ \pi^-) = (-2 \pm 9)\%$$

$$A_{CP}(K_S^*(1430)^- \pi^+ \rightarrow K_S^0 \pi^+ \pi^-) = (4 \pm 4)\%$$

$$A_{CP}(K_0^*(1430)^+ \pi^- \rightarrow K_S^0 \pi^+ \pi^-) = (12 \pm 15)\%$$

$$A_{CP}(K_2^*(1430)^- \pi^+ \rightarrow K_S^0 \pi^+ \pi^-) = (3 \pm 6)\%$$

$$A_{CP}(K_2^*(1430)^+ \pi^- \rightarrow K_S^0 \pi^+ \pi^-) = (-10 \pm 32)\%$$

$$A_{CP}(K^- \pi^+ \pi^+ \pi^-) = (0.2 \pm 0.5)\%$$

$$A_{CP}(K^+ \pi^- \pi^+ \pi^-) = (-2 \pm 4)\%$$

$$A_{CP}(K^+ K^- \pi^+ \pi^-) = (1.3 \pm 1.7)\%$$

$$A_{CP}(2K_S^0 \pi^+ \pi^-) \text{ in } D^0, \bar{D}^0 \rightarrow 2K_S^0 \pi^+ \pi^- = (-2.5 \pm 1.4) \times 10^{-2}$$

$$A_{CP}(K_1^*(1270)^+ K^- \rightarrow K^+ K^- \pi^+ \pi^-) = (-2.3 \pm 1.7)\%$$

$$A_{CP}(K_1^*(1270)^+ K^- \rightarrow K^{*0} \pi^+ K^-) = (-1 \pm 10)\%$$

$$A_{CP}(K_1^*(1270)^- K^+ \rightarrow \bar{K}^{*0} \pi^- K^+) = (-10 \pm 32)\%$$

$$A_{CP}(K_1^*(1270)^- K^+ \rightarrow K^+ K^- \pi^+ \pi^-) = (1.7 \pm 3.5)\%$$

$$A_{CP}(K_1^*(1270)^+ K^- \rightarrow \rho^0 K^+ K^-) = (-7 \pm 17)\%$$

$$A_{CP}(K_1^*(1270)^- K^+ \rightarrow \rho^0 K^- K^+) = (10 \pm 13)\%$$

$$A_{CP}(K_1(1400)^+ K^- \rightarrow K^+ K^- \pi^+ \pi^-) = (-4.4 \pm 2.1)\%$$

$$A_{CP}(K^*(1410)^+ K^- \rightarrow K^{*0} \pi^+ K^-) = (-20 \pm 17)\%$$

$$A_{CP}(K^*(1410)^- K^+ \rightarrow \bar{K}^{*0} \pi^- K^+) = (-1 \pm 14)\%$$

$$A_{CP}(K^*(1680)^+ K^- \rightarrow K^+ K^- \pi^+ \pi^-) = (-17 \pm 29)\%$$

$$A_{CP}(K^{*0} \bar{K}^{*0}) \text{ in } D^0, \bar{D}^0 \rightarrow K^{*0} \bar{K}^{*0} = (-5 \pm 14)\%$$

$$A_{CP}(K^{*0} \bar{K}^{*0} \text{ S-wave}) = (-3.9 \pm 2.2)\%$$

$$A_{CP}(\phi \rho^0) \text{ in } D^0, \bar{D}^0 \rightarrow \phi \rho^0 = (1 \pm 9)\%$$

$$A_{CP}(\phi \rho^0 \text{ S-wave}) = (-3 \pm 5)\%$$

$$A_{CP}(\phi \rho^0 \text{ D-wave}) = (-37 \pm 19)\%$$

$$A_{CP}(\phi(\pi^+ \pi^-)_{S\text{-wave}}) = (6 \pm 6)\%$$

$$A_{CP}(K^*(892)^0 (K^- \pi^+)_{S\text{-wave}}) = (-10 \pm 40)\%$$

$$A_{CP}(K^+ K^- \pi^+ \pi^- \text{ non-resonant}) = (8 \pm 20)\%$$

$$A_{CP}((K^- \pi^+)_{P\text{-wave}} (K^+ \pi^-)_{S\text{-wave}}) = (3 \pm 11)\%$$

$$A_{CP}(K^+ K^- \mu^+ \mu^-) \text{ in } D^0, \bar{D}^0 \rightarrow K^+ K^- \mu^+ \mu^- = (-2 \pm 6)\%$$

$$A_{CP}(\pi^+ \pi^- \mu^+ \mu^-) \text{ in } D^0, \bar{D}^0 \rightarrow \pi^+ \pi^- \mu^+ \mu^- = (2.9 \pm 2.1)\%$$

Meson Summary Table

CP-violation asymmetry difference

$$\Delta A_{CP} = A_{CP}(K^+ K^-) - A_{CP}(\pi^+ \pi^-) = (-0.154 \pm 0.029)\%$$

 χ^2 tests of CP-violation (CPV) p-values

$$\text{Local CPV in } D^0, \bar{D}^0 \rightarrow \pi^+ \pi^- \pi^0 = 10.6\%$$

$$\text{Local CPV in } D^0, \bar{D}^0 \rightarrow \pi^+ \pi^- \pi^+ \pi^- = (0.6 \pm 0.2)\%$$

$$\text{Local CPV in } D^0, \bar{D}^0 \rightarrow K_S^0 \pi^+ \pi^- = 96\%$$

$$\text{Local CPV in } D^0, \bar{D}^0 \rightarrow K^+ K^- \pi^0 = 16.6\%$$

$$\text{Local CPV in } D^0, \bar{D}^0 \rightarrow K^+ K^- \pi^+ \pi^- = 9.1\%$$

T-violation decay-rate asymmetry

$$A_T(K^+ K^- \pi^+ \pi^-) = (2.9 \pm 2.2) \times 10^{-3} [ij]$$

$$A_{T\text{viol}}(2K_S^0 \pi^+ \pi^-) \text{ in } D^0, \bar{D}^0 \rightarrow 2K_S^0 \pi^+ \pi^- = (-1.9 \pm 1.4) \times 10^{-2}$$

$$A_{T\text{viol}}(K_S^0 \pi^+ \pi^- \pi^0) \text{ in } D^0, \bar{D}^0 \rightarrow K_S^0 \pi^+ \pi^- \pi^0 = (-0.3 \pm 1.4) \times 10^{-3}$$

CPT-violation decay-rate asymmetry

$$A_{CPT}(K^\mp \pi^\pm) = 0.008 \pm 0.008$$

Form factors

$$r_V \equiv V(0)/A_1(0) \text{ in } D^0 \rightarrow K^*(892)^- \ell^+ \nu_\ell = 1.46 \pm 0.07$$

$$r_2 \equiv A_2(0)/A_1(0) \text{ in } D^0 \rightarrow K^*(892)^- \ell^+ \nu_\ell = 0.68 \pm 0.06$$

$$f_+(0) \text{ in } D^0 \rightarrow K^- \ell^+ \nu_\ell = 0.736 \pm 0.004$$

$$f_+(0)|V_{cs}| \text{ in } D^0 \rightarrow K^- \ell^+ \nu_\ell = 0.7166 \pm 0.0030$$

$$r_1 \equiv a_1/a_0 \text{ in } D^0 \rightarrow K^- \ell^+ \nu_\ell = -2.40 \pm 0.16$$

$$r_2 \equiv a_2/a_0 \text{ in } D^0 \rightarrow K^- \ell^+ \nu_\ell = 5 \pm 4$$

$$f_+(0) \text{ in } D^0 \rightarrow \pi^- \ell^+ \nu_\ell = 0.637 \pm 0.009$$

$$f_+(0)|V_{cd}| \text{ in } D^0 \rightarrow \pi^- \ell^+ \nu_\ell = 0.1436 \pm 0.0026 \quad (S = 1.5)$$

$$r_1 \equiv a_1/a_0 \text{ in } D^0 \rightarrow \pi^- \ell^+ \nu_\ell = -1.97 \pm 0.28 \quad (S = 1.4)$$

$$r_2 \equiv a_1/a_0 \text{ in } D^0 \rightarrow \pi^- \ell^+ \nu_\ell = -0.2 \pm 2.2 \quad (S = 1.7)$$

Most decay modes (other than the semileptonic modes) that involve a neutral K meson are now given as K_S^0 modes, not as \bar{K}^0 modes. Nearly always it is a K_S^0 that is measured, and interference between Cabibbo-allowed and doubly Cabibbo-suppressed modes can invalidate the assumption that $2\Gamma(K_S^0) = \Gamma(\bar{K}^0)$.

D⁰ DECAY MODES	Fraction (Γ_i/Γ)	Scale factor / p Confidence level (MeV/c)	
Topological modes			
0-prongs	[rr] (15 ± 6) %		–
2-prongs	(71 ± 6) %		–
4-prongs	[ss] (14.6 ± 0.5) %		–
6-prongs	[tt] (6.5 ± 1.3) × 10 ⁻⁴		–
Inclusive modes			
e ⁺ anything	[uu] (6.49 ± 0.11) %		–
μ^+ anything	(6.8 ± 0.6) %		–
K ⁻ anything	(54.7 ± 2.8) %	S=1.3	–
K_S^0 anything	(20.75 ± 0.23) %		–
K ⁺ anything	(3.4 ± 0.4) %		–
K*(892) ⁻ anything	(15 ± 9) %		–
$\bar{K}^*(892)^0$ anything	(9 ± 4) %		–
K*(892) ⁺ anything	< 3.6 %	CL=90%	–
K*(892) ⁰ anything	(2.8 ± 1.3) %		–
η anything	(9.5 ± 0.9) %		–
η' anything	(2.48 ± 0.27) %		–
ϕ anything	(1.08 ± 0.04) %		–
$\pi^+ \pi^+ \pi^-$ anything	(17.60 ± 0.25) %		–
invisibles	< 9.4 × 10 ⁻⁵	CL=90%	–
Semileptonic modes			
K ⁻ e ⁺ ν_e	(3.549 ± 0.026) %	S=1.2	867
K ⁻ μ^+ ν_μ	(3.41 ± 0.04) %		864
K*(892) ⁻ e ⁺ ν_e	(2.15 ± 0.16) %		719
K*(892) ⁻ μ^+ ν_μ	(1.89 ± 0.24) %		714
K ⁻ π^0 e ⁺ ν_e	(1.6 ± 1.3) %		861
$\bar{K}^0 \pi^-$ e ⁺ ν_e	(1.44 ± 0.04) %		860
($\bar{K}^0 \pi^-$) S-wave e ⁺ ν_e	(7.9 ± 1.7) × 10 ⁻⁴		860
K ⁻ $\pi^+ \pi^-$ e ⁺ ν_e	(2.8 ± 1.4) × 10 ⁻⁴		843
$K_1(1270)^-$ e ⁺ ν_e	(1.01 ± 0.18) × 10 ⁻³		511
K ⁻ $\pi^+ \pi^- \mu^+ \nu_\mu$	< 1.3 × 10 ⁻³	CL=90%	821
($\bar{K}^*(892) \pi^-$) $\mu^+ \nu_\mu$	< 1.5 × 10 ⁻³	CL=90%	692

$\pi^- e^+ \nu_e$	(2.91 ± 0.04) × 10 ⁻³		927
$\pi^- \mu^+ \nu_\mu$	(2.67 ± 0.12) × 10 ⁻³	S=1.3	924
$\pi^- \pi^0 e^+ \nu_e$	(1.45 ± 0.07) × 10 ⁻³		922
$\rho^- e^+ \nu_e$	(1.50 ± 0.12) × 10 ⁻³	S=1.9	771
$\rho^- \mu^+ \nu_\mu$	(1.35 ± 0.13) × 10 ⁻³		767
a(980) ⁻ e ⁺ ν_e , $a^- \rightarrow \eta \pi^-$	(1.33 ± 0.34) × 10 ⁻⁴		–
b ₁ (1235) ⁻ e ⁺ ν_e , b ₁ ⁻ → $\omega \pi^-$	< 1.12 × 10 ⁻⁴	CL=90%	–

Hadronic modes with one \bar{K}

K ⁻ π^+	(3.947 ± 0.030) %	S=1.2	861
$K_S^0 \pi^0$	(1.240 ± 0.022) %		860
$K_L^0 \pi^0$	(9.76 ± 0.32) × 10 ⁻³		860
$K_L^0 \eta$	(4.34 ± 0.16) × 10 ⁻³		772
$K_L^0 \eta'$	(8.12 ± 0.35) × 10 ⁻³	S=1.3	565
$K_L^0 \omega$	(1.16 ± 0.04) %		670
$K_S^0 \pi^+ \pi^-$	[ij] (2.80 ± 0.18) %	S=1.1	842
$K_S^0 \rho^0$	(6.3 ± 0.6) × 10 ⁻³		674
$K_S^0 \omega$, $\omega \rightarrow \pi^+ \pi^-$	(2.0 ± 0.6) × 10 ⁻⁴		670
$K_S^0 (\pi^+ \pi^-)_{S\text{-wave}}$	(3.3 ± 0.8) × 10 ⁻³		842
$K_S^0 f_0(980)$, $f_0 \rightarrow \pi^+ \pi^-$	(1.20 ± 0.40) × 10 ⁻³		549
$K_S^0 f_0(1370)$, $f_0 \rightarrow \pi^+ \pi^-$	(2.8 ± 0.9) × 10 ⁻³		†
$K_S^0 f_2(1270)$, $f_2 \rightarrow \pi^+ \pi^-$	(9 ± 10) × 10 ⁻⁵		262
K*(892) ⁻ π^+ , K* ⁻ →	(1.64 ± 0.14) %		711
$K_S^0 \pi^-$			
K*(1430) ⁻ π^+ , K ₀ ^{*-} →	(2.67 ± 0.40) × 10 ⁻³		378
$K_S^0 \pi^-$			
K*(1430) ⁻ π^+ , K ₂ ^{*-} →	(3.4 ± 1.9) × 10 ⁻⁴		367
$K_S^0 \pi^-$			
K*(1680) ⁻ π^+ , K* ⁻ →	(4.4 ± 3.5) × 10 ⁻⁴		46
$K_S^0 \pi^-$			
K*(892) ⁺ π^- , K* ⁺ →	[w] (1.13 ± 0.60) × 10 ⁻⁴		711
$K_S^0 \pi^+$			
K*(1430) ⁺ π^- , K ₀ ⁺ →	[w] < 1.4 × 10 ⁻⁵	CL=95%	–
$K_S^0 \pi^+$			
K*(1430) ⁺ π^- , K ₂ ⁺ →	[w] < 3.4 × 10 ⁻⁵	CL=95%	–
$K_S^0 \pi^+$			
$K_S^0 \pi^+ \pi^-$ nonresonant	(2.5 ± 6.0) × 10 ⁻⁴		842
K ⁻ $\pi^+ \pi^0$	[ij] (14.4 ± 0.6) %	S=2.2	844
K ⁻ ρ^+	(11.2 ± 0.7) %		675
K ⁻ $\rho(1700)^+$, $\rho^+ \rightarrow \pi^+ \pi^0$	(8.2 ± 1.8) × 10 ⁻³		†
K*(892) ⁻ π^+ , K*(892) ⁻ →	(2.31 ± 0.40) %		711
$K^- \pi^0$			
$\bar{K}^*(892)^0 \pi^0$, $\bar{K}^*(892)^0 \rightarrow$	(1.95 ± 0.25) %		711
$K^- \pi^+$			
K*(1430) ⁻ π^+ , K ₀ ^{*-} →	(4.8 ± 2.2) × 10 ⁻³		378
$K^- \pi^0$			
$\bar{K}_0^*(1430)^0 \pi^0$, $\bar{K}_0^{*0} \rightarrow$	(5.9 ± 5.0) × 10 ⁻³		379
$K^- \pi^+$			
K*(1680) ⁻ π^+ , K* ⁻ →	(1.9 ± 0.7) × 10 ⁻³		46
$K^- \pi^0$			
K ⁻ $\pi^+ \pi^0$ nonresonant	(1.15 ± 0.60) %		844
$K_S^0 2\pi^0$	(9.1 ± 1.1) × 10 ⁻³	S=2.2	843
$K_L^0 \pi^0 \pi^0$	(1.26 ± 0.06) %		843
$K_S^0 (2\pi^0)_{S\text{-wave}}$	(2.6 ± 0.7) × 10 ⁻³		–
$\bar{K}^*(892)^0 \pi^0$, $\bar{K}^{*0} \rightarrow K_S^0 \pi^0$	(8.1 ± 0.7) × 10 ⁻³		711
$\bar{K}^*(1430)^0 \pi^0$, $\bar{K}^{*0} \rightarrow$	(4 ± 23) × 10 ⁻⁵		–
$K_S^0 \pi^0$			
$\bar{K}^*(1680)^0 \pi^0$, $\bar{K}^{*0} \rightarrow$	(1.0 ± 0.4) × 10 ⁻³		–
$K_S^0 \pi^0$			
$K_S^0 f_2(1270)$, $f_2 \rightarrow 2\pi^0$	(2.3 ± 1.1) × 10 ⁻⁴		–
$2K_S^0$, one $K_S^0 \rightarrow 2\pi^0$	(3.2 ± 1.1) × 10 ⁻⁴		–
$K_S^0 3\pi^0$	(7.6 ± 0.4) × 10 ⁻³		815
K ⁻ $2\pi^+ \pi^-$	[ij] (8.22 ± 0.14) %		813
K ⁻ $\pi^+ \rho^0$ total	(6.87 ± 0.31) %		609
K ⁻ $\pi^+ \rho^0$ 3-body	(6.1 ± 1.6) × 10 ⁻³		609
$\bar{K}^*(892)^0 \rho^0$, $\bar{K}^{*0} \rightarrow$	(1.01 ± 0.05) %		416
$K^- \pi^+$			
$\bar{K}^*(892)^0 \rho^0$ transverse, $\bar{K}^{*0} \rightarrow K^- \pi^+$	(1.2 ± 0.4) %		417

Meson Summary Table

$K^- a_1(1260)^+, a_1^+ \rightarrow \rho^0 \pi^+$	$(4.32 \pm 0.32) \%$	327			
$K_1(1270)^- \pi^+, K_1^- \rightarrow K^- \pi^+ \pi^- \text{ total}$	$(3.9 \pm 0.4) \times 10^{-3}$	-			
$K_1(1270)^- \pi^+, K_1^- \rightarrow \bar{K}^*(892)^0 \pi^-, \bar{K}^{*0} \rightarrow K^- \pi^+$	$(6.6 \pm 2.3) \times 10^{-4}$	484			
$K^- 2\pi^+ \pi^- \text{ nonresonant}$	$(1.81 \pm 0.07) \%$	813			
$K_S^0 \pi^+ \pi^- \pi^0$	[xx] $(5.2 \pm 0.6) \%$	813			
$K_S^0 \eta, \eta \rightarrow \pi^+ \pi^- \pi^0$	$(1.17 \pm 0.03) \times 10^{-3}$	772			
$K_S^0 \omega, \omega \rightarrow \pi^+ \pi^- \pi^0$	$(9.9 \pm 0.6) \times 10^{-3}$	670			
$K^- \pi^+ 2\pi^0$	$(8.86 \pm 0.23) \%$	815			
$K^- \pi^+ 3\pi^0$	$(9.5 \pm 0.4) \times 10^{-3}$	774			
$K_S^0 \pi^+ \pi^- 2\pi^0$	$(1.27 \pm 0.06) \%$	773			
$K^- 2\pi^+ \pi^- \pi^0$	$(4.3 \pm 0.4) \%$	771			
$\bar{K}^*(892)^0 \pi^+ \pi^- \pi^0, \bar{K}^{*0} \rightarrow K^- \pi^+$	$(1.3 \pm 0.6) \%$	643			
$\bar{K}^*(892)^0 \omega, \bar{K}^{*0} \rightarrow K^- \pi^+, \omega \rightarrow \pi^+ \pi^- \pi^0$	$(6.5 \pm 3.0) \times 10^{-3}$	410			
$K^- \pi^+ \omega$	$(3.39 \pm 0.10) \%$	605			
$\bar{K}^*(892)^0 \omega$	$(1.1 \pm 0.5) \%$	410			
$K_S^0 \pi^0 \omega$	$(8.5 \pm 0.6) \times 10^{-3}$	605			
$K_S^0 \eta \pi^0$	$(1.01 \pm 0.05) \%$	721			
$K_S^0 a_0(980), a_0 \rightarrow \eta \pi^0$	$(1.20 \pm 0.28) \%$	-			
$\bar{K}^*(892)^0 \eta, \bar{K}^{*0} \rightarrow K_S^0 \pi^0$	$(2.9 \pm 0.7) \times 10^{-3}$	-			
$K^- \pi^+ \eta$	$(1.88 \pm 0.05) \%$	S=1.4 721			
$K^*(892)^0 \eta, K^{*0} \rightarrow K^- \pi^+$	$(8.9 \pm 0.6) \times 10^{-3}$	-			
$a_0(980)^+ K^-, a_0^+ \rightarrow \eta \pi^+$	$(7.4 \pm 0.7) \times 10^{-3}$	-			
$K_2^*(1980)^- \pi^+, K_2^{*-} \rightarrow K^- \eta$	$(2.2 \pm 1.7) \times 10^{-4}$	-			
$K^- \pi^+ \pi^0 \eta$	$(4.49 \pm 0.27) \times 10^{-3}$	656			
$K_S^0 \pi^+ \pi^- \eta$	$(2.80 \pm 0.21) \times 10^{-3}$	651			
$K_S^0 2\pi^0 \eta$	$(1.76 \pm 0.26) \times 10^{-3}$	656			
$K_S^0 2\pi^+ 2\pi^-$	$(2.66 \pm 0.30) \times 10^{-3}$	768			
$K_S^0 \rho^0 \pi^+ \pi^-, \text{ no } K^*(892)^-$	$(1.1 \pm 0.7) \times 10^{-3}$	-			
$K^*(892)^- 2\pi^+ \pi^-, K^*(892)^- \rightarrow K_S^0 \pi^-, \text{ no } \rho^0$	$(5 \pm 7) \times 10^{-4}$	642			
$K^*(892)^- \rho^0 \pi^+, K^*(892)^- \rightarrow K_S^0 \pi^-$	$(1.6 \pm 0.6) \times 10^{-3}$	230			
$K_S^0 2\pi^+ 2\pi^- \text{ nonresonant}$	$< 1.2 \times 10^{-3}$	CL=90% 768			
$K^- 3\pi^+ 2\pi^-$	$(2.2 \pm 0.6) \times 10^{-4}$	713			
Fractions of some of the following modes with resonances have already appeared above as submodes of particular charged-particle modes. These nine modes below are all corrected for unseen decays of the resonances.					
$K_S^0 \eta$	$(5.09 \pm 0.13) \times 10^{-3}$	772			
$K_S^0 \omega$	$(1.11 \pm 0.06) \%$	670			
$K_S^0 \eta'(958)$	$(9.49 \pm 0.32) \times 10^{-3}$	565			
$\bar{K}^*(892)^0 \pi^+ \pi^- \pi^0$	$(1.9 \pm 0.9) \%$	643			
$\bar{K}^*(892)^0 \eta$	$(1.41 \pm 0.12) \%$	583			
$K^- \pi^+ \eta'(958)$	$(6.43 \pm 0.34) \times 10^{-3}$	479			
$K_S^0 \eta'(958) \pi^0$	$(2.52 \pm 0.27) \times 10^{-3}$	479			
$\bar{K}^*(892)^0 \eta'(958)$	$< 1.0 \times 10^{-3}$	CL=90% 119			
Hadronic modes with three K's					
$K_S^0 K^+ K^-$	$(4.42 \pm 0.32) \times 10^{-3}$	544			
$K_S^0 a_0(980)^0, a_0^0 \rightarrow K^+ K^-$	$(2.9 \pm 0.4) \times 10^{-3}$	-			
$K^- a_0(980)^+, a_0^+ \rightarrow K^+ K^-$	$(5.9 \pm 1.8) \times 10^{-4}$	-			
$K^+ a_0(980)^-, a_0^- \rightarrow K^+ K^-$	$< 1.1 \times 10^{-4}$	CL=95% -			
$K^- K_S^0(980), f_0 \rightarrow K^+ K^-$	$< 9 \times 10^{-5}$	CL=95% -			
$K_S^0 \phi, \phi \rightarrow K^+ K^-$	$(2.03 \pm 0.15) \times 10^{-3}$	520			
$K_S^0 \phi$	$(4.14 \pm 0.23) \times 10^{-3}$	521			
$K_S^0 f_0(1370), f_0 \rightarrow K^+ K^-$	$(1.7 \pm 1.1) \times 10^{-4}$	-			
$3K_S^0$	$(7.5 \pm 0.7) \times 10^{-4}$	S=1.4 539			
$K^+ 2K^- \pi^+$	$(2.25 \pm 0.32) \times 10^{-4}$	434			
$K^+ K^- \bar{K}^*(892)^0, \bar{K}^{*0} \rightarrow K^- \pi^+$	$(4.5 \pm 1.8) \times 10^{-5}$	†			
$K^- \pi^+ \phi, \phi \rightarrow K^+ K^-$	$(4.0 \pm 1.7) \times 10^{-5}$	422			
$\phi \bar{K}^*(892)^0, \phi \rightarrow K^+ K^-, \bar{K}^{*0} \rightarrow K^- \pi^+$	$(1.08 \pm 0.21) \times 10^{-4}$	†			
$K^+ 2K^- \pi^+ \text{ nonresonant}$	$(3.4 \pm 1.5) \times 10^{-5}$	434			
$2K_S^0 K^\pm \pi^\mp$	$(5.9 \pm 1.3) \times 10^{-4}$	427			
Pionic modes					
$\pi^+ \pi^-$	$(1.454 \pm 0.024) \times 10^{-3}$	S=1.4 922			
$2\pi^0$	$(8.26 \pm 0.25) \times 10^{-4}$	923			
$\pi^+ \pi^- \pi^0$	$(1.49 \pm 0.07) \%$	S=2.3 907			
$\rho^+ \pi^-$	$(1.01 \pm 0.05) \%$	764			
$\rho^0 \pi^0$	$(3.86 \pm 0.24) \times 10^{-3}$	764			
$\rho^- \pi^+$	$(5.15 \pm 0.26) \times 10^{-3}$	764			
$\rho(1450)^+ \pi^-, \rho^+ \rightarrow \pi^+ \pi^0$	$(1.6 \pm 2.1) \times 10^{-5}$	-			
$\rho(1450)^0 \pi^0, \rho^0 \rightarrow \pi^+ \pi^-$	$(4.5 \pm 2.0) \times 10^{-5}$	-			
$\rho(1450)^- \pi^+, \rho^- \rightarrow \pi^- \pi^0$	$(2.7 \pm 0.4) \times 10^{-4}$	-			
$\rho(1700)^+ \pi^-, \rho^+ \rightarrow \pi^+ \pi^0$	$(6.1 \pm 1.5) \times 10^{-4}$	-			
$\rho(1700)^0 \pi^0, \rho^0 \rightarrow \pi^+ \pi^-$	$(7.4 \pm 1.8) \times 10^{-4}$	-			
$\rho(1700)^- \pi^+, \rho^- \rightarrow \pi^- \pi^0$	$(4.8 \pm 1.1) \times 10^{-4}$	-			
$f_0(980) \pi^0, f_0 \rightarrow \pi^+ \pi^-$	$(3.7 \pm 0.9) \times 10^{-5}$	-			
$f_0(500) \pi^0, f_0 \rightarrow \pi^+ \pi^-$	$(1.22 \pm 0.22) \times 10^{-4}$	-			
$f_0(1370) \pi^0, f_0 \rightarrow \pi^+ \pi^-$	$(5.5 \pm 2.1) \times 10^{-5}$	-			
$f_0(1500) \pi^0, f_0 \rightarrow \pi^+ \pi^-$	$(5.8 \pm 1.6) \times 10^{-5}$	-			
$f_0(1710) \pi^0, f_0 \rightarrow \pi^+ \pi^-$	$(4.6 \pm 1.6) \times 10^{-5}$	-			
$f_2(1270) \pi^0, f_2 \rightarrow \pi^+ \pi^-$	$(1.97 \pm 0.21) \times 10^{-4}$	-			
$\pi^+ \pi^- \pi^0 \text{ nonresonant}$	$(1.3 \pm 0.4) \times 10^{-4}$	907			
$3\pi^0$	$(2.0 \pm 0.5) \times 10^{-4}$	908			
$2\pi^+ 2\pi^-$	$(7.56 \pm 0.20) \times 10^{-3}$	880			
$a_1(1260)^+ \pi^-, a_1^+ \rightarrow 2\pi^+ \pi^- \text{ total}$	$(4.53 \pm 0.31) \times 10^{-3}$	-			
$a_1(1260)^+ \pi^-, a_1^+ \rightarrow \rho^0 \pi^+ S\text{-wave}$	$(3.13 \pm 0.21) \times 10^{-3}$	-			
$a_1(1260)^+ \pi^-, a_1^+ \rightarrow \rho^0 \pi^+ D\text{-wave}$	$(1.9 \pm 0.5) \times 10^{-4}$	-			
$a_1(1260)^+ \pi^-, a_1^+ \rightarrow \sigma \pi^+$	$(6.4 \pm 0.7) \times 10^{-4}$	-			
$a_1(1260)^- \pi^+, a_1^- \rightarrow \rho^0 \pi^- S\text{-wave}$	$(2.3 \pm 0.9) \times 10^{-4}$	-			
$a_1(1260)^- \pi^+, a_1^- \rightarrow \sigma \pi^-$	$(6.0 \pm 3.4) \times 10^{-5}$	-			
$\pi(1300)^+ \pi^-, \pi(1300)^+ \rightarrow \sigma \pi^+$	$(5.1 \pm 2.7) \times 10^{-4}$	-			
$\pi(1300)^- \pi^+, \pi(1300)^- \rightarrow \sigma \pi^-$	$(2.3 \pm 2.2) \times 10^{-4}$	-			
$a_1(1640)^+ \pi^-, a_1^+ \rightarrow \rho^0 \pi^+ D\text{-wave}$	$(3.2 \pm 1.6) \times 10^{-4}$	-			
$a_1(1640)^+ \pi^-, a_1^+ \rightarrow \sigma \pi^+$	$(1.8 \pm 1.4) \times 10^{-4}$	-			
$\pi_2(1670)^+ \pi^-, \pi_2^+ \rightarrow f_2(1270)^0 \pi^+, f_2^0 \rightarrow \pi^+ \pi^-$	$(2.0 \pm 0.9) \times 10^{-4}$	-			
$\pi_2(1670)^+ \pi^-, \pi_2^+ \rightarrow \sigma \pi^+$	$(2.6 \pm 1.0) \times 10^{-4}$	-			
$2\rho^0 \text{ total}$	$(1.85 \pm 0.13) \times 10^{-3}$	518			
$2\rho^0, \text{ parallel helicities}$	$(8.3 \pm 3.2) \times 10^{-5}$	-			
$2\rho^0, \text{ perpendicular helicities}$	$(4.8 \pm 0.6) \times 10^{-4}$	-			
$2\rho^0, \text{ longitudinal helicities}$	$(1.27 \pm 0.10) \times 10^{-3}$	-			
$2\rho(770)^0, S\text{-wave}$	$(1.8 \pm 1.3) \times 10^{-4}$	-			
$2\rho(770)^0, P\text{-wave}$	$(5.3 \pm 1.3) \times 10^{-4}$	-			
$2\rho(770)^0, D\text{-wave}$	$(6.2 \pm 3.0) \times 10^{-4}$	-			
$\text{Resonant } (\pi^+ \pi^-) \pi^+ \pi^-$	$(1.51 \pm 0.12) \times 10^{-3}$	-			
3-body total					
$\sigma \pi^+ \pi^-$	$(6.2 \pm 0.9) \times 10^{-4}$	-			
$\sigma \rho(770)^0$	$(5.0 \pm 2.5) \times 10^{-4}$	-			
$f_0(980) \pi^+ \pi^-, f_0 \rightarrow \pi^+ \pi^-$	$(1.8 \pm 0.5) \times 10^{-4}$	-			
$f_2(1270) \pi^+ \pi^-, f_2 \rightarrow \pi^+ \pi^-$	$(3.7 \pm 0.6) \times 10^{-4}$	-			
$2f_2(1270), f_2 \rightarrow \pi^+ \pi^-$	$(1.6 \pm 1.8) \times 10^{-4}$	-			
$f_0(1370) \sigma, f_0 \rightarrow \pi^+ \pi^-$	$(1.6 \pm 0.5) \times 10^{-3}$	-			
$\pi^+ \pi^- 2\pi^0$	$(1.002 \pm 0.031) \%$	882			
$4\pi^0$	$(7.6 \pm 1.1) \times 10^{-4}$	883			
$\eta \pi^0$	[yy] $(6.3 \pm 0.6) \times 10^{-4}$	S=1.1 846			
$\omega \pi^0$	[yy] $(1.17 \pm 0.35) \times 10^{-4}$	761			
$\omega \eta$	$(1.98 \pm 0.18) \times 10^{-3}$	S=1.1 648			
$2\pi^+ 2\pi^- \pi^0$	$(3.46 \pm 0.21) \times 10^{-3}$	844			
$\pi^+ \pi^- 3\pi^0$	$(1.53 \pm 0.21) \times 10^{-3}$	847			
$2\pi^+ 2\pi^- 2\pi^0$	$(4.8 \pm 0.4) \times 10^{-3}$	798			
$\eta \pi^+ \pi^-$	[yy] $(1.16 \pm 0.07) \times 10^{-3}$	827			
$\omega \pi^+ \pi^-$	[yy] $(1.33 \pm 0.20) \times 10^{-3}$	738			
$\omega \pi^0 \pi^0$	$< 1.10 \times 10^{-3}$	CL=90% 740			
$\eta 2\pi^0$	$(3.8 \pm 1.3) \times 10^{-4}$	829			
$\pi^+ \pi^- \pi^0 \eta$	$(3.23 \pm 0.22) \times 10^{-3}$	797			
$\eta 3\pi^0$	$(2.36 \pm 0.28) \times 10^{-3}$	799			
$\eta 2\pi^+ 2\pi^-$	$(6.0 \pm 1.2) \times 10^{-4}$	751			

Meson Summary Table

$3\pi^+ 3\pi^-$	$(4.3 \pm 1.2) \times 10^{-4}$	795	$K_1(1270)^+ K^-, K_1^+ \rightarrow$	$(1.5 \pm 0.5) \times 10^{-4}$	-
$\eta'(958)\pi^0$	$(9.2 \pm 1.0) \times 10^{-4}$	678	$K^*(1430)^0 \pi^+, K^{*0} \rightarrow$		
$\eta'(958)\pi^+ \pi^-$	$(4.5 \pm 1.7) \times 10^{-4}$	650	$K^+ \pi^-$		
2η	$(2.11 \pm 0.19) \times 10^{-3}$	S=2.2 754	$K_1(1270)^+ K^-, K_1^+ \rightarrow$	$(2.2 \pm 0.6) \times 10^{-4}$	-
$2\eta\pi^0$	$(7.3 \pm 2.2) \times 10^{-4}$	699	$\rho^0 K^+$		
$2\eta\pi^+ \pi^-$	$(8.5 \pm 1.4) \times 10^{-4}$	623	$K_1(1270)^+ K^-, K_1^+ \rightarrow$	$(1.5 \pm 1.2) \times 10^{-5}$	-
3η	$< 1.3 \times 10^{-4}$	CL=90% 421	$\omega(782) K^+, \omega \rightarrow \pi^+ \pi^-$		
$\eta\eta'(958)$	$(1.01 \pm 0.19) \times 10^{-3}$	537	$K_1(1270)^- K^+, K_1^- \rightarrow$	$(1.3 \pm 0.4) \times 10^{-4}$	-
Hadronic modes with a $K\bar{K}$ pair					
$K^+ K^-$	$(4.08 \pm 0.06) \times 10^{-3}$	S=1.6 791	$\rho^0 K^-$		
$2K_S^0$	$(1.41 \pm 0.05) \times 10^{-4}$	S=1.1 789	$K_1(1400)^+ K^-, K_1^+ \rightarrow$	$(4.6 \pm 0.4) \times 10^{-4}$	-
$K_S^0 K^- \pi^+$	$(3.3 \pm 0.5) \times 10^{-3}$	S=1.1 739	$K^*(892)^0 \pi^+, K^{*0} \rightarrow$		
$\bar{K}^*(892)^0 K_S^0, \bar{K}^{*0} \rightarrow$	$(8.2 \pm 1.6) \times 10^{-5}$	608	$K^+ \pi^-$		
$K^-(892)^+ K^-, K^{*+} \rightarrow$	$(1.89 \pm 0.30) \times 10^{-3}$	-	$K^*(1410)^- K^+, K^{*-} \rightarrow$	$(7.0 \pm 1.1) \times 10^{-5}$	-
$K_S^0 \pi^+$			$\bar{K}^{*0} \pi^-$		
$\bar{K}^*(1410)^0 K_S^0, \bar{K}^{*0} \rightarrow$	$(1.3 \pm 1.9) \times 10^{-4}$	-	$K_1(1680)^+ K^-, K_1^+ \rightarrow$	$(8.9 \pm 3.2) \times 10^{-5}$	-
$K^-(1410)^+ K^-, K^{*+} \rightarrow$	$(3.2 \pm 1.9) \times 10^{-4}$	-	$K^{*0} \pi^+, K^{*0} \rightarrow K^+ \pi^-$		
$K_S^0 \pi^+$			$K^+ K^- \pi^+ \pi^-$ non-resonant	$(2.7 \pm 0.6) \times 10^{-4}$	-
$(K^- \pi^+)_{S\text{-wave}} K_S^0$	$(6.0 \pm 2.9) \times 10^{-4}$	739	$2K_S^0 \pi^+ \pi^-$	$(5.3 \pm 0.9) \times 10^{-4}$	673
$(K_S^0 \pi^+)_{S\text{-wave}} K^-$	$(3.9 \pm 1.0) \times 10^{-4}$	739	$K_S^0 K^- \pi^+ \pi^0$	$(1.32 \pm 0.16) \times 10^{-3}$	677
$a_0(980)^- \pi^+, a_0^- \rightarrow K_S^0 K^-$	$(1.3 \pm 1.4) \times 10^{-4}$	-	$K_S^0 K^+ \pi^- \pi^0$	$(6.5 \pm 0.7) \times 10^{-4}$	677
$a_0(1450)^- \pi^+, a_0^- \rightarrow$	$(2.5 \pm 2.0) \times 10^{-5}$	-	$K_S^0 K^- 2\pi^+ \pi^-$	$< 1.4 \times 10^{-4}$	CL=90% 595
$K_S^0 K^-$			$K^+ K^- \pi^+ \pi^- \pi^0$	$(3.1 \pm 2.0) \times 10^{-3}$	600
$a_2(1320)^- \pi^+, a_2^- \rightarrow$	$(5 \pm 5) \times 10^{-6}$	-	Other $K\bar{K}X$ modes. They include all decay modes of the $\phi, \eta,$ and ω .		
$K_S^0 K^-$			$\phi\pi^0$	$(1.17 \pm 0.04) \times 10^{-3}$	645
$\rho(1450)^- \pi^+, \rho^- \rightarrow K_S^0 K^-$	$(4.6 \pm 2.5) \times 10^{-5}$	-	$\phi\eta$	$(1.8 \pm 0.5) \times 10^{-4}$	489
$K_S^0 K^+ \pi^-$	$(2.17 \pm 0.35) \times 10^{-3}$	S=1.1 739	$\phi\omega$	$(6.5 \pm 1.0) \times 10^{-4}$	238
$K^*(892)^0 K_S^0, K^{*0} \rightarrow$	$(1.12 \pm 0.21) \times 10^{-4}$	608	Radiative modes		
$K^+ \pi^-$			$\rho^0 \gamma$	$(1.82 \pm 0.32) \times 10^{-5}$	771
$K^*(892)^- K^+, K^{*-} \rightarrow$	$(6.2 \pm 1.1) \times 10^{-4}$	-	$\omega\gamma$	$< 2.4 \times 10^{-4}$	CL=90% 768
$K_S^0 \pi^-$			$\phi\gamma$	$(2.81 \pm 0.19) \times 10^{-5}$	654
$K^*(1410)^0 K_S^0, K^{*0} \rightarrow$	$(5 \pm 8) \times 10^{-5}$	-	$\bar{K}^*(892)^0 \gamma$	$(4.1 \pm 0.7) \times 10^{-4}$	719
$K^+ \pi^+$			Doubly Cabibbo suppressed (DC) modes or $\Delta C = 2$ forbidden via mixing (C2M) modes		
$K^*(1410)^- K^+, K^{*-} \rightarrow$	$(2.6 \pm 2.0) \times 10^{-4}$	-	$K^+ \ell^- \bar{\nu}_\ell$ via \bar{D}^0	$[zz] < 2.2 \times 10^{-5}$	CL=90% -
$K_S^0 \pi^-$			K^+ or $K^*(892)^+ e^- \bar{\nu}_e$ via \bar{D}^0	$< 6 \times 10^{-5}$	CL=90% -
$(K^+ \pi^-)_{S\text{-wave}} K_S^0$	$(3.7 \pm 1.9) \times 10^{-4}$	739	\bar{D}^0		
$(K_S^0 \pi^-)_{S\text{-wave}} K^+$	$(1.4 \pm 0.6) \times 10^{-4}$	739	$K^+ \pi^-$ DC	$(1.50 \pm 0.07) \times 10^{-4}$	S=3.0 861
$a_0(980)^+ \pi^-, a_0^+ \rightarrow K_S^0 K^+$	$(6 \pm 4) \times 10^{-4}$	-	$K^+ \pi^-$ via DCS	$(1.363 \pm 0.025) \times 10^{-4}$	-
$a_0(1450)^+ \pi^-, a_0^+ \rightarrow$	$(3.2 \pm 2.5) \times 10^{-5}$	-	$K^+ \pi^-$ via \bar{D}^0	$< 1.6 \times 10^{-5}$	CL=95% 861
$K_S^0 K^+$			$K_S^0 \pi^+ \pi^-$ in $D^0 \rightarrow \bar{D}^0$	$< 1.8 \times 10^{-4}$	CL=95% -
$\rho(1700)^+ \pi^-, \rho^+ \rightarrow K_S^0 K^+$	$(1.1 \pm 0.6) \times 10^{-5}$	-	$K^*(892)^+ \pi^-, K^{*+} \rightarrow$ DC	$(1.13 \pm_{0.34}^{0.60}) \times 10^{-4}$	711
$K^+ K^- \pi^0$	$(3.42 \pm 0.15) \times 10^{-3}$	743	$K_S^0 \pi^+$		
$K^*(892)^+ K^-, K^*(892)^+ \rightarrow$	$(1.52 \pm 0.08) \times 10^{-3}$	-	$K_0^*(1430)^+ \pi^-, K_0^{*+} \rightarrow$ DC	$< 1.4 \times 10^{-5}$	-
$K^+ \pi^0$			$K_S^0 \pi^+$		
$K^*(892)^- K^+, K^*(892)^- \rightarrow$	$(5.4 \pm 0.4) \times 10^{-4}$	-	$K_2^*(1430)^+ \pi^-, K_2^{*+} \rightarrow$ DC	$< 3.4 \times 10^{-5}$	-
$(K^+ \pi^0)_{S\text{-wave}} K^-$	$(2.43 \pm 0.18) \times 10^{-3}$	743	$K^+ \pi^- \pi^0$		
$(K^- \pi^0)_{S\text{-wave}} K^+$	$(1.3 \pm 0.5) \times 10^{-4}$	743	$K^+ \pi^- \pi^0$ via \bar{D}^0	$(3.06 \pm 0.16) \times 10^{-4}$	S=1.4 844
$f_0(980)\pi^0, f_0 \rightarrow K^+ K^-$	$(3.6 \pm 0.6) \times 10^{-4}$	-	$K^+ \pi^- \pi^0$ via \bar{D}^0	$(7.6 \pm_{0.6}^{0.5}) \times 10^{-4}$	-
$\phi\pi^0, \phi \rightarrow K^+ K^-$	$(6.6 \pm 0.4) \times 10^{-4}$	-	$K^+ \pi^- 2\pi^0$	$< 3.6 \times 10^{-4}$	CL=90% 815
$2K_S^0 \pi^0$	$< 1.45 \times 10^{-4}$	CL=90% 740	$K^+ \pi^+ 2\pi^-$ via DCS	$(2.49 \pm 0.07) \times 10^{-4}$	-
$K^+ K^- \eta$	$(5.9 \pm 1.9) \times 10^{-5}$	514	$K^+ \pi^+ 2\pi^-$	$(2.65 \pm 0.06) \times 10^{-4}$	813
$\phi(1020)\eta$	$(1.84 \pm 0.12) \times 10^{-4}$	489	$K^+ \pi^+ 2\pi^-$ via \bar{D}^0	$(7.9 \pm 3.0) \times 10^{-6}$	812
$K^+ K^- \eta$ nonresonant	$(9.9 \pm_{0.8}^{0.9}) \times 10^{-5}$	514	μ^- anything via \bar{D}^0	$< 4 \times 10^{-4}$	CL=90% -
$2K_S^0 \eta$	$(1.3 \pm 0.6) \times 10^{-4}$	508	$\Delta C = 1$ weak neutral current (C1) modes, Lepton Family number (LF) violating modes, Lepton (L) or Baryon (B) number violating modes		
$K^+ K^- \pi^0 \pi^0$	$(6.9 \pm 0.8) \times 10^{-4}$	681	$\gamma\gamma$	$< 8.5 \times 10^{-7}$	CL=90% 932
$K^+ K^- \pi^+ \pi^-$	$(2.47 \pm 0.11) \times 10^{-3}$	677	$e^+ e^-$	$< 7.9 \times 10^{-8}$	CL=90% 932
$\phi(\pi^+ \pi^-)_{S\text{-wave}}, \phi \rightarrow$	$(10 \pm 5) \times 10^{-5}$	614	$\mu^+ \mu^-$	$< 3.1 \times 10^{-9}$	CL=90% 926
$K^+ K^-$			$\pi^0 e^+ e^-$	$< 4 \times 10^{-6}$	CL=90% 928
$(\phi\rho^0)_{S\text{-wave}}, \phi \rightarrow K^+ K^-$	$(6.9 \pm 0.6) \times 10^{-4}$	250	$\pi^0 \mu^+ \mu^-$	$< 1.8 \times 10^{-4}$	CL=90% 915
$(\phi\rho^0)_{P\text{-wave}}, \phi \rightarrow K^+ K^-$	$(4.0 \pm 1.9) \times 10^{-5}$	-	$\pi^0 \nu \bar{\nu}$	$< 2.1 \times 10^{-4}$	CL=90% 928
$(\phi\rho^0)_{D\text{-wave}}, \phi \rightarrow K^+ K^-$	$(4.2 \pm 1.4) \times 10^{-5}$	-	$\eta e^+ e^-$	$< 3 \times 10^{-6}$	CL=90% 852
$(K^*(892)^0 \bar{K}^*(892)^0)_{S\text{-wave}},$	$(2.24 \pm 0.13) \times 10^{-4}$	-	$\eta\mu^+ \mu^-$	$< 5.3 \times 10^{-4}$	CL=90% 838
$K^{*0} \rightarrow K^\pm \pi^\mp$			$\pi^+ \pi^- e^+ e^-$	$< 7 \times 10^{-6}$	CL=90% 922
$(K^*(892)^0 \bar{K}^*(892)^0)_{P\text{-wave}},$	$(1.20 \pm 0.08) \times 10^{-4}$	-	$\rho^0 e^+ e^-$	$< 1.0 \times 10^{-4}$	CL=90% 771
$K^* \rightarrow K^\pm \pi^\mp$			$\pi^+ \pi^- \mu^+ \mu^-$	$(9.6 \pm 1.2) \times 10^{-7}$	894
$(K^*(892)^0 \bar{K}^*(892)^0)_{D\text{-wave}},$	$(4.7 \pm 0.4) \times 10^{-5}$	-	$\pi^+ \pi^- \mu^+ \mu^-$ (non-res)	$< 5.5 \times 10^{-7}$	CL=90% -
$K^* \rightarrow K^\pm \pi^\mp$			$\rho^0 \mu^+ \mu^-$	$< 2.2 \times 10^{-5}$	CL=90% 754
$K^*(892)^0 (K^- \pi^+)_{S\text{-wave}}$	$(1.4 \pm 0.6) \times 10^{-4}$	-	$\omega e^+ e^-$	$< 6 \times 10^{-6}$	CL=90% 768
3-body, $K^{*0} \rightarrow K^+ \pi^-$			$\omega\mu^+ \mu^-$	$< 8.3 \times 10^{-4}$	CL=90% 751
$K_1(1270)^+ K^-, K_1^+ \rightarrow$	$(1.4 \pm 0.9) \times 10^{-4}$	-	$K^- K^+ e^+ e^-$	$< 1.1 \times 10^{-5}$	CL=90% 791
$K^{*0} \pi^+$					

Meson Summary Table

$\phi e^+ e^-$	CI	< 5.2	$\times 10^{-5}$	CL=90%	654
$K^- K^+ \mu^+ \mu^-$	CI	(1.54 \pm 0.32)	$\times 10^{-7}$		710
$K^- K^+ \mu^+ \mu^-$ (non-res)		< 3.3	$\times 10^{-5}$	CL=90%	-
$\phi \mu^+ \mu^-$	CI	< 3.1	$\times 10^{-5}$	CL=90%	631
$\bar{K}^0 e^+ e^-$	[pp]	< 2.4	$\times 10^{-5}$	CL=90%	866
$\bar{K}^0 \mu^+ \mu^-$	[pp]	< 2.6	$\times 10^{-4}$	CL=90%	852
$K^- \pi^+ e^+ e^-$, 675 < $m_{ee} < 875$ MeV		(4.0 \pm 0.5)	$\times 10^{-6}$		-
$K^- \pi^+ e^+ e^-$, 1.005 < $m_{ee} < 1.035$ GeV		< 5	$\times 10^{-7}$	CL=90%	-
$\bar{K}^*(892)^0 e^+ e^-$	[pp]	< 4.7	$\times 10^{-5}$	CL=90%	719
$K^- \pi^+ \mu^+ \mu^-$	CI	< 3.59	$\times 10^{-4}$	CL=90%	829
$K^- \pi^+ \mu^+ \mu^-$, 675 < $m_{\mu\mu} < 875$ MeV		(4.2 \pm 0.4)	$\times 10^{-6}$		-
$\bar{K}^*(892)^0 \mu^+ \mu^-$	[pp]	< 2.4	$\times 10^{-5}$	CL=90%	700
$\pi^+ \pi^- \pi^0 \mu^+ \mu^-$	CI	< 8.1	$\times 10^{-4}$	CL=90%	863
$\mu^\pm e^\mp$	LF	[aa] < 1.3	$\times 10^{-8}$	CL=90%	929
$\pi^0 e^\pm \mu^\mp$	LF	[aa] < 8.0	$\times 10^{-7}$	CL=90%	924
$\eta e^\pm \mu^\mp$	LF	[aa] < 2.25	$\times 10^{-6}$	CL=90%	848
$\pi^+ \pi^- e^\pm \mu^\mp$	LF	[aa] < 1.71	$\times 10^{-6}$	CL=90%	911
$\rho^0 e^\pm \mu^\mp$	LF	[aa] < 5.0	$\times 10^{-7}$	CL=90%	767
$\omega e^\pm \mu^\mp$	LF	[aa] < 1.71	$\times 10^{-6}$	CL=90%	764
$K^- K^+ e^\pm \mu^\mp$	LF	[aa] < 1.00	$\times 10^{-6}$	CL=90%	754
$\phi e^\pm \mu^\mp$	LF	[aa] < 5.1	$\times 10^{-7}$	CL=90%	648
$\bar{K}^0 e^\pm \mu^\mp$	LF	[aa] < 1.74	$\times 10^{-6}$	CL=90%	863
$K^- \pi^+ e^\pm \mu^\mp$	LF	[aa] < 1.90	$\times 10^{-6}$	CL=90%	848
$\bar{K}^*(892)^0 e^\pm \mu^\mp$	LF	[aa] < 1.25	$\times 10^{-6}$	CL=90%	714
$2\pi^- 2e^+$	L	< 9.1	$\times 10^{-7}$	CL=90%	922
$2\pi^- 2\mu^+$	L	< 1.52	$\times 10^{-6}$	CL=90%	894
$K^- \pi^- 2e^+$	L	< 5.0	$\times 10^{-7}$	CL=90%	861
$K^- \pi^- 2\mu^+$	L	< 5.3	$\times 10^{-7}$	CL=90%	829
$2K^- 2e^+$	L	< 3.4	$\times 10^{-7}$	CL=90%	791
$2K^- 2\mu^+$	L	< 1.0	$\times 10^{-7}$	CL=90%	710
$\pi^- \pi^- e^+ \mu^+$	L	< 3.06	$\times 10^{-6}$	CL=90%	911
$K^- \pi^- e^+ \mu^+$	L	< 2.10	$\times 10^{-6}$	CL=90%	848
$2K^- e^+ \mu^+$	L	< 5.8	$\times 10^{-7}$	CL=90%	754
$p e^-$	L,B	< 2.2	$\times 10^{-6}$	CL=90%	696
$\bar{p} e^+$	L,B	< 1.2	$\times 10^{-6}$	CL=90%	696

 $D^*(2007)^0$

$$I(J^P) = \frac{1}{2}(1^-)$$

Mass $m = 2006.85 \pm 0.05$ MeV ($S = 1.1$) $m_{D^{*0}} - m_{D^0} = 142.014 \pm 0.030$ MeV ($S = 1.5$)Full width $\Gamma < 2.1$ MeV, CL = 90% $\bar{D}^*(2007)^0$ modes are charge conjugates of modes below.

$D^*(2007)^0$ DECAY MODES	Fraction (Γ_i/Γ)	Confidence level	ρ (MeV/c)
$D^0 \pi^0$	(64.7 \pm 0.9) %		43
$D^0 \gamma$	(35.3 \pm 0.9) %		137
$D^0 e^+ e^-$	(3.91 \pm 0.33) $\times 10^{-3}$		137
$\mu^+ \mu^-$	< 2.5	90%	998
$e^+ e^-$	< 1.7	90%	1003

 $D^*(2010)^\pm$

$$I(J^P) = \frac{1}{2}(1^-)$$

Mass $m = 2010.26 \pm 0.05$ MeV $m_{D^{*(2010)^+}} - m_{D^+} = 140.603 \pm 0.015$ MeV $m_{D^{*(2010)^+}} - m_{D^0} = 145.4258 \pm 0.0017$ MeVFull width $\Gamma = 83.4 \pm 1.8$ keV $D^*(2010)^-$ modes are charge conjugates of the modes below.

$D^*(2010)^\pm$ DECAY MODES	Fraction (Γ_i/Γ)	ρ (MeV/c)
$D^0 \pi^+$	(67.7 \pm 0.5) %	39
$D^+ \pi^0$	(30.7 \pm 0.5) %	38
$D^+ \gamma$	(1.6 \pm 0.4) %	136

 $D_0^*(2300)$

$$I(J^P) = \frac{1}{2}(0^+)$$

was $D_0^*(2400)$ Mass $m = 2343 \pm 10$ MeV ($S = 1.5$)Full width $\Gamma = 229 \pm 16$ MeV **$D_0^*(2300)$ DECAY MODES**Fraction (Γ_i/Γ) ρ (MeV/c)

$D\pi^\pm$	seen	411
------------	------	-----

 $D_1(2420)$

$$I(J^P) = \frac{1}{2}(1^+)$$

Mass $m = 2422.1 \pm 0.6$ MeV ($S = 1.7$) $m_{D_1(2420)^0} - m_{D^{*+}} = 411.8 \pm 0.6$ MeV ($S = 1.7$) $m_{D_1(2420)^\pm} - m_{D_1(2420)^0} = 4 \pm 4$ MeVFull width $\Gamma = 31.3 \pm 1.9$ MeV ($S = 2.8$) $\bar{D}_1(2420)$ modes are charge conjugates of modes below. **$D_1(2420)$ DECAY MODES**Fraction (Γ_i/Γ) ρ (MeV/c)

$D^*(2007)^0 \pi$	seen	359
-------------------	------	-----

 $D_1(2430)^0$

$$I(J^P) = \frac{1}{2}(1^+)$$

Mass $m = 2412 \pm 9$ MeVFull width $\Gamma = 314 \pm 29$ MeV **$D_1(2430)^0$ DECAY MODES**Fraction (Γ_i/Γ) ρ (MeV/c)

$D^*(2010)^+ \pi^-$	seen	345
---------------------	------	-----

 $D_2^*(2460)$

$$I(J^P) = \frac{1}{2}(2^+)$$

Mass $m = 2461.1 \pm 0.8$ MeV ($S = 6.3$) $m_{D_2^*(2460)^0} - m_{D^+} = 591.5 \pm 0.8$ MeV ($S = 6.0$) $m_{D_2^*(2460)^0} - m_{D^{*+}} = 450.9 \pm 0.8$ MeV ($S = 6.0$) $m_{D_2^*(2460)^\pm} - m_{D_2^*(2460)^0} = 2.4 \pm 1.7$ MeVFull width $\Gamma = 47.3 \pm 0.8$ MeV ($S = 1.5$) $\bar{D}_2^*(2460)$ modes are charge conjugates of modes below. **$D_2^*(2460)$ DECAY MODES**Fraction (Γ_i/Γ) ρ (MeV/c)

$D\pi^-$	seen	509
$D^*(2010)\pi^-$	seen	389

 $D_3^*(2750)$

$$I(J^P) = \frac{1}{2}(3^-)$$

Mass $m = 2763.1 \pm 3.2$ MeV ($S = 2.1$)Full width $\Gamma = 66 \pm 5$ MeV **$D_3^*(2750)$ DECAY MODES**Fraction (Γ_i/Γ) ρ (MeV/c)

$D\pi$	seen	743
$D^+ \pi^-$	seen	739
$D^0 \pi^\pm$	seen	743
$D^* \pi$	seen	639
$D^{*+} \pi^-$	seen	639

CHARMED, STRANGE MESONS

$$(C = \pm 1, S = \pm 1)$$

(including possibly non- $q\bar{q}$ states)

$$D_s^+ = c\bar{s}, D_s^- = \bar{c}s, \text{ similarly for } D_s^{* \pm}$$

 D_s^\pm

$$I(J^P) = 0(0^-)$$

Mass $m = 1968.35 \pm 0.07$ MeV $m_{D_s^\pm} - m_{D^\pm} = 98.69 \pm 0.05$ MeVMean life $\tau = (501.2 \pm 2.2) \times 10^{-15}$ s ($S = 1.3$) $c\tau = 150.3 \mu\text{m}$ **CP-violating decay-rate asymmetries**

$$A_{CP}(\mu^\pm \nu) = (-0.2 \pm 2.5)\%$$

$$A_{CP}(\tau^\pm \nu) \text{ in } D_s^+ \rightarrow \tau^+ \nu_\tau, D_s^- \rightarrow \tau^- \bar{\nu}_\tau = (3 \pm 5)\%$$

$$A_{CP}(K^\pm K_S^0) = (0.09 \pm 0.26)\%$$

$$A_{CP}(K^\pm K_L^0) \text{ in } D_s^\pm \rightarrow K^\pm K_L^0 = (-1.1 \pm 2.7) \times 10^{-2}$$

Meson Summary Table

$$A_{CP}(K^+ K^- \pi^\pm) = (-0.5 \pm 0.9)\%$$

$$A_{CP}(\phi \pi^\pm) = (-0.38 \pm 0.27)\%$$

$$A_{CP}(K^\pm K_S^0 \pi^0) = (-2 \pm 6)\%$$

$$A_{CP}(2K_S^0 \pi^\pm) = (3 \pm 5)\%$$

$$A_{CP}(K^+ K^- \pi^\pm \pi^0) = (0.0 \pm 3.0)\%$$

$$A_{CP}(K^\pm K_S^0 \pi^+ \pi^-) = (-6 \pm 5)\%$$

$$A_{CP}(K_S^0 K^\pm 2\pi^\pm) = (4.1 \pm 2.8)\%$$

$$A_{CP}(\pi^+ \pi^- \pi^\pm) = (-0.7 \pm 3.1)\%$$

$$A_{CP}(\pi^\pm \eta) = (0.32 \pm 0.31)\%$$

$$A_{CP}(\pi^\pm \eta') = (-0.06 \pm 0.22)\% \quad (S = 1.6)$$

$$A_{CP}(\eta \pi^\pm \pi^0) = (-1 \pm 4)\%$$

$$A_{CP}(\eta' \pi^\pm \pi^0) = (0 \pm 8)\%$$

$$A_{CP}(K^\pm \pi^0) = (2 \pm 4)\% \quad (S = 1.2)$$

$$A_{CP}(\bar{K}^0 / K^0 \pi^\pm) = (0.4 \pm 0.5)\%$$

$$A_{CP}(K_S^0 \pi^\pm) = (0.20 \pm 0.18)\%$$

$$A_{CP}(K^\pm \pi^+ \pi^-) = (3.7 \pm 2.7)\%$$

$$A_{CP}(K_S^0 \pi^+ \pi^0) \text{ in } D_s^\pm \rightarrow K_S^0 \pi^\pm \pi^0 = (3 \pm 6)\%$$

$$A_{CP}(K^\pm \pi^+ \pi^- \pi^0) \text{ in } D_s^\pm \rightarrow K^\pm \pi^+ \pi^- \pi^0 = (7 \pm 5) \times 10^{-2}$$

$$A_{CP}(K^\pm \eta) = (1.8 \pm 1.9)\%$$

$$A_{CP}(K^\pm \eta'(958)) = (6 \pm 19)\%$$
CP violating asymmetries of P-odd (T-odd) moments

$$\text{Local CPV in } D_s^\pm \rightarrow K^+ K^- K^\pm = 0.133$$

$$A_T(K_S^0 K^\pm \pi^+ \pi^-) = (-8 \pm 6) \times 10^{-3} [H]$$
 $D_s^+ \rightarrow \phi \ell^+ \nu_\ell$ form factors

$$r_2 = 0.83 \pm 0.08 \quad (S = 1.8)$$

$$r_V = 1.76 \pm 0.07 \quad (S = 1.1)$$

$$\Gamma_L / \Gamma_T = 0.72 \pm 0.18$$

$$f_+(0) |V_{cs}| \text{ in } D_s^+ \rightarrow \eta e^+ \nu_e = 0.452 \pm 0.010$$

$$f_+(0) |V_{cs}| \text{ in } D_s^+ \rightarrow \eta' e^+ \nu_e = 0.525 \pm 0.026$$

$$f_+(0) |V_{cd}| \text{ in } D_s^+ \rightarrow K^0 e^+ \nu_e = 0.162 \pm 0.019$$

$$r_V \equiv V(0)/A_1(0) \text{ in } D_s^+ \rightarrow K^*(892)^0 e^+ \nu_e = 1.7 \pm 0.4$$

$$r_2 \equiv A_2(0)/A_1(0) \text{ in } D_s^+ \rightarrow K^*(892)^0 e^+ \nu_e = 0.77 \pm 0.29$$

$$f_{D_s^+} |V_{cs}| \text{ in } D_s^+ \rightarrow \mu^+ \nu_\mu = 241.8 \pm 3.3 \text{ MeV}$$

$$f_{D_s^+} |V_{cs}| \text{ in } D_s^+ \rightarrow \tau^+ \nu_\tau = 246.6 \pm 2.5 \text{ MeV}$$

Unless otherwise noted, the branching fractions for modes with a resonance in the final state include all the decay modes of the resonance. D_s^- modes are charge conjugates of the modes below.

D_s^+ DECAY MODES	Fraction (Γ_i/Γ)	Scale factor/ Confidence level	p (MeV/c)
Inclusive modes			
e^+ semileptonic	[aaa] (6.33 \pm 0.15) %		—
π^+ anything	(119.3 \pm 1.4) %		—
π^- anything	(43.2 \pm 0.9) %		—
π^0 anything	(123 \pm 7) %		—
K^- anything	(18.7 \pm 0.5) %		—
K^+ anything	(28.9 \pm 0.7) %		—
K_S^0 anything	(19.0 \pm 1.1) %		—
η anything	[bbb] (29.9 \pm 2.8) %		—
ω anything	(6.1 \pm 1.4) %		—
η' anything	[ccc] (10.3 \pm 1.4) %	S=1.1	—
$f_0(980)$ anything, $f_0 \rightarrow \pi^+ \pi^-$	< 1.3 %	CL=90%	—
ϕ anything	(15.7 \pm 1.0) %		—
$K^+ K^-$ anything	(15.8 \pm 0.7) %		—
$K_S^0 K^+$ anything	(5.8 \pm 0.5) %		—
$K_S^0 K^-$ anything	(1.9 \pm 0.4) %		—
$2K_S^0$ anything	(1.70 \pm 0.32) %		—
$2K^+$ anything	< 2.6 $\times 10^{-3}$ CL=90%		—
$2K^-$ anything	< 6 $\times 10^{-4}$ CL=90%		—
$2\pi^+ \pi^-$ anything	(32.8 \pm 0.7) %		—
Leptonic and semileptonic modes			
$e^+ \nu_e$	< 8.3 $\times 10^{-5}$ CL=90%		984
$\mu^+ \nu_\mu$	(5.35 \pm 0.12) $\times 10^{-3}$		981
$\tau^+ \nu_\tau$	(5.36 \pm 0.10) %		182
$\gamma e^+ \nu_e$	< 1.3 $\times 10^{-4}$ CL=90%		984
$K^+ K^- e^+ \nu_e$	—		851
$K_S^0 K_S^0 e^+ \nu_e$	< 3.8 $\times 10^{-4}$ CL=90%		849
$\phi e^+ \nu_e$	[ddd] (2.39 \pm 0.16) %	S=1.3	720
$K_1(1270)^0 e^+ \nu_e$	< 4.1 $\times 10^{-4}$ CL=90%		585
$b_1(1235)^0 e^+ \nu_e, b_1^0 \rightarrow \omega \pi^0$	< 6.4 $\times 10^{-4}$ CL=90%		—

$\phi \mu^+ \nu_\mu$	(2.24 \pm 0.11) %		715
$\eta e^+ \nu_e + \eta'(958) e^+ \nu_e$	[ddd] (3.03 \pm 0.24) %		—
$\eta e^+ \nu_e$	[ddd] (2.26 \pm 0.06) %		908
$\eta'(958) e^+ \nu_e$	[ddd] (8.0 \pm 0.4) $\times 10^{-3}$		751
$\eta \mu^+ \nu_\mu$	(2.4 \pm 0.5) %		905
$\eta'(958) \mu^+ \nu_\mu$	(1.1 \pm 0.5) %		747
$\omega e^+ \nu_e$	[eee] < 2.0 $\times 10^{-3}$ CL=90%		829
$K^0 e^+ \nu_e$	(3.4 \pm 0.4) $\times 10^{-3}$		921
$K^*(892)^0 e^+ \nu_e$	[ddd] (2.15 \pm 0.28) $\times 10^{-3}$ S=1.1		782
$f_0(500) e^+ \nu_e, f_0 \rightarrow \pi^0 \pi^0$	< 7.3 $\times 10^{-4}$ CL=90%		—
$f_0(980) e^+ \nu_e, f_0 \rightarrow \pi^0 \pi^0$	(7.9 \pm 1.5) $\times 10^{-4}$		—
$f_0(980) \mu^+ \nu_\mu, f_0 \rightarrow K^+ K^-$	< 5.45 $\times 10^{-4}$ CL=90%		—
$a_0(980)^0 e^+ \nu_e, a_0^0 \rightarrow \pi^0 \eta$	< 1.2 $\times 10^{-4}$ CL=90%		—
$\pi^0 e^+ \nu_e$	< 6.4 $\times 10^{-5}$ CL=90%		980

Hadronic modes with a $K\bar{K}$ pair

$K^+ K_S^0$	(1.450 \pm 0.035) %		850
$K^+ K^0$	(1.49 \pm 0.06) %		850
$K^+ \bar{K}^0$	(2.95 \pm 0.14) %		850
$K^+ K^- \pi^+$	[jj] (5.37 \pm 0.10) %	S=1.1	805
$\phi \pi^+$	[ddd,fff] (4.5 \pm 0.4) %		712
$\phi \pi^+, \phi \rightarrow K^+ K^-$	[fff] (2.21 \pm 0.06) %		712
$K^+ \bar{K}^*(892)^0$	(12.7 \pm 4.0 - 3.1) %		685
$K^+ \bar{K}^*(892)^0, \bar{K}^{*0} \rightarrow$	(2.58 \pm 0.06) %		416
$K^+ \bar{K}^*(892)^0, \bar{K}^{*0} \rightarrow$	(4.8 \pm 0.5) $\times 10^{-3}$		—
$K_S^0 \pi^+$			—
$f_0(980) \pi^+, f_0 \rightarrow K^+ K^-$	(1.11 \pm 0.19) %		732
$f_0(1370) \pi^+, f_0 \rightarrow K^+ K^-$	(7.1 \pm 2.9) $\times 10^{-4}$		—
$f_0(1710) \pi^+, f_0 \rightarrow K^+ K^-$	(6.7 \pm 2.8) $\times 10^{-4}$		198
$a_0(980)^+ \pi^0, a_0^+ \rightarrow K^+ K_S^0$	(1.1 \pm 0.4) $\times 10^{-3}$		—
$a_0(1710)^+ \pi^0, a_0^+ \rightarrow$	(3.5 \pm 0.6) $\times 10^{-3}$		—
$K^+ K_S^0$			—
$K^+ \bar{K}_0^*(1430)^0, \bar{K}_0^{*0} \rightarrow$	(1.76 \pm 0.25) $\times 10^{-3}$		218
$K^+ \bar{K}_0^*(1410)^0, \bar{K}_0^{*0} \rightarrow$	(8.8 \pm 2.8) $\times 10^{-4}$		—
$K^+ K_S^0 \pi^0$	(1.47 \pm 0.07) %		805
$K^*(892)^+ K_S^0, K^{*+} \rightarrow$	(2.04 \pm 0.33) $\times 10^{-3}$		—
$2K_S^0 \pi^+$	(7.1 \pm 0.4) $\times 10^{-3}$ S=1.3		802
$f_0(980) \pi^+, f_0 \rightarrow K_S^0 K_S^0$	< 1.8 $\times 10^{-4}$ CL=90%		—
$f_0(1710) \pi^+, f_0 \rightarrow K_S^0 K_S^0$	(3.3 \pm 0.4) $\times 10^{-3}$		—
$K^*(892)^+ K_S^0, K^{*+} \rightarrow$	(3.09 \pm 0.33) $\times 10^{-3}$		683
$K_S^0 \pi^+$			—
$K^0 \bar{K}^0 \pi^+$	—		802
$K^*(892)^+ \bar{K}^0$	[ddd] (5.4 \pm 1.2) %		683
$K^+ K^- \pi^+ \pi^0$	(5.50 \pm 0.24) %	S=1.3	748
$\phi \rho^+$	[ddd] (5.59 \pm 0.34) %		401
$\bar{K}_1(1270)^0 K^+, \bar{K}_1(1270)^0 \rightarrow K^- \rho^+$	(5.7 \pm 0.6) $\times 10^{-3}$		—
$\bar{K}_1(1270)^0 K^+, \bar{K}_1(1270)^0 \rightarrow K^*(892) \pi$	(1.31 \pm 0.25) %		—
$\bar{K}_1(1400)^0 K^+, \bar{K}_1(1400)^0 \rightarrow K^*(892) \pi$	(2.0 \pm 0.4) %		—
$a_0(980)^0 \rho^+, a_0^0 \rightarrow K^+ K^-$	(1.9 \pm 0.4) $\times 10^{-3}$		—
$f_1(1420)^0 \pi^+, f_1(1420)^0 \rightarrow$	(3.9 \pm 0.7) $\times 10^{-3}$		—
$K^*(892)^+ K^\pm$			—
$f_1(1420)^0 \pi^+, f_1(1420)^0 \rightarrow$	(4.0 \pm 1.4) $\times 10^{-4}$		—
$a_0(980)^0 \pi^0, a_0(980)^0 \rightarrow$			—
$K^+ K^-$			—
$\eta(1475) \pi^+, \eta(1475) \rightarrow$	(7.0 \pm 2.8) $\times 10^{-4}$		—
$a_0(980)^0 \pi^0, a_0(980)^0 \rightarrow$			—
$K^+ K^-$			—
$K_S^0 K^- 2\pi^+$	(1.53 \pm 0.08) %	S=1.5	744
$K^+ K^- K_S^0 \pi^+$	(1.29 \pm 0.18) $\times 10^{-4}$		527
$K^*(892)^+ \bar{K}^*(892)^0$	[ddd] (5.64 \pm 0.35) %		417
$\eta(1475) K_S^0, \eta \rightarrow$	(3.4 \pm 1.0) $\times 10^{-4}$		—
$K^*(892)^0 \pi^+, K^{*0} \rightarrow$			—
$K^- \pi^+$			—
$\eta(1475) \pi^+, \eta \rightarrow$	(3.4 \pm 1.0) $\times 10^{-4}$		—
$\bar{K}^*(892)^+ K^-, \bar{K}^{*+} \rightarrow$			—
$K_S^0 \pi^+$			—
$\eta(1475) \pi^+, \eta \rightarrow$	(1.7 \pm 0.9) $\times 10^{-3}$		—
$a_0(980)^- \pi^+, a_0^- \rightarrow$			—
$K_S^0 K^-$			—

Meson Summary Table

 $D_s^{*\pm}$

$$I(J^P) = 0(1^-)$$

Mass $m = 2112.2 \pm 0.4$ MeV

$$m_{D_s^{*\pm}} - m_{D_s^\pm} = 143.8 \pm 0.4$$
 MeV

Full width $\Gamma < 1.9$ MeV, CL = 90% D_s^{*-} modes are charge conjugates of the modes below.

D_s^{*+} DECAY MODES	Fraction (Γ_i/Γ)	ρ (MeV/c)
$D_s^+ \gamma$	(93.6 \pm 0.4) %	139
$D_s^+ \pi^0$	(5.77 \pm 0.35) %	48
$D_s^+ e^+ e^-$	(6.7 \pm 1.6) $\times 10^{-3}$	139
$e^+ \nu_e$	(2.1 $^{+1.2}_{-0.9}$) $\times 10^{-5}$	1056

 $D_{s0}^*(2317)^\pm$

$$I(J^P) = 0(0^+)$$

 J, P need confirmation. J^P is natural, low mass consistent with 0^+ .See the review on "Heavy Non- $q\bar{q}$ Mesons."Mass $m = 2317.8 \pm 0.5$ MeV

$$m_{D_{s0}^*(2317)^\pm} - m_{D_s^\pm} = 349.4 \pm 0.5$$
 MeV

Full width $\Gamma < 3.8$ MeV, CL = 95% $D_{s0}^*(2317)^-$ modes are charge conjugates of modes below.

$D_{s0}^*(2317)^\pm$ DECAY MODES	Fraction (Γ_i/Γ)	Confidence level	ρ (MeV/c)
$D_s^+ \pi^0$	(100 $^{+0}_{-20}$) %		298
$D_s^+ \gamma$	< 5 %	90%	323
$D_s^*(2112)^+ \gamma$	< 6 %	90%	–
$D_s^+ \gamma \gamma$	< 18 %	95%	323
$D_s^*(2112)^+ \pi^0$	< 11 %	90%	–
$D_s^+ \pi^+ \pi^-$	< 4 $\times 10^{-3}$	90%	194
$D_s^+ \pi^0 \pi^0$	not seen		205

 $D_{s1}(2460)^\pm$

$$I(J^P) = 0(1^+)$$

See the review on "Heavy Non- $q\bar{q}$ Mesons."Mass $m = 2459.5 \pm 0.6$ MeV ($S = 1.1$)

$$m_{D_{s1}(2460)^\pm} - m_{D_s^\pm} = 347.3 \pm 0.7$$
 MeV ($S = 1.2$)

$$m_{D_{s1}(2460)^\pm} - m_{D_s^\pm} = 491.1 \pm 0.6$$
 MeV ($S = 1.1$)

Full width $\Gamma < 3.5$ MeV, CL = 95% $D_{s1}(2460)^-$ modes are charge conjugates of the modes below.

$D_{s1}(2460)^+$ DECAY MODES	Fraction (Γ_i/Γ)	Scale factor/ Confidence level	ρ (MeV/c)
$D_s^+ \pi^0$	(48 \pm 11) %		297
$D_s^+ \gamma$	(18 \pm 4) %		442
$D_s^+ \pi^+ \pi^-$	(4.3 \pm 1.3) %	$S=1.1$	363
$D_s^{*+} \gamma$	< 8 %	CL=90%	323
$D_{s0}^*(2317)^+ \gamma$	(3.7 $^{+5.0}_{-2.4}$) %		138

 $D_{s1}(2536)^\pm$

$$I(J^P) = 0(1^+)$$

 J, P need confirmation.Mass $m = 2535.11 \pm 0.06$ MeV

$$m_{D_{s1}(2536)^\pm} - m_{D_s^*(2111)} = 422.9 \pm 0.4$$
 MeV

$$m_{D_{s1}(2536)^\pm} - m_{D^*(2010)^\pm} = 524.85 \pm 0.04$$
 MeV

$$m_{D_{s1}(2536)^\pm} - m_{D^*(2007)^0} = 528.26 \pm 0.05$$
 MeV ($S = 1.1$)

Full width $\Gamma = 0.92 \pm 0.05$ MeVBranching fractions are given relative to the one **DEFINED AS 1**. $D_{s1}(2536)^-$ modes are charge conjugates of the modes below.

$D_{s1}(2536)^+$ DECAY MODES	Fraction (Γ_i/Γ)	Confidence level	ρ (MeV/c)
$D^*(2010)^+ K^0$	0.85 \pm 0.12		149
$(D^*(2010)^+ K^0)_{S-wave}$	0.61 \pm 0.09		149
$K_S^0 D^*(2010)^+$	0.48 \pm 0.07		149
$D^+ \pi^- K^+$	0.028 \pm 0.005		176

 $D^*(2007)^0 K^+$ $D^+ K^0$ $D^0 K^+$ $D_s^{*+} \gamma$ $D_s^+ \pi^+ \pi^-$ **DEFINED AS 1**

< 0.34

< 0.12

possibly seen

seen

167

381

391

388

437

 $D_{s2}^*(2573)$

$$I(J^P) = 0(2^+)$$

Mass $m = 2569.1 \pm 0.8$ MeV ($S = 2.4$)

$$m_{D_{s2}^*(2573)} - m_{D^0} = 704 \pm 3.2$$
 MeV

Full width $\Gamma = 16.9 \pm 0.7$ MeV $D_{s2}^*(2573)^-$ modes are charge conjugates of the modes below.

$D_{s2}^*(2573)^+$ DECAY MODES	Fraction (Γ_i/Γ)	ρ (MeV/c)
$D^0 K^+$	seen	431
$D^*(2007)^0 K^+$	not seen	238
$D^+ K_S^0$	seen	422
$D^{*+} K_S^0$	seen	225

 $D_{s1}^*(2700)^\pm$

$$I(J^P) = 0(1^-)$$

Mass $m = 2714 \pm 5$ MeV ($S = 1.5$)Full width $\Gamma = 122 \pm 10$ MeV

$D_{s1}^*(2700)^\pm$ DECAY MODES	Fraction (Γ_i/Γ)	ρ (MeV/c)
$D^0 K^+$	seen	579
$D^+ K_S^0$	seen	573
$D^{*0} K^+$	seen	438
$D^{*+} K_S^0$	seen	431

 $D_{s3}^*(2860)^\pm$

$$I(J^P) = 0(3^-)$$

Mass $m = 2860 \pm 7$ MeVFull width $\Gamma = 53 \pm 10$ MeV

$D_{s3}^*(2860)^\pm$ DECAY MODES	Fraction (Γ_i/Γ)	ρ (MeV/c)
$D^0 K^+$	seen	710
$D^+ K_S^0$	seen	704
$D^{*0} K^+$	seen	589
$D^{*+} K_S^0$	seen	584

BOTTOM MESONS

$$(B = \pm 1)$$

$$B^+ = u\bar{b}, B^0 = d\bar{b}, \bar{B}^0 = \bar{d}b, B^- = \bar{u}b, \text{ similarly for } B^{*s}$$

B-particle organization

Many measurements of B decays involve admixtures of B hadrons. Previously we arbitrarily included such admixtures in the B^\pm section, but because of their importance we have created two new sections: " B^\pm/B^0 Admixture" for $\Upsilon(4S)$ results and " $B^\pm/B^0/B_s^0/b$ -baryon Admixture" for results at higher energies. Most inclusive decay branching fractions and χ_b at high energy are found in the Admixture sections. B^0 - \bar{B}^0 mixing data are found in the B^0 section, while B_s^0 - \bar{B}_s^0 mixing data and B - \bar{B} mixing data for a B^0/B_s^0 admixture are found in the B_s^0 section. CP -violation data are found in the B^\pm , B^0 , and B^\pm/B^0 Admixture sections. b -baryons are found near the end of the Baryon section.

The organization of the B sections is now as follows, where bullets indicate particle sections and brackets indicate reviews.

• B^\pm mass, mean life, CP violation, branching fractions

Meson Summary Table

- B^0
mass, mean life, $B^0\text{-}\bar{B}^0$ mixing, CP violation,
branching fractions
- B^\pm/B^0 Admixtures
 CP violation, branching fractions
- $B^\pm/B^0/B_s^0/b$ -baryon Admixtures
mean life, production fractions, branching fractions
- B^* , $B_1(5721)$, $B_2^*(5747)$, $B_J(5970)$
mass, width
- B_s^0
mass, mean life, $B_s^0\text{-}\bar{B}_s^0$ mixing, CP violation,
branching fractions
- B_s^* , $B_{s1}(5830)^0$, $B_{s2}^*(5840)^0$
mass, width
- B_c^\pm
mass, mean life, branching fractions
- $B_c(2S)^\pm$
mass

At the end of Baryon Listings:

- Λ_b
mass, mean life, branching fractions
- $\Lambda_b(5912)^0$, $\Lambda_b(5920)^0$, $\Lambda_b(6070)^0$, $\Lambda_b(6146)^0$, $\Lambda_b(6152)^0$
mass, width
- Σ_b
mass
- Σ_b^* , $\Sigma_b(6097)^+$, $\Sigma_b(6097)^-$
mass, width
- Ξ_b^0 , Ξ_b^-
mass, mean life, branching fractions
- $\Xi_b^*(5935)^-$, $\Xi_b(5945)^0$, $\Xi_b(5955)^-$, $\Xi_b(6100)^-$, $\Xi_b(6227)^-$,
 $\Xi_b(6227)^0$, $\Xi_b(6327)^0$, $\Xi_b(6333)^0$
mass, width
- Ω_b^-
mass, mean life, branching fractions
- $\Omega_b(6316)^-$, $\Omega_b(6330)^-$, $\Omega_b(6340)^-$, $\Omega_b(6350)^-$
mass
- b -baryon Admixture
mean life, branching fractions

B^\pm

$$J(P) = \frac{1}{2}(0^-)$$

I , J , P need confirmation. Quantum numbers shown are quark-model predictions.

$$\begin{aligned} \text{Mass } m_{B^\pm} &= 5279.41 \pm 0.07 \text{ MeV} \\ \text{Mean life } \tau_{B^\pm} &= (1.638 \pm 0.004) \times 10^{-12} \text{ s} \\ c\tau &= 491.1 \text{ } \mu\text{m} \end{aligned}$$

CP violation

$$\begin{aligned} A_{CP}(B^+ \rightarrow J/\psi(1S)K^+) &= (1.8 \pm 3.0) \times 10^{-3} \quad (S = 1.5) \\ A_{CP}(B^+ \rightarrow J/\psi(1S)\pi^+) &= (1.8 \pm 1.2) \times 10^{-2} \quad (S = 1.3) \\ A_{CP}(B^+ \rightarrow J/\psi\rho^+) &= -0.05 \pm 0.05 \\ A_{CP}(B^+ \rightarrow J/\psi K^*(892)^+) &= -0.048 \pm 0.033 \\ A_{CP}(B^+ \rightarrow \eta_c K^+) &= 0.01 \pm 0.07 \quad (S = 2.2) \\ A_{CP}(B^+ \rightarrow \psi(2S)\pi^+) &= 0.03 \pm 0.06 \\ A_{CP}(B^+ \rightarrow \psi(2S)K^+) &= 0.012 \pm 0.020 \quad (S = 1.5) \\ A_{CP}(B^+ \rightarrow \psi(2S)K^*(892)^+) &= 0.08 \pm 0.21 \\ A_{CP}(B^+ \rightarrow \chi_{c1}(1P)\pi^+) &= 0.07 \pm 0.18 \\ A_{CP}(B^+ \rightarrow \chi_{c0}K^+) &= -0.20 \pm 0.18 \quad (S = 1.5) \\ A_{CP}(B^+ \rightarrow \chi_{c1}K^+) &= -0.009 \pm 0.033 \\ A_{CP}(B^+ \rightarrow \chi_{c1}K^*(892)^+) &= 0.5 \pm 0.5 \\ A_{CP}(B^+ \rightarrow D^0\ell^+\nu_\ell) &= (-0.14 \pm 0.20) \times 10^{-2} \\ A_{CP}(B^+ \rightarrow \bar{D}^0\pi^+) &= (-3 \pm 5) \times 10^{-3} \\ A_{CP}(B^+ \rightarrow D_{CP(+)}\pi^+) &= -0.0080 \pm 0.0024 \\ A_{CP}(B^+ \rightarrow D_{CP(-)}\pi^+) &= 0.017 \pm 0.026 \end{aligned}$$

$$\begin{aligned} A_{CP}([K^\mp\pi^\pm\pi^+\pi^-]_D\pi^+) &= 0.070 \pm 0.020 \\ A_{CP}(B^+ \rightarrow [\pi^+\pi^+\pi^-\pi^-]_D K^+) &= 0.061 \pm 0.013 \\ A_{CP}(B^+ \rightarrow [\pi^+\pi^-\pi^+\pi^-]_D K^*(892)^+) &= 0.02 \pm 0.11 \\ A_{CP}(B^+ \rightarrow [K^+K^-\pi^+\pi^-]_D K^+) &= 0.095 \pm 0.023 \\ A_{CP}(B^+ \rightarrow [K^+K^-\pi^+\pi^-]_D\pi^+) &= -0.009 \pm 0.006 \\ A_{CP}(B^+ \rightarrow \bar{D}^0 K^+) &= -0.017 \pm 0.005 \\ A_{CP}([K^\mp\pi^\pm\pi^+\pi^-]_D K^+) &= -0.32 \pm 0.04 \\ A_{CP}(B^+ \rightarrow [\pi^+\pi^+\pi^-\pi^-]_D\pi^+) &= (-8.2 \pm 3.2) \times 10^{-3} \\ A_{CP}(B^+ \rightarrow [K^-\pi^+]_D K^+) &= -0.58 \pm 0.21 \\ A_{CP}(B^+ \rightarrow [K^-\pi^+\pi^0]_D K^+) &= -0.27 \pm 0.27 \quad (S = 2.4) \\ A_{CP}(B^+ \rightarrow [K^+\pi^-\pi^0]_D K^+) &= -0.024 \pm 0.013 \\ A_{CP}(B^+ \rightarrow [K^+K^-\pi^0]_D K^+) &= 0.07 \pm 0.07 \\ A_{CP}(B^+ \rightarrow [\pi^+\pi^-\pi^0]_D K^+) &= 0.11 \pm 0.04 \\ A_{CP}(B^+ \rightarrow \bar{D}^0 K^*(892)^+) &= -0.007 \pm 0.019 \\ A_{CP}(B^+ \rightarrow [K^-\pi^+]_D K^*(892)^+) &= -0.75 \pm 0.16 \\ A_{CP}(B^+ \rightarrow [K^-\pi^+\pi^-\pi^+]_D K^*(892)^+) &= -0.45 \pm 0.25 \\ A_{CP}(B^+ \rightarrow [K^-\pi^+]_D\pi^+) &= 0.00 \pm 0.09 \\ A_{CP}(B^+ \rightarrow [K^-\pi^+\pi^0]_D\pi^+) &= 0.08 \pm 0.09 \\ A_{CP}(B^+ \rightarrow [K^+K^-\pi^0]_D\pi^+) &= -0.001 \pm 0.019 \\ A_{CP}(B^+ \rightarrow [\pi^+\pi^-\pi^0]_D\pi^+) &= 0.001 \pm 0.010 \\ A_{CP}(B^+ \rightarrow [K^-\pi^+]_D\pi^+) &= -0.09 \pm 0.27 \\ A_{CP}(B^+ \rightarrow [K^-\pi^+]_D\gamma\pi^+) &= -0.7 \pm 0.6 \\ A_{CP}(B^+ \rightarrow [K^-\pi^+]_D\pi^+ K^+) &= 0.8 \pm 0.4 \\ A_{CP}(B^+ \rightarrow [K^-\pi^+]_D\gamma K^+) &= 0.4 \pm 1.0 \\ A_{CP}(B^+ \rightarrow [\pi^+\pi^-\pi^0]_D K^+) &= -0.02 \pm 0.15 \\ A_{CP}(B^+ \rightarrow [K_S^0 K^+\pi^-]_D K^+) &= 0.00 \pm 0.09 \quad (S = 1.4) \\ A_{CP}(B^+ \rightarrow [K_S^0 K^-\pi^+]_D K^+) &= 0.00 \pm 0.07 \\ A_{CP}(B^+ \rightarrow [K_S^0 K^-\pi^+]_D\pi^+) &= -0.003 \pm 0.014 \\ A_{CP}(B^+ \rightarrow [K_S^0 K^+\pi^-]_D\pi^+) &= -0.016 \pm 0.025 \quad (S = 1.5) \\ A_{CP}(B^+ \rightarrow [K^*(892)^- K^+]_D K^+) &= 0.08 \pm 0.05 \\ A_{CP}(B^+ \rightarrow [K^*(892)^+ K^-]_D K^+) &= 0.07 \pm 0.09 \\ A_{CP}(B^+ \rightarrow [K^*(892)^+ K^-]_D\pi^+) &= 0.007 \pm 0.016 \\ A_{CP}(B^+ \rightarrow [K^*(892)^- K^+]_D\pi^+) &= -0.013 \pm 0.020 \quad (S = 1.9) \\ \mathbf{A_{CP}(B^+ \rightarrow D_{CP(+)}K^+) = 0.132 \pm 0.015} \quad (S = 1.8) \\ A_{ADS}(B^+ \rightarrow D K^+) &= -0.451 \pm 0.026 \\ A_{ADS}(B^+ \rightarrow D\pi^+) &= 0.129 \pm 0.014 \\ A_{ADS}(B^+ \rightarrow D^*(D\gamma)K^+) &= -0.6 \pm 1.3 \\ A_{ADS}(B^+ \rightarrow D^*(D\pi^0)K^+) &= 0.72 \pm 0.29 \\ A_{ADS}(B^+ \rightarrow D^*(D\gamma)\pi^+) &= 0.08 \pm 0.13 \\ A_{ADS}(B^+ \rightarrow D^*(D\pi^0)\pi^+) &= -0.14 \pm 0.06 \\ A_{ADS}(B^+ \rightarrow [K^-\pi^+]_D K^+\pi^-\pi^+) &= -0.33 \pm 0.35 \\ A_{ADS}(B^+ \rightarrow [K^-\pi^+]_D\pi^+\pi^-\pi^+) &= -0.01 \pm 0.09 \\ A_{CP}(B^+ \rightarrow D_{CP(-)}K^+) &= -0.10 \pm 0.07 \\ A_{CP}(B^+ \rightarrow [K^+K^-]_D K^+\pi^-\pi^+) &= -0.04 \pm 0.06 \\ A_{CP}(B^+ \rightarrow [\pi^+\pi^-]_D K^+\pi^-\pi^+) &= -0.05 \pm 0.10 \\ A_{CP}(B^+ \rightarrow [K^-\pi^+]_D K^+\pi^-\pi^+) &= 0.013 \pm 0.023 \\ A_{CP}(B^+ \rightarrow [K^+K^-]_D\pi^+\pi^-\pi^+) &= -0.019 \pm 0.015 \\ A_{CP}(B^+ \rightarrow [\pi^+\pi^-]_D\pi^+\pi^-\pi^+) &= -0.013 \pm 0.019 \\ A_{CP}(B^+ \rightarrow [K^-\pi^+]_D\pi^+\pi^-\pi^+) &= -0.002 \pm 0.011 \\ A_{CP}(B^+ \rightarrow \bar{D}^{*0}\pi^+) &= -0.0004 \pm 0.0021 \quad (S = 1.1) \\ A_{CP}(B^+ \rightarrow D^{*0}_{CP(+)}\pi^+) &= 0.010 \pm 0.007 \\ A_{CP}(B^+ \rightarrow D^{*0}_{CP(-)}\pi^+) &= -0.09 \pm 0.05 \\ A_{CP}(B^+ \rightarrow D^{*0}K^+) &= 0.012 \pm 0.010 \quad (S = 1.5) \\ A_{CP}(B^+ \rightarrow D^{*0}_{CP(+)}K^+) &= -0.09 \pm 0.05 \quad (S = 2.6) \\ A_{CP}(B^+ \rightarrow D^{*0}_{CP(-)}K^+) &= 0.07 \pm 0.10 \\ A_{CP}(B^+ \rightarrow D_{CP(+)}K^*(892)^+) &= 0.08 \pm 0.06 \\ A_{CP}(B^+ \rightarrow D_{CP(-)}K^*(892)^+) &= -0.23 \pm 0.22 \\ A_{CP}(B^+ \rightarrow D_s^+\phi) &= 0.0 \pm 0.4 \\ A_{CP}(B^+ \rightarrow D_s^+\bar{D}^0) &= (0.5 \pm 0.6)\% \\ A_{CP}(B^+ \rightarrow D_s^+\bar{D}^0) &= (-0.5 \pm 1.5) \times 10^{-2} \\ A_{CP}(B^+ \rightarrow D_s^+\bar{D}^{*0}) &= (1.1 \pm 1.1) \times 10^{-2} \\ A_{CP}(B^+ \rightarrow D^{*+}\bar{D}^{*0}) &= (1.3 \pm 2.6) \times 10^{-2} \\ A_{CP}(B^+ \rightarrow D^{*+}\bar{D}^0) &= (3.1 \pm 1.7) \times 10^{-2} \\ A_{CP}(B^+ \rightarrow D^+\bar{D}^{*0}) &= (0.0 \pm 2.4) \times 10^{-2} \\ A_{CP}(B^+ \rightarrow D^+\bar{D}^0) &= (2.4 \pm 1.1) \times 10^{-2} \\ A_{CP}(B^+ \rightarrow K_S^0\pi^+) &= -0.003 \pm 0.015 \quad (S = 1.1) \\ A_{CP}(B^+ \rightarrow K^+\pi^0) &= 0.027 \pm 0.012 \\ A_{CP}(B^+ \rightarrow \eta'K^+) &= 0.004 \pm 0.011 \\ A_{CP}(B^+ \rightarrow \eta'K^*(892)^+) &= -0.26 \pm 0.27 \\ A_{CP}(B^+ \rightarrow \eta'K_S^0(1430)^+) &= 0.06 \pm 0.20 \end{aligned}$$

Meson Summary Table

$$\begin{aligned}
&A_{CP}(B^+ \rightarrow \eta' K_2^*(1430)^+) = 0.15 \pm 0.13 \\
&\mathbf{A}_{CP}(B^+ \rightarrow \eta K^+) = -0.37 \pm 0.08 \\
&A_{CP}(B^+ \rightarrow \eta K^*(892)^+) = 0.02 \pm 0.06 \\
&A_{CP}(B^+ \rightarrow \eta K_0^*(1430)^+) = 0.05 \pm 0.13 \\
&A_{CP}(B^+ \rightarrow \eta K_2^*(1430)^+) = -0.45 \pm 0.30 \\
&A_{CP}(B^+ \rightarrow \omega K^+) = -0.02 \pm 0.04 \\
&A_{CP}(B^+ \rightarrow \omega K^{*+}) = 0.29 \pm 0.35 \\
&A_{CP}(B^+ \rightarrow \omega(K\pi)_0^{*+}) = -0.10 \pm 0.09 \\
&A_{CP}(B^+ \rightarrow \omega K_2^*(1430)^+) = 0.14 \pm 0.15 \\
&A_{CP}(B^+ \rightarrow K^{*0}\pi^+) = -0.021 \pm 0.032 \quad (S = 1.5) \\
&A_{CP}(B^+ \rightarrow K^*(892)^+\pi^0) = -0.39 \pm 0.21 \quad (S = 1.6) \\
&\mathbf{A}_{CP}(B^+ \rightarrow K^+\pi^-\pi^+) = 0.015 \pm 0.006 \quad (S = 1.4) \\
&A_{CP}(B^+ \rightarrow K^+K^-K^+ \text{ nonresonant}) = 0.06 \pm 0.05 \\
&A_{CP}(B^+ \rightarrow f(980)^0 K^+) = -0.08 \pm 0.09 \\
&\mathbf{A}_{CP}(B^+ \rightarrow \mathbf{f}_2(1270)K^+) = -0.68^{+0.19}_{-0.17} \\
&A_{CP}(B^+ \rightarrow f_0(1500)K^+) = 0.28 \pm 0.30 \\
&A_{CP}(B^+ \rightarrow f_2'(1525)^0 K^+) = -0.08^{+0.05}_{-0.04} \\
&\mathbf{A}_{CP}(B^+ \rightarrow \rho^0 K^+) = 0.160 \pm 0.021 \\
&A_{CP}(B^+ \rightarrow K^0\pi^+\pi^0) = 0.07 \pm 0.06 \\
&A_{CP}(B^+ \rightarrow K_0^*(1430)^0\pi^+) = 0.061 \pm 0.032 \\
&A_{CP}(B^+ \rightarrow K_0^*(1430)^+\pi^0) = 0.26^{+0.18}_{-0.14} \\
&A_{CP}(B^+ \rightarrow K_2^*(1430)^0\pi^+) = 0.05^{+0.29}_{-0.24} \\
&A_{CP}(B^+ \rightarrow K^+\pi^0\pi^0) = -0.06 \pm 0.07 \\
&A_{CP}(B^+ \rightarrow K^0\rho^+) = -0.03 \pm 0.15 \\
&A_{CP}(B^+ \rightarrow K^{*+}\pi^+\pi^-) = 0.07 \pm 0.08 \\
&A_{CP}(B^+ \rightarrow \rho^0 K^*(892)^+) = 0.31 \pm 0.13 \\
&A_{CP}(B^+ \rightarrow K^*(892)^+ f_0(980)) = -0.15 \pm 0.12 \\
&A_{CP}(B^+ \rightarrow a_1^+ K^0) = 0.12 \pm 0.11 \\
&A_{CP}(B^+ \rightarrow b_1^+ K^0) = -0.03 \pm 0.15 \\
&A_{CP}(B^+ \rightarrow K^*(892)^0\rho^+) = -0.01 \pm 0.16 \\
&A_{CP}(B^+ \rightarrow b_1^0 K^+) = -0.46 \pm 0.20 \\
&A_{CP}(B^+ \rightarrow K^0 K^+) = 0.04 \pm 0.14 \\
&A_{CP}(B^+ \rightarrow K_2^0 K^+) = -0.21 \pm 0.14 \\
&A_{CP}(B^+ \rightarrow K^+ K_S^0 K_S^0) = 0.025 \pm 0.031 \\
&\mathbf{A}_{CP}(B^+ \rightarrow K^+ K^-\pi^+) = -0.115 \pm 0.008 \\
&A_{CP}(B^+ \rightarrow K^+ K^-\pi^+ \text{ nonresonant}) = -0.11 \pm 0.06 \\
&A_{CP}(B^+ \rightarrow \pi^+ K^+ K^-, m_{K^+K^-} < 1.1 \text{ GeV}) = -0.17 \pm 0.07 \\
&A_{CP}(B^+ \rightarrow K^+ \bar{K}^*(892)^0) = 0.04 \pm 0.05 \\
&A_{CP}(B^+ \rightarrow K^+ \bar{K}_0^*(1430)^0) = 0.10 \pm 0.17 \\
&A_{CP}(B^+ \rightarrow \phi\pi^+) = 0.1 \pm 0.5 \\
&A_{CP}(B^+ \rightarrow \pi^+(K^+K^-)_{S\text{-wave}}) = -0.66 \pm 0.04 \\
&\mathbf{A}_{CP}(B^+ \rightarrow K^+K^-K^+) = -0.036 \pm 0.004 \\
&A_{CP}(B^+ \rightarrow \phi K^+) = 0.017 \pm 0.017 \quad (S = 1.8) \\
&A_{CP}(B^+ \rightarrow X_0(1550)K^+) = -0.04 \pm 0.07 \\
&A_{CP}(B^+ \rightarrow K^{*+}K^+K^-) = 0.11 \pm 0.09 \\
&A_{CP}(B^+ \rightarrow \phi K^*(892)^+) = -0.01 \pm 0.08 \\
&A_{CP}(B^+ \rightarrow \phi(K\pi)_0^{*+}) = 0.04 \pm 0.16 \\
&A_{CP}(B^+ \rightarrow \phi K_1(1270)^+) = 0.15 \pm 0.20 \\
&A_{CP}(B^+ \rightarrow \phi K_2^*(1430)^+) = -0.23 \pm 0.20 \\
&A_{CP}(B^+ \rightarrow K^+\phi\phi) = -0.08 \pm 0.07 \\
&A_{CP}(B^+ \rightarrow K^+[\phi\phi]_{\eta_c}) = 0.10 \pm 0.08 \\
&A_{CP}(B^+ \rightarrow K^*(892)^+\gamma) = 0.014 \pm 0.018 \\
&A_{CP}(B^+ \rightarrow X_S\gamma) = 0.028 \pm 0.019 \\
&A_{CP}(B^+ \rightarrow \eta K^+\gamma) = -0.12 \pm 0.07 \\
&A_{CP}(B^+ \rightarrow \phi K^+\gamma) = -0.13 \pm 0.11 \quad (S = 1.1) \\
&A_{CP}(B^+ \rightarrow \rho^+\gamma) = -0.11 \pm 0.33 \\
&A_{CP}(B^+ \rightarrow \pi^+\pi^0) = -0.01 \pm 0.04 \quad (S = 1.1) \\
&\mathbf{A}_{CP}(B^+ \rightarrow \pi^+\pi^-\pi^+) = 0.076 \pm 0.008 \quad (S = 1.5) \\
&A_{CP}(B^+ \rightarrow \pi^+\pi^0\pi^0) = (9 \pm 7) \times 10^{-2} \\
&A_{CP}(B^+ \rightarrow \rho^0\pi^+) = 0.003 \pm 0.014 \\
&A_{CP}(B^+ \rightarrow f_2(1270)\pi^+) = 0.40 \pm 0.06 \\
&A_{CP}(B^+ \rightarrow \rho^0(1450)\pi^+) = -0.11 \pm 0.05 \\
&A_{CP}(B^+ \rightarrow \rho_3(1690)\pi^+) = -0.80 \pm 0.28 \\
&\mathbf{A}_{CP}(B^+ \rightarrow \mathbf{f}_0(1370)\pi^+) = 0.72 \pm 0.22 \\
&A_{CP}(B^+ \rightarrow \pi^+\pi^-\pi^+ \text{ nonresonant}) = -0.14^{+0.23}_{-0.16} \\
&A_{CP}(B^+ \rightarrow \rho^+\pi^0) = 0.03 \pm 0.10 \\
&A_{CP}(B^+ \rightarrow X\pi^+, X \rightarrow \pi^0\pi^0) = 0.18 \pm 0.12 \\
&A_{CP}(B^+ \rightarrow \rho^+\rho^0) = -0.05 \pm 0.05 \\
&A_{CP}(B^+ \rightarrow \omega\pi^+) = -0.04 \pm 0.05 \\
&A_{CP}(B^+ \rightarrow \omega\rho^+) = -0.20 \pm 0.09 \\
&A_{CP}(B^+ \rightarrow \eta\pi^+) = -0.14 \pm 0.07 \quad (S = 1.4) \\
&A_{CP}(B^+ \rightarrow \eta\rho^+) = 0.11 \pm 0.11
\end{aligned}$$

$$\begin{aligned}
&A_{CP}(B^+ \rightarrow \eta'\pi^+) = 0.06 \pm 0.16 \\
&A_{CP}(B^+ \rightarrow \eta'\rho^+) = 0.26 \pm 0.17 \\
&A_{CP}(B^+ \rightarrow b_1^0\pi^+) = 0.05 \pm 0.16 \\
&A_{CP}(B^+ \rightarrow \rho\bar{\rho}\pi^+) = 0.00 \pm 0.04 \\
&A_{CP}(B^+ \rightarrow \rho\bar{\rho}K^+) = 0.00 \pm 0.04 \quad (S = 2.2) \\
&A_{CP}(B^+ \rightarrow \rho\bar{\rho}K^*(892)^+) = 0.21 \pm 0.16 \quad (S = 1.4) \\
&A_{CP}(B^+ \rightarrow \rho\bar{\rho}\gamma) = 0.17 \pm 0.17 \\
&A_{CP}(B^+ \rightarrow \rho\bar{\rho}\pi^0) = 0.01 \pm 0.17 \\
&A_{CP}(B^+ \rightarrow K^+\ell^+\ell^-) = -0.02 \pm 0.08 \\
&A_{CP}(B^+ \rightarrow K^+e^+e^-) = 0.14 \pm 0.14 \\
&A_{CP}(B^+ \rightarrow K^+\mu^+\mu^-) = 0.011 \pm 0.017 \\
&A_{CP}(B^+ \rightarrow \pi^+\mu^+\mu^-) = -0.11 \pm 0.12 \\
&A_{CP}(B^+ \rightarrow K^*\ell^+\ell^-) = -0.09 \pm 0.14 \\
&A_{CP}(B^+ \rightarrow K^*e^+e^-) = -0.14 \pm 0.23 \\
&A_{CP}(B^+ \rightarrow K^*\mu^+\mu^-) = -0.12 \pm 0.24 \\
&\gamma = (65.9^{+2.9}_{-3.1})^\circ \\
&\mathbf{r}_B(B^+ \rightarrow D^0 K^+) = (9.94 \pm 0.26) \times 10^{-2} \\
&\delta_B(B^+ \rightarrow D^0 K^+) = (127.7^{+3.6}_{-3.9})^\circ \\
&\mathbf{r}_B(B^+ \rightarrow D^0 K^{*+}) = 0.101^{+0.016}_{-0.034} \\
&\delta_B(B^+ \rightarrow D^0 K^{*+}) = (48^{+59}_{-16})^\circ \\
&\mathbf{r}_B(B^+ \rightarrow D^{*0} K^+) = 0.104^{+0.013}_{-0.014} \\
&\delta_B(B^+ \rightarrow D^{*0} K^+) = (314.8^{+7.9}_{-9.9})^\circ
\end{aligned}$$

B^- modes are charge conjugates of the modes below. Modes which do not identify the charge state of the B are listed in the B^\pm/B^0 ADMIXTURE section.

The branching fractions listed below assume 50% $B^0\bar{B}^0$ and 50% B^+B^- production at the $\Upsilon(4S)$. We have attempted to bring older measurements up to date by rescaling their assumed $\Upsilon(4S)$ production ratio to 50:50 and their assumed $D, D_s, D^*,$ and ψ branching ratios to current values whenever this would affect our averages and best limits significantly.

Indentation is used to indicate a subchannel of a previous reaction. All resonant subchannels have been corrected for resonance branching fractions to the final state so the sum of the subchannel branching fractions can exceed that of the final state.

For inclusive branching fractions, e.g., $B \rightarrow D^\pm X$, the values usually are multiplicities, not branching fractions. They can be greater than one.

B^+ DECAY MODES	Fraction (Γ_i/Γ)	Scale factor/ Confidence level (MeV/c)	p
Semileptonic and leptonic modes			
$\ell^+ \nu_\ell X$	[hhh] (10.99 ± 0.28) %		–
$e^+ \nu_e X_c$	(10.8 ± 0.4) %		–
$\ell^+ \nu_\ell X_u$	[hhh] (1.65 ± 0.21) × 10 ⁻³		–
$D \ell^+ \nu_\ell X$	[hhh] (9.5 ± 0.7) %		–
$\bar{D}^0 \ell^+ \nu_\ell$	[hhh] (2.21 ± 0.06) %		2310
$\bar{D}^0 \tau^+ \nu_\tau$	(7.7 ± 2.5) × 10 ⁻³		1911
$\bar{D}^*(2007)^0 \ell^+ \nu_\ell$	[hhh] (5.53 ± 0.22) %		2258
$\bar{D}^*(2007)^0 \tau^+ \nu_\tau$	(1.88 ± 0.20) %		1839
$D^{(*)} n \pi \ell^+ \nu_\ell (n \geq 1)$	[hhh] (1.83 ± 0.25) %		–
$D^-\pi^+ \ell^+ \nu_\ell$	[hhh] (3.82 ± 0.20) × 10 ⁻³		2306
$\bar{D}_2^{*0}(2460)^0 \ell^+ \nu_\ell$	[hhh] (1.59 ± 0.10) × 10 ⁻³		2065
$\bar{D}_2^{*0} \rightarrow D^-\pi^+$			
$\bar{D}_0^*(2420)^0 \ell^+ \nu_\ell$	[hhh] (9 ± 5) × 10 ⁻⁴	S=2.6	–
$\bar{D}_0^{*0} \rightarrow D^-\pi^+$			
$D^{*-}\pi^+ \ell^+ \nu_\ell$	[hhh] (5.42 ± 0.28) × 10 ⁻³		2254
$\bar{D}_1(2420)^0 \ell^+ \nu_\ell, \bar{D}_1^0 \rightarrow [hhh]$	(2.84 ± 0.17) × 10 ⁻³	S=1.1	2084
$D^{*-}\pi^+$			
$\bar{D}_1'(2430)^0 \ell^+ \nu_\ell, \bar{D}_1^0 \rightarrow [hhh]$	(1.7 ± 0.6) × 10 ⁻³	S=1.8	–
$D^{*-}\pi^+$			
$\bar{D}_2^{*0}(2460)^0 \ell^+ \nu_\ell$	[hhh] (1.06 ± 0.18) × 10 ⁻³	S=1.7	2065
$\bar{D}_2^{*0} \rightarrow D^{*-}\pi^+$			
$\bar{D}^0 \pi^+ \pi^- \ell^+ \nu_\ell$	[hhh] (1.73 ± 0.19) × 10 ⁻³		2301
$\bar{D}_1(2420)^0 \ell^+ \nu_\ell, \bar{D}_1^0 \rightarrow [hhh]$	(1.05 ± 0.14) × 10 ⁻³		–
$\bar{D}^0 \pi^+ \pi^-$			
$\bar{D}^{*0} \pi^+ \pi^- \ell^+ \nu_\ell$	[hhh] (7.0 ± 1.7) × 10 ⁻⁴		2248
$D_S^{(*)-} K^+ \ell^+ \nu_\ell$	[hhh] (6.1 ± 1.0) × 10 ⁻⁴		–
$D_S^- K^+ \ell^+ \nu_\ell$	[hhh] (3.0 ± 1.4) × 10 ⁻⁴		2242
$D_S^{*-} K^+ \ell^+ \nu_\ell$	[hhh] (2.9 ± 1.9) × 10 ⁻⁴		2185
$\pi^0 \ell^+ \nu_\ell$	[hhh] (7.80 ± 0.27) × 10 ⁻⁵		2638
$\eta \ell^+ \nu_\ell$	[hhh] (3.5 ± 0.4) × 10 ⁻⁵		2611
$\eta' \ell^+ \nu_\ell$	[hhh] (2.4 ± 0.7) × 10 ⁻⁵		2553

Meson Summary Table

$\bar{D}_3^*(2760)^0 \pi^+$	$(1.00 \pm 0.22) \times 10^{-5}$	-	$D^*(2010)^- D^*(2010)^+ K^+$	$(1.32 \pm 0.18) \times 10^{-3}$	1363
$\bar{D}_3^*(2760)^0 \pi^+ \rightarrow D^- \pi^+$			$(\bar{D} + \bar{D}^*)(D + D^*) K$	$(4.05 \pm 0.30) \%$	-
$\bar{D}_2^*(3000)^0 \pi^+$	$(2.0 \pm 1.4) \times 10^{-6}$	-	$D_s^- D_s^+ K^+$	$(1.2 \pm 0.4) \times 10^{-4}$	1429
$\bar{D}_2^*(3000)^0 \pi^+ \rightarrow D^- \pi^+$			$D_s^+ \pi^0$	$(1.6 \pm 0.5) \times 10^{-5}$	2270
$\bar{D}_2^*(2460)^0 \rho^+$	$< 4.7 \times 10^{-3}$	CL=90%	$D_s^{*+} \pi^0$	$< 2.6 \times 10^{-4}$	CL=90% 2215
$\bar{D}^0 D_s^+$	$(9.0 \pm 0.9) \times 10^{-3}$	1815	$D_s^+ \eta$	$< 1.4 \times 10^{-5}$	CL=90% 2235
$D_{s0}^*(2317)^+ \bar{D}^0, D_{s0}^{*+} \rightarrow$	$(8.0 \pm 1.6 \pm 1.3) \times 10^{-4}$	1605	$D_s^{*+} \eta$	$< 1.7 \times 10^{-5}$	CL=90% 2178
$D_{s0}^*(2317)^+ \bar{D}^0 \times$	$< 7.6 \times 10^{-4}$	CL=90%	$D_s^+ \rho^0$	$< 3.0 \times 10^{-4}$	CL=90% 2197
$B(D_{s0}(2317)^+ \rightarrow D_s^{*+} \gamma)$			$D_s^{*+} \rho^0$	$< 4 \times 10^{-4}$	CL=90% 2138
$D_{s0}(2317)^+ \bar{D}^*(2007)^0 \times$	$(9 \pm 7) \times 10^{-4}$	1511	$D_s^+ \omega$	$< 4 \times 10^{-4}$	CL=90% 2195
$B(D_{s0}(2317)^+ \rightarrow D_s^+ \pi^0)$			$D_s^{*+} \omega$	$< 6 \times 10^{-4}$	CL=90% 2136
$D_{sJ}(2457)^+ \bar{D}^0$	$(3.1 \pm 1.0 \pm 0.9) \times 10^{-3}$	-	$D_s^+ a_1(1260)^0$	$< 1.8 \times 10^{-3}$	CL=90% 2080
$D_{sJ}(2457)^+ \bar{D}^0 \times$	$(4.6 \pm 1.3 \pm 1.1) \times 10^{-4}$	-	$D_s^{*+} a_1(1260)^0$	$< 1.3 \times 10^{-3}$	CL=90% 2015
$B(D_{sJ}(2457)^+ \rightarrow D_s^+ \gamma)$			$D_s^+ K^+ K^-$	$(7.2 \pm 1.1) \times 10^{-6}$	2149
$D_{sJ}(2457)^+ \bar{D}^0 \times$	$< 2.2 \times 10^{-4}$	CL=90%	$D_s^+ \phi$	$< 4.2 \times 10^{-7}$	CL=90% 2141
$B(D_{sJ}(2457)^+ \rightarrow D_s^+ \pi^+ \pi^-)$			$D_s^{*+} \phi$	$< 1.2 \times 10^{-5}$	CL=90% 2079
$D_{sJ}(2457)^+ \bar{D}^0 \times$	$< 2.7 \times 10^{-4}$	CL=90%	$D_s^+ \bar{K}^0$	$< 3 \times 10^{-6}$	CL=90% 2242
$B(D_{sJ}(2457)^+ \rightarrow D_s^+ \pi^+ \pi^-)$			$D_s^+ \bar{K}^0$	$< 6 \times 10^{-6}$	CL=90% 2185
$D_{sJ}(2457)^+ \bar{D}^0 \times$	$< 2.7 \times 10^{-4}$	CL=90%	$D_s^+ \bar{K}^*(892)^0$	$< 4.4 \times 10^{-6}$	CL=90% 2172
$B(D_{sJ}(2457)^+ \rightarrow D_s^+ \pi^0)$			$D_s^+ K^*0$	$< 3.5 \times 10^{-6}$	CL=90% 2172
$D_{sJ}(2457)^+ \bar{D}^0 \times$	$< 9.8 \times 10^{-4}$	CL=90%	$D_s^+ \bar{K}^*(892)^0$	$< 3.5 \times 10^{-4}$	CL=90% 2112
$B(D_{sJ}(2457)^+ \rightarrow D_s^{*+} \gamma)$			$D_s^- \pi^+ K^+$	$(1.80 \pm 0.22) \times 10^{-4}$	2222
$D_{sJ}(2457)^+ \bar{D}^*(2007)^0$	$(1.20 \pm 0.30) \%$	-	$D_s^- \pi^+ K^+$	$(1.45 \pm 0.24) \times 10^{-4}$	2164
$D_{sJ}(2457)^+ \bar{D}^*(2007)^0 \times$	$(1.4 \pm 0.7 \pm 0.6) \times 10^{-3}$	-	$D_s^- \pi^+ K^*(892)^+$	$< 5 \times 10^{-3}$	CL=90% 2138
$B(D_{sJ}(2457)^+ \rightarrow D_s^+ \gamma)$			$D_s^- \pi^+ K^*(892)^+$	$< 7 \times 10^{-3}$	CL=90% 2076
$\bar{D}^0 D_{s1}(2536)^+ \times$	$(4.0 \pm 1.0) \times 10^{-4}$	1447	$D_s^- K^+ K^+$	$(9.7 \pm 2.1) \times 10^{-6}$	2149
$B(D_{s1}(2536)^+ \rightarrow$			$D_s^- K^+ K^+$	$< 1.5 \times 10^{-5}$	CL=90% 2088
$D^*(2007)^0 K^+ +$			Charmonium modes		
$D^*(2010)^+ K^0)$			$\eta_c K^+$	$(1.10 \pm 0.07) \times 10^{-3}$	S=1.1 1751
$\bar{D}^0 D_{s1}(2536)^+ \times$	$(2.2 \pm 0.7) \times 10^{-4}$	1447	$\eta_c K^*(892)^+$	$(1.2 \pm 0.5 \pm 0.4) \times 10^{-3}$	1646
$B(D_{s1}(2536)^+ \rightarrow$			$\eta_c K^+ \pi^+ \pi^-$	$< 3.9 \times 10^{-4}$	CL=90% 1684
$D^*(2007)^0 K^+)$			$\eta_c K^+ \omega(782)$	$< 5.3 \times 10^{-4}$	CL=90% 1475
$\bar{D}^*(2007)^0 D_{s1}(2536)^+ \times$	$(5.5 \pm 1.6) \times 10^{-4}$	1339	$\eta_c K^+ \eta$	$< 2.2 \times 10^{-4}$	CL=90% 1588
$B(D_{s1}(2536)^+ \rightarrow$			$\eta_c K^+ \pi^0$	$< 6.2 \times 10^{-5}$	CL=90% 1723
$D^*(2007)^0 K^+)$			$\eta_c(2S) K^+$	$(4.4 \pm 1.0) \times 10^{-4}$	1320
$\bar{D}^0 D_{s1}(2536)^+ \times$	$(2.3 \pm 1.1) \times 10^{-4}$	1447	$\eta_c(2S) K^+, \eta_c \rightarrow p \bar{p}$	$(3.5 \pm 0.8) \times 10^{-8}$	-
$B(D_{s1}(2536)^+ \rightarrow D^{*+} K^0)$			$\eta_c(2S) K^+, \eta_c \rightarrow$	$(3.4 \pm 2.3 \pm 1.6) \times 10^{-6}$	-
$\bar{D}^0 D_{sJ}(2700)^+ \times$	$(5.6 \pm 1.8) \times 10^{-4}$	S=1.7	$K_S^0 K^+ \pi^\pm$		
$B(D_{sJ}(2700)^+ \rightarrow D^0 K^+)$			$\eta_c(2S) K^+, \eta_c \rightarrow p \bar{p} \pi^+ \pi^-$	$(1.12 \pm 0.18) \times 10^{-6}$	-
$\bar{D}^{*0} D_{s1}(2536)^+, D_{s1}^+ \rightarrow$	$(3.9 \pm 2.6) \times 10^{-4}$	1339	$h_c(1P) K^+, h_c \rightarrow J/\psi \pi^+ \pi^-$	$< 3.4 \times 10^{-6}$	CL=90% 1401
$D^{*+} K^0$			$X(3730)^0 K^+, X^0 \rightarrow \eta_c \eta$	$< 4.6 \times 10^{-5}$	CL=90% -
$\bar{D}^0 D_{sJ}(2573)^+, D_{sJ}^+ \rightarrow$	$(8 \pm 15) \times 10^{-6}$	-	$X(3730)^0 K^+, X^0 \rightarrow \eta_c \pi^0$	$< 5.7 \times 10^{-6}$	CL=90% -
$D^0 K^+$			$\eta_{c2}(1D) K^+, \eta_{c2} \rightarrow h_c \gamma$	$< 3.7 \times 10^{-5}$	CL=90% -
$\bar{D}^{*0} D_{sJ}(2573), D_{sJ}^+ \rightarrow$	$< 2 \times 10^{-4}$	CL=90%	$\eta_{c2}(1D) \pi^+ K_S^0, \eta_{c2} \rightarrow h_c \gamma$	$< 1.1 \times 10^{-4}$	CL=90% -
$D^0 K^+$			$\psi_2(3823) K^+, \psi_2 \rightarrow$	$(2.8 \pm 0.6) \times 10^{-7}$	-
$\bar{D}^*(2007)^0 D_{sJ}(2573), D_{sJ}^+ \rightarrow$	$< 5 \times 10^{-4}$	CL=90%	$J/\psi \pi^+ \pi^-$		
$D^0 K^+$			$\psi_2(3823) K^+, \psi_2 \rightarrow J/\psi \eta$	$(1.2 \pm 0.7 \pm 0.5) \times 10^{-6}$	-
$\bar{D}^0 D_s^+$	$(7.6 \pm 1.6) \times 10^{-3}$	1734	$\psi_3(3842) K^+, \psi_3 \rightarrow J/\psi \eta$	$< 6.1 \times 10^{-7}$	CL=90% -
$\bar{D}^*(2007)^0 D_s^+$	$(8.2 \pm 1.7) \times 10^{-3}$	1737	$\chi_{c1}(3872) K^+$	$(2.3 \pm 0.6) \times 10^{-4}$	1141
$\bar{D}^*(2007)^0 D_s^{*+}$	$(1.71 \pm 0.24) \%$	1651	$\chi_{c0}(3915) K^+$	$< 2.8 \times 10^{-4}$	CL=90% 1100
$D_s^{(*)+} \bar{D}^{*0}$	$(2.7 \pm 1.2) \%$	-	$\chi_{c0}(3915) K^+, \chi_{c0} \rightarrow D^+ D^-$	$(8.1 \pm 3.3) \times 10^{-6}$	-
$\bar{D}^*(2007)^0 D^*(2010)^+$	$(8.1 \pm 1.7) \times 10^{-4}$	1713	$\chi_{c0}(3915) K^+, \chi_{c0} \rightarrow \eta_c \eta$	$< 4.7 \times 10^{-5}$	CL=90% -
$\bar{D}^0 D^*(2010)^+ +$	$< 1.30 \%$	CL=90%	$\chi_{c0}(3915) K^+, \chi_{c0} \rightarrow \eta_c \pi^0$	$< 1.7 \times 10^{-5}$	CL=90% -
$\bar{D}^*(2007)^0 D^+$			$X(4014)^0 K^+, X^0 \rightarrow \eta_c \eta$	$< 3.9 \times 10^{-5}$	CL=90% -
$\bar{D}^0 D^*(2010)^+$	$(3.9 \pm 0.5) \times 10^{-4}$	1792	$X(4014)^0 K^+, X^0 \rightarrow \eta_c \pi^0$	$< 1.2 \times 10^{-5}$	CL=90% -
$\bar{D}^0 D^+$	$(3.8 \pm 0.4) \times 10^{-4}$	1866	$T_{c\bar{c}1}(3900)^0 K^+, T_{c\bar{c}1}^0 \rightarrow$	$< 4.7 \times 10^{-5}$	CL=90% -
$\bar{D}^0 D^+ K^0$	$(1.55 \pm 0.21) \times 10^{-3}$	1571	$\eta_c \pi^+ \pi^-$		
$D^+ \bar{D}^*(2007)^0$	$(6.3 \pm 1.7) \times 10^{-4}$	1791	$T_{c\bar{c}1}(3900)^0 K^+, T_{c\bar{c}1}^0 \rightarrow$	$< 4.3 \times 10^{-7}$	CL=90% -
$\bar{D}^*(2007)^0 D^+ K^0$	$(2.1 \pm 0.5) \times 10^{-3}$	1475	$J/\psi \eta$		
$\bar{D}^0 D^*(2010)^+ K^0$	$(3.8 \pm 0.4) \times 10^{-3}$	1476	$T_{c\bar{c}1}(4020)^0 K^+, T_{c\bar{c}1}^0 \rightarrow$	$< 1.6 \times 10^{-5}$	CL=90% -
$\bar{D}^*(2007)^0 D^*(2010)^+ K^0$	$(9.2 \pm 1.2) \times 10^{-3}$	1362	$\eta_c \pi^+ \pi^-$		
$\bar{D}^0 D^0 K^+$	$(1.45 \pm 0.33) \times 10^{-3}$	S=2.6 1577	$\chi_{c1}(3872) K^*(892)^+$	$< 6 \times 10^{-4}$	CL=90% 940
$\bar{D}^*(2007)^0 D^0 K^+$	$(2.26 \pm 0.23) \times 10^{-3}$	1481	$\chi_{c1}(3872)^+ K^0, \chi_{c1}^+ \rightarrow$	$[nnn] < 6.1 \times 10^{-6}$	CL=90% -
$\bar{D}^0 D^*(2007)^0 K^+$	$(6.3 \pm 0.5) \times 10^{-3}$	1481	$J/\psi(1S) \pi^+ \pi^0$		
$\bar{D}^*(2007)^0 D^*(2007)^0 K^+$	$(1.12 \pm 0.13) \%$	1368	$\chi_{c1}(3872) K^0 \pi^+$	$(3.0 \pm 1.2) \times 10^{-4}$	1085
$D^- D^+ K^+$	$(2.2 \pm 0.7) \times 10^{-4}$	1571	$T_{c\bar{c}1}(4430)^+ K^0, T_{c\bar{c}1}^+ \rightarrow$	$< 1.5 \times 10^{-5}$	CL=95% -
$T_{c\bar{c}0}^*(2870)^0 D^+, T_{c\bar{c}0}^{*0} \rightarrow$	$(1.2 \pm 0.5) \times 10^{-5}$	-	$J/\psi \pi^+$		
$D^- K^+$			$T_{c\bar{c}1}(4430)^+ K^0, T_{c\bar{c}1}^+ \rightarrow$	$< 4.7 \times 10^{-5}$	CL=95% -
$T_{c\bar{c}1}^*(2900)^0 D^+, T_{c\bar{c}1}^{*0} \rightarrow$	$(6.7 \pm 2.3) \times 10^{-5}$	-	$\psi(2S) \pi^+$		
$D^- K^+$			$T_{c\bar{c}1}(4430)^0 K^+, T_{c\bar{c}1}^0 \rightarrow$	$< 1.27 \times 10^{-6}$	CL=90% -
$D^- D^+ K^+$ nonresonant	$(5.3 \pm 1.8) \times 10^{-5}$	1571	$J/\psi \eta$		
$D^- D^*(2010)^+ K^+$	$(6.3 \pm 1.1) \times 10^{-4}$	1475			
$D^*(2010)^- D^+ K^+$	$(6.0 \pm 1.3) \times 10^{-4}$	1475			

Meson Summary Table

$\psi(4230)^0 K^+, \psi^0 \rightarrow J/\psi \pi^+ \pi^-$	< 1.56	$\times 10^{-5}$	CL=95%	-	$\chi_{c0} K^*(892)^+$	< 2.1	$\times 10^{-4}$	CL=90%	1341
$\psi(4230) K^+, \psi \rightarrow J/\psi \eta$	< 3.9	$\times 10^{-7}$	CL=90%	-	$\chi_{c1}(1P) \pi^+$	(2.2 \pm 0.5)	$\times 10^{-5}$		1468
$\psi(4360) K^+, \psi \rightarrow J/\psi \eta$	< 1.24	$\times 10^{-6}$	CL=90%	-	$\chi_{c1}(1P) K^+$	(4.74 \pm 0.22)	$\times 10^{-4}$		1412
$\psi(4390) K^+, \psi \rightarrow J/\psi \eta$	< 2.41	$\times 10^{-6}$	CL=90%	-	$\chi_{c1}(1P) K^*(892)^+$	(3.0 \pm 0.6)	$\times 10^{-4}$	S=1.1	1265
$\chi_{c0}(3915) K^+, \chi_{c0} \rightarrow J/\psi \gamma$	< 1.4	$\times 10^{-5}$	CL=90%	-	$\chi_{c1}(1P) K^0 \pi^+$	(5.8 \pm 0.4)	$\times 10^{-4}$		1370
$\chi_{c0}(3915) K^+, \chi_{c0} \rightarrow \chi_{c1}(1P) \pi^0$	< 3.8	$\times 10^{-5}$	CL=90%	-	$\chi_{c1}(1P) K^+ \pi^0$	(3.29 \pm 0.35)	$\times 10^{-4}$		1373
$X(3930)^0 K^+, X^0 \rightarrow J/\psi \gamma$	< 2.5	$\times 10^{-6}$	CL=90%	-	$\chi_{c1}(1P) K^+ \pi^+ \pi^-$	(3.74 \pm 0.30)	$\times 10^{-4}$		1319
$J/\psi(1S) K^+$	(1.020 \pm 0.019)	$\times 10^{-3}$		1684	$\chi_{c1}(2P) K^+, \chi_{c1}(2P) \rightarrow \pi^+ \pi^- \chi_{c1}(1P)$	< 1.1	$\times 10^{-5}$	CL=90%	-
$J/\psi(1S) K^0 \pi^+$	(1.14 \pm 0.11)	$\times 10^{-3}$		1651	$\chi_{c2} \pi^+, \chi_{c2} \rightarrow \pi^0 \pi^0$	< 7	$\times 10^{-7}$	CL=90%	-
$J/\psi(1S) K^+ \pi^+ \pi^-$	(8.1 \pm 1.3)	$\times 10^{-4}$	S=2.5	1612	$\chi_{c2} K^+$	(1.1 \pm 0.4)	$\times 10^{-5}$		1379
$J/\psi(1S) K^+ K^- K^+$	(3.37 \pm 0.29)	$\times 10^{-5}$		1252	$\chi_{c2} K^+, \chi_{c2} \rightarrow p \bar{p} \pi^+ \pi^-$	< 1.9	$\times 10^{-7}$		-
$\chi_{c0}(3915) K^+, \chi_{c0} \rightarrow p \bar{p}$	< 7.1	$\times 10^{-8}$	CL=95%	-	$\chi_{c2} K^*(892)^+$	< 1.2	$\times 10^{-4}$	CL=90%	1228
$J/\psi(1S) K^*(892)^+$	(1.43 \pm 0.08)	$\times 10^{-3}$		1571	$\chi_{c2} K^0 \pi^+$	(1.24 \pm 0.25)	$\times 10^{-4}$		1336
$J/\psi(1S) K(1270)^+$	(1.8 \pm 0.5)	$\times 10^{-3}$		1402	$\chi_{c2} K^+ \pi^0$	< 6.2	$\times 10^{-5}$	CL=90%	1339
$J/\psi(1S) K(1400)^+$	< 5	$\times 10^{-4}$	CL=90%	1308	$\chi_{c2} K^+ \pi^+ \pi^-$	(1.34 \pm 0.19)	$\times 10^{-4}$		1284
$J/\psi(1S) \eta K^+$	(1.24 \pm 0.14)	$\times 10^{-4}$		1510	$\chi_{c2}(3930) K^+, \chi_{c2} \rightarrow D^+ D^-$	(1.6 \pm 0.6)	$\times 10^{-5}$		-
$\chi_{c1-odd}(3872) K^+, \chi_{c1-odd} \rightarrow J/\psi \eta$	< 3.8	$\times 10^{-6}$	CL=90%	-	$\chi_{c2}(3930) \pi^+, \chi_{c2} \rightarrow \pi^+ \pi^-$	< 1	$\times 10^{-7}$	CL=90%	1437
$\psi(4160) K^+, \psi \rightarrow J/\psi \eta$	< 8.7	$\times 10^{-7}$	CL=90%	-	$h_c(1P) K^+$	(3.7 \pm 1.2)	$\times 10^{-5}$		1401
$J/\psi(1S) \eta' K^+$	(3.1 \pm 0.4)	$\times 10^{-5}$		1273	$h_c(1P) K^+, h_c \rightarrow p \bar{p}$	< 6.4	$\times 10^{-8}$	CL=95%	-
$J/\psi(1S) \phi K^+$	(5.0 \pm 0.4)	$\times 10^{-5}$		1227					
$J/\psi(1S) K_1(1650), K_1 \rightarrow \phi K^+$	(6 \pm 1.0)	$\times 10^{-6}$		-	K or K* modes				
$J/\psi(1S) K^*(1680)^+, K^* \rightarrow \phi K^+$	(3.4 \pm 1.9)	$\times 10^{-6}$		-	$K^0 \pi^+$	(2.39 \pm 0.06)	$\times 10^{-5}$		2614
$J/\psi(1S) K_2^*(1980), K_2^* \rightarrow \phi K^+$	(1.5 \pm 0.9)	$\times 10^{-6}$		-	$K^+ \pi^0$	(1.32 \pm 0.04)	$\times 10^{-5}$		2615
$J/\psi(1S) K(1830)^+, K(1830)^+ \rightarrow \phi K^+$	(1.3 \pm 1.3)	$\times 10^{-6}$		-	$\eta' K^+$	(7.04 \pm 0.25)	$\times 10^{-5}$		2528
$\chi_{c1}(4140) K^+, \chi_{c1} \rightarrow J/\psi(1S) \phi$	(10 \pm 4)	$\times 10^{-6}$		-	$\eta' K^*(892)^+$	(4.8 \pm 1.8)	$\times 10^{-6}$		2472
$\chi_{c1}(4274) K^+, \chi_{c1} \rightarrow J/\psi(1S) \phi$	(3.6 \pm 2.2)	$\times 10^{-6}$		-	$\eta' K_0^*(1430)^+$	(5.2 \pm 2.1)	$\times 10^{-6}$		-
$\chi_{c0}(4500) K^+, \chi_{c0} \rightarrow J/\psi(1S) \phi$	(3.3 \pm 2.1)	$\times 10^{-6}$		-	$\eta' K_2^*(1430)^+$	(2.8 \pm 0.5)	$\times 10^{-5}$		2346
$\chi_{c0}(4700) K^+, \chi_{c0} \rightarrow J/\psi(1S) \phi$	(6 \pm 5)	$\times 10^{-6}$		-	ηK^+	(2.4 \pm 0.4)	$\times 10^{-6}$	S=1.7	2588
$J/\psi(1S) \omega K^+$	(3.20 \pm 0.60)	$\times 10^{-4}$		1388	$\eta K^*(892)^+$	(1.93 \pm 0.16)	$\times 10^{-5}$		2534
$\chi_{c0}(3915) K^+, \chi_{c0} \rightarrow J/\psi \omega$	(3.0 \pm 0.9)	$\times 10^{-5}$		1103	$\eta K_0^*(1430)^+$	(1.8 \pm 0.4)	$\times 10^{-5}$		-
$J/\psi(1S) \pi^+$	(3.92 \pm 0.09)	$\times 10^{-5}$		1728	$\eta K_2^*(1430)^+$	(9.1 \pm 3.0)	$\times 10^{-6}$		2414
$J/\psi(1S) \pi^+ \pi^+ \pi^+ \pi^- \pi^-$	(1.17 \pm 0.13)	$\times 10^{-5}$		1635	$\eta(1295) K^+ \times B(\eta(1295) \rightarrow \eta \pi \pi)$	(2.9 \pm 0.8)	$\times 10^{-6}$		2455
$\psi(2S) \pi^+ \pi^+ \pi^-$	(1.9 \pm 0.4)	$\times 10^{-5}$		1304	$\eta(1405) K^+ \times B(\eta(1405) \rightarrow \eta \pi \pi)$	< 1.3	$\times 10^{-6}$	CL=90%	2425
$J/\psi(1S) \rho^+$	(4.1 \pm 0.5)	$\times 10^{-5}$	S=1.4	1612	$\eta(1405) K^+ \times B(\eta(1405) \rightarrow K^* K)$	< 1.2	$\times 10^{-6}$	CL=90%	2425
$J/\psi(1S) \pi^+ \pi^0$ nonresonant	< 7.3	$\times 10^{-6}$	CL=90%	1717	$\eta(1475) K^+ \times B(\eta(1475) \rightarrow K^* K)$	(1.38 \pm 0.21)	$\times 10^{-5}$		2406
$J/\psi(1S) a_1(1260)^+$	< 1.2	$\times 10^{-3}$	CL=90%	1415	$f_1(1285) K^+$	< 2.0	$\times 10^{-6}$	CL=90%	2458
$J/\psi(1S) p \bar{p} \pi^+$	< 5.0	$\times 10^{-7}$	CL=90%	644	$f_1(1420) K^+ \times B(f_1(1420) \rightarrow \eta \pi \pi)$	< 2.9	$\times 10^{-6}$	CL=90%	2420
$J/\psi(1S) p \bar{p} \pi^+$	(1.46 \pm 0.12)	$\times 10^{-5}$		568	$f_1(1420) K^+ \times B(f_1(1420) \rightarrow K^* K)$	< 4.1	$\times 10^{-6}$	CL=90%	2420
$J/\psi(1S) \bar{\Sigma}^0 p$	< 1.1	$\times 10^{-5}$	CL=90%	-	$\phi(1680) K^+ \times B(\phi(1680) \rightarrow K^* K)$	< 3.4	$\times 10^{-6}$	CL=90%	2344
$J/\psi(1S) D^+$	< 1.2	$\times 10^{-4}$	CL=90%	871	$f_0(1500) K^+$	(3.7 \pm 2.2)	$\times 10^{-6}$		2393
$J/\psi(1S) \bar{D}^0 \pi^+$	< 2.5	$\times 10^{-5}$	CL=90%	665	ωK^+	(6.5 \pm 0.4)	$\times 10^{-6}$		2558
$\psi(2S) \pi^+$	(2.44 \pm 0.30)	$\times 10^{-5}$		1348	$\omega K^*(892)^+$	< 7.4	$\times 10^{-6}$	CL=90%	2503
$\psi(2S) K^+$	(6.24 \pm 0.21)	$\times 10^{-4}$		1284	$\omega(K\pi)_0^+$	(2.8 \pm 0.4)	$\times 10^{-5}$		-
$\psi(2S) K^*(892)^+$	(6.7 \pm 1.4)	$\times 10^{-4}$	S=1.3	1116	$\omega K_0^*(1430)^+$	(2.4 \pm 0.5)	$\times 10^{-5}$		-
$\psi(2S) K^+ \pi^+ \pi^-$	(4.3 \pm 0.5)	$\times 10^{-4}$		1179	$\omega K_2^*(1430)^+$	(2.1 \pm 0.4)	$\times 10^{-5}$		2379
$\psi(2S) \phi(1020) K^+$	(4.0 \pm 0.7)	$\times 10^{-6}$		418	$a_0(980)^+ K^0 \times B(a_0(980)^+ \rightarrow \eta \pi^+)$	< 3.9	$\times 10^{-6}$	CL=90%	-
$\psi(3770) K^+$	(4.3 \pm 1.1)	$\times 10^{-4}$		1218	$a_0(980)^0 K^+ \times B(a_0(980)^0 \rightarrow \eta \pi^0)$	< 2.5	$\times 10^{-6}$	CL=90%	-
$\psi(3770) K^+, \psi \rightarrow D^0 \bar{D}^0$	(1.5 \pm 0.5)	$\times 10^{-4}$	S=1.4	1218	$K^*(892)^0 \pi^+$	(1.01 \pm 0.08)	$\times 10^{-5}$		2562
$\psi(3770) K^+, \psi \rightarrow D^+ D^-$	(9.4 \pm 3.5)	$\times 10^{-5}$		1218	$K^*(892)^+ \pi^0$	(6.8 \pm 0.9)	$\times 10^{-6}$		2563
$\psi(3770) K^+, \psi \rightarrow p \bar{p}$	< 2	$\times 10^{-7}$	CL=95%	-	$K^+ \pi^- \pi^+$	(5.10 \pm 0.29)	$\times 10^{-5}$		2609
$\psi(4040) K^+$	(1.6 \pm 0.5)	$\times 10^{-3}$		1002	$K^+ \pi^- \pi^+$ nonresonant	(1.63 \pm 0.21)	$\times 10^{-5}$		2609
$\psi(4040) K^+, \psi \rightarrow D^+ D^-$	(1.1 \pm 0.5)	$\times 10^{-5}$		-	$\omega(782) K^+$	(6 \pm 9)	$\times 10^{-6}$		2558
$\psi(4160) K^+$	(5.1 \pm 2.7)	$\times 10^{-4}$		869	$K^+ f_0(980) \times B(f_0(980) \rightarrow \pi^+ \pi^-)$	(9.4 \pm 1.0)	$\times 10^{-6}$		2522
$\psi(4160) K^+, \psi \rightarrow \bar{D}^0 D^0$	(8 \pm 5)	$\times 10^{-5}$		-	$f_2(1270)^0 K^+$	(1.07 \pm 0.27)	$\times 10^{-6}$		-
$\psi(4160) K^+, \psi \rightarrow D^+ D^-$	(1.5 \pm 0.6)	$\times 10^{-5}$		-	$f_0(1370)^0 K^+ \times B(f_0(1370)^0 \rightarrow \pi^+ \pi^-)$	< 1.07	$\times 10^{-5}$	CL=90%	-
$\psi(4415) K^+, \psi \rightarrow D^+ D^-$	(2.0 \pm 0.8)	$\times 10^{-5}$		-	$\rho(14500) K^+ \times B(\rho(14500)^0 \rightarrow \pi^+ \pi^-)$	< 3.4	$\times 10^{-6}$	CL=90%	2394
$\psi(4415) K^+, \psi \rightarrow J/\psi \eta$	< 9.6	$\times 10^{-7}$	CL=90%	-	$f_2'(1525) K^+ \times B(f_2'(1525) \rightarrow \pi^+ \pi^-)$	< 3.4	$\times 10^{-6}$	CL=90%	2394
$\chi_{c0} \pi^+, \chi_{c0} \rightarrow \pi^+ \pi^-$	< 1	$\times 10^{-7}$	CL=90%	1531	$K^+ \rho^0$	(3.7 \pm 0.5)	$\times 10^{-6}$		2559
$\chi_{c0} \pi^+, \chi_{c0} \rightarrow \pi^0 \pi^0$	< 5	$\times 10^{-7}$	CL=90%	-	$K_0^*(1430)^0 \pi^+$	(3.9 \pm 0.6)	$\times 10^{-5}$	S=1.4	2445
$\chi_{c0} K^+$	(1.51 \pm 0.15)	$\times 10^{-4}$		1478	$K_2^*(1430)^0 \pi^+$	(5.6 \pm 2.2)	$\times 10^{-6}$		2445
$\chi_{c0} K^0 \pi^+$	(1.45 \pm 0.21)	$\times 10^{-3}$		1439					

Meson Summary Table

Charged particle (h^\pm) modes				Lepton Family number (LF) or Lepton number (L) or Baryon number (B) violating modes, or/and $\Delta B = 1$ weak neutral current (BI) modes			
$h^\pm = K^\pm$ or π^\pm				$\Lambda_c^+ \Xi_c^0$	< 6.5	$\times 10^{-4}$	CL=90% 1023
$h^+ \pi^0$	(1.6 ± 0.6)	$\times 10^{-5}$	2636	$\Lambda_c^+ \Xi_c(2645)^0$	< 7.9	$\times 10^{-4}$	CL=90% -
ωh^+	(1.38 ± 0.27)	$\times 10^{-5}$	2580	$\Lambda_c^+ \Xi_c(2790)^0$	(1.1 ± 0.4)	$\times 10^{-3}$	-
$h^+ X^0$ (Familon)	< 4.9	$\times 10^{-5}$	CL=90% -				
$K^+ X^0, X^0 \rightarrow \mu^+ \mu^-$	< 1	$\times 10^{-7}$	CL=95% -				
Baryon modes				Lepton Family number (LF) or Lepton number (L) or Baryon number (B) violating modes, or/and $\Delta B = 1$ weak neutral current (BI) modes			
$\rho \bar{p} \pi^+$	(1.62 ± 0.20)	$\times 10^{-6}$	2439	$\pi^+ \ell^+ \ell^-$	BI [hhh]	< 4.9	$\times 10^{-8}$ CL=90% 2638
$\rho \bar{p} \pi^+$ nonresonant	< 5.3	$\times 10^{-5}$	CL=90% 2439	$\pi^+ e^+ e^-$	BI	< 8.0	$\times 10^{-8}$ CL=90% 2638
$\rho \bar{p} \pi^+ \pi^0$	(4.6 ± 1.3)	$\times 10^{-6}$	2407	$\pi^+ \mu^+ \mu^-$	BI	(1.78 ± 0.23)	$\times 10^{-8}$ 2634
$\rho \bar{p} K^+$	(5.9 ± 0.5)	$\times 10^{-6}$	S=1.5 2348	$\pi^+ \nu \bar{\nu}$	BI	< 1.4	$\times 10^{-5}$ CL=90% 2638
$\Theta(1710)^{++} \bar{p}, \Theta^{++} \rightarrow p K^+$	[ooo] < 9.1	$\times 10^{-8}$	CL=90% -	$K^+ \ell^+ \ell^-$	BI [hhh]	(4.7 ± 0.5)	$\times 10^{-7}$ S=2.3 2617
$f_J(2220) K^+, f_J \rightarrow \rho \bar{p}$	[ooo] < 4.1	$\times 10^{-7}$	CL=90% 2135	$K^+ e^+ e^-$	BI	(5.6 ± 0.6)	$\times 10^{-7}$ 2617
$\rho \bar{p} \pi^0$	< 6.3	$\times 10^{-6}$	CL=90% 2440	$K^+ \mu^+ \mu^-$	BI	(4.53 ± 0.35)	$\times 10^{-7}$ S=1.8 2612
$\rho \bar{\Lambda}(1520)$	(3.1 ± 0.6)	$\times 10^{-7}$	2322	$K^+ \mu^+ \mu^-$ nonresonant	BI	(4.37 ± 0.27)	$\times 10^{-7}$ 2612
$\rho \bar{p} K^+$ nonresonant	< 8.9	$\times 10^{-5}$	CL=90% 2348	$K^+ \tau^+ \tau^-$	BI	< 2.25	$\times 10^{-3}$ CL=90% 1687
$\rho \bar{p} K^*(892)^+$	(3.6 ± 0.8)	$\times 10^{-6}$	2215	$K^+ \bar{\nu} \nu$	BI	< 1.6	$\times 10^{-5}$ CL=90% 2617
$f_J(2220) K^{*+}, f_J \rightarrow \rho \bar{p}$	< 7.7	$\times 10^{-7}$	CL=90% 2059	$\rho^+ \nu \bar{\nu}$	BI	< 3.0	$\times 10^{-5}$ CL=90% 2583
$\rho \bar{\Lambda}$	(2.4 ± 1.0)	$\times 10^{-7}$	2430	$K^*(892)^+ \ell^+ \ell^-$	BI [hhh]	(1.01 ± 0.11)	$\times 10^{-6}$ S=1.1 2564
$\rho \bar{\Lambda} \gamma$	(2.4 ± 0.5)	$\times 10^{-6}$	2430	$K^*(892)^+ e^+ e^-$	BI	(1.55 ± 0.40)	$\times 10^{-6}$ 2564
$\rho \bar{\Lambda} \pi^0$	(3.0 ± 0.7)	$\times 10^{-6}$	2402	$K^*(892)^+ \mu^+ \mu^-$	BI	(9.6 ± 1.0)	$\times 10^{-7}$ 2560
$\rho \Sigma(1385)^0$	< 4.7	$\times 10^{-7}$	CL=90% 2362	$K^*(892)^+ \nu \bar{\nu}$	BI	< 4.0	$\times 10^{-5}$ CL=90% 2564
$\Delta^+ \bar{\Lambda}$	< 8.2	$\times 10^{-7}$	CL=90% -	$K^+ \pi^+ \pi^- \mu^+ \mu^-$	BI	(4.3 ± 0.4)	$\times 10^{-7}$ 2593
$\rho \Sigma \gamma$	< 4.6	$\times 10^{-6}$	CL=90% 2413	$\phi K^+ \mu^+ \mu^-$	BI	(7.9 ± 2.1)	$\times 10^{-8}$ 2490
$\rho \bar{\Lambda} \pi^+ \pi^-$	(1.13 ± 0.13)	$\times 10^{-5}$	2368	$\bar{\Lambda} \rho \nu \bar{\nu}$	BI	< 3.0	$\times 10^{-5}$ CL=90% 2430
$\rho \bar{\Lambda} \pi^+ \pi^-$ nonresonant	(5.9 ± 1.1)	$\times 10^{-6}$	2368	$\pi^+ e^+ \mu^-$	LF	< 6.4	$\times 10^{-3}$ CL=90% 2637
$\rho \bar{\Lambda} \rho^0, \rho^0 \rightarrow \pi^+ \pi^-$	(4.8 ± 0.9)	$\times 10^{-6}$	2214	$\pi^+ e^- \mu^+$	LF	< 6.4	$\times 10^{-3}$ CL=90% 2637
$\rho \bar{\Lambda} f_2(1270), f_2 \rightarrow \pi^+ \pi^-$	(2.0 ± 0.8)	$\times 10^{-6}$	2026	$\pi^+ e^\pm \mu^\mp$	LF	< 1.7	$\times 10^{-7}$ CL=90% 2637
$\rho \bar{\Lambda} K^+ K^-$	(4.1 ± 0.7)	$\times 10^{-6}$	2132	$\pi^+ e^+ \tau^-$	LF	< 7.4	$\times 10^{-5}$ CL=90% 2338
$\rho \bar{\Lambda} \phi$	(8.0 ± 2.2)	$\times 10^{-7}$	2119	$\pi^+ e^- \tau^+$	LF	< 2.0	$\times 10^{-5}$ CL=90% 2338
$\bar{p} \Lambda K^+ K^-$	(3.7 ± 0.6)	$\times 10^{-6}$	2132	$\pi^+ e^\pm \tau^\mp$	LF	< 7.5	$\times 10^{-5}$ CL=90% 2338
$\Lambda \bar{\Lambda} \pi^+$	< 9.4	$\times 10^{-7}$	CL=90% 2358	$\pi^+ \mu^+ \tau^-$	LF	< 6.2	$\times 10^{-5}$ CL=90% 2334
$\Lambda \bar{\Lambda} K^+$	(3.4 ± 0.6)	$\times 10^{-6}$	2251	$\pi^+ \mu^- \tau^+$	LF	< 4.5	$\times 10^{-5}$ CL=90% 2334
$\Lambda \bar{\Lambda} K^{*+}$	(2.2 ± 1.2)	$\times 10^{-6}$	2098	$\pi^+ \mu^\pm \tau^\mp$	LF	< 7.2	$\times 10^{-5}$ CL=90% 2334
$\Lambda(1520) \bar{\Lambda} K^+$	(2.2 ± 0.7)	$\times 10^{-6}$	2126	$K^+ e^+ \mu^-$	LF	< 7.0	$\times 10^{-9}$ CL=90% 2616
$\Lambda \bar{\Lambda}(1520) K^+$	< 2.08	$\times 10^{-6}$	2126	$K^+ e^- \mu^+$	LF	< 6.4	$\times 10^{-9}$ CL=90% 2616
$\Delta^0 \rho$	< 1.38	$\times 10^{-6}$	CL=90% 2403	$K^+ e^\pm \mu^\mp$	LF	< 9.1	$\times 10^{-8}$ CL=90% 2616
$\Delta^+ \bar{p}$	< 1.4	$\times 10^{-7}$	CL=90% 2403	$K^+ e^+ \tau^-$	LF	< 1.53	$\times 10^{-5}$ CL=90% 2312
$D^+ \rho \bar{p}$	< 1.5	$\times 10^{-5}$	CL=90% 1860	$K^+ e^- \tau^+$	LF	< 1.5	$\times 10^{-5}$ CL=90% 2312
$D^*(2010)^+ \rho \bar{p}$	< 1.5	$\times 10^{-5}$	CL=90% 1786	$K^+ e^\pm \tau^\mp$	LF	< 3.0	$\times 10^{-5}$ CL=90% 2312
$\bar{D}^0 \rho \bar{p} \pi^+$	(3.72 ± 0.27)	$\times 10^{-4}$	1789	$K^+ \mu^+ \tau^-$	LF	< 2.45	$\times 10^{-5}$ CL=90% 2298
$\bar{D}^{*0} \rho \bar{p} \pi^+$	(3.73 ± 0.32)	$\times 10^{-4}$	1709	$K^+ \mu^- \tau^+$	LF	< 5.9	$\times 10^{-6}$ CL=90% 2298
$D^- \rho \bar{p} \pi^+ \pi^-$	(1.66 ± 0.30)	$\times 10^{-4}$	1705	$K^+ \mu^\pm \tau^\mp$	LF	< 4.8	$\times 10^{-5}$ CL=90% 2298
$D^{*-} \rho \bar{p} \pi^+ \pi^-$	(1.86 ± 0.25)	$\times 10^{-4}$	1621	$K^*(892)^+ e^+ \mu^-$	LF	< 1.3	$\times 10^{-6}$ CL=90% 2563
$\rho \bar{\Lambda}^0 \bar{D}^0$	(1.43 ± 0.32)	$\times 10^{-5}$	-	$K^*(892)^+ e^+ \mu^+$	LF	< 9.9	$\times 10^{-7}$ CL=90% 2563
$\rho \bar{\Lambda}^0 \bar{D}^*(2007)^0$	< 5	$\times 10^{-5}$	CL=90% -	$K^*(892)^+ e^\pm \mu^\mp$	LF	< 1.4	$\times 10^{-6}$ CL=90% 2563
$\bar{\Lambda}_c^- \rho \pi^+$	(2.3 ± 0.4)	$\times 10^{-4}$	S=2.4 1980	$\pi^- e^+ e^+$	L	< 2.3	$\times 10^{-8}$ CL=90% 2638
$\bar{\Lambda}_c^- \Delta(1232)^{++}$	< 1.9	$\times 10^{-5}$	CL=90% 1928	$\pi^- \mu^+ \mu^+$	L	< 4.0	$\times 10^{-9}$ CL=95% 2634
$\bar{\Lambda}_c^- \Delta_X(1600)^{++}$	(4.7 ± 1.0)	$\times 10^{-5}$	-	$\pi^- e^+ \mu^+$	L	< 1.5	$\times 10^{-7}$ CL=90% 2637
$\bar{\Lambda}_c^- \Delta_X(2420)^{++}$	(3.8 ± 0.8)	$\times 10^{-5}$	-	$\rho^- e^+ e^+$	L	< 1.7	$\times 10^{-7}$ CL=90% 2583
$(\bar{\Lambda}_c^- \rho)_s \pi^+$	[ppp] (3.1 ± 0.7)	$\times 10^{-5}$	-	$\rho^- \mu^+ \mu^+$	L	< 4.2	$\times 10^{-7}$ CL=90% 2578
$\bar{\Sigma}_c(2520)^0 \rho$	< 3	$\times 10^{-6}$	CL=90% 1904	$\rho^- e^+ \mu^+$	L	< 4.7	$\times 10^{-7}$ CL=90% 2582
$\bar{\Sigma}_c(2800)^0 \rho$	(2.7 ± 0.9)	$\times 10^{-5}$	-	$K^- e^+ e^+$	L	< 3.0	$\times 10^{-8}$ CL=90% 2617
$\bar{\Lambda}_c^- \rho \pi^+ \pi^0$	(1.8 ± 0.6)	$\times 10^{-3}$	1935	$K^- \mu^+ \mu^+$	L	< 4.1	$\times 10^{-8}$ CL=90% 2612
$\bar{\Lambda}_c^- \rho \pi^+ \pi^+ \pi^-$	(2.2 ± 0.7)	$\times 10^{-3}$	1880	$K^- e^+ \mu^+$	L	< 1.6	$\times 10^{-7}$ CL=90% 2616
$\bar{\Lambda}_c^- \rho \pi^+ \pi^+ \pi^- \pi^0$	< 1.34	%	CL=90% 1823	$K^*(892)^- e^+ e^+$	L	< 4.0	$\times 10^{-7}$ CL=90% 2564
$\Lambda_c^+ \Lambda_c^- K^+$	(4.9 ± 0.7)	$\times 10^{-4}$	739	$K^*(892)^- \mu^+ \mu^+$	L	< 5.9	$\times 10^{-7}$ CL=90% 2560
$\Xi_c(2930) \Lambda_c^+, \Xi_c \rightarrow K^+ \Lambda_c^-$	(1.7 ± 0.5)	$\times 10^{-4}$	-	$K^*(892)^- e^+ \mu^+$	L	< 3.0	$\times 10^{-7}$ CL=90% 2563
$\bar{\Sigma}_c(2455)^0 \rho$	(3.0 ± 0.7)	$\times 10^{-5}$	1938	$D^- e^+ e^+$	L	< 2.6	$\times 10^{-6}$ CL=90% 2309
$\bar{\Sigma}_c(2455)^0 \rho \pi^0$	(3.5 ± 1.1)	$\times 10^{-4}$	1896	$D^- e^+ \mu^+$	L	< 1.8	$\times 10^{-6}$ CL=90% 2307
$\bar{\Sigma}_c(2455)^0 \rho \pi^- \pi^+$	(3.5 ± 1.1)	$\times 10^{-4}$	1845	$D^- \mu^+ \mu^+$	L	< 6.9	$\times 10^{-7}$ CL=95% 2303
$\bar{\Sigma}_c(2455)^- \rho \pi^+ \pi^+$	(2.38 ± 0.19)	$\times 10^{-4}$	1845	$D^* \mu^+ \mu^+$	L	< 2.4	$\times 10^{-6}$ CL=95% 2251
$\bar{\Lambda}_c(2593)^- / \bar{\Lambda}_c(2625)^- \rho \pi^+$	< 1.9	$\times 10^{-4}$	CL=90% -	$D_s^- \mu^+ \mu^+$	L	< 5.8	$\times 10^{-7}$ CL=95% 2267
$\Xi_c^0 \Lambda_c^+$	(9.5 ± 2.3)	$\times 10^{-4}$	1144	$\bar{D}_s^0 \pi^- \mu^+ \mu^+$	L	< 1.5	$\times 10^{-6}$ CL=95% 2295
$\Xi_c^0 \Lambda_c^+, \Xi_c^0 \rightarrow \Xi^+ \pi^-$	(1.76 ± 0.29)	$\times 10^{-5}$	1144	$\Lambda^0 \mu^+$	L, B	< 6	$\times 10^{-8}$ CL=90% -
$\Xi_c^0 \Lambda_c^+, \Xi_c^0 \rightarrow \Lambda K^+ \pi^-$	(1.14 ± 0.26)	$\times 10^{-5}$	1144	$\Lambda^0 e^+$	L, B	< 3.2	$\times 10^{-8}$ CL=90% -
$\Xi_c^0 \Lambda_c^+, \Xi_c^0 \rightarrow p K^- K^- \pi^+$	(5.5 ± 1.9)	$\times 10^{-6}$	-	$\bar{\Lambda}^0 \mu^+$	L, B	< 6	$\times 10^{-8}$ CL=90% -
				$\bar{\Lambda}^0 e^+$	L, B	< 8	$\times 10^{-8}$ CL=90% -

Meson Summary Table

B⁰

$$I(J^P) = \frac{1}{2}(0^-)$$

I, J, P need confirmation. Quantum numbers shown are quark-model predictions.

$$\begin{aligned} \text{Mass } m_{B^0} &= 5279.72 \pm 0.08 \text{ MeV} \\ m_{B^0} - m_{B^\pm} &= 0.31 \pm 0.05 \text{ MeV} \\ \text{Mean life } \tau_{B^0} &= (1.517 \pm 0.004) \times 10^{-12} \text{ s} \\ c\tau &= 454.8 \text{ } \mu\text{m} \\ \tau_{B^+}/\tau_{B^0} &= 1.076 \pm 0.004 \quad (\text{direct measurements}) \end{aligned}$$

B⁰- \bar{B}^0 mixing parameters

$$\begin{aligned} \chi_d \text{ (} B^0\text{-}\bar{B}^0 \text{ mixing probability)} &= 0.1860 \pm 0.0011 \\ \Delta m_{B^0} = m_{B_H^0} - m_{B_L^0} &= (0.5069 \pm 0.0019) \times 10^{12} \text{ } \hbar \text{ s}^{-1} \\ &= (3.336 \pm 0.013) \times 10^{-10} \text{ MeV} \end{aligned}$$

$$\begin{aligned} x_d = \Delta m_{B^0}/\Gamma_{B^0} &= 0.7697 \pm 0.0035 \\ \text{Re}(\lambda_{CP} / |\lambda_{CP}|) \text{ Re}(z) &= 0.047 \pm 0.022 \\ \Delta\Gamma \text{ Re}(z) &= -0.007 \pm 0.004 \text{ ps}^{-1} \\ \text{Re}(z) &= (-4 \pm 4) \times 10^{-2} \quad (S = 1.4) \\ \text{Im}(z) &= (-0.8 \pm 0.4) \times 10^{-2} \end{aligned}$$

CP violation parameters

$$\begin{aligned} \text{Re}(\epsilon_{B^0})/(1+|\epsilon_{B^0}|^2) &= (-0.5 \pm 0.4) \times 10^{-3} \\ A_{T/CP}(B^0 \leftrightarrow \bar{B}^0) &= 0.005 \pm 0.018 \\ A_{CP}(B^0 \rightarrow D^*(2010)^+ D^-) &= 0.013 \pm 0.014 \\ A_{CP}(B^0 \rightarrow \bar{D}^0 \pi^0) &= (0.4 \pm 2.4) \times 10^{-2} \\ A_{CP}(B^0 \rightarrow [K^+ K^-]_D K^*(892)^0) &= -0.05 \pm 0.10 \\ A_{CP}(B^0 \rightarrow [K^+ \pi^-]_D K^*(892)^0) &= 0.047 \pm 0.029 \\ A_{CP}(B^0 \rightarrow [K^+ \pi^- \pi^+ \pi^-]_D K^*(892)^0) &= 0.037 \pm 0.034 \\ A_{CP}(B^0 \rightarrow [K^- \pi^+]_D K^*(892)^0) &= 0.19 \pm 0.19 \\ A_{CP}(B^0 \rightarrow [K^- \pi^+ \pi^+ \pi^-]_D K^*(892)^0) &= -0.01 \pm 0.24 \\ R_d^+ = \Gamma(B^0 \rightarrow [\pi^+ K^-]_D K^{*0}) / \Gamma(B^0 \rightarrow [\pi^- K^+]_D K^{*0}) &= 0.064 \pm 0.021 \\ R_d^- = \Gamma(\bar{B}^0 \rightarrow [\pi^- K^+]_D K^{*0}) / \Gamma(\bar{B}^0 \rightarrow [\pi^+ K^-]_D K^{*0}) &= 0.095 \pm 0.021 \\ A_{CP}(B^0 \rightarrow [\pi^+ \pi^-]_D K^*(892)^0) &= -0.18 \pm 0.14 \\ A_{CP}(B^0 \rightarrow [\pi^+ \pi^- \pi^+ \pi^-]_D K^*(892)^0) &= -0.03 \pm 0.15 \\ R_d^+ = \Gamma(B^0 \rightarrow [\pi^+ K^- \pi^+ \pi^-]_D K^{*0}) / \Gamma(B^0 \rightarrow [\pi^- K^+ \pi^+ \pi^-]_D K^{*0}) &= 0.074 \pm 0.026 \\ R_d^- = \Gamma(\bar{B}^0 \rightarrow [\pi^- K^+ \pi^+ \pi^-]_D K^{*0}) / \Gamma(\bar{B}^0 \rightarrow [\pi^+ K^- \pi^+ \pi^-]_D K^{*0}) &= 0.072 \pm 0.025 \\ \mathbf{A}_{CP}(B^0 \rightarrow K^+ \pi^-) &= -0.0831 \pm 0.0031 \\ A_{CP}(B^0 \rightarrow \eta' K^*(892)^0) &= -0.07 \pm 0.18 \\ A_{CP}(B^0 \rightarrow \eta' K_0^*(1430)^0) &= -0.19 \pm 0.17 \\ A_{CP}(B^0 \rightarrow \eta' K_2^*(1430)^0) &= 0.14 \pm 0.18 \\ \mathbf{A}_{CP}(B^0 \rightarrow \eta K^*(892)^0) &= 0.19 \pm 0.05 \\ A_{CP}(B^0 \rightarrow \eta K_0^*(1430)^0) &= 0.06 \pm 0.13 \\ A_{CP}(B^0 \rightarrow \eta K_2^*(1430)^0) &= -0.07 \pm 0.19 \\ A_{CP}(B^0 \rightarrow b_1 K^+) &= -0.07 \pm 0.12 \\ A_{CP}(B^0 \rightarrow \omega K^{*0}) &= 0.45 \pm 0.25 \\ A_{CP}(B^0 \rightarrow \omega (K\pi)^0) &= -0.07 \pm 0.09 \\ A_{CP}(B^0 \rightarrow \omega K_2^*(1430)^0) &= -0.37 \pm 0.17 \\ A_{CP}(B^0 \rightarrow K^+ \pi^- \pi^0) &= (0 \pm 6) \times 10^{-2} \\ A_{CP}(B^0 \rightarrow \rho^- K^+) &= 0.20 \pm 0.11 \\ A_{CP}(B^0 \rightarrow \rho(1450)^- K^+) &= -0.10 \pm 0.33 \\ A_{CP}(B^0 \rightarrow \rho(1700)^- K^+) &= -0.4 \pm 0.6 \\ A_{CP}(B^0 \rightarrow K^+ \pi^- \pi^0 \text{ nonresonant}) &= 0.10 \pm 0.18 \\ A_{CP}(B^0 \rightarrow K^0 \pi^+ \pi^-) &= -0.01 \pm 0.05 \\ \mathbf{A}_{CP}(B^0 \rightarrow K^*(892)^+ \pi^-) &= -0.27 \pm 0.04 \\ A_{CP}(B^0 \rightarrow (K\pi)^+ \pi^-) &= 0.02 \pm 0.04 \\ A_{CP}(B^0 \rightarrow K_2^*(1430)^+ \pi^-) &= -0.29 \pm 0.24 \\ A_{CP}(B^0 \rightarrow K^*(1680)^+ \pi^-) &= -0.07 \pm 0.14 \\ A_{CP}(B^0 \rightarrow f_0(980) K_S^0) &= 0.28 \pm 0.31 \\ A_{CP}(B^0 \rightarrow (K\pi)^0 \pi^0) &= -0.15 \pm 0.11 \\ A_{CP}(B^0 \rightarrow K^0 \pi^0) &= -0.15 \pm 0.13 \\ A_{CP}(B^0 \rightarrow K^*(892)^0 \pi^+ \pi^-) &= 0.07 \pm 0.05 \\ A_{CP}(B^0 \rightarrow K^*(892)^0 \rho^0) &= -0.06 \pm 0.09 \\ A_{CP}(B^0 \rightarrow K^{*0} f_0(980)) &= 0.07 \pm 0.10 \\ A_{CP}(B^0 \rightarrow K^{*+} \rho^-) &= 0.21 \pm 0.15 \\ A_{CP}(B^0 \rightarrow K^*(892)^0 K^+ K^-) &= 0.01 \pm 0.05 \\ A_{CP}(B^0 \rightarrow a_1^- K^+) &= -0.16 \pm 0.12 \\ A_{CP}(B^0 \rightarrow K^0 K^0) &= -0.6 \pm 0.7 \\ A_{CP}(B^0 \rightarrow K^*(892)^0 \phi) &= 0.00 \pm 0.04 \\ A_{CP}(B^0 \rightarrow K^*(892)^0 K^- \pi^+) &= 0.2 \pm 0.4 \end{aligned}$$

$$\begin{aligned} A_{CP}(B^0 \rightarrow \phi (K\pi)^0) &= 0.12 \pm 0.08 \\ A_{CP}(B^0 \rightarrow \phi K_2^*(1430)^0) &= -0.11 \pm 0.10 \\ A_{CP}(B^0 \rightarrow K^*(892)^0 \gamma) &= -0.006 \pm 0.011 \\ A_{CP}(B^0 \rightarrow K_2^*(1430)^0 \gamma) &= -0.08 \pm 0.15 \\ A_{CP}(B^0 \rightarrow X_s \gamma) &= -0.009 \pm 0.018 \\ A_{CP}(B^0 \rightarrow \rho^+ \pi^-) &= 0.13 \pm 0.06 \quad (S = 1.1) \\ A_{CP}(B^0 \rightarrow \rho^- \pi^+) &= -0.08 \pm 0.08 \\ A_{CP}(B^0 \rightarrow a_1(1260)^\pm \pi^\mp) &= -0.07 \pm 0.06 \\ A_{CP}(B^0 \rightarrow b_1^- \pi^+) &= -0.05 \pm 0.10 \\ A_{CP}(B^0 \rightarrow \rho \bar{\rho} K^*(892)^0) &= 0.05 \pm 0.12 \\ A_{CP}(B^0 \rightarrow \rho \bar{\Lambda} \pi^-) &= 0.04 \pm 0.07 \\ A_{CP}(B^0 \rightarrow K^{*0} \ell^+ \ell^-) &= -0.05 \pm 0.10 \\ A_{CP}(B^0 \rightarrow K^{*0} e^+ e^-) &= -0.21 \pm 0.19 \\ A_{CP}(B^0 \rightarrow K^{*0} \mu^+ \mu^-) &= -0.034 \pm 0.024 \\ C_{D^+ D^+} (B^0 \rightarrow D^*(2010)^- D^+) &= -0.02 \pm 0.08 \\ \mathbf{S}_{D^+ D^+} (B^0 \rightarrow D^*(2010)^- D^+) &= -0.83 \pm 0.09 \\ C_{D^+ D^-} (B^0 \rightarrow D^*(2010)^+ D^-) &= -0.03 \pm 0.09 \quad (S = 1.1) \\ \mathbf{S}_{D^+ D^-} (B^0 \rightarrow D^*(2010)^+ D^-) &= -0.80 \pm 0.09 \\ C_{D^+ D^*} (B^0 \rightarrow D^{*+} D^{*-}) &= 0.01 \pm 0.09 \quad (S = 1.6) \\ \mathbf{S}_{D^+ D^*} (B^0 \rightarrow D^{*+} D^{*-}) &= -0.59 \pm 0.14 \quad (S = 1.8) \\ C_+ (B^0 \rightarrow D^{*+} D^{*-}) &= 0.00 \pm 0.10 \quad (S = 1.6) \\ \mathbf{S}_+ (B^0 \rightarrow D^{*+} D^{*-}) &= -0.73 \pm 0.09 \\ C_- (B^0 \rightarrow D^{*+} D^{*-}) &= 0.19 \pm 0.31 \\ S_- (B^0 \rightarrow D^{*+} D^{*-}) &= 0.1 \pm 1.6 \quad (S = 3.5) \\ C (B^0 \rightarrow D^*(2010)^+ D^*(2010)^- K_S^0) &= 0.01 \pm 0.29 \\ S (B^0 \rightarrow D^*(2010)^+ D^*(2010)^- K_S^0) &= 0.1 \pm 0.4 \\ C_{D^+ D^-} (B^0 \rightarrow D^+ D^-) &= -0.22 \pm 0.24 \quad (S = 2.5) \\ \mathbf{S}_{D^+ D^-} (B^0 \rightarrow D^+ D^-) &= -0.76^{+0.15}_{-0.13} \quad (S = 1.2) \\ C_{J/\psi(1S) \pi^0} (B^0 \rightarrow J/\psi(1S) \pi^0) &= 0.03 \pm 0.17 \quad (S = 1.5) \\ \mathbf{S}_{J/\psi(1S) \pi^0} (B^0 \rightarrow J/\psi(1S) \pi^0) &= -0.88 \pm 0.32 \quad (S = 2.2) \\ C (B^0 \rightarrow J/\psi(1S) \rho^0) &= -0.06 \pm 0.06 \\ \mathbf{S}(B^0 \rightarrow J/\psi(1S) \rho^0) &= -0.66^{+0.16}_{-0.12} \\ C_{D_{CP}^* h^0} (B^0 \rightarrow D_{CP}^* h^0) &= -0.02 \pm 0.08 \\ \mathbf{S}_{D_{CP}^* h^0} (B^0 \rightarrow D_{CP}^* h^0) &= -0.66 \pm 0.12 \\ C_{K^0 \pi^0} (B^0 \rightarrow K^0 \pi^0) &= 0.00 \pm 0.08 \\ \mathbf{S}_{K^0 \pi^0} (B^0 \rightarrow K^0 \pi^0) &= 0.64 \pm 0.13 \\ C_{\eta(958) K_S^0} (B^0 \rightarrow \eta(958) K_S^0) &= -0.04 \pm 0.20 \quad (S = 2.5) \\ S_{\eta(958) K_S^0} (B^0 \rightarrow \eta(958) K_S^0) &= 0.43 \pm 0.17 \quad (S = 1.5) \\ C_{\eta' K^0} (B^0 \rightarrow \eta' K^0) &= -0.06 \pm 0.04 \\ \mathbf{S}_{\eta' K^0} (B^0 \rightarrow \eta' K^0) &= 0.63 \pm 0.06 \\ C_{\omega K_S^0} (B^0 \rightarrow \omega K_S^0) &= 0.0 \pm 0.4 \quad (S = 3.0) \\ S_{\omega K_S^0} (B^0 \rightarrow \omega K_S^0) &= 0.70 \pm 0.21 \\ C (B^0 \rightarrow K_S^0 \pi^0 \pi^0) &= -0.21 \pm 0.20 \\ S (B^0 \rightarrow K_S^0 \pi^0 \pi^0) &= 0.89^{+0.27}_{-0.30} \\ C_{\rho^0 K_S^0} (B^0 \rightarrow \rho^0 K_S^0) &= -0.04 \pm 0.20 \\ S_{\rho^0 K_S^0} (B^0 \rightarrow \rho^0 K_S^0) &= 0.50^{+0.17}_{-0.21} \\ C_{f_0 K_S^0} (B^0 \rightarrow f_0(980) K_S^0) &= 0.29 \pm 0.20 \\ \mathbf{S}_{f_0 K_S^0} (B^0 \rightarrow f_0(980) K_S^0) &= -0.50 \pm 0.16 \\ S_{f_2 K_S^0} (B^0 \rightarrow f_2(1270) K_S^0) &= -0.5 \pm 0.5 \\ C_{f_2 K_S^0} (B^0 \rightarrow f_2(1270) K_S^0) &= 0.3 \pm 0.4 \\ S_{f_x K_S^0} (B^0 \rightarrow f_x(1300) K_S^0) &= -0.2 \pm 0.5 \\ C_{f_x K_S^0} (B^0 \rightarrow f_x(1300) K_S^0) &= 0.13 \pm 0.35 \\ S_{K^0 \pi^+ \pi^-} (B^0 \rightarrow K^0 \pi^+ \pi^- \text{ nonresonant}) &= -0.01 \pm 0.33 \\ C_{K^0 \pi^+ \pi^-} (B^0 \rightarrow K^0 \pi^+ \pi^- \text{ nonresonant}) &= 0.01 \pm 0.26 \\ C_{K_S^0 K_S^0} (B^0 \rightarrow K_S^0 K_S^0) &= 0.0 \pm 0.4 \quad (S = 1.4) \\ S_{K_S^0 K_S^0} (B^0 \rightarrow K_S^0 K_S^0) &= -0.8 \pm 0.5 \\ C_{K^+ K^- K_S^0} (B^0 \rightarrow K^+ K^- K_S^0 \text{ nonresonant}) &= 0.06 \pm 0.08 \\ \mathbf{S}_{K^+ K^- K_S^0} (B^0 \rightarrow K^+ K^- K_S^0 \text{ nonresonant}) &= -0.66 \pm 0.11 \\ C_{K^+ K^- K_S^0} (B^0 \rightarrow K^+ K^- K_S^0 \text{ inclusive}) &= 0.01 \pm 0.09 \\ \mathbf{S}_{K^+ K^- K_S^0} (B^0 \rightarrow K^+ K^- K_S^0 \text{ inclusive}) &= -0.65 \pm 0.12 \\ C_{\phi K_S^0} (B^0 \rightarrow \phi K_S^0) &= -0.09 \pm 0.12 \\ \mathbf{S}_{\phi K_S^0} (B^0 \rightarrow \phi K_S^0) &= 0.58 \pm 0.12 \end{aligned}$$

Meson Summary Table

$$\begin{aligned}
 C_{K_S K_S K_S}(B^0 \rightarrow K_S K_S K_S) &= -0.14 \pm 0.12 \\
 S_{K_S K_S K_S}(B^0 \rightarrow K_S K_S K_S) &= -0.82 \pm 0.17 \\
 C_{K_S^0 \pi^0 \gamma}(B^0 \rightarrow K_S^0 \pi^0 \gamma) &= 0.36 \pm 0.33 \\
 S_{K_S^0 \pi^0 \gamma}(B^0 \rightarrow K_S^0 \pi^0 \gamma) &= -0.8 \pm 0.6 \\
 C_{K_S^0 \pi^+ \pi^- \gamma}(B^0 \rightarrow K_S^0 \pi^+ \pi^- \gamma) &= -0.39 \pm 0.20 \\
 S_{K_S^0 \pi^+ \pi^- \gamma}(B^0 \rightarrow K_S^0 \pi^+ \pi^- \gamma) &= 0.14 \pm 0.25 \\
 C_{K^{*0} \gamma}(B^0 \rightarrow K^*(892)^0 \gamma) &= -0.04 \pm 0.16 \quad (S = 1.2) \\
 S_{K^{*0} \gamma}(B^0 \rightarrow K^*(892)^0 \gamma) &= -0.15 \pm 0.22 \\
 C_{\eta K^0 \gamma}(B^0 \rightarrow \eta K^0 \gamma) &= 0.1 \pm 0.4 \quad (S = 1.4) \\
 S_{\eta K^0 \gamma}(B^0 \rightarrow \eta K^0 \gamma) &= -0.5 \pm 0.5 \quad (S = 1.2) \\
 C_{K^0 \phi \gamma}(B^0 \rightarrow K^0 \phi \gamma) &= -0.3 \pm 0.6 \\
 S_{K^0 \phi \gamma}(B^0 \rightarrow K^0 \phi \gamma) &= 0.7^{+0.7}_{-1.1} \\
 C(B^0 \rightarrow K_S^0 \rho^0 \gamma) &= -0.05 \pm 0.19 \\
 S(B^0 \rightarrow K_S^0 \rho^0 \gamma) &= -0.04 \pm 0.23 \\
 C(B^0 \rightarrow \rho^0 \gamma) &= 0.4 \pm 0.5 \\
 S(B^0 \rightarrow \rho^0 \gamma) &= -0.8 \pm 0.7 \\
 \mathbf{C}_{\pi\pi}(B^0 \rightarrow \pi^+ \pi^-) &= -0.314 \pm 0.030 \\
 \mathbf{S}_{\pi\pi}(B^0 \rightarrow \pi^+ \pi^-) &= -0.670 \pm 0.030 \\
 C_{\pi^0 \pi^0}(B^0 \rightarrow \pi^0 \pi^0) &= -0.30 \pm 0.20 \\
 C_{\rho\pi}(B^0 \rightarrow \rho^+ \pi^-) &= -0.03 \pm 0.07 \quad (S = 1.2) \\
 S_{\rho\pi}(B^0 \rightarrow \rho^+ \pi^-) &= 0.05 \pm 0.07 \\
 \mathbf{\Delta C}_{\rho\pi}(B^0 \rightarrow \rho^+ \pi^-) &= 0.27 \pm 0.06 \\
 \mathbf{\Delta S}_{\rho\pi}(B^0 \rightarrow \rho^+ \pi^-) &= 0.01 \pm 0.08 \\
 C_{\rho^0 \pi^0}(B^0 \rightarrow \rho^0 \pi^0) &= 0.27 \pm 0.24 \\
 S_{\rho^0 \pi^0}(B^0 \rightarrow \rho^0 \pi^0) &= -0.23 \pm 0.34 \\
 C_{a_1 \pi}(B^0 \rightarrow a_1(1260)^+ \pi^-) &= -0.05 \pm 0.11 \\
 S_{a_1 \pi}(B^0 \rightarrow a_1(1260)^+ \pi^-) &= -0.2 \pm 0.4 \quad (S = 3.2) \\
 \mathbf{\Delta C}_{a_1 \pi}(B^0 \rightarrow a_1(1260)^+ \pi^-) &= 0.43 \pm 0.14 \quad (S = 1.3) \\
 \mathbf{\Delta S}_{a_1 \pi}(B^0 \rightarrow a_1(1260)^+ \pi^-) &= -0.11 \pm 0.12 \\
 C(B^0 \rightarrow b_1^- K^+) &= -0.22 \pm 0.24 \\
 \mathbf{\Delta C}(B^0 \rightarrow b_1^- \pi^+) &= -1.04 \pm 0.24 \\
 C_{\rho^0 \rho^0}(B^0 \rightarrow \rho^0 \rho^0) &= 0.2 \pm 0.9 \\
 S_{\rho^0 \rho^0}(B^0 \rightarrow \rho^0 \rho^0) &= 0.3 \pm 0.7 \\
 C_{\rho\rho}(B^0 \rightarrow \rho^+ \rho^-) &= 0.00 \pm 0.09 \\
 S_{\rho\rho}(B^0 \rightarrow \rho^+ \rho^-) &= -0.14 \pm 0.13 \\
 |\lambda|(B^0 \rightarrow J/\psi K^*(892)^0) &< 0.25, \text{CL} = 95\% \\
 \cos 2\beta(B^0 \rightarrow J/\psi K^*(892)^0) &= 1.7^{+0.7}_{-0.9} \quad (S = 1.6) \\
 \cos 2\beta(B^0 \rightarrow [K_S^0 \pi^+ \pi^-]_{D^{(*)}} h^0) &= 0.91 \pm 0.25 \\
 (S_+ + S_-)/2(B^0 \rightarrow D^{*-} \pi^+) &= -0.039 \pm 0.011 \\
 (S_- - S_+)/2(B^0 \rightarrow D^{*-} \pi^+) &= -0.009 \pm 0.015 \\
 (S_+ + S_-)/2(B^0 \rightarrow D^- \pi^+) &= -0.046 \pm 0.023 \\
 (S_- - S_+)/2(B^0 \rightarrow D^- \pi^+) &= -0.022 \pm 0.021 \\
 S_+(B^0 \rightarrow D^- \pi^+) &= 0.058 \pm 0.023 \\
 S_-(B^0 \rightarrow D^+ \pi^-) &= 0.038 \pm 0.021 \\
 (S_+ + S_-)/2(B^0 \rightarrow D^- \rho^+) &= -0.024 \pm 0.032 \\
 (S_- - S_+)/2(B^0 \rightarrow D^- \rho^+) &= -0.10 \pm 0.06 \\
 C_{\eta_c K_S^0}(B^0 \rightarrow \eta_c K_S^0) &= 0.08 \pm 0.13 \\
 \mathbf{S}_{\eta_c K_S^0}(B^0 \rightarrow \eta_c K_S^0) &= 0.93 \pm 0.17 \\
 C_{c\bar{c}K^{(*)0}}(B^0 \rightarrow c\bar{c}K^{(*)0}) &= (-0.5 \pm 1.5) \times 10^{-2} \\
 \sin(2\beta) &= 0.709 \pm 0.011 \\
 C_{J/\psi(nS)K^0}(B^0 \rightarrow J/\psi(nS)K^0) &= (-0.8 \pm 1.7) \times 10^{-2} \\
 \mathbf{S}_{J/\psi(nS)K^0}(B^0 \rightarrow J/\psi(nS)K^0) &= 0.701 \pm 0.017 \\
 C_{J/\psi K^{*0}}(B^0 \rightarrow J/\psi K^{*0}) &= 0.03 \pm 0.10 \\
 S_{J/\psi K^{*0}}(B^0 \rightarrow J/\psi K^{*0}) &= 0.60 \pm 0.25 \\
 C_{\chi_{c0} K_S^0}(B^0 \rightarrow \chi_{c0} K_S^0) &= -0.3^{+0.5}_{-0.4} \\
 S_{\chi_{c0} K_S^0}(B^0 \rightarrow \chi_{c0} K_S^0) &= -0.7 \pm 0.5 \\
 C_{\chi_{c1} K_S^0}(B^0 \rightarrow \chi_{c1} K_S^0) &= 0.06 \pm 0.07 \\
 \mathbf{S}_{\chi_{c1} K_S^0}(B^0 \rightarrow \chi_{c1} K_S^0) &= 0.63 \pm 0.10 \\
 \sin(2\beta_{\text{eff}})(B^0 \rightarrow \phi K^0) &= 0.22 \pm 0.30 \\
 \sin(2\beta_{\text{eff}})(B^0 \rightarrow \phi K_0^*(1430)^0) &= 0.97^{+0.03}_{-0.52} \\
 \mathbf{\sin}(2\beta_{\text{eff}})(B^0 \rightarrow K^+ K^- K_S^0) &= 0.77^{+0.13}_{-0.12} \\
 \sin(2\beta_{\text{eff}})(B^0 \rightarrow [K_S^0 \pi^+ \pi^-]_{D^{(*)}} h^0) &= 0.80 \pm 0.16 \\
 \beta_{\text{eff}}(B^0 \rightarrow [K_S^0 \pi^+ \pi^-]_{D^{(*)}} h^0) &= (22 \pm 5)^\circ \\
 2\beta_{\text{eff}}(B^0 \rightarrow J/\psi \rho^0) &= (42^{+10}_{-11})^\circ \\
 |\lambda|(B^0 \rightarrow [K_S^0 \pi^+ \pi^-]_{D^{(*)}} h^0) &= 1.01 \pm 0.08
 \end{aligned}$$

$$\begin{aligned}
 |\sin(2\beta + \gamma)| &> 0.40, \text{CL} = 90\% \\
 2\beta + \gamma &= (80 \pm 60)^\circ \\
 \alpha &= (84.1^{+4.5}_{-3.8})^\circ \\
 x_+(B^0 \rightarrow DK^{*0}) &= 0.04 \pm 0.17 \\
 x_-(B^0 \rightarrow DK^{*0}) &= -0.16 \pm 0.14 \\
 y_+(B^0 \rightarrow DK^{*0}) &= -0.68 \pm 0.22 \\
 y_-(B^0 \rightarrow DK^{*0}) &= 0.20 \pm 0.25 \quad (S = 1.2) \\
 r_{B^0}(B^0 \rightarrow DK^{*0}) &= 0.257^{+0.021}_{-0.023} \\
 \delta_{B^0}(B^0 \rightarrow DK^{*0}) &= (194.1^{+9.6}_{-8.8})^\circ \\
 a_{CP}(B^0 \rightarrow p\bar{p}K^+\pi^-) &= (0.5 \pm 0.9)\% \\
 a_P(B^0 \rightarrow p\bar{p}K^+\pi^-) &= (1.5 \pm 0.9)\%
 \end{aligned}$$

\bar{B}^0 modes are charge conjugates of the modes below. Reactions indicate the weak decay vertex and do not include mixing. Modes which do not identify the charge state of the B are listed in the B^\pm/B^0 ADMIXTURE section.

The branching fractions listed below assume 50% $B^0 \bar{B}^0$ and 50% $B^+ B^-$ production at the $\Upsilon(4S)$. We have attempted to bring older measurements up to date by rescaling their assumed $\Upsilon(4S)$ production ratio to 50:50 and their assumed D, D_s, D^* , and ψ branching ratios to current values whenever this would affect our averages and best limits significantly.

Indentation is used to indicate a subchannel of a previous reaction. All resonant subchannels have been corrected for resonance branching fractions to the final state so the sum of the subchannel branching fractions can exceed that of the final state.

For inclusive branching fractions, e.g., $B \rightarrow D^\pm X$, the values usually are multiplicities, not branching fractions. They can be greater than one.

B^0 DECAY MODES	Fraction (Γ_i/Γ)	Scale factor / Confidence level	ρ (MeV/c)
$\ell^+ \nu_\ell X$	[hhh] (10.33 ± 0.28) %		—
$e^+ \nu_e X_c$	(10.1 ± 0.4) %		—
$\ell^+ \nu_\ell X_u$	[hhh] (1.51 ± 0.19) × 10 ⁻³		—
$D \ell^+ \nu_\ell X$	[hhh] (9.1 ± 0.8) %		—
$D^- \ell^+ \nu_\ell$	[hhh] (2.12 ± 0.06) %		2309
$D^- \tau^+ \nu_\tau$	(9.9 ± 2.1) × 10 ⁻³		1909
$D^*(2010)^- \ell^+ \nu_\ell$	[hhh] (4.90 ± 0.12) %		2257
$D^*(2010)^- \tau^+ \nu_\tau$	(1.45 ± 0.10) %	S=1.3	1838
$\bar{D}^{(*)} n \pi \ell^+ \nu_\ell$ ($n \geq 1$)	[hhh] (2.3 ± 0.5) %		—
$\bar{D}^0 \pi^- \ell^+ \nu_\ell$	[hhh] (3.64 ± 0.20) × 10 ⁻³		2308
$D_0^*(2300)^- \ell^+ \nu_\ell$	[hhh] < 4.4 × 10 ⁻⁴	CL=90%	—
$D_0^{*-} \rightarrow \bar{D}^0 \pi^-$			
$D_2^*(2460)^- \ell^+ \nu_\ell$	[hhh] (1.41 ± 0.20) × 10 ⁻³	S=1.7	2065
$D_2^{*-} \rightarrow \bar{D}^0 \pi^-$			
$\bar{D}^{*0} \pi^- \ell^+ \nu_\ell$	[hhh] (5.44 ± 0.28) × 10 ⁻³		2256
$D_1(2420)^- \ell^+ \nu_\ell, D_1^- \rightarrow$	[hhh] (2.85 ± 0.25) × 10 ⁻³		—
$\bar{D}^{*0} \pi^-$			
$D_1(2420)^- \ell^+ \nu_\ell, D_1^- \rightarrow$	[hhh] (1.02 ± 0.16) × 10 ⁻³		—
$D^- \pi^+ \pi^-$			
$D_1^-(2430)^- \ell^+ \nu_\ell, D_1^{*-} \rightarrow$	[hhh] (2.5 ± 0.6) × 10 ⁻³		—
$\bar{D}^{*0} \pi^-$			
$D_2^*(2460)^- \ell^+ \nu_\ell, D_2^{*-} \rightarrow$	[hhh] (6.6 ± 1.1) × 10 ⁻⁴		2065
$\bar{D}^{*0} \pi^-$			
$D^- \pi^+ \pi^- \ell^+ \nu_\ell$	[hhh] (1.45 ± 0.22) × 10 ⁻³		2299
$D^{*-} \pi^+ \pi^- \ell^+ \nu_\ell$	[hhh] (5.1 ± 2.3) × 10 ⁻⁴		2247
$\rho^- \ell^+ \nu_\ell$	[hhh] (2.94 ± 0.21) × 10 ⁻⁴		2583
$\pi^- \ell^+ \nu_\ell$	[hhh] (1.50 ± 0.06) × 10 ⁻⁴		2638
$\pi^- \tau^+ \nu_\tau$	< 2.5 × 10 ⁻⁴	CL=90%	2339
Inclusive modes			
$K^\pm X$	(78 ± 8) %		—
$D^0 X$	(8.1 ± 1.5) %		—
$\bar{D}^0 X$	(47.4 ± 2.8) %		—
$D^+ X$	< 3.9 %	CL=90%	—
$D^- X$	(36.9 ± 3.3) %		—
$D_s^+ X$	(10.3 ± 2.1) %		—
$D_s^- X$	< 2.6 %	CL=90%	—
$\Lambda_c^+ X$	< 3.1 %	CL=90%	—
$\bar{\Lambda}_c^- X$	(5.0 ± 2.1) %		—
$\bar{c} X$	(95 ± 5) %		—
$c X$	(24.6 ± 3.1) %		—
$\bar{c}/c X$	(119 ± 6) %		—
D, D*, or D_s modes			
$D^- \pi^+$	(2.51 ± 0.08) × 10 ⁻³		2306
$D^- \rho^+$	(7.6 ± 1.2) × 10 ⁻³		2235

Meson Summary Table

$D^- K^0 \pi^+$	$(4.9 \pm 0.9) \times 10^{-4}$	2259	$D_{s0}(2317)^+ D^-, D_{s0}^+ \rightarrow$	$< 9.5 \times 10^{-4}$	CL=90%	-
$D^- K^*(892)^+$	$(4.5 \pm 0.7) \times 10^{-4}$	2211	$D_s^{*+} \gamma$			
$D^- \omega \pi^+$	$(2.8 \pm 0.6) \times 10^{-3}$	2204	$D_{s0}(2317)^+ D^*(2010)^-,$	$(1.5 \pm 0.6) \times 10^{-3}$		1509
$D^- K^+$	$(2.05 \pm 0.08) \times 10^{-4}$	2279	$D_{s0}^+ \rightarrow D_s^+ \pi^0$			
$D^- K^+ \pi^+ \pi^-$	$(3.5 \pm 0.8) \times 10^{-4}$	2236	$D_{sJ}(2457)^+ D^-$	$(3.5 \pm 1.1) \times 10^{-3}$		-
$D^- K^+ \bar{K}^0$	$< 3.1 \times 10^{-4}$	2188	$D_{sJ}(2457)^+ D^-, D_{sJ}^+ \rightarrow$	$(6.5 \pm 1.7) \times 10^{-4}$		-
$D^- K^+ \bar{K}^*(892)^0$	$(8.8 \pm 1.9) \times 10^{-4}$	2070	$D_s^+ \gamma$			
$\bar{D}^0 \pi^+ \pi^-$	$(8.8 \pm 0.5) \times 10^{-4}$	2301	$D_{sJ}(2457)^+ D^-, D_{sJ}^+ \rightarrow$	$< 6.0 \times 10^{-4}$	CL=90%	-
$D^*(2010)^- \pi^+$	$(2.66 \pm 0.07) \times 10^{-3}$	2255	$D_s^+ \gamma$			
$\bar{D}^0 K^+ K^-$	$(6.1 \pm 0.5) \times 10^{-5}$	2191	$D_{sJ}(2457)^+ D^-, D_{sJ}^+ \rightarrow$	$< 2.0 \times 10^{-4}$	CL=90%	-
$D^- \pi^+ \pi^+ \pi^-$	$(6.0 \pm 0.6) \times 10^{-3}$	2287	$D_s^+ \pi^+ \pi^-$			
$(D^- \pi^+ \pi^+ \pi^-)$ nonresonant	$(3.9 \pm 1.9) \times 10^{-3}$	2287	$D_{sJ}(2457)^+ D^-, D_{sJ}^+ \rightarrow$	$< 3.6 \times 10^{-4}$	CL=90%	-
$D^- \pi^+ \rho^0$	$(1.1 \pm 1.0) \times 10^{-3}$	2206	$D_s^+ \pi^0$			
$D^- a_1(1260)^+$	$(6.0 \pm 0.8) \times 10^{-3}$	2121	$D^*(2010)^- D_{sJ}(2457)^+$	$(9.3 \pm 2.2) \times 10^{-3}$		-
$D^*(2010)^- \pi^+ \pi^0$	$(1.5 \pm 0.5) \%$	2248	$D_{sJ}(2457)^+ D^*(2010)^-, D_{sJ}^+ \rightarrow$	$(2.3 \pm 0.9) \times 10^{-3}$		-
$D^*(2010)^- \rho^+$	$(6.8 \pm 0.9) \times 10^{-3}$	2180	$D_s^+ \gamma$			
$D^*(2010)^- K^+$	$(2.16 \pm 0.08) \times 10^{-4}$	2226	$D^- D_{s1}(2536)^+, D_{s1}^+ \rightarrow$	$(2.8 \pm 0.7) \times 10^{-4}$		1444
$D^*(2010)^- K^0 \pi^+$	$(3.0 \pm 0.8) \times 10^{-4}$	2205	$D^{*0} K^+ + D^{*+} K^0$			
$D^*(2010)^- K^*(892)^+$	$(3.3 \pm 0.6) \times 10^{-4}$	2155	$D^- D_{s1}(2536)^+, D_{s1}^+ \rightarrow$	$(1.7 \pm 0.6) \times 10^{-4}$		1444
$D^*(2010)^- K^+ \bar{K}^0$	$< 4.7 \times 10^{-4}$	2131	$D^{*0} K^+$			
$D^*(2010)^- K^+ \bar{K}^*(892)^0$	$(1.29 \pm 0.33) \times 10^{-3}$	2007	$D^- D_{s1}(2536)^+, D_{s1}^+ \rightarrow$	$(2.6 \pm 1.1) \times 10^{-4}$		1444
$D^*(2010)^- \pi^+ \pi^+ \pi^-$	$(7.21 \pm 0.29) \times 10^{-3}$	2235	$D^{*+} K^0$			
$(D^*(2010)^- \pi^+ \pi^+ \pi^-)$ non-resonant	$(0.0 \pm 2.5) \times 10^{-3}$	2235	$D^*(2010)^- D_{s1}(2536)^+,$	$(5.0 \pm 1.4) \times 10^{-4}$		1336
$D^*(2010)^- \pi^+ \rho^0$	$(5.7 \pm 3.2) \times 10^{-3}$	2150	$D_{s1}^+ \rightarrow D^{*0} K^+ + D^{*+} K^0$			
$D^*(2010)^- a_1(1260)^+$	$(1.30 \pm 0.27) \%$	2061	$D^*(2010)^- D_{s1}(2536)^+,$	$(3.3 \pm 1.1) \times 10^{-4}$		1336
$\bar{D}_1(2420)^0 \pi^- \pi^+, \bar{D}_1^0 \rightarrow$	$(1.47 \pm 0.35) \times 10^{-4}$	-	$D_{s1}^+ \rightarrow D^{*0} K^+$			
$D^{*-} \pi^+$			$D^*(2010)^- D_{s1}(2536)^+,$	$(5.0 \pm 1.7) \times 10^{-4}$		1336
$D^*(2010)^- K^+ \pi^- \pi^+$	$(4.7 \pm 0.4) \times 10^{-4}$	2181	$D^{*+} K^0$			
$D^*(2010)^- \pi^+ \pi^+ \pi^- \pi^0$	$(1.76 \pm 0.27) \%$	2218	$D^*(2010)^- D_{s1}(2536)^+,$	$(3.4 \pm 1.8) \times 10^{-5}$		1414
$D^{*-} 3\pi^+ 2\pi^-$	$(4.7 \pm 0.9) \times 10^{-3}$	2195	$D_{sJ}^+ \rightarrow D^{*0} K^+$			
$D^*(2010)^- \omega \pi^+$	$(2.46 \pm 0.18) \times 10^{-3}$	2148	$D^*(2010)^- D_{sJ}(2573)^+,$	$< 2 \times 10^{-4}$	CL=90%	1304
$\bar{D}_1(2430)^0 \omega, \bar{D}_1^0 \rightarrow$	$(2.7 \pm 0.8) \times 10^{-4}$	1992	$D_{sJ}^+ \rightarrow D^0 K^+$			
$D^{*-} \pi^+$			$D^- D_{sJ}(2700)^+, D_{sJ}^+ \rightarrow$	$(7.1 \pm 1.2) \times 10^{-4}$		-
$D^{*-} \rho(1450)^+, \rho^+ \rightarrow \omega \pi^+$	$(1.07 \pm 0.40) \times 10^{-3}$	-	$D^0 K^+$			
$\bar{D}_1(2420)^0 \omega, \bar{D}_1^0 \rightarrow$	$(7.0 \pm 2.2) \times 10^{-5}$	1995	$D^+ \pi^-$	$(7.3 \pm 1.2) \times 10^{-7}$		2306
$\bar{D}_2^*(2460)^0 \omega, \bar{D}_2^0 \rightarrow$	$(4.0 \pm 1.4) \times 10^{-5}$	1975	$D_s^+ \pi^-$	$(2.03 \pm 0.18) \times 10^{-5}$		2271
$D^{*-} \pi^+$			$D_s^{*+} \pi^-$	$(2.1 \pm 0.4) \times 10^{-5}$	S=1.4	2215
$D^{*-} b_1(1235)^+, b_1^+ \rightarrow$	$< 7 \times 10^{-5}$	CL=90%	$D_s^+ \rho^-$	$< 2.4 \times 10^{-5}$	CL=90%	2197
$\bar{D}^{*-} \pi^+$			$D_s^{*+} \rho^-$	$(4.1 \pm 1.3) \times 10^{-5}$		2138
$D^*(2010)^- K^+ \pi^- \pi^+$	$(1.9 \pm 0.9) \times 10^{-3}$	-	$D_s^+ a_0^-$	$< 1.9 \times 10^{-5}$	CL=90%	-
$D_1(2420)^- \pi^+, D_1^- \rightarrow$	$(9.9 \pm 2.0) \times 10^{-5}$	-	$D_s^{*+} a_0^-$	$< 3.6 \times 10^{-5}$	CL=90%	-
$D^- \pi^+ \pi^-$			$D_s^+ a_1(1260)^-$	$< 2.1 \times 10^{-3}$	CL=90%	2080
$D_1(2420)^- \pi^+, D_1^- \rightarrow$	$< 3.3 \times 10^{-5}$	CL=90%	$D_s^{*+} a_1(1260)^-$	$< 1.7 \times 10^{-3}$	CL=90%	2015
$D^- \pi^+ \pi^-$			$D_s^+ a_2^-$	$< 1.9 \times 10^{-4}$	CL=90%	-
$\bar{D}_2^*(2460)^- \pi^+, D_2^{*-} \rightarrow$	$(2.38 \pm 0.16) \times 10^{-4}$	2062	$D_s^{*+} a_2^-$	$< 2.0 \times 10^{-4}$	CL=90%	-
$D^0 \pi^-$			$D_s^+ K^+$	$(2.7 \pm 0.5) \times 10^{-5}$	S=2.7	2242
$\bar{D}_0^*(2400)^- \pi^+, D_0^{*-} \rightarrow$	$(7.6 \pm 0.8) \times 10^{-5}$	2090	$D_s^{*-} K^+$	$(2.19 \pm 0.30) \times 10^{-5}$		2185
$D^0 \pi^-$			$D_{s1}(2536)^{\mp} K^{\pm}, D_{s1}^- \rightarrow$	$(5.1 \pm 0.6) \times 10^{-6}$		-
$D_2^*(2460)^- \pi^+, D_2^{*-} \rightarrow$	$< 2.4 \times 10^{-5}$	CL=90%	$\bar{D}^*(2007)^0 K^-$			
$D^{*-} \pi^+ \pi^-$			$D_s^- K^*(892)^+$	$(3.5 \pm 1.0) \times 10^{-5}$		2172
$\bar{D}_3^*(2460)^- \rho^+$	$< 4.9 \times 10^{-3}$	CL=90%	$D_s^- K^*(892)^+$	$(3.2 \pm 1.5) \times 10^{-5}$		2112
$D^0 \bar{D}^0$	$(1.4 \pm 0.7) \times 10^{-5}$	1868	$D_s^{*-} \pi^+ K^0$	$(9.7 \pm 1.4) \times 10^{-5}$		2222
$D^{*0} \bar{D}^0$	$< 2.9 \times 10^{-4}$	CL=90%	$D_s^{*-} \pi^+ K^0$	$< 1.10 \times 10^{-4}$	CL=90%	2164
$D^- D^+$	$(2.11 \pm 0.18) \times 10^{-4}$	1864	$D_s^- K^+ \pi^+ \pi^-$	$(1.7 \pm 0.5) \times 10^{-4}$		2198
$D^\pm D^{*\mp} (CP\text{-averaged})$	$(6.1 \pm 0.6) \times 10^{-4}$	-	$D_s^- \pi^+ K^*(892)^0$	$< 3.0 \times 10^{-3}$	CL=90%	2138
$D^- D_s^+$	$(7.2 \pm 0.8) \times 10^{-3}$	1812	$D_s^{*-} \pi^+ K^*(892)^0$	$< 1.6 \times 10^{-3}$	CL=90%	2076
$D^*(2010)^- D_s^+$	$(8.0 \pm 1.1) \times 10^{-3}$	1735	$\bar{D}^0 K^0$	$(5.5 \pm 0.4) \times 10^{-5}$		2280
$D^- D_s^{*+}$	$(7.4 \pm 1.6) \times 10^{-3}$	1732	$\bar{D}^0 K^+ \pi^-$	$(8.8 \pm 1.7) \times 10^{-5}$		2262
$D^*(2010)^- D_s^{*+}$	$(1.77 \pm 0.14) \%$	1649	$\bar{D}^0 K^*(892)^0$	$(4.5 \pm 0.6) \times 10^{-5}$		2213
$D_{s0}(2317)^- K^+, D_{s0}^- \rightarrow$	$(4.2 \pm 1.4) \times 10^{-5}$	2097	$\bar{D}^0 K^*(1410)^0$	$< 6.7 \times 10^{-5}$	CL=90%	2062
$D_s^- \pi^0$			$\bar{D}^0 K_0^*(1430)^0$	$(7 \pm 7) \times 10^{-6}$		2058
$D_{s0}(2317)^- \pi^+, D_{s0}^- \rightarrow$	$< 2.5 \times 10^{-5}$	CL=90%	$\bar{D}^0 K_2^*(1430)^0$	$(2.1 \pm 0.9) \times 10^{-5}$		2057
$D_s^- \pi^0$			$D_0^*(2300)^- K^+, D_0^{*-} \rightarrow$	$(1.9 \pm 0.9) \times 10^{-5}$		-
$D_{sJ}(2457)^- K^+, D_{sJ}^- \rightarrow$	$< 9.4 \times 10^{-6}$	CL=90%	$\bar{D}^0 \pi^-$			
$D_s^- \pi^0$			$D_2^*(2460)^- K^+, D_2^{*-} \rightarrow$	$(2.03 \pm 0.35) \times 10^{-5}$		2029
$D_{sJ}(2457)^- \pi^+, D_{sJ}^- \rightarrow$	$< 4.0 \times 10^{-6}$	CL=90%	$\bar{D}^0 \pi^-$			
$D_s^- \pi^0$			$D_3^*(2760)^- K^+, D_3^{*-} \rightarrow$	$< 1.0 \times 10^{-6}$	CL=90%	-
$D_s^- D_s^+$	$< 3.6 \times 10^{-5}$	CL=90%	$\bar{D}^0 \pi^-$			
$D_s^- D_s^+$	$< 1.3 \times 10^{-4}$	CL=90%	$\bar{D}^0 K^+ \pi^-$ nonresonant	$< 3.7 \times 10^{-5}$	CL=90%	2262
$D_s^- D_s^{*+}$	$< 2.4 \times 10^{-4}$	CL=90%	$[K^+ K^-]_D K^*(892)^0$	$(4.2 \pm 0.7) \times 10^{-5}$		-
$D_{s0}^*(2317)^+ D^-, D_{s0}^{*+} \rightarrow$	$(1.06 \pm 0.16) \times 10^{-3}$	S=1.1	$[\pi^+ \pi^-]_D K^*(892)^0$	$(6.0 \pm 1.1) \times 10^{-5}$		-
$D_s^+ \pi^0$						

Meson Summary Table

$[\pi^+ \pi^- \pi^+ \pi^-]_D K^*0$	$(4.6 \pm 0.9) \times 10^{-5}$	-	$J/\psi(1S)\rho^0$	$(2.55 \pm_{-0.16}^{+0.18}) \times 10^{-5}$	1612
$\overline{D}^0 \pi^0$	$(2.67 \pm 0.09) \times 10^{-4}$	2308	$J/\psi(1S) f_0(980), f_0 \rightarrow \pi^+ \pi^-$	$< 1.1 \times 10^{-6}$	CL=90% -
$\overline{D}^0 \rho^0$	$(3.21 \pm 0.21) \times 10^{-4}$	2237	$J/\psi(1S)\rho(1450)^0, \rho^0 \rightarrow \pi^+ \pi^-$	$(2.9 \pm_{-0.7}^{+1.6}) \times 10^{-6}$	-
$\overline{D}^0 f_2$	$(1.56 \pm 0.21) \times 10^{-4}$	-	$J/\psi(1S)\omega$	$(1.8 \pm_{-0.5}^{+0.7}) \times 10^{-5}$	1609
$\overline{D}^0 \eta$	$(2.56 \pm 0.12) \times 10^{-4}$	2274	$J/\psi(1S) K^+ K^-$	$(2.53 \pm 0.35) \times 10^{-6}$	1534
$\overline{D}^0 \eta'$	$(1.38 \pm 0.16) \times 10^{-4}$	S=1.3 2198	$J/\psi(1S) a_0(980), a_0 \rightarrow K^+ K^-$	$(4.7 \pm 3.4) \times 10^{-7}$	-
$\overline{D}^0 \omega$	$(2.54 \pm 0.16) \times 10^{-4}$	2235	$J/\psi(1S) \phi$	$< 1.1 \times 10^{-7}$	CL=90% 1520
$\overline{D}^0 \phi$	$(7.7 \pm 2.3) \times 10^{-7}$	2183	$J/\psi(1S) \eta'(958)$	$(7.6 \pm 2.4) \times 10^{-6}$	1546
$D^0 K^+ \pi^-$	$(5.3 \pm 3.2) \times 10^{-6}$	2262	$J/\psi(1S) K^0 \pi^+ \pi^-$	$(4.5 \pm 0.4) \times 10^{-4}$	1611
$D^0 K^*(892)^0$	$(3.0 \pm 0.6) \times 10^{-6}$	2213	$J/\psi(1S) K^0 K^- \pi^+ + c.c.$	$< 2.1 \times 10^{-5}$	CL=90% 1468
$\overline{D}^{*0} \gamma$	$< 2.5 \times 10^{-5}$	CL=90% 2258	$J/\psi(1S) K^0 K^+ K^-$	$(2.5 \pm 0.7) \times 10^{-5}$	S=1.8 1249
$\overline{D}^*(2007)^0 \pi^0$	$(2.2 \pm 0.6) \times 10^{-4}$	S=2.6 2256	$J/\psi(1S) K^0 \rho^0$	$(5.4 \pm 3.0) \times 10^{-4}$	1390
$\overline{D}^*(2007)^0 \rho^0$	$< 5.1 \times 10^{-4}$	CL=90% 2182	$J/\psi(1S) K^*(892)^+ \pi^-$	$(8 \pm 4) \times 10^{-4}$	1515
$\overline{D}^*(2007)^0 \eta$	$(2.3 \pm 0.6) \times 10^{-4}$	S=2.8 2220	$J/\psi(1S) \pi^+ \pi^- \pi^+ \pi^-$	$(1.44 \pm 0.12) \times 10^{-5}$	1670
$\overline{D}^*(2007)^0 \eta'$	$(1.40 \pm 0.22) \times 10^{-4}$	2141	$J/\psi(1S) \pi^+ \pi^- \pi^+ \pi^-$	$(8.4 \pm 2.1) \times 10^{-6}$	1385
$\overline{D}^*(2007)^0 \pi^+ \pi^-$	$(6.2 \pm 2.2) \times 10^{-4}$	2249	$J/\psi(1S) f_1(1285)$	$(6.6 \pm 2.2) \times 10^{-4}$	1447
$\overline{D}^*(2007)^0 K^+ \pi^-$	$(5.2 \pm 1.9) \times 10^{-5}$	2207	$J/\psi(1S) K^*(892)^0 \pi^+ \pi^-$	$< 3.5 \times 10^{-5}$	CL=90% -
$\overline{D}^*(2007)^0 K^0$	$(3.6 \pm 1.2) \times 10^{-5}$	2227	$\eta_{c2}(1D) K_S^0, \eta_{c2} \rightarrow h_c \gamma$	$< 1.0 \times 10^{-4}$	CL=90% -
$\overline{D}^*(2007)^0 K^*(892)^0$	$< 6.9 \times 10^{-5}$	CL=90% 2157	$\eta_{c2}(1D) \pi^- K^+, \eta_{c2} \rightarrow h_c \gamma$	$< 5 \times 10^{-4}$	CL=90% -
$\overline{D}^*(2007)^0 \phi$	$(2.2 \pm 0.6) \times 10^{-6}$	2125	$\chi_{c1}(3872)^- K^+$	$< 4.2 \times 10^{-6}$	CL=90% -
$D^*(2007)^0 K^*(892)^0$	$< 4.0 \times 10^{-5}$	CL=90% 2157	$\chi_{c1}(3872)^- K^+, \chi_{c1}(3872)^- \rightarrow J/\psi(1S) \pi^- \pi^0$	$(1.4 \pm 0.4) \times 10^{-4}$	S=1.1 1140
$D^*(2007)^0 \pi^+ \pi^+ \pi^- \pi^-$	$(2.7 \pm 0.5) \times 10^{-3}$	2219	$\chi_{c1}(3872) K^*(892)^0$	$(1.1 \pm 0.5) \times 10^{-4}$	940
$D^*(2010)^+ D^*(2010)^-$	$(8.0 \pm 0.6) \times 10^{-4}$	1711	$\chi_{c1}(3872) K^+ \pi^-$	$(2.2 \pm 0.7) \times 10^{-4}$	1087
$\overline{D}^*(2007)^0 \omega$	$(3.6 \pm 1.1) \times 10^{-4}$	S=3.1 2180	$\chi_{c1}(3872) \gamma$	$< 1.5 \times 10^{-5}$	CL=90% 1220
$D^*(2010)^+ D^-$	$(6.1 \pm 1.5) \times 10^{-4}$	S=1.6 1790	$T_{c\overline{c}1}(4430)^\pm K^\mp, T_{c\overline{c}1}^\pm \rightarrow \psi(2S) \pi^\pm$	$(6.0 \pm_{-2.4}^{+3.0}) \times 10^{-5}$	583
$D^*(2007)^0 \overline{D}^*(2007)^0$	$< 9 \times 10^{-5}$	CL=90% 1715	$T_{c\overline{c}1}(4430)^\pm K^\mp, T_{c\overline{c}1}^\pm \rightarrow J/\psi \pi^\pm$	$(5.4 \pm_{-1.2}^{+4.0}) \times 10^{-6}$	583
$D^- D^0 K^+$	$(1.07 \pm 0.11) \times 10^{-3}$	1574	$T_{c\overline{c}1}(3900)^\pm K^\mp, T_{c\overline{c}1}^\pm \rightarrow J/\psi \pi^\pm$	$< 9 \times 10^{-7}$	-
$D^- D^*(2007)^0 K^+$	$(3.5 \pm 0.4) \times 10^{-3}$	1478	$T_{c\overline{c}1}(4200)^\pm K^\mp, T_{c\overline{c}1}^\pm \rightarrow J/\psi \pi^\pm$	$(2.2 \pm_{-0.8}^{+1.3}) \times 10^{-5}$	-
$D^*(2010)^- D^0 K^+$	$(2.47 \pm 0.21) \times 10^{-3}$	1479	$J/\psi(1S) p\overline{p}$	$(4.5 \pm 0.6) \times 10^{-7}$	862
$D^*(2010)^- D^*(2007)^0 K^+$	$(1.06 \pm 0.09) \%$	1366	$J/\psi(1S) \gamma$	$< 1.5 \times 10^{-6}$	CL=90% 1732
$D^- D^+ K^0$	$(7.5 \pm 1.7) \times 10^{-4}$	1568	$J/\psi \mu^+ \mu^-, J/\psi \rightarrow \mu^+ \mu^-$	$< 1.0 \times 10^{-9}$	CL=95% -
$D^*(2010)^- D^+ K^0 + D^- D^*(2010)^+ K^0$	$(6.4 \pm 0.5) \times 10^{-3}$	1473	$J/\psi(1S) \overline{D}^0$	$< 1.3 \times 10^{-5}$	CL=90% 877
$D^*(2010)^- D^*(2010)^+ K^0$	$(8.1 \pm 0.7) \times 10^{-3}$	1360	$\psi(2S) \pi^0$	$(1.17 \pm 0.19) \times 10^{-5}$	1348
$D^* - D_{s1}(2536)^+, D_{s1}^+ \rightarrow D^+ K^0$	$(8.0 \pm 2.4) \times 10^{-4}$	1336	$\psi(2S) K^0$	$(5.8 \pm 0.5) \times 10^{-4}$	1283
$\overline{D}^0 D^0 K^0$	$(2.7 \pm 1.1) \times 10^{-4}$	1575	$\psi(2S) K^0 \pi^+ \pi^-$	$(2.81 \pm 0.30) \times 10^{-4}$	1177
$D^0 \overline{D}^0 K^+ \pi^-$	$(3.5 \pm 0.5) \times 10^{-4}$	1476	$\psi(3770) K^0, \psi \rightarrow \overline{D}^0 D^0$	$< 1.23 \times 10^{-4}$	CL=90% 1217
$\overline{D}^0 D^*(2007)^0 K^0 + \overline{D}^*(2007)^0 D^0 K^0$	$(1.1 \pm 0.5) \times 10^{-3}$	1478	$\psi(3770) K^0, \psi \rightarrow D^- D^+$	$< 1.88 \times 10^{-4}$	CL=90% 1217
$\overline{D}^*(2007)^0 D^*(2007)^0 K^0$	$(2.4 \pm 0.9) \times 10^{-3}$	1365	$\psi(2S) \pi^+ \pi^-$	$(2.24 \pm 0.35) \times 10^{-5}$	1332
$(\overline{D} + \overline{D}^*)(D + D^*) K$	$(3.68 \pm 0.26) \%$	-	$\psi(2S) K^+ \pi^-$	$(5.8 \pm 0.4) \times 10^{-4}$	1239
Charmonium modes					
$\eta_c K^0$	$(9.0 \pm 1.1) \times 10^{-4}$	1751	$\psi(2S) K^*(892)^0$	$(5.9 \pm 0.4) \times 10^{-4}$	1116
$\eta_c(1S) K^+ \pi^-$	$(6.5 \pm 0.7) \times 10^{-4}$	1722	$\chi_{c0} K^0$	$(1.9 \pm 0.4) \times 10^{-4}$	1478
$\eta_c(1S) K^+ \pi^- (NR)$	$(6.7 \pm 1.4) \times 10^{-5}$	-	$\chi_{c0} K^*(892)^0$	$(1.7 \pm 0.4) \times 10^{-4}$	1342
$T_{c\overline{c}}(4100)^- K^+, T_{c\overline{c}}^- \rightarrow \eta_c \pi^-$	$(2.2 \pm 1.1) \times 10^{-5}$	-	$\chi_{c1} \pi^0$	$(1.12 \pm 0.28) \times 10^{-5}$	1468
$\eta_c(1S) K^*(1410)^0$	$(2.1 \pm 1.6) \times 10^{-4}$	1395	$\chi_{c1} K^0$	$(3.95 \pm 0.27) \times 10^{-4}$	1411
$\eta_c(1S) K_0^*(1430)^0$	$(1.8 \pm 0.4) \times 10^{-4}$	1387	$\chi_{c1} \pi^- K^+$	$(4.97 \pm 0.30) \times 10^{-4}$	1372
$\eta_c(1S) K_2^*(1430)^0$	$(5.4 \pm_{-2.9}^{+2.4}) \times 10^{-5}$	1386	$\chi_{c1} K^*(892)^0$	$(2.38 \pm 0.19) \times 10^{-4}$	S=1.2 1265
$\eta_c(1S) K^*(1680)^0$	$(4 \pm 4) \times 10^{-5}$	1166	$T_{c\overline{c}}(4050)^- K^+, T_{c\overline{c}}^- \rightarrow \chi_{c1} \pi^-$	$(3.0 \pm_{-1.8}^{+4.0}) \times 10^{-5}$	-
$\eta_c(1S) K_0^*(1950)^0$	$(4.8 \pm_{-4.0}^{+3.2}) \times 10^{-5}$	-	$T_{c\overline{c}}(4250)^- K^+, T_{c\overline{c}}^- \rightarrow \chi_{c1} \pi^-$	$(4.0 \pm_{-1.0}^{+20.0}) \times 10^{-5}$	-
$\eta_c K^*(892)^0$	$(5.3 \pm_{-0.9}^{+0.8}) \times 10^{-4}$	S=1.7 1646	$\chi_{c1} \pi^+ \pi^- K^0$	$(3.2 \pm 0.5) \times 10^{-4}$	1318
$\eta_c(2S) K_S^0, \eta_c \rightarrow \rho \overline{p} \pi^+ \pi^-$	$(4.2 \pm_{-1.2}^{+1.4}) \times 10^{-7}$	-	$\chi_{c1} \pi^- \pi^0 K^+$	$(3.5 \pm 0.6) \times 10^{-4}$	1321
$\eta_c(2S) K^*0$	$< 3.9 \times 10^{-4}$	CL=90% 1159	$\chi_{c2} K^0$	$< 1.5 \times 10^{-5}$	CL=90% 1379
$h_c(1P) K_S^0$	$< 1.4 \times 10^{-5}$	1401	$\chi_{c2} K^*(892)^0$	$(4.9 \pm 1.2) \times 10^{-5}$	S=1.1 1228
$h_c(1P) K^*0$	$< 4 \times 10^{-4}$	CL=90% 1253	$\chi_{c2} \pi^- K^+$	$(7.2 \pm 1.0) \times 10^{-5}$	1338
$J/\psi(1S) K^0$	$(8.91 \pm 0.21) \times 10^{-4}$	1683	$\chi_{c2} \pi^+ \pi^- K^0$	$< 1.70 \times 10^{-4}$	CL=90% 1282
$J/\psi(1S) K^+ \pi^-$	$(1.15 \pm 0.05) \times 10^{-3}$	1652	$\chi_{c2} \pi^- \pi^0 K^+$	$< 7.4 \times 10^{-5}$	CL=90% 1286
$J/\psi(1S) K^*(892)^0$	$(1.27 \pm 0.05) \times 10^{-3}$	1572	$\psi(4660) K^0, \psi \rightarrow \Lambda_c^+ \Lambda_c^-$	$< 2.3 \times 10^{-4}$	CL=90% -
$J/\psi(1S) \eta K_S^0$	$(5.4 \pm 0.9) \times 10^{-5}$	1508	$\psi(4230)^0 K^0, \psi^0 \rightarrow J/\psi \pi^+ \pi^-$	$< 1.7 \times 10^{-5}$	CL=90% -
$J/\psi(1S) \eta' K_S^0$	$< 2.5 \times 10^{-5}$	CL=90% 1271			
$J/\psi(1S) \phi K^0$	$(4.9 \pm 1.0) \times 10^{-5}$	S=1.3 1224			
$J/\psi(1S) \omega K^0$	$(2.3 \pm 0.4) \times 10^{-4}$	1386			
$\chi_{c0}(3915), \chi_{c0} \rightarrow J/\psi \omega$	$(2.1 \pm 0.9) \times 10^{-5}$	1102			
$J/\psi(1S) K(1270)^0$	$(1.3 \pm 0.5) \times 10^{-3}$	1402			
$J/\psi(1S) \pi^0$	$(1.66 \pm 0.10) \times 10^{-5}$	1728			
$J/\psi(1S) \eta$	$(1.08 \pm 0.23) \times 10^{-5}$	S=1.5 1673			
$J/\psi(1S) \pi^+ \pi^-$	$(3.99 \pm 0.15) \times 10^{-5}$	1716			
$J/\psi(1S) \pi^+ \pi^-$ nonresonant	$< 1.2 \times 10^{-5}$	CL=90% 1716			
$J/\psi(1S) f_0(500), f_0 \rightarrow \pi \pi$	$(8.8 \pm_{-1.6}^{+1.2}) \times 10^{-6}$	-			
$J/\psi(1S) f_2$	$(3.3 \pm_{-0.6}^{+0.5}) \times 10^{-6}$	S=1.5 -			

Meson Summary Table

K or K* modes		K ⁰ \bar{K}^0		
$K^+\pi^-$	(2.00 ± 0.04) × 10 ⁻⁵	2615	(1.21 ± 0.16) × 10 ⁻⁶	2593
$K^0\pi^0$	(1.01 ± 0.04) × 10 ⁻⁵	2615	(6.7 ± 0.5) × 10 ⁻⁶	2578
$\eta'K^0$	(6.6 ± 0.4) × 10 ⁻⁵	S=1.4 2528	< 4 × 10 ⁻⁷	CL=90% 2540
$\eta'K^*(892)^0$	(2.8 ± 0.6) × 10 ⁻⁶	2472	< 9.6 × 10 ⁻⁷	CL=90% -
$\eta'K_0^*(1430)^0$	(6.3 ± 1.6) × 10 ⁻⁶	2346	(2.2 ± 0.6) × 10 ⁻⁶	2579
$\eta'K_2^*(1430)^0$	(1.37 ± 0.32) × 10 ⁻⁵	2346	< 9 × 10 ⁻⁷	CL=90% 2578
ηK^0	(1.23 ± 0.27) × 10 ⁻⁶	2587	< 1.0 × 10 ⁻⁶	CL=90% 2516
$\eta K^*(892)^0$	(1.59 ± 0.10) × 10 ⁻⁵	2534	< 2.0 × 10 ⁻⁶	CL=90% 2453
$\eta K_0^*(1430)^0$	(1.10 ± 0.22) × 10 ⁻⁵	2415	(2.68 ± 0.11) × 10 ⁻⁵	2522
$\eta K_2^*(1430)^0$	(9.6 ± 2.1) × 10 ⁻⁶	2414	(7.3 ± 0.7) × 10 ⁻⁶	2516
ωK^0	(4.8 ± 0.4) × 10 ⁻⁶	2557	$K^0\phi$	(7.0 ± 3.5) × 10 ⁻⁶
$a_0(980)^0 K^0, a_0^0 \rightarrow \eta\pi^0$	< 7.8 × 10 ⁻⁶	CL=90% -	$f_0(980)K^0, f_0 \rightarrow K^+K^-$	(7.0 ± 3.0) × 10 ⁻⁶
$b_1^0 K^0, b_1^0 \rightarrow \omega\pi^0$	< 7.8 × 10 ⁻⁶	CL=90% -	$f_0(1500)K^0$	(1.3 ± 0.7) × 10 ⁻⁵
$a_0(980)^\pm K^\mp, a_0^\pm \rightarrow \eta\pi^\pm$	< 1.9 × 10 ⁻⁶	CL=90% -	$f_2'(1525)^0 K^0$	(3 ± 5) × 10 ⁻⁷
$b_1^- K^+, b_1^- \rightarrow \omega\pi^-$	(7.4 ± 1.4) × 10 ⁻⁶	-	$f_0(1710)K^0, f_0 \rightarrow K^+K^-$	(4.4 ± 0.9) × 10 ⁻⁶
$b_1^0 K^*, b_1^0 \rightarrow \omega\pi^0$	< 8.0 × 10 ⁻⁶	CL=90% -	$K^+K^+K^-$ nonresonant	(3.3 ± 1.0) × 10 ⁻⁵
$b_1^- K^*, b_1^- \rightarrow \omega\pi^-$	< 5.0 × 10 ⁻⁶	CL=90% -	$K_S^0 K_S^0 K_S^0$	(6.0 ± 0.5) × 10 ⁻⁶
$a_0(1450)^\pm K^\mp, a_0^\pm \rightarrow \eta\pi^\pm$	< 3.1 × 10 ⁻⁶	CL=90% -	$f_0(980)K^0, f_0 \rightarrow K_S^0 K_S^0$	(2.7 ± 1.8) × 10 ⁻⁶
$K_S^0 X^0$ (Familon)	< 5.3 × 10 ⁻⁵	CL=90% -	$f_0(1710)K^0, f_0 \rightarrow K_S^0 K_S^0$	(5.0 ± 5.0) × 10 ⁻⁷
$\omega K^*(892)^0$	(2.0 ± 0.5) × 10 ⁻⁶	2503	$f_2(2010)K^0, f_2 \rightarrow K_S^0 K_S^0$	(5 ± 6) × 10 ⁻⁷
$\omega(K\pi)_0^0$	(1.84 ± 0.25) × 10 ⁻⁵	-	$K_S^0 K_S^0 K_S^0$ nonresonant	(1.33 ± 0.31) × 10 ⁻⁵
$\omega K_0^*(1430)^0$	(1.60 ± 0.34) × 10 ⁻⁵	2380	$K_S^0 K_S^0 K^0$	< 1.6 × 10 ⁻⁵
$\omega K_2^*(1430)^0$	(1.01 ± 0.23) × 10 ⁻⁵	2380	$K^*(892)^0 K^+K^-$	(2.75 ± 0.26) × 10 ⁻⁵
$\omega K^+\pi^-$ nonresonant	(5.1 ± 1.0) × 10 ⁻⁶	2542	$K^*(892)^0 \phi$	(1.00 ± 0.05) × 10 ⁻⁵
$K^+\pi^-\pi^0$	(3.78 ± 0.32) × 10 ⁻⁵	2610	$K^+K^-\pi^+\pi^-$ nonresonant	< 7.17 × 10 ⁻⁵
$K^+\rho^-$	(7.0 ± 0.9) × 10 ⁻⁶	2559	$K^*(892)^0 K^-\pi^+$	(4.5 ± 1.3) × 10 ⁻⁶
$K^+\rho(1450)^-$	(2.4 ± 1.2) × 10 ⁻⁶	-	$K^*(892)^0 \bar{K}^*(892)^0$	(8.3 ± 2.4) × 10 ⁻⁷
$K^+\rho(1700)^-$	(6 ± 7) × 10 ⁻⁷	-	$K^+K^+\pi^-\pi^-$ nonresonant	< 6.0 × 10 ⁻⁶
$(K^+\pi^-\pi^0)$ nonresonant	(2.8 ± 0.6) × 10 ⁻⁶	2610	$K^*(892)^0 K^+\pi^-$	< 2.2 × 10 ⁻⁶
$(K\pi)_0^{*+}\pi^-, (K\pi)_0^{*+} \rightarrow$	(3.4 ± 0.5) × 10 ⁻⁵	-	$K^*(892)^0 K^*(892)^0$	< 2 × 10 ⁻⁷
$(K\pi)_0^{*0}\pi^0, (K\pi)_0^{*0} \rightarrow$	(8.6 ± 1.7) × 10 ⁻⁶	-	$K^*(892)^+ K^*(892)^-$	< 2.0 × 10 ⁻⁶
$K_2^+(1430)^0\pi^0$	< 4.0 × 10 ⁻⁶	CL=90% 2445	$K_1(1400)^0\phi$	< 5.0 × 10 ⁻³
$K^*(1680)^0\pi^0$	< 7.5 × 10 ⁻⁶	CL=90% 2358	$\phi(K\pi)_0^{*0}$	(4.3 ± 0.4) × 10 ⁻⁶
$K_S^0\pi^0$ [qqq]	(6.1 ± 1.6) × 10 ⁻⁶	-	$\phi(K\pi)_0^{*0} (1.60 < m_{K\pi} < 2.15)$ [sss]	< 1.7 × 10 ⁻⁶
$K^0\pi^+\pi^-$	(4.97 ± 0.18) × 10 ⁻⁵	2609	$K_0^*(1430)^0 K^-\pi^+$	< 3.18 × 10 ⁻⁵
$K^0\pi^+\pi^-$ nonresonant	(1.39 ± 0.26) × 10 ⁻⁵	S=1.6 2609	$K_0^*(1430)^0 \bar{K}^*(892)^0$	< 3.3 × 10 ⁻⁶
$K^0\rho^0$	(3.4 ± 1.1) × 10 ⁻⁶	S=2.3 2558	$K_0^*(1430)^0 \bar{K}_0^*(1430)^0$	< 8.4 × 10 ⁻⁶
$K^*(892)^+\pi^-$	(7.5 ± 0.4) × 10 ⁻⁶	2563	$K_0^*(1430)^0 \phi$	(3.9 ± 0.8) × 10 ⁻⁶
$K_0^*(1430)^+\pi^-$	(3.3 ± 0.7) × 10 ⁻⁵	S=2.0 -	$K_0^*(1430)^0 K^*(892)^0$	< 1.7 × 10 ⁻⁶
$K_x^{*+}\pi^-$ [qqq]	(5.1 ± 1.6) × 10 ⁻⁶	-	$K_0^*(1430)^0 K_0^*(1430)^0$	< 4.7 × 10 ⁻⁶
$K^*(1410)^+\pi^-, K^{*+} \rightarrow$	< 3.8 × 10 ⁻⁶	CL=90% -	$K^*(1680)^0 \phi$	< 3.5 × 10 ⁻⁶
$(K\pi)_0^{*+}\pi^-, (K\pi)_0^{*+} \rightarrow$	(1.62 ± 0.13) × 10 ⁻⁵	-	$K^*(1780)^0 \phi$	< 2.7 × 10 ⁻⁶
$K^0\pi^+$	(8.1 ± 0.8) × 10 ⁻⁶	S=1.3 2522	$K^*(2045)^0 \phi$	< 1.53 × 10 ⁻⁵
$f_0(980)K^0, f_0 \rightarrow \pi^+\pi^-$	(1.6 ± 2.5) × 10 ⁻⁷	-	$K_2^*(1430)^0 \rho^0$	< 1.1 × 10 ⁻³
$K^0 f_0(500)$	(1.3 ± 0.8) × 10 ⁻⁶	2393	$K_2^*(1430)^0 \phi$	(6.8 ± 0.9) × 10 ⁻⁶
$K^0 f_0(1500)$	(2.7 ± 1.3) × 10 ⁻⁶	2459	$K^0\phi\phi$	(3.7 ± 0.7) × 10 ⁻⁶
$f_x(1300)K^0, f_x \rightarrow \pi^+\pi^-$	(1.8 ± 0.7) × 10 ⁻⁶	-	$\eta'\eta'K^0$	< 3.1 × 10 ⁻⁵
$K^*(892)^0\pi^0$	(3.3 ± 0.6) × 10 ⁻⁶	2563	$\eta K^0\gamma$	(7.6 ± 1.8) × 10 ⁻⁶
$K_2^*(1430)^+\pi^-$	(3.65 ± 0.34) × 10 ⁻⁶	2445	$\eta'K^0\gamma$	< 6.4 × 10 ⁻⁶
$K^*(1680)^+\pi^-$	(1.41 ± 0.10) × 10 ⁻⁵	2358	$K^0\phi\gamma$	(2.7 ± 0.7) × 10 ⁻⁶
$K^+\pi^-\pi^+\pi^-$ [rrr]	< 2.3 × 10 ⁻⁴	CL=90% 2600	$K^+\pi^-\gamma$	(4.6 ± 1.4) × 10 ⁻⁶
$\rho^0 K^+\pi^-$	(2.8 ± 0.7) × 10 ⁻⁶	2543	$K^*(892)^0\gamma$	(4.18 ± 0.25) × 10 ⁻⁵
$f_0(980)K^+\pi^-, f_0 \rightarrow \pi\pi$	(1.4 ± 0.5) × 10 ⁻⁶	2506	$K^*(1410)\gamma$	< 1.3 × 10 ⁻⁴
$K^+\pi^-\pi^+\pi^-$ nonresonant	< 2.1 × 10 ⁻⁶	CL=90% 2600	$K^+\pi^-\gamma$ nonresonant	< 2.6 × 10 ⁻⁶
$K^*(892)^0\pi^+\pi^-$	(5.5 ± 0.5) × 10 ⁻⁵	2557	$K^*(892)^0 X(214), X \rightarrow$	[ttt] < 2.26 × 10 ⁻⁸
$K^*(892)^0\rho^0$	(3.9 ± 1.3) × 10 ⁻⁶	S=1.9 2504	$\mu^+\mu^-$	
$K^*(892)^0 f_0(980), f_0 \rightarrow \pi\pi$	(3.9 ± 2.1) × 10 ⁻⁶	S=3.9 2466	$K^0\pi^+\pi^-\gamma$	(1.99 ± 0.18) × 10 ⁻⁵
$K_1(1270)^+\pi^-$	< 3.0 × 10 ⁻⁵	CL=90% 2489	$K^+\pi^-\pi^0\gamma$	(4.1 ± 0.4) × 10 ⁻⁵
$K_1(1400)^+\pi^-$	< 2.7 × 10 ⁻⁵	CL=90% 2451	$K_1(1270)^0\gamma$	< 5.8 × 10 ⁻⁵
$a_1(1260)^-K^+$ [rrr]	(1.6 ± 0.4) × 10 ⁻⁵	2471	$K_1(1400)^0\gamma$	< 1.2 × 10 ⁻⁵
$K^*(892)^+\rho^-$	(1.03 ± 0.26) × 10 ⁻⁵	2504	$K_2^*(1430)^0\gamma$	(1.24 ± 0.24) × 10 ⁻⁵
$K_0^*(1430)^+\rho^-$	(2.8 ± 1.2) × 10 ⁻⁵	-	$K^*(1680)^0\gamma$	< 2.0 × 10 ⁻³
$K_1(1400)^0\rho^0$	< 3.0 × 10 ⁻³	CL=90% 2388	$K_3^*(1780)^0\gamma$	< 8.3 × 10 ⁻⁵
$K_0^*(1430)^0\rho^0$	(2.7 ± 0.6) × 10 ⁻⁵	2381	$K_4^*(2045)^0\gamma$	< 4.3 × 10 ⁻³
$K_0^*(1430)^0 f_0(980), f_0 \rightarrow \pi\pi$	(2.7 ± 0.9) × 10 ⁻⁶	-		
$K_2^*(1430)^0 f_0(980), f_0 \rightarrow \pi\pi$	(8.6 ± 2.0) × 10 ⁻⁶	-		
$K^+\pi^-$	(7.8 ± 1.5) × 10 ⁻⁸	2593		

Light unflavored meson modes

$\rho^0\gamma$	(8.6 ± 1.5) × 10 ⁻⁷	2583
$\rho^0 X(214), X \rightarrow \mu^+\mu^-$	[ttt] < 1.73 × 10 ⁻⁸	CL=90% -
$\omega\gamma$	(4.4 ± 1.8) × 10 ⁻⁷	2582
$\phi\gamma$	< 1.0 × 10 ⁻⁷	CL=90% 2541
$f_2(1270)\gamma, f_2 \rightarrow$	< 3.1 × 10 ⁻⁷	-
$(KS)^0(KS)^0$		
$f_2'(1525)\gamma, f_2' \rightarrow$	< 2.1 × 10 ⁻⁷	-
$(KS)^0(KS)^0$		

Meson Summary Table

$\pi^+\pi^-$	$(5.37 \pm 0.20) \times 10^{-6}$	S=1.3	2636	
$\pi^0\pi^0$	$(1.55 \pm 0.17) \times 10^{-6}$	S=1.1	2636	
$\eta\pi^0$	$(4.1 \pm 1.7) \times 10^{-7}$		2610	
$\eta\eta$	$< 1.0 \times 10^{-6}$	CL=90%	2582	
$\eta'\pi^0$	$(1.2 \pm 0.6) \times 10^{-6}$	S=1.7	2551	
$\eta'\eta'$	$< 1.7 \times 10^{-6}$	CL=90%	2460	
$\eta'\eta$	$< 1.2 \times 10^{-6}$	CL=90%	2523	
$\eta'\rho^0$	$< 1.3 \times 10^{-6}$	CL=90%	2492	
$\eta'f_0(980), f_0 \rightarrow \pi^+\pi^-$	$< 9 \times 10^{-7}$	CL=90%	2454	
$\eta\rho^0$	$< 1.5 \times 10^{-6}$	CL=90%	2553	
$\eta f_0(980), f_0 \rightarrow \pi^+\pi^-$	$< 4 \times 10^{-7}$	CL=90%	2516	
$\omega\eta$	$(9.4 \pm 4.0) \times 10^{-7}$		2552	
$\omega\eta'$	$(1.0 \pm 0.5) \times 10^{-6}$		2491	
$\omega\rho^0$	$< 1.6 \times 10^{-6}$	CL=90%	2522	
$\omega f_0(980), f_0 \rightarrow \pi^+\pi^-$	$< 1.5 \times 10^{-6}$	CL=90%	2485	
$\omega\omega$	$(1.2 \pm 0.4) \times 10^{-6}$		2521	
$\phi\pi^0$	$< 1.5 \times 10^{-7}$	CL=90%	2540	
$\phi\eta$	$< 5 \times 10^{-7}$	CL=90%	2511	
$\phi\eta'$	$< 5 \times 10^{-7}$	CL=90%	2448	
$\phi\pi^+\pi^-$	$(1.8 \pm 0.5) \times 10^{-7}$		2533	
$\phi\rho^0$	$< 3.3 \times 10^{-7}$	CL=90%	2480	
$\phi f_0(980), f_0 \rightarrow \pi^+\pi^-$	$< 3.8 \times 10^{-7}$	CL=90%	2441	
$\phi\omega$	$< 7 \times 10^{-7}$	CL=90%	2479	
$\phi\phi$	$< 2.7 \times 10^{-8}$	CL=90%	2435	
$a_0(980)^\pm\pi^\mp, a_0^\pm \rightarrow \eta\pi^\pm$	$< 3.1 \times 10^{-6}$	CL=90%	-	
$a_0(1450)^\pm\pi^\mp, a_0^\pm \rightarrow \eta\pi^\pm$	$< 2.3 \times 10^{-6}$	CL=90%	-	
$\pi^+\pi^-\pi^0$	$< 7.2 \times 10^{-4}$	CL=90%	2631	
$\rho^0\pi^0$	$(2.0 \pm 0.5) \times 10^{-6}$		2581	
$\rho^\mp\pi^\pm$	[aa] $(2.30 \pm 0.23) \times 10^{-5}$		2581	
$\pi^+\pi^-\pi^+\pi^-$	$< 1.12 \times 10^{-5}$	CL=90%	2621	
$\rho^0\pi^+\pi^-$	$< 8.8 \times 10^{-6}$	CL=90%	2575	
$\rho^0\rho^0$	$(9.6 \pm 1.5) \times 10^{-7}$		2523	
$f_0(980)\pi^+\pi^-, f_0 \rightarrow \pi^+\pi^-$	$< 3.0 \times 10^{-6}$	CL=90%	-	
$\rho^0 f_0(980), f_0 \rightarrow \pi^+\pi^-$	$(7.8 \pm 2.5) \times 10^{-7}$		2486	
$f_0(980)f_0(980), f_0 \rightarrow \pi^+\pi^-$	$< 1.9 \times 10^{-7}$	CL=90%	2447	
$\pi^+\pi^-, f_0 \rightarrow \pi^+\pi^-$				
$f_0(980)f_0(980), f_0 \rightarrow \pi^+\pi^-, f_0 \rightarrow K^+K^-$	$< 2.3 \times 10^{-7}$	CL=90%	2447	
$a_1(1260)^\mp\pi^\pm$	[aa] $(2.6 \pm 0.5) \times 10^{-5}$	S=1.9	2495	
$a_2(1320)^\mp\pi^\pm$	[aa] $< 6.3 \times 10^{-6}$	CL=90%	2473	
$\pi^+\pi^-\pi^0\pi^0$	$< 3.1 \times 10^{-3}$	CL=90%	2622	
$\rho^+\rho^-$	$(2.77 \pm 0.19) \times 10^{-5}$		2523	
$a_1(1260)^0\pi^0$	$< 1.1 \times 10^{-3}$	CL=90%	2495	
$\omega\pi^0$	$< 5 \times 10^{-7}$	CL=90%	2580	
$\pi^+\pi^+\pi^-\pi^0$	$< 9.0 \times 10^{-3}$	CL=90%	2609	
$a_1(1260)^+\rho^-$	$< 6.1 \times 10^{-5}$	CL=90%	2433	
$a_1(1260)^0\rho^0$	$< 2.4 \times 10^{-3}$	CL=90%	2433	
$b_1^\mp\pi^\pm, b_1^\mp \rightarrow \omega\pi^\mp$	$(1.09 \pm 0.15) \times 10^{-5}$		-	
$b_1^0\pi^0, b_1^0 \rightarrow \omega\pi^0$	$< 1.9 \times 10^{-6}$	CL=90%	-	
$b_1^-\rho^+, b_1^- \rightarrow \omega\pi^-$	$< 1.4 \times 10^{-6}$	CL=90%	-	
$b_1^0\rho^0, b_1^0 \rightarrow \omega\pi^0$	$< 3.4 \times 10^{-6}$	CL=90%	-	
$\pi^+\pi^+\pi^+\pi^-\pi^-\pi^0$	$< 3.0 \times 10^{-3}$	CL=90%	2592	
$a_1(1260)^+ a_1(1260)^-, a_1^\pm \rightarrow 2\pi^+\pi^-, a_1^- \rightarrow 2\pi^-\pi^+$	$(1.18 \pm 0.31) \times 10^{-5}$		2336	
$\pi^+\pi^+\pi^+\pi^-\pi^-\pi^0$	< 1.1	%	CL=90%	2572
Baryon modes				
$p\bar{p}$	$(1.27 \pm 0.14) \times 10^{-8}$		2467	
$p\bar{p}\pi^+\pi^-$	$(2.87 \pm 0.19) \times 10^{-6}$		2406	
$p\bar{p}K^+\pi^-$	$(6.3 \pm 0.5) \times 10^{-6}$		2306	
$p\bar{p}K^0$	$(2.66 \pm 0.32) \times 10^{-6}$		2347	
$\Theta(1540)^+\bar{p}, \Theta^+ \rightarrow pK_S^0$	[uuu] $< 5 \times 10^{-8}$	CL=90%	2318	
$f_J(2220)K^0, f_J \rightarrow p\bar{p}$	$< 4.5 \times 10^{-7}$	CL=90%	2135	
$p\bar{p}K^*(892)^0$	$(1.24 \pm 0.28) \times 10^{-6}$		2216	
$f_J(2220)K_0^*, f_J \rightarrow p\bar{p}$	$< 1.5 \times 10^{-7}$	CL=90%	-	
$p\bar{p}K^+K^-$	$(1.21 \pm 0.32) \times 10^{-7}$		2179	
$p\bar{p}\pi^0$	$(5.0 \pm 1.9) \times 10^{-7}$		2440	
$p\bar{p}\rho\bar{p}$	$(2.2 \pm 0.4) \times 10^{-8}$		1735	
$p\bar{p}\pi^-$	$(3.16 \pm 0.24) \times 10^{-6}$		2401	
$p\bar{p}\pi^-\gamma$	$< 6.5 \times 10^{-7}$	CL=90%	2401	
$p\bar{p}\Sigma(1385)^-$	$< 2.6 \times 10^{-7}$	CL=90%	2363	
$\Delta(1232)^+\bar{p} + \Delta(1232)^-\rho$	$< 1.6 \times 10^{-6}$		-	
$\Delta^0\bar{p}$	$< 9.3 \times 10^{-7}$	CL=90%	2364	
$p\bar{p}K^-$	$< 8.2 \times 10^{-7}$	CL=90%	2308	

$p\bar{p}D^-$	$(2.5 \pm 0.4) \times 10^{-5}$		1765
$p\bar{p}D^{*-}$	$(3.4 \pm 0.8) \times 10^{-5}$		1685
$p\bar{p}\Sigma^0\pi^-$	$(1.2 \pm 0.4) \times 10^{-6}$		2383
$\bar{p}\Lambda$	$< 3.2 \times 10^{-7}$	CL=90%	2393
$\bar{p}\Lambda K^0$	$(4.8 \pm 1.0) \times 10^{-6}$		2250
$\bar{p}\Lambda K^{*0}$	$(2.5 \pm 0.9) \times 10^{-6}$		2098
$\bar{p}\Lambda D^0$	$(1.00 \pm 0.30) \times 10^{-5}$		1662
$D^0\Sigma^0\bar{p} + c.c.$	$< 3.1 \times 10^{-5}$	CL=90%	1611
$\Delta^0\bar{p}$	$< 1.5 \times 10^{-3}$	CL=90%	2335
$\Delta^{++}\bar{p}$	$< 1.1 \times 10^{-4}$	CL=90%	2335
$\bar{D}^0 p\bar{p}$	$(1.04 \pm 0.07) \times 10^{-4}$		1863
$D_s^- \bar{p}$	$(2.8 \pm 0.9) \times 10^{-5}$		1710
$\bar{D}^*(2007)^0 p\bar{p}$	$(9.9 \pm 1.1) \times 10^{-5}$		1788
$D^*(2010)^- p\bar{p}$	$(1.4 \pm 0.4) \times 10^{-3}$		1785
$D^- p\bar{p}\pi^+$	$(3.32 \pm 0.31) \times 10^{-4}$		1786
$D^*(2010)^- p\bar{p}\pi^+$	$(4.7 \pm 0.5) \times 10^{-4}$	S=1.2	1708
$\bar{D}^0 p\bar{p}\pi^+\pi^-$	$(3.0 \pm 0.5) \times 10^{-4}$		1708
$\bar{D}^{*0} p\bar{p}\pi^+\pi^-$	$(1.9 \pm 0.5) \times 10^{-4}$		1623
$\Theta_c \bar{p}\pi^+, \Theta_c \rightarrow D^- p$	$< 9 \times 10^{-6}$	CL=90%	-
$\Theta_c \bar{p}\pi^+, \Theta_c \rightarrow D^{*-} p$	$< 1.4 \times 10^{-5}$	CL=90%	-
$\Sigma_c^{--} \Delta^{++}$	$< 8 \times 10^{-4}$	CL=90%	1839
$\bar{\Lambda}_c^- p\pi^+\pi^-$	$(1.02 \pm 0.14) \times 10^{-3}$	S=1.3	1934
$\bar{\Lambda}_c^- p$	$(1.55 \pm 0.17) \times 10^{-5}$		2021
$\bar{\Lambda}_c^- p\pi^0$	$(1.55 \pm 0.18) \times 10^{-4}$		1982
$\Sigma_c(2455)^- p$	$< 2.4 \times 10^{-5}$		-
$\bar{\Lambda}_c^- p\pi^+\pi^-\pi^0$	$< 5.07 \times 10^{-3}$	CL=90%	1883
$\bar{\Lambda}_c^- p\pi^+\pi^-\pi^+\pi^-$	$< 2.74 \times 10^{-3}$	CL=90%	1821
$\bar{\Lambda}_c^- p\pi^+\pi^-$ (nonresonant)	$(5.5 \pm 1.0) \times 10^{-4}$	S=1.3	1934
$\Sigma_c(2520)^- p\pi^+$	$(1.02 \pm 0.18) \times 10^{-4}$		1860
$\Sigma_c(2520)^0 p\pi^-$	$< 3.1 \times 10^{-5}$	CL=90%	1860
$\Sigma_c(2455)^0 p\pi^-$	$(1.08 \pm 0.09) \times 10^{-4}$		1895
$\Sigma_c(2455)^0 N^0, N^0 \rightarrow$	$(6.4 \pm 1.7) \times 10^{-5}$		-
$\bar{\Sigma}_c(2455)^- p\pi^+$	$(1.89 \pm 0.15) \times 10^{-4}$		1895
$\bar{\Lambda}_c^- pK^+\pi^-$	$(3.5 \pm 0.7) \times 10^{-5}$		1786
$\bar{\Sigma}_c(2455)^- pK^+, \bar{\Sigma}_c^{--} \rightarrow$	$(8.9 \pm 2.6) \times 10^{-6}$		1754
$\bar{\Lambda}_c^- \pi^-$			
$\bar{\Lambda}_c^- pK^*(892)^0$	$< 2.42 \times 10^{-5}$	CL=90%	1647
$\bar{\Lambda}_c^- pK^+K^-$	$(2.0 \pm 0.4) \times 10^{-5}$		1588
$\bar{\Lambda}_c^- p\phi$	$< 1.0 \times 10^{-5}$	CL=90%	1567
$\bar{\Lambda}_c^- p\bar{p}p$	$< 2.8 \times 10^{-6}$		677
$\bar{\Lambda}_c^- \Lambda K^+$	$(4.8 \pm 1.1) \times 10^{-5}$		1767
$\bar{\Lambda}_c^- \Lambda_c^+$	$< 1.6 \times 10^{-5}$	CL=95%	1319
$\bar{\Lambda}_c^-(2593)^- / \bar{\Lambda}_c^-(2625)^- p$	$< 1.1 \times 10^{-4}$	CL=90%	-
$\Xi_c^+ \Lambda_c^+$	$(1.2 \pm 0.8) \times 10^{-3}$		1147
$\Xi_c^+ \Lambda_c^+, \Xi_c^+ \rightarrow \Xi^+\pi^-\pi^-$	$(2.4 \pm 1.1) \times 10^{-5}$	S=1.8	1147
$\Xi_c^+ \Lambda_c^+, \Xi_c^+ \rightarrow \bar{p}K^+\pi^-$	$(5.3 \pm 1.7) \times 10^{-6}$		-
$\Lambda_c^+ \Lambda_c^- K^0$	$(4.0 \pm 0.9) \times 10^{-4}$		732
$\bar{\Lambda}_c^-(2910)^- p, \bar{\Lambda}_c^- \rightarrow$	$(1.2 \pm 0.4) \times 10^{-5}$		-
$\bar{\Sigma}_c(2455)^- \pi^+$			
$\bar{\Lambda}_c^-(2910)^- p, \bar{\Lambda}_c^- \rightarrow$	$(10 \pm 4) \times 10^{-6}$		-
$\bar{\Sigma}_c(2455)^0 \pi^-$			
$\Xi_c^-(2930)^- \Lambda_c^+, \Xi_c^- \rightarrow \Lambda_c^- K^0$	$(2.4 \pm 0.6) \times 10^{-4}$		-
$\Lambda\psi_{DS}$	[vvv] $< 0.13-5.2 \times 10^{-5}$		-

Lepton Family number (LF) or Lepton number (L) or Baryon number (B) violating modes, or/and $\Delta B = 1$ weak neutral current (BI) modes

$\gamma\gamma$	BI	$< 3.2 \times 10^{-7}$	CL=90%	2640
e^+e^-	BI	$< 2.5 \times 10^{-9}$	CL=90%	2640
$e^+e^-\gamma$	BI	$< 1.2 \times 10^{-7}$	CL=90%	2640
$\mu^+\mu^-$	BI	$< 1.5 \times 10^{-10}$	CL=90%	2638
$\mu^+\mu^-\mu^+\mu^-$	BI	$< 1.8 \times 10^{-10}$	CL=95%	2629
$SP, S \rightarrow \mu^+\mu^-$	BI [xxx]	$< 6.0 \times 10^{-10}$	CL=95%	-
$P \rightarrow \mu^+\mu^-$				
$a a, a \rightarrow \mu^+\mu^-$	BI	$< 2.3 \times 10^{-10}$	CL=95%	-
$\tau^+\tau^-$	BI	$< 2.1 \times 10^{-3}$	CL=95%	1952
$\pi^0 \ell^+ \ell^-$	BI [hhh]	$< 5.3 \times 10^{-8}$	CL=90%	2638
$\pi^0 e^+ e^-$	BI	$< 8.4 \times 10^{-8}$	CL=90%	2638
$\pi^0 \mu^+ \mu^-$	BI	$< 6.9 \times 10^{-8}$	CL=90%	2634
$\eta \ell^+ \ell^-$	BI [hhh]	$< 6.4 \times 10^{-8}$	CL=90%	2611
$\eta e^+ e^-$	BI	$< 1.08 \times 10^{-7}$	CL=90%	2611
$\eta \mu^+ \mu^-$	BI	$< 1.12 \times 10^{-7}$	CL=90%	2607
$\pi^0 \nu \bar{\nu}$	BI	$< 9 \times 10^{-6}$	CL=90%	2638

Meson Summary Table

$K^0 \ell^+ \ell^-$	$B1$ [hhh]	$(3.3 \pm 0.6) \times 10^{-7}$		2616
$K^0 e^+ e^-$	$B1$	$(2.5 \pm_{-0.9}^{+1.1}) \times 10^{-7}$	S=1.3	2616
$K^0 \mu^+ \mu^-$	$B1$	$(3.39 \pm 0.35) \times 10^{-7}$	S=1.1	2612
$K^0 \nu \bar{\nu}$	$B1$	$< 2.6 \times 10^{-5}$	CL=90%	2616
$\rho^0 \nu \bar{\nu}$	$B1$	$< 4.0 \times 10^{-5}$	CL=90%	2583
$K^*(892)^0 \ell^+ \ell^-$	$B1$ [hhh]	$(9.9 \pm_{-1.1}^{+1.2}) \times 10^{-7}$		2565
$K^*(892)^0 e^+ e^-$	$B1$	$(1.03 \pm_{-0.17}^{+0.19}) \times 10^{-6}$		2565
$K^*(892)^0 \mu^+ \mu^-$	$B1$	$(9.4 \pm 0.5) \times 10^{-7}$		2560
$K^*(892)^0 \tau^+ \tau^-$	$B1$	$< 3.1 \times 10^{-3}$	CL=90%	1404
$\pi^+ \pi^- \mu^+ \mu^-$	$B1$	$(2.1 \pm 0.5) \times 10^{-8}$		2626
$K^*(892)^0 \nu \bar{\nu}$	$B1$	$< 1.8 \times 10^{-5}$	CL=90%	2565
invisible	$B1$	$< 2.4 \times 10^{-5}$	CL=90%	-
$\nu \bar{\nu} \gamma$	$B1$	$< 1.6 \times 10^{-5}$	CL=90%	2640
$\phi \mu^+ \mu^-$	$B1$	$< 3.2 \times 10^{-9}$	CL=90%	2537
$\phi \nu \bar{\nu}$	$B1$	$< 1.27 \times 10^{-4}$	CL=90%	2541
$e^\pm \mu^\mp$	LF [aa]	$< 1.0 \times 10^{-9}$	CL=90%	2639
$\pi^0 e^\pm \mu^\mp$	LF	$< 1.4 \times 10^{-7}$	CL=90%	2637
$K^0 e^\pm \mu^\mp$	LF	$< 3.8 \times 10^{-8}$	CL=90%	2615
$K^*(892)^0 e^+ \mu^-$	LF	$< 6.8 \times 10^{-9}$	CL=90%	2563
$K^*(892)^0 e^- \mu^+$	LF	$< 5.7 \times 10^{-9}$	CL=90%	2563
$K^*(892)^0 e^\pm \mu^\mp$	LF	$< 1.01 \times 10^{-8}$	CL=90%	2563
$K^*(892)^0 \tau^+ \mu^-$	LF	$< 1.0 \times 10^{-5}$	CL=90%	2221
$K^*(892)^0 \tau^- \mu^+$	LF	$< 8.2 \times 10^{-6}$	CL=90%	2221
$e^\pm \tau^\mp$	LF [aa]	$< 1.6 \times 10^{-5}$	CL=90%	2341
$\mu^\pm \tau^\mp$	LF [aa]	$< 1.4 \times 10^{-5}$	CL=95%	2340
$\rho \mu^-$	L, B	$< 2.6 \times 10^{-9}$	CL=90%	2555
$\Lambda_c^+ \mu^-$	L, B	$< 1.4 \times 10^{-6}$	CL=90%	2143
$\Lambda_c^+ e^-$	L, B	$< 4 \times 10^{-6}$	CL=90%	2145

 B^\pm/B^0 ADMIXTURE**CP violation**

$$\begin{aligned}
 A_{CP}(B \rightarrow K^*(892)\gamma) &= -0.003 \pm 0.011 \\
 A_{CP}(B \rightarrow s\gamma) &= 0.015 \pm 0.011 \\
 A_{CP}(B \rightarrow (s+d)\gamma) &= 0.010 \pm 0.031 \\
 A_{CP}(B \rightarrow X_s \ell^+ \ell^-) &= 0.04 \pm 0.11 \\
 A_{CP}(B \rightarrow X_s \ell^+ \ell^-) \quad (1.0 < q^2 < 6.0 \text{ GeV}^2/c^4) &= -0.06 \pm 0.22 \\
 A_{CP}(B \rightarrow X_s \ell^+ \ell^-) \quad (10.1 < q^2 < 12.9 \text{ or } q^2 > 14.2 \text{ GeV}^2/c^4) &= 0.19 \pm 0.18 \\
 A_{CP}(B \rightarrow K^* e^+ e^-) &= -0.18 \pm 0.15 \\
 A_{CP}(B \rightarrow K^* \mu^+ \mu^-) &= -0.03 \pm 0.13 \\
 A_{CP}(B \rightarrow K^* \ell^+ \ell^-) &= -0.04 \pm 0.07 \\
 A_{CP}(B \rightarrow \eta \text{ anything}) &= -0.13 \pm_{-0.05}^{+0.04} \\
 \Delta A_{CP}(X_s \gamma) = A_{CP}(B^\pm \rightarrow X_s \gamma) - A_{CP}(B^0 \rightarrow X_s \gamma) &= 0.041 \pm 0.023 \\
 \bar{A}_{CP}(B \rightarrow X_s \gamma) = (A_{CP}(B^+ \rightarrow X_s \gamma) + A_{CP}(B^0 \rightarrow X_s \gamma))/2 &= 0.009 \pm 0.012 \\
 \Delta A_{CP}(B \rightarrow K^* \gamma) = A_{CP}(B^+ \rightarrow K^{*+} \gamma) - A_{CP}(B^0 \rightarrow K^{*0} \gamma) &= 0.024 \pm 0.028 \\
 \bar{A}_{CP}(B \rightarrow K^* \gamma) = (A_{CP}(B^+ \rightarrow K^{*+} \gamma) + A_{CP}(B^0 \rightarrow K^{*0} \gamma))/2 &= -0.001 \pm 0.014
 \end{aligned}$$

The branching fraction measurements are for an admixture of B mesons at the $\Upsilon(4S)$. The values quoted assume that $B(\Upsilon(4S) \rightarrow B\bar{B}) = 100\%$.

For inclusive branching fractions, e.g., $B \rightarrow D^\pm \text{ anything}$, the treatment of multiple D 's in the final state must be defined. One possibility would be to count the number of events with one-or-more D 's and divide by the total number of B 's. Another possibility would be to count the total number of D 's and divide by the total number of B 's, which is the definition of average multiplicity. The two definitions are identical if only one D is allowed in the final state. Even though the "one-or-more" definition seems sensible, for practical reasons inclusive branching fractions are almost always measured using the multiplicity definition. For heavy final state particles, authors call their results inclusive branching fractions while for light particles some authors call their results multiplicities. In the B sections, we list all results as inclusive branching fractions, adopting a multiplicity definition. This means that inclusive branching fractions can exceed 100% and that inclusive partial widths can exceed total widths, just as inclusive cross sections can exceed total cross section.

\bar{B} modes are charge conjugates of the modes below. Reactions indicate the weak decay vertex and do not include mixing.

B DECAY MODES	Fraction (Γ_i/Γ)	Scale factor/ Confidence level (MeV/c)	p
Semileptonic and leptonic modes			
$\ell^+ \nu_\ell \text{ anything}$	[hhh,yyy]	$(10.82 \pm 0.15) \%$	-
$D^- \ell^+ \nu_\ell \text{ anything}$	[hhh]	$(2.6 \pm 0.5) \%$	-
$\bar{D}^0 \ell^+ \nu_\ell \text{ anything}$	[hhh]	$(7.2 \pm 1.5) \%$	-
$\bar{D} \ell^+ \nu_\ell$		$(2.41 \pm 0.12) \%$	2311
$D^{*-} \ell^+ \nu_\ell \text{ anything}$	[zzz]	$(6.7 \pm 1.3) \times 10^{-3}$	-
$\bar{D}^* \ell^+ \nu_\ell$	[aaaa]	$(4.95 \pm 0.11) \%$	2257
$\bar{D}^{*+} \ell^+ \nu_\ell$	[hhh,bbaa]	$(2.7 \pm 0.7) \%$	-
$\bar{D}_1(2420) \ell^+ \nu_\ell \text{ anything}$		$(3.8 \pm 1.3) \times 10^{-3}$	S=2.4
$\bar{D} \pi \ell^+ \nu_\ell \text{ anything} + \bar{D}^* \pi \ell^+ \nu_\ell \text{ anything}$		$(2.6 \pm 0.5) \%$	S=1.5
$\bar{D} \pi \ell^+ \nu_\ell \text{ anything}$		$(1.5 \pm 0.6) \%$	-
$\bar{D}^* \pi \ell^+ \nu_\ell \text{ anything}$		$(1.9 \pm 0.4) \%$	-
$\bar{D}_2^*(2460) \ell^+ \nu_\ell \text{ anything}$		$(4.4 \pm 1.6) \times 10^{-3}$	-
$D^{*-} \pi^+ \ell^+ \nu_\ell \text{ anything}$		$(1.00 \pm 0.34) \%$	-
$\bar{D} \pi^+ \pi^- \ell^+ \nu_\ell$		$(1.62 \pm 0.32) \times 10^{-3}$	2301
$\bar{D}^* \pi^+ \pi^- \ell^+ \nu_\ell$		$(9.4 \pm 3.2) \times 10^{-4}$	2247
$D_s^- \ell^+ \nu_\ell \text{ anything}$	[hhh]	$< 7 \times 10^{-3}$	CL=90%
$D_s^- \ell^+ \nu_\ell K^+ \text{ anything}$	[hhh]	$< 5 \times 10^{-3}$	CL=90%
$D_s^- \ell^+ \nu_\ell K^0 \text{ anything}$	[hhh]	$< 7 \times 10^{-3}$	CL=90%
$X_c \ell^+ \nu_\ell$		$(10.63 \pm 0.15) \%$	-
$X_u \ell^+ \nu_\ell$		$(1.88 \pm 0.27) \times 10^{-3}$	-
$X_u e^+ \nu_e$		$(1.57 \pm 0.19) \times 10^{-3}$	-
$X_u \mu^+ \nu_\mu$		$(1.62 \pm 0.21) \times 10^{-3}$	-
$K^+ \ell^+ \nu_\ell \text{ anything}$	[hhh]	$(6.3 \pm 0.5) \%$	-
$K^- \ell^+ \nu_\ell \text{ anything}$	[hhh]	$(10 \pm 4) \times 10^{-3}$	-
$K^0 / \bar{K}^0 \ell^+ \nu_\ell \text{ anything}$	[hhh]	$(4.6 \pm 0.5) \%$	-
$\bar{D} \tau^+ \nu_\tau$		$(8.6 \pm 0.8) \times 10^{-3}$	1911
$\bar{D}^* \tau^+ \nu_\tau$		$(1.40 \pm 0.07) \%$	1838

D, D*, or D_s modes

$D^\pm \text{ anything}$		$(23.1 \pm 1.2) \%$	-
$D^0 / \bar{D}^0 \text{ anything}$		$(64.6 \pm 2.1) \%$	S=1.5
$D^*(2010)^\pm \text{ anything}$		$(22.5 \pm 1.5) \%$	-
$\bar{D}^*(2007)^0 \text{ anything}$		$(26.0 \pm 2.7) \%$	-
$D_s^\pm \text{ anything}$	[aa]	$(10.6 \pm 0.6) \%$	S=1.7
$D_s^{\pm\pm} \text{ anything}$		$(6.3 \pm 1.0) \%$	-
$D_s^\pm \bar{D}^*(*)$		$(3.4 \pm 0.6) \%$	-
$\bar{D} D_{s0}(2317)$	seen		1605
$\bar{D} D_{sJ}(2457)$	seen		-
$D^*(*) \bar{D}^*(*) K^0 + D^*(*) \bar{D}^*(*) K^\pm$	[aa,ccaa]	$(7.1 \pm_{-1.7}^{+2.7}) \%$	-
$b \rightarrow c \bar{c} s$		$(22 \pm 4) \%$	-
$D_s^*(*) \bar{D}^*(*)$	[aa,ccaa]	$(5.0 \pm 0.4) \%$	-
$D^* D^*(2010)^\pm$	[aa]	$< 5.9 \times 10^{-3}$	CL=90%
$D D^*(2010)^\pm + D^* D^\pm$	[aa]	$< 5.5 \times 10^{-3}$	CL=90%
$D D^\pm$	[aa]	$< 3.1 \times 10^{-3}$	CL=90%
$D_s^*(*) \pm \bar{D}^*(*) X (n\pi^\pm)$	[aa,ccaa]	$(9 \pm_{-4}^{+5}) \%$	-
$\bar{D}^*(2010) \gamma$		$< 1.1 \times 10^{-3}$	CL=90%
$D_s^+ \pi^-, D_s^{*+} \pi^-, D_s^+ \rho^-, D_s^{*+} \rho^-, D_s^+ \pi^0, D_s^{*+} \pi^0, D_s^+ \eta, D_s^{*+} \eta, D_s^+ \rho^0, D_s^{*+} \rho^0, D_s^+ \omega, D_s^{*+} \omega$	[aa]	$< 4 \times 10^{-4}$	CL=90%
$D_{s1}(2536)^+ \text{ anything}$		$< 9.5 \times 10^{-3}$	CL=90%

Charmonium modes

$J/\psi(1S) \text{ anything}$		$(1.094 \pm 0.032) \%$	S=1.1
$J/\psi(1S) \text{ (direct) anything}$		$(7.8 \pm 0.4) \times 10^{-3}$	S=1.1
$\psi(2S) \text{ anything}$		$(3.07 \pm 0.21) \times 10^{-3}$	-
$\chi_{c1}(1P) \text{ anything}$		$(3.55 \pm 0.27) \times 10^{-3}$	S=1.3
$\chi_{c1}(1P) \text{ (direct) anything}$		$(3.08 \pm 0.19) \times 10^{-3}$	-
$\chi_{c2}(1P) \text{ anything}$		$(9.9 \pm 1.7) \times 10^{-4}$	S=1.6
$\chi_{c2}(1P) \text{ (direct) anything}$		$(7.5 \pm 1.1) \times 10^{-4}$	-
$\eta_c(1S) \text{ anything}$		$< 9 \times 10^{-3}$	CL=90%
$K \chi_{c1}(3872)$		$(2.5 \pm 0.9) \times 10^{-4}$	1141
$K X(3940), X \rightarrow D^{*0} D^0$		$< 6.7 \times 10^{-5}$	CL=90%
$K \chi_{c0}(3915), \chi_{c0} \rightarrow \omega J/\psi[ddaa]$		$(7.1 \pm 3.4) \times 10^{-5}$	1103

K or K* modes

$K^\pm \text{ anything}$	[aa]	$(78.9 \pm 2.5) \%$	-
$K^+ \text{ anything}$		$(66 \pm 5) \%$	-
$K^- \text{ anything}$		$(13 \pm 4) \%$	-
$K^0 / \bar{K}^0 \text{ anything}$	[aa]	$(64 \pm 4) \%$	-
$K^*(892)^\pm \text{ anything}$		$(18 \pm 6) \%$	-

Meson Summary Table

$K^*(892)^0/\bar{K}^*(892)^0$ anything [aa]	(14.6 ± 2.6) %	–
$K^*(892)\gamma$	(4.2 ± 0.6) × 10 ⁻⁵	2565
$\eta K\gamma$	(8.5 ± 1.8) × 10 ⁻⁶	2588
$K_1(1400)\gamma$	< 1.27 × 10 ⁻⁴	CL=90% 2454
$K_2^*(1430)\gamma$	(1.7 ± 0.6) × 10 ⁻⁵	2447
$K_2(1770)\gamma$	< 1.2 × 10 ⁻³	CL=90% 2342
$K_3^*(1780)\gamma$	< 3.7 × 10 ⁻⁵	CL=90% 2340
$K_4^*(2045)\gamma$	< 1.0 × 10 ⁻³	CL=90% 2243
$K\eta'(958)$	(8.3 ± 1.1) × 10 ⁻⁵	2528
$K^*(892)\eta'(958)$	(4.1 ± 1.1) × 10 ⁻⁶	2472
$K\eta$	< 5.2 × 10 ⁻⁶	CL=90% 2588
$K^*(892)\eta$	(1.8 ± 0.5) × 10 ⁻⁵	2534
$K\phi\phi$	(2.3 ± 0.9) × 10 ⁻⁶	2306
$\bar{b} \rightarrow \bar{s}\gamma$	(3.49 ± 0.19) × 10 ⁻⁴	–
$\bar{b} \rightarrow \bar{d}\gamma$	(9.2 ± 3.0) × 10 ⁻⁶	–
$\bar{b} \rightarrow \bar{s}$ gluon	< 6.8 %	CL=90% –
η anything	(2.6 ± 0.5) × 10 ⁻⁴	–
η' anything	(4.2 ± 0.9) × 10 ⁻⁴	–
K^+ gluon (charmless)	< 1.87 × 10 ⁻⁴	CL=90% –
K^0 gluon (charmless)	(1.9 ± 0.7) × 10 ⁻⁴	–

Light unflavored meson modes

$\rho\gamma$	(1.39 ± 0.25) × 10 ⁻⁶	S=1.2 2583
$\rho/\omega\gamma$	(1.30 ± 0.23) × 10 ⁻⁶	S=1.2 –
π^\pm anything [aa,eeaa]	(358 ± 7) %	–
π^0 anything	(235 ± 11) %	–
η anything	(17.6 ± 1.6) %	–
ρ^0 anything	(21 ± 5) %	–
ω anything	< 81 %	CL=90% –
ϕ anything	(3.43 ± 0.12) %	–
$\phi K^*(892)$	< 2.2 × 10 ⁻⁵	CL=90% 2460
π^+ gluon (charmless)	(3.7 ± 0.8) × 10 ⁻⁴	–

Baryon modes

$\Lambda_c^+/\bar{\Lambda}_c^-$ anything	(3.6 ± 0.4) %	–
Λ_c^+ anything	< 1.3 %	CL=90% –
$\bar{\Lambda}_c^-$ anything	< 7 %	CL=90% –
$\bar{\Lambda}_c^- \ell^+$ anything	< 9 × 10 ⁻⁴	CL=90% –
$\bar{\Lambda}_c^- e^+$ anything	< 1.8 × 10 ⁻³	CL=90% –
$\bar{\Lambda}_c^- \mu^+$ anything	< 1.4 × 10 ⁻³	CL=90% –
$\bar{\Lambda}_c^- p$ anything	(2.06 ± 0.33) %	–
$\bar{\Lambda}_c^- pe^+ \nu_e$	< 8 × 10 ⁻⁴	CL=90% 2021
$\bar{\Sigma}_c^{--}$ anything	(3.4 ± 1.7) × 10 ⁻³	–
$\bar{\Sigma}_c^-$ anything	< 8 × 10 ⁻³	CL=90% –
$\bar{\Sigma}_c^0$ anything	(3.7 ± 1.7) × 10 ⁻³	–
$\bar{\Sigma}_c^0 N(N = p \text{ or } n)$	< 1.2 × 10 ⁻³	CL=90% 1938
Ξ_c^0 anything, $\Xi_c^0 \rightarrow \Xi^- \pi^+$	(1.93 ± 0.30) × 10 ⁻⁴	S=1.1 –
$\Xi_c^+, \Xi_c^+ \rightarrow \Xi^- \pi^+ \pi^+$	(4.5 ± 1.3) × 10 ⁻⁴	–
ρ/\bar{p} anything [aa]	(8.0 ± 0.4) %	–
ρ/\bar{p} (direct) anything [aa]	(5.5 ± 0.5) %	–
$\bar{p}e^+ \nu_e$ anything	< 5.9 × 10 ⁻⁴	CL=90% –
$\Lambda/\bar{\Lambda}$ anything [aa]	(4.0 ± 0.5) %	–
Λ anything	seen	–
$\bar{\Lambda}$ anything	seen	–
$\Xi^-/\bar{\Xi}^+$ anything [aa]	(2.7 ± 0.6) × 10 ⁻³	–
baryons anything	(6.8 ± 0.6) %	–
$p\bar{p}$ anything	(2.47 ± 0.23) %	–
$\Lambda\bar{p}/\bar{\Lambda}p$ anything [aa]	(2.5 ± 0.4) %	–
$\Lambda\bar{\Lambda}$ anything	< 5 × 10 ⁻³	CL=90% –

Lepton Family number (LF) violating modes or $\Delta B = 1$ weak neutral current (BI) modes

$s e^+ e^-$	BI (6.7 ± 1.7) × 10 ⁻⁶	S=2.0 –
$s \mu^+ \mu^-$	BI (4.3 ± 1.0) × 10 ⁻⁶	–
$s \ell^+ \ell^-$	BI [hhh] (5.8 ± 1.3) × 10 ⁻⁶	S=1.8 –
$\pi \ell^+ \ell^-$	BI < 5.9 × 10 ⁻⁸	CL=90% 2638
$\pi e^+ e^-$	BI < 1.10 × 10 ⁻⁷	CL=90% 2638
$\pi \mu^+ \mu^-$	BI < 5.0 × 10 ⁻⁸	CL=90% 2634
$K e^+ e^-$	BI (4.4 ± 0.6) × 10 ⁻⁷	2617
$K^*(892) e^+ e^-$	BI (1.19 ± 0.20) × 10 ⁻⁶	S=1.2 2565
$K \mu^+ \mu^-$	BI (4.4 ± 0.4) × 10 ⁻⁷	2612
$K^*(892) \mu^+ \mu^-$	BI (1.06 ± 0.09) × 10 ⁻⁶	2560
$K \ell^+ \ell^-$	BI (4.8 ± 0.4) × 10 ⁻⁷	2617

$K^*(892) \ell^+ \ell^-$	BI (1.05 ± 0.10) × 10 ⁻⁶	2565
$K \nu \bar{\nu}$	BI < 1.6 × 10 ⁻⁵	CL=90% 2617
$K^* \nu \bar{\nu}$	BI < 2.7 × 10 ⁻⁵	CL=90% –
$\pi \nu \bar{\nu}$	BI < 8 × 10 ⁻⁶	CL=90% 2638
$\rho \nu \bar{\nu}$	BI < 2.8 × 10 ⁻⁵	CL=90% 2583
$s e^\pm \mu^\mp$	LF [aa] < 2.2 × 10 ⁻⁵	CL=90% –
$\pi e^\pm \mu^\mp$	LF < 9.2 × 10 ⁻⁸	CL=90% 2637
$\rho e^\pm \mu^\mp$	LF < 3.2 × 10 ⁻⁶	CL=90% 2582
$K e^\pm \mu^\mp$	LF < 3.8 × 10 ⁻⁸	CL=90% 2616
$K^*(892) e^\pm \mu^\mp$	LF < 5.1 × 10 ⁻⁷	CL=90% 2563

 $B^\pm/B^0/B_s^0/b$ -baryon ADMIXTURE

These measurements are for an admixture of bottom particles at high energy (LHC, LEP, Tevatron, $Spp\bar{S}$).

$$\text{Mean life } \tau = (1.5673 \pm 0.0029) \times 10^{-12} \text{ s}$$

$$\text{Mean life } \tau = (1.72 \pm 0.10) \times 10^{-12} \text{ s} \quad \text{Charged } b\text{-hadron admixture}$$

$$\text{Mean life } \tau = (1.58 \pm 0.14) \times 10^{-12} \text{ s} \quad \text{Neutral } b\text{-hadron admixture}$$

$$\tau_{\text{charged } b\text{-hadron}}/\tau_{\text{neutral } b\text{-hadron}} = 1.09 \pm 0.13$$

$$|\Delta\tau_b|/\tau_{b,\bar{b}} = -0.001 \pm 0.014$$

The branching fraction measurements are for an admixture of B mesons and baryons at energies above the $\Upsilon(4S)$. Only the highest energy results (LHC, LEP, Tevatron, $Spp\bar{S}$) are used in the branching fraction averages. In the following, we assume that the production fractions are the same at the LHC, LEP, and at the Tevatron.

For inclusive branching fractions, e.g., $B \rightarrow D^\pm$ anything, the values usually are multiplicities, not branching fractions. They can be greater than one.

The modes below are listed for a \bar{b} initial state. b modes are their charge conjugates. Reactions indicate the weak decay vertex and do not include mixing.

\bar{b} DECAY MODES	Fraction (Γ_i/Γ)	Scale factor / Confidence level	p (MeV/c)
-----------------------	--------------------------------	---------------------------------	-------------

PRODUCTION FRACTIONS

The production fractions for weakly decaying b -hadrons at high energy have been calculated from the best values of mean lives, mixing parameters, and branching fractions in this edition by the Heavy Flavor Averaging Group (HFAG) as described in the note “ B^0 - \bar{B}^0 Mixing” in the B^0 Particle Listings. We no longer provide world averages of the b -hadron production fractions, where results from LEP, Tevatron and LHC are averaged together; indeed the available data (from CDF and LHCb) shows that the fractions depend on the kinematics (in particular the p_T) of the produced b hadron. Hence we would like to list the fractions in Z decays instead, which are well-defined physics observables. The production fractions in $p\bar{p}$ collisions at the Tevatron are also listed at the end of the section. Values assume

$$B(\bar{b} \rightarrow B^+) = B(\bar{b} \rightarrow B^0)$$

$$B(\bar{b} \rightarrow B^+) + B(\bar{b} \rightarrow B^0) + B(\bar{b} \rightarrow B_s^0) + B(b \rightarrow b\text{-baryon}) = 100\%.$$

The correlation coefficients between production fractions are also reported:

$$\text{cor}(B_s^0, b\text{-baryon}) = 0.064$$

$$\text{cor}(B_s^0, B^\pm=B^0) = -0.633$$

$$\text{cor}(b\text{-baryon}, B^\pm=B^0) = -0.813.$$

The notation for production fractions varies in the literature ($f_B, d_{B^0}, f(b \rightarrow \bar{B}^0), \text{Br}(b \rightarrow \bar{B}^0)$). We use our own branching fraction notation here, $B(\bar{b} \rightarrow B^0)$.

Note these production fractions are b -hadronization fractions, not the conventional branching fractions of b -quark to a B -hadron, which may have considerable dependence on the initial and final state kinematic and production environment.

B^+	(40.8 ± 0.7) %	–
B^0	(40.8 ± 0.7) %	–
B_s^0	(10.0 ± 0.8) %	–
b -baryon	(8.4 ± 1.1) %	–

DECAY MODES

Semileptonic and leptonic modes

ν anything	(23.1 ± 1.5) %	–
$\ell^+ \nu_\ell$ anything [hhh]	(10.69 ± 0.22) %	–
$e^+ \nu_e$ anything	(10.86 ± 0.35) %	–
$\mu^+ \nu_\mu$ anything	(10.95 ± 0.29) %	–
$D^- \ell^+ \nu_\ell$ anything [hhh]	(2.2 ± 0.4) %	S=1.9 –
$D^- \pi^+ \ell^+ \nu_\ell$ anything	(4.9 ± 1.9) × 10 ⁻³	–

Meson Summary Table

$D^- \pi^- \ell^+ \nu_\ell$ anything	(2.6 ± 1.6) × 10 ⁻³	-
$\overline{D}^0 \ell^+ \nu_\ell$ anything	[hhh] (6.79 ± 0.34) %	-
$\overline{D}^0 \pi^- \ell^+ \nu_\ell$ anything	(1.07 ± 0.27) %	-
$\overline{D}^0 \pi^+ \ell^+ \nu_\ell$ anything	(2.3 ± 1.6) × 10 ⁻³	-
$D^{*-} \ell^+ \nu_\ell$ anything	[hhh] (2.75 ± 0.19) %	-
$D^{*-} \pi^- \ell^+ \nu_\ell$ anything	(6 ± 7) × 10 ⁻⁴	-
$D^{*-} \pi^+ \ell^+ \nu_\ell$ anything	(4.8 ± 1.0) × 10 ⁻³	-
$\overline{D}_j^0 \ell^+ \nu_\ell$ anything × B($\overline{D}_j^0 \rightarrow D^{*+} \pi^-$)	[hhh, ffaa] (2.6 ± 0.9) × 10 ⁻³	-
$D_j^- \ell^+ \nu_\ell$ anything × B($D_j^- \rightarrow D^0 \pi^-$)	[hhh, ffaa] (7.0 ± 2.3) × 10 ⁻³	-
$\overline{D}_2^*(2460)^0 \ell^+ \nu_\ell$ anything × B($\overline{D}_2^*(2460)^0 \rightarrow D^{*-} \pi^+$)	< 1.4 × 10 ⁻³ CL=90%	-
$D_2^*(2460)^- \ell^+ \nu_\ell$ anything × B($D_2^*(2460)^- \rightarrow D^0 \pi^-$)	(4.2 ± 1.5 / 1.8) × 10 ⁻³	-
$\overline{D}_2^*(2460)^0 \ell^+ \nu_\ell$ anything × B($\overline{D}_2^*(2460)^0 \rightarrow D^- \pi^+$)	(1.6 ± 0.8) × 10 ⁻³	-
charmless $\ell \overline{\nu}_\ell$	[hhh] (1.7 ± 0.5) × 10 ⁻³	-
$\tau^+ \nu_\tau$ anything	(2.41 ± 0.23) %	-
$D^{*-} \tau \nu_\tau$ anything	(9 ± 4) × 10 ⁻³	-
$\overline{c} \rightarrow \ell^+ \overline{\nu}_\ell$ anything	[hhh] (8.02 ± 0.19) %	-
$c \rightarrow \ell^+ \nu$ anything	(1.6 ± 0.4 / 0.5) %	-
Charmed meson and baryon modes		
\overline{D}^0 anything	(58.7 ± 2.8) %	-
$D^0 D_s^\pm$ anything	[aa] (9.1 ± 4.0 / 2.8) %	-
$D^\mp D_s^\pm$ anything	[aa] (4.0 ± 2.3 / 1.8) %	-
$\overline{D}^0 D^0$ anything	[aa] (5.1 ± 2.0 / 1.8) %	-
$D^0 D^\pm$ anything	[aa] (2.7 ± 1.8 / 1.6) %	-
$D^\pm D^\mp$ anything	[aa] < 9 × 10 ⁻³ CL=90%	-
D^- anything	(22.7 ± 1.6) %	-
$D^*(2010)^+$ anything	(17.3 ± 2.0) %	-
$D_1(2420)^0$ anything	(5.0 ± 1.5) %	-
$D^*(2010)^\mp D_s^\pm$ anything	[aa] (3.3 ± 1.6 / 1.3) %	-
$D^0 D^*(2010)^\pm$ anything	[aa] (3.0 ± 1.1 / 0.9) %	-
$D^*(2010)^\pm D^\mp$ anything	[aa] (2.5 ± 1.2 / 1.0) %	-
$D^*(2010)^\pm D^*(2010)^\mp$ anything	[aa] (1.2 ± 0.4) %	-
$\overline{D} D$ anything	(10 ± 11 / 10) %	-
$D_2^*(2460)^0$ anything	(4.7 ± 2.7) %	-
D_s^- anything	(14.7 ± 2.1) %	-
D_s^+ anything	(10.1 ± 3.1) %	-
Λ_c^+ anything	(7.8 ± 1.1) %	-
\overline{c}/c anything	[eeaa] (116.2 ± 3.2) %	-
Charmonium modes		
$J/\psi(1S)$ anything	(1.16 ± 0.10) %	-
$\psi(2S)$ anything	(3.06 ± 0.30) × 10 ⁻³	-
$\chi_{c0}(1P)$ anything	(1.4 ± 0.5) %	-
$\chi_{c1}(1P)$ anything	(1.4 ± 0.4) %	-
$\chi_{c2}(1P)$ anything	(5.5 ± 2.4) × 10 ⁻³	-
$\chi_c(2P)$ anything, $\chi_c \rightarrow \phi \phi$	< 2.8 × 10 ⁻⁷ CL=95%	-
$\eta_c(1S)$ anything	(5.6 ± 0.9) × 10 ⁻³	-
$\eta_c(2S)$ anything, $\eta_c \rightarrow \phi \phi$	(4.1 ± 1.7) × 10 ⁻⁷	-
$\chi_{c1}(3872)$ anything, $\chi_{c1} \rightarrow \phi \phi$	< 4.5 × 10 ⁻⁷ CL=95%	-
$\chi_{c0}(3915)$ anything, $\chi_{c0} \rightarrow \phi \phi$	< 3.1 × 10 ⁻⁷ CL=95%	-
K or K* modes		
$\overline{3}\gamma$	(3.1 ± 1.1) × 10 ⁻⁴	-
$\overline{3}\overline{\nu} \nu$	BI < 6.4 × 10 ⁻⁴ CL=90%	-
K^\pm anything	(74 ± 6) %	-
K_S^0 anything	(29.0 ± 2.9) %	-
Pion modes		
π^\pm anything	(397 ± 21) %	-
π^0 anything	[eeaa] (280 ± 60) %	-

ϕ anything	(2.82 ± 0.23) %	-
Baryon modes		
p/\overline{p} anything	(13.1 ± 1.1) %	-
$\Lambda/\overline{\Lambda}$ anything	(5.9 ± 0.6) %	-
b-baryon anything	(10.2 ± 2.8) %	-
Other modes		
charged anything	[eeaa] (497 ± 7) %	-
hadron ⁺ hadron ⁻	(1.7 ± 1.0 / 0.7) × 10 ⁻⁵	-
charmless	(7 ± 21) × 10 ⁻³	-
$\Delta B = 1$ weak neutral current (BI) modes		
$\mu^+ \mu^-$ anything	BI < 3.2 × 10 ⁻⁴ CL=90%	-

B*

$$I(J^P) = \frac{1}{2}(1^-)$$

I, J, P need confirmation.

Quantum numbers shown are quark-model predictions.

$$\begin{aligned} \text{Mass } m_{B^*} &= 5324.75 \pm 0.20 \text{ MeV} \\ m_{B^*} - m_B &= 45.18 \pm 0.20 \text{ MeV} \\ m_{B^{*+}} - m_{B^+} &= 45.34 \pm 0.20 \text{ MeV} \end{aligned}$$

B* DECAY MODES	Fraction (Γ_i/Γ)	ρ (MeV/c)
$B\gamma$	seen	45

B₁(5721)

$$I(J^P) = \frac{1}{2}(1^+)$$

I, J, P need confirmation.

$$\begin{aligned} B_1(5721)^+ \text{ mass} &= 5726.0^{+2.5}_{-2.7} \text{ MeV} \\ m_{B_1^+} - m_{B^{*0}} &= 401.2^{+2.4}_{-2.7} \text{ MeV} \\ B_1(5721)^0 \text{ mass} &= 5726.1 \pm 1.2 \text{ MeV} \quad (S = 1.2) \\ m_{B_1^0} - m_{B^+} &= 446.7 \pm 1.2 \text{ MeV} \quad (S = 1.2) \\ m_{B_1^0} - m_{B^{*+}} &= 401.4 \pm 1.2 \text{ MeV} \quad (S = 1.2) \\ \text{Full width } \Gamma(B_1(5721)^+) &= 31 \pm 6 \text{ MeV} \quad (S = 1.1) \\ \text{Full width } \Gamma(B_1(5721)^0) &= 27.5 \pm 3.4 \text{ MeV} \quad (S = 1.1) \end{aligned}$$

B₁(5721) DECAY MODES	Fraction (Γ_i/Γ)	ρ (MeV/c)
$B^* \pi$	seen	365

B₂^{*}(5747)

$$I(J^P) = \frac{1}{2}(2^+)$$

I, J, P need confirmation.

$$\begin{aligned} B_2^*(5747)^+ \text{ mass} &= 5737.3 \pm 0.7 \text{ MeV} \\ m_{B_2^{*+}} - m_{B^0} &= 457.5 \pm 0.7 \text{ MeV} \\ B_2^*(5747)^0 \text{ mass} &= 5739.6 \pm 0.7 \text{ MeV} \quad (S = 1.4) \\ m_{B_2^{*0}} - m_{B_1^0} &= 13.5 \pm 1.4 \text{ MeV} \quad (S = 1.3) \\ m_{B_2^{*0}} - m_{B^+} &= 460.2 \pm 0.6 \text{ MeV} \quad (S = 1.4) \\ \text{Full width } \Gamma(B_2^*(5747)^+) &= 20 \pm 5 \text{ MeV} \quad (S = 2.2) \\ \text{Full width } \Gamma(B_2^*(5747)^0) &= 24.2 \pm 1.7 \text{ MeV} \end{aligned}$$

B₂[*](5747) DECAY MODES	Fraction (Γ_i/Γ)	ρ (MeV/c)
$B\pi$	seen	420
$B^* \pi$	seen	376

B_J(5970)

$$I(J^P) = \frac{1}{2}(?^?)$$

I, J, P need confirmation.

$$\begin{aligned} B_J(5970)^+ \text{ mass } m &= 5965 \pm 5 \text{ MeV} \\ m_{B_J(5970)^+} - m_{B^0} &= 685 \pm 5 \text{ MeV} \\ B_J(5970)^0 \text{ mass } m &= 5971 \pm 5 \text{ MeV} \\ m_{B_J(5970)^0} - m_{B^+} &= 691 \pm 5 \text{ MeV} \\ B_J(5970)^+ \text{ full width } \Gamma &= 62 \pm 20 \text{ MeV} \\ B_J(5970)^0 \text{ full width } \Gamma &= 81 \pm 12 \text{ MeV} \end{aligned}$$

B_J(5970) DECAY MODES	Fraction (Γ_i/Γ)	ρ (MeV/c)
$B\pi$	possibly seen	633
$B^* \pi$	seen	592

Meson Summary Table

BOTTOM, STRANGE MESONS ($B = \pm 1, S = \mp 1$)

$$B_s^0 = s\bar{b}, \bar{B}_s^0 = \bar{s}b, \quad \text{similarly for } B_s^{*\prime}s$$

 B_s^0

$$J(P) = 0(0^-)$$

I, J, P need confirmation. Quantum numbers shown are quark-model predictions.

$$\text{Mass } m_{B_s^0} = 5366.93 \pm 0.10 \text{ MeV}$$

$$m_{B_s^0} - m_B = 87.37 \pm 0.12 \text{ MeV}$$

$$\text{Mean life } \tau = (1.520 \pm 0.005) \times 10^{-12} \text{ s}$$

$$c\tau = 455.7 \text{ } \mu\text{m}$$

$$\Delta\Gamma_{B_s^0} = \Gamma_{B_{sL}^0} - \Gamma_{B_{sH}^0} = (0.083 \pm 0.005) \times 10^{12} \text{ s}^{-1} \quad (S = 1.8)$$

B_s^0 - \bar{B}_s^0 mixing parameters

$$\Delta m_{B_s^0} = m_{B_{sH}^0} - m_{B_{sL}^0} = (17.765 \pm 0.006) \times 10^{12} \text{ } \hbar \text{ s}^{-1}$$

$$= (1.1693 \pm 0.0004) \times 10^{-8} \text{ MeV}$$

$$x_s = \Delta m_{B_s^0} / \Gamma_{B_s^0} = 26.99 \pm 0.09$$

$$\chi_s (B_s^0\text{-}\bar{B}_s^0 \text{ mixing parameter}) = 0.499318 \pm 0.000005$$

CP violation parameters in B_s^0

$$\text{Re}(\epsilon_{B_s^0}) / (1 + |\epsilon_{B_s^0}|^2) = (-0.15 \pm 0.70) \times 10^{-3}$$

$$C_{KK}(B_s^0 \rightarrow K^+ K^-) = 0.162 \pm 0.035$$

$$S_{KK}(B_s^0 \rightarrow K^+ K^-) = 0.14 \pm 0.05 \quad (S = 1.3)$$

$$r_B(B_s^0 \rightarrow D_s^\mp K^\pm) = 0.37 \pm_{-0.09}^{+0.10}$$

$$r_B(B_s^0 \rightarrow D_s^\mp K^\pm \pi^\pm \pi^\mp) = 0.47 \pm 0.08$$

$$\delta_B(B_s^0 \rightarrow D_s^\pm K^\mp) = (358 \pm 14)^\circ$$

$$\delta_B(B_s^0 \rightarrow D_s^\pm K^\mp \pi^\pm \pi^\mp) = (-6 \pm_{-13}^{+10})^\circ$$

$$\text{CP Violation phase } \beta_s (b \rightarrow c\bar{c}s) = (2.0 \pm 0.8) \times 10^{-2} \text{ rad}$$

$$\text{CP Violation phase } \beta_s (b \rightarrow s\bar{s}s) = (3.7 \pm 3.5) \times 10^{-2} \text{ rad}$$

$$|\lambda| (B_s^0 \rightarrow J/\psi(1S)\phi) = 0.988 \pm 0.009$$

$$|\lambda| (b \rightarrow c\bar{c}s) = 0.989 \pm 0.008$$

$$A, \text{ CP violation parameter} = -0.79 \pm 0.08$$

$$C, \text{ CP violation parameter} = 0.19 \pm 0.06$$

$$S, \text{ CP violation parameter} = 0.17 \pm 0.06$$

$$A_{CP}^L(B_s \rightarrow J/\psi \bar{K}^*(892)^0) = -0.05 \pm 0.06$$

$$A_{CP}^{\parallel}(B_s \rightarrow J/\psi \bar{K}^*(892)^0) = 0.17 \pm 0.15$$

$$A_{CP}^{\perp}(B_s \rightarrow J/\psi \bar{K}^*(892)^0) = -0.05 \pm 0.10$$

$$A_{CP}(B_s \rightarrow \pi^+ K^-) = 0.224 \pm 0.012$$

$$A_{CP}(B_s^0 \rightarrow [K^+ K^-]_D \bar{K}^*(892)^0) = -0.04 \pm 0.07$$

$$A_{CP}(B_s^0 \rightarrow [\pi^+ K^-]_D K^*(892)^0) = -0.01 \pm 0.04$$

$$A_{CP}(B_s^0 \rightarrow [\pi^+ \pi^-]_D K^*(892)^0) = 0.06 \pm 0.13$$

$$S(B_s^0 \rightarrow \phi\gamma) = 0.43 \pm 0.32$$

$$C(B_s^0 \rightarrow \phi\gamma) = 0.11 \pm 0.31$$

$$A^\Delta(B_s^0 \rightarrow \phi\gamma) = -0.7 \pm 0.4$$

$$\Delta a_{\perp} < 1.2 \times 10^{-12} \text{ GeV, CL} = 95\%$$

$$\Delta a_{\parallel} = (-0.9 \pm 1.5) \times 10^{-14} \text{ GeV}$$

$$\Delta a_X = (1.0 \pm 2.2) \times 10^{-14} \text{ GeV}$$

$$\Delta a_Y = (-3.8 \pm 2.2) \times 10^{-14} \text{ GeV}$$

$$\text{Re}(\xi) = -0.022 \pm 0.033$$

$$\text{Im}(\xi) = 0.004 \pm 0.011$$

These branching fractions all scale with $B(\bar{b} \rightarrow B_s^0)$.

The branching fraction $B(B_s^0 \rightarrow D_s^- \ell^+ \nu_\ell \text{ anything})$ is not a pure measurement since the measured product branching fraction $B(\bar{b} \rightarrow B_s^0) \times B(B_s^0 \rightarrow D_s^- \ell^+ \nu_\ell \text{ anything})$ was used to determine $B(\bar{b} \rightarrow B_s^0)$, as described in the note on " B^0 - \bar{B}^0 Mixing"

For inclusive branching fractions, e.g., $B \rightarrow D^\pm \text{ anything}$, the values usually are multiplicities, not branching fractions. They can be greater than one.

B_s^0 DECAY MODES

B_s^0 DECAY MODES	Fraction (Γ_i/Γ)	Scale factor/ Confidence level	p (MeV/c)
D_s^- anything	(62 \pm 6) %		-
D_s^\pm anything	(92 \pm 11) %		-
D^0/\bar{D}^0 anything	(38 \pm 10) %		-

$\ell \nu_\ell X$	(9.6 \pm 0.8) %	-
$e^+ \nu X^-$	(9.1 \pm 0.8) %	-
$\mu^+ \nu X^-$	(10.2 \pm 1.0) %	-
$D_s^- \ell^+ \nu_\ell \text{ anything}$	[ggaa] (8.1 \pm 1.3) %	-
$D_s^{*-} \ell^+ \nu_\ell \text{ anything}$	(5.4 \pm 1.1) %	-
$D_s^- \mu^+ \nu_\mu$	(2.31 \pm 0.21) %	2321
$D_s^{*-} \mu^+ \nu_\mu$	(5.2 \pm 0.5) %	2266
$D_{s1}(2536)^- \mu^+ \nu_\mu, D_{s1}^- \rightarrow D^{*-} K_S^0$	(2.7 \pm 0.7) $\times 10^{-3}$	-
$D_{s1}(2536)^- X \mu^+ \nu, D_{s1}^- \rightarrow \bar{D}^0 K^+$	(4.4 \pm 1.3) $\times 10^{-3}$	-
$D_{s2}(2573)^- X \mu^+ \nu, D_{s2}^- \rightarrow \bar{D}^0 K^+$	(2.7 \pm 1.0) $\times 10^{-3}$	-
$K^- \mu^+ \nu_\mu$	(1.06 \pm 0.09) $\times 10^{-4}$	2660
$D_s^- \pi^+$	(2.98 \pm 0.14) $\times 10^{-3}$	2320
$D_s^- \rho^+$	(6.8 \pm 1.4) $\times 10^{-3}$	2249
$D_s^- \pi^+ \pi^+ \pi^-$	(6.1 \pm 1.0) $\times 10^{-3}$	2301
$D_{s1}(2536)^- \pi^+, D_{s1}^- \rightarrow D_s^- \pi^+ \pi^-$	(2.4 \pm 0.8) $\times 10^{-5}$	-
$D_s^\mp K^\pm$	(2.25 \pm 0.12) $\times 10^{-4}$	2293
$D_{s1}(2536)^\mp K^\pm, D_{s1}^- \rightarrow \bar{D}^*(2007)^0 K^-$	(2.48 \pm 0.28) $\times 10^{-5}$	-
$D_s^- K^+ \pi^+ \pi^-$	(3.2 \pm 0.6) $\times 10^{-4}$	2249
$D_s^+ D_s^-$	(4.4 \pm 0.5) $\times 10^{-3}$	1824
$D_s^- D^+$	(2.8 \pm 0.5) $\times 10^{-4}$	1875
$D^+ D^-$	(2.2 \pm 0.6) $\times 10^{-4}$	1925
$D^{*+} D^{*-}$	(2.14 \pm 0.32) $\times 10^{-4}$	1778
$D^0 \bar{D}^0$	(1.9 \pm 0.5) $\times 10^{-4}$	1930
$D_s^{*-} \pi^+$	(1.9 \pm 0.5) $\times 10^{-3}$	2265
$D_s^\mp K^\pm$	(1.32 \pm 0.40) $\times 10^{-4}$	-
$D_s^{*-} \rho^+$	(9.5 \pm 2.0) $\times 10^{-3}$	2191
$D_s^+ D_s^- + D_s^{*-} D_s^+$	(1.39 \pm 0.17) %	1742
$D_s^{*+} D_s^{*-}$	(1.44 \pm 0.21) %	S=1.1 1655
$D_s^{(*)+} D_s^{(*)-}$	(4.5 \pm 1.4) %	-
$D_s^* - D_s^+$	(3.9 \pm 0.8) $\times 10^{-4}$	1801
$\bar{D}^{*0} \bar{K}^0$	(2.8 \pm 1.1) $\times 10^{-4}$	2278
$\bar{D}^0 \bar{K}^0$	(4.3 \pm 0.9) $\times 10^{-4}$	2330
$\bar{D}^0 K^- \pi^+$	(1.04 \pm 0.13) $\times 10^{-3}$	2312
$\bar{D}^*(2007)^0 K^- \pi^+$	(7.3 \pm 2.6) $\times 10^{-4}$	2259
$\bar{D}^0 \bar{K}^*(892)^0$	(4.4 \pm 0.6) $\times 10^{-4}$	2264
$\bar{D}^0 \bar{K}^*(1410)$	(3.9 \pm 3.5) $\times 10^{-4}$	2117
$\bar{D}^0 \bar{K}_0^*(1430)$	(3.0 \pm 0.7) $\times 10^{-4}$	2113
$\bar{D}^0 \bar{K}_2^*(1430)$	(1.1 \pm 0.4) $\times 10^{-4}$	2112
$\bar{D}^0 \bar{K}^*(1680)$	< 7.8 $\times 10^{-5}$	CL=90% 1997
$\bar{D}^0 \bar{K}_0^*(1950)$	< 1.1 $\times 10^{-4}$	CL=90% 1884
$\bar{D}^0 \bar{K}_3^*(1780)$	< 2.6 $\times 10^{-5}$	CL=90% 1970
$\bar{D}^0 \bar{K}_4^*(2045)$	< 3.1 $\times 10^{-5}$	CL=90% 1835
$\bar{D}^0 K^- \pi^+$ (non-resonant)	(2.1 \pm 0.8) $\times 10^{-4}$	2312
$D_{s2}^*(2573)^- \pi^+, D_{s2}^* \rightarrow \bar{D}^0 K^-$	(2.6 \pm 0.4) $\times 10^{-4}$	-
$D_{s1}^*(2700)^- \pi^+, D_{s1}^* \rightarrow \bar{D}^0 K^-$	(1.6 \pm 0.8) $\times 10^{-5}$	-
$D_{s1}^*(2860)^- \pi^+, D_{s1}^* \rightarrow \bar{D}^0 K^-$	(5 \pm 4) $\times 10^{-5}$	-
$D_{s3}^*(2860)^- \pi^+, D_{s3}^* \rightarrow \bar{D}^0 K^-$	(2.2 \pm 0.6) $\times 10^{-5}$	-
$\bar{D}^0 K^+ K^-$	(5.6 \pm 0.9) $\times 10^{-5}$	2243
$\bar{D}^0 f_0(980)$	< 3.1 $\times 10^{-6}$	CL=90% 2242
$\bar{D}^0 \phi$	(2.30 \pm 0.25) $\times 10^{-5}$	2235
$\bar{D}^{*0} \phi$	(3.2 \pm 0.4) $\times 10^{-5}$	2178
$D^{*+} \pi^\pm$	< 6.1 $\times 10^{-6}$	CL=90% -
$\eta_c \phi$	(5.0 \pm 0.9) $\times 10^{-4}$	1663
$\eta_c \pi^+ \pi^-$	(1.8 \pm 0.7) $\times 10^{-4}$	1840
$J/\psi(1S) \phi$	(1.04 \pm 0.04) $\times 10^{-3}$	1588
$J/\psi(1S) \phi \phi$	(1.20 \pm 0.14) $\times 10^{-5}$	764
$J/\psi(1S) \pi^0$	< 1.2 $\times 10^{-3}$	CL=90% 1787
$J/\psi(1S) \eta$	(4.0 \pm 0.7) $\times 10^{-4}$	S=1.4 1733
$J/\psi(1S) K_S^0$	(1.92 \pm 0.14) $\times 10^{-5}$	1743
$J/\psi(1S) \bar{K}^*(892)^0$	(4.1 \pm 0.4) $\times 10^{-5}$	1637
$J/\psi(1S) \eta'$	(3.3 \pm 0.4) $\times 10^{-4}$	1612
$J/\psi(1S) \pi^+ \pi^-$	(2.02 \pm 0.17) $\times 10^{-4}$	S=1.7 1775
$J/\psi(1S) f_0(500), f_0 \rightarrow \pi^+ \pi^-$	< 4 $\times 10^{-6}$	CL=90% -

Meson Summary Table

$J/\psi(1S) \rho, \rho \rightarrow \pi^+ \pi^-$	$< 3.4 \times 10^{-6}$	CL=90%	-	$K^0 K^+ K^-$	$(1.3 \pm 0.6) \times 10^{-6}$	2568
$J/\psi(1S) f_0(980), f_0 \rightarrow \pi^+ \pi^-$	$(1.24 \pm 0.15) \times 10^{-4}$	S=2.1	-	$\bar{K}^*(892)^0 \rho^0$	$< 7.67 \times 10^{-4}$	CL=90% 2550
$J/\psi(1S) f_2(1270), f_2 \rightarrow \pi^+ \pi^-$	$(1.0 \pm 0.4) \times 10^{-6}$		-	$\bar{K}^*(892)^0 K^*(892)^0$	$(1.11 \pm 0.27) \times 10^{-5}$	2531
$J/\psi(1S) f_2(1270)_0, f_2 \rightarrow \pi^+ \pi^-$	$(7.3 \pm 1.7) \times 10^{-7}$		-	$\phi K^*(892)^0$	$(1.14 \pm 0.30) \times 10^{-6}$	2507
$J/\psi(1S) f_2(1270)_\parallel, f_2 \rightarrow \pi^+ \pi^-$	$(1.05 \pm 0.33) \times 10^{-6}$		-	$\rho \bar{\rho}$	$< 4.4 \times 10^{-9}$	CL=90% 2514
$J/\psi(1S) f_2(1270)_\perp, f_2 \rightarrow \pi^+ \pi^-$	$(1.3 \pm 0.7) \times 10^{-6}$		-	$\rho \bar{\rho} K^+ K^-$	$(4.5 \pm 0.5) \times 10^{-6}$	2231
$J/\psi(1S) f_0(1370), f_0 \rightarrow \pi^+ \pi^-$	$(4.4 \pm 0.6) \times 10^{-5}$		-	$\rho \bar{\rho} K^+ \pi^-$	$(1.39 \pm 0.26) \times 10^{-6}$	2355
$J/\psi(1S) f_0(1500), f_0 \rightarrow \pi^+ \pi^-$	$(2.04 \pm 0.32) \times 10^{-5}$		-	$\rho \bar{\rho} \pi^+ \pi^-$	$(4.3 \pm 2.0) \times 10^{-7}$	2454
$J/\psi(1S) f'_2(1525)_0, f'_2 \rightarrow \pi^+ \pi^-$	$(1.03 \pm 0.22) \times 10^{-6}$		-	$\rho \bar{\rho} \rho \bar{\rho}$	$(2.3 \pm 1.0) \times 10^{-8}$	1797
$J/\psi(1S) f'_2(1525)_\parallel, f'_2 \rightarrow \pi^+ \pi^-$	$(1.2 \pm 2.6) \times 10^{-7}$		-	$\rho \bar{K} K^- + c.c.$	$(5.5 \pm 1.0) \times 10^{-6}$	2358
$J/\psi(1S) f'_2(1525)_\perp, f'_2 \rightarrow \pi^+ \pi^-$	$(5 \pm 4) \times 10^{-7}$		-	$\Lambda_c^- \Lambda \pi^+$	$(3.6 \pm 1.6) \times 10^{-4}$	1979
$J/\psi(1S) f_0(1790), f_0 \rightarrow \pi^+ \pi^-$	$(4.9 \pm 10.0) \times 10^{-6}$		-	$\Lambda_c^- \Lambda_c^+$	$< 8.0 \times 10^{-5}$	CL=95% 1405
$J/\psi(1S) \pi^+ \pi^-$ (nonresonant)	$(1.74 \pm 1.10) \times 10^{-5}$		1775	Lepton Family number (LF) violating modes or $\Delta B = 1$ weak neutral current (B1) modes		
$J/\psi(1S) \bar{K}^0 \pi^+ \pi^-$	$< 4.4 \times 10^{-5}$	CL=90%	1675	$\gamma \gamma$	B1	$< 3.1 \times 10^{-6}$ CL=90% 2683
$J/\psi(1S) K^+ K^-$	$(7.9 \pm 0.7) \times 10^{-4}$		1601	$\phi \gamma$	B1	$(3.4 \pm 0.4) \times 10^{-5}$ 2587
$J/\psi(1S) K^0 K^- \pi^+ + c.c.$	$(9.5 \pm 1.3) \times 10^{-4}$		1538	$\mu^+ \mu^-$	B1	$(3.34 \pm 0.27) \times 10^{-9}$ 2681
$J/\psi(1S) \bar{K}^0 K^+ K^-$	$< 1.2 \times 10^{-5}$	CL=90%	1333	$e^+ e^-$	B1	$< 9.4 \times 10^{-9}$ CL=90% 2683
$J/\psi K^*(892)^0 \bar{K}^*(892)^0$	$(1.10 \pm 0.09) \times 10^{-4}$		1083	$\tau^+ \tau^-$	B1	$< 6.8 \times 10^{-3}$ CL=95% 2011
$J/\psi(1S) f'_2(1525)$	$(2.6 \pm 0.6) \times 10^{-4}$		1310	$\mu^+ \mu^- \gamma$	B1	$< 2.0 \times 10^{-9}$ 2681
$J/\psi(1S) \rho \bar{\rho}$	$(3.6 \pm 0.4) \times 10^{-6}$		982	$\mu^+ \mu^- \mu^+ \mu^-$	B1	$< 8.6 \times 10^{-10}$ CL=95% 2673
$J/\psi(1S) \gamma$	$< 7.3 \times 10^{-6}$	CL=90%	1790	$S P, S \rightarrow \mu^+ \mu^-$	B1	[xxx] $< 2.2 \times 10^{-9}$ CL=95% -
$J/\psi(\mu^+ \mu^-), J/\psi \rightarrow \mu^+ \mu^-$	$< 2.6 \times 10^{-9}$	CL=95%	-	$P \rightarrow \mu^+ \mu^-$		
$J/\psi(1S) \pi^+ \pi^- \pi^+ \pi^-$	$(7.5 \pm 0.8) \times 10^{-5}$		1731	$a a, a \rightarrow \mu^+ \mu^-$	B1	$< 5.8 \times 10^{-10}$ CL=95% -
$J/\psi(1S) f_1(1285)$	$(7.2 \pm 1.4) \times 10^{-5}$		1460	$\phi(1020) \mu^+ \mu^-$	B1	$(8.4 \pm 0.4) \times 10^{-7}$ 2582
$\psi(2S) \eta$	$(3.3 \pm 0.9) \times 10^{-4}$		1338	$f'_2(1525) \mu^+ \mu^-$	B1	$(1.62 \pm 0.22) \times 10^{-7}$ 2464
$\psi(2S) \eta'$	$(1.29 \pm 0.35) \times 10^{-4}$		1158	$\bar{K}^*(892)^0 \mu^+ \mu^-$	B1	$(2.9 \pm 1.1) \times 10^{-8}$ 2605
$\psi(2S) \pi^+ \pi^-$	$(6.9 \pm 1.2) \times 10^{-5}$		1397	$\pi^+ \pi^- \mu^+ \mu^-$	B1	$(8.4 \pm 1.7) \times 10^{-8}$ 2670
$\psi(2S) \phi$	$(5.3 \pm 0.4) \times 10^{-4}$		1120	$\phi \nu \bar{\nu}$	B1	$< 5.4 \times 10^{-3}$ CL=90% 2587
$\psi(2S) K^0$	$(1.9 \pm 0.5) \times 10^{-5}$		1352	$e^\pm \mu^\mp$	LF [aa]	$< 5.4 \times 10^{-9}$ CL=90% 2682
$\psi(2S) K^- \pi^+$	$(3.1 \pm 0.4) \times 10^{-5}$		1310	$e^\pm \tau^\mp$	LF	$< 1.4 \times 10^{-3}$ CL=90% 2389
$\psi(2S) K^* (892)^0$	$(3.3 \pm 0.5) \times 10^{-5}$		1196	$\mu^\pm \tau^\mp$	LF	$< 4.2 \times 10^{-5}$ CL=95% 2388
$\chi_{c1} \phi$	$(1.97 \pm 0.25) \times 10^{-4}$		1275	$\phi \mu^\pm e^\mp$	LF	$< 1.6 \times 10^{-8}$ CL=90% 2586
$\chi_{c1}(3872) \phi$	$(1.22 \pm 0.35) \times 10^{-4}$		936	$\rho \mu^-$	L,B	$< 1.21 \times 10^{-8}$ CL=90% 2600
$\chi_{c1}(3872) (K^+ K^-)_{non-\phi}$	$(9.4 \pm 3.4) \times 10^{-5}$		961	B_s^* $I(J^P) = 0(1^-)$		
$\chi_{c1}(3872) \pi^+ \pi^-$	$(4.6 \pm 1.6) \times 10^{-5}$		1264	I, J, P need confirmation. Quantum numbers shown are quark-model predictions.		
$\pi^+ \pi^-$	$(7.2 \pm 1.0) \times 10^{-7}$		2680	Mass $m = 5415.4 \pm 1.4$ MeV (S = 2.6)		
$\pi^0 \pi^0$	$< 7.7 \times 10^{-6}$	CL=90%	2680	$m_{B_s^*} - m_{B_s} = 48.5 \pm 1.4$ MeV (S = 2.6)		
$\eta \pi^0$	$< 1.0 \times 10^{-3}$	CL=90%	2654	B_s^* DECAY MODES Fraction (Γ_i/Γ) ρ (MeV/c)		
$\eta \eta$	$< 1.43 \times 10^{-4}$	CL=90%	2627	$B_s \gamma$	seen	48
$\rho^0 \rho^0$	$< 3.20 \times 10^{-4}$	CL=90%	2569	$B_{s1}(5830)^0$ $I(J^P) = 0(1^+)$		
$\eta' K_S^0$	$< 8.16 \times 10^{-6}$	CL=90%	2573	I, J, P need confirmation.		
$\eta' \eta$	$< 6.5 \times 10^{-5}$	CL=90%	2568	Mass $m = 5828.73 \pm 0.20$ MeV		
$\eta' \eta'$	$(3.3 \pm 0.7) \times 10^{-5}$		2507	$m_{B_{s1}^0} - m_{B^{*+}} = 503.98 \pm 0.17$ MeV		
$\eta' \phi$	$< 8.2 \times 10^{-7}$	CL=90%	2495	Full width $\Gamma = 0.5 \pm 0.4$ MeV		
$\phi f_0(980), f_0(980) \rightarrow \pi^+ \pi^-$	$(1.12 \pm 0.21) \times 10^{-6}$		-	$B_{s1}(5830)^0$ DECAY MODES Fraction (Γ_i/Γ) ρ (MeV/c)		
$\phi f_2(1270), f_2(1270) \rightarrow \pi^+ \pi^-$	$(6.1 \pm 1.8) \times 10^{-7}$		-	$B^{*+} K^-$	seen	97
$\phi \rho^0$	$(2.7 \pm 0.8) \times 10^{-7}$		2526	$B_{s2}^*(5840)^0$ $I(J^P) = 0(2^+)$		
$\phi \pi^+ \pi^-$	$(3.5 \pm 0.5) \times 10^{-6}$		2579	I, J, P need confirmation.		
$\phi \phi$	$(1.85 \pm 0.14) \times 10^{-5}$		2482	Mass $m = 5839.88 \pm 0.12$ MeV		
$\phi \phi \phi$	$(2.2 \pm 0.6) \times 10^{-6}$		2165	$m_{B_{s2}^0} - m_{B^+} = 560.48 \pm 0.12$ MeV		
$\pi^+ K^-$	$(5.9 \pm 0.7) \times 10^{-6}$		2659	Full width $\Gamma = 1.49 \pm 0.27$ MeV		
$K^+ K^-$	$(2.72 \pm 0.23) \times 10^{-5}$		2638	Branching fractions are given relative to the one DEFINED AS 1.		
$K^0 \bar{K}^0$	$(1.76 \pm 0.31) \times 10^{-5}$		2637	$B_{s2}^*(5840)^0$ DECAY MODES Fraction (Γ_i/Γ) ρ (MeV/c)		
$K^0 \pi^+ \pi^-$	$(9.5 \pm 2.1) \times 10^{-6}$		2653	$B^+ K^-$	DEFINED AS 1	252
$K^0 K^\pm \pi^\mp$	$(8.4 \pm 0.9) \times 10^{-5}$		2622	$B^{*+} K^-$	0.093 ± 0.018	141
$K^*(892)^- \pi^+$	$(2.9 \pm 1.1) \times 10^{-6}$		2607	$B^0 K_S^0$	0.43 ± 0.11	245
$K^*(892)^\pm K^\mp$	$(1.9 \pm 0.5) \times 10^{-5}$		2585	$B^{*0} K_S^0$	0.04 ± 0.04	-
$K_0^*(1430)^\pm K^\mp$	$(3.1 \pm 2.5) \times 10^{-5}$		-			
$K_S^*(1430)^\pm K^\mp$	$(1.0 \pm 1.7) \times 10^{-5}$		-			
$K^*(892)^0 \bar{K}^0 + c.c.$	$(2.0 \pm 0.6) \times 10^{-5}$		2585			
$K_0^*(1430) \bar{K}^0 + c.c.$	$(3.3 \pm 1.0) \times 10^{-5}$		2468			
$K_S^*(1430) \bar{K}^0 + c.c.$	$(1.7 \pm 2.2) \times 10^{-5}$		2467			
$K_S^0 \bar{K}^*(892)^0 + c.c.$	$(1.6 \pm 0.4) \times 10^{-5}$		2585			

Meson Summary Table

BOTTOM, CHARMED MESONS ($B = C = \pm 1$)

$$B_c^+ = c\bar{b}, B_c^- = \bar{c}b, \quad \text{similarly for } B_c^{*s}$$

 B_c^+

$$I(J^P) = 0(0^-)$$

I, J, P need confirmation.

Quantum numbers shown are quark-model predictions.

$$\text{Mass } m = 6274.47 \pm 0.32 \text{ MeV}$$

$$m_{B_c^+} - m_{B_c^0} = 907.8 \pm 0.5 \text{ MeV}$$

$$\text{Mean life } \tau = (0.510 \pm 0.009) \times 10^{-12} \text{ s}$$

The following quantities are not pure branching ratios; rather the fractions $\Gamma_i/\Gamma \times B(\bar{b} \rightarrow B_c)$. B_c^- modes are charge conjugates of the modes below.

B_c^+ DECAY MODES $\times B(\bar{b} \rightarrow B_c)$	Fraction (Γ_i/Γ)	Confidence level	ρ (MeV/c)
$J/\psi(1S)\ell^+\nu_\ell$ anything	seen	–	–
$J/\psi(1S)\mu^+\nu_\mu$	seen	2372	–
$J/\psi(1S)\tau^+\nu_\tau$	seen	1932	–
$J/\psi(1S)\pi^+$	seen	2370	–
$J/\psi(1S)K^+$	seen	2341	–
$J/\psi(1S)\pi^+\pi^+\pi^-$	seen	2350	–
$J/\psi(1S)a_1(1260)$	not seen	2169	–
$J/\psi(1S)K^+K^-\pi^+$	seen	2203	–
$J/\psi(1S)\pi^+\pi^+\pi^+\pi^-\pi^-$	seen	2309	–
$\psi(2S)\pi^+$	seen	2051	–
$J/\psi(1S)D^0K^+$	seen	1539	–
$J/\psi(1S)D^*(2007)^0K^+$	seen	1411	–
$J/\psi(1S)D^*(2010)^+K^{*0}$	seen	919	–
$J/\psi(1S)D^+K^{*0}$	seen	1122	–
$J/\psi(1S)D_s^+$	seen	1821	–
$J/\psi(1S)D_s^{*+}$	seen	1727	–
$J/\psi(1S)p\bar{p}\pi^+$	seen	1791	–
$\chi_{c0}\pi^+$	$(2.4^{+0.9}_{-0.8}) \times 10^{-5}$	2205	–
$p\bar{p}\pi^+$	not seen	2970	–
D^0K^+	seen	2837	–
$D^0\pi^+$	not seen	2858	–
$D^{*0}\pi^+$	not seen	2814	–
$D^{*0}K^+$	not seen	2792	–
$D_s^+\bar{D}^0$	$< 7.2 \times 10^{-4}$	90%	2483
$D_s^+D^0$	$< 3.0 \times 10^{-4}$	90%	2483
$D_s^+\bar{D}^0$	$< 1.9 \times 10^{-4}$	90%	2521
D^+D^0	$< 1.4 \times 10^{-4}$	90%	2521
$D_s^{*+}\bar{D}^0$	$< 5.3 \times 10^{-4}$	90%	2425
$D_s^+\bar{D}^*(2007)^0$	$< 4.6 \times 10^{-4}$	90%	2427
$D_s^{*+}D^0$	$< 9 \times 10^{-4}$	90%	2425
$D_s^+D^*(2007)^0$	$< 6.6 \times 10^{-4}$	90%	2427
$D^*(2010)^+\bar{D}^0$	$< 3.8 \times 10^{-4}$	90%	2467
$D^*(2010)^+\bar{D}^0, D^{*+} \rightarrow D^+\pi^0/\gamma$	not seen	–	–
$D^+\bar{D}^*(2007)^0$	$< 6.5 \times 10^{-4}$	90%	2466
$D^*(2007)^+D^0$	$< 2.0 \times 10^{-4}$	90%	–
$D^*(2010)^+D^0, D^{*+} \rightarrow D^+\pi^0/\gamma$	not seen	–	2467
$D^+D^*(2007)^0$	$< 3.7 \times 10^{-4}$	90%	2466
$D_s^{*+}\bar{D}^*(2007)^0$	$< 1.3 \times 10^{-3}$	90%	2366
$D_s^{*+}D^*(2007)^0$	$< 1.3 \times 10^{-3}$	90%	2366
$D^*(2010)^+\bar{D}^*(2007)^0$	$< 1.0 \times 10^{-3}$	90%	2410
$D^*(2010)^+D^*(2007)^0$	$< 7.7 \times 10^{-4}$	90%	2410
D^+K^{*0}	not seen	2783	–
$D^+\bar{K}^{*0}$	not seen	2783	–
$D_s^+K^{*0}$	not seen	2751	–
$D_s^+\bar{K}^{*0}$	not seen	2751	–
$D_s^+\phi$	not seen	2727	–
K^+K^0	not seen	3098	–
$B_s^0\pi^+ / B(\bar{b} \rightarrow B_s)$	seen	–	–

 $B_c(2S)^\pm$

$$I(J^P) = 0(0^-)$$

$$\text{Mass } m = 6871.2 \pm 1.0 \text{ MeV}$$

The following quantities are not pure branching ratios; rather the fractions $\Gamma_i/\Gamma \times B(\bar{b} \rightarrow B_c(2S))$.

$B_c(2S)^\pm$ DECAY MODES $\times B(\bar{b} \rightarrow B_c(2S))$	Fraction (Γ_i/Γ)	ρ (MeV/c)
$B_c^+\pi^+\pi^-$	seen	504

$c\bar{c}$ MESONS (including possibly non- $q\bar{q}$ states)

 $\eta_c(1S)$

$$I^G(J^{PC}) = 0^+(0^-)$$

$$\text{Mass } m = 2984.1 \pm 0.4 \text{ MeV} \quad (S = 1.2)$$

$$\text{Full width } \Gamma = 30.5 \pm 0.5 \text{ MeV} \quad (S = 1.2)$$

$\eta_c(1S)$ DECAY MODES	Fraction (Γ_i/Γ)	Scale factor/ Confidence level	ρ (MeV/c)
--------------------------	--------------------------------	-----------------------------------	----------------

Decays involving hadronic resonances

$\eta'(958)\pi\pi$	$(2.0 \pm 0.4)\%$	S=1.4	1323
$\eta'(958)K\bar{K}$	$(1.73 \pm 0.35)\%$		1131
$\eta'(958)\eta\eta$	$(3.4 \pm 0.6) \times 10^{-3}$		1081
$\rho\rho$	$(1.8 \pm 0.4)\%$		1275
$K^*(892)^0K^-\pi^+ + \text{c.c.}$	$(1.8 \pm 0.5)\%$		1278
$K^*(892)K^*(892)$	$(7.0 \pm 1.2) \times 10^{-3}$		1196
$K^*(892)^0K^*(892)^0\pi^+\pi^-$	$(1.4 \pm 0.6)\%$		1074
ϕK^+K^-	$(3.3^{+1.2}_{-1.1}) \times 10^{-3}$		1104
$\phi\phi$	$(1.8 \pm 0.4) \times 10^{-3}$	S=2.3	1089
$\phi 2(\pi^+\pi^-)$	$< 4 \times 10^{-3}$	CL=90%	1251
$a_0(980)\pi$	seen		1327
$a_2(1320)\pi$	seen		1196
$K^*(892)K + \text{c.c.}$	$< 1.28\%$	CL=90%	1310
$f_2(1270)\eta$	seen		1145
$f_2(1270)\eta'$	seen		984
$\omega\omega$	$(2.7 \pm 0.9) \times 10^{-3}$	S=2.1	1270
$\omega\phi$	$< 2.5 \times 10^{-4}$	CL=90%	1185
$f_2(1270)f_2(1270)$	$(1.08 \pm 0.27)\%$		774
$f_2(1270)f_2'(1525)$	$(9.7 \pm 3.2) \times 10^{-3}$		524
$f_0(500)\eta$	seen		–
$f_0(500)\eta'$	seen		–
$f_0(980)\eta$	seen		1265
$f_0(980)\eta'$	seen		1130
$f_0(1500)\eta$	seen		1016
$f_0(1710)\eta'$	seen		623
$f_0(2100)\eta'$	seen		†
$f_0(2200)\eta$	seen		498
$a_0(1320)\pi$	seen		–
$a_0(1450)\pi$	seen		1140
$a_2(1700)\pi$	seen		999
$a_0(1710)\pi$	seen		994
$a_0(1950)\pi$	seen		860
$K_0^*(1430)K + \text{c.c.}$	seen		1086
$K_2^*(1430)K + \text{c.c.}$	seen		1084
$K_0^*(1950)K + \text{c.c.}$	seen		742
$K_0^*(2600)K + \text{c.c.}$	seen		–

Decays into stable hadrons

$K\bar{K}\pi$	$(7.1 \pm 0.4)\%$	S=1.1	1381
$K\bar{K}\eta$	$(1.32 \pm 0.15)\%$		1265
$\eta\pi^+\pi^-$	$(1.6 \pm 0.4)\%$		1428
$\eta 2(\pi^+\pi^-)$	$(4.3 \pm 1.3)\%$		1386
$K^+K^-\pi^+\pi^-$	$(8.3 \pm 1.8) \times 10^{-3}$	S=1.9	1345
$K^+K^-\pi^+\pi^-\pi^0$	$(3.4 \pm 0.6)\%$		1304
$K^0K^-\pi^+\pi^-\pi^+ + \text{c.c.}$	$(5.4 \pm 1.5)\%$		1302
$K^+K^-2(\pi^+\pi^-)$	$(8.4 \pm 2.4) \times 10^{-3}$		1254
$2(K^+K^-)$	$(1.4 \pm 0.4) \times 10^{-3}$	S=1.4	1056
$\pi^+\pi^-\pi^0$	$< 4 \times 10^{-4}$	CL=90%	1476
$\pi^+\pi^-\pi^0\pi^0$	$(4.6 \pm 1.0)\%$		1461
$2(\pi^+\pi^-)$	$(9.6 \pm 1.5) \times 10^{-3}$	S=1.4	1459
$2(\pi^+\pi^-\pi^0)$	$(15.9 \pm 2.0)\%$		1409
$3(\pi^+\pi^-)$	$(1.89 \pm 0.34)\%$		1407
$p\bar{p}$	$(1.33 \pm 0.11) \times 10^{-3}$	S=1.1	1160
$p\bar{p}\pi^0$	$(3.4 \pm 1.3) \times 10^{-3}$		1101
$p\bar{p}\pi^+\pi^-$	$(3.7 \pm 0.5) \times 10^{-3}$		1027

Meson Summary Table

$\Lambda\bar{\Lambda}$	$(1.10 \pm 0.28) \times 10^{-3}$	S=1.5	991	$\omega f_0(980)$	$(1.4 \pm 0.5) \times 10^{-4}$	1267
$K^+ \bar{p} \Lambda + c.c.$	$(2.5 \pm 0.4) \times 10^{-3}$		773	$\omega f_0(1710) \rightarrow \omega K \bar{K}$	$(4.8 \pm 1.1) \times 10^{-4}$	878
$\bar{\Lambda}(1520) \Lambda + c.c.$	$(3.0 \pm 1.3) \times 10^{-3}$		694	$\omega f_1(1420)$	$(6.8 \pm 2.4) \times 10^{-4}$	1060
$\Sigma^+ \bar{\Sigma}^-$	$(2.6 \pm 0.5) \times 10^{-3}$		901	$\omega f_2'(1525)$	$< 2.2 \times 10^{-4}$	CL=90% 1007
$\Xi^- \bar{\Xi}^+$	$(1.07 \pm 0.24) \times 10^{-3}$		692	$\omega X(1835) \rightarrow \omega p \bar{p}$	$< 3.9 \times 10^{-6}$	CL=95% -
				$\omega X(1835), X \rightarrow \eta' \pi^+ \pi^-$	$< 6.2 \times 10^{-5}$	-
				$\omega K^+ K^-$	$(1.52 \pm 0.31) \times 10^{-3}$	1268
				$\omega K^\pm K_S^0 \pi^\mp$	[aa] $(3.4 \pm 0.5) \times 10^{-3}$	1210
				$\omega K \bar{K}$	$(1.9 \pm 0.4) \times 10^{-3}$	1268
				$\omega K^*(892) \bar{K} + c.c.$	$(6.1 \pm 0.9) \times 10^{-3}$	1097
				$\eta' K^{*\pm} K^\mp$	$(1.48 \pm 0.13) \times 10^{-3}$	-
				$\eta' K^{*0} \bar{K}^0 + c.c.$	$(1.66 \pm 0.21) \times 10^{-3}$	1000
				$\eta' h_1(1415) \rightarrow \eta' K^* \bar{K} + c.c.$	$(2.16 \pm 0.31) \times 10^{-4}$	-
				$\eta' h_1(1415) \rightarrow \eta' K^{*\pm} K^\mp$	$(1.51 \pm 0.23) \times 10^{-4}$	-
				$\eta' h_1(1415) \rightarrow \gamma \eta' \eta'$	$(4.7 \pm 1.1) \times 10^{-7}$	-
				$\bar{K} K^*(892) + c.c.$	seen	1373
				$\bar{K} K^*(892) + c.c. \rightarrow$	$(4.8 \pm 0.5) \times 10^{-3}$	-
				$K_S^0 K^\pm \pi^\mp$		
				$K^+ K^*(892)^- + c.c.$	$(6.0 \pm 0.8) \times 10^{-3}$	S=2.9 1373
				$K^+ K^*(892)^- + c.c. \rightarrow$	$(2.69 \pm 0.13) \times 10^{-3}$	-
				$K^+ K^- \pi^0$	$(3.0 \pm 0.4) \times 10^{-3}$	-
				$K^+ K^*(892)^- + c.c. \rightarrow$		
				$K^0 K^\pm \pi^\mp + c.c.$		
				$K^0 \bar{K}^*(892)^0 + c.c.$	$(4.2 \pm 0.4) \times 10^{-3}$	1373
				$K^0 \bar{K}^*(892)^0 + c.c. \rightarrow$	$(3.2 \pm 0.4) \times 10^{-3}$	-
				$K^0 K^\pm \pi^\mp + c.c.$		
				$\bar{K}^*(892)^0 K^\pm \pi^\mp + c.c.$	$(5.7 \pm 0.8) \times 10^{-3}$	1343
				$K^*(892)^\pm K^\mp \pi^0$	$(4.1 \pm 1.3) \times 10^{-3}$	1344
				$K^*(892)^+ K_S^0 \pi^- + c.c.$	$(2.0 \pm 0.5) \times 10^{-3}$	1342
				$K^*(892)^+ K_S^0 \pi^- + c.c. \rightarrow$	$(6.7 \pm 2.2) \times 10^{-4}$	-
				$K_S^0 K_S^0 \pi^+ \pi^-$		
				$K^*(892)^0 K^- \pi^+ + c.c. \rightarrow$	$(3.8 \pm 0.5) \times 10^{-3}$	-
				$K^+ K^- \pi^+ \pi^-$		
				$K^*(892)^0 K_S^0 \rightarrow \gamma K_S^0 K_S^0$	$(6.3 \pm 0.6) \times 10^{-6}$	-
				$K^*(892)^0 K_S^0 \pi^0$	$(7 \pm 4) \times 10^{-4}$	1343
				$K^*(892)^\pm K^*(700)^\mp$	$(1.1 \pm 1.0) \times 10^{-3}$	-
				$K^*(892)^0 \bar{K}^*(892)^0$	$(2.3 \pm 0.6) \times 10^{-4}$	1266
				$K^*(892)^\pm K^*(892)^\mp$	$(1.00 \pm 0.22) \times 10^{-3}$	1266
				$K_1(1400)^\pm K^\mp$	$(3.8 \pm 1.4) \times 10^{-3}$	1170
				$K^*(1410) \bar{K} + c.c.$	seen	1165
				$K^*(1410) \bar{K} + c.c. \rightarrow$	$(7 \pm 4) \times 10^{-5}$	-
				$K^\pm K^\mp \pi^0$		
				$K^*(1410) \bar{K} + c.c. \rightarrow$	$(8 \pm 5) \times 10^{-5}$	-
				$K_S^0 K^\pm \pi^\mp$		
				$K_2^*(1430) \bar{K} + c.c.$	seen	1158
				$K_2^*(1430) \bar{K} + c.c. \rightarrow$	$(1.0 \pm 0.5) \times 10^{-4}$	-
				$K^\pm K^\mp \pi^0$		
				$K_2^*(1430) \bar{K} + c.c. \rightarrow$	$(3.8 \pm 1.0) \times 10^{-4}$	-
				$K_S^0 K^\pm \pi^\mp$		
				$\bar{K}_2^*(1430) K + c.c.$	$< 4.0 \times 10^{-3}$	CL=90% 1158
				$K_2^*(1430)^+ K^- + c.c. \rightarrow$	$(2.69 \pm 0.25) \times 10^{-4}$	-
				$K^+ K^- \pi^0$		
				$K_2^*(1430)^0 K^- \pi^+ + c.c. \rightarrow$	$(2.6 \pm 0.9) \times 10^{-3}$	-
				$K^+ K^- \pi^+ \pi^-$		
				$K_2^*(1430)^+ K_S^0 \pi^- + c.c.$	$(3.6 \pm 1.8) \times 10^{-3}$	1116
				$\bar{K}_2^*(1430)^0 K^*(892)^0 + c.c.$	$(4.67 \pm 0.29) \times 10^{-3}$	1011
				$K_2^*(1430)^- K^*(892)^+ + c.c.$	$(3.4 \pm 2.9) \times 10^{-3}$	1011
				$K_2^*(1430)^- K^*(892)^+ + c.c.$	$(4 \pm 4) \times 10^{-4}$	-
				c.c. \rightarrow		
				$K^*(892)^+ K_S^0 \pi^- + c.c.$		
				$K_2^*(1430)^0 \bar{K}_2^*(1430)^0$	$< 2.9 \times 10^{-3}$	CL=90% 601
				$\bar{K}_2^*(1770)^0 K^*(892)^0 + c.c. \rightarrow$	$(6.9 \pm 0.9) \times 10^{-4}$	-
				$K^*(892)^0 K^- \pi^+ + c.c.$		
				$K_2^*(1980)^+ K^- + c.c. \rightarrow$	$(1.10 \pm 0.60) \times 10^{-5}$	-
				$K^+ K^- \pi^0$		
				$K_4^*(2045)^+ K^- + c.c. \rightarrow$	$(6.2 \pm 2.9) \times 10^{-6}$	-
				$K^+ K^- \pi^0$		
				$K_1(1270)^\pm K^\mp$	$< 3.0 \times 10^{-3}$	CL=90% 1240
				$K_1(1270) K_S^0 \rightarrow \gamma K_S^0 K_S^0$	$(8.5 \pm 2.5) \times 10^{-7}$	-
				$a_2(1320)^\pm \pi^\mp$	[aa] $< 4.3 \times 10^{-3}$	CL=90% 1263
				$\phi \pi^0$	3×10^{-6} or 1×10^{-7}	1377
				$\phi \pi^+ \pi^-$	$(9.4 \pm 1.5) \times 10^{-4}$	S=1.7 1365
				$\phi \pi^0 \pi^0$	$(5.0 \pm 1.0) \times 10^{-4}$	1366

J/ψ(1S)

$$J^G(JPC) = 0^-(1^{--})$$

Mass $m = 3096.900 \pm 0.006$ MeVFull width $\Gamma = 92.6 \pm 1.7$ keV (S = 1.1)

J/ψ(1S) DECAY MODES	Fraction (Γ_i/Γ)	Scale factor/ Confidence level (MeV/c)	ρ
hadrons	$(87.7 \pm 0.5) \%$		-
virtual $\gamma \rightarrow$ hadrons	$(13.46 \pm 0.07) \%$		-
$g \bar{g} g$	$(64.1 \pm 1.0) \%$		-
$\gamma g g$	$(8.8 \pm 1.1) \%$		-
$e^+ e^-$	$(5.971 \pm 0.032) \%$		1548
$e^+ e^- \gamma$	[hhaa] $(8.8 \pm 1.4) \times 10^{-3}$		1548
$\mu^+ \mu^-$	$(5.961 \pm 0.033) \%$		1545
Decays involving hadronic resonances			
$\rho \pi$	$(1.88 \pm 0.12) \%$	S=2.6	1448
$\rho^0 \pi^0$	$(6.2 \pm 0.6) \times 10^{-3}$		1448
$a_2(1320)^0 \pi^+ \pi^- \rightarrow$	$(2.8 \pm 0.6) \times 10^{-3}$		-
$2(\pi^+ \pi^-) \pi^0$			
$a_2(1320)^+ \pi^- \pi^0 + c.c. \rightarrow$	$(3.7 \pm 0.7) \times 10^{-3}$		-
$2(\pi^+ \pi^-) \pi^0$			
$a_2(1320) \rho$	$(1.09 \pm 0.22) \%$		1123
$\eta \pi^+ \pi^-$	$(3.8 \pm 0.7) \times 10^{-4}$		1487
$\eta \rho$	$(1.93 \pm 0.23) \times 10^{-4}$		1396
$\eta \pi^+ \pi^- \pi^0$	$(1.17 \pm 0.20) \%$		1470
$\eta \pi^+ \pi^- 3\pi^0$	$(4.9 \pm 1.0) \times 10^{-3}$		1419
$\eta \phi f_0(980) \rightarrow$	$(1.2 \pm 0.4) \times 10^{-4}$		628
$\eta \phi \pi^+ \pi^-$			
$\eta \phi(2170) \rightarrow$	$< 2.52 \times 10^{-4}$	CL=90%	-
$\eta K^*(892)^0 \bar{K}^*(892)^0$			
$\eta K^+ K^-$	$(8.6 \pm 3.0) \times 10^{-4}$		1331
$\eta K^\pm K_S^0 \pi^\mp$	[aa] $(2.2 \pm 0.4) \times 10^{-3}$		1278
$\eta K^*(892)^0 \bar{K}^*(892)^0$	$(1.15 \pm 0.26) \times 10^{-3}$		1003
$\rho \eta'(958)$	$(8.1 \pm 0.8) \times 10^{-5}$	S=1.6	1281
$\rho^\pm \pi^\mp \pi^+ \pi^- 2\pi^0$	$(2.8 \pm 0.8) \%$		1364
$\rho^+ \rho^- \pi^+ \pi^- \pi^0$	$(6 \pm 4) \times 10^{-3}$		1186
$\rho^+ K^+ K^- \pi^- + c.c. \rightarrow$	$(3.5 \pm 0.8) \times 10^{-3}$		-
$K^+ K^- \pi^+ \pi^- \pi^0$			
$\rho^\mp K^\pm K_S^0$	$(1.9 \pm 0.4) \times 10^{-3}$		1269
$\rho(1450) \pi$	seen		1197
$\rho(1450) \pi \rightarrow \pi^+ \pi^- \pi^0$	$(2.2 \pm 1.1) \times 10^{-4}$		-
$\rho(1450)^\pm \pi^\mp \rightarrow K_S^0 K^\pm \pi^\mp$	$(3.3 \pm 0.6) \times 10^{-4}$		-
$\rho(1450)^0 \pi^0 \rightarrow K^+ K^- \pi^0$	$(2.7 \pm 0.6) \times 10^{-4}$		-
$\rho(1450) \eta'(958) \rightarrow$	$(3.3 \pm 0.7) \times 10^{-6}$		-
$\pi^+ \pi^- \eta'(958)$			
$\rho(1700) \pi$	seen		1065
$\rho(1700) \pi \rightarrow \pi^+ \pi^- \pi^0$	$(1.6 \pm 1.1) \times 10^{-4}$		-
$\rho(2150) \pi$	seen		790
$\rho(2150) \pi \rightarrow \pi^+ \pi^- \pi^0$	$(10 \pm 40) \times 10^{-6}$		-
$\omega \pi^0$	$(4.5 \pm 0.5) \times 10^{-4}$	S=1.4	1446
$\omega \pi^0 \rightarrow \pi^+ \pi^- \pi^0$	$(1.6 \pm 0.7) \times 10^{-5}$		-
$\omega \pi^+ \pi^-$	$(8.5 \pm 1.0) \times 10^{-3}$	S=1.3	1435
$\omega \pi^0 \pi^0$	$(3.4 \pm 0.8) \times 10^{-3}$		1436
$\omega 3\pi^0$	$(1.9 \pm 0.6) \times 10^{-3}$		1419
$\omega f_2(1270)$	$(4.3 \pm 0.6) \times 10^{-3}$		1142
$\omega \eta$	$(1.74 \pm 0.20) \times 10^{-3}$	S=1.6	1394
$\omega \pi^+ \pi^- \pi^0$	$(4.0 \pm 0.7) \times 10^{-3}$		1418
$\omega \pi^0 \eta$	$(3.4 \pm 1.7) \times 10^{-4}$		1363
$\omega \pi^+ \pi^+ \pi^- \pi^-$	$(8.5 \pm 3.4) \times 10^{-3}$		1392
$\omega \pi^+ \pi^- 2\pi^0$	$(3.3 \pm 0.5) \%$		1394
$\omega \eta' \pi^+ \pi^-$	$(1.12 \pm 0.13) \times 10^{-3}$		1173
$\omega \eta'(958)$	$(1.89 \pm 0.18) \times 10^{-4}$		1279

Meson Summary Table

$\phi 2(\pi^+ \pi^-)$	$(1.60 \pm 0.32) \times 10^{-3}$		1318	$K \bar{K} \pi$	$(6.1 \pm 1.0) \times 10^{-3}$	1442
$\phi \eta$	$(7.4 \pm 0.6) \times 10^{-4}$	S=1.2	1320	$K^+ K^- \pi^0$	$(2.88 \pm 0.12) \times 10^{-3}$	1442
$\phi \eta'(958)$	$(4.6 \pm 0.5) \times 10^{-4}$	S=2.2	1192	$K_S^0 K^\pm \pi^\mp$	$(5.3 \pm 0.5) \times 10^{-3}$	1440
$\phi \eta \eta'$	$(2.32 \pm 0.17) \times 10^{-4}$		885	$K_S^0 K_L^0 \pi^0$	$(2.06 \pm 0.26) \times 10^{-3}$	1440
$\phi f_0(980)$	$(3.2 \pm 0.9) \times 10^{-4}$	S=1.9	1178	$K^*(892)^0 \bar{K}^0 + \text{c.c.} \rightarrow$	$(1.21 \pm 0.18) \times 10^{-3}$	-
$\phi f_0(980) \rightarrow \phi \pi^+ \pi^-$	$(2.60 \pm 0.34) \times 10^{-4}$		-	$K_S^0 K_L^0 \pi^0$		
$\phi f_0(980) \rightarrow \phi \pi^0 \pi^0$	$(1.8 \pm 0.5) \times 10^{-4}$		-	$K_2^*(1430)^0 \bar{K}^0 + \text{c.c.} \rightarrow$	$(4.3 \pm 1.3) \times 10^{-4}$	-
$\phi \pi^0 f_0(980) \rightarrow \phi \pi^0 \pi^+ \pi^-$	$(4.5 \pm 1.0) \times 10^{-6}$		-	$K_S^0 K_L^0 \pi^0$		
$\phi \pi^0 f_0(980) \rightarrow \phi \pi^0 \rho^0 \pi^0$	$(1.7 \pm 0.6) \times 10^{-6}$		1045	$K^+ K^- \pi^+ \pi^-$	$(7.0 \pm 1.0) \times 10^{-3}$	1407
$\phi f_0(980) \eta \rightarrow \eta \phi \pi^+ \pi^-$	$(3.2 \pm 1.0) \times 10^{-4}$		-	$K^+ K^- \pi^0 \pi^0$	$(2.13 \pm 0.22) \times 10^{-3}$	1410
$\phi a_0(980)^0 \rightarrow \phi \eta \pi^0$	$(4.4 \pm 1.4) \times 10^{-6}$		-	$K^+ K^- \pi^0 \pi^0 \pi^0$	$(1.61 \pm 0.29) \times 10^{-3}$	1371
$\phi f_2(1270)$	$(3.2 \pm 0.6) \times 10^{-4}$		1036	$K_S^0 K^\pm \pi^\mp \pi^0 \pi^0$	$(5.3 \pm 0.7) \times 10^{-3}$	1369
$\phi f_1(1285)$	$(2.6 \pm 0.5) \times 10^{-4}$		1032	$K_S^0 K^\pm \pi^\mp \pi^+ \pi^-$	$(6.3 \pm 0.4) \times 10^{-3}$	1366
$\phi f_1(1285) \rightarrow$	$(9.4 \pm 2.8) \times 10^{-7}$		952	$K_S^0 K^\pm \rho(770)^\pm \pi^0$	$(2.9 \pm 0.8) \times 10^{-3}$	-
$\phi \pi^0 f_0(980) \rightarrow$				$K_S^0 K_L^0 \pi^+ \pi^-$	$(3.8 \pm 0.6) \times 10^{-3}$	1406
$\phi \pi^0 \pi^+ \pi^-$				$K_S^0 K_L^0 \pi^0 \pi^0$	$(1.9 \pm 0.4) \times 10^{-3}$	1408
$\phi f_1(1285) \rightarrow$	$(2.1 \pm 2.2) \times 10^{-7}$		955	$K_S^0 K^\pm \eta$	$(1.45 \pm 0.33) \times 10^{-3}$	1328
$\phi \pi^0 f_0(980) \rightarrow \phi 3\pi^0$				$K_S^0 K_S^0 \pi^+ \pi^-$	$(1.68 \pm 0.19) \times 10^{-3}$	1406
$\phi \eta(1405) \rightarrow \phi \eta \pi^+ \pi^-$	$(2.0 \pm 1.0) \times 10^{-5}$		946	$K^\mp K_S^0 \pi^\pm \pi^0$	$(5.7 \pm 0.5) \times 10^{-3}$	1408
$\phi f_2'(1525)$	$(8 \pm 4) \times 10^{-4}$	S=2.7	877	$K_S^0 K^\pm \pi^\mp \rho(770)^0$	$(3.1 \pm 0.5) \times 10^{-3}$	-
$\phi X(1835) \rightarrow \phi p \bar{p}$	$< 2.1 \times 10^{-7}$	CL=90%	-	$K^+ K^- 2(\pi^+ \pi^-)$	$(3.1 \pm 1.3) \times 10^{-3}$	1320
$\phi X(1835) \rightarrow \phi \eta \pi^+ \pi^-$	$< 2.8 \times 10^{-4}$	CL=90%	578	$K^+ K^- \pi^+ \pi^- \eta$	$(4.7 \pm 0.7) \times 10^{-3}$	1221
$\phi X(1870) \rightarrow \phi \eta \pi^+ \pi^-$	$< 6.13 \times 10^{-5}$	CL=90%	-	$2(K^+ K^-)$	$(7.2 \pm 0.8) \times 10^{-4}$	1131
$\phi K \bar{K}$	$(1.77 \pm 0.16) \times 10^{-3}$	S=1.3	1179	$K^+ K^- K_S^0 K_S^0$	$(4.2 \pm 0.7) \times 10^{-4}$	1127
$\phi f_0(1710) \rightarrow \phi K \bar{K}$	$(3.6 \pm 0.6) \times 10^{-4}$		875	$K_S^0 K^*(892)^0 \pi^+ \pi^-$	$(1.7 \pm 0.6) \times 10^{-3}$	1304
$\phi K^+ K^-$	$(8.3 \pm 1.1) \times 10^{-4}$		1179	$K_S^0 K^*(892)^0 \pi^0 \pi^0$	$(1.01 \pm 0.18) \times 10^{-3}$	1306
$\phi K_S^0 K_S^0$	$(5.9 \pm 1.5) \times 10^{-4}$		1176	$K^\mp K^*(892)^\pm \pi^+ \pi^-$	$(3.4 \pm 1.2) \times 10^{-3}$	1305
$\phi K^\pm K_S^0 \pi^\mp$	[$a\bar{a}$] $(7.2 \pm 0.8) \times 10^{-4}$		1114	$K^*(892)^\pm K^*(892)^0 \pi^\mp$	$(4.8 \pm 1.0) \times 10^{-3}$	1213
$\phi K^*(892) \bar{K} + \text{c.c.}$	$(2.18 \pm 0.23) \times 10^{-3}$		969	$K^\mp K^*(892)^\pm \pi^0 \pi^0$	$(1.57 \pm 0.32) \times 10^{-3}$	1308
$b_1(1235)^\pm \pi^\mp$	[$a\bar{a}$] $(3.0 \pm 0.5) \times 10^{-3}$		1300	$K^*(892)^+ K^*(892)^- \pi^0$	$(1.12 \pm 0.23) \%$	1214
$b_1(1235)^0 \pi^0$	$(2.3 \pm 0.6) \times 10^{-3}$		1300	$\rho \bar{\rho}$	$(2.120 \pm 0.029) \times 10^{-3}$	1232
$f_2'(1525) K^+ K^-$	$(1.04 \pm 0.35) \times 10^{-3}$		897	$\rho \bar{\rho} \pi^0$	$(1.19 \pm 0.08) \times 10^{-3}$	S=1.1 1176
$\Delta(1232)^+ \bar{p}$	$< 1 \times 10^{-4}$	CL=90%	1100	$\rho \bar{\rho} \pi^+ \pi^-$	$(6.0 \pm 0.5) \times 10^{-3}$	S=1.3 1107
$\Delta(1232)^{++} \bar{p} \pi^-$	$(1.6 \pm 0.5) \times 10^{-3}$		1030	$\rho \bar{\rho} \pi^+ \pi^- \pi^0$	[$j\bar{j}a$] $(2.3 \pm 0.9) \times 10^{-3}$	S=1.9 1033
$\Delta(1232)^{++} \bar{\Delta}(1232)^{-}$	$(1.10 \pm 0.29) \times 10^{-3}$		938	$\rho \bar{\rho} \eta$	$(2.00 \pm 0.12) \times 10^{-3}$	948
$\bar{\Sigma}(1385)^0 \rho K^-$	$(5.1 \pm 3.2) \times 10^{-4}$		646	$\rho \bar{\rho} \rho$	$< 3.1 \times 10^{-4}$	CL=90% 774
$\Sigma(1385)^0 \bar{\Lambda} + \text{c.c.}$	$< 8.2 \times 10^{-6}$	CL=90%	911	$\rho \bar{\rho} \omega$	$(9.8 \pm 1.0) \times 10^{-4}$	S=1.3 768
$\Sigma(1385)^- \bar{\Sigma}^+ + \text{c.c.}$	[$a\bar{a}$] $(3.0 \pm 0.7) \times 10^{-4}$		855	$\rho \bar{\rho} \eta'(958)$	$(1.29 \pm 0.14) \times 10^{-4}$	S=2.0 596
$\Sigma(1385)^+ \bar{\Sigma}^- + \text{c.c.}$	$(3.3 \pm 0.8) \times 10^{-4}$		861	$\rho \bar{\rho} \eta(958)$	$(1.29 \pm 0.14) \times 10^{-4}$	
$\Sigma(1385)^- \bar{\Sigma}(1385)^+ + \text{c.c.}$	[$a\bar{a}$] $(1.08 \pm 0.06) \times 10^{-3}$		697	$\rho \bar{\rho} a_0(980) \rightarrow \rho \bar{\rho} \pi^0 \eta$	$(6.8 \pm 1.8) \times 10^{-5}$	-
$\Sigma(1385)^+ \bar{\Sigma}(1385)^- + \text{c.c.}$	$(1.25 \pm 0.07) \times 10^{-3}$		697	$\rho \bar{\rho} \phi$	$(5.19 \pm 0.33) \times 10^{-5}$	527
$\Sigma(1385)^0 \bar{\Sigma}(1385)^0$	$(1.07 \pm 0.08) \times 10^{-3}$		697	$\rho \bar{\rho} \pi^-$	$(2.12 \pm 0.09) \times 10^{-3}$	1174
$\Lambda(1520) \bar{\Lambda} + \text{c.c.} \rightarrow \gamma \Lambda \bar{\Lambda}$	$< 4.1 \times 10^{-6}$	CL=90%	-	$n \bar{n}$	$(2.09 \pm 0.16) \times 10^{-3}$	1231
$\bar{\Lambda}(1520) \Lambda + \text{c.c.}$	$< 1.80 \times 10^{-3}$	CL=90%	807	$n \bar{n} \pi^+ \pi^-$	$(4 \pm 4) \times 10^{-3}$	1106
$\Xi(1530)^0 \Xi^0$	$(1.17 \pm 0.04) \times 10^{-3}$		818	$n N(1440)$	seen	978
$\Xi(1530)^- \Xi^+ + \text{c.c.}$	$(3.18 \pm 0.08) \times 10^{-4}$		600	$n N(1520)$	seen	928
$\Xi(1530)^0 \Xi^0$	$(3.2 \pm 1.4) \times 10^{-4}$		608	$\eta N(1535)$	seen	917
$\Theta(1540) \bar{\Theta}(1540) \rightarrow$	[$i\bar{i}a\bar{a}$] $< 1.1 \times 10^{-5}$	CL=90%	-	$\Lambda \bar{\Lambda}$	$(1.88 \pm 0.08) \times 10^{-3}$	S=2.6 1074
$K_S^0 p K^- \bar{n} + \text{c.c.}$				$\Lambda \bar{\Lambda} \pi^0$	$(3.8 \pm 0.4) \times 10^{-5}$	998
$\Theta(1540) K^- \bar{n} \rightarrow K_S^0 p K^- \bar{n}$	[$i\bar{i}a\bar{a}$] $< 2.1 \times 10^{-5}$	CL=90%	-	$\Lambda \bar{\Lambda} \pi^+ \pi^-$	$(4.3 \pm 1.0) \times 10^{-3}$	903
$\Theta(1540) K_S^0 \bar{p} \rightarrow K_S^0 \bar{p} K^+ n$	[$i\bar{i}a\bar{a}$] $< 1.6 \times 10^{-5}$	CL=90%	-	$\Lambda \bar{\Lambda} \eta$	$(1.62 \pm 0.17) \times 10^{-4}$	672
$\bar{\Theta}(1540) K^+ n \rightarrow K_S^0 \bar{p} K^+ n$	[$i\bar{i}a\bar{a}$] $< 5.6 \times 10^{-5}$	CL=90%	-	$\Lambda \bar{\Sigma}^- \pi^+ + \text{c.c.}$	[$a\bar{a}$] $(1.26 \pm 0.05) \times 10^{-3}$	S=1.2 950
$\bar{\Theta}(1540) K_S^0 p \rightarrow K_S^0 p K^- \bar{n}$	[$i\bar{i}a\bar{a}$] $< 1.1 \times 10^{-5}$	CL=90%	-	$\Lambda \bar{\Sigma}^+ \pi^- + \text{c.c.}$	[$a\bar{a}$] $(1.21 \pm 0.07) \times 10^{-3}$	S=1.8 945
Decays into stable hadrons						
$2(\pi^+ \pi^-) \pi^0$	$(4.2 \pm 0.4) \%$	S=2.1	1496	$\rho K^- \bar{\Lambda} + \text{c.c.}$	$(8.6 \pm 1.1) \times 10^{-4}$	876
$3(\pi^+ \pi^-) \pi^0$	$(2.9 \pm 0.6) \%$		1433	$\rho K^- \bar{\Sigma}^0$	$(2.9 \pm 0.8) \times 10^{-4}$	819
$\pi^+ \pi^- 3\pi^0$	$(1.9 \pm 0.9) \%$		1497	$\bar{\Lambda} n K_S^0 + \text{c.c.}$	$(6.5 \pm 1.1) \times 10^{-4}$	872
$\rho^\pm \pi^\mp \pi^0 \pi^0$	$(1.41 \pm 0.22) \%$		1421	$\Lambda \bar{\Sigma} + \text{c.c.}$	$(2.83 \pm 0.23) \times 10^{-5}$	1034
$\rho^+ \rho^- \pi^0$	$(6.0 \pm 1.1) \times 10^{-3}$		1298	$\Sigma^+ \bar{\Sigma}^-$	$(1.07 \pm 0.04) \times 10^{-3}$	992
$\pi^+ \pi^- 4\pi^0$	$(6.5 \pm 1.3) \times 10^{-3}$		1470	$\Sigma^0 \bar{\Sigma}^0$	$(1.172 \pm 0.032) \times 10^{-3}$	S=1.4 988
$\pi^+ \pi^- \pi^0$	$(2.00 \pm 0.07) \%$	S=2.0	1533	$\Sigma^+ \bar{\Sigma}^- \eta$	$(6.3 \pm 0.4) \times 10^{-5}$	498
$2(\pi^+ \pi^- \pi^0)$	$(1.61 \pm 0.20) \%$		1468	$\Xi^- \bar{\Xi}^+$	$(9.7 \pm 0.8) \times 10^{-4}$	S=1.4 807
$\pi^+ \pi^- \pi^0 K^+ K^-$	$(1.52 \pm 0.27) \%$	S=1.4	1368	$\gamma \eta_c(1S)$	$(1.41 \pm 0.14) \%$	S=1.3 111
$\pi^+ \pi^-$	$(1.47 \pm 0.14) \times 10^{-4}$		1542	$\gamma \eta_c(1S) \rightarrow 3\gamma$	seen	-
$2(\pi^+ \pi^-)$	$(3.20 \pm 0.25) \times 10^{-3}$	S=1.2	1517	$\gamma \eta_c(1S) \rightarrow \gamma \eta \eta'$	seen	-
$3(\pi^+ \pi^-)$	$(4.3 \pm 0.4) \times 10^{-3}$		1466	3γ	$(1.16 \pm 0.22) \times 10^{-5}$	1548
$2(\pi^+ \pi^-) 3\pi^0$	$(6.2 \pm 0.9) \%$		1435	4γ	$< 9 \times 10^{-6}$	CL=90% 1548
$4(\pi^+ \pi^-) \pi^0$	$(9.0 \pm 3.0) \times 10^{-3}$		1345	5γ	$< 1.5 \times 10^{-5}$	CL=90% 1548
$2(\pi^+ \pi^-) \eta$	$(2.29 \pm 0.28) \times 10^{-3}$		1446	$\gamma \pi^0$	$(3.39 \pm 0.08) \times 10^{-5}$	1546
$3(\pi^+ \pi^-) \eta$	$(7.2 \pm 1.5) \times 10^{-4}$		1379	$\gamma \pi^0 \pi^0$	$(1.15 \pm 0.05) \times 10^{-3}$	1543
$2(\pi^+ \pi^- \pi^0) \eta$	$(1.6 \pm 0.5) \times 10^{-3}$		1381	$\gamma 2\pi^+ 2\pi^-$	$(2.8 \pm 0.5) \times 10^{-3}$	S=1.9 1517
$\pi^+ \pi^- \pi^0 \pi^0 \eta$	$(2.4 \pm 0.5) \times 10^{-3}$		1448	$\gamma f_2(1270) f_2(1270)$	$(9.5 \pm 1.7) \times 10^{-4}$	878
$\rho^\pm \pi^\mp \pi^0 \eta$	$(1.9 \pm 0.8) \times 10^{-3}$		1326	$\gamma f_2(1270) f_2(1270)$ (non resonant)	$(8.2 \pm 1.9) \times 10^{-4}$	-
$K^+ K^-$	$(2.86 \pm 0.21) \times 10^{-4}$		1468	$\gamma \pi^+ \pi^- 2\pi^0$	$(8.3 \pm 3.1) \times 10^{-3}$	1518
$K_S^0 K_L^0$	$(1.95 \pm 0.11) \times 10^{-4}$	S=2.4	1466	$\gamma K_S^0 K_S^0$	$(8.1 \pm 0.4) \times 10^{-4}$	1466
$K_S^0 K_S^0$	$< 1.4 \times 10^{-8}$	CL=95%	1466			

Meson Summary Table

$\gamma(K\bar{K}\pi) [J^{PC} = 0^{-+}]$	$(7 \pm 4) \times 10^{-4}$	S=2.1	1442	$\gamma f_2(2340) \rightarrow \gamma \eta' \eta'$	$(8.7 \pm 0.9 \pm 1.8) \times 10^{-6}$	-
$\gamma K^+ K^- \pi^+ \pi^-$	$(2.1 \pm 0.6) \times 10^{-3}$		1407	$\gamma f_0(2470) \rightarrow \gamma \eta' \eta'$	$(8.2 \pm 4.0 \pm 2.8) \times 10^{-7}$	-
$\gamma K^*(892) \bar{K}^*(892)$	$(4.0 \pm 1.3) \times 10^{-3}$		1266	$\gamma X(1835) \rightarrow \gamma \pi^+ \pi^- \eta'$	$(2.7 \pm 0.6 \pm 0.8) \times 10^{-4}$	S=1.6 1006
$\gamma \eta$	$(1.090 \pm 0.013) \times 10^{-3}$		1500	$\gamma X(1835) \rightarrow \gamma \rho \bar{\rho}$	$(7.7 \pm 1.5 \pm 0.9) \times 10^{-5}$	-
$\gamma \eta \pi^0$	$(2.14 \pm 0.31) \times 10^{-5}$		1497	$\gamma X(1835) \rightarrow \gamma K_S^0 K_S^0 \eta$	$(3.3 \pm 2.0 \pm 1.3) \times 10^{-5}$	-
$\gamma a_0(980)^0 \rightarrow \gamma \eta \pi^0$	$< 2.5 \times 10^{-6}$	CL=95%	-	$\gamma X(1835) \rightarrow \gamma \gamma \gamma$	$< 3.56 \times 10^{-6}$	CL=90%
$\gamma a_2(1320)^0 \rightarrow \gamma \eta \pi^0$	$< 6.6 \times 10^{-6}$	CL=95%	-	$\gamma X(1835) \rightarrow \gamma 3(\pi^+ \pi^-)$	$(2.4 \pm 0.7 \pm 0.8) \times 10^{-5}$	-
$\gamma \eta \pi \pi$	$(6.1 \pm 1.0) \times 10^{-3}$		1487	$\gamma X(2370) \rightarrow \gamma K^+ K^- \eta'$	$(1.8 \pm 0.7) \times 10^{-5}$	-
$\gamma \eta_2(1870) \rightarrow \gamma \eta \pi^+ \pi^-$	$(6.2 \pm 2.4) \times 10^{-4}$		-	$\gamma X(2370) \rightarrow \gamma K_S^0 K_S^0 \eta'$	$(1.2 \pm 0.5) \times 10^{-5}$	-
$\gamma \eta'(958)$	$(5.28 \pm 0.06) \times 10^{-3}$	S=1.3	1400	$\gamma X(2370) \rightarrow \gamma \eta \eta'$	$< 9.2 \times 10^{-6}$	CL=90%
$\gamma \rho \rho$	$(4.5 \pm 0.8) \times 10^{-3}$		1340	$\gamma \rho \bar{\rho}$	$(3.8 \pm 1.0) \times 10^{-4}$	1232
$\gamma \rho \omega$	$< 5.4 \times 10^{-4}$	CL=90%	1338	$\gamma \rho \bar{\rho} \pi^+ \pi^-$	$< 7.9 \times 10^{-4}$	CL=90%
$\gamma \rho \phi$	$< 8.8 \times 10^{-5}$	CL=90%	1258	$\gamma \Lambda \bar{\Lambda}$	$< 1.3 \times 10^{-4}$	CL=90%
$\gamma \omega \omega$	$(1.61 \pm 0.33) \times 10^{-3}$		1336	$\gamma A^0 \rightarrow \gamma \text{invisible}$	$[kkaa] < 1.7 \times 10^{-6}$	CL=90%
$\gamma \phi \phi$	$(4.0 \pm 1.2) \times 10^{-4}$	S=2.1	1166	$\gamma A^0 \rightarrow \gamma \mu^+ \mu^-$	$[llaa] < 7.8 \times 10^{-7}$	CL=90%
$\gamma \eta(1405/1475) \rightarrow \gamma K \bar{K} \pi$	$(2.8 \pm 0.6) \times 10^{-3}$	S=1.6	1223			
$\gamma \eta(1405/1475) \rightarrow \gamma \gamma \rho^0$	$(7.8 \pm 2.0) \times 10^{-5}$	S=1.8	1223			
$\gamma \eta(1405/1475) \rightarrow \gamma \eta \pi^+ \pi^-$	$(3.0 \pm 0.5) \times 10^{-4}$		-			
$\gamma \eta(1405/1475) \rightarrow \gamma \rho^0 \rho^0$	$(1.7 \pm 0.4) \times 10^{-3}$	S=1.3	1223			
$\gamma \eta(1405/1475) \rightarrow \gamma \gamma \phi$	$< 8.2 \times 10^{-5}$	CL=95%	-			
$\gamma \eta(1405) \rightarrow \gamma \gamma \gamma$	$< 2.63 \times 10^{-6}$	CL=90%	-			
$\gamma \eta(1475) \rightarrow \gamma \gamma \gamma$	$< 1.86 \times 10^{-6}$	CL=90%	-			
$\gamma \eta(1760) \rightarrow \gamma \rho^0 \rho^0$	$(1.3 \pm 0.9) \times 10^{-4}$		1048			
$\gamma \eta(1760) \rightarrow \gamma \omega \omega$	$(1.98 \pm 0.33) \times 10^{-3}$		-			
$\gamma \eta(1760) \rightarrow \gamma \gamma \gamma$	$< 4.80 \times 10^{-6}$	CL=90%	-			
$\gamma \eta(2225)$	$(3.14 \pm 0.50 \pm 0.19) \times 10^{-4}$		752			
$\gamma f_2(1270)$	$(1.63 \pm 0.12) \times 10^{-3}$	S=1.3	1286			
$\gamma f_2(1270) \rightarrow \gamma K_S^0 K_S^0$	$(2.58 \pm 0.60 \pm 0.22) \times 10^{-5}$		-			
$\gamma f_1(1285)$	$(6.1 \pm 0.8) \times 10^{-4}$		1283			
$\gamma f_0(1370) \rightarrow \gamma K \bar{K}$	$(4.2 \pm 1.5) \times 10^{-4}$		-			
$\gamma f_0(1370) \rightarrow \gamma K_S^0 K_S^0$	$(1.1 \pm 0.4) \times 10^{-5}$		-			
$\gamma f_1(1420) \rightarrow \gamma K \bar{K} \pi$	$(7.9 \pm 1.3) \times 10^{-4}$		1220			
$\gamma f_0(1500) \rightarrow \gamma \pi \pi$	$(1.09 \pm 0.24) \times 10^{-4}$		1183			
$\gamma f_0(1500) \rightarrow \gamma \eta \eta$	$(1.7 \pm 0.6 \pm 1.4) \times 10^{-5}$		-			
$\gamma f_0(1500) \rightarrow \gamma K_S^0 K_S^0$	$(1.59 \pm 0.24 \pm 0.60) \times 10^{-5}$		-			
$\gamma f_1(1510) \rightarrow \gamma \eta \pi^+ \pi^-$	$(4.5 \pm 1.2) \times 10^{-4}$		-			
$\gamma f_2'(1525)$	$(5.7 \pm 0.8 \pm 0.5) \times 10^{-4}$	S=1.5	1177			
$\gamma f_2'(1525) \rightarrow \gamma K_S^0 K_S^0$	$(8.0 \pm 0.7 \pm 0.5) \times 10^{-5}$		-			
$\gamma f_2'(1525) \rightarrow \gamma \eta \eta$	$(3.4 \pm 1.4) \times 10^{-5}$		-			
$\gamma f_2(1640) \rightarrow \gamma \omega \omega$	$(2.8 \pm 1.8) \times 10^{-4}$		-			
$\gamma f_0(1710) \rightarrow \gamma \pi \pi$	$(3.8 \pm 0.5) \times 10^{-4}$		-			
$\gamma f_0(1710) \rightarrow \gamma K \bar{K}$	$(9.5 \pm 1.0 \pm 0.5) \times 10^{-4}$	S=1.5	1075			
$\gamma f_0(1710) \rightarrow \gamma \omega \omega$	$(3.1 \pm 1.0) \times 10^{-4}$		-			
$\gamma f_0(1710) \rightarrow \gamma \eta \eta$	$(2.4 \pm 1.2 \pm 0.7) \times 10^{-4}$		-			
$\gamma f_0(1710) \rightarrow \gamma \omega \phi$	$(2.5 \pm 0.6) \times 10^{-4}$		-			
$\gamma f_0(1770) \rightarrow \gamma K_S^0 K_S^0$	$(1.11 \pm 0.20 \pm 0.33) \times 10^{-5}$		-			
$\gamma f_2(1810) \rightarrow \gamma \eta \eta$	$(5.4 \pm 3.5 \pm 2.4) \times 10^{-5}$		-			
$\gamma \eta_1(1855) \rightarrow \gamma \eta \eta'$	$(2.7 \pm 0.4 \pm 0.5) \times 10^{-6}$		-			
$\gamma f_2(1910) \rightarrow \gamma \omega \omega$	$(2.0 \pm 1.4) \times 10^{-4}$		-			
$\gamma f_2(1950) \rightarrow$	$(7.0 \pm 2.2) \times 10^{-4}$		-			
$\gamma K^*(892) \bar{K}^*(892)$						
$\gamma f_0(2020) \rightarrow \gamma \eta' \eta'$	$(2.63 \pm 0.32 \pm 0.50) \times 10^{-4}$		-			
$\gamma f_4(2050)$	$(2.7 \pm 0.7) \times 10^{-3}$		891			
$\gamma f_0(2100) \rightarrow \gamma \eta \eta$	$(1.13 \pm 0.60 \pm 0.30) \times 10^{-4}$		-			
$\gamma f_0(2100) \rightarrow \gamma \pi \pi$	$(6.2 \pm 1.0) \times 10^{-4}$		-			
$\gamma f_0(2200)$	seen		776			
$\gamma f_0(2200) \rightarrow \gamma K \bar{K}$	$(5.9 \pm 1.3) \times 10^{-4}$		-			
$\gamma f_0(2200) \rightarrow \gamma K_S^0 K_S^0$	$(2.72 \pm 0.19 \pm 0.50) \times 10^{-4}$		-			
$\gamma f_J(2220)$	seen		745			
$\gamma f_J(2220) \rightarrow \gamma \pi \pi$	$< 3.9 \times 10^{-5}$	CL=90%	-			
$\gamma f_J(2220) \rightarrow \gamma K \bar{K}$	$< 4.1 \times 10^{-5}$	CL=90%	-			
$\gamma f_J(2220) \rightarrow \gamma \rho \bar{\rho}$	$(1.5 \pm 0.8) \times 10^{-5}$		-			
$\gamma f_0(2330) \rightarrow \gamma K_S^0 K_S^0$	$(4.9 \pm 0.7) \times 10^{-5}$		-			
$\gamma f_0(2330) \rightarrow \gamma \eta' \eta'$	$(6.1 \pm 4.0 \pm 1.8) \times 10^{-6}$		-			
$\gamma f_2(2340) \rightarrow \gamma \eta \eta$	$(5.6 \pm 2.4 \pm 2.2) \times 10^{-5}$		-			
$\gamma f_2(2340) \rightarrow \gamma K_S^0 K_S^0$	$(5.5 \pm 4.0 \pm 1.5) \times 10^{-5}$		-			
				$\pi^0 e^+ e^-$	$(7.6 \pm 1.4) \times 10^{-7}$	1546
				$\eta e^+ e^-$	$(1.42 \pm 0.08) \times 10^{-5}$	1500
				$\eta'(958) e^+ e^-$	$(6.59 \pm 0.18) \times 10^{-5}$	1400
				$X(1835) e^+ e^-, X \rightarrow$	$(3.58 \pm 0.25) \times 10^{-6}$	-
				$\pi^+ \pi^- \eta'$		
				$X(2120) e^+ e^-, X \rightarrow$	$(8.2 \pm 1.3) \times 10^{-7}$	-
				$\pi^+ \pi^- \eta'$		
				$X(2370) e^+ e^-, X \rightarrow$	$(1.08 \pm 0.17) \times 10^{-6}$	-
				$\pi^+ \pi^- \eta'$		
				$\eta U \rightarrow \eta e^+ e^-$	$[nnaa] < 9.11 \times 10^{-7}$	CL=90%
				$\eta'(958) U \rightarrow \eta'(958) e^+ e^-$	$[nnaa] < 2.0 \times 10^{-7}$	CL=90%
				$\phi e^+ e^-$	$< 1.2 \times 10^{-7}$	CL=90% 1381
				Weak decays		
				$D^- e^+ \nu_e + c.c.$	$< 7.1 \times 10^{-8}$	CL=90% 984
				$\bar{D}^0 e^+ e^- + c.c.$	$< 8.5 \times 10^{-8}$	CL=90% 987
				$D_s^- e^+ \nu_e + c.c.$	$< 1.3 \times 10^{-6}$	CL=90% 923
				$D_s^{*-} e^+ \nu_e + c.c.$	$< 1.8 \times 10^{-6}$	CL=90% 828
				$D^- \pi^+ + c.c.$	$< 7.5 \times 10^{-5}$	CL=90% 977
				$\bar{D}^0 \bar{K}^0 + c.c.$	$< 1.7 \times 10^{-4}$	CL=90% 898
				$\bar{D}^0 \bar{K}^{*0} + c.c.$	$< 2.5 \times 10^{-6}$	CL=90% 670
				$D_s^- \pi^+ + c.c.$	$< 1.3 \times 10^{-4}$	CL=90% 915
				$D_s^- \rho^+ + c.c.$	$< 1.3 \times 10^{-5}$	CL=90% 663
				Charge conjugation (C), Parity (P), Lepton Family number (LF) violating modes		
				$\gamma \gamma$	C $< 2.7 \times 10^{-7}$	CL=90% 1548
				$\gamma \phi$	C $< 1.4 \times 10^{-6}$	CL=90% 1381
				$e^\pm \mu^\mp$	LF $< 1.6 \times 10^{-7}$	CL=90% 1547
				$e^\pm \tau^\mp$	LF $< 7.5 \times 10^{-8}$	CL=90% 1039
				$\mu^\pm \tau^\mp$	LF $< 2.0 \times 10^{-6}$	CL=90% 1035
				$\Lambda_c^+ e^- + c.c.$	$< 6.9 \times 10^{-8}$	CL=90% 704
				Other decays		
				invisible	$< 7 \times 10^{-4}$	CL=90% -
				$X_{c0}(1P)$	$J^G(J^{PC}) = 0^+(0^+ +)$	
				Mass $m = 3414.71 \pm 0.30$ MeV		
				Full width $\Gamma = 10.7 \pm 0.6$ MeV (S = 1.1)		
				$X_{c0}(1P)$ DECAY MODES	Fraction (Γ_i/Γ)	Scale factor/ Confidence level
						ρ (MeV/c)
				Hadronic decays		
				$2(\pi^+ \pi^-)$	$(2.3 \pm 0.4) \%$	S=2.0 1679
				$\rho^0 \pi^+ \pi^-$	$(9.1 \pm 3.1) \times 10^{-3}$	S=1.1 1607
				$f_0(980) f_0(980)$	$(6.7 \pm 2.1) \times 10^{-4}$	1391
				$\pi^+ \pi^- \pi^0 \pi^0$	$(3.3 \pm 0.4) \%$	1680
				$\rho^+ \pi^- \pi^0 + c.c.$	$(2.9 \pm 0.4) \%$	1607
				$4\pi^0$	$(3.3 \pm 0.4) \times 10^{-3}$	1681
				$\pi^+ \pi^- K^+ K^-$	$(1.82 \pm 0.16) \%$	S=1.2 1580
				$K_0^*(1430)^0 \bar{K}_0^*(1430)^0 \rightarrow$	$(9.9 \pm 4.0 \pm 2.8) \times 10^{-4}$	-
				$\pi^+ \pi^- K^+ K^-$		
				$K_0^*(1430)^0 \bar{K}_0^*(1430)^0 + c.c. \rightarrow$	$(8.0 \pm 2.0 \pm 2.4) \times 10^{-4}$	-
				$\pi^+ \pi^- K^+ K^-$		
				$K_1(1270)^+ K^- + c.c. \rightarrow$	$(6.3 \pm 1.9) \times 10^{-3}$	-
				$\pi^+ \pi^- K^+ K^-$		

Meson Summary Table

$K_1(1400)^+ K^- + c.c. \rightarrow$ $\pi^+ \pi^- K^+ K^-$	$< 2.7 \times 10^{-3}$	CL=90%	-	$\Sigma^+ \bar{\Sigma}^-$	$(4.7 \pm 0.8) \times 10^{-4}$	S=2.6	1225
$f_0(980) f_0(980)$	$(1.6^{+1.0}_{-0.9}) \times 10^{-4}$		1391	$\Sigma^- \bar{\Sigma}^+$	$(5.1 \pm 0.5) \times 10^{-4}$		1217
$f_0(980) f_0(2200)$	$(7.9^{+2.0}_{-2.5}) \times 10^{-4}$		586	$\Sigma(1385)^+ \bar{\Sigma}(1385)^-$	$(1.6 \pm 0.6) \times 10^{-4}$		1001
$f_0(1370) f_0(1370)$	$< 2.7 \times 10^{-4}$	CL=90%	1019	$\Sigma(1385)^- \bar{\Sigma}(1385)^+$	$(2.3 \pm 0.7) \times 10^{-4}$		1001
$f_0(1370) f_0(1500)$	$< 1.7 \times 10^{-4}$	CL=90%	907	$K^- \Lambda \bar{\Sigma}^+ + c.c.$	$(1.95 \pm 0.35) \times 10^{-4}$		873
$f_0(1370) f_0(1710)$	$(6.7^{+3.5}_{-2.3}) \times 10^{-4}$		709	$\Xi^0 \bar{\Xi}^0$	$(4.5 \pm 0.5) \times 10^{-4}$	S=1.7	1089
$f_0(1500) f_0(1370)$	$< 1.3 \times 10^{-4}$	CL=90%	907	$\Xi^- \bar{\Xi}^+$	$(4.47 \pm 0.20) \times 10^{-4}$		1081
$f_0(1500) f_0(1500)$	$< 5 \times 10^{-5}$	CL=90%	774	$\Omega^- \bar{\Omega}^+$	$(3.5 \pm 0.6) \times 10^{-5}$		343
$f_0(1500) f_0(1710)$	$< 7 \times 10^{-5}$	CL=90%	515	$\eta_c \pi^+ \pi^-$	$< 7 \times 10^{-4}$	CL=90%	307
$K^+ K^- \pi^+ \pi^- \pi^0$	$(8.6 \pm 0.9) \times 10^{-3}$		1545	Radiative decays			
$K_S^0 K^\pm \pi^\mp \pi^+ \pi^-$	$(4.2 \pm 0.4) \times 10^{-3}$		1543	$\gamma J/\psi(1S)$	$(1.41 \pm 0.09) \%$	S=1.7	303
$K^+ K^- \pi^0 \pi^0$	$(5.6 \pm 0.9) \times 10^{-3}$		1582	$\gamma \rho^0$	$< 9 \times 10^{-6}$	CL=90%	1619
$K^+ \pi^- \bar{K}^0 \pi^0 + c.c.$	$(2.49 \pm 0.33) \%$		1581	$\gamma \omega$	$< 8 \times 10^{-6}$	CL=90%	1618
$\rho^+ K^- K^0 + c.c.$	$(1.21 \pm 0.21) \%$		1458	$\gamma \phi$	$< 6 \times 10^{-6}$	CL=90%	1555
$K^*(892)^- K^+ \pi^0 \rightarrow$ $K^+ \pi^- \bar{K}^0 \pi^0 + c.c.$	$(4.6 \pm 1.2) \times 10^{-3}$		-	$\gamma \gamma$	$(2.04 \pm 0.10) \times 10^{-4}$	S=1.1	1707
$K_S^0 K_S^0 \pi^+ \pi^-$	$(5.7 \pm 1.1) \times 10^{-3}$		1579	$e^+ e^- J/\psi(1S)$	$(1.34 \pm 0.30) \times 10^{-4}$		303
$K^+ K^- \eta \pi^0$	$(3.0 \pm 0.7) \times 10^{-3}$		1468	$\mu^+ \mu^- J/\psi(1S)$	$< 1.9 \times 10^{-5}$	CL=90%	226
$3(\pi^+ \pi^-)$	$(1.95 \pm 0.22) \%$	S=3.3	1633	$\chi_{c1}(1P)$			
$K^+ \bar{K}^*(892)^0 \pi^- + c.c.$	$(7.5 \pm 1.6) \times 10^{-3}$		1523	$I^G(J^{PC}) = 0^+(1^{++})$			
$K^*(892)^0 \bar{K}^*(892)^0$	$(1.7 \pm 0.6) \times 10^{-3}$		1456	Mass $m = 3510.67 \pm 0.05$ MeV (S = 1.2)			
$\pi \pi$	$(8.5 \pm 0.4) \times 10^{-3}$	S=1.2	1702	Full width $\Gamma = 0.84 \pm 0.04$ MeV (S = 1.1)			
$\pi^0 \eta$	$< 1.8 \times 10^{-4}$		1661	$\chi_{c1}(1P)$ DECAY MODES			
$\pi^0 \eta'$	$< 1.1 \times 10^{-3}$		1570	Fraction (Γ_i/Γ)			
$\pi^0 \eta_c$	$< 1.6 \times 10^{-3}$	CL=90%	383	Scale factor/ Confidence level			
$\eta \eta$	$(3.01 \pm 0.25) \times 10^{-3}$	S=1.3	1617	p (MeV/c)			
$\eta \eta'$	$(9.1 \pm 1.1) \times 10^{-5}$		1521	$e^+ e^-$	$(1.4^{+1.5}_{-1.0}) \times 10^{-7}$		1755
$\eta' \eta'$	$(2.17 \pm 0.12) \times 10^{-3}$		1413	Hadronic decays			
$\omega \omega$	$(9.7 \pm 1.1) \times 10^{-4}$		1517	$3(\pi^+ \pi^-)$	$(1.04 \pm 0.16) \%$	S=4.6	1683
$\omega \phi$	$(1.42 \pm 0.13) \times 10^{-4}$		1447	$2(\pi^+ \pi^-)$	$(7.6 \pm 2.6) \times 10^{-3}$		1728
$\omega K^+ K^-$	$(1.94 \pm 0.21) \times 10^{-3}$		1457	$\pi^+ \pi^- \pi^0 \pi^0$	$(1.19 \pm 0.15) \%$		1729
$K^+ K^-$	$(6.07 \pm 0.33) \times 10^{-3}$	S=1.1	1634	$\rho^+ \pi^- \pi^0 + c.c.$	$(1.45 \pm 0.24) \%$		1658
$K_S^0 K_S^0$	$(3.17 \pm 0.19) \times 10^{-3}$	S=1.1	1633	$\rho^0 \pi^+ \pi^-$	$(3.9 \pm 3.5) \times 10^{-3}$		1657
$\pi^+ \pi^- \eta$	$< 2.0 \times 10^{-4}$	CL=90%	1651	$4\pi^0$	$(5.4 \pm 0.8) \times 10^{-4}$		1729
$\pi^+ \pi^- \eta'$	$< 4 \times 10^{-4}$	CL=90%	1560	$\pi^+ \pi^- K^+ K^-$	$(4.5 \pm 1.0) \times 10^{-3}$		1632
$\bar{K}^0 K^+ \pi^- + c.c.$	$< 9 \times 10^{-5}$	CL=90%	1610	$K^+ K^- \pi^0 \pi^0$	$(1.12 \pm 0.27) \times 10^{-3}$		1634
$K^+ K^- \pi^0$	$< 6 \times 10^{-5}$	CL=90%	1611	$K^+ K^- \pi^+ \pi^- \pi^0$	$(1.15 \pm 0.13) \%$		1598
$K^+ K^- \eta$	$< 2.3 \times 10^{-4}$	CL=90%	1512	$K_S^0 K^\pm \pi^\mp \pi^+ \pi^-$	$(7.5 \pm 0.8) \times 10^{-3}$		1596
$K^+ K^- K_S^0 K_S^0$	$(1.4 \pm 0.5) \times 10^{-3}$		1331	$K^+ \pi^- \bar{K}^0 \pi^0 + c.c.$	$(8.6 \pm 1.4) \times 10^{-3}$		1632
$K_S^0 K_S^0 K_S^0 K_S^0$	$(5.8 \pm 0.5) \times 10^{-4}$		1327	$\rho^- K^+ \bar{K}^0 + c.c.$	$(5.0 \pm 1.2) \times 10^{-3}$		1514
$K^+ K^- K^+ K^-$	$(2.8 \pm 0.4) \times 10^{-3}$	S=1.5	1333	$K^*(892)^0 \bar{K}^0 \pi^0 \rightarrow$ $K^+ \pi^- \bar{K}^0 \pi^0 + c.c.$	$(2.3 \pm 0.6) \times 10^{-3}$		-
$K^+ K^- \phi$	$(9.7 \pm 2.5) \times 10^{-4}$		1381	$K^+ K^- \eta \pi^0$	$(1.12 \pm 0.34) \times 10^{-3}$		1523
$\bar{K}^0 K^+ \pi^- \phi + c.c.$	$(3.7 \pm 0.6) \times 10^{-3}$		1326	$\pi^+ \pi^- K_S^0 K_S^0$	$(6.9 \pm 2.9) \times 10^{-4}$		1630
$K^+ K^- \pi^0 \phi$	$(1.90 \pm 0.35) \times 10^{-3}$		1329	$K^+ K^- \eta$	$(3.2 \pm 1.0) \times 10^{-4}$		1566
$\phi \pi^+ \pi^- \pi^0$	$(1.18 \pm 0.15) \times 10^{-3}$		1525	$\bar{K}^0 K^+ \pi^- + c.c.$	$(7.0 \pm 0.6) \times 10^{-3}$	S=1.1	1661
$\phi \phi$	$(8.48 \pm 0.31) \times 10^{-4}$		1370	$K^*(892)^0 \bar{K}^0 + c.c.$	$(1.03 \pm 0.15) \times 10^{-3}$		1602
$\phi \phi \eta$	$(8.4 \pm 1.0) \times 10^{-4}$		1100	$K^*(892)^+ K^- + c.c.$	$(1.21 \pm 0.23) \times 10^{-3}$		1602
$p \bar{p}$	$(2.21 \pm 0.14) \times 10^{-4}$	S=1.6	1426	$K_S^*(1430)^0 \bar{K}^0 + c.c. \rightarrow$	$< 8 \times 10^{-4}$	CL=90%	-
$p \bar{p} \pi^0$	$(7.0 \pm 0.7) \times 10^{-4}$	S=1.3	1379	$K_S^0 K^+ \pi^- + c.c.$			
$p \bar{p} \eta$	$(3.5 \pm 0.4) \times 10^{-4}$		1187	$K_S^*(1430)^+ K^- + c.c. \rightarrow$	$< 2.1 \times 10^{-3}$	CL=90%	-
$p \bar{p} \omega$	$(5.3 \pm 0.6) \times 10^{-4}$		1043	$K_S^0 K^+ \pi^- + c.c.$			
$p \bar{p} \phi$	$(6.0 \pm 1.4) \times 10^{-5}$		876	$K^+ K^- \pi^0$	$(1.81 \pm 0.24) \times 10^{-3}$		1662
$p \bar{p} \pi^+ \pi^-$	$(2.1 \pm 0.7) \times 10^{-3}$	S=1.4	1320	$\eta \pi^+ \pi^-$	$(4.62 \pm 0.24) \times 10^{-3}$		1701
$p \bar{p} \pi^0 \pi^0$	$(1.04 \pm 0.28) \times 10^{-3}$		1324	$a_0(980)^+ \pi^- + c.c. \rightarrow \eta \pi^+ \pi^-$	$(3.2 \pm 0.4) \times 10^{-3}$	S=2.1	-
$p \bar{p} K^+ K^-$ (non-resonant)	$(1.22 \pm 0.26) \times 10^{-4}$		890	$a_2(1320)^+ \pi^- + c.c. \rightarrow \eta \pi^+ \pi^-$	$(1.76 \pm 0.24) \times 10^{-4}$		-
$p \bar{p} K_S^0 K_S^0$	$< 8.8 \times 10^{-4}$	CL=90%	884	$a_2(1700)^+ \pi^- + c.c. \rightarrow \eta \pi^+ \pi^-$	$(4.6 \pm 0.7) \times 10^{-5}$		-
$p \bar{p} \pi^-$	$(1.27 \pm 0.11) \times 10^{-3}$		1376	$f_2(1270) \eta \rightarrow \eta \pi^+ \pi^-$	$(3.5 \pm 0.6) \times 10^{-4}$		-
$\bar{p} n \pi^+$	$(1.37 \pm 0.12) \times 10^{-3}$		1376	$f_4(2050) \eta \rightarrow \eta \pi^+ \pi^-$	$(2.5 \pm 0.9) \times 10^{-5}$		-
$p \bar{p} \pi^- \pi^0$	$(2.34 \pm 0.21) \times 10^{-3}$		1321	$\pi_1(1400)^+ \pi^- + c.c. \rightarrow$ $\eta \pi^+ \pi^-$	$< 5 \times 10^{-5}$	CL=90%	-
$\bar{p} n \pi^+ \pi^0$	$(2.21 \pm 0.19) \times 10^{-3}$		1321	$\pi_1(1600)^+ \pi^- + c.c. \rightarrow$ $\eta \pi^+ \pi^-$	$< 1.5 \times 10^{-5}$	CL=90%	-
$\Lambda \bar{\Lambda}$	$(3.60 \pm 0.17) \times 10^{-4}$	S=1.1	1292	$\pi_1(2015)^+ \pi^- + c.c. \rightarrow$ $\eta \pi^+ \pi^-$	$< 8 \times 10^{-6}$	CL=90%	-
$\Lambda \bar{\Lambda} \pi^+ \pi^-$	$(1.18 \pm 0.13) \times 10^{-3}$		1153	$f_2(1270) \eta$	$(6.7 \pm 1.1) \times 10^{-4}$		1467
$\Lambda \bar{\Lambda} \pi^+ \pi^-$ (non-resonant)	$< 5 \times 10^{-4}$	CL=90%	1153	$\pi^+ \pi^- \eta'$	$(2.2 \pm 0.4) \times 10^{-3}$		1612
$\Sigma(1385)^+ \bar{\Lambda} \pi^- + c.c.$	$< 5 \times 10^{-4}$	CL=90%	1083	$K^+ K^- \eta'(958)$	$(8.8 \pm 0.9) \times 10^{-4}$		1461
$\Sigma(1385)^- \bar{\Lambda} \pi^+ + c.c.$	$< 5 \times 10^{-4}$	CL=90%	1083	$K_S^*(1430)^+ K^- + c.c.$	$(6.4^{+2.2}_{-2.8}) \times 10^{-4}$		-
$\Lambda \bar{\Lambda} \eta$	$(2.3 \pm 0.4) \times 10^{-4}$		979	$f_0(980) \eta'(958)$	$(1.6^{+1.4}_{-0.7}) \times 10^{-4}$		1460
$K^+ \bar{p} \Lambda + c.c.$	$(1.25 \pm 0.12) \times 10^{-3}$	S=1.3	1132	$f_0(1710) \eta'(958)$	$(7^{+7}_{-5}) \times 10^{-5}$		1100
$n K_S^0 \bar{\Lambda} + c.c.$	$(6.7 \pm 0.5) \times 10^{-4}$		1129	$f_2'(1525) \eta'(958)$	$(9 \pm 6) \times 10^{-5}$		1229
$K^*(892)^+ \bar{p} \Lambda + c.c.$	$(4.8 \pm 0.9) \times 10^{-4}$		845	$K_S^*(1430)^+ K^- + c.c.$	$(1.61 \pm 0.31) \times 10^{-3}$		1416
$K^+ \bar{p} \Lambda(1520) + c.c.$	$(3.0 \pm 0.8) \times 10^{-4}$		859	$K_S^*(1430) \bar{K}^0 + c.c.$	$(1.17 \pm 0.20) \times 10^{-3}$		1416
$\Lambda(1520) \bar{\Lambda}(1520)$	$(3.1 \pm 1.2) \times 10^{-4}$		780				
$\Sigma^0 \bar{\Sigma}^0$	$(4.69 \pm 0.32) \times 10^{-4}$		1222				
$\Sigma^+ \bar{p} K_S^0 + c.c.$	$(3.53 \pm 0.27) \times 10^{-4}$		1089				
$\Sigma^- \bar{p} K^+ + c.c.$	$(3.04 \pm 0.20) \times 10^{-4}$		1090				

Meson Summary Table

$\pi^0 f_0(980) \rightarrow \pi^0 \pi^+ \pi^-$	$(3.5 \pm 0.9) \times 10^{-7}$	-	
$K^+ \bar{K}^*(892)^0 \pi^- + c.c.$	$(3.2 \pm 2.1) \times 10^{-3}$	1577	
$K^*(892)^0 \bar{K}^*(892)^0$	$(1.4 \pm 0.4) \times 10^{-3}$	1512	
$K^+ K^- K_S^0 K_S^0$	$< 4 \times 10^{-4}$	CL=90%	1390
$K_S^0 K_S^0 K_S^0 K_S^0$	$(3.5 \pm 1.0) \times 10^{-5}$		1387
$K^+ K^- K^+ K^-$	$(5.4 \pm 1.1) \times 10^{-4}$		1393
$K^+ K^- \phi$	$(4.1 \pm 1.5) \times 10^{-4}$		1440
$\bar{K}^0 K^+ \pi^- \phi + c.c.$	$(3.3 \pm 0.5) \times 10^{-3}$		1387
$K^+ K^- \pi^0 \phi$	$(1.62 \pm 0.30) \times 10^{-3}$		1390
$\phi \pi^+ \pi^- \pi^0$	$(7.5 \pm 1.0) \times 10^{-4}$		1578
$\omega \omega$	$(5.7 \pm 0.7) \times 10^{-4}$		1571
$\omega K^+ K^-$	$(7.8 \pm 0.9) \times 10^{-4}$		1513
$\omega \phi$	$(2.7 \pm 0.4) \times 10^{-5}$		1503
$\phi \phi$	$(4.26 \pm 0.21) \times 10^{-4}$		1429
$\phi \phi \eta$	$(3.0 \pm 0.5) \times 10^{-4}$		1172
$\rho \bar{\rho}$	$(7.6 \pm 0.4) \times 10^{-5}$	S=1.2	1484
$\rho \bar{\rho} \pi^0$	$(1.55 \pm 0.18) \times 10^{-4}$		1438
$\rho \bar{\rho} \eta$	$(1.45 \pm 0.25) \times 10^{-4}$		1254
$\rho \bar{\rho} \omega$	$(2.12 \pm 0.31) \times 10^{-4}$		1117
$\rho \bar{\rho} \phi$	$< 1.7 \times 10^{-5}$	CL=90%	962
$\rho \bar{\rho} \pi^+ \pi^-$	$(5.0 \pm 1.9) \times 10^{-4}$		1381
$\rho \bar{\rho} \pi^0 \pi^0$	$< 5 \times 10^{-4}$	CL=90%	1385
$\rho \bar{\rho} K^+ K^-$ (non-resonant)	$(1.27 \pm 0.22) \times 10^{-4}$		974
$\rho \bar{\rho} K_S^0 K_S^0$	$< 4.5 \times 10^{-4}$	CL=90%	968
$\rho \bar{\rho} \pi^-$	$(3.8 \pm 0.5) \times 10^{-4}$		1435
$\rho \bar{\rho} \pi^+$	$(3.9 \pm 0.5) \times 10^{-4}$		1435
$\rho \bar{\rho} \pi^- \pi^0$	$(1.03 \pm 0.12) \times 10^{-3}$		1383
$\rho \bar{\rho} \pi^+ \pi^0$	$(1.01 \pm 0.12) \times 10^{-3}$		1383
$\Lambda \bar{\Lambda}$	$(1.27 \pm 0.09) \times 10^{-4}$	S=1.1	1355
$\Lambda \bar{\Lambda} \pi^+ \pi^-$	$(2.9 \pm 0.5) \times 10^{-4}$		1223
$\Lambda \bar{\Lambda} \pi^+ \pi^-$ (non-resonant)	$(2.5 \pm 0.6) \times 10^{-4}$		1223
$\Sigma(1385)^+ \bar{\Lambda} \pi^- + c.c.$	$< 1.3 \times 10^{-4}$	CL=90%	1157
$\Sigma(1385)^- \bar{\Lambda} \pi^+ + c.c.$	$< 1.3 \times 10^{-4}$	CL=90%	1157
$\Lambda \bar{\Lambda} \eta$	$(5.9 \pm 1.5) \times 10^{-5}$		1059
$K^+ \bar{p} \Lambda + c.c.$	$(4.2 \pm 0.4) \times 10^{-4}$	S=1.2	1203
$n K_S^0 \bar{\Lambda} + c.c.$	$(1.66 \pm 0.17) \times 10^{-4}$		1200
$K^*(892)^+ \bar{p} \Lambda + c.c.$	$(4.9 \pm 0.7) \times 10^{-4}$		935
$K^+ \bar{p} \Lambda(1520) + c.c.$	$(1.7 \pm 0.4) \times 10^{-4}$		951
$\Lambda(1520) \bar{\Lambda}(1520)$	$< 9 \times 10^{-5}$	CL=90%	880
$\Sigma^0 \bar{\Sigma}^0$	$(4.2 \pm 0.6) \times 10^{-5}$		1288
$\Sigma^+ \bar{p} K_S^0 + c.c.$	$(1.53 \pm 0.12) \times 10^{-4}$		1163
$\Sigma^0 \bar{p} K^+ + c.c.$	$(1.46 \pm 0.10) \times 10^{-4}$		1163
$\Sigma^+ \bar{\Sigma}^-$	$(3.6 \pm 0.7) \times 10^{-5}$		1291
$\Sigma^- \bar{\Sigma}^+$	$(5.7 \pm 1.5) \times 10^{-5}$		1283
$\Sigma(1385)^+ \bar{\Sigma}(1385)^-$	$< 9 \times 10^{-5}$	CL=90%	1081
$\Sigma(1385)^- \bar{\Sigma}(1385)^+$	$< 5 \times 10^{-5}$	CL=90%	1081
$K^- \Lambda \bar{\Xi}^+ + c.c.$	$(1.35 \pm 0.24) \times 10^{-4}$		963
$\Xi^0 \bar{\Xi}^0$	$(7.5 \pm 1.3) \times 10^{-5}$		1163
$\Xi^- \bar{\Xi}^+$	$(6.0 \pm 0.6) \times 10^{-5}$		1155
$\Omega^- \bar{\Omega}^+$	$(1.49 \pm 0.25) \times 10^{-5}$		533
$\pi^+ \pi^- + K^+ K^-$	$< 2.1 \times 10^{-3}$		-
$K_S^0 K_S^0$	$< 6 \times 10^{-5}$	CL=90%	1683
$\eta c \pi^+ \pi^-$	$< 3.2 \times 10^{-3}$	CL=90%	413

Radiative decays

$\gamma J/\psi(1S)$	$(34.3 \pm 1.3) \%$	S=1.3	389
$\gamma \rho^0$	$(2.16 \pm 0.17) \times 10^{-4}$		1670
$\gamma \omega$	$(6.8 \pm 0.8) \times 10^{-5}$		1668
$\gamma \phi$	$(2.4 \pm 0.5) \times 10^{-5}$		1607
$\gamma \gamma$	$< 6.3 \times 10^{-6}$	CL=90%	1755
$e^+ e^- J/\psi(1S)$	$(3.46 \pm 0.24) \times 10^{-3}$		389
$\mu^+ \mu^- J/\psi(1S)$	$(2.33 \pm 0.29) \times 10^{-4}$		335

 $h_c(1P)$

$$I^G(J^{PC}) = 0^-(1^+ -)$$

Mass $m = 3525.37 \pm 0.14$ MeV (S = 1.2)Full width $\Gamma = 0.78 \pm 0.28$ MeV

$h_c(1P)$ DECAY MODES	Fraction (Γ_i/Γ)	Confidence level	p (MeV/c)
$J/\psi(1S) \pi^0$	$< 5 \times 10^{-4}$	90%	382
$J/\psi(1S) \pi \pi$	not seen		312
$J/\psi(1S) \pi^+ \pi^-$	$< 2.7 \times 10^{-3}$	90%	305
$\rho \bar{\rho}$	$< 1.7 \times 10^{-4}$	90%	1492
$\rho \bar{\rho} \pi^0$	$< 8 \times 10^{-4}$	90%	1447
$\rho \bar{\rho} \pi^+ \pi^-$	$(3.3 \pm 0.6) \times 10^{-3}$		1390
$\rho \bar{\rho} \pi^0 \pi^0$	$< 6 \times 10^{-4}$	90%	1394

$\rho \bar{\rho} \pi^+ \pi^- \pi^0$	$(4.4 \pm 1.3) \times 10^{-3}$		1331
$\rho \bar{\rho} \eta$	$(7.4 \pm 2.2) \times 10^{-4}$		1264
$\pi^+ \pi^- \pi^0$	$(1.9 \pm 0.5) \times 10^{-3}$		1749
$\pi^+ \pi^- \pi^0 \eta$	$(8.3 \pm 2.4) \times 10^{-3}$		1695
$2\pi^+ 2\pi^- \pi^0$	$(9.4 \pm 1.7) \times 10^{-3}$		1716
$3\pi^+ 3\pi^- \pi^0$	$< 1.0 \%$		1661
$K^+ K^- \pi^+ \pi^-$	$< 7 \times 10^{-4}$	90%	1640
$K^+ K^- \pi^+ \pi^- \pi^0$	$(3.8 \pm 0.8) \times 10^{-3}$		1606
$K^+ K^- \pi^+ \pi^- \eta$	$< 2.7 \times 10^{-3}$	90%	1480
$K^+ K^- \pi^0$	$< 6 \times 10^{-4}$	90%	1670
$K^+ K^- \pi^0 \eta$	$< 2.4 \times 10^{-3}$	90%	1532
$K^+ K^- \eta$	$< 1.0 \times 10^{-3}$	90%	1574
$2K^+ 2K^- \pi^0$	$< 2.8 \times 10^{-4}$	90%	1339
$K_S^0 K^\pm \pi^\mp$	$< 6 \times 10^{-4}$	90%	1668
$K_S^0 K^\pm \pi^\mp \pi^+ \pi^-$	$(3.2 \pm 1.0) \times 10^{-3}$		1604

Radiative decays

$\gamma \eta$	$(4.7 \pm 2.1) \times 10^{-4}$		1720
$\gamma \eta'(958)$	$(1.5 \pm 0.4) \times 10^{-3}$		1633
$\gamma \eta c(1S)$	$(60 \pm 4) \%$		500

 $\chi_{c2}(1P)$

$$I^G(J^{PC}) = 0^+(2^+ +)$$

Mass $m = 3556.17 \pm 0.07$ MeVFull width $\Gamma = 1.98 \pm 0.09$ MeV (S = 1.1) $\chi_{c2}(1P)$ DECAY MODESScale factor/
Confidence level p (MeV/c)

$\chi_{c2}(1P)$ DECAY MODES	Fraction (Γ_i/Γ)	Confidence level	p (MeV/c)
Hadronic decays			
$2(\pi^+ \pi^-)$	$(1.00 \pm 0.13) \%$	S=1.4	1751
$\pi^+ \pi^- \pi^0$	$(1.86 \pm 0.24) \%$		1752
$\rho^+ \pi^- \pi^0 + c.c.$	$(2.22 \pm 0.35) \%$		1682
$4\pi^0$	$(1.13 \pm 0.15) \times 10^{-3}$		1752
$K^+ K^- \pi^0 \pi^0$	$(2.1 \pm 0.4) \times 10^{-3}$		1658
$K^+ \pi^- \bar{K}^0 \pi^0 + c.c.$	$(1.41 \pm 0.20) \%$		1657
$\rho^- K^+ \bar{K}^0 + c.c.$	$(4.2 \pm 1.3) \times 10^{-3}$		1540
$K^*(892)^0 K^- \pi^+ \rightarrow$ $K^- \pi^+ K^0 \pi^0 + c.c.$	$(3.0 \pm 0.8) \times 10^{-3}$		-
$K^*(892)^0 \bar{K}^0 \pi^0 \rightarrow$ $K^+ \pi^- \bar{K}^0 \pi^0 + c.c.$	$(3.9 \pm 0.9) \times 10^{-3}$		-
$K^*(892)^- K^+ \pi^0 \rightarrow$ $K^+ \pi^- \bar{K}^0 \pi^0 + c.c.$	$(3.8 \pm 0.8) \times 10^{-3}$		-
$K^*(892)^+ \bar{K}^0 \pi^- \rightarrow$ $K^+ \pi^- \bar{K}^0 \pi^0 + c.c.$	$(3.0 \pm 0.8) \times 10^{-3}$		-
$K^+ K^- \eta \pi^0$	$(1.3 \pm 0.4) \times 10^{-3}$		1549
$K^+ K^- \pi^+ \pi^-$	$(8.3 \pm 1.1) \times 10^{-3}$	S=1.2	1656
$K^+ K^- \pi^+ \pi^- \pi^0$	$(1.17 \pm 0.13) \%$		1623
$K_S^0 K^\pm \pi^\mp \pi^+ \pi^-$	$(7.3 \pm 0.8) \times 10^{-3}$		1621
$K^+ \bar{K}^*(892)^0 \pi^- + c.c.$	$(2.1 \pm 1.0) \times 10^{-3}$		1602
$K^*(892)^0 \bar{K}^*(892)^0$	$(2.2 \pm 0.9) \times 10^{-3}$	S=2.3	1538
$3(\pi^+ \pi^-)$	$(1.53 \pm 0.19) \%$	S=3.8	1707
$\phi \phi$	$(1.23 \pm 0.07) \times 10^{-3}$	S=1.9	1457
$\phi \phi \eta$	$(5.4 \pm 0.7) \times 10^{-4}$		1206
$\omega \omega$	$(8.6 \pm 1.0) \times 10^{-4}$		1597
$\omega K^+ K^-$	$(7.3 \pm 0.9) \times 10^{-4}$		1540
$\omega \phi$	$(9.7 \pm 2.8) \times 10^{-6}$		1529
$\pi \pi$	$(2.27 \pm 0.10) \times 10^{-3}$		1773
$\rho^0 \pi^+ \pi^-$	$(3.6 \pm 1.5) \times 10^{-3}$		1682
$\pi^+ \pi^- \pi^0$ (non-resonant)	$(2.0 \pm 0.4) \times 10^{-5}$		1765
$\rho(770)^\pm \pi^\mp$	$(6 \pm 4) \times 10^{-6}$		-
$\pi^+ \pi^- \eta$	$(4.9 \pm 1.3) \times 10^{-4}$		1724
$\pi^+ \pi^- \eta'$	$(5.1 \pm 1.9) \times 10^{-4}$		1636
$\eta \eta$	$(5.5 \pm 0.5) \times 10^{-4}$		1692
$K^+ K^-$	$(1.02 \pm 0.15) \times 10^{-3}$	S=2.3	1708
$K_S^0 K_S^0$	$(5.3 \pm 0.4) \times 10^{-4}$		1707
$K^*(892)^\pm K^\mp$	$(1.46 \pm 0.21) \times 10^{-4}$		1627
$K^*(892)^0 \bar{K}^0 + c.c.$	$(1.27 \pm 0.27) \times 10^{-4}$		1627
$K_2^*(1430)^\pm K^\mp$	$(1.51 \pm 0.13) \times 10^{-3}$		-
$K_2^*(1430)^0 \bar{K}^0 + c.c.$	$(1.27 \pm 0.17) \times 10^{-3}$		1443
$K_3^*(1780)^\pm K^\mp$	$(5.3 \pm 0.8) \times 10^{-4}$		-
$K_3^*(1780)^0 \bar{K}^0 + c.c.$	$(5.7 \pm 2.1) \times 10^{-4}$		1274
$a_2(1320)^0 \pi^0$	$(1.31 \pm 0.35) \times 10^{-3}$		-
$a_2(1320)^\pm \pi^\mp$	$(1.8 \pm 0.6) \times 10^{-3}$		1530
$\bar{K}^0 K^+ \pi^- + c.c.$	$(1.30 \pm 0.19) \times 10^{-3}$		1685
$K^+ K^- \pi^0$	$(3.1 \pm 0.8) \times 10^{-4}$		1686
$K^+ K^- \eta$	$< 3.3 \times 10^{-4}$	CL=90%	1592
$K^+ K^- \eta'(958)$	$(1.94 \pm 0.34) \times 10^{-4}$		1488

Meson Summary Table

$\eta\eta'$	$(2.2 \pm 0.5) \times 10^{-5}$		1600
η'/η'	$(4.6 \pm 0.6) \times 10^{-5}$		1498
$\pi^+\pi^-K_S^0K_S^0$	$(2.2 \pm 0.5) \times 10^{-3}$		1655
$K^+K^-K_S^0K_S^0$	$< 4 \times 10^{-4}$	CL=90%	1418
$K_S^0K_S^0K_S^0K_S^0$	$(1.15 \pm 0.18) \times 10^{-4}$		1415
$K^+K^-K^+K^-$	$(1.67 \pm 0.22) \times 10^{-3}$	S=1.1	1421
$K^+K^-\phi$	$(1.45 \pm 0.30) \times 10^{-3}$		1468
$\bar{K}^0K^+\pi^-\phi + c.c.$	$(4.8 \pm 0.7) \times 10^{-3}$		1416
$K^+K^-\pi^0\phi$	$(2.7 \pm 0.5) \times 10^{-3}$		1419
$\phi\pi^+\pi^-\pi^0$	$(9.3 \pm 1.2) \times 10^{-4}$		1603
$\rho\bar{\rho}$	$(7.3 \pm 0.4) \times 10^{-5}$	S=1.1	1510
$\rho\bar{\rho}\pi^0$	$(4.7 \pm 0.4) \times 10^{-4}$		1465
$\rho\bar{\rho}\eta$	$(1.77 \pm 0.25) \times 10^{-4}$		1285
$\rho\bar{\rho}\omega$	$(3.7 \pm 0.4) \times 10^{-4}$		1152
$\rho\bar{\rho}\phi$	$(2.8 \pm 0.9) \times 10^{-5}$		1002
$\rho\bar{\rho}\pi^+\pi^-$	$(1.32 \pm 0.34) \times 10^{-3}$		1410
$\rho\bar{\rho}\pi^0\pi^0$	$(8.0 \pm 2.4) \times 10^{-4}$		1414
$\rho\bar{\rho}K^+K^-$ (non-resonant)	$(1.94 \pm 0.33) \times 10^{-4}$		1013
$\rho\bar{\rho}K_S^0K_S^0$	$< 7.9 \times 10^{-4}$	CL=90%	1007
$\rho\bar{\rho}\pi^-$	$(8.7 \pm 1.0) \times 10^{-4}$		1463
$\bar{\rho}\pi\pi^+$	$(9.1 \pm 0.8) \times 10^{-4}$		1463
$\rho\bar{\rho}\pi^-\pi^0$	$(2.21 \pm 0.18) \times 10^{-3}$		1411
$\bar{\rho}\pi\pi^+\pi^0$	$(2.15 \pm 0.19) \times 10^{-3}$		1411
$\Lambda\bar{\Lambda}$	$(1.86 \pm 0.16) \times 10^{-4}$		1384
$\Lambda\bar{\Lambda}\pi^+\pi^-$	$(1.28 \pm 0.16) \times 10^{-3}$		1255
$\Lambda\bar{\Lambda}\pi^+\pi^-$ (non-resonant)	$(6.7 \pm 1.5) \times 10^{-4}$		1255
$\Sigma(1385)^+\bar{\Lambda}\pi^- + c.c.$	$< 4 \times 10^{-4}$	CL=90%	1192
$\Sigma(1385)^-\bar{\Lambda}\pi^+ + c.c.$	$< 6 \times 10^{-4}$	CL=90%	1192
$\Lambda\bar{\Lambda}\eta$	$(1.07 \pm 0.26) \times 10^{-4}$		1096
$K^+\bar{p}\Lambda + c.c.$	$(7.9 \pm 0.6) \times 10^{-4}$		1236
$nK_S^0\bar{\Lambda} + c.c.$	$(3.64 \pm 0.29) \times 10^{-4}$		1233
$K^*(892)^+\bar{p}\Lambda + c.c.$	$(8.3 \pm 1.2) \times 10^{-4}$		976
$K^+\bar{p}\Lambda(1520) + c.c.$	$(2.9 \pm 0.7) \times 10^{-4}$		992
$\Lambda(1520)\bar{\Lambda}(1520)$	$(4.7 \pm 1.5) \times 10^{-4}$		924
$\Sigma^0\bar{\Sigma}^0$	$(3.7 \pm 0.6) \times 10^{-5}$		1319
$\Sigma^+\bar{p}K_S^0 + c.c.$	$(8.4 \pm 1.0) \times 10^{-5}$		1197
$\Sigma^0\bar{p}K^+ + c.c.$	$(9.3 \pm 0.8) \times 10^{-5}$		1197
$\Sigma^+\bar{\Sigma}^-$	$(3.4 \pm 0.7) \times 10^{-5}$		1322
$\Sigma^-\bar{\Sigma}^+$	$(4.5 \pm 1.8) \times 10^{-5}$		1314
$\Sigma(1385)^+\bar{\Sigma}(1385)^-$	$< 1.6 \times 10^{-4}$	CL=90%	1118
$\Sigma(1385)^-\bar{\Sigma}(1385)^+$	$< 8 \times 10^{-5}$	CL=90%	1118
$K^-\Lambda\bar{\Xi}^+ + c.c.$	$(1.80 \pm 0.32) \times 10^{-4}$		1004
$\Xi^0\bar{\Xi}^0$	$(1.86 \pm 0.22) \times 10^{-4}$		1197
$\Xi^-\bar{\Xi}^+$	$(1.46 \pm 0.12) \times 10^{-4}$		1189
$\Omega^-\bar{\Omega}^+$	$(4.52 \pm 0.30) \times 10^{-5}$		604
$J/\psi(1S)\pi^+\pi^-\pi^0$	$< 1.5 \%$	CL=90%	185
$\pi^0\eta_c$	$< 3.2 \times 10^{-3}$	CL=90%	511
$\eta_c(1S)\pi^+\pi^-$	$< 5.4 \times 10^{-3}$	CL=90%	459

Radiative decays

$\gamma J/\psi(1S)$	$(19.5 \pm 0.8) \%$	S=1.5	430
$\gamma\rho^0$	$< 1.9 \times 10^{-5}$	CL=90%	1694
$\gamma\omega$	$< 6 \times 10^{-6}$	CL=90%	1692
$\gamma\phi$	$< 8 \times 10^{-6}$	CL=90%	1632
$\gamma\gamma$	$(2.92 \pm 0.12) \times 10^{-4}$	S=1.3	1778
$e^+e^-J/\psi(1S)$	$(2.20 \pm 0.15) \times 10^{-3}$		430
$\mu^+\mu^-J/\psi(1S)$	$(2.07 \pm 0.34) \times 10^{-4}$		381

 $\eta_c(2S)$

$$I^G(J^{PC}) = 0^+(0^-+)$$

Quantum numbers are quark model predictions.

Mass $m = 3637.7 \pm 0.9$ MeV (S = 1.2)Full width $\Gamma = 11.8 \pm 1.6$ MeV

$\eta_c(2S)$ DECAY MODES	Fraction (Γ_i/Γ)	Confidence level	ρ (MeV/c)
hadrons	seen		-
$K\bar{K}\pi$	$(1.9 \pm 1.2) \%$		1729
$K\bar{K}\eta$	$(5 \pm 4) \times 10^{-3}$		1637
$2\pi^+2\pi^-$	$< 2.1 \%$	90%	1792
$\rho^0\rho^0$	$< 1.9 \times 10^{-3}$	90%	1645
$3\pi^+3\pi^-$	$(1.3 \pm 0.9) \%$		1749
$K^+K^-\pi^+\pi^-$	$< 1.4 \%$	90%	1700
$K^*0\bar{K}^*0$	$< 2.9 \times 10^{-3}$	90%	1585
$K^+K^-\pi^+\pi^-\pi^0$	$(1.4 \pm 1.0) \%$		1668
$K^+K^-\pi^+\pi^-$	$< 1.4 \%$	90%	1627
$K_S^0K^-2\pi^+\pi^- + c.c.$	$(1.0 \pm 0.8) \%$		1666

$2K^+2K^-$	$< 1.3 \times 10^{-3}$	90%	1470
$\phi\phi$	$< 1.1 \times 10^{-3}$	90%	1506
$\rho\bar{\rho}$	$< 2.0 \times 10^{-3}$	90%	1558
$\rho\bar{\rho}\pi^+\pi^-$	seen		1461
$\gamma\gamma$	$(1.8 \pm 1.2) \times 10^{-4}$		1819
$\gamma J/\psi(1S)$	$< 1.4 \%$	90%	501
$\pi^+\pi^-\eta$	$(4.3 \pm 3.2) \times 10^{-3}$		1766
$\pi^+\pi^-\eta'$	$(2.6 \pm 1.9) \times 10^{-3}$		1680
$K_2^*(1430)\bar{K} + c.c.$	seen		1493
$K_0^*(1950)\bar{K} + c.c.$	seen		1231
$a_0(1710)\pi$	seen		1412
$a_0(1450)\pi$	seen		1531
$a_2(1700)\pi$	seen		1415
$K_0^*(2600)\bar{K} + c.c.$	seen		-
$\pi^+\pi^-\eta_c(1S)$	$< 25 \%$	90%	537

 $\psi(2S)$

$$I^G(J^{PC}) = 0^-(1^{--})$$

Mass $m = 3686.097 \pm 0.011$ MeV (S = 1.1)Full width $\Gamma = 293 \pm 9$ keV (S = 1.2)

$\psi(2S)$ DECAY MODES	Fraction (Γ_i/Γ)	Scale factor/ Confidence level	ρ (MeV/c)
hadrons	$(97.85 \pm 0.13) \%$		-
virtual $\gamma \rightarrow$ hadrons	$(1.79 \pm 0.04) \%$		-
$g\bar{g}g$	$(10.6 \pm 1.6) \%$		-
$\gamma\bar{g}g$	$(1.03 \pm 0.29) \%$		-
light hadrons	$(15.4 \pm 1.5) \%$		-
K_S^0 anything	$(16.0 \pm 1.1) \%$		-
e^+e^-	$(7.94 \pm 0.22) \times 10^{-3}$	S=1.3	1843
$\mu^+\mu^-$	$(8.0 \pm 0.6) \times 10^{-3}$		1840
$\tau^+\tau^-$	$(3.1 \pm 0.4) \times 10^{-3}$		489

Decays into $J/\psi(1S)$ and anything

$J/\psi(1S)$ anything	$(61.5 \pm 0.7) \%$	S=1.3	-
$J/\psi(1S)$ neutrals	$(25.4 \pm 0.5) \%$	S=1.6	-
$J/\psi(1S)\pi^+\pi^-$	$(34.69 \pm 0.34) \%$	S=1.1	477
$J/\psi(1S)\pi^0\pi^0$	$(18.2 \pm 0.5) \%$	S=1.6	481
$J/\psi(1S)\eta$	$(3.37 \pm 0.06) \%$	S=1.2	199
$J/\psi(1S)\pi^0$	$(1.268 \pm 0.032) \times 10^{-3}$		528

Hadronic decays

$\pi^+\pi^-$	$(7.8 \pm 2.6) \times 10^{-6}$		1838
$\pi^+\pi^-\pi^0$	$(2.01 \pm 0.17) \times 10^{-4}$	S=1.7	1830
$\rho(770)\pi \rightarrow \pi^+\pi^-\pi^0$	$(3.2 \pm 1.2) \times 10^{-5}$	S=1.8	-
$\rho(2150)\pi \rightarrow \pi^+\pi^-\pi^0$	$(1.9 \pm 1.2 \pm 0.4) \times 10^{-4}$		-
$2(\pi^+\pi^-)$	$(2.4 \pm 0.6) \times 10^{-4}$	S=2.2	1817
$\rho^0\pi^+\pi^-$	$(2.2 \pm 0.6) \times 10^{-4}$	S=1.4	1750
$2(\pi^+\pi^-)\pi^0$	$(2.9 \pm 1.0) \times 10^{-3}$	S=4.7	1799
$\rho a_2(1320)$	$(2.6 \pm 0.9) \times 10^{-4}$		1500
$\pi^+\pi^-\pi^0\pi^0\pi^0$	$(5.3 \pm 1.0) \times 10^{-3}$		1800
$\rho^\pm\pi^\mp\pi^0\pi^0$	$< 2.7 \times 10^{-3}$	CL=90%	1737
$\pi^+\pi^-4\pi^0$	$(1.4 \pm 1.0) \times 10^{-3}$		1778
$3(\pi^+\pi^-)$	$(3.5 \pm 2.0) \times 10^{-4}$	S=2.8	1774
$2(\pi^+\pi^-\pi^0)$	$(4.8 \pm 1.5) \times 10^{-3}$		1776
$3(\pi^+\pi^-)\pi^0$	$(3.5 \pm 1.6) \times 10^{-3}$		1746
$2(\pi^+\pi^-)3\pi^0$	$(1.42 \pm 0.31) \%$		1748
$\eta\pi^+\pi^-$	$< 1.6 \times 10^{-4}$	CL=90%	1791
$\eta\pi^+\pi^-\pi^0$	$(9.5 \pm 1.7) \times 10^{-4}$		1778
$\eta 2(\pi^+\pi^-)$	$(1.2 \pm 0.6) \times 10^{-3}$		1758
$\eta\pi^+\pi^-\pi^0\pi^0$	$< 4 \times 10^{-4}$	CL=90%	1760
$\eta\pi^+\pi^-3\pi^0$	$< 2.1 \times 10^{-3}$	CL=90%	1736
$\eta 2(\pi^+\pi^-\pi^0)$	$< 2.1 \times 10^{-3}$	CL=90%	1705
$\rho\eta$	$(2.2 \pm 0.6) \times 10^{-5}$	S=1.1	1717
$\eta'\pi^+\pi^-\pi^0$	$(4.5 \pm 2.1) \times 10^{-4}$		1692
$\eta'\rho$	$(1.9 \pm 1.7 \pm 1.2) \times 10^{-5}$		1625
$\omega\pi^0$	$(2.1 \pm 0.6) \times 10^{-5}$		1757
$\omega\pi^+\pi^-$	$(7.3 \pm 1.2) \times 10^{-4}$	S=2.1	1748
$\omega\pi^+\pi^-2\pi^0$	$(8.7 \pm 2.4) \times 10^{-3}$		1715
$b_1^\pm\pi^\mp$	$(4.0 \pm 0.6) \times 10^{-4}$	S=1.1	1635
$\omega f_2(1270)$	$(2.2 \pm 0.4) \times 10^{-4}$		1515
$\omega\pi^0\pi^0$	$(1.11 \pm 0.35) \times 10^{-3}$		1749
$\omega 3\pi^0$	$< 8 \times 10^{-4}$	CL=90%	1736
$b_1^0\pi^0$	$(2.4 \pm 0.6) \times 10^{-4}$		-
$\omega\eta$	$< 1.1 \times 10^{-5}$	CL=90%	1715
$\omega\eta'$	$(3.2 \pm 2.5 \pm 2.1) \times 10^{-5}$		1623

Meson Summary Table

$\phi\pi^0$	< 4	$\times 10^{-7}$	CL=90%	1699	$N(2300)\bar{p} + c.c. \rightarrow p\bar{p}\pi^0$	$(2.6 \pm_{-0.7}^{+1.2}) \times 10^{-5}$	-
$\phi\pi^+\pi^-$	(1.18 ± 0.26)	$\times 10^{-4}$	S=1.5	1690	$N(2570)\bar{p} + c.c. \rightarrow p\bar{p}\pi^0$	$(2.13 \pm_{-0.31}^{+0.40}) \times 10^{-5}$	-
$\phi f_0(980) \rightarrow \pi^+\pi^-$	(7.5 ± 3.3)	$\times 10^{-5}$	S=1.6	-	$p\bar{p}\pi^+\pi^-$	$(6.0 \pm 0.4) \times 10^{-4}$	1491
$\phi\eta$	(3.10 ± 0.31)	$\times 10^{-5}$		1654	$p\bar{p}K^+K^-$	$(2.7 \pm 0.7) \times 10^{-5}$	1118
$\eta\phi(2170), \phi(2170) \rightarrow$	< 2.2	$\times 10^{-6}$	CL=90%	-	$p\bar{p}\eta$	$(6.0 \pm 0.4) \times 10^{-5}$	1373
$\phi f_0(980), f_0 \rightarrow \pi^+\pi^-$					$N(1535)\bar{p} + c.c. \rightarrow p\bar{p}\eta$	$(4.5 \pm_{-0.6}^{+0.7}) \times 10^{-5}$	-
$\phi\eta'$	(1.54 ± 0.20)	$\times 10^{-5}$		1555	$p\bar{p}\pi^+\pi^-\pi^0$	$(7.3 \pm 0.7) \times 10^{-4}$	1435
$\phi f_1(1285)$	(3.0 ± 1.3)	$\times 10^{-5}$		1436	$p\bar{p}\rho^0$	$(5.0 \pm 2.2) \times 10^{-5}$	1252
$\phi\eta(1405) \rightarrow \phi\pi^+\pi^-\eta$	(8.5 ± 1.7)	$\times 10^{-6}$		-	$p\bar{p}\omega$	$(6.9 \pm 2.1) \times 10^{-5}$	1247
$\phi f_2'(1525)$	(4.4 ± 1.6)	$\times 10^{-5}$		1325	$p\bar{p}\eta'$	$(1.10 \pm 0.13) \times 10^{-5}$	1141
K^+K^-	(7.5 ± 0.5)	$\times 10^{-5}$		1776	$p\bar{p}\phi$	$(6.1 \pm 0.6) \times 10^{-6}$	1109
$K^+K^-\pi^+\pi^-$	(7.3 ± 0.5)	$\times 10^{-4}$		1726	$\phi X(1835) \rightarrow p\bar{p}\phi$	< 1.82	$\times 10^{-7}$ CL=90%
$K^+K^-\pi^0$	(4.07 ± 0.31)	$\times 10^{-5}$		1754	$p\bar{n}\pi^-$ or c.c.	$(2.48 \pm 0.17) \times 10^{-4}$	-
$K_S^0 K_S^0$	< 4.6	$\times 10^{-6}$		1775	$p\bar{n}\pi^-\pi^0$	$(3.2 \pm 0.7) \times 10^{-4}$	1492
$K_S^0 K_L^0$	(5.34 ± 0.33)	$\times 10^{-5}$		1775	$\Lambda\bar{\Lambda}$	$(3.81 \pm 0.13) \times 10^{-4}$	S=1.4 1467
$K_S^0 K_L^0\pi^0$	< 3.0	$\times 10^{-4}$	CL=90%	1753	$\Lambda\bar{\Lambda}\pi^0$	$(1.4 \pm 0.7) \times 10^{-6}$	1412
$K^+K^-\pi^0\pi^0$	(2.6 ± 1.3)	$\times 10^{-4}$		1728	$\Lambda\bar{\Lambda}\eta$	$(2.43 \pm 0.32) \times 10^{-5}$	1197
$K^+K^-\pi^0\pi^0\pi^0$	(6.6 ± 2.8)	$\times 10^{-4}$		1696	$\Lambda(1670)\bar{\Lambda} \rightarrow \Lambda\bar{\Lambda}\eta$	$(1.3 \pm 0.7) \times 10^{-5}$	-
$K_S^0 K^\pm\pi^\mp\pi^0\pi^0$	(1.7 ± 0.6)	$\times 10^{-3}$		1694	$\Lambda\bar{\Lambda}\eta'$	$(7.3 \pm 1.0) \times 10^{-6}$	892
$K_S^0 K^\pm\pi^\mp\pi^+\pi^-$	(2.2 ± 0.4)	$\times 10^{-3}$		1692	$\Lambda\bar{\Lambda}\omega(782)$	$(3.3 \pm 0.4) \times 10^{-5}$	1037
$K^+K^-\pi^+\pi^-\pi^0$	(1.26 ± 0.09)	$\times 10^{-3}$		1694	$\Lambda\bar{\Lambda}\pi^+\pi^-$	$(2.8 \pm 0.6) \times 10^{-4}$	1346
$\omega f_0(1710) \rightarrow \omega K^+K^-$	(5.9 ± 2.2)	$\times 10^{-5}$		-	$\Lambda\bar{p}K^+$	$(1.00 \pm 0.14) \times 10^{-4}$	1327
$K^*(892)^0 K^-\pi^+\pi^0 + c.c.$	(8.6 ± 2.2)	$\times 10^{-4}$		-	$\Lambda\bar{p}K^*(892)^+ + c.c.$	$(6.3 \pm 0.7) \times 10^{-5}$	1087
$K^*(892)^+ K^-\pi^+\pi^- + c.c.$	(9.6 ± 2.8)	$\times 10^{-4}$		-	$\Lambda\bar{p}K^+\pi^+\pi^-$	$(1.8 \pm 0.4) \times 10^{-4}$	1167
$K^*(892)^+ K^-\rho^0 + c.c.$	(7.3 ± 2.6)	$\times 10^{-4}$		-	$\bar{\Lambda}n K_S^0 + c.c.$	$(8.1 \pm 1.8) \times 10^{-5}$	1324
$K^*(892)^0 K^-\rho^+ + c.c.$	(6.1 ± 1.8)	$\times 10^{-4}$		-	$\Delta^{++}\Delta^{--}$	$(1.28 \pm 0.35) \times 10^{-4}$	1371
$K_S^0 K_S^0\pi^+\pi^-$	(2.2 ± 0.4)	$\times 10^{-4}$		1724	$\Lambda\bar{\Sigma}^+\pi^- + c.c.$	$(1.40 \pm 0.13) \times 10^{-4}$	1376
$K_S^0 K_L^0\pi^0\pi^0$	(1.3 ± 0.6)	$\times 10^{-3}$		1726	$\Lambda\bar{\Sigma}^-\pi^+ + c.c.$	$(1.54 \pm 0.14) \times 10^{-4}$	1379
$K_S^0 K^*(892)^0\pi^0\pi^0$	(3.0 ± 1.3)	$\times 10^{-4}$		1645	$\Lambda\bar{\Sigma}^0 + c.c.$	$(1.6 \pm 0.7) \times 10^{-6}$	1437
$K_S^0 K^\pm\rho(770)^\mp\pi^0$	< 7	$\times 10^{-4}$	CL=90%	-	$\Sigma^0\bar{p}K^+ + c.c.$	$(1.67 \pm 0.18) \times 10^{-5}$	1291
$K_S^0 K^\pm\pi^\mp\rho(770)^0$	< 7	$\times 10^{-4}$	CL=90%	-	$\Sigma^+\bar{\Sigma}^-$	$(2.43 \pm 0.10) \times 10^{-4}$	S=1.4 1408
$K^\mp K^*(892)^\pm\pi^0\pi^0$	(7.0 ± 2.9)	$\times 10^{-4}$		1646	$\Sigma^0\bar{\Sigma}^0$	$(2.35 \pm 0.09) \times 10^{-4}$	S=1.1 1405
$K^*(892)^+ K^*(892)^-\pi^0$	(3.6 ± 1.8)	$\times 10^{-3}$		1573	$\Sigma^-\bar{\Sigma}^+$	$(2.82 \pm 0.09) \times 10^{-4}$	1401
$K_S^0 K_L^0\eta$	(1.3 ± 0.5)	$\times 10^{-3}$		1661	$\Sigma^+\bar{\Sigma}^-\eta$	$(9.6 \pm 2.4) \times 10^{-6}$	1108
$K^+K^-\rho^0$	(2.2 ± 0.4)	$\times 10^{-4}$		1616	$\Sigma^+\bar{\Sigma}^-\omega$	$(1.89 \pm 0.28) \times 10^{-5}$	926
$K^*(892)^0 \bar{K}_2^0(1430)^0$	(1.9 ± 0.5)	$\times 10^{-4}$		1417	$\Sigma^+\bar{\Sigma}^-\phi$	$(3.0 \pm 0.7) \times 10^{-6}$	686
$K^+K^-\pi^+\pi^-\eta$	(1.3 ± 0.7)	$\times 10^{-3}$		1574	$\Sigma(1385)^+\bar{\Sigma}(1385)^-$	$(8.5 \pm 0.7) \times 10^{-5}$	1218
$K^+K^-\pi^+\pi^-$	(1.9 ± 0.9)	$\times 10^{-3}$		1654	$\Sigma(1385)^-\bar{\Sigma}(1385)^+$	$(8.5 \pm 0.8) \times 10^{-5}$	1218
$K^+K^-\pi^+\pi^-\pi^0$	(1.00 ± 0.31)	$\times 10^{-3}$		1611	$\Sigma(1385)^0\bar{\Sigma}(1385)^0$	$(6.9 \pm 0.7) \times 10^{-5}$	1218
$K^+K^*(892)^-\pi^0 + c.c.$	(2.9 ± 0.4)	$\times 10^{-5}$	S=1.2	1698	$\Xi^-\Xi^+$	$(2.87 \pm 0.11) \times 10^{-4}$	S=1.1 1284
$2(K^+K^-)$	(6.3 ± 1.3)	$\times 10^{-5}$		1499	$\Xi^0\Xi^0$	$(2.3 \pm 0.4) \times 10^{-4}$	S=4.2 1291
$2(K^+K^-)\pi^0$	(1.10 ± 0.28)	$\times 10^{-4}$		1440	$\Xi(1530)^0\Xi(1530)^0$	$(6.8 \pm 0.4) \times 10^{-5}$	1025
$K^+K^-\phi$	(7.0 ± 1.6)	$\times 10^{-5}$		1546	$\Lambda\Xi^+K^- + c.c.$	$(3.9 \pm 0.4) \times 10^{-5}$	1114
$K_S^0 K_S^0\phi$	(3.53 ± 0.29)	$\times 10^{-5}$		1543	$\Xi(1690)^-\Xi^+ \rightarrow K^-\Lambda\Xi^+ +$	$(5.2 \pm 1.6) \times 10^{-6}$	-
$K_1(1270)^\pm K^\mp$	(1.00 ± 0.28)	$\times 10^{-3}$		1588	c.c.		
$K^+\bar{K}^*(892)^0\pi^- + c.c.$	(6.7 ± 2.5)	$\times 10^{-4}$		1674	$\Xi(1820)^-\Xi^+ \rightarrow K^-\Lambda\Xi^+ +$	$(1.20 \pm 0.32) \times 10^{-5}$	-
$\eta K^+K^-, \text{ no } \eta\phi$	(3.49 ± 0.17)	$\times 10^{-5}$		1664	c.c.		
ηK^+K^-	< 2.6	$\times 10^{-4}$	CL=90%	1664	$\Xi(1530)^-\Xi(1530)^+$	$(1.15 \pm 0.07) \times 10^{-4}$	1025
$X(1750)\eta \rightarrow K^+K^-\eta$	(4.8 ± 2.8)	$\times 10^{-6}$		-	$\Xi(1530)^-\Xi^+$	$(7.0 \pm 1.2) \times 10^{-6}$	1165
$K_1(1400)^\pm K^\mp$	< 3.1	$\times 10^{-4}$	CL=90%	1532	$\Xi(1530)^0\Xi^0$	$(5.3 \pm 0.5) \times 10^{-6}$	1169
$K_2^0(1430)^\pm K^\mp$	$(7.1 \pm_{-0.9}^{+1.3})$	$\times 10^{-5}$		-	$\Sigma^0\Xi^+K^- + c.c.$	$(3.7 \pm 0.4) \times 10^{-5}$	1060
$K^*(892)^0 \bar{K}^0 + c.c.$	(1.09 ± 0.20)	$\times 10^{-4}$		1697	$\Omega^-\bar{\Omega}^+$	$(5.66 \pm 0.30) \times 10^{-5}$	S=1.3 774
ωK^+K^-	(1.62 ± 0.11)	$\times 10^{-4}$	S=1.1	1614	$\eta_c\pi^+\pi^-\pi^0$	< 1.0	$\times 10^{-3}$ CL=90%
$\omega K_S^0 K_S^0$	(7.0 ± 0.5)	$\times 10^{-5}$		1612	$h_c(1P)\pi^0$	$(7.4 \pm 0.5) \times 10^{-4}$	85
$\omega K^*(892)^+ K^- + c.c.$	(2.07 ± 0.26)	$\times 10^{-4}$		1482	$\Lambda_c^+\bar{p}e^+ + c.c.$	< 1.7	$\times 10^{-6}$ CL=90%
$\omega K_2^0(1430) + K^- + c.c.$	(6.1 ± 1.2)	$\times 10^{-5}$		1252	$\Theta(1540)\bar{\Theta}(1540) \rightarrow$	$[iiaa] < 8.8$	$\times 10^{-6}$ CL=90%
$\omega \bar{K}^*(892)^0 K^0$	(1.68 ± 0.30)	$\times 10^{-4}$		1481	$K_S^0 p K^- \bar{n} + c.c.$		
$\omega \bar{K}_2^0(1430)^0 K^0$	(5.8 ± 2.2)	$\times 10^{-5}$		1250	$\Theta(1540)K^-\bar{n} \rightarrow K_S^0 p K^- \bar{n}$	$[iiaa] < 1.0$	$\times 10^{-5}$ CL=90%
$\omega X(1440) \rightarrow \omega K_S^0 K^-\pi^+ +$	(1.6 ± 0.4)	$\times 10^{-5}$		-	$\Theta(1540)K_S^0 \bar{p} \rightarrow K_S^0 \bar{p} K^+ n$	$[iiaa] < 7.0$	$\times 10^{-6}$ CL=90%
c.c.					$\bar{\Theta}(1540)K^+ n \rightarrow K_S^0 \bar{p} K^+ n$	$[iiaa] < 2.6$	$\times 10^{-5}$ CL=90%
$\omega X(1440) \rightarrow \omega K^+K^-\pi^0$	(1.09 ± 0.26)	$\times 10^{-5}$		-	$\bar{\Theta}(1540)K_S^0 p \rightarrow K_S^0 p K^- \bar{n}$	$[iiaa] < 6.0$	$\times 10^{-6}$ CL=90%
$\omega f_1(1285) \rightarrow \omega K_S^0 K^-\pi^+ +$	(3.0 ± 1.0)	$\times 10^{-6}$		-			
c.c.							
$\omega f_1(1285) \rightarrow \omega K^+K^-\pi^0$	(1.2 ± 0.7)	$\times 10^{-6}$		-			
$p\bar{p}$	(2.94 ± 0.09)	$\times 10^{-4}$	S=1.3	1586	$\gamma\chi_{c0}(1P)$	$(9.77 \pm 0.23) \%$	S=1.1 261
$n\bar{n}$	(3.06 ± 0.15)	$\times 10^{-4}$		1586	$\gamma\chi_{c1}(1P)$	$(9.75 \pm 0.27) \%$	S=1.1 171
$p\bar{p}\pi^0$	(1.53 ± 0.07)	$\times 10^{-4}$		1543	$\gamma\chi_{c2}(1P)$	$(9.36 \pm 0.23) \%$	S=1.2 128
$N(940)\bar{p} + c.c. \rightarrow p\bar{p}\pi^0$	$(6.4 \pm_{-1.3}^{+1.8})$	$\times 10^{-5}$		-	$\gamma\eta_c(1S)$	$(3.6 \pm 0.5) \times 10^{-3}$	S=1.3 635
$N(1440)\bar{p} + c.c. \rightarrow p\bar{p}\pi^0$	$(7.3 \pm_{-1.5}^{+1.7})$	$\times 10^{-5}$	S=2.5	-	$\gamma\eta_c(2S)$	$(7 \pm 5) \times 10^{-4}$	48
$N(1520)\bar{p} + c.c. \rightarrow p\bar{p}\pi^0$	$(6.4 \pm_{-1.8}^{+2.3})$	$\times 10^{-6}$		-	$\gamma\pi^0$	$(1.04 \pm 0.22) \times 10^{-6}$	S=1.4 1841
$N(1535)\bar{p} + c.c. \rightarrow p\bar{p}\pi^0$	(2.5 ± 1.0)	$\times 10^{-5}$		-	$\gamma 2(\pi^+\pi^-)$	$(4.0 \pm 0.6) \times 10^{-4}$	1817
$N(1650)\bar{p} + c.c. \rightarrow p\bar{p}\pi^0$	$(3.8 \pm_{-1.7}^{+1.4})$	$\times 10^{-5}$		-	$\gamma 3(\pi^+\pi^-)$	< 1.7	$\times 10^{-4}$ CL=90%
$N(1720)\bar{p} + c.c. \rightarrow p\bar{p}\pi^0$	$(1.79 \pm_{-0.70}^{+0.26})$	$\times 10^{-5}$		-	$\gamma\eta'(958)$	$(1.24 \pm 0.04) \times 10^{-4}$	1719
					$\gamma f_2(1270)$	$(2.73 \pm_{-0.25}^{+0.29}) \times 10^{-4}$	S=1.8 1622
					$\gamma f_0(1370) \rightarrow \gamma K\bar{K}$	$(3.1 \pm 1.7) \times 10^{-5}$	1588
					$\gamma f_0(1500)$	$(9.3 \pm 1.9) \times 10^{-5}$	1529

Radiative decays

Meson Summary Table

$\gamma f'_2(1525)$	$(3.3 \pm 0.8) \times 10^{-5}$		1531	$K^*(892)^0 \bar{K}^0 + c.c.$	< 1.2	$\times 10^{-3}$	CL=90%	1745
$\gamma f_0(1710)$	seen		1436	$K_S^0 K_L^0$	< 1.2	$\times 10^{-5}$	CL=90%	1820
$\gamma f_0(1710) \rightarrow \gamma \pi \pi$	$(3.5 \pm 0.6) \times 10^{-5}$		-	$2(\pi^+ \pi^-)$	< 1.12	$\times 10^{-3}$	CL=90%	1861
$\gamma f_0(1710) \rightarrow \gamma K \bar{K}$	$(6.6 \pm 0.7) \times 10^{-5}$		-	$2(\pi^+ \pi^-) \pi^0$	< 1.06	$\times 10^{-3}$	CL=90%	1844
$\gamma f_0(2100) \rightarrow \gamma \pi \pi$	$(4.8 \pm 1.0) \times 10^{-6}$		1244	$2(\pi^+ \pi^-) \pi^0$	< 5.85	%	CL=90%	1821
$\gamma f_0(2200) \rightarrow \gamma K \bar{K}$	$(3.2 \pm 1.0) \times 10^{-6}$		1193	$\omega \pi^+ \pi^-$	< 6.0	$\times 10^{-4}$	CL=90%	1794
$\gamma f_J(2220) \rightarrow \gamma \pi \pi$	< 5.8	$\times 10^{-6}$	CL=90%	1168	$3(\pi^+ \pi^-)$	< 9.1	$\times 10^{-3}$	CL=90%
$\gamma f_J(2220) \rightarrow \gamma K \bar{K}$	< 9.5	$\times 10^{-6}$	CL=90%	1168	$3(\pi^+ \pi^-) \pi^0$	< 1.37	%	CL=90%
$\gamma \eta$	$(9.2 \pm 1.8) \times 10^{-7}$		1802	$3(\pi^+ \pi^-) 2\pi^0$	< 11.74	%	CL=90%	1760
$\gamma \eta \pi^+ \pi^-$	$(8.7 \pm 2.1) \times 10^{-4}$		1791	$\eta \pi^+ \pi^-$	< 1.24	$\times 10^{-3}$	CL=90%	1836
$\gamma \eta(1405)$	seen		1574	$\pi^+ \pi^- 2\pi^0$	< 8.9	$\times 10^{-3}$	CL=90%	1862
$\gamma \eta(1405) \rightarrow \gamma K \bar{K} \pi$	< 9	$\times 10^{-5}$	CL=90%	1569	$\rho^0 \pi^+ \pi^-$	< 6.9	$\times 10^{-3}$	CL=90%
$\gamma \eta(1405) \rightarrow \gamma \eta \pi^+ \pi^-$	$(3.6 \pm 2.5) \times 10^{-5}$		-	$\eta 3\pi$	< 1.34	$\times 10^{-3}$	CL=90%	1824
$\gamma \eta(1405) \rightarrow \gamma f_0(980) \pi^0$	< 5.0	$\times 10^{-7}$	CL=90%	-	$\eta 2(\pi^+ \pi^-)$	< 2.43	%	CL=90%
$\gamma \eta(1475)$	seen		1548	$\eta \rho^0 \pi^+ \pi^-$	< 1.45	%	CL=90%	1708
$\gamma \eta(1475) \rightarrow \gamma K \bar{K} \pi$	< 1.4	$\times 10^{-4}$	CL=90%	-	$\eta' 3\pi$	< 2.44	$\times 10^{-3}$	CL=90%
$\gamma \eta(1475) \rightarrow \gamma \eta \pi^+ \pi^-$	< 8.8	$\times 10^{-5}$	CL=90%	-	$K^+ K^- \pi^+ \pi^-$	< 9.0	$\times 10^{-4}$	CL=90%
$\gamma K^{*0} K^+ \pi^- + c.c.$	$(3.7 \pm 0.9) \times 10^{-4}$		1674	$\phi \pi^+ \pi^-$	< 4.1	$\times 10^{-4}$	CL=90%	1737
$\gamma K^{*0} \bar{K}^{*0}$	$(2.4 \pm 0.7) \times 10^{-4}$		1613	$K^+ K^- 2\pi^0$	< 4.2	$\times 10^{-3}$	CL=90%	1774
$\gamma K_S^0 K^+ \pi^- + c.c.$	$(2.6 \pm 0.5) \times 10^{-4}$		1753	$4(\pi^+ \pi^-)$	< 1.67	%	CL=90%	1757
$\gamma K^+ K^- \pi^+ \pi^-$	$(1.9 \pm 0.5) \times 10^{-4}$		1726	$4(\pi^+ \pi^-) \pi^0$	< 3.06	%	CL=90%	1720
$\gamma K^+ K^- 2(\pi^+ \pi^-)$	< 2.2	$\times 10^{-4}$	CL=90%	1654	$\phi f_0(980)$	< 4.5	$\times 10^{-4}$	CL=90%
$\gamma 2(K^+ K^-)$	< 4	$\times 10^{-5}$	CL=90%	1499	$K^+ K^- \pi^+ \pi^- \pi^0$	< 2.36	$\times 10^{-3}$	CL=90%
$\gamma \rho \bar{\rho}$	$(3.9 \pm 0.5) \times 10^{-5}$		S=2.0	1586	$K^+ K^- \rho^0 \pi^0$	< 8	$\times 10^{-4}$	CL=90%
$\gamma f_2(1950) \rightarrow \gamma \rho \bar{\rho}$	$(1.20 \pm 0.22) \times 10^{-5}$		-	-	$K^+ K^- \rho^+ \pi^-$	< 1.46	%	CL=90%
$\gamma f_2(2150) \rightarrow \gamma \rho \bar{\rho}$	$(7.2 \pm 1.8) \times 10^{-6}$		-	-	$\omega K^+ K^-$	< 3.4	$\times 10^{-4}$	CL=90%
$\gamma X(1835) \rightarrow \gamma \rho \bar{\rho}$	$(4.6 \pm 1.8) \times 10^{-6}$		-	-	$\phi \pi^+ \pi^- \pi^0$	< 3.8	$\times 10^{-3}$	CL=90%
$\gamma X \rightarrow \gamma \rho \bar{\rho}$	[00aa] < 2	$\times 10^{-6}$	CL=90%	-	$K^{*0} K^- \pi^+ \pi^0 + c.c.$	< 1.62	%	CL=90%
$\gamma \rho \bar{\rho} \pi^+ \pi^-$	$(2.8 \pm 1.4) \times 10^{-5}$		1491	-	$K^* K^- \pi^+ \pi^- + c.c.$	< 3.23	%	CL=90%
$\gamma \gamma$	< 1.5	$\times 10^{-4}$	CL=90%	1843	$K^+ K^- \pi^+ \pi^- 2\pi^0$	< 2.67	%	CL=90%
$\gamma \gamma J/\psi$	$(3.1 \pm 1.0) \times 10^{-4}$		542	-	$K^+ K^- 2(\pi^+ \pi^-)$	< 1.03	%	CL=90%
$e^+ e^- \eta'$	$(1.90 \pm 0.26) \times 10^{-6}$		1719	-	$K^+ K^- 2(\pi^+ \pi^-) \pi^0$	< 3.60	%	CL=90%
$e^+ e^- \eta_c(1S)$	$(3.8 \pm 0.4) \times 10^{-5}$		635	-	$\eta K^+ K^-$	< 4.1	$\times 10^{-4}$	CL=90%
$e^+ e^- \chi_{c0}(1P)$	$(1.06 \pm 0.25) \times 10^{-3}$		261	-	$\eta K^+ K^- \pi^+ \pi^-$	< 1.24	%	CL=90%
$e^+ e^- \chi_{c1}(1P)$	$(8.5 \pm 0.7) \times 10^{-4}$		171	-	$\rho^0 K^+ K^-$	< 5.0	$\times 10^{-3}$	CL=90%
$e^+ e^- \chi_{c2}(1P)$	$(6.8 \pm 0.8) \times 10^{-4}$		128	-	$2(K^+ K^-)$	< 6.0	$\times 10^{-4}$	CL=90%
					$\phi K^+ K^-$	< 7.5	$\times 10^{-4}$	CL=90%
					$2(K^+ K^-) \pi^0$	< 2.9	$\times 10^{-4}$	CL=90%
					$2(K^+ K^-) \pi^+ \pi^-$	< 3.2	$\times 10^{-3}$	CL=90%
					$K_S^0 K^- \pi^+$	< 3.2	$\times 10^{-3}$	CL=90%
					$K_S^0 K^- \pi^+ \pi^0$	< 1.33	%	CL=90%
					$K_S^0 K^- \rho^+$	< 6.6	$\times 10^{-3}$	CL=90%
					$K_S^0 K^- 2\pi^+ \pi^-$	< 8.7	$\times 10^{-3}$	CL=90%
					$K_S^0 K^- \pi^+ \rho^0$	< 1.6	%	CL=90%
					$K_S^0 K^- \pi^+ \eta$	< 1.3	%	CL=90%
					$K_S^0 K^- 2\pi^+ \pi^- \pi^0$	< 4.18	%	CL=90%
					$K_S^0 K^- 2\pi^+ \pi^- \eta$	< 4.8	%	CL=90%
					$K_S^0 K^- \pi^+ 2(\pi^+ \pi^-)$	< 1.22	%	CL=90%
					$K_S^0 K^- \pi^+ 2\pi^0$	< 2.65	%	CL=90%
					$K_S^0 K^- K^+ K^- \pi^+$	< 4.9	$\times 10^{-3}$	CL=90%
					$K_S^0 K^- K^+ K^- \pi^+ \pi^0$	< 3.0	%	CL=90%
					$K_S^0 K^- K^+ K^- \pi^+ \eta$	< 2.2	%	CL=90%
					$K^{*0} K^- \pi^+ + c.c.$	< 9.7	$\times 10^{-3}$	CL=90%
					$\rho \bar{\rho}$	not seen		1637
					$\rho \bar{\rho} \pi^0$	< 4	$\times 10^{-5}$	CL=90%
					$\rho \bar{\rho} \pi^+ \pi^-$	< 5.8	$\times 10^{-4}$	CL=90%
					$\Lambda \bar{\Lambda}$	< 1.2	$\times 10^{-4}$	CL=90%
					$\rho \bar{\rho} \pi^+ \pi^- \pi^0$	< 1.85	$\times 10^{-3}$	CL=90%
					$\omega \rho \bar{\rho}$	< 2.9	$\times 10^{-4}$	CL=90%
					$\Lambda \bar{\Lambda} \pi^0$	< 7	$\times 10^{-5}$	CL=90%
					$\rho \bar{\rho} 2(\pi^+ \pi^-)$	< 2.6	$\times 10^{-3}$	CL=90%
					$\eta \rho \bar{\rho}$	< 5.4	$\times 10^{-4}$	CL=90%
					$\eta \rho \bar{\rho} \pi^+ \pi^-$	< 3.3	$\times 10^{-3}$	CL=90%
					$\rho^0 \rho \bar{\rho}$	< 1.7	$\times 10^{-3}$	CL=90%
					$\rho \bar{\rho} K^+ K^-$	< 3.2	$\times 10^{-4}$	CL=90%
					$\eta \rho \bar{\rho} K^+ K^-$	< 6.9	$\times 10^{-3}$	CL=90%
					$\pi^0 \rho \bar{\rho} K^+ K^-$	< 1.2	$\times 10^{-3}$	CL=90%
					$\phi \rho \bar{\rho}$	< 1.3	$\times 10^{-4}$	CL=90%
					$\Lambda \bar{\Lambda} \pi^+ \pi^-$	< 2.5	$\times 10^{-4}$	CL=90%
					$\Lambda \bar{\rho} K^+$	< 2.8	$\times 10^{-4}$	CL=90%
					$\Lambda \bar{\rho} K^+ \pi^+ \pi^-$	< 6.3	$\times 10^{-4}$	CL=90%
					$\Lambda \bar{\Lambda} \eta$	< 1.9	$\times 10^{-4}$	CL=90%
					$\Sigma^+ \bar{\Sigma}^-$	< 1.0	$\times 10^{-4}$	CL=90%
					$\Sigma^0 \bar{\Sigma}^0$	< 4	$\times 10^{-5}$	CL=90%
					$\Xi^+ \bar{\Xi}^-$	< 1.5	$\times 10^{-4}$	CL=90%
					$\Xi^0 \bar{\Xi}^0$	< 1.4	$\times 10^{-4}$	CL=90%
								1353
								1347
								1263
								1234
								1387
								1405
								1469
								1310
								1490
								1522
								1544
								1595
								1637
								1722
								1214
								1427
								1491
								1742
								1658
								1570
								1703
								1670
								1621
								1740
								1665
								1773
								1799
								1426
								1494
								1598
								1552
								1666
								1624
								1712
								1661
								1702
								1705
								1693
								1694
								1723
								1664
								1623
								1624
								1741
								1597
								1720
								1757
								1774
								1737
								1773
								1741
								1796
								1862
								1836
								1760
								1792
								1820
								1794
								1821
								1844
								1861
								1820
								1

Meson Summary Table

$\Xi^- \Xi^+$	$(1.4 \pm 0.4) \times 10^{-4}$		1347
Radiative decays			
$\gamma \chi_{c2}$	$< 6.4 \times 10^{-4}$	CL=90%	211
$\gamma \chi_{c1}$	$(2.49 \pm 0.23) \times 10^{-3}$		254
$\gamma \chi_{c0}$	$(6.9 \pm 0.6) \times 10^{-3}$		342
$\gamma \eta_c$	$< 7 \times 10^{-4}$	CL=90%	707
$\gamma \eta_c(2S)$	$< 9 \times 10^{-4}$	CL=90%	133
$\gamma \eta'$	$< 1.8 \times 10^{-4}$	CL=90%	1765
$\gamma \eta$	$< 1.5 \times 10^{-4}$	CL=90%	1847
$\gamma \pi^0$	$< 2 \times 10^{-4}$	CL=90%	1884

 $\psi_2(3823)$

$$I^G(J^{PC}) = 0^-(2^{--})$$

I, J, P need confirmation.

was $\psi(3823), X(3823)$

Mass $m = 3823.51 \pm 0.34$ MeV

Full width $\Gamma < 2.9$ MeV, CL = 90%

Branching fractions are given relative to the one **DEFINED AS 1**.

$\psi_2(3823)$ DECAY MODES	Fraction (Γ_i/Γ)	Confidence level	ρ (MeV/c)
$J/\psi(1S)\pi^+\pi^-$	< 0.06	90%	607
$J/\psi(1S)\pi^0\pi^0$	< 0.11	90%	610
$J/\psi(1S)\pi^0$	< 0.030	90%	646
$J/\psi(1S)\eta$	< 0.14	90%	431
$\chi_{c0}\gamma$	< 0.24	90%	387
$\chi_{c1}\gamma$	DEFINED AS 1		300
$\chi_{c2}\gamma$	$0.28^{+0.14}_{-0.11}$		258

 $\psi_3(3842)$

$$I^G(J^{PC}) = 0^-(3^{--})$$

J, P need confirmation.

Seen by a single experiment only.

Mass $m = 3842.71 \pm 0.20$ MeV

Full width $\Gamma = 2.8 \pm 0.6$ MeV

$\psi_3(3842)$ DECAY MODES	Fraction (Γ_i/Γ)	ρ (MeV/c)
$D^+ D^-$	seen	443
$D^0 \bar{D}^0$	seen	463

 $\chi_{c1}(3872)$

$$I^G(J^{PC}) = 0^+(1^{++})$$

also known as $X(3872)$

Mass $m = 3871.64 \pm 0.06$ MeV

$m_{\chi_{c1}(3872)} - m_{J/\psi} = 775 \pm 4$ MeV

Full width $\Gamma = 1.19 \pm 0.21$ MeV ($S = 1.1$)

$\chi_{c1}(3872)$ DECAY MODES	Fraction (Γ_i/Γ)	Confidence level	ρ (MeV/c)
$e^+ e^-$	$< 2.7 \times 10^{-7}$	90%	1936
$\pi^+ \pi^- \pi^0$	$< 8 \times 10^{-3}$	90%	1924
$\pi^+ \pi^- J/\psi(1S)$	$(3.5 \pm 0.9) \%$		650
$\pi^+ \pi^- \pi^0 J/\psi(1S)$	not seen		588
$\omega \eta_c(1S)$	$< 30 \%$	90%	368
$\rho(770)^0 J/\psi(1S)$	$(2.8 \pm 0.7) \%$		-
$\omega J/\psi(1S)$	$(4.1 \pm 1.4) \%$		†
$\phi \phi$	not seen		1646
$D^0 \bar{D}^0 \pi^0$	$(45 \pm 21) \%$		116
$\bar{D}^{*0} D^0$	$(34 \pm 12) \%$		†
$\gamma \gamma$	$< 10 \%$		1936
$D^0 \bar{D}^0$	$< 26 \%$	90%	519
$D^+ D^-$	$< 17 \%$	90%	502
$\pi^0 \chi_{c2}$	$< 4 \%$	90%	273
$\pi^0 \chi_{c1}$	$(3.1 \pm 1.3) \%$		319
$\pi^0 \chi_{c0}$	$< 13 \%$	90%	411
$\pi^+ \pi^- \eta_c(1S)$	$< 13 \%$	90%	745
$\pi^0 \pi^0 \chi_{c0}$	$< 6 \%$	90%	347
$\pi^+ \pi^- \chi_{c0}$	$< 2.0 \%$	90%	340
$\pi^+ \pi^- \chi_{c1}$	$< 7 \times 10^{-3}$	90%	218
$\rho \bar{\rho}$	$< 2.2 \times 10^{-5}$	95%	1693
Radiative decays			
$\gamma D^+ D^-$	$< 3.5 \%$	90%	502
$\gamma \bar{D}^0 D^0$	$< 6 \%$	90%	519

$\gamma J/\psi$	$(7.8 \pm 2.9) \times 10^{-3}$		697
$\gamma \chi_{c1}$	$< 8 \times 10^{-3}$	90%	344
$\gamma \chi_{c2}$	$< 2.9 \%$	90%	303
$\gamma \psi(2S)$	possibly seen		181

C-violating decays

$\eta J/\psi$	$< 1.7 \%$	90%	491
---------------	------------	-----	-----

 $\chi_{c0}(3915)$

$$I^G(J^{PC}) = 0^+(0^{++})$$

was $X(3915)$

Mass $m = 3922.1 \pm 1.8$ MeV ($S = 1.5$)

Full width $\Gamma = 20 \pm 4$ MeV ($S = 1.1$)

$\chi_{c0}(3915)$ DECAY MODES	Fraction (Γ_i/Γ)	ρ (MeV/c)
$\omega J/\psi$	seen	232
$\bar{D}^{*0} D^0$	not seen	313
$D^+ D^-$	seen	592
$D_s^+ D_s^-$	seen	†
$\pi^+ \pi^- \eta_c(1S)$	not seen	788
$\eta_c \eta$	not seen	668
$\eta_c \pi^0$	not seen	817
$K \bar{K}$	not seen	1898
$\gamma \gamma$	seen	1961
$\gamma \psi(2S)$	not seen	229
$\pi^0 \chi_{c1}$	not seen	368

 $\chi_{c2}(3930)$

$$I^G(J^{PC}) = 0^+(2^{++})$$

Mass $m = 3922.5 \pm 1.0$ MeV ($S = 1.7$)

Full width $\Gamma = 35.2 \pm 2.2$ MeV ($S = 1.2$)

$\chi_{c2}(3930)$ DECAY MODES	Fraction (Γ_i/Γ)	ρ (MeV/c)
$\gamma \gamma$	seen	1961
$K \bar{K} \pi$	not seen	1878
$K^+ K^- \pi^+ \pi^- \pi^0$	not seen	1822
$D \bar{D}$	seen	607
$D^+ D^-$	seen	592
$D^0 \bar{D}^0$	seen	607
$\pi^+ \pi^- \eta_c(1S)$	not seen	788
$K \bar{K}$	not seen	1898

 $\psi(4040)$ [ppaa]

$$I^G(J^{PC}) = 0^-(1^{--})$$

Mass $m = 4040 \pm 4$ MeV

Full width $\Gamma = 84 \pm 12$ MeV

Due to the complexity of the $c\bar{c}$ threshold region, in this listing, "seen" ("not seen") means that a cross section for the mode in question has been measured at effective \sqrt{s} near this particle's central mass value, more (less) than 2σ above zero, without regard to any peaking behavior in \sqrt{s} or absence thereof. See mode listing(s) for details and references.

$\psi(4040)$ DECAY MODES	Fraction (Γ_i/Γ)	Confidence level	ρ (MeV/c)
$e^+ e^-$	$(1.02 \pm 0.17) \times 10^{-5}$		2020
$D \bar{D}$	seen		776
$D^0 \bar{D}^0$	seen		776
$D^+ D^-$	seen		764
$D^* \bar{D}^+ + c.c.$	seen		570
$D^*(2007)^0 \bar{D}^0 + c.c.$	seen		576
$D^*(2010)^+ D^- + c.c.$	seen		562
$D^* \bar{D}^*$	seen		196
$D^*(2007)^0 \bar{D}^*(2007)^0$	seen		228
$D^*(2010)^+ D^*(2010)^-$	seen		196
$D \bar{D} \pi$ (excl. $D^* \bar{D}$)	not seen		-
$D^0 D^- \pi^+ + c.c.$ (excl. $D^*(2010)^+ D^- + c.c.$)	not seen		-
$D \bar{D}^* \pi$ (excl. $D^* \bar{D}^*$)	not seen		-
$D^0 \bar{D}^{*-} \pi^+ + c.c.$ (excl. $D^*(2010)^+ D^*(2010)^-$)	seen		-
$D_s^+ D_s^-$	seen		453
$\pi^+ \pi^+ \pi^- \pi^- \pi^0$	seen		1979
$J/\psi(1S)$ hadrons	seen		-
$J/\psi \pi^+ \pi^-$	$< 4 \times 10^{-3}$	90%	795
$J/\psi \pi^0 \pi^0$	$< 2 \times 10^{-3}$	90%	797

Meson Summary Table

$J/\psi\eta$	$(5.2 \pm 0.7) \times 10^{-3}$		676
$J/\psi\pi^0$	$< 2.8 \times 10^{-4}$	90%	824
$J/\psi\pi^+\pi^-\pi^0$	$< 2 \times 10^{-3}$	90%	747
$\chi_{c1}\gamma$	$< 3.4 \times 10^{-3}$	90%	494
$\chi_{c2}\gamma$	$< 5 \times 10^{-3}$	90%	455
$\chi_{c1}\pi^+\pi^-\pi^0$	$< 1.1 \%$	90%	307
$\chi_{c2}\pi^+\pi^-\pi^0$	$< 3.2 \%$	90%	234
$h_c(1P)\pi^+\pi^-$	$< 3 \times 10^{-3}$	90%	404
$\phi\pi^+\pi^-$	$< 3 \times 10^{-3}$	90%	1880
$\Lambda\bar{\Lambda}\pi^+\pi^-$	$< 2.9 \times 10^{-4}$	90%	1579
$\Lambda\bar{\Lambda}\pi^0$	$< 9 \times 10^{-5}$	90%	1636
$\Lambda\bar{\Lambda}\eta$	$< 3.0 \times 10^{-4}$	90%	1452
$\Lambda\bar{\Lambda}$	$< 6 \times 10^{-6}$	90%	1684
$\Sigma^+\bar{\Sigma}^-$	$< 1.3 \times 10^{-4}$	90%	1632
$\Sigma^0\bar{\Sigma}^0$	$< 7 \times 10^{-5}$	90%	1630
$\Xi^+\bar{\Xi}^-$	$< 1.6 \times 10^{-4}$	90%	1527
$\Xi^0\bar{\Xi}^0$	$< 1.8 \times 10^{-4}$	90%	1533
$\Xi^-\bar{\Xi}^+$	$< 6 \times 10^{-5}$	90%	1527
$\mu^+\mu^-$	$(9 \pm 6) \times 10^{-6}$		2017

 $\chi_{c1}(4140)$

$$I^G(J^{PC}) = 0^+(1^{++})$$

was $X(4140)$

Mass $m = 4146.5 \pm 3.0$ MeV ($S = 1.3$)

Full width $\Gamma = 19^{+7}_{-5}$ MeV

$\chi_{c1}(4140)$ DECAY MODES	Fraction (Γ_i/Γ)	p (MeV/c)
$J/\psi\phi$	seen	216
$\gamma\gamma$	not seen	2073

 $\psi(4160)$ [$\rho\rho a a$]

$$I^G(J^{PC}) = 0^-(1^{--})$$

Mass $m = 4191 \pm 5$ MeV

Full width $\Gamma = 69 \pm 10$ MeV

Due to the complexity of the $c\bar{c}$ threshold region, in this listing, "seen" ("not seen") means that a cross section for the mode in question has been measured at effective \sqrt{s} near this particle's central mass value, more (less) than 2σ above zero, without regard to any peaking behavior in \sqrt{s} or absence thereof. See mode listing(s) for details and references.

$\psi(4160)$ DECAY MODES	Fraction (Γ_i/Γ)	Confidence level	p (MeV/c)
e^+e^-	$(6.9 \pm 3.3) \times 10^{-6}$		2096
$\mu^+\mu^-$	seen		2093
$D\bar{D}$	seen		956
$D^0\bar{D}^0$	seen		956
D^+D^-	seen		947
$D^*\bar{D}^+$ + c.c.	seen		798
$D^*(2007)^0\bar{D}^0$ + c.c.	seen		802
$D^*(2010)^+\bar{D}^-$ + c.c.	seen		792
$D^*\bar{D}^*$	seen		592
$D^*(2007)^0\bar{D}^*(2007)^0$	seen		604
$D^*(2010)^+D^*(2010)^-$	seen		592
$D^0D^-\pi^+$ + c.c. (excl. $D^*(2010)^+D^-$ + c.c.)	not seen		-
$D\bar{D}^*\pi$ + c.c. (excl. $D^*\bar{D}^*$)	seen		-
$D^0D^*\pi^+$ + c.c. (excl. $D^*(2010)^+D^0$)	not seen		-
$D_s^+D_s^-$	not seen		719
$D_s^*+D_s^-$ + c.c.	seen		478
$J/\psi\pi^+\pi^-$	$< 3 \times 10^{-3}$	90%	919
$J/\psi\pi^0\pi^0$	$< 3 \times 10^{-3}$	90%	921
$J/\psi K^+K^-$	$< 2 \times 10^{-3}$	90%	407
$J/\psi\eta$	$< 8 \times 10^{-3}$	90%	821
$J/\psi\pi^0$	$< 1 \times 10^{-3}$	90%	944
$J/\psi\eta'$	$< 5 \times 10^{-3}$	90%	456
$J/\psi\pi^+\pi^-\pi^0$	$< 1 \times 10^{-3}$	90%	879
$\psi(2S)\pi^+\pi^-$	$< 4 \times 10^{-3}$	90%	395
$\chi_{c1}\gamma$	$< 5 \times 10^{-3}$	90%	625
$\chi_{c2}\gamma$	$< 1.3 \%$	90%	587
$\chi_{c1}\pi^+\pi^-\pi^0$	$< 2 \times 10^{-3}$	90%	496
$\chi_{c2}\pi^+\pi^-\pi^0$	$< 8 \times 10^{-3}$	90%	444
$h_c(1P)\pi^+\pi^-$	$< 5 \times 10^{-3}$	90%	556
$h_c(1P)\pi^0\pi^0$	$< 2 \times 10^{-3}$	90%	560
$h_c(1P)\eta$	$< 2 \times 10^{-3}$	90%	348

$h_c(1P)\pi^0$	$< 4 \times 10^{-4}$	90%	600
$\omega\pi^+\pi^-$	seen		2013
$\phi\pi^+\pi^-$	$< 2 \times 10^{-3}$	90%	1961
$\gamma\chi_{c1}(3872)$	$< 1.9 \times 10^{-3}$	90%	307
$\gamma\chi_{c0}(3915) \rightarrow \gamma J/\psi\pi^+\pi^-$	$< 1.36 \times 10^{-4}$	90%	-
$\gamma X(3930) \rightarrow \gamma J/\psi\pi^+\pi^-$	$< 1.18 \times 10^{-4}$	90%	-
$\gamma X(3940) \rightarrow \gamma J/\psi\pi^+\pi^-$	$< 1.47 \times 10^{-4}$	90%	-
$\gamma\chi_{c0}(3915) \rightarrow \gamma\gamma J/\psi$	$< 1.26 \times 10^{-4}$	90%	-
$\gamma X(3930) \rightarrow \gamma\gamma J/\psi$	$< 8.8 \times 10^{-5}$	90%	-
$\gamma X(3940) \rightarrow \gamma\gamma J/\psi$	$< 1.79 \times 10^{-4}$	90%	-
$\omega\pi^0$	not seen		2020
$\omega\eta$	not seen		1984
K^+K^-	not seen		2037
$K_S^0 K_{S\mp}^0$	seen		2017
$\rho\bar{\rho}\rho\bar{\rho}$	not seen		834
$\Lambda\bar{\Lambda}$	$< 1.5 \times 10^{-6}$	90%	1774
$\Xi^-\bar{\Xi}^+$	$< 8 \times 10^{-5}$	90%	1626
$\rho K^-\bar{\Lambda}^+$ + c.c.	$< 6 \times 10^{-6}$	90%	1659

 $\psi(4230)$

$$I^G(J^{PC}) = 0^-(1^{--})$$

also known as $Y(4230)$; was $\psi(4260)$

Mass $m = 4222.1 \pm 2.3$ MeV ($S = 1.7$)

Full width $\Gamma = 49 \pm 7$ MeV ($S = 3.4$)

$\psi(4230)$ DECAY MODES	Fraction (Γ_i/Γ)	p (MeV/c)
$\mu^+\mu^-$	$(3.1 \pm 2.8) \times 10^{-5}$	2107
$\eta_c(1S)\pi^+\pi^-$	not seen	1027
$\eta_c(1S)\pi^+\pi^-\pi^0$	seen	992
$J/\psi\pi^+\pi^-$	seen	942
$J/\psi f_0(980), f_0(980) \rightarrow \pi^+\pi^-$	seen	-
$T_{c\bar{c}1}(3900)^{\pm}\pi^{\mp}, T_{c\bar{c}1}^{\pm} \rightarrow$	seen	-
$J/\psi\pi^{\pm}$		
$J/\psi\pi^0\pi^0$	seen	944
$J/\psi K^+K^-$	seen	460
$J/\psi K_S^0 K_S^0$	not seen	447
$J/\psi\eta$	seen	848
$J/\psi\pi^0$	not seen	966
$J/\psi\eta'$	seen	504
$J/\psi\pi^+\pi^-\pi^0$	not seen	904
$J/\psi\eta\pi^0$	not seen	770
$J/\psi\eta\eta$	not seen	211
$\psi(2S)\pi^+\pi^-$	seen	426
$\psi(2S)\eta$	not seen	†
$\chi_{c0}\omega$	seen	171
$\chi_{c1}\pi^+\pi^-\pi^0$	not seen	527
$\chi_{c2}\pi^+\pi^-\pi^0$	not seen	477
$h_c(1P)\pi^+\pi^-$	seen	583
$\phi\pi^+\pi^-$	not seen	1976
$\phi f_0(980) \rightarrow \phi\pi^+\pi^-$	not seen	-
ϕK^+K^-	not seen	1856
$\phi K_S^0 K_S^0$	not seen	1854
$\phi\eta$	not seen	1947
$\phi\eta'$	not seen	1864
$D\bar{D}$	not seen	987
$D^0\bar{D}^0$	not seen	987
D^+D^-	not seen	978
$D^*\bar{D}^+$ + c.c.	not seen	835
$D^*(2007)^0\bar{D}^0$ + c.c.	not seen	839
$D^*(2010)^+\bar{D}^-$ + c.c.	not seen	829
$D^*\bar{D}^*$	not seen	641
$D^*(2007)^0\bar{D}^*(2007)^0$	not seen	652
$D^*(2010)^+D^*(2010)^-$	not seen	641
$D\bar{D}\pi$ + c.c.	not seen	847
$D^0D^-\pi^+$ + c.c. (excl. $D^*(2007)^0\bar{D}^*0$ + c.c., $D^*(2010)^+D^-$ + c.c.)	not seen	-
$D\bar{D}^*\pi$ + c.c. (excl. $D^*\bar{D}^*$)	not seen	723
$D^0D^*(2010)^-\pi^+$ + c.c.	seen	650
$D_1(2420)\bar{D}^+$ + c.c.	not seen	†
$D^*\bar{D}^*\pi$	seen	367
$D^{*0}D^{*-}\pi^+$	seen	364
$D_s^+D_s^-$	not seen	760
$D_s^*+D_s^-$ + c.c.	not seen	538
$D_s^*+D_s^{*-}$	not seen	†

Meson Summary Table

$p\bar{p}$	not seen	1890
$p\bar{p}\pi^0$	not seen	1854
$p\bar{p}\eta$	not seen	1712
$\omega\pi^+\pi^-$	seen	2028
$p\bar{p}\omega$	not seen	1610
$\Xi^-\Xi^+$	not seen	1645
$\pi^+\pi^+\pi^-\pi^-$	not seen	2087
$\pi^+\pi^+\pi^-\pi^-\pi^0$	not seen	2071
$\omega\pi^0$	not seen	2035
$\omega\eta$	not seen	1999
$K_S^0 K^\pm\pi^\mp$	not seen	2032
$K_S^0 K^\pm\pi^\mp\pi^0$	not seen	2009
$K_S^0 K^\pm\pi^\mp\eta$	not seen	1917
$K^+K^-\pi^0$	not seen	2033
$K^+K^-\pi^+\pi^-$	not seen	2008
$K^+K^-\pi^+\pi^-\pi^0$	not seen	1981
$K^+K^+K^-K^-$	not seen	1813
$K^+K^+K^-K^-\pi^0$	not seen	1762
$p\bar{p}\pi^+\pi^-$	not seen	1810
$p\bar{p}\pi^+\pi^-\pi^0$	not seen	1764
$p\bar{p}p\bar{p}$	not seen	864
$\Lambda\bar{\Lambda}$	not seen	1791

Radiative decays

$\eta_c(1S)\gamma$	possibly seen	1055
$\eta_c(1S)\pi^0\gamma$	not seen	1048
$\chi_{c1}\gamma$	not seen	650
$\chi_{c2}\gamma$	not seen	612
$\chi_{c1}(3872)\gamma$	seen	334

$$\chi_{c1}(4274) \quad I^G(J^{PC}) = 0^+(1^+ +)$$

was X(4274)

$$\text{Mass } m = 4286^{+8}_9 \text{ MeV} \quad (S = 1.7)$$

$$\text{Full width } \Gamma = 51 \pm 7 \text{ MeV}$$

$\chi_{c1}(4274)$ DECAY MODES	Fraction (Γ_i/Γ)	ρ (MeV/c)
$J/\psi\phi$	seen	522

$$\psi(4360) \quad I^G(J^{PC}) = 0^-(1^- -)$$

also known as Y(4360); was X(4360)

$$\text{Mass } m = 4374 \pm 7 \text{ MeV} \quad (S = 2.4)$$

$$\text{Full width } \Gamma = 118 \pm 12 \text{ MeV} \quad (S = 2.1)$$

$\psi(4360)$ DECAY MODES	Fraction (Γ_i/Γ)	ρ (MeV/c)
e^+e^-	seen	2187
$h_c\pi^+\pi^-$	seen	723
$J/\psi\pi^+\pi^-$	seen	1064
$\psi(2S)\pi^+\pi^-$	seen	579
$\psi(3770)\pi^+\pi^-$	possibly seen	495
$\psi_2(3823)\pi^+\pi^-$	seen	444
$J/\psi\eta$	seen	983
$D^0D^{*-}\pi^+$	not seen	868
$D^+D^-\pi^+\pi^-$	seen	862
$D_1(2420)\bar{D} + \text{c.c.}$	possibly seen	431
$\phi\eta$	not seen	2030
$\omega\pi^0$	not seen	2115
$\omega\eta$	not seen	2080
$p\bar{p}\eta$	not seen	1806
$p\bar{p}\omega$	not seen	1708
$\chi_{c1}\gamma$	not seen	778
$\chi_{c2}\gamma$	not seen	741
$\Xi^-\Xi^+$	not seen	1742
$pK^-\bar{\Lambda} + \text{c.c.}$	not seen	1773

$$\psi(4415) \text{ [ppa\bar{a}]} \quad I^G(J^{PC}) = 0^-(1^- -)$$

$$\text{Mass } m = 4415 \pm 5 \text{ MeV}$$

$$\text{Full width } \Gamma = 110 \pm 22 \text{ MeV} \quad (S = 2.3)$$

Due to the complexity of the $c\bar{c}$ threshold region, in this listing, "seen" ("not seen") means that a cross section for the mode in question has been measured at effective \sqrt{s} near this particle's central mass value, more (less) than 2σ above zero, without regard to any peaking behavior in \sqrt{s} or absence thereof. See mode listing(s) for details and references.

$\psi(4415)$ DECAY MODES	Fraction (Γ_i/Γ)	Confidence level	ρ (MeV/c)
$D\bar{D}$	seen		1181
$D^0\bar{D}^0$	seen		1181
D^+D^-	seen		1173
$D^*\bar{D} + \text{c.c.}$	seen		1057
$D^*(2007)^0\bar{D}^0 + \text{c.c.}$	seen		1060
$D^*(2010)^+D^- + \text{c.c.}$	seen		1053
$D^*\bar{D}^*$	seen		912
$D^*(2007)^0\bar{D}^*(2007)^0 + \text{c.c.}$	seen		919
$D^*(2010)^+D^*(2010)^- + \text{c.c.}$	seen		912
$D^0D^-\pi^+$ (excl. $D^*(2010)^+D^-$ + c.c.)	< 2.3 %	90%	-
$D\bar{D}_2^*(2460) \rightarrow D^0D^-\pi^+ + \text{c.c.}$	(10 \pm 4) %		-
$D^0D^{*-}\pi^+ + \text{c.c.}$	< 19 %	90%	918
$D_1(2420)\bar{D} + \text{c.c.}$	possibly seen		524
$D_s^+D_s^-$	not seen		999
$\omega\chi_{c2}$	possibly seen		317
$D_s^{*+}D_s^- + \text{c.c.}$	seen		842
$D_s^{*+}D_s^{*-}$	seen		641
$\psi_2(3823)\pi^+\pi^-$	possibly seen		486
$\psi(3770)\pi^+\pi^-$	possibly seen		535
$J/\psi\eta$	< 6 $\times 10^{-3}$	90%	1017
$\chi_{c1}\gamma$	< 8 $\times 10^{-4}$	90%	812
$\chi_{c2}\gamma$	< 4 $\times 10^{-3}$	90%	775
$\Lambda\bar{\Lambda}$	< 3.1 $\times 10^{-6}$	90%	1905
$\Xi^-\Xi^+$	< 4 $\times 10^{-5}$	90%	1768
$pK^-\bar{\Lambda} + \text{c.c.}$	< 6 $\times 10^{-6}$	90%	1798
$\omega\pi^0$	not seen		2136
$\omega\eta$	not seen		2102
e^+e^-	(5.3 \pm 1.2) $\times 10^{-6}$		2207
$\mu^+\mu^-$	(1.1 \pm 0.5) $\times 10^{-5}$		2205

$$\psi(4660) \quad I^G(J^{PC}) = 0^-(1^- -)$$

also known as Y(4660); was X(4660)

$$\text{Mass } m = 4641 \pm 10 \text{ MeV} \quad (S = 2.7)$$

$$\text{Full width } \Gamma = 73^{+13}_{-11} \text{ MeV} \quad (S = 1.7)$$

$\psi(4660)$ DECAY MODES	Fraction (Γ_i/Γ)	ρ (MeV/c)
e^+e^-	not seen	2321
$\psi(2S)\pi^+\pi^-$	seen	819
$J/\psi\eta$	not seen	1201
$D^0D^{*-}\pi^+$	not seen	1165
$D^{*0}D^{*-}\pi^+$	seen	1032
$\psi_2(3823)\pi^+\pi^-$	seen	701
$\chi_{c1}\gamma$	not seen	993
$\chi_{c1}\phi$	not seen	426
$\chi_{c2}\gamma$	not seen	958
$\chi_{c2}\phi$	not seen	326
$\Lambda_c^+\Lambda_c^-$	seen	397
$D_s^+D_{s1}(2536)^-$	seen	557
$D_s^+D_{s2}^*(2573)^-$	seen	-
$\omega\pi^0$	not seen	2253
$\omega\eta$	not seen	2220
$\Xi^-\Xi^+$	not seen	1908
$pK^-\bar{\Lambda} + \text{c.c.}$	not seen	1935

$b\bar{b}$ MESONS

(including possibly non- $q\bar{q}$ states)

$$\eta_b(1S) \quad I^G(J^{PC}) = 0^+(0^- +)$$

$$\text{Mass } m = 9398.7 \pm 2.0 \text{ MeV} \quad (S = 1.5)$$

$$\text{Full width } \Gamma = 10^{+5}_{-4} \text{ MeV}$$

Meson Summary Table

$\eta_b(1S)$ DECAY MODES	Fraction (Γ_i/Γ)	Confidence level	p (MeV/c)
hadrons	seen		—
$3h^+3h^-$	not seen		4672
$2h^+2h^-$	not seen		4689
$4h^+4h^-$	not seen		4648
$\gamma\gamma$	not seen		4699
$\mu^+\mu^-$	$<9 \times 10^{-3}$	90%	4698
$\tau^+\tau^-$	$<8\%$	90%	4350

$\Upsilon(1S)$

$$J^G(J^{PC}) = 0^-(1^{--})$$

Mass $m = 9460.40 \pm 0.10$ MeV
Full width $\Gamma = 54.02 \pm 1.25$ keV

$\Upsilon(1S)$ DECAY MODES	Fraction (Γ_i/Γ)	Scale factor/ Confidence level	p (MeV/c)
$\tau^+\tau^-$	(2.60 \pm 0.10) %		4384
e^+e^-	(2.39 \pm 0.08) %		4730
$\mu^+\mu^-$	(2.48 \pm 0.04) %		4729
Hadronic decays			
ggg	(81.7 \pm 0.7) %		—
γgg	(2.2 \pm 0.6) %		—
$\eta'(958)$ anything	(2.94 \pm 0.24) %		—
$J/\psi(1S)$ anything	(5.4 \pm 0.4) $\times 10^{-4}$	S=1.4	4223
$J/\psi(1S)\eta_c$	$< 2.2 \times 10^{-6}$	CL=90%	3623
$J/\psi(1S)\chi_{c0}$	$< 3.4 \times 10^{-6}$	CL=90%	3429
$J/\psi(1S)\chi_{c1}$	(3.9 \pm 1.2) $\times 10^{-6}$		3382
$J/\psi(1S)\chi_{c2}$	$< 1.4 \times 10^{-6}$	CL=90%	3359
$J/\psi(1S)\eta_c(2S)$	$< 2.2 \times 10^{-6}$	CL=90%	3317
$J/\psi(1S)X(3940)$	$< 5.4 \times 10^{-6}$	CL=90%	3148
$J/\psi(1S)X(4160)$	$< 5.4 \times 10^{-6}$	CL=90%	3020
$X(4350)$ anything, $X \rightarrow J/\psi(1S)\phi$	$< 8.1 \times 10^{-6}$	CL=90%	—
$T_{c\bar{c}1}(3900)^\pm$ anything, $T_{c\bar{c}1} \rightarrow J/\psi(1S)\pi^\pm$	$< 1.3 \times 10^{-5}$	CL=90%	—
$T_{c\bar{c}1}(4200)^\pm$ anything, $Z_c \rightarrow J/\psi(1S)\pi^\pm$	$< 6.0 \times 10^{-5}$	CL=90%	—
$T_{c\bar{c}1}(4430)^\pm$ anything, $T_{c\bar{c}1} \rightarrow J/\psi(1S)\pi^\pm$	$< 4.9 \times 10^{-5}$	CL=90%	—
X_{cs}^\pm anything, $X \rightarrow J/\psi K^\pm$	$< 5.7 \times 10^{-6}$	CL=90%	—
$\psi(4230)$ anything, $\psi \rightarrow J/\psi(1S)\pi^+\pi^-$	$< 3.8 \times 10^{-5}$	CL=90%	—
$\psi(4230)$ anything, $\psi \rightarrow J/\psi(1S)K^+K^-$	$< 7.5 \times 10^{-6}$	CL=90%	—
$\chi_{c1}(4140)$ anything, $\chi_{c1} \rightarrow J/\psi(1S)\phi$	$< 5.2 \times 10^{-6}$	CL=90%	—
χ_{c0} anything	$< 4 \times 10^{-3}$	CL=90%	—
χ_{c1} anything	(1.90 \pm 0.35) $\times 10^{-4}$		—
$\chi_{c1}(1P)X_{tetra}$	$< 3.78 \times 10^{-5}$	CL=90%	—
χ_{c2} anything	(2.8 \pm 0.8) $\times 10^{-4}$		—
$\psi(2S)$ anything	(1.23 \pm 0.20) $\times 10^{-4}$		—
$\psi(2S)\eta_c$	$< 3.6 \times 10^{-6}$	CL=90%	3345
$\psi(2S)\chi_{c0}$	$< 6.5 \times 10^{-6}$	CL=90%	3124
$\psi(2S)\chi_{c1}$	$< 4.5 \times 10^{-6}$	CL=90%	3070
$\psi(2S)\chi_{c2}$	$< 2.1 \times 10^{-6}$	CL=90%	3043
$\psi(2S)\eta_c(2S)$	$< 3.2 \times 10^{-6}$	CL=90%	2994
$\psi(2S)X(3940)$	$< 2.9 \times 10^{-6}$	CL=90%	2797
$\psi(2S)X(4160)$	$< 2.9 \times 10^{-6}$	CL=90%	2645
$\psi(4230)$ anything, $\psi \rightarrow \psi(2S)\pi^+\pi^-$	$< 7.9 \times 10^{-5}$	CL=90%	—
$\psi(4360)$ anything, $\psi \rightarrow \psi(2S)\pi^+\pi^-$	$< 5.2 \times 10^{-5}$	CL=90%	—
$\psi(4660)$ anything, $\psi \rightarrow \psi(2S)\pi^+\pi^-$	$< 2.2 \times 10^{-5}$	CL=90%	—
$T_{c\bar{c}1}(4050)^\pm$ anything, $X \rightarrow \psi(2S)\pi^\pm$	$< 8.8 \times 10^{-5}$	CL=90%	—
$T_{c\bar{c}1}(4430)^\pm$ anything, $T_{c\bar{c}1} \rightarrow \psi(2S)\pi^\pm$	$< 6.7 \times 10^{-5}$	CL=90%	—
$\chi_{c1}(3872)$ anything	$< 2.7 \times 10^{-4}$	CL=90%	—
$T_{c\bar{c}1}(4200)^+ T_{c\bar{c}1}(4200)^-$	$< 2.23 \times 10^{-5}$	CL=90%	—
$T_{c\bar{c}1}(3900)^\pm T_{c\bar{c}1}(4200)^\mp$	$< 8.1 \times 10^{-6}$	CL=90%	—
$T_{c\bar{c}1}(3900)^+ T_{c\bar{c}1}(3900)^-$	$< 1.8 \times 10^{-6}$	CL=90%	—
$T_{c\bar{c}1}(4050)^+ T_{c\bar{c}1}(4050)^-$	$< 1.58 \times 10^{-5}$	CL=90%	—
$T_{c\bar{c}1}(4250)^+ T_{c\bar{c}1}(4250)^-$	$< 2.66 \times 10^{-5}$	CL=90%	—

$T_{c\bar{c}1}(4050)^\pm T_{c\bar{c}1}(4250)^\mp$	$< 4.42 \times 10^{-5}$	CL=90%	—
$T_{c\bar{c}1}(4430)^+ T_{c\bar{c}1}(4430)^-$	$< 2.03 \times 10^{-5}$	CL=90%	—
$T_{c\bar{c}1}(4055)^\pm T_{c\bar{c}1}(4055)^\mp$	$< 2.33 \times 10^{-5}$	CL=90%	—
$T_{c\bar{c}1}(4055)^\pm T_{c\bar{c}1}(4430)^\mp$	$< 4.55 \times 10^{-5}$	CL=90%	—
$\rho\pi$	$< 3.68 \times 10^{-6}$	CL=90%	4697
$\omega\pi^0$	$< 3.90 \times 10^{-6}$	CL=90%	4697
$\pi^+\pi^-$	$< 5 \times 10^{-4}$	CL=90%	4728
K^+K^-	$< 5 \times 10^{-4}$	CL=90%	4704
$\rho\bar{\rho}$	$< 5 \times 10^{-4}$	CL=90%	4636
$\pi^+\pi^-\pi^0$	(2.1 \pm 0.8) $\times 10^{-6}$		4725
ϕK^+K^-	(2.4 \pm 0.5) $\times 10^{-6}$		4623
$\omega\pi^+\pi^-$	(4.5 \pm 1.0) $\times 10^{-6}$		4694
$K^*(892)^0 K^- \pi^+ + c.c.$	(4.4 \pm 0.8) $\times 10^{-6}$		4667
$\phi f_2'(1525)$	$< 1.63 \times 10^{-6}$	CL=90%	4551
$\omega f_2(1270)$	$< 1.79 \times 10^{-6}$	CL=90%	4611
$\rho(770)a_2(1320)$	$< 2.24 \times 10^{-6}$	CL=90%	4605
$K^*(892)^0 K_2^*(1430)^0 + c.c.$	(3.0 \pm 0.8) $\times 10^{-6}$		4579
$K_1(1270)^\pm K^\mp$	$< 2.41 \times 10^{-6}$	CL=90%	4634
$K_1(1400)^\pm K^\mp$	(1.0 \pm 0.4) $\times 10^{-6}$		4613
$b_1(1235)^\pm \pi^\mp$	$< 1.25 \times 10^{-6}$	CL=90%	4649
$\pi^+\pi^-\pi^0$	(1.28 \pm 0.30) $\times 10^{-5}$		4720
$K_S^0 K^+ \pi^- + c.c.$	(1.6 \pm 0.4) $\times 10^{-6}$		4696
$K^*(892)^0 \bar{K}^0 + c.c.$	(2.9 \pm 0.9) $\times 10^{-6}$		4675
$K^*(892)^- K^+ + c.c.$	$< 1.11 \times 10^{-6}$	CL=90%	4675
$f_1(1285)$ anything	(4.6 \pm 3.1) $\times 10^{-3}$		—
$D^*(2010)^\pm$ anything	(2.52 \pm 0.20) %		—
$f_1(1285)X_{tetra}$	$< 6.24 \times 10^{-5}$	CL=90%	—
2H anything	(2.85 \pm 0.25) $\times 10^{-5}$		—
Sum of 100 exclusive modes	(1.200 \pm 0.017) %		—
Radiative decays			
$\gamma\pi^+\pi^-$	(6.3 \pm 1.8) $\times 10^{-5}$		4728
$\gamma\pi^0\pi^0$	(1.7 \pm 0.7) $\times 10^{-5}$		4728
$\gamma\pi\pi$ (S-wave)	(4.6 \pm 0.7) $\times 10^{-5}$		4728
$\gamma\pi^0\eta$	$< 2.4 \times 10^{-6}$	CL=90%	4713
γK^+K^-	[$qqaa$] (1.14 \pm 0.13) $\times 10^{-5}$		4704
$\gamma\rho\bar{\rho}$	[$rraa$] $< 6 \times 10^{-6}$	CL=90%	4636
$\gamma 2h^+2h^-$	(7.0 \pm 1.5) $\times 10^{-4}$		4720
$\gamma 3h^+3h^-$	(5.4 \pm 2.0) $\times 10^{-4}$		4703
$\gamma 4h^+4h^-$	(7.4 \pm 3.5) $\times 10^{-4}$		4679
$\gamma\pi^+\pi^- K^+K^-$	(2.9 \pm 0.9) $\times 10^{-4}$		4686
$\gamma 2\pi^+2\pi^-$	(2.5 \pm 0.9) $\times 10^{-4}$		4720
$\gamma 3\pi^+3\pi^-$	(2.5 \pm 1.2) $\times 10^{-4}$		4703
$\gamma 2\pi^+2\pi^- K^+K^-$	(2.4 \pm 1.2) $\times 10^{-4}$		4659
$\gamma\pi^+\pi^- \rho\bar{\rho}$	(1.5 \pm 0.6) $\times 10^{-4}$		4604
$\gamma 2\pi^+2\pi^- \rho\bar{\rho}$	(4 \pm 6) $\times 10^{-5}$		4563
$\gamma 2K^+2K^-$	(2.0 \pm 2.0) $\times 10^{-5}$		4601
$\gamma\eta'(958)$	$< 1.9 \times 10^{-6}$	CL=90%	4682
$\gamma\eta$	$< 1.0 \times 10^{-6}$	CL=90%	4714
$\gamma f_0(980)$	$< 3 \times 10^{-5}$	CL=90%	4678
$\gamma f_2'(1525)$	(2.9 \pm 0.6) $\times 10^{-5}$		4609
$\gamma f_2(1270)$	(1.01 \pm 0.06) $\times 10^{-4}$		4644
$\gamma\eta(1405)$	$< 8.2 \times 10^{-5}$	CL=90%	4625
$\gamma f_0(1500)$	$< 1.5 \times 10^{-5}$	CL=90%	4608
$\gamma f_0(1500) \rightarrow \gamma K^+K^-$	(1.0 \pm 0.4) $\times 10^{-5}$		—
$\gamma f_0(1710)$	$< 2.6 \times 10^{-4}$	CL=90%	4571
$\gamma f_0(1710) \rightarrow \gamma K^+K^-$	(1.01 \pm 0.32) $\times 10^{-5}$		—
$\gamma f_0(1710) \rightarrow \gamma\pi^+\pi^-$	(5.3 \pm 2.0) $\times 10^{-6}$		—
$\gamma f_0(1710) \rightarrow \gamma\pi^0\pi^0$	$< 1.4 \times 10^{-6}$	CL=90%	—
$\gamma f_0(1710) \rightarrow \gamma\eta\eta$	$< 1.8 \times 10^{-6}$	CL=90%	—
$\gamma f_4(2050)$	$< 5.3 \times 10^{-5}$	CL=90%	4515
$\gamma f_0(2200) \rightarrow \gamma K^+K^-$	$< 2 \times 10^{-4}$	CL=90%	4475
$\gamma f_j(2220) \rightarrow \gamma K^+K^-$	$< 8 \times 10^{-7}$	CL=90%	4469
$\gamma f_j(2220) \rightarrow \gamma\pi^+\pi^-$	$< 6 \times 10^{-7}$	CL=90%	—
$\gamma f_j(2220) \rightarrow \gamma\rho\bar{\rho}$	$< 1.1 \times 10^{-6}$	CL=90%	—
$\gamma\eta(2225) \rightarrow \gamma\phi\phi$	$< 3 \times 10^{-3}$	CL=90%	4469
$\gamma\eta_c(1S)$	$< 2.9 \times 10^{-5}$	CL=90%	4260
$\gamma\eta_c(2S)$	$< 4 \times 10^{-4}$	CL=90%	4031
$\gamma\chi_{c0}$	$< 6.6 \times 10^{-5}$	CL=90%	4114
$\gamma\chi_{c1}$	(4.7 \pm 1.9) $\times 10^{-5}$		4079
$\gamma\chi_{c2}$	$< 7.6 \times 10^{-6}$	CL=90%	4062
$\gamma\chi_{c1}(3872)$	$< 5 \times 10^{-5}$	CL=90%	3938
$\gamma\chi_{c1}(3872), \chi_{c1} \rightarrow \pi^+\pi^-\pi^0 J/\psi$	$< 2.8 \times 10^{-6}$	CL=90%	—
$\gamma\chi_{c0}(3915) \rightarrow \omega J/\psi$	$< 3.0 \times 10^{-6}$	CL=90%	—
$\gamma\chi_{c1}(4140) \rightarrow \phi J/\psi$	$< 2.2 \times 10^{-6}$	CL=90%	—
$\gamma X\bar{X} (m_X < 3.1 \text{ GeV})$	[$ssaa$] $< 1 \times 10^{-3}$	CL=90%	—

Meson Summary Table

$\gamma X \bar{X}$ ($m_X < 4.5$ GeV)	[ttaa] < 2.4	$\times 10^{-4}$	CL=90%	-
$\gamma X \rightarrow \gamma + \geq 4$ prongs	[uuaa] < 1.78	$\times 10^{-4}$	CL=95%	-
$\gamma A^0 \rightarrow \gamma \mu^+ \mu^-$	[vva] < 9	$\times 10^{-6}$	CL=90%	-
$\gamma A^0 \rightarrow \gamma \tau^+ \tau^-$	[qqa] < 1.30	$\times 10^{-4}$	CL=90%	-
$\gamma A^0 \rightarrow \gamma g g$	[xxaa] < 1	%	CL=90%	-
$\gamma A^0 \rightarrow \gamma s \bar{s}$	[xxaa] < 1	$\times 10^{-3}$	CL=90%	-

Lepton Family number (LF) violating modes

$e^\pm \mu^\mp$	LF < 3.9	$\times 10^{-7}$	CL=90%	4730
$\mu^\pm \tau^\mp$	LF < 2.7	$\times 10^{-6}$	CL=90%	4563
$e^\pm \tau^\mp$	LF < 2.7	$\times 10^{-6}$	CL=90%	4563
$\gamma e^\pm \mu^\mp$	LF < 4.2	$\times 10^{-7}$	CL=90%	4730
$\gamma \mu^\pm \tau^\mp$	LF < 6.1	$\times 10^{-6}$	CL=90%	4563
$\gamma e^\pm \tau^\mp$	LF < 6.5	$\times 10^{-6}$	CL=90%	4563

Other decays

invisible	< 3.0	$\times 10^{-4}$	CL=90%	-
hadrons	(96 \pm 4) %			-

 $\chi_{b0}(1P)$ [yyaa]

$$J^G(JPC) = 0^+(0^{++})$$

J needs confirmation.

$$\text{Mass } m = 9859.44 \pm 0.42 \pm 0.31 \text{ MeV}$$

$\chi_{b0}(1P)$ DECAY MODES	Fraction (Γ_i/Γ)	Confidence level	p (MeV/c)
$\gamma \mathcal{T}(1S)$	(1.94 \pm 0.27) %		391
$D^0 X$	< 10.4 %	90%	-
$\pi^+ \pi^- K^+ K^- \pi^0$	< 1.6 $\times 10^{-4}$	90%	4875
$2\pi^+ \pi^- K^- K_S^0$	< 5 $\times 10^{-5}$	90%	4875
$2\pi^+ \pi^- K^- K_S^0 2\pi^0$	< 5 $\times 10^{-4}$	90%	4846
$2\pi^+ 2\pi^- 2\pi^0$	< 2.1 $\times 10^{-4}$	90%	4905
$2\pi^+ 2\pi^- K^+ K^-$	(1.1 \pm 0.6) $\times 10^{-4}$		4861
$2\pi^+ 2\pi^- K^+ K^- \pi^0$	< 2.7 $\times 10^{-4}$	90%	4846
$2\pi^+ 2\pi^- K^+ K^- 2\pi^0$	< 5 $\times 10^{-4}$	90%	4828
$3\pi^+ 2\pi^- K^- K_S^0 \pi^0$	< 1.6 $\times 10^{-4}$	90%	4827
$3\pi^+ 3\pi^-$	< 8 $\times 10^{-5}$	90%	4904
$3\pi^+ 3\pi^- 2\pi^0$	< 6 $\times 10^{-4}$	90%	4881
$3\pi^+ 3\pi^- K^+ K^-$	(2.4 \pm 1.2) $\times 10^{-4}$		4827
$3\pi^+ 3\pi^- K^+ K^- \pi^0$	< 1.0 $\times 10^{-3}$	90%	4808
$4\pi^+ 4\pi^-$	< 8 $\times 10^{-5}$	90%	4880
$4\pi^+ 4\pi^- 2\pi^0$	< 2.1 $\times 10^{-3}$	90%	4850
$J/\psi J/\psi$	< 7 $\times 10^{-5}$	90%	3836
$J/\psi \psi(2S)$	< 1.2 $\times 10^{-4}$	90%	3571
$\psi(2S) \psi(2S)$	< 3.1 $\times 10^{-5}$	90%	3273
$J/\psi(1S)$ anything	< 2.3 $\times 10^{-3}$	90%	-

 $\chi_{b1}(1P)$ [yyaa]

$$J^G(JPC) = 0^+(1^{++})$$

J needs confirmation.

$$\text{Mass } m = 9892.78 \pm 0.26 \pm 0.31 \text{ MeV}$$

$\chi_{b1}(1P)$ DECAY MODES	Fraction (Γ_i/Γ)	Confidence level	p (MeV/c)
$\gamma \mathcal{T}(1S)$	(35.2 \pm 2.0) %		423
$D^0 X$	(12.6 \pm 2.2) %		-
$\pi^+ \pi^- K^+ K^- \pi^0$	(2.0 \pm 0.6) $\times 10^{-4}$		4892
$2\pi^+ \pi^- K^- K_S^0$	(1.3 \pm 0.5) $\times 10^{-4}$		4892
$2\pi^+ \pi^- K^- K_S^0 2\pi^0$	< 6 $\times 10^{-4}$	90%	4863
$2\pi^+ 2\pi^- 2\pi^0$	(8.0 \pm 2.5) $\times 10^{-4}$		4921
$2\pi^+ 2\pi^- K^+ K^-$	(1.5 \pm 0.5) $\times 10^{-4}$		4878
$2\pi^+ 2\pi^- K^+ K^- \pi^0$	(3.5 \pm 1.2) $\times 10^{-4}$		4863
$2\pi^+ 2\pi^- K^+ K^- 2\pi^0$	(8.6 \pm 3.2) $\times 10^{-4}$		4845
$3\pi^+ 2\pi^- K^- K_S^0 \pi^0$	(9.3 \pm 3.3) $\times 10^{-4}$		4844
$3\pi^+ 3\pi^-$	(1.9 \pm 0.6) $\times 10^{-4}$		4921
$3\pi^+ 3\pi^- 2\pi^0$	(1.7 \pm 0.5) $\times 10^{-3}$		4898
$3\pi^+ 3\pi^- K^+ K^-$	(2.6 \pm 0.8) $\times 10^{-4}$		4844
$3\pi^+ 3\pi^- K^+ K^- \pi^0$	(7.5 \pm 2.6) $\times 10^{-4}$		4825
$4\pi^+ 4\pi^-$	(2.6 \pm 0.9) $\times 10^{-4}$		4897
$4\pi^+ 4\pi^- 2\pi^0$	(1.4 \pm 0.6) $\times 10^{-3}$		4867
ω anything	(4.9 \pm 1.4) %		-
$\omega \chi_{tetra}$	< 4.44 $\times 10^{-4}$	90%	-
$J/\psi J/\psi$	< 2.7 $\times 10^{-5}$	90%	3857
$J/\psi \psi(2S)$	< 1.7 $\times 10^{-5}$	90%	3594
$\psi(2S) \psi(2S)$	< 6 $\times 10^{-5}$	90%	3298
$J/\psi(1S)$ anything	< 1.1 $\times 10^{-3}$	90%	-
$J/\psi(1S) \chi_{tetra}$	< 2.27 $\times 10^{-4}$	90%	-

 $h_b(1P)$

$$J^G(JPC) = 0^-(1^{+-})$$

$$\text{Mass } m = 9899.3 \pm 0.8 \text{ MeV}$$

$h_b(1P)$ DECAY MODES	Fraction (Γ_i/Γ)	p (MeV/c)
$\eta_b(1S) \gamma$	(52 $^{+6}_{-5}$) %	488

 $\chi_{b2}(1P)$ [yyaa]

$$J^G(JPC) = 0^+(2^{++})$$

J needs confirmation.

$$\text{Mass } m = 9912.21 \pm 0.26 \pm 0.31 \text{ MeV}$$

$\chi_{b2}(1P)$ DECAY MODES	Fraction (Γ_i/Γ)	Confidence level	p (MeV/c)
$\gamma \mathcal{T}(1S)$	(18.0 \pm 1.0) %		442
$D^0 X$	< 7.9 %	90%	-
$\pi^+ \pi^- K^+ K^- \pi^0$	(8 \pm 5) $\times 10^{-5}$		4902
$2\pi^+ \pi^- K^- K_S^0$	< 1.0 $\times 10^{-4}$	90%	4901
$2\pi^+ \pi^- K^- K_S^0 2\pi^0$	(5.3 \pm 2.4) $\times 10^{-4}$		4873
$2\pi^+ 2\pi^- 2\pi^0$	(3.5 \pm 1.4) $\times 10^{-4}$		4931
$2\pi^+ 2\pi^- K^+ K^-$	(1.1 \pm 0.4) $\times 10^{-4}$		4888
$2\pi^+ 2\pi^- K^+ K^- \pi^0$	(2.1 \pm 0.9) $\times 10^{-4}$		4872
$2\pi^+ 2\pi^- K^+ K^- 2\pi^0$	(3.9 \pm 1.8) $\times 10^{-4}$		4855
$3\pi^+ 2\pi^- K^- K_S^0 \pi^0$	< 5 $\times 10^{-4}$	90%	4854
$3\pi^+ 3\pi^-$	(7.0 \pm 3.1) $\times 10^{-5}$		4931
$3\pi^+ 3\pi^- 2\pi^0$	(1.0 \pm 0.4) $\times 10^{-3}$		4908
$3\pi^+ 3\pi^- K^+ K^-$	< 8 $\times 10^{-5}$	90%	4854
$3\pi^+ 3\pi^- K^+ K^- \pi^0$	(3.6 \pm 1.5) $\times 10^{-4}$		4835
$4\pi^+ 4\pi^-$	(8 \pm 4) $\times 10^{-5}$		4907
$4\pi^+ 4\pi^- 2\pi^0$	(1.8 \pm 0.7) $\times 10^{-3}$		4877
$J/\psi J/\psi$	< 4 $\times 10^{-5}$	90%	3869
$J/\psi \psi(2S)$	< 5 $\times 10^{-5}$	90%	3608
$\psi(2S) \psi(2S)$	< 1.6 $\times 10^{-5}$	90%	3313
$J/\psi(1S)$ anything	(1.5 \pm 0.4) $\times 10^{-3}$		-

 $\mathcal{T}(2S)$

$$J^G(JPC) = 0^-(1^{--})$$

$$\text{Mass } m = 10023.4 \pm 0.5 \text{ MeV}$$

$$m_{\mathcal{T}(3S)} - m_{\mathcal{T}(2S)} = 331.50 \pm 0.13 \text{ MeV}$$

$$\text{Full width } \Gamma = 31.98 \pm 2.63 \text{ keV}$$

$\mathcal{T}(2S)$ DECAY MODES	Fraction (Γ_i/Γ)	Confidence level	Scale factor / p (MeV/c)
$\mathcal{T}(1S) \pi^+ \pi^-$	(17.85 \pm 0.26) %		475
$\mathcal{T}(1S) \pi^0 \pi^0$	(8.6 \pm 0.4) %		480
$\tau^+ \tau^-$	(2.00 \pm 0.21) %		4686
$\mu^+ \mu^-$	(1.93 \pm 0.17) %	S=2.2	5011
$e^+ e^-$	(1.91 \pm 0.16) %		5012
$\mathcal{T}(1S) \pi^0$	< 4 $\times 10^{-5}$	CL=90%	531
$\mathcal{T}(1S) \eta$	(2.9 \pm 0.4) $\times 10^{-4}$	S=2.0	126
$J/\psi(1S)$ anything	< 6 $\times 10^{-3}$	CL=90%	4533
$J/\psi(1S) \eta_c$	< 5.4 $\times 10^{-6}$	CL=90%	3984
$J/\psi(1S) \chi_{c0}$	< 3.4 $\times 10^{-6}$	CL=90%	3808
$J/\psi(1S) \chi_{c1}$	< 1.2 $\times 10^{-6}$	CL=90%	3765
$J/\psi(1S) \chi_{c2}$	< 2.0 $\times 10^{-6}$	CL=90%	3745
$J/\psi(1S) \eta_c(2S)$	< 2.5 $\times 10^{-6}$	CL=90%	3707
$J/\psi(1S) X(3940)$	< 2.0 $\times 10^{-6}$	CL=90%	3555
$J/\psi(1S) X(4160)$	< 2.0 $\times 10^{-6}$	CL=90%	3442
χ_{c1} anything	(2.2 \pm 0.5) $\times 10^{-4}$		-
$\chi_{c1}(1P)^0 X_{tetra}$	< 3.67 $\times 10^{-5}$	CL=90%	-
χ_{c2} anything	(2.3 \pm 0.8) $\times 10^{-4}$		-
$\psi(2S) \eta_c$	< 5.1 $\times 10^{-6}$	CL=90%	3732
$\psi(2S) \chi_{c0}$	< 4.7 $\times 10^{-6}$	CL=90%	3536
$\psi(2S) \chi_{c1}$	< 2.5 $\times 10^{-6}$	CL=90%	3488
$\psi(2S) \chi_{c2}$	< 1.9 $\times 10^{-6}$	CL=90%	3464
$\psi(2S) \eta_c(2S)$	< 3.3 $\times 10^{-6}$	CL=90%	3422
$\psi(2S) X(3940)$	< 3.9 $\times 10^{-6}$	CL=90%	3250
$\psi(2S) X(4160)$	< 3.9 $\times 10^{-6}$	CL=90%	3120
$T_{c\bar{c}1}(3900) + T_{c\bar{c}1}(3900)^-$	< 1.0 $\times 10^{-6}$	CL=90%	-
$T_{c\bar{c}1}(4200) + T_{c\bar{c}1}(4200)^-$	< 1.67 $\times 10^{-5}$	CL=90%	-
$T_{c\bar{c}1}(3900)^\pm + T_{c\bar{c}1}(4200)^\mp$	< 7.3 $\times 10^{-6}$	CL=90%	-
$T_{c\bar{c}}(4050) + T_{c\bar{c}}(4050)^-$	< 1.35 $\times 10^{-5}$	CL=90%	-
$T_{c\bar{c}}(4250) + T_{c\bar{c}}(4250)^-$	< 2.67 $\times 10^{-5}$	CL=90%	-
$T_{c\bar{c}}(4050)^\pm + T_{c\bar{c}}(4250)^\mp$	< 2.72 $\times 10^{-5}$	CL=90%	-
$T_{c\bar{c}1}(4430) + T_{c\bar{c}1}(4430)^-$	< 2.03 $\times 10^{-5}$	CL=90%	-
$T_{c\bar{c}}(4055)^\pm + T_{c\bar{c}}(4055)^\mp$	< 1.11 $\times 10^{-5}$	CL=90%	-

Meson Summary Table

$T_{c\bar{c}}(4055)^{\pm} T_{c\bar{c}}(4430)^{\mp}$	$< 2.11 \times 10^{-5}$	CL=90%	-
2H anything	$(2.78^{+0.30}_{-0.26}) \times 10^{-5}$	S=1.2	-
hadrons	$(94 \pm 11) \%$	-	-
ggg	$(58.8 \pm 1.2) \%$	-	-
$\gamma g g$	$(1.87 \pm 0.28) \%$	-	-
$\phi K^{+} K^{-}$	$(1.6 \pm 0.4) \times 10^{-6}$	4910	-
$\omega \pi^{+} \pi^{-}$	$< 2.58 \times 10^{-6}$	CL=90%	4977
$K^{*}(892)^0 K^{-} \pi^{+}$ + c.c.	$(2.3 \pm 0.7) \times 10^{-6}$	-	4952
$\phi f_2'(1525)$	$< 1.33 \times 10^{-6}$	CL=90%	4843
$\omega f_2(1270)$	$< 5.7 \times 10^{-7}$	CL=90%	4899
$\rho(770) a_2(1320)$	$< 8.8 \times 10^{-7}$	CL=90%	4894
$K^{*}(892)^0 \bar{K}_2^*(1430)^0$ + c.c.	$(1.5 \pm 0.6) \times 10^{-6}$	-	4869
$K_1(1270)^{\pm} K^{\mp}$	$< 3.22 \times 10^{-6}$	CL=90%	4921
$K_1(1400)^{\pm} K^{\mp}$	$< 8.3 \times 10^{-7}$	CL=90%	4901
$b_1(1235)^{\pm} \pi^{\mp}$	$< 4.0 \times 10^{-7}$	CL=90%	4935
$\rho \pi$	$< 1.16 \times 10^{-6}$	CL=90%	4981
$\pi^{+} \pi^{-} \pi^0$	$< 8.0 \times 10^{-7}$	CL=90%	5007
$\omega \pi^0$	$< 1.63 \times 10^{-6}$	CL=90%	4980
$\pi^{+} \pi^{-} \pi^0 \pi^0$	$(1.30 \pm 0.28) \times 10^{-5}$	-	5002
$K_S^0 K^{+} \pi^{-}$ + c.c.	$(1.14 \pm 0.33) \times 10^{-6}$	-	4979
$K^{*}(892)^0 \bar{K}^0$ + c.c.	$< 4.22 \times 10^{-6}$	CL=90%	4959
$K^{*}(892)^{-} K^{+}$ + c.c.	$< 1.45 \times 10^{-6}$	CL=90%	4960
$f_1(1285)$ anything	$(2.2 \pm 1.6) \times 10^{-3}$	-	-
$f_1(1285) X_{tetra}$	$< 6.47 \times 10^{-5}$	CL=90%	-
$D_s^{+} D_{s1}(2536)^{-}, D_{s1}^{-} \rightarrow$ $K^{-} D^{*}(2007)^0$	$(1.6 \pm 0.4) \times 10^{-5}$	-	-
$D_s^{+} D_{s1}(2536)^{-}, D_{s1}^{-} \rightarrow$ $K_S^0 D^{*}(2010)^{-}$	$(8.4 \pm 2.3) \times 10^{-6}$	-	-
$D_s^{+} D_{s1}(2536)^{-}, D_{s1}^{-} \rightarrow$ $K^{-} D^{*}(2007)^0$	$(1.4 \pm 0.4) \times 10^{-5}$	-	-
$D_s^{+} D_{s1}(2536)^{-}, D_{s1}^{-} \rightarrow$ $K_S^0 D^{*}(2010)^{-}$	$(8.2 \pm 3.1) \times 10^{-6}$	-	-
$D_s^{+} D_{s2}^{*}(2573)^{-}, D_{s2}^{*-} \rightarrow$ $K^{-} D^0$	$(1.4 \pm 0.4) \times 10^{-5}$	-	-
$D_s^{+} D_{s2}^{*}(2573)^{-}, D_{s2}^{*-} \rightarrow$ $K_S^0 D^{-}$	$(6.9 \pm 3.0) \times 10^{-6}$	-	-
$D_s^{+} D_{s2}^{*}(2573)^{-}, D_{s2}^{*-} \rightarrow$ $K^{-} D^0$	$(9 \pm 5) \times 10^{-6}$	-	-
$D_s^{+} D_{s2}^{*}(2573)^{-}, D_{s2}^{*-} \rightarrow$ $K_S^0 D^{-}$	$(5 \pm 6) \times 10^{-6}$	-	-
Sum of 100 exclusive modes	$(2.90 \pm 0.30) \times 10^{-3}$	-	-
Radiative decays			
$\gamma \chi_{b1}(1P)$	$(6.9 \pm 0.4) \%$	130	-
$\gamma \chi_{b2}(1P)$	$(7.15 \pm 0.35) \%$	111	-
$\gamma \chi_{b0}(1P)$	$(3.8 \pm 0.4) \%$	163	-
$\gamma f_0(1710)$	$< 5.9 \times 10^{-4}$	CL=90%	4862
$\gamma f_2'(1525)$	$< 5.3 \times 10^{-4}$	CL=90%	4897
$\gamma f_2(1270)$	$< 2.41 \times 10^{-4}$	CL=90%	4931
$\gamma \eta_c(1S)$	$< 2.7 \times 10^{-5}$	CL=90%	4568
$\gamma \chi_{c0}$	$< 1.0 \times 10^{-4}$	CL=90%	4430
$\gamma \chi_{c1}$	$< 3.6 \times 10^{-6}$	CL=90%	4397
$\gamma \chi_{c2}$	$< 1.5 \times 10^{-5}$	CL=90%	4381
$\gamma \chi_{c1}(3872)$	$< 2.3 \times 10^{-5}$	CL=90%	4264
$\gamma \chi_{c1}(3872), \chi_{c1} \rightarrow$ $\pi^{+} \pi^{-} \pi^0 J/\psi$	$< 2.4 \times 10^{-6}$	CL=90%	-
$\gamma \chi_{c0}(3915) \rightarrow \omega J/\psi$	$< 2.8 \times 10^{-6}$	CL=90%	-
$\gamma \chi_{c1}(4140) \rightarrow \phi J/\psi$	$< 1.2 \times 10^{-6}$	CL=90%	-
$\gamma X(4350) \rightarrow \phi J/\psi$	$< 1.3 \times 10^{-6}$	CL=90%	-
$\gamma \eta_b(1S)$	$(5.5 \pm_{-0.9}^{1.1}) \times 10^{-4}$	S=1.2	605
$\gamma \eta_b(1S) \rightarrow \gamma$ Sum of 26 exclu- sive modes	$< 3.7 \times 10^{-6}$	CL=90%	-
$\gamma X_{b\bar{B}}$ modes $\rightarrow \gamma$ Sum of 26 exclusive modes	$< 4.9 \times 10^{-6}$	CL=90%	-
$\gamma X \rightarrow \gamma$ + ≥ 4 prongs	[zzaa] $< 1.95 \times 10^{-4}$	CL=95%	-
$\gamma A^0 \rightarrow \gamma$ hadrons	$< 8 \times 10^{-5}$	CL=90%	-
$\gamma A^0 \rightarrow \gamma \mu^{+} \mu^{-}$	$< 8.3 \times 10^{-6}$	CL=90%	-
Lepton Family number (LF) violating modes			
$e^{\pm} \tau^{\mp}$	LF $< 3.2 \times 10^{-6}$	CL=90%	4854
$\mu^{\pm} \tau^{\mp}$	LF $< 3.3 \times 10^{-6}$	CL=90%	4854

 $T_2(1D)$

$$I^G(JPC) = 0^{-}(2^{-}-)$$

was $\Upsilon(1D)$

$$\text{Mass } m = 10163.7 \pm 1.4 \text{ MeV } (S = 1.7)$$

$T_2(1D)$ DECAY MODES	Fraction (Γ_i/Γ)	ρ (MeV/c)
$\gamma \gamma \Upsilon(1S)$	seen	679
$\gamma \chi_{bJ}(1P)$	seen	300
$\eta \Upsilon(1S)$	not seen	426
$\pi^{+} \pi^{-} \Upsilon(1S)$	$(6.6 \pm 1.6) \times 10^{-3}$	623

 $\chi_{b0}(2P)$ [yyaa]

$$I^G(JPC) = 0^{+}(0^{+}+)$$

 J needs confirmation.

$$\text{Mass } m = 10232.5 \pm 0.4 \pm 0.5 \text{ MeV}$$

$\chi_{b0}(2P)$ DECAY MODES	Fraction (Γ_i/Γ)	Confidence level	ρ (MeV/c)
$\gamma \Upsilon(2S)$	$(1.38 \pm 0.30) \%$		207
$\gamma \Upsilon(1S)$	$(3.8 \pm 1.7) \times 10^{-3}$		743
$D^0 X$	$< 8.2 \%$	90%	-
$\pi^{+} \pi^{-} K^{+} K^{-} \pi^0$	$< 3.4 \times 10^{-5}$	90%	5064
$2\pi^{+} \pi^{-} K^{-} K_S^0$	$< 5 \times 10^{-5}$	90%	5063
$2\pi^{+} \pi^{-} K^{-} K_S^0 2\pi^0$	$< 2.2 \times 10^{-4}$	90%	5036
$2\pi^{+} 2\pi^{-} 2\pi^0$	$< 2.4 \times 10^{-4}$	90%	5092
$2\pi^{+} 2\pi^{-} K^{+} K^{-}$	$< 1.5 \times 10^{-4}$	90%	5050
$2\pi^{+} 2\pi^{-} K^{+} K^{-} \pi^0$	$< 2.2 \times 10^{-4}$	90%	5035
$2\pi^{+} 2\pi^{-} K^{+} K^{-} 2\pi^0$	$< 1.1 \times 10^{-3}$	90%	5019
$3\pi^{+} 2\pi^{-} K^{-} K_S^0 \pi^0$	$< 7 \times 10^{-4}$	90%	5018
$3\pi^{+} 3\pi^{-}$	$< 7 \times 10^{-5}$	90%	5091
$3\pi^{+} 3\pi^{-} 2\pi^0$	$< 1.2 \times 10^{-3}$	90%	5070
$3\pi^{+} 3\pi^{-} K^{+} K^{-}$	$< 1.5 \times 10^{-4}$	90%	5017
$3\pi^{+} 3\pi^{-} K^{+} K^{-} \pi^0$	$< 7 \times 10^{-4}$	90%	4999
$4\pi^{+} 4\pi^{-}$	$< 1.7 \times 10^{-4}$	90%	5069
$4\pi^{+} 4\pi^{-} 2\pi^0$	$< 6 \times 10^{-4}$	90%	5039

 $\chi_{b1}(2P)$ [yyaa]

$$I^G(JPC) = 0^{+}(1^{+}+)$$

 J needs confirmation.

$$\text{Mass } m = 10255.46 \pm 0.22 \pm 0.50 \text{ MeV}$$

$$m_{\chi_{b1}(2P)} - m_{\chi_{b0}(2P)} = 23.5 \pm 1.0 \text{ MeV}$$

$\chi_{b1}(2P)$ DECAY MODES	Fraction (Γ_i/Γ)	ρ (MeV/c)
$\omega \Upsilon(1S)$	$(1.63^{+0.40}_{-0.34}) \%$	134
$\gamma \Upsilon(2S)$	$(18.1 \pm 1.9) \%$	229
$\gamma \Upsilon(1S)$	$(9.9 \pm 1.0) \%$	764
$\pi \pi \chi_{b1}(1P)$	$(9.1 \pm 1.3) \times 10^{-3}$	238
$D^0 X$	$(8.8 \pm 1.7) \%$	-
$\pi^{+} \pi^{-} K^{+} K^{-} \pi^0$	$(3.1 \pm 1.0) \times 10^{-4}$	5075
$2\pi^{+} \pi^{-} K^{-} K_S^0$	$(1.1 \pm 0.5) \times 10^{-4}$	5075
$2\pi^{+} \pi^{-} K^{-} K_S^0 2\pi^0$	$(7.7 \pm 3.2) \times 10^{-4}$	5047
$2\pi^{+} 2\pi^{-} 2\pi^0$	$(5.9 \pm 2.0) \times 10^{-4}$	5104
$2\pi^{+} 2\pi^{-} K^{+} K^{-}$	$(10 \pm 4) \times 10^{-5}$	5062
$2\pi^{+} 2\pi^{-} K^{+} K^{-} \pi^0$	$(5.5 \pm 1.8) \times 10^{-4}$	5047
$2\pi^{+} 2\pi^{-} K^{+} K^{-} 2\pi^0$	$(10 \pm 4) \times 10^{-4}$	5030
$3\pi^{+} 2\pi^{-} K^{-} K_S^0 \pi^0$	$(6.7 \pm 2.6) \times 10^{-4}$	5029
$3\pi^{+} 3\pi^{-}$	$(1.2 \pm 0.4) \times 10^{-4}$	5103
$3\pi^{+} 3\pi^{-} 2\pi^0$	$(1.2 \pm 0.4) \times 10^{-3}$	5081
$3\pi^{+} 3\pi^{-} K^{+} K^{-}$	$(2.0 \pm 0.8) \times 10^{-4}$	5029
$3\pi^{+} 3\pi^{-} K^{+} K^{-} \pi^0$	$(6.1 \pm 2.2) \times 10^{-4}$	5011
$4\pi^{+} 4\pi^{-}$	$(1.7 \pm 0.6) \times 10^{-4}$	5080
$4\pi^{+} 4\pi^{-} 2\pi^0$	$(1.9 \pm 0.7) \times 10^{-3}$	5051

 $h_b(2P)$

$$I^G(JPC) = 0^{-}(1^{+}-)$$

$$\text{Mass } m = 10259.8 \pm 1.2 \text{ MeV}$$

$h_b(2P)$ DECAY MODES	Fraction (Γ_i/Γ)	ρ (MeV/c)
hadrons	not seen	-
$\eta_b(1S) \gamma$	$(22 \pm 5) \%$	825
$\eta_b(2S) \gamma$	$(48 \pm 13) \%$	257

Meson Summary Table

 $\chi_{b2}(2P)$ [yyaa] $I^G(J^{PC}) = 0^+(2^{++})$
 J needs confirmation.Mass $m = 10268.65 \pm 0.22 \pm 0.50$ MeV
 $m_{\chi_{b2}(2P)} - m_{\chi_{b1}(2P)} = 13.10 \pm 0.24$ MeV

$\chi_{b2}(2P)$ DECAY MODES	Fraction (Γ_i/Γ)	Confidence level	ρ (MeV/c)
$\omega \mathcal{T}(1S)$	$(1.10^{+0.34}_{-0.30})\%$		194
$\gamma \mathcal{T}(2S)$	$(8.9 \pm 1.2)\%$		242
$\gamma \mathcal{T}(1S)$	$(6.6 \pm 0.8)\%$		776
$\pi\pi\chi_{b2}(1P)$	$(5.1 \pm 0.9) \times 10^{-3}$		229
$D^0 X$	$< 2.4\%$	90%	–
$\pi^+\pi^-K^+K^-\pi^0$	$< 1.1 \times 10^{-4}$	90%	5082
$2\pi^+\pi^-K^-K_S^0$	$< 9 \times 10^{-5}$	90%	5082
$2\pi^+\pi^-K^-K_S^0 2\pi^0$	$< 7 \times 10^{-4}$	90%	5054
$2\pi^+2\pi^-2\pi^0$	$(3.9 \pm 1.6) \times 10^{-4}$		5110
$2\pi^+2\pi^-K^+K^-$	$(9 \pm 4) \times 10^{-5}$		5068
$2\pi^+2\pi^-K^+K^-\pi^0$	$(2.4 \pm 1.1) \times 10^{-4}$		5054
$2\pi^+2\pi^-K^+K^-2\pi^0$	$(4.7 \pm 2.3) \times 10^{-4}$		5037
$3\pi^+2\pi^-K^-K_S^0\pi^0$	$< 4 \times 10^{-4}$	90%	5036
$3\pi^+3\pi^-$	$(9 \pm 4) \times 10^{-5}$		5110
$3\pi^+3\pi^-2\pi^0$	$(1.2 \pm 0.4) \times 10^{-3}$		5088
$3\pi^+3\pi^-K^+K^-$	$(1.4 \pm 0.7) \times 10^{-4}$		5036
$3\pi^+3\pi^-K^+K^-\pi^0$	$(4.2 \pm 1.7) \times 10^{-4}$		5017
$4\pi^+4\pi^-$	$(9 \pm 5) \times 10^{-5}$		5087
$4\pi^+4\pi^-2\pi^0$	$(1.3 \pm 0.5) \times 10^{-3}$		5058

 $\mathcal{T}(3S)$ $I^G(J^{PC}) = 0^-(1^{--})$ Mass $m = 10355.1 \pm 0.5$ MeV
 $m_{\mathcal{T}(3S)} - m_{\mathcal{T}(2S)} = 331.50 \pm 0.13$ MeV
Full width $\Gamma = 20.32 \pm 1.85$ keV

$\mathcal{T}(3S)$ DECAY MODES	Fraction (Γ_i/Γ)	Scale factor/ Confidence level	ρ (MeV/c)
$\mathcal{T}(2S)$ anything	$(10.6 \pm 0.8)\%$		296
$\mathcal{T}(2S)\pi^+\pi^-$	$(2.82 \pm 0.18)\%$	S=1.6	176
$\mathcal{T}(2S)\pi^0\pi^0$	$(1.85 \pm 0.14)\%$		190
$\mathcal{T}(2S)\gamma\gamma$	$(5.0 \pm 0.7)\%$		326
$\mathcal{T}(2S)\pi^0$	$< 5.1 \times 10^{-4}$	CL=90%	298
$\mathcal{T}(1S)\pi^+\pi^-$	$(4.37 \pm 0.08)\%$		813
$\mathcal{T}(1S)\pi^0\pi^0$	$(2.20 \pm 0.13)\%$		816
$\mathcal{T}(1S)\eta$	$< 1 \times 10^{-4}$	CL=90%	677
$\mathcal{T}(1S)\pi^0$	$< 7 \times 10^{-5}$	CL=90%	846
$h_b(1P)\pi^0$	$< 1.2 \times 10^{-3}$	CL=90%	426
$h_b(1P)\pi^0 \rightarrow \gamma h_b(1S)\pi^0$	$(4.3 \pm 1.4) \times 10^{-4}$		–
$h_b(1P)\pi^+\pi^-$	$< 1.2 \times 10^{-4}$	CL=90%	352
$\tau^+\tau^-$	$(2.29 \pm 0.30)\%$		4863
$\mu^+\mu^-$	$(2.18 \pm 0.21)\%$	S=2.1	5176
e^+e^-	$(2.18 \pm 0.20)\%$		5178
hadrons	$(93 \pm 12)\%$		–
$g g g$	$(35.7 \pm 2.6)\%$		–
$\gamma g g$	$(9.7 \pm 1.8) \times 10^{-3}$		–
2H anything	$(2.33 \pm 0.33) \times 10^{-5}$		–

Radiative decays

$\gamma\chi_{b2}(2P)$	$(13.1 \pm 1.6)\%$	S=3.4	86
$\gamma\chi_{b1}(2P)$	$(12.6 \pm 1.2)\%$	S=2.4	99
$\gamma\chi_{b0}(2P)$	$(5.9 \pm 0.6)\%$	S=1.4	122
$\gamma\chi_{b2}(1P)$	$(10.0 \pm 1.0) \times 10^{-3}$	S=1.7	433
$\gamma\chi_{b1}(1P)$	$(9 \pm 5) \times 10^{-4}$	S=1.8	452
$\gamma\chi_{b0}(1P)$	$(2.7 \pm 0.4) \times 10^{-3}$		484
$\gamma h_b(2S)$	$< 6.2 \times 10^{-4}$	CL=90%	350
$\gamma h_b(1S)$	$(5.1 \pm 0.7) \times 10^{-4}$		912
$\gamma A^0 \rightarrow \gamma$ hadrons	$< 8 \times 10^{-5}$	CL=90%	–
$\gamma X \rightarrow \gamma + \geq 4$ prongs	[aabb] $< 2.2 \times 10^{-4}$	CL=95%	–
$\gamma A^0 \rightarrow \gamma\mu^+\mu^-$	$< 5.5 \times 10^{-6}$	CL=90%	–
$\gamma A^0 \rightarrow \gamma\tau^+\tau^-$	[bbbb] $< 1.6 \times 10^{-4}$	CL=90%	–

Lepton Family number (LF) violating modes

$e^\pm\tau^\mp$	LF	$< 4.2 \times 10^{-6}$	CL=90%	5025
$e^\pm\mu^\mp$	LF	$< 3.6 \times 10^{-7}$	CL=90%	5177
$\mu^\pm\tau^\mp$	LF	$< 3.1 \times 10^{-6}$	CL=90%	5025

 $\chi_{b1}(3P)$ [yyaa] $I^G(J^{PC}) = 0^+(1^{++})$ J needs confirmation.
Mass $m = 10513.4 \pm 0.7$ MeV

$\chi_{b1}(3P)$ DECAY MODES	Fraction (Γ_i/Γ)	ρ (MeV/c)
$\mathcal{T}(1S)\gamma$	seen	1000
$\mathcal{T}(2S)\gamma$	seen	479
$\mathcal{T}(3S)\gamma$	seen	157

 $\chi_{b2}(3P)$ [yyaa] $I^G(J^{PC}) = 0^+(2^{++})$ J needs confirmation.
Mass $m = 10524.0 \pm 0.8$ MeV

$\chi_{b2}(3P)$ DECAY MODES	Fraction (Γ_i/Γ)	ρ (MeV/c)
$\mathcal{T}(3S)\gamma$	seen	168

 $\mathcal{T}(4S)$ $I^G(J^{PC}) = 0^-(1^{--})$ also known as $\mathcal{T}(10580)$
Mass $m = 10579.4 \pm 1.2$ MeV
Full width $\Gamma = 20.5 \pm 2.5$ MeV

$\mathcal{T}(4S)$ DECAY MODES	Fraction (Γ_i/Γ)	Confidence level	ρ (MeV/c)
$B\bar{B}$	$> 96\%$	95%	326
B^+B^-	$(51.4 \pm 0.6)\%$		331
D^+ anything + c.c.	$(17.8 \pm 2.6)\%$		–
$B^0\bar{B}^0$	$(48.6 \pm 0.6)\%$		326
$J/\psi K_S^0 + (J/\psi, \eta_c) K_S^0$	$< 4 \times 10^{-7}$	90%	–
non- $B\bar{B}$	$< 4\%$	95%	–
e^+e^-	$(1.57 \pm 0.08) \times 10^{-5}$		5290
$\rho^+\rho^-$	$< 5.7 \times 10^{-6}$	90%	5233
$K^*(892)^0\bar{K}^0$	$< 2.0 \times 10^{-6}$	90%	5240
$J/\psi(1S)$ anything	$< 1.9 \times 10^{-4}$	95%	–
D^{*+} anything + c.c.	$< 7.4\%$	90%	5099
ϕ anything	$(7.1 \pm 0.6)\%$		5240
$\phi\eta$	$< 1.8 \times 10^{-6}$	90%	5226
$\phi\eta'$	$< 4.3 \times 10^{-6}$	90%	5196
$\rho\eta$	$< 1.3 \times 10^{-6}$	90%	5247
$\rho\eta'$	$< 2.5 \times 10^{-6}$	90%	5217
$\mathcal{T}(1S)$ anything	$< 4 \times 10^{-3}$	90%	1053
$\mathcal{T}(1S)\pi^+\pi^-$	$(8.2 \pm 0.4) \times 10^{-5}$		1026
$\mathcal{T}(1S)\eta$	$(1.81 \pm 0.18) \times 10^{-4}$		924
$\mathcal{T}(1S)\eta'$	$(3.4 \pm 0.9) \times 10^{-5}$		–
$\mathcal{T}(2S)\pi^+\pi^-$	$(8.2 \pm 0.8) \times 10^{-5}$		468
$h_b(1P)\pi^+\pi^-$	not seen		600
$h_b(1P)\eta$	$(2.18 \pm 0.21) \times 10^{-3}$		390
$\eta_b(1S)\omega$	$< 1.8 \times 10^{-4}$	90%	–
2H anything	$< 1.3 \times 10^{-5}$	90%	–

Double Radiative Decays

$\gamma\gamma \mathcal{T}(D) \rightarrow \gamma\gamma\eta \mathcal{T}(1S)$	$< 2.3 \times 10^{-5}$	90%	–
--	------------------------	-----	---

 $\mathcal{T}(10860)$ $I^G(J^{PC}) = 0^-(1^{--})$ Mass $m = 10885.2^{+2.6}_{-1.6}$ MeV
Full width $\Gamma = 37 \pm 4$ MeV

$\mathcal{T}(10860)$ DECAY MODES	Fraction (Γ_i/Γ)	Confidence level	ρ (MeV/c)
$B\bar{B}X$	$(76.2^{+2.7}_{-4.0})\%$		–
$B\bar{B}$	$(5.5 \pm 1.0)\%$		1322
$B^+\bar{B}^+ + \text{c.c.}$	$(13.7 \pm 1.6)\%$		–
$B^*\bar{B}^*$	$(38.1 \pm 3.4)\%$		1127
$B\bar{B}^*(*)\pi$	$< 19.7\%$	90%	1015
$B\bar{B}\pi$	$(0.0 \pm 1.2)\%$		1015
$B^*\bar{B}^*\pi + B\bar{B}^*\pi$	$(7.3 \pm 2.3)\%$		–
$B^*\bar{B}^*\pi$	$(1.0 \pm 1.4)\%$		739
$B\bar{B}\pi\pi$	$< 8.9\%$	90%	550
$B_s^{(*)}\bar{B}_s^{(*)}$	$(20.1 \pm 3.1)\%$		904
$B_s\bar{B}_s$	$(5 \pm 5) \times 10^{-3}$		904
$B_s\bar{B}_s^* + \text{c.c.}$	$(1.35 \pm 0.32)\%$		–

Meson Summary Table

$B_s^* \bar{B}_s^*$	(17.6 ± 2.7) %	543
no open-bottom	(3.8 $^{+5.0}_{-0.5}$) %	–
$e^+ e^-$	(8.3 ± 2.1) × 10 ⁻⁶	5443
$K^*(892)^0 \bar{K}^0$	< 1.0 × 10 ⁻⁵	90% 5395
$\Upsilon(1S) \pi^+ \pi^-$	(5.3 ± 0.6) × 10 ⁻³	1306
$\Upsilon(1S) \eta$	(8.5 ± 1.7) × 10 ⁻⁴	1229
$\Upsilon(1S) \eta'$	< 6.9 × 10 ⁻⁵	90% 985
$\Upsilon(2S) \pi^+ \pi^-$	(7.8 ± 1.3) × 10 ⁻³	783
$\Upsilon(2S) \eta$	(4.1 ± 0.6) × 10 ⁻³	639
$\Upsilon(3S) \pi^+ \pi^-$	(4.8 $^{+1.9}_{-1.7}$) × 10 ⁻³	440
$\Upsilon(1S) K^+ K^-$	(6.1 ± 1.8) × 10 ⁻⁴	959
$\eta \Upsilon_J(1D)$	(4.8 ± 1.1) × 10 ⁻³	–
$h_b(1P) \pi^+ \pi^-$	(3.5 $^{+1.0}_{-1.3}$) × 10 ⁻³	903
$h_b(2P) \pi^+ \pi^-$	(5.7 $^{+1.7}_{-2.1}$) × 10 ⁻³	544
$\chi_{bJ}(1P) \pi^+ \pi^- \pi^0$	(2.5 ± 2.3) × 10 ⁻³	894
$\chi_{b0}(1P) \pi^+ \pi^- \pi^0$	< 6.3 × 10 ⁻³	90% 894
$\chi_{b0}(1P) \omega$	< 3.9 × 10 ⁻³	90% 631
$\chi_{b0}(1P) (\pi^+ \pi^- \pi^0)_{\text{non-}\omega}$	< 4.8 × 10 ⁻³	90% –
$\chi_{b1}(1P) \pi^+ \pi^- \pi^0$	(1.85 ± 0.33) × 10 ⁻³	861
$\chi_{b1}(1P) \omega$	(1.57 ± 0.30) × 10 ⁻³	582
$\chi_{b1}(1P) (\pi^+ \pi^- \pi^0)_{\text{non-}\omega}$	(5.2 ± 1.9) × 10 ⁻⁴	–
$\chi_{b2}(1P) \pi^+ \pi^- \pi^0$	(1.17 ± 0.30) × 10 ⁻³	841
$\chi_{b2}(1P) \omega$	(6.0 ± 2.7) × 10 ⁻⁴	552
$\chi_{b2}(1P) (\pi^+ \pi^- \pi^0)_{\text{non-}\omega}$	(6 ± 4) × 10 ⁻⁴	–
$\gamma X_b \rightarrow \gamma \Upsilon(1S) \omega$	< 3.8 × 10 ⁻⁵	90% –
$\eta_b(1S) \omega$	< 1.3 × 10 ⁻³	90% 1177
$\eta_b(2S) \omega$	< 5.6 × 10 ⁻³	90% 399

Inclusive Decays.

These decay modes are submodes of one or more of the decay modes above.

ϕ anything	(13.8 $^{+2.4}_{-1.7}$) %	–
D^0 anything + c.c.	(112 ± 6) %	–
D_s anything + c.c.	(44.7 ± 2.6) %	–
J/ψ anything	(2.06 ± 0.21) %	–
B^0 anything + c.c.	(77 ± 8) %	–
B^+ anything + c.c.	(72 ± 6) %	–

 $\Upsilon(11020)$ $I^G(J^{PC}) = 0^-(1^{--})$

Mass $m = 11000 \pm 4$ MeV
Full width $\Gamma = 24^{+8}_{-6}$ MeV

$\Upsilon(11020)$ DECAY MODES	Fraction (Γ_i/Γ)	ρ (MeV/c)
$e^+ e^-$	(5.4 $^{+1.9}_{-2.1}$) × 10 ⁻⁶	5500
$\chi_{bJ}(1P) \pi^+ \pi^- \pi^0$	(9 $^{+9}_{-8}$) × 10 ⁻³	1007
$\chi_{b1}(1P) \pi^+ \pi^- \pi^0$	seen	975
$\chi_{b2}(1P) \pi^+ \pi^- \pi^0$	seen	956

OTHER MESONS

 $T_{c\bar{c}}(3900)$ $I^G(J^{PC}) = 1^+(1^{+-})$

was $Z_c(3900)$, $X(3900)$

Mass $m = 3887.1 \pm 2.6$ MeV ($S = 1.7$)
Full width $\Gamma = 28.4 \pm 2.6$ MeV

$T_{c\bar{c}}(3900)$ DECAY MODES	Fraction (Γ_i/Γ)	ρ (MeV/c)
$J/\psi \pi$	seen	699
$h_c \pi^\pm$	not seen	318
$\eta_c \pi^+ \pi^-$	not seen	758
$\eta_c(1S) \rho(770)^\pm$	seen	–
$(D \bar{D}^*)^\pm$	seen	–
$D^0 D^{*-} + \text{c.c.}$	seen	152
$D^- D^{*0} + \text{c.c.}$	seen	143
$\omega \pi^\pm$	not seen	1862
$J/\psi \eta$	not seen	510
$D^+ D^{*-} + \text{c.c.}$	seen	–
$D^0 \bar{D}^{*0} + \text{c.c.}$	seen	–

 $T_{c\bar{c}}(4020)$

$$I^G(J^{PC}) = 1^+(?^{?^-})$$

was $X(4020)$

Mass $m = 4024.1 \pm 1.9$ MeV
Full width $\Gamma = 13 \pm 5$ MeV ($S = 1.7$)

$T_{c\bar{c}}(4020)$ DECAY MODES	Fraction (Γ_i/Γ)	ρ (MeV/c)
$h_c(1P) \pi$	seen	450
$D^* \bar{D}^*$	seen	85
$D \bar{D}^* + \text{c.c.}$	not seen	542
$\eta_c \pi^+ \pi^-$	not seen	872
$J/\psi(1S) \pi^\pm$	not seen	811

 $T_{c\bar{c}}(4430)^\pm$

$$I^G(J^{PC}) = 1^+(1^{+-})$$

G, C need confirmation.

was $Z_c(4430)$, $X(4430)^\pm$

Quantum numbers not established.

Mass $m = 4478^{+15}_{-18}$ MeV
Full width $\Gamma = 181 \pm 31$ MeV

$T_{c\bar{c}}(4430)^\pm$ DECAY MODES	Fraction (Γ_i/Γ)	ρ (MeV/c)
$\pi^+ \psi(2S)$	seen	711
$\pi^+ J/\psi$	seen	1162

 $T_{b\bar{b}}(10610)$

$$I^G(J^{PC}) = 1^+(1^{+-})$$

was $Z_b(10610)$, $X(10610)$

Mass $m = 10607.2 \pm 2.0$ MeV
Mass $m = 10609 \pm 6$ MeV
Full width $\Gamma = 18.4 \pm 2.4$ MeV

$T_{b\bar{b}}(10610)$ DECAY MODES	Fraction (Γ_i/Γ)	ρ (MeV/c)
$\Upsilon(1S) \pi^+$	(5.4 $^{+1.9}_{-1.5}$) × 10 ⁻³	1077
$\Upsilon(1S) \pi^0$	not seen	1077
$\Upsilon(2S) \pi^+$	(3.6 $^{+1.1}_{-0.8}$) %	551
$\Upsilon(2S) \pi^0$	seen	552
$\Upsilon(3S) \pi^+$	(2.1 $^{+0.8}_{-0.6}$) %	207
$\Upsilon(3S) \pi^0$	seen	210
$h_b(1P) \pi^+$	(3.5 $^{+1.2}_{-0.9}$) %	671
$h_b(2P) \pi^+$	(4.7 $^{+1.7}_{-1.3}$) %	313
$B^+ \bar{B}^0$	not seen	504
$B^+ \bar{B}^{*0} + B^{*+} \bar{B}^0$	(85.6 $^{+2.1}_{-2.9}$) %	–

 $T_{b\bar{b}}(10650)^\pm$

$$I^G(J^{PC}) = 1^+(1^{+-})$$

I, G, C need confirmation.

was $Z_b(10650)$, $X(10650)^\pm$

Mass $m = 10652.2 \pm 1.5$ MeV
Full width $\Gamma = 11.5 \pm 2.2$ MeV

$T_{b\bar{b}}(10650)^\pm$ decay modes are charge conjugates of the modes below.

$T_{b\bar{b}}(10650)^\pm$ DECAY MODES	Fraction (Γ_i/Γ)	ρ (MeV/c)
$\Upsilon(1S) \pi^+$	(1.7 $^{+0.8}_{-0.6}$) × 10 ⁻³	1117
$\Upsilon(2S) \pi^+$	(1.4 $^{+0.6}_{-0.4}$) %	595
$\Upsilon(3S) \pi^+$	(1.6 $^{+0.7}_{-0.5}$) %	259
$h_b(1P) \pi^+$	(8.4 $^{+2.9}_{-2.4}$) %	714
$h_b(2P) \pi^+$	(15 ± 4) %	360
$B^+ \bar{B}^0$	not seen	703
$B^+ \bar{B}^{*0} + B^{*+} \bar{B}^0$	not seen	–
$B^{*+} \bar{B}^{*0}$	(74 $^{+4}_{-6}$) %	120

NOTES

In this Summary Table:

When a quantity has “(S = ...)” to its right, the error on the quantity has been enlarged by the “scale factor” S, defined as $S = \sqrt{\chi^2/(N-1)}$, where N is the number of measurements used in calculating the quantity. We do this when $S > 1$, which often indicates that the measurements are inconsistent. When $S > 1.25$, we also show in the Particle Listings an ideogram of the measurements. For more about S, see the Introduction.

A decay momentum p is given for each decay mode. For a 2-body decay, p is the momentum of each decay product in the rest frame of the decaying particle. For a 3-or-more-body decay, p is the largest momentum any of the products can have in this frame.

- [a] See the review on “Form Factors for Radiative Pion and Kaon Decays” for definitions and details.
- [b] Measurements of $\Gamma(e^+ \nu_e)/\Gamma(\mu^+ \nu_\mu)$ always include decays with γ 's, and measurements of $\Gamma(e^+ \nu_e \gamma)$ and $\Gamma(\mu^+ \nu_\mu \gamma)$ never include low-energy γ 's. Therefore, since no clean separation is possible, we consider the modes with γ 's to be subreactions of the modes without them, and let $[\Gamma(e^+ \nu_e) + \Gamma(\mu^+ \nu_\mu)]/\Gamma_{\text{total}} = 100\%$.
- [c] See the π^\pm Particle Listings for the energy limits used in this measurement; low-energy γ 's are not included.
- [d] Derived from an analysis of neutrino-oscillation experiments.
- [e] Forbidden by angular momentum conservation.
- [f] C parity forbids this to occur as a single-photon process.
- [g] As measured in $e^+ e^- \rightarrow \rho^0$.
- [h] The $\omega\rho$ interference is then due to $\omega\rho$ mixing only, and is expected to be small. If $e\mu$ universality holds, $\Gamma(\rho^0 \rightarrow \mu^+ \mu^-) = \Gamma(\rho^0 \rightarrow e^+ e^-) \times 0.99785$.
- [i] Our estimate. See the Particle Listings for details.
- [j] See the “Note on $a_1(1260)$ ” in the $a_1(1260)$ Particle Listings in PDG 06, Journal of Physics **G33** 1 (2006).
- [k] See also the $\omega(1650)$.
- [l] See also the $\omega(1420)$.
- [n] See the note in the K^\pm Particle Listings.
- [o] Neglecting photon channels. See, e.g., A. Pais and S.B. Treiman, Phys. Rev. **D12**, 2744 (1975).
- [p] The definition of the slope parameters of the $K \rightarrow 3\pi$ Dalitz plot is as follows (see also “Note on Dalitz Plot Parameters for $K \rightarrow 3\pi$ Decays” in the K^\pm Particle Listings):
- $$|M|^2 = 1 + g(s_3 - s_0)/m_{\pi^+}^2 + \dots$$
- [q] For more details and definitions of parameters see the Particle Listings.
- [r] See the K^\pm Particle Listings for the energy limits used in this measurement.
- [s] Most of this radiative mode, the low-momentum γ part, is also included in the parent mode listed without γ 's.
- [t] Structure-dependent part.
- [u] Direct-emission branching fraction.
- [v] Violates angular-momentum conservation.
- [x] Derived from measured values of ϕ_{+-} , ϕ_{00} , $|\eta|$, $|m_{K_L^0} - m_{K_S^0}|$, and $\tau_{K_S^0}$, as described in the introduction to “Tests of Conservation Laws.”
- [y] The CP -violation parameters are defined as follows (see also “Note on CP Violation in $K_S \rightarrow 3\pi$ ” and “Note on CP Violation in K_L^0 Decay” in the Particle Listings):

$$\eta_{+-} = |\eta_{+-}| e^{i\phi_{+-}} = \frac{A(K_L^0 \rightarrow \pi^+ \pi^-)}{A(K_S^0 \rightarrow \pi^+ \pi^-)} = \epsilon + \epsilon'$$

$$\eta_{00} = |\eta_{00}| e^{i\phi_{00}} = \frac{A(K_L^0 \rightarrow \pi^0 \pi^0)}{A(K_S^0 \rightarrow \pi^0 \pi^0)} = \epsilon - 2\epsilon'$$

$$\delta = \frac{\Gamma(K_L^0 \rightarrow \pi^- \ell^+ \nu) - \Gamma(K_L^0 \rightarrow \pi^+ \ell^- \nu)}{\Gamma(K_L^0 \rightarrow \pi^- \ell^+ \nu) + \Gamma(K_L^0 \rightarrow \pi^+ \ell^- \nu)}$$

$$\text{Im}(\eta_{+-0})^2 = \frac{\Gamma(K_S^0 \rightarrow \pi^+ \pi^- \pi^0)^{CP \text{ viol.}}}{\Gamma(K_L^0 \rightarrow \pi^+ \pi^- \pi^0)}$$

$$\text{Im}(\eta_{000})^2 = \frac{\Gamma(K_S^0 \rightarrow \pi^0 \pi^0 \pi^0)}{\Gamma(K_L^0 \rightarrow \pi^0 \pi^0 \pi^0)}$$

where for the last two relations CPT is assumed valid, i.e., $\text{Re}(\eta_{+-0}) \simeq 0$ and $\text{Re}(\eta_{000}) \simeq 0$.

- [z] See the K_S^0 Particle Listings for the energy limits used in this measurement.
- [aa] The value is for the sum of the charge states or particle/antiparticle states indicated.
- [bb] $\text{Re}(\epsilon'/\epsilon) = \epsilon'/\epsilon$ to a very good approximation provided the phases satisfy CPT invariance.
- [cc] This mode includes gammas from inner bremsstrahlung but not the direct emission mode $K_L^0 \rightarrow \pi^+ \pi^- \gamma(\text{DE})$.
- [dd] See the K_L^0 Particle Listings for the energy limits used in this measurement.
- [ee] Allowed by higher-order electroweak interactions.
- [ff] Violates CP in leading order. Test of direct CP violation since the indirect CP -violating and CP -conserving contributions are expected to be suppressed.
- [gg] See our minireview under the $K_2(1770)$ in the 2004 edition of this Review.
- [hh] This result applies to $Z^0 \rightarrow c\bar{c}$ decays only. Here ℓ^+ is an average (not a sum) of e^+ and μ^+ decays.
- [ii] See the Particle Listings for the (complicated) definition of this quantity.
- [jj] The branching fraction for this mode may differ from the sum of the submodes that contribute to it, due to interference effects. See the relevant papers in the Particle Listings.
- [kk] These subfractions of the $K^- 2\pi^+$ mode are uncertain: see the Particle Listings.
- [ll] See the listings under “ $D \rightarrow K\pi\pi$ partial wave analyses” and our 2008 Review (Physics Letters **B667** 1 (2008)) for measurements of submodes of this mode.
- [nn] The unseen decay modes of the resonances are included.
- [oo] This is *not* a test for the $\Delta C=1$ weak neutral current, but leads to the $\pi^+ \ell^+ \ell^-$ final state.
- [pp] This mode is not a useful test for a $\Delta C=1$ weak neutral current because both quarks must change flavor in this decay.
- [qq] In the 2010 Review, the values for these quantities were given using a measure of the asymmetry that was inconsistent with the usual definition.
- [rr] This value is obtained by subtracting the branching fractions for 2-, 4- and 6-prongs from unity.
- [ss] This is the sum of our $K^- 2\pi^+ \pi^-$, $K^- 2\pi^+ \pi^- \pi^0$, $\bar{K}^0 2\pi^+ 2\pi^-$, $K^+ 2K^- \pi^+$, $2\pi^+ 2\pi^-$, $2\pi^+ 2\pi^- \pi^0$, $K^+ K^- \pi^+ \pi^-$, and $K^+ K^- \pi^+ \pi^- \pi^0$, branching fractions.
- [tt] This is the sum of our $K^- 3\pi^+ 2\pi^-$ and $3\pi^+ 3\pi^-$ branching fractions.
- [uu] The branching fractions for the $K^- e^+ \nu_e$, $K^*(892)^- e^+ \nu_e$, $\pi^- e^+ \nu_e$, and $\rho^- e^+ \nu_e$ modes add up to $6.17 \pm 0.17\%$.
- [vv] This is a doubly Cabibbo-suppressed mode.
- [xx] Submodes of the $D^0 \rightarrow K_S^0 \pi^+ \pi^- \pi^0$ mode with a K^* and/or ρ were studied by COFFMAN 92B, but with only 140 events. With nothing new for 18 years, we refer to our 2008 edition, Physics Letters **B667** 1 (2008), for those results.
- [yy] This branching fraction includes all the decay modes of the resonance in the final state.
- [zz] This limit assumes the average of $B(D^0 \rightarrow K^- e^+ \nu_e)$ and $B(D^0 \rightarrow K^- \mu^+ \nu_\mu)$ for the $B(D^0 \rightarrow K^- \ell^+ \nu_\ell)$ value.
- [aaa] This is the purely e^+ semileptonic branching fraction: the e^+ fraction from τ^+ decays has been subtracted off. The sum of our (non- τ) e^+ exclusive fractions — an $e^+ \nu_e$ with an η , η' , ϕ , K^0 , or K^{*0} — is $5.99 \pm 0.31\%$.
- [bbb] This fraction includes η from η' decays.
- [ccc] The sum of our exclusive η' fractions — $\eta' e^+ \nu_e$, $\eta' \mu^+ \nu_\mu$, $\eta' \pi^+$, $\eta' \rho^+$, and $\eta' K^+$ — is $11.8 \pm 1.6\%$.
- [ddd] This branching fraction includes all the decay modes of the final-state resonance.
- [eee] A test for $\bar{u}\bar{u}$ or $d\bar{d}$ content in the D_s^+ . Neither Cabibbo-favored nor Cabibbo-suppressed decays can contribute, and $\omega - \phi$ mixing is an unlikely explanation for any fraction above about 2×10^{-4} .
- [fff] We decouple the $D_s^+ \rightarrow \phi\pi^+$ branching fraction obtained from mass projections (and used to get some of the other branching fractions) from the $D_s^+ \rightarrow \phi\pi^+$, $\phi \rightarrow K^+ K^-$ branching fraction obtained from

Meson Summary Table

- the Dalitz-plot analysis of $D_s^+ \rightarrow K^+ K^- \pi^+$. That is, the ratio of these two branching fractions is not exactly the $\phi \rightarrow K^+ K^-$ branching fraction 0.491.
- [ggg] This is the average of a model-independent and a K -matrix parametrization of the $\pi^+ \pi^-$ S -wave and is a sum over several f_0 mesons.
- [hhh] An ℓ indicates an e or a μ mode, not a sum over these modes.
- [iii] An $CP(\pm 1)$ indicates the $CP=+1$ and $CP=-1$ eigenstates of the D^0 - \bar{D}^0 system.
- [jjj] D denotes D^0 or \bar{D}^0 .
- [kkk] D_{CP+}^{*0} decays into $D^0 \pi^0$ with the D^0 reconstructed in CP -even eigenstates $K^+ K^-$ and $\pi^+ \pi^-$.
- [lll] \bar{D}^{*} represents an excited state with mass $2.2 < M < 2.8$ GeV/ c^2 .
- [nnn] $\chi_{c1}(3872)^+$ is a hypothetical charged partner of the $\chi_{c1}(3872)$.
- [ooo] $\Theta(1710)^{++}$ is a possible narrow pentaquark state and $G(2220)$ is a possible glueball resonance.
- [ppp] $(\bar{A}_c^- p)_s$ denotes a low-mass enhancement near 3.35 GeV/ c^2 .
- [qqq] Stands for the possible candidates of $K^*(1410)$, $K_0^*(1430)$ and $K_2^*(1430)$.
- [rrr] B^0 and B_s^0 contributions not separated. Limit is on weighted average of the two decay rates.
- [sss] This decay refers to the coherent sum of resonant and nonresonant $J^P = 0^+$ $K\pi$ components with $1.60 < m_{K\pi} < 2.15$ GeV/ c^2 .
- [ttt] $X(214)$ is a hypothetical particle of mass 214 MeV/ c^2 reported by the HyperCP experiment, Physical Review Letters **94** 021801 (2005)
- [uuu] $\Theta(1540)^+$ denotes a possible narrow pentaquark state.
- [vvv] ψ_{DS} is a GeV-scale dark sector antibaryon (mass range 1–4 GeV/ c^2).
- [xxx] Here S and P are the hypothetical scalar and pseudoscalar particles with masses of 2.5 GeV/ c^2 and 214.3 MeV/ c^2 , respectively.
- [yyy] These values are model dependent.
- [zzz] Here “anything” means at least one particle observed.
- [aaa] This is a $B(B^0 \rightarrow D^{*-} \ell^+ \nu_\ell)$ value.
- [baaa] D^{**} stands for the sum of the $D(1^1P_1)$, $D(1^3P_0)$, $D(1^3P_1)$, $D(1^3P_2)$, $D(2^1S_0)$, and $D(2^1S_1)$ resonances.
- [caa] $D^{(*)}\bar{D}^{(*)}$ stands for the sum of $D^* \bar{D}^*$, $D^* \bar{D}$, $D \bar{D}^*$, and $D \bar{D}$.
- [ddaa] $X(3915)$ denotes a near-threshold enhancement in the $\omega J/\psi$ mass spectrum.
- [eeaa] Inclusive branching fractions have a multiplicity definition and can be greater than 100%.
- [ffaa] D_j represents an unresolved mixture of pseudoscalar and tensor D^{**} (P -wave) states.
- [ggaa] Not a pure measurement. See note at head of B_s^0 Decay Modes.
- [hhaa] For $E_\gamma > 100$ MeV.
- [iiaa] $\Theta(1540)$ is a hypothetical pentaquark state of 1.54 GeV/ c^2 mass and a width of less than 25 MeV/ c^2 .
- [jja] Includes $p\bar{p}\pi^+\pi^-\gamma$ and excludes $p\bar{p}\eta$, $p\bar{p}\omega$, $p\bar{p}\eta'$.
- [kkaa] For a narrow state A with mass less than 960 MeV.
- [llaa] For a narrow scalar or pseudoscalar A^0 with mass 0.21–3.0 GeV.
- [naaa] For a dark photon U with mass between 100 and 2100 MeV.
- [oaaa] For a narrow resonance in the range $2.2 < M(X) < 2.8$ GeV.
- [ppaa] J^{PC} known by production in e^+e^- via single photon annihilation. I^G is not known; interpretation of this state as a single resonance is unclear because of the expectation of substantial threshold effects in this energy region.
- [qqaa] $2m_\tau < M(\tau^+\tau^-) < 9.2$ GeV
- [rraa] $2 \text{ GeV} < m_{K^+K^-} < 3$ GeV
- [ssaa] $X\bar{X}$ = vectors with $m < 3.1$ GeV
- [ttaa] X and \bar{X} = zero spin with $m < 4.5$ GeV
- [uuaa] $1.5 \text{ GeV} < m_X < 5.0$ GeV
- [vva] $201 \text{ MeV} < M(\mu^+\mu^-) < 3565$ MeV
- [xxaa] $0.5 \text{ GeV} < m_X < 9.0$ GeV, where m_X is the invariant mass of the hadronic final state.
- [yyaa] Spectroscopic labeling for these states is theoretical, pending experimental information.
- [zzaa] $1.5 \text{ GeV} < m_X < 5.0$ GeV
- [aabb] $1.5 \text{ GeV} < m_X < 5.0$ GeV
- [bbbb] For $m_{\tau^+\tau^-}$ in the ranges 4.03–9.52 and 9.61–10.10 GeV.

Meson Summary Table

See also the table of suggested $q\bar{q}$ quark-model assignments in the Quark Model section.

• Indicates particles that appear in the preceding Meson Summary Table. We do not regard the other entries as being established.

LIGHT UNFLAVORED ($S = C = B = 0$)		STRANGE ($S = \pm 1, C = B = 0$)		CHARMED, STRANGE continued $I(J^P)$		$c\bar{c}$ continued $I^G(J^{PC})$		
$I^G(J^{PC})$	$I^G(J^{PC})$	$I(J^P)$	$I(J^P)$					
• π^\pm $1^-(0^-)$	• $\rho(1700)$ $1^+(1^{--})$	• K^\pm $1/2(0^-)$	• K^\pm $1/2(0^-)$	• $D_{s0}(2590)^+$ $0(0^-)$	• $\psi(4230)$ $0^-(1^{--})$			
• π^0 $1^-(0^+)$	• $a_2(1700)$ $1^-(2^{++})$	• K^0 $1/2(0^-)$	• K^0 $1/2(0^-)$	• $D_{s1}^*(2700)^\pm$ $0(1^-)$	• $\chi_{c1}(4274)$ $0^+(1^{++})$			
• η $0^+(0^+)$	$a_0(1710)$ $1^-(0^+)$	• K_S^0 $1/2(0^-)$	• K_S^0 $1/2(0^-)$	$D_{s1}^*(2860)^\pm$ $0(1^-)$	$X(4350)$ $0^+(?^+)$			
• $f_0(500)$ $0^+(0^+)$	• $f_0(1710)$ $0^+(0^+)$	• K_L^0 $1/2(0^-)$	• K_L^0 $1/2(0^-)$	• $D_{s3}^*(2860)^\pm$ $0(3^-)$	• $\psi(4360)$ $0^-(1^{--})$			
• $\rho(770)$ $1^+(1^{--})$	$X(1750)$ $?^-(1^{--})$	• $K_0^*(700)$ $1/2(0^+)$	• $K_0^*(700)$ $1/2(0^+)$	$D_{sJ}(3040)^\pm$ $0(?^?)$	• $\psi(4415)$ $0^-(1^{--})$			
• $\omega(782)$ $0^-(1^{--})$	$\eta(1760)$ $0^+(0^+)$	• $K^*(892)$ $1/2(1^-)$	• $K^*(892)$ $1/2(1^-)$	BOTTOM ($B = \pm 1$)				
• $\eta'(958)$ $0^+(0^+)$	$f_0(1770)$ $0^+(0^+)$	• $K_1(1270)$ $1/2(1^+)$	• $K_1(1270)$ $1/2(1^+)$	• B^\pm $1/2(0^-)$	$\chi_{c0}(4500)$ $0^+(0^+)$			
• $f_0(980)$ $0^+(0^+)$	• $\pi(1800)$ $1^-(0^+)$	• $K_1^*(1400)$ $1/2(1^+)$	• $K_1^*(1400)$ $1/2(1^+)$	• B^0 $1/2(0^-)$	$X(4630)$ $0^+(?^+)$			
• $a_0(980)$ $1^-(0^+)$	$f_2(1810)$ $0^+(2^{++})$	• $K^*(1410)$ $1/2(1^-)$	• $K^*(1410)$ $1/2(1^-)$	• B^\pm/B^0 ADMIXTURE				
• $\phi(1020)$ $0^-(1^{--})$	$X(1835)$ $0^+(0^+)$	• $K_0^*(1430)$ $1/2(0^+)$	• $K_0^*(1430)$ $1/2(0^+)$	• $B^\pm/B^0/B_s^0/b$ -baryon ADMIXTURE				
• $h_1(1170)$ $0^-(1^+)$	• $\phi_3(1850)$ $0^-(3^{--})$	• $K_2^*(1430)$ $1/2(2^+)$	• $K_2^*(1430)$ $1/2(2^+)$	V_{cb} and V_{ub} CKM Ma- trix Elements				
• $b_1(1235)$ $1^+(1^+)$	$\eta_1(1855)$ $0^+(1^+)$	• $K(1460)$ $1/2(0^-)$	• $K(1460)$ $1/2(0^-)$	• B^* $1/2(1^-)$	• $\eta_b(1S)$ $0^+(0^+)$			
• $a_1(1260)$ $1^-(1^{++})$	• $\eta_2(1870)$ $0^+(2^+)$	$K_2(1580)$ $1/2(2^-)$	$K_2(1580)$ $1/2(2^-)$	• $B_1(5721)$ $1/2(1^+)$	• $\gamma(1S)$ $0^-(1^{--})$			
• $f_2(1270)$ $0^+(2^{++})$	• $\pi_2(1880)$ $1^-(2^+)$	$K(1630)$ $1/2(?^?)$	$K(1630)$ $1/2(?^?)$	• $B_J^*(5732)$ $?(?^?)$	• $\chi_{b0}(1P)$ $0^+(0^+)$			
• $f_1(1285)$ $0^+(1^+)$	$\rho(1900)$ $1^+(1^-)$	• $K_1^*(1650)$ $1/2(1^+)$	• $K_1^*(1650)$ $1/2(1^+)$	• $B_2^*(5747)$ $1/2(2^+)$	• $\chi_{b1}(1P)$ $0^+(1^+)$			
• $\eta(1295)$ $0^+(0^+)$	$f_2(1910)$ $0^+(2^+)$	• $K^*(1680)$ $1/2(1^-)$	• $K^*(1680)$ $1/2(1^-)$	• $B_J(5840)$ $1/2(?^?)$	• $h_b(1P)$ $0^-(1^+)$			
• $\pi(1300)$ $1^-(0^+)$	$a_0(1950)$ $1^-(0^+)$	• $K_2(1770)$ $1/2(2^-)$	• $K_2(1770)$ $1/2(2^-)$	• $B_J^*(5970)$ $1/2(?^?)$	• $\chi_{b2}(1P)$ $0^+(2^+)$			
• $a_2(1320)$ $1^-(2^+)$	• $f_2(1950)$ $0^+(2^+)$	• $K_3^*(1780)$ $1/2(3^-)$	• $K_3^*(1780)$ $1/2(3^-)$	BOTTOM, STRANGE ($B = \pm 1, S = \mp 1$)				
• $f_0(1370)$ $0^+(0^+)$	• $a_4(1970)$ $1^-(4^+)$	• $K_2(1820)$ $1/2(2^-)$	• $K_2(1820)$ $1/2(2^-)$	• B_s^0 $0(0^-)$	$\eta_b(2S)$ $0^+(0^+)$			
$\pi_1(1400)$ $1^-(1^+)$	$\rho_3(1990)$ $1^+(3^-)$	$K(1830)$ $1/2(0^-)$	$K(1830)$ $1/2(0^-)$	• B_s^* $0(1^-)$	• $\gamma(2S)$ $0^-(1^{--})$			
• $\eta(1405)$ $0^+(0^+)$	$\pi_2(2005)$ $1^-(2^+)$	• $K_0^*(1950)$ $1/2(0^+)$	• $K_0^*(1950)$ $1/2(0^+)$	• $B_{s1}(5830)^0$ $0(1^+)$	• $\gamma_2(1D)$ $0^-(2^{--})$			
• $h_1(1415)$ $0^-(1^+)$	• $f_2(2010)$ $0^+(2^+)$	• $K_2^*(1980)$ $1/2(2^+)$	• $K_2^*(1980)$ $1/2(2^+)$	• $B_{s2}(5840)^0$ $0(2^+)$	• $\chi_{b0}(2P)$ $0^+(0^+)$			
• $f_1(1420)$ $0^+(1^+)$	• $f_0(2020)$ $0^+(0^+)$	• $K_4^*(2045)$ $1/2(4^+)$	• $K_4^*(2045)$ $1/2(4^+)$	• $B_{sJ}^*(5850)$ $?(?^?)$	• $\chi_{b1}(2P)$ $0^+(1^+)$			
• $\omega(1420)$ $0^-(1^{--})$	• $f_4(2050)$ $0^+(4^+)$	$K_2(2250)$ $1/2(2^-)$	$K_2(2250)$ $1/2(2^-)$	• $B_{sJ}(5970)$ $0(2^?)$	• $h_b(2P)$ $0^-(1^+)$			
$f_2(1430)$ $0^+(2^{++})$	$\pi_2(2100)$ $1^-(2^+)$	$K_3(2320)$ $1/2(3^+)$	$K_3(2320)$ $1/2(3^+)$	• $B_{sJ}^*(6063)^0$ $0(2^?)$	• $\chi_{b2}(2P)$ $0^+(2^+)$			
• $a_0(1450)$ $1^-(0^+)$	$f_0(2100)$ $0^+(0^+)$	$K_5^*(2380)$ $1/2(5^-)$	$K_5^*(2380)$ $1/2(5^-)$	• $B_{sJ}(6114)^0$ $0(2^?)$	• $\gamma(3S)$ $0^-(1^{--})$			
• $\rho(1450)$ $1^+(1^-)$	$f_2(2150)$ $0^+(2^+)$	$K_4(2500)$ $1/2(4^-)$	$K_4(2500)$ $1/2(4^-)$	OTHER				
• $\eta(1475)$ $0^+(0^+)$	$\rho(2150)$ $1^+(1^-)$	$K(3100)$ $?^?(?^?)$	$K(3100)$ $?^?(?^?)$	• $T_{cs0}^*(2870)^0$ $?^+(0^+)$	• $\gamma(4S)$ $0^-(1^{--})$			
• $f_0(1500)$ $0^+(0^+)$	• $\phi(2170)$ $0^-(1^-)$	CHARMED ($C = \pm 1$)		• $\gamma(10753)$ $?^?(1^{--})$	• $\gamma(10860)$ $0^-(1^{--})$			
$f_1(1510)$ $0^+(1^+)$	$f_0(2200)$ $0^+(0^+)$	• D^\pm $1/2(0^-)$	• D^\pm $1/2(0^-)$	• $\gamma(11020)$ $0^-(1^{--})$				
• $f_2'(1525)$ $0^+(2^{++})$	$f_J(2220)$ $0^+(2^+)$	• D^0 $1/2(0^-)$	• D^0 $1/2(0^-)$	• B_c^+ $0(0^-)$				
• $f_2(1565)$ $0^+(2^{++})$	or 4^+	• $D^*(2007)^0$ $1/2(1^-)$	• $D^*(2007)^0$ $1/2(1^-)$	• $B_c(2S)^\pm$ $0(0^-)$				
$\rho(1570)$ $1^+(1^-)$	$\omega(2220)$ $0^-(1^-)$	• $D^*(2010)^\pm$ $1/2(1^-)$	• $D^*(2010)^\pm$ $1/2(1^-)$	$c\bar{c}$				
$h_1(1595)$ $0^-(1^+)$	$\eta(2225)$ $0^+(0^+)$	• $D_0^*(2300)$ $1/2(0^+)$	• $D_0^*(2300)$ $1/2(0^+)$	$I^G(J^{PC})$				
• $\pi_1(1600)$ $1^-(1^+)$	$\rho_3(2250)$ $1^+(3^-)$	• $D_1(2420)$ $1/2(1^+)$	• $D_1(2420)$ $1/2(1^+)$	• $\eta_c(1S)$ $0^+(0^+)$	• $T_{c\bar{c}1}(3900)$ $1^+(1^+)$			
• $a_1(1640)$ $1^-(1^{++})$	• $f_2(2300)$ $0^+(2^+)$	• $D_1(2430)^0$ $1/2(1^+)$	• $D_1(2430)^0$ $1/2(1^+)$	• $J/\psi(1S)$ $0^-(1^{--})$	$T_{c\bar{c}31}(4000)$ $1/2(1^+)$			
$f_2(1640)$ $0^+(2^{++})$	$f_4(2300)$ $0^+(4^+)$	• $D_2^*(2460)$ $1/2(2^+)$	• $D_2^*(2460)$ $1/2(2^+)$	• $\chi_{c0}(1P)$ $0^+(0^+)$	• $T_{c\bar{c}}(4050)^+$ $1^-(?^+)$			
• $\eta_2(1645)$ $0^+(2^+)$	$f_0(2330)$ $0^+(0^+)$	$D_0(2550)^0$ $1/2(0^-)$	$D_0(2550)^0$ $1/2(0^-)$	• $\chi_{c1}(1P)$ $0^+(1^+)$	$T_{c\bar{c}}(4055)^+$ $1^+(?^+)$			
• $\omega(1650)$ $0^-(1^-)$	• $f_2(2340)$ $0^+(2^+)$	$D_1^*(2600)^0$ $1/2(1^-)$	$D_1^*(2600)^0$ $1/2(1^-)$	• $h_c(1P)$ $0^-(1^+)$	$T_{c\bar{c}}(4100)^+$ $1^-(?^+)$			
• $\omega_3(1670)$ $0^-(3^-)$	• $\rho_5(2350)$ $1^+(5^-)$	$D^*(2640)^\pm$ $1/2(?^?)$	$D^*(2640)^\pm$ $1/2(?^?)$	• $\chi_{c2}(1P)$ $0^+(2^+)$	$T_{c\bar{c}}(4100)^+$ $1^-(?^+)$			
• $\pi_2(1670)$ $1^-(2^+)$	$X(2370)$ $?^?(?^?)$	$D_2(2740)^0$ $1/2(2^-)$	$D_2(2740)^0$ $1/2(2^-)$	• $\eta_c(2S)$ $0^+(0^+)$	$T_{c\bar{c}1}(4200)^+$ $1^+(1^+)$			
• $\phi(1680)$ $0^-(1^-)$	$f_0(2470)$ $0^+(0^+)$	• $D_3^*(2750)$ $1/2(3^-)$	• $D_3^*(2750)$ $1/2(3^-)$	• $\psi(2S)$ $0^-(1^-)$	$T_{c\bar{c}31}(4220)^+$ $1/2(1^+)$			
• $\rho_3(1690)$ $1^+(3^-)$	$f_6(2510)$ $0^+(6^+)$	$D_1^*(2760)^0$ $1/2(1^-)$	$D_1^*(2760)^0$ $1/2(1^-)$	• $\psi(3770)$ $0^-(1^-)$	$T_{c\bar{c}0}(4240)^+$ $1^+(0^-)$			
				• $D(3000)^0$ $1/2(?^?)$	• $\psi_2(3823)$ $0^-(2^-)$	$T_{c\bar{c}}(4250)^+$ $1^-(?^+)$		
				CHARMED, STRANGE ($C = \pm 1, S = \pm 1$)				
				• D_s^\pm $0(0^-)$	• $\psi_3(3842)$ $0^-(3^-)$	• $T_{c\bar{c}1}(4430)^+$ $1^+(1^+)$		
				• D_s^\pm $0(1^-)$	$\chi_{c0}(3860)$ $0^+(0^+)$	• $T_{b\bar{b}5}(5568)^+$ $1(?^?)$		
				• $D_{s0}^*(2317)^\pm$ $0(0^+)$	• $\chi_{c1}(3872)$ $0^+(1^+)$	$T_{c\bar{c}c\bar{c}}(6900)^0$ $0^+(?^+)$		
				• $D_{s1}^*(2460)^\pm$ $0(1^+)$	• $\chi_{c0}(3915)$ $0^+(0^+)$	• $T_{b\bar{b}1}(10610)$ $1^+(1^+)$		
				• $D_{s1}^*(2536)^\pm$ $0(1^+)$	• $\chi_{c2}(3930)$ $0^+(2^+)$	• $T_{b\bar{b}1}(10650)$ $1^+(1^+)$		
				• $D_{s2}^*(2573)$ $0(2^+)$	$X(3940)$ $?^?(?^?)$	Further States		
				• $\psi(4040)$ $0^-(1^-)$	• $\psi(4160)$ $0^-(1^-)$			
				• $\chi_{c1}(4140)$ $0^+(1^+)$	$X(4160)$ $?^?(?^?)$			

Baryon Summary Table

This short table gives the name, the quantum numbers (where known), and the status of baryons in the Review. Only the baryons with 3- or 4-star status are included in the Baryon Summary Table. Due to insufficient data or uncertain interpretation, the other entries in the table are not established baryons. The names with masses are of baryons that decay strongly. The spin-parity J^P (when known) is given with each particle. For the strongly decaying particles, the J^P values are considered to be part of the names.

p	$1/2^+$	****	$\Delta(1232)$	$3/2^+$	****	Σ^+	$1/2^+$	****	Λ_c^+	$1/2^+$	****	Λ_b^0	$1/2^+$	***
n	$1/2^+$	****	$\Delta(1600)$	$3/2^+$	****	Σ^0	$1/2^+$	****	$\Lambda_c(2595)^+$	$1/2^-$	***	$\Lambda_b(5912)^0$	$1/2^-$	***
$N(1440)$	$1/2^+$	****	$\Delta(1620)$	$1/2^-$	****	Σ^-	$1/2^+$	****	$\Lambda_c(2625)^+$	$3/2^-$	***	$\Lambda_b(5920)^0$	$3/2^-$	***
$N(1520)$	$3/2^-$	****	$\Delta(1700)$	$3/2^-$	****	$\Sigma(1385)$	$3/2^+$	****	$\Lambda_c(2765)^+$	*		$\Lambda_b(6070)^0$	$1/2^+$	***
$N(1535)$	$1/2^-$	****	$\Delta(1750)$	$1/2^+$	*	$\Sigma(1580)$	$3/2^-$	*	$\Lambda_c(2860)^+$	$3/2^+$	***	$\Lambda_b(6146)^0$	$3/2^+$	***
$N(1650)$	$1/2^-$	****	$\Delta(1900)$	$1/2^-$	***	$\Sigma(1620)$	$1/2^-$	*	$\Lambda_c(2880)^+$	$5/2^+$	***	$\Lambda_b(6152)^0$	$5/2^+$	***
$N(1675)$	$5/2^-$	****	$\Delta(1905)$	$5/2^+$	****	$\Sigma(1660)$	$1/2^+$	***	$\Lambda_c(2910)^+$	*		Σ_b	$1/2^+$	***
$N(1680)$	$5/2^+$	****	$\Delta(1910)$	$1/2^+$	****	$\Sigma(1670)$	$3/2^-$	****	$\Lambda_c(2940)^+$	$3/2^-$	***	Σ_b^*	$3/2^+$	***
$N(1700)$	$3/2^-$	***	$\Delta(1920)$	$3/2^+$	***	$\Sigma(1750)$	$1/2^-$	***	$\Sigma_c(2455)$	$1/2^+$	****	$\Sigma_b(6097)^+$		***
$N(1710)$	$1/2^+$	****	$\Delta(1930)$	$5/2^-$	***	$\Sigma(1775)$	$5/2^-$	****	$\Sigma_c(2520)$	$3/2^+$	***	$\Sigma_b(6097)^-$		***
$N(1720)$	$3/2^+$	****	$\Delta(1940)$	$3/2^-$	**	$\Sigma(1780)$	$3/2^+$	*	$\Sigma_c(2800)$	***		Ξ_b^-	$1/2^+$	***
$N(1860)$	$5/2^+$	**	$\Delta(1950)$	$7/2^+$	****	$\Sigma(1880)$	$1/2^+$	**	Ξ_c^+	$1/2^+$	***	Ξ_b^0	$1/2^+$	***
$N(1875)$	$3/2^-$	***	$\Delta(2000)$	$5/2^+$	**	$\Sigma(1900)$	$1/2^-$	**	Ξ_c^0	$1/2^+$	****	$\Xi_b'(5935)^-$	$1/2^+$	***
$N(1880)$	$1/2^+$	***	$\Delta(2150)$	$1/2^-$	*	$\Sigma(1910)$	$3/2^-$	***	Ξ_c^+	$1/2^+$	***	$\Xi_b(5945)^0$	$3/2^+$	***
$N(1895)$	$1/2^-$	****	$\Delta(2200)$	$7/2^-$	***	$\Sigma(1915)$	$5/2^+$	****	Ξ_c^0	$1/2^+$	***	$\Xi_b(5955)^-$	$3/2^+$	***
$N(1900)$	$3/2^+$	****	$\Delta(2300)$	$9/2^+$	**	$\Sigma(1940)$	$3/2^+$	*	Ξ_c^0	$1/2^+$	***	$\Xi_b(6087)^0$	$3/2^-$	***
$N(1990)$	$7/2^+$	**	$\Delta(2350)$	$5/2^-$	*	$\Sigma(2010)$	$3/2^-$	*	$\Xi_c(2645)$	$3/2^+$	***	$\Xi_b(6095)^0$	$3/2^-$	***
$N(2000)$	$5/2^+$	**	$\Delta(2390)$	$7/2^+$	*	$\Sigma(2030)$	$7/2^+$	****	$\Xi_c(2790)$	$1/2^-$	***	$\Xi_b(6100)^-$	$3/2^-$	***
$N(2040)$	$3/2^+$	*	$\Delta(2400)$	$9/2^-$	**	$\Sigma(2070)$	$5/2^+$	*	$\Xi_c(2815)$	$3/2^-$	***	$\Xi_b(6227)^-$		***
$N(2060)$	$5/2^-$	***	$\Delta(2420)$	$11/2^+$	****	$\Sigma(2080)$	$3/2^+$	*	$\Xi_c(2882)$	*		$\Xi_b(6227)^0$		***
$N(2100)$	$1/2^+$	****	$\Delta(2470)$	$13/2^-$	**	$\Sigma(2100)$	$7/2^-$	*	$\Xi_c(2923)$	**		$\Xi_b(6327)^0$		***
$N(2120)$	$3/2^-$	***	$\Delta(2750)$	$15/2^+$	**	$\Sigma(2110)$	$1/2^-$	*	$\Xi_c(2930)$	**		$\Xi_b(6327)^0$		***
$N(2190)$	$7/2^-$	****	$\Delta(2950)$	$15/2^+$	**	$\Sigma(2230)$	$3/2^+$	*	$\Xi_c(2970)$	$1/2^+$	***	$\Xi_b(6333)^0$		***
$N(2220)$	$9/2^+$	****	Λ	$1/2^+$	****	$\Sigma(2250)$	**		$\Xi_c(3055)$	***		Ω_b^-	$1/2^+$	***
$N(2250)$	$9/2^-$	****	$\Lambda(1380)$	$1/2^-$	**	$\Sigma(2455)$	*		$\Xi_c(3080)$	***		$\Omega_b(6316)^-$		***
$N(2300)$	$1/2^+$	**	$\Lambda(1405)$	$1/2^-$	****	$\Sigma(2620)$	*		$\Xi_c(3123)$	*		$\Omega_b(6330)^-$		***
$N(2570)$	$5/2^-$	**	$\Lambda(1520)$	$3/2^-$	****	$\Sigma(3000)$	*		Ω_c^0	$1/2^+$	***	$\Omega_b(6340)^-$		***
$N(2600)$	$11/2^-$	***	$\Lambda(1600)$	$1/2^+$	****	$\Sigma(3170)$	*		$\Omega_c(2770)^0$	$3/2^+$	***	$\Omega_b(6350)^-$		***
$N(2700)$	$13/2^+$	**	$\Lambda(1670)$	$1/2^-$	****	Ξ^0	$1/2^+$	****	$\Omega_c(3000)^0$	***		$P_{c\bar{c}}(4312)^+$	*	
			$\Lambda(1690)$	$3/2^-$	****	Ξ^-	$1/2^+$	****	$\Omega_c(3050)^0$	***		$P_{c\bar{c}s}(4338)^0$	$1/2^-$	*
			$\Lambda(1710)$	$1/2^+$	*	$\Xi(1530)$	$3/2^+$	****	$\Omega_c(3065)^0$	***		$P_{c\bar{c}}(4380)^+$	*	
			$\Lambda(1800)$	$1/2^-$	***	$\Xi(1620)$	**		$\Omega_c(3090)^0$	***		$P_{c\bar{c}}(4440)^+$	*	
			$\Lambda(1810)$	$1/2^+$	***	$\Xi(1690)$	**		$\Omega_c(3120)^0$	***		$P_{c\bar{c}}(4457)^+$	*	
			$\Lambda(1820)$	$5/2^+$	****	$\Xi(1820)$	$3/2^-$	***	$\Omega_c(3185)^0$	***		$P_{c\bar{c}s}(4459)^0$	*	
			$\Lambda(1830)$	$5/2^-$	****	$\Xi(1950)$	**		$\Omega_c(3327)^0$	***				
			$\Lambda(1890)$	$3/2^+$	****	$\Xi(2030)$	$\geq 5/2^?$	***	Ξ_c^+	*				
			$\Lambda(2000)$	$1/2^-$	*	$\Xi(2120)$	*		Ξ_c^{++}	***				
			$\Lambda(2050)$	$3/2^-$	*	$\Xi(2250)$	**		Ξ_c^{cc}	***				
			$\Lambda(2070)$	$3/2^+$	*	$\Xi(2370)$	**		Ξ_c^{cc}	***				
			$\Lambda(2080)$	$5/2^-$	*	$\Xi(2500)$	*							
			$\Lambda(2085)$	$7/2^+$	**									
			$\Lambda(2100)$	$7/2^-$	****									
			$\Lambda(2110)$	$5/2^+$	***	Ω^-	$3/2^+$	****						
			$\Lambda(2325)$	$3/2^-$	*	$\Omega(2012)^-$	$?^-$	***						
			$\Lambda(2350)$	$9/2^+$	***	$\Omega(2250)^-$		***						
			$\Lambda(2585)$	*		$\Omega(2380)^-$		**						
						$\Omega(2470)^-$		**						

**** Existence is certain, and properties are at least fairly well explored.

*** Existence ranges from very likely to certain, but further confirmation is desirable and/or quantum numbers, branching fractions, etc. are not well determined.

** Evidence of existence is only fair.

* Evidence of existence is poor.

Baryon Summary Table

N BARYONS ($S = 0, I = 1/2$)

$$p, N^+ = uud; \quad n, N^0 = udd$$

p

$$I(J^P) = \frac{1}{2}(\frac{1}{2}^+)$$

Mass $m = 1.007276466621 \pm 0.000000000053$ u
 Mass $m = 938.27208816 \pm 0.00000029$ MeV [a]
 $|m_p - m_{\bar{p}}|/m_p < 7 \times 10^{-10}$, CL = 90% [b]
 $|\frac{q_p}{m_p} - \frac{q_{\bar{p}}}{m_{\bar{p}}}| = 1.000000000003 \pm 0.000000000016$
 $|q_p + q_{\bar{p}}|/e < 7 \times 10^{-10}$, CL = 90% [b]
 $|q_p + q_e|/e < 1 \times 10^{-21}$ [c]
 Magnetic moment $\mu = 2.7928473446 \pm 0.0000000008 \mu_N$
 $(\mu_p + \mu_{\bar{p}}) / \mu_p = (0.002 \pm 0.004) \times 10^{-6}$
 Electric dipole moment $d < 0.021 \times 10^{-23}$ ecm
 Electric polarizability $\alpha = (11.2 \pm 0.4) \times 10^{-4}$ fm³
 Magnetic polarizability $\beta = (2.5 \pm 0.4) \times 10^{-4}$ fm³ ($S = 1.2$)
 Charge radius, μp Lamb shift = 0.84087 ± 0.00039 fm [d]
 Charge radius = 0.8409 ± 0.0004 fm [d]
 Magnetic radius = 0.851 ± 0.026 fm [e]
 Mean life $\tau > 9 \times 10^{29}$ years, CL = 90% ($p \rightarrow$ invisible mode)

See the "Note on Nucleon Decay" in our 1994 edition (Phys. Rev. **D50**, 1173) for a short review.

The "partial mean life" limits tabulated here are the limits on τ/B_j , where τ is the total mean life and B_j is the branching fraction for the mode in question. For N decays, p and n indicate proton and neutron partial lifetimes.

p DECAY MODES	Partial mean life (10 ³⁰ years)	Confidence level	ρ (MeV/c)
Antilepton + meson			
$N \rightarrow e^+ \pi$	> 5300 (n), > 24000 (p)	90%	459
$N \rightarrow \mu^+ \pi$	> 3500 (n), > 16000 (p)	90%	453
$N \rightarrow \nu \pi$	> 1100 (n), > 390 (p)	90%	459
$p \rightarrow e^+ \eta$	> 10000	90%	309
$p \rightarrow \mu^+ \eta$	> 4700	90%	297
$n \rightarrow \nu \eta$	> 158	90%	310
$N \rightarrow e^+ \rho$	> 217 (n), > 720 (p)	90%	149
$N \rightarrow \mu^+ \rho$	> 228 (n), > 570 (p)	90%	113
$N \rightarrow \nu \rho$	> 19 (n), > 162 (p)	90%	149
$p \rightarrow e^+ \omega$	> 1600	90%	143
$p \rightarrow \mu^+ \omega$	> 2800	90%	105
$n \rightarrow \nu \omega$	> 108	90%	144
$N \rightarrow e^+ K$	> 17 (n), > 1000 (p)	90%	339
$N \rightarrow \mu^+ K$	> 26 (n), > 4500 (p)	90%	329
$N \rightarrow \nu K$	> 86 (n), > 5900 (p)	90%	339
$n \rightarrow \nu K_S^0$	> 260	90%	338
$p \rightarrow e^+ K^*(892)^0$	> 84	90%	45
$N \rightarrow \nu K^*(892)$	> 78 (n), > 51 (p)	90%	45
Antilepton + mesons			
$p \rightarrow e^+ \pi^+ \pi^-$	> 82	90%	448
$p \rightarrow e^+ \pi^0 \pi^0$	> 147	90%	449
$n \rightarrow e^+ \pi^- \pi^0$	> 52	90%	449
$p \rightarrow \mu^+ \pi^+ \pi^-$	> 133	90%	425
$p \rightarrow \mu^+ \pi^0 \pi^0$	> 101	90%	427
$n \rightarrow \mu^+ \pi^- \pi^0$	> 74	90%	427
$n \rightarrow e^+ K^0 \pi^-$	> 18	90%	319
Lepton + meson			
$n \rightarrow e^- \pi^+$	> 65	90%	459
$n \rightarrow \mu^- \pi^+$	> 49	90%	453
$n \rightarrow e^- \rho^+$	> 62	90%	150
$n \rightarrow \mu^- \rho^+$	> 7	90%	115
$n \rightarrow e^- K^+$	> 32	90%	340
$n \rightarrow \mu^- K^+$	> 57	90%	330
Lepton + mesons			
$p \rightarrow e^- \pi^+ \pi^+$	> 30	90%	448
$n \rightarrow e^- \pi^+ \pi^0$	> 29	90%	449
$p \rightarrow \mu^- \pi^+ \pi^+$	> 17	90%	425
$n \rightarrow \mu^- \pi^+ \pi^0$	> 34	90%	427
$p \rightarrow e^- \pi^+ K^+$	> 75	90%	320
$p \rightarrow \mu^- \pi^+ K^+$	> 245	90%	279

Antilepton + photon(s)

$p \rightarrow e^+ \gamma$	> 670	90%	469
$p \rightarrow \mu^+ \gamma$	> 478	90%	463
$n \rightarrow \nu \gamma$	> 550	90%	470
$p \rightarrow e^+ \gamma \gamma$	> 100	90%	469
$n \rightarrow \nu \gamma \gamma$	> 219	90%	470

Antilepton + single massless

$p \rightarrow e^+ X$	> 790	90%	—
$p \rightarrow \mu^+ X$	> 410	90%	—

Three (or more) leptons

$p \rightarrow e^+ e^+ e^-$	> 34000	90%	469
$p \rightarrow e^+ \mu^+ \mu^-$	> 9200	90%	457
$p \rightarrow e^+ \nu \nu$	> 170	90%	469
$n \rightarrow e^+ e^- \nu$	> 257	90%	470
$n \rightarrow \mu^+ e^- \nu$	> 83	90%	464
$n \rightarrow \mu^+ \mu^- \nu$	> 79	90%	458
$p \rightarrow \mu^+ e^+ e^-$	> 23000	90%	463
$p \rightarrow \mu^- e^+ e^+$	> 19000	90%	463
$p \rightarrow \mu^+ \mu^+ \mu^-$	> 10000	90%	439
$p \rightarrow \mu^+ \nu \nu$	> 220	90%	463
$p \rightarrow e^- \mu^+ \mu^+$	> 11000	90%	457
$n \rightarrow 3\nu$	> 5×10^{-4}	90%	470

Inclusive modes

$N \rightarrow e^+$ anything	> 0.6 (n, p)	90%	—
$N \rightarrow \mu^+$ anything	> 12 (n, p)	90%	—
$N \rightarrow e^+ \pi^0$ anything	> 0.6 (n, p)	90%	—

$\Delta B = 2$ dinucleon modes

The following are lifetime limits per iron nucleus.

$p\bar{p} \rightarrow \pi^+ \pi^+$	> 72.2	90%	—
$p\bar{p} \rightarrow \pi^+ \pi^0$	> 170	90%	—
$n\bar{n} \rightarrow \pi^+ \pi^-$	> 0.7	90%	—
$n\bar{n} \rightarrow \pi^0 \pi^0$	> 404	90%	—
$p\bar{p} \rightarrow K^+ K^+$	> 170	90%	—
$p\bar{p} \rightarrow e^+ e^+$	> 5.8	90%	—
$p\bar{p} \rightarrow e^+ \mu^+$	> 3.6	90%	—
$p\bar{p} \rightarrow \mu^+ \mu^+$	> 1.7	90%	—
$p\bar{p} \rightarrow e^+ \bar{\nu}$	> 260	90%	—
$p\bar{p} \rightarrow \mu^+ \bar{\nu}$	> 200	90%	—
$p\bar{p} \rightarrow \tau^+ \bar{\nu}_\tau$	> 29	90%	—
$n\bar{n} \rightarrow$ invisible	> 1.4	90%	—
$n\bar{n} \rightarrow \nu_e \bar{\nu}_e$	> 1.4	90%	—
$n\bar{n} \rightarrow \nu_\mu \bar{\nu}_\mu$	> 1.4	90%	—
$p\bar{p} \rightarrow$ invisible	> 0.06	90%	—
$p\bar{p} \rightarrow$ invisible	> 0.11	90%	—

\bar{p} DECAY MODES

\bar{p} DECAY MODES	Partial mean life (years)	Confidence level	ρ (MeV/c)
$\bar{p} \rightarrow e^- \gamma$	> 7×10^5	90%	469
$\bar{p} \rightarrow \mu^- \gamma$	> 5×10^4	90%	463
$\bar{p} \rightarrow e^- \pi^0$	> 4×10^5	90%	459
$\bar{p} \rightarrow \mu^- \pi^0$	> 5×10^4	90%	453
$\bar{p} \rightarrow e^- \eta$	> 2×10^4	90%	309
$\bar{p} \rightarrow \mu^- \eta$	> 8×10^3	90%	297
$\bar{p} \rightarrow e^- K_S^0$	> 900	90%	337
$\bar{p} \rightarrow \mu^- K_S^0$	> 4×10^3	90%	326
$\bar{p} \rightarrow e^- K_L^0$	> 9×10^3	90%	337
$\bar{p} \rightarrow \mu^- K_L^0$	> 7×10^3	90%	326
$\bar{p} \rightarrow e^- \gamma \gamma$	> 2×10^4	90%	469
$\bar{p} \rightarrow \mu^- \gamma \gamma$	> 2×10^4	90%	463
$\bar{p} \rightarrow e^- \omega$	> 200	90%	143

n

$$I(J^P) = \frac{1}{2}(\frac{1}{2}^+)$$

Mass $m = 1.0086649160 \pm 0.0000000005$ u
 Mass $m = 939.5654205 \pm 0.0000005$ MeV [a]
 $(m_n - m_{\bar{n}})/m_n = (9 \pm 5) \times 10^{-5}$
 $m_n - m_p = 1.2933324 \pm 0.0000005$ MeV
 $= 0.00138844919(45)$ u
 Mean life $\tau = 878.4 \pm 0.5$ s ($S = 1.8$)
 $c\tau = 2.6335 \times 10^8$ km
 Magnetic moment $\mu = -1.9130427 \pm 0.0000005 \mu_N$
 Electric dipole moment $d < 0.18 \times 10^{-25}$ ecm, CL = 90%

Baryon Summary Table

Mean-square charge radius $\langle r_n^2 \rangle = -0.1155 \pm 0.0017 \text{ fm}^2$
Magnetic radius $\sqrt{\langle r_M^2 \rangle} = 0.864_{-0.008}^{+0.009} \text{ fm}$
Electric polarizability $\alpha = (11.8 \pm 1.1) \times 10^{-4} \text{ fm}^3$
Magnetic polarizability $\beta = (3.7 \pm 1.2) \times 10^{-4} \text{ fm}^3$
Charge $q = (-0.2 \pm 0.8) \times 10^{-21} e$
Mean $n\bar{n}$ -oscillation time $> 8.6 \times 10^7 \text{ s}$, CL = 90% (free n)
Mean $n\bar{\pi}$ -oscillation time $> 4.7 \times 10^8 \text{ s}$, CL = 90% [\bar{n}] (bound n)
Mean $n\bar{n}'$ -oscillation time $> 448 \text{ s}$, CL = 90% [\bar{n}]

 $p e^- \nu_e$ decay parameters [\bar{h}]

$\lambda \equiv g_A / g_V = -1.2754 \pm 0.0013$ (S = 2.7)
 $A = -0.11958 \pm 0.00021$ (S = 1.2)
 $B = 0.9807 \pm 0.0030$
 $C = -0.2377 \pm 0.0026$
 $a = -0.1049 \pm 0.0013$ (S = 1.8)
 $\phi_{AV} = (180.017 \pm 0.026)^\circ$ [I]
 $D = (-1.2 \pm 2.0) \times 10^{-4}$ [I]
 $R = 0.004 \pm 0.013$ [I]
Fierz interference term $b = 0.017 \pm 0.020$

n DECAY MODES	Fraction (Γ_i/Γ)	Confidence level	ρ (MeV/c)
$p e^- \bar{\nu}_e$	100 %		1
$p e^- \bar{\nu}_e \gamma$	[K] (9.2 ± 0.7) $\times 10^{-3}$		1
hydrogen-atom $\bar{\nu}_e$	$< 2.7 \times 10^{-3}$	95%	1.19
Charge conservation (Q) violating mode			
$p \nu_e \bar{\nu}_e$	Q $< 8 \times 10^{-27}$	68%	1

 $N(1440) 1/2^+$

$$I(J^P) = \frac{1}{2}(1/2^+)$$

Re(pole position) = 1360 to 1380 (≈ 1370) MeV
 $-2\text{Im}(\text{pole position}) = 180$ to 205 (≈ 190) MeV
Breit-Wigner mass = 1410 to 1470 (≈ 1440) MeV
Breit-Wigner full width = 250 to 450 (≈ 350) MeV

$N(1440)$ DECAY MODES	Fraction (Γ_i/Γ)	ρ (MeV/c)
$N\pi$	55–75 %	398
$N\eta$	< 1 %	†
$N\pi\pi$	17–50 %	347
$\Delta(1232)\pi$, P-wave	6–27 %	147
$N\sigma$	11–23 %	–
$p\gamma$, helicity=1/2	0.035–0.048 %	414
$n\gamma$, helicity=1/2	0.02–0.04 %	413

 $N(1520) 3/2^-$

$$I(J^P) = \frac{1}{2}(3/2^-)$$

Re(pole position) = 1505 to 1515 (≈ 1510) MeV
 $-2\text{Im}(\text{pole position}) = 105$ to 120 (≈ 110) MeV
Breit-Wigner mass = 1510 to 1520 (≈ 1515) MeV
Breit-Wigner full width = 100 to 120 (≈ 110) MeV

$N(1520)$ DECAY MODES	Fraction (Γ_i/Γ)	ρ (MeV/c)
$N\pi$	55–65 %	453
$N\eta$	0.07–0.09 %	142
$N\pi\pi$	25–35 %	410
$\Delta(1232)\pi$	22–34 %	225
$\Delta(1232)\pi$, S-wave	15–23 %	225
$\Delta(1232)\pi$, D-wave	7–11 %	225
$N\rho$	10–16 %	†
$N\rho$, S=3/2, S-wave	10–16 %	†
$N\rho$, S=1/2, D-wave	0.2–0.4 %	†
$N\sigma$	< 10 %	–
$p\gamma$	0.31–0.52 %	467
$p\gamma$, helicity=1/2	0.01–0.02 %	467
$p\gamma$, helicity=3/2	0.30–0.50 %	467
$n\gamma$	0.30–0.53 %	466
$n\gamma$, helicity=1/2	0.04–0.10 %	466
$n\gamma$, helicity=3/2	0.25–0.45 %	466

 $N(1535) 1/2^-$

$$I(J^P) = \frac{1}{2}(1/2^-)$$

Re(pole position) = 1500 to 1520 (≈ 1510) MeV
 $-2\text{Im}(\text{pole position}) = 80$ to 130 (≈ 110) MeV
Breit-Wigner mass = 1515 to 1545 (≈ 1530) MeV
Breit-Wigner full width = 125 to 175 (≈ 150) MeV

$N(1535)$ DECAY MODES	Fraction (Γ_i/Γ)	ρ (MeV/c)
$N\pi$	32–52 %	464
$N\eta$	30–55 %	176
$N\pi\pi$	4–31 %	422
$\Delta(1232)\pi$, D-wave	1–4 %	240
$N\rho$	2–17 %	†
$N\rho$, S=1/2, S-wave	2–16 %	†
$N\rho$, S=3/2, D-wave	< 1 %	†
$N\sigma$	2–10 %	–
$N(1440)\pi$	5–12 %	†
$p\gamma$, helicity=1/2	0.15–0.30 %	477
$n\gamma$, helicity=1/2	0.01–0.25 %	477

 $N(1650) 1/2^-$

$$I(J^P) = \frac{1}{2}(1/2^-)$$

Re(pole position) = 1650 to 1680 (≈ 1665) MeV
 $-2\text{Im}(\text{pole position}) = 100$ to 170 (≈ 135) MeV
Breit-Wigner mass = 1635 to 1665 (≈ 1650) MeV
Breit-Wigner full width = 100 to 150 (≈ 125) MeV

$N(1650)$ DECAY MODES	Fraction (Γ_i/Γ)	ρ (MeV/c)
$N\pi$	50–70 %	547
$N\eta$	15–35 %	348
ΛK	5–15 %	169
$N\pi\pi$	20–58 %	514
$\Delta(1232)\pi$, D-wave	6–18 %	345
$N\rho$	12–22 %	†
$N\rho$, S=1/2, S-wave	< 4 %	†
$N\rho$, S=3/2, D-wave	12–18 %	†
$N\sigma$	2–18 %	–
$N(1440)\pi$	6–26 %	150
$p\gamma$, helicity=1/2	0.04–0.20 %	558
$n\gamma$, helicity=1/2	0.003–0.17 %	557

 $N(1675) 5/2^-$

$$I(J^P) = \frac{1}{2}(5/2^-)$$

Re(pole position) = 1650 to 1660 (≈ 1655) MeV
 $-2\text{Im}(\text{pole position}) = 120$ to 150 (≈ 135) MeV
Breit-Wigner mass = 1665 to 1680 (≈ 1675) MeV
Breit-Wigner full width = 130 to 160 (≈ 145) MeV

$N(1675)$ DECAY MODES	Fraction (Γ_i/Γ)	ρ (MeV/c)
$N\pi$	38–42 %	564
$N\eta$	< 1 %	376
ΛK	< 0.04 %	216
$N\pi\pi$	25–45 %	532
$\Delta(1232)\pi$, D-wave	23–37 %	366
$N\rho$	0.1–0.9 %	†
$N\rho$, S=1/2	< 0.2 %	†
$N\rho$, S=3/2, D-wave	0.1–0.7 %	†
$N\sigma$	3–7 %	–
$p\gamma$	0–0.02 %	575
$p\gamma$, helicity=1/2	0–0.01 %	575
$p\gamma$, helicity=3/2	0–0.01 %	575
$n\gamma$	0–0.15 %	574
$n\gamma$, helicity=1/2	0–0.05 %	574
$n\gamma$, helicity=3/2	0–0.10 %	574

 $N(1680) 5/2^+$

$$I(J^P) = \frac{1}{2}(5/2^+)$$

Re(pole position) = 1660 to 1680 (≈ 1670) MeV
 $-2\text{Im}(\text{pole position}) = 110$ to 135 (≈ 120) MeV
Breit-Wigner mass = 1680 to 1690 (≈ 1685) MeV
Breit-Wigner full width = 115 to 130 (≈ 120) MeV

Baryon Summary Table

N(1680) DECAY MODES	Fraction (Γ_i/Γ)	ρ (MeV/c)
$N\pi$	60–70 %	571
$N\eta$	<1 %	386
$N\pi\pi$	28–53 %	539
$\Delta(1232)\pi$	11–23 %	374
$\Delta(1232)\pi$, <i>P</i> -wave	4–10 %	374
$\Delta(1232)\pi$, <i>F</i> -wave	1–13 %	374
$N\rho$	8–11 %	†
$N\rho$, $S=3/2$, <i>P</i> -wave	6–8 %	†
$N\rho$, $S=3/2$, <i>F</i> -wave	2–3 %	†
$N\sigma$	9–19 %	–
$p\gamma$	0.21–0.32 %	581
$p\gamma$, helicity=1/2	0.001–0.011 %	581
$p\gamma$, helicity=3/2	0.20–0.32 %	581
$n\gamma$	0.021–0.046 %	581
$n\gamma$, helicity=1/2	0.004–0.029 %	581
$n\gamma$, helicity=3/2	0.01–0.024 %	581

N(1700) $3/2^-$

$$I(J^P) = \frac{1}{2}(\frac{3}{2}^-)$$

Re(pole position) = 1650 to 1750 (\approx 1700) MeV
 $-2\text{Im}(\text{pole position}) = 100$ to 300 (\approx 200) MeV
 Breit-Wigner mass = 1650 to 1800 (\approx 1720) MeV
 Breit-Wigner full width = 100 to 300 (\approx 200) MeV

N(1700) DECAY MODES	Fraction (Γ_i/Γ)	ρ (MeV/c)
$N\pi$	7–17 %	594
$N\eta$	1–2 %	422
$N\omega$	10–34 %	†
ΛK	1–2 %	283
$N\pi\pi$	>89 %	564
$\Delta(1232)\pi$	55–85 %	402
$\Delta(1232)\pi$, <i>S</i> -wave	50–80 %	402
$\Delta(1232)\pi$, <i>D</i> -wave	4–14 %	402
$N\rho$, $S=3/2$, <i>S</i> -wave	32–44 %	74
$N\sigma$	2–14 %	–
$N(1440)\pi$	3–11 %	225
$N(1520)\pi$	<4 %	145
$p\gamma$	0.01–0.05 %	604
$p\gamma$, helicity=1/2	0.0–0.024 %	604
$p\gamma$, helicity=3/2	0.002–0.026 %	604
$n\gamma$	0.01–0.13 %	603
$n\gamma$, helicity=1/2	0.0–0.09 %	603
$n\gamma$, helicity=3/2	0.01–0.05 %	603

N(1710) $1/2^+$

$$I(J^P) = \frac{1}{2}(\frac{1}{2}^+)$$

Re(pole position) = 1650 to 1750 (\approx 1700) MeV
 $-2\text{Im}(\text{pole position}) = 80$ to 160 (\approx 120) MeV
 Breit-Wigner mass = 1680 to 1740 (\approx 1710) MeV
 Breit-Wigner full width = 80 to 200 (\approx 140) MeV

N(1710) DECAY MODES	Fraction (Γ_i/Γ)	ρ (MeV/c)
$N\pi$	5–20 %	588
$N\eta$	10–50 %	412
$N\omega$	1–5 %	†
ΛK	5–25 %	269
ΣK	seen	138
$N\pi\pi$	14–48 %	557
$\Delta(1232)\pi$, <i>P</i> -wave	3–9 %	394
$N\rho$, $S=1/2$, <i>P</i> -wave	11–23 %	†
$N\sigma$	<16 %	–
$N(1535)\pi$	9–21 %	113
$p\gamma$, helicity=1/2	0.002–0.08 %	598
$n\gamma$, helicity=1/2	0.0–0.02%	597

N(1720) $3/2^+$

$$I(J^P) = \frac{1}{2}(\frac{3}{2}^+)$$

Re(pole position) = 1660 to 1710 (\approx 1680) MeV
 $-2\text{Im}(\text{pole position}) = 150$ to 300 (\approx 200) MeV
 Breit-Wigner mass = 1680 to 1750 (\approx 1720) MeV
 Breit-Wigner full width = 150 to 400 (\approx 250) MeV

N(1720) DECAY MODES	Fraction (Γ_i/Γ)	ρ (MeV/c)
$N\pi$	8–14 %	594
$N\eta$	1–5 %	422
$N\omega$	12–40 %	†
ΛK	4–19 %	283
$N\pi\pi$	>50 %	564
$\Delta(1232)\pi$	47–89 %	402
$\Delta(1232)\pi$, <i>P</i> -wave	47–77 %	402
$\Delta(1232)\pi$, <i>F</i> -wave	<12 %	402
$N\rho$, $S=1/2$, <i>P</i> -wave	1–2 %	74
$N\sigma$	2–14 %	–
$N(1440)\pi$	<2 %	225
$N(1520)\pi$, <i>S</i> -wave	1–5 %	145
$p\gamma$	0.05–0.25 %	604
$p\gamma$, helicity=1/2	0.05–0.15 %	604
$p\gamma$, helicity=3/2	0.002–0.16 %	604
$n\gamma$	0.0–0.016 %	603
$n\gamma$, helicity=1/2	0.0–0.01 %	603
$n\gamma$, helicity=3/2	0.0–0.015 %	603

N(1875) $3/2^-$

$$I(J^P) = \frac{1}{2}(\frac{3}{2}^-)$$

was $N(2080)$

Re(pole position) = 1850 to 1950 (\approx 1900) MeV
 $-2\text{Im}(\text{pole position}) = 100$ to 220 (\approx 160) MeV
 Breit-Wigner mass = 1850 to 1920 (\approx 1875) MeV
 Breit-Wigner full width = 120 to 250 (\approx 200) MeV

N(1875) DECAY MODES	Fraction (Γ_i/Γ)	ρ (MeV/c)
$N\pi$	3–11 %	695
$N\eta$	3–16 %	559
$N\omega$	15–25 %	371
ΛK	1–2 %	454
ΣK	0.3–1.1 %	384
$N\pi\pi$	>56 %	670
$\Delta(1232)\pi$	4–44 %	520
$\Delta(1232)\pi$, <i>S</i> -wave	2–21 %	520
$\Delta(1232)\pi$, <i>D</i> -wave	2–23 %	520
$N\rho$, $S=3/2$, <i>S</i> -wave	36–56 %	379
$N\sigma$	16–60 %	–
$N(1440)\pi$	2–8 %	365
$N(1520)\pi$	<2 %	301
$\Lambda K^*(892)$	<0.2 %	†
$p\gamma$	0.001–0.025 %	703
$p\gamma$, helicity=1/2	0.001–0.021 %	703
$p\gamma$, helicity=3/2	<0.003 %	703
$n\gamma$	<0.040 %	702
$n\gamma$, helicity=1/2	<0.007 %	702
$n\gamma$, helicity=3/2	<0.033 %	702

N(1880) $1/2^+$

$$I(J^P) = \frac{1}{2}(\frac{1}{2}^+)$$

Re(pole position) = 1820 to 1900 (\approx 1860) MeV
 $-2\text{Im}(\text{pole position}) = 180$ to 280 (\approx 230) MeV
 Breit-Wigner mass = 1830 to 1930 (\approx 1880) MeV
 Breit-Wigner full width = 200 to 400 (\approx 300) MeV

N(1880) DECAY MODES	Fraction (Γ_i/Γ)	ρ (MeV/c)
$N\pi$	3–31 %	698
$N\eta$	1–55 %	563
$N\omega$	12–28 %	377
ΛK	1–3 %	459
ΣK	10–24 %	389
$N\pi\pi$	>32 %	673
$\Delta(1232)\pi$	5–42 %	524
$N\rho$, $S=1/2$, <i>P</i> -wave	19–45 %	385
$N\sigma$	8–40 %	539
$N(1535)\pi$	4–12 %	293
$N a_0(980)$	1–5 %	†
$\Lambda K^*(892)$	0.5–1.1 %	†
$p\gamma$, helicity=1/2	seen	706
$n\gamma$, helicity=1/2	0.002–0.63 %	705

Baryon Summary Table

N(2190) DECAY MODES	Fraction (Γ_i/Γ)	ρ (MeV/c)
$N\pi$	10–20 %	882
$N\eta$	1–5 %	785
$N\omega$	8–20 %	667
ΛK	0.2–0.8 %	705
$N\pi\pi$	22–51 %	864
$\Delta(1232)\pi$, <i>D</i> -wave	19–31 %	734
$N\rho$, $S=3/2$, <i>D</i> -wave	<11 %	672
$N\sigma$	3–9 %	–
$\Lambda K^*(892)$	0.2–0.8 %	423
$\rho\gamma$	<0.08 %	888
$\rho\gamma$, helicity=1/2	<0.06 %	888
$\rho\gamma$, helicity=3/2	<0.02 %	888
$n\gamma$	<0.04 %	888
$n\gamma$, helicity=1/2	<0.01 %	888
$n\gamma$, helicity=3/2	<0.03 %	888

N(2220) 9/2⁺

$$I(J^P) = \frac{1}{2}(\frac{9}{2}^+)$$

Re(pole position) = 2130 to 2200 (\approx 2150) MeV
 $-2\text{Im}(\text{pole position}) = 360$ to 480 (\approx 400) MeV
 Breit-Wigner mass = 2200 to 2300 (\approx 2250) MeV
 Breit-Wigner full width = 350 to 500 (\approx 400) MeV

N(2220) DECAY MODES	Fraction (Γ_i/Γ)	ρ (MeV/c)
$N\pi$	15–30 %	924

N(2250) 9/2⁻

$$I(J^P) = \frac{1}{2}(\frac{9}{2}^-)$$

Re(pole position) = 2100 to 2200 (\approx 2150) MeV
 $-2\text{Im}(\text{pole position}) = 350$ to 500 (\approx 420) MeV
 Breit-Wigner mass = 2250 to 2320 (\approx 2280) MeV
 Breit-Wigner full width = 300 to 600 (\approx 500) MeV

N(2250) DECAY MODES	Fraction (Γ_i/Γ)	ρ (MeV/c)
$N\pi$	5–15 %	941
$N\eta$	<5 %	852
ΛK	1–3 %	777

N(2600) 11/2⁻

$$I(J^P) = \frac{1}{2}(\frac{11}{2}^-)$$

Breit-Wigner mass = 2550 to 2750 (\approx 2600) MeV
 Breit-Wigner full width = 500 to 800 (\approx 650) MeV

N(2600) DECAY MODES	Fraction (Γ_i/Γ)	ρ (MeV/c)
$N\pi$	3–8 %	1126

Δ BARYONS

($S = 0, I = 3/2$)

$$\Delta^{++} = uuu, \quad \Delta^+ = uud, \quad \Delta^0 = udd, \quad \Delta^- = ddd$$

Δ(1232) 3/2⁺

$$I(J^P) = \frac{3}{2}(\frac{3}{2}^+)$$

Re(pole position) = 1209 to 1211 (\approx 1210) MeV
 $-2\text{Im}(\text{pole position}) = 98$ to 102 (\approx 100) MeV
 Breit-Wigner mass (mixed charges) = 1230 to 1234 (\approx 1232) MeV
 Breit-Wigner full width (mixed charges) = 114 to 120 (\approx 117) MeV

Δ(1232) DECAY MODES	Fraction (Γ_i/Γ)	ρ (MeV/c)
$N\pi$	99.4 %	229
$N\gamma$	0.55–0.65 %	259
$N\gamma$, helicity=1/2	0.11–0.13 %	259
$N\gamma$, helicity=3/2	0.44–0.52 %	259
$p e^+ e^-$	(4.2 ± 0.7) $\times 10^{-5}$	259

Δ(1600) 3/2⁺

$$I(J^P) = \frac{3}{2}(\frac{3}{2}^+)$$

Re(pole position) = 1470 to 1590 (\approx 1520) MeV
 $-2\text{Im}(\text{pole position}) = 150$ to 320 (\approx 280) MeV
 Breit-Wigner mass = 1500 to 1640 (\approx 1570) MeV
 Breit-Wigner full width = 200 to 300 (\approx 250) MeV

Δ(1600) DECAY MODES	Fraction (Γ_i/Γ)	ρ (MeV/c)
$N\pi$	8–24 %	492
$N\pi\pi$	58–84 %	454
$\Delta(1232)\pi$	58–82 %	276
$\Delta(1232)\pi$, <i>P</i> -wave	72–82 %	276
$\Delta(1232)\pi$, <i>F</i> -wave	<2 %	276
$N(1440)\pi$	17–27 %	†
$N\gamma$	0.001–0.035 %	505
$N\gamma$, helicity=1/2	0.0–0.02 %	505
$N\gamma$, helicity=3/2	0.001–0.015 %	505

Δ(1620) 1/2⁻

$$I(J^P) = \frac{3}{2}(\frac{1}{2}^-)$$

Re(pole position) = 1590 to 1610 (\approx 1600) MeV
 $-2\text{Im}(\text{pole position}) = 80$ to 140 (\approx 110) MeV
 Breit-Wigner mass = 1590 to 1630 (\approx 1610) MeV
 Breit-Wigner full width = 110 to 150 (\approx 130) MeV

Δ(1620) DECAY MODES	Fraction (Γ_i/Γ)	ρ (MeV/c)
$N\pi$	25–35 %	520
$N\pi\pi$	>67 %	484
$\Delta(1232)\pi$, <i>D</i> -wave	44–72 %	311
$N\rho$	23–32 %	†
$N\rho$, $S=1/2$, <i>S</i> -wave	23–32 %	†
$N\rho$, $S=3/2$, <i>D</i> -wave	<0.04 %	†
$N(1440)\pi$	<9 %	98
$N\gamma$, helicity=1/2	0.03–0.10 %	532

Δ(1700) 3/2⁻

$$I(J^P) = \frac{3}{2}(\frac{3}{2}^-)$$

Re(pole position) = 1640 to 1690 (\approx 1665) MeV
 $-2\text{Im}(\text{pole position}) = 200$ to 300 (\approx 250) MeV
 Breit-Wigner mass = 1690 to 1730 (\approx 1710) MeV
 Breit-Wigner full width = 220 to 380 (\approx 300) MeV

Δ(1700) DECAY MODES	Fraction (Γ_i/Γ)	ρ (MeV/c)
$N\pi$	10–20 %	588
$N\pi\pi$	>31 %	557
$\Delta(1232)\pi$	9–70 %	394
$\Delta(1232)\pi$, <i>S</i> -wave	5–54 %	394
$\Delta(1232)\pi$, <i>D</i> -wave	4–16 %	394
$N\rho$, $S=3/2$, <i>S</i> -wave	22–32 %	†
$N(1520)\pi$, <i>P</i> -wave	1–5 %	133
$N(1535)\pi$	0.5–1.5 %	113
$\Delta(1232)\eta$	3–7 %	†
$N\gamma$	0.22–0.60 %	598
$N\gamma$, helicity=1/2	0.12–0.30 %	598
$N\gamma$, helicity=3/2	0.10–0.30 %	598

Δ(1900) 1/2⁻

$$I(J^P) = \frac{3}{2}(\frac{1}{2}^-)$$

Re(pole position) = 1830 to 1900 (\approx 1865) MeV
 $-2\text{Im}(\text{pole position}) = 180$ to 300 (\approx 240) MeV
 Breit-Wigner mass = 1840 to 1920 (\approx 1860) MeV
 Breit-Wigner full width = 180 to 320 (\approx 250) MeV

Δ(1900) DECAY MODES	Fraction (Γ_i/Γ)	ρ (MeV/c)
$N\pi$	4–12 %	685
ΣK	seen	367
$N\pi\pi$	> 52 %	660
$\Delta(1232)\pi$, <i>D</i> -wave	30–70 %	509
$N\rho$	22–60 %	360
$N\rho$, $S=1/2$, <i>S</i> -wave	11–35 %	360
$N\rho$, $S=3/2$, <i>D</i> -wave	11–25 %	360

Baryon Summary Table

$N(1440)\pi$	3–32%	353
$N(1520)\pi$	2–10%	288
$\Delta(1232)\eta$	< 2%	251
$N\gamma$, helicity=1/2	0.06–0.43 %	693

 $\Delta(1905) 5/2^+$

$$I(J^P) = \frac{3}{2}(\frac{5}{2}^+)$$

Re(pole position) = 1750 to 1800 (≈ 1770) MeV
 $-2\text{Im}(\text{pole position}) = 260$ to 340 (≈ 300) MeV
 Breit-Wigner mass = 1855 to 1910 (≈ 1880) MeV
 Breit-Wigner full width = 270 to 400 (≈ 330) MeV

$\Delta(1905)$ DECAY MODES	Fraction (Γ_i/Γ)	ρ (MeV/c)
$N\pi$	9–15%	698
$N\pi\pi$	>65%	673
$\Delta(1232)\pi$	>48%	524
$\Delta(1232)\pi$, P -wave	8–43%	524
$\Delta(1232)\pi$, F -wave	40–58%	524
$N\rho$, $S=3/2$, P -wave	17–35%	385
$N(1535)\pi$	< 1%	293
$N(1680)\pi$, P -wave	5–15%	133
$\Delta(1232)\eta$	2–6%	282
$N\gamma$	0.012–0.036 %	706
$N\gamma$, helicity=1/2	0.002–0.006 %	706
$N\gamma$, helicity=3/2	0.01–0.03 %	706

 $\Delta(1910) 1/2^+$

$$I(J^P) = \frac{3}{2}(\frac{1}{2}^+)$$

Re(pole position) = 1800 to 1900 (≈ 1850) MeV
 $-2\text{Im}(\text{pole position}) = 200$ to 500 (≈ 350) MeV
 Breit-Wigner mass = 1850 to 1950 (≈ 1900) MeV
 Breit-Wigner full width = 200 to 400 (≈ 300) MeV

$\Delta(1910)$ DECAY MODES	Fraction (Γ_i/Γ)	ρ (MeV/c)
$N\pi$	10–30%	710
ΣK	4–14%	410
$\Delta(1232)\pi$	34–66%	539
$N(1440)\pi$	3–45%	386
$\Delta(1232)\eta$	5–13%	310
$N\gamma$, helicity=1/2	0.0–0.02 %	718

 $\Delta(1920) 3/2^+$

$$I(J^P) = \frac{3}{2}(\frac{3}{2}^+)$$

Re(pole position) = 1850 to 1950 (≈ 1900) MeV
 $-2\text{Im}(\text{pole position}) = 200$ to 400 (≈ 300) MeV
 Breit-Wigner mass = 1870 to 1970 (≈ 1920) MeV
 Breit-Wigner full width = 240 to 360 (≈ 300) MeV

$\Delta(1920)$ DECAY MODES	Fraction (Γ_i/Γ)	ρ (MeV/c)
$N\pi$	5–20 %	723
ΣK	2–6 %	431
$N\pi\pi$	>46 %	699
$\Delta(1232)\pi$	>46 %	553
$\Delta(1232)\pi$, P -wave	2–28 %	553
$\Delta(1232)\pi$, F -wave	44–72 %	553
$N(1440)\pi$, P -wave	4–86 %	403
$N(1520)\pi$, S -wave	<5 %	341
$N(1535)\pi$	<2 %	328
$N\omega(980)$	seen	41
$\Delta(1232)\eta$	5–17 %	336
$N\gamma$	0.01–0.84 %	731
$N\gamma$, helicity=1/2	0.0–0.42 %	731
$N\gamma$, helicity=3/2	0.01–0.42 %	731

 $\Delta(1930) 5/2^-$

$$I(J^P) = \frac{3}{2}(\frac{5}{2}^-)$$

Re(pole position) = 1820 to 1880 (≈ 1850) MeV
 $-2\text{Im}(\text{pole position}) = 300$ to 450 (≈ 320) MeV
 Breit-Wigner mass = 1900 to 2000 (≈ 1950) MeV
 Breit-Wigner full width = 200 to 400 (≈ 300) MeV

$\Delta(1930)$ DECAY MODES	Fraction (Γ_i/Γ)	ρ (MeV/c)
$N\pi$	5–15 %	742
$N\gamma$	0.0–0.01 %	749
$N\gamma$, helicity=1/2	0.0–0.005 %	749
$N\gamma$, helicity=3/2	0.0–0.004 %	749

 $\Delta(1950) 7/2^+$

$$I(J^P) = \frac{3}{2}(\frac{7}{2}^+)$$

Re(pole position) = 1870 to 1890 (≈ 1880) MeV
 $-2\text{Im}(\text{pole position}) = 220$ to 260 (≈ 240) MeV
 Breit-Wigner mass = 1915 to 1950 (≈ 1930) MeV
 Breit-Wigner full width = 235 to 335 (≈ 285) MeV

$\Delta(1950)$ DECAY MODES	Fraction (Γ_i/Γ)	ρ (MeV/c)
$N\pi$	35–45 %	729
ΣK	0.3–0.5 %	441
$N\pi\pi$	37–77 %	706
$\Delta(1232)\pi$, F -wave	1–9 %	560
$N(1680)\pi$, P -wave	3–9 %	191
$\Delta(1232)\eta$	< 0.6 %	349
$N\gamma$	0.06–0.14 %	737
$N\gamma$, helicity=1/2	0.03–0.05 %	737
$N\gamma$, helicity=3/2	0.04–0.09 %	737

 $\Delta(2200) 7/2^-$

$$I(J^P) = \frac{3}{2}(\frac{7}{2}^-)$$

Re(pole position) = 2050 to 2150 (≈ 2100) MeV
 $-2\text{Im}(\text{pole position}) = 260$ to 420 (≈ 340) MeV
 Breit-Wigner mass = 2150 to 2250 (≈ 2200) MeV
 Breit-Wigner full width = 200 to 500 (≈ 350) MeV

$\Delta(2200)$ DECAY MODES	Fraction (Γ_i/Γ)	ρ (MeV/c)
$N\pi$	2–8 %	894
ΣK	1–7 %	672
$N\pi\pi$	>45 %	876
$\Delta\pi$	>45 %	747
$\Delta\pi$, D -wave	>40 %	747
$\Delta\pi$, G -wave	5–25 %	747
$\Delta\eta$, D -wave	seen	614

 $\Delta(2420) 11/2^+$

$$I(J^P) = \frac{3}{2}(\frac{11}{2}^+)$$

Re(pole position) = 2300 to 2500 (≈ 2400) MeV
 $-2\text{Im}(\text{pole position}) = 350$ to 550 (≈ 450) MeV
 Breit-Wigner mass = 2300 to 2600 (≈ 2450) MeV
 Breit-Wigner full width = 300 to 700 (≈ 500) MeV

$\Delta(2420)$ DECAY MODES	Fraction (Γ_i/Γ)	ρ (MeV/c)
$N\pi$	5–10 %	1040

Λ BARYONS

$(S = -1, I = 0)$

$$\Lambda^0 = uds$$

 Λ

$$I(J^P) = 0(\frac{1}{2}^+)$$

Mass $m = 1115.683 \pm 0.006$ MeV
 $(m_\Lambda - m_{\bar{\Lambda}}) / m_\Lambda = (-0.1 \pm 1.1) \times 10^{-5}$ ($S = 1.6$)
 Mean life $\tau = (2.617 \pm 0.010) \times 10^{-10}$ s ($S = 1.5$)
 $(\tau_\Lambda - \tau_{\bar{\Lambda}}) / \tau_\Lambda = (0.9 \pm 3.2) \times 10^{-3}$
 $c\tau = 7.845$ cm

Magnetic moment $\mu = -0.613 \pm 0.004 \mu_N$
 Electric dipole moment $d < 1.5 \times 10^{-16}$ e cm, CL = 95%

Decay parameters

$$p\pi^- \quad \alpha_- = 0.747 \pm 0.009 \quad (S = 2.5)$$

$$\bar{p}\pi^+ \quad \alpha_+ = -0.757 \pm 0.004$$

$$\bar{\alpha}_0 \text{ FOR } \bar{\Lambda} \rightarrow \bar{n}\pi^0 = -0.692 \pm 0.017$$

Baryon Summary Table

$$\alpha_\gamma \text{ FOR } \Lambda \rightarrow n\gamma = -0.16 \pm 0.11$$

$$p\pi^- \quad \phi_- = (-6.5 \pm 3.5)^\circ$$

$$" \quad \gamma_- = 0.76 [l]$$

$$" \quad \Delta_- = (8 \pm 4)^\circ [l]$$

$$\bar{\alpha}_0 / \alpha_+ \text{ in } \bar{\Lambda} \rightarrow \bar{n}\pi^0, \bar{\Lambda} \rightarrow \bar{p}\pi^+ = 0.913 \pm 0.030$$

$$R = |G_E/G_M| \text{ in } \Lambda \rightarrow p\pi^-, \bar{\Lambda} \rightarrow \bar{p}\pi^+ = 0.96 \pm 0.14$$

$$\Delta\Phi = \Phi_E - \Phi_M \text{ in } \Lambda \rightarrow p\pi^-, \bar{\Lambda} \rightarrow \bar{p}\pi^+ = 37 \pm 13 \text{ degrees}$$

$$n\pi^0 \quad \alpha_0 = 0.75 \pm 0.05$$

$$p e^- \bar{\nu}_e \quad g_A/g_V = -0.718 \pm 0.015 [h]$$

Λ DECAY MODES	Fraction (Γ_i/Γ)	Confidence level	ρ (MeV/c)
$p\pi^-$	(64.1 \pm 0.5) %		101
$n\pi^0$	(35.9 \pm 0.5) %		104
$n\gamma$	(8.3 \pm 0.7) $\times 10^{-4}$		162
$p\pi^-\gamma$	[n] (8.5 \pm 1.4) $\times 10^{-4}$		101
$p e^- \bar{\nu}_e$	(8.34 \pm 0.14) $\times 10^{-4}$		163
$p\mu^- \bar{\nu}_\mu$	(1.51 \pm 0.19) $\times 10^{-4}$		131

Lepton (L) and/or Baryon (B) number violating decay modes

$\pi^+ e^-$	L,B	< 6	$\times 10^{-7}$	90%	549
$\pi^+ \mu^-$	L,B	< 6	$\times 10^{-7}$	90%	544
$\pi^- e^+$	L,B	< 4	$\times 10^{-7}$	90%	549
$\pi^- \mu^+$	L,B	< 6	$\times 10^{-7}$	90%	544
$K^+ e^-$	L,B	< 2	$\times 10^{-6}$	90%	449
$K^+ \mu^-$	L,B	< 3	$\times 10^{-6}$	90%	441
$K^- e^+$	L,B	< 2	$\times 10^{-6}$	90%	449
$K^- \mu^+$	L,B	< 3	$\times 10^{-6}$	90%	441
$K_S^0 \nu$	L,B	< 2	$\times 10^{-5}$	90%	447
$\bar{p}\pi^+$	B	< 9	$\times 10^{-7}$	90%	101
invisible		< 7.4	$\times 10^{-5}$	90%	-

 $\Lambda(1405) 1/2^-$

$I(J^P) = 0(\frac{1}{2}^-)$

Mass $m = 1405.1^{+1.3}_{-1.0}$ MeV
 Full width $\Gamma = 50.5 \pm 2.0$ MeV
 Below $\bar{K}N$ threshold

$\Lambda(1405)$ DECAY MODES	Fraction (Γ_i/Γ)	ρ (MeV/c)
$\Sigma\pi$	100 %	155

 $\Lambda(1520) 3/2^-$

$I(J^P) = 0(\frac{3}{2}^-)$

Mass $m = 1518$ to 1520 (≈ 1519) MeV [o]
 Full width $\Gamma = 15$ to 17 (≈ 16) MeV [o]

$\Lambda(1520)$ DECAY MODES	Fraction (Γ_i/Γ)	ρ (MeV/c)
$N\bar{K}$	(45 \pm 1) %	242
$\Sigma\pi$	(42 \pm 1) %	268
$\Lambda\pi\pi$	(10 \pm 1) %	259
$\Sigma\pi\pi$	(0.9 \pm 0.1) %	168
$\Lambda\gamma$	(0.85 \pm 0.15) %	350

 $\Lambda(1600) 1/2^+$

$I(J^P) = 0(\frac{1}{2}^+)$

Mass $m = 1570$ to 1630 (≈ 1600) MeV
 Full width $\Gamma = 150$ to 250 (≈ 200) MeV

$\Lambda(1600)$ DECAY MODES	Fraction (Γ_i/Γ)	ρ (MeV/c)
$N\bar{K}$	15-302 %	343
$\Sigma\pi$	10-60 %	338
$\Lambda\sigma$	(19 \pm 4) %	-
$\Sigma(1385)\pi$	(9 \pm 4) %	158

 $\Lambda(1670) 1/2^-$

$I(J^P) = 0(\frac{1}{2}^-)$

Mass $m = 1670$ to 1678 (≈ 1674) MeV
 Full width $\Gamma = 25$ to 35 (≈ 30) MeV

$\Lambda(1670)$ DECAY MODES	Fraction (Γ_i/Γ)	ρ (MeV/c)
$N\bar{K}$	20-30 %	418
$\Sigma\pi$	25-55 %	398

$\Lambda\eta$	10-25 %	88
$\Sigma(1385)\pi$, D-wave	(6.0 \pm 2.0) %	235
$N\bar{K}^*(892)$, S=3/2, D-wave	(5 \pm 4) %	†
$\Lambda\sigma$	(20 \pm 8) %	-

 $\Lambda(1690) 3/2^-$

$I(J^P) = 0(\frac{3}{2}^-)$

Mass $m = 1685$ to 1695 (≈ 1690) MeV
 Full width $\Gamma = 60$ to 80 (≈ 70) MeV

$\Lambda(1690)$ DECAY MODES	Fraction (Γ_i/Γ)	ρ (MeV/c)
$N\bar{K}$	20-30 %	433
$\Sigma\pi$	20-40 %	410
$\Lambda\sigma$	(5.0 \pm 2.0) %	-
$\Lambda\pi\pi$	~ 25 %	419
$\Sigma\pi\pi$	~ 20 %	358
$\Sigma(1385)\pi$, S-wave	(9 \pm 5) %	251
$\Sigma(1385)\pi$, D-wave	(3.0 \pm 2.0) %	251

 $\Lambda(1800) 1/2^-$

$I(J^P) = 0(\frac{1}{2}^-)$

Mass $m = 1750$ to 1850 (≈ 1800) MeV
 Full width $\Gamma = 150$ to 250 (≈ 200) MeV

$\Lambda(1800)$ DECAY MODES	Fraction (Γ_i/Γ)	ρ (MeV/c)
$N\bar{K}$	25-40 %	528
$\Sigma\pi$	seen	494
$\Lambda\sigma$	(15 \pm 4) %	-
$\Sigma(1385)\pi$	seen	349
$\Lambda\eta$	0.01 to 0.10	326
$N\bar{K}^*(892)$	seen	†

 $\Lambda(1810) 1/2^+$

$I(J^P) = 0(\frac{1}{2}^+)$

Mass $m = 1740$ to 1840 (≈ 1790) MeV
 Full width $\Gamma = 50$ to 170 (≈ 110) MeV

$\Lambda(1810)$ DECAY MODES	Fraction (Γ_i/Γ)	ρ (MeV/c)
$N\bar{K}$	0.05 to 0.35	520
$\Sigma\pi$	(16 \pm 5) %	487
$\Sigma(1385)\pi$	(40 \pm 15) %	340
$N\bar{K}^*(892)$	30-60 %	†

 $\Lambda(1820) 5/2^+$

$I(J^P) = 0(\frac{5}{2}^+)$

Mass $m = 1815$ to 1825 (≈ 1820) MeV
 Full width $\Gamma = 70$ to 90 (≈ 80) MeV

$\Lambda(1820)$ DECAY MODES	Fraction (Γ_i/Γ)	ρ (MeV/c)
$N\bar{K}$	55-65 %	545
$\Sigma\pi$	8-14 %	509
$\Sigma(1385)\pi$	5-10 %	366
$N\bar{K}^*(892)$, S=3/2, P-wave	(3.0 \pm 1.0) %	†

 $\Lambda(1830) 5/2^-$

$I(J^P) = 0(\frac{5}{2}^-)$

Mass $m = 1820$ to 1830 (≈ 1825) MeV
 Full width $\Gamma = 60$ to 120 (≈ 90) MeV

$\Lambda(1830)$ DECAY MODES	Fraction (Γ_i/Γ)	Scale factor	ρ (MeV/c)
$N\bar{K}$	0.04 to 0.08		549
$\Sigma\pi$	35-75 %		512
$\Sigma(1385)\pi$	>15 %		370
$\Sigma(1385)\pi$, D-wave	(40 \pm 15) %	3.2	370

 $\Lambda(1890) 3/2^+$

$I(J^P) = 0(\frac{3}{2}^+)$

Mass $m = 1870$ to 1910 (≈ 1890) MeV
 Full width $\Gamma = 80$ to 160 (≈ 120) MeV

Baryon Summary Table

$\Lambda(1890)$ DECAY MODES	Fraction (Γ_i/Γ)	ρ (MeV/c)
$N\bar{K}$	0.24 to 0.36	599
$\Sigma\pi$	3-10 %	560
$\Sigma(1385)\pi$	seen	423
$\Sigma(1385)\pi$, <i>P</i> -wave	(6.0 \pm 3.0) %	423
$\Sigma(1385)\pi$, <i>F</i> -wave	(4.0 \pm 2.0) %	423
$N\bar{K}^*(892)$	seen	236

 $\Lambda(2100) 7/2^-$

$$I(J^P) = 0(\frac{7}{2}^-)$$

Mass $m = 2090$ to 2110 (≈ 2100) MeV
Full width $\Gamma = 100$ to 250 (≈ 200) MeV

$\Lambda(2100)$ DECAY MODES	Fraction (Γ_i/Γ)	ρ (MeV/c)
$N\bar{K}$	25-35 %	751
$\Sigma\pi$	~ 5 %	705
$\Lambda\eta$	< 3 %	617
ΞK	< 3 %	491
$\Lambda\omega$	< 8 %	443
$\Sigma(1385)\pi$, <i>G</i> -wave	(1.0 \pm 1.0) %	584
$N\bar{K}^*(892)$	10-20 %	515
$N\bar{K}^*(892)$, $S=3/2$, <i>D</i> -wave	(4.0 \pm 2.0) %	515

 $\Lambda(2110) 5/2^+$

$$I(J^P) = 0(\frac{5}{2}^+)$$

Mass $m = 2050$ to 2130 (≈ 2090) MeV
Full width $\Gamma = 200$ to 300 (≈ 250) MeV

$\Lambda(2110)$ DECAY MODES	Fraction (Γ_i/Γ)	ρ (MeV/c)
$N\bar{K}$	5-25 %	744
$\Sigma\pi$	10-40 %	698
$\Lambda\omega$	seen	432
$\Lambda\omega$, $S=3/2$, <i>P</i> -wave	(5.0 \pm 2.0) %	432
$\Sigma(1385)\pi$	seen	576
$N\bar{K}^*(892)$	10-60 %	505

 $\Lambda(2350) 9/2^+$

$$I(J^P) = 0(\frac{9}{2}^+)$$

Mass $m = 2340$ to 2370 (≈ 2350) MeV
Full width $\Gamma = 100$ to 250 (≈ 150) MeV

$\Lambda(2350)$ DECAY MODES	Fraction (Γ_i/Γ)	ρ (MeV/c)
$N\bar{K}$	~ 12 %	915
$\Sigma\pi$	~ 10 %	867

 Σ BARYONS
($S = -1$, $I = 1$)

$$\Sigma^+ = uus, \quad \Sigma^0 = uds, \quad \Sigma^- = dds$$

 Σ^+

$$I(J^P) = 1(\frac{1}{2}^+)$$

Mass $m = 1189.37 \pm 0.07$ MeV ($S = 2.2$)
Mean life $\tau = (0.8018 \pm 0.0026) \times 10^{-10}$ s
 $c\tau = 2.404$ cm

$(\tau_{\Sigma^+} - \tau_{\Sigma^-}) / \tau_{\Sigma^+} = -0.0006 \pm 0.0012$
Magnetic moment $\mu = 2.458 \pm 0.010 \mu_N$ ($S = 2.1$)
 $(\mu_{\Sigma^+} + \mu_{\Sigma^-}) / \mu_{\Sigma^+} = 0.014 \pm 0.015$
 $\Gamma(\Sigma^+ \rightarrow n\ell^+\nu) / \Gamma(\Sigma^- \rightarrow n\ell^-\bar{\nu}_\ell) < 0.043$

Decay parameters

$p\pi^0$ $\alpha_0 = -0.982 \pm 0.014$
 $\bar{p}\pi^0$ $\bar{\alpha}_0 = 0.99 \pm 0.04$
 $(\alpha_0 + \bar{\alpha}_0) / (\alpha_0 - \bar{\alpha}_0) = 0.00 \pm 0.04$
 $p\pi^0$ $\phi_0 = (36 \pm 34)^\circ$
" $\gamma_0 = 0.16$ [I]

" $\Delta_0 = (187 \pm 6)^\circ$ [I]
 $n\pi^+$ $\alpha_+ = (4.89 \pm 0.26) \times 10^{-2}$
" $\phi_+ = (167 \pm 20)^\circ$ ($S = 1.1$)
 $\bar{\alpha}_-$ FOR $\bar{\Sigma}^- \rightarrow \bar{n}\pi^- = (-5.7 \pm 0.5) \times 10^{-2}$
 $\bar{\alpha}_- / \bar{\alpha}_0 = (-5.7 \pm 0.6) \times 10^{-2}$
 $(\alpha_+ + \bar{\alpha}_-) / (\alpha_+ - \bar{\alpha}_-) = (-8 \pm 6) \times 10^{-2}$
" $\gamma_+ = -0.97$ [I]
" $\Delta_+ = (-73^{+133}_{-10})^\circ$ [I]
 $p\gamma$ $\alpha_\gamma = -0.69 \pm 0.05$

 Σ^+ DECAY MODES

DECAY MODES	Fraction (Γ_i/Γ)	Confidence level	ρ (MeV/c)
$p\pi^0$	(51.57 \pm 0.30) %		189
$n\pi^+$	(48.31 \pm 0.30) %		185
$p\gamma$	(1.23 \pm 0.05) $\times 10^{-3}$		225
$n\pi^+\gamma$	[n] (4.5 \pm 0.5) $\times 10^{-4}$		185
$\Lambda e^+\nu_e$	(2.3 \pm 0.4) $\times 10^{-5}$		71

 $\Delta S = \Delta Q$ (*SQ*) violating modes or
 $\Delta S = 1$ weak neutral current (*S1*) modes

$ne^+\nu_e$	<i>SQ</i> < 5	$\times 10^{-6}$	90%	224
$n\mu^+\nu_\mu$	<i>SQ</i> < 3.0	$\times 10^{-5}$	90%	202
pe^+e^-	<i>S1</i> < 7	$\times 10^{-6}$		225
$p\mu^+\mu^-$	<i>S1</i> (2.4 \pm 1.7)	$\times 10^{-8}$		121

 Σ^0

$$I(J^P) = 1(\frac{1}{2}^+)$$

Mass $m = 1192.642 \pm 0.024$ MeV
 $m_{\Sigma^-} - m_{\Sigma^0} = 4.807 \pm 0.035$ MeV ($S = 1.1$)
 $m_{\Sigma^0} - m_\Lambda = 76.959 \pm 0.023$ MeV
Mean life $\tau = (7.4 \pm 0.7) \times 10^{-20}$ s
 $c\tau = 2.22 \times 10^{-11}$ m
Transition magnetic moment $|\mu_{\Sigma\Lambda}| = 1.61 \pm 0.08 \mu_N$

 Σ^0 DECAY MODES

DECAY MODES	Fraction (Γ_i/Γ)	Confidence level	ρ (MeV/c)
$\Lambda\gamma$	100 %		74
$\Lambda\gamma\gamma$	< 3 %	90%	74
Λe^+e^-	[p] 5×10^{-3}		74

 Σ^-

$$I(J^P) = 1(\frac{1}{2}^+)$$

Mass $m = 1197.449 \pm 0.029$ MeV ($S = 1.1$)
 $m_{\Sigma^-} - m_{\Sigma^+} = 8.08 \pm 0.08$ MeV ($S = 1.9$)
 $m_{\Sigma^-} - m_\Lambda = 81.766 \pm 0.029$ MeV ($S = 1.1$)
Mean life $\tau = (1.479 \pm 0.011) \times 10^{-10}$ s ($S = 1.3$)
 $c\tau = 4.434$ cm
Magnetic moment $\mu = -1.160 \pm 0.025 \mu_N$ ($S = 1.7$)
 Σ^- charge radius = 0.78 ± 0.10 fm

Decay parameters

$n\pi^-$ $\alpha_- = -0.068 \pm 0.008$
" $\phi_- = (10 \pm 15)^\circ$
" $\gamma_- = 0.98$ [I]
" $\Delta_- = (249^{+12}_{-120})^\circ$ [I]
 $ne^-\bar{\nu}_e$ $g_A/g_V = 0.340 \pm 0.017$ [h]
" $f_2(0)/f_1(0) = 0.97 \pm 0.14$
" $D = 0.11 \pm 0.10$
 $\Lambda e^-\bar{\nu}_e$ $g_V/g_A = 0.01 \pm 0.10$ [h] ($S = 1.5$)
" $g_{WM}/g_A = 2.4 \pm 1.7$ [h]

 Σ^- DECAY MODES

DECAY MODES	Fraction (Γ_i/Γ)	Confidence level	ρ (MeV/c)
$n\pi^-$	(99.848 \pm 0.005) %		193
$n\pi^-\gamma$	[n] (4.6 \pm 0.6) $\times 10^{-4}$		193
$ne^-\bar{\nu}_e$	(1.017 \pm 0.034) $\times 10^{-3}$		230
$n\mu^-\bar{\nu}_\mu$	(4.5 \pm 0.4) $\times 10^{-4}$		210
$\Lambda e^-\bar{\nu}_e$	(5.73 \pm 0.27) $\times 10^{-5}$		79
$\Sigma^+\chi$	< 1.2	$\times 10^{-4}$	90%

Lepton number (*L*) violating modes

pe^+e^-	<i>L</i> < 6.7	$\times 10^{-5}$	90%	231
-----------	------------------	------------------	-----	-----

Baryon Summary Table

 $\Sigma(1385) 3/2^+$

$$I(J^P) = 1(\frac{3}{2}^+)$$

$\Sigma(1385)^+$ mass $m = 1382.83 \pm 0.34$ MeV ($S = 1.9$)
 $\Sigma(1385)^0$ mass $m = 1383.7 \pm 1.0$ MeV ($S = 1.4$)
 $\Sigma(1385)^-$ mass $m = 1387.2 \pm 0.5$ MeV ($S = 2.2$)
 $\Sigma(1385)^+$ full width $\Gamma = 36.2 \pm 0.7$ MeV
 $\Sigma(1385)^0$ full width $\Gamma = 36 \pm 5$ MeV
 $\Sigma(1385)^-$ full width $\Gamma = 39.4 \pm 2.1$ MeV ($S = 1.7$)
 Below $\bar{K}N$ threshold

$\Sigma(1385)$ DECAY MODES	Fraction (Γ_i/Γ)	Confidence level	ρ (MeV/c)
$\Lambda\pi$	(87.0 \pm 1.5) %		208
$\Sigma\pi$	(11.7 \pm 1.5) %		129
$\Lambda\gamma$	(1.25 $^{+0.13}_{-0.12}$) %		241
$\Sigma^+\gamma$	(7.0 \pm 1.7) $\times 10^{-3}$		180
$\Sigma^-\gamma$	< 2.4 $\times 10^{-4}$	90%	173

 $\Sigma(1660) 1/2^+$

$$I(J^P) = 1(\frac{1}{2}^+)$$

Re(pole position) = 1585 \pm 20 MeV
 $-2\text{Im}(\text{pole position}) = 290^{+140}_{-40}$ MeV
 Mass $m = 1640$ to 1680 (≈ 1660) MeV
 Full width $\Gamma = 100$ to 300 (≈ 200) MeV

$\Sigma(1660)$ DECAY MODES	Fraction (Γ_i/Γ)	ρ (MeV/c)
$N\bar{K}$	0.05 to 0.15 (≈ 010)	405
$\Lambda\pi$	(35 \pm 12) %	440
$\Sigma\pi$	(37 \pm 10) %	387
$\Sigma\sigma$	(20 \pm 8) %	-
$\Lambda(1405)\pi$	(4.0 \pm 2.0) %	199

 $\Sigma(1670) 3/2^-$

$$I(J^P) = 1(\frac{3}{2}^-)$$

Mass $m = 1665$ to 1685 (≈ 1675) MeV
 Full width $\Gamma = 40$ to 100 (≈ 70) MeV

$\Sigma(1670)$ DECAY MODES	Fraction (Γ_i/Γ)	ρ (MeV/c)
$N\bar{K}$	0.06 to 0.12	419
$\Lambda\pi$	5-15 %	452
$\Sigma\pi$	30-60 %	398
$\Sigma\sigma$	(7.0 \pm 3.0) %	-

 $\Sigma(1750) 1/2^-$

$$I(J^P) = 1(\frac{1}{2}^-)$$

Mass $m = 1700$ to 1800 (≈ 1750) MeV
 Full width $\Gamma = 100$ to 200 (≈ 150) MeV

$\Sigma(1750)$ DECAY MODES	Fraction (Γ_i/Γ)	ρ (MeV/c)
$N\bar{K}$	0.06 to 0.12	486
$\Lambda\pi$	(14 \pm 5) %	507
$\Sigma\pi$	(16 \pm 4) %	456
$\Sigma\eta$	15-55 %	98
$\Sigma(1385)\pi$, D -wave	< 1 %	305
$\Lambda(1520)\pi$	(2.0 \pm 1.0) %	175
$N\bar{K}^*(892)$, $S=1/2$	(8 \pm 4) %	†

 $\Sigma(1775) 5/2^-$

$$I(J^P) = 1(\frac{5}{2}^-)$$

Mass $m = 1770$ to 1780 (≈ 1775) MeV
 Full width $\Gamma = 105$ to 135 (≈ 120) MeV

$\Sigma(1775)$ DECAY MODES	Fraction (Γ_i/Γ)	ρ (MeV/c)
$N\bar{K}$	37-43%	508
$\Lambda\pi$	14-20%	525
$\Sigma\pi$	2-5%	475
$\Sigma(1385)\pi$	8-12%	327
$\Lambda(1520)\pi$, P -wave	17-23%	202

 $\Sigma(1910) 3/2^-$

$$I(J^P) = 1(\frac{3}{2}^-)$$

was $\Sigma(1940)$

Mass $m = 1870$ to 1950 (≈ 1910) MeV
 Full width $\Gamma = 150$ to 300 (≈ 220) MeV

$\Sigma(1910)$ DECAY MODES	Fraction (Γ_i/Γ)	ρ (MeV/c)
$N\bar{K}$	0.01 to 0.05 (≈ 0.02)	615
$\Lambda\pi$	(6 \pm 4) %	619
$\Sigma\pi$	(86 \pm 21) %	574
$\Sigma(1385)\pi$	seen	439
$\Lambda(1520)\pi$	seen	329
$\Delta(1232)\bar{K}$	(3.0 \pm 1.0) %	377
$N\bar{K}^*(892)$	seen	274
$N\bar{K}^*(892)$, $S=1/2$, D -wave	(1.0 \pm 1.0) %	274

 $\Sigma(1915) 5/2^+$

$$I(J^P) = 1(\frac{5}{2}^+)$$

Mass $m = 1900$ to 1935 (≈ 1915) MeV
 Full width $\Gamma = 80$ to 160 (≈ 120) MeV

$\Sigma(1915)$ DECAY MODES	Fraction (Γ_i/Γ)	ρ (MeV/c)
$N\bar{K}$	0.05 to 0.15	618
$\Lambda\pi$	(6.0 \pm 2.0) %	623
$\Sigma\pi$	(10.0 \pm 2.0) %	577
$\Sigma(1385)\pi$, P -wave	(2.0 \pm 2.0) %	443
$\Sigma(1385)\pi$, F -wave	(4.0 \pm 2.0) %	443
$\Lambda(1520)\pi$, D -wave	(8.0 \pm 2.0) %	334
$N\bar{K}^*(892)$, $S=1/2$, F -wave	(5.0 \pm 3.0) %	282
$N\bar{K}^*(892)$, $S=3/2$, F -wave	(5.0 \pm 2.0) %	282
$\Delta\bar{K}$, P -wave	(16 \pm 5) %	383
$\Delta\bar{K}$, F -wave	(5.0 \pm 3.0) %	383

 $\Sigma(2030) 7/2^+$

$$I(J^P) = 1(\frac{7}{2}^+)$$

Mass $m = 2025$ to 2040 (≈ 2030) MeV
 Full width $\Gamma = 150$ to 200 (≈ 180) MeV

$\Sigma(2030)$ DECAY MODES	Fraction (Γ_i/Γ)	ρ (MeV/c)
$N\bar{K}$	17-23 %	702
$\Lambda\pi$	17-23 %	700
$\Sigma\pi$	5-10 %	657
ΞK	< 2 %	422
$\Sigma(1385)\pi$	5-15 %	532
$\Sigma(1385)\pi$, F -wave	(1.0 \pm 1.0) %	532
$\Lambda(1520)\pi$	10-20 %	431
$\Delta(1232)\bar{K}$	10-20 %	498
$\Delta(1232)\bar{K}$, F -wave	(15 \pm 5) %	498
$\Delta(1232)\bar{K}$, H -wave	(1.0 \pm 1.0) %	498
$N\bar{K}^*(892)$, $S=3/2$, F -wave	(14 \pm 8) %	439

Ξ BARYONS

($S = -2$, $I = 1/2$)

$$\Xi^0 = u s s, \quad \Xi^- = d s s$$

 Ξ^0

$$I(J^P) = \frac{1}{2}(\frac{1}{2}^+)$$

P is not yet measured; + is the quark model prediction.

Mass $m = 1314.86 \pm 0.20$ MeV

$m_{\Xi^-} - m_{\Xi^0} = 6.85 \pm 0.21$ MeV

Mean life $\tau = (2.90 \pm 0.09) \times 10^{-10}$ s

$c\tau = 8.71$ cm

Magnetic moment $\mu = -1.250 \pm 0.014 \mu_N$

Decay parameters

$\Lambda\pi^0$ $\alpha = -0.349 \pm 0.009$

α FOR $\Xi^0 \rightarrow \bar{\Lambda}\pi^0 = 0.379 \pm 0.004$

" $\phi = (0.3 \pm 0.6)^\circ$

Baryon Summary Table

ϕ ANGLE FOR $\Xi^0 \rightarrow \bar{\Lambda}\pi^0$ with $\tan\phi = \beta/\gamma = -0.3 \pm 0.6$ degrees
 $\Delta\phi_{CP}(\Xi^0) = (\phi_{\Xi^0} + \phi_{\Xi^0})/2 = 0.0 \pm 0.4$ degrees
 A_{CP} FOR $\Xi^0 \rightarrow \bar{\Lambda}\pi^0, \Xi^0 \rightarrow \bar{\Lambda}\pi^0 = (-5 \pm 7) \times 10^{-3}$
 " $\gamma = 0.85$ [l]
 " $\Delta = (218^{+12}_{-19})^\circ$ [l]
 $\Lambda\gamma$ $\alpha = -0.70 \pm 0.07$
 $\Lambda e^+ e^-$ $\alpha = -0.8 \pm 0.2$
 $\Sigma^0 \gamma$ $\alpha = -0.69 \pm 0.06$
 $\Sigma^+ e^- \bar{\nu}_e$ $g_1(0)/f_1(0) = 1.22 \pm 0.05$
 $\Sigma^+ e^- \bar{\nu}_e$ $f_2(0)/f_1(0) = 2.0 \pm 0.9$

Ξ^0 DECAY MODES	Fraction (Γ_i/Γ)	Confidence level	ρ (MeV/c)
$\Lambda\pi^0$	(99.524 ± 0.012) %		135
$\Lambda\gamma$	(1.17 ± 0.07) × 10 ⁻³		184
$\Lambda e^+ e^-$	(7.6 ± 0.6) × 10 ⁻⁶		184
$\Sigma^0 \gamma$	(3.33 ± 0.10) × 10 ⁻³		117
$\Sigma^+ e^- \bar{\nu}_e$	(2.52 ± 0.08) × 10 ⁻⁴		120
$\Sigma^+ \mu^- \bar{\nu}_\mu$	(2.33 ± 0.35) × 10 ⁻⁶		64

$\Delta S = \Delta Q$ (SQ) violating modes or
 $\Delta S = 2$ forbidden (S2) modes

$\Sigma^- e^+ \nu_e$	SQ < 1.6	× 10 ⁻⁴	90%	112
$\Sigma^- \mu^+ \nu_\mu$	SQ < 9	× 10 ⁻⁴	90%	49
$p\pi^-$	S2 < 8	× 10 ⁻⁶	90%	299
$p e^- \bar{\nu}_e$	S2 < 1.3	× 10 ⁻³		323
$p \mu^- \bar{\nu}_\mu$	S2 < 1.3	× 10 ⁻³		309

$$\Xi^- \quad I(J^P) = \frac{1}{2}(\frac{1}{2}^+)$$

P is not yet measured; + is the quark model prediction.

Mass $m = 1321.71 \pm 0.07$ MeV
 $(m_{\Xi^-} - m_{\Xi^+}) / m_{\Xi^-} = (-3 \pm 9) \times 10^{-5}$
 Mean life $\tau = (1.639 \pm 0.015) \times 10^{-10}$ s
 $c\tau = 4.91$ cm
 $(\tau_{\Xi^-} - \tau_{\Xi^+}) / \tau_{\Xi^-} = -0.01 \pm 0.07$
 Magnetic moment $\mu = -0.6507 \pm 0.0025 \mu_N$
 $(\mu_{\Xi^-} + \mu_{\Xi^+}) / |\mu_{\Xi^-}| = +0.01 \pm 0.05$

Decay parameters

$\Lambda\pi^-$ $\alpha = -0.390 \pm 0.007$ (S = 2.0)
 $\alpha(\Xi^+) \text{ for } \Xi^+ \rightarrow \bar{\Lambda}\pi^+ = 0.371 \pm 0.007$
 $(\alpha + \bar{\alpha}) / (\alpha - \bar{\alpha}) \text{ for } \Xi^- \rightarrow \Lambda\pi^-, \Xi^+ \rightarrow \bar{\Lambda}\pi^+ = (6 \pm 14) \times 10^{-3}$
 $[\alpha(\Xi^-)\alpha_-(\Lambda) - \alpha(\Xi^+)\alpha_+(\bar{\Lambda})] / [\text{sum}] = (0 \pm 7) \times 10^{-4}$
 " $\phi = (-1.2 \pm 1.0)^\circ$ (S = 1.4)
 ϕ ANGLE FOR $\Xi^+ \rightarrow \bar{\Lambda}\pi^+$ ($\tan\phi = \beta/\gamma$) = $(-1.2 \pm 1.2)^\circ$
 $\Delta\phi_{CP} = (\phi_{-} + \phi_{+})/2 = (-0.3 \pm 0.8)^\circ$
 " $\gamma = 0.89$ [l]
 " $\Delta = (175.9 \pm 1.5)^\circ$ [l]
 $\Lambda e^- \bar{\nu}_e$ $g_A/g_V = -0.25 \pm 0.05$ [h]

Ξ^- DECAY MODES	Fraction (Γ_i/Γ)	Confidence level	ρ (MeV/c)
$\Lambda\pi^-$	(99.887 ± 0.035) %		140
$\Sigma^- \gamma$	(1.27 ± 0.23) × 10 ⁻⁴		118
$\Lambda e^- \bar{\nu}_e$	(5.63 ± 0.31) × 10 ⁻⁴		190
$\Lambda \mu^- \bar{\nu}_\mu$	(3.5 ^{+3.5} _{-2.2}) × 10 ⁻⁴		163
$\Sigma^0 e^- \bar{\nu}_e$	(8.7 ± 1.7) × 10 ⁻⁵		123
$\Sigma^0 \mu^- \bar{\nu}_\mu$	< 8	× 10 ⁻⁴	90%
$\Xi^0 e^- \bar{\nu}_e$	< 2.59	× 10 ⁻⁴	90%

$\Delta S = 2$ forbidden (S2) modes

$n\pi^-$	S2 < 1.9	× 10 ⁻⁵	90%	304
$n e^- \bar{\nu}_e$	S2 < 3.2	× 10 ⁻³	90%	327
$n \mu^- \bar{\nu}_\mu$	S2 < 1.5	%	90%	314
$p\pi^- \pi^-$	S2 < 4	× 10 ⁻⁴	90%	223
$p\pi^- e^- \bar{\nu}_e$	S2 < 4	× 10 ⁻⁴	90%	305
$p\pi^- \mu^- \bar{\nu}_\mu$	S2 < 4	× 10 ⁻⁴	90%	251
$p \mu^- \bar{\nu}_\mu$	L < 4	× 10 ⁻⁸	90%	272

$$\Xi(1530) 3/2^+ \quad I(J^P) = \frac{1}{2}(\frac{3}{2}^+)$$

$\Xi(1530)^0$ mass $m = 1531.80 \pm 0.32$ MeV (S = 1.3)
 $\Xi(1530)^-$ mass $m = 1535.0 \pm 0.6$ MeV
 $\Xi(1530)^0$ full width $\Gamma = 9.1 \pm 0.5$ MeV
 $\Xi(1530)^-$ full width $\Gamma = 9.9^{+1.7}_{-1.9}$ MeV

$\Xi(1530)$ DECAY MODES	Fraction (Γ_i/Γ)	Confidence level	ρ (MeV/c)
$\Xi\pi$	100 %		158
$\Xi\gamma$	< 3.7 %	90%	202

$$\Xi(1690) \quad I(J^P) = \frac{1}{2}(\frac{1}{2}^{?})$$

Mass $m = 1690 \pm 10$ MeV [o]
 Full width $\Gamma = 20 \pm 15$ MeV

$\Xi(1690)$ DECAY MODES	Fraction (Γ_i/Γ)	ρ (MeV/c)
$\Lambda\bar{K}$	seen	240
$\Sigma\bar{K}$	seen	70
$\Xi\pi$	seen	311
$\Xi^- \pi^+ \pi^-$	possibly seen	213

$$\Xi(1820) 3/2^- \quad I(J^P) = \frac{1}{2}(\frac{3}{2}^-)$$

Mass $m = 1823 \pm 5$ MeV [o]
 Full width $\Gamma = 24^{+15}_{-10}$ MeV [o]

$\Xi(1820)$ DECAY MODES	Fraction (Γ_i/Γ)	ρ (MeV/c)
$\Lambda\bar{K}$	large	402
$\Sigma\bar{K}$	small	324
$\Xi\pi$	small	421
$\Xi(1530)\pi$	small	237

$$\Xi(1950) \quad I(J^P) = \frac{1}{2}(\frac{1}{2}^{?})$$

Mass $m = 1950 \pm 15$ MeV [o]
 Full width $\Gamma = 60 \pm 20$ MeV [o]

$\Xi(1950)$ DECAY MODES	Fraction (Γ_i/Γ)	ρ (MeV/c)
$\Lambda\bar{K}$	seen	522
$\Sigma\bar{K}$	possibly seen	460
$\Xi\pi$	seen	519

$$\Xi(2030) \quad I(J^P) = \frac{1}{2}(\geq \frac{5}{2}^?)$$

Mass $m = 2025 \pm 5$ MeV [o]
 Full width $\Gamma = 20^{+15}_{-5}$ MeV [o]

$\Xi(2030)$ DECAY MODES	Fraction (Γ_i/Γ)	ρ (MeV/c)
$\Lambda\bar{K}$	~ 20 %	585
$\Sigma\bar{K}$	~ 80 %	529
$\Xi\pi$	small	574
$\Xi(1530)\pi$	small	416
$\Lambda\bar{K}\pi$	small	499
$\Sigma\bar{K}\pi$	small	428

Ω BARYONS (S = -3, I = 0)

$$\Omega^- = sss$$

$$\Omega^- \quad I(J^P) = 0(\frac{3}{2}^+)$$

$J^P = \frac{3}{2}^+$ is the quark-model prediction; and $J = 3/2$ is fairly well established.

Mass $m = 1672.45 \pm 0.29$ MeV
 $(m_{\Omega^-} - m_{\bar{\Omega}^+}) / m_{\Omega^-} = (-1 \pm 8) \times 10^{-5}$
 Mean life $\tau = (0.821 \pm 0.011) \times 10^{-10}$ s
 $c\tau = 2.461$ cm
 $(\tau_{\Omega^-} - \tau_{\bar{\Omega}^+}) / \tau_{\Omega^-} = 0.00 \pm 0.05$
 Magnetic moment $\mu = -2.02 \pm 0.05 \mu_N$

Baryon Summary Table

Decay parameters

$\alpha(\Omega^-)$	$\alpha_-(\Lambda)$	FOR $\Omega^- \rightarrow \Lambda K^- = 0.0115 \pm 0.0015$
ΛK^-	$\alpha = 0.0154 \pm 0.0020$	
$\Lambda K^-, \bar{\Lambda} K^+$	$(\alpha + \bar{\alpha})/(\alpha - \bar{\alpha}) = -0.02 \pm 0.13$	
$\Xi^0 \pi^-$	$\alpha = 0.09 \pm 0.14$	
$\Xi^- \pi^0$	$\alpha = 0.05 \pm 0.21$	

Ω^- DECAY MODES	Fraction (Γ_i/Γ)	Scale factor/ Confidence level	p (MeV/c)
ΛK^-	$(67.7 \pm 0.7) \%$		211
$\Xi^0 \pi^-$	$(24.3 \pm 0.7) \%$	S=1.5	294
$\Xi^- \pi^0$	$(8.55 \pm 0.33) \%$		289
$\Xi^- \pi^+ \pi^-$	$(3.7^{+0.7}_{-0.6}) \times 10^{-4}$		189
$\Xi(1530)^0 \pi^-$	$< 7 \times 10^{-5}$	CL=90%	17
$\Xi^0 e^- \bar{\nu}_e$	$(5.6 \pm 2.8) \times 10^{-3}$		319
$\Xi^- \gamma$	$< 4.6 \times 10^{-4}$	CL=90%	314
$\Delta S = 2$ forbidden (S_2) modes			
$\Lambda \pi^-$	$S_2 < 2.9 \times 10^{-6}$	CL=90%	449

 $\Omega(2012)^-$

$$I(J^P) = 0(?^-)$$

Mass $m = 2012.4 \pm 0.9$ MeVFull width $\Gamma = 6.4^{+3.0}_{-2.6}$ MeV

Branching fractions are given relative to the one DEFINED AS 1.

$\Omega(2012)^-$ DECAY MODES	Fraction (Γ_i/Γ)	Confidence level	p (MeV/c)
$\Xi^0 K^-$	DEFINED AS 1		403
$\Xi^- \bar{K}^0$	0.83 ± 0.21		392
$\Xi^0 \pi^0 K^-$	< 0.30	90%	245
$\Xi^0 \pi^- \bar{K}^0$	< 0.21	90%	230
$\Xi^- \pi^0 \bar{K}^0$	< 0.7	90%	226
$\Xi^- \pi^+ K^-$	< 0.08	90%	224

 $\Omega(2250)^-$

$$I(J^P) = 0(?^-)$$

Mass $m = 2252 \pm 9$ MeVFull width $\Gamma = 55 \pm 18$ MeV

$\Omega(2250)^-$ DECAY MODES	Fraction (Γ_i/Γ)	p (MeV/c)
$\Xi^- \pi^+ K^-$	seen	532
$\Xi(1530)^0 K^-$	seen	437

CHARMED BARYONS
($C = +1$)

$$\Lambda_c^+ = udc, \quad \Sigma_c^{++} = uuc, \quad \Sigma_c^+ = udc, \quad \Sigma_c^0 = ddc,$$

$$\Xi_c^+ = usc, \quad \Xi_c^0 = dsc, \quad \Omega_c^0 = ssc$$

 Λ_c^+

$$I(J^P) = 0(\frac{1}{2}^+)$$

Mass $m = 2286.46 \pm 0.14$ MeVMean life $\tau = (202.6 \pm 1.0) \times 10^{-15}$ s $c\tau = 60.75 \mu\text{m}$

Decay asymmetry parameters

$\Lambda \pi^+$	$\alpha = -0.755 \pm 0.006$
α FOR $\Lambda_c^+ \rightarrow \Lambda \rho^+$	$= -0.76 \pm 0.07$
$\Sigma^+ \pi^0$	$\alpha = -0.484 \pm 0.027$
α FOR $\Lambda_c^+ \rightarrow \Sigma^+ \eta$	$= -0.99 \pm 0.06$
α FOR $\Lambda_c^+ \rightarrow \Sigma^+ \eta'$	$= -0.46 \pm 0.07$
α FOR $\Lambda_c^+ \rightarrow \Sigma^0 \pi^+$	$= -0.466 \pm 0.018$
α FOR $\Lambda_c^+ \rightarrow \Sigma(1385)^+ \pi^0$	$= -0.92 \pm 0.09$
α FOR $\Lambda_c^+ \rightarrow \Sigma(1385)^0 \pi^+$	$= -0.79 \pm 0.11$
$\Lambda \ell^+ \nu_\ell$	$\alpha = -0.875 \pm 0.033$
α FOR $\Lambda_c^+ \rightarrow p K_S^0$	$= 0.2 \pm 0.5$
α FOR $\Lambda_c^+ \rightarrow \Lambda K^+$	$= -0.58 \pm 0.05$
α FOR $\Lambda_c^+ \rightarrow \Sigma^0 K^+$	$= -0.54 \pm 0.20$

α FOR $\Lambda_c^+ \rightarrow \Lambda(1405) \pi^+$	$= 0.58 \pm 0.28$
α FOR $\Lambda_c^+ \rightarrow \Lambda(1520) \pi^+$	$= 0.93 \pm 0.09$
α FOR $\Lambda_c^+ \rightarrow \Lambda(1600) \pi^+$	$= 0.2 \pm 0.5$
α FOR $\Lambda_c^+ \rightarrow \Lambda(1670) \pi^+$	$= 0.82 \pm 0.08$
α FOR $\Lambda_c^+ \rightarrow \Lambda(1690) \pi^+$	$= 0.958 \pm 0.034$
α FOR $\Lambda_c^+ \rightarrow \Lambda(2000) \pi^+$	$= -0.57 \pm 0.19$
α FOR $\Lambda_c^+ \rightarrow \Delta(1232)^{++} K^-$	$= 0.55 \pm 0.04$
α FOR $\Lambda_c^+ \rightarrow \Delta(1600)^{++} K^-$	$= -0.50 \pm 0.18$
α FOR $\Lambda_c^+ \rightarrow \Delta(1700)^{++} K^-$	$= 0.22 \pm 0.08$
α FOR $\Lambda_c^+ \rightarrow \bar{K}_0^*(700)^0 p$	$= -0.1 \pm 0.7$
α FOR $\Lambda_c^+ \rightarrow \bar{K}_0^*(1430)^0 p$	$= 0.34 \pm 0.14$
$(\alpha + \bar{\alpha})/(\alpha - \bar{\alpha})$ in $\Lambda_c^+ \rightarrow \Lambda \pi^+, \bar{\Lambda}_c^- \rightarrow \bar{\Lambda} \pi^-$	$= 0.020 \pm 0.016$
$(\alpha + \bar{\alpha})/(\alpha - \bar{\alpha})$ in $\Lambda_c^+ \rightarrow \Sigma^0 \pi^+, \bar{\Lambda}_c^- \rightarrow \bar{\Sigma}^0 \pi^-$	$= -0.02 \pm 0.05$
$(\alpha + \bar{\alpha})/(\alpha - \bar{\alpha})$ in $\Lambda_c^+ \rightarrow \Lambda e^+ \nu_e, \bar{\Lambda}_c^- \rightarrow \bar{\Lambda} e^- \bar{\nu}_e$	$= 0.00 \pm 0.04$
$(\alpha + \bar{\alpha})/(\alpha - \bar{\alpha})$ in $\Lambda_c^+ \rightarrow \Lambda K^+, \bar{\Lambda}_c^- \rightarrow \bar{\Lambda} K^-$	$= -0.23 \pm 0.11$
$(\alpha + \bar{\alpha})/(\alpha - \bar{\alpha})$ in $\Lambda_c^+ \rightarrow \Sigma^0 K^+, \bar{\Lambda}_c^- \rightarrow \bar{\Sigma}^0 K^-$	$= 0.1 \pm 0.4$
$A_{CP}(\Lambda X)$ in $\Lambda_c \rightarrow \Lambda X, \bar{\Lambda}_c \rightarrow \bar{\Lambda} X$	$= (2 \pm 7) \%$
$A_{CP}(\Lambda K^+)$ in $\Lambda_c \rightarrow \Lambda K^+, \bar{\Lambda}_c \rightarrow \bar{\Lambda} K^-$	$= 0.021 \pm 0.026$
$A_{CP}(\Sigma^0 K^+)$ in $\Lambda_c \rightarrow \Sigma^0 K^+, \bar{\Lambda}_c \rightarrow \bar{\Sigma}^0 K^-$	$= 0.03 \pm 0.05$
$\Delta A_{CP} = A_{CP}(\Lambda_c^+ \rightarrow p K^+ K^-) - A_{CP}(\Lambda_c^+ \rightarrow p \pi^+ \pi^-)$	$= (0.3 \pm 1.1) \%$

Branching fractions marked with a footnote, e.g. [a], have been corrected for decay modes not observed in the experiments. For example, the sub-mode fraction $\Lambda_c^+ \rightarrow p \bar{K}^*(892)^0$ seen in $\Lambda_c^+ \rightarrow p K^- \pi^+$ has been multiplied up to include $\bar{K}^*(892)^0 \rightarrow \bar{K}^0 \pi^0$ decays.

Λ_c^+ DECAY MODES	Fraction (Γ_i/Γ)	Scale factor/ Confidence level	p (MeV/c)
Hadronic modes with a p or n: $S = -1$ final states			
$p K_S^0$	$(1.59 \pm 0.07) \%$	S=1.1	873
$p K^- \pi^+$	$(6.24 \pm 0.28) \%$	S=1.4	823
$p \bar{K}_0^*(700)^0$	$(1.9 \pm 0.6) \times 10^{-3}$		715
$p \bar{K}^*(892)^0$	[q] $(1.39 \pm 0.07) \%$		685
$p \bar{K}_0^*(1430)$	$(9.2 \pm 1.8) \times 10^{-3}$		†
$\Delta(1232)^{++} K^-$	$(1.76 \pm 0.09) \%$		710
$\Delta(1600)^{++} K^-$	$(2.8 \pm 1.0) \times 10^{-3}$		-
$\Delta(1700)^{++} K^-$	$(2.4 \pm 0.6) \times 10^{-3}$		-
$\Lambda(1405)^0 \pi^+$	$(4.8 \pm 1.9) \times 10^{-3}$		-
$\Lambda(1520) \pi^+$	[q] $(1.16 \pm 0.16) \times 10^{-3}$		628
$\Lambda(1600) \pi^+$	$(3.2 \pm 1.2) \times 10^{-3}$		571
$\Lambda(1670) \pi^+$	$(7.4 \pm 2.1) \times 10^{-4}$		516
$\Lambda(1690) \pi^+$	$(7.4 \pm 2.2) \times 10^{-4}$		504
$\Lambda(2000) \pi^+$	$(6.0 \pm 0.7) \times 10^{-3}$		234
$p K^- \pi^+$ nonresonant	$(3.5 \pm 0.4) \%$		823
$p K_S^0 \pi^0$	$(1.96 \pm 0.12) \%$		823
$n K_S^0 \pi^+$	$(1.82 \pm 0.25) \%$		821
$n K^- \pi^+ \pi^+$	$(1.90 \pm 0.12) \%$		756
$p \bar{K}^0 \eta$	$(8.8 \pm 0.6) \times 10^{-3}$	S=1.1	568
$p K_S^0 \pi^+ \pi^-$	$(1.59 \pm 0.11) \%$	S=1.1	754
$p K^- \pi^+ \pi^0$	$(4.43 \pm 0.28) \%$	S=1.5	759
$p K^*(892)^- \pi^+$	[q] $(1.4 \pm 0.5) \%$		580
$p(K^- \pi^+)$ nonresonant π^0	$(4.6 \pm 0.8) \%$		759
$\Delta(1232) \bar{K}^*(892)$	seen		419
$p K^- 2\pi^+ \pi^-$	$(1.4 \pm 0.9) \times 10^{-3}$		671
$p K^- \pi^+ 2\pi^0$	$(10 \pm 5) \times 10^{-3}$		678
Hadronic modes with a p or n: $S = 0$ final states			
$p \pi^0$	$< 8 \times 10^{-5}$	CL=90%	945
$n \pi^+$	$(6.6 \pm 1.3) \times 10^{-4}$		944
$p \eta$	$(1.57 \pm 0.12) \times 10^{-3}$		856
$p \eta'$	$(4.8 \pm 0.9) \times 10^{-4}$		639
$p \omega(782)^0$	$(1.11 \pm 0.21) \times 10^{-3}$		751
$p \pi^+ \pi^-$	$(4.59 \pm 0.25) \times 10^{-3}$		927
$p f_0(980)$	[q] $(3.4 \pm 2.3) \times 10^{-3}$		614
$n \pi^+ \pi^0$	$(6.4 \pm 0.9) \times 10^{-3}$		927
$n \pi^+ \pi^- \pi^+$	$(4.5 \pm 0.8) \times 10^{-3}$		895
$p 2\pi^+ 2\pi^-$	$(2.2 \pm 1.4) \times 10^{-3}$		852
$p K^+ K^-$	$(1.06 \pm 0.05) \times 10^{-3}$		616
$p \phi$	[q] $(1.06 \pm 0.14) \times 10^{-3}$		590
$p K^+ K^-$ non- ϕ	$(5.2 \pm 1.1) \times 10^{-4}$		616
$p K_S^0 K_S^0$	$(2.35 \pm 0.18) \times 10^{-4}$		610
$p \phi \pi^0$	$(10 \pm 4) \times 10^{-5}$		460
$p K^+ K^- \pi^0$ nonresonant	$< 6.3 \times 10^{-5}$	CL=90%	494

Baryon Summary Table

Hadronic modes with a hyperon: $S = -1$ final states			
$\Lambda\pi^+$	(1.29 ± 0.05) %	S=1.1	864
$\Lambda(1670)\pi^+, \Lambda(1670) \rightarrow \eta\Lambda$	(3.5 ± 0.5) × 10 ⁻³		-
$\Lambda\pi^+\pi^0$	(7.02 ± 0.35) %	S=1.1	844
$\Lambda\rho^+$	(4.0 ± 0.5) %		636
$\Sigma(1385)^+\pi^0, \Sigma^+ \rightarrow \Lambda\pi^+$	(5.0 ± 0.7) × 10 ⁻³		-
$\Sigma(1385)^0\pi^+, \Sigma^0 \rightarrow \Lambda\pi^0$	(5.6 ± 0.8) × 10 ⁻³		-
$\Lambda\pi^-2\pi^+$	(3.61 ± 0.26) %	S=1.4	807
$\Sigma(1385)^+\pi^+\pi^-, \Sigma^{*+} \rightarrow$	(1.0 ± 0.5) %		688
$\Lambda\pi^+$			
$\Sigma(1385)^-2\pi^+, \Sigma^{*-} \rightarrow$	(7.6 ± 1.4) × 10 ⁻³		688
$\Lambda\pi^-\rho^0$	(1.4 ± 0.6) %		524
$\Sigma(1385)^+\rho^0, \Sigma^{*+} \rightarrow \Lambda\pi^+$	(5 ± 4) × 10 ⁻³		363
$\Lambda\pi^-2\pi^+$ nonresonant	< 1.1 %	CL=90%	807
$\Lambda\pi^-\pi^02\pi^+$ total	(2.2 ± 0.8) %		757
$\Lambda\pi^+\eta$	[q] (1.84 ± 0.11) %	S=1.1	691
$\Sigma(1385)^+\eta$	[q] (9.1 ± 2.0) × 10 ⁻³		570
$\Lambda\pi^+\omega$	[q] (1.5 ± 0.5) %		517
$\Lambda\pi^-\pi^02\pi^+, \text{ no } \eta \text{ or } \omega$	< 8 × 10 ⁻³	CL=90%	757
$\Lambda K^+\bar{K}^0$	(5.6 ± 1.1) × 10 ⁻³	S=1.9	443
$\Xi(1690)^0 K^+, \Xi^{*0} \rightarrow \Lambda\bar{K}^0$	(1.6 ± 0.5) × 10 ⁻³		286
$\Sigma^0\pi^+$	(1.27 ± 0.06) %	S=1.1	825
$\Sigma^0\pi^+\eta$	(7.5 ± 0.8) × 10 ⁻³		635
$\Sigma^+\pi^0$	(1.24 ± 0.09) %		827
$\Sigma^+\eta$	(3.2 ± 0.5) × 10 ⁻³		713
$\Sigma^+\eta'$	(4.1 ± 0.8) × 10 ⁻³		391
$\Sigma^+\pi^+\pi^-$	(4.47 ± 0.22) %	S=1.2	804
$\Sigma^+\rho^0$	< 1.7 %	CL=95%	575
$\Sigma^-2\pi^+$	(1.86 ± 0.18) %		799
$\Sigma^0\pi^+\pi^0$	(3.5 ± 0.4) %		803
$\Sigma^+\pi^0\pi^0$	(1.54 ± 0.14) %		806
$\Sigma^0\pi^-2\pi^+$	(1.10 ± 0.30) %		763
$\Sigma^+\omega$	(1.69 ± 0.20) %		569
$\Sigma^-\pi^02\pi^+$	(2.1 ± 0.4) %		762
$\Sigma^+ K^+ K^-$	(3.59 ± 0.35) × 10 ⁻³	S=1.1	349
$\Sigma^+\phi$	[q] (3.9 ± 0.5) × 10 ⁻³	S=1.1	295
$\Xi(1690)^0 K^+, \Xi^{*0} \rightarrow$	(1.01 ± 0.25) × 10 ⁻³		286
$\Sigma^+ K^-$			
$\Sigma^+ K^+ K^-$ nonresonant	< 8 × 10 ⁻⁴	CL=90%	349
$\Xi^0 K^+$	(5.5 ± 0.7) × 10 ⁻³		653
$\Xi^- K^+ \pi^+$	(6.2 ± 0.5) × 10 ⁻³	S=1.1	565
$\Xi(1530)^0 K^+$	(4.3 ± 0.9) × 10 ⁻³	S=1.1	473
Hadronic modes with a hyperon: $S = 0$ final states			
ΛK^+	(6.42 ± 0.31) × 10 ⁻⁴		781
$\Lambda K^+\pi^+\pi^-$	< 5 × 10 ⁻⁴	CL=90%	637
$\Sigma^0 K^+$	(3.70 ± 0.31) × 10 ⁻⁴		735
$\Sigma^+ K_S^0$	(4.7 ± 1.4) × 10 ⁻⁴		736
$\Sigma^0 K^+\pi^+\pi^-$	< 2.5 × 10 ⁻⁴	CL=90%	574
$\Sigma^+ K^+\pi^-$	(2.00 ± 0.26) × 10 ⁻³		670
$\Sigma^+ K^*(892)^0$	[q] (3.5 ± 1.0) × 10 ⁻³		470
$\Sigma^+ K^+\pi^-\pi^0$	< 1.1 × 10 ⁻³	CL=90%	581
$\Sigma^- K^+\pi^+$	< 1.2 × 10 ⁻³	CL=90%	664
Doubly Cabibbo-suppressed modes			
$p K^+\pi^-$	(1.11 ± 0.17) × 10 ⁻⁴		823
Semileptonic modes			
$\Lambda e^+ \nu_e$	(3.56 ± 0.13) %		871
$\Lambda\pi^+\pi^- e^+ \nu_e$	< 3.9 × 10 ⁻⁴	CL=90%	843
$p K^- e^+ \nu_e$	(8.8 ± 1.8) × 10 ⁻⁴		874
$p K_S^0 \pi^- e^+ \nu_e$	< 3.3 × 10 ⁻⁴	CL=90%	821
$\Lambda(1520) e^+ \nu_e$	(1.0 ± 0.5) × 10 ⁻³		639
$\Lambda(1405)^0 e^+ \nu_e, \Lambda^0 \rightarrow p K^-$	(4.2 ± 1.9) × 10 ⁻⁴		-
$\Lambda\mu^+ \nu_\mu$	(3.48 ± 0.17) %		867
Inclusive modes			
e^+ anything	(4.06 ± 0.13) %		-
p anything	(50 ± 16) %		-
n anything	(32.6 ± 1.6) %		-
Λ anything	(38.2 ± 2.9) %		-
K_S^0 anything	(9.9 ± 0.7) %		-
3prongs	(24 ± 8) %		-

$\Delta C = 1$ weak neutral current (CI) modes, or
Lepton Family number (LF), or Lepton number (L), or
Baryon number (B) violating modes

$p e^+ e^-$	CI	< 5.5 × 10 ⁻⁶	CL=90%	951
$p \mu^+ \mu^-$ non-resonant	CI	< 7.7 × 10 ⁻⁸	CL=90%	937

$p e^+ \mu^-$	LF	< 9.9 × 10 ⁻⁶	CL=90%	947
$p e^- \mu^+$	LF	< 1.9 × 10 ⁻⁵	CL=90%	947
$\bar{p} 2e^+$	L,B	< 2.7 × 10 ⁻⁶	CL=90%	951
$\bar{p} 2\mu^+$	L,B	< 9.4 × 10 ⁻⁶	CL=90%	937
$\bar{p} e^+ \mu^+$	L,B	< 1.6 × 10 ⁻⁵	CL=90%	947
$\Sigma^- \mu^+ \mu^+$	L	< 7.0 × 10 ⁻⁴	CL=90%	812

Radiative modes

$\Sigma^+ \gamma$	< 2.5 × 10 ⁻⁴	CL=90%	834
-------------------	--------------------------	--------	-----

Exotic modes

$p \gamma D$	[r] < 8.0 × 10 ⁻⁵	CL=90%	-
--------------	------------------------------	--------	---

 $\Lambda_c(2595)^+$

$$I(J^P) = 0(\frac{1}{2}^-)$$

The spin-parity follows from the fact that $\Sigma_c(2455)\pi$ decays, with little available phase space, are dominant. This assumes that $J^P = 1/2^+$ for the $\Sigma_c(2455)$.

$$\text{Mass } m = 2592.25 \pm 0.28 \text{ MeV}$$

$$m - m_{\Lambda_c^+} = 305.79 \pm 0.24 \text{ MeV}$$

$$\text{Full width } \Gamma = 2.6 \pm 0.6 \text{ MeV}$$

$\Lambda_c^+ \pi \pi$ and its submode $\Sigma_c(2455)\pi$ — the latter just barely — are the only strong decays allowed to an excited Λ_c^+ having this mass; and the submode seems to dominate.

 $\Lambda_c(2595)^+$ DECAY MODES

Decay Mode	Fraction (Γ_i/Γ)	p (MeV/c)
$\Lambda_c^+ \pi^+ \pi^-$	[s] —	117
$\Sigma_c(2455)^{++} \pi^-$	24 ± 7 %	3
$\Sigma_c(2455)^0 \pi^+$	24 ± 7 %	3
$\Lambda_c^+ \pi^+ \pi^-$ 3-body	18 ± 10 %	117
$\Lambda_c^+ \pi^0$	[t] not seen	258
$\Lambda_c^+ \gamma$	not seen	288

 $\Lambda_c(2625)^+$

$$I(J^P) = 0(\frac{3}{2}^-)$$

J^P has not been measured; $\frac{3}{2}^-$ is the quark-model prediction.

$$\text{Mass } m = 2628.00 \pm 0.15 \text{ MeV}$$

$$m - m_{\Lambda_c^+} = 341.54 \pm 0.05 \text{ MeV}$$

$$\text{Full width } \Gamma < 0.52 \text{ MeV, CL} = 90\%$$

$\Lambda_c^+ \pi \pi$ and its submode $\Sigma(2455)\pi$ are the only strong decays allowed to an excited Λ_c^+ having this mass.

 $\Lambda_c(2625)^+$ DECAY MODES

Decay Mode	Fraction (Γ_i/Γ)	Confidence level	p (MeV/c)
$\Lambda_c^+ \pi^+ \pi^-$	[u] 66.67 %		184
$\Sigma_c(2455)^{++} \pi^-$	(3.42 ± 0.27) %		103
$\Sigma_c(2455)^0 \pi^+$	(3.46 ± 0.31) %		103
$\Lambda_c^+ \pi^+ \pi^-$ 3-body	large		184
$\Lambda_c^+ \pi^0$	[t] < 60 %	90%	293
$\Lambda_c^+ \gamma$	< 35 %	90%	319

 $\Lambda_c(2860)^+$

$$I(J^P) = 0(\frac{3}{2}^+)$$

$$\text{Mass } m = 2856.1^{+2.3}_{-6.0} \text{ MeV}$$

$$\text{Full width } \Gamma = 68^{+12}_{-22} \text{ MeV}$$

 $\Lambda_c(2860)^+$ DECAY MODES

Decay Mode	Fraction (Γ_i/Γ)	p (MeV/c)
$D^0 p$	seen	259

 $\Lambda_c(2880)^+$

$$I(J^P) = 0(\frac{5}{2}^+)$$

$$\text{Mass } m = 2881.63 \pm 0.24 \text{ MeV}$$

$$m - m_{\Lambda_c^+} = 595.17 \pm 0.28 \text{ MeV}$$

$$\text{Full width } \Gamma = 5.6^{+0.8}_{-0.6} \text{ MeV}$$

Baryon Summary Table

$\Lambda_c(2880)^+$ DECAY MODES	Fraction (Γ_i/Γ)	ρ (MeV/c)
$\Lambda_c^+ \pi^+ \pi^-$	seen	471
$\Sigma_c(2455)^{0,++} \pi^\pm$	seen	376
$\Sigma_c(2520)^{0,++} \pi^\pm$	seen	317
ρD^0	seen	316

$$\Lambda_c(2940)^+ \quad I(J^P) = 0(\frac{3}{2}^-)$$

$J^P = 3/2^-$ is favored, but is not certain

$$\text{Mass } m = 2939.6^{+1.3}_{-1.5} \text{ MeV}$$

$$\text{Full width } \Gamma = 20^{+6}_{-5} \text{ MeV}$$

$\Lambda_c(2940)^+$ DECAY MODES	Fraction (Γ_i/Γ)	ρ (MeV/c)
ρD^0	seen	420
$\Sigma_c(2455)^{0,++} \pi^\pm$	seen	-

$$\Sigma_c(2455) \quad I(J^P) = 1(\frac{1}{2}^+)$$

$$\Sigma_c(2455)^{++} \text{ mass } m = 2453.97 \pm 0.14 \text{ MeV}$$

$$\Sigma_c(2455)^+ \text{ mass } m = 2452.65^{+0.22}_{-0.16} \text{ MeV}$$

$$\Sigma_c(2455)^0 \text{ mass } m = 2453.75 \pm 0.14 \text{ MeV}$$

$$m_{\Sigma_c(2455)^{++}} - m_{\Lambda_c^+} = 167.510 \pm 0.017 \text{ MeV}$$

$$m_{\Sigma_c(2455)^+} - m_{\Lambda_c^+} = 166.19^{+0.16}_{-0.08} \text{ MeV}$$

$$m_{\Sigma_c(2455)^0} - m_{\Lambda_c^+} = 167.290 \pm 0.017 \text{ MeV}$$

$$m_{\Sigma_c(2455)^{++}} - m_{\Sigma_c(2455)^0} = 0.220 \pm 0.013 \text{ MeV}$$

$$m_{\Sigma_c(2455)^+} - m_{\Sigma_c(2455)^0} = -1.10^{+0.16}_{-0.08} \text{ MeV}$$

$$\Sigma_c(2455)^{++} \text{ full width } \Gamma = 1.89^{+0.09}_{-0.18} \text{ MeV} \quad (S = 1.1)$$

$$\Sigma_c(2455)^+ \text{ full width } \Gamma = 2.3 \pm 0.4 \text{ MeV}$$

$$\Sigma_c(2455)^0 \text{ full width } \Gamma = 1.83^{+0.11}_{-0.19} \text{ MeV} \quad (S = 1.2)$$

$\Lambda_c^+ \pi$ is the only strong decay allowed to a Σ_c having this mass.

$\Sigma_c(2455)$ DECAY MODES	Fraction (Γ_i/Γ)	ρ (MeV/c)
$\Lambda_c^+ \pi$	$\approx 100\%$	94

$$\Sigma_c(2520) \quad I(J^P) = 1(\frac{3}{2}^+)$$

J^P has not been measured; $\frac{3}{2}^+$ is the quark-model prediction.

$$\Sigma_c(2520)^{++} \text{ mass } m = 2518.41 \pm 0.22 \text{ MeV} \quad (S = 1.3)$$

$$\Sigma_c(2520)^+ \text{ mass } m = 2517.4^{+0.7}_{-0.5} \text{ MeV}$$

$$\Sigma_c(2520)^0 \text{ mass } m = 2518.48 \pm 0.21 \text{ MeV} \quad (S = 1.2)$$

$$m_{\Sigma_c(2520)^{++}} - m_{\Lambda_c^+} = 231.95 \pm 0.18 \text{ MeV} \quad (S = 1.8)$$

$$m_{\Sigma_c(2520)^+} - m_{\Lambda_c^+} = 230.9^{+0.7}_{-0.5} \text{ MeV}$$

$$m_{\Sigma_c(2520)^0} - m_{\Lambda_c^+} = 232.02 \pm 0.15 \text{ MeV} \quad (S = 1.4)$$

$$m_{\Sigma_c(2520)^{++}} - m_{\Sigma_c(2520)^0} = 0.01 \pm 0.15 \text{ MeV}$$

$$\Sigma_c(2520)^{++} \text{ full width } \Gamma = 14.78^{+0.30}_{-0.40} \text{ MeV}$$

$$\Sigma_c(2520)^+ \text{ full width } \Gamma = 17.2^{+4.0}_{-2.2} \text{ MeV}$$

$$\Sigma_c(2520)^0 \text{ full width } \Gamma = 15.3^{+0.4}_{-0.5} \text{ MeV}$$

$\Lambda_c^+ \pi$ is the only strong decay allowed to a Σ_c having this mass.

$\Sigma_c(2520)$ DECAY MODES	Fraction (Γ_i/Γ)	ρ (MeV/c)
$\Lambda_c^+ \pi$	$\approx 100\%$	179

$$\Sigma_c(2800) \quad I(J^P) = 1(?^?)$$

$$\Sigma_c(2800)^{++} \text{ mass } m = 2801^{+4}_{-6} \text{ MeV}$$

$$\Sigma_c(2800)^+ \text{ mass } m = 2792^{+14}_{-5} \text{ MeV}$$

$$\Sigma_c(2800)^0 \text{ mass } m = 2806^{+5}_{-7} \text{ MeV} \quad (S = 1.3)$$

$$m_{\Sigma_c(2800)^{++}} - m_{\Lambda_c^+} = 514^{+4}_{-6} \text{ MeV}$$

$$m_{\Sigma_c(2800)^+} - m_{\Lambda_c^+} = 505^{+14}_{-5} \text{ MeV}$$

$$m_{\Sigma_c(2800)^0} - m_{\Lambda_c^+} = 519^{+5}_{-7} \text{ MeV} \quad (S = 1.3)$$

$$\Sigma_c(2800)^{++} \text{ full width } \Gamma = 75^{+22}_{-17} \text{ MeV}$$

$$\Sigma_c(2800)^+ \text{ full width } \Gamma = 60^{+60}_{-40} \text{ MeV}$$

$$\Sigma_c(2800)^0 \text{ full width } \Gamma = 72^{+22}_{-15} \text{ MeV}$$

$\Sigma_c(2800)$ DECAY MODES	Fraction (Γ_i/Γ)	ρ (MeV/c)
$\Lambda_c^+ \pi$	seen	443

$$\Xi_c^+ \quad I(J^P) = \frac{1}{2}(\frac{1}{2}^+)$$

J^P has not been measured; $\frac{1}{2}^+$ is the quark-model prediction.

$$\text{Mass } m = 2467.71 \pm 0.23 \text{ MeV} \quad (S = 1.3)$$

$$\text{Mean life } \tau = (453 \pm 5) \times 10^{-15} \text{ s}$$

$$c\tau = 135.8 \mu\text{m}$$

Branching fractions marked with a footnote, e.g. [a], have been corrected for decay modes not observed in the experiments. For example, the sub-mode fraction $\Xi_c^+ \rightarrow \Sigma^+ \bar{K}^*(892)^0$ seen in $\Xi_c^+ \rightarrow \Sigma^+ K^- \pi^+$ has been multiplied up to include $\bar{K}^*(892)^0 \rightarrow \bar{K}^0 \pi^0$ decays.

Ξ_c^+ DECAY MODES	Fraction (Γ_i/Γ)	Scale factor / Confidence level	ρ (MeV/c)
-----------------------	--------------------------------	---------------------------------	----------------

Cabibbo-favored ($S = -2$) decays

$\rho 2K_S^0$	$(2.5 \pm 1.3) \times 10^{-3}$		766
$\Lambda \bar{K}^0 \pi^+$	—		852
$\Sigma(1385)^+ \bar{K}^0$	[q] $(2.9 \pm 2.0)\%$		746
$\Lambda K^- 2\pi^+$	$(9 \pm 4) \times 10^{-3}$		787
$\Lambda \bar{K}^*(892)^0 \pi^+$	[q] $< 5 \times 10^{-3}$	CL=90%	608
$\Sigma(1385)^+ K^- \pi^+$	[q] $< 6 \times 10^{-3}$	CL=90%	678
$\Sigma^+ K^- \pi^+$	$(2.7 \pm 1.2)\%$		810
$\Sigma^+ \bar{K}^*(892)^0$	[q] $(2.3 \pm 1.1)\%$		658
$\Sigma^0 K^- 2\pi^+$	$(8 \pm 5) \times 10^{-3}$		735
$\Xi^0 \pi^+$	$(1.6 \pm 0.8)\%$		876
$\Xi^- 2\pi^+$	$(2.9 \pm 1.3)\%$		851
$\Xi(1530)^0 \pi^+$	[q] $< 2.9 \times 10^{-3}$	CL=90%	749
$\Xi(1620)^0 \pi^+$	seen		—
$\Xi(1690)^0 \pi^+$	seen		644
$\Xi^0 \pi^+ \pi^0$	$(6.7 \pm 3.5)\%$		856
$\Xi^0 \pi^- 2\pi^+$	$(5.0 \pm 2.6)\%$		818
$\Xi^0 e^+ \nu_e$	$(7 \pm 4)\%$		884
$\Omega^- K^+ \pi^+$	$(2.0 \pm 1.5) \times 10^{-3}$		399

Cabibbo-suppressed decays

$\rho K^- \pi^+$	$(6.2 \pm 3.0) \times 10^{-3}$	S=1.5	944
$\rho \bar{K}^*(892)^0$	[q] $(3.3 \pm 1.7) \times 10^{-3}$		828
$\Sigma^+ \pi^+ \pi^-$	$(1.4 \pm 0.8)\%$		922
$\Sigma^- 2\pi^+$	$(5.1 \pm 3.4) \times 10^{-3}$		918
$\Sigma^+ K^+ K^-$	$(4.3 \pm 2.5) \times 10^{-3}$		579
$\Sigma^+ \phi$	[q] $< 3.2 \times 10^{-3}$	CL=90%	549
$\Xi(1690)^0 K^+, \Xi^0 \rightarrow \Sigma^+ K^-$	$< 1.3 \times 10^{-3}$	CL=90%	501
$\rho \phi(1020)$	$(1.2 \pm 0.6) \times 10^{-4}$		751

$$\Xi_c^0 \quad I(J^P) = \frac{1}{2}(\frac{1}{2}^+)$$

J^P has not been measured; $\frac{1}{2}^+$ is the quark-model prediction.

$$\text{Mass } m = 2470.44 \pm 0.28 \text{ MeV} \quad (S = 1.2)$$

$$m_{\Xi_c^0} - m_{\Xi_c^+} = 2.72 \pm 0.23 \text{ MeV} \quad (S = 1.1)$$

$$\text{Mean life } \tau = (150.4 \pm 2.8) \times 10^{-15} \text{ s} \quad (S = 1.4)$$

$$c\tau = 45.1 \mu\text{m}$$

Decay asymmetry parameters

$$\Xi^- \pi^+ \quad \alpha = -0.64 \pm 0.05$$

$$\alpha \text{ FOR } \Xi^0 \rightarrow \Xi^+ \pi^- = 0.61 \pm 0.05$$

$$\alpha \text{ FOR } \Xi_c^0 \rightarrow \Lambda \bar{K}^*(892)^0 = 0.15 \pm 0.22$$

$$\alpha \text{ FOR } \Xi_c^0 \rightarrow \Sigma^+ K^*(892)^- = -0.52 \pm 0.30$$

Ξ_c^0 DECAY MODES	Fraction (Γ_i/Γ)	Confidence level	ρ (MeV/c)
-----------------------	--------------------------------	------------------	----------------

Cabibbo-favored decays

$\rho K^- K^- \pi^+$	$(4.9 \pm 1.0) \times 10^{-3}$		676
$\rho K^- \bar{K}^*(892)^0, \bar{K}^{*0} \rightarrow K^- \pi^+$	$(2.0 \pm 0.6) \times 10^{-3}$		413
$\rho K^- K^- \pi^+$ (no \bar{K}^{*0})	$(3.0 \pm 0.8) \times 10^{-3}$		676
ΛK_S^0	$(3.2 \pm 0.6) \times 10^{-3}$		906
$\Lambda K^- \pi^+$	$(1.45 \pm 0.28)\%$		856
$\Lambda \bar{K}^*(892)^0$	$(2.6 \pm 0.6) \times 10^{-3}$		717
$\Lambda \bar{K}^0 \pi^+ \pi^-$	seen		786
$\Lambda K^- \pi^+ \pi^+ \pi^-$	seen		703

Baryon Summary Table

$\Sigma^0 K_S^0$	$(5.4 \pm 1.4) \times 10^{-4}$	864
$\Sigma^+ K^-$	$(1.8 \pm 0.4) \times 10^{-3}$	868
$\Sigma^0 \bar{K}^*(892)^0$	$(9.9 \pm 1.9) \times 10^{-3}$	658
$\Sigma^+ K^*(892)^-$	$(4.9 \pm 1.3) \times 10^{-3}$	661
$\Xi^- \pi^+$	$(1.43 \pm 0.27) \%$	875
$\Xi^- \pi^+ \pi^-$	$(4.8 \pm 2.3) \%$	816
$\Xi^0 \phi, \phi \rightarrow K^+ K^-$	$(5.2 \pm 1.2) \times 10^{-4}$	-
$\Xi^0 K^+ K^-$ nonresonant	$(5.6 \pm 1.2) \times 10^{-4}$	444
$\Omega^- K^+$	$(4.2 \pm 0.9) \times 10^{-3}$	522
$\Xi^- e^+ \nu_e$	$(1.05 \pm 0.20) \%$	882
$\Xi^- \mu^+ \nu_\mu$	$(1.01 \pm 0.21) \%$	878
$\Xi^0 \gamma$	$< 1.7 \times 10^{-4}$	90%

Cabibbo-suppressed decays

$\Lambda_c^+ \pi^-$	$(5.5 \pm 1.1) \times 10^{-3}$	115
$\Xi^- K^+$	$(3.9 \pm 1.1) \times 10^{-4}$	789
$\Lambda K^+ K^-$ (no ϕ)	$(4.1 \pm 1.3) \times 10^{-4}$	648
$\Lambda \phi$	$(4.9 \pm 1.3) \times 10^{-4}$	621

$$\Xi_c^{'+} \quad I(J^P) = \frac{1}{2}(\frac{1}{2}^+)$$

J^P has not been measured; $\frac{1}{2}^+$ is the quark-model prediction.

Mass $m = 2578.2 \pm 0.5$ MeV ($S = 1.1$)

$$m_{\Xi_c^{'+}} - m_{\Xi_c^+} = 110.5 \pm 0.4 \text{ MeV}$$

$$m_{\Xi_c^{'+}} - m_{\Xi_c^0} = -0.5 \pm 0.6 \text{ MeV}$$

The $\Xi_c^{'+} - \Xi_c^+$ mass difference is too small for any strong decay to occur.

$\Xi_c^{'+}$ DECAY MODES	Fraction (Γ_i/Γ)	ρ (MeV/c)
$\Xi_c^+ \gamma$	seen	108

$$\Xi_c^{'0} \quad I(J^P) = \frac{1}{2}(\frac{1}{2}^+)$$

J^P has not been measured; $\frac{1}{2}^+$ is the quark-model prediction.

Mass $m = 2578.7 \pm 0.5$ MeV

$$m_{\Xi_c^{'0}} - m_{\Xi_c^0} = 108.3 \pm 0.4 \text{ MeV}$$

The $\Xi_c^{'0} - \Xi_c^0$ mass difference is too small for any strong decay to occur.

$\Xi_c^{'0}$ DECAY MODES	Fraction (Γ_i/Γ)	ρ (MeV/c)
$\Xi_c^0 \gamma$	seen	106

$$\Xi_c(2645) \quad I(J^P) = \frac{1}{2}(\frac{3}{2}^+)$$

J^P has not been measured; $\frac{3}{2}^+$ is the quark-model prediction.

$$\Xi_c(2645)^+ \text{ mass } m = 2645.10 \pm 0.30 \text{ MeV} \quad (S = 1.2)$$

$$\Xi_c(2645)^0 \text{ mass } m = 2646.16 \pm 0.25 \text{ MeV} \quad (S = 1.3)$$

$$m_{\Xi_c(2645)^+} - m_{\Xi_c^0} = 174.67 \pm 0.09 \text{ MeV}$$

$$m_{\Xi_c(2645)^0} - m_{\Xi_c^+} = 178.45 \pm 0.10 \text{ MeV}$$

$$m_{\Xi_c(2645)^+} - m_{\Xi_c(2645)^0} = -1.06 \pm 0.27 \text{ MeV} \quad (S = 1.1)$$

$$\Xi_c(2645)^+ \text{ full width } \Gamma = 2.14 \pm 0.19 \text{ MeV} \quad (S = 1.1)$$

$$\Xi_c(2645)^0 \text{ full width } \Gamma = 2.35 \pm 0.22 \text{ MeV}$$

$\Xi_c \pi$ is the only strong decay allowed to a Ξ_c resonance having this mass.

$\Xi_c(2645)$ DECAY MODES	Fraction (Γ_i/Γ)	ρ (MeV/c)
$\Xi_c^0 \pi^+$	seen	102
$\Xi_c^+ \pi^-$	seen	106

$$\Xi_c(2790) \quad I(J^P) = \frac{1}{2}(\frac{1}{2}^-)$$

J^P has not been measured; $\frac{1}{2}^-$ is the quark-model prediction.

$$\Xi_c(2790)^+ \text{ mass } = 2791.9 \pm 0.5 \text{ MeV}$$

$$\Xi_c(2790)^0 \text{ mass } = 2793.9 \pm 0.5 \text{ MeV}$$

$$m_{\Xi_c(2790)^+} - m_{\Xi_c^0} = 213.20 \pm 0.22 \text{ MeV}$$

$$m_{\Xi_c(2790)^0} - m_{\Xi_c^+} = 215.70 \pm 0.22 \text{ MeV}$$

$$m_{\Xi_c(2790)^+} - m_{\Xi_c(2790)^0} = -2.0 \pm 0.7 \text{ MeV}$$

$$\Xi_c(2790)^+ \text{ width } = 8.9 \pm 1.0 \text{ MeV}$$

$$\Xi_c(2790)^0 \text{ width } = 10.0 \pm 1.1 \text{ MeV}$$

$\Xi_c(2790)$ DECAY MODES	Fraction (Γ_i/Γ)	ρ (MeV/c)
$\Xi_c^+ \pi^-$	seen	159
$\Lambda_c^+ K^-$	seen	98

$$\Xi_c(2815) \quad I(J^P) = \frac{1}{2}(\frac{3}{2}^-)$$

J^P has not been measured; $\frac{3}{2}^-$ is the quark-model prediction.

$$\Xi_c(2815)^+ \text{ mass } m = 2816.51 \pm 0.25 \text{ MeV} \quad (S = 1.2)$$

$$\Xi_c(2815)^0 \text{ mass } m = 2819.79 \pm 0.30 \text{ MeV} \quad (S = 1.1)$$

$$m_{\Xi_c(2815)^+} - m_{\Xi_c^+} = 348.80 \pm 0.10 \text{ MeV}$$

$$m_{\Xi_c(2815)^0} - m_{\Xi_c^0} = 349.35 \pm 0.11 \text{ MeV}$$

$$m_{\Xi_c(2815)^+} - m_{\Xi_c(2815)^0} = -3.27 \pm 0.27 \text{ MeV}$$

$$\Xi_c(2815)^+ \text{ full width } \Gamma = 2.43 \pm 0.26 \text{ MeV}$$

$$\Xi_c(2815)^0 \text{ full width } \Gamma = 2.54 \pm 0.25 \text{ MeV}$$

The $\Xi_c \pi \pi$ modes are consistent with being entirely via $\Xi_c(2645) \pi$.

$\Xi_c(2815)$ DECAY MODES	Fraction (Γ_i/Γ)	ρ (MeV/c)
$\Xi_c^+ \pi^-$	seen	188
$\Xi_c(2645) \pi$	seen	102
$\Xi_c^0 \gamma$	seen	325

$$\Xi_c(2970) \quad I(J^P) = \frac{1}{2}(\frac{1}{2}^+)$$

was $\Xi_c(2980)$

$$\Xi_c(2970)^+ \text{ } m = 2964.3 \pm 1.5 \text{ MeV} \quad (S = 3.9)$$

$$\Xi_c(2970)^0 \text{ } m = 2967.1 \pm 1.7 \text{ MeV} \quad (S = 6.7)$$

$$m_{\Xi_c(2970)^+} - m_{\Xi_c^+} = 496.6 \pm 1.5 \text{ MeV} \quad (S = 3.7)$$

$$m_{\Xi_c(2970)^0} - m_{\Xi_c^0} = 496.7 \pm 1.8 \text{ MeV} \quad (S = 5.3)$$

$$m_{\Xi_c(2970)^+} - m_{\Xi_c(2970)^0} = -2.8 \pm 1.9 \text{ MeV} \quad (S = 4.8)$$

$$\Xi_c(2970)^+ \text{ width } \Gamma = 20.9_{-3.5}^{+2.4} \text{ MeV} \quad (S = 1.2)$$

$\Xi_c(2970)$ DECAY MODES	Fraction (Γ_i/Γ)	ρ (MeV/c)
$\Lambda_c^+ \bar{K} \pi$	seen	223
$\Sigma_c(2455) \bar{K}$	seen	122
$\Lambda_c^+ \bar{K}$	not seen	410
$\Lambda_c^+ K^-$	seen	410
$\Xi_c 2\pi$	seen	381
$\Xi_c^+ \pi^-$	seen	-
$\Xi_c(2645) \pi$	seen	274

$$\Xi_c(3055) \quad I(J^P) = ?(??)$$

Mass $m = 3055.9 \pm 0.4$ MeV

Full width $\Gamma = 7.8 \pm 1.9$ MeV

$\Xi_c(3055)$ DECAY MODES	Fraction (Γ_i/Γ)	ρ (MeV/c)
$\Sigma^{++} K^-$	seen	-
ΛD^+	seen	316

$$\Xi_c(3080) \quad I(J^P) = \frac{1}{2}(??)$$

$$\Xi_c(3080)^+ \text{ } m = 3077.2 \pm 0.4 \text{ MeV}$$

$$\Xi_c(3080)^0 \text{ } m = 3079.9 \pm 1.4 \text{ MeV} \quad (S = 1.3)$$

$$\Xi_c(3080)^+ \text{ width } \Gamma = 3.6 \pm 1.1 \text{ MeV} \quad (S = 1.5)$$

$$\Xi_c(3080)^0 \text{ width } \Gamma = 5.6 \pm 2.2 \text{ MeV}$$

$\Xi_c(3080)$ DECAY MODES	Fraction (Γ_i/Γ)	ρ (MeV/c)
$\Lambda_c^+ \bar{K} \pi$	seen	415
$\Sigma_c(2455) \bar{K}$	seen	342
$\Sigma_c(2455)^{++} K^-$	seen	342
$\Sigma_c(2520)^{++} K^-$	seen	239
$\Sigma_c(2455) \bar{K} + \Sigma_c(2520) \bar{K}$	seen	-
$\Lambda_c^+ \bar{K}$	not seen	536
$\Lambda_c^+ \bar{K} \pi^+ \pi^-$	not seen	144
ΛD^+	seen	362

Baryon Summary Table

 Ω_c^0

$I(J^P) = 0(\frac{1}{2}^+)$

 J^P has not been measured; $\frac{1}{2}^+$ is the quark-model prediction.

Mass $m = 2695.2 \pm 1.7$ MeV ($S = 1.3$)

Mean life $\tau = (273 \pm 12) \times 10^{-15}$ s

$c\tau = 82$ μ m

No absolute branching fractions have been measured. The following are branching ratios relative to $\Omega^- \pi^+$.

Ω_c^0 DECAY MODES	Fraction (Γ_i/Γ)	Confidence level	ρ (MeV/c)
Cabibbo-favored ($S = -3$) decays — relative to $\Omega^- \pi^+$			
$\Omega^- \pi^+$	DEFINED AS 1		821
$\Omega^- \pi^+ \pi^0$	1.80 ± 0.33		797
$\Omega^- \rho^+$	>1.3	90%	532
$\Omega^- \pi^- 2\pi^+$	0.31 ± 0.05		753
$\Omega^- e^+ \nu_e$	1.98 ± 0.15		829
$\Omega^- \mu^+ \nu_\mu$	1.94 ± 0.21		824
$\Xi^0 \bar{K}^0$	1.64 ± 0.29		950
$\Xi^0 K^- \pi^+$	1.20 ± 0.18		901
$\Xi^0 \bar{K}^{*0}, \bar{K}^{*0} \rightarrow K^- \pi^+$	0.68 ± 0.16		764
$\Omega(2012)^- \pi^+, \Omega(2012)^- \rightarrow \Xi^0 K^-$	0.12 ± 0.05		—
$\Xi^- \bar{K}^0 \pi^+$	2.12 ± 0.28		895
$\Omega(2012)^- \pi^+, \Omega(2012)^- \rightarrow \Xi^- \bar{K}^0$	0.12 ± 0.06		—
$\Xi^- K^- 2\pi^+$	0.63 ± 0.09		830
$\Xi(1530)^0 K^- \pi^+, \Xi^{*0} \rightarrow \Xi^- \pi^+$	0.21 ± 0.06		757
$\Xi^- \bar{K}^{*0} \pi^+$	0.34 ± 0.11		653
$p K^- K^- \pi^+$	seen		864
$\Sigma^+ K^- K^- \pi^+$	<0.32	90%	689
$\Lambda \bar{K}^0 \bar{K}^0$	1.72 ± 0.35		837
Singly Cabibbo-suppressed modes — relative to $\Omega^- \pi^+$			
$\Xi^- \pi^+$	0.25 ± 0.06		—
$\Omega^- K^+$	<0.29	90%	—
Doubly Cabibbo-suppressed modes — relative to $\Omega^- \pi^+$			
$\Xi^- K^+$	<0.07	90%	—

 $\Omega_c(2770)^0$

$I(J^P) = 0(\frac{3}{2}^+)$

 J^P has not been measured; $\frac{3}{2}^+$ is the quark-model prediction.

Mass $m = 2765.9 \pm 2.0$ MeV ($S = 1.2$)

$m_{\Omega_c(2770)^0} - m_{\Omega_c^0} = 70.7_{-0.9}^{+0.8}$ MeV

The $\Omega_c(2770)^0 - \Omega_c^0$ mass difference is too small for any strong decay to occur.

$\Omega_c(2770)^0$ DECAY MODES	Fraction (Γ_i/Γ)	ρ (MeV/c)
$\Omega_c^0 \gamma$	presumably 100%	70

 $\Omega_c(3000)^0$

$I(J^P) = ?(?^?)$

Mass $m = 3000.46 \pm 0.25$ MeV

Full width $\Gamma = 3.8_{-0.4}^{+1.6}$ MeV

$\Omega_c(3000)^0$ DECAY MODES	Fraction (Γ_i/Γ)	ρ (MeV/c)
$\Xi_c^+ K^-$	seen	182

 $\Omega_c(3050)^0$

$I(J^P) = ?(?^?)$

Mass $m = 3050.17 \pm 0.19$ MeV

Full width $\Gamma < 1.8$ MeV, CL = 95%

$\Omega_c(3050)^0$ DECAY MODES	Fraction (Γ_i/Γ)	ρ (MeV/c)
$\Xi_c^+ K^-$	seen	278

 $\Omega_c(3065)^0$

$I(J^P) = ?(?^?)$

Mass $m = 3065.58 \pm 0.21$ MeV

Full width $\Gamma = 3.4_{-0.8}^{+0.7}$ MeV ($S = 1.7$)

$\Omega_c(3065)^0$ DECAY MODES	Fraction (Γ_i/Γ)	ρ (MeV/c)
$\Xi_c^+ K^-$	seen	303

 $\Omega_c(3090)^0$

$I(J^P) = ?(?^?)$

Mass $m = 3090.15 \pm 0.26$ MeV

Full width $\Gamma = 8.5_{-1.7}^{+0.8}$ MeV

$\Omega_c(3090)^0$ DECAY MODES	Fraction (Γ_i/Γ)	ρ (MeV/c)
$\Xi_c^+ K^-$	seen	340

 $\Omega_c(3120)^0$

$I(J^P) = ?(?^?)$

Mass $m = 3118.98_{-0.35}^{+0.27}$ MeV

Full width $\Gamma < 2.5$ MeV, CL = 95%

$\Omega_c(3120)^0$ DECAY MODES	Fraction (Γ_i/Γ)	ρ (MeV/c)
$\Xi_c^+ K^-$	seen	379

 $\Omega_c(3185)^0$

$I(J^P) = ?(?^?)$

Mass $m = 3185_{-1.9}^{+7.6}$ MeV

Full width $\Gamma = 50_{-21}^{+12}$ MeV

$\Omega_c(3185)^0$ DECAY MODES	Fraction (Γ_i/Γ)	ρ (MeV/c)
$\Xi_c^+ K^-$	seen	460

 $\Omega_c(3327)^0$

$I(J^P) = ?(?^?)$

Mass $m = 3327.1_{-1.8}^{+1.2}$ MeV

Full width $\Gamma = 20_{-5}^{+14}$ MeV

$\Omega_c(3327)^0$ DECAY MODES	Fraction (Γ_i/Γ)	ρ (MeV/c)
$\Xi_c^+ K^-$	seen	610

DOUBLY CHARMED BARYONS
($C = +2$)

$\Xi_{cc}^{++} = ucc, \Xi_{cc}^+ = dcc, \Omega_{cc}^+ = scc$

 Ξ_{cc}^{++}

$I(J^P) = ?(?^?)$

Mass $m = 3621.6 \pm 0.4$ MeV

Mean life $\tau = (256 \pm 27) \times 10^{-15}$ s

Ξ_{cc}^{++} DECAY MODES	Fraction (Γ_i/Γ)	Confidence level	ρ (MeV/c)
$\Lambda_c^+ K^- \pi^+ \pi^+$	DEFINED AS 1		880
$\Xi_c^+ \pi^+, \Xi_c^+ \rightarrow p K^- \pi^+$	0.0022 ± 0.0006		—
$\Xi_c^+ \pi^+, \Xi_c^+ \rightarrow \Xi_c^+ \gamma, \Xi_c^+ \rightarrow p K^- \pi^+$	0.0031 ± 0.0009		—
$D^+ p K^- \pi^+$	<0.017	90%	562

Baryon Summary Table

BOTTOM BARYONS ($B = -1$)

$$\Lambda_b^0 = udb, \Sigma_b^0 = udb, \Sigma_b^+ = uub, \Sigma_b^- = ddb$$

$$\Xi_b^0 = usb, \Xi_b^- = dsb, \Omega_b^- = ssb$$

 Λ_b^0

$$I(J^P) = 0(\frac{1}{2}^+)$$

 $I(J^P)$ not yet measured; $0(\frac{1}{2}^+)$ is the quark model prediction.

 Mass $m = 5619.60 \pm 0.17$ MeV

 $m_{\Lambda_b^0} - m_{B^0} = 339.2 \pm 1.4$ MeV

 $m_{\Lambda_b^0} - m_{B^+} = 339.72 \pm 0.28$ MeV

 Mean life $\tau = (1.471 \pm 0.009) \times 10^{-12}$ s

 $c\tau = 441.0$ μ m

 $A_{CP}(\Lambda_b \rightarrow p\pi^-) = -0.025 \pm 0.029$ ($S = 1.2$)

 $A_{CP}(\Lambda_b \rightarrow pK^-) = -0.025 \pm 0.022$
 $A_{CP}(\Lambda_b \rightarrow DpK^-) = 0.12 \pm 0.09$
 $\Delta A_{CP}(pK^-/\pi^-) = 0.014 \pm 0.024$
 $A_{CP}(\Lambda_b \rightarrow p\bar{K}^0\pi^-) = 0.22 \pm 0.13$
 $\Delta A_{CP}(J/\psi p\pi^-/K^-) = (5.7 \pm 2.7) \times 10^{-2}$
 $A_{CP}(\Lambda_b \rightarrow \Lambda K^+\pi^-) = -0.53 \pm 0.25$
 $A_{CP}(\Lambda_b \rightarrow \Lambda K^+K^-) = -0.28 \pm 0.12$
 $\Delta A_{CP}(\Lambda_b^0 \rightarrow pK^-\mu^+\mu^-) = (-4 \pm 5) \times 10^{-2}$
 $\Delta A_{CP}(\Lambda_b^0 \rightarrow p\pi^-\pi^+\pi^-) = (1.1 \pm 2.6) \times 10^{-2}$
 $\Delta A_{CP}(\Lambda_b^0 \rightarrow (p\pi^-\pi^+\pi^-)_{LBM}) = (4 \pm 4) \times 10^{-2}$
 $\Delta A_{CP}(\Lambda_b^0 \rightarrow p a_1(1260)^-) = (-1 \pm 4) \times 10^{-2}$
 $\Delta A_{CP}(\Lambda_b^0 \rightarrow N(1520)^0 \rho(770)^0) = (2 \pm 5) \times 10^{-2}$
 $\Delta A_{CP}(\Lambda_b^0 \rightarrow \Delta(1232)^{++}\pi^-\pi^-) = (0.1 \pm 3.3) \times 10^{-2}$
 $\Delta A_{CP}(\Lambda_b^0 \rightarrow pK^-\pi^+\pi^-) = (3.2 \pm 1.3) \times 10^{-2}$
 $\Delta A_{CP}(\Lambda_b^0 \rightarrow (pK^-\pi^+\pi^-)_{LBM}) = (3.5 \pm 1.6) \times 10^{-2}$
 $\Delta A_{CP}(\Lambda_b^0 \rightarrow N(1520)^0 K^*(892)^0) = (5.5 \pm 2.5) \times 10^{-2}$
 $\Delta A_{CP}(\Lambda_b^0 \rightarrow \Lambda(1520)\rho(770)^0) = (1 \pm 6) \times 10^{-2}$
 $\Delta A_{CP}(\Lambda_b^0 \rightarrow \Delta(1232)^{++}K^-\pi^-) = (4.4 \pm 2.7) \times 10^{-2}$
 $\Delta A_{CP}(\Lambda_b^0 \rightarrow pK_1(1410)^-) = (5 \pm 4) \times 10^{-2}$
 $\Delta A_{CP}(\Lambda_b^0 \rightarrow pK^-K^+\pi^-) = (-7 \pm 5) \times 10^{-2}$
 $\Delta A_{CP}(\Lambda_b^0 \rightarrow pK^-K^+K^-) = (0.2 \pm 1.9) \times 10^{-2}$
 $\Delta A_{CP}(\Lambda_b^0 \rightarrow \Lambda(1520)\phi(1020)^0) = (4 \pm 6) \times 10^{-2}$
 $\Delta A_{CP}(\Lambda_b^0 \rightarrow (pK^-)_{highmass}\phi(1020)^0) = (-0.7 \pm 3.4) \times 10^{-2}$
 $\Delta A_{CP}(\Lambda_b^0 \rightarrow (pK^-K^+K^-)_{LBM}) = (2.7 \pm 2.4) \times 10^{-2}$
 $A_{FB}^e(\mu\mu)$ in $\Lambda_b \rightarrow \Lambda\mu^+\mu^- = -0.39 \pm 0.04$
 $\Delta(A_{FB}^e(\mu\mu))$ in $\Lambda_b \rightarrow \Lambda\mu^+\mu^- = -0.05 \pm 0.09$
 $A_{FB}^h(\rho\pi)$ in $\Lambda_b \rightarrow \Lambda(\rho\pi)\mu^+\mu^- = -0.30 \pm 0.05$
 A_{FB}^h in $\Lambda_b \rightarrow \Lambda\mu^+\mu^- = 0.25 \pm 0.04$

The branching fractions $B(b\text{-baryon} \rightarrow \Lambda\ell^-\bar{\nu}_\ell\text{anything})$ and $B(\Lambda_b^0 \rightarrow \Lambda_c^+\ell^-\bar{\nu}_\ell\text{anything})$ are not pure measurements because the underlying measured products of these with $B(b \rightarrow b\text{-baryon})$ were used to determine $B(b \rightarrow b\text{-baryon})$, as described in the note "Production and Decay of b -Flavored Hadrons."

For inclusive branching fractions, e.g., $\Lambda_b \rightarrow \bar{\Lambda}_c\text{anything}$, the values usually are multiplicities, not branching fractions. They can be greater than one.

Λ_b^0 DECAY MODES	Fraction (Γ_i/Γ)	Scale factor/ Confidence level	p (MeV/c)
$J/\psi(1S)\Lambda \times B(b \rightarrow \Lambda_b^0)$	$(5.8 \pm 0.8) \times 10^{-5}$		1740
$pD^0\pi^-$	$(6.2 \pm 0.6) \times 10^{-4}$		2370
$pD^+\pi^-\pi^-$	$(2.7 \pm 0.4) \times 10^{-4}$		2332
$pD^*(2010)^+\pi^-\pi^-$	$(5.2 \pm 1.0) \times 10^{-4}$		2277
pD^0K^-	$(4.5 \pm 0.8) \times 10^{-5}$		2269
$pJ/\psi\pi^-$	$(2.6 \pm_{-0.4}^{+0.5}) \times 10^{-5}$		1755
$p\pi^-J/\psi, J/\psi \rightarrow \mu^+\mu^-$	$(1.6 \pm 0.8) \times 10^{-6}$		-
$pJ/\psi K^-$	$(3.2 \pm_{-0.5}^{+0.6}) \times 10^{-4}$		1589
$p\eta_c(1S)K^-$	$(1.06 \pm 0.26) \times 10^{-4}$		1670
$P_{c\bar{c}}(4312)^+K^-, P_{c\bar{c}}^+ \rightarrow$	$< 2.5 \times 10^{-5}$	CL=95%	-
$p\eta_c(1S)$			
$P_{c\bar{c}}(4380)^+K^-, P_{c\bar{c}}^+ \rightarrow$	[v] $(2.7 \pm 1.4) \times 10^{-5}$		-
pJ/ψ			
$P_c(4450)^+K^-, P_c \rightarrow$	[v] $(1.3 \pm 0.4) \times 10^{-5}$		-
pJ/ψ			
$\chi_{c1}(1P)pK^-$	$(7.6 \pm_{-1.3}^{+1.5}) \times 10^{-5}$		1242

$\chi_{c1}(1P)p\pi^-$	$(5.0 \pm_{-1.1}^{+1.3}) \times 10^{-6}$		1462
$\chi_{c2}(1P)pK^-$	$(7.7 \pm_{-1.4}^{+1.6}) \times 10^{-5}$		1198
$\chi_{c2}(1P)p\pi^-$	$(4.8 \pm 1.9) \times 10^{-6}$		1427
$pJ/\psi(1S)\pi^+\pi^-K^-$	$(6.6 \pm_{-1.1}^{+1.3}) \times 10^{-5}$		1410
$p\psi(2S)K^-$	$(6.6 \pm_{-1.0}^{+1.2}) \times 10^{-5}$		1063
$\chi_{c1}(3872)pK^-$	$(3.5 \pm 1.3) \times 10^{-5}$		837
$\chi_{c1}(3872)\Lambda(1520)$	$(2.0 \pm 0.9) \times 10^{-5}$		721
$\psi(2S)p\pi^-$	$(7.5 \pm_{-1.4}^{+1.6}) \times 10^{-6}$		1320
$p\bar{K}^0\pi^-$	$(1.3 \pm 0.4) \times 10^{-5}$		2693
pK^0K^-	$< 3.5 \times 10^{-6}$	CL=90%	2639
$\Lambda_c^+\pi^-$	$(4.9 \pm 0.4) \times 10^{-3}$	S=1.2	2342
$\Lambda_c^+K^-$	$(3.56 \pm 0.28) \times 10^{-4}$	S=1.2	2314
$\Lambda_c^+ a_1(1260)^-$	seen		2153
$\Lambda_c^+ D^-$	$(4.6 \pm 0.6) \times 10^{-4}$		1886
$\Lambda_c^+ D_s^-$	$(1.10 \pm 0.10) \%$		1833
$\Lambda_c^+\pi^+\pi^-\pi^-$	$(7.6 \pm 1.1) \times 10^{-3}$	S=1.1	2323
$\Lambda_c(2595)^+\pi^-$,	$(3.4 \pm 1.4) \times 10^{-4}$		2210
$\Lambda_c(2595)^+ \rightarrow \Lambda_c^+\pi^+\pi^-$			
$\Lambda_c(2625)^+\pi^-$,	$(3.3 \pm 1.3) \times 10^{-4}$		2193
$\Lambda_c(2625)^+ \rightarrow \Lambda_c^+\pi^+\pi^-$			
$\Sigma_c(2455)^0\pi^+\pi^-, \Sigma_c^0 \rightarrow$	$(5.7 \pm 2.2) \times 10^{-4}$		2265
$\Lambda_c^+\pi^-$			
$\Sigma_c(2455)^{++}\pi^-\pi^-, \Sigma_c^{++} \rightarrow$	$(3.2 \pm 1.5) \times 10^{-4}$		2265
$\Lambda_c^+\pi^+$			
$\Lambda_c^+K^+K^-\pi^-$	$(1.02 \pm 0.11) \times 10^{-3}$		2184
$\Lambda_c^+p\bar{p}\pi^-$	$(2.63 \pm 0.27) \times 10^{-4}$		1805
$\Sigma_c(2455)^0p\bar{p}, \Sigma_c^0 \rightarrow$	$(2.3 \pm 0.5) \times 10^{-5}$		-
$\Lambda_c^+\pi^-$			
$\Sigma_c(2520)^0p\bar{p}, \Sigma_c(2520)^0 \rightarrow$	$(3.1 \pm 0.7) \times 10^{-5}$		-
$\Lambda_c^+\pi^-$			
$\Lambda_c^+\ell^-\bar{\nu}_\ell\text{anything}$	[x] $(10.9 \pm 2.2) \%$		-
$\Lambda_c^+\ell^-\bar{\nu}_\ell$	$(6.2 \pm_{-1.3}^{+1.4}) \%$		2345
$\Lambda_c^+\tau^-\bar{\nu}_\tau$	$(1.9 \pm 0.5) \%$		1933
$\Lambda_c^+\pi^+\pi^-\ell^-\bar{\nu}_\ell$	$(5.6 \pm 3.1) \%$		2335
$\Lambda_c(2595)^+\ell^-\bar{\nu}_\ell$	$(7.9 \pm_{-3.5}^{+4.0}) \times 10^{-3}$		2212
$\Lambda_c(2625)^+\ell^-\bar{\nu}_\ell$	$(1.3 \pm_{-0.5}^{+0.6}) \%$		2195
$p h^-$	[y] $< 2.3 \times 10^{-5}$	CL=90%	2730
$p\pi^-$	$(4.6 \pm 0.8) \times 10^{-6}$		2730
pK^-	$(5.5 \pm 1.0) \times 10^{-6}$		2709
pD_s^-	$(1.25 \pm 0.13) \times 10^{-5}$		2364
$p\mu^-\bar{\nu}_\mu$	$(4.1 \pm 1.0) \times 10^{-4}$		2730
$\Lambda\mu^+\mu^-$	$(1.08 \pm 0.28) \times 10^{-6}$		2695
$p\pi^-\mu^+\mu^-$	$(6.9 \pm 2.5) \times 10^{-8}$		2720
$pK^-e^+e^-$	$(3.1 \pm 0.6) \times 10^{-7}$		2708
$pK^-\mu^+\mu^-$	$(2.6 \pm_{-0.4}^{+0.5}) \times 10^{-7}$		2685
$\Lambda\gamma$	$(7.1 \pm 1.7) \times 10^{-6}$		2699
$\Lambda\eta$	$(9 \pm_5^+7) \times 10^{-6}$		2670
$\Lambda\eta'(958)$	$< 3.1 \times 10^{-6}$	CL=90%	2611
$\Lambda\pi^+\pi^-$	$(4.6 \pm 1.9) \times 10^{-6}$		2692
$\Lambda K^+\pi^-$	$(5.6 \pm 1.2) \times 10^{-6}$		2660
ΛK^+K^-	$(1.60 \pm 0.21) \times 10^{-5}$		2605
$\Lambda\phi$	$(9.8 \pm 2.6) \times 10^{-6}$		2599
$p\pi^-\pi^+\pi^-$	$(2.08 \pm 0.21) \times 10^{-5}$		2715
$pK^-K^+\pi^-$	$(4.0 \pm 0.6) \times 10^{-6}$		2612
$pK^-\pi^+\pi^-$	$(5.0 \pm 0.5) \times 10^{-5}$		2675
$pK^-K^+K^-$	$(1.25 \pm 0.13) \times 10^{-5}$		2524

 $\Lambda_b(5912)^0$

$$J^P = \frac{1}{2}^-$$

 Mass $m = 5912.19 \pm 0.17$ MeV

 Full width $\Gamma < 0.25$ MeV, CL = 90%

$\Lambda_b(5912)^0$ DECAY MODES	Fraction (Γ_i/Γ)	p (MeV/c)
$\Lambda_b^0\pi^+\pi^-$	seen	86

Baryon Summary Table

$\Lambda_b(5920)^0$	$J^P = \frac{3}{2}^-$
Mass $m = 5920.09 \pm 0.17$ MeV	
Full width $\Gamma < 0.19$ MeV, CL = 90%	

$\Lambda_b(5920)^0$ DECAY MODES	Fraction (Γ_i/Γ)	ρ (MeV/c)
$\Lambda_b^0 \pi^+ \pi^-$	seen	108

$\Lambda_b(6070)^0$	$J^P = \frac{1}{2}^+$
Quantum numbers based on quark model expectations.	
Mass $m = 6072.3 \pm 2.9$ MeV	
Full width $\Gamma = 72 \pm 11$ MeV	

$\Lambda_b(6070)^0$ DECAY MODES	Fraction (Γ_i/Γ)	ρ (MeV/c)
$\Lambda_b^0 \pi^+ \pi^-$	seen	343

$\Lambda_b(6146)^0$	$J^P = \frac{3}{2}^+$
Mass $m = 6146.2 \pm 0.4$ MeV	
$m_{\Lambda_b(6146)^0} - m_{\Lambda_b^0} = 526.55 \pm 0.34$ MeV	
Full width $\Gamma = 2.9 \pm 1.3$ MeV	

$\Lambda_b(6146)^0$ DECAY MODES	Fraction (Γ_i/Γ)	ρ (MeV/c)
$\Lambda_b^0 \pi^+ \pi^-$	seen	427

$\Lambda_b(6152)^0$	$J^P = \frac{5}{2}^+$
Mass $m = 6152.5 \pm 0.4$ MeV	
$m_{\Lambda_b(6152)^0} - m_{\Lambda_b^0} = 532.89 \pm 0.28$ MeV	
$m_{\Lambda_b(6152)^0} - m_{\Lambda_b(6146)^0} = 6.34 \pm 0.32$ MeV	
Full width $\Gamma = 2.1 \pm 0.9$ MeV	

$\Lambda_b(6152)^0$ DECAY MODES	Fraction (Γ_i/Γ)	ρ (MeV/c)
$\Lambda_b^0 \pi^+ \pi^-$	seen	434

Σ_b	$I(J^P) = 1(\frac{1}{2}^+)$ I, J, P need confirmation.
Mass $m(\Sigma_b^{*+}) = 5810.56 \pm 0.25$ MeV	
Mass $m(\Sigma_b^{*-}) = 5815.64 \pm 0.27$ MeV	
$m_{\Sigma_b^{*+}} - m_{\Sigma_b^{*-}} = -5.06 \pm 0.18$ MeV	
$\Gamma(\Sigma_b^{*+}) = 5.0 \pm 0.5$ MeV	
$\Gamma(\Sigma_b^{*-}) = 5.3 \pm 0.5$ MeV	

Σ_b DECAY MODES	Fraction (Γ_i/Γ)	ρ (MeV/c)
$\Lambda_b^0 \pi$	dominant	133

Σ_b^*	$I(J^P) = 1(\frac{3}{2}^+)$ I, J, P need confirmation.
Mass $m(\Sigma_b^{*+}) = 5830.32 \pm 0.27$ MeV	
Mass $m(\Sigma_b^{*-}) = 5834.74 \pm 0.30$ MeV	
$m_{\Sigma_b^{*+}} - m_{\Sigma_b^{*-}} = -4.37 \pm 0.33$ MeV ($S = 1.6$)	
$m_{\Sigma_b^{*+}} - m_{\Sigma_b^+} = 19.73 \pm 0.18$	
$m_{\Sigma_b^{*-}} - m_{\Sigma_b^-} = 19.09 \pm 0.22$	
$\Gamma(\Sigma_b^{*+}) = 9.4 \pm 0.5$ MeV	
$\Gamma(\Sigma_b^{*-}) = 10.4 \pm 0.8$ MeV ($S = 1.3$)	
$m_{\Sigma_b^+} - m_{\Sigma_b^-} = 21.2 \pm 2.0$ MeV	

Σ_b^* DECAY MODES	Fraction (Γ_i/Γ)	ρ (MeV/c)
$\Lambda_b^0 \pi$	dominant	159

$\Sigma_b(6097)^+$	$J^P = ?^?$
Mass $m = 6095.8 \pm 1.7$ MeV	
Full width $\Gamma = 31 \pm 6$ MeV	

$\Sigma_b(6097)^+$ DECAY MODES	Fraction (Γ_i/Γ)	ρ (MeV/c)
$\Lambda_b \pi^+ \times B(b \rightarrow \Sigma_b(6097)^+)$	seen	-

$\Sigma_b(6097)^-$	$J^P = ?^?$
Mass $m = 6098.0 \pm 1.8$ MeV	
Full width $\Gamma = 29 \pm 4$ MeV	

$\Sigma_b(6097)^-$ DECAY MODES	Fraction (Γ_i/Γ)	ρ (MeV/c)
$\Lambda_b \pi^- \times B(b \rightarrow \Sigma_b(6097)^-)$	seen	-

Ξ_b^-	$I(J^P) = \frac{1}{2}(\frac{1}{2}^+)$ I, J, P need confirmation.
$m(\Xi_b^-) = 5797.0 \pm 0.6$ MeV ($S = 1.7$)	
$m_{\Xi_b^-} - m_{\Lambda_b^0} = 177.46 \pm 0.31$ MeV ($S = 1.3$)	
$m_{\Xi_b^-} - m_{\Xi_b^0} = 5.9 \pm 0.6$ MeV	
Mean life $\tau_{\Xi_b^-} = (1.572 \pm 0.040) \times 10^{-12}$ s	

Ξ_b^- DECAY MODES	Fraction (Γ_i/Γ)	Confidence level	ρ (MeV/c)
$J/\psi \Xi^- \times B(b \rightarrow \Xi_b^-)$	$(1.02^{+0.26}_{-0.21}) \times 10^{-5}$		1782
$J/\psi \Lambda K^- \times B(b \rightarrow \Xi_b^-)$	$(2.5 \pm 0.4) \times 10^{-6}$		1631
$p K^- K^- \times B(b \rightarrow \Xi_b^-)$	$(3.7 \pm 0.8) \times 10^{-8}$		2731
$p K^- K^-$	seen		2731
$p K^- \pi^-$	seen		2783
$\Lambda_b^0 \pi^- \times B(b \rightarrow \Xi_b^-)/B(b \rightarrow \Lambda_b^0)$	$(7.0 \pm 0.9) \times 10^{-4}$		99
$\Xi_c^0 \pi^-$	seen		2367
$\Sigma(1385) K^-$	$(2.6 \pm 2.3) \times 10^{-7}$		2707
$\Lambda(1405) K^-$	$(1.9 \pm 1.2) \times 10^{-7}$		2702
$\Lambda(1520) K^-$	$(7.6 \pm 3.2) \times 10^{-7}$		2673
$\Lambda(1670) K^-$	$(4.5 \pm 2.3) \times 10^{-7}$		2629
$\Sigma(1775) K^-$	$(2.2 \pm 1.5) \times 10^{-7}$		2599
$\Sigma(1915) K^-$	$(2.6 \pm 2.5) \times 10^{-7}$		2553
$\Xi^- \gamma$	$< 1.3 \times 10^{-4}$	95%	-

Ξ_b^0	$I(J^P) = \frac{1}{2}(\frac{1}{2}^+)$ I, J, P need confirmation.
$m(\Xi_b^0) = 5791.9 \pm 0.5$ MeV	
$m_{\Xi_b^0} - m_{\Lambda_b^0} = 172.5 \pm 0.4$ MeV	
Mean life $\tau_{\Xi_b^0} = (1.480 \pm 0.030) \times 10^{-12}$ s	

Ξ_b^0 DECAY MODES	Fraction (Γ_i/Γ)	Confidence level	ρ (MeV/c)
$p D^0 K^- \times B(b \rightarrow \Xi_b^0)$	$(1.7 \pm 0.5) \times 10^{-6}$		2374
$p \bar{K}^0 \pi^- \times B(b \rightarrow \Xi_b^0)/B(\bar{b} \rightarrow B^0)$	$< 1.6 \times 10^{-6}$	90%	2783
$p K^0 K^- \times B(b \rightarrow \Xi_b^0)/B(\bar{b} \rightarrow B^0)$	$< 1.1 \times 10^{-6}$	90%	2730
$\Lambda \pi^+ \pi^- \times B(b \rightarrow \Xi_b^0)/B(b \rightarrow \Lambda_b^0)$	$< 1.7 \times 10^{-6}$	90%	2781
$\Lambda K^- \pi^+ \times B(b \rightarrow \Xi_b^0)/B(b \rightarrow \Lambda_b^0)$	$< 8 \times 10^{-7}$	90%	2751
$\Lambda K^+ K^- \times B(b \rightarrow \Xi_b^0)/B(b \rightarrow \Lambda_b^0)$	$< 3 \times 10^{-7}$	90%	2698
$J/\psi \Lambda$	seen		1868
$J/\psi \Xi^0$	seen		1785
$\Lambda_c^+ K^- \times B(b \rightarrow \Xi_b^0)$	$(6 \pm 4) \times 10^{-7}$		2416
$p K^- \pi^+ \pi^- \times B(b \rightarrow \Xi_b^0)/B(b \rightarrow \Lambda_b^0)$	$(1.9 \pm 0.4) \times 10^{-6}$		2766
$p K^- K^- \pi^+ \times B(b \rightarrow \Xi_b^0)/B(b \rightarrow \Lambda_b^0)$	$(1.70 \pm 0.30) \times 10^{-6}$		2704
$p K^- K^+ K^- \times B(b \rightarrow \Xi_b^0)/B(b \rightarrow \Lambda_b^0)$	$(1.7 \pm 0.9) \times 10^{-7}$		2620

$\Xi_b'(5935)^-$	$J^P = \frac{1}{2}^+$
Mass $m = 5935.1 \pm 0.5$ MeV	
Full width $\Gamma = 0.03 \pm 0.032$ MeV	

Baryon Summary Table

$\Xi'_b(5935)^-$ DECAY MODES	Fraction (Γ_i/Γ)	ρ (MeV/c)
$\Xi_b^0 \pi^- \times B(\bar{b} \rightarrow \Xi'_b(5935)^-)/B(\bar{b} \rightarrow \Xi_b^0)$	(11.8±1.8) %	31

$$\Xi_b(5945)^0 \quad J^P = \frac{3}{2}^+$$

Mass $m = 5952.3 \pm 0.6$ MeV
Full width $\Gamma = 0.87 \pm 0.08$ MeV

$\Xi_b(5945)^0$ DECAY MODES	Fraction (Γ_i/Γ)	ρ (MeV/c)
$\Xi_b^- \pi^+$	seen	78

$$\Xi_b(5955)^- \quad J^P = \frac{3}{2}^+$$

Mass $m = 5955.7 \pm 0.5$ MeV
Full width $\Gamma = 1.43 \pm 0.11$ MeV

$\Xi_b(5955)^-$ DECAY MODES	Fraction (Γ_i/Γ)	ρ (MeV/c)
$\Xi_b^0 \pi^- \times B(\bar{b} \rightarrow \Xi_b^*(5955)^-)/B(\bar{b} \rightarrow \Xi_b^0)$	(20.7±3.5) %	84

$$\Xi_b(6087)^0 \quad I(J^P) = \frac{1}{2}(\frac{3}{2}^-)$$

J, P need confirmation.

Mass $m = 6087.2 \pm 0.5$ MeV
Full width $\Gamma = 2.4 \pm 0.5$ MeV

$\Xi_b(6087)^0$ DECAY MODES	Fraction (Γ_i/Γ)	ρ (MeV/c)
$\Xi_b^0 \pi^+ \pi^-$	seen	-

$$\Xi_b(6095)^0 \quad I(J^P) = \frac{1}{2}(\frac{3}{2}^-)$$

J, P need confirmation.

Mass $m = 6095.3 \pm 0.5$ MeV
Full width $\Gamma = 0.50 \pm 0.35$ MeV

$\Xi_b(6095)^0$ DECAY MODES	Fraction (Γ_i/Γ)	ρ (MeV/c)
$\Xi_b^0 \pi^+ \pi^-$	seen	-

$$\Xi_b(6100)^- \quad J^P = \frac{3}{2}^-$$

J, P need confirmation.

Mass $m = 6099.8 \pm 0.6$ MeV
Full width $\Gamma = 0.94 \pm 0.31$ MeV

$\Xi_b(6100)^-$ DECAY MODES	Fraction (Γ_i/Γ)	ρ (MeV/c)
$\Xi_b^- \pi^+ \pi^-$	seen	128

$$\Xi_b(6227)^- \quad J^P = ?^?$$

Mass $m = 6227.9 \pm 0.9$ MeV
Full width $\Gamma = 19.9 \pm 2.6$ MeV

$\Xi_b(6227)^-$ DECAY MODES	Fraction (Γ_i/Γ)	Scale factor	ρ (MeV/c)
$\Lambda_b^0 K^- \times B(b \rightarrow \Xi_b(6227)^-)/B(b \rightarrow \Lambda_b^0)$	(3.20±0.35) × 10 ⁻³		336
$\Xi_b^0 \pi^- \times B(b \rightarrow \Xi_b(6227)^-)/B(b \rightarrow \Xi_b^0)$	(2.8 ± 1.1) %	1.8	398

$$\Xi_b(6227)^0 \quad J^P = ?^?$$

Mass $m = 6226.8 \pm 1.6$ MeV
Full width $\Gamma = 19^{+5}_{-4}$ MeV

$\Xi_b(6227)^0$ DECAY MODES	Fraction (Γ_i/Γ)	ρ (MeV/c)
$\Xi_b^- \pi^+ \times B(b \rightarrow \Xi_b(6227)^0)/B(b \rightarrow \Xi_b^-)$	(4.5±0.9) %	398

$$\Xi_b(6327)^0 \quad J^P = ?^?$$

Mass $m = 6327.28 \pm 0.35$ MeV
Full width $\Gamma < 2.56$ MeV, CL = 95%

$\Xi_b(6327)^0$ DECAY MODES	Fraction (Γ_i/Γ)	ρ (MeV/c)
$\Lambda_b^0 K^- \pi^+$	seen	298

$$\Xi_b(6333)^0 \quad J^P = ?^?$$

Mass $m = 6332.69 \pm 0.28$ MeV
Full width $\Gamma < 1.92$ MeV, CL = 95%

$\Xi_b(6333)^0$ DECAY MODES	Fraction (Γ_i/Γ)	ρ (MeV/c)
$\Lambda_b^0 K^- \pi^+$	seen	309

$$\Omega_b^- \quad I(J^P) = 0(\frac{1}{2}^+)$$

I, J, P need confirmation.

Mass $m = 6045.8 \pm 0.8$ MeV
 $m_{\Omega_b^-} - m_{\Lambda_b^0} = 426.4 \pm 2.2$ MeV
 $m_{\Omega_b^-} - m_{\Xi_b^-} = 248.5 \pm 0.6$ MeV
Mean life $\tau = (1.64^{+0.18}_{-0.17}) \times 10^{-12}$ s
 $\tau(\Omega_b^-)/\tau(\Xi_b^-)$ mean life ratio = 1.11 ± 0.16

Ω_b^- DECAY MODES	Fraction (Γ_i/Γ)	Scale factor/ Confidence level	ρ (MeV/c)
$J/\psi \Omega^- \times B(b \rightarrow \Omega_b^-)$	(1.4 ^{+0.5} _{-0.4}) × 10 ⁻⁶	S=1.6	1805
$p K^- K^- \times B(\bar{b} \rightarrow \Omega_b^-)$	< 2.3 × 10 ⁻⁹	CL=90%	2865
$p \pi^- \pi^- \times B(\bar{b} \rightarrow \Omega_b^-)$	< 1.5 × 10 ⁻⁸	CL=90%	2943
$p K^- \pi^- \times B(\bar{b} \rightarrow \Omega_b^-)$	< 7 × 10 ⁻⁹	CL=90%	2915
$\Omega_c^0 \pi^-$	seen		2420
$\Omega_c^0 \pi^-, \Omega_c^0 \rightarrow p K^- K^- \pi^+$	seen		-
$\Xi_c^+ K^- \pi^-$	seen		2473

$$\Omega_b(6316)^- \quad I(J^P) = ?(??)$$

I, J, P need confirmation.

Mass $m = 6315.6 \pm 0.6$ MeV
Full width $\Gamma < 4.2$ MeV, CL = 95%

$\Omega_b(6316)^-$ DECAY MODES	Fraction (Γ_i/Γ)	ρ (MeV/c)
$\Xi_b^0 K^-$	seen	168

$$\Omega_b(6330)^- \quad I(J^P) = ?(??)$$

I, J, P need confirmation.

Mass $m = 6330.3 \pm 0.6$ MeV
Full width $\Gamma < 4.7$ MeV, CL = 95%

$\Omega_b(6330)^-$ DECAY MODES	Fraction (Γ_i/Γ)	ρ (MeV/c)
$\Xi_b^0 K^-$	seen	206

$$\Omega_b(6340)^- \quad I(J^P) = ?(??)$$

I, J, P need confirmation.

Mass $m = 6339.7 \pm 0.6$ MeV
Full width $\Gamma < 1.8$ MeV, CL = 95%

$\Omega_b(6340)^-$ DECAY MODES	Fraction (Γ_i/Γ)	ρ (MeV/c)
$\Xi_b^0 K^-$	seen	227

$$\Omega_b(6350)^- \quad I(J^P) = ?(??)$$

I, J, P need confirmation.

Mass $m = 6349.8 \pm 0.6$ MeV
Full width $\Gamma < 3.2$ MeV, CL = 95%

$\Omega_b(6350)^-$ DECAY MODES	Fraction (Γ_i/Γ)	ρ (MeV/c)
$\Xi_b^0 K^-$	seen	248

Baryon Summary Table

 b -baryon ADMIXTURE ($\Lambda_b, \Xi_b, \Omega_b$)

These branching fractions are actually an average over weakly decaying b -baryons weighted by their production rates at the LHC, LEP, and Tevatron, branching ratios, and detection efficiencies. They scale with the b -baryon production fraction $B(b \rightarrow b\text{-baryon})$.

The branching fractions $B(b\text{-baryon} \rightarrow \Lambda \ell^- \bar{\nu}_\ell \text{anything})$ and $B(\Lambda_b^0 \rightarrow \Lambda_c^+ \ell^- \bar{\nu}_\ell \text{anything})$ are not pure measurements because the underlying measured products of these with $B(b \rightarrow b\text{-baryon})$ were used to determine $B(b \rightarrow b\text{-baryon})$, as described in the note "Production and Decay of b -Flavored Hadrons."

For inclusive branching fractions, e.g., $B \rightarrow D^\pm \text{anything}$, the values usually are multiplicities, not branching fractions. They can be greater than one.

b -baryon ADMIXTURE DECAY MODES ($\Lambda_b, \Xi_b, \Omega_b$)	Fraction (Γ_i/Γ)	Scale factor	p (MeV/c)
$p \mu^- \bar{\nu}$ anything	$(5.8 \pm_{-2.3}^{+2.0})\%$		—
$p \ell \bar{\nu}_\ell$ anything	$(5.6 \pm 1.2)\%$		—
p anything	$(70 \pm 22)\%$		—
$\Lambda \ell^- \bar{\nu}_\ell$ anything	$(3.8 \pm 0.6)\%$		—
$\Lambda \ell^+ \nu_\ell$ anything	$(3.2 \pm 0.8)\%$		—
Λ anything	$(39 \pm 7)\%$		—
$\Xi^- \ell^- \bar{\nu}_\ell$ anything	$(4.6 \pm 1.4) \times 10^{-3}$	1.2	—

EXOTIC BARYONS **$P_{c\bar{c}s}(4338)^0$**

$$I(J^P) = 0(\frac{1}{2}^-)$$

Mass $m = 4338.2 \pm 0.8$ MeV
Full width $\Gamma = 7.0 \pm 1.8$ MeV

$P_{c\bar{c}s}(4338)^0$ DECAY MODES	Fraction (Γ_i/Γ)	p (MeV/c)
$J/\psi \Lambda$	seen	—

NOTES

This Summary Table only includes established baryons. The Particle Listings include evidence for other baryons. The masses, widths, and branching fractions for the resonances in this Table are Breit-Wigner parameters, but pole positions are also given for most of the N and Δ resonances.

For most of the resonances, the parameters come from various partial-wave analyses of more or less the same sets of data, and it is not appropriate to treat the results of the analyses as independent or to average them together. Furthermore, the systematic errors on the results are not well understood. Thus, we usually only give ranges for the parameters. We then also give a best guess for the mass (as part of the name of the resonance) and for the width. The *Note on N and Δ Resonances* and the *Note on Λ and Σ Resonances* in the Particle Listings review the partial-wave analyses.

When a quantity has "(S = ...)" to its right, the error on the quantity has been enlarged by the "scale factor" S , defined as $S = \sqrt{\chi^2/(N-1)}$, where N is the number of measurements used in calculating the quantity. We do this when $S > 1$, which often indicates that the measurements are inconsistent. When $S > 1.25$, we also show in the Particle Listings an ideogram of the measurements. For more about S , see the Introduction.

A decay momentum p is given for each decay mode. For a 2-body decay, p is the momentum of each decay product in the rest frame of the decaying particle. For a 3-or-more-body decay, p is the largest momentum any of the products can have in this frame. For any resonance, the *nominal* mass is used in calculating p . A dagger ("†") in this column indicates that the mode is forbidden when the nominal masses of resonances are used, but is in fact allowed due to the nonzero widths of the resonances.

[a] The masses of the p and n are most precisely known in u (unified atomic mass units). The conversion factor to MeV, $1 u = 931.494061(21)$ MeV, is less well known than are the masses in u .

[b] The $|m_p - m_{\bar{p}}|/m_p$ and $|q_p + q_{\bar{p}}|/e$ are not independent, and both use the more precise measurement of $|q_{\bar{p}}/m_{\bar{p}}|/(q_p/m_p)$.

[c] The limit is from neutrality-of-matter experiments; it assumes $q_n = q_p + q_e$. See also the charge of the neutron.

[d] The μp and $e p$ values for the charge radius are much too different to average them. The disagreement is not yet understood.

[e] There is a lot of disagreement about the value of the proton magnetic charge radius. See the Listings.

[f] There is some controversy about whether nuclear physics and model dependence complicate the analysis for bound neutrons (from which the best limit comes). The first limit here is from reactor experiments with free neutrons.

[g] Lee and Yang in 1956 proposed the existence of a mirror world in an attempt to restore global parity symmetry—thus a search for oscillations between the two worlds. Oscillations between the worlds would be maximal when the magnetic fields B and B' were equal. The limit for any B' in the range 0 to 12.5 μT is >12 s (95% CL).

[h] The parameters g_A, g_V , and g_{WM} for semileptonic modes are defined by $\bar{B}_f[\gamma_\lambda(g_V + g_A\gamma_5) + i(g_{WM}/m_{B_i})\sigma_{\lambda\nu}q^\nu]B_i$, and ϕ_{AV} is defined by $g_A/g_V = |g_A/g_V|e^{i\phi_{AV}}$. See the "Note on Baryon Decay Parameters" in the neutron Particle Listings.

[i] Time-reversal invariance requires this to be 0° or 180° .

[j] This coefficient is zero if time invariance is not violated.

[k] This limit is for γ energies between 0.4 and 782 keV.

[l] The decay parameters γ and Δ are calculated from α and ϕ using

$$\gamma = \sqrt{1-\alpha^2} \cos\phi, \quad \tan\Delta = -\frac{1}{\alpha} \sqrt{1-\alpha^2} \sin\phi.$$

See the "Note on Baryon Decay Parameters" in the neutron Particle Listings.

[n] See the Listings for the pion momentum range used in this measurement.

[o] Our estimate. See the Particle Listings for details.

[p] A theoretical value using QED.

[q] This branching fraction includes all the decay modes of the final-state resonance.

[r] Here γ_D stands for a dark photon.

[s] See AALTONEN 11H, Fig. 8, for the calculated ratio of $\Lambda_c^+ \pi^0 \pi^0$ and $\Lambda_c^+ \pi^+ \pi^-$ partial widths as a function of the $\Lambda_c(2595)^+ - \Lambda_c^+$ mass difference. At our value of the mass difference, the ratio is about 4.

[t] A test that the isospin is indeed 0, so that the particle is indeed a Λ_c^+ .

[u] Assuming isospin conservation, so that the other third is $\Lambda_c^+ \pi^0 \pi^0$.

[v] P_c^+ is a pentaquark-charmonium state.

[x] Not a pure measurement. See note at head of Λ_b^0 Decay Modes.

[y] Here h^- means π^- or K^- .

Searches Summary Table

SEARCHES not in other sections

Magnetic Monopole Searches

The most sensitive experiments obtain negative results.
Best cosmic-ray supermassive monopole flux limit:
 $< 1.4 \times 10^{-16} \text{ cm}^{-2} \text{sr}^{-1} \text{s}^{-1}$ for $1.1 \times 10^{-4} < \beta < 1$

Supersymmetric Particle Searches

All supersymmetric mass bounds here are model dependent.

The limits assume:

1) $\tilde{\chi}_1^0$ is the lightest supersymmetric particle; 2) R -parity is conserved, unless stated otherwise;

See the Particle Listings for a Note giving details of supersymmetry.

$\tilde{\chi}_i^0$ — neutralinos (mixtures of $\tilde{\gamma}$, \tilde{Z}^0 , and \tilde{H}_i^0)

Mass $m_{\tilde{\chi}_1^0} > 0 \text{ GeV}$, CL = 95%

[general MSSM, non-universal gaugino masses]

Mass $m_{\tilde{\chi}_1^0} > 46 \text{ GeV}$, CL = 95%

[all $\tan\beta$, all m_0 , all $m_{\tilde{\chi}_2^0} - m_{\tilde{\chi}_1^0}$]

Mass $m_{\tilde{\chi}_2^0} > 62.4 \text{ GeV}$, CL = 95%

[$1 < \tan\beta < 40$, all m_0 , all $m_{\tilde{\chi}_2^0} - m_{\tilde{\chi}_1^0}$]

Mass $m_{\tilde{\chi}_3^0} > 99.9 \text{ GeV}$, CL = 95%

[$1 < \tan\beta < 40$, all m_0 , all $m_{\tilde{\chi}_2^0} - m_{\tilde{\chi}_1^0}$]

Mass $m_{\tilde{\chi}_4^0} > 116 \text{ GeV}$, CL = 95%

[$1 < \tan\beta < 40$, all m_0 , all $m_{\tilde{\chi}_2^0} - m_{\tilde{\chi}_1^0}$]

Mass $m_{\tilde{\chi}}$ none 200–670 GeV, CL = 95% [R-Parity Violating]

[wino production, $\tilde{\chi} \rightarrow b + \ell/\nu + t/b$ via λ'_{33} coupling]

$\tilde{\chi}_i^\pm$ — charginos (mixtures of \tilde{W}^\pm and \tilde{H}_i^\pm)

Mass $m_{\tilde{\chi}_1^\pm} > 94 \text{ GeV}$, CL = 95%

[$\tan\beta < 40$, $m_{\tilde{\chi}_1^\pm} - m_{\tilde{\chi}_1^0} > 3 \text{ GeV}$, all m_0]

Mass $m_{\tilde{\chi}_1^\pm} > 1000 \text{ GeV}$, CL = 95%

[$2\ell + \cancel{E}_T$, Tchi1chi1C, $m_{\tilde{\chi}_1^0} = 0 \text{ GeV}$]

Mass $m_{\tilde{\chi}_1^\pm} > 1600 \text{ GeV}$, CL = 95% [R-Parity Violating]

[Tchi1n2l, $\tilde{\chi}_1^0 \rightarrow \ell^\pm \ell^\mp \nu$, $\lambda_{12k} \neq 0$, $m_{\tilde{\chi}_1^0} = 1200 \text{ GeV}$]

$\tilde{\chi}^\pm$ — long-lived chargino

Mass $m_{\tilde{\chi}^\pm} > 1050 \text{ GeV}$, CL = 95%

[$\tilde{\chi}^\pm \rightarrow \tilde{\chi}_1^0 \pi^\pm$, wino LSP, stable]

Mass $m_{\tilde{\chi}^\pm} > 1050 \text{ GeV}$, CL = 95%

[$\tilde{\chi}^\pm \rightarrow \tilde{\chi}_1^0 \pi^\pm$, wino LSP, $\tau = 20 \text{ ns}$]

$\tilde{\nu}$ — sneutrino

Mass $m > 41 \text{ GeV}$, CL = 95% [model independent]

Mass $m > 94 \text{ GeV}$, CL = 95%

[CMSSM, $1 \leq \tan\beta \leq 40$, $m_{\tilde{e}_R} - m_{\tilde{\chi}_1^0} > 10 \text{ GeV}$]

Mass $m > 4200 \text{ GeV}$, CL = 95% [R-Parity Violating]

[$1e + 1\mu, \nu_\tau \rightarrow e\mu, \lambda = \lambda' = 0.1$]

\tilde{e} — scalar electron (selectron)

Mass $m > 107 \text{ GeV}$, CL = 95% [all $m_{\tilde{e}_L} - m_{\tilde{\chi}_1^0}$]

Mass $m > 700 \text{ GeV}$, CL = 95%

[$2\ell + \cancel{E}_T$, $m_{\tilde{e}_R} = m_{\tilde{e}_L}$ and $\tilde{e} = \tilde{e}, \tilde{\mu}, m_{\tilde{\chi}_1^0} = 0 \text{ GeV}$]

Mass $m > 250 \text{ GeV}$, CL = 95%

[$\ell^\pm \ell^\mp + \cancel{E}_T$, \tilde{e}_R , $m_{\tilde{\chi}_1^0} = 0 \text{ GeV}$]

Mass $m > 410 \text{ GeV}$, CL = 95% [R-Parity Violating]

[$\geq 4\ell^\pm, \tilde{e} \rightarrow l\tilde{\chi}_1^0, \tilde{\chi}_1^0 \rightarrow \ell^\pm \ell^\mp \nu$]

Mass $m > 1200 \text{ GeV}$, CL = 95% [R-Parity Violating]

[$\geq 4\ell, \lambda_{12k} \neq 0, m_{\tilde{\chi}_1^0} = 900 \text{ GeV}$ (m-degenerate $\tilde{e}_L, \tilde{\nu}$)]

$\tilde{\mu}$ — scalar muon (smuon)

Mass $m > 700 \text{ GeV}$, CL = 95%

[$2\ell + \cancel{E}_T$, $m_{\tilde{\mu}_R} = m_{\tilde{\mu}_L}$ and $\tilde{\mu} = \tilde{e}, \tilde{\mu}, m_{\tilde{\chi}_1^0} = 0 \text{ GeV}$]

Mass $m > 210 \text{ GeV}$, CL = 95%

[$\ell^\pm \ell^\mp + \cancel{E}_T$, $\tilde{\mu}_R$, $m_{\tilde{\chi}_1^0} = 0 \text{ GeV}$]

Mass $m > 94 \text{ GeV}$, CL = 95%

[CMSSM, $1 \leq \tan\beta \leq 40$, $m_{\tilde{\mu}_R} - m_{\tilde{\chi}_1^0} > 10 \text{ GeV}$]

Mass $m > 410 \text{ GeV}$, CL = 95% [R-Parity Violating]

[$\geq 4\ell^\pm, \tilde{\mu} \rightarrow l\tilde{\chi}_1^0, \tilde{\chi}_1^0 \rightarrow \ell^\pm \ell^\mp \nu$]

Mass $m > 1200 \text{ GeV}$, CL = 95% [R-Parity Violating]

[$\geq 4\ell, \lambda_{12k} \neq 0, m_{\tilde{\chi}_1^0} = 900 \text{ GeV}$ (m-degenerate $\tilde{e}_L, \tilde{\nu}$)]

$\tilde{\tau}$ — scalar tau (stau)

Mass $m > 81.9 \text{ GeV}$, CL = 95%

[$m_{\tilde{\tau}_R} - m_{\tilde{\chi}_1^0} > 15 \text{ GeV}$, all θ_τ , $B(\tilde{\tau} \rightarrow \tau\tilde{\chi}_1^0) = 100\%$]

Mass $m > 400 \text{ GeV}$, CL = 95%

[2 hadronic $\tau + \cancel{E}_T$, $\tilde{\tau}_{R,L} \rightarrow \tau\tilde{\chi}_1^0$, $m_{\tilde{\chi}_1^0} = 1 \text{ GeV}$]

Mass $m > 90 \text{ GeV}$, CL = 95% [R-Parity Violating]

[$\tilde{\tau}_R$, indirect, $\Delta m > 5 \text{ GeV}$]

Mass $m > 1200 \text{ GeV}$, CL = 95% [R-Parity Violating]

[$\geq 4\ell, \lambda_{12k} \neq 0, m_{\tilde{\chi}_1^0} = 900 \text{ GeV}$ (m-degenerate $\tilde{e}_L, \tilde{\nu}$)]

Mass $m > 286 \text{ GeV}$, CL = 95% [long-lived $\tilde{\tau}$]

\tilde{q} — squarks of the first two quark generations

Mass $m > 1.220 \times 10^3 \text{ GeV}$, CL = 95%

[jets + \cancel{E}_T , Tsqk1, 1 non-degenerate \tilde{q} , $m_{\tilde{\chi}_1^0} = 0 \text{ GeV}$]

Mass $m > 1.600 \times 10^3 \text{ GeV}$, CL = 95% [R-Parity Violating]

[$\tilde{q} \rightarrow q\tilde{\chi}_1^0, \tilde{\chi}_1^0 \rightarrow \ell\ell\nu, \lambda_{121}, \lambda_{122} \neq 0, m_{\tilde{g}} = 2400 \text{ GeV}$]

\tilde{q} — long-lived squark

Mass $m > 1340 \text{ GeV}$, CL = 95% [\tilde{t} R -hadrons]

Mass $m > 1250 \text{ GeV}$, CL = 95% [\tilde{b} R -hadrons]

\tilde{b} — scalar bottom (sbottom)

Mass $m > 1.270 \times 10^3 \text{ GeV}$, CL = 95%

[b -jets + \cancel{E}_T , Tsb0t1, $m_{\tilde{\chi}_1^0} = 0 \text{ GeV}$]

Mass $m > 307 \text{ GeV}$, CL = 95% [R-Parity Violating]

[$\tilde{b} \rightarrow t d$ or $t s$, λ'_{332} or λ'_{331} coupling]

\tilde{t} — scalar top (stop)

Mass $m > 1.310 \times 10^3 \text{ GeV}$, CL = 95%

[jets + \cancel{E}_T , Tstop1, $m_{\tilde{\chi}_1^0} < 300 \text{ GeV}$]

Mass $m > 1100 \text{ GeV}$, CL = 95% [R-Parity Violating]

[$\tilde{t} \rightarrow b e$, Tstop2RPV, prompt]

Mass $m > 460 \text{ GeV}$, CL = 95%

[R-Parity Violating, long-lived \tilde{t} , $\tilde{t} \rightarrow d\bar{t}$, $0.01 \text{ cm} < c\tau < 1000 \text{ cm}$]

\tilde{g} — gluino

Mass $m > 2.300 \times 10^3 \text{ GeV}$, CL = 95%

[jets + \cancel{E}_T , Tglu1A, $m_{\tilde{\chi}_1^0} < 200 \text{ GeV}$]

Mass $m > 2.260 \times 10^3 \text{ GeV}$, CL = 95% [R-Parity Violating]

[$\geq 4\ell, \lambda_{12k} \neq 0, m_{\tilde{\chi}_1^0} > 1000 \text{ GeV}$]

Technicolor

The limits for technicolor (and top-color) particles are quite varied depending on assumptions. See the Technicolor section of the full Review (the data listings).

Quark and Lepton Compositeness, Searches for

Scale Limits Λ for Contact Interactions (the lowest dimensional interactions with four fermions)

If the Lagrangian has the form

$$\pm \frac{g^2}{2\Lambda^2} \bar{\psi}_L \gamma_\mu \psi_L \bar{\psi}_L \gamma^\mu \psi_L$$

(with $g^2/4\pi$ set equal to 1), then we define $\Lambda \equiv \Lambda_{LL}^\pm$. For the full definitions and for other forms, see the Note in the Listings on Searches for Quark and Lepton Compositeness in the full *Review* and the original literature.

$\Lambda_{LL}^+(eeee)$	> 8.3 TeV, CL = 95%
$\Lambda_{LL}^-(eeee)$	> 10.3 TeV, CL = 95%
$\Lambda_{LL}^+(ee\mu\mu)$	> 8.5 TeV, CL = 95%
$\Lambda_{LL}^-(ee\mu\mu)$	> 9.5 TeV, CL = 95%
$\Lambda_{LL}^+(ee\tau\tau)$	> 7.9 TeV, CL = 95%
$\Lambda_{LL}^-(ee\tau\tau)$	> 7.2 TeV, CL = 95%
$\Lambda_{LL}^+(\ell\ell\ell\ell)$	> 9.1 TeV, CL = 95%
$\Lambda_{LL}^-(\ell\ell\ell\ell)$	> 10.3 TeV, CL = 95%
$\Lambda_{LL}^+(eeqq)$	> 24 TeV, CL = 95%
$\Lambda_{LL}^-(eeqq)$	> 37 TeV, CL = 95%
$\Lambda_{LL}^+(eeuu)$	> 23.3 TeV, CL = 95%
$\Lambda_{LL}^-(eeuu)$	> 12.5 TeV, CL = 95%
$\Lambda_{LL}^+(eedd)$	> 11.1 TeV, CL = 95%
$\Lambda_{LL}^-(eedd)$	> 26.4 TeV, CL = 95%
$\Lambda_{LL}^+(eccc)$	> 9.4 TeV, CL = 95%
$\Lambda_{LL}^-(eccc)$	> 5.6 TeV, CL = 95%
$\Lambda_{LL}^+(eebb)$	> 9.4 TeV, CL = 95%
$\Lambda_{LL}^-(eebb)$	> 10.2 TeV, CL = 95%
$\Lambda_{LL}^+(\mu\mu qq)$	> 23.3 TeV, CL = 95%
$\Lambda_{LL}^-(\mu\mu qq)$	> 40.0 TeV, CL = 95%
$\Lambda(\ell\nu\ell\nu)$	> 3.10 TeV, CL = 90%
$\Lambda(e\nu qq)$	> 2.81 TeV, CL = 95%
$\Lambda_{LL}^+(qqqq)$	> 13.1 none 17.4–29.5 TeV, CL = 95%
$\Lambda_{LL}^-(qqqq)$	> 21.8 TeV, CL = 95%
$\Lambda_{LL}^+(\nu\nu qq)$	> 5.0 TeV, CL = 95%
$\Lambda_{LL}^-(\nu\nu qq)$	> 5.4 TeV, CL = 95%

Excited Leptons

The limits from $\ell^{*+}\ell^{*-}$ do not depend on λ (where λ is the $\ell\ell^*$ transition coupling). The λ -dependent limits assume chiral coupling.

$e^{*\pm}$ — excited electron

Mass m	> 103.2 GeV, CL = 95% (from e^*e^*)
Mass m	> 5.600×10^3 GeV, CL = 95% (from ee^*)
Mass m	> 356 GeV, CL = 95% (if $\lambda_\gamma = 1$)

$\mu^{*\pm}$ — excited muon

Mass m	> 103.2 GeV, CL = 95% (from $\mu^*\mu^*$)
Mass m	> 5.700×10^3 GeV, CL = 95% (from $\mu\mu^*$)

$\tau^{*\pm}$ — excited tau

Mass m	> 103.2 GeV, CL = 95% (from $\tau^*\tau^*$)
Mass m	> 4.600×10^3 GeV, CL = 95% (from $\tau\tau^*$)

ν^* — excited neutrino

Mass m	> 1.600×10^3 GeV, CL = 95% (from $\nu^*\nu^*$)
Mass m	> 213 GeV, CL = 95% (from ν^*X)

q^* — excited quark

Mass m	> 338 GeV, CL = 95% (from q^*q^*)
Mass m	> 6700 GeV, CL = 95% (from q^*X)

Color Sextet and Octet Particles

Color Sextet Quarks (q_6)

Mass m	> 84 GeV, CL = 95% (Stable q_6)
----------	------------------------------------

Color Octet Charged Leptons (ℓ_8)

Mass m	> 86 GeV, CL = 95% (Stable ℓ_8)
----------	---------------------------------------

Color Octet Neutrinos (ν_8)

Mass m	> 110 GeV, CL = 90% ($\nu_8 \rightarrow \nu g$)
----------	---

Extra Dimensions

Please refer to the Extra Dimensions section of the full *Review* for a discussion of the model-dependence of these bounds, and further constraints.

Constraints on the radius of the extra dimensions, for the case of two-flat dimensions of equal radii

(direct tests of Newton's law)

$$R < 3.8 \mu\text{m}, \text{CL} = 95\% \quad (pp \rightarrow jG)$$

$$R < 0.16\text{--}916 \text{ nm} \quad (\text{astrophysics; limits depend on technique and assumptions})$$

Constraints on the fundamental gravity scale

$$M_{TT} > 9.02 \text{ TeV}, \text{CL} = 95\% \quad (pp \rightarrow \text{dijet, angular distribution})$$

$$M_c > 4.16 \text{ TeV}, \text{CL} = 95\% \quad (pp \rightarrow \ell\bar{\ell})$$

Constraints on the Kaluza-Klein graviton in warped extra dimensions

$$M_G > 4.78 \text{ TeV}, \text{CL} = 95\% \quad (pp \rightarrow e^+e^-, \mu^+\mu^-)$$

Constraints on the Kaluza-Klein gluon in warped extra dimensions

$$M_{g_{KK}} > 3.8 \text{ TeV}, \text{CL} = 95\% \quad (g_{KK} \rightarrow t\bar{t})$$

WIMP and Dark Matter Searches

No confirmed evidence found for galactic

WIMPs from the GeV to the TeV mass scales and down to 1×10^{-10} pb spin independent cross section at $M = 100$ GeV.

Tests of Conservation Laws

Revised April 2024 by A. Pich (IFIC, Valencia) and M. Ramsey-Musolf (Tsung-Dao Lee Inst.; SJTU; U. Massachusetts).

In keeping with the current interest in tests of conservation laws, we collect together a Table of experimental limits on all weak and electromagnetic decays, mass differences, and moments, and on a few reactions, whose observation would violate conservation laws. The Table is given only in the full Review of Particle Physics (RPP), not in the Particle Physics Booklet, and organizes the data in two main sections: “Discrete Space-Time Symmetries”, *i.e.*, C , P , T , CP and CPT ; and “Number Conservation Laws”, *i.e.*, lepton, baryon, flavor and charge conservation. The references for these data can be found in the Particle Listings. The following text discusses the best limits among those included in the Table and gives a brief overview of the current status. For some topics, a more extensive discussion of the framework for theoretical interpretation is provided, particularly where the analogous discussion does not appear elsewhere in the RPP. References to more extensive review articles are also included where appropriate. Unless otherwise specified, all limits quoted in this review are given at a C.L. of 90%.

DISCRETE SPACE-TIME SYMMETRIES

Charge conjugation (C), parity (P) and time reversal (T) are empirically exact symmetries of the electromagnetic (QED) and strong (QCD) interactions, but they are violated by the weak forces. Owing to the left-handed nature of the $SU(2)_L \otimes U(1)_Y$ electroweak theory, C and P are maximally violated in the fermionic couplings of the W^\pm and (up to $\sin^2 \theta_W$ corrections) the Z . However, their product CP is still an exact symmetry when only one or two fermion families are considered. With three generations of fermions, CP is violated through the single complex phase present in the Cabibbo-Kobayashi-Maskawa (CKM) quark mixing matrix. An analogous CP -violating (CPV) phase appears in the lepton sector when non-vanishing neutrino masses are taken into account (plus two additional phases if neutrinos are Majorana particles). The product of the three discrete symmetries, CPT , is an exact symmetry of any local and Lorentz-invariant quantum field theory with a positive-definite hermitian Hamiltonian that preserves micro-causality [1, 2]. Therefore, the breaking of CP implies a corresponding violation of T .

Violations of charge-conjugation symmetry have never been observed in electromagnetic and strong phenomena. The most stringent limits are extracted from C -violating transitions of neutral (self-conjugate) particles such as $\text{Br}(\pi^0 \rightarrow 3\gamma) < 3.1 \times 10^{-8}$ [3] and $\text{Br}(J/\psi \rightarrow 2\gamma) < 2.7 \times 10^{-7}$ [4]. P (and CP) conservation has been also precisely tested through forbidden decays such as $\text{Br}(\eta \rightarrow 4\pi^0) < 6.9 \times 10^{-7}$ [5], but the best limits on P and T are set by the non-observation of electric dipole moments (see section 2). Obviously, the interplay of the weak interaction puts a lower bound in sensitivity for this type of tests, beyond which violations of the corresponding conservation laws should be detected.

1 Violations of CP and T

The first evidence of CP non-invariance in particle physics was the observation in 1964 of $K_L^0 \rightarrow \pi^+\pi^-$ decays [6]. For many years afterwards, the non-zero ratio

$$|\eta_{+-}| \equiv |\mathcal{M}(K_L^0 \rightarrow \pi^+\pi^-)/\mathcal{M}(K_S^0 \rightarrow \pi^+\pi^-)| \quad (1)$$

$$= (2.232 \pm 0.011) \times 10^{-3}$$

could be explained as a K^0 - \bar{K}^0 mixing effect, $\eta_{+-} = \epsilon$ (superweak CP violation), which would imply an identical ratio $\eta_{00} \equiv \mathcal{M}(K_L^0 \rightarrow \pi^0\pi^0)/\mathcal{M}(K_S^0 \rightarrow \pi^0\pi^0)$ in the neutral decay mode and successfully predicts the observed CPV semileptonic asymmetry ($A_L(e) \approx 2 \text{Re} \epsilon$)

$$A_L(e) \equiv \frac{\Gamma(K_L^0 \rightarrow \pi^- e^+ \nu_e) - \Gamma(K_L^0 \rightarrow \pi^+ e^- \bar{\nu}_e)}{\Gamma(K_L^0 \rightarrow \pi^- e^+ \nu_e) + \Gamma(K_L^0 \rightarrow \pi^+ e^- \bar{\nu}_e)} \quad (2)$$

$$= (3.34 \pm 0.07) \times 10^{-3}.$$

A tiny difference between η_{+-} and η_{00} was reported for the first time in 1988 by the CERN NA31 collaboration [7], and later es-

tablished at the 7.2σ level with the full data samples from the NA31 [8], E731 [9], NA48 [10] and KTeV [11] experiments:

$$\text{Re}(\epsilon'/\epsilon) = \frac{1}{3} (1 - |\eta_{00}/\eta_{+-}|) = (1.66 \pm 0.23) \times 10^{-3}. \quad (3)$$

This important measurement confirmed that CP violation is associated with a $\Delta S = 1$ transition, as predicted by the CKM mechanism. The Standard Model (SM) prediction, $\text{Re}(\epsilon'/\epsilon) = (1.4 \pm 0.5) \times 10^{-3}$ [12–14], is in good agreement with the measured ratio, although the theoretical uncertainty is unfortunately large.

Much larger CP asymmetries have been later measured in B meson decays, many of them involving the interference between B^0 - \bar{B}^0 mixing and the decay amplitude. They provide many successful tests of the CKM unitarity structure, validating the SM mechanism of CP violation (see the review on CP violation in the quark sector). Prominent signals of direct CP violation in the decay amplitudes have been also clearly established in several B^\pm , B_d^0 and B_s^0 decays, and, very recently, in charm decays [15, 16]:

$$\Delta a_{CP}^{\text{dir}} \equiv a_{CP}^{\text{dir}}(D^0 \rightarrow K^+K^-) - a_{CP}^{\text{dir}}(D^0 \rightarrow \pi^+\pi^-)$$

$$= (-15.7 \pm 2.9) \times 10^{-4}. \quad (4a)$$

$$a_{CP}^{\text{dir}}(D^0 \rightarrow \pi^+\pi^-) = (23.2 \pm 6.1) \times 10^{-4}. \quad (4b)$$

These direct CP asymmetries necessarily involve the presence of a strong phase-shift difference between (at least) two interfering amplitudes, which makes very challenging to perform reliable SM predictions for heavy-flavored mesons.

Global fits to neutrino oscillation data provide some hints of a non-zero mixing phase [17, 18]. Although the statistical significance is not yet compelling, they suggest that CP -violation effects in neutrino oscillations could be large (see the review on neutrino masses, mixings and oscillations). The future DUNE and Hyper-Kamiokande experiments are expected to confirm the presence of CP violation in the lepton sector or constrain the phase in the leptonic mixing matrix to be smaller than $O(10^\circ)$.

While CP violation implies a breaking of time-reversal symmetry, direct tests of T violation are much more difficult. The CPLEAR experiment observed longtime ago a non-zero difference between the oscillation probabilities of $K^0 \rightarrow \bar{K}^0$ and $\bar{K}^0 \rightarrow K^0$ [19]. Initial neutral kaons with defined strangeness were produced from proton-antiproton annihilations at rest, $p\bar{p} \rightarrow K^-\pi^+K^0, K^+\pi^-\bar{K}^0$, and tagged by the accompanying charged kaon, while the strangeness of the final neutral kaon was identified through its semileptonic decay: $K^0 \rightarrow e^+\pi^-\nu_e, \bar{K}^0 \rightarrow e^-\pi^+\bar{\nu}_e$. The average asymmetry over the time interval from 1 to 20 K_S^0 lifetimes was found to be different from zero at 4σ [19]:

$$\frac{R[\bar{K}^0(t=0) \rightarrow e^+\pi^-\nu_e(t)] - R[K^0(t=0) \rightarrow e^-\pi^+\bar{\nu}_e(t)]}{R[\bar{K}^0(t=0) \rightarrow e^+\pi^-\nu_e(t)] + R[K^0(t=0) \rightarrow e^-\pi^+\bar{\nu}_e(t)]} =$$

$$= (6.6 \pm 1.3 \pm 1.0) \times 10^{-3}. \quad (5)$$

Since this asymmetry violates also CP , its interpretation as direct evidence of T violation requires a detailed analysis of the underlying K^0 - \bar{K}^0 mixing process [20–22].

More recently, the exchange of initial and final states has been made possible in B decays, taking advantage of the entanglement of the two daughter mesons produced in the decay $\Upsilon(4S) \rightarrow B\bar{B}$ which allows for both flavor ($B^0 \rightarrow \ell^+X, \bar{B}^0 \rightarrow \ell^-X$) and CP ($B_+ \rightarrow J/\psi K_L^0, B_- \rightarrow J/\psi K_S^0$) tagging. Selecting events where one B candidate is reconstructed in a CP eigenstate and the flavor of the other B is identified, one can compare the rates of the $\bar{B}^0 \rightarrow B_\pm$ and $B^0 \rightarrow B_\pm$ transitions with their T -reversed $B_\pm \rightarrow \bar{B}^0$ and $B_\pm \rightarrow B^0$ processes, as a function of the time difference Δt between the two B decays [23–25]. Neglecting the small width difference between the two B_d^0 mass eigenstates, each of these eight transitions has a time-dependent decay rate of the form $e^{-\Gamma_d \Delta t} \{1 + S_{\alpha,\beta}^\pm \sin(\Delta m_d \Delta t) + C_{\alpha,\beta}^\pm \cos(\Delta m_d \Delta t)\}$, where Γ_d is the average decay width, Δm_d the B_d^0 mass difference, the

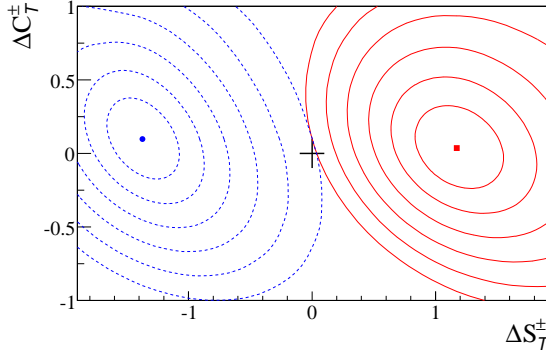


Figure 1: Measured values of ΔS_T^+ , ΔC_T^+ (blue point, dashed lines) and ΔS_T^- , ΔC_T^- (red square, solid lines) [26]. The two-dimensional contours correspond to $1 - \text{CL} = 0.317, 4.55 \times 10^{-2}, 2.70 \times 10^{-3}, 6.33 \times 10^{-5}, 5.73 \times 10^{-7}, \text{ and } 1.97 \times 10^{-9}$. The + sign indicates the T -invariant point.

subindices $\alpha = \ell^+, \ell^-$ and $\beta = K_S^0, K_L^0$ stand for the reconstructed final states of the two B mesons and the superindex + or - indicates whether the decay to the flavor final state α occurs before or after the decay to the CP final state β . Figure 1 shows confidence-level contours for the T -asymmetry parameters $\Delta S_T^\pm \equiv S_{\ell^-, K_L^0}^\mp - S_{\ell^+, K_S^0}^\pm$ and $\Delta C_T^\pm \equiv C_{\ell^-, K_L^0}^\mp - C_{\ell^+, K_S^0}^\pm$, reported by the BABAR experiment [26], which clearly demonstrate a violation of T in ΔS_T^\pm , with a significance of 14σ .

2 Electric dipole moments

Among the most powerful tests of CP invariance is the search for a permanent electric dipole moment (EDM) of an elementary fermion or non-degenerate quantum system. The EDM of an elementary spin-1/2 fermion f is defined by the effective, non-renormalizable interaction

$$\mathcal{L}_{\text{EDM}} = -\frac{i}{2} d_f \bar{f} \sigma_{\mu\nu} \gamma_5 f F^{\mu\nu} \quad (6)$$

where $F^{\mu\nu}$ is the QED field strength tensor. The values for d_f are conventionally expressed in units of $e \text{ cm}$. The interaction (6) is separately odd under T and P . In the non-relativistic limit, Eq. (6) reduces to

$$\mathcal{L}_{\text{EDM}} \rightarrow d_f \chi_f^\dagger \vec{\sigma} \chi_f \cdot \vec{E} \quad (7)$$

where χ is a two-component Pauli spinor and \vec{E} is the electric field. Note the interaction (7) is manifestly T -odd and carries no direct information on CP . The observation of a non-zero EDM of a non-relativistic (and non-degenerate) quantum system, such as the mercury atom (see below) would imply CP violation under the assumption of CPT invariance.

To date, no experimental observation of an EDM of an elementary particle or non-degenerate bound quantum system has been observed. The most stringent limits have been obtained for the EDMs of the electron, mercury atom, and neutron. A selection of the representative, most stringent limits is given in Table 1. The limits on the electron EDM are inferred from experiments involving polar molecules, paramagnetic systems with an unpaired electron spin. In contrast, the neutron and ^{199}Hg atom are diamagnetic. A variety of experimental efforts aimed at improved sensitivities are underway. For reviews of the experimental and theoretical situation, see, *e.g.* [27–30].

EDMs in the Standard Model

The SM provides two sources of d_f : the CPV phase in the CKM matrix and the P - and T -odd ‘ θ term’ in the QCD Lagrangian. The former is characterized by the Jarlskog invariant [37]

$$\mathcal{J} = \text{Im}(V_{us} V_{cs}^* V_{cb} V_{ub}^*) \sim A^2 \lambda^6 \eta < 10^{-4}, \quad (8)$$

Table 1: Most stringent limits on electric dipole moments.

EDM	Limit ($e \text{ cm}$)	Source
Electron	1.1×10^{-29} (90% C.L.)	ThO [31]
	4.1×10^{-30} (90% C.L.)	HfF ⁺ [32]
Muon	1.8×10^{-19} (95% C.L.)	[33]
Neutron	1.8×10^{-26} (90% C.L.)	[34]
^{199}Hg Atom	7.4×10^{-30} (95% C.L.)	[35]
^{129}Xe Atom	1.5×10^{-27} (95% C.L.)	[36]

while the latter is given by

$$\mathcal{L}_{\bar{\theta}} = -\frac{g_3^2}{16\pi^2} \bar{\theta} \text{Tr} (G^{\mu\nu} \tilde{G}_{\mu\nu}), \quad (9)$$

where $G_{\mu\nu}$ ($\tilde{G}_{\mu\nu} = \epsilon_{\mu\nu\alpha\beta} G^{\alpha\beta}/2$) is the QCD field strength tensor (dual).

The CKM-induced EDMs of quarks and charged leptons arise at three- and four-loop orders, respectively [38–41]. The resulting numerical impact for the experimental observables (see below) falls well below present and prospective experimental sensitivities. The most important impact of \mathcal{J} for the EDMs of the neutron and diamagnetic atoms arise via induced hadronic interactions. The resulting theoretical expectations for the electron, neutron and ^{199}Hg EDMs are

$$|d_e|_{\text{CKM}} \approx 10^{-44} e \text{ cm} \quad [41], \quad (10a)$$

$$|d_n|_{\text{CKM}} \approx (1 - 6) \times 10^{-32} e \text{ cm} \quad [42], \quad (10b)$$

$$|d_A(^{199}\text{Hg})|_{\text{CKM}} \lesssim 4 \times 10^{-34} e \text{ cm} \quad [27]. \quad (10c)$$

For d_n and $d_A(^{199}\text{Hg})$, the dominant CKM contributions arise from four-quark operators (generated after integrating out the electroweak gauge bosons) rather than from the EDMs of the individual quarks. The corresponding sensitivities to the QCD $\bar{\theta}$ parameter are given by

$$|d_n|_{\bar{\theta}} \approx (0.9 - 1.2) \times 10^{-16} \bar{\theta} e \text{ cm} \quad [42], \quad (11a)$$

$$|d_A(^{199}\text{Hg})|_{\bar{\theta}} \approx (0.07 - 8) \times 10^{-20} \bar{\theta} e \text{ cm} \quad [27, 28], \quad (11b)$$

where the ranges quoted include the impacts of hadronic, nuclear, and atomic theory uncertainties. The neutron EDM puts then a stringent limit on ‘strong’ CP violation: $\bar{\theta} \lesssim 2 \times 10^{-10}$. The corresponding limit from $d_A(^{199}\text{Hg})$ is weaker due to the large theoretical uncertainty.

EDMs Beyond the Standard Model

It is possible that the next generation of EDM searches will yield a non-zero result, arising from the θ -term interaction and/or physics beyond the SM (BSM). Most of the considered BSM scenarios involve new particles with masses well above the electroweak scale. At energies much lower than the BSM mass scale Λ , the dynamics can be described through an effective field theory (SMEFT) involving an infinite set of non-renormalizable operators $\mathcal{O}_k^{(d)}$, with dimensions $d > 4$, that are invariant under the SM gauge group:

$$\mathcal{L}_{\text{SMEFT}} = \mathcal{L}_{\text{SM}} + \sum_{k,d} \alpha_k^{(d)} \left(\frac{1}{\Lambda}\right)^{d-4} \mathcal{O}_k^{(d)}. \quad (12)$$

The operators contain only SM fields, while all short-distance information on the BSM physics is encoded in their Wilson coefficients $\alpha_k^{(d)}$. The $d = 4$ term corresponds to the SM Lagrangian.

For the systems of Table 1 and for many BSM scenarios of recent interest, it suffices to consider the leading contributions from $d = 6$ operators. Considering only the first-generation SM fermions, there exist 12 independent CPV pertinent operators. For a complete listing, see *e.g.*, Refs. [28, 43]. For a given elementary fermion f , two of these operators reduce to the EDM interaction in Eq. (6). Of the remaining, the most relevant include the chromo-electric dipole moments (cEDMs) of the quarks;

Table 2: Pertinent dimension-six EDM and cEDM sources (first generation fermions only).

System	$d = 6$ Source	Wilson Coefficient
Paramagnetic	Electron EDM	$\text{Im } C_{e\gamma}$
	Electron-quark	$C_{eq}^{(\pm)}$
Diamagnetic	Quark EDM	$\text{Im } C_{q\gamma}$
	Quark cEDM	$\text{Im } C_{qG}$
	Three gluon	$C_{\bar{G}}$
	Four quark	$\text{Im } C_{\gamma(1,8)}$
	Quark-Higgs	$\text{Im } C_{\varphi ud}$
	Electron-quark tensor*	$\text{Im } C_{\ell equ}^{(3)}$

*Applicable only to atoms.

a CP -odd three gluon operator; three semileptonic, four-fermion operators; two four-quark operators; and a CPV interaction involving two Higgs fields and a right-handed quark current. For the dipole operators, it is useful to define a rescaled Wilson coefficient $\alpha_{fV_j}^{(6)} \equiv g_j C_{fV_j}$, where V_j ($j = 1, 2, 3$) denote the gauge bosons for the three SM gauge groups with corresponding couplings g_j ; for all other $d = 6$ operators we correspondingly identify $\alpha_k^{(6)} \equiv C_k$. In this case, one has for the EDM (d_f) and cEDM (\bar{d}_q)

$$d_f = -(1.13 \times 10^{-16} \text{ e cm}) \left(\frac{v}{\Lambda}\right)^2 \text{Im } C_{f\gamma}, \quad (13a)$$

$$\bar{d}_q = -(1.13 \times 10^{-16} \text{ cm}) \left(\frac{v}{\Lambda}\right)^2 \text{Im } C_{qG}, \quad (13b)$$

with $\text{Im } C_{f\gamma} = \text{Im } C_{fB} + 3I_3^f \text{Im } C_{fW}$. As the expressions (13a,13b) illustrate, the magnitude of the BSM contributions scales with two inverse powers of the scale Λ . A similar conclusion holds for the contributions from the other $d = 6$ operators to the EDMs of Table 1.

It is important to emphasize that if the BSM mediators are light, with masses below the weak scale, the effective field theory description of Eq. (12) does not apply. For recent studies along these lines, see, *e.g.* [44, 45].

EDM Interpretation: From Short Distances to the Atomic Scale

The EDM limits in Table 1 are obtained using composite quantum systems, wherein the relevant dynamics involve physics at the hadronic, nuclear, atomic and molecular scales. The manifestation of a given CPV source (CKM, $\bar{\theta}$ term, BSM) involves an interplay of these dynamics. In all cases, one must first evolve the Wilson coefficients from the weak scale to the hadronic scale, then match onto the relevant low-energy degrees of freedom (electrons, nucleons, pions, *etc.*). At this level, the most straightforward interpretation involves the paramagnetic systems, for which two sources dominate: the electron EDM and the electron spin-dependent semileptonic interaction $\bar{e}\gamma_5 e \bar{q}q$. The latter gives rise to a spin-independent Hamiltonian, for an atom with Z electrons/protons and N neutrons,

$$\hat{H}_S = \frac{iG_F}{\sqrt{2}} \delta(\vec{r}) \left[(Z + N) C_S^{(0)} + (Z - N) C_S^{(1)} \right] \gamma_0 \gamma_5, \quad (14)$$

where $C_S^{(0)}$ ($C_S^{(1)}$) is proportional to $C_{eq}^{(+)}$ ($C_{eq}^{(-)}$). The computation of $C_S^{(0,1)}$ is relatively free from theoretical uncertainty since the operator $\bar{q}q$ essentially counts the number of quarks of flavor q in the nucleus. Experimental results for paramagnetic systems, thus, often quote bounds on

$$C_S \equiv C_S^{(0)} + \left(\frac{Z - N}{Z + N}\right) C_S^{(1)} \quad (15)$$

as well as on d_e , assuming only one of these two sources is non-vanishing. Combining results from ThO and HfF⁺ (see Figure 2) allows one to obtain the global, 90% C.L. bounds

$$|d_e| < 2.1 \times 10^{-29} \text{ e cm}, \quad |C_S| < 1.9 \times 10^{-9}. \quad (16)$$

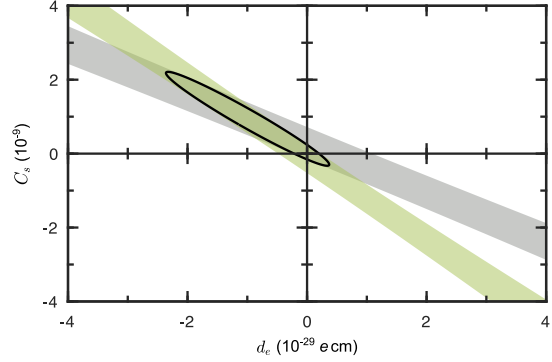


Figure 2: Constraints on d_e and C_S from EDM searches using polar molecules [32]. The green and grey bands are the 90% confidence regions from HfF⁺ and ThO, while the ellipse shows the 90% CL limits from the global fit. Parameters used in fits are from Ref. [46].

Note that the limits on d_e given in Table 1 have been obtained assuming $C_S = 0$.

For the diamagnetic systems, the situation is considerably more involved. For the neutron, a variety of approaches – including lattice QCD, chiral perturbation theory, QCD sum rules, and the quark model – have been employed to compute the relevant hadronic matrix elements of the CPV sources (see, *e.g.*, [28, 29, 47, 48]). For diamagnetic atoms, the non-leptonic sources of Table 2 give rise to the EDM of the nucleus as well as other P - and T -odd nuclear moments, as allowed by the nuclear spin. However, according to a theorem by Schiff [49], the nuclear EDM generates no contribution to the neutral-atom EDM due to screening by atomic electrons. The leading contribution from these sources, instead, arises via the nuclear Schiff moment, \vec{S} , an r^3 -weighted moment of the T - and P -odd component of the nuclear charge density. The resulting effective atomic Hamiltonian is

$$\hat{H}_{\text{Schiff}} = -4\pi \vec{\nabla} \rho_e(0) \cdot \vec{S}, \quad (17)$$

where $\vec{\nabla} \rho_e(0)$ is the gradient of the electron density at the nucleus. To date, computations of the nuclear Schiff moment have assumed that the leading contribution arises from a pion-exchange induced nuclear force, with the P - and T -odd πN interaction given by

$$\mathcal{L}_{\pi N}^{T,P} = \bar{N} \left[\bar{g}_\pi^{(0)} \vec{\tau} \cdot \vec{\pi} + \bar{g}_\pi^{(1)} \pi^0 + \bar{g}_\pi^{(2)} (3\tau_3 \pi^0 - \vec{\tau} \cdot \vec{\pi}) \right] N. \quad (18)$$

Chiral effective field theory power counting implies that in general the magnitude of $\bar{g}_\pi^{(2)}$ is suppressed with respect to the isoscalar and isovector couplings. The CPV sources then generate a diamagnetic atom EDM d_A via the sequence

$$CPV \text{ source} \longrightarrow \bar{g}_\pi^{(i)} \longrightarrow \vec{S} \longrightarrow d_A. \quad (19)$$

The steps in this sequence involve dynamics at the hadronic, nuclear, and atomic scales, respectively. In addition, d_A may receive contributions from the nuclear spin-dependent interaction generated by the semileptonic tensor interaction listed in Table 2, with the corresponding atomic Hamiltonian

$$\hat{H}_T = \frac{2iG_F}{\sqrt{2}} \delta(\vec{r}) \sum_N \left[C_T^{(0)} + C_T^{(1)} \tau_3 \right] \vec{\sigma}_N \cdot \vec{\tau}, \quad (20)$$

where σ_N is the nucleon spin Pauli matrix and $C_T^{(0,1)} \propto \text{Im } C_{\ell equ}^{(3)}$.

Given the large number of CPV sources and existing diamagnetic EDM limits, it is not possible to obtain a set of global constraints on the former. One may, however, do so for the low-energy effective parameters $\bar{g}_\pi^{(0,1)}$, $C_T^{(0,1)}$ and \bar{d}_n^{sr} , where the latter denotes a ‘short-range’ contribution to the neutron EDM [27, 50]. In this context, the dominant source of theoretical uncertainty involves computations of the nuclear Schiff moment. From the

bounds on the low-energy parameters, one may then derive constraints on the CPV sources by utilizing computations of the hadronic matrix elements. Reducing the degree of theoretical hadronic and nuclear physics uncertainty is an area of active effort.

3 Tests of CPT

CPT symmetry implies the equality of the masses and widths of a particle and its antiparticle. The most constraining limits are extracted from the neutral kaons [51, 52]:

$$\begin{aligned} 2 \frac{|m_{K^0} - m_{\bar{K}^0}|}{(m_{K^0} + m_{\bar{K}^0})} &< 6 \times 10^{-19}, \\ 2 \frac{|\Gamma_{K^0} - \Gamma_{\bar{K}^0}|}{(\Gamma_{K^0} + \Gamma_{\bar{K}^0})} &= (8 \pm 8) \times 10^{-18}. \end{aligned} \quad (21)$$

The limit on the $K^0 - \bar{K}^0$ mass difference assumes that there is no other source of CPT violation. An upper bound on CPT breaking in $K_L^0 \rightarrow 2\pi$ has been also set through the measured phase difference of the CPV ratios η_{00} and η_{+-} , $\phi_{00} - \phi_{+-} = (0.34 \pm 0.32)^\circ$, thanks to the small value of $(1 - |\eta_{00}/\eta_{+-}|)$ (see the review on CP violation in K_L^0 decays).

The measured masses and electric charges of the electron, the proton and their antiparticles provide also strong limits on CPT violation [53–56]:

$$\begin{aligned} 2 \frac{|m_{e^+} - m_{e^-}|}{m_{e^+} + m_{e^-}} &< 8 \times 10^{-9}, \quad \frac{|q_{e^+} + q_{e^-}|}{e} < 4 \times 10^{-8}, \\ \left| \frac{q_{\bar{p}}/m_{\bar{p}}}{q_p/m_p} \right| - 1 &= (0.3 \pm 1.6) \times 10^{-11}. \end{aligned} \quad (22)$$

Worth mentioning are also the tight constraints derived from the lepton and antilepton magnetic moments [57, 58],

$$\begin{aligned} 2 \frac{g_{e^+} - g_{e^-}}{g_{e^+} + g_{e^-}} &= (-0.5 \pm 2.1) \times 10^{-12}, \\ 2 \frac{g_{\mu^+} - g_{\mu^-}}{g_{\mu^+} + g_{\mu^-}} &= (-0.11 \pm 0.12) \times 10^{-8}, \end{aligned} \quad (23)$$

those of the proton and antiproton [59],

$$(\mu_p + \mu_{\bar{p}})/\mu_p = (2 \pm 4) \times 10^{-9}, \quad (24)$$

and the measurement of the 1S-2S atomic transition in antihydrogen which agrees with the corresponding frequency spectral line in hydrogen at a relative precision of 2×10^{-12} [60].

A violation of CPT in an interacting local quantum field theory would imply that Lorentz symmetry is also violated [61]. Signatures of Lorentz-invariance violation have been searched for with atomic clocks, penning traps, matter and antimatter spectroscopy, colliders and astroparticle experiments, with so far negative results [62]. A compilation of experimental bounds is given in Ref. [63], parametrized through the coefficients of the so-called Standard Model Extension (SME) Lagrangian which contains all possible Lorentz- and CPT -violating operators preserving gauge invariance, renormalizability, locality and observer causality [64].

QUANTUM-NUMBER CONSERVATION LAWS

Conservation laws of several quantum numbers have been empirically established with a very high degree of confidence. They are usually associated with some global phase symmetry. However, while some of them are deeply rooted in basic principles such as gauge invariance (charge conservation; local symmetry implies global symmetry) or Lorentz symmetry (fermion number conservation), others appear to be accidental symmetries of the SM Lagrangian and could be broken by new physics interactions.

In fact, if one only assumes the SM gauge symmetries and particle content, the most general dynamics at energies below the BSM mass scale is described by the SMEFT Lagrangian in Eq. (12). All $d = 4$ operators (*i.e.*, the SM) happen to preserve the B and

L quantum numbers, but this is no-longer true for the gauge-invariant structures of higher dimensionality. There is only one operator with $d = 5$ (up to hermitian conjugation and flavor assignments), and it violates lepton number by two units [65], giving rise to Majorana neutrino masses after the electroweak spontaneous symmetry breaking. With $d = 6$, there are five operators that violate B and L [66, 67]. Thus, violations of these quantum numbers can be generically expected, unless there is an explicit symmetry protecting them.

4 Electric charge

The conservation of electric charges is associated with the QED gauge symmetry. The most precise tests are the non-observation of the decays $e \rightarrow \nu_e \gamma$ (lifetime larger than 6.6×10^{28} yr [68]) and $n \rightarrow p \nu_e \bar{\nu}_e$ ($\text{Br} < 8 \times 10^{-27}$, 68% C.L. [69]). The neutrality of matter can be also interpreted as a test of electric charge conservation. Worth mentioning are the experimental limits on the electric charge of the neutron, $q_n/e = (-0.2 \pm 0.8) \times 10^{-21}$, and on the sum of the proton and electron charges, $|q_p + q_e|/e < 1 \times 10^{-21}$ [70].

The isotropy of the cosmic microwave background has been used to set stringent limits on a possible charge asymmetry of the Universe [71]. Assuming that charge asymmetries produced by different particles are not anticorrelated, this implies upper bounds on the photon ($|q_\gamma|/e < 1 \times 10^{-35}$) and neutrino ($|q_\nu|/e < 4 \times 10^{-35}$) electric charges. A much stronger upper bound on the photon charge ($|q_\gamma|/e < 1 \times 10^{-46}$) has been derived from the non-observation of Aharonov-Bohm phase differences in interferometric experiments with photons that have traversed cosmological distances, under the assumption that both positive and negative charged photons exist [72].

5 Lepton family numbers

In the SM with massless left-handed neutrinos there is a separate conservation number for each lepton family. However, neutrino oscillations show that neutrinos have tiny masses and there are sizable mixings among the different lepton flavors. Compelling evidence from solar, atmospheric, accelerator and reactor neutrino experiments has established a quite solid pattern of neutrino mass differences and mixing angles [17, 18]. (see the review on neutrino masses, mixings and oscillations). Nevertheless, flavor mixing among the different charged leptons has never been observed.

If neutrino masses and mixings among the three active neutrinos were the only sources of lepton-flavor violation (LFV), neutrinoless transitions from one charged lepton flavor to another would be heavily suppressed by powers of m_{ν_i} (GIM mechanism), leading to un-observably small rates; for instance [75–80],

$$\text{Br}(\mu \rightarrow e \gamma) = \frac{3\alpha}{32\pi} \left| \sum_i U_{\mu i}^* U_{ei} \frac{m_{\nu_i}^2 - m_{\nu_1}^2}{M_W^2} \right|^2 < 10^{-54}, \quad (25)$$

where U_{ia} are the relevant elements of the PMNS mixing matrix. This contribution is clearly too small to be observed in any realistic experiment, so any experimentally accessible effect would arise from BSM physics with sources of LFV not related to m_{ν_i} . The search for charged LFV (CLFV) remains an area of active interest, which has the potential to probe physics at scales much higher than the TeV.

Among the most sensitive probes are searches for the CLFV decays of the muon, $\mu \rightarrow e \gamma$ and $\mu \rightarrow 3e$, as well as the conversion process $\mu^- + A(N, Z) \rightarrow e^- + A(N, Z)$, where $A(N, Z)$ denotes a nucleus with N neutrons and Z protons. Searches for rare τ decays such as $\tau \rightarrow \ell \gamma$ ($\ell = e, \mu$) also provide interesting probes of CLFV. A variety of BSM scenarios predict that rates for these CLFV processes could be sufficiently large to be observed in the present or planned searches. To date, no observation has been reported, and the resulting null results place strong constraints on BSM scenarios. For extensive reviews of the experimental and theoretical status and prospects, see Refs. [74, 81, 82].

A detailed set of upper bounds on CLFV branching ratios is given in the listings for the muon and tau leptons. Here we

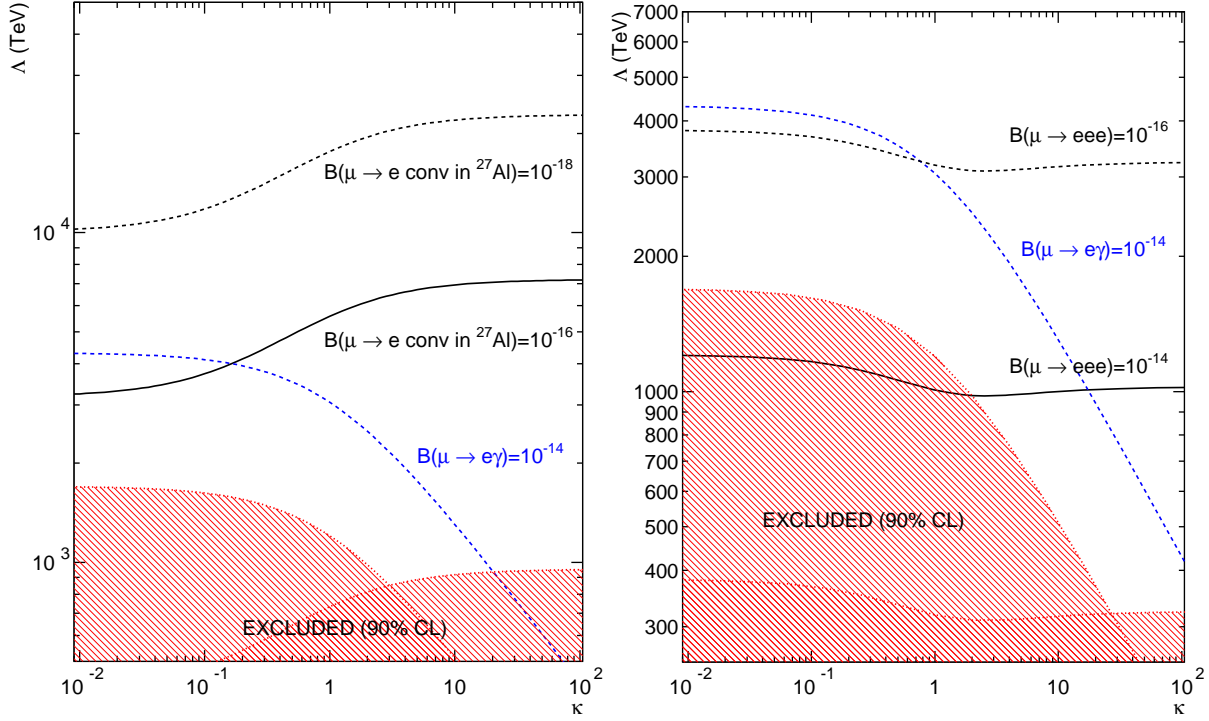


Figure 3: Model-independent CLFV sensitivities based on Eq (31). Left panel shows the comparison of present constraints with prospective future sensitivities for $\mu \rightarrow e\gamma$ and $\mu \rightarrow e$ conversion. Right panel gives analogous comparison for $\mu \rightarrow e\gamma$ and $\mu \rightarrow 3e$. Updated by [73] from Ref. [74].

emphasize those with the strongest limits:

$$\begin{aligned} \text{Br}(\mu \rightarrow e\gamma) &< 4.2 \times 10^{-13} \quad [83], \\ \text{Br}(\mu \rightarrow 3e) &< 1.0 \times 10^{-12} \quad [84] \end{aligned} \quad (26)$$

and

$$B_{\mu \rightarrow e} \equiv \frac{\Gamma(\mu^- + A(N, Z) \rightarrow e^- + A(N, Z))}{\Gamma(\mu^- + A(N, Z) \rightarrow \nu + A(N+1, Z-1))} \quad (27)$$

with the best limit so far, $B_{\mu \rightarrow e} < 7 \times 10^{-13}$ [85], obtained with gold. Several proposed experiments aim to improve these limits by several orders of magnitude with different atoms.

One may interpret both $\mu \rightarrow e\gamma$ and $\mu \rightarrow e$ conversion in terms of the amplitudes to emit a real or virtual photon:

$$\begin{aligned} \mathcal{M}_{\mu \rightarrow e\gamma^{(*)}} &= eG_{\mu} \varepsilon^{\alpha\beta} \bar{e}(p-q) \left[(q^2 \gamma_{\alpha} - \not{q} q_{\alpha}) (\tilde{A}_1^R P_R + \tilde{A}_1^L P_L) \right. \\ &\quad \left. + im_{\mu} \sigma_{\alpha\beta} q^{\beta} (\tilde{A}_2^R P_R + \tilde{A}_2^L P_L) \right] \mu(p), \end{aligned} \quad (28)$$

where it is conventional to normalize the amplitude to the Fermi constant. One then has

$$\text{Br}(\mu \rightarrow e\gamma) = 48\pi^3 \alpha \left(|\tilde{A}_2^R|^2 + |\tilde{A}_2^L|^2 \right). \quad (29)$$

For the conversion process, the virtual photon is absorbed by the quarks in the nucleus, yielding an effective four-fermion operator. In general, the exchange of other particles could lead to similar or alternate Lorentz structures, and it is not possible to distinguish between the exchange of a virtual photon or other particle. It is conventional to write the most general four-fermion amplitude, valid for energies below the electroweak scale as (adapted from Ref. [90])

$$\mathcal{M}_{\mu \rightarrow e} = G_{\mu} \sum_{n,a,q} a_{a,q}^{(n)} \bar{e} \Gamma^n P_a \mu \bar{q} \Gamma_n q, \quad (30)$$

where P_a ($a = L, R$) denote the left and right-handed projectors and Γ^n denotes $1, \gamma_5, \gamma^{\mu}, \gamma^{\mu} \gamma_5,$ and $\sigma_{\mu\nu}$. If any of the coefficients $a_{a,q}^{(n)}$ are generated by physics at a scale $\Lambda > v$, then their effects would be encoded in the SMEFT Lagrangian (12). For scenarios in which the leading CLFV operators occur at $d = 6$, the $a_{a,q}^{(n)}$ will scale as $(v/\Lambda)^2$. The corresponding decay and conversion rates will then scale as $(v/\Lambda)^4$. Note that the scalar and time component of the vector interactions are coherent over the nucleus, essentially counting the number of quarks. Consequently, these interactions typically yield the greatest sensitivities to high BSM mass scales.

It is sometimes convenient to compare the relative sensitivities of the decay and conversion processes using the following simplified effective Lagrangian [74]:

$$\begin{aligned} \mathcal{L}_{\text{eff}}^{\text{CLFV}} &= \frac{m_{\mu}}{(\kappa+1)\Lambda^2} \bar{\mu}_R \sigma_{\mu\nu} e_L F^{\mu\nu} \\ &\quad + \frac{\kappa}{(\kappa+1)\Lambda^2} \bar{\mu} \gamma_{\mu} e \sum_q \bar{q} \gamma^{\mu} q + \text{h.c.} \end{aligned} \quad (31)$$

Note that one may replace the second term in Eq. (31) by any one of the other four-fermion interactions given in Eq. (30). An analogous expression applies to the process $\mu \rightarrow 3e$ when replacing the sum over quarks by the corresponding electron bilinear. A comparison of the present and prospective sensitivities for various muon CLFV searches in this framework is shown in Figure 3.

Stringent limits have been also set on the LFV decay modes of the τ lepton [91]. As shown in Figure 4, the large τ data samples collected at the B factories have made possible to reach a 10^{-8} sensitivity for many of its leptonic ($\tau \rightarrow \ell\gamma, \tau \rightarrow \ell'\ell^+\ell^-$) and semileptonic ($\tau \rightarrow \ell P^0, \tau \rightarrow \ell V^0, \tau \rightarrow \ell P^0 P^0, \tau \rightarrow \ell P^+ P'^-$) neutrinoless LFV decays, and BELLE-II is expected to push these limits beyond the 10^{-9} level [87]. Being a third generation lepton, the τ could be more sensitive to heavier new-physics scales, which makes his LFV decays particularly interesting. Compared to the muon, the τ decay amplitudes could be enhanced by a chirality ratio $(m_{\tau}/m_{\mu})^2 \sim 280$ and/or by lepton-mixing factors such as $|U_{\tau 3}/U_{e 3}|^2 \sim 20$, but the exact relation is model dependent. In any case, the τ LFV decays provide a rich data set that is very

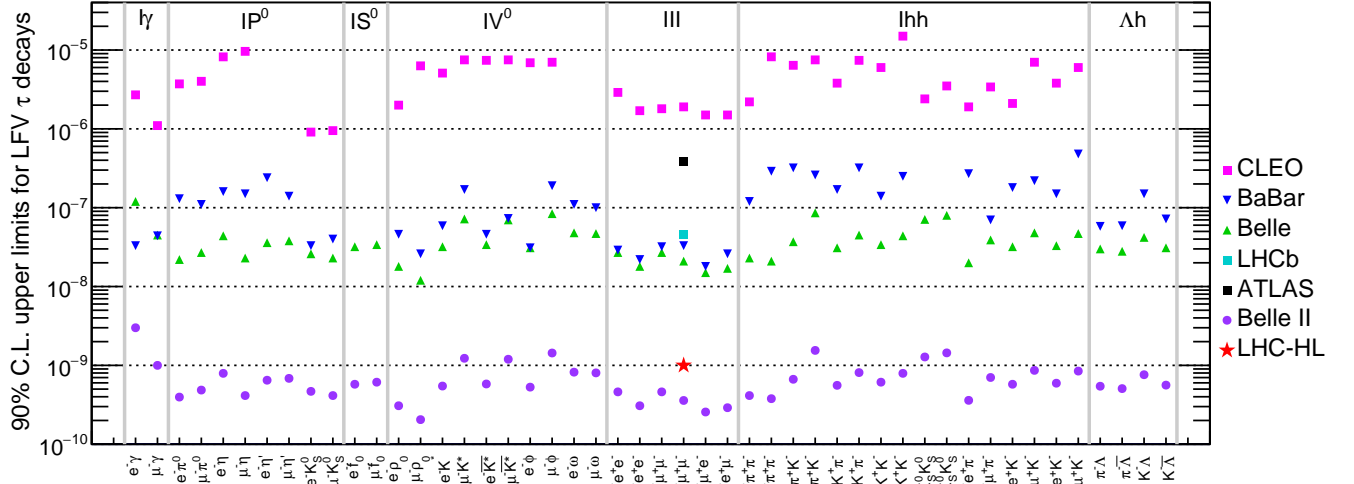


Figure 4: Current experimental limits on neutrinoless LFV τ decays [86]. Also shown are the future projections at Belle-II [87] and at the HL-LHC [88].

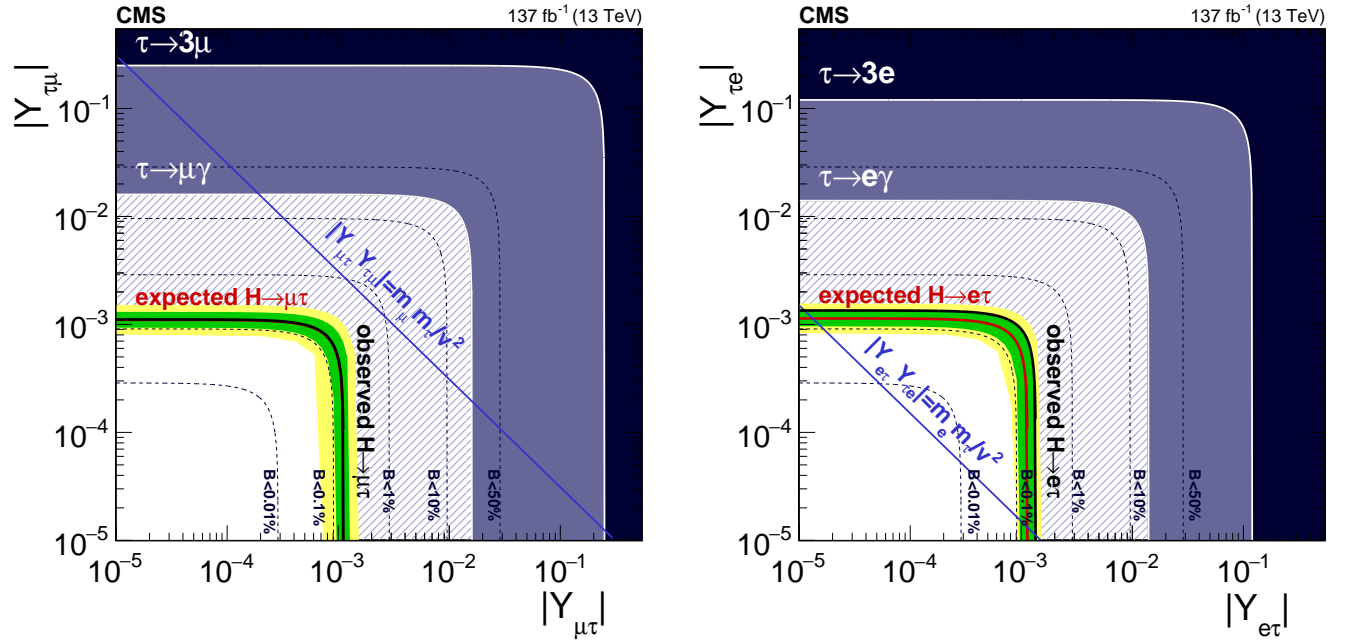


Figure 5: Current limits on the Higgs LFV τ Yukawas from direct $H^0 \rightarrow \ell^\pm \tau^\mp$ decays ($\ell = e, \mu$), and indirect constraints from τ decays [89].

complementary to the μ bounds. If LFV is finally observed, the correlations between μ and τ data, and among different LFV τ decays will allow to probe the underlying mechanism of lepton flavor breaking.

Interesting limits on LFV are also obtained in meson decays. The best bounds come from kaon experiments, e.g., $\text{Br}(K_L^0 \rightarrow e^\pm \mu^\mp) < 4.7 \times 10^{-12}$ [92], $\text{Br}(K^+ \rightarrow \pi^+ \mu^+ e^-) < 1.3 \times 10^{-11}$ [93]. Quite strong limits have also been set in decays of B and D mesons, the best upper bounds being $\text{Br}(B^0 \rightarrow e^\pm \mu^\mp) < 1.0 \times 10^{-9}$ [94] and $\text{Br}(D^0 \rightarrow e^\pm \mu^\mp) < 1.3 \times 10^{-8}$ [95].

The LFV decays of the Z boson were probed at LEP at the 10^{-5} to 10^{-6} level. Stronger (95% C.L.) limits have been set recently by the LHC ATLAS collaboration [96,97]:

$$\begin{aligned} \text{Br}(Z \rightarrow e^\pm \mu^\mp) < 2.62 \times 10^{-7}, \quad \text{Br}(Z \rightarrow e^\pm \tau^\mp) < 5.0 \times 10^{-6}, \\ \text{Br}(Z \rightarrow \mu^\pm \tau^\mp) < 6.5 \times 10^{-6}. \end{aligned} \quad (32)$$

LHC is now testing LFV in Higgs decays, within the avail-

able statistics. From the current (95% C.L.) experimental upper bounds [89,98–102],

$$\begin{aligned} \text{Br}(H^0 \rightarrow e^\pm \mu^\mp) < 4.4 \times 10^{-5}, \quad \text{Br}(H^0 \rightarrow e^\pm \tau^\mp) < 0.20\%, \\ \text{Br}(H^0 \rightarrow \mu^\pm \tau^\mp) < 0.15\%, \end{aligned} \quad (33)$$

one can derive direct limits on the LFV Yukawa couplings of the Higgs boson,

$$\mathcal{L}_Y = -H^0 \sum_{i \neq j} (Y_{\ell_i \ell_j}^2 \bar{\ell}_L^i \ell_R^j + \text{h.c.}). \quad (34)$$

From $H^0 \rightarrow e^\pm \mu^\mp$, one obtains $\sqrt{Y_{\mu e}^2 + Y_{e \mu}^2} < 1.9 \times 10^{-4}$, which is not yet competitive with the indirect limit set by $\mu \rightarrow e \gamma$ through a (one-loop) virtual Higgs exchange:

$$\sqrt{Y_{\mu e}^2 + Y_{e \mu}^2} < 3.6 \times 10^{-6}. \quad (35)$$

However, the LHC data provide at present the strongest bounds on the LFV τ Yukawas [89, 101]:

$$\sqrt{Y_{e\tau}^2 + Y_{\tau e}^2} < 1.3 \times 10^{-3}, \quad \sqrt{Y_{\mu\tau}^2 + Y_{\tau\mu}^2} < 1.11 \times 10^{-3}. \quad (36)$$

Figure 5 compares the Higgs exclusion limits on the τ Yukawas with the current indirect constraints from LFV τ decays.

6 Baryon and Lepton Number

The transitions discussed in the previous section preserve the total lepton number $L = L_e + L_\mu + L_\tau$. In the SM, conservation of $B - L$ is an accidental symmetry of the Lagrangian. At the classical level, $B + L$ is also conserved, though it is violated at the loop level by the anomaly. The latter is a topological effect that is highly suppressed at zero temperature and, moreover, does not contribute to the processes discussed in the review. Going beyond renormalizable interactions, there exists a tower of operators in the SMEFT Lagrangian (12), containing only SM fields, that break one or both of these symmetries. We briefly review these possibilities in turn.

Lepton Number

The lowest-dimension operator containing only SM fields that breaks baryon or lepton number is the $d = 5$, lepton-number-violating (LNV) ‘Weinberg’ neutrino-mass operator [65]:

$$\mathcal{L}^{\text{LNV}} = \frac{y}{\Lambda} \bar{L} C H H^T L. \quad (37)$$

When the neutral component of the Higgs field obtains its vacuum expectation value, this $\Delta L = 2$ interaction yields a Majorana mass for the light, active neutrinos. The most comprehensive approach for probing this effect is the search for neutrinoless double-beta decay ($0\nu\beta\beta$) of atomic nuclei, $(Z, A) \rightarrow (Z + 2, A) + e^- + e^-$ [103, 104] (see the review on neutrinoless double- β decay). The detection of a non-zero $0\nu\beta\beta$ signal could represent a spectacular evidence of Majorana neutrinos. The current best limit, $\tau_{1/2} > 1.07 \times 10^{26}$ yr, was obtained by the KamLAND-Zen experiment with ^{136}Xe [105].

Theoretically, the interaction (37) can arise from BSM interactions in the well-known see-saw mechanism for neutrino mass (for a review, see [106]). In this context, the conventional choice for the scale Λ is of order the GUT scale, yielding light neutrino masses of order eV and below when the couplings y are of order the charged elementary fermion Yukawa couplings. BSM theories may also give rise to LNV observables in other contexts. In these scenarios, if the LNV scale is of order 1 TeV, one may observe signatures of LNV not only in $0\nu\beta\beta$ but also in collider searches for final states containing same sign dileptons. Searches for same sign dileptons plus a di-jet pair at the LHC have placed constraints on TeV-scale LNV [107, 108] that in some cases complement those obtained from $0\nu\beta\beta$.

Stringent constraints on violations of L have been also set in $\mu^- \rightarrow e^+$ conversion in muonic atoms, the best limit being $\sigma(\mu^- \text{Ti} \rightarrow e^+ \text{Ca}) / \sigma(\mu^- \text{Ti} \rightarrow \text{all}) < 3.6 \times 10^{-11}$ [109], and at the flavor factories through L -violating decays of the τ lepton and K , D and B mesons. Some representative examples are $\text{Br}(\tau^- \rightarrow e^+ \pi^- \pi^-) < 2.0 \times 10^{-8}$ [110], $\text{Br}(K^+ \rightarrow \pi^- \mu^+ \mu^+) < 4.2 \times 10^{-11}$ [111], $\text{Br}(D^+ \rightarrow \pi^- \mu^+ \mu^+) < 1.4 \times 10^{-8}$ [112] and $\text{Br}(B^- \rightarrow \pi^+ \mu^- \mu^-) < 4.0 \times 10^{-9}$ (95% CL) [113]. All these $|\Delta L| = 2$ processes could be mediated by a massive Majorana neutrino. They provide useful bounds on the effective Majorana neutrino mass matrix $m_{\ell\ell'} \sim \sum_i U_{\ell i} U_{\ell' i} m_{\nu_i}$ [114], although not as strong as the $0\nu\beta\beta$ constraint on m_{ee} .

Baryon Number

Grand Unified Theories (GUTs) combine leptons and quarks in the same symmetry multiplets and, therefore, predict the violation of the baryon and lepton quantum numbers. Many experiments have searched for B -violating transitions, but no positive signal has been identified so far. Proton decay would be the most relevant violation of B , as it would imply the instability of matter. The current lower bound on the proton lifetime is 9×10^{29} yr [115]. Stronger limits have been set for particular decay modes, such as $\tau(p \rightarrow e^+ \pi^0) > 2.4 \times 10^{34}$ yr [116]. For a discussion of proton

decay in the context of GUTs, see the review on Grand Unified Theories.

Another spectacular signal would be neutron-antineutron oscillations. Searches have been performed for quasi-free $n-\bar{n}$ oscillations and for $n\bar{n}$ annihilation products in a nucleus. The latter would arise when the \bar{n} produced through oscillations annihilates with another neutron in the nuclear medium. The corresponding best limits, expressed in terms of the free and bound oscillation times, $\tau_{n\bar{n}}$ and τ_m , respectively, are:

$$\tau_{n\bar{n}} > 0.86 \times 10^8 \text{ s} \quad [117], \quad (38a)$$

$$\tau_m > 3.6 \times 10^{32} \text{ yr} \quad [118] \quad (38b)$$

From the latter, one may infer a bound $\tau_{n\bar{n}} > 4.7 \times 10^8$ s, as discussed below. See Ref. [119] for a recent review.

The theoretical interpretation of these bounds starts with an assumed, effective Hamiltonian for the free (anti-)neutron, \mathcal{H}_{eff} that contains a B -violating part, yielding matrix elements

$$\langle n | \mathcal{H}_{\text{eff}} | n \rangle = \langle \bar{n} | \mathcal{H}_{\text{eff}} | \bar{n} \rangle = m - i \frac{\lambda}{2}, \quad (39a)$$

$$\langle n | \mathcal{H}_{\text{eff}} | \bar{n} \rangle = \langle \bar{n} | \mathcal{H}_{\text{eff}} | n \rangle \equiv \delta m, \quad (39b)$$

where CPT is assumed to be conserved, the neutron lifetime $\tau_n = 1/\lambda$ and $\tau_{n\bar{n}} = 1/|\delta m|$. The rate for a neutron to oscillate into an antineutron after a time t is given by

$$\mathcal{P}_{n\bar{n}}(t) = \sin^2 \left(\frac{t}{\tau_{n\bar{n}}} \right) e^{-\lambda t}. \quad (40)$$

For $t \ll \tau_n \ll \tau_{n\bar{n}}$, one has

$$\mathcal{P}_{n\bar{n}}(t) \rightarrow (t/\tau_{n\bar{n}})^2. \quad (41)$$

In realistic experiments, there exist effects, such as background magnetic fields, that split the energies of the neutron and antineutron. One must ensure that the observation time is sufficiently short so that these effects do not overwhelm the small B -violating term δm and that Eq. (40) applies.

In nuclei, the interactions of neutrons and antineutrons with the surrounding medium are sufficiently distinct that one must take the corresponding matter potentials into account. In particular, the matrix elements in Eq. (39a) become

$$\langle n | \mathcal{H}_{\text{eff}} | n \rangle = m + V_n, \quad \langle \bar{n} | \mathcal{H}_{\text{eff}} | \bar{n} \rangle = m + V_{\bar{n}}, \quad (42)$$

with V_n being essentially real ($V_n \equiv V_{nR}$) and $V_{\bar{n}} = V_{\bar{n}R} - iV_{\bar{n}I}$. The imaginary part $V_{\bar{n}I}$ characterizes the annihilation of the antineutron with bound nucleons into secondary hadrons. The rate for a bound neutron to disappear is given by

$$\Gamma_m = \frac{2(\delta m)^2 |V_{\bar{n}I}|}{(V_{nR} - V_{\bar{n}R})^2 + V_{\bar{n}I}^2} \equiv (R \tau_{n\bar{n}}^2)^{-1}. \quad (43)$$

For the nuclei of experimental interest, nuclear theory computations yield $R \sim 10^{23} \text{ s}^{-1}$. Null results of bound $n-\bar{n}$ oscillation searches thus allow one to infer a bound on $\tau_{n\bar{n}}$ via Eq. (43).

From an elementary particle standpoint, $n-\bar{n}$ oscillations involve the conversion of three quarks into three antiquarks (and vice-versa). The lowest-dimension operators mediating such process arise at dimension nine in the SMEFT:

$$\mathcal{L}_{n-\bar{n}} = \frac{1}{\Lambda^5} \sum_j \alpha_j^{(9)} \mathcal{O}_j^{\text{BNV}}. \quad (44)$$

Consequently, one expects

$$\delta m \sim \alpha_j^{(9)} \frac{\Lambda_{\text{HAD}}^6}{\Lambda^5}, \quad (45)$$

where Λ_{HAD} is a hadronic scale set by the $n-\bar{n}$ matrix elements in Eq. (39b). Taking Λ_{HAD} to be of order the QCD scale and using the present bounds on $\tau_{n\bar{n}}$ yields a lower bound on the B -violating mass scale of ~ 100 TeV.

The search for B -violating decays of short-lived particles such as Z bosons, τ leptons and B mesons provides also relevant constraints. The best limits are $\text{Br}(Z \rightarrow pe, p\mu) < 1.8 \times 10^{-6}$ (95% C.L.) [120], $\text{Br}(\tau^- \rightarrow \bar{p}\mu^-\mu^+) < 1.8 \times 10^{-8}$ [121] and $\text{Br}(B^0 \rightarrow p\mu^-) < 2.6 \times 10^{-9}$ [122]

7 Quark flavors

While strong and electromagnetic forces preserve the quark flavor, the charged-current weak interactions generate transitions among the different quark species (see the review on the CKM quark-mixing matrix). Since the SM flavor-changing mechanism is associated with the W^\pm fermionic vertices, the tree-level transitions satisfy a $\Delta F = \Delta Q$ rule where ΔQ denotes the change in charge of the relevant hadrons. Remember that the flavor quantum number F is defined to be +1 for positively charged quarks ($F = U, C, T$) and -1 for quarks with negative charges ($F = D, S, B$). The strongest tests on this conservation law have been obtained in kaon decays such as $\text{Br}(K^+ \rightarrow \pi^+\pi^+e^-\bar{\nu}_e) < 1.3 \times 10^{-8}$ [123], and $(\text{Re } x, \text{Im } x) = (-0.002 \pm 0.006, 0.0012 \pm 0.0021)$ [124, 125] where $x \equiv \mathcal{M}(\bar{K}^0 \rightarrow \pi^-\ell^+\nu)/\mathcal{M}(K^0 \rightarrow \pi^-\ell^+\nu)$.

The $\Delta F = \Delta Q$ rule can be violated through quantum loop contributions giving rise to flavor-changing neutral-current transitions (FCNCs). Owing to the GIM mechanism, processes of this type are very suppressed in the SM, which makes them a superb tool in the search for new physics associated with the flavor dynamics. Within the SM itself, these transitions are also sensitive to the heavy-quark mass scales and have played a crucial role identifying the size of the charm (K^0 - \bar{K}^0 mixing) and top (B^0 - \bar{B}^0 mixing) masses before the discovery of those quarks. In addition to the well-established $\Delta F = 2$ mixings in neutral K and B mesons, $\Delta M_{K^0} \equiv M_{K_L^0} - M_{K_S^0} = (0.5293 \pm 0.0009) \times 10^{10} \text{ s}^{-1}$, $\Delta M_{B^0} \equiv M_{B_H^0} - M_{B_L^0} = (0.5069 \pm 0.0019) \times 10^{12} \text{ s}^{-1}$ and $\Delta M_{B_s^0} \equiv M_{B_{sH}^0} - M_{B_{sL}^0} = (17.765 \pm 0.006) \times 10^{12} \text{ s}^{-1}$, the mixing of the D^0 meson and its antiparticle has been recently observed with a significance of more than seven standard deviations [126], showing that there is a nonzero mass difference between the two neutral charm-meson eigenstates, of the expected size:

$$M_{D_H^0} - M_{D_L^0} = (0.997 \pm 0.116) \times 10^{10} \text{ s}^{-1}. \quad (46)$$

The SM prediction of the D_H^0 - D_L^0 mass difference is dominated by long-distance physics, because it involves virtual loops with down-type light quarks, and has unfortunately quite large uncertainties [127].

The FCNC kaon decays into lepton-antilepton pairs put stringent constraints on new flavor-changing interactions. The measured $K_L^0 \rightarrow \mu^+\mu^-$ rate, $\text{Br}(K_L^0 \rightarrow \mu^+\mu^-) = (6.84 \pm 0.11) \times 10^{-9}$, is completely dominated by the known 2γ absorptive contribution, leaving very little room for new-physics, and $\text{Br}(K_L^0 \rightarrow e^+e^-) = (9_{-4}^{+6}) \times 10^{-12}$ [128] (the tiniest branching ratio ever measured) also agrees with the SM expectation [129]. The experimental K_S^0 upper bounds on the electron, $\text{Br}(K_S^0 \rightarrow e^+e^-) < 9 \times 10^{-9}$ [130], and muon, $\text{Br}(K_S^0 \rightarrow \mu^+\mu^-) < 2.1 \times 10^{-10}$ [131], modes are still five and two orders of magnitude, respectively, larger than their SM predictions [129]. Another very clean test of FCNCs is provided by the decay $K^+ \rightarrow \pi^+\nu\bar{\nu}$. The CERN NA62 experiment has already observed 20 signal candidates, providing the first evidence of this decay [132]. This leads to $\text{Br}(K^+ \rightarrow \pi^+\nu\bar{\nu}) = (1.14_{-0.33}^{+0.40}) \times 10^{-10}$, in agreement with the predicted SM branching fraction of $(7.73 \pm 0.61) \times 10^{-11}$ [133, 134]. Even more interesting is the CP -violating neutral mode $K_L^0 \rightarrow \pi^0\nu\bar{\nu}$, expected at a rate of $(2.59 \pm 0.29) \times 10^{-11}$ [133, 134] that is still far away from the current upper bound of 3.0×10^{-9} [135]. The KOTO experiment at KEK is expected to substantially increase the sensitivity to this mode.

The strongest bound on FCNC transitions in charm decays is $\text{Br}(D^0 \rightarrow \mu^+\mu^-) < 3.1 \times 10^{-9}$ [136], while in B decays the LHC experiments have recently reached the SM sensitivity: $\text{Br}(B_d^0 \rightarrow \mu^+\mu^-) < 1.5 \times 10^{-10}$ [137] and $\text{Br}(B_s^0 \rightarrow \mu^+\mu^-) = (3.34 \pm 0.27) \times 10^{-9}$.

References

- [1] G. Luders, Kong. Dan. Vid. Sel. Mat. Fys. Med. **28N5**, 5, 1 (1954).
- [2] W. Pauli, in L. Rosenfeld and V. Weisskopf, editors, “Niels Bohr and the Development of Physics,” 30–51, McGraw-Hill, New York (1955).
- [3] J. McDonough *et al.*, Phys. Rev. **D38**, 2121 (1988).
- [4] M. Ablikim *et al.* (BESIII), Phys. Rev. **D90**, 9, 092002 (2014), [arXiv:1409.4040].
- [5] S. Prakhov *et al.* (Crystal Ball), Phys. Rev. Lett. **84**, 4802 (2000).
- [6] J. H. Christenson *et al.*, Phys. Rev. Lett. **13**, 138 (1964).
- [7] H. Burkhardt *et al.* (NA31), Phys. Lett. **B206**, 169 (1988).
- [8] G. D. Barr *et al.* (NA31), Phys. Lett. **B317**, 233 (1993).
- [9] L. K. Gibbons *et al.*, Phys. Rev. Lett. **70**, 1203 (1993).
- [10] J. R. Batley *et al.* (NA48), Phys. Lett. **B544**, 97 (2002), [hep-ex/0208009].
- [11] E. Abouzaid *et al.* (KTeV), Phys. Rev. **D83**, 092001 (2011), [arXiv:1011.0127].
- [12] H. Gisbert and A. Pich, Rept. Prog. Phys. **81**, 7, 076201 (2018), [arXiv:1712.06147].
- [13] V. Cirigliano *et al.*, JHEP **02**, 032 (2020), [arXiv:1911.01359].
- [14] R. Abbott *et al.* (RBC, UKQCD), Phys. Rev. D **102**, 5, 054509 (2020), [arXiv:2004.09440].
- [15] R. Aaij *et al.* (LHCb), Phys. Rev. Lett. **122**, 21, 211803 (2019), [arXiv:1903.08726].
- [16] R. Aaij *et al.* (LHCb), Phys. Rev. Lett. **131**, 9, 091802 (2023), [arXiv:2209.03179].
- [17] P. F. de Salas *et al.*, JHEP **02**, 071 (2021), [arXiv:2006.11237].
- [18] M. C. Gonzalez-Garcia, M. Maltoni and T. Schwetz, Universe **7**, 12, 459 (2021), [arXiv:2111.03086].
- [19] A. Angelopoulos *et al.* (CLEAR), Phys. Lett. **B444**, 43 (1998).
- [20] L. Wolfenstein, Phys. Rev. Lett. **83**, 911 (1999).
- [21] L. Alvarez-Gaume *et al.*, Phys. Lett. **B458**, 347 (1999), [hep-ph/9812326].
- [22] H. J. Gerber, Eur. Phys. J. **C35**, 195 (2004).
- [23] M. C. Bañuls and J. Bernabeu, Phys. Lett. **B464**, 117 (1999), [hep-ph/9908353].
- [24] M. C. Bañuls and J. Bernabeu, Nucl. Phys. **B590**, 19 (2000), [hep-ph/0005323].
- [25] J. Bernabeu, F. Martinez-Vidal and P. Villanueva-Perez, JHEP **08**, 064 (2012), [arXiv:1203.0171].
- [26] J. P. Lees *et al.* (BaBar), Phys. Rev. Lett. **109**, 211801 (2012), [arXiv:1207.5832].
- [27] T. Chupp *et al.*, Rev. Mod. Phys. **91**, 1, 015001 (2019), [arXiv:1710.02504].
- [28] J. Engel, M. J. Ramsey-Musolf and U. van Kolck, Prog. Part. Nucl. Phys. **71**, 21 (2013), [arXiv:1303.2371].
- [29] M. Pospelov and A. Ritz, Annals Phys. **318**, 119 (2005), [hep-ph/0504231].
- [30] J. S. M. Ginges and V. V. Flambaum, Phys. Rept. **397**, 63 (2004), [arXiv:physics/0309054].
- [31] V. Andreev *et al.* (ACME), Nature **562**, 7727, 355 (2018).
- [32] T. S. Roussy *et al.*, Science **381**, 6653, adg4084 (2023), [arXiv:2212.11841].
- [33] G. W. Bennett *et al.* (Muon (g-2)), Phys. Rev. **D80**, 052008 (2009), [arXiv:0811.1207].
- [34] C. Abel *et al.* (nEDM), Phys. Rev. Lett. **124**, 8, 081803 (2020), [arXiv:2001.11966].

- [35] B. Graner *et al.*, Phys. Rev. Lett. **116**, 16, 161601 (2016), [Erratum: Phys. Rev. Lett.119,no.11,119901(2017)], [arXiv:1601.04339].
- [36] F. Allmendinger *et al.*, Phys. Rev. **A100**, 2, 022505 (2019), [arXiv:1904.12295].
- [37] C. Jarlskog, Phys. Rev. Lett. **55**, 1039 (1985); C. Jarlskog, Z. Phys. **C29**, 491 (1985).
- [38] E. P. Shabalin, Sov. J. Nucl. Phys. **28**, 75 (1978), [Yad. Fiz.28,151(1978)].
- [39] E. P. Shabalin, Sov. Phys. Usp. **26**, 297 (1983), [Usp. Fiz. Nauk139,561(1983)].
- [40] W. Bernreuther and M. Suzuki, Rev. Mod. Phys. **63**, 313 (1991), [Erratum: Rev. Mod. Phys.64,633(1992)].
- [41] M. Pospelov and A. Ritz, Phys. Rev. **D89**, 5, 056006 (2014), [arXiv:1311.5537].
- [42] C.-Y. Seng, Phys. Rev. **C91**, 2, 025502 (2015), [arXiv:1411.1476].
- [43] B. Grzadkowski *et al.*, JHEP **10**, 085 (2010), [arXiv:1008.4884].
- [44] S. Mantry, M. Pitschmann and M. J. Ramsey-Musolf, Phys. Rev. **D90**, 5, 054016 (2014), [arXiv:1401.7339].
- [45] B. K. Sahoo, Phys. Rev. **D95**, 1, 013002 (2017), [arXiv:1612.09371].
- [46] T. Fleig and M. Jung, JHEP **07**, 012 (2018), [arXiv:1802.02171].
- [47] J. Bsaisou *et al.*, Annals Phys. **359**, 317 (2015), [arXiv:1412.5471].
- [48] J. de Vries *et al.*, Annals Phys. **338**, 50 (2013), [arXiv:1212.0990].
- [49] L. I. Schiff, Phys. Rev. **132**, 2194 (1963).
- [50] T. Chupp and M. Ramsey-Musolf, Phys. Rev. **C91**, 3, 035502 (2015), [arXiv:1407.1064].
- [51] J. Beringer *et al.* (Particle Data Group), Phys. Rev. **D86**, 010001 (2012).
- [52] A. Angelopoulos *et al.* (CLEAN), Phys. Lett. **B471**, 332 (1999).
- [53] M. S. Fee *et al.*, Phys. Rev. **A48**, 192 (1993).
- [54] R. J. Hughes and B. I. Deutch, Phys. Rev. Lett. **69**, 578 (1992).
- [55] S. Ulmer *et al.* (BASE), Nature **524**, 7564, 196 (2015).
- [56] M. J. Borchert *et al.* (BASE), Nature **601**, 7891, 53 (2022).
- [57] R. S. Van Dyck, P. B. Schwinberg and H. G. Dehmelt, Phys. Rev. Lett. **59**, 26 (1987).
- [58] G. W. Bennett *et al.* (Muon g-2), Phys. Rev. Lett. **92**, 161802 (2004), [hep-ex/0401008].
- [59] C. Smorra *et al.* (BASE), Nature **550**, 7676, 371 (2017).
- [60] M. Ahmadi *et al.*, Nature **557**, 7703, 71 (2018).
- [61] O. W. Greenberg, Phys. Rev. Lett. **89**, 231602 (2002), [hep-ph/0201258].
- [62] S. Liberati, Class. Quant. Grav. **30**, 133001 (2013), [arXiv:1304.5795].
- [63] V. A. Kostelecky and N. Russell, Rev. Mod. Phys. **83**, 11 (2011), [arXiv:0801.0287].
- [64] D. Colladay and V. A. Kostelecky, Phys. Rev. **D58**, 116002 (1998), [hep-ph/9809521].
- [65] S. Weinberg, Phys. Rev. Lett. **43**, 1566 (1979).
- [66] F. Wilczek and A. Zee, Phys. Rev. Lett. **43**, 1571 (1979).
- [67] L. F. Abbott and M. B. Wise, Phys. Rev. **D22**, 2208 (1980).
- [68] M. Agostini *et al.* (Borexino), Phys. Rev. Lett. **115**, 231802 (2015), [arXiv:1509.01223].
- [69] E. B. Norman, J. N. Bahcall and M. Goldhaber, Phys. Rev. **D53**, 4086 (1996).
- [70] G. Bressi *et al.*, Phys. Rev. **A83**, 5, 052101 (2011), [arXiv:1102.2766].
- [71] C. Caprini, S. Biller and P. G. Ferreira, JCAP **0502**, 006 (2005), [hep-ph/0310066].
- [72] B. Altschul, Phys. Rev. Lett. **98**, 261801 (2007), [hep-ph/0703126].
- [73] A. de Gouvea, Private Communication (2019).
- [74] A. de Gouvea and P. Vogel, Prog. Part. Nucl. Phys. **71**, 75 (2013), [arXiv:1303.4097].
- [75] S. T. Petcov, Sov. J. Nucl. Phys. **25**, 340 (1977), [Erratum: Yad. Fiz.25,1336(1977)].
- [76] W. J. Marciano and A. I. Sanda, Phys. Lett. **67B**, 303 (1977).
- [77] S. M. Bilenky, S. T. Petcov and B. Pontecorvo, Phys. Lett. **67B**, 309 (1977).
- [78] T.-P. Cheng and L.-F. Li, Phys. Rev. **D16**, 1425 (1977).
- [79] B. W. Lee and R. E. Shrock, Phys. Rev. **D16**, 1444 (1977).
- [80] B. W. Lee *et al.*, Phys. Rev. Lett. **38**, 937 (1977), [Erratum: Phys. Rev. Lett.38,1230(1977)].
- [81] R. H. Bernstein and P. S. Cooper, Phys. Rept. **532**, 27 (2013), [arXiv:1307.5787].
- [82] L. Calibbi and G. Signorelli, Riv. Nuovo Cim. **41**, 2, 71 (2018), [arXiv:1709.00294].
- [83] A. M. Baldini *et al.* (MEG), Eur. Phys. J. **C76**, 8, 434 (2016), [arXiv:1605.05081].
- [84] U. Bellgardt *et al.* (SINDRUM), Nucl. Phys. **B299**, 1 (1988).
- [85] W. H. Bertl *et al.* (SINDRUM II), Eur. Phys. J. **C47**, 337 (2006).
- [86] Y. S. Amhis *et al.* (HFLAV), Eur. Phys. J. C **81**, 3, 226 (2021), [arXiv:1909.12524].
- [87] W. Altmannshofer *et al.* (Belle-II), PTEP **2019**, 12, 123C01 (2019), [arXiv:1808.10567].
- [88] A. Cerri *et al.*, CERN Yellow Rep. Monogr. **7**, 867 (2019), [arXiv:1812.07638].
- [89] A. M. Sirunyan *et al.* (CMS), Phys. Rev. D **104**, 3, 032013 (2021), [arXiv:2105.03007].
- [90] R. Kitano, M. Koike and Y. Okada, Phys. Rev. **D66**, 096002 (2002), [Erratum: Phys. Rev.D76,059902(2007)], [hep-ph/0203110].
- [91] A. Pich, Prog. Part. Nucl. Phys. **75**, 41 (2014), [arXiv:1310.7922].
- [92] D. Ambrose *et al.* (BNL), Phys. Rev. Lett. **81**, 5734 (1998), [hep-ex/9811038].
- [93] A. Sher *et al.*, Phys. Rev. **D72**, 012005 (2005), [hep-ex/0502020].
- [94] R. Aaij *et al.* (LHCb), JHEP **03**, 078 (2018), [arXiv:1710.04111].
- [95] R. Aaij *et al.* (LHCb), Phys. Lett. **B754**, 167 (2016), [arXiv:1512.00322].
- [96] G. Aad *et al.* (ATLAS), Phys. Rev. D **108**, 032015 (2023), [arXiv:2204.10783].
- [97] G. Aad *et al.* (ATLAS), Nature Phys. **17**, 7, 819 (2021), [arXiv:2105.12491].
- [98] G. Aad *et al.* (ATLAS), Phys. Lett. **B801**, 135148 (2020), [arXiv:1909.10235].
- [99] G. Aad *et al.* (ATLAS), Phys. Lett. **B800**, 135069 (2020), [arXiv:1907.06131].
- [100] A. M. Sirunyan *et al.* (CMS), JHEP **06**, 001 (2018), [arXiv:1712.07173].
- [101] G. Aad *et al.* (ATLAS), JHEP **07**, 166 (2023), [arXiv:2302.05225].
- [102] A. Hayrapetyan *et al.* (CMS), Phys. Rev. D **108**, 7, 072004 (2023), [arXiv:2305.18106].

- [103] S. Dell’Oro *et al.*, Adv. High Energy Phys. **2016**, 2162659 (2016), [arXiv:1601.07512].
- [104] J. Engel and J. Menéndez, Rept. Prog. Phys. **80**, 4, 046301 (2017), [arXiv:1610.06548].
- [105] A. Gando *et al.* (KamLAND-Zen), Phys. Rev. Lett. **117**, 8, 082503 (2016), [Addendum: Phys. Rev. Lett. **117**, no.10, 109903 (2016)], [arXiv:1605.02889].
- [106] P. Fileviez Perez, Phys. Rept. **597**, 1 (2015), [arXiv:1501.01886].
- [107] G. Aad *et al.* (ATLAS), Eur. Phys. J. C **83**, 12, 1164 (2023), [arXiv:2304.09553].
- [108] A. Tumasyan *et al.* (CMS), JHEP **04**, 047 (2022), [arXiv:2112.03949].
- [109] J. Kaulard *et al.* (SINDRUM II), Phys. Lett. **B422**, 334 (1998).
- [110] Y. Miyazaki *et al.* (Belle), Phys. Lett. **B719**, 346 (2013), [arXiv:1206.5595].
- [111] E. Cortina Gil *et al.* (NA62), Phys. Lett. **B797**, 134794 (2019), [arXiv:1905.07770].
- [112] R. Aaij *et al.* (LHCb), JHEP **06**, 044 (2021), [arXiv:2011.00217].
- [113] R. Aaij *et al.* (LHCb), Phys. Rev. Lett. **112**, 13, 131802 (2014), [arXiv:1401.5361].
- [114] A. Abada *et al.*, JHEP **02**, 169 (2018), [arXiv:1712.03984].
- [115] A. Allega *et al.* (SNO+), Phys. Rev. D **105**, 11, 112012 (2022), [arXiv:2205.06400].
- [116] A. Takenaka *et al.* (Super-Kamiokande), Phys. Rev. D **102**, 11, 112011 (2020), [arXiv:2010.16098].
- [117] M. Baldo-Ceolin *et al.*, Z. Phys. **C63**, 409 (1994).
- [118] K. Abe *et al.* (Super-Kamiokande), Phys. Rev. D **103**, 1, 012008 (2021), [arXiv:2012.02607].
- [119] D. G. Phillips, II *et al.*, Phys. Rept. **612**, 1 (2016), [arXiv:1410.1100].
- [120] G. Abbiendi *et al.* (OPAL), Phys. Lett. **B447**, 157 (1999), [hep-ex/9901011].
- [121] D. Sahoo *et al.* (Belle), Phys. Rev. D **102**, 111101 (2020), [arXiv:2010.15361].
- [122] R. Aaij *et al.* (LHCb), Phys. Rev. D **108**, 1, 012021 (2023), [arXiv:2210.10412].
- [123] P. Bloch *et al.* (Geneva-Saclay), Phys. Lett. **60B**, 393 (1976).
- [124] A. Angelopoulos *et al.* (CPLEAR), Phys. Lett. **B444**, 38 (1998).
- [125] A. Angelopoulos *et al.* (CPLEAR), Eur. Phys. J. **C22**, 55 (2001).
- [126] R. Aaij *et al.* (LHCb), Phys. Rev. Lett. **127**, 11, 111801 (2021), [arXiv:2106.03744].
- [127] A. A. Petrov, Int. J. Mod. Phys. **A21**, 5686 (2006), [hep-ph/0611361].
- [128] D. Ambrose *et al.* (BNL E871), Phys. Rev. Lett. **81**, 4309 (1998), [hep-ex/9810007].
- [129] V. Cirigliano *et al.*, Rev. Mod. Phys. **84**, 399 (2012), [arXiv:1107.6001].
- [130] F. Ambrosino *et al.* (KLOE), Phys. Lett. **B672**, 203 (2009), [arXiv:0811.1007].
- [131] R. Aaij *et al.* (LHCb), Phys. Rev. Lett. **125**, 23, 231801 (2020), [arXiv:2001.10354].
- [132] E. Cortina Gil *et al.* (NA62), JHEP **06**, 093 (2021), [arXiv:2103.15389].
- [133] J. Brod, M. Gorbahn and E. Stamou, Phys. Rev. **D83**, 034030 (2011), [arXiv:1009.0947].
- [134] J. Brod, M. Gorbahn and E. Stamou, PoS **BEAUTY2020**, 056 (2021), [arXiv:2105.02868].
- [135] J. K. Ahn *et al.* (KOTO), Phys. Rev. Lett. **122**, 2, 021802 (2019), [arXiv:1810.09655].
- [136] R. Aaij *et al.* (LHCb), Phys. Rev. Lett. **131**, 4, 041804 (2023), [arXiv:2212.11203].
- [137] A. Tumasyan *et al.* (CMS), Phys. Lett. B **842**, 137955 (2023), [arXiv:2212.10311].

TESTS OF DISCRETE SPACE-TIME SYMMETRIES

CHARGE CONJUGATION (C) INVARIANCE

$\Gamma(\pi^0 \rightarrow 3\gamma)/\Gamma_{\text{total}}$	$<3.1 \times 10^{-8}$, CL = 90%
η C-nonconserving decay parameters	
$\pi^+ \pi^- \pi^0$ left-right asymmetry	$(0.09 \pm 0.11) \times 10^{-2}$
$\pi^+ \pi^- \pi^0$ sextant asymmetry	$(0.12 \pm 0.10) \times 10^{-2}$
$\pi^+ \pi^- \pi^0$ quadrant asymmetry	$(-0.09 \pm 0.09) \times 10^{-2}$
$\pi^+ \pi^- \gamma$ left-right asymmetry	$(0.9 \pm 0.4) \times 10^{-2}$
$\pi^+ \pi^- \gamma$ parameter β (D -wave)	-0.02 ± 0.07 ($S = 1.3$)
$\Gamma(\eta \rightarrow \pi^0 \gamma)/\Gamma_{\text{total}}$	[a] $<9 \times 10^{-5}$, CL = 90%
$\Gamma(\eta \rightarrow 2\pi^0 \gamma)/\Gamma_{\text{total}}$	$<5 \times 10^{-4}$, CL = 90%
$\Gamma(\eta \rightarrow 3\pi^0 \gamma)/\Gamma_{\text{total}}$	$<6 \times 10^{-5}$, CL = 90%
$\Gamma(\eta \rightarrow 3\gamma)/\Gamma_{\text{total}}$	$<1.6 \times 10^{-5}$, CL = 90%
$\Gamma(\eta \rightarrow \pi^0 e^+ e^-)/\Gamma_{\text{total}}$	[b] $<8 \times 10^{-6}$, CL = 90%
$\Gamma(\eta \rightarrow \pi^0 \mu^+ \mu^-)/\Gamma_{\text{total}}$	[b] $<5 \times 10^{-6}$, CL = 90%
$\Gamma(\omega(782) \rightarrow \eta \pi^0)/\Gamma_{\text{total}}$	$<2.1 \times 10^{-4}$, CL = 90%
$\Gamma(\omega(782) \rightarrow 2\pi^0)/\Gamma_{\text{total}}$	$<2.2 \times 10^{-4}$, CL = 90%
$\Gamma(\omega(782) \rightarrow 3\pi^0)/\Gamma_{\text{total}}$	$<2.3 \times 10^{-4}$, CL = 90%
$\eta'(958) \rightarrow \pi^+ \pi^- \gamma$ decay asymmetry parameter	-0.03 ± 0.04
$\Gamma(\eta'(958) \rightarrow \pi^0 e^+ e^-)/\Gamma_{\text{total}}$	[b] $<1.4 \times 10^{-3}$, CL = 90%
$\Gamma(\eta'(958) \rightarrow \pi^0 \rho^0)/\Gamma_{\text{total}}$	$<4 \times 10^{-2}$, CL = 90%
$\Gamma(\eta'(958) \rightarrow \eta e^+ e^-)/\Gamma_{\text{total}}$	[b] $<2.4 \times 10^{-3}$, CL = 90%
$\Gamma(\eta'(958) \rightarrow 3\gamma)/\Gamma_{\text{total}}$	$<1.0 \times 10^{-4}$, CL = 90%
$\Gamma(\eta'(958) \rightarrow \mu^+ \mu^- \pi^0)/\Gamma_{\text{total}}$	[b] $<6.0 \times 10^{-5}$, CL = 90%
$\Gamma(\eta'(958) \rightarrow \mu^+ \mu^- \eta)/\Gamma_{\text{total}}$	[b] $<1.5 \times 10^{-5}$, CL = 90%
$\Gamma(J/\psi(1S) \rightarrow \gamma \gamma)/\Gamma_{\text{total}}$	$<2.7 \times 10^{-7}$, CL = 90%
$\Gamma(J/\psi(1S) \rightarrow \gamma \phi)/\Gamma_{\text{total}}$	$<1.4 \times 10^{-6}$, CL = 90%

PARITY (P) INVARIANCE

e electric dipole moment	$<0.041 \times 10^{-28}$ ecm, CL = 90%
μ electric dipole moment $ d $	$<1.8 \times 10^{-19}$ ecm, CL = 95%
$\text{Re}(d_\tau = \tau \text{ electric dipole moment})$	$-0.185 \text{ to } 0.061 \times 10^{-16}$ ecm, CL = 95%
$\Gamma(\eta \rightarrow \pi^+ \pi^-)/\Gamma_{\text{total}}$	$<4.4 \times 10^{-6}$, CL = 90%
$\Gamma(\eta \rightarrow 2\pi^0)/\Gamma_{\text{total}}$	$<3.5 \times 10^{-4}$, CL = 90%
$\Gamma(\eta \rightarrow 4\pi^0)/\Gamma_{\text{total}}$	$<6.9 \times 10^{-7}$, CL = 90%
$\Gamma(\eta'(958) \rightarrow \pi^+ \pi^-)/\Gamma_{\text{total}}$	$<1.8 \times 10^{-5}$, CL = 90%
$\Gamma(\eta'(958) \rightarrow \pi^0 \pi^0)/\Gamma_{\text{total}}$	$<4 \times 10^{-4}$, CL = 90%
$a_P(B^0 \rightarrow \rho \bar{P} K^+ \pi^-)$	$(1.5 \pm 0.9)\%$
$\Gamma(\eta_C(1S) \rightarrow \pi^+ \pi^-)/\Gamma_{\text{total}}$	$<1.3 \times 10^{-4}$, CL = 90%
$\Gamma(\eta_C(1S) \rightarrow \pi^0 \pi^0)/\Gamma_{\text{total}}$	$<4 \times 10^{-5}$, CL = 90%
$\Gamma(\eta_C(1S) \rightarrow K^+ K^-)/\Gamma_{\text{total}}$	$<7 \times 10^{-4}$, CL = 90%
$\Gamma(\eta_C(1S) \rightarrow K_S^0 K_S^0)/\Gamma_{\text{total}}$	$<4 \times 10^{-4}$, CL = 90%
p electric dipole moment	$<0.021 \times 10^{-23}$ ecm
n electric dipole moment	$<0.18 \times 10^{-25}$ ecm, CL = 90%
Λ electric dipole moment	$<1.5 \times 10^{-16}$ ecm, CL = 95%
$a_P(\Lambda_b^0 \rightarrow \rho \pi^- \pi^+ \pi^-)$	$(-4.0 \pm 0.7)\%$
$a_P(\Lambda_b^0 \rightarrow \rho K^- \pi^+ \pi^-)$	$(-0.6 \pm 0.9)\%$
$a_P(\Lambda_b^0 \rightarrow \rho K^- K^+ \pi^-)$	$(4 \pm 5)\%$
$a_P(\Lambda_b^0 \rightarrow \rho K^- K^+ K^-)$	$(-1.6 \pm 1.5)\%$
$a_P(\Lambda_b^0 \rightarrow \rho K^- \mu^+ \mu^-)$	$(-5 \pm 5)\%$

TIME REVERSAL (T) INVARIANCE

e electric dipole moment	$<0.041 \times 10^{-28}$ ecm, CL = 90%
μ electric dipole moment $ d $	$<1.8 \times 10^{-19}$ ecm, CL = 95%
μ decay parameters	
transverse e^+ polarization normal to plane of μ spin, e^+ momentum	$(-2 \pm 8) \times 10^{-3}$
α'/A	$(-10 \pm 20) \times 10^{-3}$
β'/A	$(2 \pm 7) \times 10^{-3}$
$\text{Re}(d_\tau = \tau \text{ electric dipole moment})$	$-0.185 \text{ to } 0.061 \times 10^{-16}$ ecm, CL = 95%
P_T in $K^+ \rightarrow \pi^0 \mu^+ \nu_\mu$	$(-1.7 \pm 2.5) \times 10^{-3}$
P_T in $K^+ \rightarrow \mu^+ \nu_\mu \gamma$	$(-0.6 \pm 1.9) \times 10^{-2}$
$\text{Im}(\xi)$ in $K^+ \rightarrow \pi^0 \mu^+ \nu_\mu$ decay (from transverse μ pol.)	-0.006 ± 0.008

asymmetry A_T in $K^0 \bar{K}^0$ mixing	$(6.6 \pm 1.6) \times 10^{-3}$
$\text{Im}(\xi)$ in K^0_3 decay (from transverse μ pol.)	-0.007 ± 0.026
$A_T(D^\pm \rightarrow K_S^0 K^\pm \pi^+ \pi^-)$	[c] $(-3 \pm 8) \times 10^{-3}$ ($S = 1.1$)
$A_T(D^0 \rightarrow K^+ K^- \pi^+ \pi^-)$	[c] $(2.9 \pm 2.2) \times 10^{-3}$
$A_T(D_S^\pm \rightarrow K_S^0 K^\pm \pi^+ \pi^-)$	[c] $(-8 \pm 6) \times 10^{-3}$
$\Delta S^+_{\ell^-} (S_{\ell^-, K_S^0}^- - S_{\ell^+, K_S^0}^+)$	-1.37 ± 0.15
$\Delta S^-_{\ell^-} (S_{\ell^-, K_S^0}^+ - S_{\ell^+, K_S^0}^-)$	1.17 ± 0.21
$\Delta C^+_{\ell^-} (C_{\ell^-, K_S^0}^- - C_{\ell^+, K_S^0}^+)$	0.10 ± 0.16
$\Delta C^-_{\ell^-} (C_{\ell^-, K_S^0}^+ - C_{\ell^+, K_S^0}^-)$	0.04 ± 0.16
p electric dipole moment	$<0.021 \times 10^{-23}$ ecm
n electric dipole moment	$<0.18 \times 10^{-25}$ ecm, CL = 90%
$n \rightarrow p e^- \bar{\nu}_e$ decay parameters	
ϕ_{AV} , phase of g_A relative to g_V	[d] $(180.017 \pm 0.026)^\circ$
triple correlation coefficient D	[e] $(-1.2 \pm 2.0) \times 10^{-4}$
triple correlation coefficient R	[e] 0.004 ± 0.013
Λ electric dipole moment	$<1.5 \times 10^{-16}$ ecm, CL = 95%
triple correlation coefficient D for $\Sigma^- \rightarrow n e^- \bar{\nu}_e$	0.11 ± 0.10

CP INVARIANCE

$\text{Re}(d^W_\tau)$	$<0.50 \times 10^{-17}$ ecm, CL = 95%
$\text{Im}(d^W_\tau)$	$<1.1 \times 10^{-17}$ ecm, CL = 95%
δ (CP violating phase in neutrino mixing)	$1.19 \pm 0.22 \pi$ rad ($S = 1.2$)
$\eta \rightarrow \pi^+ \pi^- e^+ e^-$ decay-plane asymmetry	$(-0.6 \pm 3.1) \times 10^{-2}$
$\Gamma(\eta \rightarrow \pi^+ \pi^-)/\Gamma_{\text{total}}$	$<4.4 \times 10^{-6}$, CL = 90%
$\Gamma(\eta \rightarrow 2\pi^0)/\Gamma_{\text{total}}$	$<3.5 \times 10^{-4}$, CL = 90%
$\Gamma(\eta \rightarrow 4\pi^0)/\Gamma_{\text{total}}$	$<6.9 \times 10^{-7}$, CL = 90%
$\Gamma(\eta'(958) \rightarrow \pi^+ \pi^-)/\Gamma_{\text{total}}$	$<1.8 \times 10^{-5}$, CL = 90%
$\Gamma(\eta'(958) \rightarrow \pi^0 \pi^0)/\Gamma_{\text{total}}$	$<4 \times 10^{-4}$, CL = 90%
$K^\pm \rightarrow \pi^\pm e^+ e^-$ rate difference/sum	$(-2.2 \pm 1.6) \times 10^{-2}$
$K^\pm \rightarrow \pi^\pm \mu^+ \mu^-$ rate difference/sum	0.010 ± 0.023
$K^\pm \rightarrow \pi^\pm \pi^0 \gamma$ rate difference/sum	$(0.0 \pm 1.2) \times 10^{-3}$
$K^\pm \rightarrow \pi^\pm \pi^+ \pi^-$ rate difference/sum	$(0.04 \pm 0.06)\%$
$K^\pm \rightarrow \pi^\pm \pi^0 \pi^0$ rate difference/sum	$(-0.02 \pm 0.28)\%$
$K^\pm \rightarrow \pi^\pm \pi^+ \pi^- (g_+ - g_-) / (g_+ + g_-)$	$(-1.5 \pm 2.2) \times 10^{-4}$
$K^\pm \rightarrow \pi^\pm \pi^0 \pi^0 (g_+ - g_-) / (g_+ + g_-)$	$(1.8 \pm 1.8) \times 10^{-4}$
$A_S = [\Gamma(K_S^0 \rightarrow \pi^- e^+ \nu_e) - \Gamma(K_S^0 \rightarrow \pi^+ e^- \bar{\nu}_e)] / \text{SUM}$	$(-4 \pm 6) \times 10^{-3}$
$\text{Im}(\eta_{+-0}) = \text{Im}(A(K_S^0 \rightarrow \pi^+ \pi^- \pi^0, CP\text{-violating}) / A(K_L^0 \rightarrow \pi^+ \pi^- \pi^0))$	-0.002 ± 0.009
$\text{Im}(\eta_{000}) = \text{Im}(A(K_S^0 \rightarrow \pi^0 \pi^0 \pi^0) / A(K_L^0 \rightarrow \pi^0 \pi^0 \pi^0))$	-0.001 ± 0.016
$ \eta_{000} = A(K_S^0 \rightarrow 3\pi^0) / A(K_L^0 \rightarrow 3\pi^0) $	<0.0088 , CL = 90%
CP asymmetry A in $K_S^0 \rightarrow \pi^+ \pi^- e^+ e^-$	$(-0.4 \pm 0.8)\%$
$\Gamma(K_S^0 \rightarrow 3\pi^0)/\Gamma_{\text{total}}$	$<2.6 \times 10^{-8}$, CL = 90%
linear coefficient j for $K_L^0 \rightarrow \pi^+ \pi^- \pi^0$	0.0012 ± 0.0008
quadratic coefficient f for $K_L^0 \rightarrow \pi^+ \pi^- \pi^0$	0.004 ± 0.006
$ \epsilon'_{+-\gamma} /\epsilon$ for $K_L^0 \rightarrow \pi^+ \pi^- \gamma$	<0.3 , CL = 90%
$ g_{E1} $ for $K_L^0 \rightarrow \pi^+ \pi^- \gamma$	<0.21 , CL = 90%
$\Gamma(K_L^0 \rightarrow \pi^0 \mu^+ \mu^-)/\Gamma_{\text{total}}$	[f] $<3.8 \times 10^{-10}$, CL = 90%
$\Gamma(K_L^0 \rightarrow \pi^0 e^+ e^-)/\Gamma_{\text{total}}$	[f] $<2.8 \times 10^{-10}$, CL = 90%
$\Gamma(K_L^0 \rightarrow \pi^0 \nu \bar{\nu})/\Gamma_{\text{total}}$	[g] $<3.0 \times 10^{-9}$, CL = 90%
$A_{CP}(D^\pm \rightarrow \mu^\pm \nu)$	$(8 \pm 8)\%$
$A_{CP}(D^\pm \rightarrow K_L^0 e^\pm \nu)$	$(-0.6 \pm 1.6)\%$
$A_{CP}(D^\pm \rightarrow K_S^0 \pi^\pm)$	$(-0.41 \pm 0.09)\%$
$A_{CP}(D^\pm \rightarrow K^\mp 2\pi^\pm)$	$(-0.18 \pm 0.16)\%$
$A_{CP}(D^\pm \rightarrow K^\mp \pi^\pm \pi^0)$	$(-0.3 \pm 0.7)\%$
$A_{CP}(D^\pm \rightarrow K_S^0 \pi^\pm \pi^0)$	$(-0.1 \pm 0.7)\%$
$A_{CP}(D^\pm \rightarrow K_S^0 \pi^\pm \pi^+ \pi^-)$	$(0.0 \pm 1.2)\%$
$A_{CP}(D^\pm \rightarrow \pi^\pm \pi^0)$	$(0.4 \pm 1.3)\%$ ($S = 1.7$)
$A_{CP}(D^\pm \rightarrow \pi^\pm \eta)$	$(0.3 \pm 0.5)\%$
$A_{CP}(D^\pm \rightarrow \pi^\pm \eta'(958))$	$(0.41 \pm 0.23)\%$ ($S = 1.2$)
$A_{CP}(D^\pm \rightarrow \bar{K}^0 / K^0 K^\pm)$	$(0.11 \pm 0.17)\%$
$A_{CP}(D^\pm \rightarrow K_S^0 K^\pm)$	$(-0.01 \pm 0.07)\%$
$A_{CP}(D^\pm \rightarrow K^+ K^- \pi^\pm)$	$(0.37 \pm 0.29)\%$
$A_{CP}(D^\pm \rightarrow K^\pm K^*0)$	$(-0.3 \pm 0.4)\%$
$A_{CP}(D^\pm \rightarrow \phi \pi^\pm)$	$(0.01 \pm 0.09)\%$ ($S = 1.8$)

Tests of Conservation Laws

$A_{CP}(D^{\pm} \rightarrow K^{\pm} K_S^0(1430)\pi^0)$	$(8^{+7}_{-6})\%$	$A_{CP}(D^0 \rightarrow K_S^0 \pi^0)$	$(-0.20 \pm 0.17)\%$
$A_{CP}(D^{\pm} \rightarrow K^{\pm} K_S^0(1430)\pi^{\pm})$	$(43^{+20}_{-26})\%$	$A_{CP}(D^0 \rightarrow K_S^0 \eta)$	$(0.5 \pm 0.5)\%$
$A_{CP}(D^{\pm} \rightarrow K^{\pm} K_S^0(700))$	$(-12^{+18}_{-13})\%$	$A_{CP}(D^0 \rightarrow K_S^0 \eta')$	$(1.0 \pm 0.7)\%$
$A_{CP}(D^{\pm} \rightarrow a_0(1450)\pi^{\pm})$	$(-19^{+14}_{-16})\%$	$A_{CP}(D^0 \rightarrow K_S^0 \phi)$	$(-3 \pm 9)\%$
$A_{CP}(D^{\pm} \rightarrow \phi(1680)\pi^{\pm})$	$(-9 \pm 26)\%$	$A_{CP}(D^0 \rightarrow K^-\pi^+)$	$(0.2 \pm 0.5)\%$
$A_{CP}(D^{\pm} \rightarrow \pi^+\pi^-\pi^{\pm})$	$(0.5 \pm 2.0)\%$	$A_{CP}(D^0 \rightarrow K^+\pi^-)$	$(-0.9 \pm 1.4)\%$
$A_{CP}(D^{\pm} \rightarrow K_S^0 K^{\pm}\pi^{\pm})$	$(-4 \pm 7)\%$	$A_{CP}(D_{CP(\pm 1)} \rightarrow K^{\mp}\pi^{\pm})$	$(13.1 \pm 1.0)\%$
$A_{CP}(D^{\pm} \rightarrow K^{\pm}\pi^0)$	$(-3 \pm 5)\%$	$A_{CP}(D^0 \rightarrow K^-\pi^+\pi^0)$	$(0.1 \pm 0.5)\%$
Local CPV in $D^{\pm} \rightarrow \pi^+\pi^-\pi^{\pm}$	78.1%	$A_{CP}(D^0 \rightarrow K^+\pi^-\pi^0)$	$(0 \pm 5)\%$
Local CPV in $D^{\pm} \rightarrow K^+K^-\pi^{\pm}$	31%	$A_{CP}(D^0 \rightarrow K_S^0\pi^+\pi^-)$	$(-0.1 \pm 0.8)\%$
Local CPV in $D^{\pm} \rightarrow K^+K^-K^{\pm}$	31.6%	$A_{CP}(D^0 \rightarrow K^*(892)^-\pi^+ \rightarrow K_S^0\pi^+\pi^-)$	$(0.4 \pm 0.5)\%$
$ q/p $ of $D^0-\bar{D}^0$ mixing	0.995 ± 0.016	$A_{CP}(D^0 \rightarrow K^*(892)^+\pi^- \rightarrow K_S^0\pi^+\pi^-)$	$(1 \pm 6)\%$
A_{Γ} of $D^0-\bar{D}^0$ mixing	$(0.089 \pm 0.113) \times 10^{-3}$	$A_{CP}(D^0 \rightarrow K_S^0\rho^0 \rightarrow K_S^0\pi^+\pi^-)$	$(-0.1 \pm 0.5)\%$
CP-even fraction in $D^0 \rightarrow \pi^+\pi^-\pi^0$ decays	$(97.3 \pm 1.7)\%$	$A_{CP}(D^0 \rightarrow K_S^0\omega \rightarrow K_S^0\pi^+\pi^-)$	$(-13 \pm 7)\%$
CP-even fraction in $D^0 \rightarrow \pi^+\pi^-\pi^+\pi^-$ decays	$(74.6 \pm 1.6)\%$ ($S = 1.2$)	$A_{CP}(D^0 \rightarrow K_S^0 f_0(980) \rightarrow K_S^0\pi^+\pi^-)$	$(-0.4 \pm 2.7)\%$
CP-even fraction in $D^0 \rightarrow K^+K^-\pi^0$ decays	$(73 \pm 6)\%$	$A_{CP}(D^0 \rightarrow K_S^0 f_2(1270) \rightarrow K_S^0\pi^+\pi^-)$	$(-4 \pm 5)\%$
Where there is ambiguity, the CP test is labelled by the D^0 decay mode.			
$A_{CP}(D^0 \rightarrow K^+K^-)$	$(4 \pm 5) \times 10^{-4}$	$A_{CP}(D^0 \rightarrow K_S^0 f_0(1370) \rightarrow K_S^0\pi^+\pi^-)$	$(-1 \pm 9)\%$
$A_{CP}(D^0 \rightarrow K_S^0 K_S^0)$	$(-1.9 \pm 1.1)\%$ ($S = 1.1$)	$A_{CP}(D^0 \rightarrow \bar{K}^0 \rho^0(1450) \rightarrow K_S^0\pi^+\pi^-)$	$(-4 \pm 10)\%$
$A_{CP}(D^0 \rightarrow \pi^+\pi^-)$	$(0.13 \pm 0.14)\%$	$A_{CP}(D^0 \rightarrow \bar{K}^0 f_0(600) \rightarrow K_S^0\pi^+\pi^-)$	$(-3 \pm 5)\%$
$A_{CP}(D^0 \rightarrow \pi^0\pi^0)$	$(0.0 \pm 0.6)\%$	$A_{CP}(D^0 \rightarrow K^*(1410)^-\pi^+ \rightarrow K_S^0\pi^+\pi^-)$	$(-2 \pm 9)\%$
$A_{CP}(D^0 \rightarrow \rho\gamma)$	$(6 \pm 15) \times 10^{-2}$	$A_{CP}(D^0 \rightarrow K_S^0(1430)^-\pi^+ \rightarrow K_S^0\pi^+\pi^-)$	$(4 \pm 4)\%$
$A_{CP}(D^0 \rightarrow \phi\gamma)$	$(-9 \pm 7) \times 10^{-2}$	$A_{CP}(D^0 \rightarrow K_S^0(1430)^-\pi^+ \rightarrow K_S^0\pi^+\pi^-)$	$(12 \pm 15)\%$
$A_{CP}(D^0 \rightarrow \bar{K}^*(892)^0\gamma)$	$(-0.3 \pm 2.0) \times 10^{-2}$	$A_{CP}(D^0 \rightarrow K_S^0(1430)^-\pi^+ \rightarrow K_S^0\pi^+\pi^-)$	$(3 \pm 6)\%$
$A_{CP}(D^0 \rightarrow \pi^+\pi^-\pi^0)$	$(0.4 \pm 0.4)\%$	$A_{CP}(D^0 \rightarrow K_S^0(1430)^-\pi^+ \rightarrow K_S^0\pi^+\pi^-)$	$(-10 \pm 32)\%$
$A_{CP}(D^0 \rightarrow \rho(770)^+\pi^- \rightarrow \pi^+\pi^-\pi^0)$	[h] $(1.2 \pm 0.9)\%$	$A_{CP}(D^0 \rightarrow K_S^0(1430)^+\pi^- \rightarrow K_S^0\pi^+\pi^-)$	$(0.2 \pm 0.5)\%$
$A_{CP}(D^0 \rightarrow \rho(770)^0\pi^0 \rightarrow \pi^+\pi^-\pi^0)$	[h] $(-3.1 \pm 3.0)\%$	$A_{CP}(D^0 \rightarrow K^-\pi^+\pi^-\pi^-)$	$(-2 \pm 4)\%$
$A_{CP}(D^0 \rightarrow \rho(770)^-\pi^+ \rightarrow \pi^+\pi^-\pi^0)$	[h] $(-1.0 \pm 1.7)\%$	$A_{CP}(D^0 \rightarrow K^+K^-\pi^+\pi^-)$	$(1.3 \pm 1.7)\%$
$A_{CP}(D^0 \rightarrow \rho(1450)^+\pi^- \rightarrow \pi^+\pi^-\pi^0)$	[h] $(0 \pm 70)\%$	$A_{CP}(D^0 \rightarrow K_1^*(1270)^+K^- \rightarrow K^+K^-\pi^+\pi^-)$	$(-2.3 \pm 1.7)\%$
$A_{CP}(D^0 \rightarrow \rho(1450)^0\pi^0 \rightarrow \pi^+\pi^-\pi^0)$	[h] $(-20 \pm 40)\%$	$A_{CP}(D^0 \rightarrow K_1^*(1270)^+K^- \rightarrow K^*0\pi^+K^-)$	$(-1 \pm 10)\%$
$A_{CP}(D^0 \rightarrow \rho(1450)^-\pi^+ \rightarrow \pi^+\pi^-\pi^0)$	[h] $(6 \pm 9)\%$	$A_{CP}(D^0 \rightarrow K_1^*(1270)^-K^+ \rightarrow \bar{K}^*0\pi^-K^+)$	$(-10 \pm 32)\%$
$A_{CP}(D^0 \rightarrow \rho(1700)^+\pi^- \rightarrow \pi^+\pi^-\pi^0)$	[h] $(-5 \pm 14)\%$	$A_{CP}(D^0 \rightarrow K_1^*(1270)^-K^+ \rightarrow K^+K^-\pi^+\pi^-)$	$(1.7 \pm 3.5)\%$
$A_{CP}(D^0 \rightarrow \rho(1700)^0\pi^0 \rightarrow \pi^+\pi^-\pi^0)$	[h] $(13 \pm 9)\%$	$A_{CP}(D^0 \rightarrow K_1^*(1270)^+K^- \rightarrow \rho^0 K^+K^-)$	$(-7 \pm 17)\%$
$A_{CP}(D^0 \rightarrow \rho(1700)^-\pi^+ \rightarrow \pi^+\pi^-\pi^0)$	[h] $(8 \pm 11)\%$	$A_{CP}(D^0 \rightarrow K_1^*(1270)^-K^+ \rightarrow \rho^0 K^-K^+)$	$(10 \pm 13)\%$
$A_{CP}(D^0 \rightarrow f_0(980)\pi^0 \rightarrow \pi^+\pi^-\pi^0)$	[h] $(0 \pm 35)\%$	$A_{CP}(D^0 \rightarrow K_1(1400)^+K^- \rightarrow K^+K^-\pi^+\pi^-)$	$(-4.4 \pm 2.1)\%$
$A_{CP}(D^0 \rightarrow f_0(1370)\pi^0 \rightarrow \pi^+\pi^-\pi^0)$	[h] $(25 \pm 18)\%$	$A_{CP}(D^0 \rightarrow K^*(1410)^+K^- \rightarrow K^*0\pi^+K^-)$	$(-20 \pm 17)\%$
$A_{CP}(D^0 \rightarrow f_0(1500)\pi^0 \rightarrow \pi^+\pi^-\pi^0)$	[h] $(0 \pm 18)\%$	$A_{CP}(D^0 \rightarrow K^*(1410)^-K^+ \rightarrow \bar{K}^*0\pi^-K^+)$	$(-1 \pm 14)\%$
$A_{CP}(D^0 \rightarrow f_0(1710)\pi^0 \rightarrow \pi^+\pi^-\pi^0)$	[h] $(0 \pm 24)\%$	$A_{CP}(D^0 \rightarrow K^*(1680)^+K^- \rightarrow K^+K^-\pi^+\pi^-)$	$(-17 \pm 29)\%$
$A_{CP}(D^0 \rightarrow f_2(1270)\pi^0 \rightarrow \pi^+\pi^-\pi^0)$	[h] $(-4 \pm 6)\%$	$A_{CP}(K^*0\bar{K}^*0)$ in $D^0, \bar{D}^0 \rightarrow K^*0\bar{K}^*0$	$(-5 \pm 14)\%$
$A_{CP}(D^0 \rightarrow \sigma(400)\pi^0 \rightarrow \pi^+\pi^-\pi^0)$	[h] $(6 \pm 8)\%$	$A_{CP}(D^0 \rightarrow K^*0\bar{K}^*0 S\text{-wave})$	$(-3.9 \pm 2.2)\%$
$A_{CP}(\text{nonresonant } D^0 \rightarrow \pi^+\pi^-\pi^0)$	[h] $(-13 \pm 23)\%$	$A_{CP}(\phi\rho^0)$ in $D^0, \bar{D}^0 \rightarrow \phi\rho^0$	$(1 \pm 9)\%$
$A_{CP}(D^0, \bar{D}^0 \rightarrow 2\pi^+2\pi^-)$	$(0.5 \pm 1.2)\%$	$A_{CP}(D^0 \rightarrow \phi\rho^0 S\text{-wave})$	$(-3 \pm 5)\%$
$A_{CP}(D^0 \rightarrow a_1(1260)^+\pi^- \rightarrow 2\pi^+2\pi^-)$	$(5 \pm 6)\%$	$A_{CP}(D^0 \rightarrow \phi\rho^0 D\text{-wave})$	$(-37 \pm 19)\%$
$A_{CP}(D^0 \rightarrow a_1(1260)^-\pi^+ \rightarrow 2\pi^+2\pi^-)$	$(14 \pm 18)\%$	$A_{CP}(D^0 \rightarrow \phi(\pi^+\pi^-)S\text{-wave})$	$(6 \pm 6)\%$
$A_{CP}(D^0 \rightarrow \pi(1300)^+\pi^- \rightarrow 2\pi^+2\pi^-)$	$(-2 \pm 15)\%$	$A_{CP}(D^0 \rightarrow K^*(892)^0(K^-\pi^+)S\text{-wave})$	$(-10 \pm 40)\%$
$A_{CP}(D^0 \rightarrow \pi(1300)^-\pi^+ \rightarrow 2\pi^+2\pi^-)$	$(-6 \pm 30)\%$	$A_{CP}(D^0 \rightarrow K^+K^-\pi^+\pi^- \text{ non-resonant})$	$(8 \pm 20)\%$
$A_{CP}(D^0 \rightarrow a_1(1640)^+\pi^- \rightarrow 2\pi^+2\pi^-)$	$(9 \pm 26)\%$	$A_{CP}((K^-\pi^+)P\text{-wave } (K^+\pi^-)S\text{-wave})$	$(3 \pm 11)\%$
$A_{CP}(D^0 \rightarrow \pi_2(1670)^+\pi^- \rightarrow 2\pi^+2\pi^-)$	$(7 \pm 18)\%$	Local CPV p-value in $D^0, \bar{D}^0 \rightarrow \pi^+\pi^-\pi^0$	10.6%
$A_{CP}(D^0 \rightarrow \sigma f_0(1370) \rightarrow 2\pi^+2\pi^-)$	$(-15 \pm 19)\%$	Local CPV p-value in $D^0, \bar{D}^0 \rightarrow \pi^+\pi^-\pi^+\pi^-$	$(0.6 \pm 0.2)\%$
$A_{CP}(D^0 \rightarrow \sigma\rho(770)^0 \rightarrow 2\pi^+2\pi^-)$	$(3 \pm 27)\%$	Local CPV p-value in $D^0, \bar{D}^0 \rightarrow K_S^0\pi^+\pi^-$	96%
$A_{CP}(D^0 \rightarrow 2\rho(770)^0 \rightarrow 2\pi^+2\pi^-)$	$(-6 \pm 6)\%$	Local CPV p-value in $D^0, \bar{D}^0 \rightarrow K^+K^-\pi^0$	16.6%
$A_{CP}(D^0 \rightarrow 2f_2(1270) \rightarrow 2\pi^+2\pi^-)$	$(-28 \pm 24)\%$	Local CPV p-value in $D^0, \bar{D}^0 \rightarrow K^+K^-\pi^+\pi^-$	9.1%
$A_{CP}(D^0 \rightarrow K^+K^-\pi^0)$	$(-1.0 \pm 1.7)\%$	$A_{CP}(D_S^{\pm} \rightarrow \mu^{\pm}\nu)$	$(-0.2 \pm 2.5)\%$
$A_{CP}(D^0 \rightarrow K^*(892)^+K^- \rightarrow K^+K^-\pi^0)$	[h] $(-0.9 \pm 1.3)\%$		
$A_{CP}(D^0 \rightarrow K^*(1410)^+K^- \rightarrow K^+K^-\pi^0)$	[h] $(-21 \pm 24)\%$		
$A_{CP}(D^0 \rightarrow (K^+\pi^0)_S K^- \rightarrow K^+K^-\pi^0)$	[h] $(7 \pm 15)\%$		
$A_{CP}(D^0 \rightarrow \phi(1020)\pi^0 \rightarrow K^+K^-\pi^0)$	[h] $(1.1 \pm 2.2)\%$		
$A_{CP}(D^0 \rightarrow f_0(980)\pi^0 \rightarrow K^+K^-\pi^0)$	[h] $(-3 \pm 19)\%$		
$A_{CP}(D^0 \rightarrow a_0(980)\pi^0 \rightarrow K^+K^-\pi^0)$	[h] $(-5 \pm 16)\%$		
$A_{CP}(D^0 \rightarrow f'_2(1525)\pi^0 \rightarrow K^+K^-\pi^0)$	[h] $(0 \pm 160)\%$		
$A_{CP}(D^0 \rightarrow K^*(892)^-K^+ \rightarrow K^+K^-\pi^0)$	[h] $(-5 \pm 4)\%$		
$A_{CP}(D^0 \rightarrow K^*(1410)^-K^+ \rightarrow K^+K^-\pi^0)$	[h] $(-17 \pm 29)\%$		
$A_{CP}(D^0 \rightarrow (K^-\pi^0)_{S\text{-wave}} K^+ \rightarrow K^+K^-\pi^0)$	[h] $(-10 \pm 40)\%$		

Unless otherwise stated, limits are given at the 90% confidence level, while errors are given as ± 1 standard deviation.

Tests of Conservation Laws

$A_{CP}(D_S^{\pm} \rightarrow K^{\pm} K_S^0)$	$(0.09 \pm 0.26)\%$	$A_{ADS}(B^+ \rightarrow D^*(D\gamma)K^+)$	-0.6 ± 1.3
$A_{CP}(D_S^{\pm} \rightarrow K^+ K^- \pi^{\pm})$	$(-0.5 \pm 0.9)\%$	$A_{ADS}(B^+ \rightarrow D^*(D\pi^0)K^+)$	0.72 ± 0.29
$A_{CP}(D_S^{\pm} \rightarrow \phi \pi^{\pm})$	$(-0.38 \pm 0.27)\%$	$A_{ADS}(B^+ \rightarrow D^*(D\gamma)\pi^+)$	0.08 ± 0.13
$A_{CP}(D_S^{\pm} \rightarrow K^{\pm} K_S^0 \pi^0)$	$(-2 \pm 6)\%$	$A_{ADS}(B^+ \rightarrow D^*(D\pi^0)\pi^+)$	-0.14 ± 0.06
$A_{CP}(D_S^{\pm} \rightarrow 2K_S^0 \pi^{\pm})$	$(3 \pm 5)\%$	$A_{ADS}(B^+ \rightarrow [K^- \pi^+]_D K^+ \pi^- \pi^+)$	-0.33 ± 0.35
$A_{CP}(D_S^{\pm} \rightarrow K^+ K^- \pi^{\pm} \pi^0)$	$(0.0 \pm 3.0)\%$	$A_{ADS}(B^+ \rightarrow [K^- \pi^+]_D \pi^+ \pi^- \pi^+)$	-0.01 ± 0.09
$A_{CP}(D_S^{\pm} \rightarrow K^{\pm} K_S^0 \pi^{\pm} \pi^0)$	$(-6 \pm 5)\%$	$A_{CP}(B^+ \rightarrow D_{CP(-1)} K^+)$	-0.10 ± 0.07
$A_{CP}(D_S^{\pm} \rightarrow K_S^0 K^{\mp} 2\pi^{\pm})$	$(4.1 \pm 2.8)\%$	$A_{CP}(B^+ \rightarrow [K^+ K^-]_D K^+ \pi^- \pi^+)$	-0.04 ± 0.06
$A_{CP}(D_S^{\pm} \rightarrow \pi^+ \pi^- \pi^{\pm})$	$(-0.7 \pm 3.1)\%$	$A_{CP}(B^+ \rightarrow [\pi^+ \pi^-]_D K^+ \pi^- \pi^+)$	-0.05 ± 0.10
$A_{CP}(D_S^{\pm} \rightarrow \pi^{\pm} \eta)$	$(0.32 \pm 0.31)\%$	$A_{CP}(B^+ \rightarrow [K^- \pi^+]_D K^+ \pi^- \pi^+)$	0.013 ± 0.023
$A_{CP}(D_S^{\pm} \rightarrow \pi^{\pm} \eta')$	$(-0.06 \pm 0.22)\%$ ($S = 1.6$)	$A_{CP}(B^+ \rightarrow [K^+ K^-]_D \pi^+ \pi^- \pi^+)$	-0.019 ± 0.015
$A_{CP}(D_S^{\pm} \rightarrow \eta' \pi^{\pm} \pi^0)$	$(-1 \pm 4)\%$	$A_{CP}(B^+ \rightarrow [\pi^+ \pi^-]_D \pi^+ \pi^- \pi^+)$	-0.013 ± 0.019
$A_{CP}(D_S^{\pm} \rightarrow \eta' \pi^{\pm} \pi^0)$	$(0 \pm 8)\%$	$A_{CP}(B^+ \rightarrow [K^- \pi^+]_D \pi^+ \pi^- \pi^+)$	-0.002 ± 0.011
$A_{CP}(D_S^{\pm} \rightarrow K^{\pm} \pi^0)$	$(2 \pm 4)\%$ ($S = 1.2$)	$A_{CP}(B^+ \rightarrow \bar{D}^{*0} \pi^+)$	-0.0004 ± 0.0021 ($S = 1.1$)
$A_{CP}(D_S^{\pm} \rightarrow \bar{K}^0 / K^0 \pi^{\pm})$	$(0.4 \pm 0.5)\%$	$A_{CP}(B^+ \rightarrow D_{CP(+1)}^{*0} \pi^+)$	0.010 ± 0.007
$A_{CP}(D_S^{\pm} \rightarrow K_S^0 \pi^{\pm})$	$(0.20 \pm 0.18)\%$	$A_{CP}(B^+ \rightarrow D_{CP(-1)}^{*0} \pi^+)$	-0.09 ± 0.05
$A_{CP}(D_S^{\pm} \rightarrow K^{\pm} \pi^+ \pi^-)$	$(3.7 \pm 2.7)\%$	$A_{CP}(B^+ \rightarrow D^{*0} K^+)$	0.012 ± 0.010 ($S = 1.5$)
$A_{CP}(D_S^{\pm} \rightarrow K^{\pm} \eta)$	$(1.8 \pm 1.9)\%$	$A_{CP}(B^+ \rightarrow D_{CP(+1)}^{*0} K^+)$	-0.09 ± 0.05 ($S = 2.6$)
$A_{CP}(D_S^{\pm} \rightarrow K^{\pm} \eta'(958))$	$(6 \pm 19)\%$	$A_{CP}(B^+ \rightarrow D_{CP(-1)}^{*0} K^+)$	0.07 ± 0.10
$A_{CP}(B^+ \rightarrow J/\psi(1S) K^+)$	$(1.8 \pm 3.0) \times 10^{-3}$ ($S = 1.5$)	$A_{CP}(B^+ \rightarrow D_{CP(+1)} K^*(892)^+)$	0.08 ± 0.06
$A_{CP}(B^+ \rightarrow J/\psi(1S) \pi^+)$	$(1.8 \pm 1.2) \times 10^{-2}$ ($S = 1.3$)	$A_{CP}(B^+ \rightarrow D_{CP(-1)} K^*(892)^+)$	-0.23 ± 0.22
$A_{CP}(B^+ \rightarrow J/\psi \rho^+)$	-0.05 ± 0.05	$A_{CP}(B^+ \rightarrow D_S^+ \phi)$	0.0 ± 0.4
$A_{CP}(B^+ \rightarrow J/\psi K^*(892)^+)$	-0.048 ± 0.033	$A_{CP}(B^+ \rightarrow D_S^+ \bar{D}^0)$	$(0.5 \pm 0.6)\%$
$A_{CP}(B^+ \rightarrow \eta_C K^+)$	0.01 ± 0.07 ($S = 2.2$)	$A_{CP}(B^+ \rightarrow D_S^+ \bar{D}^0)$	$(-0.5 \pm 1.5) \times 10^{-2}$
$A_{CP}(B^+ \rightarrow \psi(2S) \pi^+)$	0.03 ± 0.06	$A_{CP}(B^+ \rightarrow D_S^+ \bar{D}^{*0})$	$(1.1 \pm 1.1) \times 10^{-2}$
$A_{CP}(B^+ \rightarrow \psi(2S) K^+)$	0.012 ± 0.020 ($S = 1.5$)	$A_{CP}(B^+ \rightarrow D^* \bar{D}^{*0})$	$(1.3 \pm 2.6) \times 10^{-2}$
$A_{CP}(B^+ \rightarrow \psi(2S) K^*(892)^+)$	0.08 ± 0.21	$A_{CP}(B^+ \rightarrow D^* \bar{D}^0)$	$(3.1 \pm 1.7) \times 10^{-2}$
$A_{CP}(B^+ \rightarrow \chi_{c1}(1P) \pi^+)$	0.07 ± 0.18	$A_{CP}(B^+ \rightarrow D^+ \bar{D}^{*0})$	$(0.0 \pm 2.4) \times 10^{-2}$
$A_{CP}(B^+ \rightarrow \chi_{c0} K^+)$	-0.20 ± 0.18 ($S = 1.5$)	$A_{CP}(B^+ \rightarrow D^+ \bar{D}^0)$	$(2.4 \pm 1.1) \times 10^{-2}$
$A_{CP}(B^+ \rightarrow \chi_{c1} K^+)$	-0.009 ± 0.033	$A_{CP}(B^+ \rightarrow K_S^0 \pi^+)$	-0.003 ± 0.015 ($S = 1.1$)
$A_{CP}(B^+ \rightarrow \chi_{c1} K^*(892)^+)$	0.5 ± 0.5	$A_{CP}(B^+ \rightarrow K^+ \pi^0)$	0.027 ± 0.012
$A_{CP}(B^+ \rightarrow \bar{D}^0 \pi^+)$	$(-3 \pm 5) \times 10^{-3}$	$A_{CP}(B^+ \rightarrow \eta' K^+)$	0.004 ± 0.011
$A_{CP}(B^+ \rightarrow D_{CP(+1)} \pi^+)$	-0.0080 ± 0.0024	$A_{CP}(B^+ \rightarrow \eta' K^*(892)^+)$	-0.26 ± 0.27
$A_{CP}(B^+ \rightarrow D_{CP(-1)} \pi^+)$	0.017 ± 0.026	$A_{CP}(B^+ \rightarrow \eta' K_S^0(1430)^+)$	0.06 ± 0.20
$A_{CP}([K^{\mp} \pi^{\pm} \pi^+ \pi^-]_D \pi^+)$	0.070 ± 0.020	$A_{CP}(B^+ \rightarrow \eta' K_S^0(1430)^+)$	0.15 ± 0.13
$A_{CP}(B^+ \rightarrow [\pi^+ \pi^+ \pi^- \pi^-]_D K^+)$	0.061 ± 0.013	$A_{CP}(B^+ \rightarrow \eta K^*(892)^+)$	0.02 ± 0.06
$A_{CP}(B^+ \rightarrow [\pi^+ \pi^- \pi^+ \pi^-]_D K^*(892)^+)$	0.02 ± 0.11	$A_{CP}(B^+ \rightarrow \eta K_S^0(1430)^+)$	0.05 ± 0.13
$A_{CP}(B^+ \rightarrow [K^+ K^- \pi^+ \pi^-]_D K^+)$	0.095 ± 0.023	$A_{CP}(B^+ \rightarrow \eta K_S^0(1430)^+)$	-0.45 ± 0.30
$A_{CP}(B^+ \rightarrow [K^+ K^- \pi^+ \pi^-]_D \pi^+)$	-0.009 ± 0.006	$A_{CP}(B^+ \rightarrow \omega K^+)$	-0.02 ± 0.04
$A_{CP}(B^+ \rightarrow \bar{D}^0 K^+)$	-0.017 ± 0.005	$A_{CP}(B^+ \rightarrow \omega K^{*+})$	0.29 ± 0.35
$A_{CP}([K^{\mp} \pi^{\pm} \pi^+ \pi^-]_D K^+)$	-0.32 ± 0.04	$A_{CP}(B^+ \rightarrow \omega(K\pi)_0^{*+})$	-0.10 ± 0.09
$A_{CP}(B^+ \rightarrow [\pi^+ \pi^+ \pi^- \pi^-]_D \pi^+)$	$(-8.2 \pm 3.2) \times 10^{-3}$	$A_{CP}(B^+ \rightarrow \omega K_S^0(1430)^+)$	0.14 ± 0.15
$A_{CP}(B^+ \rightarrow [K^- \pi^+]_D K^+)$	-0.58 ± 0.21	$A_{CP}(B^+ \rightarrow K^{*0} \pi^+)$	-0.021 ± 0.032 ($S = 1.5$)
$A_{CP}(B^+ \rightarrow [K^- \pi^+ \pi^0]_D K^+)$	-0.27 ± 0.27 ($S = 2.4$)	$A_{CP}(B^+ \rightarrow K^*(892)^+ \pi^0)$	-0.39 ± 0.21 ($S = 1.6$)
$A_{CP}(B^+ \rightarrow [K^+ \pi^- \pi^0]_D K^+)$	-0.024 ± 0.013	$A_{CP}(B^+ \rightarrow K^+ \pi^- \pi^+)$	0.015 ± 0.006 ($S = 1.4$)
$A_{CP}(B^+ \rightarrow [K^+ K^- \pi^0]_D K^+)$	0.07 ± 0.07	$A_{CP}(B^+ \rightarrow K^+ K^- K^+ \text{ nonresonant})$	0.06 ± 0.05
$A_{CP}(B^+ \rightarrow [\pi^+ \pi^- \pi^0]_D K^+)$	0.11 ± 0.04	$A_{CP}(B^+ \rightarrow f(980)^0 K^+)$	-0.08 ± 0.09
$A_{CP}(B^+ \rightarrow \bar{D}^0 K^*(892)^+)$	-0.007 ± 0.019	$A_{CP}(B^+ \rightarrow f_0(1500) K^+)$	0.28 ± 0.30
$A_{CP}(B^+ \rightarrow [K^- \pi^+ \pi^- \pi^+]_D K^*(892)^+)$	-0.45 ± 0.25	$A_{CP}(B^+ \rightarrow f'_2(1525)^0 K^+)$	$-0.08^{+0.05}_{-0.04}$
$A_{CP}(B^+ \rightarrow [K^- \pi^+]_D \pi^+)$	0.00 ± 0.09	$A_{CP}(B^+ \rightarrow K^0 \pi^+ \pi^0)$	0.07 ± 0.06
$A_{CP}(B^+ \rightarrow [K^- \pi^+ \pi^0]_D \pi^+)$	0.08 ± 0.09	$A_{CP}(B^+ \rightarrow K_S^0(1430)^0 \pi^+)$	0.061 ± 0.032
$A_{CP}(B^+ \rightarrow [K^+ K^- \pi^0]_D \pi^+)$	-0.001 ± 0.019	$A_{CP}(B^+ \rightarrow K_S^0(1430)^+ \pi^0)$	$0.26^{+0.18}_{-0.14}$
$A_{CP}(B^+ \rightarrow [\pi^+ \pi^- \pi^0]_D \pi^+)$	0.001 ± 0.010	$A_{CP}(B^+ \rightarrow K_S^0(1430)^0 \pi^+)$	$0.05^{+0.29}_{-0.24}$
$A_{CP}(B^+ \rightarrow [K^- \pi^+]_D \pi^+)$	-0.09 ± 0.27	$A_{CP}(B^+ \rightarrow K^+ \pi^0 \pi^0)$	-0.06 ± 0.07
$A_{CP}(B^+ \rightarrow [K^- \pi^+]_D \gamma \pi^+)$	-0.7 ± 0.6	$A_{CP}(B^+ \rightarrow K^0 \rho^+)$	-0.03 ± 0.15
$A_{CP}(B^+ \rightarrow [K^- \pi^+]_D \pi^+ K^+)$	0.8 ± 0.4	$A_{CP}(B^+ \rightarrow K^{*+} \pi^+ \pi^-)$	0.07 ± 0.08
$A_{CP}(B^+ \rightarrow [K^- \pi^+]_D \gamma K^+)$	0.4 ± 1.0	$A_{CP}(B^+ \rightarrow \rho^0 K^*(892)^+)$	0.31 ± 0.13
$A_{CP}(B^+ \rightarrow [\pi^+ \pi^- \pi^0]_D K^+)$	-0.02 ± 0.15	$A_{CP}(B^+ \rightarrow K^*(892)^+ f_0(980))$	-0.15 ± 0.12
$A_{CP}(B^+ \rightarrow [K_S^0 K^+ \pi^-]_D K^+)$	0.00 ± 0.09 ($S = 1.4$)	$A_{CP}(B^+ \rightarrow a_1^+ K^0)$	0.12 ± 0.11
$A_{CP}(B^+ \rightarrow [K_S^0 K^- \pi^+]_D K^+)$	0.00 ± 0.07	$A_{CP}(B^+ \rightarrow b_1^+ K^0)$	-0.03 ± 0.15
$A_{CP}(B^+ \rightarrow [K_S^0 K^- \pi^+]_D \pi^+)$	-0.003 ± 0.014	$A_{CP}(B^+ \rightarrow K^*(892)^0 \rho^+)$	-0.01 ± 0.16
$A_{CP}(B^+ \rightarrow [K_S^0 K^+ \pi^-]_D \pi^+)$	-0.016 ± 0.025 ($S = 1.5$)	$A_{CP}(B^+ \rightarrow b_1^0 K^+)$	-0.46 ± 0.20
$A_{CP}(B^+ \rightarrow [K^*(892)^- K^+]_D K^+)$	0.08 ± 0.05	$A_{CP}(B^+ \rightarrow K^0 K^+)$	0.04 ± 0.14
$A_{CP}(B^+ \rightarrow [K^*(892)^+ K^-]_D K^+)$	0.07 ± 0.09	$A_{CP}(B^+ \rightarrow K_S^0 K^+)$	-0.21 ± 0.14
$A_{CP}(B^+ \rightarrow [K^*(892)^+ K^-]_D \pi^+)$	0.007 ± 0.016	$A_{CP}(B^+ \rightarrow K^+ K_S^0 K_S^0)$	0.025 ± 0.031
$A_{CP}(B^+ \rightarrow [K^*(892)^- K^+]_D \pi^+)$	-0.013 ± 0.020 ($S = 1.9$)	$A_{CP}(B^+ \rightarrow K^+ K^- \pi^+ \text{ nonresonant})$	-0.11 ± 0.06
$A_{ADS}(B^+ \rightarrow D K^+)$	-0.451 ± 0.026	$A_{CP}(B^+ \rightarrow \pi^+ K^+ K^-, m_{K^+ K^-} < 1.1$	-0.17 ± 0.07
$A_{ADS}(B^+ \rightarrow D \pi^+)$	0.129 ± 0.014	GeV)	

Unless otherwise stated, limits are given at the 90% confidence level, while errors are given as ± 1 standard deviation.

Tests of Conservation Laws

$A_{CP}(B^+ \rightarrow K^+ \bar{K}^*(892)^0)$	0.04 ± 0.05	$A_{CP}(B^0 \rightarrow \omega K_2^*(1430)^0)$	-0.37 ± 0.17
$A_{CP}(B^+ \rightarrow K^+ \bar{K}_0^*(1430)^0)$	0.10 ± 0.17	$A_{CP}(B^0 \rightarrow K^+ \pi^- \pi^0)$	$(0 \pm 6) \times 10^{-2}$
$A_{CP}(B^+ \rightarrow \phi \pi^+)$	0.1 ± 0.5	$A_{CP}(B^0 \rightarrow \rho^- K^+)$	0.20 ± 0.11
$A_{CP}(B^+ \rightarrow \phi K^+)$	0.017 ± 0.017 (S = 1.8)	$A_{CP}(B^0 \rightarrow \rho(1450)^- K^+)$	-0.10 ± 0.33
$A_{CP}(B^+ \rightarrow X_0(1550) K^+)$	-0.04 ± 0.07	$A_{CP}(B^0 \rightarrow \rho(1700)^- K^+)$	-0.4 ± 0.6
$A_{CP}(B^+ \rightarrow K^{*+} K^+ K^-)$	0.11 ± 0.09	$A_{CP}(B^0 \rightarrow K^+ \pi^- \pi^0 \text{ nonresonant})$	0.10 ± 0.18
$A_{CP}(B^+ \rightarrow \phi K^*(892)^+)$	-0.01 ± 0.08	$A_{CP}(B^0 \rightarrow K^0 \pi^+ \pi^-)$	-0.01 ± 0.05
$A_{CP}(B^+ \rightarrow \phi(K\pi)_0^{*+})$	0.04 ± 0.16	$A_{CP}(B^0 \rightarrow (K\pi)_0^{*+} \pi^-)$	0.02 ± 0.04
$A_{CP}(B^+ \rightarrow \phi K_1(1270)^+)$	0.15 ± 0.20	$A_{CP}(B^0 \rightarrow K_2^*(1430)^+ \pi^-)$	-0.29 ± 0.24
$A_{CP}(B^+ \rightarrow \phi K_2^*(1430)^+)$	-0.23 ± 0.20	$A_{CP}(B^0 \rightarrow K^*(1680)^+ \pi^-)$	-0.07 ± 0.14
$A_{CP}(B^+ \rightarrow K^+ \phi \phi)$	-0.08 ± 0.07	$A_{CP}(B^0 \rightarrow f_0(980) K_S^0)$	0.28 ± 0.31
$A_{CP}(B^+ \rightarrow K^+[\phi\phi]_{\eta_c})$	0.10 ± 0.08	$A_{CP}(B^0 \rightarrow (K\pi)_0^{*0} \pi^0)$	-0.15 ± 0.11
$A_{CP}(B^+ \rightarrow K^*(892)^+ \gamma)$	0.014 ± 0.018	$A_{CP}(B^0 \rightarrow K^{*0} \pi^0)$	-0.15 ± 0.13
$A_{CP}(B^+ \rightarrow X_S \gamma)$	0.028 ± 0.019	$A_{CP}(B^0 \rightarrow K^*(892)^0 \pi^+ \pi^-)$	0.07 ± 0.05
$A_{CP}(B^+ \rightarrow \eta K^+ \gamma)$	-0.12 ± 0.07	$A_{CP}(B^0 \rightarrow K^*(892)^0 \rho^0)$	-0.06 ± 0.09
$A_{CP}(B^+ \rightarrow \phi K^+ \gamma)$	-0.13 ± 0.11 (S = 1.1)	$A_{CP}(B^0 \rightarrow K^{*0} f_0(980))$	0.07 ± 0.10
$A_{CP}(B^+ \rightarrow \rho^+ \gamma)$	-0.11 ± 0.33	$A_{CP}(B^0 \rightarrow K^{*+} \rho^-)$	0.21 ± 0.15
$A_{CP}(B^+ \rightarrow \pi^+ \pi^0)$	-0.01 ± 0.04 (S = 1.1)	$A_{CP}(B^0 \rightarrow K^*(892)^0 K^+ K^-)$	0.01 ± 0.05
$A_{CP}(B^+ \rightarrow \pi^+ \pi^0 \pi^0)$	$(9 \pm 7) \times 10^{-2}$	$A_{CP}(B^0 \rightarrow a_1^- K^+)$	-0.16 ± 0.12
$A_{CP}(B^+ \rightarrow \rho^0 \pi^+)$	0.003 ± 0.014	$A_{CP}(B^0 \rightarrow K^0 K^0)$	-0.6 ± 0.7
$A_{CP}(B^+ \rightarrow \rho^0(1450) \pi^+)$	-0.11 ± 0.05	$A_{CP}(B^0 \rightarrow K^*(892)^0 \phi)$	0.00 ± 0.04
$A_{CP}(B^+ \rightarrow \rho_3(1690) \pi^+)$	-0.80 ± 0.28	$A_{CP}(B^0 \rightarrow K^*(892)^0 K^- \pi^+)$	0.2 ± 0.4
$A_{CP}(B^+ \rightarrow f_0(1370) \pi^+)$	0.72 ± 0.22	$A_{CP}(B^0 \rightarrow \phi(K\pi)_0^{*0})$	0.12 ± 0.08
$A_{CP}(B^+ \rightarrow \pi^+ \pi^- \pi^+ \text{ nonresonant})$	$-0.14^{+0.23}_{-0.16}$	$A_{CP}(B^0 \rightarrow \phi K_2^*(1430)^0)$	-0.11 ± 0.10
$A_{CP}(B^+ \rightarrow \rho^+ \pi^0)$	0.03 ± 0.10	$A_{CP}(B^0 \rightarrow K^*(892)^0 \gamma)$	-0.006 ± 0.011
$A_{CP}(B^+ \rightarrow X \pi^+, X \rightarrow \pi^0 \pi^0)$	0.18 ± 0.12	$A_{CP}(B^0 \rightarrow K_2^*(1430)^0 \gamma)$	-0.08 ± 0.15
$A_{CP}(B^+ \rightarrow \rho^+ \rho^0)$	-0.05 ± 0.05	$A_{CP}(B^0 \rightarrow X_S \gamma)$	-0.009 ± 0.018
$A_{CP}(B^+ \rightarrow \omega \pi^+)$	-0.04 ± 0.05	$A_{CP}(B^0 \rightarrow \rho^+ \pi^-)$	0.13 ± 0.06 (S = 1.1)
$A_{CP}(B^+ \rightarrow \omega \rho^+)$	-0.20 ± 0.09	$A_{CP}(B^0 \rightarrow \rho^- \pi^+)$	-0.08 ± 0.08
$A_{CP}(B^+ \rightarrow \eta \pi^+)$	-0.14 ± 0.07 (S = 1.4)	$A_{CP}(B^0 \rightarrow a_1(1260)^\pm \pi^\mp)$	-0.07 ± 0.06
$A_{CP}(B^+ \rightarrow \eta \rho^+)$	0.11 ± 0.11	$A_{CP}(B^0 \rightarrow b_1^- \pi^+)$	-0.05 ± 0.10
$A_{CP}(B^+ \rightarrow \eta' \pi^+)$	0.06 ± 0.16	$A_{CP}(B^0 \rightarrow p \bar{p} K^*(892)^0)$	0.05 ± 0.12
$A_{CP}(B^+ \rightarrow \eta' \rho^+)$	0.26 ± 0.17	$A_{CP}(B^0 \rightarrow \rho \bar{\rho} \pi^-)$	0.04 ± 0.07
$A_{CP}(B^+ \rightarrow b_1^0 \pi^+)$	0.05 ± 0.16	$A_{CP}(B^0 \rightarrow K^{*0} \ell^+ \ell^-)$	-0.05 ± 0.10
$A_{CP}(B^+ \rightarrow p \bar{p} \pi^+)$	0.00 ± 0.04	$A_{CP}(B^0 \rightarrow K^{*0} e^+ e^-)$	-0.21 ± 0.19
$A_{CP}(B^+ \rightarrow p \bar{p} K^+)$	0.00 ± 0.04 (S = 2.2)	$A_{CP}(B^0 \rightarrow K^{*0} \mu^+ \mu^-)$	-0.034 ± 0.024
$A_{CP}(B^+ \rightarrow p \bar{p} K^*(892)^+)$	0.21 ± 0.16 (S = 1.4)	$C_{D^*(2010)^- D^+} (B^0 \rightarrow D^*(2010)^- D^+)$	-0.02 ± 0.08
$A_{CP}(B^+ \rightarrow p \bar{p} \gamma)$	0.17 ± 0.17	$C_{D^*(2010)^+ D^-} (B^0 \rightarrow D^*(2010)^+ D^-)$	-0.03 ± 0.09 (S = 1.1)
$A_{CP}(B^+ \rightarrow p \bar{p} \pi^0)$	0.01 ± 0.17	$C_{D^{*+} D^{*-}} (B^0 \rightarrow D^{*+} D^{*-})$	0.01 ± 0.09 (S = 1.6)
$A_{CP}(B^+ \rightarrow K^+ \ell^+ \ell^-)$	-0.02 ± 0.08	$C_{C^+} (B^0 \rightarrow D^{*+} D^{*-})$	0.00 ± 0.10 (S = 1.6)
$A_{CP}(B^+ \rightarrow K^+ e^+ e^-)$	0.14 ± 0.14	$C_- (B^0 \rightarrow D^{*+} D^{*-})$	0.19 ± 0.31
$A_{CP}(B^+ \rightarrow K^+ \mu^+ \mu^-)$	0.011 ± 0.017	$S_- (B^0 \rightarrow D^{*+} D^{*-})$	0.1 ± 1.6 (S = 3.5)
$A_{CP}(B^+ \rightarrow \pi^+ \mu^+ \mu^-)$	-0.11 ± 0.12	$C (B^0 \rightarrow D^*(2010)^+ D^*(2010)^- K_S^0)$	0.01 ± 0.29
$A_{CP}(B^+ \rightarrow K^{*+} \ell^+ \ell^-)$	-0.09 ± 0.14	$S (B^0 \rightarrow D^*(2010)^+ D^*(2010)^- K_S^0)$	0.1 ± 0.4
$A_{CP}(B^+ \rightarrow K^{*+} e^+ e^-)$	-0.14 ± 0.23	$C_{D^+ D^-} (B^0 \rightarrow D^+ D^-)$	-0.22 ± 0.24 (S = 2.5)
$A_{CP}(B^+ \rightarrow K^{*+} \mu^+ \mu^-)$	-0.12 ± 0.24	$C_{J/\psi(1S) \pi^0} (B^0 \rightarrow J/\psi(1S) \pi^0)$	0.03 ± 0.17 (S = 1.5)
$\text{Re}(\epsilon_{B^0})/(1+ \epsilon_{B^0} ^2)$	$(-0.5 \pm 0.4) \times 10^{-3}$	$C(B^0 \rightarrow J/\psi(1S) \rho^0)$	-0.06 ± 0.06
$A_{T/CP}(B^0 \leftrightarrow \bar{B}^0)$	0.005 ± 0.018	$C_{D_{CP}^{(*)}} h^0 (B^0 \rightarrow D_{CP}^{(*)} h^0)$	-0.02 ± 0.08
$A_{CP}(B^0 \rightarrow D^*(2010)^+ D^-)$	0.013 ± 0.014	$S_{D_{CP}^{(*)} h^0} (B^0 \rightarrow D_{CP}^{(*)} h^0)$	-0.66 ± 0.12
$A_{CP}(B^0 \rightarrow \bar{D}^0 \pi^0)$	$(0.4 \pm 2.4) \times 10^{-2}$	$C_{K^0 \pi^0} (B^0 \rightarrow K^0 \pi^0)$	0.00 ± 0.08
$A_{CP}(B^0 \rightarrow [K^+ K^-]_D K^*(892)^0)$	-0.05 ± 0.10	$C_{\eta'(958) K_S^0} (B^0 \rightarrow \eta'(958) K_S^0)$	-0.04 ± 0.20 (S = 2.5)
$A_{CP}(B^0 \rightarrow [K^+ \pi^-]_D K^*(892)^0)$	0.047 ± 0.029	$S_{\eta'(958) K_S^0} (B^0 \rightarrow \eta'(958) K_S^0)$	0.43 ± 0.17 (S = 1.5)
$A_{CP}(B^0 \rightarrow [K^+ \pi^- \pi^+ \pi^-]_D K^*(892)^0)$	0.037 ± 0.034	$C_{\eta' K^0} (B^0 \rightarrow \eta' K^0)$	-0.06 ± 0.04
$A_{CP}(B^0 \rightarrow [K^- \pi^+]_D K^*(892)^0)$	0.19 ± 0.19	$C_{\omega K_S^0} (B^0 \rightarrow \omega K_S^0)$	0.0 ± 0.4 (S = 3.0)
$A_{CP}(B^0 \rightarrow [K^- \pi^+ \pi^+ \pi^-]_D K^*(892)^0)$	-0.01 ± 0.24	$S_{\omega K_S^0} (B^0 \rightarrow \omega K_S^0)$	0.70 ± 0.21
$R_d^+(B^0 \rightarrow [\pi^\pm K^\mp]_D K^{*0})$	0.064 ± 0.021	$C (B^0 \rightarrow K_S^0 \pi^0 \pi^0)$	-0.21 ± 0.20
$R_d^-(\bar{B}^0 \rightarrow [\pi^\mp K^\pm]_D K^{*0})$	0.095 ± 0.021	$S (B^0 \rightarrow K_S^0 \pi^0 \pi^0)$	$0.89^{+0.27}_{-0.30}$
$A_{CP}(B^0 \rightarrow [\pi^+ \pi^-]_D K^*(892)^0)$	-0.18 ± 0.14	$C_{\rho^0 K_S^0} (B^0 \rightarrow \rho^0 K_S^0)$	-0.04 ± 0.20
$A_{CP}(B^0 \rightarrow [\pi^+ \pi^- \pi^+ \pi^-]_D K^*(892)^0)$	-0.03 ± 0.15	$S_{\rho^0 K_S^0} (B^0 \rightarrow \rho^0 K_S^0)$	$0.50^{+0.17}_{-0.21}$
$R_d^+(B^0 \rightarrow [\pi^\pm K^\mp \pi^\pm \pi^\mp]_D K^{*0})$	0.074 ± 0.026	$C_{f_0(980) K_S^0} (B^0 \rightarrow f_0(980) K_S^0)$	0.29 ± 0.20
$R_d^-(\bar{B}^0 \rightarrow [\pi^\mp K^\pm \pi^\pm \pi^\mp]_D K^{*0})$	0.072 ± 0.025	$S_{f_0(980) K_S^0} (B^0 \rightarrow f_0(980) K_S^0)$	-0.50 ± 0.16
$A_{CP}(B^0 \rightarrow \eta' K^*(892)^0)$	-0.07 ± 0.18	$S_{f_2(1270) K_S^0} (B^0 \rightarrow f_2(1270) K_S^0)$	-0.5 ± 0.5
$A_{CP}(B^0 \rightarrow \eta' K_0^*(1430)^0)$	-0.19 ± 0.17	$C_{f_2(1270) K_S^0} (B^0 \rightarrow f_2(1270) K_S^0)$	0.3 ± 0.4
$A_{CP}(B^0 \rightarrow \eta' K_2^*(1430)^0)$	0.14 ± 0.18		
$A_{CP}(B^0 \rightarrow \eta K_0^*(1430)^0)$	0.06 ± 0.13		
$A_{CP}(B^0 \rightarrow \eta K_2^*(1430)^0)$	-0.07 ± 0.19		
$A_{CP}(B^0 \rightarrow b_1 K^+)$	-0.07 ± 0.12		
$A_{CP}(B^0 \rightarrow \omega K^{*0})$	0.45 ± 0.25		
$A_{CP}(B^0 \rightarrow \omega(K\pi)_0^{*0})$	-0.07 ± 0.09		

Unless otherwise stated, limits are given at the 90% confidence level, while errors are given as ± 1 standard deviation.

Tests of Conservation Laws

$S_{f_x(1300)} K_S^0 (B^0 \rightarrow f_x(1300) K_S^0)$	-0.2 ± 0.5	$C_{\chi_{c1}} K_S^0 (B^0 \rightarrow \chi_{c1} K_S^0)$	0.06 ± 0.07
$C_{f_x(1300)} K_S^0 (B^0 \rightarrow f_x(1300) K_S^0)$	0.13 ± 0.35	$\sin(2\beta_{\text{eff}})(B^0 \rightarrow \phi K^0)$	0.22 ± 0.30
$S_{K^0 \pi^+ \pi^-} (B^0 \rightarrow K^0 \pi^+ \pi^- \text{ nonresonant})$	-0.01 ± 0.33	$\sin(2\beta_{\text{eff}})(B^0 \rightarrow \phi K^*(1430)^0)$	$0.97^{+0.03}_{-0.52}$
$C_{K^0 \pi^+ \pi^-} (B^0 \rightarrow K^0 \pi^+ \pi^- \text{ nonresonant})$	0.01 ± 0.26	$\sin(2\beta_{\text{eff}})(B^0 \rightarrow [K_S^0 \pi^+ \pi^-]_{D^{(*)}} h^0)$	0.80 ± 0.16
$C_{K_S^0 K_S^0} (B^0 \rightarrow K_S^0 K_S^0)$	$0.0 \pm 0.4 (S = 1.4)$	$ \lambda (B^0 \rightarrow [K_S^0 \pi^+ \pi^-]_{D^{(*)}} h^0)$	1.01 ± 0.08
$S_{K_S^0 K_S^0} (B^0 \rightarrow K_S^0 K_S^0)$	-0.8 ± 0.5	$ \sin(2\beta + \gamma) $	$>0.40, \text{CL} = 90\%$
$C_{K^+ K^- K_S^0} (B^0 \rightarrow K^+ K^- K_S^0 \text{ nonresonant})$	0.06 ± 0.08	$2\beta + \gamma$	$(80 \pm 60)^\circ$
$C_{K^+ K^- K_S^0} (B^0 \rightarrow K^+ K^- K_S^0 \text{ inclusive})$	0.01 ± 0.09	$x_+(B^0 \rightarrow D K^*0)$	0.04 ± 0.17
$C_{\phi K_S^0} (B^0 \rightarrow \phi K_S^0)$	-0.09 ± 0.12	$x_-(B^0 \rightarrow D K^*0)$	-0.16 ± 0.14
$S_{\phi K_S^0} (B^0 \rightarrow \phi K_S^0)$	0.58 ± 0.12	$y_+(B^0 \rightarrow D K^*0)$	-0.68 ± 0.22
$C_{K_S K_S K_S} (B^0 \rightarrow K_S K_S K_S)$	-0.14 ± 0.12	$y_-(B^0 \rightarrow D K^*0)$	$0.20 \pm 0.25 (S = 1.2)$
$S_{K_S K_S K_S} (B^0 \rightarrow K_S K_S K_S)$	-0.82 ± 0.17	$a_{CP}(B^0 \rightarrow p \bar{p} K^+ \pi^-)$	$(0.5 \pm 0.9)\%$
$C_{K_S^0 \pi^0 \gamma} (B^0 \rightarrow K_S^0 \pi^0 \gamma)$	0.36 ± 0.33	$A_{CP}(B \rightarrow K^*(892) \gamma)$	-0.003 ± 0.011
$S_{K_S^0 \pi^0 \gamma} (B^0 \rightarrow K_S^0 \pi^0 \gamma)$	-0.8 ± 0.6	$A_{CP}(B \rightarrow s \gamma)$	0.015 ± 0.011
$C_{K^*(892)^0 \gamma} (B^0 \rightarrow K^*(892)^0 \gamma)$	$-0.04 \pm 0.16 (S = 1.2)$	$A_{CP}(B \rightarrow (s+d) \gamma)$	0.010 ± 0.031
$S_{K^*(892)^0 \gamma} (B^0 \rightarrow K^*(892)^0 \gamma)$	-0.15 ± 0.22	$A_{CP}(B \rightarrow X_S \ell^+ \ell^-)$	0.04 ± 0.11
$C_{\eta K^0 \gamma} (B^0 \rightarrow \eta K^0 \gamma)$	$0.1 \pm 0.4 (S = 1.4)$	$A_{CP}(B \rightarrow K^* e^+ e^-)$	-0.18 ± 0.15
$S_{\eta K^0 \gamma} (B^0 \rightarrow \eta K^0 \gamma)$	$-0.5 \pm 0.5 (S = 1.2)$	$A_{CP}(B \rightarrow K^* \mu^+ \mu^-)$	-0.03 ± 0.13
$C_{K^0 \phi \gamma} (B^0 \rightarrow K^0 \phi \gamma)$	-0.3 ± 0.6	$A_{CP}(B \rightarrow K^* \ell^+ \ell^-)$	-0.04 ± 0.07
$S_{K^0 \phi \gamma} (B^0 \rightarrow K^0 \phi \gamma)$	$0.7^{+0.7}_{-1.1}$	$A_{CP}(B \rightarrow \eta \text{ anything})$	$-0.13^{+0.04}_{-0.05}$
$C(B^0 \rightarrow K_S^0 \rho^0 \gamma)$	-0.05 ± 0.19	$\Delta A_{CP}(X_S \gamma) = A_{CP}(B^\pm \rightarrow X_S \gamma) - A_{CP}(B^0 \rightarrow X_S \gamma)$	0.041 ± 0.023
$S(B^0 \rightarrow K_S^0 \rho^0 \gamma)$	-0.04 ± 0.23	$\bar{A}_{CP}(B \rightarrow X_S \gamma) = (A_{CP}(B^+ \rightarrow X_S \gamma) + A_{CP}(B^0 \rightarrow X_S \gamma))/2$	0.009 ± 0.012
$C(B^0 \rightarrow \rho^0 \gamma)$	0.4 ± 0.5	$\bar{A}_{CP}(B \rightarrow K^* \gamma) = (A_{CP}(B^+ \rightarrow K^* \gamma) + A_{CP}(B^0 \rightarrow K^* \gamma))/2$	-0.001 ± 0.014
$S(B^0 \rightarrow \rho^0 \gamma)$	-0.8 ± 0.7	$\text{Re}(\epsilon_{B_S^0}) / (1 + \epsilon_{B_S^0} ^2)$	$(-0.15 \pm 0.70) \times 10^{-3}$
$C_{\pi^0 \pi^0} (B^0 \rightarrow \pi^0 \pi^0)$	-0.30 ± 0.20	$S_{KK}(B_S^0 \rightarrow K^+ K^-)$	$0.14 \pm 0.05 (S = 1.3)$
$C_{\rho \pi} (B^0 \rightarrow \rho^+ \pi^-)$	$-0.03 \pm 0.07 (S = 1.2)$	$\delta_B(B_S^0 \rightarrow D_S^\pm K^\mp \pi^\pm \pi^\mp)$	$(-6^{+10}_{-13})^\circ$
$S_{\rho \pi} (B^0 \rightarrow \rho^+ \pi^-)$	0.05 ± 0.07	$CP \text{ Violation phase } \beta_S (b \rightarrow c \bar{c} s)$	$(2.0 \pm 0.8) \times 10^{-2} \text{ rad}$
$\Delta S_{\rho \pi} (B^0 \rightarrow \rho^+ \pi^-)$	0.01 ± 0.08	$A_{CP}^L(B_S \rightarrow J/\psi \bar{K}^*(892)^0)$	-0.05 ± 0.06
$C_{\rho^0 \pi^0} (B^0 \rightarrow \rho^0 \pi^0)$	0.27 ± 0.24	$A_{CP}^{\parallel}(B_S \rightarrow J/\psi \bar{K}^*(892)^0)$	0.17 ± 0.15
$S_{\rho^0 \pi^0} (B^0 \rightarrow \rho^0 \pi^0)$	-0.23 ± 0.34	$A_{CP}^{\perp}(B_S \rightarrow J/\psi \bar{K}^*(892)^0)$	-0.05 ± 0.10
$C_{a_1 \pi} (B^0 \rightarrow a_1(1260)^+ \pi^-)$	-0.05 ± 0.11	$A_{CP}(B_S^0 \rightarrow [K^+ K^-]_D \bar{K}^*(892)^0)$	-0.04 ± 0.07
$S_{a_1 \pi} (B^0 \rightarrow a_1(1260)^+ \pi^-)$	$-0.2 \pm 0.4 (S = 3.2)$	$A_{CP}(B_S^0 \rightarrow [\pi^+ K^-]_D K^*(892)^0)$	-0.01 ± 0.04
$\Delta C_{a_1 \pi} (B^0 \rightarrow a_1(1260)^+ \pi^-)$	$0.43 \pm 0.14 (S = 1.3)$	$A_{CP}(B_S^0 \rightarrow [\pi^+ \pi^-]_D K^*(892)^0)$	0.06 ± 0.13
$\Delta S_{a_1 \pi} (B^0 \rightarrow a_1(1260)^+ \pi^-)$	-0.11 ± 0.12	$S(B_S^0 \rightarrow \phi \gamma)$	0.43 ± 0.32
$C(B^0 \rightarrow b_1^- K^+)$	-0.22 ± 0.24	$C(B_S^0 \rightarrow \phi \gamma)$	0.11 ± 0.31
$\Delta C(B^0 \rightarrow b_1^- \pi^+)$	-1.04 ± 0.24	$\Gamma(\eta_c(1S) \rightarrow \pi^+ \pi^-) / \Gamma_{\text{total}}$	$< 1.3 \times 10^{-4}, \text{CL} = 90\%$
$C_{\rho^0 \rho^0} (B^0 \rightarrow \rho^0 \rho^0)$	0.2 ± 0.9	$\Gamma(\eta_c(1S) \rightarrow \pi^0 \pi^0) / \Gamma_{\text{total}}$	$< 4 \times 10^{-5}, \text{CL} = 90\%$
$S_{\rho^0 \rho^0} (B^0 \rightarrow \rho^0 \rho^0)$	0.3 ± 0.7	$\Gamma(\eta_c(1S) \rightarrow K^+ K^-) / \Gamma_{\text{total}}$	$< 7 \times 10^{-4}, \text{CL} = 90\%$
$C_{\rho \rho} (B^0 \rightarrow \rho^+ \rho^-)$	0.00 ± 0.09	$\Gamma(\eta_c(1S) \rightarrow K_S^0 K_S^0) / \Gamma_{\text{total}}$	$< 4 \times 10^{-4}, \text{CL} = 90\%$
$S_{\rho \rho} (B^0 \rightarrow \rho^+ \rho^-)$	-0.14 ± 0.13	$n \text{ electric dipole moment}$	$< 0.18 \times 10^{-25} \text{ ecm}, \text{CL} = 90\%$
$ \lambda (B^0 \rightarrow J/\psi K^*(892)^0)$	$< 0.25, \text{CL} = 95\%$	$(\alpha_- + \alpha_\perp) / (\alpha_- - \alpha_\perp) \text{ in } \Lambda \rightarrow p \pi^-, \bar{\Lambda} \rightarrow \bar{p} \pi^+$	$(-0.1 \pm 0.4) \times 10^{-2}$
$\cos 2\beta (B^0 \rightarrow J/\psi K^*(892)^0)$	$1.7^{+0.7}_{-0.9} (S = 1.6)$	$\frac{[\alpha(\Xi^-)\alpha(-\Lambda) - \alpha(\Xi^+)\alpha_+(\bar{\Lambda})]}{[\alpha(\Xi^-)\alpha(-\Lambda) + \alpha(\Xi^+)\alpha_+(\bar{\Lambda})]}$	$(0 \pm 7) \times 10^{-4}$
$\cos 2\beta (B^0 \rightarrow [K_S^0 \pi^+ \pi^-]_{D^{(*)}} h^0)$	0.91 ± 0.25	$(\alpha + \bar{\alpha}) / (\alpha - \bar{\alpha}) \text{ in } \Omega^- \rightarrow \Lambda K^-, \bar{\Omega}^+ \rightarrow \bar{\Lambda} K^+$	-0.02 ± 0.13
$(S_+ + S_-) / 2 (B^0 \rightarrow D^{*-} \pi^+)$	-0.039 ± 0.011	$(\alpha + \bar{\alpha}) / (\alpha - \bar{\alpha}) \text{ in } \Lambda_c^+ \rightarrow \Lambda \pi^+, \bar{\Lambda}_c^- \rightarrow \bar{\Lambda} \pi^-$	0.020 ± 0.016
$(S_- - S_+) / 2 (B^0 \rightarrow D^{*-} \pi^+)$	-0.009 ± 0.015	$(\alpha + \bar{\alpha}) / (\alpha - \bar{\alpha}) \text{ in } \Lambda_c^+ \rightarrow \Lambda e^+ \nu_e, \bar{\Lambda}_c^- \rightarrow \bar{\Lambda} e^- \bar{\nu}_e$	0.00 ± 0.04
$(S_+ + S_-) / 2 (B^0 \rightarrow D^- \pi^+)$	-0.046 ± 0.023	$A_{CP}(\Lambda_b \rightarrow p \pi^-)$	$-0.025 \pm 0.029 (S = 1.2)$
$(S_- - S_+) / 2 (B^0 \rightarrow D^- \pi^+)$	-0.022 ± 0.021	$A_{CP}(\Lambda_b \rightarrow p K^-)$	-0.025 ± 0.022
$S_+ (B^0 \rightarrow D^- \pi^+)$	0.058 ± 0.023	$A_{CP}(\Lambda_b \rightarrow D p K^-)$	0.12 ± 0.09
$S_- (B^0 \rightarrow D^+ \pi^-)$	0.038 ± 0.021	$\Delta A_{CP}(p K^- / \pi^-)$	0.014 ± 0.024
$(S_+ + S_-) / 2 (B^0 \rightarrow D^- \rho^+)$	-0.024 ± 0.032	$A_{CP}(\Lambda_b \rightarrow p \bar{K}^0 \pi^-)$	0.22 ± 0.13
$(S_- - S_+) / 2 (B^0 \rightarrow D^- \rho^+)$	-0.10 ± 0.06	$\Delta A_{CP}(J/\psi p \pi^- / K^-)$	$(5.7 \pm 2.7) \times 10^{-2}$
$C_{\eta_c K_S^0} (B^0 \rightarrow \eta_c K_S^0)$	0.08 ± 0.13	$A_{CP}(\Lambda_b \rightarrow \Lambda K^+ \pi^-)$	-0.53 ± 0.25
$C_{c \bar{c} K^{(*)0}} (B^0 \rightarrow c \bar{c} K^{(*)0})$	$(-0.5 \pm 1.5) \times 10^{-2}$	$A_{CP}(\Lambda_b \rightarrow \Lambda K^+ K^-)$	-0.28 ± 0.12
$C_{J/\psi(nS) K^0} (B^0 \rightarrow J/\psi(nS) K^0)$	$(-0.8 \pm 1.7) \times 10^{-2}$	$\Delta A_{CP}(\Lambda_b^0 \rightarrow p K^- \mu^+ \mu^-)$	$(-4 \pm 5) \times 10^{-2}$
$C_{J/\psi K^{*0}} (B^0 \rightarrow J/\psi K^{*0})$	0.03 ± 0.10	$\Delta A_{CP}(\Lambda_b^0 \rightarrow p \pi^- \pi^+ \pi^-)$	$(1.1 \pm 2.6) \times 10^{-2}$
$S_{J/\psi K^{*0}} (B^0 \rightarrow J/\psi K^{*0})$	0.60 ± 0.25	$\Delta A_{CP}(\Lambda_b^0 \rightarrow (p \pi^- \pi^+ \pi^-)_{LBM})$	$(4 \pm 4) \times 10^{-2}$
$C_{\chi_{c0}} K_S^0 (B^0 \rightarrow \chi_{c0} K_S^0)$	$-0.3^{+0.5}_{-0.4}$	$\Delta A_{CP}(\Lambda_b^0 \rightarrow p a_1(1260)^-)$	$(-1 \pm 4) \times 10^{-2}$
$S_{\chi_{c0}} K_S^0 (B^0 \rightarrow \chi_{c0} K_S^0)$	-0.7 ± 0.5	$\Delta A_{CP}(\Lambda_b^0 \rightarrow N(1520)^0 \rho(770)^0)$	$(2 \pm 5) \times 10^{-2}$
		$\Delta A_{CP}(\Lambda_b^0 \rightarrow \Delta(1232)^+ \pi^- \pi^-)$	$(0.1 \pm 3.3) \times 10^{-2}$
		$\Delta A_{CP}(\Lambda_b^0 \rightarrow p K^- \pi^+ \pi^-)$	$(3.2 \pm 1.3) \times 10^{-2}$
		$\Delta A_{CP}(\Lambda_b^0 \rightarrow (p K^- \pi^+ \pi^-)_{LBM})$	$(3.5 \pm 1.6) \times 10^{-2}$

Tests of Conservation Laws

$\Delta A_{CP}(\Lambda_b^0 \rightarrow N(1520)^0 K^*(892)^0)$	$(5.5 \pm 2.5) \times 10^{-2}$	γ	$(65.9^{+2.9}_{-3.1})^\circ$
$\Delta A_{CP}(\Lambda_b^0 \rightarrow \Lambda(1520) \rho(770)^0)$	$(1 \pm 6) \times 10^{-2}$	$\Gamma_B(B^+ \rightarrow D^0 K^+)$	$(9.94 \pm 0.26) \times 10^{-2}$
$\Delta A_{CP}(\Lambda_b^0 \rightarrow \Delta(1232)^{++} K^- \pi^-)$	$(4.4 \pm 2.7) \times 10^{-2}$	$\delta_B(B^+ \rightarrow D^0 K^+)$	$(127.7^{+3.6}_{-3.9})^\circ$
$\Delta A_{CP}(\Lambda_b^0 \rightarrow \rho K_1(1410)^-)$	$(5 \pm 4) \times 10^{-2}$	$\Gamma_B(B^+ \rightarrow D^0 K^{*+})$	$0.101^{+0.016}_{-0.034}$
$\Delta A_{CP}(\Lambda_b^0 \rightarrow \rho K^- K^+ \pi^-)$	$(-7 \pm 5) \times 10^{-2}$	$\delta_B(B^+ \rightarrow D^0 K^{*+})$	$(48^{+5.9}_{-1.6})^\circ$
$\Delta A_{CP}(\Lambda_b^0 \rightarrow \rho K^- K^+ K^-)$	$(0.2 \pm 1.9) \times 10^{-2}$	$\Gamma_B(B^+ \rightarrow D^{*0} K^+)$	$0.104^{+0.013}_{-0.014}$
$\Delta A_{CP}(\Lambda_b^0 \rightarrow \Lambda(1520) \phi(1020))$	$(4 \pm 6) \times 10^{-2}$	$\delta_B(B^+ \rightarrow D^{*0} K^+)$	$(314.8^{+7.9}_{-9.9})^\circ$
$\Delta A_{CP}(\Lambda_b^0 \rightarrow (\rho K^-)_{highmass} \phi(1020))$	$(-0.7 \pm 3.4) \times 10^{-2}$	$A_{CP}(B^0 \rightarrow K^+ \pi^-)$	-0.0831 ± 0.0031
$\Delta A_{CP}(\Lambda_b^0 \rightarrow (\rho K^- K^+ K^-)_{LBM})$	$(2.7 \pm 2.4) \times 10^{-2}$	$A_{CP}(B^0 \rightarrow \eta K^*(892)^0)$	0.19 ± 0.05
$A_c(\Lambda)$	-0.22 ± 0.13	$A_{CP}(B^0 \rightarrow K^*(892)^+ \pi^-)$	-0.27 ± 0.04
$A_s(\Lambda)$	0.13 ± 0.13	$S_{D^*(2010)^- D^+} (B^0 \rightarrow D^*(2010)^- D^+)$	-0.83 ± 0.09
$A_c(\phi)$	-0.01 ± 0.12	$S_{D^*(2010)^+ D^-} (B^0 \rightarrow D^*(2010)^+ D^-)$	-0.80 ± 0.09
$A_s(\phi)$	-0.07 ± 0.12	$S_{D^{*+} D^{*-}} (B^0 \rightarrow D^{*+} D^{*-})$	-0.59 ± 0.14 (S = 1.8)
$a_{CP}(\Lambda_b^0 \rightarrow \rho \pi^- \pi^+ \pi^-)$	$(-0.7 \pm 0.7)\%$	$S_+(B^0 \rightarrow D^{*+} D^{*-})$	-0.73 ± 0.09
$a_{CP}(\Lambda_b^0 \rightarrow \rho K^- \pi^+ \pi^-)$	$(-0.8 \pm 0.9)\%$	$S_{D^+ D^-} (B^0 \rightarrow D^+ D^-)$	$-0.76^{+0.15}_{-0.13}$ (S = 1.2)
$a_{CP}(\Lambda_b^0 \rightarrow \rho K^- K^+ \pi^-)$	$(-1 \pm 5)\%$	$S_{J/\psi(1S) \pi^0} (B^0 \rightarrow J/\psi(1S) \pi^0)$	-0.88 ± 0.32 (S = 2.2)
$a_{CP}(\Lambda_b^0 \rightarrow \rho K^- K^+ K^-)$	$(1.1 \pm 1.5)\%$	$S(B^0 \rightarrow J/\psi(1S) \rho^0)$	$-0.66^{+0.16}_{-0.12}$
$a_{CP}(\Lambda_b^0 \rightarrow \rho K^- \mu^+ \mu^-)$	$(1 \pm 5)\%$	$S_{K^0 \pi^0} (B^0 \rightarrow K^0 \pi^0)$	0.64 ± 0.13
		$S_{\eta' K^0} (B^0 \rightarrow \eta' K^0)$	0.63 ± 0.06
		$S_{K^+ K^- K_S^0} (B^0 \rightarrow K^+ K^- K_S^0)$	-0.66 ± 0.11

CP VIOLATION OBSERVED

Re(ϵ)	$(1.596 \pm 0.013) \times 10^{-3}$	$S_{K^+ K^- K_S^0} (B^0 \rightarrow K^+ K^- K_S^0)$	-0.65 ± 0.12
charge asymmetry in K_{L3}^0 decays		$S_{K^+ K^- K_S^0} (B^0 \rightarrow K^+ K^- K_S^0)$ inclusive)	-0.314 ± 0.030
$A_L =$ weighted average of $A_L(\mu)$ and $A_L(e)$	$(0.332 \pm 0.006)\%$	$C_{\pi\pi} (B^0 \rightarrow \pi^+ \pi^-)$	-0.670 ± 0.030
$A_L(\mu) = [\Gamma(\pi^- \mu^+ \nu_\mu) - \Gamma(\pi^+ \mu^- \bar{\nu}_\mu)]/\text{sum}$	$(0.304 \pm 0.025)\%$	$S_{\pi\pi} (B^0 \rightarrow \pi^+ \pi^-)$	0.27 ± 0.06
$A_L(e) = [\Gamma(\pi^- e^+ \nu_e) - \Gamma(\pi^+ e^- \bar{\nu}_e)]/\text{sum}$	$(0.334 \pm 0.007)\%$	$\Delta C_{\rho\pi} (B^0 \rightarrow \rho^+ \pi^-)$	0.93 ± 0.17
parameters for $K_L^0 \rightarrow 2\pi$ decay		$S_{\eta_c K_S^0} (B^0 \rightarrow \eta_c K_S^0)$	0.709 ± 0.011
$ \eta_{00} = A(K_L^0 \rightarrow 2\pi^0) / A(K_S^0 \rightarrow 2\pi^0) $	$(2.220 \pm 0.011) \times 10^{-3}$ (S = 1.8)	$\sin(2\beta) (B^0 \rightarrow J/\psi K_S^0)$	0.701 ± 0.017
$ \eta_{+-} = A(K_L^0 \rightarrow \pi^+ \pi^-) / A(K_S^0 \rightarrow \pi^+ \pi^-) $	$(2.232 \pm 0.011) \times 10^{-3}$ (S = 1.8)	$S_{J/\psi(nS) K^0} (B^0 \rightarrow J/\psi(nS) K^0)$	0.63 ± 0.10
$ \epsilon = (2 \eta_{+-} + \eta_{00})/3$	$(2.228 \pm 0.011) \times 10^{-3}$ (S = 1.8)	$S_{\chi_{c1} K_S^0} (B^0 \rightarrow \chi_{c1} K_S^0)$	$0.77^{+0.13}_{-0.12}$
$ \eta_{00}/\eta_{+-} $	[j] 0.9950 ± 0.0007 (S = 1.6)	$\sin(2\beta_{\text{eff}}) (B^0 \rightarrow K^+ K^- K_S^0)$	$(84.1^{+4.5}_{-3.8})^\circ$
Re(ϵ'/ϵ) = $(1 - \eta_{00}/\eta_{+-})/3$	[j] $(1.66 \pm 0.23) \times 10^{-3}$ (S = 1.6)	α	$0.257^{+0.021}_{-0.023}$
Assuming CPT		$\Gamma_{B^0} (B^0 \rightarrow D K^{*0})$	$(194.1^{+9.6}_{-8.8})^\circ$
ϕ_{+-} , phase of η_{+-}	$(43.51 \pm 0.05)^\circ$ (S = 1.2)	$\delta_{B^0} (B^0 \rightarrow D K^{*0})$	0.162 ± 0.035
ϕ_{00} , phase of η_{00}	$(43.52 \pm 0.05)^\circ$ (S = 1.2)	$C_{KK} (B_S^0 \rightarrow K^+ K^-)$	$0.37^{+0.10}_{-0.09}$
$\phi_\epsilon = (2\phi_{+-} + \phi_{00})/3$	$(43.52 \pm 0.04)^\circ$ (S = 1.2)	$\Gamma_B (B_S^0 \rightarrow D_S^\mp K^\pm)$	0.47 ± 0.08
Not assuming CPT		$\Gamma_B (B_S^0 \rightarrow D_S^\mp K^\pm \pi^\pm \pi^\mp)$	$(358 \pm 14)^\circ$
ϕ_{+-} , phase of η_{+-}	$(43.4 \pm 0.5)^\circ$ (S = 1.2)	$\delta_B (B_S^0 \rightarrow D_S^\mp K^\mp)$	0.224 ± 0.012
ϕ_{00} , phase of η_{00}	$(43.7 \pm 0.6)^\circ$ (S = 1.2)	$A_{CP}(B_S \rightarrow \pi^+ K^-)$	
$\phi_\epsilon = (2\phi_{+-} + \phi_{00})/3$	$(43.5 \pm 0.5)^\circ$ (S = 1.3)		
CP asymmetry A in $K_L^0 \rightarrow \pi^+ \pi^- e^+ e^-$	$(13.7 \pm 1.5)\%$	$(m_{W^+} - m_{W^-}) / m_{\text{average}}$	$(-3.7 \pm 3.5) \times 10^{-4}$
β_{CP} from $K_L^0 \rightarrow e^+ e^- e^+ e^-$	-0.19 ± 0.07	$(m_{e^+} - m_{e^-}) / m_{\text{average}}$	$< 8 \times 10^{-9}$, CL = 90%
γ_{CP} from $K_L^0 \rightarrow e^+ e^- e^+ e^-$	0.01 ± 0.11 (S = 1.6)	$ q_{e^+} + q_{e^-} /e$	$< 4 \times 10^{-8}$
parameters for $K_L^0 \rightarrow \pi^+ \pi^- \gamma$ decay		$(g_{e^+} - g_{e^-}) / g_{\text{average}}$	$(-0.5 \pm 2.1) \times 10^{-12}$
$ \eta_{+-\gamma} = A(K_L^0 \rightarrow \pi^+ \pi^- \gamma, CP \text{ violating}) / A(K_S^0 \rightarrow \pi^+ \pi^- \gamma) $	$(2.35 \pm 0.07) \times 10^{-3}$	$(\tau_{\mu^+} - \tau_{\mu^-}) / \tau_{\text{average}}$	$(2 \pm 8) \times 10^{-5}$
$\phi_{+-\gamma}$ = phase of $\eta_{+-\gamma}$	$(44 \pm 4)^\circ$	$(g_{\mu^+} - g_{\mu^-}) / g_{\text{average}}$	$(-0.11 \pm 0.12) \times 10^{-8}$
$\Gamma(K_L^0 \rightarrow \pi^+ \pi^-) / \Gamma_{\text{total}}$	[j] $(1.967 \pm 0.010) \times 10^{-3}$ (S = 1.5)	$(m_{\tau^+} - m_{\tau^-}) / m_{\text{average}}$	$< 2.8 \times 10^{-4}$, CL = 90%
$\Gamma(K_L^0 \rightarrow \pi^0 \pi^0) / \Gamma_{\text{total}}$	$(8.64 \pm 0.06) \times 10^{-4}$ (S = 1.8)	$\langle \Delta m_{21}^2 - \Delta \bar{m}_{21}^2 \rangle$ in neutrino mixing	$< 1.1 \times 10^{-4} \text{ eV}^2$, CL = 99.7%
$\Delta A_{CP}^D = A_{CP}(K^+ K^-) - A_{CP}(\pi^+ \pi^-)$	$(-0.154 \pm 0.029)\%$	$\langle \Delta m_{32}^2 - \Delta \bar{m}_{32}^2 \rangle$ in neutrino mixing	$(-0.12 \pm 0.25) \times 10^{-3} \text{ eV}^2$
$A_{CP}(B^+ \rightarrow [K^- \pi^+]_{\overline{D}} K^*(892)^+)$	-0.75 ± 0.16	$m_t - m_{\overline{t}}$	$-0.15 \pm 0.20 \text{ GeV}$ (S = 1.1)
$A_{CP}(B^+ \rightarrow D_{CP(+)} K^+)$	0.132 ± 0.015 (S = 1.8)	$(m_{\pi^+} - m_{\pi^-}) / m_{\text{average}}$	$(2 \pm 5) \times 10^{-4}$
$A_{ADS}(B^+ \rightarrow D K^+)$	-0.451 ± 0.026	$(\tau_{\pi^+} - \tau_{\pi^-}) / \tau_{\text{average}}$	$(6 \pm 7) \times 10^{-4}$
$A_{CP}(B^+ \rightarrow \eta K^+)$	-0.37 ± 0.08	$(m_{K^+} - m_{K^-}) / m_{\text{average}}$	$(-0.6 \pm 1.8) \times 10^{-4}$
$A_{CP}(B^+ \rightarrow K^+ \pi^- \pi^+)$	0.015 ± 0.006 (S = 1.4)	$(\tau_{K^+} - \tau_{K^-}) / \tau_{\text{average}}$	$(0.10 \pm 0.09)\%$ (S = 1.2)
$A_{CP}(B^+ \rightarrow f_2(1270) K^+)$	$-0.68^{+0.19}_{-0.17}$	$K^\pm \rightarrow \mu^\pm \nu_\mu$ rate difference/sum	$(-0.27 \pm 0.21)\%$
$A_{CP}(B^+ \rightarrow \rho^0 K^+)$	0.160 ± 0.021	$K^\pm \rightarrow \pi^\pm \pi^0$ rate difference/sum	[k] $(0.4 \pm 0.6)\%$
$A_{CP}(B^+ \rightarrow K^+ K^- \pi^+)$	-0.115 ± 0.008	δ in $K^0 - \overline{K}^0$ mixing	
$A_{CP}(B^+ \rightarrow \pi^+ (K^+ K^-)_{S\text{-wave}})$	-0.66 ± 0.04	real part of δ	$(2.5 \pm 2.3) \times 10^{-4}$
$A_{CP}(B^+ \rightarrow K^+ K^- K^+)$	-0.036 ± 0.004	imaginary part of δ	$(-1.5 \pm 1.6) \times 10^{-5}$
$A_{CP}(B^+ \rightarrow \pi^+ \pi^- \pi^+)$	0.076 ± 0.008 (S = 1.5)	Re(y), K_{e3} parameter	$(0.4 \pm 2.5) \times 10^{-3}$
$A_{CP}(B^+ \rightarrow f_2(1270) \pi^+)$	0.40 ± 0.06	Re(x), K_{e3} parameter	$(-2.9 \pm 2.0) \times 10^{-3}$
		$ m_{K^0} - m_{\overline{K}^0} / m_{\text{average}}$	[l] $< 6 \times 10^{-19}$, CL = 90%

Unless otherwise stated, limits are given at the 90% confidence level, while errors are given as ± 1 standard deviation.

Tests of Conservation Laws

$(\Gamma_{K^0} - \Gamma_{\bar{K}^0})/m_{\text{average}}$	$(8 \pm 8) \times 10^{-18}$
phase difference $\phi_{00} - \phi_{+-}$	$(0.34 \pm 0.32)^\circ$
$\text{Re}(\frac{2}{3}\eta_{+-} + \frac{1}{3}\eta_{00}) - \frac{A_{\mu}}{2}$	$(-3 \pm 35) \times 10^{-6}$
$A_{CPT}(D^0 \rightarrow K^- \pi^+)$	0.008 ± 0.008
$\Delta S_{CPT}^+(S_{\ell^+, K_S^0}^- - S_{\ell^+, K_S^0}^+)$	0.16 ± 0.23
$\Delta S_{CPT}^-(S_{\ell^+, K_S^0}^+ - S_{\ell^+, K_S^0}^-)$	-0.03 ± 0.14
$\Delta C_{CPT}^+(C_{\ell^+, K_S^0}^- - C_{\ell^+, K_S^0}^+)$	0.14 ± 0.17
$\Delta C_{CPT}^-(C_{\ell^+, K_S^0}^+ - C_{\ell^+, K_S^0}^-)$	0.03 ± 0.14
$ m_{\rho^-} - m_{\bar{\rho}^-} /m_{\rho}$	[η] $< 7 \times 10^{-10}$, CL = 90%
$(\frac{q_{\bar{\rho}^-}}{m_{\bar{\rho}^-}} - \frac{q_{\rho^-}}{m_{\rho^-}})/\frac{q_{\rho^-}}{m_{\rho^-}}$	$(0.3 \pm 1.6) \times 10^{-11}$
$ q_{\rho^-} + q_{\bar{\rho}^-} /e$	[η] $< 7 \times 10^{-10}$, CL = 90%
$(\mu_{\rho^-} + \mu_{\bar{\rho}^-})/\mu_{\rho}$	$(0.002 \pm 0.004) \times 10^{-6}$
$(m_{\eta^-} - m_{\bar{\eta}^-})/m_{\eta}$	$(9 \pm 5) \times 10^{-5}$
$(m_{\Lambda^-} - m_{\bar{\Lambda}^-})/m_{\Lambda}$	$(-0.1 \pm 1.1) \times 10^{-5}$ (S = 1.6)
$(\tau_{\Lambda^-} - \tau_{\bar{\Lambda}^-})/\tau_{\Lambda}$	$(0.9 \pm 3.2) \times 10^{-3}$
$(\tau_{\Sigma^+} - \tau_{\bar{\Sigma}^-})/\tau_{\Sigma^+}$	-0.0006 ± 0.0012
$(\mu_{\Sigma^+} + \mu_{\bar{\Sigma}^-})/\mu_{\Sigma^+}$	0.014 ± 0.015
$(m_{\Xi^-} - m_{\bar{\Xi}^+})/m_{\Xi^-}$	$(-3 \pm 9) \times 10^{-5}$
$(\tau_{\Xi^-} - \tau_{\bar{\Xi}^+})/\tau_{\Xi^-}$	-0.01 ± 0.07
$(\mu_{\Xi^-} + \mu_{\bar{\Xi}^+})/ \mu_{\Xi^-} $	$+0.01 \pm 0.05$
$(m_{\Omega^-} - m_{\bar{\Omega}^+})/m_{\Omega^-}$	$(-1 \pm 8) \times 10^{-5}$
$(\tau_{\Omega^-} - \tau_{\bar{\Omega}^+})/\tau_{\Omega^-}$	0.00 ± 0.05

TESTS OF NUMBER CONSERVATION LAWS

LEPTON FAMILY NUMBER

Lepton family number conservation means separate conservation of each of L_e, L_μ, L_τ .

$\Gamma(Z \rightarrow e^\pm \mu^\mp)/\Gamma_{\text{total}}$	[ρ] $< 2.62 \times 10^{-7}$, CL = 95%
$\Gamma(Z \rightarrow e^\pm \tau^\mp)/\Gamma_{\text{total}}$	[ρ] $< 5.0 \times 10^{-6}$, CL = 95%
$\Gamma(Z \rightarrow \mu^\pm \tau^\mp)/\Gamma_{\text{total}}$	[ρ] $< 6.5 \times 10^{-6}$, CL = 95%
$\Gamma(H \rightarrow e\mu)/\Gamma_{\text{total}}$	$< 4.4 \times 10^{-5}$, CL = 95%
$\Gamma(H \rightarrow e\tau)/\Gamma_{\text{total}}$	$< 2.0 \times 10^{-3}$, CL = 95%
$\Gamma(H \rightarrow \mu\tau)/\Gamma_{\text{total}}$	$< 1.5 \times 10^{-3}$, CL = 95%
$\sigma(e^+ e^- \rightarrow e^\pm \tau^\mp) / \sigma(e^+ e^- \rightarrow \mu^\pm \mu^-)$	$< 8.9 \times 10^{-6}$, CL = 95%
$\sigma(e^+ e^- \rightarrow \mu^\pm \tau^\mp) / \sigma(e^+ e^- \rightarrow \mu^\pm \mu^-)$	$< 4.0 \times 10^{-6}$, CL = 95%
limit on $\mu^- \rightarrow e^-$ conversion	
$\sigma(\mu^- 32S \rightarrow e^- 32S) / \sigma(\mu^- 32S \rightarrow \nu_\mu 32P^*)$	$< 7 \times 10^{-11}$, CL = 90%
$\sigma(\mu^- \text{Ti} \rightarrow e^- \text{Ti}) / \sigma(\mu^- \text{Ti} \rightarrow \text{capture})$	$< 4.3 \times 10^{-12}$, CL = 90%
$\sigma(\mu^- \text{Pb} \rightarrow e^- \text{Pb}) / \sigma(\mu^- \text{Pb} \rightarrow \text{capture})$	$< 4.6 \times 10^{-11}$, CL = 90%
$\sigma(\mu^- \text{Au} \rightarrow e^- \text{Au}) / \sigma(\mu^- \text{Au} \rightarrow \text{capture})$	$< 7 \times 10^{-13}$, CL = 90%
limit on muonium \rightarrow antimuonium conversion $R_G = G_C / G_F$	< 0.0030 , CL = 90%
$\Gamma(\mu^- \rightarrow e^- \nu_e \bar{\nu}_\mu)/\Gamma_{\text{total}}$	[ρ] $< 1.2 \times 10^{-2}$, CL = 90%
$\Gamma(\mu^- \rightarrow e^- \gamma)/\Gamma_{\text{total}}$	$< 4.2 \times 10^{-13}$, CL = 90%
$\Gamma(\mu^- \rightarrow e^- e^+ e^-)/\Gamma_{\text{total}}$	$< 1.0 \times 10^{-12}$, CL = 90%
$\Gamma(\mu^- \rightarrow e^- 2\gamma)/\Gamma_{\text{total}}$	$< 7.2 \times 10^{-11}$, CL = 90%
$\Gamma(\tau^- \rightarrow e^- \gamma)/\Gamma_{\text{total}}$	$< 3.3 \times 10^{-8}$, CL = 90%
$\Gamma(\tau^- \rightarrow e^- \gamma \gamma)/\Gamma_{\text{total}}$	$< 2.5 \times 10^{-4}$, CL = 90%
$\Gamma(\tau^- \rightarrow \mu^- \gamma)/\Gamma_{\text{total}}$	$< 4.2 \times 10^{-8}$, CL = 90%
$\Gamma(\tau^- \rightarrow \mu^- \gamma \gamma)/\Gamma_{\text{total}}$	$< 5.8 \times 10^{-4}$, CL = 90%
$\Gamma(\tau^- \rightarrow e^- \pi^0)/\Gamma_{\text{total}}$	$< 8.0 \times 10^{-8}$, CL = 90%
$\Gamma(\tau^- \rightarrow \mu^- \pi^0)/\Gamma_{\text{total}}$	$< 1.1 \times 10^{-7}$, CL = 90%
$\Gamma(\tau^- \rightarrow e^- K_S^0)/\Gamma_{\text{total}}$	$< 2.6 \times 10^{-8}$, CL = 90%
$\Gamma(\tau^- \rightarrow \mu^- K_S^0)/\Gamma_{\text{total}}$	$< 2.3 \times 10^{-8}$, CL = 90%
$\Gamma(\tau^- \rightarrow e^- \eta)/\Gamma_{\text{total}}$	$< 9.2 \times 10^{-8}$, CL = 90%
$\Gamma(\tau^- \rightarrow \mu^- \eta)/\Gamma_{\text{total}}$	$< 6.5 \times 10^{-8}$, CL = 90%

$\Gamma(\tau^- \rightarrow e^- \rho^0)/\Gamma_{\text{total}}$	$< 2.2 \times 10^{-8}$, CL = 90%
$\Gamma(\tau^- \rightarrow \mu^- \rho^0)/\Gamma_{\text{total}}$	$< 1.7 \times 10^{-8}$, CL = 90%
$\Gamma(\tau^- \rightarrow e^- \omega)/\Gamma_{\text{total}}$	$< 2.4 \times 10^{-8}$, CL = 90%
$\Gamma(\tau^- \rightarrow \mu^- \omega)/\Gamma_{\text{total}}$	$< 3.9 \times 10^{-8}$, CL = 90%
$\Gamma(\tau^- \rightarrow e^- K^*(892)^0)/\Gamma_{\text{total}}$	$< 1.9 \times 10^{-8}$, CL = 90%
$\Gamma(\tau^- \rightarrow \mu^- K^*(892)^0)/\Gamma_{\text{total}}$	$< 2.9 \times 10^{-8}$, CL = 90%
$\Gamma(\tau^- \rightarrow e^- \bar{K}^*(892)^0)/\Gamma_{\text{total}}$	$< 1.7 \times 10^{-8}$, CL = 90%
$\Gamma(\tau^- \rightarrow \mu^- \bar{K}^*(892)^0)/\Gamma_{\text{total}}$	$< 4.3 \times 10^{-8}$, CL = 90%
$\Gamma(\tau^- \rightarrow e^- \eta'(958))/\Gamma_{\text{total}}$	$< 1.6 \times 10^{-7}$, CL = 90%
$\Gamma(\tau^- \rightarrow \mu^- \eta'(958))/\Gamma_{\text{total}}$	$< 1.3 \times 10^{-7}$, CL = 90%
$\Gamma(\tau^- \rightarrow e^- f_0(980) \rightarrow e^- \pi^+ \pi^-)/\Gamma_{\text{total}}$	$< 3.2 \times 10^{-8}$, CL = 90%
$\Gamma(\tau^- \rightarrow \mu^- f_0(980) \rightarrow \mu^- \pi^+ \pi^-)/\Gamma_{\text{total}}$	$< 3.4 \times 10^{-8}$, CL = 90%
$\Gamma(\tau^- \rightarrow e^- \phi)/\Gamma_{\text{total}}$	$< 2.0 \times 10^{-8}$, CL = 90%
$\Gamma(\tau^- \rightarrow \mu^- \phi)/\Gamma_{\text{total}}$	$< 2.3 \times 10^{-8}$, CL = 90%
$\Gamma(\tau^- \rightarrow e^- e^+ e^-)/\Gamma_{\text{total}}$	$< 2.7 \times 10^{-8}$, CL = 90%
$\Gamma(\tau^- \rightarrow e^- \mu^+ \mu^-)/\Gamma_{\text{total}}$	$< 2.7 \times 10^{-8}$, CL = 90%
$\Gamma(\tau^- \rightarrow e^+ \mu^- \mu^-)/\Gamma_{\text{total}}$	$< 1.7 \times 10^{-8}$, CL = 90%
$\Gamma(\tau^- \rightarrow \mu^- e^+ e^-)/\Gamma_{\text{total}}$	$< 1.8 \times 10^{-8}$, CL = 90%
$\Gamma(\tau^- \rightarrow \mu^+ e^- e^-)/\Gamma_{\text{total}}$	$< 1.5 \times 10^{-8}$, CL = 90%
$\Gamma(\tau^- \rightarrow \mu^- \mu^+ \mu^-)/\Gamma_{\text{total}}$	$< 2.1 \times 10^{-8}$, CL = 90%
$\Gamma(\tau^- \rightarrow e^- \pi^+ \pi^-)/\Gamma_{\text{total}}$	$< 2.3 \times 10^{-8}$, CL = 90%
$\Gamma(\tau^- \rightarrow \mu^- \pi^+ \pi^-)/\Gamma_{\text{total}}$	$< 2.1 \times 10^{-8}$, CL = 90%
$\Gamma(\tau^- \rightarrow e^- \pi^+ K^-)/\Gamma_{\text{total}}$	$< 3.7 \times 10^{-8}$, CL = 90%
$\Gamma(\tau^- \rightarrow e^- \pi^- K^+)/\Gamma_{\text{total}}$	$< 3.1 \times 10^{-8}$, CL = 90%
$\Gamma(\tau^- \rightarrow e^- K_S^0 K_S^0)/\Gamma_{\text{total}}$	$< 7.1 \times 10^{-8}$, CL = 90%
$\Gamma(\tau^- \rightarrow e^- K^+ K^-)/\Gamma_{\text{total}}$	$< 3.4 \times 10^{-8}$, CL = 90%
$\Gamma(\tau^- \rightarrow \mu^- \pi^+ K^-)/\Gamma_{\text{total}}$	$< 8.6 \times 10^{-8}$, CL = 90%
$\Gamma(\tau^- \rightarrow \mu^- \pi^- K^+)/\Gamma_{\text{total}}$	$< 4.5 \times 10^{-8}$, CL = 90%
$\Gamma(\tau^- \rightarrow \mu^- K_S^0 K_S^0)/\Gamma_{\text{total}}$	$< 8.0 \times 10^{-8}$, CL = 90%
$\Gamma(\tau^- \rightarrow \mu^- K^+ K^-)/\Gamma_{\text{total}}$	$< 4.4 \times 10^{-8}$, CL = 90%
$\Gamma(\tau^- \rightarrow e^- \pi^0 \pi^0)/\Gamma_{\text{total}}$	$< 6.5 \times 10^{-6}$, CL = 90%
$\Gamma(\tau^- \rightarrow \mu^- \pi^0 \pi^0)/\Gamma_{\text{total}}$	$< 1.4 \times 10^{-5}$, CL = 90%
$\Gamma(\tau^- \rightarrow e^- \eta \eta)/\Gamma_{\text{total}}$	$< 3.5 \times 10^{-5}$, CL = 90%
$\Gamma(\tau^- \rightarrow \mu^- \eta \eta)/\Gamma_{\text{total}}$	$< 6.0 \times 10^{-5}$, CL = 90%
$\Gamma(\tau^- \rightarrow e^- \pi^0 \eta)/\Gamma_{\text{total}}$	$< 2.4 \times 10^{-5}$, CL = 90%
$\Gamma(\tau^- \rightarrow \mu^- \pi^0 \eta)/\Gamma_{\text{total}}$	$< 2.2 \times 10^{-5}$, CL = 90%
$\Gamma(\tau^- \rightarrow e^- \text{light boson})/\Gamma_{\text{total}}$	$< 9 \times 10^{-4}$, CL = 95%
$\Gamma(\tau^- \rightarrow \mu^- \text{light boson})/\Gamma_{\text{total}}$	$< 6 \times 10^{-4}$, CL = 95%

LEPTON FAMILY NUMBER VIOLATION IN NEUTRINOS

$\sin^2(\theta_{12})$	0.307 ± 0.013
Δm_{21}^2	$(7.53 \pm 0.18) \times 10^{-5} \text{ eV}^2$
$\sin^2(\theta_{23})$ (Inverted order)	$0.553^{+0.016}_{-0.024}$ (S = 1.1)
$\sin^2(\theta_{23})$ (Normal order)	$0.558^{+0.015}_{-0.021}$
Δm_{32}^2 (Inverted order)	$(-2.529 \pm 0.029) \times 10^{-3} \text{ eV}^2$
Δm_{32}^2 (Normal order)	$(2.455 \pm 0.028) \times 10^{-3} \text{ eV}^2$
$\sin^2(\theta_{13})$	$(2.19 \pm 0.07) \times 10^{-2}$ (S = 1.2)
$\Gamma(t \rightarrow e^\pm \mu^\mp c)/\Gamma_{\text{total}}$	$< 8.9 \times 10^{-7}$
$\Gamma(t \rightarrow e^\pm \mu^\mp u)/\Gamma_{\text{total}}$	$< 7 \times 10^{-8}$
$\Gamma(\pi^+ \rightarrow \mu^+ \nu_e)/\Gamma_{\text{total}}$	[q] $< 8.0 \times 10^{-3}$, CL = 90%
$\Gamma(\pi^+ \rightarrow \mu^- e^+ \nu_e)/\Gamma_{\text{total}}$	$< 1.6 \times 10^{-6}$, CL = 90%
$\Gamma(\pi^0 \rightarrow \mu^+ e^-)/\Gamma_{\text{total}}$	$< 3.8 \times 10^{-10}$, CL = 90%
$\Gamma(\pi^0 \rightarrow \mu^- e^+)/\Gamma_{\text{total}}$	$< 3.2 \times 10^{-10}$, CL = 90%
$\Gamma(\pi^0 \rightarrow \mu^+ e^- + \mu^- e^+)/\Gamma_{\text{total}}$	$< 3.6 \times 10^{-10}$, CL = 90%
$\Gamma(\eta \rightarrow \mu^+ e^- + \mu^- e^+)/\Gamma_{\text{total}}$	$< 6 \times 10^{-6}$, CL = 90%
$\Gamma(\eta'(958) \rightarrow e\mu)/\Gamma_{\text{total}}$	$< 4.7 \times 10^{-4}$, CL = 90%
$\Gamma(\phi(1020) \rightarrow e^\pm \mu^\mp)/\Gamma_{\text{total}}$	$< 2 \times 10^{-6}$, CL = 90%
$\Gamma(K^+ \rightarrow \mu^- \nu_e e^+)/\Gamma_{\text{total}}$	$< 8.1 \times 10^{-11}$, CL = 90%
$\Gamma(K^+ \rightarrow \mu^+ \nu_e)/\Gamma_{\text{total}}$	[q] $< 4 \times 10^{-3}$, CL = 90%
$\Gamma(K^+ \rightarrow \pi^+ \mu^+ e^-)/\Gamma_{\text{total}}$	$< 1.3 \times 10^{-11}$, CL = 90%
$\Gamma(K^+ \rightarrow \pi^+ \mu^- e^+)/\Gamma_{\text{total}}$	$< 6.6 \times 10^{-11}$, CL = 90%
$\Gamma(K_L^0 \rightarrow e^\pm \mu^\mp)/\Gamma_{\text{total}}$	[ρ] $< 4.7 \times 10^{-12}$, CL = 90%
$\Gamma(K_L^0 \rightarrow e^\pm e^\pm \mu^\mp \mu^\mp)/\Gamma_{\text{total}}$	[ρ] $< 4.12 \times 10^{-11}$, CL = 90%
$\Gamma(K_L^0 \rightarrow \pi^0 \mu^\pm e^\mp)/\Gamma_{\text{total}}$	[ρ] $< 7.6 \times 10^{-11}$, CL = 90%
$\Gamma(K_L^0 \rightarrow \pi^0 \pi^0 \mu^\pm e^\mp)/\Gamma_{\text{total}}$	$< 1.7 \times 10^{-10}$, CL = 90%
$\Gamma(D^+ \rightarrow \pi^+ e^+ \mu^-)/\Gamma_{\text{total}}$	$< 2.1 \times 10^{-7}$, CL = 90%
$\Gamma(D^+ \rightarrow \pi^+ e^- \mu^+)/\Gamma_{\text{total}}$	$< 2.2 \times 10^{-7}$, CL = 90%
$\Gamma(D^+ \rightarrow K^+ e^+ \mu^-)/\Gamma_{\text{total}}$	$< 7.5 \times 10^{-8}$, CL = 90%
$\Gamma(D^+ \rightarrow K^+ e^- \mu^+)/\Gamma_{\text{total}}$	$< 1.0 \times 10^{-7}$, CL = 90%
$\Gamma(D^0 \rightarrow \mu^\pm e^\mp)/\Gamma_{\text{total}}$	[ρ] $< 1.3 \times 10^{-8}$, CL = 90%
$\Gamma(D^0 \rightarrow \pi^0 e^\pm \mu^\mp)/\Gamma_{\text{total}}$	[ρ] $< 8.0 \times 10^{-7}$, CL = 90%

Tests of Conservation Laws

$\Gamma(D^0 \rightarrow \eta e^\pm \mu^\mp)/\Gamma_{\text{total}}$	[o]	$<2.25 \times 10^{-6}$, CL = 90%
$\Gamma(D^0 \rightarrow \pi^+ \pi^- e^\pm \mu^\mp)/\Gamma_{\text{total}}$	[o]	$<1.71 \times 10^{-6}$, CL = 90%
$\Gamma(D^0 \rightarrow \rho^0 e^\pm \mu^\mp)/\Gamma_{\text{total}}$	[o]	$<5.0 \times 10^{-7}$, CL = 90%
$\Gamma(D^0 \rightarrow \omega e^\pm \mu^\mp)/\Gamma_{\text{total}}$	[o]	$<1.71 \times 10^{-6}$, CL = 90%
$\Gamma(D^0 \rightarrow K^- K^+ e^\pm \mu^\mp)/\Gamma_{\text{total}}$	[o]	$<1.00 \times 10^{-6}$, CL = 90%
$\Gamma(D^0 \rightarrow \phi e^\pm \mu^\mp)/\Gamma_{\text{total}}$	[o]	$<5.1 \times 10^{-7}$, CL = 90%
$\Gamma(D^0 \rightarrow \bar{K}^0 e^\pm \mu^\mp)/\Gamma_{\text{total}}$	[o]	$<1.74 \times 10^{-6}$, CL = 90%
$\Gamma(D^0 \rightarrow K^- \pi^+ e^\pm \mu^\mp)/\Gamma_{\text{total}}$	[o]	$<1.90 \times 10^{-6}$, CL = 90%
$\Gamma(D^0 \rightarrow \bar{K}^*(892)^0 e^\pm \mu^\mp)/\Gamma_{\text{total}}$	[o]	$<1.25 \times 10^{-6}$, CL = 90%
$\Gamma(D_S^+ \rightarrow \pi^+ e^+ \mu^-)/\Gamma_{\text{total}}$		$<1.1 \times 10^{-6}$, CL = 90%
$\Gamma(D_S^+ \rightarrow \pi^+ e^- \mu^+)/\Gamma_{\text{total}}$		$<9.4 \times 10^{-7}$, CL = 90%
$\Gamma(D_S^+ \rightarrow K^+ e^+ \mu^-)/\Gamma_{\text{total}}$		$<7.9 \times 10^{-7}$, CL = 90%
$\Gamma(D_S^+ \rightarrow K^+ e^- \mu^+)/\Gamma_{\text{total}}$		$<5.6 \times 10^{-7}$, CL = 90%
$\Gamma(B^+ \rightarrow \pi^+ e^+ \mu^-)/\Gamma_{\text{total}}$		$<6.4 \times 10^{-3}$, CL = 90%
$\Gamma(B^+ \rightarrow \pi^+ e^- \mu^+)/\Gamma_{\text{total}}$		$<6.4 \times 10^{-3}$, CL = 90%
$\Gamma(B^+ \rightarrow \pi^+ e^\pm \mu^\mp)/\Gamma_{\text{total}}$		$<1.7 \times 10^{-7}$, CL = 90%
$\Gamma(B^+ \rightarrow \pi^+ e^\pm \tau^\mp)/\Gamma_{\text{total}}$		$<7.4 \times 10^{-5}$, CL = 90%
$\Gamma(B^+ \rightarrow \pi^+ e^- \tau^+)/\Gamma_{\text{total}}$		$<2.0 \times 10^{-5}$, CL = 90%
$\Gamma(B^+ \rightarrow \pi^+ e^\pm \tau^\mp)/\Gamma_{\text{total}}$		$<7.5 \times 10^{-5}$, CL = 90%
$\Gamma(B^+ \rightarrow \pi^+ \mu^+ \tau^-)/\Gamma_{\text{total}}$		$<6.2 \times 10^{-5}$, CL = 90%
$\Gamma(B^+ \rightarrow \pi^+ \mu^- \tau^+)/\Gamma_{\text{total}}$		$<4.5 \times 10^{-5}$, CL = 90%
$\Gamma(B^+ \rightarrow \pi^+ \mu^\pm \tau^\mp)/\Gamma_{\text{total}}$		$<7.2 \times 10^{-5}$, CL = 90%
$\Gamma(B^+ \rightarrow K^+ e^+ \mu^-)/\Gamma_{\text{total}}$		$<7.0 \times 10^{-9}$, CL = 90%
$\Gamma(B^+ \rightarrow K^+ e^- \mu^+)/\Gamma_{\text{total}}$		$<6.4 \times 10^{-9}$, CL = 90%
$\Gamma(B^+ \rightarrow K^+ e^\pm \mu^\mp)/\Gamma_{\text{total}}$		$<9.1 \times 10^{-8}$, CL = 90%
$\Gamma(B^+ \rightarrow K^+ e^+ \tau^-)/\Gamma_{\text{total}}$		$<1.53 \times 10^{-5}$, CL = 90%
$\Gamma(B^+ \rightarrow K^+ e^- \tau^+)/\Gamma_{\text{total}}$		$<1.5 \times 10^{-5}$, CL = 90%
$\Gamma(B^+ \rightarrow K^+ e^\pm \tau^\mp)/\Gamma_{\text{total}}$		$<3.0 \times 10^{-5}$, CL = 90%
$\Gamma(B^+ \rightarrow K^+ \mu^+ \tau^-)/\Gamma_{\text{total}}$		$<2.45 \times 10^{-5}$, CL = 90%
$\Gamma(B^+ \rightarrow K^+ \mu^- \tau^+)/\Gamma_{\text{total}}$		$<5.9 \times 10^{-6}$, CL = 90%
$\Gamma(B^+ \rightarrow K^+ \mu^\pm \tau^\mp)/\Gamma_{\text{total}}$		$<4.8 \times 10^{-5}$, CL = 90%
$\Gamma(B^+ \rightarrow K^*(892)^+ e^+ \mu^-)/\Gamma_{\text{total}}$		$<1.3 \times 10^{-6}$, CL = 90%
$\Gamma(B^+ \rightarrow K^*(892)^+ e^- \mu^+)/\Gamma_{\text{total}}$		$<9.9 \times 10^{-7}$, CL = 90%
$\Gamma(B^+ \rightarrow K^*(892)^+ e^\pm \mu^\mp)/\Gamma_{\text{total}}$		$<1.4 \times 10^{-6}$, CL = 90%
$\Gamma(B^0 \rightarrow e^\pm \mu^\mp)/\Gamma_{\text{total}}$	[o]	$<1.0 \times 10^{-9}$, CL = 90%
$\Gamma(B^0 \rightarrow \pi^0 e^\pm \mu^\mp)/\Gamma_{\text{total}}$		$<1.4 \times 10^{-7}$, CL = 90%
$\Gamma(B^0 \rightarrow K^0 e^\pm \mu^\mp)/\Gamma_{\text{total}}$		$<3.8 \times 10^{-8}$, CL = 90%
$\Gamma(B^0 \rightarrow K^*(892)^0 e^+ \mu^-)/\Gamma_{\text{total}}$		$<6.8 \times 10^{-9}$, CL = 90%
$\Gamma(B^0 \rightarrow K^*(892)^0 e^- \mu^+)/\Gamma_{\text{total}}$		$<5.7 \times 10^{-9}$, CL = 90%
$\Gamma(B^0 \rightarrow K^*(892)^0 e^\pm \mu^\mp)/\Gamma_{\text{total}}$		$<1.01 \times 10^{-8}$, CL = 90%
$\Gamma(B^0 \rightarrow K^*(892)^0 \tau^+ \mu^-)/\Gamma_{\text{total}}$		$<1.0 \times 10^{-5}$, CL = 90%
$\Gamma(B^0 \rightarrow K^*(892)^0 \tau^- \mu^+)/\Gamma_{\text{total}}$		$<8.2 \times 10^{-6}$, CL = 90%
$\Gamma(B^0 \rightarrow e^\pm \tau^\mp)/\Gamma_{\text{total}}$	[o]	$<1.6 \times 10^{-5}$, CL = 90%
$\Gamma(B^0 \rightarrow \mu^\pm \tau^\mp)/\Gamma_{\text{total}}$	[o]	$<1.4 \times 10^{-5}$, CL = 95%
$\Gamma(B \rightarrow s e^\pm \mu^\mp)/\Gamma_{\text{total}}$	[o]	$<2.2 \times 10^{-5}$, CL = 90%
$\Gamma(B \rightarrow \pi e^\pm \mu^\mp)/\Gamma_{\text{total}}$		$<9.2 \times 10^{-8}$, CL = 90%
$\Gamma(B \rightarrow \rho e^\pm \mu^\mp)/\Gamma_{\text{total}}$		$<3.2 \times 10^{-6}$, CL = 90%
$\Gamma(B \rightarrow K e^\pm \mu^\mp)/\Gamma_{\text{total}}$		$<3.8 \times 10^{-8}$, CL = 90%
$\Gamma(B \rightarrow K^*(892) e^\pm \mu^\mp)/\Gamma_{\text{total}}$		$<5.1 \times 10^{-7}$, CL = 90%
$\Gamma(B_S^0 \rightarrow e^\pm \mu^\mp)/\Gamma_{\text{total}}$	[o]	$<5.4 \times 10^{-9}$, CL = 90%
$\Gamma(B_S^0 \rightarrow e^\pm \tau^\mp)/\Gamma_{\text{total}}$		$<1.4 \times 10^{-3}$, CL = 90%
$\Gamma(B_S^0 \rightarrow \mu^\pm \tau^\mp)/\Gamma_{\text{total}}$		$<4.2 \times 10^{-5}$, CL = 95%
$\Gamma(B_S^0 \rightarrow \phi \mu^\pm e^\mp)/\Gamma_{\text{total}}$		$<1.6 \times 10^{-8}$, CL = 90%
$\Gamma(J/\psi(1S) \rightarrow e^\pm \mu^\mp)/\Gamma_{\text{total}}$		$<1.6 \times 10^{-7}$, CL = 90%
$\Gamma(J/\psi(1S) \rightarrow e^\pm \tau^\mp)/\Gamma_{\text{total}}$		$<7.5 \times 10^{-8}$, CL = 90%
$\Gamma(J/\psi(1S) \rightarrow \mu^\pm \tau^\mp)/\Gamma_{\text{total}}$		$<2.0 \times 10^{-6}$, CL = 90%
$\Gamma(\Upsilon(1S) \rightarrow e^\pm \mu^\mp)/\Gamma_{\text{total}}$		$<3.9 \times 10^{-7}$, CL = 90%
$\Gamma(\Upsilon(1S) \rightarrow \mu^\pm \tau^\mp)/\Gamma_{\text{total}}$		$<2.7 \times 10^{-6}$, CL = 90%
$\Gamma(\Upsilon(1S) \rightarrow e^\pm \tau^\mp)/\Gamma_{\text{total}}$		$<2.7 \times 10^{-6}$, CL = 90%
$\Gamma(\Upsilon(1S) \rightarrow \gamma e^\pm \mu^\mp)/\Gamma_{\text{total}}$		$<4.2 \times 10^{-7}$, CL = 90%
$\Gamma(\Upsilon(1S) \rightarrow \gamma \mu^\pm \tau^\mp)/\Gamma_{\text{total}}$		$<6.1 \times 10^{-6}$, CL = 90%
$\Gamma(\Upsilon(1S) \rightarrow \gamma e^\pm \tau^\mp)/\Gamma_{\text{total}}$		$<6.5 \times 10^{-6}$, CL = 90%
$\Gamma(\Upsilon(2S) \rightarrow e^\pm \tau^\mp)/\Gamma_{\text{total}}$		$<3.2 \times 10^{-6}$, CL = 90%
$\Gamma(\Upsilon(2S) \rightarrow \mu^\pm \tau^\mp)/\Gamma_{\text{total}}$		$<3.3 \times 10^{-6}$, CL = 90%
$\Gamma(\Upsilon(3S) \rightarrow e^\pm \tau^\mp)/\Gamma_{\text{total}}$		$<4.2 \times 10^{-6}$, CL = 90%
$\Gamma(\Upsilon(3S) \rightarrow e^\pm \mu^\mp)/\Gamma_{\text{total}}$		$<3.6 \times 10^{-7}$, CL = 90%
$\Gamma(\Upsilon(3S) \rightarrow \mu^\pm \tau^\mp)/\Gamma_{\text{total}}$		$<3.1 \times 10^{-6}$, CL = 90%
$\Gamma(\Lambda_c^+ \rightarrow p e^+ \mu^-)/\Gamma_{\text{total}}$		$<9.9 \times 10^{-6}$, CL = 90%
$\Gamma(\Lambda_c^+ \rightarrow p e^- \mu^+)/\Gamma_{\text{total}}$		$<1.9 \times 10^{-5}$, CL = 90%

TOTAL LEPTON NUMBER

Violation of total lepton number conservation also implies violation of lepton family number conservation.

$\Gamma(Z \rightarrow \nu e)/\Gamma_{\text{total}}$		$<1.8 \times 10^{-6}$, CL = 95%
$\Gamma(Z \rightarrow \nu \mu)/\Gamma_{\text{total}}$		$<1.8 \times 10^{-6}$, CL = 95%
limit on $\mu^- \rightarrow e^+$ conversion		
$\sigma(\mu^- 32S \rightarrow e^+ 32Si^*) / \sigma(\mu^- 32S \rightarrow \nu_\mu 32P^*)$		$<9 \times 10^{-10}$, CL = 90%
$\sigma(\mu^- 127I \rightarrow e^+ 127Sb^*) / \sigma(\mu^- 127I \rightarrow \text{anything})$		$<3 \times 10^{-10}$, CL = 90%
$\sigma(\mu^- \text{Ti} \rightarrow e^+ \text{Ca}) / \sigma(\mu^- \text{Ti} \rightarrow \text{capture})$		$<3.6 \times 10^{-11}$, CL = 90%
$\Gamma(\tau^- \rightarrow e^+ \pi^- \pi^-)/\Gamma_{\text{total}}$		$<2.0 \times 10^{-8}$, CL = 90%
$\Gamma(\tau^- \rightarrow \mu^+ \pi^- \pi^-)/\Gamma_{\text{total}}$		$<3.9 \times 10^{-8}$, CL = 90%
$\Gamma(\tau^- \rightarrow e^+ \pi^- K^-)/\Gamma_{\text{total}}$		$<3.2 \times 10^{-8}$, CL = 90%
$\Gamma(\tau^- \rightarrow e^+ K^- K^-)/\Gamma_{\text{total}}$		$<3.3 \times 10^{-8}$, CL = 90%
$\Gamma(\tau^- \rightarrow \mu^+ \pi^- K^-)/\Gamma_{\text{total}}$		$<4.8 \times 10^{-8}$, CL = 90%
$\Gamma(\tau^- \rightarrow \mu^+ K^- K^-)/\Gamma_{\text{total}}$		$<4.7 \times 10^{-8}$, CL = 90%
$\Gamma(\tau^- \rightarrow p e^- e^-)/\Gamma_{\text{total}}$		$<3.0 \times 10^{-8}$, CL = 90%
$\Gamma(\tau^- \rightarrow \bar{p} e^+ e^-)/\Gamma_{\text{total}}$		$<3.0 \times 10^{-8}$, CL = 90%
$\Gamma(\tau^- \rightarrow \bar{p} e^+ \mu^-)/\Gamma_{\text{total}}$		$<2.0 \times 10^{-8}$, CL = 90%
$\Gamma(\tau^- \rightarrow \bar{p} e^- \mu^+)/\Gamma_{\text{total}}$		$<1.8 \times 10^{-8}$, CL = 90%
$\Gamma(\tau^- \rightarrow p \mu^+ \mu^-)/\Gamma_{\text{total}}$		$<4.0 \times 10^{-8}$, CL = 90%
$\Gamma(\tau^- \rightarrow \bar{p} \mu^+ \mu^-)/\Gamma_{\text{total}}$		$<1.8 \times 10^{-8}$, CL = 90%
$\Gamma(\tau^- \rightarrow \bar{p} \gamma)/\Gamma_{\text{total}}$		$<3.5 \times 10^{-6}$, CL = 90%
$\Gamma(\tau^- \rightarrow \bar{p} \pi^0)/\Gamma_{\text{total}}$		$<1.5 \times 10^{-5}$, CL = 90%
$\Gamma(\tau^- \rightarrow \bar{p} 2\pi^0)/\Gamma_{\text{total}}$		$<3.3 \times 10^{-5}$, CL = 90%
$\Gamma(\tau^- \rightarrow \bar{p} \eta)/\Gamma_{\text{total}}$		$<8.9 \times 10^{-6}$, CL = 90%
$\Gamma(\tau^- \rightarrow \bar{p} \pi^0 \eta)/\Gamma_{\text{total}}$		$<2.7 \times 10^{-5}$, CL = 90%
$\Gamma(\tau^- \rightarrow \Lambda \pi^-)/\Gamma_{\text{total}}$		$<7.2 \times 10^{-8}$, CL = 90%
$\Gamma(\tau^- \rightarrow \bar{\Lambda} \pi^-)/\Gamma_{\text{total}}$		$<1.4 \times 10^{-7}$, CL = 90%
$t_{1/2}(^{76}\text{Ge} \rightarrow ^{76}\text{Se} + 2 e^-)$		$>9.0 \times 10^{25}$ yr, CL = 90%
$t_{1/2}(^{136}\text{Xe} \rightarrow ^{136}\text{Ba} + 2 e^-)$		$>10.7 \times 10^{25}$ yr, CL = 90%
$t_{1/2}(^{130}\text{Te} \rightarrow ^{130}\text{Xe} + 2 e^-)$		$>1.5 \times 10^{25}$ yr, CL = 90%
$\Gamma(\pi^+ \rightarrow \mu^+ \bar{\nu}_e)/\Gamma_{\text{total}}$	[q]	$<1.5 \times 10^{-3}$, CL = 90%
$\Gamma(K^+ \rightarrow \pi^- \mu^+ e^+)/\Gamma_{\text{total}}$		$<4.2 \times 10^{-11}$, CL = 90%
$\Gamma(K^+ \rightarrow \pi^- e^+ e^+)/\Gamma_{\text{total}}$		$<5.3 \times 10^{-11}$, CL = 90%
$\Gamma(K^+ \rightarrow \pi^- \mu^\pm \mu^\pm)/\Gamma_{\text{total}}$		$<4.2 \times 10^{-11}$, CL = 90%
$\Gamma(K^+ \rightarrow \pi^- \pi^0 e^+ e^+)/\Gamma_{\text{total}}$		$<8.5 \times 10^{-10}$, CL = 90%
$\Gamma(K^+ \rightarrow \mu^+ \bar{\nu}_e)/\Gamma_{\text{total}}$	[q]	$<3.3 \times 10^{-3}$, CL = 90%
$\Gamma(K^+ \rightarrow \pi^0 e^+ \bar{\nu}_e)/\Gamma_{\text{total}}$		$<3 \times 10^{-3}$, CL = 90%
$\Gamma(D^+ \rightarrow \pi^- 2e^+)/\Gamma_{\text{total}}$		$<5.3 \times 10^{-7}$, CL = 90%
$\Gamma(D^+ \rightarrow \pi^- 2\mu^+)/\Gamma_{\text{total}}$		$<1.4 \times 10^{-8}$, CL = 90%
$\Gamma(D^+ \rightarrow \pi^- e^+ \mu^+)/\Gamma_{\text{total}}$		$<1.3 \times 10^{-7}$, CL = 90%
$\Gamma(D^+ \rightarrow \rho^- 2\mu^+)/\Gamma_{\text{total}}$		$<5.6 \times 10^{-4}$, CL = 90%
$\Gamma(D^+ \rightarrow K^- 2e^+)/\Gamma_{\text{total}}$		$<9 \times 10^{-7}$, CL = 90%
$\Gamma(D^+ \rightarrow K^- 2\mu^+)/\Gamma_{\text{total}}$		$<1.0 \times 10^{-5}$, CL = 90%
$\Gamma(D^+ \rightarrow K^- e^+ \mu^+)/\Gamma_{\text{total}}$		$<1.9 \times 10^{-6}$, CL = 90%
$\Gamma(D^+ \rightarrow K^*(892)^- 2\mu^+)/\Gamma_{\text{total}}$		$<8.5 \times 10^{-4}$, CL = 90%
$\Gamma(D^+ \rightarrow \Lambda e^+)/\Gamma_{\text{total}}$		$<1.1 \times 10^{-6}$, CL = 90%
$\Gamma(D^+ \rightarrow \bar{\Lambda} e^+)/\Gamma_{\text{total}}$		$<6.5 \times 10^{-7}$, CL = 90%
$\Gamma(D^+ \rightarrow \Sigma^0 e^+)/\Gamma_{\text{total}}$		$<1.7 \times 10^{-6}$, CL = 90%
$\Gamma(D^+ \rightarrow \bar{\Sigma}^0 e^+)/\Gamma_{\text{total}}$		$<1.3 \times 10^{-6}$, CL = 90%
$\Gamma(D^0 \rightarrow 2\pi^- 2e^+)/\Gamma_{\text{total}}$		$<9.1 \times 10^{-7}$, CL = 90%
$\Gamma(D^0 \rightarrow 2\pi^- 2\mu^+)/\Gamma_{\text{total}}$		$<1.52 \times 10^{-6}$, CL = 90%
$\Gamma(D^0 \rightarrow K^- \pi^- 2e^+)/\Gamma_{\text{total}}$		$<5.0 \times 10^{-7}$, CL = 90%
$\Gamma(D^0 \rightarrow K^- \pi^- 2\mu^+)/\Gamma_{\text{total}}$		$<5.3 \times 10^{-7}$, CL = 90%
$\Gamma(D^0 \rightarrow 2K^- 2e^+)/\Gamma_{\text{total}}$		$<3.4 \times 10^{-7}$, CL = 90%
$\Gamma(D^0 \rightarrow 2K^- 2\mu^+)/\Gamma_{\text{total}}$		$<1.0 \times 10^{-7}$, CL = 90%
$\Gamma(D^0 \rightarrow \pi^- \pi^- e^+ \mu^+)/\Gamma_{\text{total}}$		$<3.06 \times 10^{-6}$, CL = 90%
$\Gamma(D^0 \rightarrow K^- \pi^- e^+ \mu^+)/\Gamma_{\text{total}}$		$<2.10 \times 10^{-6}$, CL = 90%
$\Gamma(D^0 \rightarrow 2K^- e^+ \mu^+)/\Gamma_{\text{total}}$		$<5.8 \times 10^{-7}$, CL = 90%
$\Gamma(D^0 \rightarrow p e^-)/\Gamma_{\text{total}}$		$<2.2 \times 10^{-6}$, CL = 90%
$\Gamma(D^0 \rightarrow \bar{p} e^+)/\Gamma_{\text{total}}$		$<1.2 \times 10^{-6}$, CL = 90%
$\Gamma(D_S^+ \rightarrow \pi^- 2e^+)/\Gamma_{\text{total}}$		$<1.4 \times 10^{-6}$, CL = 90%
$\Gamma(D_S^+ \rightarrow \pi^- 2\mu^+)/\Gamma_{\text{total}}$		$<8.6 \times 10^{-8}$, CL = 90%
$\Gamma(D_S^+ \rightarrow \pi^- e^+ \mu^+)/\Gamma_{\text{total}}$		$<6.3 \times 10^{-7}$, CL = 90%
$\Gamma(D_S^+ \rightarrow K^- 2e^+)/\Gamma_{\text{total}}$		$<7.7 \times 10^{-7}$, CL = 90%
$\Gamma(D_S^+ \rightarrow K^- 2\mu^+)/\Gamma_{\text{total}}$		$<2.6 \times 10^{-8}$, CL = 90%

Tests of Conservation Laws

$\Gamma(D_S^+ \rightarrow K^- e^+ \mu^+)/\Gamma_{\text{total}}$	$<2.6 \times 10^{-7}$, CL = 90%
$\Gamma(D_S^+ \rightarrow K^*(892)^- 2\mu^+)/\Gamma_{\text{total}}$	$<1.4 \times 10^{-3}$, CL = 90%
$\Gamma(B^+ \rightarrow \pi^- e^+ \mu^+)/\Gamma_{\text{total}}$	$<2.3 \times 10^{-8}$, CL = 90%
$\Gamma(B^+ \rightarrow \pi^- \mu^+ \mu^+)/\Gamma_{\text{total}}$	$<4.0 \times 10^{-9}$, CL = 95%
$\Gamma(B^+ \rightarrow \pi^- e^+ \mu^+)/\Gamma_{\text{total}}$	$<1.5 \times 10^{-7}$, CL = 90%
$\Gamma(B^+ \rightarrow \rho^- e^+ \mu^+)/\Gamma_{\text{total}}$	$<1.7 \times 10^{-7}$, CL = 90%
$\Gamma(B^+ \rightarrow \rho^- \mu^+ \mu^+)/\Gamma_{\text{total}}$	$<4.2 \times 10^{-7}$, CL = 90%
$\Gamma(B^+ \rightarrow \rho^- e^+ \mu^+)/\Gamma_{\text{total}}$	$<4.7 \times 10^{-7}$, CL = 90%
$\Gamma(B^+ \rightarrow K^- e^+ \mu^+)/\Gamma_{\text{total}}$	$<3.0 \times 10^{-8}$, CL = 90%
$\Gamma(B^+ \rightarrow K^- \mu^+ \mu^+)/\Gamma_{\text{total}}$	$<4.1 \times 10^{-8}$, CL = 90%
$\Gamma(B^+ \rightarrow K^- e^+ \mu^+)/\Gamma_{\text{total}}$	$<1.6 \times 10^{-7}$, CL = 90%
$\Gamma(B^+ \rightarrow K^*(892)^- e^+ \mu^+)/\Gamma_{\text{total}}$	$<4.0 \times 10^{-7}$, CL = 90%
$\Gamma(B^+ \rightarrow K^*(892)^- \mu^+ \mu^+)/\Gamma_{\text{total}}$	$<5.9 \times 10^{-7}$, CL = 90%
$\Gamma(B^+ \rightarrow K^*(892)^- e^+ \mu^+)/\Gamma_{\text{total}}$	$<3.0 \times 10^{-7}$, CL = 90%
$\Gamma(B^+ \rightarrow D^- e^+ \mu^+)/\Gamma_{\text{total}}$	$<2.6 \times 10^{-6}$, CL = 90%
$\Gamma(B^+ \rightarrow D^- e^+ \mu^+)/\Gamma_{\text{total}}$	$<1.8 \times 10^{-6}$, CL = 90%
$\Gamma(B^+ \rightarrow D^- \mu^+ \mu^+)/\Gamma_{\text{total}}$	$<6.9 \times 10^{-7}$, CL = 95%
$\Gamma(B^+ \rightarrow D^{*-} \mu^+ \mu^+)/\Gamma_{\text{total}}$	$<2.4 \times 10^{-6}$, CL = 95%
$\Gamma(B^+ \rightarrow D_S^- \mu^+ \mu^+)/\Gamma_{\text{total}}$	$<5.8 \times 10^{-7}$, CL = 95%
$\Gamma(B^+ \rightarrow \bar{D}^0 \pi^- \mu^+ \mu^+)/\Gamma_{\text{total}}$	$<1.5 \times 10^{-6}$, CL = 95%
$\Gamma(B^+ \rightarrow \Lambda^0 \mu^+)/\Gamma_{\text{total}}$	$<6 \times 10^{-8}$, CL = 90%
$\Gamma(B^+ \rightarrow \Lambda^0 e^+)/\Gamma_{\text{total}}$	$<3.2 \times 10^{-8}$, CL = 90%
$\Gamma(B^+ \rightarrow \bar{\Lambda}^0 \mu^+)/\Gamma_{\text{total}}$	$<6 \times 10^{-8}$, CL = 90%
$\Gamma(B^+ \rightarrow \bar{\Lambda}^0 e^+)/\Gamma_{\text{total}}$	$<8 \times 10^{-8}$, CL = 90%
$\Gamma(B^0 \rightarrow \rho \mu^-)/\Gamma_{\text{total}}$	$<2.6 \times 10^{-9}$, CL = 90%
$\Gamma(B^0 \rightarrow \Lambda_C^+ \mu^-)/\Gamma_{\text{total}}$	$<1.4 \times 10^{-6}$, CL = 90%
$\Gamma(B^0 \rightarrow \Lambda_C^+ e^-)/\Gamma_{\text{total}}$	$<4 \times 10^{-6}$, CL = 90%
$\Gamma(B_S^0 \rightarrow \rho \mu^-)/\Gamma_{\text{total}}$	$<1.21 \times 10^{-8}$, CL = 90%
$\Gamma(\Lambda \rightarrow \pi^+ e^-)/\Gamma_{\text{total}}$	$<6 \times 10^{-7}$, CL = 90%
$\Gamma(\Lambda \rightarrow \pi^+ \mu^-)/\Gamma_{\text{total}}$	$<6 \times 10^{-7}$, CL = 90%
$\Gamma(\Lambda \rightarrow \pi^- e^+)/\Gamma_{\text{total}}$	$<4 \times 10^{-7}$, CL = 90%
$\Gamma(\Lambda \rightarrow \pi^- \mu^+)/\Gamma_{\text{total}}$	$<6 \times 10^{-7}$, CL = 90%
$\Gamma(\Lambda \rightarrow K^+ e^-)/\Gamma_{\text{total}}$	$<2 \times 10^{-6}$, CL = 90%
$\Gamma(\Lambda \rightarrow K^+ \mu^-)/\Gamma_{\text{total}}$	$<3 \times 10^{-6}$, CL = 90%
$\Gamma(\Lambda \rightarrow K^- e^+)/\Gamma_{\text{total}}$	$<2 \times 10^{-6}$, CL = 90%
$\Gamma(\Lambda \rightarrow K^- \mu^+)/\Gamma_{\text{total}}$	$<3 \times 10^{-6}$, CL = 90%
$\Gamma(\Lambda \rightarrow K_S^0 \nu)/\Gamma_{\text{total}}$	$<2 \times 10^{-5}$, CL = 90%
$\Gamma(\Sigma^- \rightarrow p e^- e^-)/\Gamma_{\text{total}}$	$<6.7 \times 10^{-5}$, CL = 90%
$\Gamma(\Xi^- \rightarrow p \mu^- \mu^-)/\Gamma_{\text{total}}$	$<4 \times 10^{-8}$, CL = 90%
$\Gamma(\Lambda_C^+ \rightarrow \bar{p} 2e^+)/\Gamma_{\text{total}}$	$<2.7 \times 10^{-6}$, CL = 90%
$\Gamma(\Lambda_C^+ \rightarrow \bar{p} 2\mu^+)/\Gamma_{\text{total}}$	$<9.4 \times 10^{-6}$, CL = 90%
$\Gamma(\Lambda_C^+ \rightarrow \bar{p} e^+ \mu^+)/\Gamma_{\text{total}}$	$<1.6 \times 10^{-5}$, CL = 90%
$\Gamma(\Lambda_C^+ \rightarrow \Sigma^- \mu^+ \mu^+)/\Gamma_{\text{total}}$	$<7.0 \times 10^{-4}$, CL = 90%

BARYON NUMBER

$\Gamma(Z \rightarrow p e)/\Gamma_{\text{total}}$	$<1.8 \times 10^{-6}$, CL = 95%
$\Gamma(Z \rightarrow p \mu)/\Gamma_{\text{total}}$	$<1.8 \times 10^{-6}$, CL = 95%
$\Gamma(\tau^- \rightarrow p e^- e^-)/\Gamma_{\text{total}}$	$<3.0 \times 10^{-8}$, CL = 90%
$\Gamma(\tau^- \rightarrow \bar{p} e^+ e^-)/\Gamma_{\text{total}}$	$<3.0 \times 10^{-8}$, CL = 90%
$\Gamma(\tau^- \rightarrow \bar{p} e^+ \mu^-)/\Gamma_{\text{total}}$	$<2.0 \times 10^{-8}$, CL = 90%
$\Gamma(\tau^- \rightarrow \bar{p} e^- \mu^+)/\Gamma_{\text{total}}$	$<1.8 \times 10^{-8}$, CL = 90%
$\Gamma(\tau^- \rightarrow p \mu^- \mu^-)/\Gamma_{\text{total}}$	$<4.0 \times 10^{-8}$, CL = 90%
$\Gamma(\tau^- \rightarrow \bar{p} \mu^+ \mu^-)/\Gamma_{\text{total}}$	$<1.8 \times 10^{-8}$, CL = 90%
$\Gamma(\tau^- \rightarrow \bar{p} \gamma)/\Gamma_{\text{total}}$	$<3.5 \times 10^{-6}$, CL = 90%
$\Gamma(\tau^- \rightarrow \bar{p} \pi^0)/\Gamma_{\text{total}}$	$<1.5 \times 10^{-5}$, CL = 90%
$\Gamma(\tau^- \rightarrow \bar{p} 2\pi^0)/\Gamma_{\text{total}}$	$<3.3 \times 10^{-5}$, CL = 90%
$\Gamma(\tau^- \rightarrow \bar{p} \eta)/\Gamma_{\text{total}}$	$<8.9 \times 10^{-6}$, CL = 90%
$\Gamma(\tau^- \rightarrow \bar{p} \pi^0 \eta)/\Gamma_{\text{total}}$	$<2.7 \times 10^{-5}$, CL = 90%
$\Gamma(\tau^- \rightarrow \Lambda \pi^-)/\Gamma_{\text{total}}$	$<7.2 \times 10^{-8}$, CL = 90%
$\Gamma(\tau^- \rightarrow \bar{\Lambda} \pi^-)/\Gamma_{\text{total}}$	$<1.4 \times 10^{-7}$, CL = 90%
$\Gamma(D^+ \rightarrow \Lambda e^+)/\Gamma_{\text{total}}$	$<1.1 \times 10^{-6}$, CL = 90%
$\Gamma(D^+ \rightarrow \bar{\Lambda} e^+)/\Gamma_{\text{total}}$	$<6.5 \times 10^{-7}$, CL = 90%
$\Gamma(D^+ \rightarrow \Sigma^0 e^+)/\Gamma_{\text{total}}$	$<1.7 \times 10^{-6}$, CL = 90%
$\Gamma(D^+ \rightarrow \bar{\Sigma}^0 e^+)/\Gamma_{\text{total}}$	$<1.3 \times 10^{-6}$, CL = 90%
$\Gamma(D^0 \rightarrow p e^-)/\Gamma_{\text{total}}$	$<2.2 \times 10^{-6}$, CL = 90%
$\Gamma(D^0 \rightarrow \bar{p} e^+)/\Gamma_{\text{total}}$	$<1.2 \times 10^{-6}$, CL = 90%
$\Gamma(B^+ \rightarrow \Lambda^0 \mu^+)/\Gamma_{\text{total}}$	$<6 \times 10^{-8}$, CL = 90%
$\Gamma(B^+ \rightarrow \Lambda^0 e^+)/\Gamma_{\text{total}}$	$<3.2 \times 10^{-8}$, CL = 90%
$\Gamma(B^+ \rightarrow \bar{\Lambda}^0 \mu^+)/\Gamma_{\text{total}}$	$<6 \times 10^{-8}$, CL = 90%

$\Gamma(B^+ \rightarrow \bar{\Lambda}^0 e^+)/\Gamma_{\text{total}}$	$<8 \times 10^{-8}$, CL = 90%
$\Gamma(B^0 \rightarrow \rho \mu^-)/\Gamma_{\text{total}}$	$<2.6 \times 10^{-9}$, CL = 90%
$\Gamma(B^0 \rightarrow \Lambda_C^+ \mu^-)/\Gamma_{\text{total}}$	$<1.4 \times 10^{-6}$, CL = 90%
$\Gamma(B^0 \rightarrow \Lambda_C^+ e^-)/\Gamma_{\text{total}}$	$<4 \times 10^{-6}$, CL = 90%
$\Gamma(B_S^0 \rightarrow \rho \mu^-)/\Gamma_{\text{total}}$	$<1.21 \times 10^{-8}$, CL = 90%
ρ mean life	$>9 \times 10^{29}$ years, CL = 90%

A few examples of proton or bound neutron decay follow. For limits on many other nucleon decay channels, see the Baryon Summary Table.

$\tau(N \rightarrow e^+ \pi)$	> 5300 (n), > 24000 (p) $\times 10^{30}$ years, CL = 90%
$\tau(N \rightarrow \mu^+ \pi)$	> 3500 (n), > 16000 (p) $\times 10^{30}$ years, CL = 90%
$\tau(N \rightarrow e^+ K)$	> 17 (n), > 1000 (p) $\times 10^{30}$ years, CL = 90%
$\tau(N \rightarrow \mu^+ K)$	> 26 (n), > 4500 (p) $\times 10^{30}$ years, CL = 90%
Mean $n\bar{n}$ -oscillation time (free n)	$>8.6 \times 10^7$ s, CL = 90%
Mean $n\bar{n}$ -oscillation time (bound n)	[r] $>4.7 \times 10^8$ s, CL = 90%
$\Gamma(\Lambda \rightarrow \pi^+ e^-)/\Gamma_{\text{total}}$	$<6 \times 10^{-7}$, CL = 90%
$\Gamma(\Lambda \rightarrow \pi^+ \mu^-)/\Gamma_{\text{total}}$	$<6 \times 10^{-7}$, CL = 90%
$\Gamma(\Lambda \rightarrow \pi^- e^+)/\Gamma_{\text{total}}$	$<4 \times 10^{-7}$, CL = 90%
$\Gamma(\Lambda \rightarrow \pi^- \mu^+)/\Gamma_{\text{total}}$	$<6 \times 10^{-7}$, CL = 90%
$\Gamma(\Lambda \rightarrow K^+ e^-)/\Gamma_{\text{total}}$	$<2 \times 10^{-6}$, CL = 90%
$\Gamma(\Lambda \rightarrow K^+ \mu^-)/\Gamma_{\text{total}}$	$<3 \times 10^{-6}$, CL = 90%
$\Gamma(\Lambda \rightarrow K^- e^+)/\Gamma_{\text{total}}$	$<2 \times 10^{-6}$, CL = 90%
$\Gamma(\Lambda \rightarrow K^- \mu^+)/\Gamma_{\text{total}}$	$<3 \times 10^{-6}$, CL = 90%
$\Gamma(\Lambda \rightarrow K_S^0 \nu)/\Gamma_{\text{total}}$	$<2 \times 10^{-5}$, CL = 90%
$\Gamma(\Lambda \rightarrow \bar{p} \pi^+)/\Gamma_{\text{total}}$	$<9 \times 10^{-7}$, CL = 90%
$\Gamma(\Lambda_C^+ \rightarrow \bar{p} 2e^+)/\Gamma_{\text{total}}$	$<2.7 \times 10^{-6}$, CL = 90%
$\Gamma(\Lambda_C^+ \rightarrow \bar{p} 2\mu^+)/\Gamma_{\text{total}}$	$<9.4 \times 10^{-6}$, CL = 90%
$\Gamma(\Lambda_C^+ \rightarrow \bar{p} e^+ \mu^+)/\Gamma_{\text{total}}$	$<1.6 \times 10^{-5}$, CL = 90%

ELECTRIC CHARGE (Q)

γ charge (mixed)	$<1 \times 10^{-46} e$
γ charge (single)	$<1 \times 10^{-35} e$
$e \rightarrow \nu_e \gamma$ and astrophysical limits	[s] $>6.6 \times 10^{28}$ yr, CL = 90%
ν charge	$<4 \times 10^{-35} e$, CL = 95%
$ q_p + q_e /e$	[t] $<1 \times 10^{-21}$
n charge	$(-0.2 \pm 0.8) \times 10^{-21} e$
$\Gamma(n \rightarrow p \nu_e \bar{\nu}_e)/\Gamma_{\text{total}}$	$<8 \times 10^{-27}$, CL = 68%

$\Delta S = \Delta Q$ RULE

Violations allowed in second-order weak interactions.

$\Gamma(K^+ \rightarrow \pi^+ \pi^+ e^- \bar{\nu}_e)/\Gamma_{\text{total}}$	$<1.3 \times 10^{-8}$, CL = 90%
$\Gamma(K^+ \rightarrow \pi^+ \pi^+ \mu^- \bar{\nu}_\mu)/\Gamma_{\text{total}}$	$<3.0 \times 10^{-6}$, CL = 95%
Re(x_+), K_{e3} parameter	$(-0.9 \pm 3.0) \times 10^{-3}$
$x = A(\bar{K}^0 \rightarrow \pi^- \ell^+ \nu)/A(K^0 \rightarrow \pi^- \ell^+ \nu) = A(\Delta S = -\Delta Q)/A(\Delta S = \Delta Q)$	
real part of x	-0.002 ± 0.006
imaginary part of x	0.0012 ± 0.0021
$\Gamma(\Sigma^+ \rightarrow n \ell^+ \nu)/\Gamma(\Sigma^- \rightarrow n \ell^- \bar{\nu}_\ell)$	<0.043
$\Gamma(\Sigma^+ \rightarrow n e^+ \nu_e)/\Gamma_{\text{total}}$	$<5 \times 10^{-6}$, CL = 90%
$\Gamma(\Sigma^+ \rightarrow n \mu^+ \nu_\mu)/\Gamma_{\text{total}}$	$<3.0 \times 10^{-5}$, CL = 90%
$\Gamma(\Xi^0 \rightarrow \Sigma^- e^+ \nu_e)/\Gamma_{\text{total}}$	$<1.6 \times 10^{-4}$, CL = 90%
$\Gamma(\Xi^0 \rightarrow \Sigma^- \mu^+ \nu_\mu)/\Gamma_{\text{total}}$	$<9 \times 10^{-4}$, CL = 90%

$\Delta S = 2$ FORBIDDEN

Allowed in second-order weak interactions.

$\Gamma(\Xi^0 \rightarrow p \pi^-)/\Gamma_{\text{total}}$	$<8 \times 10^{-6}$, CL = 90%
$\Gamma(\Xi^0 \rightarrow p e^- \bar{\nu}_e)/\Gamma_{\text{total}}$	$<1.3 \times 10^{-3}$
$\Gamma(\Xi^0 \rightarrow p \mu^- \bar{\nu}_\mu)/\Gamma_{\text{total}}$	$<1.3 \times 10^{-3}$
$\Gamma(\Xi^- \rightarrow n \pi^-)/\Gamma_{\text{total}}$	$<1.9 \times 10^{-5}$, CL = 90%
$\Gamma(\Xi^- \rightarrow n e^- \bar{\nu}_e)/\Gamma_{\text{total}}$	$<3.2 \times 10^{-3}$, CL = 90%
$\Gamma(\Xi^- \rightarrow n \mu^- \bar{\nu}_\mu)/\Gamma_{\text{total}}$	$<1.5 \times 10^{-2}$, CL = 90%
$\Gamma(\Xi^- \rightarrow p \pi^- \pi^-)/\Gamma_{\text{total}}$	$<4 \times 10^{-4}$, CL = 90%
$\Gamma(\Xi^- \rightarrow p \pi^- e^- \bar{\nu}_e)/\Gamma_{\text{total}}$	$<4 \times 10^{-4}$, CL = 90%
$\Gamma(\Xi^- \rightarrow p \pi^- \mu^- \bar{\nu}_\mu)/\Gamma_{\text{total}}$	$<4 \times 10^{-4}$, CL = 90%

Tests of Conservation Laws

$$\Gamma(\Omega^- \rightarrow \Lambda \pi^-)/\Gamma_{\text{total}} < 2.9 \times 10^{-6}, \text{ CL} = 90\%$$

 $\Delta S = 2$ VIA MIXING

Allowed in second-order weak interactions, e.g. mixing.

$$m_{K_L^0} - m_{K_S^0} = x\Gamma \quad (0.5293 \pm 0.0009) \times 10^{10} \hbar \text{ s}^{-1} \quad (S = 1.3)$$

$$m_{K_L^0} - m_{K_S^0} = 3.484 \pm 0.006 \times 10^{-12} \text{ MeV}$$

 $\Delta C = 2$ VIA MIXING

Allowed in second-order weak interactions, e.g. mixing.

$$|m_{D_1^0} - m_{D_2^0}| = x\Gamma \quad (0.997 \pm 0.116) \times 10^{10} \hbar \text{ s}^{-1}$$

$$(\Gamma_{D_1^0} - \Gamma_{D_2^0})/\Gamma = 2\gamma \quad (1.394 \pm 0.056) \times 10^{-2}$$

 $\Delta B = 2$ VIA MIXING

Allowed in second-order weak interactions, e.g. mixing.

$$\chi_d (B^0 - \bar{B}^0 \text{ mixing probability}) \quad 0.1860 \pm 0.0011$$

$$\Delta m_{B^0} = m_{B_H^0} - m_{B_L^0} \quad (0.5069 \pm 0.0019) \times 10^{12} \hbar \text{ s}^{-1}$$

$$x_d = \Delta m_{B^0}/\Gamma_{B^0} \quad 0.7697 \pm 0.0035$$

$$\Delta m_{B_s^0} = m_{B_{sH}^0} - m_{B_{sL}^0} \quad (17.765 \pm 0.006) \times 10^{12} \hbar \text{ s}^{-1}$$

$$x_s = \Delta m_{B_s^0}/\Gamma_{B_s^0} \quad 26.99 \pm 0.09$$

$$\chi_s (B_s^0 - \bar{B}_s^0 \text{ mixing parameter}) \quad 0.499318 \pm 0.000005$$

 $\Delta S = 1$ WEAK NEUTRAL CURRENT FORBIDDEN

Allowed by higher-order electroweak interactions.

$$\Gamma(K^+ \rightarrow \pi^+ e^+ e^-)/\Gamma_{\text{total}} \quad (3.00 \pm 0.09) \times 10^{-7}$$

$$\Gamma(K^+ \rightarrow \pi^+ \mu^+ \mu^-)/\Gamma_{\text{total}} \quad (9.17 \pm 0.14) \times 10^{-8} \quad (S = 1.8)$$

$$\Gamma(K^+ \rightarrow \pi^+ \nu \bar{\nu})/\Gamma_{\text{total}} \quad (1.14 \pm 0.40) \times 10^{-10}$$

$$\Gamma(K^+ \rightarrow \pi^+ \pi^0 \nu \bar{\nu})/\Gamma_{\text{total}} \quad < 4.3 \times 10^{-5}, \text{ CL} = 90\%$$

$$\Gamma(K_S^0 \rightarrow \mu^+ \mu^-)/\Gamma_{\text{total}} \quad < 2.1 \times 10^{-10}, \text{ CL} = 90\%$$

$$\Gamma(K_S^0 \rightarrow e^+ e^-)/\Gamma_{\text{total}} \quad < 9 \times 10^{-9}, \text{ CL} = 90\%$$

$$\Gamma(K_S^0 \rightarrow \pi^0 e^+ e^-)/\Gamma_{\text{total}} \quad [u] \quad (3.0 \pm 1.5) \times 10^{-9}$$

$$\Gamma(K_S^0 \rightarrow \pi^0 \mu^+ \mu^-)/\Gamma_{\text{total}} \quad (2.9 \pm 1.5) \times 10^{-9}$$

$$\Gamma(K_L^0 \rightarrow \mu^+ \mu^-)/\Gamma_{\text{total}} \quad (6.84 \pm 0.11) \times 10^{-9}$$

$$\Gamma(K_L^0 \rightarrow e^+ e^-)/\Gamma_{\text{total}} \quad (9 \pm 4) \times 10^{-12}$$

$$\Gamma(K_L^0 \rightarrow \pi^+ \pi^- e^+ e^-)/\Gamma_{\text{total}} \quad [v] \quad (3.11 \pm 0.19) \times 10^{-7}$$

$$\Gamma(K_L^0 \rightarrow \pi^0 \pi^0 e^+ e^-)/\Gamma_{\text{total}} \quad < 6.6 \times 10^{-9}, \text{ CL} = 90\%$$

$$\Gamma(K_L^0 \rightarrow \pi^0 \pi^0 \mu^+ \mu^-)/\Gamma_{\text{total}} \quad < 9.2 \times 10^{-11}, \text{ CL} = 90\%$$

$$\Gamma(K_L^0 \rightarrow \mu^+ \mu^- e^+ e^-)/\Gamma_{\text{total}} \quad (2.69 \pm 0.27) \times 10^{-9}$$

$$\Gamma(K_L^0 \rightarrow e^+ e^- e^+ e^-)/\Gamma_{\text{total}} \quad (3.56 \pm 0.21) \times 10^{-8}$$

$$\Gamma(K_L^0 \rightarrow \pi^0 \mu^+ \mu^-)/\Gamma_{\text{total}} \quad < 3.8 \times 10^{-10}, \text{ CL} = 90\%$$

$$\Gamma(K_L^0 \rightarrow \pi^0 e^+ e^-)/\Gamma_{\text{total}} \quad < 2.8 \times 10^{-10}, \text{ CL} = 90\%$$

$$\Gamma(K_L^0 \rightarrow \pi^0 \nu \bar{\nu})/\Gamma_{\text{total}} \quad < 3.0 \times 10^{-9}, \text{ CL} = 90\%$$

$$\Gamma(K_L^0 \rightarrow \pi^0 \pi^0 \nu \bar{\nu})/\Gamma_{\text{total}} \quad < 8.1 \times 10^{-7}, \text{ CL} = 90\%$$

$$\Gamma(\Sigma^+ \rightarrow p e^+ e^-)/\Gamma_{\text{total}} \quad < 7 \times 10^{-6}$$

$$\Gamma(\Sigma^+ \rightarrow p \mu^+ \mu^-)/\Gamma_{\text{total}} \quad (2.4 \pm 1.7) \times 10^{-8}$$

 $\Delta C = 1$ WEAK NEUTRAL CURRENT FORBIDDEN

Allowed by higher-order electroweak interactions.

$$\Gamma(D^+ \rightarrow \pi^+ e^+ e^-)/\Gamma_{\text{total}} \quad < 1.1 \times 10^{-6}, \text{ CL} = 90\%$$

$$\Gamma(D^+ \rightarrow \pi^+ \mu^+ \mu^-)/\Gamma_{\text{total}} \quad < 6.7 \times 10^{-8}, \text{ CL} = 90\%$$

$$\Gamma(D^+ \rightarrow \rho^+ \mu^+ \mu^-)/\Gamma_{\text{total}} \quad < 5.6 \times 10^{-4}, \text{ CL} = 90\%$$

$$\Gamma(D^0 \rightarrow \gamma \gamma)/\Gamma_{\text{total}} \quad < 8.5 \times 10^{-7}, \text{ CL} = 90\%$$

$$\Gamma(D^0 \rightarrow e^+ e^-)/\Gamma_{\text{total}} \quad < 7.9 \times 10^{-8}, \text{ CL} = 90\%$$

$$\Gamma(D^0 \rightarrow \mu^+ \mu^-)/\Gamma_{\text{total}} \quad < 3.1 \times 10^{-9}, \text{ CL} = 90\%$$

$$\Gamma(D^0 \rightarrow \pi^0 e^+ e^-)/\Gamma_{\text{total}} \quad < 4 \times 10^{-6}, \text{ CL} = 90\%$$

$$\Gamma(D^0 \rightarrow \pi^0 \mu^+ \mu^-)/\Gamma_{\text{total}} \quad < 1.8 \times 10^{-4}, \text{ CL} = 90\%$$

$$\Gamma(D^0 \rightarrow \eta e^+ e^-)/\Gamma_{\text{total}} \quad < 3 \times 10^{-6}, \text{ CL} = 90\%$$

$$\Gamma(D^0 \rightarrow \eta \mu^+ \mu^-)/\Gamma_{\text{total}} \quad < 5.3 \times 10^{-4}, \text{ CL} = 90\%$$

$$\Gamma(D^0 \rightarrow \pi^+ \pi^- e^+ e^-)/\Gamma_{\text{total}} \quad < 7 \times 10^{-6}, \text{ CL} = 90\%$$

$$\Gamma(D^0 \rightarrow \rho^0 e^+ e^-)/\Gamma_{\text{total}} \quad < 1.0 \times 10^{-4}, \text{ CL} = 90\%$$

$$\Gamma(D^0 \rightarrow \pi^+ \pi^- \mu^+ \mu^-)/\Gamma_{\text{total}} \quad (9.6 \pm 1.2) \times 10^{-7}$$

$$\Gamma(D^0 \rightarrow \rho^0 \mu^+ \mu^-)/\Gamma_{\text{total}} \quad < 2.2 \times 10^{-5}, \text{ CL} = 90\%$$

$$\Gamma(D^0 \rightarrow \omega e^+ e^-)/\Gamma_{\text{total}} \quad < 6 \times 10^{-6}, \text{ CL} = 90\%$$

$$\Gamma(D^0 \rightarrow \omega \mu^+ \mu^-)/\Gamma_{\text{total}} \quad < 8.3 \times 10^{-4}, \text{ CL} = 90\%$$

$$\Gamma(D^0 \rightarrow K^- K^+ e^+ e^-)/\Gamma_{\text{total}} \quad < 1.1 \times 10^{-5}, \text{ CL} = 90\%$$

$$\Gamma(D^0 \rightarrow \phi e^+ e^-)/\Gamma_{\text{total}} \quad < 5.2 \times 10^{-5}, \text{ CL} = 90\%$$

$$\Gamma(D^0 \rightarrow K^- K^+ \mu^+ \mu^-)/\Gamma_{\text{total}} \quad (1.54 \pm 0.32) \times 10^{-7}$$

$$\Gamma(D^0 \rightarrow \phi \mu^+ \mu^-)/\Gamma_{\text{total}} \quad < 3.1 \times 10^{-5}, \text{ CL} = 90\%$$

$$\Gamma(D^0 \rightarrow K^- \pi^+ \mu^+ \mu^-)/\Gamma_{\text{total}} \quad < 3.59 \times 10^{-4}, \text{ CL} = 90\%$$

$$\Gamma(D^0 \rightarrow \pi^+ \pi^- \pi^0 \mu^+ \mu^-)/\Gamma_{\text{total}} \quad < 8.1 \times 10^{-4}, \text{ CL} = 90\%$$

$$\Gamma(D_s^+ \rightarrow K^+ e^+ e^-)/\Gamma_{\text{total}} \quad < 3.7 \times 10^{-6}, \text{ CL} = 90\%$$

$$\Gamma(D_s^+ \rightarrow K^+ \mu^+ \mu^-)/\Gamma_{\text{total}} \quad < 1.4 \times 10^{-7}, \text{ CL} = 90\%$$

$$\Gamma(D_s^+ \rightarrow K^*(892)^+ \mu^+ \mu^-)/\Gamma_{\text{total}} \quad < 1.4 \times 10^{-3}, \text{ CL} = 90\%$$

$$\Gamma(\Lambda_C^+ \rightarrow p e^+ e^-)/\Gamma_{\text{total}} \quad < 5.5 \times 10^{-6}, \text{ CL} = 90\%$$

$$\Gamma(\Lambda_C^+ \rightarrow p \mu^+ \mu^- \text{ non-resonant})/\Gamma_{\text{total}} \quad < 7.7 \times 10^{-8}, \text{ CL} = 90\%$$

 $\Delta B = 1$ WEAK NEUTRAL CURRENT FORBIDDEN

Allowed by higher-order electroweak interactions.

$$\Gamma(B^+ \rightarrow \pi^+ \ell^+ \ell^-)/\Gamma_{\text{total}} \quad [x] \quad < 4.9 \times 10^{-8}, \text{ CL} = 90\%$$

$$\Gamma(B^+ \rightarrow \pi^+ e^+ e^-)/\Gamma_{\text{total}} \quad < 8.0 \times 10^{-8}, \text{ CL} = 90\%$$

$$\Gamma(B^+ \rightarrow \pi^+ \mu^+ \mu^-)/\Gamma_{\text{total}} \quad (1.78 \pm 0.23) \times 10^{-8}$$

$$\Gamma(B^+ \rightarrow \pi^+ \nu \bar{\nu})/\Gamma_{\text{total}} \quad < 1.4 \times 10^{-5}, \text{ CL} = 90\%$$

$$\Gamma(B^+ \rightarrow K^+ \ell^+ \ell^-)/\Gamma_{\text{total}} \quad [x] \quad (4.7 \pm 0.5) \times 10^{-7} \quad (S = 2.3)$$

$$\Gamma(B^+ \rightarrow K^+ e^+ e^-)/\Gamma_{\text{total}} \quad (5.6 \pm 0.6) \times 10^{-7}$$

$$\Gamma(B^+ \rightarrow K^+ \mu^+ \mu^-)/\Gamma_{\text{total}} \quad (4.53 \pm 0.35) \times 10^{-7} \quad (S = 1.8)$$

$$\Gamma(B^+ \rightarrow K^+ \mu^+ \mu^- \text{ non-resonant})/\Gamma_{\text{total}} \quad (4.37 \pm 0.27) \times 10^{-7}$$

$$\Gamma(B^+ \rightarrow K^+ \tau^+ \tau^-)/\Gamma_{\text{total}} \quad < 2.25 \times 10^{-3}, \text{ CL} = 90\%$$

$$\Gamma(B^+ \rightarrow K^+ \nu \bar{\nu})/\Gamma_{\text{total}} \quad < 1.6 \times 10^{-5}, \text{ CL} = 90\%$$

$$\Gamma(B^+ \rightarrow \rho^+ \nu \bar{\nu})/\Gamma_{\text{total}} \quad < 3.0 \times 10^{-5}, \text{ CL} = 90\%$$

$$\Gamma(B^+ \rightarrow K^*(892)^+ \ell^+ \ell^-)/\Gamma_{\text{total}} \quad [x] \quad (1.01 \pm 0.11) \times 10^{-6} \quad (S = 1.1)$$

$$\Gamma(B^+ \rightarrow K^*(892)^+ e^+ e^-)/\Gamma_{\text{total}} \quad (1.55 \pm 0.40) \times 10^{-6}$$

$$\Gamma(B^+ \rightarrow K^*(892)^+ \mu^+ \mu^-)/\Gamma_{\text{total}} \quad (9.6 \pm 1.0) \times 10^{-7}$$

$$\Gamma(B^+ \rightarrow K^*(892)^+ \nu \bar{\nu})/\Gamma_{\text{total}} \quad < 4.0 \times 10^{-5}, \text{ CL} = 90\%$$

$$\Gamma(B^+ \rightarrow K^+ \pi^+ \pi^- \mu^+ \mu^-)/\Gamma_{\text{total}} \quad (4.3 \pm 0.4) \times 10^{-7}$$

$$\Gamma(B^+ \rightarrow \phi K^+ \mu^+ \mu^-)/\Gamma_{\text{total}} \quad (7.9 \pm 2.1) \times 10^{-8}$$

$$\Gamma(B^+ \rightarrow \bar{\Lambda} p \nu \bar{\nu})/\Gamma_{\text{total}} \quad < 3.0 \times 10^{-5}, \text{ CL} = 90\%$$

$$\Gamma(B^0 \rightarrow \gamma \gamma)/\Gamma_{\text{total}} \quad < 3.2 \times 10^{-7}, \text{ CL} = 90\%$$

$$\Gamma(B^0 \rightarrow e^+ e^-)/\Gamma_{\text{total}} \quad < 2.5 \times 10^{-9}, \text{ CL} = 90\%$$

$$\Gamma(B^0 \rightarrow e^+ e^- \gamma)/\Gamma_{\text{total}} \quad < 1.2 \times 10^{-7}, \text{ CL} = 90\%$$

$$\Gamma(B^0 \rightarrow \mu^+ \mu^-)/\Gamma_{\text{total}} \quad < 1.5 \times 10^{-10}, \text{ CL} = 90\%$$

$$\Gamma(B^0 \rightarrow \mu^+ \mu^- \gamma)/\Gamma_{\text{total}} \quad \text{—}$$

$$\Gamma(B^0 \rightarrow \mu^+ \mu^- \mu^+ \mu^-)/\Gamma_{\text{total}} \quad < 1.8 \times 10^{-10}, \text{ CL} = 95\%$$

$$\Gamma(B^0 \rightarrow S P, S \rightarrow \mu^+ \mu^-, P \rightarrow \mu^+ \mu^-)/\Gamma_{\text{total}} \quad [y] \quad < 6.0 \times 10^{-10}, \text{ CL} = 95\%$$

$$\Gamma(B^0 \rightarrow a a, a \rightarrow \mu^+ \mu^-)/\Gamma_{\text{total}} \quad < 2.3 \times 10^{-10}, \text{ CL} = 95\%$$

$$\Gamma(B^0 \rightarrow \tau^+ \tau^-)/\Gamma_{\text{total}} \quad < 2.1 \times 10^{-3}, \text{ CL} = 95\%$$

$$\Gamma(B^0 \rightarrow \pi^0 \ell^+ \ell^-)/\Gamma_{\text{total}} \quad [x] \quad < 5.3 \times 10^{-8}, \text{ CL} = 90\%$$

$$\Gamma(B^0 \rightarrow \pi^0 e^+ e^-)/\Gamma_{\text{total}} \quad < 8.4 \times 10^{-8}, \text{ CL} = 90\%$$

$$\Gamma(B^0 \rightarrow \pi^0 \mu^+ \mu^-)/\Gamma_{\text{total}} \quad < 6.9 \times 10^{-8}, \text{ CL} = 90\%$$

$$\Gamma(B^0 \rightarrow \eta \ell^+ \ell^-)/\Gamma_{\text{total}} \quad [x] \quad < 6.4 \times 10^{-8}, \text{ CL} = 90\%$$

$$\Gamma(B^0 \rightarrow \eta e^+ e^-)/\Gamma_{\text{total}} \quad < 1.08 \times 10^{-7}, \text{ CL} = 90\%$$

$$\Gamma(B^0 \rightarrow \eta \mu^+ \mu^-)/\Gamma_{\text{total}} \quad < 1.12 \times 10^{-7}, \text{ CL} = 90\%$$

$$\Gamma(B^0 \rightarrow \pi^0 \nu \bar{\nu})/\Gamma_{\text{total}} \quad < 9 \times 10^{-6}, \text{ CL} = 90\%$$

$$\Gamma(B^0 \rightarrow K^0 \ell^+ \ell^-)/\Gamma_{\text{total}} \quad [x] \quad (3.3 \pm 0.6) \times 10^{-7}$$

$$\Gamma(B^0 \rightarrow K^0 e^+ e^-)/\Gamma_{\text{total}} \quad (2.5 \pm 1.1) \times 10^{-7} \quad (S = 1.3)$$

$$\Gamma(B^0 \rightarrow K^0 \mu^+ \mu^-)/\Gamma_{\text{total}} \quad (3.39 \pm 0.35) \times 10^{-7} \quad (S = 1.1)$$

$$\Gamma(B^0 \rightarrow K^0 \nu \bar{\nu})/\Gamma_{\text{total}} \quad < 2.6 \times 10^{-5}, \text{ CL} = 90\%$$

$$\Gamma(B^0 \rightarrow \rho^0 \nu \bar{\nu})/\Gamma_{\text{total}} \quad < 4.0 \times 10^{-5}, \text{ CL} = 90\%$$

$$\Gamma(B^0 \rightarrow K^*(892)^0 \ell^+ \ell^-)/\Gamma_{\text{total}} \quad [x] \quad (9.9 \pm 1.2) \times 10^{-7}$$

$$\Gamma(B^0 \rightarrow K^*(892)^0 e^+ e^-)/\Gamma_{\text{total}} \quad (1.03 \pm 0.19) \times 10^{-6}$$

$$\Gamma(B^0 \rightarrow K^*(892)^0 \mu^+ \mu^-)/\Gamma_{\text{total}} \quad (9.4 \pm 0.5) \times 10^{-7}$$

$$\Gamma(B^0 \rightarrow K^*(892)^0 \chi, \chi \rightarrow \mu^+ \mu^-)/\Gamma_{\text{total}} \quad \text{—}$$

Tests of Conservation Laws

NOTES

$\Gamma(B^0 \rightarrow K^*(892)^0 \tau^+ \tau^-) / \Gamma_{\text{total}}$	$< 3.1 \times 10^{-3}$, CL = 90%
$\Gamma(B^0 \rightarrow \pi^+ \pi^- \mu^+ \mu^-) / \Gamma_{\text{total}}$	$(2.1 \pm 0.5) \times 10^{-8}$
$\Gamma(B^0 \rightarrow K^*(892)^0 \nu \bar{\nu}) / \Gamma_{\text{total}}$	$< 1.8 \times 10^{-5}$, CL = 90%
$\Gamma(B^0 \rightarrow \text{invisible}) / \Gamma_{\text{total}}$	$< 2.4 \times 10^{-5}$, CL = 90%
$\Gamma(B^0 \rightarrow \nu \bar{\nu} \gamma) / \Gamma_{\text{total}}$	$< 1.6 \times 10^{-5}$, CL = 90%
$\Gamma(B^0 \rightarrow \phi \mu^+ \mu^-) / \Gamma_{\text{total}}$	$< 3.2 \times 10^{-9}$, CL = 90%
$\Gamma(B^0 \rightarrow \phi \nu \bar{\nu}) / \Gamma_{\text{total}}$	$< 1.27 \times 10^{-4}$, CL = 90%
$\Gamma(B \rightarrow s e^+ e^-) / \Gamma_{\text{total}}$	$(6.7 \pm 1.7) \times 10^{-6}$ (S = 2.0)
$\Gamma(B \rightarrow s \mu^+ \mu^-) / \Gamma_{\text{total}}$	$(4.3 \pm 1.0) \times 10^{-6}$
$\Gamma(B \rightarrow s \ell^+ \ell^-) / \Gamma_{\text{total}}$	[x] $(5.8 \pm 1.3) \times 10^{-6}$ (S = 1.8)
$\Gamma(B \rightarrow \pi \ell^+ \ell^-) / \Gamma_{\text{total}}$	$< 5.9 \times 10^{-8}$, CL = 90%
$\Gamma(B \rightarrow \pi e^+ e^-) / \Gamma_{\text{total}}$	$< 1.10 \times 10^{-7}$, CL = 90%
$\Gamma(B \rightarrow \pi \mu^+ \mu^-) / \Gamma_{\text{total}}$	$< 5.0 \times 10^{-8}$, CL = 90%
$\Gamma(B \rightarrow K e^+ e^-) / \Gamma_{\text{total}}$	$(4.4 \pm 0.6) \times 10^{-7}$
$\Gamma(B \rightarrow K^*(892) e^+ e^-) / \Gamma_{\text{total}}$	$(1.19 \pm 0.20) \times 10^{-6}$ (S = 1.2)
$\Gamma(B \rightarrow K \mu^+ \mu^-) / \Gamma_{\text{total}}$	$(4.4 \pm 0.4) \times 10^{-7}$
$\Gamma(B \rightarrow K^*(892) \mu^+ \mu^-) / \Gamma_{\text{total}}$	$(1.06 \pm 0.09) \times 10^{-6}$
$\Gamma(B \rightarrow K \ell^+ \ell^-) / \Gamma_{\text{total}}$	$(4.8 \pm 0.4) \times 10^{-7}$
$\Gamma(B \rightarrow K^*(892) \ell^+ \ell^-) / \Gamma_{\text{total}}$	$(1.05 \pm 0.10) \times 10^{-6}$
$\Gamma(B \rightarrow K \nu \bar{\nu}) / \Gamma_{\text{total}}$	$< 1.6 \times 10^{-5}$, CL = 90%
$\Gamma(B \rightarrow K^* \nu \bar{\nu}) / \Gamma_{\text{total}}$	$< 2.7 \times 10^{-5}$, CL = 90%
$\Gamma(B \rightarrow \pi \nu \bar{\nu}) / \Gamma_{\text{total}}$	$< 8 \times 10^{-6}$, CL = 90%
$\Gamma(B \rightarrow \rho \nu \bar{\nu}) / \Gamma_{\text{total}}$	$< 2.8 \times 10^{-5}$, CL = 90%
$\Gamma(\bar{B} \rightarrow \bar{s} \nu \nu) / \Gamma_{\text{total}}$	$< 6.4 \times 10^{-4}$, CL = 90%
$\Gamma(\bar{B} \rightarrow \mu^+ \mu^- \text{anything}) / \Gamma_{\text{total}}$	$< 3.2 \times 10^{-4}$, CL = 90%
$\Gamma(B_S^0 \rightarrow \gamma \gamma) / \Gamma_{\text{total}}$	$< 3.1 \times 10^{-6}$, CL = 90%
$\Gamma(B_S^0 \rightarrow \phi \gamma) / \Gamma_{\text{total}}$	$(3.4 \pm 0.4) \times 10^{-5}$
$\Gamma(B_S^0 \rightarrow \mu^+ \mu^-) / \Gamma_{\text{total}}$	$(3.34 \pm 0.27) \times 10^{-9}$
$\Gamma(B_S^0 \rightarrow e^+ e^-) / \Gamma_{\text{total}}$	$< 9.4 \times 10^{-9}$, CL = 90%
$\Gamma(B_S^0 \rightarrow \tau^+ \tau^-) / \Gamma_{\text{total}}$	$< 6.8 \times 10^{-3}$, CL = 95%
$\Gamma(B_S^0 \rightarrow \mu^+ \mu^- \gamma) / \Gamma_{\text{total}}$	$< 2.0 \times 10^{-9}$
$\Gamma(B_S^0 \rightarrow \mu^+ \mu^- \mu^+ \mu^-) / \Gamma_{\text{total}}$	$< 8.6 \times 10^{-10}$, CL = 95%
$\Gamma(B_S^0 \rightarrow SP, S \rightarrow \mu^+ \mu^-, P \rightarrow \mu^+ \mu^-) / \Gamma_{\text{total}}$	[y] $< 2.2 \times 10^{-9}$, CL = 95%
$\Gamma(B_S^0 \rightarrow a a, a \rightarrow \mu^+ \mu^-) / \Gamma_{\text{total}}$	$< 5.8 \times 10^{-10}$, CL = 95%
$\Gamma(B_S^0 \rightarrow \phi(1020) \mu^+ \mu^-) / \Gamma_{\text{total}}$	$(8.4 \pm 0.4) \times 10^{-7}$
$\Gamma(B_S^0 \rightarrow f_2'(1525) \mu^+ \mu^-) / \Gamma_{\text{total}}$	$(1.62 \pm 0.22) \times 10^{-7}$
$\Gamma(B_S^0 \rightarrow \bar{K}^*(892)^0 \mu^+ \mu^-) / \Gamma_{\text{total}}$	$(2.9 \pm 1.1) \times 10^{-8}$
$\Gamma(B_S^0 \rightarrow \pi^+ \pi^- \mu^+ \mu^-) / \Gamma_{\text{total}}$	$(8.4 \pm 1.7) \times 10^{-8}$
$\Gamma(B_S^0 \rightarrow \phi \nu \bar{\nu}) / \Gamma_{\text{total}}$	$< 5.4 \times 10^{-3}$, CL = 90%

$\Delta T = 1$ WEAK NEUTRAL CURRENT FORBIDDEN

Allowed by higher-order electroweak interactions.

$\Gamma(t \rightarrow Z q (q=u,c)) / \Gamma_{\text{total}}$	[z] $< 1.2 \times 10^{-4}$, CL = 95%
$\Gamma(t \rightarrow H u) / \Gamma_{\text{total}}$	$< 1.9 \times 10^{-4}$, CL = 95%
$\Gamma(t \rightarrow H c) / \Gamma_{\text{total}}$	$< 4.3 \times 10^{-4}$, CL = 95%
$\Gamma(t \rightarrow \ell^+ \bar{q} q' (q=d,s,b; q'=u,c)) / \Gamma_{\text{total}}$	$< 1.6 \times 10^{-3}$, CL = 95%

In this Summary Table:

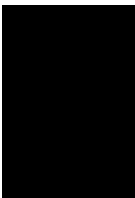
When a quantity has “(S = ...)” to its right, the error on the quantity has been enlarged by the “scale factor” S, defined as $S = \sqrt{\chi^2 / (N - 1)}$, where N is the number of measurements used in calculating the quantity. We do this when $S > 1$, which often indicates that the measurements are inconsistent. When $S > 1.25$, we also show in the Particle Listings an ideogram of the measurements. For more about S, see the Introduction.

- [a] Forbidden by angular momentum conservation.
- [b] C parity forbids this to occur as a single-photon process.
- [c] See the Particle Listings for the (complicated) definition of this quantity.
- [d] Time-reversal invariance requires this to be 0° or 180° .
- [e] This coefficient is zero if time invariance is not violated.
- [f] Allowed by higher-order electroweak interactions.
- [g] Violates CP in leading order. Test of direct CP violation since the indirect CP-violating and CP-conserving contributions are expected to be suppressed.
- [h] In the 2010 Review, the values for these quantities were given using a measure of the asymmetry that was inconsistent with the usual definition.
- [i] $\text{Re}(\epsilon'/\epsilon) = \epsilon'/\epsilon$ to a very good approximation provided the phases satisfy CPT invariance.
- [j] This mode includes gammas from inner bremsstrahlung but not the direct emission mode $K_L^0 \rightarrow \pi^+ \pi^- \gamma$ (DE).
- [k] Neglecting photon channels. See, e.g., A. Pais and S.B. Treiman, Phys. Rev. **D12**, 2744 (1975).
- [l] Derived from measured values of $\phi_{+-}, \phi_{00}, |\eta|, |m_{K_L^0} - m_{K_S^0}|$, and $\tau_{K_S^0}$, as described in the introduction to “Tests of Conservation Laws.”
- [n] The $|m_p - m_{\bar{p}}|/m_p$ and $|q_p + q_{\bar{p}}|/e$ are not independent, and both use the more precise measurement of $|q_{\bar{p}}/m_{\bar{p}}|/(q_p/m_p)$.
- [o] The value is for the sum of the charge states or particle/antiparticle states indicated.
- [p] A test of additive vs. multiplicative lepton family number conservation.
- [q] Derived from an analysis of neutrino-oscillation experiments.
- [r] There is some controversy about whether nuclear physics and model dependence complicate the analysis for bound neutrons (from which the best limit comes). The first limit here is from reactor experiments with free neutrons.
- [s] This is the best limit for the mode $e^- \rightarrow \nu \gamma$.
- [t] The limit is from neutrality-of-matter experiments; it assumes $q_n = q_p + q_e$. See also the charge of the neutron.
- [u] See the K_S^0 Particle Listings for the energy limits used in this measurement.
- [v] See the K_L^0 Particle Listings for the energy limits used in this measurement.
- [x] An ℓ indicates an e or a μ mode, not a sum over these modes.
- [y] Here S and P are the hypothetical scalar and pseudoscalar particles with masses of 2.5 GeV/c² and 214.3 MeV/c², respectively.
- [z] This limit is for $\Gamma(t \rightarrow Z q) / \Gamma(t \rightarrow W b)$.

REVIEWS, TABLES, AND PLOTS

Constants, Units, Atomic and Nuclear Properties

1. Physical constants (rev.)	137
2. Astrophysical constants and parameters (rev.)	138
3. International system of units (SI)	140
4. Periodic table of the elements (rev.)	141
5. Electronic structure of the elements (rev.)	142
6. Atomic and nuclear properties of materials (rev.)	144
7. Electromagnetic relations	146
8. Naming scheme for hadrons (rev.)	148





1. Physical Constants

Table 1.1: Revised 2024 by D. Robinson (LBNL) and P.A. Zyla (LBNL). Mainly from “CODATA Recommended Values of the Fundamental Physical Constants: 2018,” E. Tiesinga, D.B. Newell, P.J. Mohr, and B.N. Taylor, NIST SP961 (May 2019) [1].^a The electron charge magnitude e , and the Planck, Boltzmann, and Avogadro constants h , k , and N_A , now join c as having defined values; the free-space permittivity and permeability constants ϵ_0 and μ_0 are no longer exact. These changes affect practically everything else in the Table. Figures in parentheses after the values are the 1-standard-deviation uncertainties in the last digits; the fractional uncertainties in parts per 10^9 (ppb) are in the last column. The full 2018 CODATA Committee on Data for Science and Technology set of constants are found at <https://physics.nist.gov/cuu/Constants/archive2018.html>. The last set of constants (beginning with the Fermi coupling constant) comes from the Particle Data Group. See also “The International System of Units (SI),” 9th ed. (2019) of the International Bureau of Weights and Measures (BIPM), <https://www.bipm.org/utis/common/pdf/si-brochure/SI-Brochure-9-EN.pdf>.

Quantity	Symbol, equation	Value	Uncertainty (ppb)
speed of light in vacuum	c	299 792 458 m s ⁻¹	exact
Planck constant	h	6.626 070 15×10 ⁻³⁴ J s (or J/Hz) §	exact
Planck constant, reduced	$\hbar \equiv h/2\pi$	1.054 571 817... × 10 ⁻³⁴ J s = 6.582 119 569... × 10 ⁻²² MeV s	exact*
electron charge magnitude	e	1.602 176 634×10 ⁻¹⁹ C	exact
conversion constant	$\hbar c$	197.326 980 4... MeV fm	exact*
conversion constant	$(\hbar c)^2$	0.389 379 372 1... GeV ² mbarn	exact*
electron mass	m_e	0.510 998 950 00(15) MeV/c ² = 9.109 383 7015(28)×10 ⁻³¹ kg	0.30
proton mass	m_p	938.272 088 16(29) MeV/c ² = 1.672 621 923 69(51)×10 ⁻²⁷ kg = 1.007 276 466 621(53) u = 1836.152 673 43(11) m_e	0.31 0.053, 0.060
neutron mass	m_n	939.565 420 52(54) MeV/c ² = 1.008 664 915 95(49) u	0.57, 0.48
deuteron mass	m_d	1875.612 942 57(57) MeV/c ²	0.30
unified atomic mass unit**	$u = (\text{mass } ^{12}\text{C atom})/12$	931.494 102 42(28) MeV/c ² = 1.660 539 066 60(50)×10 ⁻²⁷ kg	0.30
permittivity of free space	$\epsilon_0 = 1/\mu_0 c^2$	8.854 187 8128(13) × 10 ⁻¹² F m ⁻¹	0.15
permeability of free space	$\mu_0/(4\pi \times 10^{-7})$	1.000 000 000 55(15) N A ⁻²	0.15
fine-structure constant	$\alpha = e^2/4\pi\epsilon_0\hbar c$	7.297 352 5693(11)×10 ⁻³ = 1/137.035 999 084(21) †	0.15
classical electron radius	$r_e = e^2/4\pi\epsilon_0 m_e c^2$	2.817 940 3262(13)×10 ⁻¹⁵ m	0.45
(e^- Compton wavelength)/2π	$\lambda_e = \hbar/m_e c = r_e \alpha^{-1}$	3.861 592 6796(12)×10 ⁻¹³ m	0.30
Bohr radius ($m_{\text{nucleus}} = \infty$)	$a_\infty = 4\pi\epsilon_0\hbar^2/m_e e^2 = r_e \alpha^{-2}$	0.529 177 210 903(80)×10 ⁻¹⁰ m	0.15
wavelength of 1 eV/c particle	$hc/(1 \text{ eV})$	1.239 841 984... × 10 ⁻⁶ m	exact*
Rydberg energy	$hcR_\infty = m_e e^4/2(4\pi\epsilon_0)^2 \hbar^2 = m_e c^2 \alpha^2/2$	13.605 693 122 994(26) eV	1.9×10 ⁻³
Thomson cross section	$\sigma_T = 8\pi r_e^2/3$	0.665 245 873 21(60) barn	0.91
Bohr magneton	$\mu_B = e\hbar/2m_e$	5.788 381 8060(17)×10 ⁻¹¹ MeV T ⁻¹	0.30
nuclear magneton	$\mu_N = e\hbar/2m_p$	3.152 451 258 44(96)×10 ⁻¹⁴ MeV T ⁻¹	0.31
electron cyclotron freq./field	$\omega_{\text{cycl}}^e/B = e/m_e$	1.758 820 010 76(53)×10 ¹¹ rad s ⁻¹ T ⁻¹	0.30
proton cyclotron freq./field	$\omega_{\text{cycl}}^p/B = e/m_p$	9.578 833 1560(29)×10 ⁷ rad s ⁻¹ T ⁻¹	0.31
gravitational constant‡	G_N	6.674 30(15)×10 ⁻¹¹ m ³ kg ⁻¹ s ⁻² = 6.708 83(15)×10 ⁻³⁹ $\hbar c$ (GeV/c ²) ⁻²	2.2 × 10 ⁴ 2.2 × 10 ⁴
standard gravitational accel.	g_N	9.806 65 m s ⁻²	exact
Avogadro constant	N_A	6.022 140 76×10 ²³ mol ⁻¹	exact
Boltzmann constant	k	1.380 649×10 ⁻²³ J K ⁻¹ = 8.617 333 262... × 10 ⁻⁵ eV K ⁻¹	exact*
molar volume, ideal gas at STP	$N_A k$ (273.15 K)/(101 325 Pa)	22.413 969 54... × 10 ⁻³ m ³ mol ⁻¹	exact*
Wien displacement law constant	$b = \lambda_{\text{max}} T$	2.897 771 955... × 10 ⁻³ m K	exact*
Stefan-Boltzmann constant	$\sigma = \pi^2 k^4/60\hbar^3 c^2$	5.670 374 419... × 10 ⁻⁸ W m ⁻² K ⁻⁴	exact*
Fermi coupling constant‡‡	$G_F/(\hbar c)^3$	1.166 378 8(6)×10 ⁻⁵ GeV ⁻²	510
weak-mixing angle‡‡	$\sin^2 \theta(M_Z)$ ($\overline{\text{MS}}$)	0.231 29(4)††	1.7 × 10 ⁵
W^\pm boson mass	m_W	80.3692(133) GeV/c ² ¶	1.7 × 10 ⁵
Z^0 boson mass	m_Z	91.1880(20) GeV/c ²	2.2 × 10 ⁴
strong coupling constant	$\alpha_s(m_Z)$	0.1180(9)	7.6 × 10 ⁶
$\pi = 3.141 592 653 589 793 238 \dots$ $e = 2.718 281 828 459 045 235 \dots$ $\gamma = 0.577 215 664 901 532 860 \dots$			
1 in ≡ 0.0254 m	1 G ≡ 10 ⁻⁴ T	1 eV = 1.602 176 634 × 10 ⁻¹⁹ J (exact)	kT at 300 K = [38.681 727 0718...] ⁻¹ eV (exact*)
1 Å ≡ 0.1 nm	1 dyne ≡ 10 ⁻⁵ N	(1 kg)c ² = 5.609 588 603... × 10 ³⁵ eV(exact*)	0 °C ≡ 273.15K
1 barn ≡ 10 ⁻²⁸ m ²	1 erg ≡ 10 ⁻⁷ J	1 C = 2.997 924 58 × 10 ⁹ esu	1 atmosphere ≡ 760 Torr ≡ 101 325Pa

^aUpdated values reflecting the “2022 CODATA recommended values”, released online in May 2024, will be incorporated in future editions of the *Review*.

§CODATA recommends that the unit be J/Hz to stress that in $h = E/\nu$ the frequency ν is in cycles/sec (Hz), not radians/sec.

*These are calculated from exact values and are exact to the number of places given (*i.e.* no rounding).

**The molar mass of ¹²C is 11.999 999 9958(36) g.

†CODATA recommended value at $Q^2 = 0$. At $Q^2 \approx m_W^2$, the value is $\sim 1/128$. A world average of the latest data yields $\alpha^{-1} = 137.035999178(8)$. ‡‡

‡Absolute laboratory measurements of G_N have been made only on scales of about 1 cm to 1 m.

††See the discussion in “Electroweak model and constraints on new physics” review.

‡‡The corresponding $\sin^2 \theta$ for the effective angle is $\bar{s}_\ell^2 = 0.23161(4)$. The value for the collider average is $\bar{s}_\ell^2 = 0.23149(13)$.

¶See the “Mass and width of the W boson” and “Electroweak model and constraints on new physics” reviews.

||See the “ Z boson” and “Electroweak model and constraints on new physics” reviews.

References

[1] E. Tiesinga *et al.*, Rev. Mod. Phys. **93**, 025010 (2021).

2. Astrophysical Constants and Parameters

Table 2.1: Revised August 2023 by D.E. Groom (LBNL) and D. Scott (U. of British Columbia). The figures in parentheses after some values give the $1\text{-}\sigma$ uncertainties in the last digit(s). Physical constants are from Ref. [1]. While every effort has been made to obtain the most accurate current values of the listed quantities, this table does not represent a critical review or adjustment of the constants, and is not intended as a primary reference. The values and uncertainties for the cosmological parameters depend on the exact data sets, priors, and basis parameters used in the fit. Many of the derived parameters reported in this table have non-Gaussian likelihoods and parameters may be highly correlated, so care must be taken in propagating errors. Unless otherwise specified, cosmological parameters are derived from a 6-parameter Λ CDM cosmology fit to *Planck* cosmic microwave background 2018 temperature (TT) + polarization (TE,EE+lowE) + lensing data [2]. For more information see [3] and the original papers.

Quantity	Symbol, equation	Value	Reference, footnote
Newtonian constant of gravitation	G_N	$6.674\,30(15) \times 10^{-11} \text{ m}^3 \text{ kg}^{-1} \text{ s}^{-2}$	[1]
Planck mass	$M_P = \sqrt{\hbar c/G_N}$	$1.220\,890(14) \times 10^{19} \text{ GeV}/c^2 = 2.176\,434(24) \times 10^{-8} \text{ kg}$	[1]
Planck length	$l_P = \sqrt{\hbar G_N/c^3}$	$1.616\,255(18) \times 10^{-35} \text{ m}$	[1]
tropical year (equinox to equinox, 2020)	yr	$31\,556\,925.1 \text{ s} = 365.242\,189 \text{ days}$	[4]
sidereal year (period of Earth around Sun relative to stars)		$31\,558\,149.8 \text{ s} \approx \pi \times 10^7 \text{ s}$	[4]
mean sidereal day (Earth rotation period relative to stars)		$23^{\text{h}}\,56^{\text{m}}\,04^{\text{s}}.9090\,53$	[4]
astronomical unit	au	$149\,597\,870\,700 \text{ m}$	exact [5]
parsec (1 au/1 arcsec)	pc	$3.085\,677\,581\,49 \dots \times 10^{16} \text{ m} = 3.261\,56 \dots \text{ ly}$	exact [6]
light year (deprecated unit)	ly	$0.306\,601 \dots \text{ pc} = 0.946\,073 \dots \times 10^{16} \text{ m}$	[7]
solid angle	deg^2	$(\pi/180)^2 \text{ sr} = 3.046\,17 \dots \times 10^{-4} \text{ sr}$	[8]
Schwarzschild radius of the Sun	$2G_N M_\odot/c^2$	$2.953\,250\,1 \text{ km}$	[9]
Solar mass	M_\odot	$1.988\,41(4) \times 10^{30} \text{ kg}$	[10]
nominal Solar equatorial radius	\mathcal{R}_\odot	$6.957 \times 10^8 \text{ m}$	exact [11]
nominal Solar constant	\mathcal{S}_\odot	1361 W m^{-2}	exact [11, 12]
nominal Solar photosphere temperature	T_\odot	5772 K	exact [11]
nominal Solar luminosity	\mathcal{L}_\odot	$3.828 \times 10^{26} \text{ W}$	exact [11, 13]
Schwarzschild radius of the Earth	$2G_N M_\oplus/c^2$	$8.870\,056 \text{ mm}$	[9]
Earth mass	M_\oplus	$5.972\,17(13) \times 10^{24} \text{ kg}$	[10]
nominal Earth equatorial radius	\mathcal{R}_\oplus	$6.3781 \times 10^6 \text{ m}$	exact [11]
Chandrasekhar mass	M_{Ch}	$3.097\,972 \mu^{-2} M_P^3/m_H^2 = 1.433\,77(6) (\mu/2)^{-2} M_\odot$	[14, 15]
Eddington luminosity	L_{Ed}	$1.257\,065\,179\,8(12) \times 10^{31} (M/M_\odot) \text{ W}$ $= 3.283\,869\,330\,8(31) \times 10^4 (M/M_\odot) \mathcal{L}_\odot$	[16, 17]
jansky (flux density)	Jy	$10^{-26} \text{ W m}^{-2} \text{ Hz}^{-1}$	definition
luminosity conversion	f_0	$3.0128 \times 10^{28} \times 10^{-0.4 M_{\text{Bol}}} \text{ W}$	exact [18]
flux conversion	\mathcal{F}	$(M_{\text{Bol}} = \text{absolute bolometric magnitude} = \text{bolometric magnitude at } 10 \text{ pc})$ $2.518\,021\,002 \times 10^{-8} \times 10^{-0.4 m_{\text{Bol}}} \text{ W m}^{-2}$	exact [18]
ABsolute monochromatic magnitude	AB	$(m_{\text{Bol}} = \text{apparent bolometric magnitude})$ $-2.5 \log_{10} f_\nu - 56.10 \text{ (for } f_\nu \text{ in } \text{W m}^{-2} \text{ Hz}^{-1})$ $= -2.5 \log_{10} f_\nu + 8.90 \text{ (for } f_\nu \text{ in Jy)}$	[19]
Solar distance from Galactic center	R_0	$8.275 \pm 0.009(\text{stat.}) \pm 0.033(\text{sys.}) \text{ kpc}$	[20]
local circular angular velocity	Θ_0/R_0	$28.2(10) \text{ km s}^{-1} \text{ kpc}^{-1}$	[21]
circular velocity at R_0	v_0 or Θ_0	$233.4 \pm 0.3(\text{stat.}) \pm 8.0(\text{sys.}) \text{ km s}^{-1}$	[22]
local escape velocity from the Galaxy	v_{esc}	$477 \text{ km s}^{-1} < v_{\text{esc}} < 502 \text{ km s}^{-1}$ (68%)	[23]
local disk density	ρ_{disk}	$6.6(9) \times 10^{-24} \text{ g cm}^{-3} = 3.7(5) \text{ GeV}/c^2 \text{ cm}^{-3}$	[24]
local dark matter density	ρ_χ	canonical value $0.3 \text{ GeV}/c^2 \text{ cm}^{-3}$ within factor 2-3	[25]
present-day CMB temperature	T_0	$2.7255(6) \text{ K}$	[26, 27]
present-day CMB dipole amplitude	d	$3.3621(10) \text{ mK}$	[26, 28]
Solar velocity with respect to CMB	v_\odot	$369.82(11) \text{ km s}^{-1}$ towards $(l, b) = (264.021(11)^\circ, 48.253(5)^\circ)$	[28]
Local Group velocity with respect to CMB	v_{LG}	$620(15) \text{ km s}^{-1}$ towards $(l, b) = (271.9(20)^\circ, 29.6(14)^\circ)$	[28]
number density of CMB photons	n_γ	$410.73(27) (T/2.7255 \text{ K})^3 \text{ cm}^{-3}$	[29]
density of CMB photons	ρ_γ	$4.645(4) (T/2.7255 \text{ K})^4 \times 10^{-34} \text{ g cm}^{-3} \approx 0.260 \text{ eV cm}^{-3}$	[29]
entropy density/Boltzmann constant	s/k	$2891.2 (T/2.7255 \text{ K})^3 \text{ cm}^{-3}$	[29]
present-day Hubble expansion rate	H_0	$100 h \text{ km s}^{-1} \text{ Mpc}^{-1} = h \times (9.777\,752 \text{ Gyr})^{-1}$	[30]
scaling factor for Hubble expansion rate	h	$0.674(5)$ from CMB anisotropies (<i>Planck</i>) or $0.730(10)$ from the distance ladder (SH0ES)	[2] [31, 32]
Hubble length	c/H_0	$0.925\,0629 \times 10^{26} h^{-1} \text{ m} = 1.372(11)$ or $1.267(18) \times 10^{26} \text{ m}$	[2, 31]
scaling for cosmological constant	$c^2/3H_0^2$	$2.85247 \times 10^{51} h^{-2} \text{ m}^2 = 6.29(10)$ or $5.35(15) \times 10^{51} \text{ m}^2$	[2, 31]
critical density of the Universe	$\rho_{\text{crit}} = 3H_0^2/8\pi G_N$	$1.878\,34(4) \times 10^{-29} h^2 \text{ g cm}^{-3}$ $= 1.053\,672(24) \times 10^{-5} h^2 (\text{GeV}/c^2) \text{ cm}^{-3}$ $= 2.77536627 \times 10^{11} h^2 M_\odot \text{ Mpc}^{-3}$	
baryon-to-photon ratio (from BBN)	$\eta = n_b/n_\gamma$	$6.04(12) \times 10^{-10}$	[33, 34]
number density of baryons	n_b	$2.515(17) \times 10^{-7} \text{ cm}^{-3}$ (from CMB) $2.48(5) \times 10^{-7} \text{ cm}^{-3}$ (from BBN, $\eta \times n_\gamma$)	[2, 35] [3, 33]
CMB radiation density of the Universe	$\Omega_\gamma = \rho_\gamma/\rho_{\text{crit}}$	$2.473 \times 10^{-5} (T/2.7255 \text{ K})^4 h^{-2} = 5.38(15) \times 10^{-5}$	[29]
primordial helium fraction	Y_p	$0.2448(33)$	[36]
--- <i>Planck</i> 2018 6-parameter fit to flat Λ CDM cosmology ---			
baryon density of the Universe	$\Omega_b = \rho_b/\rho_{\text{crit}}$	$\ddagger 0.02237(15) h^{-2} = \dagger 0.0493(6)$	[2, 3, 26]
cold dark matter density of the Universe	$\Omega_c = \rho_c/\rho_{\text{crit}}$	$\ddagger 0.1200(12) h^{-2} = \dagger 0.265(7)$	[2, 3, 26]
100 \times approximation to r_*/D_A	$100 \times \theta_{\text{MC}}$	$\ddagger 1.04092(31)$	[2, 3, 26]
reionization optical depth	τ	$\ddagger 0.054(7)$	[2, 3, 26]
ln(power prim. curv. pert.) ($k_0 = 0.05 \text{ Mpc}^{-1}$)	$\ln(10^{10} \Delta_{\mathcal{R}}^2)$	$\ddagger 3.044(14)$	[2, 3, 26]
scalar spectral index	n_s	$\ddagger 0.965(4)$	[2, 3, 26]
pressureless matter density parameter	$\Omega_m = \Omega_c + \Omega_b$	$\dagger 0.315(7)$	[2, 3]
dark energy density parameter	Ω_Λ	$\dagger 0.685(7)$	[2, 3]
energy density of dark energy	ρ_Λ	$\dagger 5.83(16) \times 10^{-30} \text{ g cm}^{-3}$	[2]
cosmological constant	Λ	$\dagger 1.088(30) \times 10^{-56} \text{ cm}^{-2}$	[2]
fluctuation amplitude at $8 h^{-1} \text{ Mpc}$ scale	σ_8	$\dagger 0.811(6)$	[2, 3]

Quantity	Symbol, equation.	Value	Reference, footnote
amplitude of matter fluctuations	$\sigma_8 (\Omega_m/0.3)^{0.5}$	$\dagger 0.832(13)$	[2, 3]
redshift of matter-radiation equality	z_{eq}	$\dagger 3402(26)$	[2, 37]
age at matter-radiation equality	t_{eq}	$\dagger 51.0(8)$ kyr	[2, 38]
redshift at which optical depth equals unity	z_*	$\dagger 1089.92(25)$	[2]
comoving size of sound horizon at z_*	r_*	$\dagger 144.43(26)$ Mpc	[2, 39]
age when optical depth equals unity	t_*	$\dagger 371.8(10)$ kyr	[2, 38]
redshift at half reionization	z_i	$\dagger 7.7(7)$	[2, 40]
age at half reionization	t_i	$\dagger 690(90)$ Myr	[2]
redshift when acceleration was zero	z_q	$\dagger 0.656(18)$	[2, 38]
age when acceleration was zero	t_q	$\dagger 7.70(10)$ Gyr	[2]
age of the Universe today	t_0	$\dagger 13.797(23)$ Gyr	[2]
effective number of neutrinos	N_{eff}	$\# 2.99(17)$ (CMB + BAO)	[2, 41, 42]
sum of neutrino masses	Σm_ν	$\# < 0.12$ eV (95%, CMB + BAO); ≥ 0.06 eV (mixing)	[2, 42–44]
neutrino density of the Universe	$\Omega_\nu = h^{-2} \Sigma m_\nu / 93.14$ eV	$\# < 0.003$ (95%, CMB + BAO); ≥ 0.0012 (mixing)	[2, 43, 44]
curvature	Ω_K	$\# 0.0007(19)$ (CMB + BAO)	[2]
running spectral index, $k_0 = 0.05$ Mpc $^{-1}$	$dn_s/d \ln k$	$\# -0.004(7)$	[2]
tensor-to-scalar perturbation ratio	$r_{0.05} = T/S$	$\# < 0.036$ (95%, $k_0 = 0.05$ Mpc $^{-1}$)	[2, 45–48]
dark energy equation of state parameter	w	$\# -1.028(31)$ (CMB + BAO + SNe)	[2, 49]

\dagger Parameter in 6-parameter Λ CDM fit; \ddagger derived parameter in 6-parameter Λ CDM fit; $\#$ extended model parameter, *Planck* + BAO data [2].

References

- [1] CODATA recommended 2018 values of the fundamental physical constants: physics.nist.gov/cuu/Constants/index.html.
- [2] Planck Collab. 2018 Results VI, *Astron. Astrophys.* **641**, A6 (2020), [arXiv:1807.06209].
- [3] O. Lahav and A. R. Liddle, “The Cosmological Parameters,” Sec. 25 in this *Review*.
- [4] *The Astronomical Almanac for the year 2020*.
- [5] The astronomical unit of length (au) in meters is re-defined (IAU XXVIII General Assembly 2012, Resolution B2) to be a conventional unit of length in agreement with the value adopted in IAU XXVII GA 2009, Resolution B2. It is to be used with all time scales.
- [6] The distance at which 1 au subtends 1 arc sec: 1 au divided by $\pi/648000$.
- [7] From $c \times (\text{tropical year})/\text{pc}$, $c \times (\text{tropical year})$, see IAU XVI GA 1976, Recommendations; T. Lederle, *Astron. Gesellschaft* **48**, 59 (1980).
- [8] The number of square degrees on a sphere is $360^2/\pi = 41259.9\dots$
- [9] Observationally determined mass parameter $G_N M \times 2/c^2$ [1] for either the Sun or the Earth, using the nominal values $\mathcal{G}M_\odot = 1.3271244 \times 10^{20} \text{ m}^3 \text{ s}^{-2}$ and $\mathcal{G}M_\oplus = 3.986004 \times 10^{14} \text{ m}^3 \text{ s}^{-2}$ [11]; the calligraphic symbol indicates the recommended nominal value. The combination $G_N M$ is known much more precisely than either G_N or M individually. The digits are truncated here at the point where one would need to distinguish between Barycentric Coordinate Time (TCB) and Barycentric Dynamical Time (TDB).
- [10] $G_N M \div G_N$ [1].
- [11] IAU XXIX GA 2015 Resolution B3; A. Prša *et al.*, *Astron. J.* **152**, 2, 41 (2016), [arXiv:1605.09788].
- [12] See also G. Kopp and J. L. Lean, *Geophys. Res. Lett.* **38**, L01706 (2011), who give $(1360.8 \pm 0.6) \text{ W m}^{-2}$; see paper for caveats and other measurements.
- [13] $4\pi (1 \text{ au})^2 \times \mathcal{S}_\odot$, assuming isotropic irradiance.
- [14] S. Chandrasekhar, *Astrophys. J.* **74**, 81 (1931).
- [15] This value assumes an ideal Fermi gas, using a numerical constant from the Lane-Emden equation [50], and with μ the average molecular weight per electron, defined relative to the mass of the single-proton hydrogen atom.
- [16] A. S. Eddington, *Mon. Not. Roy. Astron. Soc.* **77**, 16 (1916).
- [17] The maximum luminosity assuming pure electron scattering for the outward force arising from radiation pressure: $4\pi G_N M m_p c / \sigma_T$.
- [18] IAU XXIX GA 2015, Resolution B2; E. E. Mamajek *et al.* arXiv:1510.06262 (2015).
- [19] J. B. Oke and J. E. Gunn, *Astrophys. J.* **266**, 713 (1983).
- [20] GRAVITY Collaboration, *Astron. Astrophys.* **647**, A59 (2021), [arXiv:2101.12098].
- [21] A.-C. Eilers *et al.*, *Astrophys. J.* **871**, 1, 120 (2019), [arXiv:1810.09466]; this is representative of other published values and the systematic uncertainty here is an estimate.
- [22] Product of angular velocity and R_0 , derived from Ref. [21] with an estimate of the systematic uncertainty.
- [23] L. Necib and T. Lin, *Astrophys. J.* **926**, 2, 189 (2022), [arXiv:2102.02211].
- [24] C. F. McKee, A. Parravano and D. J. Hollenbach, *Astrophys. J.* **814**, 1, 13 (2015), [arXiv:1509.05334]; this is representative of other published estimates.
- [25] J. I. Read, *J. Phys.* **G41**, 063101 (2014), [arXiv:1404.1938]; A. M. Green, *J. Phys.* **G44**, 8, 084001 (2017), [arXiv:1703.10102]; the conclusion is $\rho_{\text{DM}}^{\text{local}} = 0.39 \pm 0.03 \text{ GeV cm}^{-3}$.
- [26] D. Scott and G. F. Smoot, “Cosmic Microwave Background,” Sec. 29 in this *Review*.
- [27] D. J. Fixsen, *Astrophys. J.* **707**, 916 (2009), [arXiv:0911.1955].
- [28] Planck Collab. 2018 Results I, *Astron. Astrophys.* **641**, A1 (2020), [arXiv:1807.06205].
- [29] $n_\gamma = \frac{2\zeta(3)}{\pi^2} \left(\frac{kT}{\hbar c}\right)^3$; $\rho_\gamma = \frac{\pi^2 kT}{15 c^2} \left(\frac{kT}{\hbar c}\right)^3$; $s/k = \frac{2.43 \cdot \pi^2}{11.45} \left(\frac{kT}{\hbar c}\right)^3$; $kT/\hbar c = 11.90235(T/2.7255)/\text{cm}$.
- [30] Conversion using length of sidereal year.
- [31] A. G. Riess *et al.*, *Astrophys. J. Lett.* **934**, 1, L7 (2022), [arXiv:2112.04510].
- [32] Distance-ladder estimates of H_0 tend to give higher values than derived from the CMB; Lahav and A. R. Liddle, “The Cosmological Parameters,” Sec. 25 in this *Review*.
- [33] T.-H. Yeh *et al.*, *J. Cosmol. Astropart. Phys.* **2022**, 10, 046 (2022), [arXiv:2207.13133].
- [34] B. D. Fields, P. Molaro and S. Sarkar, “Big-Bang Nucleosynthesis,” Sec. 24 in this *Review*.
- [35] n_b depends only upon the measured $\Omega_b h^2$, the average baryon mass at the present epoch (G. Steigman, *J. Cosmol. Astropart. Phys.*, **0610**, 016 (2006), [astro-ph/0606206]), and G_N : $n_b = (\Omega_b h^2)(h^{-2} \rho_{\text{crit}})/(0.93711 \text{ GeV}/c^2 \text{ per baryon})$.
- [36] E. Aver *et al.*, *Mon. Not. Roy. Astron. Soc.* **510**, 1, 373 (2022), [arXiv:2109.00178].
- [37] Here “radiation” includes three species of light neutrinos as well as photons.
- [38] D. Scott, A. Narimani and D. N. Page, *Phys. Canada* **70**, 258 (2014), [arXiv:1309.2381].
- [39] D. H. Weinberg and M. White, “Dark Energy,” Sec. 28 in this *Review*.
- [40] Planck Collab. Interm. Results XLVI, *Astron. Astrophys.* **596**, A107 (2016), [arXiv:1605.02985]; the range can be extended by $\Delta z \approx 1$, depending on the reionization model.
- [41] Summary Tables in this *Review* list $N_\nu = 2.984(8)$ (Standard Model fits to LEP-SLC data). Because neutrinos are not completely decoupled at e^\pm annihilation, the effective number of massless neutrino species is 3.044, rather than 3.
- [42] J. Lesgourgues and L. Verde, “Neutrinos in Cosmology,” Sec. 26 in this *Review*.
- [43] The sum is over all neutrino mass eigenstates, the lower limit following from neutrino mixing results reported in this *Review* combined with the assumptions that there are three light neutrinos and that the lightest neutrino is substantially less massive than the others.
- [44] Astrophysical determinations of Σm_ν , reported in the Full Listings of this *Review* under “Sum of the neutrino masses,” range from < 0.17 eV to < 2.3 eV in papers published since 2003.
- [45] P. A. R. Ade *et al.* (BICEP2, Keck Array), *Phys. Rev. Lett.* **121**, 221301 (2018), [arXiv:1810.05216].
- [46] M. Tristram *et al.*, *Astron. Astrophys.* **647**, A128 (2021), [arXiv:2010.01139].
- [47] BICEP/Keck Collaboration, *Phys. Rev. Lett.* **127**, 151301 (2021), [arXiv:2110.00483].
- [48] *Planck* data alone give $r < 0.056$, using all power spectra; the currently tightest constraint comes from BICEP/Keck data, using *WMAP* and *Planck* to remove foregrounds.
- [49] This constraint uses BAO and SNe data, as described in Ref. [2]; see discussion in D. H. Weinberg and M. White, “Dark Energy,” Sec. 28 in this *Review*.
- [50] G. P. Horedt, *Astrophys. Space Sci.* **126**, 2, 357 (1986).

3. International System of Units (SI)

See D.B. Newell and E. Tiesinga, ed. (2019), “The International System of Units (SI)” (National Institute of Standards and Technology, Gaithersburg, MD), NIST Special Publication **330**, 2019 edition, <https://doi.org/10.6028/NIST.SP.330-2019>; and A. Thompson and B.N. Taylor (2008), “Guide for the Use of the International System of Units (SI)” (National Institute of Standards and Technology, Gaithersburg, MD), NIST Special Publication **811**, 2008 edition, <https://doi.org/10.6028/NIST.SP.811e2008>.

SI prefixes		
10^{24}	yotta	(Y)
10^{21}	zetta	(Z)
10^{18}	exa	(E)
10^{15}	peta	(P)
10^{12}	tera	(T)
10^9	giga	(G)
10^6	mega	(M)
10^3	kilo	(k)
10^2	hecto	(h)
10	deca	(da)
10^{-1}	deci	(d)
10^{-2}	centi	(c)
10^{-3}	milli	(m)
10^{-6}	micro	(μ)
10^{-9}	nano	(n)
10^{-12}	pico	(p)
10^{-15}	femto	(f)
10^{-18}	atto	(a)
10^{-21}	zepto	(z)
10^{-24}	yocto	(y)

Physical quantity	Name of unit	Symbol
<i>Base units</i>		
length	meter	m
mass	kilogram	kg
time	second	s
electric current	ampere	A
thermodynamic temperature	kelvin	K
amount of substance	mole	mol
luminous intensity	candela	cd
<i>Derived units with special names</i>		
plane angle	radian	rad
solid angle	steradian	sr
frequency	hertz	Hz
energy	joule	J
force	newton	N
pressure	pascal	Pa
power	watt	W
electric charge	coulomb	C
electric potential	volt	V
electric resistance	ohm	Ω
electric conductance	siemens	S
electric capacitance	farad	F
magnetic flux	weber	Wb
inductance	henry	H
magnetic flux density	tesla	T
luminous flux	lumen	lm
illuminance	lux	lx
celsius temperature	degree celsius	$^{\circ}\text{C}$
activity (of a radioactive source)*	becquerel	Bq
absorbed dose (of ionizing radiation)*	gray	Gy
dose equivalent*	sievert	Sv

* See our section 37, on “Radioactivity and radiation protection.”

Table 4.1. Revised March 2024 by D.E. Groom (LBNL). The atomic number (top left) is the number of protons in the nucleus. The atomic masses (bottom) of stable elements are weighted by isotopic abundances in the Earth's surface. Atomic masses are relative to the mass of ^{12}C , defined to be exactly 12 unified atomic mass units (u). The exceptions are Th, Pa, and U, which have no stable isotopes but do have characteristic terrestrial compositions. Relative isotopic abundances often vary considerably, both in natural and commercial samples; this is reflected in the number of significant figures given for the mass. Masses may be found at <https://physics.nist.gov/cgi-bin/Compositions/stand.alone.pl>. If there is no stable isotope, the atomic mass of the most stable isotope known as of June 2019 is given in parentheses.

IUPAC announced verification of the discoveries of elements 113, 115, 117, and 118 in December 2015. The names were approved November 2016. The 7th period of the periodic table is now complete. Attempts to synthesize elements with $Z > 118$ are under way, but as of March 2024 no discoveries have been announced.

PERIODIC TABLE OF THE ELEMENTS																					
1 IA																	18 VIIIA				
1 H hydrogen 1.008	2 IIA															13 IIIA	14 IVA	15 VA	16 VIA	17 VIIA	2 He helium 4.002602
3 Li lithium 6.94	4 Be beryllium 9.012182															5 B boron 10.81	6 C carbon 12.0107	7 N nitrogen 14.007	8 O oxygen 15.999	9 F fluorine 18.998403163	10 Ne neon 20.1797
11 Na sodium 22.98976928	12 Mg magnesium 24.305	3 IIIB	4 IVB	5 VB	6 VIB	7 VIIB	8	9 VIII	10	11 IB	12 IIB	13 Al aluminum 26.9815385	14 Si silicon 28.085	15 P phosphorus 30.973761998	16 S sulfur 32.06	17 Cl chlorine 35.45	18 Ar argon 39.948				
19 K potassium 39.0983	20 Ca calcium 40.078	21 Sc scandium 44.955908	22 Ti titanium 47.867	23 V vanadium 50.9415	24 Cr chromium 51.9961	25 Mn manganese 54.938044	26 Fe iron 55.845	27 Co cobalt 58.933195	28 Ni nickel 58.6934	29 Cu copper 63.546	30 Zn zinc 65.38	31 Ga gallium 69.723	32 Ge germanium 72.630	33 As arsenic 74.921595	34 Se selenium 78.971	35 Br bromine 79.904	36 Kr krypton 83.798				
37 Rb rubidium 85.4678	38 Sr strontium 87.62	39 Y yttrium 88.90584	40 Zr zirconium 91.224	41 Nb niobium 92.90637	42 Mo molybdenum 95.95	43 Tc technetium (97.907212)	44 Ru ruthenium 101.07	45 Rh rhodium 102.90550	46 Pd palladium 106.42	47 Ag silver 107.8682	48 Cd cadmium 112.414	49 In indium 114.818	50 Sn tin 118.710	51 Sb antimony 121.760	52 Te tellurium 127.60	53 I iodine 126.90447	54 Xe xenon 131.293				
55 Cs caesium 132.90545196	56 Ba barium 137.327	57-71 LANTHANIDES	72 Hf hafnium 178.49	73 Ta tantalum 180.94788	74 W tungsten 183.84	75 Re rhenium 186.207	76 Os osmium 190.23	77 Ir iridium 192.217	78 Pt platinum 195.084	79 Au gold 196.966569	80 Hg mercury 200.592	81 Tl thallium 204.38	82 Pb lead 207.2	83 Bi bismuth 208.98040	84 Po polonium (208.98243)	85 At astatine (209.98715)	86 Rn radon (222.01758)				
87 Fr francium (223.01974)	88 Ra radium (226.02541)	89-103 ACTINIDES	104 Rf rutherford. (267.12169)	105 Db dubnium (268.12567)	106 Sg seaborgium (269.12863)	107 Bh bohrium (270.13336)	108 Hs hassium (269.13375)	109 Mt meitnerium (278.15631)	110 Ds darmstadt. (281.16451)	111 Rg roentgen. (282.16912)	112 Cn copernicium (285.17712)	113 Nh nihonium (286.18221)	114 Fl flerovium (289.19042)	115 Mc moscovium (290.19598)	116 Lv livermorium (293.20449)	117 Ts tennessine (294.21046)	118 Og oganesson (294.21392)				

Lanthanide series	57 La lanthanum 138.90547	58 Ce cerium 140.116	59 Pr praseodym. 140.90766	60 Nd neodymium 144.242	61 Pm promethium (144.91276)	62 Sm samarium 150.36	63 Eu europium 151.964	64 Gd gadolinum 157.25	65 Tb terbium 158.92535	66 Dy dysprosium 162.500	67 Ho holmium 164.93033	68 Er erbium 167.259	69 Tm thulium 168.93422	70 Yb ytterbium 173.054	71 Lu lutetium 174.9668
Actinide series	89 Ac actinium (227.02775)	90 Th thorium 232.0377	91 Pa protactinium 231.03588	92 U uranium 238.02891	93 Np neptunium (237.04817)	94 Pu plutonium (244.06420)	95 Am americium (243.06138)	96 Cm curium (247.07035)	97 Bk berkelium (247.07031)	98 Cf californium (251.07959)	99 Es einsteinium (252.08298)	100 Fm fermium (257.09511)	101 Md mendelevium (258.09844)	102 No nobelium (259.10103)	103 Lr lawrencium (262.10961)

5. Electronic Structure of the Elements

Table 5.1: Reviewed 2022 by A. Kramida (NIST). The electronic configurations, ground state levels, and ionization energies are from A. Kramida, Yu. Ralchenko, J. Reader, and NIST ASD Team (2022), “NIST Atomic Spectra Database” (ver. 5.10), [Online], Available: <https://physics.nist.gov/asd> [2023, Sept 5]. National Institute of Standards and Technology, Gaithersburg, MD. DOI: <https://doi.org/10.18434/T4W30F>. The electron configuration for, say, iron indicates an argon electronic core (see argon) plus six $3d$ electrons and two $4s$ electrons.

	Element	Electron configuration ($3d^5 =$ five $3d$ electrons, <i>etc.</i>)	Ground state $2S+1L_J$	Ionization energy (eV)	
1	H	Hydrogen	1s	$2S_{1/2}$	13.5984
2	He	Helium	$1s^2$	$1S_0$	24.5874
3	Li	Lithium	(He) 2s	$2S_{1/2}$	5.3917
4	Be	Beryllium	(He) $2s^2$	$1S_0$	9.3227
5	B	Boron	(He) $2s^2 2p$	$2P_{1/2}^o$	8.2980
6	C	Carbon	(He) $2s^2 2p^2$	$3P_0$	11.2603
7	N	Nitrogen	(He) $2s^2 2p^3$	$4S_{3/2}^o$	14.5341
8	O	Oxygen	(He) $2s^2 2p^4$	$3P_2$	13.6181
9	F	Fluorine	(He) $2s^2 2p^5$	$2P_{3/2}^o$	17.4228
10	Ne	Neon	(He) $2s^2 2p^6$	$1S_0$	21.5645
11	Na	Sodium	(Ne) 3s	$2S_{1/2}$	5.1391
12	Mg	Magnesium	(Ne) $3s^2$	$1S_0$	7.6462
13	Al	Aluminum	(Ne) $3s^2 3p$	$2P_{1/2}^o$	5.9858
14	Si	Silicon	(Ne) $3s^2 3p^2$	$3P_0$	8.1517
15	P	Phosphorus	(Ne) $3s^2 3p^3$	$4S_{3/2}^o$	10.4867
16	S	Sulfur	(Ne) $3s^2 3p^4$	$3P_2$	10.3600
17	Cl	Chlorine	(Ne) $3s^2 3p^5$	$2P_{3/2}^o$	12.9676
18	Ar	Argon	(Ne) $3s^2 3p^6$	$1S_0$	15.7596
19	K	Potassium	(Ar) 4s	$2S_{1/2}$	4.3407
20	Ca	Calcium	(Ar) $4s^2$	$1S_0$	6.1132
21	Sc	Scandium	(Ar) 3d 4s ²	T $2D_{3/2}$	6.5615
22	Ti	Titanium	(Ar) $3d^2 4s^2$	r e $3F_2$	6.8281
23	V	Vanadium	(Ar) $3d^3 4s^2$	a l $4F_{3/2}$	6.7462
24	Cr	Chromium	(Ar) $3d^5 4s$	n e $7S_3$	6.7665
25	Mn	Manganese	(Ar) $3d^5 4s^2$	s m $6S_{5/2}$	7.4340
26	Fe	Iron	(Ar) $3d^6 4s^2$	i e $5D_4$	7.9025
27	Co	Cobalt	(Ar) $3d^7 4s^2$	t n $4F_{9/2}$	7.8810
28	Ni	Nickel	(Ar) $3d^8 4s^2$	i t $3F_4$	7.6399
29	Cu	Copper	(Ar) $3d^{10} 4s$	o s $2S_{1/2}$	7.7264
30	Zn	Zinc	(Ar) $3d^{10} 4s^2$	n $1S_0$	9.3942
31	Ga	Gallium	(Ar) $3d^{10} 4s^2 4p$	$2P_{1/2}^o$	5.9993
32	Ge	Germanium	(Ar) $3d^{10} 4s^2 4p^2$	$3P_0$	7.8994
33	As	Arsenic	(Ar) $3d^{10} 4s^2 4p^3$	$4S_{3/2}^o$	9.7886
34	Se	Selenium	(Ar) $3d^{10} 4s^2 4p^4$	$3P_2$	9.7524
35	Br	Bromine	(Ar) $3d^{10} 4s^2 4p^5$	$2P_{3/2}^o$	11.8138
36	Kr	Krypton	(Ar) $3d^{10} 4s^2 4p^6$	$1S_0$	13.9996
37	Rb	Rubidium	(Kr) 5s	$2S_{1/2}$	4.1771
38	Sr	Strontium	(Kr) $5s^2$	$1S_0$	5.6949
39	Y	Yttrium	(Kr) 4d 5s ²	T $2D_{3/2}$	6.2173
40	Zr	Zirconium	(Kr) $4d^2 5s^2$	r e $3F_2$	6.6341
41	Nb	Niobium	(Kr) $4d^4 5s$	a l $6D_{1/2}$	6.7589
42	Mo	Molybdenum	(Kr) $4d^5 5s$	n e $7S_3$	7.0924
43	Tc	Technetium	(Kr) $4d^5 5s^2$	s m $6S_{5/2}$	7.1194
44	Ru	Ruthenium	(Kr) $4d^7 5s$	i e $5F_5$	7.3605
45	Rh	Rhodium	(Kr) $4d^8 5s$	t n $4F_{9/2}$	7.4589
46	Pd	Palladium	(Kr) $4d^{10}$	i t $1S_0$	8.3368
47	Ag	Silver	(Kr) $4d^{10} 5s$	o s $2S_{1/2}$	7.5762
48	Cd	Cadmium	(Kr) $4d^{10} 5s^2$	n $1S_0$	8.9938

Element			Electron configuration ($3d^5 = \text{five } 3d \text{ electrons, etc.}$)				Ground state $2S+1L_J$	Ionization energy (eV)
49	In	Indium	(Kr)	$4d^{10}$	$5s^2$	$5p$	$2P_{1/2}^o$	5.7864
50	Sn	Tin	(Kr)	$4d^{10}$	$5s^2$	$5p^2$	$3P_0$	7.3439
51	Sb	Antimony	(Kr)	$4d^{10}$	$5s^2$	$5p^3$	$4S_{3/2}^o$	8.6084
52	Te	Tellurium	(Kr)	$4d^{10}$	$5s^2$	$5p^4$	$3P_2$	9.0098
53	I	Iodine	(Kr)	$4d^{10}$	$5s^2$	$5p^5$	$2P_{3/2}^o$	10.4513
54	Xe	Xenon	(Kr)	$4d^{10}$	$5s^2$	$5p^6$	$1S_0$	12.1298
55	Cs	Cesium	(Xe)			$6s$	$2S_{1/2}$	3.8939
56	Ba	Barium	(Xe)			$6s^2$	$1S_0$	5.2117
57	La	Lanthanum	(Xe)		$5d$	$6s^2$	$2D_{3/2}$	5.5769
58	Ce	Cerium	(Xe)	$4f$	$5d$	$6s^2$	$1G_4^o$	5.5386
59	Pr	Praseodymium	(Xe)	$4f^3$		$6s^2$	$4I_{9/2}^o$	5.4702
60	Nd	Neodymium	(Xe)	$4f^4$		$6s^2$	$5I_4$	5.5250
61	Pm	Promethium	(Xe)	$4f^5$		$6s^2$	$6H_{5/2}^o$	5.5819
62	Sm	Samarium	(Xe)	$4f^6$		$6s^2$	$7F_0$	5.6437
63	Eu	Europium	(Xe)	$4f^7$		$6s^2$	$8S_{7/2}^o$	5.6704
64	Gd	Gadolinium	(Xe)	$4f^7$	$5d$	$6s^2$	$9D_2^o$	6.1498
65	Tb	Terbium	(Xe)	$4f^9$		$6s^2$	$6H_{15/2}^o$	5.8638
66	Dy	Dysprosium	(Xe)	$4f^{10}$		$6s^2$	$5I_8$	5.9391
67	Ho	Holmium	(Xe)	$4f^{11}$		$6s^2$	$4I_{15/2}^o$	6.0215
68	Er	Erbium	(Xe)	$4f^{12}$		$6s^2$	$3H_6$	6.1077
69	Tm	Thulium	(Xe)	$4f^{13}$		$6s^2$	$2F_{7/2}^o$	6.1844
70	Yb	Ytterbium	(Xe)	$4f^{14}$		$6s^2$	$1S_0$	6.2542
71	Lu	Lutetium	(Xe)	$4f^{14}$	$5d$	$6s^2$	$2D_{3/2}$	5.4259
72	Hf	Hafnium	(Xe)	$4f^{14}$	$5d^2$	$6s^2$	$3F_2$	6.8251
73	Ta	Tantalum	(Xe)	$4f^{14}$	$5d^3$	$6s^2$	$4F_{3/2}$	7.5496
74	W	Tungsten	(Xe)	$4f^{14}$	$5d^4$	$6s^2$	$5D_0$	7.8640
75	Re	Rhenium	(Xe)	$4f^{14}$	$5d^5$	$6s^2$	$6S_{5/2}$	7.8335
76	Os	Osmium	(Xe)	$4f^{14}$	$5d^6$	$6s^2$	$5D_4$	8.4382
77	Ir	Iridium	(Xe)	$4f^{14}$	$5d^7$	$6s^2$	$4F_{9/2}$	8.9670
78	Pt	Platinum	(Xe)	$4f^{14}$	$5d^9$	$6s$	$3D_3$	8.9588
79	Au	Gold	(Xe)	$4f^{14}$	$5d^{10}$	$6s$	$2S_{1/2}$	9.2256
80	Hg	Mercury	(Xe)	$4f^{14}$	$5d^{10}$	$6s^2$	$1S_0$	10.4375
81	Tl	Thallium	(Hg)	$6p$			$2P_{1/2}^o$	6.1083
82	Pb	Lead	(Hg)	$6p^2$			$3P_0$	7.4167
83	Bi	Bismuth	(Hg)	$6p^3$			$4S_{3/2}^o$	7.2855
84	Po	Polonium	(Hg)	$6p^4$			$3P_2$	8.4181
85	At	Astatine	(Hg)	$6p^5$			$2P_{3/2}^o$	9.3175
86	Rn	Radon	(Hg)	$6p^6$			$1S_0$	10.7485
87	Fr	Francium	(Rn)			$7s$	$2S_{1/2}$	4.0727
88	Ra	Radium	(Rn)			$7s^2$	$1S_0$	5.2784
89	Ac	Actinium	(Rn)		$6d$	$7s^2$	$2D_{3/2}$	5.3802
90	Th	Thorium	(Rn)		$6d^2$	$7s^2$	$3F_2$	6.3067
91	Pa	Protactinium	(Rn)	$5f^2$	$6d$	$7s^2$	$4K_{11/2}^*$	5.89
92	U	Uranium	(Rn)	$5f^3$	$6d$	$7s^2$	$5L_6^*$	6.1941
93	Np	Neptunium	(Rn)	$5f^4$	$6d$	$7s^2$	$6L_{11/2}^*$	6.2655
94	Pu	Plutonium	(Rn)	$5f^6$		$7s^2$	$7F_0$	6.0258
95	Am	Americium	(Rn)	$5f^7$		$7s^2$	$8S_{7/2}^o$	5.9738
96	Cm	Curium	(Rn)	$5f^7$	$6d$	$7s^2$	$9D_2^o$	5.9914
97	Bk	Berkelium	(Rn)	$5f^9$		$7s^2$	$6H_{15/2}^o$	6.1979
98	Cf	Californium	(Rn)	$5f^{10}$		$7s^2$	$5I_8$	6.2819
99	Es	Einsteinium	(Rn)	$5f^{11}$		$7s^2$	$4I_{15/2}^o$	6.3676
100	Fm	Fermium	(Rn)	$5f^{12}$		$7s^2$	$3H_6$	6.50
101	Md	Mendelevium	(Rn)	$5f^{13}$		$7s^2$	$2F_{7/2}^o$	6.58
102	No	Nobelium	(Rn)	$5f^{14}$		$7s^2$	$1S_0$	6.6262
103	Lr	Lawrencium	(Rn)	$5f^{14}$		$7s^2$	$2P_{1/2}^o$	4.96
104	Rf	Rutherfordium	(Rn)	$5f^{14}$	$6d^2$	$7s^2$	$3F_2$	6.02
105	Db	Dubnium	(Rn)	$5f^{14}$	$6d^3$	$7s^2$	$4F_{3/2}$	6.8
106	Sg	Seaborgium	(Rn)	$5f^{14}$	$6d^4$	$7s^2$	0	7.8
107	Bh	Bohrium	(Rn)	$5f^{14}$	$6d^5$	$7s^2$	$5/2$	7.7
108	Hs	Hassium	(Rn)	$5f^{14}$	$6d^6$	$7s^2$	4	7.6

* The usual *LS* coupling scheme does not apply for these three elements.

See the introductory note to the NIST table at https://www.nist.gov/pml/data/ion_energy.cfm.

6. Atomic and Nuclear Properties of Materials

Table 6.1: Abridged from <https://pdg.lbl.gov/current/AtomicNuclearProperties> by D.E. Groom (2023). See web pages for more detail about entries in this table and for several hundred others. Parentheses in the dE/dx and density columns indicate gases at 20° C and 1 atm. Boiling points are at 1 atm. Refractive indices n are evaluated at the sodium D line blend (589.2 nm); values $\gg 1$ in brackets indicate $(n - 1) \times 10^6$ for gases at 0° C and 1 atm.

Material	Z	A	$\langle Z/A \rangle$	Nucl.coll. length λ_T {g cm ⁻² }	Nucl.inter. length λ_I {g cm ⁻² }	Rad.len. $dE/dx _{\min}$ X_0 {g cm ⁻² }	Density {g cm ⁻³ }	Melting point (K)	Boiling point (K)	Refract. index @ Na D
H ₂	1	1.008(7)	0.99212	42.8	52.0	63.05 (4.103)	0.071(0.084)	13.81	20.28	1.11[132.]
D ₂	1	2.014101764(8)	0.49650	51.3	71.8	125.97 (2.053)	0.169(0.168)	18.7	23.65	1.11[138.]
He	2	4.002602(2)	0.49967	51.8	71.0	94.32 (1.937)	0.125(0.166)		4.220	1.02[35.0]
Li	3	6.94(2)	0.43221	52.2	71.3	82.78	1.639	0.534	453.6	1615.
Be	4	9.0121831(5)	0.44384	55.3	77.8	65.19	1.595	1.848	1560.	2744.
C diamond	6	12.0107(8)	0.49955	59.2	85.8	42.70	1.725	3.520		2.419
C graphite	6	12.0107(8)	0.49955	59.2	85.8	42.70	1.742	2.210	Sublimes at 4098. K	
N ₂	7	14.007(2)	0.49976	61.1	89.7	37.99 (1.825)	0.807(1.165)	63.15	77.29	1.20[298.]
O ₂	8	15.999(3)	0.50002	61.3	90.2	34.24 (1.801)	1.141(1.332)	54.36	90.20	1.22[271.]
F ₂	9	18.998403163(6)	0.47372	65.0	97.4	32.93 (1.676)	1.507(1.580)	53.53	85.03	[195.]
Ne	10	20.1797(6)	0.49555	65.7	99.0	28.93 (1.724)	1.204(0.839)	24.56	27.07	1.09[67.1]
Al	13	26.9815385(7)	0.48181	69.7	107.2	24.01	1.615	2.699	933.5	2792.
Si	14	28.0855(3)	0.49848	70.2	108.4	21.82	1.664	2.329	1687.	3538.
Cl ₂	17	35.453(2)	0.47951	73.8	115.7	19.28 (1.630)	1.574(2.980)	171.6	239.1	[773.]
Ar	18	39.948(1)	0.45059	75.7	119.7	19.55 (1.519)	1.396(1.662)	83.81	87.26	1.23[281.]
Ti	22	47.867(1)	0.45961	78.8	126.2	16.16	1.477	4.540	1941.	3560.
Fe	26	55.845(2)	0.46557	81.7	132.1	13.84	1.451	7.874	1811.	3134.
Cu	29	63.546(3)	0.45636	84.2	137.3	12.86	1.403	8.960	1358.	2835.
Ge	32	72.630(1)	0.44053	86.9	143.0	12.25	1.370	5.323	1211.	3106.
Sn	50	118.710(7)	0.42119	98.2	166.7	8.82	1.263	7.310	505.1	2875.
Xe	54	131.293(6)	0.41129	100.8	172.1	8.48 (1.255)	2.953(5.483)	161.4	165.1	1.39[701.]
W	74	183.84(1)	0.40252	110.4	191.9	6.76	1.145	19.300	3695.	5828.
Pt	78	195.084(9)	0.39983	112.2	195.7	6.54	1.128	21.450	2042.	4098.
Au	79	196.966569(5)	0.40108	112.5	196.3	6.46	1.134	19.320	1337.	3129.
Pb	82	207.2(1)	0.39575	114.1	199.6	6.37	1.122	11.350	600.6	2022.
U	92	[238.02891(3)]	0.38651	118.6	209.0	6.00	1.081	18.950	1408.	4404.
Air (dry, 1 atm)			0.49919	61.3	90.1	36.62 (1.815)	(1.205)		78.80	[289]
Shielding concrete			0.50274	65.1	97.5	26.57	1.711	2.300		
Borosilicate glass (Pyrex)			0.49707	64.6	96.5	28.17	1.696	2.230		
Lead glass SF5			0.44522	84.0	133.4	10.07	1.406	4.080		1.6727
Standard rock			0.50000	66.8	101.3	26.54	1.688	2.650		
Methane (CH ₄)			0.62334	54.0	73.8	46.47 (2.417)	(0.667)	90.68	111.7	[444.]
Ethane (C ₂ H ₆)			0.59861	55.0	75.9	45.66 (2.304)	(1.263)	90.36	184.5	
Propane (C ₃ H ₈)			0.58962	55.3	76.7	45.37 (2.262)	0.493(1.868)	85.52	231.0	
Butane (C ₄ H ₁₀)			0.59497	55.5	77.1	45.23 (2.278)	(2.489)	134.9	272.6	
Octane (C ₈ H ₁₈)			0.57778	55.8	77.8	45.00	2.123	0.703	214.4	398.8
Paraffin (CH ₃ (CH ₂) _n ≈23CH ₃)			0.57275	56.0	78.3	44.85	2.088	0.930		
Nylon (type 6, 6/6)			0.54790	57.5	81.6	41.92	1.973	1.18		
Polycarbonate (Lexan)			0.52697	58.3	83.6	41.50	1.886	1.20		
Polyethylene ([CH ₂ CH ₂] _n)			0.57034	56.1	78.5	44.77	2.079	0.89		
Polyethylene terephthalate (Mylar)			0.52037	58.9	84.9	39.95	1.848	1.40		
Polyimide film (Kapton)			0.51264	59.2	85.5	40.58	1.820	1.42		
Polymethylmethacrylate (acrylic)			0.53937	58.1	82.8	40.55	1.929	1.19		1.49
Polypropylene			0.55998	56.1	78.5	44.77	2.041	0.90		
Polystyrene ([C ₆ H ₅ CHCH ₂] _n)			0.53768	57.5	81.7	43.79	1.936	1.06		1.59
Polytetrafluoroethylene (Teflon)			0.47992	63.5	94.4	34.84	1.671	2.20		
Polyvinyltoluene			0.54141	57.3	81.3	43.90	1.956	1.03		1.58
Aluminum oxide (sapphire)			0.49038	65.5	98.4	27.94	1.647	3.970	2327.	3273.
Barium fluoride (BaF ₂)			0.42207	90.8	149.0	9.91	1.303	4.893	1641.	2533.
Bismuth germanate (BGO)			0.42065	96.2	159.1	7.97	1.251	7.130	1317.	2.15
Carbon dioxide gas (CO ₂)			0.49989	60.7	88.9	36.20	1.819	(1.842)		[449.]
Solid carbon dioxide (dry ice)			0.49989	60.7	88.9	36.20	1.787	1.563	Sublimes at 194.7 K	
Cesium iodide (CsI)			0.41569	100.6	171.5	8.39	1.243	4.510	894.2	1553.
Lithium fluoride (LiF)			0.46262	61.0	88.7	39.26	1.614	2.635	1121.	1946.
Lithium hydride (LiH)			0.50321	50.8	68.1	79.62	1.897	0.820	965.	
Lead tungstate (PbWO ₄)			0.41315	100.6	168.3	7.39	1.229	8.300	1403.	2.20
Silicon dioxide (SiO ₂ , fused quartz)			0.49930	65.2	97.8	27.05	1.699	2.200	1986.	3223.
Sodium chloride (NaCl)			0.47910	71.2	110.1	21.91	1.847	2.170	1075.	1738.
Sodium iodide (NaI)			0.42697	93.1	154.6	9.49	1.305	3.667	933.2	1577.
Water (H ₂ O)			0.55509	58.5	83.3	36.08	1.992	1.000	273.1	373.1
Silica aerogel			0.50093	65.0	97.3	27.25	1.740	0.200	(0.03 H ₂ O, 0.97 SiO ₂)	
Epoxy (Epotek-301-1)			0.53409	58.1	83.0	41.22	1.925	1.190		
G10			0.51166	56.8	78.4	32.17	1.762	1.800		

Material	Dielectric constant ($\kappa = \epsilon/\epsilon_0$) () is $(\kappa-1)\times 10^6$ for gas	Young's modulus [10^6 psi]	Coeff. of thermal expansion [10^{-6} cm/cm-°C]	Specific heat [cal/g-°C]	Electrical resistivity [$\mu\Omega$ cm(@°C)]	Thermal conductivity [cal/cm-°C-sec]
H ₂	(253.9)	—	—	—	—	—
He	(64)	—	—	—	—	—
Li	—	—	56	0.86	8.55(0°)	0.17
Be	—	37	12.4	0.436	5.885(0°)	0.38
C	—	0.7	0.6–4.3	0.165	1375(0°)	0.057
N ₂	(548.5)	—	—	—	—	—
O ₂	(495)	—	—	—	—	—
Ne	(127)	—	—	—	—	—
Al	—	10	23.9	0.215	2.65(20°)	0.53
Si	11.9	16	2.8–7.3	0.162	—	0.20
Ar	(517)	—	—	—	—	—
Ti	—	16.8	8.5	0.126	50(0°)	—
Fe	—	28.5	11.7	0.11	9.71(20°)	0.18
Cu	—	16	16.5	0.092	1.67(20°)	0.94
Ge	16.0	—	5.75	0.073	—	0.14
Sn	—	6	20	0.052	11.5(20°)	0.16
Xe	—	—	—	—	—	—
W	—	50	4.4	0.032	5.5(20°)	0.48
Pt	—	21	8.9	0.032	9.83(0°)	0.17
Pb	—	2.6	29.3	0.038	20.65(20°)	0.083
U	—	—	36.1	0.028	29(20°)	0.064

7. Electromagnetic Relations

Revised September 2005 by H.G. Spieler (LBNL).

Quantity	Gaussian CGS	SI
Conversion factors:		
Charge:	$2.997\,924\,58 \times 10^9$ esu	$= 1\text{ C} = 1\text{ A s}$
Potential:	$(1/299.792\,458)$ statvolt (ergs/esu)	$= 1\text{ V} = 1\text{ J C}^{-1}$
Magnetic field:	10^4 gauss $= 10^4$ dyne/esu	$= 1\text{ T} = 1\text{ N A}^{-1}\text{m}^{-1}$
	$\mathbf{F} = q(\mathbf{E} + \frac{\mathbf{v}}{c} \times \mathbf{B})$	$\mathbf{F} = q(\mathbf{E} + \mathbf{v} \times \mathbf{B})$
	$\nabla \cdot \mathbf{D} = 4\pi\rho$ $\nabla \times \mathbf{H} - \frac{1}{c} \frac{\partial \mathbf{D}}{\partial t} = \frac{4\pi}{c} \mathbf{J}$ $\nabla \cdot \mathbf{B} = 0$ $\nabla \times \mathbf{E} + \frac{1}{c} \frac{\partial \mathbf{B}}{\partial t} = 0$	$\nabla \cdot \mathbf{D} = \rho$ $\nabla \times \mathbf{H} - \frac{\partial \mathbf{D}}{\partial t} = \mathbf{J}$ $\nabla \cdot \mathbf{B} = 0$ $\nabla \times \mathbf{E} + \frac{\partial \mathbf{B}}{\partial t} = 0$
Constitutive relations:	$\mathbf{D} = \mathbf{E} + 4\pi\mathbf{P}$, $\mathbf{H} = \mathbf{B} - 4\pi\mathbf{M}$	$\mathbf{D} = \epsilon_0\mathbf{E} + \mathbf{P}$, $\mathbf{H} = \mathbf{B}/\mu_0 - \mathbf{M}$
Linear media:	$\mathbf{D} = \epsilon\mathbf{E}$, $\mathbf{H} = \mathbf{B}/\mu$ 1 1	$\mathbf{D} = \epsilon\mathbf{E}$, $\mathbf{H} = \mathbf{B}/\mu$ $\epsilon_0 = 8.854\,187 \dots \times 10^{-12}$ F m ⁻¹ $\mu_0 = 4\pi \times 10^{-7}$ N A ⁻²
	$\mathbf{E} = -\nabla V - \frac{1}{c} \frac{\partial \mathbf{A}}{\partial t}$ $\mathbf{B} = \nabla \times \mathbf{A}$	$\mathbf{E} = -\nabla V - \frac{\partial \mathbf{A}}{\partial t}$ $\mathbf{B} = \nabla \times \mathbf{A}$
	$V = \sum_{\text{charges}} \frac{q_i}{r_i} = \int \frac{\rho(\mathbf{r}')}{ \mathbf{r} - \mathbf{r}' } d^3x'$ $\mathbf{A} = \frac{1}{c} \oint \frac{I d\ell}{ \mathbf{r} - \mathbf{r}' } = \frac{1}{c} \int \frac{\mathbf{J}(\mathbf{r}')}{ \mathbf{r} - \mathbf{r}' } d^3x'$	$V = \frac{1}{4\pi\epsilon_0} \sum_{\text{charges}} \frac{q_i}{r_i} = \frac{1}{4\pi\epsilon_0} \int \frac{\rho(\mathbf{r}')}{ \mathbf{r} - \mathbf{r}' } d^3x'$ $\mathbf{A} = \frac{\mu_0}{4\pi} \oint \frac{I d\ell}{ \mathbf{r} - \mathbf{r}' } = \frac{\mu_0}{4\pi} \int \frac{\mathbf{J}(\mathbf{r}')}{ \mathbf{r} - \mathbf{r}' } d^3x'$
	$\mathbf{E}'_{\parallel} = \mathbf{E}_{\parallel}$ $\mathbf{E}'_{\perp} = \gamma(\mathbf{E}_{\perp} + \frac{1}{c} \mathbf{v} \times \mathbf{B})$ $\mathbf{B}'_{\parallel} = \mathbf{B}_{\parallel}$ $\mathbf{B}'_{\perp} = \gamma(\mathbf{B}_{\perp} - \frac{1}{c} \mathbf{v} \times \mathbf{E})$	$\mathbf{E}'_{\parallel} = \mathbf{E}_{\parallel}$ $\mathbf{E}'_{\perp} = \gamma(\mathbf{E}_{\perp} + \mathbf{v} \times \mathbf{B})$ $\mathbf{B}'_{\parallel} = \mathbf{B}_{\parallel}$ $\mathbf{B}'_{\perp} = \gamma(\mathbf{B}_{\perp} - \frac{1}{c^2} \mathbf{v} \times \mathbf{E})$
$\frac{1}{4\pi\epsilon_0} = c^2 \times 10^{-7} \text{ N A}^{-2} = 8.987\,55 \dots \times 10^9 \text{ m F}^{-1}$; $\frac{\mu_0}{4\pi} = 10^{-7} \text{ N A}^{-2}$; $c = \frac{1}{\sqrt{\mu_0\epsilon_0}} = 2.997\,924\,58 \times 10^8 \text{ m s}^{-1}$		

7.1 Impedances (SI units)

ρ = resistivity at room temperature in $10^{-8} \Omega \text{ m}$:

- ~ 1.7 for Cu ~ 5.5 for W
 - ~ 2.4 for Au ~ 73 for SS 304
 - ~ 2.8 for Al ~ 100 for Nichrome
- (Al alloys may have double the Al value.)

For alternating currents, instantaneous current I , voltage V , angular frequency ω :

$$V = V_0 e^{j\omega t} = ZI . \tag{7.1}$$

Impedance of self-inductance L : $Z = j\omega L$.

Impedance of capacitance C : $Z = 1/j\omega C$.

Impedance of free space: $Z = \sqrt{\mu_0/\epsilon_0} = 376.7 \Omega$.

High-frequency surface impedance of a good conductor:

$$Z = \frac{(1+j)\rho}{\delta} , \quad \text{where } \delta = \text{skin depth} ; \tag{7.2}$$

$$\delta = \sqrt{\frac{\rho}{\pi\nu\mu}} \approx \frac{6.6 \text{ cm}}{\sqrt{\nu \text{ (Hz)}}} \text{ for Cu} . \tag{7.3}$$

7.2 Capacitors, inductors, and transmission Lines

The capacitance between two parallel plates of area A spaced by the distance d and enclosing a medium with the dielectric constant ϵ is

$$C = K\epsilon A/d , \tag{7.4}$$

where the correction factor K depends on the extent of the fringing field. If the dielectric fills the capacitor volume without extending beyond the electrodes. The correction factor $K \approx 0.8$ for capacitors of typical geometry.

The inductance at high frequencies of a straight wire whose length ℓ is much greater than the wire diameter d is

$$L \approx 2.0 \left[\frac{\text{nH}}{\text{cm}} \right] \cdot \ell \left(\ln \left(\frac{4\ell}{d} \right) - 1 \right) . \tag{7.5}$$

For very short wires, representative of vias in a printed circuit board, the inductance is

$$L(\text{in nH}) \approx \ell/d . \tag{7.6}$$

A transmission line is a pair of conductors with inductance L and capacitance C . The characteristic impedance $Z = \sqrt{L/C}$ and the phase velocity $v_p = 1/\sqrt{LC} = 1/\sqrt{\mu\epsilon}$, which decreases with the inverse square root of the dielectric constant of the medium. Typical coaxial and ribbon cables have a propagation delay of about 5 ns/cm.

The impedance of a coaxial cable with outer diameter D and inner diameter d is

$$Z = 60 \Omega \cdot \frac{1}{\sqrt{\epsilon_r}} \ln \frac{D}{d}, \quad (7.7)$$

where the relative dielectric constant $\epsilon_r = \epsilon/\epsilon_0$. A pair of parallel wires of diameter d and spacing $a > 2.5d$ has the impedance

$$Z = 120 \Omega \cdot \frac{1}{\sqrt{\epsilon_r}} \ln \frac{2a}{d}. \quad (7.8)$$

This yields the impedance of a wire at a spacing h above a ground plane,

$$Z = 60 \Omega \cdot \frac{1}{\sqrt{\epsilon_r}} \ln \frac{4h}{d}. \quad (7.9)$$

A common configuration utilizes a thin rectangular conductor above a ground plane with an intermediate dielectric (microstrip). Detailed calculations for this and other transmission line configurations are given by Gunston [1].

7.3 Synchrotron radiation (CGS units)

For a particle of charge e , velocity $v = \beta c$, and energy $E = \gamma mc^2$, traveling in a circular orbit of radius R , the classical energy loss per revolution δE is

$$\delta E = \frac{4\pi}{3} \frac{e^2}{R} \beta^3 \gamma^4. \quad (7.10)$$

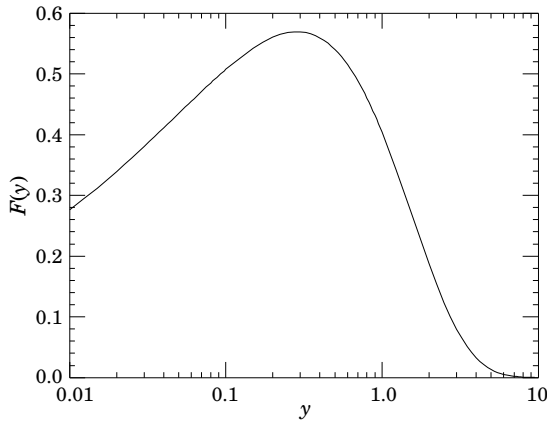


Figure 7.1: The normalized synchrotron radiation spectrum $F(y)$.

For high-energy electrons or positrons ($\beta \approx 1$), this becomes

$$\delta E \text{ (in MeV)} \approx 0.0885 [E(\text{in GeV})]^4 / R(\text{in m}). \quad (7.11)$$

For $\gamma \gg 1$, the energy radiated per revolution into the photon energy interval $d(\hbar\omega)$ is

$$dI = \frac{8\pi}{9} \alpha \gamma F(\omega/\omega_c) d(\hbar\omega), \quad (7.12)$$

where $\alpha = e^2/\hbar c$ is the fine-structure constant and

$$\omega_c = \frac{3\gamma^3 c}{2R} \quad (7.13)$$

is the critical frequency. The normalized function $F(y)$ is

$$F(y) = \frac{9}{8\pi} \sqrt{3} y \int_y^\infty K_{5/3}(x) dx, \quad (7.14)$$

where $K_{5/3}(x)$ is a modified Bessel function of the third kind. For electrons or positrons,

$$\hbar\omega_c \text{ (in keV)} \approx 2.22 [E(\text{in GeV})]^3 / R(\text{in m}). \quad (7.15)$$

For $\gamma \gg 1$ and $\omega \ll \omega_c$,

$$\frac{dI}{d(\hbar\omega)} \approx 3.3\alpha (\omega R/c)^{1/3}, \quad (7.16)$$

whereas for

$$\gamma \gg 1 \text{ and } \omega \gtrsim 3\omega_c,$$

$$\frac{dI}{d(\hbar\omega)} \approx \sqrt{\frac{3\pi}{2}} \alpha \gamma \left(\frac{\omega}{\omega_c}\right)^{1/2} e^{-\omega/\omega_c} \left[1 + \frac{55}{72} \frac{\omega_c}{\omega} + \dots\right]. \quad (7.17)$$

The radiation is confined to angles $\lesssim 1/\gamma$ relative to the instantaneous direction of motion. For $\gamma \gg 1$, where Eq. (7.12) applies, the mean number of photons emitted per revolution is

$$N_\gamma = \frac{5\pi}{\sqrt{3}} \alpha \gamma, \quad (7.18)$$

and the mean energy per photon is

$$\langle \hbar\omega \rangle = \frac{8}{15\sqrt{3}} \hbar\omega_c. \quad (7.19)$$

When $\langle \hbar\omega \rangle \gtrsim O(E)$, quantum corrections are important [2].¹

References

- [1] M.A.R. Gunston. Microwave Transmission Line Data, Noble Publishing Corp., Atlanta (1997) ISBN 1-884932-57-6, TK6565.T73G85.
- [2] J.D. Jackson, *Classical Electrodynamics*, 3rd edition (John Wiley & Sons, New York, 1998) for more formulae and details.

¹Note that earlier editions of Ref. [2] had ω_c twice as large as Eq. (7.13).

8. Naming Scheme for Hadrons

Revised August 2023 by C. Amsler (Stefan Meyer Inst.), E. Pi-anori (LBNL), D.J. Robinson (LBNL) and R.L. Workman (George Washington U.).

In the 1986 edition [1], the Particle Data Group introduced an extended and systematized naming scheme for mesons and baryons. The extensions were necessary in order to name the new particles containing c or b quarks that were then rapidly being discovered. The 1986 naming scheme has been retained in all subsequent editions, including this one. However, a number of particles were since discovered that could not be accommodated in the 1986 scheme. These include, for example the meson state originally named $Z_c(3900)^+$ (now $T_{c\bar{c}1}(3900)^+$) containing $c\bar{c}$ but with isospin $I = 1$ [2, 3]. Because of such discoveries, in the 2017 edition [4] the 1986 naming scheme was extended to cover $c\bar{c}$ and $b\bar{b}$ states with $I = 1$, including the Z_c and Z_b states.

The further discovery of various exotic hadron states—including in particular tetraquarks and pentaquarks containing $qq\bar{q}\bar{q}$ and $q\bar{q}qqq$ minimal quark content, respectively—has rendered the 2017 extension insufficient. These include, for example: the meson state $T_{cc}(3875)^+$ containing two charm quarks and with unknown isospin [5]; and the baryon state originally named $P_c(4312)^+$ (now $P_{c\bar{c}}(4312)^+$) containing minimal quark content $c\bar{c}uud$ [6]. In this edition, the 2017 scheme is revised and extended to cover all experimentally known states.

The naming scheme as a whole provides a name for each hadron, driven primarily by consideration of its quantum numbers, its minimal quark content—the smallest combination of quarks required to produce a color singlet with the required isospin, parities, strangeness, and open or hidden-heavy flavor—and its mass. While much of the naming scheme has been developed within the

context of the naive quark model, a hadron name does *not* designate the internal structure of a state per se: we make no attempt, for example, to distinguish meson states that are “mostly gluonium” from those that are “mostly $q\bar{q}$.” (Other reviews within the RPP discuss our current understanding of the nature of various hadron states). While the naming scheme conventions aim to be comprehensive, exceptions to the scheme are occasionally made for historical reasons (e.g. J/ψ , p , or n) or in cases where the spectroscopic identity of a state is considered established (e.g. $\Upsilon(1S)$). Note also the mass label used in particle names is chosen using the best information available when a name is assigned. A more accurate value of a particle mass may become available at a later time. PDG decides on a case-by-case basis whether to revise the mass label, taking into account the updated information.

8.1 Light unflavored, $c\bar{c}$, and $b\bar{b}$ mesons

Unflavored mesons—also referred to as “neutral-flavor” mesons—have zero strangeness and all heavy-flavor quantum numbers are equal to zero. Their minimal quark content is denoted $q\bar{q}$, with the understanding that for $q = u$ or d , such states may carry unit isospin: the “light unflavored” nomenclature is understood to encompass all states furnishing an isospin-1 multiplet that contains a $q\bar{q}$ neutral meson. Mesons composed of $c\bar{c}$ or $b\bar{b}$ are said to have hidden-heavy flavor.

Within the naive quark model, a neutral $q\bar{q}$ bound state has quantum numbers $P = (-1)^{L+1}$ and $C = (-1)^{L+S}$, where $S (= 0, 1)$ and L are the spin and orbital angular momentum of the $q\bar{q}$ system, respectively. The total angular momentum J satisfies $|L-S| \leq J \leq L+S$ as usual. There is thus a selection rule between the angular-momentum state $^{2S+1}L_J$ and the PC configuration, such that

$$PC = \begin{matrix} - +, & + -, & - -, & + +, \end{matrix} \quad (8.1)$$

corresponds to

$$^{2S+1}L_J = \begin{matrix} ^1(L \text{ even})_L, & ^1(L \text{ odd})_L, & ^3(L \text{ even})_{|L-1| \leq J \leq L+1}, & ^3(L \text{ odd})_{L-1, L, L+1}. \end{matrix} \quad (8.2)$$

Table 8.1 describes the naming scheme for unflavored mesons. The scheme is categorized by isospin and hidden-heavy flavor (rows) and parity/charge-conjugation configurations (columns); the first few allowed J^{PC} combinations for each column are shown in the header. Note C -parity is only well-defined for neutral unflavored mesons; the states furnishing an isospin-1 multiplet instead have a well-defined G -parity $= (-1)^{L+S+I}$; see the review on the quark model. The angular momentum J is included as a subscript to the base symbol for most unflavored mesons, but is omitted for various pseudoscalar, vector, and axial vector mesons whenever disambiguation by the J subscript is deemed superfluous. The mass is added in parentheses for mesons that decay strongly. However, for some of the familiar mesons (e.g. η' , ϕ , ω), we omit the mass.

For light unflavored mesons—i.e. those unflavored mesons formed from u , d , and s quarks—there can be two isospin-0 mesons: a prime is used to distinguish one from the other (e.g. η and η'), with the exception that vector mesons comprised of $u\bar{u} + d\bar{d}$ and $s\bar{s}$ (ideal mixing) are labeled ω and ϕ , respectively. As usual, we assign the spectroscopic name (e.g. $\Upsilon(1S)$) as the primary name to most of those ψ , Υ , and χ states whose spectroscopic identity is known. We use the form $\Upsilon(9460)$ as an alternative, and as the primary name when the spectroscopic identity is not known.

Determination of the quark content (where relevant) and the quantum numbers I , J , P , and C (or G) of an unflavored meson thus determine its symbol. For example, the light unflavored isospin-1 2^{--} meson would be the ρ_2 . Conversely, these properties may be inferred unambiguously from the symbol. The name X is used for states with still unknown quantum numbers. In some cases names are assigned when quantum numbers have not been strictly measured but have instead been inferred

Table 8.1: Base symbols for unflavored mesons (zero strangeness and heavy-flavor quantum numbers equal to zero). Each base symbol is uniquely determined by the isospin/hidden-heavy flavor and PC configuration.

J^{PC}	0^{-+}	1^{+-}	1^{--}	0^{++}
	2^{-+}	3^{+-}	2^{--}	1^{++}
	\vdots	\vdots	\vdots	\vdots
Minimal quark content				
$u\bar{d}, u\bar{u} - d\bar{d}, d\bar{u}$ ($I = 1$)	π	b	ρ	a
$d\bar{d} + u\bar{u}, s\bar{s}$	η, η'	h, h'	ω, ϕ	f, f'
and/or gluons ($I = 0$)				
$c\bar{c}$ ($I = 0$)	η_c	h_c	ψ^*	χ_c
$b\bar{b}$ ($I = 0$)	η_b	h_b	Υ	χ_b

* With the exception of the J/ψ .

from a broader context. These cases typically include an explanation in the header, such as “Quantum numbers shown are quark-model predictions.” One example is the $\psi_2(3823)$, for which the $I^G(J^{PC}) = 0^-(2^{--})$ assignment needs confirmation. Since the top quark is so heavy that it decays too rapidly to form bound states, no name is assigned to structures like $t\bar{t}$.

The selection rules in Eq. (8.2) impose restrictions on the J^{PC} quantum numbers that are allowed for $q\bar{q}$ states. These do not apply to more complicated structures such as tetraquarks, hybrid mesons, or glueballs. In particular, unflavored mesons with quantum numbers $J^{PC} = 0^{-}, 0^{+}, 1^{-+}, 2^{+-}, 3^{-+}, \dots$ cannot

be $q\bar{q}$ bound states, but might be glueballs or $q\bar{q}g$ etc. (This is distinct from light unflavored mesons with $I \geq 2$ or hidden-heavy flavor mesons with $I \geq 1$, which could be interpreted as tetraquarks). For such a “manifestly exotic” unflavored meson, the naming scheme nonetheless assigns the same base symbol as solely determined by the isospin/hidden-heavy flavor and PC in Tab. 8.1. For example, an isospin-0 light unflavored 1^{-+} meson would be denoted η_1 while an isospin-1 0^{--} light unflavored meson would be denoted ρ_0 . The exotic nature of the meson can be inferred from its PC quantum numbers—given by the symbol—and the spin J —given by the subscript.

8.2 Remarks on “neutral-flavor” mesons with hidden charm or bottom not classified as $q\bar{q}$

In the heavy-quark sector, there are several states with properties – such as masses, decay patterns, and widths – that are in disagreement with predictions from the naive quark model. For example, the vector state at 4230 MeV (the $\psi(4230)$) apparently does not decay into $D\bar{D}$, although within the naive quark model its quantum numbers would call for this decay channel to be dominant. These states were originally named X , Y , or Z , with their masses added in parentheses. This nomenclature differs from the conventions outlined in the previous section, since the meson names are not related to their quantum numbers. However, these states have properties in conflict with the naive quark model and therefore deserve some special labeling.

Since their original discovery, the properties of some of these states have become better understood and it has become possible to include them in the Listings as well as Summary Tables using the name assigned according to this review. The X -, Y -, or Z -based names used at the time of the discovery are also reported in the Listings and Summary Tables from the 2018 edition onwards as a sub-header (listed are only some examples of the particles that appear in the Summary Tables),

- the state originally named $X(3872)$ appears as ‘ $\chi_{c1}(3872)$ also known as $X(3872)$ ’;
- the state originally named $Z_c(3900)$ appears¹ as ‘ $T_{cc1}(3900)$ also known as $Z_c(3900)$ ’;
- the state originally named $Y(4260)$ appears² as ‘ $\psi(4230)$ also known as $Y(4230)$ ’;

In addition, states with quantum numbers allowed by the naive quark model but showing some peculiarities, such as an unusual decay pattern, will have the following information in the header:

This state shows properties different from a conventional $q\bar{q}$ state. A candidate for an exotic structure. See the review on (name of the proper review).

8.3 Mesons with nonzero S , C and/or B

Mesons with nonzero strangeness S or heavy flavor C and/or B are not eigenstates of charge conjugation, and in each of them one of the quarks is heavier than the other (as above, states containing top quarks are not considered). The rules have been and remain:

1. The main symbol is an upper-case italic letter indicating the heavier quark as follows:

$$s \rightarrow \bar{K} \quad c \rightarrow D \quad b \rightarrow \bar{B},$$

We use the convention that *the flavor quantum number and the charge of a quark have the same sign*. Thus the strangeness of the s quark is negative, the charm of the c quark is positive, and the bottomness of the b quark is negative. The effect of this convention is as follows: *any flavor carried by a charged meson has the same sign as its charge*. Thus the K^+ , D^+ , and B^+ have positive strangeness, charm, and bottomness, respectively, and all have positive I_3 . The D_s^+ has positive charm and strangeness. Furthermore, the

¹The name $T_{cc1}(3900)$ derives from the scheme outlined in a later section.

²This is one example where the mass label needed to be shifted given improved experimental information.

$\Delta(\text{flavor}) = \Delta Q$ rule, best known for the strange kaons, applies to every flavor.

2. If the lighter quark is not a u or a d quark, its identity is given by a subscript. The D_s^+ is an example.
3. When the spin-parity is in the natural series, $J^P = 0^+, 1^-, 2^+, \dots$, a superscript “*” is added.
4. The spin is added as a subscript except for pseudoscalar or vector mesons.

8.4 Baryons with ordinary quantum numbers

All baryons having quantum numbers consistent with a minimal quark content of three quarks are denoted by the symbols N , Δ , Λ , Σ , Ξ , and Ω introduced more than 50 years ago. These symbols are followed by J^P signifying their spin J and parity P . For those where the minimal content involves one or more heavier quarks than the light (u , d , and s) quarks, subscripts are added to their symbols, (c and b) as appropriate. The rules are:

1. Baryons with minimal content of *three* u and/or d quarks are N ’s (isospin 1/2) or Δ ’s (isospin 3/2).
2. Baryons with *two* u and/or d quarks are Λ ’s (isospin 0) or Σ ’s (isospin 1). If the third quark is a c or b quark, its identity is given by a subscript.
3. Baryons with *one* u or d quark are Ξ ’s (isospin 1/2). One or two subscripts are used if one or both of the remaining quarks are heavy: thus Ξ_c , Ξ_{cc} , Ξ_b , etc.³
4. Baryons with *no* u or d quarks are Ω ’s (isospin 0), and subscripts indicate any heavy-quark content.
5. A baryon that decays strongly has its mass in parentheses. Examples are the $\Delta(1232)$ $3/2^+$, $\Sigma(1385)$ $3/2^+$, $N(1440)$ $1/2^+$, $\Xi_c(2645)$ $3/2^+$.
6. If individual states of isospin multiplets are addressed, the electric charge is specified as a superscript. The electric charge is not necessary for isospin-0 states (Λ and Ω), as there is no ambiguity, but may still be included.
7. Antibaryons are labeled by an overline (bar) on the base symbol. For example, \bar{p} for the antiproton, or $\bar{\Lambda}_c^-$ for the antiparticle of Λ_c^+ . Alternatively, particle and antiparticle can be distinguished by including only a charge-label superscript, so long as the flavor structure of the baryon is defined solely by the base symbol (and subscripts). Thus one may also write Λ_c^- or p^- for the antiparticles of the Λ_c^+ and p^+ , but the Σ^- is not the antiparticle of Σ^+ , which is called $\bar{\Sigma}^-$.

In short, the minimal number of u plus d quarks together with the isospin determine the main symbol, and subscripts indicate any content of heavy quarks. A Σ always has isospin 1, an Ω always has isospin 0, etc.

8.5 Hadrons with a minimal quark content of $qq\bar{q}\bar{q}$ or $q\bar{q}qqq$

The naming scheme described above does not accommodate various $qq\bar{q}\bar{q}$ mesons and $q\bar{q}qqq$ baryons. In such cases, the 1986 naming scheme must be extended. Following discussion initiated by the proposal made by the LHCb collaboration [7], we adopt the notation

$$T_{\text{quarks}J}^{(*)}(\text{mass})^q \quad \text{for tetraquarks,} \quad (8.3a)$$

$$P_{\text{quarks}}(\text{mass})^q J^P \quad \text{for pentaquarks,} \quad (8.3b)$$

according to the following rules:

1. The basename T or P is chosen in cases where the minimal quark content of a state is $qq\bar{q}\bar{q}$ (tetraquark) or $q\bar{q}qqq$ (pentaquark), respectively.
2. The bottom, charm, and strange quark content (b , \bar{b} , c , \bar{c} , s , \bar{s}) is explicitly listed as a subscript, in order from the heaviest quarks and antiquarks to the lightest and listing quarks before antiquarks. The hidden-flavor $c\bar{c}$ and $b\bar{b}$ combinations

³See the “Charmed and Bottom Baryons” section of the “Quark Model” review.

Table 8.2: Names used from the 2024 edition onward compared to those in the 2022 edition. Whenever the C -parity of a charged tetraquark is specified in the Particle Listings, it refers to the C -parity of the prospective/observed neutral isospin partner. Only one member per isospin multiplet is shown (see the Listings for more information).

2024 Name	minimal quark content	$I^{(G)}(J^{P(C)})$	2022 Name	2024 Name	minimal quark content	$I^{(G)}(J^{P(C)})$	2022 Name
$T_{cs0}^*(2870)^0$	$cs\bar{u}\bar{d}$	$?(0^+)$	$X_0(2900)$	$T_{c\bar{c}1}(4430)^+$	$c\bar{c}u\bar{d}$	$1^+(1^{+-})$	$Z_c(4430)^+$
$T_{cs1}^*(2900)^0$	$cs\bar{u}\bar{d}$	$?(1^-)$	$X_1(2900)$	$T_{c\bar{c}s1}(4000)^+$	$c\bar{c}u\bar{s}$	$1/2(1^+)$	$Z_{cs}(4000)^+$
$T_{c\bar{s}0}^*(2900)^{++}$	$c\bar{s}u\bar{d}$	$1(0^+)$		$T_{c\bar{c}s1}(4220)^+$	$c\bar{c}u\bar{s}$	$1/2(1^+)$	$Z_{cs}(4220)^+$
$T_{cc}(3875)^+$	$cc\bar{u}\bar{d}$	$?(?)$		$T_{b\bar{s}}(5568)^+$	$b\bar{s}u\bar{d}$	$1(?)$	$X(5568)^+$
$T_{c\bar{c}1}(3900)^+$	$c\bar{c}u\bar{d}$	$1^+(1^{+-})$	$Z_c(3900)^+$	$T_{b\bar{b}1}(10610)^+$	$b\bar{b}u\bar{d}$	$1^+(1^{+-})$	$Z_b(10610)^+$
$T_{cc}(4020)^+$	$cc\bar{u}\bar{d}$	$1^+(?^?^-)$	$X(4020)^+$	$T_{b\bar{b}1}(10650)^+$	$b\bar{b}u\bar{d}$	$1^+(1^{+-})$	$Z_b(10650)^+$
$T_{c\bar{c}}(4050)^+$	$c\bar{c}u\bar{d}$	$1^-(?^?^+)$	$X(4050)^+$	$T_{c\bar{c}\bar{c}\bar{c}}(6900)^0$	$cc\bar{c}\bar{c}$	$0^+(?^?^+)$	$X(6900)$
$T_{cc}(4055)^+$	$cc\bar{u}\bar{d}$	$1^+(?^?^-)$	$X(4055)^+$	$P_{c\bar{c}}(4312)^+$	$c\bar{c}uud$	$1/2(?^?)$	$P_c(4312)^+$
$T_{c\bar{c}}(4100)^+$	$c\bar{c}u\bar{d}$	$1^-(?^?^+)$	$X(4100)^+$	$P_{c\bar{c}}(4380)^+$	$c\bar{c}uud$	$1/2(?^?)$	$P_c(4380)^+$
$T_{c\bar{c}1}(4200)^+$	$c\bar{c}u\bar{d}$	$1^+(1^{+-})$	$Z_c(4200)^+$	$P_{c\bar{c}}(4440)^+$	$c\bar{c}uud$	$1/2(?^?)$	$P_c(4440)^+$
$T_{c\bar{c}0}(4240)^+$	$c\bar{c}u\bar{d}$	$1^+(0^{--})$	$R_{c0}(4240)^+$	$P_{c\bar{c}}(4457)^+$	$c\bar{c}uud$	$1/2(?^?)$	$P_c(4457)^+$
$T_{c\bar{c}}(4250)^+$	$c\bar{c}u\bar{d}$	$1^-(?^?^+)$	$X(4250)^+$	$P_{c\bar{c}s}(4459)^0$	$c\bar{c}uds$	$0(?^?)$	

are listed explicitly when their presence can be inferred from production or decay patterns.

- The approximate mass of a state, in MeV/c^2 , is given in parentheses.
- The electric charge (q) can be specified as a superscript after the mass, for example when referring to a specific member of an isospin multiplet.
- Antibaryons are marked with an overline (\bar{P}). The antiparticle of a meson can be specified either with an overline or by the quark content label (e.g. the charge conjugate of $T_{cc}(3875)^+$ is $\bar{T}_{c\bar{c}}(3875)^-$, which is equivalent to $T_{c\bar{c}}(3875)^-$).
- For pentaquarks, as in the case of ordinary baryons, when known the spin-parity, J^P , of the state is included as a suffix.
- For tetraquarks, similarly to the naming scheme for mesons, the spin J is appended as a subscript after the quark content. When the spin-parity is in the natural series, $J^P = 0^+, 1^-, 2^+, \dots$, a superscript “*” is added.

Table 8.2 summarizes PDG name changes with respect to the 2022 edition [8]. We acknowledge that experiments might choose to add $I^{(G)}J^{P(C)}$ information to hadron names using experiment-

specific conventions that differ from the one utilized by the PDG.

References

- M. Aguilar-Benitez *et al.* (Particle Data Group), Phys. Lett. **170B**, 1 (1986).
- M. Ablikim *et al.* (BESIII), Phys. Rev. Lett. **110**, 252001 (2013), [arXiv:1303.5949].
- Z. Q. Liu *et al.* (Belle), Phys. Rev. Lett. **110**, 252002 (2013), [Erratum: Phys.Rev.Lett. 111, 019901 (2013)], [arXiv:1304.0121].
- M. Tanabashi *et al.* (Particle Data Group), Phys. Rev. D **98**, 3, 030001 (2018).
- R. Aaij *et al.* (LHCb), Nature Phys. **18**, 7, 751 (2022), [arXiv:2109.01038].
- R. Aaij *et al.* (LHCb), Phys. Rev. Lett. **122**, 22, 222001 (2019), [arXiv:1904.03947].
- LHCb (2022), [arXiv:2206.15233].
- R. L. Workman and Others (Particle Data Group), PTEP **2022**, 083C01 (2022).

Standard Model and Related Topics

9. Quantum chromodynamics (rev.)	153
10. Electroweak model and constraints on new physics (rev.)	185
11. Higgs boson physics, status of (rev.)	211
12. CKM quark-mixing matrix (rev.)	270
13. CP violation in the quark sector (rev.)	280
14. Neutrino masses, mixing, and oscillations (rev.)	295
15. Quark model (rev.)	322
16. Heavy-quark & soft-collinear effective theory (rev.)	341
17. Lattice quantum chromodynamics (rev.)	350
18. Structure functions (rev.)	367
19. Fragmentation functions in e^+e^- , ep and pp collisions (rev.)	389
20. High Energy Soft QCD and Diffraction (rev.)	406





9. Quantum Chromodynamics

Revised August 2023 by J. Huston (Michigan State U.), K. Rabbertz (KIT) and G. Zanderighi (MPP, Garching; München Tech. U.).

9.1	Basics	153
9.1.1	Running coupling	153
9.1.2	Quark masses	154
9.2	Structure of QCD predictions	154
9.2.1	Fully inclusive cross sections	154
9.2.2	Processes with initial-state hadrons	155
9.2.3	Cross sections with phase-space restrictions	157
9.2.4	Accuracy of predictions	161
9.3	Experimental studies of QCD	161
9.3.1	Hadronic final-state observables	162
9.3.2	QCD measurements at colliders	163
9.4	Determinations of the strong coupling constant	167
9.4.1	Hadronic τ decays and low Q^2 continuum:	168
9.4.2	Heavy quarkonia decays:	168
9.4.3	PDF fits:	169
9.4.4	Hadronic final states of e^+e^- annihilations:	169
9.4.5	Observables from hadron-induced collisions:	169
9.4.6	Electroweak precision fit:	171
9.4.7	Lattice QCD:	171
9.4.8	Determination of the world average value of $\alpha_s(m_Z^2)$:	172

9.1 Basics

Quantum Chromodynamics (QCD), the gauge field theory that describes the strong interactions of colored quarks and gluons, is the SU(3) component of the SU(3)×SU(2)×U(1) Standard Model of Particle Physics. The Lagrangian of QCD is given by

$$\mathcal{L} = \sum_q \bar{\psi}_{q,a} (i\gamma^\mu \partial_\mu \delta_{ab} - g_s \gamma^\mu t_{ab}^C A_\mu^C - m_q \delta_{ab}) \psi_{q,b} - \frac{1}{4} F_{\mu\nu}^A F^{A\mu\nu}, \quad (9.1)$$

where repeated indices are summed over. The γ^μ are the Dirac γ -matrices. The $\psi_{q,a}$ are quark-field spinors for a quark of flavor q and mass m_q , with a color-index a that runs from $a = 1$ to $N_c = 3$, *i.e.* quarks come in three “colors.” Quarks are said to be in the fundamental representation of the SU(3) color group.

The A_μ^C correspond to the gluon fields, with C running from 1 to $N_c^2 - 1 = 8$, *i.e.* there are eight kinds of gluon. Gluons transform under the adjoint representation of the SU(3) color group. The t_{ab}^C correspond to eight 3×3 matrices and are the generators of the SU(3) group (*cf.* the section on “SU(3) isoscalar factors and representation matrices” in this *Review*, with $t_{ab}^C \equiv \lambda_{ab}^C/2$). They encode the fact that a gluon’s interaction with a quark rotates the quark’s color in SU(3) space. The quantity g_s (or $\alpha_s = \frac{g_s^2}{4\pi}$) is the QCD coupling constant. Besides quark masses, which have electroweak origin, it is the only fundamental parameter of QCD. Finally, the field tensor $F_{\mu\nu}^A$ is given by

$$F_{\mu\nu}^A = \partial_\mu A_\nu^A - \partial_\nu A_\mu^A - g_s f_{ABC} A_\mu^B A_\nu^C, \quad [t^A, t^B] = i f_{ABC} t^C, \quad (9.2)$$

where the f_{ABC} are the structure constants of the SU(3) group.

Neither quarks nor gluons are observed as free particles. Hadrons are color-singlet (*i.e.* color-neutral) combinations of quarks, anti-quarks, and gluons.

Ab-initio predictive methods for QCD include lattice gauge theory and perturbative expansions in the coupling. The Feynman rules of QCD involve a quark-antiquark-gluon ($q\bar{q}g$) vertex, a 3-gluon vertex (both proportional to g_s), and a 4-gluon vertex (proportional to g_s^2). A full set of Feynman rules is to be found for example in Refs. [1, 2].

Adopting a standard notation where repeated indices are summed over, useful color-algebra relations include: $t_{ab}^A t_{bc}^A = C_F \delta_{ac}$, where $C_F \equiv (N_c^2 - 1)/(2N_c) = 4/3$ is the color factor (“Casimir”) associated with gluon emission from a quark;

$f_{ACD} f_{BCD} = C_A \delta_{AB}$, where $C_A \equiv N_c = 3$ is the color factor associated with gluon emission from a gluon; $t_{ab}^A t_{ab}^B = T_R \delta_{AB}$, where $T_R = 1/2$ is the color factor for a gluon to split to a $q\bar{q}$ pair.

There is freedom for an additional CP -violating term to be present in the QCD Lagrangian, $\theta \frac{g_s^2}{8\pi} F^A \mu\nu \tilde{F}_{\mu\nu}^A$, where θ is an additional free parameter, and $\tilde{F}_{\mu\nu}^A$ is the dual of the gluon field tensor, $\frac{1}{2} \epsilon_{\mu\nu\sigma\rho} F^A \sigma\rho$, with $\epsilon_{\mu\nu\sigma\rho}$ being the fully antisymmetric Levi-Civita symbol. Experimental limits on the electric dipole moment (EDM) of ultracold neutrons [3, 4] and atomic mercury [5] constrain the QCD vacuum angle to satisfy $|\theta| \lesssim 10^{-10}$. For an overview of current and future experiments measuring EDMs see [6]. Further discussion is to be found in Ref. [7] and in the Axions section in the Listings of this *Review*.

This section will concentrate mainly on perturbative aspects of QCD as they relate to collider physics. Related textbooks and lecture notes include Refs. [1, 2, 8–11]. Aspects specific to Monte Carlo event generators are reviewed in the dedicated section 43. Lattice QCD is also reviewed in a section of its own, Sec. 17, with further discussion of perturbative and non-perturbative aspects to be found in the sections on “Quark Masses”, “The CKM quark-mixing matrix”, “Structure functions”, “Fragmentation Functions”, “High Energy Soft QCD and Diffraction”, “Passage of Particles Through Matter” and “Heavy-Quark and Soft-Collinear Effective Theory” in this *Review*.

9.1.1 Running coupling

In the framework of perturbative QCD (pQCD), predictions for observables are expressed in terms of the renormalized coupling $\alpha_s(\mu_R^2)$, a function of an (unphysical) renormalization scale μ_R . When one takes μ_R close to the scale of the momentum transfer Q in a given process, then $\alpha_s(\mu_R^2 \simeq Q^2)$ is indicative of the effective strength of the strong interaction in that process.

The coupling satisfies the following renormalization group equation (RGE):

$$\mu_R^2 \frac{d\alpha_s}{d\mu_R^2} = \beta(\alpha_s) = -(b_0 \alpha_s^2 + b_1 \alpha_s^3 + b_2 \alpha_s^4 + \dots), \quad (9.3)$$

where $b_0 = (11C_A - 4n_f T_R)/(12\pi) = (33 - 2n_f)/(12\pi)$ is referred to as the 1-loop β -function coefficient, the 2-loop coefficient is $b_1 = (17C_A^2 - n_f T_R(10C_A + 6C_F))/(24\pi^2) = (153 - 19n_f)/(24\pi^2)$, and the 3-loop coefficient is $b_2 = (2857 - \frac{5033}{9} n_f + \frac{325}{27} n_f^2)/(128\pi^3)$ for the SU(3) values of C_A and C_F . Here n_f is the number of quark flavors. The 4-loop coefficient, b_3 , is to be found in Refs. [12, 13], while the 5-loop coefficient, b_4 , is in Refs. [14–18]. The coefficients b_2 and b_3 (and beyond) are renormalization-scheme-dependent and given here in the modified minimal subtraction scheme ($\overline{\text{MS}}$) [19], by far the most widely used scheme in QCD and the one adopted in the following.

The minus sign in Eq. (9.3) is the origin of “asymptotic freedom” [20, 21], *i.e.* the fact that the strong coupling becomes weak for processes involving large momentum transfers (“hard processes”). For momentum transfers in the 0.1–1 TeV range, $\alpha_s \sim 0.1$, while the theory is strongly interacting for scales around and below 1 GeV.

The β -function coefficients, the b_i , are given for the coupling of an *effective theory* in which n_f of the quark flavors are considered light ($m_q \ll \mu_R$), and in which the remaining heavier quark flavors decouple from the theory. One may relate the coupling for the theory with $n_f + 1$ light flavors to that with n_f flavors through an equation of the form

$$\alpha_s^{(n_f+1)}(\mu_R^2) = \alpha_s^{(n_f)}(\mu_R^2) \times \left(1 + \sum_{n=1}^{\infty} \sum_{\ell=0}^n c_{n\ell} [\alpha_s^{(n_f)}(\mu_R^2)]^n \ln^\ell \frac{\mu_R^2}{m_h^2} \right), \quad (9.4)$$

where m_h is the mass of the $(n_f + 1)^{\text{th}}$ flavor, and the first few $c_{n\ell}$ coefficients are $c_{11} = \frac{1}{6\pi}$, $c_{10} = 0$, $c_{22} = c_{11}^2$, $c_{21} = \frac{11}{24\pi^2}$, and $c_{20} = -\frac{11}{72\pi^2}$ when m_h is the $\overline{\text{MS}}$ mass at scale m_h , while

$c_{20} = \frac{7}{24\pi^2}$ when m_h is the pole mass (mass definitions are discussed below in Sec. (9.1.2) and in the review on “Quark Masses”). Terms up to $c_{4\ell}$ with $0 \leq \ell \leq 4$ are to be found in Refs. [22, 23]. Numerically, when one chooses $\mu_R = m_h$, the matching is a modest effect, owing to the zero value for the c_{10} coefficient. Relations between n_f and (n_f+2) flavors where the two heavy flavors are close in mass are given to three loops in Ref. [24].

Working in an energy range where the number of flavors is taken constant, a simple exact analytic solution exists for Eq. (9.3) only if one neglects all but the b_0 term, giving $\alpha_s(\mu_R^2) = (b_0 \ln(\mu_R^2/\Lambda^2))^{-1}$. Here Λ is a constant of integration, which corresponds to the scale where the perturbatively-defined coupling would diverge. Its value is indicative of the energy range where non-perturbative dynamics dominates. A convenient approximate analytic solution to the RGE that includes terms up to b_4 is given by solving iteratively Eq. (9.3)

$$\alpha_s(\mu_R^2) \simeq \frac{1}{b_0 t} \left(1 - \frac{b_1 \ell}{b_0^2 t} + \frac{b_1^2 (\ell^2 - \ell - 1) + b_0 b_2}{b_0^4 t^2} + \frac{b_1^3 (-2\ell^3 + 5\ell^2 + 4\ell - 1) - 6b_0 b_2 b_1 \ell + b_0^2 b_3}{2b_0^6 t^3} + \frac{18b_0 b_2 b_1^2 (2\ell^2 - \ell - 1) + b_1^4 (6\ell^4 - 26\ell^3 - 9\ell^2 + 24\ell + 7)}{6b_0^8 t^4} + \frac{-b_0^2 b_3 b_1 (12\ell + 1) + 2b_0^2 (5b_2^2 + b_0 b_4)}{6b_0^8 t^4} \right), \quad (9.5)$$

with $t \equiv \ln \frac{\mu^2}{\Lambda^2}$ and $\ell = \ln t$, again parameterized in terms of a constant Λ . Note that Eq. (9.5) is one of several possible approximate 4-loop solutions for $\alpha_s(\mu_R^2)$, and that a value for Λ only defines $\alpha_s(\mu_R^2)$ once one knows which particular approximation is being used. An alternative to the use of formulas such as Eq. (9.5) is to solve the RGE exactly, numerically (including the discontinuities, Eq. (9.4), at flavor thresholds). In such cases the quantity Λ does not directly arise (though it can be defined, cf. Eqs. (1–3) of Ref. [25]). For these reasons, in determinations of the coupling, it has become standard practice to quote the value of α_s at a given scale (typically the mass of the Z boson, m_Z) rather than to quote a value for Λ .

A discussion of determinations of the coupling and a graph illustrating its scale dependence (“running”) are to be found in Section 9.4.

9.1.2 Quark masses

Free quarks have never been observed, which is understood as a result of a long-distance, confining property of the strong QCD force: up, down, strange, charm, and bottom quarks all *hadronize*, i.e. become part of a meson or baryon, on a timescale $\sim 1/\Lambda$; the top quark instead decays before it has time to hadronize. This means that the question of what one means by the quark mass is a complex one, which requires one to adopt a specific prescription. A perturbatively defined prescription is the pole mass, m_q , which corresponds to the position of the divergence of the quark propagator. This is close to one’s physical picture of mass. However, when relating it to observable quantities, it suffers from a badly behaved perturbative series which makes it ambiguous to an amount related to Λ (see e.g. Ref. [26–28]). An alternative is the $\overline{\text{MS}}$ mass, $\overline{m}_q(\mu_R^2)$, which depends on the renormalization scale μ_R .

Results for the masses of heavier quarks are often quoted either as the pole mass or as the $\overline{\text{MS}}$ mass evaluated at a scale equal to the mass, $\overline{m}_q(\overline{m}_q^2)$; light quark masses are often quoted in the $\overline{\text{MS}}$ scheme at a scale $\mu_R \sim 2 \text{ GeV}$. The pole and $\overline{\text{MS}}$ masses are related by a series that starts as $m_q = \overline{m}_q(\overline{m}_q^2) \left(1 + \frac{4\alpha_s(\overline{m}_q^2)}{3\pi} + \mathcal{O}(\alpha_s^2) \right)$, while the scale-dependence of $\overline{\text{MS}}$ masses is given at lowest order by

$$\mu_R^2 \frac{d\overline{m}_q(\mu_R^2)}{d\mu_R^2} = \left[-\frac{\alpha_s(\mu_R^2)}{\pi} + \mathcal{O}(\alpha_s^2) \right] \overline{m}_q(\mu_R^2). \quad (9.6)$$

A more detailed discussion is to be found in a dedicated section of the *Review*, “Quark Masses”, with detailed formulas also in Ref. [29] and references therein.

In perturbative QCD calculations of scattering processes, it is customary to employ an approximation where the masses of all quarks, whose magnitudes are much smaller than the momentum transfer involved in the process, are neglected or set to zero.

9.2 Structure of QCD predictions

9.2.1 Fully inclusive cross sections

The simplest observables in perturbative QCD are those that do not depend on the initial-state hadrons and are fully inclusive, disregarding specific details of the final state. An example of such an observable is the total cross section for the process $e^+e^- \rightarrow$ hadrons at a center-of-mass energy Q . It can be expressed as follows:

$$\frac{\sigma(e^+e^- \rightarrow \text{hadrons}, Q)}{\sigma(e^+e^- \rightarrow \mu^+\mu^-, Q)} \equiv R(Q) = R_{\text{EW}}(Q)(1 + \delta_{\text{QCD}}(Q)), \quad (9.7)$$

where $R_{\text{EW}}(Q)$ is the purely electroweak prediction for the ratio and $\delta_{\text{QCD}}(Q)$ is the correction due to QCD effects.

For the sake of simplicity, we can focus on energies where $Q \ll m_Z$, where the primary contribution to the process comes from photon exchange (while disregarding electroweak and finite-quark-mass corrections) denoted as $R_{\text{EW}} = N_c \sum_q e_q^2$, with e_q representing the electric charges of the quarks. The QCD correction reads

$$\delta_{\text{QCD}}(Q) = \sum_{n=1}^{\infty} c_n \cdot \left(\frac{\alpha_s(Q^2)}{\pi} \right)^n + \mathcal{O} \left(\frac{\Lambda^4}{Q^4} \right). \quad (9.8)$$

The first four terms in the α_s series expansion are [30]

$$c_1 = 1, \quad c_2 = 1.9857 - 0.1152n_f, \quad (9.9a)$$

$$c_3 = -6.63694 - 1.20013n_f - 0.00518n_f^2 - 1.240\eta, \quad (9.9b)$$

$$c_4 = -156.61 + 18.775n_f - 0.7974n_f^2 + 0.0215n_f^3 - (17.828 - 0.575n_f)\eta, \quad (9.9c)$$

with $\eta = (\sum e_q)^2 / (N_c \sum e_q^2)$ and $N_c = 3$. For corresponding expressions including also Z exchange and finite-quark-mass effects, see Refs. [31–33].

A related series holds also for the QCD corrections to the hadronic decay width of the τ lepton, which essentially involves an integral of $R(Q)$ over the allowed range of invariant masses of the hadronic part of the τ decay (see e.g. Ref. [34]). The series expansions for QCD corrections to Higgs-boson hadronic (partial) decay widths in the limit of heavy top quark and massless light flavors at $N^4\text{LO}$ are given in Ref. [35].

One characteristic feature of Eqs. (9.8) and (9.9) is that the coefficients of α_s^n increase order by order: calculations in perturbative QCD tend to converge more slowly than would be expected based just on the size of α_s . The situation is significantly worse near thresholds or in the presence of tight kinematic cuts. Another feature is the existence of an extra “power-correction” term $\mathcal{O}(\Lambda^4/Q^4)$ in Eq. (9.8), which accounts for contributions that are fundamentally non-perturbative. All high-energy QCD predictions involve power corrections $(\Lambda/Q)^p$, although typically the suppression of these corrections with Q is smaller than given in Eq. (9.8), where $p = 4$. The exact power p depends on the observable and, for many processes and observables, it is possible to introduce an operator product expansion and associate power-suppressed terms with specific higher-dimension (non-perturbative) operators [36].

Scale dependence. In Eq. (9.8) the renormalization scale for α_s has been chosen equal to Q . The result can also be expressed in terms of the coupling at an arbitrary renormalization scale μ_R ,

$$\delta_{\text{QCD}}(Q) = \sum_{n=1}^{\infty} \bar{c}_n \left(\frac{\mu_R^2}{Q^2} \right) \cdot \left(\frac{\alpha_s(\mu_R^2)}{\pi} \right)^n + \mathcal{O} \left(\frac{\Lambda^4}{Q^4} \right), \quad (9.10)$$

where $\bar{c}_1(\mu_R^2/Q^2) \equiv c_1$, $\bar{c}_2(\mu_R^2/Q^2) = c_2 + \pi b_0 c_1 \ln(\mu_R^2/Q^2)$, $\bar{c}_3(\mu_R^2/Q^2) = c_3 + (2b_0 c_2 \pi + b_1 c_1 \pi^2) \times \ln(\mu_R^2/Q^2) + b_0^2 c_1 \pi^2 \ln^2(\mu_R^2/Q^2)$, etc. Given an infinite number of terms in the α_s expansion, the μ_R dependence of the $\bar{c}_n(\mu_R^2/Q^2)$ coefficients will exactly cancel that of $\alpha_s(\mu_R^2)$, and the final result will be independent of the choice of μ_R : physical observables do not depend on unphysical scales.¹

With just terms up to some finite $n = N$, a residual μ_R dependence will remain, which implies an uncertainty on the prediction of $R(Q)$ due to the arbitrariness of the scale choice. This uncertainty will be $\mathcal{O}(\alpha_s^{N+1})$, *i.e.* of the same order as the neglected higher-order terms. For this reason it is customary to use the scale dependence of QCD predictions as an estimate of the uncertainties due to neglected terms. One usually takes a central value for $\mu_R \sim Q$, in order to avoid the poor convergence of the perturbative series that results from the large $\ln^{n-1}(\mu_R^2/Q^2)$ terms in the \bar{c}_n coefficients when $\mu_R \ll Q$ or $\mu_R \gg Q$. Uncertainties are then commonly determined by varying μ_R by a factor of two up and down around the central scale choice. This is not a rigorous prescription for determining the uncertainty, but is motivated by the requirement that there should not be large logarithms introduced into a calculation by large ratios of scales. A more detailed discussion on the accuracy of theoretical predictions and on ways to estimate the theoretical uncertainties can be found in Section 9.2.4.

9.2.2 Processes with initial-state hadrons

Deep-Inelastic Scattering. To illustrate the key features of QCD cross sections in processes with initial-state hadrons, let us consider deep-inelastic scattering (DIS), $e + p \rightarrow e + X$, where an electron e with four-momentum k emits a highly off-shell photon (momentum q) that interacts with the proton (momentum p). For photon virtualities $Q^2 \equiv -q^2$ far above the squared proton mass (but far below the squared Z mass), the differential cross section in terms of the kinematic variables Q^2 , $x = Q^2/(2p \cdot q)$ and $y = (q \cdot p)/(k \cdot p)$ is

$$\frac{d^2\sigma}{dx dQ^2} = \frac{4\pi\alpha^2}{2xQ^4} \left[(1 + (1-y)^2) F_2(x, Q^2) - y^2 F_L(x, Q^2) \right], \quad (9.11)$$

where α is the electromagnetic coupling and $F_2(x, Q^2)$ and $F_L(x, Q^2)$ are proton structure functions, which encode the interaction between the photon and the proton. In the presence of parity-violating interactions (*e.g.* νp scattering) an additional F_3 structure function is present. For an extended review, including equations for the full electroweak and polarized cases, see Sec. 18 of this *Review*.

Structure functions are not calculable in perturbative QCD, nor is any other cross section that involves QCD interactions and initial-state hadrons. To zeroth order in α_s , the structure functions are given directly in terms of non-perturbative parton (quark or gluon) distribution functions (PDFs),

$$F_2(x, Q^2) = x \sum_q e_q^2 f_{q/p}(x), \quad F_L(x, Q^2) = 0, \quad (9.12)$$

where $f_{q/p}(x)$ is the non-perturbative PDF for quarks of type q inside the proton, *i.e.* the number density of quarks of type q inside a fast-moving proton that carry a fraction x of its longitudinal momentum.

PDFs are primarily determined from data in global fits. PDF sets are available at different orders in perturbation theory (LO, NLO and NNLO) based on the order at which cross sections used in the fits are calculated. The evolution equations for the PDFs from one scale to another matches the perturbative accuracy of the cross sections. In modern global PDF fits, data are included from

DIS, Drell-Yan (DY), jets and $t\bar{t}$ processes, and more LHC collider data, with the global PDF fits using 3000-4000 data points. There is a large change in the PDFs from LO to NLO, with a much smaller change from NLO to NNLO. LO PDFs can be unreliable for collider predictions, especially at low and high x . The uncertainties for the resulting PDFs are determined primarily from the experimental uncertainties of the data that serve as input to the global PDF fits. There is also a component due to the limitations of the parameterizations used, as discussed *e.g.* in Ref. [37], although this may be reduced with the use of more flexible forms. The PDF uncertainties can either be determined through a Hessian approach or through the use of Monte Carlo replicas. It is now relatively straightforward to convert results from one approach to the other. There has been a recent combination (PDF4LHC21) of the CT18, MSHT20 and NNPDF3.1 PDFs, each produced from a global PDF fit, that serves to provide a more comprehensive view of both the central PDFs and of their uncertainties [38]. Recently, theoretical uncertainties related to missing higher orders have been included in global PDF determinations but so far only at NLO [39–42]. By tying renormalization scales for related processes, and factorization scales for all processes, together in the global fit, an estimate of the higher order uncertainties can be added to the PDF fit. An alternative approach [43] is to attempt to deal with cross sections rather than PDFs themselves.

Another approach is to use as much available information as possible from N³LO to examine the impact of such information on the resultant PDFs [44]. The result, of course, is sensitive to the higher order information that is still missing, for example from an incomplete knowledge of the splitting functions and the N³LO matrix elements.

Since the original work of Ref. [45], one of the intriguing questions is whether lattice calculations can provide valuable insights for extracting PDFs. Despite initial debates surrounding the underlying methodologies [46, 47], it is now understood that lattice data in Euclidean space can be connected to light-cone PDFs through factorization theorems, once lattice observables have been renormalized and extrapolated to the continuum limit [48]. Initial determinations based on lattice data have begun to emerge [48–61], and the comparisons with determinations based on conventional data show great promise. However, the uncertainties in lattice-based determinations are still quite large, therefore, for practical applications, PDFs are currently derived from global fits of experimental data (*cf.* Sec. 18 of this *Review* and also Refs. [62, 63]). It is likely that lattice simulations for light-cone PDFs will have an impact in the short-medium term if they focus on flavor components (strange and charm) and on the kinematic regions that are poorly covered by the experimental data [64]. Similarly, lattice determinations of transverse momentum dependent PDF (TMDs) and generalized parton distributions (GPDs) will be more relevant for phenomenology since the experimental data for these quantities are much less abundant and precise.

The result in Eq.(9.12), with PDFs $f_{q/p}(x)$ that are independent of the scale Q , corresponds to the “quark-parton model” picture, in which the photon interacts with point-like free quarks, or equivalently, one has incoherent elastic scattering between the electron and individual constituents of the proton. As a consequence, in this picture also F_2 and F_L are independent of Q [65]. When including higher orders in pQCD, one has

$$F_2(x, Q^2) = x \sum_{n=0}^{\infty} \frac{\alpha_s^n(\mu_R^2)}{(2\pi)^n} \times \sum_{i=q,g} \int_x^1 \frac{dz}{z} C_{2,i}^{(n)}(z, Q^2, \mu_R^2, \mu_F^2) f_{i/p}\left(\frac{x}{z}, \mu_F^2\right) + \mathcal{O}\left(\frac{\Lambda^2}{Q^2}\right). \quad (9.13)$$

Just as in Eq. (9.10), we have a series in powers of $\alpha_s(\mu_R^2)$, each term involving a coefficient $C_{2,i}^{(n)}$ that can be calculated using Feynman diagrams. At variance with the parton model, the PDFs in pQCD depend on an additional scale, the factorization scale μ_F , whose significance will be discussed in the following. Another important difference is the additional integral over z .

¹ With respect to pQCD there is an important caveat to this statement: at sufficiently high orders, perturbative series generally suffer from “renormalon” divergences $\alpha_s^n n!$ (reviewed in Ref. [26]). This phenomenon is not usually visible with the limited number of perturbative terms available today. However, it is closely connected with non-perturbative contributions and sets a limit on the possible precision of perturbative predictions. The cancellation of scale dependence will also ultimately be affected by this renormalon-induced breakdown of perturbation theory.

The parton that comes from the proton can undergo a splitting before it enters the hard scattering. As a result, the $C_{2,i}^{(n)}$ coefficients are functions that depend on the ratio, z , of the parton's momentum before and after radiation, and one must integrate over that ratio. For the electromagnetic component of DIS with light quarks and gluons, the zeroth order coefficient functions are $C_{2,q}^{(0)} = e_q^2 \delta(1-z)$ and $C_{2,g}^{(0)} = 0$. Corrections are known up to $\mathcal{O}(\alpha_s^3)$ (next-to-next-to-next-to-leading order, N³LO) for both electromagnetic [66] and weak currents [67, 68]. For heavy-quark production they are known to $\mathcal{O}(\alpha_s^2)$ [69, 70] (next-to-leading order, NLO, insofar as the series starts at $\mathcal{O}(\alpha_s)$). The current status of the theoretical description of unpolarized and polarized DIS is summarized in Ref. [71]. For precise comparisons of LHC cross sections with theoretical predictions, the photon PDF of the proton is also needed. It has been computed precisely in Ref. [72, 73] and has now been implemented in most global PDF fits. More recently, the PDF for leptons has also been computed [74]. The photon PDF has an elastic and an inelastic component, where the photon is generated from the intact proton or from the splitting of quarks inside the proton, respectively, while the lepton PDF is generated by photons splitting to collinear leptons.

The majority of the emissions that modify a parton's momentum are collinear (parallel) to that parton, and do not depend on whether the parton will interact with a photon. It is natural to view these emissions as modifying the proton's structure rather than being part of the coefficient function for the parton's interaction with the photon. Technically, one uses a procedure known as *collinear factorization* to give a well-defined meaning to this distinction, most commonly through the $\overline{\text{MS}}$ factorization scheme, defined in the context of dimensional regularization. The $\overline{\text{MS}}$ factorization scheme involves an arbitrary choice of *factorization scale*, μ_F , whose meaning can be understood roughly as follows: emissions with transverse momenta above μ_F are included in the $C_{2,q}^{(n)}(z, Q^2, \mu_R^2, \mu_F^2)$; emissions with transverse momenta below μ_F are accounted for within the PDFs, $f_{i/p}(x, \mu_F^2)$. While collinear factorization is generally believed to be valid for suitable (sufficiently inclusive) observables in processes with hard scales, Ref. [75], which reviews the factorization proofs in detail, is cautious in the statements it makes about their exhaustivity, notably for the hadron-collider processes which we shall discuss below. Interesting considerations on the current status of our understanding of factorization can be found in Refs. [76, 77]. While the transverse degrees of freedom have been integrated over for collinear PDFs, it is also possible to produce transverse-momentum dependent (or unintegrated) PDFs where these degrees of freedom remain. For a recent comprehensive review of transverse-momentum-dependent parton distribution functions and fragmentation functions see Ref. [78].

For collinear PDFs, the resulting dependence on μ_F is described by the Dokshitzer-Gribov-Lipatov-Altarelli-Parisi (DGLAP) equations [79], which to leading order (LO) read²

$$\mu_F^2 \frac{\partial f_{i/p}(x, \mu_F^2)}{\partial \mu_F^2} = \sum_j \frac{\alpha_s(\mu_F^2)}{2\pi} \int_x^1 \frac{dz}{z} P_{i \leftarrow j}^{(1)}(z) f_{j/p}\left(\frac{x}{z}, \mu_F^2\right), \quad (9.14)$$

with, for example, $P_{q \leftarrow g}^{(1)}(z) = T_R(z^2 + (1-z)^2)$. The other LO splitting functions are listed in Sec. 18 of this *Review*, while results up to NLO, α_s^2 , and NNLO, α_s^3 , are given in Refs. [80] and [81] respectively. At N³LO accuracy, only partial results are currently available in Refs. [82–86]. Splitting functions for PDFs in the helicity dependent case are given in Ref. [87].

Beyond LO, the coefficient functions are also μ_F dependent, for example $C_{2,i}^{(1)}(x, Q^2, \mu_R^2, \mu_F^2) = C_{2,i}^{(1)}(x, Q^2, \mu_R^2, Q^2) - \ln\left(\frac{\mu_F^2}{Q^2}\right) \sum_j \int_x^1 \frac{dz}{z} \times C_{2,j}^{(0)}\left(\frac{x}{z}\right) P_{j \leftarrow i}^{(1)}(z)$. Progress in higher-order QED and mixed QED-QCD corrections to the splitting functions can be found in refs. [88, 89].

As with the renormalization scale, the choice of factorization scale is arbitrary, but if one has an infinite number of terms in the

perturbative series, the μ_F -dependencies of the coefficient functions and PDFs will compensate each other fully. Given only N terms of the series, a residual $\mathcal{O}(\alpha_s^{N+1})$ uncertainty is associated with the ambiguity in the choice of μ_F . As with μ_R , varying μ_F provides an input in estimating uncertainties on predictions. In inclusive DIS predictions, the default choice for the scales is usually $\mu_R = \mu_F = Q$.

As is the case for the running coupling, in DGLAP evolution one can introduce flavor thresholds near the heavy quark masses: below a given heavy quark's mass, that quark is not considered to be part of the proton's structure, while above it is considered to be part of the proton's structure and evolves with massless DGLAP splitting kernels. With appropriate parton distribution matching terms at threshold, such a variable flavor number scheme (VFNS), when used with massless coefficient functions, gives the full heavy-quark contributions at high Q^2 scales. For scales near the threshold, it is instead necessary to appropriately adapt the standard massive coefficient functions to account for the heavy-quark contribution already included in the PDFs [90–92].

At sufficiently small x and Q^2 in inclusive DIS, resummation of small x logarithms may be necessary [93, 94]. This may in fact have been observed in Refs. [95] based on HERA data [96], in a kinematic region where useful information for PDFs for collider predictions is present.

In situations, in which the center-of-mass energy \sqrt{s} is much larger than all other momentum-transfer scales in the problem (*e.g.* Q in DIS, m_b for $b\bar{b}$ production in pp collisions, *etc.*), each power of α_s beyond LO can be accompanied by a power of $\ln(s/Q^2)$ (or $\ln(s/m_b^2)$, *etc.*). This is variously referred to as the high-energy, small- x or Balitsky-Fadin-Kuraev-Lipatov (BFKL) limit [94, 97, 98]. Currently it is possible to account for the dominant and first sub-dominant [99, 100] power of such logarithms at each order of α_s , and also to estimate further sub-dominant contributions that are numerically large (see Refs. [101–104] and references therein). Progress towards NNLO is discussed in Ref. [105].

Physically, the summation of all orders in α_s can be understood as leading to a growth with s of the gluon density in the proton. At sufficiently high energies this implies non-linear effects (commonly referred to as parton saturation), whose treatment has been the subject of intense study (see for example Refs. [106–108] and references thereto).

Hadron-hadron collisions.

The extension to processes with two initial-state hadrons can be illustrated with the example of the total (inclusive) cross section for W boson production in collisions of hadrons h_1 and h_2 , which can be written as

$$\begin{aligned} \sigma(h_1 h_2 \rightarrow W + X) &= \sum_{n=0}^{\infty} \alpha_s^n(\mu_R^2) \\ &\times \sum_{i,j} \int dx_1 dx_2 f_{i/h_1}(x_1, \mu_F^2) f_{j/h_2}(x_2, \mu_F^2) \\ &\times \hat{\sigma}_{ij \rightarrow W+X}^{(n)}(x_1 x_2 s, \mu_R^2, \mu_F^2) + \mathcal{O}\left(\frac{\Lambda^2}{m_W^4}\right), \end{aligned} \quad (9.15)$$

where s is the squared center-of-mass energy of the collision. At LO, $n = 0$, the hard (partonic) cross section $\hat{\sigma}_{ij \rightarrow W+X}^{(0)}(x_1 x_2 s, \mu_R^2, \mu_F^2)$ is simply proportional to $\delta(x_1 x_2 s - m_W^2)$, in the narrow W -boson width approximation (see Sec. 51 of this *Review* for detailed expressions for this and other hard scattering cross sections). It is non-zero only for choices of i, j that can directly give a W , such as $i = u, j = \bar{d}$. At higher orders, $n \geq 1$, new partonic channels contribute, such as gq , and $x_1 x_2 s \geq m_W^2$ in the narrow W -boson width approximation.

Equation (9.15) involves a collinear factorization between the hard cross section and the PDFs, just like Eq. (9.13). As long as the same factorization scheme is used in DIS and pp or $p\bar{p}$ (usually the $\overline{\text{MS}}$ scheme), then PDFs extracted in DIS can be directly used in pp and $p\bar{p}$ predictions [75, 109] (with the anti-quark distributions

²LO is generally taken to mean the lowest order at which a quantity is non-zero.

in an anti-proton being the same as the quark distributions in a proton).

A number of fully inclusive cross-sections have been computed up to N³LO, *i.e.* including corrections up to relative order α_s^3 , in recent years. These include inclusive Higgs production through gluon fusion in the large m_t limit, calculated at N³LO in Refs. [110, 111]. Higgs boson pair production via gluon fusion in the same approximation was computed at N³LO in Ref. [112]. Calculations at this order, differential in the Higgs rapidity [113, 114] and fully differential [115] have been presented recently. Bottom-induced Higgs boson production has also been computed at N³LO [116]. Vector-boson fusion single- [117] and double-pair [118] production is also known to N³LO [117] in the factorized approximation. Neutral [119, 120] and charged [121] Drell-Yan processes, as well as associated Higgs production [116] have also been computed at N³LO. Differential rapidity distributions are available, but not yet with fiducial cuts. A number of public codes are now available which allow for phenomenological studies at N³LO [116, 117, 122–124]. The uncertainty band derived by varying the renormalization and factorization scales in the perturbative predictions is not always contained within the corresponding uncertainty band of the previous order, as might be expected from a well-behaved process. This has been ascribed to cancellations between channels at NNLO that lead to underestimates of the uncertainty at that order. This effect does not seem to be present in other processes, such as Higgs boson production through gluon-gluon fusion. Note that there is currently a mis-match in N³LO calculations in that PDFs at the same order are not yet available. Preliminary approximated N³LO PDFs [44] suggest that N³LO effects can be large, especially as far as heavy-quark distributions and low scales are concerned, as well as the gluon distribution in a region important for Higgs boson production through gluon-gluon fusion. The fully inclusive hard cross sections for several other processes are known to NNLO,³ for instance, Higgs-boson production in association with a vector boson [125], Higgs-pair production in the large m_t approximation [126], and with full m_t dependence [127], top-antitop production [128, 129], bottom-anti-bottom production [130] and vector-boson pair production [131–133]. For a comprehensive overview on other recent NNLO 2 → 2 calculations see Ref. [134, 135]. Other NNLO calculations with fiducial cuts will be discussed in Sec. 9.2.3.

Photoproduction.

γp (and $\gamma\gamma$) collisions are similar to pp collisions, with the subtlety that the photon can behave in two ways: there is “direct” photoproduction, in which the photon behaves as a point-like particle and takes part directly in the hard collision, with hard subprocesses such as $\gamma g \rightarrow q\bar{q}$; there is also resolved photoproduction, in which the photon behaves like a hadron, with non-perturbative partonic substructure and a corresponding PDF for its quark and gluon content, $f_{i/\gamma}(x, Q^2)$. While useful to understand the general structure of γp collisions, the distinction between direct and resolved photoproduction is not well defined beyond leading order, as discussed for example in Ref. [136].

9.2.3 Cross sections with phase-space restrictions

QCD final states always consist of hadrons, while perturbative QCD calculations deal with partons. Physically, an energetic parton fragments (“showers”) into many further partons, which then, on later timescales, undergo a transition to hadrons (“hadronization”). Fixed-order perturbation theory captures only a small part of these dynamics. This does not matter for the fully inclusive cross sections discussed above: the showering and hadronization stages are approximately unitary, *i.e.* they do not substantially change the overall probability of hard scattering, because they occur long after it has taken place (they introduce at most a correction proportional to a power of the ratio of timescales involved, *i.e.* a power of Λ/Q , where Q is the hard scattering scale).

Less inclusive measurements, in contrast, may be affected by the extra dynamics. For those sensitive just to the main directions

of energy flow (jet rates, event shapes, *cf.* Sec. 9.3.1) fixed-order perturbation theory is often still adequate, because showering and hadronization do not substantially change the overall energy flow. This means that one can make a prediction using just a small number of partons, which should correspond well to a measurement of the same observable carried out on hadrons. For observables that instead depend on distributions of individual hadrons (which, *e.g.*, are the inputs to detector simulations), it is mandatory to account for showering and hadronization. The range of predictive techniques available for QCD final states reflects this diversity of needs of different measurements.

While illustrating the different methods, we shall for simplicity mainly use expressions that hold for e^+e^- scattering. The extension to cases with initial-state partons will be mostly straightforward (space constraints unfortunately prevent us from addressing diffraction and exclusive hadron-production processes; extensive discussion is to be found in Sec. 20 of this *Review* and in Refs. [137, 138]).

9.2.3.1 Soft and collinear limits

Before examining specific predictive methods, it is useful to be aware of a general property of QCD matrix elements in the soft and collinear limits. Consider a squared tree-level matrix element $|M_n^2(p_1, \dots, p_n)|$ for the process $e^+e^- \rightarrow n$ partons with momenta p_1, \dots, p_n , and a corresponding phase-space integration measure $d\Phi_n$. If particle n is a gluon, which becomes collinear (parallel) to another particle i and additionally its momentum tends to zero (is “soft”), the matrix element simplifies as follows,

$$\lim_{\theta_{in} \rightarrow 0, E_n \rightarrow 0} d\Phi_n |M_n^2(p_1, \dots, p_n)| = d\Phi_{n-1} |M_{n-1}^2(p_1, \dots, p_{n-1})| \frac{\alpha_s C_i}{\pi} \frac{d\theta_{in}^2}{\theta_{in}^2} \frac{dE_n}{E_n}, \quad (9.16)$$

where $C_i = C_F$ (C_A) if i is a quark (gluon). This formula has non-integrable divergences both for the inter-parton angle $\theta_{in} \rightarrow 0$ and for the gluon energy $E_n \rightarrow 0$, which are mirrored also in the structure of divergences in loop diagrams. These divergences are important for at least two reasons: firstly, they govern the typical structure of events (inducing many emissions either with low energy or at small angle with respect to hard partons); secondly, they will determine which observables can be calculated within fixed-order perturbative QCD.

9.2.3.2 Fixed-order predictions

Let us consider an observable \mathcal{O} that is a function $\mathcal{O}_n(p_1, \dots, p_n)$ of the four-momenta of the n final-state particles in an event (either partons or hadrons). In what follows, we shall consider the cross section for events weighted with the value of the observable, $\sigma_{\mathcal{O}}$. As examples, if $\mathcal{O}_n \equiv 1$ for all n , then $\sigma_{\mathcal{O}}$ is just the total cross section; if $\mathcal{O}_n \equiv \hat{\tau}(p_1, \dots, p_n)$ where $\hat{\tau}$ is the value of the thrust for that event (see Eq. (9.22) in Sec. 9.3.1.2), then the average value of the thrust is $\langle \tau \rangle = \sigma_{\mathcal{O}} / \sigma_{\text{tot}}$; if $\mathcal{O}_n \equiv \delta(\tau - \hat{\tau}(p_1, \dots, p_n))$ then one gets the differential cross section as a function of the thrust, $\sigma_{\mathcal{O}} \equiv d\sigma/d\tau$.

In the expressions below, we shall omit to write the non-perturbative power correction term, which for most common observables is proportional to a single power of Λ/Q .

Leading Order. If the observable \mathcal{O} is non-zero only for events with at least n final-state particles, then the LO QCD prediction for the weighted cross section in e^+e^- annihilation is

$$\sigma_{\mathcal{O}}^{\text{LO}} = \alpha_s^{n-2}(\mu_R^2) \int d\Phi_n |M_n^2(p_1, \dots, p_n)| \mathcal{O}_n(p_1, \dots, p_n), \quad (9.17)$$

where the squared tree-level matrix element, $|M_n^2(p_1, \dots, p_n)|$, including relevant symmetry factors, has been summed over all subprocesses (*e.g.* $e^+e^- \rightarrow q\bar{q}q\bar{q}$, $e^+e^- \rightarrow q\bar{q}gg$) and has had all factors of α_s extracted in front. In processes other than e^+e^- collisions, the center-of-mass energy of the LO process is generally not fixed, and so the powers of the coupling are often brought inside the integrals, with the scale μ_R chosen event by event, as a function of the event kinematics.

³Processes with jets or photons in the final state have divergent cross sections unless one places a cut on the jet or (dressed) photon momentum. Accordingly, they are discussed below in Section 9.2.3.2.

Other than in the simplest cases (see the review on Cross Sections in this *Review*), the matrix elements in Eq. (9.17) are usually calculated automatically with programs such as CompHEP [139], MADGRAPH [140], ALPGEN [141], COMIX/SHERPA [142], and HELAC/PHEGAS [143]. Some of these (CompHEP, MADGRAPH) use formulas obtained from direct evaluations of Feynman diagrams. Others (ALPGEN, HELAC/PHEGAS and COMIX/SHERPA) use methods designed to be particularly efficient at high multiplicities, such as Berends-Giele recursion [144], which builds up amplitudes for complex processes from simpler ones (see also Refs. [145–147] for other tree-level calculational methods).

The phase-space integration is usually carried out by Monte Carlo sampling, because of the high dimensionality of the integration and in order to deal with the possibly involved kinematic cuts that are used in the corresponding experimental measurements. Perturbatively calculable observables should be insensitive to the emission of soft and collinear radiation. Because of the divergences in the matrix element, Eq. (9.16), at lowest order the integral converges only if the observable vanishes for kinematic configurations in which one of the n particles is arbitrarily soft or it is collinear to another particle. As an example, the cross section for producing any configuration of n partons will lead to an infinite integral, whereas a finite result will be obtained for the cross section for producing n deposits of energy (or jets, see Sec. 9.3.1.1), each above some energy threshold and well separated from each other in angle.

At a practical level, LO calculations can be carried out for $2 \rightarrow n$ processes with $n \lesssim 6 - 10$. The exact upper limit depends on the process, the method used to evaluate the matrix elements (recursive methods are more efficient), and the extent to which the phase-space integration can be optimized to work around the large variations in the values of the matrix elements.

NLO. Given an observable that is non-zero starting from n final-state particles, its prediction at NLO involves supplementing the LO result, Eq. (9.17), with the $2 \rightarrow (n+1)$ -particle squared tree-level matrix element ($|M_{n+1}^2|$), and the interference of a $2 \rightarrow n$ tree-level and $2 \rightarrow n$ 1-loop amplitude ($2\text{Re}(M_n M_{n,1\text{-loop}}^*)$),

$$\begin{aligned} \sigma_{\mathcal{O}}^{\text{NLO}} &= \sigma_{\mathcal{O}}^{\text{LO}} + \alpha_s^{n-1} (\mu_R^2) \int d\Phi_{n+1} |M_{n+1}^2(p_1, \dots, p_{n+1})| \\ &\quad \times \mathcal{O}_{n+1}(p_1, \dots, p_{n+1}) + \alpha_s^{n-1} (\mu_R^2) \\ &\quad \times \int d\Phi_n 2\text{Re} [M_n(p_1, \dots, p_n) M_{n,1\text{-loop}}^*(p_1, \dots, p_n)] \\ &\quad \times \mathcal{O}_n(p_1, \dots, p_n) . \end{aligned} \quad (9.18)$$

Relative to LO calculations, two important issues appear in the NLO calculations. Firstly, the extra complexity of loop-calculations relative to tree-level calculations means that automated calculations started to appear only about fifteen years ago (see below). Secondly, loop amplitudes are infinite in four dimensions, while tree-level amplitudes are finite, but their *integrals over the phase space* are infinite, due to the divergences of Eq. (9.16). These two sources of infinities have the same soft and collinear origins and cancel after the integration only if the observable \mathcal{O} satisfies the property of infrared and collinear safety, which means that the observable is non-sensitive to soft emissions or to collinear splittings, *i.e.*

$$\begin{aligned} \mathcal{O}_{n+1}(p_1, \dots, p_s, \dots, p_n) &\rightarrow \mathcal{O}_n(p_1, \dots, p_{s-1}, p_{s+1}, \dots, p_n) \\ &\quad \text{if } p_s \rightarrow 0 \\ \mathcal{O}_{n+1}(p_1, \dots, p_a, p_b, \dots, p_n) &\rightarrow \mathcal{O}_n(p_1, \dots, p_a + p_b, \dots, p_n) \\ &\quad \text{if } p_a \parallel p_b . \end{aligned} \quad (9.19)$$

Examples of infrared-safe quantities include event-shape distributions and jet cross sections (with appropriate jet algorithms, see below). Unsafe quantities include the distribution of the momentum of the hardest QCD particle (which is not conserved under collinear splitting), observables that require the complete ab-

sence of radiation in some region of phase space (*e.g.* rapidity gaps or 100% isolation cuts, which are affected by soft emissions), or the particle multiplicity (affected by both soft and collinear emissions). The non-cancellation of divergences at NLO due to infrared or collinear unsafety compromises the usefulness not only of the NLO calculation, but also that of a LO calculation, since LO is only an acceptable approximation if one can prove that higher-order terms are smaller. Infrared and collinear unsafety usually also implies large non-perturbative effects.

As with LO calculations, the phase-space integrals in Eq. (9.18) are usually carried out by Monte Carlo integration, so as to facilitate the study of arbitrary observables. Various methods exist to obtain numerically efficient cancellation among the different infinities. These include notably dipole [148], FKS [149] and antenna [150] subtraction.

Thanks to new ideas like the OPP method [151], generalized [152] and D -dimensional [153] unitarity, on-shell methods [154], and on-the-fly reduction algorithms [155], recent years have seen a breakthrough in the calculation of one-loop matrix elements (for reviews on unitarity based method see Ref. [156, 157]). Thanks to these innovative methods, automated tools for NLO calculations have been developed and a number of programs are available publicly: MADGRAPH5_aMC@NLO [140] and HELAC-NLO [158] provide full frameworks for NLO calculations; GoSAM [159], NJET [160], OPENLOOPS [161] and RECOLA [162] calculate just the 1-loop part and are typically interfaced with an external tool for a combination with the appropriate tree-level amplitudes. Other tools such as NLOJET++ [163], MCFM [164], VBFNLO [165], the PHOX family [166] or BLACKHAT [167] implement analytic calculations and provide full frameworks to compute NLO cross sections for selected classes of processes. Recently, a lot of attention has also been paid to the calculation of NLO electroweak corrections. Electroweak corrections are especially important for transverse momenta significantly above the W and Z masses, because they are enhanced by two powers of $\ln p_t/m_W$ for each power of the electroweak coupling, and close to Sudakov peaks⁴, where most of the data lie and the best experimental precision can be achieved. In some cases the above programs can be used to calculate also NLO electroweak or beyond-standard-model corrections [168–174].

Given the progress in QCD and EW fixed-order computations, the largest unknown from fixed-order corrections is often given by the mixed QCD-electroweak corrections of $\mathcal{O}(\alpha_s \alpha)$. These mixed two-loop corrections are often available in an approximate form [175–188]. The first complete computation of the mixed QCD–EW corrections to the neutral-current Drell–Yan process appeared recently [189–191]. For a review on EW corrections to collider processes see Ref. [192].

NNLO. NNLO is considerably more complicated than NLO as it involves a further order in α_s , consisting of: the squared $(n+2)$ -parton tree-level amplitude, the interference of the $(n+1)$ -parton tree-level and 1-loop amplitudes, the interference of the n -parton tree-level and 2-loop amplitudes, and the squared n -parton 1-loop amplitude.

Each of these elements involves large numbers of soft and collinear divergences, satisfying relations analogous to Eq. (9.16) which now involve multiple collinear or soft particles and higher loop orders (see *e.g.* Refs. [193–195]). Arranging for the cancellation of the divergences after numerical Monte Carlo integration has been one of the significant challenges of NNLO calculations, as has been the determination of the relevant 2-loop amplitudes. For the cancellations of divergences a wide range of methods has been developed. Some of them [196–205] retain the approach, inherent in NLO methods, of directly combining the separate loop and tree-level amplitudes. Others combine a suitably chosen, partially inclusive $2 \rightarrow n$ NNLO calculation with a fully differential $2 \rightarrow n+1$ NLO calculation [206–212]. The q_T -subtraction method was extended to deal with mixed QCD–QED corrections at NNLO [213]. For an overview of NNLO subtraction methods see Ref [214].

Quite a number of processes have been calculated differentially at NNLO so far. The state of the art for e^+e^- collisions is $e^+e^- \rightarrow$

⁴For the definition of Sudakov form factors or Sudakov peaks see *e.g.* Refs. [1, 2, 11].

3 jets [215–218].

For DIS, dijet production is known at NNLO [219, 220] and the description jet production has been recently pushed even to N³LO using the Projection-to-Born method [221, 222]. For hadron colliders, all $2 \rightarrow 1$ processes are known, specifically vector boson [223, 224] and Higgs boson production in the large m_t limit [206, 225]. The finite top-mass corrections at this order have also been computed [226]. This calculation eliminates one important source of theoretical uncertainty to inclusive Higgs production at the LHC. Substantial progress has been made in the years for hadron-collider $2 \rightarrow 2$ processes, with calculations having been performed for nearly all relevant processes: ZZ [132] WW [131] and WZ [227], $\gamma\gamma$ [228, 229], $Z\gamma$ [230] and $W\gamma$ [231] (many of these color singlet processes are available also in MCFM [232, 233] or MATRIX [133]), inclusive photon [234, 235], γ +jet [235, 236], W +jet [208, 237], Z +jet [236, 238, 239] H +jet [240–243], WH [244] and ZH [245], s -channel [246] and t -channel single-top [247–250], $t\bar{t}$ production [251, 252], dijet production [253, 254], W production in association with a c -jet [255, 256] and HH [126] (in large-top-mass approximation, see also the exact (two-loop) NLO result [127]). Recently, also the NNLO corrections to identified B -hadron hadro-production have been computed [257]. The frontier of NNLO calculation has now reached the complexity of $2 \rightarrow 3$ processes. The first $2 \rightarrow 3$ process known at NNLO has been Higgs production through vector-boson fusion, using an approximation in which the two underlying DIS-like $q \rightarrow qV$ scatterings are factorized, the so-called structure function approximation [211, 258]. Corrections beyond the structure function approximation are expected to be small, on the order of a percent or less [259]. More recently, first genuine $2 \rightarrow 3$ LHC processes have been described at NNLO accuracy, including three photon [260, 261], two photons and one jet [262], two jets and one photon [263], three-jets [264] and $Wb\bar{b}$ production [265]. The calculation of three-jet production might be relevant for future extractions of $\alpha_s(m_Z^2)$ from three-jet observables at the LHC [266].

Cross sections at the LHC are most often measured with fiducial cuts, for example on the transverse momenta and rapidities of the measured objects, restricting the measurement to regions where the objects have a good efficiency to be detected and are well-reconstructed. Ideally, the theoretical predictions should also be constructed at the same fiducial level; the other possibility is to extrapolate the experimental fiducial results to the full phase space. Such an extrapolation, however, requires the extrapolation (typically using a parton shower Monte Carlo) to be accurate over the full phase space.

Comparisons of fixed order predictions to fiducial measurements can sometimes result in the presence of large logarithms which degrade the accuracy of the prediction. Such is the case, for example, in the calculation of the Higgs rapidity distribution, in the diphoton final state. The imposition of transverse momenta and rapidity cuts on the two photons leads to an uncertainty notably greater at N³LO than at NNLO, due to the presence of these logs. One possible solution is to change the form of the kinematic cut on the photons, to a product of the two photon transverse momenta [267], reducing the impact of the logs; another solution is to perform a resummation of the logs, restoring the expected precision [268].

The Les Houches precision wishlist compiles predictions needed to fully exploit the data that will be taken at the High Luminosity LHC [269]. Most of the needed calculations require accuracy of at least NNLO QCD and NLO EW, and many require the prediction of $2 \rightarrow 3$ processes, such as $W/Z + \geq 2$ jets, $H + \geq 2$ jets, and $t\bar{t}H$ to NNLO. The latter process has been computed at NNLO in Ref. [270] in the approximation where the Higgs boson in the double-virtual contribution is soft. This calculation considerably reduces the theory uncertainty on this process.

As discussed in this section, calculations at NLO can now be relatively easily generated by non-experts using the programs mentioned above. By now there are also a number of publicly available tools to compute a range of processes at NNLO accuracy in QCD, such as EERAD3 [216] (for e^+e^- collisions), [206], DYNLO [224], DYTURBO [271], FEHIP [225], FEWZ [272], HTURBO [273], MATRIX [133], MCFM [233] or SUSHI [124, 274]. However, in some

cases NNLO calculations can be too complex and CPU-intensive to allow such an approach. In these cases, the relevant matrix element information for a specific observable can be stored by means of interpolation grids developed originally for cross sections at NLO [275–277] and recently extended to include electroweak corrections [278]. The application to NNLO has been demonstrated for $t\bar{t}$ and for DIS jet cross sections in Refs. [279, 280]. Each such interpolation grid corresponds to one fixed observable with specific selection criteria and binning, but is flexible with respect to the renormalization or factorization scale, the PDF, or the α_s evolution chosen for the cross-section computation. An even more flexible method, at the cost of requiring large amounts of storage space, saves huge numbers of partonic events in the form of ROOT n-tuples, which allow predictions to be generated on-the-fly for many observables of a particular process [281, 282]. Recent developments of both techniques for pp collisions at NNLO are described in Ref. [269].

9.2.3.3 Resummation

Many experimental measurements place tight constraints on emissions in the final state. For example, in e^+e^- events, that (one minus) the thrust should be less than some value $\tau \ll 1$, or, in $pp \rightarrow Z$, events that the Z -boson transverse momentum or the transverse momentum of the accompanying jet should be much smaller than the Z -boson mass. A further example is the production of heavy particles or jets near threshold (so that little energy is left over for real emissions) in DIS and pp collisions.

In such cases, the constraint vetoes a significant part of the integral over the soft and collinear divergence of Eq. (9.16). As a result, there is only a partial cancellation between real emission terms (subject to the constraint) and loop (virtual) contributions (not subject to the constraint), causing each order of α_s to be accompanied by a large coefficient $\sim L^2$, where *e.g.* $L = \ln \tau$ or $L = \ln(m_Z/p_t^2)$. One ends up with a perturbative series, whose terms go as $\sim (\alpha_s L^2)^n$. It is not uncommon that $\alpha_s L^2 \gg 1$, so that the perturbative series converges very poorly if at all.⁵ In such cases one may carry out a “resummation”, which accounts for the dominant logarithmically enhanced terms to all orders in α_s , by making use of known properties of matrix elements for multiple soft and collinear emissions, and of the all-orders properties of the divergent parts of virtual corrections, following original works such as Refs. [283–292] and also through soft-collinear effective theory [293, 294] (*cf.* also the section on “Heavy-Quark and Soft-Collinear Effective Theory” in this *Review*, as well as Ref. [295]).

For cases with double logarithmic enhancements (two powers of logarithm per power of α_s), there are two classification schemes for resummation accuracy. Writing the cross section including the constraint as $\sigma(L)$ and the unconstrained (total) cross section as σ_{tot} , the series expansion takes the form

$$\sigma(L) \simeq \sigma_{\text{tot}} \sum_{n=0}^{\infty} \sum_{k=0}^{2n} R_{nk} \alpha_s^n (\mu_R^2) L^k, \quad L \gg 1, \quad (9.20)$$

and leading log (LL) resummation means that one accounts for all terms with $k = 2n$, next-to-leading-log (NLL) includes additionally all terms with $k = 2n - 1$, *etc.* Often $\sigma(L)$ (or its Fourier or Mellin transform) *exponentiates*,⁶

$$\sigma(L) \simeq \sigma_{\text{tot}} \exp \left[\sum_{n=1}^{\infty} \sum_{k=0}^{n+1} G_{nk} \alpha_s^n (\mu_R^2) L^k \right], \quad L \gg 1, \quad (9.21)$$

where one notes the different upper limit on k ($\leq n+1$) compared to Eq. (9.20). This is a more powerful form of resummation: the

⁵To be precise one should be aware of two causes of the divergence of perturbative series. That which interests us here is associated with the presence of a new large parameter (*e.g.* ratio of scales). It is distinct from the “renormalon” induced factorial divergences of perturbation theory discussed above.

⁶Whether or not this happens depends on the quantity being resummed. A classic example involves two-jet rate in e^+e^- collisions as a function of a jet-resolution parameter y_{cut} . The logarithms of $1/y_{\text{cut}}$ exponentiate for the k_t (Durham) jet algorithm [296], but not [297] for the JADE algorithm [298] (both are discussed below in Sec. 9.3.1.1).

G_{12} term alone reproduces the full LL series in Eq. (9.20). With the form Eq. (9.21) one still uses the nomenclature LL, but this now means that all terms with $k = n + 1$ are included, and NLL implies all terms with $k = n$, *etc.*

For a large number of observables, NLL resummations are available in the sense of Eq. (9.21) (see Refs. [299–301] and references therein). NNLL has been achieved for the DY and Higgs-boson p_t distributions [302–305] (also available in the CuTe [306], HRes [307] and ResBos [308] families of programs and also differentially in vector-boson decay products [309]) and related variables [310], for the p_t of vector-boson pairs [311, 312], for the back-to-back energy-energy correlation in e^+e^- [313], the jet broadening in e^+e^- collisions [314], the jet-veto survival probability in Higgs and Z boson production in pp collisions [315–317],⁷ an event-shape type observable known as the beam thrust [318], hadron-collider jet masses in specific limits [319] (see also Ref. [320]), the production of top anti-top pairs near threshold [321–323] (and references therein), and high- p_t W and Z production [324]. Automation of NNLL jet-veto resummations for different processes has been achieved in Ref. [325] (*cf.* also the NLL automation in Ref. [326]), while automation for a certain class of e^+e^- observables has been achieved in Ref. [327]. N³LL resummations are available for the thrust variable, C-parameter and heavy-jet mass in e^+e^- annihilations [328–330], for p_t distribution of the Higgs boson [331, 332] and weak gauge bosons [333–335] and for Higgs- and vector-boson production near threshold [336]. In order to make better contact with experimental measurements, recent years have seen an increasing interest in resummations in exclusive phase-space regions and joint resummations [337–346]. Finally, there has also been considerable progress in resummed calculations for jet substructure, whose observables involve more complicated definitions than is the case for standard resummations, see *e.g.* Refs. [347–351] and references therein (see also Sec. 9.3.1.3).

9.2.3.4 Fragmentation functions

Since the parton-hadron transition is non-perturbative, it is not possible to perturbatively calculate quantities such as the energy-spectra of specific hadrons in high-energy collisions. However, one can factorize perturbative and non-perturbative contributions via the concept of fragmentation functions. These are the final-state analogue of the parton distribution functions which are used for initial-state hadrons. Like parton distribution functions, they depend on a (fragmentation) factorization scale and satisfy a DGLAP evolution equation.

It should be added that if one ignores the non-perturbative difficulties and just calculates the energy and angular spectrum of partons in perturbative QCD with some low cutoff scale $\sim \Lambda$ (using resummation to sum large logarithms of \sqrt{s}/Λ), then this reproduces many features of the corresponding hadron spectra [352]. This is often taken to suggest that hadronization is “local”, in this sense it mainly involves partons that are close both in position and in momentum.

Section 19 of this *Review* provides further information and references on these topics, including also the question of heavy-quark fragmentation.

9.2.3.5 Parton-shower Monte Carlo event generators

Parton-shower Monte Carlo (MC) event generators like PYTHIA [353–355], HERWIG [356–358], and SHERPA [359]⁸ provide fully exclusive simulations of QCD events at the level of measurable particles, the so-called “particle level” or “hadron level”. Here, “measurable” refers to color-neutral particles with mean lifetimes τ long enough to be associated with tracks or decay vertices in particle detectors. Usually, this requires mean decay lengths $c\tau$ of around 10 mm. As such MC event generators are a crucial tool for all applications that involve simulating the response of detectors

⁷A veto on the jet phase space can be severe, for example by requiring exactly zero jets above a given transverse momentum cut accompanying a Higgs boson, or relatively mild, for example by placing a transverse momentum cut of 30 GeV on the measurement of the production of a Higgs boson with one or more jets. In general, inclusive cross sections are preferable, as uncertainties on both the theoretical and experimental sides are smaller.

⁸The program ARIADNE [360] has also been widely used for simulating e^+e^- and DIS collisions.

to QCD events. Here we give only a brief outline of how they work and refer the reader to Sec. 43 and Ref. [361] for a full overview.

In general, we expect parton-shower matched predictions to differ from the underlying fixed-order results in regions where (1) there is a large sensitivity to jet shapes (for instance small R jets), (2) there is a restriction in phase space such that soft gluon resummation effects become important, (3) the observable contains multiple disparate scales, (4) there are perturbative instabilities at fixed order, *e.g.* related to kinematical cuts, and (5) the observable is sensitive to higher multiplicity states than those described by the fixed-order calculation (for an explicit study of some of these effects see *e.g.* [362]).

The MC generation of an event involves several stages. It starts with the random generation of the kinematics and partonic channels of whatever *hard scattering process* the user has requested at some high scale Q_0 (for complex processes, this may be carried out by an external program). This is followed by a *parton shower*, usually based on the successive random generation of gluon emissions (and $g \rightarrow q\bar{q}$ splittings). Leading contributions to the shower have emissions that are ordered according to some ordering variable. Common choices of scale for the ordering of emissions are virtuality, transverse momentum or angle. Each emission is generated at a scale lower than the previous emission, following a (soft and collinear resummed) perturbative QCD distribution, which depends on the momenta of all previous emissions. Parton showering stops at a scale of order 1 GeV, at which point a *hadronization model* is used to convert the resulting partons into hadrons. One widely-used model involves stretching a color “string” across quarks and gluons, and breaking it up into hadrons [363, 364]. Another breaks each gluon into a $q\bar{q}$ pair and then groups quarks and anti-quarks into colorless “clusters”, which then give the hadrons [356]. As both models are tuned primarily to LEP data, the cluster and string models provide similar results for most observables sensitive to hadronization [362]. For pp and γp processes, modeling is also needed to treat the collision between the two hadron remnants, which generates an *underlying event* (UE), usually implemented via additional $2 \rightarrow 2$ scatterings (“multiple parton interactions”, MPI) at a scale of a few GeV, following Ref. [365]. The parameter values for the MPI models must be determined from fits to minimum-bias and/or underlying-event observables of LHC collision data. As the different MC event generators are adapted to essentially the same measurements, ideally the respective MPI implementations should lead to similar predictions for each program. One complication, however, is some non-universality of the underlying event among different physics processes.

A deficiency of the soft and collinear approximations that underlie parton showers is that they may fail to reproduce the full pattern of hard wide-angle emissions, important, for example, in many new physics searches. It is therefore common to use LO multi-parton matrix elements to generate hard high-multiplicity partonic configurations as additional starting points for the showering, supplemented with some prescription (CKKW [366], MLM [367]) for consistently merging samples with different initial multiplicities. Monte Carlo generators, as described above, compute cross sections for the requested hard process that are correct at LO.

A wide variety of processes are available in MC implementations that are correct to NLO, using the MC@NLO [368] or POWHEG [369] prescriptions, through the MADGRAPH5_aMC@NLO [140], POWHEG-BOX [370] and SHERPA [142] programs. Techniques have also been developed to combine NLO plus parton shower accuracy for different multiplicities of final-state jets [371]. While NLO+PS accurate predictions can now be implemented in the above tools rather easily and are available for a range of processes, given the advances in NNLO calculations it is natural to seek for NNLO+PS accurate Monte Carlos as well. The two main approaches today are the MiNNLO [372] and Geneva [373] ones. NNLO plus shower accuracy was achieved first for Drell-Yan and Higgs production [374, 375] and is now available for several $2 \rightarrow 2$ color singlet processes [376–390], as well as for heavy-quark pair-production [391–393].

It is important to understand/verify the accuracy of the par-

ton shower predictions in the Monte Carlo programs. A general framework for assessing the logarithmic accuracy of parton-shower algorithms has been formulated, based on their ability to reproduce the singularity structure of multi-parton matrix elements, and their ability to reproduce logarithmic resummation results [394]. The dominant contributions relevant for the extension of parton showers to higher logarithmic accuracy have been computed [395–399] and included in some algorithms.

There exist ways to improve on current parton-shower algorithms [400, 401] and to demonstrate the parton shower accuracy through a comparison to analytic next-to-leading logarithmic calculations for a range of observables [401]. Considerable progress has been achieved in recent years [400–412]. References [401, 404, 405, 408, 409] introduced the first shower implementations towards NLL, but these implementations did not include spin-correlation effects and lacked full color dependence at LL level. Ref. [402] incorporated full color effects at the NLL level, while spin correlations at NLL were included in Refs. [406, 407], resulting in an NLL accurate parton shower for proton-proton collisions [410, 411]. The modifications necessary for processes such as Deep Inelastic Scattering (DIS) and Vector Boson Fusion (VBF) are addressed in [412]. The next steps involve incorporating non-perturbative effects, accounting for quark masses, and tuning NLL parton shower on experimental data.

9.2.4 Accuracy of predictions

Estimating the accuracy of perturbative QCD predictions is not an exact science. It is often said that LO calculations are accurate to within a factor of two. This is based on experience with NLO corrections in the cases where these are available. In processes involving new partonic scattering channels at NLO and/or large ratios of scales (such as jet observables in processes with vector bosons, or the production of high- p_t jets containing B -hadrons), the ratio of the NLO to LO predictions, commonly called the “ K factor”, can be substantially larger than two. NLO corrections tend to be large for processes for which there is a great deal of color annihilation in the interaction. In addition, NLO corrections tend to decrease as more final state legs are added.

For calculations beyond LO, one approach to estimate the perturbative uncertainty is to base it on the last known perturbative correction; this may lead to misleading results if new sub-processes are present at the next-higher order. A more widely used method is to estimate it from the change in the prediction when varying the renormalization and factorization scales around a central value Q that is taken close to the physical scale of the process. A conventional range of variation is $Q/2 < \mu_R, \mu_F < 2Q$, varying the two scales independently with the restriction $\frac{1}{2}\mu_R < \mu_F < 2\mu_R$ [413]. This constraint limits the risk of misleadingly small uncertainties due to fortuitous cancellations between the μ_F and μ_R dependence when both are varied together, while avoiding the appearance of large logarithms of μ_R^2/μ_F^2 when both are varied completely independently. Where possible, it can be instructive to examine the two-dimensional scale distributions (μ_R vs. μ_F) to obtain a better understanding of the interplay between μ_R and μ_F . This procedure should not be assumed to always estimate the full uncertainty from missing higher orders, but it does indicate the size of one important known source of higher-order ambiguity.⁹

Most $2 \rightarrow 2$ processes at the LHC are now known to NNLO. This typically results in a large reduction in the uncertainty from that obtained at NLO. However, care must be taken in the estimate of the uncertainty in processes containing jets, as accidental cancellations of the scale uncertainties may result an artificial reduction of the scale uncertainty; for some jet R values, the uncertainty may even be zero. There are several possibilities for providing a more realistic estimate of the scale uncertainty for such processes [362], but none have been widely adopted at the LHC.

Calculations that involve resummations usually have an additional source of uncertainty associated with the choice of argument of the logarithms being resummed, e.g. $\ln(2 \frac{p_t^Z}{m_Z})$ as opposed

to $\ln(\frac{1}{2} \frac{p_t^Z}{m_Z})$, as well as a prescription to switch off resummation effects when the logarithm is not large. In addition to varying renormalization and factorization scales, it is common practice to vary the argument of the logarithm by a suitable factor in either direction with respect to the default argument.

The accuracy of QCD predictions is limited also by non-perturbative (or hadronization) corrections, which typically scale as a power of Λ/Q .¹⁰ For measurements that are directly sensitive to the structure of the hadronic final state, the corrections are usually linear in Λ/Q . The non-perturbative corrections are further enhanced in processes with a significant underlying event (i.e. in pp and $p\bar{p}$ collisions) and the impact of non-perturbative corrections is larger in cases where the perturbative cross sections fall steeply as a function of p_t or some other kinematic variable, for example in inclusive jet p_t or dijet mass spectra. Under high-luminosity running conditions, such as 13 TeV at the LHC, there can be on the order of 50 minimum-bias interactions occurring at each beam-beam crossing. This additional energy needs to be subtracted, and is typically removed by means of a rapidity-dependent transverse energy density determined on an event-by-event basis [419]. This subtraction, of necessity, also removes the underlying event, which must be added back in by means of MC event generator modelling if one wants to restore the measured event to the particle level.

Non-perturbative corrections are commonly estimated from the difference between Monte Carlo events at the “parton level” and at particle level. Parton level refers to the stage of the parton shower, where the evolution is stopped at an energy scale of typical hadron masses of a few GeV. An issue to be aware of is that “parton level” is not a uniquely defined concept. For example, in a MC event generator such a procedure depends on an arbitrary and tunable internal cutoff scale that separates the parton showering from the hadronization. In contrast, no such cutoff scale exists in an NLO or NNLO partonic calculation. The uncertainties in these corrections are often estimated by comparing different tunes of the various MC event generators. It should be noted that such estimates are not guaranteed to fully cover the true uncertainties.

Alternative methods exist for estimating hadronization corrections, that attempt to analytically deduce non-perturbative effects in one observable based on measurements of other observables (see the reviews [26, 420]). While they directly address the problem of different possible definitions of parton level, it should also be said that they are far less flexible than Monte Carlo programs and not always able to provide equally good descriptions of the data.

One of the main issues is whether the fixed-order partonic final state of a NLO or NNLO prediction can match the parton shower in its ability to describe the experimental jet shape (minus any underlying event). Calculations at NNLO provide a better match to the parton shower predictions than do NLO ones, as might be expected from the additional gluon available to describe the jet shape. The hadronization predictions appear to work for both orders, but at an unknown accuracy.

9.3 Experimental studies of QCD

Since we are not able to directly measure partons (quarks or gluons), but only hadrons and their decay products, a central issue for every experimental study of perturbative QCD is establishing a correspondence between observables obtained at the parton and the hadron level. The only theoretically sound correspondence is achieved by means of *infrared and collinear safe* quantities, which allow one to obtain finite predictions at any order of perturbative QCD.

As stated above, the simplest case of infrared- and collinear-safe observables are inclusive cross sections. More generally, when measuring fully inclusive observables, the final state is not analyzed at all regarding its (topological, kinematical) structure or its composition. Basically the relevant information consists in the rate of a process ending up in a partonic or hadronic final state. In e^+e^- annihilation, widely used examples are the ratios of partial widths or branching ratios for the electroweak decay of particles into hadrons or leptons, such as Z or τ decays, (cf. Sec. 9.2.1).

⁹Various studies have been carried out on how to estimate uncertainties from missing higher orders that go beyond scale variations [414–418].

¹⁰In some circumstances, the scale in the denominator could be a smaller kinematic or physical scale that depends on the observable.

Such ratios are often favored over absolute cross sections or partial widths because of large cancellations of experimental and theoretical systematic uncertainties. The strong suppression of non-perturbative effects, $\mathcal{O}(\Lambda^4/Q^4)$, is one of the attractive features of such observables, however, at the same time, the sensitivity to radiative QCD corrections is small, which for example leads to a larger statistical uncertainty when using them for the determination of the strong coupling constant. In the case of τ decays not only the hadronic branching ratio is of interest, but also moments of the spectral functions of hadronic τ decays, which sample different parts of the decay spectrum and thus provide additional information. Other examples of fully inclusive observables are structure functions (and related sum rules) in DIS. These are extensively discussed in Sec. 18 of this *Review*.

On the other hand, often the structure or composition of the final state are analyzed, and cross sections differential in one or more variables characterizing this structure are of interest. Examples are jet rates, jet substructure, event shapes or transverse momentum distributions of jets or vector bosons in hadron collisions. The case of fragmentation functions, *i.e.* the measurement of hadron production as a function of the hadron momentum relative to some hard scattering scale, is discussed in Sec. 19 of this *Review*.

It is worth mentioning that, besides the correspondence between the parton and hadron level, also a correspondence between the hadron level and the actually measured quantities in the detector has to be established. The simplest examples are corrections for finite experimental acceptance and efficiencies. Whereas acceptance corrections essentially are of theoretical nature, since they involve extrapolations from the measurable (partial) to the full phase space, other corrections such as for efficiency, resolution and response are of experimental nature. For example, measurements of differential cross sections such as jet rates require corrections in order to relate, *e.g.*, the energy deposits in a calorimeter to the jets at the hadron level. Typically detector simulations and/or data-driven methods are used in order to obtain these corrections. Care should be taken here in order to have a clear separation between the parton-to-hadron level and hadron-to-detector level corrections. Finally, for the sake of an easy comparison to the results of other experiments and/or theoretical calculations, it is suggested to provide, whenever possible, measurements corrected for detector effects and/or all necessary information related to the detector response (*e.g.*, the detector response matrix). Any fiducial phase space for measurements should be defined as close as possible to the detector-level selection in order to minimize model-dependent extrapolations. A versatile repository for storing such information is the use of Rivet routines [421].

9.3.1 Hadronic final-state observables

9.3.1.1 Jets

In hard interactions, final-state partons and hadrons appear predominantly in collimated bunches, which are generically called *jets*. To a first approximation, a jet can be thought of as a hard parton that has undergone soft and collinear showering and then hadronization. Jets are used both for testing our understanding and predictions of high-energy QCD processes, and also for identifying the hard partonic structure of decays of massive particles such as top quarks and W, Z and Higgs bosons.

In order to map observed hadrons onto a set of jets, one uses a *jet definition*. The mapping involves explicit choices: for example when a gluon is radiated from a quark, for what range of kinematics should the gluon be part of the quark jet, or instead form a separate jet? Good jet definitions are infrared and collinear safe, simple to use in theoretical and experimental contexts, applicable to any type of inputs (parton or hadron momenta, charged particle tracks, and/or energy deposits in the detectors) and lead to jets that are not too sensitive to non-perturbative effects.

An extensive treatment of the topic of jet definitions is given in Ref. [422] (for e^+e^- collisions) and Refs. [423–425]. Here we briefly review the two main classes: cone algorithms, extensively used at hadron colliders before the LHC, and sequential recombination algorithms, more widespread in e^+e^- and ep colliders and at the LHC.

Very generically, most (iterative) cone algorithms start with

some seed particle i , sum the momenta of all particles j within a cone of opening-angle R , typically defined in terms of differences in rapidity and azimuthal angle. They then take the direction of this sum as a new seed and repeat until the direction of the cone is stable, and call the contents of the resulting stable cone a jet if its transverse momentum is above some threshold $p_{t,\min}$. The parameters R and $p_{t,\min}$ should be chosen according to the needs of a given analysis.

There are many variants of the cone algorithm, and they differ in the set of seeds they use and the manner in which they ensure a one-to-one mapping of particles to jets, given that two stable cones may share particles (“overlap”). The use of seed particles is a problem w.r.t. infrared and collinear safety. Seeded algorithms are generally not compatible with higher-order (or sometimes even leading-order) QCD calculations, especially in multi-jet contexts, as well as potentially subject to large non-perturbative corrections and instabilities. Seeded algorithms (JetCLU, MidPoint, and various other experiment-specific iterative cone algorithms) are therefore to be deprecated. Such algorithms are not used at the LHC, but were at the Fermilab Tevatron, where data still provide useful information, for example for global PDF fits.¹¹ A modern alternative is to use a seedless variant, SIScone [427].

Sequential recombination algorithms at hadron colliders (and in DIS) are characterized by a distance $d_{ij} = \min(k_{t,i}^{2p}, k_{t,j}^{2p})\Delta_{ij}^2/R^2$ between all pairs of particles i, j , where Δ_{ij} is their separation in the rapidity-azimuthal plane, $k_{t,i}$ is the transverse momentum w.r.t. the incoming beams, and R is a free parameter. At the LHC, R is typically in the range from 0.4 to 0.8, although analyses can also use jet sizes up to 1.0–1.2. They also involve a “beam” distance $d_{iB} = k_{t,i}^{2p}$. One identifies the smallest of all the d_{ij} and d_{iB} , and if it is a d_{ij} , then i and j are merged into a new pseudo-particle (with some prescription, a recombination scheme, for the definition of the merged four-momentum). If the smallest distance is a d_{iB} , then i is removed from the list of particles and called a jet. As with cone algorithms, one usually considers only jets above some transverse-momentum threshold $p_{t,\min}$. The parameter p determines the kind of algorithm: $p = 1$ corresponds to the (*inclusive*-) k_t algorithm [296, 428, 429], $p = 0$ defines the *Cambridge-Aachen* algorithm [430, 431], while for the *anti*- k_t algorithm $p = -1$ [432]. All these variants are infrared and collinear safe. Whereas the former two lead to irregularly shaped jet boundaries, the latter results in cone-like boundaries, except in situations where there are nearby jets. The *anti*- k_t algorithm has become the de-facto standard for the LHC experiments.

In e^+e^- annihilation the k_t algorithm [296] uses $y_{ij} = 2 \min(E_i^2, E_j^2)(1 - \cos\theta_{ij})/Q^2$ as distance measure between two particles/partons i and j and repeatedly merges the pair with smallest y_{ij} , until all y_{ij} distances are above some threshold y_{cut} , the jet resolution parameter. Q is a measure of the overall hardness of the event. The (pseudo)-particles that remain at this point are called the jets. Here it is y_{cut} (rather than R and $p_{t,\min}$) that should be chosen according to the needs of the analysis. The two-jet rate in the k_t algorithm has the property that logarithms $\ln(1/y_{\text{cut}})$ exponentiate. This is one reason why it is preferred over the earlier JADE algorithm [298], which uses the distance measure $y_{ij} = 2 E_i E_j (1 - \cos\theta_{ij})/Q^2$. Note that other variants of sequential recombination algorithms for e^+e^- annihilations, using different definitions of the resolution measure y_{ij} , exhibit much larger sensitivities to fragmentation and hadronization effects than the k_t and JADE algorithms [433]. Efficient implementations of the above algorithms are available through the *FastJet* package [434].

While building infrared (IR) safe jets is generally considered a solved problem, this is not quite the case when one also wishes to assign a flavor to a jet. In fact, the general experimental definition considers a flavored-jet to be a jet that contains at least one flavor tag (such as a B or D meson) above a given transverse momentum threshold. Because of collinear or soft wide-angle $g \rightarrow q\bar{q}$ splittings, it is easy to see that such a definition is neither collinear nor infrared safe. This problem was addressed

¹¹In the data, the difference between the use of the Midpoint algorithm and the use of the SIScone algorithm is small [426], allowing the use of the SIScone algorithm for any theory comparisons at higher order in QCD.

in Ref. [435, 436] in the context of heavy-flavor production at the Tevatron. However, the jet-algorithm proposed in that work was impractical to implement experimentally because it was based on the k_t -algorithm. Furthermore, it required tagging two nearby flavored hadrons and involved a rather complex beam-distance measure. Since most experimental studies instead rely on the anti- k_t algorithm, recent investigations have focused on developing algorithms that preserve the anti- k_t kinematics of the jets while assigning jet flavors in an infrared safe way [437–439]. It turns out that the problem is more involved than anticipated, and a formulation of infrared-safe anti- k_t -like jets could only be achieved by introducing an interleaved flavor neutralization procedure [440]. An unfolding procedure will be necessary to convert experimental measurements of flavor- k_t jets to a form that can be directly compared to theoretical predictions.

9.3.1.2 Event Shapes

Event-shape variables are functions of the four momenta of the particles in the final state and characterize the topology of an event’s energy flow. They are sensitive to QCD radiation (and correspondingly to the strong coupling) insofar as gluon emission changes the shape of the energy flow.

The classic example of an event shape is the *thrust* [441, 442] in e^+e^- annihilations, defined as

$$\hat{\tau} = \max_{\vec{n}_\tau} \frac{\sum_i |\vec{p}_i \cdot \vec{n}_\tau|}{\sum_i |\vec{p}_i|}, \quad (9.22)$$

where \vec{p}_i are the momenta of the particles or the jets in the final-state and the maximum is obtained for the thrust axis \vec{n}_τ . In the Born limit of the production of a perfect back-to-back $q\bar{q}$ pair, the limit $\hat{\tau} \rightarrow 1$ is obtained, whereas a perfectly spherical many-particle configuration leads to $\hat{\tau} \rightarrow 1/2$. Further event shapes of similar nature have been extensively measured at LEP and at HERA, and for their definitions and reviews we refer to Refs. [1, 8, 420, 443, 444]. The energy-energy correlation function [445], namely the energy-weighted angular distribution of produced hadron pairs, and its associated asymmetry are further shape variables which have been studied in detail at e^+e^- colliders. For hadron colliders the appropriate modification consists in only taking the transverse momentum component [446]. The event shape variable *N-jettiness* has been proposed [447], that measures the degree to which the hadrons in the final state are aligned along N jet axes or the beam direction. It vanishes in the limit of exactly N infinitely narrow jets.

Phenomenological discussions of event shapes at hadron colliders can be found in Refs. [447–451]. Measurements of hadronic event-shape distributions have been published by CDF [452], ATLAS [453–459] and CMS [460–463].

Event shapes are used for many purposes. These include measuring the strong coupling (see *e.g.* Ref. [459]), tuning the parameters of Monte Carlo programs, investigating analytical models of hadronization and distinguishing QCD events from events that might involve decays of new particles (giving event-shape values closer to the spherical limit).

9.3.1.3 Jet substructure, quark vs. gluon jets

Jet substructure, which can be resolved by finding subjets or by measuring jet shapes, is sensitive to the details of QCD radiation in the shower development inside a jet and has been extensively used to study differences in the properties of quark and gluon induced jets, strongly related to their different color charges. There is clear experimental evidence that gluon jets have a softer particle spectrum and are “broader” than (light-) quark jets (as expected from perturbative QCD) when looking at observables such as the jet shape $\Psi(r/R)$ (see *e.g.* Ref. [464]). This is the fraction of transverse momentum contained within a sub-cone of cone-size r for jets of cone-size R . It is sensitive to the relative fractions of quark and gluon jets in an inclusive jet sample and receives contributions from soft-gluon initial-state radiation and the underlying event. Therefore, it has been widely employed for validation and tuning of Monte Carlo parton-shower models. Furthermore, this quantity turns out to be sensitive to the modification of the gluon radiation pattern in heavy ion collisions (see *e.g.* Ref. [465]).

Jet shape measurements using proton-proton collision data have been presented for inclusive jet samples [466–468] and for top-quark production [469]. Further discussions, references and summaries can be found in Refs. [444, 470–472] and Sec. 4 of Ref. [473].

The use of jet substructure has also been investigated in order to distinguish QCD jets from jets that originate from hadronic decays of boosted massive particles (high- p_t electroweak bosons, top quarks and hypothesized new particles). A considerable number of experimental studies have been carried out with Tevatron and LHC data, in order to investigate the performance of the proposed algorithms for resolving jet substructure and to apply them to searches for new physics, as well as to the reconstruction of boosted top quarks, vector bosons and the Higgs boson. For reviews of this rapidly growing field, see Sec. 5.3 of Ref. [423], Refs. [350, 351, 473–479] and references thereto. One convenient representation for visualizing jet substructure is through the Lund plane [480]. From a theoretical perspective, the Lund plane would be constructed using quarks and gluons, but similar observables can be constructed through the use of jets, as described in detail in Ref. [481].

Neural network techniques and deep learning methods have also been applied to jet and top physics and jet substructure, see *e.g.* Refs. [482–485]. Perhaps no other sub-field has benefited as much from machine learning techniques as the study of jet substructure. As a jet can have $O(100)$ constituents each with kinematic and other information, jet substructure analysis is naturally a highly multivariate problem. Deep learning techniques can use all of the available information to study jets in their natural high dimensionality. Such techniques have not only improved discrimination between different final states/types of jets, but have also improved our understanding of perturbative QCD. See for example the review in Ref. [349].

9.3.2 QCD measurements at colliders

There exists a wealth of data on QCD-related measurements in e^+e^- , ep , pp , and $p\bar{p}$ collisions, to which a short overview like this would not be able to do any justice. Reviews of the subject have been published in Refs. [443, 444] for e^+e^- colliders and in Ref. [486] for ep scattering, whereas for hadron colliders overviews are given in, *e.g.*, Refs. [424, 471] and Refs. [2, 11, 487–489].

Below we concentrate our discussion on measurements that are most sensitive to hard QCD processes with focus on jet production.

9.3.2.1 e^+e^- colliders

Analyses of jet production in e^+e^- collisions are mostly based on data from the JADE experiment at center-of-mass energies between 14 and 44 GeV, as well as on LEP collider data at the Z resonance and up to 209 GeV. The analyses cover the measurements of (differential or exclusive) jet rates (with multiplicities typically up to 4, 5 or 6 jets), the study of three-jet events and particle production between the jets, as well as four-jet production and angular correlations in four-jet events.

Event-shape distributions from e^+e^- data have been an important input to the tuning of parton shower MC models, typically matched to matrix elements for three-jet production. In general these models provide good descriptions of the available, highly precise data. Especially for the large LEP data sample at the Z peak, the statistical uncertainties are mostly negligible and the experimental systematic uncertainties are at the percent level or even below. These are usually dominated by the uncertainties related to the MC model dependence of the efficiency and acceptance corrections (often referred to as “detector corrections”).

Observables measured in e^+e^- collisions have been used for determinations of the strong coupling constant (*cf.* Section 9.4 below) and for putting constraints on the QCD color factors (*cf.* Sec. 9.1 for their definitions), thus probing the non-Abelian nature of QCD. Angular correlations in four-jet events are sensitive at leading order. Some sensitivity to these color factors, although only at NLO, is also obtained from event-shape distributions. Scaling violations of fragmentation functions and the different subjet structure in quark and gluon induced jets also give access to these color factors. A compilation of results [444] quotes world average values of $C_A = 2.89 \pm 0.03$ (stat) ± 0.21 (syst)

and $C_F = 1.30 \pm 0.01$ (stat) ± 0.09 (syst), with a correlation coefficient of 82%. These results are in perfect agreement with the expectations from SU(3) of $C_A = 3$ and $C_F = 4/3$.

9.3.2.2 DIS and photoproduction

Jet measurements in ep collisions, both in the DIS and photoproduction regimes, allow for tests of QCD factorization (as they involve only one initial state proton and thus one PDF function), and provide sensitivity to both the gluon PDF and to the strong coupling constant. Calculations are available at NNLO in both regimes [219, 220]. An N³LO calculation using the Projection-to-Born method was also presented in Ref. [221, 222]. Experimental uncertainties of the order of 5–10% have been achieved, whereas statistical uncertainties are negligible to a large extent. For comparison to theoretical predictions, at large jet p_t the PDF uncertainty dominates the theoretical uncertainty (typically of order 5–10%, in some regions of phase space up to 20%), therefore jet observables become useful inputs for PDF fits.

In general, the data are well described by the NLO and NNLO matrix-element calculations, combined with DGLAP evolution equations, in particular at large Q^2 and central values of jet pseudo-rapidity. At low values of Q^2 and x , in particular for large jet pseudo-rapidities, certain features of the data have been interpreted as requiring BFKL-type evolution, though the predictions for such schemes are still limited. It is worth noting that there is no indication that the BKFL approximation is needed within the currently probed phase space in the x, Q^2 plane, and an alternative approach [490], which implements the merging of LO matrix-element based event generation with a parton shower (using the SHERPA framework), successfully describes the data in all kinematical regions, including the low Q^2 , low x domain. At moderately small x values, it should perhaps not be surprising that the BFKL approach and fixed-order matrix-element merging with parton showers may both provide adequate descriptions of the data, because some part of the multi-parton phase space that they model is common to both approaches.

In the case of photoproduction, a wealth of measurements with low p_t jets were performed in order to constrain the photon content of the proton (which is by now determined with percent accuracy thanks to the LUX approach [72, 73]). A few examples of measurements can be found in Refs. [491–495] for photoproduction and in Refs. [496–505] for DIS.

9.3.2.3 Hadron-hadron colliders

The spectrum of observables and the number of measurements performed at hadron colliders is enormous, probing many regions of phase space and covering a huge range of cross sections, as exemplified in Fig. 9.1 for a wide class of processes by the ATLAS experiment, and specialised to top-quark related processes by the CMS experiment at the LHC. In general, the theory agreement with data is excellent for a wide variety of processes, indicating the success of perturbative QCD with the PDF and the strong coupling as inputs. For the sake of brevity, in the following only certain classes of those measurements will be discussed, which permit various aspects of the QCD studies to be addressed. Most of our discussion will focus on LHC results, which are available for center-of-mass energies of 2.76, 5, 7, 8 and 13 TeV with integrated luminosities of up to 140 fb^{-1} . As of writing of this update, new results at 13.6 TeV are starting to appear. Generally speaking, besides representing precision tests of the Standard Model and QCD in particular, these measurements serve several purposes, such as: (i) probing pQCD and its various approximations and implementations in MC models to quantify the order of magnitude of not yet calculated contributions and to gauge their precision when used as background predictions to searches for new physics, or (ii) extracting/constraining model parameters such as the strong coupling constant or PDFs.

The final states measured at the LHC include single, double and triple gauge boson production, top production (single top, top pair and four top production), Higgs boson production, alone and in conjunction with a W or Z boson, and with a top quark pair. Many/most of these events are accompanied by additional jets. So far only limits have been placed on double Higgs production. The volume of LHC results prohibits a comprehensive description

in this *Review*; hence, only a few highlights will be presented.

Among the most important cross sections measured, and the one with the largest dynamic range, is the inclusive jet spectrum as a function of the jet transverse momentum (p_t), for several rapidity regions and for p_t up to 700 GeV at the Tevatron and ~ 3.5 TeV at the LHC. It is worth noting that this latter upper limit in p_t corresponds to a distance scale of $\sim 10^{-19}$ m: no other experiment so far is able to directly probe smaller distance scales of nature than this measurement. The Tevatron inclusive jet measurements in Run 2 (Refs. [508–511]) were carried out with the MidPoint jet clustering algorithm (or its equivalent) and, in a few cases, with the k_t jet clustering algorithm. Most of the LHC measurements use the *anti- k_t* algorithm, with a variety of jet radii. The use of multiple jet radii in the same analysis allows a better understanding of the underlying QCD dynamics. Measurements by ALICE, ATLAS and CMS have been published in Refs. [512–522].

In general, we observe a good description of the data by the NLO and NNLO QCD predictions over about 11 orders of magnitude in cross section, as long as care is taken for the functional form of the central scale choice [523]. The experimental systematic uncertainties are dominated by the jet energy scale uncertainty, quoted to be in the range of a few percent (see for instance the review in Ref. [524]), leading to uncertainties of $\sim 5 - 30\%$ on the cross section, increasing with p_t and rapidity. The PDF uncertainties dominate the theoretical uncertainty at large p_t and rapidity. In fact, inclusive jet data are one of the most important inputs to global PDF fits, in particular for constraining the high- x gluon PDF [525–527]. Constraints on the PDFs can also be obtained from ratios of inclusive cross sections at different center-of-mass energies [513, 518]. Ratios of jet cross sections are a means to (at least partially) cancel the jet energy scale uncertainties and thus provide jet observables with significantly improved precision.

Dijet events are typically analyzed in terms of their invariant mass or average dijet p_t and angular distributions, which allows for tests of NLO and NNLO QCD predictions (see *e.g.* Refs. [517, 528, 529] for recent LHC results), and for setting stringent limits on deviations from the Standard Model, such as quark compositeness or contact interactions (some examples can be found in Refs. [520, 530–536]). Furthermore, dijet azimuthal correlations between the two leading jets, normalized to the total dijet cross section, are an extremely valuable tool for studying the spectrum of gluon radiation in the event. The azimuthal separation of the two leading jets is sensitive to multi-jet production, avoiding at the same time large systematic uncertainties from the jet energy calibration. For example, results from the Tevatron [537, 538] and the LHC [458, 539–543] show that the LO (non-trivial) prediction for this observable, with at most three partons in the final state, is not able to describe the data for an azimuthal separation below $2\pi/3$, where NLO contributions (with 4 partons) restore the agreement with data. In addition, this observable can be employed to tune Monte Carlo predictions of soft gluon radiation. Further examples of dijet observables that probe special corners of phase space are those that involve forward (large rapidity) jets and where a large rapidity separation, possibly also a rapidity gap, is required between the two jets. Reviews of such measurements can be found in Ref. [471], showing that no single prediction is capable of describing the data in all phase-space regions. In particular, no conclusive evidence for BFKL effects in these observables has been established so far.

Beyond dijet final states, measurements of the production of three or more jets, including cross section ratios, have been performed (see Refs. [471, 544] for recent reviews), as a means of testing perturbative QCD predictions, determining the strong coupling constant, and probing/tuning MC models, in particular those combining multi-parton matrix elements with parton showers [459, 545]. The calculation of three-jet production to NNLO [264] will allow more precise predictions of the three-jet to two-jet ratio, and thus the extraction of $\alpha_s(m_Z^2)$ from this observable. This calculation also allows for the use of transverse energy-energy correlations (TEEC) for the determination of $\alpha_s(m_Z^2)$ [459].

W and Z production serve as benchmark cross sections at the

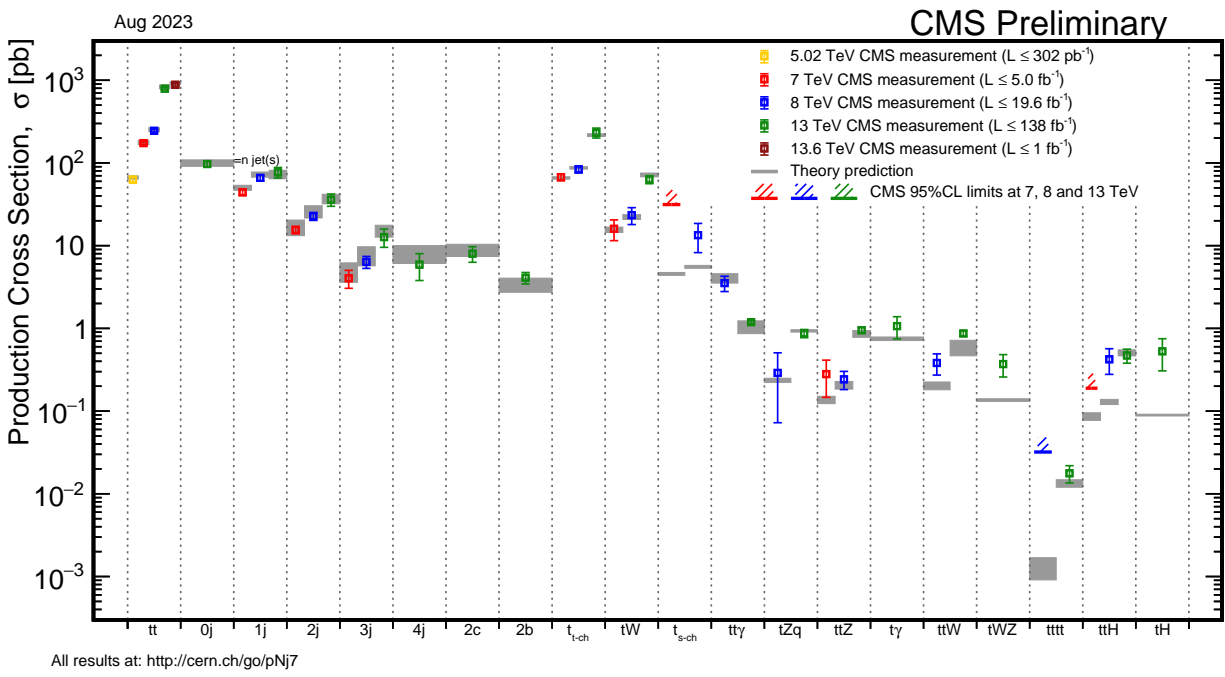
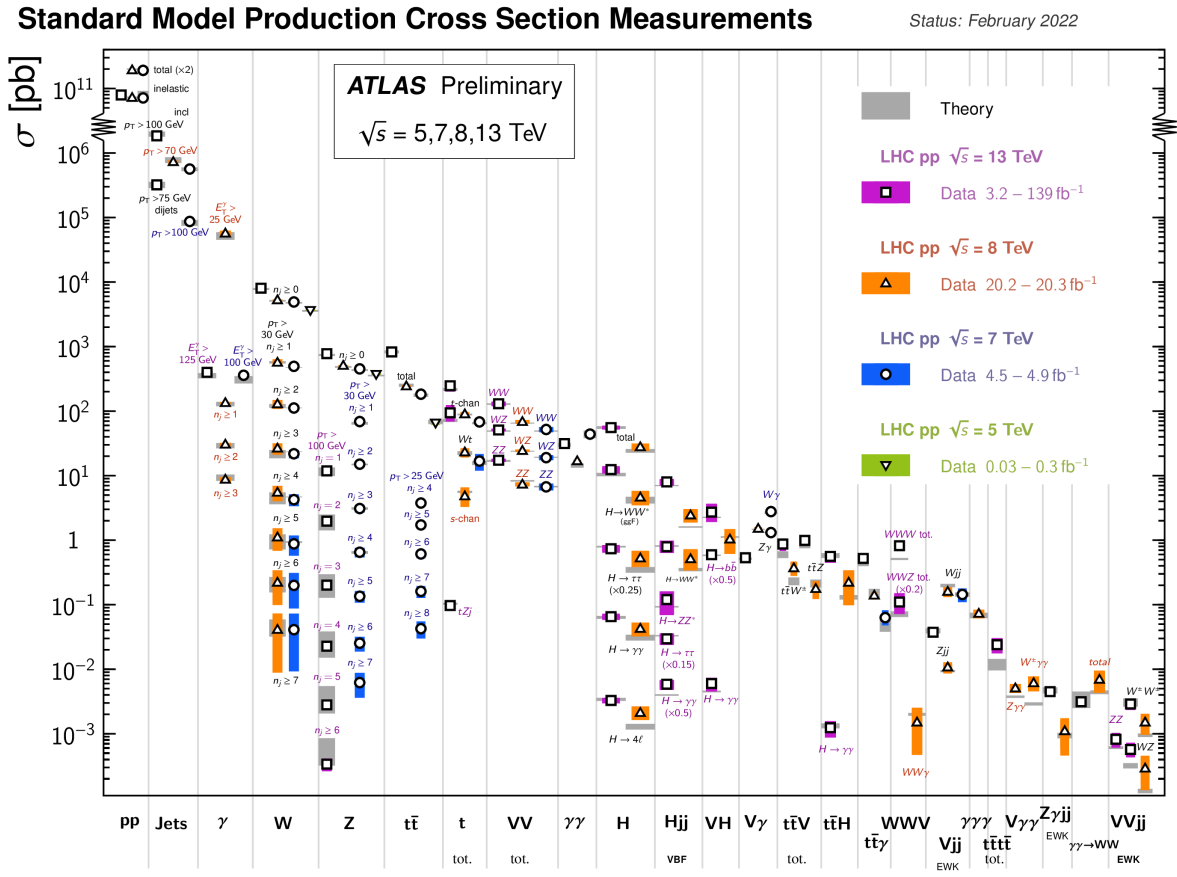


Figure 9.1: Overview of cross section measurements for a wide class of processes by the ATLAS [506] experiment, and specialised to top-quark related processes by the CMS [507] experiment at the LHC, for center-of-mass energies of 5, 7, 8, 13, and 13.6 TeV. Also shown are the theoretical predictions and their uncertainties.

LHC. The large boson mass stabilizes perturbative predictions, which results in better theoretical accuracy. In terms of experimental precision, measurements of inclusive vector boson (W, Z) production provide the most precisely determined observables at hadron colliders so far. This is because the experimental signatures are based on charged leptons which are measured much more accurately than jets or photons. At the LHC [546–553], the dominant uncertainty stems from the luminosity determination ($\leq 2\text{--}4\%$), while other uncertainties (*e.g.* statistical or from lepton efficiencies) are controlled at the $\sim 0.5\text{--}3\%$ level. The uncertainty from the acceptance correction of about $\sim 1\text{--}2\%$ can be reduced by measuring so-called fiducial cross sections, *i.e.* by applying kinematic cuts also to the particle level of the theoretical predictions. Measurements combining the electron and muon final states were able to achieve a precision a few per mille level in the dilepton final state for the normalized cross section for p_T^l less than 30 GeV [554, 555]. This level of precision can also be achieved by measuring cross section ratios (W/Z or W^+/W^-). On the theory side, as discussed earlier in this *Review*, the production of these color-singlet states has been calculated to N³LO [119–121]. Since the dominant theoretical uncertainty is related to the choice of PDFs, these high-precision data provide useful handles for PDF determinations.

Further insights are obtained from measurements of differential vector boson production, as a function of the invariant dilepton mass, the boson’s rapidity or its transverse momentum. For example, the dilepton invariant mass distribution has been measured [556–561] for masses between 15 and 3000 GeV, covering more than 8 orders of magnitude in cross section. NNLO QCD predictions, together with modern PDF sets and including higher-order electroweak and QED final-state radiation corrections, describe the data to within 5–10% over this large range, whereas NLO predictions show larger deviations, unless matched to a parton shower.

Similar conclusions can be drawn from the observed rapidity distribution of the dilepton system (see *e.g.* Refs. [546, 557, 562]) or, in the case of W production, from the observed charged lepton rapidity distribution and its charge asymmetry. The latter is particularly sensitive to differences among PDF sets [546, 563–565], also thanks to the high precision achieved by the ATLAS and CMS experiments for central rapidity ranges. These measurements are extended to the very forward region, up to 4.5 in lepton rapidity, by the LHCb experiment [552, 553, 566].

An overview of these kinds of measurement can be found in Ref. [471]. There one can also find a discussion of and references to LHC results from studies of the vector boson’s transverse momentum distribution, p_T^V (see also Refs. [567–569]). This observable covers a wide kinematic range and probes different aspects of higher-order QCD effects. It is sensitive to jet production in association with the vector boson, without suffering from the large jet energy scale uncertainties. In the p_T^V region of several tens of GeV to over 1 TeV, the NNLO predictions for V+jet can be used to predict the high- p_T boson production cross section.¹² The NNLO predictions agree with the data to within about 10%, and agree somewhat better at high transverse momentum than do the NLO predictions [570]. At transverse momenta below ~ 20 GeV, the fixed-order predictions fail and soft-gluon resummation is needed to restore the agreement with data. The soft gluon resummation can either be performed analytically, or effectively using parton showering implemented in Monte Carlo programs. While analytic approaches reach a higher perturbative precision, they typically refer to inclusive measurements without fiducial cuts.

The addition of further jets to the final state extends the kinematic range as well as increasing the complexity of the calculation/measurements. The number of results obtained both at the Tevatron and at the LHC is extensive, summaries can be found in Refs. [471, 571], and more recent results can be found in Refs. [570, 572–575]. The measurements cover a very large phase space, *e.g.* with jet transverse momenta between 30 GeV and ~ 1.5 TeV and jet rapidities up to $|y| < 4.4$ [570, 576]. Jet

multiplicities as high as seven jets accompanying the vector boson have already been probed at the LHC, together with a substantial number of other kinematical observables, such as angular correlations among the various jets or among the jets and the vector boson, or the sum of jet transverse momenta, H_T . Whereas the jet p_T and H_T distributions are dominated by jet energy scale uncertainties at levels similar to those discussed above for inclusive jet production, angular correlations and jet multiplicity ratios have been measured with a precision of $\sim 10\%$, see *e.g.* Refs. [461, 577].

NLO calculations for up to five jets [578] in addition to the vector boson are in good agreement with the data over that phase space, where the calculations are applicable. Predictions for V+jet at NNLO improve the description of the data for distributions involving the vector boson or the leading jet. MC models that implement parton shower matching to matrix elements (either at LO or NLO) have mixed results.

The challenges get even more severe in the case of vector boson plus heavy quark (b, c) production: on the theory side because an additional scale is introduced by the heavy quark mass, and different schemes exist for the handling of heavy quarks and their mass effects in the initial and/or final state; and on the experimental side because additional uncertainties related to the heavy-flavor tagging must be considered [579] (see also the discussion regarding flavor-jet definition in Sec. 9.3.1.1). A review of heavy quark production at the LHC is presented in Ref. [580], where the di- b -jet p_T and mass spectra are found to be well modeled within uncertainties by most generators for b -jet production with or without associated W and Z bosons. However, sizable differences between data and predictions are seen in the modeling of events with single b jets, particularly at large b -jet p_T , where gluon splitting processes become dominant, as also confirmed by studies of b -hadron and b -jet angular correlations.

The precision reached in photon measurements is in between that for lepton and jet measurements. The photon energy and angles can be measured at about the same precision as the lepton energy and angles in Drell-Yan production, but there are greater challenges encountered in photon reconstruction (for example isolation) and in purity determination. Note, though, that the photon purity approaches unity as the photon p_T increases. At high p_T , it becomes increasingly difficult for a jet to fragment into an isolated neutral electromagnetic cluster which mimics the photon signature. The inclusive photon cross section can be measured [528, 581–584], as well as the production of a photon accompanied by one or more jets [584–586, 586–590]. The kinematic range for photon production is less than that for jet production because of the presence of the electromagnetic coupling, but still reaches about 2 TeV. Better agreement is obtained with NNLO predictions for photon production than for NLO predictions, except when the latter are matched to matrix element plus parton shower predictions. Photon production in association with a heavy-flavor jet is a useful input for the determination of the b and c quark PDFs [591].

Electroweak corrections are expected to become more and more relevant now that the TeV energy range starts to be explored, and EW corrections can now also be computed automatically [171]. For a comprehensive review on electroweak corrections see Ref. [192]. For example, such corrections were found [592, 593] to be sizable (tens of percent) when studying the ratio $(d\sigma^\gamma/dp_{T\ell})/(d\sigma^Z/dp_{T\ell})$ in $\gamma(Z)$ +jet production, $p_{T\ell}$ being the boson’s transverse momentum, and might account for (some of) the differences observed in a CMS measurement [594] of this quantity.

A number of interesting developments, in terms of probing higher-order QCD effects, have occurred in the sector of diboson production, in particular for the WW and $\gamma\gamma$ cases. Regarding the former, an early disagreement of about 10% between the LHC measurements and the NLO predictions had led to a number of speculations of possible new physics effects in this channel. However, more recent ATLAS and CMS measurements [595–598] are in agreement with the NNLO prediction [131]. The statistical reach of the LHC has resulted in the discovery of triple massive gauge boson production [599–601].

In the case of diphoton production, ATLAS [602–604] and CMS [605] have provided accurate measurements, in particular

¹²For these calculations, there is a requirement of the presence of a jet, but the p_T cut is typically small (30 GeV) compared to the high p_T region being discussed here.

for phase-space regions that are sensitive to radiative QCD corrections (multi-jet production), such as small azimuthal photon separation. While there are large deviations between data and NLO predictions in this region, a calculation [228] at NNLO accuracy manages to mostly fill this gap. This is an interesting example where scale variations can not provide a reliable estimate of missing contributions beyond NLO, since at NNLO new channels appear in the initial state (gluon fusion in this case). These missing channels can be included in a matrix element plus parton shower calculation in which two additional jets are included at NLO. The result exhibits a similar level of agreement as that obtained at NNLO. Three-photon production has also been measured [606] and is in good agreement with NNLO theory predictions [260, 261].

In terms of heaviest particle involved, top-quark production at the LHC has become an important tool for probing higher-order QCD calculations, thanks to very impressive achievements both on the experimental and theoretical side, as extensively summarized in Ref. [607]. Regarding $t\bar{t}$ production, the most precise inclusive cross section measurements are achieved using the dilepton ($e\mu$) final state, with a total uncertainty of 4% [608–612]. This is of about the same size as the uncertainty on the most advanced theoretical predictions [128, 129, 613, 614], obtained at NNLO with additional soft-gluon resummation at NNLL accuracy [615]. There is excellent agreement between data and the QCD predictions.

The $t\bar{t}$ final state allows multiple observables to be measured. A large number of differential cross section measurements have been performed at 7, 8 and 13 TeV center-of-mass energy, studying distributions such as the top-quark p_t and rapidity, the transverse momentum and invariant mass of the $t\bar{t}$ system (probing the TeV range), or the number of additional jets. These measurements have been compared to a wide range of predictions, at fixed order up to NNLO as well as using LO or NLO matrix elements matched to parton showers. Each of the observables provides information on the high x gluon. However, there are tensions among the multiple observables that can lead to difficulties in PDF fits. Four top production has been measured in multi-lepton final states [616] by the ATLAS and CMS collaboration, with results consistent with the standard model prediction [617].

Thanks to both the precise measurements of, and predictions for, the inclusive top-pair cross section, which is sensitive to the strong coupling constant and the top-quark mass, this observable has been used to measure the strong coupling constant at NNLO accuracy from hadron collider data [618, 619] (*cf.* Section 9.4 below), as well as to obtain a measurement of the top-quark’s pole mass without employing direct reconstruction methods [618, 620, 621].

The Higgs boson provides a tool for QCD studies, especially as the dominant production mechanism is gg fusion, which is subject to very large QCD corrections. Higgs boson production has been measured in the ZZ , $\gamma\gamma$, $b\bar{b}$, WW and $\tau\tau$ decay channels. A measurement of the cross section in the ZZ and $\gamma\gamma$ channels is one of the first measurements at 13.6 TeV to be published [622]. The experimental cross section is now known with a precision approaching 10% [623, 624], similar to the size of the theoretical uncertainty [625], of which the PDF+ α_s uncertainty is the largest component. Part of this systematic is the mis-match in orders between the PDF determination (NNLO) and the cross section evaluation (N³LO), as discussed earlier. The experimental precision has allowed detailed fiducial and differential cross section measurements. For example, with the diphoton final state, the transverse momentum of the Higgs boson can be measured out to the order of 650 GeV [626–629], where top quark mass effects become important. The production of a Higgs boson with up to 4 jets has been measured [624, 626]. The experimental cross sections have been compared to NNLO predictions (for $H \rightarrow \geq 1$ jet), NLO for 2 and 3 jets, and NNLO+NNLL for the transverse momentum distribution. In addition, finite top quark mass effects have been taken into account at NLO. The use of the boosted $H \rightarrow b\bar{b}$ topology allows probes of Higgs boson transverse momenta on the order of 600 GeV and greater [624]. So far the agreement with the perturbative QCD corrections is good.

9.4 Determinations of the strong coupling constant

Beside the quark masses, the only free parameter in the QCD Lagrangian is the strong coupling constant α_s . The coupling constant in itself is not a physical observable, but rather a quantity defined in the context of perturbation theory, which enters predictions for experimentally measurable observables, such as R in Eq. (9.7). The value of the strong coupling constant must be inferred from such measurements and is subject to experimental and theoretical uncertainties. The incomplete knowledge of α_s propagates into uncertainties in numerous precision tests of the Standard Model. Here, we present an update of the 2022 PDG average value of $\alpha_s(m_Z^2)$ and its uncertainty [630].

Many experimental observables are used to determine α_s . A number of recent determinations are collected in Refs. [631, 632]. Further discussions and considerations on determinations of α_s can also be found in Refs. [633–635]. Such considerations include:

- The observable’s sensitivity to α_s as compared to the experimental precision. For example, for the e^+e^- cross section to hadrons (*cf.* R in Sec. 9.2.1), QCD effects are only a small correction, since the perturbative series starts at order α_s^0 ; three-jet production or event shapes in e^+e^- annihilations are directly sensitive to α_s since they start at order α_s ; the hadronic decay width of heavy quarkonia, $\Gamma(\mathcal{T} \rightarrow \text{hadrons})$, is very sensitive to α_s since its leading order term is $\propto \alpha_s^3$.
- The accuracy of the perturbative prediction, or equivalently of the relation between α_s and the value of the observable. Several observables have been known to NNLO for quite some time. These include, for instance, inclusive observables, as well as three-jet rates and event shapes in e^+e^- collisions, inclusive jet and dijet production in DIS, and inclusive jet, dijet, $t\bar{t}$, W/Z +jet and three-jet production cross sections in pp or $p\bar{p}$ collisions. The e^+e^- hadronic cross section and τ , W and Z branching fractions to hadrons are even known to N³LO, if one denotes the LO as the first non-trivial term. In certain cases, fixed-order predictions are supplemented with resummation. The precise magnitude of the associated theory uncertainties usually is estimated as discussed in Sec. 9.2.4.
- The size of non-perturbative effects. Sufficiently inclusive quantities, like the e^+e^- cross section to hadrons, have small non-perturbative contributions $\sim \Lambda^4/Q^4$. Others, such as event-shape distributions, have typically contributions $\sim \Lambda/Q$.
- The scale at which the measurement is performed. An uncertainty δ on a measurement of $\alpha_s(Q^2)$, at a scale Q , translates to an uncertainty $\delta' = (\alpha_s^2(m_Z^2)/\alpha_s^2(Q^2)) \cdot \delta$ on $\alpha_s(m_Z^2)$. For example, this enhances the already important impact of precise low- Q measurements, such as from τ decays, in combinations performed at the m_Z scale.

The selection of results from which to determine the world average value of $\alpha_s(m_Z^2)$ is restricted to those that are

- published in a peer-reviewed journal at the time of writing this report,
- based on the most complete perturbative QCD predictions of at least NNLO accuracy,
- accompanied by reliable estimates of all experimental and theoretical uncertainties.

Numerous measurements from jet production in DIS and at hadron colliders are still excluded from the average presented here, because the determination of $\alpha_s(m_Z^2)$ from those data sets has not yet been upgraded to NNLO. A few new results did appear comparing to theory at NNLO and are included in the corresponding section. NLO analyses will still be discussed in this *Review*, as they are important ingredients for the experimental evidence of the energy dependence of α_s , *i.e.* for asymptotic freedom, one of the key features of QCD.

In order to calculate the world average value of $\alpha_s(m_Z^2)$, we apply, as in earlier editions, an intermediate step of pre-averaging results within the sub-fields now labeled “Hadronic τ decays and low Q^2 continuum” (τ decays and low Q^2), “Heavy quarkonia decays”

($Q\bar{Q}$ bound states), “PDF fits” (PDF fits), “Hadronic final states of e^+e^- annihilations” (e^+e^- jets & shapes), “Observables from hadron-induced collisions” (hadron colliders), and “Electroweak precision fit” (electroweak) as explained in the following sections. For each sub-field, the *unweighted average* of all selected results is taken as the pre-average value of $\alpha_s(m_Z^2)$, and the *unweighted average* of the quoted total uncertainties is assigned to be the respective overall error of this pre-average. Asymmetric total uncertainties are symmetrised beforehand by adopting the larger of the two values as the (\pm) uncertainty. For the “Lattice QCD” (lattice) sub-field we do not perform a pre-averaging; instead, we adopt for this sub-field the $\alpha_s(m_Z^2)$ estimate and uncertainty derived by the Flavour Lattice Averaging Group (FLAG) in Ref. [636].

Assuming that the six sub-fields (excluding lattice) are largely independent of each other, we determine a non-lattice world average value using a ‘ χ^2 averaging’ method. In a last step we perform an unweighted average of the values and uncertainties of $\alpha_s(m_Z^2)$ from our non-lattice result and the lattice result presented in the FLAG 2021 report [636].

9.4.1 Hadronic τ decays and low Q^2 continuum:

Based on complete N^3 LO predictions [34], analyses of the τ hadronic decay width and spectral functions have been performed, *e.g.* in Refs. [34, 637–642], and lead to precise determinations of α_s at the energy scale of m_τ^2 . They are based on different approaches to treat perturbative and non-perturbative contributions, the impacts of which have been a matter of intense discussions for a long time, see *e.g.* Refs. [641–644]. In particular, in τ decays there is a significant difference between results obtained using fixed-order (FOPT) or contour-improved perturbation theory (CIPT), such that analyses based on CIPT generally arrive at larger values of $\alpha_s(m_\tau^2)$ than those based on FOPT.

In addition, some results show discrepancies in $\alpha_s(m_\tau^2)$ among groups of authors using the same data sets and perturbative calculations, most likely due to different treatments of the non-perturbative contributions, *cf.* Ref. [642] with Refs. [641, 645]. References [646, 647] question the validity of using a truncated operator product expansion (OPE) at $Q^2 = m_\tau^2$ based on the disagreement found between experimental values of the spectral moments and the theory representations based on the truncated OPE fits at $Q^2 > m_\tau^2$.

Recent developments now have shed light on the disagreement between FOPT- and CIPT-based analyses. References [648–650] argue that CIPT-based calculations require a dedicated estimation of non-perturbative effects instead of “standard” ones used so far. Otherwise an asymptotic separation between results using the two perturbative approaches would remain. Potential ways forward are suggested in Refs. [651, 652]. As a consequence we remove for the time being determinations of the strong coupling constant based on CIPT from the derivation of the central value and the uncertainty of $\alpha_s(m_Z^2)$.

We determine the pre-average value of $\alpha_s(m_Z^2)$ for this sub-field only from studies that employ FOPT expansions and remove any eventual averaging with CIPT central values or increased uncertainties due to the differences in CIPT vs. FOPT. As the results from Refs. [34, 644, 645] are not totally independent, we pre-averaged as a first step these three results in the previous edition of this *Review*. Lacking, however, an estimate of the theory uncertainty for the FOPT method, Ref. [645] had to be left out, such that the first entry to this category of α_s determinations is pre-averaged from $\alpha_s(m_Z^2) = 0.1183 \pm 0.0026$ [34] and $\alpha_s(m_Z^2) = 0.1181 \pm 0.0015$ [644] to $\alpha_s(m_Z^2) = 0.1182 \pm 0.0021$ (summarized as BP 2008-16 FO in Fig. 9.2).

Subsequently, this is combined with $\alpha_s(m_Z^2) = 0.1158 \pm 0.0022$ [653] and $\alpha_s(m_Z^2) = 0.1171 \pm 0.0010$ [654], which replaces the previous result from Ref. [642]. We also include the result from τ decay and lifetime measurements, obtained in Sec. *Electroweak Model and constraints on New Physics* of the 2022 edition of this *Review* [630], $\alpha_s(m_Z^2) = 0.1171 \pm 0.0018$. The latter result, being a global fit of τ data, involves some correlations with the other extractions of this category. However, since we perform an unweighted average of the central value and uncertainty, the effects of the potential correlations are reduced. Finally, a new

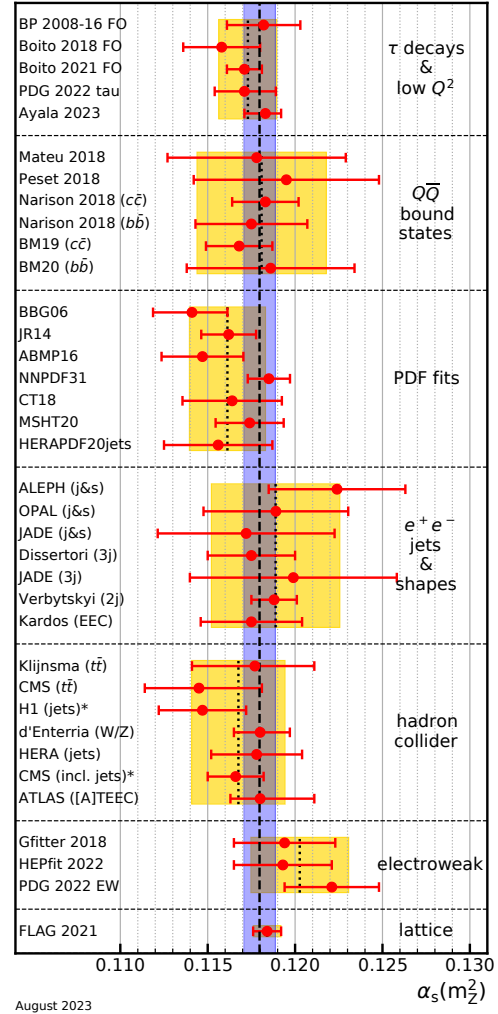


Figure 9.2: Summary of determinations of $\alpha_s(m_Z^2)$ with uncertainty in the seven sub-fields as discussed in the text. The yellow (light shaded) bands and dotted lines indicate the pre-average values of each sub-field. The dashed line and blue (dark shaded) band represent the final world average value of $\alpha_s(m_Z^2)$. The “*” symbol within the “hadron colliders” sub-field indicates a determination including a simultaneous fit of PDFs.

determination reported in Ref. [655] is added to this category: $\alpha_s(m_Z^2) = 0.1183^{+0.0009}_{-0.0012}$. A recent publication evaluating data on R_{had} in the continuum below the charm threshold exhibits huge experimental uncertainties and therefore has not been considered [656].

All these results are summarized in Fig. 9.2. Determining the unweighted average of the central values and their overall uncertainties, we arrive at $\alpha_s(m_Z^2) = 0.1173 \pm 0.0017$, which we will use as the first input for determining the world average value of $\alpha_s(m_Z^2)$. This corresponds to $\alpha_s(m_\tau^2) = 0.314 \pm 0.014$.

9.4.2 Heavy quarkonia decays:

Two determinations of $\alpha_s(m_Z^2)$ have been performed [657, 658] that are based on N^3 LO accurate predictions. Reference [657] performs a simultaneous fit of the strong coupling and the bottom mass \bar{m}_b , including states with principal quantum number up to $n \leq 2$ in order to break the degeneracy between α_s and \bar{m}_b , finding $\alpha_s(m_Z^2) = 0.1178 \pm 0.0051$. Reference [658] instead uses as input of the fit the renormalon-free combination of masses of the meson B_c , the bottomonium η_b and the charmonium η_c , $M_{B_c} - M_{\eta_b}/2 - M_{\eta_c}/2$, which is weakly dependent on the heavy quark masses, but shows a good dependence on α_s . Using this observable, they obtain $\alpha_s(m_Z^2) = 0.1195 \pm 0.0053$.

Two further values are derived at NNLO in Ref. [659,660] from mass splittings and sum rules giving $\alpha_s(m_Z^2) = 0.1183 \pm 0.0019$ and $\alpha_s(m_Z^2) = 0.1175 \pm 0.0032$ when evolved from the relevant charmonium respectively bottomonium mass scales to m_Z^2 . Finally, by means of quarkonium sum rules, Refs. [661,662] quote $\alpha_s(m_Z^2) = 0.1168 \pm 0.0019$ and $\alpha_s(m_Z^2) = 0.1186 \pm 0.0048$ for charmonium and bottomonium respectively. These six determinations satisfy our criteria to be included in the heavy-quarkonia category of the world average. Their unweighted combination leads to the pre-average for this category of $\alpha_s(m_Z^2) = 0.1181 \pm 0.0037$.

9.4.3 PDF fits:

Another class of studies, analyzing structure functions at NNLO QCD (and partly beyond), provide results that serve as relevant inputs for the world average of α_s . Some of these studies do *not*, however, explicitly include estimates of theoretical uncertainties when quoting fit results of α_s . In such cases we add, in quadrature, half of the difference between the results obtained in NNLO and NLO to the quoted errors.

A combined analysis of non-singlet structure functions from DIS [663], based on QCD predictions up to N³LO in some of its parts, results in $\alpha_s(m_Z^2) = 0.1141 \pm 0.0022$ (BBG). Studies of singlet and non-singlet structure functions, based on NNLO predictions, result in $\alpha_s(m_Z^2) = 0.1162 \pm 0.0017$ [664] (JR14). The AMBP group [665,666] determined a set of parton distribution functions using data from HERA, NOMAD, CHORUS, from the Tevatron and the LHC using the Drell-Yan process and the hadro-production of single-top and top-quark pairs, and determined $\alpha_s(m_Z^2) = 0.1147 \pm 0.0024$ [665].

The MSHT group [667], also including hadron collider data, determined a set of parton density functions (MSHT20) together with $\alpha_s(m_Z^2) = 0.1174 \pm 0.0013$. Similarly, the CT group [37] determined the CT18 parton density set together with $\alpha_s(m_Z^2) = 0.1164 \pm 0.0026$. The NNPDF group [668] presented NNPDF3.1 parton distribution functions together with $\alpha_s(m_Z^2) = 0.1185 \pm 0.0012$. New in this category is the result of $\alpha_s(m_Z^2) = 0.1156 \pm 0.0031$ reported as HERAPDF2.0Jets in Ref. [669]. In addition to DIS data from HERA also jet cross sections are considered in the fit to theory at NNLO.

We note that criticism has been expressed on some of the above extractions. Among the issues raised, we mention the neglect of singlet contributions at $x \geq 0.3$ in pure non-singlet fits [670], the impact and detailed treatment of particular classes of data in the fits [670,671], possible biases due to insufficiently flexible parameterizations of the PDFs [672] and the use of a fixed-flavor number scheme [673,674]. For recent more extensive discussions see *e.g.* Ref. [38].

Summarizing the results from world data on structure functions, taking the *unweighted average* of the central values and errors of all selected results, leads to a pre-average value of $\alpha_s(m_Z^2) = 0.1161 \pm 0.0022$, see also Fig. 9.2.

9.4.4 Hadronic final states of e^+e^- annihilations:

Re-analyses of jets and event shapes in e^+e^- annihilation (j&ks), measured around the Z peak and at LEP2 center-of-mass energies up to 209 GeV, using NNLO predictions matched to NLL resummation and Monte Carlo models to correct for hadronization effects, resulted in $\alpha_s(m_Z^2) = 0.1224 \pm 0.0039$ (ALEPH) [675], and in $\alpha_s(m_Z^2) = 0.1189 \pm 0.0043$ (OPAL) [676]. Similarly, an analysis of JADE data [677] at center-of-mass energies between 14 and 46 GeV gives $\alpha_s(m_Z^2) = 0.1172 \pm 0.0051$, with contributions from the hadronization model and from perturbative QCD uncertainties of 0.0035 and 0.0030, respectively. Precise determinations of α_s from three-jet production alone (3j), at NNLO, resulted in $\alpha_s(m_Z^2) = 0.1175 \pm 0.0025$ [678] from ALEPH data and in $\alpha_s(m_Z^2) = 0.1199 \pm 0.0059$ [679] from JADE. A recent determination is based on an NNLO+NNLL accurate calculation that allows to fit the region of lower three-jet rate (2j) using data collected at LEP and PETRA at different energies. This fit gives $\alpha_s(m_Z^2) = 0.1188 \pm 0.0013$ [680], where the dominant uncertainty is the hadronization uncertainty, which is estimated from Monte Carlo simulations. A fit of energy-energy-correlation (EEC), also based on an NNLO+NNLL calculation, together with

a Monte Carlo based modeling of hadronization corrections gives $\alpha_s(m_Z^2) = 0.1175 \pm 0.0029$ [681]. These results are summarized in the e^+e^- sector of Fig. 9.2.

Another class of α_s determinations is based on analytic modeling of non-perturbative and hadronization effects, rather than on Monte Carlo models [682–685], using methods like power corrections, factorization of soft-collinear effective field theory, dispersive models and low scale QCD effective couplings. In these studies, the world data on thrust distributions (T), or the C-parameter distributions (C), are analyzed and fitted to perturbative QCD predictions at NNLO matched with resummation of leading logs up to N³LL accuracy, see Sec. 9.2.3.3. The results are $\alpha_s(m_Z^2) = 0.1135 \pm 0.0011$ [683] and $\alpha_s(m_Z^2) = 0.1134^{+0.0031}_{-0.0025}$ [684] from thrust, and $\alpha_s(m_Z^2) = 0.1123 \pm 0.0015$ [685] from C-parameter.

A long-standing question was why this latter class of determinations led systematically to rather small values of $\alpha_s(m_Z^2)$ as compared to the former one based on Monte Carlo models to correct for hadronization effects. New insights have now been gained in this regard. In a recent calculation of the leading non-perturbative contribution to the C-parameter in the three-jet symmetric limit based on an effective coupling approach it was found that it differs by a factor of two from the one in the two-jet limit [686]. Subsequently, using the same effective coupling approach, the leading $1/Q$ power correction was computed for thrust and the C-parameter in the full three-jet region under the assumption of a large (negative) n_f limit [687]. Expanding on this approach, Ref. [688] extended the calculation of non-perturbative corrections to include the heavy-jet mass, the difference of jet masses, wide broadening, and, with some caveat, the three-jet resolution variable in the Durham algorithm. The key finding in Ref. [688] is that non-perturbative corrections computed in the three-jet region significantly deviate from those computed in the two-jet limit and hence the aforementioned fits based on power corrections in the two-jet limit result in smaller values of $\alpha_s(m_Z^2)$. Another important observation is that the inclusion of resummation effects introduces a relatively substantial ambiguity outside the two-jet limit. Additionally, other factors such as the choice of mass-scheme used to extend the definition of event shapes to massive hadrons can have significant effects.

These findings are inconsistent with the very small experimental, hadronization, and theoretical uncertainties of only 2, 5, and 9 per-mille, respectively, as reported in Refs. [683,685]. For these reasons, we exclude the results of Refs. [683–685] from the average. Determinations based on corrections for non-perturbative hadronization effects using QCD-inspired Monte Carlo generators have also faced criticism due to the differing nature of parton-level simulations compared to fixed-order calculations. However, these determinations typically exhibit a more conservative theoretical uncertainty.

Not included in the computation of the world average but worth mentioning are a computation of the NLO corrections to 5-jet production and comparison to the measured 5-jet rates at LEP [689], giving $\alpha_s(m_Z^2) = 0.1156^{+0.0041}_{-0.0034}$, and a computation of non-perturbative and perturbative QCD contributions to the scale evolution of quark and gluon jet multiplicities, including resummation, resulting in $\alpha_s(m_Z^2) = 0.1199 \pm 0.0026$ [690].

The unweighted average of the considered determinations as shown in the e^+e^- sector of Fig. 9.2 yields $\alpha_s(m_Z^2) = 0.1189 \pm 0.0037$.

9.4.5 Observables from hadron-induced collisions:

Until recently, determinations of α_s using hadron collider data, mostly from jet or $t\bar{t}$ production processes, could be performed at NLO only. NNLO calculations have now become available for $t\bar{t}$ [128, 613, 614] and for inclusive jet, dijet, and three-jet production [253, 264, 266, 691, 692]. For $t\bar{t}$ production, in addition, logarithms to NNLL have been resummed [615]. Both should be supplemented by electroweak corrections [693–696], which become important for high- p_T collisions at the LHC. Z+jet production, studied with respect to an α_s determination at NLO from multi-jet events in Ref. [697], is also known at NNLO for the 1-jet case [239, 698].

Determinations of α_s from production cross sections at hadron colliders also require a knowledge of the relevant PDFs for those α_s values. Two strategies are pursued for the extraction of α_s , one using pre-determined PDFs as input and a second strategy fitting the proton PDFs together with the strong coupling constant. Each global PDF group produces PDF sets not only for a value of 0.118 that is close to the world average, but also for a wide range above and below in increments of 0.001, which can be used in such determinations. The latter technique of simultaneously fitting α_s and the PDFs is technically more accurate, given that the new data used in the determination of α_s may modify the PDFs in a manner not taken into account by the α_s -variation PDFs provided by the fitting collaborations. The former technique may result in a bias of unknown magnitude [699]. As the LHC experiments have the ability to combine a PDF fit with the α_s determination, for example with tools like described in Ref. [700], we expect more experimental joint determinations of PDFs and of α_s for future iterations of this review.

The first determination of α_s at NNLO accuracy in QCD has been reported by CMS from the $t\bar{t}$ production cross section at $\sqrt{s} = 7$ TeV [618]. In former *Reviews* this opened up a new sub-field on its own. In the meantime, multiple datasets on $t\bar{t}$ production from Tevatron at $\sqrt{s} = 1.96$ TeV and from LHC at $\sqrt{s} = 7, 8,$ and 13 TeV have been analyzed simultaneously to determine α_s [619] to $\alpha_s(m_Z^2) = 0.1177^{+0.0034}_{-0.0036}$, where the largest uncertainties are associated with missing higher orders and with PDFs, and where an additional complication arises from the top-mass dependence. Since this combined analysis contains among other things an updated measurement as compared to the dataset used by CMS, the latter is replaced in the averaging by this combined result. A second entry into this sub-field is given by an analysis of $t\bar{t}$ production data at $\sqrt{s} = 13$ TeV from the CMS Collaboration [610]. From the four values derived for different PDF sets, the unweighted average is taken: $\alpha_s(m_Z^2) = 0.1145^{+0.0036}_{-0.0031}$. A second analysis by CMS using differential distributions of $t\bar{t}$ production [611] has been performed at NLO only and is not further considered.

From collisions at HERA the α_s determination at NNLO using inclusive jet and dijet measurements in addition to DIS data of the H1 Collaboration [505] has been corrected for an issue with the theory prediction reported in Ref. [220]. We choose the result $\alpha_s(m_Z^2) = 0.1147 \pm 0.0025$ that is derived from a simultaneous fit of the strong coupling constant together with proton PDFs. We note that results of this section derived from such a simultaneous fit will be marked with a “*” in the corresponding figures. A second determination [280] combines multiple datasets on inclusive jet production of the H1 and ZEUS collaborations into one fit using interpolation grids at NNLO. The result of $\alpha_s(m_Z^2) = 0.1178 \pm 0.0026$ has been updated for the same issue reported above [220] and is included in the unweighted average, although some of the inclusive jet data have already been used in the previous analysis. We note that the ZEUS Collaboration has presented preliminary results from a new inclusive jet measurement [701].

A first new determination of $\alpha_s(m_Z^2)$ at NNLO from inclusive jet production at the LHC has been presented by the CMS Collaboration [522]. A simultaneous fit of the strong coupling constant and the proton PDFs to the HERA DIS and the new LHC jet data gives: $\alpha_s(m_Z^2) = 0.1166 \pm 0.0016$. The ATLAS Collaboration has published an extraction of $\alpha_s(m_Z^2)$ at NNLO from the transverse energy-energy correlation (TEEC) and its asymmetry (ATEEC) [459]. The results of this first derivation from an event shape observable requiring three-jet predictions at NNLO are $\alpha_s(m_Z^2) = 0.1175^{+0.0035}_{-0.0018}$ for the TEEC and $\alpha_s(m_Z^2) = 0.1185^{+0.0027}_{-0.0015}$ for the ATEEC, respectively. We include the unweighted average of the two numbers $\alpha_s(m_Z^2) = 0.1180^{+0.0031}_{-0.0017}$ as a new result in this category. Very recently, two preliminary determinations of the strong coupling constant, albeit at NLO, have been reported by CMS from energy correlators inside jets and from azimuthal correlations among jets [702,703].

Finally, Ref. [704] extracts the strong coupling constant from a fit at NNLO to measurements of inclusive Z and W boson

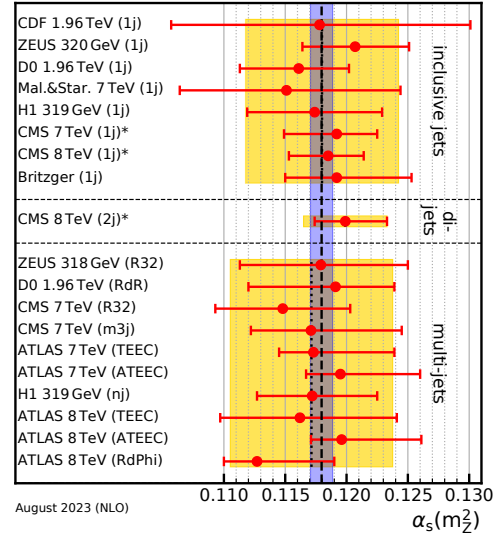


Figure 9.3: Summary of determinations of $\alpha_s(m_Z^2)$ at NLO from inclusive jet, dijet, and multi-jet measurements at hadron colliders. The uncertainty is dominated by estimates of the impact of missing higher orders. The yellow (light shaded) bands and dotted lines indicate average values for each sub-field. The dashed line and blue (dark shaded) band represent the final world average value of $\alpha_s(m_Z^2)$. The “*” symbol indicates determinations including a simultaneous fit of PDFs.

production by experiments at the LHC and Tevatron colliders. From the four values quoted for different PDF sets we include the unweighted average for the CT14 and MMHT14 PDFs $\alpha_s(m_Z^2) = 0.1180^{+0.0017}_{-0.0015}$. The other results suffer from either a bad fit quality or $\alpha_s(m_Z^2)$ values outside the range of validity for the PDF set. Furthermore, two determinations using measurements of the Z boson’s recoil at low p_T have been submitted using data of the CDF respectively ATLAS experiments [705,706]. The very small size of the estimated uncertainties has stimulated some discussion.

As unweighted pre-average for this sub-field we now obtain $\alpha_s(m_Z^2) = 0.1168 \pm 0.0027$. If the stricter requirement of simultaneous fits with PDFs is imposed, then only the H1 and CMS results are left giving $\alpha_s(m_Z^2) = 0.1157 \pm 0.0021$ for this sub-field. In sect. 9.4.8 below, we will also report the outcome for this choice.

Many further α_s determinations from jet measurements have not yet been advanced to NNLO accuracy. A selection of results from inclusive jet [504, 518, 707–712], dijet [529], and multi-jet measurements [455, 457, 458, 504, 713–717] is presented in Fig. 9.3, where the uncertainty in most cases is dominated by the impact of missing higher orders estimated through scale variations. From the CMS Collaboration we quote for the inclusive jet production at $\sqrt{s} = 7$ and 8 TeV, and for dijet production at 8 TeV the values that have been derived in a simultaneous fit with the PDFs and marked with “*” in the figure. The last point of the inclusive jet sub-field from Ref. [712] is derived from a simultaneous fit to six datasets from different experiments and partially includes data used already for the other data points, *e.g.* the CMS result at 7 TeV.

The multi-jet α_s determinations are based on three-jet cross sections (m3j), three- to two-jet cross-section ratios (R32), dijet angular decorrelations (RdR, RdPhi), and the aforementioned transverse energy-energy-correlations, but at $\sqrt{s} = 7$ and 8 TeV only. The H1 result is extracted from a fit to inclusive one-, two-, and three-jet cross sections (nj) simultaneously.

All NLO results are within their large uncertainties in agreement with the world average and the associated analyses provide valuable new values for the scale dependence of α_s at energy scales now extending beyond 2.0 TeV as shown in Fig. 9.5.

9.4.6 Electroweak precision fit:

For this category, we take the global electroweak fit of Ref. [718], which includes kinematic top quark and W boson mass measurements from the LHC, determinations of the effective leptonic electroweak mixing angles from the Tevatron, a Higgs mass measurement from ATLAS and CMS, and an evaluation of the hadronic contribution to the running of the electromagnetic coupling at the Z -boson mass. We also consider the fit of $\alpha_s(m_Z^2)$ from the global fit to electroweak data presented in the supplemental material of Ref. [719]. We choose to include the result of their “conservative scenario”¹³ in accounting for the uncertainties of m_t and m_W , which avoids a potential bias from inconsistencies between the world average of the W boson mass and the new measurement reported by the CDF Collaboration in Ref. [721]. In addition, we use the newer results of the electroweak fit at the Z mass pole from LEP and SLC data presented in Sec. *Electroweak Model and constraints on New Physics* of the 2022 edition of this Review. All three determinations, $\alpha_s(m_Z^2) = 0.1194 \pm 0.0029$ [718], $\alpha_s(m_Z^2) = 0.1193 \pm 0.0028$ [719], and $\alpha_s(m_Z^2) = 0.1221 \pm 0.0027$ [630], are also in perfect agreement with the original result obtained from LEP and SLD data [722]. Our pre-averaging gives $\alpha_s(m_Z^2) = 0.1203 \pm 0.0028$.

We note, however, that results from electroweak precision data strongly depend on the strict validity of Standard Model predictions and the existence of the minimal Higgs mechanism to implement electroweak symmetry breaking. Any - even small - deviation of nature from this model could strongly influence this extraction of α_s .

9.4.7 Lattice QCD:

Several methods exist to extract the strong coupling constant from lattice QCD, as reviewed also in Sec. *Lattice QCD* of this Review and in Ref. [723]. The Flavour Lattice Averaging Group has considered the most up-to-date determinations and combined them to produce an updated $\alpha_s(m_Z^2)$ estimate [636]. Their final result is obtained by considering a multitude of possible input calculations and by retaining in their final estimate only those that fulfill their predefined quality criteria, detailed in the Sec. 9.2.1 of Ref. [636]. In summary, a determination of α_s needs to satisfy the following requirements:

- The determination of α_s should be based on a comparison of a short-distance quantity Q at scale μ with a well-defined continuum limit, which does not involve UV or IR divergences, when the quantity is expressed by using an expansion in terms of a short distance definition of the strong coupling (*e.g.* in the \overline{MS} scheme);
- The scale μ , at which the determination is carried out, has to be sufficiently large such that the error associated with the perturbative truncation remains small enough;
- If Q is defined by physical quantities in infinite volume, one needs to satisfy the constraints $L/a \gg \mu/\Lambda_{\text{QCD}}$, where L is the lattice size and a the lattice spacing;
- Only results for $n_f \geq 3$ are considered.
- As is the case for the PDG average, a calculation must be published in a peer-reviewed journal to be eligible for inclusion into the FLAG estimate.

We note that the FLAG criteria applied now are unchanged compared to the FLAG 2019 Review [724] and are considered to be relatively loose. More stringent criteria have already been formulated by FLAG, and it is likely that in future their estimate includes only those results that satisfy these stricter criteria.

Altogether, from a large number of old and new results six from the 2019 Review also enter the final FLAG 2021 estimate [725–729]¹⁴ and three new ones qualify for inclusion [730–732]. These determinations, together with their uncertainties, are displayed in Fig. 9.4. The yellow (light shaded) band and dotted line indicate the FLAG 2021 estimate, while the dashed line and blue (dark shaded) band represent the world average.

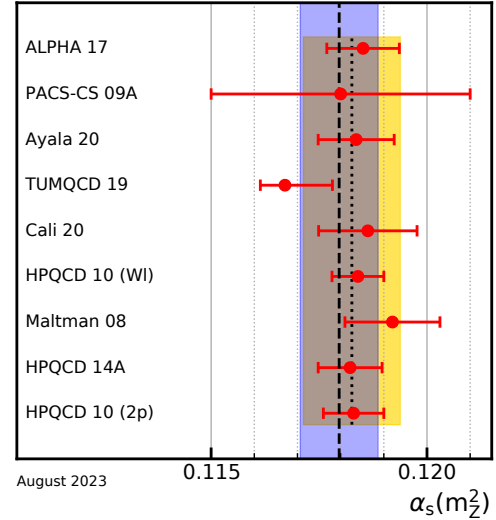


Figure 9.4: Lattice determinations that enter the FLAG 2021 estimate. The yellow (light shaded) band and dotted line indicate the *unweighted average* value for this sub-field. The dashed line and blue (dark shaded) band represent our final world average value of $\alpha_s(m_Z^2)$.

shaded) band represent the world average (see later). The level of agreement of individual results to the world average, or to the non-lattice world average is very similar.

Similarly to what is done here, the FLAG Collaboration built pre-averages of results within the various classes. The five categories that contribute to their final estimate are: step-scaling methods ($\alpha_s(m_Z^2) = 0.11848 \pm 0.00081$), the potential at short distances ($\alpha_s(m_Z^2) = 0.11782 \pm 0.00165$), Wilson loops ($\alpha_s(m_Z^2) = 0.11871 \pm 0.00128$), heavy-quark current two-point functions ($\alpha_s(m_Z^2) = 0.11826 \pm 0.00200$) and, for the first time, light quark vacuum polarization ($\alpha_s(m_Z^2) = 0.11863 \pm 0.00360$). Other categories such as the calculation of QCD vertices, or of the eigenvalue spectrum of the Dirac operator have not yet published results that fulfill all requirements.

We note that, in addition to presenting new results and improvements on previous works, the ALPHA Collaboration [733] has introduced a novel approach to non-perturbative renormalization called decoupling. This strategy shifts the perspective on results involving unphysical flavor numbers, particularly $n_f = 0$. By performing a non-perturbative matching calculation, these results can be non-perturbatively related to results with $n_f > 0$. Consequently, obtaining precise and controlled $n_f = 0$ results becomes of great importance, with significant implications for future FLAG reports.

The final value is obtained by performing a *weighted average* of the pre-averages. The final uncertainty however is not the combined uncertainty of the pre-averages (which is 0.0006), since the errors on almost all determinations are dominated by the perturbative truncation error. Instead, the error on the pre-range for α_s from the step-scaling method is taken, since perturbative truncation errors are sub-dominant in this method. The final FLAG 2021 estimate (rounded to four digits) is

$$\alpha_s(m_Z^2) = 0.1184 \pm 0.0008 \quad (\text{FLAG 2021 estimate}), \quad (9.23)$$

which is fully compatible with the FLAG 2019 result of $\alpha_s(m_Z^2) = 0.1182 \pm 0.0008$.

We believe that this result expresses to a large extent the consensus of the lattice community and that the imposed criteria and the rigorous assessment of systematic uncertainties qualify for a direct inclusion of this FLAG estimate here. As in the previous review, we therefore adopt the FLAG estimate with its uncertainty as our value of α_s for the lattice category. Moreover, this lattice result will not be directly combined with any other sub-field

¹³We note that this result agrees with the previous fit in the “conservative scenario” of Ref. [720], which precedes the latest CDF W mass determination.

¹⁴Reference [727] contains two results.

Table 9.1: Unweighted and weighted pre-averages of $\alpha_s(m_Z^2)$ for each sub-field in columns two and three. The bottom line corresponds to the combined result (without lattice gauge theory) using the χ^2 averaging method. The same χ^2 averaging is used for column four combining all unweighted averages except for the sub-field of column one. See text for more details.

averages per sub-field	unweighted	weighted	unweighted without subfield
τ decays & low Q^2	0.1173 ± 0.0017	0.1174 ± 0.0009	0.1177 ± 0.0013
$Q\bar{Q}$ bound states	0.1181 ± 0.0037	0.1177 ± 0.0011	0.1175 ± 0.0011
PDF fits	0.1161 ± 0.0022	0.1168 ± 0.0014	0.1179 ± 0.0011
e^+e^- jets & shapes	0.1189 ± 0.0037	0.1187 ± 0.0017	0.1174 ± 0.0011
hadron colliders	0.1168 ± 0.0027	0.1169 ± 0.0014	0.1177 ± 0.0011
electroweak	0.1203 ± 0.0028	0.1203 ± 0.0016	0.1171 ± 0.0011
PDG 2023 (without lattice)	0.1175 ± 0.0010	0.1178 ± 0.0005	n/a

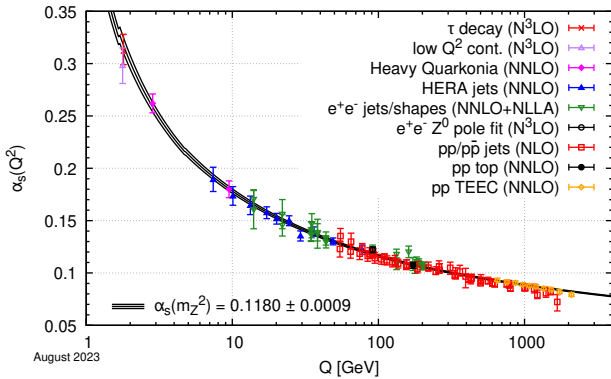


Figure 9.5: Summary of determinations of α_s as a function of the energy scale Q compared to the running of the coupling computed at five loops taking as an input the current PDG average, $\alpha_s(m_Z^2) = 0.1180 \pm 0.0009$. Compared to the previous edition, numerous points have been updated or added.

average, but with our non-lattice average to give our final world average value for α_s .

9.4.8 Determination of the world average value of $\alpha_s(m_Z^2)$:

Obtaining a world average value for $\alpha_s(m_Z^2)$ is a non-trivial exercise. A certain arbitrariness and subjective component is inevitable because of the choice of measurements to be included in the average, the treatment of (non-Gaussian) systematic uncertainties of mostly theoretical nature, as well as the treatment of correlations among the various inputs, of theoretical as well as experimental origin.

We have chosen to determine pre-averages for sub-fields of measurements that are considered to exhibit a maximum degree of independence among each other, considering experimental as well as theoretical issues. The six pre-averages, illustrated also in Fig. 9.2, are listed in column two of Table 9.1. We recall that these are exclusively obtained from extractions that are based on (at least) NNLO QCD predictions, and are published in peer-reviewed journals at the time of completing this *Review*. To obtain our final world average, we first combine these six pre-averages, excluding the lattice result, using a χ^2 averaging method. This gives

$$\alpha_s(m_Z^2) = 0.1175 \pm 0.0010 \quad (\text{PDG 2023 without lattice}). \quad (9.24)$$

This result is fully compatible with the lattice estimate Eq. (9.23) and has a comparable error. To avoid a possible over-reduction, we combine these two numbers using an unweighted average and take as an uncertainty the average between these two uncertainties. This gives our final world average value

$$\alpha_s(m_Z^2) = 0.1180 \pm 0.0009 \quad (\text{PDG 2023 average}). \quad (9.25)$$

If for the sub-field of hadron colliders we are more restrictive and instead only accept results from a simultaneous fit of PDFs, we arrive at 0.1157 ± 0.0021 for this sub-field leading to $0.1172 \pm$

0.0010 (without lattice) and $\alpha_s(m_Z^2) = 0.1178 \pm 0.0009$ for the final average. Both the new world average value and the restricted result are compatible with each other and changed only marginally as compared to the values reported in the last edition of this *Review*.

It also stands to question whether the sub-fields of PDF fits and hadron colliders still are as independent as originally assumed. To test the potential impact, the fit has been repeated while grouping all $\alpha_s(m_Z^2)$ determinations of both sub-fields into a common one. We obtain 0.1164 ± 0.0024 for the new larger sub-field and 0.1178 ± 0.0011 for the combination with all other sub-fields except lattice, which is well within the estimated uncertainties. Moreover, we present in column four of Table 9.1 the combined result for $\alpha_s(m_Z^2)$ when the respective sub-field is omitted from the combination. The variation in values obtained for $\alpha_s(m_Z^2)$ is ± 0.0004 , which is less than half our estimated uncertainty.

Since two long-standing issues causing offsets among determinations of $\alpha_s(m_Z^2)$ in the sub-fields of τ decays and low Q^2 and e^+e^- jets & shapes have been resolved, it may be argued that a weighted fit among the non-lattice sub-fields may be warranted. We compare the outcome of weighted fits with our standard procedure in columns two and three of Table 9.1. We observe that the weighted averages are rather close to the unweighted ones. However, the uncertainties become significantly smaller. This approach may be too aggressive as it ignores the correlations among the data, methods, and theory ingredients of the various determinations. We feel that the uncertainty of ± 0.0005 is an underestimation of the true error. We also note that in the unweighted combination the estimated uncertainty for each sub-field is larger than the spread of the results as given by the standard deviation. In the weighted fit this crosscheck fails in four out of six cases.

The last several years have seen clarification of some persistent concerns and a wealth of new results at NNLO, providing not only a rather precise and reasonably stable world average value of $\alpha_s(m_Z^2)$, but also a clear signature and proof of the energy dependence of α_s in full agreement with the QCD prediction of asymptotic freedom. This is demonstrated in Fig. 9.5, where results of $\alpha_s(Q^2)$ obtained at discrete energy scales Q are summarized, which now mostly include those based on NNLO QCD.¹⁵ Thanks to the results from the LHC, the energy scales, at which α_s is determined, now extend even beyond 2 TeV.¹⁶ The points in this plot are extracted from Refs. [280, 458, 459, 518, 619, 630, 653, 660, 675–677, 679, 709, 715, 716].

In this combination, as in past combinations, we have considered lattice QCD calculations of α_s independently of experimental/phenomenological determinations. In the future, when the lattice continuum extrapolations are under better control, it may be useful to group lattice QCD determinations of α_s with experimental determinations of α_s that have systematics of similar

¹⁵The uncertainties of the HERA jets points were, by mistake, shown at only half their size. The uncertainties of the ALEPH points of the e^+e^- jets/shapes sub-field now correspond to the total uncertainty.

¹⁶We note, however, that the relevant energy scale of a measurement is not uniquely defined. In addition to being multiplied by factors of *e.g.* 1/2 or 2, for instance in studies of the ratio of three- to two-jet cross sections at the LHC, the relevant scale can be taken to be the average of the transverse momenta of the two leading jets [714], or alternatively might be chosen to be the transverse momentum of the 3^{rd} jet.

origin, in a similar manner as we currently group, for example, hadron collider results together [723].

References

- [1] R. K. Ellis, W. J. Stirling and B. R. Webber, *Camb. Monogr. Part. Phys. Nucl. Phys. Cosmol.* **8**, 1 (1996).
- [2] J. Campbell, J. Huston, F. Krauss “*The Black Book of Quantum Chromodynamics, a Primer for the QCD Era*,” Oxford University Press, UK (2017).
- [3] C. A. Baker *et al.*, *Phys. Rev. Lett.* **97**, 131801 (2006), [hep-ex/0602020].
- [4] J. M. Pendlebury *et al.*, *Phys. Rev.* **D92**, 9, 092003 (2015), [arXiv:1509.04411].
- [5] B. Graner *et al.*, *Phys. Rev. Lett.* **116**, 16, 161601 (2016), [Erratum: *Phys. Rev. Lett.* 119, no.11, 119901 (2017)], [arXiv:1601.04339].
- [6] <https://www.psi.ch/en/nedm/edms-world-wide>.
- [7] J. E. Kim and G. Carosi, *Rev. Mod. Phys.* **82**, 557 (2010), [arXiv:0807.3125].
- [8] G. Dissertori, I. G. Knowles and M. Schmelling, *High energy experiments and theory*, Oxford, UK: Clarendon (2003).
- [9] R. Brock *et al.* (CTEQ), *Rev. Mod. Phys.* **67**, 157 (1995).
- [10] K. Melnikov, CERN Yellow Rep. School Proc. **3**, 37 (2018).
- [11] F. Gross *et al.* (2022), [arXiv:2212.11107].
- [12] T. van Ritbergen, J. A. M. Vermaseren and S. A. Larin, *Phys. Lett.* **B400**, 379 (1997), [hep-ph/9701390].
- [13] M. Czakon, *Nucl. Phys.* **B710**, 485 (2005), [hep-ph/0411261].
- [14] P. A. Baikov, K. G. Chetyrkin and J. H. Kühn, *Phys. Rev. Lett.* **118**, 8, 082002 (2017), [arXiv:1606.08659].
- [15] T. Luthe *et al.*, *JHEP* **07**, 127 (2016), [arXiv:1606.08662].
- [16] F. Herzog *et al.*, *JHEP* **02**, 090 (2017), [arXiv:1701.01404].
- [17] T. Luthe *et al.*, *JHEP* **10**, 166 (2017), [arXiv:1709.07718].
- [18] K. G. Chetyrkin *et al.*, *JHEP* **10**, 179 (2017), [Addendum: *JHEP* 12, 006 (2017)], [arXiv:1709.08541].
- [19] W. A. Bardeen *et al.*, *Phys. Rev.* **D18**, 3998 (1978).
- [20] D. J. Gross and F. Wilczek, *Phys. Rev. Lett.* **30**, 1343 (1973), [271(1973)].
- [21] H. D. Politzer, *Phys. Rev. Lett.* **30**, 1346 (1973), [274(1973)].
- [22] Y. Schroder and M. Steinhauser, *JHEP* **01**, 051 (2006), [hep-ph/0512058].
- [23] K. G. Chetyrkin, J. H. Kuhn and C. Sturm, *Nucl. Phys.* **B744**, 121 (2006), [hep-ph/0512060].
- [24] A. G. Grozin *et al.*, *JHEP* **09**, 066 (2011), [arXiv:1107.5970].
- [25] M. Dalla Brida *et al.* (ALPHA), *Phys. Rev. Lett.* **117**, 18, 182001 (2016), [arXiv:1604.06193].
- [26] M. Beneke, *Phys. Rept.* **317**, 1 (1999), [hep-ph/9807443].
- [27] M. Beneke *et al.*, *Phys. Lett.* **B775**, 63 (2017), [arXiv:1605.03609].
- [28] A. H. Hoang, C. Lepenik and M. Preisser, *JHEP* **09**, 099 (2017), [arXiv:1706.08526].
- [29] P. Marquard *et al.*, *Phys. Rev. Lett.* **114**, 14, 142002 (2015), [arXiv:1502.01030].
- [30] P. A. Baikov *et al.*, *Phys. Lett.* **B714**, 62 (2012), [arXiv:1206.1288].
- [31] K. G. Chetyrkin, J. H. Kuhn and A. Kwiatkowski (1996), [Phys. Rept. 277, 189 (1996)], [hep-ph/9503396].
- [32] Y. Kiyo *et al.*, *Nucl. Phys.* **B823**, 269 (2009), [arXiv:0907.2120].
- [33] P. A. Baikov *et al.*, *Phys. Rev. Lett.* **108**, 222003 (2012), [arXiv:1201.5804].
- [34] P. A. Baikov, K. G. Chetyrkin and J. H. Kuhn, *Phys. Rev. Lett.* **101**, 012002 (2008), [arXiv:0801.1821].
- [35] F. Herzog *et al.*, *JHEP* **08**, 113 (2017), [arXiv:1707.01044].
- [36] V. A. Novikov *et al.*, *Nucl. Phys.* **B174**, 378 (1980).
- [37] T.-J. Hou *et al.*, *Phys. Rev. D* **103**, 1, 014013 (2021), [arXiv:1912.10053].
- [38] R. D. Ball *et al.* (PDF4LHC Working Group), *J. Phys. G* **49**, 8, 080501 (2022), [arXiv:2203.05506].
- [39] R. Abdul Khalek *et al.* (NNPDF), *Eur. Phys. J. C* **79**, 838 (2019), [arXiv:1905.04311].
- [40] R. Abdul Khalek *et al.* (NNPDF), *Eur. Phys. J. C* **79**, 11, 931 (2019), [arXiv:1906.10698].
- [41] R. D. Ball and R. L. Pearson, *Eur. Phys. J. C* **81**, 9, 830 (2021), [arXiv:2105.05114].
- [42] Z. Kassabov, M. Ubiali and C. Voisey, *JHEP* **03**, 148 (2023), [arXiv:2207.07616].
- [43] L. A. Harland-Lang and R. S. Thorne, *Eur. Phys. J. C* **79**, 3, 225 (2019), [arXiv:1811.08434].
- [44] J. McGowan *et al.*, *Eur. Phys. J. C* **83**, 3, 185 (2023), [Erratum: *Eur. Phys. J. C* 83, 302 (2023)], [arXiv:2207.04739].
- [45] X. Ji, *Phys. Rev. Lett.* **110**, 262002 (2013), [arXiv:1305.1539].
- [46] G. C. Rossi and M. Testa, *Phys. Rev.* **D96**, 1, 014507 (2017), [arXiv:1706.04428].
- [47] G. Rossi and M. Testa, *Phys. Rev. D* **98**, 5, 054028 (2018), [arXiv:1806.00808].
- [48] L. Del Debbio, T. Giani and C. J. Monahan, *JHEP* **09**, 021 (2020), [arXiv:2007.02131].
- [49] H.-W. Lin *et al.*, *Phys. Rev.* **D91**, 054510 (2015), [arXiv:1402.1462]; C. Alexandrou *et al.*, *Phys. Rev.* **D92**, 014502 (2015), [arXiv:1504.07455].
- [50] H.-W. Lin *et al.*, *Prog. Part. Nucl. Phys.* **100**, 107 (2018), [arXiv:1711.07916].
- [51] C. Alexandrou *et al.*, *Phys. Rev. Lett.* **121**, 11, 112001 (2018), [arXiv:1803.02685].
- [52] J.-W. Chen *et al.* (2018), [arXiv:1803.04393].
- [53] K. Cichy, L. Del Debbio and T. Giani, *JHEP* **10**, 137 (2019), [arXiv:1907.06037].
- [54] K. Cichy and M. Constantinou, *Adv. High Energy Phys.* **2019**, 3036904 (2019), [arXiv:1811.07248].
- [55] M. A. Ebert, I. W. Stewart and Y. Zhao, *JHEP* **09**, 037 (2019), [arXiv:1901.03685].
- [56] M. Constantinou, *Eur. Phys. J. A* **57**, 2, 77 (2021), [arXiv:2010.02445].
- [57] M. Constantinou *et al.*, *Prog. Part. Nucl. Phys.* **121**, 103908 (2021), [arXiv:2006.08636].
- [58] L. Del Debbio *et al.*, *JHEP* **02**, 138 (2021), [arXiv:2010.03996].
- [59] Z. Fan, R. Zhang and H.-W. Lin, *Int. J. Mod. Phys. A* **36**, 13, 2150080 (2021), [arXiv:2007.16113].
- [60] T. Khan *et al.* (HadStruc), *Phys. Rev. D* **104**, 9, 094516 (2021), [arXiv:2107.08960].
- [61] Z. Fan, W. Good and H.-W. Lin (2022), [arXiv:2210.09985].
- [62] J. Gao, L. Harland-Lang and J. Rojo, *Phys. Rept.* **742**, 1 (2018), [arXiv:1709.04922].
- [63] K. Kovařík, P. M. Nadolsky and D. E. Soper, *Rev. Mod. Phys.* **92**, 4, 045003 (2020), [arXiv:1905.06957].
- [64] T.-J. Hou *et al.*, *Phys. Rev. D* **107**, 7, 076018 (2023), [arXiv:2211.11064].
- [65] J. D. Bjorken and E. A. Paschos, *Phys. Rev.* **185**, 1975 (1969).
- [66] J. A. M. Vermaseren, A. Vogt and S. Moch, *Nucl. Phys.* **B724**, 3 (2005), [hep-ph/0504242].
- [67] S. Moch, J. A. M. Vermaseren and A. Vogt, *Nucl. Phys.* **B813**, 220 (2009), [arXiv:0812.4168].

- [68] J. Davies *et al.*, PoS **DIS2016**, 059 (2016), [arXiv:1606.08907].
- [69] E. Laenen *et al.*, Nucl. Phys. **B392**, 162 (1993); S. Riemersma, J. Smith and W. L. van Neerven, Phys. Lett. **B347**, 143 (1995), [hep-ph/9411431].
- [70] J. Blümlein *et al.* (2019), [arXiv:1903.06155].
- [71] J. Blümlein (2023), [arXiv:2306.01362].
- [72] A. Manohar *et al.*, Phys. Rev. Lett. **117**, 24, 242002 (2016), [arXiv:1607.04266].
- [73] A. V. Manohar *et al.*, JHEP **12**, 046 (2017), [arXiv:1708.01256].
- [74] L. Buonocore *et al.*, JHEP **08**, 08, 019 (2020), [arXiv:2005.06477].
- [75] J. C. Collins, D. E. Soper and G. F. Sterman, Adv. Ser. Direct. High Energy Phys. **5**, 1 (1989), [hep-ph/0409313].
- [76] J. Collins and J.-W. Qiu, Phys. Rev. D **75**, 114014 (2007), [arXiv:0705.2141].
- [77] G. Sterman, in “Snowmass 2021,” (2022), [arXiv:2207.06507].
- [78] R. Boussarie *et al.* (2023), [arXiv:2304.03302].
- [79] V. N. Gribov and L. N. Lipatov, Sov. J. Nucl. Phys. **15**, 438 (1972), [Yad. Fiz.15,781(1972)]; L. N. Lipatov, Sov. J. Nucl. Phys. **20**, 94 (1975), [Yad. Fiz.20,181(1974)]; G. Altarelli and G. Parisi, Nucl. Phys. **B126**, 298 (1977); Y. L. Dokshitzer, Sov. Phys. JETP **46**, 641 (1977), [Zh. Eksp. Teor. Fiz.73,1216(1977)].
- [80] G. Curci, W. Furmanski and R. Petronzio, Nucl. Phys. **B175**, 27 (1980); W. Furmanski and R. Petronzio, Phys. Lett. **97B**, 437 (1980).
- [81] A. Vogt, S. Moch and J. A. M. Vermaseren, Nucl. Phys. **B691**, 129 (2004), [hep-ph/0404111]; S. Moch, J. A. M. Vermaseren and A. Vogt, Nucl. Phys. **B688**, 101 (2004), [hep-ph/0403192].
- [82] J. Davies *et al.*, Nucl. Phys. B **915**, 335 (2017), [arXiv:1610.07477].
- [83] S. Moch *et al.*, JHEP **10**, 041 (2017), [arXiv:1707.08315].
- [84] A. Vogt *et al.*, PoS **RADCOR2017**, 046 (2018), [arXiv:1801.06085].
- [85] A. Vogt *et al.*, PoS **LL2018**, 050 (2018), [arXiv:1808.08981].
- [86] G. Falcioni *et al.*, Phys. Lett. B **842**, 137944 (2023), [arXiv:2302.07593].
- [87] S. Moch, J. A. M. Vermaseren and A. Vogt, Nucl. Phys. **B889**, 351 (2014), [arXiv:1409.5131].
- [88] D. de Florian, G. F. R. Sborlini and G. Rodrigo, Eur. Phys. J. **C76**, 5, 282 (2016), [arXiv:1512.00612]; D. de Florian, G. F. R. Sborlini and G. Rodrigo, JHEP **10**, 056 (2016), [arXiv:1606.02887].
- [89] D. de Florian and L. P. Conte (2023), [arXiv:2305.14144].
- [90] R. S. Thorne, Phys. Rev. **D73**, 054019 (2006), [hep-ph/0601245].
- [91] S. Forte *et al.*, Nucl. Phys. **B834**, 116 (2010), [arXiv:1001.2312].
- [92] M. Guzzi *et al.*, Phys. Rev. **D86**, 053005 (2012), [arXiv:1108.5112].
- [93] V. S. Fadin, E. A. Kuraev and L. N. Lipatov, Phys. Lett. **60B**, 50 (1975).
- [94] I. I. Balitsky and L. N. Lipatov, Sov. J. Nucl. Phys. **28**, 822 (1978), [Yad. Fiz.28,1597(1978)].
- [95] R. D. Ball *et al.*, Eur. Phys. J. **C78**, 4, 321 (2018), [arXiv:1710.05935].
- [96] H. Abramowicz *et al.* (H1, ZEUS), Eur. Phys. J. **C75**, 12, 580 (2015), [arXiv:1506.06042].
- [97] L. N. Lipatov, Sov. J. Nucl. Phys. **23**, 338 (1976), [Yad. Fiz.23,642(1976)].
- [98] E. A. Kuraev, L. N. Lipatov and V. S. Fadin, Sov. Phys. JETP **45**, 199 (1977), [Zh. Eksp. Teor. Fiz.72,377(1977)].
- [99] V. S. Fadin and L. N. Lipatov, Phys. Lett. **B429**, 127 (1998), [hep-ph/9802290].
- [100] M. Ciafaloni and G. Camici, Phys. Lett. **B430**, 349 (1998), [hep-ph/9803389].
- [101] G. Altarelli, R. D. Ball and S. Forte, Nucl. Phys. **B799**, 199 (2008), [arXiv:0802.0032].
- [102] M. Ciafaloni *et al.*, JHEP **08**, 046 (2007), [arXiv:0707.1453].
- [103] C. D. White and R. S. Thorne, Phys. Rev. **D75**, 034005 (2007), [hep-ph/0611204].
- [104] E. Iancu *et al.*, Phys. Lett. **B744**, 293 (2015), [arXiv:1502.05642].
- [105] N. Gromov, F. Levkovich-Maslyuk and G. Sizov, Phys. Rev. Lett. **115**, 25, 251601 (2015), [arXiv:1507.04010]; V. N. Velizhanin (2015), [arXiv:1508.02857]; S. Caron-Huot and M. Herranen, JHEP **02**, 058 (2018), [arXiv:1604.07417]; V. Fadin, *Chapter 4: BFKL — Past and Future*, 63–90 (2021), [arXiv:2012.11931].
- [106] I. Balitsky, Nucl. Phys. **B463**, 99 (1996), [hep-ph/9509348].
- [107] Y. V. Kovchegov, Phys. Rev. **D60**, 034008 (1999), [hep-ph/9901281].
- [108] M. Davier *et al.*, Eur. Phys. J. C **56**, 305 (2008), [arXiv:0803.0979].
- [109] J. C. Collins, D. E. Soper and G. F. Sterman, Nucl. Phys. **B261**, 104 (1985).
- [110] C. Anastasiou *et al.*, Phys. Rev. Lett. **114**, 212001 (2015), [arXiv:1503.06056]; C. Anastasiou *et al.*, JHEP **05**, 058 (2016), [arXiv:1602.00695].
- [111] B. Mistlberger, JHEP **05**, 028 (2018), [arXiv:1802.00833].
- [112] L.-B. Chen *et al.*, Phys. Lett. B **803**, 135292 (2020), [arXiv:1909.06808].
- [113] F. Dulat, B. Mistlberger and A. Pelloni, Phys. Rev. **D99**, 3, 034004 (2019), [arXiv:1810.09462].
- [114] L. Cieri *et al.*, JHEP **02**, 096 (2019), [arXiv:1807.11501].
- [115] X. Chen *et al.* (2021), [arXiv:2102.07607].
- [116] J. Baglio *et al.*, JHEP **12**, 066 (2022), [arXiv:2209.06138].
- [117] F. A. Dreyer and A. Karlberg, Phys. Rev. Lett. **117**, 7, 072001 (2016), [arXiv:1606.00840].
- [118] F. A. Dreyer and A. Karlberg, Phys. Rev. D **98**, 11, 114016 (2018), [arXiv:1811.07906].
- [119] C. Duhr, F. Dulat and B. Mistlberger, Phys. Rev. Lett. **125**, 17, 172001 (2020), [arXiv:2001.07717].
- [120] X. Chen *et al.* (2021), [arXiv:2107.09085].
- [121] C. Duhr, F. Dulat and B. Mistlberger, JHEP **11**, 143 (2020), [arXiv:2007.13313].
- [122] M. Bonvini *et al.*, JHEP **08**, 105 (2016), [arXiv:1603.08000].
- [123] F. Dulat, A. Lazopoulos and B. Mistlberger, Comput. Phys. Commun. **233**, 243 (2018), [arXiv:1802.00827].
- [124] R. V. Harlander, S. Liebler and H. Mantler, Comput. Phys. Commun. **212**, 239 (2017), [arXiv:1605.03190].
- [125] O. Brein, A. Djouadi and R. Harlander, Phys. Lett. **B579**, 149 (2004), [hep-ph/0307206].
- [126] D. de Florian and J. Mazzitelli, Phys. Rev. Lett. **111**, 201801 (2013), [arXiv:1309.6594].
- [127] S. Borowka *et al.*, Phys. Rev. Lett. **117**, 1, 012001 (2016), [Erratum: Phys. Rev. Lett.117,no.7,079901(2016)], [arXiv:1604.06447].
- [128] M. Czakon, P. Fiedler and A. Mitov, Phys. Rev. Lett. **110**, 252004 (2013), [arXiv:1303.6254].
- [129] S. Catani *et al.*, Phys. Rev. **D99**, 5, 051501 (2019), [arXiv:1901.04005].
- [130] S. Catani *et al.*, JHEP **03**, 029 (2021), [arXiv:2010.11906].

- [131] T. Gehrmann *et al.*, Phys. Rev. Lett. **113**, 21, 212001 (2014), [arXiv:1408.5243].
- [132] F. Cascioli *et al.*, Phys. Lett. **B735**, 311 (2014), [arXiv:1405.2219].
- [133] M. Grazzini, S. Kallweit and M. Wiesemann, Eur. Phys. J. **C78**, 7, 537 (2018), [arXiv:1711.06631].
- [134] G. Heinrich, Phys. Rept. **922**, 1 (2021), [arXiv:2009.00516].
- [135] A. Huss *et al.*, J. Phys. G **50**, 4, 043001 (2023), [arXiv:2207.02122].
- [136] M. Greco and A. Vicini, Nucl. Phys. **B415**, 386 (1994).
- [137] A. Hebecker, Phys. Rept. **331**, 1 (2000), [hep-ph/9905226].
- [138] A. V. Belitsky and A. V. Radyushkin, Phys. Rept. **418**, 1 (2005), [hep-ph/0504030].
- [139] E. Boos *et al.* (CompHEP), Nucl. Instrum. Meth. **A534**, 250 (2004), [hep-ph/0403113].
- [140] J. Alwall *et al.*, JHEP **07**, 079 (2014), [arXiv:1405.0301]; <https://launchpad.net/mg5amcnlo>.
- [141] M. L. Mangano *et al.*, JHEP **07**, 001 (2003), [hep-ph/0206293]; <http://cern.ch/mlm/alpgen/>.
- [142] T. Gleisberg and S. Hoeche, JHEP **12**, 039 (2008), [arXiv:0808.3674]; <https://sherpa-team.gitlab.io/>.
- [143] A. Cafarella, C. G. Papadopoulos and M. Worek, Comput. Phys. Commun. **180**, 1941 (2009), [arXiv:0710.2427]; <http://cern.ch/helac-phegas/>.
- [144] F. A. Berends and W. T. Giele, Nucl. Phys. **B306**, 759 (1988).
- [145] L. J. Dixon, in “QCD and beyond. Proceedings, Theoretical Advanced Study Institute in Elementary Particle Physics, TASI-95, Boulder, USA, June 4-30, 1995,” 539–584 (1996), [hep-ph/9601359], URL <http://www-public.slac.stanford.edu/sciDoc/docMeta.aspx?slacPubNumber=SLAC-PUB-7106>.
- [146] R. Britto, F. Cachazo and B. Feng, Nucl. Phys. **B715**, 499 (2005), [hep-th/0412308].
- [147] F. Cachazo, P. Svrcek and E. Witten, JHEP **09**, 006 (2004), [hep-th/0403047].
- [148] S. Catani and M. H. Seymour, Nucl. Phys. **B485**, 291 (1997), [Erratum: Nucl. Phys. **B510**, 503 (1998)], [hep-ph/9605323].
- [149] S. Frixione, Z. Kunszt and A. Signer, Nucl. Phys. **B467**, 399 (1996), [hep-ph/9512328].
- [150] D. A. Kosower, Phys. Rev. **D57**, 5410 (1998), [hep-ph/9710213]; J. M. Campbell, M. A. Cullen and E. W. N. Glover, Eur. Phys. J. **C9**, 245 (1999), [hep-ph/9809429]; D. A. Kosower, Phys. Rev. **D71**, 045016 (2005), [hep-ph/0311272].
- [151] G. Ossola, C. G. Papadopoulos and R. Pittau, Nucl. Phys. **B763**, 147 (2007), [hep-ph/0609007].
- [152] R. Britto, F. Cachazo and B. Feng, Nucl. Phys. **B725**, 275 (2005), [hep-th/0412103].
- [153] R. K. Ellis *et al.*, Nucl. Phys. **B822**, 270 (2009), [arXiv:0806.3467].
- [154] C. F. Berger and D. Forde, Ann. Rev. Nucl. Part. Sci. **60**, 181 (2010), [arXiv:0912.3534].
- [155] F. Cascioli, P. Maierhofer and S. Pozzorini, Phys. Rev. Lett. **108**, 111601 (2012), [arXiv:1111.5206].
- [156] Z. Bern, L. J. Dixon and D. A. Kosower, Annals Phys. **322**, 1587 (2007), [arXiv:0704.2798].
- [157] R. K. Ellis *et al.*, Phys. Rept. **518**, 141 (2012), [arXiv:1105.4319].
- [158] G. Bevilacqua *et al.*, Comput. Phys. Commun. **184**, 986 (2013), [arXiv:1110.1499]; <http://cern.ch/helac-phegas/>.
- [159] G. Cullen *et al.*, Eur. Phys. J. **C74**, 8, 3001 (2014), [arXiv:1404.7096]; <http://gosam.hepforge.org/>.
- [160] S. Badger *et al.*, Comput. Phys. Commun. **184**, 1981 (2013), [arXiv:1209.0100]; <https://bitbucket.org/njet/wiki/Home/>.
- [161] F. Buccioni, S. Pozzorini and M. Zoller, Eur. Phys. J. **C78**, 1, 70 (2018), [arXiv:1710.11452]; <https://openloops.hepforge.org/>.
- [162] S. Actis *et al.*, Comput. Phys. Commun. **214**, 140 (2017), [arXiv:1605.01090].
- [163] Z. Nagy, Phys. Rev. **D68**, 094002 (2003), [hep-ph/0307268]; <http://www.desy.de/~znagy/Site/NLOJet++.html>.
- [164] J. M. Campbell and R. K. Ellis, Phys. Rev. **D62**, 114012 (2000), [hep-ph/0006304].
- [165] J. Baglio *et al.* (2011), [arXiv:1107.4038]; <http://www-itp.particle.uni-karlsruhe.de/~vbfnlweb>.
- [166] T. Binoth *et al.*, Eur. Phys. J. **C16**, 311 (2000), [hep-ph/9911340]; http://laph.in2p3.fr/PHOX_FAMILY/.
- [167] Z. Bern *et al.*, PoS **LL2012**, 018 (2012), [arXiv:1210.6684].
- [168] G. Cullen, N. Greiner and G. Heinrich, Eur. Phys. J. **C73**, 4, 2388 (2013), [arXiv:1212.5154].
- [169] S. Kallweit *et al.*, JHEP **04**, 012 (2015), [arXiv:1412.5157].
- [170] A. Denner *et al.*, JHEP **04**, 018 (2015), [arXiv:1412.7421].
- [171] M. Chiesa, N. Greiner and F. Tramontano, J. Phys. **G43**, 1, 013002 (2016), [arXiv:1507.08579].
- [172] S. Frixione *et al.*, JHEP **06**, 184 (2015), [arXiv:1504.03446].
- [173] B. Biedermann *et al.*, Eur. Phys. J. **C77**, 492 (2017), [arXiv:1704.05783].
- [174] R. Frederix *et al.*, JHEP **07**, 185 (2018), [Erratum: JHEP **11**, 085 (2021)], [arXiv:1804.10017].
- [175] C. Anastasiou, R. Boughezal and F. Petriello, JHEP **04**, 003 (2009), [arXiv:0811.3458].
- [176] S. Dittmaier, A. Huss and C. Schwinn, Nucl. Phys. **B885**, 318 (2014), [arXiv:1403.3216].
- [177] S. Dittmaier, A. Huss and C. Schwinn, Nucl. Phys. **B904**, 216 (2016), [arXiv:1511.08016].
- [178] D. de Florian, M. Der and I. Fabre, Phys. Rev. **D98**, 9, 094008 (2018), [arXiv:1805.12214].
- [179] M. Bonetti, K. Melnikov and L. Tancredi, Phys. Rev. **D97**, 3, 034004 (2018), [arXiv:1711.11113].
- [180] M. Bonetti, K. Melnikov and L. Tancredi, Phys. Rev. **D97**, 5, 056017 (2018), [Erratum: Phys. Rev. **D97**, no.9, 099906 (2018)], [arXiv:1801.10403].
- [181] C. Anastasiou *et al.*, JHEP **03**, 162 (2019), [arXiv:1811.11211].
- [182] V. Hirschi, S. Lionetti and A. Schweitzer, JHEP **05**, 002 (2019), [arXiv:1902.10167].
- [183] M. Becchetti *et al.*, Phys. Rev. D **103**, 5, 054037 (2021), [arXiv:2010.09451].
- [184] M. Bonetti *et al.*, JHEP **11**, 045 (2020), [arXiv:2007.09813].
- [185] A. Behring *et al.*, Phys. Rev. D **103**, 1, 013008 (2021), [arXiv:2009.10386].
- [186] S. Dittmaier, T. Schmidt and J. Schwarz, JHEP **12**, 201 (2020), [arXiv:2009.02229].
- [187] F. Buccioni *et al.*, Phys. Lett. B **811**, 135969 (2020), [arXiv:2005.10221].
- [188] L. Buonocore *et al.*, Phys. Rev. D **103**, 114012 (2021), [arXiv:2102.12539].
- [189] R. Bonciani *et al.*, Phys. Rev. Lett. **128**, 1, 012002 (2022), [arXiv:2106.11953].
- [190] T. Armadillo *et al.*, JHEP **05**, 072 (2022), [arXiv:2201.01754].
- [191] F. Buccioni *et al.*, JHEP **06**, 022 (2022), [arXiv:2203.11237].
- [192] A. Denner and S. Dittmaier, Phys. Rept. **864**, 1 (2020), [arXiv:1912.06823].

- [193] Z. Bern *et al.*, Nucl. Phys. **B425**, 217 (1994), [hep-ph/9403226].
- [194] J. M. Campbell and E. W. N. Glover, Nucl. Phys. **B527**, 264 (1998), [hep-ph/9710255].
- [195] S. Catani and M. Grazzini, Phys. Lett. **B446**, 143 (1999), [hep-ph/9810389].
- [196] T. Binoth and G. Heinrich, Nucl. Phys. **B585**, 741 (2000), [hep-ph/0004013].
- [197] C. Anastasiou, K. Melnikov and F. Petriello, Phys. Rev. **D69**, 076010 (2004), [hep-ph/0311311].
- [198] A. Gehrmann-De Ridder, T. Gehrmann and E. W. N. Glover, JHEP **09**, 056 (2005), [hep-ph/0505111].
- [199] G. Somogyi, Z. Trocsanyi and V. Del Duca, JHEP **01**, 070 (2007), [hep-ph/0609042].
- [200] M. Czakon, Phys. Lett. **B693**, 259 (2010), [arXiv:1005.0274].
- [201] F. Caola, K. Melnikov and R. Röntsch, Eur. Phys. J. C **77**, 4, 248 (2017), [arXiv:1702.01352].
- [202] L. Magnea *et al.*, JHEP **12**, 107 (2018), [Erratum: JHEP 06, 013 (2019)], [arXiv:1806.09570].
- [203] R. M. Prisco and F. Tramontano, JHEP **06**, 089 (2021), [arXiv:2012.05012].
- [204] G. Bertolotti *et al.* (2022), [arXiv:2212.11190].
- [205] C. Anastasiou and G. Sterman, JHEP **05**, 242 (2023), [arXiv:2212.12162].
- [206] S. Catani and M. Grazzini, Phys. Rev. Lett. **98**, 222002 (2007), [hep-ph/0703012]; <http://theory.fi.infn.it/grazzini/codes.html>.
- [207] R. Bonciani *et al.*, Eur. Phys. J. C **75**, 12, 581 (2015), [arXiv:1508.03585].
- [208] R. Boughezal *et al.*, Phys. Rev. Lett. **115**, 6, 062002 (2015), [arXiv:1504.02131].
- [209] R. Boughezal, X. Liu and F. Petriello, Phys. Rev. D **91**, 9, 094035 (2015), [arXiv:1504.02540].
- [210] J. Gaunt *et al.*, JHEP **09**, 058 (2015), [arXiv:1505.04794].
- [211] M. Cacciari *et al.*, Phys. Rev. Lett. **115**, 8, 082002 (2015), [Erratum: Phys. Rev. Lett.120,no.13,139901(2018)], [arXiv:1506.02660].
- [212] Z. Capatti, V. Hirschi and B. Ruijl, JHEP **10**, 120 (2022), [arXiv:2203.11038].
- [213] L. Cieri *et al.*, JHEP **09**, 155 (2020), [arXiv:2005.01315].
- [214] W. J. Torres Bobadilla *et al.*, Eur. Phys. J. C **81**, 3, 250 (2021), [arXiv:2012.02567].
- [215] A. Gehrmann-De Ridder *et al.*, Phys. Rev. Lett. **99**, 132002 (2007), [arXiv:0707.1285]; A. Gehrmann-De Ridder *et al.*, JHEP **12**, 094 (2007), [arXiv:0711.4711]; A. Gehrmann-De Ridder *et al.*, Phys. Rev. Lett. **100**, 172001 (2008), [arXiv:0802.0813].
- [216] A. Gehrmann-De Ridder *et al.*, Comput. Phys. Commun. **185**, 3331 (2014), [arXiv:1402.4140]; <https://eeraad3.hepforge.org/>.
- [217] S. Weinzierl, Phys. Rev. Lett. **101**, 162001 (2008), [arXiv:0807.3241]; S. Weinzierl, JHEP **06**, 041 (2009), [arXiv:0904.1077].
- [218] V. Del Duca *et al.*, Phys. Rev. D **94**, 7, 074019 (2016), [arXiv:1606.03453]; V. Del Duca *et al.*, Phys. Rev. Lett. **117**, 15, 152004 (2016), [arXiv:1603.08927].
- [219] J. Currie, T. Gehrmann and J. Niehues, Phys. Rev. Lett. **117**, 4, 042001 (2016), [arXiv:1606.03991].
- [220] J. Currie *et al.*, JHEP **07**, 018 (2017), [Erratum: JHEP 12, 042 (2020)], [arXiv:1703.05977].
- [221] J. Currie *et al.*, JHEP **05**, 209 (2018), [arXiv:1803.09973].
- [222] T. Gehrmann *et al.*, Phys. Lett. **B792**, 182 (2019), [arXiv:1812.06104].
- [223] K. Melnikov and F. Petriello, Phys. Rev. **D74**, 114017 (2006), [hep-ph/0609070]; <http://gate.hep.anl.gov/fpetriello/FEWZ.html>.
- [224] S. Catani *et al.*, Phys. Rev. Lett. **103**, 082001 (2009), [arXiv:0903.2120]; <http://theory.fi.infn.it/gazzani/dy.html>.
- [225] C. Anastasiou, K. Melnikov and F. Petriello, Nucl. Phys. **B724**, 197 (2005), [hep-ph/0501130]; <http://www.phys.ethz.ch/~pheno/fehipro/>.
- [226] M. Czakon *et al.* (2021), [arXiv:2105.04436].
- [227] M. Grazzini *et al.*, JHEP **05**, 139 (2017), [arXiv:1703.09065].
- [228] S. Catani *et al.*, Phys. Rev. Lett. **108**, 072001 (2012), [Erratum: Phys. Rev. Lett.117,no.8,089901(2016)], [arXiv:1110.2375].
- [229] J. M. Campbell *et al.*, JHEP **07**, 148 (2016), [arXiv:1603.02663].
- [230] M. Grazzini *et al.*, Phys. Lett. **B731**, 204 (2014), [arXiv:1309.7000].
- [231] M. Grazzini, S. Kallweit and D. Rathlev, JHEP **07**, 085 (2015), [arXiv:1504.01330].
- [232] J. M. Campbell and R. K. Ellis, Phys. Rev. D **60**, 113006 (1999), [hep-ph/9905386].
- [233] R. Boughezal *et al.*, Eur. Phys. J. **C77**, 1, 7 (2017), [arXiv:1605.08011].
- [234] J. M. Campbell, R. K. Ellis and C. Williams, Phys. Rev. Lett. **118**, 22, 222001 (2017), [arXiv:1612.04333].
- [235] X. Chen *et al.*, Submitted to: J. High Energy Phys. (2019), [arXiv:1904.01044].
- [236] J. M. Campbell, R. K. Ellis and C. Williams, Phys. Rev. **D96**, 1, 014037 (2017), [arXiv:1703.10109].
- [237] A. Gehrmann-De Ridder *et al.*, Phys. Rev. Lett. **120**, 12, 122001 (2018), [arXiv:1712.07543].
- [238] A. Gehrmann-De Ridder *et al.*, Phys. Rev. Lett. **117**, 2, 022001 (2016), [arXiv:1507.02850].
- [239] R. Boughezal *et al.*, Phys. Rev. Lett. **116**, 15, 152001 (2016), [arXiv:1512.01291].
- [240] R. Boughezal *et al.*, Phys. Rev. Lett. **115**, 8, 082003 (2015), [arXiv:1504.07922].
- [241] R. Boughezal *et al.*, Phys. Lett. **B748**, 5 (2015), [arXiv:1505.03893].
- [242] F. Caola, K. Melnikov and M. Schulze, Phys. Rev. **D92**, 7, 074032 (2015), [arXiv:1508.02684].
- [243] X. Chen *et al.*, JHEP **10**, 066 (2016), [arXiv:1607.08817].
- [244] G. Ferrera, M. Grazzini and F. Tramontano, Phys. Rev. Lett. **107**, 152003 (2011), [arXiv:1107.1164].
- [245] G. Ferrera, M. Grazzini and F. Tramontano, Phys. Lett. **B740**, 51 (2015), [arXiv:1407.4747].
- [246] Z. L. Liu and J. Gao, Phys. Rev. D **98**, 7, 071501 (2018), [arXiv:1807.03835].
- [247] M. Brucherseifer, F. Caola and K. Melnikov, Phys. Lett. **B736**, 58 (2014), [arXiv:1404.7116].
- [248] E. L. Berger *et al.*, Phys. Rev. **D94**, 7, 071501 (2016), [arXiv:1606.08463].
- [249] E. L. Berger, J. Gao and H. X. Zhu, JHEP **11**, 158 (2017), [arXiv:1708.09405].
- [250] J. Campbell, T. Neumann and Z. Sullivan, JHEP **02**, 040 (2021), [arXiv:2012.01574].
- [251] M. Czakon, P. Fiedler and A. Mitov, Phys. Rev. Lett. **115**, 5, 052001 (2015), [arXiv:1411.3007].
- [252] M. Czakon *et al.*, JHEP **05**, 034 (2016), [arXiv:1601.05375].
- [253] J. Currie, E. W. N. Glover and J. Pires, Phys. Rev. Lett. **118**, 7, 072002 (2017), [arXiv:1611.01460].
- [254] X. Chen *et al.*, JHEP **09**, 025 (2022), [arXiv:2204.10173].

- [255] M. Czakon *et al.* (2020), [arXiv:2011.01011].
- [256] M. Czakon *et al.*, JHEP **02**, 241 (2023), [arXiv:2212.00467].
- [257] M. L. Czakon *et al.* (2021), [arXiv:2102.08267].
- [258] J. Cruz-Martinez *et al.*, Phys. Lett. **B781**, 672 (2018), [arXiv:1802.02445].
- [259] T. Liu, K. Melnikov and A. A. Penin (2019), [arXiv:1906.10899].
- [260] H. A. Chawdhry *et al.*, JHEP **02**, 057 (2020), [arXiv:1911.00479].
- [261] S. Kallweit, V. Sotnikov and M. Wiesemann, Phys. Lett. B **812**, 136013 (2021), [arXiv:2010.04681].
- [262] H. A. Chawdhry *et al.*, JHEP **09**, 093 (2021), [arXiv:2105.06940].
- [263] S. Badger *et al.* (2023), [arXiv:2304.06682].
- [264] M. Czakon, A. Mitov and R. Poncelet, Phys. Rev. Lett. **127**, 15, 152001 (2021), [Erratum: Phys.Rev.Lett. 129, 119901 (2022)], [arXiv:2106.05331].
- [265] H. B. Hartanto *et al.*, Phys. Rev. D **106**, 7, 074016 (2022), [arXiv:2205.01687].
- [266] M. Alvarez *et al.*, JHEP **03**, 129 (2023), [arXiv:2301.01086].
- [267] G. P. Salam and E. Slade, JHEP **11**, 220 (2021), [arXiv:2106.08329].
- [268] M. A. Ebert *et al.*, JHEP **04**, 102 (2021), [arXiv:2006.11382].
- [269] S. Amoroso *et al.*, in “11th Les Houches Workshop on Physics at TeV Colliders: PhysTeV Les Houches,” (2020), [arXiv:2003.01700].
- [270] S. Catani *et al.*, Phys. Rev. Lett. **130**, 11, 111902 (2023), [arXiv:2210.07846].
- [271] S. Camarda *et al.*, Eur. Phys. J. C **80**, 3, 251 (2020), [Erratum: Eur.Phys.J.C 80, 440 (2020)], [arXiv:1910.07049].
- [272] R. Gavin *et al.*, Comput. Phys. Commun. **182**, 2388 (2011), [arXiv:1011.3540].
- [273] S. Camarda *et al.*, Eur. Phys. J. C **82**, 5, 492 (2022), [arXiv:2202.10343].
- [274] R. V. Harlander, S. Liebler and H. Mantler, Comput. Phys. Commun. **184**, 1605 (2013), [arXiv:1212.3249].
- [275] T. Carli *et al.*, Eur. Phys. J. C **66**, 503 (2010), [arXiv:0911.2985].
- [276] T. Kluge, K. Rabbertz and M. Wobisch, in “14th International Workshop on Deep Inelastic Scattering (DIS 2006),” 483, Tsukuba, Japan, April 20-24 (2006), [hep-ph/0609285].
- [277] D. Britzger *et al.*, in “Proceedings, XX. International Workshop on Deep-Inelastic Scattering and Related Subjects (DIS 2012),” 217, Bonn, Germany, March 26-30 (2012), [arXiv:1208.3641].
- [278] S. Carrazza *et al.*, JHEP **12**, 108 (2020), [arXiv:2008.12789].
- [279] M. Czakon, D. Heymes and A. Mitov (2017), [arXiv:1704.08551].
- [280] D. Britzger *et al.*, Eur. Phys. J. C **79**, 10, 845 (2019), [Erratum: Eur.Phys.J.C 81, 957 (2021)], [arXiv:1906.05303].
- [281] D. Maître, J. Phys. Conf. Ser. **1525**, 1, 012014 (2020).
- [282] D. Maître, G. Heinrich and M. Johnson, PoS **LL2016**, 016 (2016), [arXiv:1607.06259].
- [283] Y. L. Dokshitzer, D. Diakonov and S. I. Troian, Phys. Rept. **58**, 269 (1980).
- [284] G. Parisi and R. Petronzio, Nucl. Phys. **B154**, 427 (1979).
- [285] G. Curci, M. Greco and Y. Srivastava, Nucl. Phys. **B159**, 451 (1979).
- [286] A. Bassetto, M. Ciafaloni and G. Marchesini, Nucl. Phys. **B163**, 477 (1980).
- [287] J. C. Collins and D. E. Soper, Nucl. Phys. **B193**, 381 (1981), [Erratum: Nucl. Phys.B213,545(1983)].
- [288] J. C. Collins and D. E. Soper, Nucl. Phys. **B197**, 446 (1982).
- [289] J. Kodaira and L. Trentadue, Phys. Lett. **112B**, 66 (1982).
- [290] J. Kodaira and L. Trentadue, Phys. Lett. **123B**, 335 (1983).
- [291] J. C. Collins, D. E. Soper and G. F. Sterman, Nucl. Phys. **B250**, 199 (1985).
- [292] S. Catani *et al.*, Nucl. Phys. **B407**, 3 (1993).
- [293] C. W. Bauer *et al.*, Phys. Rev. **D63**, 114020 (2001), [hep-ph/0011336].
- [294] C. W. Bauer, D. Pirjol and I. W. Stewart, Phys. Rev. **D65**, 054022 (2002), [hep-ph/0109045].
- [295] T. Becher, A. Broggio and A. Ferroglia, Lect. Notes Phys. **896**, pp.1 (2015), [arXiv:1410.1892].
- [296] S. Catani *et al.*, Phys. Lett. **B269**, 432 (1991).
- [297] N. Brown and W. J. Stirling, Phys. Lett. **B252**, 657 (1990).
- [298] W. Bartel *et al.* (JADE), Z. Phys. **C33**, 23 (1986), [53(1986)].
- [299] N. Kidonakis, G. Oderda and G. F. Sterman, Nucl. Phys. **B531**, 365 (1998), [hep-ph/9803241].
- [300] R. Bonciani *et al.*, Phys. Lett. **B575**, 268 (2003), [hep-ph/0307035].
- [301] A. Banfi, G. P. Salam and G. Zanderighi, JHEP **03**, 073 (2005), [hep-ph/0407286].
- [302] D. de Florian and M. Grazzini, Phys. Rev. Lett. **85**, 4678 (2000), [hep-ph/0008152].
- [303] G. Bozzi *et al.*, Nucl. Phys. **B737**, 73 (2006), [hep-ph/0508068]; <http://theory.fi.infn.it/grazzini/codes.html>.
- [304] G. Bozzi *et al.*, Phys. Lett. **B696**, 207 (2011), [arXiv:1007.2351].
- [305] T. Becher and M. Neubert, Eur. Phys. J. **C71**, 1665 (2011), [arXiv:1007.4005].
- [306] <http://cute.hepforge.org/>.
- [307] D. de Florian *et al.*, JHEP **06**, 132 (2012), [arXiv:1203.6321]; <http://theory.fi.infn.it/grazzini/codes.html>.
- [308] C. Balazs and C. P. Yuan, Phys. Rev. **D56**, 5558 (1997), [hep-ph/9704258].
- [309] S. Catani *et al.*, JHEP **12**, 047 (2015), [arXiv:1507.06937].
- [310] A. Banfi *et al.*, Phys. Lett. **B715**, 152 (2012), [arXiv:1205.4760].
- [311] M. Grazzini *et al.*, JHEP **08**, 154 (2015), [arXiv:1507.02565].
- [312] J. M. Campbell *et al.*, JHEP **03**, 080 (2023), [arXiv:2210.10724].
- [313] D. de Florian and M. Grazzini, Nucl. Phys. **B704**, 387 (2005), [hep-ph/0407241].
- [314] T. Becher and G. Bell, JHEP **11**, 126 (2012), [arXiv:1210.0580].
- [315] A. Banfi *et al.*, Phys. Rev. Lett. **109**, 202001 (2012), [arXiv:1206.4998]; T. Becher, M. Neubert and L. Rothen, JHEP **10**, 125 (2013), [arXiv:1307.0025].
- [316] I. W. Stewart *et al.*, Phys. Rev. D **89**, 5, 054001 (2014), [arXiv:1307.1808].
- [317] J. M. Campbell *et al.*, JHEP **04**, 106 (2023), [arXiv:2301.11768].
- [318] I. W. Stewart, F. J. Tackmann and W. J. Waalewijn, Phys. Rev. Lett. **106**, 032001 (2011), [arXiv:1005.4060].
- [319] Y.-T. Chien *et al.*, Phys. Rev. **D87**, 1, 014010 (2013), [arXiv:1208.0010]; T. T. Jouttenus *et al.*, Phys. Rev. **D88**, 5, 054031 (2013), [arXiv:1302.0846].
- [320] M. Dasgupta *et al.*, JHEP **10**, 126 (2012), [arXiv:1207.1640].
- [321] V. Ahrens *et al.*, JHEP **09**, 097 (2010), [arXiv:1003.5827].

- [322] M. Aliev *et al.*, *Comput. Phys. Commun.* **182**, 1034 (2011), [arXiv:1007.1327].
- [323] N. Kidonakis, *Phys. Rev.* **D82**, 114030 (2010), [arXiv:1009.4935].
- [324] T. Becher, C. Lorentzen and M. D. Schwartz, *Phys. Rev. Lett.* **108**, 012001 (2012), [arXiv:1106.4310].
- [325] T. Becher *et al.*, *Eur. Phys. J.* **C75**, 4, 154 (2015), [arXiv:1412.8408].
- [326] E. Gerwick *et al.*, *JHEP* **02**, 106 (2015), [arXiv:1411.7325].
- [327] A. Banfi *et al.*, *JHEP* **05**, 102 (2015), [arXiv:1412.2126].
- [328] T. Becher and M. D. Schwartz, *JHEP* **07**, 034 (2008), [arXiv:0803.0342].
- [329] A. H. Hoang *et al.*, *Phys. Rev.* **D91**, 9, 094017 (2015), [arXiv:1411.6633].
- [330] Y.-T. Chien and M. D. Schwartz, *JHEP* **08**, 058 (2010), [arXiv:1005.1644].
- [331] W. Bizon *et al.*, *JHEP* **02**, 108 (2018), [arXiv:1705.09127].
- [332] X. Chen *et al.*, *Phys. Lett. B* **788**, 425 (2019), [arXiv:1805.00736].
- [333] W. Bizon *et al.*, *Eur. Phys. J. C* **79**, 10, 868 (2019), [arXiv:1905.05171].
- [334] T. Neumann and J. Campbell, *Phys. Rev. D* **107**, 1, L011506 (2023), [arXiv:2207.07056].
- [335] E. Re, L. Rottoli and P. Torrielli (2021), [arXiv:2104.07509].
- [336] S. Catani *et al.*, *Nucl. Phys.* **B888**, 75 (2014), [arXiv:1405.4827].
- [337] A. Banfi *et al.*, *JHEP* **04**, 049 (2016), [arXiv:1511.02886].
- [338] A. J. Larkoski and I. Moulton, *Phys. Rev.* **D93**, 014017 (2016), [arXiv:1510.08459].
- [339] G. Lustermsans, W. J. Waalewijn and L. Zeune, *Phys. Lett.* **B762**, 447 (2016), [arXiv:1605.02740].
- [340] C. Muselli, S. Forte and G. Ridolfi, *JHEP* **03**, 106 (2017), [arXiv:1701.01464].
- [341] W. Bizoń *et al.*, *JHEP* **12**, 132 (2018), [arXiv:1805.05916].
- [342] M. Bonvini and S. Marzani, *Phys. Rev. Lett.* **120**, 20, 202003 (2018), [arXiv:1802.07758].
- [343] M. Procura, W. J. Waalewijn and L. Zeune, *JHEP* **10**, 098 (2018), [arXiv:1806.10622].
- [344] G. Lustermsans *et al.*, *JHEP* **03**, 124 (2019), [arXiv:1901.03331].
- [345] P. F. Monni, L. Rottoli and P. Torrielli, *Phys. Rev. Lett.* **124**, 25, 252001 (2020), [arXiv:1909.04704].
- [346] T. Becher and T. Neumann, *JHEP* **03**, 199 (2021), [arXiv:2009.11437].
- [347] M. Dasgupta *et al.*, *JHEP* **09**, 029 (2013), [arXiv:1307.0007].
- [348] A. J. Larkoski *et al.*, *JHEP* **05**, 146 (2014), [arXiv:1402.2657].
- [349] A. J. Larkoski, I. Moulton and B. Nachman, *Phys. Rept.* **841**, 1 (2020), [arXiv:1709.04464].
- [350] S. Marzani, G. Soyez and M. Spannowsky (2019), [Lect. Notes Phys. 958, pp.(2019)], [arXiv:1901.10342].
- [351] R. Kogler *et al.*, *Rev. Mod. Phys.* **91**, 4, 045003 (2019), [arXiv:1803.06991].
- [352] Yu.L. Dokshitzer *et al.*, “*Basics of perturbative QCD*,” Gif-sur-Yvette, France: Éditions frontières (1991), see also <http://www.lpthe.jussieu.fr/~yuri/BPQCD/cover.html>.
- [353] T. Sjostrand *et al.*, *Comput. Phys. Commun.* **135**, 238 (2001), [hep-ph/0010017].
- [354] T. Sjostrand, S. Mrenna and P. Z. Skands, *JHEP* **05**, 026 (2006), [hep-ph/0603175]; <http://projects.hepforge.org/pythia6/>.
- [355] T. Sjostrand *et al.*, *Comput. Phys. Commun.* **191**, 159 (2015), [arXiv:1410.3012]; <http://home.thep.lu.se/~torbjorn/Pythia.html>.
- [356] B. R. Webber, *Nucl. Phys.* **B238**, 492 (1984).
- [357] G. Corcella *et al.*, *JHEP* **01**, 010 (2001), [hep-ph/0011363]; <http://www.hep.phy.cam.ac.uk/theory/webber/Herwig/>.
- [358] M. Bahr *et al.*, *Eur. Phys. J.* **C58**, 639 (2008), [arXiv:0803.0883]; <http://projects.hepforge.org/herwig/>.
- [359] T. Gleisberg *et al.*, *JHEP* **02**, 007 (2009), [arXiv:0811.4622].
- [360] L. Lonnblad, *Comput. Phys. Commun.* **71**, 15 (1992).
- [361] A. Buckley *et al.*, *Phys. Rept.* **504**, 145 (2011), [arXiv:1101.2599].
- [362] J. Bellm *et al.*, *Eur. Phys. J. C* **80**, 2, 93 (2020), [arXiv:1903.12563].
- [363] B. Andersson *et al.*, *Phys. Rept.* **97**, 31 (1983).
- [364] T. Sjostrand, *Nucl. Phys.* **B248**, 469 (1984).
- [365] T. Sjostrand and M. van Zijl, *Phys. Rev.* **D36**, 2019 (1987).
- [366] S. Catani *et al.*, *JHEP* **11**, 063 (2001), [hep-ph/0109231].
- [367] J. Alwall *et al.*, *Eur. Phys. J.* **C53**, 473 (2008), [arXiv:0706.2569].
- [368] S. Frixione and B. R. Webber, *JHEP* **06**, 029 (2002), [hep-ph/0204244].
- [369] P. Nason, *JHEP* **11**, 040 (2004), [hep-ph/0409146].
- [370] S. Alioli *et al.*, *JHEP* **06**, 043 (2010), [arXiv:1002.2581]; <http://powhegbox.mib.infn.it/>.
- [371] S. Plätzer, *JHEP* **08**, 114 (2013), [arXiv:1211.5467]; R. Frederix and S. Frixione, *JHEP* **12**, 061 (2012), [arXiv:1209.6215]; K. Hamilton *et al.*, *JHEP* **05**, 082 (2013), [arXiv:1212.4504].
- [372] P. F. Monni *et al.*, *JHEP* **05**, 143 (2020), [arXiv:1908.06987].
- [373] S. Alioli *et al.*, *JHEP* **06**, 089 (2014), [arXiv:1311.0286].
- [374] K. Hamilton *et al.*, *JHEP* **10**, 222 (2013), [arXiv:1309.0017].
- [375] A. Karlberg, E. Re and G. Zanderighi, *JHEP* **09**, 134 (2014), [arXiv:1407.2940]; S. Höche, Y. Li and S. Prestel, *Phys. Rev.* **D91**, 7, 074015 (2015), [arXiv:1405.3607]; S. Höche, Y. Li and S. Prestel, *Phys. Rev.* **D90**, 5, 054011 (2014), [arXiv:1407.3773]; S. Alioli *et al.*, *Phys. Rev.* **D92**, 9, 094020 (2015), [arXiv:1508.01475]; S. Alioli *et al.* (2021), [arXiv:2102.08390]; S. Alioli *et al.*, *JHEP* **05**, 128 (2023), [arXiv:2301.11875].
- [376] W. Astill *et al.*, *JHEP* **06**, 154 (2016), [arXiv:1603.01620].
- [377] W. Astill *et al.*, *JHEP* **11**, 157 (2018), [arXiv:1804.08141].
- [378] E. Re, M. Wiesemann and G. Zanderighi, *JHEP* **12**, 121 (2018), [arXiv:1805.09857].
- [379] S. Alioli *et al.*, *Phys. Rev. D* **100**, 9, 096016 (2019), [arXiv:1909.02026].
- [380] D. Lombardi, M. Wiesemann and G. Zanderighi (2020), [arXiv:2010.10478].
- [381] D. Lombardi, M. Wiesemann and G. Zanderighi, *Phys. Lett. B* **824**, 136846 (2022), [arXiv:2108.11315].
- [382] S. Alioli *et al.*, *JHEP* **04**, 041 (2021), [arXiv:2010.10498].
- [383] D. Lombardi, M. Wiesemann and G. Zanderighi (2021), [arXiv:2103.12077].
- [384] S. Alioli *et al.*, *Phys. Lett. B* **818**, 136380 (2021), [arXiv:2103.01214].
- [385] S. Alioli *et al.* (2022), [arXiv:2212.10489].
- [386] J. M. Lindert *et al.*, *JHEP* **11**, 036 (2022), [arXiv:2208.12660].
- [387] A. Gavardi, C. Oleari and E. Re, *JHEP* **09**, 061 (2022), [arXiv:2204.12602].
- [388] L. Buonocore *et al.*, *JHEP* **01**, 072 (2022), [arXiv:2108.05337].

- [389] U. Haisch *et al.*, JHEP **07**, 054 (2022), [arXiv:2204.00663].
- [390] S. Zanolini *et al.*, JHEP **07**, 008 (2022), [arXiv:2112.04168].
- [391] J. Mazzitelli *et al.* (2020), [arXiv:2012.14267].
- [392] J. Mazzitelli *et al.*, JHEP **04**, 079 (2022), [arXiv:2112.12135].
- [393] J. Mazzitelli *et al.*, Phys. Lett. B **843**, 137991 (2023), [arXiv:2302.01645].
- [394] M. Dasgupta *et al.*, JHEP **09**, 033 (2018), [Erratum: JHEP **03**, 083 (2020)], [arXiv:1805.09327].
- [395] L. Hartgring, E. Laenen and P. Skands, JHEP **10**, 127 (2013), [arXiv:1303.4974].
- [396] H. T. Li and P. Skands, Phys. Lett. B **771**, 59 (2017), [arXiv:1611.00013].
- [397] S. Höche and S. Prestel, Phys. Rev. D **96**, 7, 074017 (2017), [arXiv:1705.00742].
- [398] F. Dulat, S. Höche and S. Prestel, Phys. Rev. D **98**, 7, 074013 (2018), [arXiv:1805.03757].
- [399] A. Banfi, B. K. El-Menoufi and P. F. Monni, JHEP **01**, 083 (2019), [arXiv:1807.11487].
- [400] G. Bewick *et al.*, JHEP **04**, 019 (2020), [arXiv:1904.11866].
- [401] M. Dasgupta *et al.*, Phys. Rev. Lett. **125**, 5, 052002 (2020), [arXiv:2002.11114].
- [402] K. Hamilton *et al.*, JHEP **03**, 041, 041 (2021), [arXiv:2011.10054].
- [403] J. R. Forshaw, J. Holguin and S. Plätzer, JHEP **09**, 014 (2020), [arXiv:2003.06400].
- [404] Z. Nagy and D. E. Soper, Phys. Rev. D **104**, 5, 054049 (2021), [arXiv:2011.04773].
- [405] Z. Nagy and D. E. Soper (2020), [arXiv:2011.04777].
- [406] A. Karlberg *et al.*, Eur. Phys. J. C **81**, 8, 681 (2021), [arXiv:2103.16526].
- [407] K. Hamilton *et al.*, JHEP **03**, 193 (2022), [arXiv:2111.01161].
- [408] F. Herren *et al.* (2022), [arXiv:2208.06057].
- [409] Z. Nagy and D. E. Soper, Phys. Rev. D **106**, 1, 014024 (2022), [arXiv:2204.05631].
- [410] M. van Beekveld *et al.*, JHEP **11**, 019 (2022), [arXiv:2205.02237].
- [411] M. van Beekveld *et al.*, JHEP **11**, 020 (2022), [arXiv:2207.09467].
- [412] M. van Beekveld and S. Ferrario Ravasio (2023), [arXiv:2305.08645].
- [413] M. Cacciari *et al.*, JHEP **04**, 068 (2004), [hep-ph/0303085].
- [414] M. Cacciari and N. Houdeau, JHEP **09**, 039 (2011), [arXiv:1105.5152].
- [415] A. David and G. Passarino, Phys. Lett. **B726**, 266 (2013), [arXiv:1307.1843].
- [416] E. Bagnaschi *et al.*, JHEP **02**, 133 (2015), [arXiv:1409.5036].
- [417] C. Duhr *et al.*, JHEP **09**, 122 (2021), [arXiv:2106.04585].
- [418] A. Ghosh *et al.* (2022), [arXiv:2210.15167].
- [419] G. Soyez *et al.*, Phys. Rev. Lett. **110**, 16, 162001 (2013), [arXiv:1211.2811].
- [420] M. Dasgupta and G. P. Salam, J. Phys. **G30**, R143 (2004), [hep-ph/0312283].
- [421] C. Bierlich *et al.*, SciPost Phys. **8**, 026 (2020), [arXiv:1912.05451].
- [422] S. Moretti, L. Lonnblad and T. Sjostrand, JHEP **08**, 001 (1998), [hep-ph/9804296].
- [423] G. P. Salam, Eur. Phys. J. **C67**, 637 (2010), [arXiv:0906.1833].
- [424] S. D. Ellis *et al.*, Prog. Part. Nucl. Phys. **60**, 484 (2008), [arXiv:0712.2447].
- [425] M. Cacciari, Int. J. Mod. Phys. **A30**, 31, 1546001 (2015), [arXiv:1509.02272].
- [426] A. Abulencia *et al.* (CDF), Phys. Rev. D **74**, 071103 (2006), [hep-ex/0512020].
- [427] G. P. Salam and G. Soyez, JHEP **05**, 086 (2007), [arXiv:0704.0292].
- [428] S. Catani *et al.*, Nucl. Phys. **B406**, 187 (1993).
- [429] S. D. Ellis and D. E. Soper, Phys. Rev. **D48**, 3160 (1993), [hep-ph/9305266].
- [430] Y. L. Dokshitzer *et al.*, JHEP **08**, 001 (1997), [hep-ph/9707323].
- [431] M. Wobisch and T. Wengler, in “Monte Carlo generators for HERA physics. Proceedings, Workshop, Hamburg, Germany, 1998-1999,” 270–279 (1998), [hep-ph/9907280].
- [432] M. Cacciari, G. P. Salam and G. Soyez, JHEP **04**, 063 (2008), [arXiv:0802.1189].
- [433] S. Bethke *et al.*, Nucl. Phys. **B370**, 310 (1992), [Erratum: Nucl. Phys. **B523**, 681 (1998)].
- [434] M. Cacciari and G. P. Salam, Phys. Lett. **B641**, 57 (2006), [hep-ph/0512210]; M. Cacciari, G. P. Salam and G. Soyez, Eur. Phys. J. **C72**, 1896 (2012), [arXiv:1111.6097].
- [435] A. Banfi, G. P. Salam and G. Zanderighi, Eur. Phys. J. C **47**, 113 (2006), [hep-ph/0601139].
- [436] A. Banfi, G. P. Salam and G. Zanderighi, JHEP **07**, 026 (2007), [arXiv:0704.2999].
- [437] M. Czakon, A. Mitov and R. Poncelet, JHEP **04**, 138 (2023), [arXiv:2205.11879].
- [438] R. Gauld, A. Huss and G. Stagnitto, Phys. Rev. Lett. **130**, 16, 161901 (2023), [arXiv:2208.11138].
- [439] S. Caletti *et al.*, JHEP **10**, 158 (2022), [arXiv:2205.01117].
- [440] F. Caola *et al.* (2023), [arXiv:2306.07314].
- [441] S. Brandt *et al.*, Phys. Lett. **12**, 57 (1964).
- [442] E. Farhi, Phys. Rev. Lett. **39**, 1587 (1977).
- [443] O. Biebel, Phys. Rept. **340**, 165 (2001).
- [444] S. Kluth, Rept. Prog. Phys. **69**, 1771 (2006), [hep-ex/0603011].
- [445] C. L. Basham *et al.*, Phys. Rev. Lett. **41**, 1585 (1978).
- [446] A. Ali, E. Pietarinen and W. J. Stirling, Phys. Lett. **141B**, 447 (1984).
- [447] I. W. Stewart, F. J. Tackmann and W. J. Waalewijn, Phys. Rev. Lett. **105**, 092002 (2010), [arXiv:1004.2489].
- [448] A. Banfi, G. P. Salam and G. Zanderighi, JHEP **08**, 062 (2004), [hep-ph/0407287].
- [449] A. Banfi, G. P. Salam and G. Zanderighi, JHEP **06**, 038 (2010), [arXiv:1001.4082].
- [450] T. Becher, X. Garcia i Tormo and J. Piclum, Phys. Rev. **D93**, 5, 054038 (2016), [Erratum: Phys. Rev. **D93**, no. 7, 079905 (2016)], [arXiv:1512.00022].
- [451] A. Gao *et al.*, Phys. Rev. Lett. **123**, 6, 062001 (2019), [arXiv:1901.04497].
- [452] T. Aaltonen *et al.* (CDF), Phys. Rev. **D83**, 112007 (2011), [arXiv:1103.5143].
- [453] G. Aad *et al.* (ATLAS), Eur. Phys. J. **C72**, 2211 (2012), [arXiv:1206.2135].
- [454] G. Aad *et al.* (ATLAS), Phys. Rev. **D88**, 3, 032004 (2013), [arXiv:1207.6915].
- [455] G. Aad *et al.* (ATLAS), Phys. Lett. **B750**, 427 (2015), [arXiv:1508.01579].
- [456] G. Aad *et al.* (ATLAS), Eur. Phys. J. **C76**, 7, 375 (2016), [arXiv:1602.08980].
- [457] M. Aaboud *et al.* (ATLAS), Eur. Phys. J. **C77**, 12, 872 (2017), [arXiv:1707.02562].
- [458] M. Aaboud *et al.* (ATLAS), Phys. Rev. **D98**, 9, 092004 (2018), [arXiv:1805.04691].

- [459] G. Aad *et al.* (ATLAS), JHEP **07**, 085 (2023), [arXiv:2301.09351].
- [460] V. Khachatryan *et al.* (CMS), Phys. Lett. **B699**, 48 (2011), [arXiv:1102.0068].
- [461] S. Chatrchyan *et al.* (CMS), Phys. Lett. **B722**, 238 (2013), [arXiv:1301.1646].
- [462] V. Khachatryan *et al.* (CMS), JHEP **10**, 87 (2014), [arXiv:1407.2856].
- [463] A. M. Sirunyan *et al.* (CMS), JHEP **12**, 117 (2018), [arXiv:1811.00588].
- [464] A. Ali and G. Kramer, Eur. Phys. J. H **36**, 245 (2011), [arXiv:1012.2288].
- [465] S. Chatrchyan *et al.* (CMS), Phys. Lett. **B730**, 243 (2014), [arXiv:1310.0878].
- [466] G. Aad *et al.* (ATLAS), Phys. Rev. **D83**, 052003 (2011), [arXiv:1101.0070].
- [467] S. Chatrchyan *et al.* (CMS), JHEP **06**, 160 (2012), [arXiv:1204.3170].
- [468] B. B. Abelev *et al.* (ALICE), Phys. Rev. **D91**, 11, 112012 (2015), [arXiv:1411.4969].
- [469] G. Aad *et al.* (ATLAS), Eur. Phys. J. **C73**, 12, 2676 (2013), [arXiv:1307.5749].
- [470] C. Glasman (H1, ZEUS), Nucl. Phys. Proc. Suppl. **191**, 121 (2009), [arXiv:0812.0757].
- [471] T. Carli, K. Rabbertz and S. Schumann, in T. Schörner-Sadenius, editor, “The Large Hadron Collider: Harvest of Run 1,” 139–194 (2015), [arXiv:1506.03239].
- [472] P. Gras *et al.*, JHEP **07**, 091 (2017), [arXiv:1704.03878].
- [473] A. Abdesselam *et al.*, Eur. Phys. J. **C71**, 1661 (2011), [arXiv:1012.5412].
- [474] D. Krohn, J. Thaler and L.-T. Wang, JHEP **02**, 084 (2010), [arXiv:0912.1342].
- [475] A. Altheimer *et al.*, J. Phys. **G39**, 063001 (2012), [arXiv:1201.0008].
- [476] A. Altheimer *et al.*, Eur. Phys. J. **C74**, 3, 2792 (2014), [arXiv:1311.2708].
- [477] P. C. Stichel and W. J. Zakrzewski, Eur. Phys. J. **C75**, 1, 9 (2015), [arXiv:1409.1363].
- [478] D. Adams *et al.*, Eur. Phys. J. **C75**, 9, 409 (2015), [arXiv:1504.00679].
- [479] L. de Oliveira *et al.*, JHEP **07**, 069 (2016), [arXiv:1511.05190].
- [480] F. A. Dreyer, G. P. Salam and G. Soyez, JHEP **12**, 064 (2018), [arXiv:1807.04758].
- [481] G. Aad *et al.* (ATLAS), Phys. Rev. Lett. **124**, 22, 222002 (2020), [arXiv:2004.03540].
- [482] G. Louppe *et al.*, JHEP **01**, 057 (2019), [arXiv:1702.00748].
- [483] D. Guest, K. Cranmer and D. Whiteson, Ann. Rev. Nucl. Part. Sci. **68**, 161 (2018), [arXiv:1806.11484].
- [484] A. Butter *et al.*, SciPost Phys. **7**, 014 (2019), [arXiv:1902.09914].
- [485] P. T. Komiske, E. M. Metodiev and J. Thaler, JHEP **01**, 121 (2019), [arXiv:1810.05165].
- [486] T. Schorner-Sadenius, Eur. Phys. J. **C72**, 2060 (2012), [Erratum: Eur. Phys. J. **C72**, 2133 (2012)].
- [487] J. M. Campbell, J. W. Huston and W. J. Stirling, Rept. Prog. Phys. **70**, 89 (2007), [hep-ph/0611148].
- [488] M. L. Mangano, Phys. Usp. **53**, 109 (2010), [Usp. Fiz. Nauk180,113(2010)].
- [489] J. M. Butterworth, G. Dissertori and G. P. Salam, Ann. Rev. Nucl. Part. Sci. **62**, 387 (2012), [arXiv:1202.0583].
- [490] T. Carli, T. Gehrmann and S. Hoeche, Eur. Phys. J. **C67**, 73 (2010), [arXiv:0912.3715].
- [491] S. Chekanov *et al.* (ZEUS), Nucl. Phys. **B792**, 1 (2008), [arXiv:0707.3749].
- [492] S. Chekanov *et al.* (ZEUS), Phys. Rev. **D76**, 072011 (2007), [arXiv:0706.3809].
- [493] A. Aktas *et al.* (H1), Phys. Lett. **B639**, 21 (2006), [hep-ex/0603014].
- [494] H. Abramowicz *et al.* (ZEUS), Eur. Phys. J. **C71**, 1659 (2011), [arXiv:1104.5444].
- [495] H. Abramowicz *et al.* (ZEUS), Nucl. Phys. **B864**, 1 (2012), [arXiv:1205.6153].
- [496] F. D. Aaron *et al.* (H1), Eur. Phys. J. **C65**, 363 (2010), [arXiv:0904.3870].
- [497] F. D. Aaron *et al.* (H1), Eur. Phys. J. **C54**, 389 (2008), [arXiv:0711.2606].
- [498] S. Chekanov *et al.* (ZEUS), Eur. Phys. J. **C52**, 515 (2007), [arXiv:0707.3093].
- [499] S. Chekanov *et al.* (ZEUS), Phys. Rev. **D78**, 032004 (2008), [arXiv:0802.3955].
- [500] H. Abramowicz *et al.* (ZEUS), Eur. Phys. J. **C70**, 965 (2010), [arXiv:1010.6167].
- [501] H. Abramowicz *et al.* (ZEUS), Phys. Lett. **B691**, 127 (2010), [arXiv:1003.2923].
- [502] S. Chekanov *et al.* (ZEUS), Phys. Rev. **D85**, 052008 (2012), [arXiv:0808.3783].
- [503] F. D. Aaron *et al.* (H1), Eur. Phys. J. **C67**, 1 (2010), [arXiv:0911.5678].
- [504] V. Andreev *et al.* (H1), Eur. Phys. J. **C75**, 2, 65 (2015), [arXiv:1406.4709].
- [505] V. Andreev *et al.* (H1), Eur. Phys. J. **C77**, 11, 791 (2017), [Erratum: Eur. Phys. J. **C81**, 8, 738 (2021)], [arXiv:1709.07251].
- [506] <http://atlas.web.cern.ch/Atlas/GROUPS/PHYSICS/CombinedSummaryPlots/SM>.
- [507] <http://twiki.cern.ch/twiki/bin/view/CMSPublic/PhysicsResultsCombined>.
- [508] A. Abulencia *et al.* (CDF), Phys. Rev. **D75**, 092006 (2007), [Erratum: Phys. Rev. **D75**, 119901 (2007)], [hep-ex/0701051].
- [509] T. Aaltonen *et al.* (CDF), Phys. Rev. **D78**, 052006 (2008), [Erratum: Phys. Rev. **D79**, 119902 (2009)], [arXiv:0807.2204].
- [510] V. M. Abazov *et al.* (D0), Phys. Rev. Lett. **101**, 062001 (2008), [arXiv:0802.2400].
- [511] V. M. Abazov *et al.* (D0), Phys. Rev. **D85**, 052006 (2012), [arXiv:1110.3771].
- [512] B. Abelev *et al.* (ALICE), Phys. Lett. **B722**, 262 (2013), [arXiv:1301.3475].
- [513] G. Aad *et al.* (ATLAS), Eur. Phys. J. **C73**, 8, 2509 (2013), [arXiv:1304.4739].
- [514] G. Aad *et al.* (ATLAS), JHEP **02**, 153 (2015), [Erratum: JHEP09,141(2015)], [arXiv:1410.8857].
- [515] M. Aaboud *et al.* (ATLAS), JHEP **09**, 020 (2017), [arXiv:1706.03192].
- [516] V. Khachatryan *et al.* (CMS), Eur. Phys. J. **C76**, 5, 265 (2016), [arXiv:1512.06212].
- [517] S. Chatrchyan *et al.* (CMS), Phys. Rev. **D87**, 11, 112002 (2013), [Erratum: Phys. Rev. **D87**, no.11, 119902 (2013)], [arXiv:1212.6660].
- [518] V. Khachatryan *et al.* (CMS), JHEP **03**, 156 (2017), [arXiv:1609.05331].
- [519] V. Khachatryan *et al.* (CMS), Eur. Phys. J. **C76**, 8, 451 (2016), [arXiv:1605.04436].
- [520] M. Aaboud *et al.* (ATLAS), JHEP **05**, 195 (2018), [arXiv:1711.02692].
- [521] A. M. Sirunyan *et al.* (CMS), JHEP **12**, 082 (2020), [arXiv:2005.05159].

- [522] A. Tumasyan *et al.* (CMS), JHEP **02**, 142 (2022), [Addendum: JHEP 12, 035 (2022)], [arXiv:2111.10431].
- [523] J. Currie *et al.*, JHEP **10**, 155 (2018), [arXiv:1807.03692].
- [524] A. Schwartzman, Int. J. Mod. Phys. **A30**, 31, 1546002 (2015), [arXiv:1509.05459].
- [525] T.-J. Hou *et al.* (2019), [arXiv:1908.11238].
- [526] R. Abdul Khalek *et al.*, Eur. Phys. J. C **80**, 8, 797 (2020), [arXiv:2005.11327].
- [527] X. Jing *et al.* (2023), [arXiv:2306.03918].
- [528] G. Aad *et al.* (ATLAS), JHEP **05**, 059 (2014), [arXiv:1312.3524].
- [529] A. M. Sirunyan *et al.* (CMS), Eur. Phys. J. **C77**, 11, 746 (2017), [arXiv:1705.02628].
- [530] T. Aaltonen *et al.* (CDF), Phys. Rev. **D79**, 112002 (2009), [arXiv:0812.4036].
- [531] V. M. Abazov *et al.* (D0), Phys. Rev. Lett. **103**, 191803 (2009), [arXiv:0906.4819].
- [532] S. Chatrchyan *et al.* (CMS), JHEP **05**, 055 (2012), [arXiv:1202.5535].
- [533] V. Khachatryan *et al.* (CMS), Phys. Lett. **B746**, 79 (2015), [arXiv:1411.2646].
- [534] A. M. Sirunyan *et al.* (CMS), JHEP **07**, 013 (2017), [arXiv:1703.09986].
- [535] G. Aad *et al.* (ATLAS), JHEP **01**, 029 (2013), [arXiv:1210.1718].
- [536] M. Aaboud *et al.* (ATLAS), Phys. Rev. **D96**, 5, 052004 (2017), [arXiv:1703.09127].
- [537] V. M. Abazov *et al.* (D0), Phys. Rev. Lett. **94**, 221801 (2005), [hep-ex/0409040].
- [538] V. M. Abazov *et al.* (D0), Phys. Lett. **B721**, 212 (2013), [arXiv:1212.1842].
- [539] G. Aad *et al.* (ATLAS), Phys. Rev. Lett. **106**, 172002 (2011), [arXiv:1102.2696].
- [540] V. Khachatryan *et al.* (CMS), Phys. Rev. Lett. **106**, 122003 (2011), [arXiv:1101.5029].
- [541] V. Khachatryan *et al.* (CMS), Eur. Phys. J. **C76**, 10, 536 (2016), [arXiv:1602.04384].
- [542] A. M. Sirunyan *et al.* (CMS), Eur. Phys. J. **C78**, 7, 566 (2018), [arXiv:1712.05471].
- [543] A. M. Sirunyan *et al.* (CMS) (2019), [arXiv:1902.04374].
- [544] P. Kokkas, Int. J. Mod. Phys. **A30**, 31, 1546004 (2015), [arXiv:1509.02144].
- [545] G. Aad *et al.* (ATLAS), JHEP **01**, 188 (2021), [Erratum: JHEP 12, 053 (2021)], [arXiv:2007.12600].
- [546] M. Aaboud *et al.* (ATLAS), Eur. Phys. J. **C77**, 6, 367 (2017), [arXiv:1612.03016].
- [547] G. Aad *et al.* (ATLAS), Phys. Lett. **B759**, 601 (2016), [arXiv:1603.09222].
- [548] R. Aaij *et al.* (LHCb), JHEP **08**, 039 (2015), [arXiv:1505.07024].
- [549] S. Chatrchyan *et al.* (CMS), JHEP **10**, 132 (2011), [arXiv:1107.4789].
- [550] S. Chatrchyan *et al.* (CMS), Phys. Rev. Lett. **112**, 191802 (2014), [arXiv:1402.0923].
- [551] R. Aaij *et al.* (LHCb), JHEP **06**, 058 (2012), [arXiv:1204.1620].
- [552] R. Aaij *et al.* (LHCb), JHEP **01**, 155 (2016), [arXiv:1511.08039].
- [553] R. Aaij *et al.* (LHCb), JHEP **09**, 136 (2016), [arXiv:1607.06495].
- [554] G. Aad *et al.* (ATLAS), Eur. Phys. J. C **80**, 7, 616 (2020), [arXiv:1912.02844].
- [555] A. M. Sirunyan *et al.* (CMS), JHEP **12**, 061 (2019), [arXiv:1909.04133].
- [556] S. Chatrchyan *et al.* (CMS), JHEP **10**, 007 (2011), [arXiv:1108.0566].
- [557] V. Khachatryan *et al.* (CMS), Eur. Phys. J. **C75**, 4, 147 (2015), [arXiv:1412.1115].
- [558] G. Aad *et al.* (ATLAS), Phys. Lett. **B725**, 223 (2013), [arXiv:1305.4192].
- [559] G. Aad *et al.* (ATLAS), JHEP **06**, 112 (2014), [arXiv:1404.1212].
- [560] G. Aad *et al.* (ATLAS), JHEP **08**, 009 (2016), [arXiv:1606.01736].
- [561] A. M. Sirunyan *et al.* (CMS), Submitted to: JHEP (2018), [arXiv:1812.10529].
- [562] M. Aaboud *et al.* (ATLAS), JHEP **12**, 059 (2017), [arXiv:1710.05167].
- [563] S. Chatrchyan *et al.* (CMS), Phys. Rev. **D90**, 3, 032004 (2014), [arXiv:1312.6283].
- [564] V. Khachatryan *et al.* (CMS), Eur. Phys. J. **C76**, 8, 469 (2016), [arXiv:1603.01803].
- [565] G. Aad *et al.* (ATLAS), Submitted to: Eur. Phys. J. (2019), [arXiv:1904.05631].
- [566] R. Aaij *et al.* (LHCb), JHEP **10**, 030 (2016), [arXiv:1608.01484].
- [567] G. Aad *et al.* (ATLAS), Eur. Phys. J. **C76**, 5, 291 (2016), [arXiv:1512.02192].
- [568] V. Khachatryan *et al.* (CMS), JHEP **02**, 096 (2017), [arXiv:1606.05864].
- [569] A. M. Sirunyan *et al.* (CMS), JHEP **03**, 172 (2018), [arXiv:1710.07955].
- [570] M. Aaboud *et al.* (ATLAS), JHEP **05**, 077 (2018), [arXiv:1711.03296].
- [571] U. Blumenschein, Int. J. Mod. Phys. **A30**, 31, 1546007 (2015), [arXiv:1509.04885].
- [572] G. Aad *et al.* (ATLAS) (2019), [arXiv:1907.06728].
- [573] V. Khachatryan *et al.* (CMS), Phys. Rev. **D95**, 052002 (2017), [arXiv:1610.04222].
- [574] A. M. Sirunyan *et al.* (CMS), Phys. Rev. **D96**, 7, 072005 (2017), [arXiv:1707.05979].
- [575] A. M. Sirunyan *et al.* (CMS), Eur. Phys. J. **C78**, 11, 965 (2018), [arXiv:1804.05252].
- [576] G. Aad *et al.* (ATLAS), JHEP **06**, 080 (2023), [arXiv:2205.02597].
- [577] G. Aad *et al.* (ATLAS), JHEP **07**, 032 (2013), [arXiv:1304.7098].
- [578] Z. Bern *et al.*, Phys. Rev. **D88**, 1, 014025 (2013), [arXiv:1304.1253].
- [579] (2022), [arXiv:2204.12355].
- [580] M. Voutilainen, Int. J. Mod. Phys. **A30**, 31, 1546008 (2015), [arXiv:1509.05026].
- [581] G. Aad *et al.* (ATLAS), JHEP **08**, 005 (2016), [arXiv:1605.03495].
- [582] G. Aad *et al.* (ATLAS), JHEP **10**, 203 (2019), [arXiv:1908.02746].
- [583] S. Chatrchyan *et al.* (CMS), Phys. Rev. **D84**, 052011 (2011), [arXiv:1108.2044].
- [584] S. Chatrchyan *et al.* (CMS), JHEP **06**, 009 (2014), [arXiv:1311.6141].
- [585] G. Aad *et al.* (ATLAS), Phys. Rev. **D89**, 5, 052004 (2014), [arXiv:1311.1440].
- [586] M. Aaboud *et al.* (ATLAS), Phys. Lett. **B780**, 578 (2018), [arXiv:1801.00112].
- [587] M. Aaboud *et al.* (ATLAS), Nucl. Phys. **B918**, 257 (2017), [arXiv:1611.06586].
- [588] A. M. Sirunyan *et al.* (CMS), Eur. Phys. J. **C79**, 1, 20 (2019), [arXiv:1807.00782].

- [589] A. M. Sirunyan *et al.* (CMS) (2019), [arXiv:1907.08155].
- [590] G. Aad *et al.* (ATLAS), JHEP **03**, 179 (2020), [arXiv:1912.09866].
- [591] M. Aaboud *et al.* (ATLAS), Phys. Lett. **B776**, 295 (2018), [arXiv:1710.09560].
- [592] J. H. Kuhn *et al.*, JHEP **03**, 059 (2006), [hep-ph/0508253].
- [593] J. M. Lindert *et al.*, Eur. Phys. J. C **77**, 12, 829 (2017), [arXiv:1705.04664].
- [594] V. Khachatryan *et al.* (CMS), JHEP **10**, 128 (2015), [Erratum: JHEP04,010(2016)], [arXiv:1505.06520].
- [595] G. Aad *et al.* (ATLAS), JHEP **09**, 029 (2016), [arXiv:1603.01702].
- [596] M. Aaboud *et al.* (ATLAS), Phys. Lett. **B773**, 354 (2017), [arXiv:1702.04519].
- [597] M. Aaboud *et al.* (ATLAS) (2019), [arXiv:1905.04242].
- [598] V. Khachatryan *et al.* (CMS), Eur. Phys. J. **C76**, 7, 401 (2016), [arXiv:1507.03268].
- [599] G. Aad *et al.* (ATLAS), Phys. Lett. B **798**, 134913 (2019), [arXiv:1903.10415].
- [600] G. Aad *et al.* (ATLAS), Phys. Rev. Lett. **129**, 6, 061803 (2022), [arXiv:2201.13045].
- [601] A. M. Sirunyan *et al.* (CMS), Phys. Rev. Lett. **125**, 15, 151802 (2020), [arXiv:2006.11191].
- [602] G. Aad *et al.* (ATLAS), JHEP **01**, 086 (2013), [arXiv:1211.1913].
- [603] M. Aaboud *et al.* (ATLAS), Phys. Rev. **D95**, 11, 112005 (2017), [arXiv:1704.03839].
- [604] G. Aad *et al.* (ATLAS), JHEP **11**, 169 (2021), [arXiv:2107.09330].
- [605] S. Chatrchyan *et al.* (CMS), Eur. Phys. J. **C74**, 11, 3129 (2014), [arXiv:1405.7225].
- [606] M. Aaboud *et al.* (ATLAS), Phys. Lett. **B781**, 55 (2018), [arXiv:1712.07291].
- [607] K. Kröninger, A. B. Meyer and P. Uwer, in T. Schörner-Sadenius, editor, “The Large Hadron Collider: Harvest of Run 1,” 259–300 (2015), [arXiv:1506.02800].
- [608] M. Aaboud *et al.* (ATLAS), Phys. Rev. **D94**, 9, 092003 (2016), [arXiv:1607.07281].
- [609] M. Aaboud *et al.* (ATLAS), Eur. Phys. J. **C77**, 5, 292 (2017), [arXiv:1612.05220].
- [610] A. M. Sirunyan *et al.* (CMS), Eur. Phys. J. **C79**, 5, 368 (2019), [arXiv:1812.10505].
- [611] A. M. Sirunyan *et al.* (CMS), Eur. Phys. J. C **80**, 7, 658 (2020), [arXiv:1904.05237].
- [612] G. Aad *et al.* (ATLAS), JHEP **07**, 141 (2023), [arXiv:2303.15340].
- [613] M. Czakon, D. Heymes and A. Mitov, Phys. Rev. Lett. **116**, 8, 082003 (2016), [arXiv:1511.00549].
- [614] S. Catani *et al.*, JHEP **07**, 100 (2019), [arXiv:1906.06535].
- [615] M. Czakon *et al.*, JHEP **05**, 149 (2018), [arXiv:1803.07623].
- [616] G. Aad *et al.* (ATLAS), Eur. Phys. J. C **83**, 6, 496 (2023), [arXiv:2303.15061].
- [617] G. Bevilacqua and M. Worek, JHEP **07**, 111 (2012), [arXiv:1206.3064].
- [618] S. Chatrchyan *et al.* (CMS), Phys. Lett. **B728**, 496 (2014), [Erratum: Phys. Lett. B738,526(2014)], [arXiv:1307.1907].
- [619] T. Klijnsma *et al.*, Eur. Phys. J. **C77**, 11, 778 (2017), [arXiv:1708.07495].
- [620] G. Aad *et al.* (ATLAS), Eur. Phys. J. C **74**, 10, 3109 (2014), [Addendum: Eur.Phys.J.C 76, 642 (2016)], [arXiv:1406.5375].
- [621] A. M. Sirunyan *et al.* (CMS), JHEP **09**, 051 (2017), [arXiv:1701.06228].
- [622] G. Aad *et al.* (ATLAS) (2023), [arXiv:2306.11379].
- [623] M. Aaboud *et al.* (ATLAS), Phys. Lett. **B786**, 114 (2018), [arXiv:1805.10197].
- [624] A. M. Sirunyan *et al.* (CMS), Phys. Lett. **B792**, 369 (2019), [arXiv:1812.06504].
- [625] D. de Florian *et al.* (LHC Higgs Cross Section Working Group) (2016), [arXiv:1610.07922].
- [626] M. Aaboud *et al.* (ATLAS), Phys. Rev. **D98**, 052005 (2018), [arXiv:1802.04146].
- [627] A. M. Sirunyan *et al.* (CMS), JHEP **01**, 183 (2019), [arXiv:1807.03825].
- [628] G. Aad *et al.* (ATLAS), JHEP **08**, 027 (2022), [arXiv:2202.00487].
- [629] A. Tumasyan *et al.* (CMS), JHEP **07**, 091 (2023), [arXiv:2208.12279].
- [630] R. L. Workman *et al.* (Particle Data Group), PTEP **2022**, 083C01 (2022).
- [631] D. d’Enterria *et al.*, in “Workshop on precision measurements of the QCD coupling constant (alphas-2019) Trento, Trentino, Italy, February 11-15, 2019,” (2019), [arXiv:1907.01435].
- [632] D. d’Enterria *et al.* (2022), [arXiv:2203.08271].
- [633] G. P. Salam, in A. Levy, S. Forte and G. Ridolfi, editors, “From My Vast Repertoire ...: Guido Altarelli’s Legacy,” 101–121 (2019), [arXiv:1712.05165].
- [634] A. Pich *et al.*, in “13th Conference on Quark Confinement and the Hadron Spectrum (Confinement XIII) Maynooth, Ireland, July 31-August 6, 2018,” (2018), [arXiv:1811.11801].
- [635] A. Pich, Prog. Part. Nucl. Phys. **117**, 103846 (2021), [arXiv:2012.04716].
- [636] Y. Aoki *et al.* (Flavour Lattice Averaging Group (FLAG)), Eur. Phys. J. C **82**, 10, 869 (2022), [arXiv:2111.09849].
- [637] M. Beneke and M. Jamin, JHEP **09**, 044 (2008), [arXiv:0806.3156].
- [638] K. Maltman and T. Yavin, Phys. Rev. **D78**, 094020 (2008), [arXiv:0807.0650].
- [639] S. Narison, Phys. Lett. **B673**, 30 (2009), [arXiv:0901.3823].
- [640] I. Caprini and J. Fischer, Eur. Phys. J. **C64**, 35 (2009), [arXiv:0906.5211].
- [641] A. Pich, Prog. Part. Nucl. Phys. **75**, 41 (2014), [arXiv:1310.7922].
- [642] D. Boito *et al.*, Phys. Rev. **D91**, 3, 034003 (2015), [arXiv:1410.3528].
- [643] G. Altarelli, PoS **Corfu2012**, 002 (2013), [arXiv:1303.6065].
- [644] A. Pich and A. Rodríguez-Sánchez, Phys. Rev. **D94**, 3, 034027 (2016), [arXiv:1605.06830].
- [645] M. Davier *et al.*, Eur. Phys. J. **C74**, 3, 2803 (2014), [arXiv:1312.1501].
- [646] D. Boito *et al.*, Phys. Rev. **D95**, 3, 034024 (2017), [arXiv:1611.03457].
- [647] D. Boito *et al.*, Phys. Rev. **D100**, 7, 074009 (2019), [arXiv:1907.03360].
- [648] A. H. Hoang and C. Regner, Phys. Rev. D **105**, 9, 096023 (2022), [arXiv:2008.00578].
- [649] A. H. Hoang and C. Regner, Eur. Phys. J. ST **230**, 12-13, 2625 (2021), [arXiv:2105.11222].
- [650] M. Golterman, K. Maltman and S. Peris, Phys. Rev. D **108**, 1, 014007 (2023), [arXiv:2305.10386].
- [651] M. A. Benitez-Rathgeb *et al.*, JHEP **09**, 223 (2022), [arXiv:2207.01116].
- [652] M. A. Benitez-Rathgeb *et al.*, JHEP **07**, 016 (2022), [arXiv:2202.10957].

- [653] D. Boito *et al.*, Phys. Rev. **D98**, 7, 074030 (2018), [arXiv:1805.08176].
- [654] D. Boito *et al.*, Phys. Rev. D **103**, 3, 034028 (2021), [arXiv:2012.10440].
- [655] C. Ayala, G. Cvetič and D. Teca, J. Phys. G **50**, 4, 045004 (2023), [arXiv:2206.05631].
- [656] J.-M. Shen *et al.*, JHEP **07**, 109 (2023), [arXiv:2303.11782].
- [657] V. Mateu and P. G. Ortega, JHEP **01**, 122 (2018), [arXiv:1711.05755].
- [658] C. Peset, A. Pineda and J. Segovia, JHEP **09**, 167 (2018), [arXiv:1806.05197].
- [659] S. Narison, Int. J. Mod. Phys. A **33**, 10, 1850045 (2018), [Addendum: Int. J. Mod. Phys. A **33**, 1850045 (2018)], [arXiv:1801.00592].
- [660] S. Narison, Int. J. Mod. Phys. A **33**, 33, 1892004 (2018), [arXiv:1812.09360].
- [661] D. Boito and V. Mateu, Phys. Lett. B **806**, 135482 (2020), [arXiv:1912.06237].
- [662] D. Boito and V. Mateu, JHEP **03**, 094 (2020), [arXiv:2001.11041].
- [663] J. Blümlein, H. Bottcher and A. Guffanti, Nucl. Phys. **B774**, 182 (2007), [hep-ph/0607200].
- [664] P. Jimenez-Delgado and E. Reya, Phys. Rev. **D89**, 7, 074049 (2014), [arXiv:1403.1852].
- [665] S. Alekhin *et al.*, Phys. Rev. **D96**, 1, 014011 (2017), [arXiv:1701.05838].
- [666] S. Alekhin, J. Blümlein and S. Moch, Eur. Phys. J. **C78**, 6, 477 (2018), [arXiv:1803.07537].
- [667] T. Cridge *et al.* (2021), [arXiv:2106.10289].
- [668] R. D. Ball *et al.* (NNPDF), Eur. Phys. J. **C78**, 5, 408 (2018), [arXiv:1802.03398].
- [669] I. Abt *et al.* (H1, ZEUS), Eur. Phys. J. C **82**, 3, 243 (2022), [arXiv:2112.01120].
- [670] R. S. Thorne and G. Watt, JHEP **08**, 100 (2011), [arXiv:1106.5789].
- [671] S. Alekhin, J. Blümlein and S. Moch, Eur. Phys. J. **C71**, 1723 (2011), [arXiv:1101.5261].
- [672] R. D. Ball *et al.* (NNPDF), Phys. Lett. **B704**, 36 (2011), [arXiv:1102.3182].
- [673] R. D. Ball *et al.* (NNPDF), Phys. Lett. **B723**, 330 (2013), [arXiv:1303.1189].
- [674] R. S. Thorne, PoS **DIS2013**, 042 (2013), [arXiv:1306.3907].
- [675] G. Dissertori *et al.*, JHEP **08**, 036 (2009), [arXiv:0906.3436].
- [676] G. Abbiendi *et al.* (OPAL), Eur. Phys. J. **C71**, 1733 (2011), [arXiv:1101.1470].
- [677] S. Bethke *et al.* (JADE), Eur. Phys. J. **C64**, 351 (2009), [arXiv:0810.1389].
- [678] G. Dissertori *et al.*, Phys. Rev. Lett. **104**, 072002 (2010), [arXiv:0910.4283].
- [679] J. Schieck *et al.* (JADE), Eur. Phys. J. **C73**, 3, 2332 (2013), [arXiv:1205.3714].
- [680] A. Verbytskyi *et al.*, JHEP **08**, 129 (2019), [arXiv:1902.08158].
- [681] A. Kardos *et al.*, Eur. Phys. J. **C78**, 6, 498 (2018), [arXiv:1804.09146].
- [682] R. A. Davison and B. R. Webber, Eur. Phys. J. **C59**, 13 (2009), [arXiv:0809.3326].
- [683] R. Abbate *et al.*, Phys. Rev. **D83**, 074021 (2011), [arXiv:1006.3080].
- [684] T. Gehrmann, G. Luisoni and P. F. Monni, Eur. Phys. J. **C73**, 1, 2265 (2013), [arXiv:1210.6945].
- [685] A. H. Hoang *et al.*, Phys. Rev. **D91**, 9, 094018 (2015), [arXiv:1501.04111].
- [686] G. Luisoni, P. F. Monni and G. P. Salam, Eur. Phys. J. C **81**, 2, 158 (2021), [arXiv:2012.00622].
- [687] F. Caola *et al.*, JHEP **01**, 093 (2022), [arXiv:2108.08897]; F. Caola *et al.*, JHEP **12**, 062 (2022), [arXiv:2204.02247].
- [688] P. Nason and G. Zanderighi, JHEP **06**, 058 (2023), [arXiv:2301.03607].
- [689] R. Frederix *et al.*, JHEP **11**, 050 (2010), [arXiv:1008.5313].
- [690] P. Bolzoni, B. A. Kniehl and A. V. Kotikov, Nucl. Phys. **B875**, 18 (2013), [arXiv:1305.6017].
- [691] J. Currie *et al.*, Phys. Rev. Lett. **119**, 15, 152001 (2017), [arXiv:1705.10271].
- [692] M. Czakon *et al.* (2019), [arXiv:1907.12911].
- [693] S. Dittmaier, A. Huss and C. Speckner, JHEP **11**, 095 (2012), [arXiv:1210.0438].
- [694] R. Frederix *et al.*, JHEP **04**, 076 (2017), [arXiv:1612.06548].
- [695] M. Czakon *et al.*, JHEP **10**, 186 (2017), [arXiv:1705.04105].
- [696] M. Reyer, M. Schönherr and S. Schumann, Eur. Phys. J. C **79**, 4, 321 (2019), [arXiv:1902.01763].
- [697] M. Johnson and D. Maître, Phys. Rev. **D97**, 5, 054013 (2018), [arXiv:1711.01408].
- [698] A. Gehrmann-De Ridder *et al.*, JHEP **07**, 133 (2016), [arXiv:1605.04295].
- [699] S. Forte and Z. Kassabov, Eur. Phys. J. C **80**, 3, 182 (2020), [arXiv:2001.04986].
- [700] S. Alekhin *et al.*, Eur. Phys. J. C **75**, 304 (2015), [arXiv:1410.4412].
- [701] F. Lorkowski (ZEUS), Acta Phys. Polon. Supp. **16**, 5, 35 (2023).
- [702] A. Hayrapetyan *et al.* (CMS) (2024), [arXiv:2402.13864].
- [703] CMS Collaboration (CMS), CMS Physics Analysis Summary CMS-PAS-SMP-22-005 (2023), URL <http://cds.cern.ch/record/2868568>.
- [704] D. d'Enterria and A. Poldaru, JHEP **06**, 016 (2020), [arXiv:1912.11733].
- [705] S. Camarda, G. Ferrera and M. Schott, Eur. Phys. J. C **84**, 1, 39 (2024), [arXiv:2203.05394].
- [706] G. Aad *et al.* (ATLAS) (2023), [arXiv:2309.12986].
- [707] T. Affolder *et al.* (CDF), Phys. Rev. Lett. **88**, 042001 (2002), [hep-ex/0108034].
- [708] S. Chekanov *et al.* (ZEUS), Phys. Lett. B **649**, 12 (2007), [hep-ex/0701039].
- [709] V. M. Abazov *et al.* (D0), Phys. Rev. **D80**, 111107 (2009), [arXiv:0911.2710].
- [710] B. Malaescu and P. Starovoitov, Eur. Phys. J. **C72**, 2041 (2012), [arXiv:1203.5416].
- [711] V. Khachatryan *et al.* (CMS), Eur. Phys. J. **C75**, 6, 288 (2015), [arXiv:1410.6765].
- [712] D. Britzger *et al.*, Eur. Phys. J. **C79**, 1, 68 (2019), [arXiv:1712.00480].
- [713] S. Chekanov *et al.* (ZEUS), Eur. Phys. J. **C44**, 183 (2005), [hep-ex/0502007].
- [714] S. Chatrchyan *et al.* (CMS), Eur. Phys. J. **C73**, 10, 2604 (2013), [arXiv:1304.7498].
- [715] V. M. Abazov *et al.* (D0), Phys. Lett. **B718**, 56 (2012), [arXiv:1207.4957].
- [716] V. Khachatryan *et al.* (CMS), Eur. Phys. J. **C75**, 5, 186 (2015), [arXiv:1412.1633].
- [717] V. Andreev *et al.* (H1), Eur. Phys. J. C **77**, 4, 215 (2017), [arXiv:1611.03421].
- [718] J. Haller *et al.*, Eur. Phys. J. **C78**, 8, 675 (2018), [arXiv:1803.01853].
- [719] J. de Blas *et al.*, Phys. Rev. Lett. **129**, 27, 271801 (2022), [Supplemental Material: Phys.Rev.Lett. **129**, 271801 (2022)], [arXiv:2204.04204].

- [720] J. de Blas *et al.*, Phys. Rev. D **106**, 3, 033003 (2022), [arXiv:2112.07274].
- [721] T. Aaltonen *et al.* (CDF), Science **376**, 6589, 170 (2022).
- [722] S. Schael *et al.* (ALEPH, DELPHI, L3, OPAL, SLD, LEP Electroweak Working Group, SLD Electroweak Group, SLD Heavy Flavour Group), Phys. Rept. **427**, 257 (2006), [hep-ex/0509008].
- [723] L. Del Debbio and A. Ramos, Physics Reports **920**, 1 (2021), ISSN 0370-1573, [arXiv:2101.04762].
- [724] S. Aoki *et al.* (Flavour Lattice Averaging Group), Eur. Phys. J. C **80**, 2, 113 (2020), [arXiv:1902.08191].
- [725] M. Bruno *et al.* (ALPHA), Phys. Rev. Lett. **119**, 10, 102001 (2017), [arXiv:1706.03821].
- [726] S. Aoki *et al.* (PACS-CS), JHEP **10**, 053 (2009), [arXiv:0906.3906].
- [727] C. McNeile *et al.*, Phys. Rev. **D82**, 034512 (2010), [arXiv:1004.4285].
- [728] K. Maltman *et al.*, Phys. Rev. **D78**, 114504 (2008), [arXiv:0807.2020].
- [729] B. Chakraborty *et al.*, Phys. Rev. **D91**, 5, 054508 (2015), [arXiv:1408.4169].
- [730] C. Ayala, X. Lobregat and A. Pineda, JHEP **09**, 016 (2020), [arXiv:2005.12301].
- [731] A. Bazavov *et al.* (TUMQCD), Phys. Rev. D **100**, 11, 114511 (2019), [arXiv:1907.11747].
- [732] S. Cali *et al.*, Phys. Rev. Lett. **125**, 242002 (2020), [arXiv:2003.05781].
- [733] M. Dalla Brida *et al.* (ALPHA), Phys. Lett. B **807**, 135571 (2020), [arXiv:1912.06001].

10. Electroweak Model and Constraints on New Physics

Revised April 2024 by J. Eler (KPH, JGU Mainz) and A. Freitas (Pittsburgh U.).

10.1	Introduction	185
10.2	Renormalization and radiative corrections	185
10.2.1	The Fermi constant	186
10.2.2	The electromagnetic coupling	186
10.2.3	Quark masses	187
10.2.4	The weak mixing angle	187
10.2.5	Radiative corrections	189
10.3	Low energy electroweak observables	189
10.3.1	Neutrino scattering	189
10.3.2	Parity violating lepton scattering	190
10.3.3	Atomic parity violation	191
10.4	Precision flavor physics	192
10.4.1	The τ lifetime	192
10.4.2	The muon anomalous magnetic moment	193
10.5	Physics of the massive electroweak bosons	193
10.5.1	The Z boson mass	194
10.5.2	Electroweak physics off the Z pole	194
10.5.3	Z pole physics	195
10.5.4	W and Z decays	197
10.6	Global fit results	198
10.7	Constraints on new physics	200
10.8	Alternative scenarios	203

10.1 Introduction

The standard model of the electroweak interactions (SM) [1–4] is based on the gauge group $SU(2) \times U(1)$, with gauge bosons W_μ^i , $i = 1, 2, 3$, and B_μ for the $SU(2)$ and $U(1)$ factors, respectively, and the corresponding gauge coupling constants g and g' . The left-handed fermion fields of the i^{th} fermion family transform as doublets $\Psi_i = \begin{pmatrix} \nu_i \\ d_i^- \end{pmatrix}$ and $\begin{pmatrix} u_i \\ d_i^+ \end{pmatrix}$ under $SU(2)$, where $d_i^\pm \equiv \sum_j V_{ij} d_j$, and V is the Cabibbo-Kobayashi-Maskawa mixing [5, 6] matrix. The right-handed fields are $SU(2)$ singlets. From Higgs and electroweak precision data it is known that there are precisely three sequential fermion families. Constraints on V and tests of universality are discussed in Ref. [7] and in Section 12 on the ‘‘CKM Quark-Mixing Matrix’’ in this *Review*. The extension of the formalism to allow an analogous leptonic mixing matrix is discussed in Section 14 on ‘‘Neutrino Masses, Mixing, and Oscillations’’ in this *Review*.

A complex scalar Higgs doublet, ϕ , is added to the model for mass generation through spontaneous symmetry breaking with potential¹ given by,

$$V(\phi) = \mu^2 \phi^\dagger \phi + \frac{\lambda^2}{2} (\phi^\dagger \phi)^2, \quad \phi \equiv \begin{pmatrix} \phi^+ \\ \phi^0 \end{pmatrix}. \quad (10.1)$$

For μ^2 negative, ϕ develops a vacuum expectation value, $v/\sqrt{2} = |\mu|/\lambda$, where $v = 246.22$ GeV, breaking part of the electroweak (EW) gauge symmetry, after which only one neutral Higgs scalar, H , remains in the physical particle spectrum. In non-minimal models there are additional charged and neutral scalar Higgs particles. Higgs boson physics is reviewed in Section 11 on the ‘‘Status of Higgs Boson Physics’’ in this *Review*.

After symmetry breaking the Lagrangian for the fermion fields, ψ_i , is

$$\begin{aligned} \mathcal{L}_F = & \sum_i \bar{\psi}_i \left(i \not{\partial} - m_i - \frac{m_i H}{v} \right) \psi_i \\ & - \frac{g}{2\sqrt{2}} \sum_i \bar{\psi}_i \gamma^\mu (1 - \gamma^5) (T^+ W_\mu^+ + T^- W_\mu^-) \Psi_i \end{aligned}$$

¹There is no generally accepted convention to write the quartic term. Our numerical coefficient simplifies Eq. (10.5a) below and the squared coupling preserves the relation between the number of external legs and the power counting of couplings at a given loop order. This structure also naturally emerges from physics beyond the SM, such as Supersymmetry.

$$\begin{aligned} & - e \sum_i Q_i \bar{\psi}_i \gamma^\mu \psi_i A_\mu \\ & - \frac{g}{2 \cos \theta_W} \sum_i \bar{\psi}_i \gamma^\mu (g_V^i - g_A^i \gamma^5) \psi_i Z_\mu. \end{aligned} \quad (10.2)$$

Here $\theta_W \equiv \tan^{-1}(g'/g)$ is the weak mixing angle and $e = g \sin \theta_W$ is the positron electric charge. Furthermore,

$$A_\mu \equiv B_\mu \cos \theta_W + W_\mu^3 \sin \theta_W, \quad (10.3a)$$

$$W_\mu^\pm \equiv \frac{W_\mu^1 \mp i W_\mu^2}{\sqrt{2}}, \quad (10.3b)$$

$$Z_\mu \equiv -B_\mu \sin \theta_W + W_\mu^3 \cos \theta_W, \quad (10.3c)$$

are the photon field (γ) and the charged (W^\pm) and neutral (Z) weak boson fields, respectively.

The Yukawa coupling of H to ψ_i in the first term in \mathcal{L}_F , which is flavor diagonal in the minimal model, is $gm_i/2M_W$. From the bosonic interaction Lagrangian,

$$\begin{aligned} \mathcal{L}_{HV} = & \frac{1}{2} (v + H)^2 \left[\frac{g^2}{2} W_\mu^+ W_\mu^- + \frac{g^2 + g'^2}{4} Z_\mu Z^\mu \right] \\ & - V \left(\frac{v + H}{\sqrt{2}} \right), \end{aligned} \quad (10.4)$$

one obtains the EW boson masses (at tree level, *i.e.*, to lowest order in perturbation theory)

$$M_H = \lambda v, \quad (10.5a)$$

$$M_W = \frac{gv}{2} = \frac{ev}{2 \sin \theta_W}, \quad (10.5b)$$

$$M_Z = \sqrt{g^2 + g'^2} \frac{v}{2} = \frac{ev}{2 \sin \theta_W \cos \theta_W}, \quad (10.5c)$$

$$M_\gamma = 0. \quad (10.5d)$$

The second term in \mathcal{L}_F represents the charged-current weak interaction [8–10], where T^+ and T^- are the weak isospin raising and lowering operators. For example, the coupling of a W to an electron and a neutrino is

$$- \frac{e}{2\sqrt{2} \sin \theta_W} \left[W_\mu^- \bar{e} \gamma^\mu (1 - \gamma^5) \nu + W_\mu^+ \bar{\nu} \gamma^\mu (1 - \gamma^5) e \right]. \quad (10.6)$$

For momenta small compared to M_W , this term gives rise to the effective four-fermion interaction with the Fermi constant given by $G_F/\sqrt{2} = 1/2v^2 = g^2/8M_W^2$. CP violation is incorporated into the EW model by a single observable phase in V_{ij} .

The third term in \mathcal{L}_F describes electromagnetic interactions (QED) [11, 12], and the last is the weak neutral-current interaction [9, 10, 13]. The vector and axial-vector couplings are

$$g_V^i \equiv t_{3L}(i) - 2Q_i \sin^2 \theta_W, \quad (10.7a)$$

$$g_A^i \equiv t_{3L}(i), \quad (10.7b)$$

where $t_{3L}(i)$ is the weak isospin of fermion i (+1/2 for u_i and ν_i ; $-1/2$ for d_i and e_i) and Q_i is the charge of ψ_i in units of e .

The first term in Eq. (10.2) also gives rise to fermion masses, and in the presence of right-handed neutrinos to Dirac neutrino masses. The possibility of Majorana masses is discussed in Section 14 on ‘‘Neutrino Mass, Mixing, and Oscillations’’ in this *Review*.

10.2 Renormalization and radiative corrections

In addition to the Higgs boson mass, M_H , the fermion masses and mixings, and the strong coupling constant, α_s , the SM has three parameters. The set with the smallest experimental errors contains the Z mass², the Fermi constant, and the fine structure constant. The latter two will be discussed in more detail in

²We emphasize that in the fits described in Sec. 10.6 and Sec. 10.7 the values of the SM parameters are affected by all observables that depend on

the next two subsections. (The numerical values quoted in Sections 10.2–10.4 correspond to the main fit result in Table 10.7.)

10.2.1 The Fermi constant

The Fermi constant,

$$G_F = 1.1663788(6) \times 10^{-5} \text{ GeV}^{-2}, \quad (10.8)$$

is derived from the μ lifetime formula³,

$$\frac{\hbar}{\tau_\mu} = \frac{G_F^2 m_\mu^5}{192\pi^3} F(\rho) \left[1 + H_1(\rho) \frac{\widehat{\alpha}(m_\mu)}{\pi} + H_2(\rho) \frac{\widehat{\alpha}^2(m_\mu)}{\pi^2} + H_3 \frac{\widehat{\alpha}^3(m_\mu)}{\pi^3} \right], \quad (10.9)$$

where $\rho = m_e^2/m_\mu^2$, and where

$$F(\rho) = 1 - 8\rho + 8\rho^3 - \rho^4 - 12\rho^2 \ln \rho = 0.99981295, \quad (10.10a)$$

$$H_1(\rho) = \frac{25}{8} - \frac{\pi^2}{2} - (9 + 4\pi^2 + 12 \ln \rho) \rho + 16\pi^2 \rho^{3/2} + \mathcal{O}(\rho^2) = -1.80793, \quad (10.10b)$$

$$H_2(\rho) = \frac{156815}{5184} - \frac{518}{81}\pi^2 - \frac{895}{36}\zeta(3) + \frac{67}{720}\pi^4 + \frac{53}{6}\pi^2 \ln 2 - (0.042 \pm 0.002)_{\text{had}} - \frac{5}{4}\pi^2 \sqrt{\rho} + \mathcal{O}(\rho) = 6.64, \quad (10.10c)$$

$$\widehat{\alpha}(m_\mu)^{-1} = \alpha^{-1} + \frac{1}{3\pi} \ln \rho + \mathcal{O}(\alpha) = 135.901. \quad (10.10d)$$

H_1 and H_2 capture the QED corrections within the Fermi model. The results for $\rho = 0$ have been obtained in Refs. [16] and [17, 18] for H_1 and H_2 , respectively, where the term in parentheses is from the hadronic vacuum polarization [17]. The mass corrections to H_1 have been known for some time [19], while those to H_2 are more recent [20]. Notice the term linear in m_e in H_2 whose appearance was unforeseen and can be traced to the use of the muon pole mass in the prefactor [20]. The coefficient $H_3 = -15.3 \pm 2.3$ has been estimated in Refs. [21–23]. The remaining uncertainty in G_F is mostly experimental and has been reduced by an order of magnitude by the MuLan collaboration [15] at the PSI.

10.2.2 The electromagnetic coupling

The fine structure constant, α , can be extracted from the anomalous magnetic moment of the electron, $a_e = (1159652180.59 \pm 0.13) \times 10^{-12}$ [24]. Application of QED corrections up to five loop order [25–27] allows to extract the value $\alpha^{-1} = 137.035999166(15)$. (Here the number in parentheses denotes the uncertainty in the last digits shown.) Another approach combines measurements of the Rydberg constant and atomic masses with interferometry of atomic recoil kinematics. Applied to ^{87}Rb [28] and ^{133}Cs [29], this method implies the results $\alpha^{-1} = 137.035999206(11)$ and $\alpha^{-1} = 137.035999046(27)$, respectively, which differ by 5.5σ from each other, and when combined would give $\alpha^{-1} = 137.035999183(10)$. Finally, combining the anomalous magnetic moment and atomic interferometry methods, which unlike in the past are now in agreement, leads to the world average,

$$\alpha^{-1} = 137.035999178(8). \quad (10.11)$$

them. This is of no practical consequence for α and G_F , however, since they are very precisely known. Also note that other choices for the three SM input parameters (see *e.g.* Ref. [14]) will lead to equivalent fit results within theoretical uncertainties.

³In the spirit of the Fermi theory, we incorporated the small propagator correction, $3/5 m_\mu^2/M_W^2$, into Δr (see below). This is also the convention adopted by the MuLan collaboration [15]. While this breaks with historical consistency, the numerical difference was negligible in the past.

This combination differs from the value in Section 1 (“Physical Constants”) in this *Review*, which does not use the latest experimental inputs.

In most EW renormalization schemes it is convenient to define a running α dependent on the energy scale of the process, with $\alpha^{-1} \approx 137.036$ appropriate at very low energy, *i.e.* close to the Thomson limit. The OPAL [30] and L3 [31] collaborations at LEP could also observe the running directly in small and large angle Bhabha scattering, respectively. For scales above a few hundred MeV the low energy hadronic contribution to vacuum polarization introduces a theoretical uncertainty in α . In the modified minimal subtraction ($\overline{\text{MS}}$) scheme⁴ [32] (used for this *Review*), and with $\alpha_s(M_Z) = 0.1187 \pm 0.0017$ we have $\widehat{\alpha}^{(4)}(m_\tau)^{-1} = 133.450 \pm 0.006$ and $\widehat{\alpha}^{(5)}(M_Z)^{-1} = 127.930 \pm 0.008$. The latter corresponds to a quark sector contribution (without the top) to the conventional (on-shell) QED coupling,

$$\alpha(M_Z) = \frac{\alpha}{1 - \Delta\alpha(M_Z)}, \quad (10.12)$$

of $\Delta\alpha_{\text{had}}^{(5)}(M_Z) = 0.02783 \pm 0.00006$. These values are updated with respect to Ref. [33] with the uncertainty reduced (partly due to a more precise charm quark mass). Various evaluations of $\Delta\alpha_{\text{had}}^{(5)}(M_Z)$ are summarized in Table 10.1, where the relation⁵ between the $\overline{\text{MS}}$ and on-shell definitions (obtained using Refs. [37, 38]) is given by,

$$\begin{aligned} & \Delta\widehat{\alpha}(M_Z) - \Delta\alpha(M_Z) \\ &= \frac{\alpha}{\pi} \left[\frac{100}{27} - \frac{1}{6} - \frac{7}{4} \ln \frac{M_Z^2}{M_W^2} + \frac{\alpha_s(M_Z)}{\pi} \left(\frac{605}{108} - \frac{44}{9} \zeta(3) \right) \right. \\ &+ \frac{\alpha_s^2}{\pi^2} \left(\frac{976481}{23328} - \frac{253}{36} \zeta(2) - \frac{781}{18} \zeta(3) + \frac{275}{27} \zeta(5) \right) \\ &+ \frac{\alpha_s^3}{\pi^3} \left(\frac{1483517111}{3359232} - \frac{22781}{144} \zeta(2) - \frac{3972649}{7776} \zeta(3) - \frac{31}{81} \zeta(2)^2 \right. \\ &\left. \left. + \frac{521255}{7776} \zeta(5) - \frac{7315}{324} \zeta(7) + \frac{5819}{54} \zeta(2)\zeta(3) + \frac{14675}{162} \zeta(3)^2 \right) \right] \\ &= 0.007122(2)(5), \end{aligned} \quad (10.13)$$

and where the first entry of the lowest order term is from fermions and the other two are from W^\pm loops, which are usually excluded from the on-shell definition. Fermion mass effects and corrections of $\mathcal{O}(\alpha^2)$ contributing to Eq. (10.13) are small, partly cancel each other and are not included here. The first error in Eq. (10.13) is parametric (from α_s) and the second is from the truncation of the perturbative expansion. The most recent results of $\Delta\alpha_{\text{had}}^{(5)}(M_Z)$ [39–42] typically assume the validity of perturbative QCD (PQCD) at scales of ~ 2 GeV and above and are in good agreement with each other. In regions where PQCD is not trusted, one can use $e^+e^- \rightarrow$ hadrons cross-section data (for a list of references see, *e.g.*, Ref. [41]) and isospin rotated information derived from τ decay spectral functions [43], where the latter derive from OPAL [44], CLEO [45], ALEPH [46], and Belle [47]. Very recently new results appeared from the CMD-3 experiment [48] at the e^+e^- collider VEPP-2000. There is noticeable spread in the results, with lattice QCD [49] and CMD-3 (KLOE) suggesting stronger (weaker) running. While VEPP-2000 and VEPP-4M scanned center-of-mass (CM) energies up to 2 GeV and between about 3 and 4 GeV, respectively, the BaBar collaboration studied multi-hadron events radiatively returned from the $\Upsilon(4S)$, reconstructing the radiated photon and normalizing to $\mu^\pm\gamma$ final states.

We include all of this information by using as actual input (fit constraint) instead of $\Delta\alpha_{\text{had}}^{(5)}(M_Z)$ the low energy contribution by

⁴In this Section we denote quantities defined in the $\overline{\text{MS}}$ scheme by a caret; the exception is the strong coupling constant, α_s , which will always correspond to the $\overline{\text{MS}}$ definition and where the caret will be dropped. Furthermore, $\alpha^{(n)}$ and $\alpha_s^{(n)}$ denote the running couplings with n quark flavors.

⁵In practice, $\alpha(M_Z)$ is directly evaluated in the $\overline{\text{MS}}$ scheme using the FORTRAN package GAPP [34], including the QED contributions of both leptons and quarks. The leptonic three-loop [35] and four-loop [36] contributions in the on-shell scheme have also been obtained.

the three light quarks,

$$\Delta\alpha_{\text{had}}^{(3)}(2.0 \text{ GeV}) = (60.30 \pm 0.43) \times 10^{-4}, \quad (10.14)$$

which we obtained relying on the analysis in Ref. [41], with τ decay data and the latest CMD-3 results added following Ref. [50]. Its correlation (86% [51]) with a_μ discussed in Sec. 10.4.2, is included in the fits. The non-linear α_s dependence of $\hat{\alpha}(M_Z)$ and the resulting correlation with the input variable α_s are fully taken into account by calculating the perturbative and heavy quark contributions to $\hat{\alpha}(M_Z)$ in each call of the fits according to Ref. [33]. Part of the uncertainty ($\pm 0.37 \times 10^{-4}$) in $\Delta\alpha_{\text{had}}^{(5)}(M_Z)$ is from the combination of e^+e^- annihilation data, τ decays into two-pion final states, and constraints from lattice QCD (LQCD), but un-calculated higher order perturbative QCD corrections ($\pm 0.21 \times 10^{-4}$) and the $\overline{\text{MS}}$ quark mass values (see below) also contribute.

10.2.3 Quark masses

Further free parameters entering into Eq. (10.2) are the quark and lepton masses, where m_i is the mass of the i^{th} fermion ψ_i . For the light quarks, as described in Section 60 on “Quark Masses” in this *Review*, $\hat{m}_u = 2.16^{+0.49}_{-0.26}$ MeV, $\hat{m}_d = 4.67^{+0.48}_{-0.17}$ MeV, and $\hat{m}_s = 93.4^{+8.6}_{-3.4}$ MeV. These are running $\overline{\text{MS}}$ masses evaluated at the scale $\mu = 2$ GeV. For the charm mass we use the constraint [58],

$$\hat{m}_c(\hat{m}_c) = 1274 \pm 8 + 2616 [\alpha_s(M_Z) - 0.1182] \text{ MeV}, \quad (10.15)$$

which is based on QCD sum rules [59,60], and recalculate \hat{m}_c in each call of our fits to account for its α_s dependence. Similarly, for the bottom quark mass we use [61],

$$\hat{m}_b(\hat{m}_b) = 4180 \pm 8 - 108 [\alpha_s(M_Z) - 0.1182] \text{ MeV}, \quad (10.16)$$

with a theoretical correlation of about 60% arising from the PQCD truncation uncertainty which is similar for $\hat{m}_c(\hat{m}_c)$ and $\hat{m}_b(\hat{m}_b)$. To improve the precisions in $\hat{m}_c(\hat{m}_c)$ and $\hat{m}_b(\hat{m}_b)$ in the future it would help to remeasure the threshold regions of the heavy quarks, as well as the electronic decay widths of the narrow $c\bar{c}$ and $b\bar{b}$ resonances. It would also be important to obtain data on the R -ratio in e^+e^- annihilation for center-of-mass energies $\gtrsim 11.2$ GeV, as in this region QCD perturbation theory cannot be sufficiently relied upon for b quarks [61].

The top quark “pole” mass (the quotation marks are a reminder that the experiments do not strictly measure the pole mass and that quarks do not form asymptotic states) has been kinematically reconstructed by the Tevatron collaborations, CDF and D0, in leptonic, hadronic, and mixed channels with the result [62],

$$m_t = 174.30 \pm 0.35_{\text{stat.}} \pm 0.54_{\text{syst.}} \text{ GeV (Tevatron)}. \quad (10.17)$$

Likewise, using data from CM energies $\sqrt{s} = 7$ and 8 TeV (Run 1), ATLAS and CMS (including alternative technique measurements) at the LHC obtained [63],

$$m_t = 172.52 \pm 0.14_{\text{stat.}} \pm 0.30_{\text{syst.}} \text{ GeV (LHC Run 1)}. \quad (10.18)$$

In addition, there are results derived from $\sqrt{s} = 13$ TeV data (Run 2). The CMS collaboration obtained $m_t = 171.77 \pm 0.04_{\text{stat.}} \pm 0.37_{\text{syst.}} \text{ GeV}$ [64] in the lepton + jets channel, $m_t = 172.33 \pm 0.14_{\text{stat.}} \pm 0.69_{\text{syst.}} \text{ GeV}$ [65] in the di-lepton channel, $m_t = 172.34 \pm 0.20_{\text{mostly stat.}} \pm 0.70_{\text{syst.}} \text{ GeV}$ [66] in the all-jets channel, and $m_t = 172.13 \pm 0.32_{\text{stat.}} \pm 0.70_{\text{syst.}} \text{ GeV}$ [67] in t -channel single top events (leptonic decays). ATLAS quotes $m_t = 174.41 \pm 0.39_{\text{stat.}} \pm 0.71_{\text{syst.}} \text{ GeV}$ [68] from the lepton + jets channel and $m_t = 172.21 \pm 0.20_{\text{stat.}} \pm 0.78_{\text{syst.}} \text{ GeV}$ [69] from the di-lepton channel. Assuming that the correlation matrix for individual channels of the Run 1 combination [63] is approximately applicable also at Run 2 (and that the same applies to the effective 9% correlation between ATLAS and CMS which can also be extracted from Ref. [63]), we arrive at the result,

$$m_t = 172.13 \pm 0.06_{\text{stat.}} \pm 0.30_{\text{syst.}} \text{ GeV (LHC Run 2)}. \quad (10.19)$$

To combine the two LHC runs, we use the largest correlation coefficient (0.51) between 7 TeV and 8 TeV results from the same experiment and channel in Ref. [63], and obtain,

$$m_t = 172.30 \pm 0.07_{\text{stat.}} \pm 0.27_{\text{syst.}} \text{ GeV (LHC)}. \quad (10.20)$$

This treatment is highly conservative in view of the fact that for their lepton + jets channels novel leptonic invariant mass and profile likelihood approaches were used by ATLAS and CMS, respectively, implying reduced correlations with the more traditional analyses at Run 1. Note that the statistical uncertainty of the combination (0.07 GeV) is larger than that of the CMS lepton+jets measurement at 13 TeV (0.04 GeV) [64] because the latter has a relatively large systematic uncertainty and thus gets a small weight in the average. See Ref. [70] for a detailed discussion.

The Tevatron and LHC average values, (10.17) with (10.20), differ by 2.8σ . In the inter-collider combination we treat them as uncorrelated, yielding

$$m_t = 172.61 \pm 0.25_{\text{exp.}} \text{ GeV} + \Delta m_{\text{MC}}, \quad (10.21)$$

where Δm_{MC} is defined to account for any difference between the top pole mass, m_t , and the mass parameter implemented in the Monte Carlo event generators employed by the experimental groups. Δm_{MC} is expected to be of order $\alpha_s(Q_0)Q_0$ with a low scale $Q_0 \sim \mathcal{O}(1 \text{ GeV})$ [71], but its value is unknown in hadron collider environments so that we will treat it as an uncertainty instead⁶, and choose for definiteness $Q_0 = \Gamma_t = 1.42 \text{ GeV}$ to arrive at $\Delta m_{\text{MC}} = 0 \pm 0.52 \text{ GeV}$. We further assume that an uncertainty [74] of $\pm 0.32 \text{ GeV}$ in the relation [75] between m_t and the $\overline{\text{MS}}$ definition, $\hat{m}_t(\hat{m}_t)$, entering electroweak radiative correction libraries, including the renormalon ambiguity [76], is already included in Δm_{MC} , as m_t merely serves as an intermediate book-keeping device in Ref. [71]. A promising future direction to arrive at a competitive independent constraint on m_t is to analyze differential top quark pair production cross-sections at next-to-next-to-leading order (NNLO) [77,78] as m_t extraction based on them are easier to interpret, and experimentally they have become much more precise recently [79–82]. The combination in Eq. (10.21) differs slightly from the average, $m_t = 172.57 \pm 0.29_{\text{exp.}} \text{ GeV}$, which appears in the Top Quark Listings in this *Review*, and which is based exclusively on published results and assumes vanishing correlations. For more details and references, see Section 61 on the “Top Quark” and the Quarks Listings in this *Review*.

10.2.4 The weak mixing angle

The observables $\sin^2 \theta_W$ and M_W can be calculated from M_Z , $\hat{\alpha}(M_Z)$, and G_F , when values for m_t and M_H are given, or conversely, M_H can be constrained by $\sin^2 \theta_W$ and M_W . The value of $\sin^2 \theta_W$ is extracted from neutral-current processes (see Sec. 10.3) and Z pole observables (see Sec. 10.5.4) and depends on the renormalization prescription. There are a number of popular schemes [9] leading to values which differ by small factors depending on m_t and M_H . The notation for these schemes is shown in Table 10.2.

- (i) The on-shell scheme [84] promotes the tree-level formula $\sin^2 \theta_W = 1 - M_W^2/M_Z^2$ to a definition of the renormalized $\sin^2 \theta_W$ to all orders in perturbation theory, *i.e.*,

$$\sin^2 \theta_W \rightarrow s_W^2 \equiv 1 - \frac{M_W^2}{M_Z^2}, \quad (10.22a)$$

$$M_W = \frac{A_0}{s_W(1 - \Delta r)^{1/2}}, \quad M_Z = \frac{M_W}{c_W}, \quad (10.22b)$$

where $c_W \equiv \cos \theta_W$, $A_0 = (\pi\alpha/\sqrt{2}G_F)^{1/2} = 37.28038(1) \text{ GeV}$, and Δr includes the radiative corrections relating α , $\alpha(M_Z)$, G_F , M_W , and M_Z . One finds $\Delta r \sim$

⁶However, see Ref. [72,73] for proposed procedures to calibrate the Monte-Carlo mass parameter at hadron colliders.

Table 10.1: Evaluations of the on-shell $\Delta\alpha_{\text{had}}^{(5)}(M_Z)$ by different groups (for a more complete list of evaluations see the 2012 edition of this *Review*). For better comparison we adjusted central values and errors to correspond to a common and fixed value of $\alpha_s(M_Z) = 0.120$, except for Ref. [49], for which α_s is not an explicit input. References quoting results without the top quark decoupled are converted to the five flavor definition. Ref. [52] uses $\Lambda_{\text{QCD}} = 380 \pm 60$ MeV; for the conversion we assumed $\alpha_s(M_Z) = 0.118 \pm 0.003$.

Reference	Result	Comment
Krasnikov, Rodenberg [53]	0.02737 ± 0.00039	PQCD for $\sqrt{s} > 2.3$ GeV
Kühn & Steinhauser [54]	0.02778 ± 0.00016	full $\mathcal{O}(\alpha_s^2)$ for $\sqrt{s} > 1.8$ GeV
Groote <i>et al.</i> [52]	0.02787 ± 0.00032	use of QCD sum rules
Martin <i>et al.</i> [55]	0.02741 ± 0.00019	incl. new BES data
de Troconiz, Yndurain [56]	0.02754 ± 0.00010	PQCD for $s > 2$ GeV ²
Burkhardt, Pietrzyk [57]	0.02750 ± 0.00033	PQCD for $\sqrt{s} > 12$ GeV
Erlar, Ferro-Hernández [39]	0.02761 ± 0.00010	conv. from $\overline{\text{MS}}$ scheme
Jegerlehner [40]	0.02755 ± 0.00013	Euclidean split technique
Davier <i>et al.</i> [41]	0.02760 ± 0.00010	PQCD for $\sqrt{s} = 1.8\text{--}3.7$ & > 5 GeV
Keshavarzi <i>et al.</i> [42]	0.02761 ± 0.00011	PQCD for $\sqrt{s} > 11.2$ GeV
Cè <i>et al.</i> [49]	0.02773 ± 0.00015	LQCD for Euclidian $Q^2 < 5$ GeV ²

Table 10.2: Notations used to indicate the various $\sin^2\theta_W$ schemes discussed in the text. Numerical values and the uncertainties induced by the imperfectly known SM parameters and unknown higher orders [83] are also given for illustration.

Scheme	Notation	Value	Uncertainty
On-shell	s_W^2	0.22348	± 0.00010
$\overline{\text{MS}}$	\widehat{s}_Z^2	0.23129	± 0.00004
$\overline{\text{MS}}$ (ND)	$\widehat{s}_{\text{ND}}^2$	0.23147	± 0.00004
$\overline{\text{MS}}$	\widehat{s}_0^2	0.23873	± 0.00005
Effective angle	\widehat{s}_ℓ^2	0.23161	± 0.00004

$\Delta r_0 - \rho_t \tan^{-2}\theta_W$, where $\Delta r_0 = 1 - \alpha/\widehat{\alpha}(M_Z) = 0.06646(6)$ is due to the running of α , and

$$\rho_t = \frac{3G_F m_t^2}{8\sqrt{2}\pi^2} = 0.00934 \times \frac{m_t^2}{(172.61 \text{ GeV})^2}, \quad (10.23)$$

represents the dominant (quadratic) m_t dependence. There are additional contributions to Δr from bosonic loops, including those which depend logarithmically on M_H and higher-order corrections⁷. One has $\Delta r = 0.03685 \mp 0.00020 \pm 0.00006$, where the first uncertainty is from m_t (the \mp sign indicates that increasing m_t has the effect of decreasing Δr) and the second is from $\alpha(M_Z)$. Thus the value of s_W^2 extracted from M_Z includes an uncertainty (∓ 0.00007) from the currently allowed range of m_t . This scheme is simple conceptually. However, the relatively large ($\sim 3\%$) correction from ρ_t causes large spurious contributions in higher orders. s_W^2 depends not only on the gauge couplings but also on the spontaneous-symmetry breaking, and it is awkward in the presence of any extension of the SM which perturbs the value of M_Z (or M_W). Other definitions are motivated by the tree-level coupling constant definition $\theta_W = \tan^{-1}(g'/g)$:

- (ii) In particular, the $\overline{\text{MS}}$ scheme introduces the quantity,

$$\sin^2\widehat{\theta}_W(\mu) \equiv \frac{\widehat{g}'^2(\mu)}{\widehat{g}^2(\mu) + \widehat{g}'^2(\mu)}, \quad (10.24)$$

where the couplings \widehat{g} and \widehat{g}' are defined by modified minimal subtraction and the scale μ is conveniently chosen to be M_Z for many EW processes. The value of $\widehat{s}_Z^2 \equiv \sin^2\widehat{\theta}_W(M_Z)$ extracted from M_Z is less sensitive than s_W^2 to m_t (by a factor of $\tan^2\theta_W$), and is less sensitive to most types of new physics. It is also very useful for comparing with the predictions of grand unification. There are actually several variant definitions of $\sin^2\widehat{\theta}_W(M_Z)$, differing according

to whether or how finite $\alpha \ln(m_t/M_Z)$ terms are decoupled (subtracted from the couplings). One cannot entirely decouple the $\alpha \ln(m_t/M_Z)$ terms from all EW quantities because $m_t \gg m_b$ breaks SU(2) symmetry. The scheme that will be adopted here decouples the $\alpha \ln(m_t/M_Z)$ terms from the γ - Z mixing [32, 85], essentially eliminating any $\ln(m_t/M_Z)$ dependence in the formulae for asymmetries at the Z pole when written in terms of \widehat{s}_Z^2 . (A similar definition is used for $\widehat{\alpha}$.) The on-shell and $\overline{\text{MS}}$ definitions are related by

$$\widehat{s}_Z^2 = c(m_t, M_H) s_W^2 = (1.0349 \pm 0.0003) s_W^2. \quad (10.25)$$

The quadratic m_t dependence is given by $c \sim 1 + \rho_t/\tan^2\theta_W$. The expressions for M_W and M_Z in the $\overline{\text{MS}}$ scheme are

$$M_W = \frac{A_0}{\widehat{s}_Z(1 - \Delta\widehat{r}_W)^{1/2}}, \quad M_Z = \frac{M_W}{\widehat{\rho}^{1/2} c_Z}, \quad (10.26)$$

and one predicts $\Delta\widehat{r}_W = 0.06937 \pm 0.00006$. $\Delta\widehat{r}_W$ has no quadratic m_t dependence, because shifts in M_W are absorbed into the observed G_F , so that the error in $\Delta\widehat{r}_W$ is almost entirely due to $\Delta r_0 = 1 - \alpha/\widehat{\alpha}(M_Z)$. The quadratic m_t dependence has been shifted into $\widehat{\rho} \sim 1 + \rho_t$, where including bosonic loops, $\widehat{\rho} = 1.01016 \pm 0.00009$.

- (iii) A variant $\overline{\text{MS}}$ quantity $\widehat{s}_{\text{ND}}^2$ (used in the 1992 edition of this *Review*) does not decouple the $\alpha \ln(m_t/M_Z)$ terms [86]. It is related to \widehat{s}_Z^2 by

$$\widehat{s}_Z^2 = \frac{\widehat{s}_{\text{ND}}^2}{1 + \frac{\alpha}{\pi} d}, \quad d = \frac{1}{3} \left(\frac{1}{\widehat{s}_Z^2} - \frac{8}{3} \right) \left[\left(1 + \frac{\alpha_s}{\pi} \right) \ln \frac{m_t}{M_Z} - \frac{15\alpha_s}{8\pi} \right]. \quad (10.27)$$

Thus, $\widehat{s}_Z^2 - \widehat{s}_{\text{ND}}^2 = -0.0002$.

- (iv) Some of the low-energy experiments discussed in the next section are sensitive to the weak mixing angle at almost van-

⁷All explicit numbers quoted here and below include the two- and three-loop corrections described near the end of Sec. 10.2.

ishing momentum transfer [39, 87–89]. Thus, Table 10.2 also includes $\widehat{s}_0^2 \equiv \sin^2 \widehat{\theta}_W(0)$.

- (v) Yet another definition, the effective angle [90, 91], $\widehat{s}_f^2 \equiv \sin^2 \theta_{\text{eff}}^f$, for the Z vector coupling to fermion f , is based on Z pole observables and described in Sec. 10.5.

10.2.5 Radiative corrections

Experiments are at such level of precision [83] that complete one-loop, dominant two-loop, and partial three and four-loop radiative corrections must be applied. For neutral-current and Z pole processes, these corrections are conveniently divided into two classes:

1. QED diagrams involving the emission of real photons or the exchange of virtual photons in loops, but not including vacuum polarization diagrams. These graphs often yield finite and gauge-invariant contributions to observable processes. However, they are dependent on energies, experimental cuts, *etc.*, and must be calculated individually for each experiment.
2. EW corrections, including $\gamma\gamma$, γZ , ZZ , and WW vacuum polarization diagrams, as well as vertex corrections, box graphs, *etc.*, involving virtual W and Z bosons. One-loop corrections [92] are included for all processes, and many two-loop corrections are also important. In particular, two-loop corrections involving the top quark modify ρ_t in $\widehat{\rho}$, Δr , and elsewhere by

$$\rho_t \rightarrow \rho_t \left[1 + R(M_H, m_t) \frac{\rho_t}{3} \right]. \quad (10.28)$$

$R(M_H, m_t)$ can be described as an expansion in M_Z^2/m_t^2 , for which the leading m_t^4/M_Z^4 [93, 94] and next-to-leading m_t^2/M_Z^2 [95, 96] terms are known. The complete two-loop calculation of Δr (without further approximation) has been performed in Refs. [97–101]. More recently, Ref. [102] obtained the $\overline{\text{MS}}$ quantities $\Delta \widehat{r}_W$ and $\widehat{\rho}$ to two-loop accuracy, confirming the prediction of M_W in the on-shell scheme from Refs. [99, 103] within about 4 MeV. Similarly, the EW two-loop corrections for the relation between $\widehat{s}_{\ell,b}^2$ and s_W^2 are known [104–109], as well as for the partial decay and total decay widths and the effective couplings of the Z boson [110–113]. For $\widehat{s}_{s,c}$ only two-loop corrections from diagrams with closed fermion loops are available [114], but given the experimental precision this is more than adequate.

The mixed QCD-EW contributions to gauge boson self-energies of order $\alpha\alpha_s m_t^2$ [115, 116], $\alpha\alpha_s^2 m_t^2$ [117, 118], and $\alpha\alpha_s^3 m_t^2$ [119–121] increase the predicted value of m_t by 6%. This is, however, almost entirely an artifact of using the pole mass definition for m_t . The equivalent corrections when using the $\overline{\text{MS}}$ definition $\widehat{m}_t(\widehat{m}_t)$ increase m_t by less than 0.5%. The sub-leading $\alpha\alpha_s$ corrections [122–125] are also included. Further three-loop corrections of order $\alpha\alpha_s^2$ [126, 127], $\alpha^3 m_t^6$, $\alpha^2 \alpha_s m_t^4$ [128, 129], α_f^3 and $\alpha_f^2 \alpha_s$ [130, 131] are rather small (here α_f denotes electroweak corrections with a closed fermion loop). The same is true for $\alpha^3 M_H^4$ [132] corrections unless M_H approaches 1 TeV. The theoretical uncertainty from unknown higher-order corrections [83] is estimated to amount to 4 MeV for the prediction of M_W [103] and 4.5×10^{-5} for \widehat{s}_ℓ^2 [114].

Throughout this *Review* we utilize EW radiative corrections from the program GAPP [34], which works entirely in the $\overline{\text{MS}}$ scheme, and which is independent of the ZFITTER [133] and GRIFFIN [134] packages.

10.3 Low energy electroweak observables

In the following we discuss EW precision observables obtained at low momentum transfers [135], *i.e.*, $Q^2 \ll M_Z^2$. It is convenient to write the four-fermion interactions relevant to ν -hadron, ν - e , as well as parity violating e -hadron and e - e neutral-current processes, in a form that is valid in an arbitrary gauge theory (assuming

Table 10.3: SM tree level expressions for the neutral-current parameters for ν -hadron, ν - e , and e^- scattering processes. To obtain the SM values in the last column, the tree level expressions have to be multiplied by the low-energy neutral-current ρ parameter, $\rho_{\text{NC}} = 1.00060$, and further vertex and box corrections need to be added as detailed in Ref. [13]. The dominant m_t dependence is again given by $\rho_{\text{NC}} \sim 1 + \rho_t$.

Quantity	SM tree level	SM value
$g_{LV}^{\nu\mu e}$	$-\frac{1}{2} + 2\widehat{s}_0^2$	-0.0395
$g_{LA}^{\nu\mu e}$	$-\frac{1}{2}$	-0.5063
$g_{LL}^{\nu\mu u}$	$\frac{1}{2} - \frac{2}{3}\widehat{s}_0^2$	0.3457
$g_{LL}^{\nu\mu d}$	$-\frac{1}{2} + \frac{1}{3}\widehat{s}_0^2$	-0.4288
$g_{LR}^{\nu\mu u}$	$-\frac{2}{3}\widehat{s}_0^2$	-0.1553
$g_{LR}^{\nu\mu d}$	$\frac{1}{3}\widehat{s}_0^2$	0.0777
g_{AV}^{ee}	$\frac{1}{2} - 2\widehat{s}_0^2$	0.0224
g_{AV}^{eu}	$-\frac{1}{2} + \frac{4}{3}\widehat{s}_0^2$	-0.1886
g_{AV}^{ed}	$\frac{1}{2} - \frac{2}{3}\widehat{s}_0^2$	0.3418
g_{VA}^{eu}	$-\frac{1}{2} + 2\widehat{s}_0^2$	-0.0349
g_{VA}^{ed}	$\frac{1}{2} - 2\widehat{s}_0^2$	0.0246

massless left-handed neutrinos). One has⁸,

$$-\mathcal{L}^{\nu e} = \frac{G_F}{\sqrt{2}} \bar{\nu} \gamma_\mu (1 - \gamma^5) \nu \bar{e} \gamma^\mu (g_{LV}^{\nu e} - g_{LA}^{\nu e} \gamma^5) e, \quad (10.29a)$$

$$-\mathcal{L}^{\nu h} = \frac{G_F}{\sqrt{2}} \bar{\nu} \gamma_\mu (1 - \gamma^5) \nu \sum_q \left[g_{LL}^{\nu q} \bar{q} \gamma^\mu (1 - \gamma^5) q + g_{LR}^{\nu q} \bar{q} \gamma^\mu (1 + \gamma^5) q \right], \quad (10.29b)$$

$$-\mathcal{L}^{ee} = -\frac{G_F}{\sqrt{2}} g_{AV}^{ee} \bar{e} \gamma_\mu \gamma^5 e \bar{e} \gamma^\mu e, \quad (10.29c)$$

$$-\mathcal{L}^{eh} = -\frac{G_F}{\sqrt{2}} \sum_q \left[g_{AV}^{eq} \bar{e} \gamma_\mu \gamma^5 e \bar{q} \gamma^\mu q + g_{VA}^{eq} \bar{e} \gamma_\mu e \bar{q} \gamma^\mu \gamma^5 q \right], \quad (10.29d)$$

where one must include the charged-current contribution for ν_e - e and $\bar{\nu}_e$ - e and the parity conserving QED contribution for electron scattering. The SM tree level expressions for the four-Fermi couplings are given in Table 10.3. Note that they differ from the respective products of the gauge couplings in (10.7) in the radiative corrections and in the presence of possible physics beyond the SM.

10.3.1 Neutrino scattering

The cross-section in the laboratory system for $\nu_\mu e \rightarrow \nu_\mu e$ or $\bar{\nu}_\mu e \rightarrow \bar{\nu}_\mu e$ elastic scattering [9, 136] is (in this subsection we drop the redundant index L in the effective neutrino couplings),

$$\frac{d\sigma_{\nu,\bar{\nu}}}{dy} = \frac{G_F^2 m_e E_\nu}{2\pi} \left[(g_V^{\nu e} \pm g_A^{\nu e})^2 + (g_V^{\nu e} \mp g_A^{\nu e})^2 (1-y)^2 - (g_V^{\nu e 2} - g_A^{\nu e 2}) \frac{y m_e}{E_\nu} \right], \quad (10.30)$$

where the upper (lower) sign refers to $\nu_\mu(\bar{\nu}_\mu)$, and $y \equiv T_e/E_\nu$ (which runs from 0 to $(1 + m_e/2E_\nu)^{-1}$) is the ratio of the kinetic energy of the recoil electron to the incident ν or $\bar{\nu}$ energy. For

⁸We use here slightly different definitions (and to avoid confusion also a different notation) for the coefficients of these four-Fermi operators than we did in previous editions of this *Review*. The new couplings [13] are defined in the static limit, $Q^2 \rightarrow 0$, with specific radiative corrections included, while others (more experiment specific ones) are assumed to be removed by the experimentalist. They are convenient in that their determinations from very different types of processes can be straightforwardly combined.

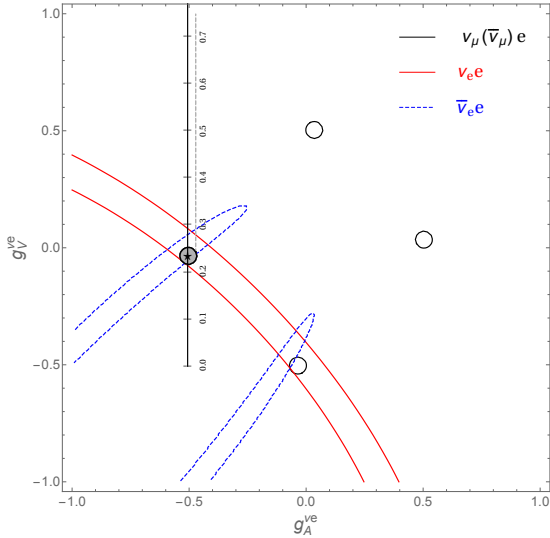


Figure 10.1: Allowed contours in $g_A^{\nu e}$ vs. $g_V^{\nu e}$ from neutrino-electron scattering and the SM prediction as a function of \widehat{s}_Z^2 . (The SM best fit value, $\widehat{s}_Z^2 = 0.23129$, is also indicated.) The $\nu_e e$ [140, 141] and $\bar{\nu}_e e$ [142] constraints are at 1σ , while each of the four equivalent $\nu_\mu(\bar{\nu}_\mu) e$ [137–139] solutions ($g_{V,A} \rightarrow -g_{V,A}$ and $g_{V,A} \rightarrow g_{A,V}$) are at the 90% CL. The global best fit region (shaded) almost exactly coincides with the corresponding $\nu_\mu(\bar{\nu}_\mu) e$ region. The solution near $g_A = 0$ and $g_V = -0.5$ is eliminated by $e^+e^- \rightarrow \ell^+\ell^-$ data under the weak additional assumption that the neutral current is dominated by the exchange of a single Z boson.

$E_\nu \gg m_e$ this yields a total cross-section

$$\sigma = \frac{G_F^2 m_e E_\nu}{2\pi} \left[(g_V^{\nu e} \pm g_A^{\nu e})^2 + \frac{1}{3} (g_V^{\nu e} \mp g_A^{\nu e})^2 \right]. \quad (10.31)$$

The most accurate measurements of $\sin^2 \theta_W$ from ν -lepton scattering (see Sec. 10.6) are from the ratio $R \equiv \sigma_{\nu_\mu e} / \sigma_{\bar{\nu}_\mu e}$, in which many of the systematic uncertainties cancel. The results are $\sin^2 \theta_W = 0.211 \pm 0.037$ [137], $\sin^2 \theta_W = 0.195 \pm 0.022$ [138], and $\sin^2 \theta_W = 0.2324 \pm 0.0083$ [139], where radiative corrections (other than m_t effects) are small compared to the precision of present experiments and have negligible effect. As shown in Fig. 10.1, one can determine $g_{V,A}^{\nu e}$ from the experimental data as well. The cross-sections for $\nu_e e$ and $\bar{\nu}_e e$ may be obtained from Eq. (10.30) by replacing $g_{V,A}^{\nu e}$ by $g_{V,A}^{\nu e} + 1$, where the 1 is due to the charged-current contribution.

A precise determination of the on-shell s_W^2 , which depends only very weakly on m_t and M_H , is obtained from deep inelastic scattering (DIS) of neutrinos [136, 143] from (approximately) isoscalar targets. The ratio $R_\nu \equiv \sigma_{\nu N}^{NC} / \sigma_{\nu N}^{CC}$ of neutral-to-charged-current cross-sections has been measured to 1% accuracy by CDHS [144] and CHARM [145] at CERN. CCFR [146] at Fermilab has obtained an even more precise result, so it is important to obtain theoretical expressions for R_ν and $R_{\bar{\nu}} \equiv \sigma_{\bar{\nu} N}^{NC} / \sigma_{\bar{\nu} N}^{CC}$ to comparable accuracy. Fortunately, many of the uncertainties from the strong interactions and neutrino spectra cancel in the ratio. A large theoretical uncertainty is associated with the c -threshold, which mainly affects σ^{CC} . Using the slow rescaling prescription [147, 148] the central value of $\sin^2 \theta_W$ from CCFR varies as $0.0111(m_c/\text{GeV} - 1.31)$, where m_c is the effective mass which is numerically close to the $\overline{\text{MS}}$ mass $\widehat{m}_c(\widehat{m}_c)$, but their exact relation is unknown at higher orders. For $m_c = 1.31 \pm 0.24$ GeV, which was determined from ν -induced di-muon production [149], this contributes ± 0.003 to the total error of $\Delta \sin^2 \theta_W = \pm 0.004$ (the experimental uncertainty was also ± 0.003). This uncertainty

largely cancels, however, in the Paschos-Wolfenstein ratio [150],

$$R^- = \frac{\sigma_{\nu N}^{NC} - \sigma_{\bar{\nu} N}^{NC}}{\sigma_{\nu N}^{CC} - \sigma_{\bar{\nu} N}^{CC}}. \quad (10.32)$$

It was measured by Fermilab's NuTeV collaboration [151] for the first time, and required a high-intensity and high-energy anti-neutrino beam.

A simple zeroth-order approximation is,

$$R_\nu = g_L^2 + g_R^2, \quad R_{\bar{\nu}} = g_L^2 + \frac{g_R^2}{r}, \quad (10.33a)$$

$$R^- = g_L^2 - g_R^2, \quad r \equiv \frac{\sigma_{\bar{\nu} N}^{CC}}{\sigma_{\nu N}^{CC}}, \quad (10.33b)$$

where r is the ratio of $\bar{\nu}$ to ν charged-current cross-sections which can be measured directly⁹, and

$$g_L^2 \equiv (g_{LL}^{\nu u})^2 + (g_{LL}^{\nu d})^2 \approx \frac{1}{2} - \sin^2 \theta_W + \frac{5}{9} \sin^4 \theta_W, \quad (10.34a)$$

$$g_R^2 \equiv (g_{LR}^{\nu u})^2 + (g_{LR}^{\nu d})^2 \approx \frac{5}{9} \sin^4 \theta_W. \quad (10.34b)$$

In practice, Eq. (10.33b) must be corrected for quark mixing, quark sea effects, c quark threshold effects, non-isoscalarity, W - Z propagator differences, the finite muon mass, QED and EW radiative corrections. Details of the neutrino spectra, experimental cuts, x and Q^2 dependence of structure functions, and longitudinal structure functions, enter only at the level of these corrections and therefore lead to very small uncertainties. CCFR quotes $s_W^2 = 0.2236 \pm 0.0041$ for the reference values (m_t, M_H) = (175, 150) GeV with very little sensitivity to (m_t, M_H).

The NuTeV collaboration found $s_W^2 = 0.2277 \pm 0.0016$ (for the same reference values), which was 3.0σ higher than the SM prediction [151]. However, since then several groups have raised concerns about the interpretation of the NuTeV result, which could affect the extracted $g_{L,R}^2$ (and thus s_W^2) including their uncertainties and correlation. These include the assumption of symmetric strange and anti-strange sea quark distributions, the electron neutrino contamination from K_{e3} decays, isospin symmetry violation in the parton distribution functions and from QED splitting effects, nuclear shadowing effects, and a more complete treatment of EW and QCD radiative corrections. A more detailed discussion and a list of references can be found in the 2016 edition of this *Review*. The precise impact of these effects would need to be evaluated carefully by the collaboration, but in the absence of such an effort we do not include the ν DIS constraints in our default set of fits.

Recently, the COHERENT collaboration was the first to observe the coherent elastic neutrino nucleus scattering (CE ν NS) process [152] on a target consisting mostly of ^{133}Cs and ^{127}I , and at the opposite end of the kinematic scale where the momentum transfer is significantly smaller than the inverse of the nuclear radius. Subsequently, COHERENT [153] observed CE ν NS using a liquid ^{40}Ar detector, as well. The coherence enhances the process roughly proportional to the square of the number of neutrons in the nuclei, but the process is difficult to observe as the experimental signature is a mere keV scale nuclear recoil.

10.3.2 Parity violating lepton scattering

Reviews on weak polarized electron scattering may be found in Refs. [9, 154]. The SLAC polarized electron-deuteron DIS (eDIS) experiment [155] measured the parity violating right-left asymmetry,

$$A_{RL} \equiv \frac{\sigma_R - \sigma_L}{\sigma_R + \sigma_L}, \quad (10.35)$$

where $\sigma_{R,L}$ is the cross-section for the deep-inelastic scattering of a right- or left-handed electron, $e_{R,L}N \rightarrow eX$. In the quark

⁹In the simple parton model, ignoring hadron energy cuts, $r \approx (1 + 3\epsilon)/(3 + \epsilon)$, where $\epsilon \sim 0.125$ is the ratio of the fraction of the nucleon's momentum carried by anti-quarks to that carried by quarks.

parton model,

$$\frac{A_{RL}}{Q^2} = a_1 + a_2 \frac{1 - (1 - y)^2}{1 + (1 - y)^2}, \quad (10.36)$$

where $Q^2 > 0$ is the momentum transfer and y is the fractional energy transfer from the electron to the hadrons. For the deuteron or other isoscalar targets, one has, neglecting the s quark and anti-quarks,

$$a_1 = \frac{3G_F}{5\sqrt{2}\pi\alpha} \left(g_{AV}^{eu} - \frac{1}{2}g_{AV}^{ed} \right) \approx \frac{3G_F}{5\sqrt{2}\pi\alpha} \left(-\frac{3}{4} + \frac{5}{3}\hat{s}_0^2 \right), \quad (10.37a)$$

$$a_2 = \frac{3G_F}{5\sqrt{2}\pi\alpha} \left(g_{VA}^{eu} - \frac{1}{2}g_{VA}^{ed} \right) \approx \frac{9G_F}{5\sqrt{2}\pi\alpha} \left(\hat{s}_0^2 - \frac{1}{4} \right). \quad (10.37b)$$

The Jefferson Lab Hall A collaboration [156, 157] improved on the SLAC result by measuring A_{RL} at $Q^2 = 1.085 \text{ GeV}^2$ and 1.901 GeV^2 , and determined the weak mixing angle to 2% precision, $\hat{s}_Z^2 = 0.2299 \pm 0.0043$. In another polarized electron scattering experiment on deuterons, but in the quasi-elastic kinematic regime, the SAMPLE experiment [158, 159] at MIT-Bates extracted the combination $g_{VA}^{eu} - g_{VA}^{ed}$ at Q^2 values of 0.038 GeV^2 and 0.091 GeV^2 . What was actually determined were nucleon form factors from which the quoted results were obtained by the removal of a multi-quark radiative correction [160]. Other linear combinations of the effective couplings have been determined in polarized lepton scattering at CERN in μ - ^{12}C DIS [161] (the observable was the double charge-helicity cross-section asymmetry), at Mainz in e - ^9Be (quasi-elastic) [162], and at Bates in e - ^{12}C (elastic) [163]. More recent polarized electron scattering experiments, *i.e.*, SAMPLE, the PVA4 experiment at Mainz, and the HAPPEX and $G0$ experiments at Jefferson Lab, have focussed on the strange quark content of the nucleon [164].

A_{RL} can also be measured in fixed target polarized Møller scattering, $e^-e^- \rightarrow e^-e^-$, and reads [165],

$$\frac{A_{RL}}{Q^2} = -2g_{AV}^{ee} \frac{G_F}{\sqrt{2}\pi\alpha} \frac{1 - y}{1 + y^4 + (1 - y)^4}. \quad (10.38)$$

It has been determined at low $Q^2 = 0.026 \text{ GeV}^2$ in the SLAC E158 experiment [166], with the result, $A_{RL} = (-1.31 \pm 0.14_{\text{stat.}} \pm 0.10_{\text{syst.}}) \times 10^{-7}$. Expressed in terms of the weak mixing angle in the $\overline{\text{MS}}$ scheme this yields $\hat{s}^2(161 \text{ MeV}) = 0.2403 \pm 0.0013$, and as shown in Fig. 10.2 established the scale dependence of the weak mixing angle at the level of 6.4σ . One also extracts the model-independent effective coupling, $g_{AV}^{ee} = 0.0190 \pm 0.0027$ [13]. One-loop radiative corrections and implications are discussed in Ref. [87].

In a similar experiment and at about the same $Q^2 = 0.0248 \text{ GeV}^2$, the Q_{weak} collaboration at Jefferson Lab obtained $A_{RL} = (-2.265 \pm 0.073_{\text{stat.}} \pm 0.058_{\text{syst.}}) \times 10^{-7}$ [167, 168] in elastic $e^-p \rightarrow e^-p$ scattering. To extract the physical quantity of interest, the weak charge of the proton [169], a large ($\approx 30\%$) correction had to be applied to A_{RL} arising from electromagnetic, strange, and axial form factors. This was achieved by performing a global fit [170] including a large number of A_{RL} data points at larger Q^2 , dominated by the HAPPEX result at $Q^2 = 0.109 \text{ GeV}^2$ [171]. Finally, the constraint, $2g_{AV}^{eu} + g_{AV}^{ed} = 0.0356 \pm 0.0023$, which translates into a weak mixing angle measurement of $\hat{s}^2(157 \text{ MeV}) = 0.2382 \pm 0.0011$, could be deduced, after correcting for a relatively large and uncertain contribution from the γZ box diagram [172–175].

10.3.3 Atomic parity violation

There are precise measurements of atomic parity violation (APV) [9, 176, 177] in ^{133}Cs [178, 179] (at the 0.4% level [178]), ^{205}Tl [180, 181], ^{208}Pb [182], and ^{209}Bi [183]. The EW physics is contained in the nuclear weak charges $Q_W(Z, N)$, where Z and N are the numbers of protons and neutrons in the nucleus. In terms

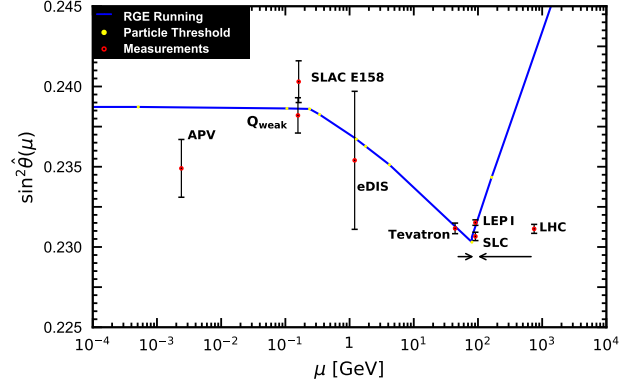


Figure 10.2: Scale dependence of the weak mixing angle defined in the $\overline{\text{MS}}$ scheme [39, 88] (for the scale dependence in a mass-dependent renormalization scheme, see Ref. [87]). The minimum of the curve corresponds to $\mu = M_W$, below which we switch to an effective theory with the W^\pm bosons integrated out, and where the β -function for $\hat{s}^2(\mu)$ changes sign. At M_W and each fermion mass there are also discontinuities arising from scheme dependent matching terms, which are necessary to ensure that the various effective field theories within a given loop order describe the same physics. However, in the $\overline{\text{MS}}$ scheme these are very small numerically and barely visible in the figure provided one decouples quarks at $\mu = \hat{m}_q$. The width of the curve exceeds the theory uncertainty from strong interaction effects which at low energies is at the level of $\pm 2 \times 10^{-5}$ [39]. The Tevatron and LHC measurements are strongly dominated by invariant masses of the final-state di-lepton pair of $\mathcal{O}(M_Z)$ and can thus be considered as additional Z pole data points. For clarity we displayed the Tevatron and LHC points horizontally to the left and right, respectively.

of the nucleon vector couplings,

$$g_{AV}^{ep} \equiv 2g_{AV}^{eu} + g_{AV}^{ed} \approx -\frac{1}{2} + 2\hat{s}_0^2, \quad (10.39a)$$

$$g_{AV}^{en} \equiv g_{AV}^{eu} + 2g_{AV}^{ed} \approx +\frac{1}{2}, \quad (10.39b)$$

one has,

$$Q_W(Z, N) \equiv -2 \left[Z(g_{AV}^{ep} + 0.00005) + N(g_{AV}^{en} + 0.00006) \right] \left(1 - \frac{\alpha}{2\pi} \right), \quad (10.40)$$

where the numerically small adjustments are discussed in Ref. [13] and include the result of the γZ -box correction from Ref. [184].

E.g., $Q_W(^{133}\text{Cs})$ is extracted by measuring experimentally the ratio of the parity violating amplitude, E_{PNC} , to the Stark vector transition polarizability, β , and by calculating theoretically E_{PNC} in terms of Q_W . One can then write,

$$Q_W(^{133}\text{Cs}) = N \left(\frac{\text{Im } E_{\text{PNC}}}{\beta} \right)_{\text{exp.}} \left(\frac{|e| a_B}{\text{Im } E_{\text{PNC}}} \frac{Q_W}{N} \right)_{\text{th.}} \times \left(\frac{\beta}{a_B^3} \right)_{\text{exp.+th.}} \left(\frac{a_B^2}{|e|} \right), \quad (10.41)$$

where a_B is the Bohr radius. There are currently two semi-empirical approaches to β of similar precision. The ratio of the off-diagonal hyperfine amplitude to the vector polarizability was measured directly by the Boulder group [185]. Combined with the hyperfine amplitude, computed precisely in Ref. [186], one finds $\beta = (26.957 \pm 0.044_{\text{exp.}} \pm 0.027_{\text{th.}}) a_B^3$. Alternatively, one can combine [187] the measurement of the ratio of scalar to vector transition polarizabilities [188] with the recent calculation of the scalar polarizability [189] to obtain $\beta = (26.887 \pm 0.030_{\text{exp.}} \pm 0.021_{\text{th.}}) a_B^3$, in agreement with earlier results [190, 191] based on this approach. The two determinations average to $\beta = (26.911 \pm 0.025_{\text{exp.}} \pm 0.017_{\text{th.}}) a_B^3$.

The uncertainties associated with the atomic wave function calculations are relatively small for cesium [9, 192–194]. State-of-the-art many-body atomic structure computations of the parity non-conserving amplitude, $\text{Im } E_{\text{PNC}} = (0.8977 \pm 0.0040) \times 10^{-11} |e| a_B Q_W / N$ [195–200], together with the measurements [178, 179] which can be combined to give $\text{Im } E_{\text{PNC}} / \beta = -1.5924 \pm 0.0055$ mV/cm, imply,

$$Q_W(^{133}_{78}\text{Cs}) = -72.41 \pm 0.26_{\text{exp.}} \pm 0.33_{\text{th.}}, \quad (10.42)$$

or equivalently the constraint, $55g_{AV}^{ep} + 78g_{AV}^{en} = 36.25 \pm 0.21$. Within the SM this can also be translated into a determination of the weak mixing angle, $\hat{s}^2(2.4 \text{ MeV}) = 0.2349 \pm 0.0018$, where the scale setting follows the estimate in Ref. [201] for the typical momentum transfer for parity violation experiments in Cs (the corresponding estimate for Tl amounts to 8 MeV). By comparing different hyperfine transitions, the Boulder experiment in cesium also observed the parity violating weak corrections to the nuclear electromagnetic vertex, called the nuclear anapole moment [202–204].

The theoretical atomic structure uncertainties are 3% for thallium [205] and even larger for the other atoms. However, they mostly cancel if one takes ratios of parity violation in different isotopes [206]. The first result of this type of experiment was announced recently by the Mainz group [207], who studied APV in ^{100}Yb , ^{102}Yb , ^{104}Yb , and ^{106}Yb , at the 0.5% level. The resulting three ratios can be interpreted as a measurement of $\hat{s}_0^2 = 0.258 \pm 0.052$, and represent a very complementary approach to search for BSM physics [208]. If the precision increases in the future, one would ultimately face uncertainties from differences in the neutron charge radii [209, 210]. These can be constrained experimentally [211], *e.g.*, by measuring A_{RL} in heavier nuclei as done by the PREX collaboration at Jefferson Lab on ^{208}Pb [212] and ^{48}Ca [213].

10.4 Precision flavor physics

In addition to cross-sections, asymmetries, parity violation, W , Z , Higgs and other collider physics, there is a large number of experiments and observables testing the flavor structure of the SM. These are addressed elsewhere in this *Review*, and are generally not included in this Section. However, we identify three precision observables with sensitivity to similar types of new physics as the other processes discussed here. The branching fraction of the flavor changing transition $b \rightarrow s\gamma$ is of comparatively low precision, but since it is a loop-level process (in the SM) its sensitivity to new physics (and SM parameters, such as heavy quark masses) is enhanced. A discussion can be found in the 2010 edition of this *Review*.

The τ lepton lifetime and leptonic branching ratios are primarily sensitive to α_s and not affected significantly by many types of new physics. However, having an independent and reliable low energy measurement of α_s in a global analysis allows the comparison with the Z lineshape determination of α_s which shifts easily in the presence of new physics contributions. By far the most precise observable discussed here is the anomalous magnetic moment of the muon. Its combined experimental and theoretical uncertainty is smaller than typical electroweak scale contributions. The electron magnetic moment is measured to even greater precision, and as discussed in Sec. 10.2.2 can be used to determine α . Its new physics sensitivity, however, is suppressed by an additional factor of m_e^2/m_μ^2 , unless there is a new light degree of freedom such as a dark Z [214] boson.

10.4.1 The τ lifetime

The extraction of α_s from the τ lifetime τ_τ [215, 216] is standing out from other determinations because of a variety of independent reasons:

- (i) The τ -scale is low, so that upon extrapolation to the Z scale (where it can be compared to the theoretically clean Z lineshape determinations) the α_s error shrinks by about an order of magnitude.
- (ii) Yet, this scale is high enough that perturbation theory and the operator product expansion (OPE) can be applied.

- (iii) These observables are fully inclusive and thus free of fragmentation and hadronization effects that would have to be modeled or measured.
- (iv) Duality violation (DV) effects are most problematic near the branch cut but there they are suppressed by a double zero at $s = m_\tau^2$.
- (v) There are data [44, 46, 217] to constrain non-perturbative effects both within and breaking the OPE.
- (vi) A complete four-loop order QCD calculation is available [218–222] in the massless limit.
- (vii) Large effects associated with the QCD β -function can be re-summed [223] in what has become known as contour improved perturbation theory (CIPT).

However, while CIPT certainly shows faster convergence in the lower (calculable) orders, doubts have been cast on the method by the observation of discrepancies in a specific model [224] and the realization that CIPT appears to be incompatible with the OPE [225, 226]. Moreover, it has been found that the construction of a renormalon-free scheme for the gluon condensate brings the CIPT results in agreement with ordinary fixed order perturbation theory (FOPT), without significantly modifying the latter [227, 228]. We therefore use the FOPT expressions [60, 222, 229],

$$\tau_\tau = \hbar \frac{1 - \mathcal{B}_\tau^s}{\Gamma_\tau^e + \Gamma_\tau^\mu + \Gamma_\tau^{ud}} = 290.75 \pm 0.36 \text{ fs}, \quad (10.43)$$

and

$$\Gamma_\tau^{ud} = \frac{G_F^2 m_\tau^5 |V_{ud}|^2}{64\pi^3} S(m_\tau, M_Z) \left(1 + \frac{3}{5} \frac{m_\tau^2 - m_\mu^2}{M_W^2} \right) \times \left[1 + \frac{\alpha_s(m_\tau)}{\pi} + 5.202 \frac{\alpha_s^2}{\pi^2} + 26.37 \frac{\alpha_s^3}{\pi^3} + 127.1 \frac{\alpha_s^4}{\pi^4} + \frac{\hat{\alpha}}{\pi} \left(\frac{85}{24} - \frac{\pi^2}{2} \right) + \delta_{\text{NP}} \right], \quad (10.44)$$

where Γ_τ^e and Γ_τ^μ can be taken from Eq. (10.9) with obvious replacements. The relative fraction of strangeness changing ($\Delta S = -1$) decays, $\mathcal{B}_\tau^s = 0.0292 \pm 0.0004$, is based on experimental data since the value for the strange quark mass, $\hat{m}_s(m_\tau)$, is not well known and the QCD expansion proportional to \hat{m}_s^2 converges poorly and cannot be trusted. $S(m_\tau, M_Z) = 1.01908 \pm 0.0003$ is a logarithmically enhanced EW correction factor [230] with higher orders re-summed [231].

δ_{NP} collects non-perturbative and quark-mass suppressed contributions, including the dimension four, six and eight terms in the OPE, as well as DV effects. We use the average $\delta_{\text{NP}} = 0.0141 \pm 0.0072$ derived from the τ decay spectral functions provided by OPAL [44] and ALEPH [46, 217], which give $\delta_{\text{NP}} = 0.000 \pm 0.012$ and $\delta_{\text{NP}} = 0.022 \pm 0.009$, respectively. These numbers are based on the original analyses in Refs. [232, 233], but are modified to correspond to a strict FOPT analysis as is appropriate for our purpose¹⁰ (for alternative analyses, see Section 9 on “Quantum Chromodynamics” in this *Review*).

The dominant uncertainty arises from the truncation of the FOPT series and is conservatively taken as the α_s^4 term (this is re-calculated in each call of the fits, leading to an α_s -dependent and thus asymmetric error) until a better understanding of the numerical differences between FOPT and CIPT has been gained. Our perturbative error covers almost the entire range from using CIPT to assuming that the nearly geometric series in Eq. (10.44) continues to higher orders. The experimental uncertainty in Eq. (10.43) is from the combination of the two leptonic branching ratios with the direct τ_τ . Included are also various smaller uncertainties (± 0.16 fs) from other sources. Based on the method of Refs. [60, 234], we obtain in total

$$\alpha_s^{(4)}(m_\tau) = 0.312_{-0.013}^{+0.016}, \quad \alpha_s^{(5)}(M_Z) = 0.1171_{-0.0017}^{+0.0018}, \quad (10.45)$$

¹⁰We are indebted to Diogo Boito, Maarten Golterman, Kim Maltman and Santiago Peris for privately communicating these results to us.

which represents a 1.5% determination of $\alpha_s(M_Z)$. For more details, see Refs. [232,233] where the τ spectral functions themselves and an estimate of the unknown α_s^5 term were used as additional inputs.

10.4.2 The muon anomalous magnetic moment

The world average of the muon anomalous magnetic moment¹¹,

$$a_\mu^{\text{exp}} = \frac{g_\mu - 2}{2} = (1165920.59 \pm 0.22) \times 10^{-9}, \quad (10.46)$$

is the combination of the final result of the BNL E821 collaboration [235] and the recent result of the Muon $g - 2$ collaboration at Fermilab [236]. The QED contribution has been calculated to five loops [25, 27, 237–239] (fully analytic to three loops [240–244]). The estimated SM EW contribution [245–250], $a_\mu^{\text{EW}} = (1.54 \pm 0.01) \times 10^{-9}$, includes two-loop [251–255] and leading three-loop [256,257] corrections and is at the level of more than four times the current total uncertainty.

The limiting factor in the interpretation of the result are the uncertainties from hadronic effects. The most recent evaluations of the leading-order (two-loop) hadronic vacuum polarization contribution using data from $e^+e^- \rightarrow$ hadrons obtained $a_\mu^{\text{had,VP}}(\alpha^2) = (68.81 \pm 0.41) \times 10^{-9}$ [258], $a_\mu^{\text{had,VP}}(\alpha^2) = (69.23 \pm 0.33) \times 10^{-9}$ [259], $a_\mu^{\text{had,VP}}(\alpha^2) = (69.40 \pm 0.40) \times 10^{-9}$ [41], and $a_\mu^{\text{had,VP}}(\alpha^2) = (69.28 \pm 0.24) \times 10^{-9}$ [42]. Our analysis is based on the e^+e^- data compiled in Ref. [41], where by utilizing the assessment in Ref. [50], we add τ -decay information and the very recent CMD-3 result [48] to estimate the dominant pion form factor contribution. We complement the contributions up to $\sqrt{s} = 2$ GeV, for which we find $a_\mu^{\text{had,VP}}(\alpha^2, 2 \text{ GeV}) = (65.12 \pm 0.30) \times 10^{-9}$, with analytical PQCD expressions for energies beyond 2 GeV and for the c and b quark contributions [244,260].

By now there are also precise results for $a_\mu^{\text{had,VP}}(\alpha^2)$ from lattice QCD calculations [261]. We use the constraint, $a_\mu^{\text{had,VP}}(\alpha^2, 2 \text{ GeV}) = (65.71 \pm 0.55) \times 10^{-9}$, obtained from the result with the smallest quoted uncertainty (by the BMW collaboration [262]), $a_\mu^{\text{had,VP}}(\alpha^2) = (70.75 \pm 0.55) \times 10^{-9}$, by subtracting the perturbative QCD contribution including from charm and bottom quarks. It is important to note that there is a strong correlation (estimated to 86% in Ref. [51]) between $a_\mu^{\text{had,VP}}(\alpha^2, 1.8 \text{ GeV})$ and $\Delta\alpha_{\text{had}}^{(3)}(1.8 \text{ GeV})$ discussed in Sec. 10.2.2. As a result, using the lattice calculation from Ref. [49] as a constraint for $\Delta\alpha_{\text{had}}$ has an impact on $a_\mu^{\text{had,VP}}$ by slightly increasing it¹². Incorporating this effect together with the BMW result, $a_\mu^{\text{had,VP}}(\alpha^2, 2 \text{ GeV}) = (65.71 \pm 0.55) \times 10^{-9}$, and the data-driven value, $a_\mu^{\text{had,VP}}(\alpha^2, 2 \text{ GeV}) = (65.12 \pm 0.30) \times 10^{-9}$, we obtain

$$a_\mu^{\text{had,VP}}(\alpha^2, 2 \text{ GeV}) = (65.44 \pm 0.25) \times 10^{-9}, \quad (10.47)$$

which we use as an input to our fits. The BMW result is roughly 2 σ higher than the value derived from the KLOE data [263], is slightly lower than that from CMD-3 [48], and agrees well with τ decays. In fact, the discrepancy between KLOE and CMD-3 cross-sections exceeds 5σ locally, and amounts to 3.3σ if one considers the entire overlap region of the two experiments [50]. A more detailed analysis [264, 265] of the difference between BMW and the data-driven evaluation using KLOE input suggests that it originates mostly from hadronic contributions below 2 GeV to the vacuum polarization. The BMW result for this hadronic window is supported by findings from other lattice collaborations [266–272]. Possible explanations for this discrepancy include underestimated systematic uncertainties in the analysis of some

of the available experimental data and higher-order initial-state radiation effects [50].

Sub-leading hadronic vacuum polarization effects at three-loop [273] and four-loop order [274] contribute $a_\mu^{\text{had,VP}}(\alpha^3) = (-0.983 \pm 0.004) \times 10^{-9}$ [42] and $a_\mu^{\text{had,VP}}(\alpha^4) = (0.124 \pm 0.001) \times 10^{-9}$ [274], respectively. To account for the larger vacuum polarization effects suggested by lattice QCD, we increase both $a_\mu^{\text{had,VP}}(\alpha^3)$ and $a_\mu^{\text{had,VP}}(\alpha^4)$ by 1%. The correlations with the two-loop hadronic contribution and with $\Delta\alpha(M_Z)$ (see Sec. 10.2) were considered in Ref. [244].

The other hadronic uncertainty is induced by the three-loop light-by-light scattering amplitude, where a number of independent model calculations yield results which are in reasonable agreement with each other, $a_\mu^{\text{had,\gamma}\times\gamma}(\alpha^3) = (1.36 \pm 0.25) \times 10^{-9}$ [275], $a_\mu^{\text{had,\gamma}\times\gamma}(\alpha^3) = 1.37_{-0.27}^{+0.15} \times 10^{-9}$ [276], $a_\mu^{\text{had,\gamma}\times\gamma}(\alpha^3) = (1.05 \pm 0.26) \times 10^{-9}$ [277], and $a_\mu^{\text{had,\gamma}\times\gamma}(\alpha^3) = (1.03 \pm 0.29) \times 10^{-9}$ [258], but the sign of this effect is opposite [278] to the one quoted in the 2002 edition of this *Review*. There is also an upper bound given by $a_\mu^{\text{had,\gamma}\times\gamma}(\alpha^3) < 1.59 \times 10^{-9}$ [276] but this requires an *ad hoc* assumption, too. Efforts to improve the evaluation by using experimental input where available yield the lower values, $a_\mu^{\text{had,\gamma}\times\gamma}(\alpha^3) = (0.87 \pm 0.13) \times 10^{-9}$ [279] and $a_\mu^{\text{had,\gamma}\times\gamma}(\alpha^3) = (0.92 \pm 0.19) \times 10^{-9}$ [261]. See also Ref. [280] for a recent discussion of the axial-vector contribution and short-distance constraints. Lattice calculations have reached similar levels of precision, $a_\mu^{\text{had,\gamma}\times\gamma}(\alpha^3) = (1.10 \pm 0.15) \times 10^{-9}$ [281,282] and $a_\mu^{\text{had,\gamma}\times\gamma}(\alpha^3) = (1.25 \pm 0.15) \times 10^{-9}$ [283], and are consistent with the model and data-driven calculations. For our fits we average the two lattice results (with the systematic errors considered as fully correlated) and combine them with the data-driven result [261] to obtain,

$$a_\mu^{\text{had,\gamma}\times\gamma}(\alpha^3) = (1.11 \pm 0.10) \times 10^{-9}, \quad (10.48)$$

which we have shifted by 1×10^{-11} to account for the perturbative charm quark treatment of Ref. [276]. Higher-order contributions with a hadronic light-by-light scattering subgraph have been estimated in Ref. [284] with the result, $a_\mu^{\text{had,\gamma}\times\gamma}(\alpha^4) = (0.02 \pm 0.01) \times 10^{-9}$ [261].

Altogether, the SM prediction is

$$a_\mu^{\text{theory}} = (1165919.46 \pm 0.27) \times 10^{-9}, \quad (10.49)$$

where the error is from the hadronic uncertainties excluding parametric ones, such as from α_s and the heavy quark masses. We evaluate the correlation of the total (experimental plus theoretical) uncertainty in a_μ with $\Delta\alpha(M_Z)$ to amount to 43%. The overall 3.2 σ discrepancy between the experimental value (10.46) and the SM prediction,

$$a_\mu^{\text{exp}} - a_\mu^{\text{theory}} = (1.13 \pm 0.35) \times 10^{-9}, \quad (10.50)$$

could be due to fluctuations (a_μ^{exp} is statistics dominated) or underestimates of the theoretical uncertainties. On the other hand, the deviation could also arise from physics beyond the SM, such as supersymmetric models with large $\tan\beta$ and moderately light superparticle masses [285], or a dark Z boson [214].

10.5 Physics of the massive electroweak bosons

If the CM energy \sqrt{s} is large compared to the fermion mass m_f , the unpolarized Born cross-section for $e^+e^- \rightarrow f\bar{f}$ [286] can be written as,

$$\frac{d\sigma}{d\cos\theta} = \frac{\pi\alpha^2(s)}{2s} [F_1(1 + \cos^2\theta) + 2F_2\cos\theta] + B, \quad (10.51a)$$

$$F_1 = Q_e^2 Q_f^2 - 2\chi Q_e Q_f \bar{g}_V^e \bar{g}_V^f \cos\delta_R + \chi^2 (\bar{g}_V^{e2} + \bar{g}_A^{e2}) (\bar{g}_V^{f2} + \bar{g}_A^{f2}), \quad (10.51b)$$

$$F_2 = -2\chi Q_e Q_f \bar{g}_A^e \bar{g}_A^f \cos\delta_R + 4\chi^2 \bar{g}_V^e \bar{g}_A^e \bar{g}_V^f \bar{g}_A^f, \quad (10.51c)$$

¹¹In what follows, we summarize the most important aspects of a_μ and give some details on the evaluation in our fits. For more details and references, see Section 56 of the ‘‘Muon Anomalous Magnetic Moment’’ in this *Review*. There are some numerical differences, which are well understood and arise because internal consistency of the fits requires the calculation of all observables from analytical expressions and common inputs and fit parameters, so that an independent evaluation is necessary for this Section.

¹²Conversely, adding the BMW constraint for $a_\mu^{\text{had,VP}}$ has the effect of increasing $\Delta\alpha_{\text{had}}^{(3)}(2 \text{ GeV})$.

where

$$\tan \delta_R = \frac{\overline{M}_Z \overline{\Gamma}_Z}{\overline{M}_Z^2 - s}, \quad \chi = \frac{G_F}{2\sqrt{2}\pi\alpha(s)} \frac{s\overline{M}_Z^2}{\left[(\overline{M}_Z^2 - s)^2 + \overline{M}_Z^2 \overline{\Gamma}_Z^2\right]^{1/2}}. \quad (10.52)$$

B accounts for box graphs involving virtual Z and W bosons, and the $\overline{g}_{V,A}^f$ are defined in Eq. (10.53) below. \overline{M}_Z and $\overline{\Gamma}_Z$ correspond to mass and width definitions based on a Breit-Wigner shape with an energy-independent width (see Section 55 on the “ Z Boson” in this *Review*). The differential cross-section receives important corrections from QED effects in the initial and final states, and interference between the two [287]. For $q\bar{q}$ production, there are additional final-state QCD corrections, which are relatively large. Note also that the equations above are written in the CM frame of the incident e^+e^- system, which may be boosted due to the initial-state QED radiation.

Some of the leading virtual EW corrections are captured by the running QED coupling $\alpha(s)$ and the Fermi constant G_F . The remaining corrections to the Zff interactions are absorbed by replacing the tree-level couplings in Eq. (10.7) with the s -dependent *effective couplings* [288],

$$\overline{g}_V^f = \sqrt{\rho_f} (t_{3L}^f - 2Q_f \kappa_f \sin^2 \theta_W), \quad (10.53a)$$

$$\overline{g}_A^f = \sqrt{\rho_f} t_{3L}^f. \quad (10.53b)$$

In these equations, the effective couplings are to be taken at the scale \sqrt{s} , but for notational simplicity we do not show this explicitly. At tree-level, $\rho_f = \kappa_f = 1$, but inclusion of EW radiative corrections leads to $\rho_f \neq 1$ and $\kappa_f \neq 1$, which depend on the fermion f and on the renormalization scheme. In the on-shell scheme, the quadratic m_t dependence is given by,

$$\rho_f \sim 1 + \rho_t, \quad \kappa_f \sim 1 + \frac{\rho_t}{\tan^2 \theta_W}, \quad (10.54)$$

while in $\overline{\text{MS}}$, $\widehat{\rho}_f \sim \widehat{\kappa}_f \sim 1$, for $f \neq b$, and

$$\widehat{\rho}_b \sim 1 - \frac{4}{3}\rho_t, \quad \widehat{\kappa}_b \sim 1 + \frac{2}{3}\rho_t. \quad (10.55)$$

In the $\overline{\text{MS}}$ scheme the normalization is changed according to $G_F M_Z^2 / 2\sqrt{2}\pi \rightarrow \widehat{\alpha} / 4\widehat{s}_Z^2 \widehat{c}_Z^2$ in the second Eq. (10.52).

As reviewed in Sec. 10.2.5, for the high precision Z pole observables discussed below, many additional bosonic and fermionic loop effects, vertex corrections, and higher order contributions, *etc.*, must be included. For example, in the $\overline{\text{MS}}$ scheme one then has $\widehat{\rho}_\ell = 0.9977$, $\widehat{\kappa}_\ell = 1.0014$, $\widehat{\rho}_b = 0.9867$, and $\widehat{\kappa}_b = 1.0068$.

To connect to measured quantities, it is convenient to define an effective angle

$$\overline{s}_f^2 \equiv \sin^2 \overline{\theta}_{Wf} \equiv \widehat{\kappa}_f \widehat{s}_Z^2 = \kappa_f s_W^2, \quad (10.56)$$

in terms of which \overline{g}_V^f and \overline{g}_A^f are given by $\sqrt{\rho_f}$ times their tree-level formulae. One finds that the $\widehat{\kappa}_f$ ($f \neq b$) are almost independent of m_t and M_H , and thus one can write,

$$\overline{s}_\ell^2 = \widehat{s}_Z^2 + 0.00032, \quad (10.57)$$

while the κ_f for the on-shell scheme are m_t dependent.

10.5.1 The Z boson mass

The mass of the Z boson, $M_Z = 91.1876 \pm 0.0021$ GeV, has been determined from the Z lineshape scan at LEP 1 [288]. Very recently the CDF collaboration at the Tevatron [289] determined M_Z from fits to the dimuon and dielectron mass distributions. The dimuon channel strongly dominates so that our combination, $M_Z = 91.192 \pm 0.007$ GeV, is insensitive (at the level of the quoted digits) to variations in the assumption concerning possible cross-channel correlations. Combined we find the world average,

$$M_Z = 91.1880 \pm 0.0020 \text{ GeV}. \quad (10.58)$$

These values correspond to a definition based on a Breit-Wigner shape with an energy-dependent width, which differs from \overline{M}_Z in eq. (10.52)¹³.

10.5.2 Electroweak physics off the Z pole

Experiments at PEP, PETRA and TRISTAN have measured the unpolarized forward-backward asymmetry, A_{FB} , and the total cross-section relative to pure QED, R , for $e^+e^- \rightarrow \ell^+\ell^-$, $\ell = \mu$ or τ at CM energies $\sqrt{s} < M_Z$. They are defined as

$$A_{FB} \equiv \frac{\sigma_F - \sigma_B}{\sigma_F + \sigma_B}, \quad R = \frac{\sigma}{\mathcal{R}_{\text{ini}} \otimes \sigma_{\text{QED}}}, \quad (10.59)$$

where σ_F (σ_B) is the cross-section for ℓ^- to travel forward (backward) with respect to the e^- direction, σ_{QED} is the tree-level cross-section from s-channel photon exchange, and $\mathcal{R}_{\text{ini}} \otimes$ denotes convolution with initial-state QED corrections. Neglecting box graph contributions, they are given by,

$$A_{FB} = \frac{3}{4} \frac{F_2}{F_1}, \quad R = F_1. \quad (10.60)$$

For the available data, it is sufficient to approximate the EW corrections through the leading running $\alpha(s)$ and quadratic m_t contributions [290], as described above. Reviews and formulae for $e^+e^- \rightarrow$ hadrons may be found in [9, 291, 292].

LEP 2 [294] ran at several energies above the Z pole up to ~ 209 GeV. Measurements were made of a number of observables, including the total production cross-sections of $f\bar{f}$ pairs for $f = \mu, \tau$, and q (hadrons), of four-fermion final states, of $\gamma\gamma$, ZZ , WW and $WW\gamma$. The differential cross-sections for all three lepton flavors, and the leptonic and hadronic W branching ratios were also extracted.

Among the most important LEP 2 results were the measurements [294] of the W boson mass, M_W , which were dominated by kinematic reconstruction, but included the complementary albeit statistics limited and thus much less precise determination from a WW threshold cross-section measurement. The kinematic method was also employed at the Tevatron [301] and by ATLAS [302] and LHCb [296] at the LHC. A recent combination [298] of all available M_W measurements, using a careful calibration of simulation tools and PDFs, obtained the world average,

$$M_W = 80.3946 \pm 0.0115 \text{ GeV}. \quad (10.61)$$

However, the χ^2 probability of this combination is 0.5% or less, depending on the chosen PDF set, which is mostly due to the W mass measurement by CDF from Run II at the Tevatron [289], $M_W = 80.432 \pm 0.016$ GeV (adjusted to the common PDF set CT18 [303] in Ref. [298]). It differs by almost 4 σ from the other measurements of M_W , while the latter agree well among each other, with the average [298]

$$M_W = 80.3692 \pm 0.0133 \text{ GeV}, \quad (10.62)$$

without CDF II. Subsequently, the ATLAS result has been updated [295], resulting in a significant downward shift of M_W . It also included a measurement of the W boson width, Γ_W , together with a strong 30% anticorrelation with M_W . The new ATLAS Γ_W value differs by about 2 σ from the Tevatron width result [299] and the SM prediction. To include it in the global fit, instead of employing (10.62) *verbatim*, we combine (i) the adjusted results for $D\mathcal{O}$ and LHCb quoted in Ref. [298], (ii) LEP [294], (iii) the new ATLAS results [295], and (iv) the Tevatron width determination [299], keeping the approximate 49% PDF anticorrelation between ATLAS and LHCb. Including further small correlations between $D\mathcal{O}$ and the LHC experiments, this results in the updated overall averages (without M_W from CDF as recommended

¹³Note that \overline{M}_Z is defined through the complex pole of the propagator, which ensures that it is gauge-invariant and theoretically consistent, and which leads to a Breit-Wigner shape with a constant width. The two definitions differ numerically, and this difference has to be accounted for in theoretical calculations.

Table 10.4: Non- Z pole observables, compared with the SM best fit predictions. The SM prediction for Γ_H is without electroweak corrections as in Ref. [293]. The first and second M_W and Γ_W values are from LEP 2 [294] and ATLAS [295], respectively. The remaining M_W values are from LHCb [296], DØ [297], and CDF [289], respectively, adjusted according to Ref. [298], and where the last one [in brackets] is omitted from the fits (see text and Sec. 10.8). The third Γ_W is the Tevatron combination [299], shifted to correspond to the current SM prediction of M_W (what is actually measured is a linear combination containing an M_W term). The hadronic branching ratio for W decays combines LEP 2 [294] and CMS [300] and assumes lepton flavor universality. The world averages for $g_{V,A}^{\nu e}$ are dominated by the CHARM II [139] results, $g_V^{\nu e} = -0.035 \pm 0.017$ and $g_A^{\nu e} = -0.503 \pm 0.017$. The τ_τ value is the τ lifetime world average computed by combining the direct measurements with values derived from the leptonic branching ratios [60]; in this case, the theory error is included in the SM prediction. In all other SM predictions, the uncertainty is parametric from M_Z , M_H , m_t , m_b , m_c , $\hat{\alpha}(M_Z)$, and α_s , and theoretical from unknown higher orders [83], where correlations due to both types have been accounted for. The column denoted by Pull gives the standard deviations.

Quantity	Value	Standard Model	Pull
m_t [GeV]	172.61 ± 0.58	172.85 ± 0.55	-0.4
M_H [GeV]	125.10 ± 0.09	125.10 ± 0.09	0.0
Γ_H [MeV]	3.5 ± 1.5	4.09 ± 0.05	-0.4
M_W [GeV]	80.376 ± 0.033	80.356 ± 0.005	0.6
	80.355 ± 0.016		-0.1
	80.347 ± 0.033		-0.3
	80.372 ± 0.026		0.6
	$[80.432 \pm 0.016]$		—
Γ_W [GeV]	2.195 ± 0.083	2.089 ± 0.001	1.3
	2.198 ± 0.049		2.2
	2.059 ± 0.049		-0.6
$\mathcal{B}(W \rightarrow \text{hadrons})$	0.6736 ± 0.0018	0.6751 ± 0.0001	-0.8
$g_V^{\nu e}$	-0.040 ± 0.015	-0.0395 ± 0.0001	0.0
$g_A^{\nu e}$	-0.507 ± 0.014	-0.5063	0.0
$Q_W(e)$	-0.0403 ± 0.0053	-0.0469 ± 0.0002	1.3
$Q_W(p)$	0.0719 ± 0.0045	0.0705 ± 0.0002	0.3
$Q_W(\text{Cs})$	-72.41 ± 0.42	-73.26 ± 0.01	2.0
$Q_W(\text{Tl})$	-116.4 ± 3.6	-116.93 ± 0.01	0.1
$\hat{s}_Z^2(\text{eDIS})$	0.2299 ± 0.0043	0.23129 ± 0.00004	-0.3
τ_τ [fs]	290.75 ± 0.36	288.59 ± 2.31	0.9
$\frac{1}{2}(g_\mu - 2 - \frac{\alpha}{\pi})$	$(4510.86 \pm 0.35) \times 10^{-9}$	$(4509.73 \pm 0.03) \times 10^{-9}$	3.2

by the authors of Ref. [298]¹⁴,

$$M_W = 80.360 \pm 0.012 \text{ GeV} , \quad (10.63)$$

$$\Gamma_W = 2.136 \pm 0.032 \text{ GeV} , \quad (10.64)$$

with a correlation coefficient of close to -0.3 . Alternatively, fixing Γ_W to the SM prediction gives

$$M_W = 80.366 \pm 0.012 \text{ GeV} . \quad (10.65)$$

For details and references, see Section 54 on the “Mass and Width of the W Boson” in this *Review*.

Strong constraints on anomalous triple and quartic gauge couplings have been obtained at LEP 2, the Tevatron, and the LHC. These are described in detail in “Extraction of Triple Gauge Couplings (TGCs)”, “Anomalous W/Z Quartic Couplings (QGCs)” notes in the W particle listing and in “Anomalous $ZZ\gamma$, $Z\gamma\gamma$, and ZZV Couplings” note in the Z particle listing.

After their discovery of the Higgs boson [304, 305], the LHC experiments are now performing high precision measurements of its mass, M_H . We average the results, $M_H = 125.11 \pm 0.09_{\text{stat.}} \pm 0.06_{\text{syst.}}$ GeV from ATLAS [306], and $M_H = 125.08 \pm 0.10_{\text{stat.}} \pm 0.07_{\text{syst.}}$ GeV from CMS [307], by treating the smaller systematic error as common among the two determinations, and arrive at,

$$M_H = 125.10 \pm 0.07_{\text{stat.}} \pm 0.06_{\text{syst.}} \text{ GeV (LHC)} . \quad (10.66)$$

There are also first measurements of the Higgs boson width, $\Gamma_H = 2.9^{+1.9}_{-1.4}$ MeV from CMS [307] and $\Gamma_H = 4.5^{+3.3}_{-2.5}$ MeV from ATLAS [308]. We perform a simple Gaussian average using the upper error of CMS and the lower error of ATLAS. For further references and

more details on Higgs boson properties, see Section 11 on the “Status of Higgs Boson Physics” in this *Review*.

The principal non- Z pole observables discussed here and in Sections 10.2–10.4 are summarized in Table 10.4.

10.5.3 Z pole physics

High precision measurements of various Z pole ($\sqrt{s} \approx M_Z$) observables [9, 318, 319] have been performed at LEP 1 and SLC [288, 315, 316, 320, 321], as summarized in Table 10.5. These include the Z mass and total width, Γ_Z , and partial widths $\Gamma_{f\bar{f}}$ for $Z \rightarrow f\bar{f}$, where $f = e, \mu, \tau$, light hadrons, b , and c . It is convenient to use the variables M_Z, Γ_Z ,

$$\sigma_{\text{had}} \equiv \frac{12\pi\Gamma_{e^+e^-}\Gamma_{\text{had}}}{M_Z^2\Gamma_Z^2} , \quad R_\ell \equiv \frac{\Gamma_{\text{had}}}{\Gamma_{\ell^+\ell^-}} , \quad R_q \equiv \frac{\Gamma_{q\bar{q}}}{\Gamma_{\text{had}}} , \quad (10.67)$$

for $\ell = e, \mu$ or τ , and $q = b$ or c , where Γ_{had} is the partial decay width into hadrons. Most of these are weakly correlated experimentally. The three values for R_ℓ are consistent with lepton universality¹⁵ (although R_τ is somewhat low compared to R_e and R_μ), but we use the general analysis in which the three observables are treated as independent. Similar remarks apply to $A_{FB}^{0,\ell}$ defined through Eq. (10.68) with $P_e = 0$, where $A_{FB}^{0,\tau}$ is somewhat high. Initial-state radiation reduces the peak cross-section by more than 25%, where $\mathcal{O}(\alpha^3)$ QED effects induce a large anti-correlation (-30%) between Γ_Z and σ_{had} . The anti-correlation between R_b and R_c amounts to -18% [288]. The R_ℓ are insensitive to m_t except for the $Z \rightarrow b\bar{b}$ vertex, final-state corrections,

¹⁵The ratio of branching fractions for Z bosons decaying into e^+e^- relative to $\mu^+\mu^-$ final states has also been measured by ATLAS [322], obtaining $R_{e/\mu} = 1.0026 \pm 0.0050$, in perfect agreement with lepton universality.

¹⁴See Sec. 10.8 for the impact of including the CDF W mass result.

Table 10.5: Principal Z pole observables and their SM predictions (*cf.* Table 10.4). The first M_Z is from LEP 1 [288] and the second from CDF [289]. The first \bar{s}_ℓ^2 is the effective weak mixing angle extracted from the hadronic charge asymmetry at LEP 1 [288], the second is the combined value from the Tevatron [309], and the third is from the LHC [310–314]. The values of A_e are (i) from A_{LR} for hadronic final states [315]; (ii) from A_{LR} for leptonic final states and from polarized Bhabha scattering [316]; and (iii) from the angular distribution of the τ polarization at LEP 1 [288]. The A_τ values are from SLD [316], the total τ polarization from LEP [288], and from CMS [317], respectively. Note that the SM errors in Γ_Z , the R_ℓ , and σ_{had} are largely dominated by the uncertainty in α_s .

Quantity	Value	Standard Model	Pull
M_Z [GeV]	91.1876 ± 0.0021	91.1884 ± 0.0019	−0.4
	91.192 ± 0.007		0.6
Γ_Z [GeV]	2.4955 ± 0.0023	2.4940 ± 0.0009	0.7
σ_{had} [nb]	41.481 ± 0.033	41.481 ± 0.009	0.0
R_e	20.804 ± 0.050	20.736 ± 0.010	1.4
R_μ	20.784 ± 0.034	20.736 ± 0.010	1.4
R_τ	20.764 ± 0.045	20.781 ± 0.010	−0.4
R_b	0.21629 ± 0.00066	0.21583 ± 0.00002	0.7
R_c	0.1721 ± 0.0030	0.17221 ± 0.00003	0.0
$A_{FB}^{(0,e)}$	0.0145 ± 0.0025	0.01606 ± 0.00006	−0.6
$A_{FB}^{(0,\mu)}$	0.0169 ± 0.0013		0.6
$A_{FB}^{(0,\tau)}$	0.0188 ± 0.0017		1.6
$A_{FB}^{(0,b)}$	0.0996 ± 0.0016	0.1026 ± 0.0002	−1.8
$A_{FB}^{(0,c)}$	0.0707 ± 0.0035	0.0732 ± 0.0002	−0.7
$A_{FB}^{(0,s)}$	0.0976 ± 0.0114	0.1027 ± 0.0002	−0.4
\bar{s}_ℓ^2	0.2324 ± 0.0012	0.23161 ± 0.00004	0.7
	0.23148 ± 0.00033		−0.4
	0.23145 ± 0.00028		−0.6
A_e	0.15138 ± 0.00216	0.1463 ± 0.0003	2.3
	0.1544 ± 0.0060		1.3
	0.1498 ± 0.0049		0.7
A_μ	0.142 ± 0.015		−0.3
A_τ	0.136 ± 0.015		−0.7
	0.1439 ± 0.0043		−0.6
	0.144 ± 0.015		−0.2
A_b	0.923 ± 0.020	0.9347	−0.6
A_c	0.670 ± 0.027	0.6674 ± 0.0001	0.1
A_s	0.895 ± 0.091	0.9356	−0.4

and the implicit dependence through $\sin^2 \theta_W$. Thus, they are especially useful for constraining α_s .

Very important constraints follow from measurements of various Z pole asymmetries. These include the forward-backward asymmetry, A_{FB} , and the polarization or left-right asymmetry, A_{LR} , defined analogously to Eq. (10.35). The latter was measured precisely by the SLD collaboration at the SLC [315], and has the advantages of being very sensitive to \bar{s}_ℓ^2 and that systematic uncertainties largely cancel. After removing initial-state QED corrections and contributions from photon exchange, γ - Z interference, as well as the EW boxes in Eq. (10.51a), one can use the effective tree-level expressions,

$$A_{LR} = A_e P_e, \quad A_{FB} = \frac{3}{4} A_f \frac{A_e + P_e}{1 + P_e A_e}, \quad (10.68)$$

where,

$$A_f \equiv \frac{2\bar{g}_V^f \bar{g}_A^f}{\bar{g}_V^{f2} + \bar{g}_A^{f2}} = \frac{1 - 4|Q_f| \bar{s}_f^2}{1 - 4|Q_f| \bar{s}_f^2 + 8Q_f^2 \bar{s}_f^4}. \quad (10.69)$$

P_e is the initial e^- polarization, so that the second equality in Eq. (10.70) is reproduced for $P_e = 1$, and the Z pole forward-backward asymmetries at LEP 1 ($P_e = 0$) are given by $A_{FB}^{(0,f)} = \frac{3}{4} A_e A_f$ for $f = e, \mu, \tau, b, c, s$ [288], and q , and where $A_{FB}^{(0,q)}$ refers to the hadronic charge asymmetry. Corrections for t -channel exchange and s/t -channel interference cause $A_{FB}^{(0,e)}$ to

be strongly anti-correlated with R_e (−37%). Recently, the m_b -dependence [323] of the $\mathcal{O}(\alpha_s^2)$ QCD correction [324], affecting the reference axis of the b quark asymmetry [325], increased the extracted¹⁶ $A_{FB}^{(0,b)}$ by about 0.2σ . The correlation between $A_{FB}^{(0,b)}$ and $A_{FB}^{(0,c)}$ amounts to 15%.

In addition, SLD extracted the final-state couplings A_b , A_c [288], A_s [320], A_τ , and A_μ [316], from left-right forward-backward asymmetries, using

$$A_{LR}^{FB}(f) = \frac{\sigma_{LF}^f - \sigma_{LB}^f - \sigma_{RF}^f + \sigma_{RB}^f}{\sigma_{LF}^f + \sigma_{LB}^f + \sigma_{RF}^f + \sigma_{RB}^f} = \frac{3}{4} A_f, \quad (10.70)$$

where, for example, σ_{LF}^f is the cross-section for a left-handed incident electron to produce a fermion f traveling in the forward hemisphere. Similarly, A_τ and A_e were measured at LEP 1 [288] (A_τ also very recently by CMS [317]) through the τ polarization, \mathcal{P}_τ , as a function of the scattering angle θ , which can be written as,

$$\mathcal{P}_\tau = -\frac{A_\tau(1 + \cos^2 \theta) + 2A_e \cos \theta}{(1 + \cos^2 \theta) + 2A_\tau A_e \cos \theta}. \quad (10.71)$$

The average polarization, $\langle \mathcal{P}_\tau \rangle$, obtained by integrating over $\cos \theta$ in the numerator and denominator of Eq. (10.71), yields

¹⁶We are grateful to Werner Bernreuther and Long Chen for the recalculation of their result employing the more appropriate $\overline{\text{MS}}$ mixing angle, \bar{s}_Z^2 , instead of the on-shell quantity, s_W^2 .

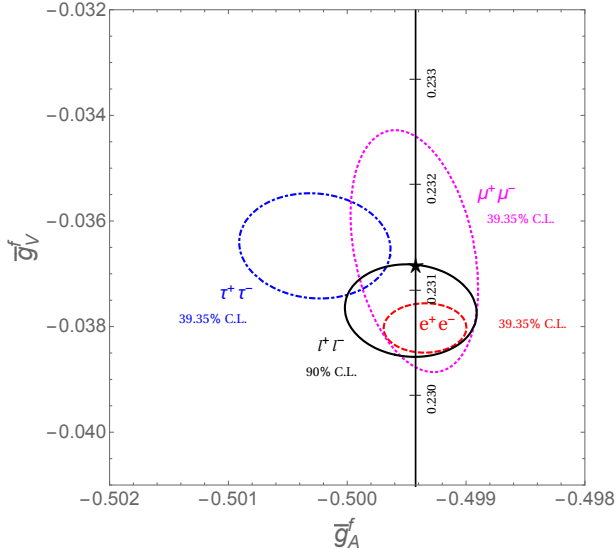


Figure 10.3: 1σ (39.35% CL) contours of the effective couplings \bar{g}_A^f and \bar{g}_V^f for $f = e, \mu$ and τ from LEP and SLC, compared to the SM expectation as a function of \hat{s}_Z^2 . (The SM best fit value $\hat{s}_Z^2 = 0.23129$ is also indicated.) Also shown is the 90% CL allowed region in $\bar{g}_{A,V}^\ell$ obtained assuming lepton universality.

$\langle \mathcal{P}_\tau \rangle = -A_\tau$, and A_e can be extracted from the \mathcal{P}_τ angular distribution. The initial-state coupling, A_e , was also determined through the left-right charge asymmetry [321] and in polarized Bhabha scattering [316] at the SLC. Because \bar{g}_V^ℓ is very small, not only $A_{LR}^0 = A_e$, $A_{FB}^{(0,\ell)}$, and \mathcal{P}_τ , but also $A_{FB}^{(0,q)}$ for $q = b, c$, and s , as well as the hadronic asymmetries are mainly sensitive to \bar{s}_ℓ^2 . The combination of all LEP and SLC asymmetries (but excluding other observables such as R_ℓ) yields,

$$\bar{s}_\ell^2 = 0.23151 \pm 0.00016 \text{ (LEP + SLC)}. \quad (10.72)$$

As an example of the precision of the Z pole observables, the values of \bar{g}_A^f and \bar{g}_V^f for $f = e, \mu, \tau$, and ℓ , extracted from the LEP and SLC lineshape and asymmetry data, are shown in Fig. 10.3. It may be compared with Fig. 10.1 as the two sets of parameters coincide at the SM at tree-level.

As for hadron colliders, the forward-backward asymmetry, A_{FB} , for e^+e^- and $\mu^+\mu^-$ final states (with invariant masses restricted to or dominated by values around M_Z) in $p\bar{p}$ collisions has been measured by the CDF [326] and DØ [327] collaborations, and the values $\bar{s}_\ell^2 = 0.23221 \pm 0.00046$ and $\bar{s}_\ell^2 = 0.23095 \pm 0.00040$ were extracted, respectively. The combination of these measurements (which differ by more than 2σ) yields [309],

$$\bar{s}_\ell^2 = 0.23148 \pm 0.00033 \text{ (Tevatron)}. \quad (10.73)$$

By varying the invariant mass and the scattering angle (and assuming the electron couplings), information on the effective Z couplings to light quarks, $\bar{g}_{V,A}^{u,d}$, could also be obtained [328, 329], but with large uncertainties, mutual correlations, and not independently of \bar{s}_ℓ^2 above. Similar analyses have also been reported by the H1 [330] and ZEUS [331] collaborations at HERA and by the LEP collaborations [288]. This kind of measurement is harder in the pp environment due to the difficulty to assign the initial quark and antiquark in the underlying Drell-Yan process to the protons, thus requiring excellent control of uncertainties from parton distribution functions. ATLAS obtained $\bar{s}_\ell^2 = 0.2308 \pm 0.0012$ using 7 TeV data [310] and a preliminary result $\bar{s}_\ell^2 = 0.23140 \pm 0.00036$ at 8 TeV [311], while CMS measured $\bar{s}_\ell^2 = 0.23101 \pm 0.00053$ (8 TeV) [312] and a preliminary result $\bar{s}_\ell^2 = 0.23157 \pm 0.00031$ (13 TeV) [313], and LHCb reported $\bar{s}_\ell^2 = 0.23142 \pm 0.00106$ (from both 7 and 8 TeV data, but only analyzing $\mu^+\mu^-$ final

state) [314]. Assuming that the smallest theoretical and PDF uncertainty (± 0.00024 from ATLAS [311]) is fully correlated among the five determinations, they combine to

$$\bar{s}_\ell^2 = 0.23145 \pm 0.00028 \text{ (LHC)}. \quad (10.74)$$

Combining Eqs. (10.72), (10.73), and (10.74) gives,

$$\bar{s}_\ell^2 = 0.23149 \pm 0.00013 \text{ (collider average)}. \quad (10.75)$$

10.5.4 W and Z decays

The partial decay widths for gauge bosons to decay into massless fermions $f_1\bar{f}_2$ (the numerical values include the small EW radiative corrections and final-state mass effects) are given by,

$$\Gamma(W^+ \rightarrow e^+\nu_e) = \frac{M_W^3}{12\pi v^2} = 226.29 \pm 0.04 \text{ MeV}, \quad (10.76a)$$

$$\Gamma(W^+ \rightarrow u_i\bar{d}_j) = \frac{M_W^3}{12\pi v^2} |V_{ij}|^2 \mathcal{R}_V^q = (705.3 \pm 0.4 \text{ MeV}) |V_{ij}|^2, \quad (10.76b)$$

$$\Gamma(Z \rightarrow f\bar{f}) = \frac{M_Z^3}{12\pi v^2} [\mathcal{R}_V^f \bar{g}_V^f + \mathcal{R}_A^f \bar{g}_A^f], \quad (10.76c)$$

where the result for the latter are shown in Table 10.6. Final-state QED and QCD corrections [333] to the vector and axial-vector form factors are given by,

$$\mathcal{R}_{V,A}^f = N_C \left[1 + \frac{3}{4} \left(Q_f^2 \frac{\alpha(s)}{\pi} + \frac{N_C^2 - 1}{2N_C} \frac{\alpha_s(s)}{\pi} \right) + \dots \right], \quad (10.77)$$

where $N_C = 3$ (1) is the color factor for quarks (leptons) and the dots indicate finite fermion mass effects proportional to m_f^2/s which are different for \mathcal{R}_V^f and \mathcal{R}_A^f , as well as higher-order QCD corrections [334], which are known to $\mathcal{O}(\alpha_s^4)$ [222]. For the Z boson, these include singlet contributions starting from two-loop order which are large, strongly top quark mass dependent, family universal, and flavor non-universal [335–339]. The $\mathcal{O}(\alpha^2)$ self-energy corrections from Ref. [340] are also taken into account.

For the W decay into quarks, Eq. (10.76b), only the universal massless part (non-singlet and $m_q = 0$) of the final-state QCD radiator function in \mathcal{R}_V from Eq. (10.77) is used, and the QED corrections are modified. Expressing the widths in terms of $G_F M_{W,Z}^3$ incorporates the largest radiative corrections from the running QED coupling. EW corrections to the Z widths are then taken into account through the effective couplings $\bar{g}_{V,A}^{i,2}$. Hence, in the on-shell scheme the Z widths are proportional to $\rho_i \sim 1 + \rho_t$. There is additional (negative) quadratic m_t dependence in the $Z \rightarrow b\bar{b}$ vertex corrections [341, 342] which causes $\Gamma_{b\bar{b}}$ to decrease with m_t . The dominant effect is to multiply $\Gamma_{b\bar{b}}$ by the vertex correction $1 + \delta\rho_{b\bar{b}}$, where $\delta\rho_{b\bar{b}} \sim 10^{-2}(-\frac{1}{2}m_t^2/M_Z^2 + \frac{1}{5})$. In practice, the corrections are included in $\hat{\rho}_b$ and $\hat{\kappa}_b$, as discussed in Sec. 10.5.

Starting at $\mathcal{O}(\alpha\alpha_s)$, the factorized form indicated in Eq. (10.76) is violated and corrections need to be included [343–345]. They add coherently, resulting in a sizable effect, and shift $\alpha_s(M_Z)$ when extracted from Z lineshape observables by about $+0.0007$. Similar non-factorizable corrections are also known for mixed QED-EW corrections [111, 112, 114, 346].

For three fermion families the total widths of the Z [347–351] and W [352, 353] bosons are predicted to be,

$$\Gamma_Z = 2.4940 \pm 0.0009 \text{ GeV}, \quad \Gamma_W = 2.0892 \pm 0.0008 \text{ GeV}. \quad (10.78)$$

The uncertainties in these predictions are almost entirely induced by the parametric error in $\alpha_s(M_Z) = 0.1187 \pm 0.0017$ from the global fit. These predictions can be compared with the experimental results, $\Gamma_Z = 2.4955 \pm 0.0023 \text{ GeV}$ [288, 332] and $\Gamma_W = 2.137 \pm 0.032 \text{ GeV}$ in (10.78). Note regarding the latter that in this Section we include the very recent result from ATLAS [295] and an updated value of the Tevatron result [299],

Table 10.6: Results derived from Table 10.5 and the corresponding covariance matrices [288, 332], and the SM predictions for the partial and total Z decay widths [in MeV]. In the (second) third column lepton universality is (not) assumed.

Quantity	Value	Value (universal)	Standard Model
$\Gamma_{e^+e^-}$	83.87 ± 0.12	83.942 ± 0.085	83.955 ± 0.009
$\Gamma_{\mu^+\mu^-}$	83.95 ± 0.18	83.941 ± 0.085	83.955 ± 0.009
$\Gamma_{\tau^+\tau^-}$	84.03 ± 0.21	83.759 ± 0.085	83.772 ± 0.009
Γ_{inv}	498.9 ± 2.5	500.5 ± 1.5	501.435 ± 0.045
$\Gamma_{u\bar{u}}$	—	—	299.87 ± 0.20
$\Gamma_{c\bar{c}}$	300.3 ± 5.3	300.0 ± 5.2	299.81 ± 0.20
$\Gamma_{d\bar{d}}, \Gamma_{s\bar{s}}$	—	—	382.75 ± 0.14
$\Gamma_{b\bar{b}}$	377.4 ± 1.3	377.0 ± 1.2	375.73 ∓ 0.18
Γ_{had}	1744.8 ± 2.6	1743.2 ± 1.9	1740.88 ± 0.86
Γ_Z	2495.5 ± 2.3	2495.5 ± 2.3	2494.00 ± 0.87

which differ from the treatment in the Gauge & Higgs Bosons Particle Listings and Section 54 on the “Mass and Width of the W Boson” in this *Review*. The hadronic branching ratio of the W boson, $\mathcal{B}(W \rightarrow \text{hadrons})$ has been measured by both LEP 2 [294] and CMS [300]. The measurements of the total and partial widths are generally in good agreement with the SM. The exceptions are Γ_W , which is 1.5σ larger than the SM prediction, and the branching ratio $W \rightarrow \tau + \nu_\tau$ from LEP 2, which is 2.6σ larger than the electron-muon average [294]¹⁷.

The invisible decay width, $\Gamma_{\text{inv}} = \Gamma_Z - \Gamma_{e^+e^-} - \Gamma_{\mu^+\mu^-} - \Gamma_{\tau^+\tau^-} - \Gamma_{\text{had}}$, can be used to determine the number of neutrino flavors, N_ν , much lighter than $M_Z/2$. The hadronic peak cross-section, and therefore the extracted Γ_{had} , depends strongly on the knowledge of the LEP 1 luminosity derived from small-angle Bhabha scattering. However, the prediction for the Bhabha cross-section was recently found to be overestimated, and consequently the luminosity underestimated [332]. The updated analysis involved an improved Z lineshape fit, significantly reducing σ_{had} , while slightly increasing Γ_Z , with the result, $N_\nu = 2.9963 \pm 0.0074$ [332]. In practice, we determine N_ν by allowing it as an additional fit parameter and obtain,

$$N_\nu = 3.0025 \pm 0.0061, \quad (10.79)$$

which is now in perfect agreement with the observed number of fermion generations and $N_\nu = 3$ (a 1.3σ deviation was observed in the 2018 edition of this *Review* before including the correction in the luminosity determination).

10.6 Global fit results

In this section, we present the results of global fits, subject to the experimental data and theoretical constraints discussed in Section 10.2–10.5. For earlier analyses, see Refs. [83, 288, 355–358] and previous editions of this *Review*. Recent global fits by other groups [359–361] find a similar pattern of agreement as discussed below, with some discrepancies beyond the 2σ level for a few quantities entering into the fit. They differ, however, from the fit presented here by (i) not including inputs from low-energy parity-violation data and the muon magnetic moment¹⁸; (ii) the set of input data; (iii) the implementation of radiative corrections; and (iv) the fitting tools used.

For the results in this *Review*, the values for m_t (see Sec. 10.2.3), M_H [364, 365], Γ_H [308, 366], M_W [295, 298], Γ_W [294, 295, 299], $\mathcal{B}(W \rightarrow \text{hadrons})$ [294, 300], the weak charges of the electron [166], the proton [167], cesium [178, 179] and thallium [180, 181], the weak mixing angle extracted from eDIS [156], $\nu_\mu(\bar{\nu}_\mu)$ -e scattering [137–139], the τ lifetime, and the μ anomalous magnetic moment [367] are listed in Table 10.4. Likewise, Table 10.5 summa-

rizes the principal Z pole observables, where the LEP 1 averages of the ALEPH, DELPHI, L3, and OPAL results include common systematic uncertainties and correlations [288, 332]. The heavy flavor results [288, 323] of LEP 1 and SLD are based on common inputs, and are thus correlated, as well.

Also shown in both tables are the SM predictions for the values of M_Z , $\alpha_s(M_Z)$, $\Delta\alpha_{\text{had}}^{(3)}$ and the heavy quark masses shown in Table 10.7. The predictions result from a global least-square (χ^2) fit to all data using the minimization package MINUIT [368] and the EW library GAPP [34]. In most cases, we treat all input errors (the uncertainties of the values) as Gaussian. The reason is not that we assume that theoretical and systematic errors are intrinsically bell-shaped (which they are not) but because in most cases the input errors are either dominated by the statistical components or they are combinations of many different (including statistical) error sources, which should yield approximately Gaussian *combined* errors by the large number theorem. An exception is the theory dominated error on the τ lifetime, which we recalculate in each χ^2 -function call since it depends itself on α_s . Sizes and shapes of the output errors (the uncertainties of the predictions and the SM fit parameters) are fully determined by the fit, and 1σ errors are defined to correspond to $\Delta\chi^2 = \chi^2 - \chi_{\text{min}}^2 = 1$, and do not necessarily correspond to the 68.3% probability range or the 39.3% probability contour (for 2 parameters).

The agreement is generally very good. Despite the few discrepancies addressed in the following, the global electroweak fit describes the data well, with a very good $\chi^2/\text{d.o.f.} = 49.5/47$. The probability of a larger χ^2 is 37%, and only $g_\mu - 2$ is currently showing a larger (3.2σ) conflict. In addition, A_{LR}^0 (SLD) from hadronic final states, $A_{FB}^{(0,b)}$ (LEP 1), Γ_W (ATLAS) and $Q_W(\text{Cs})$ deviate at the 2σ level. g_L^2 from NuTeV is nominally in conflict with the SM, as well, but the precise status is unresolved (see Sec. 10.3.1). Also, there is currently no understanding as to why the M_W value reported by the CDF collaboration is significantly larger than the findings by other groups. In this context, we refer to Sec. 10.8 for a discussion of fits involving alternative data inputs. We also emphasize that there are a number of discrepancies among individual measurements of certain quantities, as discussed in previous sections, but that they are not reflected in the overall χ^2 of the fit as only the corresponding combinations are used as constraints.

A_b can be extracted from $A_{FB}^{(0,b)}$ when $A_e = 0.1501 \pm 0.0016$ is taken from a fit to leptonic asymmetries (using lepton universality). The result, $A_b = 0.885 \pm 0.017$, is 2.9σ below the SM prediction¹⁹ and also 1.4σ below $A_b = 0.923 \pm 0.020$ obtained from $A_{LR}^{FB}(b)$ at SLD. Thus, it appears that at least some of the problem in A_b is due to a statistical fluctuation or other experimental effect in one of the asymmetries. Note, however, that the uncertainty in $A_{FB}^{(0,b)}$ is strongly statistics dominated. The combined value, $A_b = 0.901 \pm 0.013$ deviates by 2.6σ .

¹⁷ W -boson branching ratio measurements from CMS and ATLAS are in good agreement with lepton universality and slightly more precise than LEP-2 [300, 354].

¹⁸Refs. [51, 362, 363] report on specialized fits to study the impact of a shift of the hadronic vacuum polarization in the running of the electromagnetic coupling, where such shift is motivated by the apparent mismatch of the direct measurement and the data-driven SM prediction of $g_\mu - 2$, but they do not include $g_\mu - 2$ itself in the fit.

¹⁹Alternatively, one can use $A_\ell = 0.1481 \pm 0.0027$, which is from LEP 1 alone and in excellent agreement with the SM, and obtain $A_b = 0.897 \pm 0.022$ which is 1.7σ low. This illustrates that some of the discrepancy is related to the one in A_{LR} .

Table 10.7: Principal electroweak SM fit result including mutual correlations.

M_Z [GeV]	91.1884 ± 0.0019	1.00	-0.08	0.00	0.00	0.02	0.02
$\widehat{m}_t(\widehat{m}_t)$ [GeV]	163.18 ± 0.54	-0.08	1.00	0.00	-0.12	-0.23	0.04
$\widehat{m}_b(\widehat{m}_b)$ [GeV]	4.180 ± 0.008	0.00	0.00	1.00	0.19	-0.02	0.01
$\widehat{m}_c(\widehat{m}_c)$ [GeV]	1.274 ± 0.009	0.00	-0.12	0.19	1.00	0.48	0.01
$\alpha_s(M_Z)$	0.1187 ± 0.0017	0.02	-0.23	-0.02	0.48	1.00	-0.04
$\Delta\alpha_{\text{had}}^{(3)}(2 \text{ GeV})$	0.00608 ± 0.00004	0.02	0.04	0.01	0.01	-0.04	1.00

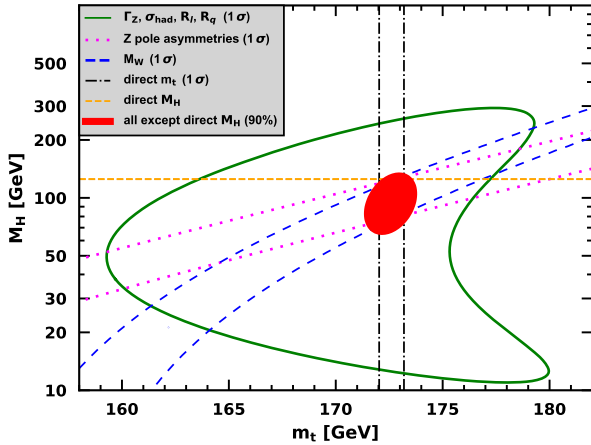


Figure 10.4: Fit result and one-standard-deviation (approximately 39.35% for the closed contours and 68% for the others) uncertainties in M_H as a function of m_t for various inputs, and the 90% CL region ($\Delta\chi^2 = 4.605$) allowed by all data. $\alpha_s(M_Z) = 0.1187$ is assumed except for the fits including the Z lineshape. The width of the horizontal dashed band is not visible on the scale of the plot.

The left-right asymmetry, $A_{LR}^0 = 0.15138 \pm 0.00216$ [315], from hadronic decays at SLD, differs by 2.3σ from the SM expectation of 0.1463 ± 0.0003 . The combined value of $A_\ell = 0.1513 \pm 0.0021$ from SLD (using lepton-family universality and including correlations) is also 2.4σ above the SM prediction; but there is experimental agreement between this SLD value and the LEP 1 value, $A_\ell = 0.1481 \pm 0.0027$, obtained from a fit to $A_{FB}^{(0,\ell)}$, $A_e(\mathcal{P}_\tau)$, and $A_\tau(\mathcal{P}_\tau)$, again assuming universality.

The observables in Table 10.4 and Table 10.5, as well as some other less precise observables, are used in the global fits described below. In all fits, the errors include full statistical, systematic, and theoretical uncertainties. The correlations from the LEP 1 lineshape and τ polarization measurements, the LEP/SLD heavy flavor observables, the SLD lepton asymmetries, and the ν - e scattering observables, are included. The theoretical correlations between $\Delta\alpha_{\text{had}}^{(5)}$, \widehat{s}_0^2 , and $g_\mu - 2$, and between the M_W and Γ_W extractions from the LHC and the Tevatron, are also accounted for.

The electroweak data allow a simultaneous determination of M_Z , m_t , and $\alpha_s(M_Z)$. The direct measurements of M_H at the LHC [364, 365] have reached a precision that the global fit result for M_H coincides with the constraint in Eq. (10.66) with negligible correlations with the other fit parameters. \widehat{m}_c , \widehat{m}_b , and $\Delta\alpha_{\text{had}}^{(3)}$ are also allowed to float in the fits, subject to the theoretical constraints [33, 58] described in Sec. 10.2, and are correlated with α_s , which in turn is determined mainly through R_ℓ , Γ_Z , σ_{had} , and τ_τ , but Γ_W and $\mathcal{B}(W \rightarrow \text{hadrons})$ also have an impact. The global fit to all data, including the hadron collider m_t average in Eq. (10.21), yields the results in Table 10.7, while those for the weak mixing angle in various schemes are summarized in Table 10.2.

Removing the kinematic constraint on M_H from LHC gives the

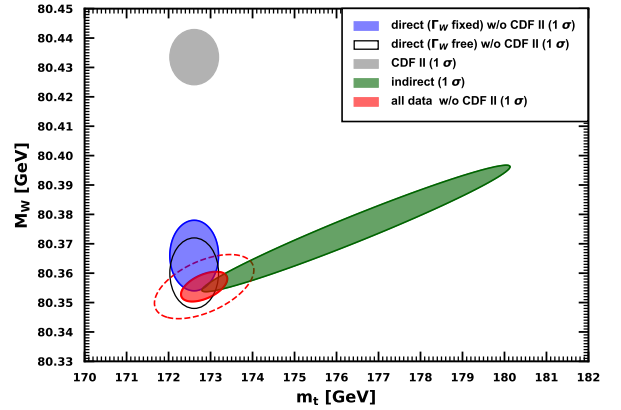


Figure 10.5: One-standard-deviation (39.35%) regions in M_W as a function of m_t for the indirect data from the fit (green), the direct data for m_t and M_W without the CDF II measurement (blue and black contour, respectively, for two differently treatments of the W -boson width), and the combination thereof (red). For the combination, the 90% CL region ($\Delta\chi^2 = 4.605$) is also shown as a red dashed contour. The grey region uses only the M_W value from CDF II. Compared to previous editions of this *Review*, this plot additionally includes theoretical uncertainties and subleading parameter dependencies.

loop-level determination from the precision data,

$$M_H = 97_{-16}^{+18} \text{ GeV} , \quad (10.80)$$

which is 1.6σ below the value in Eq. (10.66). The latter is just inside the 90% central confidence range,

$$71 \text{ GeV} < M_H < 126 \text{ GeV} . \quad (10.81)$$

It is instructive to study the effect of doubling the uncertainty in Eq. (10.14) on the loop-level determination of the Higgs boson mass. The result, $M_H = 94_{-16}^{+19} \text{ GeV}$, reduces the small tension compared to Eq. (10.80) only slightly (1.5σ) and demonstrates that the uncertainty in $\Delta\alpha_{\text{had}}$ is currently of only secondary importance. In fact, even removing $\Delta\alpha_{\text{had}}^{(3)}(2 \text{ GeV})$ altogether as a fit constraint still gives the bound $M_H < 135 \text{ GeV}$ at the 95% CL. The hadronic contribution to $\alpha(M_Z)$ is correlated with $g_\mu - 2$ (see Sec. 10.4). The measurement of the latter is higher than the SM prediction, and its inclusion in the fit favors a larger $\alpha(M_Z)$ and a lower M_H from the precision data (currently by 3.2 GeV).

Alternatively, one can carry out a fit without including the direct constraint from the hadron colliders. One obtains $m_t = 175.2 \pm 1.8 \text{ GeV}$, which is 1.4σ higher than the collider average $m_t = 172.61 \pm 0.58 \text{ GeV}$, and a reflection of the low value in Eq. (10.80). (The indirect prediction is for the $\overline{\text{MS}}$ mass definition, $\widehat{m}_t(\widehat{m}_t) = 165.4 \pm 1.7 \text{ GeV}$, which is in the end converted to the pole mass.) Finally, one can remove the explicit M_W and Γ_W constraints from the global fit and use $M_H = 125.10 \pm 0.09 \text{ GeV}$ to obtain $M_W = 80.353 \pm 0.006 \text{ GeV}$, in very good agreement with the experimental measurements except the one from CDF II. The situation is summarized in Fig. 10.4 and in Fig. 10.5, showing the m_t dependence of M_H and M_W , respectively.

Table 10.8: Values of \widehat{s}_Z^2 , s_W^2 , α_s , m_t and M_H for various data sets. In the fit to the LHC data, the α_s constraint is from an NNLO analysis of the transverse momentum distribution of Z bosons [369]. For the Tevatron fit we use the α_s result from the inclusive jet cross-section at $D\bar{O}$ [370] and add the M_W result from CDF [289] as adjusted in Ref. [298].

data set	\widehat{s}_Z^2	s_W^2	$\alpha_s(M_Z)$	m_t [GeV]	M_H [GeV]
all data	0.23129(4)	0.22348(10)	0.1187(17)	172.9 ± 0.6	125
all data except M_H	0.23118(8)	0.22327(18)	0.1190(17)	172.6 ± 0.6	97_{-16}^{+18}
all data except M_Z	0.23121(6)	0.22346(10)	0.1187(17)	172.6 ± 0.6	125
all data except M_W, Γ_W	0.23130(4)	0.22353(11)	0.1188(17)	172.7 ± 0.6	125
all data except m_t	0.23123(6)	0.22324(20)	0.1191(17)	175.2 ± 1.8	125
$M_{H,Z} + \Gamma_{H,Z} + m_t$	0.23134(8)	0.22361(16)	0.1221(45)	172.6 ± 0.6	125
LHC	0.23122(8)	0.22349(11)	0.1183 (9)	172.3 ± 0.6	125
Tevatron	0.23085(13)	0.22254(28)	0.1159(45)	174.4 ± 0.8	67_{-20}^{+25}
LEP 1 + LEP 2	0.23138(19)	0.22350(46)	0.1233(29)	177 ± 11	173_{-96}^{+237}
LEP 1 + SLD	0.23116(17)	0.22340(58)	0.1221(27)	169 ± 10	71_{-33}^{+87}
SLD + $M_Z + \Gamma_Z + m_t$	0.23064(29)	0.22224(54)	0.1196(52)	172.6 ± 0.6	31_{-22}^{+27}
$A_{FB}^{(b,c)} + M_Z + \Gamma_Z + m_t$	0.23190(30)	0.22492(70)	0.1279(49)	172.6 ± 0.6	306_{-111}^{+164}
$M_{W,Z} + \Gamma_{W,Z} + m_t$	0.23119(11)	0.22329(23)	0.1212(42)	172.6 ± 0.6	96_{-20}^{+23}
low energy + $M_{H,Z}$	0.23173(94)	0.2252(35)	0.1172(18)	159 ± 29	125

Table 10.9: Values of model-independent neutral-current parameters, compared with the SM predictions, where the uncertainties in the latter are $\lesssim 0.0001$, throughout.

Quantity	Experimental Value	Standard Model	Correlation
$g_{LV}^{\nu e}$	-0.040 ± 0.015	-0.0395	-0.05
$g_{LA}^{\nu e}$	-0.507 ± 0.014	-0.5063	
$g_{AV}^{eu} + 2g_{AV}^{ed}$	0.4927 ± 0.0031	0.4950	-0.88 0.20
$2g_{AV}^{eu} - g_{AV}^{ed}$	-0.7165 ± 0.0068	-0.7189	-0.22
$2g_{VA}^{eu} - g_{VA}^{ed}$	-0.13 ± 0.06	-0.0944	
g_{VA}^{ee}	0.0190 ± 0.0027	0.0224	

The weak mixing angle can be determined from Z pole observables, M_W , and a variety of neutral-current processes spanning a very wide Q^2 range. The results (for older low energy neutral-current data see Refs. [355–358], as well as earlier editions of this *Review*) shown in Table 10.8 are in reasonable agreement with each other, indicating the quantitative success of the SM. One of the largest discrepancies is the value $\widehat{s}_Z^2 = 0.23064 \pm 0.00028$ from the SLD asymmetries (combined with M_Z , Γ_Z , and m_t), which is 2.3σ below the value 0.23129 ± 0.00004 from the global fit to all data. On the other hand, $\widehat{s}_Z^2 = 0.23176 \pm 0.00027$ from $A_{FB}^{(0,b)}$ and $A_{FB}^{(0,c)}$ is 1.7σ high.

The extracted Z pole value of $\alpha_s(M_Z)$ is based on a formula with negligible theoretical uncertainty if one assumes the exact validity of the SM. One should keep in mind, however, that this value, $\alpha_s(M_Z) = 0.1221 \pm 0.0027$, which increased after the updated analysis in Ref. [332], is very sensitive to certain types of new physics such as non-universal vertex corrections. A fit to the wider set of high-energy data, *i.e.*, including W -decays but without τ_τ and $g_\mu - 2$, returns $\alpha_s(M_Z) = 0.1211 \pm 0.0025$. In contrast, the value derived from τ decays, $\alpha_s(M_Z) = 0.1171_{-0.0017}^{+0.0018}$, is theory dominated but less sensitive to new physics. The agreement between these values is only marginal, but the latter does agree well with the averages deduced from heavy quarkonia spectroscopy (0.1181 ± 0.0037), DIS and global PDF fits (0.1161 ± 0.0022), hadronic final states of e^+e^- annihilations (0.1189 ± 0.0037), hadron colliders (0.1168 ± 0.0027), as well as lattice QCD simulations (0.1184 ± 0.0008). For more details, other determinations, and references, see Section 9 on “Quantum Chromodynamics” in this *Review*. We also provide the values, computed with five-loop beta functions and four-loop matching,

$$\alpha_s^{(4)}(m_\tau) = 0.325 \pm 0.014, \quad (10.82)$$

$$\alpha_s^{(5)}(M_W) = 0.1210 \pm 0.0017, \quad (10.83)$$

$$\alpha_s^{(5)}(M_H) = 0.1132 \pm 0.0015, \quad (10.84)$$

$$\alpha_s^{(6)}(\widehat{m}_t) = 0.1090 \pm 0.0014, \quad (10.85)$$

to be used in precision calculations.

Using $\alpha(M_Z)$ and \widehat{s}_Z^2 as inputs, one can predict $\alpha_s(M_Z)$ assuming grand unification. One finds $\alpha_s(M_Z) = 0.13 \pm 0.01$ [371, 372] for the simplest theories based on the minimal supersymmetric extension of the SM, where the uncertainty is from the unknown particle thresholds. This is slightly larger, but consistent with $\alpha_s(M_Z) = 0.1187 \pm 0.0017$ from our fit and most other determinations, while minimal non-supersymmetric theories predict much lower and excluded values (see Section 93 on “Grand Unified Theories” in this *Review*).

Most of the parameters relevant to ν -hadron, ν - e , e -hadron, and e - e processes are determined uniquely and precisely from the data in “model-independent” fits, *i.e.*, fits allowing for an arbitrary EW gauge theory. The values for the parameters defined in Eq. (10.29) are given in Table 10.9 along with the predictions of the SM. The agreement is very good. (The ν -hadron results including NuTeV [151] and other ν -DIS data can be found in the 2006 edition of this *Review*, and fits with modified NuTeV constraints in the 2008 and 2010 editions.)

10.7 Constraints on new physics

The masses and decay properties of the electroweak bosons and low energy data can be used to search for and set limits on deviations from the SM. We will mainly discuss the effects of exotic particles (with heavy masses $M_{\text{new}} \gg M_Z$ in an expansion in M_Z/M_{new}) on the gauge boson self-energies. (Brief remarks are made on new physics which is not of this type.) Most of the effects on precision measurements can be described by three gauge self-energy parameters S , T , and U . We will define these, as well as

the related parameters ρ_0 and $\widehat{\epsilon}_i$, to arise from new physics only. In other words, they are equal to zero ($\rho_0 = 1$) exactly in the SM, and do not include any (loop induced) contributions that depend on m_t or M_H , which are treated separately. Our treatment differs from most of the original papers.

The dominant effect of many extensions of the SM can be described by the ρ_0 parameter,

$$\rho_0 \equiv \frac{M_W^2}{M_Z^2 \widehat{c}_Z^2 \widehat{\rho}}, \quad (10.86)$$

which describes new sources of SU(2) breaking that cannot be accounted for by the SM Higgs doublet or by m_t effects. $\widehat{\rho}$ is calculated as in Eq. (10.26) assuming the validity of the SM. In the presence of $\rho_0 \neq 1$, Eq. (10.86) generalizes the second Eq. (10.26) while the first remains unchanged. Provided that the new physics which yields $\rho_0 \neq 1$ is a small perturbation which does not significantly affect other radiative corrections, ρ_0 can be regarded as a phenomenological parameter which multiplies G_F in Eqs. (10.29) and (10.52), as well as Γ_Z in Eq. (10.76c). From the global fit,

$$\rho_0 = 1.00031 \pm 0.00019, \quad (10.87a)$$

$$\alpha_s(M_Z) = 0.1189 \pm 0.0017, \quad (10.87b)$$

where as before the uncertainty is from the experimental inputs and includes an estimate of the error from unknown higher-order electroweak corrections. The result in Eq. (10.87a) is 1.6 σ above the SM expectation, $\rho_0 = 1$, and not unrelated to the small tension observed in the context with Eq. (10.80). It can be used to constrain higher-dimensional Higgs representations to have vacuum expectation values of less than a few percent of those of the doublets. Indeed, the relation between M_W and M_Z is modified if there are Higgs multiplets with weak isospin $> 1/2$ and significant vacuum expectation values. For a general (charge-conserving) Higgs structure,

$$\rho_0 = \frac{\sum_i [t_i(t_i + 1) - t_{3i}^2] |v_i|^2}{2 \sum_i t_{3i}^2 |v_i|^2}, \quad (10.88)$$

where v_i is the expectation value of the neutral component of a Higgs multiplet with weak isospin t_i and third component t_{3i} . In order to calculate to higher orders in such theories one must define a set of four fundamental renormalized parameters which one may conveniently choose to be α , G_F , M_Z , and M_W , since M_W and M_Z are directly measurable. Then \widehat{s}_Z^2 and ρ_0 can be considered dependent parameters.

Eq. (10.87a) can also be used to constrain other types of new physics. For example, non-degenerate multiplets of heavy fermions or scalars break the vector part of weak SU(2) and lead to a decrease in the value of M_Z/M_W . Each non-degenerate SU(2) doublet $\begin{pmatrix} f_1 \\ f_2 \end{pmatrix}$ yields a positive contribution to ρ_0 [373–375] of

$$\frac{N_C G_F}{8\sqrt{2}\pi^2} \Delta m^2, \quad (10.89)$$

where

$$\Delta m^2 \equiv m_1^2 + m_2^2 - \frac{4m_1^2 m_2^2}{m_1^2 - m_2^2} \ln \frac{m_1}{m_2} \geq (m_1 - m_2)^2, \quad (10.90)$$

and $N_C = 1$ (3) for color singlets (triplets). Eq. (10.87a) taken together with Eq. (10.89) implies the following constraint on the mass splitting at the 90% CL,

$$(2 \text{ GeV})^2 < \sum_i \frac{N_C^i}{3} \Delta m_i^2 < (44 \text{ GeV})^2, \quad (10.91)$$

where the sum runs over all new-physics doublets, for example fourth-family quarks or leptons, $\begin{pmatrix} t' \\ b' \end{pmatrix}$ or $\begin{pmatrix} \nu' \\ \ell' \end{pmatrix}$, vector-like fermion doublets (which contribute to the sum in Eq. (10.91) with an extra factor of 2), and scalar doublets such as $\begin{pmatrix} \hat{t} \\ \hat{b} \end{pmatrix}$ in Supersymmetry (in the absence of L - R mixing).

Non-degenerate multiplets usually imply $\rho_0 > 1$. Similarly, heavy Z' bosons decrease the prediction for M_Z due to mixing and generally lead to $\rho_0 > 1$ [376]. On the other hand, extra Higgs doublets participating in spontaneous symmetry breaking [377–379] or heavy lepton doublets involving Majorana neutrinos [380], both of which have more complicated expressions, and the v_i of higher-dimensional Higgs representations can contribute to ρ_0 with either sign.

A number of authors [381–383] have considered the general effects on neutral-current, Z and W boson observables of various types of heavy (*i.e.*, $M_{\text{new}} \gg M_Z$) physics which contribute to the W and Z self-energies but which do not have any direct coupling to the ordinary fermions (an alternative formulation is given by Ref. [384]). In addition to non-degenerate multiplets, which break the vector part of weak SU(2), these include heavy degenerate multiplets of chiral fermions which break the axial generators.

Such effects can be described by just three parameters, S , T , and U [385], at the (EW) one-loop level²⁰. T is proportional to the difference between the W and Z self-energies at $Q^2 = 0$ (*i.e.*, vector SU(2)-breaking), while S ($S + U$) is associated with the difference between the Z (W) self-energy at $Q^2 = M_{Z,W}^2$ and $Q^2 = 0$ (axial SU(2)-breaking). Denoting the contributions of new physics to the various self-energies by Π_{ij}^{new} , we have

$$\widehat{\alpha}(M_Z)T \equiv \frac{\Pi_{WW}^{\text{new}}(0)}{M_W^2} - \frac{\Pi_{ZZ}^{\text{new}}(0)}{M_Z^2}, \quad (10.92a)$$

$$\begin{aligned} \frac{\widehat{\alpha}(M_Z)}{4\widehat{s}_Z^2\widehat{c}_Z^2}S &\equiv \frac{\Pi_{ZZ}^{\text{new}}(M_Z^2) - \Pi_{ZZ}^{\text{new}}(0)}{M_Z^2} \\ &\quad - \frac{\widehat{c}_Z^2 - \widehat{s}_Z^2}{\widehat{c}_Z\widehat{s}_Z} \frac{\Pi_{Z\gamma}^{\text{new}}(M_Z^2)}{M_Z^2} - \frac{\Pi_{\gamma\gamma}^{\text{new}}(M_Z^2)}{M_Z^2}, \end{aligned} \quad (10.92b)$$

$$\begin{aligned} \frac{\widehat{\alpha}(M_Z)}{4\widehat{s}_Z^2}(S+U) &\equiv \frac{\Pi_{WW}^{\text{new}}(M_W^2) - \Pi_{WW}^{\text{new}}(0)}{M_W^2} \\ &\quad - \frac{\widehat{c}_Z}{\widehat{s}_Z} \frac{\Pi_{Z\gamma}^{\text{new}}(M_Z^2)}{M_Z^2} - \frac{\Pi_{\gamma\gamma}^{\text{new}}(M_Z^2)}{M_Z^2}. \end{aligned} \quad (10.92c)$$

S , T , and U are defined with a factor proportional to $\widehat{\alpha}$ removed, so that they are expected to be of order unity in the presence of new physics. In the $\overline{\text{MS}}$ scheme as defined in Ref. [85], the last two terms in Eqs. (10.92b) and (10.92c) can be omitted, as was done in some earlier editions of this *Review*. These parameters are related to other parameter sets, S_i [85], $\widehat{\epsilon}_i$ [389], and h_i [390], by

$$T = h_V = \frac{\widehat{\epsilon}_1}{\widehat{\alpha}(M_Z)}, \quad (10.93a)$$

$$S = h_{AZ} = S_Z = 4\widehat{s}_Z^2 \frac{\widehat{\epsilon}_3}{\widehat{\alpha}(M_Z)}, \quad (10.93b)$$

$$U = h_{AW} - h_{AZ} = S_W - S_Z = -4\widehat{s}_Z^2 \frac{\widehat{\epsilon}_2}{\widehat{\alpha}(M_Z)}. \quad (10.93c)$$

A heavy non-degenerate multiplet of fermions or scalars contributes positively to T as

$$\rho_0 - 1 = \frac{1}{1 - \widehat{\alpha}(M_Z)T} - 1 \approx \widehat{\alpha}(M_Z)T, \quad (10.94)$$

where $\rho_0 - 1$ is given in Eq. (10.89). The effects of non-standard Higgs representations cannot be separated from heavy non-degenerate multiplets unless the new physics has other consequences, such as vertex corrections. Most of the original papers defined T to include the effects of loops only. However, we

²⁰Three additional parameters are needed if the new physics scale is comparable to M_Z [386]. Further generalizations, including effects relevant to LEP 2 and Drell-Yan production at the LHC, are described in Refs. [387] and [388], respectively.

will redefine T to include all new sources of SU(2) breaking, including non-standard Higgs, so that T and ρ_0 are equivalent by Eq. (10.94).

A multiplet of heavy degenerate chiral fermions yields

$$S = \frac{N_C}{3\pi} \sum_i (t_{3i}^L - t_{3i}^R)^2, \quad (10.95)$$

where $t_{3i}^{L,R}$ is the 3rd component of weak isospin of the left-(right)-handed component of fermion i . For example, a heavy degenerate ordinary or mirror family would contribute $2/3\pi$ to S . In models with warped extra dimensions [391], sizeable corrections to the S parameter are generated through mixing between the SM gauge bosons and their Kaluza-Klein (KK) excitations, and one finds $S \approx 30 v^2 M_{KK}^{-2}$ [392], where M_{KK} is the mass scale of the KK gauge bosons. Large positive values of S can also be generated in models with dynamical electroweak symmetry breaking, where the Higgs boson is composite. In simple composite Higgs models, the dominant contribution stems from heavy spin-1 resonances of the strong dynamics leading to $S \approx 4\pi v^2 (M_V^{-2} + M_A^{-2})$, where $M_{V,A}$ are the masses of the lightest vector and axial-vector resonances, respectively [393].

Negative values of S are possible, for example, in composite Higgs models with larger gauge group representations [394,395], or from loops involving scalars or Majorana particles [396–398]. The simplest origin of $S < 0$ would probably be an additional heavy Z' boson [376]. Supersymmetric extensions of the SM [399,400] generally give very small effects. For more details and references, see Refs. [401–410] and Sections 88,89 on ‘‘Supersymmetry’’ in this Review. Most simple types of new physics yield $U = 0$, although there are counter-examples, such as the effects of anomalous triple gauge vertices [389].

The SM expressions for observables are replaced by,

$$M_Z^2 = M_{Z0}^2 \frac{1 - \hat{\alpha}(M_Z)T}{1 - G_F M_{Z0}^2 S / 2\sqrt{2}\pi}, \quad (10.96a)$$

$$M_W^2 = M_{W0}^2 \frac{1}{1 - G_F M_{W0}^2 (S + U) / 2\sqrt{2}\pi}, \quad (10.96b)$$

where M_{Z0} and M_{W0} are the SM expressions (as functions of m_t and M_H) in the $\overline{\text{MS}}$ scheme. Furthermore,

$$\Gamma_Z = \frac{M_Z^3 \beta_Z}{1 - \hat{\alpha}(M_Z)T}, \quad (10.97a)$$

$$\Gamma_W = M_W^3 \beta_W, \quad (10.97b)$$

$$A_i = \frac{A_{i0}}{1 - \hat{\alpha}(M_Z)T}, \quad (10.97c)$$

where $\beta_{Z,W}$ are the SM expressions for the reduced widths Γ_{Z0}/M_{Z0}^3 and Γ_{W0}/M_{W0}^3 , M_Z and M_W are the physical masses, and A_i (A_{i0}) is a neutral-current amplitude (in the SM).

The data allows for a simultaneous determination of M_H and m_t (from the hadron colliders), S (from M_Z), T (mainly from Γ_Z), U (from M_W), $\hat{s}_Z^2 = 0.23113 \pm 0.00013$ (from the Z pole asymmetries), and $\alpha_s(M_Z) = 0.1191 \pm 0.0018$ (mostly from R_ℓ , σ_{had} , and τ_r), giving,

$$S = -0.04 \pm 0.10, \quad (10.98a)$$

$$T = 0.01 \pm 0.12, \quad (10.98b)$$

$$U = -0.01 \pm 0.09, \quad (10.98c)$$

where the correlations among the SM parameters are similar to those in Table 10.7, and where the uncertainties are from unknown higher orders in the SM predictions and the inputs. The parameters in Eq. (10.98), which by definition are due to new physics only, are in excellent agreement with the SM values of zero. Fixing $U = 0$, which is motivated by the fact that U is suppressed by an additional factor M_{new}^2/M_Z^2 compared to S and T [411],

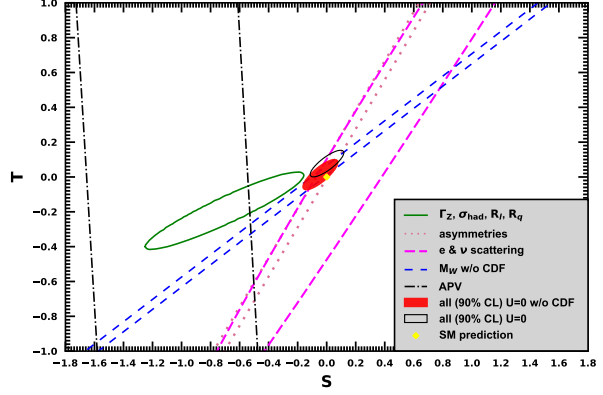


Figure 10.6: 1σ constraints (39.35% for the closed contours and 68% for the others) on S and T (for $U = 0$) from various inputs combined with M_Z . S and T represent the contributions of new physics only. Data sets not involving M_W or Γ_W are insensitive to U . With the exception of the fit to all data, we fix $\alpha_s = 0.1187$. The yellow dot indicates the Standard Model values $S = T = 0$. The fits to all data are at the 90% CL, with the open black ellipse corresponding to the alternative scenario discussed in Sec. 10.8, *i.e.* including the M_W result from CDF.

greatly improves the precision on S and particularly T ,

$$S = -0.05 \pm 0.07, \quad (10.99a)$$

$$T = 0.00 \pm 0.06. \quad (10.99b)$$

Using Eq. (10.94), the value of ρ_0 corresponding to T in Eq. (10.98b) is 1.0001 ± 0.0009 , while the one corresponding to Eq. (10.99b) is 1.0000 ± 0.0005 . Thus, the multi-parameter fits are consistent with $\rho_0 = 1$, in contrast to the fit with $S = U = 0$ in Eq. (10.87a). There is a strong correlation (93%) between the S and T parameters. The U parameter is -70% (-87%) anti-correlated with S (T). The allowed regions in S – T (for $U = 0$) are shown in Fig. 10.6. From Eqs. (10.98) one obtains $S \leq 0.11$ and $T \leq 0.20$ at 95% CL, where the former puts the constraint $M_{KK} \gtrsim 4$ TeV on the masses of KK gauge bosons in warped extra dimensions. In minimal composite Higgs models, the bound on S requires $M_V \gtrsim 4.8$ TeV, which is obtained from a one-sided 95% CL bound on $S > 0$ for $T = 0$ and using Weinberg sum rules [412]. However, this constraint can be relaxed, *e.g.*, if the fermionic sector is also allowed to be partially composite [413,414] and in soft-wall models [415].

The S parameter can also be used to constrain the number of fermion families, *under the assumption* that there are no new contributions to T or U and therefore that any new families are degenerate; then an extra generation of SM fermions is excluded with almost 9σ confidence, corresponding to $N_F = 2.75 \pm 0.14$. This can be compared to the fit to the number of light neutrinos given in Eq. (10.79), $N_\nu = 3.0025 \pm 0.0061$, but the S parameter fits are valid even for a very heavy fourth family neutrino. Allowing T to vary as well, the constraint on a fourth family is weaker [416]. However, a heavy fourth family would increase the Higgs production cross-section through gluon fusion by a factor of about 9 [417], which is in considerable tension with the observed Higgs signal at the LHC [418]. Combining the limits from electroweak precision data with the measured Higgs production rate and limits from direct searches for heavy quarks [419], a fourth family of chiral fermions is now excluded by more than five standard deviations [420,421]. Similar remarks apply to a heavy mirror family [422] involving right-handed SU(2) doublets and left-handed singlets. In contrast, new doublets that receive most of their mass from a different source than the Higgs vacuum expectation value, such as vector-like fermion doublets or scalar doublets in Supersymmetry, give small or no contribution to S , T , U , and the Higgs production cross-section and are therefore still allowed. Partial or complete vector-like fermion families are predicted in

many Grand Unified Theories [423] (see Section 93 on “Grand Unified Theories” in this *Review*), and many other models including supersymmetric and superstring inspired ones [424–427].

As discussed in Sec. 10.6, there is a 3.6% deviation in the asymmetry parameter A_b . Assuming that this is due to new physics affecting preferentially the third generation, we can perform a fit allowing additional $Z \rightarrow b\bar{b}$ vertex corrections ρ_b and κ_b as in Eq. (10.53) (here defined to be due to new physics only with the SM contributions removed), as well as S , T , U , and the SM parameters, with the result,

$$\rho_b = 0.057 \pm 0.020 , \quad (10.100a)$$

$$\kappa_b = 0.183 \pm 0.067 , \quad (10.100b)$$

with an almost perfect correlation of 99% (because R_b is much better determined than A_b). The central values of the oblique parameters are consistent with their SM values of zero (note, however, that $S = -0.10 \pm 0.10$ is slightly outside its 1σ range), and there is little change in the SM parameters, except that the value of $\alpha_s(M_Z)$ is lower by 0.0009 compared to the SM fit. Given that an $\mathcal{O}(20\%)$ correction to κ_b would be necessary, it would be difficult to account for the deviation in A_b by new physics that enters only at the level of radiative corrections. Thus, if it is due to new physics, it is most likely of tree-level type affecting preferentially the third generation. Examples include the decay of a scalar neutrino resonance [428], mixing of the b quark with heavy exotics [429], and a heavy Z' with family non-universal couplings [430,431]. It is difficult, however, to simultaneously account for R_b without tuning, which has been measured on the Z peak and off-peak [432] at LEP 1.

There is no simple parametrization to describe the effects of every type of new physics on every possible observable. The S , T , and U formalism describes many types of heavy physics which affect only the gauge self-energies, and it can be applied to all precision observables. However, new physics which couples directly to ordinary fermions cannot be fully parametrized in this framework. Examples include heavy Z' bosons [376], mixing with exotic fermions [9, 433, 434], leptoquark exchange [294, 435, 436], supersymmetric models, strong EW dynamics [413], Little Higgs models [437, 438], and TeV-scale extra spatial dimensions [439–442] (for more details and references, see Section 85 on “Extra Dimensions” in this *Review*). These types of new physics can be parametrized in a model-independent way by using an effective field theory description [443–446]. Here the SM is extended by a set of higher-dimensional operators, denoted \mathcal{O}_i ,

$$\mathcal{L} = \mathcal{L}_{\text{SM}} + \sum_{d>4} \sum_i \frac{C_i}{\Lambda^{d-4}} \mathcal{O}_i , \quad (10.101)$$

where Λ is the characteristic scale of the new physics sector, which is assumed to satisfy $\Lambda \gg v$. For EW precision observables, the leading new operators enter at dimension $d = 6$. Note that S and T can be identified with two of these operators (or linear combinations thereof, depending on the chosen operator basis), while U corresponds to a dimension-8 operator [411, 447]. With current data on M_W and Z pole observables, Λ is constrained to be larger than $\mathcal{O}(\text{TeV})$ if the Wilson coefficients C_i are of order unity [448–454].

Limits on new four-Fermi operators and on leptoquarks using LEP 2 and lower energy data are given in Refs. [294, 455–457], while constraints on various types of new physics are addressed in Refs. [9, 169, 319, 458, 459]. For a particularly well motivated and explored type of physics beyond the SM, see Section 87 on “ Z' -Boson Searches” in this *Review*.

10.8 Alternative scenarios

For our evaluation of $g_\mu - 2$ and $\Delta\alpha_{\text{had}}^{(5)}(M_Z)$ we took the recent vacuum polarization constraints from CMD-3 [48] and LQCD into account. Both have the effect to move the SM prediction of $g_\mu - 2$ closer to the new measurement result in Ref. [236], while reducing the indirect determination of M_H and slightly increasing the small tension with the direct LHC measurements [306, 307]. The discrepancies of CMD-3 and LQCD with some of the older

data (especially KLOE) is presently not understood. Thus, it is illustrative to repeat the global fit by replacing $\Delta\alpha_{\text{had}}^{(3)}(2 \text{ GeV}) = (60.30 \pm 0.43) \times 10^{-4}$ and $a_\mu^{\text{had,VP}}(\alpha^2) = (65.44 \pm 0.25) \times 10^{-9}$ with the values that we used for the 2022 edition of this *Review*, $\Delta\alpha_{\text{had}}^{(3)}(2 \text{ GeV}) = (58.84 \pm 0.51) \times 10^{-4}$ and $a_\mu^{\text{had,VP}}(\alpha^2) = (64.49 \pm 0.33) \times 10^{-9}$. As a result, the discrepancy between the SM prediction and the measurement of a_μ would become 5.1σ , and Eq. (10.50) would change to

$$a_\mu^{\text{exp}} - a_\mu^{\text{theory}} = (2.08 \pm 0.41) \times 10^{-9} . \quad (10.102)$$

On the other hand, the result for the indirect determination of M_H in Eq. (10.80) would now read

$$M_H = 103_{-17}^{+18} \text{ GeV} . \quad (10.103)$$

The global fit reported in Sec. 10.6 excluded the recent M_W result by the CDF collaboration [289], because there is a roughly 4σ discrepancy with other measurements whose origin is currently not understood (Ref. [289] also contains the first high-precision measurement of M_Z at a hadron collider shown in Table 10.5, in perfect agreement with LEP). Here we study the effect of including this measurement as an additional constraint, using $M_W = 80.432 \pm 0.016 \text{ GeV}$ (see Table 10.4), which is the result of the adjustment to the common PDF set CT18 [303] in Ref. [298]. The quality of the global fit deteriorates sharply with a $\chi^2/\text{d.o.f.} = 70.1/48$ and a probability of a larger χ^2 of only 2%. The increase in χ^2 amounts to more than 20 for 1 additional degree of freedom. Removing M_H from the LHC as a constraint gives a somewhat improved fit quality with a $\chi^2/\text{d.o.f.} = 60.1/47$, but with

$$M_H = 75_{-12}^{+14} \text{ GeV} , \quad (10.104)$$

driven to very low and excluded values. More acceptable is the ρ_0 fit as in Eq. (10.87a) with a $\chi^2/\text{d.o.f.} = 58.5/47$ (12%), and

$$\rho_0 = 1.00059 \pm 0.00016 , \quad (10.105)$$

corresponding to $T = 0.08 \pm 0.02$. Thus, if one views the discrepancies in the M_W measurements as statistical fluctuations, then ample parameter space would open up, allowing, *e.g.*, additional non-degenerate SU(2) doublets, as reviewed in Sec. 10.7. In the STU fit,

$$S = -0.04 \pm 0.10 , \quad (10.106a)$$

$$T = 0.01 \pm 0.12 , \quad (10.106b)$$

$$U = 0.05 \pm 0.09 , \quad (10.106c)$$

the effect is mostly moved to the U parameter when compared to Eqs. (10.98). S , T and U are highly correlated and despite appearances the probability of all vanishing simultaneously is just 0.3%. Finally, Eq. (10.99) changes only moderately (see also the open black ellipse in Fig. 10.6),

$$S = -0.00 \pm 0.07 , \quad (10.107a)$$

$$T = 0.07 \pm 0.05 . \quad (10.107b)$$

Of course, more drastic changes would be observed with the constraint, $M_W = 80.4335 \pm 9.4 \text{ GeV}$ from the original publication [289] with its much smaller quoted uncertainty. For related discussions of this issue, see Refs. [361, 460–463].

Acknowledgments

It is a pleasure to thank Rodolfo Ferro-Hernández for discussions, for performing some of the calculations and checks, and for updating the plots. A.F. is supported in part by the National Science Foundation under grant no. PHY-2112829.

References

- [1] S. Glashow, Nucl. Phys. **22**, 579 (1961).
- [2] S. Weinberg, Phys. Rev. Lett. **19**, 1264 (1967).
- [3] A. Salam, Conf. Proc. C **680519**, 367 (1968).
- [4] S. Glashow, J. Iliopoulos and L. Maiani, Phys. Rev. D **2**, 1285 (1970).

- [5] N. Cabibbo, Phys. Rev. Lett. **10**, 531 (1963).
- [6] M. Kobayashi and T. Maskawa, Prog. Theor. Phys. **49**, 652 (1973).
- [7] S. Descotes-Genon and P. Koppenburg, Ann. Rev. Nucl. Part. Sci. **67**, 97 (2017), [arXiv:1702.08834].
- [8] E. Commins and P. Bucksbaum, *Weak Interactions of Leptons and Quarks*, Cambridge Univ. Pr., Cambridge, USA (1983), ISBN 978-0-521-27370-1.
- [9] P. Langacker, editor, *Precision tests of the standard electroweak model*, volume 14, WSP, Singapore (1996).
- [10] P. Langacker, *The standard model and beyond*, CRC Pr., Boca Raton, USA (2010), ISBN 978-1-4200-7906-7.
- [11] T. Kinoshita, editor, *Quantum electrodynamics*, volume 7, WSP, Singapore (1990).
- [12] S. G. Karshenboim, Phys. Rept. **422**, 1 (2005), [hep-ph/0509010].
- [13] J. Erler and S. Su, Prog. Part. Nucl. Phys. **71**, 119 (2013), [arXiv:1303.5522].
- [14] I. Brivio *et al.* (2021), [arXiv:2111.12515].
- [15] D. Webber *et al.* (MuLan), Phys. Rev. Lett. **106**, 041803 (2011), [arXiv:1010.0991].
- [16] T. Kinoshita and A. Sirlin, Phys. Rev. **113**, 1652 (1959).
- [17] T. van Ritbergen and R. G. Stuart, Nucl. Phys. B **564**, 343 (2000), [hep-ph/9904240].
- [18] M. Steinhauser and T. Seidensticker, Phys. Lett. B **467**, 271 (1999), [hep-ph/9909436].
- [19] Y. Nir, Phys. Lett. B **221**, 184 (1989).
- [20] A. Pak and A. Czarnecki, Phys. Rev. Lett. **100**, 241807 (2008), [arXiv:0803.0960].
- [21] A. Ferroglia, G. Ossola and A. Sirlin, Nucl. Phys. B **560**, 23 (1999), [hep-ph/9905442].
- [22] M. Fael, K. Schönwald and M. Steinhauser, Phys. Rev. D **104**, 1, 016003 (2021), [arXiv:2011.13654].
- [23] M. Czakon, A. Czarnecki and M. Dowling, Phys. Rev. D **103**, L111301 (2021), [arXiv:2104.05804].
- [24] X. Fan *et al.*, Phys. Rev. Lett. **130**, 7, 071801 (2023), [arXiv:2209.13084].
- [25] T. Aoyama *et al.*, Phys. Rev. Lett. **109**, 111808 (2012), [arXiv:1205.5370].
- [26] T. Aoyama, T. Kinoshita and M. Nio, Atoms **7**, 1, 28 (2019).
- [27] S. Volkov (2024), [arXiv:2404.00649].
- [28] L. Morel *et al.*, Nature **588**, 7836, 61 (2020).
- [29] R. H. Parker *et al.*, Science **360**, 191 (2018), [arXiv:1812.04130].
- [30] G. Abbiendi *et al.* (OPAL), Eur. Phys. J. C **45**, 1 (2006), [hep-ex/0505072].
- [31] P. Achard *et al.* (L3), Phys. Lett. B **623**, 26 (2005), [hep-ex/0507078].
- [32] S. Fanchiotti, B. A. Kniehl and A. Sirlin, Phys. Rev. D **48**, 307 (1993), [hep-ph/9212285].
- [33] J. Erler, Phys. Rev. D **59**, 054008 (1999), [hep-ph/9803453].
- [34] J. Erler (1999), [hep-ph/0005084].
- [35] M. Steinhauser, Phys. Lett. B **429**, 158 (1998), [hep-ph/9803313].
- [36] C. Sturm, Nucl. Phys. B **874**, 698 (2013), [arXiv:1305.0581].
- [37] K. Chetyrkin, J. H. Kuhn and M. Steinhauser, Nucl. Phys. B **482**, 213 (1996), [hep-ph/9606230].
- [38] A. V. Nesterenko, *Strong interactions in spacelike and time-like domains: dispersive approach*, Elsevier (2016), ISBN 978-0-12-803448-4.
- [39] J. Erler and R. Ferro-Hernández, JHEP **03**, 196 (2018), [arXiv:1712.09146].
- [40] A. Blondel *et al.*, editors, *Theory for the FCC-ee: Report on the 11th FCC-ee Workshop Theory and Experiments*, volume 3/2020 of *CERN Yellow Reports: Monographs*, CERN, Geneva (2019), [arXiv:1905.05078].
- [41] M. Davier *et al.*, Eur. Phys. J. C **80**, 3, 241 (2020), [arXiv:1908.00921].
- [42] A. Keshavarzi, D. Nomura and T. Teubner, Phys. Rev. D **101**, 1, 014029 (2020), [arXiv:1911.00367].
- [43] M. Davier *et al.*, Eur. Phys. J. C **71**, 1515 (2011), [Erratum: Eur.Phys.J.C 72, 1874 (2012)], [arXiv:1010.4180].
- [44] K. Ackerstaff *et al.* (OPAL), Eur. Phys. J. C **7**, 571 (1999), [hep-ex/9808019].
- [45] S. Anderson *et al.* (CLEO), Phys. Rev. D **61**, 112002 (2000), [hep-ex/9910046].
- [46] S. Schael *et al.* (ALEPH), Phys. Rept. **421**, 191 (2005), [hep-ex/0506072].
- [47] M. Fujikawa *et al.* (Belle), Phys. Rev. D **78**, 072006 (2008), [arXiv:0805.3773].
- [48] F. V. Ignatov *et al.* (CMD-3) (2023), [arXiv:2302.08834].
- [49] M. Cè *et al.*, JHEP **08**, 220 (2022), [arXiv:2203.08676].
- [50] M. Davier *et al.* (2023), [arXiv:2312.02053].
- [51] B. Malaescu and M. Schott, Eur. Phys. J. C **81**, 1, 46 (2021), [arXiv:2008.08107].
- [52] S. Groote *et al.*, Phys. Lett. B **440**, 375 (1998), [hep-ph/9802374].
- [53] N. Krasnikov and R. Rodenberg, Nuovo Cim. A **111**, 217 (1998), [hep-ph/9711367].
- [54] J. H. Kuhn and M. Steinhauser, Phys. Lett. B **437**, 425 (1998), [hep-ph/9802241].
- [55] A. D. Martin, J. Outhwaite and M. Ryskin, Phys. Lett. B **492**, 69 (2000), [hep-ph/0008078].
- [56] J. de Troconiz and F. Yndurain, Phys. Rev. D **65**, 093002 (2002), [hep-ph/0107318].
- [57] H. Burkhardt and B. Pietrzyk, Phys. Rev. D **84**, 037502 (2011), [arXiv:1106.2991].
- [58] J. Erler, P. Masjuan and H. Spiesberger, Eur. Phys. J. C **77**, 2, 99 (2017), [arXiv:1610.08531].
- [59] V. Novikov *et al.*, Phys. Rept. **41**, 1 (1978).
- [60] J. Erler and M. Luo, Phys. Lett. B **558**, 125 (2003), [hep-ph/0207114].
- [61] J. Erler, P. Masjuan and H. Spiesberger, Eur. Phys. J. C **82**, 11, 1023 (2022), [arXiv:2203.02348].
- [62] T. Aaltonen *et al.* (CDF, DØ, Tevatron Electroweak Working Group) (2016), [arXiv:1608.01881].
- [63] A. Hayrapetyan *et al.* (ATLAS, CMS) (2023), [arXiv:2402.08713].
- [64] A. Tumasyan *et al.* (CMS), Eur. Phys. J. C **83**, 10, 963 (2023), [arXiv:2302.01967].
- [65] A. M. Sirunyan *et al.* (CMS), Eur. Phys. J. C **79**, 5, 368 (2019), [arXiv:1812.10505].
- [66] A. M. Sirunyan *et al.* (CMS), Eur. Phys. J. C **79**, 4, 313 (2019), [arXiv:1812.10534].
- [67] A. Tumasyan *et al.* (CMS), JHEP **12**, 161 (2021), [arXiv:2108.10407].
- [68] G. Aad *et al.* (ATLAS), JHEP **06**, 019 (2023), [arXiv:2209.00583].
- [69] Technical Report ATLAS-CONF-2023-058, CERN, Geneva (2022), URL <http://cds.cern.ch/record/2826701>.
- [70] J. Erler, Eur. Phys. J. C **75**, 9, 453 (2015), [arXiv:1507.08210].
- [71] A. H. Hoang, S. Plätzer and D. Samitz, JHEP **10**, 200 (2018), [arXiv:1807.06617].
- [72] J. Kieseler, K. Lipka and S.-O. Moch, Phys. Rev. Lett. **116**, 16, 162001 (2016), [arXiv:1511.00841].

- [73] B. Dehnadi *et al.*, JHEP **12**, 065 (2023), [arXiv:2309.00547].
- [74] M. Beneke *et al.*, Phys. Lett. B **775**, 63 (2017), [arXiv:1605.03609].
- [75] P. Marquard *et al.*, Phys. Rev. Lett. **114**, 14, 142002 (2015), [arXiv:1502.01030].
- [76] M. Beneke, Phys. Rept. **317**, 1 (1999), [hep-ph/9807443].
- [77] S. Catani *et al.*, JHEP **07**, 100 (2019), [arXiv:1906.06535].
- [78] S. Catani *et al.*, Eur. Phys. J. C **81**, 6, 491 (2021), [arXiv:2102.03256].
- [79] A. M. Sirunyan *et al.* (CMS), Eur. Phys. J. C **80**, 7, 658 (2020), [arXiv:1904.05237].
- [80] G. Aad *et al.* (ATLAS), JHEP **11**, 150 (2019), [arXiv:1905.02302].
- [81] A. Tumasyan *et al.* (CMS), JHEP **07**, 077 (2023), [arXiv:2207.02270].
- [82] G. Aad *et al.* (ATLAS, CMS), JHEP **07**, 213 (2023), [arXiv:2205.13830].
- [83] J. Erler and M. Schott, Prog. Part. Nucl. Phys. **106**, 68 (2019), [arXiv:1902.05142].
- [84] A. Sirlin, Phys. Rev. D **22**, 971 (1980).
- [85] W. J. Marciano and J. L. Rosner, Phys. Rev. Lett. **65**, 2963 (1990), [Erratum: Phys.Rev.Lett. 68, 898 (1992)].
- [86] G. Degrossi, S. Fanchiotti and A. Sirlin, Nucl. Phys. B **351**, 49 (1991).
- [87] A. Czarnecki and W. J. Marciano, Int. J. Mod. Phys. A **15**, 2365 (2000), [hep-ph/0003049].
- [88] J. Erler and M. J. Ramsey-Musolf, Phys. Rev. D **72**, 073003 (2005), [hep-ph/0409169].
- [89] K. Kumar *et al.*, Ann. Rev. Nucl. Part. Sci. **63**, 237 (2013), [arXiv:1302.6263].
- [90] G. Degrossi and A. Sirlin, Nucl. Phys. B **352**, 342 (1991).
- [91] P. Gambino and A. Sirlin, Phys. Rev. D **49**, 1160 (1994), [hep-ph/9309326].
- [92] W. Hollik, Fortsch. Phys. **38**, 165 (1990).
- [93] R. Barbieri *et al.*, Nucl. Phys. B **409**, 105 (1993).
- [94] J. Fleischer, O. Tarasov and F. Jegerlehner, Phys. Lett. B **319**, 249 (1993).
- [95] G. Degrossi, P. Gambino and A. Vicini, Phys. Lett. B **383**, 219 (1996), [hep-ph/9603374].
- [96] G. Degrossi, P. Gambino and A. Sirlin, Phys. Lett. B **394**, 188 (1997), [hep-ph/9611363].
- [97] A. Freitas *et al.*, Phys. Lett. B **495**, 338 (2000), [Erratum: Phys.Lett.B 570, 265 (2003)], [hep-ph/0007091].
- [98] M. Awramik and M. Czakon, Phys. Lett. B **568**, 48 (2003), [hep-ph/0305248].
- [99] A. Freitas *et al.*, Nucl. Phys. B **632**, 189 (2002), [Erratum: Nucl.Phys.B 666, 305–307 (2003)], [hep-ph/0202131].
- [100] M. Awramik and M. Czakon, Phys. Rev. Lett. **89**, 241801 (2002), [hep-ph/0208113].
- [101] A. Onishchenko and O. Veretin, Phys. Lett. B **551**, 111 (2003), [hep-ph/0209010].
- [102] G. Degrossi, P. Gambino and P. P. Giardino, JHEP **05**, 154 (2015), [arXiv:1411.7040].
- [103] M. Awramik *et al.*, Phys. Rev. D **69**, 053006 (2004), [hep-ph/0311148].
- [104] M. Awramik *et al.*, Phys. Rev. Lett. **93**, 201805 (2004), [hep-ph/0407317].
- [105] W. Hollik, U. Meier and S. Uccirati, Nucl. Phys. B **731**, 213 (2005), [hep-ph/0507158].
- [106] M. Awramik, M. Czakon and A. Freitas, Phys. Lett. B **642**, 563 (2006), [hep-ph/0605339].
- [107] W. Hollik, U. Meier and S. Uccirati, Nucl. Phys. B **765**, 154 (2007), [hep-ph/0610312].
- [108] M. Awramik *et al.*, Nucl. Phys. B **813**, 174 (2009), [arXiv:0811.1364].
- [109] I. Dubovyk *et al.*, Phys. Lett. B **762**, 184 (2016), [arXiv:1607.08375].
- [110] A. Freitas, Phys. Lett. B **730**, 50 (2014), [arXiv:1310.2256].
- [111] A. Freitas, JHEP **04**, 070 (2014), [arXiv:1401.2447].
- [112] I. Dubovyk *et al.*, Phys. Lett. B **783**, 86 (2018), [arXiv:1804.10236].
- [113] I. Dubovyk *et al.*, JHEP **08**, 113 (2019), [arXiv:1906.08815].
- [114] M. Awramik, M. Czakon and A. Freitas, JHEP **11**, 048 (2006), [hep-ph/0608099].
- [115] A. Djouadi and C. Verzegnassi, Phys. Lett. B **195**, 265 (1987).
- [116] A. Djouadi, Nuovo Cim. A **100**, 357 (1988).
- [117] K. Chetyrkin, J. H. Kuhn and M. Steinhauser, Phys. Lett. B **351**, 331 (1995), [hep-ph/9502291].
- [118] L. Avdeev *et al.*, Phys. Lett. B **336**, 560 (1994), [Erratum: Phys.Lett.B 349, 597–598 (1995)], [hep-ph/9406363].
- [119] Y. Schroder and M. Steinhauser, Phys. Lett. B **622**, 124 (2005), [hep-ph/0504055].
- [120] K. Chetyrkin *et al.*, Phys. Rev. Lett. **97**, 102003 (2006), [hep-ph/0605201].
- [121] R. Boughezal and M. Czakon, Nucl. Phys. B **755**, 221 (2006), [hep-ph/0606232].
- [122] B. A. Kniehl, J. H. Kuhn and R. Stuart, Phys. Lett. B **214**, 621 (1988).
- [123] B. A. Kniehl, Nucl. Phys. B **347**, 86 (1990).
- [124] F. Halzen and B. A. Kniehl, Nucl. Phys. B **353**, 567 (1991).
- [125] A. Djouadi and P. Gambino, Phys. Rev. D **49**, 3499 (1994), [Erratum: Phys.Rev.D 53, 4111 (1996)], [hep-ph/9309298].
- [126] A. Anselm, N. Dombey and E. Leader, Phys. Lett. B **312**, 232 (1993).
- [127] K. Chetyrkin, J. H. Kuhn and M. Steinhauser, Phys. Rev. Lett. **75**, 3394 (1995), [hep-ph/9504413].
- [128] J. van der Bij *et al.*, Phys. Lett. B **498**, 156 (2001), [hep-ph/0011373].
- [129] M. Faisst *et al.*, Nucl. Phys. B **665**, 649 (2003), [hep-ph/0302275].
- [130] L. Chen and A. Freitas, JHEP **07**, 210 (2020), [arXiv:2002.05845].
- [131] L. Chen and A. Freitas, JHEP **03**, 215 (2021), [arXiv:2012.08605].
- [132] R. Boughezal, J. Tausk and J. van der Bij, Nucl. Phys. B **725**, 3 (2005), [hep-ph/0504092].
- [133] A. Arbuzov *et al.*, Comput. Phys. Commun. **174**, 728 (2006), [hep-ph/0507146].
- [134] L. Chen and A. Freitas, SciPost Phys. Codeb. **2023**, 18 (2023), [arXiv:2211.16272].
- [135] J. Erler and M. J. Ramsey-Musolf, Prog. Part. Nucl. Phys. **54**, 351 (2005), [hep-ph/0404291].
- [136] J. Formaggio and G. Zeller, Rev. Mod. Phys. **84**, 1307 (2012), [arXiv:1305.7513].
- [137] J. Dorenbosch *et al.* (CHARM), Z. Phys. C **41**, 567 (1989), [Erratum: Z.Phys.C 51, 142 (1991)].
- [138] L. Ahrens *et al.*, Phys. Rev. D **41**, 3297 (1990).
- [139] P. Vilain *et al.* (CHARM-II), Phys. Lett. B **335**, 246 (1994).
- [140] R. Allen *et al.*, Phys. Rev. D **47**, 11 (1993).
- [141] L. Auerbach *et al.* (LSND), Phys. Rev. D **63**, 112001 (2001), [hep-ex/0101039].
- [142] M. Deniz *et al.* (TEXONO), Phys. Rev. D **81**, 072001 (2010), [arXiv:0911.1597].
- [143] J. M. Conrad, M. H. Shaevitz and T. Bolton, Rev. Mod. Phys. **70**, 1341 (1998), [hep-ex/9707015].

- [144] A. Blondel *et al.*, Z. Phys. C **45**, 361 (1990).
- [145] J. Allaby *et al.* (CHARM), Z. Phys. C **36**, 611 (1987).
- [146] K. S. McFarland *et al.* (CCFR, E744, E770), Eur. Phys. J. C **1**, 509 (1998), [hep-ex/9701010].
- [147] R. Barnett, Phys. Rev. D **14**, 70 (1976).
- [148] H. Georgi and H. Politzer, Phys. Rev. D **14**, 1829 (1976).
- [149] S. Rabinowitz *et al.*, Phys. Rev. Lett. **70**, 134 (1993).
- [150] E. Paschos and L. Wolfenstein, Phys. Rev. D **7**, 91 (1973).
- [151] G. Zeller *et al.* (NuTeV), Phys. Rev. Lett. **88**, 091802 (2002), [Erratum: Phys.Rev.Lett. 90, 239902 (2003)], [hep-ex/0110059].
- [152] D. Akimov *et al.* (COHERENT), Science **357**, 6356, 1123 (2017), [arXiv:1708.01294].
- [153] D. Akimov *et al.* (COHERENT), Phys. Rev. Lett. **126**, 1, 012002 (2021), [arXiv:2003.10630].
- [154] J. Erler *et al.*, Ann. Rev. Nucl. Part. Sci. **64**, 269 (2014), [arXiv:1401.6199].
- [155] C. Prescott *et al.*, Phys. Lett. B **84**, 524 (1979).
- [156] D. Wang *et al.* (PVDIS), Nature **506**, 7486, 67 (2014).
- [157] D. Wang *et al.*, Phys. Rev. C **91**, 4, 045506 (2015), [arXiv:1411.3200].
- [158] R. Hasty *et al.* (SAMPLE), Science **290**, 2117 (2000), [arXiv:nucl-ex/0102001].
- [159] E. Beise, M. Pitt and D. Spayde, Prog. Part. Nucl. Phys. **54**, 289 (2005), [arXiv:nucl-ex/0412054].
- [160] S.-L. Zhu *et al.*, Phys. Rev. D **62**, 033008 (2000), [hep-ph/0002252].
- [161] A. Argento *et al.*, Phys. Lett. B **120**, 245 (1983).
- [162] W. Heil *et al.*, Nucl. Phys. B **327**, 1 (1989).
- [163] P. Souder *et al.*, Phys. Rev. Lett. **65**, 694 (1990).
- [164] D. Armstrong and R. McKeown, Ann. Rev. Nucl. Part. Sci. **62**, 337 (2012), [arXiv:1207.5238].
- [165] E. Derman and W. J. Marciano, Annals Phys. **121**, 147 (1979).
- [166] P. Anthony *et al.* (SLAC E158), Phys. Rev. Lett. **95**, 081601 (2005), [hep-ex/0504049].
- [167] D. Androić *et al.* (Qweak), Nature **557**, 7704, 207 (2018), [arXiv:1905.08283].
- [168] R. D. Carlini *et al.*, Ann. Rev. Nucl. Part. Sci. **69**, 191 (2019).
- [169] J. Erler, A. Kurylov and M. J. Ramsey-Musolf, Phys. Rev. D **68**, 016006 (2003), [hep-ph/0302149].
- [170] R. D. Young *et al.*, Phys. Rev. Lett. **99**, 122003 (2007), [arXiv:0704.2618].
- [171] A. Acha *et al.* (HAPPEX), Phys. Rev. Lett. **98**, 032301 (2007), [arXiv:nucl-ex/0609002].
- [172] M. Gorchtein and C. Horowitz, Phys. Rev. Lett. **102**, 091806 (2009), [arXiv:0811.0614].
- [173] M. Gorchtein, C. Horowitz and M. J. Ramsey-Musolf, Phys. Rev. C **84**, 015502 (2011), [arXiv:1102.3910].
- [174] N. Hall *et al.*, Phys. Lett. B **753**, 221 (2016), [arXiv:1504.03973].
- [175] J. Erler *et al.*, Phys. Rev. D **100**, 5, 053007 (2019), [arXiv:1907.07928].
- [176] M. Bouchiat and C. Bouchiat, Phys. Lett. B **48**, 111 (1974).
- [177] M. Safronova *et al.*, Rev. Mod. Phys. **90**, 2, 025008 (2018), [arXiv:1710.01833].
- [178] C. Wood *et al.*, Science **275**, 1759 (1997).
- [179] J. Guena, M. Lintz and M. Bouchiat, Phys. Rev. A **71**, 042108 (2005), [arXiv:physics/0412017].
- [180] N. Edwards *et al.*, Phys. Rev. Lett. **74**, 2654 (1995).
- [181] P. Vetter *et al.*, Phys. Rev. Lett. **74**, 2658 (1995).
- [182] D. Meekhof *et al.*, Phys. Rev. Lett. **71**, 3442 (1993).
- [183] M. Macpherson *et al.*, Phys. Rev. Lett. **67**, 20, 2784 (1991).
- [184] P. Blunden, W. Melnitchouk and A. Thomas, Phys. Rev. Lett. **109**, 262301 (2012), [arXiv:1208.4310].
- [185] S. Bennett and C. E. Wieman, Phys. Rev. Lett. **82**, 2484 (1999), [Erratum: Phys.Rev.Lett. 82, 4153 (1999), Erratum: Phys.Rev.Lett. 83, 889 (1999)], [hep-ex/9903022].
- [186] V. Dzuba and V. Flambaum., Phys. Rev. A **62**, 052101 (2000), [arXiv:physics/0005038].
- [187] V. Dzuba, V. Flambaum and O. Sushkov, Phys. Rev. A **56**, 4357 (1997), [hep-ph/9709251].
- [188] D. Cho *et al.*, Phys. Rev. A **55**, 1007 (1997).
- [189] H. B. Tran Tan, D. Xiao and A. Derevianko, Phys. Rev. A **108**, 2, 022808 (2023), [arXiv:2306.09573].
- [190] A. A. Vasilyev *et al.*, Phys. Rev. A **66**, 020101 (2002).
- [191] V. Dzuba, V. Flambaum and J. Ginges, Phys. Rev. D **66**, 076013 (2002), [hep-ph/0204134].
- [192] J. Ginges and V. Flambaum, Phys. Rept. **397**, 63 (2004), [arXiv:physics/0309054].
- [193] A. Derevianko and S. G. Porsev, Eur. Phys. J. A **32**, 4, 517 (2007), [hep-ph/0608178].
- [194] B. Roberts, V. Dzuba and V. Flambaum, Ann. Rev. Nucl. Part. Sci. **65**, 63 (2015), [arXiv:1412.6644].
- [195] A. Derevianko, Phys. Rev. Lett. **85**, 1618 (2000), [hep-ph/0005274].
- [196] W. Johnson, I. Bednyakov and G. Soff, Phys. Rev. Lett. **87**, 233001 (2001), [Erratum: Phys.Rev.Lett. 88, 079903 (2002)], [hep-ph/0110262].
- [197] M. Kuchiev and V. Flambaum, Phys. Rev. Lett. **89**, 283002 (2002), [hep-ph/0206124].
- [198] A. Milstein, O. Sushkov and I. Terekhov, Phys. Rev. Lett. **89**, 283003 (2002), [hep-ph/0208227].
- [199] S. Porsev, K. Beloy and A. Derevianko, Phys. Rev. Lett. **102**, 181601 (2009), [arXiv:0902.0335].
- [200] V. Dzuba *et al.*, Phys. Rev. Lett. **109**, 203003 (2012), [arXiv:1207.5864].
- [201] C. Bouchiat and C. Piketty, Phys. Lett. B **128**, 73 (1983).
- [202] I. Zel'dovich, J. Exp. Theor. Phys. **6**, 1184 (1958).
- [203] V. Flambaum and D. Murray, Phys. Rev. C **56**, 1641 (1997), [arXiv:nucl-th/9703050].
- [204] W. Haxton and C. E. Wieman, Ann. Rev. Nucl. Part. Sci. **51**, 261 (2001), [arXiv:nucl-th/0104026].
- [205] V. Dzuba *et al.*, J. Phys. B **20**, 3297 (1987).
- [206] J. L. Rosner, Phys. Rev. D **53**, 2724 (1996), [hep-ph/9507375].
- [207] D. Antypas *et al.*, Nature Phys. **15**, 2, 120 (2019), [arXiv:1804.05747].
- [208] M. Ramsey-Musolf, Phys. Rev. C **60**, 015501 (1999), [hep-ph/9903264].
- [209] S. Pollock, E. Fortson and L. Wilets, Phys. Rev. C **46**, 2587 (1992), [arXiv:nucl-th/9211004].
- [210] B. Chen and P. Vogel, Phys. Rev. C **48**, 1392 (1993), [arXiv:nucl-th/9303003].
- [211] C. Horowitz *et al.*, Phys. Rev. C **63**, 025501 (2001), [arXiv:nucl-th/9912038].
- [212] D. Adhikari *et al.* (PREX), Phys. Rev. Lett. **126**, 17, 172502 (2021), [arXiv:2102.10767].
- [213] D. Adhikari *et al.* (CREX), Phys. Rev. Lett. **129**, 4, 042501 (2022), [arXiv:2205.11593].
- [214] H. Davoudiasl, H.-S. Lee and W. J. Marciano, Phys. Rev. D **86**, 095009 (2012), [arXiv:1208.2973].
- [215] E. Braaten, S. Narison and A. Pich, Nucl. Phys. B **373**, 581 (1992).

- [216] A. Pich, *Prog. Part. Nucl. Phys.* **75**, 41 (2014), [arXiv:1310.7922].
- [217] M. Davier *et al.*, *Eur. Phys. J. C* **74**, 3, 2803 (2014), [arXiv:1312.1501].
- [218] K. Chetyrkin, A. Kataev and F. Tkachov, *Phys. Lett. B* **85**, 277 (1979).
- [219] M. Dine and J. Sapiirstein, *Phys. Rev. Lett.* **43**, 668 (1979).
- [220] S. Gorishnii, A. Kataev and S. Larin, *Phys. Lett. B* **259**, 144 (1991).
- [221] L. R. Surguladze and M. A. Samuel, *Phys. Rev. Lett.* **66**, 560 (1991), [Erratum: *Phys.Rev.Lett.* 66, 2416 (1991)].
- [222] P. Baikov, K. Chetyrkin and J. H. Kuhn, *Phys. Rev. Lett.* **101**, 012002 (2008), [arXiv:0801.1821].
- [223] F. Le Diberder and A. Pich, *Phys. Lett. B* **286**, 147 (1992).
- [224] M. Beneke and M. Jamin, *JHEP* **09**, 044 (2008), [arXiv:0806.3156].
- [225] A. H. Hoang and C. Regner, *Phys. Rev. D* **105**, 9, 096023 (2022), [arXiv:2008.00578].
- [226] M. Golterman, K. Maltman and S. Peris, *Phys. Rev. D* **108**, 1, 014007 (2023), [arXiv:2305.10386].
- [227] M. A. Benitez-Rathgeb *et al.*, *JHEP* **09**, 223 (2022), [arXiv:2207.01116].
- [228] M. Beneke and H. Takaura, in “16th International Symposium on Radiative Corrections: Applications of Quantum Field Theory to Phenomenology,” (2023), [arXiv:2309.10853].
- [229] E. Braaten and C.-S. Li, *Phys. Rev. D* **42**, 3888 (1990).
- [230] W. Marciano and A. Sirlin, *Phys. Rev. Lett.* **61**, 1815 (1988).
- [231] J. Erler, *Rev. Mex. Fis.* **50**, 200 (2004), [hep-ph/0211345].
- [232] D. Boito *et al.*, *Phys. Rev. D* **85**, 093015 (2012), [arXiv:1203.3146].
- [233] D. Boito *et al.*, *Phys. Rev. D* **91**, 3, 034003 (2015), [arXiv:1410.3528].
- [234] J. Erler (2011), [arXiv:1102.5520].
- [235] G. Bennett *et al.* (Muon g-2), *Phys. Rev. Lett.* **92**, 161802 (2004), [hep-ex/0401008].
- [236] D. P. Aguillard *et al.* (Muon g-2), *Phys. Rev. Lett.* **131**, 16, 161802 (2023), [arXiv:2308.06230].
- [237] T. Aoyama *et al.*, *PTEP* **2012**, 01A107 (2012).
- [238] P. Baikov, A. Maier and P. Marquard, *Nucl. Phys. B* **877**, 647 (2013), [arXiv:1307.6105].
- [239] S. Laporta, *Phys. Lett. B* **772**, 232 (2017), [arXiv:1704.06996].
- [240] G. Li, R. Mendel and M. A. Samuel, *Phys. Rev. D* **47**, 1723 (1993).
- [241] S. Laporta and E. Remiddi, *Phys. Lett. B* **301**, 440 (1993).
- [242] S. Laporta and E. Remiddi, *Phys. Lett. B* **379**, 283 (1996), [hep-ph/9602417].
- [243] A. Czarnecki and M. Skrzypek, *Phys. Lett. B* **449**, 354 (1999), [hep-ph/9812394].
- [244] J. Erler and M. Luo, *Phys. Rev. Lett.* **87**, 071804 (2001), [hep-ph/0101010].
- [245] S. J. Brodsky and J. D. Sullivan, *Phys. Rev.* **156**, 1644 (1967).
- [246] T. Burnett and M. Levine, *Phys. Lett. B* **24**, 467 (1967).
- [247] R. Jackiw and S. Weinberg, *Phys. Rev. D* **5**, 2396 (1972).
- [248] I. Bars and M. Yoshimura, *Phys. Rev. D* **6**, 374 (1972).
- [249] K. Fujikawa, B. Lee and A. Sanda, *Phys. Rev. D* **6**, 2923 (1972).
- [250] W. A. Bardeen, R. Gastmans and B. Lautrup, *Nucl. Phys. B* **46**, 319 (1972).
- [251] T. Kukhto *et al.*, *Nucl. Phys. B* **371**, 567 (1992).
- [252] S. Peris, M. Perrottet and E. de Rafael, *Phys. Lett. B* **355**, 523 (1995), [hep-ph/9505405].
- [253] A. Czarnecki, B. Krause and W. J. Marciano, *Phys. Rev. D* **52**, 2619 (1995), [hep-ph/9506256].
- [254] A. Czarnecki, B. Krause and W. J. Marciano, *Phys. Rev. Lett.* **76**, 3267 (1996), [hep-ph/9512369].
- [255] C. Gnendiger, D. Stöckinger and H. Stöckinger-Kim, *Phys. Rev. D* **88**, 053005 (2013), [arXiv:1306.5546].
- [256] G. Degrossi and G. Giudice, *Phys. Rev. D* **58**, 053007 (1998), [hep-ph/9803384].
- [257] A. Czarnecki, W. J. Marciano and A. Vainshtein, *Phys. Rev. D* **67**, 073006 (2003), [Erratum: *Phys.Rev.D* 73, 119901 (2006)], [hep-ph/0212229].
- [258] F. Jegerlehner, *EPJ Web Conf.* **166**, 00022 (2018), [arXiv:1705.00263].
- [259] M. Hoferichter, B.-L. Hoid and B. Kubis, *JHEP* **08**, 137 (2019), [arXiv:1907.01556].
- [260] P. D. Kennedy, J. Erler and H. Spiesberger (2021), [arXiv:2111.13016].
- [261] T. Aoyama *et al.*, *Phys. Rept.* **887**, 1 (2020), [arXiv:2006.04822].
- [262] S. Borsanyi *et al.*, *Nature* **593**, 7857, 51 (2021), [arXiv:2002.12347].
- [263] A. Anastasi *et al.* (KLOE-2), *JHEP* **03**, 173 (2018), [arXiv:1711.03085].
- [264] M. Davier *et al.*, *Phys. Rev. D* **109**, 7, 076019 (2024), [arXiv:2308.04221].
- [265] G. Benton *et al.*, *Phys. Rev. D* **109**, 3, 036010 (2024), [arXiv:2311.09523].
- [266] C. Lehner and A. S. Meyer, *Phys. Rev. D* **101**, 074515 (2020), [arXiv:2003.04177].
- [267] G. Wang *et al.* (chiQCD), *Phys. Rev. D* **107**, 3, 034513 (2023), [arXiv:2204.01280].
- [268] C. Aubin *et al.*, *Phys. Rev. D* **106**, 5, 054503 (2022), [arXiv:2204.12256].
- [269] M. Cè *et al.*, *Phys. Rev. D* **106**, 11, 114502 (2022), [arXiv:2206.06582].
- [270] C. Alexandrou *et al.* (Extended Twisted Mass), *Phys. Rev. D* **107**, 7, 074506 (2023), [arXiv:2206.15084].
- [271] T. Blum *et al.* (RBC, UKQCD), *Phys. Rev. D* **108**, 5, 054507 (2023), [arXiv:2301.08696].
- [272] A. Bazavov *et al.* (Fermilab Lattice, HPQCD, MILC), *Phys. Rev. D* **107**, 11, 114514 (2023), [arXiv:2301.08274].
- [273] B. Krause, *Phys. Lett. B* **390**, 392 (1997), [hep-ph/9607259].
- [274] A. Kurz *et al.*, *Phys. Lett. B* **734**, 144 (2014), [arXiv:1403.6400].
- [275] K. Melnikov and A. Vainshtein, *Phys. Rev. D* **70**, 113006 (2004), [hep-ph/0312226].
- [276] J. Erler and G. Toledo Sanchez, *Phys. Rev. Lett.* **97**, 161801 (2006), [hep-ph/0605052].
- [277] J. Prades, E. de Rafael and A. Vainshtein **20**, 303 (2009), [arXiv:0901.0306].
- [278] M. Knecht and A. Nyffeler, *Phys. Rev. D* **65**, 073034 (2002), [hep-ph/0111058].
- [279] I. Danilkin, C. F. Redmer and M. Vanderhaeghen, *Prog. Part. Nucl. Phys.* **107**, 20 (2019), [arXiv:1901.10346].
- [280] P. Masjuan and P. Roig, in “20th International Conference on Hadron Spectroscopy and Structure,” (2024), [arXiv:2401.05666].
- [281] E.-H. Chao *et al.*, *Eur. Phys. J. C* **81**, 7, 651 (2021), [arXiv:2104.02632].
- [282] E.-H. Chao *et al.*, *Eur. Phys. J. C* **82**, 8, 664 (2022), [arXiv:2204.08844].
- [283] T. Blum *et al.* (2023), [arXiv:2304.04423].

- [284] G. Colangelo *et al.*, Phys. Lett. B **735**, 90 (2014), [arXiv:1403.7512].
- [285] J. L. Lopez, D. V. Nanopoulos and X. Wang, Phys. Rev. D **49**, 366 (1994), [hep-ph/9308336].
- [286] G. Passarino and M. Veltman, Nucl. Phys. B **160**, 151 (1979).
- [287] W. Hollik and G. Duckeck, Springer Tracts Mod. Phys. **162**, 1 (2000).
- [288] S. Schael *et al.* (ALEPH, DELPHI, L3, OPAL, SLD, LEP Electroweak Working Group, SLD Electroweak Group, SLD Heavy Flavour Group), Phys. Rept. **427**, 257 (2006), [hep-ex/0509008].
- [289] T. Aaltonen *et al.* (CDF), Science **376**, 6589, 170 (2022).
- [290] B. Lynn and R. Stuart, Nucl. Phys. B **253**, 216 (1985).
- [291] S. L. Wu, Phys. Rept. **107**, 59 (1984).
- [292] R. Marshall, Z. Phys. C **43**, 607 (1989).
- [293] D. de Florian *et al.* (LHC Higgs Cross Section Working Group) (2016), [arXiv:1610.07922].
- [294] S. Schael *et al.* (ALEPH, DELPHI, L3, OPAL, LEP Electroweak), Phys. Rept. **532**, 119 (2013), [arXiv:1302.3415].
- [295] G. Aad *et al.* (ATLAS) (2024), [arXiv:2403.15085].
- [296] R. Aaij *et al.* (LHCb), JHEP **01**, 036 (2022), [arXiv:2109.01113].
- [297] V. M. Abazov *et al.* (D0), Phys. Rev. Lett. **108**, 151804 (2012), [arXiv:1203.0293].
- [298] S. Amoroso *et al.* (LHC-TeV MW Working Group) (2023), [arXiv:2308.09417].
- [299] Technical Report TEVEWWG/WZ 2010/01, FERMI LAB, Batavia (2010), [arXiv:1003.2826], URL <https://www-d0.fnal.gov/Run2Physics/WWW/results/prelim/EW/E34>.
- [300] A. Tumasyan *et al.* (CMS), Phys. Rev. D **105**, 7, 072008 (2022), [arXiv:2201.07861].
- [301] T. A. Aaltonen *et al.* (CDF, DØ), Phys. Rev. D **88**, 5, 052018 (2013), [arXiv:1307.7627].
- [302] M. Aaboud *et al.* (ATLAS), Eur. Phys. J. C **78**, 2, 110 (2018), [Erratum: Eur.Phys.J.C 78, 898 (2018)], [arXiv:1701.07240].
- [303] T.-J. Hou *et al.* (2019), [arXiv:1908.11394].
- [304] G. Aad *et al.* (ATLAS), Phys. Lett. B **716**, 1 (2012), [arXiv:1207.7214].
- [305] S. Chatrchyan *et al.* (CMS), Phys. Lett. B **716**, 30 (2012), [arXiv:1207.7235].
- [306] G. Aad *et al.* (ATLAS), Phys. Rev. Lett. **131**, 25, 251802 (2023), [arXiv:2308.04775].
- [307] Technical Report CMS-PAS-HIG-21-019, CERN, Geneva (2023), URL <http://cds.cern.ch/record/2871702>.
- [308] G. Aad *et al.* (ATLAS), Phys. Lett. B **846**, 138223 (2023), [arXiv:2304.01532].
- [309] T. A. Aaltonen *et al.* (CDF, DØ), Phys. Rev. D **97**, 11, 112007 (2018), [arXiv:1801.06283].
- [310] G. Aad *et al.* (ATLAS), JHEP **09**, 049 (2015), [arXiv:1503.03709].
- [311] Technical Report ATLAS-CONF-2018-037, CERN, Geneva (2018), URL <https://cds.cern.ch/record/2630340>.
- [312] A. M. Sirunyan *et al.* (CMS), Eur. Phys. J. C **78**, 9, 701 (2018), [arXiv:1806.00863].
- [313] Technical Report CMS-PAS-SMP-22-010, CERN, Geneva (2024), URL <http://cds.cern.ch/record/2893842>.
- [314] R. Aaij *et al.* (LHCb), JHEP **11**, 190 (2015), [arXiv:1509.07645].
- [315] K. Abe *et al.* (SLD), Phys. Rev. Lett. **84**, 5945 (2000), [hep-ex/0004026].
- [316] K. Abe *et al.* (SLD), Phys. Rev. Lett. **86**, 1162 (2001), [hep-ex/0010015].
- [317] A. Hayrapetyan *et al.* (CMS), JHEP **01**, 101 (2024), [arXiv:2309.12408].
- [318] D. Kennedy *et al.*, Nucl. Phys. B **321**, 83 (1989).
- [319] S. Riemann, Rept. Prog. Phys. **73**, 126201 (2010).
- [320] K. Abe *et al.* (SLD), Phys. Rev. Lett. **85**, 5059 (2000), [hep-ex/0006019].
- [321] K. Abe *et al.* (SLD), Phys. Rev. Lett. **78**, 17 (1997), [hep-ex/9609019].
- [322] M. Aaboud *et al.* (ATLAS), Eur. Phys. J. C **77**, 6, 367 (2017), [arXiv:1612.03016].
- [323] W. Bernreuther *et al.*, JHEP **01**, 053 (2017), [arXiv:1611.07942].
- [324] S. Catani and M. H. Seymour, JHEP **07**, 023 (1999), [hep-ph/9905424].
- [325] A. Djouadi, J. H. Kuhn and P. Zerwas, Z. Phys. C **46**, 411 (1990).
- [326] T. A. Aaltonen *et al.* (CDF), Phys. Rev. D **93**, 11, 112016 (2016), [Addendum: Phys.Rev.D 95, 119901 (2017)], [arXiv:1605.02719].
- [327] V. M. Abazov *et al.* (DØ), Phys. Rev. Lett. **120**, 24, 241802 (2018), [arXiv:1710.03951].
- [328] V. Abazov *et al.* (DØ), Phys. Rev. D **84**, 012007 (2011), [arXiv:1104.4590].
- [329] D. Acosta *et al.* (CDF), Phys. Rev. D **71**, 052002 (2005), [hep-ex/0411059].
- [330] V. Andreev *et al.* (H1), Eur. Phys. J. C **78**, 9, 777 (2018), [arXiv:1806.01176].
- [331] H. Abramowicz *et al.* (ZEUS), Phys. Rev. D **93**, 9, 092002 (2016), [arXiv:1603.09628].
- [332] P. Janot and S. Jadach, Phys. Lett. B **803**, 135319 (2020), [arXiv:1912.02067].
- [333] D. Albert *et al.*, Nucl. Phys. B **166**, 460 (1980).
- [334] K. Chetyrkin, J. H. Kuhn and A. Kwiatkowski, Phys. Rept. **277**, 189 (1996), [hep-ph/9503396].
- [335] B. A. Kniehl and J. H. Kuhn, Nucl. Phys. B **329**, 547 (1990).
- [336] K. Chetyrkin and A. Kwiatkowski, Phys. Lett. B **319**, 307 (1993), [hep-ph/9310229].
- [337] S. Larin, T. van Ritbergen and J. Vermaseren, Phys. Lett. B **320**, 159 (1994), [hep-ph/9310378].
- [338] K. Chetyrkin and O. Tarasov, Phys. Lett. B **327**, 114 (1994), [hep-ph/9312323].
- [339] P. Baikov *et al.*, Phys. Rev. Lett. **108**, 222003 (2012), [arXiv:1201.5804].
- [340] A. Kataev, Phys. Lett. B **287**, 209 (1992).
- [341] B. W. Lynn and R. G. Stuart, Phys. Lett. B **252**, 676 (1990).
- [342] J. Bernabeu, A. Pich and A. Santamaria, Nucl. Phys. B **363**, 326 (1991).
- [343] A. Czarnecki and J. H. Kuhn, Phys. Rev. Lett. **77**, 3955 (1996), [hep-ph/9608366].
- [344] R. Harlander, T. Seidensticker and M. Steinhauser, Phys. Lett. B **426**, 125 (1998), [hep-ph/9712228].
- [345] J. Fleischer *et al.*, Phys. Lett. B **459**, 625 (1999), [hep-ph/9904256].
- [346] P. A. Grassi, B. A. Kniehl and A. Sirlin, Phys. Rev. Lett. **86**, 389 (2001), [hep-th/0005149].
- [347] A. Akhundov, D. Bardin and T. Riemann, Nucl. Phys. B **276**, 1 (1986).
- [348] F. Jegerlehner, Z. Phys. C **32**, 425 (1986), [Erratum: Z.Phys.C 38, 519 (1988)].
- [349] W. Beenakker and W. Hollik, Z. Phys. C **40**, 141 (1988).
- [350] D. Bardin *et al.*, Z. Phys. C **44**, 493 (1989).
- [351] A. Borrelli *et al.*, Nucl. Phys. B **333**, 357 (1990).
- [352] A. Denner and T. Sack, Z. Phys. C **46**, 653 (1990).

- [353] A. Denner, *Fortsch. Phys.* **41**, 307 (1993), [arXiv:0709.1075].
- [354] G. Aad *et al.* (ATLAS), *Nature Phys.* **17**, 7, 813 (2021), [arXiv:2007.14040].
- [355] U. Amaldi *et al.*, *Phys. Rev. D* **36**, 1385 (1987).
- [356] G. Costa *et al.*, *Nucl. Phys. B* **297**, 244 (1988).
- [357] P. Langacker and M. Luo, *Phys. Rev. D* **44**, 817 (1991).
- [358] J. Erler and P. Langacker, *Phys. Rev. D* **52**, 441 (1995), [hep-ph/9411203].
- [359] J. Haller *et al.*, *Eur. Phys. J. C* **78**, 8, 675 (2018), [arXiv:1803.01853].
- [360] J. de Blas *et al.*, *Phys. Rev. D* **106**, 3, 033003 (2022), [arXiv:2112.07274].
- [361] J. de Blas *et al.*, *Phys. Rev. Lett.* **129**, 27, 271801 (2022), [arXiv:2204.04204].
- [362] A. Crivellin *et al.*, *Phys. Rev. Lett.* **125**, 9, 091801 (2020), [arXiv:2003.04886].
- [363] A. Keshavarzi *et al.*, *Phys. Rev. D* **102**, 3, 033002 (2020), [arXiv:2006.12666].
- [364] M. Aaboud *et al.* (ATLAS), *Phys. Lett. B* **784**, 345 (2018), [arXiv:1806.00242].
- [365] A. M. Sirunyan *et al.* (CMS), *Phys. Lett. B* **805**, 135425 (2020), [arXiv:2002.06398].
- [366] A. Tumasyan *et al.* (CMS) (2022), [arXiv:2202.06923].
- [367] B. Abi *et al.* (Muon $g-2$), *Phys. Rev. Lett.* **126**, 14, 141801 (2021), [arXiv:2104.03281].
- [368] F. James and M. Roos, *Comput. Phys. Commun.* **10**, 343 (1975).
- [369] G. Aad *et al.* (ATLAS) (2023), [arXiv:2309.12986].
- [370] V. Abazov *et al.* (DØ), *Phys. Rev. D* **80**, 111107 (2009), [arXiv:0911.2710].
- [371] J. Bagger, K. T. Matchev and D. Pierce, *Phys. Lett. B* **348**, 443 (1995), [hep-ph/9501277].
- [372] P. Langacker and N. Polonsky, *Phys. Rev. D* **52**, 3081 (1995), [hep-ph/9503214].
- [373] M. Veltman, *Nucl. Phys. B* **123**, 89 (1977).
- [374] M. S. Chanowitz, M. Furman and I. Hinchliffe, *Phys. Lett. B* **78**, 285 (1978).
- [375] J. van der Bij and F. Hoogeveen, *Nucl. Phys. B* **283**, 477 (1987).
- [376] P. Langacker and M. Luo, *Phys. Rev. D* **45**, 278 (1992).
- [377] A. Denner, R. Guth and J. H. Kuhn, *Phys. Lett. B* **240**, 438 (1990).
- [378] W. Grimus *et al.*, *J. Phys. G* **35**, 075001 (2008), [arXiv:0711.4022].
- [379] H. E. Haber and D. O’Neil, *Phys. Rev. D* **83**, 055017 (2011), [arXiv:1011.6188].
- [380] S. Bertolini and A. Sirlin, *Phys. Lett. B* **257**, 179 (1991).
- [381] M. Golden and L. Randall, *Nucl. Phys. B* **361**, 3 (1991).
- [382] B. Holdom and J. Terning, *Phys. Lett. B* **247**, 88 (1990).
- [383] M. E. Peskin and T. Takeuchi, *Phys. Rev. Lett.* **65**, 964 (1990).
- [384] K. Hagiwara *et al.*, *Z. Phys. C* **64**, 559 (1994), [Erratum: *Z. Phys. C* **68**, 352 (1995)], [hep-ph/9409380].
- [385] M. E. Peskin and T. Takeuchi, *Phys. Rev. D* **46**, 381 (1992).
- [386] I. Maksymyk, C. Burgess and D. London, *Phys. Rev. D* **50**, 529 (1994), [hep-ph/9306267].
- [387] R. Barbieri *et al.*, *Nucl. Phys. B* **703**, 127 (2004), [hep-ph/0405040].
- [388] M. Farina *et al.*, *Phys. Lett. B* **772**, 210 (2017), [arXiv:1609.08157].
- [389] G. Altarelli and R. Barbieri, *Phys. Lett. B* **253**, 161 (1991).
- [390] D. Kennedy and P. Langacker, *Phys. Rev. D* **44**, 1591 (1991).
- [391] L. Randall and R. Sundrum, *Phys. Rev. Lett.* **83**, 3370 (1999), [hep-ph/9905221].
- [392] M. Carena *et al.*, *Nucl. Phys. B* **759**, 202 (2006), [hep-ph/0607106].
- [393] R. Contino, in “Theoretical Advanced Study Institute in Elementary Particle Physics: Physics of the Large and the Small,” 235–306 (2011), [arXiv:1005.4269].
- [394] D. D. Dietrich, F. Sannino and K. Tuominen, *Phys. Rev. D* **72**, 055001 (2005), [hep-ph/0505059].
- [395] M. T. Frandsen and M. Rosenlyst, *JHEP* **03**, 222 (2023), [arXiv:2207.01465].
- [396] E. Gates and J. Terning, *Phys. Rev. Lett.* **67**, 1840 (1991).
- [397] H. Georgi, *Nucl. Phys. B* **363**, 301 (1991).
- [398] M. J. Dugan and L. Randall, *Phys. Lett. B* **264**, 154 (1991).
- [399] H. E. Haber and G. L. Kane, *Phys. Rept.* **117**, 75 (1985).
- [400] A. Djouadi, *Phys. Rept.* **459**, 1 (2008), [hep-ph/0503173].
- [401] R. Barbieri *et al.*, *Nucl. Phys. B* **341**, 309 (1990).
- [402] R. Barbieri, M. Frigeni and F. Caravaglios, *Phys. Lett. B* **279**, 169 (1992).
- [403] J. Erler and D. M. Pierce, *Nucl. Phys. B* **526**, 53 (1998), [hep-ph/9801238].
- [404] G.-C. Cho and K. Hagiwara, *Nucl. Phys. B* **574**, 623 (2000), [hep-ph/9912260].
- [405] G. Altarelli *et al.*, *JHEP* **06**, 018 (2001), [hep-ph/0106029].
- [406] S. Heinemeyer, W. Hollik and G. Weiglein, *Phys. Rept.* **425**, 265 (2006), [hep-ph/0412214].
- [407] S. P. Martin, K. Tobe and J. D. Wells, *Phys. Rev. D* **71**, 073014 (2005), [hep-ph/0412424].
- [408] M. Ramsey-Musolf and S. Su, *Phys. Rept.* **456**, 1 (2008), [hep-ph/0612057].
- [409] S. Heinemeyer *et al.*, *JHEP* **04**, 039 (2008), [arXiv:0710.2972].
- [410] O. Buchmueller *et al.*, *Eur. Phys. J. C* **72**, 2020 (2012), [arXiv:1112.3564].
- [411] B. Grinstein and M. B. Wise, *Phys. Lett. B* **265**, 326 (1991).
- [412] A. Pich, I. Rosell and J. Sanz-Cillero, *JHEP* **01**, 157 (2014), [arXiv:1310.3121].
- [413] C. T. Hill and E. H. Simmons, *Phys. Rept.* **381**, 235 (2003), [Erratum: *Phys. Rept.* **390**, 553–554 (2004)], [hep-ph/0203079].
- [414] G. Panico and A. Wulzer, *The Composite Nambu-Goldstone Higgs*, volume 913, Springer (2016), [arXiv:1506.01961].
- [415] J. A. Cabrer, G. von Gersdorff and M. Quiros, *JHEP* **05**, 083 (2011), [arXiv:1103.1388].
- [416] J. Erler and P. Langacker, *Phys. Rev. Lett.* **105**, 031801 (2010), [arXiv:1003.3211].
- [417] J. Gunion, D. W. McKay and H. Pois, *Phys. Rev. D* **53**, 1616 (1996), [hep-ph/9507323].
- [418] A. Lenz, *Adv. High Energy Phys.* **2013**, 910275 (2013).
- [419] S. Chatrchyan *et al.* (CMS), *Phys. Rev. D* **86**, 112003 (2012), [arXiv:1209.1062].
- [420] A. Djouadi and A. Lenz, *Phys. Lett. B* **715**, 310 (2012), [arXiv:1204.1252].
- [421] O. Eberhardt *et al.*, *Phys. Rev. Lett.* **109**, 241802 (2012), [arXiv:1209.1101].
- [422] J. Maalampi and M. Roos, *Phys. Rept.* **186**, 53 (1990).
- [423] P. Langacker, *Phys. Rept.* **72**, 185 (1981).
- [424] J. L. Hewett and T. G. Rizzo, *Phys. Rept.* **183**, 193 (1989).
- [425] J. Kang, P. Langacker and B. D. Nelson, *Phys. Rev. D* **77**, 035003 (2008), [arXiv:0708.2701].
- [426] S. P. Martin, *Phys. Rev. D* **81**, 035004 (2010), [arXiv:0910.2732].

- [427] P. W. Graham *et al.*, Phys. Rev. D **81**, 055016 (2010), [arXiv:0910.3020].
- [428] J. Erler, J. L. Feng and N. Polonsky, Phys. Rev. Lett. **78**, 3063 (1997), [hep-ph/9612397].
- [429] D. Choudhury, T. M. Tait and C. Wagner, Phys. Rev. D **65**, 053002 (2002), [hep-ph/0109097].
- [430] J. Erler and P. Langacker, Phys. Rev. Lett. **84**, 212 (2000), [hep-ph/9910315].
- [431] P. Langacker and M. Plumacher, Phys. Rev. D **62**, 013006 (2000), [hep-ph/0001204].
- [432] P. Abreu *et al.* (DELPHI), Eur. Phys. J. C **10**, 415 (1999).
- [433] P. Langacker and D. London, Phys. Rev. D **38**, 886 (1988).
- [434] F. del Aguila, J. de Blas and M. Perez-Victoria, Phys. Rev. D **78**, 013010 (2008), [arXiv:0803.4008].
- [435] M. Chemtob, Prog. Part. Nucl. Phys. **54**, 71 (2005), [hep-ph/0406029].
- [436] R. Barbier *et al.*, Phys. Rept. **420**, 1 (2005), [hep-ph/0406039].
- [437] T. Han, H. E. Logan and L.-T. Wang, JHEP **01**, 099 (2006), [hep-ph/0506313].
- [438] M. Pospelov, Prog. Part. Nucl. Phys. **58**, 247 (2007), [hep-ph/0512128].
- [439] I. Antoniadis, in “Supergravity, Superstrings and M-Theory,” (2001), [hep-th/0102202].
- [440] M. Carena *et al.*, Phys. Rev. D **68**, 035010 (2003), [hep-ph/0305188].
- [441] K. Agashe *et al.*, JHEP **08**, 050 (2003), [hep-ph/0308036].
- [442] I. Gogoladze and C. Macesanu, Phys. Rev. D **74**, 093012 (2006), [hep-ph/0605207].
- [443] S. Weinberg, Phys. Rev. Lett. **43**, 1566 (1979).
- [444] W. Buchmuller and D. Wyler, Nucl. Phys. B **268**, 621 (1986).
- [445] B. Grzadkowski *et al.*, JHEP **10**, 085 (2010), [arXiv:1008.4884].
- [446] R. Contino *et al.*, JHEP **07**, 035 (2013), [arXiv:1303.3876].
- [447] K. Hagiwara *et al.*, Phys. Rev. D **48**, 2182 (1993).
- [448] A. Pomarol and F. Riva, JHEP **01**, 151 (2014), [arXiv:1308.2803].
- [449] J. Ellis, V. Sanz and T. You, JHEP **03**, 157 (2015), [arXiv:1410.7703].
- [450] A. Efrati, A. Falkowski and Y. Soreq, JHEP **07**, 018 (2015), [arXiv:1503.07872].
- [451] J. de Blas *et al.*, PoS **EPS-HEP2017**, 467 (2017), [arXiv:1710.05402].
- [452] E. da Silva Almeida *et al.*, Phys. Rev. D **99**, 3, 033001 (2019), [arXiv:1812.01009].
- [453] S. Dawson and P. P. Giardino, Phys. Rev. D **101**, 1, 013001 (2020), [arXiv:1909.02000].
- [454] T. Corbett *et al.*, Phys. Rev. D **107**, 11, 115013 (2023), [arXiv:2304.03305].
- [455] G.-C. Cho, K. Hagiwara and S. Matsumoto, Eur. Phys. J. C **5**, 155 (1998), [hep-ph/9707334].
- [456] K. Cheung, Phys. Lett. B **517**, 167 (2001), [hep-ph/0106251].
- [457] Z. Han and W. Skiba, Phys. Rev. D **71**, 075009 (2005), [hep-ph/0412166].
- [458] P. Langacker, M. Luo and A. K. Mann, Rev. Mod. Phys. **64**, 87 (1992).
- [459] P. Langacker, Rev. Mod. Phys. **81**, 1199 (2009), [arXiv:0801.1345].
- [460] P. Asadi *et al.*, Phys. Rev. D **108**, 5, 055026 (2023), [arXiv:2204.05283].
- [461] E. Bagnaschi *et al.*, JHEP **08**, 308 (2022), [arXiv:2204.05260].
- [462] J. Gu *et al.*, Chin. Phys. C **46**, 12, 123107 (2022), [arXiv:2204.05296].
- [463] A. Paul and M. Valli, Phys. Rev. D **106**, 1, 013008 (2022), [arXiv:2204.05267].

11. Status of Higgs Boson Physics

Revised August 2023 by M. Carena (FNAL; Chicago U.; Chicago U., Kavli Inst.), C. Grojean (DESY, Hamburg; Physik, Humboldt U.), M. Kado (MPP, Garching) and V. Sharma (UC San Diego).

11.1	Introduction	211
11.2	The Standard Model and the mechanism of electroweak symmetry breaking	212
11.2.1	The SM Higgs boson mass, couplings and quantum numbers	212
11.2.2	The SM custodial symmetry	213
11.2.3	Stability of the Higgs potential	213
11.2.4	Higgs boson production and decay mechanisms	213
11.3	The experimental profile of the Higgs boson	218
11.3.1	The principal decay channels of the Higgs boson	218
11.3.2	The Higgs boson decay to vector bosons	218
11.3.3	Measurement of the Higgs boson mass	219
11.3.4	Higgs decays to third generation fermions ($b\bar{b}$ and $\tau^+\tau^-$)	220
11.3.5	Higgs boson production in association with top quarks	222
11.3.6	Combining the main channels	223
11.3.7	Probing the Higgs boson coupling to the second generation	225
11.3.8	Searches for rare decays of the Higgs boson	226
11.3.9	Higgs boson pair production and self-coupling	228
11.3.10	Beyond the main Higgs boson production modes	230
11.3.11	First results on the main production and decay channels at 13.6 TeV	230
11.4	Main quantum numbers and width of the Higgs boson	231
11.4.1	Main quantum numbers J^{PC}	231
11.4.2	Off-shell couplings of the Higgs boson	234
11.4.3	The Higgs boson width	235
11.5	Probing the coupling properties of the Higgs boson	236
11.5.1	Probing coupling properties	236
11.5.2	Effective Lagrangian framework	240
11.6	New physics models of EWSB in the light of the Higgs boson discovery	242
11.6.1	Higgs bosons in the minimal supersymmetric standard model (MSSM)	243
11.6.2	Supersymmetry with singlet extensions	246
11.6.3	Supersymmetry with extended gauge sectors	246
11.6.4	Effects of CP violation	247
11.6.5	Non-supersymmetric extensions of the Higgs sector	248
11.6.6	Composite Higgs models	250
11.6.7	Searches for signatures of extended Higgs sectors	253
11.7	Summary and outlook	258

11.1 Introduction

Understanding how the masses of the known elementary particles are generated has been one of the fundamental endeavours in particle physics for several decades. The chiral nature of the weak interactions forbids an intrinsic mass terms for the quarks and leptons at high energy, and their masses can only appear as emergent quantities after the spontaneous symmetry of the electroweak symmetry. The discovery in 2012 by the ATLAS [1] and the CMS [2] collaborations of a new resonance with a mass of approximately 125 GeV and the subsequent studies of its properties with the full data set from Run 1, from 2009 to 2012, with a centre-of-mass energy of 7 TeV and 8 TeV, conclusively provided a first sketch of the Electroweak Symmetry Breaking (EWSB) mechanism. The much larger dataset collected during the LHC Run 2, from 2015 to 2018, with a higher centre-of-mass energy of 13 TeV, demonstrated the compatibility of the measured resonance with the Higgs boson of the Standard Model (SM) [3] and strongly challenged other contenders. The LHC started its Run 3

in 2022 and this data taking phase is expected to comprise of four years of operations until 2026. By then the LHC is expected to deliver proton-proton collision data corresponding to an integrated luminosity of approximately 250 fb^{-1} per experiment.

In the SM, the electroweak interactions are described by a gauge field theory invariant under the $SU(2)_L \times U(1)_Y$ symmetry group. The mechanism of EWSB [4] provides a general framework to keep untouched the structure of these gauge interactions at high energies and still generate the observed masses of the W and Z gauge bosons as well as those of the quarks and charged leptons. The EWSB mechanism posits a self-interacting complex EW doublet scalar field, whose CP -even neutral component acquires a vacuum expectation value (VEV) $v \approx 246\text{ GeV}$, which sets the scale of the symmetry breaking. Three massless Goldstone bosons are generated and are absorbed to give masses to the W and Z gauge bosons. The remaining component of the complex doublet becomes the Higgs boson – a new, and so far unique, fundamental scalar particle. The masses of all fermions are also a consequence of EWSB since the Higgs doublet is postulated to couple to the fermions through Yukawa interactions in a way consistent with all the gauge symmetries of the SM.

The initial measurements during the LHC Run 1 were accessible mainly through production and decay channels related to the couplings of the Higgs boson to the vector gauge bosons. The outstanding performance of the LHC Run 2, made it possible for the ATLAS and CMS experiments to independently and unambiguously establish the couplings of the Higgs boson to the charged fermions of the third generation (the top quark, the bottom quark, and the tau lepton). In all observed production and decay modes measured so far, the rates and differential measurements are found to be consistent, within experimental and theoretical uncertainties, with the SM predictions. In high mass resolution decay channels, such as the ones with four leptons (electrons or muons) or diphoton final states, the mass of the Higgs boson has been measured at the permill precision level. And, from the search for Higgs boson decays to muons, there are tentativing experimental evidences for Yukawa interactions of the Higgs boson to the second generation of fermions. Nevertheless, several Higgs boson decay channels are very challenging experimentally at the LHC. The couplings of the Higgs boson to the first generation of fermions, at the level expected in the Standard Model, remain so far out of reach at the LHC.

Within the current precision, a more complex Higgs sector with additional states, although significantly constrained, is not ruled out. Nor has it been established whether the Higgs boson is an elementary particle or whether it has an internal structure like any other scalar particle observed before it. Therefore, Higgs physics remains a vivid and intense field of research on the experimental and theoretical fronts.

Without the Higgs boson, the calculability of the SM would have been spoiled. In particular, perturbative unitarity [5] would be lost at high energies since the longitudinal W/Z boson scattering amplitude would grow with the centre-of-mass energy. In addition, the radiative corrections to the gauge boson self-energies would exhibit dangerous logarithmic divergences that would be difficult to reconcile with EW precision data. With the discovery of the Higgs boson, the SM is a spontaneously broken gauge theory and, as such, it could a priori be consistently extrapolated well above the masses of the W and Z bosons. Hence, formally there is no need for new physics at the EW scale. However, as the SM Higgs boson is a scalar particle, it has sensitivity to possible new physics scales. Quite generally, the Higgs boson mass is affected by the presence of heavy particles and it receives large quantum corrections which destabilise the weak scale barring a large fine-tuning of unrelated parameters. This is known as the Higgs naturalness or hierarchy problem [6], and it has been the prime argument for expecting new physics right at the TeV scale. To remedy to his unsatisfactory feature, theoretically motivated paradigms have been explored for several decades, such as a new fermion-boson symmetry called supersymmetry (SUSY) [7] (for recent reviews, see Refs. [8, 9]), or the existence of strong interactions at a scale of the order of a TeV from which the Higgs boson would emerge as a composite state [10] (see Refs. [11, 12]

for recent reviews). Alternatively, new agents stabilising the weak scale could also be light but elusive, like in models of neutral naturalness [13, 14]. And it was recently appreciated [15, 16] that the cosmological evolution of the Universe could drive the Higgs boson mass to a value much smaller than the cutoff of the theory, alleviating the hierarchy problem without the need for TeV scale new physics, even though there might still be interesting and spectacular signatures [15, 17]. This new approach spurs a change in perspective invoking our Universe as part of a multiverse that should be treated as a quantum statistical system [18].

The Higgs boson is special and, in the eleven years since its discovery, it became a powerful tool to explore the manifestations of the SM and to probe the physics landscape beyond it.

This review is organised as follows. Section 11.2 is a theoretical introduction to the SM Higgs boson, its properties, production mechanisms and decay rates. The experimental measurements are described in Section 11.3. In Section 11.3.6, the combination of the main Higgs boson production and decay channels is presented. In Section 11.4, measurements of the main quantum numbers and CP properties of the Higgs boson are reported and the bounds on its total width are discussed. In Section 11.5, a general theoretical framework to describe the deviations of the Higgs boson couplings from the SM predictions is introduced and the experimental measurements of these Higgs couplings are reviewed. Measurements of differential cross sections are also outlined. Section 11.6 presents, in detail, some interesting models with an extended Higgs sector, addressing the hierarchy problem or not, and considers their experimental signatures. Section 11.7 provides a short summary and a brief outlook.

11.2 The Standard Model and the mechanism of electroweak symmetry breaking

In the SM [3], electroweak symmetry breaking [4] is responsible for generating a mass for the W and Z gauge bosons rendering the weak interactions short ranged. The SM scalar potential reads:

$$V(\Phi) = m^2 \Phi^\dagger \Phi + \lambda (\Phi^\dagger \Phi)^2 \quad (11.1)$$

with the Higgs field Φ being a self-interacting $SU(2)_L$ complex doublet (four real degrees of freedom) with weak hypercharge $Y=1$ (the hypercharge is normalised such that $Q = T_{3L} + Y/2$, Q being the electric charge and T_{3L} the eigenvalue of the diagonal generator of $SU(2)_L$):

$$\Phi = \frac{1}{\sqrt{2}} \begin{pmatrix} \sqrt{2}\phi^+ \\ \phi^0 + ia^0 \end{pmatrix}, \quad (11.2)$$

where ϕ^0 and a^0 are the CP -even and CP -odd neutral components, and ϕ^+ is the complex charged component of the Higgs doublet, respectively. $V(\Phi)$ is the most general renormalisable scalar potential invariant under $SU(2)_L \times U(1)_Y$. If the quadratic term is negative, the neutral component of the scalar doublet acquires a non-zero (real) vacuum expectation value (VEV)

$$\langle \Phi \rangle = \frac{1}{\sqrt{2}} \begin{pmatrix} 0 \\ v \end{pmatrix}, \quad (11.3)$$

with $\phi^0 = H + \langle \phi^0 \rangle$ and $\langle \phi^0 \rangle \equiv v$, inducing the spontaneous breaking of the SM gauge symmetry $SU(3)_C \times SU(2)_L \times U(1)_Y$ into $SU(3)_C \times U(1)_{\text{em}}$. The global minimum of the theory defines the ground state, and spontaneous symmetry breaking implies that there is a (global and/or local) symmetry of the system that is not respected by the ground state. From the four generators of the $SU(2)_L \times U(1)_Y$ SM gauge group, three are spontaneously broken, i.e., they do not leave the ground state invariant. This breaking implies the existence of three massless Goldstone bosons identified with three of the four Higgs field degrees of freedom. The Higgs field couples to the W_μ and B_μ gauge fields associated with the $SU(2)_L \times U(1)_Y$ local symmetry through the covariant derivative appearing in the kinetic term of the Higgs Lagrangian,

$$\mathcal{L}_{\text{Higgs}} = (D_\mu \Phi)^\dagger (D^\mu \Phi) - V(\Phi), \quad (11.4)$$

where $D_\mu \Phi = (\partial_\mu + ig\sigma^a W_\mu^a/2 + ig'Y B_\mu/2)\Phi$, g and g' are the $SU(2)_L$ and $U(1)_Y$ gauge couplings, respectively, and $\sigma^a, a = 1, 2, 3$ are the usual Pauli matrices. As a result, the neutral

and the two charged massless Goldstone degrees of freedom mix with the gauge fields corresponding to the broken generators of $SU(2)_L \times U(1)_Y$ and become, in the unitarity gauge, the longitudinal components of the Z and W physical gauge bosons, respectively. The Z and W gauge bosons acquire masses,

$$m_W^2 = \frac{g^2 v^2}{4}, \quad m_Z^2 = \frac{(g'^2 + g^2)v^2}{4}. \quad (11.5)$$

The fourth generator remains unbroken since it is the one associated to the conserved $U(1)_{\text{em}}$ gauge symmetry, and its corresponding gauge field, the photon, remains massless. Similarly, the eight color gauge bosons, the gluons, corresponding to the conserved $SU(3)_C$ gauge symmetry with 8 unbroken generators, also remain massless (though confined inside hadrons and mesons as the result of the asymptotic freedom behaviour of Quantum ChromoDynamics (QCD)). Hence, from the initial four degrees of freedom of the Higgs field, two are absorbed by the W^\pm gauge bosons, one by the Z gauge boson, and there is one remaining degree of freedom, H , that is the physical Higgs boson — a new scalar particle first imagined by P. Higgs [4]. The Higgs boson is neutral under the electromagnetic interactions and transforms as a singlet under $SU(3)_C$ and hence does not couple at tree level to the massless photons and gluons.

The fermions of the SM acquire a mass through renormalisable and gauge invariant interactions between the Higgs field and the fermions: the Yukawa interactions,

$$\mathcal{L}_{\text{Yukawa}} = -\hat{h}_{d_{ij}} \bar{q}_{L_i} \Phi d_{R_j} - \hat{h}_{u_{ij}} \bar{q}_{L_i} \tilde{\Phi} u_{R_j} - \hat{h}_{l_{ij}} \bar{l}_{L_i} \Phi e_{R_j} + h.c., \quad (11.6)$$

which respect the symmetries of the SM but generate fermion masses once EWSB occurs. In the Lagrangian above, $\tilde{\Phi} = i\sigma_2 \Phi^*$ and q_L (l_L) and u_R , d_R (e_R) are the quark (lepton) $SU(2)_L$ doublets and singlets, respectively, while in each term, $\hat{h}_{f_{ij}}$, $f = u, d, l$ is parametrised by a 3×3 matrix in family space. The mass term for neutrinos is omitted, but could be added in an analogous manner to the up-type quarks when right-handed neutrinos are supplementing the SM particle content (neutrinos can also acquire Majorana masses via non-renormalisable dimension-5 interactions with the Higgs field [19]). Once the Higgs field acquires a VEV, and after rotation to the fermion mass eigenstate basis that also diagonalises the Higgs-fermion interactions, $\hat{h}_{f_{ij}} \rightarrow h_{f_i} \delta_{ij}$ (the diagonal Yukawa coupling h_{f_i} is often denoted as y_{f_i}), all fermions acquire a mass given by $m_{f_i} = h_{f_i} v / \sqrt{2}$. The indices $i, j = 1, 2, 3$ refer to the three families in the up-quark, down-quark or charged lepton sectors. Remarkably, if the Yukawa interactions Eq. (11.6) are indeed fully responsible for the fermion masses, the Higgs interactions do not mediate flavour changing neutral currents at tree-level. It should be further noted that the EWSB mechanism provides no additional insight on possible underlying reasons for the large variety of mass values of the fermions, often referred to as the flavour hierarchy. The fermion masses, accounting for a large number of the free parameters of the SM, are simply translated into Yukawa couplings.

11.2.1 The SM Higgs boson mass, couplings and quantum numbers

The SM Higgs boson is a CP -even scalar of spin 0. Its mass is given by $m_H = \sqrt{2\lambda} v$, where λ is the self-coupling parameter in $V(\Phi)$. The expectation value of the Higgs field, $v = (\sqrt{2}G_F)^{-1/2} \approx 246$ GeV, is fixed by the Fermi coupling G_F , which is determined with a precision of 0.6 ppm from muon decay measurements [20]. The quartic coupling λ is a free parameter in the SM, and hence, there is no a priori prediction for the Higgs mass. Moreover the sign of the quadratic coupling, $m^2 = -\lambda v^2$, in the Higgs field potential $V(\Phi)$ has to be negative for the EW symmetry breaking to take place, but there is no a priori understanding of what decides of this sign. The experimentally measured Higgs boson mass, $m_H \simeq 125$ GeV [20], implies that $\lambda \simeq 0.13$ and $|m| \simeq 88.4$ GeV.

The Higgs boson couplings to the fundamental particles are set by their masses. This is a new type of interaction; very weak for light particles, such as up and down quarks, and electrons, but strong for heavy particles such as the W and Z bosons and

the top quark. More precisely, the SM Higgs couplings to fundamental fermions are linearly proportional to the fermion masses, whereas the couplings to bosons are proportional to the square of the boson masses. The SM Higgs boson couplings to gauge bosons and fermions, as well as the Higgs boson self coupling, are summarised in the following Lagrangian:

$$\mathcal{L} = -g_{Hf\bar{f}}\bar{f}fH + \frac{g_{HHH}}{6}H^3 + \frac{g_{HHHH}}{24}H^4 + \delta_V V_\mu V^\mu \left(g_{HVV}H + \frac{g_{HHVV}}{2}H^2 \right) \quad (11.7)$$

with

$$g_{Hf\bar{f}} = \frac{m_f}{v}, \quad g_{HVV} = \frac{2m_V^2}{v}, \quad g_{HHVV} = \frac{2m_V^2}{v^2}, \quad (11.8)$$

$$g_{HHH} = \frac{3m_H^2}{v}, \quad g_{HHHH} = \frac{3m_H^2}{v^2},$$

where $V = W^\pm$ or Z and $\delta_W = 1, \delta_Z = 1/2$. As a result, the dominant mechanisms for Higgs boson production and decay involve the coupling of H to W, Z and/or the third generation quarks and leptons. The Higgs boson coupling to gluons [21,22] is induced at leading order by a one-loop process in which H couples to a virtual $t\bar{t}$ pair (with minor contributions from the other lighter quarks). Likewise, the Higgs boson coupling to photons is also generated via loops, although in this case the one-loop graph with a virtual W^+W^- pair provides the dominant contribution [23] and it is interfering destructively with the smaller contribution involving a virtual $t\bar{t}$ pair (as such, the Higgs coupling to photons is sensitive to the relative phase of the interactions between bosons and fermions).

11.2.2 The SM custodial symmetry

The SM Higgs Lagrangian, $\mathcal{L}_{\text{Higgs}} + \mathcal{L}_{\text{Yukawa}}$ of Eq. (11.4) and Eq. (11.6), is, by construction, $SU(2)_L \times U(1)_Y$ gauge invariant, but it also has an approximate global symmetry. In the limit $g' \rightarrow 0$ and $h_f \rightarrow 0$, a global $SU(2)_R$ symmetry emerges. This symmetry is preserved for non-vanishing Yukawa couplings provided $\hat{h}_u = \hat{h}_d$. Once the Higgs field acquires a VEV, both the $SU(2)_L$ and $SU(2)_R$ symmetry groups are broken but the diagonal subgroup $SU(2)_{L+R}$ remains unbroken and it is this subgroup that defines the custodial symmetry of the SM [24].

In the limit $g' \rightarrow 0$, the W^\pm and Z gauge bosons have equal mass and form a triplet of the $SU(2)_{L+R}$ unbroken global symmetry. Using the expressions for the W and Z gauge boson masses in term of the gauge couplings, one obtains at tree level

$$\frac{m_W^2}{m_Z^2} = \frac{g^2}{g^2 + g'^2} \equiv \cos^2 \theta_W \quad \text{i.e.} \quad \rho \equiv \frac{m_W^2}{m_Z^2 \cos^2 \theta_W} = 1. \quad (11.9)$$

The custodial symmetry protects the above relation from large radiative corrections. All corrections to the ρ parameter are therefore proportional to terms that break the custodial symmetry. For instance, radiative corrections involving the Higgs boson are proportional to $\sin^2 \theta_W$, $\delta\rho = -11G_F m_Z^2 \sin^2 \theta_W \log(m_H^2/m_Z^2)/(24\sqrt{2}\pi^2)$, and vanish in the limit $g' \rightarrow 0$. Since $m_t \neq m_b$, there are also relevant radiative corrections generated by massive fermions. They are proportional to $m_t^2 + m_b^2 - 2(m_t^2 m_b^2) \log(m_t^2/m_b^2)/(m_t^2 - m_b^2)$ and would indeed vanish for $m_t = m_b$ [25].

11.2.3 Stability of the Higgs potential

The discovery of the Higgs boson with $m_H \approx 125$ GeV has far reaching consequences within the SM framework. In particular, the precise value of m_H determines the value of the quartic coupling λ at the electroweak scale and makes it possible to study its behavior up to high energy scales. A larger value of m_H would have implied that the self coupling λ would become non-perturbative at some scale Λ that could be well below the Planck scale [26].

However, for the value of Higgs boson mass experimentally measured, the EW vacuum of the Higgs potential is most likely metastable [27]. The high-energy evolution of λ shows that it becomes negative at energies $\Lambda = \mathcal{O}(10^{11})$ GeV (even though λ

could remain positive till higher energy, maybe all the way to the Planck scale, if the top quark mass exceeds its current measured value by 3σ). When this occurs, the SM Higgs potential develops an instability and the long term existence of the EW vacuum is challenged. This behaviour may call for new physics at an intermediate scale before the instability develops, i.e., below M_{Planck} , even though new physics at M_{Planck} could influence the stability of the EW vacuum and possibly modify this conclusion [28]. The consequences of the instability of the EW vacuum on high-scale inflation have been discussed in Ref. [29]. It was also noticed that Higgs field fluctuations during inflation could seed the formation of primordial black holes, possibly making up the Dark Matter relic abundance [30] or they could produce a stochastic background of gravitational waves with characteristic structures [31], offering a probe of the EW vacuum near criticality.

The lifetime of the EW metastable vacuum is determined by the rate of quantum tunnelling from this vacuum into the true vacuum of the theory (for the most recent computation of the EW vacuum lifetime within the SM, see Ref. [32]). Within the SM, the running of the Higgs self coupling slows down at high energies with a cancellation of its β -function at energies just one to two orders of magnitude below the Planck scale [33]. This slow evolution of the quartic coupling is responsible for saving the EW vacuum from premature collapse. It might also help the Higgs boson to play the role of an inflaton [34] (see, however, Ref. [35] for potential issues with this Higgs-boson-as-an-inflaton idea).

11.2.4 Higgs boson production and decay mechanisms

Comprehensive reviews of the SM Higgs boson properties and phenomenology, with an emphasis on the impact of loop corrections to the Higgs boson decay rates and cross sections, can be found in Refs. [36–40]. The main results are summarised here.

11.2.4.1 Production mechanisms at hadron colliders

The main production mechanisms at the Tevatron collider and the LHC are gluon fusion (ggF), weak-boson fusion (VBF), associated production with a gauge boson (VH), and associated production with a $t\bar{t}$ pair ($t\bar{t}H$) or with a single top quark (tHq). Figure 11.1 depicts representative diagrams for these dominant Higgs boson production processes.

The state-of-the-art of the theoretical calculations in the main different production channels is summarised in Table 11.1.

Table 11.1: State-of-the-art of the theoretical calculations in the main Higgs boson production channels in the SM, and, when publicly available, the major MC tools used in the simulations. Furthermore, all the Higgs-boson production modes have been interfaced with parton-shower event generators at NLO QCD like *Poweg-Box*, *MG5_aMC@NLO* or *Sherpa* (the entries “—” indicate cases when the results are implemented in codes that are not yet public). For ggF and VH NNLO matched simulations now also exist. Differential NNLO QCD results exist for $t\bar{t}H$ [41] (though the exact 2-loop virtual corrections are still missing) and have been implemented in *MATRIX* [42].

ggF	VBF	VH	$t\bar{t}H$
Inclusive:	Inclusive:	Inclusive:	Inclusive:
N3LO QCD + NLO EW (iHixs)	N3LO QCD proVBFH	N3LO QCD (n3loxz)	NNLO QCD —
N3LO QCD ggHiggs		NNLO QCD (VH@NNLO)	
Differential:	Differential:	Differential:	Differential:
NNLO+N3LL QCD (Radish+NNLOJET)	NNLO QCD	NNLO QCD	NLO QCD+EW (MG5_aMC@NLO)
N3LO+N3LL' QCD (TROLL)	NLO QCD + EW (HAWK)	NLO QCD + EW (HAWK)	

The cross sections for the production of a SM Higgs boson as a function of \sqrt{s} , the center of mass energy, for pp collisions, including bands indicating the theoretical uncertainties, are summarised in Fig. 11.2 (left) [43]. A detailed discussion, including uncertainties in the theoretical calculations due to missing higher-order effects and experimental uncertainties on the determination

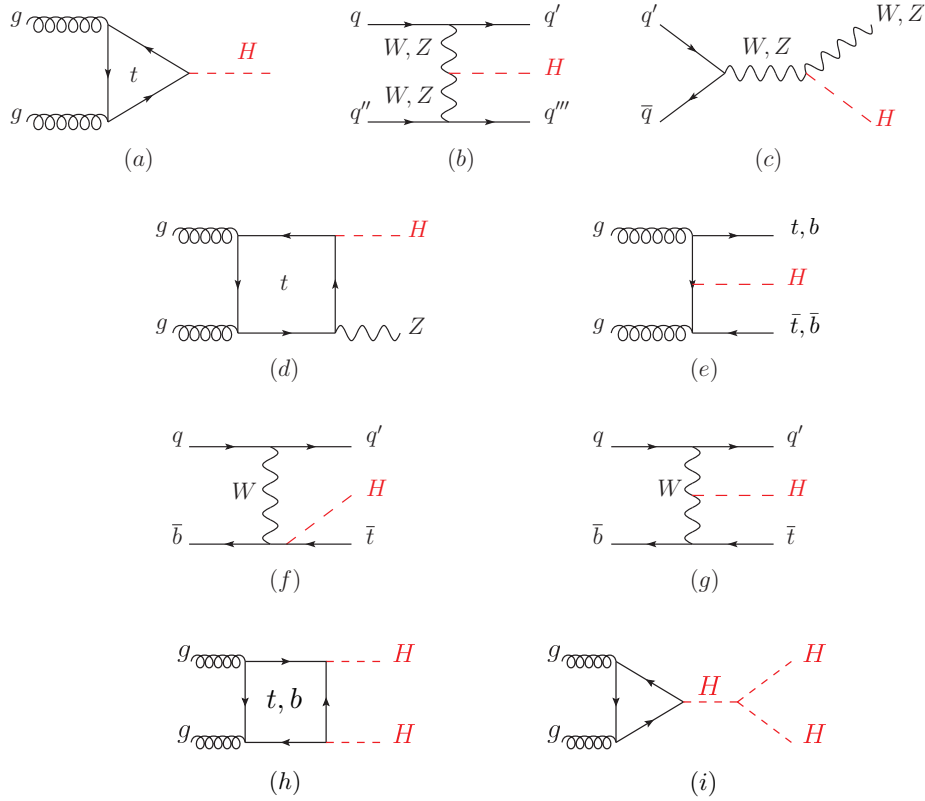


Figure 11.1: Main leading order Feynman diagrams contributing to the single Higgs boson production in (a) gluon fusion, (b) Vector-boson fusion, (c) Higgs-strahlung (or associated production with a gauge boson at tree level from a quark-quark interaction), (d) associated production with a gauge boson (at loop level from a gluon-gluon interaction), (e) associated production with a pair of top/bottom quarks, (f-g) production in association with a single top quark, and double Higgs production through (h) a top- and bottom-quark loop, (i) the self coupling of the Higgs boson.

of SM parameters involved in the calculations, can be found in Refs. [37–40]. These references also contain state-of-the-art discussions on the impact of PDF uncertainties, QCD scale uncertainties and uncertainties due to different procedures for including higher-order corrections matched to parton shower simulations, as well as uncertainties due to hadronisation and parton-shower events.

Table 11.2 summarises the Higgs boson production cross sections and relative uncertainties for a Higgs boson mass of 125 GeV, for $\sqrt{s} = 7, 8, 13, 13.6$ and 14 TeV.

i. Gluon fusion production mechanism

At high-energy hadron colliders, the Higgs boson production mechanism with the largest cross section is the gluon-fusion process, $gg \rightarrow H + X$, mediated by the exchange of a virtual, heavy top quark [45]. Contributions from lighter quarks propagating in the loop are suppressed proportionally to m_q^2 . QCD radiative corrections to the gluon-fusion process are very important and have been studied in detail. Including the full dependence on the (top, bottom, charm) quark and Higgs boson masses, the cross section has been calculated at the next-to-leading order (NLO) in α_s [46, 47]. To a very good approximation, the leading top-quark contribution can be evaluated in the limit $m_t \rightarrow \infty$ by matching the SM to an effective theory. The gluon-fusion amplitude is then evaluated from an effective Lagrangian containing a local $HG_{\mu\nu}^a G^{a\mu\nu}$ operator [21, 22]. In this approximation, the cross section is known at next-to-next-to-next-to-leading order in α_s expansion (N3LO QCD) [48]. The validity of the effective theory with infinite m_t is greatly enhanced by rescaling the result by the exact LO result: $\sigma = (\sigma_{m_t}^{\text{LO}}/\sigma_{m_t=\infty}^{\text{LO}}) \times \sigma_{m_t=\infty}$ [40]. The large top-quark mass approximation, after this rescaling of the cross section, yields a next-to-next-to-leading order (NNLO) QCD result that has been established to be at the percent level accuracy [49]. Fur-

ther progress was made to include full top mass dependence at NNLO QCD [50]. And the bottom and light quark contributions to the Higgs production have been reassessed in Refs. [51–53].

The LO contribution and NLO QCD corrections [54] amount to about 80% of the total N3LO QCD cross section. The NNLO QCD corrections [55] further enhance the cross section by approximately 30% of the LO plus NLO result (at $\mu_f = \mu_r = m_H/2$). Electroweak radiative corrections have been computed at NLO and increase the LO cross section by about 5% for $m_H \simeq 125$ GeV [56]. Mixed QCD-EW corrections are now being investigated with encouraging results on the computation of the exact 3-loop amplitude [57] complementing the results obtained in either limit of heavy [58] or massless [59] gauge bosons. The mixed QCD-EW corrections still have to be evaluated at large pt .

At N3LO QCD, the perturbation series is rather stable with a mere enhancement of 3% of the total cross section, with a central value quite insensitive to threshold resummation effects with the scale choice mentioned above ($\mu_f = \mu_r = m_H/2$) [40, 48, 60, 61]. At the LHC with a center-of-mass energy of 13 TeV, the most up-to-date value for the production cross section of a 125 GeV Higgs boson amounts to [40]

$$\sigma_{\text{ggF}}^{\text{N3LO}} = 48.6^{+2.2(4.6\%)}_{-3.3(6.7\%)} (\text{theory}) \pm 1.6(3.2\%) (\text{PDF} + \alpha_s) \text{ pb.} \quad (11.10)$$

This cross-section was first computed in terms of an expansion around the production threshold of the Higgs boson. This approximation was overcome in Ref. [61]. The PDF uncertainty of order 1-2% quoted above has been questioned as the first global analysis of PDFs at approximate N3LO QCD was presented, suggesting an unexpected decrease of the cross-section central value by more than 5% [62].

Besides considering the inclusive Higgs boson production cross section at the LHC, it is important to study differential distri-

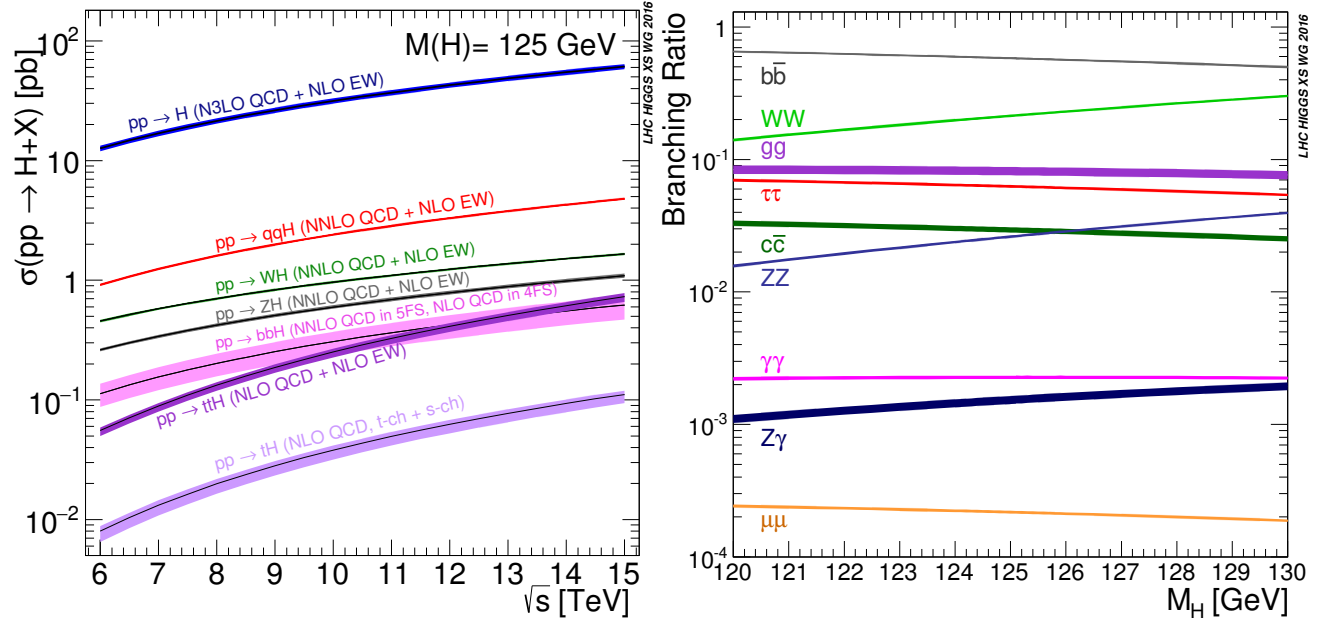


Figure 11.2: (Left) The SM Higgs boson production cross sections as a function of the center of mass energy, \sqrt{s} , for pp collisions [43]. The VBF process is indicated here as qqH . (Right) The branching ratios for the main decays of the SM Higgs boson near $m_H = 125$ GeV [39, 40]. The theoretical uncertainties are indicated as bands.

butions in order to probe the properties of the Higgs boson in a detailed way. The Higgs boson rapidity distribution has been computed at the N3LO QCD order in Ref. [63]. And fully differential N3LO QCD predictions for Higgs production in gluon fusion have been obtained by combining N3LO QCD predictions for Higgs rapidity distribution with NNLO QCD predictions for H +jet [64]. A more exclusive account of Higgs boson production is also required because experimental analyses often impose cuts on the final states in order to improve the signal-to-background ratio. Using soft-collinear effective theory, large fiducial power corrections induced by fiducial cuts have been resummed at N3LO+N3LL/QCD accuracy, i.e. at next-to-next-to-next-leading-log, incorporating the complete $\mathcal{O}(\alpha_s^3)$ singular structure for $q_T \rightarrow 0$ allowing one to consistently match to N3LO QCD [65]. This is the most accurate result that can be directly compared with fiducial measurements. Different fiducial cuts are explored to suppress these fiducial effects. In addition, progress has been made to improve the calculation of the Higgs boson production cross section with a jet veto (the “0-jet bin” or in the presence of a veto bounding the transverse momentum of the hardest accompanying jet) [66], reaching NNLL accuracy matched to N3LO QCD. These accurate predictions for the jet-veto cross section are required, e.g., to suppress the $t\bar{t}$ background in the $H \rightarrow WW$ channel [67].

ii. Vector boson fusion production mechanism

The SM Higgs boson production mode with the second-largest cross section at the LHC is vector boson fusion. At the Tevatron collider, VBF also occurred, but for $m_H = 125$ GeV had a smaller cross section than Higgs boson production in association with a W or Z boson. Higgs boson production via VBF, $qq \rightarrow qqH$, proceeds by the scattering of two (anti-)quarks, mediated by t - or u -channel exchange of a W or Z boson, with the Higgs boson radiated off the weak-boson propagator. The scattered quarks give rise to two hard jets in the forward and backward regions of the detector with a large rapidity gap [68]. Because of the color-singlet nature of the weak-gauge boson exchange, gluon radiation from the central-rapidity regions is strongly suppressed. These characteristic features of VBF processes can be exploited to distinguish them from overwhelming QCD backgrounds, including gluon-fusion induced Higgs boson + 2 jet production, and from s -channel WH or ZH production with a hadronically decaying weak gauge boson. After the application of specific selection cuts,

the VBF channel provides a clean environment, not only for the Higgs boson searches originally performed, but also for the subsequent determination of Higgs boson couplings at the LHC.

The cross-section is known at N3LO QCD at the inclusive level [69] and at NNLO enforcing the VBF cuts [70] with a residual uncertainty of the order of few permill. However, this result is obtained in the DIS/factorized approximation [71] where the fusing gauge bosons are emitted from the two quark legs independently. While, the exact NNLO QCD VBF calculation will remain out-of-reach in the near future, the leading non-factorisable contributions with two forward jets have been estimated [72] and the impact of non-factorizable effects have been studied in Ref. [73]. They give some corrections, also of the order of few permill, to inclusive quantities, but they are an order of magnitude larger for differential observables. Overall, the residual uncertainty is of the order of a few percent but is quite sensitive to the tagging jet cuts and jet radius modelling [74]. Extensive studies on VBF at fixed order and with parton shower matched computations can be found in Ref. [75]. In addition, EW corrections have been included and the VBF process is known at NLO QCD+EW order for some time [76, 77].

iii. WH and ZH associated production mechanism

The next most relevant Higgs boson production mechanisms are associated production with W and Z gauge bosons. The cross sections for the associated production processes, $pp \rightarrow VH + X$, with $V = W^\pm, Z$ receive contributions at NLO QCD given by NLO QCD corrections to the Drell–Yan cross section [78, 79] and from NLO EW corrections. The latter, unlike the QCD corrections, do not respect the factorisation into Drell–Yan production since there are irreducible box contributions already at one loop [76, 80]. At NNLO QCD, the Drell–Yan-like corrections to WH production also give the bulk of the corrections to ZH production [81]. For ZH production there are, however, gluon-gluon induced contributions that do not involve a virtual Z gauge boson but are such that the Z gauge boson and H boson couple to gluons via top-quark loops [82], see diagram (d) in Fig. 11.1. NLO QCD virtual corrections to the partonic cross section for $gg \rightarrow ZH$, in the high-energy and large top mass limits are available in Refs. [83]. In addition, WH and ZH production receive non Drell–Yan-like corrections in the $q\bar{q}'$ and $q\bar{q}$ initiated channels, respectively, at the NNLO level in QCD, where the Higgs boson is radiated off

Table 11.2: The SM Higgs boson production cross sections for $m_H = 125$ GeV in pp collisions ($p\bar{p}$ collisions at $\sqrt{s} = 1.96$ TeV for the Tevatron), as a function of the center of mass energy, \sqrt{s} . The predictions for the LHC energies are taken from Refs. [37–40, 43], the ones for the Tevatron energy are the ones used in Ref. [44]. The predictions for the ggF channel at the LHC include the latest N3LO QCD + NLO EW results. The uncertainties are estimated assuming no correlation between α_S and PDF uncertainties. The uncertainties on the total cross sections are dominated by the ones on the gluon fusion process.

\sqrt{s} (TeV)	Production cross section (in pb) for $m_H = 125$ GeV					
	ggF	VBF	WH	ZH	$t\bar{t}H$	total
1.96	$0.95^{+17\%}_{-17\%}$	$0.065^{+8\%}_{-7\%}$	$0.13^{+8\%}_{-8\%}$	$0.079^{+8\%}_{-8\%}$	$0.004^{+10\%}_{-10\%}$	$1.23^{+15\%}_{-15\%}$
7	$16.9^{+5.5\%}_{-7.6\%}$	$1.24^{+2.2\%}_{-2.2\%}$	$0.58^{+2.2\%}_{-2.3\%}$	$0.34^{+3.1\%}_{-3.0\%}$	$0.09^{+5.6\%}_{-10.2\%}$	$19.1^{+5\%}_{-7\%}$
8	$21.4^{+5.4\%}_{-7.6\%}$	$1.60^{+2.1\%}_{-2.1\%}$	$0.70^{+2.1\%}_{-2.2\%}$	$0.42^{+3.4\%}_{-2.9\%}$	$0.13^{+5.9\%}_{-10.1\%}$	$24.2^{+5\%}_{-7\%}$
13	$48.6^{+5.6\%}_{-7.4\%}$	$3.78^{+2.1\%}_{-2.1\%}$	$1.37^{+2.0\%}_{-2.0\%}$	$0.88^{+4.1\%}_{-3.5\%}$	$0.50^{+6.8\%}_{-9.9\%}$	$55.1^{+5\%}_{-7\%}$
13.6	$52.2^{+5.6\%}_{-7.4\%}$	$4.1^{+2.1\%}_{-1.5\%}$	$1.46^{+1.8\%}_{-1.9\%}$	$0.95^{+4.0\%}_{-3.6\%}$	$0.57^{+6.9\%}_{-9.9\%}$	$59.2^{+5\%}_{-7\%}$
14	$54.7^{+5.6\%}_{-7.4\%}$	$4.28^{+2.1\%}_{-2.1\%}$	$1.51^{+1.8\%}_{-1.9\%}$	$0.99^{+4.1\%}_{-3.7\%}$	$0.61^{+6.9\%}_{-9.8\%}$	$62.1^{+5\%}_{-7\%}$

top-quark loops [84]. The full QCD corrections up to NNLO order, the NLO EW corrections and the NLO corrections to the gluon-gluon channel are available in VH@NNLO [85]. NNLO QCD corrections to $pp \rightarrow WH + \text{jet}$ are important for signal modelling. NLO corrections to cross section inclusive in the number of jets show excellent convergence while NNLO QCD corrections to exclusive single jet cross section are much more significant [86].

As neither the Higgs boson nor the weak gauge bosons are stable particles, their decays also have to be taken into account. Providing full kinematical information for the decay products can furthermore help in the suppression of large QCD backgrounds. Differential distributions for the processes $pp \rightarrow WH \rightarrow \bar{\nu}_\ell \ell H$ and $pp \rightarrow ZH \rightarrow \ell^+ \ell^- H / \nu_\ell \bar{\nu}_\ell H$, including NLO QCD and EW corrections, have been presented in Ref. [87]. The NNLO QCD corrections to differential observables for WH production at the LHC, including the leptonic decays of the W boson and the decay of the Higgs boson into a $b\bar{b}$ pair, are presented in Ref. [88]. Calculations at the same level, including also the ZH process have been performed [89]. The WH production mode has also been matched to a parton shower at NNLO QCD accuracy [90]. Full NNLO QCD results for both the production and decay are available [91] and show a large impact of radiation from the final-state bottoms. The WH and ZH production modes, especially in the boosted regime, provide a relatively clean environment for studying the decay of the Higgs boson into bottom quarks [92]. Bottom mass effects have been computed at NNLO [93, 94] and tend to increase the rates by 6–7%.

The inclusive cross section for associated Higgs boson production with a massive gauge boson is recently known up to N3LO QCD too [95].

iv. Higgs boson production in association with $t\bar{t}$

Higgs boson radiation off top quarks, $pp \rightarrow t\bar{t}H$, provides a direct probe of the top-Higgs Yukawa coupling. The LO cross section for this production process was computed in Ref. [96]. Later, the NLO QCD [97] and NLO EW corrections [98] were evaluated yielding a moderate increase in the total cross section of at most 20%, but significantly reducing the scale dependence of the inclusive cross section. The EW corrections can be enhanced by large electroweak Sudakov logarithms in particular in the boosted regime often used in the phenomenological analyses [99]. The re-

summation of soft gluon contributions close to the partonic kinematical threshold are considered in Refs. [100] to reach a result at NLO+NNLL QCD order. Full off-shell calculations with decaying top quarks are computed at NLO QCD [101] and NLO QCD + EW [102] order, respectively. The fixed-order NLO QCD calculation has been interfaced with the standard parton shower Monte-Carlo generators in Refs. [103], allowing an accurate description of the $t\bar{t}H$ signal, from the energy scale of the hard scattering to the hadronisation energy scale. These programs provide the most flexible tools to date for the computation of differential distributions, including experimental selection cuts and vetoes on the final-state particles and their decay products. The exploitation of this $t\bar{t}H$ channel requires, however, a proper description of the background, in particular $t\bar{t}b\bar{b}$, which exhibits a huge k-factor¹ enhancement from shower effects, see Ref. [40] for a detailed discussion. While the $H \rightarrow b\bar{b}$ decay mode was first considered, the focus has been broadened and other modes have been studied too, in particular the multilepton channel and other backgrounds such as $t\bar{t}W$ and $t\bar{t}Z$ have become relevant and intensively analyzed.

The total theoretical uncertainties, estimated by combining the ones from factorisation and renormalisation scales, strong gauge coupling, and parton distributions, amount to 10–15% of the corresponding inclusive cross section. To match the experimental precision envisioned at the end of HL-LHC, NNLO QCD predictions are required. Using the q_T subtraction formalism for $t\bar{t}H$ production, Ref. [104] presented the first quantitative results at NNLO. The calculation is accurate at NLO in QCD and agrees with the results obtained using the conventional subtraction methods. The NNLO corrections are computed for the flavour off-diagonal partonic channels but their contribution turn out to be at the permill level. The results for the diagonal channels have been obtained in Ref. [41]. The two-loop amplitudes are not yet known, but they have been reliably evaluated by using a soft Higgs boson approximation. At the 13 TeV centre-of-mass energy, the NNLO corrections increase the NLO result for the total cross section by about 4% and lead to a significant reduction of perturbative uncertainties. Also recently, the fragmentation and splitting functions for the production of a Higgs boson have been computed at order $y_t^2 \alpha_s$ and they can be used to compute dif-

¹the k-factor is defined as the ratio of a physical quantity with and without radiative corrections included.

differential cross sections with arbitrary top-quark and Higgs-boson masses directly from the results in the massless limit [105].

v. Other single Higgs boson production mechanisms at the LHC

The Higgs boson production in association with a single top quark, though subdominant, can bring valuable information, in particular regarding the sign of the top Yukawa coupling. This is due to an almost totally destructive interference between two large contributions, one where the Higgs boson couples to a space-like W boson and the other where it couples to the top quark. This process has been computed at NLO QCD in a five-flavour scheme [106] and amounts to about 90 fb at $\sqrt{s} = 14$ TeV (with the opposite sign of the top Yukawa coupling, the cross section increases by one order of magnitude while the cross section for associated production with a pair of top quarks is unaffected). Recently, the tHj (and tZj) process has been computed at NLO QCD+EW accuracy [107]. The NLO EW correction is found to be within the NLO QCD theory uncertainties if the 4 vs 5 flavour scheme uncertainty is taken into account. The EW corrections reduce the total cross section by 3-4%.

The Higgs boson production in association with a pair of bottom quarks ($b\bar{b}H$) has been computed at the N3LO QCD order in the 5-flavour scheme [108], while the production with one/two b-jets, defined by specific kinematic cuts, is known respectively at NLO QCD in the 4-flavour scheme and at NNLO QCD in the 5-flavour scheme [109–111]. The coupling of the Higgs boson to a b -quark is suppressed in the SM by the bottom-quark mass over the Higgs VEV, m_b/v , implying that associated production of a SM Higgs boson with b -quarks is small at the LHC. Yet, at high energy, large logarithms are present and need to be resummed, leading to an enhancement of the inclusive cross section. At $\sqrt{s} = 14$ TeV, the $b\bar{b}H$ cross section can be as large as 550 fb, still two orders of magnitude below the ggF production cross section. Furthermore, the overwhelming ZH and VBF backgrounds (at the inclusive but also differential levels) make it challenging to extract genuine bottom Yukawa signal in a traditional cut-based analysis [112] but innovative machine-learning techniques are a promising avenue to obtain information complementary to the ones extracted from $gg \rightarrow h \rightarrow b\bar{b}$, in particular for what concerns the phase of the bottom Yukawa coupling [113]. In a two Higgs doublet model or a SUSY model, which will be discussed in Section 11.6, this coupling is proportional to the ratio of neutral Higgs boson vacuum expectation values, $\tan\beta$, and can be significantly enhanced for large values of this ratio. Consequently, the $b\bar{b}H$ mode can even become the dominant production process for the Higgs boson, unlike in the SM.

The Higgs boson production in association with charm quarks is also known at NNLO QCD and its cross section is approximately 85 fb at $\sqrt{s} = 13$ TeV [40].

vi. Double Higgs boson production at the LHC

The main interest in the double Higgs boson production is that it can provide invaluable information on the Higgs potential. In particular, it gives access to the Higgs trilinear self coupling. The dominant production is via gluon fusion $gg \rightarrow HH$ (slightly more than 31 fb at 13 TeV) and it accounts for more than 90% of the total inclusive cross-section, the sub-leading production mechanisms are VBF $HHjj$ (around 1.7 fb at 13 TeV), HHW (0.50 fb), HHZ (0.36 fb) and $t\bar{t}HH$ (0.8 fb). The fixed order QCD corrections, computed in the infinite top mass limit, are large, typically doubling the cross section from LO to NLO QCD [114], further enhancing it by 20% and reducing the scale uncertainty by a factor 2-3 from NLO to NNLO QCD [115], with a milder increase of order 3% at N3LO [116] to finally reach at 13 TeV

$$\sigma(gg \rightarrow HH)_{\text{ggF}, m_t \rightarrow \infty}^{\text{N3LO}} = 31.31^{+0.66\%}_{-2.8\%} \text{ fb}. \quad (11.11)$$

Recently, the complete NLO corrections with all top quark mass effects also became available numerically [117], intriguingly revealing a k -factor much less flat than predicted in the large top mass approximations. The non-trivial dependence of the results on the renormalisation scheme and scale for the top quark mass

questions the assessment of the scale uncertainty and would warrant a proper NNLO computation that will however remain out of reach for quite some time. At the differential level, the destructive interference between the box and the triangle contributions complicates the predictions made in the infinite top mass limit for both the HH invariant mass and the leading Higgs boson p_T distributions. With an inclusive cross section of about 35 fb at $\sqrt{s} = 13$ TeV and a difficult signal vs background discrimination, the double Higgs boson production remains a challenging channel to probe and will greatly benefit from the high-luminosity run of the LHC and the combination of various decay modes [118]. The double Higgs channel is definitively a prime target on the Higgs physics agenda and the forthcoming analyses will greatly benefit from the solidification of the fixed order predictions and the detailed uncertainty budget estimate that is underway [119].

11.2.4.2 Production mechanisms at e^+e^- colliders

The dominant Higgs boson production cross sections at an e^+e^- collider are from the Higgs-strahlung process [21, 120], $e^+e^- \rightarrow ZH$, and the WW fusion process [121], $e^+e^- \rightarrow \bar{\nu}_e \nu_e W^* W^* \rightarrow \bar{\nu}_e \nu_e H$. The cross-section for the Higgs-strahlung process scales as the inverse of the collision centre-of-mass squared energy, s , and is predominant at low energies, while the cross-section for the WW fusion process scales as $\ln(s/m_H^2)$ and dominates at high energies [122]. The ZZ fusion mechanism, $e^+e^- \rightarrow e^+e^- Z^* Z^* \rightarrow e^+e^- H$, also contributes to the Higgs boson production, with a cross-section suppressed by an order of magnitude with respect to that of WW fusion. The process $e^+e^- \rightarrow t\bar{t}H$ [123] becomes important for $\sqrt{s} \geq 500$ GeV. For a more detailed discussion of Higgs boson production properties at lepton colliders, see for example Refs. [124]. Interesting progress has been made recently [125] to accurately account for beamstrahlung and initial state radiation using the factorisation approach primarily developed for hadron colliders and this method is being implemented in Monte Carlo event generators. Further information about Higgs physics at an e^+e^- collider can be found in Ref. [126].

11.2.4.3 SM Higgs boson branching ratios and total width

For the understanding and interpretation of the experimental results, the computation of all relevant Higgs boson decay widths is essential, including an estimate of their uncertainties and, when appropriate, the effects of Higgs boson decays into off-shell particles with successive decays into lighter SM ones. A Higgs boson mass of about 125 GeV allows to explore the Higgs boson couplings to many SM particles. In particular the dominant decay modes are $H \rightarrow b\bar{b}$ and $H \rightarrow WW^*$, followed by $H \rightarrow gg$, $H \rightarrow \tau^+\tau^-$, $H \rightarrow c\bar{c}$ and $H \rightarrow ZZ^*$. With much smaller rates follow the Higgs boson decays into $H \rightarrow \gamma\gamma$, $H \rightarrow \gamma Z$ and $H \rightarrow \mu^+\mu^-$. Since the decays into gluons, diphotons and $Z\gamma$ are loop induced, they provide indirect information on the Higgs boson couplings to WW , ZZ and $t\bar{t}$ in different combinations. The uncertainties in the branching ratios include the missing higher-order corrections in the theoretical calculations as well as the errors in the SM input parameters, in particular fermion masses and the QCD gauge coupling, involved in the decay. In the following the state-of-the-art of the theoretical calculations compiled by the LHC Higgs Working Group [43] will be discussed and the reader is referred to Refs. [37–40, 127] for detail.

The evaluation of the radiative corrections to the fermionic decays of the SM Higgs boson are implemented in HDECAY [128] at different levels of accuracy. The computations of the $H \rightarrow b\bar{b}$ and $H \rightarrow c\bar{c}$ decays include the complete massless QCD corrections up to N4LO, with a corresponding scale dependence of about 0.1% [129]. Both the electroweak corrections to $H \rightarrow b\bar{b}$, $c\bar{c}$ as well as $H \rightarrow \tau^+\tau^-$ are known at NLO [130] providing predictions with an overall accuracy of about 1–2% for $m_H \simeq 125$ GeV.

The loop induced decays of the SM Higgs boson are known fully at NLO and partially beyond that approximation. For $H \rightarrow gg$, the QCD corrections are known up to N3LO in the limit of heavy top quarks [47, 131] and the uncertainty from the scale dependence is about 3%. For the $H \rightarrow \gamma\gamma$, the full NLO QCD corrections are available [47, 132] and the three-loop QCD corrections have also been evaluated [133]. The NLO electroweak corrections to

$H \rightarrow gg$ and $H \rightarrow \gamma\gamma$ have been computed in Ref. [134]. All these corrections are implemented in HDECAY [128]. For $m_H \simeq 125$ GeV, the overall impact of known QCD and EW radiative effects turns out to be well below 1%. In addition, the contribution of the $H \rightarrow \gamma e^+ e^-$ decay via virtual photon conversion has been computed in Ref. [135]. The partial decay width $H \rightarrow Z\gamma$ is only implemented at LO in HDECAY, including the virtual W , top-, bottom-, and τ -loop contributions. The QCD corrections have been calculated and are at the percent level [136]. The theoretical uncertainty due to unknown electroweak corrections is estimated to be less than 5%, an accuracy that will be hard to achieve in the measurement of this process at the LHC.

Table 11.3: The branching ratios and the relative uncertainty for a SM Higgs boson with $m_H = 125$ GeV [39, 40].

Decay channel	Branching ratio	Rel. uncertainty
$H \rightarrow \gamma\gamma$	2.27×10^{-3}	2.1%
$H \rightarrow ZZ$	2.62×10^{-2}	$\pm 1.5\%$
$H \rightarrow W^+W^-$	2.14×10^{-1}	$\pm 1.5\%$
$H \rightarrow \tau^+\tau^-$	6.27×10^{-2}	$\pm 1.6\%$
$H \rightarrow b\bar{b}$	5.82×10^{-1}	+1.2% -1.3%
$H \rightarrow c\bar{c}$	2.89×10^{-2}	+5.5% -2.0%
$H \rightarrow Z\gamma$	1.53×10^{-3}	$\pm 5.8\%$
$H \rightarrow \mu^+\mu^-$	2.18×10^{-4}	$\pm 1.7\%$

The decays $H \rightarrow WW/ZZ \rightarrow 4f$ can be simulated with the Prophecy4f Monte-Carlo generator [137] that includes complete NLO QCD and EW corrections for Higgs decays into any possible four-fermion final state. All calculations are consistently performed with off-shell gauge bosons, without any on-shell approximation. For the SM Higgs boson, the missing higher-order corrections are estimated to be roughly 0.5%. Such uncertainties will have to be combined with the parametric uncertainties, in particular those associated to the bottom-quark mass and the strong gauge coupling, to arrive at the full theory uncertainty. A detailed treatment of the differential distributions for a Higgs boson decay into four charged leptons in the final state is discussed in Refs. [39, 138].

The total width of a 125 GeV SM Higgs boson is $\Gamma_H = 4.07 \times 10^{-3}$ GeV, with a relative uncertainty of $^{+4.0\%}_{-3.9\%}$. The branching ratios for the most relevant decay modes of the SM Higgs boson as a function of m_H , including the most recent theoretical uncertainties, are shown in Fig. 11.2 (right) and listed for $m_H = 125$ GeV in Table 11.3. Further details of these calculations can be found in the reviews [37–40] and references therein.

11.3 The experimental profile of the Higgs boson

The observation [1, 2] at the LHC of a narrow resonance with a mass of about 125 GeV was an important landmark in the decades-long direct search [44, 139] for the SM Higgs boson. This observation is being followed by a detailed exploration of properties of the Higgs boson at the different runs of the LHC at $\sqrt{s} = 7, 8, 13$ and 13.6 TeV.

The dataset at $\sqrt{s} = 13$ TeV collected during the Run-2 phase of the LHC operation is the largest analysed dataset so far and corresponds to an integrated luminosity of about 160 fb^{-1} delivered to the ATLAS and CMS experiments, see Table 11.4 [140]. The datasets effectively useful for analysis need to take into account the data-taking efficiency with fully operational detectors and the data quality efficiency. The typical total inefficiency for both ATLAS and CMS is approximately 10%, where approximately half

is due to the data acquisition inefficiency and the other half from data quality requirements.

In this section, most of the references for the Run-1 measurements that have been updated with the data delivered in Run 2 are given in the previous version of this review [141] and are not repeated herein.

Table 11.4: The LHC pp collision centre-of-mass energies and approximate collision samples delivered to ATLAS & CMS experiments.

Year	\sqrt{s} (TeV)	$\int \text{L.dt}$ (fb^{-1})	Period
2010	7.0	0.04	Run 1
2011	7.0	6	Run 1
2012	8.0	23	Run 1
2015	13.0	4	Run 2
2016	13.0	39	Run 2
2017	13.0	51	Run 2
2018	13.0	61	Run 2
2022	13.6	39	Run 3
2023	13.6	32	Run 3

11.3.1 The principal decay channels of the Higgs boson

For a given m_H , the sensitivity of a channel depends on the production cross section of the Higgs boson, its decay branching fraction, the reconstructed mass resolution, the selection efficiency and the level of background in the final state. It is defined typically as the expected significance for the observation of a given process or in terms of expected upper limit at 95% Confidence Level (CL). At the LHC, for a Higgs boson with a mass close to 125 GeV, five decay channels play an important role. In the $H \rightarrow \gamma\gamma$ and $H \rightarrow ZZ^* \rightarrow 4\ell$ channels, all final state particles can be very precisely measured and the reconstructed m_H resolution is excellent (typically 1–2%). The $H \rightarrow W^\pm W^\mp(\gamma) \rightarrow \ell^+ \nu_\ell \ell'^- \bar{\nu}_{\ell'}$ channel has a relatively large branching fraction. However, the presence of neutrinos, which are not reconstructed in the final state, means that the m_H resolution, obtained through observables sensitive to the Higgs boson mass such as the transverse mass, is poor (approximately 20%). The $H \rightarrow b\bar{b}$ and the $H \rightarrow \tau^+\tau^-$ (with the tau subsequently decaying to electrons or muons and two neutrinos $\tau \rightarrow \ell\nu\bar{\nu}$ or to hadrons and one neutrino $\tau \rightarrow \text{hadrons}\nu$) channels suffer from large backgrounds and lead to an intermediate mass resolution of about 10% and 15% respectively.

With the increase in the size of datasets, measurements in the most sensitive channels are now carried out differentially or in exclusive modes depending on specific production characteristics. These measurements are discussed in Section 11.5.1.5.

The candidate events in each Higgs boson decay channel are split into several mutually exclusive categories (or event tags) based on the specific topological, kinematic or other features present in the event. The categorization of events increases the sensitivity of the overall analysis and allows a separation of different Higgs boson production processes. Most categories are dominated by signal from one Higgs boson decay mode but contain an admixture of various Higgs boson production processes. For example, a typical VBF selection requires Higgs boson candidates to be accompanied by two energetic jets (≥ 30 GeV) with a large dijet mass (≥ 400 GeV) and separated by a large pseudo-rapidity ($\Delta\eta_{jj} \geq 3.5$) [142]. While such a category is enriched in Higgs bosons produced via VBF, the contamination from the ggF or VH production mechanisms can be significant. Hence, a measurement of the signal rate in the VBF category is not equivalent to a measurement of VBF production cross section since one cannot resolve the contamination from ggF. Simulations are used to determine the relative contributions of the various Higgs boson production modes in each of the specific categories.

11.3.2 The Higgs boson decay to vector bosons

11.3.2.1 $H \rightarrow \gamma\gamma$

In the diphoton channel, the measurement of a narrow peak over a smoothly falling background in the invariant mass distribution of two high p_T photons is performed. The background in

this channel is conspicuous and stems from prompt $\gamma\gamma$ processes for the irreducible backgrounds, and the γ +jet and dijet processes for the reducible backgrounds where one jet fragments typically into a leading π^0 . In order to optimise search sensitivity and also to separate the various Higgs boson production modes, ATLAS and CMS split events into several mutually exclusive categories. Diphoton events containing high p_T muons or electrons, or missing energy (E_T^{miss}) consistent with the decay of a W or Z boson, are tagged in the VH production category. Diphoton events containing energetic dijets with a large mass and pseudo-rapidity difference are assigned to the VBF production category, and events with two jets compatible with the hadronic decay of a W or a Z are considered in the VH category. While the leptonic VH category is relatively pure, the VBF category has significant contamination from the gluon fusion process. Finally more complex topologies aiming at selecting events from the $t\bar{t}H$ production mode in the semi-leptonic and fully hadronic top decays are also considered and discussed in more detail in Section 11.3.5.1 Events are also further categorised according to their expected $m_{\gamma\gamma}$ resolution and signal-to-background ratio. Categories with good m_H resolution and larger signal-to-background ratio contribute most to the sensitivity of the search.

Both ATLAS and CMS have studied in detail the calibration of the energy response of photons, in particular using $Z \rightarrow e^+e^-$, $Z \rightarrow \mu^+\mu^-$ and the response of muons in the calorimeter (for ATLAS) from $Z \rightarrow \mu^+\mu^-$ events. This information is used to correct the simulated signal mass line-shapes. In each category, parametric signal models are adjusted to these line-shapes to provide a functional form for the signal. Simple functional forms of the backgrounds are determined by a fit to the $m_{\gamma\gamma}$ distribution in each category (typically exponential, Bernstein polynomials, Laurent series or power laws). All categories are fitted simultaneously to determine the signal yield at a given Higgs boson mass hypothesis.

The results are expressed in terms of signal strength, which can be defined as $\mu = (\sigma \cdot \text{BR})_{\text{obs}} / (\sigma \cdot \text{BR})_{\text{SM}}$, the observed product of the Higgs boson production cross section (σ) and its branching ratio (BR) normalised to the corresponding SM values. A more detailed definition is given in Section 11.3.6 and Eq. 11.14. The signal strength overall for this channel and for specific production processes are summarised in Fig. 11.3. All results are in agreement with the SM expectation within the overall measurement precisions of approximately 9% for both experiments.

11.3.2.2 $H \rightarrow ZZ^* \rightarrow \ell^+\ell^-\ell'^+\ell'^-$

In the $H \rightarrow ZZ^* \rightarrow \ell^+\ell^-\ell'^+\ell'^-$ channel, a search is performed for a narrow mass peak over a small continuous background dominated by non-resonant ZZ^* production from $q\bar{q}$ annihilation and gg fusion processes. The contribution and the shape of this irreducible background is taken from simulation. The subdominant and reducible backgrounds stem from $Z+bb$, $t\bar{t}$ and Z +jets events. Their contribution is suppressed by requirements on lepton isolation and lepton impact parameter and their yield is estimated from control samples in data.

To distinguish the Higgs boson signal from the dominant non-resonant ZZ^* background, both ATLAS and CMS use multivariate techniques as well as a matrix element likelihood approach to construct a kinematic discriminant built for each 4ℓ event based on the ratio of complete leading-order matrix elements $|\mathcal{M}_{\text{sig}}^2/\mathcal{M}_{\text{bkg}}^2|$ for the signal ($gg \rightarrow H \rightarrow 4\ell, q\bar{q} \rightarrow VH (\rightarrow 4\ell)$ and $q\bar{q} \rightarrow q\bar{q}H (\rightarrow 4\ell)$) and background ($q\bar{q} \rightarrow ZZ \rightarrow 4\ell$) hypotheses.

To improve the sensitivity to more exclusive production processes such as VBF, VH , and $t\bar{t}H$, the experiments divide 4ℓ events into mutually exclusive categories. Events are categorised in terms of the number of reconstructed jets, the number of additional leptons (from the decay of a vector boson in the associated production mode), number of jet tagged as containing a b -hadron, the transverse momentum of the Higgs boson (or e.g. its associated vector boson) and missing transverse momentum. Dijets with a large mass and pseudo-rapidity difference populate the VBF category. ATLAS requires the presence of an additional lepton in the VH category. In events with less than two jets, CMS uses the $p_T^{4\ell}$ to distinguish between production via the gluon fu-

sion and the VH/VBF processes.

Since the $m_{4\ell}$ resolutions and the reducible background levels are different in the 4μ , $4e$ and $2e2\mu$ sub-channels, they are analysed separately and statistically combined to produce the final results.

The results for this channel, overall and in specific production processes are summarised in Fig. 11.3. All results are in agreement with the SM expectation within the overall measurement precisions of approximately 9% and 12% for the ATLAS and CMS experiments respectively.

11.3.2.3 $H \rightarrow W^+W^- \rightarrow \ell^+\nu\ell'^-$

In this challenging channel, experiments search for an excess of events with two leptons (electrons or muons) of opposite charge accompanied by missing energy and/or jets. A typical event selection is described below in order to give an idea of the main intricacies. Specific selections vary between experiments and between Run-1 and Run-2 analyses. Events are divided into several categories depending on the lepton flavour combination (e^+e^- , $\mu^+\mu^-$ and $e^\pm\mu^\mp$) and the number of accompanying jets ($N_{\text{jet}} = 0, 1, \geq 2$). The $N_{\text{jet}} \geq 2$ category is optimised for the VBF production process by selecting two leading jets with a large pseudo-rapidity difference and with a large mass (typically $m_{jj} > 500$ GeV).

Backgrounds contributing to this channel are numerous and depend on the category of selected events. Reducing them and accurately estimating the remainder is a major challenge in this analysis. For events with opposite-flavour leptons and no accompanying high p_T jets, the dominant background stems from non-resonant WW production. Events with same-flavour leptons suffer from large Drell–Yan contamination (note that also the opposite-flavour leptons analysis has Drell–Yan $\tau\bar{\tau}$ background in 0-jet category). The $t\bar{t}$, tW and W +jets (with the jet misidentified as a lepton) events contaminate all categories. Non-resonant WZ , ZZ and $W\gamma$ processes also contribute to the background at a sub-leading level.

A requirement of large missing transverse energy (E_T^{miss}) is used to reduce the Drell–Yan and multi-jet backgrounds. In the e^+e^- and $\mu^+\mu^-$ categories, events with $m_{\ell\ell}$ consistent with the Z mass are vetoed. The $t\bar{t}$ background is suppressed by a veto against identified b -jets and tight isolation requirements diminish the W +jets background. The scalar nature of the Higgs boson and the $V-A$ nature of the W boson decay implies that the two charged leptons in the final state are preferentially emitted at small angles with respect to each other. Therefore the dilepton invariant mass ($m_{\ell\ell}$) and the azimuthal angle difference between the leptons ($\Delta\phi_{\ell\ell}$) are used to discriminate between the signal and non-resonant WW events [143]. The transverse mass, constructed from the dilepton p_T ($p_T^{\ell\ell}$), E_T^{miss} and the azimuthal angle between E_T^{miss} and $p_T^{\ell\ell}$, is defined as

$$m_T = \sqrt{2p_T^{\ell\ell}E_T^{\text{miss}}(1 - \cos\Delta\phi_{E_T^{\text{miss}}\ell\ell})}$$

and serves as an effective discriminant against backgrounds. The transverse mass variable also tracks the Higgs boson mass but with a poor mass resolution. Background rates except for the small contributions typically from non-resonant WZ , ZZ and $W\gamma$ are evaluated from data control samples with floating normalization.

ATLAS and CMS have also searched for the associated Higgs boson production in this channel. The signal consists of up to three (WH) or four (ZH) high p_T isolated leptons with missing transverse energy and low hadronic activity. The major backgrounds stem from triboson and diboson production where each boson decays leptonically.

Measurements by ATLAS and CMS, in terms of signal strengths, for the five largest Higgs boson production modes are displayed in Fig. 11.3. All measurements are in agreement with the SM expectation within the overall measurement precisions of approximately 12% and 9% for ATLAS and CMS respectively.

11.3.3 Measurement of the Higgs boson mass

To measure the mass of the Higgs boson, ATLAS and CMS collaborations rely on the two high mass-resolution channels, $\gamma\gamma$ and $ZZ^*/4\ell$. The ATLAS and CMS approaches are very similar in these two analyses with small differences on the usage of cat-

egories, additional discriminating variables and per-event errors. In these two channels, the mass resolutions range from 1.4 GeV to 2 GeV for ATLAS and from 1.0 GeV to 2.8 GeV for CMS (see Ref. [144] and the reconstruction-performance references therein). An excellent mass resolution is obtained for both experiments in the diphoton channel for central diphoton pairs (typically for events where both photons are not converted). However, the best precision in this measurement at Run 2 is obtained using the four lepton channel and in particular in the sub-channel of four muons (followed, in precision, by the two-electrons and two muons channel where the mass resolution is driven by the reconstruction of the lower mass di-lepton pair with typically lower transverse momentum leptons).

Both ATLAS and CMS have produced several Higgs boson mass measurements, including the individual and combined Run-1 measurements [144] and several Run-2 measurements by ATLAS [145, 146] and CMS [147, 148] for both the 4ℓ and the diphoton channels. The measurements performed by ATLAS include the full Run-2 dataset whereas in the case of CMS, the mass measurements were done with a fraction of the Run-2 data corresponding to the data collected in 2016. An overall combination of all available measurements has not yet been performed. The Run-1 combination including both ATLAS and CMS measurements yielded [144]:

$$m_H = 125.09 \pm 0.21 \text{ (stat.)} \pm 0.11 \text{ (syst.) GeV.}$$

The current most precise di-photon channel result is obtained by ATLAS using the full Run-2 dataset and a combination with the Run-1 measurements in the $H \rightarrow \gamma\gamma$ yielding a measurement of [149]:

$$m_H = 125.22 \pm 0.11 \text{ (stat.)} \pm 0.09 \text{ (syst.) GeV.}$$

The systematic uncertainty of 90 MeV is worth noting, as it results from a very challenging calibration and estimates of the amount of material upstream of the calorimeter to extrapolate the calorimeter energy response calibration from electrons in Z boson decays to photons. This result is promising for prospects in precision measurements in this channel. In Ref. [149], ATLAS has also estimated the expected effect of the interference between the signal and the gluon fusion continuum di-photon background to be of 24 MeV. This ATLAS measurement is significantly more precise than the full Run-2 measurement in the 4ℓ channel, however the latter is dominated by the statistical uncertainty of 170 MeV with a systematic uncertainty of 30 MeV [150]. The ATLAS diphoton channel measurement reached the same sensitivity as the early Run-2 and Run-1 combined measurement of CMS, which uses both channels but with a much smaller amount of Run-2 data, corresponding only to the 2016 LHC run, which yielded [148]:

$$m_H = 125.38 \pm 0.11 \text{ (stat.)} \pm 0.08 \text{ (syst.) GeV.}$$

ATLAS has also combined its results in the diphoton and the four-lepton channels yielding the current most precise measurement with a precision of 0.09% [151]:

$$m_H = 125.11 \pm 0.09 \text{ (stat.)} \pm 0.06 \text{ (syst.) GeV.}$$

The most precise single channel result has very recently been obtained by CMS in the 4ℓ channel with the full Run 2 dataset [152]:

$$m_H = 125.08 \pm 0.12 \text{ GeV.}$$

The analysis of the entire Run-2 dataset and the LHC combination of the two experiments will be of great interest and important for the combination of all Higgs boson measurements across experiments.

11.3.4 Higgs decays to third generation fermions ($b\bar{b}$ and $\tau^+\tau^-$)

In the SM, fermions acquire a mass through gauge invariant interactions with the Higgs field which is also responsible for the electroweak symmetry breaking and thus for generating the masses of gauge bosons (see Section 11.2 for more details). While

this minimal solution is very elegant, there is no fundamental reason for it to be the case, and probing the couplings of the Higgs boson to fermions is therefore of fundamental importance, in particular since BSM physics can largely change the SM predictions.

The discovery of the Higgs boson was made essentially through the bosonic final states. These decays probed mostly the couplings of the Higgs boson to vector bosons (the decay of the Higgs boson to photons occurring only through loops is also dominated in the SM by the coupling of the Higgs boson to W bosons). However, the predominant Higgs boson production mode is the gluon fusion, occurring only through loops dominated by the coupling of the Higgs boson to fermions. The observation of the Higgs boson in the two photons or two gluons decay modes is also an indirect evidence for the coupling of the Higgs boson to fermions (and in particular to the top quark). Nevertheless, the observation of either decays to fermions or production modes which unambiguously proceed through fermion couplings provide direct probes of the coupling of the Higgs boson to fermions and is thus of fundamental importance.

At hadron colliders, the most promising channel for probing the coupling of the Higgs field to the quarks and leptons are $H \rightarrow b\bar{b}$ and $H \rightarrow \tau^+\tau^-$, respectively. For a Higgs boson with $m_H \approx 125$ GeV, the branching fraction to $b\bar{b}$ is about 58% and to $\tau^+\tau^-$ is about 6%. Nevertheless, the presence of very large backgrounds makes the measurement of a Higgs boson signal in these channels challenging.

One of the most prominent goals of the LHC Run-2 physics program was the direct observation of the Yukawa coupling of the Higgs boson to fermions of the third generation (bottom quarks, tau leptons and top quarks). This goal has been reached independently by both ATLAS and CMS and with only partial Run-2 datasets.

11.3.4.1 $H \rightarrow \tau^+\tau^-$

In the $H \rightarrow \tau^+\tau^-$ search, τ leptons decaying to electrons (τ_e), muons (τ_μ) and hadrons (τ_{had}) are considered. The $\tau^+\tau^-$ invariant mass ($m_{\tau\tau}$) is reconstructed from a kinematic fit of the visible products from the two τ leptons and the missing energy observed in the event. Due to the presence of missing neutrinos, the $m_{\tau\tau}$ resolution is poor ($\approx 10\% - 15\%$). As a result, a broad excess over the expected background in the $m_{\tau\tau}$ distribution is searched for. The major sources of background stem from Drell-Yan $Z \rightarrow \tau^+\tau^-$ and $Z \rightarrow e^+e^-$, W +jets, $t\bar{t}$ and multijet production. Events in all sub-channels are divided into categories based on the number and kinematic properties of additional energetic jets in the event and the transverse momentum of the reconstructed Higgs boson and the distance ΔR distance between the two τ 's. The sensitivity of the search is generally higher for categories with one or more additional jets. The VBF category, consisting of a τ pair with two energetic jets separated by a large pseudo-rapidity, has the best signal-to-background ratio and search sensitivity, followed by the $\tau^+\tau^- + 1$ jet category. The signal to background discrimination relies in part on the $m_{\tau\tau}$ resolution, which improves with the boost of the Higgs boson. The non-VBF categories are further subdivided according to the observed boost of the $\tau^+\tau^-$ system. ATLAS and CMS combine various kinematic properties of each event categories with multivariate techniques to build the final discriminant.

Searches for $H \rightarrow \tau^+\tau^-$ decays in the VH production mode are also performed in final states where the W or Z boson decays into leptons or jets. The irreducible background in this search arises from non-resonant WZ and ZZ diboson production. The reducible backgrounds originate from W , Z , and $t\bar{t}$ events that contain at least one fake lepton in the final state due to a misidentified jet. The shape and yield of the major backgrounds in each category are estimated from control samples in data. Contributions from non-resonant WZ and ZZ diboson production are estimated from simulations but corrected for reconstruction efficiency using control samples formed from observed data.

The first clear evidence of direct decays of the Higgs boson to taus was achieved by ATLAS and CMS in combination [153], with the observation of an excess with a significance of 5.5σ and the combined signal strength is $\mu = 1.11^{+0.24}_{-0.22}$, consistent with the SM expectation. The early Run-2 data fully corroborated these

results to establish an unambiguous observation in each experiment independently. ATLAS [154] and CMS [155, 156] analysed an early Run-2 dataset to provide independent observations, with significances of 4.4σ and 4.9σ respectively.

Both ATLAS [157] and CMS [158, 159] have then completed the analyses of the full Run-2 dataset in various production channels. These results are summarised in Fig. 11.3. These results perform simultaneously measurements of the VBF production, the gluon fusion mode where the Higgs boson has a sizeable boost, and the associated production with a vector boson as well as the associated production with a pair of top quarks. It is interesting to note that the with the current measurements the gluon fusion channels have a sensitivity which is very close to the VBF production.

11.3.4.2 $H \rightarrow b\bar{b}$

To measure the decays of the Higgs boson to a pair of b -quarks, the most sensitive production modes are the associated WH and ZH processes allowing use of the leptonic W and Z decays which are helpful for triggering the events and to reject QCD backgrounds. The W bosons are reconstructed via their leptonic decay $W \rightarrow \ell\bar{\nu}_\ell$ where $\ell = e, \mu$ or τ . The Z bosons are reconstructed via their decay into e^+e^- , $\mu^+\mu^-$ or $\nu\bar{\nu}$. The Higgs boson candidate mass is reconstructed from two b -tagged jets in the event. Backgrounds arise from production of W and Z bosons in association with gluon, light and heavy-flavoured jets (V +jets), $t\bar{t}$, diboson (ZZ and WZ with $Z \rightarrow b\bar{b}$) and QCD multi-jet processes. Due to the limited $m_{b\bar{b}}$ mass resolution, a SM Higgs boson signal is expected to appear as a relatively broad enhancement in the reconstructed dijet mass distribution. The crucial elements in this search are b -jet tagging with high efficiency and low fake rate, accurate estimate of b -jet momentum and estimate of backgrounds from various signal depleted control samples constructed from data.

At the Tevatron, the $H \rightarrow b\bar{b}$ channel contributed the majority of the Higgs boson search sensitivity below $m_H = 130$ GeV. To separate signal from background, CDF and D0 used multivariate analysis (MVA) techniques that combined several discriminating variables into a single final discriminant. Each channel was divided into exclusive sub-channels according to various lepton, jet multiplicity, and b -tagging characteristics in order to group events with similar signal-to-background ratio and thus optimise the overall search sensitivity. The combined CDF and D0 data showed [44, 160] an excess of events with respect to the predicted background in the 115–140 GeV mass range in the most sensitive bins of the discriminant distributions suggesting the potential presence of a signal. At $m_H = 125$ GeV, the observed signal strength was $\mu = 1.59^{+0.69}_{-0.72}$.

At the LHC, in order to reduce the dominant V +jets background, following Ref. [92], experiments select a region in the VH production phase space where the vector boson is significantly boosted and recoils from the $H \rightarrow b\bar{b}$ candidate with a large azimuthal angle $\Delta\phi_{VH}$. For each channel, events are categorised into different $p_T(V)$ regions with varying signal/background ratios. Events with higher $p_T(V)$ have smaller backgrounds and better $m_{b\bar{b}}$ resolution. Experiments use MVA classifiers based on kinematic, topological and quality of b -jet tagging and trained on different values of m_H to separate Higgs boson signal in each category from backgrounds. The main discriminating variables in this analysis are the transverse momentum of the vector boson and the di- b -jet invariant mass.

The direct observation of the Higgs boson decaying to a pair of b -quarks, a major result of Run 2, was obtained by both ATLAS and CMS independently after the update of their search with similar analyses as those performed at Run 1 but with a larger dataset of approximately 80 fb^{-1} of data collected in 2015, 2016 and 2017. The increase in signal cross sections of nearly a factor of 3 at the centre-of-mass energy of 13 TeV with respect to 7 TeV, has also been instrumental in bringing the two experiments to the required sensitivity to claim an evidence for this decay mode in the VH production mode (in the high transverse momentum of the vector boson fiducial region of interest for this channel). The expected significance for a SM Higgs boson was 4.3σ for ATLAS [161] and 4.9σ for CMS [162]. Both ATLAS and CMS observed significant excesses corresponding to 4.9σ and 4.8σ respectively with Run-2

data only. When combined with results obtained in Run 1, the observed (expected) significance of the excesses were 5.4σ (5.5σ) and 5.6σ (5.5σ) respectively. These results provided direct and unambiguous observation for the $H \rightarrow b\bar{b}$ decay through the VH production mode.

Since these important observations, both experiments have completed the analysis of the full Run-2 dataset using two reconstruction techniques. The first is based on the reconstruction of the Higgs boson with two jets is referred to as *resolved*. The second is based on the reconstruction of the Higgs boson as a large radius jet and is referred to as *boosted*. These measurements expand the range of measurements of the Higgs boson decays to b -quarks in association with a vector boson at higher transverse momentum, above 400 GeV. These results are summarised in Fig. 11.3. It should be noted that the sensitivity of these analyses are already limited by systematic uncertainties.

Also, the LHCb collaboration has performed a search for the VH production with subsequent decay of the Higgs boson to a pair of b -quarks [163] with 1.98 fb^{-1} of data taken at a centre-of-mass energy of 8 TeV. The final state is required to have two reconstructed b quarks and one lepton in the LHCb acceptance of $2 < \eta < 5$. The sensitivity of this search is an expected 95% CL exclusion of 84 times the SM production rate. This analysis is also used to set a limit on the VH production with the subsequent decay of the Higgs boson in a pair of c quarks with a 95% CL limit at 6.4×10^3 times the SM production rate, while the expected sensitivity corresponds to an exclusion of 7.9×10^3 times the SM production rate.

ATLAS and CMS have also searched for $H \rightarrow b\bar{b}$ in the VBF production mode. The event topology consists of two VBF-tagging energetic light-quark jets in the forward and backward direction relative to the beam direction and two b -tagged jets in the central region of the detector. Due to the electroweak nature of the process, for the signal events, no additional energetic jet activity (excluding that from the Higgs boson) is expected in the rapidity gap between the two VBF-tagging jets. The dominant background in this search stems from QCD production of multi-jet events and the hadronic decays of vector bosons accompanied by additional jets. A contribution of Higgs boson events produced in the ggF process but with two or more associated jets is expected in the signal sample. The signal is expected as a relatively broad enhancement in the $m_{b\bar{b}}$ distribution over the smoothly falling contribution from the SM background processes. Both ATLAS [164] and CMS [165] have produced results in this channel with Run-1 data, but with limited sensitivity. Both experiments performed a similar analysis with Run-2 data [166, 167].

Two of the main difficulties for the VBF production mode are the large QCD background and the difficulty in triggering fully hadronic events. Both difficulties are addressed, by the proposal made in Ref. [168], where the requirement of an additional photon in the final state reduces the background through an interference effect and enhances the possibilities for triggering. This analysis has been carried out by ATLAS at Run 2 [169] and its result combined with the standard VBF channel. The sensitivity in this channel is smaller than in the fully hadronic mode. Through the combination of these channels ATLAS has reached a first evidence at 3 standard deviations of the Higgs boson decaying to a pair of b quarks in the VBF production mode. The results are reported below

$$\text{ATLAS } \mu_{VBF(\gamma)}^{b\bar{b}} = 0.99^{+0.30}_{-0.30} (\text{stat})^{+0.18}_{-0.16} (\text{syst}), \quad (11.12)$$

$$\text{CMS } \mu_{VBF}^{b\bar{b}} = 1.01 \pm 0.36 (\text{stat})^{+0.40}_{-0.27} (\text{syst}).$$

The sensitivity in the inclusive search for the Higgs boson in the ggF production mode with $H \rightarrow b\bar{b}$ is limited by the overwhelming background from the inclusive production of $pp \rightarrow b\bar{b} + X$ via the strong interaction. With the increase in centre-of-mass energy to 13 TeV, and taking advantage of the harder transverse momentum spectrum of the $gg \rightarrow H$ production mode with respect to the QCD background, a search for high p_T Higgs boson decaying to a pair of b quarks in association with an energetic Initial State

Radiation (ISR) jet. Considerable efforts have been made using state-of-the-art deep learning techniques to improve the performance of the identification of a Higgs boson decaying to b quarks and reconstructed as a large radius jet at high transverse momentum. In order to gain sensitivity in this channel and reconstruct the Higgs boson within one jet of radius 0.8 or 1.0 a lower cut at 450 GeV of transverse momentum is required. This analysis was performed by both ATLAS [170] and CMS [171] with the entire Run-2 data dataset. As in the case of VH production mode, this analysis is sensitive also to the inclusive $Z \rightarrow b\bar{b}$ production, which is an important step in the validation of the analysis chain. The $Z \rightarrow b\bar{b}$ decay is observed with a significance in excess of five standard deviations, in agreement with the expected rate from the Standard Model. This estimate has a non negligible uncertainty from the precise estimate of the fiducial signal cross section in the specific acceptance of this analysis. CMS observes an excesses at $m_H = 125$ GeV of 1.2σ [171] with a sensitivity of 0.9σ . It should be noted that the estimates of the signal expectation in this remote region of phase space at high transverse momentum for the production are highly non-trivial and subject to fairly large theoretical and statistical uncertainties:

$$\begin{aligned} \text{ATLAS } \mu_{\text{inclusive}}^{b\bar{b}} &= -0.1 \pm 3.5 \quad (1.0 \pm 3.4 \text{ expected}), \\ \text{CMS } \mu_{\text{inclusive}}^{b\bar{b}} &= 2.1^{+1.9}_{-1.7}. \end{aligned} \quad (11.13)$$

In addition to the inclusive production, in [171] CMS has also performed a search sensitive to the VBF production in the boosted Higgs regime, yielding a sensitivity of 0.9σ . In this channel a broad excess has been observed which results in an observed excess with a significance of 3.0σ . These results are particularly interesting as these measurements will bring a strong complement to the main channels in the high transverse momentum regime.

Another important production mode sensitive to the decay of the Higgs boson to bottom quarks, is the associated production with a pair of top quarks. The results of the searches for this process have been combined with the channels described above, to provide an additional constraint on the Yukawa coupling of the Higgs boson to bottom quarks. The channels corresponding to this production mode are described in Section 11.3.5.

11.3.5 Higgs boson production in association with top quarks

11.3.5.1 The associated production with top quark pairs

As discussed in Section 11.2, the coupling of the Higgs boson to top quarks plays a special role in the electroweak symmetry breaking mechanism in the SM, as well as in its possible extensions. Substantial indirect evidence of this coupling is provided by the compatibility of observed rates of the Higgs boson in the principal discovery channels, given that the main production process – gluon fusion – is dominated by a top quark loop. Direct evidence of this coupling at the LHC and the future e^+e^- colliders will be mainly available through the $t\bar{t}H$ final state and will permit a clean measurement of the top quark-Higgs boson Yukawa coupling. The $t\bar{t}H$ production cross section at the LHC is small in comparison with the ggF or even VH production modes. The production cross section for a 125 GeV Higgs boson in pp collisions at $\sqrt{s} = 8$ TeV of about 130 fb made it challenging to measure the $t\bar{t}H$ process with the LHC Run-1 dataset. However, at Run 2, the increase in cross section at $\sqrt{s} = 13$ TeV is substantial, reaching approximately 500 fb.

The analysis channels for such complex final states can be separated in four classes according to the decays of the Higgs boson. In each of these classes, most of the decay final states of the top quarks are considered (fully hadronic, semi-leptonic and dilepton decay final states).

The first analysis is the search for $t\bar{t}H$ production in the $H \rightarrow \gamma\gamma$ channel. This analysis relies on the search for a narrow mass peak in the $m_{\gamma\gamma}$ distribution. The background is estimated from the $m_{\gamma\gamma}$ sidebands. The sensitivity in this channel is mostly limited by the available statistics.

The second analysis is the search for the Higgs boson decaying to ZZ^* and subsequently to four leptons (electrons and/or muons). This channel is currently limited by the low statistics

due to the small branching fraction of the Z decays to leptons.

In the third analysis the W^+W^- , $\tau^+\tau^-$ and ZZ^* final states are searched for inclusively in multilepton event topologies (but not including the resonant $H \rightarrow 4\ell$ channel that is covered in the specific analysis described in Section 11.3.2). The corresponding $t\bar{t}H$ modes can be decomposed in terms of the decays of the Higgs boson and those of the top quarks as having two b -quarks and four W bosons (or two W and two taus, or two W and two Z) in the final state.

The fourth channel is the search in the $H \rightarrow b\bar{b}$ channel. This search is intricate due to the large backgrounds, both physical and combinatorial in resolving the $b\bar{b}$ system from the Higgs boson decay, in events with six jets and four b -tagged jets. Already with the Run-1 dataset, the sensitivity of this analysis was strongly impacted by the systematic uncertainties on the background predictions.

Prior to its start, it was unclear if this process would at all be observable at the LHC. A first milestone was reached with the completion of the Run-1 analyses by ATLAS and CMS with a complete set of results in these channels and their combination [172, 173]. These results are reported in Table 11.5. However the sensitivity remained very limited. The breakthrough in the search for this process of fundamental importance came with the Run-2 data at a higher centre-of-mass energy of 13 TeV and the increase of a factor of nearly four of the production cross section of the $t\bar{t}H$ associated production process.

Using only a partial Run-2 dataset, ATLAS and CMS were able to independently make an unambiguous observation of this process. For these results ATLAS and CMS had different strategies. ATLAS relied mostly in the $t\bar{t}(H \rightarrow \gamma\gamma)$ channel where a narrow peak over a continuous background is searched for. It is interesting to note that the rapid evolution of the sensitivity in the diphoton channel owes not only to the large increase in cross section, but also to the fact that high mass diphoton events in an environment with additional leptons, jets and b -tagged jets the search for a pair of photon at high mass has a low background. In contrast with the inclusive search for $H \rightarrow \gamma\gamma$, the analyses in this channel reached a signal-to-background ratio in excess of unity. This channel, which is characterised by a narrow peak over a continuous background, also has the advantage of being less prone to systematic uncertainties than channels where the assessment of backgrounds cannot be made through the use of sidebands. ATLAS used up to 79.8 fb^{-1} of Run-2 data to reach an expected sensitivity of 4.9σ and an observed significance of 5.8σ with the Run-2 partial dataset alone, and 6.3σ (with 5.1σ expected) in combination with the Run-1 results [174]. CMS instead relied on a smaller dataset of 35.9 fb^{-1} and relied on all channels. The most sensitive in this case was the $t\bar{t}H(bb)$ whose sensitivity was limited by systematic uncertainties. CMS reached a sensitivity of 4.2σ and observed an excess with respect to the background-only hypothesis of 5.2σ , combining the Run-1 and Run-2 results [175].

This direct observation of the Yukawa coupling of the Higgs boson to top quarks was particularly important in comparison to the indirect evidence through the gluon fusion production process dominated by the top quark loop

Since the observation of this important process, with few exceptions, all channels have been updated with the full Run-2 dataset, by both experiments.

For the principal decays of the Higgs boson in the diphoton and four lepton channels, the measurements are done in the framework of ‘Simplified Template Cross Section’ discussed in Section 11.5.1.5). The diphoton channels were updated by both the ATLAS and CMS experiments in Refs. [176, 177]. The four lepton decays of the Higgs boson in the associated production with a pair of top quarks is a search for a narrow peak in the busy $t\bar{t}H$ environment. It was also performed by ATLAS [176] and CMS [177] with the full Run-2 datasets. These results are reported in Table 11.5. This channel has currently very low statistic but also very high purity, reaching signal-to-background ratios in excess of 10.

To address the WW , ZZ and $\tau\tau$ decay modes, an approach based on multiple channels with electrons, muons and taus decaying hadronically, the so-called ‘multi-lepton’, is adopted by both

experiments. This analysis excludes the $H \rightarrow 4\ell$ channel. CMS has analysed the Full Run-2 dataset [178] and ATLAS only part of it [179]. In a preliminary release of this analysis using a larger, but not full Run-2 dataset corresponding to an integrated luminosity of approximately 80 fb^{-1} , the ATLAS experiment found that the normalisation of the $t\bar{t}W$ background was larger than expected from SM calculations by factors ranging from 1.3 to 1.7 and modelling issues were observed in analysis regions where the $t\bar{t}W$ process is dominant [179]. The search for Higgs boson decays to tau leptons in association with a pair of top quarks was carried out by ATLAS with the full Run-2 dataset and discussed in 11.3.4.1 [180]. Using the full dataset in this channel CMS obtained an observation of the Higgs boson production in association with top quarks with an observed significance of 4.7 standard deviations (5.2σ expected). The results are reported in Table 11.5. The rate of the $t\bar{t}W$ background in this analysis is also high by a factor of approximately 1.4.

Both ATLAS and CMS have performed the analysis of Higgs bosons decaying to b-quarks in the $t\bar{t}H$ production mode with the full Run-2 dataset. In ATLAS, this analysis was performed in the semi-leptonic and di-leptonic channels [181], including a resolved mode where the Higgs boson is reconstructed as two standard jets and a boosted mode where the Higgs boson is reconstructed as a single large radius jet. CMS also performed this analysis with the full Run-2 dataset, including in addition the fully hadronic mode where both W bosons from top decays subsequently decay hadronically [182]. The results reported in Table 11.5. It should be noted that in this channel a deficit in observed Higgs boson decays is observed. This deficit is rather significant and in tension with the observation of the other $t\bar{t}H$ modes as well as the observation of the Higgs boson in the $b\bar{b}$ channels.

The discrepancies observed in both the multilepton and the $H \rightarrow b\bar{b}$ channels will require further studies.

A combination of all available channels has been performed by ATLAS [183] and CMS [184] and is reported in Fig. 11.3. It should be noted that the latest $t\bar{t}H(\rightarrow b\bar{b})$ channel from CMS with the full Run 2 data has not yet been included in the combination. A fit of individual decay modes in the $t\bar{t}H$ production is also given therein.

11.3.5.2 The associated production with a single top quark

An additional production mode of the Higgs boson in association with a top quark is the single top associated production mode. There is an interesting similarity between this production mode and the $H \rightarrow \gamma\gamma$ decay mode. Both processes proceed through either the top Yukawa coupling or the interaction of the Higgs boson with the W boson, with a negative interference between the two. Representative Feynman diagrams for this production process are shown in Fig. 11.1. Contrary to the diphoton decay channel, in this production mode the interference occurs at the tree level and is dominant. This process can therefore be used to further discriminate a negative relative sign between the couplings of the Higgs boson to fermions and its couplings to gauge bosons [185].

ATLAS and CMS have produced specific searches for the tH production mode with the Run-1 and Run-2 data exploiting a variety of Higgs boson decay modes resulting in final states with photons, bottom quarks, and multiple charged leptons, including tau leptons. In particular, with the Run-2 data, CMS has searched for multi-leptonic decay signatures from the $H \rightarrow WW^*$, $H \rightarrow \tau^+\tau^-$ and $H \rightarrow ZZ^*$ modes [186]. This analysis restricts values of κ_t , the top-Higgs coupling normalised to its SM value, to $[-1.25, 1.60]$ at 95% CL. CMS has also performed an analysis of the 2015 dataset to search for the $H \rightarrow b\bar{b}$ mode [187], yielding much less stringent constraints.

The diphoton channel has also been used to search specifically for this production mode by ATLAS using Run-1 data, yielding the restricted range of allowed values of κ_t at the 95% CL to $[-1.3, 8]$.

The strongest constraint on the negative (relative) sign of κ_t was obtained by CMS using the recent analysis of the full dataset [178] in the multilepton ($H \rightarrow WW$, $H \rightarrow ZZ$, $H \rightarrow \tau\tau$) discussed in 11.3.5.1, negative values of κ_t are disfavoured and the

only non excluded negative values of κ_t at 95% CL. range between -0.9 and -0.7.

11.3.6 Combining the main channels

The analysis strategy used by the LHC experiments to perform the searches for the Higgs boson has been based on the Higgs boson decay modes. It is a natural choice given that it focusses on the decay products of the object searched for. However, for each channel, exclusive sub-channels have been defined to target different production modes and kinematic regimes, and these sub-channels have been combined. The natural extension of this approach in order to probe further the production and decay modes of the Higgs boson is to combine the analysis channels together. Such a combination is also used in Section 11.5 to further measure the coupling properties of the Higgs boson.

At the LHC, the total cross section cannot be measured independently of the decay branching fractions. As a consequence, the total width of the Higgs boson cannot be directly measured. However, a combined measurement of the large number of categories described above with different sensitivities to various production and decay modes, permits a wide variety of measurements of the production, decay and coupling properties. These measurements, however, rely on assumptions.

Combining Higgs observation channels requires that measurements in all channels are done under the same Higgs boson mass hypothesis. This is always the case within experiments but is not necessarily the case across experiments. At Run 1, prior to combining the measurements of rates in ATLAS and CMS, a common and thus combined Higgs boson mass measurement was made. Only thereafter were the ATLAS and CMS measurements combined [153]. The Run 1 full combination results were derived by the two collaborations, taking rigorously into account all correlations in the systematic uncertainties and in the large number of channels and their categories. For a review of the Run-1 combined results see former PDG reviews in [188] and references therein.

It is important to note that, between the Run-1 and the Run-2 results, the signal theoretical systematic uncertainties have improved significantly.

At Run 2, ATLAS [183] and CMS [184] have already produced combined measurements of the coupling properties and production cross section ratios of the Higgs boson.

In this section, only the results on the main Higgs boson production and decay modes will be discussed. Only a brief presentation of the combination framework is given here (a more detailed description is given in Ref. [189]). This framework will also be used in Section 11.5 to discuss the measurements of the coupling properties of the Higgs boson.

11.3.6.1 Principles of the combination

The combination of the Higgs boson analysis channels in each experiment and for the two experiments together was done using a fit of a signal and background model to the data. As described above, the data was made of a large number of categories, aiming at reconstructing exclusive production and decay modes. In the combination of ATLAS and CMS [153], there were approximately 600 categories. The combination was a simultaneous fit to the data across all these categories, using a reduced number of parameters of interest and the Higgs boson mass fixed to its measured value at Run 1 [144]. The much larger number of categories present in the ATLAS and CMS combination [153] is due to additional separation in terms of finer exclusive production regions, decay channels of the Z and the W bosons, and taus, control regions where little-to-no signal is present, and different center-of-mass energies.

In their Run-2 individual combinations, ATLAS and CMS have not considered the $Z\gamma$ channel. Both ATLAS and CMS experiment have included the $\mu\mu$ channel based on a partial Run-2 dataset corresponding to an integrated luminosity of 36 fb^{-1} only.

The key to understanding how the combination of channels works relies on the combination master formula, which expresses for each category, indexed by c , of a given channel (typically a category covers mostly one decay mode, but possibly various production modes), the measured number of signal events n_c^s as a

Table 11.5: Summary of the results of searches for a Higgs boson in association with a top quark pair by ATLAS and CMS. The results are given in terms of a measured signal strength.

$t\bar{t}H$	ATLAS Run 1	CMS Run 1	ATLAS Run 2	CMS Run 2
$H \rightarrow \gamma\gamma$	$1.3^{+2.6}_{-1.7}{}^{+2.5}_{-1.7}$	$1.2^{+2.5}_{-1.7}{}^{+2.6}_{-1.8}$	$1.38^{+0.33}_{-0.31}{}^{+0.26}_{-0.18}$	$2.27^{+0.86}_{-0.74}$
$H \rightarrow 4\ell$	—	—	$1.2^{+1.4}_{-0.8}$	$0.00^{+0.91}_{-0.00}$
$H \rightarrow WW/\tau\tau/ZZ$	$1.4 \pm 0.6 \pm 1.0$	3.3 ± 1.4	$1.56^{+0.30}_{-0.29}{}^{+0.30}_{-0.27}$	$0.92^{+0.26}_{-0.23}$
$H \rightarrow b\bar{b}$	$1.4 \pm 1.0 \pm 0.6$	$1.6^{+1.6}_{-1.5}$	$0.35 \pm 0.20 \pm 0.30$	$0.33 \pm 0.16 \pm 0.21$
Combination	$1.7 \pm 0.5 \pm 0.8$	$2.6^{+1.0}_{-0.9}$	$0.97 \pm 0.14^{+0.14}_{-0.13}$	$0.94 \pm 0.20^{+0.09}_{-0.14}$

function of a limited number of parameters as follows:

$$n_s^c = \left(\sum_{i,f} \mu_i \sigma_i^{\text{SM}} \times A_{i,f}^c \times \varepsilon_{i,f}^c \times \mu_f \text{BR}_f^{\text{SM}} \right) \times \mathcal{L}^c. \quad (11.14)$$

The production index is defined as $i \in \{\text{ggF}, \text{VBF}, \text{ZH}, \text{WH}, \text{t}\bar{t}H, \text{tH}, \dots\}$ (including specific modes and regions of phase space) and the decay index is defined as $f \in \{\gamma\gamma, \text{WW}, \text{ZZ}, \text{bb}, \tau\tau, \mu\mu, \text{Z}\gamma\}$, while σ_i^{SM} and BR_f^{SM} are the corresponding production cross sections and decay branching fractions, estimated as described in Section 11.2, assuming that the Higgs boson is that of the SM. $A_{i,f}^c$ and $\varepsilon_{i,f}^c$ are the signal acceptance and the reconstruction efficiency for the given production and decay modes in the category c . \mathcal{L}^c is the integrated luminosity used for that specific category. For the purpose of this review, these parameters can be considered as fixed².

The parameters of interest in the master formula are the signal strength parameters μ_i and μ_f . It is important to note that the formula relies on the factorisation of the production cross section and decay branching fraction, which assumes the narrow width approximation. The width of the Higgs boson will be discussed in Section 11.4, however, for the precision needed here, the fact that the Higgs boson has been observed in decay channels with high mass resolution as a resonance is sufficient to validate this hypothesis. It is also manifest in the above equation that the ten parameters for the production modes (μ_i) and decay modes (μ_f) cannot be determined simultaneously. This illustrates that total cross sections or branching fractions cannot be measured without further assumptions in this fit.

The master formula also illustrates an important caveat to the measurement of signal strength parameters. In case these are interpreted as scale factors of the production cross sections or branching fractions, then all the other quantities such as the acceptances and efficiencies, $A_{i,f}^c$ and $\varepsilon_{i,f}^c$, need to be assumed as independent and fixed to their estimated values for the SM Higgs boson. An additional important caveat to note concerning these combined results is that only the normalisation is varied, while the discriminating variables for the signal are not modified and are still used in the fit. These caveats are of particular importance in the use of the combination to measure the coupling properties of the Higgs boson, as discussed in Section 11.5. For relatively small perturbations of the couplings of the Higgs boson from the SM values, this hypothesis is valid.

However, the products $\mu_i \times \mu_f$ can be considered as free parameters and in principle measurable (if there is sufficient sensitivity from specific categories). Measuring the products of signal strengths can be viewed as measuring the cross sections times the branching fraction, $\sigma \cdot \text{BR}$. Measurements by ATLAS and CMS of $\sigma \cdot \text{BR}$, normalised to the SM predictions, for the five largest Higgs boson production modes and five major Higgs decay modes are displayed in Fig. 11.3.

²In the combination performed by ATLAS and CMS, the systematic uncertainties on these parameters are taken into account by allowing these parameters to vary within their constraints in the fit.

Other fits involving ratios of cross sections, which are less sensitive to theory uncertainties, are performed and reported in Ref. [189].

The most constrained fit in the combination allows for only one single parameter to vary, i.e., $\forall(i, f), \mu_i = \mu_f = \mu$. This global-signal-strength model provides the simplest probe of the compatibility of the signal with the SM Higgs boson. Indeed, it is sensitive to any deviation from the SM Higgs boson couplings provided that these deviations do not cancel overall. The full Run-1 combination determines the global signal strength to be

$$\mu = 1.09 \pm 0.11 = 1.09 \pm 0.07 \text{ (stat.)} \pm 0.04 \text{ (expt.)} \pm 0.03 \text{ (th. bkg.)} \pm 0.07 \text{ (th. sig.)}, \quad (11.15)$$

where the statistical, experimental uncertainties as well as the theoretical uncertainties on the background and on the signal are reported separately. The ATLAS Run-2 combination of the global signal strength yields [183]:

$$\mu = 1.05 \pm 0.06 = 1.05 \pm 0.03 \text{ (stat.)} \pm 0.03 \text{ (exp.)} \pm 0.02 \text{ (th. bkg.)} \pm 0.04 \text{ (th. sig.)}, \quad (11.16)$$

while the CMS Run-2 combination yields [184] $\mu = 1.002 \pm 0.057$.

These overall signal strengths are fully compatible with the SM expectation, $\mu = 1$, with a precision of 6%. It is interesting to note that the main uncertainty in these measurements arises from the limited precision in the theoretical predictions for the signal production processes. The precision reached with the individual experiments combinations using partial Run-2 data sets have already exceeded the full Run-1 ATLAS and CMS combination precision.

11.3.6.2 Main decay modes

Despite the large number of decay channels, since the cross sections cannot be independently measured, from the measurements described in this section it is impossible to measure the decay branching fractions without a loss of generality. The simplest assumption that can be made is that the production cross sections are those of the SM, which is equivalent to assume that, for all i indices, $\mu_i = 1$. All branching fractions μ_f can then be measured in a simple 7 parameter fit. Results of these measurements are reported in Fig. 11.3.

11.3.6.3 Main production modes

Most analysis channels are divided into exclusive categories allowing for an increased overall sensitivity and permitting to access the various Higgs boson production modes. The cross sections of the main production modes can be measured assuming that the branching fractions are those of the SM, i.e., for all f indices $\mu_f = 1$. These assumptions lead to a 6 parameter combination.

The gluon fusion production process is the dominant production mode. Although no numerical estimate of combined significance of observation for this process has been given by the experiments, it is considered as established due to the overwhelming evidence from the three main discovery channels. At the LHC, all production modes have been unambiguously observed. The intricate VH production mode has been unambiguously observed by ATLAS

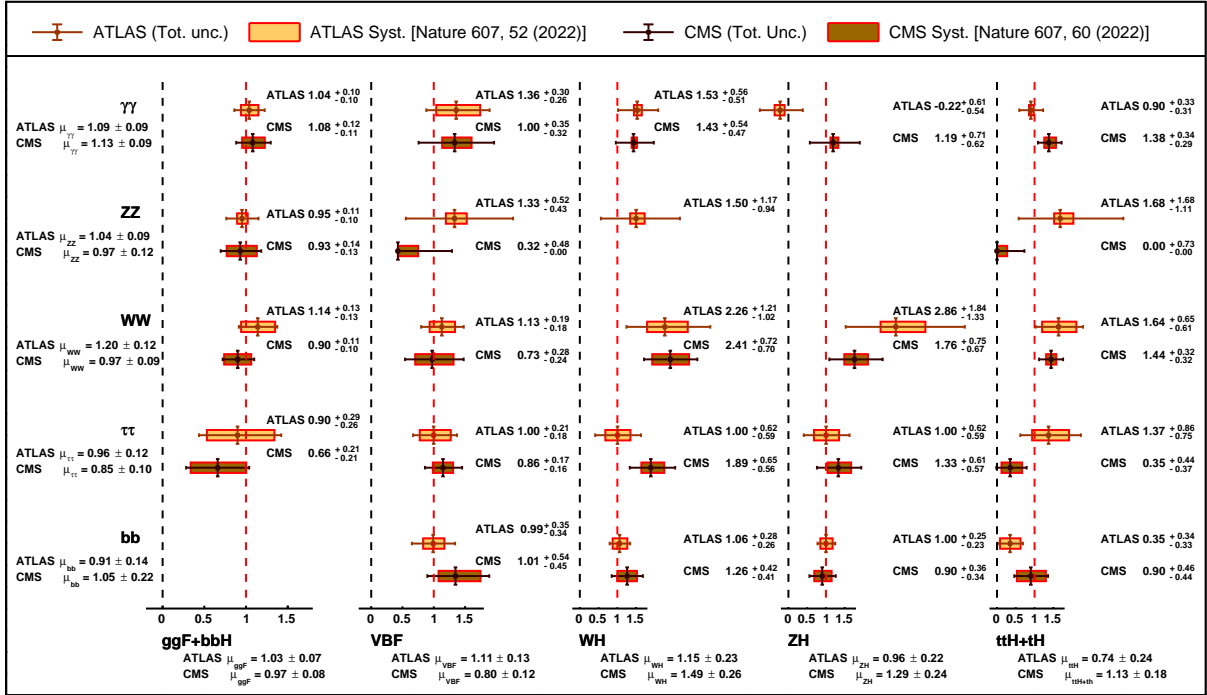


Figure 11.3: Combined measurements by ATLAS [183] and CMS [184] of the products $\sigma \cdot \text{BR}$, normalised to the SM predictions, for the five main production and five main decay modes.

and CMS independently (as discussed in Section 11.3.4) through the $V(H \rightarrow b\bar{b})$ channel. The results of these measurements are reported in Fig. 11.3.

With the Run-2 data, all the main production processes have been established, and in particular the $pp \rightarrow t\bar{t}H$ process, which provides direct evidence of the coupling of the Higgs boson to top quarks. This is another milestone in the LHC physics program.

11.3.7 Probing the Higgs boson coupling to the second generation

11.3.7.1 First evidence for $H \rightarrow \mu^+\mu^-$

The branching fraction in the $H \rightarrow \mu^+\mu^-$ channel for a 125 GeV SM Higgs boson is 2.2×10^{-4} , about ten times smaller than that for $H \rightarrow \gamma\gamma$. The major challenge in this channel is the extremely small, permil level, signal-to-background ratio. The dominant and irreducible background arises from the $Z/\gamma^* \rightarrow \mu^+\mu^-$ process which has a rate several orders of magnitude larger than that from the SM Higgs boson signal. Due to the precise muon momentum measurement achieved by ATLAS and CMS, the $m_{\mu^+\mu^-}$ mass resolution is very good ($\approx 2\text{--}4\%$ for ATLAS and $\approx 1\text{--}3\%$ for CMS depending on the selected categories; a better resolution is expected for CMS due its higher magnetic field strength in the inner detector). A search is performed for a narrow peak over a large but smoothly falling background. For optimal search sensitivity, events are divided into several categories. Either taking advantage of the superior muon momentum measurement in the central region, events can be subdivided by the pseudo-rapidity of the muons, or designing selections aiming at specific production processes such in particular as the vector boson fusion.

ATLAS and CMS analyses target the main production modes such as gluon fusion, associated production with a vector boson (including in the vector boson leptonic decay modes), vector boson fusion and associated production with a top-quark pair. The analyses use multivariate and deep machine learning methods to discriminate signal from background in these Higgs production categories. The signal in both experiments is extracted from a fit to the di-muon invariant mass spectrum and the background is modeled using a suite of analytical functions, except in the case of the most sensitive channel (VBF) in the CMS analysis where the distribution of a discriminant Deep Neural Network output is used.

With the Run-2 dataset, ATLAS measured [190] a signal strengths of $\mu = 1.2 \pm 0.6$ with an observed (expected) significance of $2.0(1.7)\sigma$. The 95% CL limit on $pp \rightarrow H \rightarrow \mu^+\mu^-$ was set at 2.2 times the SM prediction while the expected limit on a $H \rightarrow \mu^+\mu^-$ signal assuming the absence (presence) of a SM signal was 1.1 (2.0). CMS reported [191] the first evidence for $H \rightarrow \mu^+\mu^-$ at 3σ level with a signal strength of $\mu = 1.19 \pm 0.40$ (stat.) ± 0.15 (syst.) and an expected analysis sensitivity of 2.5σ . These measurements provide the first direct evidence for the decay $H \rightarrow \mu^+\mu^-$ and thus of the Yukawa coupling of the Higgs boson to second generation fermions.

11.3.7.2 Constraints on Higgs boson coupling to charm quarks

The possibility of probing the Yukawa coupling to the charm has been discussed early in Ref. [192] where indirect bounds are estimated from a combined fit to the Higgs data and the importance of using charm tagging is emphasised. A SM decay rate in standard production was long thought to be out of reach at the LHC. However recent results, in particular from CMS have shown that a different perspective might be emerging [193].

The channels which are currently foreseen to be most sensitive are similar to those aiming at the b -quark Yukawa coupling, and pertain to the VH production mode. As was discussed in [188], the typical sensitivity of these analysis using the LHC Run-2 data on the production times branching fraction was approximately a factor of 30 times the expected rate in the Standard Model.

The key aspect to bring sensitivity to the charm coupling is the ability of flavour tagging algorithms to discriminate charm quark initiated jets from both b quark and light quark jets. Significant progress was recently made in development of parton flavour taggers using state-of-the-art machine learning techniques [194] and additional information to these algorithms. Novel algorithms have also been used to identify pairs of charm quarks resulting from the decay of a Higgs boson, in particular in a regime where the Higgs boson is reconstructed as a large radius jets with a distinctive substructure. These new techniques have resulted in impressive improvements which have led to the first observation of Z boson decays to charm quarks at a hadron collider with a significance of 5.7 standard deviations [193] and an expected sensitivity to the exclusion of a Higgs boson signal decaying to a pair of charm quarks of 7.6 times the Standard Model rate. The observed limit

for CMS is at 14 times the SM rate. This led CMS to set limits on the absolute value of κ_c , the Yukawa coupling of the Higgs boson to charm quarks with respect to its value in the Standard Model.

The expected 95% CL interval is $|\kappa_c| < 3.4$. The observed 95% CL interval is the following:

$$1.1 < |\kappa_c| < 5.5 \quad (11.17)$$

This is the most stringent constraint today. The ATLAS analysis [195], in contrast, is still relying on traditional techniques and sets an observed (expected) limit at 26 (31) times the SM rate, using the VH production mode where the vector boson decays to leptons.

CMS complemented this search in the VH production mode with an inclusive search for the Higgs boson produced at high transverse momentum (in excess of 450 GeV) and decaying to a pair of charm quarks [196]. The observed (expected) limit at 95% CL is 47 (39) times the SM rate, which is also an impressive result as it is almost comparable to the previous results obtained in the more sensitive VH channel.

With this striking improvement in sensitivity, CMS reappraised their prospect for the search of Higgs boson decays to charm quarks at the HL-LHC and showed that a CMS could reach a relative precision on the the production rate of approximately 80%. In combination with ATLAS and potential improvements in the analysis, this is bringing the Yukawa coupling of the Higgs boson closer to being at reach at the HL-LHC.

11.3.8 Searches for rare decays of the Higgs boson

11.3.8.1 Combined evidence for $H \rightarrow Z\gamma$ and the first evidence for the Dalitz $H \rightarrow \ell^+\ell^-\gamma$ decay

The search for $H \rightarrow Z\gamma$ is performed in the final states where the Z boson decays into opposite sign and same flavour leptons ($\ell^+\ell^-$), ℓ here refers to e or μ . While the branching fraction for $H \rightarrow Z\gamma$ is comparable to $H \rightarrow \gamma\gamma$ (about 10^{-3}) at $m_H = 125$ GeV, the observable signal yield is brought down by the small branching ratio of $Z \rightarrow (e^+e^- + \mu^+\mu^-) = 6.7 \times 10^{-2}$. In these channels, the $m_{\ell\ell\gamma}$ mass resolution is excellent (1–3%), therefore the analyses search for a narrow mass peak over a continuous background. The major backgrounds arise from the $Z + \gamma$ final state radiation in Drell–Yan decays and from the $Z +$ jets processes where a jet is misidentified as a photon. The ratio of signal over background in this channel is typically of the order of 0.5%. In a narrow window of a few GeV around 125 GeV, several hundreds of events are expected in a Run-2 dataset corresponding to approximately 36 fb^{-1} . Events are divided into mutually exclusive categories on the basis either of the expected $m_{Z\gamma}$ resolution or exclusive production mode categories.

With the full Run-2 dataset, ATLAS observes an excess with a significance of 2.2σ while an excess with a significance of 1.2σ is expected. CMS observes an excess with a significance of 2.6σ while 1.2σ is expected. ATLAS and CMS have jointly published a combination of these results, yielding a first evidence for the Higgs boson decay to a Z boson and a photon at the LHC with an observed significance of 3.4σ and an expected sensitivity of 1.6σ [197]. This combined result is compatible with the SM hypothesis at 1.9σ .

Both ATLAS and CMS experiments have extended the search for the so-called Dalitz Higgs boson decays $H \rightarrow \gamma^*\gamma \rightarrow \ell^+\ell^-\gamma$ in the low mass γ^* range of approximately 20–30 GeV. This decay mode has a substantially larger branching fraction compared to the $Z\gamma$ decay, as $\Gamma(H \rightarrow \gamma^*\gamma \rightarrow e^+e^-\gamma) \sim 3.5\% \times \Gamma(H \rightarrow \gamma\gamma)$ and $\Gamma(H \rightarrow \gamma^*\gamma \rightarrow \mu^+\mu^-\gamma) \sim 1.7\% \times \Gamma(H \rightarrow \gamma\gamma)$, while $\Gamma(H \rightarrow Z\gamma) = 2.3\% \times \Gamma(H \rightarrow \gamma\gamma)$ (which does not account for the subsequent decay of the Z boson to electrons or muons). With the Run-1 dataset, CMS observes an upper limit of 6.7 times the SM branching ratio [198]. With a partial Run-2 dataset, in the $\gamma^*\gamma$ CMS obtained a much more stringent limits on the cross section times the corresponding branching fractions of 1.4 (6.1) times the SM cross section [199]. CMS also performed a combination of this mode with $H \rightarrow Z\gamma$, obtaining a combined observed (expected) limit of 3.9 (2.0) times the SM branching fractions.

Using the full Run-2 dataset corresponding to 139 fb^{-1} , ATLAS obtained the first evidence for Higgs boson decays to a low-mass

dilepton pair and a photon with a significance of 3.2 (2.1) standard deviations (expected) [200]. The invariant mass requirement on the di-lepton is $m_{\ell\ell} < 30$ GeV. The corresponding signal strength is $\mu = 1.5 \pm 0.5$, compatible with the SM expectation.

11.3.8.2 Higgs coupling to first generation, search for $H \rightarrow e^+e^-$

Probing the Yukawa couplings to the first generation fermions is extremely challenging at the LHC given the overwhelming backgrounds and very small signal rates.

A search similar to the $H \rightarrow \mu^+\mu^-$ is performed in the non-VBF categories by CMS in the di-electron channel [201]. In this search, the contribution from the peaking background from Higgs boson decays to diphotons mis-identified as di-electrons (when converted photons are faking electrons) needs to be carefully assessed. The sensitivity to the SM Higgs decays is negligible given the extremely small branching fraction to e^+e^- , approximately 40,000 times smaller than the branching fraction to dimuons. It is nevertheless interesting to probe this decay channel to search for potential large anomalous couplings. Assuming a SM Higgs boson production cross section, the observed limit on the $H \rightarrow e^+e^-$ branching fraction at the 95% CL is 3.0×10^{-4} , more than five orders of magnitude larger than the expected SM prediction. ATLAS has also performed a search for the $H \rightarrow e^+e^-$ decay mode with the Run-2 dataset, placing a limit of 3.6×10^{-4} on the branching fraction [202].

It is important to note that processes not depending on the electron Yukawa coupling such as the $H \rightarrow e^+e^-\gamma$ (where the photon is soft), are sizeably larger than the direct Yukawa coupling process, but also much smaller than the current constraints, making any interpretation in terms of constraint on the electron Yukawa couplings far from straightforward.

11.3.8.3 Invisible decays of the Higgs boson

The discovery of the Higgs boson immediately raised the question of its couplings to DM and how it could be used to reveal at colliders the existence of a dark sector coupled to the SM via the Higgs boson portal, see Ref. [203] and references therein. If kinematically accessible and with a sufficiently large coupling to the Higgs boson, DM particles, such as, e.g., neutralinos in SUSY models, graviscalars in models with extra dimensions or heavy neutrinos in the context of four-generation fermion models, would manifest themselves as invisible decays of the Higgs boson, thus strongly motivating searches for the invisible decays of the Higgs boson.

It should be noted that in the Standard Model the branching fraction of a Higgs boson into invisible decays through the $H \rightarrow ZZ^* \rightarrow \nu\bar{\nu}\nu\bar{\nu}$ process has a branching fraction of 0.12%.

To identify an invisibly decaying Higgs boson at the LHC, it must be produced in association with other particles. Searches for invisible decays of the Higgs boson at the LHC have been carried out in the three associated production modes of the Higgs boson with the highest SM cross sections and target events with large missing energy.

The ggF production mode has the largest SM cross section but it usually results in the Higgs boson being created alone and hence leaving no characteristic signature in the detector of its invisible decay. One way to search for invisible decays in ggF production mode is to look for events with the monojet topology arising from initial state gluon radiation and containing missing energy. The major irreducible background in such searches stems from $Z +$ jets events where the Z boson decays into a pair of neutrinos [204]. The analysis with the best sensitivity targets the VBF production topology but it suffers from large backgrounds arising from events with two jets and large missing energy. The VH mode has much smaller cross section but the presence of a W or Z boson allows a variety of final states that can be tagged with relatively low background.

ATLAS and CMS have searched for such final states at Run 1 and have observed no significant excess over the predicted backgrounds (for references, see the previous edition of this review [141]). Table 11.6 summarises the 95% CL limits on the invisible decays of the Higgs boson assuming a SM Higgs boson production cross section and the corresponding detector acceptances.

Table 11.6: Summary of the channels searched for and the corresponding 95% CL limits from ATLAS and CMS on the branching fraction for the Higgs boson decay to invisible particles assuming a SM Higgs boson production cross section. The results in parentheses are the expected exclusions.

	ATLAS (Run 1)	ATLAS (Run 2)	CMS (Run 1)	CMS (Run 2)
ggF (monojet); $H \rightarrow \text{inv.}$	–	33 (38) %	67 (71) %	49 (32)%
VBF; $H \rightarrow \text{inv.}$	28 (31) %	14.5 (10.3) %	57 (40) %	18 (10) %
$\bar{Z}H$; $Z \rightarrow \ell^+\ell^-$; $H \rightarrow \text{inv.}$	75 (62)%	18.5 (18.5) %	75 (91) %	–
VH; $Z, W \rightarrow jj$; $H \rightarrow \text{inv.}$	78 (86)%	83 (58) %	–	21 (18)%
$\bar{Z}H$; $Z \rightarrow b\bar{b}$; $H \rightarrow \text{inv.}$	–	–	182 (189)%	–
$t\bar{t}H$; $H \rightarrow \text{inv.}$	–	38 (30)%	–	26 (30)%
Run 1 & 2 Combination	10.7 (7.7)%		15 (8)%	

ATLAS and CMS have performed the search for invisible decays of the Higgs boson at Run 2 with the full dataset in all the aforementioned channels [205–207]. The results are summarised in Table 11.6.

These constraints can then be further used to probe Higgs portal models to DM [203], where an additional weakly interacting particle χ with mass lower than $m_H/2$ is introduced as DM candidate and where the Higgs boson is considered as the only mediator between the SM particles and DM. In this model, it is interesting to express the limit on the invisible branching fraction in terms of strength of interaction of DM with standard matter, i.e., in terms of its interaction cross section with nucleons $\sigma_{\chi-N}$. In this model, the couplings of the Higgs boson to SM particles are assumed to be those of the SM and the interaction of the Higgs boson with the nucleon is parametrised in a Higgs-Nucleon form factor estimated using lattice QCD calculations [203]. The results for the ATLAS limits are shown in Fig. 11.4.

11.3.8.4 Exclusive Higgs boson decays

A possibility to access the charm Yukawa coupling has been discussed in Ref. [208]. It relies on the decays of the Higgs boson to a final state with quarkonia. Searches have been performed in several channels including $H \rightarrow \Upsilon\gamma, J/\Psi\gamma, \phi\gamma, \rho\gamma$ these processes can provide indirect constraints on the Higgs boson Yukawa coupling to b , charm, strange and light quarks. The limits obtained so far in these channels [209, 210] are reported in the Higgs particle listings [188]. Limits on branching fractions range between 10^{-3} – 10^{-4} .

CMS has also performed a search of the decays of the Higgs boson in the $J/\Psi J/\Psi$ and $\Upsilon\Upsilon$ final states to cover the cases where the photon in the $J/\Psi\gamma$ decay is virtual and transforms into a J/Ψ meson, These decays provide an additional channel potentially sensitive to BSM phenomena [211].

More recently a search for Higgs boson decays to mesons and a photon in the channels $H \rightarrow \omega\gamma$ and $H \rightarrow K^*\gamma$ have been carried out by the ATLAS experiment [212]. The limits on these processes are of 1.5×10^{-4} and 8.5×10^{-5} on the $\omega\gamma$ and the $K^*\gamma$ respectively.

Another class of searches for exclusive decays of the Higgs boson is $H \rightarrow ZQ$ where Q is a quarkonium state. This decay results from the interference of two contributions, one where the Higgs boson couples to a quark-anti-quark pair which forms a quarkonium and radiates a Z boson at leading order, and another one from the off-shell decay $H \rightarrow ZZ^*$ or $H \rightarrow Z\gamma^*$ and the conversion of the off-shell Z or photon into a quarkonium. A search was carried out by ATLAS in the ZJ/Ψ and Z/η_c channel in the $Z \rightarrow \ell^+\ell^-$ and a light hadronically decaying resonance signature [213] and by CMS in the ZJ/Ψ and ZJ/Υ channels in fully leptonic final states [214].

11.3.8.5 Lepton flavour violating (LFV) Higgs boson decays

Given the Yukawa suppression of the couplings of the Higgs boson to quarks and leptons of the first two generations and the small total width of the Higgs boson, new physics decay modes could easily have sizeable branching fractions. One very interesting possibility is the Lepton Flavour Violating (LFV) decays of the Higgs boson, in particular in the $\tau\mu$ and τe modes. These decays are suppressed in the SM but they could easily be enhanced in theories such as two-Higgs-doublet models (discussed

in Section 11.6). Indirect constraints on the LFV Yukawa couplings $|Y_{\tau\mu}|$ can be obtained from channels such as the $\tau \rightarrow 3\mu$ or $\tau \rightarrow \mu\gamma$, or a re-interpretation of the search for Higgs boson decays to $\tau^+\tau^-$. A direct search at the LHC, however, complements these indirect limits.

The search for LFV decays in the $\tau\mu$, τe and μe channels were carried out with the Run-1 and early Run-2 datasets in several channels according to the subsequent decay of the τ [215–220]. The limits on LFV decays of the Higgs boson are reviewed in this volume of the particle listings [188] and reached 0.15% in the $\tau\mu$ channel and 0.22% in the τe channel.

ATLAS [221] has performed the analysis with the full Run-2 dataset, yielding limits of 0.20% and 0.18% on the $e\tau$ and $\mu\tau$ channels respectively. CMS [222] has performed analyses with the full Run-2 dataset of the $e\mu$ channel reaching a limit of 4.4×10^{-5} at 95% CL.

The CMS search in the $e\mu$ channel was done not only at the specific Higgs boson mass, but in a wider mass domain between 110 GeV and 160 GeV. A mild excess with a global significance of 2.8 standard deviations is observed for a mass hypothesis of approximately 146 GeV.

11.3.8.6 Flavour changing neutral current decays of the top quark

The discovery of the Higgs boson at a mass smaller than the top quark mass opened a new decay channel for the top quark. The decays of the top quark to a Higgs boson and a charm or an up quark proceed through a Flavour Changing Neutral Current (FCNC) which are forbidden in the Standard Model at tree level and suppressed at higher orders through the Glashow–Iliopoulos–Maiani (GIM) mechanism [3]. The SM prediction for these branching fractions is $\text{BR}(t \rightarrow Hc) = 10^{-15}$ and two orders of magnitude less for the Hu final state. These decay channels of the top quark are, therefore, very interesting to probe possible FCNC interactions in the Yukawa couplings to the quark sector, see Section 11.6.

ATLAS has searched for FCNC top decays specifically in channels involving a Higgs boson that subsequently decays into a pair of b quarks, two photons, a tau pair or two W bosons [223]. It has also reinterpreted a search for the $t\bar{t}H$ production in the multi-lepton final state (discussed in Section 11.3.5.1) [173]. The latter channel covers Higgs boson decays to a pair of W bosons and a pair of taus. No significant excess was observed in any of the specific channels (as discussed in Section 11.3.5.1, a slight excess is observed in the $t\bar{t}H$ multi-lepton channel) and 95% CL upper limits are set on $\text{BR}(t \rightarrow Hc) < 0.46\%$ with an expected sensitivity of 0.25% and $\text{BR}(t \rightarrow Hu) < 0.45\%$ with an expected sensitivity of 0.29%. CMS has performed a search for these FCNC top decays in the diphoton and multi-lepton channels [224], placing a 95% CL upper limit on $\text{BR}(t \rightarrow Hc) < 0.40\%$ with an expected sensitivity of 0.43%.

From these limits on branching fractions, constraints on non-flavour-diagonal Yukawa couplings of a FCNC Lagrangian of the form:

$$\mathcal{L}_{\text{FCNC}} = \lambda_{tcH}\bar{t}Hc + \lambda_{tuH}\bar{t}Hu + h.c. \quad (11.18)$$

can be derived. The 95% CL observed (expected) upper limits from ATLAS on the $|\lambda_{tcH}|$ and $|\lambda_{tuH}|$ couplings are 0.13 (0.10) and 0.13 (0.10), respectively.

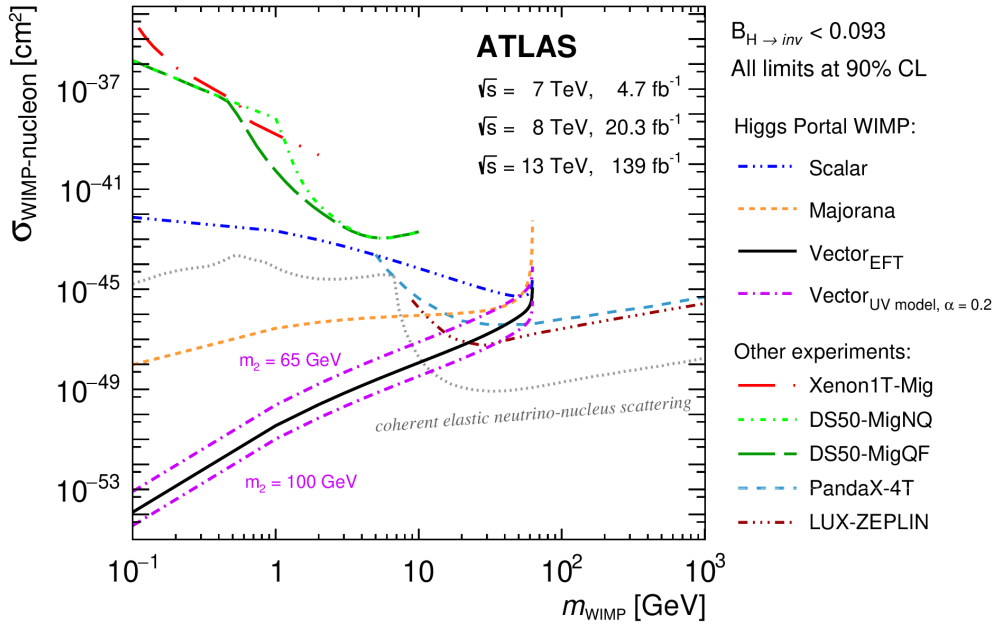


Figure 11.4: 90% CL upper limits on the spin-independent WIMP-nucleon scattering cross section as a function of the DM particle mass for direct detection experiments and the interpretation of the $H \rightarrow \text{invisible}$ combination result in models where the Higgs boson is a portal between the SM matter and the Dark Sector. For the vector UV-model, m_2 are two representative values of the predicted Dark Higgs particle with mixing angle α . The regions above the limit contours are excluded in the range shown in the plot. From Ref. [205].

The results above are derived from the combination of several channels for searches performed with Run-1 data. Both ATLAS and CMS have produced updates of individual channels with Run-2 data. ATLAS has searched for FCNC top decays with subsequent decays of the Higgs boson to a pair of photons [225], yielding a 95% CL upper limit on $\text{BR}(t \rightarrow Hc) < 0.22\%$ with an expected sensitivity of 0.16%. CMS has searched for FCNC top decays with subsequent decays of the Higgs boson to a pair of b -quarks [226], yielding a 95% CL upper limit on $\text{BR}(t \rightarrow Hu) < 0.079\%$ with an expected sensitivity of 0.011% and on $\text{BR}(t \rightarrow Hc) < 0.094\%$ with an expected sensitivity of 0.086%.

11.3.8.7 Exotic Higgs boson decays

The 125 GeV Higgs boson serves not only as a probe for potential DM candidates, but also to search for other exotic particles arising from fields associated with a low-mass hidden sector (for a review, see for instance Ref. [227]). Such hidden sectors are composed of fields that are singlet under the SM gauge group $SU(3) \times SU(2) \times U(1)$. These models are referred to as hidden valley models [228]. Since a light Higgs boson is a particle with a narrow width, even modest couplings to new states can give rise to a significant modification of the Higgs boson phenomenology through exotic decays. Simple hidden valley models exist in which the Higgs boson decays to an invisible fundamental particle, which has a long lifetime to decay back to SM particles through a small mixing with the SM Higgs boson, see Ref. [228] for a concrete example. The Higgs boson may also decay to a pair of hidden valley “ v -quarks,” which subsequently hadronise in the hidden sector, forming “ v -mesons.” These mesons often prefer to decay to the heaviest state kinematically available, so that a possible signature is $H \rightarrow 4b$. Some of the v -mesons may be stable, implying a mixed missing energy plus heavy flavour final state. In other cases, the v -mesons may decay to leptons, implying the presence of low mass lepton resonances in high- H_T events [229]. Other scenarios have been studied [230] in which the Higgs boson decays predominantly into light hidden sector particles, either directly, or through light SUSY states, and with subsequent cascades that increase the multiplicity of hidden sector particles. In such scenarios, the high-multiplicity hidden-sector particles, after decaying back into the SM, appear in the detector as clusters of collimated leptons known as “lepton jets”.

A variety of models have been investigated searching for final states involving dark photons and hidden valley scalars. The resulting topologies typically have leptons or light hadrons which in some cases can be prompt (i.e., originating from the hard process interaction point) or not and are in some cases collimated and reconstructed as jets [231, 232], and long-lived weakly interacting particles. The latter occur not only in hidden valley scenarios, but also in gauge-mediated extensions of the minimal SUSY standard model (MSSM), the MSSM with R-parity violation, and inelastic DM scenarios [233]. Finally, CMS has performed a search for pair production of light bosons [234]. Such a scenario can occur in SUSY models with additional hidden (or dark) valleys.

11.3.9 Higgs boson pair production and self-coupling

Higgs boson pair production in the SM is a rare but very important mode to measure and search for. The measurement of Higgs boson pair production is essential to directly constrain the trilinear Higgs boson self coupling and the search for Higgs boson pair resonances is key in a variety of BSM models. The latter searches are discussed in Section 11.6.7.

In the SM, the main non-resonant production mode of two Higgs bosons proceeds through a loop, mainly of top quarks, see Fig. 11.1(h). Another production mode is via the trilinear coupling of the Higgs boson, see Fig. 11.1(i), whose amplitude is not negligible compared to the former. These diagrams interfere negatively, making the overall production rate smaller than what would be expected in the absence of a trilinear coupling.

11.3.9.1 Searches for Higgs boson pair production

The searches for Higgs boson pair production both resonant and non-resonant are important probes for a variety of BSM theories, and they can be done in a large number of Higgs boson decay channels. At Run 1, ATLAS and CMS have searched for both resonant and non resonant Higgs boson pair production in the following channels: (i) $HH \rightarrow b\bar{b}\gamma\gamma$; (ii) $HH \rightarrow b\bar{b}\tau^+\tau^-$; (iii) $HH \rightarrow b\bar{b}b\bar{b}$; (iv) $HH \rightarrow b\bar{b}4\ell$; (v) $HH \rightarrow WW^*\gamma\gamma$; (vi) in final states containing multiple leptons (electrons or muons) covering the WW^*WW^* , WW^*ZZ^* , ZZ^*ZZ^* , $ZZ^*\tau^+\tau^-$, $WW^*\tau^+\tau^-$, $ZZ^*b\bar{b}$, $\tau^+\tau^-\tau^+\tau^-$ channels; and (vi) $\gamma\gamma\tau^+\tau^-$ channels.

At Run 2, similarly to the $t\bar{t}H$ production process, the di-Higgs production profits from a significant increase in production cross section of a factor in excess of 3 from 8 TeV to 13 TeV, and most

of these channels have been updated both by ATLAS [235] and CMS [184, 236]. The detailed description of the various analyses used can be found in the references therein. All the results and their combinations are summarised in Table 11.7 and in Fig. 11.5 (left). The channels (i)-(iii) are the most sensitive to the HH production. These three channels have been updated with the full Run-2 dataset except the $HH \rightarrow b\bar{b}\tau^+\tau^-$ channel by CMS and the $HH \rightarrow b\bar{b}b\bar{b}$ channel by ATLAS which have both been analysed using a partial Run-2 dataset.

In several of these analysis channels the VBF production mode is searched for separately providing sensitivity to the coupling involving two vector bosons and two Higgs bosons HHVV which is an expected coupling in the Standard Model.

Table 11.7: Summary of the final states investigated in the search for Higgs boson pair production by ATLAS and CMS, the results reported in bold are based on the full Run-2 dataset. For ATLAS, the result indicated by (*) uses mostly the $b\bar{b}W^+W^-$ channel. Results are 95% CL upper limits on the observed (expected) signal strengths.

Channel	ATLAS	CMS
$b\bar{b}\gamma\gamma$	4.2 (5.7)	8.4 (5.5)
$b\bar{b}b\bar{b}$	5.4 (8.1)	7.2 (4.2)
$b\bar{b}\tau^+\tau^-$	4.7 (3.9)	3.3 (5.2)
$b\bar{b}4\ell$	-	32 (40)
$W^+W^-W^+W^-$	160 (120)	-
$W^+W^-\gamma\gamma$	230 (170)	97 (52)
$b\bar{b}VV$	305 (305)*	14 (18)
Multi-lepton	-	19 (21)
Combination	2.4 (2.9)	3.4 (2.5)

The current single channel most stringent limits obtained on the HHVV coupling modifier denoted κ_{2V} are obtained from the analysis performed by CMS [237] in the $b\bar{b}b\bar{b}$:

$$-0.1 < \kappa_{2V} < 2.2 \text{ (observed)}, \quad -0.4 < \kappa_{2V} < 2.5 \text{ (expected)}$$

and for the overall most stringent constraints are obtained through the combination of channels in ATLAS, yielding [235]:

$$-0.1 < \kappa_{2V} < 2.0 \text{ (observed)}, \quad 0.0 < \kappa_{2V} < 2.1 \text{ (expected)}$$

11.3.9.2 The Higgs boson self coupling

The Higgs boson self coupling is an extremely important direct probe of the Higgs potential with implications on our understanding of the electroweak phase transition. Constraints on the trilinear self coupling from HH processes is an outstanding long term goal of the LHC and the reach in sensitivity has been reappraised in the light of the recent HH analyses from ATLAS and CMS, shedding a different light on the achievable sensitivity [118]. Constraints from the HHH final state on the quartic Higgs boson self coupling are out of reach at the LHC due mostly to the very small production rates and intricate final states.

In the SM, the Higgs boson pair production through the trilinear Higgs boson self coupling has an on-shell component and a large off-shell component. The on-shell $H \rightarrow H^*H^*$ is strongly disfavoured, requiring two off-shell Higgs bosons in the final state. The sensitivity region to the trilinear coupling production as in Fig. 11.1 (i), is mainly in the kinematic region where the two Higgs boson in the final state are on-shell and the Higgs boson acts as a propagator (off-shell). As discussed in the introduction to this section, this process interferes negatively with the background Higgs

boson pair production (Fig. 11.1 (h)). The extraction of the trilinear component of the di-Higgs production measurements is very similar to the extraction of the off-shell component of the Higgs coupling to vector bosons discussed in Section 11.4.2.

The measurement of the trilinear coupling requires separating the contributions of the diagram of Fig. 11.1 (i) from the box diagram of Fig. 11.1 (h), and therefore a precise knowledge of the top-Yukawa coupling is needed. Each diagram alone would produce a rather distinct m_{HH} distribution. And, for values of the trilinear coupling close to the SM value, an additional discriminating feature of the signal with respect to one obtained with the box contribution alone is a deficit in the number of events. With large variations of the trilinear coupling, an excess of events over the SM prediction would be observed (for a value of the trilinear coupling about 6 times larger than its SM value, the number of events is equal to the SM expectation). Additional sensitivity to the trilinear coupling is also obtained from the kinematical distributions of the signal taking in particular into account the effect of the HH mass distribution which discriminates the main contributions of Fig. 11.1. This further discrimination is instrumental in resolving the degeneracy in the total cross section mentioned above. Bounds on the trilinear coupling are obtained from limits on the HH production as a function of the trilinear coupling factor κ_λ as illustrated in Fig. 11.5. As the sensitivity in this channel grows it will be interesting to more closely look at the combined and individual likelihoods as a function of the trilinear coupling to quantify the exclusion of the secondary minimum induced by the degeneracy between the value of κ_λ yielding the same overall HH rate as the Standard Model (*i.e.* $\kappa_\lambda = 1$). The results obtained by ATLAS [235] and CMS [184] are the following:

$$\begin{aligned} \text{(ATLAS)} \quad & -0.6 < \kappa_\lambda < 6.6 \text{ (observed)}, \\ & -2.1 < \kappa_\lambda < 7.8 \text{ (expected)}, \\ \text{(CMS)} \quad & -1.2 < \kappa_\lambda < 6.5 \text{ (observed)}, \end{aligned} \quad (11.19)$$

where κ_λ is the ratio between the trilinear coupling value left free in the fit and its expected value in the SM ($\kappa_\lambda = 1$ corresponds to the SM). For the CMS result the expected excluded range is not specified in [184], however its illustration in the exclusion figure therein shows that it is compatible with the observation. The so-called κ formalism is discussed in more detail in Section 11.5.1.1. These results are also illustrated in Fig. 11.5.

Single Higgs production can indirectly also be used to further constrain the trilinear coupling of the Higgs boson, both using inclusive total or differential cross sections. A combination of di-Higgs and single-Higgs boson production results has been performed by the ATLAS collaboration yielding the following limits [235]:

$$-0.4 < \kappa_\lambda < 6.3 \text{ (observed)},$$

It is interesting to note that currently the *direct* ($-0.6 < \kappa_\lambda < 6.6$) and *indirect* constraints ($-4.0 < \kappa_\lambda < 10.3$) on the Higgs boson trilinear self-coupling are of comparable strength. However, the double Higgs boson measurements are dominated by statistical uncertainties and are expected to improve more rapidly than the precision on single Higgs boson measurements. It should also be stressed that the constraints on the trilinear self-coupling obtained via the NLO fit of single Higgs boson data are model-dependent since the NLO effects induced by a shift of the trilinear self-coupling compete with possible LO effects sourced by the deviations of the Higgs boson couplings to the other SM particles. The different effects can be disentangled by the measurements of various kinematical differential distributions in addition to the study of the inclusive rates [238], but the expected sensitivity obtained in such global fits are not as strong as when only the Higgs boson self-coupling is allowed to deviate from its SM value [119]. It should also be noted that in this fit the parameters κ_t , κ_b , κ_τ and κ_V are fit simultaneously.

The analyses performed at Run 2 bring substantial improvements from those of Run 1, and they were first used to reappraise the sensitivity of the LHC in the High Luminosity regime in the framework of the update of the European Strategy for Particle Physics [118]. The result in terms of bounds on the trilinear coupling indicated that the significance of the observation of the HH

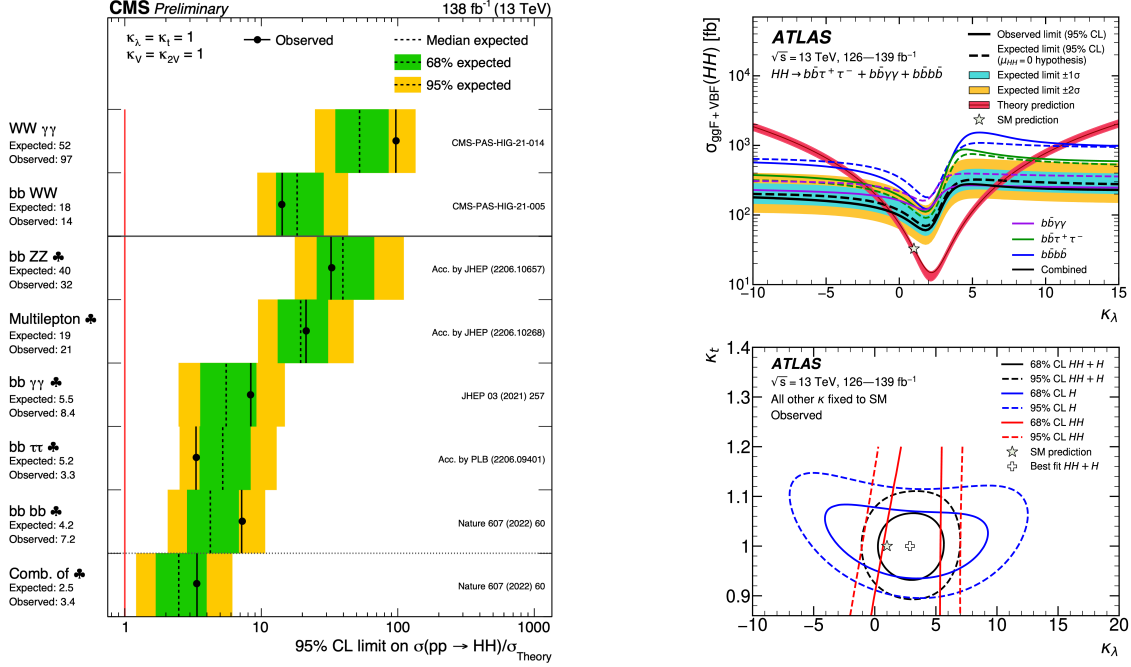


Figure 11.5: (Left) Upper limits obtained by CMS on the total $pp \rightarrow HH$ production cross section. (Top right) Upper limits obtained by ATLAS on the total $pp \rightarrow HH$ production cross section as a function of the trilinear coupling modifier κ_λ . The variation of the limit corresponds to variations in the signal acceptance. The expected total production cross section is also illustrated (red). (Bottom right) Likelihood contours for the ATLAS di-Higgs and single-Higgs combined results as a function of κ_λ and κ_t .

process reaches 4σ . It is also apparent that the degeneracy of secondary minimum at intermediate values of κ_λ is resolved by the use of the kinematic discriminants. This secondary minimum was expected to be excluded at 99.4% CL and at HL-LHC, the foreseen precision on κ_λ was estimated to reach approximately 50%. These studies were based on early LHC Run-2 analyses [239] and more recently using the latest HH searches results, these projections have been updated. Both experiments have reappraised their studies at HL-LHC [240], to reach individually a sensitivity of approximately 3.5σ , a significant improvement compared to the sensitivities estimated between 2.5σ and 3σ in [118]. These studies indicate that a sensitivity of 5σ in combination of the two experiments should be reached at HL-LHC.

Higher precisions can be reached at pp colliders (and e^+e^- colliders) at higher centre-of-mass energies. The foreseen precision for a High-Energy (HE) LHC at a centre-of-mass energy of 27 TeV is expected to be within 10% to 20% [118]. At a very large hadron collider at a centre-of-mass energy of 100 TeV, a 5% sensitivity is expected to be reached, provided that the theoretical and parametric uncertainties are kept at the 1% level [241].

One of the main open questions in particle physics is related to the precise history of the EWSB mechanism. This in turn can be of relevance to provide a mechanism for generating the matter-antimatter asymmetry of the universe at the electroweak scale, the so called electroweak baryogenesis (EWBG) (see Refs. [242, 243] for some reviews). In the SM EWBG is ruled out, but new physics models, in particular those additional scalar particles coupled/mixed with the Higgs boson, can provide a successful alternative. Given that di-Higgs production will become an excellent probe of trilinear Higgs coupling modifications, it will provide a unique window into the history of EWSB and will become a powerful test of EWBG models.

11.3.10 Beyond the main Higgs boson production modes

Most of the production modes illustrated in Fig.11.1 have been investigated at the LHC so far. These processes are often referred to as the 'main production modes'. Beyond these production modes, two additional SM processes involving the Higgs boson

have been investigated and are worth noting.

The first is the four top production mode which is closely related to the $t\bar{t}H$ mode. This process has recently been unambiguously observed at the LHC by both ATLAS [244] and CMS [245]. This production mode has a non trivial contribution from the exchange of a Higgs boson. A first limit on the Yukawa coupling of the Higgs boson has thus been derived using this four top process, $|\kappa_t| < 1.8(1.6)$, under the assumption that the Yukawa coupling of the Higgs boson to top quarks in CP even [244].

Another process beyond the main production modes is the associated WH production through Vector Boson Fusion (VBF) yielding a topology of events with two jets in the forward region with a large rapidity gap, a W boson and a Higgs boson. This process is particularly interesting as it is sensitive to the relative sign of the coupling of the Higgs boson to the W and Z boson through the interference of the processes where the Higgs boson couples either to the W or the Z bosons in the vector boson fusion process. ATLAS has carried out analyses targeting at the decay of the Higgs boson to $b\bar{b}$ and W^+W^- for this process, resulting in the exclusion of the opposite sign hypothesis by 8 standard deviations and an upper limit corresponding to 11.2 times the cross section expected in the Standard Model [246].

11.3.11 First results on the main production and decay channels at 13.6 TeV

After a long shutdown between 2019 and 2022, devoted to the upgrades of the experiments and the machine to prepare for the High Luminosity phase, in the Spring 2022 the LHC delivered pp collisions data at an enhanced centre-of-mass energy of 13.6 TeV. During this high-energy run, ATLAS and CMS have collected datasets corresponding to integrated luminosities of approximately 60 fb^{-1} each. The first preliminary measurements of Higgs boson production at this increased centre-of-mass energy using the two high-resolution channels $H \rightarrow \gamma\gamma$ and $H \rightarrow ZZ^* \rightarrow \ell^+\ell^-\ell'^+\ell'^-$ have been carried out by ATLAS [247], see Fig. 11.6. The measurements are in good agreement within the precision with the theoretical prediction which display the expected increase of approximately 7% in inclusive cross section from the increase in centre-of-mass energy.

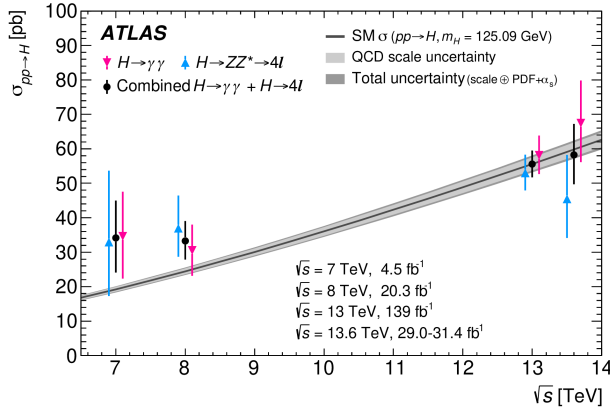


Figure 11.6: Higgs boson production cross sections as a function of the pp centre-of-mass energy. The SM predictions are shown by the shaded band.

11.4 Main quantum numbers and width of the Higgs boson

11.4.1 Main quantum numbers J^{PC}

Probing the Higgs boson quantum numbers is essential to further unveiling its coupling properties. The measurements of the signal event yields in all the channels discussed in Section 11.3 and their compatibility with the SM Higgs boson predictions, give a qualitative but, nonetheless, compelling indication of its nature. For the observed particle not to be of spin 0 and +1 parity would require an improbable conspiracy of effects. It is nevertheless important to test this hypothesis independently, in particular since the measurements of coupling properties of the Higgs boson assume that it is a CP -even state.

This qualitative picture is further complemented by the implications of the observation of the particle in the diphoton channel. According to the Landau–Yang theorem [248], the observation made in the diphoton channel excludes the spin-1 hypothesis and restricts possibilities for the spin to 0 or 2.

The Landau–Yang theorem does not apply if the observed state is not decaying to a pair of photons but to a pair of scalars subsequently decaying to two very collimated pairs of photons (as for example in the case of $H \rightarrow a_1 a_1 \rightarrow 4\gamma$). This possibility has not been rigorously excluded but is not experimentally favoured since tight selection criteria are applied on the electromagnetic shower shapes of the reconstructed photons. A more systematic analysis of shower shapes and the fraction of conversions could be performed to further discriminate between the single prompt photon and the two overlapping photons hypotheses. There are also potential theoretical loopholes concerning the applicability of the Landau–Yang theorem, such as off-shell vector boson decays.

The spin 1 hypothesis has therefore been investigated quantitatively with the LHC Run-1 dataset and has been excluded at more than 95% CL through the analysis of the Higgs boson decays to WW^* and ZZ^* channels. These results are reported in previous versions of this review and will not be covered herein. [188].

11.4.1.1 Charge conjugation

The charge conjugation quantum number is multiplicative, therefore given that the Higgs-like particle is observed in the $H \rightarrow \gamma\gamma$ channel, and given that photons are C -odd eigenstates, assuming C conservation, the observed neutral particle should be C -even.

11.4.1.2 Spin and parity

To probe the spin and parity quantum numbers of the discovered particle, a systematic analysis of its production and decay processes is performed in several analyses. These analyses are designed to be independent of the measured event yields and they rely instead on the production and the decay angles, and on the threshold distributions as long as a significant signal is observed,

i.e., in situations when an excess over the expected background can be used to further discriminate between signal hypotheses. These analyses are based on probing various alternative models of spin and parity [249]. These models can be expressed in terms of an effective Lagrangian [250] or in terms of helicity amplitudes [251]. The two approaches are equivalent.

i. Spin-0 models

The interaction Lagrangian relevant for the analysis of spin-0 particle interaction with a pair of W or Z bosons with either fixed or mixed SM and BSM CP -even couplings or CP -odd couplings, is the following [252]:

$$\begin{aligned} \mathcal{L}_0^{W,Z} \supset & \left\{ \cos(\alpha) \kappa_{\text{SM}} \left[\frac{1}{2} g_{HZZ} Z_\mu Z^\mu + g_{HWW} W_\mu^+ W^{-\mu} \right] \right. \\ & - \frac{1}{4\Lambda} \left[\cos(\alpha) \kappa_{HZZ} Z_{\mu\nu} Z^{\mu\nu} + \sin(\alpha) \kappa_{AZZ} Z_{\mu\nu} \tilde{Z}^{\mu\nu} \right] \\ & \left. - \frac{1}{2\Lambda} \left[\cos(\alpha) \kappa_{HWW} W_{\mu\nu}^+ W^{-\mu\nu} + \sin(\alpha) \kappa_{AWW} W_{\mu\nu}^+ \tilde{W}^{-\mu\nu} \right] \right\} H, \end{aligned} \quad (11.20)$$

where $V^\mu = Z^\mu, W^{+\mu}$ are the vector boson fields, $V^{\pm\mu\nu}$ are the reduced field tensors, $\tilde{V}^{\pm\mu\nu} = 1/2 \varepsilon^{\mu\nu\rho\sigma} V_{\rho\sigma}$ are the dual tensor fields, and Λ defines an effective theory energy scale. The factors $\kappa_{\text{SM}}, \kappa_{HZZ}, \kappa_{HWW}, \kappa_{AZZ}, \kappa_{AWW}$ denote the coupling constants corresponding to the coupling of the SM and BSM CP -even and CP -odd components of the Higgs boson to the W and Z fields. The mixing angle α allows for the production of a CP -mixed state and the CP -symmetry is broken when $\alpha \neq 0, \pi$.

This formalism can be used to probe both CP -mixing for a spin-0 state, as discussed in Section 11.4.1.5 or specific alternative hypotheses, as discussed below, such as a pure CP -odd state ($J^P = 0^-$) corresponding to $\alpha = \pi/2$, $\kappa_{\text{SM}} = \kappa_{HVV} = 0$ and $\kappa_{AVV} = 1$. A BSM CP -even state $J^P = 0^+$ corresponds to $\alpha = 0$, $\kappa_{AVV} = 0$, $\kappa_{HVV} = 1$ and κ_{SM} arbitrary. These hypotheses are compared to the SM Higgs boson hypothesis corresponding to $\alpha = 0$ and $\kappa_{HVV} = \kappa_{AVV} = 0$ and $\kappa_{\text{SM}} = 1$. This formalism has been adopted by the ATLAS experiment.

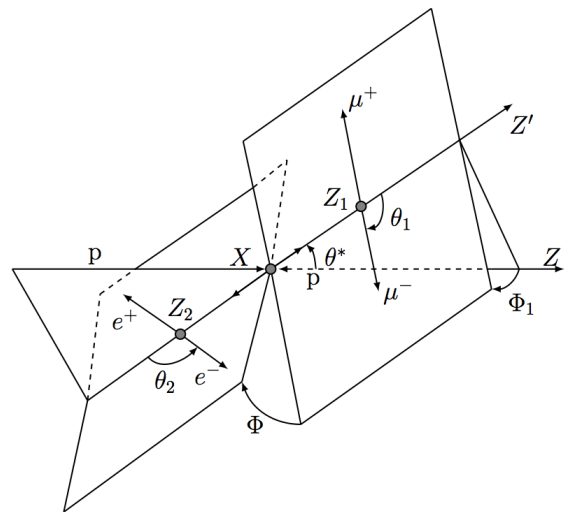


Figure 11.7: Definition of the production and decay angles defined for the $H \rightarrow ZZ^{(*)} \rightarrow 4l$ final state.

A different parametrisation of anomalous couplings of a spin-zero boson with two gauge bosons VV can also be expressed in the

general form of the scattering amplitude A :

$$A \sim \left[a_1^{VV} - \frac{\kappa_1^{VV} q_1^2 + \kappa_2^{VV} q_2^2}{(\Lambda_1^{VV})^2} - \frac{\kappa_3^{VV} (q_1 + q_2)^2}{(\Lambda_Q^{VV})^2} \right] m_{V_1}^2 \varepsilon_{V_1}^* \varepsilon_{V_2}^* + a_2^{VV} f_{\mu\nu}^{*(1)} f^{*(2)\mu\nu} + a_3^{VV} f_{\mu\nu}^{*(1)} \tilde{f}^{*(2)\mu\nu} \quad (11.21)$$

where ε_i is the polarization vector of the boson V_i , $f_{\mu\nu}^{*(i)} = \varepsilon_i^\mu q^\nu - \varepsilon_i^\nu q^\mu$ is a scalar tensor constructed from the vector boson V_i polarization and four momentum, $\tilde{f}_{\mu\nu}^{*(i)} = \frac{1}{2} \varepsilon_{\mu\nu\rho\sigma} f^{*(i)\rho\sigma}$ is the corresponding pseudo-scalar tensor. Λ_1 and Λ_Q are new physics scales, $a_{1,2,3}$ are coupling strength modifiers and $|\kappa_{(1,2,3)}^{VV}| = 0$ or 1. This parametrisation can be used both for gluons, photons and electroweak vector bosons, as well as the $Z\gamma$ coupling. In the case of the W and Z bosons, the custodial symmetry would require that $a^{WW} = a^{ZZ}$ and, at tree-level, the only non-zero contributions would come from the a_1 term. It is fully equivalent to the interaction Lagrangian approach described above. This formalism has been adopted by the CMS experiment.

Finally, CP -odd interactions can also be expressed in the framework of the Standard Model Effective Field Theory (SMEFT) in various possible bases (as discussed in Section 11.5.2). This formalism is more in line with analyses of a broader ensemble of observable probing the Standard Model. In this case the effective Lagrangian is defined as a function of the $\Phi^\dagger \Phi$ gauge invariant and the gauge field tensors before the electroweak symmetry breaking $W_{\mu\nu}^I$ and $B_{\mu\nu}$ with three operators, $\Phi^\dagger \Phi \tilde{W}_{\mu\nu}^I W^{I\mu\nu}$, $\Phi^\dagger \Phi \tilde{W}_{\mu\nu}^I B^{\mu\nu}$, and $\Phi^\dagger \Phi \tilde{B}_{\mu\nu} B^{\mu\nu}$, and their corresponding Wilson coefficients $c_{H\tilde{W}}$, $c_{H\tilde{W}B}$, and $c_{H\tilde{B}}$ respectively.

It is important to note that, as is apparant in Eq. (11.20), CP -odd couplings of the Higgs boson to vector boson are not allowed at tree level and are therefore suppressed at higher order by the scale Λ . Instead, CP -odd couplings of the Higgs boson to fermions are allowed at tree level, these can be parametrised in a somewhat simpler fashion with the following Lagrangian which accounts only for an additional pseudo-scalar term:

$$\mathcal{L}_0^{\psi_f} \supset \frac{\lambda_f}{\sqrt{2}} \left(\kappa_f H \bar{\psi}_f \psi_f + i \tilde{\kappa}_f H \bar{\psi}_f \gamma_5 \psi_f \right). \quad (11.22)$$

This formulation is equivalent to a definition a CP -mixing angle $\varphi_f = \tan \frac{\tilde{\kappa}_f}{\kappa_f}$.

It is interesting to note that CP -odd Higgs couplings to fermions could have a significant impact on the very clean and precisely measured low energy observables as the electron EDM [253]. Owing to its large Yukawa couplings, the CP -odd top Yukawa is strongly constrained by the stringent electron EDM limits to better than $\tilde{\kappa}_t < 0.001$ [253]. This makes it very challenging at the LHC to surpass. However, one should keep in mind that EDM experiments provide an indirect constraint on the SM Yukawa couplings, in particular in this case they constrain the product $\kappa_e \times \tilde{\kappa}_t$, and one needs to make assumptions on the value of κ_e , a quantity that remains out of reach experimentally. The limits on the tau Yukawa coupling from the electron EDM constraints are much less stringent and at the level of $\tilde{\kappa}_\tau < 0.3$ [253]. This makes the possibility of measuring CP mixing of the fermion Higgs Yukawa couplings particularly interesting in the tau channels since these can be accessed from the Higgs decays directly using tau polarisation sensitive variable and will be discussed herein. For more details on the searches for CP -odd couplings of the Higgs boson to vector bosons please see previous versions of this review [188].

ii. Spin-2 model

The graviton-inspired interaction Lagrangian for a spin-2 boson $X^{\mu\nu}$ that does not carry any color, weak and electromagnetic charge and that uniquely interacts with the energy momentum tensor $\mathcal{T}^{V,f}$ of vector bosons V or fermions f , can be written as follows [252]:

$$\mathcal{L}_2 \supset \frac{1}{\Lambda} \left[\sum_V \xi_V \mathcal{T}_{\mu\nu}^V X^{\mu\nu} + \sum_f \xi_f \mathcal{T}_{\mu\nu}^f X^{\mu\nu} \right], \quad (11.23)$$

where the strength of the interaction is determined by the couplings ξ_V and ξ_f . The simplest scenarios, referred to as universal couplings (UC), correspond to $\xi_V = \xi_f$. They predict a large branching ratio to photons (of approximately 5%) and negligible couplings to massive gauge bosons (W and Z). They are therefore disfavoured, and other models are investigated where the couplings of the W , Z and γ are assumed to be independent. Universality of the couplings refers to $\xi_g = \xi_q$. Two other scenarios are considered: $\xi_q = 0$ and $\xi_q = 2\xi_g$. In these scenarios, a large enhancement of the tail of the transverse momentum of the spin-2 state is expected and requires a further selection requirement in order to probe the models within the range of validity of the effective field theory. Two requirements are considered, $p_T^X < 300$ GeV and $p_T^X < 125$ GeV [250].

11.4.1.3 The VH production at $D0$

The mass of the VH system is a powerful discriminant to distinguish a $J^P = 0^+$, with a threshold behaviour in $d\sigma/dM^2 \sim \beta, \beta^3, \beta^5$ from a $0^+, 0^-$ and 2^+ state, respectively [254]. The VH mass observable not only discriminates signal hypotheses, but also has an increased separation between the 0^- and 2^+ hypotheses with respect to the backgrounds, thus allowing, with a small and not yet significant signal yield, to exclude that the observed state is 0^- at 98% CL [255] and 2^+ at the 99.9% CL [256], assuming a signal produced with their best fit signal strength (which was $\mu = 1.23$).

11.4.1.4 Probing the spin in the $\gamma\gamma$ channel at the LHC

In the $H \rightarrow \gamma\gamma$ channel, the analysis is performed inclusively using the production angle $\cos\theta_{CS}^*$ and the transverse momentum of the diphoton pair [250]. The polar angle in the rest frame is defined with respect to the bisector axis of the momenta of the incoming protons and is referred to as the polar angle in the Collins–Soper frame [257]. The SM Higgs boson signal distribution is expected to be uniform with a cutoff due to the selection requirements on the photons transverse momentum. The $H \rightarrow \gamma\gamma$ channel is mostly sensitive to the gluon-initiated spin-2 production scenarios, which yield a $\cos\theta_{CS}^*$ distribution peaking at values close to 1. The ATLAS limits are derived from a fit of the signal in bins of $\cos\theta_{CS}^*$ and diphoton transverse momentum. The data is compatible with the SM 0^+ hypothesis and contributes strongly to the exclusion of several spin-2 scenarios. The conclusions are the same from CMS results [251].

11.4.1.5 Probing CP -mixing and anomalous HVV couplings

The careful study of the kinematic properties of angular distributions in events observed in the $H \rightarrow ZZ^{(*)} \rightarrow 4\ell$ and $H \rightarrow WW^{(*)} \rightarrow \ell\nu\ell\nu$ channel, as well as the analysis of production observables sensitive to anomalous HVV interactions in the VBF or VH production have been used to set limits wither on CP -mixing parameters, amplitude terms or Wilson coefficients in the framework of SMEFT. These analysis assume that the observed particle is a spin-0 state, several results were obtained by the ATLAS [258] and CMS [251] collaborations, all show a good agreement with the Standard Model CP -even hypothesis. Recent specific examples are given here.

In the $H \rightarrow WW^{(*)} \rightarrow \ell\nu\ell\nu$ channel, the production and decay angles cannot be easily reconstructed due to the presence of neutrinos in the final state, however, sensitivity arises from the $V - A$ structure of the decay of the W bosons. A scalar state thus yields a clear spin correlation pattern that implies that the charged leptons e or μ from the decays of the W bosons are produced close to one another in the transverse plane. This feature impacts observables such as the azimuthal angle between the two leptons $\Delta\Phi_{\ell\ell}$ or their invariant mass $m_{\ell\ell}$ in addition to the threshold behaviour of the decay. It can be used to discriminate between various spin and parity hypotheses.

The $H \rightarrow ZZ^{(*)} \rightarrow 4\ell$ coupling analysis, as described in Section 11.3, also uses a discriminant based on the 0^+ nature of the Higgs boson to further separate signal and background. In this analysis, this feature is used to discriminate between signal hypotheses. The observables sensitive to the spin and parity have first been identified in Ref. [249, 259, 260] the masses of the two Z bosons (due to the threshold dependence of the mass of the

off-shell Z boson [249, 261]), two production angles θ^* and Φ_1 , and three decay angles, Φ , θ_1 and θ_2 . The production and decay angles are defined as:

- θ_1 and θ_2 , the angles between the negative final state lepton and the direction of flight of Z_1 and Z_2 in the rest frame.
- Φ , the angle between the decay planes of the four final state leptons expressed in the four lepton rest frame.
- Φ_1 , the angle defined between the decay plane of the leading lepton pair and a plane defined by the vector of the Z_1 in the four lepton rest frame and the positive direction of the proton axis.
- θ^* , the production angle of the Z_1 defined in the four lepton rest frame with respect to the proton axis.

These angles are illustrated in Fig. 11.7 [260].

These analyses are sensitive to various J^P hypotheses and in particular discriminate the 0^+ hypothesis from the 0^- . In all scenarios investigated, and for both ATLAS and CMS, the data is compatible with the 0^+ hypothesis. ATLAS and CMS exclude a pure pseudo-scalar nature of the observed boson at CL_S levels of 98% and 99.8% [251].

An individual ZZ^* channel measurement has also been carried out with a partial Run-2 dataset by ATLAS [258]. CMS has performed a CP -mixing analysis of a partial Run-2 dataset of 36 pb^{-1} combined with the full Run-1 data using the ZZ^* channel [262]. In this analysis the CMS experiment sets constraints on the parameters defined in the parametrisation (11.21) of the scattering amplitude.

With the full Run-2 dataset, analyses have started exploiting in combination both the production and decay modes of the Higgs boson as exemplified by the analysis carried out by ATLAS using the $H \rightarrow ZZ^* \rightarrow 4\ell$ analysis taking advantage of the production and decay angles of the process and VBF production sensitive observables [263]. Very similar analyses have been carried out in CMS as well. The analysis uses optimal observables constructed from matrix elements of the SMEFT. These optimal observables are defined from the ratio of the interference term between the Standard Model and the SMEFT matrix elements (normalised to the Standard Model) for given values of the Wilson coefficients $c_{H\bar{W}}$, $c_{H\bar{W}B}$, and $c_{H\bar{B}}$ below Eq. (11.21). As illustrated in Fig. 11.8, all measurements are in agreement with the Standard Model. ATLAS has also performed a similar analysis with the Higgs boson decaying to two photons analysing the VBF production mode [264] which can then be used to constrain the $c_{H\bar{W}}$ parameter as shown in Fig. 11.8.

An analysis of Higgs boson anomalous couplings HVV (as well as pseudo-scalar Yukawa coupling to the top) in the $H \rightarrow 4\ell$ channel was also carried out by CMS [265].

ATLAS has also performed an analysis using optimal observables [266], defined as the ratio of the interference between the CP -odd and the SM contributions normalised to the SM matrix element squared, using the Run-1 data. In this study, the CP -mixing contributions are described in the framework of an effective field theory governed by a single parameter \bar{d} , found to be consistent with its SM value of $\bar{d} = 0$ and constrained to the interval $[-0.11, 0.05]$ at the 68% CL.

CP invariance in the HVV coupling can also be probed with the VBF production process in the $H \rightarrow \tau^+\tau^-$ channel or similarly to the D0 analysis in the VH channels. CMS has performed an analysis in this channel and has combined its results with the aforementioned ZZ^* channel using the same dataset [267].

Finally two additional specific measurements as for example in $H \rightarrow WW^*jj$ [268] by ATLAS and using the $H \rightarrow \tau^+\tau^-$ final state [269] by CMS in several production modes have also been used to set limits on both anomalous CP -even and CP -odd couplings.

These measurements show the complementarity of the study of production and decay modes, separately and in combination, and underscores the importance of a synthetic approach that combines all the available information.

11.4.1.6 Probing $Hf\bar{f}$ coupling CP properties in $pp \rightarrow t\bar{t}H$ production

Although EDM limits disfavour large CP -odd effects in the top Yukawa coupling of the Higgs boson, these indirect limits are model dependent. It is therefore important to further probe these

effects directly. This can be achieved using the $pp \rightarrow t\bar{t}H$ process. The increased sensitivity to the this process at Run 2 in particular in the channels where the Higgs boson decays to a pair of photons provide a good sensitivity to the CP properties of the coupling through kinematics and angular distributions between the Higgs boson and the top quarks produced in the final state.

With the full Run-2 dataset, several Higgs boson decay channels have been investigated. ATLAS [270] excludes CP -mixing angles φ_t greater than 43° and smaller than -43° at 95% confidence level in the $H \rightarrow \gamma\gamma$ channel and has recently published constraints using the $H \rightarrow b\bar{b}$ channel with a measurement of $\varphi_t = 11^\circ_{-73^\circ}^{+52^\circ}$ [271].

Also using the full Run-2 dataset, CMS [272] measures the CP -odd fraction defined as follows:

$$f_{CP} = \frac{|\tilde{\kappa}_t|^2}{|\kappa_t|^2 + |\tilde{\kappa}_t|^2} \times \text{sign}(\tilde{\kappa}_t/\kappa_t)$$

in the diphoton channel to be $f_{CP} = 0.00 \pm 0.33$. CMS also derived a constraint on the CP -odd fraction using the $H \rightarrow 4\ell$ channel [265]. More recently CMS has analysed the $t\bar{t}H$ multi-lepton channel, sensitive both to the $H \rightarrow WW$ and $H \rightarrow \tau^+\tau^-$ decays, to probe the top Yukawa CP properties [273], and combined its results with the two aforementioned channels to yield the following constraint on the CP -odd fraction:

$$|f_{CP}| = 0.28_{-0.28}^{+0.27}$$

Both the ATLAS and CMS experiments used multivariate analyses in order to maximize the sensitivity to the measurement of the CP properties of the $Hf\bar{f}$ coupling. Both experiments used leptonic and hadronic decays of the top quarks.

11.4.1.7 Probing $Hf\bar{f}$ coupling CP properties in $H \rightarrow \tau^+\tau^-$ decays

As discussed in Section 11.4.1, it is interesting to investigate the CP properties of the $Hf\bar{f}$ coupling is the Higgs decay to taus through tau polarisation sensitive variables.

CMS performed a first analysis with the full Run-2 dataset [274] of the transverse spin correlations between the tau leptons in the final state which are sensitive to the CP mixing angle or relative component of the scalar and pseudo scalar couplings of the Higgs boson to taus. These transverse spin correlations are in turn related to the direction of the decay products of the taus.

In the case of the two-body decay of a tau to a charged pion and a neutrino, the transverse momentum component of the charged pions are typically anti-aligned for the case of a scalar decay and aligned for the pseudo-scalar case. The angle between the decay planes as illustrated in Fig. 11.9-(left) is therefore sensitive to the CP -mixing. Given that the tau direction cannot be measured directly, the impact parameter direction is used instead as a proxy, where the impact parameter direction is defined as the direction between the interaction point and the point of closest approach of the pion track. This direction in the rest frame of the Higgs boson are denoted λ^\pm , as shown in Fig. 11.9-(centre). In the case of three-body or more decays of the taus as for example the decays to an intermediate rho or an $a_1(1260)$ vector mesons which subsequently decay to $\rho \rightarrow \pi^+\pi^0$ and $a_1 \rightarrow \pi^+\pi^0\pi^0$ respectively, the planes are defined as either as the (π^+, π^0) plane as shown in Fig. 11.9-(centre) in the case of the ρ decay, or the plane formed by the charged pion and a combination of the two neutral pions in the case of the a_1 decay. The discrimination obtained, showing the two extreme fully scalar and pseudo-scalar cases are illustrated in Fig. 11.9-(right). ATLAS performed a similar analysis [275]. The results obtained are the following:

$$\begin{array}{ll} \text{ATLAS} & \varphi_\tau = 9^\circ \pm 16^\circ \quad (0^\circ \pm 28^\circ) \quad [274] \\ \text{CMS} & \varphi_\tau = -1^\circ \pm 19^\circ \quad (0^\circ \pm 21^\circ) \quad [275] \end{array}$$

It is interesting to note that the precision reached by both experiments is already at the level that was foreseen for HL-LHC by initial studies [276], which yielded a precision ranging between $\pm 18^\circ$ and $\pm 30^\circ$.

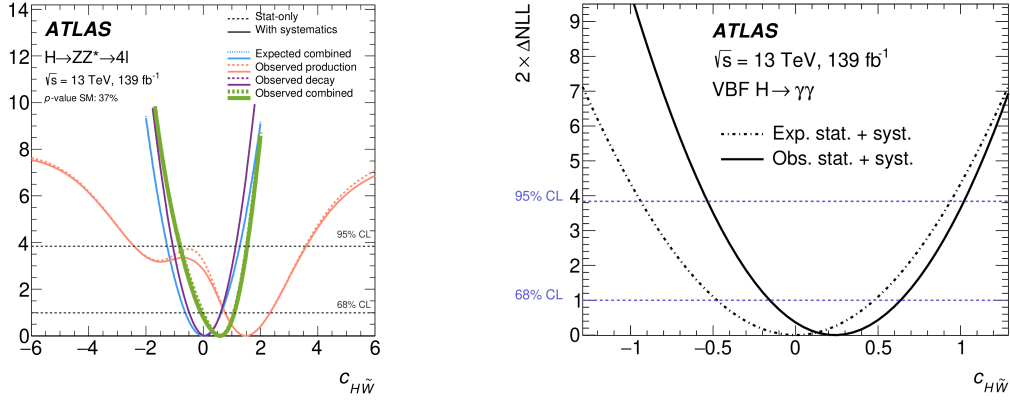


Figure 11.8: The measurement of the $c_{H\tilde{W}}$ Wilson coefficient based on the optimal observable sensitive to the Higgs boson production, its decay and their combination (left) for the ATLAS $H \rightarrow ZZ^* \rightarrow 4\ell$ analysis. The measurement of the $c_{H\tilde{W}}$ Wilson coefficient based on optimal observable sensitive to the Higgs boson production in the VBF channel (right) for the ATLAS $H \rightarrow \gamma\gamma$.

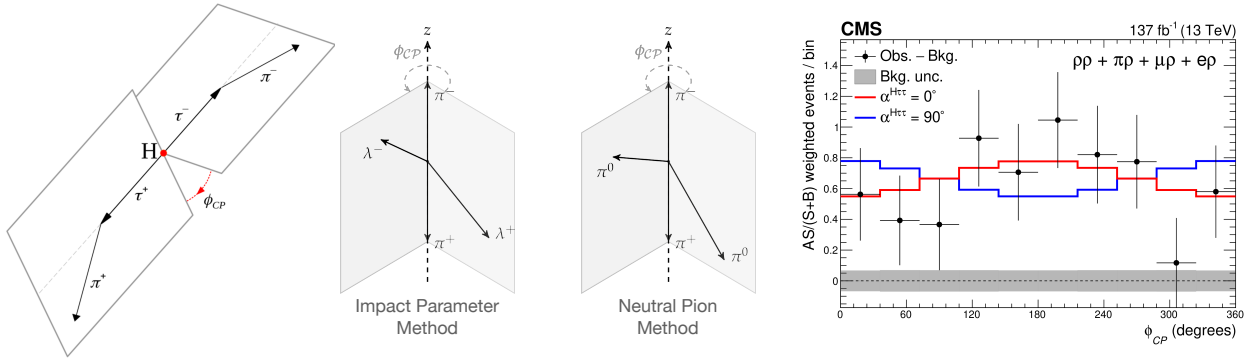


Figure 11.9: Sketch of the definition of the φ_{CP} angle for the decays $\tau^\pm \rightarrow \pi^\pm \nu_\tau$ (left) and the definition at reconstruction level of φ_{CP} observables (center). The distribution weighted per tau decay categories of the φ_{CP} observables, including the expected distributions for the expected pure scalar or pure pseudo scalar cases.

11.4.2 Off-shell couplings of the Higgs boson

In the dominant ggF production mode with a subsequent decay of the Higgs boson into a pair of electroweak vector bosons, the production cross section of an off-shell Higgs boson is known to be sizeable. This follows as a consequence of the enhanced couplings of the Higgs boson to the longitudinal polarization of the massive vector bosons at high energy.

The off-shell to on-shell cross section ratio is approximately 8% in the SM [277]. This part of the 'off-shell' regime corresponding to the exchange of a Higgs boson as a propagator and not as a narrow mass state is very interesting as it is sensitive to physics beyond the SM. Still, the Higgs contribution to VV production at large invariant mass remains small compared to the background. In addition, the difficulty in the off-shell VV analysis, beyond the small signal-to-background ratio, is due to a large negative interference between the signal and the $gg \rightarrow VV$ background.

The resulting presence of a SM Higgs boson signal in the far off-shell domain results in a deficit of events with respect to the expectation from background only events. It is only when the off-shell couplings of the Higgs boson are larger than expected in the SM that the presence of a signal appears as an excess over the background expectation. One additional intricacy arises from the precision in the prediction of the rate for $gg \rightarrow VV$, a loop process at lowest order, and its interference with the signal.

Besides this 'continuum' $gg \rightarrow VV$ background with which the 'off-shell' Higgs process interferes, the largest background comes from the $qq \rightarrow VV$ production, making this analysis very challenging.

It is interesting to note that, in this regime, the Higgs boson is

studied as a propagator and not as a particle. The measurement of its off-shell couplings is therefore absolute and does not rely on the knowledge of the total Higgs boson width. The off-shell coupling constraints can then be used to indirectly constrain the width of the Higgs boson, under specific assumptions detailed in Section 11.4.3.3.

This measurement has been carried out in the $H \rightarrow ZZ \rightarrow 4\ell$, $H \rightarrow ZZ \rightarrow \ell\nu\nu$ and $H \rightarrow WW \rightarrow \ell\nu\nu$ channels, via the ggF , VBF and VH production modes. To enhance the sensitivity of the analysis, the knowledge of the full kinematics of the events is important. In particular the signal and the background can be further distinguished by the invariant mass of the VV system, which is more accurately accessible in the $H \rightarrow ZZ \rightarrow 4\ell$ channel. Angular distributions also play an important role in this analysis. For these reasons, the $H \rightarrow ZZ^{(*)} \rightarrow 4\ell$ channel is significantly more sensitive than $H \rightarrow WW^{(*)} \rightarrow \ell\nu\nu$.

Limits on the off-shell rates have been reported for the two channels by ATLAS [278] and CMS [279] with Run-1 data. The combined results, assuming that the off-shell rates in the ZZ and WW channels scale equally, are given for two different hypotheses on the VBF production rate: fixing it to its SM value or scaling it as the gluon fusion rate. The observed (expected) limits on the off-shell rate fraction with respect to its SM expectation is 6.7 (9.1) for ATLAS [278] with the VBF rate fixed to its SM value and 2.4 (6.2) for CMS [279] where no assumption is made on the relative production rates of gluon-fusion and VBF. In both cases, the custodial symmetry is assumed and the ratio of the rates in the ZZ and WW decays are fixed to those of the SM. Results without this assumption have also been reported in Ref. [279].

The situation using the Run-2 data has significantly changed. Both ATLAS [280] and CMS [281] have performed off-shell Higgs boson analyses to constrain the off-shell Higgs boson production rates with the full Run-2 datasets using the $H \rightarrow ZZ^*$ channel. The results obtained have already reached an impressive sensitivity. Both experiments have considered two independent off-shell contributions, the first corresponding to the ggF production denoted $\mu_{g,\text{off-shell}}$ and the second corresponding to the VBF and VH denoted $\mu_{V,\text{off-shell}}$. For simplicity we will report only the results considering $\mu_{g,\text{off-shell}} = \mu_{V,\text{off-shell}} = \mu_{\text{off-shell}}$ here.

The first striking result is that both experiments exclude the background-only hypothesis $\mu_{\text{off-shell}} = 0$ with a significance of 3.2σ (2.2σ) observed (expected) for ATLAS [280] and 3.6σ for CMS [281]. This corresponds to a first evidence for the off-shell production of a Higgs boson, through the measurement of a significant deficit in the overall $gg \rightarrow VV$ production.

The measured off-shell signal strengths $\mu_{\text{off-shell}}$ are the following:

$$(\text{ATLAS}) \quad \mu_{\text{off-shell}} = 1.1_{-0.6}^{+0.7} (\text{obs}) \quad [1.00_{-0.9}^{+0.9} (\text{exp})], \quad (11.24)$$

$$(\text{CMS}) \quad \mu_{\text{off-shell}} = 0.74_{-0.38}^{+0.56} (\text{obs}) \quad [1.00_{-0.84}^{+1.00} (\text{exp})].$$

11.4.3 The Higgs boson width

In the SM, the Higgs boson width is very precisely predicted once the Higgs boson mass is known. For a mass of 125 GeV, the Higgs boson has a very narrow width of 4.1 MeV [40]. It is dominated by the fermionic decays partial width at approximately 75%, while the vector boson modes are suppressed and contribute 25% only.

At the LHC or the Tevatron, in all production modes, only the cross sections times branching fractions can be measured. As a consequence, the total width of the Higgs boson cannot be directly derived from the measurements of Higgs boson rates without additional assumptions. Direct constraints on the Higgs boson width are much larger than the expected width of the SM Higgs boson.

11.4.3.1 Direct constraints

Analyses of the reconstructed mass line-shape in the two channels with a good mass resolution, the $H \rightarrow \gamma\gamma$ and $H \rightarrow ZZ^{(*)} \rightarrow 4\ell$ channels, allow for a direct measurement of the width of the SM Higgs boson. The intrinsic mass resolution in these channels is about 1–2 GeV, much larger than the expected width of the SM Higgs boson. As a result, only upper limits on the Higgs boson width have been set by ATLAS [282] and more recently CMS [152]. The two main challenges of direct constraints on the width through the measurement of the line-shape are: (i) the modelling of resolution uncertainties and (ii) the modelling of the interference between the signal and the continuum background which can be sizeable for large widths, in particular in the range where direct constraints are set. These challenges affect mostly the diphoton channel. Given that these interference effects are small with respect to the individual channels sensitivity, they are neglected in deriving constraints on the total width. The combined constraints, however, being more precise, could be affected by the interference. Direct lineshape measurements provide the most unambiguous access to the Higgs boson width, however constraints are still two orders of magnitude larger than the expected SM width. The current results are fully compatible with the SM hypothesis. The most stringent limit is obtained by CMS of 330 MeV at 95% CL [152].

Another direct constraint on the Higgs boson width can be obtained, in the $H \rightarrow ZZ^{(*)} \rightarrow 4\ell$ channel, from the measurement of the average lifetime of the Higgs boson calculated from the displacement of the four-lepton vertex from the beam spot. This analysis has been carried out by CMS (see references in Ref. [141]), using the measured decay length. The measured $c\tau_H$ is $2_{-2}^{+25} \mu\text{m}$, yielding an observed (and expected) limit at the 95% CL of $c\tau_H < 57(56) \mu\text{m}$. From this upper limit on the lifetime of the Higgs boson, the 95% CL lower limit on its width is $\Gamma_H > 3.5 \times 10^{-12} \text{ GeV}$.

11.4.3.2 Indirect constraints from mass shift in the diphoton channel

In the diphoton channel, it was noticed in Ref. [283], that the effect of the interference between the main signal $gg \rightarrow H \rightarrow \gamma\gamma$ and the continuum irreducible background $gg \rightarrow \gamma\gamma$, taking into account detector resolution effects, is responsible for a non negligible mass shift. The size of the mass shift depends on the total width of the Higgs boson and it was suggested that measuring this mass shift could provide a constraint on the width [283]. It was further noticed that the mass shift has a dependence also on the diphoton transverse momentum. The total width of the Higgs boson could therefore be constrained using the diphoton channel alone.

Further studies were performed by ATLAS to estimate the size of the expected mass shift [284]. The expected shift in mass in the diphoton channel is $35 \pm 9 \text{ MeV}$ for the SM Higgs boson. Very preliminary studies of the sensitivity of this method to estimate the width of the Higgs boson in the High-Luminosity regime have been made by ATLAS [285] and yield an expected 95% CL upper limit on the total width of approximately 200 MeV from 3 ab^{-1} of 14 TeV data.

11.4.3.3 Indirect constraints from on-shell rate in the diphoton channel

In the diphoton channel, it was noticed in Ref. [286], that the interference between the main signal $gg \rightarrow H \rightarrow \gamma\gamma$ amplitude and the continuum irreducible background $gg \rightarrow \gamma\gamma$ amplitude generates non-negligible change in the on-shell cross sections, as a result of the existence of a relative phase between these amplitudes. The size of this on-shell interference effect depends on the total width of the Higgs boson and it was suggested that measuring this on-shell cross section precisely could provide a constraint on the Higgs total width. This interference effect yields a reduction of around 2% for the $gg \rightarrow H \rightarrow \gamma\gamma$ cross section measurement in the SM. The current evaluation of this interference effect is performed at NLO and has a $^{+50\%}_{-30\%}$ uncertainty, due to the fact that the large relative phase is driven by the two-loop $gg \rightarrow \gamma\gamma$ background amplitude [283, 286]. This on-shell interference effect has a dependence on the p_T of the diphoton system and the photon polar angle in the diphoton rest frame, which can be further exploited to improve the measurement to constrain the Higgs total width.

Taking the ratios of the on-shell cross section of Higgs boson to diphoton channel and the cross section of Higgs boson to four-leptons channel where the interference effect is negligible could put a bound on the Higgs boson total width. This ratio is free from many dominant sources of systematic uncertainties for cross section measurements, i.e., PDF uncertainty and luminosity uncertainty, and can be further improved by the accumulation of the LHC data. From this cross section ratio measurement alone, a preliminary estimation of the current limit from this interference effect with current 30% precision puts an upper bound of 800 MeV on the Higgs boson total width and the limit improves to 60 MeV with 3 ab^{-1} of 14 TeV data [286, 287].

11.4.3.4 Indirect constraints from off-shell couplings

Using simultaneously on-shell and off-shell measurements in the VV channels, it was noticed [277, 288] that the total width of the Higgs boson could be constrained. This can be illustrated from the parametrisation of the signal strength measurements both on-shell ($\mu_{\text{on-shell}}$) and off-shell ($\mu_{\text{off-shell}}$) as a function of the couplings modifiers κ_g and κ_V parameterizing the main process $gg \rightarrow H \rightarrow VV$ (see Section 11.5.1 for the definition of these coupling modifiers). The on-shell and off-shell signal strengths can be written as:

$$\begin{aligned} \mu_{\text{on-shell}} &= \frac{\kappa_{g,\text{on-shell}}^2 \kappa_{V,\text{on-shell}}^2}{\Gamma_H / \Gamma_{\text{SM}}}, \\ \mu_{\text{off-shell}} &= \kappa_{g,\text{off-shell}}^2 \kappa_{V,\text{off-shell}}^2. \end{aligned} \quad (11.25)$$

A bound on the Higgs boson width can then be obtained from the measurements of the on-shell and off-shell signal strengths. This assumes that no new physics alters the Higgs boson couplings in

the off-shell regime, i.e., that the running of its couplings in this energy range does not differ from the Standard Model [289, 290].

Both ATLAS [278] and CMS [281] have used their very strong off-shell production analyses described above, with kinematic event characteristics to further gain in sensitivity to discriminate between the signal and background.

In addition, in the CMS analysis, results are also derived allowing for anomalous couplings of the Higgs boson, therefore reducing the discriminating power of the kinematic variables used in the analysis but reducing the model dependence. The sensitivity already reached at Run 2 is remarkable:

$$(\text{ATLAS}) \quad \Gamma_H = 4.5_{-2.5}^{+3.3} [4.1_{-3.8}^{+3.8} (\text{exp})] \text{ MeV}, \quad (11.26)$$

$$(\text{CMS}) \quad \Gamma_H = 3.2_{-1.7}^{+2.4} [4.1_{-3.5}^{+4.0} (\text{exp})] \text{ MeV}. \quad (11.27)$$

ATLAS and CMS have also performed a study of the prospects for measuring the Higgs boson width mainly in the four lepton channel. Projecting to a luminosity of 3 ab^{-1} , it was concluded that, within assumptions similar to the ones mentioned above and assuming the SM central value, the width of the Higgs boson could be constrained with the following precision [118]:

$$\Gamma_H = 4.1_{-0.8}^{+0.7} \text{ MeV}. \quad (11.28)$$

11.5 Probing the coupling properties of the Higgs boson

As discussed in Section 11.2, within the SM, all the Higgs boson couplings are fixed unambiguously once all the particle masses are known. Any deviation in the measurement of the couplings of the Higgs boson could therefore signal BSM physics.

Measuring the Higgs boson couplings without relying on the SM assumption requires a general framework treating deviations from the SM coherently at the quantum level in order to provide theoretical predictions for relevant observables to be confronted with experimental data. An attempt in that direction has been formalised in the so-called κ -formalism [291], following earlier attempts [292] and initial phenomenological studies of the first hints of the existence of the Higgs boson [293]. In this LO-inspired approach, the SM Higgs boson couplings are rescaled by arbitrary factors, κ 's, keeping the same Lorentz structure of the interactions. This formalism allows for simple interpretation of the signal strengths measured in the various Higgs channels. It has been utilised to test various physics scenarios, like the existence of additional new particles contributing to the radiative Higgs boson production and decays, or to probe various symmetries of the SM itself, as for example the custodial symmetry. It only compares the experimental measurements to their best SM predictions and does not require any new BSM computations per se. And, from a more theoretical perspective, its relevance arises from the fact that it actually fully captures the leading effects in single Higgs processes of well motivated scenarios. Still, the κ -formalism has obvious limitations and certainly does not capture the most general deformations of the SM, even under the assumptions of heavy and decoupling new physics. A particularly acute shortcoming at the time Higgs physics is entering a precision era is the lack of proficiency to assert the richness of kinematical distributions beyond simple signal strength measurements. Several extensions and alternative approaches are being developed as part of the activities of the LHC Higgs Cross Section Working Group [43].

The Higgs Pseudo-Observable (HPO) approach [294] allows one to report the data in terms of a finite set of on-shell form factors parametrisating amplitudes of physical processes subject to constraints from Lorentz invariance and other general requirements like analyticity, unitarity, and crossing symmetry. These form factors are expanded in powers of kinematical invariants of the process around the known poles of SM particles, assuming that poles from BSM particles are absent in the relevant energy regime. A set of HPOs have been proposed to characterise both the Higgs boson decays and the EW Higgs boson production channels, thus exploring different kinematical regimes. Prospective studies concluded that these HPOs can be measured/bounded at the percent level at the HL-LHC and could therefore be used to constrain some explicit models of new physics.

Another systematic and popular approach to characterise the possible Higgs boson coupling deviations induced by BSM physics is the use of Effective Field Theories (EFT) [295, 296]. This approach assumes again that the new physics degrees of freedom are sufficiently heavy to be integrated out, and they give rise to effective interactions among the light SM particles. By construction, an EFT approach cannot systematically account for deviations in Higgs physics induced by light degrees of freedom unless they are added themselves as extra fields in the effective Lagrangians, requiring to know about these light fields beforehand. In Section 11.6, several examples of models with light degrees of freedom affecting Higgs boson production and decay rates will be presented. Like in explicit UV models and unlike the κ -approach, the main advantage of EFTs is their prowess to relate different observables in different sectors and at different energies to constrain a finite set of effective interactions among the SM degrees of freedom. In an EFT, the SM Lagrangian is extended by a set of higher-dimensional operators, and it reproduces the low-energy limit of a more fundamental UV description. It will be assumed that the Higgs boson is part of a CP -even EW doublet, Φ , and that the Lagrangian is an analytic function of the gauge invariant $\Phi^\dagger \Phi$. This scenario is commonly referred as SMEFT. Even though it is not fully established experimentally, this set-up is motivated by the measurements of the Higgs couplings to the different SM particles that show an alignment with their masses, such an alignment naturally follows under this assumption of a linear realisation of the $SU(2)_L \times U(1)_Y$ symmetry of the SM. General Lagrangians bypassing this linear assumption have been explicitly written down, see for instance Ref. [297], and connections with explicit UV models made [298, 299]. They rely on a chiral expansion with a specific power-counting, effectively resumming the expansion in powers of the Higgs field, usually referred as HEFT as opposed to SMEFT.

11.5.1 Probing coupling properties

11.5.1.1 From effective Lagrangians to Higgs observables

The κ framework, described in detail in Ref. [39, 291], facilitates the characterisation of Higgs coupling properties in terms of a series of Higgs coupling strength modifier parameters κ_i , which are defined as the ratios of the couplings of the Higgs bosons to particles i to their corresponding SM values. The κ framework assumes a single narrow resonance so that the zero-width approximation can be used to decompose the cross section as a product of two factors characterising the production and the decay of the Higgs boson. The κ parameters are introduced by expressing each of these factors as their SM expectation multiplied by the square of a coupling strength modifier for the corresponding process at leading order:

$$\begin{aligned} (\sigma \cdot \text{BR})(i \rightarrow H \rightarrow f) &= \frac{\sigma_i^{\text{SM}} \kappa_i^2 \cdot \Gamma_f^{\text{SM}} \kappa_f^2}{\Gamma_H^{\text{SM}} \kappa_H^2} \rightarrow \\ &\rightarrow \mu_i^f \equiv \frac{\sigma \cdot \text{BR}}{\sigma_{\text{SM}} \cdot \text{BR}_{\text{SM}}} = \frac{\kappa_i^2 \cdot \kappa_f^2}{\kappa_H^2}, \end{aligned} \quad (11.29)$$

where μ_i^f is the rate relative to the SM expectation and κ_H^2 is an expression that adjusts the SM Higgs width to take into account the modifications induced by the deformed Higgs boson couplings. When all κ_i are set to 1, the SM is reproduced. For loop-induced processes, e.g. $H \rightarrow \gamma\gamma$, there is a choice of either resolving the coupling strength modification in its SM expectation, i.e., $\kappa_\gamma(\kappa_t, \kappa_W)$ or keeping κ_γ as an effective coupling strength parameter.

The κ -framework is the simplest parametrisation directly related to experimental measurements of the Higgs boson production and decay modes. For this reason, it has been widely used by the community. It can also be connected to the SMEFT formalism as follows. Restricting to the EFT directions not probed outside Higgs physics [300], the Higgs boson couplings are written

in the unitary gauge as:

$$\begin{aligned}
\mathcal{L} = & \kappa_Z \frac{m_Z^2}{v} Z_\mu Z^\mu H + \kappa_W \frac{2m_W^2}{v} W_\mu^+ W^{-\mu} H \\
& + \kappa_{VV} \frac{\alpha}{2\pi v} \left(\cos^2 \theta_W Z_{\mu\nu} Z^{\mu\nu} + 2W_{\mu\nu}^+ W^{-\mu\nu} \right) H \\
& + \kappa_g \frac{\alpha_s}{12\pi v} G_{\mu\nu}^a G^{a\mu\nu} H + \kappa_\gamma \frac{2\alpha}{9\pi v} A_{\mu\nu} A^{\mu\nu} H + \kappa_{Z\gamma} \frac{\alpha}{\pi v} A_{\mu\nu} Z^{\mu\nu} H \\
& - \sum_F \kappa_F \frac{m_F}{v} \bar{F} F H + \kappa_3 \frac{m_H^2}{2v} H^3 + \dots
\end{aligned} \tag{11.30}$$

The exact correspondence between the effective coefficients of the dimension-6 operators and the κ 's can be found for instance in Ref. [40]. In the SM, the Higgs boson does not couple to massless gauge bosons at tree level, hence $\kappa_g = \kappa_\gamma = \kappa_{Z\gamma} = 0$. Nonetheless, the contact operators are generated radiatively by SM particle loops. In particular, the top quark gives a contribution to the 3 coefficients $\kappa_g, \kappa_\gamma, \kappa_{Z\gamma}$ that does not decouple in the infinite top mass limit (for instance, in that heavy limit, the top quark contribution amounts to $\Delta\kappa_\gamma = \Delta\kappa_g = 1$ [21, 22, 301], while the W^\pm also contributes to κ_γ). Depending on the nature of new physics, these effective couplings can be generated at tree level or only at the radiative/loop level, see Refs. [295, 302–304] for further discussions.

The coefficient for the contact interactions of the Higgs boson to the W and Z field strengths is not independent but obeys the relation

$$(1 - \cos^4 \theta_W) \kappa_{VV} = \sin 2\theta_W \kappa_{Z\gamma} + \sin^2 \theta_W \kappa_{\gamma\gamma}. \tag{11.31}$$

This relation is a general consequence of the custodial symmetry [305], which also imposes $\kappa_Z = \kappa_W$ at leading order ($\kappa_Z/\kappa_W - 1$ is a measure of custodial symmetry breaking and, as such, is already constrained by electroweak precision data and the bounds on anomalous gauge couplings). When the Higgs boson is part of an $SU(2)_L$ doublet, the custodial symmetry in the bosonic sector could only be broken by the $\mathcal{O}_T = \frac{1}{2} (\Phi^\dagger \overleftrightarrow{D}^\mu \Phi)^2$ operator at the level of dimension-6 operators and it is accidentally realised among the interactions with four derivatives, like the contact interactions considered.

The coefficient κ_3 is the trilinear Higgs boson self-coupling parameter which corresponds to the more generic κ_λ self-coupling parameter discussed in Section 11.3.9.1. Before the associated production of a Higgs boson with a pair of top quarks was observed, the Higgs boson coupling to the top quark was only probed indirectly via the one-loop gluon fusion production or the radiative decay into two photons. However, these two processes are only sensitive to the combinations of couplings $(\kappa_t + \kappa_g)$ and $(\kappa_t + \kappa_\gamma)$ and not to the individual couplings. Therefore a deviation in the Higgs boson coupling to the top quark can in principle always be masked by new contact interactions to photons and gluons (and this is precisely what is happening in minimal incarnations of composite Higgs models [306]). The current and still limited sensitivity, of the order of 20%, in the $t\bar{t}H$ channel leaves elongated ellipses in the direction $\kappa_g = \kappa_\gamma = 1 - \kappa_t$.

The operators already bounded by EW precision data and the limits on anomalous gauge couplings modify in general the Lorentz structure of the Higgs couplings and hence induce some modifications of the kinematical differential distributions [307]. A promising way to have a direct access to the effective coefficients of these operators in Higgs physics is to study the VH associated production with a W or a Z at large invariant mass of the VH system [308]. These differential distributions could also be a way to test the hypothesis that the Higgs boson belongs to a $SU(2)_L$ doublet together with the longitudinal components of the massive electroweak gauge bosons.

11.5.1.2 Measurements of the Higgs boson coupling properties

As described in Section 11.3, a framework was developed by ATLAS and CMS [153], individually and together, to combine the very large number of exclusive categories aimed at reconstructing the five main decay modes and the five main production modes

of the Higgs boson. The general conclusion of this combination, illustrating the compatibility of the observation with the SM expectations, is given in Section 11.3. The same framework with its master formula, Eq. (11.14), can be used to further measure coupling properties of the Higgs boson under specific additional assumptions.

i. Interpretations of the experimental data

The measurements of the coupling properties of the Higgs boson are entirely based on the formalism of the effective Lagrangian described above. Measurements of coupling properties in this framework implies assessing the parameters of the model Eq. (11.30) or combinations of these parameters with different sets of assumptions.

These measurements are carried out with the combination framework described in Section 11.3.6, where the μ_i and μ_f signal strength parameters are further interpreted in terms of modifiers of the SM couplings κ_k where $k \in \{Z, W, f, g, \gamma, Z\gamma\}$ as in Eq. (11.30). The number of signal events per category for the various production modes are typically estimated at higher orders in the analyses but are scaled by these single LO-inspired factors, thus not taking into account possible intricacies and correlations of these parameters through the higher-order corrections. This approximation is valid within the level of precision of current results and their compatibility with the SM expectation.

In this formalism, further assumptions are explicitly made: (i) the signals observed in the different search channels originate from a single narrow resonance with a mass of 125 GeV; (ii) similarly to the combination described in Section 11.3.6, the narrow width approximation is assumed (to allow the decomposition of signal yields into products of production and decay signal strengths); (iii) the tensor structure of the couplings is assumed to be the same as that of a SM Higgs boson. This means in particular that the observed state is assumed to be a CP -even scalar as in the SM.

Loop-level couplings such as the $gg \rightarrow H$, $H \rightarrow \gamma\gamma$ and $H \rightarrow Z\gamma$ can either be treated effectively, with κ_g , κ_γ and $\kappa_{Z\gamma}$ as free parameters in the fit or these parameters can be expressed in terms of the know SM field content and as a function of the SM coupling modifiers, in the following way [309] by either scaling cross sections (for κ_g given for a centre-of-mass energy of 13 TeV and a Higgs boson mass of 125 GeV) or partial widths (for κ_γ and $\kappa_{Z\gamma}$ for a Higgs boson mass of 125 GeV):

$$\begin{aligned}
\kappa_g^2(\kappa_t, \kappa_b, \kappa_c) &= 1.042 \kappa_t^2 - 0.040 \kappa_t \kappa_b + 0.002 \kappa_b^2 \\
&\quad - 0.005 \kappa_t \kappa_c + 0.0005 \kappa_b \kappa_c + 0.00002 \kappa_c^2, \\
\kappa_\gamma^2(\kappa_t, \kappa_W) &= 1.59 \kappa_W^2 - 0.66 \kappa_W \kappa_t + 0.07 \kappa_t^2, \\
\kappa_{Z\gamma}^2(\kappa_t, \kappa_W) &= 1.12 \kappa_W^2 - 0.15 \kappa_W \kappa_t + 0.03 \kappa_t^2.
\end{aligned} \tag{11.32}$$

It should be noted that the parametrisation of the gluon coupling modifier could also be used to scale the $H \rightarrow gg$ partial width and would be different from the cross section parametrisation. However when considered effectively, i.e., without resolving the content of the loop in terms of SM fields, it can be assumed that the scaling behaviour of the production cross section and partial width will be very similar.

The parametrisations are given for a Higgs boson mass hypothesis of 125 GeV (and in the last two expressions, all the Higgs-fermion couplings are assumed to be rescaled by an universal multiplicative factor κ_F). It can be noted from the expression of κ_γ that the coupling of the Higgs boson to photons is dominated by the loop of W bosons, and it is affected by the top quark loop mostly through its interference with the W loop. The sensitivity of the current measurements to the relative sign of the fermion and vector boson couplings to the Higgs boson is due to this large negative interference term. The κ_g parameter is expressed in terms of the scaling of production cross sections and therefore also depends on the pp collisions centre-of-mass energy. The parametrisations of κ_γ and $\kappa_{Z\gamma}$ are obtained from the scaling of partial widths and are only dependent on the Higgs boson mass hypothesis. Experiments use a more complete parametri-

sation with the contributions from the b -quarks, τ -leptons in the loops [39, 291].

The global fit is then performed expressing the μ_i and μ_f parameters in terms of a limited number of κ_k parameters or their ratios, under various assumptions. The parametrisation for the main production modes are: (i) $\mu_{ggF} = \kappa_g^2$ for the gluon fusion and an effective coupling of the Higgs boson to the gluons; (ii) $\mu_{VBF, VH} = \kappa_V^2$ for the VBF and VH processes when the W and Z couplings are assumed to scale equally, and $\mu_{VBF}^2(\kappa_W, \kappa_Z) = (\kappa_W^2 \sigma_{WWH} + \kappa_Z^2 \sigma_{ZZH}) / (\sigma_{WWH} + \sigma_{ZZH})$, when the couplings to the W and Z bosons are varied independently (σ_{WWH} and σ_{ZZH} denote the VBF cross sections via the fusion of a W and a Z boson respectively, the small interference term is neglected); (iii) $\mu_{t\bar{t}H} = \kappa_t^2$ for the $t\bar{t}H$ production mode. Numerically the production modes signal strengths as a function of the coupling modifiers to the SM fields for a centre-of-mass energy of 13 TeV and Higgs boson mass of 125 GeV are:

$$\begin{aligned} \mu_{ggF} &= 1.040\kappa_t^2 + 0.002\kappa_b^2 - 0.038\kappa_t\kappa_b, \quad \text{and} \\ \mu_{VBF} &= 0.73\kappa_W^2 + 0.27\kappa_Z^2. \end{aligned} \quad (11.33)$$

The decay mode signal strengths are parametrised as $\mu_k = \kappa_k^2 / \kappa_H^2$ where $k \in \{Z, W, f, g, \gamma, Z\gamma\}$ denotes the decay mode and κ_H , the overall modifier of the total width that affects all the signal yields. κ_H is a priori an independent parameter. However, when it is assumed that the Higgs boson cannot decay to new particles beyond those of the SM, κ_H can also be treated as an effective parameter and expressed in terms of the coupling modifiers to the SM field content. Its general expression is:

$$\begin{aligned} \kappa_H^2 &= 0.57\kappa_b^2 + 0.06\kappa_\tau^2 + 0.03\kappa_c^2 + 0.22\kappa_W^2 + 0.03\kappa_Z^2 + 0.09\kappa_g^2 \\ &\quad + 0.0023\kappa_\gamma^2. \end{aligned} \quad (11.34)$$

The general expression of the total width of the Higgs boson can be written as follows:

$$\Gamma_H = \frac{\kappa_H^2 \Gamma_H^{\text{SM}}}{1 - \text{BR}_{\text{BSM}}} \quad (11.35)$$

where Γ_H^{SM} is the total width of the SM Higgs boson and BR_{BSM} is the branching fraction of the Higgs boson to new particles beyond the SM.

It is worth reminding that, in the absence of a measurement of the Higgs width which can be accessed through Off-Shell couplings measurements as discussed in Section 11.4.2, LHC requires some hypotheses in order to extract the Higgs couplings from the measured Higgs signal strengths. In particular, one can assume either (i) no BSM particles in the decay, or (ii) any BSM particles in the decay would give rise to invisible signatures and thus be detectable through invisible Higgs boson channels (or in other terms that there is no BSM undetected contribution), or (iii) $|\kappa_V| \leq 1$. These scenarios will be examined below.

Specific parametrisations will be made in order to address the following aspects of the coupling properties of the Higgs boson under different assumptions, depending essentially on two assumptions concerning either the natural width of the Higgs boson, whether it consists of partial width from Standard Model particles only or not, or the effective couplings of the Higgs boson to photons, gluons, $Z\gamma$ and $\gamma^*\gamma$, whether these contributions are parametrised as function of the Standard Model field content in the loops or whether these couplings are considered as effective.

Negative values of couplings are not excluded a priori, but would imply the existence of new physics at a light scale and would also raise questions about the validity of the perturbative treatment of the SM deformations and also about the stability of the vacuum [310]. Since the results are only sensitive to the relative sign of vector bosons with respect to fermions, by convention negative coupling values will only be considered for vector boson couplings. Among the five main Higgs boson decay channels, only the $\gamma\gamma$ is sensitive to the sign of κ_F (or κ_V) through the interference of the W and t loops as shown in Eq. (11.32). The current global fit disfavors a negative value of κ_F at more than

five standard deviations. A specific analysis for the Higgs boson production in association with a single top quark has been proposed in order to more directly probe the sign of κ_F (see references in Ref. [141]). All available experimental data show a fair agreement of the SM prediction of the couplings of the Higgs boson to fermions and gauge bosons.

ii. Coupling measurements and probing BSM physics in loops and in the decay

Measuring Higgs boson couplings to other Standard Model fields requires either assumptions on the total Higgs boson width, or an assumption on the coupling of the Higgs boson to vector bosons, or a direct constraint on the Higgs boson width as the one obtained from the ratio of off-shell to on-shell Higgs boson couplings. These three cases will be discussed briefly. With the precision reached by analyses discussed in Section 11.3.1, strong assumptions on the BSM content of the loop-induced couplings of the Higgs boson to vector bosons as Hgg , $H\gamma\gamma$ or $HZ\gamma$ are not needed and these couplings can be considered as effective and provide a stringent probe of new fields potentially entering the loop.

Using the full Run-2 dataset and the formalism described in Section 11.3.1, ATLAS [183] and CMS [184], have performed interpretations of the results presented in Section 11.3.6 to derive measurements of the Higgs boson couplings. These results are summarised in Table 11.8.

The results above are obtained under the assumption that the Higgs boson decays only to SM particles. The degeneracy that originates from the fact that at LHC only production cross sections times branching fractions are measured is embodied in the degeneracy between all κ factors and κ_H . It is interesting to note that in order to measure all couplings to be in agreement with the Standard Model model value requires that any deviation in the Higgs boson total width or κ_H be precisely compensated by all couplings to Standard Model fields in the same fashion. This is often referred to a flat direction, meaning that all the couplings are scaled by a factor α and the Higgs boson width by a factor α^2 . A model realising such flat direction is given in [311]. It requires the introduction of a scalar field which decays for instance light hadrons which would not be detectable in the current experimental setups and are referred to as 'undetected'. It cannot be 'invisible' as it would otherwise be constrained by direct invisible Higgs boson constraints. The model parameters would also have to lead to couplings of the Higgs to Standard Model fields to be larger than in the Standard Model and a coupling of the Higgs boson to the scalar which will have to match the scaling of the Standard Model couplings. The former condition is exotic and the latter requires a 'conspiracy'.

As we have previously discussed, the flat direction can however be removed in two ways. The first is to impose $\kappa_V \leq 1$. This will induce a constraint on κ_H which can be seen for instance from processes such as VBF Higgs production with subsequent decays to two vector bosons which are proportional to κ_V^4 / κ_H^2 . As was discussed, BSM scenarios yielding $\kappa_V > 1$ can be considered exotic. The measurements using this constraints from the ATLAS experiment are shown in Fig. 11.10 (left). The second is to use the Higgs boson width derived from the off-shell Higgs boson production measurements. In this specific interpretation, the flat off-shell Higgs measurement constrain the visible, invisible and undetected branching fractions. The 'visible' branching fraction corresponds to the Higgs branchings to Standard Model fields. The invisible branching fraction is constrained from 'invisible' Higgs searches. The flat direction is therefore represented by the 'undetected' branching fraction which is then constrained by the off-shell Higgs boson measurements. This constraint was used in previous Higgs boson couplings measurements (see references for example the partial Run-2 combination performed in [312]).

Interpretations which are less sensitive to modelling systematic uncertainties and require no constraints on the natural width of the Higgs bosons have been considered, either through the ratio of cross section and branching ratios (see results in Ref. [141]) or through a more generic approach to avoid the degeneracy in the measurement of the coupling modifiers, probing the coupling properties of the Higgs boson through ratio of couplings. In the

Table 11.8: Coupling modifier combined measurements assuming the absence of perceptible new physics in the decay of the Higgs boson. No assumption is made for the loop level couplings of the Higgs boson to gluons and photons which are considered as effective. The last column gives the expected precision at the HL-LHC [118].

	LHC Run 1	ATLAS Run 2	CMS Run 2	HL-LHC (expected)
κ_γ	$0.87^{+0.14}_{-0.09}$	1.01 ± 0.06	1.10 ± 0.08	1.8%
κ_W	$0.87^{+0.13}_{-0.09}$	1.05 ± 0.06	1.02 ± 0.08	1.7%
κ_Z	-0.98 ± 0.10	0.99 ± 0.06	1.04 ± 0.07	1.5%
κ_g	$0.78^{+0.13}_{-0.10}$	0.95 ± 0.07	0.92 ± 0.08	2.5%
κ_t	$1.40^{+0.24}_{-0.21}$	0.94 ± 0.11	1.01 ± 0.11	3.4%
κ_b	$0.49^{+0.27}_{-0.15}$	0.89 ± 0.11	0.99 ± 0.16	3.7%
κ_τ	$0.84^{+0.15}_{-0.11}$	0.93 ± 0.07	0.92 ± 0.08	1.9%
κ_μ	—	$1.06^{+0.25}_{-0.30}$	1.12 ± 0.21	4.3%
$\kappa_{Z\gamma}$	—	$1.38^{+0.31}_{-0.36}$	1.65 ± 0.34	9.8%

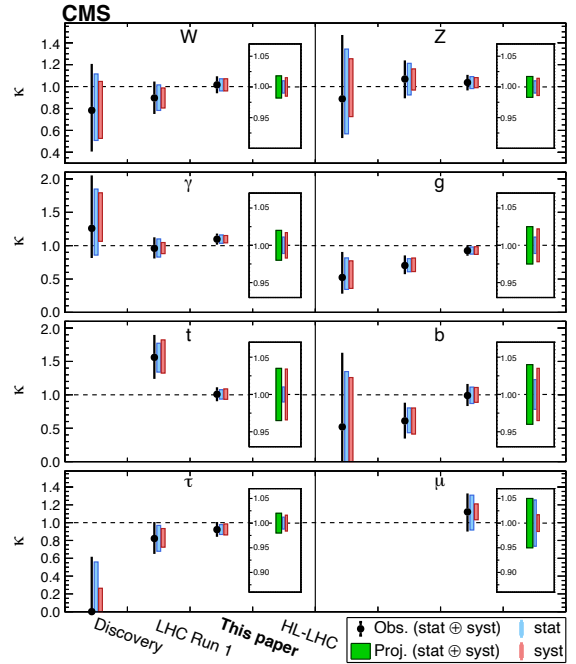
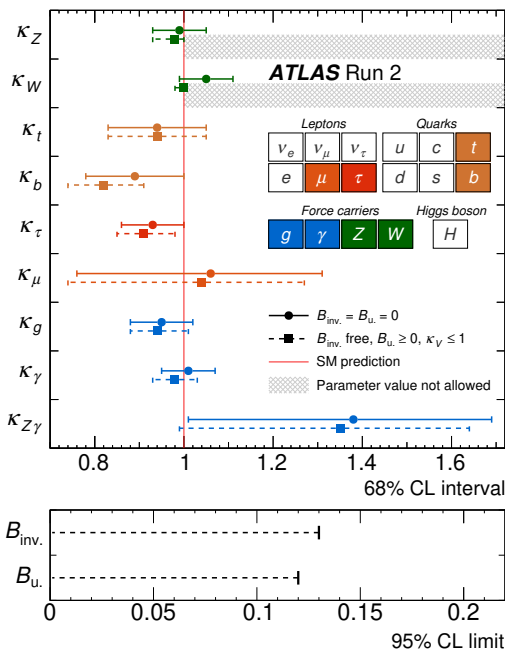


Figure 11.10: ATLAS [183] (left) and CMS [184] (right) combined measurements of coupling modifiers with various assumptions. The ATLAS measurements also use the off-shell Higgs measurements.

latter model, the cross section times branching fraction of the $gg \rightarrow H \rightarrow ZZ$ process is parametrised as a function of a single coupling modifier:

$$\kappa_{gZ} = \kappa_g \times \frac{\kappa_Z}{\kappa_H}. \quad (11.36)$$

Then all combination signals can be parametrised with the following ratios of coupling modifiers: (i) the $\lambda_{Zg} = \kappa_Z/\kappa_g$ ratio which is mainly probed by the measurements of the VBF and ZH production; (ii) the $\lambda_{tg} = \kappa_t/\kappa_g$ ratio constrained by the $t\bar{t}H$ production process; (iii) the $\lambda_{WZ} = \kappa_W/\kappa_Z$ ratio mainly probed by the WW and ZZ decay modes; (iv) the $\lambda_{\tau Z} = \kappa_\tau/\kappa_Z$ ratio constrained by the $\tau^+\tau^-$ channel; (v) the $\lambda_{bZ} = \kappa_b/\kappa_Z$ ratio probed mainly by the $VH(b\bar{b})$ channels; and (vi) the $\lambda_{\gamma Z} = \kappa_\gamma/\kappa_Z$ ratio constrained by the diphoton channel. In this parametrisation, the ZZ channel plays an important normalisation role (the results are discussed in detail in the previous edition of this review [141]).

11.5.1.3 Differential cross sections

To further characterise the production and decay properties of the Higgs boson, with the increase in size of the LHC datasets, measurements of fiducial and differential cross sections are being carried out by ATLAS and CMS both at Run 1 (the references can be found in the previous edition of this review [141]) and Run 2 and in several channels [313–316]: the diphoton, the four leptons, the WW , $b\bar{b}$ and $\tau^+\tau^-$ channels.

The definition of a fiducial volume as close as possible to the reconstruction level selection criteria is very important, as it will minimise the model dependence from possible variations in the signal reconstruction efficiencies. Minimising model dependence of unfolded fiducial differential cross section measurements is also key to ensure their usefulness to further probe and tune more accurate models in the future.

While strict fiducial requirements are key to minimise model dependence, if the decay products are part of the fiducial volume definition, these make combinations of decay channels impossible. To gain precision in the measurement of the production properties

of the Higgs boson, the fiducial volume can be defined in terms of the Higgs boson distributions, while its decay channels and properties are fully integrated. This has been used to combine differential cross section for instance in the transverse momentum of the Higgs boson. Such hybrid approaches are also discussed in Section 11.5.1.5.

A large number of observables have been studied aiming at probing the accuracy of the modelling of the Higgs boson production simulations as well as measuring the properties of the Higgs boson.

The measured differential cross section in the Higgs boson transverse momentum by ATLAS and CMS using the full Run-2 datasets are illustrated in Fig. 11.11 [314, 315, 317].

The Higgs boson transverse momentum distribution is of particular importance to probe new physics in the Higgs production. An example of interpretations that can be made using these measurements is the constraints on the b and charm quark Yukawa couplings through their impact on the production, both via the loop-level gluon fusion contribution or the $gg \rightarrow b\bar{b}H, c\bar{c}H$ processes. These results are also combined with the direct search for the $VH(b\bar{b})$ process and shown in Fig. 11.12. It is interesting to compare the constraint, $|\kappa_c| < 8.5$, from the $VH(c\bar{c})$ production analysis alone and the limit obtained using only the differential distribution which is approximately the double of the direct search limit as well as the limit that also uses the normalisation which yields $|\kappa_c| < 2.3$. The latter indirect limits assume that $\kappa_b = 1$. This shows the already good strength of the shape analysis as well as the limit coming from the parametrisation of the normalisation in the $H \rightarrow \gamma\gamma, 4\ell$ decay channels. The constraint coming from the normalisation is due to the modification of the total width from the charm and b quark couplings [314].

11.5.1.4 Constraints on non-SM Higgs boson interactions in an effective Lagrangian

An example of the possible use of differential cross sections in constraining non-SM Higgs boson couplings in an EFT is given by ATLAS [318]. In this analysis, differential cross section measured in the diphoton channel are used to constrain an effective Lagrangian where the SM is supplemented by dimension six CP -even operators of the Strongly Interacting Light Higgs (SILH) formulation [295] and corresponding CP -odd operators. The diphoton differential cross sections are mainly sensitive to the operators that affect the Higgs boson interactions with gauge bosons. CMS has also recently analysed [313] the Higgs boson transverse momentum distribution to constrain the Higgs boson couplings to top, bottom, and charm quarks as well as the effective coupling to gluons. This analysis is, however, not performed in an EFT framework.

The differential distributions used in this combination are: (i) the transverse momentum of the Higgs boson, (ii) the number of reconstructed jets produced in association with the diphoton pair, (iii) the invariant mass of the diphoton system and (iv) the difference in azimuthal angle of the leading and sub-leading jets in events with two or more jets. This analysis shows how differential information significantly improves the sensitivity to dimension-6 operators.

11.5.1.5 Simplified Template Cross Sections (STXS)

An overarching subject of discussion between the theory and experimental communities in the field of Higgs physics has been how experimentalists could best communicate their results to be most efficiently used by others for further interpretation. The commonly used practice is that results are given at particle level within a well-defined fiducial volume of phase space. The fiducial volume is usually defined close enough to the experimental reconstruction to minimise the possible variations of the reconstruction efficiency within the particle level fiducial volume. In this way, results minimise their dependence on theoretical uncertainties.

ATLAS and CMS have produced fiducial and unfolded cross sections based on all objects reconstructed in the events. These measurements could be used for further interpretation. However, performing a proper combination of channels taking into account all experimental systematic uncertainties is non trivial and given the number of channels, combinations are very involved. A pro-

posal [40, 319] was made by the LHC Higgs Working Group to produce results in each decay channel with a well defined fiducial phase space of the Higgs boson (and not its decay products) and for other associated objects pertaining to all channels, such as jets and missing transverse momentum (MET). The definition of the fiducial regions is motivated by maximising the experimental sensitivity, isolating possible BSM effects, and minimising the dependence on theoretical uncertainties. The number of regions is also minimised to avoid the loss of experimental sensitivity. The observables that are measured in this approach are still the standard production cross sections (the gluon fusion, the vector boson fusion, the VH and $t\bar{t}H$ associated production modes) within the defined fiducial volumes.

This approach is hybrid. It is fiducial on specific objects to reduce the theory dependence and inclusive in the Higgs kinematics in order to allow for a more straightforward combination. This approach also allows the use of multivariate techniques to enhance the sensitivity within given fiducial regions, at the expense of a greater extrapolation and therefore increased model dependence.

The currently used Simplified Template Cross Sections (STXS) scheme covers, with a limited number of bins, the ggF process in four categories in number of jets (0, 1, 2 and 2 VBF-like jets, where VBF-like means a selection of two high invariant mass jets with large pseudo rapidity difference) further subdivided in four transverse momentum categories covering the full spectrum with the last bin being inclusive for $p_T > 200$ GeV. The VH process is subdivided in two categories depending on the number of reconstructed charged leptons corresponding to the decays of either a W boson or a Z boson, and two bins in transverse momentum. VBF and hadronic VH categories are defined using jet cuts and two bins in transverse momentum.

Measurements in this framework have been made in various decay channels. The first measurements have been performed in the main Higgs boson discovery channels. ATLAS and CMS have produced measurements of the diphoton and the 4ℓ channels with Run-2 data [258, 314, 320–325].

The ATLAS and CMS collaborations have also performed measurements of the STXS in the $H \rightarrow W^+W^-$ decay channel [326, 327].

CMS has also carried out a measurement of the STXS in the $H \rightarrow \tau^+\tau^-$ decay channel targeting the high transverse momentum of the Higgs boson [156], in particular in the channel where the Higgs boson is produced with one jet of transverse energy in excess of 200 GeV.

ATLAS [328] has made a measurement of the STXS aiming at the VH production mode in the $H \rightarrow b\bar{b}$ decay mode at high transverse momentum of the vector boson above 250 GeV, where the discrimination of the background further increases.

A combination of STXS across decay channels has also been carried out by ATLAS with the full Run-2 dataset [183, 329, 330].

11.5.2 Effective Lagrangian framework

The SMEFT has the same field content and it respects the same linearly-realised $SU(3)_C \times SU(2)_L \times U(1)_Y$ local symmetry as the SM. The difference is the presence of operators with canonical mass-dimension d larger than 4. These are organised in a systematic expansion in d , where each consecutive term is suppressed by a larger power of a high mass scale. Assuming baryon and lepton number conservation, the most general Lagrangian takes the form

$$\mathcal{L}_{\text{eff}} = \mathcal{L}_{\text{SM}} + \sum_i c_i^{(6)} \mathcal{O}_i^{(6)} + \sum_j c_j^{(8)} \mathcal{O}_j^{(8)} + \dots \quad (11.37)$$

The contribution of the higher order operators of dimension d to physical amplitudes is suppressed by $(E/\Lambda)^{d-4}$, where E is the relevant energy scale of the process and Λ is the energy scale suppressing the higher-dimensional operators. The Wilson coefficients $c_i^{(d)}$ encode the virtual effects of the heavy new physics in low-energy observables. Their precise forms in terms of masses and couplings of the new particles can be obtained via matching with the ultraviolet (UV) completion of the SM [331–334], or inferred using specific power-counting rules [295, 335].

The list of dimension-6 operators was first classified in a systematic way in Ref. [336] after the works of Ref. [337]. Subsequent

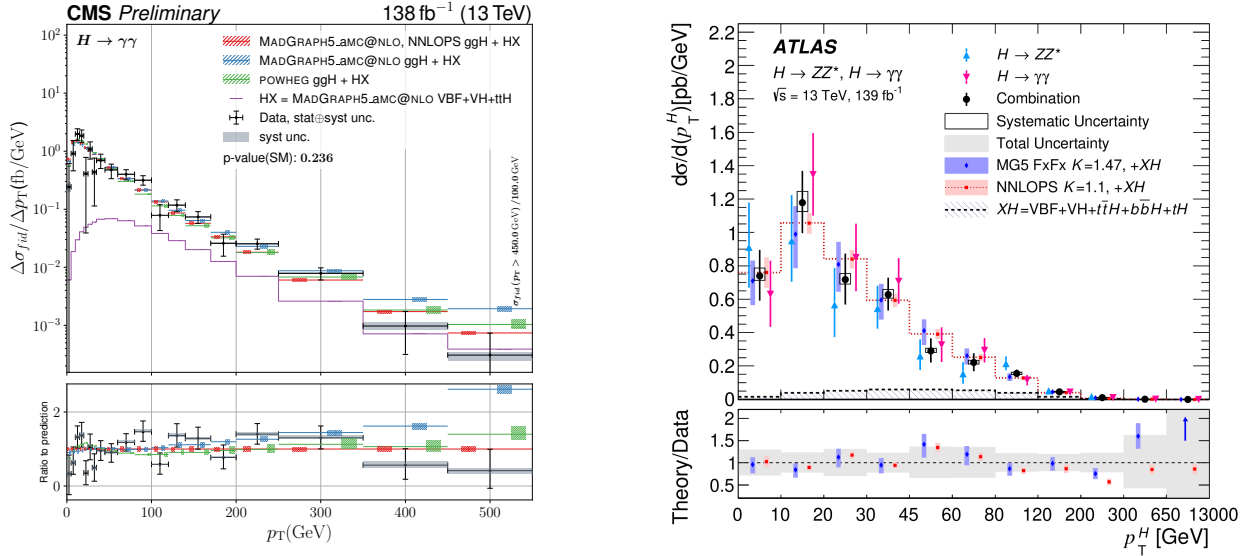


Figure 11.11: (Left) Fiducial differential cross sections in Higgs boson transverse momentum in the $H \rightarrow \gamma\gamma$ channel from the CMS experiment [315]. (Right) Partially fiducial combined cross sections using the $H \rightarrow \gamma\gamma$ and $H \rightarrow 4\ell$ channels from the ATLAS experiment [314].

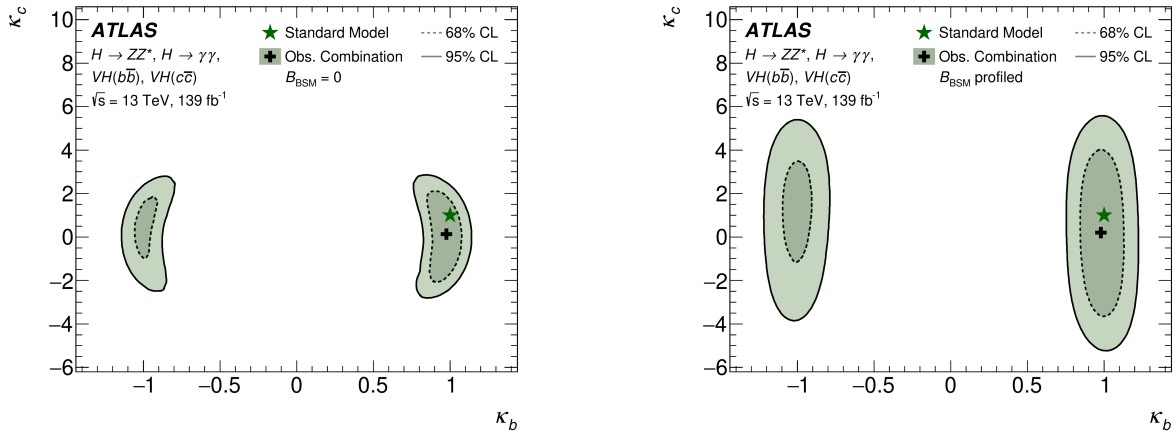


Figure 11.12: Measured likelihood contours for the κ_b and κ_c parameters from a simultaneous fit of the direct search for $VH(\bar{b}b, c\bar{c})$ analyses and the measurement of the differential cross section in transverse momentum in the $H \rightarrow \gamma\gamma, 4\ell$ channels, using the overall normalisation of the cross sections parametrised as a function of the κ_b and κ_c couplings and assuming no non-Standard Model contributions to the total width of the Higgs boson (left) and using only the differential shape in transverse momentum [314].

analyses pointed out the presence of redundant operators, and a minimal and complete list of operators was finally provided in Ref. [338]³. For a single family of fermions, there are 76 real ways to deform the SM generated by 59 independent operators. With the 3 families of fermions of the SM, flavour indices can be added to these 59 operators, and furthermore, new operator structures, that have been dismissed by means of Fierz transformations in the single family case, have to be considered, for a total of 2499 real deformations [341].

The numbers of operators to constrain can be reduced by imposing suitable flavour assumptions. Inspired by flavour physics, a $U(2)_q \times U(2)_u \times U(2)_d \times U(3)_l \times U(3)_e$ symmetry can be enforced to impose a flavour symmetry in the first two quark generations

and all three lepton generations. ATLAS performed a detailed analysis of Higgs and EW data from LEP/SLD and LHC. Under the previous flavour assumption, 22 operators are affecting Higgs observables alone, 22 operators are affecting EW precision observables alone and 11 operators are affecting both sets of observables simultaneously. Dedicated samples representing SM, linear, and quadratic effects of dimension-six operators are generated at leading order using `MadGraph5_aMC@NLO` and `SMEFTsim`. Events are interfaced to `Pythia8` to simulate parton shower and hadronization. The decays of bottom and charm hadrons are performed by `EvtGen`. For the loop-induced processes, calculations are performed with `SMEFTatNLO`, which allows for the calculation of NLO QCD corrections, instead of `SMEFTsim`. Effects of dimension-six operators on background processes are usually not taken into account except in the analysis of VBF Z measurement and of WW production. The results are displayed in Fig. 11.14 [342]. The current measurements cannot currently constrain simultaneously

³Complete enumerations of $d=8$ operators have been obtained [339] and some preliminary constraints on peculiar subsets of these operators have been derived from experimental measurements [340]. Still, in this review, the EFT Lagrangians will be truncated at the level of dimension-6 operators.

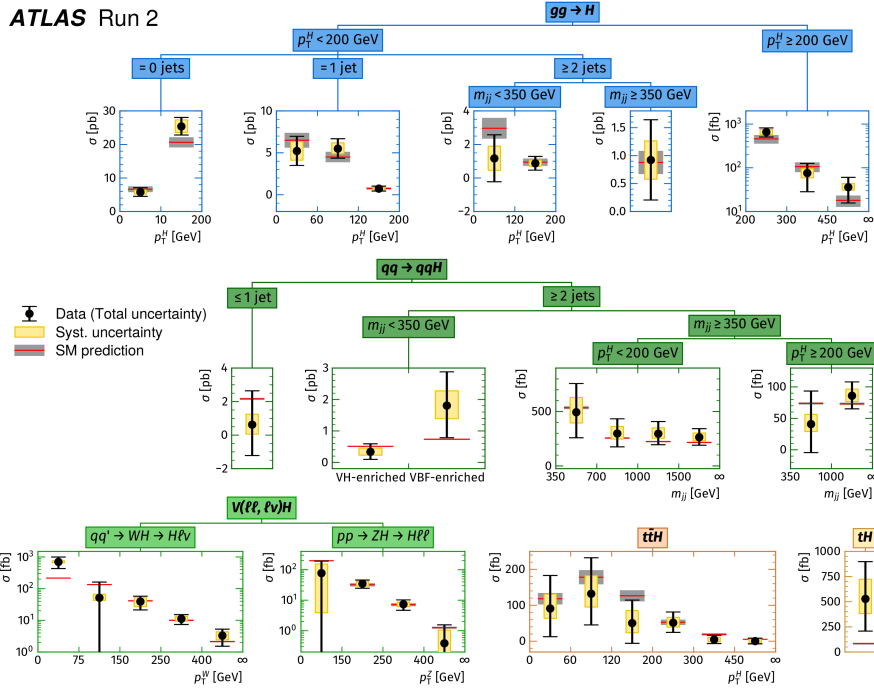


Figure 11.13: Simultaneous combined measurement of simplified template cross sections assuming SM branching fractions of the Higgs boson [183].

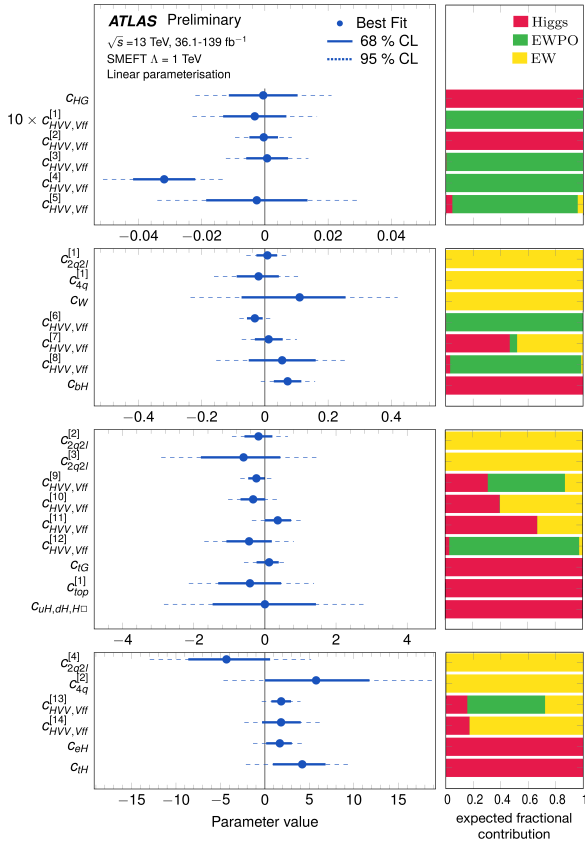


Figure 11.14: Constraints on Wilson coefficients from the combined LHC+EWPO analysis, presented in four blocks with different x -axis ranges. Right-hand side panel shows the contribution of each input measurement group to the eigenvector constraint in the Gaussian approximation.

all SMEFT Wilson coefficients as numerous degrees of freedom are not constrained by the data. One option is to fit a limited (typically one) coefficient while fixing the others. Another approach as shown in Fig. 11.14 is to perform a Principal Component Analysis (PCA) which will identify the sensitive and the flat directions of the likelihood and compute a modified basis corresponding to a linear combination of the SMEFT coefficients [342]. For this reason the results displayed in Fig. 11.14 illustrate coefficients with several indices, which correspond to the main Wilson coefficients represented in a given direction of the PCA analysis. The superscript represent a numbering of different linear combinations with similar coefficients. These results show the excellent agreement between measurements and the Standard Model expectations projected onto SMEFT sensitive directions. The largest discrepancy is observed for the $c_{HVV,Vff}^{[4]}$ coefficient which is driven by the longstanding discrepancy in the $A_{FB}^{0,b}$ measurements at LEP. In this paper [342], ATLAS has performed both fits in the linear and quadratic parametrisations of SMEFT effects corresponding to taking into account the interference between SM and SMEFT only or the entire SMEFT effect (including the quadratic SMEFT contributions) respectively.

Phenomenological studies [343, 344] have also combined Higgs, diboson, and top quark production and decay measurements from the LHC and LEP to produce global fit of SMEFT at the dimension-6 order. Automated codes like `Matchete` [334] or `Matchmakereft` [333] allows one to match explicit UV models onto SMEFT and hence to interpret the global EFT fit to directly constrain these UV models.

11.6 New physics models of EWSB in the light of the Higgs boson discovery

The discovery of a light scalar with couplings to gauge bosons and fermions that are consistent with SM predictions, together with the slow running of the Higgs boson self-coupling at high energies allow one to consider the SM as a valid perturbative description of nature all the way to the Planck scale. This picture is admittedly very attractive, but it posits that the Higgs boson is an elementary scalar field, whose mass has quantum sensitivity to possible new physics scales. This EW/Higgs naturalness problem [6] has become much more definite after the Higgs boson discovery.

There are two broad classes of models addressing the naturalness problem⁴. One is based on SUSY [7] (for recent reviews, see Refs. [8, 9]). This is a weakly coupled approach to EWSB, maintaining the perturbativity of the SM, and, the Higgs boson remains elementary and the corrections to its mass are screened at the scale at which SUSY is broken so the value of the weak scale remains insensitive to the details of the physics at higher scales. These theories predict at least three neutral Higgs particles and a pair of charged Higgs particles [23]. One of the neutral Higgs bosons, most often the lightest CP -even one, has properties that can resemble those of the SM Higgs boson (at least in some regions of the parameter space referred to as the alignment limit [346, 347], which in the case of sufficiently heavy additional Higgs bosons is dubbed the decoupling limit [348, 349]). Such scalar is referred to as a SM-like Higgs boson, meaning that its couplings are close to the ones predicted in the SM. The other approach invokes the existence of strong interactions at a scale of the order of one TeV or above and these new interactions induce the breaking of the electroweak symmetry [350]. In the original incarnation, dubbed technicolor, the strong interactions themselves trigger EWSB without the need of a Higgs boson. Another possibility, more compatible with the ATLAS and CMS discovery, is that the strong interactions produce four light resonances identified with the Higgs doublet and EWSB proceeds through vacuum misalignment [10] (see Refs. [11, 12] for recent reviews). In that case, the Higgs boson itself has a finite size and thus never feels the UV degrees of freedom that would otherwise have dragged its mass to much higher scales. The Higgs boson could also correspond to the Goldstone boson associated with the spontaneous breaking of scale invariance, see Ref. [351] and references therein. However, this dilaton/radion scenario now requires a jumbled model-building to be consistent with the constraints from the coupling measurements. All these BSM scenarios can have important effects on the phenomenology of the Higgs boson. Also, in each case, the role of the Higgs boson in the unitarisation of scattering amplitudes is shared by other particles which remain targets of experimental searches.

The realisation of SUSY at low energies has many good qualities that render it attractive as a model of new physics. First of all since, for every SM degree of freedom, there is a superpartner of different spin but of equal mass and effective coupling to the SM-like Higgs boson, in the case of exact SUSY, an automatic cancellation of quantum corrections to the Higgs mass parameter holds. In practice, it is known that SUSY must be broken since no superpartners of the SM particles have been observed so far. The mass difference between the precise value of the mass of any particle and that of its corresponding superpartner is proportional to the correlated soft SUSY breaking parameter, generically called M_{SUSY} . The quantum corrections to the Higgs boson mass parameter are proportional to M_{SUSY}^2 , and provided M_{SUSY} is of order of a few TeV, the low energy mass parameters of the Higgs sector become insensitive to physics at the GUT or Planck scale. Another interesting feature of SUSY theories is related to the dynamical generation of EWSB [352]. In the SM, a negative Higgs mass parameter, m^2 , needs to be inserted by hand to induce EWSB, see Eq. (11.1). In SUSY, instead, even if the relevant Higgs mass parameter is positive in the ultraviolet, it may become negative and induce EWSB radiatively through the strong effect of the top quark-Higgs boson coupling in its renormalisation group evolution [352].

In the following, the Higgs sector will be explored in specific SUSY models. In all of them, it is often possible to find regions of the parameter space that accommodate one neutral Higgs boson with properties that resemble those of the SM Higgs boson, whereas additional neutral and charged Higgs bosons are also predicted and are intensively being sought for at the LHC (see Section 11.6.7). In the simplest SUSY model, accommodating a SM-like Higgs boson mass of about 125 GeV results in constraints on the stop sector, with at least one stop mass in the few TeV mass range. In non-minimal SUSY extensions of the SM (details

and related references can be found in the 2018 edition of this review [141]), a SM-like Higgs boson with mass of 125 GeV can be accommodated with less restrictions on the stop sector. While naturalness dictates relatively light stops and - at the two loop level - also gluinos, the first and second generation of squarks and sleptons couple weakly to the Higgs sector and may be heavy. Moreover, small values of the μ parameter and therefore light Higgsinos, the fermionic superpartners of the Higgs bosons, would be a signature of a natural realization of electroweak symmetry breaking [353]. Such SUSY spectra, consisting of TeV range stop masses and light Higgsinos, continue to be under intense scrutiny by the experimental collaborations [354], in order to understand if such natural SUSY scenarios endure and can explain why the Higgs boson remains light.

In the context of weakly coupled models of EWSB, one can also consider multiple Higgs $SU(2)_L$ doublets as well as additional Higgs singlets, triplets or even more complicated multiplet structures, with or without low energy SUSY. In general, for such models, one needs to take into account experimental constraints from precision measurements and flavour changing neutral currents. The LHC signatures of such extended Higgs sectors are largely shaped by the role of the exotic scalar fields in EWSB.

The idea that the Higgs boson itself could be a composite bound state emerging from a new strongly-coupled sector has been reconsidered thanks to the insights gained from the AdS/CFT duality. The composite Higgs boson idea is an incarnation of EWSB via strong dynamics that smoothly interpolates between the standard technicolor approach and the true SM limit. To avoid the usual conflict with EW data, it is sufficient, if not necessary, that a mass gap separates the Higgs resonance from the other resonances of the strong sector. Such a mass gap can naturally follow from dynamics if the strongly-interacting sector exhibits a global symmetry, G , broken dynamically to a subgroup H at the scale f , such that, in addition to the three Nambu-Goldstone bosons of $SO(4)/SO(3)$ that describe the longitudinal components of the massive W and Z , the coset G/H contains a fourth Nambu-Goldstone boson that can be identified with the physical Higgs boson. Simple examples of such a coset are $SU(3)/SU(2)$ or $SO(5)/SO(4)$, the latter being favoured since it is invariant under the custodial symmetry. It is also possible to have non-minimal custodial cosets with extra Goldstone bosons leading to additional Higgs bosons in the spectrum, see for instance Ref. [355]. Modern incarnations of composite Higgs models have been recently investigated in the framework of 5D warped models where, according to the principles of the AdS/CFT correspondence, the holographic composite Higgs boson then originates from a component of a gauge field along the 5th dimension with appropriate boundary conditions.

A last crucial ingredient in the construction of viable composite Higgs boson models is the concept of partial compositeness [356], i.e., the idea that there are only linear mass mixings between elementary fields and composite states. After diagonalisation of the mass matrices, the SM particles, fermions and gauge bosons, are admixtures of elementary and composite states and thus they interact with the strong sector, and in particular with the Higgs boson, through their composite component. This setup has important consequences on the flavour properties, chiefly the suppression of large flavour changing neutral currents involving light fermions. It also plays an important role in dynamically generating a potential for the would-be Goldstone bosons. Partial compositeness also links the properties of the Higgs boson to the spectrum of the fermionic resonances, i.e., the partners of the top quark. As in the MSSM, these top partners are really the agents that trigger the EWSB and also generate the mass of the Higgs boson that otherwise would remain an exact Goldstone boson and hence massless. The bounds from the direct searches for the top partners, in addition to the usual constraints from EW precision data, force the minimal composite Higgs models into some unnatural corners of their parameter spaces [357].

11.6.1 Higgs bosons in the minimal supersymmetric standard model (MSSM)

The particle masses and interactions in a SUSY theory are uniquely defined as a function of the superpotential and the Kähler potential [9]. A fundamental theory of SUSY breaking, how-

⁴Another solution to the naturalness problem is to lower the fundamental scale of quantum gravity, like for instance in models with large extra-dimensions, see Ref. [345].

ever, is unknown at this time. Nevertheless, one can parametrise the low-energy theory in terms of the most general set of soft SUSY-breaking operators [9]. The simplest realistic model of low-energy SUSY is the minimal SUSY extension of the SM (MSSM) [9, 358], that associates a SUSY partner to each gauge boson and chiral fermion of the SM, and provides a realistic model of physics at the weak scale. However, in this minimal model, with the most general set of soft SUSY-breaking terms, more than 100 new parameters are introduced. Nevertheless, only a subset of these parameters impact the Higgs boson phenomenology either directly at tree-level or through quantum effects.

The MSSM contains the particle spectrum of a two-Higgs-doublet model (2HDM) extension of the SM and the corresponding SUSY partners. Two Higgs doublets, Φ_1 and Φ_2 , with hypercharge $Y = -1$ and $Y = 1$, respectively, are required to ensure an anomaly-free SUSY extension of the SM and to generate mass for down-type quarks/charged leptons (Φ_1) and up-type quarks (Φ_2) [23]. The Higgs potential reads

$$\begin{aligned} V = & m_1^2 \Phi_1^\dagger \Phi_1 + m_2^2 \Phi_2^\dagger \Phi_2 - m_3^2 (\Phi_1^T i \sigma_2 \Phi_2 + \text{h.c.}) \\ & + \frac{1}{2} \lambda_1 (\Phi_1^\dagger \Phi_1)^2 + \frac{1}{2} \lambda_2 (\Phi_2^\dagger \Phi_2)^2 + \lambda_3 (\Phi_1^\dagger \Phi_1) (\Phi_2^\dagger \Phi_2) \\ & + \lambda_4 |\Phi_1^T i \sigma_2 \Phi_2|^2 + \frac{1}{2} \lambda_5 [(\Phi_1^T i \sigma_2 \Phi_2)^2 + \text{h.c.}] \\ & + [[\lambda_6 (\Phi_1^\dagger \Phi_1) + \lambda_7 (\Phi_2^\dagger \Phi_2)] \Phi_1^T i \sigma_2 \Phi_2 + \text{h.c.}], \end{aligned} \quad (11.38)$$

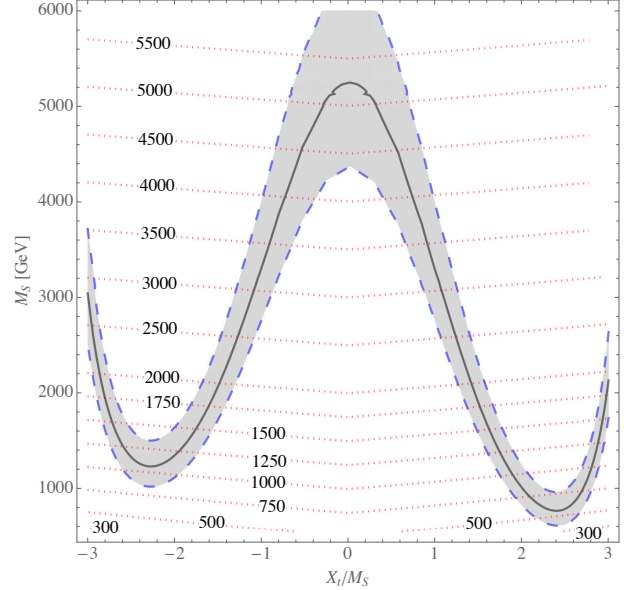
where $m_i^2 = \mu^2 + m_{H_i}^2$ ($i = 1, 2$), with μ being the supersymmetric Higgsino mass parameter and m_{H_i} the soft supersymmetric breaking mass parameters of the two Higgs doublets; $m_3^2 \equiv B\mu$ is associated to the B-term soft SUSY breaking parameter; and λ_i , for $i = 1$ to 7, are all the Higgs quartic couplings.

After the spontaneous breaking of the electroweak symmetry, five physical Higgs particles are left in the MSSM spectrum: one charged Higgs pair, H^\pm , one CP -odd neutral scalar, A , and two CP -even neutral states, H and h , with h being the lightest.⁵ The Higgs sector at tree level depends on the electroweak gauge coupling constants and the vacuum expectation value v – or equivalently the Z gauge boson mass – and is determined by only two free parameters: $\tan\beta$ – the ratio of the two Higgs doublets' vacuum expectation values v_2/v_1 – and one Higgs boson mass, conventionally chosen to be the CP -odd Higgs boson mass, m_A . The other tree-level Higgs boson masses are then given in terms of these parameters. The tree level value of m_h is maximised not only for $m_A \gg m_Z$ but also for $\tan\beta \gg 1$. For $m_A \gg m_Z$ it acquires a maximum value $m_h = m_Z \cos 2\beta$.

Radiative corrections have a significant impact on the values of Higgs boson masses and couplings in the MSSM. The dominant radiative effects to the SM-like Higgs boson mass arise from the incomplete cancellation between top and scalar-top (stop) loops and at large $\tan\beta$ also from sbottom and stau loops. The stop, sbottom and stau masses and mixing angles depend on the SUSY Higgsino mass parameter μ and on the soft-SUSY-breaking parameters [9, 358]: M_Q, M_U, M_D, M_L, M_E , and A_t, A_b, A_τ . The first three of these are the left-chiral and the right-chiral top and bottom scalar quark mass parameters. The next two are the left-chiral stau/sneutrino and the right-chiral stau mass parameters, and the last three are the trilinear parameters that enter in the off-diagonal squark/slepton mixing elements: $X_t \equiv A_t - \mu \cot\beta$ and $X_{b,\tau} \equiv A_{b,\tau} - \mu \tan\beta$. At one-loop, the electroweak gauginos yield a small contribution to the Higgs boson mass, and at the two-loop level, the masses of the gluinos also enter in the calculations. Radiative corrections to the Higgs boson masses have been computed using a number of techniques, with a variety of approximations, see Ref. [359] for a recent review.

⁵Observe that in the SM sections of this review, H denotes the SM Higgs boson, whereas in the sections about SUSY, or extensions of the SM with two Higgs doublets, H is used for the heaviest CP -even Higgs boson, since this is the standard notation in the literature, and the 125 GeV SM-like light Higgs boson will be denoted by h . Generically, in the MSSM, the lightest CP -even Higgs boson is indeed SM-like and thus it is naturally identified with the 125 GeV Higgs boson discovered by ATLAS and CMS, while in general 2HDM extensions, with or without SUSY, there could still be lighter scalar states below 125 GeV.

Figure 11.15: Values of the SUSY mass scale $M_{\text{SUSY}} = M_S$ versus the stop mixing parameter normalised by the SUSY mass scale X_t/M_{SUSY} , for fixed $\tan\beta = 20$, $\mu = 200$ GeV and $A_t = A_b = A_\tau$. The solid black line corresponds to $m_h = 125$ GeV while in the grey band m_h varies by ± 1 GeV. The red dotted lines are iso-values of the stop mass in GeV. This figure is based on Ref. [360].



The discovered SM-like Higgs boson, if interpreted as the lightest MSSM Higgs boson with a mass of about 125 GeV, provides information on the possible MSSM parameter space, see Fig. 11.15.

The phenomenology of the Higgs sector depends on the couplings of the Higgs bosons to gauge bosons and fermions. At tree-level, the couplings of the two CP -even Higgs bosons to W and Z bosons are given in terms of the angles α , that diagonalises the CP -even Higgs boson squared-mass matrix, and β

$$g_{hVV} = g_V m_V \sin(\beta - \alpha), \quad g_{HVV} = g_V m_V \cos(\beta - \alpha), \quad (11.39)$$

where $g_V \equiv 2m_V/v$, for $V = W$ or Z ($g_V m_V$ is the SM hVV coupling). Observe that in the limit $\cos(\beta - \alpha) \rightarrow 0$, the lightest CP -even Higgs boson h behaves as the SM Higgs boson. This situation is called alignment and is achieved in specific regions of parameter space for $m_A \geq m_Z$ [348] or in the large $m_A \gg m_Z$ limit, in which alignment is achieved through decoupling [348, 349]. There are no tree-level couplings of A or H^\pm to VV . The couplings of the Z boson to two neutral Higgs bosons are given by $g_{\phi AZ}(p_\phi - p_A)$, where $\phi = H$ or h , the momenta p_ϕ and p_A point into the vertex, and

$$g_{hAZ} = g_Z \cos(\beta - \alpha)/2, \quad g_{HAZ} = -g_Z \sin(\beta - \alpha)/2. \quad (11.40)$$

The expressions of the couplings between a charged Higgs boson, a neutral Higgs boson and the W boson as well as the expressions of the four-point couplings of vector bosons and Higgs bosons can be found in Ref. [23].

The tree-level Higgs boson couplings to fermions obey the following property: the neutral components of one Higgs doublet, Φ_1 , couple exclusively to down-type fermion pairs while the neutral components of the other doublet, Φ_2 , couple exclusively to up-type fermion pairs [23]. This Higgs-fermion coupling structure defines the Type-II 2HDM. In the MSSM, fermion masses are generated when both neutral Higgs components acquire a vacuum expectation value, and the relations between Yukawa couplings and fermion masses are (in third-generation notation)

$$h_{b,\tau} = \sqrt{2} m_{b,\tau} / (v \cos\beta), \quad h_t = \sqrt{2} m_t / (v \sin\beta). \quad (11.41)$$

The couplings of the neutral Higgs bosons to $f\bar{f}$, relative to their SM values, $g m_f/(2m_W)$, are therefore given by

$$\begin{aligned} h\bar{b}b &: -\sin\alpha/\cos\beta, & h\bar{t}t &: \cos\alpha/\sin\beta, \\ H\bar{b}b &: \cos\alpha/\cos\beta, & H\bar{t}t &: \sin\alpha/\sin\beta, \\ A\bar{b}b &: \gamma_5 \tan\beta, & A\bar{t}t &: \gamma_5 \cot\beta. \end{aligned} \quad (11.42)$$

In each relation above, the factor listed for $b\bar{b}$ also pertains to $\tau^+\tau^-$. The charged Higgs boson couplings to fermion pairs, normalised to $g/(\sqrt{2}m_W)$, are given by

$$\begin{aligned} g_{H-t\bar{b}} &: m_t \cot\beta \frac{1+\gamma_5}{2} + m_b \tan\beta \frac{1-\gamma_5}{2}, \\ g_{H-\tau^+\nu} &: m_\tau \tan\beta \frac{1-\gamma_5}{2}. \end{aligned} \quad (11.43)$$

The non-standard neutral Higgs bosons have significantly enhanced couplings to down-type fermions at sizeable $\tan\beta$. Radiative corrections can modify significantly the values of the Higgs boson couplings to fermion pairs and to vector boson pairs, through a radiatively-corrected value for $\cos(\beta-\alpha)$ as well as from the one-loop vertex corrections to tree-level Higgs-fermion Yukawa couplings, see Ref. [9] and references therein, for a detailed discussion.

11.6.1.1 MSSM Higgs boson phenomenology

The MSSM parameters have to be arranged such that the mass, the CP properties, the decay and production properties of one of the neutral Higgs bosons agree with the LHC Higgs data. Given that present data allows only for moderate departures from the SM predictions, it implies that some degree of alignment is necessary.

The SM-like branching ratios of h can be modified if decays into SUSY particles are kinematically allowed, and, in particular, decays into a pair of the lightest SUSY particles – i.e., the lightest neutralinos, $\tilde{\chi}_1^0$ – can become dominant and would be invisible if R -parity is conserved [361]. Moreover, if light superpartners exist and couple to photons and/or gluons, the h loop-induced coupling to gg and $\gamma\gamma$ could deviate sizeably from the corresponding SM predictions (see for instance the review [362]), and would be in conflict with present data (see Section 11.3). For the heavier Higgs states, there are two possibilities to be considered⁶:

- i) Alignment triggered by decoupling, hence $m_A \geq$ several hundred GeV: The HWW and HZZ couplings are very small. The dominant H, A decay branching ratios strongly depend on $\tan\beta$. The decay modes $H, A \rightarrow b\bar{b}, \tau^+\tau^-$ dominate when $\tan\beta$ is large (this holds even away from decoupling). For small $\tan\beta$, the $t\bar{t}$ decay mode dominates above its kinematic threshold. For the charged Higgs boson, $H^+ \rightarrow t\bar{b}$ dominates.
- ii) Some degree of alignment without decoupling, hence $m_A \leq$ a few hundred GeV: The main difference with the previous case is that, in the low $\tan\beta$ regime ($\tan\beta \leq 5$), additional decay channels may be allowed which involve decays into the lightest SM-like Higgs boson; $A \rightarrow Zh, H \rightarrow hh$ as well as $H \rightarrow WW/ZZ$ decay modes are available (they are suppressed in the strict alignment limit). When kinematically open, the decays $A/H \rightarrow t\bar{t}$ become relevant or even dominant for sufficiently small $\tan\beta$. For the charged Higgs boson, $H^+ \rightarrow \tau^+\nu_\tau$ dominates below the $t\bar{b}$ threshold, and also $H^\pm \rightarrow W^\pm h$ may be searched for.

In both cases i) and ii), the heavier Higgs states, H, A and H^\pm , are roughly mass degenerate (with masses ± 20 GeV or less apart). If kinematically allowed, the heavy Higgs boson decays into charginos, neutralinos and third-generation squarks and sleptons can be important [365].

At hadron colliders, the dominant neutral Higgs boson production mechanism at moderate values of $\tan\beta$ is gluon fusion, mediated by loops containing heavy top and bottom quarks and the corresponding SUSY partners. The effect of light stops that may

contribute to the gluon fusion production can be partially cancelled by mixing effects. Higgs boson radiation off bottom quarks becomes important for large $\tan\beta$, where at least two of the three neutral Higgs bosons have enhanced couplings to bottom-type fermions [366, 367]. Detailed discussions of the impact of radiative corrections in these search modes are presented for instance in Ref. [368]. The vector boson fusion and Higgs-strahlung production of the CP -even Higgs bosons as well as the associated production of neutral Higgs bosons with top quark pairs have lower production cross sections by at least an order of magnitude with respect to the dominant ones, depending on the precise region of MSSM parameter space [37–40]. Higgs boson pair production of non-standard MSSM Higgs bosons has been studied in Ref. [369]. For a discussion of charged Higgs boson production at LHC, see Refs. [38, 39, 370].

Strong production of a heavy neutral Higgs boson followed by its decay into top-quark pairs is a challenging channel, only most recently being searched for by ATLAS and CMS. Interference effects between the signal and the SM $t\bar{t}$ background need to be carefully taken into account [371, 372].

Summarising, the additional Higgs bosons are sought for mainly via the channels:

$$\begin{aligned} pp &\rightarrow A/H \rightarrow \tau^+\tau^- \text{ (inclusive)}, \\ b\bar{b}A/H, A/H &\rightarrow \tau^+\tau^- \text{ (with } b\text{-tag)}, \\ b\bar{b}A/H, A/H &\rightarrow b\bar{b} \text{ (with } b\text{-tag)}, \\ pp &\rightarrow t\bar{t} \rightarrow H^\pm W^\mp b\bar{b}, H^\pm \rightarrow \tau^+\nu_\tau(\tau^-\bar{\nu}_\tau) \text{ or } t\bar{b}(b\bar{t}), \\ gb &\rightarrow H^-t \text{ or } g\bar{b} \rightarrow H^+\bar{t}, H^\pm \rightarrow \tau^+\nu_\tau(\tau^-\bar{\nu}_\tau) \text{ or } t\bar{b}(b\bar{t}). \end{aligned} \quad (11.44)$$

After the Higgs boson discovery, updated MSSM benchmark scenarios have been defined to highlight interesting conditions for the MSSM Higgs boson searches [39, 364] and are scrutinised by the LHC Higgs Working Group [373]. The latest benchmark scenarios update [364], partly based in MSSM parameter space discussions in Ref. [374], considers six benchmarks to illustrate different aspects of Higgs phenomenology in the MSSM. They include one case with complex parameters, but they all assume R -parity conservation and no flavour mixing. Each scenario contains one CP -even scalar with mass around 125 GeV and SM-like couplings. These scenarios include a M_h^{125} scenario with relatively heavy superparticles, so the Higgs phenomenology at the LHC resembles that of a 2HDM with MSSM-inspired Higgs boson couplings. Other two scenarios are characterised by some of the superparticles – staus or electroweakinos – being relatively light, that in turn is of relevance for heavy neutral Higgs boson searches. In particular, the traditional $A/H \rightarrow \tau^+\tau^-$ search channel varies depending on the values of μ and M_2 , that may enable the A/H decays into electroweakinos. Another two scenarios are characterised by the phenomenon of alignment without decoupling, in which one of the two neutral CP -even scalars has SM-like couplings independently of the mass spectrum of the remaining Higgs bosons, hence allowing for all the Higgs bosons to have relatively low mass values (about few hundred GeV). Finally, there is one scenario which incorporates CP violation in the Higgs sector and gives rise to a strong admixture of the two heavier neutral states. All the above scenarios assume all parameters in the mass range from 1 to a few TeV, hence they are not applicable for values of $\tan\beta$ of order a few, for which a Higgs boson mass value of 125 GeV is out of reach. An additional study [375], relying on an EFT approach in the MSSM, focusses on two scenarios specifically designed for the low $\tan\beta$ region and ensures a 125 GeV Higgs boson mass in almost the entire parameter space by employing a flexible supersymmetric mass scale, reaching values of up to 10^{16} GeV.

An alternative approach to reduce the large number of parameters relevant to the Higgs sector is to consider that, in the Higgs basis, the only important radiative corrections are those affecting the Higgs boson mass [376]. This approximation is called hMSSM and works well in large regions of parameter space but it breaks down for sizeable values of μ and A_t , and moderate values of $\tan\beta$, for which the radiative corrections to the mixing between the two CP even eigenstates become relevant. The effect of such radiative corrections is to allow for alignment for small to intermediate

⁶In very special regions of the parameter space, there is still the possibility that the heavier CP -even Higgs state is identified with the 125 GeV Higgs boson discovered by ATLAS and CMS, see for instance the discussion in Ref. [363] and the benchmark M_H^{125} defined in Ref. [364].

values of $\tan\beta$, independent of the specific value of m_A [346]. In addition, the hMSSM assumption that the right value of the Higgs boson mass may be obtained for all values of m_A and $\tan\beta$ is in conflict with the MSSM predictions for the Higgs boson mass for small values of m_A and $\tan\beta \simeq \mathcal{O}(1)$. The recent M_h^{25} [364] and EFTMSSM benchmarks [375], are designed to address the limitations of the hMSSM, in particular the low $\tan\beta$ region for the EFTMSSM.

The compatibility between the predicted and measured Higgs boson mass sets stringent constraints on the parameter space of BSM models. The predictions are illustrated in Fig. 11.16 for two concrete scenarios. Note that to use the predicted Higgs boson mass as a constraint (exclusion at nearly constant $\tan\beta$ at high M_A in the $(M_A, \tan\beta)$ plane), it is important to account for the theoretical uncertainty on the prediction which is in excess of an order of magnitude larger than the experimental uncertainty on the measured mass of the Higgs boson. The theoretical uncertainty depends itself on the specific SUSY spectrum for a given MSSM parameter set and should be estimated accordingly, however, a more generic estimate of ± 3 GeV is made and found to be a conservative choice [359].

Reviews of the properties and phenomenology of the Higgs bosons of the MSSM can be found for example in Refs. [9,362,378]. Future precision measurements of the Higgs boson couplings to fermions and gauge bosons together with information on heavy Higgs boson searches will provide powerful information on the SUSY parameter space [379].

Improvements in our understanding of B -physics observables put indirect constraints on additional Higgs bosons in mass ranges that would be accessible in direct LHC searches. In particular, $\text{BR}(B_s \rightarrow \mu^+ \mu^-)$, $\text{BR}(b \rightarrow s\gamma)$, and $\text{BR}(B_u \rightarrow \tau\nu)$ play an important role within minimal flavour-violating (MFV) models [380], in which flavour effects proportional to the CKM matrix elements are induced as in the SM [381].

11.6.2 Supersymmetry with singlet extensions

The Higgs mass parameter μ is a SUSY parameter, and as such, it should naturally be of order M_{GUT} or M_{Planck} . The fact that phenomenologically it is required that μ be at the electroweak/TeV scale is known as the μ problem [382]. SUSY models with additional singlets can provide a solution to the μ problem, by promoting the μ parameter to a dynamical singlet superfield S that only interacts with the MSSM Higgs doublets through a coupling λ_S at the level of the superpotential. An effective μ is generated when the real scalar component of S acquires a vacuum expectation value v_S , yielding $\mu_{eff} = \lambda_S v_S$. After the minimization of the Higgs potential, the vacuum state relates the vacuum expectation values of the three CP -even neutral scalars, v_1 , v_2 and v_S , to the scalar doublet and singlet soft SUSY breaking masses, hence, one expects that these VEVs should all be of order M_{SUSY} and therefore the μ problem is solved.

The addition of a singlet superfield to the MSSM may come along with additional symmetries imposed to the theory. Depending on such symmetries, different models with singlet extensions of the MSSM (xMSSM) have been proposed, see Ref. [383] for a general review. Among the most studied examples are the NMSSM with an additional discrete Z_3 symmetry (first introduced in Ref. [384]), the Nearly-Minimal SUSY SM (nMSSM), with additional discrete Z_5^R , and Z_7^R symmetries [385], and the $U(1)'$ -extended MSSM (UMSSM) [386]. A Secluded $U(1)'$ -extended MSSM (sMSSM) [387] contains three singlets in addition to the standard UMSSM Higgs boson singlet; this model is equivalent to the nMSSM in the limit that the additional singlet VEV's are large, and the trilinear singlet coupling, λ_S , is small [388]. The non-zero neutrino masses provide also a motivation for a particular extension of the MSSM, $\mu\nu$ SMS [389], which also happens to address the mu problem. The computation of the Higgs boson spectrum in these various models has been reviewed in Ref. [359].

A singlet extended SUSY Higgs sector opens new avenues for discovery. Since the singlet pseudoscalar particle may be identified as the pseudo-Goldstone boson of a spontaneously broken Peccei–Quinn symmetry, it may become naturally light [390]. Generally, there is mixing of the singlet sector with the MSSM Higgs sector, and for a sufficiently light, singlet-dominated scalar or pseu-

doscalar, h_S or A_S , respectively, the SM-like Higgs boson h may decay to pairs of h_S or A_S . The light scalar and/or pseudoscalar may subsequently decay to $\tau\tau$ or $b\bar{b}$ pairs. Such cascade decays are more difficult to detect than in standard searches due to the potentially soft decay products. There is also a rich phenomenology for the decays of the heavy CP -even and CP -odd doublets, H and A into two lighter Higgs bosons such as $H \rightarrow hh_S$, hh , $h_S h_S$ or $A \rightarrow A_S h_S$, $A_S h$ as well as into a light Higgs boson and a gauge boson: $H \rightarrow A_S Z$; $A \rightarrow h_S Z$, hZ . If kinematically allowed, the heavy Higgs bosons decay into $t\bar{t}$. If the singlet-dominated scalar or pseudoscalar are somewhat heavier, the decays $h_S \rightarrow WW$ or $A_S \rightarrow h_S Z$ will be allowed.

In addition, the light singlet scenario in the NMSSM or nMSSM is typically associated with a light singlino-dominated neutralino. The 125 GeV SM-like Higgs boson can then decay to pairs of this neutralino [391], opening an invisible decay mode that is not excluded by present data. All of the Higgs bosons can decay into electroweakinos depending on kinematics and on the singlino or Higgsino composition of the electroweakinos.

In models with extended singlets, at low $\tan\beta$, it is possible to trade the requirement of a large stop mixing by a sizeable trilinear Higgs-singlet Higgs coupling λ_S , rendering more freedom on the requirements for gluon fusion production. As in the MSSM, mixing in the Higgs sector – additionally triggered by the extra new parameter λ_S – can produce variations in the Higgs- $b\bar{b}$ and Higgs- $\tau^-\tau^+$ couplings that can alter the Higgs to ZZ / WW and to diphoton rates. Light charginos at low $\tan\beta$ can independently contribute to enhance the di-photon rate, without altering any other of the Higgs boson decay rates, see for instance Ref. [392].

There is much activity in exploring the NMSSM phenomenology in the light of the 125 GeV Higgs boson as well as in defining benchmark scenarios with new topologies including Higgs decay chains, see Refs. [40,393] and references therein. An analytic understanding of the alignment condition in the NMSSM is presented in Ref. [347]. The NMSSM with a Higgs boson of mass 125 GeV can be compatible with stop masses of order of the electroweak/TeV scale, thereby reducing the degree of fine-tuning necessary to achieve electroweak symmetry breaking. Interestingly, the alignment conditions point toward a more natural region of parameter space for electroweak symmetry breaking, while allowing for perturbativity of the theory up to the Planck scale and yielding a rich and interesting Higgs boson phenomenology at the LHC.

11.6.3 Supersymmetry with extended gauge sectors

In the MSSM, the tree-level value of the lightest CP -even Higgs boson mass originates from the D-term dependence of the scalar potential that comes from the SUSY kinetic terms in the Kähler potential. The D-terms lead to tree-level quartic couplings which are governed by the squares of the gauge couplings of the weak interactions, under which the Higgs boson has non-trivial charges. Hence, the lightest Higgs mass is bounded to be smaller than M_Z . In the presence of new gauge interactions at the TeV scale, and if the Higgs fields had non-trivial charges under them, new D-term contributions would lead to an enhancement of the tree-level Higgs boson mass value. Since the low energy gauge interactions reduce to the known $SU(3)_c \times SU(2)_L \times U(1)_Y$ ones, in order for this mechanism to work, the extended gauge and Higgs sectors should be integrated out in a non-SUSY way. This means that there must be SUSY breaking terms that are of the order of, or larger than, the new gauge boson masses. The tree-level quartic couplings would then be enhanced through their dependence on the square of the gauge couplings of the extended Higgs sector. This effect will be suppressed when the heavy gauge boson masses are larger than the SUSY breaking scale and will acquire its full potential only for large values of this scale.

One of the simplest possibilities is to extend the weak interactions to a $SU(2)_1 \times SU(2)_2$ sector, such that the known weak interactions are obtained after the spontaneous breaking of these groups to $SU(2)_L$ [394]. This example is briefly summarised in the previous editions of this review [141]. Assuming SUSY breaking terms of the order of the new gauge boson masses, enhancements of order 50% of the MSSM D-term contribution to the Higgs boson mass may be obtained. Such enhancements are sufficient to obtain

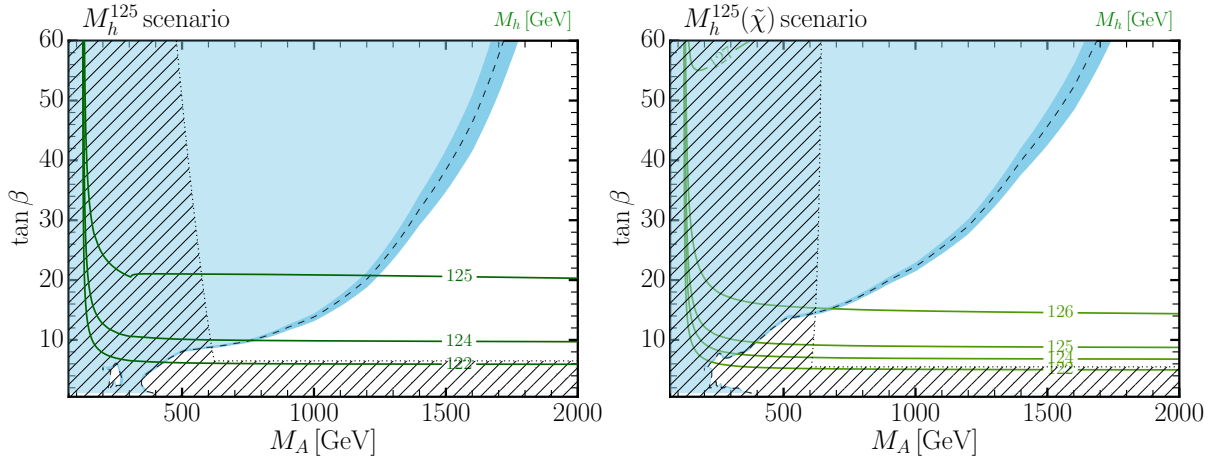


Figure 11.16: The 95% CL exclusion contours in the $(M_A, \tan \beta)$ parameter space for the M_h^{125} (right) and $M_h^{125}(\tilde{\chi})$ (left) benchmark scenarios [377]. The M_h^{125} benchmark assumes that super partners are heavy, so that the phenomenology of the observed Higgs boson is not altered except in its couplings due to the existence of another doublet. The $M_h^{125}(\tilde{\chi})$ scenario on the other hand considers light electroweakinos and therefore the heavy Higgs bosons H and A can have sizeable decay rates to charginos and neutralinos, consequently suppressing the $\tau^+\tau^-$ decay rate. The nearly vertical dotted line illustrates the lower limit on the mass of the A boson from precision measurements of the Higgs boson couplings and the close-to horizontal dotted line represents the limit on $\tan \beta$ from the compatibility of the measured mass of the observed Higgs boson and the prediction using radiative corrections (mostly from the stop sector).

the measured Higgs mass value without the need for very heavy stops or large stop mixing parameters. This gauge extension leads to new, heavy gauge and Higgs bosons, as well as new neutralinos and charginos, that depending on the region of parameter space can induce novel phenomenology at the LHC. Gauge extensions including new Abelian gauge groups have also been considered.

Gauge extensions of the MSSM can also lead to an enhancement of the Higgs boson mass value by modifying the renormalisation group evolution of the Higgs quartic coupling to low energies. In the MSSM, the evolution of the quartic coupling is governed by the top-quark Yukawa interactions and depends on the fourth power of the top-quark Yukawa coupling. The neutralino and chargino contributions, which depend on the fourth power of the weak gauge couplings, are small due to the smallness of these couplings. Depending on the values of the soft SUSY breaking parameters in the gaugino and Higgsino sectors, the $SU(2)_1$ gauginos may become light, with masses of the order of the weak scale. Since the $SU(2)_1$ coupling may be significantly larger than the $SU(2)_L$ one, for small values of the Higgsino mass parameter μ , the associated charginos and neutralinos may modify the evolution of the quartic coupling in a significant way [395]. This may lead to a significant increase of the lightest CP -even Higgs boson mass, even for small values of $\tan \beta \simeq 1$ for which the D-term contributions become small. Radiative corrections should be properly taken into account in this scenario as they might modify the tree-level result.

11.6.4 Effects of CP violation

SUSY scenarios with CP -violation (CPV) phases are theoretically appealing, since additional CPV beyond that observed in the K , D , and B meson systems is required to explain the observed cosmic matter-antimatter asymmetry. In the MSSM, CP -violation effects in the Higgs sector appear at the quantum level, while in singlet extensions of the MSSM CP -violation effects can already be effective at tree level. In general, CP -violation effects in the Higgs sector have significant constraints from electric dipole moments data [396].

In the MSSM, the gaugino mass parameters $(M_{1,2,3})$, the Higgsino mass parameter, μ , the bilinear Higgs squared-mass parameter, m_{12}^2 , and the trilinear couplings of the squark and slepton fields to the Higgs fields, A_f , may carry non-trivial phases. The two parameter combinations $\arg[\mu A_f (m_{12}^2)^*]$ and $\arg[\mu M_i (m_{12}^2)^*]$ are invariant under phase redefinitions of the MSSM fields [397, 398]. Therefore, if one of these quantities is non-zero, there would be new sources of CP -violation affecting the Higgs sector through radiative corrections, see Ref. [399] and

references therein. The mixing of the neutral CP -odd and CP -even Higgs boson states is no longer forbidden. Hence, m_A is no longer a physical parameter. However, the charged Higgs boson mass m_{H^\pm} is still physical and can be used as an input for the computation of the neutral Higgs boson spectrum of the theory. For large values of m_{H^\pm} , corresponding to the decoupling limit, the properties of the lightest neutral Higgs boson state approach those of the SM Higgs boson. In particular, the upper bound on the lightest neutral Higgs boson mass takes the same value as in the CP -conserving case [398]. Nevertheless, there still can be significant mixing between the two heavier neutral mass eigenstates. For a detailed study of the Higgs boson mass spectrum and parametric dependence of the associated radiative corrections, see Ref. [399] and references therein.

Major variations to the Higgs boson phenomenology occur in the presence of explicit CPV phases. In the CPV case, vector boson pairs couple to all three neutral Higgs boson mass eigenstates, H_i ($i = 1, 2, 3$), with couplings

$$\begin{aligned} g_{H_i V V} &= \cos \beta \mathcal{O}_{1i} + \sin \beta \mathcal{O}_{2i}, \\ g_{H_i H_j Z} &= \mathcal{O}_{3i} (\cos \beta \mathcal{O}_{2j} - \sin \beta \mathcal{O}_{1j}) \\ &\quad - \mathcal{O}_{3j} (\cos \beta \mathcal{O}_{2i} - \sin \beta \mathcal{O}_{1i}), \end{aligned} \quad (11.45)$$

where the $g_{H_i V V}$ couplings are normalised to the analogous SM coupling and the $g_{H_i H_j Z}$ have been normalised to $g_Z^{\text{SM}}/2$. The orthogonal matrix \mathcal{O}_{ij} , only defined in the $p^2 \rightarrow 0$ limit, is relating the weak eigenstates to the mass eigenstates. It has non-zero off-diagonal entries mixing the CP -even and CP -odd components of the weak eigenstates. Moreover, CPV phases imply that all neutral Higgs bosons can couple to both scalar and pseudoscalar fermion bilinear densities. The couplings of the mass eigenstates H_i to fermions depend on the loop-corrected fermion Yukawa couplings (similarly to the CP conserving (CPC) case), on $\tan \beta$ and on \mathcal{O}_{ji} [400].

The production processes of neutral MSSM Higgs bosons in the CPV scenario are similar to those in the CPC scenario. Regarding the decay properties, the lightest mass eigenstate, H_1 , predominantly decays to $b\bar{b}$ if kinematically allowed, with a smaller fraction decaying to $\tau^+\tau^-$. If kinematically allowed, a SM-like neutral Higgs boson, H_2 or H_3 can decay predominantly to $H_1 H_1$ leading to many new interesting signals both at lepton and hadron colliders; otherwise it will decay preferentially to $b\bar{b}$.

The discovery of a 125 GeV Higgs boson has put strong constraints on the realisation of the CPV scenario within the MSSM. This is partly due to the fact that the observed Higgs boson rates

are close to the SM values, and a large CP -violating component would necessarily induce a large variation in the rate of the SM-like Higgs boson decays into the weak gauge bosons W^\pm and Z . The measured Higgs mass imposes additional constraints on the realisation of this scenario. Once all effects are considered, the CP -odd Higgs boson A component of the lightest Higgs boson tends to be smaller than about 10% [401]. This restriction can be alleviated in the NMSSM or more general two Higgs doublet models. CP -violating effects can still be significant in the heavy Higgs sector. For instance, the Higgs bosons H_2 and H_3 may be admixtures of CP -even and CP -odd scalars, and therefore both may be able to decay into pairs of weak gauge bosons. The observation of such decays would be a clear signal of CP -violation. In the MSSM, the proximity of the masses of H_2 and H_3 makes the measurement of such effect quite challenging, but in generic two Higgs doublet models, the mass splitting between the two heavy mass eigenstates may become larger, facilitating the detection of CP -violating effects at collider experiments [402].

11.6.5 Non-supersymmetric extensions of the Higgs sector

There are many ways to extend the minimal Higgs sector of the SM. In the preceding sections the phenomenology of SUSY Higgs sectors is considered, which at tree level implies a constrained type-II 2HDM (with restrictions on the Higgs boson masses and couplings). In the following discussion, more generic 2HDM's are presented (for some comprehensive reviews, see the reviews [403]). These models are theoretically less compelling since they do not provide an explanation for the SM Higgs naturalness problem, but can lead to different patterns of Higgs-fermion couplings, hence, to different phenomenology. It is also possible to consider models with a SM Higgs boson and one or more additional scalar $SU(2)$ doublets that acquire no VEV and hence play no role in the EWSB mechanism. Such models are dubbed Inert Higgs Doublet Models (IHD) [404]. Without a VEV associated to it, a Higgs boson from an inert doublet has no tree-level coupling to gauge bosons and hence cannot decay into a pair of them. Moreover, imposing a Z_2 symmetry that prevents them from coupling to the fermions, it follows that, if the lightest inert Higgs boson is neutral, it becomes a good DM candidate with interesting associated collider signals. Various studies of IHD models in the light of a 125 GeV Higgs boson have been performed, see for instance Ref. [405], showing an interesting interplay between collider and direct DM detection signals.

An interesting type of 2HDMs are those in which an Abelian flavour symmetry broken at the electroweak scales creates the fermion mass hierarchies and mixing angles [406]. This idea is based on the Froggatt–Nielsen model [407], where a flavon field couples differently to the SM fermions of different flavour charges. Such flavon acquires a vacuum expectation value, breaking the flavour symmetry but leaving both the flavour breaking and the new physics scales undetermined. In Refs. [408], it was proposed to relate the flavour breaking scale to the electroweak scale by identifying the flavon with the modulus square of the Higgs field. A 2HDM, however, provides a more compelling realisation of the electroweak scale flavour breaking idea. In the most ambitious constructions of two Higgs doublet flavour models (2HDFM), the textures of the Yukawa couplings are a result of an Abelian flavour symmetry that only allows renormalisable Yukawa couplings of the top quark to the Higgs bosons. All other Yukawa couplings are generated by higher dimensional operators that produce hierarchical entries of the Yukawa matrices, explaining the observed quark masses and mixing angles. Flavour observables, LHC Higgs signal strength measurements, electroweak precision measurements, unitarity and perturbativity bounds, as well as collider searches for new scalar resonances result in precise predictions for the parameters of these 2HDFMs. In particular, correlated departures from SM Higgs boson couplings, as well as additional Higgs bosons with masses < 700 GeV must be observed at the LHC. Other incarnations of 2HDFMs can aim at only partially explaining the fermion mass hierarchies but are therefore less restrictive.

Other extensions of the Higgs sector can include multiple copies of $SU(2)_L$ doublets [409], additional Higgs singlets [410], triplets or more complicated combinations of Higgs multiplets. It is also possible to enlarge the gauge symmetry beyond $SU(2)_L \times U(1)_Y$

along with the necessary Higgs field structure to generate gauge boson and fermion masses. There are two main experimental constraints on these extensions: (i) precision measurements which constrain $\rho = m_W^2/(m_Z^2 \cos^2 \theta_W)$ to be very close to 1 and (ii) flavour changing neutral current (FCNC) effects. In electroweak models based on the SM gauge group, the tree-level value of ρ is determined by the Higgs multiplet structure. By suitable choices for the hypercharges, and in some cases the mass splitting between the charged and neutral Higgs sector or the vacuum expectation values of the Higgs fields, it is possible to obtain a richer combination of singlets, doublets, triplets and higher multiplets compatible with precision measurements. Concerning the constraints coming from FCNC effects, the Glashow–Weinberg (GW) criterion [411] states that, in the presence of multiple Higgs doublets, the tree-level FCNC's mediated by neutral Higgs bosons will be absent if all fermions of a given electric charge couple to no more than one Higgs doublet. An alternative way of suppressing FCNC in a two Higgs doublet model has been considered in Ref. [412], where it is shown that it is possible to have tree level FCNC completely fixed by the CKM matrix, as a result of an Abelian symmetry.

There is a lot of activity on the study of non-supersymmetric models with an extended Higgs sector with an intense collaboration between theorists and experimentalists, in particular inside the LHC Higgs Working Group [373].

11.6.5.1 Two-Higgs-doublet models

General two Higgs doublet models [403] can have a more diverse Higgs-fermion coupling structure than in SUSY, and can be viewed as a simple extension of the SM to realise the spontaneous breakdown of $SU(2)_L \times U(1)_Y$ to $U(1)_{\text{em}}$. Quite generally, if the two Higgs doublets contain opposite hypercharges, the scalar potential will contain mixing mass parameters of the kind $m_{12}^2 \Phi_1^T i\sigma_2 \Phi_2 + h.c.$. In the presence of such terms, both Higgs doublets will acquire vacuum expectation values, $v_1/\sqrt{2}$ and $v_2/\sqrt{2}$, respectively, and the gauge boson masses will keep their SM expressions with the Higgs VEV v replaced by $\sqrt{v_1^2 + v_2^2}$. Apart from the mass terms, the most generic renormalisable and gauge invariant scalar potential for two Higgs doublets with opposite hypercharges contains seven quartic couplings, as presented in Eq. (11.38).

Just as in the MSSM case, after electroweak symmetry breaking and in the absence of CP -violation, the physical spectrum contains a pair of charged Higgs bosons H^\pm , a CP -odd Higgs boson A and two neutral CP -even Higgs bosons, h and H . The angles α and β diagonalise the CP -even, and the CP -odd and charged Higgs sectors, respectively. The complete 2HDM is defined only after considering the interactions of the Higgs fields to fermions. Yukawa couplings of the generic form

$$- h_{ij}^a \bar{\Psi}_L^i H_a \Psi_R^j + h.c. \quad (11.46)$$

may be added to the renormalisable Lagrangian of the theory. Contrary to the SM, the two Higgs doublet structure does not ensure the alignment of the fermion mass terms $m_{ij} = h_{ij}^a v_a/\sqrt{2}$ with the Yukawa couplings h_{ij}^a . This implies that quite generally the neutral Higgs boson will mediate flavour changing interactions between the different mass eigenstates of the fermion fields. Such flavour changing interactions should be suppressed in order to describe properly the Kaon, D and B meson phenomenology. Based on the Glashow–Weinberg criterion, it is clear that the simplest way of avoiding such transitions is to assume the existence of a symmetry that ensures the couplings of the fermions of each given quantum number (up-type and down-type quarks, charged and neutral leptons) to only one of the two Higgs doublets. Different models may be defined depending on which of these fermion fields couple to a given Higgs boson, see Table 11.9. Models of type-I are those in which all SM fermions couple to a single Higgs field. In type-II models, down-type quarks and charged leptons couple to a common Higgs field, while the up-type quarks and neutral leptons couple to the other. In models of type-III (lepton-specific), quarks couple to one of the Higgs bosons, while leptons couple to the other. Finally, in models of type-IV (flipped), up-type quarks and charged leptons couple to one of the Higgs fields

while down-quarks and neutral leptons couple to the other.

Table 11.9: Higgs boson couplings to up, down and charged lepton-type $SU(2)_L$ singlet fermions in the four discrete types of 2HDM models that satisfy the Glashow–Weinberg criterion.

Model	2HDM I	2HDM II	2HDM III	2HDM IV
u	Φ_2	Φ_2	Φ_2	Φ_2
d	Φ_2	Φ_1	Φ_2	Φ_1
e	Φ_2	Φ_1	Φ_1	Φ_2

The two Higgs doublet model phenomenology depends strongly on the size of the mixing angle α and therefore on the quartic couplings. For large values of m_A , $\sin \alpha \rightarrow -\cos \beta$, $\cos \alpha \rightarrow \sin \beta$, $\cos(\beta - \alpha) \rightarrow 0$, and the lightest CP -even Higgs boson h behaves as the SM Higgs boson. The same behaviour is obtained if the quartic couplings are such that $\mathcal{M}_{12}^2 \sin \beta = -(\mathcal{M}_{11}^2 - m_h^2) \cos \beta$. The latter condition represents a situation in which the couplings of h to fermions and weak gauge bosons become the same as in the SM, without decoupling the rest of the non-standard scalars and it is of particular interest due to the fact that the discovered Higgs boson has SM-like properties. This situation will be referred to as alignment, as in the MSSM case.

In analogy to the effects of CP violation in the SUSY 2HDM, some parameters of the Higgs potential can be complex and one has a model that is explicitly CP violating. The three neutral mass eigenstates mixed with each other and the Higgs phenomenology is analogous to the one described for the SUSY case above, with the caveat that when considering the neutral Higgs boson couplings to the scalar and pseudoscalar fermion bilinear densities, the proper weight should be considered for the respective 2HDM's.

In type-II Higgs doublet models, at large values of $\tan \beta$ and moderate values of m_A , the non-standard Higgs bosons H , A and H^\pm couple strongly to bottom quarks and τ leptons. Hence, the decay modes of the non-standard Higgs bosons tend to be dominated by the b -quark and τ -lepton modes, including top quarks or neutrinos in the case of the charged Higgs boson. However, for large and negative values of λ_4 , the charged Higgs boson mass may be sufficiently heavy to allow on-shell decays $H^\pm \rightarrow W^\pm + (H, A)$, via a trilinear coupling

$$g_{H^\pm W^\mp H, A} \simeq \frac{M_W}{v} \sin(\beta - \alpha)(p_{H^+} - p_{H, A}), \quad (11.47)$$

where p_{H^+} and $p_{H, A}$ are the charged and neutral scalar Higgs boson momenta pointing into the vertex. On the other hand, for large and positive values of λ_5 , the above charged Higgs boson decay into a W^\pm and the CP -odd Higgs boson may be allowed, but the heavy Higgs boson H may be sufficiently heavy to decay into a CP -odd Higgs boson and an on-shell Z , $H \rightarrow Z + A$, via

$$g_{HZ A} \simeq \frac{M_Z}{v} \sin(\beta - \alpha)(p_H - p_A). \quad (11.48)$$

The decay $H^\pm \rightarrow W^\pm + H$, on the other hand may be allowed only if $\lambda_4 < -\lambda_5$. The couplings controlling all the above decay modes are proportional to $\sin(\beta - \alpha)$ and therefore they are unsuppressed in the alignment limit. Moreover, these could still be the dominant decay modes at moderate values of $\tan \beta$, offering a way to evade the current bounds obtained assuming a dominant decay into b -quarks or τ -leptons.

The quartic couplings are restricted by the condition of stability of the effective potential as well as by the restriction of obtaining the proper value of the lightest CP -even Higgs boson mass. Close to the alignment limit, the lightest CP -even Higgs boson mass becomes

$$m_h^2 \simeq v^2(\lambda_1 \cos^4 \beta + \lambda_2 \sin^4 \beta + 2\tilde{\lambda}_3 v^2 \cos^2 \beta \sin^2 \beta + 4\lambda_6 \cos^3 \beta \sin \beta + 4\lambda_7 \sin^3 \beta \cos \beta), \quad (11.49)$$

where $\tilde{\lambda}_3 = \lambda_3 + \lambda_4 + \lambda_5$.

The stability conditions imply the positiveness of all masses, as well as the avoidance of run-away solutions to large negative values of the fields in the scalar potential. These conditions imply

$$\begin{aligned} \lambda_1 &\geq 0, \quad \lambda_2 \geq 0, \quad \lambda_3 + \lambda_4 - |\lambda_5| \geq -\sqrt{\lambda_1 \lambda_2}, \quad \lambda_3 \geq -\sqrt{\lambda_1 \lambda_2}, \\ 2|\lambda_6 + \lambda_7| &< \frac{\lambda_1 + \lambda_2}{2} + \tilde{\lambda}_3, \end{aligned} \quad (11.50)$$

where the first four conditions are necessary and sufficient conditions in the case of $\lambda_6 = \lambda_7 = 0$, while the last one is a necessary condition in the case all couplings are non-zero. Therefore, to obtain the conditions that allow the decays $H^\pm \rightarrow W^\pm H$, A and $H \rightarrow ZA$, λ_3 should take large positive values in order to compensate for the effects of λ_4 and λ_5 . For more detailed discussions about 2HDM phenomenology, see for example Refs. [40, 403].

11.6.5.2 Higgs triplets

Electroweak triplet scalars are the simplest non-doublet extension of the SM that can participate in the spontaneous breakdown of $SU(2)_L \times U(1)_Y$ to $U(1)_{em}$. Two types of model have been developed in enough detail to make a meaningful comparison to LHC data: the Higgs triplet model (HTM) [413] and the Georgi–Machacek model (GM) [414].

The Higgs triplet model extends the SM by the addition of a complex $SU(2)_L$ triplet scalar field Δ with hypercharge $Y = 2$, and a general gauge-invariant renormalisable potential $V(\Phi, \Delta)$ for Δ and the SM Higgs doublet Φ . The components of the triplet field can be parameterised as

$$\Delta = \frac{1}{\sqrt{2}} \begin{pmatrix} \Delta^+ & \sqrt{2}\Delta^{++} \\ v_\Delta + \delta + i\xi & -\Delta^+ \end{pmatrix}. \quad (11.51)$$

where Δ^+ is a singly-charged field, Δ^{++} is a doubly-charged field, δ is a neutral CP -even scalar, ξ is a neutral CP -odd scalar, and v_Δ is the triplet VEV. The general scalar potential mixes the doublet and triplet components. After electroweak symmetry breaking there are seven physical mass eigenstates, denoted $H^{\pm\pm}$, H^\pm , A , H , and h .

A distinguishing feature of the HTM is that it violates the custodial symmetry of the SM; thus the ρ parameter deviates from 1 even at tree level. Letting x denote the ratio of triplet and doublet VEVs, the tree level expression is

$$\rho = \frac{1 + 2x^2}{1 + 4x^2}. \quad (11.52)$$

The measured value of the ρ parameter then limits the triplet VEV to be quite small, $x \lesssim 0.03$, or $v_\Delta < 8$ GeV. This constraint severely limits the role of the triplet scalar in the EWSB mechanism.

The small VEV of the Higgs triplet in the HTM is a virtue from the point of view of generating neutrino masses without the necessity for introducing right-handed neutrino fields. The gauge invariant dimension four interaction

$$h_{\nu_{ij}} \ell_i^T C^{-1} i\sigma_2 \Delta \ell_j, \quad (11.53)$$

where ℓ_i are the lepton doublets, C is the charge conjugation matrix, and $h_{\nu_{ij}}$ is a complex symmetric coupling matrix, generates a Majorana mass matrix for the neutrinos:

$$m_{\nu_{ij}} = \sqrt{2} h_{\nu_{ij}} v_\Delta. \quad (11.54)$$

This can be combined with the usual neutrino seesaw to produce what is known as the type-II seesaw [415].

The HTM suggests the exciting possibility of measuring parameters of the neutrino mass matrix at the LHC. If the doubly-charged Higgs boson is light enough and/or its couplings to W^+W^+ are sufficiently suppressed, then its primary decay is into same-sign lepton pairs: $H^{++} \rightarrow \ell_i^+ \ell_j^+$; from Eq. (11.53) and Eq. (11.54), it is apparent that these decays are in general lepton-flavour violating with branchings proportional to elements of the neutrino mass matrix [416].

Precision electroweak data constrain the mass spectrum as well as the triplet VEV of the HTM [417]. These constraints favour a spectrum where H^{++} is the lightest of the exotic bosons, and where the mass difference between H^+ and H^{++} is a few hundred GeV. The favoured triplet VEV is a few GeV, which also favours H^{++} decays into W^+W^+ over same-sign dileptons.

The GM model addresses the ρ parameter constraint directly by building in a custodial symmetry (it was however argued that large corrections to $\rho = 1$ are generated at one-loop [418], requiring some fine-tuning to preserve agreement with EW precision data). Writing the complex scalar doublet of the SM as a $(2, 2)$ under $SU(2)_L \times SU(2)_R$, it is obvious that the next simplest construction respecting custodial symmetry is a scalar transforming like a $(3, 3)$ [419]. These nine real degrees of freedom correspond to a complex electroweak triplet combined with a real triplet, with the scalar potential required to be invariant under $SU(2)_R$. Under the custodial $SU(2)_{L+R}$, they transform as $1 \oplus 3 \oplus 5$, with a CP -even neutral scalar as the custodial singlet (thus matching the SM Higgs boson), a CP -odd neutral scalar in the custodial triplet, and another CP -even neutral scalar in the custodial 5-plet.

The scalar components can be decomposed as

$$\Xi = \begin{pmatrix} \chi_3^* & \xi_1 & \chi_1 \\ -\chi_2^* & \xi_2 & \chi_2 \\ \chi_1^* & -\xi_1^* & \chi_3 \end{pmatrix}, \quad (11.55)$$

where ξ_2 is a real scalar and the others are complex scalars. Linear combinations of these scalars account for the neutral custodial singlet, a neutral and singly-charged field making up the custodial triplet, and neutral, singly-charged, and doubly-charged fields making up the custodial 5-plet.

When combined with the usual SM doublet field Φ , the electroweak scale v is now related to the doublet and triplet VEVs by

$$v^2 = v_\Phi^2 + 8v_\Xi^2. \quad (11.56)$$

Note that the GM triplets by themselves are sufficient to explain electroweak symmetry breaking and the existence of a 125 GeV neutral boson along with a custodial triplet of Goldstone bosons; the complex doublet field in the GM model is required to generate fermion masses via the usual dimension four Yukawa couplings. This raises the question of whether one can rule out the possibility that the 125 GeV boson is the neutral member of a custodial 5-plet rather than a custodial singlet, without invoking decays to fermions. A conclusive answer is given by observing that the ratio of the branching fractions to W versus Z bosons is completely determined by the custodial symmetry properties of the boson. For a custodial 5-plet, the ratio of the signal strength to WW over that to ZZ is predicted to be $1/4$ that of a SM Higgs boson [419], and thus already ruled out by the experimental results presented in Section 11.5.

Another interesting general feature of Higgs triplet models is that, after mixing, the SM-like neutral boson can have stronger couplings to WW and ZZ than predicted by the SM [420]; this is in contrast to mixing with additional doublets and singlet, which can only reduce the WW and ZZ couplings versus the SM. This emphasises that LHC Higgs data cannot extract model independent coupling strengths for the Higgs boson [291].

Because of the built-in custodial symmetry, the triplet VEV in the GM model can be large compared to the doublet VEV. The custodial singlet neutral boson from the triplets mixes with the neutral boson from the doublet. Two interesting special cases are (i) the triplet VEV is small and the 125 GeV boson is SM-like except for small deviations, and (ii) the 125 GeV boson is mostly the custodial singlet neutral boson from the electroweak triplets. The phenomenology of the doubly-charged and singly-charged bosons is similar to that of the HTM. The constraints on the GM model from precision electroweak data, LEP data, and current LHC data are summarised in Ref. [40].

11.6.6 Composite Higgs models

Within the SM, EWSB is posited but has no dynamical origin. Furthermore, the Higgs boson appears to be unnaturally light. A scenario that remedies these two catches is to consider the Higgs boson as a bound state of new dynamics becoming strong around

the weak scale. The Higgs boson can be made significantly lighter than the other resonances of the strong sector if it appears as a pseudo-Nambu–Goldstone boson, see Refs. [11] for reviews.

11.6.6.1 Little Higgs models

The idea behind the Little Higgs boson models [421] is to identify the Higgs doublet as a (pseudo) Nambu–Goldstone boson while keeping some sizeable non-derivative interactions, in particular a largish Higgs quartic interaction. By analogy with QCD where the pions $\pi^{\pm,0}$ appear as Nambu–Goldstone bosons associated to the breaking of the chiral symmetry $SU(2)_L \times SU(2)_R/SU(2)$, switching on some interactions that break explicitly the global symmetry will generate masses for the would-be massless Nambu–Goldstone bosons of the order of $g\Lambda_{G/H}/(4\pi)$, where g is the coupling of the symmetry breaking interaction and $\Lambda_{G/H} = 4\pi f_{G/H}$ is the dynamical scale of the global symmetry breaking G/H . In the case of the Higgs boson, the top Yukawa interaction or the gauge interactions themselves will certainly break explicitly (part of) the global symmetry since they act non-linearly on the Higgs boson. Therefore, obtaining a Higgs boson mass around 125 GeV would demand a dynamical scale $\Lambda_{G/H}$ of the order of 1 TeV, which is known to lead to too large oblique corrections. Raising the strong dynamical scale by at least one order of magnitude requires an additional selection rule to ensure that a Higgs boson mass is generated at the 2-loop level only

$$m_H^2 = \frac{g^2}{16\pi^2} \Lambda_{G/H}^2 \rightarrow m_H^2 = \frac{g_1^2 g_2^2}{(16\pi^2)^2} \Lambda_{G/H}^2. \quad (11.57)$$

The way to enforce this selection rule is through a “collective breaking” of the global symmetry:

$$\mathcal{L} = \mathcal{L}_{G/H} + g_1 \mathcal{L}_1 + g_2 \mathcal{L}_2. \quad (11.58)$$

Each interaction \mathcal{L}_1 or \mathcal{L}_2 individually preserves a subset of the global symmetry such that the Higgs boson remains an exact Nambu–Goldstone boson whenever either g_1 or g_2 is vanishing. A mass term for the Higgs boson can be generated only by diagrams involving simultaneously both interactions. At one-loop, such diagrams are not quadratically divergent, so the Higgs boson mass is not UV sensitive. Explicitly, the cancellation of the SM quadratic divergences is achieved by a set of new particles around the Fermi scale: gauge bosons, vector-like quarks, and extra massive scalars, which are related, by the original global symmetry, to the SM particles with the same spin. Contrary to SUSY, the cancellation of the quadratic divergences is achieved by same-spin particles. These new particles, with definite couplings to SM particles as dictated by the global symmetries of the theory, are perfect goals for the LHC.

The simplest incarnation of the collective breaking idea, the so-called littlest Higgs boson model, is based on a non-linear σ -model describing the spontaneous breaking $SU(5)$ down to $SO(5)$. A subgroup $SU(2)_1 \times U(1)_1 \times SU(2)_2 \times U(1)_2$ is weakly gauged. This model contains a weak doublet, that is identified with the Higgs doublet, and a complex weak triplet whose mass is not protected by collective breaking. Other popular little Higgs models are based on different coset spaces: minimal moose ($SU(3)^2/SU(3)$), the simplest little Higgs ($SU(3)^2/SU(2)^2$), the bestest little Higgs ($SO(6)^2/SO(6)$). For comprehensive reviews, see Ref. [422].

Generically, oblique corrections in Little Higgs models are reduced either by increasing the coupling of one of the gauge groups (in the case of product group models) or by increasing the masses of the W and Z partners, leading ultimately to a fine-tuning of the order of a few percents (see for instance Ref. [423] and references therein). The compatibility of Little Higgs models with experimental data is significantly improved when the global symmetry involves a custodial symmetry as well as a T -parity [424] under which, in analogy with R -parity in SUSY models, the SM particles are even and their partners are odd. Such Little Higgs models would therefore appear in colliders as jet(s) with missing transverse energy [425] and the ATLAS and CMS searches for squarks and gluinos can be recast to obtain limits on the masses of the heavy vector-like quarks. The T -even top partner, with an expected mass below 1 TeV to cancel the top loop quadratic divergence without too much fine-tuning, would decay dominantly into

a $t+Z$ pair or into a $b+W$ pair or even into $t+H$. The latest CMS and ATLAS direct searches [426] for vector-like top partners put a lower bound around 1.1–1.3 TeV (for various branching fraction combinations), excluding the most natural region of the parameter space of these models, i.e., imposing a fine-tuning below the percent level.

The motivation for Little Higgs models is to solve the little hierarchy problem, i.e., to push the need for new physics (responsible for the stability of the weak scale) up to around 10 TeV. Per se, Little Higgs models are effective theories valid up to their cut-off scale $\Lambda_{G/H}$. Their UV completions could either be weakly or strongly coupled.

11.6.6.2 Models of partial compositeness

Even in composite models, the Higgs boson cannot appear as a regular resonance of the strong sector without endangering the viability of the setup when confronted to data. The way out is that the Higgs boson appears as a pseudo Nambu–Goldstone boson: the new strongly coupled sector is supposed to be invariant under a global symmetry G spontaneously broken to a subgroup H at the scale f (the typical mass scale of the resonances of the strong sector is $m_\rho \sim g_\rho f$ with g_ρ the characteristic coupling of the strong sector). To avoid conflict with EW precision measurements, the strong interactions themselves should better not break the EW symmetry. Hence the SM gauge symmetry itself should be contained in H . See Table 11.10 for a few examples of coset spaces.

Table 11.10: Global symmetry breaking patterns and the corresponding Goldstone boson contents of the SM, the minimal composite Higgs model, the next to minimal composite Higgs model, and the minimal composite two Higgs doublet model. Note that the SU(3) model does not have a custodial invariance. a denotes a CP -odd scalar while h and H are CP -even scalars.

Model	Symmetry Pattern	Goldstones
SM	SO(4)/SO(3)	W_L, Z_L
–	SU(3)/SU(2)×U(1)	W_L, Z_L, H
MCHM	SO(5)/SO(4)	W_L, Z_L, H
NMCHM	SO(6)/SO(5)	W_L, Z_L, H, a
MC2HM	SO(6)/SO(4)×SO(2)	W_L, Z_L, h, H, H^\pm, a

The SM (light) fermions and gauge bosons cannot be part of the strong sector itself since LEP data have already put stringent bounds on the compositeness scale of these particles far above the TeV scale. The gauge bosons couple to the strong sector by a weak gauging of a SU(2)×U(1) subgroup of the global symmetry G . Inspiration for the construction of such models comes from the AdS/CFT correspondence: the components of a gauge field along an extra warped space dimension can be interpreted as the Goldstone bosons resulting from the breaking of global symmetry of the strong sector. The couplings of the SM fermions to the strong sector could a priori take two different forms:

- (i) a bilinear coupling of two SM fermions to a composite scalar operator, \mathcal{O} , of the form $\mathcal{L} = y \bar{q}_L u_R \mathcal{O} + h.c.$, in simple analogy with the SM Yukawa interactions. This is the way fermion masses were introduced in technicolor theories and it generically comes with severe flavour problems and calls for extended model-building gymnastics [12] to circumvent them;
- (ii) a linear mass mixing with fermionic vector-like operators: $\mathcal{L} = \lambda_L \bar{q}_L \mathcal{Q}_R + \lambda_R \bar{U}_L u_R$. \mathcal{Q} and \mathcal{U} are two fermionic composite operators of mass M_Q and M_U .

Being part of the composite sector, the composite fermionic operators can have a direct coupling of generic order Y_* to the Higgs boson. In analogy with the photon- ρ mixing in QCD, once the linear mixings are diagonalised, the physical states are a linear combination of elementary and composite fields. Effective Yukawa couplings are generated and read for instance for the up-type quark

$$y = Y_* \sin \theta_L \sin \theta_R \quad (11.59)$$

where $\sin \theta_i = \lambda_i / \sqrt{M_{Q,U}^2 + \lambda_i^2}$, $i = L, R$, measure the amount of compositeness of the SM left- and right-handed up-type quark. If the strong sector is flavour-anarchic, i.e., if the couplings of the Higgs boson to the composite fermions does not exhibit any particular flavour structure, the relation Eq. (11.59) implies that the light fermions are mostly elementary states ($\sin \theta_i \ll 1$), while the third generation quarks need to have a sizable degree of compositeness. The partial compositeness paradigm offers an appealing dynamical explanation of the hierarchies in the fermion masses. In fact, assuming the strong sector to be almost conformal above the confinement scale, the low-energy values of the mass-mixing parameters $\lambda_{L,R}$ are determined by the (constant) anomalous dimension of the composite operator they mix with. If the UV scale at which the linear mixings are generated is large, then $\mathcal{O}(1)$ differences in the anomalous dimensions can generate naturally large hierarchies in the fermion masses via renormalisation group running [427]. While the introduction of partial compositeness greatly ameliorated the flavour problem of the original composite Higgs models, nevertheless, it did not solve the issue completely, at least in the case where the strong sector is assumed to be flavour-anarchic [428]. While the partial compositeness set-up naturally emerges in models built in space-times with extra dimensions, no fully realistic microscopic realisation of partial compositeness has been proposed in the literature.

Another nice aspect of the partial compositeness structure is the dynamical generation of the Higgs potential that is not arbitrary like in the SM. The Higgs boson being a pseudo-Nambu–Goldstone boson, its mass does not receive any contribution from the strong sector itself but it is generated at the one-loop level via the couplings of the SM particles to the strong sector since these interactions are breaking the global symmetries under which the Higgs doublet transforms non-linearly. Obtaining $v \ll f$, as required phenomenologically, requires some degree of tuning, which scales like $\xi \equiv v^2/f^2$. A mild tuning of the order of 10% ($\xi \approx 0.1$) is typically enough to comply with electroweak precision constraints. This is an important point: in partial compositeness models, the entire Higgs potential is generated at one loop, therefore the separation between v and f can only be obtained at a price of a tuning. This marks a difference with respect to the Little Higgs models which realise a parametric hierarchy between the quartic and mass terms through the collective symmetry breaking mechanism. In fact in Little Higgs models, the quartic coupling is a tree-level effect, leading to a potential

$$V(H) \approx \frac{g_{\text{SM}}^2}{16\pi^2} m_\rho^2 H^2 + g_{\text{SM}}^2 H^4, \quad (11.60)$$

where g_{SM} generically denotes the SM couplings. The minimisation condition reads $v^2/f^2 \sim g_\rho^2/(16\pi^2)$, therefore v is formally loop suppressed with respect to f . This is the major achievement of the Little Higgs constructions, which however comes at the price of the presence of sub-TeV vectors carrying EW quantum numbers and therefore giving rise generically to large oblique corrections to the propagators of the W and the Z gauge bosons.

After minimisation, the dynamically generated potential leads to an estimate of the Higgs boson mass as

$$m_H^2 \approx g_\rho^3 y_t 2\pi^2 v^2. \quad (11.61)$$

It follows that the limit $f \rightarrow \infty$, i.e., $\xi \rightarrow 0$, is a true decoupling limit: all the resonances of the strong sector become heavy but the Higgs boson whose mass is protected by the symmetries of the coset G/H . When compared to the experimentally measured Higgs boson mass, this estimate puts an upper bound on the strength of the strong interactions: $g_\rho \lesssim 2$. In this limit of not so large coupling, the Higgs potential receives additional contributions. In particular, the fermionic resonances in the top sector which follow from the global symmetry structure of the new physics sector can help raising the Higgs boson mass. Using some dispersion relation techniques, the mass of the Higgs is connected to the resonance masses. In the minimal SO(5)/SO(4) model, it was shown [429] that a 125 GeV mass can be obtained if at least one of the fermionic resonances is lighter than $\sim 1.4f$. As in SUSY scenarios, the top sector is playing a crucial role in the

dynamics of EWSB and can provide the first direct signs of new physics. The direct searches for these top partners, in particular the ones with exotic electric charges $5/3$, are already exploring the natural parameter spaces of these models [430].

The main physics properties of a pseudo Nambu–Goldstone Higgs boson can be captured in a model-independent way by a small number of higher-dimensional operators. Indeed, the strong dynamics at the origin of the composite Higgs boson singles out a few operators among the complete list discussed earlier in Section 11.5: these are the operators that involve extra powers of the Higgs doublets, and they are therefore generically suppressed by a factor $1/f^2$ as opposed to the operators that involve extra derivatives or gauge bosons that are suppressed by a factor $1/(g_\rho^2 f^2)$. The relevant effective Lagrangian describing a strongly interacting light Higgs boson is:

$$\begin{aligned} \mathcal{L}_{\text{SILH}} = & \frac{c_H}{2f^2} (\partial_\mu (\Phi^\dagger \Phi))^2 + \frac{c_T}{2f^2} (\Phi^\dagger \overleftrightarrow{D}^\mu \Phi)^2 - \frac{c_6 \lambda}{f^2} (\Phi^\dagger \Phi)^3 \\ & + \left(\sum_f \frac{c_f y_f}{f^2} \Phi^\dagger \Phi \bar{f}_L \Phi f_R + \text{h.c.} \right). \end{aligned} \quad (11.62)$$

Typically, these new interactions induce deviations in the Higgs boson couplings that scale like $\mathcal{O}(v^2/f^2)$. Hence, the measurements of the Higgs boson couplings can be translated into some constraints on the compositeness scale, $4\pi f$, of the Higgs boson. The peculiarity of these composite models is that, due to the Goldstone nature of the Higgs boson, the direct couplings to photons and gluons are further suppressed and generically the coupling modifiers scale like

$$\begin{aligned} \kappa_{W,Z,f} & \sim 1 + \mathcal{O}\left(\frac{v^2}{f^2}\right), \quad \kappa_{Z\gamma} \sim \mathcal{O}\left(\frac{v^2}{f^2}\right), \\ \kappa_{\gamma,g} & \sim \mathcal{O}\left(\frac{v^2}{f^2} \times \frac{y_t^2}{g_\rho^2}\right), \end{aligned} \quad (11.63)$$

where g_ρ denotes the typical coupling strength among the states of the strongly coupled sector and y_t is the top Yukawa coupling, the largest interaction that breaks the Goldstone symmetry. The $\kappa_{Z\gamma,\gamma,g}$ coupling modifiers are not generated by the strong coupling operators of Eq. (11.62) but by some subleading form-factor operator generated by loops of heavy resonances of the strong sector. The coupling modifiers also receive additional contributions from the other resonances of the strong sector, in particular the fermionic resonances of the top sector that are required to be light to generate a 125 GeV Higgs boson mass. Some indirect information on the resonance spectrum could thus be inferred by a precise measurement of the Higgs boson coupling deviations. However, it was realised, see in particular Ref. [306], that the task is actually complicated by the fact that, in the minimal models, these top partners give a contribution to both κ_t (resulting from a modification of the top Yukawa coupling) and κ_γ and κ_g (resulting from new heavy particles running into the loops) and the structure of interactions is such that the net effect vanishes for inclusive quantities like $\sigma(gg \rightarrow H)$ or $\Gamma(H \rightarrow \gamma\gamma)$ as a consequence of the Higgs low energy theorem [21, 22, 301]. So, one would need to rely on differential distribution, like the Higgs boson p_T distribution discussed in Section 11.2.4.1, to see the top partner effects in Higgs data [431]. The off-shell channel $gg \rightarrow H^* \rightarrow 4l$ [290] and the double Higgs boson production $gg \rightarrow HH$ [432] can also help to resolve the gluon loop and separate the top and top-partner contributions.

11.6.6.3 Minimal composite Higgs models

The minimal composite Higgs models (MCHM) are concrete examples of the partial compositeness paradigm. The Higgs doublet is described by the coset space $\text{SO}(5)/\text{SO}(4)$ where a subgroup $\text{SU}(2)_L \times \text{U}(1)_Y$ is weakly gauged and under which the four Goldstone bosons transform as a doublet of hypercharge 1. There is some freedom on how the global symmetry is acting on the SM fermions: in MCHM4 the quarks and leptons are embedded into spinorial representations of $\text{SO}(5)$, while in MCHM5

they are part of fundamental representations (it might also be interesting phenomenologically to consider larger representations like MCHM14 [433] with the SM fermions inside a representation of dimension 14). It is also possible to consider that fermions of different chirality and flavour are in different representations of $\text{SO}(5)$, leading to a more varied phenomenology [434]. The non-linearly realised symmetry acting on the Goldstone bosons leads to general predictions of the coupling of the Higgs boson to the EW gauge bosons. For instance, it can be shown that the quadratic terms in the W and Z bosons read

$$m_W^2(H) \left(W_\mu W^\mu + \frac{1}{2 \cos^2 \theta_W} Z_\mu Z^\mu \right), \quad (11.64)$$

with $m_W(H) = \frac{gf}{2} \sin \frac{H}{f}$. Expanding around the EW vacuum, the expression of the weak scale is $v = f \sin(\langle H \rangle / f)$. And the values of the modified Higgs boson couplings to the W and Z become:

$$g_{HVV} = \frac{2m_V^2}{v} \sqrt{1 - v^2/f^2}, \quad g_{HHVV} = \frac{2m_V^2}{v^2} (1 - 2v^2/f^2). \quad (11.65)$$

Note that the Higgs boson couplings to gauge bosons is always suppressed compared to the SM prediction. This is a general result [435] that holds as long as the coset space is compact.

The Higgs boson couplings to the fermions depend on the representation which the SM fermions are embedded into. The most commonly used embeddings consider all fermion doublets and singlets in the same representations. While, in MCHM4 and MCHM5, the modifications of the couplings depend only on the Higgs boson compositeness scale, in MCHM14 the leading corrections depend also on the mass spectrum of the resonances [433]. This is due to the fact that more than one $\text{SO}(5)$ invariant gives rise to SM fermion masses. The (κ_V, κ_f) experimental fit of the Higgs boson couplings can be used to derive a lower bound on the Higgs boson compositeness scale $4\pi f \gtrsim 9 \text{ TeV}$, which is less stringent than the indirect bound obtained from EW precision data, $4\pi f \gtrsim 15 \text{ TeV}$ [436] but more robust and less subject on assumptions [437].

11.6.6.4 Twin Higgs models

In all composite models presented above, the particles responsible for canceling the quadratic divergences in the Higgs boson mass are charged under the SM gauge symmetries. In particular, the top partner carries color charge, implying a reasonably large minimal production cross section at the LHC. An alternative scenario, which is experimentally quite challenging and might explain the null result in various new physics searches, is the case nowadays referred to as “neutral naturalness” [13, 14], where the particles canceling the 1-loop quadratic divergences are neutral under the SM. The canonical example for such theories is the Twin Higgs model of Ref. [13]. This is an example of a pseudo-Goldstone boson model with an approximate global $\text{SU}(4)$ symmetry broken to $\text{SU}(3)$. The Twin Higgs model is obtained by gauging the $\text{SU}(2)_A \times \text{SU}(2)_B$ subgroup of $\text{SU}(4)$, where $\text{SU}(2)_A$ is identified with the SM $\text{SU}(2)_L$, while $\text{SU}(2)_B$ is the twin $\text{SU}(2)$ group. Gauging this subgroup breaks the $\text{SU}(4)$ symmetry explicitly, but quadratically divergent corrections do not involve the Higgs boson when the gauge couplings of the two $\text{SU}(2)$ subgroups are equal, $g_A = g_B$. The $\text{SU}(4) \rightarrow \text{SU}(3)$ breaking will also result in the breaking of the twin $\text{SU}(2)_B$ group and, as a result, three of the seven Goldstone bosons will be eaten, leaving 4 Goldstone bosons corresponding to the SM Higgs doublet. In fact, imposing the Z_2 symmetry on the full model will ensure the cancellation of all 1-loop quadratic divergences to the Higgs boson mass. Logarithmically divergent terms can, however, arise for example from gauge loops, leading to a Higgs boson mass of order $g^2 f / 4\pi$, which is of the order of the physical Higgs boson mass for $f \sim 1 \text{ TeV}$. The quadratic divergences from the top sector can be eliminated if the Z_2 protecting the Higgs boson mass remains unbroken by the couplings that result in the top Yukawa coupling. This can be achieved by introducing top partners charged under a twin $\text{SU}(3)_C$. In this case, the quadratic divergences are cancelled by top partners that are neutral under the SM gauge symmetries.

Twin Higgs models are low-energy effective theories valid up to a cutoff scale of order $\Lambda \sim 4\pi f \sim 5\text{--}10\text{ TeV}$, beyond which a UV completion has to be specified. The simplest such possibility is to also make the Higgs boson composite, and to UV complete the twin Higgs model via gauge and top partners at masses of the order of a few TeV. A concrete implementation is the holographic twin Higgs model [438], which also incorporates a custodial symmetry to protect the T -parameter from large corrections. It is based on a warped extra dimensional theory with a bulk $\text{SO}(8)$ gauge group, which incorporates the $\text{SU}(4)$ global symmetry discussed above enlarged to contain the $\text{SU}(2)_L \times \text{SU}(2)_R$ custodial symmetry. In addition, the bulk contains either a full $\text{SU}(7)$ group or an $\text{SU}(3) \times \text{SU}(3) \times \text{U}(1) \times \text{U}(1) \times \text{Z}_2$ subgroup of it to incorporate the QCD, its twin, and the hypercharge local symmetries. The breaking on the UV brane is to the SM symmetries and their twin symmetries, while on the IR brane $\text{SO}(8) \rightarrow \text{SO}(7)$, giving rise to the 7 Goldstone bosons, three of which will be again eaten by the twin W, Z . The main difference compared to ordinary composite Higgs models is that, in composite twin Higgs models, the cancellation of the one-loop quadratic divergences is achieved by the twin partners. They have a mass of order $700\text{ GeV--}1\text{ TeV}$ and they are uncharged under the SM gauge group. This allows the IR scale of the warped extra dimension to be raised to the multi-TeV range without reintroducing the hierarchy problem. The role of the composite partners is to UV complete the theory, rather than to cancel the one-loop quadratic divergences. For more details about the composite twin Higgs models, see Refs. [439].

11.6.7 Searches for signatures of extended Higgs sectors

The measurements described in Sections 11.3 to 11.5 have established the existence of one state of the electroweak symmetry breaking sector, compatible with a SM Higgs boson, but not that it is the only one. As was discussed above, several classes of models beyond the SM require extended Higgs sectors. The searches are typically designed to be as model-independent as possible⁷ and can be categorised in the classes summarised as follows:

- (i) the search for an additional CP -even state mostly in the high mass domain decaying to vector bosons, which would correspond either to the heavy CP -even state in a generic 2HDM where the light state would be the discovered Higgs boson at 125 GeV or to a generic additional singlet;
- (ii) the search for a state in the high mass domain decaying to pairs of fermions, which would correspond to the CP -odd A or the heavy CP -even state H in a generic 2HDM;
- (iii) the search for charged Higgs bosons, which also appear in generic 2HDMs;
- (iv) the search for a CP -odd state a in the low mass region which appears in the NMSSM in a variety of final states, e.g., with one or two a bosons decaying to pairs of photons, muons, taus, and b -quarks;
- (v) the search for doubly charged Higgs bosons which are expected in extensions of the Higgs sector with triplets.

Below is a concise description of the most recent searches performed at the LHC and elsewhere. A summary of these searches in terms of final states is given in Table 11.11 where the corresponding references are given for more details.

11.6.7.1 Searches for an additional CP -even state

(a) Exclusion limits from LEP

The searches for the SM Higgs boson at LEP provided an absolute lower limit of 114 GeV on its mass. These searches are also relevant for non-SM Higgs bosons. These searches were interpreted as 95% CL upper bounds on the ratio of the coupling g_{HZZ} to its SM prediction as a function of the Higgs boson mass [139, 523]. These results have an impact on MSSM benchmarks such as the low- m_H scenario where the heavy CP -even Higgs boson is the discovered 125 GeV boson [374], which is also nearly ruled out by

⁷Still, most non-SUSY models are likely to include further states and dynamics above the weak scale to stabilise the scalar sector and this new and unknown physics may influence the searches described in this section in a way difficult to estimate.

current direct constraints and charged Higgs boson limits from LHC. These results also impact scenarios of light CP -even Higgs boson of the NMSSM which are constrained to project predominantly onto the EW singlet component. Additional interest for these scenarios is due to the slight excess observed at LEP [139] at a Higgs boson mass hypothesis of approximately 98 GeV , bolstered by a possible excess in the diphoton channel at 96 GeV in Run-2 data of CMS [445].

(b) Searches at the LHC

At the LHC, the searches for the SM Higgs boson before the 2012 discovery covered a wide range of mass hypotheses up to approximately 1 TeV . After the discovery, the SM Higgs boson searches have been reappraised to search for a heavy CP -even state, extending progressively the search mass range beyond 1 TeV . This state could be the heavy CP -even Higgs boson of a 2HDM, or a generic additional singlet. In both cases, the natural width of the additional H state can be very different from that of the SM Higgs boson. To preserve unitarity of the longitudinal vector boson scattering and the longitudinal vector boson scattering into fermion pairs, the couplings of the additional CP -even Higgs boson to gauge bosons and fermions should not be too large and should constrain the natural width to be smaller than that of a unique Higgs boson at high mass with couplings to fermions and gauge bosons as predicted by the SM (and provided that trilinear and quartic couplings are not too large and that no new state affects the heavy state total width). It is therefore reasonable to consider total widths for the high mass CP -even state smaller than the equivalent SM width. Two specific cases have been considered: (i) the SM width using the complex pole scheme (CPS), and (ii) the narrow width approximation. For the sake of generality, these searches are now done as a function of the Higgs boson mass and total width.

Searches for the Higgs boson in the channels $H \rightarrow \gamma\gamma$, $H \rightarrow Z\gamma$, $H \rightarrow WW^{(*)}$ leptonic and semi-leptonic, and in the $H \rightarrow ZZ^{(*)}$ searches in the 4ℓ , $\ell\ell q\bar{q}$ and $\ell\ell\nu\nu$ channels have also been done, but some of them are simple reinterpretations of the SM Higgs boson search in the CPS scheme. References for these searches are summarised in Table 11.11.

(c) Searches for an additional resonance decaying to a pair of Higgs bosons

In addition to the rare and expected Higgs boson pair production mode, high mass CP -even Higgs bosons can be searched for in the resonant double Higgs boson mode. Searches for such processes, where the Higgs boson is used as a tool for searches for BSM phenomena, have been carried out in a variety of distinct modes depending on the subsequent decays of each Higgs bosons. ATLAS and CMS have searched for the $H \rightarrow hh \rightarrow b\bar{b}\tau\tau$, $b\bar{b}\gamma\gamma$, $H \rightarrow hh \rightarrow 4b$, $H \rightarrow hh \rightarrow \gamma\gamma WW^*$, $H \rightarrow hh \rightarrow b\bar{b}WW^*$, $H \rightarrow hh \rightarrow WW^* WW^*$ and $H \rightarrow hh \rightarrow b\bar{b}ZZ^*$ final states. For mass hypotheses of an additional Higgs boson below 500 GeV , the two dominant search channels are the $b\bar{b}\gamma\gamma$ and the $b\bar{b}\tau\tau$ channels. For masses above 500 GeV , the most powerful search is with the $4b$ final state. As illustrated in Fig. 11.17, these searches provide useful limits in the low $\tan\beta$ and high mass domain. The list of references for these searches is given in Table 11.11.

(d) Searches for an additional state with the presence of the Higgs boson

In the post-discovery era, analyses searching for additional Higgs bosons need to take into account the presence of the 125 GeV Higgs boson. For searches with sufficiently high mass resolution to disentangle the additional states which are not degenerate in mass, the strength of the observed state and limits on the signal strength of a potential additional state can be set independently, as discussed in the next section. However, in some cases where channels do not have a sufficiently fine mass resolution to resolve states nearly degenerate in mass, specific analyses need to be designed. There are two examples of such analyses: (i) the search for an additional state in the $H \rightarrow WW^{(*)} \rightarrow \ell\nu\ell\nu$ channel in ATLAS, and (ii) the search for nearly degenerate states in the $H \rightarrow \gamma\gamma$ channel with the CMS detector.

Table 11.11: Summary of references to the searches for additional states from extended Higgs sectors. (BBr) denotes the BaBar experiment and (TeV), the Tevatron experiments. V denotes either the W or the Z boson. Only Run-2 searches references are indicated except when searches have been carried out using Run-1 data only. References for Run-1 searches are available in Ref. [141].

	ATLAS	CMS	Other experiments
<i>CP-even H</i>			
$H \rightarrow \gamma\gamma$	[440, 441]	[442, 443]	—
$H \rightarrow \gamma\gamma$ (low mass)	[444]	[445]	—
$H \rightarrow Z\gamma$	[446, 447]	[448]	—
$H \rightarrow ZZ \rightarrow 4\ell$	[449]	[450]	—
$H \rightarrow ZZ \rightarrow \ell\ell\nu\nu$	[449]	[451]	—
$H \rightarrow WZ \rightarrow \ell\ell\nu$	—	[452]	—
$H \rightarrow ZZ \rightarrow \ell\ell q\bar{q}$	[453]	[454, 455]	—
$H \rightarrow ZZ \rightarrow \nu\nu q\bar{q}$	[456]	—	—
$H \rightarrow WW \rightarrow \ell\nu\ell\nu$	[457]	[458]	—
$H \rightarrow WW \rightarrow \ell\nu q\bar{q}$	[459]	[458]	—
$H \rightarrow VV \rightarrow q\bar{q}q\bar{q}$ (JJ)	[460, 461]	—	—
$H \rightarrow VV$ combination	[462]	—	—
$H \rightarrow hh \rightarrow b\bar{b}\tau\tau, b\bar{b}\gamma\gamma, 4b,$ $\gamma\gamma WW^*, bbWW^*, WW^*WW^*, bbZZ^*$	[463–465]	[455, 466, 467]	—
<i>CP-odd A (and/or CP-even H)</i>			
$H, A \rightarrow \tau^+\tau^-$	[468]	[469, 470]	[471, 472] (TeV) [473] (LHCb)
$A \rightarrow \tau^+\tau^-$ (low mass)	—	[474]	—
$H, A \rightarrow \mu^+\mu^-$	[475]	[476]	—
$H \rightarrow \mu\tau, e\tau$ LFV	—	[477]	—
$bj\mu^+\mu^-$ (low $\mu^+\mu^-$ mass)	[478]	[479]	—
$H, A \rightarrow t\bar{t}$	[461, 480]	[481]	—
$H, A \rightarrow b\bar{b}$	[482]	[483]	[484, 485] (TeV)
$A \rightarrow hV \rightarrow b\bar{b}q\bar{q}', b\bar{b}\ell\nu, b\bar{b}\ell\ell, \ell\ell\tau\tau, \nu\bar{\nu}b\bar{b}$	[486, 487]	[488, 489]	—
$A \rightarrow ZH$	[490]	[491]	—
$H \rightarrow ZA \rightarrow b\bar{b}\ell^+\ell^-$	[213]	[492]	—
<i>Charged H^\pm</i>			
$H^\pm \rightarrow \tau^\pm\nu$	[493, 494]	[495]	—
$H^\pm \rightarrow cs$	[496]	[497]	—
$H^\pm \rightarrow tb$	[498]	[499]	—
$H^\pm \rightarrow W^\pm Z$	[500]	[501, 502]	—
$H^\pm \rightarrow W^\pm A$	—	[503]	—
$H^\pm \rightarrow HW^\pm$	—	[504]	—
$H^\pm \rightarrow cb$	—	[505]	—
<i>CP-odd a</i>			
$a \rightarrow \mu^+\mu^-$	[506]	[507]	—
$h \rightarrow aa \rightarrow 4\mu, 4\tau, 2\mu 2\tau, 4\gamma$	[508]	[509–512]	[513] (LEP)
[514] (TeV) $h \rightarrow aa \rightarrow b\bar{b}\mu\mu, b\bar{b}\tau\tau, 4b$	[515, 516]	[517, 518]	—
$\Upsilon_{1s,3s} \rightarrow a\gamma$	—	—	[519, 520] (BBr)
Doubly charged $H^{\pm\pm}$	[521]	[502, 522]	—

In the $H \rightarrow WW^{(*)} \rightarrow \ell\nu\ell\nu$ channel, the search for an additional state is done using a boosted decision tree combining several discriminating kinematic characteristics to separate both the signal from the background and a high mass signal H from the lower mass state h [524]. A simultaneous fit of the two states h and H is then made to test the presence of an additional state. In this case, the usual null hypothesis of background includes the SM signal.

The CMS search for nearly degenerate mass states decaying to a pair of photons [525] is more generic and could for instance apply to CP -odd Higgs bosons as well. It consists of a fit to the diphoton mass spectrum using two nearly degenerate mass templates.

(e) Type I 2HDM and fermiophobia

The measurements of coupling properties of the 125 GeV Higgs boson directly establish its couplings to fermions. However, the presence of an additional fermiophobic state, as predicted by Type I 2HDMs, is not excluded. Prior to the discovery, ATLAS and CMS have performed searches for a fermiophobic Higgs boson, i.e., produced through couplings with vector bosons only (VBF and VH) and decaying in two photons. CMS has further combined these results with searches in the W^+W^- and ZZ channels, assuming fermiophobic production and decay. This way,

CMS excluded a fermiophobic Higgs boson in the range $110 \text{ GeV} < m_H < 188 \text{ GeV}$ at the 95% CL. References for these Run-1 measurements can be found in Ref. [141]

11.6.7.2 Searches for additional neutral states ($\phi \equiv h, H, A$) decaying to fermions

(a) Exclusion limits from LEP

In e^+e^- collisions, around the centre-of-mass energies reached by LEP, the main production mechanisms of the neutral MSSM Higgs bosons were the Higgs-strahlung processes $e^+e^- \rightarrow hZ, HZ$ and the pair production processes $e^+e^- \rightarrow hA, HA$, while the vector boson fusion processes played a marginal role. Higgs boson decays to $b\bar{b}$ and $\tau^+\tau^-$ were used in these searches.

The searches and limits from the four LEP experiments are described in Refs. [526]. The combined LEP data did not contain any excess of events which would imply the production of a Higgs boson. Combined limits were derived [523]. For $m_A \gg M_Z$, the limit on m_h is nearly that of the SM searches, as $\sin^2(\beta - \alpha) \approx 1$. For high values of $\tan\beta$ and low m_A ($m_A \leq m_h^{max}$), the $e^+e^- \rightarrow hA$ searches become the most important, and the lightest Higgs boson h is non SM-like. In this region, the 95% CL mass bounds are $m_h > 92.8 \text{ GeV}$ and $m_A > 93.4 \text{ GeV}$. In the m_h^{max}

scenario [527], values of $\tan\beta$ from 0.7 to 2.0 are excluded taking $m_t = 174.3$ GeV, while a much larger $\tan\beta$ region is excluded for other benchmark scenarios such as the no-mixing one.

A flavour-independent limit for Higgs bosons in the Higgs-strahlung process at LEP has also been set at 112 GeV [528].

Neutral Higgs bosons may also be produced by Yukawa processes $e^+e^- \rightarrow f\bar{f}\phi$, where the Higgs particle $\phi \equiv h, H, A$, is radiated off a massive fermion ($f \equiv b$ or τ^\pm). These processes can be dominant at low masses, and whenever the $e^+e^- \rightarrow hZ$ and hA processes are suppressed. The corresponding ratios of the $f\bar{f}h$ and $f\bar{f}A$ couplings to the SM coupling are $-\sin\alpha/\cos\beta$ and $\tan\beta$, respectively. The LEP data have been used to search for $b\bar{b}b\bar{b}$, $b\bar{b}\tau^+\tau^-$, and $\tau^+\tau^-\tau^+\tau^-$ final states [529]. Regions of low mass and high enhancement factors are excluded by these searches.

The searches for the Higgs boson at LEP also included the case where it does not predominantly decay to a pair of b quarks. All four collaborations conducted dedicated searches for the Higgs boson with reduced model dependence, assuming it is produced via the Higgs-strahlung process, and not addressing its flavour of decay, a lower limit on the Higgs boson mass of 112.9 GeV is set by combining the data of all four experiments [528].

Using an effective Lagrangian approach and combining results sensitive to the $h\gamma\gamma$, $hZ\gamma$ and hZZ couplings, an interpretation of several searches for the Higgs boson was made and set a lower limit of 106.7 GeV on the mass of a Higgs boson that can couple anomalously to photons [528].

(b) Searches at the Tevatron and the LHC

The best sensitivity is in the regime with low to moderate m_A and with large $\tan\beta$ which enhances the couplings of the Higgs bosons to down-type fermions. The corresponding limits on the Higgs boson production cross section times the branching ratio of the Higgs boson into down-type fermions can be interpreted in MSSM benchmark scenarios [530]. The most promising channels at the Tevatron are the inclusive $p\bar{p} \rightarrow \phi \rightarrow \tau^+\tau^-$ process ($\phi = A, H, h$), with contributions from both $gg \rightarrow \phi$ and $b\bar{b}\phi$ production, and $b\bar{b}\phi$, $\phi \rightarrow \tau^+\tau^-$ or $\phi \rightarrow b\bar{b}$, with $b\tau\tau$ or three tagged b -jets in the final state, respectively. Although the Higgs boson production via gluon fusion has a higher cross section in general than via associated production, it cannot be used to study the $\phi \rightarrow b\bar{b}$ decay mode since the signal is overwhelmed by the QCD background.

CDF and D0 have searched for neutral Higgs bosons produced in association with bottom quarks and which decay into $b\bar{b}$ [484, 485], or into $\tau^+\tau^-$ [471, 472]. The most recent searches in the $b\bar{b}\phi$ channel with $\phi \rightarrow b\bar{b}$ analyse approximately 2.6 fb^{-1} (CDF) and 5.2 fb^{-1} (D0) of data, seeking events with at least three b -tagged jets. The cross section is defined such that at least one b quark not from ϕ decay is required to have $p_T > 20$ GeV and $|\eta| < 5$. The invariant mass of the two leading jets as well as b -tagging variables are used to discriminate the signal from the backgrounds. The QCD background rates and shapes are inferred from data control samples, in particular, the sample with two b -tagged jets and a third, untagged jet. Separate-signal hypotheses are tested and limits are placed on $\sigma(p\bar{p} \rightarrow b\bar{b}\phi) \times \text{BR}(\phi \rightarrow b\bar{b})$. A local excess of approximately 2.5σ significance has been observed in the mass range of 130–160 GeV, but D0's search is more sensitive and sets stronger limits. The D0 result had a $\mathcal{O}(2\sigma)$ local upward fluctuation in the 110 to 125 GeV mass range. These results have been superseded by the LHC searches and the excess seen by D0 has not been confirmed elsewhere.

A substantially larger sensitivity in the search for the $\phi \rightarrow \tau^+\tau^-$ is obtained with the ATLAS and CMS analyses. The higher centre-of-mass energy reached at the Run 2 brings a substantial, though not excessively large, increase in sensitivity due to the intermediate masses probed. Both ATLAS and CMS have reported the result of their searches in this important channel with the full 2016 dataset. The searches are performed in categories of the decays of the two tau leptons: $e\tau_{\text{had}}$, $\mu\tau_{\text{had}}$, $e\mu$, and $\mu\mu$, where τ_{had} denotes a tau lepton which decays to one or more hadrons plus a tau neutrino, e denotes $\tau \rightarrow e\nu\nu$, and μ denotes $\tau \rightarrow \mu\nu\nu$. The dominant background comes from $Z \rightarrow \tau^+\tau^-$ decays, although $t\bar{t}$,

W +jets and Z +jets events contribute as well. Separating events into categories based on the number of b -tagged jets improves the sensitivity in the MSSM. The $b\bar{b}$ annihilation process and radiation of a Higgs boson from a b quark gives rise to events in which the Higgs boson is accompanied by a $b\bar{b}$ pair in the final state. Requiring the presence of one or more b -jets reduces the background from Z +jets. Data control samples are used to constrain background rates. The rates for jets to be identified as a hadronically decaying tau lepton are measured in dijet samples, and W +jets samples provide a measurement of the rate of events that, with a fake hadronic tau, can pass the signal selection requirements. Lepton fake rates are measured using samples of isolated lepton candidates and same-sign lepton candidates. Constraints from the ATLAS searches are shown in Fig. 11.17 (left) in the hMSSM approximation defined in Ref. [376]. The neutral Higgs boson searches consider the contributions of both the CP -odd and CP -even neutral Higgs bosons with enhanced couplings to bottom quarks, similarly to what was done for the Tevatron results. In Fig. 11.17, decays of the charged Higgs boson into $\tau\nu$ and decays of the heavy Higgs boson into a pair of SM-like Higgs bosons or gauge bosons, or decays of A into hZ are also being constrained. In addition, decays of the neutral Higgs bosons into muon pairs are also being explored. In the $m_h^{\text{mod+}}$ scenario, the region of $\tan\beta$ lower than 5 does not allow for a Higgs boson mass m_h close to 125 GeV. For the hMSSM scenario, instead, the SM-like Higgs boson mass is fixed as an input and hence the requirement that it is close to 125 GeV is always fulfilled, although this may imply other limitations as discussed in Section 11.6.1.1.

A search for $\phi \rightarrow \mu^+\mu^-$ has also been performed by ATLAS [475] and CMS [476] and no significant deviations from the SM expectation were observed, allowing to set model-independent limit on the product of the branching fraction for the decay into a muon pair and the cross section for the production of a scalar neutral boson, either via gluon fusion, or in association with b quarks, in the mass range from 130 to 1000 GeV.

Finally, searches for a resonance decaying to a top quark pair were done by ATLAS [480, 531] and CMS [481, 532]. These searches were interpreted as searches for scalar resonances by ATLAS [480], however, an important component of these searches is an accurate treatment of the interference effects between the signal and the continuum background. These effects can yield a dip and peak structure instead of a simple peak [372]. ATLAS has performed a search for a high mass state decaying to a pair of top quarks taking into account the deformation in mass shape of the signal in the presence of the continuum background [533].

The LHC has the potential to explore a broad range of SUSY parameter space through the search for non-SM-like Higgs bosons. As illustrated in Fig. 11.17, the parameter space corresponding to large $\tan\beta$ values and large masses of the A boson are covered mostly by the searches in the $A, H \rightarrow \tau^+\tau^-$ channel. A projection of the combined sensitivity of ATLAS and CMS at the HL-LHC has been performed in Ref. [118], showing that, compared to the current sensitivity, the full HL-LHC luminosity can expand the exclusion domain by nearly 1 TeV. In the low $\tan\beta$ limit, the parameter space spanning large A boson masses is best excluded indirectly from the observed Higgs boson measurements. This is illustrated in the M_h^{125} scenario by the nearly horizontal exclusion which is due to the compatibility of the Higgs boson mass measurement with its prediction from radiative corrections (mostly from the stop sector). Nevertheless, Fig. 11.17 (right) shows a broad region with intermediate $\tan\beta$ and large values of m_A that is not accessed by current searches, and in which the most promising channel is the very difficult search for $t\bar{t}$ decays with its aforementioned intricacies [379]. In this region of parameter space, it is possible that only the SM-like Higgs boson can be within the LHC's reach. If no other state of the EWSB sector than the 125 GeV state is discovered, it may be challenging to determine only from the Higgs sector whether there is a SUSY extension of the SM in nature.

11.6.7.3 Searches for a CP -odd state decaying to hZ

Similarly, to the search for a CP -even high mass Higgs boson decaying to a pair of Higgs bosons, the search for a CP -odd states decaying to hZ was carried out at the LHC by ATLAS and CMS

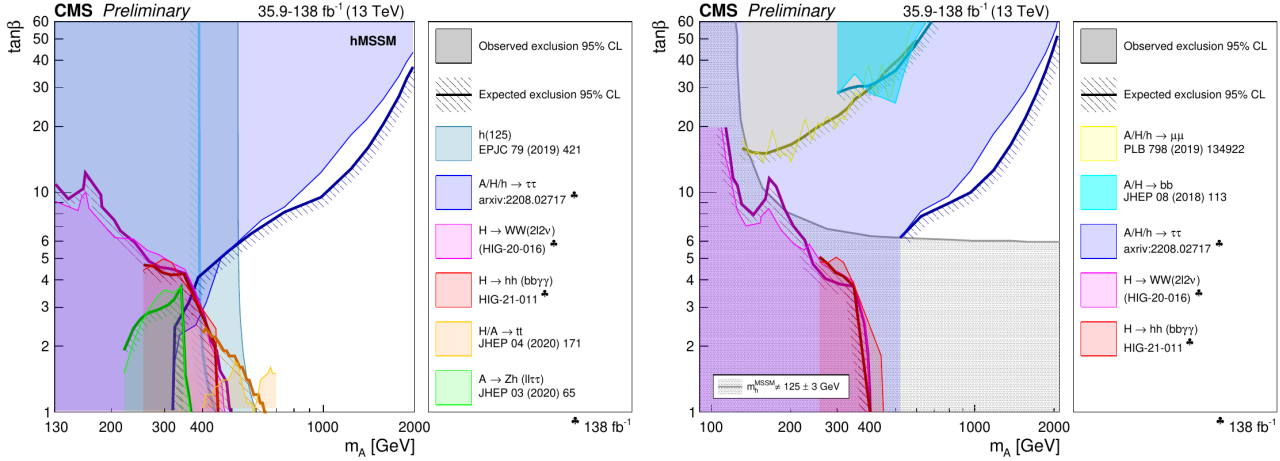


Figure 11.17: The 95% CL exclusion contours in the $(M_A, \tan\beta)$ parameter space for: (left) a summary of CMS Run-2 searches in the hMSSM and (right) in the M_h^{125} scenario.

in various channels: (i) $(Z \rightarrow \ell\ell)(h \rightarrow b\bar{b})$, (ii) $(Z \rightarrow \nu\nu)(h \rightarrow b\bar{b})$, (iii) $(Z \rightarrow \ell\ell)(h \rightarrow \tau\tau)$, and (iv) $(Z \rightarrow \ell\ell)(h \rightarrow \tau\tau)$. The searches where the A boson decays to a pair of b quarks have been performed both in the regime where both b -jets are resolved and in the boosted regime where the two b -jets are merged in a single larger radius jet. These searches have been used to constrain the parameter space of 2HDMs. In the MSSM, these searches place limits on small values of $\tan\beta$ for masses of A between 220 GeV and 360 GeV.

11.6.7.4 Searches for low mass states

Searches for pseudo-scalar Higgs boson at intermediate to low masses, below the Z mass (in the 25 GeV to 80 GeV mass range) have been performed by CMS both in the $\tau^+\tau^-$ [534] and the $\mu^+\mu^-$ [535] decay channels. A light pseudo-scalar in this mass range is excluded by current direct constraints in the MSSM but not in general 2HDMs [536]. These searches are done in the decay channels where the pseudo-scalar Higgs boson is produced in association with a pair of b -quarks and decays into a pair of taus or muons.

CMS has also reported an anomaly observed in the search for $\mu^+\mu^-$ resonances produced with one jet tagged as containing a b -hadron and a forward jet in the Run-1 data. A mild excess appeared in the di-muon mass distribution at approximately 28 GeV. Another very mild excess was then also found in the 2016 Run-2 data [479]. ATLAS then performed a similar analysis with the full Run-2 dataset corresponding to an integrated luminosity of approximately 139 fb^{-1} , and no significant excess was found [478].

Searches for low mass Higgs bosons were also performed in the diphoton channel by both ATLAS and CMS [537, 538] at Run 1. ATLAS and CMS have updated the results of this search with Run-2 data [440, 442]. A modest excess has been observed by CMS at a mass of 95.4 GeV with a local significance of 2.9σ (the corresponding global significance is 1.3σ). A slight excess was also seen by ATLAS at the same mass of 95.4 GeV with a local significance of 1.7σ . No significant excess has been observed in this region by ATLAS at Run 1. This mildly significant excess also coincides in mass with the excess observed at LEP and discussed in Section 11.6.7.1. It is interesting to note that the sensitivity of searches at masses very near that of the Z boson, require a very strong rejection of events where electrons are misidentified as photons. Dedicated experimental methods have been developed to reduce the vulnerability of the analysis in this specific mass region to this background. It has therefore raised interest and speculations on its possible nature, see for instance Ref. [539] and references therein.

11.6.7.5 Searches for charged Higgs bosons H^\pm

At e^+e^- colliders, charged Higgs bosons can be pair produced in the s -channel via γ or Z boson exchange. This process is dominant in the LEP centre-of-mass energies range, i.e., up to 209 GeV. At higher centre-of-mass energies, other processes can play an important role such as the production in top quark decays via $t \rightarrow b + H^\pm$ if $m_{H^\pm} < m_t - m_b$ or via the one-loop process $e^+e^- \rightarrow W^\pm H^\mp$ [540, 541], which allows the production of a charged Higgs boson with $m_{H^\pm} > \sqrt{s}/2$, even when H^+H^- production is kinematically forbidden. Other single charged Higgs boson production mechanisms include $t\bar{b}H^+/\bar{t}bH^+$ production [123], $\tau^+\nu H^-/\tau^-\bar{\nu}H^+$ production [542], and a variety of processes in which H^\pm is produced in association with a one or two other gauge and/or Higgs bosons [543].

At hadron colliders, charged Higgs bosons can be produced in several different modes depending on the value of its mass with respect to the top-quark mass. For light values of the charged Higgs boson mass, defined by Higgs boson masses smaller than the mass of the top quark (with experimental analyses typically considering masses up to $m_{H^\pm} \leq 160 \text{ GeV}$), the top-quark decay $t \rightarrow Hb$ is allowed and the charged Higgs boson is light enough so that top-quark off-shell effects can be neglected. The cross section for the production of a light charged Higgs boson is simply given by the product of the top-pair production cross section and the branching ratio of a top quark into a charged Higgs boson. The top-pair production cross section is known up to NNLO in perturbative QCD [544], and relevant QCD and SUSY-QCD including NLO corrections to the branching ratio for $t \rightarrow H^+b$ have been computed in the literature, see Refs. [545–547] and references therein. At present, the theoretical accuracy for the production of a light charged Higgs boson is at the few percent level. For the intermediate mass range, values of m_{H^\pm} near m_t , the finite top-width effects as well as the interplay between top-quark resonant and non-resonant diagrams cannot be neglected. Hence, the full process $pp \rightarrow H^\pm W^\mp b\bar{b}$ (with massive b -quarks) must be considered to perform a reliable perturbative calculation of the charged Higgs boson production cross section [547]. For heavy charged Higgs boson scenarios, with charged Higgs boson masses larger than the top-quark mass (typically above 180 GeV), the dominant charged Higgs boson production channel is the associated production with a top quark/antiquark and a (possibly low transverse momentum) bottom antiquark/quark. Theoretical calculation at NLO have been computed both at the inclusive and fully-differential level in the five-flavour scheme and in the four-flavour scheme, see Ref. [40] and references therein. Charged Higgs bosons can also be produced via associated production with W^\pm bosons through $b\bar{b}$ annihilation and gg -fusion annihilation [548].

For charged Higgs boson production cross section predictions

for the Tevatron and the LHC, see Refs. [38, 39, 370].

(a) *Exclusion limits from LEP*

Charged Higgs bosons have been searched for at LEP, where the combined data of the four experiments, ALEPH, DELPHI, L3, and OPAL, were sensitive to masses of up to about 90 GeV [523] in two decay channels, $\tau\nu$ and $c\bar{s}$. The combined LEP data exclude, at 95% CL, charged Higgs bosons with mass below 80 GeV (Type II scenario) or 72.5 GeV (Type I scenario) [549].

(b) *Exclusion limits from Tevatron*

Compared to the mass domain covered by LEP searches, the Tevatron covered a complementary range of charged Higgs boson masses. CDF and D0 have also searched for charged Higgs bosons in top quark decays with subsequent decays to $\tau\nu$ or $c\bar{s}$ [550]. For the $H^+ \rightarrow c\bar{s}$ channel, the limits on $\text{BR}(t \rightarrow H^+b)$ from CDF and D0 are $\approx 20\%$ in the mass range $90 \text{ GeV} < m_{H^+} < 160 \text{ GeV}$ and assuming a branching fraction of 100% in this specific final state. $H^+ \rightarrow \tau^+\nu_\tau$ channel, D0's limits on $\text{BR}(t \rightarrow H^+b)$ are also $\approx 20\%$ in the same mass range and assuming a branching fraction of 100% in this final state. These limits are valid in general 2HDMs, and they have also been interpreted in terms of the MSSM [550].

(c) *Exclusion limits from LHC*

Similarly, to the Tevatron, at the LHC, light charged Higgs bosons can be searched for in the decays of top quarks. The main initial production mode for light charged Higgs bosons ($m_{H^\pm} < m_t - m_b$) is top pair production. The subsequent decay modes of the charged Higgs boson for these searches are $\tau\nu$ and $c\bar{s}$. More recently, ATLAS and CMS have also searched for higher mass charged Higgs bosons ($m_{H^\pm} > m_t + m_b$) in $H^+ \rightarrow t\bar{b}$. The main production modes are the associated production of a charged Higgs boson in association with a top and a bottom quark or in association with a top quark only.

The decay $H^+ \rightarrow \tau^+\nu_\tau$ is searched typically in three final state topologies:

- (i) lepton+jets: with $t\bar{t} \rightarrow \bar{b}WH^+ \rightarrow b\bar{b}(q\bar{q}')(\tau_{\text{lep}}\nu)$, i.e., the W boson decays hadronically and the tau decays into an electron or a muon, with two neutrinos;
- (ii) τ +lepton: with $t\bar{t} \rightarrow \bar{b}WH^+ \rightarrow b\bar{b}(\ell\nu)(\tau_{\text{had}}\nu)$, i.e., the W boson decays leptonically (with $\ell = e, \mu$) and the tau decays hadronically;
- (iii) τ +jets: $t\bar{t} \rightarrow \bar{b}WH^+ \rightarrow b\bar{b}(q\bar{q}')(\tau_{\text{had}}\nu)$, i.e., both the W boson and the τ decay hadronically.

CMS has also searched for the charged Higgs boson in the decay products of top quark pairs: $t\bar{t} \rightarrow H^\pm W^\mp b\bar{b}$ and $t\bar{t} \rightarrow H^+ H^- b\bar{b}$ as well. Three types of final states with large missing transverse energy and jets originating from b -quark hadronisation have been analysed: the fully-hadronic channel with a hadronically decaying tau in association with jets, the dilepton channel with a hadronically decaying tau in association with an electron or muon and the dilepton channel with an electron-muon pair. The results of the searches at the LHC are illustrated in Figure 11.17.

Both ATLAS and CMS have also searched for high mass charged Higgs bosons decaying to a top and bottom quarks. The main production mode for this search is the associated production with one top quark (5-flavour scheme) or a top quark and a bottom quark (4-flavour scheme) in the final state. The s -channel production mode where the charged Higgs boson is produced alone in the final state at tree level is also considered. This search is particularly intricate and it is sensitive to the modelling of the top pair production background produced in association with additional partons and in particular b -quarks. No excess was found and the results are expressed in terms of exclusion limits of cross section times branching fractions.

ATLAS and CMS have also searched for charged Higgs bosons in top quark decays assuming $\text{BR}(H^+ \rightarrow c\bar{s}) = 100\%$ [496, 551], and sets limits of $\approx 20\%$ on $\text{BR}(t \rightarrow H^+b)$ in the $90 \text{ GeV} < m_{H^+} < 160 \text{ GeV}$ mass range.

In 2HDMs, the decay of the charged Higgs boson to a W and a Z boson is allowed only at loop level and is therefore suppressed.

However the $H^\pm \rightarrow W^\pm Z$ decay channel is allowed in Higgs triplet models. ATLAS [500] has searched for such decays, requiring that the charged Higgs boson is produced through the fusion of vector bosons. No excess with respect to the SM backgrounds has been observed in this channel, and the results are interpreted in the Georgi–Machacek model [414] discussed in Section 11.6.5.2.

At the LHC, various other channels still remain to be explored, in particular searches involving additional neutral scalars in particular in the WH , WA channels (A is the pseudo-scalar MSSM Higgs boson), and in the Wa channel (a is the light CP -odd scalars of the NMSSM).

11.6.7.6 *Interpretation of the measurements of the coupling properties of the Higgs boson*

The 125 GeV Higgs boson being part of any hypothetically extended EWSB sector, it can be used through the compatibility of its measured couplings and mass with those predicted in specific models to provide constraints on these specific models parameters.

As discussed in Section 11.6.1.1, the mass of the Higgs boson limits drastically the MSSM parameter space and can be used to set limits on specific MSSM benchmarks. This is the case for the Mh125 scenario as illustrated in Fig. 11.16 and in Fig. 11.17, corresponding approximately to a lower limit on $\tan\beta$ in this model [118].

The measurements of the Higgs boson couplings, discussed in Section 11.5, can be interpreted in the framework of a constrained model where the couplings of the Higgs boson to vector bosons, up-type quarks, down-type quarks and leptons, are varied. In 2HDMs, these couplings are functions of the mixing angle α between the observed Higgs boson and the heavy CP -even neutral scalar, and of the ratio of the vacuum expectation values of the two doublets, $\tan\beta$. In the case of the MSSM, the two parameters are the A boson mass and $\tan\beta$ (the sole two parameters needed to describe the MSSM Higgs sector at tree level). The coupling measurements have been interpreted both by ATLAS [312] and CMS [552] in specific MSSM benchmarks and in 2HDMs. The exclusion contour in the hMSSM for the ATLAS combination [312] is illustrated in Fig. 11.17.

11.6.7.7 *Searches for a light CP-odd Higgs boson*

A light pseudo-scalar boson a is present in any two Higgs doublet model enhanced with an additional singlet field. A prominent example is the NMSSM. The theoretical motivations for singlet extensions of the MSSM are discussed in Section 11.6.2. There is also a variety of other models with light additional spin-0 bosons such as two Higgs doublet models with a scalar, Little Higgs models or light scalar mediator to a dark sector.

In the framework of the NMSSM, the searches now focus on the low a mass region for several reasons:

- (i) in the NMSSM, the light pseudo-scalar a boson can, as a pseudo-Goldstone boson, be a natural candidate for an axion;
- (ii) scenarios where $m_a > 2m_b$ and a CP -even state h decaying to a pair of a ($m_h > 2m_a$) are excluded by direct searches at LEP in the four b 's channel [514, 523, 553];
- (iii) in the pre-discovery era, LEP limits on a CP -even Higgs boson resulted in fine-tuning MSSM constraints [554] which could be evaded through non standard decays of the Higgs boson to aa ;
- (iv) in the NMSSM, a CP -odd a boson with a mass in the range 9.2–12 GeV can also account for the difference observed between the measured anomalous muon magnetic moment and its prediction [555].

The benchmark scenarios have also changed in the light of the Higgs boson discovery. The 125 GeV state could be the lightest or the next-to-lightest of the three CP -even states of the NMSSM. Light pseudo-scalar scenarios are still very interesting in particular for the potential axion candidate. There are three main types of direct searches for the light a boson:

- (i) for masses below the Υ resonance, the search is for radiative decays $\Upsilon \rightarrow a\gamma$ at B-factories;
- (ii) the inclusive search in high energy pp collisions at the LHC;

- (iii) the search for decays of the observed CP -even Higgs h boson into a pair of a bosons;

Radiative decays $\Upsilon \rightarrow a\gamma$ have been searched for in various colliders, the most recent results are searches for radiative decays of the $\Upsilon(1s)$ to $a\gamma$ with a subsequent decay of the a boson to a pair of taus at CLEO [556], and the radiative decays of the $\Upsilon(1s, 2s, 3s)$ to $a\gamma$ with subsequent decays to a pair of muons or taus by BaBar [519, 520].

Direct inclusive searches for the light pseudo scalar a boson were performed in the $a \rightarrow \mu\mu$ channel at the Tevatron by D0 [514] and by ATLAS [506], CMS [507], and LHCb [164] at the LHC.

Finally, searches for the decays of the Higgs boson to a pair of a bosons were performed with subsequent decays to four photons, in the four muons final state, in the two muons and two taus final state, and in the four taus final state.

No significant excess in the searches for a light CP -odd a boson was found and limits on the production times branching fractions of the a boson have been set.

References for all these searches are summarised in Table 11.11.

11.6.7.8 Searches in Higgs decays

Dark-photons or axion-like particles searches can also be carried out within the decays of the Higgs boson to four leptons through dilepton pair resonances. Such search has been carried out by ATLAS and CMS [557]. Alternatively signatures of dark photons escaping detection with missing transverse momentum signatures have also been searched for by ATLAS [558].

11.6.7.9 Searches for doubly charged Higgs bosons $H^{\pm\pm}$

As discussed in Section 11.6.5, the generation of small neutrino masses via the standard EWSB mechanism described in Section 11.2 requires unnaturally small Yukawa couplings, provided that neutrinos are Dirac-type fermions. A Majorana mass term with a see-saw mechanism for neutrinos, would allow for naturally small masses and would also yield a framework for the appealing scenario of leptogenesis. However, within the SM, Majorana mass terms correspond to (non-renormalizable) dimension-5 operators. Such effective interactions can be generated via renormalisable interactions with an electroweak triplet of complex scalar fields (corresponding to a type-II see-saw mechanism). Other models such as the Zee–Babu model, with the introduction of two $SU(2)_L$ singlets, also generate Majorana mass terms. The signature of such models would be the presence of doubly charged Higgs bosons $H^{\pm\pm}$.

The main production mechanisms of $H^{\pm\pm}$ bosons at hadron colliders are the pair production in the s -channel through the exchange of a Z boson or a photon and the associated production with a charged Higgs boson through the exchange of a W boson. Various searches for doubly charged Higgs bosons have been performed by ATLAS and CMS at Run 1 [559] and Run 2 [521, 522]. Typically, these searches aim at low values of the Higgs triplet vacuum expectation for which the doubly charged Higgs boson will decay mostly to leptons (for high values, the decay to W bosons will become predominant). These searches assume that the coupling to W bosons is negligible and that the main production mode is through the Drell–Yan process.

11.6.7.10 Searches for non-standard production processes of the Higgs boson

The discovery of the Higgs boson has also allowed for searches of BSM processes involving standard decays of the Higgs boson. One example directly pertaining to the search for additional states of the EWSB sector is the search for Higgs bosons in the cascade decay of a heavy CP -even Higgs boson decaying to charged Higgs boson and a W boson, and the charged Higgs boson subsequently decaying to H and another W boson. This search has been performed by ATLAS in $b\bar{b}$ decays of the 125 GeV Higgs boson [560].

11.6.7.11 Outlook on searches for additional states

The LHC program of searches for additional states covers a large variety of decay and production channels. Since the Higgs boson discovery, many new channels have been explored at the LHC, e.g., the searches for additional states decaying into hh or Vh or ZA . The search for charged Higgs bosons has been ex-

tended to include the WZ , WA and the very difficult $t\bar{b}$ decay channel.

11.7 Summary and outlook

Summary– The discovery of the Higgs boson is a major milestone in the history of particle physics as well as an extraordinary achievement of the LHC machine and the ATLAS and CMS experiments. Eleven years after the discovery, substantial progress in the field of Higgs boson physics has been accomplished and a significant number of measurements probing the nature of this unique particle have been made. They are revealing an increasingly precise profile of the Higgs boson.

The LHC has concluded its Run 2 in 2018, delivering a dataset of 13 TeV pp collisions corresponding to an integrated luminosity of more than 150 fb^{-1} of data collected by ATLAS and CMS. The Run 3 started in 2022 at 13.6 TeV and more than 70 fb^{-1} of additional data were delivered. First cross section measurements at this new centre-of-mass energy have been presented and are reported herein. With the substantial increase in production rates at the higher center-of-mass energy (mostly from Run 1 to Run 2) and the larger datasets, new landmark results in Higgs physics have been achieved. They are highlighted in the 10th anniversary papers of the Higgs boson discovery [183, 184].

Three new results of fundamental importance have been achieved with Run-2 datasets by ATLAS and CMS independently: (i) the clear and unambiguous observation of the Higgs boson decay to taus; (ii) the clear and unambiguous observation of the Higgs boson decay to a pair of b quarks; (iii) the clear and unambiguous observation of the production of the Higgs boson through the $t\bar{t}H$ process. These results provide direct evidence for the Yukawa coupling of the Higgs boson to fermions of the third generation: taus, bottom quarks and top quarks, at rates compatible with those expected in the SM. In addition, the evidence for the decay of the Higgs boson to muons is being consolidated. These, and all other experimental measurements, are consistent with the EWSB mechanism of the SM.

New theoretical calculations and developments in Monte-Carlo simulations pertaining to Higgs physics are still occurring at a rapid pace. For example, the theoretical prediction for the dominant gluon fusion production mode now includes the latest N3LO result at the inclusive and differential levels, which is twice as precise as previous N2LO calculations. With these improvements in the state-of-the-art theory predictions and the increase in luminosity and center-of-mass energy, Higgs physics has definitively entered a precision era. Its impact can already be seen on the latest Run-2 combined measurements of the Higgs boson couplings (see Section 11.5).

Since the discovery of the Higgs boson, new ideas have emerged to probe its rare decays and production modes, as well as to indirectly measure the Higgs boson width through the study of its off-shell couplings, or via on-shell interference effects. The Higgs boson has now become part of the standard toolkit in searches for new physics, with Higgs measurements being used in SMEFT global fits.

Many extensions of the SM at higher energies call for an enlargement of the EWSB sector. Hence, direct searches for additional scalar states can provide valuable insights on the dynamics of the EWSB mechanism. The ATLAS and CMS experiments have searched for additional Higgs bosons in the Run-2 data, and have imposed constraints in broad ranges of mass and couplings for various scenarios with an extended Higgs sector.

The landscape of Higgs physics has been scrutinized extensively since its discovery. The current precisions on the measurements of the couplings of the Higgs boson to gauge bosons and third generation fermions are typically of the order of 10–20%. The uncertainty on the Higgs boson coupling to the muon shrank below 50%, and the upper limits on the branching fraction to new invisible particles are approximately 10%. Sensitivity to the Higgs boson self-coupling has not reached the SM value yet, and there is no information on how the Higgs field acquired its VEV in the early times of the Universe. However, significant progress in being made through exploration of di-Higgs production, including new analyses based on machine learning algorithms. This situation allows for new challenges to ultimately increase further the reach in

precision and it also widens the possibilities of unveiling the true nature and the dynamics of the electroweak symmetry breaking mechanism.

Outlook– The unitarisation of the vector boson scattering (VBS) amplitudes, dominated at high energies by their longitudinal polarisation, has been the basis of the *no lose* theorem at the LHC, and was a determining consideration in the building of the accelerator and detectors. It motivated the existence of a Higgs boson or the observability of manifestations of strong dynamics at the TeV scale. Now that a Higgs boson has been found and its couplings to gauge bosons are – within current accuracy – consistent with the SM predictions, perturbative unitarity is preserved to a large extent with the sole exchange of the Higgs boson, and without the need for any additional states. VBS remains still an important channel to further investigate in order to better understand the nature of the Higgs sector and the possible completion of the SM at the TeV scale. In association with the double Higgs boson production channel by vector boson fusion, VBS could, for instance, confirm that the Higgs boson is part of a weak doublet and also establish whether it is an elementary object or a composite state that could emerge as a pseudo-Nambu–Goldstone boson from a new underlying broken symmetry.

The fermion-Higgs boson couplings are not governed by local gauge symmetry. Thus, in addition to a new particle, the LHC has also discovered a new force, different in nature from the other fundamental interactions since it is non-universal and distinguishes between the three families of quarks and leptons. The existence of the Higgs boson embodies the problem of an unnatural cancellation among the quantum corrections to its mass if new physics is present at scales significantly higher than the EW scale. The non-observation of additional states which could stabilise the Higgs boson mass is a challenge for natural scenarios like Supersymmetry or models with a new strong interaction in which the Higgs boson is not a fundamental particle. This increasingly pressing paradox starts questioning the principle of naturalness and it also inspires new solutions tied to the cosmological evolution of the Universe.

The search for the Higgs boson has occupied the particle physics community for the last 50 years. Its discovery has shaped and sharpened the physics programs of the LHC and of prospective future accelerators [126, 561]. With respect to current data, at the HL-LHC the precision will improve by a factor of approximately 5–10 depending on the observables considered. Table 11.8 displays the expected sensitivities in the characterization of the Higgs boson at HL-LHC: in this table, the parameters κ_i specify by how much the coupling of the Higgs boson to a given particle i deviates from the SM expectation. The only channels which are expected to be limited by data statistics are the rare decays to muons and $Z\gamma$. In all other cases, the experimental systematic uncertainties are similar to the statistical uncertainties, but the dominant source of uncertainty arises from theory, and this remains the case even after assuming that, by the end of the HL-LHC run, the theory uncertainties can be reduced by a factor two compared to the current uncertainties, a hypothesis that appears realistic but still requires dedicated and concerted work [118]. For both hadron and lepton colliders, some theoretical progress is crucial to fully exploit and capitalise on the experimental data. In particular, the expected HL-LHC data together with rapid ongoing progress in theoretical calculations are defining a new era of precision Higgs boson measurements.

Acknowledgements

We would like to thank many of our colleagues for proofreading this review, for useful criticism and for their input in general: W. Altmannshofer, J. de Blas, G. Branco, G. Buchalla, J. Campbell, F. Caola, F. Cerutti, C. Csáki, R. Contino, J. Conway, N. Craig, A. David, S. Dawson, J.B. De Vivie, J. D’Hondt, G. Durieux, C. Englert, J.R. Espinosa, A. Falkowski, L. Fayard, W. Fischer, S. Forte, S. Gori, M. Grazzini, J. Gu, H. Haber, B. Heinemann, S. Heinemeyer, J. Hubisz, A. Korytov, B. Jäger, H. Ji, T. Junk, P. Langacker, J. Lykken, F. Maltoni, M.L. Mangano, B. Mansoulié, M. McCullough, R. Mishra, M. Mühlleitner, B. Murray, M. Neubert, A. Nisati, Y. Paul,

G. Perez, G. Petrucciani, A. Pomarol, E. Pontón, R. Rattazzi, D. Rebuffi, L. Reina, F. Riva, R. Salerno, J. Santiago, E. Salvioni, N. Shah, G. Shaughnessy, M. Spira, A. Strumia, K. Tackmann, R. Tanaka, J. Terning, A. Vartak, C. Wagner, N. Wardle, A. Weiler, A. Wulzer, and G. Zanderighi. We are also most grateful to the ATLAS, CDF, CMS and D0 collaborations for their help with this review.

M.C. is supported by Fermilab, that is operated by Fermi Research Alliance, LLC under Contract No. DE-AC02-07CH11359 with the United States Department of Energy. C.G. is supported by the Helmholtz Association and by the Deutsche Forschungsgemeinschaft under Germany’s Excellence Strategy – EXC 2121 “Quantum Universe” – 390833306. V.S. is supported by the grant DE-SC0009919 of the United States Department of Energy.

References

- [1] G. Aad *et al.* (ATLAS), Phys. Lett. **B716**, 1 (2012), [arXiv:1207.7214].
- [2] S. Chatrchyan *et al.* (CMS), Phys. Lett. **B716**, 30 (2012), [arXiv:1207.7235].
- [3] S.L. Glashow, Nucl. Phys. **20**, 579 (1961); S. Weinberg, Phys. Rev. Lett. **19**, 1264 (1967); A. Salam, *Elementary Particle Theory*, eds.: Svartholm, Almquist and Wiksells, Stockholm, 1968; S. L. Glashow, J. Iliopoulos and L. Maiani, Phys. Rev. **D2**, 1285 (1970).
- [4] F. Englert and R. Brout, Phys. Rev. Lett. **13**, 321 (1964), [157(1964)]; P. W. Higgs, Phys. Rev. **145**, 1156 (1966); G. S. Guralnik, C. R. Hagen and T. W. B. Kibble, Phys. Rev. Lett. **13**, 585 (1964), [162(1964)].
- [5] J. M. Cornwall, D. N. Levin and G. Tiktopoulos, Phys. Rev. Lett. **30**, 1268 (1973), [Erratum: Phys. Rev. Lett. **31**, 572 (1973)]; J. M. Cornwall, D. N. Levin and G. Tiktopoulos, Phys. Rev. **D10**, 1145 (1974), [Erratum: Phys. Rev. **D11**, 972 (1975)]; C. H. Llewellyn Smith, Phys. Lett. **46B**, 233 (1973); B. W. Lee, C. Quigg and H. B. Thacker, Phys. Rev. **D16**, 1519 (1977).
- [6] K. G. Wilson, Phys. Rev. **D3**, 1818 (1971); G. ’t Hooft, in *Proc. of 1979 Cargèse Institute on Recent Developments in Gauge Theories*, p. 135 Press, New York 1980; For a modern discussion, see the GGI Tea Break’s Seminar by G.F. Giudice and R. Rattazzi, <https://is.gd/nUnjAr> (2021).
- [7] J. Wess and B. Zumino, Phys. Lett. **49B**, 52 (1974).
- [8] S. P. Martin, Adv. Ser. Direct. High Energy Phys. 1–98 (1998), [hep-ph/9709356].
- [9] B.C. Allanach and H.E. Haber, *Supersymmetry, Part I (Theory)*, in this volume.
- [10] D. B. Kaplan and H. Georgi, Phys. Lett. **136B**, 183 (1984).
- [11] B. Bellazzini, C. Csaki and J. Serra, Eur. Phys. J. **C74**, 5, 2766 (2014), [arXiv:1401.2457]; G. Panico and A. Wulzer, Lect. Notes Phys. **913**, pp.1 (2016), [arXiv:1506.01961]; C. Csaki, C. Grojean and J. Terning, Rev. Mod. Phys. **88**, 4, 045001 (2016), [arXiv:1512.00468].
- [12] K.M. Black, R.S. Chivukula and M. Narain, *Dynamical Electroweak Symmetry Breaking: Implications of the H0*, in this volume.
- [13] Z. Chacko, H.-S. Goh and R. Harnik, Phys. Rev. Lett. **96**, 231802 (2006), [hep-ph/0506256]; Z. Chacko, H.-S. Goh and R. Harnik, JHEP **01**, 108 (2006), [hep-ph/0512088].
- [14] N. Craig *et al.*, JHEP **07**, 105 (2015), [arXiv:1501.05310]; N. Craig, S. Knapen and P. Longhi, Phys. Rev. Lett. **114**, 6, 061803 (2015), [arXiv:1410.6808].
- [15] P. W. Graham, D. E. Kaplan and S. Rajendran, Phys. Rev. Lett. **115**, 22, 221801 (2015), [arXiv:1504.07551]; J. R. Espinosa *et al.*, Phys. Rev. Lett. **115**, 25, 251803 (2015), [arXiv:1506.09217]; G. Dvali (2019), [arXiv:1908.05984].
- [16] C. Csaki *et al.*, Phys. Rev. Lett. **126**, 091801 (2021), [arXiv:2007.14396]; N. Arkani-Hamed, R. Tito D’agnolo and H. D. Kim (2020), [arXiv:2012.04652]; R. Tito D’agnolo and D. Teresi (2021), [arXiv:2106.04591].

- [17] T. Flacke *et al.*, JHEP **06**, 050 (2017), [arXiv:1610.02025].
- [18] J. Khoury and O. Parrikar, JCAP **12**, 014 (2019), [arXiv:1907.07693]; G. F. Giudice, M. McCullough and T. You (2021), [arXiv:2105.08617].
- [19] S. Weinberg, Phys. Rev. Lett. **43**, 1566 (1979).
- [20] See the particle listing section at <http://pdg.lbl.gov>.
- [21] J. R. Ellis, M. K. Gaillard and D. V. Nanopoulos, Nucl. Phys. **B106**, 292 (1976).
- [22] M. A. Shifman *et al.*, Sov. J. Nucl. Phys. **30**, 711 (1979), [Yad. Fiz.30,1368(1979)].
- [23] J. F. Gunion *et al.*, *The Higgs Hunter's Guide*, Addison-Wesley (1990).
- [24] P. Sikivie *et al.*, Nucl. Phys. **B173**, 189 (1980); H. Georgi, Ann. Rev. Nucl. Part. Sci. **43**, 209 (1993).
- [25] M. J. G. Veltman, Nucl. Phys. **B123**, 89 (1977).
- [26] M. Lüscher and P. Weisz, Nucl. Phys. **B290**, 25 (1987); M. Lüscher and P. Weisz, Nucl. Phys. **B295**, 65 (1988).
- [27] G. Degrandi *et al.*, JHEP **08**, 098 (2012), [arXiv:1205.6497]; S. Alekhin, A. Djouadi and S. Moch, Phys. Lett. **B716**, 214 (2012), [arXiv:1207.0980]; D. Buttazzo *et al.*, JHEP **12**, 089 (2013), [arXiv:1307.3536].
- [28] V. Branchina, E. Messina and M. Sher, Phys. Rev. **D91**, 013003 (2015), [arXiv:1408.5302].
- [29] A. Hook *et al.*, JHEP **01**, 061 (2015), [arXiv:1404.5953]; J. Kearney, H. Yoo and K. M. Zurek, Phys. Rev. **D91**, 12, 123537 (2015), [arXiv:1503.05193].
- [30] J. R. Espinosa, D. Racco and A. Riotto, Phys. Rev. Lett. **120**, 12, 121301 (2018), [arXiv:1710.11196].
- [31] J. R. Espinosa, D. Racco and A. Riotto, JCAP **1809**, 09, 012 (2018), [arXiv:1804.07732].
- [32] A. Andreassen, W. Frost and M. D. Schwartz, Phys. Rev. **D97**, 5, 056006 (2018), [arXiv:1707.08124]; S. Chigusa, T. Moroi and Y. Shoji, Phys. Rev. Lett. **119**, 21, 211801 (2017), [arXiv:1707.09301].
- [33] M. Shaposhnikov and C. Wetterich, Phys. Lett. **B683**, 196 (2010), [arXiv:0912.0208]; M. Holthausen, K. S. Lim and M. Lindner, JHEP **02**, 037 (2012), [arXiv:1112.2415].
- [34] F. L. Bezrukov and M. Shaposhnikov, Phys. Lett. **B659**, 703 (2008), [arXiv:0710.3755]; F. L. Bezrukov, A. Magnin and M. Shaposhnikov, Phys. Lett. **B675**, 88 (2009), [arXiv:0812.4950].
- [35] C. P. Burgess, H. M. Lee and M. Trott, JHEP **09**, 103 (2009), [arXiv:0902.4465]; J. L. F. Barbon and J. R. Espinosa, Phys. Rev. **D79**, 081302 (2009), [arXiv:0903.0355]; M. P. Hertzberg, JHEP **11**, 023 (2010), [arXiv:1002.2995].
- [36] A. Djouadi, Phys. Rept. **457**, 1 (2008), [hep-ph/0503172].
- [37] S. Dittmaier *et al.* (LHC Higgs Cross Section Working Group), CERN Report **2011-002** (2011), [arXiv:1101.0593].
- [38] S. Dittmaier *et al.* (LHC Higgs Cross Section Working Group), CERN Report **2012-002** (2012), [arXiv:1201.3084].
- [39] S. Heinemeyer *et al.* (LHC Higgs Cross Section Working Group), CERN Report **2013-004** (2013), [arXiv:1307.1347].
- [40] D. de Florian *et al.* (LHC Higgs Cross Section Working Group), CERN Report **2017-002** (2016), [arXiv:1610.07922].
- [41] S. Catani *et al.*, Phys. Rev. Lett. **130**, 11, 111902 (2023), [arXiv:2210.07846].
- [42] M. Grazzini, S. Kallweit and M. Wiesemann, Eur. Phys. J. C **78**, 7, 537 (2018), [arXiv:1711.06631].
- [43] LHC Higgs Working Group, <https://twiki.cern.ch/twiki/bin/view/LHCPhysics/LHCHWG>.
- [44] T. Aaltonen *et al.* (CDF, D0), Phys. Rev. **D88**, 5, 052014 (2013), [arXiv:1303.6346].
- [45] H. M. Georgi *et al.*, Phys. Rev. Lett. **40**, 692 (1978).
- [46] D. Graudenz, M. Spira and P. M. Zerwas, Phys. Rev. Lett. **70**, 1372 (1993).
- [47] M. Spira *et al.*, Nucl. Phys. **B453**, 17 (1995), [hep-ph/9504378].
- [48] C. Anastasiou *et al.*, Phys. Rev. Lett. **114**, 212001 (2015), [arXiv:1503.06056]; C. Anastasiou *et al.*, JHEP **05**, 058 (2016), [arXiv:1602.00695].
- [49] R. V. Harlander and K. J. Ozeren, JHEP **11**, 088 (2009), [arXiv:0909.3420]; A. Pak, M. Rogal and M. Steinhauser, JHEP **02**, 025 (2010), [arXiv:0911.4662].
- [50] J. Davies *et al.*, Phys. Rev. **D100**, 3, 034017 (2019), [arXiv:1906.00982]; M. Czakon *et al.* (2021), [arXiv:2105.04436].
- [51] F. Caola *et al.*, JHEP **09**, 035 (2018), [arXiv:1804.07632].
- [52] K. Melnikov and A. Penin, JHEP **05**, 172 (2016), [arXiv:1602.09020].
- [53] C. Anastasiou and A. Penin, JHEP **07**, 195 (2020), [Erratum: JHEP 01, 164 (2021)], [arXiv:2004.03602].
- [54] S. Dawson, Nucl. Phys. **B359**, 283 (1991); A. Djouadi, M. Spira and P. M. Zerwas, Phys. Lett. **B264**, 440 (1991).
- [55] R. V. Harlander and W. B. Kilgore, Phys. Rev. Lett. **88**, 201801 (2002), [hep-ph/0201206]; C. Anastasiou and K. Melnikov, Nucl. Phys. **B646**, 220 (2002), [hep-ph/0207004]; V. Ravindran, J. Smith and W. L. van Neerven, Nucl. Phys. **B665**, 325 (2003), [hep-ph/0302135].
- [56] A. Djouadi and P. Gambino, Phys. Rev. Lett. **73**, 2528 (1994), [hep-ph/9406432]; S. Actis *et al.*, Phys. Lett. **B670**, 12 (2008), [arXiv:0809.1301]; U. Aglietti *et al.*, Phys. Lett. **B595**, 432 (2004), [hep-ph/0404071]; G. Degrandi and F. Maltoni, Phys. Lett. **B600**, 255 (2004), [hep-ph/0407249].
- [57] M. Bonetti, K. Melnikov and L. Tancredi, Phys. Rev. **D97**, 5, 056017 (2018), [Erratum: Phys. Rev. **D97**, 9, 099906 (2018)], [arXiv:1801.10403]; M. Bonetti *et al.*, JHEP **11**, 045 (2020), [arXiv:2007.09813]; M. Becchetti *et al.*, Phys. Rev. D **103**, 5, 054037 (2021), [arXiv:2010.09451].
- [58] C. Anastasiou, R. Boughezal and F. Petriello, JHEP **04**, 003 (2009), [arXiv:0811.3458].
- [59] C. Anastasiou *et al.*, JHEP **03**, 162 (2019), [arXiv:1811.11211].
- [60] M. Bonvini *et al.*, JHEP **08**, 105 (2016), [arXiv:1603.08000].
- [61] B. Mistlberger, JHEP **05**, 028 (2018), [arXiv:1802.00833].
- [62] J. McGowan *et al.*, Eur. Phys. J. C **83**, 3, 185 (2023), [Erratum: Eur.Phys.J.C 83, 302 (2023)], [arXiv:2207.04739].
- [63] F. Dulat, B. Mistlberger and A. Pelloni, Phys. Rev. D **99**, 3, 034004 (2019), [arXiv:1810.09462].
- [64] X. Chen *et al.*, Phys. Rev. Lett. **127**, 7, 072002 (2021), [arXiv:2102.07607].
- [65] G. Billis *et al.*, Phys. Rev. Lett. **127**, 7, 072001 (2021), [arXiv:2102.08039].
- [66] A. Banfi, G. P. Salam and G. Zanderighi, JHEP **06**, 159 (2012), [arXiv:1203.5773]; T. Becher, M. Neubert and D. Wilhelm, JHEP **05**, 110 (2013), [arXiv:1212.2621]; A. Banfi *et al.*, JHEP **04**, 049 (2016), [arXiv:1511.02886]; J. K. L. Michel, P. Pietrulewicz and F. J. Tackmann, JHEP **04**, 142 (2019), [arXiv:1810.12911]; P. F. Monni, L. Rottoli and P. Torrielli, Phys. Rev. Lett. **124**, 25, 252001 (2020), [arXiv:1909.04704].
- [67] I. Moulton and I. W. Stewart, JHEP **09**, 129 (2014), [arXiv:1405.5534].
- [68] V. D. Barger *et al.*, Phys. Rev. **D44**, 1426 (1991).
- [69] F. A. Dreyer and A. Karlberg, Phys. Rev. Lett. **117**, 7, 072001 (2016), [arXiv:1606.00840].

- [70] M. Cacciari *et al.*, Phys. Rev. Lett. **115**, 8, 082002 (2015), [Erratum: Phys. Rev. Lett. **120**, 13,139901 (2018)], [arXiv:1506.02660]; J. Cruz-Martinez *et al.*, Phys. Lett. **B781**, 672 (2018), [arXiv:1802.02445].
- [71] T. Han, G. Valencia and S. Willenbrock, Phys. Rev. Lett. **69**, 3274 (1992), [hep-ph/9206246].
- [72] T. Liu, K. Melnikov and A. A. Penin, Phys. Rev. Lett. **123**, 12, 122002 (2019), [arXiv:1906.10899].
- [73] F. A. Dreyer, A. Karlberg and L. Tancredi, JHEP **10**, 131 (2020), [arXiv:2005.11334].
- [74] M. Rauch and D. Zeppenfeld, Phys. Rev. **D95**, 11, 114015 (2017), [arXiv:1703.05676].
- [75] A. Buckley *et al.* (2021), [arXiv:2105.11399].
- [76] A. Denner *et al.*, JHEP **03**, 075 (2012), [arXiv:1112.5142].
- [77] A. Denner *et al.*, Comput. Phys. Commun. **195**, 161 (2015), [arXiv:1412.5390].
- [78] S. L. Glashow, D. V. Nanopoulos and A. Yildiz, Phys. Rev. **D18**, 1724 (1978); T. Han and S. Willenbrock, Phys. Lett. **B273**, 167 (1991); T. Han, G. Valencia, and S. Willenbrock, Phys. Rev. Lett. **69**, 3274 (1992); H. Baer, B. Bailey and J. F. Owens, Phys. Rev. **D47**, 2730 (1993); J. Ohnemus and W. J. Stirling, Phys. Rev. **D47**, 2722 (1993).
- [79] A. Stange, W. J. Marciano and S. Willenbrock, Phys. Rev. **D49**, 1354 (1994), [hep-ph/9309294]; A. Stange, W. J. Marciano and S. Willenbrock, Phys. Rev. **D50**, 4491 (1994), [hep-ph/9404247].
- [80] M. L. Ciccolini, S. Dittmaier and M. Krämer, Phys. Rev. **D68**, 073003 (2003), [hep-ph/0306234].
- [81] R. Hamberg, W. L. van Neerven and T. Matsuura, Nucl. Phys. **B359**, 343 (1991), [Erratum: Nucl. Phys. **B644**, 403 (2002)].
- [82] O. Brein, A. Djouadi and R. Harlander, Phys. Lett. **B579**, 149 (2004), [hep-ph/0307206]; L. Altenkamp *et al.*, JHEP **02**, 078 (2013), [arXiv:1211.5015].
- [83] J. Davies, G. Mishima and M. Steinhauser, JHEP **03**, 034 (2021), [arXiv:2011.12314]; L. Chen *et al.*, JHEP **03**, 125 (2021), [arXiv:2011.12325].
- [84] O. Brein *et al.*, Eur. Phys. J. **C72**, 1868 (2012), [arXiv:1111.0761].
- [85] O. Brein, R. V. Harlander and T. J. E. Zirke, Comput. Phys. Commun. **184**, 998 (2013), [arXiv:1210.5347]; R. V. Harlander *et al.*, JHEP **05**, 089 (2018), [arXiv:1802.04817].
- [86] R. Gauld *et al.*, Phys. Lett. B **817**, 136335 (2021), [arXiv:2009.14209].
- [87] A. Denner *et al.*, JHEP **03**, 075 (2012), [arXiv:1112.5142].
- [88] G. Ferrera, M. Grazzini, and F. Tramontano, Phys. Rev. Lett. **107**, 152003 (2011).
- [89] G. Ferrera, M. Grazzini and F. Tramontano, Phys. Lett. **B740**, 51 (2015), [arXiv:1407.4747]; J. M. Campbell, R. K. Ellis and C. Williams, JHEP **06**, 179 (2016), [arXiv:1601.00658].
- [90] W. Astill *et al.*, JHEP **06**, 154 (2016), [arXiv:1603.01620].
- [91] F. Caola *et al.*, Phys. Rev. **D97**, 7, 074022 (2018), [arXiv:1712.06954]; R. Gauld *et al.*, JHEP **10**, 002 (2019), [arXiv:1907.05836].
- [92] J. M. Butterworth *et al.*, Phys. Rev. Lett. **100**, 242001 (2008), [arXiv:0802.2470].
- [93] A. Behring *et al.*, Phys. Rev. D **101**, 11, 114012 (2020), [arXiv:2003.08321].
- [94] W. Bizon *et al.* (2021), [arXiv:2106.06328].
- [95] J. Baglio *et al.*, JHEP **12**, 066 (2022), [arXiv:2209.06138].
- [96] R. Raitio and W. W. Wada, Phys. Rev. **D19**, 941 (1979); Z. Kunszt, Nucl. Phys. **B247**, 339 (1984); J. N. Ng and P. Zakarauskas, Phys. Rev. D **29**, 876 (1984); J. F. Gunion, Phys. Lett. **B261**, 510 (1991); W. J. Marciano and F. E. Paige, Phys. Rev. Lett. **66**, 2433 (1991).
- [97] W. Beenakker *et al.*, Phys. Rev. Lett. **87**, 201805 (2001), [hep-ph/0107081]; L. Reina and S. Dawson, Phys. Rev. Lett. **87**, 201804 (2001), [hep-ph/0107101]; L. Reina, S. Dawson and D. Wackerroth, Phys. Rev. D **65**, 053017 (2002), [hep-ph/0109066]; S. Dawson *et al.*, Phys. Rev. **D67**, 071503 (2003), [hep-ph/0211438]; W. Beenakker *et al.*, Nucl. Phys. **B653**, 151 (2003), [hep-ph/0211352]; S. Dawson *et al.*, Phys. Rev. **D68**, 034022 (2003), [hep-ph/0305087].
- [98] Y. Zhang *et al.*, Phys. Lett. **B738**, 1 (2014), [arXiv:1407.1110]; S. Frixione *et al.*, JHEP **09**, 065 (2014), [arXiv:1407.0823]; S. Frixione *et al.*, JHEP **06**, 184 (2015), [arXiv:1504.03446].
- [99] T. Plehn, G. P. Salam and M. Spannowsky, Phys. Rev. Lett. **104**, 111801 (2010), [arXiv:0910.5472].
- [100] A. Kulesza *et al.*, JHEP **03**, 065 (2016), [arXiv:1509.02780]; A. Broggio *et al.*, JHEP **03**, 124 (2016), [arXiv:1510.01914]; A. Broggio *et al.*, JHEP **02**, 126 (2017), [arXiv:1611.00049]; A. Kulesza *et al.*, Phys. Rev. D **97**, 11, 114007 (2018), [arXiv:1704.03363]; A. Broggio *et al.*, JHEP **08**, 039 (2019), [arXiv:1907.04343]; A. Kulesza *et al.*, Eur. Phys. J. C **80**, 5, 428 (2020), [arXiv:2001.03031].
- [101] A. Denner and R. Feger, JHEP **11**, 209 (2015), [arXiv:1506.07448].
- [102] A. Denner *et al.*, JHEP **02**, 053 (2017), [arXiv:1612.07138].
- [103] R. Frederix *et al.*, Phys. Lett. **B701**, 427 (2011), [arXiv:1104.5613]; H. B. Hartanto *et al.*, Phys. Rev. D **91**, 9, 094003 (2015), [arXiv:1501.04498].
- [104] S. Catani *et al.*, Eur. Phys. J. C **81**, 6, 491 (2021), [arXiv:2102.03256].
- [105] C. Branchiaccio *et al.*, JHEP **08**, 145 (2021), [arXiv:2106.06516].
- [106] F. Demartin *et al.*, Eur. Phys. J. **C75**, 6, 267 (2015), [arXiv:1504.00611].
- [107] D. Pagani, I. Tsinikos and E. Vryonidou, JHEP **08**, 082 (2020), [arXiv:2006.10086].
- [108] C. Duhr *et al.*, JHEP **08**, 08, 017 (2020), [arXiv:2004.04752].
- [109] K.A. Assamagan *et al.*, [Higgs Working Group, "Physics at TeV Colliders" workshop, Les Houches, 2003], arXiv:hep-ph/0406152 (2004).
- [110] R. V. Harlander and W. B. Kilgore, Phys. Rev. **D68**, 013001 (2003), [hep-ph/0304035]; J. M. Campbell *et al.*, Phys. Rev. **D67**, 095002 (2003), [hep-ph/0204093]; S. Dawson *et al.*, Phys. Rev. Lett. **94**, 031802 (2005), [hep-ph/0408077]; S. Dittmaier, M. Krämer and M. Spira, Phys. Rev. **D70**, 074010 (2004), [hep-ph/0309204]; S. Dawson *et al.*, Phys. Rev. **D69**, 074027 (2004), [hep-ph/0311067].
- [111] W. J. Stirling and D. J. Summers, Phys. Lett. **B283**, 411 (1992); F. Maltoni *et al.*, Phys. Rev. **D64**, 094023 (2001), [hep-ph/0106293].
- [112] D. Pagani, H.-S. Shao and M. Zaro, JHEP **11**, 036 (2020), [arXiv:2005.10277].
- [113] C. Grojean, A. Paul and Z. Qian, JHEP **04**, 139 (2021), [arXiv:2011.13945].
- [114] S. Dawson, S. Dittmaier and M. Spira, Phys. Rev. **D58**, 115012 (1998), [hep-ph/9805244].
- [115] D. de Florian and J. Mazzitelli, Phys. Rev. Lett. **111**, 201801 (2013), [arXiv:1309.6594].
- [116] L.-B. Chen *et al.*, Phys. Lett. B **803**, 135292 (2020), [arXiv:1909.06808].
- [117] S. Borowka *et al.*, Phys. Rev. Lett. **117**, 1, 012001 (2016), [Erratum: Phys. Rev. Lett. **117**, 7, 079901 (2016)], [arXiv:1604.06447]; J. Baglio *et al.*, Eur. Phys. J. **C79**, 6, 459 (2019), [arXiv:1811.05692]; J. Davies *et al.*, JHEP **11**, 024 (2019), [arXiv:1907.06408].
- [118] M. Cepeda *et al.* (HL/HE-LHC WG2 group) (2019), [arXiv:1902.00134].

- [119] J. Alision *et al.*, *Rev. Phys.* **5**, 100045 (2020), [arXiv:1910.00012].
- [120] B.L. Ioffe and V.A. Khoze, *Sov. J. Nucl. Phys.* **9**, 50 (1978).
- [121] D. R. T. Jones and S. T. Petcov, *Phys. Lett.* **84B**, 440 (1979); R. N. Cahn and S. Dawson, *Phys. Lett.* **136B**, 196 (1984), [Erratum: *Phys. Lett.* **138B**, 464 (1984)]; G. L. Kane, W. W. Repko and W. B. Rolnick, *Phys. Lett.* **148B**, 367 (1984); G. Altarelli, B. Mele and F. Pitolli, *Nucl. Phys.* **B287**, 205 (1987); W. Kilian, M. Krämer and P. M. Zerwas, *Phys. Lett.* **B373**, 135 (1996), [hep-ph/9512355].
- [122] B. A. Kniehl, *Z. Phys.* **C55**, 605 (1992); J. Fleischer and F. Jegerlehner, *Nucl. Phys.* **B216**, 469 (1983); A. Denner *et al.*, *Z. Phys.* **C56**, 261 (1992); B. A. Kniehl, *Int. J. Mod. Phys.* **A17**, 1457 (2002), [hep-ph/0112023].
- [123] K. J. F. Gaemers and G. J. Gounaris, *Phys. Lett.* **77B**, 379 (1978); A. Djouadi, J. Kalinowski and P. M. Zerwas, *Z. Phys.* **C54**, 255 (1992); B. A. Kniehl, F. Madricardo and M. Steinhauser, *Phys. Rev.* **D66**, 054016 (2002), [hep-ph/0205312]; S. Dittmaier *et al.*, *Phys. Lett.* **B441**, 383 (1998), [hep-ph/9808433]; S. Dittmaier *et al.*, *Phys. Lett.* **B478**, 247 (2000), [hep-ph/0002035]; S. Dawson and L. Reina, *Phys. Rev.* **D59**, 054012 (1999), [hep-ph/9808443].
- [124] A. Arbey *et al.*, *Eur. Phys. J.* **C75**, 8, 371 (2015), [arXiv:1504.01726]; A. Freitas *et al.* (2019), [arXiv:1906.05379].
- [125] S. Frixione *et al.* (2021), [arXiv:2108.10261].
- [126] J. de Blas *et al.*, *JHEP* **01**, 139 (2020), [arXiv:1905.03764].
- [127] A. Denner *et al.*, *Eur. Phys. J.* **C71**, 1753 (2011), [arXiv:1107.5909].
- [128] A. Djouadi, J. Kalinowski, and M. Spira, *Comp. Phys. Comm.* **108**, 56 (1998); A. Djouadi *et al.*, arXiv:1003.1643 [hep-ph] (2010).
- [129] S. G. Gorishnii *et al.*, *Mod. Phys. Lett.* **A5**, 2703 (1990); S. G. Gorishnii *et al.*, *Phys. Rev.* **D43**, 1633 (1991); A. L. Kataev and V. T. Kim, *Mod. Phys. Lett.* **A9**, 1309 (1994); L. R. Surguladze, *Phys. Lett.* **B341**, 60 (1994), [hep-ph/9405325]; S. A. Larin, T. van Ritbergen and J. A. M. Vermaseren, *Phys. Lett.* **B362**, 134 (1995), [hep-ph/9506465]; K. G. Chetyrkin and A. Kwiatkowski, *Nucl. Phys.* **B461**, 3 (1996), [hep-ph/9505358]; K. G. Chetyrkin, *Phys. Lett.* **B390**, 309 (1997), [hep-ph/9608318]; P. A. Baikov, K. G. Chetyrkin and J. H. Kuhn, *Phys. Rev. Lett.* **96**, 012003 (2006), [hep-ph/0511063].
- [130] J. Fleischer and F. Jegerlehner, *Phys. Rev.* **D23**, 2001 (1981); D. Yu. Bardin, B. M. Vilensky and P. K. Khristova, *Sov. J. Nucl. Phys.* **53**, 152 (1991), [*Yad. Fiz.*53,240(1991)]; A. Dabelstein and W. Hollik, *Z. Phys.* **C53**, 507 (1992); B. A. Kniehl, *Nucl. Phys.* **B376**, 3 (1992); A. Djouadi *et al.*, in "In *Munich/Annecy/Hamburg 1991, Proceedings, e+ e-collisions at 500 GeV, pt. A* 11-30," (1991).
- [131] T. Inami, T. Kubota and Y. Okada, *Z. Phys.* **C18**, 69 (1983); K. G. Chetyrkin, B. A. Kniehl and M. Steinhauser, *Phys. Rev. Lett.* **79**, 353 (1997), [hep-ph/9705240]; P. A. Baikov and K. G. Chetyrkin, *Phys. Rev. Lett.* **97**, 061803 (2006), [hep-ph/0604194].
- [132] H.-Q. Zheng and D.-D. Wu, *Phys. Rev.* **D42**, 3760 (1990); A. Djouadi *et al.*, *Phys. Lett.* **B257**, 187 (1991); S. Dawson and R. P. Kauffman, *Phys. Rev.* **D47**, 1264 (1993); A. Djouadi, M. Spira and P. M. Zerwas, *Phys. Lett.* **B311**, 255 (1993), [hep-ph/9305335]; K. Melnikov and O. I. Yakovlev, *Phys. Lett.* **B312**, 179 (1993), [hep-ph/9302281]; M. Inoue *et al.*, *Mod. Phys. Lett.* **A9**, 1189 (1994).
- [133] P. Maierhöfer and P. Marquard, *Phys. Lett.* **B721**, 131 (2013), [arXiv:1212.6233].
- [134] U. Aglietti *et al.*, *Phys. Lett.* **B595**, 432 (2004), [hep-ph/0404071]; G. Degrossi and F. Maltoni, *Phys. Lett.* **B600**, 255 (2004), [hep-ph/0407249]; S. Actis *et al.*, *Phys. Lett.* **B670**, 12 (2008), [arXiv:0809.1301]; U. Aglietti *et al.*, *Phys. Lett.* **B600**, 57 (2004), [hep-ph/0407162]; G. Degrossi and F. Maltoni, *Nucl. Phys.* **B724**, 183 (2005), [hep-ph/0504137]; U. Aglietti *et al.*, FERMILAB-CONF (2006), [hep-ph/0612172].
- [135] A. Abbasabadi *et al.*, *Phys. Rev.* **D55**, 5647 (1997), [hep-ph/9611209]; A. Abbasabadi and W. W. Repko, *Phys. Rev.* **D71**, 017304 (2005), [hep-ph/0411152]; A. Abbasabadi and W. W. Repko, *JHEP* **08**, 048 (2006), [hep-ph/0602087]; D. A. Dicus and W. W. Repko, *Phys. Rev.* **D87**, 7, 077301 (2013), [arXiv:1302.2159]; L.-B. Chen, C.-F. Qiao and R.-L. Zhu, *Phys. Lett.* **B726**, 306 (2013), [arXiv:1211.6058]; Y. Sun, H.-R. Chang and D.-N. Gao, *JHEP* **05**, 061 (2013), [arXiv:1303.2230]; G. Passarino, *Phys. Lett.* **B727**, 424 (2013), [arXiv:1308.0422].
- [136] M. Spira, A. Djouadi and P. M. Zerwas, *Phys. Lett.* **B276**, 350 (1992).
- [137] A. Bredenstein *et al.*, *Phys. Rev.* **D74**, 013004 (2006), [hep-ph/0604011]; A. Bredenstein *et al.*, *JHEP* **02**, 080 (2007), [hep-ph/0611234]; A. Bredenstein *et al.*, *Prophecy4f: A Monte Carlo generator for a proper description of the Higgs decay into 4 fermions*, <http://omnibus.uni-freiburg.de/~sd565/programs/prophecy4f/prophecy4f.html>.
- [138] A. Ghinculov, *Phys. Lett.* **B337**, 137 (1994), [Erratum: *Phys. Lett.* **B346**, 426 (1995)], [hep-ph/9405394]; L. Durand, B. A. Kniehl and K. Riesselmann, *Phys. Rev.* **D51**, 5007 (1995), [hep-ph/9412311]; L. Durand, K. Riesselmann and B. A. Kniehl, *Phys. Rev. Lett.* **72**, 2534 (1994), [Erratum: *Phys. Rev. Lett.* **74**, 1699 (1995)].
- [139] R. Barate *et al.* (LEP Working Group for Higgs boson searches, ALEPH, DELPHI, L3, OPAL), *Phys. Lett.* **B565**, 61 (2003), [hep-ex/0306033].
- [140] LHC Programme Coordination, "LHC Delivered Luminosities", <https://lpc.web.cern.ch>.
- [141] M. Tanabashi *et al.* (Particle Data Group), *Phys. Rev.* **D98**, 3, 030001 (2018).
- [142] Y. L. Dokshitzer, S. I. Troian and V. A. Khoze, *Sov. J. Nucl. Phys.* **46**, 712 (1987), [*Yad. Fiz.*46,1220(1987)].
- [143] M. Dittmar and H. K. Dreiner, *Phys. Rev.* **D55**, 167 (1997), [hep-ph/9608317].
- [144] G. Aad *et al.* (ATLAS, CMS), *Phys. Rev. Lett.* **114**, 191803 (2015), [arXiv:1503.07589].
- [145] M. Aaboud *et al.* (ATLAS), *Phys. Lett.* **B784**, 345 (2018), [arXiv:1806.00242].
- [146] ATLAS Collaboration, ATLAS-CONF-2020-005 (2020).
- [147] A. M. Sirunyan *et al.* (CMS), *JHEP* **11**, 047 (2017), [arXiv:1706.09936].
- [148] A. M. Sirunyan *et al.* (CMS), *Phys. Lett. B* **805**, 135425 (2020), [arXiv:2002.06398].
- [149] G. Aad *et al.* (ATLAS) (2023), [arXiv:2308.07216].
- [150] G. Aad *et al.* (ATLAS), *Phys. Lett. B* **843**, 137880 (2023), [arXiv:2207.00320].
- [151] G. Aad *et al.* (ATLAS) (2023), [arXiv:2308.04775].
- [152] CMS Collaboration, CMS-PAS-HIG-21-019 (2023).
- [153] G. Aad *et al.* (ATLAS, CMS), *JHEP* **08**, 045 (2016), [arXiv:1606.02266].
- [154] M. Aaboud *et al.* (ATLAS), *Phys. Rev.* **D99**, 072001 (2019), [arXiv:1811.08856].
- [155] A. M. Sirunyan *et al.* (CMS), *Phys. Lett.* **B779**, 283 (2018), [arXiv:1708.00373].
- [156] CMS Collaboration, CMS-PAS-HIG-18-032 (2019).
- [157] G. Aad *et al.* (ATLAS), *JHEP* **08**, 175 (2022), [arXiv:2201.08269].
- [158] A. Tumasyan *et al.* (CMS), *Eur. Phys. J. C* **83**, 7, 562 (2023), [arXiv:2204.12957].
- [159] A. Tumasyan *et al.* (CMS), *Phys. Rev. Lett.* **128**, 8, 081805 (2022), [arXiv:2107.11486].

- [160] T. Aaltonen *et al.* (CDF, D0), Phys. Rev. Lett. **109**, 071804 (2012), [arXiv:1207.6436].
- [161] M. Aaboud *et al.* (ATLAS), Phys. Lett. **B786**, 59 (2018), [arXiv:1808.08238].
- [162] A. M. Sirunyan *et al.* (CMS), Phys. Rev. Lett. **121**, 12, 121801 (2018), [arXiv:1808.08242].
- [163] LHCb-CONF-2016-006, CERN-LHCb-CONF-2016-006.
- [164] M. Aaboud *et al.* (ATLAS), JHEP **11**, 112 (2016), [arXiv:1606.02181].
- [165] V. Khachatryan *et al.* (CMS), Phys. Rev. **D92**, 3, 032008 (2015), [arXiv:1506.01010].
- [166] G. Aad *et al.* (ATLAS), Eur. Phys. J. C **81**, 6, 537 (2021), [arXiv:2011.08280].
- [167] A. Hayrapetyan *et al.* (CMS) (2023), [arXiv:2308.01253].
- [168] E. Gabrielli *et al.*, Nucl. Phys. **B781**, 64 (2007), [hep-ph/0702119].
- [169] G. Aad *et al.* (ATLAS), JHEP **03**, 268 (2021), [arXiv:2010.13651].
- [170] G. Aad *et al.* (ATLAS), Phys. Rev. D **105**, 9, 092003 (2022), [arXiv:2111.08340].
- [171] CMS Collaboration, CMS-PAS-HIG-21-020 (2023).
- [172] V. Khachatryan *et al.* (CMS), Eur. Phys. J. **C75**, 6, 251 (2015), [arXiv:1502.02485].
- [173] G. Aad *et al.* (ATLAS), Phys. Lett. **B749**, 519 (2015), [arXiv:1506.05988].
- [174] M. Aaboud *et al.* (ATLAS), Phys. Lett. B **784**, 173 (2018), [arXiv:1806.00425].
- [175] A. M. Sirunyan *et al.* (CMS), Phys. Rev. Lett. **120**, 23, 231801 (2018), [arXiv:1804.02610].
- [176] G. Aad *et al.* (ATLAS), Eur. Phys. J. C **80**, 10, 957 (2020), [Erratum: Eur.Phys.J.C 81, 29 (2021), Erratum: Eur.Phys.J.C 81, 398 (2021)], [arXiv:2004.03447].
- [177] A. M. Sirunyan *et al.* (CMS), Eur. Phys. J. C **81**, 6, 488 (2021), [arXiv:2103.04956].
- [178] A. M. Sirunyan *et al.* (CMS), Eur. Phys. J. C **81**, 4, 378 (2021), [arXiv:2011.03652].
- [179] ATLAS Collaboration, ATLAS-CONF-2019-045 (2019).
- [180] ATLAS Collaboration, ATLAS-CONF-2021-044 (2021).
- [181] G. Aad *et al.* (ATLAS), JHEP **06**, 097 (2022), [arXiv:2111.06712].
- [182] CMS Collaboration, CMS-PAS-HIG-19-011 (2023).
- [183] Nature **607**, 7917, 52 (2022), [Erratum: Nature 612, E24 (2022)], [arXiv:2207.00092].
- [184] A. Tumasyan *et al.* (CMS), Nature **607**, 7917, 60 (2022), [arXiv:2207.00043].
- [185] M. Farina *et al.*, JHEP **05**, 022 (2013), [arXiv:1211.3736].
- [186] CMS Collaboration, CMS-PAS-HIG-17-005 (2017).
- [187] CMS Collaboration, CMS-PAS-HIG-16-019 (2016).
- [188] R. L. Workman *et al.* (Particle Data Group), PTEP **2022**, 083C01 (2022).
- [189] C. Patrignani *et al.* (Particle Data Group), Chin. Phys. **C40**, 10, 100001 (2016).
- [190] G. Aad *et al.*, Physics Letters B **812**, 135980 (2021), ISSN 0370-2693, URL <https://www.sciencedirect.com/science/article/pii/S0370269320307838>.
- [191] A. M. Sirunyan *et al.* (CMS), JHEP **01**, 148 (2021), [arXiv:2009.04363].
- [192] C. Delaunay *et al.*, Phys. Rev. **D89**, 3, 033014 (2014), [arXiv:1310.7029].
- [193] (2022), [arXiv:2205.05550].
- [194] H. Qu and L. Gouskos, Phys. Rev. D **101**, 056019 (2020), URL <https://link.aps.org/doi/10.1103/PhysRevD.101.056019>.
- [195] G. Aad *et al.* (ATLAS), Eur. Phys. J. C **82**, 717 (2022), [arXiv:2201.11428].
- [196] A. Tumasyan *et al.* (CMS), Phys. Rev. Lett. **131**, 4, 041801 (2023), [arXiv:2211.14181].
- [197] G. Aad *et al.* (CMS, ATLAS) (2023), [arXiv:2309.03501].
- [198] V. Khachatryan *et al.* (CMS), Phys. Lett. **B753**, 341 (2016), [arXiv:1507.03031].
- [199] A. M. Sirunyan *et al.* (CMS), JHEP **11**, 152 (2018), [arXiv:1806.05996].
- [200] G. Aad *et al.* (ATLAS), Phys. Lett. B **819**, 136412 (2021), [arXiv:2103.10322].
- [201] A. M. Sirunyan *et al.* (CMS) (2022), [arXiv:2208.00265].
- [202] G. Aad *et al.* (ATLAS), Phys. Lett. B **801**, 135148 (2020), [arXiv:1909.10235].
- [203] A. Djouadi *et al.*, Eur. Phys. J. **C73**, 6, 2455 (2013), [arXiv:1205.3169].
- [204] O. J. P. Eboli and D. Zeppenfeld, Phys. Lett. **B495**, 147 (2000), [hep-ph/0009158].
- [205] Phys. Lett. B **842**, 137963 (2023), [arXiv:2301.10731].
- [206] (2023), [arXiv:2303.01214].
- [207] A. Tumasyan *et al.* (CMS), Phys. Rev. D **105**, 9, 092007 (2022), [arXiv:2201.11585].
- [208] G. Isidori, A. V. Manohar and M. Trott, Phys. Lett. **B728**, 131 (2014), [arXiv:1305.0663]; G. T. Bodwin *et al.*, Phys. Rev. **D88**, 5, 053003 (2013), [arXiv:1306.5770]; M. König and M. Neubert, JHEP **08**, 012 (2015), [arXiv:1505.03870].
- [209] G. Aad *et al.* (ATLAS), Phys. Rev. Lett. **114**, 12, 121801 (2015), [arXiv:1501.03276].
- [210] G. Aad *et al.* (ATLAS), Eur. Phys. J. C **83**, 9, 781 (2023), [arXiv:2208.03122].
- [211] A. M. Sirunyan *et al.* (CMS), Phys. Lett. **B797**, 134811 (2019), [arXiv:1905.10408].
- [212] (2023), [arXiv:2301.09938].
- [213] G. Aad *et al.* (ATLAS), Phys. Rev. Lett. **125**, 22, 221802 (2020), [arXiv:2004.01678].
- [214] CMS Collaboration, CMS-PAS-HIG-20-008 (2022).
- [215] A. M. Sirunyan *et al.* (CMS), Phys. Rev. D **104**, 3, 032013 (2021), [arXiv:2105.03007].
- [216] G. Aad *et al.* (ATLAS), JHEP **11**, 211 (2015), [arXiv:1508.03372].
- [217] G. Aad *et al.* (ATLAS), Eur. Phys. J. **C77**, 2, 70 (2017), [arXiv:1604.07730].
- [218] V. Khachatryan *et al.* (CMS), Phys. Lett. **B763**, 472 (2016), [arXiv:1607.03561].
- [219] G. Aad *et al.* (ATLAS) (2019), [arXiv:1907.06131].
- [220] A. M. Sirunyan *et al.* (CMS), JHEP **06**, 001 (2018), [arXiv:1712.07173].
- [221] G. Aad *et al.* (ATLAS), JHEP **07**, 166 (2023), [arXiv:2302.05225].
- [222] A. Hayrapetyan *et al.* (CMS) (2023), [arXiv:2305.18106].
- [223] G. Aad *et al.* (ATLAS), JHEP **12**, 061 (2015), [arXiv:1509.06047].
- [224] V. Khachatryan *et al.* (CMS), JHEP **02**, 079 (2017), [arXiv:1610.04857].
- [225] ATLAS Collaboration, JHEP **129**, 010 (2017).
- [226] A. Tumasyan *et al.* (CMS), JHEP **02**, 169 (2022), [arXiv:2112.09734].
- [227] D. Curtin *et al.*, Phys. Rev. D **90**, 7, 075004 (2014), [arXiv:1312.4992].
- [228] M. J. Strassler and K. M. Zurek, Phys. Lett. **B651**, 374 (2007), [hep-ph/0604261]; M. J. Strassler and K. M. Zurek, Phys. Lett. **B661**, 263 (2008), [hep-ph/0605193].
- [229] T. Han *et al.*, JHEP **07**, 008 (2008), [arXiv:0712.2041].

- [230] A. Falkowski *et al.*, Phys. Rev. Lett. **105**, 241801 (2010), [arXiv:1007.3496].
- [231] G. Aad *et al.* (ATLAS), Eur. Phys. J. C **80**, 5, 450 (2020), [arXiv:1909.01246].
- [232] CMS Collaboration, CMS-PAS-EXO-19-007 (2019).
- [233] D. Tucker-Smith and N. Weiner, Phys. Rev. **D64**, 043502 (2001), [hep-ph/0101138].
- [234] S. Chatrchyan *et al.* (CMS), Phys. Lett. **B726**, 564 (2013), [arXiv:1210.7619].
- [235] G. Aad *et al.* (ATLAS), Phys. Lett. B **843**, 137745 (2023), [arXiv:2211.01216].
- [236] A. Tumasyan *et al.* (CMS), Phys. Lett. B **842**, 137531 (2023), [arXiv:2206.09401].
- [237] A. Tumasyan *et al.* (CMS), Phys. Rev. Lett. **129**, 8, 081802 (2022), [arXiv:2202.09617].
- [238] S. Di Vita *et al.*, JHEP **09**, 069 (2017), [arXiv:1704.01953]; F. Maltoni *et al.*, Eur. Phys. J. **C77**, 12, 887 (2017), [arXiv:1709.08649].
- [239] S. Dawson *et al.*, in “Snowmass 2021,” (2022), [arXiv:2209.07510].
- [240] ATLAS Collaboration, ATLAS-PHYS-PUB-2022-005 (2022).
- [241] M. L. Mangano, G. Ortona and M. Selvaggi, Eur. Phys. J. C **80**, 11, 1030 (2020), [arXiv:2004.03505].
- [242] A. Riotto and M. Trodden, Ann. Rev. Nucl. Part. Sci. **49**, 35 (1999), [hep-ph/9901362].
- [243] D. E. Morrissey and M. J. Ramsey-Musolf, New J. Phys. **14**, 125003 (2012), [arXiv:1206.2942].
- [244] G. Aad *et al.* (ATLAS), Eur. Phys. J. C **83**, 6, 496 (2023), [arXiv:2303.15061].
- [245] A. Hayrapetyan *et al.* (CMS) (2023), [arXiv:2305.13439].
- [246] ATLAS Collaboration, ATLAS-CONF-2023-057 (2023).
- [247] ATLAS Collaboration, ATLAS-CONF-2022-012 (2023).
- [248] L. D. Landau, Dokl. Akad. Nauk Ser. Fiz. **60**, 2, 207 (1948); C.-N. Yang, Phys. Rev. **77**, 242 (1950).
- [249] S. Bolognesi *et al.*, Phys. Rev. **D86**, 095031 (2012), [arXiv:1208.4018].
- [250] G. Aad *et al.* (ATLAS), Eur. Phys. J. **C75**, 10, 476 (2015), [Erratum: Eur. Phys. J. **C76**, 3, 152 (2016)], [arXiv:1506.05669].
- [251] V. Khachatryan *et al.* (CMS), Phys. Rev. **D92**, 1, 012004 (2015), [arXiv:1411.3441]; G. Aad *et al.* (ATLAS), Phys. Lett. **B726**, 120 (2013), [arXiv:1307.1432].
- [252] P. Artoisenet *et al.*, JHEP **11**, 043 (2013), [arXiv:1306.6464].
- [253] J. Brod, U. Haisch and J. Zupan, JHEP **11**, 180 (2013), [arXiv:1310.1385].
- [254] J. Ellis *et al.*, JHEP **11**, 134 (2012), [arXiv:1208.6002].
- [255] D0 Collaboration, Note 6387-CONF (2013).
- [256] D0 Collaboration, Note 6406-CONF (2013).
- [257] J. C. Collins and D. E. Soper, Phys. Rev. **D16**, 2219 (1977).
- [258] ATLAS Collaboration, ATLAS-CONF-2017-043 (2017).
- [259] S. Y. Choi *et al.*, Phys. Lett. B **553**, 61 (2003), [hep-ph/0210077].
- [260] Y. Gao *et al.*, Phys. Rev. D **81**, 075022 (2010), [arXiv:1001.3396].
- [261] A. De Rujula *et al.*, Phys. Rev. **D82**, 013003 (2010), [arXiv:1001.5300].
- [262] A. M. Sirunyan *et al.* (CMS), Phys. Rev. **D99**, 11, 112003 (2019), [arXiv:1901.00174].
- [263] G. Aad *et al.* (ATLAS) (2023), [arXiv:2304.09612].
- [264] G. Aad *et al.* (ATLAS), Phys. Rev. Lett. **131**, 6, 061802 (2023), [arXiv:2208.02338].
- [265] A. M. Sirunyan *et al.* (CMS), Phys. Rev. D **104**, 5, 052004 (2021), [arXiv:2104.12152].
- [266] G. Aad *et al.* (ATLAS), Eur. Phys. J. **C76**, 12, 658 (2016), [arXiv:1602.04516].
- [267] A. M. Sirunyan *et al.* (CMS), Submitted to: Phys. Rev. (2019), [arXiv:1903.06973].
- [268] G. Aad *et al.* (ATLAS), Eur. Phys. J. C **82**, 7, 622 (2022), [arXiv:2109.13808].
- [269] A. Tumasyan *et al.* (CMS), Phys. Rev. D **108**, 3, 032013 (2023), [arXiv:2205.05120].
- [270] G. Aad *et al.* (ATLAS), Phys. Rev. Lett. **125**, 6, 061802 (2020), [arXiv:2004.04545].
- [271] (2023), [arXiv:2303.05974].
- [272] A. M. Sirunyan *et al.* (CMS), Phys. Rev. Lett. **125**, 6, 061801 (2020), [arXiv:2003.10866].
- [273] A. Tumasyan *et al.* (CMS), JHEP **07**, 092 (2023), [arXiv:2208.02686].
- [274] A. Tumasyan *et al.* (CMS), JHEP **06**, 012 (2022), [arXiv:2110.04836].
- [275] G. Aad *et al.* (ATLAS), Eur. Phys. J. C **83**, 7, 563 (2023), [arXiv:2212.05833].
- [276] ATLAS Collaboration, ATL-PHYS-PUB-2019-008 (2019).
- [277] N. Kauer and G. Passarino, JHEP **08**, 116 (2012), [arXiv:1206.4803].
- [278] G. Aad *et al.* (ATLAS), Eur. Phys. J. **C75**, 7, 335 (2015), [arXiv:1503.01060].
- [279] V. Khachatryan *et al.* (CMS), JHEP **09**, 051 (2016), [arXiv:1605.02329].
- [280] G. Aad *et al.* (ATLAS) (2023), [arXiv:2304.01532].
- [281] A. Tumasyan *et al.* (CMS), Nature Phys. **18**, 11, 1329 (2022), [arXiv:2202.06923].
- [282] G. Aad *et al.* (ATLAS), Phys. Rev. **D90**, 5, 052004 (2014), [arXiv:1406.3827].
- [283] L. J. Dixon and M. S. Siu, Phys. Rev. Lett. **90**, 252001 (2003), [hep-ph/0302233]; S. P. Martin, Phys. Rev. **D86**, 073016 (2012), [arXiv:1208.1533]; L. J. Dixon and Y. Li, Phys. Rev. Lett. **111**, 111802 (2013), [arXiv:1305.3854].
- [284] ATLAS Collaboration, ATL-PHYS-PUB-2016-009 (2016).
- [285] ATLAS Collaboration, ATL-PHYS-PUB-2013-014 (2013).
- [286] J. Campbell *et al.*, Phys. Rev. Lett. **119**, 18, 181801 (2017), [Addendum: Phys. Rev. Lett. **119**, 19, 199901 (2017)], [arXiv:1704.08259].
- [287] ATLAS Collaboration, ATL-PHYS-PUB-2014-016 (2014).
- [288] F. Caola and K. Melnikov, Phys. Rev. **D88**, 054024 (2013), [arXiv:1307.4935]; J. M. Campbell, R. K. Ellis and C. Williams, JHEP **04**, 060 (2014), [arXiv:1311.3589]; J. M. Campbell, R. K. Ellis and C. Williams, Phys. Rev. **D89**, 5, 053011 (2014), [arXiv:1312.1628].
- [289] C. Englert and M. Spannowsky, Phys. Rev. **D90**, 053003 (2014), [arXiv:1405.0285].
- [290] A. Azatov *et al.*, Zh. Eksp. Teor. Fiz. **147**, 410 (2015), [J. Exp. Theor. Phys. **120**, 354 (2015)], [arXiv:1406.6338]; A. Azatov *et al.*, JHEP **09**, 123 (2016), [arXiv:1608.00977].
- [291] A. David *et al.* (LHC Higgs Cross Section Working Group), LHC HXSWG interim recommendations to explore the coupling structure of a Higgs-like particle (2012), [arXiv:1209.0040].
- [292] M. Dührssen, Prospects for the measurement of Higgs boson coupling parameters in the mass range from 110–190 GeV (2003); M. Dührssen *et al.*, Phys. Rev. **D70**, 113009 (2004), [hep-ph/0406323]; R. Lafaye *et al.*, JHEP **08**, 009 (2009), [arXiv:0904.3866].

- [293] J. R. Espinosa *et al.*, JHEP **05**, 097 (2012), [arXiv:1202.3697]; A. Azatov, R. Contino and J. Galloway, JHEP **04**, 127 (2012), [Erratum: JHEP **04**, 140 (2013)], [arXiv:1202.3415]; D. Carmi *et al.*, JHEP **07**, 136 (2012), [arXiv:1202.3144]; J. R. Espinosa *et al.*, JHEP **12**, 045 (2012), [arXiv:1207.1717].
- [294] M. Gonzalez-Alonso *et al.*, Eur. Phys. J. **C75**, 128 (2015), [arXiv:1412.6038]; A. Greljo *et al.*, Eur. Phys. J. **C76**, 3, 158 (2016), [arXiv:1512.06135].
- [295] G. F. Giudice *et al.*, JHEP **06**, 045 (2007), [hep-ph/0703164].
- [296] S. Willenbrock and C. Zhang, Ann. Rev. Nucl. Part. Sci. **64**, 83 (2014), [arXiv:1401.0470]; I. Brivio and M. Trott, Phys. Rept. **793**, 1 (2019), [arXiv:1706.08945]; S. Dawson, C. Englert and T. Plehn, Phys. Rept. **816**, 1 (2019), [arXiv:1808.01324]; T. Cohen, PoS **TASI2018**, 011 (2019), [arXiv:1903.03622].
- [297] F. Feruglio, Int. J. Mod. Phys. **A8**, 4937 (1993), [hep-ph/9301281]; G. Buchalla, O. Catà and C. Krause, Nucl. Phys. **B880**, 552 (2014), [Erratum: Nucl. Phys. **B913**, 475 (2016)], [arXiv:1307.5017]; A. V. Manohar, in “Les Houches summer school: EFT in Particle Physics and Cosmology Les Houches, Chamonix Valley, France, July 3-28, 2017,” (2018), [arXiv:1804.05863]; I. Brivio *et al.*, JHEP **03**, 024 (2014), [arXiv:1311.1823].
- [298] T. Cohen *et al.*, JHEP **03**, 237 (2021), [arXiv:2008.08597].
- [299] I. Banta *et al.*, JHEP **02**, 029 (2022), [arXiv:2110.02967].
- [300] R. S. Gupta, A. Pomarol and F. Riva, Phys. Rev. **D91**, 3, 035001 (2015), [arXiv:1405.0181].
- [301] B. A. Kniehl and M. Spira, Z. Phys. **C69**, 77 (1995), [hep-ph/9505225].
- [302] J. Elias-Miró *et al.*, JHEP **08**, 033 (2013), [arXiv:1302.5661].
- [303] G. Buchalla *et al.*, Phys. Lett. B **750**, 298 (2015), [arXiv:1504.01707].
- [304] N. Craig *et al.*, JHEP **08**, 086 (2020), [arXiv:2001.00017].
- [305] R. Contino *et al.*, JHEP **07**, 035 (2013), [arXiv:1303.3876].
- [306] A. Azatov and J. Galloway, Phys. Rev. **D85**, 055013 (2012), [arXiv:1110.5646].
- [307] G. Isidori and M. Trott, JHEP **02**, 082 (2014), [arXiv:1307.4051]; A. Pomarol and F. Riva, JHEP **01**, 151 (2014), [arXiv:1308.2803].
- [308] J. Ellis, V. Sanz and T. You, JHEP **07**, 036 (2014), [arXiv:1404.3667]; A. Biekötter *et al.*, Phys. Rev. **D91**, 055029 (2015), [arXiv:1406.7320].
- [309] LHC Higgs Cross Section Working Group, <https://twiki.cern.ch/twiki/bin/view/LHCPhysics/LHCHWG2KAPPA>.
- [310] M. Reece, New J. Phys. **15**, 043003 (2013), [arXiv:1208.1765].
- [311] A. Azatov *et al.* (2022), [arXiv:2203.02418].
- [312] G. Aad *et al.* (ATLAS), Phys. Rev. D **101**, 1, 012002 (2020), [arXiv:1909.02845].
- [313] A. M. Sirunyan *et al.* (CMS), Phys. Lett. **B792**, 369 (2019), [arXiv:1812.06504].
- [314] G. Aad *et al.* (ATLAS), JHEP **05**, 028 (2023), [arXiv:2207.08615].
- [315] A. Hayrapetyan *et al.* (CMS) (2023), [arXiv:2305.07532].
- [316] A. Tumasyan *et al.* (CMS) (2021), [arXiv:2107.11486].
- [317] (2022), [arXiv:2208.12279].
- [318] G. Aad *et al.* (ATLAS), Phys. Lett. **B753**, 69 (2016), [arXiv:1508.02507].
- [319] N. Berger *et al.* (2019), [arXiv:1906.02754].
- [320] ATLAS Collaboration, ATLAS-CONF-2017-045 (2017).
- [321] CMS Collaboration, CMS-PAS-HIG-16-040 (2017).
- [322] CMS Collaboration, CMS-PAS-HIG-16-041 (2017).
- [323] ATLAS Collaboration, ATLAS-CONF-2018-028 (2018).
- [324] A. M. Sirunyan *et al.* (CMS), JHEP **07**, 027 (2021), [arXiv:2103.06956].
- [325] CMS Collaboration, CMS-PAS-HIG-19-001 (2019).
- [326] G. Aad *et al.* (ATLAS), Phys. Rev. D **108**, 032005 (2023), [arXiv:2207.00338].
- [327] A. Tumasyan *et al.* (CMS), Eur. Phys. J. C **83**, 7, 667 (2023), [arXiv:2206.09466].
- [328] M. Aaboud *et al.* (ATLAS), JHEP **05**, 141 (2019), [arXiv:1903.04618].
- [329] ATLAS Collaboration, ATLAS-CONF-2020-027 (2020).
- [330] ATLAS Collaboration, ATLAS-CONF-2020-053 (2020).
- [331] J. de Blas *et al.*, JHEP **03**, 109 (2018), [arXiv:1711.10391].
- [332] I. Brivio *et al.*, SciPost Phys. **12**, 1, 036 (2022), [arXiv:2108.01094].
- [333] A. Carmona *et al.*, SciPost Phys. **12**, 6, 198 (2022), [arXiv:2112.10787].
- [334] J. Fuentes-Martín *et al.*, Eur. Phys. J. C **83**, 7, 662 (2023), [arXiv:2212.04510].
- [335] A. Manohar and H. Georgi, Nucl. Phys. **B234**, 189 (1984); M. A. Luty, Phys. Rev. **D57**, 1531 (1998), [hep-ph/9706235]; D. Liu *et al.*, JHEP **11**, 141 (2016), [arXiv:1603.03064].
- [336] W. Buchmuller and D. Wyler, Nucl. Phys. **B268**, 621 (1986).
- [337] C. J. C. Burges and H. J. Schnitzer, Nucl. Phys. **B228**, 464 (1983); C. N. Leung, S. T. Love and S. Rao, Z. Phys. **C31**, 433 (1986).
- [338] B. Grzadkowski *et al.*, JHEP **10**, 085 (2010), [arXiv:1008.4884].
- [339] L. Lehman and A. Martin, JHEP **02**, 081 (2016), [arXiv:1510.00372]; B. Henning *et al.*, JHEP **08**, 016 (2017), [arXiv:1512.03433].
- [340] C. Hays *et al.*, JHEP **02**, 123 (2019), [arXiv:1808.00442].
- [341] R. Alonso *et al.*, JHEP **04**, 159 (2014), [arXiv:1312.2014].
- [342] ATLAS Collaboration, ATLAS-CONF-2022-037 (2022).
- [343] J. Ellis *et al.*, JHEP **04**, 279 (2021), [arXiv:2012.02779].
- [344] J. J. Ethier *et al.* (SMEFT), JHEP **11**, 089 (2021), [arXiv:2105.00006].
- [345] Y. Gershtein, and A. Pomarol, *Extra Dimensions*, in this volume.
- [346] M. Carena *et al.*, Phys. Rev. **D91**, 3, 035003 (2015), [arXiv:1410.4969].
- [347] M. Carena *et al.*, Phys. Rev. **D93**, 3, 035013 (2016), [arXiv:1510.09137].
- [348] J. F. Gunion and H. E. Haber, Phys. Rev. **D67**, 075019 (2003), [hep-ph/0207010].
- [349] H. E. Haber and Y. Nir, Nucl. Phys. **B335**, 363 (1990).
- [350] S. Weinberg, Phys. Rev. **D13**, 974 (1976), [Addendum: Phys. Rev. **D19**, 1277 (1979)]; L. Susskind, Phys. Rev. **D20**, 2619 (1979); For a review, see C. T. Hill and E. H. Simmons, Phys. Reports **381**, 235 (2003) [Erratum: 390, 553 (2004)], [arXiv:hep-ph/0203079].
- [351] Z. Chacko, R. Franceschini and R. K. Mishra, JHEP **04**, 015 (2013), [arXiv:1209.3259].
- [352] L. E. Ibanez and G. G. Ross, Phys. Lett. **110B**, 215 (1982); L. E. Ibanez, Phys. Lett. **118B**, 73 (1982); J. R. Ellis, D. V. Nanopoulos and K. Tamvakis, Phys. Lett. **121B**, 123 (1983); L. Alvarez-Gaume, J. Polchinski and M. B. Wise, Nucl. Phys. **B221**, 495 (1983).
- [353] S. Dimopoulos and G. F. Giudice, Phys. Lett. **B357**, 573 (1995), [hep-ph/9507282]; M. Papucci, J. T. Ruderman and A. Weiler, JHEP **09**, 035 (2012), [arXiv:1110.6926].

- [354] ATLAS Collaboration, <https://twiki.cern.ch/twiki/bin/view/AtlasPublic/Publications>; CMS Collaboration, <http://cms-results.web.cern.ch/cms-results/public-results/publications/SUS/STOP.html>.
- [355] J. Mrazek *et al.*, Nucl. Phys. **B853**, 1 (2011), [arXiv:1105.5403].
- [356] D. B. Kaplan, Nucl. Phys. **B365**, 259 (1991).
- [357] G. Panico *et al.*, JHEP **03**, 051 (2013), [arXiv:1210.7114].
- [358] H. E. Haber and G. L. Kane, Phys. Rept. **117**, 75 (1985).
- [359] P. Slavich *et al.*, Eur. Phys. J. C **81**, 5, 450 (2021), [arXiv:2012.15629].
- [360] P. Draper, G. Lee and C. E. M. Wagner, Phys. Rev. **D89**, 5, 055023 (2014), [arXiv:1312.5743].
- [361] E. L. Berger *et al.*, Phys. Rev. **D66**, 095001 (2002), [hep-ph/0205342].
- [362] A. Djouadi, Phys. Rept. **459**, 1 (2008), [hep-ph/0503173].
- [363] P. Bechtle *et al.*, Eur. Phys. J. **C77**, 2, 67 (2017), [arXiv:1608.00638].
- [364] E. Bagnaschi *et al.*, Eur. Phys. J. **C79**, 7, 617 (2019), [arXiv:1808.07542].
- [365] A. Djouadi, J. Kalinowski and P. M. Zerwas, Z. Phys. **C57**, 569 (1993).
- [366] G. Lee and C. E. M. Wagner, Phys. Rev. **D92**, 7, 075032 (2015), [arXiv:1508.00576].
- [367] D. Dicus *et al.*, Phys. Rev. **D59**, 094016 (1999), [hep-ph/9811492].
- [368] M. Carena *et al.*, JHEP **07**, 091 (2012), [arXiv:1203.1041].
- [369] A. A. Barrientos Bendezu and B. A. Kniehl, Phys. Rev. **D64**, 035006 (2001), [hep-ph/0103018].
- [370] LHC Higgs Working Group, <https://twiki.cern.ch/twiki/bin/view/LHCPhysics/LHCHWGMSSMCharged>.
- [371] D. Dicus, A. Stange and S. Willenbrock, Phys. Lett. B **333**, 126 (1994), [hep-ph/9404359]; N. Craig *et al.*, JHEP **06**, 137 (2015), [arXiv:1504.04630]; S. Gori *et al.*, Phys. Rev. D **93**, 7, 075038 (2016), [arXiv:1602.02782].
- [372] A. Djouadi, J. Ellis and J. Quevillon, JHEP **07**, 105 (2016), [arXiv:1605.00542]; M. Carena and Z. Liu, JHEP **11**, 159 (2016), [arXiv:1608.07282].
- [373] LHC Higgs Working Group for BSM Higgs, <https://twiki.cern.ch/twiki/bin/view/LHCPhysics/LHCHWG3>.
- [374] M. Carena *et al.*, Eur. Phys. J. **C73**, 9, 2552 (2013), [arXiv:1302.7033].
- [375] H. Bahl, S. Liebler and T. Stefaniak, Eur. Phys. J. **C79**, 3, 279 (2019), [arXiv:1901.05933].
- [376] L. Maiani, A. D. Polosa and V. Riquer, Phys. Lett. **B718**, 465 (2012), [arXiv:1209.4816]; A. Djouadi and J. Quevillon, JHEP **10**, 028 (2013), [arXiv:1304.1787]; A. Djouadi *et al.*, Eur. Phys. J. **C73**, 2650 (2013), [arXiv:1307.5205].
- [377] E. Bagnaschi *et al.*, Eur. Phys. J. C **79**, 7, 617 (2019), [arXiv:1808.07542].
- [378] M. Carena and H. E. Haber, Prog. Part. Nucl. Phys. **50**, 63 (2003), [hep-ph/0208209].
- [379] H. Bahl *et al.*, Eur. Phys. J. C **80**, 10, 916 (2020), [arXiv:2005.14536].
- [380] R. S. Chivukula and H. Georgi, Phys. Lett. **B188**, 99 (1987); L. J. Hall and L. Randall, Phys. Rev. Lett. **65**, 2939 (1990); A. J. Buras *et al.*, Phys. Lett. **B500**, 161 (2001), [hep-ph/0007085]; G. D'Ambrosio *et al.*, Nucl. Phys. **B645**, 155 (2002), [hep-ph/0207036].
- [381] M. Misiak and M. Steinhauser, Eur. Phys. J. C **77**, 3, 201 (2017), [arXiv:1702.04571].
- [382] L. J. Hall, J. D. Lykken and S. Weinberg, Phys. Rev. **D27**, 2359 (1983); J. E. Kim and H. P. Nilles, Phys. Lett. **138B**, 150 (1984); G. F. Giudice and A. Masiero, Phys. Lett. **B206**, 480 (1988).
- [383] U. Ellwanger, C. Hugonie and A. M. Teixeira, Phys. Rept. **496**, 1 (2010), [arXiv:0910.1785].
- [384] P. Fayet, Nucl. Phys. **B90**, 104 (1975).
- [385] C. Panagiotakopoulos and K. Tamvakis, Phys. Lett. **B469**, 145 (1999), [hep-ph/9908351]; A. Dedes *et al.*, Phys. Rev. **D63**, 055009 (2001), [hep-ph/0009125]; A. Menon, D. E. Morrissey and C. E. M. Wagner, Phys. Rev. **D70**, 035005 (2004), [hep-ph/0404184].
- [386] M. Cvetič *et al.*, Phys. Rev. **D56**, 2861 (1997), [Erratum: Phys. Rev. **D58**, 119905 (1998)], [hep-ph/9703317]; P. Langacker and J. Wang, Phys. Rev. **D58**, 115010 (1998), [hep-ph/9804428].
- [387] J. Erler, P. Langacker and T.-j. Li, Phys. Rev. **D66**, 015002 (2002), [hep-ph/0205001]; T. Han, P. Langacker and B. McElrath, Phys. Rev. **D70**, 115006 (2004), [hep-ph/0405244]; V. Barger *et al.*, Phys. Rev. **D73**, 115010 (2006), [hep-ph/0603247].
- [388] V. Barger, P. Langacker and G. Shaughnessy, Phys. Rev. **D75**, 055013 (2007), [hep-ph/0611239].
- [389] D. E. Lopez-Fogliani and C. Munoz, Phys. Rev. Lett. **97**, 041801 (2006), [hep-ph/0508297].
- [390] B. A. Dobrescu, G. L. Landsberg and K. T. Matchev, Phys. Rev. **D63**, 075003 (2001), [hep-ph/0005308]; R. Dermisek and J. F. Gunion, Phys. Rev. Lett. **95**, 041801 (2005), [hep-ph/0502105].
- [391] O. J. P. Eboli and D. Zeppenfeld, Phys. Lett. **B495**, 147 (2000), [hep-ph/0009158]; H. Davoudiasl, T. Han and H. E. Logan, Phys. Rev. **D71**, 115007 (2005), [hep-ph/0412269].
- [392] J.-J. Cao *et al.*, JHEP **03**, 086 (2012), [arXiv:1202.5821].
- [393] LHC Higgs Working Group, Beyond the Standard Model Higgs – NMSSM, <https://twiki.cern.ch/twiki/bin/view/LHCPhysics/LHCHWGMSSM>.
- [394] P. Batra *et al.*, JHEP **02**, 043 (2004), [hep-ph/0309149].
- [395] R. Huo *et al.*, Phys. Rev. **D87**, 5, 055011 (2013), [arXiv:1212.0560].
- [396] J. Engel, M. J. Ramsey-Musolf and U. van Kolck, Prog. Part. Nucl. Phys. **71**, 21 (2013), [arXiv:1303.2371].
- [397] S. Dimopoulos and S. D. Thomas, Nucl. Phys. **B465**, 23 (1996), [hep-ph/9510220]; S. D. Thomas, Int. J. Mod. Phys. **A13**, 2307 (1998), [hep-ph/9803420].
- [398] A. Pilaftsis and C. E. M. Wagner, Nucl. Phys. **B553**, 3 (1999), [hep-ph/9902371].
- [399] M. Frank *et al.*, JHEP **02**, 047 (2007), [hep-ph/0611326].
- [400] M. Carena *et al.*, Nucl. Phys. **B586**, 92 (2000), [hep-ph/0003180].
- [401] B. Li and C. E. M. Wagner, Phys. Rev. **D91**, 095019 (2015), [arXiv:1502.02210].
- [402] M. D. Goodsell and F. Staub, Eur. Phys. J. **C77**, 1, 46 (2017), [arXiv:1604.05335]; A. Chakraborty *et al.*, Phys. Rev. **D90**, 5, 055005 (2014), [arXiv:1301.2745]; M. Carena *et al.*, JHEP **02**, 123 (2016), [arXiv:1512.00437].
- [403] J. F. Gunion and H. E. Haber, Phys. Rev. **D67**, 075019 (2003), [hep-ph/0207010]; G. C. Branco *et al.*, Phys. Rept. **516**, 1 (2012), [arXiv:1106.0034].
- [404] N. G. Deshpande and E. Ma, Phys. Rev. **D18**, 2574 (1978).
- [405] A. Goudelis, B. Herrmann and S. O., JHEP **09**, 106 (2013), [arXiv:1303.3010].
- [406] M. Bauer, M. Carena and K. Gemmler, JHEP **11**, 016 (2015), [arXiv:1506.01719]; M. Bauer, M. Carena and K. Gemmler, Phys. Rev. **D94**, 11, 115030 (2016), [arXiv:1512.03458].
- [407] C. D. Froggatt and H. B. Nielsen, Nucl. Phys. **B147**, 277 (1979).
- [408] K. S. Babu and S. Nandi, Phys. Rev. **D62**, 033002 (2000), [hep-ph/9907213]; G. F. Giudice and O. Lebedev, Phys. Lett. **B665**, 79 (2008), [arXiv:0804.1753].

- [409] E. Accomando *et al.*, CERN Report **2006-009** (2006), [hep-ph/0608079].
- [410] T. Robens and T. Stefaniak, Eur. Phys. J. **C75**, 104 (2015), [arXiv:1501.02234].
- [411] S. L. Glashow and S. Weinberg, Phys. Rev. **D15**, 1958 (1977); E. A. Paschos, Phys. Rev. **D15**, 1966 (1977).
- [412] G. C. Branco, W. Grimus and L. Lavoura, Phys. Lett. **B380**, 119 (1996), [hep-ph/9601383]; F. J. Botella, G. C. Branco and M. N. Rebelo, Phys. Lett. **B687**, 194 (2010), [arXiv:0911.1753].
- [413] J. Schechter and J. W. F. Valle, Phys. Rev. **D22**, 2227 (1980); T. P. Cheng and L.-F. Li, Phys. Rev. **D22**, 2860 (1980).
- [414] H. Georgi and M. Machacek, Nucl. Phys. **B262**, 463 (1985); M. S. Chanowitz and M. Golden, Phys. Lett. **165B**, 105 (1985); J. F. Gunion, R. Vega and J. Wudka, Phys. Rev. **D42**, 1673 (1990).
- [415] P. Nath *et al.*, Nucl. Phys. Proc. Suppl. **200-202**, 185 (2010), [arXiv:1001.2693].
- [416] J. Garayoa and T. Schwetz, JHEP **03**, 009 (2008), [arXiv:0712.1453].
- [417] H. E. Haber and H. E. Logan, Phys. Rev. **D62**, 015011 (2000), [hep-ph/9909335]; S. Kanemura and K. Yagyu, Phys. Rev. **D85**, 115009 (2012), [arXiv:1201.6287].
- [418] J. F. Gunion, R. Vega and J. Wudka, Phys. Rev. **D43**, 2322 (1991).
- [419] I. Low and J. Lykken, JHEP **10**, 053 (2010), [arXiv:1005.0872]; I. Low, J. Lykken and G. Shaughnessy, Phys. Rev. **D86**, 093012 (2012), [arXiv:1207.1093].
- [420] H. E. Logan and M.-A. Roy, Phys. Rev. **D82**, 115011 (2010), [arXiv:1008.4869]; A. Falkowski, S. Rychkov and A. Urbano, JHEP **04**, 073 (2012), [arXiv:1202.1532].
- [421] N. Arkani-Hamed *et al.*, JHEP **07**, 034 (2002), [hep-ph/0206021]; N. Arkani-Hamed, A. G. Cohen and H. Georgi, Phys. Lett. **B513**, 232 (2001), [hep-ph/0105239].
- [422] M. Perelstein, Prog. Part. Nucl. Phys. **58**, 247 (2007), [hep-ph/0512128]; M. Schmaltz and D. Tucker-Smith, Ann. Rev. Nucl. Part. Sci. **55**, 229 (2005), [hep-ph/0502182].
- [423] J. A. Casas, J. R. Espinosa and I. Hidalgo, JHEP **03**, 038 (2005), [hep-ph/0502066].
- [424] H.-C. Cheng and I. Low, JHEP **09**, 051 (2003), [hep-ph/0308199].
- [425] M. Carena *et al.*, Phys. Rev. **D75**, 091701 (2007), [hep-ph/0610156].
- [426] M. Aaboud *et al.* (ATLAS), Phys. Rev. Lett. **121**, 211801 (2018), [arXiv:1808.02343]; A. M. Sirunyan *et al.* (CMS), Eur. Phys. J. **C79**, 4, 364 (2019), [arXiv:1812.09768].
- [427] H. Georgi, A. E. Nelson and A. Manohar, Phys. Lett. **126B**, 169 (1983); A. E. Nelson and M. J. Strassler, JHEP **09**, 030 (2000), [hep-ph/0006251]; S. Davidson, G. Isidori and S. Uhlig, Phys. Lett. **B663**, 73 (2008), [arXiv:0711.3376].
- [428] C. Csaki, A. Falkowski and A. Weiler, JHEP **09**, 008 (2008), [arXiv:0804.1954]; B. Keren-Zur *et al.*, Nucl. Phys. **B867**, 394 (2013), [arXiv:1205.5803].
- [429] O. Matsedonskyi, G. Panico and A. Wulzer, JHEP **01**, 164 (2013), [arXiv:1204.6333]; M. Redi and A. Tesi, JHEP **10**, 166 (2012), [arXiv:1205.0232]; D. Marzocca, M. Serone and J. Shu, JHEP **08**, 013 (2012), [arXiv:1205.0770]; A. Pomarol and F. Riva, JHEP **08**, 135 (2012), [arXiv:1205.6434].
- [430] R. Contino and G. Servant, JHEP **06**, 026 (2008), [arXiv:0801.1679]; J. Mrazek and A. Wulzer, Phys. Rev. **D81**, 075006 (2010), [arXiv:0909.3977]; A. De Simone *et al.*, JHEP **04**, 004 (2013), [arXiv:1211.5663]; A. Azatov *et al.*, Phys. Rev. **D89**, 7, 075001 (2014), [arXiv:1308.6601].
- [431] A. Banfi, A. Martin and V. Sanz, JHEP **08**, 053 (2014), [arXiv:1308.4771]; A. Azatov and A. Paul, JHEP **01**, 014 (2014), [arXiv:1309.5273]; C. Grojean *et al.*, JHEP **05**, 022 (2014), [arXiv:1312.3317].
- [432] A. Azatov *et al.*, Phys. Rev. **D92**, 3, 035001 (2015), [arXiv:1502.00539].
- [433] K. Agashe, R. Contino and A. Pomarol, Nucl. Phys. **B719**, 165 (2005), [hep-ph/0412089]; R. Contino, L. Da Rold and A. Pomarol, Phys. Rev. **D75**, 055014 (2007), [hep-ph/0612048]; D. Pappadopulo, A. Thamm and R. Torre, JHEP **07**, 058 (2013), [arXiv:1303.3062]; M. Montull *et al.*, Phys. Rev. **D88**, 095006 (2013), [arXiv:1308.0559].
- [434] M. Carena, L. Da Rold and E. Pontón, JHEP **06**, 159 (2014), [arXiv:1402.2987]; D. Liu, I. Low and C. E. M. Wagner, Phys. Rev. **D96**, 3, 035013 (2017), [arXiv:1703.07791].
- [435] I. Low, R. Rattazzi and A. Vichi, JHEP **04**, 126 (2010), [arXiv:0907.5413].
- [436] M. Ciuchini *et al.*, JHEP **08**, 106 (2013), [arXiv:1306.4644].
- [437] C. Grojean, O. Matsedonskyi and G. Panico, JHEP **10**, 160 (2013), [arXiv:1306.4655].
- [438] M. Geller and O. Telem, Phys. Rev. Lett. **114**, 191801 (2015), [arXiv:1411.2974].
- [439] P. Batra and Z. Chacko, Phys. Rev. **D79**, 095012 (2009), [arXiv:0811.0394]; R. Barbieri *et al.*, JHEP **08**, 161 (2015), [arXiv:1501.07803]; M. Low, A. Tesi and L.-T. Wang, Phys. Rev. **D91**, 095012 (2015), [arXiv:1501.07890].
- [440] ATLAS Collaboration, ATLAS-CONF-2023-035 (2023).
- [441] G. Aad *et al.* (ATLAS), JHEP **07**, 155 (2023), [arXiv:2211.04172].
- [442] CMS Collaboration, CMS-PAS-HIG-20-002 (2023).
- [443] CMS Collaboration, CMS-PAS-HIG-17-13 (2017).
- [444] M. Aaboud *et al.* (ATLAS), Phys. Lett. **B775**, 105 (2017), [arXiv:1707.04147].
- [445] A. M. Sirunyan *et al.* (CMS), Phys. Lett. B **793**, 320 (2019), [arXiv:1811.08459].
- [446] ATLAS Collaboration, ATLAS-CONF-2023-030 (2023).
- [447] M. Aaboud *et al.* (ATLAS), JHEP **10**, 112 (2017), [arXiv:1708.00212].
- [448] CMS Collaboration, CMS-PAS-HIG-16-014 (2016).
- [449] G. Aad *et al.* (ATLAS), Eur. Phys. J. C **81**, 4, 332 (2021), [arXiv:2009.14791].
- [450] CMS Collaboration, CMS-PAS-HIG-16-033 (2016).
- [451] CMS Collaboration, CMS-PAS-HIG-16-023 (2016).
- [452] G. Aad *et al.* (ATLAS), Eur. Phys. J. C **83**, 7, 633 (2023), [arXiv:2207.03925].
- [453] G. Aad *et al.* (ATLAS), Eur. Phys. J. C **80**, 12, 1165 (2020), [arXiv:2004.14636].
- [454] CMS Collaboration, CMS-PAS-HIG-16-034 (2017).
- [455] A. M. Sirunyan *et al.* (CMS), Phys. Rev. D **102**, 3, 032003 (2020), [arXiv:2006.06391].
- [456] ATLAS Collaboration, ATLAS-CONF-2016-082 (2016).
- [457] ATLAS Collaboration, ATLAS-CONF-2013-067 (2013).
- [458] A. M. Sirunyan *et al.* (CMS), JHEP **03**, 034 (2020), [arXiv:1912.01594].
- [459] ATLAS Collaboration, ATLAS-CONF-2012-018 (2012).
- [460] M. Aaboud *et al.* (ATLAS), Phys. Lett. **B777**, 91 (2018), [arXiv:1708.04445].
- [461] G. Aad *et al.* (ATLAS), JHEP **09**, 091 (2019), [arXiv:1906.08589].
- [462] M. Aaboud *et al.* (ATLAS), Phys. Rev. **D98**, 5, 052008 (2018), [arXiv:1808.02380].
- [463] G. Aad *et al.* (ATLAS), Phys. Rev. D **106**, 5, 052001 (2022), [arXiv:2112.11876].

- [464] ATLAS Collaboration, ATLAS-CONF-2016-004 (2016); M. Aaboud *et al.* (ATLAS), JHEP **05**, 124 (2019), [arXiv:1811.11028]; M. Aaboud *et al.* (ATLAS), Eur. Phys. J. **C78**, 12, 1007 (2018), [arXiv:1807.08567].
- [465] ATLAS Collaboration, ATLAS-CONF-2019-030 (2019); M. Aaboud *et al.* (ATLAS), Phys. Rev. Lett. **121**, 19, 191801 (2018), [Erratum: Phys. Rev. Lett. **122**, 089901 (2019)], [arXiv:1808.00336]; G. Aad *et al.* (ATLAS) (2019), [arXiv:1908.06765].
- [466] A. M. Sirunyan *et al.* (CMS), Phys. Lett. B **788**, 7 (2019), [arXiv:1806.00408].
- [467] V. Khachatryan *et al.* (CMS), Phys. Lett. **B755**, 217 (2016), [arXiv:1510.01181].
- [468] G. Aad *et al.* (ATLAS), Phys. Rev. Lett. **125**, 5, 051801 (2020), [arXiv:2002.12223].
- [469] A. Tumasyan *et al.* (CMS), JHEP **07**, 073 (2023), [arXiv:2208.02717].
- [470] A. M. Sirunyan *et al.* (CMS), JHEP **09**, 007 (2018), [arXiv:1803.06553].
- [471] V. M. Abazov *et al.* (D0), Phys. Rev. Lett. **104**, 151801 (2010), [arXiv:0912.0968].
- [472] D0 Collaboration, D0Note 5974-CONF (2011).
- [473] R. Aaij *et al.* (LHCb), JHEP **05**, 132 (2013), [arXiv:1304.2591].
- [474] A. M. Sirunyan *et al.* (CMS), JHEP **05**, 210 (2019), [arXiv:1903.10228].
- [475] M. Aaboud *et al.* (ATLAS), JHEP **07**, 117 (2019), [arXiv:1901.08144].
- [476] A. M. Sirunyan *et al.* (CMS) (2019), [arXiv:1907.03152].
- [477] A. M. Sirunyan *et al.* (CMS), JHEP **03**, 103 (2020), [arXiv:1911.10267].
- [478] ATLAS Collaboration, ATLAS-CONF-2019-036 (2019).
- [479] A. M. Sirunyan *et al.* (CMS), JHEP **11**, 161 (2018), [arXiv:1808.01890].
- [480] G. Aad *et al.* (ATLAS), JHEP **08**, 148 (2015), [arXiv:1505.07018].
- [481] A. M. Sirunyan *et al.* (CMS), JHEP **04**, 171 (2020), [arXiv:1908.01115].
- [482] G. Aad *et al.* (ATLAS), Phys. Rev. D **102**, 3, 032004 (2020), [arXiv:1907.02749].
- [483] S. Chatrchyan *et al.* (CMS), Phys. Lett. **B722**, 207 (2013), [arXiv:1302.2892]; CMS Collaboration, CMS-PAS-HIG-16-025 (2016); A. M. Sirunyan *et al.* (CMS), JHEP **08**, 113 (2018), [arXiv:1805.12191].
- [484] V. M. Abazov *et al.* (D0), Phys. Lett. **B698**, 97 (2011), [arXiv:1011.1931].
- [485] T. Aaltonen *et al.* (CDF), Phys. Rev. **D85**, 032005 (2012), [arXiv:1106.4782].
- [486] ATLAS Collaboration, ATLAS-CONF-2017-055 (2017).
- [487] G. Aad *et al.* (ATLAS), Phys. Rev. D **102**, 11, 112008 (2020), [arXiv:2007.05293]; G. Aad *et al.* (ATLAS), Phys. Lett. **B744**, 163 (2015), [arXiv:1502.04478].
- [488] A. M. Sirunyan *et al.* (CMS), JHEP **03**, 065 (2020), [arXiv:1910.11634].
- [489] A. M. Sirunyan *et al.* (CMS), Eur. Phys. J. **C79**, 7, 564 (2019), [arXiv:1903.00941].
- [490] M. Aaboud *et al.* (ATLAS), Phys. Lett. B **783**, 392 (2018), [arXiv:1804.01126].
- [491] V. Khachatryan *et al.* (CMS), Phys. Lett. B **759**, 369 (2016), [arXiv:1603.02991].
- [492] A. M. Sirunyan *et al.* (CMS), JHEP **03**, 055 (2020), [arXiv:1911.03781].
- [493] M. Aaboud *et al.* (ATLAS), Phys. Lett. **B759**, 555 (2016), [arXiv:1603.09203].
- [494] M. Aaboud *et al.* (ATLAS), JHEP **09**, 139 (2018), [arXiv:1807.07915].
- [495] CMS Collaboration, CMS-PAS-HIG-16-031 (2016); A. M. Sirunyan *et al.* (CMS), JHEP **07**, 142 (2019), [arXiv:1903.04560].
- [496] ATLAS Collaboration, ATLAS-CONF-2012-010 (2012).
- [497] A. M. Sirunyan *et al.* (CMS), Phys. Rev. D **102**, 7, 072001 (2020), [arXiv:2005.08900].
- [498] G. Aad *et al.* (ATLAS), JHEP **06**, 145 (2021), [arXiv:2102.10076].
- [499] A. M. Sirunyan *et al.* (CMS), JHEP **07**, 126 (2020), [arXiv:2001.07763]; V. Khachatryan *et al.* (CMS), JHEP **11**, 018 (2015), [arXiv:1508.07774]; A. M. Sirunyan *et al.* (CMS) (2019), [arXiv:1908.09206].
- [500] G. Aad *et al.* (ATLAS), Phys. Rev. Lett. **114**, 23, 231801 (2015), [arXiv:1503.04233].
- [501] A. M. Sirunyan *et al.* (CMS), Phys. Rev. Lett. **119**, 14, 141802 (2017), [arXiv:1705.02942].
- [502] A. M. Sirunyan *et al.* (CMS), Eur. Phys. J. C **81**, 8, 723 (2021), [arXiv:2104.04762].
- [503] A. M. Sirunyan *et al.* (CMS), Phys. Rev. Lett. **123**, 13, 131802 (2019), [arXiv:1905.07453].
- [504] A. Tumasyan *et al.* (CMS), JHEP **09**, 032 (2023), [arXiv:2207.01046].
- [505] A. M. Sirunyan *et al.* (CMS), JHEP **11**, 115 (2018), [arXiv:1808.06575].
- [506] ATLAS Collaboration, ATLAS-CONF-2011-020 (2011).
- [507] A. M. Sirunyan *et al.* (CMS), JHEP **11**, 010 (2017), [arXiv:1707.07283].
- [508] G. Aad *et al.* (ATLAS), Phys. Rev. **D92**, 5, 052002 (2015), [arXiv:1505.01609]; ATLAS Collaboration, ATLAS-CONF-2012-079 (2012).
- [509] A. Tumasyan *et al.* (CMS), JHEP **07**, 148 (2023), [arXiv:2208.01469].
- [510] A. Tumasyan *et al.* (CMS), Phys. Rev. Lett. **131**, 101801 (2023), [arXiv:2209.06197].
- [511] A. Tumasyan *et al.* (CMS), JHEP **11**, 057 (2021), [arXiv:2106.10361].
- [512] A. M. Sirunyan *et al.* (CMS), JHEP **08**, 139 (2020), [arXiv:2005.08694]; V. Khachatryan *et al.* (CMS), JHEP **10**, 076 (2017), [arXiv:1701.02032]; A. M. Sirunyan *et al.* (CMS), Phys. Lett. **B795**, 398 (2019), [arXiv:1812.06359]; A. M. Sirunyan *et al.* (CMS), Phys. Lett. **B796**, 131 (2019), [arXiv:1812.00380]; A. M. Sirunyan *et al.* (CMS) (2019), [arXiv:1907.07235]; A. M. Sirunyan *et al.* (CMS), Phys. Lett. **B785**, 462 (2018), [arXiv:1805.10191]; A. M. Sirunyan *et al.* (CMS), JHEP **11**, 018 (2018), [arXiv:1805.04865]; CMS Collaboration, CMS-PAS-HIG-18-015 (2019).
- [513] S. Schael *et al.* (ALEPH), JHEP **05**, 049 (2010), [arXiv:1003.0705].
- [514] V. M. Abazov *et al.* (D0), Phys. Rev. Lett. **103**, 061801 (2009), [arXiv:0905.3381].
- [515] G. Aad *et al.* (ATLAS), Phys. Rev. D **105**, 1, 012006 (2022), [arXiv:2110.00313].
- [516] M. Aaboud *et al.* (ATLAS), JHEP **10**, 031 (2018), [arXiv:1806.07355].
- [517] A. M. Sirunyan *et al.* (CMS), Phys. Lett. B **795**, 398 (2019), [arXiv:1812.06359].
- [518] A. M. Sirunyan *et al.* (CMS), Phys. Lett. B **785**, 462 (2018), [arXiv:1805.10191].
- [519] B. Aubert *et al.* (BaBar), Phys. Rev. Lett. **103**, 081803 (2009), [arXiv:0905.4539].
- [520] B. Aubert *et al.* (BaBar), Phys. Rev. Lett. **103**, 181801 (2009), [arXiv:0906.2219].

- [521] ATLAS Collaboration, ATLAS-CONF-2016-051 (2016); ATLAS Collaboration, ATLAS-CONF-2017-053 (2017); M. Aaboud *et al.* (ATLAS), Eur. Phys. J. **C79**, 1, 58 (2019), [arXiv:1808.01899].
- [522] CMS Collaboration, CMS-PAS-HIG-16-036 (2017).
- [523] S. Schael *et al.* (ALEPH, DELPHI, L3, OPAL, LEP Working Group for Higgs Boson Searches), Eur. Phys. J. **C47**, 547 (2006), [hep-ex/0602042].
- [524] ATLAS Collaboration, ATLAS-CONF-2013-027 (2013).
- [525] CMS Collaboration, CMS-PAS-HIG-13-016 (2013).
- [526] A. Heister *et al.* (ALEPH), Phys. Lett. **B526**, 191 (2002), [hep-ex/0201014]; P. Achard *et al.* (L3), Phys. Lett. **B545**, 30 (2002), [hep-ex/0208042].
- [527] M. Carena *et al.* (1999), [hep-ph/9912223].
- [528] M. M. Kado and C. G. Tully, Ann. Rev. Nucl. Part. Sci. **52**, 65 (2002).
- [529] G. Abbiendi *et al.* (OPAL), Eur. Phys. J. **C23**, 397 (2002), [hep-ex/0111010]; J. Abdallah *et al.* (DELPHI), Eur. Phys. J. **C38**, 1 (2004), [hep-ex/0410017].
- [530] M. Carena *et al.*, Eur. Phys. J. **C45**, 797 (2006), [hep-ph/0511023].
- [531] ATLAS Collaboration, ATLAS-CONF-2016-104 (2016).
- [532] S. Chatrchyan *et al.* (CMS), JHEP **09**, 029 (2012), [Erratum: JHEP **03**, 132 (2014)], [arXiv:1204.2488].
- [533] M. Aaboud *et al.* (ATLAS), Phys. Rev. Lett. **119**, 19, 191803 (2017), [arXiv:1707.06025].
- [534] V. Khachatryan *et al.* (CMS), Phys. Lett. **B758**, 296 (2016), [arXiv:1511.03610].
- [535] A. M. Sirunyan *et al.* (CMS), JHEP **11**, 010 (2017), [arXiv:1707.07283].
- [536] J. Bernon *et al.*, Phys. Rev. **D91**, 7, 075019 (2015), [arXiv:1412.3385].
- [537] G. Aad *et al.* (ATLAS), Phys. Rev. Lett. **113**, 17, 171801 (2014), [arXiv:1407.6583].
- [538] CMS Collaboration, CMS-PAS-HIG-14-037 (2015).
- [539] T. Biekötter, S. Heinemeyer and G. Weiglein (2023), [arXiv:2306.03889].
- [540] S. H. Zhu, arXiv preprint (1999), [hep-ph/9901221].
- [541] H. E. Logan and S.-f. Su, Phys. Rev. **D66**, 035001 (2002), [hep-ph/0203270].
- [542] A. Gutierrez-Rodriguez and O. A. Sampayo, Phys. Rev. **D62**, 055004 (2000).
- [543] S. Kanemura, S. Moretti and K. Odagiri, JHEP **02**, 011 (2001), [hep-ph/0012030].
- [544] M. Czakon, P. Fiedler and A. Mitov, Phys. Rev. Lett. **110**, 252004 (2013), [arXiv:1303.6254].
- [545] M. Carena *et al.*, Nucl. Phys. **B577**, 88 (2000), [hep-ph/9912516].
- [546] J. M. Campbell, R. K. Ellis and F. Tramontano, Phys. Rev. **D70**, 094012 (2004), [hep-ph/0408158].
- [547] C. Degrande *et al.*, Phys. Lett. **B772**, 87 (2017), [arXiv:1607.05291].
- [548] A. A. Barrientos Bendezu and B. A. Kniehl, Phys. Rev. **D63**, 015009 (2001), [hep-ph/0007336]; A. A. Barrientos Bendezu and B. A. Kniehl, Nucl. Phys. **B568**, 305 (2000), [hep-ph/9908385].
- [549] G. Abbiendi *et al.* (ALEPH, DELPHI, L3, OPAL, LEP), Eur. Phys. J. **C73**, 2463 (2013), [arXiv:1301.6065].
- [550] B. Abbott *et al.* (D0), Phys. Rev. Lett. **82**, 4975 (1999), [hep-ex/9902028]; A. Abulencia *et al.* (CDF), Phys. Rev. Lett. **96**, 042003 (2006), [hep-ex/0510065]; V. M. Abazov *et al.* (D0), Phys. Lett. **B682**, 278 (2009), [arXiv:0908.1811].
- [551] V. Khachatryan *et al.* (CMS), JHEP **12**, 178 (2015), [arXiv:1510.04252].
- [552] A. M. Sirunyan *et al.* (CMS), Eur. Phys. J. **C79**, 5, 421 (2019), [arXiv:1809.10733].
- [553] J. Abdallah *et al.* (DELPHI), Eur. Phys. J. **C54**, 1 (2008), [Erratum: Eur. Phys. J. **C56**, 165 (2008)], [arXiv:0801.3586].
- [554] R. Dermisek, Mod. Phys. Lett. **A24**, 1631 (2009), [arXiv:0907.0297].
- [555] J. F. Gunion, JHEP **08**, 032 (2009), [arXiv:0808.2509].
- [556] W. Love *et al.* (CLEO), Phys. Rev. Lett. **101**, 151802 (2008), [arXiv:0807.1427].
- [557] G. Aad *et al.* (ATLAS), JHEP **03**, 041 (2022), [arXiv:2110.13673]; A. Tumasyan *et al.* (CMS), Eur. Phys. J. C **82**, 4, 290 (2022), [arXiv:2111.01299].
- [558] G. Aad *et al.* (ATLAS), JHEP **07**, 133 (2023), [arXiv:2212.09649].
- [559] G. Aad *et al.* (ATLAS), Eur. Phys. J. **C72**, 2244 (2012), [arXiv:1210.5070]; S. Chatrchyan *et al.* (CMS), Eur. Phys. J. **C72**, 2189 (2012), [arXiv:1207.2666].
- [560] G. Aad *et al.* (ATLAS), Phys. Rev. **D89**, 3, 032002 (2014), [arXiv:1312.1956].
- [561] J. de Blas *et al.*, in “Snowmass 2021,” (2022), [arXiv:2206.08326].

12. CKM Quark-Mixing Matrix

Revised April 2024 by A. Ceccucci (CERN), Z. Ligeti (LBNL) and Y. Sakai (KEK).

12.1 Introduction

The masses and mixings of quarks have a common origin in the Standard Model (SM). They arise from the Yukawa interactions with the Higgs condensate,

$$\mathcal{L}_Y = -Y_{ij}^d \overline{Q_{Li}^I} \phi d_{Rj}^I - Y_{ij}^u \overline{Q_{Li}^I} \epsilon \phi^* u_{Rj}^I + \text{h.c.}, \quad (12.1)$$

where $Y^{u,d}$ are 3×3 complex matrices, ϕ is the Higgs field, i, j are generation labels, and ϵ is the 2×2 antisymmetric tensor. Q_L^I are left-handed quark doublets, and d_R^I and u_R^I are right-handed down- and up-type quark singlets, respectively, in the weak-eigenstate basis. When ϕ acquires a vacuum expectation value, $\langle \phi \rangle = (0, v/\sqrt{2})$, Eq. (12.1) yields mass terms for the quarks. The physical states are obtained by diagonalizing $Y^{u,d}$

by four unitary matrices, $V_{L,R}^{u,d}$, as $M_{\text{diag}}^f = V_L^f Y^f V_R^{f\dagger} (v/\sqrt{2})$, $f = u, d$. As a result, the charged-current W^\pm interactions couple to the physical u_{Lj} and d_{Lk} quarks with couplings given by

$$\frac{-g}{\sqrt{2}} (\overline{u}_L, \overline{c}_L, \overline{t}_L) \gamma^\mu W_\mu^+ V_{\text{CKM}} \begin{pmatrix} d_L \\ s_L \\ b_L \end{pmatrix} + \text{h.c.}, \quad (12.2)$$

$$V_{\text{CKM}} \equiv V_L^u V_L^{d\dagger} = \begin{pmatrix} V_{ud} & V_{us} & V_{ub} \\ V_{cd} & V_{cs} & V_{cb} \\ V_{td} & V_{ts} & V_{tb} \end{pmatrix}.$$

This Cabibbo-Kobayashi-Maskawa (CKM) matrix [1,2] is a 3×3 unitary matrix. It can be parameterized by three mixing angles and the CP -violating KM phase [2]. Of the many possible conventions, a standard choice has become [3]

$$V_{\text{CKM}} = \begin{pmatrix} 1 & 0 & 0 \\ 0 & c_{23} & s_{23} \\ 0 & -s_{23} & c_{23} \end{pmatrix} \begin{pmatrix} c_{13} & 0 & s_{13} e^{-i\delta} \\ 0 & 1 & 0 \\ -s_{13} e^{i\delta} & 0 & c_{13} \end{pmatrix} \begin{pmatrix} c_{12} & s_{12} & 0 \\ -s_{12} & c_{12} & 0 \\ 0 & 0 & 1 \end{pmatrix} \quad (12.3)$$

$$= \begin{pmatrix} c_{12} c_{13} & s_{12} c_{13} & s_{13} e^{-i\delta} \\ -s_{12} c_{23} - c_{12} s_{23} s_{13} e^{i\delta} & c_{12} c_{23} - s_{12} s_{23} s_{13} e^{i\delta} & s_{23} c_{13} \\ s_{12} s_{23} - c_{12} c_{23} s_{13} e^{i\delta} & -c_{12} s_{23} - s_{12} c_{23} s_{13} e^{i\delta} & c_{23} c_{13} \end{pmatrix},$$

where $s_{ij} = \sin \theta_{ij}$, $c_{ij} = \cos \theta_{ij}$, and δ is the phase responsible for all CP -violating phenomena in flavor-changing processes in the SM. The angles θ_{ij} can be chosen to lie in the first quadrant, so $s_{ij}, c_{ij} \geq 0$.

It is known experimentally that $s_{13} \ll s_{23} \ll s_{12} \ll 1$, and it is convenient to exhibit this hierarchy using the Wolfenstein parameterization. We define [4–6]

$$s_{12} = \lambda = \frac{|V_{us}|}{\sqrt{|V_{ud}|^2 + |V_{us}|^2}}, \quad s_{23} = A\lambda^2 = \lambda \left| \frac{V_{cb}}{V_{us}} \right|,$$

$$s_{13} e^{i\delta} = V_{ub}^* = A\lambda^3 (\rho + i\eta) = \frac{A\lambda^3 (\bar{\rho} + i\bar{\eta}) \sqrt{1 - A^2 \lambda^4}}{\sqrt{1 - \lambda^2} [1 - A^2 \lambda^4 (\bar{\rho} + i\bar{\eta})]}. \quad (12.4)$$

These relations ensure that $\bar{\rho} + i\bar{\eta} = -(V_{ud} V_{ub}^*) / (V_{cd} V_{cb}^*)$ is phase convention independent, and the CKM matrix written in terms of $\lambda, A, \bar{\rho}$, and $\bar{\eta}$ is unitary to all orders in λ . The definitions of $\bar{\rho}, \bar{\eta}$ reproduce all approximate results in the literature; *i.e.*, $\bar{\rho} = \rho(1 - \lambda^2/2 + \dots)$ and $\bar{\eta} = \eta(1 - \lambda^2/2 + \dots)$, and one can write V_{CKM} to $\mathcal{O}(\lambda^4)$ either in terms of $\bar{\rho}, \bar{\eta}$ or, traditionally,

$$V_{\text{CKM}} = \begin{pmatrix} 1 - \lambda^2/2 & \lambda & A\lambda^3 (\rho - i\eta) \\ -\lambda & 1 - \lambda^2/2 & A\lambda^2 \\ A\lambda^3 (1 - \rho - i\eta) & -A\lambda^2 & 1 \end{pmatrix} + \mathcal{O}(\lambda^4). \quad (12.5)$$

The CKM matrix elements are fundamental parameters of the SM, so their precise determination is important. The unitarity of the CKM matrix imposes $\sum_i V_{ij} V_{ik}^* = \delta_{jk}$ and $\sum_j V_{ij} V_{kj}^* = \delta_{ik}$. The six vanishing combinations can be represented as triangles in a complex plane, of which those obtained by taking scalar products of neighboring rows or columns are nearly degenerate. The areas of all triangles are the same, half of the Jarlskog invariant, J [7], which is a phase-convention-independent measure of CP violation, defined by $\text{Im}[V_{ij} V_{kl} V_{il}^* V_{kj}^*] = J \sum_{m,n} \varepsilon_{ikm} \varepsilon_{jln}$.

The most commonly used unitarity triangle arises from

$$V_{ud} V_{ub}^* + V_{cd} V_{cb}^* + V_{td} V_{tb}^* = 0, \quad (12.6)$$

by dividing each side by $V_{cd} V_{cb}^*$ (see Fig. 12.1). Its vertices are exactly $(0,0)$, $(1,0)$, and, due to the definition in Eq. (12.4), $(\bar{\rho}, \bar{\eta})$. An important goal of flavor physics is to overconstrain the CKM elements, and many measurements can be conveniently displayed and compared in the $\bar{\rho}, \bar{\eta}$ plane. While the Lagrangian in Eq. (12.1) is renormalized, and the CKM matrix has a well-known

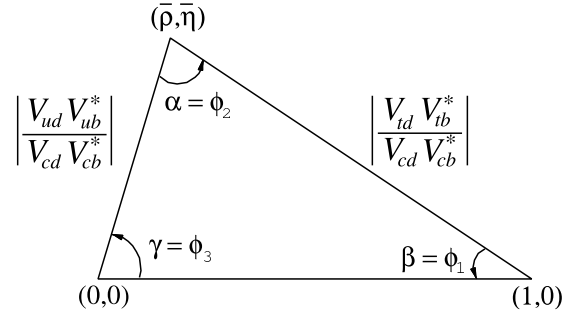


Figure 12.1: Sketch of the unitarity triangle.

scale dependence above the weak scale [8], below $\mu = m_W$ the CKM elements can be treated as constants, with all μ -dependence contained in the running of quark masses and higher-dimension operators.

Unless explicitly stated otherwise, we describe all measurements assuming the SM, to extract magnitudes and phases of CKM elements in Sec. 12.2 and 12.3. Processes dominated by loop-level contributions in the SM are particularly sensitive to new physics beyond the SM (BSM). We give the global fit results for the CKM elements in Sec. 12.4, and discuss some implications for beyond standard model physics in Sec. 12.5.

12.2 Magnitudes of CKM elements

12.2.1 $|V_{ud}|$

The most precise determination of $|V_{ud}|$ comes from the study of superallowed $0^+ \rightarrow 0^+$ nuclear beta decays, which are pure vector transitions. Taking the average of the fifteen most precise determinations [9] yields [10]

$$|V_{ud}| = 0.97367 \pm 0.00032. \quad (12.7)$$

This uncertainty is slightly more than twice as large as that in the 2020 edition, due to a more conservative estimate of the nuclear structure uncertainties. A less precise determination of $|V_{ud}|$ can be obtained from the measurement of the neutron lifetime. The theoretical uncertainties are very small, but the determination is limited by the knowledge of the ratio of the axial-vector and vector couplings, $g_A = G_A/G_V$ [10]. The PIBETA experiment [11] has improved the measurement of the $\pi^+ \rightarrow \pi^0 e^+ \nu$ branching ratio to 0.6%, and Ref. [12] quotes $|V_{ud}| = 0.9739 \pm 0.0027$, in

agreement with the more precise result listed above. The interest in this measurement is that the determination of $|V_{ud}|$ is very clean theoretically, because it is a pure vector transition and is free from nuclear-structure uncertainties.

12.2.2 $|V_{us}|$

The product of $|V_{us}|$ and the form factor at $q^2 = 0$, $|V_{us}| f_+(0)$, has been extracted traditionally from $K_L^0 \rightarrow \pi e \nu$ decays in order to avoid isospin-breaking corrections ($\pi^0 - \eta$ mixing) that affect K^\pm semileptonic decay, and the complications induced by a second (scalar) form factor present in the muonic decays. The last round of measurements has led to enough experimental constraints to justify the comparison between different decay modes. Systematic errors related to the experimental quantities, *e.g.*, the lifetime of neutral or charged kaons, and the form factor determinations for electron and muonic decays, differ among decay modes, and the consistency between different determinations enhances the confidence in the final result. For this reason, we follow the prescription [13] to average $K_L^0 \rightarrow \pi e \nu$, $K_L^0 \rightarrow \pi \mu \nu$, $K^\pm \rightarrow \pi^0 e^\pm \nu$, $K^\pm \rightarrow \pi^0 \mu^\pm \nu$ and $K_S^0 \rightarrow \pi e \nu$. The average of these five decay modes yields $|V_{us}| f_+(0) = 0.21656 \pm 0.00035$. Results obtained from each decay mode, and exhaustive references to the experimental data, are listed for instance in Ref. [10]. The form factor average $f_+(0) = 0.9698 \pm 0.0017$ [14] from $N_f = 2 + 1 + 1$ lattice QCD calculations gives $|V_{us}| = 0.2233 \pm 0.0005$ [10].¹ The broadly used classic calculation of $f_+(0)$ [16] is in good agreement with this value, while other calculations [18] differ by as much as 2%.

The calculation of the ratio of the kaon and pion decay constants enables one to extract $|V_{us}/V_{ud}|$ from $K \rightarrow \mu \nu(\gamma)$ and $\pi \rightarrow \mu \nu(\gamma)$, where (γ) indicates that radiative decays are included [19]. The value of $\Gamma(K \rightarrow \mu \nu(\gamma))$ [10] derived from the KLOE measurement of the corresponding branching ratio [20], combined with the lattice QCD result, $f_K/f_\pi = 1.1932 \pm 0.0021$ [14], leads to $|V_{us}| = 0.2250 \pm 0.0004$, where the accuracy is limited by the knowledge of the ratio of the decay constants. The average of these two determinations, with the error scaled according to the PDG prescription [21] by $\sqrt{\chi^2} = 2.5$, is quoted as [10]

$$|V_{us}| = 0.22431 \pm 0.00085. \quad (12.8)$$

It is important to include both QED and QCD sources of isospin violations in the lattice QCD calculations.

The latest determination from hyperon decays can be found in Ref. [22]. The authors focus on the analysis of the vector form factor, protected from first order flavor $SU(3)$ breaking effects by the Ademollo-Gatto theorem [23], and treat the ratio between the axial and vector form factors g_1/f_1 as experimental input, thus avoiding first order $SU(3)$ breaking effects in the axial-vector contribution. They find $|V_{us}| = 0.2250 \pm 0.0027$, although this does not include an estimate of the theoretical uncertainty due to second-order $SU(3)$ breaking, contrary to Eq. (12.8). Concerning hadronic τ decays to strange particles, averaging the inclusive decay and the exclusive $\tau \rightarrow h \nu$ ($h = \pi, K$) measurements yields $|V_{us}| = 0.2207 \pm 0.0014$ [24].

12.2.3 $|V_{cd}|$

The magnitude of V_{cd} can be extracted from semileptonic charm decays, using theoretical knowledge of the form factors. In semileptonic D decays, lattice QCD calculations have predicted the normalization of the $D \rightarrow \pi \ell \nu$ and $D \rightarrow K \ell \nu$ form factors [14]. The dependence on the invariant mass of the lepton pair, q^2 , is determined from lattice QCD and theoretical constraints from analyticity [15]. Using $N_f = 2 + 1 + 1$ lattice QCD calculations for $D \rightarrow \pi \ell \nu$, $f_+^{D\pi}(0) = 0.612 \pm 0.035$ [14], and the average [24] of the measurements of $D \rightarrow \pi \ell \nu$ decays by *BABAR* [25], BESIII [26], CLEO-c [27], and Belle [28], one obtains $|V_{cd}| = 0.2330 \pm 0.0029 \pm 0.0133$, where the first uncertainty is experimental, and the second is from the theoretical uncertainty of the form factor.

¹For lattice QCD inputs, we use the averages from Ref. [14], unless the minireviews [10,15] choose different values. We only use unquenched results, and if both $N_f = 2 + 1 + 1$ and $2 + 1$ calculations are available, we use the former.

The determination of $|V_{cd}|$ is also possible from the leptonic decay $D^+ \rightarrow \mu^+ \nu$ and $\tau^+ \nu$. The experimental uncertainties have not decreased significantly recently. Averaging the BESIII [29] and earlier CLEO [30] for $\mu^+ \nu$ and BESIII [31] for $\tau^+ \nu$ measurements, and using the $N_f = 2 + 1 + 1$ lattice QCD result, $f_D = 212.0 \pm 0.7$ MeV [14], yields $|V_{cd}| = 0.2181 \pm 0.0049 \pm 0.0007$ [24].²

Earlier determinations of $|V_{cd}|$ came from neutrino scattering data. The difference of the ratio of double-muon to single-muon production by neutrino and antineutrino beams is proportional to the charm cross section off valence d quarks, and therefore to $|V_{cd}|^2$ times the average semileptonic branching ratio of charm mesons, \mathcal{B}_μ . The method was used first by CDHS [32] and then by CCFR [33] and CHARM II [34]. Averaging these results is complicated, because it requires assumptions about the scale of the QCD corrections, and because \mathcal{B}_μ is an effective quantity, which depends on the specific neutrino beam characteristics. With no recent experimental input available, we quote the average from a past review, $\mathcal{B}_\mu |V_{cd}|^2 = (0.463 \pm 0.034) \times 10^{-2}$ [35]. Analysis cuts make these experiments insensitive to neutrino energies smaller than 30 GeV. Thus, \mathcal{B}_μ should be computed using only neutrino interactions with visible energy larger than 30 GeV. An appraisal [36] based on charm-production fractions measured in neutrino interactions [37] gives $\mathcal{B}_\mu = 0.088 \pm 0.006$. Data from the CHORUS experiment [38] are sufficiently precise to extract \mathcal{B}_μ directly, by comparing the number of charm decays with a muon to the total number of charmed hadrons found in the nuclear emulsions. Requiring the visible energy to be larger than 30 GeV, CHORUS found $\mathcal{B}_\mu = 0.085 \pm 0.009 \pm 0.006$. We use the average of these two determinations, $\mathcal{B}_\mu = 0.087 \pm 0.005$, and obtain $|V_{cd}| = 0.230 \pm 0.011$. Averaging the three determinations above, we find

$$|V_{cd}| = 0.221 \pm 0.004. \quad (12.9)$$

12.2.4 $|V_{cs}|$

The direct determination of $|V_{cs}|$ is possible from semileptonic D or leptonic D_s decays, using lattice QCD calculations of the semileptonic D form factor or the D_s decay constant. For muonic decays, the average of Belle [39], CLEO-c [40], *BABAR* [41], and BESIII [42,43] is $\mathcal{B}(D_s^+ \rightarrow \mu^+ \nu) = (5.43 \pm 0.16) \times 10^{-3}$ [24]. For decays to τ leptons, the average of CLEO-c [40,44], *BABAR* [41], Belle [39], and BESIII [42] gives $\mathcal{B}(D_s^+ \rightarrow \tau^+ \nu) = (5.40 \pm 0.23) \times 10^{-2}$ [24]. From each of these values, determinations of $|V_{cs}|$ can be obtained using the PDG values for the mass and lifetime of the D_s , the masses of the leptons, and $f_{D_s} = (249.9 \pm 0.5)$ MeV [14]. The average of these determinations gives $|V_{cs}| = 0.984 \pm 0.012$, where the error is dominated by the experimental uncertainty. In semileptonic D decays, lattice QCD calculations of the $D \rightarrow K \ell \nu$ form factor are available [14]. Using $f_+^{DK}(0) = 0.7385 \pm 0.0044$ and the average [24] of CLEO-c [27], Belle [28], *BABAR* [45], and recent BESIII [26,46] measurements of $D \rightarrow K \ell \nu$ decays, one obtains $|V_{cs}| = 0.972 \pm 0.007$, where the dominant uncertainty is from the theoretical calculation of the form factor. Averaging the determinations from leptonic and semileptonic decays, we find

$$|V_{cs}| = 0.975 \pm 0.006. \quad (12.10)$$

Measurements of on-shell W^\pm decays sensitive to $|V_{cs}|$ were made by LEP-2. The W branching ratios depend on the six CKM elements involving only the quarks lighter than m_W . The W branching ratio to each lepton flavor is $1/\mathcal{B}(W \rightarrow \ell \bar{\nu}_\ell) = 3 [1 + \sum_{u,c,d,s,b} |V_{ij}|^2 (1 + \alpha_s(m_W)/\pi) + \dots]$. Assuming lepton universality, the measurement $\mathcal{B}(W \rightarrow \ell \bar{\nu}_\ell) = (10.83 \pm 0.07 \pm 0.07)\%$ [47] implies $\sum_{u,c,d,s,b} |V_{ij}|^2 = 2.002 \pm 0.027$. This is a precise test of unitarity; however, only flavor-tagged W -decays determine $|V_{cs}|$ directly, such as DELPHI's tagged $W^+ \rightarrow c \bar{s}$ analysis, yielding $|V_{cs}| = 0.94_{-0.26}^{+0.32} \pm 0.13$ [48].

12.2.5 $|V_{cb}|$

This matrix element can be determined from exclusive and inclusive semileptonic decays of B mesons to charm. The in-

²Hereafter the first error is statistical and the second is systematic, unless mentioned otherwise.

clusive determinations use the semileptonic decay rate measurement, together with (certain moments of) the lepton energy and the hadronic invariant-mass spectra. The theoretical basis is the operator product expansion [49, 50], which allows calculation of the decay rate and various spectra as expansions in α_s and inverse powers of the heavy-quark mass. The dependence on m_b , m_c , and the parameters that occur at subleading order is different for different moments. The measurements of many moments overconstrain these parameters, and also test the consistency of their determination. The precise extraction of $|V_{cb}|$ requires using a “threshold” quark mass definition [51, 52]. Inclusive measurements have been performed using B mesons from Z^0 decays at LEP, and at e^+e^- colliders operated at the $\Upsilon(4S)$. At LEP, the large boost of B mesons from the Z^0 decay allows the determination of the moments throughout phase space, which is not possible otherwise, but the large statistics available at the B factories lead to more precise determinations. An average of the measurements and a compilation of the references are provided in Ref. [15]: $|V_{cb}| = (42.2 \pm 0.5) \times 10^{-3}$.

Complementary determinations are based on exclusive semileptonic B decays to D and D^* . In the $m_{b,c} \gg \Lambda_{\text{QCD}}$ limit, all form factors are given by a single Isgur-Wise function [53], which depends on the product of the four-velocities of the B and $D^{(*)}$ mesons, $w = v \cdot v'$. Heavy-quark symmetry determines the rate (in the symmetry limit) at $w = 1$, the point in phase space at which the invariant mass of the $\ell\bar{\nu}$ pair is maximal; $|V_{cb}|$ is obtained from extrapolating a fit to the spectrum to $w = 1$. The current update of the V_{cb} and V_{ub} minireview quotes from exclusive decays $|V_{cb}| = (39.8 \pm 0.6) \times 10^{-3}$ [15], based on the only unfolded measurement of $B \rightarrow D^*$ semileptonic decay distributions [54], and using a more general fit [55] than in earlier B factory measurements. With the uncertainty scaled by $\sqrt{\chi^2} = 3.0$, this yields the combination [15],

$$|V_{cb}| = (41.1 \pm 1.2) \times 10^{-3}. \quad (12.11)$$

Determinations of $|V_{cb}|$ that are currently less precise and not included in this average, can be obtained from the measurement of $B_s \rightarrow D_s^{(*)} \mu\bar{\nu}$ decays [56]. In addition, semileptonic decays to τ leptons measured in $B \rightarrow D^{(*)} \tau\bar{\nu}$ and related modes are also sensitive to $|V_{cb}|$. The most precise data involving τ leptons are the $|V_{cb}|$ -independent ratios, $\mathcal{B}(B \rightarrow D^{(*)} \tau\bar{\nu})/\mathcal{B}(B \rightarrow D^{(*)} \ell\bar{\nu})$ measured by BaBar, Belle, and LHCb. If the current, approximately 3.3σ [24] hint of lepton non-universality prevails, the determination of $|V_{cb}|$ becomes more complicated.

12.2.6 $|V_{ub}|$

The determination of $|V_{ub}|$ from inclusive $B \rightarrow X_u \ell\bar{\nu}$ decay is complicated due to large $B \rightarrow X_c \ell\bar{\nu}$ backgrounds. In most regions of phase space where the charm background is kinematically forbidden, the hadronic physics enters via unknown nonperturbative functions, so-called shape functions. (By contrast, the nonperturbative physics for $|V_{cb}|$ is encoded in a few parameters.) At leading order in Λ_{QCD}/m_b , there is only one shape function, which can be extracted from the photon energy spectrum in $B \rightarrow X_s \gamma$ [57, 58], and applied to several spectra in $B \rightarrow X_u \ell\bar{\nu}$. The subleading shape functions are modeled in the current determinations. Phase space cuts for which the rate has only subleading dependence on the shape function are also possible [59]. The measurements of both the hadronic and the leptonic systems are important for an optimal choice of phase space. A different approach is to make the measurements more inclusive by extending them deeper into the $B \rightarrow X_c \ell\bar{\nu}$ region, and thus reduce the theoretical uncertainties. Analyses of the electron-energy endpoint from CLEO [60], BABAR [61], and Belle [62] quote $B \rightarrow X_u e\bar{\nu}$ partial rates for $|\vec{p}_e| \geq 2.0$ GeV and 1.9 GeV, which are well below the charm endpoint. The large and pure $B\bar{B}$ samples at the B factories permit the selection of $B \rightarrow X_u \ell\bar{\nu}$ decays in events where the other B is fully reconstructed [63]. With this full-reconstruction tag method, the four-momenta of both the leptonic and the hadronic final states can be measured. It also gives access to a wider kinematic region, because of improved signal purity. Ref. [15] quotes the inclusive average, $|V_{ub}| = (4.13 \pm 0.12 \text{ }^{+0.13}_{-0.14} \pm 0.18) \times 10^{-3}$, where the first error is experimental, the second arises from the

model dependence quoted by the individual measurements, and the third is an additional one estimated in Ref. [15].

To extract $|V_{ub}|$ from exclusive decays, the form factors have to be known. Experimentally, better signal-to-background ratios are offset by smaller yields. The $B \rightarrow \pi \ell\bar{\nu}$ branching ratio is now known to 5%. Lattice QCD calculations of the $B \rightarrow \pi \ell\bar{\nu}$ form factor are available [64] for the high q^2 region ($q^2 > 16$ or 18 GeV²). A fit to the experimental partial rates and lattice QCD results versus q^2 yields $|V_{ub}| = (3.70 \pm 0.10 \pm 0.12) \times 10^{-3}$ [24]. Using additional input from light-cone QCD sum rules (which are thought to be reliable in the small q^2 region), yield a combination, $|V_{ub}| = (3.67 \pm 0.09 \pm 0.12) \times 10^{-3}$ [15, 24].

The uncertainties in extracting $|V_{ub}|$ from inclusive and exclusive decays are different to a large extent. An average of these determinations, with the uncertainty scaled by $\sqrt{\chi^2} = 1.4$, is [15]

$$|V_{ub}| = (3.82 \pm 0.20) \times 10^{-3}. \quad (12.12)$$

A determination of $|V_{ub}|$ not included in this average can be obtained from $\mathcal{B}(B \rightarrow \tau\bar{\nu}) = (1.09 \pm 0.21) \times 10^{-4}$ [24]. Using $f_B = (190.0 \pm 1.3)$ MeV [14] and $\tau_{B^\pm} = (1.638 \pm 0.004)$ ps [65], we find the remarkably consistent result, $|V_{ub}| = (4.11 \pm 0.39) \times 10^{-3}$. This decay is sensitive, for example, to tree-level charged Higgs contributions, and the measured rate is consistent with the SM expectation. The LHCb measurement $|V_{ub}/V_{cb}| = 0.083 \pm 0.004$ [15] from the ratios of $\Lambda_b \rightarrow p^+ \mu^- \bar{\nu}$ and $\Lambda_b \rightarrow \Lambda_c^+ \mu^- \bar{\nu}$ [66] and $B_s^0 \rightarrow K^- \mu^+ \nu$ and $B_s^0 \rightarrow D_s^- \mu^+ \nu$ [67] in different regions of q^2 , provides another complementary determination.

12.2.7 $|V_{td}|$ and $|V_{ts}|$

The CKM elements $|V_{td}|$ and $|V_{ts}|$ are not likely to be precisely measurable in tree-level processes involving top quarks, so one has to rely on determinations from $B^0 - \bar{B}^0$ mixing, dominated by box diagrams with top quarks, or loop-mediated rare K and B decays. Theoretical uncertainties in hadronic effects limit the accuracy of the current determinations. These can be reduced by taking ratios of processes that are equal in the flavor $SU(3)$ limit to determine $|V_{td}|/|V_{ts}|$.

The phenomenon of $B^0 - \bar{B}^0$ mixing was discovered by ARGUS [68], and the mass difference is now precisely measured as $\Delta m_d = (0.5069 \pm 0.0019)$ ps⁻¹ [69]. In the B_s^0 system, Δm_s was first measured significantly by CDF [70] and the world average, dominated by an LHCb measurement [71], is $\Delta m_s = (17.765 \pm 0.006)$ ps⁻¹ [69]. Neglecting corrections suppressed by $|V_{tb}| - 1$, and using the lattice QCD results $f_{B_d} \sqrt{\widehat{B}_{B_d}} = (210.6 \pm 5.5)$ MeV and $f_{B_s} \sqrt{\widehat{B}_{B_s}} = (256.1 \pm 5.7)$ MeV [14],

$$|V_{td}| = (8.6 \pm 0.2) \times 10^{-3}, \quad |V_{ts}| = (41.5 \pm 0.9) \times 10^{-3}. \quad (12.13)$$

The uncertainties are dominated by lattice QCD. Several uncertainties are reduced in the calculation of the ratio $\xi = (f_{B_s} \sqrt{\widehat{B}_{B_s}})/(f_{B_d} \sqrt{\widehat{B}_{B_d}}) = 1.216 \pm 0.016$ [14] and therefore the constraint on $|V_{td}|/|V_{ts}|$ from $\Delta m_d/\Delta m_s$ is more reliable theoretically. These provide a theoretically clean and significantly improved determination,

$$|V_{td}|/|V_{ts}| = 0.207 \pm 0.001 \pm 0.003. \quad (12.14)$$

The inclusive branching ratio $\mathcal{B}(B \rightarrow X_s \gamma) = (3.49 \pm 0.19) \times 10^{-4}$ extrapolated to $E_\gamma > E_0 = 1.6$ GeV [24] is also sensitive to $|V_{tb}V_{ts}|$. In addition to t -quark penguins, a substantial part of the rate comes from charm contributions proportional to $V_{cb}V_{cs}^*$ via the application of 3×3 CKM unitarity (which is used here). With the NNLO calculation of $\mathcal{B}(B \rightarrow X_s \gamma)_{E_\gamma > E_0}/\mathcal{B}(B \rightarrow X_c e\bar{\nu})$ [72], we obtain $|V_{ts}/V_{cb}| = 1.00 \pm 0.04$. The $B_s \rightarrow \mu^+ \mu^-$ rate is also proportional to $|V_{tb}V_{ts}|^2$ in the SM, and the world average, $\mathcal{B}(B_s \rightarrow \mu^+ \mu^-) = (3.01 \pm 0.35) \times 10^{-9}$ [65], is consistent with the SM, with sizable uncertainties.

A complementary determination of $|V_{td}|/|V_{ts}|$ is possible from the ratio of $B \rightarrow \rho\gamma$ and $K^*\gamma$ rates. The ratio of the neutral modes is theoretically cleaner than that of the charged ones, because the poorly known spectator-interaction contribution is expected to be

smaller (W -exchange vs. weak annihilation). For now, because of low statistics, we average the charged and neutral rates assuming the isospin symmetry and heavy-quark limit motivated relation, $|V_{td}/V_{ts}|^2/\xi_\gamma^2 = [\Gamma(B^+ \rightarrow \rho^+\gamma) + 2\Gamma(B^0 \rightarrow \rho^0\gamma)]/[\Gamma(B^+ \rightarrow K^{*+}\gamma) + \Gamma(B^0 \rightarrow K^{*0}\gamma)] = (3.35 \pm 0.48)\%$ [24, 73]. Here ξ_γ contains the poorly known hadronic physics. Using $\xi_\gamma = 1.2 \pm 0.2$ [74] gives $|V_{td}/V_{ts}| = 0.220 \pm 0.016 \pm 0.037$, where the first uncertainty is experimental and the second is theoretical.

A theoretically clean determination of $|V_{td}V_{ts}^*|$ is possible from $K^+ \rightarrow \pi^+\nu\bar{\nu}$ decay [75]. Experimentally, more than 20 candidates have been observed [76, 77] and the rate is consistent with the SM within errors. Much more data are needed for a precision measurement.

12.2.8 $|V_{tb}|$

The determination of $|V_{tb}|$ from top decays uses the ratio of branching fractions $R = \mathcal{B}(t \rightarrow Wb)/\mathcal{B}(t \rightarrow Wq) = |V_{tb}|^2/(\sum_q |V_{tq}|^2) = |V_{tb}|^2$, where $q = b, s, d$. The CDF and DØ measurements performed on data collected during Run II of the Tevatron give $|V_{tb}| > 0.85$ [78] and $0.99 > |V_{tb}| > 0.90$ [79], respectively, at 95% CL. CMS measured the same quantity at 8 TeV and obtained $|V_{tb}| > 0.975$ [80] at 95% CL.

The direct determination of $|V_{tb}|$, without assuming unitarity, is possible from the single top quark production cross section. The $(3.30_{-0.40}^{+0.52})$ pb combined cross section [81] of DØ and CDF measurements implies $|V_{tb}| = 1.02_{-0.05}^{+0.06}$. The LHC experiments, ATLAS and CMS, have measured single top quark production cross sections (and extracted $|V_{tb}|$) in t -channel, Wt -channel, and s -channel at 7 TeV, 8 TeV, and 13 TeV [82]. The average of these $|V_{tb}|$ values is calculated to be $|V_{tb}| = 1.007 \pm 0.030$, where all systematic errors and theoretical errors are treated to be fully correlated. The average of Tevatron and LHC values gives

$$|V_{tb}| = 1.010 \pm 0.027. \quad (12.15)$$

The experimental systematic uncertainties dominate, and a dedicated combination would be welcome.

A weak constraint on $|V_{tb}|$ can be obtained from precision electroweak data, where top quarks enter in loops. The sensitivity is best in $\Gamma(Z \rightarrow b\bar{b})$ and yields $|V_{tb}| = 0.77_{-0.24}^{+0.18}$ [83].

12.3 Phases of CKM elements

As can be seen from Fig. 12.1, the angles of the unitarity triangle are

$$\begin{aligned} \beta = \phi_1 &= \arg\left(-\frac{V_{cd}V_{cb}^*}{V_{td}V_{tb}^*}\right), \\ \alpha = \phi_2 &= \arg\left(-\frac{V_{td}V_{tb}^*}{V_{ud}V_{ub}^*}\right), \\ \gamma = \phi_3 &= \arg\left(-\frac{V_{ud}V_{ub}^*}{V_{cd}V_{cb}^*}\right). \end{aligned} \quad (12.16)$$

Since CP violation involves phases of CKM elements, many measurements of CP -violating observables can be used to constrain these angles and the $\bar{\rho}, \bar{\eta}$ parameters.

12.3.1 ϵ and ϵ'

The measurement of CP violation in $K^0-\bar{K}^0$ mixing, $|\epsilon| = (2.228 \pm 0.011) \times 10^{-3}$ [84], provides important information about the CKM matrix. The phase of ϵ is determined by long-distance physics, $\epsilon = \frac{1}{2} e^{i\phi_\epsilon} \sin\phi_\epsilon \arg(-M_{12}/\Gamma_{12})$, where $\phi_\epsilon = \arctan[2\Delta m_K/\Delta\Gamma_K] \simeq 43.5^\circ$. The SM prediction can be written as

$$\begin{aligned} \epsilon &= \kappa_\epsilon e^{i\phi_\epsilon} \frac{G_F^2 m_W^2 m_K}{12\sqrt{2}\pi^2 \Delta m_K} f_K^2 \widehat{B}_K \left\{ \eta_{tt} S(x_t) \text{Im}[(V_{ts}V_{td}^*)^2] \right. \\ &\quad \left. + 2\eta_{ct} S(x_c, x_t) \text{Im}(V_{cs}V_{cd}^*V_{ts}V_{td}^*) + \eta_{cc} x_c \text{Im}[(V_{cs}V_{cd}^*)^2] \right\}, \end{aligned} \quad (12.17)$$

where $\kappa_\epsilon \simeq 0.94 \pm 0.02$ [85] includes the effects of strangeness changing $\Delta S = 1$ operators and additional dependence on $\phi_\epsilon \neq$

$\pi/4$ (see also Ref. [86]). The displayed terms are the short-distance $\Delta S = 2$ contribution to $\text{Im}M_{12}$ in the usual phase convention, S is an Inami-Lim function [87], $x_q = m_q^2/m_W^2$, and η_{ij} are perturbative QCD corrections. The constraint from ϵ in the $\bar{\rho}, \bar{\eta}$ plane is bounded by approximate hyperbolas. Lattice QCD determined the bag parameter $\widehat{B}_K = 0.717 \pm 0.024$ [14] and the main uncertainties are from $(V_{ts}V_{td}^*)^2$ (approximately given by that of $|V_{cb}|^4$ or A^4), the η_{ij} coefficients, and estimates of κ_ϵ .

The measurement of $6\text{Re}(\epsilon'/\epsilon) = 1 - |\eta_{00}/\eta_{+-}|^2$, where each $\eta_{ij} = \langle \pi^i \pi^j | \mathcal{H} | K_L \rangle / \langle \pi^i \pi^j | \mathcal{H} | K_S \rangle$ violates CP , provides a qualitative test of the CKM mechanism, and strong constraints on many BSM scenarios. Its nonzero value, $\text{Re}(\epsilon'/\epsilon) = (1.67 \pm 0.23) \times 10^{-3}$ [84], demonstrated the existence of direct CP violation, a prediction of the KM ansatz. While $\text{Re}(\epsilon'/\epsilon) \propto \text{Im}(V_{td}V_{ts}^*)$, this quantity cannot easily be used to extract CKM parameters, because cancellations between the electromagnetic and gluonic penguin contributions for large m_t [88] enhance the hadronic uncertainties. Most SM estimates [89] agree with the observed value, indicating that $\bar{\eta}$ is positive. Progress in lattice QCD [90] may yield a precise SM prediction in the future, and trigger new work on assessing the consistency of the SM with the measured value [91, 92].

12.3.2 β / ϕ_1

12.3.2.1 Charmonium modes

CP -violation measurements in B -meson decays provide direct information on the angles of the unitarity triangle, shown in Fig. 12.1. These overconstraining measurements serve to improve the determination of the CKM elements, and to reveal possible effects beyond the SM.

The time-dependent CP asymmetry of neutral B decays to a final state f common to B^0 and \bar{B}^0 is given by [93–95]

$$\begin{aligned} \mathcal{A}_f &= \frac{\Gamma(\bar{B}^0(t) \rightarrow f) - \Gamma(B^0(t) \rightarrow f)}{\Gamma(\bar{B}^0(t) \rightarrow f) + \Gamma(B^0(t) \rightarrow f)}, \\ &= S_f \sin(\Delta m_d t) - C_f \cos(\Delta m_d t), \end{aligned} \quad (12.18)$$

where

$$S_f = \frac{2\text{Im}\lambda_f}{1 + |\lambda_f|^2}, \quad C_f = \frac{1 - |\lambda_f|^2}{1 + |\lambda_f|^2}, \quad \lambda_f = \frac{q}{p} \frac{\bar{A}_f}{A_f}. \quad (12.19)$$

Here, q/p describes $B^0-\bar{B}^0$ mixing and, to a good approximation in the SM, $q/p = V_{tb}^*V_{td}/V_{tb}V_{td}^* = e^{-2i\beta + \mathcal{O}(\lambda^4)}$ in the usual phase convention. A_f (\bar{A}_f) is the amplitude of the $B^0 \rightarrow f$ ($\bar{B}^0 \rightarrow f$) decay. If f is a CP eigenstate, and amplitudes with one CKM phase dominate the decay, then $|A_f| = |\bar{A}_f|$, $C_f = 0$, and $S_f = \sin(\arg\lambda_f) = \eta_f \sin 2\phi$, where η_f is the CP eigenvalue of f and 2ϕ is the phase difference between the $B^0 \rightarrow f$ and $B^0 \rightarrow \bar{B}^0 \rightarrow f$ decay paths. A contribution of another amplitude to the decay with a different CKM phase makes the value of S_f sensitive to relative strong-interaction phases between the decay amplitudes (it also makes $C_f \neq 0$ possible).

The $b \rightarrow c\bar{c}s$ decays to CP eigenstates ($B^0 \rightarrow$ charmonium $K_{S,L}^0$) give currently the most precise measurements of $S_f = -\eta_f \sin 2\beta$. The $b \rightarrow s$ penguin amplitudes have dominantly the same weak phase as the $b \rightarrow c\bar{c}s$ tree amplitude. Since only λ^2 -suppressed penguin amplitudes introduce a different CP -violating phase, amplitudes with a single weak phase dominate, and we expect $|\bar{A}_{\psi K}/A_{\psi K} - 1| < 0.01$. The e^+e^- asymmetric-energy B -factory experiments, $BABAR$ [96] and Belle [97], and LHCb [98] provided precise measurements. The world average, including some other measurements, is [24, 95, 99]

$$\sin 2\beta = 0.709 \pm 0.011. \quad (12.20)$$

This measurement has a four-fold ambiguity in β , which can be resolved by a global fit as mentioned in Sec. 12.4. Experimentally, the two-fold ambiguity $\beta \rightarrow \pi/2 - \beta$ (but not $\beta \rightarrow \pi + \beta$) can be resolved by a time-dependent angular analysis of $B^0 \rightarrow J/\psi K^{*0}$ [100, 101], or a time-dependent Dalitz plot analysis of $B^0 \rightarrow \bar{D}^0 h^0$. The time-dependent Dalitz plot analysis of $B^0 \rightarrow \bar{D}^0 h^0$ ($h^0 = \pi^0, \eta, \omega$) with $\bar{D}^0 \rightarrow K_S^0 \pi^+ \pi^-$, jointly performed by Belle and $BABAR$, excludes the $\pi/2 - \beta$ solution with

7.3 σ confidence level [102]. These results exclude the negative $\cos 2\beta$ solutions, in agreement with the global CKM fit, which is no longer shown in Fig. 12.2.

The $b \rightarrow c\bar{c}d$ mediated transitions, such as $B^0 \rightarrow J/\psi\pi^0$ and $B^0 \rightarrow D^{(*)+}D^{(*)-}$, also measure approximately $\sin 2\beta$. However, the dominant component of the $b \rightarrow d$ penguin amplitude has a different CKM phase ($V_{tb}^*V_{td}$) than the tree amplitude ($V_{cb}^*V_{cd}$), and their magnitudes are of the same order in λ . Therefore, the effect of penguins could be large, resulting in $S_f \neq -\eta_f \sin 2\beta$ and $C_f \neq 0$. Such decay modes have been measured by *BABAR*, Belle, and LHCb. The world averages [24], $S_{J/\psi\pi^0} = -0.86 \pm 0.14$, $S_{J/\psi\rho^0} = -0.66_{-0.12}^{+0.16}$, $S_{D^+D^-} = -0.84 \pm 0.12$, and $S_{D^{*+}D^{*-}} = -0.71 \pm 0.09$ (where $\eta_f = +1$ for the $J/\psi\pi^0$ and D^+D^- modes, while $J/\psi\rho^0$ and $D^{*+}D^{*-}$ are mixtures of CP even and odd states), are consistent with $\sin 2\beta$ obtained from $B^0 \rightarrow$ charmium K^0 decays, and the C_f 's are consistent with zero, although the uncertainties are sizable.

The $b \rightarrow c\bar{u}d$ decays $B^0 \rightarrow \bar{D}^0(*)h^0$, with $\bar{D}^0 \rightarrow CP$ eigenstates and $\bar{D}^0 \rightarrow K_S^0\pi^+\pi^-$ with Dalitz plot analysis, have no penguin contributions, and provide theoretically clean $\sin 2\beta$ measurements. The average of joint analyses of *BABAR* and Belle data [102, 103] give $\sin 2\beta = 0.71 \pm 0.09$ [24].

12.3.2.2 Penguin-dominated modes

The $b \rightarrow s\bar{q}q$ penguin-dominated decays have the same CKM phase as the $b \rightarrow c\bar{s}$ tree level decays, up to corrections suppressed by λ^2 , since $V_{tb}^*V_{ts} = -V_{cb}^*V_{cs}[1 + \mathcal{O}(\lambda^2)]$. Therefore, decays such as $B^0 \rightarrow \phi K^0$ and $\eta'K^0$ provide $\sin 2\beta$ measurements in the SM. Any BSM contribution to the amplitude with a different weak phase would give rise to $S_f \neq -\eta_f \sin 2\beta$, and possibly $C_f \neq 0$. Therefore, the main interest in these modes is not simply to measure $\sin 2\beta$, but to search for new physics. Measurements of many other decay modes in this category, such as $B \rightarrow \pi^0 K_S^0$, $K_S^0 K_S^0 K_S^0$, etc., have also been performed by *BABAR* and Belle. The results and their uncertainties are summarized in Fig. 13.3 and Table 13.1 of Ref. [94]. The comparison of CP violation measurements between tree-dominated and penguin-dominated modes in B_s^0 decays provides similar sensitivity to new physics.

12.3.3 α / ϕ_2

Since α is the phase between $V_{tb}^*V_{td}$ and $V_{ub}^*V_{ud}$, only time-dependent CP asymmetries in decay modes dominated by $b \rightarrow u\bar{u}d$ transitions can directly measure $\sin 2\alpha$, in contrast to $\sin 2\beta$, where several different quark-level transitions can be used. Since $b \rightarrow d$ penguin amplitudes have a different CKM phase than $b \rightarrow u\bar{u}d$ tree amplitudes, and their magnitudes are of the same order in λ , the penguin contribution can be sizable, which makes the determination of α complicated. To date, α has been measured in $B \rightarrow \pi\pi$, $\rho\pi$ and $\rho\rho$ decay modes.

12.3.3.1 $B \rightarrow \pi\pi$

It is well-established from the data that there is a sizable contribution of $b \rightarrow d$ penguin amplitudes in $B \rightarrow \pi\pi$ decays. Thus, $S_{\pi^+\pi^-}$ in the time-dependent $B^0 \rightarrow \pi^+\pi^-$ analysis does not measure $\sin 2\alpha$, but

$$S_{\pi^+\pi^-} = \sqrt{1 - C_{\pi^+\pi^-}^2} \sin(2\alpha + 2\Delta\alpha), \quad (12.21)$$

where $2\Delta\alpha$ is the phase difference between $e^{2i\gamma}\bar{A}_{\pi^+\pi^-}$ and $A_{\pi^+\pi^-}$. The value of $\Delta\alpha$, and hence α , can be extracted using the isospin relation among the amplitudes of $B^0 \rightarrow \pi^+\pi^-$, $B^0 \rightarrow \pi^0\pi^0$, and $B^+ \rightarrow \pi^+\pi^0$ decays [104],

$$\frac{1}{\sqrt{2}} A_{\pi^+\pi^-} + A_{\pi^0\pi^0} - A_{\pi^+\pi^0} = 0, \quad (12.22)$$

and a similar expression for the $\bar{A}_{\pi\pi}$'s. This method utilizes the fact that a pair of pions from $B \rightarrow \pi\pi$ decay must be in a zero angular momentum state, and, because of Bose statistics, they must have even isospin. Consequently, $\pi^+\pi^0$ is in a pure isospin-2 state, while the penguin amplitudes only contribute to the isospin-0 final state. The latter does not hold for the electroweak penguin amplitudes, but their effect is expected to be small. The isospin

analysis uses the world averages of *BABAR*, Belle, and LHCb measurements, $S_{\pi^+\pi^-} = -0.666 \pm 0.029$, $C_{\pi^+\pi^-} = -0.311 \pm 0.030$, the decay widths of all three modes, and the direct CP asymmetry $C_{\pi^0\pi^0} = -0.33 \pm 0.22$ [24]. This analysis leads to 16 mirror solutions for $0 \leq \alpha < 2\pi$. Because of this, and due to the experimental uncertainties, some of these solutions are not well separated [95].

12.3.3.2 $B \rightarrow \rho\rho$

The decay $B^0 \rightarrow \rho^+\rho^-$ contains two vector mesons in the final state, and so in general is a mixture of CP -even and CP -odd components. At the current level of precision, it simplifies the analysis that the longitudinal polarization fractions in $B^+ \rightarrow \rho^+\rho^0$ and $B^0 \rightarrow \rho^+\rho^-$ decays were measured to be close to unity [105], which implies that the final states are almost purely CP -even. Furthermore, $\mathcal{B}(B^0 \rightarrow \rho^0\rho^0) = (0.96 \pm 0.15) \times 10^{-6}$ is much smaller than $\mathcal{B}(B^0 \rightarrow \rho^+\rho^-) = (27.5 \pm 1.7) \times 10^{-6}$ and $\mathcal{B}(B^+ \rightarrow \rho^+\rho^0) = (23.8 \pm 1.7) \times 10^{-6}$ [24], which implies that the effect of the penguin contributions is small. The isospin analysis using the world averages, $S_{\rho^+\rho^-} = -0.14 \pm 0.13$ and $C_{\rho^+\rho^-} = 0.00 \pm 0.09$ [24], together with the time-dependent CP asymmetry, $S_{\rho^0\rho^0} = -0.3 \pm 0.7$ and $C_{\rho^0\rho^0} = -0.2 \pm 0.9$ [106], and the above mentioned branching fractions and longitudinal polarization fractions, gives two solutions (with mirror solutions at $3\pi/2 - \alpha$) [95]. A possible small violation of Eq. (12.22) due to the finite width of the ρ [107] is so far neglected.

12.3.3.3 $B \rightarrow \rho\pi$

The final state in $B^0 \rightarrow \rho^+\pi^-$ decay is not a CP eigenstate, but this decay proceeds via the same quark-level diagrams as $B^0 \rightarrow \pi^+\pi^-$, and both B^0 and \bar{B}^0 can decay to $\rho^+\pi^-$, while the final state in $B^0 \rightarrow \rho^0\pi^0$ is a CP eigenstate. Consequently, mixing-induced CP violation can occur in B^0 and \bar{B}^0 decays to $\rho^\pm\pi^\mp$ and $\rho^0\pi^0$. The time-dependent Dalitz plot analysis of $B^0 \rightarrow \pi^+\pi^-\pi^0$ decays permits the extraction of α with a single discrete ambiguity, $\alpha \rightarrow \alpha + \pi$, since one knows the variation of the strong phases in the interference regions of the $\rho^+\pi^-$, $\rho^-\pi^+$, and $\rho^0\pi^0$ amplitudes in the Dalitz plot [108]. The combination of Belle [109] and *BABAR* [110] measurements gives only moderate constraints [95].

Combining the $B \rightarrow \pi\pi$, $\rho\pi$, and $\rho\rho$ decay modes [24, 95, 99], α is constrained as

$$\alpha = (84.1_{-3.8}^{+4.5})^\circ. \quad (12.23)$$

Similar results can be found in Refs. [111, 112].

12.3.4 γ / ϕ_3

By virtue of Eq. (12.16), γ does not depend on CKM elements involving the top quark, so it can be measured in tree-level B decays. This is an important distinction from the measurements of α and β , and implies that measurements of γ are unlikely to be affected by physics beyond the SM.

12.3.4.1 $B_{(s)} \rightarrow D_{(s)}K^{(*)}$

The interference of $B^- \rightarrow D^0K^-$ ($b \rightarrow c\bar{u}s$) and $B^- \rightarrow \bar{D}^0K^-$ ($b \rightarrow u\bar{c}s$) transitions can be studied in final states accessible in both D^0 and \bar{D}^0 decays [93]. In principle, it is possible to extract the B and D decay amplitudes, the relative strong phases, and the weak phase γ from the data [95].

A practical complication is that the precision depends sensitively on the ratio of the interfering amplitudes

$$r_B = \left| A(B^- \rightarrow \bar{D}^0K^-) / A(B^- \rightarrow D^0K^-) \right|, \quad (12.24)$$

which is around 0.1. The original GLW method [113, 114] considers D decays to CP eigenstates, such as $B^\pm \rightarrow D_{CP}^{(*)}(\rightarrow \pi^+\pi^-)K^{(*)\pm}$. To alleviate the smallness of r_B and make the interfering amplitudes (which are products of the B and D decay amplitudes) comparable in magnitude, the ADS method [115] considers final states where Cabibbo-allowed \bar{D}^0 and doubly-Cabibbo-suppressed D^0 decays interfere. Measurements have been made by the B factories, CDF, and LHCb, using both methods [24]. The GLW method currently gives only a loose constraint on γ , while the ADS method provides a moderate constraint.

The BPGGSZ method [116, 117] utilizes the fact that both D^0 and \bar{D}^0 can have large branching fractions to CP self-conjugate

three- and four-body final states, such as $K_s^0 \pi^+ \pi^-$, and the analysis can be optimized by studying the Dalitz plot dependence of the interferences. The best present determination of γ comes from this method, dominated by 3-body D decay modes. Combining results in 3-body decay modes from Belle [118], *BABAR* [119], and the most precise LHCb [120] one, $\gamma = (70.0 \pm 4.0)^\circ$ is obtained [95]. The uncertainty is sensitive to the central value of the amplitude ratio r_B (and r_B^* for the $D^* K$ mode), for which Belle found somewhat larger central values than *BABAR* and LHCb. The same values of $r_B^{(*)}$ enter the ADS analyses, and the data (including 4-body D decays [121]) can be combined to fit for $r_B^{(*)}$ and γ . The effect of $D^0 - \bar{D}^0$ mixing on γ is either below the present experimental accuracy or can be taken into account in the analysis [122] (even if $D^0 - \bar{D}^0$ mixing is due to CP -violating new physics [123]).

The amplitude ratio is much larger in the analogous $B_s^0 \rightarrow D_s^\pm K^\mp$ decays, which allows a model-independent extraction of $\gamma - 2\beta_s$ [124] (here $\beta_s = \arg(-V_{ts} V_{tb}^* / V_{cs} V_{cb}^*)$ is related to the phase of B_s mixing). Measurements by LHCb with $B_s^0 \rightarrow D_s^\pm K^\mp$ [125] and $B_s^0 \rightarrow D_s^\pm K^\mp \pi^+ \pi^-$ [126] give $\gamma = (79_{-21}^{+19})^\circ$ using a constraint on $2\beta_s$ (see Sec. 12.5).

Combining all the above measurements [24, 95, 99], γ is constrained as

$$\gamma = (65.7 \pm 3.0)^\circ. \quad (12.25)$$

Similar results can be found in Refs. [111, 112].

12.3.4.2 $B^0 \rightarrow D^{(*)\pm} \pi^\mp$

The interference of $b \rightarrow u$ and $b \rightarrow c$ transitions can be studied in $\bar{B}^0 \rightarrow D^{(*)+} \pi^-$ ($b \rightarrow c \bar{u} d$) and $\bar{B}^0 \rightarrow B^0 \rightarrow D^{(*)+} \pi^-$ ($\bar{b} \rightarrow \bar{u} c d$) decays and their CP conjugates, since both B^0 and \bar{B}^0 decay to $D^{(*)\pm} \pi^\mp$ (or $D^\pm \rho^\mp$, etc.). Since there are only tree and no penguin contributions to these decays, in principle, it is possible to extract from the four time-dependent rates the magnitudes of the two hadronic amplitudes, their relative strong phase, and the weak phase between the two decay paths, which is $2\beta + \gamma$.

A complication is that the ratio of the interfering amplitudes is very small, $r_{D\pi} = A(B^0 \rightarrow D^+ \pi^-) / A(\bar{B}^0 \rightarrow D^+ \pi^-) = \mathcal{O}(0.01)$ (and similarly for $r_{D^* \pi}$ and $r_{D\rho}$), and therefore it has not been possible to measure it. To obtain $2\beta + \gamma$, $SU(3)$ flavor symmetry and dynamical assumptions have been used to relate $A(\bar{B}^0 \rightarrow D^+ \pi^-)$ to $A(\bar{B}^0 \rightarrow D_s^- \pi^+)$, so this measurement is not model independent at present. Combining the $D^\pm \pi^\mp$, $D^{*\pm} \pi^\mp$ and $D^\pm \rho^\mp$ measurements [127] gives $\sin(2\beta + \gamma) > 0.68$ at 68% CL [111], consistent with the previously discussed results for β and γ .

12.4 Global fit in the Standard Model

Using the independently measured CKM elements mentioned in the previous sections, the unitarity of the CKM matrix can be checked. We obtain $|V_{ud}|^2 + |V_{us}|^2 + |V_{ub}|^2 = 0.9984 \pm 0.0007$ (1st row), $|V_{cd}|^2 + |V_{cs}|^2 + |V_{cb}|^2 = 1.001 \pm 0.012$ (2nd row), $|V_{ud}|^2 + |V_{cd}|^2 + |V_{td}|^2 = 0.9971 \pm 0.0020$ (1st column), and $|V_{us}|^2 + |V_{cs}|^2 + |V_{ts}|^2 = 1.003 \pm 0.012$ (2nd column), respectively. Due to the recent reduction of the value of $|V_{ud}|$, there is a 2.3σ tension with unitarity in the 1st row, leading also to poor consistency of the SM fit below. The uncertainties in the second row and column are dominated by that of $|V_{cs}|$. For the second row, another check is obtained from the measurement of $\sum_{u,c,d,s,b} |V_{ij}|^2$ in Sec. 12.2.4, minus the sum in the first row above: $|V_{cd}|^2 + |V_{cs}|^2 + |V_{cb}|^2 = 1.002 \pm 0.027$. These provide strong tests of the unitarity of the CKM matrix. With the significantly improved direct determination of $|V_{tb}|$, the unitarity checks for the third row and column have also become fairly precise, leaving decreasing room for mixing with other states. The sum of the three angles of the unitarity triangle, $\alpha + \beta + \gamma = (172 \pm 5)^\circ$, is also consistent with the SM expectation.

The CKM matrix elements can be most precisely determined using a global fit to all available measurements and imposing the SM constraints (*i.e.*, three generation unitarity). The fit must also use theory predictions for hadronic matrix elements, which sometimes have significant uncertainties. There are several approaches to combining the experimental data. CKMfitter [6, 111] and Ref. [128] (which develops [129, 130] further) use frequentist

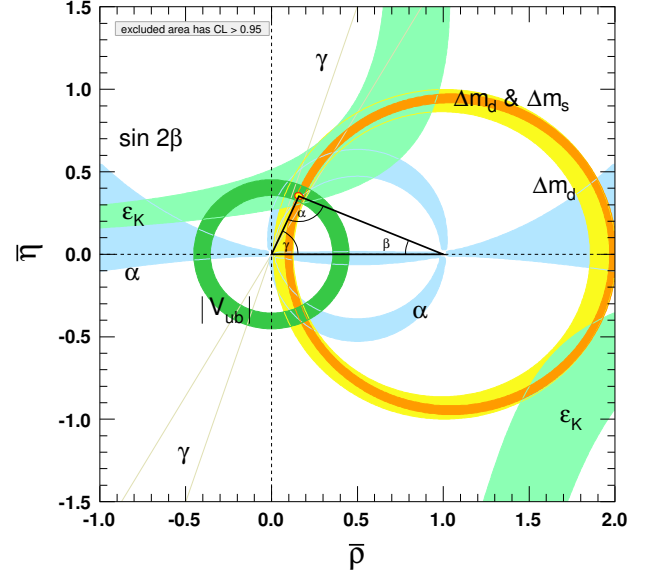


Figure 12.2: Constraints on the $\bar{\rho}, \bar{\eta}$ plane. The shaded areas have 95% CL.

statistics, while UTfit [112, 131] uses a Bayesian approach. These approaches provide similar results.

The constraints implied by the unitarity of the three generation CKM matrix significantly reduce the allowed range of some of the CKM elements. The fit for the Wolfenstein parameters defined in Eq. (12.4) gives

$$\begin{aligned} \lambda &= 0.22501 \pm 0.00068, & A &= 0.826_{-0.015}^{+0.016}, \\ \bar{\rho} &= 0.1591 \pm 0.0094, & \bar{\eta} &= 0.3523_{-0.0071}^{+0.0073}. \end{aligned} \quad (12.26)$$

These values are obtained using the method of Refs. [6, 111]. The prescription of Refs. [112, 131] gives $\lambda = 0.22497 \pm 0.00070$, $A = 0.839 \pm 0.011$, $\bar{\rho} = 0.1581 \pm 0.0092$, and $\bar{\eta} = 0.3548 \pm 0.0072$ [132]; these results are now very close to one another. The fit results for the magnitudes of all nine CKM elements are

$$|V_{\text{CKM}}| = \begin{pmatrix} 0.97435 \pm 0.00016 & 0.22501 \pm 0.00068 & 0.003732_{-0.000085}^{+0.000090} \\ 0.22487 \pm 0.00068 & 0.97349 \pm 0.00016 & 0.04183_{-0.00069}^{+0.00079} \\ 0.00858_{-0.00017}^{+0.00019} & 0.04111_{-0.00068}^{+0.00077} & 0.999118_{-0.000034}^{+0.000029} \end{pmatrix}, \quad (12.27)$$

and the Jarlskog invariant is $J = (3.12_{-0.12}^{+0.13}) \times 10^{-5}$. The parameters in Eq. (12.3) are

$$\begin{aligned} \sin \theta_{12} &= 0.22501 \pm 0.00068, & \sin \theta_{13} &= 0.003732_{-0.000085}^{+0.000090}, \\ \sin \theta_{23} &= 0.04183_{-0.00069}^{+0.00079}, & \delta &= 1.147 \pm 0.026. \end{aligned} \quad (12.28)$$

Fig. 12.2 illustrates the constraints on the $\bar{\rho}, \bar{\eta}$ plane from various measurements, and the global fit result. The shaded 95% CL regions all overlap consistently around the global fit region.

If one uses only tree-level inputs (magnitudes of CKM elements not coupling to the top quark and the angle γ), the resulting fit is almost identical for λ in Eq. (12.26), while the other parameters' central values can change by about a sigma and their uncertainties double, yielding $\lambda = 0.22509 \pm 0.00068$, $A = 0.811 \pm 0.024$, $\bar{\rho} = 0.166_{-0.021}^{+0.022}$, and $\bar{\eta} = 0.367_{-0.023}^{+0.024}$. This illustrates how the constraints can be less tight in the presence of BSM physics.

12.5 Implications beyond the SM

The effects in B, B_s, K , and D decays and mixings due to high-scale physics (W, Z, t, H in the SM, and unknown heavier particles) can be parameterized by operators composed of SM

fields, obeying the $SU(3) \times SU(2) \times U(1)$ gauge symmetry. Flavor-changing neutral currents, suppressed in the SM, are especially sensitive to beyond SM contributions. Processes studied in great detail, both experimentally and theoretically, include neutral meson mixings, $B_{(s)} \rightarrow X\gamma$, $X\ell^+\ell^-$, $\ell^+\ell^-$, $K \rightarrow \pi\nu\bar{\nu}$, etc. The BSM contributions to these operators are suppressed by powers of the scale at which they are generated. Already at lowest order, there are many dimension-6 operators, and the observable effects of BSM interactions are encoded in their coefficients. In the SM, these coefficients are determined by just the four CKM parameters, and the W , Z , and quark masses. For example, Δm_d , $\Gamma(B \rightarrow \rho\gamma)$, $\Gamma(B \rightarrow \pi\ell^+\ell^-)$, and $\Gamma(B \rightarrow \ell^+\ell^-)$ are all proportional to $|V_{td}V_{tb}|^2$ in the SM, however, they may receive unrelated BSM contributions. These BSM contributions may or may not obey the SM relations. (For example, the flavor sector of the MSSM contains 69 CP -conserving parameters and 41 CP -violating phases, *i.e.*, 40 new ones [133]). Thus, similar to the measurements of $\sin 2\beta$ in tree- and loop-dominated decay modes, overconstraining measurements of the magnitudes and phases of flavor-changing neutral-current amplitudes gives good sensitivity to BSM.

To illustrate the level of suppression required for BSM contributions, consider a class of models in which the unitarity of the CKM matrix is maintained, and the dominant BSM effects modify the neutral meson mixing amplitudes [134] by $(z_{ij}/\Lambda^2)(\bar{q}_i\gamma^\mu P_L q_j)^2$, where z_{ij} is an unknown coefficient and Λ is the scale suppressing this BSM contribution (see, [135, 136]). It is only known since the first measurements of γ and α that the SM gives the leading contribution to $B^0 - \bar{B}^0$ mixing [6, 137]. Nevertheless, new physics with a generic weak phase may still contribute to neutral meson mixings at a significant fraction of the SM [131, 138, 139]. The existing data imply that $\Lambda/|z_{ij}|^{1/2}$ has to exceed about 10^4 TeV for $K^0 - \bar{K}^0$ mixing, 10^3 TeV for $D^0 - \bar{D}^0$ mixing, 500 TeV for $B^0 - \bar{B}^0$ mixing, and 100 TeV for $B_s^0 - \bar{B}_s^0$ mixing [131, 136]. (Some other operators are even better constrained [131].) The constraints are the strongest in the kaon sector, because the CKM suppression is the most severe. Thus, if there is new physics at the TeV scale, $|z_{ij}| \ll 1$ is required. Even if $|z_{ij}|$ are suppressed by a loop factor and $|V_{ti}^*V_{tj}|^2$ (in the down quark sector), similar to the SM, one expects percent-level effects, which may be observable in forthcoming flavor physics experiments. To constrain such extensions of the SM, many measurements irrelevant for the SM-CKM fit, such as the CP asymmetry in semileptonic $B_{d,s}^0$ decays, $A_{SL}^{d,s}$, are important [140]. The current world averages [24] are consistent with the SM, with experimental uncertainties far greater than those of the theory predictions.

There are many key measurements sensitive to BSM physics, which do not constrain the unitarity triangle in Fig. 12.1. For example, a key quantity in the B_s system is $\beta_s = \arg(-V_{ts}V_{tb}^*/V_{cs}V_{cb}^*)$, which is the small, λ^2 -suppressed, angle of a “squashed” unitarity triangle, obtained by taking the scalar product of the second and third columns of the CKM matrix. This angle can be measured via time-dependent CP violation in $B_s^0 \rightarrow J/\psi\phi$, similar to β in $B^0 \rightarrow J/\psi K^0$. Since the $J/\psi\phi$ final state is not a CP eigenstate, an angular analysis of the decay products is needed to separate the CP -even and CP -odd components, which give opposite asymmetries. In the SM, the asymmetry for the CP -even part is $2\beta_s$, when one neglects subdominant amplitudes with a weak phase V_{ub} . (Sometimes the notation $\phi_s = -2\beta_s$ plus a possible BSM contribution to the B_s mixing phase is used.) Testing if the data agree with the SM prediction, $2\beta_s = 0.03726_{-0.00077}^{+0.00078}$ [111], is another sensitive probe of the SM. The current world average, dominated by LHC measurements including the $B_s \rightarrow J/\psi K^+ K^-$ and $J/\psi \pi^+ \pi^-$ decay modes, is $2\beta_s = 0.040 \pm 0.016$ [69]. Since the uncertainty is much larger than that in the SM, a lot will be learned from more precise future measurements. Searches for CP violation in the charm sector, in particular in $D^0 - \bar{D}^0$ mixing, provide complementary sensitivity to BSM.

In the kaon sector, the CP -violating observables, ϵ and ϵ' , are tiny, so models in which all sources of CP violation are small were viable before the B -factory measurements. Since the measurement of $\sin 2\beta$, we know that CP violation can be an $\mathcal{O}(1)$ ef-

fect, and only flavor mixing is suppressed between the three quark generations. Thus, many models with spontaneous CP violation were excluded. In the kaon sector, clean tests of the SM can come from measurements of $K^+ \rightarrow \pi^+ \nu \bar{\nu}$ [77] and $K_L^0 \rightarrow \pi^0 \nu \bar{\nu}$ [141]. These loop-induced rare decays are sensitive to BSM, and will allow precise tests [142] of the CKM paradigm, independent of B decays.

The CKM elements are fundamental parameters, so they should be measured as precisely as possible. The overconstraining measurements of CP asymmetries, mixing, semileptonic, and rare decays severely constrain the magnitudes and phases of possible BSM contributions to flavor-changing interactions. If new particles are observed at the LHC, it will be important to explore their flavor parameters as precisely as possible to understand the underlying physics.

References

- [1] N. Cabibbo, Phys. Rev. Lett. **10**, 531 (1963).
- [2] M. Kobayashi and T. Maskawa, Prog. Theor. Phys. **49**, 652 (1973).
- [3] L.-L. Chau and W.-Y. Keung, Phys. Rev. Lett. **53**, 1802 (1984).
- [4] L. Wolfenstein, Phys. Rev. Lett. **51**, 1945 (1983).
- [5] A. J. Buras, M. E. Lautenbacher and G. Ostermaier, Phys. Rev. **D50**, 3433 (1994), [hep-ph/9403384].
- [6] J. Charles *et al.* (CKMfitter Group), Eur. Phys. J. **C41**, 1, 1 (2005), [hep-ph/0406184].
- [7] C. Jarlskog, Phys. Rev. Lett. **55**, 1039 (1985).
- [8] W. J. Marciano and A. Sirlin, Nucl. Phys. **B93**, 303 (1975); K. S. Babu, Z. Phys. **C35**, 69 (1987).
- [9] J. C. Hardy and I. S. Towner, Phys. Rev. C **102**, 4, 045501 (2020).
- [10] E. Blucher, G. D’Ambrosio, and W.J. Marciano, “ V_{ud} , V_{us} , the Cabibbo Angle and CKM Unitarity,” in this *Review*.
- [11] D. Poganic *et al.*, Phys. Rev. Lett. **93**, 181803 (2004), [hep-ex/0312030].
- [12] A. Czarnecki, W. J. Marciano and A. Sirlin, Phys. Rev. D **101**, 9, 091301 (2020), [arXiv:1911.04685].
- [13] M. Antonelli *et al.* (FlaviaNet Working Group on Kaon Decays), Eur. Phys. J. **C69**, 399 (2010), [arXiv:1005.2323]; see also <http://www.lnf.infn.it/wg/vus>.
- [14] S. Aoki *et al.* (Flavour Lattice Averaging Group) “FLAG Review 2021 (March 24, 2023 update)”, <http://flag.unibe.ch/2021>; The original papers that led to the quoted averages are cited in this reference.
- [15] T. Mannel and P. Urquijo, “Semileptonic b -Hadron Decays, Determination of V_{cb} and V_{ub} ,” in this *Review*.
- [16] H. Leutwyler and M. Roos, Z. Phys. **C25**, 91 (1984); For earlier fits for $|V_{ud}|$ and $|V_{us}|$ in the 3-generation SM, see Ref. [17].
- [17] R. E. Shrock and L.-L. Wang, Phys. Rev. Lett. **41**, 1692 (1978).
- [18] J. Bijnens and P. Talavera, Nucl. Phys. **B669**, 341 (2003), [hep-ph/0303103]; M. Jamin, J. A. Oller and A. Pich, JHEP **02**, 047 (2004), [hep-ph/0401080]; V. Cirigliano *et al.*, JHEP **04**, 006 (2005), [hep-ph/0503108]; C. Dawson *et al.*, PoS **LAT2005**, 337 (2006), [hep-lat/0510018]; N. Tsutsui *et al.* (JLQCD), PoS **LAT2005**, 357 (2006), [hep-lat/0510068]; M. Okamoto (Fermilab Lattice, MILC, HPQCD), in “3rd Conference on Flavor Physics and CP Violation (FPCP 2004) Daegu, Korea, October 4-9, 2004,” (2004), [hep-lat/0412044].
- [19] W. J. Marciano, Phys. Rev. Lett. **93**, 231803 (2004), [hep-ph/0402299].
- [20] F. Ambrosino *et al.* (KLOE), Phys. Lett. **B632**, 76 (2006), [hep-ex/0509045].
- [21] See Sec. 5.2, “Averages and fits,” in the Introduction to this *Review*, <https://pdg.lbl.gov/2023/reviews/rpp2023-rev-rpp-intro.pdf>.

- [22] N. Cabibbo, E. C. Swallow and R. Winston, *Ann. Rev. Nucl. Part. Sci.* **53**, 39 (2003), [hep-ph/0307298]; N. Cabibbo, E. C. Swallow and R. Winston, *Phys. Rev. Lett.* **92**, 251803 (2004), [hep-ph/0307214].
- [23] M. Ademollo and R. Gatto, *Phys. Rev. Lett.* **13**, 264 (1964).
- [24] Y. S. Amhis *et al.* (HFLAV), *Phys. Rev. D* **107**, 5, 052008 (2023), [arXiv:2206.07501]; and updates at <https://hflav.web.cern.ch/>.
- [25] J. P. Lees *et al.* (BaBar), *Phys. Rev. D* **91**, 5, 052022 (2015), [arXiv:1412.5502].
- [26] M. Ablikim *et al.* (BESIII), *Phys. Rev. D* **92**, 7, 072012 (2015), [arXiv:1508.07560]; M. Ablikim *et al.* (BESIII), *Phys. Rev. D* **96**, 1, 012002 (2017), [arXiv:1703.09084].
- [27] D. Besson *et al.* (CLEO), *Phys. Rev. D* **80**, 032005 (2009), [arXiv:0906.2983].
- [28] L. Widhalm *et al.* (Belle), *Phys. Rev. Lett.* **97**, 061804 (2006), [hep-ex/0604049].
- [29] M. Ablikim *et al.* (BESIII), *Phys. Rev. D* **89**, 5, 051104 (2014), [arXiv:1312.0374].
- [30] B. I. Eisenstein *et al.* (CLEO), *Phys. Rev. D* **78**, 052003 (2008), [arXiv:0806.2112].
- [31] M. Ablikim *et al.* (BESIII), *Phys. Rev. Lett.* **123**, 21, 211802 (2019), [arXiv:1908.08877].
- [32] H. Abramowicz *et al.*, *Z. Phys.* **C15**, 19 (1982).
- [33] S. A. Rabinowitz *et al.*, *Phys. Rev. Lett.* **70**, 134 (1993); A. O. Bazarko *et al.* (CCFR), *Z. Phys.* **C65**, 189 (1995), [hep-ex/9406007].
- [34] P. Vilain *et al.* (CHARM II), *Eur. Phys. J.* **C11**, 19 (1999).
- [35] F. J. Gilman, K. Kleinknecht and B. Renk (2004).
- [36] G. De Lellis, P. Migliozi and P. Santorelli, *Phys. Rept.* **399**, 227 (2004), [Erratum: *Phys. Rept.* 411,323(2005)].
- [37] N. Ushida *et al.* (Fermilab E531), *Phys. Lett.* **B206**, 380 (1988); T. Bolton (1997), [hep-ex/9708014].
- [38] A. Kayis-Topaksu *et al.* (CHORUS), *Phys. Lett.* **B626**, 24 (2005).
- [39] A. Zupanc *et al.* (Belle), *JHEP* **09**, 139 (2013), [arXiv:1307.6240].
- [40] J. P. Alexander *et al.* (CLEO), *Phys. Rev. D* **79**, 052001 (2009), [arXiv:0901.1216].
- [41] P. del Amo Sanchez *et al.* (BaBar), *Phys. Rev. D* **82**, 091103 (2010), [Erratum: *Phys. Rev. D* 91, no.1, 019901(2015)], [arXiv:1008.4080].
- [42] M. Ablikim *et al.* (BESIII), *Phys. Rev. D* **94**, 7, 072004 (2016), [arXiv:1608.06732].
- [43] M. Ablikim *et al.* (BESIII), *Phys. Rev. D* **104**, 5, 052009 (2021), [arXiv:2102.11734].
- [44] P. U. E. Onyisi *et al.* (CLEO), *Phys. Rev. D* **79**, 052002 (2009), [arXiv:0901.1147]; P. Naik *et al.* (CLEO), *Phys. Rev. D* **80**, 112004 (2009), [arXiv:0910.3602].
- [45] B. Aubert *et al.* (BaBar), *Phys. Rev. D* **76**, 052005 (2007), [arXiv:0704.0020].
- [46] M. Ablikim *et al.* (BESIII), *Phys. Rev. Lett.* **122**, 1, 011804 (2019), [arXiv:1810.03127].
- [47] LEP *W* branching fraction results for this Review of Particle Physics, LEPEWWG/XSEC/2005-01, <http://lepewwg.web.cern.ch/LEPEWWG/lepww/4f/Winter05>.
- [48] P. Abreu *et al.* (DELPHI), *Phys. Lett.* **B439**, 209 (1998).
- [49] I. I. Y. Bigi *et al.*, *Phys. Rev. Lett.* **71**, 496 (1993), [hep-ph/9304225].
- [50] A. V. Manohar and M. B. Wise, *Phys. Rev. D* **49**, 1310 (1994), [hep-ph/9308246].
- [51] I. I. Y. Bigi *et al.*, *Phys. Rev. D* **56**, 4017 (1997), [hep-ph/9704245].
- [52] A. H. Hoang, Z. Ligeti and A. V. Manohar, *Phys. Rev. D* **59**, 074017 (1999), [hep-ph/9811239]; A. H. Hoang, Z. Ligeti and A. V. Manohar, *Phys. Rev. Lett.* **82**, 277 (1999), [hep-ph/9809423]; A. H. Hoang and T. Teubner, *Phys. Rev. D* **60**, 114027 (1999), [hep-ph/9904468].
- [53] N. Isgur and M. B. Wise, *Phys. Lett.* **B237**, 527 (1990); N. Isgur and M. B. Wise, *Phys. Lett.* **B232**, 113 (1989).
- [54] A. Abdesselam *et al.* (Belle) (2017), [arXiv:1702.01521].
- [55] C. G. Boyd, B. Grinstein and R. F. Lebed, *Phys. Rev. D* **56**, 6895 (1997), [hep-ph/9705252]; C. G. Boyd, B. Grinstein and R. F. Lebed, *Nucl. Phys.* **B461**, 493 (1996), [hep-ph/9508211].
- [56] R. Aaij *et al.* (LHCb), *Phys. Rev. D* **101**, 7, 072004 (2020), [arXiv:2001.03225].
- [57] M. Neubert, *Phys. Rev. D* **49**, 3392 (1994), [hep-ph/9311325]; M. Neubert, *Phys. Rev. D* **49**, 4623 (1994), [hep-ph/9312311].
- [58] I. I. Y. Bigi *et al.*, *Int. J. Mod. Phys.* **A9**, 2467 (1994), [hep-ph/9312359].
- [59] C. W. Bauer, Z. Ligeti and M. E. Luke, *Phys. Lett.* **B479**, 395 (2000), [hep-ph/0002161]; C. W. Bauer, Z. Ligeti and M. E. Luke, *Phys. Rev. D* **64**, 113004 (2001), [hep-ph/0107074].
- [60] A. Bornheim *et al.* (CLEO), *Phys. Rev. Lett.* **88**, 231803 (2002), [hep-ex/0202019].
- [61] B. Aubert *et al.* (BaBar), *Phys. Rev. D* **73**, 012006 (2006), [hep-ex/0509040].
- [62] A. Limosani *et al.* (Belle), *Phys. Lett.* **B621**, 28 (2005), [hep-ex/0504046].
- [63] P. Urquijo *et al.* (Belle), *Phys. Rev. Lett.* **104**, 021801 (2010), [arXiv:0907.0379]; J. P. Lees *et al.* (BaBar), *Phys. Rev. D* **86**, 032004 (2012), [arXiv:1112.0702].
- [64] J. A. Bailey *et al.* (Fermilab Lattice, MILC), *Phys. Rev. D* **92**, 1, 014024 (2015), [arXiv:1503.07839]; J. M. Flynn *et al.*, *Phys. Rev. D* **91**, 7, 074510 (2015), [arXiv:1501.05373]; B. Colquhoun *et al.*, *Phys. Rev. D* **93**, 3, 034502 (2016), [arXiv:1510.07446].
- [65] Particle listing, in this *Review*.
- [66] R. Aaij *et al.* (LHCb), *Nature Phys.* **11**, 743 (2015), [arXiv:1504.01568].
- [67] R. Aaij *et al.* (LHCb), *Phys. Rev. Lett.* **126**, 8, 081804 (2021), [arXiv:2012.05143].
- [68] H. Albrecht *et al.* (ARGUS), *Phys. Lett.* **B192**, 245 (1987).
- [69] O. Schneider, “ B^0 – \bar{B}^0 mixing,” in this *Review*.
- [70] A. Abulencia *et al.* (CDF), *Phys. Rev. Lett.* **97**, 242003 (2006), [hep-ex/0609040].
- [71] R. Aaij *et al.* (LHCb), *Nature Phys.* **18**, 1, 1 (2022), [arXiv:2104.04421].
- [72] M. Misiak *et al.*, *Phys. Rev. Lett.* **114**, 22, 221801 (2015), [arXiv:1503.01789]; P. Czakon, MichaŁeand Fiedler *et al.*, *JHEP* **04**, 168 (2015), [arXiv:1503.01791].
- [73] Heavy Flavor Averaging Group [24] *CP Asymmetries in Charmless B Decay*, End of April 2023, <https://hflav-eos.web.cern.ch/hflav-eos/rare/Apr2023/html/index.html>.
- [74] B. Grinstein and D. Pirjol, *Phys. Rev. D* **62**, 093002 (2000), [hep-ph/0002216]; A. Ali, E. Lunghi and A. Ya. Parkhomenko, *Phys. Lett.* **B595**, 323 (2004), [hep-ph/0405075]; M. Beneke, T. Feldmann and D. Seidel, *Nucl. Phys.* **B612**, 25 (2001), [hep-ph/0106067]; S. W. Bosch and G. Buchalla, *Nucl. Phys.* **B621**, 459 (2002), [hep-ph/0106081]; Z. Ligeti and M. B. Wise, *Phys. Rev. D* **60**, 117506 (1999), [hep-ph/9905277]; D. Becirevic *et al.*, *JHEP* **05**, 007 (2003), [hep-lat/0301020]; P. Ball, G. W. Jones and R. Zwicky, *Phys. Rev. D* **75**, 054004 (2007), [hep-ph/0612081]; W. Wang, R.-H. Li and C.-D. Lu (2007), [arXiv:0711.0432]; C.-D. Lu, W. Wang and Z.-T. Wei, *Phys. Rev. D* **76**, 014013 (2007), [hep-ph/0701265].

- [75] A. J. Buras *et al.*, Phys. Rev. Lett. **95**, 261805 (2005), [hep-ph/0508165].
- [76] A. V. Artamonov *et al.* (E949), Phys. Rev. Lett. **101**, 191802 (2008), [arXiv:0808.2459]; A. V. Artamonov *et al.* (BNL-E949), Phys. Rev. **D79**, 092004 (2009), [arXiv:0903.0030].
- [77] E. Cortina Gil *et al.* (NA62), JHEP **06**, 093 (2021), [arXiv:2103.15389].
- [78] T. A. Aaltonen *et al.* (CDF), Phys. Rev. Lett. **112**, 22, 221801 (2014), [arXiv:1404.3392].
- [79] V. M. Abazov *et al.* (D0), Phys. Rev. Lett. **107**, 121802 (2011), [arXiv:1106.5436].
- [80] V. Khachatryan *et al.* (CMS), Phys. Lett. **B736**, 33 (2014), [arXiv:1404.2292].
- [81] T. A. Aaltonen *et al.* (CDF, D0), Phys. Rev. Lett. **115**, 15, 152003 (2015), [arXiv:1503.05027].
- [82] LHC Top Working Group summary plots, single top quark production, November 2023, <https://twiki.cern.ch/twiki/bin/view/LHCPhysics/LHCtopWGSummaryPlots>.
- [83] J. Swain and L. Taylor, Phys. Rev. **D58**, 093006 (1998), [hep-ph/9712420].
- [84] “ K_L^0 meson” particle listing, in this *Review*.
- [85] A. J. Buras, D. Guadagnoli and G. Isidori, Phys. Lett. **B688**, 309 (2010), [arXiv:1002.3612]; For earlier discussions, see Ref. [86].
- [86] E. A. Andriyash, G. G. Ovanesyan and M. I. Vysotsky, Phys. Lett. **B599**, 253 (2004), [hep-ph/0310314]; K. Anikeev *et al.*, in “Workshop on B Physics at the Tevatron: Run II and Beyond Batavia, Illinois, September 23-25, 1999,” (2001), [hep-ph/0201071]; A. J. Buras and D. Guadagnoli, Phys. Rev. **D78**, 033005 (2008), [arXiv:0805.3887].
- [87] T. Inami and C. S. Lim, Prog. Theor. Phys. **65**, 297 (1981), [Erratum: Prog. Theor. Phys.65,1772(1981)].
- [88] J. M. Flynn and L. Randall, Phys. Lett. **B224**, 221 (1989), [Erratum: Phys. Lett.B235,412(1990)]; G. Buchalla, A. J. Buras and M. K. Harlander, Nucl. Phys. **B337**, 313 (1990).
- [89] M. Ciuchini *et al.*, Phys. Lett. **B301**, 263 (1993), [hep-ph/9212203]; A. J. Buras, M. Jamin and M. E. Lautenbacher, Nucl. Phys. **B408**, 209 (1993), [hep-ph/9303284]; T. Hambye *et al.*, Nucl. Phys. **B564**, 391 (2000), [hep-ph/9906434]; S. Bertolini, J. O. Eeg and M. Fabbrichesi, Phys. Rev. **D63**, 056009 (2001), [hep-ph/0002234]; V. Cirigliano *et al.*, Phys. Rev. Lett. **91**, 162001 (2003), [hep-ph/0307030].
- [90] R. Abbott *et al.* (RBC, UKQCD), Phys. Rev. D **102**, 5, 054509 (2020), [arXiv:2004.09440].
- [91] A. J. Buras *et al.*, JHEP **11**, 202 (2015), [arXiv:1507.06345].
- [92] V. Cirigliano *et al.*, JHEP **02**, 032 (2020), [arXiv:1911.01359].
- [93] A. B. Carter and A. I. Sanda, Phys. Rev. Lett. **45**, 952 (1980); A. B. Carter and A. I. Sanda, Phys. Rev. **D23**, 1567 (1981).
- [94] A more detailed discussion and references can be found in: T. Gershon and Y. Nir, “ CP violation in meson decays,” in this *Review*.
- [95] T. Gershon, M. Kenzie and K. Trabelsi, “Determination of CKM angles from B hadrons,” in this *Review*.
- [96] B. Aubert *et al.* (BaBar), Phys. Rev. **D79**, 072009 (2009), [arXiv:0902.1708].
- [97] I. Adachi *et al.* (Belle), Phys. Rev. Lett. **108**, 171802 (2012), [arXiv:1201.4643].
- [98] R. Aaij *et al.* (LHCb), Phys. Rev. Lett. **132**, 2, 021801 (2024), [arXiv:2309.09728].
- [99] Heavy Flavor Averaging Group [24], Results on Time-Dependent CP Violation and Measurements Related to the Angles of the Unitarity Triangle: Winter conferences (Moriond, etc.) 2024: <https://hflav-eos.web.cern.ch/hflav-eos/triangle/moriond2024/>.
- [100] B. Aubert *et al.* (BaBar), Phys. Rev. **D71**, 032005 (2005), [hep-ex/0411016].
- [101] R. Itoh *et al.* (Belle), Phys. Rev. Lett. **95**, 091601 (2005), [hep-ex/0504030].
- [102] I. Adachi *et al.* (BaBar, Belle), Phys. Rev. Lett. **121**, 26, 261801 (2018), [arXiv:1804.06152]; I. Adachi *et al.* (BaBar, Belle), Phys. Rev. **D98**, 11, 112012 (2018), [arXiv:1804.06153].
- [103] A. Abdesselam *et al.* (BaBar, Belle), Phys. Rev. Lett. **115**, 12, 121604 (2015), [arXiv:1505.04147].
- [104] M. Gronau and D. London, Phys. Rev. Lett. **65**, 3381 (1990).
- [105] J. Zhang *et al.* (Belle), Phys. Rev. Lett. **91**, 221801 (2003), [hep-ex/0306007]; A. Somov *et al.* (Belle), Phys. Rev. Lett. **96**, 171801 (2006), [hep-ex/0601024]; B. Aubert *et al.* (BaBar), Phys. Rev. Lett. **97**, 261801 (2006), [hep-ex/0607092]; B. Aubert *et al.* (BaBar), Phys. Rev. **D76**, 052007 (2007), [arXiv:0705.2157].
- [106] B. Aubert *et al.* (BaBar), Phys. Rev. **D78**, 071104 (2008), [arXiv:0807.4977].
- [107] A. F. Falk *et al.*, Phys. Rev. **D69**, 011502 (2004), [hep-ph/0310242].
- [108] A. E. Snyder and H. R. Quinn, Phys. Rev. **D48**, 2139 (1993).
- [109] A. Kusaka *et al.* (Belle), Phys. Rev. Lett. **98**, 221602 (2007), [hep-ex/0701015].
- [110] J. P. Lees *et al.* (BaBar), Phys. Rev. **D88**, 1, 012003 (2013), [arXiv:1304.3503].
- [111] A. Hocker *et al.*, Eur. Phys. J. **C21**, 225 (2001), [hep-ph/0104062]; and updates at <http://ckmfitter.in2p3.fr/>.
- [112] M. Bona *et al.* (UTfit), JHEP **07**, 028 (2005), [hep-ph/0501199]; and updates at <http://www.utfit.org>.
- [113] M. Gronau and D. London, Phys. Lett. **B253**, 483 (1991).
- [114] M. Gronau and D. Wyler, Phys. Lett. **B265**, 172 (1991).
- [115] D. Atwood, I. Dunietz and A. Soni, Phys. Rev. Lett. **78**, 3257 (1997), [hep-ph/9612433]; D. Atwood, I. Dunietz and A. Soni, Phys. Rev. **D63**, 036005 (2001), [hep-ph/0008090].
- [116] A. Bondar, talk at the Belle analysis workshop, Novosibirsk, September 2002; A. Poluektov *et al.* (Belle), Phys. Rev. **D70**, 072003 (2004), [hep-ex/0406067].
- [117] A. Giri *et al.*, Phys. Rev. **D68**, 054018 (2003), [hep-ph/0303187].
- [118] A. Poluektov *et al.* (Belle), Phys. Rev. **D81**, 112002 (2010), [arXiv:1003.3360].
- [119] P. del Amo Sanchez *et al.* (BaBar), Phys. Rev. Lett. **105**, 121801 (2010), [arXiv:1005.1096].
- [120] R. Aaij *et al.* (LHCb), JHEP **02**, 169 (2021), [arXiv:2010.08483].
- [121] R. Aaij *et al.* (LHCb), JHEP **07**, 138 (2023), [arXiv:2209.03692]; R. Aaij *et al.* (LHCb), Eur. Phys. J. C **83**, 6, 547 (2023), [Erratum: Eur.Phys.J.C 83, 672 (2023)], [arXiv:2301.10328].
- [122] Y. Grossman, A. Soffer and J. Zupan, Phys. Rev. **D72**, 031501 (2005), [hep-ph/0505270]; M. Rama, Phys. Rev. D **89**, 1, 014021 (2014), [arXiv:1307.4384].
- [123] A. Amorim, M. G. Santos and J. P. Silva, Phys. Rev. **D59**, 056001 (1999), [hep-ph/9807364].
- [124] R. Aleksan, I. Dunietz and B. Kayser, Z. Phys. **C54**, 653 (1992).
- [125] R. Aaij *et al.* (LHCb), JHEP **03**, 059 (2018), [arXiv:1712.07428].
- [126] R. Aaij *et al.* (LHCb), JHEP **03**, 137 (2021), [arXiv:2011.12041].

- [127] B. Aubert *et al.* (BaBar), Phys. Rev. **D71**, 112003 (2005), [hep-ex/0504035]; B. Aubert *et al.* (BaBar), Phys. Rev. **D73**, 111101 (2006), [hep-ex/0602049]; F. J. Ronga *et al.* (Belle), Phys. Rev. **D73**, 092003 (2006), [hep-ex/0604013]; S. Bahinipati *et al.* (Belle), Phys. Rev. **D84**, 021101 (2011), [arXiv:1102.0888]; R. Aaij *et al.* (LHCb), JHEP **06**, 084 (2018), [arXiv:1805.03448].
- [128] G. P. Dubois-Felsmann *et al.*, *Sensitivity of CKM fits to theoretical uncertainties and their representation* (2003), [hep-ph/0308262]; G. Eigen *et al.*, Phys. Rev. **D89**, 3, 033004 (2014), [arXiv:1301.5867].
- [129] D. Boutigny *et al.* (BaBar), in “Workshop on Physics at an Asymmetric B Factory (BaBar Collaboration Meeting) Pasadena, California, September 22-24, 1997,” (1998), URL <http://www-public.slac.stanford.edu/sciDoc/docMeta.aspx?slacPubNumber=SLAC-R-504>.
- [130] S. Plaszczynski and M.-H. Schune hf8/019 (1999), [PoShf8,019(1999)], [hep-ph/9911280].
- [131] M. Bona *et al.* (UTfit), JHEP **03**, 049 (2008), [arXiv:0707.0636].
- [132] We thank the CKMfitter and UTfit groups for performing fits and preparing plots using input values from this *Review*.
- [133] H. E. Haber, Nucl. Phys. Proc. Suppl. **62**, 469 (1998), [hep-ph/9709450]; Y. Nir, *CP violation: A New era* (2001), [hep-ph/0109090].
- [134] J. M. Soares and L. Wolfenstein, Phys. Rev. **D47**, 1021 (1993); T. Goto *et al.*, Phys. Rev. **D53**, 6662 (1996), [hep-ph/9506311]; J. P. Silva and L. Wolfenstein, Phys. Rev. **D55**, 5331 (1997), [hep-ph/9610208].
- [135] Y. Grossman, Z. Ligeti and Y. Nir, Prog. Theor. Phys. **122**, 125 (2009), [arXiv:0904.4262].
- [136] G. Isidori, Y. Nir and G. Perez, Ann. Rev. Nucl. Part. Sci. **60**, 355 (2010), [arXiv:1002.0900]; G. Isidori, in “Proceedings, 2012 European School of High-Energy Physics (ES-HEP 2012): La Pommeraye, Anjou, France, June 06-19, 2012,” 69–105 (2014), [arXiv:1302.0661].
- [137] Z. Ligeti, Int. J. Mod. Phys. **A20**, 5105 (2005), [hep-ph/0408267].
- [138] J. Charles *et al.*, Phys. Rev. **D89**, 3, 033016 (2014), [arXiv:1309.2293].
- [139] K. Agashe *et al.* (2005), [hep-ph/0509117].
- [140] S. Laplace *et al.*, Phys. Rev. **D65**, 094040 (2002), [hep-ph/0202010].
- [141] J. K. Ahn *et al.* (KOTO), Phys. Rev. Lett. **122**, 2, 021802 (2019), [arXiv:1810.09655]; J. K. Ahn *et al.* (KOTO), Phys. Rev. Lett. **126**, 12, 121801 (2021), [arXiv:2012.07571].
- [142] A. J. Buras *et al.*, JHEP **11**, 033 (2015), [arXiv:1503.02693].

13. CP Violation in the Quark Sector

Revised August 2023 by T. Gershon (Warwick U.) and Y. Nir (Weizmann Inst.).

The CP transformation combines charge conjugation C with parity P . Under C , particles and antiparticles are interchanged, by conjugating all internal quantum numbers, *e.g.*, $Q \rightarrow -Q$ for electromagnetic charge. Under P , the handedness of space is reversed, $\vec{x} \rightarrow -\vec{x}$. Thus, for example, a left-handed electron e_L^- is transformed under CP into a right-handed positron, e_R^+ .

If CP were an exact symmetry, the laws of nature would be the same for matter and for antimatter. We observe that most phenomena are C - and P -symmetric, and therefore, also CP -symmetric. In particular, these symmetries are respected by the electromagnetic and strong interactions. The weak interactions, on the other hand, violate C and P in the strongest possible way. For example, the W bosons couple to left-handed electrons, e_L^- , and to their CP -conjugate right-handed positrons, e_R^+ , but to neither their C -conjugate left-handed positrons, e_L^+ , nor their P -conjugate right-handed electrons, e_R^- . While weak interactions violate C and P separately, CP is still preserved in most weak interaction processes. The CP symmetry is, however, violated in certain processes involving interference effects, as discovered in neutral K decays in 1964 [1], and established later in B (2001) and D (2019) decays. For example, as discovered in 1967, a K_L meson decays more often to $\pi^- e^+ \nu_e$ than to $\pi^+ e^- \bar{\nu}_e$, thus allowing electrons and positrons to be unambiguously distinguished, but the decay-rate asymmetry is only at the 0.003 level. The CP -violating effects observed in the B system are larger: the parameter describing the CP asymmetry in the decay time distribution of B^0/\bar{B}^0 meson transitions to CP eigenstates like $J/\psi K_S^0$ is about 0.7 [2, 3]. These effects are related to $K^0-\bar{K}^0$ and $B^0-\bar{B}^0$ mixing, but CP violation arising solely from decay amplitudes has also been observed, first in $K \rightarrow \pi\pi$ decays [4–6], subsequently in B^0 [7, 8], B^+ [9–11], and B_s^0 [12] decays, and most recently in charm decays [13]. All of these observed CP asymmetries are consistent with the Standard Model predictions. Similar effects could also occur in decays of baryons, but have not yet been observed. Given that neutrino masses and lepton mixing have been established, it is expected that CP is violated also in the lepton sector [14]. Discovering CP violation in the lepton sector is one of the main goals of current and near-future experiments. CP violation has not yet been observed in processes involving the top quark, nor in flavor-conserving processes such as electric dipole moments; for these, any significant observation would be a clear indication of physics beyond the Standard Model.

In addition to parity and to continuous Lorentz transformations, there is one other spacetime operation that could be a symmetry of the interactions: time reversal T , $t \rightarrow -t$. Violations of T symmetry have been observed in neutral K decays [15]. More recently, T violation has been observed between states that are not CP -conjugate [16], exploiting the fact that for neutral B mesons both flavor tagging and CP tagging can be used [17]. Moreover, T violation is expected as a corollary of CP violation if the combined CPT transformation is a fundamental symmetry of nature [18]. All observations indicate that CPT is indeed a symmetry of nature [15]. Furthermore, one cannot build a locally Lorentz-invariant quantum field theory with a Hermitian Hamiltonian that violates CPT . (At several points in our discussion, we avoid assumptions about CPT , in order to identify cases where evidence for CP violation relies on assumptions about CPT .)

Within the Standard Model, CP symmetry is broken by complex phases in the Yukawa couplings (that is, the couplings of the Higgs scalar to quarks). When all transformations to remove unphysical phases in this model are exhausted, a single CP -violating parameter remains [19]. In the basis of mass eigenstates, this single phase appears in the 3×3 unitary matrix that gives the W -boson couplings to an up-type antiquark and a down-type quark. (If the Standard Model is supplemented with Majorana mass terms for the neutrinos, the analogous mixing matrix for leptons has three CP -violating phases.) The beautifully consistent and economical Standard-Model description of CP violation in terms of Yukawa couplings, known as the Kobayashi-Maskawa (KM) mechanism [19], agrees with all measurements to date. Fur-

thermore, one can fit the data allowing contributions from beyond the Standard Model (referred to subsequently as new physics) to loop processes to compete with, or even dominate over, the Standard Model amplitudes [20, 21]. Such an analysis provides model-independent proof that the KM phase is different from zero, and that the matrix of three-generation quark mixing is the dominant source of CP violation in meson decays.

The current level of experimental accuracy and the theoretical uncertainties involved in the interpretation of the various observations leave room, however, for additional subdominant sources of CP violation from new physics. Indeed, almost all extensions of the Standard Model imply that there are such additional sources. Moreover, CP violation is a necessary condition for baryogenesis, the process of dynamically generating the matter-antimatter asymmetry of the Universe [22]. Despite the phenomenological success of the KM mechanism, it fails (by several orders of magnitude) to accommodate the observed asymmetry [23]. This discrepancy strongly suggests that nature provides additional sources of CP violation beyond the KM mechanism. The evidence for neutrino masses implies that CP can be violated also in the lepton sector. This situation makes leptogenesis [24, 25], a scenario where CP -violating phases in the Yukawa couplings of the neutrinos play a crucial role in the generation of the baryon asymmetry, a very attractive possibility. The expectation of new sources motivates the large ongoing experimental effort to find deviations from the predictions of the KM mechanism.

CP violation can be experimentally searched for in a variety of processes, such as hadron decays, electric dipole moments of neutrons, electrons and nuclei, and neutrino oscillations. Hadron decays via the weak interaction probe flavor-changing CP violation. The search for electric dipole moments may find (or constrain) sources of CP violation that, unlike the KM phase, are not related to flavor-changing couplings. Following the discovery of the Higgs boson [26, 27], searches for CP violation in the Higgs sector are becoming feasible. Future searches for CP violation in neutrino oscillations might provide further input on leptogenesis.

The present measurements of CP asymmetries provide some of the strongest constraints on the weak couplings of quarks. Future measurements of CP violation in K , D , B , and B_s^0 meson decays will provide additional constraints on the flavor parameters of the Standard Model, and can probe new physics. In this review, we give the formalism and basic physics motivations that are relevant to present and near future measurements of CP violation in the quark sector.

13.1 Formalism

The phenomenology of CP violation for neutral flavored mesons is particularly interesting, since many of the observables can be cleanly interpreted. Although the phenomenology is superficially different for K^0 , D^0 , B^0 , and B_s^0 decays, this is primarily because each of these systems is governed by a different balance between decay rates, oscillations, and lifetime splitting. However, the general considerations presented in this section are identical for all flavored neutral pseudoscalar mesons. The phenomenology of CP violation for neutral mesons that do not carry flavor quantum numbers (such as the $\eta^{(\prime)}$ state) is quite different: such states are their own antiparticles and have definite CP eigenvalues, so the signature of CP violation is simply the decay to a final state with the opposite CP . Such decays are mediated by the electromagnetic or (OZI-suppressed [28–30]) strong interaction, where CP violation is not expected and has not yet been observed. In the remainder of this review, we restrict ourselves to considerations of weakly decaying hadrons.

In this section, we present a general formalism for, and classification of, CP violation in the decay of a weakly decaying hadron, denoted M . We pay particular attention to the case that M is a K^0 , D^0 , B^0 , or B_s^0 meson. Subsequent sections describe the CP -violating phenomenology, approximations, and alternative formalisms that are specific to each system.

13.1.1 Charged- and neutral-hadron decays

We define decay amplitudes of M (which could be charged or neutral) and its CP conjugate \bar{M} to a multi-particle final state f

and its CP conjugate \bar{f} as

$$A_f = \langle f | \mathcal{H} | M \rangle, \quad \bar{A}_f = \langle f | \mathcal{H} | \bar{M} \rangle, \quad (13.1a)$$

$$A_{\bar{f}} = \langle \bar{f} | \mathcal{H} | M \rangle, \quad \bar{A}_{\bar{f}} = \langle \bar{f} | \mathcal{H} | \bar{M} \rangle, \quad (13.1b)$$

where \mathcal{H} is the Hamiltonian governing weak interactions. The action of CP on these states introduces phases ξ_M and ξ_f that depend on their flavor content, according to

$$CP|M\rangle = e^{+i\xi_M} |\bar{M}\rangle, \quad CP|f\rangle = e^{+i\xi_f} |\bar{f}\rangle, \quad (13.2a)$$

$$CP|\bar{M}\rangle = e^{-i\xi_M} |M\rangle, \quad CP|\bar{f}\rangle = e^{-i\xi_f} |f\rangle, \quad (13.2b)$$

so that $(CP)^2 = 1$. The phases ξ_M and ξ_f are arbitrary and unobservable because of the flavor symmetry of the strong interaction. If CP is conserved by the dynamics, $[CP, \mathcal{H}] = 0$, then A_f and $\bar{A}_{\bar{f}}$ have the same magnitude and an arbitrary unphysical relative phase

$$\bar{A}_{\bar{f}} = e^{i(\xi_f - \xi_M)} A_f. \quad (13.3)$$

13.1.2 Neutral-meson mixing

A state that is initially a superposition of M^0 and \bar{M}^0 , say

$$|\psi(0)\rangle = a(0)|M^0\rangle + b(0)|\bar{M}^0\rangle, \quad (13.4)$$

will evolve in time acquiring components that describe all possible decay final states $\{f_1, f_2, \dots\}$, that is,

$$|\psi(t)\rangle = a(t)|M^0\rangle + b(t)|\bar{M}^0\rangle + c_1(t)|f_1\rangle + c_2(t)|f_2\rangle + \dots \quad (13.5)$$

If we are interested in computing only the values of $a(t)$ and $b(t)$ (and not the values of all $c_i(t)$), and if the times t under study are much larger than the typical strong interaction scale, then we can use a much simplified formalism [31]. The simplified time evolution is determined by a 2×2 effective Hamiltonian \mathbf{H} that is not Hermitian, since otherwise the mesons would only oscillate and not decay. Any complex matrix, such as \mathbf{H} , can be written in terms of Hermitian matrices \mathbf{M} and $\mathbf{\Gamma}$ as

$$\mathbf{H} = \mathbf{M} - \frac{i}{2} \mathbf{\Gamma}. \quad (13.6)$$

\mathbf{M} and $\mathbf{\Gamma}$ are associated with $(M^0, \bar{M}^0) \leftrightarrow (M^0, \bar{M}^0)$ transitions via off-shell (dispersive), and on-shell (absorptive) intermediate states, respectively. Diagonal elements of \mathbf{M} and $\mathbf{\Gamma}$ are associated with the flavor-conserving transitions $M^0 \rightarrow M^0$ and $\bar{M}^0 \rightarrow \bar{M}^0$, while off-diagonal elements are associated with flavor-changing transitions $M^0 \leftrightarrow \bar{M}^0$.

The eigenvectors of \mathbf{H} have well-defined masses and decay widths. To specify the components of the strong interaction eigenstates, M^0 and \bar{M}^0 , in the light (M_L) and heavy (M_H) mass eigenstates, we introduce three complex parameters: p , q , and, for the case that both CP and CPT are violated in mixing, z . Then

$$|M_L\rangle \propto p\sqrt{1-z}|M^0\rangle + q\sqrt{1+z}|\bar{M}^0\rangle, \quad (13.7a)$$

$$|M_H\rangle \propto p\sqrt{1+z}|M^0\rangle - q\sqrt{1-z}|\bar{M}^0\rangle, \quad (13.7b)$$

with the normalization $|q|^2 + |p|^2 = 1$ when $z = 0$. (Another possible choice of labeling, which is in standard usage for K mesons, defines the mass eigenstates according to their lifetimes: K_S for the short-lived and K_L for the long-lived state. The K_L is experimentally found to be the heavier state. Yet another choice is often used for the D mesons [32]: the eigenstates are labeled according to their dominant CP content.)

The real and imaginary parts of the eigenvalues $\omega_{L,H}$ corresponding to $|M_{L,H}\rangle$ represent their masses and decay widths, respectively. The mass and width splittings are

$$\Delta m \equiv m_H - m_L = \text{Re}(\omega_H - \omega_L), \quad (13.8a)$$

$$\Delta\Gamma \equiv \Gamma_H - \Gamma_L = -2\text{Im}(\omega_H - \omega_L). \quad (13.8b)$$

Note that here Δm is positive by definition, while the sign of $\Delta\Gamma$ must be experimentally determined. The sign of $\Delta\Gamma$ has not yet been established for B^0 mesons, while $\Delta\Gamma < 0$ is established for K

and B_s^0 mesons. The Standard Model predicts $\Gamma_L > \Gamma_H$ for $B_{(s)}^0$ mesons; for this reason, $\Delta\Gamma = \Gamma_L - \Gamma_H$, which is still a signed quantity, is often used in the $B_{(s)}^0$ literature and is the convention used in the PDG experimental summaries.

Solving the eigenvalue problem for \mathbf{H} yields

$$\left(\frac{q}{p}\right)^2 = \frac{\mathbf{M}_{12}^* - (i/2)\mathbf{\Gamma}_{12}^*}{\mathbf{M}_{12} - (i/2)\mathbf{\Gamma}_{12}} \quad (13.9)$$

and

$$z \equiv \frac{\delta m - (i/2)\delta\Gamma}{\Delta m - (i/2)\Delta\Gamma}, \quad (13.10)$$

where

$$\delta m \equiv \mathbf{M}_{11} - \mathbf{M}_{22}, \quad \delta\Gamma \equiv \mathbf{\Gamma}_{11} - \mathbf{\Gamma}_{22} \quad (13.11)$$

are the differences in effective mass and decay-rate expectation values for the strong interaction states M^0 and \bar{M}^0 .

If either CP or CPT is a symmetry of \mathbf{H} (independently of whether T is conserved or violated), then the values of δm and $\delta\Gamma$ are both zero, and hence $z = 0$. We also find that

$$\omega_H - \omega_L = 2\sqrt{\left(\mathbf{M}_{12} - \frac{i}{2}\mathbf{\Gamma}_{12}\right)\left(\mathbf{M}_{12}^* - \frac{i}{2}\mathbf{\Gamma}_{12}^*\right)}. \quad (13.12)$$

If either CP or T is a symmetry of \mathbf{H} (independently of whether CPT is conserved or violated), then $\mathbf{\Gamma}_{12}/\mathbf{M}_{12}$ is real, leading to

$$\left(\frac{q}{p}\right)^2 = e^{2i\xi_M} \Rightarrow \left|\frac{q}{p}\right| = 1, \quad (13.13)$$

where ξ_M is the arbitrary unphysical phase introduced in Eq. (13.2). If, and only if, CP is a symmetry of \mathbf{H} (independently of CPT and T), then both of the above conditions hold, with the result that the mass eigenstates are orthogonal

$$\langle M_H | M_L \rangle = |p|^2 - |q|^2 = 0. \quad (13.14)$$

13.1.3 CP-violating observables

All CP -violating observables in M and \bar{M} decays to final states f and \bar{f} can be expressed in terms of phase-convention-independent combinations of A_f , \bar{A}_f , $A_{\bar{f}}$, and $\bar{A}_{\bar{f}}$, together with, for neutral meson decays only, q/p . CP violation in charged meson and all baryon decays depends only on the combination $|\bar{A}_{\bar{f}}/A_f|$, while CP violation in flavored neutral meson decays is enriched by $M^0 \leftrightarrow \bar{M}^0$ oscillations, and depends, additionally, on $|q/p|$ and on $\lambda_f \equiv (q/p)(\bar{A}_f/A_f)$.

The decay rates of the two neutral kaon mass eigenstates, K_S and K_L , are different enough ($\Gamma_S/\Gamma_L \sim 500$) that one can, in most cases, actually study their decays independently. For D^0 , B^0 , and B_s^0 mesons, however, values of $\Delta\Gamma/\Gamma$ (where $\Gamma \equiv (\Gamma_H + \Gamma_L)/2$) are relatively small, and so both mass eigenstates must be considered in their evolution. We denote the state of an initially pure $|M^0\rangle$ or $|\bar{M}^0\rangle$ after an elapsed proper time t as $|M_{\text{phys}}^0(t)\rangle$ or $|\bar{M}_{\text{phys}}^0(t)\rangle$, respectively. Using the effective Hamiltonian approximation, but not assuming CPT to be a good symmetry, we obtain

$$|M_{\text{phys}}^0(t)\rangle = (g_+(t) + z g_-(t)) |M^0\rangle - \sqrt{1-z^2} \frac{q}{p} g_-(t) |\bar{M}^0\rangle, \quad (13.15a)$$

$$|\bar{M}_{\text{phys}}^0(t)\rangle = (g_+(t) - z g_-(t)) |\bar{M}^0\rangle - \sqrt{1-z^2} \frac{p}{q} g_-(t) |M^0\rangle, \quad (13.15b)$$

where

$$g_{\pm}(t) \equiv \frac{1}{2} \left[\exp\left(-im_H t - \frac{1}{2}\Gamma_H t\right) \pm \exp\left(-im_L t - \frac{1}{2}\Gamma_L t\right) \right] \quad (13.16)$$

and $z = 0$ if either CPT or CP is conserved.

Defining $x \equiv \Delta m/\Gamma$ and $y \equiv \Delta\Gamma/(2\Gamma)$, and assuming $z = 0$, one obtains the following time-dependent decay rates:

$$\begin{aligned} \frac{d\Gamma[M_{\text{phys}}^0(t) \rightarrow f]}{e^{-\Gamma t}\mathcal{N}_f} &= (|A_f|^2 + |(q/p)\bar{A}_f|^2) \cosh(y\Gamma t) \\ &+ (|A_f|^2 - |(q/p)\bar{A}_f|^2) \cos(x\Gamma t) \\ &+ 2\mathcal{R}e((q/p)A_f^*\bar{A}_f) \sinh(y\Gamma t) \\ &- 2\mathcal{I}m((q/p)A_f^*\bar{A}_f) \sin(x\Gamma t), \end{aligned} \quad (13.17a)$$

$$\begin{aligned} \frac{d\Gamma[\bar{M}_{\text{phys}}^0(t) \rightarrow f]}{e^{-\Gamma t}\mathcal{N}_f} &= (|(p/q)A_f|^2 + |\bar{A}_f|^2) \cosh(y\Gamma t) \\ &- (|(p/q)A_f|^2 - |\bar{A}_f|^2) \cos(x\Gamma t) \\ &+ 2\mathcal{R}e((p/q)A_f\bar{A}_f^*) \sinh(y\Gamma t) \\ &- 2\mathcal{I}m((p/q)A_f\bar{A}_f^*) \sin(x\Gamma t), \end{aligned} \quad (13.17b)$$

where \mathcal{N}_f is a common, time-independent, normalization factor that can be determined bearing in mind that the range of t is $0 < t < \infty$. Decay rates to the CP -conjugate final state \bar{f} are obtained analogously, with $\mathcal{N}_f = \mathcal{N}_{\bar{f}}$ and the substitutions $A_f \rightarrow A_{\bar{f}}$ and $\bar{A}_f \rightarrow \bar{A}_{\bar{f}}$ in Eqs. (13.17a) and (13.17b). Terms proportional to $|A_f|^2$ or $|\bar{A}_f|^2$ are associated with decays that occur without any net $M^0 \leftrightarrow \bar{M}^0$ oscillation, while terms proportional to $|(q/p)\bar{A}_f|^2$ or $|(p/q)A_f|^2$ are associated with decays following a net oscillation. The $\sinh(y\Gamma t)$ and $\sin(x\Gamma t)$ terms of Eqs. (13.17a) and (13.17b) are associated with the interference between these two cases. Note that, in multi-body decays such as $D^0 \rightarrow K_S\pi^+\pi^-$ or $B^0 \rightarrow \pi^+\pi^-\pi^+\pi^-$, amplitudes are functions of variables that describe the phase-space of the final state. Interference may be present in some regions but not others, and is strongly influenced by resonant substructure.

When neutral pseudoscalar mesons are produced coherently in pairs from the decay of a vector resonance, $V \rightarrow M^0\bar{M}^0$ (for example, $\Upsilon(4S) \rightarrow B^0\bar{B}^0$, $\psi(3770) \rightarrow D^0\bar{D}^0$ or $\phi \rightarrow K^0\bar{K}^0$), the time-dependence of their subsequent decays to final states f_1 and f_2 has a similar form to Eqs. (13.17a) and (13.17b):

$$\begin{aligned} \frac{d\Gamma[V_{\text{phys}}(t_1, t_2) \rightarrow f_1 f_2]/d(\Delta t)}{e^{-\Gamma|\Delta t|}\mathcal{N}_{f_1 f_2}} &= (|a_+|^2 + |a_-|^2) \cosh(y\Gamma\Delta t) \\ &+ (|a_+|^2 - |a_-|^2) \cos(x\Gamma\Delta t) \\ &- 2\mathcal{R}e(a_+^*a_-) \sinh(y\Gamma\Delta t) \\ &+ 2\mathcal{I}m(a_+^*a_-) \sin(x\Gamma\Delta t), \end{aligned} \quad (13.18)$$

where $\Delta t \equiv t_2 - t_1$ is the difference in the production times, t_1 and t_2 , of f_1 and f_2 , respectively, and the dependence on the average decay time and on decay angles has been integrated out. The normalization factor $\mathcal{N}_{f_1 f_2}$ can be evaluated, noting that the range of Δt is $-\infty < \Delta t < \infty$. The coefficients in Eq. (13.18) are determined by the amplitudes for no net oscillation from $t_1 \rightarrow t_2$, $\bar{A}_{f_1}A_{f_2}$, and $A_{f_1}\bar{A}_{f_2}$, and for a net oscillation, $(q/p)\bar{A}_{f_1}A_{f_2}$ and $(p/q)A_{f_1}\bar{A}_{f_2}$, via

$$a_+ \equiv \bar{A}_{f_1}A_{f_2} - A_{f_1}\bar{A}_{f_2}, \quad (13.19a)$$

$$\begin{aligned} a_- &\equiv -\sqrt{1-z^2} \left(\frac{q}{p}\bar{A}_{f_1}\bar{A}_{f_2} - \frac{p}{q}A_{f_1}A_{f_2} \right) \\ &+ z (\bar{A}_{f_1}A_{f_2} + A_{f_1}\bar{A}_{f_2}). \end{aligned} \quad (13.19b)$$

Assuming CPT conservation, $z = 0$, and identifying $\Delta t \rightarrow t$ and $f_2 \rightarrow f$, we find that Eqs. (13.18) and (13.19) reduce to Eq. (13.17a) with $A_{f_1} = 0$, $\bar{A}_{f_1} = 1$, or to Eq. (13.17b) with $\bar{A}_{f_1} = 0$, $A_{f_1} = 1$. Indeed, this plays an important role in experiments that exploit the coherence of $V \rightarrow M^0\bar{M}^0$ production. Final states f_1 with $A_{f_1} = 0$ or $\bar{A}_{f_1} = 0$ are called tagging states,

because they identify the decaying pseudoscalar meson as, respectively, \bar{M}^0 or M^0 . Before one of M^0 or \bar{M}^0 decays, they evolve in phase, so that there is always one M^0 and one \bar{M}^0 present. A tagging decay of one meson sets the clock for the time evolution of the other: it starts at t_1 as purely M^0 or \bar{M}^0 , with time evolution that depends only on $t_2 - t_1$.

When f_1 is a state that both M^0 and \bar{M}^0 can decay into, then Eq. (13.18) contains interference terms proportional to $A_{f_1}\bar{A}_{f_1} \neq 0$ that are not present in Eqs. (13.17a) and (13.17b). Even when f_1 is dominantly produced by M^0 decays rather than \bar{M}^0 decays, or vice versa, $A_{f_1}\bar{A}_{f_1}$ can be non-zero owing to doubly-CKM-suppressed decays (with amplitudes suppressed by at least two powers of λ relative to the dominant amplitude, in the language of Section 13.3), and these terms should be considered for precision studies of CP violation in coherent $V \rightarrow M^0\bar{M}^0$ decays [33]. The correlations in $V \rightarrow M^0\bar{M}^0$ decays can also be exploited to determine phase differences between favored and suppressed decay amplitudes [34, 35].

13.1.4 Classification of CP-violating effects

We distinguish three types of CP -violating effects that can occur in the quark sector:

- I. CP violation in decay is defined by

$$|\bar{A}_{\bar{f}}/A_f| \neq 1. \quad (13.20)$$

In charged meson (and all baryon) decays, where mixing effects are absent, this is the only possible source of CP asymmetries:

$$A_{f\pm} \equiv \frac{\Gamma(M^- \rightarrow f^-) - \Gamma(M^+ \rightarrow f^+)}{\Gamma(M^- \rightarrow f^-) + \Gamma(M^+ \rightarrow f^+)} = \frac{|\bar{A}_{f-}/A_{f+}|^2 - 1}{|\bar{A}_{f-}/A_{f+}|^2 + 1}. \quad (13.21)$$

Note that the usual sign convention for CP asymmetries of hadrons is for the difference between the rate involving the particle that contains a heavy quark and that which contains an antiquark. Hence, Eq. (13.21) corresponds to the definition for B^\pm mesons, but the opposite sign is used for $D_{(s)}^\pm$ decays.

- II. CP (and T) violation in mixing is defined by

$$|q/p| \neq 1. \quad (13.22)$$

In charged-current semileptonic neutral meson decays $M, \bar{M} \rightarrow \ell^\pm X^\mp$ (taking $|A_{\ell^+ X^-}| = |\bar{A}_{\ell^- X^+}|$ and $A_{\ell^+ X^-} + \bar{A}_{\ell^- X^+} = 0$, as is the case in the Standard Model, to lowest order in G_F , and in most of its extensions), this is the only source of CP violation, and can be measured via the asymmetry of “wrong-sign” decays induced by oscillations:

$$\begin{aligned} A_{\text{SL}}(t) &\equiv \frac{d\Gamma/dt[\bar{M}_{\text{phys}}^0(t) \rightarrow \ell^+ X^-] - d\Gamma/dt[M_{\text{phys}}^0(t) \rightarrow \ell^- X^+]}{d\Gamma/dt[\bar{M}_{\text{phys}}^0(t) \rightarrow \ell^+ X^-] + d\Gamma/dt[M_{\text{phys}}^0(t) \rightarrow \ell^- X^+]}, \end{aligned} \quad (13.23a)$$

$$= \frac{1 - |q/p|^4}{1 + |q/p|^4}. \quad (13.23b)$$

Note that this asymmetry of time-dependent decay rates is actually time-independent.

- III. CP violation in interference between a decay without mixing, $M^0 \rightarrow f$, and a decay with mixing, $M^0 \rightarrow \bar{M}^0 \rightarrow f$ (such an effect occurs only in decays to final states that are common to M^0 and \bar{M}^0 , including all CP eigenstates), is defined by

$$\arg(\lambda_f) + \arg(\lambda_{\bar{f}}) \neq 0, \quad \text{with} \quad \lambda_f \equiv \frac{q}{p} \frac{\bar{A}_f}{A_f}. \quad (13.24)$$

For final CP eigenstates, f_{CP} , the condition Eq. (13.24) simplifies to

$$\mathcal{I}m(\lambda_{f_{CP}}) \neq 0, \quad (13.25)$$

This form of CP violation can be observed, for example, using the asymmetry of neutral meson decay rates into CP eigenstates

$$\begin{aligned} \mathcal{A}_{fCP}(t) &\equiv \\ &\equiv \frac{d\Gamma/dt[\overline{M}_{\text{phys}}^0(t) \rightarrow f_{CP}] - d\Gamma/dt[M_{\text{phys}}^0(t) \rightarrow f_{CP}]}{d\Gamma/dt[\overline{M}_{\text{phys}}^0(t) \rightarrow f_{CP}] + d\Gamma/dt[M_{\text{phys}}^0(t) \rightarrow f_{CP}]} . \end{aligned} \quad (13.26)$$

If $\Delta\Gamma = 0$, as expected to a good approximation for B^0 mesons but not for K^0 and B_s^0 mesons, and $|q/p| = 1$, then \mathcal{A}_{fCP} has a particularly simple form (see Eq. (13.75), below). If, in addition, the decay amplitudes fulfill $|\overline{A}_{fCP}| = |A_{fCP}|$, the interference between decays with and without mixing is the only source of asymmetry and $\mathcal{A}_{fCP}(t) = \text{Im}(\lambda_{fCP}) \sin(x\Gamma t)$.

Examples of these three types of CP violation will be given in Sections 13.4, 13.5, and 13.6.

13.2 Theoretical Interpretation: General Considerations

Consider the $M \rightarrow f$ decay amplitude A_f , and the CP conjugate process, $\overline{M} \rightarrow \overline{f}$, with decay amplitude $\overline{A}_{\overline{f}}$. There are two types of phases that may appear in these decay amplitudes. Complex parameters in any Lagrangian term that contributes to the amplitude will appear in complex conjugate form in the CP -conjugate amplitude. Thus, their phases appear in A_f and $\overline{A}_{\overline{f}}$ with opposite signs. In the Standard Model, these phases occur only in the couplings of the W^\pm bosons, and hence, are often called “weak phases.” The weak phase of any single term is convention-dependent. However, the difference between the weak phases in two different terms in A_f is convention-independent. A second type of phase can appear in scattering or decay amplitudes, even when the Lagrangian is real. This phase originates from the possible contribution from intermediate on-shell states in the decay process. Since such phases are generated by CP -invariant interactions, they are the same in A_f and $\overline{A}_{\overline{f}}$. Usually the dominant rescattering is due to strong interactions; hence the designation “strong phases” for the phase shifts so induced. Again, only the relative strong phases between different terms in the amplitude are physically meaningful.

The “weak” and “strong” phases discussed here appear in addition to the spurious CP -transformation phases of Eq. (13.3). Those spurious phases are due to an arbitrary choice of phase convention, and do not originate from any dynamics or induce any CP violation. For simplicity, we set them to zero from here on.

It is useful to write each contribution a_i to A_f in three parts: its magnitude $|a_i|$, its weak phase ϕ_i , and its strong phase δ_i . If, for example, there are two such contributions, $A_f = a_1 + a_2$, we have

$$A_f = |a_1|e^{i(\delta_1+\phi_1)} + |a_2|e^{i(\delta_2+\phi_2)}, \quad (13.27a)$$

$$\overline{A}_{\overline{f}} = |a_1|e^{i(\delta_1-\phi_1)} + |a_2|e^{i(\delta_2-\phi_2)}. \quad (13.27b)$$

Similarly, for neutral mesons, it is useful to write

$$\mathbf{M}_{12} = |\mathbf{M}_{12}|e^{i\phi_M}, \quad \mathbf{\Gamma}_{12} = |\mathbf{\Gamma}_{12}|e^{i\phi_\Gamma}. \quad (13.28)$$

Each of the phases appearing in Eqs. (13.27) and (13.28) is convention-dependent, but combinations such as $\delta_1 - \delta_2$, $\phi_1 - \phi_2$, $\phi_M - \phi_\Gamma$, and $\phi_M + \phi_1 - \phi_1$ (where ϕ_1 is a weak phase contributing to $\overline{A}_{\overline{f}}$) are physical.

It is now straightforward to evaluate the various asymmetries in terms of the theoretical parameters introduced here. We will do so with approximations that are often relevant to the most interesting measured asymmetries.

1. The CP asymmetry in charged meson and all baryon decays

[Eq. (13.21)] is given by

$$\mathcal{A}_f = - \frac{2|a_1 a_2| \sin(\delta_2 - \delta_1) \sin(\phi_2 - \phi_1)}{|a_1|^2 + |a_2|^2 + 2|a_1 a_2| \cos(\delta_2 - \delta_1) \cos(\phi_2 - \phi_1)}. \quad (13.29)$$

The quantity of most interest to theory is the weak phase difference $\phi_2 - \phi_1$. Its extraction from the asymmetry requires, however, that the amplitude ratio $|a_2/a_1|$ and the strong phase difference $\delta_2 - \delta_1$ are known. Both quantities depend on non-perturbative hadronic parameters that are difficult to calculate, but in some cases can be obtained from experiment.

2. In the approximation that $|\mathbf{\Gamma}_{12}/\mathbf{M}_{12}| \ll 1$ (valid for B^0 and B_s^0 mesons), the CP asymmetry in semileptonic neutral-meson decays [Eq. (13.23)] is given by

$$\mathcal{A}_{\text{SL}} = - \left| \frac{\mathbf{\Gamma}_{12}}{\mathbf{M}_{12}} \right| \sin(\phi_M - \phi_\Gamma). \quad (13.30)$$

The quantity of most interest to theory is the weak phase $\phi_M - \phi_\Gamma$. Its extraction from the asymmetry requires, however, that $|\mathbf{\Gamma}_{12}/\mathbf{M}_{12}|$ is known. State of the art calculations of this quantity for the B^0 and B_s^0 mesons have uncertainties of around 10% [36].

3. In the approximations that only a single weak phase contributes to decay, $A_f = |a_f|e^{i(\delta_f+\phi_f)}$, and that $|\mathbf{\Gamma}_{12}/\mathbf{M}_{12}| = 0$, we obtain $|\lambda_f| = 1$, and the CP asymmetries in decays to a final CP eigenstate f [Eq. (13.26)] with eigenvalue $\eta_f = \pm 1$ are given by

$$\mathcal{A}_{fCP}(t) = \text{Im}(\lambda_f) \sin(\Delta m t) \quad \text{with} \quad \text{Im}(\lambda_f) = \eta_f \sin(\phi_M + 2\phi_f). \quad (13.31)$$

Note that the phase measured is purely a weak phase, and no hadronic parameters are involved in the extraction of its value from $\text{Im}(\lambda_f)$.

The discussion above allows us to introduce another classification of CP -violating effects:

1. *Indirect CP violation* is consistent with taking $\phi_M \neq 0$ and setting all other CP violating phases to zero. CP violation in mixing (type II) belongs to this class.
2. *Direct CP violation* cannot be accounted for by just $\phi_M \neq 0$. CP violation in decay (type I) belongs to this class.

The historical significance of this classification is related to theory. In superweak models [37], CP violation appears only in diagrams that contribute to \mathbf{M}_{12} , hence predicting no direct CP violation. In most models and, in particular, in the Standard Model, CP violation is both direct and indirect. As concerns type III CP violation, a single observation of such an effect would be consistent with indirect CP violation, but observing $\eta_{f_1} \text{Im}(\lambda_{f_1}) \neq \eta_{f_2} \text{Im}(\lambda_{f_2})$ (for the same decaying meson and two different final CP eigenstates f_1 and f_2) would establish direct CP violation. The experimental observation of $\epsilon' \neq 0$, which was achieved by establishing that $\text{Im}(\lambda_{\pi^+\pi^-}) \neq \text{Im}(\lambda_{\pi^0\pi^0})$ (see Section 13.4), excluded the superweak scenario.

13.3 Theoretical Interpretation: The KM Mechanism

Of all the Standard Model quark parameters, only the Kobayashi-Maskawa (KM) phase is CP -violating. Having a single source of CP violation, the Standard Model is very predictive for CP asymmetries: some vanish, and those that do not are correlated.

To be precise, CP could be violated also by strong interactions. The experimental upper bound on the electric-dipole moment of the neutron [38] implies, however, that θ_{QCD} , the non-perturbative parameter that determines the strength of this type of CP violation, is tiny, if not zero [39]. The smallness of θ_{QCD} constitutes a theoretical puzzle, known as “the strong CP problem.” This, however, is irrelevant to our discussion of hadron decays.

The charged current interactions (that is, the W^\pm interactions) for quarks are given by

$$-\mathcal{L}_{W^\pm} = \frac{g}{\sqrt{2}} \overline{u_{Li}} \gamma^\mu (V_{\text{CKM}})_{ij} d_{Lj} W_\mu^\pm + \text{h.c.} \quad (13.32)$$

Here $i, j = 1, 2, 3$ are generation numbers. The Cabibbo-Kobayashi-Maskawa (CKM) mixing matrix for quarks is a 3×3 unitary matrix [40]. Ordering the quarks by their masses, *i.e.*, $(u_1, u_2, u_3) \rightarrow (u, c, t)$ and $(d_1, d_2, d_3) \rightarrow (d, s, b)$, the elements of V_{CKM} are written as follows:

$$V_{\text{CKM}} = \begin{pmatrix} V_{ud} & V_{us} & V_{ub} \\ V_{cd} & V_{cs} & V_{cb} \\ V_{td} & V_{ts} & V_{tb} \end{pmatrix}. \quad (13.33)$$

While a general 3×3 unitary matrix depends on three real angles

$$V_{\text{CKM}} = \begin{pmatrix} 1 - \frac{1}{2}\lambda^2 - \frac{1}{8}\lambda^4 & \lambda & A\lambda^3(\rho - i\eta) \\ -\lambda + \frac{1}{2}A^2\lambda^5[1 - 2(\rho + i\eta)] & 1 - \frac{1}{2}\lambda^2 - \frac{1}{8}\lambda^4(1 + 4A^2) & A\lambda^2 \\ A\lambda^3[1 - (1 - \frac{1}{2}\lambda^2)(\rho + i\eta)] & -A\lambda^2 + \frac{1}{2}A\lambda^4[1 - 2(\rho + i\eta)] & 1 - \frac{1}{2}A^2\lambda^4 \end{pmatrix}. \quad (13.34)$$

Here $\lambda \approx 0.23$ (not to be confused with λ_f), the sine of the Cabibbo angle, plays the role of an expansion parameter, and η represents the CP -violating phase. Terms of $\mathcal{O}(\lambda^6)$ have been neglected.

The unitarity of the CKM matrix, $(VV^\dagger)_{ij} = (V^\dagger V)_{ij} = \delta_{ij}$, leads to twelve distinct complex relations among the matrix elements. The six relations with $i \neq j$ can be represented geometrically as triangles in the complex plane. Two of these,

$$V_{ud}V_{ub}^* + V_{cd}V_{cb}^* + V_{td}V_{tb}^* = 0, \quad (13.35a)$$

$$V_{td}V_{ud}^* + V_{ts}V_{us}^* + V_{tb}V_{ub}^* = 0, \quad (13.35b)$$

have terms of equal order, $\mathcal{O}(A\lambda^3)$, and so have corresponding triangles whose interior angles are all $\mathcal{O}(1)$ physical quantities that can be independently measured. The angles of the first triangle (see Fig. 13.1) are given by

$$\alpha \equiv \varphi_2 \equiv \arg\left(-\frac{V_{td}V_{tb}^*}{V_{ud}V_{ub}^*}\right) \simeq \arg\left(-\frac{1 - \rho - i\eta}{\rho + i\eta}\right), \quad (13.36a)$$

$$\beta \equiv \varphi_1 \equiv \arg\left(-\frac{V_{cd}V_{cb}^*}{V_{td}V_{tb}^*}\right) \simeq \arg\left(\frac{1}{1 - \rho - i\eta}\right), \quad (13.36b)$$

$$\gamma \equiv \varphi_3 \equiv \arg\left(-\frac{V_{ud}V_{ub}^*}{V_{cd}V_{cb}^*}\right) \simeq \arg(\rho + i\eta). \quad (13.36c)$$

The angles of the second triangle are equal to (α, β, γ) up to corrections of $\mathcal{O}(\lambda^2)$. The notations (α, β, γ) and $(\varphi_1, \varphi_2, \varphi_3)$ are both in common usage but, for convenience, we only use the first convention in the following.

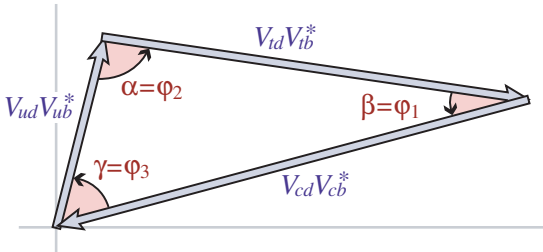


Figure 13.1: Graphical representation of the unitarity constraint $V_{ud}V_{ub}^* + V_{cd}V_{cb}^* + V_{td}V_{tb}^* = 0$ as a triangle in the complex plane.

Another relation that can be represented as a triangle,

$$V_{us}V_{ub}^* + V_{cs}V_{cb}^* + V_{ts}V_{tb}^* = 0, \quad (13.37)$$

and, in particular, its small angle, of $\mathcal{O}(\lambda^2)$,

$$\beta_s \equiv \arg\left(-\frac{V_{ts}V_{tb}^*}{V_{cs}V_{cb}^*}\right), \quad (13.38)$$

is convenient for analyzing CP violation in the B_s^0 sector.

and six phases, the freedom to redefine the phases of the quark mass eigenstates can be used to remove five of the phases, leaving a single physical phase, the Kobayashi-Maskawa phase, that is responsible for all CP violation in the Standard Model.

The fact that one can parameterize V_{CKM} by three real and only one imaginary physical parameters can be made manifest by choosing an explicit parametrization. The Wolfenstein parametrization [41, 42] is particularly useful:

All unitarity triangles have the same area, commonly denoted by $J/2$ [43]. If CP is violated, J is different from zero and can be taken as the single CP -violating parameter. In the Wolfenstein parametrization of Eq. (13.34), $J \simeq \lambda^6 A^2 \eta$.

13.4 Kaons

CP violation was discovered in $K \rightarrow \pi\pi$ decays in 1964 [1]. The same mode provided the first observation of direct CP violation [4–6].

The decay amplitudes actually measured in neutral K decays refer to the mass eigenstates K_L and K_S , rather than to the K and \bar{K} states referred to in Eq. (13.1). The final $\pi^+\pi^-$ and $\pi^0\pi^0$ states are CP -even. In the CP conservation limit, K_S (K_L) would be CP -even (odd), and therefore would (would not) decay to two pions. We define CP -violating amplitude ratios for two-pion final states,

$$\eta_{00} \equiv \frac{\langle \pi^0\pi^0 | \mathcal{H} | K_L \rangle}{\langle \pi^0\pi^0 | \mathcal{H} | K_S \rangle}, \quad \eta_{+-} \equiv \frac{\langle \pi^+\pi^- | \mathcal{H} | K_L \rangle}{\langle \pi^+\pi^- | \mathcal{H} | K_S \rangle}. \quad (13.39)$$

Another important observable is the asymmetry of time-integrated semileptonic decay rates:

$$\delta_L \equiv \frac{\Gamma(K_L \rightarrow \ell^+\nu_\ell\pi^-) - \Gamma(K_L \rightarrow \ell^-\bar{\nu}_\ell\pi^+)}{\Gamma(K_L \rightarrow \ell^+\nu_\ell\pi^-) + \Gamma(K_L \rightarrow \ell^-\bar{\nu}_\ell\pi^+)}. \quad (13.40)$$

CP violation has been observed as an appearance of K_L decays to two-pion final states [44],

$$|\eta_{00}| = (2.220 \pm 0.011) \times 10^{-3}, \quad (13.41a)$$

$$|\eta_{+-}| = (2.232 \pm 0.011) \times 10^{-3}, \quad (13.41b)$$

$$|\eta_{00}/\eta_{+-}| = 0.9950 \pm 0.0007, \quad (13.41c)$$

where the CP -conserving phases ϕ_{ij} of the amplitude ratios η_{ij} have been determined both assuming CPT invariance:

$$\phi_{00} = (43.52 \pm 0.05)^\circ, \quad \phi_{+-} = (43.51 \pm 0.05)^\circ, \quad (13.42)$$

and without assuming CPT invariance:

$$\phi_{00} = (43.7 \pm 0.6)^\circ, \quad \phi_{+-} = (43.4 \pm 0.5)^\circ. \quad (13.43)$$

CP violation has also been observed in semileptonic K_L decays [44]

$$\delta_L = (3.32 \pm 0.06) \times 10^{-3}, \quad (13.44)$$

where δ_L is a weighted average of muon and electron measurements, as well as in K_L decays to $\pi^+\pi^-\gamma$ and $\pi^+\pi^-e^+e^-$ [44]. CP violation in $K \rightarrow 3\pi$ decays has not yet been observed [44, 45].

Historically, CP violation in neutral K decays has been described in terms of the complex parameters ϵ and ϵ' . The observables η_{00} , η_{+-} , and δ_L are related to these parameters, and to

those of Section 13.1, by

$$\eta_{00} = \frac{1 - \lambda_{\pi^0\pi^0}}{1 + \lambda_{\pi^0\pi^0}} = \epsilon - 2\epsilon', \quad (13.45a)$$

$$\eta_{+-} = \frac{1 - \lambda_{\pi^+\pi^-}}{1 + \lambda_{\pi^+\pi^-}} = \epsilon + \epsilon', \quad (13.45b)$$

$$\delta_L = \frac{1 - |q/p|^2}{1 + |q/p|^2} = \frac{2\mathcal{R}e(\epsilon)}{1 + |\epsilon|^2}, \quad (13.45c)$$

where, in the last line, we have assumed that $|A_{\ell^+\nu_\ell\pi^-}| = |\bar{A}_{\ell^-\bar{\nu}_\ell\pi^+}|$ and $|A_{\ell^-\bar{\nu}_\ell\pi^+}| = |\bar{A}_{\ell^+\nu_\ell\pi^-}| = 0$. (The convention-dependent parameter $\tilde{\epsilon} \equiv (1 - q/p)/(1 + q/p)$, sometimes used in the literature, is, in general, different from ϵ but yields a similar expression, $\delta_L = 2\mathcal{R}e(\tilde{\epsilon})/(1 + |\tilde{\epsilon}|^2)$.) A fit to the $K \rightarrow \pi\pi$ data yields [44]

$$|\epsilon| = (2.228 \pm 0.011) \times 10^{-3}, \quad (13.46a)$$

$$\mathcal{R}e(\epsilon'/\epsilon) = (1.66 \pm 0.23) \times 10^{-3}. \quad (13.46b)$$

In discussing two-pion final states, it is useful to express the amplitudes $A_{\pi^0\pi^0}$ and $A_{\pi^+\pi^-}$ in terms of their isospin components via

$$A_{\pi^0\pi^0} = \sqrt{\frac{1}{3}} |A_0| e^{i(\delta_0 + \phi_0)} - \sqrt{\frac{2}{3}} |A_2| e^{i(\delta_2 + \phi_2)}, \quad (13.47a)$$

$$A_{\pi^+\pi^-} = \sqrt{\frac{2}{3}} |A_0| e^{i(\delta_0 + \phi_0)} + \sqrt{\frac{1}{3}} |A_2| e^{i(\delta_2 + \phi_2)}, \quad (13.47b)$$

where we parameterize the amplitude $A_I(\bar{A}_I)$ for $K^0(\bar{K}^0)$ decay into two pions with total isospin $I = 0$ or 2 as

$$A_I \equiv \langle (\pi\pi)_I | \mathcal{H} | K^0 \rangle = |A_I| e^{i(\delta_I + \phi_I)}, \quad (13.48a)$$

$$\bar{A}_I \equiv \langle (\pi\pi)_I | \mathcal{H} | \bar{K}^0 \rangle = |A_I| e^{i(\delta_I - \phi_I)}. \quad (13.48b)$$

The smallness of $|\eta_{00}|$ and $|\eta_{+-}|$ allows us to approximate

$$\epsilon \simeq \frac{1}{2}(1 - \lambda_{(\pi\pi)_{I=0}}), \quad \epsilon' \simeq \frac{1}{6}(\lambda_{\pi^0\pi^0} - \lambda_{\pi^+\pi^-}). \quad (13.49)$$

The parameter ϵ represents indirect CP violation, while ϵ' parameterizes direct CP violation: $\mathcal{R}e(\epsilon')$ measures CP violation in decay (type I), $\mathcal{R}e(\epsilon)$ measures CP violation in mixing (type II), and $\mathcal{I}m(\epsilon)$ and $\mathcal{I}m(\epsilon')$ measure the interference between decays with and without mixing (type III).

The following expressions for ϵ and ϵ' are useful for theoretical evaluations:

$$\epsilon \simeq \frac{e^{i\pi/4} \mathcal{I}m(\mathbf{M}_{12})}{\sqrt{2} \Delta m}, \quad \epsilon' \simeq \frac{i}{\sqrt{2}} \left| \frac{A_2}{A_0} \right| e^{i(\delta_2 - \delta_0)} \sin(\phi_2 - \phi_0). \quad (13.50)$$

The expression for ϵ is only valid in a phase convention where $\phi_2 = 0$, corresponding to a real $V_{ud}^* V_{us}$, and in the approximation that also $\phi_0 = 0$. The phase of ϵ , $\arg(\epsilon) \approx \arctan(-2\Delta m/\Delta\Gamma)$, is determined by non-perturbative QCD dynamics and is experimentally determined to be about $\pi/4$. The calculation of ϵ benefits from the fact that $\mathcal{I}m(\mathbf{M}_{12})$ is dominated by short distance physics. Consequently, the main sources of uncertainty in theoretical interpretations of ϵ are the values of matrix elements, such as $\langle K^0 | (\bar{s}d)_{V-A} (\bar{s}d)_{V-A} | \bar{K}^0 \rangle$. The expression for ϵ' is valid to first order in $|A_2/A_0| \sim 1/20$. The phase of ϵ' is experimentally determined, $\pi/2 + \delta_2 - \delta_0 \approx \pi/4$, and is independent of the model of electroweak interactions. Note that, accidentally, ϵ'/ϵ is real to a good approximation. Determination of weak phase information from the measurement of $\mathcal{R}e(\epsilon'/\epsilon)$ given in Eq. (13.46) has until now been precluded by uncertainties in the hadronic parameters, but recent advances in lattice QCD calculations and other theoretical approaches [46–48] suggest that it may become possible.

A future measurement of much interest is that of CP violation in the rare $K \rightarrow \pi\nu\bar{\nu}$ decays. The signal for CP violation is simply observing the $K_L \rightarrow \pi^0\nu\bar{\nu}$ decay. The effect here is that

of interference between decays with and without mixing (type III) [49]:

$$\frac{\Gamma(K_L \rightarrow \pi^0\nu\bar{\nu})}{\Gamma(K^+ \rightarrow \pi^+\nu\bar{\nu})} = \frac{1}{2} \left[1 + |\lambda_{\pi\nu\bar{\nu}}|^2 - 2\mathcal{R}e(\lambda_{\pi\nu\bar{\nu}}) \right] \simeq 1 - \mathcal{R}e(\lambda_{\pi\nu\bar{\nu}}), \quad (13.51)$$

where in the last equation we neglect CP violation in decay and in mixing (expected, model-independently, to be of order 10^{-5} and 10^{-3} , respectively). Such a measurement is experimentally very challenging but would be theoretically very rewarding [50]. Similar to the CP asymmetry in $B^0 \rightarrow J/\psi K_S$, the CP violation in $K \rightarrow \pi\nu\bar{\nu}$ decay is predicted to be large (that is, the ratio in Eq. (13.51) is neither CKM- nor loop-suppressed) and can be very cleanly interpreted. In particular, the independent determinations of the CKM parameters via B -meson and K -meson decays and mixing will over-constrain the unitarity triangle and provide a stringent test of the KM mechanism.

Within the Standard Model, the $K_L \rightarrow \pi^0\nu\bar{\nu}$ decay is dominated by an intermediate top quark contribution and, consequently, can be interpreted in terms of CKM parameters [51]. (For the charged mode, $K^+ \rightarrow \pi^+\nu\bar{\nu}$, the contribution from an intermediate charm quark is not negligible, and constitutes a source of hadronic uncertainty.) In particular, $\mathcal{B}(K_L \rightarrow \pi^0\nu\bar{\nu})$ provides a theoretically clean way to determine the Wolfenstein parameter η [52]:

$$\mathcal{B}(K_L \rightarrow \pi^0\nu\bar{\nu}) = \kappa_L [X(m_t^2/m_W^2)]^2 A^4 \eta^2, \quad (13.52)$$

where the hadronic parameter $\kappa_L \sim 2 \times 10^{-10}$ incorporates the value of the four-fermion matrix element which is deduced, using isospin relations, from $\mathcal{B}(K^+ \rightarrow \pi^0 e^+ \nu_e)$, and $X(m_t^2/m_W^2)$ is a known function of the top mass. An explicit calculation gives $\mathcal{B}(K_L \rightarrow \pi^0\nu\bar{\nu}) = (3.00 \pm 0.30) \times 10^{-11}$ [53].

Currently the most stringent experimental limit is $\mathcal{B}(K_L \rightarrow \pi^0\nu\bar{\nu}) < 3.0 \times 10^{-9}$ [54, 55], which does not yet reach the bound that can be derived from Eq. (13.51), $\mathcal{B}(K_L \rightarrow \pi^0\nu\bar{\nu}) < 4.4 \times \mathcal{B}(K^+ \rightarrow \pi^+\nu\bar{\nu})$ [49], with the most precise result for the charged kaon decay being $\mathcal{B}(K^+ \rightarrow \pi^+\nu\bar{\nu}) = (10.6^{+4.0}_{-3.4} \pm 0.9) \times 10^{-11}$ [56]. Significant further progress is anticipated from experiments searching for $K \rightarrow \pi\nu\bar{\nu}$ decays in the next few years.

13.5 Charm

The existence of $D^0\text{--}\bar{D}^0$ mixing is well established [57–61], with the latest experimental constraints giving [62, 63] $x \equiv \Delta m/\Gamma = (0.407 \pm 0.044) \times 10^{-2}$ and $y \equiv \Delta\Gamma/(2\Gamma) = (0.647 \pm 0.024) \times 10^{-2}$. Long-distance contributions make it difficult to calculate Standard Model predictions for the $D^0\text{--}\bar{D}^0$ mixing parameters. Therefore, the goal of the search for $D^0\text{--}\bar{D}^0$ mixing is not to constrain the CKM parameters, but rather to probe new physics. Here CP violation plays an important role. Within the Standard Model, the CP -violating effects are predicted to be small, since the mixing and the relevant decays are described, to an excellent approximation, by the physics of the first two generations only. The expectation is that the Standard Model size of CP violation in D decays is $\mathcal{O}(10^{-3})$ or less. At present, the most sensitive searches involve the $D^0 \rightarrow K^+K^-$, $D^0 \rightarrow \pi^+\pi^-$ and $D^0 \rightarrow K^\pm\pi^\mp$ modes.

The neutral D mesons decay via a singly-Cabibbo-suppressed transition to the CP eigenstates K^+K^- and $\pi^+\pi^-$. These decays are dominated by Standard-Model tree diagrams. Thus, we can write, for $f = K^+K^-$ or $\pi^+\pi^-$,

$$A_f = A_f^T e^{+i\phi_f^T} [1 + r_f e^{i(\delta_f + \phi_f)}], \quad (13.53a)$$

$$\bar{A}_f = A_f^T e^{-i\phi_f^T} [1 + r_f e^{i(\delta_f - \phi_f)}], \quad (13.53b)$$

where $A_f^T e^{\pm i\phi_f^T}$ is the Standard Model tree-level contribution, ϕ_f^T and ϕ_f are weak, CP violating phases, δ_f is a strong phase difference, and r_f is the ratio between a subleading ($r_f \ll 1$) contribution with a weak phase different from ϕ_f^T and the Standard

Model tree-level contribution. Neglecting r_f , λ_f is universal, and we can define an observable phase ϕ_D via

$$\lambda_f \equiv -|q/p|e^{i\phi_D}. \quad (13.54)$$

(In the limit of CP conservation, choosing $\phi_D = 0$ is equivalent to defining the mass eigenstates by their CP eigenvalue: $|D_{\mp}\rangle = p|D^0\rangle \pm q|\bar{D}^0\rangle$, with D_- (D_+) being the CP -odd (CP -even) state; that is, the state that does not (does) decay into K^+K^- .)

We define the time integrated CP asymmetry for a final CP eigenstate f as follows:

$$a_f \equiv \frac{\int_0^\infty \Gamma(D_{\text{phys}}^0(t) \rightarrow f)dt - \int_0^\infty \Gamma(\bar{D}_{\text{phys}}^0(t) \rightarrow f)dt}{\int_0^\infty \Gamma(D_{\text{phys}}^0(t) \rightarrow f)dt + \int_0^\infty \Gamma(\bar{D}_{\text{phys}}^0(t) \rightarrow f)dt}. \quad (13.55)$$

(This expression corresponds to the D meson being tagged at production, hence the integration goes from 0 to $+\infty$; measurements are also possible with $\psi(3770) \rightarrow D^0\bar{D}^0$, in which case the integration goes from $-\infty$ to $+\infty$ giving slightly different results; see the discussion in Section 13.1.3.) We take $x, y, r_f \ll 1$ and expand to leading order in these parameters. We can then separate the contribution to a_f into three parts [64],

$$a_f = a_f^d + a_f^m + a_f^i, \quad (13.56)$$

with the following underlying mechanisms:

1. a_f^d signals CP violation in decay (similar to Eq. (13.21)):

$$a_f^d = 2r_f \sin \phi_f \sin \delta_f. \quad (13.57)$$

2. a_f^m signals CP violation in mixing (similar to Eq. (13.30)). With our approximations, it is universal:

$$a^m = -\frac{y}{2} \left(\left| \frac{q}{p} \right| - \left| \frac{p}{q} \right| \right) \cos \phi_D. \quad (13.58)$$

3. a_f^i signals CP violation in the interference of mixing and decay (similar to Eq. (13.31)). With our approximations, it is universal:

$$a^i = \frac{x}{2} \left(\left| \frac{q}{p} \right| + \left| \frac{p}{q} \right| \right) \sin \phi_D. \quad (13.59)$$

In the SM, both a^m and a^i are $\mathcal{O}(10^{-5})$ or less, while a^d could be up to two orders of magnitude larger.

One can isolate the effects of direct CP violation by taking the difference between the CP asymmetries in the K^+K^- and $\pi^+\pi^-$ modes:

$$\Delta a_{CP} \equiv a_{K^+K^-} - a_{\pi^+\pi^-} = a_{K^+K^-}^d - a_{\pi^+\pi^-}^d, \quad (13.60)$$

where we neglected a residual, experiment-dependent, contribution from indirect CP violation due to the fact that there may be a decay time-dependent acceptance function that can be different for the K^+K^- and $\pi^+\pi^-$ channels. The current average gives [13, 62]:

$$a_{K^+K^-}^d - a_{\pi^+\pi^-}^d = (-0.161 \pm 0.028) \times 10^{-2}, \quad (13.61)$$

demonstrating CP violation in charm decay. While the asymmetry is somewhat larger than the theoretical predictions that preceded the measurement, it can in principle be explained by non-perturbative QCD effects.

One can also isolate the effects of indirect CP violation in the following way. Consider the time-dependent decay rates in Eq. (13.17a) and Eq. (13.17b). The mixing processes modify the time dependence from a pure exponential. However, given the small values of x and y , the time dependences can be recast, to a good approximation, into purely exponential form, but with modified decay-rate parameters [65, 66] (given here for the K^+K^- final state):

$$\Gamma_{D^0 \rightarrow K^+K^-} = \Gamma \times [1 + |q/p| (y \cos \phi_D - x \sin \phi_D)], \quad (13.62a)$$

$$\Gamma_{\bar{D}^0 \rightarrow K^+K^-} = \Gamma \times [1 + |p/q| (y \cos \phi_D + x \sin \phi_D)]. \quad (13.62b)$$

One can define CP -conserving and CP -violating combinations of these two observables (normalized to the true width Γ):

$$y_{CP} \equiv \frac{\Gamma_{\bar{D}^0 \rightarrow K^+K^-} + \Gamma_{D^0 \rightarrow K^+K^-}}{2\Gamma} - 1$$

$$= (y/2) (|q/p| + |p/q|) \cos \phi_D - (x/2) (|q/p| - |p/q|) \sin \phi_D, \quad (13.63a)$$

$$A_\Gamma \equiv \frac{\Gamma_{D^0 \rightarrow K^+K^-} - \Gamma_{\bar{D}^0 \rightarrow K^+K^-}}{2\Gamma}$$

$$= -(a^m + a^i). \quad (13.63b)$$

In the limit of CP conservation (and, in particular, within the Standard Model), $y_{CP} = (\Gamma_+ - \Gamma_-)/2\Gamma = y$ (where Γ_+ (Γ_-) is the decay width of the CP -even (-odd) mass eigenstate) and $A_\Gamma = 0$. Indeed, present measurements imply that CP violation is small [62],

$$y_{CP} - y_{CP}(K\pi) = (+0.697 \pm 0.028) \times 10^{-2}, \quad (13.64a)$$

$$A_\Gamma = (0.009 \pm 0.011) \times 10^{-2}, \quad (13.64b)$$

where the correction $y_{CP}(K\pi)$ is necessary at high precision since experimentally the denominator of the relative widths in Eq. (13.63a) is measured with the $D^0 \rightarrow K^-\pi^+$ mode [67, 68].

The $K^\pm\pi^\mp$ states are not CP eigenstates, but they are still common final states for D^0 and \bar{D}^0 decays. Since $D^0(\bar{D}^0) \rightarrow K^-\pi^+$ is a Cabibbo-favored (doubly-Cabibbo-suppressed) process, these processes are particularly sensitive to x and/or $y = \mathcal{O}(\lambda^2)$. Taking into account that $|\lambda_{K^-\pi^+}|, |\lambda_{K^+\pi^-}^{-1}| \ll 1$ and $x, y \ll 1$, assuming that there is no direct CP violation (these are Standard Model tree-level decays dominated by a single weak phase, and there is no contribution from penguin-like and chromomagnetic operators), and expanding the time-dependent rates for $xt, yt \lesssim \Gamma^{-1}$, one obtains

$$\Gamma[D_{\text{phys}}^0(t) \rightarrow K^+\pi^-] = e^{-\Gamma t} |\bar{A}_{K^-\pi^+}|^2$$

$$\times \left[r_d^2 + r_d \left| \frac{q}{p} \right| (y' \cos \phi_D - x' \sin \phi_D) \Gamma t + \left| \frac{q}{p} \right|^2 \frac{y^2 + x^2}{4} (\Gamma t)^2 \right], \quad (13.65a)$$

$$\Gamma[\bar{D}_{\text{phys}}^0(t) \rightarrow K^-\pi^+] = e^{-\Gamma t} |\bar{A}_{K^-\pi^+}|^2$$

$$\times \left[r_d^2 + r_d \left| \frac{p}{q} \right| (y' \cos \phi_D + x' \sin \phi_D) \Gamma t + \left| \frac{p}{q} \right|^2 \frac{y^2 + x^2}{4} (\Gamma t)^2 \right], \quad (13.65b)$$

where

$$y' \equiv y \cos \delta - x \sin \delta \quad \text{and} \quad x' \equiv x \cos \delta + y \sin \delta. \quad (13.66)$$

The weak phase ϕ_D is the same as that of Eq. (13.54) (a consequence of neglecting direct CP violation) and $r_d = \mathcal{O}(\tan^2 \theta_c)$ is the amplitude ratio, $r_d = |\bar{A}_{K^-\pi^+}/A_{K^-\pi^+}| = |A_{K^+\pi^-}/\bar{A}_{K^+\pi^-}|$, that is, $\lambda_{K^-\pi^+} = r_d|q/p|e^{-i(\delta-\phi_D)}$ and $\lambda_{K^+\pi^-}^{-1} = r_d|p/q|e^{-i(\delta+\phi_D)}$. The parameter δ is a strong-phase difference for these processes, that can be obtained from measurements of quantum correlated $\psi(3770) \rightarrow D^0\bar{D}^0$ decays [69, 70]. By fitting to the six coefficients of the various time-dependences, one can determine r_d , $|q/p|$, $(x^2 + y^2)$, $y' \cos \phi_D$, and $x' \sin \phi_D$. In particular, finding CP violation ($|q/p| \neq 1$ and/or $\sin \phi_D \neq 0$) at a level much higher than 10^{-3} would constitute evidence for new physics. The most stringent constraints to date on CP violation in charm mixing have been obtained with this method [71] and from the A_Γ measurement [72].

A fit to all data [62], including also results from time-dependent analyses of $D^0 \rightarrow K_S\pi^+\pi^-$ decays, from which $x, y, |q/p|$ and ϕ_D can be determined directly, yields no evidence for indirect CP violation:

$$1 - |q/p| = +0.006_{-0.016}^{+0.015}, \quad (13.67a)$$

$$\phi_D = (-2.6 \pm 1.1)^\circ. \quad (13.67b)$$

With the additional assumption of no direct CP violation in doubly-Cabibbo-suppressed D decays [73–75], more stringent constraints are obtained:

$$1 - |q/p| = -0.005 \pm 0.007, \quad (13.68a)$$

$$\phi_D = (-0.2 \pm 0.3)^\circ. \quad (13.68b)$$

More details on various theoretical and experimental aspects of $D^0\text{--}\bar{D}^0$ mixing can be found in Ref. [32].

Searches for CP violation in charged $D_{(s)}$ decays have been performed in many modes. Searches in decays mediated by Cabibbo-suppressed amplitudes are particularly interesting, since in other channels effects are likely to be too small to be observable in current experiments. Examples of relevant two-body modes are $D^+ \rightarrow \pi^+\pi^0$, $K_S K^+$, $\phi\pi^+$ and $D_s^+ \rightarrow K^+\pi^0$, $K_S\pi^+$, ϕK^+ . The most precise results are $\mathcal{A}_{D^+ \rightarrow K_S K^+} = +0.0011 \pm 0.0017$ and $\mathcal{A}_{D_s^+ \rightarrow K_S \pi^+} = +0.0038 \pm 0.0048$ [62]. The precision of experiments is now sufficient that the effect from CP violation in the neutral kaon system can be seen in $D^+ \rightarrow K_S \pi^+$ decays [76, 77].

Three- and four-body final states provide additional possibilities to search for CP violation, since effects may vary over the phase-space [78]. A number of methods have been proposed to exploit this feature and search for CP violation in ways that do not require modelling of the decay distribution [79–82]. Such methods are useful for analysis of charm decays since they are less sensitive to biases from production asymmetries, and are well suited to address the issue of whether or not CP violation effects are present. They can also be applied to tagged neutral D meson as well as to charged $D_{(s)}$ decays (flavor tagging is typically achieved from the charge of the pion produced in $D^{*+} \rightarrow D^0\pi^+$ decays). The results of all searches to date are consistent with the absence of CP violation, with the most significant hint at the level of 2.7σ [83].

13.6 Beauty

13.6.1 CP violation in mixing of B^0 and B_s^0 mesons

The upper bound on the CP asymmetry in semileptonic B decays [84] implies that CP violation in $B^0\text{--}\bar{B}^0$ mixing is a small effect (we use $\mathcal{A}_{\text{SL}}/2 \approx 1 - |q/p|$, see Eq. (13.23)):

$$\mathcal{A}_{\text{SL}}^d = (-2.1 \pm 1.7) \times 10^{-3} \implies |q/p| = 1.0010 \pm 0.0008. \quad (13.69)$$

The Standard Model prediction is

$$\mathcal{A}_{\text{SL}}^d = \mathcal{O} \left[(m_c^2/m_t^2) \sin \beta \right] \lesssim 0.001. \quad (13.70)$$

An explicit calculation gives $(-4.73 \pm 0.42) \times 10^{-4}$ [36].

The experimental constraint on CP violation in $B_s^0\text{--}\bar{B}_s^0$ mixing is somewhat weaker than that in the $B^0\text{--}\bar{B}^0$ system [84]

$$\mathcal{A}_{\text{SL}}^s = (-0.6 \pm 2.8) \times 10^{-3} \implies |q/p| = 1.0003 \pm 0.0014. \quad (13.71)$$

The Standard Model prediction is $\mathcal{A}_{\text{SL}}^s = \mathcal{O} \left[(m_c^2/m_t^2) \sin \beta_s \right] \lesssim 10^{-4}$, with an explicit calculation giving $(2.06 \pm 0.18) \times 10^{-5}$ [36].

The fit to experimental data that results in the averages quoted above has a χ^2 probability of 4.5% indicating some tension between the different measurements [62]. This originates in part from a result from the D0 collaboration for the inclusive same-sign dimuon asymmetry that deviates from the Standard Model prediction by 3.6σ [85]. As yet, this has not been confirmed by independent studies.

In models where $\Gamma_{12}/\mathbf{M}_{12}$ is approximately real, such as the Standard Model, an upper bound on $\Delta\Gamma/\Delta m \approx \mathcal{R}e(\Gamma_{12}/\mathbf{M}_{12})$ provides yet another upper bound on the deviation of $|q/p|$ from one. This constraint does not hold if $\Gamma_{12}/\mathbf{M}_{12}$ is approximately imaginary. (An alternative parameterization uses $q/p = (1 - \bar{\epsilon}_B)/(1 + \bar{\epsilon}_B)$, leading to $\mathcal{A}_{\text{SL}} \simeq 4\mathcal{R}e(\bar{\epsilon}_B)$.)

13.6.2 CP violation in interference of B^0 decays with and without mixing

The small deviation (less than one percent) of $|q/p|$ from 1 implies that, at the present level of experimental precision, CP violation in B^0 mixing is a negligible effect. Thus, for the purpose of analyzing CP asymmetries in hadronic B^0 decays, we can use

$$\lambda_f = e^{-i\phi_M(B^0)} (\bar{A}_f/A_f), \quad (13.72)$$

where $\phi_M(B^0)$ refers to the phase of \mathbf{M}_{12} appearing in Eq. (13.28) that is appropriate for $B^0\text{--}\bar{B}^0$ oscillations. Within the Standard Model, the corresponding phase factor is given by

$$e^{-i\phi_M(B^0)} = (V_{tb}^* V_{td}) / (V_{tb} V_{td}^*). \quad (13.73)$$

The class of CP violation effects in interference between mixing and decay is studied with final states that are common to B^0 and \bar{B}^0 decays [86–88]. It is convenient to rewrite Eq. (13.26) for B^0 decays as [89–91]

$$\mathcal{A}_f(t) = S_f \sin(\Delta m t) - C_f \cos(\Delta m t), \quad (13.74)$$

$$S_f \equiv \frac{2\mathcal{I}m(\lambda_f)}{1 + |\lambda_f|^2}, \quad C_f \equiv \frac{1 - |\lambda_f|^2}{1 + |\lambda_f|^2}, \quad (13.75)$$

where we assume that $\Delta\Gamma = 0$ and $|q/p| = 1$. An alternative notation in use is $A_f \equiv -C_f$ – this A_f should not be confused with the A_f of Eq. (13.1), but in the limit that $|q/p| = 1$ is equivalent with the \mathcal{A}_f of Eq. (13.21).

A large class of interesting processes proceed via quark transitions of the form $\bar{b} \rightarrow \bar{q}q\bar{q}'$ with $q' = s$ or d . For $q = c$ or u , there are contributions from both tree (t) and penguin (p^{qu}), where $qu = u, c, t$ is the quark in the loop diagrams (see Fig. 13.2) which carry different weak phases:

$$A_f = (V_{qb}^* V_{qq'}) t_f + \sum_{qu=u,c,t} (V_{qb}^* V_{quq'}) p_f^{qu}. \quad (13.76)$$

(The distinction between tree and penguin contributions is a heuristic one; the separation by the operator that enters is more precise. A more detailed discussion of the operator product expansion approach, which also includes higher order QCD corrections, can be found in Ref. [92, 93] for example.) Using CKM unitarity, the various decay amplitudes can always be written in terms of just two CKM combinations. For example, for $f = \pi\pi$, which proceeds via a $\bar{b} \rightarrow \bar{u}u\bar{d}$ transition, we can write

$$A_{\pi\pi} = (V_{ub}^* V_{ud}) T_{\pi\pi} + (V_{tb}^* V_{td}) P_{\pi\pi}^t, \quad (13.77)$$

where $T_{\pi\pi} = t_{\pi\pi} + p_{\pi\pi}^u - p_{\pi\pi}^c$ and $P_{\pi\pi}^t = p_{\pi\pi}^t - p_{\pi\pi}^c$. CP -violating phases in Eq. (13.77) appear only in the CKM elements, so that

$$\frac{\bar{A}_{\pi\pi}}{A_{\pi\pi}} = \frac{(V_{ub} V_{ud}^*) T_{\pi\pi} + (V_{tb} V_{td}^*) P_{\pi\pi}^t}{(V_{ub}^* V_{ud}) T_{\pi\pi} + (V_{tb}^* V_{td}) P_{\pi\pi}^t}. \quad (13.78)$$

For $f = J/\psi K$, which proceeds via a $\bar{b} \rightarrow \bar{c}c\bar{s}$ transition, we can write

$$A_{\psi K} = (V_{cb}^* V_{cs}) T_{\psi K} + (V_{ub}^* V_{us}) P_{\psi K}^u, \quad (13.79)$$

where $T_{\psi K} = t_{\psi K} + p_{\psi K}^c - p_{\psi K}^t$ and $P_{\psi K}^u = p_{\psi K}^u - p_{\psi K}^t$. A subtlety arises in this decay that is related to the fact that B^0 decays into a final $J/\psi K^0$ state while \bar{B}^0 decays into a final $J/\psi \bar{K}^0$ state. A common final state, e.g., $J/\psi K_S$, is reached only via $K^0\text{--}\bar{K}^0$ mixing. Consequently, the phase factor (defined in Eq. (13.28)) corresponding to neutral K mixing, $e^{-i\phi_M(K)} = (V_{cd}^* V_{cs}) / (V_{cd} V_{cs}^*)$, plays a role:

$$\frac{\bar{A}_{\psi K_S}}{A_{\psi K_S}} = - \frac{(V_{cb} V_{cs}^*) T_{\psi K} + (V_{ub} V_{us}^*) P_{\psi K}^u}{(V_{cb}^* V_{cs}) T_{\psi K} + (V_{ub}^* V_{us}) P_{\psi K}^u} \times \frac{V_{cd}^* V_{cs}}{V_{cd} V_{cs}^*}. \quad (13.80)$$

For $q = s$ or d , there are only penguin contributions to A_f , that is, $t_f = 0$ in Eq. (13.76). (The tree $\bar{b} \rightarrow \bar{u}u\bar{q}'$ transition followed by $\bar{u}u \rightarrow \bar{q}q$ rescattering is included below in the P^u terms.) Again, CKM unitarity allows us to write A_f in terms of two CKM combinations. For example, for $f = \phi K_S$, which proceeds via a $\bar{b} \rightarrow \bar{s}s\bar{s}$ transition, we can write

$$\frac{\bar{A}_{\phi K_S}}{A_{\phi K_S}} = - \frac{(V_{cb} V_{cs}^*) P_{\phi K}^c + (V_{ub} V_{us}^*) P_{\phi K}^u}{(V_{cb}^* V_{cs}) P_{\phi K}^c + (V_{ub}^* V_{us}) P_{\phi K}^u} \times \frac{V_{cd}^* V_{cs}}{V_{cd} V_{cs}^*}, \quad (13.81)$$

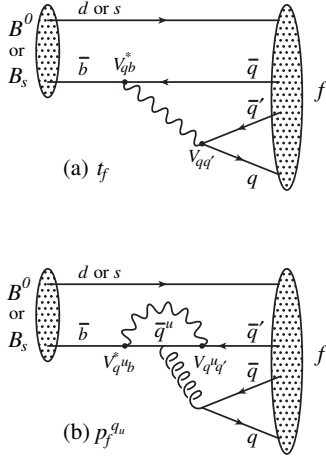


Figure 13.2: Feynman diagrams for (a) tree and (b) penguin amplitudes contributing to $B^0 \rightarrow f$ or $B_s^0 \rightarrow f$ via a $\bar{b} \rightarrow \bar{q} q'$ quark-level process.

where $P_{\phi K}^c = p_{\phi K}^c - p_{\phi K}^t$ and $P_{\phi K}^u = p_{\phi K}^u - p_{\phi K}^t$.

Since in general the amplitude A_f involves two different weak phases, the corresponding decays can exhibit both CP violation in the interference of decays with and without mixing, $S_f \neq 0$, and CP violation in decay, $C_f \neq 0$. (At the present level of experimental precision, the contribution to C_f from CP violation in mixing is negligible, see Eq. (13.69).) If the contribution from a second weak phase is suppressed, then the interpretation of S_f in terms of Lagrangian CP -violating parameters is clean, while C_f is small. If such a second contribution is not suppressed, S_f depends on hadronic parameters and, if the relevant strong phase difference is large, C_f is large.

A summary of $\bar{b} \rightarrow \bar{q} q'$ modes with $q' = s$ or d is given in Table 13.1. The $\bar{b} \rightarrow \bar{d} d \bar{q}$ transitions lead to final states that are similar to those from $\bar{b} \rightarrow \bar{u} u \bar{q}$ transitions and have similar phase dependence. Final states that consist of two vector mesons ($\psi\phi$ and $\phi\phi$) are not CP eigenstates, and angular analysis is needed to separate the CP -even from the CP -odd contributions.

The cleanliness of the theoretical interpretation of S_f can be assessed from the information in the last column of Table 13.1. In case of small uncertainties, the expression for S_f in terms of CKM phases can be deduced from the fourth column of Table 13.1 in combination with Eq. (13.73) (and, for $b \rightarrow q \bar{q} s$ decays, the example in Eq. (13.80)). Here we consider several interesting examples.

For $B^0 \rightarrow J/\psi K_S$ and other $\bar{b} \rightarrow \bar{c} c \bar{s}$ processes, we can neglect the P^u contribution to A_f , in the Standard Model, to an approximation that is better than one percent, giving

$$\lambda_{\psi K_S} = -e^{-2i\beta} \Rightarrow S_{\psi K_S} = \sin(2\beta), \quad C_{\psi K_S} = 0. \quad (13.82)$$

It is important to verify experimentally the level of suppression of the penguin contribution. Methods based on flavor symmetries [94–97] allow limits to be obtained. All are currently consistent with the P^u term being negligible. Explicit calculations [97–100] also support this conclusion.

In the presence of new physics, A_f is still likely to be dominated by the T term, but the mixing amplitude might be modified. Thus, model-independently, $C_f \approx 0$ while S_f cleanly determines the mixing phase ($\phi_M - 2 \arg(V_{cb} V_{cd}^*)$). The experimental measurement gave the first precision test of the Kobayashi-Maskawa mechanism. The latest world average [62] is

$$S_{\psi K^0} = +0.709 \pm 0.011. \quad (13.83)$$

(We use K^0 throughout to denote results that combine K_S and K_L modes, but use the sign appropriate to K_S .) The consistency of this measurement with the predictions for $\sin 2\beta$ makes it very likely that this mechanism is indeed the dominant source of CP violation in the quark sector.

For $B^0 \rightarrow \phi K_S$ and other $\bar{b} \rightarrow \bar{s} s \bar{s}$ processes (as well as some $\bar{b} \rightarrow \bar{u} u \bar{s}$ processes), we can neglect the subdominant contributions, in the Standard Model, to an approximation that is good to the order of a few percent:

$$\lambda_{\phi K_S} = -e^{-2i\beta} \Rightarrow S_{\phi K_S} = \sin 2\beta, \quad C_{\phi K_S} = 0. \quad (13.84)$$

A review of explicit calculations of the effects of subleading amplitudes can be found in Ref. [101]. In the presence of new physics, both A_f and M_{12} can have contributions that are comparable in size to those of the Standard Model and carry new weak phases. Such a situation gives several interesting consequences for penguin-dominated $\bar{b} \rightarrow \bar{q} q \bar{s}$ decays ($q = u, d, s$) to a final state f :

1. The value of $-\eta_f S_f$ may be different from $S_{\psi K_S}$ by more than a few percent, where η_f is the CP eigenvalue of the final state.
2. The values of $\eta_f S_f$ for different final states f may be different from each other by more than a few percent (for example, $S_{\phi K_S} \neq S_{\eta' K_S}$).
3. The value of C_f may be different from zero by more than a few percent.

While a clear interpretation of such signals in terms of Lagrangian parameters will be difficult because, under these circumstances, hadronic parameters play a role, any of the above three options will clearly signal new physics. In addition, flavor symmetry relations, such as those that relate observables in $B \rightarrow K\pi$ decays [102,103] can be used to provide further tests of the Standard Model. Fig. 13.3 summarizes the present experimental results: none of the possible signatures listed above is unambiguously established, but there is definitely still room for new physics.

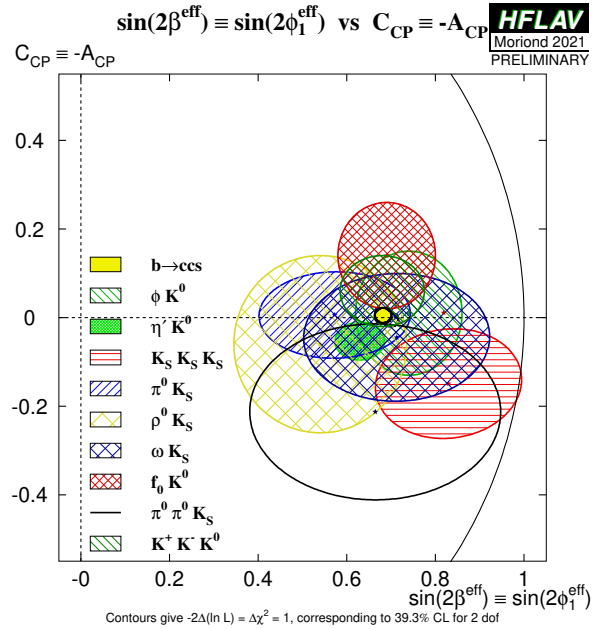


Figure 13.3: Summary of the results [62] of time-dependent analyses of $b \rightarrow \bar{q} q \bar{s}$ decays, which are potentially sensitive to new physics.

For the $\bar{b} \rightarrow \bar{u} u \bar{d}$ process $B \rightarrow \pi\pi$ and other related channels, the penguin-to-tree ratio can be estimated using $SU(3)$ relations and experimental data on related $B \rightarrow K\pi$ decays. The result (for $\pi\pi$) is that the suppression is at the level of 0.2–0.3 and so cannot be neglected. The expressions for $S_{\pi\pi}$ and $C_{\pi\pi}$ to leading order in $R_{PT} \equiv (|V_{tb} V_{td}| P_{\pi\pi}^t) / (|V_{ub} V_{ud}| T_{\pi\pi})$ are:

$$\lambda_{\pi\pi} = e^{2i\alpha} \left[(1 - R_{PT} e^{-i\alpha}) / (1 - R_{PT} e^{+i\alpha}) \right] \Rightarrow \quad (13.85)$$

$$S_{\pi\pi} \approx \sin 2\alpha + 2 \operatorname{Re}(R_{PT}) \cos 2\alpha \sin \alpha, \quad C_{\pi\pi} \approx 2 \operatorname{Im}(R_{PT}) \sin \alpha. \quad (13.86)$$

Table 13.1: Summary of $\bar{b} \rightarrow \bar{q}q\bar{q}'$ modes with $q' = s$ or d . The second and third columns give examples of hadronic final states (usually those which are experimentally most convenient to study). The fourth column gives the CKM dependence of the amplitude A_f , using the notation of Eqs. ((13.77), (13.79), (13.81)), with the dominant term first and the subdominant second. The suppression factor of the second term compared to the first is given in the last column. “Loop” refers to a penguin versus tree-suppression factor (it is mode-dependent and roughly $\mathcal{O}(0.2 - 0.3)$) and $\lambda \simeq 0.23$ is the expansion parameter of Eq. (13.34).

$\bar{b} \rightarrow \bar{q}q\bar{q}'$	$B^0 \rightarrow f$	$B_s^0 \rightarrow f$	CKM dependence of A_f	Suppression
$\bar{b} \rightarrow \bar{c}c\bar{s}$	ψK_S	$\psi\phi$	$(V_{cb}^*V_{cs})T + (V_{ub}^*V_{us})P^u$	loop $\times \lambda^2$
$\bar{b} \rightarrow \bar{s}s\bar{s}$	ϕK_S	$\phi\phi$	$(V_{cb}^*V_{cs})P^c + (V_{ub}^*V_{us})P^u$	λ^2
$\bar{b} \rightarrow \bar{u}u\bar{s}$	$\pi^0 K_S$	K^+K^-	$(V_{cb}^*V_{cs})P^c + (V_{ub}^*V_{us})T$	λ^2/loop
$\bar{b} \rightarrow \bar{c}c\bar{d}$	D^+D^-	ψK_S	$(V_{cb}^*V_{cd})T + (V_{tb}^*V_{td})P^t$	loop
$\bar{b} \rightarrow \bar{s}s\bar{d}$	$K_S K_S$	ϕK_S	$(V_{tb}^*V_{td})P^t + (V_{cb}^*V_{cd})P^c$	$\lesssim 1$
$\bar{b} \rightarrow \bar{u}u\bar{d}$	$\pi^+\pi^-$	$\rho^0 K_S$	$(V_{ub}^*V_{ud})T + (V_{tb}^*V_{td})P^t$	loop
$\bar{b} \rightarrow \bar{c}u\bar{d}$	$D_{CP}\pi^0$	$D_{CP}K_S$	$(V_{cb}^*V_{ud})T + (V_{ub}^*V_{cd})T'$	λ^2
$\bar{b} \rightarrow \bar{c}u\bar{s}$	$D_{CP}K_S$	$D_{CP}\phi$	$(V_{cb}^*V_{us})T + (V_{ub}^*V_{cs})T'$	$\lesssim 1$

Note that R_{PT} is mode-dependent and, in particular, could be different for $\pi^+\pi^-$ and $\pi^0\pi^0$. If strong phases can be neglected, then R_{PT} is real, resulting in $C_{\pi\pi} = 0$. The size of $C_{\pi\pi}$ is an indicator of how large the strong phase is. The present experimental average is $C_{\pi^+\pi^-} = -0.311 \pm 0.030$ [62]. As concerns $S_{\pi\pi}$, it is clear from Eq. (13.86) that the relative size or strong phase of the penguin contribution must be known to extract α . The theoretical uncertainty stemming from $|R_{PT}| \ll 1$ is referred to in the literature as penguin pollution.

The cleanest solution involves isospin relations among the $B \rightarrow \pi\pi$ amplitudes [104]:

$$\frac{1}{\sqrt{2}}A_{\pi^+\pi^-} + A_{\pi^0\pi^0} = A_{\pi^+\pi^0}. \quad (13.87)$$

The method exploits the fact that the penguin contribution to $P_{\pi\pi}^t$ is pure $\Delta I = 1/2$ (this is not true for the electroweak penguins which, however, are expected to be small), while the tree contribution to $T_{\pi\pi}$ contains amplitudes that are both $\Delta I = 1/2$ and $\Delta I = 3/2$. A simple geometric construction then allows one to find R_{PT} and extract α cleanly from $S_{\pi^+\pi^-}$. The key experimental difficulty is that one must measure accurately the separate rates for B^0 and $\bar{B}^0 \rightarrow \pi^0\pi^0$.

CP asymmetries in $B \rightarrow \rho\pi$ and $B \rightarrow \rho\rho$ can also be used to determine α . In particular, the $B \rightarrow \rho\rho$ measurements are presently very significant in constraining α . The extraction proceeds via isospin analysis similar to that of $B \rightarrow \pi\pi$. There are, however, several important differences. First, due to the finite width of the ρ mesons, a final $(\rho\rho)_{I=1}$ state is possible [105]. The effect is, however, of the order of $(\Gamma_\rho/m_\rho)^2 \sim 0.04$. Second, due to the presence of three helicity states for the two vector mesons, angular analysis is needed to separate the CP -even and CP -odd components. The theoretical expectation is that the CP -odd component is small. This is supported by experiments which find that the $\rho^+\rho^-$ and $\rho^\pm\rho^0$ modes are dominantly longitudinally polarized. Third, an important advantage of the $\rho\rho$ modes is that the penguin contribution is expected to be small due to different hadronic dynamics. This expectation is confirmed by the smallness of $\mathcal{B}(B^0 \rightarrow \rho^0\rho^0) = (0.95 \pm 0.16) \times 10^{-6}$ compared to $\mathcal{B}(B^0 \rightarrow \rho^+\rho^-) = (24.2 \pm 3.1) \times 10^{-6}$ [62]. Thus, $S_{\rho^+\rho^-}$ is not far from $\sin 2\alpha$. Finally, both $S_{\rho^0\rho^0}$ and $C_{\rho^0\rho^0}$ are experimentally accessible, which may allow a precise determination of α . However, a full isospin analysis should allow that the fractions of longitudinal polarization in B and \bar{B} decays may differ, which has not yet been done by the experiments.

Detailed discussion of the determination of α with these methods can be found in Refs. [106, 107]. The latest world average is

$$\alpha = (84.1_{-3.8}^{+4.5})^\circ. \quad (13.88)$$

The consistency between the range of α determined by the $B \rightarrow \pi\pi$, $\rho\pi$ and $\rho\rho$ measurements and the range allowed by CKM fits (excluding these direct determinations) provides further support to the Kobayashi-Maskawa mechanism.

All modes discussed in this Section so far have possible contributions from penguin amplitudes. As shown in Table 13.1, CP

violation can also be studied with final states, typically containing charmed mesons, where no such contribution is possible. The neutral charmed meson must be reconstructed in a final state, such as a CP eigenstate, common to D^0 and \bar{D}^0 so that the amplitudes for the B and \bar{B} meson decays interfere. Although there is a second tree amplitude with a different weak phase, the contributions of the different diagrams can in many cases be separated experimentally (for example by exploiting different decays of the neutral D mesons) making these channels very clean theoretically. The first determination of $\sin(2\beta)$, with significance of CP violation over 5σ , with this method has recently been reported [108]. Moreover, the interference between the two tree diagrams gives sensitivity to γ , as will be discussed in Section 13.6.4.

13.6.3 CP violation in interference of B_s^0 decays with and without mixing

As discussed in Section 13.6.1, the world average for $|q/p|$ in the B_s^0 system currently deviates from the Standard Model expectation due to an anomalous value of the dimuon asymmetry. Attributing the dimuon asymmetry result to a fluctuation, we again neglect the deviation of $|q/p|$ from 1, and use

$$\lambda_f = e^{-i\phi_M(B_s^0)}(\bar{A}_f/A_f). \quad (13.89)$$

Within the Standard Model,

$$e^{-i\phi_M(B_s^0)} = (V_{tb}^*V_{ts})/(V_{tb}V_{ts}^*). \quad (13.90)$$

Note that in the B_s^0 system, and with the sign convention of Eq. (13.8b), $\Delta\Gamma/\Gamma = -0.126 \pm 0.007$ [62] and therefore y should not be put to zero in Eqs. (13.17a) and (13.17b). However, $|q/p| = 1$ is expected to hold to an even better approximation than for B^0 mesons. One therefore obtains

$$A_f(t) = \frac{S_f \sin(\Delta mt) - C_f \cos(\Delta mt)}{\cosh(\Delta\Gamma t/2) - A_f^{\Delta\Gamma} \sinh(\Delta\Gamma t/2)}, \quad (13.91)$$

$$A_f^{\Delta\Gamma} \equiv \frac{-2\mathcal{R}\epsilon(\lambda_f)}{1 + |\lambda_f|^2}. \quad (13.92)$$

The presence of the $A_f^{\Delta\Gamma}$ term implies that information on λ_f can be obtained from analyses that do not use tagging of the initial flavor, through so-called effective lifetime measurements [109].

The $B_s^0 \rightarrow J/\psi\phi$ decay proceeds via the $\bar{b} \rightarrow \bar{c}c\bar{s}$ transition. The CP asymmetry in this mode thus determines (with angular analysis to disentangle the CP -even and CP -odd components of the final state) $\sin 2\beta_s$, where β_s is defined in Eq. (13.38) [110]. The $B_s^0 \rightarrow J/\psi\pi^+\pi^-$ decay, which has a large contribution from $J/\psi f_0(980)$ and is assumed to also proceed dominantly via the $\bar{b} \rightarrow \bar{c}c\bar{s}$ transition, has also been used to determine β_s . In this case no angular analysis is necessary, since the final state has been shown to be dominated by the CP -odd component [111]. The combination of measurements yields [62]

$$2\beta_s = 0.049 \pm 0.019, \quad (13.93)$$

consistent with the Standard Model prediction, assuming negligible penguin contributions, $\beta_s = 0.0184 \pm 0.0004$ [20].

A time-dependent CP asymmetry was established in $B_s^0 \rightarrow K^+K^-$ decay, which proceeds via the $\bar{b} \rightarrow \bar{u}u\bar{s}$ transition [112]:

$$C_{KK} = +0.172 \pm 0.031, \quad S_{KK} = +0.139 \pm 0.032. \quad (13.94)$$

For both C_{KK} and S_{KK} , the hadronic ratio (T/P^c) plays an important role (see Table 13.1), making a clean theoretical interpretation challenging. First results on the $\bar{b} \rightarrow \bar{q}q\bar{s}$ decays $B_s^0 \rightarrow \phi\phi$ and $K^{*0}\bar{K}^{*0}$ have also been reported. Parameters of CP violation have also been determined from the decay-time distributions of $B_s^0 \rightarrow D_s^\mp K^\pm$ and $D_s^\mp K^\pm \pi^+ \pi^-$ decays, involving interference between $\bar{b} \rightarrow \bar{c}u\bar{s}$ and $\bar{b} \rightarrow \bar{c}\bar{s}$ amplitudes.

13.6.4 Direct CP violation in the B system

An interesting class of decay modes is that of the tree-level decays $B^\pm \rightarrow D^{(*)}K^\pm$, which allow a theoretically pristine determination of the angle γ [113–118]. The method uses the decays $B^+ \rightarrow D^0K^+$, which proceeds via the quark transition $\bar{b} \rightarrow \bar{u}c\bar{s}$, and $B^+ \rightarrow \bar{D}^0K^+$, which proceeds via the quark transition $\bar{b} \rightarrow \bar{c}u\bar{s}$, with the D^0 and \bar{D}^0 decaying into a common final state. The decays into common final states, such $(\pi^0 K_S)DK^+$, involve interference effects between the two amplitudes, with sensitivity to the relative phase, $\delta + \gamma$ (δ is the relevant strong phase difference). The CP -conjugate processes are sensitive to $\delta - \gamma$. Measurements of branching ratios and CP asymmetries allow the determination of γ and δ from amplitude triangle relations. The method suffers from discrete ambiguities but, since all hadronic parameters can be determined from the data, has negligible theoretical uncertainty [119].

Unfortunately, the smallness of the CKM-suppressed $b \rightarrow u$ transitions makes it difficult to use the simplest methods alone [113–115] to determine γ . These difficulties are overcome (and the discrete ambiguities are removed) by performing a Dalitz plot analysis for multi-body D decays [116–118]. Detailed discussion of the determination of γ with these methods can be found in Ref. [107].

Constraints on γ from combinations of results on various $B \rightarrow D^{(*)}K^{(*)}$ processes have been obtained by experiments [120, 121]. The latest world average is [62, 107]

$$\gamma = (65.9_{-3.1}^{+2.9})^\circ. \quad (13.95)$$

The consistency between the range of γ determined by the $B \rightarrow DK$ measurements and the range allowed by CKM fits (excluding these direct determinations) provides further support to the Kobayashi-Maskawa mechanism. As more data become available, determinations of γ from $B_s^0 \rightarrow D_s^\mp K^\pm$ [122, 123] and $B^0 \rightarrow DK^{*0}$ [124–128] are expected to also give competitive measurements.

Decays to the final state $K^\mp \pi^\pm$ provided the first observations of direct CP violation in both B^0 and B_s^0 systems. The asymmetry arises due to interference between tree and penguin diagrams [129], similar to the effect discussed in Section 13.6.2. In principle, measurements of $\mathcal{A}_{B^0 \rightarrow K^+ \pi^-}$ and $\mathcal{A}_{B_s^0 \rightarrow K^- \pi^+}$ could be used to determine the weak phase difference γ , but lack of knowledge of the relative magnitude and strong phase of the contributing amplitudes limits the achievable precision. The uncertainties on these hadronic parameters can be reduced by exploiting flavor symmetries, which predict a number of relations between asymmetries in different modes. One such relation is that the partial rate differences for B^0 and B_s^0 decays to $K^\mp \pi^\pm$ are expected to be approximately equal and opposite [130], which is consistent with current data. It is also expected that the partial rate asymmetries for $B^0 \rightarrow K^+ \pi^-$ and $B^+ \rightarrow K^+ \pi^0$ should be approximately equal; however, the experimental results currently show a significant discrepancy [62]:

$$\mathcal{A}_{B^0 \rightarrow K^+ \pi^-} = -0.0836 \pm 0.0032, \quad \mathcal{A}_{B^+ \rightarrow K^+ \pi^0} = +0.029 \pm 0.012. \quad (13.96)$$

It is therefore of great interest to understand whether this originates from Standard Model QCD corrections, or whether it is a signature of new dynamics. Improved tests of a more precise

relation between the partial rate differences of all four $K\pi$ final states [131–134], currently limited by knowledge of the CP asymmetry in $\bar{B}^0 \rightarrow K_S \pi^0$ decays, may help to resolve the situation.

It is also of interest to investigate whether similar patterns appear among the CP violating asymmetries in B meson decays to final states containing one pseudoscalar and one vector meson. Since the vector resonance decays to two particles, such channels can be studied through Dalitz plot analysis of the three-body final state. Model-independent analyses of $B^+ \rightarrow K^+ K^- K^+$, $\pi^+ \pi^- K^+$, $\pi^+ \pi^- \pi^+$ and $K^+ K^- \pi^+$ decays have revealed large CP violation effects in certain regions of phase space [135]. For the $B^+ \rightarrow K^+ K^- \pi^+$ decay, an amplitude analysis has established a large CP violation effect associated with $\pi\pi \leftrightarrow KK$ S-wave rescattering [136]. In $B^+ \rightarrow \pi^+ \pi^- \pi^+$ decays, amplitude analysis has established CP violation effects in the decay amplitude involving the $f_2(1270)$ resonance, in the $\pi^+ \pi^-$ S-wave at low invariant mass, and in the interference between the $\pi^+ \pi^-$ S-wave and the P-wave $B^+ \rightarrow \rho(770)^0 \pi^+$ amplitude [137, 138]. For the other channels it remains to be seen whether the CP violation effects are associated to particular resonances or to interference effects, which will be necessary to understand the underlying dynamics.

13.7 Summary and Outlook

CP violation has been experimentally established in K , D and B meson decays. A full list of CP asymmetries that have been measured at a level higher than 5σ is given in Section 13.8. In Section 13.1.4 we introduced three types of CP -violating effects. Examples of these three types include the following:

1. All three types of CP violation have been observed in $K \rightarrow \pi\pi$ decays:

$$\begin{aligned} \text{Re}(\epsilon') &= \frac{1}{6} \left(\left| \frac{\bar{A}_{\pi^0 \pi^0}}{A_{\pi^0 \pi^0}} \right| - \left| \frac{\bar{A}_{\pi^+ \pi^-}}{A_{\pi^+ \pi^-}} \right| \right) \\ &= (2.5 \pm 0.4) \times 10^{-6}, \end{aligned} \quad (\text{I}) \quad (13.97a)$$

$$\begin{aligned} \text{Re}(\epsilon) &= \frac{1}{2} \left(1 - \left| \frac{q}{p} \right| \right) \\ &= (1.66 \pm 0.02) \times 10^{-3}, \end{aligned} \quad (\text{II}) \quad (13.97b)$$

$$\begin{aligned} \text{Im}(\epsilon) &= -\frac{1}{2} \text{Im}(\lambda_{(\pi\pi)_{I=0}}) \\ &= (1.57 \pm 0.02) \times 10^{-3}. \end{aligned} \quad (\text{III}) \quad (13.97c)$$

2. For D mesons, CP violation in decay has been established in the difference of asymmetries for $D^0 \rightarrow K^+ K^-$ and $D^0 \rightarrow \pi^+ \pi^-$ decays.

$$\begin{aligned} \Delta a_{CP} &= \frac{|\bar{A}_{K^+ K^-} / A_{K^+ K^-}|^2 - 1}{|\bar{A}_{K^+ K^-} / A_{K^+ K^-}|^2 + 1} - \frac{|\bar{A}_{\pi^+ \pi^-} / A_{\pi^+ \pi^-}|^2 - 1}{|\bar{A}_{\pi^+ \pi^-} / A_{\pi^+ \pi^-}|^2 + 1} \\ &= (-0.161 \pm 0.028) \times 10^{-2}, \end{aligned} \quad (\text{I}) \quad (13.98)$$

3. In the B meson system, CP violation in decay has been observed in, for example, $B^0 \rightarrow K^+ \pi^-$ transitions, while CP violation in interference of decays with and without mixing has been observed in, for example, the $B^0 \rightarrow J/\psi K_S$ channel:

$$\begin{aligned} \mathcal{A}_{K^+ \pi^-} &= \frac{|\bar{A}_{K^- \pi^+} / A_{K^+ \pi^-}|^2 - 1}{|\bar{A}_{K^- \pi^+} / A_{K^+ \pi^-}|^2 + 1} \\ &= -0.0836 \pm 0.0032, \end{aligned} \quad (\text{I}) \quad (13.99a)$$

$$\begin{aligned} S_{\psi K^0} &= \text{Im}(\lambda_{\psi K^0}) \\ &= +0.709 \pm 0.011. \end{aligned} \quad (\text{III}) \quad (13.99b)$$

Based on Standard Model predictions, further observations of CP violation in B^0 , B^+ and B_s^0 decays seem likely in the near future, at both LHCb and its upgrades [139–141] as well as the Belle II experiment [142]. The first observation of CP violation in b baryons is also likely to be within reach of LHCb. Further improvements in the sensitivity to CP violation effects in the charm sector can also be anticipated, though uncertainty in the Standard Model predictions makes it difficult to forecast whether or

not additional discoveries will be forthcoming. A number of upcoming experiments have potential to make significant progress on rare kaon decays. Observables that are subject to clean theoretical interpretation, such as β from $S_{\psi K_S}$, β_s from $B_s^0 \rightarrow J/\psi\phi$, $B(K_L \rightarrow \pi^0\nu\bar{\nu})$ and γ from CP violation in $B \rightarrow DK$ decays, are of particular value for constraining the values of the CKM parameters and probing the flavor sector of extensions to the Standard Model. Progress in lattice QCD calculations is also needed to complement the anticipated experimental results. Other probes of CP violation now being pursued experimentally include the electric dipole moments of the neutron and electron, and the decays of tau leptons. Additional processes that are likely to play an important role in future CP studies include top-quark production and decay, Higgs boson decays and neutrino oscillations.

All measurements of CP violation to date are consistent with the predictions of the Kobayashi-Maskawa mechanism of the Standard Model. In fact, it is now established that the KM mechanism plays a dominant role in the CP violation measured in the quark sector. However, a dynamically-generated matter-antimatter asymmetry of the universe requires additional sources of CP violation, and such sources are naturally generated by extensions to the Standard Model. New sources might eventually reveal themselves as small deviations from the predictions of the KM mechanism, or else might not be observable in the quark sector at all, but observable with future probes such as neutrino oscillations or electric dipole moments. The fundamental nature of CP violation demands a vigorous search.

A number of excellent reviews of CP violation are available [143–150], where the interested reader may find a detailed discussion of the various topics that are briefly reviewed here.

We thank David Kirkby for significant contributions to earlier versions of this review.

13.8 Observed CP violation effects

We conclude by listing the observables where CP violation has been observed at a level above 5σ [44, 62, 84]:

- Indirect CP violation in $K \rightarrow \pi\pi$ and $K \rightarrow \pi\ell\nu$ decays, and in the $K_L \rightarrow \pi^+\pi^-e^+e^-$ decay, is given by

$$|\epsilon| = (2.228 \pm 0.011) \times 10^{-3}. \quad (13.100)$$

- Direct CP violation in $K \rightarrow \pi\pi$ decays is given by

$$\mathcal{R}e(\epsilon'/\epsilon) = (1.65 \pm 0.26) \times 10^{-3}. \quad (13.101)$$

- CP violation in the interference of mixing and decay in the tree-dominated $b \rightarrow c\bar{c}s$ transitions, such as $B^0 \rightarrow \psi K^0$, is given by:

$$S_{\psi K^0} = +0.709 \pm 0.011. \quad (13.102)$$

- CP violation in the interference of mixing and decay in modes governed by the tree-dominated $b \rightarrow c\bar{u}d$ transitions is given by

$$S_{D^{(*)}h^0} = +0.71 \pm 0.09, \quad (13.103)$$

- CP violation in the interference of mixing and decay in various modes related to $b \rightarrow c\bar{c}d$ transitions is given by

$$\begin{aligned} S_{\psi\pi^0} &= -0.86 \pm 0.14, \\ S_{D^+D^-} &= -0.84 \pm 0.12, \\ S_{D^{*+}D^{*-}} &= -0.81 \pm 0.06, \\ S_{D^{*+}D^{*-}} &= -0.71 \pm 0.09. \end{aligned} \quad (13.104)$$

- CP violation in the interference of mixing and decay in various modes related to $b \rightarrow q\bar{q}s$ (penguin) transitions is given by

$$\begin{aligned} S_{\phi K^0} &= +0.74_{-0.13}^{+0.11}, \\ S_{\eta' K^0} &= +0.63 \pm 0.06, \\ S_{f_0 K^0} &= +0.69_{-0.12}^{+0.10}, \\ S_{K^+K^-K_S} &= +0.68_{-0.10}^{+0.09}. \end{aligned} \quad (13.105)$$

- CP violation in the interference of mixing and decay in the $B^0 \rightarrow \pi^+\pi^-$ mode is given by

$$S_{\pi^+\pi^-} = -0.666 \pm 0.029. \quad (13.106)$$

- Direct CP violation in the $B^0 \rightarrow \pi^+\pi^-$ mode is given by

$$C_{\pi^+\pi^-} = -0.311 \pm 0.030. \quad (13.107)$$

- Direct CP violation in the $B_s^0 \rightarrow K^+K^-$ mode is given by

$$C_{K^+K^-} = 0.172 \pm 0.031. \quad (13.108)$$

- Direct CP violation in $B^+ \rightarrow D_+^{(*)}K^+$ decays ($D_+^{(*)}$ is the CP -even neutral $D^{(*)}$ state) are given by

$$\begin{aligned} \mathcal{A}_{B^+ \rightarrow D_+ K^+} &= +0.139 \pm 0.009 \quad \text{and} \\ \mathcal{A}_{B^+ \rightarrow D_+^* K^+} &= -0.109 \pm 0.019, \end{aligned} \quad (13.109)$$

while the corresponding quantity in the case that the neutral D meson is reconstructed in the suppressed $K^-\pi^+$ final state is

$$\mathcal{A}_{B^+ \rightarrow D_{K^-\pi^+} K^+} = -0.453 \pm 0.026, \quad (13.110)$$

- Direct CP violation has also been observed in $B^+ \rightarrow DK^+$ decays through differences between the phase-space distributions of subsequent $D \rightarrow K_S\pi^+\pi^-$ and $D \rightarrow K^-\pi^+\pi^+\pi^-$ decays.

- Direct CP violation in the $B^0 \rightarrow K^+\pi^-$ mode is given by

$$\mathcal{A}_{B^0 \rightarrow K^+\pi^-} = -0.0836 \pm 0.0032. \quad (13.111)$$

- Direct CP violation in the $B_s^0 \rightarrow K^-\pi^+$ mode is given by

$$\mathcal{A}_{B_s^0 \rightarrow K^-\pi^+} = +0.225 \pm 0.012. \quad (13.112)$$

- Direct CP violation in $B^+ \rightarrow K^+K^-\pi^+$, $B^+ \rightarrow K^+K^-K^+$ and $B^+ \rightarrow \pi^+\pi^-\pi^+$ decays is given by

$$\begin{aligned} \mathcal{A}_{B^+ \rightarrow K^+K^-\pi^+} &= -0.115 \pm 0.008, \\ \mathcal{A}_{B^+ \rightarrow K^+K^-K^+} &= -0.0365 \pm 0.0036, \\ \mathcal{A}_{B^+ \rightarrow \pi^+\pi^-\pi^+} &= 0.076 \pm 0.005, \end{aligned} \quad (13.113)$$

- Large CP violation effects have been observed model-independently in certain regions of the phase space of $B^+ \rightarrow K^+K^-K^+$, $K^+K^-\pi^+$, $\pi^+\pi^-K^+$ and $\pi^+\pi^-\pi^+$ decays. An amplitude analysis has established a large CP violation effect associated with $\pi\pi \leftrightarrow KK$ S-wave rescattering in $B^+ \rightarrow K^+K^-\pi^+$ decays. In $B^+ \rightarrow \pi^+\pi^-\pi^+$ decays, amplitude analysis has established CP violation effects in the decay amplitude involving the $f_2(1270)$ resonance, in the $\pi^+\pi^-$ S-wave at low invariant mass, and in the interference between the $\pi^+\pi^-$ S-wave and the P-wave $B^+ \rightarrow \rho(770)^0\pi^+$ amplitude.

- Direct CP violation has been established in the difference of asymmetries for $D^0 \rightarrow K^+K^-$ and $D^0 \rightarrow \pi^+\pi^-$ decays

$$\Delta a_{CP} = (-0.161 \pm 0.028) \times 10^{-2}. \quad (13.114)$$

References

- [1] J. H. Christenson *et al.*, Phys. Rev. Lett. **13**, 138 (1964).
- [2] B. Aubert *et al.* (BaBar), Phys. Rev. Lett. **87**, 091801 (2001), [hep-ex/0107013].
- [3] K. Abe *et al.* (Belle), Phys. Rev. Lett. **87**, 091802 (2001), [hep-ex/0107061].
- [4] H. Burkhardt *et al.* (NA31), Phys. Lett. **B206**, 169 (1988).
- [5] V. Fanti *et al.* (NA48), Phys. Lett. **B465**, 335 (1999), [hep-ex/9909022].
- [6] A. Alavi-Harati *et al.* (KTeV), Phys. Rev. Lett. **83**, 22 (1999), [hep-ex/9905060].
- [7] B. Aubert *et al.* (BaBar), Phys. Rev. Lett. **93**, 131801 (2004), [hep-ex/0407057].
- [8] Y. Chao *et al.* (Belle), Phys. Rev. Lett. **93**, 191802 (2004), [hep-ex/0408100].
- [9] A. Poluektov *et al.* (Belle), Phys. Rev. **D81**, 112002 (2010), [arXiv:1003.3360].

- [10] P. del Amo Sanchez *et al.* (BaBar), Phys. Rev. **D82**, 072004 (2010), [arXiv:1007.0504].
- [11] R. Aaij *et al.* (LHCb), Phys. Lett. **B712**, 203 (2012), [Erratum-ibid. **B713**, 351 (2012)], [arXiv:1203.3662].
- [12] R. Aaij *et al.* (LHCb), Phys. Rev. Lett. **110**, 221601 (2013), [arXiv:1304.6173].
- [13] R. Aaij *et al.* (LHCb), Phys. Rev. Lett. **122**, 211803 (2019), [arXiv:1903.08726].
- [14] See the review on “Neutrino Masses, Mixing, and Oscillations,” in this *Review*.
- [15] See the review on “Tests of Conservation Laws,” in this *Review*.
- [16] J. P. Lees *et al.* (BaBar), Phys. Rev. Lett. **109**, 211801 (2012), [arXiv:1207.5832].
- [17] J. Bernabeu, F. Martinez-Vidal and P. Villanueva-Perez, JHEP **08**, 064 (2012), [arXiv:1203.0171].
- [18] See, for example, R. F. Streater and A. S. Wightman, *CPT, Spin and Statistics, and All That*, reprinted by Addison-Wesley, New York (1989).
- [19] M. Kobayashi and T. Maskawa, Prog. Theor. Phys. **49**, 652 (1973).
- [20] J. Charles *et al.* (CKMfitter Group), Eur. Phys. J. **C41**, 1 (2005), updated results and plots available at: <http://ckmfitter.in2p3.fr>, [hep-ph/0406184].
- [21] M. Bona *et al.* (UTfit), JHEP **10**, 081 (2006), updated results and plots available at: <http://www.utfit.org/UTfit>, [hep-ph/0606167].
- [22] A. D. Sakharov, Pisma Zh. Eksp. Teor. Fiz. **5**, 32 (1967), [Usp. Fiz. Nauk161,no.5,61(1991)].
- [23] A. Riotto, in “Proceedings, Summer School in High-energy physics and cosmology: Trieste, Italy, June 29-July 17, 1998,” 326–436 (1998), [hep-ph/9807454].
- [24] M. Fukugita and T. Yanagida, Phys. Lett. **B174**, 45 (1986).
- [25] S. Davidson, E. Nardi and Y. Nir, Phys. Rept. **466**, 105 (2008), [arXiv:0802.2962].
- [26] G. Aad *et al.* (ATLAS), Phys. Lett. **B716**, 1 (2012), [arXiv:1207.7214].
- [27] S. Chatrchyan *et al.* (CMS), Phys. Lett. **B716**, 30 (2012), [arXiv:1207.7235].
- [28] S. Okubo, Phys. Lett. **5**, 165 (1963).
- [29] G. Zweig (1964), *An SU₃ model for strong interaction symmetry and its breaking; Version 2*, CERN-TH-412.
- [30] J. Iizuka, Prog. Theor. Phys. Suppl. **37**, 21 (1966).
- [31] V. Weisskopf and E. P. Wigner, Z. Phys. **63**, 54 (1930).
- [32] See the review on “ $D^0-\bar{D}^0$ Mixing” in this *Review*.
- [33] O. Long *et al.*, Phys. Rev. **D68**, 034010 (2003), [hep-ex/0303030].
- [34] M. Gronau, Y. Grossman and J. L. Rosner, Phys. Lett. **B508**, 37 (2001), [hep-ph/0103110].
- [35] D. Atwood and A. Soni, Phys. Rev. **D68**, 033003 (2003), [hep-ph/0304085].
- [36] A. Lenz and G. Tetlalmatzi-Xolocotzi, JHEP **07**, 177 (2020), [arXiv:1912.07621].
- [37] L. Wolfenstein, Phys. Rev. Lett. **13**, 562 (1964).
- [38] C. Abel *et al.* (nEDM), Phys. Rev. Lett. **124**, 081803 (2020), [arXiv:2001.11966].
- [39] R. J. Crewther *et al.*, Phys. Lett. **B88**, 123 (1979), [Erratum-ibid. **B91**, 487 (1980)].
- [40] See the review on “Cabibbo-Kobayashi-Maskawa Mixing Matrix,” in this *Review*.
- [41] L. Wolfenstein, Phys. Rev. Lett. **51**, 1945 (1983).
- [42] A. J. Buras, M. E. Lautenbacher and G. Ostermaier, Phys. Rev. **D50**, 3433 (1994), [hep-ph/9403384].
- [43] C. Jarlskog, Phys. Rev. Lett. **55**, 1039 (1985).
- [44] See the K -meson Listings in this *Review*.
- [45] See the review on “ CP violation in $K_S \rightarrow 3\pi$,” in this *Review*.
- [46] R. Abbott *et al.* (RBC, UKQCD), Phys. Rev. **D102**, 5, 054509 (2020), [arXiv:2004.09440].
- [47] V. Cirigliano *et al.*, JHEP **02**, 032 (2020), [arXiv:1911.01359].
- [48] A. J. Buras, Acta Phys. Polon. **B52**, 1, 7 (2021), [arXiv:2101.00020].
- [49] Y. Grossman and Y. Nir, Phys. Lett. **B398**, 163 (1997), [hep-ph/9701313].
- [50] L. S. Littenberg, Phys. Rev. **D39**, 3322 (1989).
- [51] A. J. Buras, Phys. Lett. **B333**, 476 (1994), [hep-ph/9405368].
- [52] G. Buchalla and A. J. Buras, Nucl. Phys. **B400**, 225 (1993).
- [53] A. J. Buras *et al.*, JHEP **11**, 033 (2015), [arXiv:1503.02693].
- [54] J. K. Ahn *et al.* (KOTO), Phys. Rev. Lett. **122**, 021802 (2019), [arXiv:1810.09655].
- [55] J. K. Ahn *et al.* (KOTO), Phys. Rev. Lett. **126**, 121801 (2021), [arXiv:2012.07571].
- [56] E. Cortina Gil *et al.* (NA62), JHEP **06**, 093 (2021), [arXiv:2103.15389].
- [57] B. Aubert *et al.* (BaBar), Phys. Rev. Lett. **98**, 211802 (2007), [hep-ex/0703020].
- [58] M. Staric *et al.* (Belle), Phys. Rev. Lett. **98**, 211803 (2007), [hep-ex/0703036].
- [59] T. Aaltonen *et al.* (CDF), Phys. Rev. Lett. **100**, 121802 (2008), [arXiv:0712.1567].
- [60] R. Aaij *et al.* (LHCb), Phys. Rev. Lett. **110**, 101802 (2013), [arXiv:1211.1230].
- [61] R. Aaij *et al.* (LHCb), Phys. Rev. Lett. **127**, 11, 111801 (2021), [arXiv:2106.03744].
- [62] Y. S. Amhis *et al.* (HFLAV), Eur. Phys. J. **C81**, 226 (2021), updated results and plots available at <https://hflav.web.cern.ch/>, [arXiv:1909.12524].
- [63] See the D -meson Listings in this *Review*.
- [64] Y. Grossman, A. L. Kagan and Y. Nir, Phys. Rev. **D75**, 036008 (2007), [hep-ph/0609178].
- [65] S. Bergmann *et al.*, Phys. Lett. **B486**, 418 (2000), [hep-ph/0005181].
- [66] M. Gersabeck *et al.*, J. Phys. **G39**, 045005 (2012), [arXiv:1111.6515].
- [67] T. Pajero and M. J. Morello, JHEP **03**, 162 (2022), [arXiv:2106.02014].
- [68] R. Aaij *et al.* (LHCb), Phys. Rev. **D105**, 9, 092013 (2022), [arXiv:2202.09106].
- [69] D. M. Asner *et al.* (CLEO), Phys. Rev. **D78**, 012001 (2008), [arXiv:0802.2268].
- [70] M. Ablikim *et al.* (BESIII), Phys. Lett. **B734**, 227 (2014), [arXiv:1404.4691].
- [71] R. Aaij *et al.* (LHCb), Phys. Rev. **D97**, 3, 031101 (2018), [arXiv:1712.03220].
- [72] R. Aaij *et al.* (LHCb), Phys. Rev. **D104**, 7, 072010 (2021), [arXiv:2105.09889].
- [73] M. Ciuchini *et al.*, Phys. Lett. **B655**, 162 (2007), [hep-ph/0703204].
- [74] Y. Grossman, Y. Nir and G. Perez, Phys. Rev. Lett. **103**, 071602 (2009), [arXiv:0904.0305].
- [75] A. L. Kagan and M. D. Sokoloff, Phys. Rev. **D80**, 076008 (2009), [arXiv:0907.3917].
- [76] Y. Grossman and Y. Nir, JHEP **04**, 002 (2012), [arXiv:1110.3790].

- [77] B. R. Ko *et al.* (Belle), Phys. Rev. Lett. **109**, 021601 (2012), [Erratum-ibid. **109**, 119903 (2012)], [arXiv:1203.6409].
- [78] See the “Review of Multibody Charm Analyses” in this *Review*.
- [79] B. Aubert *et al.* (BaBar), Phys. Rev. **D78**, 051102 (2008), [arXiv:0802.4035].
- [80] I. Bediaga *et al.*, Phys. Rev. **D80**, 096006 (2009), [arXiv:0905.4233].
- [81] I. Bediaga *et al.*, Phys. Rev. **D86**, 036005 (2012), [arXiv:1205.3036].
- [82] M. Williams, Phys. Rev. **D84**, 054015 (2011), [arXiv:1105.5338].
- [83] R. Aaij *et al.* (LHCb), Phys. Lett. **B769**, 345 (2017), [arXiv:1612.03207].
- [84] See the *B*-meson Listings in this *Review*.
- [85] V. M. Abazov *et al.* (D0), Phys. Rev. **D82**, 032001 (2010), [arXiv:1005.2757].
- [86] A. B. Carter and A. I. Sanda, Phys. Rev. Lett. **45**, 952 (1980).
- [87] A. B. Carter and A. I. Sanda, Phys. Rev. **D23**, 1567 (1981).
- [88] I. I. Y. Bigi and A. I. Sanda, Nucl. Phys. **B193**, 85 (1981).
- [89] I. Dunietz and J. L. Rosner, Phys. Rev. **D34**, 1404 (1986).
- [90] Y. I. Azimov, N. G. Uraltsev and V. A. Khoze, Sov. J. Nucl. Phys. **45**, 878 (1987), [Yad. Fiz. **45**, 1412 (1987)].
- [91] I. I. Y. Bigi and A. I. Sanda, Nucl. Phys. **B281**, 41 (1987).
- [92] G. Buchalla, A. J. Buras and M. E. Lautenbacher, Rev. Mod. Phys. **68**, 1125 (1996), [hep-ph/9512380].
- [93] A. J. Buras and L. Silvestrini, Nucl. Phys. **B569**, 3 (2000), [hep-ph/9812392].
- [94] R. Fleischer, Eur. Phys. J. **C10**, 299 (1999), [hep-ph/9903455].
- [95] M. Ciuchini, M. Pierini and L. Silvestrini, Phys. Rev. Lett. **95**, 221804 (2005), [hep-ph/0507290].
- [96] S. Faller *et al.*, Phys. Rev. **D79**, 014030 (2009), [arXiv:0809.0842].
- [97] M. Jung, Phys. Rev. **D86**, 053008 (2012), [arXiv:1206.2050].
- [98] H.-n. Li and S. Mishima, JHEP **03**, 009 (2007), [hep-ph/0610120].
- [99] K. De Bruyn and R. Fleischer, JHEP **03**, 145 (2015), [arXiv:1412.6834].
- [100] P. Frings, U. Nierste and M. Wiebusch, Phys. Rev. Lett. **115**, 061802 (2015), [arXiv:1503.00859].
- [101] L. Silvestrini, Ann. Rev. Nucl. Part. Sci. **57**, 405 (2007), [arXiv:0705.1624].
- [102] R. Fleischer *et al.*, Phys. Rev. **D78**, 111501 (2008), [arXiv:0806.2900].
- [103] R. Fleischer *et al.*, Eur. Phys. J. **C78**, 943 (2018), [arXiv:1806.08783].
- [104] M. Gronau and D. London, Phys. Rev. Lett. **65**, 3381 (1990).
- [105] A. F. Falk *et al.*, Phys. Rev. **D69**, 011502 (2004), [hep-ph/0310242].
- [106] J. Charles *et al.*, Eur. Phys. J. **C77**, 574 (2017), [arXiv:1705.02981].
- [107] See the review on “Determination of CKM Angles from *B* hadrons,” in this *Review*.
- [108] A. Abdesselam *et al.* (BaBar, Belle), Phys. Rev. Lett. **115**, 121604 (2015), [arXiv:1505.04147].
- [109] R. Fleischer and R. Knegjens, Eur. Phys. J. **C71**, 1789 (2011), [arXiv:1109.5115].
- [110] A. S. Dighe, I. Dunietz and R. Fleischer, Eur. Phys. J. **C6**, 647 (1999), [hep-ph/9804253].
- [111] R. Aaij *et al.* (LHCb), Phys. Rev. **D89**, 092006 (2014), [arXiv:1402.6248].
- [112] R. Aaij *et al.* (LHCb), JHEP **03**, 075 (2021), [arXiv:2012.05319].
- [113] M. Gronau and D. London, Phys. Lett. **B253**, 483 (1991).
- [114] M. Gronau and D. Wyler, Phys. Lett. **B265**, 172 (1991).
- [115] D. Atwood, I. Dunietz and A. Soni, Phys. Rev. Lett. **78**, 3257 (1997), [hep-ph/9612433].
- [116] D. Atwood, I. Dunietz and A. Soni, Phys. Rev. **D63**, 036005 (2001), [hep-ph/0008090].
- [117] A. Giri *et al.*, Phys. Rev. **D68**, 054018 (2003), [hep-ph/0303187].
- [118] A. Bondar, *Proceedings of BINP special analysis meeting on Dalitz analysis*, 24-26 Sep. 2002, unpublished.
- [119] J. Brod and J. Zupan, JHEP **01**, 051 (2014), [arXiv:1308.5663].
- [120] J. P. Lees *et al.* (BaBar), Phys. Rev. **D87**, 052015 (2013), [arXiv:1301.1029].
- [121] R. Aaij *et al.* (LHCb), JHEP **12**, 087 (2016), [arXiv:1611.03076].
- [122] R. Aleksan, I. Dunietz and B. Kayser, Z. Phys. **C54**, 653 (1992).
- [123] R. Fleischer, Nucl. Phys. **B671**, 459 (2003), [hep-ph/0304027].
- [124] I. Dunietz, Phys. Lett. **B270**, 75 (1991).
- [125] M. Gronau, Phys. Lett. **B557**, 198 (2003), [hep-ph/0211282].
- [126] T. Gershon, Phys. Rev. **D79**, 051301 (2009), [arXiv:0810.2706].
- [127] T. Gershon and M. Williams, Phys. Rev. **D80**, 092002 (2009), [arXiv:0909.1495].
- [128] T. Gershon and A. Poluektov, Phys. Rev. **D81**, 014025 (2010), [arXiv:0910.5437].
- [129] M. Bander, D. Silverman and A. Soni, Phys. Rev. Lett. **43**, 242 (1979).
- [130] X.-G. He, Eur. Phys. J. **C9**, 443 (1999), [hep-ph/9810397].
- [131] D. Atwood and A. Soni, Phys. Rev. **D58**, 036005 (1998), [hep-ph/9712287].
- [132] M. Gronau and J. L. Rosner, Phys. Rev. **D59**, 113002 (1999), [hep-ph/9809384].
- [133] H. J. Lipkin, Phys. Lett. **B445**, 403 (1999), [hep-ph/9810351].
- [134] M. Gronau, Phys. Lett. **B627**, 82 (2005), [hep-ph/0508047].
- [135] R. Aaij *et al.* (LHCb), Phys. Rev. **D90**, 112004 (2014), [arXiv:1408.5373].
- [136] R. Aaij *et al.* (LHCb), Phys. Rev. Lett. **123**, 231802 (2019), [arXiv:1905.09244].
- [137] R. Aaij *et al.* (LHCb), Phys. Rev. Lett. **124**, 031801 (2020), [arXiv:1909.05211].
- [138] R. Aaij *et al.* (LHCb), Phys. Rev. **D101**, 012006 (2020), [arXiv:1909.05212].
- [139] A. A. Alves, Jr. *et al.* (LHCb), JINST **3**, S08005 (2008).
- [140] I. Bediaga *et al.* (LHCb) (2012), CERN-LHCC-2012-007.
- [141] R. Aaij *et al.* (LHCb) (2017), CERN-LHCC-2017-003.
- [142] W. Altmannshofer *et al.* (Belle-II), PTEP **2019**, 123C01 (2019), [Erratum-ibid. **2020**, 029201 (2020)], [arXiv:1808.10567].
- [143] G. C. Branco, L. Lavoura and J. P. Silva, Int. Ser. Monogr. Phys. **103**, 1 (1999).
- [144] I. I. Bigi and A. I. Sanda (2000), [Camb. Monogr. Part. Phys. Nucl. Phys. Cosmol.9,1(2009)].
- [145] A. J. Bevan *et al.* (BaBar, Belle), Eur. Phys. J. **C74**, 3026 (2014), [arXiv:1406.6311].

- [146] H.R. Quinn and Y. Nir, *“The Mystery of the Missing Antimatter,”* Princeton University Press, Princeton (2008).
- [147] T. E. Browder *et al.*, Rev. Mod. Phys. **81**, 1887 (2009), [arXiv:0802.3201].
- [148] M. Ciuchini and A. Stocchi, Ann. Rev. Nucl. Part. Sci. **61**, 491 (2011), [arXiv:1110.3920].
- [149] R. Aaij *et al.* (LHCb), Eur. Phys. J. **C73**, 2373 (2013), [arXiv:1208.3355].
- [150] T. Gershon and V. V. Gligorov, Rept. Prog. Phys. **80**, 046201 (2017), [arXiv:1607.06746].

14. Neutrino Masses, Mixing, and Oscillations

Revised September 2023 by M.C. Gonzalez-Garcia (YITP, Stony Brook; ICREA, Barcelona; ICC, U. of Barcelona) and M. Yokoyama (UTokyo; Kavli IPMU (WPI), UTokyo).

14.1	Neutrinos in the Standard Model: Massless Neutrinos	295
14.2	Extending the Standard Model to Introduce Massive Neutrinos	296
14.2.1	Dirac Neutrinos	296
14.2.2	The See-saw Mechanism	296
14.2.3	Light Sterile Neutrinos	297
14.2.4	Neutrino Masses from Generic New Physics	297
14.3	Lepton Mixing	297
14.4	Mass-Induced Flavour Oscillations in Vacuum	298
14.5	Propagation of Massive Neutrinos in Matter	299
14.5.1	The Mikheyev-Smirnov-Wolfenstein Effect for Solar Neutrinos	301
14.6	Experimental Study of Neutrino Oscillations	301
14.6.1	Solar Neutrinos	302
14.6.2	Atmospheric Neutrinos	303
14.6.3	Accelerator Neutrinos	304
14.6.4	Reactor Antineutrinos	308
14.7	Combined Analysis of Experimental Results: The 3ν Paradigm	310
14.7.1	3ν Oscillation Probabilities	311
14.7.2	3ν Oscillation Analysis	312
14.7.3	Convention-independent Measures of Leptonic CP Violation in 3ν Mixing	312
14.8	Beyond 3ν : Additional Neutrinos at the eV Scale	313
14.9	Laboratory Probes of ν Mass Scale and its Nature	315
14.9.1	Constraints from Kinematics of Weak Decays	315
14.9.2	Dirac vs. Majorana: Neutrinoless Double-beta Decay	316
14.9.3	Experimental Search for Neutrinoless Double-beta Decay	317

14.1 Neutrinos in the Standard Model: Massless Neutrinos

The gauge symmetry principle is one of the pillars of the great success of modern particle physics as it establishes an unambiguous connection between local (gauge) symmetries and forces mediated by spin-1 particles. In the Standard Model (SM) of particle physics the strong, weak, and electromagnetic interactions are connected to gauge symmetry under $SU(3)_C \times SU(2)_L \times U(1)_Y$ where C stands for colour, L for left-handedness, and Y for hypercharge. The SM gauge symmetry is spontaneously broken to $SU(3)_C \times U(1)_{EM}$ where $U(1)_{EM}$ couples to the electromagnetic charge $Q_{EM} = T_{L3} + Y$ (T_{L3} is the weak isospin which is the third generator of $SU(2)_L$). The model explains all the interactions of the known fermions once they are assigned to a well defined representation of the gauge group. The construction and tests of the Standard Model as a gauge theory are covered in Chapter 9 “Quantum chromodynamics” and Chapter 10 “Electroweak model and constraints on new physics” of this *Review*. Here we emphasize that the gauge invariance principle requires that all terms in the Lagrangian, including the mass terms, respect the local symmetry. This has important implications for the neutrino and in particular for the question of the neutrino mass ¹.

In the SM, neutrinos are fermions that do not have strong nor electromagnetic interactions. Consequently, they are singlets of the subgroup $SU(3)_C \times U(1)_{EM}$. They are part of the lepton doublets $L_{L\ell} = \begin{pmatrix} \nu_\ell \\ \ell \end{pmatrix}_L$ where f_L is the left-handed component of the fermion f , $f_L = P_L f \equiv \frac{1-\gamma_5}{2} f$. In what follows we will refer as *active* neutrinos to neutrinos that are part of these lepton doublets. In the SM there is one active neutrino for each charged

leptons, $\ell = e, \mu, \tau$. $SU(2)_L$ gauge invariance dictates the form of weak charged current (CC) interactions between the neutrinos and their corresponding charged leptons and neutral current (NC) among themselves to be:

$$-\mathcal{L}_{CC} = \frac{g}{\sqrt{2}} \sum_{\ell} \bar{\nu}_{L\ell} \gamma^{\mu} \ell_L^{-} W_{\mu}^{+} + \text{h.c.}, \quad (14.1)$$

$$-\mathcal{L}_{NC} = \frac{g}{2 \cos \theta_W} \sum_{\ell} \bar{\nu}_{L\ell} \gamma^{\mu} \nu_{L\ell} Z_{\mu}^0. \quad (14.2)$$

In the above equations, g is the coupling constant associated with $SU(2)$ and θ_W is the Weinberg angle. Equations (14.1) and (14.2) describe all the neutrino interactions in the SM. In particular, Eq. (14.2) determines the decay width of the Z boson into light ($m_{\nu} \leq m_Z/2$) left-handed neutrinos states. Thus from the measurement of the total decay width of the Z one can infer the number of such states. At present the measurement implies $N_{\nu} = 2.984 \pm 0.008$ (see Particle Listing). As a result any extension of the SM should contain three, and only three, light active neutrinos.

Sterile neutrinos are defined as having no SM gauge interactions, that is, they are singlets of the complete SM gauge group. Thus the SM, as the gauge theory able to describe all known particle interactions, contains no sterile neutrinos.

The SM with its gauge symmetry and the particle content required for the gauge interactions, that is, in the absence of SM singlets, respects an accidental global symmetry that is not imposed but appears as a consequence of the gauge symmetry and the representation of the matter fields:

$$G_{SM}^{\text{global}} = U(1)_B \times U(1)_{L_e} \times U(1)_{L_{\mu}} \times U(1)_{L_{\tau}}, \quad (14.3)$$

where $U(1)_B$ is the baryon number symmetry, and $U(1)_{L_e, L_{\mu}, L_{\tau}}$ are the three lepton flavour symmetries. The total lepton number, $L_e + L_{\mu} + L_{\tau}$, is then also an accidental symmetry since it is a subgroup of G_{SM}^{global} . This fact has consequences that are relevant to the question of the neutrino mass as we argue next.

In the SM, the masses of the fermions are generated via a Yukawa coupling of the scalar Higgs doublet ϕ with a fermion right-handed and left-handed component. The former is an $SU(2)_L$ singlet, the latter is part of a doublet. For leptons, we can build such a term coupling the left-handed lepton doublets L_L with the right-handed charged lepton fields E_R :

$$-\mathcal{L}_{\text{Yukawa,lep}} = Y_{ij}^{\ell} \bar{L}_{Li} \phi E_{Rj} + \text{h.c.} \quad (14.4)$$

After spontaneous symmetry breaking these terms lead to charged lepton masses

$$m_{ij}^{\ell} = Y_{ij}^{\ell} \frac{v}{\sqrt{2}}, \quad (14.5)$$

where v is the vacuum expectation value of the Higgs field. However, since the model does not contain right-handed neutrinos, no such Yukawa interaction can be built for the neutrinos, which are consequently massless at the Lagrangian level.

In principle, a neutrino mass term could be generated at loop level. With the particle content of the SM the only possible neutrino mass term that could be constructed is the bilinear $\bar{L}_L L_L^c$, where L_L^c is the charge conjugated field, $L_L^c = C \bar{L}_L^T$ and C is the charge conjugation matrix. However this term is forbidden in the SM because it violates the total lepton symmetry by two units and therefore it cannot be induced by loop corrections because it breaks the accidental symmetry of the model. Also, because $U(1)_{B-L}$ is a non-anomalous subgroup of G_{SM}^{global} , the bilinear $\bar{L}_L L_L^c$, cannot be induced by nonperturbative corrections either since it breaks $B-L$.

We conclude that within the SM neutrinos are precisely massless. Consequently one must go beyond the SM in order to add a mass to the neutrino.

¹The physics of massive neutrinos has been the subject of excellent books such as [1–5] and multiple review articles. The contents of the present review is built upon the structure and the contents of the review articles [6, 7].

14.2 Extending the Standard Model to Introduce Massive Neutrinos

From the above discussion, we conclude that it is not possible to construct a renormalizable mass term for the neutrinos with the fermionic content and gauge symmetry of the SM. The obvious consequence is that in order to introduce a neutrino mass in the theory one must extend the particle content of the model, depart from gauge invariance and/or renormalizability, or do both.

As a matter of fact, neutrino mass terms can be constructed in different ways. In the following we shall assume to maintain the gauge symmetry and explore the different possibilities to introduce a neutrino mass term adding to the SM an arbitrary number of sterile neutrinos ν_{si} ($i = 1, \dots, m$).

In the SM extended with the addition of m number of sterile neutrinos one can construct two gauge invariant renormalizable operators leading to two types of mass terms

$$-\mathcal{L}_{M_\nu} = M_{Dij} \bar{\nu}_{si} \nu_{Lj} + \frac{1}{2} M_{Nij} \bar{\nu}_{si} \nu_{sj}^c + \text{h.c.}, \quad (14.6)$$

where ν^c is the neutrino charge conjugated field (defined in section 14.1). M_D is a complex matrix of dimension $m \times 3$ and M_N is a symmetric $m \times m$ matrix.

The first term is generated after spontaneous electroweak symmetry breaking from Yukawa interactions,

$$Y_{ij}^\nu \bar{\nu}_{si} \tilde{\phi}^\dagger L_{Lj} \Rightarrow M_{Dij} = Y_{ij}^\nu \frac{v}{\sqrt{2}}, \quad (14.7)$$

in a similar way to Eqs.(14.4) and (14.5) for the charged fermion masses. It is correspondingly called a Dirac mass term. It conserves total lepton number but it can break the lepton flavour number symmetries.

The second term in Eq.(14.6) is a Majorana mass term and it differs from the Dirac mass terms in several relevant aspects. First, it is a singlet of the SM gauge group and, as such, it can appear as a bare mass term in the Lagrangian. Second, since it involves two neutrino fields (right-handed in this case), it breaks lepton number by two units. In general, such a term is not allowed if the neutrinos carry any additive conserved charge.

It is possible to rewrite Eq.(14.6) as:

$$-\mathcal{L}_{M_\nu} = \frac{1}{2} (\bar{\nu}_L^c, \bar{\nu}_s) \begin{pmatrix} 0 & M_D^T \\ M_D & M_N \end{pmatrix} \begin{pmatrix} \bar{\nu}_L \\ \bar{\nu}_s^c \end{pmatrix} + \text{h.c.} \equiv \bar{\nu}^c M_\nu \bar{\nu} + \text{h.c.}, \quad (14.8)$$

where $\bar{\nu} = (\bar{\nu}_L, \bar{\nu}_s^c)^T$ is a $(3+m)$ -dimensional vector. The matrix M_ν is complex and symmetric². Thus it can be diagonalized by a unitary matrix V^ν of dimension $(3+m)$, so

$$(V^\nu)^T M_\nu V^\nu = \text{diag}(m_1, m_2, \dots, m_{3+m}). \quad (14.9)$$

One can express the original weak eigenstates in terms of the resulting $3+m$ mass eigenstates

$$\bar{\nu}_{\text{mass}} = (V^\nu)^\dagger \bar{\nu}, \quad (14.10)$$

and in terms of the mass eigenstates, Eq.(14.8) takes the form:

$$\begin{aligned} -\mathcal{L}_{M_\nu} &= \frac{1}{2} \sum_{k=1}^{3+m} m_k \left(\bar{\nu}_{\text{mass},k}^c \nu_{\text{mass},k} + \bar{\nu}_{\text{mass},k} \nu_{\text{mass},k}^c \right) \\ &= \frac{1}{2} \sum_{k=1}^{3+m} m_k \bar{\nu}_{Mk} \nu_{Mk}, \end{aligned} \quad (14.11)$$

where

$$\nu_{Mk} = \nu_{\text{mass},k} + \nu_{\text{mass},k}^c = (V^\nu)^\dagger \bar{\nu}_k + (V^\nu)^\dagger \bar{\nu}_k^c. \quad (14.12)$$

²Notice that Eq.(14.8) corresponds to the tree-level neutrino mass matrix. Corrections are induced at the loop level, which in particular lead to non-vanishing $\bar{\nu}_L^c \nu_L$ entry [8].

So these states obey the Majorana condition

$$\nu_M = \nu_M^c, \quad (14.13)$$

and are referred to as Majorana neutrinos. The Majorana condition implies that only one field describes both neutrino and antineutrino states, unlike the case of a charged fermion for which particles and antiparticles are described by two different fields. So a Majorana neutrino can be described by a two-component spinor unlike the charged fermions, which are Dirac particles, and are represented by four-component spinors.

Inverting Eq.(14.12) we can write the weak-doublet components of the neutrino fields as:

$$\nu_{Li} = P_L \sum_{j=1}^{3+m} V_{ij}^\nu \nu_{Mj} \quad i = 1, 2, 3, \quad (14.14)$$

where P_L is the left projector.

In the following, we will discuss some interesting particular cases of this general framework: light Dirac neutrinos in Sec.14.2.1, and light Majorana neutrinos and the see-saw mechanism in Sec.14.2.2. A special case of the second example is the possibility of light-sterile neutrinos discussed in Sec.14.2.3. In Sec.14.2.4 we shall discuss the effective generation of neutrino masses from non-renormalizable operators (of which the see-saw mechanism is a particular realization).

14.2.1 Dirac Neutrinos

Imposing $M_N = 0$ is equivalent to imposing lepton number symmetry on the model. In doing this only the first term in Eq.(14.6), the Dirac mass term, is allowed. If there are only three sterile ($m = 3$), we can identify them with the right-handed component of a four-spinor neutrino field. In this case the Dirac mass term can be diagonalized with two 3×3 unitary matrices, V^ν and V_R^ν as:

$$V_R^{\nu\dagger} M_D V^\nu = \text{diag}(m_1, m_2, m_3). \quad (14.15)$$

The neutrino mass term can be written as:

$$-\mathcal{L}_{M_\nu} = \sum_{k=1}^3 m_k \bar{\nu}_{Dk} \nu_{Dk}, \quad (14.16)$$

where

$$\nu_{Dk} = (V^\nu)^\dagger \bar{\nu}_L)_k + (V_R^{\nu\dagger} \bar{\nu}_s)_k, \quad (14.17)$$

so the weak-doublet components of the neutrino fields are

$$\nu_{Li} = P_L \sum_{j=1}^3 V_{ij}^\nu \nu_{Dj}. \quad i = 1, 2, 3. \quad (14.18)$$

Let us stress that in this case both the low-energy matter content and the assumed symmetries are different from those of the SM. Consequently, the SM is not even a good low-energy effective theory. Furthermore, this scenario does not explain the fact that neutrinos are much lighter than the corresponding charged fermions, because all of them acquire their mass via the same mechanism.

14.2.2 The See-saw Mechanism

If the mass eigenvalues of M_N are much higher than the scale of electroweak symmetry breaking v , the diagonalization of M_ν leads to three light neutrinos, ν_l , and m heavy neutrinos, N :

$$-\mathcal{L}_{M_\nu} = \frac{1}{2} \bar{\nu}_l M^l \nu_l + \frac{1}{2} \bar{N} M^h N, \quad (14.19)$$

with

$$M^l \simeq -V_l^T M_D^T M_N^{-1} M_D V_l, \quad M^h \simeq V_h^T M_N V_h, \quad (14.20)$$

and

$$V^\nu \simeq \begin{bmatrix} \left(1 - \frac{1}{2} M_D^\dagger M_N^* - 1 M_N^{-1} M_D\right) V_l & M_D^\dagger M_N^* V_h \\ -M_N^{-1} M_D V_l & \left(1 - \frac{1}{2} M_N^{-1} M_D M_D^\dagger M_N^* - 1\right) V_h \end{bmatrix}, \quad (14.21)$$

where V_l and V_h are 3×3 and $m \times m$ unitary matrices respectively. From Eq.(14.20) we see that the masses of the heavier states are proportional to M_N while those of the lighter ones to M_N^{-1} , hence the name *see-saw mechanism* [9–13]. Also, as seen from Eq.(14.21), the heavy states are mostly right-handed while the light ones are mostly left-handed. Both the light and the heavy neutrinos are Majorana particles. Two well-known examples of extensions of the SM leading to a see-saw mechanism for neutrino masses are SO(10) Grand Unified Theories [10, 11] and left-right symmetric models [13].

In this case, the SM is a good effective low energy theory. Indeed the see-saw mechanism is a particular example of a full theory whose low energy effective realization is the SM with three light Majorana neutrinos which we describe in Sec.14.2.4.

14.2.3 Light Sterile Neutrinos

If the scale of some $n_s \leq m$ eigenvalues of M_N are not higher than the electroweak scale, the low energy spectrum contains n_s additional light states with a large admixture of sterile component. As in the case with Dirac Neutrinos, the SM is not a good low energy effective theory: there are more than three ($3+n_s$) light neutrinos, and they are admixtures of doublet and singlet fields. As in the general case, both light and heavy neutrinos are Majorana particles.

14.2.4 Neutrino Masses from Generic New Physics

Under the generic hypothesis that new physics (NP) beyond the SM only manifests itself directly above some scale Λ_{NP} , we can consider that the SM is an effective low energy theory which is valid to describe the physical world at energies well below Λ_{NP} with the same gauge group, fermionic spectrum, and the pattern of spontaneous symmetry breaking of the SM. However, this is an effective theory, holding only till energy below Λ_{NP} , and consequently does not need to be renormalizable. In this case, the low energy Lagrangian can contain non-renormalizable higher dimensional terms whose effect will be suppressed by powers $1/\Lambda_{\text{NP}}^{\text{dim}-4}$.

In this approach, the least suppressed NP effects at low energy are expected to come from $\text{dim}=5$ operators. With the SM fields and gauge symmetry one can only construct the following set of dimension-five terms

$$\mathcal{O}_5 = \frac{Z_{ij}^\nu}{\Lambda_{\text{NP}}} (\bar{L}_{Li} \tilde{\phi}) (\tilde{\phi}^T L_{Lj}^C) + \text{h.c.} \quad (14.22)$$

This set violates (14.3), which poses no problem since, in general, there is no reason for the NP to respect the accidental symmetries of the SM. In particular, it violates the total lepton number by two units, and after spontaneous symmetry breaking it generates a bilinear neutrino field term:

$$-\mathcal{L}_{M_\nu} = \frac{Z_{ij}^\nu}{2} \frac{v^2}{\Lambda_{\text{NP}}} \bar{\nu}_{Li} \nu_{Lj}^c + \text{h.c.} \quad (14.23)$$

This is a Majorana mass term (see Eq.(14.8)). It is built with the left-handed neutrino fields and with mass matrix:

$$(M_\nu)_{ij} = Z_{ij}^\nu \frac{v^2}{\Lambda_{\text{NP}}}. \quad (14.24)$$

We conclude that Eq.(14.24) would arise in a generic extension of the SM and that neutrino masses are very likely to appear if there is NP. Comparing Eq.(14.24) and Eq.(14.5), we also find that the scale of neutrino masses is suppressed by v/Λ_{NP} when compared to the scale of charged fermion masses, which provides an explanation for their smallness. Furthermore, both total lepton number and the lepton flavour symmetry $U(1)_e \times U(1)_\mu \times U(1)_\tau$ are broken by Eq.(14.24), which means that, generically, in the absence of additional symmetries on the coefficients Z_{ij} , we can expect lepton flavour mixing and CP violation as we discuss in the next section.

Finally, we notice that, as mentioned in Sec.14.2.2, a theory where the NP is composed of m heavy sterile neutrinos, provides an specific example of a theory which at low energy contains three light mass eigenstates with an effective dim-5 interaction of the form (14.22) with $\Lambda_{\text{NP}} = M_N$. In this case, the NP scale is the characteristic mass scale of the heavy sterile neutrinos.

14.3 Lepton Mixing

Let us start by considering $n = 3 + m$ massive neutrino states and denote the neutrino mass eigenstates by $(\nu_1, \nu_2, \nu_3, \dots, \nu_n)$. The neutrino interaction eigenstates are denoted by $\vec{\nu} = (\nu_{Le}, \nu_{L\mu}, \nu_{L\tau}, \nu_{s1}, \dots, \nu_{sm})$. We label the corresponding mass and interaction eigenstates for the charged leptons as (e, μ, τ) and (e^I, μ^I, τ^I) , respectively. The Lagrangian for the leptonic charged current interactions in the mass basis takes the form:

$$-\mathcal{L}_{\text{CC}} = \frac{g}{\sqrt{2}} (\bar{e}_L, \bar{\mu}_L, \bar{\tau}_L) \gamma^\mu U \begin{pmatrix} \nu_1 \\ \nu_2 \\ \nu_3 \\ \vdots \\ \nu_n \end{pmatrix} W_\mu^+ + \text{h.c.}, \quad (14.25)$$

where U is a $3 \times n$ matrix [14–16]. It satisfies the unitary condition

$$UU^\dagger = I_{3 \times 3}. \quad (14.26)$$

However, in general $U^\dagger U \neq I_{n \times n}$.

In the interaction basis, the mass terms for the leptons are:

$$-\mathcal{L}_M = [(\bar{e}_L^I, \bar{\mu}_L^I, \bar{\tau}_L^I) M_\ell \begin{pmatrix} e_R^I \\ \mu_R^I \\ \tau_R^I \end{pmatrix} + \text{h.c.}] - \mathcal{L}_{M_\nu}, \quad (14.27)$$

with \mathcal{L}_{M_ν} given in Eq.(14.8). M_ℓ can be diagonalized with two 3×3 unitary matrices V^ℓ and V_R^ℓ which satisfy

$$V^{\ell\dagger} M_\ell V_R^\ell = \text{diag}(m_e, m_\mu, m_\tau). \quad (14.28)$$

Then for the charged leptons we have

$$-\mathcal{L}_{M_\ell} = \sum_{k=1}^3 m_{\ell_k} \bar{\ell}_k \ell_k, \quad (14.29)$$

with

$$\ell_k = (V^{\ell\dagger} \ell_L^I)_k + (V_R^\ell \ell_R^I)_k. \quad (14.30)$$

Inverting the equation above we find that the weak-doublet components of the charged lepton fields are

$$\ell_{Li}^I = P_L \sum_{j=1}^3 V_{ij}^\ell \ell_j. \quad i = 1, 2, 3 \quad (14.31)$$

From Eqs.(14.14), (14.18) and (14.31) we find that the mixing matrix U can be expressed as:

$$U_{ij} = \mathcal{P}_{\ell,ii} V_{ik}^{\ell\dagger} V_{kj}^\nu (\mathcal{P}_{\nu,jj}). \quad (14.32)$$

The matrix $V^{\ell\dagger} V^\nu$ contains a number of phases that are not physical. Three of them are eliminated by the diagonal 3×3 phase matrix \mathcal{P}_ℓ that absorbs them in the charged lepton mass eigenstates. If neutrinos are Dirac states, further $n - 1$ are similarly eliminated by absorbing them in the neutrino mass eigenstates with the diagonal $n \times n$ phase matrix \mathcal{P}_ν . For Majorana neutrinos, $\mathcal{P}_\nu = I_{n \times n}$ because one cannot rotate by an arbitrary phase a Majorana field without physical effects. If one rotates a Majorana neutrino by a phase, this phase will appear in its mass term, which will no longer be real. Consequently, the number of phases that can be absorbed by redefining the mass eigenstates

depends on whether the neutrinos are Dirac or Majorana particles. Altogether for $n \geq 3$ Majorana [Dirac] neutrinos, the U matrix contains a total of $6(n-2)$ [$5n-11$] real parameters, of which $3(n-2)$ are angles, and $3(n-2)$ [$2n-5$] can be interpreted as physical phases.

The possibility of arbitrary mixing between massive neutrino states was first discussed in the context of two neutrinos in Ref. [17] (the possibility of two mixed massless flavour neutrino states had been previously considered in the literature [18], and the possibility of mixing between neutrino and antineutrino states even

earlier, in the seminal paper of Pontecorvo [19]). For the case where only mixing between two generations is considered with $n=2$ distinct neutrino masses, the U matrix is 2×2 and contains one mixing angle if the neutrinos are Dirac and an additional physical phase if they are Majorana.

If there are only $n=3$ Majorana neutrinos, U is a 3×3 matrix analogous to the CKM matrix for the quarks [20, 21], but due to the Majorana nature of the neutrinos it depends on six independent parameters: three mixing angles and three phases. In this case the mixing matrix can be conveniently parameterized as:

$$U = \begin{pmatrix} 1 & 0 & 0 \\ 0 & c_{23} & s_{23} \\ 0 & -s_{23} & c_{23} \end{pmatrix} \cdot \begin{pmatrix} c_{13} & 0 & s_{13}e^{-i\delta_{\text{CP}}} \\ 0 & 1 & 0 \\ -s_{13}e^{i\delta_{\text{CP}}} & 0 & c_{13} \end{pmatrix} \cdot \begin{pmatrix} c_{12} & s_{12} & 0 \\ -s_{12} & c_{12} & 0 \\ 0 & 0 & 1 \end{pmatrix} \cdot \begin{pmatrix} e^{i\eta_1} & 0 & 0 \\ 0 & e^{i\eta_2} & 0 \\ 0 & 0 & 1 \end{pmatrix}, \quad (14.33)$$

where $c_{ij} \equiv \cos \theta_{ij}$ and $s_{ij} \equiv \sin \theta_{ij}$. The angles θ_{ij} can be taken without loss of generality to lie in the first quadrant, $\theta_{ij} \in [0, \pi/2]$ and the phases $\delta_{\text{CP}}, \eta_i \in [0, 2\pi]$. This is to be compared to the case of three Dirac neutrinos. In this case, the Majorana phases,

η_1 and η_2 , can be absorbed in the neutrino states so the number of physical phases is one (similar to the CKM matrix). Thus we can write U as:

$$U = \begin{pmatrix} c_{12}c_{13} & s_{12}c_{13} & s_{13}e^{-i\delta_{\text{CP}}} \\ -s_{12}c_{23} - c_{12}s_{13}s_{23}e^{i\delta_{\text{CP}}} & c_{12}c_{23} - s_{12}s_{13}s_{23}e^{i\delta_{\text{CP}}} & c_{13}s_{23} \\ s_{12}s_{23} - c_{12}s_{13}c_{23}e^{i\delta_{\text{CP}}} & -c_{12}s_{23} - s_{12}s_{13}c_{23}e^{i\delta_{\text{CP}}} & c_{13}c_{23} \end{pmatrix}. \quad (14.34)$$

This matrix is often called the Pontecorvo-Maki-Nakagawa-Sakata (PMNS) mixing matrix.

Notice that when the charged leptons have no other interactions than the SM ones, one can identify their interaction eigenstates with the corresponding mass eigenstates up to phase redefinition. This implies that, in this case, U is just a $3 \times n$ sub-matrix of the unitary neutrino mass diagonalizing matrix V^ν .

Finally, let us point out that for the case of 3 light Dirac neutrinos, the procedure above leads to a unitary U matrix for the light states. But for three light Majorana neutrinos, this is not the case since the full spectrum contains states which are heavy and are not in the low energy spectrum as seen, for example, in Eq.(14.21). This implies that, strictly speaking, the parametrization in Eq.(14.33) is not valid to describe the flavour mixing of the three light Majorana neutrinos in the see-saw mechanism. The violation of unitarity, however, is rather small, of the order $\mathcal{O}(M_D/M_N)$ as seen in Eq.(14.21). It is also severely constrained experimentally [22, 23]. For all these reasons, for all practical purposes, we will consider the U matrix for the 3ν mixing case to be unitary independently of whether neutrinos are Dirac or Majorana particles.

14.4 Mass-Induced Flavour Oscillations in Vacuum

If neutrinos have masses and lepton flavours are mixed in the weak CC interactions, lepton flavour is not conserved in neutrino propagation [19, 24]. This phenomenon is usually referred to as *neutrino oscillations*. In brief, a weak eigenstates, ν_α , which by default is the state produced in the weak CC interaction of a charged lepton ℓ_α , is the linear combination determined by the mixing matrix U

$$|\nu_\alpha\rangle = \sum_{i=1}^n U_{\alpha i}^* |\nu_i\rangle, \quad (14.35)$$

where ν_i are the mass eigenstates, and here n is the number of light neutrino species (implicit in our definition of the state $|\nu\rangle$ is its energy-momentum and space-time dependence). After traveling a distance L ($L \simeq ct$ for relativistic neutrinos), that state evolves as:

$$|\nu_\alpha(t)\rangle = \sum_{i=1}^n U_{\alpha i}^* |\nu_i(t)\rangle. \quad (14.36)$$

This neutrino can then undergo a charged-current (CC) interaction producing a charge lepton ℓ_β , $\nu_\alpha(t)N' \rightarrow \ell_\beta N$, with a

probability

$$P_{\alpha\beta} = |\langle \nu_\beta | \nu_\alpha(t) \rangle|^2 = \left| \sum_{i=1}^n \sum_{j=1}^n U_{\alpha i}^* U_{\beta j} \langle \nu_j | \nu_i(t) \rangle \right|^2. \quad (14.37)$$

Assuming that $|\nu\rangle$ is a plane wave, $|\nu_i(t)\rangle = e^{-iE_i t} |\nu_i(0)\rangle$,³ with $E_i = \sqrt{p_i^2 + m_i^2}$ and m_i being, respectively, the energy and the mass of the neutrino mass eigenstate ν_i . In all practical cases neutrinos are very relativistic, so $p_i \simeq p_j \equiv p \simeq E$. We can then write

$$E_i = \sqrt{p_i^2 + m_i^2} \simeq p + \frac{m_i^2}{2E}, \quad (14.38)$$

and use the orthogonality of the mass eigenstates, $\langle \nu_j | \nu_i \rangle = \delta_{ij}$, to arrive to the following form for $P_{\alpha\beta}$:

$$P_{\alpha\beta} = \delta_{\alpha\beta} - 4 \sum_{i<j} \text{Re}[U_{\alpha i} U_{\beta i}^* U_{\alpha j}^* U_{\beta j}] \sin^2 X_{ij} + 2 \sum_{i<j} \text{Im}[U_{\alpha i} U_{\beta i}^* U_{\alpha j}^* U_{\beta j}] \sin 2X_{ij}, \quad (14.39)$$

where

$$X_{ij} = \frac{(m_i^2 - m_j^2)L}{4E} = 1.267 \frac{\Delta m_{ij}^2}{\text{eV}^2} \frac{L/E}{\text{m/MeV}}. \quad (14.40)$$

If we had made the same derivation for antineutrino states, we would have ended with a similar expression but with the exchange $U \rightarrow U^*$. Consequently, we conclude that the first term in the right-hand-side of Eq.(14.39) is CP conserving since it is the same for neutrinos and antineutrinos, while the last one is CP violating because it has opposite signs for neutrinos and antineutrinos.

Equation (14.39) is oscillatory in distance with oscillation lengths

$$L_{0,ij}^{\text{osc}} = \frac{4\pi E}{|\Delta m_{ij}^2|}, \quad (14.41)$$

and with amplitudes proportional to products of elements in the mixing matrix. Thus, neutrinos must have different masses

³ For a pedagogical discussion of the quantum mechanical description of flavour oscillations in the wave package approach see for example Ref. [3]. A recent review of the quantum mechanical aspects and subtleties on neutrino oscillations can be found in Ref. [25].

Table 14.1: Characteristic values of L and E for experiments performed using various neutrino sources and the corresponding ranges of $|\Delta m^2|$ to which they can be most sensitive to flavour oscillations in vacuum. SBL stands for Short Baseline, VSBL stands for Very Short Baseline, MBL stands for Medium Baseline, and LBL for Long Baseline.

Experiment		L (m)	E (MeV)	$ \Delta m^2 $ (eV^2)
Solar		10^{10}	1	10^{-10}
Atmospheric		$10^4 - 10^7$	$10^2 - 10^5$	$10^{-1} - 10^{-4}$
Reactor	VSBL-SBL-MBL	$10 - 10^3$	1	$1 - 10^{-3}$
	LBL	$10^4 - 10^5$		$10^{-4} - 10^{-5}$
Accelerator	SBL	10^2	$10^3 - 10^4$	> 0.1
	LBL	$10^5 - 10^6$	$10^3 - 10^4$	$10^{-2} - 10^{-3}$

($\Delta m_{ij}^2 \neq 0$) and they must have not vanishing mixing ($U_{\alpha i} U_{\beta i} \neq 0$) in order to undergo flavour oscillations. Also, from Eq.(14.39) we see that the Majorana phases cancel out in the oscillation probability. This is expected because flavour oscillation is a total lepton number conserving process.

Ideally, a neutrino oscillation experiment would like to measure an oscillation probability over a distance L between the source and the detector, for neutrinos of a definite energy E . In practice, neutrino beams, both from natural or artificial sources, are never monoenergetic but have an energy spectrum $\Phi(E)$. In addition, each detector has a finite energy resolution. Under these circumstances what is measured is an average probability

$$\begin{aligned} \langle P_{\alpha\beta} \rangle &= \frac{\int dE \frac{d\Phi}{dE} \sigma(E) P_{\alpha\beta}(E) \epsilon(E)}{\int dE \frac{d\Phi}{dE} \sigma_{CC}(E) \epsilon(E)} \\ &= \delta_{\alpha\beta} - 4 \sum_{i < j}^n \text{Re}[U_{\alpha i} U_{\beta i}^* U_{\alpha j}^* U_{\beta j}] \langle \sin^2 X_{ij} \rangle \\ &\quad + 2 \sum_{i < j}^n \text{Im}[U_{\alpha i} U_{\beta i}^* U_{\alpha j}^* U_{\beta j}] \langle \sin 2X_{ij} \rangle. \end{aligned} \quad (14.42)$$

σ is the cross-section for the process in which the neutrino flavour is detected, and $\epsilon(E)$ is the detection efficiency. The minimal range of the energy integral is determined by the energy resolution of the experiment.

It is clear from the above expression that if $(E/L) \gg |\Delta m_{ij}^2|$ ($L \ll L_{0,ij}^{\text{osc}}$) so $\sin^2 X_{ij} \ll 1$, the oscillation phase does not give any appreciable effect. Conversely, if $L \gg L_{0,ij}^{\text{osc}}$, many oscillation cycles occur between production and detection, so the oscillating term is averaged to $\langle \sin^2 X_{ij} \rangle = 1/2$.

We summarize in Table 14.1 the typical values of L/E for different types of neutrino sources and experiments and the corresponding ranges of Δm^2 to which they can be most sensitive.

Historically, the results of neutrino oscillation experiments were interpreted assuming two-neutrino states so there is only one oscillating phase; the mixing matrix depends on a single mixing angle θ , and no CP violation effect in oscillations is possible. At present, as we will discuss in Sec.14.7, we need at least the mixing among three-neutrino states to fully describe the bulk of experimental results. However, in many cases, the observed results can be understood in terms of oscillations dominantly driven by one Δm^2 . In this limit $P_{\alpha\beta}$ of Eq.(14.39) takes the form [24]

$$P_{\alpha\beta} = \delta_{\alpha\beta} - (2\delta_{\alpha\beta} - 1) \sin^2 2\theta \sin^2 X. \quad (14.43)$$

In this effective $2 - \nu$ limit, changing the sign of the mass difference, $\Delta m^2 \rightarrow -\Delta m^2$, and changing the octant of the mixing angle, $\theta \rightarrow \frac{\pi}{2} - \theta$, is just redefining the mass eigenstates, $\nu_1 \leftrightarrow \nu_2$: $P_{\alpha\beta}$ must be invariant under such transformation. So the physical parameter space can be covered with either $\Delta m^2 \geq 0$ with $0 \leq \theta \leq \frac{\pi}{2}$, or, alternatively, $0 \leq \theta \leq \frac{\pi}{4}$ with either sign for Δm^2 .

However, from Eq.(14.43) we see that $P_{\alpha\beta}$ is actually invariant under the change of sign of the mass splitting and the change of octant of the mixing angle separately. This implies that there is a two-fold discrete ambiguity since the two different sets of physical parameters, $(\Delta m^2, \theta)$ and $(\Delta m^2, \frac{\pi}{2} - \theta)$, give the same

transition probability in vacuum. In other words, one could not tell from a measurement of, say, $P_{e\mu}$ in vacuum whether the larger component of ν_e resides in the heavier or in the lighter neutrino mass eigenstate. This symmetry is broken when one considers mixing of three or more neutrinos in the flavour evolution and or when the neutrinos traverse regions of dense matter as we describe in Sec.14.7.1 and Sec.14.5, respectively.

14.5 Propagation of Massive Neutrinos in Matter

Neutrinos propagating in a dense medium can interact with the particles in the medium. The probability of an incoherent inelastic scattering is very small. For example the characteristic cross section for ν -proton scattering is of the order

$$\sigma \sim \frac{G_F^2 s}{\pi} \sim 10^{-43} \text{ cm}^2 \left(\frac{E}{\text{MeV}} \right)^2, \quad (14.44)$$

where G_F is the Fermi constant and s is the square of the center of mass energy of the collision.

But when neutrinos propagate in dense matter, they can also interact coherently with the particles in the medium. By definition, in coherent interactions, the medium remains unchanged so it is possible to have interference of the forward scattered and the unscattered neutrino waves which enhances the effect of matter in the neutrino propagation. In this case, the effect of the medium is not on the intensity of the propagating neutrino beam, which remains unchanged, but on the phase velocity of the neutrino wave, and for this reason the effect is proportional to G_F , instead of the G_F^2 dependence of the incoherent scattering. Coherence also allows decoupling the evolution equation of the neutrinos from those of the medium. In this limit, the effect of the medium is introduced in the evolution equation for the neutrinos in the form of an effective potential which depends on the density and composition of the matter [26].

As an example, let us consider the evolution of ν_e in a medium with electrons, protons, and neutrons with corresponding n_e , n_p , and n_n number densities. The effective low-energy Hamiltonian describing the relevant neutrino interactions at point x is given by

$$H_W = \frac{G_F}{\sqrt{2}} \left[J^{(+)\alpha}(x) J_\alpha^{(-)}(x) + \frac{1}{4} J^{(N)\alpha}(x) J_\alpha^{(N)}(x) \right], \quad (14.45)$$

where the J_α 's are the standard fermionic currents

$$J_\alpha^{(+)}(x) = \bar{\nu}_e(x) \gamma_\alpha (1 - \gamma_5) e(x), \quad (14.46)$$

$$J_\alpha^{(-)}(x) = \bar{e}(x) \gamma_\alpha (1 - \gamma_5) \nu_e(x), \quad (14.47)$$

$$\begin{aligned} J_\alpha^{(N)}(x) &= \bar{\nu}_e(x) \gamma_\alpha (1 - \gamma_5) \nu_e(x) \\ &\quad - \bar{e}(x) [\gamma_\alpha (1 - \gamma_5) - 4 \sin^2 \theta_W \gamma_\alpha] e(x) \\ &\quad + \bar{p}(x) [\gamma_\alpha (1 - g_A^{(p)} \gamma_5) - 4 \sin^2 \theta_W \gamma_\alpha] p(x) \\ &\quad - \bar{n}(x) \gamma_\alpha (1 - g_A^{(n)} \gamma_5) n(x), \end{aligned} \quad (14.48)$$

and $g_A^{(n,p)}$ are the axial couplings for neutrons and protons, respectively.

Let us focus first on the effect of the charged current inter-

actions. The effective CC Hamiltonian due to electrons in the medium is

$$\begin{aligned} H_C^{(e)} &= \frac{G_F}{\sqrt{2}} \int d^3 p_e f(E_e, T) \times \left\langle \langle e(s, p_e) | \bar{e}(x) \gamma^\alpha (1 - \gamma_5) \nu_e(x) \bar{\nu}_e(x) \gamma_\alpha (1 - \gamma_5) e(x) | e(s, p_e) \rangle \right\rangle \\ &= \frac{G_F}{\sqrt{2}} \bar{\nu}_e(x) \gamma_\alpha (1 - \gamma_5) \nu_e(x) \int d^3 p_e f(E_e, T) \left\langle \langle e(s, p_e) | \bar{e}(x) \gamma_\alpha (1 - \gamma_5) e(x) | e(s, p_e) \rangle \right\rangle. \end{aligned} \quad (14.49)$$

In the above equation, we denote by s the electron spin, and by p_e its momentum, and $f(E_e, T)$ is the energy distribution function of the electrons in the medium which is assumed to be homogeneous and isotropic and is normalized as

$$\int d^3 p_e f(E_e, T) = 1. \quad (14.50)$$

We denote by $\langle \dots \rangle$ the averaging over electron spinors and summing over all electrons in the medium. Coherence dictates that s, p_e are the same for initial and final electrons. The axial current reduces to the spin in the non-relativistic limit and therefore averages to zero for a background of non-relativistic electrons. The spatial components of the vector current cancel because of isotropy. Therefore, the only non-trivial average is

$$\int d^3 p_e f(E_e, T) \left\langle \langle e(s, p_e) | \bar{e}(x) \gamma_0 e(x) | e(s, p_e) \rangle \right\rangle = n_e(x), \quad (14.51)$$

which gives a contribution to the effective Hamiltonian

$$H_C^{(e)} = \sqrt{2} G_F n_e \bar{\nu}_{eL}(x) \gamma_0 \nu_{eL}(x). \quad (14.52)$$

This can be interpreted as a contribution to the ν_{eL} potential energy

$$V_C = \sqrt{2} G_F n_e. \quad (14.53)$$

Should we have considered antineutrino states, we would have ended up with $V_C = -\sqrt{2} G_F n_e$. For a more detailed derivation of the matter potentials see, for example, Ref. [3].

With an equivalent derivation, we find that for ν_μ and ν_τ , the potential due to its CC interactions is zero for most media since neither μ 's nor τ 's are present, while the effective potential for any active neutrino due to the neutral current interactions is found to be

$$V_{NC} = \frac{\sqrt{2}}{2} G_F [-n_e(1 - 4 \sin^2 \theta_w) + n_p(1 - 4 \sin^2 \theta_w) - n_n]. \quad (14.54)$$

In neutral matter, $n_e = n_p$ and the contribution from electrons and protons cancel each other. So we are left only with the neutron contribution

$$V_{NC} = -1/\sqrt{2} G_F n_n. \quad (14.55)$$

After including these effects, the evolution equation for n ultrarelativistic neutrinos propagating in matter written in the mass basis is (see for instance Ref. [27–29] for the derivation):

$$i \frac{d\vec{\nu}}{dx} = H \vec{\nu}, \quad H = H_m + U^\nu \dagger V U^\nu. \quad (14.56)$$

Here $\vec{\nu} \equiv (\nu_1, \nu_2, \dots, \nu_n)^T$, H_m is the kinetic Hamiltonian,

$$H_m = \frac{1}{2E} \text{diag}(m_1^2, m_2^2, \dots, m_n^2), \quad (14.57)$$

and V is the effective neutrino potential in the interaction basis. U^ν is the $n \times n$ submatrix of the unitary V^ν matrix corresponding to the n ultrarelativistic neutrino states. For the three SM active neutrinos with purely SM interactions crossing a neutral medium with electrons, protons and neutrons, the evolution equation takes the form (14.56) with $U^\nu \equiv U$, and the effective potential:

$$V = \text{diag}(\pm \sqrt{2} G_F n_e(x), 0, 0) \equiv \text{diag}(V_e, 0, 0). \quad (14.58)$$

The sign $+$ ($-$) in Eq.(14.58) applies to neutrinos (antineutrinos), and $n_e(x)$ is the electron number density in the medium, which in general is not constant along the neutrino trajectory so the potential is not constant. The characteristic value of the potential at the Earth core is $V_e \sim 10^{-13}$ eV, while at the solar core $V_e \sim 10^{-12}$ eV. Since the neutral current potential Eq.(14.55) is flavour diagonal, it can be eliminated from the evolution equation as it only contributes to an overall unobservable phase.

The instantaneous mass eigenstates in matter, ν_i^m , are the eigenstates of the Hamiltonian H in (14.56) for a fixed value of x , and they are related to the interaction basis by

$$\vec{\nu} = \tilde{U}(x) \nu^{\vec{m}}. \quad (14.59)$$

The corresponding instantaneous eigenvalues of H are $\mu_i(x)^2/(2E)$ with $\mu_i(x)$ being the instantaneous effective neutrino masses.

Let us take for simplicity a neutrino state which is an admixture of only two neutrino species $|\nu_\alpha\rangle$ and $|\nu_\beta\rangle$, so the two instantaneous mass eigenstates in matter ν_1^m and ν_2^m have instantaneous effective neutrino masses

$$\mu_{1,2}^2(x) = \frac{m_1^2 + m_2^2}{2} + E[V_\alpha + V_\beta] \quad (14.60)$$

$$\mp \frac{1}{2} \sqrt{[\Delta m^2 \cos 2\theta - A]^2 + [\Delta m^2 \sin 2\theta]^2},$$

and $\tilde{U}(x)$ is a 2x2 rotation matrix with the instantaneous mixing angle in matter given by

$$\tan 2\theta_m = \frac{\Delta m^2 \sin 2\theta}{\Delta m^2 \cos 2\theta - A}. \quad (14.61)$$

In the Eqs.(14.60) and (14.61) A is

$$A \equiv 2E(V_\alpha - V_\beta), \quad (14.62)$$

and its sign depends on the composition of the medium and on the flavour composition of the neutrino state considered. From the expressions above, we see that for a given sign of A the mixing angle in matter is larger(smaller) than in vacuum if this last one is in the first (second) octant. We see that the symmetry about $\theta = 45^\circ$ which exists in vacuum oscillations between two neutrino states is broken by the matter potential in propagation in a medium. The expressions above show that significant effects are present when A , is close to $\Delta m^2 \cos 2\theta$. In particular, as seen in Eq.(14.61), the tangent of the mixing angle changes sign if, along its path, the neutrino passes by some matter density region satisfying, for its energy, the *resonance condition*

$$A_R = \Delta m^2 \cos 2\theta. \quad (14.63)$$

This implies that if the neutrino is created in a region where the relevant potential satisfies $A_0 > A_R$ (A_0 here is the value of the relevant potential at the production point), then the effective mixing angle in matter at the production point is such that $\text{sgn}(\cos 2\theta_{m,0}) = -\text{sgn}(\cos 2\theta)$. So the flavour component of the mass eigenstates is inverted as compared to their composition in vacuum. In particular, if at the production point we have $A_0 = 2A_R$, then $\theta_{m,0} = \frac{\pi}{2} - \theta$. Asymptotically, for $A_0 \gg A_R$, $\theta_{m,0} \rightarrow \frac{\pi}{2}$. In other words, if in vacuum the lightest (heaviest) mass eigenstate has a larger projection on the flavour α (β), inside a matter with density and composition such that $A > A_R$,

the opposite holds. So if the neutrino system is traveling across a monotonically varying matter potential, the dominant flavour component of a given mass eigenstate changes when crossing the region with $A = A_R$. This phenomenon is known as *level crossing*.

Taking the derivative of Eq.(14.59) with respect to x and using Eq.(14.56), we find that in the instantaneous mass basis the evolution equation reads:

$$i \frac{d\vec{\nu}^m}{dx} = \left[\frac{1}{2E} \text{diag} (\mu_1^2(x), \mu_2^2(x), \dots, \mu_n^2(x)) - i \tilde{U}^\dagger(x) \frac{d\tilde{U}(x)}{dx} \right] \vec{\nu}^m. \quad (14.64)$$

The presence of the last term, Eq.(14.64) implies that this is a system of coupled equations. So, in general, the instantaneous mass eigenstates, ν_i^m are not energy eigenstates. For constant or slowly enough varying matter potential this last term can be neglected and the instantaneous mass eigenstates, ν_i^m , behave approximately as energy eigenstates, and they do not mix in the evolution. This is the *adiabatic* transition approximation. On the contrary, when the last term in Eq.(14.64) cannot be neglected, the instantaneous mass eigenstates mix along the neutrino path. This implies there can be *level-jumping* [30–33], and the evolution is *non-adiabatic*.

For adiabatic evolution in matter, the oscillation probability take a form very similar to the vacuum oscillation expression, Eq.(14.39). For example, neglecting CP violation:

$$P_{\alpha\beta} = \left| \sum_i \tilde{U}_{\alpha i}(0) \tilde{U}_{\beta i}(L) \exp \left(-\frac{i}{2E} \int_0^L \mu_i^2(x') dx' \right) \right|^2. \quad (14.65)$$

To compute $P_{\alpha\beta}$ in a varying potential, one can always solve the evolution equation numerically. Also, several analytic approximations for specific profiles of the matter potential can be found in the literature [34].

14.5.1 The Mikheyev-Smirnov-Wolfenstein Effect for Solar Neutrinos

The matter effects discussed in the previous section are of special relevance for solar neutrinos. As the Sun produces ν_e 's in its core, we consider the propagation of a $\nu_e - \nu_X$ neutrino system (X is some superposition of μ and τ , which is arbitrary because ν_μ and ν_τ have only and equal neutral current interactions) in the matter density of the Sun.

The density of solar matter is a monotonically decreasing function of the distance R from the center of the Sun, and it can be approximated by an exponential for $R < 0.9R_\odot$

$$n_e(R) = n_e(0) \exp(-R/r_0), \quad (14.66)$$

with $r_0 = R_\odot/10.54 = 6.6 \times 10^7 \text{ m} = 3.3 \times 10^{14} \text{ eV}^{-1}$.

As mentioned above, the nuclear reactions in the Sun produce electron neutrinos. After crossing the Sun, the composition of the neutrino state exiting the Sun will depend on the relative size of $\Delta m^2 \cos 2\theta$ versus $A_0 = 2EG_F n_{e,0}$ (where 0 refers to the neutrino production point, which is near but not exactly at the center of the Sun, $R = 0$).

If the relevant matter potential at production is well below the resonant value, $A_R = \Delta m^2 \cos 2\theta \gg A_0$, matter effects are negligible. With the characteristic matter density and energy of the solar neutrinos, this condition is fulfilled for values of Δm^2 such that $\Delta m^2/E \gg L_{\text{Sun-Earth}}$. So the propagation occurs as in vacuum with the oscillating phase averaged to 1/2 and the survival probability at the exposed surface of the Earth is

$$P_{ee}(\Delta m^2 \cos 2\theta \gg A_0) = 1 - \frac{1}{2} \sin^2 2\theta > \frac{1}{2}. \quad (14.67)$$

If the relevant matter potential at production is only slightly below the resonant value, $A_R = \Delta m^2 \cos 2\theta \gtrsim A_0$, the neutrino does not cross a region with resonant density, but matter effects are sizable enough to modify the mixing. The oscillating phase is

averaged in the propagation between the Sun and the Earth. This regime is well described by an adiabatic propagation, Eq.(14.65). Using that $\tilde{U}(0)$ is a 2x2 rotation of angle $\theta_{m,0}$ – the mixing angle in matter at the neutrino production point–, and $\tilde{U}(L)$ is the corresponding rotation with vacuum mixing angle θ , we get

$$\begin{aligned} P_{ee}(\Delta m^2 \cos 2\theta \geq A_0) &= \cos^2 \theta_{m,0} \cos^2 \theta + \sin^2 \theta_{m,0} \sin^2 \theta \\ &= \frac{1}{2} [1 + \cos 2\theta_{m,0} \cos 2\theta]. \end{aligned} \quad (14.68)$$

This expression reflects that an electron neutrino produced at A_0 is an admixture of ν_1 with fraction $P_{e1,0} = \cos^2 \theta_{m,0}$ and ν_2 with fraction $P_{e2,0} = \sin^2 \theta_{m,0}$. On exiting the Sun, ν_1 consists of ν_e with fraction $P_{1e} = \cos^2 \theta$, and ν_2 consists of ν_e with fraction $P_{2e} = \sin^2 \theta$ so $P_{ee} = P_{e1,0}P_{1e} + P_{e2,0}P_{2e} = \cos^2 \theta_{m,0} \cos^2 \theta + \sin^2 \theta_{m,0} \sin^2 \theta$ [35–37], exactly as given in Eq.(14.68). Since $A_0 < A_R$ the resonance is not crossed so $\cos 2\theta_{m,0}$ has the same sign as $\cos 2\theta$ and still $P_{ee} \geq 1/2$.

Finally, in the case that $A_R = \Delta m^2 \cos 2\theta < A_0$, the neutrino can cross the resonance on its way out. In the convention of $\Delta m^2 > 0$ this occurs if $\cos 2\theta > 0$ ($\theta < \pi/4$), which means that in vacuum ν_e is a combination of ν_1 and ν_2 with a larger ν_1 component, while at the production point ν_e is a combination of ν_1^m and ν_2^m with larger ν_2^m component. In particular, if the density at the production point is much higher than the resonant density, $\Delta m^2 \cos 2\theta \ll A_0$,

$$\theta_{m,0} = \frac{\pi}{2} \Rightarrow \cos 2\theta_{m,0} = -1, \quad (14.69)$$

and the produced ν_e is purely ν_2^m .

In this regime, the evolution of the neutrino ensemble can be adiabatic or non-adiabatic depending on the particular values of Δm^2 and the mixing angle. The oscillation parameters (see Secs.14.6.1 and 14.7) happen to be such that the transition is adiabatic in all ranges of solar neutrino energies. Thus the survival probability at the exposed surface of the Earth is given by Eq.(14.68) but now with mixing angle (14.69) so

$$P_{ee}(\Delta m^2 \cos 2\theta < A_0) = \frac{1}{2} [1 + \cos 2\theta_{m,0} \cos 2\theta] = \sin^2 \theta. \quad (14.70)$$

So, in this case, P_{ee} can be much smaller than 1/2 because $\cos 2\theta_{m,0}$ and $\cos 2\theta$ have opposite signs. This is referred to as the Mikheyev-Smirnov-Wolfenstein (MSW) effect [26, 38], which plays a fundamental role in the interpretation of the solar neutrino data.

The resulting energy dependence of the survival probability of solar neutrinos is shown in Fig.14.3 (together with a compilation of data from solar experiments). The plotted curve corresponds to $\Delta m^2 \sim 7.5 \times 10^{-5} \text{ eV}^2$ and $\sin^2 \theta \sim 0.3$ (the so-called large mixing angle, LMA, solution). The figure illustrates the regimes described above. For these values of the oscillation parameters, neutrinos with $E \ll 1 \text{ MeV}$ are in the regime with $\Delta m^2 \cos 2\theta \gg A_0$ so the curve represents the value of vacuum averaged survival probability, Eq.(14.67), and therefore $P_{ee} > 0.5$. For $E > 10 \text{ MeV}$, on the contrary, $\Delta m^2 \cos 2\theta \ll A_0$ and the survival probability is given by Eq.(14.70), so $P_{ee} = \sin^2 \theta \sim 0.3$. In between, the survival probability is given by Eq.(14.68) with θ_0 changing rapidly from its vacuum value to the asymptotic matter value (14.69), 90° .

14.6 Experimental Study of Neutrino Oscillations

Neutrino flavour transitions, or neutrino oscillations, have been experimentally studied using various neutrino sources and detection techniques. Intense sources and large detectors are mandatory because of a large distance necessary for observable oscillation effects in addition to the tiny cross-sections. Also, the relevant neutrino flux before oscillations should be known with sufficient precision for a definitive measurement. Here, the experimental status of neutrino oscillations with the different neutrino sources: the Sun, Earth's atmosphere, accelerators, and nuclear reactors are reviewed.

14.6.1 Solar Neutrinos

14.6.1.1 Solar neutrino flux

In the Sun, electron neutrinos are produced in the thermonuclear reactions which generate solar energy. These reactions occur via two main chains, the pp chain and the CNO cycle. The pp chain includes reactions $p+p \rightarrow d+e^++\nu$ (pp), $p+e^-+p \rightarrow d+\nu$ (pep), ${}^3\text{He}+p \rightarrow {}^4\text{He}+e^++\nu$ (hep), ${}^7\text{Be}+e^- \rightarrow {}^7\text{Li}+\nu(+\gamma)$ (${}^7\text{Be}$), and ${}^8\text{B} \rightarrow {}^8\text{Be}^*+e^++\nu$ (${}^8\text{B}$). The CNO cycle involves ${}^{13}\text{N} \rightarrow {}^{13}\text{C}+e^++\nu$ (${}^{13}\text{N}$), ${}^{15}\text{O} \rightarrow {}^{15}\text{N}+e^++\nu$ (${}^{15}\text{O}$), and ${}^{17}\text{F} \rightarrow {}^{17}\text{O}+e^++\nu$ (${}^{17}\text{F}$). Those reactions result in the overall fusion of protons into ${}^4\text{He}$, $4p \rightarrow {}^4\text{He}+2e^++2\nu_e$, where the energy released in the reaction, $Q = 4m_p - m_{{}^4\text{He}} - 2m_e \sim 26$ MeV, is mostly radiated through the photons and only a small fraction is carried by the neutrinos, $(E_{2\nu_e}) = 0.59$ MeV. In addition, electron capture on ${}^{13}\text{N}$, ${}^{15}\text{O}$, and ${}^{17}\text{F}$ produces line spectra of neutrinos called ecCNO neutrinos. Dividing the solar luminosity by the energy released per neutrino production, the total neutrino flux can be estimated. At Earth, the pp solar neutrino flux is about $6 \times 10^{10} \text{ cm}^{-2}\text{s}^{-1}$.

The solar neutrino flux has been calculated based on the Standard Solar Model (SSM). The SSM describes the structure and evolution of the Sun based on a variety of inputs such as the mass, luminosity, radius, surface temperature, age, and surface elemental abundances. In addition, the knowledge of the absolute nuclear reaction cross sections for relevant fusion reactions and radiative opacities are necessary. John Bahcall and his collaborators continuously updated the SSM calculations over several decades [39,40]. Figure 14.1 shows the solar neutrino fluxes predicted by the SSM calculation in [41] and ecCNO neutrinos in [42].

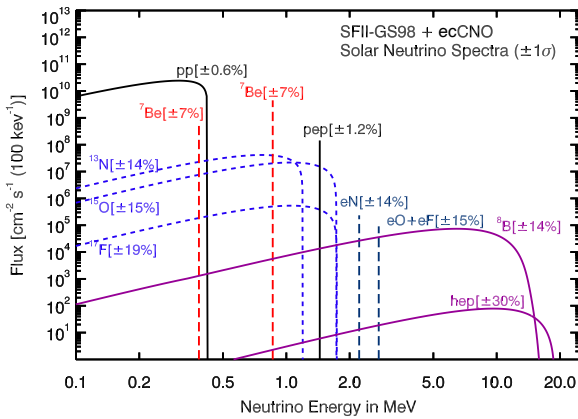


Figure 14.1: Spectrum of solar neutrino fluxes predicted by SSM calculation in [41]. In addition to standard fluxes, ecCNO neutrinos have been added based on [42]. Electron capture fluxes are given in $\text{cm}^{-2}\text{s}^{-1}$. Taken from [43].

14.6.1.2 Detection of solar neutrinos and the solar neutrino problem

Experiments that observed solar neutrinos are summarized in Table 14.2. A pioneering solar neutrino experiment was carried out by R. Davis, Jr. and collaborators at Homestake starting in the late 1960s [44]. The Davis' experiment utilizes the reaction $\nu_e + {}^{37}\text{Cl} \rightarrow e^- + {}^{37}\text{Ar}$. Because this process has an energy threshold of 814 keV, the most relevant fluxes are the ${}^7\text{Be}$ and ${}^8\text{B}$ neutrinos. The detector contained ~ 615 t of C_2Cl_4 . The produced ${}^{37}\text{Ar}$, which has a half-life of 34.8 days, was chemically extracted and introduced into a low-background proportional chamber every few months. The Auger electrons from electron capture of ${}^{37}\text{Ar}$ were counted to determine the reaction rate.

From the beginning, the observed number of neutrinos in the Homestake mine experiment was significantly smaller than the prediction by SSM — it was almost one-third. After thorough checks of both experimental and theoretical work, the discrepancy remained. This became to be known as the solar neutrino problem. The final result from the Homestake experiment is $2.56 \pm 0.16 \pm 0.16$ SNU [45], where SNU (solar neutrino unit)

is a unit of event rate, $1 \text{ SNU} = 10^{-36}$ captures/(s atom). On the other hand, prediction based on SSM is $8.46_{-0.88}^{+0.87}$ SNU [46].

The detection of neutrinos from other production processes was recognized as an important input to investigate the origin of the solar neutrino problem. In particular, the pp neutrino is most abundant, and its flux prediction has the smallest uncertainty. Using the radiochemical technique with gallium, the reaction $\nu_e + {}^{71}\text{Ga} \rightarrow e^- + {}^{71}\text{Ge}$ has an energy threshold of 233 keV and can be used for the pp neutrino detection. According to the SSM, more than half of the events on ${}^{71}\text{Ga}$ are due to the pp neutrinos, with the second dominant contribution coming from the ${}^7\text{Be}$ neutrinos. ${}^{71}\text{Ge}$ decays via electron capture with a half-life of 11.4 days. The SAGE experiment in Baksan [47] used about 50 t of liquid metallic gallium as a target. The GALLEX experiment in LNGS [48] used 101 t of GaCl_3 , containing 30.3 t of gallium. Both experiments used natural gallium, containing 39.9% of ${}^{71}\text{Ga}$ isotope. GALLEX was followed by its successor GNO experiment. The measured capture rate is $69.3 \pm 4.1 \pm 3.6$ SNU for GALLEX+GNO [49] and $65.4_{-3.0}^{+3.1+2.6}$ SNU for SAGE [50]. A SSM prediction is $127.9_{-8.2}^{+8.1}$ SNU [46].

The radiochemical detectors measure the reaction rate integrated between extractions. The real-time measurement of solar neutrinos was realized by the Kamiokande experiment [51]. The Kamiokande detector was a 3,000-t water-Cherenkov detector in the Kamioka mine. Super-Kamiokande, the successor of Kamiokande, started operation in 1996. It is a large upright cylindrical water Cherenkov detector containing 50 kt of pure water⁴. An inner detector volume corresponding to 32 kt water mass is viewed by more than 11,000 inward-facing 50 cm diameter photomultiplier tubes (PMTs). Kamiokande and Super-Kamiokande can observe solar neutrinos using ν_e - e elastic scattering (ES), $\nu_x + e^- \rightarrow \nu_x + e^-$. The ES reaction occurs via both charged and neutral current interactions. Consequently, it is sensitive to all active neutrino flavours, although the cross-section for ν_e , which is the only flavour to interact via charged current, is about six times larger than that for ν_μ or ν_τ . Because the energy threshold is 6.5 MeV for Kamiokande and 3.5 MeV for the present Super-Kamiokande (for the kinetic energy of recoil electron), these experiments are sensitive to primarily to ${}^8\text{B}$ neutrinos.

The results from Kamiokande [52] and Super-Kamiokande [53] showed significantly smaller numbers of observed solar neutrinos compared to the prediction. The latest solar neutrino flux observed by Super-Kamiokande is $(2.345 \pm 0.014 \pm 0.036) \times 10^6 \text{ cm}^{-2}\text{s}^{-1}$ [54], while a prediction based on the SSM is $(5.46 \pm 0.66) \times 10^6 \text{ cm}^{-2}\text{s}^{-1}$ [55]. In addition, no significant zenith angle variation nor spectrum distortion were observed in the initial phase of Super-Kamiokande, which placed strong constraints on the solution of the solar neutrino problem [56].

14.6.1.3 Solution of the solar neutrino problem

The SNO experiment in Canada used 1,000 t of heavy water (D_2O) contained in a spherical acrylic vessel which was surrounded by an H_2O shield. An array of PMTs installed on a stainless steel structure detected Cherenkov radiation produced in both the D_2O and H_2O . The SNO detector observed ${}^8\text{B}$ neutrinos via three different reactions. In addition to the ES scattering with an electron, with D_2O target the CC $\nu_e + d \rightarrow e^- + p + p$ and the NC $\nu_x + d \rightarrow \nu_x + p + n$ interactions are possible. The CC reaction is sensitive to only ν_e , while NC reaction is sensitive to all active flavours of neutrinos with equal cross-sections. Therefore, by comparing the measurements of different reactions, SNO could provide a model-independent test of the neutrino flavour change [57].

In 2001, SNO reported the initial result of CC measurement [60]. Combined with the high statistics measurement of ν_e - e elastic scattering from Super-Kamiokande [61], it provided a direct evidence for the existence of non- ν_e component in solar neutrino flux. The result of the NC measurement in 2002 [62] established it with 5.3σ of statistical significance. Figure 14.2 shows the fluxes of electron neutrinos ($\phi(\nu_e)$) and muon and tau

⁴Recently, gadolinium (0.01% by weight in 2020, 0.03% in 2022) is loaded in the water.

Table 14.2: List of solar neutrino experiments

Name	Target material	Energy threshold (MeV)	Mass (ton)	Years
Homestake	C ₂ Cl ₄	0.814	615	1970–1994
SAGE	Ga	0.233	50	1989–
GALLEX	GaCl ₃	0.233	100 [30.3 for Ga]	1991–1997
GNO	GaCl ₃	0.233	100 [30.3 for Ga]	1998–2003
Kamiokande	H ₂ O	6.5	3,000	1987–1995
Super-Kamiokande	H ₂ O	3.5	50,000	1996–
SNO	D ₂ O	3.5	1,000	1999–2006
KamLAND	Liquid scintillator	0.5/5.5	1,000	2001–
Borexino	Liquid scintillator	0.19	300	2007–2021

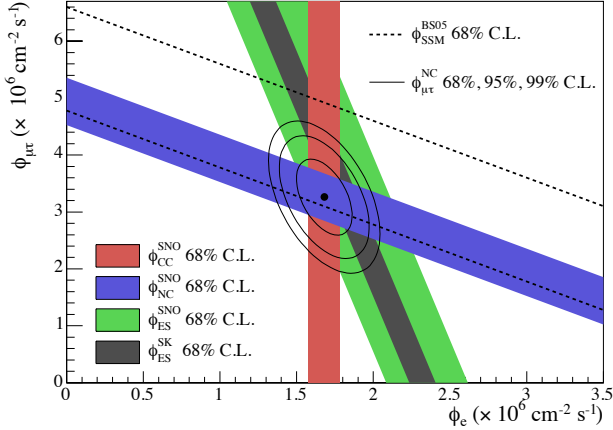


Figure 14.2: Fluxes of ^8B solar neutrinos, $\phi(\nu_e)$, and $\phi(\nu_{\mu,\tau})$, deduced from the SNO’s CC, ES, and NC results [58]. The Super-Kamiokande ES flux is from [59]. The BS05(OP) standard solar model prediction [40] is also shown. The bands represent the 1σ error. The contours show the 68%, 95%, and 99% joint probability for $\phi(\nu_e)$ and $\phi(\nu_{\mu,\tau})$. The figure is from [58].

neutrinos ($\phi(\nu_{\mu,\tau})$) with the 68%, 95%, and 99% joint probability contours obtained with the SNO data. Finally, together with the reactor neutrino experiment KamLAND (see Sec.14.6.4), the solution of solar neutrino problem was found to be the MSW adiabatic flavour transitions in the solar matter, the so-called large mixing angle (LMA) solution. From a combined result of three phases of SNO [63], the total flux of ^8B solar neutrino is found to be $(5.25 \pm 0.16^{+0.11}_{-0.13}) \text{ cm}^{-2}\text{s}^{-1}$, consistent with the SSM prediction. This consistency is one of the major accomplishments of SSM.

In order to understand the SSM as well as to study the MSW effect for the solar neutrino, measurements of solar neutrinos other than ^8B are important. The Borexino experiment at Gran Sasso detected solar neutrino via ν -e scattering in real-time with a low energy threshold. The Borexino detector consisted of 300 t of ultra-pure liquid scintillator, which achieved 0.19 MeV of energy threshold and 5% energy resolution at 1 MeV. Borexino reported the first real-time detection of ^7Be solar neutrinos [65]. They also measured the fluxes of pep [66], pp [67], and CNO [68] neutrino for the first time. Together with ^8B [69] neutrino measurement, Borexino provides important data to study the MSW effect. The KamLAND experiment also measured solar neutrinos [70, 71].

Figure 14.3 shows the survival probability of solar ν_e as a function of neutrino energy. The data points are from the Borexino results [72, 73] and the SNO+SK ^8B data. The theoretical curve shows the prediction of the MSW-LMA solution. All the data shown in this plot are consistent with the theoretically calculated curve. This indicates that these solar neutrino measurements are consistent with the MSW-LMA solution of the solar neutrino problem.

The matter effects can also be relevant to the propagation of solar neutrinos through the Earth. Because solar neutrinos go

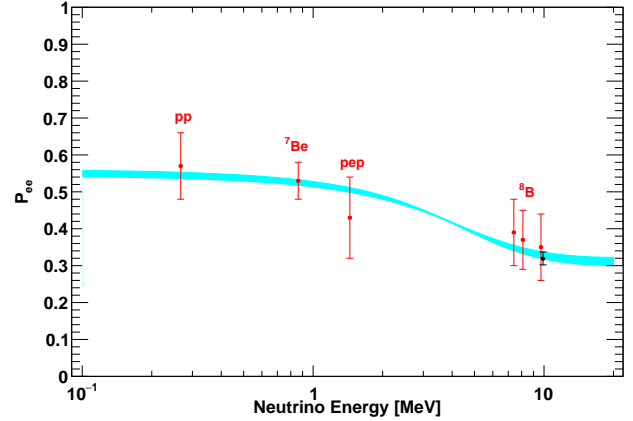


Figure 14.3: Electron neutrino survival probability as a function of neutrino energy. The points represent, from left to right, the Borexino pp , ^7Be , pep , and ^8B data (red points) and the SNO+SK ^8B data (black point). The three Borexino ^8B data points correspond, from left to right, to the low-energy (LE) range, LE+HE range, and the high-energy (HE) range. The electron neutrino survival probabilities from experimental points are determined using a high metallicity SSM from [55]. The error bars represent the $\pm 1\sigma$ experimental + theoretical uncertainties. The curve corresponds to the $\pm 1\sigma$ prediction of the MSW-LMA solution using the parameter values given in [64]. This figure is provided by A. Ianni.

through the Earth before interaction in the detector during the nighttime, a comparison of measured event rate between daytime and nighttime provides a clean and direct test of matter effects on neutrino oscillations. Super-Kamiokande reported the indication of the day/night asymmetry in ^8B solar neutrinos [54]. The measured asymmetry, defined as the difference of the average day rate and average night rate divided by the average of those two rates, is $(-3.3 \pm 1.0 \pm 0.5)\%$, corresponding to a statistical significance of 2.9σ .

14.6.2 Atmospheric Neutrinos

14.6.2.1 Atmospheric neutrino flux

Atmospheric neutrinos are produced by the decays of pions and kaons generated in the interaction of cosmic rays and nucleons in the Earth’s atmosphere. They have a broad range of energy ($\sim 0.1 \text{ GeV}$ to $> \text{TeV}$) and long travel distances before detection (~ 10 to $\sim 10^4 \text{ km}$), and contain all the flavours of neutrinos and antineutrinos.

Considering their dominant production modes, some generic relations for flux ratios of different flavours of neutrinos can be derived without detailed calculations. From the decay chain of a charged pion $\pi^+ \rightarrow \mu^+ \nu_\mu$ followed by $\mu^+ \rightarrow e^+ \nu_e \bar{\nu}_\mu$ (and the charge conjugate for π^-), the ratio $(\nu_\mu + \bar{\nu}_\mu)/(\nu_e + \bar{\nu}_e)$ is expected to be around 2 at low energies ($\sim 1 \text{ GeV}$), where most muons decay in the atmosphere. For higher energies, some muons reach the Earth before they decay and the ratio increases. One can also

expect that the zenith angle distributions of atmospheric neutrinos are symmetric between upward-going and downward-going neutrinos. It is true for the energy above 1 GeV, but at lower energies, the Earth's geomagnetic field induces up-down asymmetries in the primary cosmic ray. The zenith angle corresponds to the flight length of atmospheric neutrinos. Vertically upward-going neutrinos come from the other side of the Earth with flight lengths of $\sim 10^4$ km, while downward-going neutrinos produced just above the experimental site travel ~ 10 km before detection.

The atmospheric neutrino fluxes are calculated in detail based on the energy spectrum and composition of primary cosmic rays and their hadronic interactions in the atmosphere. The effects of solar activity and geomagnetic field are also taken into account. Results of calculations by several groups are available [74–77]. A typical uncertainty of the absolute flux is 10–20%, while the ratio of fluxes between different flavour has much smaller uncertainty (< 5%).

14.6.2.2 Observation of atmospheric neutrino oscillations

The first detection of atmospheric neutrinos was reported in the 1960's by the underground experiments in the Kolar Gold Field experiment in India [78] and in South Africa [79]. In the 1980's, experiments searching for nucleon decays started operation. They used large underground detectors which could also observe atmospheric neutrinos that were studied as backgrounds to nucleon decays. Among the early experiments were Kamiokande [80] and IMB [81] using water Cherenkov detectors, and Frejus [82] and NUSEX [83] using iron tracking calorimeters.

The flavour of an atmospheric neutrino can be identified in charged current interaction with nuclei, which produces the corresponding charged lepton. Those detectors originally designed for nucleon decay search had the capability to distinguish muons and electrons. For example, a water Cherenkov detector can utilize the information from Cherenkov ring patterns for particle identification; e -like particles (e^\pm , γ) produce more diffuse ring than μ -like particles (μ^\pm , π^\pm) because of electromagnetic cascades and multiple Coulomb scattering effects.

To reduce the uncertainty, in early results the flux ratio $\nu_\mu/\nu_e \equiv (\nu_\mu + \bar{\nu}_\mu)/(\nu_e + \bar{\nu}_e)$ was measured, and the double ratio between observation and expectation $(\nu_\mu/\nu_e)_{\text{obs}}/(\nu_\mu/\nu_e)_{\text{exp}}$ was reported. The Kamiokande experiment reported an indication of a deficit of $(\nu_\mu + \bar{\nu}_\mu)$ flux [80]. IMB also observed a similar deficit [81], but measurements by Frejus [82] and NUSEX [83] were consistent with the expectations. This was called the atmospheric neutrino anomaly. Kamiokande reported studies with an increased data set of the sub-GeV (< 1.33 GeV) [84] as well as the multi-GeV (> 1.33 GeV) [85] samples. In the latter, they reported an analysis of zenith angle distributions, which showed an indication that the muon disappearance probability is dependent on the zenith angle, hence the travel length of neutrinos. However, the statistical significance was not sufficient to provide a conclusive interpretation.

The solution to the atmospheric neutrino anomaly was brought by Super-Kamiokande, which reported compelling evidence for neutrino oscillations in atmospheric neutrinos in 1998 [86]. The zenith angle (θ_z , with $\theta_z = 0$ for vertically downward-going) distributions of μ -like events showed a clear deficit of upward-going events, while no significant asymmetry was observed for e -like events. The asymmetry is defined as $A = (U - D)/(U + D)$, where U is the number of upward-going ($-1 < \cos \theta_z < -0.2$) events and D is the number of downward-going ($0.2 < \cos \theta_z < 1.0$) events. With multi-GeV (visible energy > 1.33 GeV) μ -like events alone, the measured asymmetry was $A = -0.296 \pm 0.048 \pm 0.001$, deviating from zero by more than 6σ . The sub-GeV (< 1.33 GeV) μ -like, upward through going, and upward stopping μ samples which correspond to different energy ranges of neutrinos, showed the consistent behaviour which strengthens the credibility of the observation. Super-Kamiokande's results were confirmed by other atmospheric neutrino observations MACRO [87] and Soudan2 [88].

Although the energy and zenith-angle-dependent muon neutrino disappearance observed with atmospheric neutrinos could be consistently explained by the neutrino oscillations predominantly between ν_μ and ν_τ , other exotic explanations such as neutrino decay [89] or decoherence [90] were not initially ruled out. By using a selected sample from Super-Kamiokande's atmospheric

data with good L/E resolution, the L/E dependence of the survival probability was measured [91]. The observed dip in the L/E distribution was consistent with the expectation from neutrino oscillation, while alternative models were strongly disfavored.

As an experimental proof of ν_μ - ν_τ oscillation, an appearance signal of ν_τ was searched for in the atmospheric neutrino data. Because of the high energy threshold (> 3.5 GeV) of ν_τ CC interaction and the short lifetime of τ lepton (0.3 ps), identifying the appearance of ν_τ experimentally is challenging. Super-Kamiokande reported evidence of tau neutrino appearance using atmospheric neutrino data with 4.6σ significance [92]. The definitive observation of ν_τ appearance was made by the long-baseline experiment, OPERA (See Sec.14.6.3.3), and recently IceCube also reported the ν_τ appearance analysis [93] using atmospheric neutrinos.

14.6.2.3 Neutrino oscillation measurements using atmospheric neutrinos

Figure 14.4 shows the zenith angle distributions of atmospheric neutrino data from Super-Kamiokande. For a wide range of neutrino energy and path length, the observed distributions are consistent with the expectation from neutrino oscillation. Atmospheric neutrinos in the energy region of a few to ~ 10 GeV provide information for the determination of the neutrino mass ordering [94].

The neutrino telescopes primarily built for high-energy neutrino astronomy such as ANTARES and IceCube can also measure neutrino oscillations with atmospheric neutrinos. ANTARES consists of a sparse array of PMTs deployed under the Mediterranean Sea at a depth of about 2.5 km to instrument a 10^5 m³ volume. IceCube is a detector deployed in ice in Antarctica at the South Pole, at a depth between 1.45 and 2.45 km. In the bottom center of IceCube there is a region of $\sim 10^7$ m³ volume with denser PMT spacing called DeepCore to extend the observable energies to the lower energy region. By observing the charged current interaction of up-going ν_μ , they measure the ν_μ disappearance. ANTARES reported a measurement of ν_μ disappearance with 20 GeV threshold [95]. The ν_μ disappearance measurements from IceCube DeepCore [96] provided a precision comparable to the measurements by Super-Kamiokande and long-baseline accelerator neutrino experiments.

There are several projects for atmospheric neutrino observations either proposed or under preparation. The atmospheric neutrino observation program is included in the plans for future neutrino telescopes such as ORCA in the KM3NeT project [97] in the Mediterranean Sea and the IceCube Upgrade [98]. In India, a 50 kt magnetized iron tracking calorimeter ICAL is planned at the INO [99]. Future large underground detectors, Hyper-Kamiokande in Japan [100] and DUNE in US [101] can also study the atmospheric neutrinos.

14.6.3 Accelerator Neutrinos

14.6.3.1 Accelerator neutrino beams

A comprehensive description of the accelerator neutrino beams is found in [102]. Conventional neutrino beams from accelerators are produced by colliding high-energy protons onto a target, producing π and K , which then decay into neutrinos. Undecayed mesons and muons are stopped in a beam dump and soil. Because pions are the most abundant product of the high energy collisions, a conventional neutrino beam contains a dominant amount of muon-type neutrinos (or antineutrinos).

Focusing devices called magnetic horns are used to concentrate the neutrino beam flux towards the desired direction [103]. A magnetic horn is a pulsed electromagnet with toroidal magnetic fields to focus charged particles that are parents of neutrinos. One can choose the dominant component of the beam to be either neutrinos or antineutrinos by selecting the direction of current in the magnetic horns. Even with the focusing with horns, *wrong sign* neutrinos contaminate in the beam. Also, there is a small amount of contamination of ν_e and $\bar{\nu}_e$ coming primarily from kaon and muon decays.

In order to maximize the sensitivity of the experiment, the ratio of baseline and neutrino energy (L/E) should be chosen to match the oscillation effects to be studied. In addition to maximizing the flux of neutrinos with relevant energy, neutrinos with irrele-

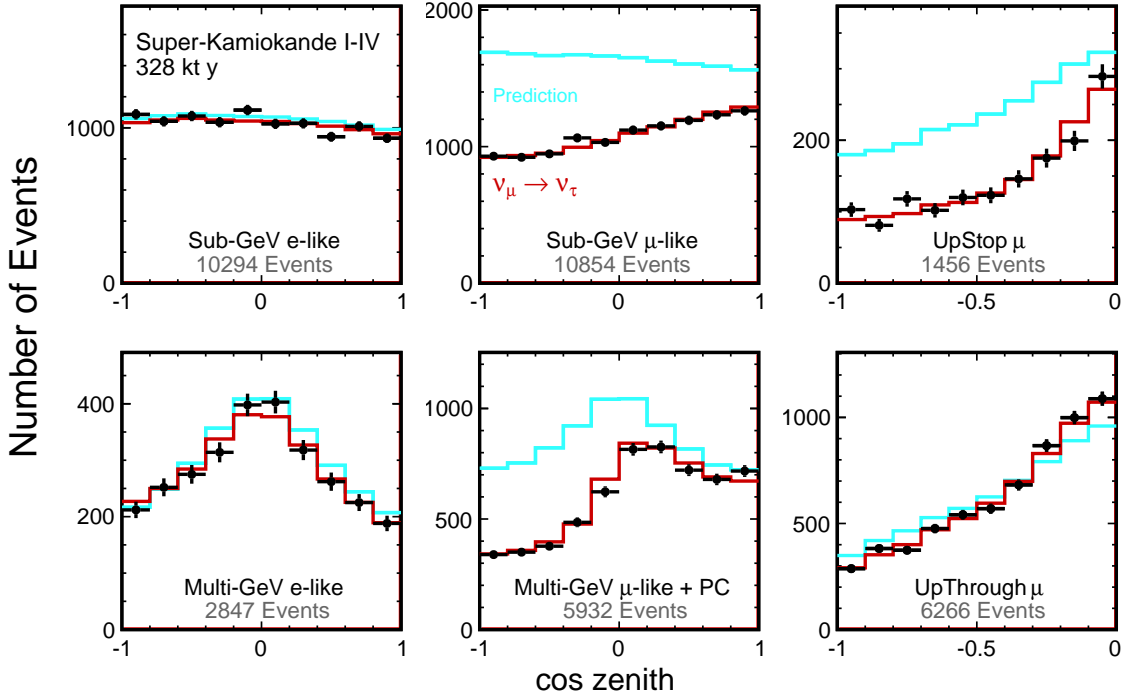


Figure 14.4: The zenith angle distributions of Super-Kamiokande atmospheric neutrino events. A data set corresponding to 328 kton-years of exposure is used. Fully contained 1-ring e -like and μ -like events with visible energy < 1.33 GeV (sub-GeV) and > 1.33 GeV (multi-GeV), as well as upward stopping and upward through going μ samples are shown. Partially contained (PC) events are combined with multi-GeV μ -like events. The blue histograms show the non-oscillated Monte Carlo events, and the red histograms show the best-fit expectations for neutrino oscillations. (This figure is provided by the Super-Kamiokande Collaboration)

vant energy that result in unwanted background process should be suppressed. The energy of a neutrino from a pion decay is

$$E_\nu = \frac{[1 - (m_\mu/m_\pi)^2]E_\pi}{1 + \gamma^2\theta^2}, \quad (14.71)$$

where E_ν and E_π are the energy of neutrino and pion, respectively, θ is the angle between the pion and neutrino direction, and $\gamma = E_\pi/m_\pi$. For $\theta = 0$, the energy of neutrino is linearly proportional to the energy of pion. In this case, a narrow band beam can be made by selecting the momentum of pions. On the other hand, for $\theta \neq 0$, the energy of neutrino is not strongly dependent on the parent energy for a wide range of pion energy, but dependent on the off-axis angle θ . Using this relation, a neutrino beam with narrow energy spectrum, around the energy determined by θ , can be produced. This off-axis beam method was first introduced for BNL E889 proposal [104] and adopted in T2K and NOvA experiments. For a list of neutrino beamlines, see also Chapter 33 of this *Review*, “Neutrino Beam Lines at High-Energy Proton Synchrotrons.”

As indicated in Table 14.1, there are two different scales of baselines for accelerator-based experiments to study different ranges of Δm^2 . The atmospheric mass splitting $\Delta m^2 \sim 2.5 \times 10^{-3} \text{ eV}^2$ gives rise to the first oscillation maximum at $L/E \sim 500 \text{ GeV/km}$. In order to study this parameter region with a $\sim 1 \text{ GeV}$ accelerator neutrino beam, a long baseline of a few hundred to a thousand km is necessary. On the other hand, there have been reports of possible neutrino oscillations at the $\sim 1 \text{ eV}^2$ scale, which can be studied at $\sim 1 \text{ km}$ baseline with neutrinos from accelerators. These experiments are called short-baseline oscillation experiments.

The flux of a neutrino beam is calculated using Monte Carlo simulation based on the configuration of the beamline. An important ingredient of the neutrino flux prediction is the hadron production cross-section. Data from dedicated hadron production experiments [105–108] are used to tune the beam simulation and constrain the uncertainty. The uncertainty of predicted neutrino flux for the most relevant energy region is 5–10% with the latest hadron production data [109–111].

14.6.3.2 Near detectors and neutrino interaction cross sections

Many long-baseline experiments use two detectors to reduce the systematic uncertainties arising from neutrino flux and neutrino-nucleus interactions. The near detectors either use the same technology as the far detector or consist of sub-detectors with complementary functions to obtain detailed information of the neutrino beam and interactions. The near detectors provide information for the neutrino flux, energy spectrum, and the interaction cross-sections, which is used as input to make predictions of observables at the far detector. However, even with the two-detector configuration, one should note that the neutrino flux is inevitably different between the near and the far detectors. In addition to the fact that the neutrino source looks like a line source for the near detector while it looks like a point source for the far detector, the neutrino oscillations alter the flavour composition of the neutrino beam quite significantly, as the design of a neutrino oscillation experiment requires.

For the precision measurements of neutrino oscillations with long-baseline experiments, the understanding of the neutrino-nucleus interaction becomes crucial. Because heavy nuclei are used as the interaction target, the nuclear effects complicate the understanding of the neutrino-nucleus interaction. For more information on the neutrino cross-sections, see also Chapter 52 of this *Review*, “Neutrino Cross Section Measurements.”

14.6.3.3 Long-baseline experiments

Long-baseline neutrino oscillation experiments are summarized in Table 14.3. The first long-baseline experiment was the K2K experiment which used a neutrino beam from the KEK 12 GeV proton synchrotron directed towards Super-Kamiokande with a baseline of 250 km. The beam had an average energy of 1.3 GeV. The K2K near detectors, located 300 m downstream of the production target, consisted of a combination of a 1 kt water Cherenkov detector and a set of fine-grained detectors. K2K confirmed the muon neutrino disappearance originally reported by Super-Kamiokande atmospheric neutrino observation [112].

The MINOS experiment used a beam from Fermilab and a de-

Table 14.3: List of long-baseline neutrino oscillation experiments

Name	Beamline	Far Detector	L (km)	E_ν (GeV)	Year
K2K	KEK-PS	Water Cherenkov	250	1.3	1999–2004
MINOS	NuMI	Iron-scintillator	735	3	2005–2013
MINOS+	NuMI	Iron-scintillator	735	7	2013–2016
OPERA	CNGS	Emulsion hybrid	730	17	2008–2012
ICARUS	CNGS	Liquid argon TPC	730	17	2010–2012
T2K	J-PARC	Water Cherenkov	295	0.6	2010–
NOvA	NuMI	Liquid scint. tracking calorimeter	810	2	2014–
DUNE	LBNF	Liquid argon TPC	1300	2–3	
Hyper-Kamiokande	J-PARC	Water Cherenkov	295	0.6	

tector in the Soudan mine 735 km away. The neutrino beam is produced in the NuMI beamline with a 120 GeV proton beam from the Main Injector. The MINOS detectors were both iron-scintillator tracking calorimeters with toroidal magnetic fields. The far detector was 5.4 kt, while the near detector had a total mass of 0.98 kt and was located 1 km downstream of the production target. The energy spectrum of the NuMI beamline can be varied by changing the relative position of the target and horns. Most of MINOS data were taken with the “low energy” configuration with a peak energy of around 3 GeV. Since 2013, NuMI was operated with a “medium energy” configuration with the peak neutrino energy of around 7 GeV. The experiment for this period was called MINOS+. MINOS and MINOS+ combined accelerator and atmospheric neutrino data in both disappearance and appearance modes to measure oscillation parameters [113, 114].

In Europe, the CNGS neutrino beamline provided a beam with mean energy of 17 GeV from CERN to LNGS for long-baseline experiments with about 730 km of baseline. The beam energy was chosen so that CC interaction of ν_τ can occur for direct confirmation of ν_τ appearance. There was no near detector in CNGS because it was not necessary for the ν_τ appearance search. The OPERA experiment used a detector consisting of an emulsion/lead target with about 1.25 kt total mass, complemented by electronic detectors. The excellent spatial resolution of the emulsion enabled the event-by-event identification of τ leptons. OPERA observed ten ν_τ CC candidate events with 2.0 ± 0.4 expected background [115] and confirmed $\nu_\mu \rightarrow \nu_\tau$ oscillation in appearance mode with a statistical significance of 6.1σ . Another neutrino experiment, ICARUS [116], which used 600 t liquid argon time projection chambers (TPCs), was operated in Gran Sasso from 2010 to 2012.

The first generation of long-baseline experiments confirmed the existence of neutrino oscillation. The major initial goal of second-generation experiments was the observation of $\nu_\mu \rightarrow \nu_e$ oscillation. Using this appearance mode, and by comparison of neutrino and antineutrino oscillation probabilities, search for CP violation in the neutrino mixing and measurement of the mass ordering and the octant of θ_{23} become possible.

The T2K experiment started in 2010 using a newly constructed high-intensity proton synchrotron J-PARC and the Super-Kamiokande detector. It is the first long-baseline experiment to employ the off-axis neutrino beam. The off-axis angle of 2.5° was chosen to set the peak of the neutrino energy spectrum at 0.6 GeV, matching the first maximum of oscillation probability at the 295 km baseline for $\Delta m^2 \sim 2.5 \times 10^{-3} \text{ eV}^2$. T2K employs a set of near detectors at about 280 m from the production target. In 2011, T2K reported the first indication of $\nu_\mu \rightarrow \nu_e$ oscillation with a statistical significance of 2.5σ [117]. In the framework of 3ν mixing, it corresponds to detecting non-zero amplitude generated by the mixing angle θ_{13} (see Eq.14.33). Later $\nu_\mu \rightarrow \nu_e$ oscillation was established by T2K with more than 7σ in 2014 [118]. Figure 14.5 shows the observed kinematic distributions from T2K, for neutrino and antineutrino beam mode and also for muon and electron candidates. By a combined analysis of the neutrino and antineutrino data, T2K reported a hint of CP violation at the 2σ level [119].

The NOvA experiment uses the upgraded NuMI beamline with an off-axis configuration. The 14 kt NOvA far detector is lo-

cated near Ash River, Minnesota, 810 km away from the source. At 14.6 mrad off-axis from the central axis of the NuMI beam, the neutrino energy spectrum at the far detector has a peak of around 2 GeV. The near detector, located around 1 km from the source, has a functionally identical design to the far detector with a total mass of 290 t. Both detectors are tracking calorimeters consisting of planes of polyvinyl chloride cells alternating in vertical and horizontal orientation filled with liquid scintillator. The physics run of NOvA was started in 2014. After confirmation of ν_e appearance from ν_μ beam [120], NOvA started data taking with antineutrino beam in 2016. Using the antineutrino beam data, NOvA has reported the observation of $\bar{\nu}_e$ appearance from $\bar{\nu}_\mu$ beam with 4.4σ significance [121]. Figure 14.6 shows the reconstructed neutrino energy distributions from NOvA [122]. The NOvA data do not show a strong asymmetry in the rate of ν_e versus $\bar{\nu}_e$ appearance, excluding $\delta_{CP} = 90^\circ$ for the inverted mass ordering ($m_3 < m_2 < m_1$, see Sec.14.7 for definitions) with $> 3\sigma$ and disfavoring $\delta_{CP} = 270^\circ$ for the case of normal mass ordering ($m_1 < m_2 < m_3$, see Sec.14.7 for definitions) with $> 2\sigma$.

Two large-scale long-baseline experiments are under construction. DUNE [101] will be a 1,300 km long-baseline experiment based in the US. The DUNE far detector will consist of four modules of at least 10 kt fiducial mass liquid argon time projection chambers, located 1.5 km underground at the Sanford Underground Research Facility in South Dakota. The beamline for DUNE, 1.2 MW at start and upgradable to 2.4 MW, as well as the facility for near detectors will be newly constructed at Fermilab. The Hyper-Kamiokande detector [100] in Japan will be the successor of the Super-Kamiokande detector. It will be a water Cherenkov detector with 260 kt total water mass. With upgrades to the existing accelerator and beamline, J-PARC will provide a 1.3 MW neutrino beam to Hyper-Kamiokande with a baseline of 295 km. Both DUNE and Hyper-Kamiokande will have a rich physics program besides the long-baseline experiment, such as searches for nucleon decays and study of supernova neutrinos.

14.6.3.4 Short-baseline experiments

The LSND experiment searched for neutrino oscillation using neutrinos from stopped pions at Los Alamos. A 800 MeV linac was used to produce pions that stopped in the target. Most of π^- s are absorbed by the nuclei inside the target, while π^+ s and their daughter μ^+ s decay and produce neutrinos. Therefore, the produced neutrinos are mostly ν_μ , $\bar{\nu}_\mu$, and ν_e with minimal contamination of $\bar{\nu}_e$. The detector was a tank filled with 167 t of diluted liquid scintillator, located about 30 m from the neutrino source. LSND searched for $\bar{\nu}_\mu \rightarrow \bar{\nu}_e$ appearance using the inverse beta decay process, $\bar{\nu}_e + p \rightarrow e^+ + n$, and found an excess of $87.9 \pm 22.4 \pm 6.0$ events over the expected background [123].

The KARMEN experiment was performed at the neutron spallation facility ISIS of the Rutherford Appleton Laboratory. The KARMEN 2 detector was a segmented liquid scintillation calorimeter with a total volume of 65 m^3 located at a mean distance of 17.7 m from the ISIS target. KARMEN found a number of events consistent with the total background expectation, showing no signal for $\bar{\nu}_\mu \rightarrow \bar{\nu}_e$ oscillations [124]. The resulting limits exclude large regions of the parameter area favored by LSND.

The MiniBooNE experiment at Fermilab used a conventional neutrino beam to search for ν_e and $\bar{\nu}_e$ appearance in the same

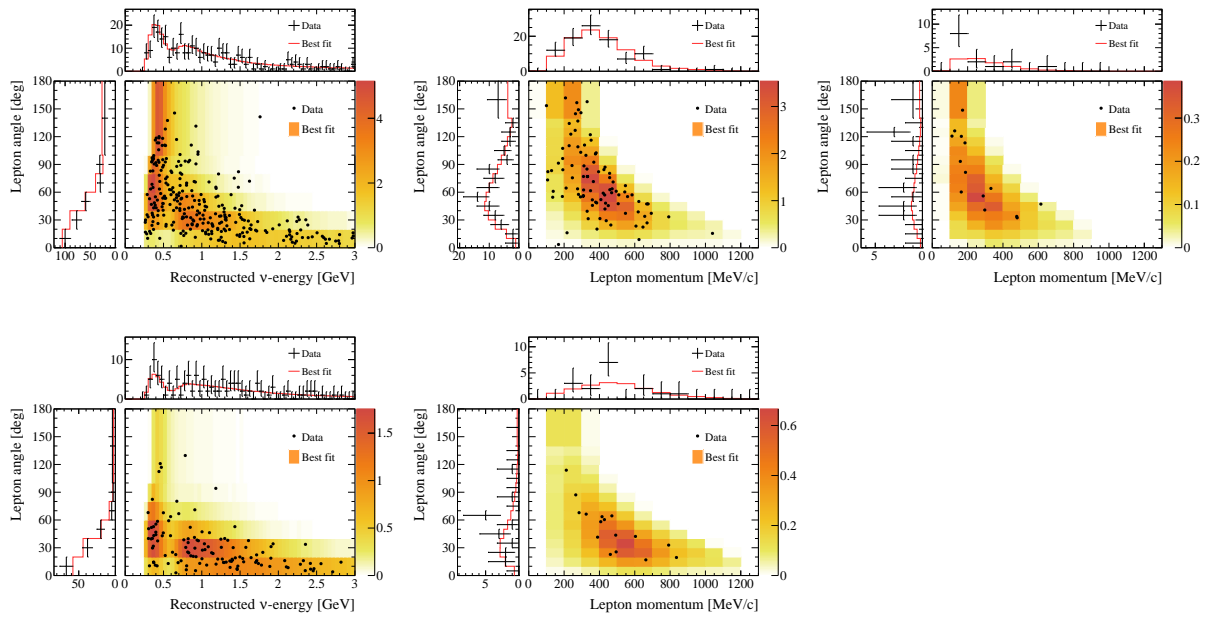


Figure 14.5: Observed kinematic distributions from T2K compared to the expectations with the best-fit parameters [119]. Top and bottom panels correspond to data from neutrino and antineutrino beam mode, respectively. Left, middle, and right panels show distributions for single ring μ -like events, single ring e -like events with no associated decay electron, and single ring e -like events with one associated decay electron (only for neutrino beam mode data), respectively.

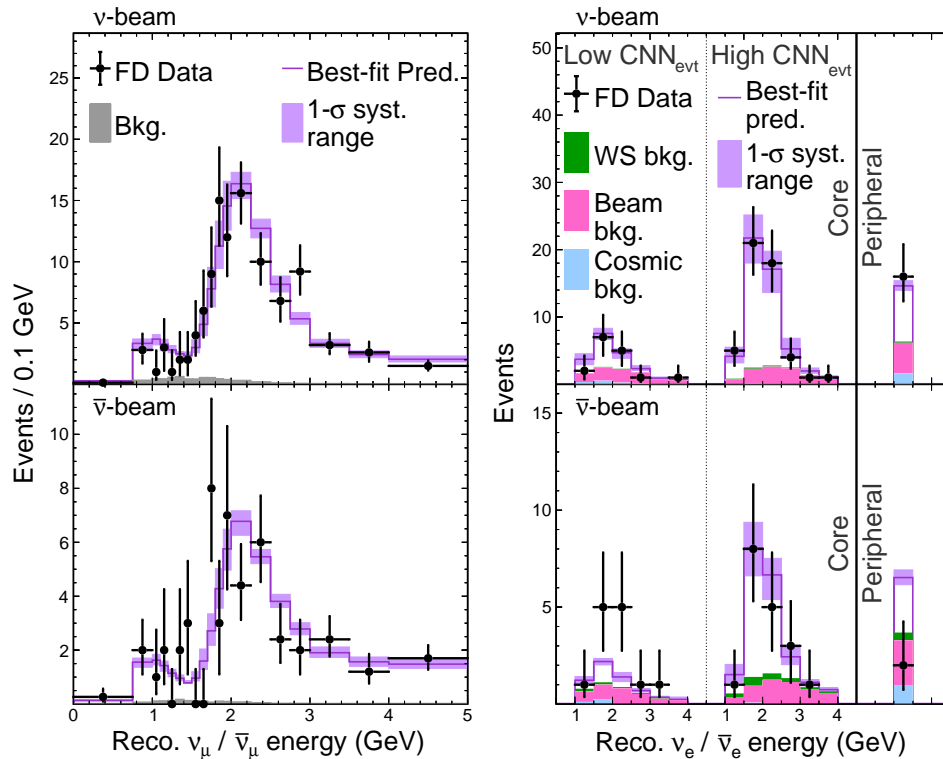


Figure 14.6: Reconstructed neutrino energy distributions from the NOvA far detector [122]. Top plots are for neutrino beam mode, and bottom plots are for antineutrino beam mode. Left: muon-type candidates. Right: electron-type candidates, split into a low and high purity sample as well as the event counts in the peripheral sample which occurred near the edge of the detector.

parameter region as LSND. The booster neutrino beamline (BNB) with a single magnetic horn uses an 8 GeV proton beam from the Fermilab booster to produce a neutrino (antineutrino) beam with an energy spectrum peak of 600 (400) MeV. The MiniBooNE detector consists of a 12.2 m diameter sphere filled with 818 t of mineral and oil located 541 m from the target. MiniBooNE reported ν_e and $\bar{\nu}_e$ event excess in both neutrino and antineutrino running modes. In total, $638.0 \pm 52.1 \pm 122.2$ excess events are observed over the expected backgrounds, corresponding to 4.8σ significance [125].

Both LSND and MiniBooNE are single detector experiments. The short-baseline neutrino (SBN) program at Fermilab BNB [126] is further investigating the reported excess with a multi-detector configuration. The SBN program comprises three liquid argon time projection chambers at different baselines in the same neutrino beamline. The 85 t MicroBooNE detector was operated at 470 m from the target. The 112 t Short-Baseline Near Detector is located at 110 m from the target. The ICARUS detector was transported from Europe after refurbishment at CERN and is located at a baseline of 600 m as the SBN Far Detector. As of the writing of this review, MicroBooNE is the only experiment that has presented results from SBN, observing no excess of ν_e events [127] and no evidence of light sterile neutrino oscillations [128].

JSNS² experiment at J-PARC has started the search for neutrino oscillations with $\Delta m^2 \sim 1 \text{ eV}^2$ [129]. 1MW proton beam from the 3 GeV Rapid Cycling Synchrotron of J-PARC produces neutrinos from muon decay at rest. With a detector filled with a gadolinium-loaded liquid scintillator of 17 t fiducial mass at 24 m from the target, JSNS² is aiming to provide a direct test of the LSND anomaly. The second phase with an additional second detector at 48 m is under preparation.

14.6.4 Reactor Antineutrinos

14.6.4.1 Reactor antineutrino flux

Nuclear reactors are very intense sources of $\bar{\nu}_e$'s in the MeV energy region, which are generated in nuclear fission of heavy isotopes (mainly ²³⁵U, ²³⁸U, ²³⁹Pu, and ²⁴¹Pu). The $\bar{\nu}_e$ flux from a reactor can be estimated based on the thermal power output and fuel composition as a function of time. On average, about six $\bar{\nu}_e$'s are emitted, and about 200 MeV of energy is released per fission. Therefore, a 1 GW_{th} (thermal power) reactor produces about 2×10^{20} $\bar{\nu}_e$'s per second.

The detailed estimate of $\bar{\nu}_e$ flux and energy spectrum can be obtained by either summing up the spectra of beta decays involved using available nuclear data information of each fission fragment and its decays, or by using measurements of cumulative electron spectra associated with the beta decays of fission fragments. Because the fission of four main fuel isotopes involves thousands of beta-decay branches, a complete *ab initio* calculation is challenging. The cumulative electron spectra for ²³⁵U, ²³⁹Pu, and ²⁴¹Pu were measured at the Institut Laue-Langevin (ILL) reactor in Grenoble, France in the 1980s [130–132]. For the prediction of $\bar{\nu}_e$ flux from ²³⁸U, a summation calculation in [133] was often used together with the ILL results.

A recent calculation of the reactor $\bar{\nu}_e$ flux [134] uses an improved *ab initio* approach for ²³⁸U and combined information from nuclear databases and electron spectra measured at ILL for ²³⁵U, ²³⁹Pu, and ²⁴¹Pu. Another calculation [135] is provided for ²³⁵U, ²³⁹Pu, and ²⁴¹Pu based on the ILL measurement of electron spectra, taking into account higher-order corrections and minimizing the use of nuclear databases. Both calculations predict a few percent higher normalization for the energy-averaged antineutrino fluxes of ²³⁵U, ²³⁹Pu, and ²⁴¹Pu compared to the original analyses of ILL data. However, the reactor antineutrino flux measurement at Daya Bay [136] is consistent with the old flux predictions and the flux measurement results. Also, an excess of $\bar{\nu}_e$ flux around 5 MeV, compared to the prediction, has been observed by recent reactor experiments [137–139].

14.6.4.2 Reactor antineutrino oscillation experiments

Charged current interaction cannot happen if a reactor $\bar{\nu}_e$ changes its flavour to $\bar{\nu}_\mu$ or $\bar{\nu}_\tau$, because its energy is not sufficient to produce heavier charged leptons. Thus, $\bar{\nu}_e$ disappear-

ance is the only channel to study neutrino flavour change with reactor experiments. The inverse beta decay $\bar{\nu}_e + p \rightarrow e^+ + n$ provides a way to detect $\bar{\nu}_e$ in the relevant energy region. The energy of prompt signal from e^+ , E_p , is related to the energy of $\bar{\nu}_e$, $E_{\bar{\nu}} \sim E_p + 0.8 \text{ MeV}$. The delayed coincidence with the signal from γ ray emitted by neutron capture on nucleus after thermalization very efficiently suppresses the backgrounds. A liquid scintillator is often used to realize large detectors containing hydrogen as the target of inverse beta decay. In order to increase the neutron detection efficiency, a liquid scintillator is sometimes loaded with gadolinium because of a large neutron capture cross-section and higher energy of emitted γ rays, the total energy of about 8 MeV, by gadolinium, in contrast to 2.2 MeV for the capture by hydrogen.

Table 14.4 shows a list of reactor antineutrino experiments measuring neutrino oscillations. As was also shown in Table 14.1, experiments are designed with different baselines because of the different scale of mass splittings found by solar and atmospheric neutrino experiments. Experiments with O(100) km baseline are sensitive to Δm^2 of 10^{-4} – 10^{-5} eV^2 , while $\sim 1 \text{ km}$ of baseline results in a sensitivity in the range of 10^{-2} – 10^{-3} eV^2 .

The KamLAND detector consists of 1,000 t of ultra-pure liquid scintillator contained in a 13-m diameter spherical balloon [140]. The detector is located in the original Kamiokande cavern, where the $\bar{\nu}_e$ flux was dominated by a few reactors at an average distance of $\sim 180 \text{ km}$ until 2011. KamLAND reported the first results in 2002 showing that the ratio of the observed number of $\bar{\nu}_e$ events and expectation without disappearance is $0.611 \pm 0.085 \pm 0.041$, evidence for reactor $\bar{\nu}_e$ disappearance at the 99.95% confidence level [140]. It confirmed a large value of the mixing angle corresponding to the LMA solution, which was reported by solar neutrino experiments. KamLAND also showed the evidence of $\bar{\nu}_e$ spectrum distortion consistent with the expectation from neutrino oscillations [141]. Figure 14.7 shows the ratio of observed $\bar{\nu}_e$ spectrum to the expectation for no-oscillation as a function of L_0/E ($L_0 = 180 \text{ km}$) for the KamLAND data. A clear oscillatory signature can be seen.

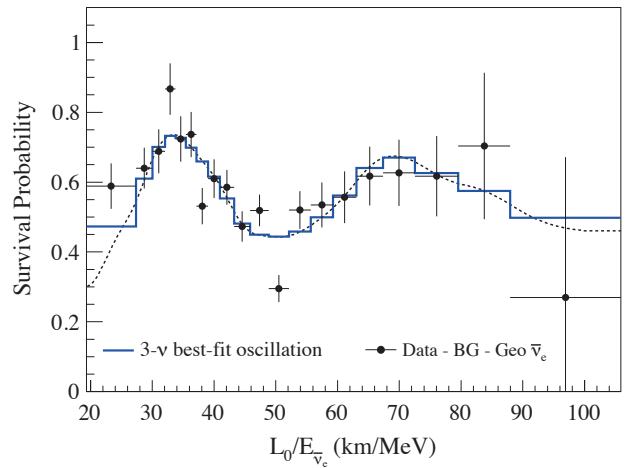


Figure 14.7: Ratio of the observed $\bar{\nu}_e$ spectrum to the expectation for no-oscillation versus L_0/E for the KamLAND data. $L_0 = 180 \text{ km}$ is the flux-weighted average reactor baseline. The 3- ν histogram is the best-fit survival probability curve from the three-flavour unbinned maximum-likelihood analysis using only the KamLAND data. This figure is taken from [142].

Following the establishment of neutrino oscillations with atmospheric, solar, accelerator, and reactor experiments, the measurement of the remaining mixing angle θ_{13} was recognized as the next major milestone. A reactor neutrino experiment with a baseline of $\sim 1 \text{ km}$ can make an almost pure measurement of $\sin^2 2\theta_{13}$ from the disappearance of $\bar{\nu}_e$. To be sensitive to a small value of θ_{13} , experiments with two detectors were proposed. Among several proposals, three experiments have been realized: Double Chooz

Table 14.4: List of reactor antineutrino oscillation experiments

Name	Reactor power (GW _{th})	Baseline (km)	Detector mass (t)	Year
KamLAND	various	180 (ave.)	1,000	2001–
Double Chooz	4.25×2	1.05	8.3	2011–2018
Daya Bay	2.9×6	1.65	20×4	2011–2020
RENO	2.8×6	1.38	16	2011–
JUNO	26.6 (total)	53	20,000	

in France, Daya Bay in China, and RENO in Korea.

These three experiments employ a similar detector design optimized for the precise measurement of a reactor antineutrino. An antineutrino detector consists of a cylindrical stainless steel vessel that houses two nested acrylic cylindrical vessels. The innermost vessel is filled with gadolinium-doped liquid scintillator as the primary antineutrino target. It is surrounded by a liquid scintillator layer to contain γ rays from the target volume. A buffer layer of mineral oil is placed outside to shield inner volumes from radioactivity of PMTs and surrounding rock. The light from liquid scintillator is detected by an array of PMTs mounted on the stainless steel vessel. Optically separated by the stainless steel vessel, the outside region is instrumented as a veto detector with either liquid scintillator (Double Chooz) or water Cherenkov (Daya Bay and RENO) detector.

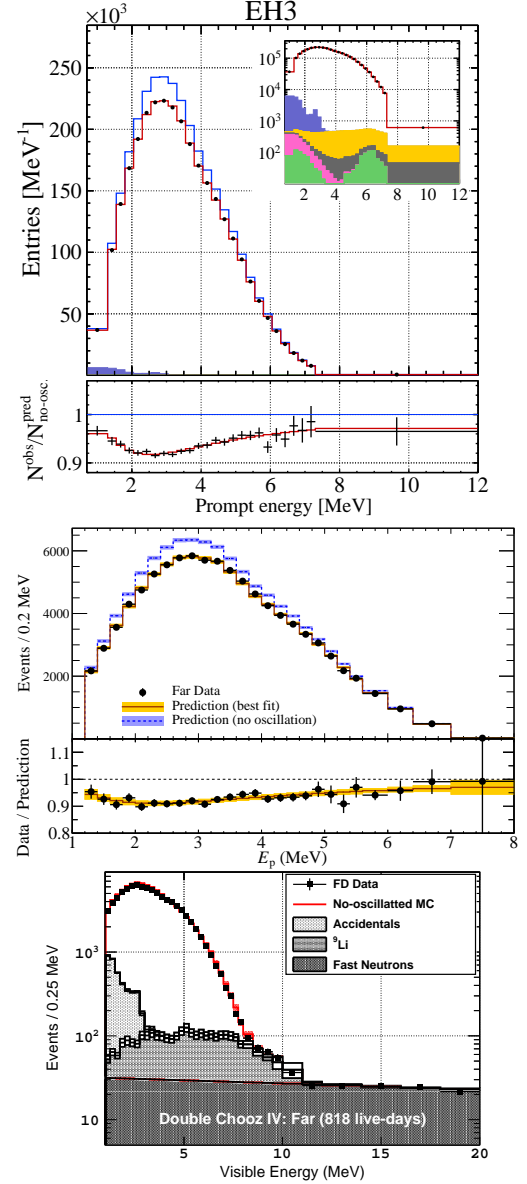
The Double Chooz detector has a gadolinium-doped liquid scintillator with a mass of 8.3 t. The far detector at a baseline of ~ 1050 m from the two 4.25 GW_{th} reactors started physics data taking in 2011. The near detector, located at ~ 400 m from the reactors, was completed in the end of 2014. Double Chooz finished data taking in early 2018. Daya Bay has two near (flux-weighted baseline 470 m and 576 m), and one far (1648 m) underground experimental halls near six reactors with 2.9 GW_{th} each. Daya Bay has eight antineutrino detectors in total; two detectors in each of the near detector halls, and four detectors in the far detector hall. Each detector contains 20 t of gadolinium-loaded liquid scintillator. RENO has two identical detectors located at 294 m and 1383 m from the center of an array of six 2.8 GW_{th} reactors. The mass of the gadolinium-loaded liquid scintillator is 16 t per detector. RENO started data taking with both near and far detectors in August 2011.

All three reactor neutrino experiments published their first results in 2012. First, Double Chooz reported an indication of reactor electron antineutrino disappearance with the ratio of observed to expected events of $R = 0.944 \pm 0.016 \pm 0.04$, ruling out the no-oscillation hypothesis at the 94.6% CL [143]. Daya Bay observed $R = 0.940 \pm 0.011 \pm 0.004$, corresponding to 5.2σ significance of non-zero value of θ_{13} [144]. RENO also reported $R = 0.920 \pm 0.009 \pm 0.014$, indicating a non-zero value of θ_{13} with a significance of 4.9σ [145]. These results established a non-zero value of θ_{13} .

Both Daya Bay [146] and RENO [137] report results constraining mass-squared difference as well as the mixing angle by using both relative $\bar{\nu}_e$ rate and energy spectra information. Double Chooz has reported the analysis based on both far and near detectors [138] for the mixing angle, using neutron capture on any elements (primarily gadolinium and hydrogen) to increase the effective target mass. Figure 14.8 shows the energy spectra of the prompt signals observed in the far detector of three experiments.

In all three experiments, an excess of $\bar{\nu}_e$ events over the expected energy spectrum has been observed around 5 MeV, as mentioned earlier. This excess is observed in both near and far detectors and scales with the reactor power. Thanks to the cancellation between the near and far detectors, the neutrino oscillation measurements are not affected in a multi-detector setup.

With a baseline of ~ 50 km and an excellent energy measurement, reactor antineutrino experiments have significant sensitivity to the mass ordering. The JUNO detector, which is under construction, will consist of a 20 kt liquid scintillator and be located at 53 km from two nuclear power plants in China [147]. The JUNO experiment aims to determine the mass ordering with this technique as its primary goal. It can also provide precision

**Figure 14.8:** Energy spectra for prompt events at the far detectors for Daya Bay [146], RENO [137], and Double Chooz [138].

measurements of neutrino mixing parameters as well as a broad non-oscillation science program.

14.6.4.3 Reactor experiments sensitive to $O(1)$ eV^2 oscillations

Possible hints of neutrino oscillation at a scale of $\Delta m^2 \sim 1$ eV^2 (see Sec.14.8) have motivated reactor experiments at a distance of ~ 10 m from the core. Recent experiments searching for ~ 1 eV^2 oscillation at reactors are summarized in Table 14.5.

As the antineutrino source, some use commercial reactors, which can provide a large flux leading to high statistical preci-

Table 14.5: List of reactor antineutrino experiments for $O(\text{eV}^2)$ oscillations

Name	Reactor power (MW _{th})	Baseline (m)	Detector mass (t)	Detector technology	σ_E/E @1 MeV(%)	S/B
NEOS	2,800	24	1	Gd-LS	5	22
DANSS	3,100	10–13	0.9	Gd-PS	34	~30
STEREO	57	9–11	1.7	Gd-LS	10	0.9
PROSPECT	85	7–9	4	⁶ Li-LS	4.5	1.3
NEUTRINO-4	100	6–12	1.5	Gd-LS	16	0.5
SoLid	80	6–9	1.6	⁶ Li-PS	14	

sion. On the other hand, though the flux is orders of magnitude smaller, a research reactor could have favorable conditions such as relatively easier access to a short baseline, simpler fuel composition, and compact core size.

The detectors are based on organic scintillators, either liquid scintillator (LS) or solid plastic scintillator (PS), which contain hydrogen as the target for inverse beta decay ($\bar{\nu}_e + p \rightarrow e^+ + n$). To identify the signal, neutron capture on either gadolinium (Gd) or ⁶Li is detected with delayed coincidence. When a neutron is captured by Gd, γ rays with a total energy of 8 MeV are emitted. After neutron capture, ⁶Li decays into triton and α . The effect of neutrino oscillation appears as a distortion of energy spectrum. To be independent from the reactor neutrino spectrum uncertainties, some experiments compare the spectra at different baselines by using a segmented detector or moving the detector.

NEOS [139,148] uses about 1 t of gadolinium-loaded liquid scintillator in an unsegmented detector. It is located at 23.7 m from the center of a commercial reactor and covered by an overburden of about 20 meters of water equivalent.

DANSS [149] is another experiment using a commercial reactor. The detector is highly segmented, consisting of 2,500 plastic scintillator strips, each with the size of $1 \times 4 \times 100 \text{ cm}^3$ and coated with a thin gadolinium-loaded reflective layer. The detector is placed on a movable platform below the reactor core, which varies the distance to the core from 10.7 to 12.7 m.

The STEREO detector [150,151] has six identical target cells of 37 cm length, $\sim 2 \text{ m}^3$ of volume in total, filled with gadolinium-loaded liquid scintillator. They are placed from 9.4 to 11.1 m from the compact (80 cm high, 40 cm diameter) core of the ILL research reactor.

The PROSPECT detector [152] consists of a segmented 4 t ⁶Li-doped liquid scintillator detector. It covers a baseline range of 7–9 m from the highly ²³⁵U enriched reactor core of the High Flux Isotope Reactor (HFIR) at Oak Ridge National Laboratory. Thin reflecting panels divide the LS volume into an 11×14 two-dimensional array of 154 optically isolated rectangular segments ($14.5 \times 14.5 \times 117.6 \text{ cm}^3$).

NEUTRINO-4 [153,154] uses a gadolinium-loaded liquid scintillator detector segmented in 10×5 sections with a total volume of 1.8 m^3 . The detector is installed on a movable platform and moved to various positions with baselines of 6–12 m from the SM-3 reactor core in Russia.

The SoLid detector [155] is a finely segmented detector made of $5 \times 5 \times 5 \text{ cm}^3$ plastic scintillator cubes and ⁶LiF:ZnS sheets. Using the difference of time constant of scintillation between ZnS and the plastic scintillator a n - γ separation capability is achieved. A detector with 1.6 t of active volume is installed at a distance of 6–9 m from the research reactor core in the BR2 reactor, Belgium.

14.7 Combined Analysis of Experimental Results: The 3ν Paradigm

From the experimental situation described in Sec.14.6 we conclude that

- Atmospheric ν_μ and $\bar{\nu}_\mu$ disappear most likely converting to ν_τ and $\bar{\nu}_\tau$. The results show an energy and distance dependence perfectly described by mass-induced oscillations.
- Accelerator ν_μ and $\bar{\nu}_\mu$ disappear over distances of ~ 200 to 800 km. The energy spectrum of the results show a clear oscillatory behavior also in accordance with mass-induced

oscillations with a wavelength in agreement with the effect observed in atmospheric neutrinos.

- Accelerator ν_μ and $\bar{\nu}_\mu$ appear as ν_e and $\bar{\nu}_e$ at distances ~ 200 to 800 km.
- Solar ν_e convert to ν_μ and/or ν_τ . The observed energy dependence of the effect is well described by massive neutrino conversion in the Sun matter according to the MSW effect
- Reactor $\bar{\nu}_e$ disappear over distances of ~ 200 km and ~ 1.5 km with different probabilities. The observed energy spectra show two different mass-induced oscillation wavelengths: at short distances in agreement with the one observed in accelerator ν_μ disappearance, and a long distance compatible with the required parameters for MSW conversion in the Sun.

The minimum scenario to describe these results requires the mixing between the three flavour neutrinos of the standard model in three distinct mass eigenstates. In this case U in Eq. (14.32) is a 3×3 matrix analogous to the CKM matrix for the quarks [21], but due to the possible Majorana nature of the neutrinos it can depend on six independent parameters: three mixing angles and three phases. There are several possible conventions for the ranges of the angles and ordering of the states. The community finally agreed to a parametrization of the leptonic mixing matrix as in Eq. (14.33). The angles θ_{ij} can be taken without loss of generality to lie in the first quadrant, $\theta_{ij} \in [0, \pi/2]$, and the phase $\delta_{CP} \in [0, 2\pi]$. Values of δ_{CP} different from 0 and π imply CP violation in neutrino oscillations in vacuum [156–158]. The Majorana phases η_1 and η_2 play no role in neutrino oscillations [157,159]. Hence for the study of neutrino oscillations in the 3ν mixing scenario one can use the parametrization in Eq. (14.34) irrespective of whether neutrinos are Dirac or Majorana particles. Indeed, Majorana phases are very hard to measure since they are only physical if neutrino mass is non-zero, and therefore, the amplitude of any process involving them is suppressed by a factor m_ν/E to some power where E is the energy involved in the process, which is typically much larger than the neutrino mass. The most sensitive experimental probe of Majorana phases is the rate of neutrinoless $\beta\beta$ decay discussed in Secs. 14.9.3 and 14.9.2.

In this convention there are two non-equivalent orderings for the spectrum of neutrino masses:

- Spectrum with Normal Ordering (NO) with $m_1 < m_2 < m_3$
- Spectrum Inverted ordering (IO) with $m_3 < m_1 < m_2$.

Furthermore, the data show a hierarchy between the mass splittings, $\Delta m_{21}^2 \ll |\Delta m_{31}^2| \simeq |\Delta m_{32}^2|$ with $\Delta m_{ij}^2 \equiv m_i^2 - m_j^2$.

In this section, we follow the convention used in the listing section of the PDG and discuss the results for both, NO and IO, using Δm_{21}^2 , which is always the smallest mass splitting, and Δm_{32}^2 , which up to a sign, is the largest mass splitting for IO, while for NO the largest mass splitting is $\Delta m_{31}^2 = \Delta m_{32}^2 + \Delta m_{21}^2$.

With what we know of the mass differences (see table 14.7) and the neutrino mass scale (see Sec. 14.9), depending on the value of the lightest neutrino mass, the neutrino mass spectrum can be further classified in:

- Normal Hierarchical Spectrum (NH): $m_1 \ll m_2 < m_3$,
 $\Rightarrow m_2 \simeq \sqrt{\Delta m_{21}^2} \sim 8.6 \times 10^{-3} \text{ eV}$, $m_3 \simeq \sqrt{\Delta m_{32}^2 + \Delta m_{21}^2} \sim 0.05 \text{ eV}$,

- Inverted Hierarchical Spectrum (IH): $m_3 \ll m_1 < m_2$,
 $\Rightarrow m_1 \simeq \sqrt{|\Delta m_{32}^2 + \Delta m_{21}^2|} \sim 0.0492\text{eV}, m_2 \simeq \sqrt{|\Delta m_{32}^2|} \sim 0.05\text{eV},$
- Quasidegenerate Spectrum (QD): $m_1 \simeq m_2 \simeq m_3 \gg \sqrt{|\Delta m_{32}^2|}.$

Sometimes in the literature the determination of the neutrino mass spectrum is referred to as determination of the neutrino hierarchy. However, as described above, with what we know so far of the neutrino mass scale, the neutrino spectrum may or may not be hierarchical. Therefore determination of neutrino mass ordering is a more precise expression, and it is the one used in this review.

In total, the 3ν oscillation analysis of the existing data involves six parameters: 2 mass differences (one of which can be positive or negative), 3 mixing angles, and the CP phase. The different experiments described in Sec.14.6 provide information on different subsets of these parameters. The precise statistical analysis of the data requires the numerical evaluation of the corresponding oscillation probabilities by solving the evolution equation of the neutrino ensemble from their source to the experiment. Nevertheless, the dominant effects in the different experiments can be qualitatively understood in terms of approximate expressions for the oscillation probabilities which, for convenience, we briefly summarize here.

14.7.1 3ν Oscillation Probabilities

The relevant survival probabilities for solar and KamLAND experiments in the framework of three neutrino oscillations can be written as:

$$P_{ee}^{3\nu} = \sin^4 \theta_{13} + \cos^4 \theta_{13} P_{ee}^{2\nu}(\Delta m_{21}^2, \theta_{12}), \quad (14.72)$$

where we have used the fact that $L_{0,32}^{\text{osc}} = 4\pi E_\nu / \Delta m_{32}^2$ is much shorter than the distance traveled by both solar and KamLAND neutrinos, so that the oscillations related to $L_{0,32}^{\text{osc}}$ are averaged. In the presence of matter effects $P_{ee}^{2\nu}(\Delta m_{21}^2, \theta_{12})$ should be calculated, taking into account the evolution in an effective matter density $n_e^{\text{eff}} = n_e \cos^2 \theta_{13}$. For $10^{-5} \lesssim \Delta m^2 / \text{eV}^2 \lesssim 10^{-4}$, $P_{ee}^{2\nu}(\Delta m_{21}^2, \theta_{12})$ presents the following asymptotic behaviors [160]:

$$P_{ee}^{2\nu, \text{sun}} \simeq 1 - \frac{1}{2} \sin^2(2\theta_{12}) \quad \text{for } E_\nu \lesssim \text{few} \times 100 \text{ keV}, \quad (14.73)$$

$$P_{ee}^{2\nu, \text{sun}} \simeq \sin^2(\theta_{12}) \quad \text{for } E_\nu \gtrsim \text{few} \times 1 \text{ MeV}, \quad (14.74)$$

$$P_{ee}^{2\nu, \text{kam}} = 1 - \sin^2(2\theta_{12}) \sin^2 \frac{\Delta m_{21}^2 L}{4E_\nu}. \quad (14.75)$$

At present most of the precision of the solar analysis is provided by SNO and SK, for which the relevant MSW survival probability provides a direct measurement of $\sin^2 \theta_{12}$, as seen in Eq. (14.74). In the MSW regime, the determination of Δm_{21}^2 in solar experiments comes dominantly from the ratio between the solar potential and the Δm_{21}^2 term required to simultaneously describe the CC/NC data at SNO and the undistorted spectra of ^8B neutrinos as measured in both SK and SNO. Conversely, KamLAND $\bar{\nu}_e$ survival probability proceeds dominantly as vacuum oscillations and provides a most precise determination of Δm_{21}^2 via the strong effect of the oscillating phase in the distortion of the reactor energy spectrum. On the contrary, it yields a weaker constraint on θ_{12} as the vacuum oscillation probability depends on the double-valued and “flatter” function $\sin^2(2\theta_{12})$.

In what respects the interpretation of ν_μ disappearance data, at LBL experiments, the ν_μ survival probability can be expanded in the small parameters $\sin \theta_{13}$ and $\alpha \equiv \Delta m_{21}^2 / \Delta m_{31}^2$ to good

accuracy as [161, 162]

$$\begin{aligned} P_{\nu_\mu \rightarrow \nu_\mu} &\approx 1 - \sin^2 2\theta_{\mu\mu} \sin^2 \frac{\Delta m_{\mu\mu}^2 L}{4E_\nu} \\ &\approx 1 - \cos^2 \theta_{13} \sin^2(2\theta_{23}) \sin^2 \frac{\Delta m_{32}^2 L}{4E_\nu} + \mathcal{O}(\alpha, s_{13}^2), \end{aligned} \quad (14.76)$$

with

$$\begin{aligned} \sin^2 \theta_{\mu\mu} &= \cos^2 \theta_{13} \sin^2 \theta_{23}, \\ \Delta m_{\mu\mu}^2 &= \sin^2 \theta_{12} \Delta m_{31}^2 + \cos^2 \theta_{12} \Delta m_{32}^2 \\ &\quad + \cos \delta_{\text{CP}} \sin \theta_{13} \sin 2\theta_{12} \tan \theta_{23} \Delta m_{21}^2. \end{aligned}$$

At present ν_μ disappearance results at LBL provide the best determination of $|\Delta m_{32}^2|$ and θ_{23} , but as seen above, the probability is symmetric with respect to the octant of $\theta_{\mu\mu}$, which implies symmetry around $s_{23}^2 = 0.5/c_{13}^2$.

The relevant oscillation probability for ν_e appearance at LBL experiments can be expanded at the second order in the small parameters $\sin \theta_{13}$ and α , and assuming a constant matter density it takes the form [163–165]:

$$\begin{aligned} P_{\nu_\mu \rightarrow \nu_e, (\bar{\nu}_\mu \rightarrow \bar{\nu}_e)} &\approx 4 \sin^2 \theta_{13} \sin^2 \theta_{23} \frac{\sin^2 \Delta(1-A)}{(1-A)^2} \\ &\quad + \alpha^2 \sin^2 2\theta_{12} \cos^2 \theta_{23} \frac{\sin^2 A \Delta}{A^2} \\ &\quad + 8\alpha J_{\text{CP}}^{\text{max}} \cos(\Delta \pm \delta_{\text{CP}}) \frac{\sin \Delta A}{A} \frac{\sin \Delta(1-A)}{1-A}, \end{aligned} \quad (14.77)$$

with

$$J_{\text{CP}}^{\text{max}} = \cos \theta_{12} \sin \theta_{12} \cos \theta_{23} \sin \theta_{23} \cos^2 \theta_{13} \sin \theta_{13}, \quad (14.78)$$

and

$$\Delta \equiv \frac{\Delta m_{31}^2 L}{4E_\nu}, \quad A \equiv \frac{2E_\nu V}{\Delta m_{31}^2}, \quad (14.79)$$

where V is the effective matter potential in the Earth’s crust. Results on ν_e appearance at LBL provide us with the dominant information on leptonic CP violation. Furthermore, α , Δ , and A are sensitive to the sign of Δm_{32}^2 (*i.e.*, the type of the neutrino mass ordering). The plus (minus) sign in Eq. (14.77) applies for neutrinos (antineutrinos), and for antineutrinos $V \rightarrow -V$, which implies $A \rightarrow -A$. Numerically one finds for a typical Earth crust matter density of 3 g/cm^3 that at T2K with $E \sim 0.7 \text{ GeV}$, matter effects cause $\sim \pm 10\%$ differences in the rates, whereas in NOvA with $E \sim 2 \text{ GeV}$, we can have $|A| \sim 0.2$. Also, $\alpha^2 \approx 10^{-3}$, which implies that the second term in the first line of Eq. (14.77) gives a very small contribution compared to the other terms. Also, the first term in Eq. (14.77) (which dominates for large θ_{13}) depends on $\sin^2 \theta_{23}$ and therefore is sensitive to the octant.

The ν_e survival probability relevant for reactor experiments with medium baseline (MBL), $L \sim 1 \text{ km}$, can be approximated as [162, 166]:

$$P_{\nu_e \rightarrow \nu_e} = 1 - \sin^2 2\theta_{13} \sin^2 \frac{\Delta m_{ee}^2 L}{4E_\nu} + \mathcal{O}(\alpha^2), \quad (14.80)$$

where

$$\Delta m_{ee}^2 = \cos^2 \theta_{12} \Delta m_{31}^2 + \sin^2 \theta_{12} \Delta m_{32}^2. \quad (14.81)$$

These MBL reactor experiments provide the most precise determination of θ_{13} . Furthermore there is an additional effect sensitive to the mass ordering when comparing the disappearance of ν_μ at LBL experiments – which is symmetric with respect to the sign of $\Delta m_{\mu\mu}^2$ given in Eq.(14.7.1) – with that of ν_e disappearance at MBL reactors which is symmetric with respect to the slightly different effective mass-squared difference Δm_{ee}^2 given in Eq. (14.81).

Finally, for atmospheric neutrinos, the fluxes contain ν_e , ν_μ , $\bar{\nu}_e$, and $\bar{\nu}_\mu$, and for a good fraction of the events, neutrinos travel through the Earth’s matter. In the context of 3ν mixing, the

Table 14.6: Experiments contributing to the present determination of the oscillation parameters.

Experiment	Dominant	Important
Solar Experiments	θ_{12}	$\Delta m_{21}^2, \theta_{13}$
Reactor LBL (KamLAND)	Δm_{21}^2	θ_{12}, θ_{13}
Reactor MBL (Daya-Bay, Reno, D-Chooz)	$\theta_{13}, \Delta m_{31,32}^2 $	
Atmospheric Experiments (SK, IC-DC)		$\theta_{23}, \Delta m_{31,32}^2 , \theta_{13}, \delta_{CP}$
Accel LBL $\nu_\mu, \bar{\nu}_\mu$, Disapp (K2K, MINOS, T2K, NO ν A)	$ \Delta m_{31,32}^2 , \theta_{23}$	
Accel LBL $\nu_e, \bar{\nu}_e$ App (MINOS, T2K, NO ν A)	δ_{CP}	θ_{13}, θ_{23}

dominant oscillation channel of atmospheric neutrinos is $\nu_\mu \rightarrow \nu_\tau$ driven by $|\Delta m_{32}^2|$ with an amplitude controlled by θ_{23} with sub-leading oscillation modes, triggered by Δm_{21}^2 and/or θ_{13} , which depend on the octant of θ_{23} , on the mass ordering, and on δ_{CP} . In that respect, an interesting observable is the deviation of e -like events relative to the no-oscillation prediction N_e^0 , since in the two-flavour limit one expects $N_e = N_e^0$. Such deviation can be written in the following way (see, *e.g.*, [167]):

$$\begin{aligned} \frac{N_e}{N_e^0} - 1 &\approx (r \sin^2 \theta_{23} - 1) P_{2\nu}(\Delta m_{32}^2, \theta_{13}) \\ &+ (r \cos^2 \theta_{23} - 1) P_{2\nu}(\Delta m_{21}^2, \theta_{12}) \\ &- \sin \theta_{13} \sin 2\theta_{23} r \Re(A_{ee}^* A_{\mu e}). \end{aligned} \quad (14.82)$$

Here $r \equiv \Phi_\mu / \Phi_e$ is the flux ratio with $r \approx 2$ in the sub-GeV range and $r \approx 2.6 \rightarrow 4.5$ in the multi-GeV range. $P_{2\nu}(\Delta m^2, \theta)$ is an effective two-flavour oscillation probability, and $A_{ee}, A_{\mu e}$ are elements of a transition amplitude matrix. The three terms appearing in Eq. (14.82) have a well-defined physical interpretation. The first term is important in the multi-GeV range and is controlled by the mixing angle θ_{13} in $P_{2\nu}(\Delta m_{32}^2, \theta_{13})$. This probability can be strongly affected by resonant matter effects [168–173]. Depending on the mass ordering, the resonance will occur either for neutrinos or antineutrinos. The second term is important for sub-GeV events, and it takes into account the effect of oscillations due to Δm_{21}^2 and θ_{12} [174–177]. Via the pre-factor containing the flux ratio r both, the first and second terms in Eq. (14.82) depend on the octant of θ_{23} , though in opposite directions: the multi-GeV (sub-GeV) excess is suppressed (enhanced) for $\theta_{23} < 45^\circ$. Finally, the last term in Eq. (14.82) is an interference term between θ_{13} and Δm_{21}^2 amplitudes and this term shows also dependence on the CP phase δ_{CP} [167, 177].

Subdominant three neutrino effects can also affect μ -like events. For example, for multi-GeV muon events one can write the excess in μ -like events as [178, 179]

$$\begin{aligned} \frac{N_\mu}{N_\mu^0} - 1 &\approx \sin^2 \theta_{23} \left(\frac{1}{r} - \sin^2 \theta_{23} \right) P_{2\nu}(\Delta m_{32}^2, \theta_{13}) \\ &- \frac{1}{2} \sin^2 2\theta_{23} [1 - \Re(A_{33})]. \end{aligned} \quad (14.83)$$

The first term is controlled by θ_{13} and is subject to resonant matter effects, similar to the first term in Eq. (14.82), though with a different dependence on θ_{23} and the flux ratio. In the second term, A_{33} is a probability amplitude satisfying $P_{2\nu}(\Delta m_{32}^2, \theta_{13}) = 1 - |A_{33}|^2$. In the limit $\theta_{13} = 0$ we have $\Re(A_{33}) = \cos(\Delta m_{32}^2 L/2E)$, such that the second term in Eq. (14.83) just describes two-flavour $\nu_\mu \rightarrow \nu_\mu$ vacuum oscillations.

14.7.2 3ν Oscillation Analysis

We summarize in Table 14.6 the different experiments which dominantly contribute to the present determination of the different parameters in the chosen convention.

The table illustrates that the determination of the leptonic parameters requires global analyses of the data from the different experiments. Over the years, these analyses have been in the hands of a few phenomenological groups. We show in Table 14.7 the results from the latest analyses in Refs. [180–183]. For the sake of comparison, all results are presented in the convention of the listing section as described above.

The table illustrates the dependence of the present determination of the parameters on variations of the statistical analysis

performed by the different groups and on the data samples included. In that last respect, the main difference resides in the results from Super-Kamiokande atmospheric data [94] which, at present, can only be included in this analysis by directly adding the χ^2 tabulated χ^2 map provided by the experiment.

Altogether the different analyses find consistent results, in particular on the better-known parameters, θ_{12} , θ_{13} and Δm_{21}^2 and $|\Delta m_{32}^2|$. The issues which still require clarification are the mass ordering discrimination, the determination of θ_{23} and the leptonic CP phase δ_{CP} :

- In all analyses the best fit is for the normal mass ordering. Inverted ordering is disfavoured with a $\Delta\chi^2$, which ranges from slightly above 1.5σ – driven by the interplay of long-baseline accelerator and short-baseline reactor data – to 2.5σ when adding the atmospheric χ^2 table from Ref. [184].
- There is no statistically significant preference for the octant of θ_{23} in any of the analysis.
- The best fit for the complex phase in NO is at $\delta_{CP} \sim 200^\circ$. CP conservation (for $\delta_{CP} \sim 180^\circ$) is allowed at a confidence level (CL) of $1-2\sigma$.

14.7.3 Convention-independent Measures of Leptonic CP Violation in 3ν Mixing

In the framework of 3ν mixing leptonic CP violation can also be quantified in terms of the leptonic Jarlskog invariant [185], defined by:

$$\begin{aligned} \Im[U_{\alpha i} U_{\alpha j}^* U_{\beta i} U_{\beta j}] &\equiv \sum_{\gamma=e,\mu,\tau} \sum_{k=1,2,3} J_{CP} \epsilon_{\alpha\beta\gamma} \epsilon_{ijk} \\ &\equiv J_{CP}^{\max} \sin \delta_{CP}. \end{aligned} \quad (14.84)$$

With the convention in Eq. (14.33) J_{CP}^{\max} is the combination of mixing angles in Eq. (14.78). For example, from the analysis in Ref. [180, 181]

$$J_{CP}^{\max} = 0.0330 \pm 0.0006 (\pm 0.0019), \quad (14.85)$$

at 1σ (3σ) for both orderings, and the preference of the present data for non-zero δ_{CP} implies a small non-zero best fit value $J_{CP}^{\text{best}} = -0.009$.

The status of the determination of leptonic CP violation can also be graphically displayed by projecting the results of the global analysis in terms of leptonic unitarity triangles [186–188]. Since in the analysis U is unitary by construction, any given pair of rows or columns can be used to define a triangle in the complex plane. There are a total of six possible triangles corresponding to the unitary conditions

$$\sum_{i=1,2,3} U_{\alpha i} U_{\beta i}^* = 0 \text{ with } \alpha \neq \beta, \quad \sum_{\alpha=e,\mu,\tau} U_{\alpha i} U_{\alpha j}^* = 0 \text{ with } i \neq j. \quad (14.86)$$

As an illustration we show in Fig. 14.9 the recasting of the allowed regions of the analysis in Ref. [180, 181] in terms of one leptonic unitarity triangle. We show the triangle corresponding to the unitarity conditions on the first and third columns (after the shown rescaling), which is the equivalent to the one usually shown for the quark sector. In this figure, the absence of CP violation would imply a flat triangle, *i.e.*, $\Im(z) = 0$. So the CL at which leptonic CP violation is being observed would be given by the CL at which the region crosses the horizontal axis. Notice however, that this representation is made *under the assumption*

Table 14.7: 3ν oscillation parameters obtained from different global analyses of neutrino data. In all cases, the numbers labeled as NO (IO) are obtained assuming NO (IO), *i.e.*, relative to the respective local minimum. SK-ATM makes reference to the tabulated χ^2 map from the Super-Kamiokande analysis of their data in Ref. [184].

	Ref. [181] w/o SK-ATM		Ref. [181] w SK-ATM		Ref. [182] w SK-ATM		Ref. [183] w SK-ATM	
NO	Best Fit Ordering		Best Fit Ordering		Best Fit Ordering		Best Fit Ordering	
Param	bfp $\pm 1\sigma$	3σ range	bfp $\pm 1\sigma$	3σ range	bfp $\pm 1\sigma$	3σ range	bfp $\pm 1\sigma$	3σ range
$\frac{\sin^2 \theta_{12}}{10^{-1}}$	$3.03^{+0.12}_{-0.11}$	2.70 \rightarrow 3.41	$3.03^{+0.12}_{-0.12}$	2.70 \rightarrow 3.41	$3.03^{+0.13}_{-0.13}$	2.63 \rightarrow 3.45	$3.18^{+0.16}_{-0.16}$	2.71 \rightarrow 3.69
$\theta_{12}/^\circ$	$33.41^{+0.75}_{-0.72}$	31.31 \rightarrow 35.74	$33.41^{+0.75}_{-0.72}$	31.31 \rightarrow 35.74	$33.40^{+0.80}_{-0.82}$	30.85 \rightarrow 35.97	$34.3^{+1.0}_{-1.0}$	31.4 \rightarrow 37.4
$\frac{\sin^2 \theta_{23}}{10^{-1}}$	$5.72^{+0.18}_{-0.23}$	4.06 \rightarrow 6.20	$4.51^{+0.19}_{-0.16}$	4.08 \rightarrow 6.03	$4.55^{+0.18}_{-0.15}$	4.16 \rightarrow 5.99	$5.74^{+0.14}_{-0.14}$	4.34 \rightarrow 6.10
$\theta_{23}/^\circ$	$49.1^{+1.0}_{-1.3}$	39.6 \rightarrow 51.9	$42.2^{+1.1}_{-0.9}$	39.7 \rightarrow 51.0	$42.4^{+1.0}_{-0.9}$	40.2 \rightarrow 50.7	$49.3^{+0.8}_{-0.8}$	41.2 \rightarrow 51.3
$\frac{\sin^2 \theta_{13}}{10^{-2}}$	$2.203^{+0.056}_{-0.059}$	2.029 \rightarrow 2.391	$2.225^{+0.056}_{-0.059}$	2.052 \rightarrow 2.398	$2.23^{+0.07}_{-0.06}$	2.04 \rightarrow 2.44	$2.200^{+0.069}_{-0.062}$	2.00 \rightarrow 2.405
$\theta_{13}/^\circ$	$8.54^{+0.11}_{-0.12}$	8.19 \rightarrow 8.89	$8.58^{+0.11}_{-0.11}$	8.23 \rightarrow 8.91	$8.59^{+0.13}_{-0.12}$	8.21 \rightarrow 8.99	$8.53^{+0.13}_{-0.12}$	8.13 \rightarrow 8.92
$\delta_{CP}/^\circ$	197^{+42}_{-25}	108 \rightarrow 404	232^{+36}_{-26}	144 \rightarrow 350	223^{+32}_{-23}	139 \rightarrow 355	194^{+24}_{-22}	128 \rightarrow 359
$\frac{\Delta m_{21}^2}{10^{-5} \text{ eV}^2}$	$7.41^{+0.21}_{-0.20}$	6.82 \rightarrow 8.03	$7.41^{+0.21}_{-0.20}$	6.82 \rightarrow 8.03	$7.36^{+0.16}_{-0.15}$	6.93 \rightarrow 7.93	$7.50^{+0.22}_{-0.20}$	6.94 \rightarrow 8.14
$\frac{\Delta m_{32}^2}{10^{-3} \text{ eV}^2}$	$2.437^{+0.028}_{-0.027}$	2.354 \rightarrow 2.523	$2.433^{+0.026}_{-0.027}$	2.353 \rightarrow 2.516	$2.448^{+0.023}_{-0.031}$	2.367 \rightarrow 2.521	$2.47^{+0.02}_{-0.03}$	2.40 \rightarrow 2.46
IO	$\Delta\chi^2 = 2.3$		$\Delta\chi^2 = 6.4$		$\Delta\chi^2 = 6.5$		$\Delta\chi^2 = 6.4$	
$\frac{\sin^2 \theta_{12}}{10^{-1}}$	$3.03^{+0.12}_{-0.11}$	2.70 \rightarrow 3.41	$3.03^{+0.12}_{-0.12}$	2.70 \rightarrow 3.41	$3.03^{+0.13}_{-0.13}$	2.63 \rightarrow 3.45	$3.18^{+0.16}_{-0.16}$	2.71 \rightarrow 3.69
$\theta_{12}/^\circ$	$33.41^{+0.75}_{-0.72}$	31.31 \rightarrow 35.74	$33.41^{+0.75}_{-0.72}$	31.31 \rightarrow 35.74	$33.40^{+0.80}_{-0.82}$	30.85 \rightarrow 35.97	$34.3^{+1.0}_{-1.0}$	31.4 \rightarrow 37.4
$\frac{\sin^2 \theta_{23}}{10^{-1}}$	$5.78^{+0.16}_{-0.21}$	4.12 \rightarrow 6.23	$5.69^{+0.16}_{-0.21}$	4.12 \rightarrow 6.13	$5.69^{+0.13}_{-0.21}$	4.17 \rightarrow 6.06	$5.78^{+0.10}_{-0.17}$	4.33 \rightarrow 6.08
$\theta_{23}/^\circ$	$49.5^{+0.9}_{-1.2}$	39.9 \rightarrow 52.1	$49.0^{+1.0}_{-1.2}$	39.9 \rightarrow 51.5	$49.0^{+0.7}_{-1.4}$	40.2 \rightarrow 51.1	$49.5^{+0.6}_{-1.0}$	41.2 \rightarrow 51.2
$\frac{\sin^2 \theta_{13}}{10^{-2}}$	$2.219^{+0.060}_{-0.057}$	2.047 \rightarrow 2.396	$2.223^{+0.058}_{-0.058}$	2.048 \rightarrow 2.416	$2.23^{+0.06}_{-0.06}$	2.03 \rightarrow 2.45	$2.225^{+0.064}_{-0.070}$	2.02 \rightarrow 2.42
$\theta_{13}/^\circ$	$8.57^{+0.12}_{-0.11}$	8.23 \rightarrow 8.90	$8.57^{+0.11}_{-0.11}$	8.23 \rightarrow 8.94	$8.59^{+0.13}_{-0.12}$	8.19 \rightarrow 9.00	$8.58^{+0.12}_{-0.14}$	8.17 \rightarrow 8.96
$\delta_{CP}/^\circ$	286^{+27}_{-32}	192 \rightarrow 360	276^{+22}_{-29}	194 \rightarrow 344	274^{+25}_{-27}	193 \rightarrow 342	284^{+26}_{-28}	200 \rightarrow 353
$\frac{\Delta m_{21}^2}{10^{-5} \text{ eV}^2}$	$7.41^{+0.21}_{-0.20}$	6.82 \rightarrow 8.03	$7.41^{+0.21}_{-0.20}$	6.82 \rightarrow 8.03	$7.36^{+0.16}_{-0.15}$	6.93 \rightarrow 7.93	$7.50^{+0.22}_{-0.20}$	6.94 \rightarrow 8.14
$\frac{\Delta m_{32}^2}{10^{-3} \text{ eV}^2}$	$-2.498^{+0.032}_{-0.025}$	-2.581 \rightarrow -2.408	$-2.486^{+0.028}_{-0.025}$	-2.570 \rightarrow -2.406	$-2.492^{+0.025}_{-0.030}$	-2.578 \rightarrow -2.413	$-2.52^{+0.03}_{-0.02}$	-2.60 \rightarrow -2.44

of a unitary U matrix and therefore does not provide any test of unitarity in the leptonic sector.

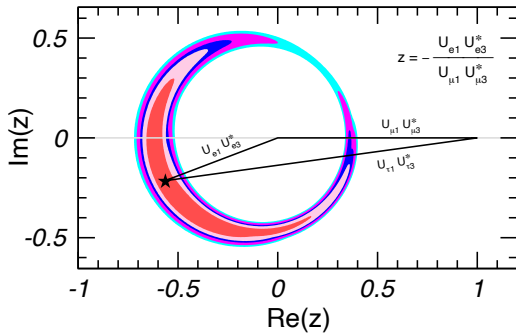


Figure 14.9: Leptonic unitarity triangle for the first and third columns of the mixing matrix. After scaling and rotating the triangle so that two of its vertices always coincide with (0,0) and (1,0) the figure shows the 1σ , 90% , 2σ , 99% , 3σ CL (2 dof) allowed regions of the third vertex for the NO from the analysis in Ref. [180, 181].

14.8 Beyond 3ν : Additional Neutrinos at the eV Scale

Besides the huge success of three-flavour oscillations described in Sec.14.7, as mentioned in Secs.14.6.3 and 14.6.4, there are some anomalies which cannot be explained within the 3ν framework and which have been interpreted as hints for the existence of additional neutrino states with masses at the eV scale. In brief:

- the LSND experiment [123] reported evidence for $\bar{\nu}_\mu \rightarrow \bar{\nu}_e$ transitions with $E/L \sim 1 \text{ eV}^2$, where E and L are the neu-

trino energy and the distance between source and detector, respectively (see *Short Baseline Experiments* subsection of Sec.14.6.3).

- this effect was further explored by the MiniBooNE experiment [189], which reported a yet unexplained event excess in the low-energy region of the electron neutrino and antineutrino event spectra. No significant excess is found at higher neutrino energies. Interpreting the data in terms of oscillations, parameter values consistent with the ones from LSND were obtained, though the test was not definitive;
- radioactive source experiments at the Gallium solar neutrino experiments both in SAGE and GALLEX/GNO obtained an event rate that is somewhat lower than expected. This result was recently confirmed by the BEST experiment [190]. If not due to uncertainties in the interaction cross-section, this effect by itself can be explained by the hypothesis of ν_e disappearance due to oscillations with $\Delta m^2 \gtrsim 1 \text{ eV}^2$ (“Gallium anomaly”) [191–193];
- the calculations of the neutrino flux emitted by nuclear reactors in Refs. [134, 135] predicted a neutrino rate that is a few percent higher than observed in short-baseline ($L \lesssim 100 \text{ m}$) reactor experiments. This “reactor anomaly” could be explained by assuming $\bar{\nu}_e$ disappearance due to oscillations with $\Delta m^2 \sim 1 \text{ eV}^2$ [194]. The flux predictions from [134, 135] were not supported by the reactor antineutrino flux measurement at Daya Bay [195, 196] which was consistent with the older (lower) flux predictions and the flux measurement results in the short-baseline reactor neutrino oscillation experiments. In the last years the reactor flux calculations have been revisited [197–199] and in most cases lower fluxes are predicted, in agreement with the flux measurement at Daya Bay. These new fluxes, correspondingly reduce the significance of the anomaly [200].

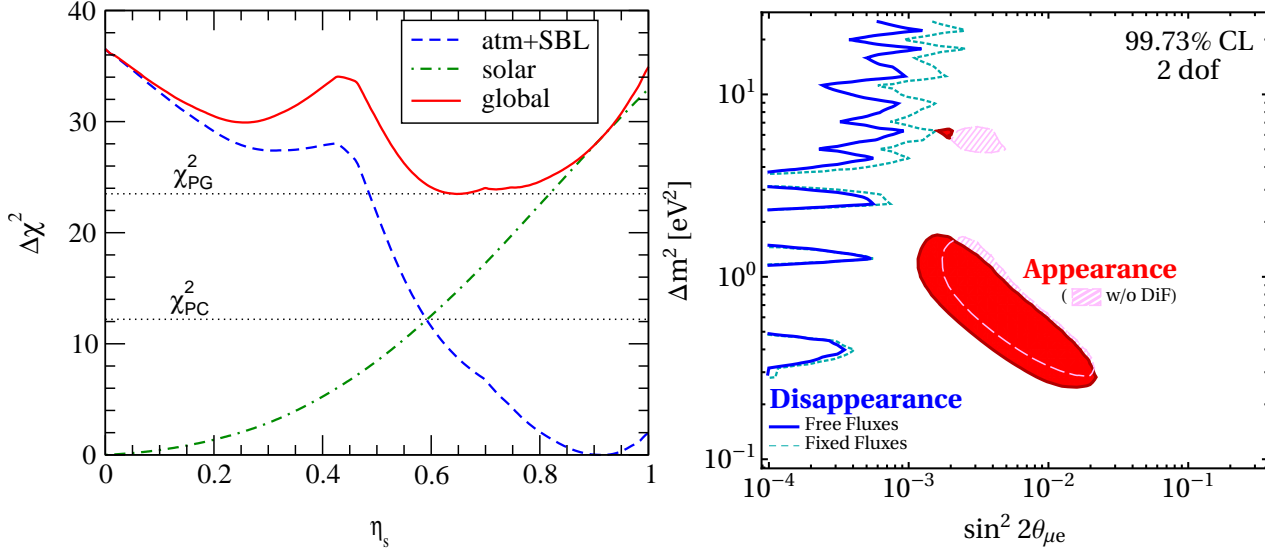


Figure 14.10: *Left:* Status of the 2+2 oscillation scenarios from Ref. [201] ($\eta_S = \sum_i |U_{is}|^2$ where i runs over the two massive states mostly relevant for solar neutrino oscillations). In the figure also shown are the values of χ_{PC}^2 and χ_{PG}^2 relevant for parameter consistency test and parameter goodness of fit, respectively. *Right:* Present status of 3+1 oscillation scenarios from Ref. [202].

These anomalies are under study by the experimental community with a set of follow-up measurements performed at SBL both at reactors and accelerators (see the corresponding subsections in Sec.14.6.4 and Sec.14.6.3).

As mentioned in Sec.14.1, whatever the extension of the SM we want to consider, it must contain only three light active neutrinos. Therefore if we need more than three light massive neutrinos, we must add sterile neutrinos to the particle content of the model.

The most immediate question as these anomalies were reported was whether they could all be consistently described in combination with the rest of the neutrino data – in particular with the negative results on the disappearance of ν_μ at short distances – if one adds those additional sterile states. Quantitatively one can start by adding a fourth massive neutrino state to the spectrum and perform a global data analysis to answer this question. Although the answer is always the same, the physical reason behind it depends on ordering assumed for the states. In brief, there are six possible four-neutrino schemes that can, in principle, accommodate the results of solar+KamLAND and atmospheric+LBL neutrino experiments as well as the SBL result. They can be divided into two classes: (2+2) and (3+1). In the (3+1) schemes, there is a group of three close-by neutrino masses (as on the 3ν schemes described in the previous section) that is separated from the fourth one by a gap of the order of 1 eV, which is responsible for the SBL oscillations. In (2+2) schemes, there are two pairs of close masses (one pair responsible for solar results and the other for atmospheric [203]) separated by the $\mathcal{O}(\text{eV})$ gap. The main difference between these two classes is the following: if a (2+2)-spectrum is realized in nature, the transition into the sterile neutrino is a solution of either the solar or the atmospheric neutrino problem, or the sterile neutrino takes part in both. Consequently, a (2+2)-spectrum is easier to test because the required mixing of sterile neutrinos in either solar and/or atmospheric oscillations would modify their effective matter potential in the Sun and in the Earth, giving distinctive effects in the solar and/or atmospheric neutrino observables. Those distinctive effects were not observed so oscillations into sterile neutrinos did not describe well either solar or atmospheric data. Consequently, as soon as the early 2000's 2+2 spectra could be ruled out already beyond 3-4 σ as seen in the left panel in Fig.14.10 taken from Ref. [201].

On the contrary, for a (3+1)-spectrum (and more generally for a 3+ N -spectrum with an arbitrary N number of sterile states), the sterile neutrino(s) could be only slightly mixed with the active ones and mainly provide a description of the SBL results. In

this case, the oscillation probabilities for experiments working at $E/L \sim 1 \text{ eV}^2$ take a simple form:

$$P_{\alpha\alpha} = 1 - \sin^2 2\theta_{\alpha\alpha} \sin^2 \Delta, \quad P_{\mu e} = \sin^2 2\theta_{\mu e} \sin^2 \Delta, \quad (14.87)$$

where $\Delta \equiv \Delta m_{41}^2 L/4E$ and one can define effective mixing angles

$$\sin^2 2\theta_{\alpha\alpha} \equiv 4|U_{\alpha 4}|^2(1 - |U_{\alpha 4}|^2), \quad \sin^2 2\theta_{\mu e} \equiv 4|U_{\mu 4}|^2|U_{e 4}|^2. \quad (14.88)$$

In here $\alpha = e, \mu$ and $U_{\alpha 4}$ are the elements of the lepton mixing matrix describing the mixing of the 4th neutrino mass state with the electron and muon flavour. In this scenario, there is no sensitivity to CP violation in the Δ driven oscillations, so the relations above are valid for both neutrinos and antineutrinos. At linear order in the mixing elements one can derive a relation between the amplitudes of appearance and disappearance probabilities:

$$4 \sin^2 2\theta_{\mu e} \approx \sin^2 2\theta_{ee} \sin^2 2\theta_{\mu\mu}. \quad (14.89)$$

This relation implies a constraint between the possible results in disappearance and appearance experiments. Consequently, it is not trivial to find a consistent description to all the SBL anomalies. Over the years, different groups have performed a variety of such global analyses leading to different quantitative conclusions on the statistical quality of the global fit (see for example [202, 204–208], see also Refs. [209, 210] for recent reviews on the subject). Generically, the results of the global analysis show that there is significant tension between groups of different data sets – in particular between appearance and disappearance results – and Eq.(14.89) makes it difficult to obtain a good global fit as illustrated in the right panel in Fig.14.10 taken from Ref. [202] which concluded that 3+1 scenario is excluded at 4.7σ level.

A straightforward question to ask is whether the situation improves if more neutrino states at the eV scale are introduced. The simplest extension is the introduction of 2 states with eV scale mass splittings, ν_4 and ν_5 . The ordering of the states can be such that Δm_{41}^2 and Δm_{51}^2 are both positive (“3+2”), or one of them is negative (“1+3+1”). From the point of view of the description of the data, the most important new qualitative feature is that now, non-zero CP violation at $E/L \sim \text{eV}^2$ is possibly observable [206, 211–213]. This allows some additional freedom in fitting neutrino versus antineutrino data from LSND and MiniBooNE together. However, it still holds that a non-zero $\nu_\mu \rightarrow \nu_e$ appearance at SBL necessarily predicts SBL disappearance for both ν_e and ν_μ . So, generically, the tension between appearance and

disappearance results remains, though differences in the methodology of statistical quantification of the degree of agreement/disagreement in these scenarios can lead to different conclusions on whether they can provide a successful description of all the data [202,209,210]. Cosmological observations can provide complementary information on the number of relativistic neutrino states in thermal equilibrium in the early Universe and on the sum of their masses, which sets further constraints on light sterile neutrino scenarios (see Chapter 26 of this *Review*, “Neutrinos in cosmology”).

14.9 Laboratory Probes of ν Mass Scale and its Nature

As described in Secs.14.4 and 14.5, neutrino flavour oscillations in vacuum and flavour transitions in matter only depend on the differences between the neutrino masses-squared, Δm_{ij}^2 , and on the mixing matrix elements, U_{ij} . However, they are insensitive to the absolute mass scale for the neutrinos, m_i . They also give us no information on whether they are Dirac or Majorana particles.

Clearly, the observation of flavour oscillations implies a lower bound on the mass of the heavier neutrino in Δm_{ij}^2 , $|m_i| \geq \sqrt{\Delta m_{ij}^2}$ for $\Delta m_{ij}^2 > 0$. However, there is no upper bound on m_i . In particular, oscillation results allow the neutrino spectrum to be approximately degenerate at a mass scale that is much higher than the $\sqrt{\Delta m_{ij}^2}$ that they determine. Information of the mass scale of the neutrino is provided by other types of experiments. Here we briefly summarize the most sensitive laboratory probes of the neutrino mass scale and on whether they are Dirac or Majorana particles. Cosmological observations provide, albeit indirectly, complementary information on the neutrino mass scale as it is reviewed in Chapter 26 of this *Review*, “Neutrinos in cosmology”.

14.9.1 Constraints from Kinematics of Weak Decays

The only model-independent information on the neutrino masses, rather than mass differences, can be extracted from energy-momentum conservation relation in reactions in which a neutrino or an antineutrino is involved.

Historically these bounds were labeled as limits on the mass of the flavour neutrino states corresponding to the charged flavour involved in the decay. Fermi proposed in 1933 such a kinematic search for the ν_e neutrino mass (which we will label here as $m_{\nu_e}^{\text{eff}}$) in the end part of the beta spectra in ${}^3\text{H}$ beta decay ${}^3\text{H} \rightarrow {}^3\text{He} + e^- + \bar{\nu}_e$.

Because ${}^3\text{H}$ beta decay is a superallowed transition, the nuclear matrix elements are energy independent, so the electron spectrum is determined exclusively by the phase space

$$\begin{aligned} \frac{dN}{dE} &= C p E (Q - T) \sqrt{(Q - T)^2 - (m_{\nu_e}^{\text{eff}})^2} F(E) \\ &\equiv R(E) \sqrt{(E_0 - E)^2 - (m_{\nu_e}^{\text{eff}})^2}. \end{aligned} \quad (14.90)$$

E_0 is the mass difference between the initial and final nucleus, $E = T + m_e$ is the total electron energy, p its momentum, $Q \equiv E_0 - m_e$ is the maximum kinetic energy of the electron and Final state Coulomb interactions are contained in the Fermi function $F(E)$. $R(E)$ in the second equality contains all the m_{ν_e} -independent factors.

The Kurie function is defined as $K(T) \equiv \sqrt{\frac{dN}{dE} \frac{1}{pEF(E)}}$. From Eq.(14.90), we see that if $m_{\nu_e}^{\text{eff}}=0$ $K(T)$ would depend linearly on T . A non-vanishing neutrino mass then provokes a distortion from the straight-line T -dependence at the endpoint, So for $m_{\nu_e}^{\text{eff}} = 0$, $T_{\text{max}} = Q$, while for $m_{\nu_e}^{\text{eff}} \neq 0$, $T_{\text{max}} = Q - m_{\nu_e}^{\text{eff}}$. In ${}^3\text{H}$ beta decay $Q = 18.6$ KeV is very small and therefore, this decay is more sensitive to this $m_{\nu_e}^{\text{eff}}$ -induced distortion.

The most recent result on the kinematic search for neutrino mass in tritium decay is from KATRIN [214], an experiment which has found so far no indication of $m_{\nu_e} \neq 0$ and sets an upper limit

$$m_{\nu_e}^{\text{eff}} < 0.8 \text{ eV}, \quad (14.91)$$

at 90% CL improving over the previous bound from the Mainz [215] and Troitsk [216] experiments which constrained

$m_{\nu_e}^{\text{eff}} < 2.2$ eV at 95% CL. KATRIN continues running with an estimated sensitivity limit of $m_{\nu_e}^{\text{eff}} \sim 0.2$ eV. Project 8 is exploring a new technique for β -spectrometry based on cyclotron radiation [217].

An alternative isotope to Tritium is ${}^{163}\text{Ho}$ [218] which presents the advantage of a smaller $Q = 2.8$ KeV. It decays via electron capture to ${}^{163}\text{Dy}$. Currently, there are three experiments exploring this decay to probe the neutrino mass: ECHO [219], HOLMES [220], and NuMECS [221]. These experiments are complementary to tritium-based searches from a technical point of view. Also, the decay of ${}^{163}\text{Ho}$ determines the effective electron neutrino mass as opposed to antineutrino in Tritium.

For the other flavours the present limits compiled in the listing section of the PDG read

$$m_{\nu_\mu}^{\text{eff}} < 190 \text{ keV (90\% CL)} \quad \text{from} \quad \pi^- \rightarrow \mu^- + \bar{\nu}_\mu, \quad (14.92)$$

$$m_{\nu_\tau}^{\text{eff}} < 18.2 \text{ MeV (95\% CL)} \quad \text{from} \quad \tau^- \rightarrow n\pi + \nu_\tau. \quad (14.93)$$

In the presence of mixing and for neutrinos with small mass differences, the distortion of the beta spectrum is given by the sum of the individual spectra generated incoherently by each neutrino massive state weighted with the relevant mixing matrix element squared [222]:

$$\frac{dN}{dE} = R(E) \sum_i |U_{ei}|^2 \sqrt{(E_0 - E)^2 - m_i^2} \Theta(E_0 - E - m_i). \quad (14.94)$$

The step function $\Theta(E_0 - E - m_i)$ arises because a neutrino with a given mass m_i can only be produced if the available energy is larger than its mass. Equation (14.94) shows the two main effects of the neutrino masses and mixings on the electron energy spectrum: First, kinks appear at the electron energies $E_e^{(i)} = E \sim E_0 - m_i$ with sizes that are determined by $|U_{ei}|^2$. Second, the endpoint shifts to $E_{\text{ep}} = E_0 - m_0$, where m_0 is the lightest neutrino mass. Corrections are induced once the energy resolution of the experiment is considered. [223,224]

In the 3ν mixing scenario, the distortion of the spectrum can still be effectively described by a single parameter – which we will still denote as m_{ν_e} – if for all neutrino states $E_0 - E = Q - T \gg m_i$. In this case, one can expand Eq.(14.94) as:

$$\frac{dN}{dE} \simeq R(E) \sum_i |U_{ei}|^2 \sqrt{(E_0 - E)^2 - (m_{\nu_e}^{\text{eff}})^2}, \quad (14.95)$$

with

$$(m_{\nu_e}^{\text{eff}})^2 = \frac{\sum_i m_i^2 |U_{ei}|^2}{\sum_i |U_{ei}|^2} = \sum_i m_i^2 |U_{ei}|^2, \quad (14.96)$$

where unitarity is assumed in the second equality. In this approximation, the distortion of the endpoint of the spectrum is described by a single parameter, and with the present results from KATRIN, it is bounded to be

$$\begin{aligned} 1.1 \text{ eV} &\geq m_{\nu_e}^{\text{eff}} = \sqrt{\sum_i m_i^2 |U_{ei}|^2} \\ &= \begin{cases} \sqrt{m_0^2 + \Delta m_{21}^2 (1 - c_{13}^2 c_{12}^2) + \Delta m_{32}^2 s_{13}^2} & \text{in NO,} \\ \sqrt{m_0^2 + \Delta m_{21}^2 c_{13}^2 c_{12}^2 - \Delta m_{32}^2 c_{13}^2} & \text{in IO,} \end{cases} \end{aligned} \quad (14.97)$$

where $m_0 = m_1 (m_3)$ is the lightest neutrino mass in the NO (IO) spectrum. Correspondingly the bounds in Eqs.(14.92) and (14.93) apply to the combinations $\sum_i m_i^2 |U_{\alpha i}|^2$ for $\alpha = \mu$ and τ respectively. So with the values known of the mixing matrix elements, the strongest constraint on the absolute value of the neutrino mass comes from Tritium beta decay.

From Eq.(14.97) we see that, given the present knowledge of the neutrino mass differences and their mixing from oscillation experiments, it is possible to translate the experimental information of m_{ν_e} on a corresponding range for the lightest neutrino mass and

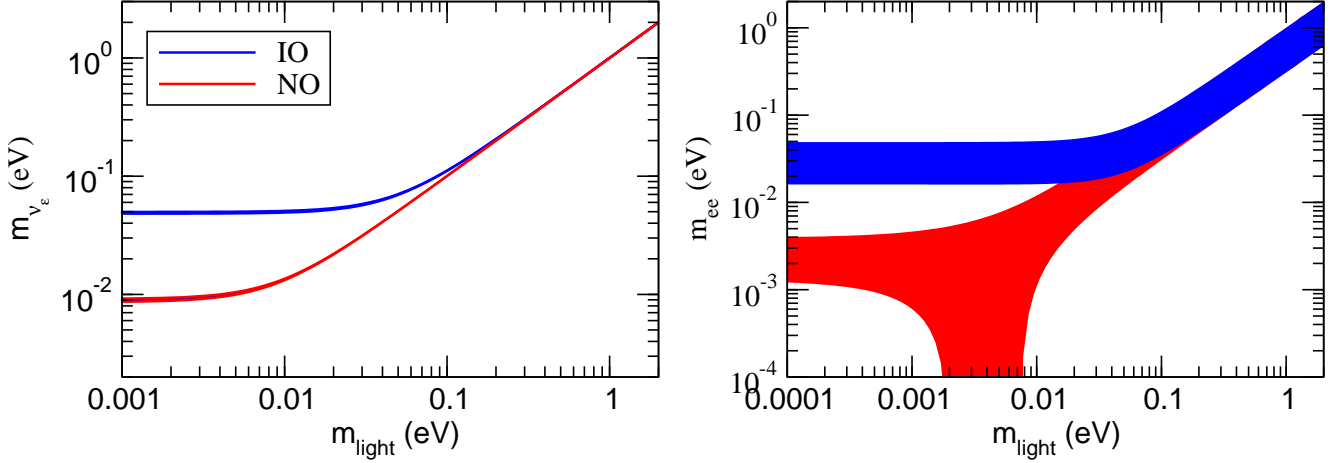


Figure 14.11: Allowed 95% CL ranges (1 dof) for the neutrino mass observable determined in ${}^3\text{H}$ beta decay (left panel) and in $0\nu\beta\beta$ (right panel) in the framework of 3ν mixing as a function of the lightest neutrino mass. The ranges are obtained by projecting the results of the global analysis of oscillation data (w/o SK-atm) in Ref. [180, 181]. The region for each ordering is defined with respect to its local minimum.

that such relation depends on the ordering of the states. We plot in Fig.14.11 the recasting of the allowed regions of the analysis in Ref. [180, 181] in terms of the allowed range m_{ν_e} as a function of $m_{\text{light}} \equiv m_0$. In particular, one finds that the results of oscillation experiments imply a lower bound on $m_{\nu_e} > 0.048$ (0.0085) eV for IO (NO) at 95% CL.

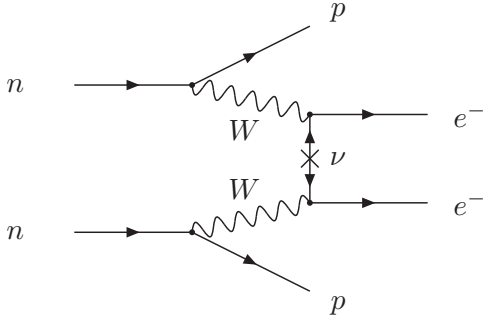


Figure 14.12: Feynman diagram for neutrinoless double-beta decay.

14.9.2 Dirac vs. Majorana: Neutrinoless Double-beta Decay

The most sensitive probe to whether neutrinos are Dirac or Majorana states is the neutrinoless double beta decay ($0\nu\beta\beta$):

$$(A, Z) \rightarrow (A, Z + 2) + e^- + e^-. \quad (14.98)$$

In the presence of neutrino masses and mixing, the process in Eq.(14.98) can be generated at lower order in perturbation theory by the term represented in Fig.14.12. The corresponding amplitude is proportional to the product of the two leptonic currents

$$M_{\alpha\beta} \propto [\bar{e}\gamma_\alpha(1 - \gamma_5)\nu_e] [\bar{e}\gamma_\beta(1 - \gamma_5)\nu_e] \propto \sum_i (U_{ei})^2 [\bar{e}\gamma_\alpha(1 - \gamma_5)\nu_i] [\bar{e}\gamma_\beta(1 - \gamma_5)\nu_i]. \quad (14.99)$$

$$m_{ee} = \left| \sum_i m_i U_{ei}^2 \right| = \begin{cases} \left| m_0 c_{12}^2 c_{13}^2 + \sqrt{\Delta m_{21}^2 + m_0^2} s_{12}^2 c_{13}^2 e^{2i(\eta_2 - \eta_1)} + \sqrt{\Delta m_{32}^2 + \Delta m_{21}^2 + m_0^2} s_{13}^2 e^{-2i(\delta_{\text{CP}} + \eta_1)} \right| & \text{in NO,} \\ \left| m_0 s_{13}^2 + \sqrt{m_0^2 - \Delta m_{32}^2} s_{12}^2 c_{13}^2 e^{2i(\eta_2 + \delta_{\text{CP}})} + \sqrt{m_0^2 - \Delta m_{32}^2 - \Delta m_{21}^2} c_{12}^2 c_{13}^2 e^{2i(\eta_1 + \delta_{\text{CP}})} \right| & \text{in IO,} \end{cases} \quad (14.101)$$

The neutrino propagator in Fig.14.12 can only arise from the contraction $\langle 0 | \nu_i(x) \nu_i(y)^T | 0 \rangle$. However, if the neutrino is a Dirac particle ν_i field annihilates a neutrino state and creates an antineutrino state, and neutrino and antineutrino states are different, so the contraction $\langle 0 | \nu_i(x) \nu_i(y)^T | 0 \rangle = 0$ and $M_{\alpha\beta} = 0$. On the other hand, if ν_i is a Majorana particle, neutrino and antineutrino are described by the same field and $\langle 0 | \nu_i(x) \nu_i(y)^T | 0 \rangle \neq 0$.

The conclusion is that in order to induce the $0\nu\beta\beta$ decay, neutrinos must be Majorana particles. This is consistent with the fact that the process (14.98) violates the total lepton number by two units. Conversely, if $0\nu\beta\beta$ decay is observed, massive neutrinos cannot be Dirac states [225].

It is important to stress that neutrinoless double-beta decay could be dominantly induced by other new physics effects beyond that of Majorana neutrino masses. Consequently, the connection between the observation or limitation of the neutrinoless double beta decay and the neutrino mass can only be made under some assumption about the source of total lepton number violation in the model.

The observable determined by the experiments is the half-life of the decay. Under the assumption that the Majorana neutrino mass is the only source of lepton number violation at low energies, the decay half-life is given by:

$$(T_{1/2}^{0\nu})^{-1} = G^{0\nu} |M^{0\nu}|^2 \left(\frac{m_{ee}}{m_e} \right)^2, \quad (14.100)$$

where $G^{0\nu}$ is the phase space integral taking into account the final atomic state, $|M^{0\nu}|$ is the nuclear matrix element of the transition, and m_{ee} is the *effective Majorana mass* of ν_e ,

which, in addition to the masses and mixing parameters that affect the tritium beta decay spectrum, also depends on the leptonic CP -violating phases. We plot in Fig.14.11 the recasting of the allowed regions of the analysis in Ref. [180,181] in terms of the allowed range m_{ee} as a function of $m_{\text{light}} \equiv m_0$ for the two orderings. As a consequence of the dependence on the unknown Majorana phases, the allowed range of m_{ee} for a given value of m_{light} and ordering is substantially broader than that of m_{ν_e} . Nevertheless, the results of oscillation experiments imply a lower bound on the effective Majorana mass for the IO, which at 95%CL reads $m_{ee} > 0.016$ eV.

From Eq.(14.100) we see that nuclear structure details enter relation between the decay rate (or lifetime) and the effective Majorana mass. As a consequence, uncertainties in the nuclear structure calculations result in a spread of m_{ee} values for a given $T_{1/2}^{0\nu}$ by a factor of 2–3 [226].

We present in Sec.14.9.3 a brief description of the experimental searches for neutrinoless double-beta decay. At the time of writing of this review, the strongest bound on $0\nu\beta\beta$ decay lifetimes came for Xenon and Germanium from the KamLAND-Zen [227] and GERDA [228] experiments, respectively. They have set a bound on the corresponding half-lives of $T_{1/2}^{0\nu} > 2.3 \times 10^{26}$ yr, and $T_{1/2}^{0\nu} > 1.8 \times 10^{26}$ yr, at 90% CL. Using a variety of nuclear matrix element calculations, the corresponding upper bounds on the effective Majorana mass are

$$m_{ee} < 36 - 156 \text{ meV} \quad (14.102)$$

$$m_{ee} < 79 - 180 \text{ meV} . \quad (14.103)$$

14.9.3 Experimental Search for Neutrinoless Double-beta Decay

There are 35 candidate nuclei for double-beta decay. Currently, experiments using ^{136}Xe and ^{76}Ge have reported the most sensitive results of $0\nu\beta\beta$ search. Because of the uncertainties related to the nuclear matrix element, the complementarity of technologies, different backgrounds, and the investigation of the mechanism behind the $0\nu\beta\beta$ in case of a positive signal, it is important to pursue the searches with as many isotopes as possible.

The signature of $0\nu\beta\beta$ is that the sum of the energy of two electrons is equal to the Q -value of the nuclear transition. The energy from electrons is measured with either ionization, scintillation, or through phonons. In some experiments, a combination of two techniques is used to enhance the sensitivity. In the case of background-free measurement, the sensitivity to the half-life is proportional to the product of the detection efficiency of the signal ε , the source mass M , and the measurement time t . If background exists, it is proportional to $\varepsilon\sqrt{\frac{Mt}{b\Delta E}}$, where b is the background rate, and ΔE is the energy resolution.

Among the experiments using ionization detection, ultra-high-purity germanium detector provides the best sensitivity thanks to high energy resolution and low background. GERDA achieved a background level of $(5.2^{+1.6}_{-1.3}) \times 10^{-4}$ counts/(keV·kg·year) [228], which enabled a background-free search. The final result from GERDA for the half-life limit for $0\nu\beta\beta$ decay of ^{76}Ge is $T_{1/2} > 1.8 \times 10^{26}$ years at 90% CL. The Majorana Demonstrator achieved energy resolution of 2.5 keV FWHM (full width at half maximum) at the Q -value (2.039 MeV) [229] and set a half-life limit of $T_{1/2} > 8.3 \times 10^{25}$ years at 90% CL. GERDA and Majorana collaborations have united and formed, together with new groups, the LEGEND collaboration. LEGEND has adopted a phased approach toward the deployment of a tonne of enriched Ge detectors [230]. The first phase of LEGEND based on approximately 200 kg of enriched Ge, using the GERDA infrastructure at LNGS, has started and first data are being taken. The second phase of LEGEND has been approved as a one ton experiment in a new cryostat reaching a discovery sensitivity of half-lives beyond 10^{28} years. In China, CDEX-300 ν using 225 kg of enriched Ge detector is under preparation [231] in the existing CEDX-DM infrastructure at the China Jinping Underground Laboratory.

Liquid scintillator detectors have a simple structure and can utilize existing large detectors with low background environments. By adding an inner balloon to contain xenon-loaded liquid scintillator to the KamLAND detector, KamLAND-Zen uses 745 kg of

xenon with 90.9% enrichment in ^{136}Xe . KamLAND-Zen reported the half-life limit of 2.3×10^{26} years at 90% CL [227]. The SNO detector has also been upgraded to be filled with a liquid scintillator in the SNO+ experiment [232]. The SNO+ detector will be loaded with 0.5% natural tellurium, corresponding to approximately 1.3 t of ^{130}Te , to search for $0\nu\beta\beta$.

With a time projection chamber, one can utilize both ionization and scintillation. EXO-200 used a liquid xenon time projection chamber with enriched Xe and reported a half-life limit of $T_{1/2} > 3.5 \times 10^{25}$ years at 90% CL [233] for ^{136}Xe . Based on the technology validated by EXO-200, nEXO plans to use about 5,000 kg of enriched xenon [234]. NEXT has been developing a high-pressure xenon gas time projection chamber with electroluminescent amplification and optical readouts. An energy resolution of 1% FWHM at the Q -value of ^{136}Xe $0\nu\beta\beta$ is demonstrated with NEXT-White detector [235].

CUORE uses a cryogenic bolometer to measure the energy in a calorimetric way. The detector composed of 988 TeO_2 bolometers for a total mass of 742 kg, corresponding to 206 kg of ^{130}Te , was operated at 10 mK. CUORE set a half-life limit of $T_{1/2} > 2.2 \times 10^{25}$ years at 90% CL for ^{130}Te [236]. For further reduction of background towards future search based on the CUORE technology, CUPID proposes to simultaneously measure the calorimetric signal and the scintillation light with a tonne-scale bolometric detector. Using the prototype the technology is demonstrated, and $0\nu\beta\beta$ is also searched for with ^{82}Se [237] and ^{100}Mo [238].

AMoRE also uses the simultaneous detection of heat and scintillation. Six ^{100}Mo -enriched and ^{48}Ca -depleted CaMoO_4 crystals with a total mass of 1.9 kg (AMoRE-Pilot) were operated in Yangyang underground laboratory located in South Korea, searching for $0\nu\beta\beta$ of ^{100}Mo [239]. Currently, AMoRE-I experiment [240] is under operation in Yemilab.

A tracker-calorimeter technique is employed in NEMO. Source isotopes are hosted in thin foils surrounded by a tracking detector, which in turn is surrounded by a calorimeter. Full topological event reconstruction with this configuration enables background rejection and gives additional information after discovery. The NEMO-3 experiment used 7 isotopes, with the largest mass comprised of ^{100}Mo (7 kg) [241].

References

- [1] J. N. Bahcall, *NEUTRINO ASTROPHYSICS* (1989), ISBN 9780521379755.
- [2] R. N. Mohapatra and P. B. Pal, World Sci. Lect. Notes Phys. **60**, 1 (1998), [World Sci. Lect. Notes Phys.72,1(2004)].
- [3] C. W. Kim and A. Pevsner, Contemp. Concepts Phys. **8**, 1 (1993).
- [4] B. Kayser, F. Gibrat-Debu and F. Perrier, World Sci. Lect. Notes Phys. **25**, 1 (1989).
- [5] C. Giunti and C. W. Kim, *Fundamentals of Neutrino Physics and Astrophysics* (2007), ISBN 9780198508717.
- [6] M. C. Gonzalez-Garcia and Y. Nir, Rev. Mod. Phys. **75**, 345 (2003), [hep-ph/0202058].
- [7] M. C. Gonzalez-Garcia and M. Maltoni, Phys. Rept. **460**, 1 (2008), [arXiv:0704.1800].
- [8] A. Pilaftsis, Z. Phys. **C55**, 275 (1992), [hep-ph/9901206].
- [9] P. Minkowski, Phys. Lett. **67B**, 421 (1977).
- [10] P. Ramond, in “International Symposium on Fundamentals of Quantum Theory and Quantum Field Theory,” (1979), [hep-ph/9809459].
- [11] M. Gell-Mann, P. Ramond and R. Slansky, Conf. Proc. **C790927**, 315 (1979), [arXiv:1306.4669].
- [12] T. Yanagida, Conf. Proc. C **7902131**, 95 (1979).
- [13] R. N. Mohapatra and G. Senjanovic, Phys. Rev. Lett. **44**, 912 (1980).
- [14] J. Schechter and J. W. F. Valle, Phys. Rev. **D21**, 309 (1980).
- [15] J. Schechter and J. W. F. Valle, Phys. Rev. **D22**, 2227 (1980).

- [16] J. Schechter and J. W. F. Valle, Phys. Rev. **D24**, 1883 (1981), [Erratum: Phys. Rev. **D25**, 283(1982)].
- [17] Z. Maki, M. Nakagawa and S. Sakata, Prog. Theor. Phys. **28**, 870 (1962).
- [18] Y. Katayama *et al.*, Prog. Theor. Phys. **28**, 675 (1962).
- [19] B. Pontecorvo, Zh. Eksp. Teor. Fiz. **53**, 1717 (1967).
- [20] N. Cabibbo, Phys. Rev. Lett. **10**, 531 (1963).
- [21] M. Kobayashi and T. Maskawa, Prog. Theor. Phys. **49**, 652 (1973).
- [22] S. Antusch *et al.*, JHEP **10**, 084 (2006), [hep-ph/0607020].
- [23] S. Antusch and O. Fischer, JHEP **10**, 094 (2014), [arXiv:1407.6607].
- [24] V. N. Gribov and B. Pontecorvo, Phys. Lett. **28B**, 493 (1969).
- [25] E. Akhmedov, in “International Conference on History of the Neutrino: 1930-2018 Paris, France, September 5-7, 2018,” (2019), [arXiv:1901.05232].
- [26] L. Wolfenstein, Phys. Rev. D **17**, 2369 (1978).
- [27] A. Halprin, Phys. Rev. **D34**, 3462 (1986).
- [28] A. J. Baltz and J. Weneser, Phys. Rev. **D37**, 3364 (1988).
- [29] P. D. Mannheim, Phys. Rev. **D37**, 1935 (1988).
- [30] L. Landau, Phys. Z. Sov. **2**, 46 (1932).
- [31] C. Zener, Proc. Roy. Soc. Lond. **A137**, 696 (1932).
- [32] E. Majorana, Nuovo Cim. **9**, 43 (1932).
- [33] E. C. G. Stueckelberg, Helv. Phys. Acta **5**, 369 (1932).
- [34] T.-K. Kuo and J. T. Pantaleone, Rev. Mod. Phys. **61**, 937 (1989).
- [35] S. J. Parke, Phys. Rev. Lett. **57**, 1275 (1986).
- [36] W. C. Haxton, Phys. Rev. Lett. **57**, 1271 (1986).
- [37] S. T. Petcov, Phys. Lett. B **191**, 299 (1987).
- [38] S. P. Mikheyev and A. Y. Smirnov, Sov. J. Nucl. Phys. **42**, 913 (1985).
- [39] J. N. Bahcall *et al.*, Rev. Mod. Phys. **54**, 767 (1982).
- [40] J. N. Bahcall, A. M. Serenelli and S. Basu, Astrophys. J. **621**, L85 (2005), [arXiv:astro-ph/0412440].
- [41] A. M. Serenelli, W. C. Haxton and C. Pena-Garay, Astrophys. J. **743**, 24 (2011), [arXiv:1104.1639].
- [42] F. L. Villante, Phys. Lett. **B742**, 279 (2015), [arXiv:1410.2796].
- [43] A. Serenelli, Eur. Phys. J. **A52**, 4, 78 (2016), [arXiv:1601.07179].
- [44] R. Davis, Jr., D. S. Harmer and K. C. Hoffman, Phys. Rev. Lett. **20**, 1205 (1968).
- [45] B. T. Cleveland *et al.*, Astrophys. J. **496**, 505 (1998).
- [46] C. Pena-Garay and A. Serenelli (2008), [arXiv:0811.2424].
- [47] J. N. Abdurashitov *et al.* (SAGE), J. Exp. Theor. Phys. **95**, 181 (2002), [Zh. Eksp. Teor. Fiz. **122**, 211(2002)], [arXiv:astro-ph/0204245].
- [48] W. Hampel *et al.* (GALLEX), Phys. Lett. **B447**, 127 (1999).
- [49] M. Altmann *et al.* (GNO), Phys. Lett. **B616**, 174 (2005), [hep-ex/0504037].
- [50] J. N. Abdurashitov *et al.* (SAGE), Phys. Rev. **C80**, 015807 (2009), [arXiv:0901.2200].
- [51] K. S. Hirata *et al.* (Kamiokande-II), Phys. Rev. Lett. **63**, 16 (1989).
- [52] Y. Fukuda *et al.* (Kamiokande), Phys. Rev. Lett. **77**, 1683 (1996).
- [53] Y. Fukuda *et al.* (Super-Kamiokande), Phys. Rev. Lett. **81**, 1158 (1998), [Erratum: Phys. Rev. Lett. **81**, 4279 (1998)], [hep-ex/9805021].
- [54] K. Abe *et al.* (Super-Kamiokande), Phys. Rev. D **94**, 5, 052010 (2016), [arXiv:1606.07538].
- [55] N. Vinyoles *et al.*, Astrophys. J. **835**, 2, 202 (2017), [arXiv:1611.09867].
- [56] S. Fukuda *et al.* (Super-Kamiokande), Phys. Rev. Lett. **86**, 5656 (2001), [hep-ex/0103033].
- [57] H. H. Chen, Phys. Rev. Lett. **55**, 1534 (1985).
- [58] B. Aharmim *et al.* (SNO), Phys. Rev. **C72**, 055502 (2005), [arXiv:nucl-ex/0502021].
- [59] S. Fukuda *et al.* (Super-Kamiokande), Phys. Lett. **B539**, 179 (2002), [hep-ex/0205075].
- [60] Q. R. Ahmad *et al.* (SNO), Phys. Rev. Lett. **87**, 071301 (2001), [arXiv:nucl-ex/0106015].
- [61] S. Fukuda *et al.* (Super-Kamiokande), Phys. Rev. Lett. **86**, 5651 (2001), [hep-ex/0103032].
- [62] Q. R. Ahmad *et al.* (SNO), Phys. Rev. Lett. **89**, 011301 (2002), [arXiv:nucl-ex/0204008].
- [63] B. Aharmim *et al.* (SNO), Phys. Rev. **C88**, 025501 (2013), [arXiv:1109.0763].
- [64] J. Bergstrom *et al.*, JHEP **03**, 132 (2016), [arXiv:1601.00972].
- [65] C. Arpesella *et al.* (Borexino), Phys. Lett. B **658**, 101 (2008), [arXiv:0708.2251].
- [66] G. Bellini *et al.* (Borexino), Phys. Rev. Lett. **108**, 051302 (2012), [arXiv:1110.3230].
- [67] M. Agostini *et al.* (BOREXINO), Nature **562**, 7728, 505 (2018).
- [68] M. Agostini *et al.* (BOREXINO), Nature **587**, 577 (2020), [arXiv:2006.15115].
- [69] G. Bellini *et al.* (Borexino), Phys. Rev. D **82**, 033006 (2010), [arXiv:0808.2868].
- [70] S. Abe *et al.* (KamLAND), Phys. Rev. **C84**, 035804 (2011), [arXiv:1106.0861].
- [71] A. Gando *et al.* (KamLAND), Phys. Rev. **C92**, 5, 055808 (2015), [arXiv:1405.6190].
- [72] M. Agostini *et al.* (Borexino), Phys. Rev. D **100**, 8, 082004 (2019), [arXiv:1707.09279].
- [73] M. Agostini *et al.* (Borexino), Phys. Rev. D **101**, 6, 062001 (2020), [arXiv:1709.00756].
- [74] M. Honda *et al.*, Phys. Rev. **D92**, 2, 023004 (2015), [arXiv:1502.03916].
- [75] G. D. Barr *et al.*, Phys. Rev. **D74**, 094009 (2006), [arXiv:astro-ph/0611266].
- [76] G. Battistoni *et al.*, Astropart. Phys. **19**, 269 (2003), [Erratum: Astropart. Phys. **19**, 291(2003)], [hep-ph/0207035].
- [77] J. Evans *et al.*, Phys. Rev. **D95**, 2, 023012 (2017), [arXiv:1612.03219].
- [78] C. V. Achar *et al.*, Phys. Lett. **18**, 196 (1965).
- [79] F. Reines *et al.*, Phys. Rev. Lett. **15**, 429 (1965).
- [80] K. S. Hirata *et al.* (Kamiokande-II), Phys. Lett. B **205**, 416 (1988).
- [81] D. Casper *et al.*, Phys. Rev. Lett. **66**, 2561 (1991).
- [82] K. Daum *et al.* (Frejus), Z. Phys. **C66**, 417 (1995).
- [83] M. Aglietta *et al.* (NUSEX), Europhys. Lett. **8**, 611 (1989).
- [84] K. S. Hirata *et al.* (Kamiokande-II), Phys. Lett. **B280**, 146 (1992).
- [85] Y. Fukuda *et al.* (Kamiokande), Phys. Lett. **B335**, 237 (1994).
- [86] Y. Fukuda *et al.* (Super-Kamiokande), Phys. Rev. Lett. **81**, 1562 (1998), [hep-ex/9807003].
- [87] M. Ambrosio *et al.* (MACRO), Phys. Lett. **B517**, 59 (2001), [hep-ex/0106049].
- [88] M. C. Sanchez *et al.* (Soudan 2), Phys. Rev. **D68**, 113004 (2003), [hep-ex/0307069].

- [89] V. D. Barger *et al.*, Phys. Rev. Lett. **82**, 2640 (1999), [arXiv:astro-ph/9810121].
- [90] E. Lisi, A. Marrone and D. Montanino, Phys. Rev. Lett. **85**, 1166 (2000), [hep-ph/0002053].
- [91] Y. Ashie *et al.* (Super-Kamiokande), Phys. Rev. Lett. **93**, 101801 (2004), [hep-ex/0404034].
- [92] Z. Li *et al.* (Super-Kamiokande), Phys. Rev. **D98**, 5, 052006 (2018), [arXiv:1711.09436].
- [93] M. G. Aartsen *et al.* (IceCube), Phys. Rev. **D99**, 3, 032007 (2019), [arXiv:1901.05366].
- [94] K. Abe *et al.* (Super-Kamiokande), Phys. Rev. **D97**, 7, 072001 (2018), [arXiv:1710.09126].
- [95] A. Albert *et al.* (ANTARES), JHEP **06**, 113 (2019), [arXiv:1812.08650].
- [96] R. Abbasi *et al.* (IceCube), Phys. Rev. D **108**, 1, 012014 (2023), [arXiv:2304.12236].
- [97] S. Adrian-Martinez *et al.* (KM3Net), J. Phys. **G43**, 8, 084001 (2016), [arXiv:1601.07459].
- [98] M. G. Aartsen *et al.* (IceCube-Gen2), J. Phys. G **48**, 6, 060501 (2021), [arXiv:2008.04323].
- [99] S. Ahmed *et al.* (ICAL), Pramana **88**, 5, 79 (2017), [arXiv:1505.07380].
- [100] K. Abe *et al.* (Hyper-Kamiokande) (2018), [arXiv:1805.04163].
- [101] B. Abi *et al.* (DUNE), JINST **15**, 08, T08008 (2020), [arXiv:2002.02967].
- [102] S. E. Kopp, Phys. Rept. **439**, 101 (2007), [arXiv:physics/0609129].
- [103] S. van der Meer (1961), CERN-61-07.
- [104] D. Beavis *et al.* (E899) (1995), BNL-52459.
- [105] M. G. Catanesi *et al.* (HARP), Nucl. Instrum. Meth. **A571**, 527 (2007).
- [106] J. M. Paley *et al.* (MIPP), Phys. Rev. **D90**, 3, 032001 (2014), [arXiv:1404.5882].
- [107] N. Abgrall *et al.* (NA61), JINST **9**, P06005 (2014), [arXiv:1401.4699].
- [108] M. Pavin *et al.* (EMPHATIC), Phys. Rev. D **106**, 11, 112008 (2022), [arXiv:2106.15723].
- [109] N. Abgrall *et al.* (NA61/SHINE), Eur. Phys. J. C **76**, 2, 84 (2016), [arXiv:1510.02703].
- [110] N. Abgrall *et al.* (NA61/SHINE), Eur. Phys. J. C **79**, 2, 100 (2019), [arXiv:1808.04927].
- [111] H. Adhikary *et al.* (NA61/SHINE) (2023), [arXiv:2306.02961].
- [112] M. H. Ahn *et al.* (K2K), Phys. Rev. **D74**, 072003 (2006), [hep-ex/0606032].
- [113] P. Adamson *et al.* (MINOS), Phys. Rev. Lett. **112**, 191801 (2014), [arXiv:1403.0867].
- [114] P. Adamson *et al.* (MINOS+), Phys. Rev. Lett. **125**, 13, 131802 (2020), [arXiv:2006.15208].
- [115] N. Agafonova *et al.* (OPERA), Phys. Rev. Lett. **120**, 21, 211801 (2018), [Erratum: Phys. Rev. Lett. **121**, no. 13, 139901 (2018)], [arXiv:1804.04912].
- [116] C. Rubbia *et al.*, JINST **6**, P07011 (2011), [arXiv:1106.0975].
- [117] K. Abe *et al.* (T2K), Phys. Rev. Lett. **107**, 041801 (2011), [arXiv:1106.2822].
- [118] K. Abe *et al.* (T2K), Phys. Rev. Lett. **112**, 061802 (2014), [arXiv:1311.4750].
- [119] K. Abe *et al.* (T2K), Eur. Phys. J. C **83**, 9, 782 (2023), [arXiv:2303.03222].
- [120] P. Adamson *et al.* (NOvA), Phys. Rev. Lett. **118**, 23, 231801 (2017), [arXiv:1703.03328].
- [121] M. A. Acero *et al.* (NOvA), Phys. Rev. Lett. **123**, 15, 151803 (2019), [arXiv:1906.04907].
- [122] M. A. Acero *et al.* (NOvA), Phys. Rev. D **106**, 3, 032004 (2022), [arXiv:2108.08219].
- [123] A. Aguilar-Arevalo *et al.* (LSND), Phys. Rev. **D64**, 112007 (2001), [hep-ex/0104049].
- [124] B. Armbruster *et al.* (KARMEN), Phys. Rev. **D65**, 112001 (2002), [hep-ex/0203021].
- [125] A. A. Aguilar-Arevalo *et al.* (MiniBooNE), Phys. Rev. D **103**, 5, 052002 (2021), [arXiv:2006.16883].
- [126] M. Antonello *et al.* (MicroBooNE, LAr1-ND, ICARUS-WA104) (2015), [arXiv:1503.01520].
- [127] P. Abratenko *et al.* (MicroBooNE), Phys. Rev. Lett. **128**, 24, 241801 (2022), [arXiv:2110.14054].
- [128] P. Abratenko *et al.* (MicroBooNE), Phys. Rev. Lett. **130**, 1, 011801 (2023), [arXiv:2210.10216].
- [129] S. Ajimura *et al.* (JSNS2), Nucl. Instrum. Meth. A **1014**, 165742 (2021), [arXiv:2104.13169].
- [130] F. Von Feilitzsch, A. A. Hahn and K. Schreckenbach, Phys. Lett. **118B**, 162 (1982).
- [131] K. Schreckenbach *et al.*, Phys. Lett. **160B**, 325 (1985).
- [132] A. A. Hahn *et al.*, Phys. Lett. **B218**, 365 (1989).
- [133] P. Vogel *et al.*, Phys. Rev. **C24**, 1543 (1981).
- [134] T. A. Mueller *et al.*, Phys. Rev. **C83**, 054615 (2011), [arXiv:1101.2663].
- [135] P. Huber, Phys. Rev. **C84**, 024617 (2011), [Erratum: Phys. Rev. **C85**, 029901 (2012)], [arXiv:1106.0687].
- [136] D. Adey *et al.* (Daya Bay), Phys. Rev. D **100**, 5, 052004 (2019), [arXiv:1808.10836].
- [137] G. Bak *et al.* (RENO), Phys. Rev. Lett. **121**, 20, 201801 (2018), [arXiv:1806.00248].
- [138] H. de Kerret *et al.* (Double Chooz), Nature Phys. **16**, 5, 558 (2020), [arXiv:1901.09445].
- [139] Y. J. Ko *et al.* (NEOS), Phys. Rev. Lett. **118**, 12, 121802 (2017), [arXiv:1610.05134].
- [140] K. Eguchi *et al.* (KamLAND), Phys. Rev. Lett. **90**, 021802 (2003), [hep-ex/0212021].
- [141] T. Araki *et al.* (KamLAND), Phys. Rev. Lett. **94**, 081801 (2005), [hep-ex/0406035].
- [142] A. Gando *et al.* (KamLAND), Phys. Rev. **D88**, 3, 033001 (2013), [arXiv:1303.4667].
- [143] Y. Abe *et al.* (Double Chooz), Phys. Rev. Lett. **108**, 131801 (2012), [arXiv:1112.6353].
- [144] F. P. An *et al.* (Daya Bay), Phys. Rev. Lett. **108**, 171803 (2012), [arXiv:1203.1669].
- [145] J. K. Ahn *et al.* (RENO), Phys. Rev. Lett. **108**, 191802 (2012), [arXiv:1204.0626].
- [146] F. P. An *et al.* (Daya Bay), Phys. Rev. Lett. **130**, 16, 161802 (2023), [arXiv:2211.14988].
- [147] A. Abusleme *et al.* (JUNO), Prog. Part. Nucl. Phys. **123**, 103927 (2022), [arXiv:2104.02565].
- [148] Z. Atif *et al.* (RENO, NEOS), Phys. Rev. D **105**, 11, L111101 (2022), [arXiv:2011.00896].
- [149] I. Alekseev *et al.* (DANSS), Phys. Lett. **B787**, 56 (2018), [arXiv:1804.04046].
- [150] H. Almazán *et al.* (STEREO), Phys. Rev. D **102**, 5, 052002 (2020), [arXiv:1912.06582].
- [151] H. Almazán *et al.* (STEREO), Nature **613**, 7943, 257 (2023), [arXiv:2210.07664].
- [152] M. Andriamirado *et al.* (PROSPECT), Phys. Rev. D **103**, 3, 032001 (2021), [arXiv:2006.11210].
- [153] A. P. Serebrov *et al.* (NEUTRINO-4), Pisma Zh. Eksp. Teor. Fiz. **109**, 4, 209 (2019), [JETP Lett. **109**, no. 4, 213 (2019)], [arXiv:1809.10561].

- [154] A. P. Serebrov *et al.*, Phys. Rev. D **104**, 3, 032003 (2021), [arXiv:2005.05301].
- [155] Y. Abreu *et al.* (SoLid), JINST **16**, 02, P02025 (2021), [arXiv:2002.05914].
- [156] N. Cabibbo, Phys. Lett. **72B**, 333 (1978).
- [157] S. M. Bilenky, J. Hosek and S. T. Petcov, Phys. Lett. **94B**, 495 (1980).
- [158] V. D. Barger, K. Whisnant and R. J. N. Phillips, Phys. Rev. Lett. **45**, 2084 (1980).
- [159] P. Langacker *et al.*, Nucl. Phys. **B282**, 589 (1987).
- [160] S. Goswami and A. Yu. Smirnov, Phys. Rev. **D72**, 053011 (2005), [hep-ph/0411359].
- [161] N. Okamura, Prog. Theor. Phys. **114**, 1045 (2006), [hep-ph/0411388].
- [162] H. Nunokawa, S. J. Parke and R. Zukanovich Funchal, Phys. Rev. **D72**, 013009 (2005), [hep-ph/0503283].
- [163] A. Cervera *et al.*, Nucl. Phys. **B579**, 17 (2000), [Erratum: Nucl. Phys. **B593**, 731 (2001)], [hep-ph/0002108].
- [164] M. Freund, Phys. Rev. **D64**, 053003 (2001), [hep-ph/0103300].
- [165] E. K. Akhmedov *et al.*, JHEP **04**, 078 (2004), [hep-ph/0402175].
- [166] H. Minakata *et al.*, Phys. Rev. **D74**, 053008 (2006), [hep-ph/0607284].
- [167] O. L. G. Peres and A. Yu. Smirnov, Nucl. Phys. **B680**, 479 (2004), [hep-ph/0309312].
- [168] S. Petcov, Phys. Lett. **B434**, 321 (1998), [hep-ph/9805262].
- [169] E. K. Akhmedov *et al.*, Nucl. Phys. **B542**, 3 (1999), [hep-ph/9808270].
- [170] E. K. Akhmedov, Nucl. Phys. **B538**, 25 (1999), [hep-ph/9805272].
- [171] M. Chizhov, M. Maris and S. Petcov (1998), SISSA-53-98-EP, [hep-ph/9810501].
- [172] M. Chizhov and S. Petcov, Phys. Rev. Lett. **83**, 1096 (1999), [hep-ph/9903399].
- [173] E. K. Akhmedov, M. Maltoni and A. Y. Smirnov, JHEP **0705**, 077 (2007), [hep-ph/0612285].
- [174] C. Kim and U. Lee, Phys. Lett. **B444**, 204 (1998), [hep-ph/9809491].
- [175] O. Peres and A. Y. Smirnov, Phys. Lett. **B456**, 204 (1999), [hep-ph/9902312].
- [176] M. Gonzalez-Garcia, M. Maltoni and A. Y. Smirnov, Phys. Rev. **D70**, 093005 (2004), [hep-ph/0408170].
- [177] E. K. Akhmedov, M. Maltoni and A. Y. Smirnov, JHEP **0806**, 072 (2008), [arXiv:0804.1466].
- [178] J. Bernabeu, S. Palomares Ruiz and S. Petcov, Nucl. Phys. **B669**, 255 (2003), [hep-ph/0305152].
- [179] S. Petcov and T. Schwetz, Nucl. Phys. **B740**, 1 (2006), [hep-ph/0511277].
- [180] I. Esteban *et al.*, JHEP **09**, 178 (2020), [arXiv:2007.14792].
- [181] I. Esteban *et al.*, NuFIT5.2 at NuFit webpage <http://www.nu-fit.org>.
- [182] F. Capozzi *et al.*, Phys. Rev. D **104**, 8, 083031 (2021), [arXiv:2107.00532].
- [183] P. F. de Salas *et al.*, JHEP **02**, 071 (2021), [arXiv:2006.11237].
- [184] Super-Kamiokande, Atmospheric Oscillation Analysis 2020 (preliminary) results. Link to data release <https://www-sk.icrr.u-tokyo.ac.jp/sk/publications/data/sk.atm.data.release.tar.gz>.
- [185] C. Jarlskog, Phys. Rev. Lett. **55**, 1039 (1985).
- [186] M. C. Gonzalez-Garcia, M. Maltoni and T. Schwetz, JHEP **11**, 052 (2014), [arXiv:1409.5439].
- [187] Y. Farzan and A. Yu. Smirnov, Phys. Rev. **D65**, 113001 (2002), [hep-ph/0201105].
- [188] A. Dueck, S. Petcov and W. Rodejohann, Phys. Rev. **D82**, 013005 (2010), [arXiv:1006.0227].
- [189] A. Aguilar-Arevalo *et al.* (MiniBooNE) (2012), [arXiv:1207.4809].
- [190] V. V. Barinov *et al.*, Phys. Rev. Lett. **128**, 23, 232501 (2022), [arXiv:2109.11482].
- [191] M. A. Acero, C. Giunti and M. Laveder, Phys. Rev. **D78**, 073009 (2008), [arXiv:0711.4222].
- [192] C. Giunti and M. Laveder, Phys. Rev. **C83**, 065504 (2011), [arXiv:1006.3244].
- [193] C. Giunti *et al.*, JHEP **10**, 164 (2022), [arXiv:2209.00916].
- [194] G. Mention *et al.*, Phys. Rev. **D83**, 073006 (2011), [arXiv:1101.2755].
- [195] F. P. An *et al.* (Daya Bay), Phys. Rev. Lett. **116**, 6, 061801 (2016), [Erratum: Phys. Rev. Lett. **118**, no. 9, 099902 (2017)], [arXiv:1508.04233].
- [196] F. P. An *et al.* (Daya Bay), Phys. Rev. Lett. **118**, 25, 251801 (2017), [arXiv:1704.01082].
- [197] V. Kopeikin, M. Skorokhvatov and O. Titov, Phys. Rev. D **104**, 7, L071301 (2021), [arXiv:2103.01684].
- [198] M. Estienne *et al.*, Phys. Rev. Lett. **123**, 2, 022502 (2019), [arXiv:1904.09358].
- [199] L. Hayen *et al.*, Phys. Rev. C **100**, 5, 054323 (2019), [arXiv:1908.08302].
- [200] C. Giunti *et al.*, Phys. Lett. B **829**, 137054 (2022), [arXiv:2110.06820].
- [201] M. Maltoni *et al.*, Nucl. Phys. **B643**, 321 (2002), [hep-ph/0207157].
- [202] M. Dentler *et al.*, JHEP **08**, 010 (2018), [arXiv:1803.10661].
- [203] J. J. Gomez-Cadenas and M. C. Gonzalez-Garcia, Z. Phys. **C71**, 443 (1996), [hep-ph/9504246].
- [204] C. Giunti and M. Laveder, Phys. Rev. **D84**, 093006 (2011), [arXiv:1109.4033].
- [205] J. M. Conrad *et al.*, Adv. High Energy Phys. **2013**, 163897 (2013), [arXiv:1207.4765].
- [206] J. Kopp *et al.*, JHEP **05**, 050 (2013), [arXiv:1303.3011].
- [207] G. H. Collin *et al.*, Phys. Rev. Lett. **117**, 22, 221801 (2016), [arXiv:1607.00011].
- [208] S. Gariazzo *et al.*, JHEP **06**, 135 (2017), [arXiv:1703.00860].
- [209] A. Diaz *et al.*, Phys. Rept. **884**, 1 (2020), [arXiv:1906.00045].
- [210] S. Böser *et al.*, Prog. Part. Nucl. Phys. **111**, 103736 (2020), [arXiv:1906.01739].
- [211] G. Karagiorgi *et al.*, Phys. Rev. **D75**, 013011 (2007), [Erratum: Phys. Rev. **D80**, 099902 (2009)], [hep-ph/0609177].
- [212] M. Maltoni and T. Schwetz, Phys. Rev. **D76**, 093005 (2007), [arXiv:0705.0107].
- [213] C. Giunti and M. Laveder, Phys. Rev. **D84**, 073008 (2011), [arXiv:1107.1452].
- [214] M. Aker *et al.* (KATRIN), Nature Phys. **18**, 2, 160 (2022), [arXiv:2105.08533].
- [215] J. Bonn *et al.*, Nucl. Phys. B Proc. Suppl. **91**, 273 (2001).
- [216] V. M. Lobashev *et al.*, Nucl. Phys. B Proc. Suppl. **91**, 280 (2001).
- [217] B. Monreal and J. A. Formaggio, Phys. Rev. **D80**, 051301 (2009), [arXiv:0904.2860].
- [218] A. De Rujula and M. Lusignoli, Phys. Lett. **118B**, 429 (1982).
- [219] L. Gastaldo *et al.*, J. Low Temp. Phys. **176**, 5-6, 876 (2014), [arXiv:1309.5214].
- [220] B. Alpert *et al.*, Eur. Phys. J. **C75**, 3, 112 (2015), [arXiv:1412.5060].

- [221] M. P. Croce *et al.*, *J. Low. Temp. Phys.* **184**, 3-4, 958 (2016), [arXiv:1510.03874].
- [222] R. E. Shrock, *Phys. Lett.* **96B**, 159 (1980).
- [223] F. Vissani, *Nucl. Phys. B Proc. Suppl.* **100**, 273 (2001), [hep-ph/0012018].
- [224] Y. Farzan, O. L. G. Peres and A. Yu. Smirnov, *Nucl. Phys.* **B612**, 59 (2001), [hep-ph/0105105].
- [225] J. Schechter and J. W. F. Valle, *Phys. Rev. D* **25**, 2951 (1982).
- [226] J. Engel and J. Menendez, *Rept. Prog. Phys.* **80**, 4, 046301 (2017), [arXiv:1610.06548].
- [227] S. Abe *et al.* (KamLAND-Zen), *Phys. Rev. Lett.* **130**, 5, 051801 (2023), [arXiv:2203.02139].
- [228] M. Agostini *et al.* (GERDA), *Phys. Rev. Lett.* **125**, 25, 252502 (2020), [arXiv:2009.06079].
- [229] I. J. Arnquist *et al.* (Majorana), *Phys. Rev. Lett.* **130**, 6, 062501 (2023), [arXiv:2207.07638].
- [230] N. Abgrall *et al.* (LEGEND) (2021), [arXiv:2107.11462].
- [231] W. H. Dai *et al.* (CDEX), *Phys. Rev. D* **106**, 3, 032012 (2022), [arXiv:2205.10718].
- [232] V. Albanese *et al.* (SNO+), *JINST* **16**, 08, P08059 (2021), [arXiv:2104.11687].
- [233] G. Anton *et al.* (EXO-200), *Phys. Rev. Lett.* **123**, 16, 161802 (2019), [arXiv:1906.02723].
- [234] G. Adhikari *et al.* (nEXO), *J. Phys. G* **49**, 1, 015104 (2022), [arXiv:2106.16243].
- [235] J. Renner *et al.* (NEXT), *JINST* **13**, 10, P10020 (2018), [arXiv:1808.01804].
- [236] D. Q. Adams *et al.* (CUORE), *Nature* **604**, 7904, 53 (2022), [arXiv:2104.06906].
- [237] O. Azzolini *et al.* (CUPID), *Phys. Rev. Lett.* **129**, 11, 111801 (2022), [arXiv:2206.05130].
- [238] C. Augier *et al.* (CUPID), *Eur. Phys. J. C* **82**, 11, 1033 (2022), [arXiv:2202.08716].
- [239] V. Alenkov *et al.* (AMoRE), *Eur. Phys. J. C* **79**, 9, 791 (2019), [arXiv:1903.09483].
- [240] M. H. Lee (AMoRE), *JINST* **15**, 08, C08010 (2020), [arXiv:2005.05567].
- [241] R. Arnold *et al.* (NEMO-3), *Phys. Rev.* **D92**, 7, 072011 (2015), [arXiv:1506.05825].

15. Quark Model

Revised August 2023 by C. Amsler (Stefan Meyer Inst.), V. Crede (Florida State U.) and T. DeGrand (Colorado U., Boulder).

- 15.1 Introduction 322
- 15.2 Quantum numbers of the quarks 322
- 15.3 Mesons 323
- 15.4 Exotic mesons 326
 - 15.4.1 Tetraquarks 326
 - 15.4.2 Glueballs 326
 - 15.4.3 Hybrids 327
- 15.5 Baryons: qqq states 327
 - 15.5.1 Light baryons 327
 - 15.5.2 Charmed and bottom baryons 330
- 15.6 Magnetic moments 332
- 15.7 Dynamics 333
- 15.8 Lattice Calculations of Hadronic Spectroscopy . 334
 - 15.8.1 Spectroscopy of low-lying states 334
 - 15.8.2 Excited state spectroscopy 334
 - 15.8.3 Electromagnetic effects 337

15.1 Introduction

Quantum chromodynamics (QCD) is the theory of strong interactions. QCD is a quantum field theory with an $SU(N_c)$ local “color” gauge symmetry with $N_c = 3$ colors and a collection of N_f “flavors” of colored fermions, the quarks. It involves a set of $N_c^2 - 1 = 8$ non-Abelian gauge fields, the gluons. QCD is believed to confine, that is, its physical states are color singlets with internal quark and gluon degrees of freedom. This review is concerned with the description of the properties (masses and matrix elements for couplings to electromagnetism and the weak interactions) of the low lying bound states of QCD. The shorthand expression for describing this physics is called the “quark model”.

The spectrum of strongly interacting particles consists of a tower of many states, which can be either bosons (labelled as “mesons”) or fermions (labelled as “baryons”). The spectrum of baryons and mesons exhibits a high degree of regularity. The organizational principle which best categorizes this regularity is encoded in the quark model. All descriptions of strongly interacting states use the language of the quark model. At the same time, the language is not precise. The quark model exists on many levels: at the simplest level, it is an almost dynamics-free picture of strongly interacting particles as bound states of quarks and antiquarks. As one refines the description, the quark model can become a framework with more detailed descriptions of dynamics. At its most fundamental level, it might be a description of QCD. In effective field theories of QCD at low energies the hadron spectrum is not simply given by a series of states but is the manifestation of a complex dynamics involving various types of states [1].

At its heart, the quark model assumes that mesons are bound states of quark - antiquark pairs, and baryons are bound states of three quarks. These are the minimal particle content states which can be color singlets in an $SU(3)$ gauge theory. This approach cannot be justified directly from QCD; however, there is indirect evidence that this description has some fundamental validity from the version of QCD where the number of colors N_c is taken to infinity [2–4]. In that limit, mesons are dominantly narrow (width proportional to $1/N_c$) bound states of a quark - antiquark pair, and baryons have a mass which scales as N_c .

A better justification is that this approach works. Indeed, the quark model is much older than QCD as a theory of the strong interactions (1973-1974, see the article on “50 Years of Quantum Chromodynamics” [5]). In fact, the principal issue (circa 1963-64) in strong interaction physics before QCD was to justify the success of the quark model in systemizing the properties of mesons and baryons in terms of some more fundamental dynamics (QCD).

Today one knows that this is not the whole story. There are experimentally observed states which either cannot be described, or have an uncomfortable description, as minimal quark number states. Some of them have “exotic” (non- $q\bar{q}$ or qqq) quantum

numbers. Given the successes of the quark model, these are classified as “tetraquarks” ($qq\bar{q}\bar{q}$), “pentaquarks” ($qqqq\bar{q}$) or “glueballs”, bound states of gluons, the gluonic degrees of freedom in QCD. Of course, such labels are imprecise: bound states with the same overall quantum numbers can mix, regardless of their internal degrees of freedom.

This review has several parts. We start by describing the properties of strongly interacting particles in terms of the properties of states made of a minimal number of quark fields which can be coupled into a color singlet – two fields (a quark and an antiquark) for the mesons, and three quarks, for a baryon. Quarks come in six flavors. We describe the properties of mesons as $\bar{q}q$ systems and baryons as qqq systems. Along the way we discuss hadronic bound states which do not fit into this classification.

Finally, at the end of this review, we present results from lattice simulations of QCD, a direct approach to the solution of QCD from its Lagrangian, without reference to models. Lattice simulations interact with the quark model in (at least) two ways: first, the interpolating fields which are used in lattice simulations are usually directly based on quark model constructions. That is the simplest way to create states with the desired quantum numbers, which can then be processed by the lattice calculation. The second way that lattice calculations interact with the quark model comes when one wishes to put the lattice calculations into some context: without the quark model, there are simply the results from the lattice calculations, and the results from experiment, and no way to understand why they are similar or different. The quark model is the framework which is almost universally used to generate that context. Of course, that statement is equally valid when one tries to systemize actual experimental data: the context is always some variation of a quark model.

15.2 Quantum numbers of the quarks

As gluons carry no intrinsic quantum numbers beyond color charge, and because color is believed to be permanently confined, the quantum numbers of strongly interacting particles are given by the quantum numbers of their constituent quarks and antiquarks.

Quarks are strongly interacting fermions with spin 1/2 and, by convention, positive parity. Antiquarks have negative parity. Quarks have the additive baryon number 1/3, antiquarks $-1/3$. Table 15.1 gives the other additive quantum numbers (flavors) for the three generations of quarks. They are related to the charge Q (in units of the elementary charge e) through the generalized Gell-Mann-Nishijima formula

$$Q = I_z + \frac{B + S + C + B + T}{2}, \quad (15.1)$$

where B is the baryon number. The convention is that the quark flavor (I_z , S , C , B , or T) has the same sign as its charge Q . Antiquarks have the opposite flavor signs. With this convention, any flavor carried by a charged meson has the same sign as its charge, *e.g.*, the strangeness of the K^+ ($c\bar{s}$) is +1, the bottomness of the B^+ ($u\bar{b}$) is +1, and the charm and strangeness of the D_s^- ($s\bar{c}$) are each -1 .

Table 15.1: Quark quantum numbers.

	d	u	s	c	b	t
Q – electric charge	$-\frac{1}{3}$	$+\frac{2}{3}$	$-\frac{1}{3}$	$+\frac{2}{3}$	$-\frac{1}{3}$	$+\frac{2}{3}$
I – isospin	$\frac{1}{2}$	$\frac{1}{2}$	0	0	0	0
I_z – isospin z -component	$-\frac{1}{2}$	$+\frac{1}{2}$	0	0	0	0
S – strangeness	0	0	-1	0	0	0
C – charm	0	0	0	$+1$	0	0
B – bottomness	0	0	0	0	-1	0
T – topness	0	0	0	0	0	$+1$

The hypercharge is defined as

$$Y = B + S - \frac{C - B + T}{3}. \quad (15.2)$$

Thus Y is equal to $\frac{1}{3}$ for the u and d quarks, $-\frac{2}{3}$ for the s quark, and 0 for all other quarks. More details and derivations on

the quark structure of mesons and baryons can be found *e.g.* in Ref. [6].

The naming scheme for hadrons has been updated by the Particle Data Group in 2023, to include the heavy “exotic” states discovered recently, the tetraquark ($qq\bar{q}\bar{q}$) and pentaquark ($qqq\bar{q}\bar{q}$) candidates (see “Naming Scheme for Hadrons” in this *Review*).

15.3 Mesons

Mesons have baryon number $\mathcal{B} = 0$. In the quark model, they are $q\bar{q}'$ bound states of quarks q and antiquarks \bar{q}' (the flavors of q and q' may be different).

If the orbital angular momentum of the $q\bar{q}'$ state is ℓ , then the parity P is $(-1)^{\ell+1}$. The meson spin J is given by the usual relation $|\ell - s| \leq J \leq |\ell + s|$, where $s = 0$ (antiparallel quark spins) or $s = 1$ (parallel quark spins). The charge conjugation, or C -parity $C = (-1)^{\ell+s}$, is defined only for states made of quarks and their own antiquarks. The C -parity can be generalized to the G -parity $G = (-1)^{I+\ell+s}$ for mesons made of quarks and their own antiquarks (isospin $I_z = 0$), and for the charged $u\bar{d}$ and $d\bar{u}$ states (isospin $I = 1$).

The mesons are classified in J^{PC} multiplets. The $\ell = 0$ states are the pseudoscalars (0^{-+}) and the vectors (1^{--}). The orbital excitations $\ell = 1$ are the scalars (0^{++}), the axial vectors (1^{+-}) and (1^{+0}) *aka* pseudovectors, and the tensors (2^{++}). Assignments for many of the known mesons are given in Tables 15.2, 15.3 and 15.4. Radial excitations are denoted by the principal quantum number n . The very short lifetime of the t quark ($\rightarrow W^+b$) makes it likely that bound-state hadrons containing t quarks and/or antiquarks do not exist.

States in the natural spin-parity series $P = (-1)^J$ must, according to the above, have $s = 1$ and hence, $CP = +1$. Thus, mesons with natural spin-parity and $CP = -1$ (0^{+-} , 1^{-+} , 2^{+-} , 3^{-+} , *etc.*) are forbidden in the $q\bar{q}'$ model. The $J^{PC} = 0^{- -}$ state is forbidden as well. Mesons with such *exotic* quantum numbers may exist, but would lie outside the $q\bar{q}'$ model (see section 15.4 below on exotic mesons).

Following SU(3), the nine possible $q\bar{q}'$ combinations containing the light u , d , and s quarks are grouped into an octet and a singlet of light quark mesons:

$$3 \otimes \bar{3} = 8 \oplus 1. \quad (15.3)$$

A fourth quark such as charm c can be included by extending SU(3) to SU(4). However, SU(4) is badly broken owing to the much heavier c quark. Nevertheless, in an SU(4) classification, the sixteen mesons are grouped into a 15-plet and a singlet:

$$4 \otimes \bar{4} = 15 \oplus 1. \quad (15.4)$$

The *weight diagrams* for the ground-state pseudoscalar (0^{-+}) and vector (1^{--}) mesons are depicted in Fig. 15.1. The light quark mesons are members of nonets building the middle plane in Fig. 15.1(a) and (b).

Isoscalar states with the same J^{PC} mix, but mixing between the two light quark isoscalar mesons, and the much heavier charmonium and bottomonium states, are generally assumed to be negligible. In the following, we shall use the generic names a for the $I = 1$, K for the $I = 1/2$, f and f' for the $I = 0$ members of the light quark nonets. Thus, the physical isoscalars are mixtures of the SU(3) wave function ψ_8 and ψ_1 :

$$f' = \psi_8 \cos \theta - \psi_1 \sin \theta, \quad (15.5)$$

$$f = \psi_8 \sin \theta + \psi_1 \cos \theta, \quad (15.6)$$

where θ is the nonet mixing angle and

$$\psi_8 = \frac{1}{\sqrt{6}}(u\bar{u} + d\bar{d} - 2s\bar{s}), \quad (15.7)$$

$$\psi_1 = \frac{1}{\sqrt{3}}(u\bar{u} + d\bar{d} + s\bar{s}). \quad (15.8)$$

The mixing relations are often rewritten to exhibit the $u\bar{u} + d\bar{d}$ and $s\bar{s}$ components which decouple for the “ideal” mixing angle

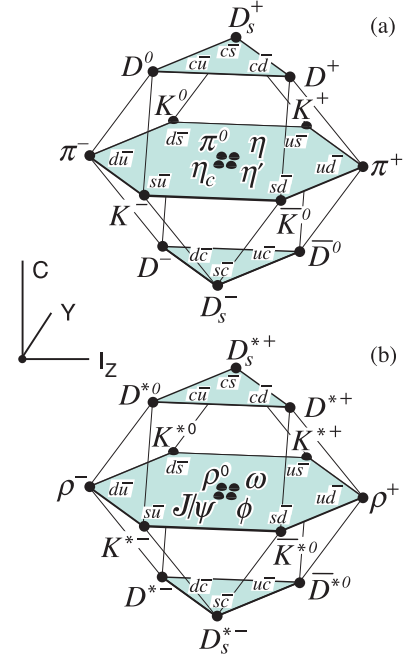


Figure 15.1: SU(4) weight diagram showing the 16-plets for the pseudoscalar (a) and vector mesons (b) made of the u , d , s , and c quarks as a function of isospin I_z , charm C , and hypercharge $Y = \mathcal{B} + S - \frac{C}{3}$. The nonets of light mesons occupy the central planes to which the $c\bar{c}$ states have been added.

θ_i , such that $\tan \theta_i = 1/\sqrt{2}$ (or $\theta_i = 35.3^\circ$). Defining $\alpha = \theta + 54.7^\circ$, one obtains the physical isoscalar state in the flavor basis

$$f' = \frac{1}{\sqrt{2}}(u\bar{u} + d\bar{d}) \cos \alpha - s\bar{s} \sin \alpha, \quad (15.9)$$

and its orthogonal partner f (replace α by $\alpha - 90^\circ$). Thus for ideal mixing ($\alpha_i = 90^\circ$), the f' becomes pure $s\bar{s}$ and the f pure $u\bar{u} + d\bar{d}$. The mixing angle θ can be derived by diagonalizing the mass matrix

$$\begin{pmatrix} m_8 & m_{81} \\ m_{18} & m_1 \end{pmatrix}. \quad (15.10)$$

The mass eigenvalues are $m_{f'}$ and m_f . The mixing angle is given by

$$\tan \theta = \frac{m_8 - m_{f'}}{m_{81}}. \quad (15.11)$$

Calculating m_8 and m_{81} from the wave functions Eq. (15.7) and Eq. (15.8), and expressing the quark masses as a function of the $I = 1/2$ and $I = 1$ meson masses, one obtains

$$\tan \theta = \frac{4m_K - m_a - 3m_{f'}}{2\sqrt{2}(m_a - m_K)}, \quad (15.12)$$

which also determines the sign of θ . Alternatively, one can express the mixing angle as a function of all nonet masses. The octet mass is given by

$$m_8 = m_{f'} \cos^2 \theta + m_f \sin^2 \theta \quad (15.13)$$

whence

$$\tan^2 \theta = \frac{4m_K - m_a - 3m_{f'}}{-4m_K + m_a + 3m_{f'}}. \quad (15.14)$$

Eliminating θ from Eq. (15.12) and Eq. (15.14) leads to the sum rule [14]

$$(m_f + m_{f'})(4m_K - m_a) - 3m_f m_{f'} = 8m_K^2 - 8m_K m_a + 3m_a^2. \quad (15.15)$$

This relation is verified for the ground-state vector mesons. We identify the $\phi(1020)$ with the f' and the $\omega(783)$ with the f . Thus

$$\phi(1020) = \psi_8 \cos \theta_V - \psi_1 \sin \theta_V, \quad (15.16)$$

$$\omega(782) = \psi_8 \sin \theta_V + \psi_1 \cos \theta_V, \quad (15.17)$$

Table 15.2: Suggested $q\bar{q}$ quark-model assignments for the lightest mesons made of u , d and s quarks. Mesons in boldface are included in the Summary Table. The wave functions f and f' are given in the text (Eq. (15.9)) and the singlet-octet mixing angles in Table 15.5 below for the well established nonets. The classification of the 0^{++} mesons is controversial: (i) the scalars $a_0(980)$, $K_0^*(700)$, $f_0(980)$ and $f_0(500)$, omitted from the table, are often considered to be four-quark states, but are also proposed for the ground state scalar nonet (see the chapter “Scalar Mesons below 1 GeV” in this *Review*); (ii) there are three isoscalar 0^{++} mesons, $f_0(1370)$, $f_0(1500)$ and $f_0(1710)$, both $f_0(1500)$ and $f_0(1710)$ being proposed as glueballs. The three states are expected to mix. The isoscalar assignments in the 2^1S_0 (0^{-+}) nonet are also tentative. Details and alternative schemes can be found in “Spectroscopy of Light Meson Resonances” in this *Review*.

^a The $1^{+\pm}$ and $2^{-\pm}$ isospin $\frac{1}{2}$ states mix. In particular, the K_{1A} and K_{1B} are nearly equal mixtures of the $K_1(1270)$ and $K_1(1400)$ [7]. The $2^{-\pm}$ mixed partner of the $K_2(1770)$ is the established $K_2(1820)$.

^b The physical vector mesons are mixtures of 1^3D_1 and 2^3S_1 (for a discussion see [8]).

^c This state has also been proposed as a tetraquark state [9].

^d The $\eta(1475)$ and $\eta(1405)$ (not shown) may be manifestations of a single state [10].

^e This state has also been proposed as the ground state tensor glueball [11,12].

$n^{2s+1}\ell_J$	J^{PC}	$l = 1$	$l = \frac{1}{2}$	$l = 0$	$l = 0$
		$u\bar{d}, \bar{u}d,$ $\frac{1}{\sqrt{2}}(d\bar{d} - u\bar{u})$	$u\bar{s}, d\bar{s};$ $\bar{d}s, \bar{u}s$	f'	f
1^1S_0	0^{-+}	π	K	η	$\eta'(958)$
1^3S_1	1^{--}	$\rho(770)$	$K^*(892)$	$\phi(1020)$	$\omega(782)$
1^3P_0	0^{++}	$a_0(1450)$	$K_0^*(1430)$	$f_0(1370, 1500, 1710)$	
1^1P_1	1^{+-}	$b_1(1235)$	K_{1B}^a	$h_1(1415)$	$h_1(1170)$
1^3P_1	1^{++}	$a_1(1260)$	K_{1A}^a	$f_1(1420)$	$f_1(1285)$
1^3P_2	2^{++}	$a_2(1320)$	$K_2^*(1430)$	$f_2'(1525)$	$f_2(1270)$
1^3D_1	1^{--}	$\rho(1700)$	$K^*(1680)^b$	$\phi(2170)^c$	$\omega(1650)$
1^1D_2	2^{-+}	$\pi_2(1670)$	$K_2(1770)^a$	$\eta_2(1870)$	$\eta_2(1645)$
1^3D_3	3^{--}	$\rho_3(1690)$	$K_3^*(1780)$	$\phi_3(1850)$	$\omega_3(1670)$
1^3F_4	4^{++}	$a_4(1970)$	$K_4^*(2045)$	$f_4(2300)$	$f_4(2050)$
1^3G_5	5^{--}	$\rho_5(2350)$	$K_5^*(2380)$		
2^1S_0	0^{-+}	$\pi(1300)$	$K(1460)$	$\eta(1475)^d$	$\eta(1295)$
2^3S_1	1^{--}	$\rho(1450)$	$K^*(1410)^b$	$\phi(1680)$	$\omega(1420)$
2^3P_1	1^{++}	$a_1(1640)$	$K_1(1650)$		
2^3P_2	2^{++}	$a_2(1700)$	$K_2^*(1980)$	$f_2(1950)^e$	$f_2(1640)$
2^1D_2	2^{-+}	$\pi_2(1880)$			
3^1S_0	0^{-+}	$\pi(1800)$	$K(1830)$		$\eta(1760)$

Table 15.3: $c\bar{c}$ quark-model assignments for the charmonium mesons with established J^{PC} and their corresponding open charm mesons. Mesons in boldface are included in the Meson Summary Table. The open flavor states in the 1^{+-} and 1^{++} rows are mixtures of the $1^{+\pm}$ states.

^a In unitarized chiral perturbation theory this meson splits into two states at 2105 and 2451 MeV [1,13].

^b The masses are considerably smaller than most theoretical predictions. They have also been considered as tetraquark or $D^{(*)}K$ molecular states.

^c This meson splits into two states at 2247 and 2555 MeV [1].

^d Mixtures of the 1^3D_1 and 2^3S_1 states.

$n^{2s+1}\ell_J$	J^{PC}	$l = 0$	$l = \frac{1}{2}$	$l = 0$
		$c\bar{c}$	$c\bar{u}, c\bar{d};$ $\bar{c}u, \bar{c}d$	$c\bar{s};$ $\bar{c}s$
1^1S_0	0^{-+}	$\eta_c(1S)$	D	D_s^\pm
1^3S_1	1^{--}	$J/\psi(1S)$	D^*	$D_s^{*\pm}$
1^3P_0	0^{++}	$\chi_{c0}(1P)$	$D_0^*(2300)^a$	$D_{s0}^*(2317)^{\pm b}$
1^3P_1	1^{++}	$\chi_{c1}(1P)$	$D_1(2430)^c$	$D_{s1}(2460)^{\pm b}$
1^1P_1	1^{+-}	$h_c(1P)$	$D_1(2420)$	$D_{s1}(2536)^\pm$
1^3P_2	2^{++}	$\chi_{c2}(1P)$	$D_2^*(2460)$	$D_{s2}^*(2573)^\pm$
2^1S_0	0^{-+}	$\eta_c(2S)$	$D_0(2550)^0$	$D_{s0}(2590)^+$
2^3S_1	1^{--}	$\psi(2S)$	$D_1^*(2600)^0$	$D_{s1}^*(2700)^{\pm d}$
1^3D_1	1^{--}	$\psi(3770)$	$D_1^*(2760)^0$	$D_{s1}^*(2860)^{\pm d}$
1^3D_2	2^{--}	$\psi_2(3823)$	$D_2(2740)^0$	
2^3P_J	0^{++}	$\chi_{c0}(3860)$		
	2^{++}	$\chi_{c2}(3930)$		
3^3S_1	1^{--}	$\psi(4040)$		
2^3D_1	1^{--}	$\psi(4160)$		
4^3S_1	1^{--}	$\psi(4415)$		
1^3D_3	3^{--}	$\psi_3(3842)$	$D_3^*(2750)$	$D_{s3}^*(2860)^\pm$

Table 15.4: $b\bar{b}$ quark-model assignments for the bottomonium mesons with established J^{PC} and their corresponding open bottom mesons.

$n^{2s+1}\ell_J$	J^{PC}	$I = 0$ $b\bar{b}$	$I = \frac{1}{2}$ $b\bar{u}, b\bar{d};$ $\bar{b}u, \bar{b}d$	$I = 0$ $b\bar{s};$ $\bar{b}s$	$I = 0$ $b\bar{c};$ $\bar{b}c$
1^1S_0	0^{-+}	$\eta_b(1S)$	B	B_s^0	B_c^\pm
1^3S_1	1^{--}	$\Upsilon(1S)$	B^*	B_s^*	
1^3P_0	0^{++}	$\chi_{b0}(1P)$			
1^3P_1	1^{++}	$\chi_{b1}(1P)$			
1^1P_1	1^{+-}	$h_b(1P)$	$B_1(5721)$	$B_{s1}(5830)^0$	
1^3P_2	2^{++}	$\chi_{b2}(1P)$	$B_2^*(5747)$	$B_{s2}^*(5840)^0$	
2^1S_0	0^{-+}	$\eta_b(2S)$			$B_c(2S)^\pm$
2^3S_1	1^{--}	$\Upsilon(2S)$			
1^3D_2	2^{--}	$\Upsilon_2(1D)$			
2^3P_J	$0, 1, 2^{++}$	$\chi_{b0,1,2}(2P)$			
2^1P_1	1^{+-}	$h_b(2P)$			
3^3S_1	1^{--}	$\Upsilon(3S)$			
3^3P_J	$0, 1, 2^{++}$	$\chi_{b1,2}(3P)$			
4^3S_1	1^{--}	$\Upsilon(4S)$			

with the vector mixing angle $\theta_V = 36.5^\circ$ from Eq. (15.14), very close to ideal mixing. Thus $\phi(1020)$ is nearly pure $s\bar{s}$. For ideal mixing, Eq. (15.12) and Eq. (15.14) lead to the relations

$$m_K = \frac{m_f + m_{f'}}{2}, \quad m_a = m_f, \quad (15.18)$$

which are satisfied for the vector mesons.

The situation for the pseudoscalar and scalar mesons is not so clear cut, either theoretically or experimentally. For the pseudoscalars, the mixing angle is small. This can be understood qualitatively via gluon-line counting of the mixing process. The size of the mixing process between the nonstrange and strange mass bases scales as α_s^2 , not α_s^3 , because of two rather than three gluon exchange as it does for the vector mesons. It may also be that the lightest isoscalar pseudoscalars mix more strongly with excited states or with states of substantial non- $q\bar{q}$ content, as will be discussed below.

In fact a large mixing from hadronic loops is expected for scalar mesons, no matter what model is assumed for $q\bar{q}$ pair production [15]. A variety of analysis methods lead to similar results: First, for these states, Eq. (15.15) is satisfied only approximately. Then Eq. (15.12) and Eq. (15.14) lead to somewhat different values for the mixing angle. Identifying the η with the f' one gets

$$\eta = \psi_8 \cos\theta_P - \psi_1 \sin\theta_P, \quad (15.19)$$

$$\eta' = \psi_8 \sin\theta_P + \psi_1 \cos\theta_P. \quad (15.20)$$

Following chiral perturbation theory, the meson masses in the mass formulae (Eq. (15.12) and Eq. (15.14)) might be replaced by their squares. Table 15.5 lists the mixing angle θ_{lin} from Eq. (15.14) (using the neutral members of the nonets) and the corresponding θ_{quad} obtained by replacing the meson masses by their squares throughout. The mixing angles in the 1^{--} , 2^{++} and 3^{--} nonets are not far from ideal, while larger $s\bar{s}$ -($u\bar{u} + d\bar{d}$) mixing is predicted from hadronic loops in the 0^{++} , 0^{-+} and 1^\pm nonets [15].

The pseudoscalar mixing angle θ_P can also be measured by comparing the partial widths for radiative J/ψ decay into a vector and a pseudoscalar [16], radiative $\phi(1020)$ decay into η and η' [17], radiative decays between pseudoscalar and vector mesons [18], or $p\bar{p}$ annihilation at rest into a pair of vector and pseudoscalar or into two pseudoscalars [19, 20]. One obtains a mixing angle between -10° and -20° . More recently, a lattice QCD simulation, Ref. [21], has successfully reproduced the masses of the η and η' , and as a byproduct find a mixing angle $\theta_{\text{lin}} = -14.1(2.8)^\circ$. We return to this point in Sec. 15.8.

The nonet mixing angles can be measured in $\gamma\gamma$ collisions, *e.g.*, for the 0^{-+} , 0^{++} , and 2^{++} nonets. In the quark model, the amplitude for the coupling of neutral mesons to two photons is proportional to $\sum_i Q_i^2$, where Q_i is the charge of the i -th quark.

Table 15.5: Singlet-octet mixing angles for the well established nonets from the linear mass formula Eq. (15.14) and its quadratic version in which the masses are squared. The 1^{++} and 1^{+-} nonet mixing angles depend on the mixing angle θ_{K_1} between K_{1A} and K_{1B} . The recommended values are $\sim 23^\circ$ and $\sim 28^\circ$ for 1^{++} and 1^{+-} , respectively, with $\theta_{K_1} \sim 35^\circ$ [7].

$n^{2s+1}\ell_J$	J^{PC}	θ_{quad} [$^\circ$]	θ_{lin} [$^\circ$]
1^1S_0	0^{-+}	-11.3	-24.5
1^3S_1	1^{--}	39.2	36.5
1^3P_2	2^{++}	29.6	28.0
1^3D_3	3^{--}	31.8	30.8

The 2γ partial width of an isoscalar meson with mass m is then given in terms of the mixing angle α by

$$\Gamma_{2\gamma} = C(5 \cos\alpha - \sqrt{2} \sin\alpha)^2 m^3, \quad (15.21)$$

for f' and f ($\alpha \rightarrow \alpha - 90^\circ$). The coupling C may depend on the meson mass. It is often assumed to be a constant in the nonet. For the isovector a , one finds $\Gamma_{2\gamma} = 9Cm^3$. Thus the members of an ideally mixed nonet couple to 2γ with partial widths in the ratios $f : f' : a = 25 : 2 : 9$. For tensor mesons, one finds from the ratios of the measured 2γ partial widths for the $f_2(1270)$ and $f_2'(1525)$ mesons a mixing angle α_T of $(81 \pm 1)^\circ$, or $\theta_T = (27 \pm 1)^\circ$, in accord with the linear mass formula. For the pseudoscalars, one finds from the ratios of partial widths $\Gamma(\eta' \rightarrow 2\gamma)/\Gamma(\eta \rightarrow 2\gamma)$ a mixing angle $\theta_P = (-18 \pm 2)^\circ$, while the ratio $\Gamma(\eta' \rightarrow 2\gamma)/\Gamma(\pi^0 \rightarrow 2\gamma)$ leads to $\sim -24^\circ$. SU(3) breaking effects for pseudoscalars are discussed in [22].

The partial width Γ for the decay of a scalar or a tensor meson into a pair of pseudoscalar mesons is model-dependent. Following Ref. [23],

$$\Gamma = C \times \gamma^2 \times |F(q)|^2 \times q, \quad (15.22)$$

where C is a nonet constant, q the momentum of the decay products, $F(q)$ a form factor, and γ^2 the SU(3) coupling. Details and explicit expressions for γ^2 and $F(q)$ are given in "Spectroscopy of Light Meson Resonances". The decay of a $q\bar{q}$ meson into a pair of mesons involves the creation of a $q\bar{q}$ pair, and SU(3) symmetry assumes that the matrix elements for the creation of $s\bar{s}$, $u\bar{u}$, and $d\bar{d}$ pairs are equal. An excellent fit to the tensor meson decay widths is obtained assuming SU(3) symmetry and a pseudoscalar mixing angle $\theta_P \simeq -17^\circ$ [23].

The analysis of resonances is complicated by the presence of thresholds such as $K\bar{K}$ in $a_0(980) \rightarrow \eta\pi$ or $f_0(980) \rightarrow \pi\pi$, which

affect the resonance masses and widths. A particularly nasty kinematic effect is the triangle singularity in which one of the primary decay daughters in turn decays and is emitted backwards, catching up and scattering with the second primary product. This mechanism generates fake peaks in the final state and has been proposed as alternative explanation for several meson (and baryon) signals. Prominent examples are the $\eta(1475) \rightarrow K^*(\rightarrow K\pi)K$ and $\eta(1410) \rightarrow a_0(980)(\rightarrow \eta\pi)\pi$ signals which could be due to one single state [10] (as shown in Table 15.2).

Furthermore, to parametrize resonances, many data analyses resort to Breit-Wigner amplitudes which are not suitable to describe broad interfering mesons with the same quantum numbers, as they violate unitarity. This is in particular the case in the mass range above 1500 MeV where radial and orbital excitations, e.g. of broad scalar and tensor mesons, start to accumulate. A better approach is to determine the T-matrix poles in the complex plane, where resonances are usually located on the second Riemann sheet.

15.4 Exotic mesons

There are two classes of colorless exotic mesons allowed in QCD: multiquark states (section 15.4.1) and mesons with active gluons, bound states of gluons (the glueballs, section 15.4.2) and $q\bar{q}$ states with “valence” gluons (the hybrids, section 15.4.3). The first class contains the simplest system consisting of two quarks and two antiquarks (tetraquarks). Compact tetraquarks (also called “diquonium” in the older literature) are made of diquarks and antidiquarks. Hadroquarkonia consist of a pair of heavy quark and antiquark in a compact core surrounded by a light-quark cloud. In hadronic “molecules” the building blocks are color-neutral hadrons bound by meson exchanges.

15.4.1 Tetraquarks

The existence of a light nonet composed of four quarks (tetraquarks) with masses below 1 GeV was suggested a long time ago [24, 25]. Coupling two triplets of light quarks u , d , and s , one obtains nine states, of which the six symmetric (uu , dd , ss , $ud+du$, $us+su$, $ds+sd$) form the six dimensional representation $\mathbf{6}$, while the three antisymmetric ($ud-du$, $us-su$, $ds-sd$) form the three dimensional representation $\bar{\mathbf{3}}$ of SU(3):

$$\mathbf{3} \otimes \mathbf{3} = \mathbf{6} \oplus \bar{\mathbf{3}}. \quad (15.23)$$

Hence for tetraquarks one gets the reduction

$$\begin{aligned} \mathbf{3} \otimes \mathbf{3} \otimes \bar{\mathbf{3}} \otimes \bar{\mathbf{3}} &= \mathbf{6} \oplus \bar{\mathbf{3}} \otimes \bar{\mathbf{6}} \otimes \bar{\mathbf{3}} \\ &= \bar{\mathbf{3}} \otimes \mathbf{3} \oplus \mathbf{6} \oplus \bar{\mathbf{6}} \oplus \mathbf{6} \oplus \bar{\mathbf{3}} \oplus \bar{\mathbf{6}} \\ &= \mathbf{9} \oplus \mathbf{36} \oplus \mathbf{18} \oplus \bar{\mathbf{18}}. \end{aligned} \quad (15.24)$$

Combining with spin and color and requiring antisymmetry for diquarks and antidiquarks, one finds for ground states (zero angular momenta) that the most deeply bound tetraquarks (and hence the lightest ones) form a nonet and are scalar mesons (see also [6]). The masses are estimated to be below 900 MeV. The strange quark determines the mass splittings and one obtains a mass inverted spectrum with a light isosinglet ($f_0(500)$), a medium heavy isodoublet ($K_0^*(700)$) and a heavy isotriplet ($a_0(980)$) + isosinglet ($f_0(980)$). In alternative schemes these states build the lightest $q\bar{q}$ scalar nonet (for details see “Scalar mesons below 1 GeV” in this “Review”).

A plethora of new heavy multiquark candidates have been reported in the charmonium spectrum (Fig. 15.2). Details and references can be found in the review “Heavy non- $q\bar{q}$ Mesons”, see also Refs. [26–28].

The most prominent one is the $\chi_{c1}(3872)$ (was $X(3872)$), first observed by BELLE in 2003 in B -decays in the final state $J/\psi\pi^+\pi^-$ [29] and firmly established by many experiments (Babar, BESIII, CDF, D0, LHCb) in several production modes (e^+e^- , A_b decay, $p\bar{p}$, pp). This narrow state (< 1 MeV) decays mainly into $D^0\bar{D}^{0*}$ and is right at the $D^0\bar{D}^{0*}$ threshold. Its composition is believed to be mostly molecular, bound by pion exchange. Its existence was already predicted in 1991 [30]. Many non- $c\bar{c}$ candidates have been reported since then above the open

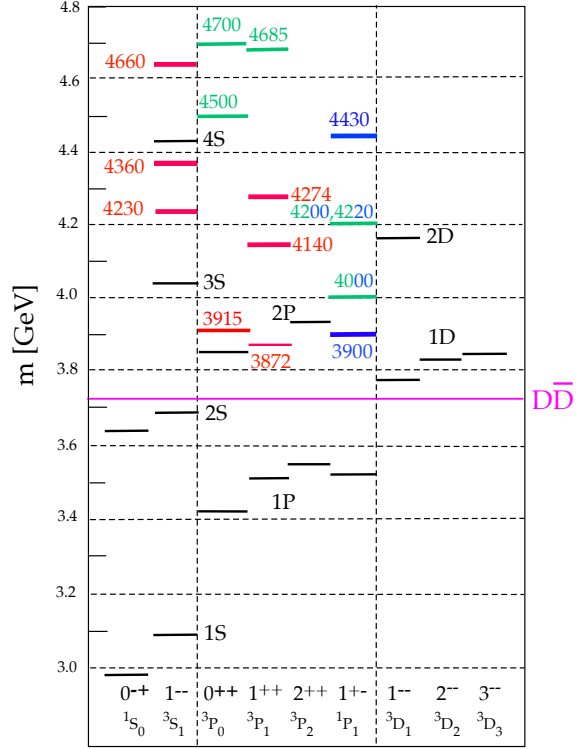


Figure 15.2: Mass spectrum with known $I^G(J^{PC})$ observed in the charmonium region. The $D\bar{D}$ line shows the open charm threshold. The well-known $c\bar{c}$ mesons are shown in black. (The $1^1D_2 \eta_{c2}$, expected around 3800 MeV, has not been seen yet.) The established additional observed states are shown in red, and the states needing confirmation (i.e. omitted from the Summary Tables) are labeled in green. The blue color denotes exotic isovectors.

charm threshold, with quantum numbers compatible with $c\bar{c}$, but which are not expected in the pure charmonium spectrum. In addition, one observes isovector (charged) mesons decaying into $c\bar{c}$ states plus a charged pion or kaon. (They are listed in this Review under “Other mesons”.) For example, the $1^{+-} T_{c\bar{c}1}(3900)^+$ (was $Z_c(3900)^+$) and $T_{c\bar{c}s1}(4000)^+$ (was $Z_{cs}(4000)^-$) cannot be pure charmonia, but are compatible with $c\bar{c}u\bar{d}$ and $c\bar{c}s\bar{u}$, respectively. They could belong to the same nonet, hence identifying the other multiplet members might shed light on the structure of such states.

Even more remarkable are the observations by LHCb of a doubly charmed state $T_{cc}(3875)^+$ ($ccu\bar{d}$) [31] at the $D_0D_0^*$ threshold and of a $T_{cc\bar{c}\bar{c}}(6900)$ [32] decaying into a pair of $J/\psi(1S)$. Similar states begin to emerge also in the bottomonium spectrum, such as the $1^{+-} T_{b\bar{b}1}(10610)^+$ (was $Z_b(10610)^+$) and $T_{b\bar{b}1}(10650)^+$ (was $Z_b(10650)^+$), both $b\bar{b}u\bar{d}$. Many of these states may be hadronic modules made of charge conjugated pairs of mesons such as $D^{(*)}$, $D_s^{(*)}$ or their excitations, and their B and B^* counterparts. They could also be mimicked by kinematical effects such as triangle singularities.

15.4.2 Glueballs

QCD predicts the existence of extra isoscalar mesons which cannot be addressed by the quark model. In the pure gauge theory they contain only gluons. The ground state glueball is predicted by lattice gauge theories to be 0^{++} , the first excited state 2^{++} . Errors on the mass predictions are large. From Ref. [33] one obtains 1750 (50) (80) MeV for the mass of the lightest 0^{++} glueball from quenched QCD. As an example for the glueball mass spectrum, we show in Fig. 15.3 a calculation from [34]. A mass of 1710 MeV is predicted for the ground state, also with an error of about 100 MeV. Earlier work by other groups produced masses at 1650 MeV [35] and 1550 MeV [36] (see also [37]). The first excited

state has a mass of about 2.4 GeV, and the lightest glueball with exotic quantum numbers (2^{+-}) has a mass of about 4 GeV.

These calculations are made in the so-called “quenched approximation” which neglects $q\bar{q}$ loops. However, both glue and $q\bar{q}$ states couple to singlet scalar mesons. Therefore glueballs will mix with nearby $q\bar{q}$ states of the same quantum numbers. The first results from lattice calculations, which include these effects, indicate that the mass shifts are small. We return to a discussion of this point in Sec. 15.8, see also Fig. 15.15.

The existence of three singlet scalar mesons around 1.5 GeV suggests additional degrees of freedom such as glue, since only two mesons are predicted in this mass range (as indicated in Table 15.2). The $f_0(1500)$ [23, 38] or, alternatively, the $f_0(1710)$ [35], have been proposed as candidates for the scalar glueball, both states having considerable mixing also with the $f_0(1370)$. Following Ref. [39] the glue is distributed among the 0^{++} isoscalars $q\bar{q}$ mesons around 2 GeV. Other mixing schemes, in particular with the $f_0(500)$ and the $f_0(980)$, have also been proposed [40]. According to a holographic model of low-energy QCD scalar glueballs decay strongly into kaons and η mesons, in good agreement with data on the $f_0(1710)$ [41]. Details can be found in the review “Spectroscopy of Light Meson Resonances” and in Ref. [42]. See also the review “Scalar Mesons below 1 GeV” in this *Review*.

15.4.3 Hybrids

Mesons made of $q\bar{q}$ pairs bound by excited gluons ($q\bar{q}g$) are also predicted. Early model estimates placed them in the 1.9 GeV mass region, according to gluon flux tube models [43]. In the bag model there are four nonets, among them an exotic 1^{-+} , around or above 1.4 GeV [44, 45].

Lattice QCD calculations show that the lightest hybrid is an exotic 1^{-+} state, at a mass around 2 GeV [46–48]. Fig. 15.13 will show an example of the spectroscopy from one group’s [48] simulation.

There are so far two candidates for exotic states with quantum numbers 1^{-+} , the $\pi_1(1400)$ and $\pi_1(1600)$, which could be hybrids or four-quark states. However, a recent combined re-analysis of π_1 production in diffractive π^-p interaction and low energy $\bar{p}p$ annihilation leads to a single pole at ~ 1560 MeV with a width of ~ 390 MeV, although a two-pole scenario cannot be excluded [49]. Recently BESIII has reported evidence for the existence of a 1^{-+} $\eta_1(1855) \rightarrow \eta\eta'$ [50] which could be one of the isoscalar partners of the $\pi_1(1600)$ in the 1^{-+} hybrid nonet [51]. (For details and references, see the review “Spectroscopy of Light Meson Resonances” in this *Review*.)

15.5 Baryons: qqq states

Baryons are fermions with baryon number $\mathcal{B} = 1$, *i.e.*, in the most general case, they are composed of three quarks plus any number of quark - antiquark pairs. Until recently, all established baryons were consistent with 3-quark (qqq) configurations, which we mainly discuss in this section. However, in 2015 the LHCb collaboration published first evidence for charmed ‘pentaquark’ states of minimal quark content $c\bar{c}uud$ at invariant masses close to 4.4 GeV [52]. More refined LHCb experiments have revealed evidence for four such states called $P_{c\bar{c}}(4312)^+$, $P_{c\bar{c}}(4380)^+$, $P_{c\bar{c}}(4440)^+$, and $P_{c\bar{c}}(4457)^+$ [53]. These states are located close to the thresholds of the production of ordinary baryon-meson pairs like $\Sigma_c^+ \bar{D}^0$ and $\Sigma_c^+ \bar{D}^{*0}$ and are consistent with the predictions in terms of molecular-like states [54, 55]. A nice overview on the discussion of pentaquark and tetraquark states is given in Ref. [56]. See also the article on “Pentaquarks” in this *Review*.

The color part of the baryon wave function is an SU(3) singlet, a completely antisymmetric state of the three colors. Since the quarks are fermions, the wave function must be antisymmetric under interchange of any two equal-mass quarks (up and down quarks in the limit of isospin symmetry). Thus, it can be written as

$$|qqq\rangle_A = |\text{color}\rangle_A \times |\text{space, spin, flavor}\rangle_S, \quad (15.25)$$

where the subscripts S and A indicate symmetry or antisymmetry under interchange of any two equal-mass quarks. Note the contrast with the state function for the three nucleons in ^3H or ^3He :

$$|NNN\rangle_A = |\text{space, spin, isospin}\rangle_A. \quad (15.26)$$

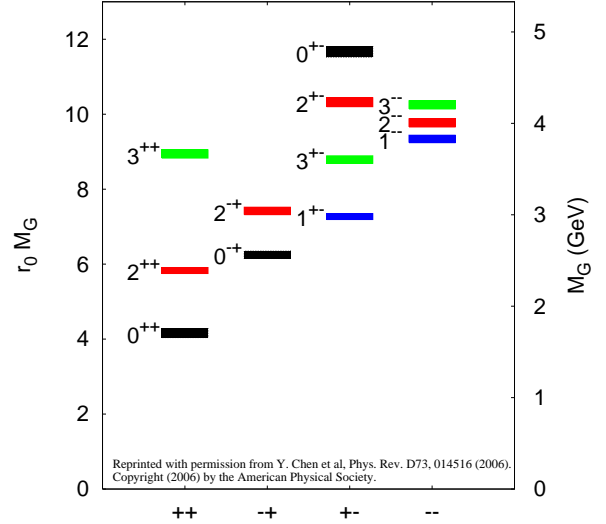


Figure 15.3: Predicted glueball spectrum from the lattice in quenched approximation (from [34]).

This difference has major implications for the internal structure, magnetic moments, *etc.* (For a nice discussion, see [57].)

15.5.1 Light baryons

The “ordinary” light-flavor baryons are made up of u , d , and s quarks. The three flavors imply an approximate SU(3) flavor symmetry, which requires that baryons made of these quarks belong to the multiplets on the right side of

$$\mathbf{3} \otimes \mathbf{3} \otimes \mathbf{3} = \mathbf{10}_S \oplus \mathbf{8}_M \oplus \mathbf{8}_M \oplus \mathbf{1}_A \quad (15.27)$$

(see the section on “SU(n) Multiplets and Young Diagrams” in this *Review*). Here the subscripts indicate symmetric, mixed-symmetry, or antisymmetric states under interchange of any two quarks. The $\mathbf{1}$ is a $|uds\rangle$ singlet state (A_1), and the octet contains a similar state (A_8). If these have the same spin and parity, they can mix. The mechanism is the same as for the mesons (see above). In the ground state multiplet, the SU(3) flavor singlet A_1 is forbidden by Fermi statistics. The section on “SU(3) Isoscalar Factors and Representation Matrices,” shows how relative decay rates in, say, $\mathbf{10} \rightarrow \mathbf{8} \otimes \mathbf{8}$ decays may be calculated.

For the light-flavor baryons (no c or b quark), flavor and spin may be combined in an approximate flavor-spin SU(6), in which the six basic states are $d \uparrow, d \downarrow, \dots, s \downarrow$ ($\uparrow, \downarrow =$ spin up, down). Then the baryons belong to the multiplets on the right side of

$$\mathbf{6} \otimes \mathbf{6} \otimes \mathbf{6} = \mathbf{56}_S \oplus \mathbf{70}_M \oplus \mathbf{70}_M \oplus \mathbf{20}_A. \quad (15.28)$$

These SU(6) multiplets decompose into flavor SU(3) multiplets as follows:

$$\mathbf{56} = \mathbf{4}\mathbf{10} \oplus \mathbf{2}\mathbf{8} \quad (15.29a)$$

$$\mathbf{70} = \mathbf{2}\mathbf{10} \oplus \mathbf{4}\mathbf{8} \oplus \mathbf{2}\mathbf{8} \oplus \mathbf{2}\mathbf{1} \quad (15.29b)$$

$$\mathbf{20} = \mathbf{2}\mathbf{8} \oplus \mathbf{4}\mathbf{1}, \quad (15.29c)$$

where the superscript ($2S+1$) gives the net spin S of the quarks for each particle in the SU(3) multiplet. The $J^P = 1/2^+$ octet containing the nucleon and the $J^P = 3/2^+$ decuplet containing the $\Delta(1232)$ together make up the “ground-state” 56-plet, in which the orbital angular momenta between the quark pairs are zero (so that the spatial part of the state function is trivially symmetric). The $\mathbf{70}$ and $\mathbf{20}$ require some excitation of the spatial part of the wave function in order to make the overall wave function symmetric. States with nonzero orbital angular momenta are classified in SU(6) \otimes O(3) supermultiplets.

It is useful to classify the baryons into bands that have the same number N of quanta of excitation. Each band consists of a number of supermultiplets, specified by (D, L_N^P) , where D is the dimensionality of the SU(6) representation, L is the total quark

orbital angular momentum, and P is the total parity. Supermultiplets contained in bands up to $N = 12$ are given in [58]. The $N = 0$ band (with positive parity), which contains the nucleon and $\Delta(1232)$, consists only of the $(56, 0_0^+)$ supermultiplet. The $N = 1$ band (with negative parity) consists only of the $(70, 1_1^-)$ multiplet and contains the negative-parity baryons with masses below about 1.9 GeV. The $N = 2$ band (with positive parity) contains five supermultiplets: $(56, 0_2^+)$, $(70, 0_2^+)$, $(56, 2_2^+)$, $(70, 2_2^+)$, and $(20, 1_2^+)$, where the $(56, 0_0^+)$ represents the multiplet that contains the first radial excitations having the same quantum numbers as the ground state.

The wave functions of the non-strange baryons in the harmonic oscillator basis are often labeled by $|X^2S^{+1}L_\pi J^P\rangle$, where S, L, J, P are as above, $X = N$ or Δ , and $\pi = S, M$ or A denotes the symmetry of the spatial wave function. The possible model states for the bands with $N=0,1,2$ are given in Table 15.7. The assignment of experimentally observed states is only complete and well established up to the $N=1$ band. Some more tentative assignments for higher multiplets are suggested in [59].

In Table 15.6, quark-model assignments are given for many of the established baryons whose $SU(6) \otimes O(3)$ compositions are relatively unmixed. Apart from the mixing of the Λ singlet and octet states, one must, however, keep in mind that states with same J^P but different L, S combinations can also mix. In the quark model with one-gluon exchange motivated interactions, the size of the mixing is determined by the relative strength of the tensor term with respect to the contact term (see below). The mixing is more important for the decay patterns of the states than for their positions. An example are the lowest lying $(70, 1_1^-)$ states with $J^P = 1/2^-$ and $3/2^-$. The physical states are

$$|N(1535)1/2^-\rangle = \cos(\Theta_S)|N^2P_M1/2^-\rangle - \sin(\Theta_S)|N^4P_M1/2^-\rangle \quad (15.30)$$

$$|N(1520)3/2^-\rangle = \cos(\Theta_D)|N^2P_M3/2^-\rangle - \sin(\Theta_D)|N^4P_M3/2^-\rangle \quad (15.31)$$

and the orthogonal combinations for $N(1650)1/2^-$ and $N(1700)3/2^-$. The mixing is large for the $J^P = 1/2^-$ states ($\Theta_S \approx -32^\circ$), but small for the $J^P = 3/2^-$ states ($\Theta_D \approx +6^\circ$) [61–63].

All baryons of the ground state multiplets are known. Many of their properties, in particular their masses, are in good agreement with even the most basic versions of the quark model, including harmonic (or linear) confinement and a spin-spin interaction, which is responsible for the octet - decuplet mass shifts. A consistent description of the ground-state electroweak properties, however, requires refined relativistic constituent quark models.

The situation for the excited states is much less clear. The assignment of some experimentally observed states with strange quarks to model configurations is only tentative and in many cases candidates are completely missing. Melde, Plessas and Sengl [60] have calculated baryon properties in relativistic constituent quark models, using one-gluon exchange and Goldstone-boson exchange for the modeling of the hyperfine interactions (see Sec. 15.7 on Dynamics). Both types of models give qualitatively comparable results and in general, underestimate experimentally observed decay widths. Nevertheless, in particular on the basis of the observed decay patterns, the authors have assigned some additional states with strangeness to the $SU(3)$ multiplets and suggest re-assignments for a few others. Among the new assignments are states with weak experimental evidence (two or three star ratings) and partly without firm spin/parity assignments, so that further experimental efforts are necessary before final conclusions can be drawn. We have added their suggestions in Table 15.6.

In the non-strange sector there are two main problems which are illustrated in Fig. 15.4, where the experimentally observed excitation spectrum of the nucleon (N and Δ resonances) is compared to the results of a typical quark model calculation [64]. The lowest states from the $N=2$ band, the $N(1440)1/2^+$, and the $\Delta(1600)3/2^+$, appear lower than the negative parity states from the $N=1$ band (see Table 15.7) and much lower than predicted by most models. Also negative parity Δ states from the $N=3$ band ($\Delta(1900)1/2^-$, $\Delta(1940)3/2^-$, and $\Delta(1930)5/2^-$) are too low in energy. The low lying states show a clustering in groups of levels around 1700 MeV and 1900 MeV for N^* states and around

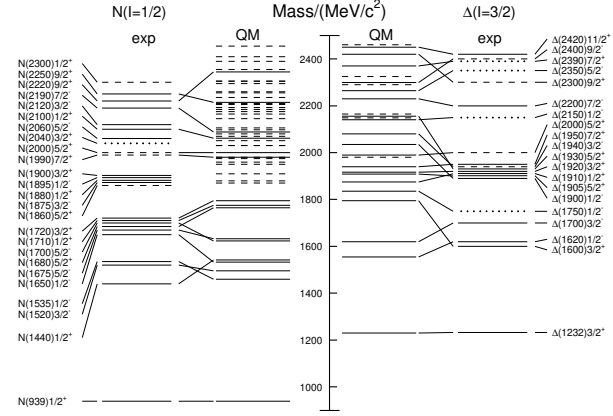


Figure 15.4: Excitation spectrum of the nucleon. Compared are the positions of the excited states identified in experiment, to those predicted by a relativized quark model calculation. Left hand side: isospin $I = 1/2$ N -states, right hand side: isospin $I = 3/2$ Δ -states. Experimental: (columns labeled 'exp'), three- and four-star states are indicated by full lines (two-star dashed lines, one-star dotted lines). At the very left and right of the figure, the spectroscopic notation of these states is given. Quark model [64, 65]: (columns labeled 'QM'), all states for the $N=1,2$ bands, low-lying states for the $N=3,4,5$ bands. Full lines: at least tentative assignment to observed states, dashed lines: so far no observed counterparts. Many of the assignments between predicted and observed states are highly tentative.

1900 MeV for Δ states which is not reflected in models.

Furthermore, many more states are predicted than observed. This has been known for a long time as the 'missing resonance' problem [61]. Up to an excitation energy of 2.4 GeV, about 45 N states are predicted, but only 20 are established (four- or three-star; see Note on N and Δ Resonances for the rating of the status of resonances) and 5 are tentative (two- or one-star). However, there is some recent progress. For the $N=2$ band, candidates have been identified for almost all predicted states with the exception of the $(20, 1_2^+)$. The total number of states has perhaps not significantly changed but the number of states with four- or three-star rating has increased from 14 to 20 compared to the 2018 PDG particle listings. Most of this progress is due to the programs concentrating on the study of meson photoproduction reactions, while the most recent partial wave analysis of elastic pion scattering and charge exchange data by Arndt and collaborators [66] found no evidence for almost half of the states listed in this review (and included in Fig. 15.4). Such analyses are of course biased against resonances which couple only weakly to the $N\pi$ channel. Quark model predictions for the couplings to other hadronic channels and to photons are given in Ref. [64]. The large experimental effort ongoing at several electron accelerators to study the baryon resonance spectrum with real and virtual photon-induced meson production reactions includes the search for as-yet-unobserved states, as well as detailed studies of the properties of the low lying states (decay patterns, electromagnetic couplings, magnetic moments, etc.) (see Ref. [67] for reviews). There are two major new aspects of this program. The investigation of single and double polarization observables allows, via the study of interference terms, access to small partial waves that do not leave a footprint in unpolarized cross sections. An example for the impact of such data is given by a comparison of results from different multipole analyses of pion photoproduction [68]. It shows clearly that with the inclusion of polarization observables the reaction model results start to converge. This will in the near future much improve the database for excited baryons in the light quark sector.

The other aspect is the study of final states with meson pairs, in particular $\pi\pi$ and $\pi\eta$ pairs, which has made much progress during the last few years. This is important for higher lying states, which in the quark model may have both possible oscillations ex-

Table 15.6: Quark-model assignments for some of the known baryons in terms of a flavor-spin SU(6) basis. Only the dominant representation is listed. Assignments for several states, especially for the $\Lambda(1810)$, $\Lambda(2350)$, $\Xi(1620)$, $\Xi(1690)$, $\Xi(1820)$, and $\Xi(2030)$, are merely educated guesses. † suggestions for assignments and re-assignments from Ref. [60].

J^P	(D, L^P_N)	S	Octet members				Singlets
$1/2^+$	$(56, 0_0^+)$	$1/2$	$N(939)$	$\Lambda(1116)$	$\Sigma(1193)$	$\Xi(1318)$	
$1/2^+$	$(56, 0_2^+)$	$1/2$	$N(1440)$	$\Lambda(1600)$	$\Sigma(1660)$		
$1/2^-$	$(70, 1_1^-)$	$1/2$	$N(1535)$	$\Lambda(1670)$	$\Sigma(1620)$	$\Xi(1620)$	$\Lambda(1405)$
					$\Sigma(1560)^\dagger$		
$3/2^-$	$(70, 1_1^-)$	$1/2$	$N(1520)$	$\Lambda(1690)$	$\Sigma(1670)$	$\Xi(1820)$	$\Lambda(1520)$
$1/2^-$	$(70, 1_1^-)$	$3/2$	$N(1650)$	$\Lambda(1800)$	$\Sigma(1750)$	$\Xi(1690)$	
					$\Sigma(1620)^\dagger$		
$3/2^-$	$(70, 1_1^-)$	$3/2$	$N(1700)$	$\Lambda(?)$	$\Sigma(1940)^\dagger$	$\Xi(?)$	
$5/2^-$	$(70, 1_1^-)$	$3/2$	$N(1675)$	$\Lambda(1830)$	$\Sigma(1775)$	$\Xi(1950)^\dagger$	
$1/2^+$	$(70, 0_2^+)$	$1/2$	$N(1710)$	$\Lambda(1810)$	$\Sigma(1880)$	$\Xi(?)$	$\Lambda(1810)^\dagger$
$3/2^+$	$(56, 2_3^+)$	$1/2$	$N(1720)$	$\Lambda(1890)$	$\Sigma(?)$	$\Xi(?)$	
$5/2^+$	$(56, 2_2^+)$	$1/2$	$N(1680)$	$\Lambda(1820)$	$\Sigma(1915)$	$\Xi(2030)$	
$7/2^-$	$(70, 3_3^-)$	$1/2$	$N(2190)$	$\Lambda(?)$	$\Sigma(?)$	$\Xi(?)$	$\Lambda(2100)$
$9/2^-$	$(70, 3_3^-)$	$3/2$	$N(2250)$	$\Lambda(?)$	$\Sigma(?)$	$\Xi(?)$	
$9/2^+$	$(56, 4_4^+)$	$1/2$	$N(2220)$	$\Lambda(2350)$	$\Sigma(?)$	$\Xi(?)$	

Decuplet members						
$3/2^+$	$(56, 0_0^+)$	$3/2$	$\Delta(1232)$	$\Sigma(1385)$	$\Xi(1530)$	$\Omega(1672)$
$3/2^+$	$(56, 0_2^+)$	$3/2$	$\Delta(1600)$	$\Sigma(1690)^\dagger$	$\Xi(?)$	$\Omega(?)$
$1/2^-$	$(70, 1_1^-)$	$1/2$	$\Delta(1620)$	$\Sigma(1750)^\dagger$	$\Xi(?)$	$\Omega(?)$
$3/2^-$	$(70, 1_1^-)$	$1/2$	$\Delta(1700)$	$\Sigma(?)$	$\Xi(?)$	$\Omega(2012)$
$5/2^+$	$(56, 2_2^+)$	$3/2$	$\Delta(1905)$	$\Sigma(?)$	$\Xi(?)$	$\Omega(?)$
$7/2^+$	$(56, 2_2^+)$	$3/2$	$\Delta(1950)$	$\Sigma(2030)$	$\Xi(?)$	$\Omega(?)$
$11/2^+$	$(56, 4_4^+)$	$3/2$	$\Delta(2420)$	$\Sigma(?)$	$\Xi(?)$	$\Omega(?)$

Table 15.7: N and Δ states in the $N=0,1,2$ harmonic oscillator bands. L^P denotes angular momentum and parity, S the three-quark spin and ‘sym’=A,S,M the symmetry of the spatial wave function. Listed are all possible spin/parity combinations and assignments of experimentally observed states. Only dominant components are indicated. Assignments in the $N=2$ band are partly tentative.

\bar{N}	sym	L^P	S	$N(I = 1/2)$			
2	A	1^+	$1/2$	$1/2^+$	$3/2^+$	-	-
2	M	2^+	$3/2$	$1/2^+$	$3/2^+$	$5/2^+$	$7/2^+$
2	M	2^+	$1/2$	-	$3/2^+$	$5/2^+$	-
2	M	0^+	$3/2$	-	$3/2^+$	-	-
2	M	0^+	$1/2$	$1/2^+$ $N(1710)$	-	-	-
2	S	2^+	$3/2$	-	-	-	-
2	S	2^+	$1/2$	-	$3/2^+$ $N(1720)$	$5/2^+$ $N(1680)$	-
2	S	0^+	$3/2$	-	-	-	-
2	S	0^+	$1/2$	$1/2^+$ $N(1440)$	-	-	-
1	M	1^-	$3/2$	$1/2^-$ $N(1650)$	$3/2^-$ $N(1700)$	$5/2^-$ $N(1675)$	-
1	M	1^-	$1/2$	$1/2^-$ $N(1535)$	$3/2^-$ $N(1520)$	-	-
0	S	0^+	$3/2$	-	-	-	-
0	S	0^+	$1/2$	$1/2^+$ $N(938)$	-	-	-

\bar{N}	sym	L^P	S	$\Delta(I = 3/2)$			
2	A	1^+	$1/2$	-	-	-	-
2	M	2^+	$3/2$	-	-	-	-
2	M	2^+	$1/2$	-	$3/2^+$	$5/2^+$	-
2	M	0^+	$3/2$	-	-	-	-
2	M	0^+	$1/2$	$1/2^+$ $\Delta(1750)$	-	-	-
2	S	2^+	$3/2$	$1/2^+$ $\Delta(1910)$	$3/2^+$ $\Delta(1920)$	$5/2^+$ $\Delta(1905)$	$7/2^+$ $\Delta(1950)$
2	S	2^+	$1/2$	-	-	-	-
2	S	0^+	$3/2$	-	$3/2^+$ $\Delta(1600)$	-	-
2	S	0^+	$1/2$	-	-	-	-
1	M	1^-	$3/2$	-	-	-	-
1	M	1^-	$1/2$	$1/2^-$ $\Delta(1620)$	$3/2^-$ $\Delta(1700)$	-	-
0	S	0^+	$3/2$	-	$3/2^+$ $\Delta(1232)$	-	-
0	S	0^+	$1/2$	-	-	-	-

made of u , d , or s quarks, is

$$\mathbf{3} \otimes \mathbf{3} = \bar{\mathbf{3}}_A \oplus \mathbf{6}_S. \quad (15.33)$$

For ground-state baryons, the overall antisymmetry of baryon wave function (including color) requires the light diquark to be symmetric under the exchange of spin and flavor, hence both symmetric or both antisymmetric, that is spin 1 for the $\mathbf{6}_S$ and spin 0 for the $\bar{\mathbf{3}}_A$. The $\bar{\mathbf{3}}$ then combines with the c quark to form the $J^P = 1/2^+$ states, while the $\mathbf{6}$ combines to form $J^P = 1/2^+$ or $J^P = 3/2^+$. The weight diagrams of the $\bar{\mathbf{3}}$ and $\mathbf{6}$ ground-state representations are shown in Fig. 15.6. Within each multiplet the $C = 1$ baryons obey isospin and $SU(3)_f$ mass relations at the expected orders.

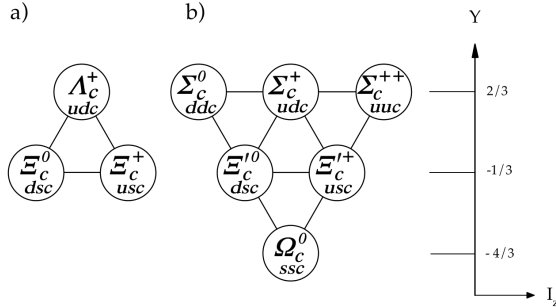


Figure 15.6: The $SU(3)_f$ $\bar{\mathbf{3}}$ (a) and $\mathbf{6}$ (b) ground state $J^P = 1/2^+$ representations. The structure of the $\mathbf{6}$ ground state with $J^P = 3/2^+$ is identical to the one in (b).

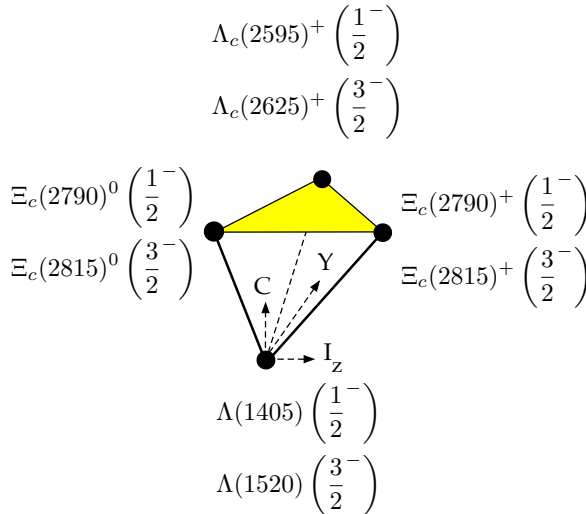


Figure 15.7: Weight diagram of the $\bar{\mathbf{4}}$ $SU(4)_f$ multiplet with the experimentally observed negative parity baryons.

The antisymmetric quadruplet in (15.32) does not exist in the ground state but is realized for the first orbital excitations ($L = 1$). Figure 15.7 shows the weight diagram with the experimentally observed states. In the quark model the quadruplet consists of four baryons with spins coupling to $\frac{1}{2}$, leading to four $L = 1$ excitations with $J^P = \frac{1}{2}^-$ and four excitations with $\frac{3}{2}^-$. The charmed ones are the partners of the $\Lambda(1405)$ and $\Lambda(1520)$ singlets of $SU(3)_f$.

For a detailed review on charmed baryons see Ref. [77]. Quark model predictions for baryons with two heavy quarks are given in Ref. [89] and lattice results for doubly and triply charmed states are discussed in Sec. 15.8 of this *Review*.

The $C = 1$ ground state baryons have all been observed. Due to their relatively narrow widths the states are much easier to isolate than the light quark baryon resonances which require intricate

partial wave analyses. The production cross sections are small, but the recent measurements at the e^+e^- B-factories, at the $p\bar{p}$ Tevatron collider, and at LHCb have boosted the field. The LHCb collaboration has published evidence for five new narrow Ω_c^0 states (css) [90] in proton-proton collisions. Four of these states have been confirmed by the Belle experiment in e^+e^- collisions [91]. Their quantum numbers are still unknown, but they could correspond to the $L = 1$ ssc orbital excitations. Constituent quark models, lattice QCD, quark-diquark models, molecular models, and pentaquark states, have been discussed to describe their structure (see e.g. [92] for references). In the meantime, also four Ω_b^- states of the bss type have been reported from LHCb [92]. They lie in a narrow range between 6316 - 6350 MeV, but since their intrinsic widths are on the order of just a few MeV, they are well separated in the invariant mass spectra. Spectroscopy and theory in this field is rapidly evolving.

LHCb has also reported a doubly charmed Ξ_{cc}^{++} (ccu) baryon [93]. The quantum numbers of this state are undetermined, but its significance is already rated three stars in the current compilation. Doubly charmed baryons have a very different structure from light baryons, more resembling heavy ‘double-star’ systems with attached light ‘planets’, which opens a new window for QCD properties. The first candidate for a doubly charmed baryon Ξ_{cc}^+ (ccd) had been reported earlier by the SELEX experiment [94, 95]. A significance of 6.3σ was claimed for the $\Lambda_c^+ K^- \pi^+$ decay and 4.8σ for $pD^+ K^-$ but searches by other experiments have not confirmed it so far (see e.g. [96] and Refs. therein) and it is not included in the particle listings. The SELEX and LHCb masses lie in the predicted 3500 – 3700 MeV mass range (see e.g. [89]). The LHCb Ξ_{cc}^{++} state lies about 100 MeV above the SELEX one, with a mass splitting far too large for ucc and dcc isospin partners. However, it has also been discussed that due to the different production mechanisms this is not necessarily a contradiction [97].

Figure 15.8 shows the spectrum of the established singly-charmed baryons (3^* and 4^* baryons in the *Listings* with known quantum numbers). The parity of the Λ_c^+ is that of the c quark, defined as positive. Spin and parity have not been determined experimentally for most of the states. They follow the ordering and expectation from the quark model. Candidates for $L = 2$ orbital excitations of the Λ_c (with $J^P = \frac{3}{2}^+$ and $J^P = \frac{5}{2}^+$) have already been observed, as well as a $\frac{3}{2}^-$ state at 2940 MeV, possibly a radial $L = 1$ excitation [98].

The same $SU(4)_f$ multiplets can be constructed for the bottom baryons by replacing the c quark by a b quark. The established 3^* and 4^* bottom baryons are shown in Fig. 15.8. The quadruplet $\bar{\mathbf{4}}$ contains the two negative parity candidates $\Lambda_b(5912)^0$ and $\Lambda_b(5920)^0$. It appears that the confining potential is only weakly flavour dependent. For example, the mass difference between the Ξ_b and the Λ_b is roughly the same as that between the Ξ_c and the Λ_c , the mass splitting between the spin- $\frac{1}{2}$ Ω_b and the Λ_b close to that between the spin- $\frac{1}{2}$ Ω_c and the Λ_c . The spin- $\frac{3}{2}$ states are also heavier than the spin- $\frac{1}{2}$ ones, in agreement with expectations from the spin-spin force.

The bottom hadrons can also be embedded in a larger $SU(5)_f$ group that accounts for all baryons constructed from the five quark flavors. (The existence of baryons with t -quarks is very unlikely due to the short lifetime of the t -quark.) One predicts the decomposition

$$\mathbf{5} \otimes \mathbf{5} \otimes \mathbf{5} = \bar{\mathbf{10}}_A \oplus \mathbf{40}_{MS} \oplus \mathbf{40}_{MA} \oplus \mathbf{35}_S. \quad (15.34)$$

The decuplet is not realized in the ground state. The two 40-plets have mixed symmetry ($\frac{1}{2}$ -spin) and the 35-plet is symmetric ($\frac{3}{2}$ -spin). The $SU(4)_f$ spin- $\frac{1}{2}$ multiplet in Fig. 15.5 contains 20 spin- $\frac{1}{2}$ baryons and the corresponding one with bottom quarks an additional 12, giving together 32 states. Similarly there are 30 spin- $\frac{3}{2}$ baryons. One expects 75 ground state mesons from (15.34). Thus 13 ground state baryons containing both b and c quarks are predicted (8 spin- $\frac{1}{2}$ [$4\Omega + 4\Xi$] and 5 spin- $\frac{3}{2}$ [$3\Omega + 2\Xi$]).

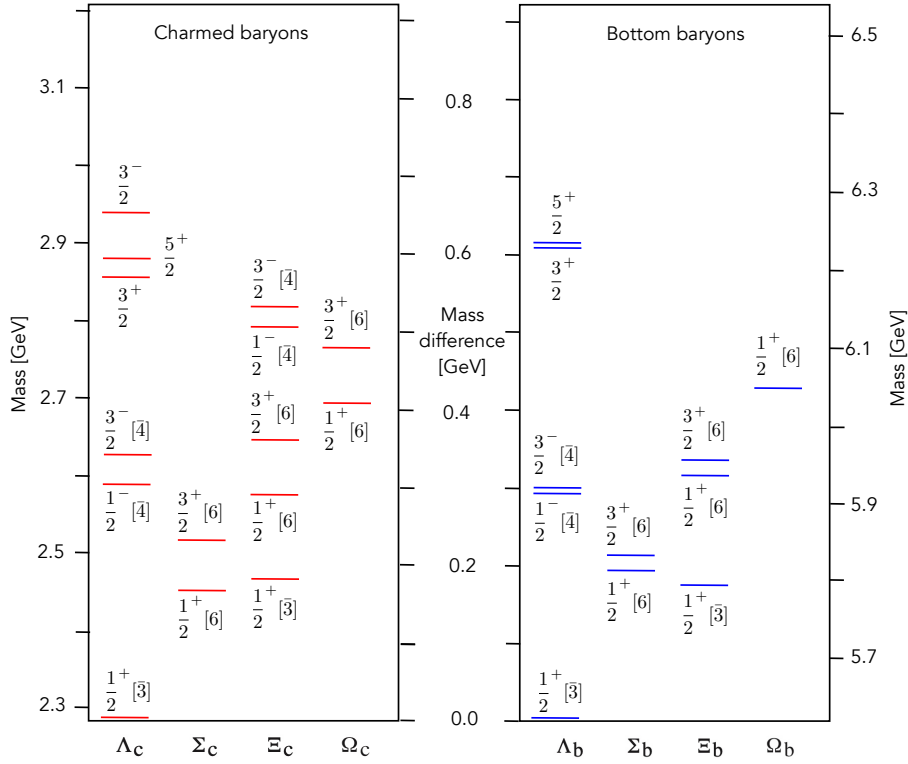


Figure 15.8: Mass spectrum of the established $C = 1$ charmed and $B = -1$ bottom baryons with known J^P . The flavor symmetry assignments are given by the square brackets. According to their isospins the $\Sigma_{c,b}$ ($\Xi_{c,b}$) consist of three (two) charged or neutral states that are nearly degenerate.

15.6 Magnetic moments

The magnetic dipole moment of a baryon is conventionally written relative to the mass of the proton:

$$\vec{\mu}_B = g_B \mu_N \vec{s}, \quad (15.35)$$

where $\mu_N = \frac{e}{2m_p}$ is the nuclear magneton (in natural units). The factor g_B is calculated by adding the quark contributions. The magnetic moment of quark i with charge $q_i e$ and constituent mass m_i is $\vec{\mu}_i = 2(\frac{q_i e}{2m_i})\vec{s}$, hence for the three light quarks,

$$\mu_u = \frac{2}{3}\kappa_u, \quad \mu_d = -\frac{1}{3}\kappa_d, \quad \mu_s = -\frac{1}{3}\kappa_s, \quad \text{with } \kappa_i \equiv \frac{e}{2m_i}. \quad (15.36)$$

The magnetic dipole moment of a baryon is then given by

$$\mu_B = \sum_{i=1}^3 \langle B \uparrow | \mu_i \sigma_{zi} | B \uparrow \rangle, \quad (15.37)$$

where $|B \uparrow\rangle$ is the wavefunction for a baryon with its spin along the z -axis and $\vec{s} = 2\vec{s}$. Since the quark model uses the totally symmetric SU(6) wavefunctions (flavor SU(3) \times spin SU(2)) one predicts for the proton:

$$\mu_p = \frac{4}{3}\mu_u - \frac{1}{3}\mu_d = \frac{e}{2m} \equiv \kappa, \quad (15.38)$$

assuming $m_u = m_d \simeq m$ (for the detailed derivation see *e.g.* Ref. [6]). For the magnetic moment of the neutron one obtains likewise

$$\mu_n = -\frac{1}{3}\mu_u + \frac{4}{3}\mu_d = -\frac{2}{3}\kappa, \quad (15.39)$$

which leads to the simple prediction $\mu_n/\mu_p = g_n/g_p = -2/3$.

The famous Frisch and Stern experiment showed for the first time that $g_p \sim 5.58 \gg 2$. Modern measurements are performed in electromagnetic traps, see the *Listings*, while the magnetic moment of the neutron is measured with cold neutron beams. The

experimental ratio $\mu_n/\mu_p = -0.6849793 \pm 0.0000003$ is impressively close to the prediction of the quark model (note that using instead the *antisymmetric* SU(6) wavefunctions would lead to $\mu_n/\mu_p = -2$ [6]). The constituent mass m of the u and d quarks can be estimated from (15.35) and (15.38): $m = 2m_p/g_p \simeq 336$ MeV.

The magnetic moment of the Λ is easy to predict: the diquark ud has isospin $i = 0$, since $i(s) = 0$ and $i(\Lambda) = 0$, and is therefore an antisymmetric isospin state. The symmetric quark model then also requires the spin to be zero, so that the magnetic moment of the Λ stems from the s quark:

$$\mu_\Lambda = \mu_s = -\frac{1}{3}\kappa_s. \quad (15.40)$$

The magnetic moment of the Λ is obtained from the Larmor precession frequency of the polarization vector in an homogeneous magnetic field. The latter is derived from the asymmetric distribution of the proton in $\Lambda \rightarrow \pi^- p$ [99]. The experimental result is listed in Table 15.8. The constituent mass of the s quark is then $m_s = -m\mu_p/3\mu_\Lambda = 509$ MeV.

The magnetic moments of the other baryons (Table 15.8) are predicted from κ and κ_s . The magnetic moment of the Σ^+ is obtained by replacing the d quark in (15.38) by an s quark, and for the Σ^- the u quark by an s quark in (15.39). The magnetic moment of the Σ^+ has also been measured with the precession method using its decay into $p\pi^0$ [100], that of the $\Sigma^- \rightarrow n\pi^-$ likewise, or by detecting the X-rays emitted by cascading Σ^- captured in the Coulomb shells of target atoms. The magnetic moment is then derived from the fine-structure splitting [101].

The magnetic moments of the Ξ^0 , Ξ^- and Ω^- are obtained from the polarization of the Λ in the decays $\Lambda\pi^0$, $\Lambda\pi^-$ and ΛK^- , respectively. The SU(6) wavefunction of the (spin 3/2) Ω^- is the product of the two symmetric SU(3) flavor and SU(2) spin

Table 15.8: Quark model predictions and measured magnetic dipole moments of the ground state baryons in units of μ_N ; $\kappa \equiv \frac{e}{2m} = 2.793 \mu_N$ and $\kappa_s \equiv \frac{e}{2m_s} = -3\mu_A = 1.84 \mu_N$. $\dagger \Sigma^0 \rightarrow \Lambda$ transition magnetic moment.

Baryon	κ	Quark model	Experimental value		
p		input	2.793		
n	$-\frac{2}{3}\kappa$	=	-1.86	-1.913	
Λ	$-\frac{1}{3}\kappa_s$	input	-0.6138	\pm	0.0047
Σ^+	$\frac{8}{9}\kappa + \frac{1}{9}\kappa_s$	=	2.68	2.458	\pm 0.010
Σ^0	$\frac{2}{9}\kappa + \frac{1}{9}\kappa_s$	=	0.82		
$\Sigma^{0\dagger}$	$-\frac{1}{\sqrt{3}}\kappa$	=	-1.61	-1.61	\pm 0.08
Σ^-	$-\frac{4}{9}\kappa + \frac{1}{9}\kappa_s$	=	-1.04	-1.160	\pm 0.025
Ξ^0	$-\frac{2}{9}\kappa - \frac{4}{9}\kappa_s$	=	-1.44	-1.250	\pm 0.014
Ξ^-	$\frac{1}{9}\kappa - \frac{4}{9}\kappa_s$	=	-0.51	-0.6507	\pm 0.0025
Ω^-	$-\kappa_s$	=	-1.84	-2.024	\pm 0.056
Δ^{++}	2κ	=	5.58	4.52	\pm 0.67
Δ^+	κ	=	2.79	2.3	- 4.5

wavefunctions. Summing over the three s quarks one gets

$$\mu_{\Omega^-} = \sum_{i=1}^3 \langle \Omega^- \uparrow | \mu_i \sigma_{zi} | \Omega^- \uparrow \rangle = 3\mu_s = 3\mu_A. \quad (15.41)$$

The magnetic moment of the Ω^- is hard to measure, because the Ω^- is unpolarized at high energies, in contrast to the other hyperons. Polarized Ω^- hyperons have been obtained from polarized Λ and Ξ^0 impinging on a nuclear target [102].

In quark models with full isospin symmetry the magnetic moments of the Δ -resonances are simply related to the magnetic moment of the proton by $\mu_\Delta = Q_\Delta \cdot \mu_N$, ($Q_\Delta =$ charge) i.e. the moment of the Δ^+ should equal the proton moment and the moment of the Δ^{++} should be twice as large (sum of the three u -quarks). Magnetic moments of the decuplet baryons (with the exception of the Ω^-) are very difficult to measure because their lifetimes are so short that spin precession techniques cannot be used. For the Δ one can profit from an electromagnetic spin-orientation transition inside the large width of the state. This leads to the emission of a magnetic dipole photon in reactions like $\pi^+ p \rightarrow \pi^+ p \gamma$ or $\gamma p \rightarrow \pi^0 p \gamma'$ which is related to the magnetic moment of the resonance. The first reaction has been used to study the magnetic moment of the Δ^{++} by measuring the left-right asymmetry with polarized protons [103]. The second one was used for the Δ^+ state [104, 105]. Taking all experimental and systematic uncertainties into account the result spans the range from $(2.3 - 4.5)\mu_N$, covering the quark model prediction of $\approx 2.8\mu_N$, but is not very precise.

Table 15.8 lists the current experimental values for the magnetic moments of the ground state baryons, together with the predictions from the quark model. There are significant discrepancies, but given its crudeness, the quark model performs surprisingly well.

15.7 Dynamics

Quantum chromodynamics (QCD) is well-established as the theory for the strong interactions. As such, one of the goals of QCD is to predict the spectrum of strongly-interacting particles. To date, the only first-principles calculations of spectroscopy from QCD use lattice methods. These are the subject of Sec. 15.8. These calculations are difficult and unwieldy, and many interesting questions do not have a good lattice-based method of solution. Therefore, it is natural to build models, whose ingredients are abstracted from QCD, or from the low-energy limit of QCD (such as chiral Lagrangians) or from the data itself.

Phenomenological models for light quark systems typically include

1. A confining interaction, which is generally spin-independent (*e.g.*, harmonic oscillator or linear confinement);
2. A strange quark mass somewhat larger than the up and down quark masses, in order to split the SU(3) multiplets;
3. Different types of spin-dependent interactions:

a) commonly used is a color-magnetic flavor-independent interaction modeled after the effects of gluon exchange in QCD (see *e.g.*, Ref. [106]). For example, in the S -wave states, there is a spin-spin hyperfine interaction of the form

$$H_{HF} = -\alpha_S M \sum_{i>j} (\vec{\sigma}\lambda_a)_i (\vec{\sigma}\lambda_a)_j, \quad (15.42)$$

where M is a constant with units of energy, λ_a ($a = 1, \dots, 8$) is the set of SU(3) unitary spin matrices, defined in the review ‘‘SU(3) Isoscalar Factors and Representation Matrices,’’ and the sum runs over constituent quarks or antiquarks. Spin-orbit interactions, although allowed, seem to be small in general, but a tensor term is responsible for the mixing of states with the same J^P but different L, S combinations.

b) other approaches include flavor-dependent short-range quark forces from instanton effects (see *e.g.*, [107, 108]). This interaction acts only on scalar, isoscalar pairs of quarks in a relative S -wave state:

$$\langle q^2; S, L, T | W | q^2; S, L, T \rangle = -4g\delta_{S,0}\delta_{L,0}\delta_{I,0}\mathcal{W} \quad (15.43)$$

where \mathcal{W} is the radial matrix element of the contact interaction.

c) a rather different and somewhat controversial approach is based on flavor-dependent spin-spin forces arising from one-boson exchange. The interaction term is of the form:

$$H_{HF} \propto \sum_{i<j} V(\vec{r}_{ij}) \lambda_i^F \cdot \lambda_j^F \vec{\sigma}_i \cdot \vec{\sigma}_j \quad (15.44)$$

where the λ_i^F are in flavor space (see *e.g.*, Ref. [109]).

4. In the case of spin-spin interactions, a flavor-symmetric interaction for mixing $q\bar{q}$ configurations of different flavors (*e.g.*, $u\bar{u} \leftrightarrow d\bar{d} \leftrightarrow s\bar{s}$), in isoscalar channels, so as to reproduce *e.g.*, the $\eta - \eta'$ and $\omega - \phi$ mesons.

Systems with heavy quarks have their own approaches. Besides potential models to deal with $Q\bar{Q}$ spectroscopy (which are similar to what we have just described for light quarks) there are a variety of effective field theories built on QCD. Nonrelativistic QCD or NRQCD is a nonrelativistic reduction of the QCD Lagrangian, written as an expansion in powers of the heavy quarks' velocities. Its expressions are often used in lattice calculations. Terms in the Lagrangian have obvious quark model analogs, but are derived directly from QCD. For example, the heavy quark potential is a derived quantity, extracted from simulations.

There are also many versions of heavy quark effective theory (HQET), an expansion in the inverse mass of the heavy constituent. The physics input is one of decoupling of scales: the interactions of the heavy quarks take place at short distance while the light degrees of freedom involve long distance dynamics, so to some degree they decouple. The form of terms in the expansion is fixed (often by symmetry) but the coefficients are not. These approaches allow one to interpolate from the charm sector to the bottom one, or from masses of mesons to baryons. For example, a Hamiltonian for one or more heavy quarks bound to light degrees of freedom could be written as

$$H_l^Q = m_Q + e_l + \frac{\kappa_l}{2m_Q} + \frac{s_l}{2m_Q} \vec{S} \cdot \vec{j}_l + \dots \quad (15.45)$$

where m_Q is the mass of the heavy quark (or heavy quarks where the heavy quarks are treated as a single dynamical object) and \vec{S} is the angular momentum carried by the heavy degrees of freedom. e_l , κ_l and \vec{j}_l involve the light degrees of freedom. We will see an example of the use of this formula in the next section.

15.8 Lattice Calculations of Hadronic Spectroscopy

Lattice calculations are a major source of information about QCD masses and matrix elements. The necessary theoretical background is given in Sec. 17 of this *Review*. Here we confine ourselves to some general comments and illustrations of lattice calculations for spectroscopy.

It might seem a bit out of place to have a section about lattice calculations in a review of the quark model, since to many readers, the quark model is just a model while QCD could be thought of as a construct which is something deeper than a model. But this review is, despite its title, actually an introduction to the spectroscopy and related quantities of the strong interactions. From that perspective, a presentation of lattice results is entirely appropriate.

The input to lattice calculations is a discretized version of the QCD Lagrangian. Lattice calculations measure correlation functions via Monte Carlo simulation and physical observables are determined through fits of the lattice data to theoretical expectations. It is fair to say that all lattice calculations make extensive use of quark model ideas – for example, the operators used to create and annihilate hadrons are almost always based on the quark model.

There is only a sporadic literature connecting lattice results to the quark model (one recent example is [110]) but of course the qualitative understanding of lattice results depends as heavily on quark model ideas as does the qualitative understanding of experimental data.

In general, the cleanest lattice results come from computations of processes in which there is only one particle in the simulation volume. These quantities include masses of hadrons, simple decay constants, like pseudoscalar meson decay constants, and semileptonic form factors (such as the ones appropriate to $B \rightarrow D\nu\ell$, $K\nu\ell$, $\pi\nu\ell$). The cleanest predictions for masses are for states which are far below any thresholds to open channels, since the effects of final state interactions are not yet under complete control on the lattice. As a simple corollary, the lightest state in a channel is easier to study than the heavier ones.

Good-quality modern lattice calculations will present multi-part error budgets with their predictions. Part of the uncertainty is statistical, from sample size. Typically, the quoted statistical uncertainty includes uncertainty from a fit: it is rare that a simulation computes one global quantity which is the desired observable. Simulations which include virtual quark-antiquark pairs (also known as “dynamical quarks” or “sea quarks”) are often done at up and down quark mass values heavier than the experimental ones, and it is then necessary to extrapolate in these quark masses. Simulations can be carried out at the physical values of the heavier quarks’ masses. They are always done at nonzero lattice spacing, and so it is necessary to extrapolate to zero lattice spacing. Some theoretical input is needed to do this. Much of the uncertainty in these extrapolations is systematic, from the choice of fitting function. Other systematics include the effect of finite simulation volume, the number of flavors of dynamical quarks actually simulated, and technical issues with how these dynamical quarks are included. The particular choice of a fiducial mass (to normalize other predictions) is not standardized; there are many possible choices, each with its own set of strengths and weaknesses, and determining it usually requires a second lattice simulation from that used to calculate the quantity under consideration.

A systematic error of major historical interest is the “quenched approximation,” in which dynamical quarks are simply left out of the simulation. This was done because the addition of these virtual pairs presented an expensive computational problem. No generally-accepted methodology has ever allowed one to correct for quenching effects, short of redoing all calculations with dynamical quarks. (All light degrees of freedom must be included in any realistic simulation of a quantum field theory.) Advances in algorithms and computer hardware have rendered it obsolete.

With these brief remarks, we turn to examples. The field of lattice QCD simulations is vast, and so it is not possible to give a comprehensive review of them in a small space. The history of lattice QCD simulations is a story of thirty years of incremental

improvements in physical understanding, algorithm development, and ever faster computers, which have combined to bring the field to a present state where it is possible to carry out very high quality calculations. We present a few representative illustrations, to show the current state of the art.

15.8.1 Spectroscopy of low-lying states

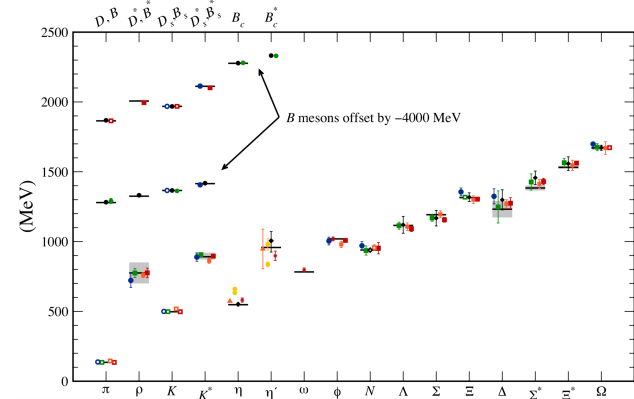


Figure 15.9: Hadron spectrum from lattice QCD. Comprehensive results for mesons and baryons are from MILC [111, 112], PACS-CS [113], BMW [114], QCDSF [115], and ETM [116]. Results for η and η' are from RBC & UKQCD [21], Hadron Spectrum [117] (also the only ω mass), UKQCD [118], and Michael, Otnad, and Urbach [119]. Results for heavy-light hadrons from Fermilab-MILC [120], HPQCD [121, 122], and Mohler and Woloshyn [123]. Circles, squares, diamonds, and triangles stand for staggered, Wilson, twisted-mass Wilson, and chiral sea quarks, respectively. Asterisks represent anisotropic lattices. Open symbols denote the masses used to fix parameters. Filled symbols (and asterisks) denote results. Red, orange, yellow, green, and blue stand for increasing numbers of ensembles (i.e., lattice spacing and sea quark mass) Black symbols stand for results with 2+1+1 flavors of sea quarks. Horizontal bars (gray boxes) denote experimentally measured masses (widths). b -flavored meson masses are offset by -4000 MeV.

One of the first goals of large scale lattice simulations was to compute masses of the lightest states in all of the “conventional” $q\bar{q}$ and qqq channels. We illustrate results from many groups in Fig. 15.9, a comprehensive summary from 2012 provided by A. Kronfeld (private communication; see also [124]).

Mesons with a valence structure of identical quark - antiquark pairs such as the eta or eta-prime, $|\eta\rangle \sim \alpha|\bar{u}u + \bar{d}d\rangle + \beta|\bar{s}s\rangle$, present more of a challenge, because one must include the effects of “annihilation graphs” for the valence q and \bar{q} . Many groups, among them Refs. [21, 118, 125, 126], have reported calculations of the η and η' mesons. The most recent calculation is that of Ref. [126], which finds masses of 554.7 ± 9.2 and 930 ± 21 MeV for the η and η' .

The spectroscopy of mesons containing heavy quarks is truly a high-precision endeavor. These simulations typically use NRQCD for $Q\bar{Q}$ bound states. Figs. 15.10 and 15.11 show the low lying mass spectrum for charmonium and bottomonium states from several different groups [122, 127–130]. Most, but not all, of the results are for the lightest state with a given value of quantum numbers. We return to this point below.

Fig. 15.12 shows a compilation of lattice results for doubly and triply charmed baryons, provided by S. Meinel [138]. The position of the observed Ξ_{cc}^+ [93] is also shown. Note that the lattice calculations for the mass of this state were predictions, not post-dictions.

15.8.2 Excited state spectroscopy

A close look at Fig. 15.9 reveals an issue: while many of the states shown in it are stable under the strong interactions, some of them (the vector mesons, the Delta) are not. They are resonances. And so are all the excited states of hadrons listed in the PDG be

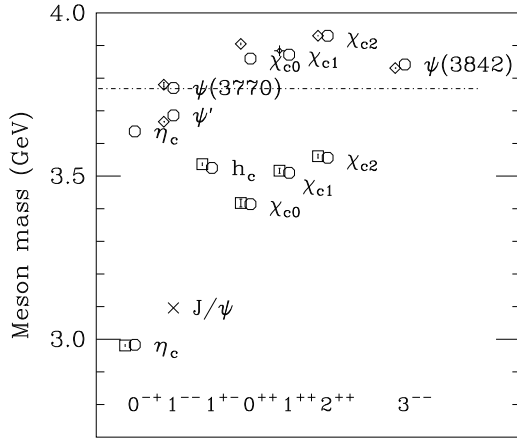


Figure 15.10: Selected spectroscopy of the $\bar{c}c$ spectrum, compared to lattice data from Ref. [127] in squares, from Refs. [128, 129] in diamonds, and from Ref. [130] as a fancy diamond. Particles whose masses are used to fix lattice parameters by Ref. [127] are shown with crosses; octagons label experimental values. The upper χ_{c1} state is also known as $X(3872)$. The dotted line shows the threshold value for two charmed mesons.

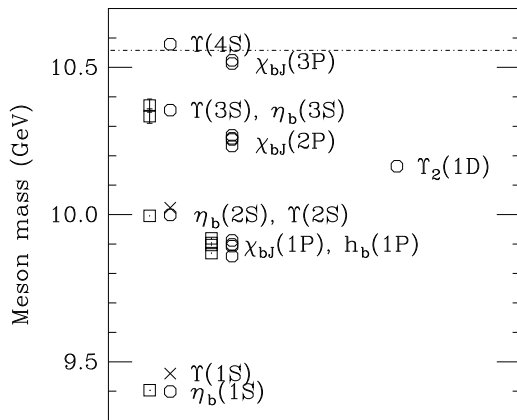


Figure 15.11: Spectroscopy of the $\bar{b}b$ system, adapted from Ref. [122]. Particles whose masses are used to fix lattice parameters are shown with crosses; octagons label experimental values, and lattice results are shown as squares. The dotted line shows the threshold value for two bottom mesons.

they “ordinary,” or “exotic.” How do lattice calculations deal with such states? This is actually a complicated business, which is an active area of research.

There are two issues involving excited state spectroscopy, which are entangled in any lattice calculation:

1. There are many states with the same quantum numbers, all of which contribute to lattice observables
2. In finite volume, states do not decay, they only mix.

To explain what is going on, we have to describe how a lattice calculation determines a mass. This is done by measuring an observable which involves the creation of a set of quark and gluon fields at some point on the lattice and their annihilation at other points on the lattice. To find the energies of zero momentum states, the operators are averaged over position and the observable is

$$C_{ij}(t) = \sum_x \langle O_i(x, t) O_j(0, 0) \rangle \propto \sum_n \langle 0 | O_i | n \rangle \langle n | O_j | 0 \rangle \exp(-E_n t). \quad (15.46)$$

E_n is the energy of the n th hadronic state with the quantum numbers of the source or sink. The reader can see that by taking t large, the correlator is dominated by the contribution from the

lightest state, decaying with t as $\exp(-E_{min}t)$. This is a positive thing if one is interested in the ground state, but the contribution of excited states is exponentially suppressed at large t . The size of a given state’s contribution, $\langle 0 | O_i | n \rangle$, can provide information about the content of the state.

As we move away from hadrons which can be created by the simplest quark model operators (appropriate to the lightest meson and baryon multiplets) we encounter a host of new problems: either no good interpolating fields, or too many possible interpolating fields, and many states with the same quantum numbers. Techniques for dealing with these interrelated problems vary from collaboration to collaboration, but all share common features: typically, correlation functions from many different interpolating fields are used, and the signal is extracted in what amounts to a variational calculation using the chosen operator basis. In addition to mass spectra, wave function information can be garnered from the form of the best variational wave function.

These calculations give towers of excited states, but the states are not resonances. Lattice calculations do not see decays directly because they are done in boxes of some finite size. Generally, the energies of the single particle states do not depend strongly on the box size. Multiple particle states, such as two particle states with equal and opposite momenta, are different, though. The finite box size quantizes the allowed values of momentum and the spectrum of states, which would be a continuum in infinite volume, is just a discrete tower. As the box size is varied, some of these states can approach the energies of single particle states, and the nearby states will mix and split, participating in a quantum mechanical avoided level crossing. The mixing and splitting of single and multiparticle states is the finite volume data which is used to infer how states in the continuum interact.

As a simple example, two positive energy but interacting particles in a one dimensional box have a spatial wave function which looks like $\cos(k|z| + \delta)$ where δ is the phase shift due to their interaction. Periodic boundary conditions in a finite box of length L give a quantization condition to the allowed momentum of the state ($kL + 2\delta(E) = 0 \pmod{2\pi}$, for example) which involves the phase shift. Simulations with many values of L and operators for states carrying many values of momentum can be combined into information about phase shifts, and then to statements about the location(s) of singularities in the complex energy plane.

The techniques for studying excited states of mesons and baryons, glueballs, and exotics are similar. They all use a large basis of trial states: the progression with time started with minimum quark content states, then added more complicated states (pairs of mesons or tetraquark states), then carried out simulations with multiple volumes with the goal of extracting resonance properties. The older single volume studies typically presented results for many quantum numbers, which give a broad (though incomplete) view of the QCD spectrum.

An example of meson spectroscopy where this is done, by [48], is shown in Fig. 15.13. The quark masses are still heavier than their physical values, so the pion is at 392 MeV. The authors can assign a relative composition of nonstrange and strange quark content to their states, observing, for example, a nonstrange ω and a strange ϕ . Some states also have a substantial component of gluonic excitation. Note especially the three exotic channels $J^{PC} = 1^{-+}, 0^{+-},$ and 2^{+-} , with states around 2 GeV. These calculations will become more realistic as the quark masses are carried lower and resonance effects are included.

The interesting physics questions of excited baryon spectroscopy to be addressed are precisely those enumerated in the last section. An example of a calculation involving only single particle states in a single volume, due to Ref. [139], is shown in Fig. 15.14. Notice that the pion is not yet at its physical value. The lightest positive parity state is the nucleon, and the Roper resonance has not yet appeared as a light state.

Glueballs present similar issues. In Fig. 15.3 we showed a figure from [34] presenting a lattice prediction for the glueball mass spectrum in quenched approximation. A true QCD prediction of the glueball spectrum requires dynamical light quarks, some way to deal with the mixing of glue states and quark-antiquark (and beyond) states and (because glueball operators are intrinsically

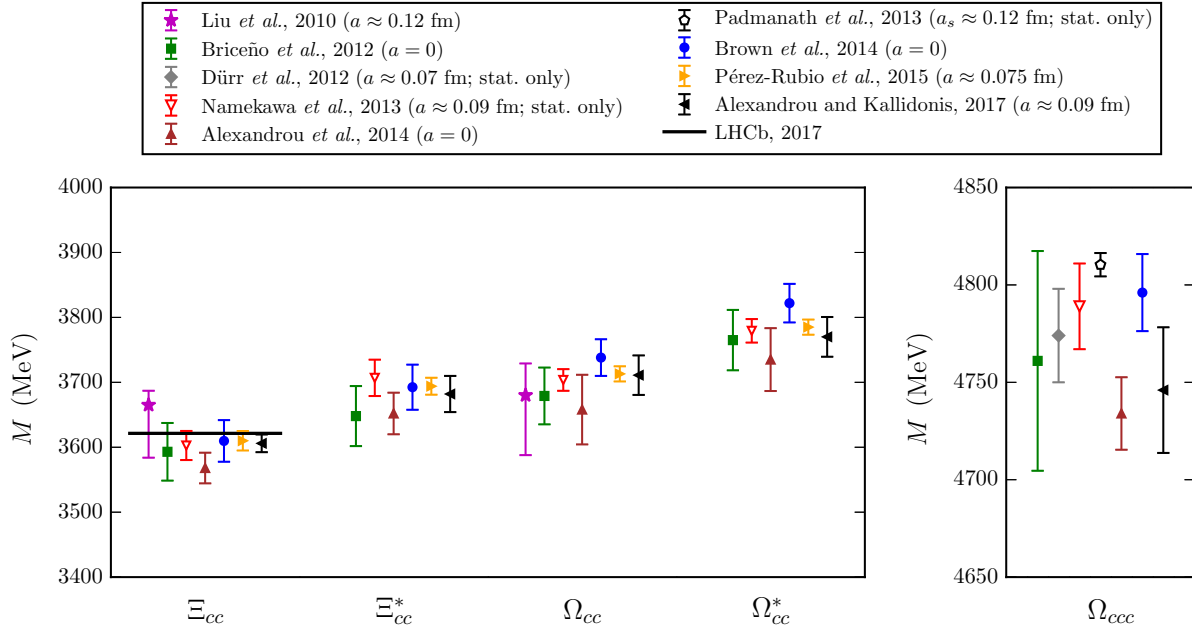


Figure 15.12: Comparison of lattice QCD results for the doubly and triply charmed baryon masses. Labels are Liu, *et al.*, [131]; Briceño, *et al.*, [132]; Namekawa, *et al.*, [133]; Padmanath, *et al.*, [134]; Alexandrou, *et al.*, [116]; Brown, *et al.*, [135]; Pérez-Rubio *et al.*, [136]; Alexandrou and Kallidonis 2017, [137]. Only calculations with dynamical light quarks are included; for the doubly charmed baryons, only calculations were performed at or extrapolated to the physical pion mass are shown. Results without estimates of systematic uncertainties are labeled “stat. only”. The lattice spacing values used in the calculations are also given; $a = 0$ indicates that the results have been extrapolated to the continuum limit. In the plot of the doubly charmed baryons, the position of the experimentally observed Ξ_{cc}^+ state [93] is shown with a horizontal line.

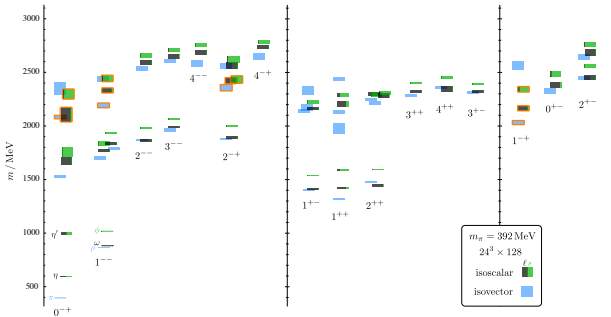


Figure 15.13: Isoscalar (green and black) and isovector (blue) spectrum from Ref. [48]. States are labeled J^{PC} . The quark mass is heavier than its physical value; $m_\pi = 392$ MeV. The vertical height of each box indicates the statistical uncertainty in the mass. Black and green indicate relative nonstrange and strange composition. Orange outlines show states with a large chromomagnetic component to their wave function, which the authors argue are hybrid states. Note the exotic states in the three right-most columns.

noisy) high statistics. Early studies which include the 0^{++} channel are Refs. [140, 141]. Fig. 15.15 shows results from [140], done with dynamical u , d and s quarks at two lattice spacings, 0.123 and 0.092 fm, with pion masses at 280 and 360 MeV respectively, along with comparisons to the quenched lattice calculation of [33] and to experimental isosinglet mesons. This study shows that the effects of quenching seem to be small at its relatively heavy pion masses.

Calculations of resonance properties are more recent. Two body decays with a single open channel, such as the rho coupled to two pions, have a large literature. A review [142] summarizes the situation, and example of a calculation of the rho meson decay width is [143]. (See also [144].) The mass and decay width of the $f_0(500)$ have recently been computed in [145] and [146] and those

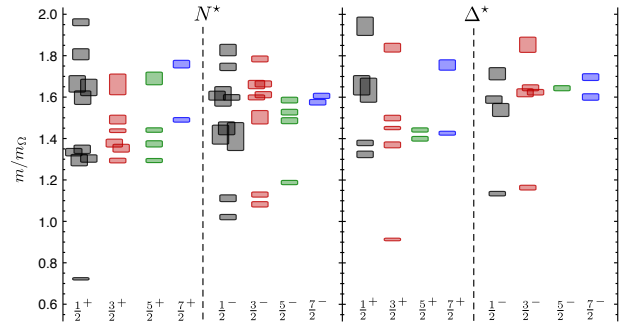


Figure 15.14: Spin-identified spectrum of nucleons and deltas, from lattices where $m_\pi = 396$ MeV, in units of the calculated Ω mass, from Ref. [139]. The colors just correspond to the different J assignments: grey for $J = 1/2$, red for $J = 3/2$, green for $J = 5/2$, blue for $J = 7/2$.

of other mesons in [147]. Ref. [148] studies the decay width of the $\Delta(1238)$.

Studies which observe a large basis of states across many volumes can probe excited state spectroscopy as resonances. These calculations are just beginning and the ones we know about are still performed at unphysically heavy quark masses. Examples include the decays of an exotic $J^{PC} = 1^{-+}$ resonance [149] and the spectroscopy of J^{--} resonances [150]. The results of Refs. [128, 129] in Fig. 15.10 come from similar analyses. We expect to see considerable progress in this area over the next few years.

We conclude this section with some remarks about unusual states containing heavy quarks. Lattice calculations relevant to the extra states observed in the charmonium and bottomonium spectrum (Sec. 15.4) are difficult, because the states sit high in the spectrum of most channels, because of the number of nearby multiparticle states, and because it is necessary to have the technology to study heavy and light quarks together.

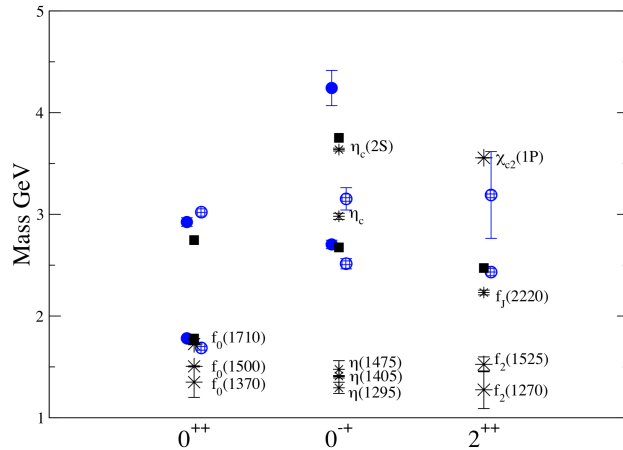


Figure 15.15: Lattice QCD predictions for glueball masses. The open and closed circles are the larger and smaller lattice spacing data of the full QCD calculation of glueball masses of Ref. [140], at pion masses of 280 and 360 MeV. Squares are the quenched data for glueball masses of Ref. [33]. The bursts labeled by particle names are experimental states with the appropriate quantum numbers.

Some lattice calculations are used as input for phenomenological studies of hybrids. The theoretical motivation is that one can imagine states made of a heavy $Q\bar{Q}$ pair along with excitations of light degrees of freedom, viewed as an excited state of the string connecting them. The analogy is to an excited state of a diatomic molecule. The heavy quark potential, the potential from orbitally excited gluon configurations, and the “string breaking” potential (from the interaction between static sources and static-light mesons) are used as inputs in Born - Oppenheimer and coupled channel calculations for systems whose constituents include heavy quarks and antiquarks. Examples of such calculations include Refs. [151–153].

The system with the largest lattice literature is a bound state of two heavy quarks and two light antiquarks, for example $b\bar{b}\bar{u}\bar{d}$. The story begins with the spectroscopy of doubly and triply charmed baryons in Fig. 15.12; the lattice calculations in that figure were performed in 2010 - 2017. In 2017 two groups of authors [154,155] realized that one could extrapolate from the masses of $Q\bar{q}$, Qqq , and QQq states (Q for a heavy quark, \bar{q} for a light antiquark) to predict the mass of a $QQ\bar{q}\bar{q}$ tetraquark. The $QQ\bar{q}\bar{q}$ state would be stable if the mass of the Q were heavy enough. (This basically arises because the QQ diquark is in an attractive color-triplet state and the effective binding energy scales as $\alpha_s^2 m_Q$.) The $J^P = 1^+ b\bar{b}\bar{u}\bar{d}$ state was expected to be stable. Simultaneously, a lattice calculation [156] of the mass of a $b\bar{b}\bar{u}\bar{d}$ state showed that it was below threshold to fall apart into a pair of B mesons. The $I(J^P) = 0(1^+)$ state is predicted to be stable by about 128(26) MeV [157] or 189(10) MeV [156]. (These authors put the $b\bar{b}\bar{u}\bar{d}$ state at 98 MeV below threshold.) These numbers are in reasonable agreement with phenomenological estimates from Refs. [154,155].

These states are easier for the lattice theorist to study than other exotics because they are the lightest single particle states in their channels. They are difficult because they are just barely bound, and the usual approximation for a lattice calculation of unphysically heavy light quarks tends to raise their mass. The calculations have to include multiple trial states: the tetraquark itself plus pairs of mesons.

The situation with regard to the recently discovered $T_{cc}(3875)^+$ [158] is still unsettled. Both lattice calculations and HQET estimates put a $cc\bar{u}\bar{d}$ state right at threshold, which is a difficult place to explore on the lattice (or by any other method, for that matter). The $T_{cc}(3875)^+$ is seen in $D^0 D^0 \pi^+$ and researchers studying three body decays on the lattice (an open problem, at present) mark it as an obvious research target.

15.8.3 Electromagnetic effects

As a final part of spectroscopy we mention electromagnetic mass splittings (such as the neutron - proton mass difference). They are interesting but difficult. These calculations are important for determining the values of the quark masses (for a discussion see Sec. 60 in this Review). Knowing that the neutron is heavier than the proton tells us that these splittings have a complicated origin. One part of the shift is because the up and down quarks have slightly different masses. The second is that the quarks have (different) charges. Phenomenologists (compare Ref. [159]) combine Coulomb forces and spin-dependent electromagnetic hyperfine interactions to model their charge effects. In order to compute hadronic mass differences on the lattice, electromagnetic interactions must be included in the simulations. This creates a host of technical issues. An important one is that electromagnetic interactions are long range, but lattice simulations are done in finite volumes. The theoretical situation is summarized in the recent Flavour Lattice Averaging Group (FLAG) review [160]. A 2014 calculation, Ref. [161], presented the first results for electromagnetic mass splittings in the baryon octet, with good agreement with observation. Refs. [162–164] have performed calculations for meson splittings.

There is a small lattice literature associated with magnetic moments of baryons. The calculations are done by including a static magnetic field in the simulation and computing the energy difference between baryons in different spin states. We are aware of no calculations at physical quark masses. A recent calculation [165] used 800 and 450 MeV pions. When expressed in units of the nucleon magneton at the simulation point ($e/(2M_N(m_\pi))$) the moments are in reasonable agreement with experiment and with quark model expectations.

References

- [1] M.-L. Du *et al.*, Phys. Rev. D **98**, 094018 (2018), [arXiv:1712.07957].
- [2] G. 't Hooft, Nucl. Phys. B **72**, 461 (1974).
- [3] G. 't Hooft, Nucl. Phys. B **75**, 461 (1974).
- [4] E. Witten, Nucl. Phys. B **160**, 57 (1979).
- [5] F. Gross *et al.*, Eur. Phys. J. C **83**, 1125 (2023), [arXiv:2212.11107].
- [6] C. Amsler in the Quark Structure of Hadrons, Lecture Notes in Physics **949** (2018), ed. Springer.
- [7] H.-Y. Cheng, Physics Letters B **707**, 116 (2012), [arXiv:1110.2249].
- [8] J.-C. Feng *et al.*, Phys. Rev. D **104**, 054027 (2021), [arXiv:2104.01339].
- [9] H.-W. Ke and X.-Q. Li, Phys. Rev. D **99**, 036014 (2019), [arXiv:1810.07912].
- [10] M.-C. Du and Q. Zhao, Phys. Rev. D **100**, 036005 (2019), [arXiv:1905.04207].
- [11] A. A. Godizov, Eur. Phys. J. C **76**, 361 (2016), [arXiv:1604.01689].
- [12] S. Donnachie *et al.*, *Pomeron Physics and QCD*, Cambridge Monographs on Particle Physics, Nuclear Physics and Cosmology, Cambridge University Press, p. 85 (2002).
- [13] M.-L. Du *et al.*, Phys. Rev. Lett. **126**, 192001 (2021), [arXiv:2012.04599].
- [14] J. Schwinger, Phys. Rev. **135**, B816 (1964).
- [15] H. J. Lipkin and B.-s. Zou, Phys. Rev. D **53**, 6693 (1996).
- [16] A. Bramon, R. Escribano and M. D. Scadron, Phys. Lett. **B403**, 339 (1997), [hep-ph/9703313].
- [17] A. Aloisio *et al.* (KLOE), Phys. Lett. **B541**, 45 (2002), [hep-ex/0206010].
- [18] F. Ambrosino *et al.*, JHEP **07**, 105 (2009), [arXiv:0906.3819].
- [19] C. Amsler *et al.* (Crystal Barrel), Phys. Lett. **B294**, 451 (1992).
- [20] C. Amsler, Rev. Mod. Phys. **70**, 1293 (1998), [hep-ex/9708025].

- [21] N. H. Christ *et al.*, Phys. Rev. Lett. **105**, 241601 (2010), [arXiv:1002.2999].
- [22] T. Feldmann, Int. J. Mod. Phys. **A915**, 159 (2000).
- [23] C. Amsler and F. E. Close, Phys. Rev. **D53**, 295 (1996), [hep-ph/9507326].
- [24] R. L. Jaffe, Phys. Rev. **D15**, 267 (1977).
- [25] R. L. Jaffe, Phys. Rev. **D15**, 281 (1977).
- [26] S.L. Olsen, Front. Phys. **10**, 121 (2015), [arXiv:1411.7738].
- [27] S. L. Olsen, T. Skwarnicki and D. Zieminska, Rev. Mod. Phys. **90**, 015003 (2018), [arXiv:1708.04012].
- [28] N. Brambilla *et al.*, Physics Reports **873**, 1 (2020), [arXiv:1907.07583].
- [29] S. K. Choi *et al.*, Physical Review Letters **91**, 262001 (2003), [hep-ex/0309032].
- [30] N. A. Törnqvist, Physical Review Letters **67**, 556 (1991).
- [31] R. Aaij *et al.*, Nature Physics **18**, 751 (2022), [arXiv:2109.01038].
- [32] R. Aaij *et al.*, Science Bulletin **65**, 1983 (2020), [arXiv:2006.16957].
- [33] C. J. Morningstar and M. J. Peardon, Phys. Rev. **D60**, 034509 (1999), [hep-lat/9901004].
- [34] Y. Chen *et al.*, Phys. Rev. **D73**, 014516 (2006), [hep-lat/0510074].
- [35] W.-J. Lee and D. Weingarten, Phys. Rev. **D61**, 014015 (2000), [hep-lat/9910008].
- [36] G. S. Bali *et al.* (UKQCD), Phys. Lett. **B309**, 378 (1993), [hep-lat/9304012].
- [37] C. Michael, AIP Conf. Proc. **432**, 657 (1998), [hep-ph/9710502].
- [38] F. E. Close and A. Kirk, Eur. Phys. J. **C21**, 531 (2001), [hep-ph/0103173].
- [39] A. V. Sarantsev *et al.*, Physics Letters B **816**, 136227 (2021), [arXiv:2103.09680].
- [40] W. Ochs, J. Phys. **G40**, 043001 (2013), [arXiv:1301.5183].
- [41] F. Brünner and A. Rebhan, Phys. Rev. Lett. **115**, 131601 (2015), [arXiv:1504.05815].
- [42] C. Amsler and N. A. Tornqvist, Phys. Rept. **389**, 61 (2004).
- [43] N. Isgur and J. E. Paton, Phys. Rev. **D31**, 2910 (1985).
- [44] M. S. Chanowitz and S. R. Sharpe, Nucl. Phys. **B222**, 211 (1983), [Erratum: Nucl. Phys. B228,588(1983)].
- [45] T. Barnes *et al.*, Nucl. Phys. **B224**, 241 (1983).
- [46] P. Lacey *et al.* (UKQCD), Phys. Lett. **B401**, 308 (1997), [hep-lat/9611011].
- [47] J. J. Dudek, Phys. Rev. D **84**, 074023 (2011), [arXiv:1106.5515].
- [48] J. J. Dudek *et al.* (Hadron Spectrum), Phys. Rev. **D88**, 094505 (2013), [arXiv:1309.2608].
- [49] B. Kopf *et al.*, The European Physical Journal C **81**, 1056 (2021), [arXiv:2008.11566].
- [50] M. Ablikim *et al.* (BESIII), Phys. Rev. Lett. **129**, 192002 (2022), [Erratum: Phys.Rev.Lett. 130, 159901 (2023)], [arXiv:2202.00621].
- [51] E. S. Swanson, Physical Review D **107**, 074028 (2023), [arXiv:2302.01372].
- [52] R. Aaij *et al.* (LHCb), Phys. Rev. Lett. **115**, 072001 (2015), [arXiv:1507.03414].
- [53] R. Aaij *et al.* (LHCb), Phys. Rev. Lett. **122**, 222001 (2019), [arXiv:1904.03947].
- [54] J.-J. Wu *et al.*, Phys. Rev. Lett. **105**, 232001 (2010), [arXiv:1007.0573].
- [55] J.-J. Wu, T.-S. H. Lee and B. S. Zou, Phys. Rev. C **85**, 044002 (2012), [arXiv:1202.1036].
- [56] Y.-R. Liu *et al.*, Prog. Part. Nucl. Phys. **107**, 237 (2019), [arXiv:1903.11976].
- [57] F.E. Close, in *Quarks and Nuclear Forces* (Springer-Verlag, 1982), p. 56.
- [58] R.H. Dalitz and L.J. Reinders, in “Hadron Structure as Known from Electromagnetic and Strong Interactions,” *Proceedings of the Hadron ’77 Conference* (Veda, 1979), p. 11.
- [59] E. Klempt and J.-M. Richard, Rev. Mod. Phys. **82**, 1095 (2010), [arXiv:0901.2055].
- [60] T. Melde, W. Plessas and B. Sengl, Phys. Rev. **D77**, 114002 (2008), [arXiv:0806.1454].
- [61] N. Isgur and G. Karl, Phys. Rev. **D18**, 4187 (1978).
- [62] N. Isgur and G. Karl, Phys. Rev. **D19**, 2653 (1979), [Erratum: Phys. Rev. D23,817(1981)].
- [63] S. Capstick and W. Roberts, Prog. Part. Nucl. Phys. **45**, S241 (2000), [arXiv:nucl-th/0008028].
- [64] S. Capstick and W. Roberts, Phys. Rev. **D58**, 074011 (1998), [arXiv:nucl-th/9804070].
- [65] S. Capstick, Phys. Rev. **D46**, 2864 (1992).
- [66] R. A. Arndt *et al.*, Phys. Rev. **C74**, 045205 (2006), [arXiv:nucl-th/0605082].
- [67] B. Krusche and S. Schadmand, Prog. Part. Nucl. Phys. **51**, 399 (2003), [arXiv:nucl-ex/0306023].
- [68] A. V. Anisovich *et al.*, Eur. Phys. J. **A52**, 284 (2016), [arXiv:1604.05704].
- [69] E. Gutz *et al.* (CBELSA/TAPS), Eur. Phys. J. **A50**, 74 (2014), [arXiv:1402.4125].
- [70] V. Sokhoyan *et al.* (CBELSA/TAPS), Eur. Phys. J. **A51**, 95 (2015), [Erratum: Eur. Phys. J. A51,no.12,187(2015)], [arXiv:1507.02488].
- [71] E. Klempt *et al.*, Eur. Phys. J. **A56**, 261 (2020), [arXiv:2007.04232].
- [72] J. Yelton *et al.* (Belle), Phys. Rev. Lett. **121**, 5, 052003 (2018), [arXiv:1805.09384].
- [73] M. Sumihama *et al.* (Belle Collaboration), Phys. Rev. Lett. **122**, 072501 (2019), [arXiv:1810.06181].
- [74] G. Barucca *et al.*, Eur. Phys. J. **A57**, 149 (2021).
- [75] G. Barucca *et al.*, Eur. Phys. J. **A57**, 154 (2021).
- [76] S. Capstick and W. Roberts, Prog. in Part. Nucl. Phys. **45**, 241 (2000), [arXiv:nucl-th/0008028].
- [77] V. Crede and W. Roberts, Rept. on Prog. in Phys. **76**, 076301 (2013), [arXiv:1302.7299].
- [78] M. Ferraris *et al.*, Phys. Lett. **B364**, 231 (1995).
- [79] M. M. Giannini and E. Santopinto, Chin. J. Phys. **53**, 020301 (2015), [arXiv:1501.03722].
- [80] M. Anselmino *et al.*, Rev. Mod. Phys. **65**, 1199 (1993).
- [81] R. Bijker, F. Iachello and A. Leviatan, Annals Phys. **236**, 69 (1994), [arXiv:nucl-th/9402012].
- [82] S. Capstick and P. R. Page, Phys. Rev. **C66**, 065204 (2002), [arXiv:nucl-th/0207027].
- [83] R. L. Jaffe, D. Pirjol and A. Scardicchio, Phys. Rept. **435**, 157 (2006), [hep-ph/0602010].
- [84] G. Eichmann *et al.*, Prog. Part. Nucl. Phys. **91**, 1 (2016), [arXiv:1606.09602].
- [85] G. Eichmann and C. S. Fischer, Few Body Syst. **60**, 2 (2019).
- [86] A. Bashir *et al.*, Commun. Theor. Phys. **58**, 79 (2012), [arXiv:1201.3366].
- [87] C. D. Roberts, IRMA Lect. Math. Theor. Phys. **21**, 355 (2015).
- [88] R. Slansky, Phys. Rept. **79**, 1 (1981).
- [89] M. Karliner and J. L. Rosner, Phys. Rev. **D90**, 094007 (2014), [arXiv:1408.5877].

- [90] R. Aaij *et al.* (LHCb), Phys. Rev. Lett. **118**, 182001 (2017), [arXiv:1703.04639].
- [91] Y. Yelton *et al.*, Phys. Rev. **D97**, 051102(R) (2018).
- [92] R. Aaij *et al.*, Phys. Rev. Lett. **124**, 082002 (2020).
- [93] R. Aaij *et al.* (LHCb), Phys. Rev. Lett. **119**, 112001 (2017), [arXiv:1707.01621].
- [94] M. Mattson *et al.* (SELEX), Phys. Rev. Lett. **89**, 112001 (2002), [hep-ex/0208014].
- [95] A. Ocherashvili *et al.* (SELEX), Phys. Lett. **B628**, 18 (2005), [hep-ex/0406033].
- [96] R. Aaij *et al.* (LHCb), Sci. China Phys. Mech. Astron. **63**, 221062 (2020), [arXiv:1909.12273].
- [97] S. Brodsky, S. Groote and S. Koshkarev, Eur. Phys. J. **C78**, 483 (2018).
- [98] R. Aaij *et al.* (LHCb), JHEP **05**, 030 (2017), [arXiv:1701.07873].
- [99] L. Schachinger *et al.*, Phys. Rev. Lett. **41**, 1348 (1978).
- [100] A. Morelos Pineda *et al.* (E761), Phys. Rev. Lett. **71**, 3417 (1993).
- [101] D. W. Hertzog *et al.*, Phys. Rev. D **37**, 1142 (1988).
- [102] N. B. Wallace *et al.*, Phys. Rev. Lett. **74**, 3732 (1995).
- [103] A. Bosshard *et al.*, Phys. Rev. D **44**, 1962 (1991).
- [104] M. Kotulla *et al.*, Phys. Rev. Lett. **27**, 272001 (2002).
- [105] S. Schumann *et al.*, The European Physical Journal A **43**, 269 (2010).
- [106] A. De Rujula, H. Georgi and S. L. Glashow, Phys. Rev. **D12**, 147 (1975).
- [107] W. H. Blask *et al.*, Z. Phys. **A337**, 327 (1990).
- [108] U. Loring *et al.*, Eur. Phys. J. **A10**, 309 (2001), [hep-ph/0103287].
- [109] L. Ya. Glozman and D. O. Riska, Phys. Rept. **268**, 263 (1996), [hep-ph/9505422].
- [110] T. DeGrand and E. T. Neil, Phys. Rev. D **101**, 034504 (2020), [arXiv:1910.08561].
- [111] C. Aubin *et al.*, Phys. Rev. **D70**, 094505 (2004), [hep-lat/0402030].
- [112] A. Bazavov *et al.* (MILC), Rev. Mod. Phys. **82**, 1349 (2010), [arXiv:0903.3598].
- [113] S. Aoki *et al.* (PACS-CS), Phys. Rev. **D79**, 034503 (2009), [arXiv:0807.1661].
- [114] S. Durr *et al.*, Science **322**, 1224 (2008), [arXiv:0906.3599].
- [115] W. Bietenholz *et al.*, Phys. Rev. **D84**, 054509 (2011), [arXiv:1102.5300].
- [116] C. Alexandrou *et al.*, Phys. Rev. **D90**, 074501 (2014), [arXiv:1406.4310].
- [117] J. J. Dudek *et al.*, Phys. Rev. **D83**, 111502 (2011), [arXiv:1102.4299].
- [118] E. B. Gregory *et al.* (UKQCD), Phys. Rev. **D86**, 014504 (2012), [arXiv:1112.4384].
- [119] C. Michael, K. Ottnad and C. Urbach (ETM), Phys. Rev. Lett. **111**, 181602 (2013), [arXiv:1310.1207].
- [120] C. Bernard *et al.* (Fermilab Lattice, MILC), Phys. Rev. **D83**, 034503 (2011), [arXiv:1003.1937].
- [121] E. B. Gregory *et al.*, Phys. Rev. **D83**, 014506 (2011), [arXiv:1010.3848].
- [122] R. J. Dowdall *et al.*, Phys. Rev. **D86**, 094510 (2012), [arXiv:1207.5149].
- [123] D. Mohler and R. M. Woloshyn, Phys. Rev. **D84**, 054505 (2011), [arXiv:1103.5506].
- [124] A. S. Kronfeld, Ann. Rev. Nucl. Part. Sci. **62**, 265 (2012), [arXiv:1203.1204].
- [125] K. Ottnad, C. Urbach and F. Zimmermann (OTM), Nucl. Phys. **B896**, 470 (2015), [arXiv:1501.02645].
- [126] G. S. Bali *et al.* (RQCD), JHEP **08**, 137 (2021), [arXiv:2106.05398].
- [127] C. DeTar *et al.* (Fermilab Lattice, MILC), Phys. Rev. D **99**, 034509 (2019), [arXiv:1810.09983].
- [128] S. Piemonte *et al.*, Phys. Rev. D **100**, 074505 (2019), [arXiv:1905.03506].
- [129] S. Prelovsek *et al.*, JHEP **06**, 035 (2021), [arXiv:2011.02542].
- [130] M. Padmanath, C. B. Lang and S. Prelovsek, Phys. Rev. D **92**, 034501 (2015), [arXiv:1503.03257].
- [131] L. Liu *et al.*, Phys. Rev. **D81**, 094505 (2010), [arXiv:0909.3294].
- [132] R. A. Briceno, H.-W. Lin and D. R. Bolton, Phys. Rev. **D86**, 094504 (2012), [arXiv:1207.3536].
- [133] Y. Namekawa *et al.* (PACS-CS), Phys. Rev. **D87**, 094512 (2013), [arXiv:1301.4743].
- [134] M. Padmanath *et al.*, Phys. Rev. **D90**, 074504 (2014), [arXiv:1307.7022].
- [135] Z. S. Brown *et al.*, Phys. Rev. **D90**, 094507 (2014), [arXiv:1409.0497].
- [136] P. Pérez-Rubio, S. Collins and G. S. Bali, Phys. Rev. **D92**, 034504 (2015), [arXiv:1503.08440].
- [137] C. Alexandrou and C. Kallidonis, Phys. Rev. **D96**, 034511 (2017), [arXiv:1704.02647].
- [138] S. Meinel, private communication.
- [139] R. G. Edwards *et al.*, Phys. Rev. **D84**, 074508 (2011), [arXiv:1104.5152].
- [140] C. M. Richards *et al.* (UKQCD), Phys. Rev. **D82**, 034501 (2010), [arXiv:1005.2473].
- [141] E. Gregory *et al.*, JHEP **10**, 170 (2012), [arXiv:1208.1858].
- [142] R. A. Briceno, J. J. Dudek and R. D. Young, Rev. Mod. Phys. **90**, 025001 (2018), [arXiv:1706.06223].
- [143] J. Bulava *et al.*, Nucl. Phys. **B910**, 842 (2016), [arXiv:1604.05593].
- [144] A. Rodas, J. J. Dudek and R. G. Edwards (Hadron Spectrum), Phys. Rev. D **108**, 3, 034513 (2023), [arXiv:2303.10701].
- [145] R. A. Briceno *et al.*, Phys. Rev. Lett. **118**, 022002 (2017), [arXiv:1607.05900].
- [146] D. Guo *et al.*, Phys. Rev. D **98**, 014507 (2018), [arXiv:1803.02897].
- [147] R. A. Briceno *et al.*, Phys. Rev. D **97**, 5, 054513 (2018), [arXiv:1708.06667].
- [148] J. Bulava *et al.*, Nucl. Phys. B **987**, 116105 (2023), [arXiv:2208.03867].
- [149] A. J. Woss *et al.* (Hadron Spectrum), Phys. Rev. D **103**, 054502 (2021), [arXiv:2009.10034].
- [150] C. T. Johnson and J. J. Dudek (Hadron Spectrum), Phys. Rev. D **103**, 074502 (2021), [arXiv:2012.00518].
- [151] R. Bruschini and P. González, Phys. Rev. D **102**, 074002 (2020), [arXiv:2007.07693].
- [152] R. Bruschini and P. González, Phys. Rev. D **103**, 074009 (2021), [arXiv:2101.04636].
- [153] R. F. Lebed, R. E. Mitchell and E. S. Swanson, Prog. Part. Nucl. Phys. **93**, 143 (2017), [arXiv:1610.04528].
- [154] E. J. Eichten and C. Quigg, Phys. Rev. Lett. **119**, 202002 (2017), [arXiv:1707.09575].
- [155] M. Karliner and J. L. Rosner, Phys. Rev. Lett. **119**, 202001 (2017), [arXiv:1707.07666].
- [156] A. Francis *et al.*, Phys. Rev. Lett. **118**, 142001 (2017), [arXiv:1607.05214].
- [157] L. Leskovec *et al.*, Phys. Rev. D **100**, 014503 (2019), [arXiv:1904.04197].

- [158] R. Aaij *et al.* (LHCb), *Nature Phys.* **18**, 751 (2022), [arXiv:2109.01038].
- [159] M. Karliner and J. L. Rosner **100**, 073006 (2019), [arXiv:1906.07799].
- [160] Y. Aoki *et al.* (Flavour Lattice Averaging Group (FLAG)), *Eur. Phys. J. C* **82**, 869 (2022), [arXiv:2111.09849].
- [161] S. Borsanyi *et al.*, *Science* **347**, 1452 (2015), [arXiv:1406.4088].
- [162] G. M. de Divitiis *et al.* (RM123), *Phys. Rev. D* **87**, 114505 (2013), [arXiv:1303.4896].
- [163] D. Giusti *et al.*, *Phys. Rev.* **D95**, 114504 (2017), [arXiv:1704.06561].
- [164] S. Basak *et al.* (MILC), *Phys. Rev. D* **99**, 034503 (2019), [arXiv:1807.05556].
- [165] A. Parreno *et al.*, *Phys. Rev. D* **95**, 114513 (2017), [arXiv:1609.03985].

16. Heavy-Quark and Soft-Collinear Effective Theory

Revised August 2023 by C.W. Bauer (LBNL) and M. Neubert (PRISMA, Mainz Inst. for Theor. Physics, JG U.).

16.1 Effective Field Theories

Quantum field theories provide the most precise computational tools for describing physics at the highest energies. One of their characteristic features is that they almost inevitably involve multiple length scales. When trying to determine the value of an observable, quantum field theory demands that all possible virtual states and hence all particles be included in the calculation. Since these particles have widely different masses, the final prediction is sensitive to many scales. This fact represents a formidable challenge from a practical point of view. No realistic quantum field theories can be solved exactly, so that one needs to resort to approximation schemes; these, however, are typically most straightforward when only a single scale is involved at a time.

Effective field theories (EFTs) provide a general theoretical framework to deal with the multi-scale problems of realistic quantum field theories. This framework aims at reducing such problems to a combination of separate and simpler single-scale problems; simultaneously, however, it provides an organization scheme whereby the other scales are not omitted but allowed to play their role in a separate step of the computation. The philosophy and basic principles of this approach are very generic, and correspondingly EFTs represent a widely used method in many different areas of high-energy physics, from the low-energy scales of atomic and nuclear physics to the high-energy scales of (partly yet unknown) elementary-particle physics, see [1–3] for some early references. EFTs can play a role both within analytic perturbative computations and in the context of non-perturbative numerical simulations. One of the simplest applications of EFTs to particle physics concerns the description of an underlying theory that is only probed at energy scales $E < \Lambda$. Any particle with mass $m > \Lambda$ cannot be produced as a real state and therefore only leads to short-distance virtual effects. Thus, one can construct an effective theory in which the quantum fluctuations of such heavy particles are “integrated out” from the generating functional for Green functions. This results in a simpler theory containing only those degrees of freedom that are relevant to the energy scales under consideration. In fact, the standard model of particle physics itself is widely viewed as an EFT of some yet unknown, more fundamental theory [4, 5].

The development of any effective theory starts by identifying the degrees of freedom that are relevant to describe the physics at a given energy (or length) scale and constructing the Lagrangian describing the interactions among these fields. Short-distance quantum fluctuations associated with much smaller length scales are absorbed into the coefficients of the various operators in the effective theory. These coefficients are determined in a matching procedure, by requiring that the EFT reproduces the matrix elements of the full theory up to power corrections. In many cases the effective Lagrangian exhibits enhanced symmetries compared with the fundamental theory, giving non-trivial relations between different observables.

16.2 Heavy-Quark Effective Theory

Heavy-quark systems provide prime examples for applications of the EFT technology, because the hierarchy $m_Q \gg \Lambda_{\text{QCD}}$ (with $Q = b, c$) provides a natural separation of scales. Physics at the scale m_Q is of a short-distance nature and can be treated perturbatively, while for heavy-quark systems there is always also some hadronic physics governed by the confinement scale Λ_{QCD} of the strong interaction. Being able to separate the short-distance and long-distance effects associated with these two scales is crucial for any quantitative description. For instance, if the long-distance hadronic matrix elements are obtained from lattice QCD, then it is necessary to analytically compute the effects of short-wavelength modes that do not fit on the lattice. In many other instances, the long-distance physics can be encoded in a small number of hadronic parameters.

16.2.1 General idea and derivation of the effective Lagrangian

The simplest effective theory for heavy-quark systems is the heavy-quark effective theory (HQET) [6–9] (see [10, 11] for detailed discussions). It provides a simplified description of the soft interactions of a single heavy quark with light partons. This includes the interactions that bind the heavy quark with other light partons inside heavy mesons and baryons.

A softly interacting heavy quark is nearly on-shell. Its momentum may be decomposed as $p_Q = m_Q v + k$, where v is the 4-velocity of the hadron containing the heavy quark. The “residual momentum” k results from the soft interactions of the heavy quark with its environment and satisfies $v \cdot k \sim \Lambda_{\text{QCD}}$ and $k^2 \sim \Lambda_{\text{QCD}}^2$, which in the rest frame of the heavy hadron reduces to $k^\mu \sim \Lambda_{\text{QCD}}$. In the limit $m_Q \gg \Lambda_{\text{QCD}}$, the soft interactions do not change the 4-velocity of the heavy quark, which is therefore a conserved quantum number that is often used as a label on the effective heavy-quark fields.

A nearly on-shell Dirac spinor has two large and two small components. We define

$$Q(x) = e^{-im_Q v \cdot x} [h_v(x) + H_v(x)], \quad (16.1)$$

where

$$h_v(x) = e^{im_Q v \cdot x} \frac{1 + \not{v}}{2} Q(x), \quad H_v(x) = e^{im_Q v \cdot x} \frac{1 - \not{v}}{2} Q(x) \quad (16.2)$$

are the large (“upper”) and small (“lower”) components of the spinor field, respectively. The extraction of the phase factor in (16.1) implies that the fields h_v and H_v carry the residual momentum k . The field H_v is $1/m_Q$ suppressed relative to h_v and describes quantum fluctuations far off the mass shell. Integrating it out using its equations of motion yields the HQET Lagrangian

$$\begin{aligned} \mathcal{L}_{\text{HQET}} = & \bar{h}_v i v \cdot D_s h_v \\ & + \frac{1}{2m_Q} \left[\bar{h}_v (iD_s)^2 h_v + C_{\text{mag}}(\mu) \frac{g}{2} \bar{h}_v \sigma_{\mu\nu} G_s^{\mu\nu} h_v \right] + \dots \end{aligned} \quad (16.3)$$

The covariant derivative $iD_s^\mu = i\partial^\mu + gA_s^\mu$ and the field strength $G_s^{\mu\nu}$ contain only the soft gluon field. Hard gluons have been integrated out, and their effects are contained in the Wilson coefficients of the operators in the effective Lagrangian. From the leading operator one derives the Feynman rules of HQET. The new operators entering at subleading order are referred to as the “kinetic energy” and “chromo-magnetic interaction”. The kinetic-energy operator corresponds to the first correction term in the Taylor expansion of the relativistic energy $E = m_Q + \vec{p}^2/2m_Q + \dots$. Lorentz invariance, which is encoded as a reparametrization invariance of the effective Lagrangian [12], ensures that its Wilson coefficient is not renormalized ($C_{\text{kin}} \equiv 1$). The coefficient C_{mag} of the chromo-magnetic operator receives corrections starting at one-loop order [6].

16.2.2 Spin-flavor symmetry

The leading term in the HQET Lagrangian exhibits a global spin-flavor symmetry. Its physical meaning is that, in the infinite mass limit, the properties of hadronic systems containing a single heavy quark are insensitive to the spin and flavor of the heavy quark [13, 14]. The spin symmetry results from the fact that there are no Dirac matrices in the leading term of the effective Lagrangian in (16.3), implying that the interactions of the heavy quark with soft gluons leave its spin unchanged. The flavor symmetry arises since the mass of the heavy quark does not appear at leading order. For n_Q heavy quarks moving at the same velocity, one can simply extend (16.3) by summing over n_Q identical terms for heavy-quark fields h_v^i . The result is invariant under rotations in flavor space. When combined with the spin symmetry, the symmetry group becomes promoted to $SU(2n_Q)$. These symmetries are broken by the operators at subleading power in the $1/m_Q$ expansion.

The spin-flavor symmetry leads to many interesting relations between the properties of hadrons containing a heavy quark. The

most direct consequences concern the spectroscopy of such states [15]. In the heavy-quark limit, the spin of the heavy quark and the total angular momentum j of the light degrees of freedom are separately conserved by the strong interactions. Because of heavy-quark symmetry, the dynamics is independent of the spin and mass of the heavy quark. Hadronic states can thus be classified by the quantum numbers (flavor, spin, parity, etc.) of the light degrees of freedom. The spin symmetry predicts that, for fixed $j \neq 0$, there is a doublet of degenerate states with total spin $J = j \pm \frac{1}{2}$. The flavor symmetry relates the properties of states with different heavy-quark flavor.

16.2.3 Weak decay form factors

Of particular interest are the relations between the weak decay form factors of heavy mesons, which parametrize hadronic matrix elements of currents between two mesons containing a heavy quark. These relations have been derived by Isgur and Wise [14], generalizing ideas developed by Nussinov and Wetzel [16] and Voloshin and Shifman [17]. For the purpose of this discussion, it is convenient to work with a mass-independent normalization of meson states and use velocity rather than momentum variables.

Consider the elastic scattering of a pseudoscalar meson, $P(v) \rightarrow P(v')$, induced by an external vector current coupled to the heavy quark contained in P , which acts as a color source moving with the meson's velocity v . The action of the current is to replace instantaneously the color source by one moving at velocity v' . Soft gluons need to be exchanged in order to rearrange the light degrees of freedom and build up the final state meson moving at velocity v' . This rearrangement leads to a form-factor suppression. The important observation is that, in the $m_Q \rightarrow \infty$ limit, the form factor can only depend on the Lorentz boost $\gamma = v \cdot v'$ connecting the rest frames of the initial and final-state mesons (as long as $\gamma = \mathcal{O}(1)$). In the effective theory the hadronic matrix element describing the scattering process can therefore be written as

$$\langle P(v') | \bar{h}_{v'} \gamma^\mu h_v | P(v) \rangle = \xi(v \cdot v') (v + v')^\mu, \quad (16.4)$$

with a form factor $\xi(v \cdot v')$ that is real and independent of m_Q . By flavor symmetry, the form factor remains identical when one replaces the heavy quark Q in one of the meson states by a heavy quark Q' of a different flavor, thereby turning P into another pseudoscalar meson P' . At the same time, the current becomes a flavor-changing vector current. This universal form factor is called the Isgur-Wise function [14]. For equal velocities the vector current $J^\mu = \bar{h}_v \gamma^\mu h_v$ is conserved in the effective theory, irrespective of the flavor of the heavy quarks. The corresponding conserved charges are the generators of the flavor symmetry. It follows that the Isgur-Wise function is normalized at the point of equal velocities: $\xi(1) = 1$. Since the recoil energy of the daughter meson P' in the rest frame of the parent meson P is $E_{\text{recoil}} = m_{P'} (v \cdot v' - 1)$, the point $v \cdot v' = 1$ is referred to as the zero-recoil limit. The heavy-quark spin symmetry leads to additional relations among weak decay form factors. It can be used to relate matrix elements involving vector mesons to those involving pseudoscalar mesons, which once again can be described completely in terms of the universal Isgur-Wise function.

The form factor relations imposed by heavy-quark symmetry describe the semileptonic decay processes $\bar{B} \rightarrow D \ell \bar{\nu}$ and $\bar{B} \rightarrow D^* \ell \bar{\nu}$ in the limit of infinite heavy-quark masses. They are model-independent consequences of QCD. The known normalization of the Isgur-Wise function at zero recoil can be used to obtain a model-independent measurement of the element $|V_{cb}|$ of the Cabibbo-Kobayashi-Maskawa (CKM) matrix. The semileptonic decay $\bar{B} \rightarrow D^* \ell \bar{\nu}$ is particularly well suited for this purpose [18]. Experimentally this is a very clean mode, since the reconstruction of the D^* meson mass provides a powerful rejection against background. From the theoretical point of view, it is ideal since the decay rate at zero recoil is protected by Luke's theorem against first-order power corrections in $1/m_Q$ [19]. This is described in more detail in Section 12. Corrections to the heavy-quark symmetry relations for the $\bar{B} \rightarrow D^{(*)}$ form factors near zero recoil can also be constrained using sum rules derived in the small-velocity limit [20, 21].

16.2.4 Decoupling transformation

At leading order in $1/m_Q$, the couplings of soft gluons to heavy quarks in the effective Lagrangian (16.3) can be removed by the field redefinition $h_v(x) = Y_v(x) \bar{h}_v^{(0)}(x)$, where $Y_v(x)$ is a soft Wilson line along the direction of v , extending from minus infinity to the point x . In terms of the new fields the leading-order HQET Lagrangian becomes $\mathcal{L}_{\text{HQET}} = \bar{h}_v^{(0)} i v \cdot \partial h_v^{(0)}$. It describes a free theory as far as the strong interactions of heavy quarks are concerned. However, the theory is nevertheless non-trivial in the presence of external sources. Consider, e.g., the case of a weak-interaction heavy-quark current

$$\bar{h}_{v'} \gamma^\mu (1 - \gamma_5) h_v = \bar{h}_{v'}^{(0)} \gamma^\mu (1 - \gamma_5) Y_{v'}^\dagger Y_v h_v^{(0)}, \quad (16.5)$$

where v and v' are the velocities of the heavy mesons containing the heavy quarks. Unless the two velocities are equal, corresponding to the zero-recoil limit discussed above, the object $Y_{v'}^\dagger Y_v$ is non-trivial, and hence the soft gluons do not decouple from the heavy quarks inside the current operator. One may interpret $Y_{v'}^\dagger Y_v$ as a Wilson loop with a cusp at the point x , where the two paths parallel to the different velocity vectors intersect. The presence of the cusp leads to non-trivial ultra-violet behavior (for $v \neq v'$), which is described by a cusp anomalous dimension $\Gamma_{\text{cusp}}(v \cdot v')$ that was calculated at two-loop order in [22]. It coincides with the velocity-dependent anomalous dimension of heavy-quark currents, which was introduced in the context of HQET in [23]. The interpretation of heavy quarks as Wilson lines is a useful tool, which was put forward in one of the very first papers on the subject [6]. This technology will be useful in the study of the interactions of heavy quarks with collinear degrees of freedom discussed later in this review.

16.2.5 Heavy-quark expansion for inclusive decays

The theoretical description of inclusive decays of hadrons containing a heavy quark exploits two observations [24–28]: bound-state effects related to the initial state can be calculated using the heavy-quark expansion, and the fact that the final state consists of a sum over many hadronic channels eliminates the sensitivity to the properties of individual final-state hadrons. The second feature rests on the hypothesis of quark-hadron duality, i.e. the assumption that decay rates are calculable in QCD after a smearing procedure has been applied [29]. In semileptonic decays, the integration over the lepton spectrum provides a smearing over the invariant hadronic mass of the final state (global duality). For nonleptonic decays, where the total hadronic mass is fixed, the summation over many hadronic final states provides an averaging (local duality). Since global duality is a much weaker assumption, the theoretical control of inclusive semileptonic decays is on firmer footing.

Using the optical theorem, the inclusive decay width of a hadron H_b containing a b quark can be written in the form

$$\Gamma(H_b) = \frac{1}{M_{H_b}} \text{Im} \langle H_b | i \int d^4x T \{ \mathcal{H}_{\text{eff}}(x), \mathcal{H}_{\text{eff}}(0) \} | H_b \rangle. \quad (16.6)$$

The effective weak Hamiltonian for b -quark decays consists of dimension-6 four-fermion operators and dipole operators [30]. Because of the large mass of the b quark, it follows that the separation of fields in the time-ordered product in (16.6) is small, of order $x \sim 1/m_b$. It is thus possible to construct an operator-product expansion (OPE) for the time-ordered product, in which it is represented as a series of local operators in HQET. The leading operator $\bar{h}_v h_v$ has a trivial matrix element. The next contributions arise at $\mathcal{O}(1/m_b^2)$ and give rise to two parameters $\mu_\pi^2(H_b)$ and $\mu_G^2(H_b)$, which are defined as the matrix elements of the heavy-quark kinetic energy and chromo-magnetic interaction inside the hadron H_b , respectively [31]. For the ground-state heavy mesons and baryons, one has $\mu_G^2(B) = 3(m_{B^*}^2 - m_B^2)/4 \simeq 0.36 \text{ GeV}^2$ and $\mu_G^2(\Lambda_b) = 0$. Thus, the total inclusive decay rate of a hadron H_b

can be written as [25, 26]

$$\Gamma(H_b) = \frac{G_F^2 m_b^5 |V_{cb}|^2}{192\pi^3} \left[c_1 + c_2 \frac{\mu_\pi^2(H_b)}{2m_b^2} + c_3 \frac{\mu_G^2(H_b)}{2m_b^2} + \mathcal{O}\left(\frac{1}{m_b^3}\right) + \dots \right], \quad (16.7)$$

where the prefactor arises from the loop integrations and is proportional to the fifth power of the b -quark mass. The coefficient functions c_i are calculable order by order in perturbation theory. While c_1 corresponds to the decay rate of a free heavy quark, the higher-order coefficients systematically account for bound-state effects. The coefficients of the subleading operators and of the leading operator at third order in $1/m_b$ have been calculated at NLO [32–36]. At tree level the heavy-quark expansion has been performed up to fifth order in $1/m_b$ [37].

From the fully inclusive width in (16.7) one can obtain the lifetime of a heavy hadron via $\tau(H_b) = 1/\Gamma(H_b)$. Due to the universality of the leading term in the heavy-quark expansion, lifetime ratios such as $\tau(B^-)/\tau(\bar{B}^0)$, $\tau(\bar{B}_s^0)/\tau(B^0)$ and $\tau(\Lambda_b)/\tau(\bar{B}^0)$ are particularly sensitive to the hadronic parameters determining the power corrections in the expansion. In order to understand these ratios theoretically, it is necessary to include phase-space enhanced power corrections of order $(\Lambda_{\text{QCD}}/m_b)^3$ [38, 39] as well as short-distance perturbative effects [40] in the calculation (see [41] for a discussion of the corresponding calculations).

A formula analogous to (16.7) can be derived for differential distributions in specific inclusive decay processes, assuming that these distributions are integrated over a sufficiently large region of phase space to ensure quark-hadron duality. Important examples are the distributions in the lepton energy and the lepton invariant mass, as well as moments of the invariant hadronic mass distribution in the semileptonic processes $\bar{B} \rightarrow X_u \ell \bar{\nu}$ and $\bar{B} \rightarrow X_c \ell \bar{\nu}$. A global fit of semileptonic decay distributions can be used to determine the CKM matrix elements $|V_{ub}|$ and $|V_{cb}|$ along with heavy-quark parameters such as the masses m_b , m_c and the hadronic parameters $\mu_\pi^2(B)$, $\mu_G^2(B)$. These determinations provide some of the most accurate values for these parameters (see e.g. [42–45]).

16.2.6 Shape functions and non-local power corrections

In certain regions of phase space, in which the hadronic final state in an inclusive heavy-hadron decay is made up of light energetic partons, the local OPE for inclusive decays must be replaced by a more complicated expansion involving hadronic matrix elements of non-local light-ray operators [46, 47]. Prominent examples are the radiative decay $\bar{B} \rightarrow X_s \gamma$ for large photon energy E_γ near $m_B/2$, and the semileptonic decay $\bar{B} \rightarrow X_u \ell \bar{\nu}$ at large lepton energy or small hadronic invariant mass. In these cases, the differential decay rates at leading order in the heavy-quark expansion can be written in the factorized form $d\Gamma = H J \otimes S$ [48], where the hard function H and the jet function J are calculable in perturbation theory. The characteristic scales for these functions are set by m_b and $(m_b \Lambda_{\text{QCD}})^{1/2}$, respectively. The soft function

$$S(\omega) = \int \frac{dt}{4\pi} e^{-i\omega t} \langle \bar{B}(v) | \bar{h}_v(tn) Y_n(tn) Y_n^\dagger(0) h_v(0) | \bar{B}(v) \rangle \quad (16.8)$$

is a non-perturbative object called the shape function [46, 47]. Here Y_n are soft Wilson lines along a light-like direction n aligned with the momentum of the hadronic final-state jet. The jet function and the shape function share a common variable $\omega \sim \Lambda_{\text{QCD}}$, and the symbol \otimes denotes a convolution in this variable.

While the hard functions are different for the decays $\bar{B} \rightarrow X_s \gamma$ and $\bar{B} \rightarrow X_u \ell \bar{\nu}$, the jet and soft functions are identical at leading order in Λ_{QCD}/m_Q . This is particularly important for the shape function, which introduces non-perturbative physics into the theoretical predictions for the decay rates in the regions of experimental interest. The fact that both processes depend on the same non-perturbative function makes it possible to use the measured shape of the $\bar{B} \rightarrow X_s \gamma$ photon spectrum to reduce the theoretical uncertainties in the determination of the CKM element $|V_{ub}|$ from semileptonic decays. In higher orders of the heavy-quark

expansion, an increasing number of subleading jet and soft functions are required to describe the decay distributions [49]. These have been analyzed in detail at order $1/m_b$ [50–52]. In the case of $\bar{B} \rightarrow X_s \gamma$ (and also in the related case of $\bar{B} \rightarrow X_s \ell \bar{\ell}$), some of these non-local effects survive in the total decay rate and give rise to irreducible hadronic uncertainties [53]. The technology for deriving the corresponding factorization theorems relies on the soft-collinear effective theory, to which we now turn.

16.3 Soft-Collinear Effective Theory

As discussed in the previous section, soft gluons that bind a heavy quark inside a heavy meson cannot change the virtuality of that heavy quark by a significant amount. The ratio Λ_{QCD}/m_Q provides the expansion parameter in HQET, which is a small parameter since $m_Q \gg \Lambda_{\text{QCD}}$. This obviously does not work when considering light quarks. However, if the energy Q (not to be confused with the flavor of a heavy quark) of the quarks is large, the ratio Λ_{QCD}/Q provides a small parameter, which can be used to construct an effective theory. One major difference to HQET is that light energetic quarks cannot only emit soft gluons, but they can also emit collinear gluons (an energetic gluon in the same direction as the original quark), without parametrically changing their virtuality. Thus, to fully reproduce the long-distance physics of energetic quarks requires that one includes their interactions with both soft and collinear particles. The resulting effective theory is therefore called soft-collinear effective theory (SCET) [54–57] (see [58] for a review).

A single energetic particle can always be boosted to a frame where all momentum components have similar size, in which case there is no small expansion parameter. Thus, the presence of energetic particles must refer to a reference frame defined by external kinematics. SCET has a wide range of applications; some examples are the production of energetic, light states in the decay of a heavy particle in its rest frame, the production of energetic jets in collider environments, and the scattering of energetic particles off a target at rest. In this brief review we will outline the main features of this effective theory and mention a few selected applications.

16.3.1 General idea of the expansion

Consider a quark with virtuality much less than its energy Q , moving along the direction \bar{n} . It is convenient to parameterize the momentum p_n of this particle in terms of its light-cone components, defined by $(p_n^-, p_n^+, p_n^\perp) = (\bar{n} \cdot p_n, n \cdot p_n, p_n^\perp)$, where $n^\mu = (1, \bar{n})$ and $\bar{n}^\mu = (1, -\bar{n})$ are light-like reference vectors, and $n \cdot p_n^\perp = \bar{n} \cdot p_n^\perp = 0$. The subscript n on the momentum indicates the direction of the collinear particle. In terms of these light-cone components, the virtuality satisfies $p_n^2 = p_n^+ p_n^- + p_n^{\perp 2}$. The individual components of the momentum obey

$$(p_n^-, p_n^+, p_n^\perp) \sim Q(1, \lambda^2, \lambda), \quad (16.9)$$

where $\lambda^2 = p^2/Q^2$ is the expansion parameter of SCET. The virtuality of such an energetic particle remains parametrically unchanged if it interacts with energetic particles in the same direction n , or with soft particles with momentum scaling as

$$(p_s^-, p_s^+, p_s^\perp) \sim Q(\lambda^2, \lambda^2, \lambda^2). \quad (16.10)$$

SCET is constructed in such a way as to reproduce the long-distance dynamics arising from the interactions of collinear and soft degrees of freedom.

In the above power counting the transverse momenta of soft degrees of freedom scale as $p_s^\perp \sim Q\lambda^2$, which is much smaller than the transverse momenta $p_c^\perp \sim Q\lambda$ of collinear fields. This theory is usually called SCET_I. If the external kinematics require that the transverse momenta of both soft and collinear fields are of the same size, $p_c^\perp \sim p_s^\perp$, then the appropriate degrees of freedom have the scaling $p_c \sim Q(1, \lambda^2, \lambda)$ and $p_s \sim Q(\lambda, \lambda, \lambda)$. This theory is usually called SCET_{II} and is required, e.g., for exclusive hadronic decays such as $\bar{B} \rightarrow D\pi$, where the virtuality of both collinear and soft degrees of freedom are set by Λ_{QCD} , or for the description of transverse-momentum distributions at colliders. SCET_I power counting is assumed in the following sections, while SCET_{II} is discussed in more detail in 16.3.6.

16.3.2 Leading-order Lagrangian

The derivation of the SCET Lagrangian follows similar steps as described for HQET in Section 16.2.1. One begins by deriving the Lagrangian for a theory containing only a single collinear sector. Similar to HQET, one separates the full QCD field into two components, $q_n(x) = \psi_n(x) + \eta_n(x)$, where (with $n \cdot \bar{n} = 2$)

$$\psi_n(x) = \frac{\not{n}\not{\bar{n}}}{4} q_n(x), \quad \eta_n(x) = \frac{\not{\bar{n}}\not{n}}{4} q_n(x). \quad (16.11)$$

The degrees of freedom described by the field η_n are far off shell and can therefore be eliminated using its equation of motion. This gives

$$\mathcal{L}_n = \bar{\psi}_n(x) \left[in \cdot D + i\not{D}^\perp \frac{1}{i\bar{n} \cdot D} i\not{D}^\perp \right] \frac{\not{n}}{2} \psi_n(x). \quad (16.12)$$

As a next step, one separates the large and small momentum components by decomposing the collinear momentum into a ‘‘label’’ and a residual momentum, $p^\mu = P^\mu + k^\mu$ with $n \cdot P = 0$. One then performs a phase redefinition on the collinear fields, such that $\psi_n(x) = e^{-iP \cdot x} \xi_n(x)$. Derivatives acting on the fields $\xi_n(x)$ now only pick out the residual momentum. Since unlike in HQET the label momentum in SCET is not conserved, one defines a label operator \mathcal{P}^μ acting as $\mathcal{P}^\mu \xi_n(x) = P^\mu \xi_n(x)$ [56], as well as a corresponding covariant label operator $i\not{D}_n^\mu = \mathcal{P}^\mu + gA_n^\mu(x)$. Note that at leading order in power counting $i\not{D}_n^\mu$ does not contain the soft gluon field. This leads to the final SCET Lagrangian [56,57,59,60]

$$\mathcal{L}_n = \bar{\xi}_n(x) \left[in \cdot D_n + gn \cdot A_s + i\not{D}_n^\perp \frac{1}{i\bar{n} \cdot \mathcal{D}_n} i\not{D}_n^\perp \right] \frac{\not{n}}{2} \xi_n(x) + \dots, \quad (16.13)$$

where we have split $in \cdot D$ into a collinear piece $in \cdot D_n = in \cdot \partial + gn \cdot A_n$ and a soft piece $gn \cdot A_s$. This latter term gives rise to the only interaction between a collinear quark and soft gluons at leading power in λ . The ellipses represent higher-order interactions between soft and collinear particles.

The Lagrangian describing collinear fields in different light-like directions is simply given by the sum of the Lagrangians for each direction n , i.e. $\mathcal{L} = \sum_n \mathcal{L}_n$. The soft gluons are the same in each individual Lagrangian. An alternative way to understand the separation between large and small momentum components is to derive the Lagrangian of SCET in position space [60]. In this case no label operators are required, but the collinear field operators are separated by a light-like distance. An important difference between SCET and HQET is that the SCET Lagrangian is not corrected by short distance fluctuations. The physical reason is that in the construction described above no high-momentum modes have been integrated out [60]. Such hard modes arise when different collinear sectors are coupled via some external current (e.g. in jet production at e^+e^- or hadron colliders), or when collinear particles are produced in the rest frame of a decaying heavy object (such as in B decays). Short-distance effects are then incorporated in the Wilson coefficients of the external source operators.

16.3.3 Collinear gauge invariance and Wilson lines

An important aspect of SCET concerns the implementation of local gauge invariance. Because the effective field operators describe modes with certain momentum scalings, the effective Lagrangian respects only residual gauge symmetries. One of them satisfies the collinear scaling

$$(\bar{n} \cdot \partial, n \cdot \partial, \partial^\perp) U_n(x) \sim Q(1, \lambda^2, \lambda) U_n(x), \quad (16.14)$$

and one the soft scaling

$$(\bar{n} \cdot \partial, n \cdot \partial, \partial^\perp) U_s(x) \sim Q(\lambda^2, \lambda^2, \lambda^2) U_s(x). \quad (16.15)$$

While the soft gauge transformation is common for all fields, collinear fields in different directions each transform under their own collinear gauge transformation. In other words, each collinear sector has to be separately gauge invariant under its collinear gauge transformation. This requires the introduction of collinear Wilson lines [56]

$$W_n(x) = \text{P exp} \left[-ig \int_{-\infty}^0 ds \bar{n} \cdot A_n(s\bar{n} + x) \right], \quad (16.16)$$

which transform under collinear gauge transformations according to $W_n \rightarrow U_n W_n$. Thus, the combination $\chi_n \equiv W_n^\dagger \psi_n$ is gauge invariant. In a similar manner, one can define the gauge-invariant gluon field $B_n^\mu = g^{-1} W_n^\dagger iD_n^\mu W_n$ [61, 62]. Collinear operators in SCET are typically constructed from such collinearly gauge-invariant building blocks.

16.3.4 Derivation of factorization theorems

One of the important applications of SCET is to understand how to factorize cross sections or decay rates involving energetic particles moving in different directions into simpler quantities that can either be calculated perturbatively or determined from data. For the purpose of this discussion, we focus on factorization in the context of collider physics. Note that factorization theorems have been around for much longer than SCET (see [63] for a review). However, the effective theory allows for a conceptually simpler understanding of certain classes of factorization theorems [61], since most simplifications happen already at the level of the Lagrangian. The discussion in this section is valid to leading order in the power counting of the effective theory.

As discussed in the previous section, the Lagrangian of SCET does not involve any direct couplings between collinear particles moving in different directions. A process involving highly energetic initial- and/or final-state particles moving along different directions n_i is therefore described in SCET by operators involving gauge-invariant collinear building blocks for each direction, which only interact amongst each other via soft gluon exchange. At leading power, soft gluons couple to collinear quarks only through the term $\bar{\xi}_n gn \cdot A_s (\not{n}/2) \xi_n$ in the effective Lagrangian in (16.13), which is similar to the coupling of soft gluons to heavy quarks in HQET, see Section 16.2.4. This coupling, and the corresponding coupling to collinear gluons can be removed by means of the field redefinitions [57]

$$\psi_n(x) = Y_n(x) \psi_n^{(0)}(x), \quad A_n^a(x) = Y_n^{ab}(x) A_n^{b(0)}(x), \quad (16.17)$$

where the soft Wilson lines Y_n and Y_n^{ab} live in the fundamental and adjoint representations of $SU(3)$, respectively. Each collinear building block gives rise to a soft Wilson line. After this decoupling, the different collinear sectors no longer interact with each other and the soft interactions are entirely encoded in the product of soft Wilson lines. This is the basis of factorization proofs in SCET.

The simplest applications of this formalism concern inclusive processes, such as the Drell-Yan production of electroweak bosons in the threshold region, $pp \rightarrow Z/H + X_s$, where X_s is a final state containing only soft particles, and event shape distributions in e^+e^- collisions in the two-jet limit. For Drell-Yan the factorization formula is given by [61, 64]

$$\begin{aligned} \sigma(pp \rightarrow ZX_s) &= \sum_q H_q(\mu) \left[f_{q/p}(\mu) f_{\bar{q}/p}(\mu) \right] \otimes S_F(\mu), \\ \sigma(pp \rightarrow HX_s) &= H_g(\mu) \left[f_{g/p}(\mu) f_{g/p}(\mu) \right] \otimes S_A(\mu), \end{aligned} \quad (16.18)$$

where the collinear matrix elements give rise to the parton distributions $f_{a/p}(\mu)$, the soft function are vacuum matrix element of the soft Wilson lines in the fundamental or adjoint representation, and the hard functions are the squares of the Wilson coefficients of the relevant SCET operators. The convolution symbol indicates a convolution over the longitudinal momentum fractions of the colliding partons. The objects in the factorization theorem depend on the renormalization scale μ , whereas the cross sections are scale independent. Solving the renormalization group equations (RGE) allows to resum large logarithms in the cross section (see below).

For event shapes such as thrust T , no initial-state partons are present, and the factorization formula takes the form (with $\tau = 1 - T$) [65, 66]

$$\frac{d\sigma}{d\tau} = H(\mu) \left[J_n(\mu) J_{\bar{n}}(\mu) \right] \otimes S_{n\bar{n}}(\mu), \quad (16.19)$$

where the the jet functions are vacuum matrix elements of the outgoing collinear quark fields, which are convoluted with the soft

function $S_{n\bar{n}}$ defined as another vacuum matrix element of the soft Wilson lines.

For a more general high-energy scattering process such as $pp \rightarrow N$ jets, where the incoming protons move along directions $n_{a,b}$ and the jets define directions n_1, \dots, n_N , the factorization theorem for the differential cross section can be written as

$$d\sigma \sim \sum_{ab} H_{ab\dots N}(\mu) [B_{a/p}(\mu) B_{b/p}(\mu)] \otimes [J_1(\mu) \dots J_N(\mu)] \otimes S_{ab\dots N}(\mu). \quad (16.20)$$

where the beam functions are generalized parton distributions [67] and the jet functions depend on the algorithm used to define the jets. It should be mentioned that the most difficult part of traditional factorization proofs involves showing that so-called Glauber gluons do not spoil the above factorization theorem [68]. The description of Glauber effects within SCET [69] has been developed in [70], where a closed form for the effective Lagrangian describing these interactions was derived. The formalism has been extended to Glauber quarks in [71]. In this context, a proof of factorization requires demonstrating that this Lagrangian has no impact on a particular cross section. If an observable is non-global, in the sense that energetic radiation is restricted to certain regions in phase space, the above factorization theorem needs to be generalized [72–74].

16.3.5 Resummation of large logarithms

Many processes of interest depend on multiple scales which can be widely separated. The perturbative series of such processes depends logarithmically on large scale ratios. For high-energy processes involving soft and collinear particles, there can be up to two powers of large logarithms for each power of the coupling constant. These double logarithms are referred to as Sudakov logarithms and can spoil the perturbative expansion.

SCET can be used to sum large logarithms L using renormalization-group equations. This reorganizes the perturbative series in such a way that the product $\alpha_s L$ is treated as an $\mathcal{O}(1)$ parameter. In many cases, one can write a perturbative series for the logarithm of a cross section, such that

$$\sigma \sim \exp [L g_0(\alpha_s L) + g_1(\alpha_s L) + \alpha_s g_2(\alpha_s L) + \dots], \quad (16.21)$$

with functions $g_n(x)$ that need to be determined. Note that each term in this series in the exponent is one power of α_s suppressed relative to the previous term.

The important ingredient in achieving this resummation is the fact that SCET factorizes a given cross section into simpler pieces, each of which depends on a single physical scale. The only dependence on that scale can arise through logarithms of its ratio with the renormalization scale μ . Thus, for each of the components in the factorization theorem one can choose a renormalization scale μ for which the large logarithmic terms are absent. Of course, the factorization formula requires a common renormalization scale μ in all its components, and one therefore has to use the renormalization group (RG) to evolve the various component functions from their preferred scale to the common scale μ . A novel feature of RG equations in SCET, as opposed to other EFTs, is that the anomalous dimensions entering the evolution equations of the hard, beam, jet and soft functions in a factorization formula such as (16.20) contain a single power of the logarithm of the relevant energy scale. For example, the anomalous dimension γ_H of the hard function has the form

$$\gamma_H(\mu) = c_H \Gamma_{\text{cusp}}(\alpha_s) \ln \frac{Q^2}{\mu^2} + \gamma(\alpha_s), \quad (16.22)$$

where c_H is a process-dependent coefficient and Γ_{cusp} denotes the so-called cusp anomalous dimension [22, 75]. Collinear and soft functions have similar anomalous dimensions, which also involve a cusp and a non-cusp part. The non-cusp part γ of the anomalous dimensions is process (and observable) dependent. The presence of a logarithm in the anomalous dimension is characteristic of Sudakov problems and arises since the perturbative series contains double logarithms of scale ratios.

Solving the RG equations one can systematically resum all large logarithms of scale ratios in the factorized cross section and express the functions $g_n(\alpha_s L)$ introduced above in terms of ratios of running coupling constants. In order to compute the first two terms $L g_0(\alpha_s L) + g_1(\alpha_s L)$ in $\ln \sigma$, corresponding to the next-to-leading logarithmic (NLL) approximation, one needs two-loop expressions for the cusp anomalous dimension and β function, one-loop expressions for the non-cusp pieces in the anomalous dimensions, and tree-level matching conditions for all component functions at their characteristic scales. To calculate the next term $\alpha_s g_2(\alpha_s L)$ in the expansion, corresponding to NNLL order, one needs to go one order higher in the loop expansion, and so on.

16.3.6 Factorization and resummation in SCET_{II}

The effective theory SCET_{II} contains collinear and soft particles with momenta scaling as $(p_n^-, p_n^+, p_n^\perp) \sim Q(1, \lambda^2, \lambda)$ and $(p_s^-, p_s^+, p_s^\perp) \sim Q(\lambda, \lambda, \lambda)$. They have the same small virtuality ($p_n^\pm \sim p_s^\pm \sim Q^2 \lambda^2$) but differ in their rapidities. An important class of observables, for which this scaling is relevant, contains cross sections for processes in which the transverse momenta of particles are constrained by external kinematics. The prime example are the transverse-momentum distributions of electroweak gauge bosons or Higgs bosons produced at hadron colliders. The parton transverse momenta are constrained by the fact that their vector sum must be equal and opposite to the transverse momentum q_T of the boson. Standard RG evolution in the effective theory controls the logarithms arising from the fact that the virtualities of the collinear and soft modes are much smaller than the hard scale Q in the process (the boson mass). However, additional large logarithms arise since the rapidities of collinear and soft modes are parametrically different, such that $e^{|y_c - y_s|} \sim 1/\lambda$. These logarithms can be traced to a new source of divergences and an unusual failure of dimensional regularization. They need to be factorized in the cross section and resummed by other means.

Two approaches exist for how to deal with the additional rapidity logarithms in SCET. In the approach of [76], they are interpreted as a consequence of a ‘‘collinear anomaly’’ of the effective theory SCET_{II}, resulting from the fact that a classical rescaling symmetry of the effective Lagrangian is broken by quantum effects. The extra large logarithms can be resummed by means of simple differential equations, which typically state that, to all orders in perturbation theory (and in an appropriate space), the logarithm of the cross section contains only a single extra logarithm of $\lambda \sim q_T/Q$ not contained in the hard function. Another approach to resum the rapidity logarithms uses the ‘‘rapidity renormalization group’’ [77], in which the relevant differential equations are obtained by considering a new type of scale variation in a parameter ν , which separates the phase space for collinear and soft particles along a hyperbola in the (p_-, p_+) plane. In contrast to the standard RG, there is no running coupling involved in the ν evolution, since the different contributions live at the same virtuality.

As an important application, consider the Higgs-boson production cross section in gluon fusion at the LHC, defined with a jet veto stating that no jet in the final state has transverse momentum above a threshold p_T^{veto} , which can be factorized in the form [78, 79]

$$\begin{aligned} \sigma(p_T^{\text{veto}}) = & H(m_H, \mu) \left(\frac{\nu_B}{\nu_S} \right)^{-2F_{gg}(R, p_T^{\text{veto}}, \mu)} S_{gg}(R, p_T^{\text{veto}}, \mu, \frac{\nu_S}{p_T^{\text{veto}}}) \\ & \times \int_\tau^1 \frac{dz}{z} B_{g/P} \left(z, R, p_T^{\text{veto}}, \mu, \frac{\nu_B}{m_H} \right) B_{g/P} \left(\frac{\tau}{z}, R, p_T^{\text{veto}}, \mu, \frac{\nu_B}{m_H} \right), \end{aligned} \quad (16.23)$$

where $\tau = m_H^2/s$, and $\mu \sim p_T^{\text{veto}}$ is a common factorization scale. The beam functions $B_{g/P}$, the soft function S_{gg} and the exponent F_{gg} all depend on the jet radius R as well as the jet clustering algorithm. The scale dependence of the hard function H is controlled by standard RG evolution in SCET. The beam functions can be factorized further into calculable collinear kernels convoluted with parton distribution functions. In addition to the renormalization scale μ , the beam and soft functions depend on

two rapidity scales $\nu_B \sim m_H$ and $\nu_S \sim p_T^{\text{veto}}$, respectively. In [78] the default values $\nu_B = m_H$ and $\nu_S = p_T^{\text{veto}}$ are used for these scales, and the soft function S_{gg} is absorbed into the beam functions. In [79] the exponent F_{gg} is called $-\gamma_g^S/2$. The second factor on the right-hand side of the factorization formula (16.23), which resums large rapidity logarithms, implies that the logarithm of the jet-veto cross section contains a single large logarithm $\ln \sigma = -2F_{gg}(R, p_T^{\text{veto}}, \mu) \ln(m_H/p_T^{\text{veto}}) + \dots$ not contained in the hard function. Its coefficient can be calculated in fixed-order perturbation theory.

SCET_{II} also plays an important role in the study of factorization for a variety of exclusive B meson decays, such as $\bar{B} \rightarrow \pi \ell \bar{\nu}$, $\bar{B} \rightarrow K^* \gamma$ and $\bar{B} \rightarrow \pi \pi$, for which the virtualities of energetic (collinear) final-state particles are of order Λ_{QCD} , which is also the scale for the soft light degrees of freedom contained in the initial-state B meson.

16.3.7 Applications

Most of the applications of SCET are either in flavor physics, where the decay of a heavy B meson can give rise to energetic light partons, or in collider physics, where the presence of jets naturally leads to collimated sets of energetic particles. For some of these applications alternative approaches existed before the invention of SCET, but the effective theory has opened up alternative ways to understand the physics of these processes. For many examples, however, SCET has allowed new insights and new applications.

The investigation of heavy-to-light form factors has been instrumental for understanding factorization in exclusive semileptonic B decays [80]. SCET has also provided a field-theoretic basis for the QCD factorization approach to exclusive, non-leptonic decays of B mesons [81]. Using SCET methods, proofs of factorization were derived for the color-allowed decay $\bar{B}^0 \rightarrow D^+ \pi^-$ [82], the color-suppressed decay $\bar{B}^0 \rightarrow D^0 \pi^0$ [83], and the radiative decay $\bar{B} \rightarrow K^* \gamma$ [84]. In recent years, the factorization approach has been extended to include QED effects [85, 86]. Further examples are factorization theorems and the resummation of endpoint logarithms for quarkonia production [87], the resummation of large logarithmic terms for the thrust [88] and jet broadening [89] distributions in e^+e^- annihilation beyond NLL order, the development of new factorizable observables to veto extra jets [67, 90], all-order factorization theorems for processes containing electroweak Sudakov logarithms [91], and the resummation of threshold (soft gluon) logarithms in momentum space for several important processes at hadron colliders [64, 92, 93]. There has also been a lot of activity describing p_T -based resummation at hadron colliders. Prominent examples are the transverse-momentum distributions of electroweak bosons [76, 77, 94], which give access to the p_T -dependent parton distribution functions. Higher-order resummations of event shape distributions [88], combined with two-loop fixed-order expressions [95, 96] and including nonperturbative effects by means of a shape function, have been used for an accurate determination of the strong coupling constant α_s [97, 98]. A method based on N -jettiness (\mathcal{T}_N) slicing [99, 100] has provided a new way of performing the IR subtractions needed for precise fixed-order calculations, using the fact that the singular dependence on \mathcal{T}_N can be calculated using SCET at NNLO. This has been used to compute various processes with final states containing up to one hard, colored particle [101–105]. Calculations of the leading power corrections in \mathcal{T}_0/Q [106, 107] have helped to improve the numerical stability of the method. The N -jettiness slicing method has also been used in the combination of higher-order resummation with parton showers [108–110]. Finally, SCET has given new insights into the jet substructure methods (see [111] for a review).

A novel type of SCET factorization theorem is needed to describe non-global observables, in which energetic radiation is limited to certain regions of phase space, e.g. inside jets. Jet events play a prominent role in collider physics, because they closely mirror the underlying short-distance dynamics. In the theoretical description of such observables one encounters so-called “non-global” logarithms (NGLs) [112, 113], whose resummation cannot be performed using standard techniques. Using SCET, this problem has been reduced to the solution of a RG evolution equation derived from a novel type of factorization theorem, in which the

hard and soft functions are operators in color space and in the (infinite) space of parton multiplicities [72, 74] (see also [73, 114]). In e^+e^- collisions, solving the RGE in the large- N_c limit using parton-shower techniques [115] gives a result that agrees with the solution of the BSM integral equation for the NGLs [116]. The first application of this formalism was to the light jet mass distribution [117], and the extension of the resummation to NLL accuracy has been accomplished in [118, 119]. Non-global observables at hadron colliders are yet more intricate, since Glauber-gluon exchange between the colliding partons lead to a new type of double logarithmic corrections in high orders of perturbation theory, the so-called superleading logarithms (SLLs) [120, 121]. Based on the corresponding SCET factorization theorem, the all-order resummation of SLLs has been accomplished for arbitrary $pp \rightarrow n$ jet processes [122].

Recent years have seen a strong effort to push the applications of SCET factorization and resummation techniques to next-to-leading power (NLP) in the expansion in λ . The subleading SCET Lagrangian [60, 123, 124] and current operators arising in B -meson decays and their anomalous dimensions [59, 60, 125–127] have been studied a long time ago. For important collider processes, such as Drell-Yan or Higgs production, the general sets of operators have been identified [128–130], and several of their anomalous dimensions have been calculated [130, 131]. Resummed results at subleading power have been presented for event shapes [132] and the Drell-Yan process [133]. More applications of SCET can be found in Section 6.4 of the review article [134].

16.4 Open issues and perspectives

HQET has successfully passed many experimental tests, and there are not many open questions that still need to be addressed. One concept that has not been derived from first principles is the notion of quark-hadron duality, which underlies the application of HQET to the description of inclusive decays of B mesons. The validity of global duality (at energies even lower than those relevant in B decays) has been tested experimentally using high-precision data on semileptonic B decays and on hadronic τ decays. However, assigning a theoretical uncertainty due to possible duality violations remains a difficult task. Another known issue is that the measured values of the CKM elements $|V_{ub}|$ and $|V_{cb}|$ extracted from exclusive or inclusive decays of B mesons differ from each other by several standard deviations (see Section 76). This measurement relies on the heavy-quark limit, and the uncertainty quoted includes a theoretical estimate of the effect of power corrections arising from the finite b -quark mass. It remains an open question whether the discrepancy is due to underestimated theoretical or experimental uncertainties.

SCET, on the other hand, is still an active field of research, and new results are being obtained regularly. In particular, it has been realized that at NLP SCET factorization theorems generically suffer from endpoint-divergent convolution integrals [135–140]. To remove these divergences, one uses exact D -dimensional refactorization conditions, which relate different terms in the NLP factorization theorem in the singular limits, to rearrange these terms in such a way that the endpoint divergences are systematically removed. Successful applications of this technique include the NLP factorization theorem for the b -quark induced contribution to the diphoton decay amplitude of the Higgs boson [139, 141] and the $gg \rightarrow H$ production amplitude [142], the “off-diagonal gluon thrust” in e^+e^- collisions [143], and the NLP factorization theorems for some exclusive [144, 145] and inclusive [146] B -meson decays. On the other hand, for some other processes, such as electron-muon backward scattering [147], the factorization of endpoint singularities is still a subject of ongoing research.

Another active field concerns the further study and applications of Glauber gluons and quarks in SCET and their relation to the BFKL equation familiar from small- x physics [114, 148]. The theoretical formalism developed in [70, 71] sets the basis for a solid understanding of the impact of Glauber exchanges on factorization theorems. Moreover, using the rapidity renormalization group one can derive the BFKL equation in the presence of a single Glauber exchange describing forward scattering [70, 148] and for small x resummation in deep inelastic scattering [149]. Glauber gluons play an important role in SCET-based analysis of

jet propagation in dense QCD media [150–152], which gives rise to the jet-quenching phenomenon in heavy-ion collisions. They are also a crucial ingredient in studies of violations of collinear factorization at hadron colliders [69, 153–157].

We close this short review by mentioning a particularly nice application combining the methods of heavy-particle EFTs such as HQET and non-relativistic QCD with SCET in the context of describing the interactions of heavy dark matter (with mass $M \gg v$) with SM particles. In [158] it was realized that the interactions of heavy, weakly interacting massive particles (WIMPs) with nuclear targets can be described in a model-independent way using heavy-particle EFTs. The WIMPs are charged under $SU(2)_L$ and can interact with electroweak gauge bosons and the Higgs boson. The WIMP EFT was later extended by describing the produced, highly energetic electroweak gauge bosons in terms of soft or collinear fields in SCET [159–161]. This allows one to systematically separate all relevant mass scales, resum electroweak Sudakov logarithms and disentangle the so-called Sommerfeld enhancement from the short-distance hard annihilation process.

References

- [1] E. Witten, Nucl. Phys. **B122**, 109 (1977).
- [2] S. Weinberg, Phys. Lett. **91B**, 51 (1980).
- [3] L. J. Hall, Nucl. Phys. **B178**, 75 (1981).
- [4] W. Buchmuller and D. Wyler, Nucl. Phys. B **268**, 621 (1986).
- [5] B. Grzadkowski *et al.*, JHEP **10**, 085 (2010), [arXiv:1008.4884].
- [6] E. Eichten and B. R. Hill, Phys. Lett. B **234**, 511 (1990).
- [7] H. Georgi, Phys. Lett. **B240**, 447 (1990).
- [8] B. Grinstein, Nucl. Phys. **B339**, 253 (1990).
- [9] T. Mannel, W. Roberts and Z. Ryzak, Nucl. Phys. **B368**, 204 (1992).
- [10] M. Neubert, Phys. Rept. **245**, 259 (1994), [hep-ph/9306320].
- [11] A. V. Manohar and M. B. Wise, Camb. Monogr. Part. Phys. Nucl. Phys. Cosmol. **10**, 1 (2000).
- [12] M. E. Luke and A. V. Manohar, Phys. Lett. **B286**, 348 (1992), [hep-ph/9205228].
- [13] E. V. Shuryak, Phys. Lett. **93B**, 134 (1980).
- [14] N. Isgur and M. B. Wise, Phys. Lett. **B232**, 113 (1989).
- [15] N. Isgur and M. B. Wise, Phys. Rev. Lett. **66**, 1130 (1991).
- [16] S. Nussinov and W. Wetzel, Phys. Rev. **D36**, 130 (1987).
- [17] M. A. Shifman and M. B. Voloshin, Sov. J. Nucl. Phys. **45**, 292 (1987), [Yad. Fiz.45,463(1987)].
- [18] M. Neubert, Phys. Lett. **B264**, 455 (1991).
- [19] M. E. Luke, Phys. Lett. **B252**, 447 (1990).
- [20] I. I. Y. Bigi *et al.*, Phys. Rev. **D52**, 196 (1995), [hep-ph/9405410].
- [21] N. Uraltsev, Phys. Lett. **B501**, 86 (2001), [,195(2000)], [hep-ph/0011124].
- [22] G. P. Korchemsky and A. V. Radyushkin, Nucl. Phys. **B283**, 342 (1987).
- [23] A. F. Falk *et al.*, Nucl. Phys. **B343**, 1 (1990).
- [24] J. Chay, H. Georgi and B. Grinstein, Phys. Lett. **B247**, 399 (1990).
- [25] I. I. Y. Bigi, N. G. Uraltsev and A. I. Vainshtein, Phys. Lett. **B293**, 430 (1992), [Erratum: Phys. Lett. B297,477(1992)], [hep-ph/9207214].
- [26] A. V. Manohar and M. B. Wise, Phys. Rev. **D49**, 1310 (1994), [hep-ph/9308246].
- [27] T. Mannel, Nucl. Phys. **B413**, 396 (1994), [hep-ph/9308262].
- [28] A. F. Falk, M. E. Luke and M. J. Savage, Phys. Rev. **D49**, 3367 (1994), [hep-ph/9308288].
- [29] E. C. Poggio, H. R. Quinn and S. Weinberg, Phys. Rev. **D13**, 1958 (1976).
- [30] G. Buchalla, A. J. Buras and M. E. Lautenbacher, Rev. Mod. Phys. **68**, 1125 (1996), [hep-ph/9512380].
- [31] A. F. Falk and M. Neubert, Phys. Rev. **D47**, 2965 (1993), [hep-ph/9209268].
- [32] T. Becher, H. Boos and E. Lunghi, JHEP **12**, 062 (2007), [arXiv:0708.0855].
- [33] A. Alberti, P. Gambino and S. Nandi, JHEP **01**, 147 (2014), [arXiv:1311.7381].
- [34] T. Mannel, A. A. Pivovarov and D. Rosenthal, Phys. Lett. **B741**, 290 (2015), [arXiv:1405.5072].
- [35] T. Mannel, A. A. Pivovarov and D. Rosenthal, Phys. Rev. **D92**, 5, 054025 (2015), [arXiv:1506.08167].
- [36] T. Mannel and A. A. Pivovarov, Phys. Rev. **D100**, 9, 093001 (2019), [arXiv:1907.09187].
- [37] T. Mannel, S. Turczyk and N. Uraltsev, JHEP **11**, 109 (2010), [arXiv:1009.4622].
- [38] M. Neubert and C. T. Sachrajda, Nucl. Phys. **B483**, 339 (1997), [hep-ph/9603202].
- [39] M. Beneke, G. Buchalla and I. Dunietz, Phys. Rev. **D54**, 4419 (1996), [Erratum: Phys. Rev. D83,119902(2011)], [hep-ph/9605259].
- [40] M. Beneke *et al.*, Phys. Lett. **B459**, 631 (1999), [hep-ph/9808385].
- [41] M. Kirk, A. Lenz and T. Rauh, JHEP **12**, 068 (2017), [arXiv:1711.02100].
- [42] C. W. Bauer *et al.*, Phys. Rev. D **70**, 094017 (2004), [hep-ph/0408002].
- [43] P. Gambino and C. Schwanda, Phys. Rev. **D89**, 1, 014022 (2014), [arXiv:1307.4551].
- [44] F. U. Bernlochner *et al.* (SIMBA), Phys. Rev. Lett. **127**, 10, 102001 (2021), [arXiv:2007.04320].
- [45] Y. S. Amhis *et al.* (HFLAV), Phys. Rev. D **107**, 052008 (2023), [arXiv:2206.07501].
- [46] M. Neubert, Phys. Rev. **D49**, 3392 (1994), [hep-ph/9311325].
- [47] I. I. Y. Bigi *et al.*, Int. J. Mod. Phys. **A9**, 2467 (1994), [hep-ph/9312359].
- [48] G. P. Korchemsky and G. F. Sterman, Phys. Lett. **B340**, 96 (1994), [hep-ph/9407344].
- [49] C. W. Bauer, M. E. Luke and T. Mannel, Phys. Rev. **D68**, 094001 (2003), [hep-ph/0102089].
- [50] K. S. M. Lee and I. W. Stewart, Nucl. Phys. **B721**, 325 (2005), [hep-ph/0409045].
- [51] S. W. Bosch, M. Neubert and G. Paz, JHEP **11**, 073 (2004), [hep-ph/0409115].
- [52] M. Beneke *et al.*, JHEP **06**, 071 (2005), [hep-ph/0411395].
- [53] M. Benzke *et al.*, JHEP **08**, 099 (2010), [arXiv:1003.5012].
- [54] C. W. Bauer, S. Fleming and M. E. Luke, Phys. Rev. **D63**, 014006 (2000), [hep-ph/0005275].
- [55] C. W. Bauer *et al.*, Phys. Rev. **D63**, 114020 (2001), [hep-ph/0011336].
- [56] C. W. Bauer and I. W. Stewart, Phys. Lett. **B516**, 134 (2001), [hep-ph/0107001].
- [57] C. W. Bauer, D. Pirjol and I. W. Stewart, Phys. Rev. **D65**, 054022 (2002), [hep-ph/0109045].
- [58] T. Becher, A. Broggio and A. Ferroglia, Lect. Notes Phys. **896**, pp.1 (2015), [arXiv:1410.1892].
- [59] J. Chay and C. Kim, Phys. Rev. **D65**, 114016 (2002), [hep-ph/0201197].
- [60] M. Beneke *et al.*, Nucl. Phys. **B643**, 431 (2002), [hep-ph/0206152].

- [61] C. W. Bauer *et al.*, Phys. Rev. **D66**, 014017 (2002), [hep-ph/0202088].
- [62] R. J. Hill and M. Neubert, Nucl. Phys. **B657**, 229 (2003), [hep-ph/0211018].
- [63] J. C. Collins, D. E. Soper and G. F. Sterman, Adv. Ser. Direct. High Energy Phys. **5**, 1 (1989), [hep-ph/0409313].
- [64] T. Becher, M. Neubert and G. Xu, JHEP **07**, 030 (2008), [arXiv:0710.0680].
- [65] S. Fleming *et al.*, Phys. Rev. D **77**, 074010 (2008), [hep-ph/0703207].
- [66] M. D. Schwartz, Phys. Rev. D **77**, 014026 (2008), [arXiv:0709.2709].
- [67] I. W. Stewart, F. J. Tackmann and W. J. Waalewijn, Phys. Rev. D **81**, 094035 (2010), [arXiv:0910.0467].
- [68] J. C. Collins, D. E. Soper and G. F. Sterman, Nucl. Phys. **B261**, 104 (1985).
- [69] C. W. Bauer, B. O. Lange and G. Ovanesyan, JHEP **07**, 077 (2011), [arXiv:1010.1027].
- [70] I. Z. Rothstein and I. W. Stewart, JHEP **08**, 025 (2016), [arXiv:1601.04695].
- [71] I. Moulton *et al.*, JHEP **02**, 134 (2018), [arXiv:1709.09174].
- [72] T. Becher *et al.*, Phys. Rev. Lett. **116**, 19, 192001 (2016), [arXiv:1508.06645].
- [73] A. J. Larkoski, I. Moulton and D. Neill, JHEP **09**, 143 (2015), [arXiv:1501.04596].
- [74] T. Becher *et al.*, JHEP **11**, 019 (2016), [Erratum: JHEP05,154(2017)], [arXiv:1605.02737].
- [75] I. A. Korchemskaya and G. P. Korchemsky, Phys. Lett. **B287**, 169 (1992).
- [76] T. Becher and M. Neubert, Eur. Phys. J. **C71**, 1665 (2011), [arXiv:1007.4005].
- [77] J.-Y. Chiu *et al.*, JHEP **05**, 084 (2012), [arXiv:1202.0814].
- [78] T. Becher and M. Neubert, JHEP **07**, 108 (2012), [arXiv:1205.3806].
- [79] I. W. Stewart *et al.*, Phys. Rev. **D89**, 5, 054001 (2014), [arXiv:1307.1808].
- [80] M. Beneke and T. Feldmann, Nucl. Phys. **B685**, 249 (2004), [hep-ph/0311335].
- [81] M. Beneke *et al.*, Phys. Rev. Lett. **83**, 1914 (1999), [hep-ph/9905312].
- [82] C. W. Bauer, D. Pirjol and I. W. Stewart, Phys. Rev. Lett. **87**, 201806 (2001), [hep-ph/0107002].
- [83] S. Mantry, D. Pirjol and I. W. Stewart, Phys. Rev. **D68**, 114009 (2003), [hep-ph/0306254].
- [84] T. Becher, R. J. Hill and M. Neubert, Phys. Rev. **D72**, 094017 (2005), [hep-ph/0503263].
- [85] M. Beneke, C. Bobeth and R. Szafron, JHEP **10**, 232 (2019), [Erratum: JHEP 11, 099 (2022)], [arXiv:1908.07011].
- [86] M. Beneke *et al.*, JHEP **10**, 223 (2021), [arXiv:2107.03819].
- [87] S. Fleming, A. K. Leibovich and T. Mehen, Phys. Rev. **D68**, 094011 (2003), [hep-ph/0306139].
- [88] T. Becher and M. D. Schwartz, JHEP **07**, 034 (2008), [arXiv:0803.0342].
- [89] T. Becher and G. Bell, JHEP **11**, 126 (2012), [arXiv:1210.0580].
- [90] I. W. Stewart, F. J. Tackmann and W. J. Waalewijn, Phys. Rev. Lett. **105**, 092002 (2010), [arXiv:1004.2489].
- [91] J.-y. Chiu, R. Kelley and A. V. Manohar, Phys. Rev. **D78**, 073006 (2008), [arXiv:0806.1240].
- [92] V. Ahrens *et al.*, Eur. Phys. J. **C62**, 333 (2009), [arXiv:0809.4283].
- [93] X. Liu, S. Mantry and F. Petriello, Phys. Rev. **D86**, 074004 (2012), [arXiv:1205.4465].
- [94] M. G. Echevarria, A. Idilbi and I. Scimemi, JHEP **07**, 002 (2012), [arXiv:1111.4996].
- [95] A. Gehrmann-De Ridder *et al.*, Phys. Rev. Lett. **99**, 132002 (2007), [arXiv:0707.1285].
- [96] S. Weinzierl, Phys. Rev. Lett. **101**, 162001 (2008), [arXiv:0807.3241].
- [97] R. Abbate *et al.*, Phys. Rev. **D83**, 074021 (2011), [arXiv:1006.3080].
- [98] A. H. Hoang *et al.*, Phys. Rev. **D91**, 9, 094018 (2015), [arXiv:1501.04111].
- [99] R. Boughezal, X. Liu and F. Petriello, Phys. Rev. **D91**, 9, 094035 (2015), [arXiv:1504.02540].
- [100] J. Gaunt *et al.*, JHEP **09**, 058 (2015), [arXiv:1505.04794].
- [101] R. Boughezal *et al.*, Phys. Lett. **B748**, 5 (2015), [arXiv:1505.03893].
- [102] R. Boughezal *et al.*, Phys. Rev. Lett. **116**, 15, 152001 (2016), [arXiv:1512.01291].
- [103] J. M. Campbell, R. K. Ellis and C. Williams, JHEP **06**, 179 (2016), [arXiv:1601.00658].
- [104] J. M. Campbell *et al.*, JHEP **07**, 148 (2016), [arXiv:1603.02663].
- [105] G. Heinrich *et al.*, JHEP **03**, 142 (2018), [arXiv:1710.06294].
- [106] I. Moulton *et al.*, Phys. Rev. **D95**, 7, 074023 (2017), [arXiv:1612.00450].
- [107] R. Boughezal, X. Liu and F. Petriello, JHEP **03**, 160 (2017), [arXiv:1612.02911].
- [108] S. Alioli *et al.*, JHEP **09**, 120 (2013), [arXiv:1211.7049].
- [109] S. Alioli *et al.*, Phys. Rev. **D92**, 9, 094020 (2015), [arXiv:1508.01475].
- [110] S. Alioli *et al.*, Phys. Rev. D **104**, 9, 094020 (2021), [arXiv:2102.08390].
- [111] A. J. Larkoski, I. Moulton and B. Nachman (2017), [arXiv:1709.04464].
- [112] M. Dasgupta and G. P. Salam, Phys. Lett. **B512**, 323 (2001), [hep-ph/0104277].
- [113] R. B. Appleby and M. H. Seymour, JHEP **12**, 063 (2002), [hep-ph/0211426].
- [114] S. Caron-Huot, JHEP **03**, 036 (2018), [arXiv:1501.03754].
- [115] M. Balsiger, T. Becher and D. Y. Shao, JHEP **08**, 104 (2018), [arXiv:1803.07045].
- [116] A. Banfi, G. Marchesini and G. Smye, JHEP **08**, 006 (2002), [hep-ph/0206076].
- [117] T. Becher, B. D. Pecjak and D. Y. Shao, JHEP **12**, 018 (2016), [arXiv:1610.01608].
- [118] M. Balsiger, T. Becher and D. Y. Shao, JHEP **04**, 020 (2019), [arXiv:1901.09038].
- [119] T. Becher, T. Rauh and X. Xu, JHEP **08**, 134 (2022), [arXiv:2112.02108].
- [120] J. R. Forshaw, A. Kyrieleis and M. H. Seymour, JHEP **08**, 059 (2006), [hep-ph/0604094].
- [121] J. R. Forshaw, A. Kyrieleis and M. H. Seymour, JHEP **09**, 128 (2008), [arXiv:0808.1269].
- [122] T. Becher, M. Neubert and D. Y. Shao, Phys. Rev. Lett. **127**, 21, 212002 (2021), [arXiv:2107.01212].
- [123] M. Beneke and T. Feldmann, Phys. Lett. B **553**, 267 (2003), [hep-ph/0211358].
- [124] C. W. Bauer, D. Pirjol and I. W. Stewart, Phys. Rev. **D68**, 034021 (2003), [hep-ph/0303156].
- [125] D. Pirjol and I. W. Stewart, Phys. Rev. **D67**, 094005 (2003), [Erratum: Phys. Rev. D69,019903(2004)], [hep-ph/0211251].
- [126] R. J. Hill *et al.*, JHEP **07**, 081 (2004), [hep-ph/0404217].
- [127] M. Beneke and D. Yang, Nucl. Phys. **B736**, 34 (2006), [hep-ph/0508250].

- [128] I. Moult, I. W. Stewart and G. Vita, JHEP **07**, 067 (2017), [arXiv:1703.03408].
- [129] I. Feige *et al.*, JHEP **11**, 142 (2017), [arXiv:1703.03411].
- [130] M. Beneke *et al.*, JHEP **03**, 001 (2018), [arXiv:1712.04416].
- [131] S. Alte, M. König and M. Neubert, JHEP **08**, 095 (2018), [arXiv:1806.01278].
- [132] I. Moult *et al.*, JHEP **08**, 013 (2018), [arXiv:1804.04665].
- [133] M. Beneke *et al.*, JHEP **03**, 043 (2019), [arXiv:1809.10631].
- [134] F. Gross *et al.* (2022), [arXiv:2212.11107].
- [135] I. Moult, I. W. Stewart and G. Vita, JHEP **11**, 153 (2019), [arXiv:1905.07411].
- [136] M. Beneke *et al.*, JHEP **09**, 101 (2019), [arXiv:1907.05463].
- [137] I. Moult *et al.*, JHEP **05**, 089 (2020), [arXiv:1910.14038].
- [138] M. Beneke *et al.*, JHEP **07**, 078 (2020), [arXiv:1912.01585].
- [139] Z. L. Liu and M. Neubert, JHEP **04**, 033 (2020), [arXiv:1912.08818].
- [140] M. Beneke *et al.*, JHEP **10**, 196 (2020), [arXiv:2008.04943].
- [141] Z. L. Liu *et al.*, JHEP **01**, 077 (2021), [arXiv:2009.06779].
- [142] Z. L. Liu *et al.*, JHEP **06**, 183 (2023), [arXiv:2212.10447].
- [143] M. Beneke *et al.*, JHEP **07**, 144 (2022), [arXiv:2205.04479].
- [144] T. Feldmann *et al.*, Phys. Rev. D **107**, 1, 013007 (2023), [arXiv:2211.04209].
- [145] C. Cornella, M. König and M. Neubert, Phys. Rev. D **108**, 3, L031502 (2023), [arXiv:2212.14430].
- [146] T. Hurth and R. Szafron, Nucl. Phys. B **991**, 116200 (2023), [arXiv:2301.01739].
- [147] G. Bell, P. Böer and T. Feldmann, JHEP **09**, 183 (2022), [arXiv:2205.06021].
- [148] S. Fleming, Phys. Lett. **B735**, 266 (2014), [arXiv:1404.5672].
- [149] D. Neill, A. Pathak and I. W. Stewart, JHEP **09**, 089 (2023), [arXiv:2303.13710].
- [150] A. Idilbi and A. Majumder, Phys. Rev. **D80**, 054022 (2009), [arXiv:0808.1087].
- [151] G. Ovanesyan and I. Vitev, JHEP **06**, 080 (2011), [arXiv:1103.1074].
- [152] V. Vaidya, JHEP **11**, 064 (2021), [arXiv:2010.00028].
- [153] S. Catani, D. de Florian and G. Rodrigo, JHEP **07**, 026 (2012), [arXiv:1112.4405].
- [154] J. R. Forshaw, M. H. Seymour and A. Siodmok, JHEP **11**, 066 (2012), [arXiv:1206.6363].
- [155] J. R. Gaunt, JHEP **07**, 110 (2014), [arXiv:1405.2080].
- [156] M. Zeng, JHEP **10**, 189 (2015), [arXiv:1507.01652].
- [157] M. D. Schwartz, K. Yan and H. X. Zhu, Phys. Rev. D **96**, 5, 056005 (2017), [arXiv:1703.08572].
- [158] R. J. Hill and M. P. Solon, Phys. Lett. **B707**, 539 (2012), [arXiv:1111.0016].
- [159] M. Bauer *et al.*, JHEP **01**, 099 (2015), [arXiv:1409.7392].
- [160] M. Baumgart, I. Z. Rothstein and V. Vaidya, Phys. Rev. Lett. **114**, 211301 (2015), [arXiv:1409.4415].
- [161] G. Ovanesyan, T. R. Slatyer and I. W. Stewart, Phys. Rev. Lett. **114**, 21, 211302 (2015), [arXiv:1409.8294].

17. Lattice Quantum Chromodynamics

Revised August 2023 by S. Hashimoto (KEK) and S.R. Sharpe (U. Washington), written September 2011 with J. Laiho (Syracuse U.)

17.1	Lattice regularization of QCD	350
17.1.1	Gauge invariance, gluon fields and the gluon action	350
17.1.2	Lattice fermions	351
17.1.3	Heavy quarks on the lattice	352
17.1.4	QED on the lattice	353
17.1.5	Basic inputs for lattice calculations	353
17.1.6	Sources of systematic error	354
17.2	Methods and status	355
17.2.1	Monte-Carlo method	355
17.2.2	Two-point functions	356
17.2.3	Three-point functions	356
17.2.4	Scattering amplitudes and resonances	357
17.2.5	Status of LQCD simulations	357
17.3	Physics applications	357
17.3.1	Spectrum	358
17.3.2	Decay constants and bag parameters	358
17.3.3	Form factors ($K \rightarrow \pi \ell \nu$, $D \rightarrow K \ell \nu$, $B \rightarrow \pi \ell \nu$, $B \rightarrow D^{(*)} \ell \nu$, etc.)	358
17.3.4	Strong gauge coupling	359
17.3.5	Quark masses	359
17.3.6	Other physical quantities of interest	360
17.3.7	Other applications of lattice QCD	360
17.4	Outlook	360
17.5	Acknowledgments	361

Many physical processes considered in the Review of Particle Properties (RPP) involve hadrons. The properties of hadrons—which are composed of quarks and gluons—are governed primarily by Quantum Chromodynamics (QCD) (with small corrections from Quantum Electrodynamics [QED]). Theoretical calculations of these properties require non-perturbative methods, and Lattice Quantum Chromodynamics (LQCD) is a tool to carry out such calculations. It has been successfully applied to many properties of hadrons. Most important for the RPP are the calculation of electroweak decay constants and form factors, which are needed to extract Cabibbo-Kobayashi-Maskawa (CKM) matrix elements when combined with the corresponding experimental measurements. LQCD has also been used to determine other fundamental parameters of the standard model, in particular the strong gauge coupling and quark masses, as well as to predict hadronic contributions to the anomalous magnetic moment of the muon, $g_\mu - 2$.

This review describes the theoretical foundations of LQCD and sketches the methods used to calculate the quantities relevant for the RPP. It also describes the various sources of error that must be controlled in a LQCD calculation. Results for hadronic quantities are found in the corresponding dedicated reviews.

17.1 Lattice regularization of QCD

Gauge theories form the building blocks of the Standard Model. While the SU(2) and U(1) parts have weak couplings and can be studied accurately with perturbative methods, the SU(3) component—QCD—is only amenable to a perturbative treatment at high energies. The growth of the gauge coupling in the infrared—the flip-side of asymptotic freedom—requires the use of non-perturbative methods to determine the low energy properties of QCD. Lattice gauge theory, proposed by K. Wilson in 1974 [1], provides such a method, for it gives a non-perturbative definition of vector-like gauge field theories such as QCD. In lattice regularized QCD—commonly called lattice QCD or LQCD—Euclidean space-time is discretized, usually on a hypercubic lattice with lattice spacing a , with quark fields placed on sites and gauge fields on the links between sites. The lattice spacing plays the role of the ultraviolet regulator, rendering the quantum field theory finite. The continuum theory is recovered by taking the limit of vanishing lattice spacing, which can be reached by tuning the bare gauge coupling to zero according to the renormalization group.

Unlike dimensional regularization, which is commonly used in continuum QCD calculations, the definition of LQCD does not

rely on the perturbative expansion. Indeed, LQCD allows non-perturbative calculations by numerical evaluation of the path integral that defines the theory.

Practical LQCD calculations are limited by the availability of computational resources and the efficiency of algorithms. Because of this, LQCD results come with both statistical and systematic errors, the former arising from the use of Monte-Carlo integration, the latter, for example, from the use of non-zero values of a . There are also different ways in which the QCD action can be discretized, and all must give consistent results in the continuum limit, $a \rightarrow 0$. It is the purpose of this review to provide an outline of the methods of LQCD, with particular focus on applications to particle physics, and an overview of the various sources of error. This should allow the reader to better understand the LQCD results that are presented in other reviews, primarily those on “Quark Masses,” “Quark Model,” “Quantum Chromodynamics,” “CKM quark-mixing matrix,” “ V_{ud} , V_{us} , Cabibbo angle and CKM Unitarity,” “Leptonic Decays of Charged Pseudoscalar Mesons,” “ B^0 - \bar{B}^0 Mixing,” and “Semileptonic b -Hadron Decays, Determination of V_{cb} and V_{ub} .” For more extensive explanations the reader should consult the available textbooks or lecture notes, the most up-to-date of which are Refs. [2–4].

17.1.1 Gauge invariance, gluon fields and the gluon action

A key feature of the lattice formulation of QCD is that it preserves gauge invariance. This is in contrast to perturbative calculations, where gauge fixing is an essential step. The preservation of gauge invariance leads to considerable simplifications, e.g., restricting the form of operators that can mix under renormalization.

The gauge transformations of lattice quark fields are just as in the continuum: $q(x) \rightarrow V(x)q(x)$ and $\bar{q}(x) \rightarrow \bar{q}(x)V^\dagger(x)$, with $V(x)$ an arbitrary element of SU(3). The only difference is that the Euclidean space-time positions x are restricted to lie on the sites of the lattice, i.e. $x = a(n_1, n_2, n_3, n_4)$ for a hypercubic lattice, with the n_j being integers. Quark bilinears involving different lattice points can be made gauge invariant by introducing the gluon field $U_\mu(x)$. For example, for adjacent points the bilinear is $\bar{q}(x)U_\mu(x)q(x+a\hat{\mu})$, with $\hat{\mu}$ the unit vector in the μ 'th direction. (This form is used in the construction of the lattice covariant derivative.) This is illustrated in Fig. 17.1. The gluon field (or “gauge link”) is an element of the group, SU(3), in contrast to the continuum field A_μ which takes values in the Lie algebra. The bilinear is invariant if U_μ transforms as $U_\mu(x) \rightarrow V(x)U_\mu(x)V^\dagger(x+a\hat{\mu})$. The lattice gluon field is naturally associated with the link joining x and $x+a\hat{\mu}$, and corresponds in the continuum to a Wilson line connecting these two points, $P \exp(i \int_x^{x+a\hat{\mu}} dx_\mu A_\mu^{\text{cont}}(x))$ (where P indicates a path-ordered integral, and the superscript on A_μ indicates that it is a continuum field). The trace of a product of the $U_\mu(x)$ around any closed loop is easily seen to be gauge invariant and is the lattice version of a Wilson loop.

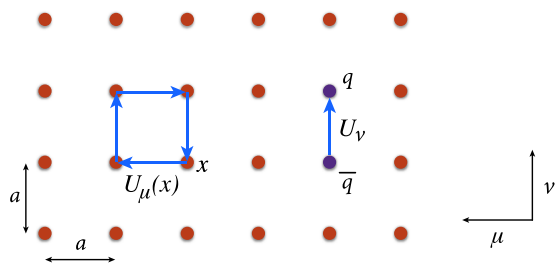


Figure 17.1: Sketch of a two-dimensional slice through the μ - ν plane of a lattice, showing gluon fields lying on links and forming either the plaquette product appearing in the gauge action or a component of the covariant derivative connecting quark and antiquark fields.

The simplest possible gauge action, usually called the Wilson gauge action, is given by the product of gauge links around ele-

mentary plaquettes:

$$S_g = \beta \sum_{x, \mu < \nu} \left[1 - \frac{1}{3} \text{ReTr}[U_\mu(x)U_\nu(x+a\hat{\mu})U_\mu^\dagger(x+a\hat{\nu})U_\nu^\dagger(x)] \right]. \quad (17.1)$$

This is illustrated in Fig. 17.1. For small a , assuming that the fields are slowly varying, one can expand the action in powers of a using $U_\mu(x) = \exp(iaA_\mu(x))$. Keeping only the leading non-vanishing term, and replacing the sum with an integral, one finds the continuum form,

$$S_g \longrightarrow \int d^4x \frac{1}{4g_{\text{lat}}^2} \text{Tr}[F_{\mu\nu}^2(x)], \quad (17.2)$$

$$(F_{\mu\nu} = \partial_\mu A_\nu - \partial_\nu A_\mu + i[A_\mu, A_\nu])$$

as long as one chooses $\beta = 6/g_{\text{lat}}^2$ for the lattice coupling. In this expression, g_{lat} is the bare gauge coupling in the lattice scheme, which can be related (by combining continuum and lattice perturbation theory) to a more conventional gauge coupling such as that in the $\overline{\text{MS}}$ scheme (see Sec. 17.3.4 below).

In practice, the lattice spacing a is non-zero, leading to discretization errors. In particular, the lattice breaks Euclidean rotational invariance (which is the Euclidean version of Lorentz invariance) down to a discrete hypercubic subgroup. One wants to reduce discretization errors as much as possible. A very useful tool for understanding and then reducing discretization errors is the Symanzik effective action: the interactions of quarks and gluons with momenta low compared to the lattice cutoff ($|p| \ll 1/a$) are described by a continuum action consisting of the standard continuum terms (e.g., the gauge action given in Eq. (17.2)) augmented by higher dimensional operators suppressed by powers of a [5]. For the Wilson lattice gauge action, the leading corrections to the continuum terms come in at $\mathcal{O}(a^2)$. They take the form $\sum_j a^2 c_j O_6^{(j)}$, with the sum running over all dimension-six operators $O_6^{(j)}$ allowed by the lattice symmetries, and c_j unknown coefficients. Some of these operators violate Euclidean rotational invariance, and all of them lead to discretization errors of the form $a^2 \Lambda^2$ (up to $\log(a)$ corrections that will be discussed below), where Λ is a typical momentum scale for the quantity being calculated. These errors can, however, be reduced by adding corresponding operators to the lattice action and tuning their coefficients to eliminate the dimension-six operators in the effective action to a given order in perturbation theory or even non-perturbatively. This is the idea of the Symanzik improvement program [5]. In the case of the gauge action, one adds Wilson loops involving six gauge links (as opposed to the four links needed for the original plaquette action, Eq. (17.1)) to define the $\mathcal{O}(a^2)$ improved (or “Symanzik”) action [6]. In practical implementations, the improvement is either at tree-level (so that residual errors are proportional to $\alpha_s a^2$, where the coupling is evaluated at a scale $\sim 1/a$), or at one-loop order (errors proportional to $\alpha_s^2 a^2$). Another popular choice is motivated by studies of renormalization group (RG) flow. It has the same terms as the $\mathcal{O}(a^2)$ improved action but with different coefficients, and is called the RG-improved or “Iwasaki” action [7].

17.1.2 Lattice fermions

Discretizing the fermion action turns out to involve subtle issues, and the range of actions being used is more extensive than for gauge fields. Recall that the continuum fermion action is $S_f = \int d^4x \bar{q}[D_\mu \gamma_\mu + m_q]q$, where $D_\mu = \partial_\mu + iA_\mu$ is the gauge-covariant derivative. The simplest discretization replaces the derivative with a symmetric difference:

$$D_\mu q(x) \longrightarrow \frac{1}{2a} [U_\mu(x)q(x+a\hat{\mu}) - U_\mu(x-a\hat{\mu})^\dagger q(x-a\hat{\mu})]. \quad (17.3)$$

The factors of U_μ ensure that $D_\mu q(x)$ transforms under gauge transformations in the same way as $q(x)$, so that the discretized version of $\bar{q}(x)\gamma_\mu D_\mu q(x)$ is gauge invariant. The choice in Eq. (17.3) leads to the so-called naive fermion action. This, however, suffers from the fermion doubling problem—in d dimensions it describes 2^d equivalent fermion fields in the continuum

limit. The appearance of the extra “doubler” fermions is related to the deeper theoretical problem of formulating chirally symmetric fermions on the lattice. This is encapsulated by the Nielsen-Ninomiya theorem [8]: one cannot define lattice fermions having exact chiral symmetry of the standard form $\delta q = \epsilon \gamma_5 q$, $\delta \bar{q} = \epsilon \bar{q} \gamma_5$ (ϵ is infinitesimal) without producing doublers. Naive lattice fermions do have chiral symmetry but at the cost of introducing 15 unwanted doublers (for $d = 4$).

There are a number of different strategies for dealing with the doubling problem, each with their own theoretical and computational advantages and disadvantages. Wilson fermions [1] add a term proportional to $a\bar{q}\Delta q$ to the fermion action (the “Wilson term”—in which Δ is a covariant lattice Laplacian). This gives a mass of $\mathcal{O}(1/a)$ to the doublers, so that they decouple in the continuum limit. The Wilson term, however, violates chiral symmetry at non-zero lattice spacing, and introduces discretization errors linear in a . A commonly used variant that eliminates the $\mathcal{O}(a)$ discretization error is the $\mathcal{O}(a)$ -improved Wilson (or “clover”) action [9]. In this application of Symanzik improvement, methods have been developed to remove $\mathcal{O}(a)$ terms non-perturbatively using auxiliary simulations to tune parameters [10]. Such “non-perturbative improvement” is of great practical importance as it brings the discretization error from the fermion action down to the same level as that from the gauge action.

The advantages of Wilson fermions are their theoretical simplicity and relatively low computational cost. Their main disadvantage is the lack of chiral symmetry, which makes them difficult to use in cases where mixing with wrong chirality operators can occur, particularly if this involves divergences proportional to powers of $1/a$. A related problem is the presence of potential numerical instabilities due to spurious near-zero modes of the lattice Dirac operator. There are, however, studies that successfully ameliorate the problems due to the lack of chiral symmetry and increase the range of quantities for which Wilson fermions can be used (see, e.g., Refs. [11–13]).

Twisted-mass fermions [14] are a variant of Wilson fermions in which two flavors are treated together with an isospin-breaking mass term (the “twisted mass” term). The main advantage of this approach is that all errors linear in a are automatically removed (without the need for tuning of parameters) by a clever choice of twisted mass and operators [15]. A disadvantage is the presence of isospin breaking effects (such as a splitting between charged and neutral pion masses even when up and down quarks are degenerate), which, however, vanish as $a^2 \Lambda^2$ in the continuum limit. Strange and charm quarks can be added as a second pair, with a term added to split their masses [16, 17].

Staggered fermions are a reduced version of naive fermions in which there is only a single fermion Dirac component on each lattice site, with the full Dirac structure built up from neighboring sites [18]. They have the advantages of being somewhat faster to simulate than Wilson-like fermions, of preserving some chiral symmetry, and of having discretization errors of $\mathcal{O}(a^2)$. Their disadvantage is that they retain some of the doublers (3 for $d = 4$). The action thus describes four degenerate fermions in the continuum limit. These are usually called “tastes”, to distinguish them from physical flavors, and the corresponding $\text{SU}(4)$ symmetry is referred to as the “taste symmetry”. The preserved chiral symmetry in this formulation has non-singlet taste. Practical applications usually introduce one staggered fermion for each physical flavor, and remove contributions from the unwanted tastes by taking the fourth-root of the fermion determinant appearing in the path integral. The validity of this “rooting” procedure is not obvious because taste symmetry is violated for non-zero lattice spacing. Theoretical arguments, supported by numerical evidence, suggest that the procedure is valid as long as one takes the continuum limit before approaching the light quark mass region [19]. Additional issues arise for the valence quarks (those appearing in quark propagators, as described in Sec. 17.2 below), where rooting is not possible, and one must ignore the extra tastes, or account for them by including appropriate factors [20], which can be nontrivial in applications involving baryons [21].

Just as for Wilson fermions, the staggered action can be improved, so as to reduce discretization errors. The Asqtad (a -

squared tadpole improved) action [22] was used until recently in many large scale simulations [23]. More recent calculations use the HISQ (highly improved staggered quark) action, introduced in Ref. [24]. At tree-level it removes both $\mathcal{O}(a^2)$ errors and, to lowest order in the quark speed v/c , $\mathcal{O}([am]^4)$ errors. It also substantially reduces effects caused by taste-symmetry breaking. This makes it attractive not only for light quarks, but means that it is also quite accurate for heavy quarks because it suppresses $(am)^n$ errors. It is being used to directly simulate charm quarks and to approach direct simulations of bottom quarks (for early studies, see, e.g., [25–27]).

There is an important class of lattice fermions, “Ginsparg-Wilson fermions,” that possess a continuum-like chiral symmetry without introducing unwanted doublers. The lattice Dirac operator D for these fermions satisfies the Ginsparg-Wilson relation $D\gamma_5 + \gamma_5 D = aD\gamma_5 D$ [28]. In the continuum, the right-hand-side vanishes, leading to chiral symmetry. On the lattice, it is non-vanishing, but with a particular form (with two factors of D) that restricts the violations of chiral symmetry in Ward-Takahashi identities to short-distance terms that do not contribute to physical matrix elements [29]. In fact, one can define a modified chiral transformation on the lattice (by including dependence on the gauge fields) such that Ginsparg-Wilson fermions have an exact chiral symmetry for on-shell quantities [30]. The net result is that such fermions essentially have the same properties under chiral transformations as do continuum fermions, including the index theorem [29]. Their leading discretization errors are of $\mathcal{O}(a^2)$.

Two types of Ginsparg-Wilson fermions are currently being used in large-scale numerical simulations. The first is Domain-wall fermions (DWF). These are defined on a five-dimensional space, in which the fifth dimension is fictitious [31]. The action is chosen so that the low-lying modes are chiral, with left- and right-handed modes localized on opposite four-dimensional surfaces. For an infinite fifth dimension, these fermions satisfy the Ginsparg-Wilson relation. In practice, the fifth dimension is kept finite, and there remains a small, controllable violation of chiral symmetry. The second type is Overlap fermions. These appeared from a completely different context and have an explicit form that exactly satisfies the Ginsparg-Wilson relation [32]. Their numerical implementation requires an approximation of the matrix sign function of a Wilson-like fermion operator, and various approaches are being used. In fact, it is possible to rewrite these approximations in terms of a five-dimensional formulation, showing that the DWF and Overlap approaches are essentially equivalent [33, 34]. Numerically, the five-dimensional approach appears to be more computationally efficient.

The various lattice fermion formulations are often combined with the technique of link smearing. Here one couples the fermions to a smoother gauge link, defined by averaging with adjacent links in a gauge invariant manner. Several closely related implementations are being used. All reduce the coupling of fermions to the short-distance fluctuations in the gauge field, leading to an improvement in the numerical stability and speed of algorithms. One cannot perform this smearing too aggressively, however, since the smearing may distort short distance physics and enhance discretization errors.

As noted above, each fermion formulation has its own advantages and disadvantages. For instance, domain-wall and overlap fermions are theoretically preferred as they have chiral symmetry without doublers, but their computational cost is greater than for other choices. If the physics application of interest and the target precision do not require near-exact chiral symmetry, there is no strong motivation to use these expensive formulations. On the other hand, there is a class of applications (including the calculation of the $\Delta I = 1/2$ amplitude for $K \rightarrow \pi\pi$ decays [35–37] and the S -parameter [38]) where chiral symmetry plays an essential role and for which the use of Ginsparg-Wilson fermions is strongly favored.

17.1.3 Heavy quarks on the lattice

The fermion formulations described in the previous subsection can be used straightforwardly only for quarks whose masses are small compared to the lattice cutoff, $m_q \lesssim 1/a$. This is because there are discretization errors proportional to powers of am_q , and

if $am_q \gtrsim 1$ these errors are large and uncontrolled. Present LQCD simulations typically have cutoffs in the range of $1/a = 2\text{--}5$ GeV (corresponding to $a \approx 0.1\text{--}0.04$ fm). Thus, while for the up, down and strange quarks one has $am_q \ll 1$, for bottom quarks (with $m_b \approx 4.5$ GeV) one must use alternative approaches. Charm quarks ($m_c \approx 1.5$ GeV) are an intermediate case, allowing simulations using both direct and alternative approaches, although increasingly the direct approach is being used.

For the charm quark, the straightforward approach is to simultaneously reduce the lattice spacing and to improve the fermion action so as to reduce the size of errors proportional to powers of am_c . This approach has been followed successfully using the HISQ, twisted-mass and domain-wall actions [24, 25, 27, 39–41]. It is important to note, however, that reducing a increases the computational cost because an increased number of lattice points are needed for the same physical volume. One cannot reduce the spatial size below 2–3 fm without introducing significant finite volume errors. Present lattices have typical sizes of $\sim 64^3 \times 128$ (with the long direction being Euclidean time), and thus allow a lattice cutoff up to $1/a \sim 4\text{--}6$ GeV.

This approach can, to some extent, be extended to the bottom quark, by the use of simulations with small lattice spacings [26, 42]. This has been pursued with the HISQ action [43], using lattices of size up to $144^3 \times 288$ and lattice spacings down to $a \approx 0.03$ fm ($1/a \approx 6.6$ GeV). Extrapolation in m_b is still needed [44], however, and this makes use of the mass dependence predicted by Heavy Quark Effective Theory (HQET). Small lattice spacings are also helpful for the simulations of quarkonium for which a different heavy-quark mass scaling is expected. See Ref. [45] for a recent study.

Alternative approaches for discretizing heavy quarks are motivated by effective field theories. For a bottom quark in heavy-light hadrons, one can use HQET to expand about the infinite quark-mass limit. In this limit, the bottom quark is a static color source, and one can straightforwardly write the corresponding lattice action [46]. Corrections, proportional to powers of $1/m_b$, can be introduced as operator insertions, with coefficients that can be determined non-perturbatively using existing techniques [47]. This method allows the continuum limit to be taken controlling all $1/m_b$ corrections.

Another way of introducing the $1/m_b$ corrections is to include the relevant terms in the effective action. This leads to a non-relativistic QCD (NRQCD) action, in which the heavy quark is described by a two-component spinor [48]. This approach has the advantage over HQET that it can also be used for heavy-heavy systems, such as the Upsilon states. Moreover, the bottom quark can be treated without any extrapolation in m_b . A disadvantage is that some of the parameters in this effective theory are determined perturbatively (at tree-level or at one-loop [49]), which limits the precision of the final results. Although discretization effects can be controlled with good numerical precision for a range of lattice spacings, these artifacts cannot be extrapolated away by taking the lattice spacing to zero. This is because NRQCD is a non-relativistic effective field theory and so ceases to work when the cutoff π/a becomes much larger than the heavy-quark mass. In practice these effects are accounted for in the error budget.

This problem can be avoided if one uses HQET power counting to analyze and reduce discretization effects for heavy quarks while using conventional fermion actions [50]. For instance, one can tune the parameters of an improved Wilson quark action so that the leading HQET corrections to the static quark limit are correctly accounted for. As the lattice spacing becomes finer, the action smoothly goes over to that of a light Wilson quark action, where the continuum limit can be taken as usual. In principle, one can improve the action in the heavy quark regime up to arbitrarily high orders using HQET, but so far large-scale simulations have typically used clover improved Wilson quarks, where tuning the parameters of the action corresponds to including all corrections through next-to-leading order in HQET. Three different methods for tuning the parameters of the clover action are being used: the Fermilab [50], Tsukuba [51] and Columbia [52] approaches. An advantage of this HQET approach is that the c and b quarks can be treated on the same footing. Parameter tuning has been done

perturbatively, as in NRQCD, or using non-perturbative tuning of some of the parameters [53, 54]. One can improve the effective theory including the terms beyond the next-to-leading order. The Oktay-Kronfeld action that includes dimension-six and -seven operators has been constructed [55] and used in large-scale numerical calculations [56].

Another approach is the “ratio method” introduced in Ref. [57]. Here one uses quarks with masses lying at, or slightly above, the charm mass m_c , which can be simulated with a relativistic action, and extrapolates to m_b incorporating the behavior predicted by HQET. The particular implementation relies on the use of ratios. As an example, consider the B meson decay constant f_B . According to HQET, this scales as $1/\sqrt{m_B}$ for $m_B \gg \Lambda_{\text{QCD}}$, up to a logarithmic dependence that is calculable in perturbative QCD (but will be suppressed in the following). Here m_B is the B meson mass, which differs from m_b by $\sim \Lambda_{\text{QCD}}$. One considers the ratio $y(\lambda, m_{b'}) \equiv f_{B''} \sqrt{m_{B''}} / f_{B'} \sqrt{m_{B'}}$ for fictitious B mesons containing b quarks with unphysical masses $m_{b'}$ and $m_{b''} = \lambda m_{b'}$. HQET implies that $y(\lambda, m_{b'})$ approaches unity for large $m_{b'}$ and any fixed $\lambda > 1$. The ratios are evaluated on the lattice for the sequence of masses $m_{b'} = m_c, \lambda m_c, \lambda^2 m_c$, all well below the physical m_b , and for each the continuum limit is taken. The form of the ratio for larger values of $m_{b'}$ is obtained by fitting, incorporating the constraints implied by HQET. The result for $f_B \sqrt{m_B}$ is then obtained as a product of y 's with $f_D \sqrt{m_D}$ [58].

17.1.4 QED on the lattice

Quarks in nature are electrically charged, and the resultant coupling to photons leads to shifts in the properties of hadrons that are generically of $\mathcal{O}(\alpha_{\text{EM}})$. Thus, for example, the proton mass is increased by ~ 1 MeV relative to that of the neutron due to its overall charge although this effect is more than compensated for by the ~ 2.5 MeV relative decrease due to the up quark being lighter than the down quark [59]. This example shows that once pure QCD, isospin-symmetric lattice calculations reach percent-level accuracy, further improvement requires the inclusion of effects due to both electromagnetism and the up-down mass difference. This level of accuracy has in fact been obtained for various quantities, e.g., light hadron masses and decay constants (see Ref. [60]), and simulations including isospin-breaking and QED effects are becoming more common.

One approach for including QED is to treat electromagnetic gauge fields in a similar fashion to those of QCD. This extension is straightforward, although some new subtleties arise. The essential change is that the quark must now propagate through a background field containing both gluons and photons. The gauge field U_μ that appears in the covariant derivative of Eq. (17.3) is extended from an SU(3) matrix to one living in U(3): $U_\mu \rightarrow U_\mu e^{iaq_e A_\mu^{\text{EM}}}$. Here A_μ^{EM} is the photon field, e the electromagnetic coupling, and q the charge of the quark, e.g., $q = 2/3$ for up and $-1/3$ for down and strange quarks. The lattice action for the photon that is typically used is a discretized version of the continuum action Eq. (17.2), rather than the form used for the gluons, Eq. (17.1). This “non-compact” action has the advantage that it is quadratic in A_μ^{EM} , which simplifies the QED part of the generation of configurations.

One subtlety that arises is that Gauss’ law forbids a charged particle in a box with periodic boundary conditions. This can be overcome by including a uniform background charge, which can be shown to be equivalent to removing the zero-momentum mode from the photon field, an approach denoted QED_L [61]. However, this modification leads to enhanced finite-volume dependence for physical quantities, scaling as $1/L^n$ with $n = 1, 2, \dots$. This should be compared to the $\exp(-m_\pi L)$ dependence expected for many quantities (as discussed in Sec. 17.1.6.2 below). Methods to remove the leading few powers of $1/L$ have been developed [62, 63], and there is a promising alternative approach in which QED effects are calculated analytically in infinite volume [64]. Finally we note that there is an alternative approach using so-called C^* boundary conditions that avoids the Gauss’ law issue altogether, although the numerical application is still at an early stage [65, 66].

Substantial progress on including QED and isospin-breaking effects has been made over the last few years. The direct approach

of using different up and down-quark masses and simulating QED has been successfully carried out for a range of quark masses approaching the physical values [59, 67–69]. Alternative approaches have also been used: reweighting the QCD fields *a posteriori* [70], using a massive photon [71], and keeping only the linear term in an expansion in α_{EM} about the QCD only case [72, 73], with the latter approach by now the most popular. Most calculations to date have included QED effects for the valence quarks but not the sea quarks (the “electro-quenched approximation”). [41, 74–77].

The QED corrections to processes including leptons, such as the leptonic and semileptonic decays of hadrons, involve additional diagrams in which a photon propagator bridges between a hadron and a lepton. Such diagrams induce infrared divergences that cancel against soft photon radiation (Bloch-Nordsieck theorem [78]). Methods have been developed to implement this cancellation in lattice calculations, treating the soft photon analytically [62], and results have been reported for leptonic pion and kaon decays [79–81]. An application to semi-leptonic decays has been developed [64, 82].

17.1.5 Basic inputs for lattice calculations

Since LQCD is nothing but a regularization of QCD, the renormalizability of QCD implies that the number of input parameters in LQCD is the same as for continuum QCD—the strong gauge coupling $\alpha_s = g^2/(4\pi)$, the quark masses for each flavor, and the CP violating phase θ . The θ parameter is usually assumed to be zero, while the other parameters must be determined using experimental inputs.

17.1.5.1 Lattice spacing

In QCD, the gauge coupling is a function of scale. With lattice regularization, this scale is the inverse lattice spacing $1/a$, and choosing the bare gauge coupling is equivalent to fixing the lattice spacing.

In principle, a can be determined using any dimensionful quantity measured accurately by experiments. For example, using the mass of hadron H one has $a = (am_H)^{\text{lat}}/m_H^{\text{exp}}$. One chooses quantities that can be calculated accurately on the lattice, and that are only weakly dependent on the quark masses. The latter property minimizes errors from extrapolating or interpolating to the physical light quark masses or from mistuning of other quark masses.

Commonly used choices are the spin-averaged 1S-1P or 1S-2S splittings in the Upsilon system, the masses of the Ξ and Ω^- baryons, and the pion decay constant f_π . Ultimately, all choices must give consistent results for a , and that this is the case provides a highly non-trivial check of both the calculational method and of QCD.

Many recent lattice calculations use intermediate length scales in place of a direct determination of the lattice spacing. These length scales, which we denote \mathcal{R} , have the advantage that they can be precisely, and relatively cheaply, computed numerically. Examples are r_0 , derived from the heavy quark potential [83], and t_0 and w_0 , determined from the gradient flow of the gauge field [84]. These scales are used in the following manner, explained here in the context of calculating a quantity Q with mass dimension d (e.g. a decay constant for which $d = 1$). In the first step, one calculates the dimensionless quantities $a^d Q$ and \mathcal{R}/a in a given lattice calculation, and forms the product $(a^d Q) \times (\mathcal{R}/a)^d = Q\mathcal{R}^d$. In a second step, one uses results available from previous dedicated lattice calculations that have determined \mathcal{R} in physical units (i.e. fm) by relating them to physical quantities as discussed above. Then one obtains $Q = (Q\mathcal{R}^d)/\mathcal{R}^d$. The use of intermediate quantities is reviewed in the latest edition of the Flavor Lattice Averaging Group (FLAG) report [85].

17.1.5.2 Light quark masses

In LQCD simulations, the up, down and strange quarks are usually referred to as the light quarks, in the sense that $m_q < \Lambda_{\text{QCD}}$. (The standard definition of Λ_{QCD} is given in the “Quantum Chromodynamics” review; in this review we are using it only to indicate the approximate non-perturbative scale of QCD.) This condition is stronger than that used above to distinguish quarks with small discretization errors, $m_q < 1/a$. Loop effects from light quarks must be included in the simulations to accurately represent QCD.

At present, most simulations are done in the isospin symmetric limit $m_u = m_d \equiv m_\ell < m_s$, with charm-quark loops either excluded (referred to as “ $N_f = 2 + 1$ ” simulations) or included (denoted “ $N_f = 2 + 1 + 1$ ” simulations). As noted above, precision is now reaching the point where isospin breaking effects must be included. To do so without approximation requires simulating with non-degenerate up and down quarks (leading to $N_f = 1 + 1 + 1$ or $1 + 1 + 1 + 1$ simulations) as well as including electromagnetism (as described above).

We now describe the tuning of m_ℓ , m_s and m_c to their physical values. (For brevity, we ignore isospin violation in the following discussion.) The most commonly used quantities for these tunings are, respectively, m_π , m_K and m_{η_c} . If the scale is being set by m_Ω , then one adjusts the lattice quark masses until the ratios m_π/m_Ω , m_K/m_Ω and m_{η_c}/m_Ω take their physical values. In the past, most calculations needed to extrapolate to the physical value of m_ℓ (typically using forms based on chiral perturbation theory [ChPT]), while simulating directly at or near to the physical values of m_s and m_c . Present calculations are increasingly done with physical or near physical values of m_ℓ , requiring at most only a short extrapolation or interpolation.

17.1.5.3 Heavy quark masses

The b quark is usually treated only as a valence quark, with no loop effects included. The errors introduced by this approximation can be estimated to be $\sim \alpha_s(m_b)A_{\text{QCD}}^2/m_b^2$ and are likely to be very small. In the past, the same approximation has been made for the c quark, leading to errors $\sim \alpha_s(m_c)A_{\text{QCD}}^2/m_c^2$. (See Ref. [86] for a quantitative estimate of the effects of including the charm quark on some low energy physical quantities, and Ref. [87] for similar estimates for B -meson matrix elements.) For high precision, however, dynamical charm quarks are necessary, and some of the most recent simulations now include them.

The b quark mass can be tuned by setting heavy-heavy (\mathcal{T}) or heavy-light (B) meson masses to their experimental values. Consistency between these two determinations provides an important check that the determination of parameters in the heavy quark lattice formulations is being done correctly (see, e.g., Ref. [26,88,89]). For instance, the b quark masses obtained from heavy-light [44] and heavy-heavy [77] mesons are in excellent agreement within the precision of 0.5%.

17.1.6 Sources of systematic error

Lattice results have statistical and systematic errors that must be quantified for any calculation in order for the result to be a useful input to phenomenology. The statistical error is due to the use of Monte Carlo importance sampling to evaluate the path integral (a method discussed below). There are, in addition, a number of systematic errors that are always present to some degree in lattice calculations, although the size of any given error depends on the particular quantity under consideration and the parameters of the ensembles being used. The most common lattice errors are reviewed below.

Although not strictly a systematic error, it is important to note that the presence of long auto-correlations in the sequence of lattice configurations generated by the Monte Carlo method can lead to underestimates of statistical errors [90]. It is known that the global topological charge of the gauge fields decorrelates very slowly with certain algorithms [90,91]. The effect of poorly sampling topological charge is expected to be most significant for the pion mass and related quantities [92–94]. This issue becomes more relevant as the precision of the final results improves. The problem of slow decorrelation of topology can be mitigated using open boundary conditions, for which the global topological charge is not quantized [95].

17.1.6.1 Continuum limit

Physical results are obtained in the limit that the lattice spacing a goes to zero. The Symanzik effective theory (SET) determines the scaling of lattice artefacts with a . Most lattice calculations use improved actions with leading discretization errors of $\mathcal{O}(\alpha_s a \Lambda)$, $\mathcal{O}(a^2 \Lambda^2)$, or $\mathcal{O}(\alpha_s a^2 \Lambda^2)$, where Λ is a typical momentum scale in the system. Knowledge of the scaling of the leading discretization errors allows controlled extrapolation to $a = 0$ when multiple

lattice spacings are available, as in current state-of-the-art calculations. Residual errors arise from the exclusion of sub-leading a dependence from the fits, either that due to prefactors containing powers of $\log(a)$, or from higher powers of a . The former can, in principle, be understood using the SET, and first studies of this have been undertaken [96–98].

For many quantities the typical momentum scale in the system is $\sim \Lambda_{\text{QCD}} \approx 300$ MeV. Discretization errors are expected to be larger for quantities involving larger scales, for example form factors or decays involving particles with momenta or masses larger than Λ_{QCD} .

17.1.6.2 Infinite volume limit

LQCD calculations are necessarily carried out in finite space-time boxes, leading to departures of physical quantities (masses, decay constants, etc.) from their measured, infinite volume values. These finite-volume shifts are an important systematic that must be estimated and minimized.

Typical lattices are asymmetric, with N_s points in the three spatial directions and N_t in the (Euclidean) temporal direction. The spatial and temporal sizes in physical units are thus $L_s = aN_s$ and $L_t = aN_t$, respectively. (Anisotropic lattice spacings are also sometimes used, as discussed below in Sec. 17.2.2.) Typically, $L_t \geq 2L_s$, a longer temporal direction being used to allow excited-state contributions to correlators to decay. This means that the dominant impact of using finite volume is from the presence of a finite spatial box.

The highest-precision LQCD calculations are of quantities involving no more than a single strongly-interacting particle in initial and final states. For such quantities, once the volume exceeds about 2 fm (so that the particle is not “squeezed”), the dominant finite-volume effect comes from virtual pions wrapping around the lattice in the spatial directions. This effect is exponentially suppressed as the volume becomes large, roughly as $\sim \exp(-m_\pi L_s)$, and has been estimated using ChPT [99] or other methods [100]. These estimates suggest that finite volume shifts are sub-percent effects when $m_\pi L_s \gtrsim 4$, and most large-scale simulations use lattices satisfying this condition. (See also Sec. 2.1.1 of the FLAG report [85] for more detailed discussion concerning the conditions required to control finite volume effects.) This becomes challenging as one approaches the physical pion mass, for which $L_s \gtrsim 5$ fm is required.

Finite volume errors are usually determined by repeating the simulations on two or more different volumes (with other parameters fixed). If different volumes are not available, the ChPT estimate can be used, often inflated to account for the fact that the ChPT calculation is truncated at some order.

In the future, LQCD calculations involving more than a single hadron will become increasingly precise. Examples include the calculation of resonance parameters and the $K \rightarrow \pi\pi$ amplitudes. Finite volume effects are much larger in these cases, with power-law terms (e.g., $1/L_s^3$) in addition to exponential dependence. Indeed, as will be discussed in Sec. 17.2.4, one can use the volume dependence to indirectly extract infinite-volume quantities such as scattering lengths. Doing so, however, requires a set of lattice volumes satisfying $m_\pi L_s \gtrsim 4$ and is thus more challenging than for single-particle quantities.

17.1.6.3 Chiral extrapolation

Until recently, an important source of systematic error in LQCD calculations was the need to extrapolate in m_u and m_d (or, equivalently, in m_π). This extrapolation was usually done using functional forms based on ChPT, or with analytic functions, with the difference between different fits used as an estimate of the systematic error, which was often substantial. Increasingly, however, calculations work directly at, or very close to, the physical quark masses. This either removes entirely, or greatly reduces, the uncertainties in the extrapolation, such that this error is subdominant.

17.1.6.4 Operator matching

Many of the quantities that LQCD can precisely calculate involve hadronic matrix elements of operators from the electroweak Hamiltonian. Examples include the pion and kaon decay constants, semileptonic form factors and the kaon mixing parameter

B_K (the latter defined in Eq. (17.13)). The operators in the lattice matrix elements are defined in the lattice regularization scheme. To be used in tests of the Standard Model, however, they must be matched to the continuum regularization scheme in which the corresponding Wilson coefficients have been calculated. The only case in which such matching is not needed is if the operator is a conserved or partially conserved current. Similar matching is also needed for the conversion of lattice bare quark masses to those in the continuum $\overline{\text{MS}}$ scheme.

Several methods are used to calculate the matching factors: perturbation theory (usually to one- or two-loop order), non-perturbative renormalization (NPR) using Landau-gauge quark and gluon external states [101], NPR using gauge-invariant methods based on the Schrödinger functional [102], NPR using gauge-invariant short-distance hadron correlators [103], and NPR using gauge-invariant heavy-heavy correlators [27, 104]. The NPR methods replace truncation errors (which can only be approximately estimated) by statistical and systematic errors that can be determined reliably and systematically reduced.

An issue that arises in some of such calculations (e.g., for quark masses and B_K) is that, using NPR with Landau-gauge quark and gluon external states, one ends up with operators regularized in a MOM-like scheme (or a Schrödinger-functional scheme), rather than the $\overline{\text{MS}}$ scheme mostly used for calculating the Wilson coefficients. To make contact with this scheme requires a purely continuum perturbative matching calculation supplemented by the operator product expansion (OPE). (The importance of power corrections is emphasized in [105].) The resultant truncation error of perturbative expansion and OPE can be minimized by pushing up the momentum scale at which the matching is done using step-scaling techniques as part of the NPR calculation [106].

It should also be noted that this final step in the conversion to the $\overline{\text{MS}}$ scheme could be avoided if continuum calculations used a MOM-like scheme or if one imposes a renormalization condition for quantities that are calculable both in the $\overline{\text{MS}}$ scheme and in LQCD, such as the hadron correlators at short distances (see, e.g., Ref. [107]).

17.2 Methods and status

Once the lattice action is chosen, it is straightforward to define the quantum theory using the path integral formulation. The Euclidean-space partition function is

$$Z = \int [dU] \prod_f [dq_f][d\bar{q}_f] e^{-S_g[U] - \sum_f \bar{q}_f (D[U] + m_f) q_f}, \quad (17.4)$$

where link variables are integrated over the SU(3) manifold, q_f and \bar{q}_f are Grassmann (anti-commuting) quark and antiquark fields of flavor f , and $D[U]$ is the chosen lattice Dirac operator with m_f the quark mass in lattice units. Integrating out the quark and antiquark fields, one arrives at a form suitable for simulation:

$$Z = \int [dU] e^{-S_g[U]} \prod_f \det(D[U] + m_f). \quad (17.5)$$

The building blocks for calculations are expectation values of multi-local gauge-invariant operators, also known as “correlation functions”,

$$\begin{aligned} \langle \mathcal{O}(U, q, \bar{q}) \rangle = \\ (1/Z) \int [dU] \prod_f [dq_f][d\bar{q}_f] \mathcal{O}(U, q, \bar{q}) e^{-S_g[U] - \sum_f \bar{q}_f (D[U] + m_f) q_f}. \end{aligned} \quad (17.6)$$

If the operators depend on the (anti-)quark fields q_f and \bar{q}_f , then integrating these fields out leads not only to the fermion determinant but also, through Wick’s theorem, to a series of quark “propagators”, $(D[U] + m_f)^{-1}$, connecting the positions of the fields.

This set-up allows one to choose, by hand, the masses of the quarks in the determinant (the sea quarks) differently from those in the propagators (valence quarks). This is called “partial

quenching”, and is used by some calculations as a way of obtaining more data points from which to extrapolate both sea and valence quarks to their physical values.

17.2.1 Monte-Carlo method

Since the number of integration variables U is huge ($N_s^3 \times N_t \times 4 \times 8$), direct numerical integration is impractical and one has to use Monte-Carlo techniques. In this method, one generates a Markov chain of gauge configurations (a “configuration” being the set of U ’s on all links) distributed according to the probability measure $[dU] e^{-S_g[U]} \prod_f \det(D[U] + m_f)$. Once the configurations are generated, expectation values $\langle \mathcal{O}(U, q, \bar{q}) \rangle$ are calculated by averaging over those configurations. In this way the configurations can be used for many different calculations, and there are several large collections of ensembles of configurations (with a range of values of a , lattice sizes and quark masses) that are publicly available through the International Lattice Data Grid (ILDG) [108]. As the number of the configurations, N , is increased, the error decreases as $1/\sqrt{N}$.

The most challenging part of the generation of gauge configurations is the need to include the fermion determinant. Direct evaluation of the determinant is not feasible, as it requires $\mathcal{O}((N_s^3 \times N_t)^3)$ computations. Instead, one rewrites it in terms of “pseudo-fermion” fields ϕ (auxiliary fermion fields with bosonic statistics). For example, for two degenerate quarks one has

$$\det(D[U] + m_f)^2 = \int [d\phi] e^{-\phi^\dagger (D[U] + m_f) (D[U] + m_f)^\dagger \phi}. \quad (17.7)$$

By treating the pseudo-fermions as additional integration variables in the path integral, one obtains a totally bosonic representation. The price one pays is that the pseudo-fermion effective action is highly non-local since it includes the inverse Dirac operator $(D[U] + m_f)^{-1}$. Thus, the large sparse matrix $(D[U] + m)$ has to be inverted every time one needs an evaluation of the effective action.

Present simulations generate gauge configurations using the Hybrid Monte Carlo (HMC) algorithm [109], or variants thereof. This algorithm combines molecular dynamics (MD) evolution [110–112] in a fictitious time (which is also discretized) with a Metropolis “accept-reject” step [113]. It makes a global update of the configuration, and is made exact by the Metropolis step. In its original form it can be used only for two degenerate flavors, but extensions (particularly the rational HMC [114]) are available for single flavors. Considerable speed-up of the algorithms has been achieved over the last two decades using a variety of techniques.

All these algorithms spend the bulk of their computational time on the repeated inversion of $(D[U] + m)$ acting on a source (which is required at every step of the MD evolution). Inversions are done using a variety of iterative algorithms, e.g., the conjugate gradient algorithm. In this class of algorithms, computational cost is determined by the condition number of the matrix, which is the ratio of maximum and minimum eigenvalues. For $(D[U] + m)$ the smallest eigenvalue is $\approx m$, and the cost is inversely proportional to the quark mass. This is a major reason why simulations at the physical light quark masses are challenging.

Algorithmic improvements have significantly reduced this problem. The main idea is to separate different length scales [115, 116]. Since the low eigenvalues of $(D[U] + m)$ are associated with long wavelength quark modes, one may project the problem onto that of a coarse-grained lattice by averaging the field within a block of sublattices and carrying out the inversion on this coarse lattice. The result is then fed back to the original lattice as an efficient *preconditioner* for the iterative solver, and the whole procedure may be nested multiple times. Variants of such methods have been implemented, specifically domain-decomposition [117, 118], deflation [119–122] and multigrid [123, 124]. They are increasingly used in large-scale lattice simulations.

A practical concern is the inevitable presence of correlations between configurations in the Markov chain. These are characterized by an auto-correlation length in the fictitious MD time. One aims to use configurations separated in MD time by greater than this auto-correlation length. In practice, it is difficult to

measure this length accurately, see, e.g., [125], and this leads to some uncertainty in the resulting statistical errors, as well as the possibility of insufficient equilibration.

The computational cost of gauge generation grows with the lattice volume, $V_{\text{lat}} = N_s^3 N_t$, as $V_{\text{lat}}^{1+\delta}$. Here $\delta = 1/4$ for the HMC algorithm [126] and can be reduced slightly using modern variants. Such growth with V_{lat} provides a (time-dependent) limit on the largest lattice volumes that can be simulated. At present, the largest lattices being used have $N_s = 144$ and $N_t = 288$ or $N_s = N_T = 160$. Typically, one aims to create an ensemble of $\sim 10^3$ statistically independent configurations at each choice of parameters (a , m_q and V_{lat}). For most physical quantities of interest, this is sufficient to make the resulting statistical errors smaller than or comparable to the systematic errors. Recently, the master-field approach is being investigated [13, 127, 128]. It aims to create a large-volume ensemble and repeat the calculation of physical quantities in different small patches of the entire lattice. Translational invariance guarantees that the correct average is obtained with fewer configurations than in the traditional approach, with the advantage of reduced finite-volume effects [129].

In the past, the cost of generating gauge configurations was larger than that of performing “measurements” on those configurations. However, as the number of quantities being calculated and their complexity has increased, the balance has shifted to the point that the total cost of measurements exceeds that of generation. Sharing the configurations, e.g. through the ILDG, has become more common, and a number of groups are utilizing them to compute a wide variety of quantities, as partly covered by the following sections.

17.2.2 Two-point functions

One can extract properties of stable hadrons from two-point correlation functions, $\langle O_X(x) O_Y^\dagger(0) \rangle$. Here $O_{X,Y}(x)$ are operators that have non-zero overlaps with the hadronic state of interest $|H\rangle$, i.e. $\langle 0|O_{X,Y}(x)|H\rangle \neq 0$. On the lattice, the two-point correlation function can be constructed, using Wick’s theorem, from the quark propagators $(D[U] + m_f)_{x0}^{-1}$ from the insertion point of the source operator $O_Y(0)$ to the sink operator $O_X(x)$. An average over gauge configurations yields the estimate of $\langle O_X(x) O_Y^\dagger(0) \rangle$.

One usually Fourier transforms in the spatial directions and considers correlators as a function of Euclidean time:

$$C_{XY}(t; \mathbf{p}) = \sum_{\mathbf{x}} \langle O_X(t, \mathbf{x}) O_Y^\dagger(0) \rangle e^{-i\mathbf{p}\cdot\mathbf{x}}. \quad (17.8)$$

(Here and throughout this section all quantities are expressed in dimensionless lattice units, so that, for example, $\mathbf{p} = a\mathbf{p}_{\text{phys}}$.) By inserting a complete set of states having spatial momentum \mathbf{p} , the two-point function can be written as

$$C_{XY}(t; \mathbf{p}) = \sum_{i=0}^{\infty} \frac{1}{2E_i(\mathbf{p})} \langle 0|O_X(0)|H_i(\mathbf{p})\rangle \langle H_i(\mathbf{p})|O_Y^\dagger(0)|0\rangle e^{-E_i(\mathbf{p})t}, \quad (17.9)$$

where the energy of the i -th state $E_i(\mathbf{p})$ appears in the eigenvalue of the Euclidean time evolution operator e^{-Ht} , $e^{-E_i(\mathbf{p})t}$. The factor of $1/[2E_i(\mathbf{p})]$ is due to the relativistic normalization used for the states. For large enough t , the dominant contribution is that of the lowest energy state $|H_0(\mathbf{p})\rangle$:

$$C_{XY}(t) \xrightarrow{t \rightarrow \infty} \frac{1}{2E_0(\mathbf{p})} \langle 0|O_X(0)|H_0(\mathbf{p})\rangle \langle H_0(\mathbf{p})|O_Y^\dagger(0)|0\rangle e^{-E_0(\mathbf{p})t}. \quad (17.10)$$

One can thus obtain the energy $E_0(\mathbf{p})$, which equals the hadron mass m_H when $\mathbf{p} = 0$, and the product of matrix elements $\langle 0|O_X(0)|H_i(\mathbf{p})\rangle \langle H_i(\mathbf{p})|O_Y^\dagger(0)|0\rangle$.

This method can be used to determine the masses of all the stable (in QCD) mesons and baryons by making appropriate choices of operators. For example, if one uses the axial current, $O_X = O_Y = A_\mu = \bar{d}\gamma_\mu\gamma_5 u$, then one can determine m_{π^+} from the rate of exponential fall-off, and in addition the decay constant f_π from the coefficient of the exponential.

The expression given in (17.9) for the correlator $C_{XY}(t; \mathbf{p})$ shows how, in principle, one can determine the energies of the excited hadron states having the same quantum numbers as the operators $O_{X,Y}$, by fitting the correlation function to a sum of exponentials, including both ground-state and excited-state contributions. It is important to do this in order to obtain accurate results for the ground-state parameters. To reliably identify excited-state parameters in practice, one often needs to use a large basis of operators with a variety of overlaps, $\langle 0|O|H\rangle$, with the different states, and to adopt a variational approach, such as that of [130]. Use of an anisotropic lattices in which a_t , the lattice spacing in the time direction, is smaller than its spatial counterpart, a_s , allows more temporal samples of the correlation function at small times where there is a signal for excited states. Using these and other technical improvements, extensive excited-state spectra have been obtained [131–136].

A complication arises for states with high spins ($j \geq 4$ for bosons) because the spatial rotation group on the lattice is a discrete subgroup of the continuum group $\text{SO}(3)$. This implies that lattice operators, even when chosen to lie in irreducible representations of the lattice rotation group, have overlap with states that have a number of values of j in the continuum limit [137]. For example $j = 0$ operators can also create mesons with $j = 4$. Methods to overcome this problem in practice are available [131, 138] and have been used successfully.

The two-point function (17.8) contains, in principle, information on all possible states having the quantum numbers of the operator O . Thus, if O is chosen to be a vector current, it can be used to estimate the hadronic vacuum polarization function contribution to the muon anomalous magnetic moment, as discussed in Sec. 17.3.6.

17.2.3 Three-point functions

Hadronic matrix elements needed to calculate semileptonic form factors and neutral meson mixing amplitudes can be computed from three-point correlation functions. We discuss here, as a representative example, the $D \rightarrow K$ amplitude. As in the case of two-point correlation functions one constructs operators O_D and O_K having overlap, respectively, with the D and K mesons. We are interested in calculating the matrix element $\langle K|V_\mu|D\rangle$, with $V_\mu = \bar{c}\gamma_\mu s$ the flavor-changing vector current.

To obtain this, we use the three-point correlator

$$C_{KV_\mu D}(t_x, t_y; \mathbf{p}) = \sum_{\mathbf{x}, \mathbf{y}} \langle O_K(t_x, \mathbf{x}) V_\mu(0) O_D^\dagger(t_y, \mathbf{y}) \rangle e^{-i\mathbf{p}\cdot\mathbf{x}}, \quad (17.11)$$

and focus on the limit $t_x \rightarrow \infty$, $t_y \rightarrow -\infty$. In this example we set the D -meson at rest while the kaon carries three-momentum \mathbf{p} . Momentum conservation then implies that the weak operator V_μ inserts three-momentum $-\mathbf{p}$. Inserting a complete set of states between each pair of operators, we find

$$C_{KV_\mu D}(t_x, t_y; \mathbf{p}) = \sum_{i,j} \frac{1}{2m_{D_i} 2E_{K_j}(\mathbf{p})} e^{-m_{D_i} t_x - E_{K_j}(\mathbf{p}) |t_y|} \times \langle 0|O_K(0)|K_j(\mathbf{p})\rangle \langle K_j(\mathbf{p})|V_\mu(0)|D_i(\mathbf{0})\rangle \langle D_i(\mathbf{0})|O_D^\dagger(0)|0\rangle. \quad (17.12)$$

The matrix element $\langle K_i(\mathbf{p})|V_\mu(0)|D_j(\mathbf{0})\rangle$ can then be extracted, since all other quantities in this expression can be obtained from two-point correlation functions. Typically, one is interested in the weak matrix elements of ground states, such as the lightest pseudo-scalar mesons. In the limit of large separation between the three operators in Euclidean time, the three-point correlation function yields the weak matrix element of the transition between ground states. The extraction of the ground state is not always straightforward, especially when a significant contribution is expected from states with an extra pion. An example relevant to $B \rightarrow \pi l \nu$ decay is discussed in Ref. [139].

From (17.12) the matrix element $\langle K_i(\mathbf{p})|V_\mu(0)|D_j(\mathbf{0})\rangle$ is obtained at several discretized values of momentum \mathbf{p} , given by a multiple of $2\pi/L$ in each spatial direction. Each momentum corresponds to a certain value of the momentum transfer

$q^2 = (m_D - E_K(\mathbf{p}))^2 - \mathbf{p}^2$. The restriction on the available momentum can be relaxed by introducing twisted boundary conditions [140–142], which are a generalization of (anti-)periodic boundary conditions in the spatial directions that allows a general $U(1)$ phase upon translation by distance L . The choice of phase leads to a quark momentum that does not have to be a multiple of $2\pi/L$. The method has been applied in a number of lattice calculations.

To interpolate in q^2 , the so-called z parametrization [143–146] is often employed. It takes account of the analytic structure of the form factor in the complex q^2 plane, and a polynomial expansion in z is justified.

17.2.4 Scattering amplitudes and resonances

The methods described thus far yield matrix elements involving single, stable particles (where by stable we mean here absolutely stable to strong interaction decays). Most of the particles listed in the Review of Particle Properties are, however, unstable—they are resonances decaying into final states consisting of multiple strongly interacting particles. LQCD simulations cannot directly calculate resonance properties, but methods have been developed to do so indirectly for resonances coupled to two-particle final states in the elastic regime, starting from the seminal work of Lüscher [147].

The difficulty faced by LQCD calculations is that, to obtain resonance properties, or, more generally, scattering phase-shifts, one must calculate multi-particle scattering amplitudes in momentum space and put the external particles on their mass-shells. This requires analytically continuing from Euclidean to Minkowski momenta. Although it is straightforward in LQCD to generalize the methods described above to calculate four- and higher-point correlation functions, one necessarily obtains them at a discrete and finite set of Euclidean momenta. Analytic continuation to $p_E^2 = -m^2$ is then an ill-posed and numerically unstable problem. The same problem arises for single-particle states, but can be largely overcome by picking out the exponential fall-off of the Euclidean correlator, as described above. With a multi-particle state there is no corresponding trick, except for two particles at threshold [148], although recent ideas using smeared correlators and advanced spectral-reconstruction methods offer hope for future progress [149, 150].

What LQCD can calculate are the energies of the eigenstates of the QCD Hamiltonian in a finite box. The energies of states containing two stable particles, e.g., two pions, clearly depend on the interactions between the particles. It is possible to invert this dependence and, with plausible assumptions, determine the scattering phase-shifts at a discrete set of momenta from a calculation of the two-particle energy levels for a variety of spatial volumes [147]. This is a challenging calculation, but it has been carried through in several channels with quark masses approaching physical values. Channels studied include $\pi\pi$ (for $I = 2, 1$ and 0), $\bar{K}K$, $K\pi$, $\pi\omega$, $\pi\phi$, KD , DD^* , $B\pi$, and $N\pi$. For recent comprehensive reviews see [151, 152]. Extensions to nucleon interactions are being actively studied [153]. The formalism has been generalized to three particles (both identical and non-degenerate, and including spin) [154], and has been applied in lattice calculations of $3\pi^+$, $2\pi^+ + K^+$, $\pi^+ + 2K^+$, and $3K^*$ systems [155] as well as to the $I = 1$ three-pion channel [156]. For recent reviews, see [152, 157].

It is also possible to extend the methodology to calculate electroweak decay amplitudes to two particles below the inelastic threshold, e.g., $A(K \rightarrow \pi\pi)$ [158]. Results for both the $\Delta I = 3/2$ and $1/2$ amplitudes with physical quark masses have been obtained [35–37, 159], the former now including a controlled continuum limit [160]. First results for the CP -violating quantity ϵ' have been obtained [35, 36].

Partial extensions of the formalism above the elastic threshold have been worked out, in particular for the case of multiple two-particle channels [161]. Another theoretical extension is to allow the calculation of form factors between a stable particle and a resonance [162], and between two resonances [163]. The former has been used to calculate the $\gamma\pi \rightarrow \rho$ amplitude, albeit for unphysically large quark masses [164, 165], as well as $\gamma K \rightarrow K^*$ [166]. Finally, the formalism for using LQCD to calculate electroweak

decays or transitions to three particles, e.g. $\gamma^* \rightarrow 3\pi$ and $K \rightarrow 3\pi$, has recently been worked out [167, 168].

While a systematic extension to decays with many multi-particle channels, e.g., hadronic B decays, has, however, yet to be formulated, some interesting new ideas have been proposed [150, 169, 170], including a method to compute inclusive decay rates or cross sections [171, 172]. The latter represents the inclusive processes using the Compton amplitude, in which two currents are inserted and all possible final states are created between the two [150]. The relative weight among different final states depends on the Euclidean time separation between the current, from which one can extract the inclusive rates. First calculations have been reported [173, 174]. A related approach has been recently applied to provide a lattice determination of the inclusive semileptonic τ decay rate [175].

17.2.5 Status of LQCD simulations

Until the 1990s, most large-scale lattice simulations were limited to the “quenched” approximation, wherein the fermion determinant is omitted from the path integral. While much of the basic methodology was developed in this era, the results obtained had uncontrolled systematic errors and were not suitable for use in placing precision constraints on the Standard Model. During the 1990s, more extensive simulations including the fermion determinant (also known as simulations with “dynamical” or “sea” quarks) were begun, but with unphysically heavy quark masses ($m_\ell \sim 50 - 100$ MeV), such that the extrapolation to the physical light quark masses was a source of large systematic errors [176]. During the 2000s, advances in both algorithms and computers allowed simulations to reach much smaller quark masses ($m_\ell \sim 10 - 20$ MeV) such that LQCD calculations of selected quantities with all sources of error controlled and small became available. Their results played an important role in constraints on the CKM matrix and other phenomenological analyses. In the last decade, simulations directly at the physical isospin-symmetric light quark masses have become standard, removing the need for a chiral extrapolation and thus significantly reducing the overall error. The present frontier, as noted above, is the inclusion of isospin breaking. This will be needed to push the accuracy of calculations below the percent level.

On a more qualitative level, analytic and numerical results from LQCD have demonstrated that QCD confines color and spontaneously breaks chiral symmetry. Confinement can be seen as a linearly rising potential between heavy quark and anti-quark in the absence of quark loops. Analytically, this can be shown in the strong coupling limit $g_{\text{lat}} \rightarrow \infty$ [1]. At weaker couplings there are precise numerical calculations of the potential that clearly show that this behavior persists in the continuum limit [177–179].

Chiral symmetry breaking was also demonstrated in the strong coupling limit on the lattice [18, 180], and there have been a number of numerical studies showing that this holds also in the continuum limit. The accumulation of low-lying modes of the Dirac operator, which is the analog of Cooper pair condensation in superconductors, has been observed, yielding a determination of the chiral condensate [181–187]. Many relations among physical quantities that can be derived under the assumption of broken chiral symmetry have been confirmed by a number of lattice groups [188].

17.3 Physics applications

In this section we describe the main applications of LQCD that are both computationally mature and relevant for the determination of particle properties.

A general feature to keep in mind is that, since there are many different choices for lattice actions, all of which lead to the same continuum theory, a crucial test is that results for any given quantity are consistent. In many cases, different lattice calculations are completely independent and often have very different systematic errors. Thus, final agreement, if found, is a highly non-trivial check, just as it is for different experimental measurements.

The number, variety and precision of the calculations has progressed to the point that an international collaboration, FLAG, has been formed, which aims to collect all lattice results of relevance for a variety of phenomenologically interesting quantities

and provide averages of those results that pass appropriate quality criteria. The averages attempt to account for possible correlations between results (which can arise, for example, if they use common gauge configurations). The quantities considered are those we discuss in this section, with the exception of the hadron spectrum, as well as the intermediate scale-setting quantities discussed earlier. The most recent FLAG review is from 2021 [85] (see also older editions, Refs. [60, 188]). The interested reader can consult this review for very extensive discussions of the details of the calculations and of the sources of systematic errors.

We stress that the results we quote below are those obtained using the physical complement of light quarks (i.e. $N_f = 2 + 1$ or $2 + 1 + 1$ simulations).

17.3.1 Spectrum

The most basic prediction of LQCD is of the hadron spectrum. Once the input parameters are fixed as described in Sec. 17.1.5, the masses or resonance parameters of all other states can be predicted. This includes hadrons composed of light (u , d and s) quarks, as well as heavy-light and heavy-heavy hadrons. It also includes quark-model exotics (e.g., $J^{PC} = 1^{-+}$ mesons) and glueballs. Thus, in principle, LQCD calculations should be able to reproduce many of the experimental results compiled in the Review of Particle Properties. Doing so would test both that the error budgets of LQCD calculations are accurate and that QCD indeed describes the strong interactions in the low-energy domain. The importance of the latter test can hardly be overstated.

What is the status of this fundamental test? As discussed in Sec. 1.2, LQCD calculations are most straightforward for stable, low-lying hadrons. Calculations of the properties of resonances that can decay into only two particles are more challenging, but are becoming standard in the meson sector, with the frontier being decays involving baryons. As noted above, the formalism for resonances decaying to three particles exists, but has yet to be applied to resonant channels other than in pioneering calculations. It is also more technically challenging to calculate masses of flavor singlet states (which can annihilate into purely gluonic intermediate states) than those of flavor non-singlets, although again algorithmic and computational advances have begun to make such calculations accessible, including first calculations that reach physical quark masses [189].

The present status for light hadrons is that fully controlled results are available for the masses of the octet light baryons, while results with less than complete control are available for the decuplet baryon resonances, the vector meson resonances and the η and η' . This is discussed in the “Quark Model” review—see, in particular, Fig. 15.9. In addition, it has been possible to calculate the isospin splitting in light mesons and baryons (due to the up-down mass difference and the incorporation of QED). There are also extensive results for heavy-light (D and B systems) and heavy-heavy (J/ψ and Υ systems). All present results, which are discussed in the “Quark Model” review, are consistent with experimental values, and several predictions have been made. We refer the reader to that review for references to the relevant work.

17.3.2 Decay constants and bag parameters

The pseudo-scalar decay constants can be determined from two-point correlation functions involving the axial-vector current, as discussed in Sec. 17.2.2. The decay constant f_P of a meson P is extracted from the weak matrix element involving the axial-vector current using the definition $\langle 0|A_\mu(x)|P(p)\rangle = f_P p_\mu \exp(-ip \cdot x)$, where p_μ is the momentum of P and $A_\mu(x)$ is the axial-vector current. (In practice, results with the smallest errors are obtained using the pseudo-scalar density $P(x) = \bar{q}(x)\gamma_5 q(x)$ instead of $A_\mu(x)$.) Since they are among the simplest quantities to calculate, decay constants provide good benchmarks for lattice methods, in addition to being important inputs for flavor physics phenomenology in their own right. Results from several lattice groups for the pion and kaon decay constants now have sub-percent errors. The decay constants in the charm and bottom sectors, f_D , f_{D_s} , f_B , and f_{B_s} , have also been calculated using the various heavy quark formulations on the lattice outlined in Sec. 17.1.3. The precision has reached sub-percent errors for charmed mesons, and percent-level errors for bottom mesons. Lattice results for all of these

decay constants are discussed in detail in the review “Leptonic Decays of Charged Pseudoscalar Mesons.”

Another important lattice quantity is the kaon bag parameter, B_K , which is needed to turn the precise measurement of CP -violation in kaon mixing into a constraint on the Standard Model. It is defined by

$$\frac{8}{3} m_K^2 f_K^2 B_K(\mu) = \langle \bar{K}^0 | Q_{\Delta S=2}(\mu) | K^0 \rangle, \quad (17.13)$$

where m_K is the kaon mass, f_K is the kaon decay constant, $Q_{\Delta S=2} = \bar{s}\gamma_\mu(1-\gamma_5)d\bar{s}\gamma_\mu(1-\gamma_5)d$ is the four-quark operator of the effective electroweak Hamiltonian and μ is the renormalization scale. The short distance contribution to the electroweak Hamiltonian can be calculated perturbatively, but the hadronic matrix element parameterized by B_K must be computed using non-perturbative methods. In order to be of use to phenomenology, the renormalization factor of the four-quark operator must be matched to a continuum renormalization scheme, e.g., to $\overline{\text{MS}}$, as described in Sec. 17.1.6.4. Determinations with percent-level precision using different fermion actions and $N_f = 2 + 1$ light sea quarks are now available using DWF [190], staggered fermions [191], DWF valence on staggered sea quarks [192], and Wilson fermions [11]. The results are all consistent, and the present FLAG average is $\hat{B}_K = 0.7625(97)$ [85] for its renormalization group invariant definition (for original papers, see [11, 192–194]).

The bag parameters for B and B_s meson mixing are defined analogously to that for kaon mixing. The B and B_s mesons contain a valence b -quark so that calculations of these quantities must use one of the methods for heavy quarks described above. Calculations have been done using NRQCD [195, 196], the Fermilab formalism [87], and static heavy quarks [197]. All results are consistent. The FLAG averages for the quantities relevant for B_s and B mixing with $N_f = 2 + 1$, which are based on results from Refs. [87, 195, 197], are $f_{B_s} \sqrt{\hat{B}_{B_s}} = 274(8)$ MeV and $f_B \sqrt{\hat{B}_B} = 225(9)$ MeV, with their ratio (which is somewhat better determined) being $\xi = 1.206(17)$. FLAG also quotes an “average” for $N_f = 2 + 1 + 1$, which comes from a single calculation [196] and gives $f_{B_s} \sqrt{\hat{B}_{B_s}} = 256(6)$ MeV $f_B \sqrt{\hat{B}_B} = 211(6)$ MeV, and $\xi = 1.216(16)$. These are consistent with the $N_f = 2 + 1$ results at the 2σ level. Errors for quantities involving b quarks are typically larger than those for quantities involving only light quarks, although the difference has steadily decreased in recent years.

For the K , D and B systems, one can also consider the matrix elements of four-fermion operators that arise in beyond-the-standard-model (BSM) theories, which can have a different chiral structure. Knowledge of these matrix elements allows one to constrain the parameters of the BSM theories, and is complementary to direct searches at the LHC. Reliable results are now available from lattice calculations, and are reviewed by FLAG in the case of kaon mixing [85]. Complete results for D and B mixing are presented in Ref. [198, 199] and Ref. [87, 200], respectively.

The results for mixing matrix elements are used in the reviews “The CKM Quark-Mixing Matrix,” and “ $B^0 - \bar{B}^0$ Mixing.”

17.3.3 Form factors ($K \rightarrow \pi l\nu$, $D \rightarrow K l\nu$, $B \rightarrow \pi l\nu$, $B \rightarrow D^{(*)} l\nu$, etc.)

Semileptonic decay rates can be used to extract CKM matrix elements once the semileptonic form factors are known from lattice calculations. For example, the matrix element of a pseudo-scalar meson P undergoing semileptonic decay to another pseudo-scalar meson D is mediated by the vector current, and can be written in terms of form factors as

$$\langle D(p_D) | V_\mu | P(p_P) \rangle = f_+(q^2)(p_D + p_P - \Delta)_\mu + f_0(q^2)\Delta_\mu, \quad (17.14)$$

where $q = p_D - p_P$, $\Delta_\mu = (m_D^2 - m_P^2)q_\mu/q^2$ and V_μ is the quark vector current. For K and D meson decays, the shapes of the form factors are well determined by experiment and the value of $f_+(q^2)$ at some reference value of q^2 is needed from the lattice in order to extract CKM matrix elements. Lattice calculations of the form factor shapes may provide further consistency checks. Typically, $f_+(q^2)$ dominates the decay rate, since the contribution from $f_0(q^2)$ is suppressed when the final state lepton is light.

The form factor $f_+(0)$ for $K \rightarrow \pi \ell \nu$ decays is highly constrained by the Ademollo-Gatto theorem [201] and chiral symmetry. Old estimates using chiral perturbation theory combined with quark models quote sub-percent precision [202], though they suffer from some model dependence. Utilizing the constraint from the vector current conservation that $f_+(0)$ is normalized to unity in the limit of degenerate up and strange quark masses, the lattice calculation can be made very precise and has now matched the precision of the phenomenological estimates [203–210]. The present FLAG average (from $N_f = 2 + 1 + 1$ simulations) is $f_+(0) = 0.9698(17)$, based on Refs. [210].

Charmed meson semileptonic decays have been calculated by different groups using methods similar to those used for charm decay constants, and results are steadily improving in precision [211–216]. Charmed baryon decays have also been computed using a similar method [217, 218].

For semileptonic decays involving a bottom quark, one can use HQET or NRQCD to control the discretization errors of the bottom quark. HQET is also used to constrain the extrapolation of the lattice results obtained in the lower heavy-quark mass region using relativistic lattice fermion actions.

The form factors for the semileptonic decay $B \rightarrow \pi \ell \nu$ (and the similar decay $B_s \rightarrow K \ell \nu$) have been calculated in unquenched lattice QCD by a number of groups [219–228]. These B semileptonic form factors are difficult to calculate at low q^2 , *i.e.* when the mass of the B -meson must be balanced by a large pion momentum, in order to transfer a large momentum to the lepton pair. The low q^2 region has large discretization errors and very large statistical errors, while the high q^2 region is much more accessible to the lattice. For experiment, the opposite is true. To combine lattice and experimental results it has proved helpful to use the z -parameter expansion [143–146]. This provides a theoretically constrained parameterization of the entire q^2 range, and allows one to obtain $|V_{ub}|$ without model dependence [229]. Analyticity and unitarity can be used to obtain further constraints, including extra information on susceptibilities relevant to the form factors in the time-like region [146, 230–233].

The semileptonic decays $B \rightarrow D \ell \nu$ and $B \rightarrow D^* \ell \nu$ (and the similar decays $B_s \rightarrow D_s \ell \nu$ and $B_s \rightarrow D_s^* \ell \nu$) can be used to extract $|V_{cb}|$ once the corresponding form factors are known. The lattice calculation is most precise at zero recoil since the bulk of the systematic error cancels for appropriate ratios between $B \rightarrow D^{(*)}$ and $B \rightarrow B$ or $D^{(*)} \rightarrow D^{(*)}$ [234]. The unquenched calculation of the $B \rightarrow D^{(*)} \ell \nu$ form factor at zero recoil has been performed with various formulations for the heavy quark [235]. Calculations at non-zero recoil have also now been performed to constrain the functional form of the form factor, which can be used to extrapolate the experimental data to the zero-recoil point or to determine $|V_{cb}|$ directly at the non-zero recoil points [42, 236–241]. The range of q^2 that can be handled for B -meson decays in lattice QCD is growing as more accurate results become available on finer lattices. Comparison of the shape of the form factors between lattice calculations and experiments provides non-trivial cross checks. Semileptonic decays of the Λ_b baryon can also be used to constrain $|V_{cb}|$ and $|V_{ub}|$ using lattice calculations of the relevant form factors [242].

The rare decays $B \rightarrow K \ell^+ \ell^-$ involve matrix elements similar to those needed for semileptonic decays, Eq. (17.14), except that the vector current V_μ is replaced by the operators $\bar{s} \gamma^\mu (1 - \gamma_5) b$ or $\bar{s} \sigma^{\mu\nu} (1 + \gamma_5) b$. Lattice calculations of the corresponding form factors involve similar techniques to those for the semileptonic form factors. The range of q^2 for which lattice calculations can be done is being extended, as above, but here there is an intermediate q^2 region where $c\bar{c}$ resonances are present and this must be avoided. Recent lattice calculations [223, 243, 244] suggest some tension with the experimentally observed decay rate. In these calculations, the long-distance contribution from decay chain $b \rightarrow s c \bar{c} \rightarrow s \ell^+ \ell^-$ is ignored. Systematic errors including such long-distance contributions need to be carefully studied before drawing any definite conclusions. A similar study for baryonic decay mode $\Lambda_b \rightarrow \Lambda \ell^+ \ell^-$ can be found in Ref. [245].

The results discussed in this section are used in the reviews “The CKM Quark-Mixing Matrix,” “ V_{ud} , V_{us} , the Cabibbo Angle and

CKM Unitarity,” and “Semileptonic b -hadron decays, determination of V_{cb} , V_{ub} .”

17.3.4 Strong gauge coupling

As explained in Sec. 17.1.5.1, for a given lattice action, the choice of bare lattice gauge coupling, g_{lat} , determines the lattice spacing a . If one then calculates a as described in Sec. 17.1.5.1, one knows the strong gauge coupling in the bare lattice scheme at the scale $1/a$, $\alpha_{\text{lat}} = g_{\text{lat}}^2/(4\pi)$. This is not, however, useful for comparing to results for α_s obtained from other inputs, such as deep inelastic scattering or jet shape variables. This is because the latter results give α_s in the $\overline{\text{MS}}$ scheme, which is commonly used in such analyses, and the conversion factor between the lattice and $\overline{\text{MS}}$ schemes is known to converge extremely poorly in perturbation theory. Instead, one must use a method which directly determines α_s on the lattice in a scheme closer to $\overline{\text{MS}}$.

Several such methods have been used, all following a similar strategy. One calculates a short-distance quantity K both perturbatively (K^{PT}) and non-perturbatively (K^{NP}) on the lattice, and requires equality: $K^{\text{NP}} = K^{\text{PT}} = \sum_{i=0}^n c_i \alpha_s^i$. Solving this equation one obtains α_s at a scale related to the quantity being used. Often, α_s thus obtained is not defined in the conventional $\overline{\text{MS}}$ scheme, and one has to convert among the different schemes using perturbation theory. Unlike for the bare lattice scheme, the required conversion factors are reasonably convergent. As a final step, one uses the renormalization group to run the resulting coupling to a canonical scale (such as M_Z).

In the work of the HPQCD collaboration [246, 247], the short-distance quantities are Wilson loops of several sizes and their ratios. These quantities are perturbatively calculated through $\mathcal{O}(\alpha_s^3)$ using the V -scheme defined through the heavy quark potential. The coefficients of even higher orders are estimated using the data at various values of a . In addition, this work obtains a result for α_s by matching with α_{lat} in a tadpole-improved scheme that improves convergence.

Another choice of short-distance quantities is to use current-current correlators. Appropriate moments of these correlators are ultraviolet finite, and by matching lattice results to the *continuum* perturbative predictions, one can directly extract the $\overline{\text{MS}}$ coupling [248]. The method can be applied for light meson correlators [249–252] as well as heavy meson correlators [40, 247, 253–256]. Yet another choice of short-distance quantity is the static-quark potential, where the lattice result for the potential is compared to perturbative calculations; this method was used to compute α_s within 2+1 flavor QCD [257–262]. There is also a determination of α_s from a comparison of lattice data for the ghost-gluon coupling with that of perturbation theory [263, 264].

With a definition of α_s given using the Schrödinger functional, one can non-perturbatively control the evolution of α_s to high-energy scales, such as 100 GeV, where the perturbative expansion converges very well. This method developed by the ALPHA collaboration [106] has been applied to 2+1-flavor QCD in [265–267].

The various lattice methods for calculating α_s have significantly different sources of systematic error. The FLAG review [85] reports an estimate $\alpha_{\overline{\text{MS}}}^{(5)}(M_Z) = 0.1184(8)$, based on Refs. [247, 252, 254, 262, 265, 267–269]. A comparison to other phenomenological determinations can be found in the “Quantum Chromodynamics” review.

17.3.5 Quark masses

Once the quark mass parameters are tuned in the lattice action, the remaining task is to convert them to those of the conventional definition. Since the quarks do not appear as asymptotic states due to confinement, the pole mass of the quark propagator is not a physical quantity. Instead, one defines the quark mass after subtracting the ultra-violet divergences in some particular way. The conventional choice is again the $\overline{\text{MS}}$ scheme at a canonical scale such as 2 or 3 GeV. Ratios such as m_c/m_s and m_b/m_c are also useful as they are free from multiplicative renormalization (in a mass-independent scheme), and can be computed precisely in lattice QCD, with a precision of 0.2% for m_c/m_s [44] and 0.3% for m_b/m_c [77].

As discussed in Sec. 17.1.6.4, one must convert the lattice bare quark mass to that in the $\overline{\text{MS}}$ scheme. Older calculations did so

directly using low-order perturbation theory; most recent calculations use an intermediate NPR method (e.g., RI/MOM or RI/S-MOM) which is then converted to the $\overline{\text{MS}}$ scheme using three-loop perturbation theory (see, e.g., [41, 190, 270–274]).

Alternatively, one can use a definition based on the Schrödinger functional, which allows one to evolve the quark mass to a high scale non-perturbatively [275, 276], where perturbative matching to the $\overline{\text{MS}}$ scheme can be done accurately.

Other approaches available for heavy quarks are to match current-current correlators at short distances calculated on the lattice to those obtained in continuum perturbation theory in the $\overline{\text{MS}}$ scheme [40, 77, 247, 253–255], or to use HQET mass relations [273, 277]. This has allowed an accurate determination of m_c and m_b [104, 247, 254].

The ratio method for heavy quarks (discussed earlier) can also be used to determine m_b [278].

Results are summarized in the review of “Quark Masses.”

17.3.6 Other physical quantities of interest

In some physics applications, one is interested in the two-point correlation function $\langle O_X(x)O_Y^\dagger(0) \rangle$ for all values of the separation x , not just its asymptotic form for large separations (which is used to determine the hadron spectrum as sketched in Sec. 17.2.2). A topical example, related to the evaluation of the Standard Model contribution to the muon anomalous magnetic moment $g-2$, is the hadronic vacuum polarization function $\Pi_{\mu\nu}(x) = \langle V_\mu(x)V_\nu(0) \rangle$ and its Fourier transform $\Pi_{\mu\nu}(q^2)$. Since the lattice is in Euclidean space-time, only space-like momenta, $q^2 = -Q^2 < 0$, are accessible. Nevertheless, this quantity is of significant interest. It determines the running of the QED coupling constant α_{QED} , for which non-perturbative effects arise from quark loops. First lattice calculations appeared recently [279, 280]. It is also related by a dispersion relation to the cross section for $e^+e^- \rightarrow \text{hadrons}$, and is needed for a first-principles calculation of the “hadronic vacuum polarization” contribution to the muon anomalous magnetic moment a_μ . Following the pioneering work or Ref. [281], there have been many lattice calculations of this contribution. The status as of March 2020 is summarized in the White Paper of the $g-2$ Theory Initiative [282]. More recent calculations are those of Refs. [283–285].

Since the relevant scale is set by the muon mass m_μ , this quantity is most sensitive to the low-energy region $Q^2 \simeq m_\mu^2$ of $\Pi_{\mu\nu}(-Q^2)$, where the long-range contribution of multi-body states become relevant. The lattice calculation is challenging because of this and also because the necessary precision is high (below 0.5%). Many systematic effects must be carefully studied and controlled in order to achieve this precision, including finite volume errors [286], errors from the chiral-continuum extrapolations [285], isospin breaking [287, 288], quark-line disconnected diagrams [288, 289], and QED corrections [288, 290, 291]. One lattice calculation has achieved the required sub-percent precision [283], a level that is comparable to the determination of the HVP contribution using dispersion relations based on e^+e^- scattering data (the “data-driven” approach). The lattice result is in tension with the data-driven approach by 2.1σ . In order to facilitate the comparison among different lattice calculations with controlled systematic errors, the so-called “intermediate window quantity” was introduced [288]. It essentially eliminates short-distance and long-distance contributions to the hadronic vacuum polarization and focuses in the region where the lattice calculation provides the best accuracy. The results from various lattice collaborations [283, 291–293] are in good agreement but disagree with the corresponding data-driven estimate at the level of 3.8σ . This discrepancy between the lattice and data-driven results needs to be understood before drawing any conclusion about new-physics contribution to the muon $g-2$.

Calculations of the light-by-light scattering contribution to a_μ have been performed. These involve the calculations of four-point correlation functions with various external momenta. Ingenious methods to evaluate the contribution to a_μ have been developed by two groups and the results are in good agreement [294].

There are other quantities for which lattice calculations can make a significant contribution to establishing a quantitative un-

derstanding of hadronic processes. One example is the long-distance contribution to the neutral kaon mass splitting, ΔM_K . This also requires the evaluation of a four-point function, constructed from the two-point functions described above by the insertion of two electroweak Hamiltonians [295, 296]. Another example is the long-distance contribution to ϵ_K , which provides a correction to the contribution of the mixing parameter B_K , and has also been computed recently [297]. Rare kaon decays $K \rightarrow \pi\ell^+\ell^-$ and $K \rightarrow \pi\nu\bar{\nu}$ are also important processes for which first lattice studies have appeared [298]. A related process is $\pi^0 \rightarrow e^+e^-$, which has recently been studied on the lattice [299]. Radiative leptonic decays $\pi \rightarrow \ell\nu\gamma^{(*)}$, $K \rightarrow \ell\nu\gamma^{(*)}$, and $D \rightarrow \ell\nu\gamma^{(*)}$ also include two operator insertions, i.e. an electroweak Hamiltonian and an electromagnetic current, and similar techniques developed for the rare decays can be applied. First lattice results have appeared [64, 300]. Finally, we note that similar lattice methods allow the calculation of the γW box contribution to the radiative corrections to semileptonic decays of pions and kaons [301]. The extension to neutron β decay is an important next step, as this promises to reduce the theoretical uncertainty in the extraction of $|V_{ud}|$ from neutron decays. First results have appeared recently [302].

17.3.7 Other applications of lattice QCD

In this review we have concentrated on applications of LQCD that are relevant to the quantities discussed in the Review of Particle Properties. We have not considered at all several other applications that are being actively pursued by simulations. Here we list the major such applications. The reader can consult the aforementioned texts [2–4] for further details, as well as the proceedings of recent lattice conferences [303], and several recent white papers [304].

LQCD can be used, in principle, to simulate QCD at non-zero temperature and density, and in particular to study how confinement and chiral-symmetry breaking are lost as T and μ (the chemical potential) are increased. For example, as T is increased at $\mu = 0$, it is found that, for the physical values of the quark masses, the deconfinement and chiral-symmetry-restoration transitions are smooth crossovers, rather than phase transitions, and that they occur together. This is of relevance to heavy-ion collisions, the early Universe and neutron-star structure. In practice, finite temperature simulations are computationally tractable and relatively mature, while simulations at finite μ suffer from a “sign problem” and are at a rudimentary stage.

Another topic under active investigation is nucleon structure and inter-nucleon interactions. The simplest nucleon matrix elements are calculable with a precision that is now starting to rival that for some mesonic quantities. Of particular interest are those of the axial current (leading to g_A) and of the scalar density (with $\langle N|\bar{s}s|N \rangle$ needed for dark matter searches), both of which are reviewed by FLAG [85]. Other such matrix elements provide information on the parton distribution functions (PDFs), including their low moments. Recently, methods to directly access PDFs have been developed (see Ref. [305] for a recent review). Also, neutrino-nucleon scattering matrix elements play a crucial role in the estimate of the expected event rate in the current and future neutrino experiments, such as T2K and DUNE. The lattice computation of the matrix elements is similar to those of the meson semi-leptonic decays and the lattice results are reaching the required precision as summarized in [306].

Finally, we note that there is much recent interest in studying QCD-like theories with more fermions, possibly in other representations of the gauge group (see, e.g., [307]). The main interest is to find nearly conformal theories which might be candidates for “walking technicolor” models.

17.4 Outlook

While LQCD calculations have made major strides in the last decade, and are now playing an important role in constraining the Standard Model, there are many calculations that could be done in principle but are not yet mature due to limitations in computational resources. As we move to exascale resources (10^{18} floating point operations per second), the list of mature calculations will grow. Examples that we expect to mature in the next few years

are results for B meson and Λ_b baryon form factors covering the full range of q^2 ; results for excited hadrons, including quark-model exotics, at close to physical light-quark masses; results for structure functions and related parton distribution functions; results for a variety of nucleon matrix elements; $K \rightarrow \pi\pi$ amplitudes (allowing a precise prediction of ϵ'/ϵ from the Standard Model); hadronic vacuum polarization contributions to $g_\mu - 2$, the running of α_{EM} and α_s (the status of the first of which was discussed in Sec. 17.3.6); $\pi \rightarrow \gamma\gamma$ and related amplitudes; long-distance contributions to $\bar{K} \leftrightarrow K$ mixing; the light-by-light contribution to $g_\mu - 2$; and determinations of long distance contributions to rare kaon decays such as $K \rightarrow \pi\nu\bar{\nu}$. There will also be steady improvement in the precision attained for the mature quantities discussed above. As already noted, for several of these quantities, attaining the desired precision will require the inclusion of isospin-breaking and electromagnetic effects.

17.5 Acknowledgments

We are grateful to Jack Laiho for his collaboration on previous editions of this review, and to Christine Davies, Takashi Kaneko, and Stefan Meinel for comments and suggestions.

References

- [1] K. G. Wilson, Phys. Rev. **D10**, 2445 (1974).
- [2] T. DeGrand & C. DeTar, “Lattice Methods for Quantum Chromodynamics,” World Scientific (2006).
- [3] C. Gattringer & C.B. Lang, “Quantum Chromodynamics on the Lattice: An Introductory Presentation,” Springer (2009).
- [4] “Modern Perspectives in Lattice QCD: quantum field theory and high performance computing” (Lecture notes of the Les Houches Summer School, Vol. 93) eds. L. Lellouch *et al.*, Oxford Univ. Press. (Aug. 2011).
- [5] W. Zimmermann, in “Lectures on Elementary Particles and Quantum Field Theory”, ed. S. Deser *et al.*, MIT Press, Cambridge, MA (1971); K. Symanzik, Nucl. Phys. **B226**, 187 (1983); K. Symanzik, Nucl. Phys. **B226**, 205 (1983).
- [6] M. Lüscher and P. Weisz, Commun. Math. Phys. **97**, 59 (1985), [Erratum: Commun. Math. Phys. 98, 433(1985)].
- [7] Y. Iwasaki (1983), UT-HEP-118, [arXiv:1111.7054].
- [8] H. B. Nielsen and M. Ninomiya, Phys. Lett. **105B**, 219 (1981).
- [9] B. Sheikholeslami and R. Wohlert, Nucl. Phys. **B259**, 572 (1985).
- [10] K. Jansen *et al.*, Phys. Lett. **B372**, 275 (1996), [hep-lat/9512009].
- [11] S. Dürr *et al.*, Phys. Lett. B **705**, 477 (2011), [arXiv:1106.3230].
- [12] N. Ishizuka *et al.*, Phys. Rev. **D92**, 7, 074503 (2015), [arXiv:1505.05289].
- [13] A. Francis *et al.*, Comput. Phys. Commun. **255**, 107355 (2020), [arXiv:1911.04533].
- [14] R. Frezzotti *et al.* (Alpha), JHEP **08**, 058 (2001), [hep-lat/0101001].
- [15] R. Frezzotti and G. C. Rossi, JHEP **08**, 007 (2004), [hep-lat/0306014].
- [16] R. Frezzotti and G. C. Rossi, Nucl. Phys. Proc. Suppl. **128**, 193 (2004), [hep-lat/0311008].
- [17] R. Frezzotti and G. C. Rossi, JHEP **10**, 070 (2004), [hep-lat/0407002].
- [18] L. Susskind, Phys. Rev. **D16**, 3031 (1977); N. Kawamoto and J. Smit, Nucl. Phys. B **192**, 100 (1981); H. S. Sharatchandra, H. J. Thun and P. Weisz, Nucl. Phys. B **192**, 205 (1981).
- [19] M. Golterman, PoS **CONFINEMENT8**, 014 (2008), [arXiv:0812.3110].
- [20] C. Bernard, Phys. Rev. **D73**, 114503 (2006), [hep-lat/0603011]; S. R. Sharpe, PoS **LAT2006**, 022 (2006), [hep-lat/0610094].
- [21] J. A. Bailey, Phys. Rev. D **75**, 114505 (2007), [hep-lat/0611023]; Y. Lin *et al.*, Phys. Rev. D **103**, 5, 054510 (2021), [arXiv:2010.10455].
- [22] G. P. Lepage, Phys. Rev. **D59**, 074502 (1999), [hep-lat/9809157].
- [23] A. Bazavov *et al.* (MILC), Rev. Mod. Phys. **82**, 1349 (2010), [arXiv:0903.3598].
- [24] E. Follana *et al.* (HPQCD, UKQCD), Phys. Rev. **D75**, 054502 (2007), [hep-lat/0610092].
- [25] C. T. H. Davies *et al.*, Phys. Rev. **D82**, 114504 (2010), [arXiv:1008.4018].
- [26] C. McNeile *et al.*, Phys. Rev. **D85**, 031503 (2012), [arXiv:1110.4510].
- [27] G. C. Donald *et al.*, Phys. Rev. **D86**, 094501 (2012), [arXiv:1208.2855].
- [28] P. H. Ginsparg and K. G. Wilson, Phys. Rev. **D25**, 2649 (1982).
- [29] P. Hasenfratz, V. Laliena and F. Niedermayer, Phys. Lett. **B427**, 125 (1998), [hep-lat/9801021].
- [30] M. Lüscher, Phys. Lett. **B428**, 342 (1998), [hep-lat/9802011].
- [31] D. B. Kaplan, Phys. Lett. **B288**, 342 (1992), [hep-lat/9206013]; Y. Shamir, Nucl. Phys. **B406**, 90 (1993), [hep-lat/9303005]; Y. Shamir, Nucl. Phys. **B417**, 167 (1994), [hep-lat/9310006].
- [32] H. Neuberger, Phys. Lett. **B417**, 141 (1998), [hep-lat/9707022]; H. Neuberger, Phys. Lett. **B427**, 353 (1998), [hep-lat/9801031].
- [33] A. Borici, NATO Sci. Ser. C **553**, 41 (2000), [hep-lat/9912040].
- [34] A. D. Kennedy (2006), [hep-lat/0607038].
- [35] Z. Bai *et al.* (RBC, UKQCD), Phys. Rev. Lett. **115**, 21, 212001 (2015), [arXiv:1505.07863].
- [36] R. Abbott *et al.* (RBC, UKQCD), Phys. Rev. D **102**, 5, 054509 (2020), [arXiv:2004.09440].
- [37] T. Blum *et al.* (2023), [arXiv:2306.06781].
- [38] E. Shintani *et al.* (JLQCD), Phys. Rev. Lett. **101**, 242001 (2008), [arXiv:0806.4222].
- [39] P. A. Boyle *et al.*, JHEP **12**, 008 (2017), [arXiv:1701.02644].
- [40] K. Nakayama, B. Fahy and S. Hashimoto, Phys. Rev. **D94**, 5, 054507 (2016), [arXiv:1606.01002].
- [41] D. Hatton *et al.* (HPQCD), Phys. Rev. D **102**, 5, 054511 (2020), [arXiv:2005.01845].
- [42] J. Harrison and C. T. H. Davies (HPQCD), Phys. Rev. D **105**, 9, 094506 (2022), [arXiv:2105.11433].
- [43] A. Bazavov *et al.*, Phys. Rev. **D98**, 7, 074512 (2018), [arXiv:1712.09262].
- [44] A. Bazavov *et al.* (Fermilab Lattice, MILC, TUMQCD), Phys. Rev. **D98**, 5, 054517 (2018), [arXiv:1802.04248].
- [45] D. Hatton *et al.*, Phys. Rev. D **103**, 5, 054512 (2021), [arXiv:2101.08103].
- [46] E. Eichten and B. R. Hill, Phys. Lett. **B234**, 511 (1990).
- [47] J. Heitger and R. Sommer (ALPHA), JHEP **02**, 022 (2004), [hep-lat/0310035]; B. Blossier *et al.* (ALPHA), JHEP **12**, 039 (2010), [arXiv:1006.5816].
- [48] B. A. Thacker and G. P. Lepage, Phys. Rev. **D43**, 196 (1991); G. P. Lepage *et al.*, Phys. Rev. **D46**, 4052 (1992), [hep-lat/9205007].
- [49] R. J. Dowdall *et al.* (HPQCD), Phys. Rev. **D85**, 054509 (2012), [arXiv:1110.6887].
- [50] A. X. El-Khadra, A. S. Kronfeld and P. B. Mackenzie, Phys. Rev. **D55**, 3933 (1997), [hep-lat/9604004].
- [51] S. Aoki, Y. Kuramashi and S.-i. Tominaga, Prog. Theor. Phys. **109**, 383 (2003), [hep-lat/0107009].

- [52] N. H. Christ, M. Li and H.-W. Lin, Phys. Rev. **D76**, 074505 (2007), [hep-lat/0608006].
- [53] Y. Aoki *et al.* (RBC, UKQCD), Phys. Rev. **D86**, 116003 (2012), [arXiv:1206.2554].
- [54] N. H. Christ *et al.*, Phys. Rev. **D91**, 5, 054502 (2015), [arXiv:1404.4670].
- [55] M. B. Oktay and A. S. Kronfeld, Phys. Rev. **D78**, 014504 (2008), [arXiv:0803.0523].
- [56] J. A. Bailey *et al.*, Eur. Phys. J. **C77**, 11, 768 (2017), [arXiv:1701.00345].
- [57] B. Blossier *et al.* (ETM), JHEP **04**, 049 (2010), [arXiv:0909.3187].
- [58] A. Bussone *et al.* (ETM), Phys. Rev. D **93**, 11, 114505 (2016), [arXiv:1603.04306].
- [59] S. Borsanyi *et al.*, Science **347**, 1452 (2015), [arXiv:1406.4088].
- [60] S. Aoki *et al.* (Flavour Lattice Averaging Group), Eur. Phys. J. C **80**, 2, 113 (2020), [arXiv:1902.08191].
- [61] M. Hayakawa and S. Uno, Prog. Theor. Phys. **120**, 413 (2008), [arXiv:0804.2044].
- [62] N. Carrasco *et al.*, Phys. Rev. **D91**, 7, 074506 (2015), [arXiv:1502.00257].
- [63] M. Di Carlo *et al.*, Phys. Rev. D **105**, 7, 074509 (2022), [arXiv:2109.05002].
- [64] N. H. Christ *et al.*, Phys. Rev. D **108**, 1, 014501 (2023), [arXiv:2304.08026].
- [65] B. Lucini *et al.*, JHEP **02**, 076 (2016), [arXiv:1509.01636].
- [66] L. Bushnaq *et al.* (RCstar), JHEP **03**, 012 (2023), [arXiv:2209.13183].
- [67] R. Horsley *et al.*, J. Phys. G **43**, 10, 10LT02 (2016), [arXiv:1508.06401].
- [68] R. Horsley *et al.* (CSSM, QCDSF, UKQCD), J. Phys. G **46**, 115004 (2019), [arXiv:1904.02304].
- [69] Z. R. Kordov *et al.* (CSSM/QCDSF/UKQCD), Phys. Rev. D **101**, 3, 034517 (2020), [arXiv:1911.02186].
- [70] T. Ishikawa *et al.*, Phys. Rev. Lett. **109**, 072002 (2012), [arXiv:1202.6018].
- [71] M. G. Endres *et al.*, Phys. Rev. Lett. **117**, 7, 072002 (2016), [arXiv:1507.08916].
- [72] G. M. de Divitiis *et al.* (RM123), Phys. Rev. **D87**, 11, 114505 (2013), [arXiv:1303.4896].
- [73] D. Giusti *et al.*, Phys. Rev. **D95**, 11, 114504 (2017), [arXiv:1704.06561].
- [74] P. Boyle *et al.*, JHEP **09**, 153 (2017), [arXiv:1706.05293].
- [75] S. Basak *et al.* (MILC), Phys. Rev. D **99**, 3, 034503 (2019), [arXiv:1807.05556].
- [76] D. Hatton, C. T. H. Davies and G. P. Lepage, Phys. Rev. D **102**, 9, 094514 (2020), [arXiv:2009.07667].
- [77] D. Hatton *et al.*, Phys. Rev. D **103**, 11, 114508 (2021), [arXiv:2102.09609].
- [78] F. Bloch and A. Nordsieck, Phys. Rev. **52**, 54 (1937).
- [79] D. Giusti *et al.*, Phys. Rev. Lett. **120**, 7, 072001 (2018), [arXiv:1711.06537].
- [80] M. Di Carlo *et al.*, Phys. Rev. D **100**, 3, 034514 (2019), [arXiv:1904.08731].
- [81] P. Boyle *et al.*, JHEP **02**, 242 (2023), [arXiv:2211.12865].
- [82] C. T. Sachrajda *et al.*, PoS **LATTICE2019**, 162 (2019), [arXiv:1910.07342]; C.-Y. Seng *et al.*, JHEP **10**, 179 (2020), [arXiv:2009.00459].
- [83] R. Sommer, Nucl. Phys. B **411**, 839 (1994), [hep-lat/9310022].
- [84] M. Lüscher, JHEP **08**, 071 (2010), [Erratum: JHEP 03, 092 (2014)], [arXiv:1006.4518].
- [85] Y. Aoki *et al.* (Flavour Lattice Averaging Group (FLAG)), Eur. Phys. J. C **82**, 10, 869 (2022), [arXiv:2111.09849].
- [86] M. Bruno *et al.* (ALPHA), Phys. Rev. Lett. **114**, 10, 102001 (2015), [arXiv:1410.8374].
- [87] A. Bazavov *et al.* (Fermilab Lattice, MILC), Phys. Rev. **D93**, 11, 113016 (2016), [arXiv:1602.03560].
- [88] R. J. Dowdall *et al.*, Phys. Rev. **D86**, 094510 (2012), [arXiv:1207.5149].
- [89] C. McNeile *et al.*, Phys. Rev. **D86**, 074503 (2012), [arXiv:1207.0994].
- [90] S. Schaefer, R. Sommer and F. Virota (ALPHA), Nucl. Phys. **B845**, 93 (2011), [arXiv:1009.5228].
- [91] M. Lüscher, PoS **LATTICE2010**, 015 (2010), [arXiv:1009.5877].
- [92] R. Brower *et al.*, Phys. Lett. **B560**, 64 (2003), [hep-lat/0302005].
- [93] S. Aoki *et al.*, Phys. Rev. **D76**, 054508 (2007), [arXiv:0707.0396].
- [94] C. Bernard and D. Toussaint (MILC), Phys. Rev. D **97**, 7, 074502 (2018), [arXiv:1707.05430].
- [95] M. Luscher and S. Schaefer, JHEP **07**, 036 (2011), [arXiv:1105.4749].
- [96] N. Husung, P. Marquard and R. Sommer, Eur. Phys. J. C **80**, 3, 200 (2020), [arXiv:1912.08498].
- [97] N. Husung, P. Marquard and R. Sommer, Phys. Lett. B **829**, 137069 (2022), [arXiv:2111.02347].
- [98] N. Husung, Eur. Phys. J. C **83**, 2, 142 (2023), [arXiv:2206.03536].
- [99] G. Colangelo, S. Dürr and C. Haefeli, Nucl. Phys. **B721**, 136 (2005), [hep-lat/0503014].
- [100] M. Lüscher, Commun. Math. Phys. **104**, 177 (1986).
- [101] G. Martinelli *et al.*, Nucl. Phys. **B445**, 81 (1995), [hep-lat/9411010].
- [102] M. Lüscher *et al.*, Nucl. Phys. **B384**, 168 (1992), [hep-lat/9207009].
- [103] G. Martinelli *et al.*, Phys. Lett. **B411**, 141 (1997), [hep-lat/9705018].
- [104] B. Colquhoun *et al.*, Phys. Rev. **D91**, 7, 074514 (2015), [arXiv:1408.5768].
- [105] D. Hatton *et al.* (HPQCD), Phys. Rev. D **100**, 11, 114513 (2019), [arXiv:1909.00756].
- [106] M. Lüscher *et al.*, Nucl. Phys. **B413**, 481 (1994), [hep-lat/9309005]; M. Della Morte *et al.* (ALPHA), Nucl. Phys. **B713**, 378 (2005), [hep-lat/0411025].
- [107] M. Tomii *et al.* (JLQCD), Phys. Rev. **D94**, 5, 054504 (2016), [arXiv:1604.08702].
- [108] F. Karsch, H. Simma and T. Yoshie, PoS **LATTICE2022**, 244 (2023), [arXiv:2212.08392].
- [109] S. Duane *et al.*, Phys. Lett. **B195**, 216 (1987).
- [110] D. J. E. Callaway and A. Rahman, Phys. Rev. Lett. **49**, 613 (1982).
- [111] D. J. E. Callaway and A. Rahman, Phys. Rev. D **28**, 1506 (1983).
- [112] J. Polonyi and H. W. Wyld, Phys. Rev. Lett. **51**, 2257 (1983), [Erratum: Phys.Rev.Lett. 52, 401 (1984)].
- [113] N. Metropolis *et al.*, J. Chem. Phys. **21**, 1087 (1953).
- [114] M. A. Clark and A. D. Kennedy, Phys. Rev. Lett. **98**, 051601 (2007), [hep-lat/0608015].
- [115] J. C. Sexton and D. H. Weingarten, Nucl. Phys. B **380**, 665 (1992).
- [116] M. Hasenbusch, Phys. Lett. **B519**, 177 (2001), [hep-lat/0107019].
- [117] M. Lüscher, JHEP **05**, 052 (2003), [hep-lat/0304007].

- [118] M. Lüscher, *Comput. Phys. Commun.* **156**, 209 (2004), [hep-lat/0310048].
- [119] M. Lüscher, *JHEP* **07**, 081 (2007), [arXiv:0706.2298].
- [120] M. Lüscher, *JHEP* **12**, 011 (2007), [arXiv:0710.5417].
- [121] A. Stathopoulos and K. Orginos, *SIAM J. Sci. Comput.* **32**, 439 (2010), [arXiv:0707.0131].
- [122] P. A. Boyle (2014), [arXiv:1402.2585].
- [123] R. Babich *et al.*, *Phys. Rev. Lett.* **105**, 201602 (2010), [arXiv:1005.3043].
- [124] A. Frommer *et al.*, *SIAM J. Sci. Comput.* **36**, A1581 (2014), [arXiv:1303.1377].
- [125] M. Bruno, S. Schaefer and R. Sommer (ALPHA), *JHEP* **08**, 150 (2014), [arXiv:1406.5363].
- [126] M. Creutz, *Phys. Rev.* **D38**, 1228 (1988); R. Gupta, G. W. Kilcup and S. R. Sharpe, *Phys. Rev.* **D38**, 1278 (1988).
- [127] P. Fritzsche *et al.*, *PoS LATTICE2021*, 465 (2022), [arXiv:2111.11544].
- [128] M. Cè *et al.*, *PoS LATTICE2021*, 383 (2022), [arXiv:2110.15375].
- [129] M. Lüscher, *EPJ Web Conf.* **175**, 01002 (2018), [arXiv:1707.09758].
- [130] M. Lüscher and U. Wolff, *Nucl. Phys.* **B339**, 222 (1990).
- [131] J. J. Dudek *et al.*, *Phys. Rev.* **D82**, 034508 (2010), [arXiv:1004.4930]; J. J. Dudek *et al.*, *Phys. Rev.* **D83**, 111502 (2011), [arXiv:1102.4299]; R. G. Edwards *et al.*, *Phys. Rev.* **D84**, 074508 (2011), [arXiv:1104.5152].
- [132] G. P. Engel *et al.* (BGR [Bern-Graz-Regensburg]), *Phys. Rev.* **D82**, 034505 (2010), [arXiv:1005.1748]; D. Mohler *et al.*, *Phys. Rev. Lett.* **111**, 22, 222001 (2013), [arXiv:1308.3175].
- [133] M. S. Mahbub *et al.*, *Annals Phys.* **342**, 270 (2014), [arXiv:1310.6803].
- [134] J. Bulava *et al.*, *Nucl. Phys.* **B910**, 842 (2016), [arXiv:1604.05593].
- [135] R. Brett *et al.*, *Nucl. Phys.* **B932**, 29 (2018), [arXiv:1802.03100].
- [136] B. Hörz and A. Hanlon, *Phys. Rev. Lett.* **123**, 14, 142002 (2019), [arXiv:1905.04277].
- [137] J. E. Mandula, G. Zweig and J. Govaerts, *Nucl. Phys.* **B228**, 91 (1983); J. E. Mandula and E. Shpiz, *Nucl. Phys.* **B232**, 180 (1984).
- [138] H. B. Meyer and M. J. Teper, *Nucl. Phys.* **B658**, 113 (2003), [hep-lat/0212026].
- [139] O. Bar, A. Broll and R. Sommer, *Eur. Phys. J. C* **83**, 8, 757 (2023), [arXiv:2306.02703].
- [140] P. F. Bedaque, *Phys. Lett. B* **593**, 82 (2004), [arXiv:nucl-th/0402051].
- [141] P. F. Bedaque and J.-W. Chen, *Phys. Lett. B* **616**, 208 (2005), [hep-lat/0412023].
- [142] G. M. de Divitiis, R. Petronzio and N. Tantalo, *Phys. Lett. B* **595**, 408 (2004), [hep-lat/0405002].
- [143] C. Bourrely, B. Machet and E. de Rafael, *Nucl. Phys.* **B189**, 157 (1981).
- [144] C. G. Boyd, B. Grinstein and R. F. Lebed, *Phys. Rev. Lett.* **74**, 4603 (1995), [hep-ph/9412324].
- [145] T. Becher and R. J. Hill, *Phys. Lett.* **B633**, 61 (2006), [hep-ph/0509090].
- [146] C. Bourrely, I. Caprini and L. Lellouch, *Phys. Rev.* **D79**, 013008 (2009), [Erratum: *Phys. Rev.* **D82**, 099902(2010)], [arXiv:0807.2722].
- [147] M. Lüscher, *Commun. Math. Phys.* **105**, 153 (1986); M. Lüscher, *Nucl. Phys.* **B364**, 237 (1991).
- [148] L. Maiani and M. Testa, *Phys. Lett.* **B245**, 585 (1990).
- [149] M. T. Hansen, H. B. Meyer and D. Robaina, *Phys. Rev.* **D96**, 9, 094513 (2017), [arXiv:1704.08993].
- [150] M. Hansen, A. Lupo and N. Tantalo, *Phys. Rev.* **D99**, 9, 094508 (2019), [arXiv:1903.06476]; J. Bulava and M. T. Hansen, *Phys. Rev. D* **100**, 3, 034521 (2019), [arXiv:1903.11735]; M. Bruno and M. T. Hansen, *JHEP* **06**, 043 (2021), [arXiv:2012.11488].
- [151] R. A. Briceño, J. J. Dudek and R. D. Young, *Rev. Mod. Phys.* **90**, 2, 025001 (2018), [arXiv:1706.06223]; N. Brambilla *et al.* (2019), [arXiv:1907.07583].
- [152] F. Romero-López, *PoS LATTICE2022*, 235 (2023), [arXiv:2212.13793]; L. Liu, *PoS LATTICE2022*, 234 (2023).
- [153] M. J. Savage, *Prog. Part. Nucl. Phys.* **67**, 140 (2012), [arXiv:1110.5943]; T. Inoue *et al.* (HAL QCD), *Phys. Rev.* **C91**, 1, 011001 (2015), [arXiv:1408.4892]; B. Hörz *et al.*, *Phys. Rev. C* **103**, 1, 014003 (2021), [arXiv:2009.11825].
- [154] K. Polejaeva and A. Rusetsky, *Eur. Phys. J.* **A48**, 67 (2012), [arXiv:1203.1241]; R. A. Briceño and Z. Davoudi, *Phys. Rev.* **D87**, 9, 094507 (2013), [arXiv:1212.3398]; M. T. Hansen and S. R. Sharpe, *Phys. Rev.* **D90**, 11, 116003 (2014), [arXiv:1408.5933]; M. T. Hansen and S. R. Sharpe, *Phys. Rev.* **D92**, 11, 114509 (2015), [arXiv:1504.04248]; R. Briceño, M. T. Hansen and S. R. Sharpe, *Phys. Rev.* **D95**, 7, 074510 (2017), [arXiv:1701.07465]; H. W. Hammer, J. Y. Pang and A. Rusetsky, *JHEP* **10**, 115 (2017), [arXiv:1707.02176]; R. A. Briceño, M. T. Hansen and S. R. Sharpe, *Phys. Rev.* **D99**, 1, 014516 (2019), [arXiv:1810.01429]; M. Mai and M. Döring, *Eur. Phys. J.* **A53**, 12, 240 (2017), [arXiv:1709.08222]; M. T. Hansen, F. Romero-López and S. R. Sharpe, *JHEP* **07**, 047 (2020), [Erratum: *JHEP* **02**, 014 (2021)], [arXiv:2003.10974]; T. D. Blanton and S. R. Sharpe, *Phys. Rev. D* **103**, 5, 054503 (2021), [arXiv:2011.05520]; T. D. Blanton and S. R. Sharpe, *Phys. Rev. D* **104**, 3, 034509 (2021), [arXiv:2105.12094]; Z. T. Draper *et al.*, *JHEP* **07**, 226 (2023), [arXiv:2303.10219].
- [155] T. D. Blanton, F. Romero-López and S. R. Sharpe, *Phys. Rev. Lett.* **124**, 3, 032001 (2020), [arXiv:1909.02973]; C. Culver *et al.*, *Phys. Rev. D* **101**, 11, 114507 (2020), [arXiv:1911.09047]; A. Alexandru *et al.*, *Phys. Rev. D* **102**, 11, 114523 (2020), [arXiv:2009.12358]; R. Brett *et al.*, *Phys. Rev. D* **104**, 1, 014501 (2021), [arXiv:2101.06144]; Z. T. Draper *et al.*, *JHEP* **05**, 137 (2023), [arXiv:2302.13587].
- [156] M. Mai *et al.* (GWQCD), *Phys. Rev. Lett.* **127**, 22, 222001 (2021), [arXiv:2107.03973].
- [157] M. T. Hansen and S. R. Sharpe, *Ann. Rev. Nucl. Part. Sci.* **69**, 65 (2019), [arXiv:1901.00483]; M. Mai, M. Döring and A. Rusetsky, *Eur. Phys. J. ST* **230**, 6, 1623 (2021), [arXiv:2103.00577].
- [158] L. Lellouch and M. Lüscher, *Commun. Math. Phys.* **219**, 31 (2001), [hep-lat/0003023].
- [159] T. Blum *et al.*, *Phys. Rev. Lett.* **108**, 141601 (2012), [arXiv:1111.1699]; T. Blum *et al.*, *Phys. Rev.* **D86**, 074513 (2012), [arXiv:1206.5142].
- [160] T. Blum *et al.*, *Phys. Rev.* **D91**, 7, 074502 (2015), [arXiv:1502.00263].
- [161] V. Bernard *et al.*, *JHEP* **01**, 019 (2011), [arXiv:1010.6018]; M. Doring *et al.*, *Eur. Phys. J.* **A47**, 139 (2011), [arXiv:1107.3988]; M. T. Hansen and S. R. Sharpe, *Phys. Rev.* **D86**, 016007 (2012), [arXiv:1204.0826]; R. A. Briceño and Z. Davoudi, *Phys. Rev.* **D88**, 9, 094507 (2013), [arXiv:1204.1110].
- [162] R. Briceño, M. T. Hansen and A. Walker-Loud, *Phys. Rev.* **D91**, 3, 034501 (2015), [arXiv:1406.5965].
- [163] R. Briceño and M. T. Hansen, *Phys. Rev.* **D94**, 1, 013008 (2016), [arXiv:1509.08507].
- [164] R. Briceño *et al.*, *Phys. Rev.* **D93**, 11, 114508 (2016), [arXiv:1604.03530].

- [165] C. Alexandrou *et al.*, Phys. Rev. D **98**, 7, 074502 (2018), [Erratum: Phys.Rev.D 105, 019902 (2022)], [arXiv:1807.08357].
- [166] A. Radhakrishnan, J. J. Dudek and R. G. Edwards (Hadron Spectrum), Phys. Rev. D **106**, 11, 114513 (2022), [arXiv:2208.13755].
- [167] F. Müller and A. Rusetsky, JHEP **03**, 152 (2021), [arXiv:2012.13957].
- [168] M. T. Hansen, F. Romero-López and S. R. Sharpe, JHEP **04**, 113 (2021), [arXiv:2101.10246].
- [169] D. Agadjanov *et al.*, JHEP **06**, 043 (2016), [arXiv:1603.07205].
- [170] S. Hashimoto, PTEP **2017**, 5, 053B03 (2017), [arXiv:1703.01881].
- [171] P. Gambino and S. Hashimoto, Phys. Rev. Lett. **125**, 3, 032001 (2020), [arXiv:2005.13730].
- [172] H. Fukaya *et al.*, Phys. Rev. D **102**, 11, 114516 (2020), [arXiv:2010.01253].
- [173] P. Gambino *et al.*, JHEP **07**, 083 (2022), [arXiv:2203.11762].
- [174] A. Barone *et al.*, JHEP **07**, 145 (2023), [arXiv:2305.14092].
- [175] A. Evangelista *et al.* (2023), [arXiv:2308.03125].
- [176] C. Bernard *et al.*, Nucl. Phys. Proc. Suppl. **119**, 170 (2003), [hep-lat/0209086].
- [177] S. Perantonis and C. Michael, Nucl. Phys. **B347**, 854 (1990).
- [178] G. S. Bali and K. Schilling, Phys. Rev. **D46**, 2636 (1992).
- [179] S. Necco and R. Sommer, Nucl. Phys. **B622**, 328 (2002), [hep-lat/0108008].
- [180] J. M. Blairon *et al.*, Nucl. Phys. **B180**, 439 (1981).
- [181] H. Fukaya *et al.* (JLQCD), Phys. Rev. Lett. **104**, 122002 (2010), [Erratum: Phys. Rev. Lett.105,159901(2010)], [arXiv:0911.5555].
- [182] H. Fukaya *et al.* (JLQCD, TWQCD), Phys. Rev. **D83**, 074501 (2011), [arXiv:1012.4052].
- [183] L. Giusti and M. Lüscher, JHEP **03**, 013 (2009), [arXiv:0812.3638].
- [184] K. Cichy, E. Garcia-Ramos and K. Jansen, JHEP **10**, 175 (2013), [arXiv:1303.1954].
- [185] G. P. Engel *et al.*, Phys. Rev. Lett. **114**, 11, 112001 (2015), [arXiv:1406.4987].
- [186] G. P. Engel *et al.*, Phys. Rev. **D91**, 5, 054505 (2015), [arXiv:1411.6386].
- [187] G. Cossu *et al.*, PTEP **2016**, 9, 093B06 (2016), [arXiv:1607.01099].
- [188] S. Aoki *et al.*, Eur. Phys. J. **C77**, 2, 112 (2017), [arXiv:1607.00299].
- [189] G. S. Bali *et al.* (RQCD), JHEP **08**, 137 (2021), [arXiv:2106.05398].
- [190] T. Blum *et al.* (RBC, UKQCD), Phys. Rev. **D93**, 7, 074505 (2016), [arXiv:1411.7017].
- [191] B. J. Choi *et al.* (SWME), Phys. Rev. **D93**, 1, 014511 (2016), [arXiv:1509.00592].
- [192] J. Laiho and R. S. Van de Water, PoS **LATTICE2011**, 293 (2011), [arXiv:1112.4861].
- [193] T. Blum *et al.* (RBC, UKQCD), Phys. Rev. D **93**, 7, 074505 (2016), [arXiv:1411.7017].
- [194] B. J. Choi *et al.* (SWME), Phys. Rev. D **93**, 1, 014511 (2016), [arXiv:1509.00592].
- [195] E. Gamiz *et al.* (HPQCD), Phys. Rev. **D80**, 014503 (2009), [arXiv:0902.1815].
- [196] R. J. Dowdall *et al.*, Phys. Rev. D **100**, 9, 094508 (2019), [arXiv:1907.01025].
- [197] Y. Aoki *et al.*, Phys. Rev. **D91**, 11, 114505 (2015), [arXiv:1406.6192].
- [198] N. Carrasco *et al.* (ETM), Phys. Rev. D **92**, 3, 034516 (2015), [arXiv:1505.06639].
- [199] A. Bazavov *et al.*, Phys. Rev. **D97**, 3, 034513 (2018), [arXiv:1706.04622].
- [200] C. T. H. Davies *et al.* (HPQCD), Phys. Rev. Lett. **124**, 8, 082001 (2020), [arXiv:1910.00970].
- [201] M. Ademollo and R. Gatto, Phys. Rev. Lett. **13**, 264 (1964).
- [202] H. Leutwyler and M. Roos, Z. Phys. **C25**, 91 (1984).
- [203] P. A. Boyle *et al.*, Phys. Rev. Lett. **100**, 141601 (2008), [arXiv:0710.5136].
- [204] V. Lubicz *et al.* (ETM), Phys. Rev. **D80**, 111502 (2009), [arXiv:0906.4728]; V. Lubicz *et al.* (ETM), PoS **LATTICE2010**, 316 (2010), [arXiv:1012.3573].
- [205] P. A. Boyle *et al.* (RBC-UKQCD), Eur. Phys. J. **C69**, 159 (2010), [arXiv:1004.0886].
- [206] A. Bazavov *et al.*, Phys. Rev. **D87**, 073012 (2013), [arXiv:1212.4993].
- [207] T. Kaneko *et al.* (JLQCD), PoS **LATTICE2012**, 111 (2012), [arXiv:1211.6180].
- [208] P. A. Boyle *et al.*, JHEP **08**, 132 (2013), [arXiv:1305.7217].
- [209] P. A. Boyle *et al.* (RBC/UKQCD), JHEP **06**, 164 (2015), [arXiv:1504.01692].
- [210] N. Carrasco *et al.*, Phys. Rev. **D93**, 11, 114512 (2016), [arXiv:1602.04113]; A. Bazavov *et al.* (Fermilab Lattice, MILC), Phys. Rev. D **99**, 11, 114509 (2019), [arXiv:1809.02827].
- [211] H. Na *et al.*, Phys. Rev. **D82**, 114506 (2010), [arXiv:1008.4562].
- [212] H. Na *et al.*, Phys. Rev. **D84**, 114505 (2011), [arXiv:1109.1501].
- [213] V. Lubicz *et al.* (ETM), Phys. Rev. **D96**, 5, 054514 (2017), [Erratum: Phys. Rev. D99, 099902(2019)], [arXiv:1706.03017].
- [214] T. Kaneko *et al.* (JLQCD), EPJ Web Conf. **175**, 13007 (2018), [arXiv:1711.11235].
- [215] B. Chakraborty *et al.* ((HPQCD Collaboration)§, HPQCD), Phys. Rev. D **104**, 3, 034505 (2021), [arXiv:2104.09883].
- [216] A. Bazavov *et al.* (Fermilab Lattice, MILC), Phys. Rev. D **107**, 9, 094516 (2023), [arXiv:2212.12648].
- [217] S. Meinel, Phys. Rev. Lett. **118**, 8, 082001 (2017), [arXiv:1611.09696].
- [218] S. Meinel, Phys. Rev. D **97**, 3, 034511 (2018), [arXiv:1712.05783].
- [219] E. Dalgic *et al.*, Phys. Rev. **D73**, 074502 (2006), [Erratum: Phys. Rev. D75,119906(2007)], [hep-lat/0601021].
- [220] J. M. Flynn *et al.*, Phys. Rev. **D91**, 7, 074510 (2015), [arXiv:1501.05373].
- [221] J. A. Bailey *et al.* (Fermilab Lattice, MILC), Phys. Rev. **D92**, 1, 014024 (2015), [arXiv:1503.07839].
- [222] B. Colquhoun *et al.*, Phys. Rev. **D93**, 3, 034502 (2016), [arXiv:1510.07446].
- [223] Z. Gelzer *et al.*, EPJ Web Conf. **175**, 13024 (2018), [arXiv:1710.09442].
- [224] B. Colquhoun *et al.* (JLQCD), Phys. Rev. D **106**, 5, 054502 (2022), [arXiv:2203.04938].
- [225] C. M. Bouchard *et al.*, Phys. Rev. D **90**, 054506 (2014), [arXiv:1406.2279].
- [226] C. J. Monahan *et al.*, Phys. Rev. D **98**, 11, 114509 (2018), [arXiv:1808.09285].
- [227] A. Bazavov *et al.* (Fermilab Lattice, MILC), Phys. Rev. D **100**, 3, 034501 (2019), [arXiv:1901.02561].

- [228] J. M. Flynn *et al.* (RBC/UKQCD), Phys. Rev. D **107**, 11, 114512 (2023), [arXiv:2303.11280].
- [229] M. C. Arnesen *et al.*, Phys. Rev. Lett. **95**, 071802 (2005), [hep-ph/0504209]; J. A. Bailey *et al.*, Phys. Rev. **D79**, 054507 (2009), [arXiv:0811.3640].
- [230] L. Lellouch, Nucl. Phys. B **479**, 353 (1996), [hep-ph/9509358].
- [231] M. Di Carlo *et al.*, Phys. Rev. D **104**, 5, 054502 (2021), [arXiv:2105.02497].
- [232] G. Martinelli, S. Simula and L. Vittorio, JHEP **08**, 022 (2022), [arXiv:2202.10285].
- [233] J. M. Flynn, A. Jüttner and J. T. Tsang (2023), [arXiv:2303.11285].
- [234] S. Hashimoto *et al.*, Phys. Rev. **D61**, 014502 (1999), [hep-ph/9906376]; S. Hashimoto *et al.*, Phys. Rev. **D66**, 014503 (2002), [hep-ph/0110253].
- [235] C. Bernard *et al.*, Phys. Rev. **D79**, 014506 (2009), [arXiv:0808.2519]; J. A. Bailey *et al.* (Fermilab Lattice, MILC), Phys. Rev. **D89**, 11, 114504 (2014), [arXiv:1403.0635]; J. Harrison, C. Davies and M. Wingate (HPQCD), Phys. Rev. **D97**, 5, 054502 (2018), [arXiv:1711.11013]; E. McLean *et al.*, Phys. Rev. **D99**, 11, 114512 (2019), [arXiv:1904.02046]; T. Bhattacharya *et al.* (LANL/SWME), PoS **LATTICE2018**, 283 (2018).
- [236] J. A. Bailey *et al.* (MILC), Phys. Rev. **D92**, 3, 034506 (2015), [arXiv:1503.07237].
- [237] H. Na *et al.* (HPQCD), Phys. Rev. **D92**, 5, 054510 (2015), [Erratum: Phys. Rev. **D93**, 19906(2016)], [arXiv:1505.03925].
- [238] E. McLean *et al.*, Phys. Rev. D **101**, 7, 074513 (2020), [arXiv:1906.00701].
- [239] A. Bazavov *et al.* (Fermilab Lattice, MILC, Fermilab Lattice, MILC), Eur. Phys. J. C **82**, 12, 1141 (2022), [Erratum: Eur.Phys.J.C 83, 21 (2023)], [arXiv:2105.14019].
- [240] J. Harrison and C. T. H. Davies (2023), [arXiv:2304.03137].
- [241] Y. Aoki *et al.* (JLQCD) (2023), [arXiv:2306.05657].
- [242] W. Detmold, C. Lehner and S. Meinel, Phys. Rev. **D92**, 3, 034503 (2015), [arXiv:1503.01421].
- [243] R. R. Horgan *et al.*, Phys. Rev. **D89**, 9, 094501 (2014), [arXiv:1310.3722]; J. A. Bailey *et al.*, Phys. Rev. **D93**, 2, 025026 (2016), [arXiv:1509.06235]; D. Du *et al.*, Phys. Rev. **D93**, 3, 034005 (2016), [arXiv:1510.02349].
- [244] W. G. Parrott, C. Bouchard and C. T. H. Davies ((HPQCD collaboration)§, HPQCD), Phys. Rev. D **107**, 1, 014510 (2023), [arXiv:2207.12468].
- [245] W. Detmold and S. Meinel, Phys. Rev. **D93**, 7, 074501 (2016), [arXiv:1602.01399].
- [246] C. T. H. Davies *et al.* (HPQCD), Phys. Rev. **D78**, 114507 (2008), [arXiv:0807.1687].
- [247] C. McNeile *et al.*, Phys. Rev. **D82**, 034512 (2010), [arXiv:1004.4285].
- [248] A. Bochkarev and P. de Forcrand, Nucl. Phys. B **477**, 489 (1996), [hep-lat/9505025].
- [249] E. Shintani *et al.*, Phys. Rev. **D82**, 7, 074505 (2010), [Erratum: Phys. Rev. **D89**, 099903(2014)], [arXiv:1002.0371].
- [250] R. J. Hudspith *et al.*, Mod. Phys. Lett. **A31**, 32, 1630037 (2016).
- [251] R. J. Hudspith *et al.* (2018), [arXiv:1804.10286].
- [252] S. Cali *et al.*, Phys. Rev. Lett. **125**, 242002 (2020), [arXiv:2003.05781].
- [253] I. Allison *et al.* (HPQCD), Phys. Rev. **D78**, 054513 (2008), [arXiv:0805.2999].
- [254] B. Chakraborty *et al.*, Phys. Rev. **D91**, 5, 054508 (2015), [arXiv:1408.4169].
- [255] Y. Maezawa and P. Petreczky, Phys. Rev. **D94**, 3, 034507 (2016), [arXiv:1606.08798].
- [256] P. Petreczky and J. H. Weber, Phys. Rev. D **100**, 3, 034519 (2019), [arXiv:1901.06424].
- [257] Q. Mason *et al.* (HPQCD, UKQCD), Phys. Rev. Lett. **95**, 052002 (2005), [hep-lat/0503005].
- [258] A. Bazavov *et al.*, Phys. Rev. **D86**, 114031 (2012), [arXiv:1205.6155].
- [259] A. Bazavov *et al.*, Phys. Rev. **D90**, 7, 074038 (2014), [arXiv:1407.8437].
- [260] F. Karbstein, M. Wagner and M. Weber, Phys. Rev. **D98**, 11, 114506 (2018), [arXiv:1804.10909].
- [261] H. Takaura *et al.*, JHEP **04**, 155 (2019), [arXiv:1808.01643].
- [262] A. Bazavov *et al.* (TUMQCD), Phys. Rev. D **100**, 11, 114511 (2019), [arXiv:1907.11747].
- [263] B. Blossier *et al.*, Phys. Rev. **D85**, 034503 (2012), [arXiv:1110.5829]; B. Blossier *et al.*, Phys. Rev. Lett. **108**, 262002 (2012), [arXiv:1201.5770].
- [264] S. Zafeiropoulos *et al.*, Phys. Rev. Lett. **122**, 16, 162002 (2019), [arXiv:1902.08148].
- [265] S. Aoki *et al.* (PACS-CS), JHEP **10**, 053 (2009), [arXiv:0906.3906].
- [266] P. Fritzsche *et al.*, PoS **LATTICE2014**, 291 (2014), [arXiv:1411.7648].
- [267] M. Bruno *et al.* (ALPHA), Phys. Rev. Lett. **119**, 10, 102001 (2017), [arXiv:1706.03821].
- [268] C. Ayala, X. Lobregat and A. Pineda, JHEP **09**, 016 (2020), [arXiv:2005.12301].
- [269] K. Maltman *et al.*, Phys. Rev. D **78**, 114504 (2008), [arXiv:0807.2020].
- [270] S. Dürr *et al.*, Phys. Lett. **B701**, 265 (2011), [arXiv:1011.2403].
- [271] S. Dürr *et al.*, JHEP **08**, 148 (2011), [arXiv:1011.2711].
- [272] A. T. Lytle *et al.* (HPQCD), Phys. Rev. D **98**, 1, 014513 (2018), [arXiv:1805.06225].
- [273] A. Bazavov *et al.* (Fermilab Lattice, MILC, TUMQCD), Phys. Rev. D **98**, 5, 054517 (2018), [arXiv:1802.04248].
- [274] C. Alexandrou *et al.* (Extended Twisted Mass), Phys. Rev. D **104**, 7, 074515 (2021), [arXiv:2104.13408].
- [275] S. Capitani *et al.*, Nucl. Phys. **B544**, 669 (1999), [Erratum: Nucl. Phys. **B582**, 762(2000)], [hep-lat/9810063].
- [276] M. Bruno *et al.* (ALPHA), PoS **LATTICE2018**, 220 (2019), [arXiv:1903.04094].
- [277] J. Komijani, JHEP **08**, 062 (2017), [arXiv:1701.00347]; N. Brambilla *et al.* (TUMQCD), Phys. Rev. D **97**, 3, 034503 (2018), [arXiv:1712.04983].
- [278] A. Bussone *et al.* (ETM), Phys. Rev. **D93**, 11, 114505 (2016), [arXiv:1603.04306].
- [279] F. Burger *et al.*, JHEP **11**, 215 (2015), [arXiv:1505.03283].
- [280] M. Cè *et al.*, JHEP **08**, 220 (2022), [arXiv:2203.08676].
- [281] T. Blum, Phys. Rev. Lett. **91**, 052001 (2003), [hep-lat/0212018].
- [282] T. Aoyama *et al.*, Phys. Rept. **887**, 1 (2020), [arXiv:2006.04822].
- [283] S. Borsanyi *et al.*, Nature **593**, 7857, 51 (2021), [arXiv:2002.12347].
- [284] C. Lehner and A. S. Meyer, Phys. Rev. D **101**, 074515 (2020), [arXiv:2003.04177].
- [285] C. Aubin *et al.*, Phys. Rev. D **106**, 5, 054503 (2022), [arXiv:2204.12256].
- [286] T. Izubuchi *et al.* (PACS), Phys. Rev. D **98**, 5, 054505 (2018), [arXiv:1805.04250]; E. Shintani and Y. Kuramashi (PACS), Phys. Rev. D **100**, 3, 034517 (2019), [arXiv:1902.00885].
- [287] B. Chakraborty *et al.* (Fermilab Lattice, HPQCD, MILC), Phys. Rev. Lett. **120**, 15, 152001 (2018), [arXiv:1710.11212].

- [288] T. Blum *et al.* (RBC, UKQCD), Phys. Rev. Lett. **121**, 2, 022003 (2018), [arXiv:1801.07224]; D. Giusti *et al.*, Phys. Rev. D **99**, 11, 114502 (2019), [arXiv:1901.10462].
- [289] B. Chakraborty *et al.*, Phys. Rev. **D93**, 7, 074509 (2016), [arXiv:1512.03270].
- [290] G. Ray *et al.*, PoS **LATTICE2022**, 329 (2023), [arXiv:2212.12031].
- [291] M. Cè *et al.*, Phys. Rev. D **106**, 11, 114502 (2022), [arXiv:2206.06582].
- [292] C. Alexandrou *et al.* (Extended Twisted Mass), Phys. Rev. D **107**, 7, 074506 (2023), [arXiv:2206.15084].
- [293] E.-H. Chao, H. B. Meyer and J. Parrino, Phys. Rev. D **107**, 5, 054505 (2023), [arXiv:2211.15581]; T. Blum *et al.* (RBC, UKQCD), Phys. Rev. D **108**, 5, 054507 (2023), [arXiv:2301.08696]; G. Wang *et al.* (chiQCD), Phys. Rev. D **107**, 3, 034513 (2023), [arXiv:2204.01280]; A. Bazavov *et al.* (Fermilab Lattice, HPQCD, MILC), Phys. Rev. D **107**, 11, 114514 (2023), [arXiv:2301.08274].
- [294] T. Blum *et al.*, Phys. Rev. Lett. **114**, 1, 012001 (2015), [arXiv:1407.2923]; T. Blum *et al.*, Phys. Rev. **D93**, 1, 014503 (2016), [arXiv:1510.07100]; J. Green *et al.*, Phys. Rev. Lett. **115**, 22, 222003 (2015), [arXiv:1507.01577]; T. Blum *et al.*, Phys. Rev. Lett. **118**, 2, 022005 (2017), [arXiv:1610.04603]; T. Blum *et al.*, Phys. Rev. **D96**, 3, 034515 (2017), [arXiv:1705.01067]; T. Blum *et al.*, Phys. Rev. Lett. **124**, 13, 132002 (2020), [arXiv:1911.08123]; E.-H. Chao *et al.*, Eur. Phys. J. C **80**, 9, 869 (2020), [arXiv:2006.16224]; E.-H. Chao *et al.*, Eur. Phys. J. C **81**, 7, 651 (2021), [arXiv:2104.02632]; T. Blum *et al.* (2023), [arXiv:2304.04423].
- [295] Z. Bai *et al.*, Phys. Rev. Lett. **113**, 112003 (2014), [arXiv:1406.0916].
- [296] N. H. Christ *et al.*, Phys. Rev. D **91**, 11, 114510 (2015), [arXiv:1504.01170].
- [297] Z. Bai *et al.* (2023), [arXiv:2309.01193].
- [298] N. H. Christ *et al.* (RBC, UKQCD), Phys. Rev. **D92**, 9, 094512 (2015), [arXiv:1507.03094]; N. H. Christ *et al.* (RBC, UKQCD), Phys. Rev. **D93**, 11, 114517 (2016), [arXiv:1605.04442]; N. H. Christ *et al.*, Phys. Rev. **D94**, 11, 114516 (2016), [arXiv:1608.07585]; Z. Bai *et al.*, Phys. Rev. Lett. **118**, 25, 252001 (2017), [arXiv:1701.02858]; Z. Bai *et al.*, Phys. Rev. **D98**, 7, 074509 (2018), [arXiv:1806.11520]; N. H. Christ *et al.* (RBC, UKQCD), Phys. Rev. D **100**, 11, 114506 (2019), [arXiv:1910.10644].
- [299] N. Christ *et al.*, Phys. Rev. Lett. **130**, 19, 191901 (2023), [arXiv:2208.03834].
- [300] D. Giusti *et al.*, Phys. Rev. D **107**, 7, 074507 (2023), [arXiv:2302.01298]; A. Desiderio *et al.*, Phys. Rev. D **103**, 1, 014502 (2021), [arXiv:2006.05358]; G. Gagliardi *et al.*, Phys. Rev. D **105**, 11, 114507 (2022), [arXiv:2202.03833].
- [301] P.-X. Ma *et al.*, Phys. Rev. D **103**, 114503 (2021), [arXiv:2102.12048]; J.-S. Yoo *et al.*, Phys. Rev. D **108**, 3, 034508 (2023), [arXiv:2305.03198].
- [302] P.-X. Ma *et al.* (2023), [arXiv:2308.16755].
- [303] *Proceedings, 39th International Symposium on Lattice Field Theory*, volume PoS **LATTICE2022** (2022), URL <https://pos.sissa.it/430/>.
- [304] A. S. Kronfeld *et al.* (USQCD) (2022), [arXiv:2207.07641]; P. Boyle *et al.*, in “Snowmass 2021,” (2022), [arXiv:2204.00039]; D. Boyda *et al.*, in “Snowmass 2021,” (2022), [arXiv:2202.05838]; Z. Davoudi *et al.*, in “Snowmass 2021,” (2022), [arXiv:2209.10758].
- [305] M. Constantinou *et al.* (2022), [arXiv:2202.07193].
- [306] A. S. Meyer, A. Walker-Loud and C. Wilkinson, Ann. Rev. Nucl. Part. Sci. **72**, 205 (2022), [arXiv:2201.01839].
- [307] R. C. Brower *et al.* (USQCD) (2019), [arXiv:1904.09964].

18. Structure Functions

Revised August 2023 by E.C. Aschenauer (BNL), R.S. Thorne (UCL) and R. Yoshida (ANL).

18.1 Deep inelastic scattering

High-energy lepton-nucleon scattering plays a key role in determining the partonic structure of the proton. The process $\ell N \rightarrow \ell' X$ is illustrated in Fig. 18.1. The filled circle in this figure represents the internal structure of the proton which can be expressed in terms of structure functions.

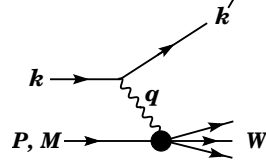


Figure 18.1: Kinematic quantities for the description of deep inelastic scattering. The quantities k and k' are the four-momenta of the incoming and outgoing leptons, P is the four-momentum of a nucleon with mass M , and W is the mass of the recoiling system X . The exchanged particle is a γ , W^\pm , or Z ; it transfers four-momentum $q = k - k'$ to the nucleon.

Invariant quantities:

$\nu = \frac{q \cdot P}{M} = E - E'$ is the lepton's energy loss in the nucleon rest frame (in earlier literature sometimes $\nu = q \cdot P$). Here, E and E' are the initial and final lepton energies in the nucleon rest frame.

$Q^2 = -q^2 = 2(E E' - \vec{k} \cdot \vec{k}') - m_\ell^2 - m_{\ell'}^2$, where m_ℓ ($m_{\ell'}$) is the initial (final) lepton mass. If $E E' \sin^2(\theta/2) \gg m_\ell^2, m_{\ell'}^2$, then

$\approx 4E E' \sin^2(\theta/2)$, where θ is the lepton's scattering angle with respect to the lepton beam direction.

$x = \frac{Q^2}{2M\nu}$ where, in the parton model, x is the fraction of the nucleon's momentum carried by the struck quark. Beyond leading order the equation remains the definition of x , but this is no longer identical to nucleon momentum fraction.

$y = \frac{q \cdot P}{k \cdot P} = \frac{\nu}{E}$ is the fraction of the lepton's energy lost in the nucleon rest frame.

$W^2 = (P + q)^2 = M^2 + 2M\nu - Q^2$ is the mass squared of the system X recoiling against the scattered lepton.

$s = (k + P)^2 = \frac{Q^2}{xy} + M^2 + m_\ell^2$ is the center-of-mass energy squared of the lepton-nucleon system.

The process in Fig. 18.1 is called deep ($Q^2 \gg M^2$) inelastic ($W^2 \gg M^2$) scattering (DIS). In what follows, the masses of the initial and scattered leptons, m_ℓ and $m_{\ell'}$, are neglected.

18.1.1 DIS cross sections

The double-differential cross section for deep inelastic scattering can be expressed in terms of kinematic variables in several ways.

$$\frac{d^2\sigma}{dx dy} = x(s - M^2) \frac{d^2\sigma}{dx dQ^2} = \frac{2\pi M\nu}{E'} \frac{d^2\sigma}{d\Omega_{N\text{rest}} dE'} \quad (18.1)$$

In lowest-order perturbation theory, the cross section for the scattering of polarized leptons on polarized nucleons can be expressed in terms of the products of leptonic and hadronic tensors associated with the coupling of the exchanged bosons at the upper and lower vertices in Fig. 18.1 (see Refs. [1–4])

$$\frac{d^2\sigma}{dx dy} = \frac{2\pi y \alpha^2}{Q^4} \sum_j \eta_j L_j^{\mu\nu} W_{\mu\nu}^j \quad (18.2)$$

For neutral-current processes, the summation is over $j = \gamma, Z$ and γZ representing photon and Z exchange and the interference

between them, whereas for charged-current interactions there is only W exchange, $j = W$. (For transverse nucleon polarization, there is a dependence on the azimuthal angle of the scattered lepton.) The lepton tensor $L_{\mu\nu}$ is associated with the coupling of the exchange boson to the leptons. For incoming leptons of charge $e = \pm 1$ and helicity $\lambda = \pm 1$,

$$\begin{aligned} L_{\mu\nu}^\gamma &= 2(k_\mu k'_\nu + k'_\mu k_\nu - (k \cdot k' - m_\ell^2)g_{\mu\nu} - i\lambda \varepsilon_{\mu\nu\alpha\beta} k^\alpha k'^\beta), \\ L_{\mu\nu}^{\gamma Z} &= (g_V^e + e\lambda g_A^e) L_{\mu\nu}^\gamma, \quad L_{\mu\nu}^Z = (g_V^e + e\lambda g_A^e)^2 L_{\mu\nu}^\gamma, \\ L_{\mu\nu}^W &= (1 + e\lambda)^2 L_{\mu\nu}^\gamma, \end{aligned} \quad (18.3)$$

where $g_V^e = -\frac{1}{2} + 2\sin^2\theta_W$, $g_A^e = -\frac{1}{2}$.

Although here the helicity basis is adopted, an alternative approach is to express the tensors in Eq. (18.3) in terms of the polarization of the lepton.

The factors η_j in Eq. (18.2) denote the ratios of the corresponding propagators and couplings to the photon propagator and coupling squared

$$\begin{aligned} \eta_\gamma &= 1; \quad \eta_{\gamma Z} = \left(\frac{G_F M_Z^2}{2\sqrt{2}\pi\alpha} \right) \left(\frac{Q^2}{Q^2 + M_Z^2} \right); \\ \eta_Z &= \eta_{\gamma Z}^2; \quad \eta_W = \frac{1}{2} \left(\frac{G_F M_W^2}{4\pi\alpha} \frac{Q^2}{Q^2 + M_W^2} \right)^2. \end{aligned} \quad (18.4)$$

The hadronic tensor, which describes the interaction of the appropriate electroweak currents with the target nucleon, is given by

$$W_{\mu\nu} = \frac{1}{4\pi} \int d^4z e^{iq \cdot z} \langle P, S | [J_\mu^\dagger(z), J_\nu(0)] | P, S \rangle, \quad (18.5)$$

where J_α is the hadronic contribution to the electromagnetic, or weak current and S denotes the nucleon-spin 4-vector, with $S^2 = -M^2$ and $S \cdot P = 0$.

18.2 Structure functions of the proton

The structure functions are defined in terms of the hadronic tensor (see Refs. [1–3])

$$\begin{aligned} W_{\mu\nu} &= \left(-g_{\mu\nu} + \frac{q_\mu q_\nu}{q^2} \right) F_1(x, Q^2) + \frac{\hat{P}_\mu \hat{P}_\nu}{P \cdot q} F_2(x, Q^2) \\ &- i\varepsilon_{\mu\nu\alpha\beta} \frac{q^\alpha P^\beta}{2P \cdot q} F_3(x, Q^2) \\ &+ i\varepsilon_{\mu\nu\alpha\beta} \frac{q^\alpha}{P \cdot q} \left[S^\beta g_1(x, Q^2) + \left(S^\beta - \frac{S \cdot q}{P \cdot q} P^\beta \right) g_2(x, Q^2) \right] \\ &+ \frac{1}{P \cdot q} \left[\frac{1}{2} (\hat{P}_\mu \hat{S}_\nu + \hat{S}_\mu \hat{P}_\nu) - \frac{S \cdot q}{P \cdot q} \hat{P}_\mu \hat{P}_\nu \right] g_3(x, Q^2) \\ &+ \frac{S \cdot q}{P \cdot q} \left[\frac{\hat{P}_\mu \hat{P}_\nu}{P \cdot q} g_4(x, Q^2) + \left(-g_{\mu\nu} + \frac{q_\mu q_\nu}{q^2} \right) g_5(x, Q^2) \right] \end{aligned} \quad (18.6)$$

where

$$\hat{P}_\mu = P_\mu - \frac{P \cdot q}{q^2} q_\mu, \quad \hat{S}_\mu = S_\mu - \frac{S \cdot q}{q^2} q_\mu \quad (18.7)$$

In [2], the definition of $W_{\mu\nu}$ with $\mu \leftrightarrow \nu$ is adopted, which changes the sign of the $\varepsilon_{\mu\nu\alpha\beta}$ terms in Eq. (18.6), although the formulae given below are unchanged. Ref. [1] tabulates the relation between the structure functions defined in Eq. (18.6) and other choices available in the literature.

The cross sections for neutral- and charged-current deep inelastic scattering on unpolarized nucleons can be written in terms of

the structure functions in the generic form

$$\begin{aligned} \frac{d^2\sigma^i}{dx dy} &= \frac{4\pi\alpha^2}{xyQ^2} \eta^i \left\{ \left(1 - y - \frac{x^2 y^2 M^2}{Q^2} \right) F_2^i \right. \\ &\quad \left. + y^2 x F_1^i \mp \left(y - \frac{y^2}{2} \right) x F_3^i \right\}, \end{aligned} \quad (18.8)$$

where $i = \text{NC, CC}$ corresponds to neutral-current ($eN \rightarrow eX$) or charged-current ($eN \rightarrow \nu X$ or $\nu N \rightarrow eX$) processes, respectively. For incoming neutrinos, $L_{\mu\nu}^W$ of Eq. (18.3) is still true, but with e, λ corresponding to the outgoing charged lepton. In the last term of Eq. (18.8), the $-$ sign is taken for an incoming e^+ or $\bar{\nu}$ and the $+$ sign for an incoming e^- or ν . The factor $\eta^{\text{NC}} = 1$ for unpolarized e^\pm beams, whereas

$$\eta^{\text{CC}} = (1 \pm \lambda)^2 \eta_W \quad (18.9)$$

with \pm for ℓ^\pm ; and where λ is the helicity of the incoming lepton and η_W is defined in Eq. (18.4); for incoming neutrinos $\eta^{\text{CC}} = 4\eta_W$. The CC structure functions, which derive exclusively from W exchange, are

$$F_1^{\text{CC}} = F_1^W, \quad F_2^{\text{CC}} = F_2^W, \quad xF_3^{\text{CC}} = xF_3^W. \quad (18.10)$$

The NC structure functions $F_2^\gamma, F_2^{\gamma Z}, F_2^Z$ are, for $e^\pm N \rightarrow e^\pm X$, given by [5],

$$F_2^{\text{NC}} = F_2^\gamma - (g_V^e \pm \lambda g_A^e) \eta_{\gamma Z} F_2^{\gamma Z} + (g_V^e \mp g_A^e \pm 2\lambda g_V^e g_A^e) \eta_Z F_2^Z \quad (18.11)$$

and similarly for F_1^{NC} , whereas

$$xF_3^{\text{NC}} = -(g_A^e \pm \lambda g_V^e) \eta_{\gamma Z} x F_3^{\gamma Z} + [2g_V^e g_A^e \pm \lambda (g_V^e \mp g_A^e)] \eta_Z x F_3^Z. \quad (18.12)$$

The polarized cross-section difference

$$\Delta\sigma = \sigma(\lambda_n = -1, \lambda_\ell) - \sigma(\lambda_n = 1, \lambda_\ell), \quad (18.13)$$

where λ_ℓ, λ_n are the helicities (± 1) of the incoming lepton and nucleon, respectively, may be expressed in terms of the five structure functions $g_{1,\dots,5}(x, Q^2)$ of Eq. (18.6). Explicitly,

$$\begin{aligned} \frac{d^2\Delta\sigma^i}{dx dy} &= \frac{8\pi\alpha^2}{xyQ^2} \eta^i \left\{ -\lambda_\ell y \left(2 - y - 2x^2 y^2 \frac{M^2}{Q^2} \right) x g_1^i \right. \\ &\quad \left. + \lambda_\ell 4x^3 y^2 \frac{M^2}{Q^2} g_2^i + 2x^2 y \frac{M^2}{Q^2} \left(1 - y - x^2 y^2 \frac{M^2}{Q^2} \right) g_3^i \right. \\ &\quad \left. - \left(1 + 2x^2 y \frac{M^2}{Q^2} \right) \left[\left(1 - y - x^2 y^2 \frac{M^2}{Q^2} \right) g_4^i + x y^2 g_5^i \right] \right\} \end{aligned} \quad (18.14)$$

with $i = \text{NC or CC}$ as before. The Eq. (18.13) corresponds to the difference of antiparallel minus parallel spins of the incoming particles for e^- or ν initiated reactions, but the difference of parallel minus antiparallel for e^+ or $\bar{\nu}$ initiated processes. For longitudinal nucleon polarization, the contributions of g_2 and g_3 are suppressed by powers of M^2/Q^2 . These structure functions give an unsuppressed contribution to the cross section for transverse polarization [1], but in this case the cross-section difference vanishes as $M/Q \rightarrow 0$.

Because the same tensor structure occurs in the spin-dependent and spin-independent parts of the hadronic tensor of Eq. (18.6) in the $M^2/Q^2 \rightarrow 0$ limit, the differential cross-section difference of Eq. (18.14) may be obtained from the differential cross section Eq. (18.8) by replacing

$$F_1 \rightarrow -g_5, \quad F_2 \rightarrow -g_4, \quad F_3 \rightarrow 2g_1, \quad (18.15)$$

and multiplying by two, since the total cross section is the average over the initial-state polarizations. In this limit, Eq. (18.8) and Eq. (18.14) may be written in the form

$$\begin{aligned} \frac{d^2\sigma^i}{dx dy} &= \frac{2\pi\alpha^2}{xyQ^2} \eta^i \left[Y_+ F_2^i \mp Y_- x F_3^i - y^2 F_L^i \right], \\ \frac{d^2\Delta\sigma^i}{dx dy} &= \frac{4\pi\alpha^2}{xyQ^2} \eta^i \left[-Y_+ g_4^i \mp Y_- 2x g_1^i + y^2 g_5^i \right], \end{aligned} \quad (18.16)$$

with $i = \text{NC or CC}$, where $Y_\pm = 1 \pm (1-y)^2$ and

$$F_L^i = F_2^i - 2x F_1^i, \quad g_L^i = g_4^i - 2x g_5^i. \quad (18.17)$$

In the naive quark-parton model, the analogy with the Callan-Gross relations $[6] F_L^i = 0$, are the Dicus relations [7] $g_L^i = 0$. Therefore, there are only two independent polarized structure functions: g_1 (parity conserving) and g_5 (parity violating), in analogy with the unpolarized structure functions F_1 and F_3 .

18.2.1 Structure functions in the quark parton model

In the naive quark-parton model [8, 9], contributions to the structure functions F^i and g^i can be expressed in terms of the quark distribution functions $q(x, Q^2)$ of the proton, where $q = u, \bar{u}, d, \bar{d}$ etc. The quantity $q(x, Q^2) dx$ is the number of quarks (or antiquarks) of designated flavor that carry a momentum fraction between x and $x + dx$ of the proton's momentum in a frame in which the proton momentum is large. One of the most striking predictions of the quark-parton model is that the structure functions F_i, g_i scale, i.e., $F_i(x, Q^2) \rightarrow F_i(x)$ in the Bjorken limit that Q^2 and $\nu \rightarrow \infty$ with x fixed [10]. This property is related to the assumption that the transverse momentum of the partons in the infinite-momentum frame of the proton is small.

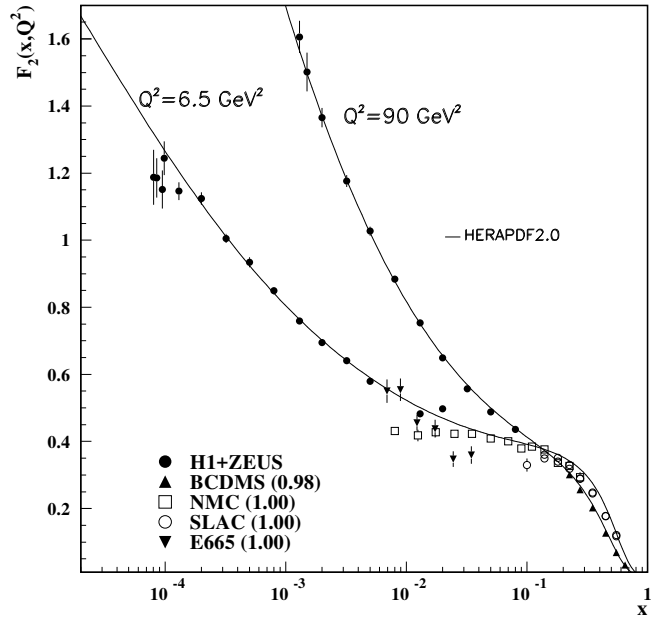


Figure 18.2: The proton structure function F_2^p given at two Q^2 values (6.5 GeV^2 and 90 GeV^2), which exhibit scaling at the ‘pivot’ point $x \sim 0.14$. See the captions in Fig. 18.10 and Fig. 18.12 for the references of the data. The various data sets have been renormalized by the factors shown in brackets in the key to the plot, which were globally determined in a previous HERAPDF analysis [11]. The curves were obtained using the PDFs from the HERAPDF analysis [12]. In practice, data for the reduced cross section, $F_2(x, Q^2) - (y^2/Y_+)F_L(x, Q^2)$, were fitted, rather than F_2 and F_L separately. The agreement between data and theory at low Q^2 and x can be improved by a positive higher-twist correction to $F_L(x, Q^2)$ [13, 14] (see Fig. 8 of Ref. [14]), or small- x resummation [15, 16].

For the neutral-current processes $ep \rightarrow eX$,

$$\begin{aligned} [F_2^\gamma, F_2^{\gamma Z}, F_2^Z] &= x \sum_q [e_q^2, 2e_q g_V^q, g_V^{q^2} + g_A^{q^2}] (q + \bar{q}), \\ [F_3^\gamma, F_3^{\gamma Z}, F_3^Z] &= \sum_q [0, 2e_q g_A^q, 2g_V^q g_A^q] (q - \bar{q}), \\ [g_1^\gamma, g_1^{\gamma Z}, g_1^Z] &= \frac{1}{2} \sum_q [e_q^2, 2e_q g_V^q, g_V^{q^2} + g_A^{q^2}] (\Delta q + \Delta \bar{q}), \\ [g_5^\gamma, g_5^{\gamma Z}, g_5^Z] &= \sum_q [0, e_q g_A^q, g_V^q g_A^q] (\Delta \bar{q} - \Delta q), \end{aligned} \quad (18.18)$$

where $g_V^q = \pm \frac{1}{2} - 2e_q \sin^2 \theta_W$ and $g_A^q = \pm \frac{1}{2}$, with \pm according to whether q is a u - or d -type quark respectively. The quantity Δq is the difference $q \uparrow - q \downarrow$ of the distributions with the quark spin parallel and antiparallel to the proton spin.

For the charged-current processes $e^-p \rightarrow \nu X$ and $\bar{\nu}p \rightarrow e^+X$, the structure functions are:

$$\begin{aligned} F_2^{W^-} &= 2x(u + \bar{d} + \bar{s} + c \dots), \\ F_3^{W^-} &= 2(u - \bar{d} - \bar{s} + c \dots), \\ g_1^{W^-} &= (\Delta u + \Delta \bar{d} + \Delta \bar{s} + \Delta c \dots), \\ g_5^{W^-} &= (-\Delta u + \Delta \bar{d} + \Delta \bar{s} - \Delta c \dots), \end{aligned} \quad (18.19)$$

where only the active flavors have been kept and where CKM mixing has been neglected. For $e^+p \rightarrow \bar{\nu}X$ and $\nu p \rightarrow e^-X$, the structure functions F^{W^+}, g^{W^+} are obtained by the flavor interchanges $d \leftrightarrow u, s \leftrightarrow c$ in the expressions for F^{W^-}, g^{W^-} . The structure functions for scattering on a neutron are obtained from those of the proton by the interchange $u \leftrightarrow d$. For both the neutral- and charged-current processes, the quark-parton model predicts $2xF_1^i = F_2^i$ and $g_4^i = 2xg_5^i$.

Neglecting masses, the structure functions g_2 and g_3 contribute only to scattering from transversely polarized nucleons, and have no simple interpretation in terms of the quark-parton model. They arise from off-diagonal matrix elements $\langle P, \lambda' | [J_\mu^\dagger(z), J_\nu(0)] | P, \lambda \rangle$, where the proton helicities satisfy $\lambda' \neq \lambda$. In fact, the leading-twist contributions to both g_2 and g_3 are both twist-2 and twist-3, which contribute at the same order of Q^2 . The Wandzura-Wilczek relation [17] expresses the twist-2 part of g_2 in terms of g_1 as

$$g_2^i(x) = -g_1^i(x) + \int_x^1 \frac{dy}{y} g_1^i(y). \quad (18.20)$$

However, the twist-3 component of g_2 is unknown. Similarly, there is a relation expressing the twist-2 part of g_3 in terms of g_4 . A complete set of relations, including M^2/Q^2 effects, can be found in [18].

18.2.2 Structure functions and QCD

In QCD, there are perturbative corrections to the partonic cross sections defining structure functions. Also, the radiation of hard gluons from the quarks violates the assumption that the transverse momentum of the partons is small, leading to logarithmic scaling violations, which are particularly large at small x , see Fig. 18.2. The radiation of gluons produces the evolution of the partons and structure functions. As Q^2 increases, more and more gluons are radiated, which in turn split into $q\bar{q}$ pairs. This process leads both to the softening of the initial quark momentum distributions and to the growth of the gluon density and the $q\bar{q}$ sea as x decreases.

For $Q^2 \gg M^2$, the structure functions satisfy the factorization theorem [19],

$$F_i = \sum_a C_i^a \otimes f_a + \mathcal{O}(M^2/Q^2), \quad (18.21)$$

where \otimes denotes the convolution integral

$$C \otimes f = \int_x^1 \frac{dy}{y} C(y) f\left(\frac{x}{y}\right), \quad (18.22)$$

and where the coefficient functions C_i^a , where $a = g$ or q , are given as a power series in α_s . The scale-dependent parton distribution $f_a(x, \mu^2)$ corresponds, at a given x , to the density of parton a in the proton integrated over transverse momentum k_t up to the factorization scale μ . Typically, μ is the scale of the probe Q . For parton distributions x always refers to the nucleon momentum fraction of the parton, whereas for structure functions it retains the definition in Sec. 18.1. The parton evolution in μ is described in QCD by a DGLAP equation (see Refs. [20–23]) which has the schematic form

$$\frac{\partial f_a}{\partial \ln \mu^2} \sim \frac{\alpha_s(\mu^2)}{2\pi} \sum_b (P_{ab} \otimes f_b), \quad (18.23)$$

where the P_{ab} , which describe the parton splitting $b \rightarrow a$, are also given as a power series in α_s . Although perturbative QCD can predict, via Eq. (18.23), the evolution of the parton distribution functions from a particular scale, μ_0 , these DGLAP equations cannot predict them *a priori* at any particular μ_0 . Thus they must be measured at a starting point μ_0 before the predictions of QCD can be compared to the data at other scales, μ . In general, all observables involving a hard hadronic interaction (such as structure functions) can be expressed as a convolution of calculable, process-dependent coefficient functions and these universal parton distributions, e.g. Eq. (18.21).

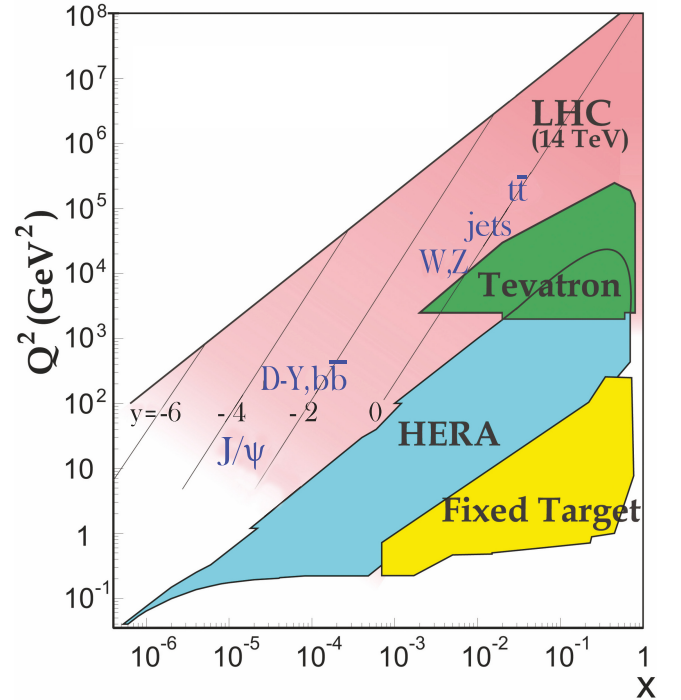


Figure 18.3: Kinematic domains in x and Q^2 probed by fixed-target and collider experiments, where here Q^2 can refer either to the literal Q^2 for deep inelastic scattering, or the hard scale of the process in hadron-hadron collisions, e.g. invariant mass or transverse momentum p_T^2 . Some of the final states accessible at the LHC are indicated in the appropriate regions, where y is the rapidity. The incoming partons have $x_{1,2} = (Q/14 \text{ TeV})e^{\pm y}$ where Q is the hard scale of the process shown in blue in the figure. For example, open charm production [24] and exclusive J/ψ and Υ production [25] at high $|y|$ at the LHC may probe the gluon PDF down to $x \sim 10^{-5}$.

Table 18.1: The main processes relevant to global PDF analyses, ordered in three groups: fixed-target experiments, HERA and the $p\bar{p}$ Tevatron / pp LHC. For each process we give an indication of their dominant partonic subprocesses, the primary partons which are probed and the approximate range of x constrained by the data. This list expands as more processes are measured and calculated with sufficient precision.

Process	Subprocess	Partons	x range
$\ell^\pm \{p, n\} \rightarrow \ell^\pm X$	$\gamma^* q \rightarrow q$	q, \bar{q}, g	$x \gtrsim 0.01$
$\ell^\pm n/p \rightarrow \ell^\pm X$	$\gamma^* d/u \rightarrow d/u$	d/u	$x \gtrsim 0.01$
$pp \rightarrow \mu^+ \mu^- X$	$u\bar{u}, d\bar{d} \rightarrow \gamma^*$	\bar{q}	$0.015 \lesssim x \lesssim 0.35$
$pm/pp \rightarrow \mu^+ \mu^- X$	$(u\bar{d})/(u\bar{u}) \rightarrow \gamma^*$	\bar{d}/\bar{u}	$0.015 \lesssim x \lesssim 0.35$
$\nu(\bar{\nu}) N \rightarrow \mu^-(\mu^+) X$	$W^* q \rightarrow q'$	q, \bar{q}	$0.01 \lesssim x \lesssim 0.5$
$\nu N \rightarrow \mu^- \mu^+ X$	$W^* s \rightarrow c$	s	$0.01 \lesssim x \lesssim 0.2$
$\bar{\nu} N \rightarrow \mu^+ \mu^- X$	$W^* \bar{s} \rightarrow \bar{c}$	\bar{s}	$0.01 \lesssim x \lesssim 0.2$
$e^\pm p \rightarrow e^\pm X$	$\gamma^* q \rightarrow q$	g, q, \bar{q}	$10^{-4} \lesssim x \lesssim 0.1$
$e^+ p \rightarrow \bar{\nu} X$	$W^+ \{d, s\} \rightarrow \{u, c\}$	d, s	$x \gtrsim 0.01$
$e^\pm p \rightarrow e^\pm c\bar{c}X, e^\pm b\bar{b}X$	$\gamma^* c \rightarrow c, \gamma^* g \rightarrow c\bar{c}$	c, b, g	$10^{-4} \lesssim x \lesssim 0.01$
$e^\pm p \rightarrow \text{jet}+X$	$\gamma^* g \rightarrow q\bar{q}$	g	$0.01 \lesssim x \lesssim 0.1$
$p\bar{p}, pp \rightarrow \text{jet}(\text{dijet})+X$	$gg, qg, qq \rightarrow 2j$	g, q	$0.00005 \lesssim x \lesssim 0.5$
$p\bar{p} \rightarrow (W^\pm \rightarrow \ell^\pm \nu) X$	$ud \rightarrow W^+, \bar{u}\bar{d} \rightarrow W^-$	$u, d, s, \bar{u}, \bar{d}, \bar{s}$	$x \gtrsim 0.05$
$pp \rightarrow (W^\pm \rightarrow \ell^\pm \nu) X$	$u\bar{d} \rightarrow W^+, d\bar{u} \rightarrow W^-$	$u, d, s, \bar{u}, \bar{d}, \bar{s}, g$	$x \gtrsim 0.001$
$p\bar{p}(pp) \rightarrow (Z \rightarrow \ell^+ \ell^-) X$	$uu, dd, \dots (u\bar{u}, \dots) \rightarrow Z$	$u, d, s, \dots (g)$	$x \gtrsim 0.001$
$pp \rightarrow W^- c, W^+ \bar{c}$	$gs \rightarrow W^- c$	s, \bar{s}	$x \sim 0.01$
$pp \rightarrow (\gamma^* \rightarrow \ell^+ \ell^-) X$	$u\bar{u}, d\bar{d}, \dots \rightarrow \gamma^*$	\bar{q}, g	$x \gtrsim 10^{-5}$
$pp \rightarrow (\gamma^* \rightarrow \ell^+ \ell^-) X$	$u\gamma, d\gamma, \dots \rightarrow \gamma^*$	γ	$x \gtrsim 10^{-2}$
$pp \rightarrow b\bar{b} X, t\bar{t} X$	$gg \rightarrow b\bar{b}, t\bar{t}$	g	$x \gtrsim 10^{-5}, 10^{-2}$
$pp \rightarrow t(\bar{t}) X,$	$bu(\bar{b}d) \rightarrow td(\bar{t}u)$	$b, d/u$	$x \gtrsim 10^{-2}$
$pp \rightarrow \text{exclusive } J/\psi, \Upsilon$	$\gamma^*(gg) \rightarrow J/\psi, \Upsilon$	g	$x \gtrsim 10^{-5}, 10^{-4}$
$pp \rightarrow \gamma X$	$gq \rightarrow \gamma q, g\bar{q} \rightarrow \gamma \bar{q}$	g	$x \gtrsim 0.005$

It is often convenient to write the evolution equations in terms of the gluon, non-singlet (q^{NS}) and singlet (q^S) quark distributions, such that

$$q^{NS} = q_i - \bar{q}_i \quad (\text{or } q_i - q_j), \quad q^S = \sum_i (q_i + \bar{q}_i). \quad (18.24)$$

The non-singlet distributions have non-zero values of flavor quantum numbers, such as isospin and baryon number. The DGLAP evolution equations then take the form

$$\frac{\partial q^{NS}}{\partial \ln \mu^2} = \frac{\alpha_s(\mu^2)}{2\pi} P_{qq} \otimes q^{NS},$$

$$\frac{\partial}{\partial \ln \mu^2} \begin{pmatrix} q^S \\ g \end{pmatrix} = \frac{\alpha_s(\mu^2)}{2\pi} \begin{pmatrix} P_{qq} & 2n_f P_{qg} \\ P_{gq} & P_{gg} \end{pmatrix} \otimes \begin{pmatrix} q^S \\ g \end{pmatrix}, \quad (18.25)$$

where P are splitting functions that describe the probability of a given parton splitting into two others, and n_f is the number of (active) quark flavors. The leading-order Altarelli-Parisi [22] splitting functions are

$$P_{qq} = \frac{4}{3} \left[\frac{1+x^2}{(1-x)} \right]_+ = \frac{4}{3} \left[\frac{1+x^2}{(1-x)_+} \right] + 2\delta(1-x), \quad (18.26)$$

$$P_{qg} = \frac{1}{2} [x^2 + (1-x)^2], \quad P_{gq} = \frac{4}{3} \left[\frac{1+(1-x)^2}{x} \right], \quad (18.27)$$

$$P_{gg} = 6 \left[\frac{1-x}{x} + x(1-x) + \frac{x}{(1-x)_+} \right] + \left[\frac{11}{2} - \frac{n_f}{3} \right] \delta(1-x), \quad (18.28)$$

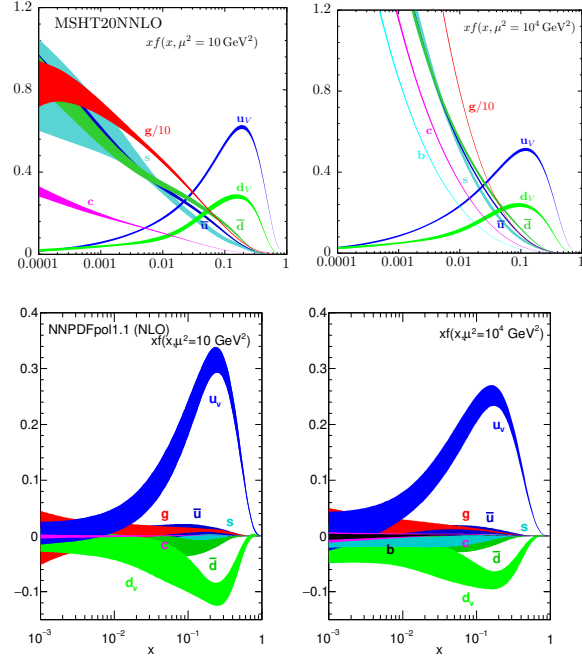


Figure 18.4: The bands are x times the unpolarized parton distributions $f(x)$ (where $f = u_v, d_v, \bar{u}, \bar{d}, s \simeq \bar{s}, c = \bar{c}, b = \bar{b}, g$) obtained in the NNLO MSHT20 global analysis [26] (top) at scales $\mu^2 = 10 \text{ GeV}^2$ (left) and $\mu^2 = 10^4 \text{ GeV}^2$ (right), with $\alpha_s(M_Z^2) = 0.118$. The polarized parton distributions $f(x)$ obtained in the NLO NNPDFpol1.1 fit [27] (bottom).

where the notation $[F(x)]_+$ defines a distribution such that for any sufficiently regular function, $f(x)$,

$$\int_0^1 dx f(x) [F(x)]_+ = \int_0^1 dx (f(x) - f(1)) F(x). \quad (18.29)$$

In general, the splitting functions can be expressed as a power series in α_s . The series contains both terms proportional to $\ln \mu^2$ and to $\ln(1/x)$ and $\ln(1-x)$. The leading-order DGLAP evolution sums up the $(\alpha_s \ln \mu^2)^n$ contributions, while at next-to-leading order (NLO) the sum over the $\alpha_s (\alpha_s \ln \mu^2)^{n-1}$ terms is included [28, 29]. The NNLO contributions to the splitting functions and the DIS coefficient functions are also all known [30–32], as are the N³LO corrections to the coefficient functions [33]. Some Mellin moments of the N³LO splitting functions are also known [34], together with some other pieces of specific information.

In the kinematic region of very small x , one may also sum leading terms in $\ln(1/x)$, independent of the value of $\ln \mu^2$. At leading order, LLx, this is done by the BFKL equation for the unintegrated distributions (see Refs. [35, 36]). The leading-order $(\alpha_s \ln(1/x))^n$ terms result in a power-like growth, $x^{-\omega}$ with $\omega = (12\alpha_s \ln 2)/\pi$, at asymptotic values of $\ln 1/x$. The next-to-leading $\ln 1/x$ (NLLx) contributions are also available [37, 38]. They are so large (and negative) that the results initially appeared to be perturbatively unstable. Methods, based on a combination of collinear and small- x resummations, have been developed which reorganize the perturbative series into a more stable hierarchy [39–42], and this has been used as the basis for a framework for including the corrections in phenomenological studies [43, 44]. There are some limited indications that small- x resummations become necessary for sufficient precision for $x \lesssim 10^{-3}$ at low scales [15, 16]. At sufficiently small x it is expected that evolution should also be affected by non-linear/saturation effects due to a high density of partons, i.e. the gluon density would be so high that gluon-gluon recombination effects would become significant, see [45–47] for reviews. However, there is not yet any very convincing indication for a non-linear regime for $Q^2 \gtrsim 2 \text{ GeV}^2$ in hadron DIS. Better evidence for saturation may be found in more exclu-

sive final states such as dihadron correlations in proton-nucleus collisions, e.g. [48, 49].

The precision of the experimental data demands that at least NLO, and preferably NNLO, DGLAP evolution be used in comparisons between QCD theory and experiment. Beyond the leading order, it is necessary to specify, and to use consistently, both a renormalization and a factorization scheme. The renormalization scheme used almost universally is the modified minimal subtraction ($\overline{\text{MS}}$) scheme [50, 51]. The most popular choices for the factorization scheme is also $\overline{\text{MS}}$ [52]. Historically, sometimes the DIS [53] scheme was adopted, in which there are no higher-order corrections to the F_2 structure function, and this was extended to a specific definition appropriate to small x [54], assimilated in the parton distribution functions.

The discussion above relates to the Q^2 behavior of leading-twist (twist-2) contributions to the structure functions. Higher-twist terms, which involve their own non-perturbative input, exist. These die off as powers of Q ; specifically twist- n terms are damped by $1/Q^{n-2}$. Provided a cut, say $W^2 > 15 \text{ GeV}^2$ is imposed, the higher-twist terms appear to be numerically unimportant for Q^2 above a few GeV^2 , except possibly for very small x and more definitively for x close to 1 [55–57], though it is important to note that they are likely to be larger in $x F_3(x, Q^2)$ than in $F_2(x, Q^2)$ (see e.g. [58]) due to a lack of a constraining sum rule for $x F_3(x, Q^2)$.

18.3 Determination of parton distributions

The parton distribution functions (PDFs) can be determined from an analysis of data for deep inelastic lepton-nucleon scattering and for related hard-scattering processes initiated by nucleons; see Refs. [59–65] for reviews. Table 18.1 highlights some of the processes and their primary sensitivity to PDFs. LHC data are playing an increasing role [66], and new processes are continually being added to the list. Fixed-target and collider experiments have complementary kinematic reach (as is shown in Fig. 18.3), which enables the determination of PDFs over a wide range in x and μ^2 . As more precise LHC data for W^\pm , Z , γ , jet, $b\bar{b}$ and $t\bar{t}$ production become available, tighter constraints on the PDFs are expected in a wider kinematic range. At present about half the constraint on PDFs comes from LHC data [26], but much of the constraint still comes from structure functions.

Recent determinations and releases of the unpolarized PDFs up to NNLO have been made by five groups: MSHT [26], NNPDF [67], CT [68], ATLAS [69] and ABMP [70]. The CJ group produce PDFs at NLO and concentrate on the high x , low Q^2 regime, including data with lower kinematic cuts [71]. All groups start evolution at $Q_0^2 = 1 - 4 \text{ GeV}^2$. Most groups use input PDFs of the form $xf = x^a(\dots)(1-x)^b$ with 14–32 free parameters in total. In these cases the PDF uncertainties are made available using the “Hessian” formulation. The free parameters are expanded around their best fit values, and orthogonal eigenvector sets of PDFs depending on linear combinations of the parameter variations are obtained. The uncertainty is then the quadratic sum of the uncertainties arising from each eigenvector. The NNPDF group combines a Monte Carlo representation of the probability measure in the space of PDFs with the use of neural networks. Fits are performed to a very large number of “replica” data sets obtained by allowing individual data points to fluctuate randomly by amounts determined by the size of the data uncertainties. This results in a set of replicas of unbiased PDF sets. In this case the best prediction is the average obtained using all PDF replicas and the uncertainty is the standard deviation over all replicas. It is possible to convert the eigenvectors of Hessian-based PDFs to Monte Carlo replicas [72] and *vice versa* [73]. Recently accumulated information on N^3LO calculation has been used by MSHT in order to produce a first set of approximate N^3LO global PDFs [74] together with theoretical uncertainties, and an alternative approach to theoretical uncertainty has been made in [75].

In these analyses, the u , d and s quarks are taken to be massless, but the treatment of the heavy c and b quark masses, m_Q , differs, and has a long history, which may be traced from Refs. [76–87]. The MSHT, CT, NNPDF and HERAPDF analyses use different variants of the General-Mass Variable-Flavour-Number Scheme (GM-VFNS). This combines fixed-order contributions to the co-

efficient functions (or partonic cross sections) calculated with the full m_Q dependence, with the all-order resummation of contributions via DGLAP evolution in which the heavy quarks are treated as massless after starting evolution at some transition point. Transition matrix elements are computed, following [79], which provide the boundary conditions between n_f and $n_f + 1$ PDFs. The ABMP analysis uses for structure function calculations a FFNS where only the three light (massless) quarks enter the evolution, while the heavy quarks enter the partonic cross sections with their full m_Q dependence. The GM-VFNS and FFNS approaches yield different results: in particular $\alpha_s(M_Z^2)$ and the large- x gluon PDF at large Q^2 are both significantly smaller in the FFNS. It has been argued [56, 57, 86] that the difference is due to the slow convergence of the $\ln^n(Q^2/m_Q^2)$ terms in certain regions in a FFNS. The final HERA combination of heavy flavour structure function data has been published [88], and the evolution of these measurements and their interpretation may be traced in [89].

The recent determinations of the groups fitting a variety of data and using a GM-VFNS (MSHT, NNPDF and CT) have converged, so that now a good agreement has been achieved between the resulting PDFs. Indeed, the recent global fit PDF sets, CT18 [68], MSHT2018 [26], and NNPDF3.1 [90], have been combined [91] using the Monte Carlo approach [72] mentioned above. The single combined set of PDFs is discussed in detail in Ref. [92].

For illustration, we show in Fig. 18.4 the PDFs obtained in the NNLO MSHT analysis [26] at scales $\mu^2 = 10$ and 10^4 GeV^2 (and an equivalent plot for polarized PDFs from NNPDF [27]). The values of α_s found by MSHT [93] may be taken as representative of those resulting from the GM-VFNS analyses

$$\text{NLO} : \alpha_s(M_Z^2) = 0.1203 \pm 0.0015,$$

$$\text{NNLO} : \alpha_s(M_Z^2) = 0.1174 \pm 0.0013,$$

where the error (at 68% C.L.) corresponds to the uncertainties resulting from the data fitted (the uncertainty that might be expected from the neglect of higher orders is at least as large). A similar results is found by the NNPDF group [94], who find $\alpha_s(M_Z^2) = 0.1185 \pm 0.0012$ at NNLO and the CT group [68], who obtain $\alpha_s(M_Z^2) = 0.1164 \pm 0.0026$. The ABMP analysis [70], which uses a FFNS, finds $\alpha_s(M_Z^2) = 0.1147 \pm 0.0011$ at NNLO.

As a first step towards the inclusion of higher order electroweak corrections a recent development has been a vastly increased understanding of the photon content of the proton. Sets of PDFs with a photon contribution were considered in Refs. [95–97]. However, due to weak data constraints, the uncertainty was extremely large. Subsequently, there has been a much improved understanding of the separation into elastic and inelastic contributions [98–100]. This gives much more theoretical precision, since the elastic contribution, arising from coherent emission of a photon from the proton, can be directly related to the well-known proton electric and magnetic form factors; the model dependence of the inelastic (incoherent) contribution, related to the quark PDFs, is at the level of tens of percent. A final and decisive development directly relating the entire photon contribution to the proton structure function [101] resulted in a determination of the photon content of the proton as precise as that of the light quarks. The framework has been applied within global fits to PDFs via an iterative procedure in [102] and to provide the low-scale input photon PDF in [103, 104]. A further development is the calculation of photon-initiated collider processes directly from structure functions [105].

There are also some calculations of PDFs using lattice QCD, see [106, 107] for a recent review. There has been significant recent progress in the development of efficient algorithms for generating ensembles of gauge field configurations and in tools for extracting the required information from correlation functions. However, there remain a number of sources of systematic uncertainty; discretization effects, pion mass dependence, finite volume effects, excited state contamination and renormalization, which need to be determined and ideally minimised. Moreover, PDFs cannot be determined directly in Euclidean lattice QCD because they depend on quantum fields at light-like separations. Traditionally

the lattice has been used to determine matrix elements of twist two operators which can be related to integer moments of PDFs. Until recently these did not always agree well with determinations using global fit PDFs [106]. However, there have been recent improvements [108–110], though uncertainties are still relatively large. An alternative approach [111] suggested the computation of the matrix elements of frame-dependent, equal-time correlators in the large momentum limit. This leads to so-called Quasi-PDFs, which in the infinite momentum frame can be related to light-cone PDFs via a matching procedure, and there is the closely related pseudo PDF approach [112]. Recent results using physical values of the light quark masses are in [113–117].

Comprehensive sets of PDFs are available from the LHAPDF library [118], which can be linked directly into a user’s programme to provide access to recent PDFs in a standard format. This also includes many nuclear and polarized PDFs.

Nuclear PDFs: The study of the parton distributions for nucleons within nuclei, so-called nuclear parton distribution functions (nPDFs), is now reaching a level of maturity and sophistication similar to nucleon PDFs (and some nuclear target data is often included in determinations of nucleon PDFs), though they are still typically performed at NLO in perturbative QCD. The PDFs are also a function of the nucleon number of the nucleus, A . The nPDFs are obtained via fits to deep inelastic scattering data and dilepton (Drell-Yan) and pion production from proton-nucleus, and most recently also from jet and heavy flavour production data. There are a number of recent examples of NLO analyses, TUJU21 [119], nCTEQ15HQ(HiX) [120, 121], EPPS21 [122], nNNPDF3.0 [123], while NNLO analyses with a smaller selection of data types now also exist [119, 124, 125]. A comparison of the nuclear modification factors for nCTEQ15HQ [120], EPPS21 [122] and nNNPDF3.0 [123] is shown in Fig. 18.6 where, for example, for the up quark $R_u^{Pb} = (Z_{Pb}u_{Pb} + (A_{Pb} - Z_{Pb})d_{Pb}) / (Z_{Pb}u_p + (A_{Pb} - Z_{Pb})d_p)$ i.e. it involves “physical” nuclear PDFs and is normalised such that $R_u^{Pb} = 1$ corresponds to no nuclear effects.

Much of the heavy-nucleus data included are in the form of ratios to proton or deuteron measurements. Initially most nuclear PDFs were related to a particular proton PDF via a nuclear modification factor, i.e.

$$f_i^{p/A}(x, Q^2) = R_i^A(x, Q^2) f_i^p(x, Q^2). \quad (18.30)$$

However, it is now common to parameterise the nuclear PDFs directly but so that they become equal to proton PDFs in the limit $A = 1$, and this approach has been adopted in [119–121, 123]. There is some variation in whether charged current neutrino DIS data is used as well as neutral current DIS data since there is no clear compatibility in the modification factors obtained [126, 127]. Recently, LHC data from vector boson production [128–131] in proton-lead collisions has been used along with DIS data in most fits, though the most recent data [132] shows some tendency to require NNLO corrections. LHC jet data [133] has been included in some fits [122, 123] giving extra constraint on the gluon within nuclei. Further information at smaller x values is also obtained from heavy meson production at LHCb [134]. Single inclusive hadron production e.g. [135, 136], is already sometimes used. All the PDF extractions above are based on the Hessian formulation, except for the NNPDF studies which use Monte Carlo replicas. Agreement between the different nuclear PDFs is generally good, though uncertainty is still large compared to proton PDFs. As well as improved constraints from further LHC data, nPDFs would be very significantly improved by data from a potential high-energy Electron-Ion Collider [137–139].

Double Parton Distributions Double parton scattering (DPS) occurs when two pairs of partons initiate two distinct hard scattering processes in a single collision. It becomes more prevalent at higher collider energies as the parton flux increases. Hence, it is becoming relevant at the LHC, and even more so for planning of higher energy colliders. It has a long theoretical history [140–144], and in recent years experimental studies have

started. DPS is often suppressed, but this is less the case in certain kinematic regions, e.g. when the total transverse momentum of the two hard-scattering processes is small [145–148], when they have a large rapidity separation [149, 150], or when single particle production is suppressed by coupling constants, e.g. like-sign W production [151]. There have been results with some evidence for DPS found from both the Tevatron [152, 153] involving final states with multijets and photons, and at the LHC [154–156] in states with multiple vector bosons or mesons. Recent developments have been involved in putting the theoretical foundations of DPS on a much more rigorous footing and describing it in terms of well-defined double parton distributions (DPDs) which extend the concept of parton distribution functions (PDFs) to the case of two partons [145–148, 157–159]. The current knowledge of DPDs is still limited, though there are a number of attempts to impose theoretical constraints as a limit on the forms [160–162]. The DPDs can be calculated quite accurately when the transverse separation of the two partons is small, since in this limit the observed partons are produced by a splitting from a single parton. This limit is complicated by potential double counting [148], and an approach to deal with this has been devised [159]. The full splitting functions for DPS have been calculated at LO [148], and there is progress at NLO, e.g. [163].

Polarized PDFs: For spin-dependent structure functions, data exists for a more restricted range of Q^2 and has lower precision, so that the scaling violations are not seen so clearly. However, spin-dependent (or polarized) parton distributions have been extracted by comparison to data using NLO global analyses which include measurements of the g_1 structure function in inclusive polarized DIS, ‘flavour-tagged’ semi-inclusive DIS data, open-charm production in DIS and results from polarized pp scattering at RHIC. There are recent results on DIS from JLAB [164] (for g_1^n/F_1^n), COMPASS [165, 166] and CLAS [167]. NLO analyses are given in Refs. [168–171] and more recent extractions [172, 173]. Improved parton-to-hadron fragmentation functions, needed to describe the semi-inclusive DIS (SIDIS) data, can be found in Refs. [174–177].

The DSSV collaboration includes in their NLO analysis to extract polarized PDFs all the world data, inclusive and semi-inclusive DIS, double spin asymmetries in jet [178], dijet [179] and inclusive π^0 -production [180], but not yet the single spin asymmetries in W^\pm, Z^0 production [181, 182]. A determination [183], using the NNPDF methodology, concentrates just on the inclusive polarized DIS data, and finds the uncertainties on the polarized gluon PDF have been underestimated in the earlier analyses. An update to this [27], where jet and W^\pm data from pp collisions

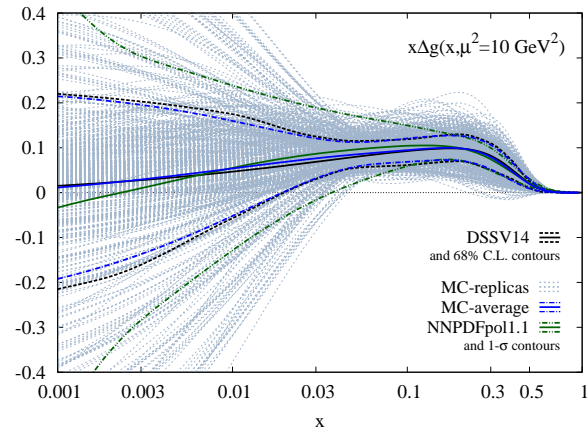


Figure 18.5: Ensemble of replicas (dotted blue lines) for the NLO gluon helicity density $\Delta g(x, Q^2)$ at $Q^2 = 10 \text{ GeV}^2$ shown along with its statistical average (solid blue line) and variance (dot-dashed blue lines). The corresponding results from the DSSV14 fit (black lines) [172] and the NNPDFpol1.1 analysis (green lines) [27] are shown for comparison. Figure taken from Ref. [184].

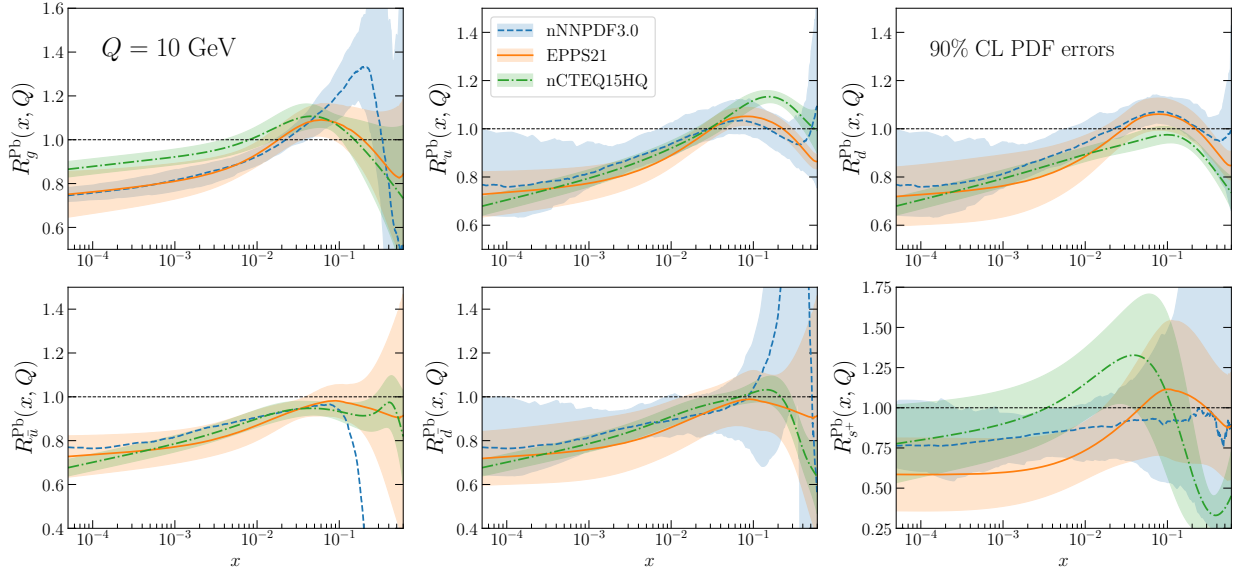


Figure 18.6: Comparison of the nNNPDF3.0, nCTEQ15HQ and EPPS21 nuclear PDFs. The curves shown are ratios to the result in the limit of no nuclear corrections. Plot from NNPDF collaboration (Juan Rojo – private communication).

and open-charm DIS data have been included via reweighting, reduces the uncertainty and suggests a positive polarized gluon PDF. The evidence for a positive gluon polarization is strengthened by the most recent jet [185–187] and inclusive π^0 [188] data. The DSSV group has recently implemented a Monte Carlo sampling strategy to extract helicity parton densities and their uncertainties from a reference set of longitudinally polarized scattering data [184]. A simultaneous extraction of spin-dependent parton distributions and fragmentation functions has recently also been performed [189]. Calculations of polarised PDFs on the lattice are frequently produced by the same studies as for unpolarised PDFs. These are usually in better agreement with the corresponding moments obtained from global fits, than the unpolarised PDFs, and also tend to have much more competitive uncertainties, see [106, 107] for a review and e.g. [109, 190] for more recent results.

A comparison of the polarized gluon PDFs obtained in the NLO analyses of NNPDF [27] and DSSV [184] is shown in Fig. 18.5 at scale $\mu^2 = 10 \text{ GeV}^2$. The world data of the inclusive structure function g_1 for proton and deuteron included in these analysis are shown in Fig. 18.16 and Fig. 18.17.

18.4 The hadronic structure of the photon

Besides the *direct* interactions of the photon, it is possible for it to fluctuate into a hadronic state via the process $\gamma \rightarrow q\bar{q}$. While in this state, the partonic content of the photon may be *resolved*, for example, through the process $e^+e^- \rightarrow e^+e^-\gamma^*\gamma \rightarrow e^+e^-X$, where the virtual photon emitted by the DIS lepton probes the hadronic structure of the quasi-real photon emitted by the other lepton. The perturbative LO QED contributions to this process with $\gamma \rightarrow q\bar{q}$ in conjunction with $\gamma^*q(\bar{q}) \rightarrow q(\bar{q})$, are subject to QCD corrections due to the radiation of gluons from these quarks.

Often the equivalent-photon approximation is used to express the differential cross section for deep inelastic electron–photon scattering in terms of the structure functions of the transverse quasi-real photon times a flux factor N_γ^T (for these incoming quasi-real photons of transverse polarization)

$$\frac{d^2\sigma}{dx dQ^2} = N_\gamma^T \frac{2\pi\alpha^2}{xQ^4} \left[(1 + (1-y)^2) F_2^\gamma(x, Q^2) - y^2 F_L^\gamma(x, Q^2) \right], \quad (18.31)$$

where we have used $F_2^\gamma = 2xF_T^\gamma + F_L^\gamma$ (where F_T is the transverse structure function), not to be confused with F_2^γ of Sec. 18.2. Complete formulae are given, for example, in the comprehensive review of [191].

The hadronic photon structure function, F_2^γ , evolves with in-

creasing Q^2 from the ‘hadron-like’ behavior, calculable via the vector-meson-dominance model, to the dominating ‘point-like’ behaviour, calculable in perturbative QCD. Due to the point-like coupling, the logarithmic evolution of F_2^γ with Q^2 has a *positive* slope for all values of x , see Fig. 18.18. The ‘loss’ of quarks at large x due to gluon radiation is over-compensated by the ‘creation’ of quarks via the point-like $\gamma \rightarrow q\bar{q}$ coupling. The logarithmic evolution was first predicted in the quark–parton model ($\gamma^*\gamma \rightarrow q\bar{q}$) [192, 193], and then an improved expression was obtained using QCD corrections in the limit of large Q^2 [194]. The evolution is now known to NLO [195–197]. The NLO data analyses to determine the parton densities of the photon can be found in Refs. [198–200].

18.5 Diffractive DIS (DDIS)

Some 10% of DIS events are diffractive, $\gamma^*p \rightarrow X + p$, in which the slightly deflected proton and the cluster X of outgoing hadrons are well-separated in rapidity [201]. Besides x and Q^2 , two extra

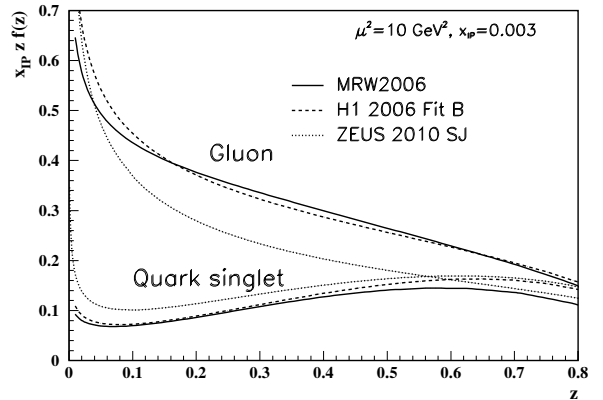


Figure 18.7: Diffractive parton distributions, $x_{IP} z f_{a/p}^D$, obtained from fitting to the ZEUS data with $Q^2 > 5 \text{ GeV}^2$ [202], H1 data with $Q^2 > 8.5 \text{ GeV}^2$ assuming Regge factorization [203], and from MRW2006 [204] using a more perturbative QCD approach [204]. Only the Pomeron contributions are shown and not the secondary Reggeon contributions, which are negligible at the value of $x_{IP} = 0.003$ chosen here. The H1 2007 Jets distribution [205] is similar to H1 2006 Fit B.

variables are needed to describe a DDIS event: the fraction x_{IP} of

the proton's momentum transferred across the rapidity gap and t , the square of the 4-momentum transfer of the proton. The DDIS data [206, 207] are usually analysed using two levels of factorization. First, the diffractive structure function F_2^D satisfies *collinear factorization*, and can be expressed as the convolution [208]

$$F_2^D = \sum_{a=q,g} C_2^a \otimes f_{a/p}^D, \quad (18.32)$$

with the same coefficient functions as in DIS (see Eq. (18.21)), and where the diffractive parton distributions $f_{a/p}^D$ ($a = q, g$) satisfy DGLAP evolution. Second, *Regge factorization* is assumed [209],

$$f_{a/p}^D(x_{IP}, t, z, \mu^2) = f_{IP/p}(x_{IP}, t) f_{a/IP}(z, \mu^2), \quad (18.33)$$

where $f_{a/IP}$ are the parton densities of the Pomeron, which itself is treated like a hadron, and $z \in [x/x_{IP}, 1]$ is the fraction of the Pomeron's momentum carried by the parton entering the hard subprocess. The Pomeron flux factor $f_{IP/p}(x_{IP}, t)$ is taken from Regge phenomenology. There are also secondary Reggeon contributions to Eq. (18.33). A sample of the t -integrated diffractive parton densities, obtained in this way, is shown in Fig. 18.7. A more recent extraction of the parton densities may be found in [210].

Although collinear factorization holds as $\mu^2 \rightarrow \infty$, there are non-negligible corrections for finite μ^2 and small x_{IP} . Besides the *resolved* interactions of the Pomeron, the perturbative QCD Pomeron may also interact *directly* with the hard subprocess, giving rise to an inhomogeneous evolution equation for the diffractive parton densities analogous to the photon case. The results of the MRW analysis [204], which includes these contributions, are also shown in Fig. 18.7.

Unlike the inclusive case, the diffractive parton densities cannot be directly used to calculate diffractive hadron-hadron cross sections, since account must first be taken of ‘‘soft’’ rescattering effects.

18.6 Three-dimensional structure of hadrons

Generalized parton distributions (GPDs) and their complement, transverse momentum dependent distributions (TMDs) describe the three-dimensional structure of hadrons. While GPDs encode the transverse position of a parton in a nucleon, TMDs, encompassing both the parton distributions (TMD PDF) and fragmentation functions (TMD FF), encode their transverse momenta and lead to observable transverse momenta in the final state. Both TMDs and GPDs derive, via integration over the appropriate variable, from Wigner distributions [211–213] that depend on the average transverse momentum and position of partons.

18.6.1 Generalized parton distributions

The parton distributions of the proton of Sec. 18.3 are given by the diagonal matrix elements $\langle P, \lambda | \hat{O} | P, \lambda \rangle$, where P and λ are the 4-momentum and helicity of the proton, and \hat{O} is a twist-2 quark or gluon operator. However, there is new information in the so-called generalised parton distributions (GPDs) defined in terms of the off-diagonal matrix elements $\langle P', \lambda' | \hat{O} | P, \lambda \rangle$; see Refs. [214–219] for reviews. Unlike the diagonal PDFs, the GPDs cannot be regarded as parton densities, but are to be interpreted as probability amplitudes.

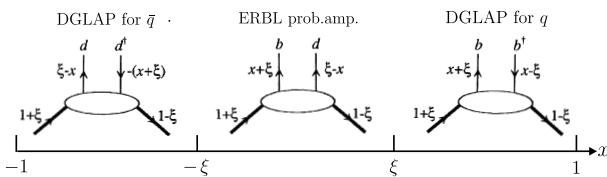


Figure 18.8: Schematic diagrams of the three distinct kinematic regions of the imaginary part of H_q . The proton and quark momentum fractions refer to \bar{P}^+ , and x covers the interval $(-1, 1)$. In the ERBL domain the GPDs are generalisations of distribution amplitudes which occur in processes such as $p\bar{p} \rightarrow J/\psi$.

The physical significance of GPDs is best seen using light-cone coordinates, $z^\pm = (z^0 \pm z^3)/\sqrt{2}$, and in the light-cone gauge, $A^+ = 0$. It is conventional to define the generalised quark distributions in terms of quark operators at light-like separation

$$F_q(x, \xi, t) = \frac{1}{2} \int \frac{dz^-}{2\pi} e^{ix\bar{P}^+ z^-} \langle P' | \bar{\psi}(-z/2) \gamma^+ \psi(z/2) | P \rangle \Big|_{z^+ = z^1 = z^2 = 0} \\ = \frac{1}{2\bar{P}^+} \\ \times \left(H_q(x, \xi, t) \bar{u}(P') \gamma^+ u(P) + E_q(x, \xi, t) \bar{u}(P') \frac{i\sigma^{+\alpha} \Delta_\alpha}{2m} u(P) \right) \quad (18.34)$$

with $\bar{P} = (P + P')/2$ and $\Delta = P' - P$, and where we have suppressed the helicity labels of the protons and spinors. We now have two extra kinematic variables:

$$t = \Delta^2, \quad \xi = -\Delta^+ / (P + P')^+. \quad (18.35)$$

We see that $-1 \leq \xi \leq 1$. Similarly, we may define GPDs \tilde{H}_q and \tilde{E}_q with an additional γ_5 between the quark operators in Eq. (18.34); and also an analogous set of gluon GPDs, H_g, E_g, \tilde{H}_g and \tilde{E}_g . After a Fourier transform with respect to the transverse components of Δ , we are able to describe the spatial distribution of partons in the impact parameter plane in terms of GPDs [220, 221].

For $P' = P, \lambda' = \lambda$ the matrix elements reduce to the ordinary PDFs of Sec. 18.2.1

$$H_q(x, 0, 0) = q(x), \quad H_q(-x, 0, 0) = -\bar{q}(x), \quad H_g(x, 0, 0) = xg(x), \quad (18.36)$$

$$\tilde{H}_q(x, 0, 0) = \Delta q(x), \quad \tilde{H}_q(-x, 0, 0) = \Delta \bar{q}(x), \quad \tilde{H}_g(x, 0, 0) = x\Delta g(x), \quad (18.37)$$

where $\Delta q = q \uparrow - q \downarrow$ as in Eq. (18.18). No corresponding relations exist for E, \tilde{E} as they decouple in the forward limit, $\Delta = 0$.

The functions H_g, E_g are even in x , and \tilde{H}_g, \tilde{E}_g are odd functions of x . We can introduce valence and ‘singlet’ quark distributions which are even and odd functions of x respectively. For example

$$H_q^V(x, \xi, t) \equiv H_q(x, \xi, t) + H_q(-x, \xi, t) = H_q^V(-x, \xi, t), \quad (18.38)$$

$$H_q^S(x, \xi, t) \equiv H_q(x, \xi, t) - H_q(-x, \xi, t) = -H_q^S(-x, \xi, t). \quad (18.39)$$

All the GPDs satisfy relations of the form

$$H(x, -\xi, t) = H(x, \xi, t) \quad \text{and} \quad H(x, -\xi, t)^* = H(x, \xi, t), \quad (18.40)$$

and so are real-valued functions. Moreover, the moments of GPDs, that is the x integrals of $x^n H_q$ etc., are *polynomials* in ξ of order $n + 1$. Another important property of GPDs are Ji’s sum rule [214]

$$\frac{1}{2} \int_{-1}^1 dx \, x (H_q(x, \xi, t) + E_q(x, \xi, t)) = J_q(t), \quad (18.41)$$

where $J_q(0)$ is the total angular momentum carried by quarks and antiquarks of flavour q , with a similar relation for gluons.

To visualize the physical content of H_q , we Fourier expand ψ and $\bar{\psi}$ in terms of quark, antiquark creation (b, d) and annihilation (b^\dagger, d^\dagger) operators, and sketch the result in Fig. 18.8. There are two types of domain: (i) the time-like or ‘annihilation’ domain, with $|x| < |\xi|$, where the GPDs describe the wave functions of a t -channel $q\bar{q}$ (or gluon) pair and evolve according to modified ERBL equations [222, 223]; (ii) the space-like or ‘scattering’ domain, with $|x| > |\xi|$, where the GPDs generalise the familiar \bar{q}, q (and gluon) PDFs and describe processes such as ‘deeply virtual Compton scattering’ ($\gamma^* p \rightarrow \gamma p$), $\gamma p \rightarrow J/\psi p$, etc., and evolve according to modified DGLAP equations. The splitting functions for the evolution of GPDs are known to NLO [224–226].

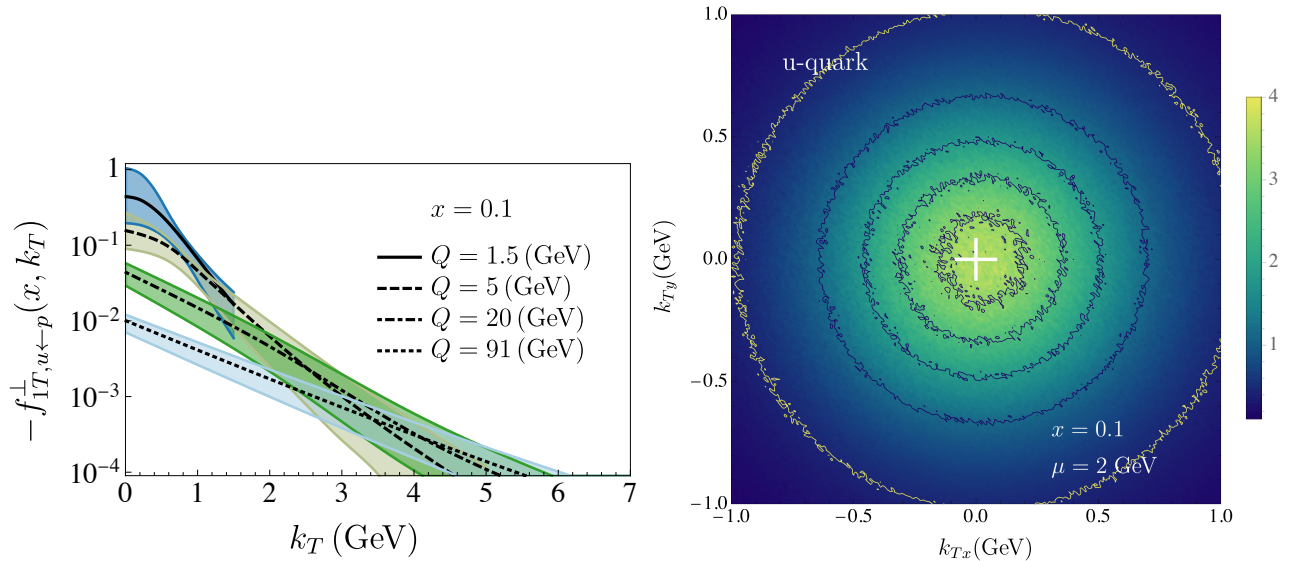


Figure 18.9: (Left) Siverson function in the momentum space for u quark [227] at $x = 0.1$ as a function of transverse momentum k_T for different values of Q . The bands are 68%CI. (Right) Momentum space density function as defined in [227] for the unpolarized u quark in a proton totally polarized in the y direction. The white cross indicates the origin with respect to which a shift of the distribution along the x -direction due to the Siverson function can be seen. The width of the patterns in the plot roughly indicates the uncertainty of the extraction.

GPDs describe new aspects of proton structure and must be determined from experiment. We can parametrise them in terms of ‘double distributions’ [228,229], which reduce to diagonal PDFs as $\xi \rightarrow 0$. Alternatively, flexible $SO(3)$ -based parametrisations have been used to determine GPDs from DVCS data [230,231]; a more recent summary may be found in Ref. [232,233].

18.6.2 Transverse momentum dependent distributions

For a proton, there are eight independent transverse dependent distribution (TMD) PDFs, at leading twist, three of which correspond to the usual unpolarized, longitudinally polarized and transversely polarized quark parton distributions [234,235]. The novel TMD PDFs have physical interpretations. For example, the Siverson function [236] represents the distribution of unpolarized partons inside a transversely polarized hadron. For (pseudo)scalar particles, such as kaon and pions, there are two independent leading-twist TMD FFs, one being the ordinary unpolarized fragmentation function and the other the Collins FF [237] which is related to the probability of a polarized quark fragmenting into an unpolarized hadron.

Factorization of TMDs has been shown for semi-inclusive DIS, for the Drell-Yan process as well as for electron-positron annihilation into dihadrons [238–243]. Recently first TMD global fits have become available [244–252], although potential problems with consistent descriptions are highlighted in remain [253–255]. The results of a recent extraction of Siverson function from a global fit to polarized Semi-Inclusive DIS, polarized pion-induced Drell-Yan and $W^{+/-}$ Z boson production data is shown in Fig. 18.9 [227].

Because TMD PDFs encode nonperturbative information about transverse momentum and polarization degrees of freedom, they are important for descriptions of multi-scale, non-inclusive collider observables, for example, production of electroweak gauge bosons at LHC [256] and can have an effect on determination of the W boson mass [257]. The combination of TMD PDFs and FFs can give consistent global description of spin and azimuthal asymmetries and provide predictions. Some recent reviews of this rapidly developing field are given here [256,258–261].

References

- [1] J. Blumlein and N. Kochelev, Nucl. Phys. **B498**, 285 (1997), [hep-ph/9612318].
- [2] S. Forte, M. L. Mangano and G. Ridolfi, Nucl. Phys. **B602**, 585 (2001), [hep-ph/0101192].
- [3] M. Anselmino, P. Gambino and J. Kalinowski, Z. Phys. **C64**, 267 (1994), [hep-ph/9401264].
- [4] M. Anselmino, A. Efremov and E. Leader, Phys. Rept. **261**, 1 (1995), [Erratum: Phys. Rept.281,399(1997)], [hep-ph/9501369].
- [5] M. Klein and T. Riemann, Z. Phys. **C24**, 151 (1984).
- [6] C. G. Callan, Jr. and D. J. Gross, Phys. Rev. Lett. **22**, 156 (1969).
- [7] D. A. Dicus, Phys. Rev. **D5**, 1367 (1972).
- [8] J. D. Bjorken and E. A. Paschos, Phys. Rev. **185**, 1975 (1969).
- [9] R.P. Feynman, Photon Hadron Interactions (Benjamin, New York, 1972).
- [10] J. D. Bjorken, Phys. Rev. **179**, 1547 (1969).
- [11] A.M. Cooper-Sarkar, private communication.
- [12] H. Abramowicz *et al.* (H1, ZEUS), Eur. Phys. J. **C75**, 12, 580 (2015), [arXiv:1506.06042].
- [13] L. A. Harland-Lang *et al.*, Eur. Phys. J. **C76**, 4, 186 (2016), [arXiv:1601.03413].
- [14] I. Abt *et al.*, Phys. Rev. **D94**, 3, 034032 (2016), [arXiv:1604.02299].
- [15] R. D. Ball *et al.*, Eur. Phys. J. **C78**, 4, 321 (2018), [arXiv:1710.05935].
- [16] H. Abdolmaleki *et al.* (xFitter Developers’ Team), Eur. Phys. J. **C78**, 8, 621 (2018), [arXiv:1802.00064].
- [17] S. Wandzura and F. Wilczek, Phys. Lett. **72B**, 195 (1977).
- [18] J. Blumlein and A. Tkabladze, Nucl. Phys. **B553**, 427 (1999), [hep-ph/9812478].
- [19] J. C. Collins, D. E. Soper and G. F. Sterman, Adv. Ser. Direct. High Energy Phys. **5**, 1 (1989), [hep-ph/0409313].
- [20] V. N. Gribov and L. N. Lipatov, Sov. J. Nucl. Phys. **15**, 438 (1972), [Yad. Fiz.15,781(1972)].
- [21] L.N. Lipatov, Sov. J. Nucl. Phys. **20**, 95 (1975).
- [22] G. Altarelli and G. Parisi, Nucl. Phys. **B126**, 298 (1977).
- [23] Y. L. Dokshitzer, Sov. Phys. JETP **46**, 641 (1977), [Zh. Eksp. Teor. Fiz.73,1216(1977)].

- [24] V. Bertone, R. Gauld and J. Rojo, JHEP **01**, 217 (2019), [arXiv:1808.02034].
- [25] R. Aaij *et al.* (LHCb), JHEP **10**, 167 (2018), [arXiv:1806.04079].
- [26] S. Bailey *et al.*, Eur. Phys. J. C **81**, 4, 341 (2021), [arXiv:2012.04684].
- [27] E. R. Nocera *et al.* (NNPDF), Nucl. Phys. **B887**, 276 (2014), [arXiv:1406.5539].
- [28] G. Curci, W. Furmanski and R. Petronzio, Nucl. Phys. **B175**, 27 (1980); W. Furmanski and R. Petronzio, Phys. Lett. **97B**, 437 (1980).
- [29] R.K. Ellis *et al.*, QCD and Collider Physics (Cambridge UP, 1996).
- [30] W. L. van Neerven and E. B. Zijlstra, Phys. Lett. **B272**, 127 (1991); E. B. Zijlstra and W. L. van Neerven, Phys. Lett. **B273**, 476 (1991); E. B. Zijlstra and W. L. van Neerven, Phys. Lett. **B297**, 377 (1992); E. B. Zijlstra and W. L. van Neerven, Nucl. Phys. **B383**, 525 (1992).
- [31] S. Moch and J. A. M. Vermaseren, Nucl. Phys. **B573**, 853 (2000), [hep-ph/9912355].
- [32] S. Moch, J. A. M. Vermaseren and A. Vogt, Nucl. Phys. **B688**, 101 (2004), [hep-ph/0403192]; A. Vogt, S. Moch and J. A. M. Vermaseren, Nucl. Phys. **B691**, 129 (2004), [hep-ph/0404111]; S. Moch, J. A. M. Vermaseren and A. Vogt, Phys. Lett. **B606**, 123 (2005), [hep-ph/0411112].
- [33] J. A. M. Vermaseren, A. Vogt and S. Moch, Nucl. Phys. **B724**, 3 (2005), [hep-ph/0504242].
- [34] S. Moch *et al.*, Phys. Lett. B **825**, 136853 (2022), [arXiv:2111.15561]; G. Falcioni *et al.*, Phys. Lett. B **842**, 137944 (2023), [arXiv:2302.07593].
- [35] V. S. Fadin, E. A. Kuraev and L. N. Lipatov, Phys. Lett. **60B**, 50 (1975); E. A. Kuraev, L. N. Lipatov and V. S. Fadin, Sov. Phys. JETP **44**, 443 (1976), [Zh. Eksp. Teor. Fiz.71,840(1976)]; E. A. Kuraev, L. N. Lipatov and V. S. Fadin, Sov. Phys. JETP **45**, 199 (1977), [Zh. Eksp. Teor. Fiz.72,377(1977)].
- [36] I. I. Balitsky and L. N. Lipatov, Sov. J. Nucl. Phys. **28**, 822 (1978), [Yad. Fiz.28,1597(1978)].
- [37] V. S. Fadin and L. N. Lipatov, Phys. Lett. **B429**, 127 (1998), [hep-ph/9802290].
- [38] G. Camici and M. Ciafaloni, Phys. Lett. **B412**, 396 (1997), [Erratum: Phys. Lett. B417,390(1998)], [hep-ph/9707390]; M. Ciafaloni and G. Camici, Phys. Lett. **B430**, 349 (1998), [hep-ph/9803389].
- [39] M. Ciafaloni, D. Colferai and G. P. Salam, Phys. Rev. **D60**, 114036 (1999), [hep-ph/9905566]; M. Ciafaloni, D. Colferai and G. P. Salam, JHEP **07**, 054 (2000), [hep-ph/0007240].
- [40] M. Ciafaloni *et al.*, Phys. Lett. **B576**, 143 (2003), [hep-ph/0305254]; M. Ciafaloni *et al.*, Phys. Rev. **D68**, 114003 (2003), [hep-ph/0307188].
- [41] G. Altarelli, R. D. Ball and S. Forte, Nucl. Phys. **B742**, 1 (2006), [hep-ph/0512237]; G. Altarelli, R. D. Ball and S. Forte, Nucl. Phys. **B799**, 199 (2008), [arXiv:0802.0032].
- [42] C. D. White and R. S. Thorne, Phys. Rev. **D75**, 034005 (2007), [hep-ph/0611204].
- [43] M. Bonvini, S. Marzani and T. Peraro, Eur. Phys. J. **C76**, 11, 597 (2016), [arXiv:1607.02153].
- [44] M. Bonvini, S. Marzani and C. Muselli, JHEP **12**, 117 (2017), [arXiv:1708.07510].
- [45] Y. V. Kovchegov and E. Levin, *Quantum chromodynamics at high energy*, volume 33, Cambridge University Press (2012), ISBN 978-0-521-11257-4, 978-1-139-55768-9.
- [46] J. L. Albacete and C. Marquet, Prog. Part. Nucl. Phys. **76**, 1 (2014), [arXiv:1401.4866].
- [47] A. Morreale and F. Salazar, Universe **7**, 8, 312 (2021), [arXiv:2108.08254].
- [48] G. Giacalone and C. Marquet, Nucl. Phys. A **982**, 291 (2019), [arXiv:1807.06388].
- [49] X. Chu (STAR), in “28th International Workshop on Deep Inelastic Scattering and Related Subjects,” (2021), [arXiv:2110.03731].
- [50] G. 't Hooft and M. J. G. Veltman, Nucl. Phys. **B44**, 189 (1972).
- [51] G. 't Hooft, Nucl. Phys. **B61**, 455 (1973).
- [52] W. A. Bardeen *et al.*, Phys. Rev. **D18**, 3998 (1978).
- [53] G. Altarelli, R. K. Ellis and G. Martinelli, Nucl. Phys. **B143**, 521 (1978), [Erratum: Nucl. Phys. B146,544(1978)].
- [54] S. Catani, Z. Phys. C **70**, 263 (1996), [hep-ph/9506357].
- [55] A. D. Martin *et al.*, Eur. Phys. J. **C35**, 325 (2004), [hep-ph/0308087].
- [56] R. D. Ball *et al.* (NNPDF), Phys. Lett. **B723**, 330 (2013), [arXiv:1303.1189].
- [57] R. S. Thorne, Eur. Phys. J. **C74**, 7, 2958 (2014), [arXiv:1402.3536].
- [58] M. Dasgupta and B. R. Webber, Phys. Lett. **B382**, 273 (1996), [hep-ph/9604388].
- [59] A. De Roeck and R. S. Thorne, Prog. Part. Nucl. Phys. **66**, 727 (2011), [arXiv:1103.0555].
- [60] S. Forte and G. Watt, Ann. Rev. Nucl. Part. Sci. **63**, 291 (2013), [arXiv:1301.6754].
- [61] J. Blumlein, Prog. Part. Nucl. Phys. **69**, 28 (2013), [arXiv:1208.6087].
- [62] E. Perez and E. Rizvi, Rept. Prog. Phys. **76**, 046201 (2013), [arXiv:1208.1178].
- [63] R. D. Ball *et al.*, JHEP **04**, 125 (2013), [arXiv:1211.5142].
- [64] J. Gao, L. Harland-Lang and J. Rojo, Phys. Rept. **742**, 1 (2018), [arXiv:1709.04922].
- [65] J. J. Ethier and E. R. Nocera, Ann. Rev. Nucl. Part. Sci. **70**, 43 (2020), [arXiv:2001.07722].
- [66] J. Rojo *et al.*, J. Phys. **G42**, 103103 (2015), [arXiv:1507.00556].
- [67] R. D. Ball *et al.* (NNPDF), Eur. Phys. J. C **82**, 5, 428 (2022), [arXiv:2109.02653].
- [68] T.-J. Hou *et al.*, Phys. Rev. D **103**, 1, 014013 (2021), [arXiv:1912.10053].
- [69] G. Aad *et al.* (ATLAS), Eur. Phys. J. C **82**, 5, 438 (2022), [arXiv:2112.11266].
- [70] S. Alekhin *et al.*, Phys. Rev. **D96**, 1, 014011 (2017), [arXiv:1701.05838].
- [71] A. Accardi *et al.*, Phys. Rev. D **93**, 11, 114017 (2016), [arXiv:1602.03154].
- [72] G. Watt and R. S. Thorne, JHEP **08**, 052 (2012), [arXiv:1205.4024].
- [73] S. Carrazza *et al.*, Eur. Phys. J. **C75**, 8, 369 (2015), [arXiv:1505.06736].
- [74] J. McGowan *et al.*, Eur. Phys. J. C **83**, 3, 185 (2023), [Erratum: Eur.Phys.J.C 83, 302 (2023)], [arXiv:2207.04739].
- [75] R. Abdul Khalek *et al.* (NNPDF), Eur. Phys. J. C **79**, 11, 931 (2019), [arXiv:1906.10698].
- [76] J. C. Collins, F. Wilczek and A. Zee, Phys. Rev. **D18**, 242 (1978).
- [77] E. Laenen *et al.*, Nucl. Phys. **B392**, 162 (1993).
- [78] M. A. G. Aivazis *et al.*, Phys. Rev. **D50**, 3102 (1994), [hep-ph/9312319].
- [79] M. Buza *et al.*, Eur. Phys. J. **C1**, 301 (1998), [hep-ph/9612398].
- [80] J. C. Collins, Phys. Rev. **D58**, 094002 (1998), [hep-ph/9806259].
- [81] A. Chuvakin, J. Smith and W. L. van Neerven, Phys. Rev. **D61**, 096004 (2000), [hep-ph/9910250].

- [82] R. S. Thorne, Phys. Rev. **D73**, 054019 (2006), [hep-ph/0601245].
- [83] R. S. Thorne and W. K. Tung, in “Proceedings, HERA and the LHC Workshop Series on the implications of HERA for LHC physics: 2006-2008,” 332–351 (2008), [2(2008)], [arXiv:0809.0714].
- [84] S. Alekhin and S. Moch, Phys. Lett. **B699**, 345 (2011), [arXiv:1011.5790].
- [85] S. Forte *et al.*, Nucl. Phys. **B834**, 116 (2010), [arXiv:1001.2312].
- [86] R. S. Thorne, Phys. Rev. **D86**, 074017 (2012), [arXiv:1201.6180].
- [87] E. G. de Oliveira *et al.*, Eur. Phys. J. **C73**, 10, 2616 (2013), [arXiv:1307.3508].
- [88] H. Abramowicz *et al.* (H1, ZEUS), Eur. Phys. J. **C78**, 6, 473 (2018), [arXiv:1804.01019].
- [89] O. Behnke, A. Geiser and M. Lisovsky, Prog. Part. Nucl. Phys. **84**, 1 (2015), [arXiv:1506.07519].
- [90] R. D. Ball *et al.* (NNPDF), Eur. Phys. J. **C77**, 10, 663 (2017), [arXiv:1706.00428].
- [91] J. Butterworth *et al.*, J. Phys. **G43**, 023001 (2016), [arXiv:1510.03865].
- [92] R. D. Ball *et al.* (PDF4LHC Working Group), J. Phys. **G49**, 8, 080501 (2022), [arXiv:2203.05506].
- [93] T. Cridge *et al.*, Eur. Phys. J. **C81**, 744 (2021), [arXiv:2106.10289].
- [94] R. D. Ball *et al.* (NNPDF), Eur. Phys. J. **C78**, 5, 408 (2018), [arXiv:1802.03398].
- [95] A. D. Martin *et al.*, Eur. Phys. J. **C39**, 155 (2005), [hep-ph/0411040].
- [96] R. D. Ball *et al.* (NNPDF), Nucl. Phys. **B877**, 290 (2013), [arXiv:1308.0598].
- [97] C. Schmidt *et al.*, Phys. Rev. **D93**, 11, 114015 (2016), [arXiv:1509.02905].
- [98] M. Gluck, C. Pisano and E. Reya, Phys. Lett. **B540**, 75 (2002), [hep-ph/0206126].
- [99] A. D. Martin and M. G. Ryskin, Eur. Phys. J. **C74**, 3040 (2014), [arXiv:1406.2118].
- [100] L. A. Harland-Lang, V. A. Khoze and M. G. Ryskin, Phys. Rev. **D94**, 7, 074008 (2016), [arXiv:1607.04635].
- [101] A. Manohar *et al.*, Phys. Rev. Lett. **117**, 24, 242002 (2016), [arXiv:1607.04266].
- [102] V. Bertone *et al.* (NNPDF), SciPost Phys. **5**, 1, 008 (2018), [arXiv:1712.07053].
- [103] L. A. Harland-Lang *et al.*, Eur. Phys. J. **C79**, 10, 811 (2019), [arXiv:1907.02750].
- [104] K. Xie *et al.* (CTEQ-TEA), Phys. Rev. D **105**, 5, 054006 (2022), [arXiv:2106.10299].
- [105] L. A. Harland-Lang, JHEP **03**, 128 (2020), [arXiv:1910.10178].
- [106] H.-W. Lin *et al.*, Prog. Part. Nucl. Phys. **100**, 107 (2018), [arXiv:1711.07916].
- [107] M. Constantinou *et al.*, Prog. Part. Nucl. Phys. **121**, 103908 (2021), [arXiv:2006.08636].
- [108] Y.-B. Yang *et al.*, Phys. Rev. Lett. **121**, 21, 212001 (2018), [arXiv:1808.08677].
- [109] C. Alexandrou *et al.*, Phys. Rev. D **101**, 9, 094513 (2020), [arXiv:2003.08486].
- [110] Z. Fan, H.-W. Lin and M. Zeilbeck, Phys. Rev. D **107**, 3, 034505 (2023), [arXiv:2208.00980].
- [111] X. Ji, Phys. Rev. Lett. **110**, 262002 (2013), [arXiv:1305.1539].
- [112] A. V. Radyushkin, Phys. Rev. D **96**, 3, 034025 (2017), [arXiv:1705.01488].
- [113] C. Alexandrou *et al.*, Phys. Rev. Lett. **121**, 11, 112001 (2018), [arXiv:1803.02685].
- [114] R. Zhang, H.-W. Lin and B. Yoon, Phys. Rev. D **104**, 9, 094511 (2021), [arXiv:2005.01124].
- [115] Z. Fan, W. Good and H.-W. Lin, Phys. Rev. D **108**, 1, 014508 (2023), [arXiv:2210.09985].
- [116] M. Bhat *et al.*, Phys. Rev. D **103**, 3, 034510 (2021), [arXiv:2005.02102].
- [117] B. Joó *et al.*, Phys. Rev. Lett. **125**, 23, 232003 (2020), [arXiv:2004.01687].
- [118] A. Buckley *et al.*, Eur. Phys. J. **C75**, 132 (2015), [arXiv:1412.7420].
- [119] I. Helenius, M. Walt and W. Vogelsang, Phys. Rev. D **105**, 9, 094031 (2022), [arXiv:2112.11904].
- [120] P. Duwentäster *et al.*, Phys. Rev. D **105**, 11, 114043 (2022), [arXiv:2204.09982].
- [121] E. P. Segarra *et al.*, Phys. Rev. D **103**, 11, 114015 (2021), [arXiv:2012.11566].
- [122] K. J. Eskola *et al.*, Eur. Phys. J. **C82**, 5, 413 (2022), [arXiv:2112.12462].
- [123] R. Abdul Khalek *et al.*, Eur. Phys. J. **C82**, 6, 507 (2022), [arXiv:2201.12363].
- [124] R. Abdul Khalek, J. J. Ethier and J. Rojo (NNPDF), Eur. Phys. J. **C79**, 6, 471 (2019), [arXiv:1904.00018].
- [125] H. Khanpour *et al.*, Phys. Rev. D **104**, 3, 034010 (2021), [arXiv:2010.00555].
- [126] K. Kovarik *et al.*, Phys. Rev. Lett. **106**, 122301 (2011), [arXiv:1012.0286].
- [127] H. Paukkunen and C. A. Salgado, Phys. Rev. Lett. **110**, 21, 212301 (2013), [arXiv:1302.2001].
- [128] G. Aad *et al.* (ATLAS), Phys. Rev. **C92**, 4, 044915 (2015), [arXiv:1507.06232].
- [129] V. Khachatryan *et al.* (CMS), Phys. Lett. **B750**, 565 (2015), [arXiv:1503.05825].
- [130] V. Khachatryan *et al.* (CMS), Phys. Lett. **B759**, 36 (2016), [arXiv:1512.06461].
- [131] A. M. Sirunyan *et al.* (CMS), Phys. Lett. **B800**, 135048 (2020), [arXiv:1905.01486].
- [132] A. M. Sirunyan *et al.* (CMS), JHEP **05**, 182 (2021), [arXiv:2102.13648].
- [133] A. M. Sirunyan *et al.* (CMS), Phys. Rev. Lett. **121**, 6, 062002 (2018), [arXiv:1805.04736].
- [134] R. Aaij *et al.* (LHCb), JHEP **10**, 090 (2017), [arXiv:1707.02750].
- [135] S. Acharya *et al.* (ALICE), Eur. Phys. J. **C78**, 8, 624 (2018), [arXiv:1801.07051].
- [136] S. S. Adler *et al.* (PHENIX), Phys. Rev. Lett. **98**, 172302 (2007), [arXiv:nucl-ex/0610036].
- [137] E. C. Aschenauer *et al.*, Phys. Rev. **D96**, 11, 114005 (2017), [arXiv:1708.05654].
- [138] R. Abdul Khalek *et al.*, Nucl. Phys. A **1026**, 122447 (2022), [arXiv:2103.05419].
- [139] R. A. Khalek *et al.*, Phys. Rev. D **103**, 9, 096005 (2021), [arXiv:2102.00018].
- [140] P. V. Landshoff and J. C. Polkinghorne, Phys. Rev. D **18**, 3344 (1978).
- [141] R. Kirschner, Phys. Lett. **B84**, 266 (1979).
- [142] N. Paver and D. Treleani, Nuovo Cim. A **70**, 215 (1982).
- [143] V. P. Shelest, A. M. Snigirev and G. M. Zinovev, Phys. Lett. **B113**, 325 (1982).
- [144] M. Mekhfi, Phys. Rev. D **32**, 2371 (1985).
- [145] B. Blok *et al.*, Phys. Rev. D **83**, 071501 (2011), [arXiv:1009.2714].

- [146] M. Diehl and A. Schafer, Phys. Lett. B **698**, 389 (2011), [arXiv:1102.3081].
- [147] B. Blok *et al.*, Eur. Phys. J. C **72**, 1963 (2012), [arXiv:1106.5533].
- [148] M. Diehl, D. Ostermeier and A. Schafer, JHEP **03**, 089 (2012), [Erratum: JHEP 03, 001 (2016)], [arXiv:1111.0910].
- [149] C. H. Kom, A. Kulesza and W. J. Stirling, Phys. Rev. Lett. **107**, 082002 (2011), [arXiv:1105.4186].
- [150] C. H. Kom, A. Kulesza and W. J. Stirling, Eur. Phys. J. C **71**, 1802 (2011), [arXiv:1109.0309].
- [151] J. R. Gaunt *et al.*, Eur. Phys. J. C **69**, 53 (2010), [arXiv:1003.3953].
- [152] F. Abe *et al.* (CDF), Phys. Rev. D **56**, 3811 (1997).
- [153] V. M. Abazov *et al.* (D0), Phys. Rev. D **93**, 5, 052008 (2016), [arXiv:1512.05291].
- [154] R. Aaij *et al.* (LHCb), JHEP **06**, 047 (2017), [Erratum: JHEP 10, 068 (2017)], [arXiv:1612.07451].
- [155] M. Aaboud *et al.* (ATLAS), Phys. Lett. B **790**, 595 (2019), [arXiv:1811.11094].
- [156] A. M. Sirunyan *et al.* (CMS), Eur. Phys. J. C **80**, 1, 41 (2020), [arXiv:1909.06265].
- [157] A. V. Manohar and W. J. Waalewijn, Phys. Rev. D **85**, 114009 (2012), [arXiv:1202.3794].
- [158] B. Blok *et al.*, Eur. Phys. J. C **74**, 2926 (2014), [arXiv:1306.3763].
- [159] M. Diehl, J. R. Gaunt and K. Schönwald, JHEP **06**, 083 (2017), [arXiv:1702.06486].
- [160] J. R. Gaunt and W. J. Stirling, JHEP **03**, 005 (2010), [arXiv:0910.4347].
- [161] K. Golec-Biernat *et al.*, Phys. Lett. B **750**, 559 (2015), [arXiv:1507.08583].
- [162] M. Diehl *et al.*, Eur. Phys. J. C **80**, 5, 468 (2020), [arXiv:2001.10428].
- [163] M. Diehl, J. R. Gaunt and P. Ploessl, JHEP **08**, 040 (2021), [arXiv:2105.08425].
- [164] D. Flay *et al.* (Jefferson Lab Hall A), Phys. Rev. **D94**, 5, 052003 (2016), [arXiv:1603.03612].
- [165] C. Adolph *et al.* (COMPASS), Phys. Lett. **B753**, 18 (2016), [arXiv:1503.08935].
- [166] C. Adolph *et al.* (COMPASS), Phys. Lett. **B769**, 34 (2017), [arXiv:1612.00620].
- [167] R. Fersch *et al.* (CLAS), Phys. Rev. **C96**, 6, 065208 (2017), [arXiv:1706.10289].
- [168] M. Hirai and S. Kumano (Asymmetry Analysis), Nucl. Phys. **B813**, 106 (2009), [arXiv:0808.0413].
- [169] D. de Florian *et al.*, Phys. Rev. Lett. **101**, 072001 (2008), [arXiv:0804.0422]; D. de Florian *et al.*, Phys. Rev. **D80**, 034030 (2009), [arXiv:0904.3821].
- [170] E. Leader, A. V. Sidorov and D. B. Stamenov, Phys. Rev. **D82**, 114018 (2010), [arXiv:1010.0574].
- [171] J. Blumlein and H. Bottcher, Nucl. Phys. **B841**, 205 (2010), [arXiv:1005.3113].
- [172] D. de Florian *et al.*, Phys. Rev. Lett. **113**, 1, 012001 (2014), [arXiv:1404.4293].
- [173] N. Sato *et al.* (Jefferson Lab Angular Momentum), Phys. Rev. **D93**, 7, 074005 (2016), [arXiv:1601.07782].
- [174] D. de Florian *et al.*, Phys. Rev. **D91**, 1, 014035 (2015), [arXiv:1410.6027].
- [175] D. de Florian *et al.*, Phys. Rev. **D95**, 9, 094019 (2017), [arXiv:1702.06353].
- [176] V. Bertone *et al.* (NNPDF), Eur. Phys. J. **C77**, 8, 516 (2017), [arXiv:1706.07049].
- [177] V. Bertone *et al.* (NNPDF), Eur. Phys. J. **C78**, 8, 651 (2018), [arXiv:1807.03310].
- [178] L. Adamczyk *et al.* (STAR), Phys. Rev. Lett. **115**, 9, 092002 (2015), [arXiv:1405.5134].
- [179] L. Adamczyk *et al.* (STAR), Phys. Rev. D **95**, 7, 071103 (2017), [arXiv:1610.06616].
- [180] A. Adare *et al.* (PHENIX), Phys. Rev. D **90**, 1, 012007 (2014), [arXiv:1402.6296].
- [181] J. Adam *et al.* (STAR), Phys. Rev. D **99**, 5, 051102 (2019), [arXiv:1812.04817].
- [182] A. Adare *et al.* (PHENIX), Phys. Rev. D **98**, 3, 032007 (2018), [arXiv:1804.04181].
- [183] R. D. Ball *et al.* (NNPDF), Nucl. Phys. **B874**, 36 (2013), [arXiv:1303.7236].
- [184] D. De Florian *et al.*, Phys. Rev. D **100**, 11, 114027 (2019), [arXiv:1902.10548].
- [185] J. Adam *et al.* (STAR), Phys. Rev. D **100**, 5, 052005 (2019), [arXiv:1906.02740].
- [186] M. Abdallah *et al.* (STAR), Phys. Rev. D **103**, 9, L091103 (2021), [arXiv:2103.05571].
- [187] M. S. Abdallah *et al.* (STAR), Phys. Rev. D **105**, 9, 092011 (2022), [arXiv:2110.11020].
- [188] A. Adare *et al.* (PHENIX), Phys. Rev. D **93**, 1, 011501 (2016), [arXiv:1510.02317].
- [189] C. Cocuzza *et al.* (Jefferson Lab Angular Momentum (JAM)), Phys. Rev. D **106**, 3, L031502 (2022), [arXiv:2202.03372].
- [190] J. Liang *et al.*, Phys. Rev. D **98**, 7, 074505 (2018), [arXiv:1806.08366].
- [191] R. Nisius, Phys. Rept. **332**, 165 (2000), [hep-ex/9912049].
- [192] T. F. Walsh and P. M. Zerwas, Phys. Lett. **44B**, 195 (1973).
- [193] R. L. Kingsley, Nucl. Phys. **B60**, 45 (1973).
- [194] E. Witten, Nucl. Phys. **B120**, 189 (1977).
- [195] W. A. Bardeen and A. J. Buras, Phys. Rev. **D20**, 166 (1979), [Erratum: Phys. Rev. D21, 2041 (1980)].
- [196] M. Fontannaz and E. Pilon, Phys. Rev. **D45**, 382 (1992).
- [197] M. Gluck, E. Reya and A. Vogt, Phys. Rev. **D45**, 3986 (1992).
- [198] F. Cornet, P. Jankowski and M. Krawczyk, Phys. Rev. **D70**, 093004 (2004), [hep-ph/0404063].
- [199] P. Aurenche, M. Fontannaz and J. P. Guillet, Eur. Phys. J. **C44**, 395 (2005), [hep-ph/0503259].
- [200] W. Slominski, H. Abramowicz and A. Levy, Eur. Phys. J. **C45**, 633 (2006), [hep-ph/0504003].
- [201] H. Abramowicz and A. Caldwell, Rev. Mod. Phys. **71**, 1275 (1999), [hep-ex/9903037].
- [202] S. Chekanov *et al.* (ZEUS), Nucl. Phys. **B831**, 1 (2010), [arXiv:0911.4119].
- [203] A. Aktas *et al.* (H1), Eur. Phys. J. **C48**, 715 (2006), [hep-ex/0606004].
- [204] A. D. Martin, M. G. Ryskin and G. Watt, Phys. Lett. **B644**, 131 (2007), [hep-ph/0609273].
- [205] A. Aktas *et al.* (H1), JHEP **10**, 042 (2007), [arXiv:0708.3217].
- [206] F. D. Aaron *et al.* (H1, ZEUS), Eur. Phys. J. **C72**, 2175 (2012), [arXiv:1207.4864].
- [207] F. D. Aaron *et al.* (H1), Eur. Phys. J. **C72**, 2074 (2012), [arXiv:1203.4495].
- [208] J. C. Collins, Phys. Rev. **D57**, 3051 (1998), [Erratum: Phys. Rev. D61, 019902 (2000)], [hep-ph/9709499].
- [209] G. Ingelman and P. E. Schlein, Phys. Lett. **152B**, 256 (1985).
- [210] M. Goharipour, H. Khanpour and V. Guzey, Eur. Phys. J. **C78**, 4, 309 (2018), [arXiv:1802.01363].
- [211] X. Ji, Phys. Rev. Lett. **91**, 062001 (2003), [hep-ph/0304037].

- [212] A. V. Belitsky, X. Ji and F. Yuan, Phys. Rev. **D69**, 074014 (2004), [hep-ph/0307383].
- [213] C. Lorce, B. Pasquini and M. Vanderhaeghen, JHEP **05**, 041 (2011), [arXiv:1102.4704].
- [214] X.-D. Ji, J. Phys. **G24**, 1181 (1998), [hep-ph/9807358].
- [215] K. Goeke, M. V. Polyakov and M. Vanderhaeghen, Prog. Part. Nucl. Phys. **47**, 401 (2001), [hep-ph/0106012].
- [216] M. Diehl, Phys. Rept. **388**, 41 (2003), [hep-ph/0307382].
- [217] A. V. Belitsky and A. V. Radyushkin, Phys. Rept. **418**, 1 (2005), [hep-ph/0504030].
- [218] S. Boffi and B. Pasquini, Riv. Nuovo Cim. **30**, 387 (2007), [arXiv:0711.2625].
- [219] K. Kumericki, S. Liuti and H. Moutarde, Eur. Phys. J. **A52**, 6, 157 (2016), [arXiv:1602.02763].
- [220] M. Burkardt, Int. J. Mod. Phys. **A18**, 173 (2003), [hep-ph/0207047].
- [221] M. Diehl, Eur. Phys. J. **C25**, 223 (2002), [Erratum: Eur. Phys. J. **C31**, 277(2003)], [hep-ph/0205208].
- [222] A. V. Efremov and A. V. Radyushkin, Phys. Lett. **94B**, 245 (1980).
- [223] G. P. Lepage and S. J. Brodsky, Phys. Rev. **D22**, 2157 (1980).
- [224] A. V. Belitsky, A. Freund and D. Mueller, Phys. Lett. **B493**, 341 (2000), [hep-ph/0008005].
- [225] A. V. Belitsky, A. Freund and D. Mueller, Nucl. Phys. **B574**, 347 (2000), [hep-ph/9912379].
- [226] V. M. Braun *et al.*, JHEP **06**, 037 (2017), [arXiv:1703.09532].
- [227] M. Bury, A. Prokudin and A. Vladimirov, JHEP **05**, 151 (2021), [arXiv:2103.03270].
- [228] A. V. Radyushkin, Phys. Rev. **D59**, 014030 (1999), [hep-ph/9805342].
- [229] A. V. Radyushkin, Phys. Lett. **B449**, 81 (1999), [hep-ph/9810466].
- [230] K. Kumericki and D. Mueller, Nucl. Phys. **B841**, 1 (2010), [arXiv:0904.0458].
- [231] N. d'Hose, S. Niccolai and A. Rostomyan, Eur. Phys. J. **A52**, 6, 151 (2016).
- [232] M. Guidal, H. Moutarde and M. Vanderhaeghen, Rept. Prog. Phys. **76**, 066202 (2013), [arXiv:1303.6600].
- [233] M. Anselmino, M. Guidal and P. Rossi, The European Physical Journal A **52**, 6, 149 (2016), ISSN 1434-601X, URL <https://doi.org/10.1140/epja/i2016-16164-4>.
- [234] P. J. Mulders and R. D. Tangerman, Nucl. Phys. **B461**, 197 (1996), [Erratum: Nucl. Phys. **B484**, 538(1997)], [hep-ph/9510301].
- [235] D. Boer and P. J. Mulders, Phys. Rev. **D57**, 5780 (1998), [hep-ph/9711485].
- [236] D. W. Sivers, Phys. Rev. **D41**, 83 (1990).
- [237] J. C. Collins, Nucl. Phys. **B396**, 161 (1993), [hep-ph/9208213].
- [238] X. Ji, J. Ma and F. Yuan, Phys. Rev. **D71**, 034005 (2005), [hep-ph/0404183].
- [239] J. Collins, Foundations of perturbative QCD Camb. Monogr. Part. Phys. Nucl. Phys. Cosmol. **32** (2011) 1-624 and references therein.
- [240] S. M. Aybat and T. C. Rogers, Phys. Rev. **D83**, 114042 (2011), [arXiv:1101.5057].
- [241] M. G. Echevarria, A. Idilbi and I. Scimemi, JHEP **07**, 002 (2012), [arXiv:1111.4996].
- [242] M. G. A. Buffing, A. Mukherjee and P. J. Mulders, Phys. Rev. **D88**, 054027 (2013), [arXiv:1306.5897].
- [243] T. C. Rogers and P. J. Mulders, Phys. Rev. **D81**, 094006 (2010), [arXiv:1001.2977].
- [244] A. Signori *et al.*, JHEP **11**, 194 (2013), [arXiv:1309.3507].
- [245] M. Anselmino *et al.*, JHEP **04**, 005 (2014), [arXiv:1312.6261].
- [246] U. D'Alesio *et al.*, JHEP **11**, 098 (2014), [arXiv:1407.3311].
- [247] P. Sun *et al.*, Int. J. Mod. Phys. **A33**, 11, 1841006 (2018), [arXiv:1406.3073].
- [248] V. Bertone, I. Scimemi and A. Vladimirov, JHEP **06**, 028 (2019), [arXiv:1902.08474].
- [249] I. Scimemi and A. Vladimirov, JHEP **06**, 137 (2020), [arXiv:1912.06532].
- [250] M. G. Echevarria, Z.-B. Kang and J. Terry, JHEP **01**, 126 (2021), [arXiv:2009.10710].
- [251] A. Bacchetta *et al.*, Phys. Lett. B **827**, 136961 (2022), [arXiv:2004.14278].
- [252] A. Bacchetta *et al.* (MAP (Multi-dimensional Analyses of Partonic distributions)), JHEP **10**, 127 (2022), [arXiv:2206.07598].
- [253] J. O. Gonzalez-Hernandez *et al.*, Phys. Rev. **D98**, 11, 114005 (2018), [arXiv:1808.04396].
- [254] A. Bacchetta *et al.*, Phys. Rev. **D100**, 1, 014018 (2019), [arXiv:1901.06916].
- [255] M. Bury *et al.*, JHEP **10**, 118 (2022), [arXiv:2201.07114].
- [256] R. Angeles-Martinez *et al.*, Acta Phys. Polon. **B46**, 12, 2501 (2015), [arXiv:1507.05267].
- [257] A. Bacchetta *et al.*, Phys. Lett. **B788**, 542 (2019), [arXiv:1807.02101].
- [258] M. Diehl, Eur. Phys. J. **A52**, 6, 149 (2016), [arXiv:1512.01328].
- [259] A. Bacchetta, Eur. Phys. J. **A52**, 6, 163 (2016).
- [260] <http://hepdata.cedar.ac.uk/pdfs>.
- [261] I. Scimemi, Adv. High Energy Phys. **2019**, 3142510 (2019), [arXiv:1901.08398].

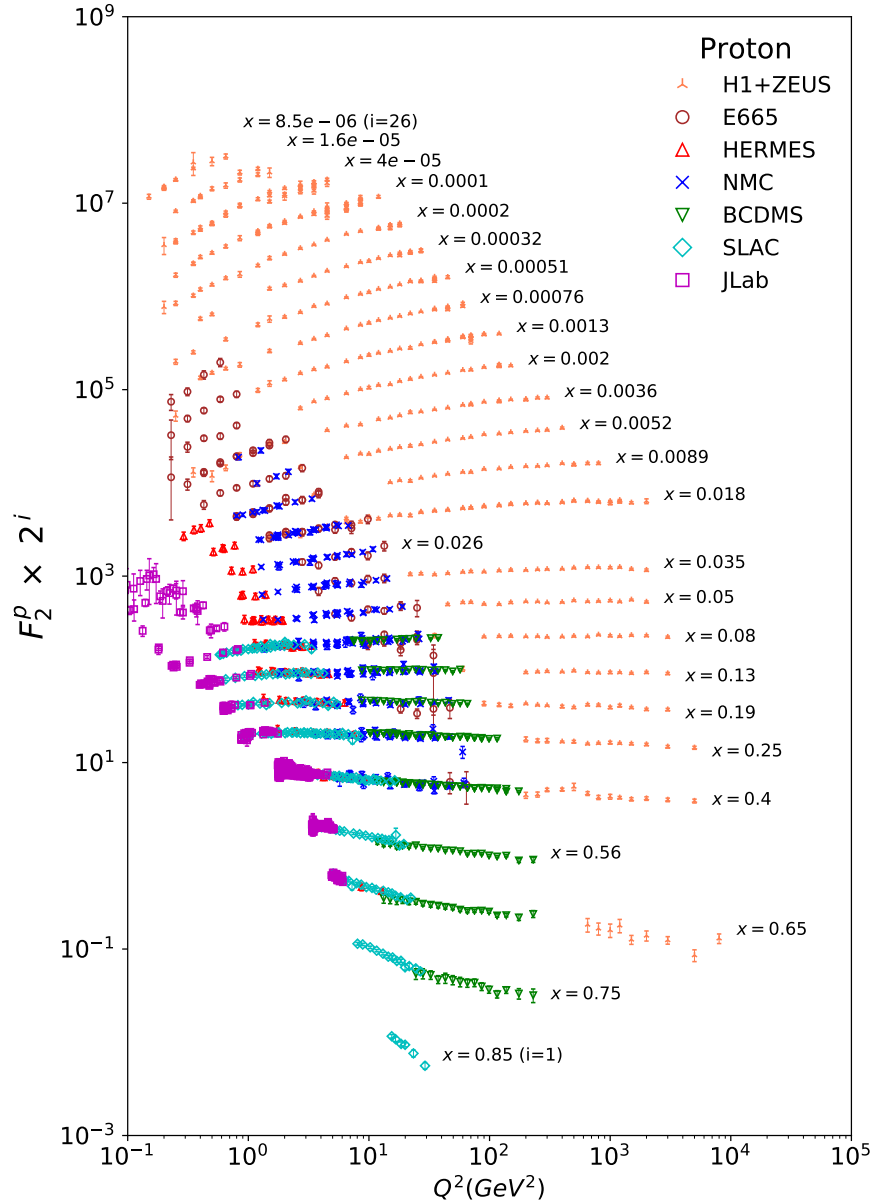


Figure 18.10: The proton structure function F_2^p measured in electromagnetic scattering of electrons and positrons on protons, and for electrons/positrons (SLAC,HERMES,JLAB) and muons (BCDMS, E665, NMC) on a fixed target. Statistical and systematic errors added in quadrature are shown. The H1+ZEUS combined values are obtained from the measured reduced cross section and converted to F_2^p with a HERAPDF NLO fit, for all measured points where the predicted ratio of F_2^p to reduced cross-section was within 10% of unity. The data are plotted as a function of Q^2 in bins of fixed x . Some points have been slightly offset in Q^2 for clarity. The H1+ZEUS combined binning in x is used in this plot; all other data are rebinned to the x values of these data. For the purpose of plotting, F_2^p has been multiplied by 2^{i_x} , where i_x is the number of the x bin, ranging from $i_x = 1$ ($x = 0.85$) to $i_x = 26$ ($x = 0.0000085$). Only data with $W^2 > 3.5$ GeV² is included. Plot from CJ collaboration (Shujie Li – private communication).

References: **H1 and ZEUS**—H. Abramowicz *et al.*, Eur. Phys. J. **C75**, 580 (2015) (for both data and HERAPDF parameterization); **BCDMS**—A.C. Benvenuti *et al.*, Phys. Lett. **B223**, 485 (1989) (as given in [260]) **E665**—M.R. Adams *et al.*, Phys. Rev. **D54**, 3006 (1996); **NMC**—M. Arneodo *et al.*, Nucl. Phys. **B483**, 3 (1997); **SLAC**—L.W. Whitlow *et al.*, Phys. Lett. **B282**, 475 (1992); **HERMES**—A. Airapetian *et al.*, JHEP **1105**, 126 (2011); **JLAB**—Y. Liang *et al.*, Jefferson Lab Hall C E94-110 collaboration, nucl-ex/0410027, M.E. Christy *et al.*, Jefferson Lab Hall C E94-110 Collaboration, Phys. Rev. **C70**, 015206 (2004), S. Malace *et al.*, Jefferson Lab Hall C E00-116 Collaboration, Phys. Rev. **C80**, 035207 (2009), V. Tvaskis *et al.*, Jefferson Lab Hall C E99-118 Collaboration, Phys. Rev. **C81**, 055207 (2010), M. Osipenko *et al.*, Jefferson Lab Hall B CLAS6 Collaboration, Phys. Rev. **D67**, 092001 (2003).

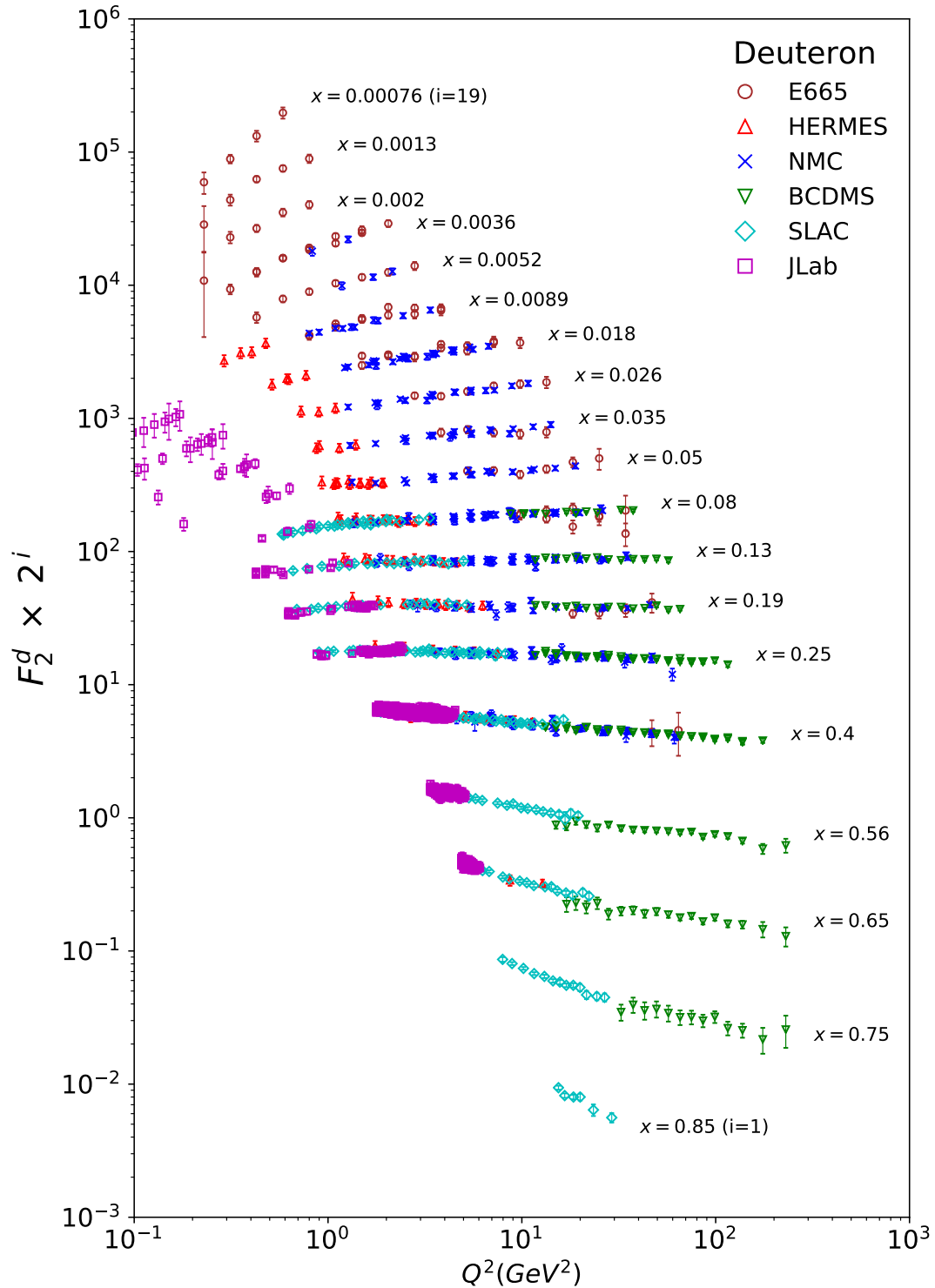


Figure 18.11: The deuteron structure function F_2^d measured in electromagnetic scattering of electrons/positrons (SLAC, HERMES, JLAB) and muons (BCDMS, E665, NMC) on a fixed target, shown as a function of Q^2 for bins of fixed x . Statistical and systematic errors added in quadrature are shown. For the purpose of plotting, F_2^d has been multiplied by 2^{i_x} , where i_x is the number of the x bin, ranging from 1 ($x = 0.85$) to 29 ($x = 0.00076$). Only data with $W^2 > 3.5 \text{ GeV}^2$ is included. Plot from CJ collaboration (Shujie Li – private communication) References: **BCDMS**—A.C. Benvenuti *et al.*, Phys. Lett. **B237**, 592 (1990). **E665**, **NMC**, **SLAC**, **HERMES**—same references as Fig. 18.10; **JLAB**—S. Malace *et al.*, Jefferson Lab Hall C E00-116 Collaboration, Phys. Rev. **C80**, 035207 (2009), V. Tvaskis *et al.*, Jefferson Lab Hall C E99-118 Collaboration, Phys. Rev. **C81**, 055207 (2010), J. Seely (MIT, LNS) *et al.*, Jefferson Lab Hall C E03-103 Collaboration, Phys. Rev. Lett. **103**, 202301 (2009), M. Osipenko *et al.*, Jefferson Lab Hall B CLAS6 Collaboration, Phys. Rev. **C73**, 045205 (2006).

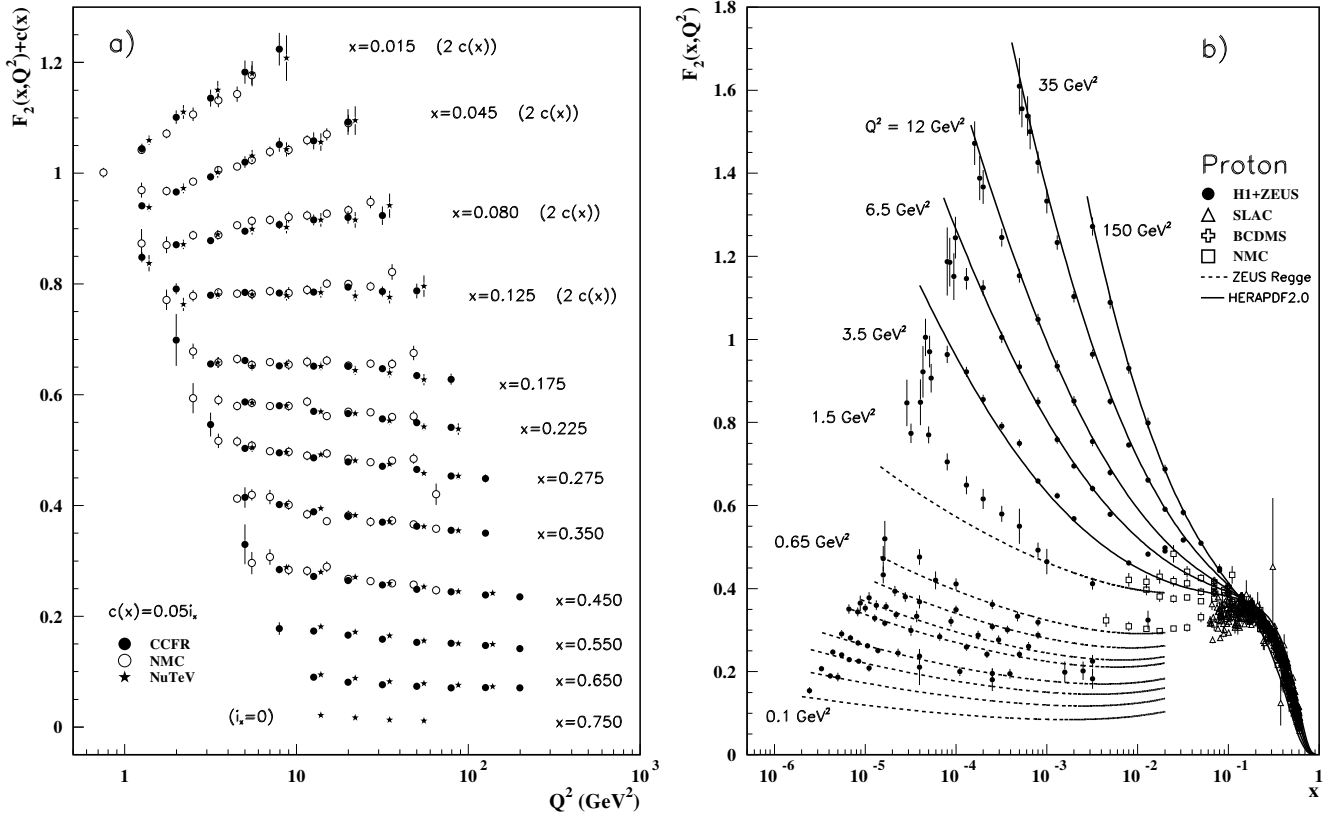


Figure 18.12: a) The deuteron structure function F_2 measured in deep inelastic scattering of muons on a fixed target (NMC) is compared to the structure function F_2 from neutrino-iron scattering (CCFR and NuTeV) using $F_2^\mu = (5/18)F_2^\nu - x(s + \bar{s})/6$, where heavy-target effects have been taken into account. The data are shown versus Q^2 , for bins of fixed x . The NMC data have been rebinned to CCFR and NuTeV x values. For the purpose of plotting, a constant $c(x) = 0.05i_x$ is added to F_2 , where i_x is the number of the x bin, ranging from 0 ($x = 0.75$) to 7 ($x = 0.175$). For $i_x = 8$ ($x = 0.125$) to 11 ($x = 0.015$), $2c(x)$ has been added. References: NMC—M. Arneodo *et al.*, Nucl. Phys. **B483**, 3 (1997); CCFR/NuTeV—U.K. Yang *et al.*, Phys. Rev. Lett. **86**, 2741 (2001); NuTeV—M. Tzanov *et al.*, Phys. Rev. **D74**, 012008 (2006). b) The proton structure function F_2^p mostly at small x and Q^2 , measured in electromagnetic scattering of electrons and positrons (H1, ZEUS), electrons (SLAC), and muons (BCDMS, NMC) on protons. Lines are ZEUS Regge and HERAPDF parameterizations for lower and higher Q^2 , respectively. The width of the bins can be up to 10% of the stated Q^2 . Some points have been slightly offset in x for clarity. The H1+ZEUS combined values for $Q^2 \geq 3.5$ GeV² are obtained from the measured reduced cross section and converted to F_2^p with a HERAPDF NLO fit, for all measured points where the predicted ratio of F_2^p to reduced cross-section was within 10% of unity. A turn-over is visible in the low- x points at medium Q^2 (3.5 GeV² and 6 GeV²) for the H1+ZEUS combined values. In order to obtain F_2^p from the measured reduced cross-section, F_L must be estimated; for the points shown, this estimate is obtained from HERAPDF2.0. No F_L value consistent with the HERA data can eliminate the turn-over. This may indicate that at low x and Q^2 there are contributions to the structure functions that cannot be described in standard DGLAP evolution.

References: H1 and ZEUS—F.D. Aaron *et al.*, JHEP **1001**, 109 (2010) (data for $Q^2 < 3.5$ GeV²), H. Abramowicz *et al.*, Eur. Phys. J. **C75**, 580 (2015) (data for $Q^2 \geq 3.5$ GeV² and HERAPDF parameterization); ZEUS—J. Breitweg *et al.*, Phys. Lett. **B487**, 53 (2000) (ZEUS Regge parameterization); BCDMS, NMC, SLAC—same references as Fig. 18.10. Statistical and systematic errors added in quadrature are shown for both plots.

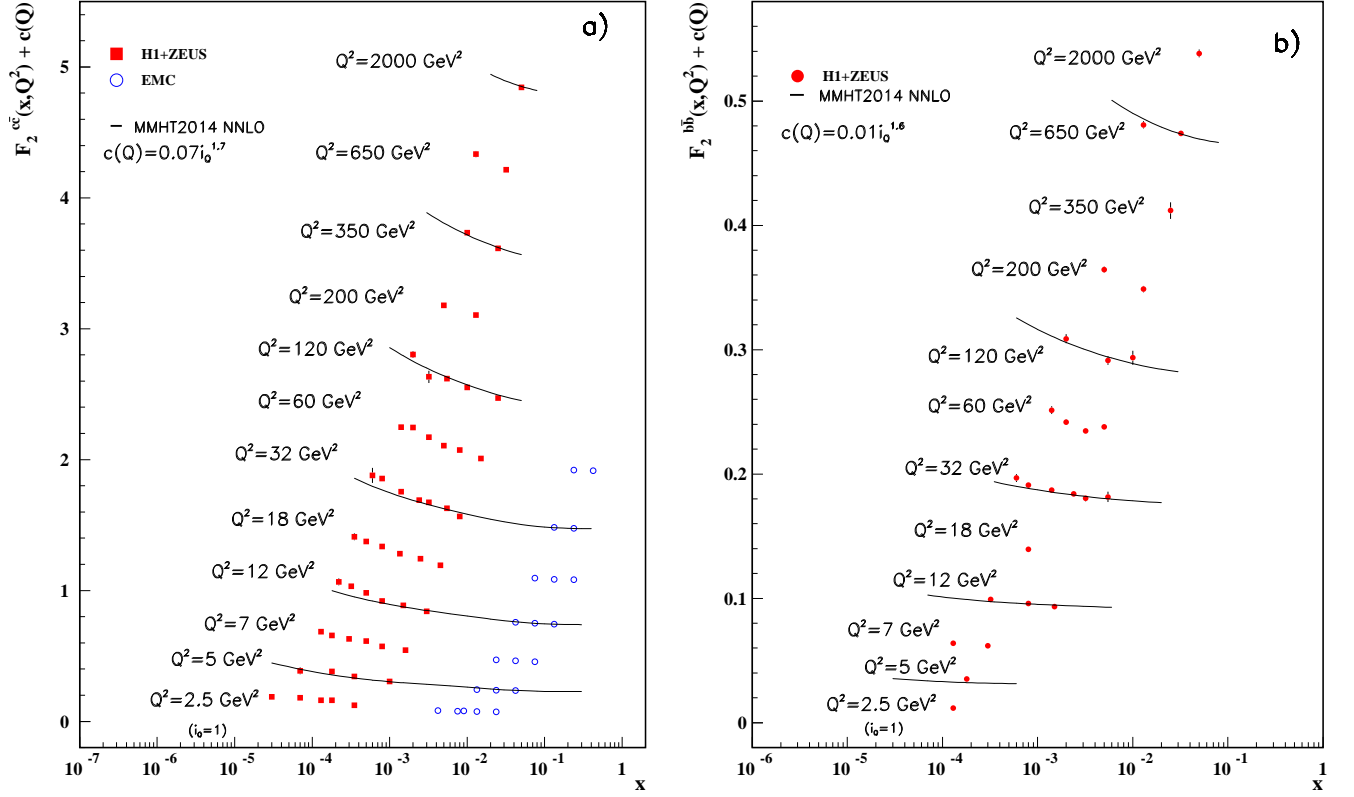


Figure 18.13: a) The charm-quark structure function $F_2^{c\bar{c}}(x)$, i.e. that part of the inclusive structure function F_2^p arising from the production of charm quarks, measured in electromagnetic scattering of positrons on protons (H1, ZEUS) (the values are obtained from the measured reduced cross section and converted to $F_2^{c\bar{c}}$ using the PDFs from the MMHT NNLO fit) and muons on iron (EMC). For the purpose of plotting, a constant $c(Q) = 0.07 i_Q^{1.7}$ is added to $F_2^{c\bar{c}}$ where i_Q is the number of the Q^2 bin, ranging from 1 ($Q^2 = 2.5 \text{ GeV}^2$) to 12 ($Q^2 = 2000 \text{ GeV}^2$). References: **H1 and ZEUS run I +II combination**—H. Abramowicz *et al.*, *Eur. Phys. J.* **C78**, 473 (2018); **EMC**—J.J. Aubert *et al.*, *Nucl. Phys.* **B213**, 31 (1983).

b) The bottom-quark structure function $F_2^{b\bar{b}}(x)$. For the purpose of plotting, a constant $c(Q) = 0.01 i_Q^{1.6}$ is added to $F_2^{b\bar{b}}$ where i_Q is the number of the Q^2 bin, ranging from 1 ($Q^2 = 2.5 \text{ GeV}^2$) to 12 ($Q^2 = 2000 \text{ GeV}^2$). References: **H1 and ZEUS run I combination**—H. Abramowicz *et al.*, *Eur. Phys. J.* **C78**, 473 (2018).

For both plots, statistical and systematic errors added in quadrature are shown. The data are given as a function of x in bins of Q^2 . Points may have been slightly offset in x for clarity. Some data have been rebinned to common Q^2 values. Also shown is the MMHT2014 parameterization given at several Q^2 values (L. A. Harland-Lang *et al.*, *Eur. Phys. J.* **C75**, 204 (2015)).

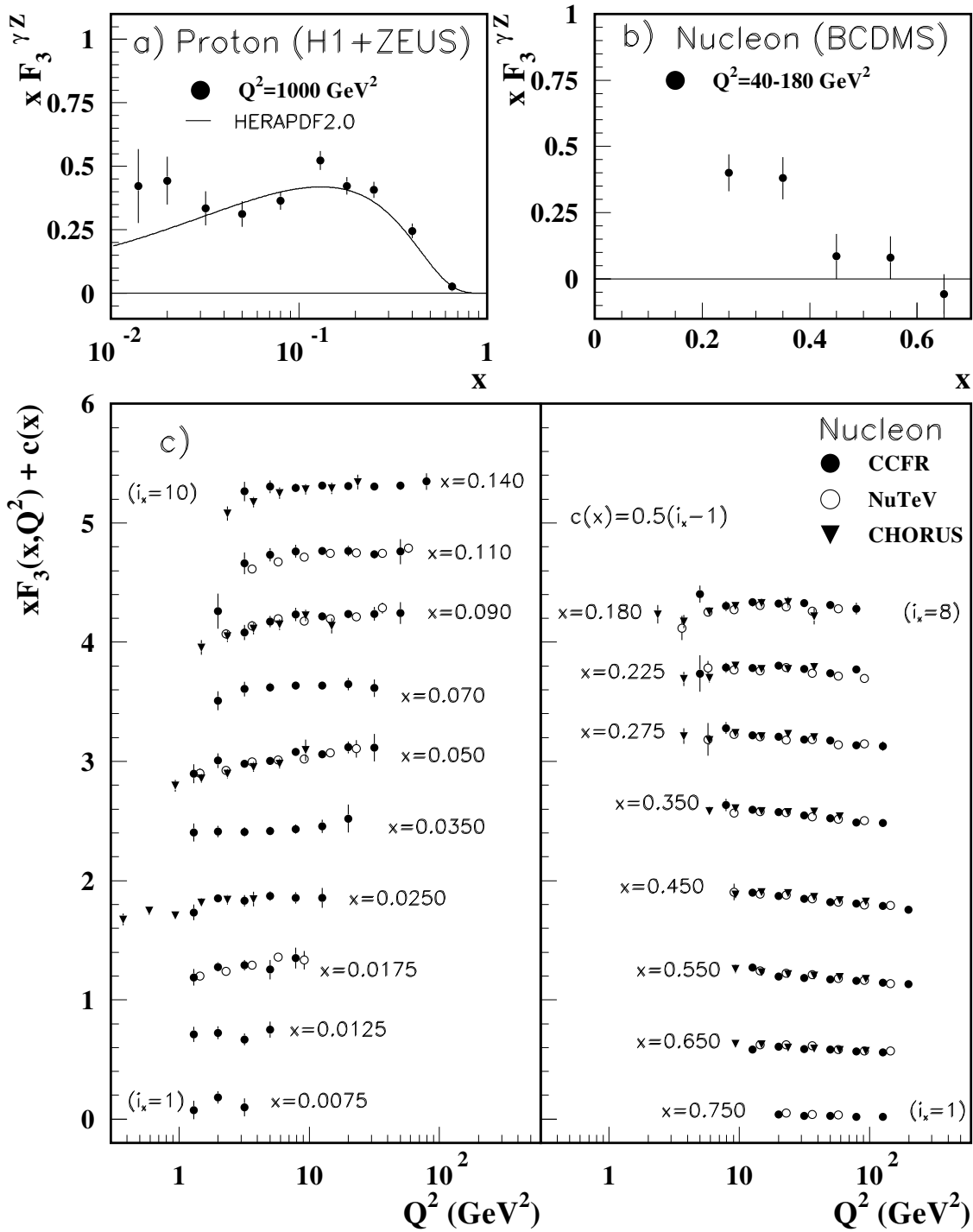


Figure 18.14: The structure function $x F_3^{\gamma Z}$ measured in electroweak scattering of **a)** electrons on protons (H1 and ZEUS) and **b)** muons on carbon (BCDMS). The line in **a)** is the HERAPDF parameterization. References: **H1 and ZEUS**—H. Abramowicz *et al.*, Eur. Phys. J. **C75**, 580 (2015) (for both data and HERAPDF parameterization); **BCDMS**—A. Argento *et al.*, Phys. Lett. **B140**, 142 (1984). **c)** The structure function $x F_3$ of the nucleon measured in ν -Fe scattering. The data are plotted as a function of Q^2 in bins of fixed x . For the purpose of plotting, a constant $c(x) = 0.5(i_x - 1)$ is added to $x F_3$, where i_x is the number of the x bin as shown in the plot. The NuTeV and CHORUS points have been shifted to the nearest corresponding x bin as given in the plot and slightly offset in Q^2 for clarity. References: **CCFR**—W.G. Seligman *et al.*, Phys. Rev. Lett. **79**, 1213 (1997); **NuTeV**—M. Tzanov *et al.*, Phys. Rev. **D74**, 012008 (2006); **CHORUS**—G. Öngüt *et al.*, Phys. Lett. **B632**, 65 (2006).

Statistical and systematic errors added in quadrature are shown for all plots.

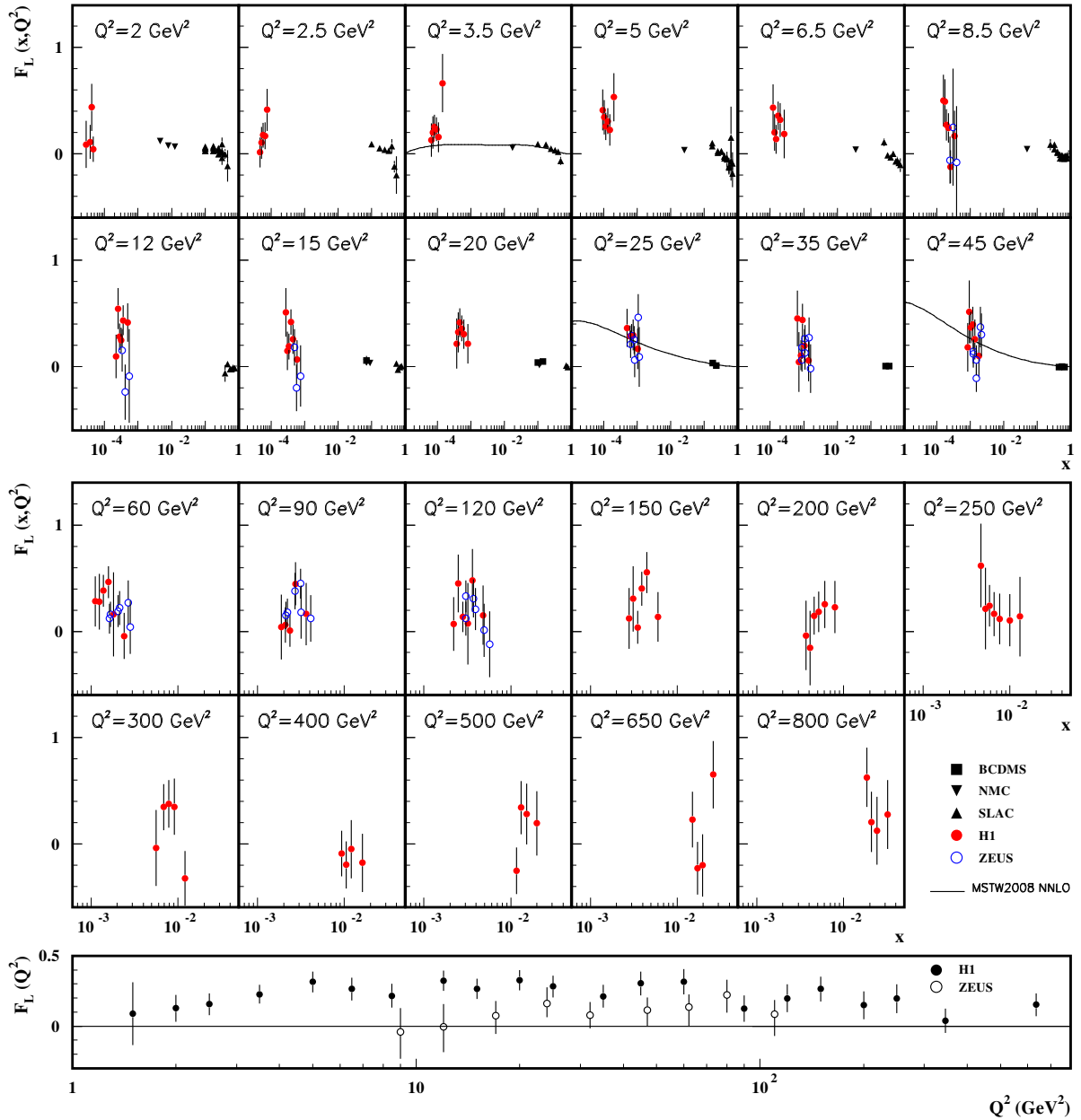


Figure 18.15: Top panels: The longitudinal structure function F_L as a function of x in bins of fixed Q^2 measured on the proton (except for the SLAC data which also contain deuterium data). BCDMS, NMC, and SLAC results are from measurements of R (the ratio of longitudinal to transverse photon absorption cross sections) which are converted to F_L by using the BDCMS parameterization of F_2 (A.C. Benvenuti *et al.*, Phys. Lett. **B223**, 485 (1989)). It is assumed that the Q^2 dependence of the fixed-target data is small within a given Q^2 bin. Some of the other data may have been rebinned to common Q^2 values. Some points have been slightly offset in x for clarity. Also shown is the MSTW2008 parameterization given at three Q^2 values (A.D. Martin *et al.*, Eur. Phys. J. **C63**, 189 (2009)). References: **H1**—V. Andreev *et al.*, Eur. Phys. J. **C74**, 2814 (2014); **ZEUS**—S. Chekanov *et al.*, Phys. Lett. **B682**, 8 (2009); H. Abramowicz *et al.*, Phys. Rev. **D90**, 072002 (2014); **BCDMS**—A. Benvenuti *et al.*, Phys. Lett. **B223**, 485 (1989); **NMC**—M. Arneodo *et al.*, Nucl. Phys. **B483**, 3 (1997); **SLAC**—L.W. Whitlow *et al.*, Phys. Lett. **B250**, 193 (1990) and numerical values from the thesis of L.W. Whitlow (SLAC-357). Bottom panel: The longitudinal structure function F_L as a function of Q^2 . Some points have been slightly offset in Q^2 for clarity. References: **H1**—V. Andreev *et al.*, Eur. Phys. J. **C74**, 2814 (2014); **ZEUS**—H. Abramowicz *et al.*, Phys. Rev. **D90**, 072002 (2014). The results shown in the bottom plot require the assumption of the validity of the QCD form for the F_2 structure function in order to extract F_L . Statistical and systematic errors added in quadrature are shown for both plots.

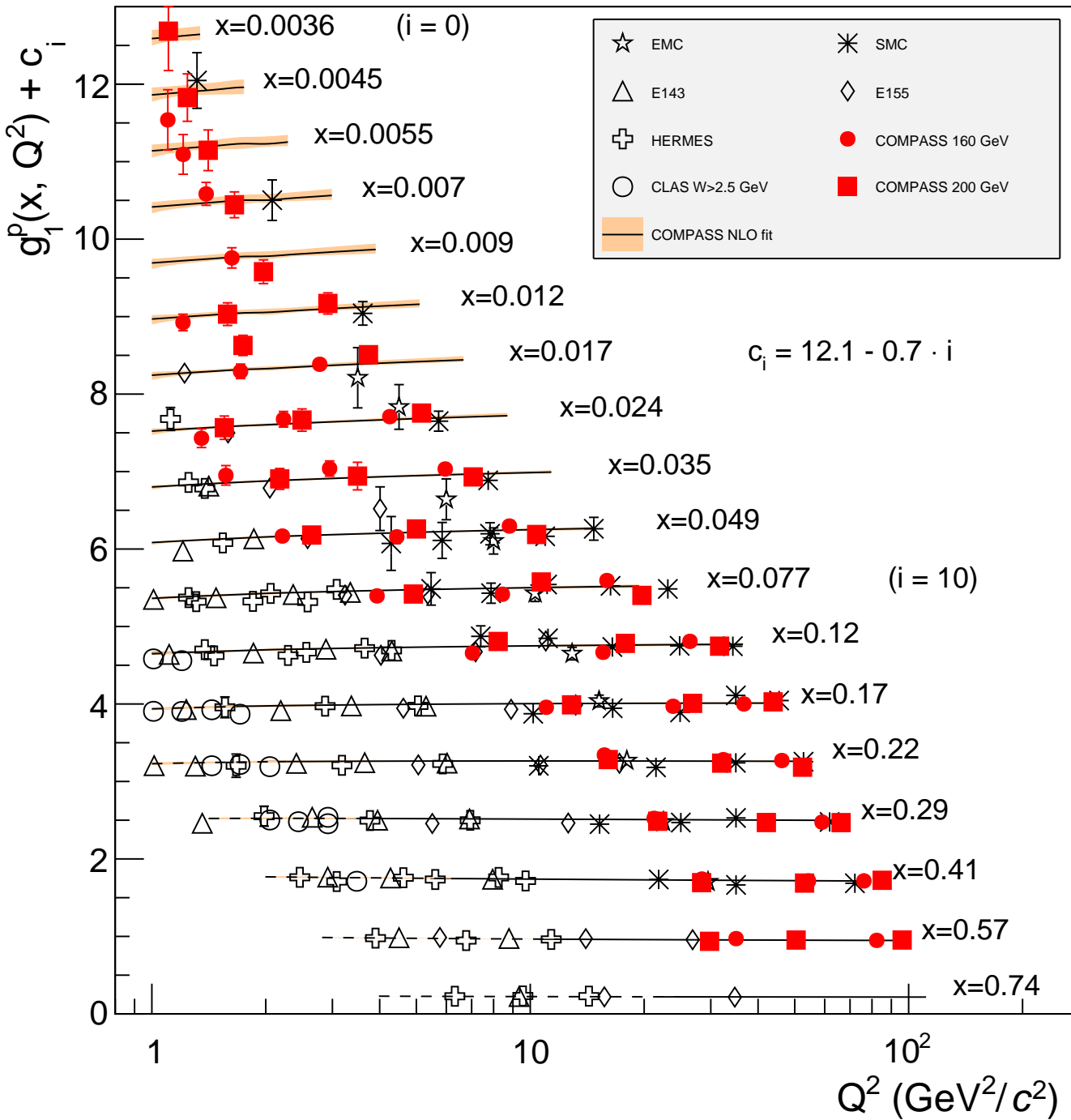


Figure 18.16: World data on the spin-dependent structure function g_1^p as a function of Q^2 for various values of x . The lines represent the Q^2 dependence for each value of x , as determined from a NLO QCD fit. The dashed ranges represent the region with $W^2 < 10$ (GeV/c^2)². References: **EMC**—J. Ashman *et al.*, Phys. Lett. **B206**, 363 (1988); Nucl. Phys. **B328**, 1 (1989); **E143**—K. Abe *et al.*, Phys. Rev. **D58**, 112003 (1998); **SMC**—B. Adeva *et al.*, Phys. Rev. **D58**, 112001 (1998); **HERMES**—A. Airapetian *et al.*, Phys. Rev. **D75**, 012007 (2007); **E155**—P.L. Anthony *et al.*, Phys. Lett. **B493**, 19 (2000); **COMPASS**—M.G. Alekseev *et al.*, Phys. Lett. **B690**, 466 (2010), C. Adolph, *et al.*, Phys. Lett. **B753**, 18 (2016); **CLAS**—K.V. Dharmawardane *et al.*, Phys. Lett. **B641**, 11 (2006) (which also includes resonance region data not shown on this plot — there is also low W^2 CLAS data in Y. Prok *et al.*, Phys. Rev. **C90**, 025212 (2014) and N. Guler *et al.*, Phys. Rev. **C92**, 055201 (2015)).

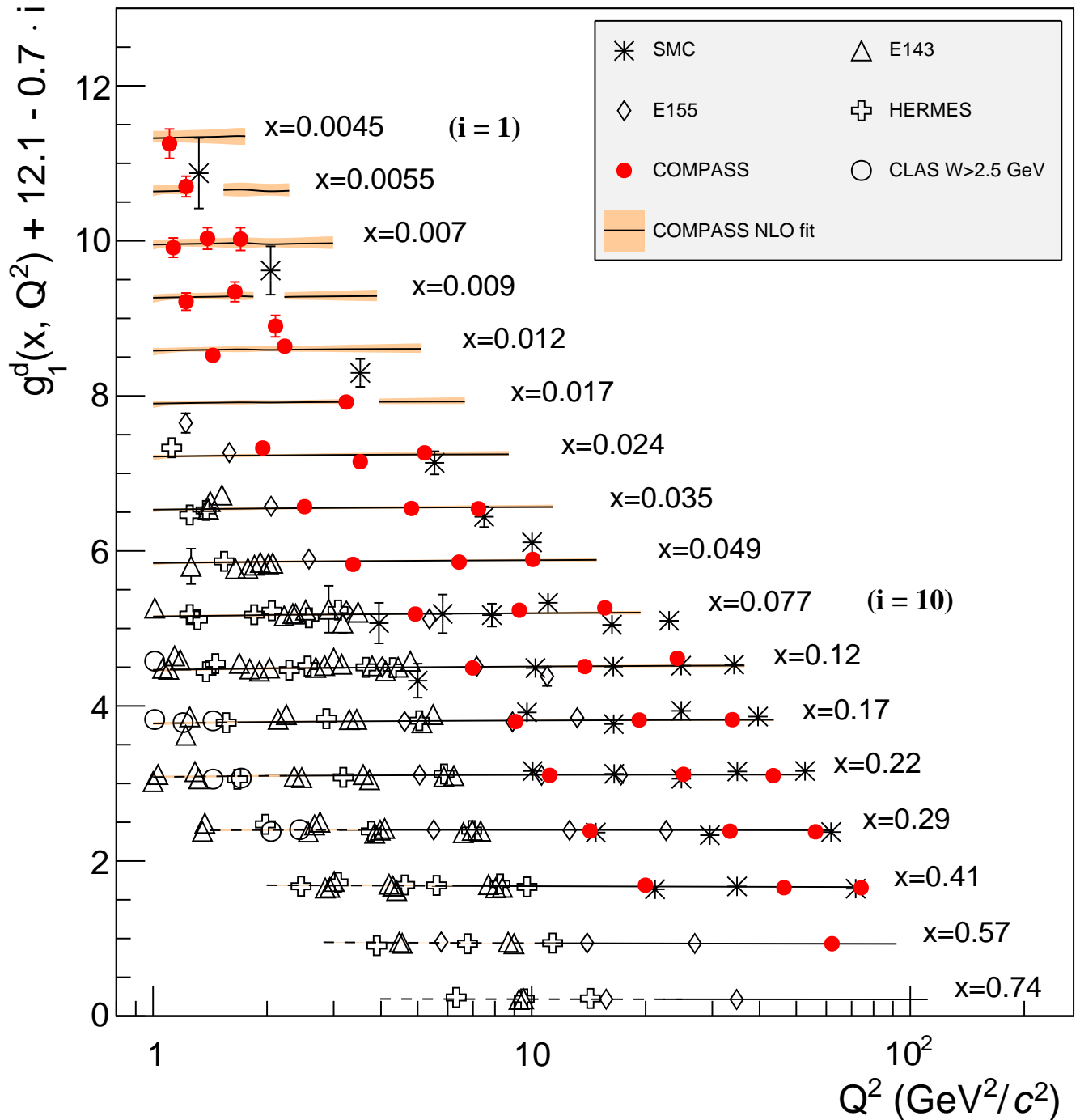


Figure 18.17: World data on the spin-dependent structure function g_1^d as a function of Q^2 for various values of x . The lines represent the Q^2 dependence for each value of x , as determined from a NLO QCD fit. The dashed ranges represent the region with $W^2 < 10$ (GeV/c^2) 2 . **CLAS**—K.V. Dharmawardane *et al.*, Phys. Lett. **B641**, 11 (2006) **HERMES**—A. Airapetian *et al.*, Phys. Rev. **D75**, 012007 (2007); **SMC**—B. Adeva *et al.*, Phys. Rev. **D58**, 112001 (1998); **E155**—P.L. Anthony *et al.*, Phys. Lett. **B463**, 339 (1999); **E143**—K. Abe *et al.*, Phys. Rev. **D58**, 112003 (1998); **COMPASS**—C. Adolph, *et al.*, Phys. Lett. **B769**, 34 (2017);

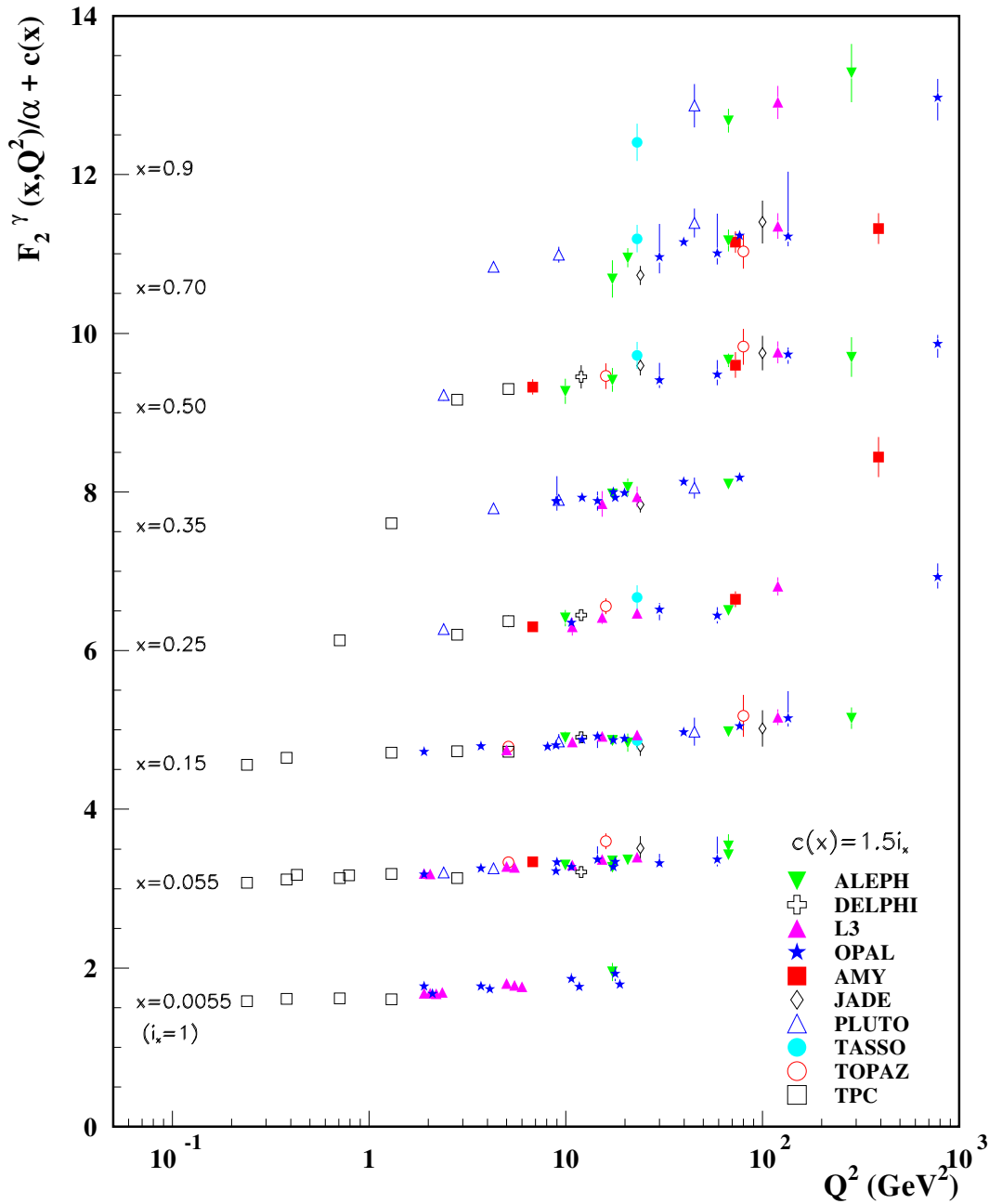


Figure 18.18: The hadronic structure function of the photon F_2^γ divided by the fine structure constant α measured in e^+e^- scattering, shown as a function of Q^2 for bins of x . Data points have been shifted to the nearest corresponding x bin as given in the plot. Some points have been offset in Q^2 for clarity. Statistical and systematic errors added in quadrature are shown. For the purpose of plotting, a constant $c(x) = 1.5i_x$ is added to F_2^γ/α where i_x is the number of the x bin, ranging from 1 ($x = 0.0055$) to 8 ($x = 0.9$). References: **ALEPH**—R. Barate *et al.*, Phys. Lett. **B458**, 152 (1999); A. Heister *et al.*, Eur. Phys. J. **C30**, 145 (2003); **DELPHI**—P. Abreu *et al.*, Z. Phys. **C69**, 223 (1995); **L3**—M. Acciarri *et al.*, Phys. Lett. **B436**, 403 (1998); M. Acciarri *et al.*, Phys. Lett. **B447**, 147 (1999); M. Acciarri *et al.*, Phys. Lett. **B483**, 373 (2000); **OPAL**—A. Ackerstaff *et al.*, Phys. Lett. **B411**, 387 (1997); A. Ackerstaff *et al.*, Z. Phys. **C74**, 33 (1997); G. Abbiendi *et al.*, Eur. Phys. J. **C18**, 15 (2000); G. Abbiendi *et al.*, Phys. Lett. **B533**, 207 (2002) (note that there is overlap of the data samples in these last two papers); **AMY**—S.K. Sahu *et al.*, Phys. Lett. **B346**, 208 (1995); T. Kojima *et al.*, Phys. Lett. **B400**, 395 (1997); **JADE**—W. Bartel *et al.*, Z. Phys. **C24**, 231 (1984); **PLUTO**—C. Berger *et al.*, Phys. Lett. **142B**, 111 (1984); C. Berger *et al.*, Nucl. Phys. **B281**, 365 (1987); **TASSO**—M. Althoff *et al.*, Z. Phys. **C31**, 527 (1986); **TOPAZ**—K. Muramatsu *et al.*, Phys. Lett. **B332**, 477 (1994); **TPC/Two Gamma**—H. Aihara *et al.*, Z. Phys. **C34**, 1 (1987).

19. Fragmentation Functions in e^+e^- , ep , and pp Collisions

Revised August 2023 by O. Biebel (Ludwig-Maximilians U.), D. de Florian (ICAS and ICIFI, UNSAM), D. Milstead (Stockholm U.) and W. Vogelsang (Tübingen U.).

19.1 Introduction to fragmentation

Quarks and gluons produced in hard-scattering reactions will ultimately give rise to the colorless hadronic bound states that may be observed in the detector. The associated hadronization process is described by fragmentation functions $D_i^h(x, \mu^2)$ ($i = q, \bar{q}, g$) which are universal functions representing, in the simplest picture, a measure of the probability density that an outgoing parton produces a hadron h . Here, x is the fraction of the parton's momentum transferred to the hadron, and μ is a 'resolution' scale known as factorization scale. The $D_i^h(x, \mu^2)$ may be viewed as the final-state analogs of the initial-state parton distribution functions (PDFs) addressed in Section 18 of this *Review*. They are also sometimes referred to as *timelike* distributions since they are primarily accessed in e^+e^- annihilation via a timelike intermediate boson. (See Refs. [1,2] for introductory reviews, and Refs. [3–5] for summaries of experimental and theoretical research in this field).

The cleanest laboratory for the study of fragmentation functions is provided by semi-inclusive electron-positron annihilation, $e^+e^- \rightarrow \gamma/Z \rightarrow h+X$. The cross section for this reaction may be expressed in terms of 'fragmentation structure functions' $F_{T,L,A}$ that are directly related to the fragmentation functions. At center-of-mass (CM) energy $\sqrt{s} = q^2$ we have

$$\frac{1}{\sigma_0} \frac{d^2\sigma^h}{dx d\cos\theta} = \frac{3}{8}(1 + \cos^2\theta)F_T^h(x, q^2) + \frac{3}{4}\sin^2\theta F_L^h(x, q^2) + \frac{3}{4}\cos\theta F_A^h(x, q^2). \quad (19.1)$$

Here, q is the four-momentum of the intermediate photon or Z -boson, with $q^2 > 0$, and $x = 2P_h \cdot q/q^2$ with the hadron's four-momentum P_h is the fragmentation counterpart of the familiar DIS Bjorken variable. (Note that $x = 2E_h/\sqrt{s} \leq 1$ in terms of the energy E_h of the produced hadron in the CM frame of the electron positron pair.) Furthermore, in the same frame, θ is the hadron's angle relative to the electron beam direction. Eq. (19.1) is the most general form for unpolarized inclusive single-particle production via vector bosons [6]. The fragmentation structure functions F_T and F_L represent the contributions from γ/Z polarizations transverse or longitudinal with respect to the direction of motion of the hadron. The parity-violating term with the asymmetric fragmentation function F_A arises from the interference between vector and axial-vector contributions. Various normalization factors σ_0 are used in the literature, ranging from the total cross section σ_{tot} for $e^+e^- \rightarrow \text{hadrons}$, including all weak and QCD contributions, to $\sigma_0 = 4\pi\alpha^2 N_c/3s$ with $N_c = 3$, the lowest-order QED cross section for $e^+e^- \rightarrow \mu^+\mu^-$ times the number of colors N_c . LEP1 measurements of the three fragmentation structure functions are shown in Fig. 19.1.

Integration of Eq. (19.1) over all θ yields the total fragmentation structure function $F^h = F_T^h + F_L^h$:

$$\frac{1}{\sigma_0} \frac{d\sigma^h}{dx} = F^h(x, q^2) = \sum_i \int_x^1 \frac{dz}{z} C_i \left(z, \alpha_s(\mu), \frac{q^2}{\mu^2} \right) D_i^h \left(\frac{x}{z}, \mu^2 \right). \quad (19.2)$$

On the right we have written the factorized expression for the structure function in terms of a sum over convolutions of the fragmentation functions D_i^h for partons $i = u, \bar{u}, d, \bar{d}, \dots, g$ with perturbative coefficient functions C_i . Since photons and Z bosons do not distinguish between quarks and antiquarks, e^+e^- annihilation primarily constrains the combinations $D_q^h + D_{\bar{q}}^h$. Gluon fragmentation contributes only at higher order in perturbation theory or by scaling violations. Corrections to the factorized expression in Eq. (19.2) are suppressed by inverse powers of q^2 . They arise from quark and hadron mass terms and from non-perturbative effects.

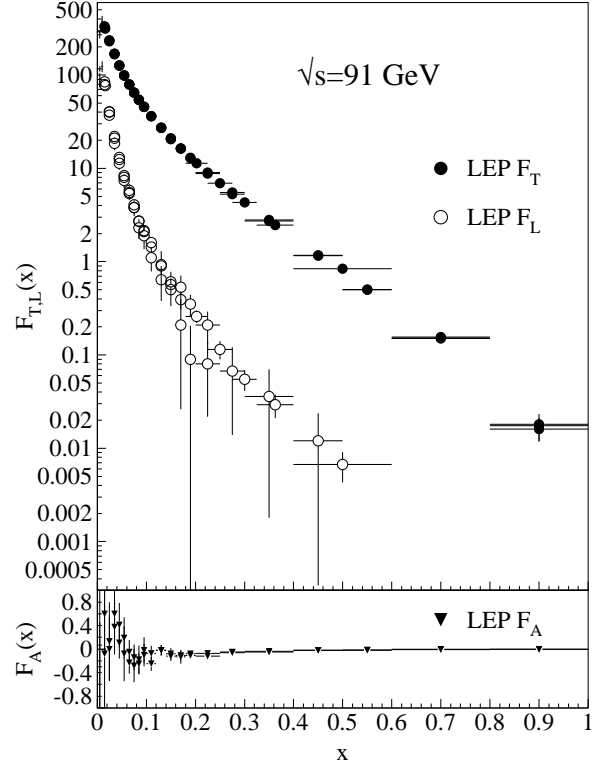


Figure 19.1: LEP1 measurements of total transverse (F_T), longitudinal (F_L), and asymmetric (F_A) fragmentation structure functions [7]. Data points with relative errors greater than 100% are omitted.

Analogous factorized expressions as in Eq. (19.2) may be written for each of the structure functions $F_{T,L,A}$ individually.

The fragmentation functions obey the momentum sum rule constraint

$$\sum_h \int_0^1 dx x D_i^h(x, \mu^2) = 1, \quad (19.3)$$

separately for each flavor i . Note that the sum rule involves a sum over all possible produced hadrons. The dependence of the functions D_i^h on the factorization scale μ^2 will be discussed in the next section.

Measurements of hadron production in deeply-inelastic lepton-proton scattering and hadron-hadron scattering are complementary to those in e^+e^- annihilation. The former process, $\ell p \rightarrow \ell' + h + X$, is known as *semi-inclusive deep-inelastic scattering* (SIDIS). Here, in analogy with Eq. (19.2), the high virtuality of the photon in DIS also permits factorization of the cross section in terms of fragmentation functions, PDFs for the incoming proton, and perturbative hard-scattering cross sections. Likewise, factorization also occurs for $pp \rightarrow h + X$ at large transverse momentum of the produced hadron, and for $pp \rightarrow \text{jet}(h) + X$, where the hadron is part of a fully reconstructed jet. The fragmentation functions contributing to $e^+e^- \rightarrow h + X$, $\ell p \rightarrow \ell' + h + X$, and $pp \rightarrow h + X$, $pp \rightarrow \text{jet}(h) + X$ are universal in the sense that the same functions appear in the factorized expressions for the three reactions. Modern QCD analyses of fragmentation functions “globally” take into account experimental data sets for all three types of processes in order to obtain optimal sets of fragmentation functions.

Electron-positron annihilation has the advantage that there is no hadronic initial state and hence no beam remnant. This is in contrast to $\ell p \rightarrow \ell' + h + X$ or $pp \rightarrow h + X$, which are affected by hadron remnant contributions associated with the partons of the initial-state hadron(s) which are collaterally involved in the hard lepton-parton or parton-parton collision. On the other hand,

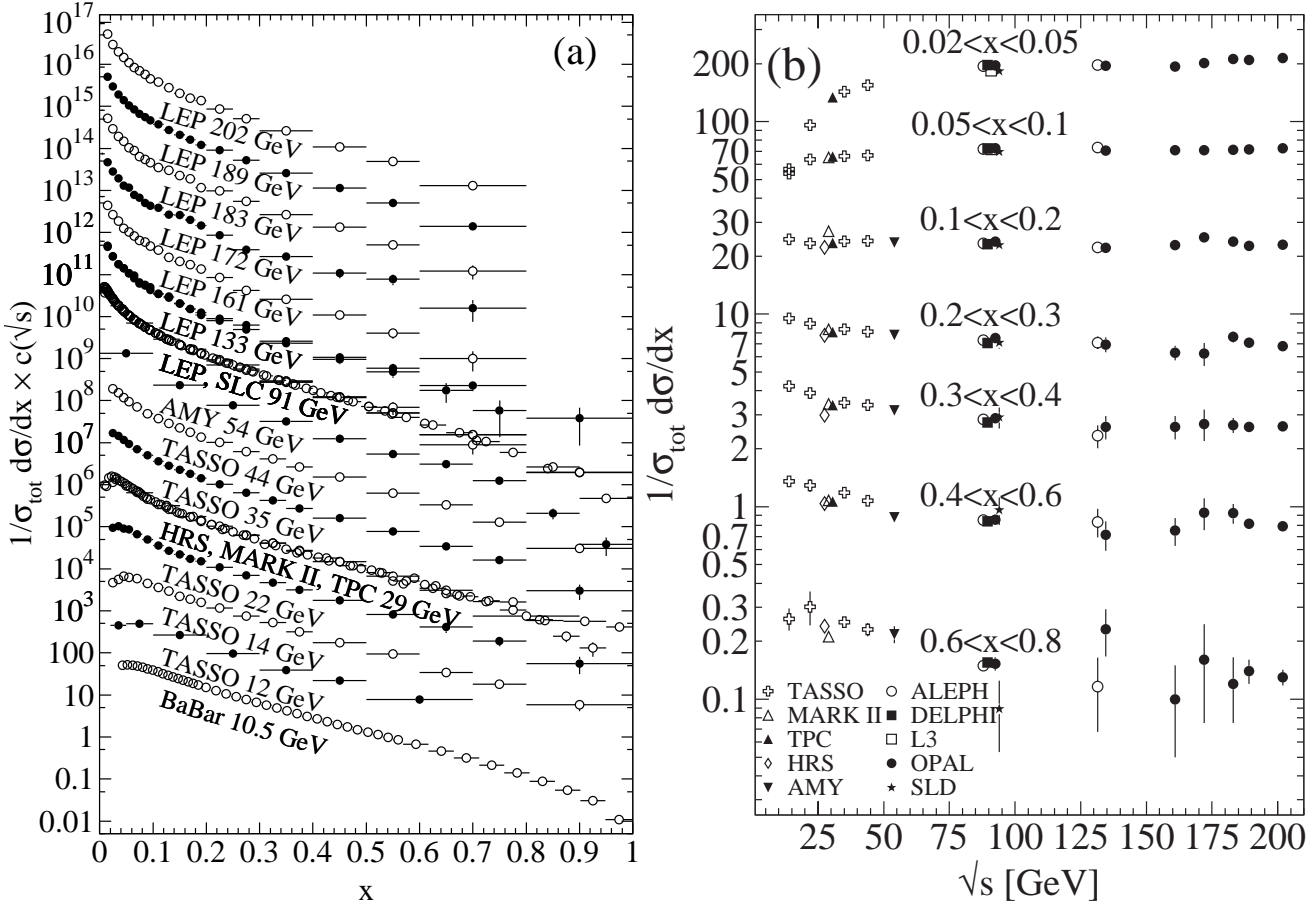


Figure 19.2: Cross section for $e^+e^- \rightarrow h + X$ for all charged hadrons [8–26], (a) for different CM energies \sqrt{s} versus x , and (b) for various ranges of x versus \sqrt{s} . For (a) the distributions have been scaled by $c(\sqrt{s}) = 10^i$ with i ranging from $i = 0$ ($\sqrt{s} = 12$ GeV) to $i = 13$ ($\sqrt{s} = 202$ GeV).

$e^+e^- \rightarrow h + X$ has little sensitivity to D_q^h and is insensitive to the charge asymmetries $D_q^h - D_{\bar{q}}^h$. These quantities are best constrained in proton-(anti-)proton and electron-proton scattering, respectively. Especially the latter provides an environment that allows the study of the influence of initial-state QCD radiation on the fragmentation process, of the partonic and spin structure of the hadron target, and of the target remnant system. (See Ref. [27] for a comprehensive review of the measurements and models of fragmentation in lepton-hadron scattering).

Moreover, unlike e^+e^- annihilation where $q^2 = s$ is fixed by the collider energy, lepton-hadron scattering has two independent scales, $Q^2 = -q^2$ and the invariant mass squared, $W^2 \approx Q^2(1-x)/x$, of the hadronic final state, which both can vary by several orders of magnitudes for a given CM energy, thus allowing the study of fragmentation in different environments by a single experiment. For example, in photoproduction the exchanged photon is quasi-real ($Q^2 \approx 0$), leading to processes akin to hadron-hadron scattering. In DIS ($Q^2 \gg 1$ GeV²), using factorization, the hadronic fragments of the struck quark can be directly compared with quark fragmentation in e^+e^- in a suitable frame. Results from lepton-hadron experiments quoted in this report primarily concern fragmentation in the DIS regime. Studies performed by lepton-hadron experiments of fragmentation with photoproduction data containing high transverse momentum jets or particles are also reported, when these are directly comparable to DIS and e^+e^- results.

Fragmentation studies in lepton-hadron collisions are usually performed in one of two frames in which the target hadron and the exchanged boson are collinear. The hadronic center-of-mass frame (HCMS) is defined as the rest system of the exchanged boson and incoming hadron, with the z^* -axis defined along the direction of the exchanged boson. The positive z^* direction de-

fines the so-called current fragmentation region. Fragmentation measurements performed in the HCMS often use the Feynman- x variable $x_F = 2p_z^*/W$, where p_z^* is the longitudinal momentum of the particle in this frame. As W is the invariant mass of the hadronic final state, x_F ranges between -1 and 1 .

The Breit system [28, 29] is related to the HCMS by a longitudinal boost such that the time component of q vanishes, i.e., $q = (0, 0, 0, -Q)$. In the parton model, the struck parton then has the longitudinal momentum $Q/2$ which becomes $-Q/2$ after the collision. As compared with the HCMS, the current fragmentation region of the Breit frame is more closely matched to the partonic scattering process, and is thus appropriate for direct comparisons of fragmentation functions in DIS with those from e^+e^- annihilation. The variable $x_p = 2p^*/Q$, where p^* is the particle's momentum in the current region of the Breit frame, is used at HERA for measurements in the Breit frame, enabling rather direct comparisons of DIS and e^+e^- results.

19.2 Scaling violations and QCD corrections

As mentioned, the coefficient functions for the fragmentation structure functions in $e^+e^- \rightarrow h + X$ are amenable to QCD perturbation theory. For each of the structure functions $F_{T,L,A}(x, q^2)$ in Eq. (19.1) (and hence for the total structure function F^h in Eq. (19.2)) the coefficient function has an expansion of the form

$$C_{a,i} \left(z, \alpha_s(\mu), \frac{q^2}{\mu^2} \right) = (1 - \delta_{aL}) \delta_{iq} \delta(1-z) + \frac{\alpha_s(\mu)}{2\pi} c_{a,i}^{(1)} \left(z, \frac{q^2}{\mu^2} \right) + \left(\frac{\alpha_s(\mu)}{2\pi} \right)^2 c_{a,i}^{(2)} \left(z, \frac{q^2}{\mu^2} \right) + \dots \quad (19.4)$$

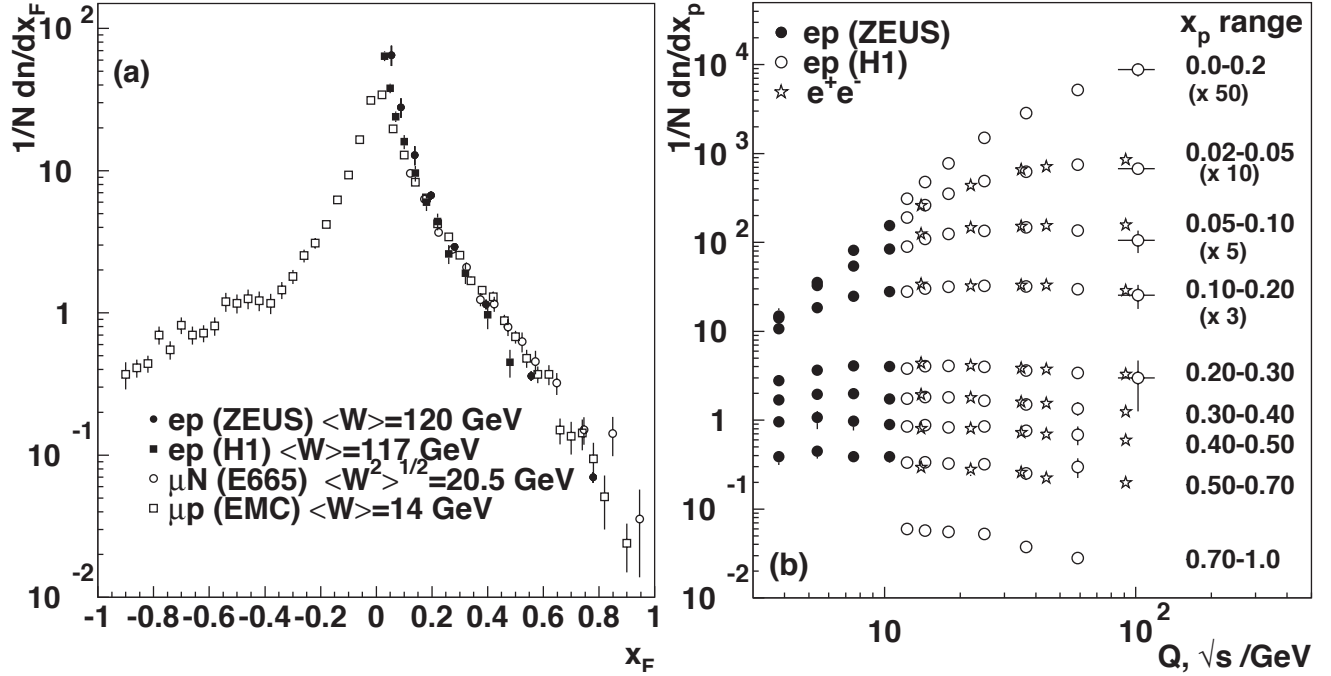


Figure 19.3: (a) The distribution $1/N \cdot dN/dx_F$ for all charged particles in DIS lepton-hadron experiments at different values of W , measured in the HCMS [30–33]. (b) Scaling violations of the fragmentation structure function for all charged particles in the current region of the Breit frame of DIS [34, 35] and in e^+e^- interactions [19, 36]. The data are shown as a function of \sqrt{s} for e^+e^- results, and as a function of Q for the DIS results, each within the same indicated intervals of the scaled momentum x_p . The data for the four lowest intervals of x_p are multiplied by factors 50, 10, 5, and 3, respectively for better visibility.

where $a = T, L, A$. At the zeroth order in the strong coupling α_s the coefficient functions C_g for gluons vanish, while for (anti-)quarks $C_i = g_i(s) \delta(1-z)$ (except for F_L for which the leading contribution is of order α_s , as indicated in Eq. (19.4)). Here $g_i(s)$ is the appropriate electroweak coupling. In particular, $g_i(s)$ is proportional to the squared charge of the quark i at $s \ll M_Z^2$, when weak effects can be neglected. The full electroweak prefactors $g_i(s)$ can be found in Ref. [6]. The first-order QCD corrections to the coefficient functions have been calculated in Refs. [37, 38], and the second-order terms in [39–41]. Thus, the coefficient functions are known to NNLO, except for F_L . We note that beyond the leading order the coefficient functions, and hence the fragmentation functions, start to depend on the choice of factorization scheme. The standard choice in the literature is the $\overline{\text{MS}}$ scheme.

The simplest parton-model approach would predict scale-independent (‘scaling’) x -distributions for both the structure function F^h and the parton fragmentation functions D_i^h . Perturbative QCD corrections lead to logarithmic scaling violations via the evolution equations [42]

$$\frac{\partial}{\partial \ln \mu^2} D_i^h(x, \mu^2) = \sum_j \int_x^1 \frac{dz}{z} P_{ji}(z, \alpha_s(\mu^2)) D_j^h\left(\frac{x}{z}, \mu^2\right), \quad (19.5)$$

where the functions $P_{ij}(z, \alpha_s(\mu^2))$ describe the splitting process $i \rightarrow j + X$, where parton j carries the longitudinal momentum fraction z of parton i . Note that for fragmentation the relevant splitting functions are P_{ji} (rather than P_{ij} as for the PDFs) since D_j^h represents the fragmentation of the final parton. Usually the system of evolution equations is decomposed into a 2×2 flavor-singlet sector comprising the gluon and the sum of all quark and antiquark fragmentation functions, and scalar (‘non-singlet’) equations for quark-antiquark and flavor differences.

The splitting functions in Eq. (19.5) have the perturbative expansion

$$P_{ji}(z, \alpha_s) = \frac{\alpha_s}{2\pi} P_{ji}^{(0)}(z) + \left(\frac{\alpha_s}{2\pi}\right)^2 P_{ji}^{(1)}(z) + \left(\frac{\alpha_s}{2\pi}\right)^3 P_{ji}^{(2)}(z) + \dots, \quad (19.6)$$

where the leading-order (LO) functions $P^{(0)}(z)$ [42, 43] are the same as those for the initial-state parton distributions. The next-to-leading order (NLO) corrections $P^{(1)}(z)$ have been calculated in Refs. [44–48] (there are well-known misprints in the journal version of Ref. [45]). Ref. [48] also includes the spin-dependent case. The timelike functions are different from, but related to, their spacelike counterparts, see also Ref. [49]. The connections between the two sets of functions has facilitated recent calculations of the next-to-next-to-leading order (NNLO) quantities $P_{qq}^{(2)}(z)$ and $P_{gg}^{(2)}(z)$ in Eq. (19.6) [40, 50]. In the same way, the corresponding off-diagonal quantities $P_{qg}^{(2)}$ and $P_{gq}^{(2)}$ were recently obtained in Ref. [51] with the help of constraints from the momentum sum rule Eq. (19.3) [50] and of the limit of $C_A = C_F = n_f$ for which QCD becomes supersymmetric. An uncertainty still remains for the $P_{qg}^{(2)}$ kernel, which however does not affect the logarithmic behavior at small and large momentum fractions. With the exception of Ref. [47], all these higher-order results refer to the standard $\overline{\text{MS}}$ scheme with a fixed number n_f of light flavors. When the threshold for the production of a heavier quark flavor is crossed in the course of the scale evolution, fragmentation functions change. The NLO treatment of these flavor thresholds in the evolution has been addressed in Ref. [52].

The phenomenological effect of scale evolution is similar in the timelike and spacelike cases: As the scale increases, one observes a scaling violation in which the x -distribution is shifted towards lower values. This can be seen from Fig. 19.2 where a set of measurements of the total fragmentation structure function in e^+e^- annihilation are shown. In particular, the figure on the right exhibits the dependence on $\sqrt{q^2} = \sqrt{s}$ at fixed values of x . QCD analyses of these data are discussed in Section 19.5 below.

The NLO coefficient functions for SIDIS, $ep \rightarrow e + h + X$, have been presented in Refs. [37, 38] Corresponding results have also been obtained for the case that a non-vanishing hadron transverse momentum is required in the HCMS frame [53, 54].

Scaling violations in DIS are shown in Fig. 19.3 for both the HCMS and the Breit frames. In Fig. 19.3(a) the distribution in terms of $x_F = 2p_z^*/W$ shows a steeper slope in ep data than for the lower-energy μp data for $x_F > 0.15$, indicating the scaling

violations. At smaller values of x_F in the current jet region, the multiplicity of particles substantially increases with W , owing to the increased phase space available for the fragmentation process. The EMC data access both the current region and the region of the fragmenting target remnant system. At higher values of $|x_F|$, due to the extended nature of the remnant, the multiplicity in the target region far exceeds that in the current region. For acceptance reasons the remnant hemisphere of the HCMS is only accessible by the lower-energy fixed-target experiments.

Using hadrons from the current hemisphere in the Breit frame, measurements of fragmentation functions and the production properties of particles in ep scattering have been reported in Refs. [34, 35, 55–58]. Fig. 19.3(b) compares results from ep scattering and e^+e^- experiments; the latter results have been divided by two as they cover both event hemispheres. The agreement between the DIS and e^+e^- results is fairly good. However, processes in DIS which are not present in e^+e^- annihilation, such as boson-gluon fusion and initial-state QCD radiation, can depopulate the current region. These effects become most prominent at low values of Q and x_p . Hence, when compared with e^+e^- annihilation data at $\sqrt{s} = 5.2, 6.5$ GeV [59] not shown here, the DIS particle rates tend to lie below those observed in e^+e^- annihilation. A ZEUS study [60] finds that the direct comparability of the ep data to e^+e^- results at low scales is improved if twice the energy in the current hemisphere of the Breit frame, $2E_B^{cr}$, is used instead of $Q/2$ as the fragmentation scale. Choosing $2E_B^{cr}$ for the fragmentation scale approximates QCD radiation effects relevant at low scales, as detailed in Ref. [29].

19.3 Fragmentation functions for small particle momenta

The higher-order timelike splitting functions in Eq. (19.6) are singular at small values of x . They show a double-logarithmic enhancement, with leading terms of the form $\alpha_s^k (\ln^{2k-2} x)/x$ at the k th order of perturbation theory, corresponding to poles $\alpha_s^k (N-1)^{1-2k}$ for the Mellin moments

$$P^{(k)}(N) = \int_0^1 dx x^{N-1} P^{(k)}(x). \quad (19.7)$$

Despite large cancellations between leading and non-leading logarithms at non-asymptotic values of x , the resulting small- x rise in the timelike splitting functions dwarfs that of their spacelike counterparts for the evolution of the parton distributions in Section 18 of this *Review*, see Fig. 1 of Ref. [50]. Consequently, in fragmentation the fixed-order approximation to the evolution breaks down orders of magnitude earlier in x than in DIS.

The pattern of the known coefficients and other considerations suggest that the double-logarithmic terms sum to all-order expressions without any pole at $N = 1$, such as [61, 62]

$$P_{gg}^{LL}(N) = -\frac{1}{4} \left(N - 1 - \sqrt{(N-1)^2 \cdot 24 \alpha_s / \pi} \right) \quad (19.8)$$

for the gluon-to-gluon splitting function at leading logarithmic order. Keeping the first three terms in the resulting expansion of Eq. (19.5) around $N = 1$ and taking the Mellin inverse yields a Gaussian in the variable $\xi = \ln(1/x)$ for the small- x fragmentation functions,

$$xD(x, q^2 = s) \propto \exp \left[-\frac{1}{2\sigma^2} (\xi - \xi_p)^2 \right], \quad (19.9)$$

with the peak position and width varying with the energy as [63] (see also Ref. [2])

$$\xi_p \simeq \frac{1}{4} \ln \left(\frac{s}{\Lambda^2} \right), \quad \sigma \propto \left[\ln \left(\frac{s}{\Lambda^2} \right) \right]^{3/4}. \quad (19.10)$$

Next-to-leading logarithmic corrections to the above predictions have been calculated [64]. In the method of Ref. [65], see also Refs. [66, 67], the corrections are included in an analytical form known as the ‘modified leading logarithmic approximation’ (MLLA). Alternatively they can be used to compute higher-moment correc-

tions to the shape in Eq. (19.9) [68]. The small- x resummation of the coefficient functions for semi-inclusive e^+e^- annihilation and of the timelike spitting functions in the standard $\overline{\text{MS}}$ scheme was extended in Refs. [69–73] and has reached full next-to-next-to-leading logarithmic accuracy. Applications of these results to gluon and quark jet multiplicities have been presented in Refs. [74].

Fig. 19.4 shows the ξ distribution for charged particles produced in the current region of the Breit frame in DIS and in e^+e^- annihilation. Consistently with Eq. (19.9) (the ‘hump backed plateau’) and Eq. (19.10) the distributions have a Gaussian shape, with the peak position and area increasing with CM energy (e^+e^-) and Q^2 (DIS).

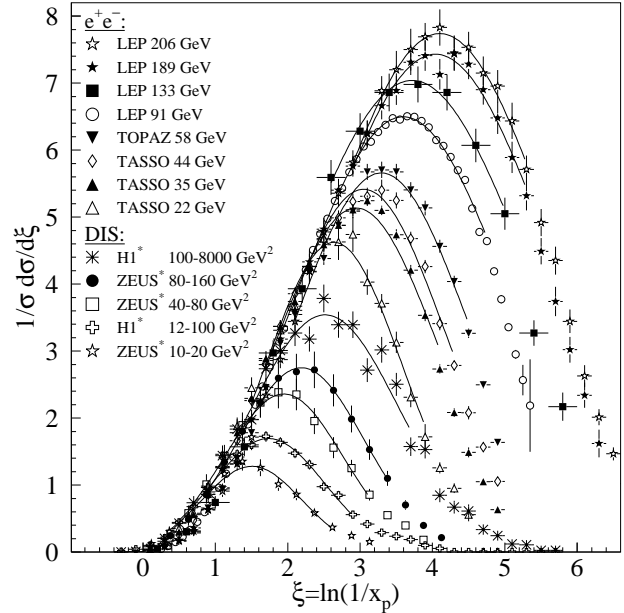


Figure 19.4: Distribution of the normalized fragmentation cross sections in $\xi = \ln(1/x_p)$ at several CM energies (e^+e^-) [10, 11, 16–19, 57, 58, 75–78] and for intervals of Q^2 (DIS). At each energy only one representative measurement is displayed. For clarity some measurements at intermediate CM energies (e^+e^-) or Q^2 ranges (DIS) are not shown. The DIS measurements (*) have been scaled by a factor of 2 for direct comparability with the e^+e^- results. Fits of simple Gaussian functions are overlaid for illustration.

The predicted energy dependence of the peak in the ξ distribution (see Eq. (19.10)) is explained by soft gluon coherence (angular ordering), *i.e.*, the destructive interference of the color wavefunction of low energy gluon radiation, which correctly predicts the suppression of hadron production at small x . Of course, a decrease at very small x is expected on purely kinematical grounds, but this would occur at particle energies proportional to their masses, *i.e.*, at $x \propto m/\sqrt{s}$ and hence $\xi \sim \frac{1}{2} \ln s$. Thus, if the suppression were purely kinematic, the peak position ξ_p would vary twice as rapidly with the energy, which is ruled out by the data in Fig. 19.5. The e^+e^- and DIS data agree well with each other, demonstrating the universality of hadronization and the MLLA prediction. Measurements of the higher moments of the ξ distribution in e^+e^- [19, 78–80] and DIS [58] have also been performed and show consistency with each other.

The average charged-particle multiplicity is another observable sensitive to fragmentation functions for small particle momenta. Perturbative predictions using both NLO [89] and MLLA [90, 91] have been obtained by solving Eq. (19.5) yielding

$$\langle n_G(Q^2) \rangle \propto \alpha_s^b(Q^2) \cdot \exp \left[\frac{c}{4\pi b_0 \sqrt{\alpha_s(Q^2)}} \cdot \left(1 + 6a_2 \frac{\alpha_s(Q^2)}{\pi} \right) \right], \quad (19.11)$$

where $b = \frac{1}{4} + \frac{10}{27} \frac{n_f}{4\pi b_0}$, $c = \sqrt{96\pi}$, with $b_0 = (33 - 2n_f)/(12\pi)$,

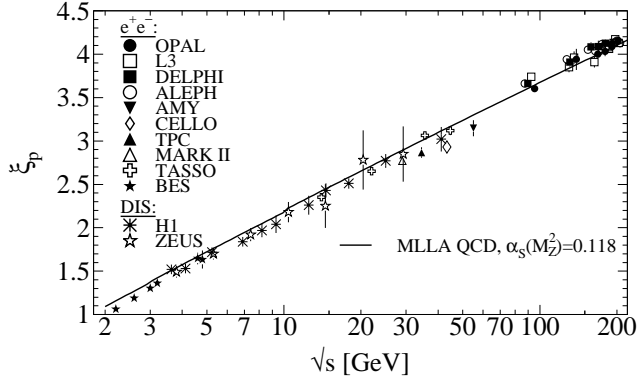


Figure 19.5: Evolution of the peak position, ξ_p , of the ξ distribution with the CM energy \sqrt{s} . The MLLA QCD prediction using $\alpha_s(s = M_Z^2) = 0.118$ is superimposed to the data of Refs. [10, 12, 15, 19, 56, 57, 76, 77, 80–88].

cf. Section 9 of this Review, for n_f contributing quark flavors. Higher-order corrections to Eq. (19.11) are known up to next-to-next-to-leading order (N³LO), for details and references see [92]. The term proportional to $a_2 \approx -0.502 + 0.0421 n_f - 0.00036 n_f^2$ in Eq. (19.11) is the contribution due to NNLO corrections [93]. The quantity $\langle n_G(Q^2) \rangle$ refers to the average number of gluons, while for $\langle n_q(Q^2) \rangle$ for quarks a correction factor $1/r$ is required due to the different color factors in quark and gluon couplings, so that $\langle n_q(Q^2) \rangle = \langle n_G(Q^2) \rangle / r$. The correction factor depends only weakly on Q^2 ; higher-order corrections up to N³LO on the asymptotic value $r = C_A/C_F = 9/4$ [94] are quoted in [92].

Employing the hypothesis of ‘Local Parton-Hadron Duality’ (LPHD) [90], *i.e.*, that the color charge of partons is balanced locally in phase space and, hence, their hadronization occurs locally such that (Mellin transformed) parton and hadron inclusive distributions directly correspond, Eq. (19.11) can be applied to describe average charged particle multiplicities obtained in e^+e^- annihilation. The equation can also be applied to $e^\pm p$ scattering if the current fragmentation region of the Breit frame is considered for measuring the average charged-particle multiplicity. Fig. 19.6 shows corresponding data and fits of Eq. (19.11) where apart from an LPHD normalization factor a constant offset has been allowed for, so that $\langle n_{\text{ch}}(Q) \rangle = K_{\text{LHPD}} \cdot \langle n_G(Q) \rangle / r + n_0$.

In hadron-hadron collisions beam remnants, *e.g.* from single-diffractive (SD) scattering where one colliding proton is negligibly deflected while hadrons related with the other colliding proton are well-separated in rapidity from the former proton, contribute to the measurement of the hadron multiplicity from a hard parton-parton scattering, making interpretation of the data more model dependent. Experimental results are usually given for inelastic processes or for non-single diffractive processes (NSD). Due to the large beam particle momenta at Tevatron and LHC, not all final state particles can be detected within the limited detector acceptance. Therefore, experiments at Tevatron and LHC quote particle multiplicities for limited ranges of pseudo-rapidity $\eta = -\ln \tan(\vartheta/2)$ or at central rapidity, *i.e.* $\eta = 0$, as shown in Fig. 19.6.

A universality of the average particle multiplicities in e^+e^- and $p(\bar{p})$ processes has been reported in Ref. [124] when considering an effective collision energy $Q_{\text{eff}} = \sqrt{s}/k$ in $p(\bar{p})$ reduced by a factor of $k \approx 3$, plus a constant offset of $n_0 \approx 2$. A more detailed review is available in Ref. [125]. According to the investigations presented in Ref. [126] the universality of the energy dependence of average particle multiplicities also applies to hadron-hadron and nucleus-nucleus collisions for both full and central rapidity multiplicities. Evidence for this universality is given by the good agreement for the energy dependence of Eq. (19.11) when fit to the $p(\bar{p})$ data as shown in Fig. 19.6.

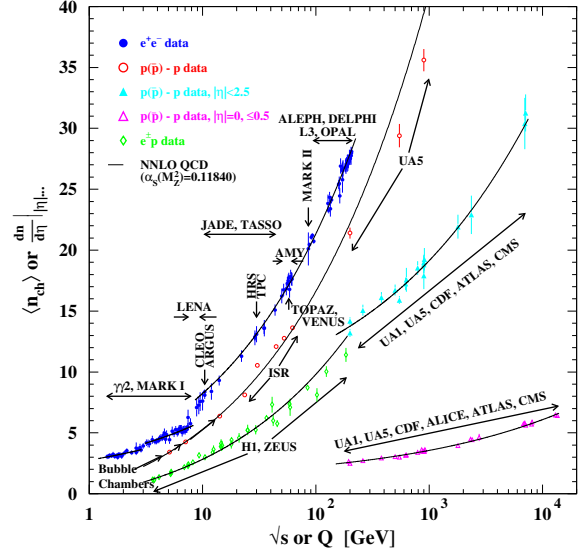


Figure 19.6: Average charged-particle multiplicity $\langle n_{\text{ch}} \rangle$ as a function of \sqrt{s} or Q for e^+e^- and $p\bar{p}$ annihilations, and pp and ep collisions. The indicated errors are statistical and systematic uncertainties added in quadrature, except when no systematic uncertainties are given. All NNLO QCD curves are from Eq. (19.11) with fitted normalization, K_{LHPD} , and offset, n_0 , using a fixed $\alpha_s(M_Z^2) = 0.1184$ [95] and for e^+e^- annihilation data $n_f = 3, 4$, or 5 depending on \sqrt{s} , else $n_f = 3$. e^+e^- : Contributions from K_S^0 and Λ decays included. Data compiled from Refs. [8, 10, 16, 16, 22, 77, 83, 96–106]; $e^\pm p$: Multiplicities have been measured in the current fragmentation region of the Breit frame. Data compiled from Refs. [35, 57, 58, 60, 107]; $p(\bar{p})$: Measured values above 20 GeV refer to non-single diffractive (NSD) processes. Central pseudorapidity multiplicities $(dn/d\eta)|_{|\eta| \dots}$ refer to either $|\eta| < 2.5$ (CMS: $|\eta| < 2.4$) or $|\eta| = 0$ (UA5, CMS, ALICE: $|\eta| < 0.5$). Data compiled from Refs. [108–123].

19.4 Fragmentation models

Although the scaling violations can be calculated perturbatively, the actual form of the parton fragmentation functions is non-perturbative. Perturbative evolution gives rise to a shower of quarks and gluons (partons). Multi-parton final states from leading and higher order matrix element calculations are linked to these parton showers using factorization prescriptions, also called matching schemes, see Ref. [127] for an overview.

Phenomenological schemes are then used to model the carry-over of parton momenta and flavor to the hadrons. Implemented in Monte Carlo event generators (see Section 43 of this Review), these schemes have been tuned using e^+e^- data and provide good description of hadron collisions as well, thus providing evidence of the universality of fragmentation. However, e^+e^- mainly fix the quark jet fragmentation while it provides less constraints for modelling the gluon jet fragmentation.

19.5 Phenomenology of quark and gluon fragmentation functions

The fragmentation functions are solutions to the evolution equations Eq. (19.5), but need to be specified at some initial scale μ_0^2 (usually around 1 GeV² for light quarks and gluons, and at m_Q^2 for heavy quarks). A typical parameterization for a given light hadron is [128, 131–139]

$$D_i^h(x, \mu_0^2) = N_i x^{\alpha_i} (1-x)^{\beta_i} (1 + \gamma_i(1-x)^{\delta_i}), \quad (19.12)$$

where as indicated the normalization N_i , and the parameters α_i , β_i , γ_i and δ_i depend on the type i of the fragmenting parton. Heavy flavor fragmentation into heavy mesons is discussed in Sec. 19.8 below. The parameters of Eq. (19.12) are obtained by

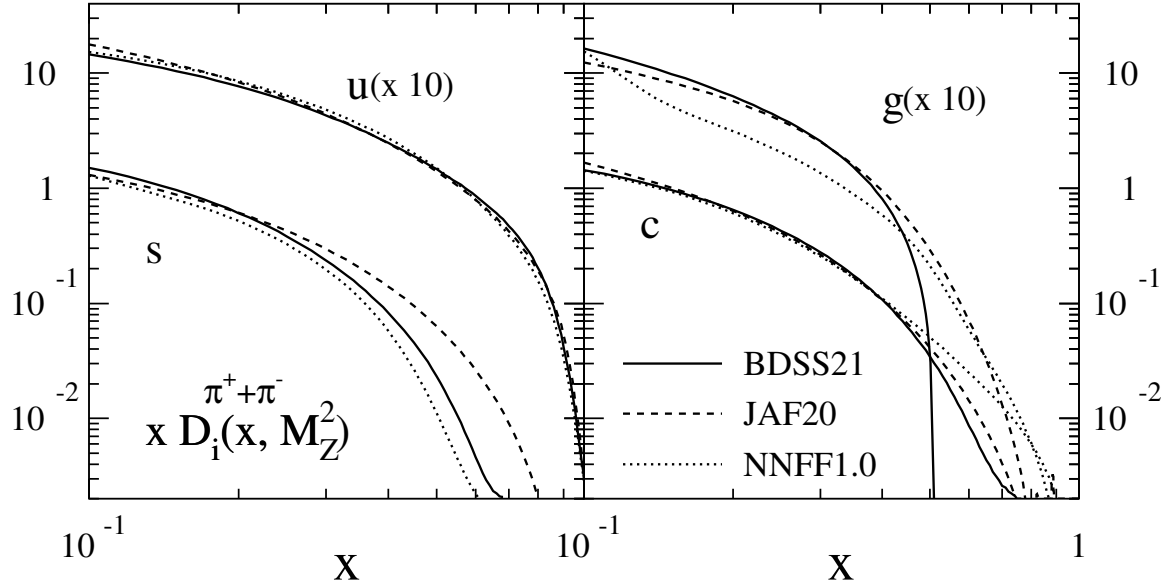


Figure 19.7: Comparison of up, strange, charm and gluon NLO fragmentation functions for $\pi^+ + \pi^-$ at the mass of the Z . The different lines correspond to the results of the analyses performed in Refs. [128–130].

performing global fits to data on various hadron types for different combinations of partons and hadrons in e^+e^- , lepton-hadron and hadron-hadron collisions. We note that the choice of parameterization of the fragmentation functions at the initial scale necessarily introduces a bias since it imposes a certain form of the functions. This bias is largely avoided in neural network approaches which offer a wide flexibility of the initial functions and have recently been applied to fragmentation functions as well [130]. Sets of fragmentation functions are now available for pions, kaons, protons, neutrons, η mesons, Λ baryons, and charged hadrons [129, 130, 132–144]. They are all at NLO level, except for Refs. [130, 141, 144] which have been performed at NNLO level. The latter sets are restricted to the analysis of e^+e^- annihilation data. Recently, data from hadron-hadron collisions have been added in the framework of the neural network approach at NLO accuracy for charged hadrons [145]. It is noteworthy that the NNLO effects lead to an improvement in the theoretical description of the data in e^+e^- annihilation.

Data from e^+e^- annihilation present the cleanest experimental source for the measurement of fragmentation functions, but cannot be used to disentangle quark from antiquark fragmentation. Since the bulk of the e^+e^- annihilation data is obtained at the mass of the Z -boson, where the electroweak couplings are roughly the same for the different partons, it provides the most precise determination of the flavor-singlet combination of quark and antiquark fragmentation functions. Flavor-tagged results [146], distinguishing between the light quark, charm and bottom contributions are of particular value for flavor decomposition, even though those measurements cannot be unambiguously interpreted in perturbative QCD.

The most relevant source for quark-antiquark (and also flavor) separation is provided by SIDIS data. Semi-inclusive measurements are usually performed at much lower scales than for e^+e^- annihilation. The inclusion of SIDIS data in global fits allows for a wider coverage in the evolution of the fragmentation functions, resulting at the same time in a stringent test of the universality of the distributions. Charged-hadron production data in hadronic collisions also have sensitivity to (anti-)quark fragmentation functions. A recent analysis [129] performs a simultaneous extraction of parton distributions and fragmentation functions based on SIDIS data.

The gluon fragmentation function $D_g^h(x)$ can be extracted, in

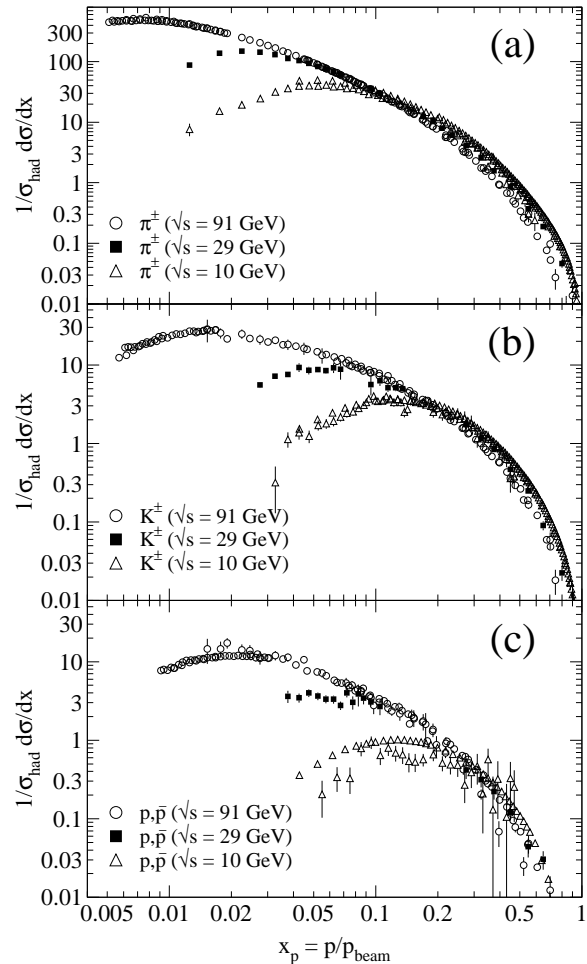


Figure 19.8: Scaled momentum spectra of (a) π^\pm , (b) K^\pm , and (c) p, \bar{p} at $\sqrt{s} = 10, 29, \text{ and } 91$ GeV [24, 26, 85, 147, 148].

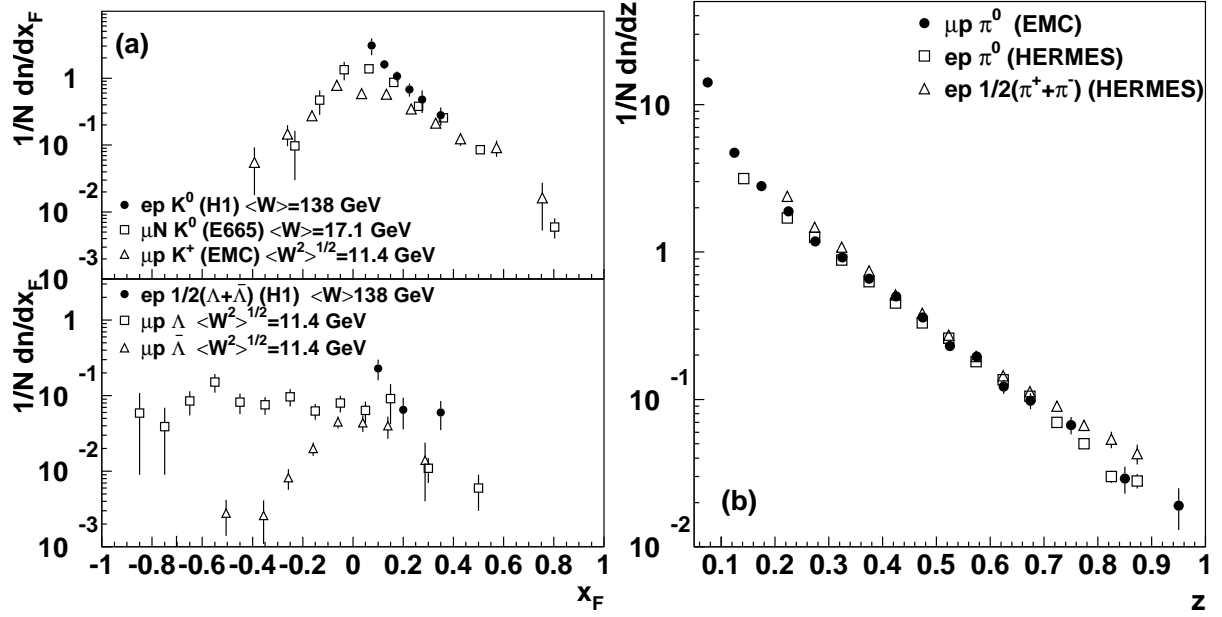


Figure 19.9: (a) $1/N \cdot dn/dx_F$ for identified strange particles in DIS at various values of W [149–151]. (b) $1/N \cdot dn/dz$ for measurements of pions in fixed-target DIS experiments [152–154].

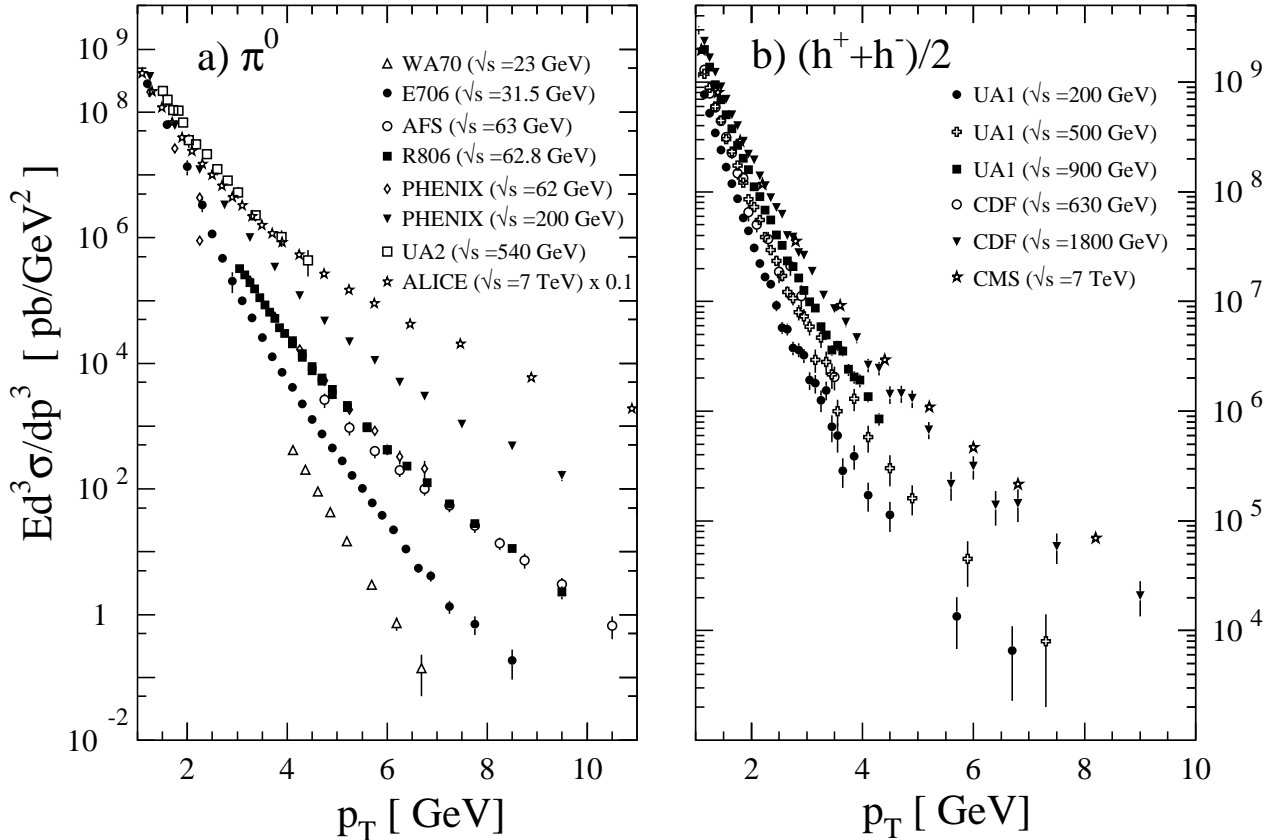


Figure 19.10: Selection of inclusive (a) π^0 and (b) charged-hadron production data from pp [118, 155–160] and $p\bar{p}$ [114, 161, 162] collisions.

principle, from the longitudinal fragmentation structure function F_L in Eq. (19.2), as the coefficient functions $C_{L,i}$ for quarks and gluons are comparable to order α_s . However at NLO, *i.e.*, including the $\mathcal{O}(\alpha_s^2)$ coefficient functions $C_{L,i}^{(2)}$ [39], quark fragmentation is dominant in F_L over a large part of the kinematic range, reducing the sensitivity to D_g^h . This distribution could be determined also by analyzing the scale evolution of the fragmentation func-

tions. This possibility is limited by the lack of sufficiently precise data at energy scales away from the Z -resonance and the dominance of the quark contributions at medium and large values of x . In e^+e^- annihilation, D_g^h can also be deduced from the study of three-jet events in which the gluon jet is identified, for example, by tagging the other two jets with heavy quark decays. To leading order, the measured distributions of $x = E_{\text{had}}/E_{\text{jet}}$ for

Table 19.1: Classification of spin- and transverse-momentum dependent quark fragmentation functions. For simplicity we have left out the ubiquitous label for flavor i of the fragmenting quark and for hadron species h . Each of the functions carries the argument $(x, x^2 k_T^2)$ (plus dependence on a factorization scale), where $xk_T = p_T^h$ is the hadron’s transverse momentum. λ and Λ are the quark’s and hadron’s helicities, respectively, and \vec{s}_T and \vec{S}_T are their transverse spin vectors. We have defined $[\vec{a} \times \vec{b}] \equiv a^1 b^2 - a^2 b^1$. Finally, m_h is the mass of the produced hadron.

hadron pol.	quark polarization		
	unpolarized	long. polarized	transv. polarized
unpol.	D	–	$\frac{[\vec{k}_T \times \vec{s}_T]}{m_h} H^\perp$
long. pol.	–	$\lambda \Lambda G_L$	$\frac{\vec{k}_T \cdot \vec{s}_T}{m_h} \Lambda H_L^\perp$
transv. pol.	$\frac{[\vec{k}_T \times \vec{S}_T]}{m_h} D_T^\perp$	$\frac{\vec{k}_T \cdot \vec{S}_T}{m_h} \lambda G_T^\perp$	$(\vec{s}_T \cdot \vec{S}_T) H_T + \frac{\vec{k}_T \cdot \vec{S}_T}{m_h} \frac{\vec{k}_T \cdot \vec{s}_T}{m_h} H_T^\perp$

particles in gluon jets can be identified directly with the gluon fragmentation function $D_g^h(x)$.

Data for $p(\bar{p}) \rightarrow h + X$ provide much more direct constraint on D_g^h . At variance with e^+e^- annihilation and SIDIS, here gluon fragmentation contributes already at the lowest order in the coupling constant. At large $x \gtrsim 0.5$, where information from e^+e^- is sparse, data from hadronic colliders significantly improve extractions of D_g^h [131, 132, 138, 140]. Recent LHC data has been included in the NLO analyses [128, 138, 139] of pion-fragmentation functions; see Sec.(17.7) for more details. Note that these analyses are currently the only ones that ‘globally’ incorporate available data from all sources, $e^+e^- \rightarrow h + X$, $ep \rightarrow e'h + X$ and $pp \rightarrow h + X$.

We note that recently a ‘hybrid’ type of high- p_T jet/hadron observable has also been considered both theoretically [163–169] and experimentally [170–177]. It is defined by an identified specific hadron found inside a fully reconstructed jet. This gives rise to a *same-side* hadron-jet momentum correlation that may be addressed using perturbative methods. One of several relevant kinematical variables (see [168] for an overview) is $z_h \equiv (\vec{p}_T^h \cdot \vec{p}_T^{\text{jet}})/(p_T^{\text{jet}})^2$, where \vec{p}_T^h and \vec{p}_T^{jet} are the transverse momenta of the hadron and the jet, respectively. The observable provides an alternative window on fragmentation functions in a more exclusive setting, enabling novel tests of the universality of fragmentation functions. Varying z_h and/or the hadron species, one can map out the fragmentation functions ‘locally’ as functions of x . This is in contrast to the single-inclusive observable $pp \rightarrow h + X$, which inevitably samples over a broad range of x . Although hadron-in-jet data are not yet routinely included in analysis of fragmentation functions, a ‘proof-of-principle’ analysis does exist [178] that shows the potential of the observable in providing constraint on fragmentation functions.

A comparison of recent NLO fits of fragmentation functions for $\pi^+ + \pi^-$ obtained by the updated version of BDSS21 [128], JAF20 [129] and NNPDF1.0 [130] is shown in Fig. 19.7. Differences among the functions for these sets are visible, especially for the gluon fragmentation function over the full range of x and for the quark functions at large momentum fractions. The differences are even larger for other species of hadrons like kaons and protons [131, 132, 136, 140]. Recent analyses [128–130, 136, 138, 139, 179, 180] estimate the uncertainties involved in the extraction of fragmentation functions.

Photonic fragmentation functions play a relevant role in the theoretical understanding of inclusive photon production in (leptonic and hadronic) high energy processes. In the spirit of the analogy between parton fragmentation functions and parton distribution functions, also photonic fragmentation functions are analogous to the photon structure function F_2^γ and to the proton’s photonic parton distributions (see review on structure functions in Section 18 of this *Review*). Since photons have a pointlike coupling to quarks [181], the corresponding fragmentation functions obey inhomogeneous evolution equations and are generally decomposed into a perturbative and a non-perturbative compo-

nent [135, 182, 183]. The hadronic part, sometimes approximated by the Vector Meson Dominance Model, can in principle be obtained by performing a global analysis to the available prompt photon production data [7, 12, 15, 19–21, 85, 147, 184, 185], although in practice this has not been done. We note that also the cross section for photons produced in fully reconstructed jets has been proposed [186] as a new tool for obtaining access to photon fragmentation functions, in analogy to the hadron-in-jet cross section discussed above.

19.6 Identified particles in e^+e^- and semi-inclusive DIS

There is a great wealth of measurements of e^+e^- fragmentation into identified particles. A collection of references for data on fragmentation into identified particles is provided in Table 53.1 of this *Review*. As a representative example, Figure 19.8 shows differential charged-hadron spectra as functions of the scaled hadron momentum at several CM energies.

Quantitative results of studies of scaling violations in e^+e^- fragmentation have been reported in [7, 21, 187, 188]. Scaling violations may be used to extract a value of α_s ; the values obtained are consistent with the world average (see review on QCD in Section 9 of this *Review*).

Many studies have been made of production of identified particles in lepton-hadron scattering, although fewer particle species have been measured than in e^+e^- collisions. References [149, 150, 152–154, 189–191] and [151, 192–197] are representative of the data from fixed target and ep collider experiments, respectively. QCD calculations performed at NLO provide an overall good description of the HERA data [33, 34, 58, 197–199], both for SIDIS [200] and for the hadron transverse momentum distribution [53, 201] in the kinematic regions in which the calculations are predictive. Threshold corrections to SIDIS have been computed at NNLO [202] and even at one order higher [203]. Very recently, the full set of NNLO QCD corrections to the corresponding coefficient functions were obtained in [204, 205].

Fig. 19.9(a) compares lower-energy fixed-target and HERA data on strangeness production, showing that the HERA spectra have substantially increased multiplicities, albeit with statistical precision that is insufficient to study scaling violations. The fixed-target data show that the Λ rate substantially exceeds the $\bar{\Lambda}$ rate in the remnant region, owing to the conserved baryon number from the baryon target. Fig. 19.9(b) shows $1/N \cdot dn/dz$ for neutral and charged pion production, where z is defined as the ratio of the pion energy to that of the exchanged boson, both measured in the laboratory frame. Results are shown from the HERMES and the EMC experiments, where the HERMES data have been evolved to $\langle Q^2 \rangle = 25 \text{ GeV}^2$ at NLO QCD, in order to be comparable with the EMC data. Each of the experiments uses various kinematic cuts to ensure that the measured particles lie in the region that is expected to be associated with the struck quark. In the DIS kinematic regime accessed at these experiments, and over the range in z shown in Fig. 19.9, the z and x_F variables

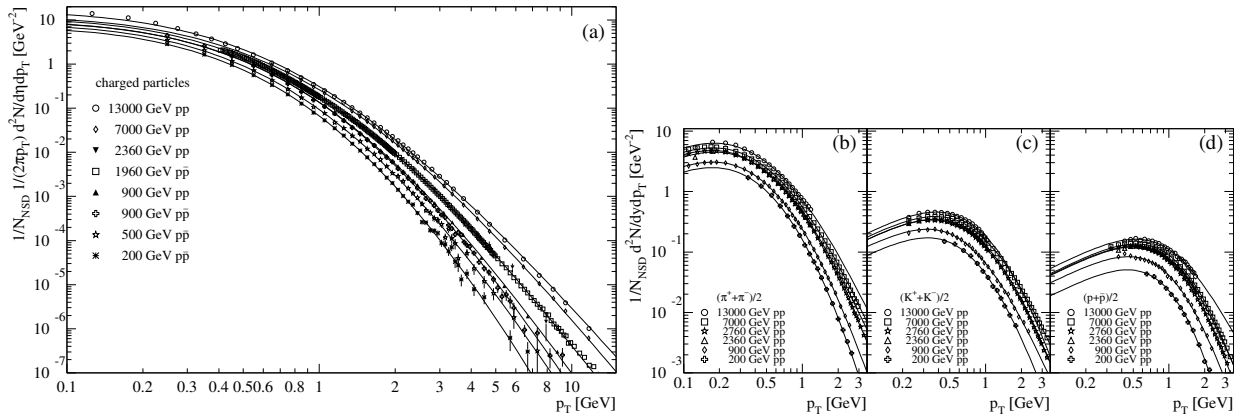


Figure 19.11: (a) Selection of inclusive charged-particle transverse momentum spectra [114, 117, 119, 121, 161, 206, 207], normalized to the non-single diffractive cross section (NSD). (b)–(d) Selection of identified charged-particle transverse momentum spectra [208–213] normalized to the NSD cross section. All spectra are scaled to the NSD cross-section using measurements of total, inelastic, elastic, single, or non-single diffractive cross sections from [214–218, 218–220]. The overall normalization uncertainty of about 3% is not shown. Superimposed are fits of the Tsallis distribution in Eq. (19.13).

have similar values [30]. The precision data on identified particles can be used in the study of the quark flavor content of the proton [179, 221, 222].

Data on identified particle production can aid the investigation of the universality of jet fragmentation in e^+e^- and DIS. The strangeness suppression factor γ_s , as derived principally from tuning the Lund string model [223] within JETSET [224], is typically found to be around 0.3 in e^+e^- experiments [75], although values closer to 0.2 [225] have also been obtained. A number of measurements of so-called V^0 -particles (K^0 , Λ^0) and the relative rates of V^0 's and inclusively produced charged particles have been performed at HERA [151, 192, 226] and fixed target experiments [149]. These typically favour a stronger suppression ($\gamma_s \approx 0.2$) than usually obtained from e^+e^- data, although values close to 0.3 have also been obtained [227, 228].

However, when comparing the description of QCD-based models for lepton-hadron interactions and e^+e^- collisions, it is important to note that the overall description by event generators of inclusively produced hadronic final states is more accurate in e^+e^- collisions than in lepton-hadron interactions [229]. Predictions of particle rates in lepton-hadron scattering are affected by uncertainties in the modelling of the parton composition of the proton and photon, the extended target remnant, and initial and final-state QCD radiation. Furthermore, the tuning of event generators for e^+e^- collisions is typically based on a larger set of parameters and uses more observables [75] than are used when optimizing models for lepton-hadron data [230].

19.7 Fragmentation in hadron-hadron collisions

An extensive set on high-transverse momentum (p_T) single-inclusive hadron data has been collected in $h_1 h_2 \rightarrow hX$ scattering processes, both at high energy colliders and fixed-target experiments [155–162, 185, 231–253]. Fig. 19.10 shows the invariant cross sections $E d^3\sigma/dp^3$ for a compilation of neutral-pion and charged-hadron production data for energies in the range $\sqrt{s} \approx 23 - 7000$ GeV.

The differential cross section for high-transverse momentum hadron production has been computed to NLO accuracy in perturbative QCD [254]. The NLO corrections are typically large and can even double the prediction for the cross section at fixed-target energies. Nevertheless, the NLO calculations significantly under-predict the cross-section for several fixed-target energy data sets [249, 255, 256]. Different strategies have been developed to ameliorate the theoretical description at fixed-target energies. A possible phenomenological approach involves the introduction of a non-perturbative intrinsic partonic transverse momentum [160, 249, 257, 258]. Furthermore, the resummation of the dominant higher order corrections at threshold produces an enhancement of the theoretical calculation that significantly improves the description of the data [259, 260].

Data collected at high energy colliders are either included in global fit analyses or used as a test for the universality of fragmentation functions. A certain tension has been observed between data sets from RHIC and the LHC [261]. The tension can be largely resolved [128] by taking properly into account the theoretical scale dependence in the global analysis, allowing factorization and renormalization scales to vary according to the kinematics of each experiment within a conventional range.

Transverse momentum distributions can usually be fit by power laws [262]. An approach to describe the low p_T particle spectra is the Tsallis distribution [263–265], which is based on a non-extensive generalization of the Boltzmann-Gibbs statistics. The functional form [266]

$$\frac{d^2N}{dp_T dy} = p_T \frac{dN}{dy} \frac{(n-1)(n-2)}{nT(nT + m_0(n-2))} \left[1 + \frac{m_T - m_0}{nT} \right]^{-n} \quad (19.13)$$

is frequently used to fit the transverse momentum spectra, where dN/dy is the particle's multiplicity, T and n are fit parameters of the Tsallis distribution, m_0 is the either the mass of the most abundant particle, i.e. the pion for inclusive spectra, or the mass of an identified particle, and $m_T = \sqrt{p_T^2 + m_0^2}$. The parameter n is related to the non-extensive parameter $q = n/(n-1)$ of the original Tsallis formula [267], and T is connected to the temperature in the Boltzmann-Gibbs statistics. The Tsallis distribution has been very successfully fit to measured transverse momentum distributions of both inclusive charged particles and identified particle spectra for hadron-hadron collisions, see for example [268–270], for collisions of heavy nuclei, see for example [271], and also for e^+e^- collisions, see for example [272]. The energy dependence of the fitted Tsallis parameters has also been investigated in detail, see [266, 273]. Fig. 19.11 shows examples of hadron production data in pp and $p\bar{p}$ collisions compared to Tsallis distributions.

Hadron production provides a critical observable for probing the high energy-density matter produced in heavy-ion collisions. Measurements at colliders show a suppression of inclusive hadron yields at high transverse momentum for AA collisions compared to pp scattering, indicating the formation of a dense medium opaque to quark and gluons, see e.g. [274].

19.8 Heavy quark fragmentation

It was recognized very early [275] that a heavy flavored meson should retain a large fraction of the momentum of the primordial heavy quark, and therefore its fragmentation function should be much harder than that of a light hadron. In the limit of a very heavy quark, one expects the fragmentation function for a heavy quark to go into any heavy hadron to be peaked near $x = 1$.

When the heavy quark is produced at a momentum much larger than its mass, one expects important perturbative effects, enhanced by powers of the logarithm of the transverse momentum

over the heavy quark mass, to intervene and modify the shape of the fragmentation function. In leading logarithmic order (*i.e.*, including all powers of $\alpha_s \log(m_Q/p_T)$), the total (*i.e.*, summed over all hadron types) perturbative fragmentation function is simply obtained by solving the leading evolution equation for fragmentation functions, Eq. (19.5), with the initial condition due to the finite mass of the heavy quark given by $D_Q(x, \mu^2)|_{\mu^2=m_Q^2} = \delta(1-x)$ and $D_i(x, \mu^2)|_{\mu^2=m_Q^2} = 0$ for $i \neq Q$ (here $D_i(x, \mu^2)$, stands for the probability to produce a heavy quark Q from parton i with a fraction x of the parton momentum).

Several extensions of the leading logarithmic result have appeared in the literature. Next-to-leading-log (NLL) order results for the perturbative heavy quark fragmentation function have been obtained in [279]. The resummation of the dominant logarithmic contributions at large x was performed in [280] to next-to-leading-log accuracy. Fixed-order calculations of the fragmentation function at order α_s^2 in e^+e^- annihilation have appeared in [281] while the initial condition for the perturbative heavy quark fragmentation function has been extended to NNLO in [282].

Inclusion of non-perturbative effects in the calculation of the heavy-quark fragmentation function is done by convoluting the perturbative result with a phenomenological non-perturbative form. This form follows from the simple kinematical consideration that the formation of a hadron by attaching light quarks/antiquarks to the heavy quark will slightly decelerate the heavy quark. Thus, its shape will show a peak that becomes increasingly centered next to $x = 1$ the higher the quark mass. Among the most popular parameterizations we have the following:

$$\text{Peterson } et al. [283]: D_{np}(x) \propto \frac{1}{x} \left(1 - \frac{1}{x} - \frac{\epsilon}{1-x}\right)^{-2}, \quad (19.14)$$

$$\text{Kartvelishvili } et al. [284]: D_{np}(x) \propto x^\alpha(1-x), \quad (19.15)$$

$$\text{Collins \& Spiller [285]: } D_{np}(x) \propto \left(\frac{1-x}{x} + \frac{(2-x)\epsilon_C}{1-x}\right) \times (1+x^2) \times \left(1 - \frac{1}{x} - \frac{\epsilon_C}{1-x}\right)^{-2} \quad (19.16)$$

$$\text{Colangelo \& Nason [286]: } D_{np}(x) \propto (1-x)^\alpha x^\beta \quad (19.17)$$

$$\text{Bowler [287]: } D_{np}(x) \propto x^{-(1+bm_{h,\perp}^2)} \times (1-x)^a \exp\left(-\frac{bm_{h,\perp}^2}{x}\right) \quad (19.18)$$

$$\text{Braaten } et al. [288]: \text{ (see Eqs. (31), (32) in [288]) } \quad (19.19)$$

where ϵ , ϵ_C , a , $bm_{h,\perp}^2$, α , and β are non-perturbative parameters that depend on the heavy hadron considered. The parameters entering the non-perturbative forms are fitted together with some model of hard radiation, which can be either a shower Monte Carlo, a leading-log or NLL calculation (which may or may not include Sudakov resummation), or a fixed order calculation. In [281], for example, the Peterson *et al.* [283] ϵ parameter for charm and bottom production is fitted from the measured distributions of Refs. [289, 290] for charm, and of [291] for bottom. If the leading-logarithmic approximation (LLA) is used for the perturbative part, one finds $\epsilon_c \approx 0.05$ and $\epsilon_b \approx 0.006$; if a second order calculation is used one finds $\epsilon_c \approx 0.035$ and $\epsilon_b \approx 0.0033$; if a NLL improved fixed order $\mathcal{O}(\alpha_s^2)$ calculation is used instead of NLO $\mathcal{O}(\alpha_s)$ one finds $\epsilon_c \approx 0.022$ and $\epsilon_b \approx 0.0023$. The larger values found in the LL approximation are consistent with what is obtained in the context of parton shower models [292], as expected. The ϵ parameter for charm and bottom scales roughly with the inverse square of the heavy flavor mass. This behavior can be justified by several arguments [275, 293, 294]. It can be used to relate the non-perturbative parts of the fragmentation

functions of charm and bottom quarks [281, 286, 295].

A more conventional approach [296] involves the introduction of a unique set of heavy quark fragmentation functions of non-perturbative nature that obey the usual massless evolution equations in Eq. (19.5). Finite mass terms of the form $(m_Q/p_T)^n$ are kept in the corresponding short distance coefficient function for each scattering process. Within this approach, the initial condition for the perturbative fragmentation function provides the term needed to define the correct subtraction scheme to match the massless limit for the coefficient function (see e.g. [297]). Such an implementation is in line with the variable flavor number scheme introduced for parton distributions functions, as described in Section 18 of this *Review*.

High statistics data for charmed-meson production near the Υ resonance (excluding decay products of B mesons) have been published [276, 277]. They include results for D and D^* , D_s (see also [298, 299]) and Λ_c . Shown in Fig. 19.12(a) are the CLEO and BELLE inclusive cross-sections times branching ratio \mathcal{B} , $s\mathcal{B}d\sigma/dx_p$, for the production of D^0 and D^{*+} . The variable x_p approximates the light-cone momentum fraction x , but is not identical to it. The two measurements are consistent with each other.

The branching ratio \mathcal{B} represents $D^0 \rightarrow K^-\pi^+$ for the D^0 results and for the D^{*+} the product of the branching fractions for $D^{*+} \rightarrow D^0\pi^+$ and $D^0 \rightarrow K^-\pi^+$. Given the high precision of CLEO's and BELLE's data, a superposition of different parametric forms for the non-perturbative contribution is needed to obtain a good fit [52]. Older studies are reported in Refs. [290, 300, 301]. Charmed meson spectra on the Z peak have been published by OPAL and ALEPH [302, 303].

Charm quark production has also been extensively studied at HERA by the H1 and ZEUS collaborations. Measurements have been made of $D^{*\pm}$, D^\pm , and D_s^\pm mesons and the Λ_c baryon. See, for example, Refs. [304, 305].

Experimental studies of the fragmentation function for b quarks, shown in Fig. 19.12(b), have been performed at LEP and SLD [278, 291, 306]. Commonly used methods identify the B meson through its semileptonic decay or based upon tracks emerging from the B secondary vertex. Heavy flavor contributions from gluon splitting are usually explicitly removed before fitting for the fragmentation functions. The studies in [278] fit the B spectrum using a Monte Carlo shower model supplemented with non-perturbative fragmentation functions yielding consistent results.

The experiments measure primarily the spectrum of B mesons. This defines a fragmentation function that includes the effect of the decay of higher mass excitations, like the B^* and B^{**} . In the literature (cf. details in Ref. [307]), there is sometimes ambiguity in what is defined to be the bottom fragmentation function. Instead of using what is directly measured (*i.e.*, the B meson spectrum), in some cases corrections are applied to account for B^* or B^{**} production.

Heavy-flavor production in e^+e^- collisions is the primary source of information for the role of fragmentation effects in heavy-flavor production in hadron-hadron and lepton-hadron collisions. The QCD calculations tend to underestimate the data in certain regions of phase space. Some experimental results from LHC summarized in [308] show such deviations e.g. at high transverse jet momentum and also at low di-jet separation angles, see [309] for details, and were already theoretically investigated in [310].

Both bottomed- and charmed-meson spectra have been measured at the Tevatron with unprecedented accuracy [311]. The measured spectra are in good agreement with QCD calculations (including non-perturbative fragmentation effects inferred from e^+e^- data [312]).

The HERA collaborations have produced a number of measurements of beauty production; see, for example, Refs. [304, 313–316]. As for the Tevatron data, the HERA results are described well by QCD-based calculations using fragmentation models optimized with e^+e^- data.

Besides degrading the fragmentation function by gluon radiation, QCD evolution can also generate soft heavy quarks, increasing in the small x region as \sqrt{s} increases. Several theoretical studies are available on the issue of how often $b\bar{b}$ or $c\bar{c}$ pairs are

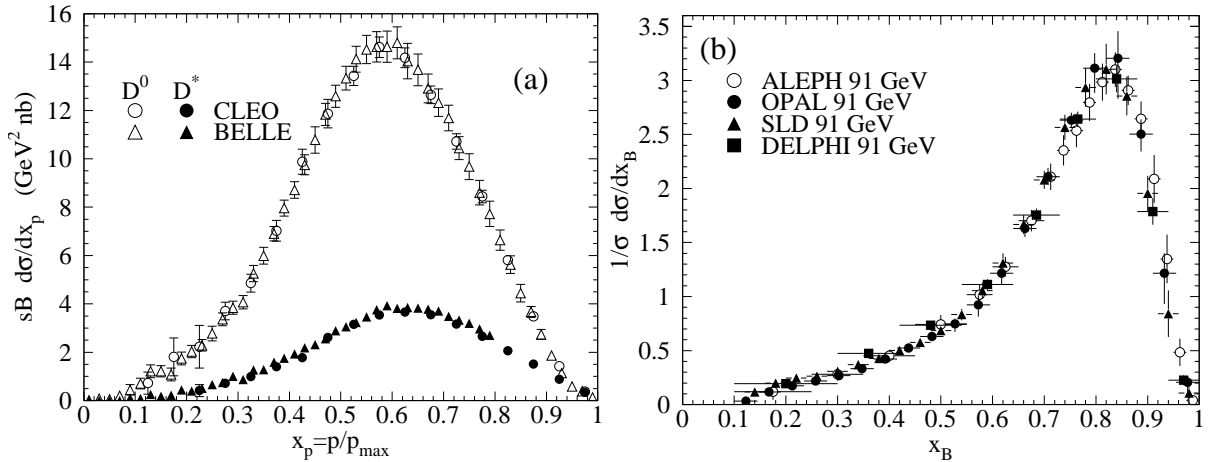


Figure 19.12: (a) Efficiency-corrected inclusive cross-section measurements for the production of D^0 and D^{*+} in e^+e^- measurements at $\sqrt{s} \approx 10.6$ GeV, excluding B decay products [276] [277]. (b) Measured e^+e^- fragmentation function of b quarks into B hadrons at $\sqrt{s} \approx 91$ GeV [278].

produced indirectly via a gluon splitting mechanism [317–319]. Experimental results from studies on charm and bottom production via gluon splitting, given in [303, 320–324], yield weighted averages of $\bar{n}_{g \rightarrow c\bar{c}} = 3.05 \pm 0.45\%$ and $\bar{n}_{g \rightarrow b\bar{b}} = 0.277 \pm 0.072\%$, respectively. The production of bottom-antibottom quark pairs via gluon splitting has also been investigated at hadron colliders, see for example [325–327].

19.9 Spin-dependent and transverse-momentum dependent fragmentation functions

The fragmentation functions we have considered so far apply to the spin-averaged case in which the polarization of the produced hadron is not observed, or the hadron has spin-0. We have also only considered ‘collinear’ fragmentation functions $D_i^h(x, \mu^2)$ which carry only one kinematical variable, the momentum fraction x . New insights into fragmentation and hadronization become available when also the dependence of fragmentation functions on the spin of the produced hadron and/or its relative transverse momentum with respect to the fragmenting parton are considered. In the latter case, one refers to the fragmentation functions as ‘transverse-momentum dependent (TMD)’ fragmentation functions.

Staying first with collinear fragmentation functions, two types of spin-dependent fragmentation functions to spin-1/2 hadrons can be considered. The helicity-dependent fragmentation function measures the transfer of longitudinal spin from the fragmenting parton to the hadron [38, 328–331]. It is given by

$$\Delta D_i^h(x, \mu^2) \equiv D_{i+}^{h+}(x, \mu^2) - D_{i+}^{h-}(x, \mu^2), \quad (19.20)$$

where the superscripts \pm refer to the helicities of the parton and hadron. Λ hyperons are ideally suited for measurements of the ΔD_i^h , thanks to their self-analyzing weak decay $\Lambda \rightarrow \pi p$. Measurements of the longitudinal spin transfer to Lambda hyperons have been presented in e^+e^- (on the Z resonance), ℓp , and pp scattering in Refs. [332–338]. One may readily extend Eq. (19.20) to the case of transverse polarization of hadrons and quarks [339], where the corresponding fragmentation functions are known as ‘transversity’ fragmentation functions. There are also measurements constraining these fragmentation functions [333, 340, 341]. A recent phenomenological analysis was presented in [342].

If the transverse-momentum (k_T) dependence of fragmentation functions is considered, there are eight types of leading-twist functions, defined by the correlations among the hadronic and partonic spin vectors and transverse-momentum vectors they represent. (For review, see [5]). We note that the eight fragmentation functions given in the table below exist separately for each quark and antiquark flavor, and a similar set may be introduced for gluons. Upon integration over the transverse momentum k_T the collinear unpolarized, helicity, and transversity fragmentation functions are

reproduced.

The various fragmentation functions may be obtained from spin asymmetries and angular distributions in hadron production processes. There is a large body of precision data by now on transverse-momentum distributions in e^+e^- annihilation [343] and SIDIS [190, 344] that provide constraints on the unpolarized TMD fragmentation functions D_i^h , which have been analyzed theoretically, partly also including TMD evolution effects and high orders of perturbation theory [345–352].

Besides the unpolarized functions D most of the attention in experiment and theory has been on the function H^\perp which describes the production of unpolarized (or spin-0) hadrons by transversely polarized quarks. This function is known as the ‘Collins function’ [353]. Its importance also derives from the fact that it may be used to probe the quark transversity PDF of the nucleon [354] which gives the probability of finding a transversely polarized quark with its spin aligned or anti-aligned with the spin of a transversely polarized nucleon. The transversity function is chiral-odd, and therefore not accessible through measurements of inclusive lepton-hadron scattering. The Collins effect in semi-inclusive DIS, on the other hand, provides an avenue for accessing transversity. The Collins fragmentation function is chiral-odd and T-odd, leading to a characteristic single-spin asymmetry in the azimuthal angular distribution of the produced hadron in the hadron scattering plane. A number of SIDIS [355–366] and e^+e^- experiments [367–371] have performed measurements of the Collins effect, for charged pions and kaons. These have been analyzed theoretically [372, 373], leading to an extraction of the nucleon’s transversity distributions [373]. The Collins effect has also been studied in pp scattering, where one considers azimuthal transverse single-spin asymmetries for distributions of hadrons inside jets [177, 374, 375].

In the context of extractions of transversity PDFs also fragmentation functions for same-side pairs of hadrons with small invariant mass, *dihadrons*, have been introduced and studied [376–384]. Compared to the Collins effect, dihadron fragmentation functions have the advantage that they may be defined purely in collinear factorization. The relevant spin-dependent dihadron fragmentation function exploits a correlation between the transverse polarization of the fragmenting quark and the relative momentum of the two hadrons. In SIDIS with a transversely polarized hadron beam, the dihadron cross section then contains a specific modulation in the azimuthal orientation of the plane containing the momenta of the two hadrons. The coefficient of this modulation is a product of the spin-dependent dihadron fragmentation function and the target’s transversity PDF. The dihadron fragmentation functions may be separately extracted from measurements in e^+e^- annihilation, and the Belle experiment has presented data [385] that have been analyzed theoretically [386, 387].

In lepton scattering, HERMES [388] and COMPASS [389, 390] have reported data sensitive to the spin-dependent dihadron fragmentation functions, and recently the STAR experiment at RHIC has presented data in the azimuthal distribution of $\pi^+\pi^-$ pairs produced in pp scattering with one transversely polarized proton [391]. The results have been successfully used for the extraction of transversity PDFs [387, 392–394].

References

- [1] G. Altarelli, Phys. Rept. **81**, 1 (1982).
- [2] R.K. Ellis *et al.*, *QCD and Collider Physics*, Cambridge University Press (1996).
- [3] S. Albino *et al.* (2008), [arXiv:0804.2021].
- [4] F. Arleo, Eur. Phys. J. **C61**, 603 (2009), [arXiv:0810.1193].
- [5] A. Metz and A. Vossen, Prog. Part. Nucl. Phys. **91**, 136 (2016), [arXiv:1607.02521].
- [6] P. Nason and B. R. Webber, Nucl. Phys. **B421**, 473 (1994), [Erratum: Nucl. Phys. **B480**, 755 (1996)].
- [7] D. Buskulic *et al.* (ALEPH), Phys. Lett. **B357**, 487 (1995), [Erratum: Phys. Lett. **B364**, 247 (1995)].
- [8] P. Abreu *et al.* (DELPHI), Eur. Phys. J. **C6**, 19 (1999).
- [9] R. Barate *et al.* (ALEPH), Phys. Rept. **294**, 1 (1998).
- [10] D. Buskulic *et al.* (ALEPH), Z. Phys. **C73**, 409 (1997).
- [11] B. Adeva *et al.* (L3), Phys. Lett. **B259**, 199 (1991).
- [12] Y. K. Li *et al.* (AMY), Phys. Rev. **D41**, 2675 (1990).
- [13] D. Bender *et al.*, Phys. Rev. **D31**, 1 (1985).
- [14] G. S. Abrams *et al.*, Phys. Rev. Lett. **64**, 1334 (1990).
- [15] A. Petersen *et al.*, Phys. Rev. **D37**, 1 (1988).
- [16] G. Alexander *et al.* (OPAL), Z. Phys. **C72**, 191 (1996).
- [17] K. Ackerstaff *et al.* (OPAL), Z. Phys. **C75**, 193 (1997).
- [18] G. Abbiendi *et al.* (OPAL), Eur. Phys. J. **C16**, 185 (2000), [hep-ex/0002012].
- [19] W. Braunschweig *et al.* (TASSO), Z. Phys. **C47**, 187 (1990).
- [20] K. Ackerstaff *et al.* (OPAL), Eur. Phys. J. **C7**, 369 (1999), [hep-ex/9807004].
- [21] P. Abreu *et al.* (DELPHI), Phys. Lett. **B398**, 194 (1997).
- [22] G. Abbiendi *et al.* (OPAL), Eur. Phys. J. **C37**, 1, 25 (2004), [hep-ex/0404026].
- [23] R. Brandelik *et al.* (TASSO), Phys. Lett. **114B**, 65 (1982).
- [24] K. Abe *et al.* (SLD), Phys. Rev. **D69**, 072003 (2004), [hep-ex/0310017].
- [25] H. Aihara *et al.* (TPC/Two Gamma), Phys. Rev. Lett. **61**, 1263 (1988).
- [26] M. Leitgab *et al.* (Belle), Phys. Rev. Lett. **111**, 062002 (2013), [arXiv:1301.6183].
- [27] W. Kittel and E.A. De Wolf, *Soft Multihadron Dynamics*, World Scientific (2005).
- [28] H.F. Jones, Nuovo Cimento **40A**, 1018 (1965).
- [29] K. H. Streng, T. F. Walsh and P. M. Zerwas, Z. Phys. **C2**, 237 (1979).
- [30] M. R. Adams *et al.* (E-665), Phys. Lett. **B272**, 163 (1991).
- [31] M. Arneodo *et al.* (European Muon), Z. Phys. **C35**, 417 (1987).
- [32] I. Abt *et al.* (H1), Z. Phys. **C63**, 377 (1994).
- [33] M. Derrick *et al.* (ZEUS), Z. Phys. **C70**, 1 (1996), [hep-ex/9511010].
- [34] J. Breitweg *et al.* (ZEUS), Phys. Lett. **B414**, 428 (1997), [hep-ex/9710011].
- [35] F. D. Aaron *et al.* (H1), Phys. Lett. **B654**, 148 (2007), [arXiv:0706.2456].
- [36] P. Abreu *et al.* (DELPHI), Phys. Lett. **B311**, 408 (1993).
- [37] G. Altarelli *et al.*, Nucl. Phys. **B160**, 301 (1979); R. Baier and K. Fey, Z. Phys. **C2**, 339 (1979).
- [38] D. de Florian, M. Stratmann and W. Vogelsang, Phys. Rev. **D57**, 5811 (1998), [hep-ph/9711387].
- [39] P. J. Rijken and W. L. van Neerven, Phys. Lett. **B386**, 422 (1996), [hep-ph/9604436]; P. J. Rijken and W. L. van Neerven, Phys. Lett. **B392**, 207 (1997), [hep-ph/9609379]; P. J. Rijken and W. L. van Neerven, Nucl. Phys. **B487**, 233 (1997), [hep-ph/9609377].
- [40] A. Mitov, S. Moch and A. Vogt, Phys. Lett. **B638**, 61 (2006), [hep-ph/0604053].
- [41] A. Mitov and S.-O. Moch, Nucl. Phys. **B751**, 18 (2006), [hep-ph/0604160].
- [42] V. N. Gribov and L. N. Lipatov, Sov. J. Nucl. Phys. **15**, 438 (1972), [Yad. Fiz. **15**, 781 (1972)]; V. N. Gribov and L. N. Lipatov, Sov. J. Nucl. Phys. **15**, 675 (1972), [Yad. Fiz. **15**, 1218 (1972)]; L.N. Lipatov, Sov. J. Nucl. Phys. **20**, 95 (1975); Yu.L. Dokshitzer, Sov. Phys. JETP Lett. **46**, 641 (1977); G. Altarelli and G. Parisi, Nucl. Phys. **B126**, 298 (1977).
- [43] H. Georgi and H. D. Politzer, Nucl. Phys. **B136**, 445 (1978); J. F. Owens, Phys. Lett. **76B**, 85 (1978); T. Uematsu, Phys. Lett. **79B**, 97 (1978).
- [44] G. Curci, W. Furmanski and R. Petronzio, Nucl. Phys. **B175**, 27 (1980).
- [45] W. Furmanski and R. Petronzio, Phys. Lett. **97B**, 437 (1980).
- [46] E. G. Floratos, C. Kounnas and R. Lacaze, Nucl. Phys. **B192**, 417 (1981).
- [47] J. Kalinowski, K. Konishi and T. R. Taylor, Nucl. Phys. **B181**, 221 (1981).
- [48] M. Stratmann and W. Vogelsang, Nucl. Phys. **B496**, 41 (1997), [hep-ph/9612250].
- [49] Yu. L. Dokshitzer, G. Marchesini and G. P. Salam, Phys. Lett. **B634**, 504 (2006), [hep-ph/0511302].
- [50] S. Moch and A. Vogt, Phys. Lett. **B659**, 290 (2008), [arXiv:0709.3899].
- [51] A. A. Almasy, S. Moch and A. Vogt, Nucl. Phys. **B854**, 133 (2012), [arXiv:1107.2263].
- [52] M. Cacciari, P. Nason and C. Oleari, JHEP **04**, 006 (2006), [hep-ph/0510032]; M. Cacciari, P. Nason and C. Oleari, JHEP **10**, 034 (2005), [hep-ph/0504192].
- [53] P. Aurenche *et al.*, Eur. Phys. J. **C34**, 277 (2004), [hep-ph/0312359]; A. Daleo, D. de Florian and R. Sassot, Phys. Rev. **D71**, 034013 (2005), [hep-ph/0411212]; B. A. Kniehl, G. Kramer and M. Maniatis, Nucl. Phys. **B711**, 345 (2005), [Erratum: Nucl. Phys. **B720**, 231 (2005)], [hep-ph/0411300].
- [54] B. Wang *et al.*, Phys. Rev. **D99**, 9, 094029 (2019), [arXiv:1903.01529].
- [55] S. Aid *et al.* (H1), Nucl. Phys. **B445**, 3 (1995), [hep-ex/9505003].
- [56] M. Derrick *et al.* (ZEUS), Z. Phys. **C67**, 93 (1995), [hep-ex/9501012].
- [57] C. Adloff *et al.* (H1), Nucl. Phys. **B504**, 3 (1997), [hep-ex/9707005].
- [58] J. Breitweg *et al.* (ZEUS), Eur. Phys. J. **C11**, 251 (1999), [hep-ex/9903056].
- [59] J. F. Patrick *et al.*, Phys. Rev. Lett. **49**, 1232 (1982).
- [60] S. Chekanov *et al.* (ZEUS), JHEP **06**, 061 (2008), [arXiv:0803.3878].
- [61] A. H. Mueller, Phys. Lett. **104B**, 161 (1981).
- [62] A. Bassetto *et al.*, Nucl. Phys. **B207**, 189 (1982).
- [63] Yu.L. Dokshitzer *et al.*, Z. Phys. **C15**, 324 (1982).
- [64] A. H. Mueller, Nucl. Phys. **B213**, 85 (1983); A. H. Mueller, Nucl. Phys. **B241**, 141 (1984).
- [65] Y. L. Dokshitzer, V. A. Khoze and S. I. Troian, Int. J. Mod. Phys. **A7**, 1875 (1992).

- [66] Yu.L. Dokshitzer *et al.*, *Basics of Perturbative QCD*, Editions Frontières (1991).
- [67] V. A. Khoze and W. Ochs, *Int. J. Mod. Phys. A* **12**, 2949 (1997), [hep-ph/9701421].
- [68] C. P. Fong and B. R. Webber, *Nucl. Phys. B* **355**, 54 (1991).
- [69] S. Albino *et al.*, *Phys. Rev. Lett.* **95**, 232002 (2005), [hep-ph/0503170].
- [70] S. Albino *et al.*, *Phys. Rev. D* **73**, 054020 (2006), [hep-ph/0510319].
- [71] S. Albino *et al.*, *Nucl. Phys. B* **851**, 86 (2011), [arXiv:1104.3018]; S. Albino *et al.*, *Nucl. Phys. B* **855**, 801 (2012), [arXiv:1108.3948].
- [72] A. Vogt, *JHEP* **10**, 025 (2011), [arXiv:1108.2993]; C. H. Kom, A. Vogt and K. Yeats, *JHEP* **10**, 033 (2012), [arXiv:1207.5631].
- [73] D. P. Anderle *et al.*, *Phys. Rev. D* **95**, 5, 054003 (2017), [arXiv:1611.03371].
- [74] P. Bolzoni, B. A. Kniehl and A. V. Kotikov, *Phys. Rev. Lett.* **109**, 242002 (2012), [arXiv:1209.5914]; P. Bolzoni, B. A. Kniehl and A. V. Kotikov, *Nucl. Phys. B* **875**, 18 (2013), [arXiv:1305.6017].
- [75] P. Abreu *et al.* (DELPHI), *Z. Phys. C* **73**, 11 (1996).
- [76] P. Abreu *et al.* (DELPHI), *Z. Phys. C* **73**, 229 (1997).
- [77] P. Achard *et al.* (L3), *Phys. Rept.* **399**, 71 (2004), [hep-ex/0406049].
- [78] R. Itoh *et al.* (TOPAZ), *Phys. Lett. B* **345**, 335 (1995), [hep-ex/9412015].
- [79] M. Althoff *et al.* (TASSO), *Z. Phys. C* **22**, 307 (1984).
- [80] M. Z. Akrawy *et al.* (OPAL), *Phys. Lett. B* **247**, 617 (1990).
- [81] W. Dunwoodie *et al.* (BES), *Phys. Rev. D* **69**, 072002 (2004), [hep-ex/0306055].
- [82] D. Buskulic *et al.* (ALEPH), *Z. Phys. C* **55**, 209 (1992).
- [83] A. Heister *et al.* (ALEPH), *Eur. Phys. J. C* **35**, 457 (2004).
- [84] P. Abreu *et al.* (DELPHI), *Phys. Lett. B* **275**, 231 (1992).
- [85] P. Abreu *et al.* (DELPHI), *Eur. Phys. J. C* **5**, 585 (1998).
- [86] P. Abreu *et al.* (DELPHI), *Phys. Lett. B* **459**, 397 (1999).
- [87] M. Acciarri *et al.* (L3), *Phys. Lett. B* **444**, 569 (1998).
- [88] TPC/TWO-GAMMA Collab.: H. Aihara *et al.*, LBL 23737.
- [89] B. R. Webber, *Phys. Lett. B* **143B**, 501 (1984).
- [90] Y. I. Azimov *et al.*, *Z. Phys. C* **27**, 65 (1985).
- [91] Y. I. Azimov *et al.*, *Z. Phys. C* **31**, 213 (1986).
- [92] I. M. Dremin and J. W. Gary, *Phys. Rept.* **349**, 301 (2001), [hep-ph/0004215].
- [93] I. M. Dremin and V. A. Nechitailo, *Mod. Phys. Lett. A* **9**, 1471 (1994), [hep-ex/9406002].
- [94] S. J. Brodsky and J. F. Gunion, *Phys. Rev. Lett.* **37**, 402 (1976).
- [95] J. Beringer *et al.* (Particle Data Group), *Phys. Rev. D* **86**, 010001 (2012).
- [96] R. Akers *et al.* (OPAL), *Z. Phys. C* **68**, 203 (1995).
- [97] P. D. Acton *et al.* (OPAL), *Z. Phys. C* **53**, 539 (1992).
- [98] D. Buskulic *et al.* (ALEPH), *Z. Phys. C* **69**, 15 (1995).
- [99] P. Abreu *et al.* (DELPHI), *Phys. Lett. B* **372**, 172 (1996).
- [100] P. Abreu *et al.* (DELPHI), *Phys. Lett. B* **416**, 233 (1998).
- [101] P. Abreu *et al.* (DELPHI), *Eur. Phys. J. C* **18**, 203 (2000), [Erratum: *Eur. Phys. J. C* **25**, 493 (2002)], [hep-ex/0103031].
- [102] M. Acciarri *et al.* (L3), *Phys. Lett. B* **371**, 137 (1996).
- [103] M. Acciarri *et al.* (L3), *Phys. Lett. B* **404**, 390 (1997).
- [104] K. Nakabayashi *et al.* (TOPAZ), *Phys. Lett. B* **413**, 447 (1997).
- [105] K. Okabe *et al.* (VENUS), *Phys. Lett. B* **423**, 407 (1998).
- [106] H. Albrecht *et al.* (ARGUS), *Z. Phys. C* **54**, 13 (1992).
- [107] S. Chekanov *et al.* (ZEUS), *Phys. Lett. B* **510**, 36 (2001), [hep-ex/0104036].
- [108] J. Benecke *et al.* (Bonn-Hamburg-Munich), *Nucl. Phys. B* **76**, 29 (1974).
- [109] W. M. Morse *et al.*, *Phys. Rev. D* **15**, 66 (1977).
- [110] W. Thome *et al.* (Aachen-CERN-Heidelberg-Munich), *Nucl. Phys. B* **129**, 365 (1977).
- [111] A. Breakstone *et al.* (Ames-Bologna-CERN-Dortmund-Heidelberg-Warsaw), *Phys. Rev. D* **30**, 528 (1984).
- [112] G. J. Alner *et al.* (UA5), *Phys. Rept.* **154**, 247 (1987).
- [113] R. E. Ansorge *et al.* (UA5), *Z. Phys. C* **43**, 357 (1989).
- [114] C. Albajar *et al.* (UA1), *Nucl. Phys. B* **335**, 261 (1990).
- [115] F. Abe *et al.* (CDF), *Phys. Rev. D* **41**, 2330 (1990), [119(1989)].
- [116] K. Aamodt *et al.* (ALICE), *Eur. Phys. J. C* **68**, 89 (2010), [arXiv:1004.3034].
- [117] V. Khachatryan *et al.* (CMS), *JHEP* **02**, 041 (2010), [arXiv:1002.0621].
- [118] V. Khachatryan *et al.* (CMS), *JHEP* **01**, 079 (2011), [arXiv:1011.5531].
- [119] V. Khachatryan *et al.* (CMS), *Phys. Rev. Lett.* **105**, 022002 (2010), [arXiv:1005.3299].
- [120] G. Aad *et al.* (ATLAS), *Eur. Phys. J. C* **76**, 7, 403 (2016), [arXiv:1603.02439].
- [121] M. Aaboud *et al.* (ATLAS), *Eur. Phys. J. C* **76**, 9, 502 (2016), [arXiv:1606.01133].
- [122] J. Adam *et al.* (ALICE), *Phys. Lett. B* **753**, 319 (2016), [arXiv:1509.08734].
- [123] J. Adam *et al.* (ALICE), *Eur. Phys. J. C* **77**, 1, 33 (2017), [arXiv:1509.07541].
- [124] P. V. Chliapnikov and V. A. Uvarov, *Phys. Lett. B* **251**, 192 (1990).
- [125] J. F. Grosse-Oetringhaus and K. Reyggers, *J. Phys. G* **37**, 083001 (2010), [arXiv:0912.0023].
- [126] E. K. G. Sarkisyan and A. S. Sakharov (2004), [hep-ph/0410324]; E. K. G. Sarkisyan and A. S. Sakharov, *AIP Conf. Proc.* **828**, 1, 35 (2006), [hep-ph/0510191]; E. K. G. Sarkisyan and A. S. Sakharov, *Eur. Phys. J. C* **70**, 533 (2010), [arXiv:1004.4390].
- [127] S. Hoeche *et al.*, in “HERA and the LHC: A Workshop on the implications of HERA for LHC physics: Proceedings Part A,” 288–289 (2005), [hep-ph/0602031]; S. Mrenna and P. Richardson, *JHEP* **05**, 040 (2004), [hep-ph/0312274]; J. Alwall *et al.*, *Eur. Phys. J. C* **53**, 473 (2008), [arXiv:0706.2569].
- [128] I. Borsa *et al.* (2021), [arXiv:2110.14015].
- [129] E. Moffat *et al.* (Jefferson Lab Angular Momentum (JAM)), *Phys. Rev. D* **104**, 1, 016015 (2021), [arXiv:2101.04664].
- [130] V. Bertone *et al.* (NNPDF), *Eur. Phys. J. C* **77**, 8, 516 (2017), [arXiv:1706.07049].
- [131] D. de Florian, R. Sassot and M. Stratmann, *Phys. Rev. D* **76**, 074033 (2007), [arXiv:0707.1506].
- [132] S. Albino, B. A. Kniehl and G. Kramer, *Nucl. Phys. B* **803**, 42 (2008), [arXiv:0803.2768].
- [133] S. Kretzer, E. Leader and E. Christova, *Eur. Phys. J. C* **22**, 269 (2001), [hep-ph/0108055].
- [134] S. Kretzer, *Phys. Rev. D* **62**, 054001 (2000), [hep-ph/0003177].
- [135] L. Bourhis *et al.*, *Eur. Phys. J. C* **19**, 89 (2001), [hep-ph/0009101].
- [136] M. Hirai *et al.*, *Phys. Rev. D* **75**, 094009 (2007), [hep-ph/0702250].

- [137] C. A. Aidala *et al.*, Phys. Rev. **D83**, 034002 (2011), [arXiv:1009.6145].
- [138] D. de Florian *et al.*, Phys. Rev. **D91**, 1, 014035 (2015), [arXiv:1410.6027].
- [139] D. de Florian *et al.*, Phys. Rev. **D95**, 9, 094019 (2017), [arXiv:1702.06353].
- [140] D. de Florian, R. Sassot and M. Stratmann, Phys. Rev. **D75**, 114010 (2007), [hep-ph/0703242].
- [141] D. P. Anderle, F. Ringer and M. Stratmann, Phys. Rev. **D92**, 11, 114017 (2015), [arXiv:1510.05845].
- [142] E. Leader, A. V. Sidorov and D. B. Stamenov, Phys. Rev. **D93**, 7, 074026 (2016), [arXiv:1506.06381].
- [143] R. A. Khalek, V. Bertone and E. R. Nocera (2021), [arXiv:2105.08725].
- [144] H. Abdolmaleki *et al.* (xFitter) (2021), [arXiv:2105.11306].
- [145] V. Bertone *et al.* (NNPDF), Eur. Phys. J. **C78**, 8, 651 (2018), [arXiv:1807.03310].
- [146] R. Barate *et al.* (ALEPH), Eur. Phys. J. **C17**, 1 (2000); R. Akers *et al.* (OPAL), Z. Phys. **C68**, 179 (1995); G. Abbiendi *et al.* (OPAL), Eur. Phys. J. **C11**, 217 (1999), [hep-ex/9903027].
- [147] K. Abe *et al.* (SLD), Phys. Rev. **D59**, 052001 (1999), [hep-ex/9805029].
- [148] D. Buskalic *et al.* (ALEPH), Z. Phys. **C66**, 355 (1995); H. Albrecht *et al.* (ARGUS), Z. Phys. **C44**, 547 (1989); R. Akers *et al.* (OPAL), Z. Phys. **C63**, 181 (1994).
- [149] M. R. Adams *et al.* (E665), Z. Phys. **C61**, 539 (1994).
- [150] M. Arneodo *et al.* (European Muon), Z. Phys. **C34**, 283 (1987).
- [151] S. Aid *et al.* (H1), Nucl. Phys. **B480**, 3 (1996), [hep-ex/9607010].
- [152] J. J. Aubert *et al.* (European Muon), Z. Phys. **C18**, 189 (1983).
- [153] A. Airapetian *et al.* (HERMES), Eur. Phys. J. **C21**, 599 (2001), [hep-ex/0104004].
- [154] T. P. McPharlin *et al.*, Phys. Lett. **90B**, 479 (1980).
- [155] S. S. Adler *et al.* (PHENIX), Phys. Rev. Lett. **91**, 241803 (2003), [hep-ex/0304038].
- [156] B. Abelev *et al.* (ALICE), Phys. Lett. **B717**, 162 (2012), [arXiv:1205.5724].
- [157] M. Bonesini *et al.* (WA70), Z. Phys. **C38**, 371 (1988).
- [158] T. Akesson *et al.* (Axial Field Spectrometer), Sov. J. Nucl. Phys. **51**, 836 (1990), [Yad. Fiz.51,1314(1990)].
- [159] C. Kourkoumelis *et al.*, Z. Phys. **C5**, 95 (1980).
- [160] L. Apanasevich *et al.* (Fermilab E706), Phys. Rev. **D68**, 052001 (2003), [hep-ex/0204031].
- [161] F. Abe *et al.* (CDF), Phys. Rev. Lett. **61**, 1819 (1988).
- [162] M. Banner *et al.* (UA2), Phys. Lett. **115B**, 59 (1982).
- [163] M. Procura and I. W. Stewart, Phys. Rev. **D81**, 074009 (2010), [Erratum: Phys. Rev.D83,039902(2011)], [arXiv:0911.4980].
- [164] A. Jain, M. Procura and W. J. Waalewijn, JHEP **05**, 035 (2011), [arXiv:1101.4953].
- [165] M. Procura and W. J. Waalewijn, Phys. Rev. **D85**, 114041 (2012), [arXiv:1111.6605].
- [166] F. Arleo *et al.*, JHEP **04**, 147 (2014), [arXiv:1311.7356].
- [167] M. Ritzmann and W. J. Waalewijn, Phys. Rev. **D90**, 5, 054029 (2014), [arXiv:1407.3272].
- [168] T. Kaufmann, A. Mukherjee and W. Vogelsang, Phys. Rev. **D92**, 5, 054015 (2015), [arXiv:1506.01415].
- [169] Y.-T. Chien *et al.*, JHEP **05**, 125 (2016), [arXiv:1512.06851].
- [170] F. Abe *et al.* (CDF), Phys. Rev. Lett. **65**, 968 (1990).
- [171] T. A. collaboration (ATLAS) (2015).
- [172] S. Chatrchyan *et al.* (CMS), JHEP **10**, 087 (2012), [arXiv:1205.5872].
- [173] X. Lu (ALICE), Nucl. Phys. **A931**, 428 (2014), [arXiv:1407.8385].
- [174] C. Bianchin (ALICE), J. Phys. Conf. Ser. **612**, 1, 012020 (2015).
- [175] F. Krizek (ALICE), J. Phys. Conf. Ser. **668**, 1, 012018 (2016), [arXiv:1509.02024].
- [176] M. Aaboud *et al.* (ATLAS), Nucl. Phys. **A978**, 65 (2018), [arXiv:1706.02859].
- [177] L. Adamczyk *et al.* (STAR), Phys. Rev. **D97**, 3, 032004 (2018), [arXiv:1708.07080].
- [178] D. P. Anderle *et al.*, Phys. Rev. **D96**, 3, 034028 (2017), [arXiv:1706.09857].
- [179] N. Sato *et al.* (JAM) (2019), [arXiv:1905.03788].
- [180] M. Epele *et al.*, Phys. Rev. **D86**, 074028 (2012), [arXiv:1209.3240].
- [181] E. Witten, Nucl. Phys. **210**, 189 (1977).
- [182] L. Bourhis, M. Fontannaz and J. P. Guillet, Eur. Phys. J. **C2**, 529 (1998), [hep-ph/9704447].
- [183] M. Gluck, E. Reya and A. Vogt, Phys. Rev. **D48**, 116 (1993), [Erratum: Phys. Rev.D51,1427(1995)]; Erratum *ibid.* **D51**, 1427 (1995).
- [184] G. Abbiendi *et al.* (OPAL), Eur. Phys. J. **C27**, 467 (2003), [hep-ex/0209048].
- [185] G. Bocquet *et al.*, Phys. Lett. **B366**, 434 (1996).
- [186] T. Kaufmann, A. Mukherjee and W. Vogelsang, Phys. Rev. **D93**, 11, 114021 (2016), [arXiv:1604.07175].
- [187] P. Abreu *et al.* (DELPHI), Eur. Phys. J. **C13**, 573 (2000).
- [188] B. A. Kniehl, G. Kramer and B. Potter, Phys. Rev. Lett. **85**, 5288 (2000), [hep-ph/0003297].
- [189] M. Arneodo *et al.* (European Muon), Z. Phys. **C33**, 167 (1986).
- [190] A. Airapetian *et al.* (HERMES), Phys. Rev. **D87**, 074029 (2013), [arXiv:1212.5407].
- [191] C. Adolph *et al.* (COMPASS), Phys. Lett. **B764**, 1 (2017), [arXiv:1604.02695].
- [192] F. D. Aaron *et al.* (H1), Phys. Lett. **B673**, 119 (2009), [arXiv:0901.0477].
- [193] M. Derrick *et al.* (ZEUS), Z. Phys. **C68**, 29 (1995), [hep-ex/9505011].
- [194] S. Chekanov *et al.* (ZEUS), Phys. Lett. **B553**, 141 (2003), [hep-ex/0211025].
- [195] S. Chekanov *et al.* (ZEUS), Nucl. Phys. **B786**, 181 (2007), [arXiv:0705.3770].
- [196] F. D. Aaron *et al.* (H1), Eur. Phys. J. **C61**, 185 (2009), [arXiv:0810.4036].
- [197] A. Aktas *et al.* (H1), Eur. Phys. J. **C36**, 413 (2004), [hep-ex/0403056].
- [198] P. Dixon, D. Kant and G. Thompson, J. Phys. **G25**, 1453 (1999).
- [199] C. Adloff *et al.* (H1), Phys. Lett. **B462**, 440 (1999), [hep-ex/9907030].
- [200] D. Graudenz, Fortsch. Phys. **45**, 629 (1997), [hep-ph/9701334].
- [201] P. M. Nadolsky, D. R. Stump and C. P. Yuan, Phys. Rev. **D61**, 014003 (2000), [Erratum: Phys. Rev.D64,059903(2001)], [hep-ph/9906280].
- [202] M. Abele, D. de Florian and W. Vogelsang, Phys. Rev. D **104**, 9, 094046 (2021), [arXiv:2109.00847].
- [203] M. Abele, D. de Florian and W. Vogelsang, Phys. Rev. D **106**, 1, 014015 (2022), [arXiv:2203.07928].

- [204] L. Bonino, T. Gehrmann and G. Stagnitto (2024), [arXiv:2401.16281].
- [205] S. Goyal *et al.* (2023), [arXiv:2312.17711].
- [206] T. Aaltonen *et al.* (CDF), Phys. Rev. **D79**, 112005 (2009), [Erratum: Phys. Rev. D82,119903(2010)], [arXiv:0904.1098].
- [207] G. Aad *et al.* (ATLAS), New J. Phys. **13**, 053033 (2011), [arXiv:1012.5104].
- [208] B. I. Abelev *et al.* (STAR), Phys. Rev. **C75**, 064901 (2007), [arXiv:nucl-ex/0607033].
- [209] K. Aamodt *et al.* (ALICE), Eur. Phys. J. **C71**, 1655 (2011), [arXiv:1101.4110].
- [210] B. B. Abelev *et al.* (ALICE), Phys. Lett. **B736**, 196 (2014), [arXiv:1401.1250].
- [211] J. Adam *et al.* (ALICE), Eur. Phys. J. **C75**, 5, 226 (2015), [arXiv:1504.00024].
- [212] S. Chatrchyan *et al.* (CMS), Eur. Phys. J. **C72**, 2164 (2012), [arXiv:1207.4724].
- [213] A. M. Sirunyan *et al.* (CMS), Phys. Rev. **D96**, 11, 112003 (2017), [arXiv:1706.10194].
- [214] G. J. Alner *et al.* (UA5), Z. Phys. **C32**, 153 (1986).
- [215] B. Abelev *et al.* (ALICE), Eur. Phys. J. **C73**, 6, 2456 (2013), [arXiv:1208.4968].
- [216] G. Antchev *et al.* (TOTEM), EPL **101**, 2, 21004 (2013).
- [217] A. M. Sirunyan *et al.* (CMS), JHEP **07**, 161 (2018), [arXiv:1802.02613].
- [218] F. Abe *et al.* (CDF), Phys. Rev. **D50**, 5550 (1994).
- [219] F. Abe *et al.* (CDF), Phys. Rev. **D50**, 5518 (1994).
- [220] S. S. Adler *et al.* (PHENIX), Phys. Rev. **C74**, 024904 (2006), [arXiv:nucl-ex/0603010].
- [221] S. Albino *et al.*, Phys. Rev. **D75**, 034018 (2007), [hep-ph/0611029].
- [222] I. Borsa, R. Sassot and M. Stratmann, Phys. Rev. **D96**, 9, 094020 (2017), [arXiv:1708.01630].
- [223] B. Andersson *et al.*, Phys. Rept. **97**, 31 (1983).
- [224] T. Sjostrand and M. Bengtsson, Comput. Phys. Commun. **43**, 367 (1987); T. Sjostrand, Comput. Phys. Commun. **82**, 74 (1994).
- [225] P. D. Acton *et al.* (OPAL), Phys. Lett. **B305**, 407 (1993).
- [226] J. Breitweg *et al.* (ZEUS), Eur. Phys. J. **C2**, 77 (1998), [hep-ex/9711018].
- [227] D. DeProspero *et al.* (E632), Phys. Rev. **D50**, 6691 (1994).
- [228] S. Chekanov *et al.* (ZEUS), Eur. Phys. J. **C51**, 1 (2007), [hep-ex/0612023].
- [229] G. Grindhammer *et al.*, in: *Proceedings of the Workshop on Monte Carlo Generators for HERA Physics*, Hamburg, Germany, 1998/1999.
- [230] N. Brook *et al.*, in: *Proceedings of the Workshop for Future HERA Physics at HERA*, Hamburg, Germany, 1996.
- [231] D. Acosta *et al.* (CDF), Phys. Rev. **D72**, 052001 (2005), [hep-ex/0504048].
- [232] G. Arnison *et al.* (UA1), Phys. Lett. **118B**, 167 (1982).
- [233] M. Banner *et al.* (UA2), Phys. Lett. **122B**, 322 (1983).
- [234] M. Banner *et al.* (UA2, Bern-CERN-Copenhagen-Orsay-Pavia-Saclay), Z. Phys. **C27**, 329 (1985).
- [235] A. Adare *et al.* (PHENIX), Phys. Rev. **D76**, 051106 (2007), [arXiv:0704.3599].
- [236] A. Adare *et al.* (PHENIX), Phys. Rev. **D83**, 032001 (2011), [arXiv:1009.6224].
- [237] A. Adare *et al.* (PHENIX), Phys. Rev. **D86**, 092006 (2012), [arXiv:1202.4020].
- [238] A. Adare *et al.* (PHENIX), Phys. Rev. **D88**, 3, 032006 (2013), [arXiv:1209.3283].
- [239] A. Adare *et al.* (PHENIX), Phys. Rev. **D91**, 3, 032001 (2015), [arXiv:1409.1907].
- [240] A. Adare *et al.* (PHENIX), Phys. Rev. **D90**, 7, 072008 (2014), [arXiv:1406.3541].
- [241] A. Adare *et al.* (PHENIX), Phys. Rev. **D93**, 1, 011501 (2016), [arXiv:1510.02317].
- [242] I. Arsene *et al.* (BRAHMS), Phys. Rev. Lett. **98**, 252001 (2007), [hep-ex/0701041].
- [243] J. Adams *et al.* (STAR), Phys. Rev. Lett. **97**, 152302 (2006), [arXiv:nucl-ex/0602011].
- [244] J. Adams *et al.* (STAR), Phys. Lett. **B637**, 161 (2006), [arXiv:nucl-ex/0601033].
- [245] B. I. Abelev *et al.* (STAR), Phys. Rev. **D80**, 111108 (2009), [arXiv:0911.2773].
- [246] G. Agakishiev *et al.* (STAR), Phys. Rev. Lett. **108**, 072302 (2012), [arXiv:1110.0579].
- [247] L. Adamczyk *et al.* (STAR), Phys. Rev. **D89**, 1, 012001 (2014), [arXiv:1309.1800].
- [248] B. B. Abelev *et al.* (ALICE), Eur. Phys. J. **C73**, 12, 2662 (2013), [arXiv:1307.1093].
- [249] L. Apanasevich *et al.* (Fermilab E706), Phys. Rev. Lett. **81**, 2642 (1998), [hep-ex/9711017].
- [250] G. Balocchi *et al.* (UA6), Phys. Lett. **B436**, 222 (1998).
- [251] K. Aamodt *et al.* (ALICE), Eur. Phys. J. **C71**, 1594 (2011), [arXiv:1012.3257].
- [252] R. Aaij *et al.* (LHCb), Phys. Lett. **B703**, 267 (2011), [arXiv:1107.3935].
- [253] G. Aad *et al.* (ATLAS), Phys. Lett. **B758**, 67 (2016), [arXiv:1602.01633].
- [254] F. Aversa *et al.*, Nucl. Phys. **B327**, 105 (1989); D. de Florian, Phys. Rev. **D67**, 054004 (2003), [hep-ph/0210442]; B. Jager *et al.*, Phys. Rev. **D67**, 054005 (2003), [hep-ph/0211007].
- [255] U. Baur *et al.*, in “QCD and weak boson physics in Run II. Proceedings, Batavia, USA, March 4-6, June 3-4, November 4-6, 1999,” 115–164 (2000), [115(2000)], [hep-ph/0005226], URL <http://lss.fnal.gov/archive/preprint/fermilab-conf-00-411-ae.shtml>.
- [256] P. Aurenche *et al.*, Eur. Phys. J. **C13**, 347 (2000), [hep-ph/9910252].
- [257] L. Apanasevich *et al.*, Phys. Rev. **D59**, 074007 (1999), [hep-ph/9808467].
- [258] U. D’Alesio and F. Murgia, Phys. Rev. **D70**, 074009 (2004), [hep-ph/0408092].
- [259] D. de Florian and W. Vogelsang, Phys. Rev. **D71**, 114004 (2005), [hep-ph/0501258].
- [260] P. Hinderer *et al.*, Phys. Rev. **D99**, 5, 054019 (2019), [arXiv:1812.00915].
- [261] D. d’Enterria *et al.*, Nucl. Phys. **B883**, 615 (2014), [arXiv:1311.1415].
- [262] G. Wilk and Z. Włodarczyk, Eur. Phys. J. **A40**, 299 (2009), [arXiv:0810.2939].
- [263] C. Tsallis, J. Statist. Phys. **52**, 479 (1988).
- [264] C. Tsallis, Braz. J. Phys. **29**, 1 (1999).
- [265] C. Tsallis, Eur. Phys. J. **A40**, 257 (2009), [arXiv:0812.4370].
- [266] M. D. Azmi and J. Cleymans, J. Phys. **G41**, 065001 (2014), [arXiv:1401.4835].
- [267] G. Wilk and Z. Włodarczyk, Phys. Rev. Lett. **84**, 2770 (2000), [hep-ph/9908459].
- [268] T. Bhattacharyya *et al.*, J. Phys. **G45**, 5, 055001 (2018), [arXiv:1709.07376].
- [269] S. Grigoryan, Phys. Rev. **D95**, 5, 056021 (2017), [arXiv:1702.04110].
- [270] T. Wibig, Int. J. Mod. Phys. **A29**, 1450021 (2014).

- [271] K. Saraswat, P. Shukla and V. Singh, *J. Phys. Comm.* **2**, 3, 035003 (2018), [arXiv:1706.04860].
- [272] K. Urmosy, G. G. Barnafoldi and T. S. Biro, *Phys. Lett.* **B701**, 111 (2011), [arXiv:1101.3023].
- [273] A. S. Parvan, O. V. Teryaev and J. Cleymans, *Eur. Phys. J.* **A53**, 5, 102 (2017), [arXiv:1607.01956].
- [274] K. Adcox *et al.* (PHENIX), *Phys. Rev. Lett.* **88**, 022301 (2002), [arXiv:nucl-ex/0109003]; C. Adler *et al.* (STAR), *Phys. Rev. Lett.* **90**, 082302 (2003), [arXiv:nucl-ex/0210033].
- [275] V.A. Khoze *et al.*, *Proceedings, Conference on High-Energy Physics, Tbilisi 1976*; J. D. Bjorken, *Phys. Rev.* **D17**, 171 (1978).
- [276] M. Artuso *et al.* (CLEO), *Phys. Rev.* **D70**, 112001 (2004), [hep-ex/0402040].
- [277] R. Seuster *et al.* (Belle), *Phys. Rev.* **D73**, 032002 (2006), [hep-ex/0506068].
- [278] A. Heister *et al.* (ALEPH), *Phys. Lett.* **B512**, 30 (2001), [hep-ex/0106051]; J. Abdallah *et al.* (DELPHI), *Eur. Phys. J.* **C71**, 1557 (2011), [arXiv:1102.4748]; G. Abbiendi *et al.* (OPAL), *Eur. Phys. J.* **C29**, 463 (2003), [hep-ex/0210031]; K. Abe *et al.* (SLD), *Phys. Rev.* **D65**, 092006 (2002), [Erratum: *Phys. Rev.* **D66**, 079905 (2002)], [hep-ex/0202031].
- [279] B. Mele and P. Nason, *Phys. Lett.* **B245**, 635 (1990); B. Mele and P. Nason, *Nucl. Phys.* **B361**, 626 (1991), [Erratum: *Nucl. Phys.* **B921**, 841 (2017)].
- [280] M. Cacciari and S. Catani, *Nucl. Phys.* **B617**, 253 (2001), [hep-ph/0107138].
- [281] P. Nason and C. Oleari, *Phys. Lett.* **B418**, 199 (1998), [hep-ph/9709358]; P. Nason and C. Oleari, *Phys. Lett.* **B447**, 327 (1999), [hep-ph/9811206]; P. Nason and C. Oleari, *Nucl. Phys.* **B565**, 245 (2000), [hep-ph/9903541].
- [282] K. Melnikov and A. Mitov, *Phys. Rev.* **D70**, 034027 (2004), [hep-ph/0404143].
- [283] C. Peterson *et al.*, *Phys. Rev.* **D27**, 105 (1983).
- [284] V. G. Kartvelishvili, A. K. Likhoded and V. A. Petrov, *Phys. Lett.* **78B**, 615 (1978).
- [285] P. D. B. Collins and T. P. Spiller, *J. Phys.* **G11**, 1289 (1985).
- [286] G. Colangelo and P. Nason, *Phys. Lett.* **B285**, 167 (1992).
- [287] M. G. Bowler, *Z. Phys.* **C11**, 169 (1981).
- [288] E. Braaten *et al.*, *Phys. Rev.* **D51**, 4819 (1995), [hep-ph/9409316].
- [289] R. Akers *et al.* (OPAL), *Z. Phys.* **C67**, 27 (1995).
- [290] H. Albrecht *et al.* (ARGUS), *Z. Phys.* **C52**, 353 (1991).
- [291] D. Buskulic *et al.* (ALEPH), *Phys. Lett.* **B357**, 699 (1995).
- [292] J. Chrin, *Z. Phys.* **C36**, 163 (1987).
- [293] R. L. Jaffe and L. Randall, *Nucl. Phys.* **B412**, 79 (1994), [hep-ph/9306201].
- [294] M. Cacciari and E. Gardi, *Nucl. Phys.* **B664**, 299 (2003), [hep-ph/0301047].
- [295] L. Randall and N. Rius, *Nucl. Phys.* **B441**, 167 (1995), [hep-ph/9405217].
- [296] J. C. Collins, *Phys. Rev.* **D58**, 094002 (1998), [hep-ph/9806259].
- [297] B. A. Kniehl *et al.*, *Eur. Phys. J.* **C41**, 199 (2005), [hep-ph/0502194].
- [298] S. Ahmed *et al.* (CLEO), *Phys. Rev.* **D62**, 112003 (2000), [hep-ex/0008015].
- [299] B. Aubert *et al.* (BaBar), *Phys. Rev.* **D65**, 091104 (2002), [hep-ex/0201041].
- [300] D. Bortoletto *et al.* (CLEO), *Phys. Rev.* **D37**, 1719 (1988), [Erratum: *Phys. Rev.* **D39**, 1471 (1989)].
- [301] H. Albrecht *et al.* (ARGUS), *Z. Phys.* **C54**, 1 (1992).
- [302] G. Alexander *et al.* (OPAL), *Z. Phys.* **C69**, 543 (1996).
- [303] A. Heister *et al.* (ALEPH), *Phys. Lett.* **B561**, 213 (2003), [hep-ex/0302003].
- [304] F. D. Aaron *et al.* (H1), *Eur. Phys. J.* **C65**, 89 (2010), [arXiv:0907.2643].
- [305] S. Chekanov *et al.* (ZEUS), *JHEP* **07**, 074 (2007), [arXiv:0704.3562]; ZEUS Collab: H. Abramowicz *et al.*, *JHEP*, 1309 (2013); A. Aktas *et al.* (H1), *Eur. Phys. J.* **C51**, 271 (2007), [hep-ex/0701023]; F. D. Aaron *et al.* (H1), *Eur. Phys. J.* **C59**, 589 (2009), [arXiv:0808.1003].
- [306] B. Adeva *et al.* (L3), *Phys. Lett.* **B261**, 177 (1991).
- [307] O. Biebel, P. Nason and B. R. Webber (2001), [hep-ph/0109282].
- [308] H. Evans (ALICE, ATLAS, CMS, LHCb), in “Proceedings, 14th International Conference on Hadron spectroscopy (Hadron 2011): Munich, Germany, June 13-17, 2011,” (2011), [arXiv:1110.5294]; E. Aguilo, in “Proceedings, 47th Rencontres de Moriond on QCD and High Energy Interactions: La Thuile, France, March 10-17, 2012,” 115–120 (2012), [arXiv:1205.5678]; F. Simonetto, *Journal of Physics: Conference Series* **347**, 012014 (2012).
- [309] V. Khachatryan *et al.* (CMS), *JHEP* **03**, 136 (2011), [arXiv:1102.3194]; G. Aad *et al.* (ATLAS), *Eur. Phys. J.* **C71**, 1846 (2011), [arXiv:1109.6833]; S. Chatrchyan *et al.* (CMS), *JHEP* **04**, 084 (2012), [arXiv:1202.4617]; G. Aad *et al.* (ATLAS), *Eur. Phys. J.* **C73**, 2, 2301 (2013), [arXiv:1210.0441].
- [310] H. Jung *et al.*, *Phys. Rev.* **D85**, 034035 (2012), [arXiv:1111.1942].
- [311] D. Acosta *et al.* (CDF), *Phys. Rev. Lett.* **91**, 241804 (2003), [hep-ex/0307080]; D. Acosta *et al.* (CDF), *Phys. Rev.* **D71**, 032001 (2005), [hep-ex/0412071].
- [312] M. Cacciari and P. Nason, *JHEP* **09**, 006 (2003), [hep-ph/0306212]; M. Cacciari *et al.*, *JHEP* **07**, 033 (2004), [hep-ph/0312132]; B. A. Kniehl *et al.*, *Phys. Rev. Lett.* **96**, 012001 (2006), [hep-ph/0508129].
- [313] H. Abramowicz *et al.* (ZEUS), *Eur. Phys. J.* **C71**, 1573 (2011), [arXiv:1101.3692].
- [314] S. Chekanov *et al.* (ZEUS), *Phys. Rev.* **D78**, 072001 (2008), [arXiv:0805.4390].
- [315] S. Chekanov *et al.* (ZEUS), *JHEP* **02**, 032 (2009), [arXiv:0811.0894].
- [316] F. D. Aaron *et al.* (H1), *Eur. Phys. J.* **C72**, 2148 (2012), [arXiv:1206.4346].
- [317] M. L. Mangano and P. Nason, *Phys. Lett.* **B285**, 160 (1992).
- [318] M. H. Seymour, *Nucl. Phys.* **B436**, 163 (1995).
- [319] D. J. Miller and M. H. Seymour, *Phys. Lett.* **B435**, 213 (1998), [hep-ph/9805414].
- [320] R. Barate *et al.* (ALEPH), *Phys. Lett.* **B434**, 437 (1998).
- [321] P. Abreu *et al.* (DELPHI), *Phys. Lett.* **B405**, 202 (1997).
- [322] M. Acciarri *et al.* (L3), *Phys. Lett.* **B476**, 243 (2000), [hep-ex/9911016].
- [323] G. Abbiendi *et al.* (OPAL), *Eur. Phys. J.* **C13**, 1 (2000), [hep-ex/9908001].
- [324] K. Abe *et al.* (SLD) (1999), [hep-ex/9908028], URL <http://www-public.slac.stanford.edu/sciDoc/docMeta.aspx?slacPubNumber=SLAC-PUB-8157>.
- [325] C. Albajar *et al.* (UA1 Collaboration), *Z. Phys. C* **61**, 41 (1993), URL <http://cds.cern.ch/record/253028>.
- [326] R. Aaij *et al.* (LHCb), *JHEP* **11**, 030 (2017), [arXiv:1708.05994].
- [327] M. Aaboud *et al.* (ATLAS), *Phys. Rev.* **D99**, 5, 052004 (2019), [arXiv:1812.09283].
- [328] M. Burkardt and R. L. Jaffe, *Phys. Rev. Lett.* **70**, 2537 (1993), [hep-ph/9302232].

- [329] P. J. Mulders and R. D. Tangerman, Nucl. Phys. **B461**, 197 (1996), [Erratum: Nucl. Phys.B484,538(1997)], [hep-ph/9510301].
- [330] R. Jakob, Nucl. Phys. **A711**, 35 (2002), [hep-ph/0206271].
- [331] D. de Florian, M. Stratmann and W. Vogelsang, Phys. Rev. Lett. **81**, 530 (1998), [hep-ph/9802432].
- [332] D. Buskulic *et al.* (ALEPH), Phys. Lett. **B374**, 319 (1996).
- [333] K. Ackerstaff *et al.* (OPAL), Eur. Phys. J. **C2**, 49 (1998), [hep-ex/9708027].
- [334] G. Abbiendi *et al.* (OPAL), Phys. Lett. **B444**, 539 (1998), [hep-ex/9808006].
- [335] M. Alekseev *et al.* (COMPASS), Eur. Phys. J. **C64**, 171 (2009), [arXiv:0907.0388].
- [336] A. Airapetian *et al.* (HERMES), Phys. Rev. **D74**, 072004 (2006), [hep-ex/0607004].
- [337] G. Karyan (HERMES), Int. J. Mod. Phys. Conf. Ser. **40**, 1660067 (2016).
- [338] J. Adam *et al.* (STAR), Phys. Rev. **D98**, 11, 112009 (2018), [arXiv:1808.07634].
- [339] R. L. Jaffe, Phys. Rev. **D54**, 11, R6581 (1996), [hep-ph/9605456].
- [340] A. Airapetian *et al.* (HERMES), Phys. Rev. **D76**, 092008 (2007), [arXiv:0704.3133].
- [341] A. Moretti (COMPASS), PoS **SPIN2018**, 138 (2018), [arXiv:1901.01735].
- [342] L. Gamberg *et al.*, Phys. Lett. B **818**, 136371 (2021), [arXiv:2102.05553].
- [343] R. Seidl *et al.* (Belle), Phys. Rev. **D99**, 11, 112006 (2019), [arXiv:1902.01552].
- [344] C. Adolph *et al.* (COMPASS), Eur. Phys. J. **C73**, 8, 2531 (2013), [Erratum: Eur. Phys. J.C75,no.2,94(2015)], [arXiv:1305.7317].
- [345] A. Signori *et al.*, JHEP **11**, 194 (2013), [arXiv:1309.3507].
- [346] M. Anselmino *et al.*, JHEP **04**, 005 (2014), [arXiv:1312.6261].
- [347] M. G. Echevarria *et al.*, Phys. Rev. **D89**, 074013 (2014), [arXiv:1401.5078].
- [348] M. G. Echevarria, I. Scimemi and A. Vladimirov, Phys. Rev. **D93**, 1, 011502 (2016), [Erratum: Phys. Rev.D94,no.9,099904(2016)], [arXiv:1509.06392].
- [349] M. G. Echevarria, I. Scimemi and A. Vladimirov, JHEP **09**, 004 (2016), [arXiv:1604.07869].
- [350] A. Bacchetta *et al.*, JHEP **06**, 081 (2017), [Erratum: JHEP06,051(2019)], [arXiv:1703.10157].
- [351] M. A. Ebert, B. Mistlberger and G. Vita, JHEP **07**, 121 (2021), [arXiv:2012.07853].
- [352] M.-x. Luo *et al.*, JHEP **06**, 115 (2021), [arXiv:2012.03256].
- [353] J. C. Collins, Nucl. Phys. **B396**, 161 (1993), [hep-ph/9208213].
- [354] J. P. Ralston and D. E. Soper, Nucl. Phys. **B152**, 109 (1979).
- [355] H. Avakian *et al.* (CLAS), Phys. Rev. **D69**, 112004 (2004), [hep-ex/0301005].
- [356] A. Airapetian *et al.* (HERMES), Phys. Rev. Lett. **84**, 4047 (2000), [hep-ex/9910062].
- [357] A. Airapetian *et al.* (HERMES), Phys. Rev. **D64**, 097101 (2001), [hep-ex/0104005].
- [358] A. Airapetian *et al.* (HERMES), Phys. Rev. Lett. **94**, 012002 (2005), [hep-ex/0408013].
- [359] A. Airapetian *et al.* (HERMES), Phys. Lett. **B693**, 11 (2010), [arXiv:1006.4221].
- [360] V. Yu. Alexakhin *et al.* (COMPASS), Phys. Rev. Lett. **94**, 202002 (2005), [hep-ex/0503002].
- [361] E. S. Ageev *et al.* (COMPASS), Nucl. Phys. **B765**, 31 (2007), [hep-ex/0610068].
- [362] M. Alekseev *et al.* (COMPASS), Phys. Lett. **B673**, 127 (2009), [arXiv:0802.2160].
- [363] M. G. Alekseev *et al.* (COMPASS), Phys. Lett. **B692**, 240 (2010), [arXiv:1005.5609].
- [364] M. G. Alekseev *et al.* (COMPASS), Eur. Phys. J. **C70**, 39 (2010), [arXiv:1007.1562].
- [365] C. Adolph *et al.* (COMPASS), Phys. Lett. **B717**, 376 (2012), [arXiv:1205.5121].
- [366] C. Adolph *et al.* (COMPASS), Phys. Lett. **B744**, 250 (2015), [arXiv:1408.4405].
- [367] K. Abe *et al.* (Belle), Phys. Rev. Lett. **96**, 232002 (2006), [hep-ex/0507063].
- [368] R. Seidl *et al.* (Belle), Phys. Rev. **D78**, 032011 (2008), [Erratum: Phys. Rev.D86,039905(2012)], [arXiv:0805.2975].
- [369] J. P. Lees *et al.* (BaBar), Phys. Rev. **D90**, 5, 052003 (2014), [arXiv:1309.5278].
- [370] J. P. Lees *et al.* (BaBar), Phys. Rev. **D92**, 11, 111101 (2015), [arXiv:1506.05864].
- [371] M. Ablikim *et al.* (BESIII), Phys. Rev. Lett. **116**, 4, 042001 (2016), [arXiv:1507.06824].
- [372] M. Anselmino *et al.*, Phys. Rev. **D92**, 11, 114023 (2015), [arXiv:1510.05389].
- [373] Z.-B. Kang *et al.*, Phys. Rev. **D93**, 1, 014009 (2016), [arXiv:1505.05589].
- [374] F. Yuan, Phys. Rev. Lett. **100**, 032003 (2008), [arXiv:0709.3272].
- [375] Z.-B. Kang *et al.*, JHEP **11**, 068 (2017), [arXiv:1705.08443].
- [376] K. Konishi, A. Ukawa and G. Veneziano, Phys. Lett. **78B**, 243 (1978).
- [377] I. Vendramin, Nuovo Cim. **A66**, 339 (1981).
- [378] J. C. Collins, S. F. Heppelmann and G. A. Ladinsky, Nucl. Phys. **B420**, 565 (1994), [hep-ph/9305309].
- [379] R. L. Jaffe, X.-m. Jin and J. Tang, Phys. Rev. Lett. **80**, 1166 (1998), [hep-ph/9709322].
- [380] R. L. Jaffe, X.-m. Jin and J.-a. Tang, Phys. Rev. **D57**, 5920 (1998), [hep-ph/9710561].
- [381] A. Bianconi *et al.*, Phys. Rev. **D62**, 034008 (2000), [hep-ph/9907475].
- [382] M. Radici, R. Jakob and A. Bianconi, Phys. Rev. **D65**, 074031 (2002), [hep-ph/0110252].
- [383] D. de Florian and L. Vanni, Phys. Lett. **B578**, 139 (2004), [hep-ph/0310196].
- [384] A. Bacchetta and M. Radici, Phys. Rev. **D67**, 094002 (2003), [hep-ph/0212300].
- [385] A. Vossen *et al.* (Belle), Phys. Rev. Lett. **107**, 072004 (2011), [arXiv:1104.2425].
- [386] A. Courtoy *et al.*, Phys. Rev. **D85**, 114023 (2012), [arXiv:1202.0323].
- [387] M. Radici *et al.*, JHEP **05**, 123 (2015), [arXiv:1503.03495].
- [388] A. Airapetian *et al.* (HERMES), JHEP **06**, 017 (2008), [arXiv:0803.2367].
- [389] C. Adolph *et al.* (COMPASS), Phys. Lett. **B713**, 10 (2012), [arXiv:1202.6150].
- [390] C. Adolph *et al.* (COMPASS), Phys. Lett. **B736**, 124 (2014), [arXiv:1401.7873].
- [391] L. Adamczyk *et al.* (STAR), Phys. Rev. Lett. **115**, 242501 (2015), [arXiv:1504.00415].
- [392] A. Bacchetta, A. Courtoy and M. Radici, Phys. Rev. Lett. **107**, 012001 (2011), [arXiv:1104.3855].
- [393] A. Bacchetta, A. Courtoy and M. Radici, JHEP **03**, 119 (2013), [arXiv:1212.3568].
- [394] M. Radici and A. Bacchetta, Phys. Rev. Lett. **120**, 19, 192001 (2018), [arXiv:1802.05212].

20. High Energy Soft QCD and Diffraction

Revised August 2023 by V.A. Khoze (Durham U.), M.G. Ryskin (Petersburg Nuclear Phys. Inst.) and M. Taševský (Prague, Inst. Phys.).

20.1 Introduction

Despite the enormous successes of Quantum Chromodynamics (QCD) (see Section 9 in [1] and [2]) there remain a number of deep questions to be answered in the domain of strong interaction physics. These concern first of all small momentum transfer processes which are generically called soft interactions.

One of the most challenging problems is the high-energy behaviour of hadronic scattering processes. At high collision energies, \sqrt{s} , soft interactions play a dominant role. Unfortunately, soft interactions cannot be described in terms of perturbative QCD. These are non-perturbative phenomena related to confinement which are generally considered in the context of the analytic S -matrix, based on *first principles*, such as analyticity, crossing symmetry and unitarity of partial waves, see e.g. [3, 4]. At high energies the most self-consistent way to perform the calculations and to describe the data is the Regge approach (see for example [5–7]), which will be considered below. As discussed in Section 20.5, this formalism could be smoothly matched with perturbative QCD calculations at larger transverse momenta. Therefore, here we will concentrate on the properties of high energy soft interactions that can be expected from the extension of the perturbative QCD domain.

The main aim of this review is to present the well-established theoretical framework, based on Regge theory and QCD, used for describing high-energy collisions. A limited number of some new experimental results, mainly from the LHC, are shown in order to demonstrate that the gross features of the data are in agreement with this approach. We are not focussing on any particular phenomenological or Monte Carlo model, which are covered in the dedicated reviews and books, see e.g. Section 43 in [1], [2, 8–14] and Chapter 2 in [15].

Typically, in multiparticle production, the secondaries¹ fill the whole available rapidity interval.² However, there exists an important class of events in which a large interval of rapidity (typically at least 4 units) is devoid of any hadronic activity. Such an interval is called a Large Rapidity Gap (LRG). The most frequent case with a LRG is elastic scattering. There are also events in which one of the incoming protons (or both) is transformed (dissociates) into a set of two or more final state particles with the mass $M \ll \sqrt{s}$ and proton quantum number. All these events have properties similar to those of the well-known from optics pattern of diffraction of a beam of light on an obstacle. By analogy, in high-energy physics, the corresponding processes are usually called diffractive. The classic example is the elastic scattering of hadrons on nuclei (see e.g. [16]), which manifests an angular distribution with a series of minima and maxima, analogous to the diffraction of light on a black disk. At LHC energies diffractive processes constitute up to 40% of the total (pp) cross section, σ_{tot} . Therefore, we will pay special attention to the description of the elastic scattering amplitude and proton diffractive dissociation. Diffraction dissociation can be considered as a quantum mechanical process caused by the fact that different components of the incoming hadron wave function have different probabilities for interaction with a target [17]. This feature allows us to probe the transverse size of the interaction region.

Note that besides being of a fundamental interest in their own right for understanding the high energy behaviour of the QCD amplitude, there are several reasons why it is important to study soft and diffractive processes. Firstly, soft interactions unavoidably give an underlying component to rare ‘hard’ events, from which we hope to extract signals for New Physics. Secondly, we should be able to estimate the probability that rapidity gaps, which oc-

cur in ‘hard’ diffractive events, survive rescattering effects, that is, survive the population of the gaps by the secondary particles from the underlying event. Thirdly, an understanding of diffractive processes is very important for evaluation of pile-up backgrounds in high-luminosity pp collisions, which have a direct impact on various experimental measurements. Pile-up corresponds to soft independent interactions in the same bunch crossing whose number rises with increasing instantaneous luminosity. And, finally, studies of diffractive processes should help in the understanding of the structure of high-energy cosmic ray cascades, which requires a very detailed knowledge of the spectra of particles carrying a large fraction x of the incoming momentum in proton-air and nucleus-air interactions, see for instance [18].

Experimentally, diffractive processes are selected using two distinct features:

1. large regions (typically at least $\Delta\eta > 4$) in the detector are devoid of hadronic activity (LRG) and/or
2. one or both incoming particles stay intact after collision and are registered by the dedicated forward detectors placed a few hundred meters from the interaction point. The momentum loss of the initial particle, $\xi = 1 - x$, is typically smaller than 0.15.

Thus, in the case of proton-proton collisions, diffractive events correspond to elastic $pp \rightarrow pp$ scattering and to $pp \rightarrow p + X$ (Single Dissociation, SD) and $pp \rightarrow X + Y$ (Double Dissociation, DD) processes, where the + sign denotes a large rapidity gap. Note that strictly speaking in high energy physics it is impossible to define (and select) rigorously purely diffractive events. We can always have some admixture of events of different origin. As a rule we call ‘diffractive’ the events with sufficiently large gap (with say $\Delta y > 4$, see above) and the vacuum quantum numbers transferred across the gap. Typically at the LHC the integrated cross sections of diffractive dissociation, σ_{SD} , σ_{DD} , are of the order of 5–10 mb depending on the gap size. Schematic diagrams of all discussed processes are shown in Fig. 20.1.

20.2 Regge pole approach

In pre-QCD times, in order to describe the behaviour of scattering amplitudes at high energy, \sqrt{s} , and small momentum-transfer squared, $-t$, Regge theory was developed and successfully applied in a wide range of energies. The Regge approach [5–7] is based on the singularities of amplitudes in the complex angular momentum, j , plane.

For instance, the measured $\pi^- p \rightarrow \pi^0 n$ amplitude behaves as

$$T_{\pi p}(s, t) \propto s^{\alpha_\rho(t)}, \quad (20.1)$$

where the process is described by the exchange of the ρ -trajectory, $j = \alpha_\rho(t) \simeq 0.5 + 0.9t$ (with $t = (p_{\pi^-} - p_{\pi^0})^2$ in GeV^2). This trajectory passes through the spin-1 ρ -meson resonance in the ‘crossed’ t -channel $\pi^- \pi^0 \rightarrow \bar{p} n$; that is, $\alpha_\rho(t = m_\rho^2) = 1$. The corresponding cross section decreases with increasing s .

On the other hand, high-energy total and elastic pp cross sections are observed to grow slowly with energy (see e.g. Section 53 in [1]) and in terms of Regge theory are dominated by the exchange of a trajectory with vacuum quantum numbers, $\sigma_{\text{tot}} \propto s^{j-1}$. The simplest possibility is to assume that the rightmost singularity in the j -plane, which drives the high-energy behaviour of the cross section, is the leading (at $t \leq 0$) Regge pole at $j = \alpha(t)$. Then the pp elastic amplitude reads

$$T_{\text{el}}(s, t) \propto s^{\alpha_{\mathbb{P}}(t)}. \quad (20.2)$$

The total cross section can then be conveniently expressed using the so called optical theorem which states that

$$s\sigma_{\text{tot}} = \text{Im}T_{\text{el}}(s, t = 0), \quad (20.3)$$

as illustrated in the upper part of Fig. 20.2, and thus

$$\sigma_{\text{tot}} \propto s^{\alpha_{\mathbb{P}}(0)-1}. \quad (20.4)$$

¹Here and in what follows, we call secondaries the new particles produced in the course of the interaction.

²For definition of particle rapidity (pseudorapidity), see Section 49.5.2 in [1]; $y = \frac{1}{2} \ln \frac{E+p_z}{E-p_z}$ ($\eta = -\ln(\tan(\theta/2))$); the correct variable is the rapidity y , however, experimentally it is simpler to use the pseudorapidity η which does not require identifying the particles, setting $m = 0$. For $p_T \gg m$, $\eta \simeq y$.

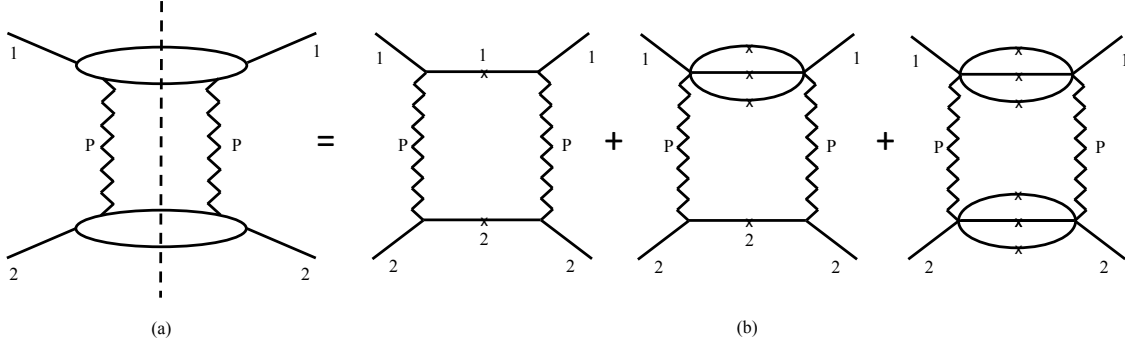


Figure 20.3: Two-Pomeron exchange in the t channel expressed as a sum over all diffractive intermediate states in the s -channel. The crosses indicate that the particles are on the mass shell.

with $S = I + iT$. If we were to focus, for example, on the unitarity for elastic and quasielastic processes, then *disc* T would simply denote a cut in s -channel between incoming and outgoing particles as visualized by crosses in Fig. 20.3.

At high energies, the s -channel unitarity relation is diagonal in the b basis such that

$$2\text{Im} T_{\text{el}}(s, b) = |T_{\text{el}}(s, b)|^2 + G_{\text{inel}}(s, b) \quad (20.9)$$

with

$$\sigma_{\text{tot}} = 2 \int d^2b \text{Im} T_{\text{el}}(s, b) \quad (20.10)$$

$$\sigma_{\text{el}} = \int d^2b |T_{\text{el}}(s, b)|^2 \quad (20.11)$$

$$\sigma_{\text{inel}} = \int d^2b [2\text{Im} T_{\text{el}}(s, b) - |T_{\text{el}}(s, b)|^2]. \quad (20.12)$$

The general solution of Eq. (20.9) is

$$T_{\text{el}}(b) = i(1 - e^{-\Omega(b)/2}) \quad (20.13)$$

and

$$G_{\text{inel}}(s, b) = 1 - e^{-\text{Re}\Omega(b)} = 1 - P_{\text{nointer}}(s, b), \quad (20.14)$$

where G_{inel} is the sum over all inelastic intermediate states and P_{nointer} is a probability to have no inelastic interactions. $G_{\text{inel}}(s, b)$ describes the b -profile of inelastic particle collisions. It satisfies the condition $0 \leq G_{\text{inel}} \leq 1$ and determines how absorptive the interaction region is at a given impact parameter (with $G_{\text{inel}} = 1$ for full absorption and $G_{\text{inel}} = 0$ for the complete dominance of elastic scattering). As seen from Eq. (20.14), $\exp(-\text{Re}\Omega(s, b))$ is the probability that no inelastic interactions occur at impact parameter b . Ω ($\text{Re}\Omega \geq 0$) is called the opacity (optical density) or eikonal. The quantity

$$S^2(b) \equiv e^{-\text{Re}\Omega(b)} = P_{\text{nointer}}(b) \quad (20.15)$$

is the so-called survival factor, which enables us to calculate the probability that the LRG survives soft rescattering.

In terms of the opacity the elastic cross section takes the form

$$\begin{aligned} \frac{d\sigma_{\text{el}}}{dt} &= \frac{1}{16\pi s^2} |T_{\text{el}}(s, t)|^2 = \frac{1}{4\pi} \left| \int d^2b e^{i\vec{q}_t \cdot \vec{b}} (1 - e^{-\Omega(b)/2}) \right|^2 \\ &= \pi \left| \int b db J_0(q_t b) (1 - e^{-\Omega(b)/2}) \right|^2, \end{aligned} \quad (20.16)$$

where $q_t = \sqrt{|t|}$ and J_0 is the zeroth-order Bessel function.

To describe the elastic scattering at one fixed energy we can always find an appropriate parameterization for the opacity $\Omega(b)$ and tune the parameters to reproduce the observed $d\sigma_{\text{el}}/dt$ cross

section. Moreover, we can fix the form of the parameterization, but choose, at each particular energy, the corresponding values of parameters; see, e.g. [39]. Alternatively, we may simply take the Fourier-Bessel transform from the experimental data [33, 40, 41]

$$\text{Im} T_{\text{el}}(b) = \int \frac{q_t dq_t}{4\pi} \sqrt{\frac{d\sigma_{\text{el}}}{dt} \frac{16\pi}{1 + \rho^2}} J_0(q_t b), \quad (20.17)$$

where the square root represents $\text{Im} T_{\text{el}}(q_t)$, with $\rho \equiv \text{Re} T_{\text{el}} / \text{Im} T_{\text{el}}$. In this way, we first determine T_{el} from the data for $d\sigma_{\text{el}}/dt$, and then calculate $\Omega(b)$ using Eq. (20.13), assuming in accordance with data that ρ is small (or $\rho(t) = \text{constant}$).

At high energies $\rho^2 \ll 1$, which is usually well justified except in the diffractive dip region (see Section 20.3.3.1 for discussion of the dip region).

The value of ρ can be derived via the dispersion relation, see [3]:

$$\frac{1}{s} \text{Re} T_{\text{el}}(s) = \frac{1}{\pi} \int_{-\infty}^{+\infty} \frac{ds'}{s' - s} \sigma_{\text{tot}}(|s'|) = \frac{1}{\pi} \int_0^{\infty} \sigma_{\text{tot}}(s') \frac{2s ds'}{s'^2 - s^2}. \quad (20.18)$$

Since we consider just the charge-parity C -even amplitude, here for negative s' we put $\sigma_{p\bar{p}} = \sigma_{pp}$. That is, for negative s' , which corresponds to the interaction with an *antiparticle*, we use the same $\sigma_{pp}(|s'|)$. The major contribution comes from $s' \simeq s$. Thus, with a good accuracy we can evaluate $\rho(t=0)$ as

$$\rho \simeq \frac{\pi}{2} \frac{\partial \ln \sigma_{\text{tot}}(s)}{\partial \ln s}. \quad (20.19)$$

20.3.2 Diffractive dissociation

The elastic cross section probes the optical density of the proton. The well known example of scattering on a black disk, with $G_{\text{inel}} = 1$ for $b < R$, gives $\sigma_{\text{el}} = \sigma_{\text{inel}} = \pi R^2$ and $\sigma_{\text{tot}} = 2\pi R^2$. In general, the absorption of the initial wave (due to inelastic channels) leads, via s -channel unitarity, to elastic scattering.

Inelastic diffraction (i.e. proton dissociation) is a consequence of the *internal structure* of hadrons. This can be conveniently described at high energies, where the lifetimes of each particular Fock component of the incoming hadron/proton wave function (the hadronic fluctuations) are large, $\tau \sim E/m^2$, and during these time intervals the corresponding Fock states can be considered as ‘frozen’. Each hadronic constituent can undergo a scattering with its own probability and thus destroys coherence of the fluctuations⁴. As a result, the outgoing superposition of states will be different from the incident particle, and will most likely contain multiparticle states, so we will have *inelastic*, as well as elastic scattering.

To calculate diffractive dissociation we can enlarge the set of intermediate states (p, N_a^*), from just the single elastic channel, and introduce a multichannel eikonal. However, it is more convenient

⁴ At high energies the configurations with different transverse separation, r , between the quarks (valence partons) can serve as an example of such Fock states. An interaction with the QCD Pomeron does not change the value of r , while the cross section $\sigma \propto \alpha_s^2 r^2$ (see Section 20.4.2 and [42–44]).

to follow Good and Walker [45], and to introduce states ϕ_k diagonalising the T matrix (which e.g. in the proton case describes different $p \rightarrow N^*$, $N_a^* \rightarrow N_b^*$ transitions). Such eigenstates only undergo elastic scattering. Since there are no off-diagonal transitions,

$$\langle \phi_i | T | \phi_k \rangle = 0 \quad \text{for } i \neq k, \quad (20.20)$$

a state k cannot diffractively dissociate into a state $j \neq k$. Working in terms of the Good-Walker eigenstates ϕ_i , we have a simple one-channel eikonal for each state. We denote the orthogonal matrix which diagonalizes T by a , so that

$$T = a F a^T \quad \text{with} \quad \langle \phi_i | F | \phi_k \rangle = F_k \delta_{ik}, \quad (20.21)$$

where F_k is the probability amplitude of the hadronic process proceeding via the diffractive eigenstate ϕ_k .

Now consider the diffractive dissociation of an incoming state $|h\rangle$. We can write

$$|h\rangle = \sum_k a_{hk} |\phi_k\rangle. \quad (20.22)$$

The elastic scattering amplitude satisfies

$$\langle h | T | h \rangle = \sum_k |a_{hk}|^2 F_k = \langle F \rangle, \quad (20.23)$$

where $F_k \equiv \langle \phi_k | F | \phi_k \rangle$ and where the brackets of $\langle F \rangle$ mean that we take the average of F over the initial probability distribution of diffractive eigenstates. After the diffractive scattering described by T_{fh} , the final state $|f\rangle$ will, in general, be a different superposition of eigenstates from that of $|h\rangle$, which was shown in Eq. (20.22). Neglecting the real parts, for the cross sections at a given impact parameter b , we have

$$\begin{aligned} \frac{d\sigma_{\text{tot}}}{d^2b} &= 2 \text{Im} \langle h | T | h \rangle = 2 \sum_k |a_{hk}|^2 \text{Im} F_k = 2 \langle \text{Im} F \rangle \\ \frac{d\sigma_{\text{el}}}{d^2b} &= |\langle h | T | h \rangle|^2 = \left| \sum_k |a_{hk}|^2 F_k \right|^2 = \langle |F|^2 \rangle \\ \frac{d\sigma_{\text{el}} + \text{SD}}{d^2b} &= \sum_k |\langle \phi_k | T | h \rangle|^2 = \sum_k |a_{hk}|^2 |F_k|^2 = \langle |F|^2 \rangle. \end{aligned} \quad (20.24)$$

It follows that the cross section for the single diffractive dissociation of a proton,

$$\frac{d\sigma_{\text{SD}}}{d^2b} = \langle |F|^2 \rangle - \langle |F| \rangle^2, \quad (20.25)$$

is given by the statistical dispersion in the absorption probabilities of the diffractive eigenstates. Here the average is taken over the components k of the incoming proton which dissociates. If the averages are taken over the components of both of the incoming particles, then Eq. (20.25) is the sum of the cross sections for single and double dissociation, see Fig. 20.3.

Note that if all the components ϕ_k of the incoming proton $|h\rangle$ were absorbed equally, then the diffracted superposition would be proportional to the incident one and the probability of the inelastic diffraction would be zero. Thus if, at very high energies, the amplitudes F_k at small impact parameters are equal to the black disk limit, $F_k = i$, then diffractive production will be equal to zero in this impact parameter domain, and so will only occur in the peripheral b region where the edge of the disk becomes not completely black. Hence the impact parameter structure of diffractive dissociation and elastic scattering is drastically different in the presence of absorptive s -channel unitarity effects (see the G_{inel} term in Eq. (20.9)). Under the assumption that amplitudes F_k at high energies cannot exceed the black disk limit, $\text{Im} F_k \leq 1$, equations 20.24 lead to the following bound

$$\frac{d\sigma_{\text{el}} + \text{SD}_1 + \text{SD}_2 + \text{DD}}{d^2b} \leq \frac{1}{2} \frac{d\sigma_{\text{tot}}}{d^2b}. \quad (20.26)$$

known as the Pumplin bound [46]⁵.

20.3.3 Diffraction from the t -channel viewpoint

The t -channel approach is based on the Regge model (see Section 20.2), where high-energy diffractive processes are mediated by the exchange of a Pomeron (\mathbb{P}). In the case of the elastic pp -scattering amplitude in the eikonal model (see Eq. (20.13)), the opacity corresponding to the exchange of one Pomeron is

$$\Omega(s, b) = \int \frac{d^2q_t}{4\pi^2} \Omega(s, q_t) e^{i\vec{q}_t \cdot \vec{b}} \quad (20.27)$$

with

$$\Omega(s, q_t) = \frac{1}{s} T'_{\text{el}} = -i\eta_P(t) g_N(t) g_N(t) \left(\frac{s}{s_0} \right)^{\alpha_{\mathbb{P}}(t)-1}, \quad (20.28)$$

where T'_{el} is the two-particle s -channel irreducible elastic amplitude, cf. Eq. (20.5), and $g_N(t)$ is the proton-Pomeron coupling.

If we assume an exponential t -dependence of the coupling, $g_N(t) = g_N(0) \exp(B_0 t)$, and neglect the Pomeron phase, then the opacity is

$$\Omega(s, q_t) = g_N(0) g_N(0) \left(\frac{s}{s_0} \right)^{\alpha_{\mathbb{P}}(0)-1} e^{Bt}, \quad (20.29)$$

with the t -slope given by

$$B = 2B_0 + \alpha'_{\mathbb{P}} \ln \left(\frac{s}{s_0} \right). \quad (20.30)$$

At high energies the opacity has a Gaussian form in the b -space:

$$\Omega(s, b) = \frac{g_N^2(0)}{4\pi B} \left(\frac{s}{s_0} \right)^{\alpha_{\mathbb{P}}(0)-1} e^{-b^2/4B}. \quad (20.31)$$

In terms of opacity the effective radius of interaction increases at high energies as $\sqrt{\alpha'_{\mathbb{P}} \ln(s/s_0)}$. This means that with energy increasing the differential cross section becomes steeper (the so called *shrinkage* of the diffractive peak).

If we were to take for the Pomeron the DL parametrisation [25, 26], that is to keep just the first, $T(b) = \Omega(b)/2$, term in the elastic amplitude (Eq. (20.13)) then, at LHC energies, the Gaussian would exceed the black disk limit at small b . However, the eikonal unitarization reduces the power growth of the one-Pomeron exchange cross section. Thus, in Eq. (20.31) $\Omega(s, b) \propto (s/s_0)^{\alpha_{\mathbb{P}}-1}$ gives an amplitude $\text{Im} T_{\text{el}}(s, b) = 1 - e^{-\Omega/2} < 1$. Hence the total cross section is limited by the size of the effective interaction area $\sigma_{\text{tot}} < 2\pi R^2$, where the interaction radius R can be estimated from Eq. (20.31) as the value of b where $\text{Re}\Omega(b)$ becomes ~ 1 .

For the parameterization of Eq. (20.31) the corresponding radius grows at very large energies as

$$b^2 = R^2 = 4B \ln \left[\frac{g_N^2(0)}{4\pi B} \left(\frac{s}{s_0} \right)^{\alpha_{\mathbb{P}}(0)-1} \right] \simeq 4\Delta \alpha'_{\mathbb{P}} \ln^2(s/s_0). \quad (20.32)$$

That is for $\Delta = 0.1$ and $\alpha'_{\mathbb{P}} = 0.25 \text{ GeV}^{-2}$ we may expect that the cross section increases as

$$\sigma_{\text{tot}} = 2\pi R^2 \simeq c \cdot \ln^2 s, \quad (20.33)$$

with $c = 8\pi \Delta \alpha'_{\mathbb{P}} = 0.24 \text{ mb}$. This value is close to that obtained by the COMPETE parameterization ($c = 0.27 \text{ mb}$ [22, 24]) but much smaller than the Froissart-Lukaszk-Martin (FLM) bound [47–49]. With $c^{\text{FLM}} = \pi/m_{\pi}^2 \simeq 60 \text{ mb}$, see Section 20.7,

$$\sigma_{\text{tot}} \leq \frac{\pi}{m_{\pi}^2} \ln^2 \left(\frac{s}{s_0} \right). \quad (20.34)$$

⁵Strictly speaking the proof of the Pumplin bound is justified only for low mass dissociation. When the masses $M_{1,2}$ become so large (say, $M_i^2 > \sqrt{s s_0}$) that the Good-Walker states $|\phi_i\rangle$, corresponding to two incoming protons overlap, we may face double counting. Therefore, the high mass dissociation will be considered in the next Section, in terms of the multi-Pomeron diagram. Here and in what follows s_0 is a constant which should be defined for a particular theoretical model or fitted from experiment.

The fact that $c=(0.24-0.27)$ mb $\ll c^{\text{FLM}} = 60$ mb demonstrates that even at the LHC we are very far from true high-energy asymptotics⁶, and the observed growth of the cross section is driven by the interactions at relatively large transverse momenta $k_t \gg m_\pi$ rather than the smallest hadron mass m_π in the denominator of Eq. (20.34).

20.3.3.1 The t -slope and dip in the elastic cross section

We first start with a relatively small one-Pomeron amplitude and consider the two-Pomeron contribution corresponding to the Ω^2 term in the expansion of the eikonal $1 - \exp(-\Omega/2)$. In this term the momentum transferred, $q_t = \sqrt{|t|}$, is divided between the two Pomerons so that each Pomeron carries about a momentum $q_t/2$. Correspondingly, the t dependence of the whole ‘two-Pomeron’ amplitude will be $\exp(2B(t/4)) = \exp(Bt/2)$ ⁷.

Since the two-Pomeron contribution has an opposite sign in comparison with the one-Pomeron exchange, their interference will result in the appearance of the first diffractive minimum which moves to smaller $|t|$ with energy increasing. Such interference effects are largely responsible for the zero in the imaginary part of the amplitude (with the minimum filled by the real part).

It is worth mentioning that the one-channel eikonal discussed so far is a rather oversimplified approximation. It provides some indications about the behaviour we may expect for the elastic cross section, but clearly it does not give the whole story. Moreover, even within the framework of the one-channel eikonal, the expectation for the elastic slope t -dependence could be masked by other effects. Firstly, there is no reason why the t -dependence of the proton-Pomeron coupling $g_N(t)$ has to be a pure exponent. Next, there exists a two-pion singularity at $t = 4m_\pi^2$ (close to the physical region) in the Pomeron trajectory which generates some curvature in the behaviour of $d\sigma_{el}/dt$ [50–52]. So there may be some compensation between the effects caused by the eikonal (arising from the interference between the different multi-Pomeron contributions), and the curvatures coming from the form of the proton-Pomeron coupling and the two-pion singularity of the Pomeron trajectory. However, an exact compensation looks quite non-trivial and a *pure* exponential behaviour of $d\sigma_{el}/dt$ looks highly unlikely.

Indeed, the measurements by the TOTEM collaboration at 8 TeV [53] and at 13 TeV [54] clearly demonstrate that the local slope of the elastic pp cross section,

$$B = d[\ln(d\sigma_{el}/dt)]/dt, \quad (20.35)$$

at $-t \lesssim 0.3$ GeV² varies with t .

20.3.3.2 High mass dissociation

Let us turn to inelastic diffractive processes that is, to single and double proton dissociations, $pp \rightarrow X+p$ and $pp \rightarrow X_1+X_2$, where the $+$ sign denotes the presence of a LRG in the distribution of final state particles. For example, for the diffractive dissociation of a proton into a system of mass M , the rapidity gap between the incoming proton and the remaining hadrons is

$$\Delta y = \ln\left(\frac{s}{M^2}\right) = \ln\left(\frac{1}{\xi}\right), \quad (20.36)$$

where $\xi = 1-x$ and x is the initial momentum fraction (Feynman variable) carried by the outgoing proton. The masses, M , of the diffractively excited states, produced in high \sqrt{s} collisions, can be large. To separate dissociation from the common inelastic process, usually the condition $M^2 \ll s$ is imposed.

The simplest multi-Pomeron diagram used to describe the diffractive dissociation is the so-called triple-Pomeron graph, shown at the end of Fig. 20.2.

In the Regge pole model, the cross section for the inclusive single diffractive (SD) dissociation process [55–57] can be written

in the form (see Fig. 20.2)

$$\begin{aligned} \frac{\xi d\sigma_{\text{SD}}}{dt d\xi} &= \frac{M^2 d\sigma_{\text{SD}}}{dt dM^2} \\ &= \frac{g_{3\mathbb{P}}(t)g_N(0)g_N^2(t)}{16\pi^2} \left(\frac{s}{M^2}\right)^{2\alpha_{\mathbb{P}}(t)-2} \left(\frac{M^2}{s_0}\right)^{\alpha_{\mathbb{P}}(0)-1}, \end{aligned} \quad (20.37)$$

where $g_{3\mathbb{P}}(t)$ is the triple-Pomeron coupling. The value of the coupling $g_{3\mathbb{P}}$ is usually obtained from a triple-Regge analysis of lower energy data (see e.g. [34]).

In an analogous way the cross section for double dissociation reads

$$\begin{aligned} \frac{\xi_1 \xi_2 d\sigma_{\text{DD}}}{dt d\xi_1 d\xi_2} &= \frac{M_1^2 M_2^2 d\sigma_{\text{DD}}}{dt dM_1^2 dM_2^2} \\ &= \frac{g_{3\mathbb{P}}^2(t)g_N^2(0)}{16\pi^3} \left(\frac{ss_0}{M_1^2 M_2^2}\right)^{2\alpha_{\mathbb{P}}(t)-2} \left(\frac{M_1^2 M_2^2}{s_0^2}\right)^{\alpha_{\mathbb{P}}(0)-1}, \end{aligned} \quad (20.38)$$

where t is the momentum squared transferred through the LRG. As discussed in Section 20.5, from a microscopic point of view the

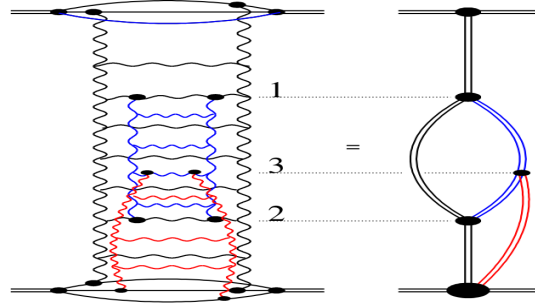


Figure 20.4: Pomeron exchange with schematic diagrams for the enhanced and semi-enhanced exchanges.

Pomeron exchange is described by a set of ladder-type diagrams (see [58–60]), which can lead to a rescattering of the intermediate partons (produced inside this ladder during the evolution), see Fig. 20.4. The left plot shows the Pomeron exchange complemented with the rescattering of partons 1 and 2 and the scattering of a parton 3 on the target. In terms of multi-Pomeron exchanges this corresponds to the diagram on the right hand side, where the Pomeron exchange is shown by the double line of a corresponding colour. The blue one is called ‘enhanced’ (its contribution is integrated over the rapidities of both upper and lower vertices, i.e. of partons 1 and 2). The loop formed by the Pomerons shown in red is called ‘semi-enhanced’ (it is integrated over the rapidity of one intermediate parton).

While the rescattering of the incoming hadron (proton) is already embedded in the eikonal formula (Eq. (20.13)), the rescattering of the intermediate partons in RFT is accounted for by the so-called enhanced diagrams⁸ with multi-Pomeron vertices, g_m^n , which couple m to n Pomerons. It is quite a challenging task to resum all the enhanced diagrams, however this was successfully performed within the framework of the QGSJET Monte Carlo [61]. An elegant approach to sum up all enhanced diagrams in the case when each extra effective Pomeron contribution is very large was proposed in [62], assuming the analyticity of the g_m^n vertices in n and m in the right half of the complex n - and m -planes. The resulting amplitude becomes a black disk.

The simplest triple-Pomeron vertex $g_2^1 = g_{3\mathbb{P}}$ produces the first multi-Pomeron graph considered above (see the end of Fig. 20.2). However, numerically the multi-Pomeron vertices are relatively small. Note also that the value of $g_{3\mathbb{P}}$, determined from the fit to

⁶As usual, we assume $s_0 = 1$ GeV², but the qualitative conclusion does not depend on any realistic choice of s_0 .

⁷The two-Pomeron contribution has a factor of two smaller t -slope, and in terms of the impact parameter, the $\Omega^2(b)$ term is concentrated in the domain of a smaller radius. In such a simplified picture, the impact parameters corresponding to an exchange of n Pomerons will rapidly decrease with n increasing.

⁸This contribution is *enhanced* due to the large parton multiplicity.

experimental data (e.g. [63]), is actually an effective vertex with coupling

$$g_{\text{eff}} = g_{3\mathbb{P}} \langle S^2 \rangle, \quad (20.39)$$

which already includes the survival factor $S^2(b)$, see Eq. (20.15).

Since the opacity Ω increases with energy, at large Ω the number of multiple interactions grows as $N \propto \Omega$, leading to a smaller S^2 . An explicit analysis [64] accounting for the survival effects gives a coupling $g_{3\mathbb{P}}$ about a factor of 3 larger than g_{eff} , namely $g_{3\mathbb{P}} \simeq 0.2g_N$.

Recall that the Pomeron exchange simultaneously describes both the elastic scattering amplitude, T_{el} , and the multiparticle production cross section, G_{inel} . The discontinuity (*disc* T_{el}) of the ladder diagram corresponds to the production of secondary particles, practically homogeneously distributed over the whole available rapidity interval covered by the Pomeron, as illustrated by the right-hand diagram in Fig. 20.5.

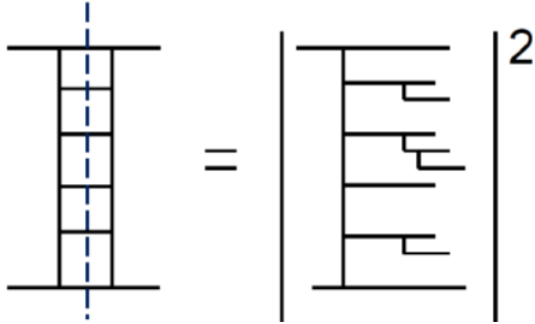


Figure 20.5: Cut Pomeron contribution to the inelastic cross section.

For the one-Pomeron case this discontinuity is called the ‘‘cut Pomeron’’. Correspondingly each multi-Pomeron diagram describes a series of different processes. Cutting k Pomerons in the diagram with n Pomerons we get the inelastic interaction with the multiplicity (density of secondaries) k times larger than that, N_0 , produced by one cut Pomeron, $dN/dy = k \cdot N_0$. The remaining $n - k$ (elastic) Pomerons account for the absorptive corrections to the subprocess with k cut Pomerons. Indeed, the contribution of the diagram with n Pomerons includes also the processes with larger, $(k + i) \cdot N_0$ multiplicities (cut Pomerons), where $(i = 1, 2, \dots, n - k)$. Absorptive corrections, described by the remaining elastic Pomerons, play a role of the survival factor S^2 for the process with the fixed particle density $k \cdot N_0$. They ensure probability conservation (the sum of the probabilities of all possible different channels is equal to one) and restore unitarity. Note that the multi-Pomeron diagrams represent all possible interactions between partons from the protons and partons from the Pomerons. In the case of Monte Carlo generators, the non-enhanced multi-Pomeron contributions are included in terms of the multiple parton interaction (MPI) option, see [13,65] and Section 7.2 in [2]. However, as a rule, this option accounts mainly for the multiple interactions between the partons from the protons (incoming hadrons). The energy-momentum sharing between the various inelastic rescattering processes (including the cut and uncut Pomerons) was performed at the amplitude level within the EPOS Monte Carlo [66].

20.3.3.3 AGK cutting rules

The relation between the cross sections of subprocesses with a different number of cut Pomerons within a given diagram with n Pomerons is given by the AGK (Abramovsky-Gribov-Kancheli [67]) cutting rules. These rules include also the cut *between* the Pomerons with $k = 0$ which corresponds to the contribution of the particular diagram to the elastic cross section. By applying these rules, it is possible to show the self-consistency of the approach, which was lacking in the pure Regge-pole model.

Consider a diagram where the elastic scattering amplitude is mediated by an exchange of n Pomerons. The AGK cutting rules specify the coefficients c_n^k arising when k of these Pomerons are cut. Recall that the Pomeron cut discontinuities give the

corresponding inelastic contributions to σ_{tot} . The terms with $k = 0$ correspond to the diffractive cutting of the diagram (that is, the cut is between the Pomeron exchanges, and not through the Pomerons themselves), while the terms with $k = 1, 2, \dots$ describe the processes with k cut Pomerons. The coefficients $c_n^k = \sigma_n^k / |\sigma_{\text{tot}}^{(n)}|$ are ⁹

$$c_n^{k=0} = (-1)^n (2^{n-1} - 1), \quad c_n^{k \neq 0} = (-2)^{n-1} \frac{(-1)^{k-1} n!}{k!(n-k)!} \quad (20.40)$$

where $\sigma_{\text{tot}}^{(n)}$ denotes the contribution of the n -Pomeron diagram to the total cross section. Note the alternating sign of $\sigma_{\text{tot}}^{(n)}$ expressed as $(-1)^{n-1}$.

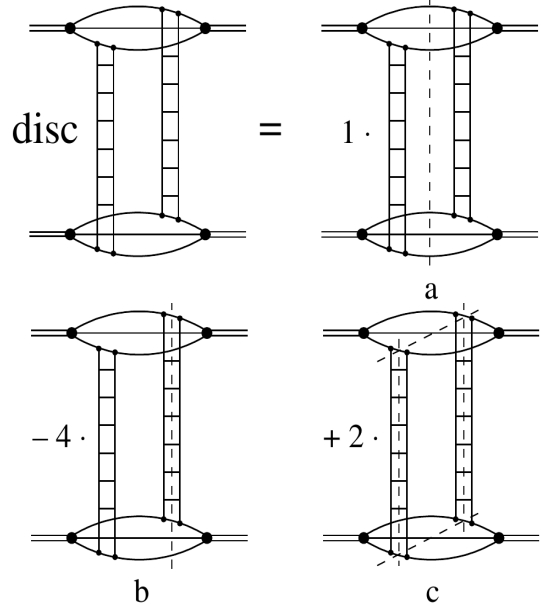


Figure 20.6: Two-Pomeron exchange diagram as a sum of different AGK cuts shown by the dashed lines.

For the two-Pomeron exchange, $n = 2$, the coefficients are $+1$, -4 , or $+2$ according to whether $k = 0, 1$ or 2 Pomerons are cut, respectively. As shown in Fig. 20.6, the amplitude of the two-Pomeron exchange corresponds to a sum of three processes: i) inelastic interaction with particle density twice that caused by one Pomeron (see Fig. 20.6(c)) which enters with the coefficient ‘2’, ii) shadowing (absorptive) correction to the one-Pomeron exchange contribution, which corresponds to events with a single Pomeron density (only one Pomeron is cut), see Fig. 20.6(b), which enters with a factor ‘-4’, and iii) diffractive elastic scattering or proton dissociation (when different components of the proton wave function correspond to different interaction cross sections), caused by the distortion of the incoming plane wave, see Fig. 20.6(a).

Note that the inclusive cross section is not affected by the multi-Pomeron contribution: $2 \times (2) + 1 \times (-4) = 0$. This is a general property of the AGK rules valid for any number of Pomerons n . Thus in order to calculate the inclusive single-particle cross section, it is sufficient to consider just the *one*-Pomeron exchange diagram.

Let us emphasize that the AGK rules provide a framework to consistently work with multi-Pomeron diagrams, that is, with the Regge cuts, accounting for their contributions to different processes (elastic scattering and diffractive dissociation, inelastic events with different densities, dN/dy , of secondaries, etc.).

Measurements of diffractive dissociation cross sections have been made in a wide range of pre-LHC energies, see e.g. [68–73]. At the LHC, cross sections of events with a LRG were measured by the ATLAS, CMS and ALICE collaborations at 7 and 8 TeV,

⁹In their complete form the AGK cutting rules were implemented in the QGSJET Monte Carlo [61].

see [74–77]. ATLAS [78] and CMS and TOTEM [79] presented first measurements of SD cross sections at 8 TeV with a tagged forward proton. While ATLAS measured inclusive SD cross section, CMS and TOTEM studied SD dijet production. Note that in [78] the measured slope $B = 7.65 \pm 0.34 \text{ GeV}^{-2}$ of the inclusive SD cross section as well as the differential distributions $\frac{d\sigma_{\text{SD}}}{dt d\xi}$ for $0.0001 \leq \xi \leq 0.025$ are (within the experimental uncertainties) in a good agreement with the theoretical expectations [29,80]. Moreover a relatively small (in comparison with the $d\sigma_{\text{el}}/dt$) slope B indicates that the size of the triple-Pomeron vertex is much smaller than the proton size.

20.3.4 Central Diffractive processes

Processes $pp \rightarrow p + X + p$, where an object X , produced in the central rapidity region, is separated from the outgoing protons by a LRG on each side, are called Central Exclusive Production (CEP). They are described by the double Pomeron exchange (DPE) diagrams. When the mass of the central system, M_X , is large and the interaction in the M_X region can be described by Pomeron exchange, the corresponding cross section reads

$$\frac{\xi_1 \xi_2 d\sigma^{\text{CEP}}}{d\xi_1 dt_1 d\xi_2 dt_2} = \frac{g_N^2(t_1) g_N^2(t_2)}{(16\pi^2)^2} \left(\frac{1}{\xi_1}\right)^{2\alpha_{\mathbb{P}}(t_1)-2} \left(\frac{1}{\xi_2}\right)^{2\alpha_{\mathbb{P}}(t_2)-2} \times g_{3\mathbb{P}}^2(0) \left(\frac{M_X^2}{s_0}\right)^{\alpha_{\mathbb{P}}(0)-1}. \quad (20.41)$$

If the mass M_X is not too large or for the cases (such as exclusive Higgs boson or dijet production) where the mass M_X is comparable with the corresponding hard scale, the last factor $g_{3\mathbb{P}}^2(0)(M_X^2/s_0)^{\alpha_{\mathbb{P}}(0)-1}$ should be replaced by the corresponding ‘Pomeron-Pomeron cross section’, see for instance [81,82].

Note that equations (20.37), (20.38) and (20.41) are written in a simplified way without accounting for absorptive corrections. That is, the cross sections in equations (20.37) (20.38) and (20.41) should be multiplied by the gap survival factor S^2 (see Eq. (20.15)).

Since the QCD Pomeron is built mainly from gluons it is natural to search for glueballs in double Pomeron exchange processes, and in particular, in CEP.

Resonance production in the Pomeron-Pomeron fusion was extensively studied at the CERN ISR at \sqrt{s} from 22 GeV to 63 GeV (see for reviews [82–84]) and, after the ISR closure in 1983, in fixed target experiments at the CERN SPS [85] and E690 at the Tevatron [86,87]. Glueballs were actively searched for and the properties of the f_0 and f_2 production studied in detail using multiparticle spectrometers, such as the Omega facility at the CERN SPS experiments (WA76, WA91 and WA102), see for a review [85].

An important property of CEP processes, which can be expected from matching with the perturbative QCD LO (leading order) calculation, is the $J_z = 0$ dominance. Perturbatively, for the CEP of a heavy object, the leading contribution comes from a configuration with the projection of this object spin onto the beam axis $J_z = 0$ [81]. Note that the CEP cross section is suppressed at large M_X by a strong bremsstrahlung off the incoming gluons (from the Pomeron) which would violate the ‘exclusivity’. The small probability of not having such radiation is described by the Sudakov suppression factor, T_{Sud} , [88], see [81] for details.

20.3.5 Diffractive parton distributions

Selecting in Deep Inelastic Scattering (DIS) events with a LRG (see e.g. [89,90]) or detecting the leading proton (see Section V.C. in the review [91]) we can study the parton (quark and gluon) distributions of the Pomeron¹⁰. In other words, such events can be treated as DIS on the Pomeron target with the incoming Pomeron flux given by

$$f_{\mathbb{P}}(x_{\mathbb{P}}) = \int dt \frac{g_N^2(t)}{16\pi^2} x_{\mathbb{P}}^{2(1-\alpha_{\mathbb{P}}(t))}, \quad (20.42)$$

¹⁰see also Section 18.5 in [1]

where the proton momentum fraction transferred through the Pomeron $x_{\mathbb{P}} = \xi = M^2/s$.

These Pomeron PDFs were extracted from the HERA measurements of ep scattering with leading protons or a LRG and can be used to describe the inclusive production of high E_T dijets or another hard process based on the collinear factorization theorem in the same way as that in non-diffractive collisions (see [91]). The inclusive measurements of these PDFs are described in [92–94], with the combined H1 and ZEUS data using tagged protons analyzed in [95]. The impact of diffractive jet measurements is addressed e.g. in [96] and the measured charm contribution is presented in [97,98]. As far as the parton distributions are known, we can calculate the corresponding inelastic cross section of the Pomeron-proton interaction using one of the ‘general purpose’ Monte Carlo generators (see e.g. [13]), multiply it by the Pomeron flux and compare the obtained result with the Regge formula in Eq. (20.37). This approach provides another way to evaluate the triple-Pomeron vertex $g_{3\mathbb{P}}$. The corresponding analysis was performed in [99] and leads to practically the same (within the error bars) value of $g_{3\mathbb{P}} = 0.2g_N(0)$.

It is worth mentioning that in DIS at large Q^2 we are dealing with small-size objects and the rescattering effects are small. Therefore, the survival factor $S^2 \simeq 1$ and does not affect the results.

20.4 Experimental data on diffraction at high energies

20.4.1 Total and elastic cross sections

The elastic scattering of protons is a process with a special and rather simple experimental signature: the central detector is empty while the incoming protons after the collisions are detected in the dedicated forward proton detectors (FPD) placed far from the interaction point (IP). Elastic scattering data are taken in special runs in order to be able to reach different ranges of t -values and thanks to the very large value of the cross section the data can be collected with a relatively low instantaneous luminosity and hence a negligible pile-up.¹¹

These special runs usually have very few proton bunches and differ in the t range covered, which is governed roughly by the relation $t_{\text{min}} \propto d^2/\beta^*$. Here d is the distance, expressed in multiples of the beam size at the detector, from the centre of the LHC beam and β^* is defined as the distance from the IP to the point where the transverse area of the beam is twice as wide as that at the IP (see Section 31 in [1]). Note that if we work at large β^* , the incoming protons have very small angular divergence leading to small average transverse momentum, which allows us to measure very small $|t|$ values. The lowest $|t|$ values measured so far at the LHC are $4 \times 10^{-4} \text{ GeV}^2$ (ALFA) and $6 \times 10^{-4} \text{ GeV}^2$ (TOTEM) reached with the 8 TeV LHC beam configured with $\beta^* = 1 \text{ km}$ optics. The largest t values of about 4 GeV² were measured by TOTEM at 8 and 13 TeV with $\beta^* = 90 \text{ m}$ thanks to special triggers. Other β^* values used in special runs are 3.5 m, 11 m and 2.5 km.

There are four ways to determine the σ_{tot} value:

1. **Elastic and Inelastic.** This method does not require the optical theorem and hence no extrapolation of $d\sigma_{\text{el}}/dt$ to $t = 0$ and no ρ (defined below Eq. (20.17)) but rather the luminosity and measuring rates N_{el} (elastic) and N_{inel} (inelastic). The total cross section is then simply:

$$\sigma_{\text{tot}} = \frac{1}{\mathcal{L}} (N_{\text{el}} + N_{\text{inel}}). \quad (20.43)$$

Of course, both N_{el} and N_{inel} should be corrected for the detector acceptance and efficiency. This is especially important for N_{inel} since the detectors never cover the whole rapidity region (i.e. the whole 4π).

2. **Elastic only.** This approach necessitates measuring $d\sigma_{\text{el}}/dt$ and using the optical theorem with a known value of ρ . As explained in Section 20.2, the optical theorem states that

¹¹The pile-up is formed by additional pp collisions which typically produce low- p_T particles. These may affect the signal sample and worsen various reconstruction and identification efficiencies.

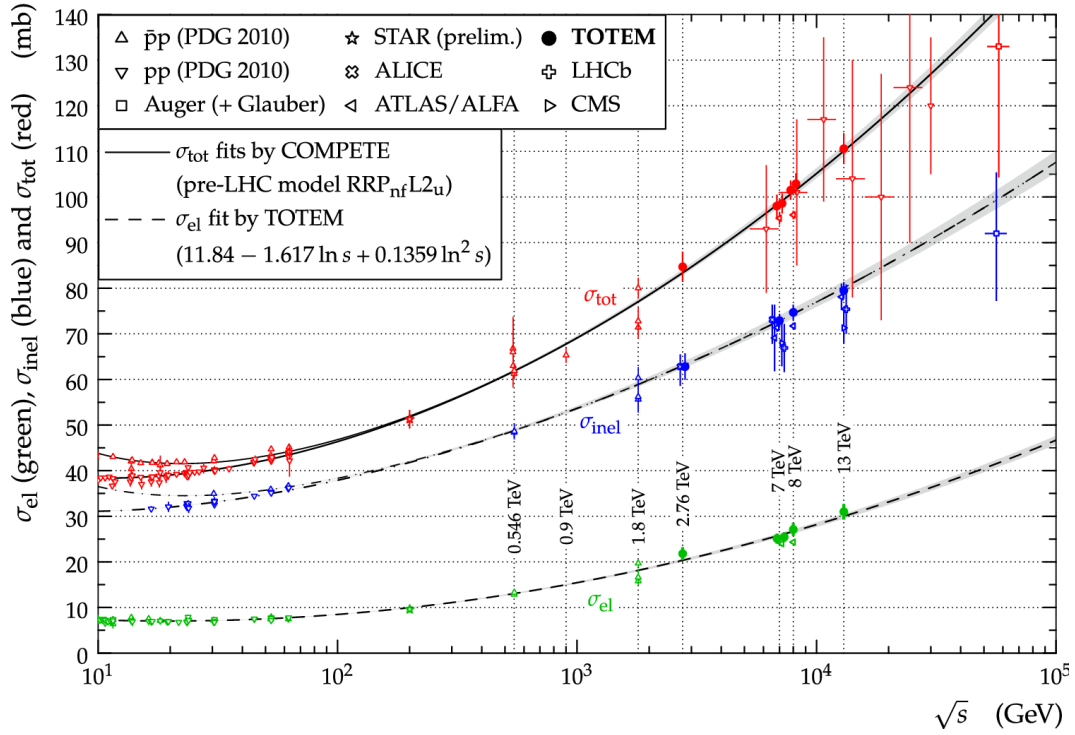


Figure 20.7: Overview of elastic (σ_{el}), inelastic (σ_{inel}) and total (σ_{tot}) cross section data for pp and $p\bar{p}$ collisions as a function of \sqrt{s} . The continuous black lines (lower for pp , upper for $p\bar{p}$) represent the best fits of the total cross section data by the COMPETE collaboration [22]. The dashed line is a fit of the elastic cross section data. The dashed-dotted lines refer to the inelastic cross section and are obtained from the difference between the continuous and dashed lines. Figure from Ref. [100].

$\sigma_{\text{tot}} \propto \text{Im}[T_{\text{el}}(t \rightarrow 0)]$, see Eq. (20.3). Since in practice it is not possible to measure down to $t = 0$, we need to extrapolate. To minimize the model dependence when extrapolating, it is vital to measure down to as low $|t|$ values as possible (i.e. high β^*). This method requires an independent luminosity measurement. Once the luminosity is known, $d\sigma_{\text{el}}/dt$ can be normalized and used to extract σ_{tot} using the formula:

$$\sigma_{\text{tot}}^2 = \frac{16\pi}{1 + \rho^2} \left. \frac{d\sigma_{\text{el}}}{dt} \right|_{t \rightarrow 0}. \quad (20.44)$$

3. **Coulomb normalization.** Similarly to the previous method, this approach relies on the elastic observables only and requires a measurement of the elastic cross section at very low values of $|t|$, where it is sensitive to the theoretically well known Coulomb QED contribution $4\pi\alpha_{\text{QED}}^2/t^2$. The normalization of $d\sigma_{\text{el}}/dt$ is then determined by fitting the experimental data at very low $|t|$ using a formula including the Coulomb amplitude and its interference with the strongly interacting (the so-called nuclear) term. This method has been successfully used by UA4/2 [101] and TOTEM [102].

4. **Luminosity-independent.** This method does not rely on the knowledge of luminosity but rather on the knowledge of N_{el} and N_{inel} and on the optical theorem: combining equations (20.43) and (20.44) with $\frac{d\sigma_{\text{el}}}{dt} = \frac{1}{\mathcal{L}} \frac{dN_{\text{el}}}{dt}$ we get

$$\sigma_{\text{tot}} = \frac{16\pi}{1 + \rho^2} \frac{dN_{\text{el}}/dt|_{t=0}}{N_{\text{el}} + N_{\text{inel}}}, \quad (20.45)$$

where $dN_{\text{el}}/dt|_{t=0}$ corresponds to the extrapolation to $t = 0$ of the nuclear term only. By independently and simultaneously measuring N_{el} and N_{inel} , and applying the optical theorem, we can also determine the luminosity.

The TOTEM [100, 103–105] and ATLAS [106, 107] collaborations at CERN have covered an energy range from $\sqrt{s}=2.76$ TeV to 13 TeV. A compilation of high energy total pp and $p\bar{p}$ cross section measurements is shown in Fig. 20.7 (for discussion of the pre-LHC elastic scattering data see review [108]).

Despite some tension between the Tevatron CDF [109] and E811 [110] data¹² and to a lesser extent between the TOTEM [104, 105] and ATLAS [106, 107] measurements, the data clearly indicate that in the Tevatron – LHC energy interval the total cross section starts to grow *faster* than the power-law parametrization [26] describing the data below the Tevatron energy. In particular, while the DL fit [26] predicts $\sigma_{\text{tot}} = 90.7$ mb at $\sqrt{s} = 7$ TeV, the TOTEM experiment observes 98.6 ± 2.2 mb [104].

A compilation of the high-energy data on the elastic slope is shown in Fig. 20.8. It is clearly seen that in the TeV energy range the slope increases with \sqrt{s} more rapidly than the logarithmic behaviour expected in the case of one-Pomeron exchange, see Eq. (20.30). Such an acceleration of the t -slope derivative, $dB/d \ln s$, is a clear manifestation of the increasing role of the multi-Pomeron exchanges, where asymptotically the slope should rise as $\ln^2 s$, see [117]. Finally, Fig. 20.9 illustrates the energy dependence of the differential elastic pp cross section. As expected (see Section 20.3.3.1), the diffractive dip moves to smaller $|t|$ with increasing energy.

20.4.2 Diffractive vector meson production

The exclusive production of vector mesons was studied in detail at HERA (see for a review [91]). It is well described within the ‘dipole model’ (see for review and references [120]), where the incoming photon first fluctuates into a quark-antiquark, which then interacts with the target proton and, finally, with the probability given by the overlap integral between the vector meson wave function and the outgoing $q\bar{q}$ -pair, the vector meson is produced. The crucial quantity is the value of cross section, $\sigma(q\bar{q} - p)$, of elastic scattering of the $q\bar{q}$ -pair on the proton. The energy behaviour of $\sigma(q\bar{q} - p)$ is driven by the intercept, $\alpha_{\text{eff}}(0)$, of the effective Pomeron¹³ (rightmost singularity in the j -plane), while

¹²The CDF 1.8 TeV point [109] is 2.8σ higher than the corresponding E811 result [110].

¹³Effective Pomeron means that this is not an original pole in the j -plane, but it includes the corrections (renormalizations) caused by the enhanced diagrams (see e.g. [121]).

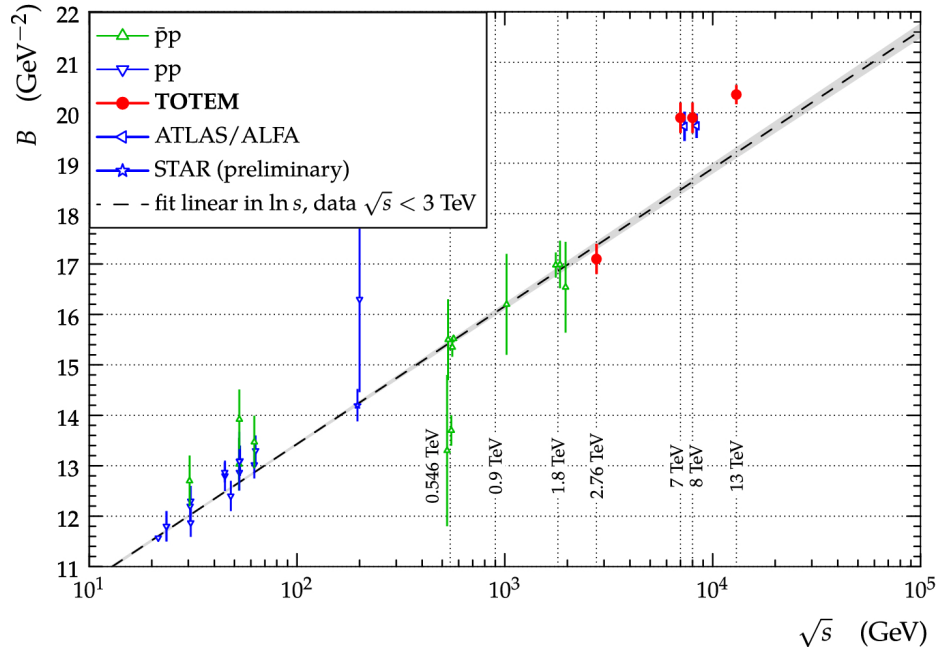


Figure 20.8: The diffractive slope B for pp and $p\bar{p}$ elastic scattering as a function of \sqrt{s} . The experimental uncertainties represent the quadratic sum of statistical and systematic uncertainties. The dashed line is a result of a linear fit to data at $\sqrt{s} < 3$ TeV. The data points come from [103–107, 111–113]. Figure from Ref. [100].

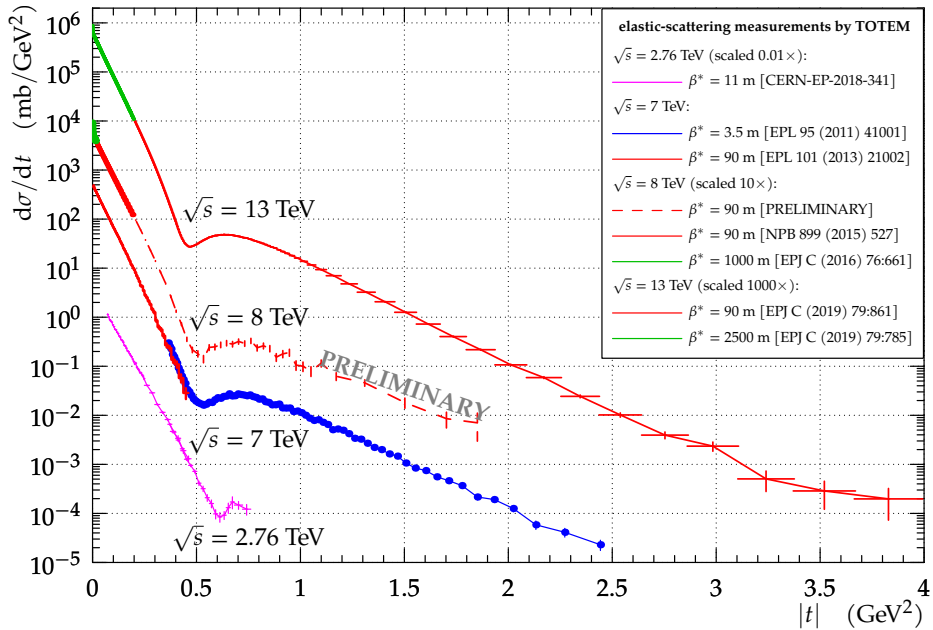


Figure 20.9: The t -dependence of the pp elastic cross section for collision energies $\sqrt{s} = 2.76$ TeV [103], 7 TeV [104, 114], 8 TeV [53, 115, 116] and 13 TeV [54, 102]. The experimental uncertainties represent the quadratic sum of statistical and systematic uncertainties. Figure from Ref. [116].

the value of the cross section depends on the quark separation, r , in the transverse plane, $\sigma(q\bar{q} - p) \propto \alpha_s^2 \langle r^2 \rangle$ [43, 44]. Thus different processes with the same $\langle r^2 \rangle$ are driven by the same $\sigma(q\bar{q} - p)$ cross section.

In the DIS case this separation in turn is controlled by the photon virtuality, Q^2 , and the quark mass, m_q : $\langle r^2 \rangle \simeq 1/(z(1-z)Q^2 + m_q^2)$ (z is the photon momentum fraction carried by the quark). Indeed, the cross section of the ρ meson diffractive production in DIS at $Q^2 = M_{J/\psi}^2$ is close (up to the difference in the quark electric charges) to that for the J/ψ photoproduction, see Fig. 20.10 (Left).

The production cross section depends non-trivially on W , the

energy of the γ^*p center of mass system. It increases with W as W^n , where $n = 0.2$ for ρ, ω and ϕ (light quark)-mesons but $n = 0.8$ for J/ψ . Note that in the J/ψ case the energy dependence is close to that of the BFKL (Balitsky-Fadin-Kuraev-Lipatov) Pomeron [59, 122, 123], that is, the singularity calculated within the leading (and next-to-leading) approximation in perturbative QCD. But at lower scales the absorptive (multi-Pomeron) corrections tame the growth which leads to smaller values of n ([124–127]), see Fig. 20.10 (Right).

A similar situation reveals in the dependence of α_{eff} on Q^2 , as can be seen in Fig. 47 of [91]. At a large scale $\mu^2 = (Q^2 + M_V^2)/4$ the value of $\alpha_{\text{eff}} \simeq 1.3$ is close to the prediction for the QCD

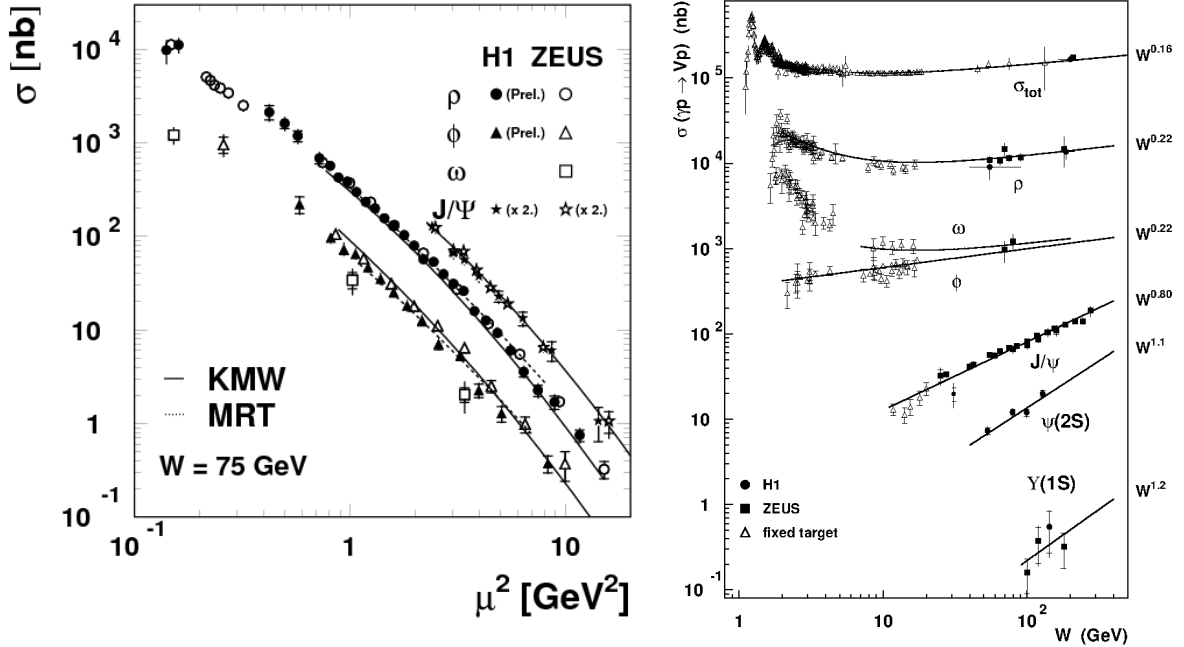


Figure 20.10: (Left) The ρ , ω , ϕ and J/ψ elastic production cross sections as a function of the scale $\mu^2 = (Q^2 + M_V^2)/4$. For readability of the figure, the J/ψ cross sections are multiplied by a factor 2. Figure from Ref. [118]. (Right) Compilation of photoproduction cross section measurements as a function of the γp centre-of-mass energy, W . The total cross section and various vector meson production cross sections are included, with the approximate power law dependences $\sigma \propto W^\delta$ indicated for each process. Figure from Ref. [119].

Pomeron, while for a smaller scale, the absorptive corrections described by the multi-Pomeron diagrams start to reduce the cross section, and α_{eff} decreases.

20.5 Pomeron in QCD

All features described in the previous Sections were based on *first principles*, such as analyticity (based on causality), unitarity, crossing symmetry, etc. Since QCD theory satisfies all these principles it should reveal a corresponding ‘‘Regge’’ behaviour. Indeed, within perturbative QCD there is a Pomeron: an even-signature singularity in the j -plane with vacuum quantum numbers. While in the old Regge theory the Regge trajectories and their couplings were phenomenological numbers fitted from experiment, perturbative QCD allows one to calculate the positions of the singularities and the corresponding couplings with $O(\alpha_s)$ and even with $O(\alpha_s^2)$ accuracy [59, 122, 123, 128–131].

In terms of Feynman diagrams, the QCD Pomeron may be viewed as a sum of multi-particle ladders built by the exchange of two t -channel (reggeized¹⁴) gluons, see the left-hand side of Fig. 20.5.

The sum of ladder diagrams of the type of Fig. 20.5 is the simplest multiparticle structure which reproduces the power-like s^α behaviour of the Pomeron pole. In other words it corresponds to a sum of completely inelastic $2 \rightarrow n$ processes, that is, to the last term $G_{\text{inel}} = 1 - \exp(-\Omega)$ in the unitarity equation (20.9). This set of diagrams was resummed in the limit of a small QCD coupling, $\alpha_s \ll 1$, but large energy, such that $\alpha_s \ln(s/s_0) \sim O(1)$ [59]. The summation results in the rightmost singularity at $j = 1 + \omega_0 > 1$. After accounting for the next-to-leading logarithmic (NLL) corrections, the position of the singularity (Pomeron intercept) corresponds to $\omega_0 = 0.25\text{--}0.3$ depending only weakly on the scale [122, 123, 132–136], whose value is characterized by the transverse momentum, k_t , of gluons in the ladder.

It was demonstrated (see e.g. [137]) that the resummation of

the $(\alpha_s \ln(1/x))^n$ terms based on the QCD Pomeron results essentially improves the description of low- x inclusive HERA data within the framework of the NNLO DGLAP evolution.

At this stage the singularity is the cut in the j -plane. However we have to account for the boundary conditions at relatively small k_t . Imposing a reasonable boundary, we arrive at a series of Regge poles in the interval from $j = 1$ to $j = 1 + \omega_0$ instead of the cut [134]. Note that the first (corresponding to the rightmost pole in the j -plane, i.e. to the pole with the largest $\text{Re } j$) eigenfunction consists of gluons with relatively small k_t , while for the next poles the k_t increases. DIS inclusive $\gamma^* p$ cross sections were fitted in [135] using the QCD based approach in which Pomeron is represented by series of Regge poles obtained within the perturbative QCD BFKL approach. It was concluded that the first pole has a small coupling to the proton. It is possible that this small value of the coupling to the proton is related to the fact that the enhanced multi-Pomeron diagrams (i.e. the rescattering of intermediate partons) were neglected in the fit. The main effect of this enhanced contribution is the ‘‘renormalization’’ of the intercept which diminishes the effective value of ω_0 . Besides this, the enhanced diagrams provide a saturation by reducing the rise of the parton densities in the (b, k_t, y) -space (see e.g. [138, 139]).

Note that perturbative QCD allows us to understand why the values of the phenomenological multi-Pomeron vertices and the shift, ω_0 , of the intercept, are small (due to $\alpha_s \ll 1$ and some numerical factors such as N_c and π). Indeed, at the lowest α_s orders we get for the ω_0 value and the simplest multi-Pomeron vertices (see e.g. [59, 139, 140]):

$$\omega_0 \propto \frac{N_c \alpha_s}{\pi}, \quad g_{3\mathbb{P}} \propto \frac{N_c \alpha_s^2}{(N_c^2 - 1)\pi^2} \quad \text{and} \quad g_2^2 \propto \frac{N_c \alpha_s}{(N_c^2 - 1)^2}, \quad (20.46)$$

where g_2^2 is the coupling corresponding to the transition of 2 into 2 Pomerons.

20.5.1 BFKL evolution in the ‘dipole’ representation

It was shown in [141–144] that the LO BFKL Pomeron equation [59] can be written in terms of the evolution of the dipole

¹⁴That is, the virtual loop corrections to the one-gluon exchanges are included. These corrections are important in order to provide infrared stability of the results.

density, $N(x_d, y_d; y)$, in rapidity y (here x_d and y_d are the transverse coordinates of two t -channel gluons which form the colour singlet dipole). Indeed, after the emission of a new gluon at point z_d , the initial colour dipole with coordinates (x_d, y_d) turns into a pair of dipoles (x_d, z_d) and (z_d, y_d) . This can be considered as a development of a ‘dipole cascade’. Moreover in this formalism it is easy to include the non-linear absorptive corrections (last term in the square brackets in Eq. (20.47)), which accounts for the rescattering of the intermediate partons (gluons) on the target proton. The corresponding contribution is described by the so-called ‘fan’ diagrams and these are the most important corrections to the linear DGLAP (Dokshitzer-Gribov-Lipatov-Altarelli-Parisi) evolution [145] in the case of DIS at not large scales but at very small momentum fraction [139].

The resulting non-linear evolution (Balitsky-Kovchegov equation [146–148]) reads

$$\begin{aligned} \frac{d}{dy} N(x_d, y_d; y) &= \frac{\alpha_s N_c}{2\pi^2} \int d^2 z_d \frac{(x_d - y_d)^2}{(x_d - z_d)^2 (y_d - z_d)^2} \\ &\times [N(x_d, z_d; y) + N(y_d, z_d; y) - N(x_d, y_d; y) \\ &\quad - N(x_d, z_d; y)N(y_d, z_d; y)] . \end{aligned} \quad (20.47)$$

For a small density N the last term in the square brackets can be neglected, and the first three terms in Eq. (20.47) reproduce the conventional BFKL equation in the coordinate representation. However, for large $N \rightarrow 1$ the right-hand side of Eq. (20.47) vanishes and we reach the saturation $N = 1$. It is worth mentioning that, as shown in [149], in terms of ‘dipole’ formalism, with the triple-Pomeron vertex generated by the ‘one dipole to two dipoles’ transition, it is possible to relate the Good-Walker approach to high mass diffraction with the triple-Pomeron diagram.

20.5.2 Distribution of secondaries: theory versus experiment

As already discussed, in terms of Feynman diagrams the cut Pomeron can be viewed as a set of ladder diagrams corresponding to a sum of completely inelastic $2 \rightarrow n$ processes, that is, to the last term $G_{\text{inel}} = 1 - \exp(-\Omega)$ in the unitarity equation (20.9). Here $n > 2$ means the production of additional $(n - 2)$ gluons which, after hadronization, form minijets.¹⁵ Therefore, in the final state driven by one Pomeron, we expect to observe gluon minijets with a flat rapidity distribution in the central (plateau) rapidity region. This would correspond to a flat pseudorapidity distribution of produced particles if they were massless. A typical pseudorapidity distribution of charged particles in inclusive events (up to $|\eta| = 7$) is shown in Fig. 20.11 (left) [150] (see also Fig. 5.3.1 in [1]). The central part ($|\eta| < 2.5$) was measured by CMS, while the forward region was covered by TOTEM. The dip observed at $\eta = 0$ is explained by the presence of massive particles (the Jacobian $J(p_T, m, \eta) = p_T/E \rightarrow p_T/\sqrt{p_T^2 + m^2}$ at $\eta = 0$). A photon energy spectrum is shown in Fig. 20.11 (right) [151], measured by LHCf inclusively and in events with a diffraction topology, i.e. no charged particles with $p_T > 100$ MeV and $|\eta| < 2.5$ observed by ATLAS. As expected in diffractive events the energy flow decreases with E_γ more slowly than that in the inclusive case.

The energy dependence of the particle density $dN_{\text{ch}}/d\eta$ at $\eta = 0$ is shown in Fig. 20.12 (left). Neglecting absorptive corrections given by the enhanced diagrams (which mainly change (‘renormalize’) the effective Pomeron intercept $\alpha_{\text{eff}}(0) = 1 + \Delta$ [121]), we conclude that according to the AGK rules the plateau height $d\sigma/d\eta \propto s^\Delta$ is driven just by the one-Pomeron exchange with effective $\Delta \sim 0.2$ (see Section 20.3.3.3). That is, the density of secondaries observed in the inclusive process increases with increasing energy faster than the total cross section, whose growth is tamed by the multi-Pomeron diagrams. Indeed, as is seen from Fig. 20.12 (left), in the interval of collider energies $dN_{\text{ch}}/d\eta = (1/\sigma_{\text{inel}})d\sigma/d\eta \propto s^{0.115}$ (i.e. $d\sigma/d\eta \propto s^{0.215}$), while $\sigma_{\text{inel}} \propto s^{0.1}$.

¹⁵Minijets result from hadronization of partons emitted from the cut QCD Pomeron. Typically these are groups of hadrons with comparatively low overall $E_T \lesssim 5\text{--}10$ GeV.

Contrary to the ‘old’ Regge theory where it was *assumed* (based on the experimental data existing in the 1950s and 1960s) that all transverse momenta are limited, in QCD the k_t distributions of jets (charged particles) have a long k_t tail ($d\sigma/dk_t^2 \propto \alpha_s^2(k_t^2)/k_t^4$ at large k_t and very large energy $s \gg k_t^2$). An example of the p_T distribution of charged secondaries is shown in Fig. 20.12 (right).

Note that the mean transverse momentum of secondaries, produced via jet fragmentation, slowly increases with collision energy, see Fig. 20.13 (right). This is caused by the stronger absorption (at larger \sqrt{s}) of the gluons with a smaller k_t ($\sigma^{\text{abs}} \propto 1/k_t^2$). The growth of $\langle p_T \rangle$ with multiplicity (see Fig. 20.13 (left)) can be explained by the fact that events with larger N_{ch} correspond to a smaller impact parameter, b , where the absorption of a low k_t component is stronger and, next, larger multiplicity can be originated by the events with jets/minijets with higher p_T . Since the mean p_T of secondaries grows with \sqrt{s} , the increase with \sqrt{s} of transverse energy flow is a bit faster than that of particle density.

The model [162] based on a modification of the classic RFT allows one to trace the smooth transition from the pure perturbative, large k_t , region into the *soft* domain. A strong absorption of the low k_t partons plays a crucial role here since it produces an effective infrared cutoff, k_{sat} , and provides the possibility of extending the parton approach, used for ‘hard’ processes, to also describe high-energy soft and semihard interactions. This approach combines a description of soft physics and diffraction with jet physics in a coherent self-consistent way.

Another way is to include the soft and hard components independently [37, 66, 163, 164]. In this approach the soft part is described in terms of RFT with the phenomenological ‘soft’ Pomeron pole while the hard part is calculated in terms of the parton model for minijet production with the energy dependent cutoff $k_t > k_0(s)$. A combined description of soft and hard processes in hadronic collisions is reached within the QGSJET Monte Carlo model (e.g. [61]) in the framework of the so-called ‘semihard Pomeron’ approach (see e.g. [165]).

In [166] a model was constructed, which incorporated the attractive features of the two successful theoretical approaches to high energy QCD: BFKL Pomeron calculus [59,60] and the Colour Glass Condensate/saturation [167].

20.5.2.1 Correlations

All LHC experiments routinely measure tracks with $p_T > p_{\text{min}}$, where p_{min} can vary in different studies. Typically, $p_{\text{min}} = 200$ MeV, where tracking reconstruction efficiencies are larger than 70%. In order to identify particle species, each experiment has sophisticated identification procedures usually based on the ionization energy loss, dE/dx , or other techniques, with different regions of applicability for different particle species. Thanks to usually relatively large cross sections of soft QCD processes, most of the results below come from event samples with very low or negligible pile-up.

Following the notation in [168], symmetrized inclusive particle number densities for q points at y_1, \dots, y_q (where y_i represents the 4-momentum of the i th particle), $\rho_q(y_1, \dots, y_q)$, are related to the inclusive differential cross section by

$$\frac{1}{\sigma_{\text{inel}}} d\sigma = \rho_1(y)dy, \quad \frac{1}{\sigma_{\text{inel}}} d^2\sigma = \rho_2(y_1, y_2)dy_1 dy_2 \quad \text{etc.} \quad (20.48)$$

By integrating we get

$$\int \rho_1(y)dy = \langle n \rangle, \quad \iint \rho_2(y_1, y_2)dy_1 dy_2 = \langle n(n-1) \rangle \quad \text{etc.}, \quad (20.49)$$

where the angular brackets denote averaging over the event sample and n is the particle multiplicity.

Since the inclusive q -particle densities in general contain trivial contributions from lower-order densities, it is convenient to consider quantities C_q which vanish when one of their arguments becomes statistically independent of (uncorrelated with) the others. These quantities C_q , called correlation functions (or cumulant

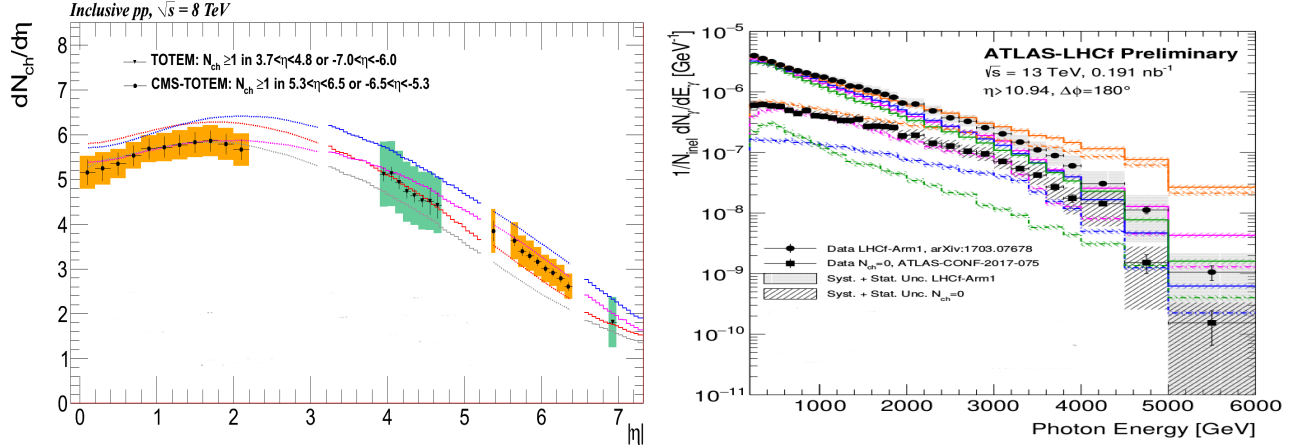


Figure 20.11: (Left) Charged-particle pseudorapidity distribution for inclusive events measured by CMS and TOTEM [150]. The error bars represent the statistical and uncorrelated systematic uncertainties between neighboring bins, while the shaded areas denote the combined statistical and full systematic uncertainties. The coloured lines indicate model predictions. (Right) Photon energy spectrum measured by LHCf at $|\eta| > 10.94$. The filled circles show the inclusive photon spectrum measured by LHCf [152] and filled squares the spectrum for $N_{ch} = 0$ events where no charged particles with $p_T > 100$ MeV and $|\eta| < 2.5$ are observed by ATLAS [153]. The coloured lines indicate model predictions. The error bars correspond to the statistical uncertainties and the shaded areas denote the combined statistical and systematic uncertainties. Figure from Ref. [151].

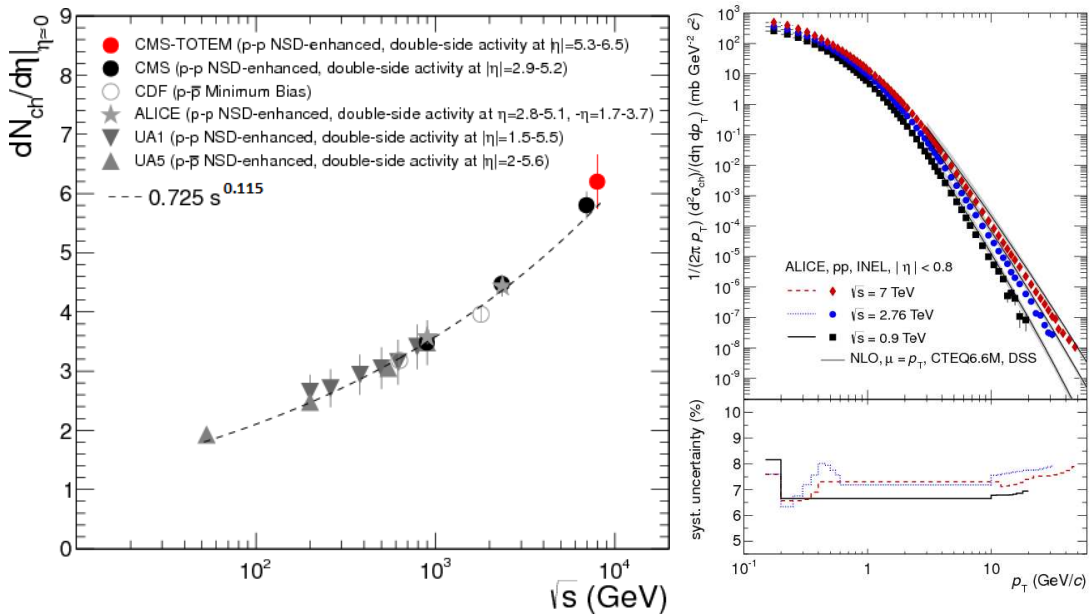


Figure 20.12: (Left) Energy dependence of the charged particle density $dN_{ch}/d\eta$ at $\eta \approx 0$ for pp and $p\bar{p}$ collisions. Shown are measurements performed with different Non-SD event selections from UA1 [154], UA5 [155], CDF [156,157], ALICE [158] and CMS [159]. The dashed line is a power-law fit to the data. Figure from Ref. [150]. (Right) Differential cross section of charged particles with $|\eta| < 0.8$ in inelastic pp collisions at $\sqrt{s} = 0.9, 2.76$ and 7 TeV as a function of p_T . Only statistical uncertainties are shown. Figure from Ref. [160].

functions), are defined as:

$$\begin{aligned}
 C_2(1, 2) &= \rho_2(1, 2) - \rho_1(1)\rho_1(2), \quad C_3(1, 2, 3) \\
 &= \rho_3(1, 2, 3) - \sum_{(3)} \rho_1(1)\rho_2(2, 3) + 2\rho_1(1)\rho_1(2)\rho_1(3), \\
 C_4(1, 2, 3, 4) &= \rho_4(1, 2, 3, 4) - \sum_{(4)} \rho_1(1)\rho_3(1, 2, 3) \\
 &\quad - \sum_{(3)} \rho_2(1, 2)\rho_2(3, 4) + 2 \sum_{(6)} \rho_1(1)\rho_1(2)\rho_2(3, 4) \\
 &\quad - 6\rho_1(1)\rho_1(2)\rho_1(3)\rho_1(4).
 \end{aligned} \tag{20.50}$$

The 2D two-particle correlation function is defined as

$$C(\Delta\eta, \Delta\phi) = \frac{\rho_2(\Delta\eta, \Delta\phi)}{\rho_1(\eta_a, \phi_a)\rho_1(\eta_b, \phi_b)}. \tag{20.51}$$

The distribution $\rho_2(\Delta\eta, \Delta\phi)$ is usually interpreted as a conditional probability to observe a particle a at the phase-space point (η_a, ϕ_a) if a particle b at (η_b, ϕ_b) is observed as well, and $\Delta\eta = \eta_a - \eta_b$ and $\Delta\phi = \phi_a - \phi_b$. The distributions $\rho_1(\eta_a, \phi_a)$ and $\rho_1(\eta_b, \phi_b)$ are probabilities to observe a single particle at (η_a, ϕ_a) and (η_b, ϕ_b) , respectively. The denominator of Eq. (20.51) is constructed as a product of two single-particle distributions using an event mixing technique, where each particle in the pair comes from a different event. Experimentally, each reconstructed track is weighted by the inverse of an efficiency factor which accounts

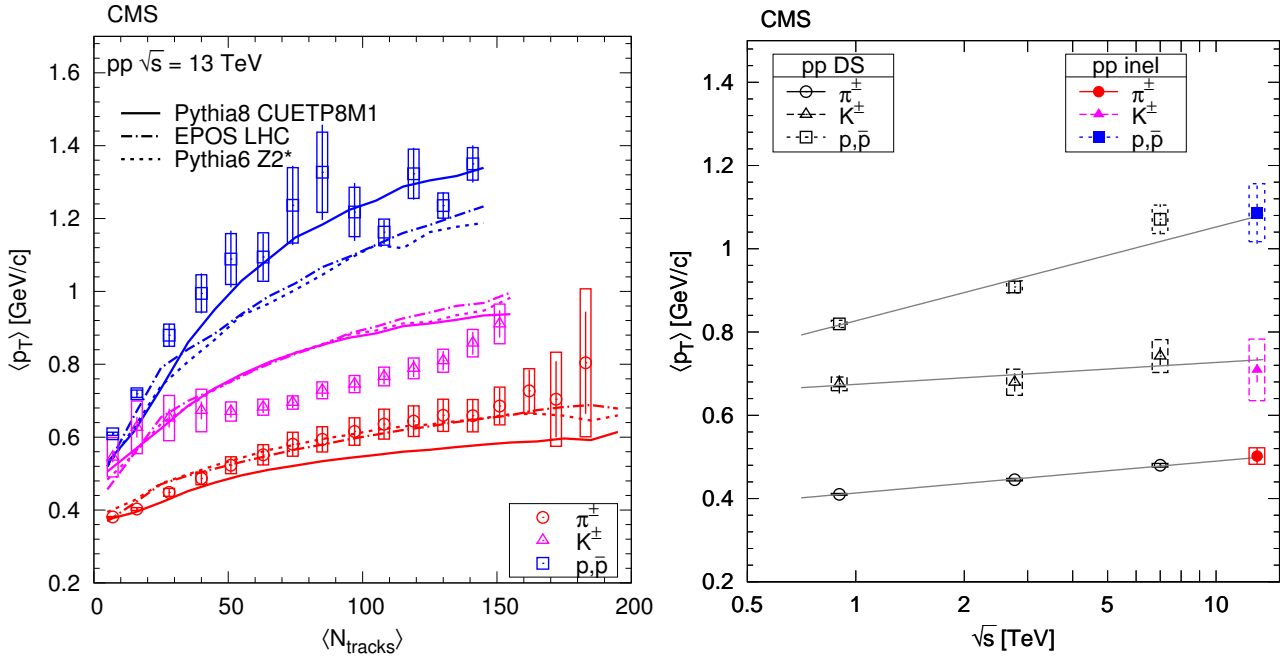


Figure 20.13: Average p_T of pions, kaons and protons in the range $|\eta| < 1.0$ as a function of (left) track multiplicity at $|\eta| < 2.4$ and (right) of center-of-mass energy where the curves show linear fits using lns. The error bars indicate the uncorrelated combined uncertainties, while the boxes show the uncorrelated systematic uncertainties. Figures from Ref. [161].

for the detector acceptance, the reconstruction and particle identification efficiencies, the contamination by secondary particles and the fraction of misreconstructed tracks.

An example of two-particle correlation functions measured in pp collisions at 7 TeV is shown in Fig. 20.14 for identical-particle pairs (right panel) and for particle-anti-particle pairs (left panel) [169].

We observe two distinct features which can be explained by short-range (in rapidity) correlations: 1) a near-side peak at $\Delta\phi \approx 0$ and 2) an away-side peak or rather a ridge at $\Delta\phi \approx \pi$. The near-side peak is considered to be caused by at least three effects:

- *fragmentation of partons scattered at a hard scale.* These relatively high p_T partons produce showers which after the hadronization form the mini-jets which create a broad structure extending over at least one unit in $\Delta\eta$ and $\Delta\phi$.
- *resonance decays.* The decay of resonances contributes to the near-side peak at $\Delta\eta \sim 0$ and extended in $\Delta\phi$ [170–172], depending on the released kinetic energy of the given resonance. This effect is mostly visible for unlike-sign particle pairs.
- *femtoscopic correlations.* The term ‘‘femtoscopic’’ refers to a length scale of the order of 10^{-15} m. These correlations are present at low relative momenta of the particles in a pair (representing a very small phase-space corner, so they are practically invisible in terms of $(\Delta\eta, \Delta\phi)$) and give rise to an enhancement of the correlation function (due to Bose-Einstein quantum statistics for identical bosons) or its suppression (due to Fermi-Dirac quantum statistics for identical fermions). Besides this, at low relative momenta there are correlations caused by Coulomb and/or other final state interactions. The shape of all these effects in $(\Delta\eta, \Delta\phi)$ space depend strongly on the mass of the particle type as well as on the size of the particle-emitting system. The latter is traditionally measured in Bose-Einstein correlation (BEC) analyses and is not part of this review.

The away-side peak originates from energy-momentum conservation which manifests itself by the quark and the anti-quark going back-to-back in ϕ . In this case the rapidity width of the away-side peak is much larger than the near-side peak since in the original matrix element the quark and the antiquark can be separated by some $\Delta\eta$ interval.

As discussed in Sections 20.3.3.2 and 20.3.3.3, there may be several cut Pomerons in the same event, each giving rise to particle sets which are, in general, independent of each other (except for small Bose-Einstein correlations). This leads to long-range (in rapidity) correlations. Since the density of secondaries, dN/dy , is proportional to the number of cut Pomerons, k , the probability to observe at least one particle is proportional to $\langle k \rangle$, while the probability to observe simultaneously two particles separated by some (rather large) rapidity interval is proportional to $\langle k^2 \rangle$. Thus the long-range correlations are predicted to be $C_2 = \langle k^2 \rangle / \langle k \rangle^2 - 1 > 0$ which depends weakly on the separation $\Delta\eta$ between the two particles [173, 174]. In the case of the pure eikonal approach, neglecting the enhanced diagrams and the conservation law effects in the proton fragmentation region, we expect that these long-range correlations,

$$C_2(\Delta y) = \frac{\sigma_{\text{inel}} d^2\sigma/dy_1 dy_2}{d\sigma/dy_1 d\sigma/dy_2} - 1 \sim \text{const}, \quad (20.52)$$

do not depend on the rapidity separation, $\Delta y = |y_1 - y_2|$, between the two particles. The contribution of the processes with more cut Pomerons also results in a much wider multiplicity distribution and in a larger density of soft particles coming from the ‘underlying event’.

20.5.2.2 Color reconnection

In this context, we have to mention also the so-called ‘colour reconnection’ phenomenon. This is a pure ‘soft QCD’ effect. The point is that after a number of coloured secondary partons are produced, there are different possibilities to form the colour flow between these partons and to group the partons into colourless clusters. In the process of reconnection, one rearranges the colour flow in such a way as to minimize the size of the clusters. This is especially important when dealing with MPI contributions. The reconnection between the different cut Pomerons diminishes the final multiplicity and can change the form of the N_{ch} distributions (see e.g. Section 43.3.2 of [1] and [2, 13, 177, 178]).

20.5.2.3 Double parton scattering

The probability of MPI depends on the spatial distribution of partons in the incoming protons. The effects of MPI are suppressed if the density of partons is low and the partons from the incoming beam particles are separated from each other by a large

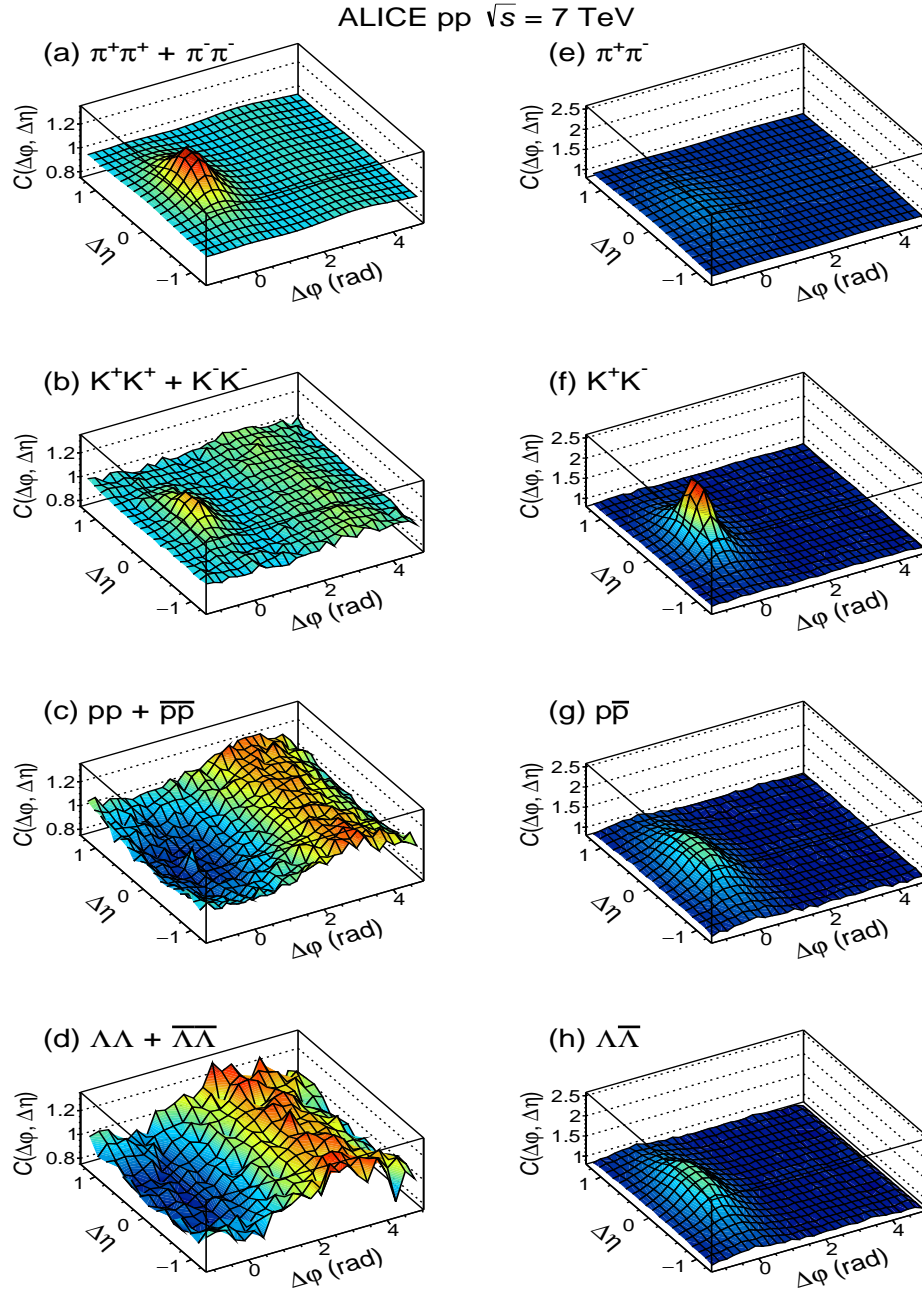


Figure 20.14: Two-particle correlation functions for identical-particle pairs: $\pi^+\pi^+ + \pi^-\pi^-$, $K^+K^+ + K^-K^-$, $pp + \bar{p}\bar{p}$, and $\Lambda\Lambda + \bar{\Lambda}\bar{\Lambda}$ (left panel) and particle-anti-particle pairs: $\pi^+\pi^-$, K^+K^- , $p\bar{p}$ and $\Lambda\bar{\Lambda}$ (right panel). Figure from Ref. [169].

interval in transverse coordinate space \vec{x}_t . Events in which two hard subprocesses, caused by interactions of two different parton pairs (say, (a_1b_1) and (a_2b_2)), take place simultaneously, are called Double Parton Scattering (DPS). The DPS cross section is driven by the ‘double parton distributions’, $D(y_{a_1}, y_{a_2}, \dots)$, where y_{a_1} and y_{a_2} are momentum fractions carried by the partons from the proton a and the dots denote all other coordinates. As a rule, experiments study DPS processes at relatively small momentum fractions y_i . Here, correlations due to momentum conservation (like $y_{a_1} + y_{a_2} < 1$) are not so important, and with a reasonable accuracy we can assume a factorization

$$D(y_{a_1}, y_{a_2}, \dots) \propto F(y_{a_1}) \cdot F(y_{a_2}), \quad (20.53)$$

where $F(y_{a_i})$ are the single parton distributions. In such a case the DPS cross section takes the form

$$\sigma^{\text{DPS}} = c \cdot \frac{\sigma_{a_1b_1} \sigma_{a_2b_2}}{\sigma_{\text{eff}}}, \quad (20.54)$$

where $\sigma_{a_1b_1}$ and $\sigma_{a_2b_2}$ are cross sections for the two *independent* hard processes, while σ_{eff} characterizes the mean area occupied by the partons a_1 and b_1 ; the constant factor $c = 1/2$ if both hard processes (a_1b_1) and (a_2b_2) are identical, otherwise $c = 1$. Thus the DPS cross section is sensitive to the spatial separations between partons in the proton (see Section 7.2.3 in [2] and [179, 180] for more explanations and reviews).

One problem is that within this approach we *assume* that the partons a_1 and a_2 are produced by two independent parton showers (and similarly for the other incoming proton). On the other hand, there is a probability that from the beginning we start with the evolution of a single shower which further splits into two different branches. In this case the separation between the two partons (two shower branches) becomes very small – of the order of the inverse scale ($\sim 1/\sqrt{q^2}$) at which the splitting occurs. The exact value of this ‘splitting’ scale q^2 depends on the particular kinematics of the DPS process. So, different experiments (with

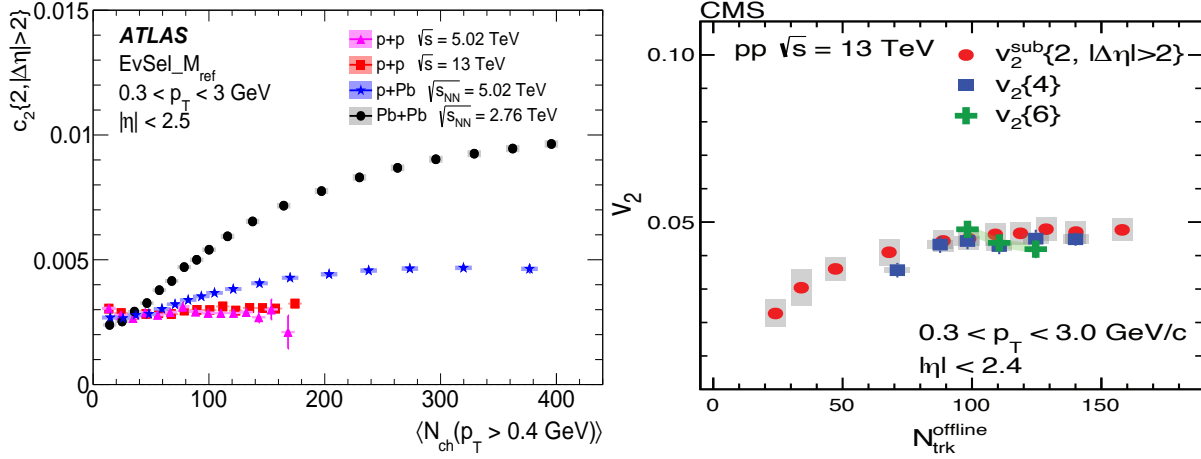


Figure 20.15: (Left) The two-particle cumulant, $c_2\{2, |\Delta\eta| > 2\}$, as a function of $\langle N_{\text{ch}}(p_T > 0.4 \text{ GeV}) \rangle$ for pp collisions at $\sqrt{s} = 5.02$ and 13 TeV , pPb collisions at $\sqrt{s_{NN}} = 5.02 \text{ TeV}$ and low-multiplicity $PbPb$ collisions at $\sqrt{s_{NN}} = 2.76 \text{ TeV}$. The data are constructed from particles with $0.3 < p_T < 3.0 \text{ GeV}$. Figure from Ref. [175]. (Right) The $v_2\{2, |\Delta\eta| > 2\}$, $v_2\{4\}$ and $v_2\{6\}$ values as a function of number of charged particles, averaged over $0.3 < p_T < 3.0 \text{ GeV}$ and $|\eta| < 2.4$, in pp collisions at $\sqrt{s} = 13 \text{ TeV}$. Figure from Ref. [176]. The error bars correspond to the statistical uncertainties, while the shaded areas denote the systematic uncertainties.

different kinematical conditions) can give somewhat different values of σ_{eff} . In general, the value of σ_{eff} depends on the following features: a) on the measured process since the spatial (b_t) distributions of different incoming partons (light quarks, heavy quarks, gluons) can be different; b) on the splitting scale, $\sqrt{q^2}$, of one parton cascade into two branches. The typically high value of the splitting scale then explains the fact that the experimentally measured values of $\sigma_{\text{eff}} \sim 7\text{--}25 \text{ mb}$ (see Fig. 4 of [181]) are smaller than σ_{tot} or mostly even lower than the proton area $\pi R_p^2 \sim 22\text{--}24 \text{ mb}$ (see e.g. [182]); c) on the p_T balance, k_T , in the individual hard process (e.g. for two dijet productions $k_T = |\vec{p}_{T1} + \vec{p}_{T2}|$ where p_{T1} and p_{T2} are jet p_T 's of the first hard process (similarly for the second hard process)). A small value of k_T indicates that there were no splittings or the splitting scale $\sqrt{q^2}$ was small and, therefore, we expect larger σ_{eff} ; d) on the contribution of single parton scatterings misidentified as DPS. For a lower scale of the hard process this contribution is larger (see [183] for more detailed discussion).

20.5.2.4 Final state interactions

The formalism of the RFT does not include ‘final state interactions’¹⁶. Therefore, besides the correlations considered in the previous Section 20.5.2.1 we have to expect the correlation caused by partons and hadrons rescattering in the final state. These effects are not crucial at lower energies, but become more important at high LHC energies, in particular in heavy-ion collisions where the particle density is large. For example, the final state interactions (FSI) lead to the formation of the collective flow of secondaries (see e.g. [185] for a review), especially in high-multiplicity events. To study the collective flow experimentally, one has to subtract correlations coming from few-particle sources such as resonance decays, mini-jets, multi-jets and BEC (so called ‘non-flow’). The non-flow can efficiently be suppressed using the sub-event method, that is by studying the azimuthal correlations between particles separated in η [186], or subtracted using the multi-particle correlation (or cumulant) techniques.

The cumulant method is based on calculating $2k$ -particle azimuthal correlations, $\text{corr}_n\{2k\}$, and cumulants $c_n\{2k\}$ (where $k = 1, 2, \dots$), for n th Fourier harmonics. The $\text{corr}_n\{2k\}$ are defined as [187, 188]:

$$\langle\langle \text{corr}_n\{2\} \rangle\rangle = \langle\langle e^{in(\phi_1 - \phi_2)} \rangle\rangle, \quad \langle\langle \text{corr}_n\{4\} \rangle\rangle = \langle\langle e^{in(\phi_1 + \phi_2 - \phi_3 - \phi_4)} \rangle\rangle,$$

$$\langle\langle \text{corr}_n\{6\} \rangle\rangle = \langle\langle e^{in(\phi_1 + \phi_2 + \phi_3 - \phi_4 - \phi_5 - \phi_6)} \rangle\rangle$$

and similarly for higher numbers of correlated particles. The double-brackets $\langle\langle \rangle\rangle$ denote averaging first over particles in an event and then over events within a given event class. For every event, the average is taken over all possible combinations of azimuthal angles ϕ_l ($l = 1, \dots, 2k$) of the $2k$ particles. The cumulants are then obtained from multi-particle azimuthal correlations after subtracting correlations between $2(k-1)$ particles according to the following formulae [187, 188]:

$$c_n\{2\} = \langle\langle \text{corr}_n\{2\} \rangle\rangle, \quad c_n\{4\} = \langle\langle \text{corr}_n\{4\} \rangle\rangle - 2\langle\langle \text{corr}_n\{2\} \rangle\rangle^2, \\ c_n\{6\} = \langle\langle \text{corr}_n\{6\} \rangle\rangle - 9\langle\langle \text{corr}_n\{2\} \rangle\rangle \times \langle\langle \text{corr}_n\{4\} \rangle\rangle + 12\langle\langle \text{corr}_n\{2\} \rangle\rangle^3.$$

The cumulants for higher particle multiplicities are calculated in [187, 188]. The cumulants then serve to estimate the Fourier harmonics v_n as follows [187]:

$$v_n\{2\} = \sqrt{c_n\{2\}}, \quad v_n\{4\} = \sqrt[4]{-c_n\{4\}}, \quad v_n\{6\} = \sqrt[6]{c_n\{6\}/4}.$$

Some of the long-range correlation ($|\Delta\eta| > 2$) results obtained on a sample of charged particles with $0.3 < p_T < 3.0 \text{ GeV}$ and $|\eta| < 2.4$ are summarized in Fig. 20.15. The left plot shows the cumulant c_2 measured for pp , pPb and $PbPb$ collisions [175], while the right plot shows the elliptical harmonics v_2 measured for pp collisions [176], both as functions of multiplicities of charged particles. The two-particle correlations are observed to be strongest and rising with N_{ch} for $PbPb$ collisions, and weakest and rather flat for pp collisions. The elliptical-flow harmonics for 4- and 6-particle correlations show again a rather flat multiplicity dependence (at least for large multiplicities). Within experimental uncertainties, the values of $v_2\{2\}$, $v_2\{4\}$ and $v_2\{6\}$ measured in pp collisions at 13 TeV are consistent with each other. The similarity between $v_2\{4\}$ and $v_2\{6\}$ suggests that some collective effects are occurring in pp collisions at high multiplicity and the observations are similar to those in $PbPb$ collisions, where the $v_2\{4\}$ values were measured to be close to $v_2\{6\}$ but they are both lower than $v_2\{2\}$ (not shown here).

Another example of long-range correlations is the so-called ‘ridge effect’. Here not only the ‘back-to-back’ jet correlations are registered, but also an excess of particles going in the same (in the azimuthal plane) direction as the leading (relatively high p_T) hadron. Moreover, this excess is seen at the rapidities separated from the leading hadron by a rather large interval (see e.g. [189] for a review).

It is popular to describe such FSI effects within the hydrodynamic model [190], which operates with collective (thermodynamic) variables. In terms of microscopic interactions, the collec-

¹⁶In general, final state interactions can be included into the detailed structure of the multi-Pomeron vertices. However these vertices are phenomenological objects which are not well known experimentally.

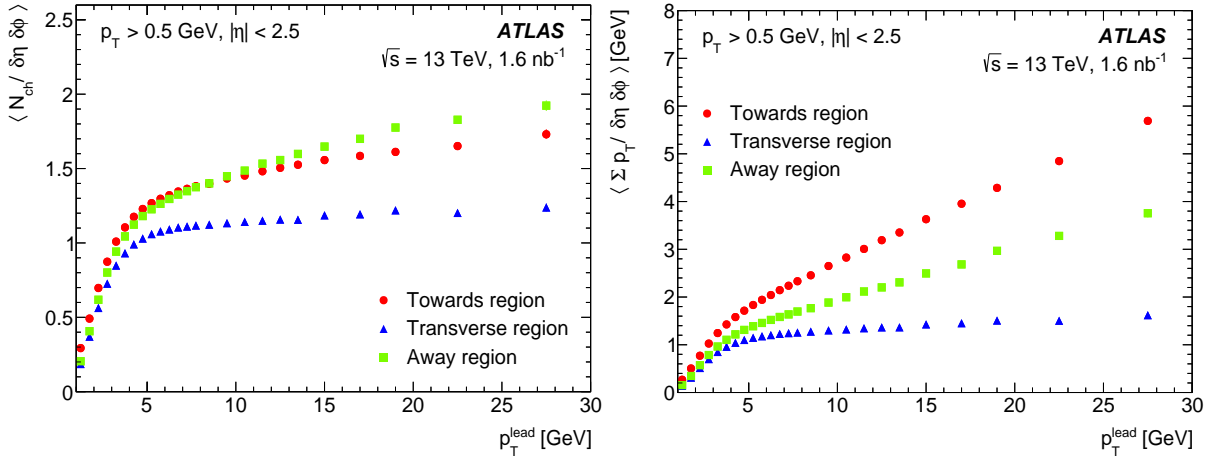


Figure 20.16: Mean charged particle density (left) and the sum of transverse momenta of secondaries (right) in events with the ‘leading’ high p_T particle as a function of p_T^{lead} in the transverse, towards and away azimuthal regions. Secondaries with $p_T > 0.5$ GeV and $|\eta| < 2.5$ are registered. The error bars (mostly hidden by the data markers) represent combined statistical and systematic uncertainties. Figures from [184].

tive flow can be caused by the geometry of a particular collision (the absorption is smaller for the secondaries flying in the direction orthogonal to the impact parameter vector \vec{b} [191, 192]), or by the colour reconnection at the hadronization stage [193], or accounting for the rescattering of secondaries directly, as was done, for example, in the AMPT model [194].

20.5.3 The underlying event

Except for the exclusive case, any ‘hard’ subprocess is accompanied by soft secondaries coming from initial state radiation (ISR), final state radiation (FSR) and multiple parton interaction (MPI), see Subsection 7.2.2 in [2]. These extra particles distort the signal we are looking for. In particular, they affect the isolation criteria applied to photons and charged leptons and the vertex reconstruction efficiency. In general, also the effects of colour reconnection (discussed in Section 20.5.2.2) contribute to the underlying event.

The usual procedure of estimating the amount of underlying event (UE) is to spatially divide tracks in each event according to their azimuthal angle into the Toward region (where the highest p_T jet points), the Away region (opposite to the Toward region) and to two Transverse regions. The standard observables are the average track multiplicity per unit area and the average scalar sum of track p_T per unit area. Figure 20.16 shows the particle density and the sum of p_T for the UE in ATLAS events containing at least one charged particle with $p_T > 0.5$ GeV and $|\eta| < 2.5$ [184].

Note that by construction the largest values of $\langle p_T \rangle$ are observed in the ‘Toward’ region, while in the ‘Away’ region we observe a slightly larger density than in the Toward region. These are results of the ‘leading’ and ‘backward’ jet fragmentation. In the transverse region, mostly filled by particles from the UE, the particle density and sum of p_T per unit $(\Delta\eta, \Delta\phi)$ area practically do not depend on the p_T^{lead} since these secondaries come from the other cut Pomeron(s), that is, from other ‘multiple interactions’. For low $p_T^{\text{lead}} < 2$ GeV the distributions in all three regions are close to each other. These events actually do not contain a ‘hard’ subprocess. Moreover, for a very small $p_T^{\text{lead}} \rightarrow 1$ GeV we start to select soft events with abnormally low $p_T < p_T^{\text{lead}}$ particles. Since only particles with $p_T > 0.5$ GeV are registered, the signal drops fast for $p_T^{\text{lead}} \rightarrow 1$ GeV. As a function of collision energy \sqrt{s} , the energy flow in the transverse region increases as $\sum p_T \sim s^{0.2}$ (as follows from Fig. 7 (right) in [184]) due to the larger number of MPI collisions and larger $\langle p_T \rangle$ in each collision¹⁷. As follows from this and other UE-dedicated LHC studies [195], from the comparisons of the data to the models with and without MPI, the necessity of MPI is convincingly demonstrated.

¹⁷Recall the stronger absorption of the low k_t partons.

20.6 The Odderon

Apart from the even-signature singularity (Pomeron), in QCD with $N_c = 3$ there exists its counterpart, the odd-signature singularity placed at $j \simeq 1$ and formed by three t-channel reggeized gluons connected in colour space by the symmetric d^{abc} tensor of the colour $SU(3)$ group [200, 201]. This object is called the Odderon. The Odderon exchange amplitude has opposite sign for pp and $p\bar{p}$ scatterings. Its intercept is predicted to be very close to $j = 1$ [202–204], while according to perturbative estimates the coupling to the nucleon is rather small [205, 206]. The corresponding amplitude is mainly real and is about 100 times smaller than the imaginary part of the Pomeron exchange amplitude. Calculating the elastic amplitude via the eikonal formula (20.13) we have to replace the opacity $\Omega(b)$ by the sum $\Omega = \Omega_{\text{even}} + \Omega_{\text{odd}}$, where Ω_{even} is mainly real and Ω_{odd} is imaginary. Note that at $t = 0$ this QCD Odderon does not couple to mesons, and the t -slope of the Odderon amplitude is expected to be smaller than that for the Pomeron; instead of the singularity at $t = 4m_\pi^2$ in the Pomeron case, the nearest singularity in the Odderon channel is at $t = 9m_\pi^2$, see for instance [204]. Thus, in the impact parameter b space the QCD Odderon occupies an area of a smaller radius, see e.g. [207].

Experimentally an indication in favour of a manifestation of the high energy C -odd amplitude was observed by comparing the elastic pp and $p\bar{p}$ cross sections in the dip region (where the contribution from the C -even amplitude has a minimum) at the CERN-ISR [197], see Fig. 20.17 (left)¹⁸.

To get a better understanding of the Odderon effects it would be very instructive to have the $d\sigma_{el}/dt$ data for both pp and $p\bar{p}$ reactions at the same but higher energy ~ 1 TeV (ideally in the same apparatus) and, in the ideal case, to study the energy dependence.

At the moment we can only compare the pp cross section measured by TOTEM at $\sqrt{s} = 2.76$ TeV [103] with the $d\sigma/dt$ values measured by the D0 collaboration at 1.96 TeV in $p\bar{p}$ collisions [199], see Fig. 20.17 (right).

The situation looks quite intriguing, but needs further investigation. Note that in the TeV energy range the ω, ρ and $\omega P, \rho P$ exchange contributions, which may be responsible for the difference between the pp and $p\bar{p}$ cross sections in the dip region at the ISR energies, are practically negligible.

Another way to search for the Odderon is to measure the real part of the elastic pp scattering amplitude via the interference with the pure QED one-photon exchange. Since the one-photon

¹⁸Note that a qualitatively similar behaviour to the $p\bar{p}$ ISR data, namely a filling in of the dip in the t -distribution, was observed by the UA4 collaboration at the CERN SppS collider at $\sqrt{s} = 546$ and 630 GeV (see [208, 209] and in particular Fig. 2 in [209]) and by the D0 collaboration at the Tevatron at 1.96 TeV [199].

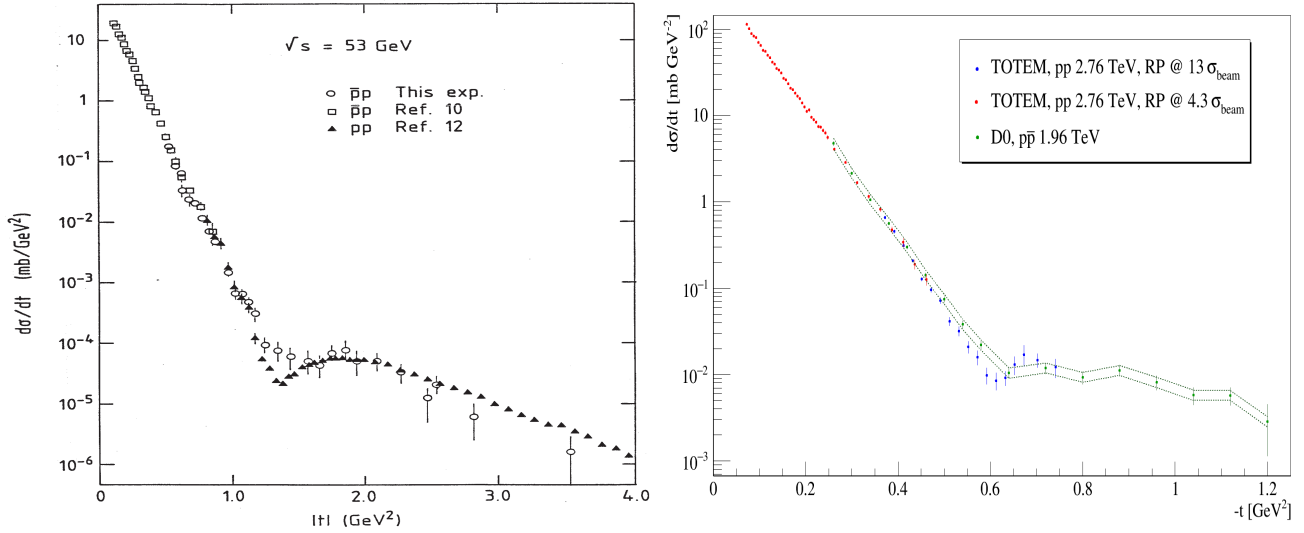


Figure 20.17: Comparison of the t -dependence of the elastic cross sections from pp and $p\bar{p}$ collisions. (Left) Data from the ISR energy of 53 GeV are shown by closed triangles [196] for pp collisions and by open circles [197] and open squares [198] for $p\bar{p}$ collisions. Only t -dependent uncertainties are shown and the systematic scale uncertainty is estimated to be $\pm 30\%$. Figure from Ref. [197]. (Right) Data from the D0 experiment at 1.96 TeV [199] are compared with data from the TOTEM experiment [103]. The green dashed line indicates the normalization uncertainty of the D0 measurement. Figure from Ref. [103].

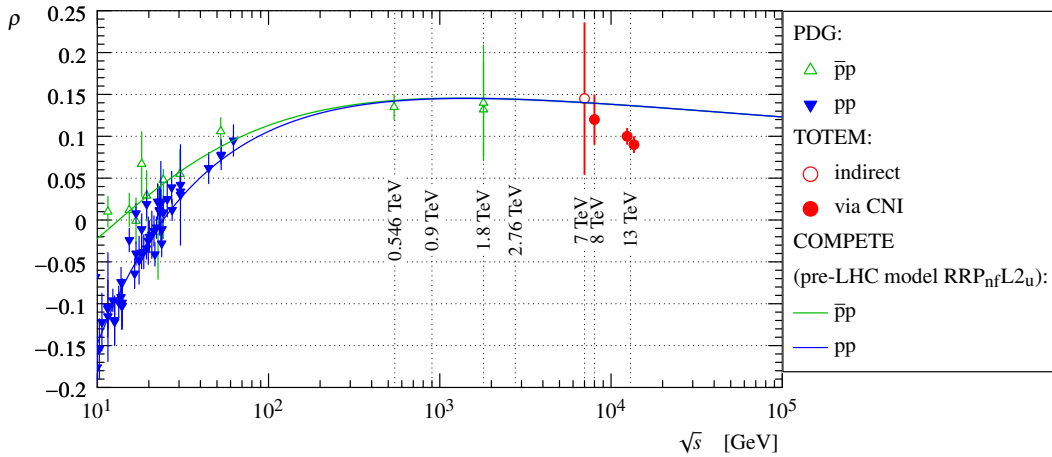


Figure 20.18: The dependence of the ρ parameter on the collision energy. The pp (blue) and $p\bar{p}$ (green) data are taken from [1]. The TOTEM measurements are marked in red. The two points at 13 TeV correspond to two fit cases, discussed in [102], using the same data. The lines represent fits to the data using the COMPETE parameterization [22]. Figure from Ref. [102].

exchange amplitude contribution is sizeable only at very small $|t|$, this way we can study the Odderon at or near to $t = 0$. Indeed, the value of the ratio $\rho \equiv \text{Re}T_{el}/\text{Im}T_{el}$, obtained by TOTEM at 13 TeV ($\rho = 0.10 \pm 0.01$ [102]), turns out to be smaller than that expected for the pure even-signature amplitude, see Fig. 20.18.

Based on dispersion relations and assuming the C -even contribution only, from the known total cross sections we would rather expect $\rho \simeq 0.13$ – 0.14 . The difference could indicate that the rise of the total cross section at energies above those of the LHC slows down (see the dispersion relation, Eq. (20.19)) or this could be attributed to an Odderon contribution (see e.g. [210]). However, the Odderon exchange amplitude extracted in this analysis has opposite sign to that for the lowest- α_s -order QCD Odderon, see e.g. [205, 206, 211, 212]. Besides this, the Odderon contribution to ρ , obtained in [210], grows with \sqrt{s} (for $\sqrt{s} > 0.5$ TeV), while in QCD we expect that the Odderon contribution to ρ decreases with energy, since the QCD Odderon intercept is smaller than that of the QCD Pomeron. Note also that recently the ATLAS Collaboration has published new results on elastic pp scattering at 13 TeV using the ALFA proton spectrometer [213]. While the measured value of $\rho = 0.098 \pm 0.011$ appears to be in a good agreement, a smaller total cross-section (with a smaller error bar)

$\sigma_{\text{tot}} = 104.7 \pm 1.1$ mb, is obtained when both are compared with TOTEM results at 13 TeV [102].

The values of σ_{tot} measured by ATLAS at 7, 8, and 13 TeV are found systematically lower than the TOTEM numbers. We note that if we used these ALFA values in dispersion relations, we would obtain a smaller ρ ratio for the C -even amplitude as well. Indeed, as shown in Figure 3 of Ref. [214], a good description of both, the σ_{tot} and ρ measurements, is achieved based on a global fit to the data performed using a damped $\ln^2 s$ amplitude and without an assumption of the Odderon. A good description of the ATLAS-ALFA data ($\chi^2/\text{n.d.f.} = 0.85$, see table 11 of Ref. [213]) of both σ_{tot} and ρ without an assumption of the Odderon is also obtained in the KMR model [215].

It is worth mentioning also that the Odderon contribution is strongly screened by the multi-Pomeron diagrams, which facilitate the falling-off of ρ with energy increasing, see [216, 217]. On the other hand, analyzing the whole ensemble of high energy elastic pp ($p\bar{p}$) low $|t|$ data, a reasonable description can be obtained using the even-signature amplitude only, that is, without the Odderon. In particular, the RR(PL2)qc model/version of the COMPETE parameterization is consistent with the TOTEM 13 TeV data on

σ_{tot} and ρ within 1σ ¹⁹. Another example is the recent analysis in [212] of the low $|t| < 0.1 \text{ GeV}^2$ elastic data. Fitting all the low- t pp and $p\bar{p}$ data in the range of \sqrt{s} between 13 GeV and 13 TeV without Odderon, Donnachie and Landshoff [212] succeeded to describe the TOTEM cross section with less than 1σ deviation in each $d\sigma_{\text{el}}/dt$ point (see Fig. 8 of [212]). Note that in this analysis, they get a larger value of ρ close to 0.14 at 13 TeV.

It was proposed also to search for the Odderon in exclusive C -even meson ($\pi^0, \eta, f_2, \eta_c, \dots$) photoproduction (see e.g. [218, 219]). However the expected cross sections are small (e.g. for η_c) and in each channel there is a large background caused either by Pomeron-Pomeron fusion (such as CEP of the f_2 meson production in pp or pPb collisions) or due to the vector meson radiative decay (such as $\omega \rightarrow \pi^0\gamma$ for the case of pion) [220]. Up to now, no definitive Odderon signal in the C -even meson production has been observed. At the moment there exist only upper limits on the photoproduction cross sections obtained in the measurements at HERA at $\sqrt{s} \simeq 200 \text{ GeV}$ [221–223].

To conclude, let us emphasize that the existence of the C -odd singularity with intercept $\alpha_{\text{odd}}(0) \simeq 1$ is a firm prediction of QCD. At least in the high k_t region there is a well established C -odd three-gluon contribution to the scattering amplitude. However the expected coupling of such an Odderon singularity is numerically very small. Therefore it is quite challenging to observe its manifestation experimentally. Currently it seems to be a bit premature to draw any definite conclusion about an experimental observation of the Odderon signal.

20.7 Asymptotics

The high-energy behaviour of total hadronic cross sections has been one of the oldest problems of strong interactions over many decades, beginning from Heisenberg [224]. The most important bound obtained based on general analytical properties of scattering amplitudes is the FLM bound [47–49]. It states that the growth of the total hadronic cross section with energy does not exceed $\ln^2 s$, see Eq. (20.34).

Recall that we neglected the photon contribution as well as the whole electro-weak sector, and that the parameter in Eq. (20.34) s_0 is an *a priori* unknown scale. However, if we were to assume a reasonable hadronic scale, $s_0 \simeq 1 \text{ GeV}^2$, we would find that Eq. (20.34) implies an unrealistically high upper bound in comparison with the cross sections observed at present collider energies. Nevertheless there is a common trend in the literature (see for instance, reviews [225, 226] and references therein) to fit phenomenologically the total cross section with $\ln^2 s$, keeping in mind the saturation of the FLM bound. Such an asymptotic behaviour is assumed also by the COMPETE collaboration [22], which achieved a comprehensive description of all soft pre-LHC data measured at $\sqrt{s} \geq 4 \text{ GeV}$ as well as total pp cross sections from the LHC available in the first half of 2015 (see Section 51 in [24]).

It is interesting that the Froissart-type $\ln^2 s$ asymptotics of the pp total cross section are also supported by numerical results in lattice QCD [227]. Such a behaviour is also observed in the approach [228] based on Colour Glass Condensate saturation.

Finally, it is worth mentioning that the possibility that *asymptotically* the Pomeron intercept becomes smaller than 1, $\alpha_{\mathbb{P}}(0) < 1$, and at very high energies the total cross section starts to decrease with energy, though highly unlikely, is not yet completely rejected. For instance, such a behaviour is expected in a theory with only the triple-Pomeron coupling, $g_{3\mathbb{P}}$, and which neglects the more complicated multi-Pomeron vertices g_m^n , such as the $2 \rightarrow 2$ Pomeron coupling [229, 230].

It was also argued that in the case of an increasing (with energy) cross section the only regime consistent asymptotically with both the s - and the t -channel unitarities is that of a *black* disc whose radius increases as $R = c \cdot \ln s$ [231] (i.e. $R \propto (\ln s)^\gamma$, with $\gamma = 1$ exactly).

20.8 Acknowledgements

It is a pleasure to thank Michael Albrow, Robert Cahn, Robert Ciesielski, Per Grafstrom, Frank Krauss, Paul Newman, Sergey

Ostapchenko and Edward Sarkisyan-Grinbaum for discussions, suggestions and comments on this review. Special thanks to Graeme Watt who read the article through and helped to improve the presentation. MT is supported by MEYS of the Czech Republic within project LTT17018. VAK thanks the Institute of Physics of the Czech Academy of Sciences in Prague for hospitality.

References

- [1] M. Tanabashi *et al.* (Particle Data Group), Phys. Rev. **D98**, 3, 030001 (2018).
- [2] J. Campbell, J. Huston and F. Krauss, *The Black Book of Quantum Chromodynamics*, Oxford University Press (2017), ISBN 9780199652747, URL <https://global.oup.com/academic/product/the-black-book-of-quantum-chromodynamics-9780199652747>.
- [3] R. J. Eden *et al.*, *The analytic S-matrix*, Cambridge Univ. Press, Cambridge (1966).
- [4] A. Martin, Lect. Notes Phys. **3**, 1 (1969).
- [5] P. D. B. Collins, *An Introduction to Regge Theory and High-Energy Physics*, Cambridge Monographs on Mathematical Physics, Cambridge Univ. Press, Cambridge, UK (2009), ISBN 9780521110358, URL <http://www-spires.fnal.gov/spires/find/books/www?c1=QC793.3.R4C695>.
- [6] S. Donnachie *et al.*, Camb. Monogr. Part. Phys. Nucl. Phys. Cosmol. **19**, 1 (2002).
- [7] V. N. Gribov, *The theory of complex angular momenta: Gribov lectures on theoretical physics*, Cambridge Monographs on Mathematical Physics, Cambridge University Press (2007), ISBN 9780521037037, 9780521818346, 9780511055041, URL <http://www.cambridge.org/uk/catalogue/catalogue.asp?isbn=0521307848>.
- [8] S. Ostapchenko, in “25th European Cosmic Ray Symposium (ECRS 2016) Turin, Italy, September 04-09, 2016,” (2016), [arXiv:1612.09461].
- [9] T. Sjostrand, Int. J. Mod. Phys. **A3**, 751 (1988).
- [10] B. Andersson, Camb. Monogr. Part. Phys. Nucl. Phys. Cosmol. **7**, 1 (1997).
- [11] W. Kittel and E. A. De Wolf, *Soft multihadron dynamics* (2005), ISBN 9789812562951.
- [12] I. M. Dremin and A. B. Kaidalov, Phys. Usp. **49**, 263 (2006), [Usp. Fiz. Nauk176,275(2006)].
- [13] A. Buckley *et al.*, Phys. Rept. **504**, 145 (2011), [arXiv:1101.2599].
- [14] R. Ciesielski and K. Goulianos, PoS **ICHEP2012**, 301 (2013), [arXiv:1205.1446].
- [15] K. Akiba *et al.* (LHC Forward Physics Working Group), J. Phys. **G43**, 110201 (2016), [arXiv:1611.05079].
- [16] G. D. Alkhalov, S. L. Belostotsky and A. A. Vorobev, Phys. Rept. **42**, 89 (1978).
- [17] E. L. Feinberg and I. Y. Pomeranchuk, Doklady Akad. Nauk SSSR **93**, 439 (1953); E. L. Feinberg and I. Y. Pomeranchuk, Suppl. Nuovo Cimento **III**, serie X, 652 (1956).
- [18] R. Engel, D. Heck and T. Pierog, Ann. Rev. Nucl. Part. Sci. **61**, 467 (2011).
- [19] M. Gell-Mann, in “High-energy physics. Proceedings, 11th International Conference, ICHEP’62, Geneva, Switzerland, Jul 4-11, 1962,” 533–542 (1962).
- [20] S. Frautschi, M. Gell-Mann and F. Zachariasen, Phys. Rev. **126**, 6, 2204 (1962).
- [21] K. G. Boreskov, A. B. Kaidalov and O. V. Kancheli, Phys. Atom. Nucl. **69**, 1765 (2006), [Yad. Fiz.69,1802(2006)].
- [22] J. R. Cudell *et al.* (COMPETE), Phys. Rev. Lett. **89**, 201801 (2002), [hep-ph/0206172].
- [23] C. Bourrely, J. Soffer and T. T. Wu, Eur. Phys. J. **C28**, 97 (2003), [hep-ph/0210264].

¹⁹We thank Jean-Rene Cudell for clarifying this issue.

- [24] C. Patrignani *et al.* (Particle Data Group), *Chin. Phys.* **C40**, 10, 100001 (2016).
- [25] A. Donnachie and P. V. Landshoff, *Nucl. Phys.* **B231**, 189 (1984).
- [26] A. Donnachie and P. V. Landshoff, *Phys. Lett.* **B296**, 227 (1992), [hep-ph/9209205].
- [27] S. Mandelstam, *Nuovo Cim.* **30**, 1148 (1963).
- [28] V. N. Gribov, I. Ya. Pomeranchuk and K. A. Ter-Martirosian, *Phys. Lett.* **9**, 269 (1964).
- [29] V. A. Khoze, A. D. Martin and M. G. Ryskin, *Int. J. Mod. Phys.* **A30**, 08, 1542004 (2015), [arXiv:1402.2778].
- [30] E. Gotsman, E. Levin and U. Maor, *Int. J. Mod. Phys.* **A30**, 08, 1542005 (2015), [arXiv:1403.4531].
- [31] S. Ostapchenko, *Phys. Rev.* **D81**, 114028 (2010), [arXiv:1003.0196].
- [32] V. N. Gribov, *Sov. Phys. JETP* **26**, 414 (1968), [*Zh. Eksp. Teor. Fiz.* 53,654(1967)].
- [33] U. Amaldi, M. Jacob and G. Matthiae, *Ann. Rev. Nucl. Part. Sci.* **26**, 385 (1976).
- [34] A. B. Kaidalov, *Phys. Rept.* **50**, 157 (1979).
- [35] V. Barone and E. Predazzi, *High-Energy Particle Diffraction*, volume v.565 of *Texts and Monographs in Physics*, Springer-Verlag, Berlin Heidelberg (2002), ISBN 3540421076, URL <http://www-spires.fnal.gov/spires/find/books/www?cl=QC794.6.C6B37::2002>.
- [36] A. B. Kaidalov *et al.*, *Acta Phys. Polon.* **B34**, 3163 (2003), [hep-ph/0303111].
- [37] L. Frankfurt and M. Strikman, in E. M. Henley and S. D. Ellis, editors, "100 Years of Subatomic Physics," 363–423 (2013), [arXiv:1304.4308].
- [38] V. A. Khoze *et al.*, *Eur. Phys. J.* **C69**, 85 (2010), [arXiv:1005.4839].
- [39] D. A. Fagundes *et al.*, *Phys. Rev.* **D88**, 9, 094019 (2013), [arXiv:1306.0452].
- [40] R. Fiore *et al.*, *Int. J. Mod. Phys.* **A24**, 2551 (2009), [arXiv:0810.2902].
- [41] I. M. Dremin, *Phys. Usp.* **56**, 3 (2013), [*Usp. Fiz. Nauk* 183, 3 (2013)], [arXiv:1206.5474].
- [42] L. Frankfurt *et al.*, *Phys. Rev. Lett.* **101**, 202003 (2008), [arXiv:0808.0182].
- [43] G. Bertsch *et al.*, *Phys. Rev. Lett.* **47**, 297 (1981).
- [44] B. Z. Kopeliovich, L. I. Lapidus and A. B. Zamolodchikov, *JETP Lett.* **33**, 595 (1981), [*Pisma Zh. Eksp. Teor. Fiz.* 33, 612 (1981)].
- [45] M. L. Good and W. D. Walker, *Phys. Rev.* **120**, 1855 (1960).
- [46] J. Pumplin, *Phys. Rev.* **D8**, 2899 (1973).
- [47] M. Froissart, *Phys. Rev.* **123**, 1053 (1961).
- [48] A. Martin, *Nuovo Cim.* **A42**, 930 (1965).
- [49] L. Lukaszuk and A. Martin, *Nuovo Cim.* **A52**, 122 (1967).
- [50] A. A. Anselm and V. N. Gribov, *Phys. Lett.* **40B**, 487 (1972).
- [51] G. Cohen-Tannoudji, V. V. Ilyin and L. L. Jenkovszky, *Lett. Nuovo Cim.* **5S2**, 957 (1972), [*Lett. Nuovo Cim.* 5,957(1972)].
- [52] V. A. Khoze, A. D. Martin and M. G. Ryskin, *Eur. Phys. J.* **C18**, 167 (2000), [hep-ph/0007359].
- [53] G. Antchev *et al.* (TOTEM), *Nucl. Phys.* **B899**, 527 (2015), [arXiv:1503.08111].
- [54] G. Antchev *et al.* (TOTEM), *Eur. Phys. J.* **C79**, 10, 861 (2019), [arXiv:1812.08283].
- [55] L. Caneschi and A. Pignotti, *Phys. Rev. Lett.* **22**, 1219 (1969).
- [56] O. V. Kancheli, *JETP Lett.* **11**, 267 (1970), [*Pisma Zh. Eksp. Teor. Fiz.* 11, 397 (1970)].
- [57] A. H. Mueller, *Phys. Rev.* **D4**, 150 (1971).
- [58] D. Amati, A. Stanghellini and S. Fubini, *Nuovo Cim.* **26**, 896 (1962).
- [59] V. S. Fadin, E. A. Kuraev and L. N. Lipatov, *Phys. Lett.* **60B**, 50 (1975); E. A. Kuraev, L. N. Lipatov and V. S. Fadin, *Sov. Phys. JETP* **44**, 443 (1976), [*Zh. Eksp. Teor. Fiz.* 71,840(1976)]; E. A. Kuraev, L. N. Lipatov and V. S. Fadin, *Sov. Phys. JETP* **45**, 199 (1977), [*Zh. Eksp. Teor. Fiz.* 72,377(1977)]; I. I. Balitsky and L. N. Lipatov, *Sov. J. Nucl. Phys.* **28**, 822 (1978), [*Yad. Fiz.* 28,1597(1978)].
- [60] B. L. Ioffe, V. S. Fadin and L. N. Lipatov, *Quantum chromodynamics: Perturbative and nonperturbative aspects*, volume 30, Cambridge Univ. Press (2010), ISBN 9781107424753, 9780521631488, 9780511717444, URL <http://www.cambridge.org/de/knowledge/isbn/item2710695>.
- [61] S. Ostapchenko, *Phys. Rev.* **D83**, 014018 (2011), [arXiv:1010.1869].
- [62] J. L. Cardy, *Nucl. Phys.* **B75**, 413 (1974).
- [63] A. B. Kaidalov *et al.*, *Phys. Lett.* **45B**, 493 (1973).
- [64] E. G. S. Luna *et al.*, *Eur. Phys. J.* **C59**, 1 (2009), [arXiv:0807.4115].
- [65] T. Sjöstrand, *Adv. Ser. Direct. High Energy Phys.* **29**, 191 (2018), [arXiv:1706.02166].
- [66] K. Werner, F.-M. Liu and T. Pierog, *Phys. Rev.* **C74**, 044902 (2006), [hep-ph/0506232].
- [67] V. A. Abramovsky, V. N. Gribov and O. V. Kancheli, *Yad. Fiz.* **18**, 595 (1973), [*Sov. J. Nucl. Phys.* 18, 308 (1974)].
- [68] G. Alberi and G. Goggi, *Phys. Rept.* **74**, 1 (1981).
- [69] K. A. Goulianos, *Phys. Rept.* **101**, 169 (1983).
- [70] D. Bernard *et al.* (UA4), *Phys. Lett.* **B186**, 227 (1987).
- [71] R. E. Ansorge *et al.* (UA5), *Z. Phys.* **C33**, 175 (1986).
- [72] N. A. Amos *et al.* (E710), *Phys. Lett.* **B301**, 313 (1993).
- [73] F. Abe *et al.* (CDF), *Phys. Rev.* **D50**, 5535 (1994).
- [74] G. Aad *et al.* (ATLAS), *Eur. Phys. J.* **C72**, 1926 (2012), [arXiv:1201.2808].
- [75] V. Khachatryan *et al.* (CMS), *Phys. Rev.* **D92**, 1, 012003 (2015), [arXiv:1503.08689].
- [76] B. Abelev *et al.* (ALICE), *Eur. Phys. J.* **C73**, 6, 2456 (2013), [arXiv:1208.4968].
- [77] G. Aad *et al.* (ATLAS), *Phys. Lett.* **B754**, 214 (2016), [arXiv:1511.00502].
- [78] G. Aad *et al.* (ATLAS), *JHEP* **02**, 042 (2020), [arXiv:1911.00453].
- [79] A. M. Sirunyan *et al.* (CMS and TOTEM) (2020), [arXiv:2002.12146].
- [80] V. A. Khoze, A. D. Martin and M. G. Ryskin, *Eur. Phys. J.* **C73**, 2503 (2013), [arXiv:1306.2149].
- [81] V. A. Khoze, A. D. Martin and M. G. Ryskin, *Eur. Phys. J.* **C23**, 311 (2002), [hep-ph/0111078].
- [82] M. G. Albrow, T. D. Coughlin and J. R. Forshaw, *Prog. Part. Nucl. Phys.* **65**, 149 (2010), [arXiv:1006.1289].
- [83] M. Albrow, *Int. J. Mod. Phys.* **A29**, 1402006 (2014).
- [84] H. G. Fischer, W. Geist and M. Makariev, *Int. J. Mod. Phys.* **A29**, 28, 1446005 (2014).
- [85] A. Kirk, *Int. J. Mod. Phys.* **A29**, 28, 1446001 (2014), [arXiv:1408.1196].
- [86] M. A. Reyes *et al.* (E690), *Phys. Rev. Lett.* **81**, 4079 (1998).
- [87] G. Gutierrez and M. A. Reyes, *Int. J. Mod. Phys.* **A29**, 28, 1446008 (2014), [arXiv:1409.8243].
- [88] Y. L. Dokshitzer, D. Diakonov and S. I. Troian, *Phys. Rept.* **58**, 269 (1980).
- [89] M. Derrick *et al.* (ZEUS), *Phys. Lett.* **B315**, 481 (1993).

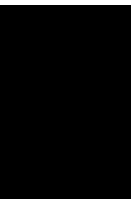
- [90] T. Ahmed *et al.* (H1), Nucl. Phys. **B429**, 477 (1994).
- [91] P. Newman and M. Wing, Rev. Mod. Phys. **86**, 3, 1037 (2014), [arXiv:1308.3368].
- [92] A. Aktas *et al.* (H1), Eur. Phys. J. **C48**, 715 (2006), [hep-ex/0606004].
- [93] S. Chekanov *et al.* (ZEUS), Nucl. Phys. **B816**, 1 (2009), [arXiv:0812.2003].
- [94] F. D. Aaron *et al.* (H1), Eur. Phys. J. **C72**, 2074 (2012), [arXiv:1203.4495].
- [95] F. D. Aaron *et al.* (H1, ZEUS), Eur. Phys. J. **C72**, 2175 (2012), [arXiv:1207.4864].
- [96] A. Aktas *et al.* (H1), JHEP **10**, 042 (2007), [arXiv:0708.3217].
- [97] A. Aktas *et al.* (H1), Eur. Phys. J. **C50**, 1 (2007), [hep-ex/0610076].
- [98] S. Chekanov *et al.* (ZEUS), Nucl. Phys. **B672**, 3 (2003), [hep-ex/0307068].
- [99] E. G. de Oliveira, A. D. Martin and M. G. Ryskin, Phys. Lett. **B695**, 162 (2011), [arXiv:1010.1366].
- [100] G. Antchev *et al.* (TOTEM), Eur. Phys. J. **C79**, 2, 103 (2019), [arXiv:1712.06153].
- [101] C. Augier *et al.* (UA4/2), Phys. Lett. **B316**, 448 (1993).
- [102] G. Antchev *et al.* (TOTEM), Eur. Phys. J. **C79**, 9, 785 (2019), [arXiv:1812.04732].
- [103] G. Antchev *et al.* (TOTEM), Eur. Phys. J. **C80**, 2, 91 (2020), [arXiv:1812.08610].
- [104] G. Antchev *et al.* (TOTEM), EPL **101**, 2, 21002 (2013).
- [105] G. Antchev *et al.* (TOTEM), Phys. Rev. Lett. **111**, 1, 012001 (2013).
- [106] G. Aad *et al.* (ATLAS), Nucl. Phys. **B889**, 486 (2014), [arXiv:1408.5778].
- [107] M. Aaboud *et al.* (ATLAS), Phys. Lett. **B761**, 158 (2016), [arXiv:1607.06605].
- [108] M. M. Block and R. N. Cahn, Rev. Mod. Phys. **57**, 563 (1985).
- [109] F. Abe *et al.* (CDF), Phys. Rev. **D50**, 5550 (1994).
- [110] C. Avila *et al.* (E811), Phys. Lett. **B445**, 419 (1999).
- [111] W. Guryan, Invited talk at the Workshop on Diffraction and Low-x Physics, Reggio Calabria, Italy, August 26th–September 1st, 2018; J. Adam *et al.* (STAR), Phys. Lett. B **808**, 135663 (2020), [arXiv:2003.12136].
- [112] K. Nakamura *et al.* (Particle Data Group), J. Phys. **G37**, 075021 (2010).
- [113] F. J. Nemes, PoS **DIS2017**, 059 (2018).
- [114] G. Antchev *et al.* (TOTEM), EPL **95**, 4, 41001 (2011), [arXiv:1110.1385].
- [115] G. Antchev *et al.* (TOTEM), Eur. Phys. J. **C76**, 12, 661 (2016), [arXiv:1610.00603].
- [116] J. Kaspar, Invited talk at the meeting of the LHC Working Group on Forward Physics and Diffraction, CERN, Switzerland, December 16-17th, 2019.
- [117] V. A. Schegelsky and M. G. Ryskin, Phys. Rev. **D85**, 094024 (2012), [arXiv:1112.3243].
- [118] A. Bruni, X. Janssen and P. Marage, in “Proceedings, HERA and the LHC Workshop Series on the implications of HERA for LHC physics: 2006-2008,” 427–439 (2008), [arXiv:0812.0539].
- [119] A. Levy, in “Proceedings, 17th International Workshop on Deep-Inelastic Scattering and Related Subjects (DIS 2009): Madrid, Spain, April 26-30, 2009,” 177 (2009), [arXiv:0907.2178].
- [120] J. R. Forshaw, R. Sandapen and G. Shaw, JHEP **11**, 025 (2006), [hep-ph/0608161].
- [121] A. Capella *et al.*, Nucl. Phys. **B593**, 336 (2001), [hep-ph/0005049].
- [122] V. S. Fadin and L. N. Lipatov, Phys. Lett. **B429**, 127 (1998), [hep-ph/9802290].
- [123] M. Ciafaloni and G. Camici, Phys. Lett. **B430**, 349 (1998), [hep-ph/9803389].
- [124] F. D. Aaron *et al.* (H1), JHEP **05**, 032 (2010), [arXiv:0910.5831].
- [125] C. Adloff *et al.* (H1), Eur. Phys. J. **C13**, 371 (2000), [hep-ex/9902019].
- [126] J. Breitweg *et al.* (ZEUS), Eur. Phys. J. **C6**, 603 (1999), [hep-ex/9808020].
- [127] S. Chekanov *et al.* (ZEUS), PMC Phys. **A1**, 6 (2007), [arXiv:0708.1478].
- [128] M. Ciafaloni, Nucl. Phys. **B296**, 49 (1988).
- [129] S. Catani, F. Fiorani and G. Marchesini, Phys. Lett. **B234**, 339 (1990).
- [130] S. Catani, F. Fiorani and G. Marchesini, Nucl. Phys. **B336**, 18 (1990).
- [131] G. Marchesini, Nucl. Phys. **B445**, 49 (1995), [hep-ph/9412327].
- [132] G. P. Salam, JHEP **07**, 019 (1998), [hep-ph/9806482].
- [133] M. Ciafaloni and D. Colferai, Phys. Lett. **B452**, 372 (1999), [hep-ph/9812366].
- [134] H. Kowalski, L. N. Lipatov and D. A. Ross, Eur. Phys. J. **C76**, 1, 23 (2016), [arXiv:1508.05744].
- [135] H. Kowalski *et al.*, Eur. Phys. J. **C77**, 11, 777 (2017), [arXiv:1707.01460].
- [136] S. J. Brodsky *et al.*, JETP Lett. **70**, 155 (1999), [hep-ph/9901229].
- [137] R. D. Ball *et al.*, Eur. Phys. J. **C78**, 4, 321 (2018), [arXiv:1710.05935].
- [138] E. M. Levin and M. G. Ryskin, Phys. Rept. **189**, 267 (1990).
- [139] L. V. Gribov, E. M. Levin and M. G. Ryskin, Phys. Rept. **100**, 1 (1983).
- [140] E. M. Levin, M. G. Ryskin and A. G. Shuvaev, Nucl. Phys. **B387**, 589 (1992).
- [141] A. H. Mueller, Phys. Rept. **73**, 237 (1981).
- [142] A. H. Mueller, Nucl. Phys. **B415**, 373 (1994).
- [143] A. H. Mueller and B. Patel, Nucl. Phys. **B425**, 471 (1994), [hep-ph/9403256].
- [144] N. N. Nikolaev, B. G. Zakharov and V. R. Zoller, JETP Lett. **59**, 6 (1994), [hep-ph/9312268].
- [145] V. N. Gribov and L. N. Lipatov, Sov. J. Nucl. Phys. **15**, 438 (1972), [Yad. Fiz.15,781(1972)]; G. Altarelli and G. Parisi, Nucl. Phys. **B126**, 298 (1977); Y. L. Dokshitzer, Sov. Phys. JETP **46**, 641 (1977), [Zh. Eksp. Teor. Fiz. 73, 1216 (1977)].
- [146] I. Balitsky, Nucl. Phys. **B463**, 99 (1996), [hep-ph/9509348].
- [147] I. Balitsky, Phys. Rev. **D60**, 014020 (1999), [hep-ph/9812311].
- [148] Y. V. Kovchegov, Phys. Rev. **D60**, 034008 (1999), [hep-ph/9901281].
- [149] G. Gustafson, Phys. Lett. **B718**, 1054 (2013), [arXiv:1206.1733].
- [150] S. Chatrchyan *et al.* (CMS, TOTEM), Eur. Phys. J. **C74**, 10, 3053 (2014), [arXiv:1405.0722].
- [151] Q.-D. Zhou (LHCF, ATLAS), EPJ Web Conf. **208**, 05008 (2019).
- [152] O. Adriani *et al.* (LHCF), Phys. Lett. **B780**, 233 (2018), [arXiv:1703.07678].
- [153] M. Aaboud *et al.* (ATLAS), ATLAS-CONF-2017-075.
- [154] C. Albajar *et al.* (UA1), Nucl. Phys. **B335**, 261 (1990).
- [155] G. J. Alner *et al.* (UA5), Z. Phys. **C33**, 1 (1986).

- [156] T. Aaltonen *et al.* (CDF), Phys. Rev. **D79**, 112005 (2009), [Erratum: Phys. Rev. **D82**, 119903(2010)], [arXiv:0904.1098].
- [157] F. Abe *et al.* (CDF), Phys. Rev. **D41**, 2330 (1990), [119(1989)].
- [158] K. Aamodt *et al.* (ALICE), Eur. Phys. J. **C68**, 89 (2010), [arXiv:1004.3034].
- [159] V. Khachatryan *et al.* (CMS), Phys. Rev. Lett. **105**, 022002 (2010), [arXiv:1005.3299].
- [160] B. B. Abelev *et al.* (ALICE), Eur. Phys. J. **C73**, 12, 2662 (2013), [arXiv:1307.1093].
- [161] A. M. Sirunyan *et al.* (CMS), Phys. Rev. **D96**, 11, 112003 (2017), [arXiv:1706.10194].
- [162] M. G. Ryskin, A. D. Martin and V. A. Khoze, Eur. Phys. J. **C71**, 1617 (2011), [arXiv:1102.2844].
- [163] X.-N. Wang, Phys. Rept. **280**, 287 (1997), [hep-ph/9605214].
- [164] S. Ostapchenko and M. Bleicher, Universe **5**, 5, 106 (2019).
- [165] F. M. Liu *et al.*, J. Phys. **G28**, 2597 (2002), [hep-ph/0109104].
- [166] E. Gotsman, E. Levin and U. Maor, Acta Phys. Polon. Supp. **8**, 777 (2015).
- [167] Y. V. Kovchegov and E. Levin, Camb. Monogr. Part. Phys. Nucl. Phys. Cosmol. **33**, 1 (2012).
- [168] E. A. De Wolf, I. M. Dremin and W. Kittel, Phys. Rept. **270**, 1 (1996), [hep-ph/9508325].
- [169] J. Adam *et al.* (ALICE), Eur. Phys. J. **C77**, 8, 569 (2017), [arXiv:1612.08975].
- [170] V. Khachatryan *et al.* (CMS), JHEP **09**, 091 (2010), [arXiv:1009.4122].
- [171] K. Eggert *et al.*, Nucl. Phys. **B86**, 201 (1975).
- [172] B. Alver *et al.* (PHOBOS), Phys. Rev. **C75**, 054913 (2007), [arXiv:0704.0966].
- [173] E. M. Levin and M. G. Ryskin, Sov. J. Nucl. Phys. **20**, 280 (1975), [Yad. Fiz. **20**, 519(1974)].
- [174] A. Capella and A. Krzywicki, Phys. Rev. **D18**, 4120 (1978).
- [175] M. Aaboud *et al.* (ATLAS), Eur. Phys. J. **C77**, 6, 428 (2017), [arXiv:1705.04176].
- [176] V. Khachatryan *et al.* (CMS), Phys. Lett. **B765**, 193 (2017), [arXiv:1606.06198].
- [177] S. Gieseke, Invited talk at the Workshop on Multiple Partonic Interactions at the LHC, Prague, Czech Republic, November 18th–26th, 2019.
- [178] S. Kundu, B. Mohanty and D. Mallick (2019), [arXiv:1912.05176].
- [179] M. Diehl, D. Ostermeier and A. Schafer, JHEP **03**, 089 (2012), [Erratum: JHEP **03**, 001(2016)], [arXiv:1111.0910].
- [180] T. Sjostrand and P. Z. Skands, JHEP **03**, 053 (2004), [hep-ph/0402078].
- [181] M. Aaboud *et al.* (ATLAS), Phys. Lett. **B790**, 595 (2019), [Phys. Lett. **790**, 595(2019)], [arXiv:1811.11094].
- [182] M. G. Ryskin and A. M. Snigirev, Phys. Rev. **D83**, 114047 (2011), [arXiv:1103.3495].
- [183] B. Blok *et al.*, Eur. Phys. J. **C74**, 2926 (2014), [arXiv:1306.3763].
- [184] M. Aaboud *et al.* (ATLAS), JHEP **03**, 157 (2017), [arXiv:1701.05390].
- [185] R. Snellings, New J. Phys. **13**, 055008 (2011), [arXiv:1102.3010].
- [186] M. Aaboud *et al.* (ATLAS), Phys. Rev. **C97**, 2, 024904 (2018), [arXiv:1708.03559].
- [187] N. Borghini, P. M. Dinh and J.-Y. Ollitrault, Phys. Rev. **C63**, 054906 (2001), [arXiv:nucl-th/0007063].
- [188] A. Bilandzic, R. Snellings and S. Voloshin, Phys. Rev. **C83**, 044913 (2011), [arXiv:1010.0233].
- [189] W. Li, Mod. Phys. Lett. **A27**, 1230018 (2012), [arXiv:1206.0148].
- [190] B. Schenke, J. Phys. **G38**, 124009 (2011), [arXiv:1106.6012].
- [191] K. G. Boreskov, A. B. Kaidalov and O. V. Kancheli, Eur. Phys. J. **C58**, 445 (2008), [arXiv:0809.0625].
- [192] K. G. Boreskov, A. B. Kaidalov and O. V. Kancheli, Phys. Atom. Nucl. **72**, 361 (2009), [Yad. Fiz. **72**, 390(2009)].
- [193] C. Bierlich and J. R. Christiansen, Phys. Rev. **D92**, 9, 094010 (2015), [arXiv:1507.02091].
- [194] Z.-W. Lin *et al.*, Phys. Rev. **C72**, 064901 (2005), [arXiv:nucl-th/0411110].
- [195] V. Khachatryan *et al.* (CMS), CMS-PAS-FSQ-16-008.
- [196] E. Nagy *et al.*, Nucl. Phys. **B150**, 221 (1979).
- [197] A. Breakstone *et al.*, Phys. Rev. Lett. **54**, 2180 (1985).
- [198] A. Breakstone *et al.* (AMES-BOLOGNA-CERN-DORTMUND-HEIDELBERG-WARSAW), Nucl. Phys. **B248**, 253 (1984).
- [199] V. M. Abazov *et al.* (D0), Phys. Rev. **D86**, 012009 (2012), [arXiv:1206.0687].
- [200] J. Bartels, Nucl. Phys. **B175**, 365 (1980).
- [201] J. Kwiecinski and M. Praszalowicz, Phys. Lett. **94B**, 413 (1980).
- [202] M. A. Braun (1998), [hep-ph/9805394].
- [203] J. Bartels, L. N. Lipatov and G. P. Vacca, Phys. Lett. **B477**, 178 (2000), [hep-ph/9912423].
- [204] C. Ewerz (2003), [hep-ph/0306137].
- [205] M. Fukugita and J. Kwiecinski, Phys. Lett. **83B**, 119 (1979), [625(1979)].
- [206] M. G. Ryskin, Sov. J. Nucl. Phys. **46**, 337 (1987), [Yad. Fiz. **46**, 611(1987)].
- [207] J. Bartels, C. Contreras and G. P. Vacca, JHEP **04**, 183 (2020), [arXiv:1910.04588].
- [208] M. Bozzo *et al.* (UA4), Phys. Lett. **155B**, 197 (1985).
- [209] D. Bernard *et al.* (UA4), Phys. Lett. **B171**, 142 (1986).
- [210] E. Martynov and B. Nicolescu, Eur. Phys. J. **C79**, 6, 461 (2019), [arXiv:1808.08580].
- [211] A. Donnachie and P. V. Landshoff, Phys. Lett. **123B**, 345 (1983).
- [212] A. Donnachie and P. V. Landshoff, Phys. Lett. **B798**, 135008 (2019), [arXiv:1904.11218].
- [213] G. Aad *et al.* (ATLAS), Eur. Phys. J. **C 83**, 5, 441 (2023), [arXiv:2207.12246].
- [214] S. Valentinetti (ATLAS), Acta Phys. Polon. Supp. **16**, 5, 11 (2023).
- [215] V. A. Khoze, A. D. Martin and M. G. Ryskin, Phys. Lett. **B 784**, 192 (2018), [arXiv:1806.05970].
- [216] J. Finkelstein *et al.*, Phys. Lett. **B232**, 257 (1989).
- [217] V. A. Khoze, A. D. Martin and M. G. Ryskin, Phys. Lett. **B780**, 352 (2018), [arXiv:1801.07065].
- [218] W. Kilian and O. Nachtmann, Eur. Phys. J. **C5**, 317 (1998), [hep-ph/9712371].
- [219] J. Bartels *et al.*, Eur. Phys. J. **C20**, 323 (2001), [hep-ph/0102221].
- [220] L. A. Harland-Lang *et al.*, Phys. Rev. **D99**, 3, 034011 (2019), [arXiv:1811.12705].
- [221] J. Olsson (H1), in “New trends in high-energy physics: Experiment, phenomenology, theory. Proceedings, International Conference, Yalta, Crimea, Ukraine, September 22-29, 2001,” 79–87 (2001), [hep-ex/0112012].
- [222] C. Adloff *et al.* (H1), Phys. Lett. **B544**, 35 (2002), [hep-ex/0206073].
- [223] T. Berndt (H1), Acta Phys. Polon. **B33**, 3499 (2002), [182(2002)].

- [224] W. Heisenberg, Z. Phys. **133**, 65 (1952).
- [225] G. Pancheri and Y. N. Srivastava, Eur. Phys. J. **C77**, 3, 150 (2017), [arXiv:1610.10038].
- [226] M. M. Block, Phys. Rept. **436**, 71 (2006), [hep-ph/0606215].
- [227] M. Giordano, E. Meggiolaro and N. Moretti, JHEP **09**, 031 (2012), [arXiv:1203.0961].
- [228] E. Ferreira *et al.*, Nucl. Phys. **A710**, 373 (2002), [hep-ph/0206241].
- [229] P. Grassberger and K. Sundermeyer, Phys. Lett. **77B**, 220 (1978).
- [230] K. G. Boreskov, in M. Olshanetsky and A. Vainshtein, editors, “Multiple facets of quantization and supersymmetry,” 322–351 (2001), [hep-ph/0112325].
- [231] V. A. Khoze, A. D. Martin and M. G. Ryskin, Phys. Lett. **B787**, 167 (2018), [arXiv:1809.10406].

Astrophysics and Cosmology

21. Experimental tests of gravitational theory (rev.)	431
22. Big-Bang cosmology (rev.)	444
23. Inflation (rev.)	457
24. Big-Bang nucleosynthesis (rev.)	474
25. Cosmological parameters (rev.)	482
26. Neutrinos in cosmology (rev.)	491
27. Dark matter (rev.)	499
28. Dark energy (rev.)	515
29. Cosmic microwave background (rev.)	524
30. Cosmic rays (rev.)	535





21. Experimental Tests of Gravitational Theory

Revised August 2023 by T. Damour (IHES, Bures-sur-Yvette).

21.1 General Relativity

Einstein's theory of General Relativity (GR), the current “standard” theory of gravitation, describes gravity as a universal deformation of the Minkowski metric:

$$g_{\mu\nu}(x^\lambda) = \eta_{\mu\nu} + h_{\mu\nu}(x^\lambda), \text{ where } \eta_{\mu\nu} = \text{diag}(-1, +1, +1, +1). \quad (21.1)$$

GR is classically defined by two postulates, embodied in the total action defining the theory:

$$S_{\text{tot}}[g_{\mu\nu}, \psi, A_\mu, H] = c^{-1} \int d^4x (\mathcal{L}_{\text{Ein}} + \mathcal{L}_{\text{SM}}). \quad (21.2)$$

The first postulate states that the Lagrangian density describing the propagation and self-interaction of the gravitational field is

$$\mathcal{L}_{\text{Ein}}[g_{\alpha\beta}] = \frac{c^4}{16\pi G} \sqrt{g} g^{\mu\nu} R_{\mu\nu}(g_{\alpha\beta}), \quad (21.3)$$

where G denotes Newton's constant, $g = -\det(g_{\mu\nu})$, $g^{\mu\nu}$ is the matrix inverse of $g_{\mu\nu}$, and where the Ricci tensor $R_{\mu\nu} \equiv R^\alpha{}_{\mu\alpha\nu}$ is the only independent trace of the curvature tensor

$$R^\alpha{}_{\mu\beta\nu} = \partial_\beta \Gamma_{\mu\nu}^\alpha - \partial_\nu \Gamma_{\mu\beta}^\alpha + \Gamma_{\sigma\beta}^\alpha \Gamma_{\mu\nu}^\sigma - \Gamma_{\sigma\nu}^\alpha \Gamma_{\mu\beta}^\sigma, \quad (21.4)$$

$$\Gamma_{\mu\nu}^\lambda = \frac{1}{2} g^{\lambda\sigma} (\partial_\mu g_{\nu\sigma} + \partial_\nu g_{\mu\sigma} - \partial_\sigma g_{\mu\nu}). \quad (21.5)$$

The second postulate states that $g_{\mu\nu}$ (and its associated connection) couples universally, and minimally, to all the bosonic (respectively fermionic) fields of the Standard Model by replacing everywhere the Minkowski metric $\eta_{\mu\nu}$ (respectively the flat Minkowski connection). Schematically (suppressing matrix indices and labels for the various gauge fields and fermions and for the Higgs doublet),

$$\begin{aligned} \mathcal{L}_{\text{SM}}[\psi, A_\mu, H, g_{\mu\nu}] = & \\ & - \frac{1}{4} \sum \sqrt{g} g^{\mu\alpha} g^{\nu\beta} F_{\mu\nu}^\alpha F_{\alpha\beta}^\nu - \sum \sqrt{g} \bar{\psi} \gamma^\mu (D_\mu + \frac{1}{4} \omega_{ij\mu} \gamma^{ij}) \psi \\ & - \frac{1}{2} \sqrt{g} g^{\mu\nu} \bar{D}_\mu \bar{H} D_\nu H - \sqrt{g} V(H) - \sum \lambda \sqrt{g} \bar{\psi} H \psi. \end{aligned} \quad (21.6)$$

Here $F_{\mu\nu}^\alpha = \partial_\mu A_\nu^\alpha - \partial_\nu A_\mu^\alpha + g_A f_{bc}^\alpha A_\mu^b A_\nu^c$ and the (representation-dependent) gauge-field covariant derivative $D_\mu = \partial_\mu + g_A A_\mu^\alpha T_\alpha^{\text{rep}}$ are defined as in Special Relativity, while the derivative of spin- $\frac{1}{2}$ fermions also includes a coupling to the gravitational “spin-connection” $\omega_{ij\mu} = -\omega_{ji\mu}$, via its contraction with $\gamma^{ij} = \frac{1}{2}(\gamma^i \gamma^j - \gamma^j \gamma^i)$, where $i, j = 0, 1, 2, 3$ and $\gamma^i = e^\mu{}_{i\mu} \gamma^\mu$ are usual (numerical) Dirac matrices satisfying $\gamma^i \gamma^j + \gamma^j \gamma^i = 2\eta^{ij}$. The connection components $\omega_{ij\mu}$ are defined in terms of the local orthonormal frame (vierbein) $e^i{}_\mu$ (such that $g_{\mu\nu} = \eta_{ij} e^i{}_\mu e^j{}_\nu$) used to describe the components of the various fermions ψ , and of its inverse $e_i{}^\mu$ (such that $e_i{}^\mu e^j{}_\mu = \delta_i^j$), by $\omega_{ij\mu} = \frac{1}{2} (C_{i[jk]} + C_{j[ki]} - C_{k[ij]}) e_k{}^\mu$ where $C_{i[jk]} = \eta_{is} C^s{}_{[jk]}$, with $C^i{}_{[jk]} \equiv (\partial_\mu e^i{}_\nu - \partial_\nu e^i{}_\mu) e_j{}^\mu e_k{}^\nu$. From the total action follow Einstein's field equations,

$$R_{\mu\nu} - \frac{1}{2} R g_{\mu\nu} = \frac{8\pi G}{c^4} T_{\mu\nu}. \quad (21.7)$$

Here $R = g^{\mu\nu} R_{\mu\nu}$ is the scalar curvature, and $T_{\mu\nu} \equiv g_{\mu\alpha} g_{\nu\beta} T^{\alpha\beta}$ where $T^{\mu\nu} = (2/\sqrt{g}) \delta \mathcal{L}_{\text{SM}} / \delta g_{\mu\nu}$ is the (symmetric) energy-momentum tensor of the Standard Model matter. The theory is invariant under arbitrary coordinate transformations: $x^\mu = f^\mu(x^\nu)$ (as well as under arbitrary local $\text{SO}(3,1)$ rotations of the vierbein, $e^i{}_\mu = \Lambda^i{}_j(x) e'^j{}_\mu$). To solve the field equations Eq. (21.7), one needs to fix the coordinate gauge freedom, e.g., the “harmonic gauge” (which is the analogue of the Lorenz gauge, $\partial_\mu A^\mu = 0$, in electromagnetism) corresponds to imposing the condition $\partial_\nu (\sqrt{g} g^{\mu\nu}) = 0$.

In this *Review*, we only consider the classical limit of gravitation (i.e. classical matter and classical gravity). Quantum

gravitational effects are expected (when considered at low energy) to correct the classical action Eq. (21.2) by additional terms involving quadratic and higher powers of the curvature tensor. This suggests that the validity of classical gravity extends (at most) down to length scales of order the Planck length $L_P = \sqrt{\hbar G/c^3} \simeq 1.62 \times 10^{-33}$ cm, i.e., up to energy scales of order the Planck energy $E_P = \sqrt{\hbar c^5/G} \simeq 1.22 \times 10^{19}$ GeV. Considering quantum matter in a classical gravitational background also poses interesting challenges, notably the possibility that the zero-point fluctuations of the matter fields generate a nonvanishing vacuum energy density ρ_{vac} , corresponding to a term $-\sqrt{g} \rho_{\text{vac}}$ in \mathcal{L}_{SM} [1]. This is equivalent to adding a “cosmological constant” term $+\Lambda g_{\mu\nu}$ on the left-hand side of Einstein's equations, Eq. (21.7), with $\Lambda = 8\pi G \rho_{\text{vac}}/c^4$. Recent cosmological observations (see the following *Reviews*) suggest a positive value of Λ corresponding to $\rho_{\text{vac}} \approx (2.3 \times 10^{-3} \text{eV})^4$. Such a small value has a negligible effect on the non-cosmological tests discussed below.

21.2 Key features and predictions of GR

The definition of GR recalled above makes predictions both about the coupling of gravity to matter, and about the structure of the gravitational field beyond its previously known Newtonian aspects.

21.2.1 Equivalence Principle

First, the universal nature of the coupling between $g_{\mu\nu}$ and the Standard Model matter postulated in Eq. (21.6) entails many observable consequences that go under the generic name of “Equivalence Principle”.

A first aspect of the Equivalence Principle is that the outcome of a local non-gravitational experiment, referred to local standards, should not depend on where, when, and in which locally inertial frame, the experiment is performed. This means, for instance, that local experiments should neither feel the cosmological evolution of the Universe (constancy of the “constants”), nor exhibit preferred directions in spacetime (isotropy of space, local Lorentz invariance).

A second aspect of the Equivalence Principle is that the kinetic terms, $g^{\mu\nu} \partial_\mu \phi \partial_\nu \phi$ or $\bar{\psi} \gamma^i e_i{}^\mu \partial_\mu \psi$, of all the fields of Nature (including the gravitational field itself) are universally coupled to the same curved spacetime metric $g_{\mu\nu}(x) = \eta_{ij} e^i{}_\mu e^j{}_\nu$. This implies in particular that all massless fields should propagate with the same speed.

A third aspect of the Equivalence Principle is that two (electrically neutral) test bodies dropped at the same location and with the same velocity in an external gravitational field should fall in the same way, independently of their masses and compositions (“universality of free fall” or “Weak Equivalence Principle”). In addition, the study (using the nonlinear structure of GR) of the motion, in an external gravitational field, of bodies having a non-negligible, or even strong, self-gravity (such as planets, neutron stars, or black holes) has shown that the latter property of free-fall universality holds equally well for self-gravitating bodies (“Strong Equivalence Principle”).

A last aspect of the Equivalence Principle concerns various universality features of the gravitational redshift of clock rates. GR predicts that, when intercomparing them by means of electromagnetic signals, two (non gravity-based) clocks located along two different spacetime worldlines should exhibit a universal difference in clock rate that depends on their worldlines, but that is independent of their nature and constitution. For instance, two clocks located at two different positions in a static external Newtonian potential $U(\mathbf{x}) = \sum Gm/r$ should exhibit, when intercompared by electromagnetic signals, the difference in clock rate, $\tau_1/\tau_2 = \nu_2/\nu_1 = 1 + [U(\mathbf{x}_1) - U(\mathbf{x}_2)]/c^2 + O(1/c^4)$, (“universal gravitational redshift of clock rates”). Similarly, the comparison of atomic-transition frequencies when observing on Earth a transition that took place on a far-away galaxy should involve (at lowest order in cosmological perturbations) the universal cosmological redshift factor $1+z = a(t_{\text{reception}})/a(t_{\text{emission}})$ between the Friedmann scale factors $a(t)$ (see below).

21.2.2 Quasi-stationary, weak-field (post-Newtonian) gravity

When applied to quasi-stationary, weak-field gravitational fields, Einstein equations, Eq. (21.7), entail a spacetime structure which predicts deviations from Newtonian gravity of the first post-Newtonian (1PN) order, *i.e.*, fractionally smaller than Newtonian effects by a factor $O(v^2/c^2) \sim O(GM/(c^2 r))$. The 1PN-accurate solution of Eq. (21.7) reads (in harmonic gauge)

$$\begin{aligned} g_{00} &= -1 + \frac{2}{c^2}V - \frac{2}{c^4}V^2 + O\left(\frac{1}{c^6}\right), \\ g_{0i} &= -\frac{4}{c^3}V_i + O\left(\frac{1}{c^5}\right), \\ g_{ij} &= \delta_{ij}\left[1 + \frac{2}{c^2}V\right] + O\left(\frac{1}{c^4}\right), \end{aligned} \quad (21.8)$$

where $x^0 = ct$, $i, j = 1, 2, 3$, and where the scalar, V , and vector, V_i , (retarded) potentials are defined in terms of the sources $\sigma = \frac{T^{00} + T^{ii}}{c^2}$, $\sigma_i = \frac{T^{0i}}{c}$ by

$$V = \square_{\text{ret}}^{-1}[-4\pi G\sigma]; \quad V_i = \square_{\text{ret}}^{-1}[-4\pi G\sigma_i]. \quad (21.9)$$

In GR the gravitational interaction of N moving point masses (labeled by $A = 1, \dots, N$) is described by a reduced (classical) action that admits a diagrammatic expansion:

$$S_{\text{reduced}} = S^{\text{free}} + S^{\text{tree-level}} + S^{\text{one-loop}} + \dots \quad (21.10)$$

where the free (special-relativistic) action reads

$$\begin{aligned} S^{\text{free}} &= -\sum_A \int m_A c \sqrt{-\eta_{\mu\nu} dx_A^\mu dx_A^\nu} \\ &= -\sum_A \int dt m_A c^2 \sqrt{1 - \mathbf{v}_A^2/c^2}, \end{aligned} \quad (21.11)$$

while the tree-level (one-graviton-exchange) interaction term reads

$$S^{\text{tree-level}} = -\frac{8\pi G}{c^4} \int d^4x T^{\mu\nu} \square^{-1}(T_{\mu\nu} - \frac{1}{2}T\eta_{\mu\nu}) = \int dt L^{(2)}. \quad (21.12)$$

Corresponding to the 1PN-accurate metric of Eq. (21.8), the 1PN-accurate expansion of the latter tree-level, two-body interaction Lagrangian $L^{(2)}$ reads (with $r_{AB} \equiv |\mathbf{x}_A - \mathbf{x}_B|$, $\mathbf{n}_{AB} \equiv (\mathbf{x}_A - \mathbf{x}_B)/r_{AB}$)

$$\begin{aligned} L^{(2)} &= \frac{1}{2} \sum_{A \neq B} \frac{G m_A m_B}{r_{AB}} \left[1 + \frac{3}{2c^2}(v_A^2 + v_B^2) - \frac{7}{2c^2}(\mathbf{v}_A \cdot \mathbf{v}_B) \right. \\ &\quad \left. - \frac{1}{2c^2}(\mathbf{n}_{AB} \cdot \mathbf{v}_A)(\mathbf{n}_{AB} \cdot \mathbf{v}_B) + O\left(\frac{1}{c^4}\right) \right] \end{aligned} \quad (21.13)$$

The two-body interactions, Eq. (21.13), exhibit v^2/c^2 corrections to Newton's $1/r$ potential induced by spin-2 exchange ("gravitomagnetism"). Consistency at the 1PN level, $v^2/c^2 \sim Gm/rc^2$, requires that one also considers the three-body interactions contained in the one-loop contribution $S^{\text{one-loop}}$, corresponding to terms induced by some of the three-graviton vertices and other non-linearities (terms $O(h^2)$ and $O(hT)$ in Eq. (21.15) below), *i.e.*, to the $O(V^2)$ term in Eq. (21.8):

$$L^{(3)} = -\frac{1}{2} \sum_{B \neq A \neq C} \frac{G^2 m_A m_B m_C}{r_{AB} r_{AC} c^2} + O\left(\frac{1}{c^4}\right). \quad (21.14)$$

21.2.3 Gravitational Waves in GR

The linearized approximation to Einstein's field equations, Eq. (21.7), in harmonic gauge $\partial^\nu(h_{\mu\nu} - \frac{1}{2}h\eta_{\mu\nu}) = 0$ (with $h \equiv \eta^{\mu\nu}h_{\mu\nu}$), reads

$$\square h_{\mu\nu} = -\frac{16\pi G}{c^4}(T_{\mu\nu} - \frac{1}{2}T\eta_{\mu\nu}) + O(h^2) + O(hT). \quad (21.15)$$

Outside of any source (*i.e.*, when $T_{\mu\nu} = 0$), this yields $\square h_{\mu\nu} = 0$, with $\partial^\nu(h_{\mu\nu} - \frac{1}{2}h\eta_{\mu\nu}) = 0$. The generic linearized solution (modulo the diffeomorphism freedom) of the latter vacuum Einstein equations can be written as (with $k^2 = k \cdot k = \eta_{\mu\nu}k^\mu k^\nu$, $k \cdot x = k_\mu x^\mu$)

$$h_{\mu\nu}(x) = \int d^4k \delta(k^2) \epsilon_{\mu\nu}(k) e^{ik \cdot x}, \quad (21.16)$$

where the polarization tensor $\epsilon_{\mu\nu}(k)$ must be transverse ($\epsilon_{\mu\nu}k^\nu = 0$) and traceless ($\eta^{\mu\nu}\epsilon_{\mu\nu} = 0$). In addition, $\epsilon_{\mu\nu}(k)$ can be freely submitted to the gauge freedom $\epsilon'_{\mu\nu} = \epsilon_{\mu\nu} + \xi_\mu k_\nu + \xi_\nu k_\mu$. This implies that gravitational waves (GW) propagate with the speed of light, and (like electromagnetic waves) have only two independent polarizations. In a frame where, say, $k^\mu = (ck, 0, 0, k)$, the two independent linear polarization tensors can be taken to have components only in the transverse 1-2 plane, of the following form: $\epsilon_{11}^+ = -\epsilon_{22}^+ = \epsilon^+$, with $\epsilon_{12}^+ = \epsilon_{21}^+ = 0$; or $\epsilon_{11}^\times = +\epsilon_{22}^\times = \epsilon^\times$, with $\epsilon_{12}^\times = \epsilon_{21}^\times = 0$. Under a little-group rotation of angle θ in the 1-2 plane, the two circular polarization amplitudes $\epsilon^{(\pm)} = \epsilon^+ \mp i\epsilon^\times$ vary as $\epsilon'^{(\pm)} = e^{\pm 2i\theta} \epsilon^{(\pm)}$, thereby characterizing the helicity-2 nature of GWs.

When solving the inhomogeneous equation Eq. (21.15), taking into account the nonlinear contributions $O(h^2) + O(hT)$, one finds that, to lowest order, the GW amplitude emitted at large distances by a matter distribution is given by the following "quadrupole formula"

$$h_{ij}^{\text{TT}}(T, \mathbf{X}) \approx \frac{2G}{c^4} P_{ijab}^{\text{TT}}(\mathbf{N}) \frac{\ddot{Q}_{ab}(T - R/c)}{R}, \quad (21.17)$$

where $Q_{ij}(t) = \int d^3x \sigma(t, \mathbf{x})(x^i x^j - \frac{1}{3}\delta_{ij} \mathbf{x}^2)$ ($a, b, i, j = 1, 2, 3$) is the quadrupole moment of the source, $R = |\mathbf{X}|$ the distance to the source, $\mathbf{N} = \mathbf{X}/R$ the unit direction from the source to the observer, and $P_{ijab}^{\text{TT}}(\mathbf{N}) = (\delta_{ia} - N_i N_a)(\delta_{jb} - N_j N_b) - \frac{1}{2}(\delta_{ij} - N_i N_j)(\delta_{ab} - N_a N_b)$ the transverse-traceless projector onto the 2-plane orthogonal to \mathbf{N} .

21.2.4 Strong gravitational fields: neutron stars and black holes

The nonlinear structure of Einstein's equations implies many predictions for strong gravitational fields that distinguish GR from Newtonian gravity. For instance, in Newtonian gravity, there is no upper limit to the dimensionless gravitational potential U/c^2 , with U satisfying Poisson's equation $\Delta U = -4\pi G\rho$, where ρ denotes the Newtonian mass density. By contrast, in GR, the dimensionless surface gravitational potential $GM/(c^2 R)$ of a spherically symmetric (perfect fluid) body cannot exceed $\frac{4}{9}[2]$.

Given an equation of state $p = f(\rho)$ modeling the interior of a (cold) spherically symmetric body (say a non-rotating neutron star), Einstein equations, Eq. (21.7), with $T^{\mu\nu} = (\rho + p)u^\mu u^\nu + pg^{\mu\nu}$, and

$$g_{\mu\nu} dx^\mu dx^\nu = -e^{2\Phi(r)} c^2 dt^2 + \frac{dr^2}{1 - \frac{2GM(r)}{c^2 r}} + r^2 (d\theta^2 + \sin^2 \theta d\phi^2), \quad (21.18)$$

yield the following Tolman-Oppenheimer-Volkoff radial equations:

$$p'(r) = -\frac{G(\rho + p/c^2)(M(r) + 4\pi r^3 p/c^2)}{r^2(1 - 2GM(r)/(c^2 r))}; \quad (21.19)$$

$$M'(r) = 4\pi r^2 \rho; \quad (21.20)$$

$$\Phi'(r) = \frac{G(M(r) + 4\pi r^3 p/c^2)}{r^2(1 - 2GM(r)/(c^2 r))}. \quad (21.21)$$

In the exterior of the star ($r \geq R$), the metric takes the Schwarzschild form

$$\begin{aligned} g_{\mu\nu} dx^\mu dx^\nu &= -\left(1 - \frac{2GM}{c^2 r}\right) c^2 dt^2 + \frac{dr^2}{1 - \frac{2GM}{c^2 r}} \\ &\quad + r^2 (d\theta^2 + \sin^2 \theta d\phi^2), \end{aligned} \quad (21.22)$$

where $M \equiv M(R)$ is the total gravitational mass of the star. GR predicts, for any given $p = f(\rho)$, several (in principle) observable

features of neutron stars, such as: (i) the maximum mass of a neutron star; (ii) the relation between the radius R and the total mass M ; (iii) the dimensionless surface gravitational potential $GM/(c^2R)$ (linked to the surface redshift $\sqrt{-g_{00}} = \sqrt{1 - \frac{2GM}{c^2R}}$ measured by an observer at infinity); (iv) the moment of inertia; and (v) the Love number (tidal polarizability). The current uncertainty on the equation of state of a neutron star yields the GR-predicted approximate range for the maximum mass of non-rotating neutron stars $1.5 M_\odot \lesssim M_{\max} \lesssim 2.5 M_\odot$, and the absolute upper bound $M_{\max} < 3 M_\odot$ [3]. The surface gravitational potential of a typical neutron star is $GM/c^2 R_{\text{NS}} \simeq 0.17$, which is a factor $\sim 10^8$ higher than the surface potential of the Earth, and a mere factor 3 below the black hole limit $GM/c^2 R_{\text{BH}} = \frac{1}{2}$ to be discussed next.

The existence of a maximum mass for a neutron star led Oppenheimer and Snyder [4] to predict that the end point of stellar evolution for sufficiently heavy stars, after exhaustion of all thermonuclear sources of energy, will be what are now called “black holes.” The latter are solutions of Einstein’s equations whose past structure involves a gravitationally collapsing star, but whose presently observable structure is essentially described (for non-rotating black holes) by the vacuum Schwarzschild solution Eq. (21.22). It took many years for theoretical (and mathematical) physicists to understand that the apparent singularity of the Schwarzschild solution at $r = \frac{2GM}{c^2}$ was a coordinate singularity and that the Schwarzschild spacetime was regular at the “black hole horizon”, $R_{\text{BH}} \equiv \frac{2GM}{c^2}$. The rotating analog of the Schwarzschild spacetime is the Kerr black hole [5].

Black holes are outstanding consequences of GR which enjoy many remarkable properties, notably: (i) presence of a one-way surface (the horizon) for all waves and particles; (ii) absence of “hair” (*i.e.*, barring a possible electric charge, their structure is fully described by only two parameters, total mass, M , and total angular momentum, $J \leq GM^2/c$); (iii) existence of a spectrum of damped quasi-normal vibrational modes; and (iv) a behavior under external perturbations similar to ordinary physical objects satisfying the laws of (dissipative) thermodynamics. Moreover, though no classical waves or particles can get out of the horizon, black holes are predicted to slowly evaporate via quantum particle creation.

21.2.5 Cosmology

To complete our short tour of the main predictions of GR, let us mention that GR offers the current standard framework for describing the large-scale structure of the Cosmos, from the nearly homogeneous Big Bang (and its plausible inflationary beginning) to the current inhomogeneous Universe undergoing an accelerated expansion. The spacetime structure on large (temporal and spatial) scales is well described by a solution of Einstein’s equations of the form

$$ds^2 = -(1 + 2\Phi(t, \mathbf{x}))c^2 dt^2 + 2W_i(t, \mathbf{x})dt dx^i + a^2(t)((1 - 2\Psi(t, \mathbf{x}))\delta_{ij} + h_{ij}(t, \mathbf{x}))dx^i dx^j, \quad (21.23)$$

where, after a suitable gauge-fixing [6], $W_i(t, \mathbf{x})$ is transverse, while $h_{ij}(t, \mathbf{x})$ is transverse and traceless. The source $T^{\mu\nu}$ must involve a certain number of postulated ingredients: an inflaton field; the matter of the Standard Model; a dark matter component; and a cosmological constant contribution $T_\Lambda^{\mu\nu} = -\rho_{\text{vac}}g^{\mu\nu}$, with $\rho_{\text{vac}} \equiv c^4\Lambda/(8\pi G)$. The scale factor $a(t)$ of the Friedmann background metric $ds_0^2 = -c^2 dt^2 + a^2(t)\delta_{ij}dx^i dx^j$ satisfies the GR-predicted Friedmann equations (with vanishing spatial curvature $k = 0$),

$$H^2 \equiv \left(\frac{\dot{a}}{a}\right)^2 = \frac{8\pi G}{3}\rho_{\text{tot}}, \quad (21.24)$$

$$\frac{\ddot{a}}{a} = -\frac{4\pi G}{3}\left(\rho_{\text{tot}} + \frac{3}{c^2}p_{\text{tot}}\right), \quad (21.25)$$

while the scalar $(\Phi(t, \mathbf{x}), \Psi(t, \mathbf{x}))$, vector $(W_i(t, \mathbf{x}))$, and tensor $(h_{ij}(t, \mathbf{x}))$ inhomogeneous perturbations satisfy some GR-predicted propagation equations (coupled to matter perturbations); see [6] and the following *Reviews*. When the cosmic fluid is

well approximated by a perfect fluid, Einstein’s equations predict the following link between the scalar perturbations

$$\Phi(t, \mathbf{x}) = \Psi(t, \mathbf{x}). \quad (21.26)$$

21.3 A roadmap of parametrizations of deviations from GR, and of modified gravity

As will be discussed below, all currently performed gravitational experiments are compatible with GR. However, similarly to what is done in discussions of precision electroweak experiments, it is useful to quantify the significance of precision gravitational experiments by parameterizing possible deviations from GR. One can distinguish two main approaches to considering, and parameterizing, deviations from GR: (i) theory-agnostic phenomenological approaches; or, (ii) the study of the predictions of specific classes of alternative theories of gravity. Both types have led to useful ways of discussing tests of gravity. Both types also have their limitations. Considering them together leads to cross-fertilization.

21.3.1 Theory-agnostic phenomenological approaches to parameterizing deviations from GR

The theory-agnostic phenomenological approach is the oldest, and, arguably, the most robust one. It essentially consists in starting from specific observable predictions within the considered standard theory, and of deforming them by introducing some free parameters measuring either deviations from effects already present within the standard theory, or new effects absent from the standard theory. A classic example is the periastron advance of Mercury (and the other planets). When working within Newtonian gravity as a standard theory of gravity, the rate of periastron advance of Mercury, $\dot{\omega}$, is (when neglecting the quadrupole moment of the Sun) a calculable function of the masses and semi-major axes of the other planets of the solar system, say $\dot{\omega}^{\text{Newton}}(m_i, a_i)$. However, $\dot{\omega}$ is also a directly observable quantity, so that one can parameterize the periastron advance of Mercury by writing

$$\dot{\omega}^{\text{obs}} = \dot{\omega}^{\text{Newton}}(m_i, a_i) + \Delta\dot{\omega}. \quad (21.27)$$

Using other observable data to determine some “observed” values of the m_i ’s and a_i ’s, one can then measure the anomalous periastron precession $\Delta\dot{\omega}$ and see whether it is compatible with zero, or not. As is well-known, Leverrier used such a methodology and, in 1859, measured an anomalous periastron precession of about $\Delta\dot{\omega} \simeq 38$ arcsec/century (later re-estimated at 43 arcsec/century), which was explained in 1915 as a GR prediction. Let us discuss further examples of the use of such theory-agnostic approaches for discussing deviations from GR.

21.3.2 Parameterized post-Newtonian (PPN) formalism.

When considering the weak-field slow-motion limit appropriate to describing gravitational experiments in the solar system, it has been traditional to parameterize possible (long-range) deviations from the GR-predicted 1PN metric by introducing extra dimensionless coefficients in the various terms of the metric of Eq. (21.8). The minimal version of the parameterized post-Newtonian (PPN) formalism (essentially due to Eddington) involves only two parameters β and γ , namely

$$g_{00} = -1 + \frac{2}{c^2}V - \frac{2\beta}{c^4}V^2 + O\left(\frac{1}{c^6}\right), \quad (21.28)$$

$$g_{0i} = -\frac{2(\gamma+1)}{c^3}V_i + O\left(\frac{1}{c^5}\right), \quad (21.29)$$

$$g_{ij} = \delta_{ij}\left[1 + \frac{2\gamma}{c^2}V\right] + O\left(\frac{1}{c^4}\right), \quad (21.30)$$

with V and V_i defined by Eq. (21.9), with the same vectorial source $\sigma_i = \frac{T^{0i}}{c}$, but a modified scalar source

$$\sigma^{\text{PPN}} = \frac{1}{c^2}\left[\left(1 + (3\gamma - 2\beta - 1)\frac{V}{c^2}\right)T^{00} + \gamma T^{ii}\right]. \quad (21.31)$$

In GR, $\beta^{\text{GR}} = 1$ and $\gamma^{\text{GR}} = 1$, so that deviations from GR are parameterized by $\bar{\beta} \equiv \beta - 1$ and $\bar{\gamma} \equiv \gamma - 1$. Richer versions of the

PPN formalism (involving up to ten parameters) were developed in interaction with the study of classes of alternative theories of gravity [7, 8]. This led to parameterizing new types of contributions to the IPN metric that are absent in the GR framework.

When deriving the IPN-accurate dynamics of N point masses predicted by the PPN-modified metric, Eq. (21.28), one finds that the free Lagrangian is not modified (because we are considering here a Lorentz-invariant subclass of PPN metrics), while there are modifications of both the two-body Lagrangian, $L^{(2)}$, Eq. (21.13), and the three-body one, $L^{(3)}$, Eq. (21.14). More precisely, denoting $\eta \equiv 4\bar{\beta} - \bar{\gamma}$, the Newtonian interaction energy term in Eq. (21.13) is modified into $G_{AB}m_A m_B/r_{AB}$, with a body-dependent gravitational “constant”

$$G_{AB} = G[1 + \eta(E_A^{\text{grav}}/m_A c^2 + E_B^{\text{grav}}/m_B c^2) + O(1/c^4)], \quad (21.32)$$

where E_A^{grav} denotes the gravitational binding energy of body A . In addition, there is the additional contribution $+\bar{\gamma}(\mathbf{v}_A - \mathbf{v}_B)^2/c^2$ in the brackets on the right-hand side of $L^{(2)}$, Eq. (21.13). As for the three-body interaction term $L^{(3)}$, Eq. (21.14), it is modified by the overall factor $1 + 2\bar{\beta}$.

These results show how the introduction of the two minimal PPN deviation parameters $\bar{\beta} \equiv \beta - 1$ and $\bar{\gamma} \equiv \gamma - 1$ suffices to introduce many different observable effects. Some of them (the ones linked with $\bar{\gamma}$) concern deviations at the linearized (one-graviton-exchange) level (and affect, for instance, light deflection and time-delay effects), while the deviation parameter $\bar{\beta}$ parameterizes effects linked to the cubic vertex of Einstein’s gravity (and affects, for instance, periastron precession). Of particular interest is the fact that Eq. (21.32) shows that the combination $\eta \equiv 4\bar{\beta} - \bar{\gamma}$ parameterizes a violation of the Strong Equivalence Principle, because the gravitational interaction between self-gravitating bodies is seen to be influenced by the gravitational binding energy of each body [9]. As stated above, this effect is absent in GR (where $\eta^{\text{GR}} = 0$). This is an example where the fact of contrasting GR with some deviations from it gives physical significance to a null effect in GR (namely the universality of free fall of self-gravitating bodies).

Finally, one can extend the PPN formalism by allowing for a slow, phenomenological time variation of Newton’s constant:

$$G(t) = G_0 \left[1 + \frac{\dot{G}_0}{G_0}(t - t_0) \right]. \quad (21.33)$$

Here, one assumes that there exist units in which the masses, m_i , of elementary particles stay constant, and that G is measured in such units. A possible time variation of G then corresponds to a possible common variation of the dimensionless couplings $Gm_i^2/(\hbar c)$.

21.3.3 Parameterized post-Keplerian (PPK) formalism.

The discovery of pulsars (*i.e.*, rotating neutron stars emitting a beam of radio noise) in gravitationally bound orbits [10, 11] has given us our first experimental handle on a regime of relativistic gravity going significantly beyond the uniformly weak-field, and quasi-stationary regime of solar-system gravity. Binary pulsars allow us to probe some radiative effects, and also some strong-gravitational-field effects. In these systems, the finite speed of propagation of the gravitational interaction between the pulsar and its companion generates damping-like terms at order $(v/c)^5$ in the equations of motion [12]. These damping forces are the local counterparts of the gravitational radiation emitted at infinity by the system (“gravitational radiation reaction”). They cause the binary orbit to shrink and its orbital period P_b to decrease. The remarkable stability of pulsar clocks has allowed one to measure the corresponding very small orbital period decay $\dot{P}_b \equiv dP_b/dt \sim -(v/c)^5 \sim -10^{-12} - 10^{-14}$ in several binary systems, thereby giving us a direct experimental handle on the propagation properties of the gravitational field. In addition, the large surface gravitational potential of a neutron star allows one to probe the quasi-static strong-gravitational-field regime, as is discussed below.

It is possible to extract phenomenological (theory-independent) tests of gravity from binary pulsar data by using the parameter-

ized post-Keplerian (PPK) formalism [13]. The basis of this formalism is the fact that, after correcting for the Earth’s motion around the Sun and for the dispersion due to propagation in the interstellar plasma, the time of arrival of the N th pulse t_N can be described by a generic, parameterized “timing formula” [13, 14], whose functional form is common to the whole class of tensor-scalar gravitation theories:

$$t_N - t_0 = F[T_N(\nu_p, \dot{\nu}_p, \ddot{\nu}_p); \{p^K\}; \{p^{PK}\}]. \quad (21.34)$$

Here, T_N is the pulsar proper time corresponding to the N th turn given by $N/2\pi = \nu_p T_N + \frac{1}{2}\dot{\nu}_p T_N^2 + \frac{1}{6}\ddot{\nu}_p T_N^3$ (with $\nu_p \equiv 1/P_p$ the spin frequency of the pulsar, *etc.*), $\{p^K\} = \{P_b, T_0, e, \omega_0, x\}$ is the set of “Keplerian” parameters (notably, orbital period P_b , eccentricity e , periastron longitude ω_0 and projected semi-major axis $x = a \sin i/c$), and $\{p^{PK}\} = \{k, \gamma_{\text{timing}}, \dot{P}_b, r, s, \delta_\theta, \dot{e}, \dot{x}\}$ denotes the set of (separately measurable) “post-Keplerian” parameters. Most important among these are: the fractional periastron advance per orbit $k \equiv \dot{\omega} P_b / 2\pi$; a dimensionful time-dilation parameter γ_{timing} ; the orbital period derivative \dot{P}_b ; and the “range” and “shape” parameters of the gravitational time delay caused by the companion, r and s .

Without assuming any specific theory of gravity, one can phenomenologically analyze the data from any binary pulsar by least-squares fitting the observed sequence of pulse arrival times to the timing formula of Eq. (21.34). This fit yields the “measured” values of the parameters $\{\nu_p, \dot{\nu}_p, \ddot{\nu}_p\}$, $\{p^K\}$, $\{p^{PK}\}$. Now, each specific relativistic theory of gravity predicts that, for instance, k , γ_{timing} , \dot{P}_b , r , and s (to quote parameters that have been successfully measured from some binary pulsar data) are some theory-dependent functions of the Keplerian parameters and of the (unknown) masses m_1 , m_2 of the pulsar and its companion. For instance, in GR, one finds (with $M \equiv m_1 + m_2$, $n \equiv 2\pi/P_b$),

$$\begin{aligned} k^{\text{GR}}(m_1, m_2) &= 3(1 - e^2)^{-1}(GMn/c^3)^{2/3}, \\ \gamma_{\text{timing}}^{\text{GR}}(m_1, m_2) &= en^{-1}(GMn/c^3)^{2/3}m_2(m_1 + 2m_2)/M^2, \\ \dot{P}_b^{\text{GR}}(m_1, m_2) &= -(192\pi/5)(1 - e^2)^{-7/2} \left(1 + \frac{73}{24}e^2 + \frac{37}{96}e^4 \right) \\ &\quad \times (GMn/c^3)^{5/3}m_1m_2/M^2, \\ r^{\text{GR}}(m_1, m_2) &= Gm_2/c^3, \\ s^{\text{GR}}(m_1, m_2) &= nx(GMn/c^3)^{-1/3}M/m_2. \end{aligned} \quad (21.35)$$

In alternative gravity theories each of the functions $k^{\text{theory}}(m_1, m_2)$, $\gamma_{\text{timing}}^{\text{theory}}(m_1, m_2)$, $\dot{P}_b^{\text{theory}}(m_1, m_2)$, *etc.*, is modified by quasi-static strong field effects (associated with the self-gravities of the pulsar and its companion), while the particular function $\dot{P}_b^{\text{theory}}(m_1, m_2)$ is further modified by radiative effects [15–18]. If one measures $N > 2$ PPK parameters from the data of a specific binary pulsar, these N measurements determine, for each given theory, N curves (defined by the N equations $k_i^{\text{theory}}(m_1, m_2) = k_i^{\text{obs}}$) in the two-dimensional mass plane (m_1, m_2) . This yields $N - 2$ tests of the specified theory, according to whether the N curves (or strips) have one point in common, as they should.

21.3.4 Parameterized-post-Friedmannian (PPF) formalisms.

We have recalled above that, in GR, the two functions, $\Phi(t, \mathbf{x})$, and $\Psi(t, \mathbf{x})$, parameterizing (in the “longitudinal gauge”) the scalar perturbations of the background Friedmann metric are related (in absence of anisotropic stresses) by Eq. (21.26). Several authors [19–28] have defined various types of parameterized-post-Friedmannian (PPF) formalisms involving (generally space and time dependent) phenomenological parameters. The simplest versions of these formalisms involve two phenomenological parameters measuring: (i) the ratio between $\Phi(t, \mathbf{x})$, and $\Psi(t, \mathbf{x})$, say (using a parametrization which parallels the usual PPN parametrization)

$$\Psi(t, \mathbf{x}) = \gamma_{\text{cosmo}}(t, \mathbf{x})\Phi(t, \mathbf{x}); \quad (21.36)$$

and (ii) the effective gravitational constant entering the Poisson equation for $\Phi(t, \mathbf{x})$, say

$$\Delta\Phi(t, \mathbf{x}) = 4\pi G_{\Phi}(t, \mathbf{x})\delta\rho(t, \mathbf{x}). \quad (21.37)$$

However, the peculiarities of cosmological observables limit the domain of applicability of such phenomenological approaches [26] (notably because the strong dependence of cosmological probes on epochs and scales obliges one to rely on specific parameterizations of the functions $\gamma_{\text{cosmo}}(t, \mathbf{x})$ and $G_{\Phi}(t, \mathbf{x})$, e.g., [25, 28]). Approaches based on specific classes of modified-gravity theories allow for a more complete treatment involving, in principle, all existing cosmological observables: Big Bang nucleosynthesis, cosmic microwave background, large-scale structure, Hubble diagram, weak lensing, etc. Discussing the current cosmological tests using either such PPF formalisms, or comparisons with the predictions of modified-gravity theories, is beyond the scope of this review. See [29] for a comprehensive recent discussion. The bottom line is that all present cosmological data have been found to be compatible with GR (within the Friedmann-Lemaître-based Λ CDM model). Beyond the quantitative limits on various parameterized theoretical models [29], one should remember the striking (strong-field-type) qualitative verification of GR embodied in the fact that relativistic cosmological models give an accurate picture of the Universe over a period during which the spatial metric has been blown up by a gigantic factor, say $(1+z)^2 \sim 10^{19}$ between Big Bang nucleosynthesis and now.

21.3.5 Various phenomenological tests of GR from gravitational wave (GW) data

The observations by the US-based Laser Interferometer Gravitational-wave Observatory (LIGO), later joined by the Europe-based Virgo detector, of gravitational-wave (GW) signals [30–34], have opened up a novel testing ground for relativistic gravity. The first three observing runs (O1, O2, O3a and O3b) of the LIGO-Virgo collaboration, recently joined by the Japan-based KAGRA detector (LVK collaboration), have led to the confident detection of 93 GW signals, most of which come from binary black-hole coalescences. These observations are summarized in three GW transient catalogs: GWTC-1 [35], GWTC-2 [36] and GWTC-3 [37].

Several approaches have been used to either test consistency with GR, or to look for special types of possible deviations. Making accurate predictions for GW signals from coalescing black holes within GR took years of both analytical [38, 39] and numerical [40] work. Some works have started (both analytically [15, 41–45] and numerically [46–48]) to derive the corresponding predictions within some modified-gravity theories. Phenomenological approaches are very useful for parameterizing general, conceivable deviations from GR when analyzing the GW signals emitted by coalescing black holes or neutron stars.

A first phenomenological, global consistency test simply consists of measuring the noise-weighted correlation \mathcal{C} between each detected strain signal and the corresponding best-fit GR-predicted waveform. \mathcal{C}^{obs} should be equal to 1, modulo statistical (and/or systematic) errors.

Various other phenomenological tests of the structure of the GR-predicted waveforms emitted by coalescing compact binaries have been suggested. One general idea [49–51] (dubbed “parameterized post-Einsteinian formalism” in [52]) is to modify the GR-predicted Fourier-domain value $\psi(f)$ of the phase of black-hole coalescence GW signals $h(f) = A(f)e^{i\psi(f)}$ by introducing GR-deviation parameters, say

$$\psi(f) = \sum_i \left[p_i^{\text{GR,NS}}(m_1, m_2)(1 + \delta\hat{p}_i) + p_i^{\text{GR,S}}(m_1, m_2, S_1, S_2) \right] \times u_i(f). \quad (21.38)$$

Here, the $u_i(f)$ ’s define a basis of functions of the GW frequency f , and the superscript NS refers to the nonspinning contribution, while the superscript S refers to the spinning one. Such a GR-modification directly applies to the phenomenological representation [53] of $\psi(f)$, and can be generalized to any waveform model by adding the non-GR phase term $\sum_i p_i^{\text{GR,NS}}(m_1, m_2)\delta\hat{p}_i u_i(f)$

to the corresponding GR-predicted Fourier-domain phase $\psi(f)$ [54]. For instance, the leading-order (LO), quadrupolar term in the GR phase evolution during the early inspiral corresponds to $u_0(f) = f^{-5/3}$ and $p_0^{\text{GR}} = \frac{3(m_1+m_2)^2}{128m_1m_2}(\pi G(m_1+m_2)/c^3)^{-5/3}$, while the next-to-leading-order (NLO) term is a $O(v^2/c^2)$ correction $p_2^{\text{GR}}u_2(f)$ with $u_2(f) = f^{-1}$. In the phenomenological model [53] these terms (as well as the other inspiral contributions) are cut-off beyond the frequency $G(m_1+m_2)f/c^3 = 0.018$.

Each dimensionless parameter $\delta\hat{p}_i$ introduces a fractional deviation from the corresponding individual phasing GR effect having the frequency dependence $u_i(f)$, and can, in principle, be extracted by fitting the inspiral part of the observed waveform to the deformed template of Eq. (21.38). However, one must also use this deformed template for simultaneously extracting the values of m_1, m_2, S_1 , and S_2 . Together with signal-to-noise ratio (SNR) considerations, and parameter-correlation issues, this limits the applicability of such a test to introducing only one deformation parameter $\delta\hat{p}_i$ at a time. A particularly meaningful deformation [49] is to leave undeformed the LO and NLO terms $p_0^{\text{GR}}u_0(f) + p_2^{\text{GR}}u_2(f)$ and to vary the third coefficient p_3 parameterizing the next, “GW tail”-related $O(v^3/c^3)$ correction, with $u_3(f) = f^{-2/3}$. Another well-motivated test [52] is to introduce a new coefficient $\delta\hat{p}_{-2}$, which is absent in GR, and which parameterizes an $O((\frac{v}{c})^{-2})$ fractional correction to the LO, quadrupolar term, thereby allowing for a possible dipolar GW flux (indeed, dipolar GW radiation generally exists in theories containing scalar excitations). As p_2^{GR} vanishes, $\delta\hat{p}_{-2}$ is added as an absolute deviation, scaled by the LO term p_0^{GR} .

The coalescence of two black holes, or of a black hole and a neutron star (or of two heavy-enough neutron stars) leads to the formation of a black hole that is initially formed in a perturbed state. The relaxation of the latter perturbed black hole into its stationary, equilibrium state leads to the emission of characteristic (rapidly decaying) ringing GW modes (a.k.a. quasi-normal modes) [55, 56], whose frequencies and decay times are functions of the mass (M_f) and spin ($S_f \equiv GM_f^2 a_f/c$) of the final black hole, say

$$\omega_a = (c^3/GM_f)[2\pi\hat{f}_a^{\text{QNM}}(a_f) - i/\hat{\tau}_a^{\text{QNM}}(a_f)], \quad (21.39)$$

where $a = 1, 2, \dots$ labels the various ringing modes, starting from the least-damped one. In principle, if the SNR is large enough, one can directly test for the presence of one or several of these modes in the post-merger signal, and measure both $\text{Re}(\omega_a)$ and $\text{Im}(\omega_a)$ in a theory-independent way. These phenomenological measurements then lead to null tests of GR, from which one can extract theoretical information about eventual deviations from GR [57, 58].

As recalled above, GR predicts that GWs propagate (in vacuum) at exactly the same speed as light (i.e., they have the same dispersion law $g^{\mu\nu}k_\mu k_\nu = 0$ in curved spacetime). Deviations from such a universal, scale-free dispersion law can be phenomenologically parameterized in several ways. If one phenomenologically assumes that the graviton dispersion law includes a mass term, say $g^{\mu\nu}k_\mu k_\nu + m_g^2/h^2 = 0$, or some more general type of frequency-dependent modification, such changes affect the phasing of the inspiral GW signal and can be directly tested [59]. When one observes both GWs and electromagnetic waves emitted by the same system, one can also directly test whether both types of waves propagate in the same way.

Let us now present some examples of theory-dependent discussions of experimental tests based on considering specific classes of alternative theories. The most conservative deviations from Einstein’s pure spin-2 theory are defined by adding new, bosonic, light or massless, macroscopically coupled fields.

21.3.6 Gravity tests within classes of tensor-scalar theories of gravity

The possible existence of new gravitational-strength couplings leading to deviations from Einsteinian (and Newtonian) gravity has been suggested by many natural extensions of GR, starting with the classic Kaluza-Klein idea, and continuing up to now with the study of extended supergravity theories, and of (super-

)string theory. In particular, a recurrent suggestion of such theories (which dates back to pioneering work by Jordan, and by Fierz [60]) is the existence of a scalar field φ coupled both to the scalar curvature R and to the various $F_{\mu\nu}^a{}^2$ gauge-field actions. Such fields (“dilaton” or “moduli”) generically appear in string theory and are massless at the tree-level, but could acquire a self-interaction potential $V(\varphi)$ beyond the tree-level.

The exchange of such a dilaton-like field leads to several types of observational deviations from GR. For experimental limits on the gravitational inverse-square-law (down to the micrometer range) see Refs. [61–65]. If the potential $V(\varphi)$ is zero or negligible for the considered range, the coupling of φ to $F_{\mu\nu}^a{}^2$ leads to apparent violations of the weak equivalence principle, with rather specific composition-dependence [66]. Next, when neglecting the fractionally small composition-dependent effects, such a field approximately couples to the trace of the energy-momentum tensor $T = g_{\mu\nu}T^{\mu\nu}$. The most general such theory contains (after suitable field redefinitions) two arbitrary functions of the scalar field, namely the self-interaction potential $V(\varphi)$, and a matter-coupling function $a(\varphi)$:

$$\mathcal{L}_{\text{tot}}[g_{\mu\nu}, \varphi, \psi, A_\mu, H] = \frac{c^4}{16\pi G_*} \sqrt{g}(R(g_{\mu\nu}) - 2g^{\mu\nu} \partial_\mu \varphi \partial_\nu \varphi) - \sqrt{g}V(\varphi) + \mathcal{L}_{\text{SM}}[\psi, A_\mu, H, \tilde{g}_{\mu\nu}]. \quad (21.40)$$

Here G_* is a “bare” Newton constant, and the Standard Model matter is coupled not to the “Einstein” (pure spin-2) metric $g_{\mu\nu}$, but to the conformally related (“Jordan-Fierz”) metric

$$\tilde{g}_{\mu\nu} = \exp(2a(\varphi))g_{\mu\nu}. \quad (21.41)$$

The scalar field equation

$$\square_g \varphi = \frac{4\pi G}{c^4} \left(-\alpha(\varphi)T + \frac{\partial V(\varphi)}{\partial \varphi} \right), \quad (21.42)$$

features

$$\alpha(\varphi) \equiv \partial a(\varphi)/\partial \varphi, \quad (21.43)$$

as the basic (field-dependent) coupling between φ and matter [15, 67]. The best-known, special case of these theories is the one-parameter (ω) Jordan-Fierz-Brans-Dicke theory [68], with $V(\varphi) = 0$ and $a(\varphi) = \alpha_0 \varphi$, leading to a field-independent coupling $\alpha(\varphi) = \alpha_0$ (with $\alpha_0^2 = 1/(2\omega + 3)$). More generally, if we consider the massless theories ($V(\varphi) = 0$) with arbitrary (non-linear) coupling function $a(\varphi)$, they modify Einstein’s predictions in the weak-field slow-motion limit appropriate to describing gravitational experiments in the solar system (1PN approximation) only through the appearance of exactly the same two “post-Einstein” dimensionless parameters $\bar{\gamma} = \gamma - 1$ and $\bar{\beta} = \beta - 1$ that entered the minimal (Eddington) PPN formalism presented above. However, we now have the following theoretical expressions relating the latter phenomenological parameters to the coupling functions entering the tensor-scalar action Eq. (21.40):

$$\bar{\gamma} = -2 \frac{\alpha_0^2}{1 + \alpha_0^2}; \quad (21.44)$$

$$\bar{\beta} = +\frac{1}{2} \frac{\beta_0 \alpha_0^2}{(1 + \alpha_0^2)^2}. \quad (21.45)$$

Here $\alpha_0 \equiv \alpha(\varphi_0)$, and $\beta_0 \equiv \partial \alpha(\varphi_0)/\partial \varphi_0$, with φ_0 denoting the vacuum expectation value (VEV) of φ around the solar system. In addition, the observable value G^{obs} of the gravitational constant is found to be field-dependent and given (at a place where $\varphi = \varphi_0$) by

$$G^{\text{obs}} = G(\varphi_0) \equiv G_* \exp[2a(\varphi_0)](1 + \alpha_0^2). \quad (21.46)$$

This makes it clear that the parameter $\bar{\gamma}$ is the basic post-Einstein parameter, which measures the admixture of an additional field (here a spin-0 field) to the pure spin-2 GR. One also sees how the parameter $\bar{\beta}$ is linked to non-linear effects (here coupling terms

$\beta_0(\varphi - \varphi_0)^2 T$ in the action), and how the Nordtvedt parameter $\eta \equiv 4\bar{\beta} - \bar{\gamma}$ is related to the field-dependence of G^{obs} ($\eta = (\alpha_0/(1 + \alpha_0^2))\partial \ln G(\varphi_0)/\partial \varphi_0$).

The advantage of a theory-dependent approach, such as Eq. (21.40), over the phenomenological minimal PPN approach of Eq. (21.28), is that it allows one to consistently predict the observational deviations from GR in all possible gravity regimes: the quasi-stationary weak-field regime; the wavelike weak-field regime; the strong-field regime; the cosmological regime, etc. All such observational deviations can be consistently worked out once one chooses specific forms of the coupling function $a(\varphi)$, and of $V(\varphi)$. The simple choice of a two-parameter quadratic coupling function, say $a(\varphi) = \alpha_0(\varphi - \varphi_0) + \frac{1}{2}\beta_0(\varphi - \varphi_0)^2$, has been found useful for describing many possible observable deviations from GR.

The observable consequences for binary pulsar observations of the strong-field and radiative effects linked to the coupling to φ have been explicitly worked out in Refs. [15, 44] in the case where φ is massless (see Ref. [69] for the case where φ is massive). In particular, the strong-field nature of the pulsar tests is demonstrated by the fact that some tensor-scalar theories can be as close as desired to GR in the weak-field regime of the solar-system (*i.e.*, $\bar{\gamma}$ and $\bar{\beta}$ can be as small as desired, or even exactly zero), while developing (via a “spontaneous scalarization” mechanism) differences of order unity with GR in binary pulsar experiments [17, 18].

21.3.7 Attractor and screening mechanisms in modified gravity

As will follow from the discussion of experimental data below, the comparison between the predictions of general massless tensor-scalar theories and current data shows that the basic coupling parameter α_0 must be tuned to a small value (especially when allowing for composition-dependent effects). This raises the issue of the naturalness of such small coupling parameters. It has been shown in this respect that, in many tensor-scalar theories, there is an *attractor mechanism* by which the cosmological evolution naturally drives the VEV $\varphi_0(t)$ towards a value for which the coupling parameter $\alpha_0 = \alpha(\varphi_0)$ vanishes, thereby making it natural to expect only small deviations from GR (at least for the weak-field regime) at our current cosmological epoch [70, 71].

There are other theoretical mechanisms (generically called “screening mechanisms”) that could explain why a theory of gravity whose theoretical content significantly differs from that of GR could naturally pass all the stringent, GR-compatible experimental limits that will be discussed below. In particular, when considering a self-interacting scalar field ($V(\varphi) \neq 0$), the interplay between the two terms on the right-hand side of Eq. (21.42) tends to drive the local VEV φ_0 of φ to a density-dependent value. In turn, this leads to a corresponding density-dependent effective mass $m_0(\varphi_0) = \sqrt{4\pi G \partial^2 V(\varphi_0)/\partial \varphi_0^2}$ of the φ field, and to density-dependent matter couplings [72]. Various choices of the functions $V(\varphi)$ and $a(\varphi)$ can then reduce the φ -induced deviations from GR in dense environments while still allowing for significant deviations in different (*e.g.*, cosmological) regimes [73–77].

Other screening mechanisms have been invoked, based on an environment dependence mediated by (first or second) derivatives of a scalar degree of freedom. Roughly speaking, such mechanisms involve a (possibly effective) scalar degree of freedom φ that satisfies a field equation that is more general than Eq. (21.42) in that the left-hand side, $\square_g \varphi$, is replaced by a non-linear function of φ , $\partial \varphi$ and $\partial^2 \varphi$. The presence of non-linear derivative self-interactions of φ can weaken the effective coupling of φ to matter. A simple toy-model showing this weakening would be to replace Eq. (21.42) by an equation of the form

$$Z(\varphi, \partial \varphi, \partial^2 \varphi) \square_g \varphi = \frac{4\pi G}{c^4} \left(-\alpha(\varphi)T + \frac{\partial V(\varphi)}{\partial \varphi} \right). \quad (21.47)$$

Such an equation is equivalent, at a first level of approximation, to replacing the gravitational constant G entering Eq. (21.42) by $G_{\text{eff}}(\varphi_0, \partial \varphi_0, \partial^2 \varphi_0) \equiv G/Z_0$, where $Z_0 \equiv Z(\varphi_0, \partial \varphi_0, \partial^2 \varphi_0)$. This has a screening effect if $Z_0 \gg 1$. Indeed, the replacement $G \rightarrow G_{\text{eff}}$ diminishes the strength of the interaction potential due to φ exchange by a factor of $1/Z_0$. In addition, the range of this

interaction is also affected: $m_0(\varphi_0) = \sqrt{4\pi G \partial^2 V(\varphi_0)/\partial \varphi_0^2} \rightarrow m_{0\text{eff}}(\varphi_0, \partial \varphi_0, \partial^2 \varphi_0) = \sqrt{4\pi G_{\text{eff}} \partial^2 V(\varphi_0)/\partial \varphi_0^2} = Z_0^{-1/2} m_0$.

Screening mechanisms based on such non-linear derivative self-interactions are often referred to as being ‘‘Vainshtein-like’’ because a similar mechanism was first invoked in Ref. [78] as a conjectural way to ensure that the extra degrees of freedom associated with a massive (rather than massless) graviton become effectively weakly coupled to matter within a large domain around gravitational sources. Here, one is considering massive deformations of the massless spin-2 metric field of GR by a very small mass, possibly of cosmological scale: $m_g \sim \hbar H_0 \sim 10^{-33}$ eV. The construction of ghost-free potential terms for a spin-2 field has turned out to be a delicate matter [79]. The phenomenology of a very-low-mass graviton is still partly uncontrolled, both because of the unknown extent to which the Vainshtein screening is really active, and because of subtle constraints linked to an eventual UV completion of the theory beyond the unusually low energy scale where it becomes strongly coupled:

$$\Lambda_{\text{strong coupling}} \sim (M_{\text{Planck}} m_0^2)^{1/3} \sim 10^{-13} \left(\frac{m_0}{\hbar H_0} \right)^{2/3} \text{ eV}. \quad (21.48)$$

The search for modified gravity theories incorporating an extra scalar degree of freedom potentially able to yield a Vainshtein-like screening led to writing down the following general class of tensor-scalar Lagrangian [80, 81]:

$$\begin{aligned} L_{\text{tot}}[g_{\mu\nu}, \varphi, \psi] = & G_2(\varphi, X) - G_3(\varphi, X) \square_g \varphi + G_4(\varphi, X) R \\ & + G_{4X}(\varphi, X) [(\square_g \varphi)^2 - \varphi^{\mu\nu} \varphi_{\mu\nu}] \\ & + G_5(\varphi, X) G^{\mu\nu} \varphi_{\mu\nu} - \frac{1}{6} G_{5X}(\varphi, X) (\square_g \varphi)^3 \\ & - 3 \square_g \varphi \varphi^{\mu\nu} + 2 \varphi_{\mu\nu} \varphi^{\mu\lambda} \varphi_{\lambda}^{\nu} + L_{\text{matter}}[g_{\mu\nu}, \psi]. \end{aligned} \quad (21.49)$$

Here $g_{\mu\nu}$ denotes the matter-coupled metric, $X \equiv -\frac{1}{2} g^{\mu\nu} \partial_\mu \varphi \partial_\nu \varphi$, $\varphi_{\mu\nu} \equiv \nabla_\mu \nabla_\nu \varphi$, $G^{\mu\nu} \equiv R^{\mu\nu} - \frac{1}{2} R g^{\mu\nu}$, and the various coefficients $G_n(\varphi, X)$ are arbitrary functions of two variables (with $G_{nX} \equiv \partial G_n / \partial X$). The field equations derived from the Lagrangian of Eq. (21.49) are only of second order in derivatives in spite of the non-linear structure of L_{tot} . This implies that the tensor-scalar theories defined by Eq. (21.49) feature three degrees of freedom, corresponding to a massless spin-2 excitation (GW) and a spin-0 excitation. Contrary to the simpler tensor-scalar theories of Eq. (21.40), it is found that the speed of propagation of GWs implied by Eq. (21.49) is generically different from the speed of light:

$$\frac{c_{\text{GW}}^2}{c^2} = \frac{G_4 - X(\ddot{\varphi} G_{5X} + G_{5\varphi})}{G_4 - 2XG_{4X} - X(H\dot{\varphi}G_{5X} - G_{5\varphi})}. \quad (21.50)$$

More general modified gravity models have been proposed (see, *e.g.* Refs. [82, 83]). Apart from the simplest of them, most of these models have a rather artificial flavor, and do not lead to convincing alternative explanations either of dark matter or of dark energy. In addition, many of them do not lead (contrary to GR) to mathematically ‘‘well-posed’’ evolution problems [84–86]. This entails a serious challenge to deriving strong-field predictions for such models. It has been argued that many of these (dark-energy motivated) models should be viewed as effective field theory (EFT) approximations that need some sort of UV completion at an unusually low frequency scale [87]. In spite of these shortcomings, such models are conceptually interesting because they give examples of deviations for various predictions of GR, existing independently from each other, in various regimes. For instance, some special tensor-scalar models lead to black hole solutions modified by scalar-hair [88–90]. For other types of black holes with scalar-hair, see Ref. [91]. This shows the interest of phenomenologically testing, in a democratic and agnostic way, all conceivable deviations from GR.

Let us now turn to briefly presenting current experimental results of various phenomenological tests of the main GR predictions recalled in Section 21.2 above.

21.4 Experimental tests of the Equivalence Principle (*i.e.*, of the matter-gravity coupling)

21.4.1 Tests of the constancy of constants

Stringent limits on a possible time variation of the basic coupling constants have been obtained by analyzing a natural fission reactor phenomenon that took place at Oklo, Gabon, two billion years ago [92, 93]. These limits are at the 1×10^{-8} level for the fractional variation of the fine-structure constant α_{em} [93], and at the 4×10^{-9} level for the fractional variation of the ratio m_q/Λ_{QCD} between the light quark masses and Λ_{QCD} [94]. The determination of the lifetime of Rhenium 187 from isotopic measurements of some meteorites dating back to the formation of the solar system (about 4.6 Gyr ago) yields comparably strong limits [95]. Measurements of absorption lines in astronomical spectra also give stringent limits on the variability of both α_{em} and $\mu = m_p/m_e$ at cosmological redshifts, *e.g.*,

$$\Delta\alpha_{\text{em}}/\alpha_{\text{em}} = (1.2 \pm 1.7_{\text{stat}} \pm 0.9_{\text{sys}}) \times 10^{-6}, \quad (21.51)$$

at redshifts $z = 1.0\text{--}2.4$ [96], and

$$|\Delta\mu/\mu| < 4 \times 10^{-7} (95\% \text{ C.L.}), \quad (21.52)$$

at a redshift $z = 0.88582$ [97]. There are also significant limits on the variation of α_{em} and $\mu = m_p/m_e$ at redshift $z \sim 10^3$ from cosmic microwave background data, *e.g.*, $\Delta\alpha_{\text{em}}/\alpha_{\text{em}} = (3.6 \pm 3.7) \times 10^{-3}$ [98]. Direct laboratory limits (based on monitoring the frequency ratio of several different atomic clocks) on the present time variation of α_{em} , and $\mu = m_p/m_e$ have reached the levels [99, 100]

$$\begin{aligned} d \ln(\alpha_{\text{em}})/dt &= (1.8 \pm 2.5) \times 10^{-19} \text{ yr}^{-1}, \\ d \ln(\mu)/dt &= (-8 \pm 36) \times 10^{-18} \text{ yr}^{-1}. \end{aligned} \quad (21.53)$$

There are also experimental limits on a possible dependence of coupling constants on the gravitational potential [99, 100].

Experimental limits on the present time variation of the gravitational constant, Eq. (21.33), have been derived from planetary ephemerides [101], lunar laser ranging [102], and binary-pulsar data [103, 104]. The most stringent limits come from lunar-laser-ranging data [102]:

$$\frac{\dot{G}_0}{G_0} = (7.1 \pm 7.6) \times 10^{-14} \text{ yr}^{-1}. \quad (21.54)$$

21.4.2 Tests of the isotropy of space and of Local Lorentz invariance

The highest precision tests of the isotropy of space have been performed by looking for possible quadrupolar shifts of nuclear energy levels [105]. The (null) results can be interpreted as testing the fact that the various pieces in the matter Lagrangian, Eq. (21.6), are indeed coupled to the same external metric $g_{\mu\nu}$ to the 10^{-29} level.

Stringent tests of possible violations of local Lorentz invariance in gravitational interactions have been obtained both from solar-system data [8] and pulsar data [106, 107]. For astrophysical constraints on possible Planck-scale violations of Lorentz invariance, see Ref. [108].

21.4.3 Tests of the universality of free fall (weak, and strong equivalence principles)

The universality of the acceleration of free fall has been verified, for laboratory bodies, both on the ground [109, 110] (at the 10^{-13} level), and in space [111, 112] (at the 10^{-15} level):

$$\begin{aligned} (\Delta a/a)_{\text{BeTi}} &= (0.3 \pm 1.8) \times 10^{-13}; \\ (\Delta a/a)_{\text{BeAl}} &= (-0.7 \pm 1.3) \times 10^{-13}; \\ (\Delta a/a)_{\text{TiPt}} &= (-1.5 \pm 2.3(\text{stat}) \pm 1.5(\text{syst})) \times 10^{-15}. \end{aligned} \quad (21.55)$$

The universality of free fall has also been verified when comparing the fall of classical and quantum objects (at the 6×10^{-9} level

[113]), or of two quantum objects (at the $(0.3 \pm 5.4) \times 10^{-7}$ [114], and $(1 \pm 1.4) \times 10^{-9}$, levels [115]).

The universality of free fall of self-gravitating bodies (strong equivalence principle) has been verified in both the weak-gravity, and the strong-gravity regimes. The gravitational accelerations of the Earth and the Moon toward the Sun have been checked to agree at the 10^{-13} level [102]

$$(\Delta a/a)_{\text{EarthMoon}} = (-3 \pm 5) \times 10^{-14}. \quad (21.56)$$

The latter result constrains the Nordtvedt PPN parameter [9] $\eta \equiv 4\bar{\beta} - \bar{\gamma}$ to the 10^{-4} level:

$$\eta = (-0.2 \pm 1.1) \times 10^{-4}. \quad (21.57)$$

See below for strong-field tests of the strong equivalence principle.

Finally, the universality of the gravitational redshift of clock rates has been verified at the 10^{-4} level by comparing a hydrogen-maser clock flying on a rocket up to an altitude of about 10,000 km to a similar clock on the ground [116]. The redshift due to a height change of only 33 cm has been detected by comparing two optical clocks based on $^{27}\text{Al}^+$ ions [117]. The gravitational redshift has also been detected in the orbit of a star near the supermassive black hole at the center of our Galaxy [118, 119], and its universality has been verified at the 5% level [120].

21.5 Tests of quasi-stationary, weak-field gravity

All currently performed gravitational experiments in the solar system, including perihelion advances of planetary orbits, the bending and delay of electromagnetic signals passing near the Sun, and very accurate ranging data to the Moon obtained by laser echoes, are compatible with the post-Newtonian results of Eq. (21.15), Eq. (21.13), and Eq. (21.14). The “gravito-magnetic” interactions $\propto v_A v_B$ contained in Eq. (21.13) are involved in many of these experimental tests. They have been particularly tested in lunar-laser-ranging data [121], in the combined LAGEOS-LARES satellite data [122, 123], and in the dedicated Gravity Probe B mission [124].

To assess in a quantitative manner the results of the various solar-system tests of gravity it is convenient to express them in terms of the PPN parameters defined above. The best current limit on the post-Einstein parameter $\bar{\gamma} \equiv \gamma - 1$ is

$$\bar{\gamma} = (2.1 \pm 2.3) \times 10^{-5}, \quad (21.58)$$

as deduced from the additional Doppler shift experienced by radio-wave beams connecting the Earth to the Cassini spacecraft when they passed near the Sun [125].

The (cubic-vertex-related) post-Einstein parameter $\bar{\beta} \equiv \beta - 1$ is constrained at the 10^{-4} level both from a study of the global sensitivity of planetary ephemerides to post-Einstein parameters [101],

$$|\bar{\beta}| < 7 \times 10^{-5}, \quad (21.59)$$

and from lunar-laser-ranging data [102]

$$\bar{\beta} = (-4.5 \pm 5.6) \times 10^{-5}. \quad (21.60)$$

The periastron advance of the star S2 around the Galactic center massive black hole has been observed to agree with GR within 20% [126]. More stringent limits on $\bar{\gamma}$ (*i.e.* the coupling of φ to matter) are obtained in dilaton-like models where scalar couplings violate the Equivalence Principle [127].

21.6 Tests of strong-field gravity (neutron stars and black holes)

Experimental tests of strong-field gravity have been obtained in various physical systems, notably binary pulsars and coalescing binary black holes.

It is convenient to quantitatively express binary-pulsar tests of strong-field gravity by using the PPK formalism defined above. We recall that the measurement of N phenomenological PPK parameters leads to $N - 2$ tests of strong-field gravity. In all, *thirteen* tests of strong-field and/or radiative gravity have been obtained in the four different (double neutron-star) binary pulsar systems PSR1913+16 [10, 11, 128], PSR1534+12 [129–131],

PSR J1141–6545 [132–135], and PSR J0737–3039 A,B [136–140]. These consist of $N - 2 = 5 - 2 = 3$ tests from PSR1913+16 ; $5 - 2 = 3$ tests from PSR1534+12; $4 - 2 = 2$ tests from PSR J1141–6545; and $7 - 2 = 5$ tests from PSR J0737–3039 (see, also, Ref. [141] for additional, less accurate tests of relativistic gravity). Among these tests, four of them (those involving the measurement of the PPK parameter \dot{P}_b) probe radiative effects, and will be discussed in the following section. The four binary pulsar systems PSR1913+16, PSR1534+12, PSR J1141–6545, and PSR J0737–3039 A,B have given nine tests of quasi-static, strong-field gravity. GR passes all these tests within the measurement accuracy. Let us only highlight here some of the most accurate strong-field tests.

In the binary pulsar PSR 1534+12 [129] one has measured *five* post-Keplerian parameters: k , γ_{timing} , r , s , and (with less accuracy) \dot{P}_b [130, 131]. This yields *three* tests of relativistic gravity. Among these tests, the two involving the measurements of k , γ_{timing} , r , and s accurately probe strong field gravity, without mixing of radiative effects [130]. The most precise (10^{-3} level) of these pure strong-field tests is the one obtained by combining the measurements of k , γ_{timing} , and s ; namely, [131],

$$\left[\frac{s^{\text{obs}}}{s^{\text{GR}}[k^{\text{obs}}, \gamma_{\text{timing}}^{\text{obs}}]} \right]_{1534+12} = 1.002 \pm 0.002. \quad (21.61)$$

The discovery of the remarkable *double* binary pulsar PSR J0737–3039 A and B [136, 137] has led to the measurement of *seven* independent parameters [138–140]: five of them are the post-Keplerian parameters k , γ_{timing} , r , s , and \dot{P}_b entering the relativistic timing formula of the fast-spinning pulsar PSR J0737–3039 A; a sixth is the ratio $R = x_B/x_A$ between the projected semi-major axis of the more slowly spinning companion pulsar PSR J0737–3039 B, and that of PSR J0737–3039 A (the theoretical prediction for the ratio $R = x_B/x_A$, considered as a function of the (inertial) masses $m_1 = m_A$ and $m_2 = m_B$, is $R^{\text{theory}} = m_1/m_2 + O((v/c)^4)$ [13, 14], independently of the gravitational theory considered). Finally, the seventh parameter $\Omega_{\text{SO,B}}$ is the angular rate of (spin-orbit) precession of PSR J0737–3039 B around the total angular momentum vector [139, 140]. These seven measurements give us *five* tests of relativistic gravity [138, 142, 143], four of which are quasi-static, strong-field tests. GR passes all those tests with flying colors [144]. The most accurate is at the 2×10^{-4} level:

$$\left[\frac{s^{\text{obs}}}{s^{\text{GR}}[k^{\text{obs}}, \gamma_{\text{timing}}^{\text{obs}}]} \right]_{0737-3039} = 1.00009 \pm 0.00018. \quad (21.62)$$

Binary pulsar data on other types of pulsar systems can be used to test strong-field aspects of the “strong equivalence principle,” namely the GR prediction that strong-self-gravity objects (such as neutron stars) should fall with the same acceleration as weak-self-gravity objects (such as white-dwarfs) in the (external) gravitational field created by other objects (such as the Galaxy, or another white dwarf). The first binary-pulsar tests of this property have been obtained in nearby circular binary systems (made of a neutron star and a white dwarf) falling in the field of the Galaxy, and have led to strong-field confirmations (at the 2×10^{-3} level) of the strong equivalence principle [104, 145–147]. The remarkable discovery of the pulsar PSR J0337+1715 in a hierarchical triple system [148] has allowed one to derive a much more accurate test of the strong equivalence principle because the inner binary (comprising a pulsar and a close white-dwarf companion) falls toward the outer white-dwarf companion with an acceleration that is 10^8 times larger than the Galactic acceleration. This leads to a 95% confidence level limit on a possible fractional difference in free-fall acceleration of the pulsar and its close companion of [149, 150]

$$|\Delta a/a| < 2.05 \times 10^{-6} \text{ (95\% C.L.)}. \quad (21.63)$$

This limit yields strong constraints on tensor-scalar gravity models.

Measurements over several years of the pulse profiles of various pulsars have detected secular changes compatible with the prediction [151] that the general relativistic spin-orbit coupling should

cause a secular change in the orientation of the pulsar beam with respect to the line of sight (“geodetic precession”). Such confirmations of general-relativistic spin-orbit effects were obtained in PSR 1913+16 [152], PSR B1534+12 [131], PSR J1141–6545 [153], PSR J0737–3039 [139, 140], and PSR J1906+0746 [154, 155]. In some cases (notably PSR 1913+16 and PSR J1906+0746) the secular change in the orientation of the pulsar beam is expected to lead to the disappearance of the beam (as seen on the Earth) on a human time scale (the second pulsar in the double system PSR J0737–3039 already disappeared in March 2008 and is expected to reappear around 2035 [140]).

Recently, the ultimate strong-field regime of black holes has started to be quantitatively probed via GW observations. The LIGO-Virgo(-Kagra) collaboration has detected (starting in September 2015) GW signals [35], which, besides testing the radiative structure of gravity (see next section), are in excellent qualitative and quantitative agreement with the structure and dynamics of black-hole horizons in GR. Because of the mixing of strong-field effects with radiative effects during the coalescence of two black holes, and because of the lack of detailed alternative-theory predictions for this process (see, however, Refs. [46–48]), it is not easy to set quantitative limits on possible strong-field deviations from GR, independently of radiative effects. Direct tests of the existence of black-hole horizons are scarce (see, however, Sec. VIII B of [156] which reports the lack of any statistical evidence for GW echoes).

Let us also mention that the Event Horizon Telescope collaboration has obtained event-horizon-scale images of the supermassive black hole candidates in the center of the giant elliptical galaxy M87, and in the center of our Galaxy. These images are consistent with GR models of accreting Kerr black holes [157, 158]. For discussions of the corresponding constraints on the black hole geometry in the vicinity of the light ring see Refs. [159–161].

21.7 Tests of radiative gravity (both in binary-pulsar data and in GW data)

Experimental confirmations of the GR predictions for the radiative structure of gravity have been obtained both in binary-pulsar data and in the observation of GW signals from coalescing compact binaries (binary black holes and binary neutron stars).

Binary-pulsar observations involving the measurement of the orbital period derivative \dot{P}_b give *direct* experimental tests of the reality of gravitational radiation, and, in particular, an experimental confirmation that the speed of propagation of gravity c_g is equal to the speed of light c (indeed, as recalled above, \dot{P}_b is a consequence of the propagation of the gravitational interaction between the two neutron stars [12]). Even in the presence of screening mechanisms within the binary system, the value of \dot{P}_b yields a measurement of the speed of propagation of GWs at the 10^{-2} level [162]. The currently most accurate binary-pulsar tests of the radiative properties of gravity come from the binary neutron-star systems PSR1913+16 and PSR J0737–3039 A,B, as well as from several neutron-star-white-dwarf systems, notably PSR J1738+0333.

After subtracting a small ($\sim 10^{-14}$ level in $\dot{P}_b^{\text{obs}} = (-2.423 \pm 0.001) \times 10^{-12}$), but significant, “Galactic” perturbing effect (linked to Galactic accelerations and to the pulsar proper motion) [163], one finds that the phenomenological test obtained by combining the measurements of the three PPK parameters ($k - \gamma_{\text{timing}} - \dot{P}_b$)₁₉₁₃₊₁₆ is passed by GR with complete success [128]:

$$\left[\frac{\dot{P}_b^{\text{obs}} - \dot{P}_b^{\text{gal}}}{\dot{P}_b^{\text{GR}}[k^{\text{obs}}, \gamma_{\text{timing}}^{\text{obs}}]} \right]_{1913+16} = 0.9983 \pm 0.0016. \quad (21.64)$$

Here $\dot{P}_b^{\text{GR}}[k^{\text{obs}}, \gamma_{\text{timing}}^{\text{obs}}]$ is the result of inserting in $\dot{P}_b^{\text{GR}}(m_1, m_2)$ the values of the masses predicted by the two equations $k^{\text{obs}} = k^{\text{GR}}(m_1, m_2)$, and $\gamma_{\text{timing}}^{\text{obs}} = \gamma_{\text{timing}}^{\text{GR}}(m_1, m_2)$. This yields experimental evidence for the reality of gravitational radiation damping forces at the $(-1.7 \pm 1.6) \times 10^{-3}$ level.

An even better experimental test of the radiative structure of gravity (6×10^{-5} level) has been recently obtained from the com-

bined measurement in PSR J0737–3039 A,B of the three parameters k , s , and \dot{P}_b [144]:

$$\left[\frac{\dot{P}_b^{\text{obs}} - \dot{P}_b^{\text{gal}}}{\dot{P}_b^{\text{GR}}[k^{\text{obs}}, s^{\text{obs}}]} \right]_{0737-3039} = 0.999963 \pm 0.000063. \quad (21.65)$$

In addition to the above tests, further very stringent tests of radiative gravity follow from the measurement of the orbital period decay \dot{P}_b of low-eccentricity pulsar-white dwarf systems. Notably, the system PSR J1738+0333 yields an intrinsic orbital decay of [164]

$$\left[\dot{P}_b^{\text{obs}} - \dot{P}_b^{\text{gal}} \right]_{1738+0333} = (-25.9 \pm 3.2) \times 10^{-15}, \quad (21.66)$$

to be compared to

$$\left[\dot{P}_b^{\text{GR}} \right]_{1738+0333} = (-27.7_{-1.9}^{+1.5}) \times 10^{-15}. \quad (21.67)$$

The fractional agreement between the (corrected) observed period decay and the GR-predicted one seems to be quantitatively less impressive than the double-neutron-star results cited above, but the crucial point is that asymmetric binary systems (such as neutron-star-white-dwarf ones) are strong emitters of dipolar gravitational radiation in tensor-scalar theories, with \dot{P}_b scaling (modulo matter-scalar couplings) like $m_1 m_2 / (m_1 + m_2)^2 (v/c)^3$, instead of the parametrically smaller GR-predicted quadrupolar radiation $\dot{P}_b \sim (v/c)^5$ [7, 15]. In view of the very small absolute value of \dot{P}_b , this makes such systems (and notably PSR J1738+0333) very sensitive probes of tensor-scalar gravity [103, 164–168]. It is then useful to turn to a theory-dependent analysis of pulsar data. Such an analysis (see, e.g., [17, 130, 164, 167, 168]) leads to excluding a large portion of the parameter space of tensor-scalar gravity allowed by solar-system tests. As a result, the basic matter-scalar coupling α_0^2 is more strongly constrained, over most of the parameter space, than the best current solar-system limits of Eq. (21.58) (namely below the 10^{-5} level) [164, 167].

We now turn to the tests of radiative gravity that can be deduced from the GW data gathered from the first three observing runs of the LIGO-Virgo-Kagra collaboration. All currently detected GW signals are consistent with GR predictions. Several phenomenological approaches were used and led to setting limits on possible deviations from GR [51, 156, 169, 170].

A theory-agnostic quantitative assessment on possible deviations from GR is given by measuring the agreement between the full observed GW signal of coalescing binary black holes, and the GR-predicted one. One of the strongest results was obtained with the first event: GW150914, which had an SNR of 24. The noise-weighted correlation between the GW150914 signal and the best-fit GR-predicted waveform was found to be $\geq 97\%$ [51, 169]. In other words, GR-violation effects that cannot be reabsorbed in a redefinition of physical parameters are limited (in a noise-weighted sense) to less than 3%.

Besides checking the agreement between the *full* observed GW signals and the corresponding best-fit full signals predicted by GR, one also tested the consistency between separate parts of the signals. A first approach [156, 169, 170] separates: (i) the lower-frequency signal emitted during the *inspiral* phase (considered up to the innermost stable circular orbit); and (ii) the higher-frequency remaining signal emitted during the *postinspiral* phase, comprising the late-*inspiral*, the *merger*, and the *ringdown*. Separately fitting each of these partial signals to GR-based templates then yields separate estimates of the binary’s parameters, leading to separate estimates of the mass M_f and dimensionless spin parameter $a_f = J_f / (GM_f^2)$ of the final black hole that would be formed (in GR) by the coalescence of the two initial black holes. The consistency with GR then consists in testing whether the two estimates $(M_f, a_f)_{\text{insp}}$ and $(M_f, a_f)_{\text{postinsp}}$ are compatible with each other. They were found to be compatible for all events whose corresponding separate SNRs made such an analysis meaningful (see Figs. 3 and 4 in [170] and Fig.3 in [156]). Quantitatively, the

(population-marginalized) fractional differences

$$\begin{aligned}\frac{\Delta M_f}{\bar{M}_f} &= 2 \frac{M_f^{\text{insp}} - M_f^{\text{postinsp}}}{M_f^{\text{insp}} + M_f^{\text{postinsp}}}, \\ \frac{\Delta a_f}{\bar{a}_f} &= 2 \frac{a_f^{\text{insp}} - a_f^{\text{postinsp}}}{a_f^{\text{insp}} + a_f^{\text{postinsp}}},\end{aligned}\quad (21.68)$$

between the two estimates were found to be consistent with zero (*i.e.* with GR) [156]

$$\begin{aligned}\frac{\Delta M_f}{\bar{M}_f} &= -0.02_{-0.06}^{+0.07}, \\ \frac{\Delta a_f}{\bar{a}_f} &= -0.06_{-0.07}^{+0.10}.\end{aligned}\quad (21.69)$$

A second approach studies the consistency of the ringdown GW signal (emitted by the final, vibrating black hole) with GR predictions. See, in particular, section VIII A, and Figs. 13 and 14, of [156]. The results are rather sensitive to various data analysis assumptions (notably the use of complete waveform models versus an analysis using only the ringdown signal). Though there is no clear sign of any deviations from GR, the current SNRs do not yield strong theory-agnostic evidence for the presence of ringing overtones.

The parametrization of Eq. (21.38) for possible deviations in the frequency dependence of the Fourier-domain phase $\psi(f)$ of the black hole coalescence GW signal was used to measure best-fit values for each fractional deviation parameter $\delta\hat{p}_i$, considered separately (the other ones being set to zero). In all cases, the posterior distribution for each $\delta\hat{p}_i$ is consistent with the GR value, *i.e.*, $\delta\hat{p}_i^{\text{GR}} = 0$ (see Fig. 6 in [156]). The current limits on $\delta\hat{p}_i$ are (roughly) of order unity, except for the two parameters highlighted above: $\delta\hat{p}_3$ (parameterizing the $O((\frac{v}{c})^3)$ fractional correction to the LO, quadrupolar term); and $\delta\hat{p}_{-2}$ (parameterizing a possible dipolar-radiation-related $O((\frac{v}{c})^{-2})$ fractional correction to the LO, quadrupolar term). Ref. [170] gives 90%-credible intervals for $\delta\hat{p}_3$ of $-0.02_{-0.10}^{+0.11}$ (when using a phenomenological model [53]), and $-0.01_{-0.10}^{+0.10}$ (when using an effective one-body model [38]). Ref. [156] gives a 90%-credible upper bound for a possible dipolar term of $|\delta\hat{p}_{-2}| \leq 7.3 \times 10^{-4}$.

As recalled above, GR predicts that the polarization content of GWs is pure helicity-2, *i.e.* described by the two independent components of a traceless tensor transverse to the propagation direction. A (massless) scalar excitation would add a pure-trace “breathing mode” in the plane transverse to the propagation direction. A phenomenological approach to generic metric theories of gravity would allow for up to six polarizations for a GW [171], namely two tensor, two vector and two scalar modes. The LVK collaboration tested possible polarization deviations from GR in various ways [33, 156, 169]. Recent results are given in section VII of [156]. Though pure-scalar, pure-vector and vector-scalar hypotheses are significantly disfavored, any mixed hypothesis involving tensor modes (*i.e.*, tensor-scalar, tensor-vector, and tensor-vector-scalar) cannot be ruled out conclusively.

GR also predicts that GWs are non dispersive, and propagate at the same speed as light. One can phenomenologically modify the GR-predicted GW phase evolution by adding the putative effect of an anomalous dispersion relation of the form $E^2 = p^2 c^2 + A p^\alpha c^\alpha$. GW data have been used to set bounds on the anomalous coefficient A for various values of the exponent α . The case $\alpha = 0$ is equivalent to assuming that gravitons disperse as a massive particle [59]. The current (90%-credibility) phenomenological GW limit on the graviton mass is $m_g \leq 1.27 \times 10^{-23} \text{eV}/c^2$ [156]. This is 2.5 times more stringent than the Solar System bound of $3.16 \times 10^{-23} \text{eV}/c^2$ [65].

Finally, a very constraining bound on the speed of propagation of gravity c_{GW} was derived from the observed time delay of 1.7 s between GW170817 and the associated γ -ray burst. Namely, the fractional difference between c_{GW} and $c_{\text{light}} \equiv c$ is constrained to

be [172]

$$-3 \times 10^{-15} < \frac{c_{\text{GW}} - c}{c} < +7 \times 10^{-16}. \quad (21.70)$$

When comparing the latter bound to the prediction Eq. (21.50) from general second-order tensor-scalar theories, Eq. (21.49), one is led to conclude that the coupling function $G_5(\varphi, X)$ has to be ignored and that the coupling function $G_4(\varphi, X)$ has to be restricted to depend only on φ . This drastically reduces the viable tensor-scalar modified-gravity models [173–176].

Let us finally mention that four pulsar timing arrays have recently given tantalizing evidence for the existence of a stochastic background of gravitational waves with frequency $\sim 10^{-9}$ Hz [177–180].

21.8 Conclusions

All present experimental tests are compatible with the predictions of the current “standard” theory of gravitation, Einstein’s General Relativity. Let us recap the main tests. The universality of the coupling between matter and gravity (Equivalence Principle) has been verified at around the 10^{-15} level. Solar system experiments have tested the weak-field predictions of Einstein’s theory at the few times 10^{-5} level. The propagation properties (in the near zone) of relativistic gravity, as well as several of its static strong-field aspects, have been verified at the 10^{-4} level (or better) in several binary pulsar experiments. Interferometric detectors of gravitational radiation have given direct observational proofs of the existence, and properties, of gravitational waves (in the wave zone), and of the existence of coalescing black holes, and they have already set strong limits on possible deviations; in particular: an upper bound $|\delta\hat{p}_{-2}| < 7.3 \times 10^{-4}$ on a possible dipolar contribution to the GW flux; the $O(10^{-15})$ bound of Eq. (21.70) on the speed of gravity; and confirmation of the tensor polarization structure of gravitational waves. In addition, laboratory experiments have set strong constraints on sub-millimeter modifications of Newtonian gravity, while many different cosmological data sets have been used to set limits on possible GR deviations on cosmological scales [29]. In spite of the uneasiness of having to assume the existence of dark matter, and the presence of an unnaturally small cosmological constant (as dark energy), General Relativity stands out as a uniquely successful description of gravity on all the scales that have been explored so far. There are no modified-gravity models which naturally pass all existing experimental tests, while either explaining away the need for dark matter or for dark energy.

References

- [1] S. Weinberg, *Rev. Mod. Phys.* **61**, 1 (1989).
- [2] H. A. Buchdahl, *Phys. Rev.* **116**, 1027 (1959).
- [3] N. Chamel *et al.*, *Int. J. Mod. Phys. E* **22**, 1330018 (2013), [arXiv:1307.3995].
- [4] J. R. Oppenheimer and H. Snyder, *Phys. Rev.* **56**, 455 (1939).
- [5] R. P. Kerr, *Phys. Rev. Lett.* **11**, 237 (1963).
- [6] V. F. Mukhanov, H. A. Feldman and R. H. Brandenberger, *Phys. Rept.* **215**, 203 (1992).
- [7] C. M. Will, *Theory and Experiment in Gravitational Physics*, Cambridge University Press (2018).
- [8] C. M. Will, *Living Rev. Rel.* **17**, 4 (2014), [arXiv:1403.7377].
- [9] K. Nordtvedt, *Phys. Rev.* **170**, 1186 (1968).
- [10] R. A. Hulse, *Rev. Mod. Phys.* **66**, 699 (1994).
- [11] J. H. Taylor, *Rev. Mod. Phys.* **66**, 711 (1994).
- [12] T. Damour and N. Deruelle, *Phys. Lett.* **A87**, 81 (1981); T. Damour, *C.R. Acad. Sci. Paris* **294**, 1335 (1982).
- [13] T. Damour and J. H. Taylor, *Phys. Rev.* **D45**, 1840 (1992).
- [14] T. Damour and N. Deruelle, *Ann. Inst. H. Poincaré A*, **44**, 263 (1986).
- [15] T. Damour and G. Esposito-Farese, *Class. Quant. Grav.* **9**, 2093 (1992).

- [16] C. M. Will and H. W. Zaglauer, *Astrophys. J.* **346**, 366 (1989).
- [17] T. Damour and G. Esposito-Farese, *Phys. Rev.* **D54**, 1474 (1996), [arXiv:gr-qc/9602056].
- [18] T. Damour and G. Esposito-Farese, *Phys. Rev.* **D58**, 042001 (1998), [arXiv:gr-qc/9803031].
- [19] J.-P. Uzan, *Gen. Rel. Grav.* **39**, 307 (2007), [arXiv:astro-ph/0605313].
- [20] R. Caldwell, A. Cooray and A. Melchiorri, *Phys. Rev.* **D76**, 023507 (2007), [arXiv:astro-ph/0703375].
- [21] P. Zhang *et al.*, *Phys. Rev. Lett.* **99**, 141302 (2007), [arXiv:0704.1932].
- [22] L. Amendola, M. Kunz and D. Sapone, *JCAP* **0804**, 013 (2008), [arXiv:0704.2421].
- [23] W. Hu and I. Sawicki, *Phys. Rev.* **D76**, 104043 (2007), [arXiv:0708.1190].
- [24] S. F. Daniel *et al.*, *Phys. Rev.* **D77**, 103513 (2008), [arXiv:0802.1068].
- [25] G.-B. Zhao *et al.*, *Phys. Rev.* **D79**, 083513 (2009), [arXiv:0809.3791].
- [26] J.-P. Uzan, *Gen. Rel. Grav.* **42**, 2219 (2010), [arXiv:0908.2243].
- [27] E. Bertschinger, *Phil. Trans. Roy. Soc. Lond.* **A369**, 4947 (2011), [arXiv:1111.4659].
- [28] T. Baker, P. G. Ferreira and C. Skordis, *Phys. Rev.* **D87**, 2, 024015 (2013), [arXiv:1209.2117].
- [29] M. Ishak, *Living Rev. Rel.* **22**, 1, 1 (2019), [arXiv:1806.10122].
- [30] B. P. Abbott *et al.* (LIGO Scientific, Virgo), *Phys. Rev. Lett.* **116**, 6, 061102 (2016), [arXiv:1602.03837].
- [31] B. P. Abbott *et al.* (LIGO Scientific, Virgo), *Phys. Rev. Lett.* **116**, 24, 241103 (2016), [arXiv:1606.04855].
- [32] B. P. Abbott *et al.* (LIGO Scientific, VIRGO), *Phys. Rev. Lett.* **118**, 22, 221101 (2017), [Erratum: *Phys. Rev. Lett.* **121**, no.12, 129901 (2018)], [arXiv:1706.01812].
- [33] B. P. Abbott *et al.* (LIGO Scientific, Virgo), *Phys. Rev. Lett.* **119**, 14, 141101 (2017), [arXiv:1709.09660].
- [34] B. P. Abbott *et al.* (LIGO Scientific, Virgo), *Phys. Rev. Lett.* **119**, 16, 161101 (2017), [arXiv:1710.05832].
- [35] B. P. Abbott *et al.* (LIGO Scientific, Virgo), *Phys. Rev.* **X9**, 3, 031040 (2019), [arXiv:1811.12907].
- [36] R. Abbott *et al.* (LIGO Scientific, Virgo), *Phys. Rev. X* **11**, 021053 (2021), [arXiv:2010.14527].
- [37] R. Abbott *et al.* (LIGO Scientific, VIRGO, KAGRA) (2021), [arXiv:2111.03606].
- [38] A. Buonanno and T. Damour, *Phys. Rev.* **D62**, 064015 (2000), [arXiv:gr-qc/0001013].
- [39] L. Blanchet, *Living Rev. Rel.* **17**, 2 (2014), [arXiv:1310.1528].
- [40] F. Pretorius, *Phys. Rev. Lett.* **95**, 121101 (2005), [arXiv:gr-qc/0507014]; M. Campanelli *et al.*, *Phys. Rev. Lett.* **96**, 111101 (2006), [arXiv:gr-qc/0511048]; J. G. Baker *et al.*, *Phys. Rev. Lett.* **96**, 111102 (2006), [arXiv:gr-qc/0511103].
- [41] K. Yagi *et al.*, *Phys. Rev.* **D85**, 064022 (2012), [Erratum: *Phys. Rev.* **D93**, no.2, 029902 (2016)], [arXiv:1110.5950].
- [42] K. Yagi, L. C. Stein and N. Yunes, *Phys. Rev.* **D93**, 2, 024010 (2016), [arXiv:1510.02152].
- [43] K. Prabhu and L. C. Stein, *Phys. Rev.* **D98**, 2, 021503 (2018), [arXiv:1805.02668].
- [44] L. Bernard, *Phys. Rev.* **D98**, 4, 044004 (2018), [arXiv:1802.10201].
- [45] F.-L. Julié and E. Berti, *Phys. Rev. D* **100**, 10, 104061 (2019), [arXiv:1909.05258].
- [46] M. Okounkova *et al.*, *Phys. Rev.* **D96**, 4, 044020 (2017), [arXiv:1705.07924].
- [47] H. Witek *et al.*, *Phys. Rev.* **D99**, 6, 064035 (2019), [arXiv:1810.05177].
- [48] M. Okounkova *et al.* (2019), [arXiv:1906.08789].
- [49] L. Blanchet and B. S. Sathyaprakash, *Phys. Rev. Lett.* **74**, 1067 (1995).
- [50] K. G. Arun *et al.*, *Phys. Rev.* **D74**, 024006 (2006), [arXiv:gr-qc/0604067].
- [51] B. P. Abbott *et al.* (LIGO Scientific, Virgo), *Phys. Rev. Lett.* **116**, 22, 221101 (2016), [Erratum: *Phys. Rev. Lett.* **121**, no.12, 129902 (2018)], [arXiv:1602.03841].
- [52] N. Yunes and F. Pretorius, *Phys. Rev.* **D80**, 122003 (2009), [arXiv:0909.3328].
- [53] S. Khan *et al.*, *Phys. Rev.* **D93**, 4, 044007 (2016), [arXiv:1508.07253].
- [54] B. P. Abbott *et al.* (LIGO Scientific, Virgo), *Phys. Rev. Lett.* **123**, 1, 011102 (2019), [arXiv:1811.00364].
- [55] C. V. Vishveshwara, *Nature* **227**, 936 (1970).
- [56] S. L. Detweiler, *Astrophys. J.* **239**, 292 (1980).
- [57] V. Cardoso *et al.*, *Phys. Rev.* **D99**, 10, 104077 (2019), [arXiv:1901.01265].
- [58] R. McManus *et al.*, *Phys. Rev.* **D100**, 4, 044061 (2019), [arXiv:1906.05155].
- [59] C. M. Will, *Phys. Rev.* **D57**, 2061 (1998), [arXiv:gr-qc/9709011].
- [60] M. Fierz, *Helv. Phys. Acta* **29**, 128 (1956).
- [61] E. G. Adelberger, B. R. Heckel and A. E. Nelson, *Ann. Rev. Nucl. Part. Sci.* **53**, 77 (2003), [hep-ph/0307284].
- [62] D. J. Kapner *et al.*, *Phys. Rev. Lett.* **98**, 021101 (2007), [hep-ph/0611184].
- [63] A. O. Sushkov *et al.*, *Phys. Rev. Lett.* **107**, 171101 (2011), [arXiv:1108.2547].
- [64] W.-H. Tan *et al.*, *Phys. Rev. Lett.* **124**, 5, 051301 (2020).
- [65] L. Bernus *et al.*, *Phys. Rev. D* **102**, 2, 021501 (2020), [arXiv:2006.12304].
- [66] T. Damour and J. F. Donoghue, *Phys. Rev.* **D82**, 084033 (2010), [arXiv:1007.2792].
- [67] R. V. Wagoner, *Phys. Rev.* **D1**, 3209 (1970).
- [68] C. Brans and R. H. Dicke, *Phys. Rev.* **124**, 925 (1961), [142(1961)].
- [69] J. Alsing *et al.*, *Phys. Rev.* **D85**, 064041 (2012), [arXiv:1112.4903].
- [70] T. Damour and K. Nordtvedt, *Phys. Rev. Lett.* **70**, 2217 (1993).
- [71] T. Damour and A. M. Polyakov, *Nucl. Phys.* **B423**, 532 (1994), [hep-th/9401069].
- [72] K. A. Olive and M. Pospelov, *Phys. Rev.* **D77**, 043524 (2008), [arXiv:0709.3825].
- [73] J. Khoury and A. Weltman, *Phys. Rev. Lett.* **93**, 171104 (2004), [arXiv:astro-ph/0309300].
- [74] K. Hinterbichler and J. Khoury, *Phys. Rev. Lett.* **104**, 231301 (2010), [arXiv:1001.4525].
- [75] P. Brax *et al.*, *Phys. Rev.* **D82**, 063519 (2010), [arXiv:1005.3735].
- [76] A. Joyce *et al.*, *Phys. Rept.* **568**, 1 (2015), [arXiv:1407.0059].
- [77] C. Burrage and J. Sakstein, *Living Rev. Rel.* **21**, 1, 1 (2018), [arXiv:1709.09071].
- [78] A. I. Vainshtein, *Phys. Lett.* **39B**, 393 (1972).
- [79] C. de Rham, *Living Rev. Rel.* **17**, 7 (2014), [arXiv:1401.4173].
- [80] G. W. Horndeski, *Int. J. Theor. Phys.* **10**, 363 (1974).
- [81] C. Deffayet *et al.*, *Phys. Rev.* **D84**, 064039 (2011), [arXiv:1103.3260].

- [82] L. Heisenberg, Phys. Rept. **796**, 1 (2019), [arXiv:1807.01725].
- [83] T. Kobayashi, Rept. Prog. Phys. **82**, 8, 086901 (2019), [arXiv:1901.07183].
- [84] G. Papallo and H. S. Reall, Phys. Rev. **D96**, 4, 044019 (2017), [arXiv:1705.04370].
- [85] L. Bernard, L. Lehner and R. Luna, Phys. Rev. **D100**, 2, 024011 (2019), [arXiv:1904.12866].
- [86] A. D. Kovács, Phys. Rev. **D100**, 2, 024005 (2019), [arXiv:1904.00963].
- [87] C. de Rham and S. Melville, Phys. Rev. Lett. **121**, 22, 221101 (2018), [arXiv:1806.09417].
- [88] D. D. Doneva and S. S. Yazadjiev, Phys. Rev. Lett. **120**, 13, 131103 (2018), [arXiv:1711.01187].
- [89] H. O. Silva *et al.*, Phys. Rev. Lett. **120**, 13, 131104 (2018), [arXiv:1711.02080].
- [90] G. Antoniou *et al.*, Phys. Rev. D **104**, 4, 044002 (2021), [arXiv:2105.04479].
- [91] C. A. R. Herdeiro and E. Radu, Int. J. Mod. Phys. **D24**, 09, 1542014 (2015), [arXiv:1504.08209].
- [92] A.I. Shlyakhter, Nature **264**, 340 (1976).
- [93] T. Damour and F. Dyson, Nucl. Phys. **B480**, 37 (1996), [hep-ph/9606486]; C. R. Gould, E. I. Sharapov and S. K. Lamoreaux, Phys. Rev. **C74**, 024607 (2006), [arXiv:nuclex/0701019]; E. D. Davis and L. Hamdan, Phys. Rev. **C92**, 1, 014319 (2015), [arXiv:1503.06011]; Yu. V. Petrov *et al.*, Phys. Rev. **C74**, 064610 (2006), [hep-ph/0506186].
- [94] V. V. Flambaum and R. B. Wiringa, Phys. Rev. **C79**, 034302 (2009), [arXiv:0807.4943].
- [95] K. A. Olive *et al.*, Phys. Rev. **D69**, 027701 (2004), [arXiv:astro-ph/0309252].
- [96] M. T. Murphy, A. L. Malec and J. X. Prochaska, Mon. Not. Roy. Astron. Soc. **461**, 3, 2461 (2016), [arXiv:1606.06293].
- [97] N. Kanekar *et al.*, Mon. Not. Roy. Astron. Soc. **448**, 1, L104 (2015), [arXiv:1412.7757].
- [98] P. A. R. Ade *et al.* (Planck), Astron. Astrophys. **580**, A22 (2015), [arXiv:1406.7482].
- [99] R. Lange *et al.*, Phys. Rev. Lett. **126**, 1, 011102 (2021), [arXiv:2010.06620].
- [100] M. Filzinger *et al.*, Phys. Rev. Lett. **130**, 25, 253001 (2023), [arXiv:2301.03433].
- [101] A. Fienga *et al.*, Cel. Mech. Dyn. Astr. **123**, Issue 2, 1 (2015).
- [102] F. Hofmann and J. Müller, Class. Quant. Grav. **35**, 3, 035015 (2018).
- [103] K. Lazaridis *et al.*, Mon. Not. R. Astron. Soc. **400**, 805 (2009), [arXiv:0908.0285].
- [104] W. W. Zhu *et al.*, Mon. Not. Roy. Astron. Soc. **482**, 3, 3249 (2019), [arXiv:1802.09206].
- [105] M. Smiciklas *et al.*, Phys. Rev. Lett. **107**, 171604 (2011), [arXiv:1106.0738].
- [106] J. F. Bell and T. Damour, Class. Quant. Grav. **13**, 3121 (1996), [arXiv:gr-qc/9606062].
- [107] L. Shao and N. Wex, Class. Quant. Grav. **29**, 215018 (2012), [arXiv:1209.4503].
- [108] S. Liberati, J. Phys. Conf. Ser. **631**, 1, 012011 (2015).
- [109] S. Schlamminger *et al.*, Phys. Rev. Lett. **100**, 041101 (2008), [arXiv:0712.0607].
- [110] T. A. Wagner *et al.*, Class. Quant. Grav. **29**, 184002 (2012), [arXiv:1207.2442].
- [111] P. Touboul *et al.* (MICROSCOPE), Phys. Rev. Lett. **129**, 12, 121102 (2022), [arXiv:2209.15487].
- [112] P. Touboul *et al.*, Class. Quant. Grav. **39**, 20, 204009 (2022), [arXiv:2209.15488].
- [113] S. Merlet *et al.*, Metrologia, **47**, L9-L11 (2010).
- [114] D. Schlippert *et al.*, Phys. Rev. Lett. **112**, 203002 (2014), [arXiv:1406.4979].
- [115] G. Rosi *et al.*, Nature Commun. **8**, 5529 (2017), [arXiv:1704.02296].
- [116] R.F.C. Vessot and M.W. Levine, Gen. Rel. Grav. **10**, 181 (1978); R. F. C. Vessot *et al.*, Phys. Rev. Lett. **45**, 2081 (1980).
- [117] C. W. Chou *et al.*, Science **329**, 1630 (2010).
- [118] R. Abuter *et al.* (GRAVITY), Astron. Astrophys. **615**, L15 (2018), [arXiv:1807.09409].
- [119] T. Do *et al.*, Science **365**, 6454, 664 (2019), [arXiv:1907.10731].
- [120] A. Amorim *et al.* (GRAVITY), Phys. Rev. Lett. **122**, 10, 101102 (2019), [arXiv:1902.04193].
- [121] J.G. Williams, S.G. Turyshev, and D.H. Boggs, Class. Quantum Grav. **29**, 184004 (2012).
- [122] I. Ciufolini and E. C. Pavlis, Nature **431**, 958 (2004).
- [123] I. Ciufolini *et al.*, Eur. Phys. J. **C76**, 3, 120 (2016), [arXiv:1603.09674].
- [124] C. W. F. Everitt *et al.*, Phys. Rev. Lett. **106**, 221101 (2011), [arXiv:1105.3456].
- [125] B. Bertotti, L. Iess and P. Tortora, Nature **425**, 374 (2003).
- [126] R. Abuter *et al.* (GRAVITY), Astron. Astrophys. **636**, L5 (2020), [arXiv:2004.07187].
- [127] J. Bergé *et al.*, Phys. Rev. Lett. **120**, 14, 141101 (2018), [arXiv:1712.00483].
- [128] J. M. Weisberg and Y. Huang, Astrophys. J. **829**, 1, 55 (2016), [arXiv:1606.02744].
- [129] A. Wolszczan, Nature **350**, 688 (1991).
- [130] J. N. Taylor, A. Wolszczan and T. Damour, Nature **355**, 132 (1993).
- [131] E. Fonseca, I. H. Stairs and S. E. Thorsett, Astrophys. J. **787**, 82 (2014), [arXiv:1402.4836].
- [132] V. M. Kaspi *et al.*, Astrophys. J. **528**, 445 (2000), [arXiv:astro-ph/9906373].
- [133] S. M. Ord, M. Bailes and W. van Straten, Astrophys. J. **574**, L75 (2002), [arXiv:astro-ph/0204421].
- [134] M. Bailes *et al.*, Astrophys. J. **595**, L49 (2003), [arXiv:astro-ph/0307468].
- [135] N. D. R. Bhat, M. Bailes and J. P. W. Verbiest, Phys. Rev. **D77**, 124017 (2008), [arXiv:0804.0956].
- [136] M. Burgay *et al.*, Nature **426**, 531 (2003), [arXiv:astro-ph/0312071].
- [137] A. G. Lyne *et al.*, Science **303**, 1153 (2004), [arXiv:astro-ph/0401086].
- [138] M. Kramer *et al.*, Science **314**, 97 (2006), [arXiv:astro-ph/0609417].
- [139] R. P. Breton *et al.*, Science **321**, 104 (2008), [arXiv:0807.2644].
- [140] B. Perera *et al.*, Astrophys. J. **721**, 1193 (2010), [arXiv:1008.1097].
- [141] R. D. Ferdman *et al.*, Mon. Not. Roy. Astron. Soc. **443**, 3, 2183 (2014), [arXiv:1406.5507].
- [142] M. Kramer and N. Wex, Class. Quant. Grav. **26**, 073001 (2009).
- [143] M. Kramer, IAU Symp. **291**, 19 (2013), [arXiv:1211.2457].
- [144] M. Kramer *et al.*, Phys. Rev. X **11**, 4, 041050 (2021), [arXiv:2112.06795].
- [145] T. Damour and G. Schaefer, Phys. Rev. Lett. **66**, 2549 (1991).
- [146] M. E. Gonzalez *et al.*, Astrophys. J. **743**, 102 (2011), [arXiv:1109.5638].

- [147] P. C. C. Freire, M. Kramer and N. Wex, *Class. Quant. Grav.* **29**, 184007 (2012), [arXiv:1205.3751].
- [148] S. M. Ransom *et al.*, *Nature* **505**, 520 (2014), [arXiv:1401.0535].
- [149] A. M. Archibald *et al.*, *Nature* **559**, 7712, 73 (2018), [arXiv:1807.02059].
- [150] G. Voisin *et al.*, *Astron. Astrophys.* **638**, A24 (2020), [arXiv:2005.01388].
- [151] T. Damour and R. Ruffini, *C. R. Acad. Sc. Paris* **279**, série A, 971 (1974); B. M. Barker and R. F. O'Connell, *Phys. Rev. D* **12**, 329 (1975).
- [152] M. Kramer, *Astrophys. J.* **509**, 856 (1998), [arXiv:astro-ph/9808127]; J. M. Weisberg and J. H. Taylor, *Astrophys. J.* **576**, 942 (2002), [arXiv:astro-ph/0205280].
- [153] R. N. Manchester *et al.*, *Astrophys. J.* **710**, 1694 (2010), [arXiv:1001.1483].
- [154] J. van Leeuwen *et al.*, *Astrophys. J.* **798**, 2, 118 (2015), [arXiv:1411.1518].
- [155] G. Desvignes *et al.*, *Science* **365**, 6457, 1013 (2019).
- [156] R. Abbott *et al.* (LIGO Scientific, VIRGO, KAGRA) (2021), [arXiv:2112.06861].
- [157] K. Akiyama *et al.* (Event Horizon Telescope), *Astrophys. J.* **875**, 1, L1 (2019), [arXiv:1906.11238].
- [158] K. Akiyama *et al.* (Event Horizon Telescope), *Astrophys. J. Lett.* **930**, 2, L12 (2022).
- [159] D. Psaltis *et al.* (Event Horizon Telescope), *Phys. Rev. Lett.* **125**, 14, 141104 (2020), [arXiv:2010.01055].
- [160] S. H. Völkel *et al.* (2020), [arXiv:2011.06812].
- [161] K. Akiyama *et al.* (Event Horizon Telescope), *Astrophys. J. Lett.* **930**, 2, L17 (2022).
- [162] J. Beltran Jimenez, F. Piazza and H. Velten, *Phys. Rev. Lett.* **116**, 6, 061101 (2016), [arXiv:1507.05047].
- [163] T. Damour and J. H. Taylor, *Astrophys. J.* **366**, 501 (1991).
- [164] P. C. C. Freire *et al.*, *Mon. Not. Roy. Astron. Soc.* **423**, 3328 (2012), [arXiv:1205.1450].
- [165] J. Antoniadis *et al.*, *Science* **340**, 6131 (2013), [arXiv:1304.6875].
- [166] W. W. Zhu *et al.*, *Astrophys. J.* **809**, 1, 41 (2015), [arXiv:1504.00662].
- [167] L. Shao *et al.*, *Phys. Rev. X* **7**, 4, 041025 (2017), [arXiv:1704.07561].
- [168] N. Wex and M. Kramer, *Universe* **6**, 9, 156 (2020).
- [169] B. P. Abbott *et al.* (LIGO Scientific, Virgo), *Phys. Rev. D* **100**, 10, 104036 (2019), [arXiv:1903.04467].
- [170] R. Abbott *et al.* (LIGO Scientific, Virgo), *Phys. Rev. D* **103**, 12, 122002 (2021), [arXiv:2010.14529].
- [171] D. M. Eardley, D. L. Lee and A. P. Lightman, *Phys. Rev. D* **8**, 3308 (1973).
- [172] B. P. Abbott *et al.* (LIGO Scientific, Virgo, Fermi-GBM, INTEGRAL), *Astrophys. J.* **848**, 2, L13 (2017), [arXiv:1710.05834].
- [173] T. Baker *et al.*, *Phys. Rev. Lett.* **119**, 25, 251301 (2017), [arXiv:1710.06394].
- [174] P. Creminelli and F. Vernizzi, *Phys. Rev. Lett.* **119**, 25, 251302 (2017), [arXiv:1710.05877].
- [175] J. Sakstein and B. Jain, *Phys. Rev. Lett.* **119**, 25, 251303 (2017), [arXiv:1710.05893].
- [176] J. M. Ezquiaga and M. Zumalacárregui, *Phys. Rev. Lett.* **119**, 25, 251304 (2017), [arXiv:1710.05901].
- [177] G. Agazie *et al.* (NANOGrav), *Astrophys. J. Lett.* **951**, 1, L8 (2023), [arXiv:2306.16213].
- [178] J. Antoniadis *et al.* (EPTA) (2023), [arXiv:2306.16214].
- [179] D. J. Reardon *et al.*, *Astrophys. J. Lett.* **951**, 1, L6 (2023), [arXiv:2306.16215].
- [180] H. Xu *et al.*, *Res. Astron. Astrophys.* **23**, 7, 075024 (2023), [arXiv:2306.16216].

22. Big-Bang Cosmology

Revised August 2023 by K.A. Olive (Minnesota U.) and J.A. Peacock (Edinburgh U.).

22.1 Introduction to the standard big-bang model

The observed expansion of the Universe [1–3] is a natural (almost inevitable) result of any homogeneous and isotropic cosmological model based on general relativity. However, by itself, the Hubble expansion does not provide sufficient evidence for what we generally refer to as the Big-Bang model of cosmology. While general relativity is in principle capable of describing the cosmology of any given distribution of matter, it is extremely fortunate that our Universe appears to be homogeneous and isotropic on large scales. Together, homogeneity and isotropy allow us to extend the Copernican Principle to the Cosmological Principle, stating that all spatial positions in the Universe are essentially equivalent.

The formulation of the Big-Bang model began in the 1940s with the work of George Gamow and his collaborators, Ralph Alpher and Robert Herman. In order to account for the possibility that the abundances of the elements had a cosmological origin, they proposed that the early Universe was once very hot and dense (enough so as to allow for the nucleosynthetic processing of hydrogen), and has subsequently expanded and cooled to its present state [4, 5]. In 1948, Alpher and Herman predicted that a direct consequence of this model is the presence of a relic background radiation with a temperature of order a few kelvin [6, 7]. Of course this radiation was observed 16 years later as the cosmic microwave background (CMB) [8]. Indeed, it was the observation of this radiation that singled out the Big-Bang model as the prime candidate to describe our Universe. Subsequent work on Big-Bang nucleosynthesis further confirmed the necessity of our hot and dense past. See Sec. 22.3.7 for a brief discussion of BBN, and Sec. 24 of this *Review* for a detailed discussion of BBN. These relativistic cosmological models face severe problems with their initial conditions, to which the best modern solution is inflationary cosmology, discussed in Sec. 22.3.5 and in – Sec. 23 of this *Review*. If correct, these ideas would strictly render the term ‘Big Bang’ redundant, since it was first coined by Hoyle to represent a criticism of the lack of understanding of the initial conditions.

22.1.1 The Robertson-Walker Universe

The observed homogeneity and isotropy enable us to describe the overall geometry and evolution of the Universe in terms of two cosmological parameters accounting for the spatial curvature and the overall expansion (or contraction) of the Universe. These two quantities appear in the most general expression for a space-time metric that has a (3D) maximally symmetric subspace of a 4D space-time, known as the Robertson-Walker metric:

$$ds^2 = dt^2 - R^2(t) \left[\frac{dr^2}{1 - kr^2} + r^2 (d\theta^2 + \sin^2 \theta d\phi^2) \right]. \quad (22.1)$$

Note that we adopt $c = 1$ throughout. By rescaling the radial coordinate, we can choose the curvature constant k to take only the discrete values $+1$, -1 , or 0 corresponding to closed, open, or spatially flat geometries. In this case, it is often more convenient to re-express the metric as

$$ds^2 = dt^2 - R^2(t) [d\chi^2 + S_k^2(\chi) (d\theta^2 + \sin^2 \theta d\phi^2)], \quad (22.2)$$

where the function $S_k(\chi)$ is $(\sin \chi, \chi, \sinh \chi)$ for $k = (+1, 0, -1)$. The coordinate r [in Eq. (22.1)] and the ‘angle’ χ [in Eq. (22.2)] are both dimensionless; the dimensions are carried by the cosmological scale factor, $R(t)$, which determines proper distances in terms of the comoving coordinates. A common alternative is to define a dimensionless scale factor, $a(t) = R(t)/R_0$, where $R_0 \equiv R(t_0)$ is R at the present epoch. It is also sometimes convenient to define a dimensionless or conformal time coordinate, η , by $d\eta = dt/R(t)$. Along constant spatial sections, the proper time is defined by the time coordinate, t . Similarly, for $dt = d\theta = d\phi = 0$, the proper distance is given by $R(t)\chi$. For standard texts on cosmological models see *e.g.*, Refs. [9–16].

22.1.2 The redshift

The cosmological redshift is a direct consequence of the Hubble expansion, determined by $R(t)$. A local observer detecting light from a distant emitter sees a redshift in frequency. We can define the redshift as

$$z \equiv \frac{\nu_1 - \nu_2}{\nu_2} \simeq v_{12}, \quad (22.3)$$

where ν_1 is the frequency of the emitted light, ν_2 is the observed frequency, and v_{12} is the relative velocity between the emitter and the observer. While the definition, $z = (\nu_1 - \nu_2)/\nu_2$ is valid in general, relating the redshift to a simple relative velocity is only correct on small scales (*i.e.*, less than cosmological scales) such that the expansion velocity is non-relativistic. For light signals, we can use the metric given by Eq. (22.1) and $ds^2 = 0$ to write

$$v_{12} = \dot{R} \delta r = \frac{\dot{R}}{R} \delta t = \frac{\delta R}{R} = \frac{R_2 - R_1}{R_1}, \quad (22.4)$$

where $\delta r(\delta t)$ is the radial coordinate (temporal) separation between the emitter and observer. Noting that physical distance, D , is $R\delta r$ or δt , Eq. (22.4) gives us Hubble’s law, $v = HD$. In addition, we obtain a simple relation between the redshift and the scale factor:

$$1 + z = \frac{\nu_1}{\nu_2} = \frac{R_2}{R_1}. \quad (22.5)$$

This result does not depend on the non-relativistic approximation.

22.1.3 The Friedmann equations of motion

The cosmological equations of motion are derived from Einstein’s equations:

$$\mathcal{R}_{\mu\nu} - \frac{1}{2} g_{\mu\nu} \mathcal{R} = 8\pi G_N T_{\mu\nu} + \Lambda g_{\mu\nu}. \quad (22.6)$$

Gliner [17] and Zeldovich [18] pioneered the modern view, in which the Λ term is set on the rhs and interpreted as an effective energy-momentum tensor $T_{\mu\nu}$ for the vacuum of $\Lambda g_{\mu\nu}/8\pi G_N$. It is common to assume that the matter content of the Universe is a perfect fluid, for which

$$T_{\mu\nu} = -p g_{\mu\nu} + (p + \rho) u_\mu u_\nu, \quad (22.7)$$

where $g_{\mu\nu}$ is the space-time metric described by Eq. (22.1), p is the isotropic pressure, ρ is the energy density and $u = (1, 0, 0, 0)$ is the velocity vector for the isotropic fluid in co-moving coordinates. With the perfect fluid source, Einstein’s equations lead to the Friedmann equations:

$$H^2 \equiv \left(\frac{\dot{R}}{R} \right)^2 = \frac{8\pi G_N \rho}{3} - \frac{k}{R^2} + \frac{\Lambda}{3}, \quad (22.8)$$

and

$$\frac{\ddot{R}}{R} = \frac{\Lambda}{3} - \frac{4\pi G_N}{3} (\rho + 3p), \quad (22.9)$$

where $H(t)$ is the Hubble parameter and Λ is the cosmological constant. The first of these is sometimes called *the* Friedmann equation. Energy conservation via $T^{\mu\nu}_{;\mu} = 0$, leads to a third useful equation [which can also be derived from Eq. (22.8) and Eq. (22.9)]:

$$\dot{\rho} = -3H(\rho + p). \quad (22.10)$$

Equation (22.10) can also be simply derived as a consequence of the first law of thermodynamics.

Equation (22.8) has a simple classical mechanical analog if we neglect (for the moment) the cosmological term Λ . By interpreting $-k/R^2$ Newtonianly as a ‘total energy’, then we see that the evolution of the Universe is governed by a competition between the potential energy, $8\pi G_N \rho/3$, and the kinetic term $(\dot{R}/R)^2$. For $\Lambda = 0$, it is clear that the Universe must be expanding or contracting (except at the turning point prior to collapse in a closed Universe). The ultimate fate of the Universe is determined by the curvature constant k . For $k = +1$, the Universe will recollapse in a finite time, whereas for $k = 0, -1$, the Universe will expand indefinitely. These simple conclusions can be altered when $\Lambda \neq 0$ or more generally with some component with $(\rho + 3p) < 0$.

22.1.4 Definition of cosmological parameters

In addition to the Hubble parameter, it is useful to define several other measurable cosmological parameters. The Friedmann equation can be used to define a critical density such that $k = 0$ when $\Lambda = 0$:

$$\begin{aligned}\rho_c &\equiv \frac{3H^2}{8\pi G_N} = 1.88 \times 10^{-26} h^2 \text{ kg m}^{-3} \\ &= 1.05 \times 10^{-5} h^2 \text{ GeV cm}^{-3},\end{aligned}\quad (22.11)$$

where the scaled Hubble parameter, h , is defined by

$$\begin{aligned}H &\equiv 100 h \text{ km s}^{-1} \text{ Mpc}^{-1} \\ \Rightarrow H^{-1} &= 9.778 h^{-1} \text{ Gyr} \\ &= 2998 h^{-1} \text{ Mpc}.\end{aligned}\quad (22.12)$$

The cosmological density parameter Ω_{tot} is defined as the energy density relative to the critical density:

$$\Omega_{\text{tot}} = \rho/\rho_c. \quad (22.13)$$

Note that one can now rewrite the Friedmann equation as

$$k/R^2 = H^2(\Omega_{\text{tot}} - 1). \quad (22.14)$$

From Eq. (22.14), one can see that when $\Omega_{\text{tot}} > 1$, $k = +1$ and the Universe is closed, when $\Omega_{\text{tot}} < 1$, $k = -1$ and the Universe is open, and when $\Omega_{\text{tot}} = 1$, $k = 0$, and the Universe is spatially flat.

It is often necessary to distinguish different contributions to the density. It is therefore convenient to define present-day density parameters for pressureless matter (Ω_m) and relativistic particles (Ω_r), plus the quantity $\Omega_\Lambda = \Lambda/3H^2$. In more general models, we may wish to drop the assumption that the vacuum energy density is constant, and we therefore denote the present-day density parameter of the vacuum by Ω_v . The Friedmann equation then becomes

$$k/R_0^2 = H_0^2(\Omega_m + \Omega_r + \Omega_v - 1), \quad (22.15)$$

where the subscript 0 indicates present-day values. Thus, it is the sum of the densities in matter, relativistic particles, and vacuum that determines the overall sign of the curvature. Note that the quantity $-k/R_0^2 H_0^2$ is sometimes referred to as Ω_K . This usage is unfortunate: it encourages one to think of curvature as a contribution to the energy density of the Universe, which is not correct.

22.1.5 Standard Model solutions

Much of the history of the Universe in the standard Big-Bang model can be easily described by assuming that either matter or radiation dominates the total energy density. During inflation and again today the expansion rate for the Universe is accelerating, and we should allow for domination by a cosmological constant or some other form of dark energy. In the following, we shall delineate the solutions to the Friedmann equation when a single component dominates the energy density. Each component is distinguished by an equation of state parameter $w = p/\rho$. We concentrate on solutions that expand at early times, although the Friedmann equation also permits a time-reversed contracting solution.

22.1.5.1 Solutions for a general equation of state

Let us first assume a general equation of state parameter for a single component, w , which is constant. In this case, Eq. (22.10) can be written as $\dot{\rho} = -3(1+w)\rho\dot{R}/R$ and is easily integrated to yield

$$\rho \propto R^{-3(1+w)}. \quad (22.16)$$

Note that at early times when R is small, the less singular curvature term k/R^2 in the Friedmann equation can be neglected so long as $w > -1/3$. Curvature domination occurs at rather late times (if a cosmological constant term does not dominate sooner). For $w \neq -1$, one can insert this result into the Friedmann equation Eq. (22.8), and if one neglects the curvature and cosmological constant terms, it is easy to integrate the equation to obtain

$$R(t) \propto t^{2/[3(1+w)]}. \quad (22.17)$$

22.1.5.2 A Radiation-dominated Universe

In the early hot and dense Universe, it is appropriate to assume an equation of state corresponding to a gas of radiation (or relativistic particles) for which $w = 1/3$. In this case, Eq. (22.16) becomes $\rho \propto R^{-4}$. The ‘extra’ factor of $1/R$ is due to the cosmological redshift; not only is the number density of particles in the radiation background decreasing as R^{-3} since volume scales as R^3 , but in addition each particle’s energy is decreasing as $E \propto \nu \propto R^{-1}$. Similarly, one can substitute $w = 1/3$ into Eq. (22.17) to obtain

$$R(t) \propto t^{1/2}; \quad H = 1/2t. \quad (22.18)$$

22.1.5.3 A Matter-dominated Universe

At relatively late times, non-relativistic matter eventually dominates the energy density over radiation [see Eq. (22.3.8)]. A pressureless gas ($w = 0$) leads to the expected dependence $\rho \propto R^{-3}$ from Eq. (22.16) and, if $k = 0$, we obtain

$$R(t) \propto t^{2/3}; \quad H = 2/3t. \quad (22.19)$$

22.1.5.4 A Universe dominated by vacuum energy

If there is a dominant source of vacuum energy, V_0 , it would act as a cosmological constant with $\Lambda = 8\pi G_N V_0$ and equation of state $w = -1$. In this case, the solution to the Friedmann equation when curvature is neglected is particularly simple and leads to an exponential expansion of the Universe:

$$R(t) \propto e^{\sqrt{\Lambda/3}t}. \quad (22.20)$$

More generally we could write

$$a(t) = \sinh^{2/3}(\sqrt{3\Lambda}t/2), \quad (22.21)$$

which describes a flat Universe containing both matter and vacuum energy, with $a(t)$ being the scale factor normalized to unity when both components are equal.

A key parameter is the equation of state of the vacuum, $w \equiv p/\rho$; this need not be the $w = -1$ of Λ , and may not even be constant [19–21]. There is much interest in the more general possibility of a dynamically evolving vacuum energy, for which the name ‘dark energy’ has become commonly used. A variety of techniques exist whereby the vacuum density as a function of time may be measured, usually expressed as the value of w as a function of epoch [22, 23]. The best current measurement for the equation of state (assumed constant, but without assuming zero curvature) is $w = -1.028 \pm 0.031$ [24]. Unless stated otherwise, we will assume that the vacuum energy is a cosmological constant with $w = -1$ exactly.

The presence of vacuum energy can dramatically alter the fate of the Universe. For example, if $\Lambda < 0$, the Universe will eventually recollapse independent of the sign of k . For large values of $\Lambda > 0$ (larger than the Einstein static value needed to halt any cosmological expansion or contraction), even a closed Universe will expand forever. One way to quantify this is the deceleration parameter, q_0 , defined as

$$q_0 = - \left. \frac{R\ddot{R}}{\dot{R}^2} \right|_0 = \frac{1}{2}\Omega_m + \Omega_r + \frac{(1+3w)}{2}\Omega_v. \quad (22.22)$$

This equation shows us that $w < -1/3$ for the vacuum may lead to an accelerating expansion. To the continuing astonishment of cosmologists, such an effect has been observed: one piece of direct evidence is the supernova Hubble diagram [25–30] (see Fig. 22.1 below). Current data indicate that vacuum energy is indeed the largest contributor to the cosmological density budget, with $\Omega_v = 0.685 \pm 0.007$ and $\Omega_m = 0.315 \pm 0.007$ if $k = 0$ is assumed [24].

The existence of this constituent is without doubt the greatest puzzle raised by the current cosmological model; the final section of this review discusses some of the ways in which the vacuum-energy problem is being addressed. For more details, see Dark Energy – Sec. 28 of this *Review*.

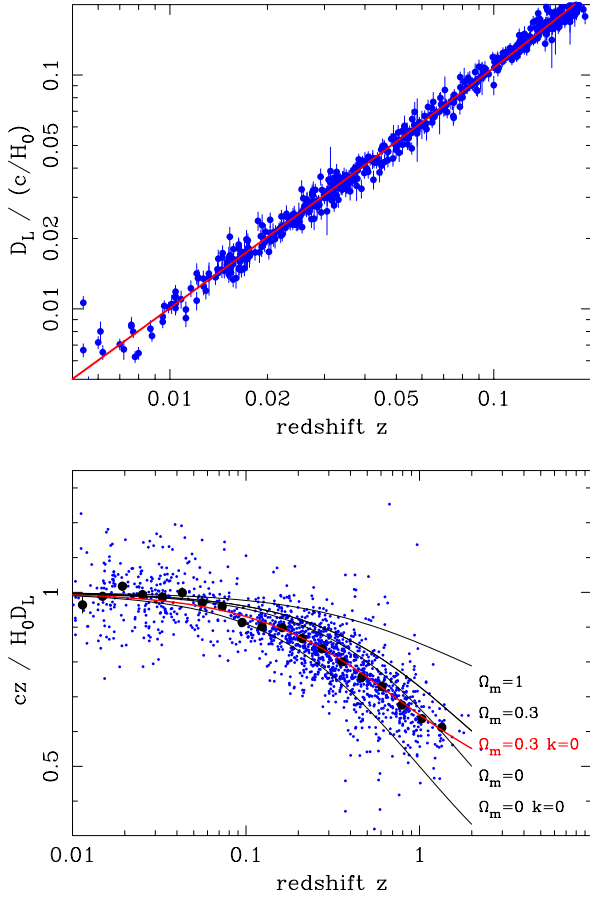


Figure 22.1: The type Ia supernova Hubble diagram, based on 1650 publicly available supernova distance estimates [28–30]. The first panel shows that for $z \ll 1$ the large-scale Hubble flow is indeed linear and uniform; the second panel shows an expanded scale, with the linear trend divided out, and with the redshift range extended to show how the Hubble law becomes nonlinear ($\Omega_r = 0$ is assumed). Larger points with errors show median values in redshift bins. Comparison with the prediction of Friedmann models favors a vacuum-dominated Universe.

22.2 Introduction to observational cosmology

22.2.1 Fluxes, luminosities, and distances

The key quantities for observational cosmology can be deduced quite directly from the metric.

(1) The *proper* transverse size of an object seen by us to subtend an angle $d\psi$ is its comoving size $d\psi S_k(\chi)$ times the scale factor at the time of emission:

$$d\ell = d\psi R_0 S_k(\chi)/(1+z). \quad (22.23)$$

(2) The apparent flux density of an object is deduced by allowing its photons to flow through a sphere of current radius $R_0 S_k(\chi)$; but photon energies and arrival rates are redshifted, and the bandwidth $d\nu$ is reduced. The observed photons at frequency ν_0 were emitted at frequency $\nu_0(1+z)$, so the flux density is the luminosity at this frequency, divided by the total area, divided by $1+z$:

$$S_\nu(\nu_0) = \frac{L_\nu([1+z]\nu_0)}{4\pi R_0^2 S_k^2(\chi)(1+z)}. \quad (22.24)$$

These relations lead to the following common definitions:

$$\begin{aligned} \text{angular-diameter distance} \quad D_A &= (1+z)^{-1} R_0 S_k(\chi); \\ \text{luminosity distance} \quad D_L &= (1+z) R_0 S_k(\chi). \end{aligned} \quad (22.25)$$

These distance-redshift relations are expressed in terms of observables by using the equation of a null radial geodesic ($R(t)d\chi = dt$) plus the Friedmann equation:

$$\begin{aligned} R_0 d\chi &= \frac{1}{H(z)} dz = \frac{1}{H_0} [(1 - \Omega_m - \Omega_v - \Omega_r)(1+z)^2 \\ &\quad + \Omega_v(1+z)^{3+3w} + \Omega_m(1+z)^3 \\ &\quad + \Omega_r(1+z)^4]^{-1/2} dz. \end{aligned} \quad (22.26)$$

The main scale for the distance here is the Hubble length, $1/H_0$. The flux density is the product of the specific intensity I_ν and the solid angle $d\Omega$ subtended by the source: $S_\nu = I_\nu d\Omega$. Combining the angular size and flux-density relations thus gives the relativistic version of surface-brightness conservation:

$$I_\nu(\nu_0) = \frac{B_\nu([1+z]\nu_0)}{(1+z)^3}, \quad (22.27)$$

where B_ν is surface brightness (luminosity emitted into unit solid angle per unit area of source). We can integrate over ν_0 to obtain the corresponding total or bolometric formula:

$$I_{\text{tot}} = \frac{B_{\text{tot}}}{(1+z)^4}. \quad (22.28)$$

This cosmology-independent form expresses Liouville's Theorem: photon phase-space density is conserved along rays.

22.2.2 Distance data and geometrical tests of cosmology

In order to confront these theoretical predictions with data, we have to bridge the divide between two extremes. Nearby objects may have their distances measured quite easily, but their radial velocities are dominated by deviations from the ideal Hubble flow, which typically have a magnitude of several hundred km s^{-1} . On the other hand, objects at redshifts $z \gtrsim 0.01$ will have observed recession velocities that differ from their ideal values by $\lesssim 10\%$, but absolute distances are much harder to supply in this case. The traditional solution to this problem is the construction of the distance ladder: an interlocking set of methods for obtaining relative distances between various classes of object, which begins with absolute distances at the 10 to 100 pc level, and terminates at galaxies at significant redshifts. This is discussed in the article on Cosmological Parameters – Sec. 25 of this *Review*.

One of the key developments in this area has been the use of type Ia supernovae (SNe), which now allow measurement of relative distances with 5% precision. In combination with improved Cepheid data from the *HST* plus improved measurements of the distance to the LMC (or alternatively a direct geometrical distance to the maser galaxy NGC4258), SNe results extend the distance ladder to the point where deviations from uniform expansion are negligible, leading to the best existing Cepheid-based value for H_0 : $(73.0 \pm 1.0) \text{ km s}^{-1} \text{ Mpc}^{-1}$ [31]. Better still, the analysis of high- z SNe has allowed a simple and direct test of cosmological geometry to be carried out: as shown in Fig. 22.1 and Fig. 22.2, supernova data and measurements of CMB anisotropies strongly favor a $k = 0$ model dominated by vacuum energy. It is worth noting that there is some tension (4.2σ) between the Cepheid and CMB determinations of H_0 (the latter is $(67.4 \pm 0.5) \text{ km s}^{-1} \text{ Mpc}^{-1}$ [24]). While it is remarkable that the two very different methods give such similar results, the formal disagreement shows that either there are unidentified systematic errors or that some new post-CDM physics is required; there is no current consensus in the community on these alternatives. We do note that a recent analysis of SNe Ia with a calibration of the tip of the red-giant branch gives a result close to that of the CMB: $(69.8 \pm 0.6 \text{ (stat.)} \pm 1.6 \text{ (sys.)}) \text{ km s}^{-1} \text{ Mpc}^{-1}$ [32, 33]. See Cosmological Parameters – Sec. 25 of this *Review* for a more comprehensive review of Hubble parameter determinations.

22.2.3 Age of the Universe

The most striking conclusion of relativistic cosmology is that the Universe has not existed forever. The dynamical result for

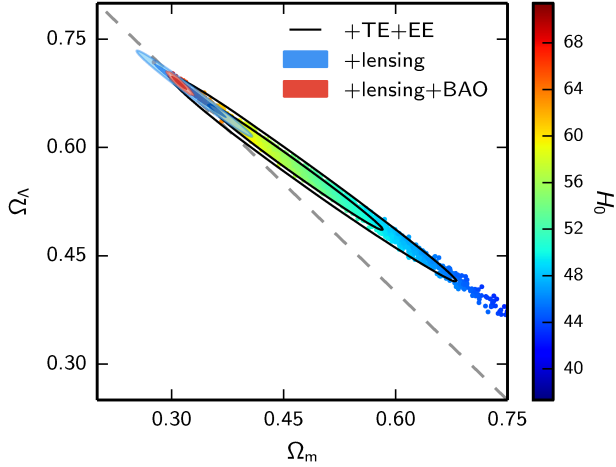


Figure 22.2: Likelihood-based probability densities over the plane Ω_Λ (*i.e.*, Ω_ν assuming $w = -1$) versus Ω_m . The colored locus derives from *Planck* [34] and shows that the CMB alone requires a flat Universe $\Omega_\nu + \Omega_m \simeq 1$ if the Hubble constant is not too high. The SNe Ia results [35] very nearly constrain the orthogonal combination $\Omega_\nu - \Omega_m$, and the intersection of these constraints directly favors a flat model with $\Omega_m \simeq 0.3$, as does the measurement of the baryon acoustic oscillation lengthscale (for which a joint constraint is shown on this plot). The CMB alone is capable of breaking the degeneracy with H_0 by using the measurements of gravitational lensing that can be made with modern high-resolution CMB data.

the age of the Universe may be written as

$$\begin{aligned} H_0 t_0 &= \int_0^\infty \frac{dz}{(1+z)H(z)} \\ &= \int_0^\infty \frac{dz}{(1+z) [(1+z)^2(1+\Omega_m z) - z(2+z)\Omega_\nu]^{1/2}}, \end{aligned} \quad (22.29)$$

where we have neglected Ω_r and chosen $w = -1$. Over the range of interest ($0.1 \lesssim \Omega_m \lesssim 1$, $|\Omega_\nu| \lesssim 1$), this exact answer may be approximated to a few per cent accuracy by

$$H_0 t_0 \simeq \frac{2}{3} (0.7\Omega_m + 0.3 - 0.3\Omega_\nu)^{-0.3}. \quad (22.30)$$

For the special case that $\Omega_m + \Omega_\nu = 1$, the integral in Eq. (22.29) can be expressed analytically as

$$H_0 t_0 = \frac{2}{3\sqrt{\Omega_\nu}} \ln \frac{1 + \sqrt{\Omega_\nu}}{\sqrt{1 - \Omega_\nu}} \quad (\Omega_m < 1). \quad (22.31)$$

The most accurate means of obtaining ages for astronomical objects is based on the natural clocks provided by radioactive decay. The use of these clocks is complicated by a lack of knowledge of the initial conditions of the decay. In the Solar System, chemical fractionation of different elements helps pin down a precise age for the pre-Solar nebula of 4.6 Gyr, but for stars it is necessary to attempt an a priori calculation of the relative abundances of nuclei that result from supernova explosions. In this way, a lower limit for the age of stars in the local part of the Milky Way of about 11 Gyr is obtained [36, 37].

The other major means of obtaining cosmological age estimates is based on the theory of stellar evolution. In principle, the main-sequence turnoff point in the color-magnitude diagram of a globular cluster should yield a reliable age. But these have been controversial, owing to theoretical uncertainties in the evolution model – as well as observational uncertainties in the distance, dust extinction, and metallicity of clusters. The present consensus favors ages for the oldest clusters of about 13 Gyr [38].

These methods are all consistent with the age deduced from studies of structure formation, using the microwave background and large-scale structure: $t_0 = (13.80 \pm 0.02)$ Gyr [24], where

the extra accuracy comes at the price of assuming the simple 6-parameter Λ CDM model to be true.

22.2.4 Horizon, isotropy, flatness problems

For photons, the radial equation of motion is just $c dt = R d\chi$. How far can a photon get in a given time? The answer is clearly

$$\Delta\chi = \int_{t_1}^{t_2} \frac{dt}{R(t)} \equiv \Delta\eta, \quad (22.32)$$

i.e., just the interval of conformal time. We can replace dt by dR/\dot{R} , which the Friedmann equation says is $\propto dR/\sqrt{\rho R^2}$ at early times. Thus, this integral converges if $\rho R^2 \rightarrow \infty$ as $t_1 \rightarrow 0$, otherwise it diverges. Provided the equation of state is such that ρ changes faster than R^{-2} , light signals can only propagate a finite distance between the Big Bang and the present; there is then said to be a particle horizon. Such a horizon therefore exists in conventional Big-Bang models, which are dominated by radiation ($\rho \propto R^{-4}$) at early times.

At late times, the integral for the horizon is largely determined by the matter-dominated phase, for which

$$D_H = R_0 \chi_H \equiv R_0 \int_0^{t(z)} \frac{dt}{R(t)} \simeq \frac{6000}{\sqrt{\Omega_m z}} h^{-1} \text{Mpc} \quad (z \gg 1). \quad (22.33)$$

The horizon at the time of formation of the microwave background (‘last scattering’: $z \simeq 1100$) was thus of order 100 *Mpc* in size, subtending an angle of about 1° . Why then are the large number of causally disconnected regions we see on the microwave sky all at the same temperature? The Universe is very nearly isotropic and homogeneous, even though the initial conditions appear not to permit such a state to be constructed.

A related problem is that the $\Omega = 1$ Universe is unstable:

$$\Omega(a) - 1 = \frac{\Omega - 1}{1 - \Omega + \Omega_\nu a^2 + \Omega_m a^{-1} + \Omega_r a^{-2}}, \quad (22.34)$$

where Ω with no subscript is the total density parameter, and $a(t) = R(t)/R_0$. This requires $\Omega(t)$ to be unity to arbitrary precision as the initial time tends to zero; a Universe of non-zero curvature today requires very finely tuned initial conditions.

22.3 The Hot Thermal Universe

22.3.1 Thermodynamics of the early Universe

As alluded to above, we expect that much of the early Universe can be described by a radiation-dominated equation of state. In addition, through much of the radiation-dominated period, thermal equilibrium is established by the rapid rate of particle interactions relative to the expansion rate of the Universe (see Sec. 22.3.3 below). In equilibrium, it is straightforward to compute the thermodynamic quantities, ρ , p , and the entropy density, s . In general, the energy density for a given particle type i can be written as

$$\rho_i = \int E_i dn_{q_i}, \quad (22.35)$$

with the density of states given by

$$dn_{q_i} = \frac{g_i}{2\pi^2} (\exp[(E_{q_i} - \mu_i)/T_i] \pm 1)^{-1} q_i^2 dq_i, \quad (22.36)$$

where g_i counts the number of degrees of freedom for particle type i , $E_{q_i}^2 = m_i^2 + q_i^2$, μ_i is the chemical potential, and the \pm corresponds to either Fermi or Bose statistics. Similarly, we can define the pressure of a perfect gas as

$$p_i = \frac{1}{3} \int \frac{q_i^2}{E_i} dn_{q_i}. \quad (22.37)$$

The number density of species i is simply

$$n_i = \int dn_{q_i}, \quad (22.38)$$

and the entropy density is

$$s_i = \frac{\rho_i + p_i - \mu_i n_i}{T_i}. \quad (22.39)$$

In the Standard Model, a chemical potential is often associated with baryon number, and since the net baryon density relative to the photon density is known to be very small (of order 10^{-9}), we can neglect any such chemical potential when computing total thermodynamic quantities.

For photons, we can compute all of the thermodynamic quantities rather easily. Taking $g_i = 2$ for the 2 photon polarization states, we have (in units where $\hbar = k_B = 1$)

$$\rho_\gamma = \frac{\pi^2}{15} T^4, \quad p_\gamma = \frac{1}{3} \rho_\gamma, \quad s_\gamma = \frac{4\rho_\gamma}{3T}, \quad n_\gamma = \frac{2\zeta(3)}{\pi^2} T^3, \quad (22.40)$$

with $2\zeta(3)/\pi^2 \simeq 0.2436$. Note that Eq. (22.10) can be converted into an equation for entropy conservation. Recognizing that $\dot{p} = s\dot{T}$, Eq. (22.10) becomes

$$d(sR^3)/dt = 0. \quad (22.41)$$

For radiation, this corresponds to the relationship between expansion and cooling, $T \propto R^{-1}$ in an adiabatically expanding Universe. Note also that both s and n_γ scale as T^3 .

22.3.2 Radiation content of the Early Universe

At the very high temperatures associated with the early Universe, massive particles are pair produced, and are part of the thermal bath. If for a given particle species i we have $T \gg m_i$, then we can neglect the mass in Eq. (22.35) to Eq. (22.39), and the thermodynamic quantities are easily computed as in Eq. (22.40). In general, we can approximate the energy density (at high temperatures) by including only those particles with $m_i \ll T$. In this case, we have

$$\rho = \left(\sum_B g_B + \frac{7}{8} \sum_F g_F \right) \frac{\pi^2}{30} T^4 \equiv \frac{\pi^2}{30} N(T) T^4, \quad (22.42)$$

where $g_{B(F)}$ is the number of degrees of freedom of each boson (fermion) and the sum runs over all boson and fermion states with $m \ll T$. The factor of $7/8$ is due to the difference between the Fermi and Bose integrals. Eq. (22.42) defines the effective number of degrees of freedom, $N(T)$, by taking into account new particle degrees of freedom as the temperature is raised. This quantity, calculated from high temperature lattice QCD, is plotted in Fig. 22.3 [39]. Near the QCD transition, there is a slight difference between the coefficient of T^4 for ρ and the coefficient of T^3 for the entropy density $s = (2\pi^2/45)N_s(T)T^3$ [40], as seen in the figure.

The value of $N(T)$ at any given temperature depends on the particle physics model. In the standard $SU(3) \times SU(2) \times U(1)$ model, we can specify $N(T)$ up to temperatures of $O(100)$ GeV. The change in N (ignoring mass effects) can be seen in the table below.

Temperature	New Particles	$4N(T)$
$T < m_e$	γ 's + ν 's	29
$m_e < T < m_\mu$	e^\pm	43
$m_\mu < T < m_\pi$	μ^\pm	57
$m_\pi < T < T_c^\dagger$	π 's	69
$T_c < T < m_{\text{strange}}$	π 's + u, \bar{u}, d, \bar{d} + gluons	205
$m_s < T < m_{\text{charm}}$	s, \bar{s}	247
$m_c < T < m_\tau$	c, \bar{c}	289
$m_\tau < T < m_{\text{bottom}}$	τ^\pm	303
$m_b < T < m_{W,Z}$	b, \bar{b}	345
$m_{W,Z} < T < m_{\text{Higgs}}$	W^\pm, Z	381
$m_H < T < m_{\text{top}}$	H^0	385
$m_t < T$	t, \bar{t}	427

$^\dagger T_c$ corresponds to the confinement-deconfinement transition between quarks and hadrons.

At higher temperatures, $N(T)$ will be model-dependent. For example, in the minimal $SU(5)$ model, one needs to add 24 states to $N(T)$ for the charged and colored X and Y gauge bosons,

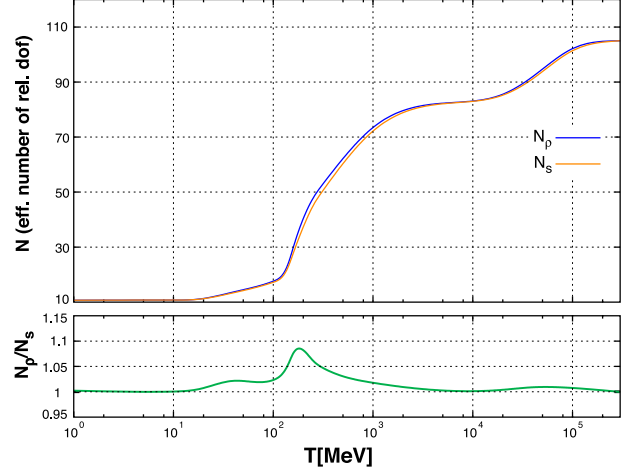


Figure 22.3: The effective numbers of relativistic degrees of freedom as a function of temperature. The sharp drop corresponds to the quark-hadron transition. The bottom panel shows the relative ratio between the number of degrees of freedom characterizing the energy density and the entropy.

another 24 from the adjoint Higgs, and another six scalar degrees of freedom (in addition to the four associated with the complex Higgs doublet already counted in the longitudinal components of W^\pm and Z , and in H) from the $\bar{5}$ of Higgs. Hence for $T > m_X$ in minimal $SU(5)$, $N(T) = 160.75$. In a supersymmetric model this would at least double.

In the radiation-dominated epoch, Eq. (22.10) can be integrated (neglecting the T -dependence of N), giving us a relationship between the age of the Universe and its temperature:

$$t = \left(\frac{90}{32\pi^3 G_N N(T)} \right)^{1/2} T^{-2}. \quad (22.43)$$

This can be expressed more conveniently in the form

$$t T_{\text{MeV}}^2 = 2.4 [N(T)]^{-1/2}, \quad (22.44)$$

where t is measured in seconds and T_{MeV} in units of MeV.

22.3.3 Neutrinos and equilibrium

Due to the expansion of the Universe, certain rates may be too slow to either establish or maintain equilibrium. Quantitatively, for each particle i , a minimal condition for equilibrium requires that the interaction rate Γ_i involving that type of particle should be larger than the expansion rate of the Universe:

$$\Gamma_i > H. \quad (22.45)$$

Recalling that the age of the Universe is determined by H^{-1} , this condition is equivalent to requiring that on average, at least one interaction has occurred over the lifetime of the Universe.

A good example for a process that goes in and out of equilibrium is the weak interaction of neutrinos. On dimensional grounds, one can estimate the thermally averaged scattering cross-section:

$$\langle \sigma v \rangle \sim O(10^{-2}) T^2 / m_W^4 \quad (22.46)$$

for $T \lesssim m_W$. Recalling that the number density of leptons is $n \propto T^3$, we can compare the weak interaction rate, $\Gamma_{\text{wk}} \sim n \langle \sigma v \rangle$, with the expansion rate and so obtain

$$H = \left(\frac{8\pi G_N \rho}{3} \right)^{1/2} = \left(\frac{8\pi^3}{90} N(T) \right)^{1/2} T^2 / M_{\text{P}} \quad (22.47) \\ \simeq 1.66 N(T)^{1/2} T^2 / M_{\text{P}},$$

where the Planck mass $M_{\text{P}} = G_N^{-1/2} = 1.22 \times 10^{19}$ GeV.

Neutrinos will be in equilibrium when $\Gamma_{\text{wk}} > H$ or

$$T > (500 m_W^4 / M_{\text{P}})^{1/3} \sim 1 \text{ MeV}. \quad (22.48)$$

However, this condition assumes $T \ll m_W$; for higher temperatures, we should write $\langle \sigma v \rangle \sim O(10^{-2})/T^2$, so that $\Gamma \sim 10^{-2}T$. Thus, in the very early stages of expansion, at temperatures $T \gtrsim 10^{-2}M_P/\sqrt{N}$, equilibrium will not have been established.

Having attained a quasi-equilibrium stage, the Universe then cools further to the point where the interaction and expansion timescales match once again. The temperature at which these rates are equal is commonly referred to as the neutrino decoupling or freeze-out temperature and is defined by $\Gamma_{\text{wk}}(T_d) = H(T_d)$. For $T < T_d$, neutrinos drop out of equilibrium. The Universe becomes transparent to neutrinos and their momenta simply redshift with the cosmic expansion. The effective neutrino temperature will simply fall with $T \propto 1/R$.

Soon after decoupling, e^\pm pairs in the thermal background begin to annihilate (when $T \lesssim m_e$). Because the neutrinos are decoupled, the energy released due to annihilation heats up the photon background relative to the neutrinos. The change in the photon temperature can be easily computed from entropy conservation. The neutrino entropy must be conserved separately from the entropy of interacting particles. A straightforward computation yields

$$T_\nu = (4/11)^{1/3} T_\gamma \simeq 1.9 \text{ K}. \quad (22.49)$$

The total entropy density is therefore given by the contribution from photons and three flavors of neutrinos:

$$s = \frac{4}{3} \frac{\pi^2}{30} \left(2 + \frac{21}{4} (T_\nu/T_\gamma)^3 \right) T_\gamma^3 = \frac{4}{3} \frac{\pi^2}{30} \left(2 + \frac{21}{11} \right) T_\gamma^3 = 7.04 n_\gamma. \quad (22.50)$$

Similarly, the total relativistic energy density is given by

$$\rho_r = \frac{\pi^2}{30} \left[2 + \frac{21}{4} (T_\nu/T_\gamma)^4 \right] T_\gamma^4 \simeq 1.68 \rho_\gamma. \quad (22.51)$$

In practice, a small correction is needed to this, since neutrinos are not totally decoupled at e^\pm annihilation: the effective number of massless neutrino species is 3.044, rather than 3 [41].

This expression ignores neutrino rest masses, but current oscillation data require at least one neutrino eigenstate to have a mass exceeding 0.06 eV. In this minimal case, $\Omega_\nu h^2 = 6 \times 10^{-4}$, so the neutrino contribution to the matter budget would be negligibly small (which is our normal assumption). However, a nearly degenerate pattern of mass eigenstates could allow larger densities, since oscillation experiments only measure differences in m^2 values. Note that a 0.06-eV neutrino has $T_\nu = m_\nu$ at $z \simeq 357$, so the above expression for the total present relativistic density is really only an extrapolation. However, neutrinos are almost certainly relativistic at all epochs where the radiation content of the Universe is dynamically significant. Combining *Planck* data with data from large-scale structure surveys such as DES [42] provides an upper limit to the sum of neutrino masses, $\Sigma m_\nu < 0.13$ eV, and may provide the first measurement of a neutrino mass (as opposed to a difference of neutrino mass² from oscillation data) from future surveys. See Neutrinos in Cosmology – Sec. 26 of this *Review* for a detailed discussion of neutrinos in cosmology.

22.3.4 Field theory and phase transitions

It is very likely that the Universe has undergone one or more phase transitions during the course of its evolution [43–46]. Our current vacuum state is described by $SU(3)_c \times U(1)_{\text{em}}$, which in the Standard Model is a remnant of an unbroken $SU(3)_c \times SU(2)_L \times U(1)_Y$ gauge symmetry. Symmetry breaking occurs when a non-singlet gauge field (the Higgs field in the Standard Model) picks up a non-vanishing vacuum expectation value, determined by a scalar potential. For example, a simple (non-gauged) potential describing symmetry breaking is $V(\phi) = \frac{1}{4} \lambda \phi^4 - \frac{1}{2} \mu^2 \phi^2 + V(0)$. The resulting expectation value is simply $\langle \phi \rangle = \mu/\sqrt{\lambda}$.

In the early Universe, finite temperature radiative corrections typically add terms to the potential of the form $\phi^2 T^2$. Thus, at very high temperatures, the symmetry is restored and $\langle \phi \rangle = 0$. As the Universe cools, depending on the details of the potential, symmetry breaking will occur via a first-order phase transition in which the field tunnels through a potential barrier, or via a second-order transition in which the field evolves smoothly from

one state to another (as would be the case for the above example potential).

The evolution of scalar fields can have a profound impact on the early Universe. The equation of motion for a scalar field ϕ can be derived from the energy-momentum tensor:

$$T_{\mu\nu} = \partial_\mu \phi \partial_\nu \phi - \frac{1}{2} g_{\mu\nu} \partial_\rho \phi \partial^\rho \phi - g_{\mu\nu} V(\phi). \quad (22.52)$$

By associating $\rho = T_{00}$ and $p = R^{-2}(t)T_{ii}$ we have

$$\begin{aligned} \rho &= \frac{1}{2} \dot{\phi}^2 + \frac{1}{2} R^{-2}(t) (\nabla \phi)^2 + V(\phi); \\ p &= \frac{1}{2} \dot{\phi}^2 - \frac{1}{6} R^{-2}(t) (\nabla \phi)^2 - V(\phi), \end{aligned} \quad (22.53)$$

and from Eq. (22.10) we can write the equation of motion as follows (by considering a homogeneous region, we can ignore the gradient terms):

$$\ddot{\phi} + 3H\dot{\phi} = -\partial V/\partial \phi. \quad (22.54)$$

22.3.5 Inflation

In Sec. 22.2.4, we discussed some of the problems associated with the standard Big-Bang model. However, during a phase transition, our assumptions of an adiabatically expanding Universe are generally not valid. If, for example, a phase transition occurred in the early Universe such that the field evolved slowly from the symmetric state to the global minimum, the Universe may have been dominated by the vacuum energy density associated with the potential near $\phi \simeq 0$. During this period of slow evolution, the energy density due to radiation will fall below the vacuum energy density, $\rho \ll V(0)$. When this happens, the expansion rate will be dominated by the constant $V(0)$, and we obtain the exponentially expanding solution given in Eq. (22.20). When the field evolves towards the global minimum it will begin to oscillate about that minimum, energy will be released during its decay, and a hot thermal Universe will be restored. If released fast enough, it will produce radiation at a temperature $NT_R^4 \lesssim V(0)$. In this reheating process, entropy has been created and the final value of RT is greater than the initial value of RT . Thus, we see that, during a phase transition, the relation $RT \sim \text{constant}$ need not hold true. This is the basis of the inflationary Universe scenario [47–49].

If, during the phase transition, the value of RT changed by a factor of $O(10^{29})$, the cosmological problems discussed above would be solved. The observed isotropy would be generated by the immense expansion; one small causal region could get blown up, and thus our entire visible Universe would have been in thermal contact some time in the past. In addition, the density parameter Ω would have been driven to 1 (with exponential precision). Density perturbations will be stretched by the expansion, $\lambda \propto R(t)$. Thus it will appear that $\lambda \gg H^{-1}$ or that the perturbations have left the horizon, where in fact the size of the causally connected region is now no longer simply H^{-1} . However, not only does inflation offer an explanation for large scale perturbations, it also offers a source for the perturbations themselves through quantum fluctuations.

Problems with early models of inflation based on either a first-order [50] or second-order [51, 52] phase transition of a Grand Unified Theory led to models invoking a completely new scalar field: the inflaton, ϕ . The potential of this field, $V(\phi)$, needs to have a very low gradient and curvature in order to match observed metric fluctuations. For a more thorough discussion of the problems of early models and a host of current models being studied see the review on inflation – Sec. 23 of this *Review*. In most current inflation models, reheated bubbles typically do not percolate, so inflation is ‘eternal’ and continues with exponential expansion in the region outside the bubbles. These causally disconnected bubble Universes constitute a ‘multiverse’, where low-energy physics can vary between different bubbles. This has led to a controversial ‘anthropic’ approach to cosmology [53–55], where observer selection within the multiverse can be introduced as a means of understanding *e.g.* why the observed level of vacuum energy is so low (because larger values suppress growth of structure).

22.3.6 Baryogenesis

The Universe appears to be populated exclusively with matter rather than antimatter [56, 57]. Indeed antimatter is only detected in accelerators or in cosmic rays. However, the presence of antimatter in the latter is understood to be the result of collisions of primary particles in the interstellar medium. There is in fact strong evidence against primary forms of antimatter in the Universe. Furthermore, the density of baryons compared to the density of photons is extremely small, $\eta \sim 10^{-9}$.

The production of a net baryon asymmetry requires baryon number violating interactions, C and CP violation, and a departure from thermal equilibrium [58]. The first two of these ingredients are expected to be contained in Grand Unified Theories (GUTs) as well as in the non-perturbative sector of the Standard Model; the third can be realized in an expanding Universe where, as we have seen, interactions come in and out of equilibrium.

There are several interesting and viable mechanisms for the production of the baryon asymmetry. While we cannot review any of them here in any detail, we mention some of the important scenarios. In all cases, all three ingredients listed above are incorporated. One of the first mechanisms was based on the out of equilibrium decay of a massive particle such as a superheavy GUT gauge or Higgs boson [59, 60]. A novel mechanism involving the decay of flat directions in supersymmetric models is known as the Affleck-Dine scenario [61]. There is also the possibility of generating the baryon asymmetry at the electroweak scale using the non-perturbative interactions of sphalerons [62]. Because these interactions conserve the sum of baryon and lepton number, $B + L$, it is possible to first generate a lepton asymmetry (*e.g.*, by the out-of-equilibrium decay of a superheavy right-handed neutrino), which is converted to a baryon asymmetry at the electroweak scale [63]. This mechanism is known as leptobaryogenesis, or simply leptogenesis.

22.3.7 Nucleosynthesis

An essential element of the standard cosmological model is Big-Bang nucleosynthesis (BBN), the theory that predicts the abundances of the light element isotopes D, ^3He , ^4He , and ^7Li . Nucleosynthesis takes place at a temperature scale of order 1 MeV. The nuclear processes lead primarily to ^4He , with a primordial mass fraction of about 25%. Lesser amounts of the other light elements are produced: about 10^{-5} of D and ^3He and about 10^{-10} of ^7Li by number relative to H. The abundances of the light elements depend almost solely on one key parameter, the baryon-to-photon ratio, η . The nucleosynthesis predictions can be compared with observational determinations of the abundances of the light elements. Consistency between theory and observations, driven primarily by recent D/H measurements [64, 65], leads to a range of [66]

$$5.8 \times 10^{-10} < \eta < 6.3 \times 10^{-10}. \quad (22.55)$$

The value of η is related to the baryon density as follows:

$$\Omega_b = 3.66 \times 10^7 \eta h^{-2}, \quad (22.56)$$

or $10^{10} \eta = 274 \Omega_b h^2$. The *Planck* result [24] for $\Omega_b h^2$ of 0.0224 ± 0.0002 translates into a value of $\eta = 6.12 \pm 0.04$. This result can be used to ‘predict’ the light element abundances, which can in turn be compared with observation [67]. The resulting D/H abundance is in excellent agreement with that found in quasar absorption systems. It is in reasonable agreement with the helium abundance observed in extragalactic HII regions (once systematic uncertainties are accounted for). The BBN predicted Li abundance is systematically higher than the Li abundance observed in the atmospheres of halo dwarf stars [68], but there is mounting evidence that effects of stellar depletion cannot be ignored so that the stellar abundances of Li may not correspond to the primordial abundance [69]. See BBN – Sec. 24 of this *Review* for a detailed discussion of BBN, in addition to references [66, 70–74].

22.3.8 The transition to a matter-dominated Universe

In the Standard Model, the temperature (or redshift) at which the Universe undergoes a transition from a radiation-dominated to a matter-dominated Universe is determined by the amount of dark matter. Assuming three nearly massless neutrinos, the energy

density in radiation at temperatures $T \ll 1$ MeV, is given by

$$\rho_r = \frac{\pi^2}{30} \left[2 + \frac{21}{4} \left(\frac{4}{11} \right)^{4/3} \right] T^4. \quad (22.57)$$

In the absence of non-baryonic dark matter, the matter density can be written as

$$\rho_m = m_N \eta n_\gamma, \quad (22.58)$$

where m_N is the nucleon mass. Recalling that $n_\gamma \propto T^3$ [cf. Eq. (22.40)], we can solve for the temperature or redshift at the matter-radiation equality when $\rho_r = \rho_m$:

$$T_{\text{eq}} = 0.22 m_N \eta \quad \text{or} \quad (1 + z_{\text{eq}}) = 0.22 \eta \frac{m_N}{T_0}, \quad (22.59)$$

where T_0 is the present temperature of the microwave background. For $\eta = 6.1 \times 10^{-10}$, this corresponds to a temperature $T_{\text{eq}} \simeq 0.13$ eV or $(1 + z_{\text{eq}}) \simeq 550$. A transition this late would be problematic for structure formation (see Sec. 22.4.5).

The redshift of matter domination can be pushed back significantly if non-baryonic dark matter is present. If instead of Eq. (22.58), we write

$$\rho_m = \Omega_m \rho_c \left(\frac{T}{T_0} \right)^3, \quad (22.60)$$

we find that

$$T_{\text{eq}} = 0.9 \frac{\Omega_m \rho_c}{T_0^3} \quad \text{or} \quad (1 + z_{\text{eq}}) = 2.4 \times 10^4 \Omega_m h^2. \quad (22.61)$$

22.4 The Universe at late times

22.4.1 The CMB

One form of the infamous Olbers’ paradox says that, in Euclidean space, surface brightness is independent of distance. Every line of sight will terminate on matter that is hot enough to be ionized and so scatter photons: $T \gtrsim 10^3$ K, and the sky should therefore shine as brightly as the surface of the Sun. The reason the night sky is dark is entirely due to the expansion, which cools the radiation temperature to 2.73 K. This gives a Planck function peaking at around 1 mm to produce the CMB.

The CMB spectrum is a very accurate match to a Planck function [75]; see also CMB – Sec. 29 of this *Review*. The COBE estimate of the temperature is [76]

$$T = (2.7255 \pm 0.0006) \text{ K}. \quad (22.62)$$

The lack of any distortion of the Planck spectrum is a strong physical constraint. It is very difficult to account for in any expanding Universe other than one that passes through a hot stage. Alternative schemes for generating the radiation, such as thermalization of starlight by dust grains, inevitably generate a superposition of temperatures. What is required in addition to thermal equilibrium is that $T \propto 1/R$, so that radiation from different parts of space arrive at an observer with the same apparent temperature.

Although it is common to speak of the CMB as originating at ‘recombination’, a more accurate terminology is the era of ‘last scattering’. In practice, this takes place at $z \simeq 1100$, almost independently of the main cosmological parameters, at which time the fractional ionization is very small. This occurred when the age of the Universe was about 370,000 years. But the CMB photons themselves were not generated at this point, and were the result of thermalization at $z \sim 10^7$. See CMB – Sec. 29 of this *Review* for a full discussion of the CMB.

22.4.2 Matter in the Universe

One of the main tasks of cosmology is to measure the density of the Universe, and how this is divided between dark matter and baryons. The baryons consist partly of stars, with $0.002 \lesssim \Omega_* \lesssim 0.003$ [77] but mainly inhabit the intergalactic medium (IGM). One powerful way in which this can be studied is via the absorption of light from distant luminous objects such as quasars. Even very small amounts of neutral hydrogen can

absorb rest-frame UV photons (the Gunn-Peterson effect), and should suppress the continuum by a factor $\exp(-\tau)$, where

$$\tau \simeq 10^{4.62} h^{-1} \left[\frac{n_{\text{HI}}(z)/m^{-3}}{(1+z)\sqrt{1+\Omega_m z}} \right], \quad (22.63)$$

and this expression applies while the Universe is matter dominated ($z \gtrsim 1$ in the $\Omega_m = 0.3$ $\Omega_v = 0.7$ model). At $z < 6$, the dominant effect on quasar spectra is a ‘forest’ of narrow absorption lines, which produce a mean $\tau = 1$ in the Ly α forest at about $z = 3$, and so we have $\Omega_{\text{HI}} \simeq 10^{-6.7} h^{-1}$. This is such a small number that the IGM must be very highly ionized at these redshifts, apart from a few high-density clumps. But at $z > 6$ there is good evidence for a ‘reionization’ era at which the general IGM is not so strongly ionized [78]. As discussed below, this ionized IGM at low z is also detectable via the secondary Compton scattering of CMB photons.

The Ly α forest is of great importance in pinning down the abundance of deuterium. Because electrons in deuterium differ in reduced mass by about 1 part in 4000 compared to hydrogen, each absorption system in the Ly α forest is accompanied by an offset deuterium line. By careful selection of systems with an optimal HI column density, a measurement of the D/H ratio can be made. This has now been done with high accuracy in 10 quasars, with consistent results [64]. Combining these determinations with the theory of primordial nucleosynthesis yields a baryon density of $\Omega_b h^2 = 0.021\text{--}0.023$ (95% confidence) in excellent agreement with the *Planck* result. For more details, see BBN – Sec. 24 of this *Review*.

Ionized IGM can also be detected in emission when it is densely clumped, via bremsstrahlung radiation. This generates the spectacular X-ray emission from rich clusters of galaxies. Studies of this phenomenon allow us to achieve an accounting of the total baryonic material in clusters. Within the central $\simeq 1$ Mpc, the masses in stars, X-ray emitting gas, and total dark matter can be determined with reasonable accuracy (perhaps 20% rms), and this allows a minimum baryon fraction to be determined [79, 80]:

$$\frac{M_{\text{baryons}}}{M_{\text{total}}} \gtrsim 0.009 + (0.066 \pm 0.003) h^{-3/2}. \quad (22.64)$$

Because clusters are the largest collapsed structures, it is reasonable to take this as applying to the Universe as a whole. This equation implies a minimum baryon fraction of perhaps 12% (for reasonable h), which is too high for $\Omega_m = 1$ if we take $\Omega_b h^2 \simeq 0.02$ from nucleosynthesis. This is therefore one of the more robust arguments in favor of $\Omega_m \simeq 0.3$; for more details, see Cosmological Parameters – Sec. 25 of this *Review*. This argument is also consistent with the inference on Ω_m that can be made from Fig. 22.2.

This method is much more robust than the older classical technique for weighing the Universe: ‘ $L \times M/L$ ’. The overall light density of the Universe is reasonably well determined from redshift surveys of galaxies, so that a good determination of mass M and luminosity L for a single object suffices to determine Ω_m – but only *if* the mass-to-light ratio were universal.

22.4.3 Gravitational lensing

A robust method for determining masses in cosmology is to use gravitational light deflection. Most systems can be treated as a geometrically thin gravitational lens, where the light bending is assumed to take place only at a single distance. Simple geometry then determines a mapping between the coordinates in the intrinsic source plane (S) and the observed image plane (I):

$$\alpha(D_I \theta_I) = \frac{D_S}{D_{LS}} (\theta_I - \theta_S), \quad (22.65)$$

where the angles θ_I, θ_S , and α are in general two-dimensional vectors on the sky. The distances D_{LS} etc. are given by an extension of the usual distance-redshift formula:

$$D_{LS} = \frac{R_0 S_k (\chi_S - \chi_L)}{1 + z_S}. \quad (22.66)$$

This is the angular-diameter distance for objects on the source plane as perceived by an observer on the lens.

Solutions of this equation divide into weak lensing, where the mapping between source plane and image plane is one-to-one, and strong lensing, in which multiple imaging is possible. For circularly-symmetric lenses, an on-axis source is multiply imaged into a ‘caustic’ ring, whose radius is the Einstein radius:

$$\begin{aligned} \theta_E &= \left(4GM \frac{D_{LS}}{D_L D_S} \right)^{1/2} \\ &= \left(\frac{M}{10^{11.09} M_\odot} \right)^{1/2} \left(\frac{D_L D_S / D_{LS}}{\text{Gpc}} \right)^{-1/2} \text{ arcsec}. \end{aligned} \quad (22.67)$$

The observation of ‘arcs’ (segments of near-perfect Einstein rings) in rich clusters of galaxies has thus given very accurate masses for the central parts of clusters – generally in good agreement with other indicators, such as analysis of X-ray emission from the cluster IGM [81, 82].

Gravitational lensing has also developed into a particularly promising probe of cosmological structure on 10-Mpc to 100-Mpc scales. Weak image distortions manifest themselves as an additional ellipticity of galaxy images (‘shear’), which can be observed by averaging many images together (the corresponding flux amplification is less readily detected). The result is a ‘cosmic shear’ field of order 1% ellipticity, coherent over scales of around 30 arcmin, which is directly related to the cosmic mass field. For this reason, weak lensing is seen as potentially the cleanest probe of matter fluctuations, next to the CMB. Already, impressive results have been obtained in measuring cosmological parameters, based on survey data from only $\sim 10^3$ deg² [83, 84]. A particular strength of lensing is its ability to measure the amplitude of mass fluctuations; this can be deduced from the amplitude of CMB fluctuations, but only with low precision on account of the poorly-known optical depth due to Compton scattering after reionization. However, the effect of weak lensing on the CMB map itself can be detected via the induced non-Gaussian signal, and this gives the CMB greater internal power [85]. The main difficulty of principle with lensing is that part of the signal is generated by small-scale density fluctuations; thus a model is required for nonlinear evolution, including astrophysical effects that separate baryons and dark matter. In this respect, the CMB is a cleaner probe of the primordial fluctuations.

22.4.4 Density fluctuations

The overall properties of the Universe are very close to being homogeneous; and yet telescopes reveal a wealth of detail on scales varying from single galaxies to large-scale structures of size exceeding 100 Mpc. The existence of these structures must be telling us something important about the initial conditions of the Big Bang, and about the physical processes that have operated subsequently. This motivates the study of the density perturbation field, defined as

$$\delta(\mathbf{x}) \equiv \frac{\rho(\mathbf{x}) - \langle \rho \rangle}{\langle \rho \rangle}. \quad (22.68)$$

A critical feature of the δ field is that it inhabits a Universe that is isotropic and homogeneous in its large-scale properties. This suggests that the statistical properties of δ should also be statistically homogeneous – *i.e.*, it is a stationary random process.

It is often convenient to describe δ as a Fourier superposition:

$$\delta(\mathbf{x}) = \sum \delta_{\mathbf{k}} e^{-i\mathbf{k} \cdot \mathbf{x}}. \quad (22.69)$$

We avoid difficulties with an infinite Universe by applying periodic boundary conditions in a cube of some large volume V . The cross-terms vanish when we compute the variance in the field, which is just a sum over modes of the power spectrum:

$$\langle \delta^2 \rangle = \sum |\delta_{\mathbf{k}}|^2 \equiv \sum P(k). \quad (22.70)$$

Note that the statistical nature of the fluctuations must be isotropic, so we write $P(k)$ rather than $P(\mathbf{k})$. The $\langle \dots \rangle$ average here is a volume average. Cosmological density fields are an example of an ergodic process, in which the average over a large

volume tends to the same answer as the average over a statistical ensemble.

The statistical properties of discrete objects sampled from the density field are often described in terms of N -point correlation functions, which represent the excess probability over random for finding one particle in each of N boxes in a given configuration. For the 2-point case, the correlation function is readily shown to be identical to the autocorrelation function of the δ field: $\xi(r) = \langle \delta(x)\delta(x+r) \rangle$.

The power spectrum and correlation function are Fourier conjugates, and thus are equivalent descriptions of the density field (similarly, k -space equivalents exist for the higher-order correlations). It is convenient to take the limit $V \rightarrow \infty$ and use k -space integrals, defining a dimensionless power spectrum, which measures the contribution to the fractional variance in density per unit logarithmic range of scale, as $\Delta^2(k) = d\langle \delta^2 \rangle / d \ln k = V k^3 P(k) / 2\pi^2$:

$$\xi(r) = \int \Delta^2(k) \frac{\sin kr}{kr} d \ln k; \quad \Delta^2(k) = \frac{2}{\pi} k^3 \int_0^\infty \xi(r) \frac{\sin kr}{kr} r^2 dr. \quad (22.71)$$

For many years, an adequate approximation to observational data on galaxies was $\xi = (r/r_0)^{-\gamma}$, with $\gamma \simeq 1.8$ and $r_0 \simeq 5 h^{-1}$ Mpc. Modern surveys are now able to probe into the large-scale linear regime where unaltered traces of the curved post-recombination spectrum can be detected [86–88].

22.4.5 Formation of cosmological structure

The simplest model for the generation of cosmological structure is gravitational instability acting on some low-amplitude initial fluctuations (for the origin of which a theory such as inflation is required). If the perturbations are adiabatic (*i.e.*, fractionally perturb number densities of photons and matter equally), the linear growth law for matter fluctuations is simple:

$$\delta \propto \begin{cases} a^2(t) & (\text{radiation domination; } \Omega_r = 1); \\ a(t) & (\text{matter domination; } \Omega_m = 1). \end{cases} \quad (22.72)$$

For low-density Universes, the growth is slower:

$$d \ln \delta / d \ln a \simeq \Omega_m^{-\gamma}(a), \quad (22.73)$$

where the parameter γ is close to 0.55 independent of the vacuum density [89, 90].

The alternative perturbation mode is isocurvature: only the equation of state changes, and the total density is initially unperturbed. These modes perturb the total entropy density, and thus induce additional large-scale CMB anisotropies [91]. Although the character of perturbations in the simplest inflationary theories are purely adiabatic, correlated adiabatic and isocurvature modes are predicted in many models; the simplest example is the curvaton, which is a scalar field that decays to yield a perturbed radiation density. If the matter content already exists at this time, the overall perturbation field will have a significant isocurvature component. Such a prediction is inconsistent with current CMB data [92], and most analyses of CMB and large-scale structure (LSS) data assume the adiabatic case to hold exactly.

Linear evolution preserves the shape of the power spectrum. However, a variety of processes mean that growth actually depends on the matter content.

1. Pressure opposes gravity effectively for wavelengths below the horizon length while the Universe is radiation dominated. The *comoving* horizon size at z_{eq} is therefore an important scale:

$$D_H(z_{\text{eq}}) = \frac{2(\sqrt{2}-1)}{(\Omega_m z_{\text{eq}})^{1/2} H_0} = \frac{16.0}{\Omega_m h^2} \text{Mpc}. \quad (22.74)$$

2. At early times, dark matter particles will undergo free streaming at the speed of light, and so erase all scales up to the horizon – a process that only ceases when the particles go nonrelativistic. For light massive neutrinos, this happens at z_{eq} ; all structure up to the horizon-scale power-spectrum

break is in fact erased. Hot(cold) dark matter models are thus sometimes dubbed large(small)-scale damping models.

3. A further important scale arises where photon diffusion can erase perturbations in the matter – radiation fluid; this process is named Silk damping.

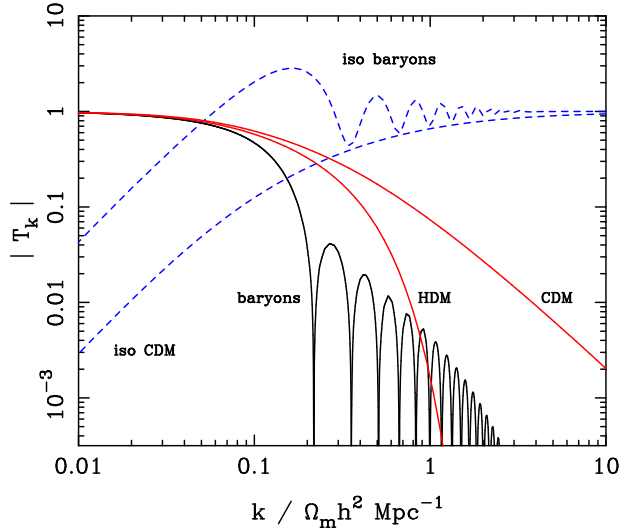


Figure 22.4: A plot of transfer functions for various models. For adiabatic models, $T_k \rightarrow 1$ at small k , whereas the opposite is true for isocurvature models. For dark-matter models, the characteristic wavenumber scales proportional to $\Omega_m h^2$. The scaling for baryonic models does not obey this exactly; the plotted cases correspond to $\Omega_m = 1$, $h = 0.5$.

The overall effect is encapsulated in the transfer function, which gives the ratio of the late-time amplitude of a mode to its initial value (see Fig. 22.4). The overall power spectrum is thus the primordial scalar-mode power law, times the square of the transfer function:

$$P(k) \propto k^{n_s} T_k^2. \quad (22.75)$$

The most generic power-law index is $n_s = 1$: the ‘Zeldovich’ or ‘scale-invariant’ spectrum. Inflationary models tend to predict a small ‘tilt’: $|n_s - 1| \lesssim 0.05$ [12, 13]. On the assumption that the dark matter is cold, the power spectrum then depends on five parameters: n_s , h , Ω_b , Ω_c ($\equiv \Omega_m - \Omega_b$), and an overall amplitude. The latter is often specified as σ_8 , the linear-theory fractional rms in density when a spherical filter of radius $8 h^{-1}$ Mpc is applied in linear theory. This scale can be probed directly via weak gravitational lensing, and also via its effect on the abundance of rich galaxy clusters. The normalization derived from samples of X-ray clusters has been given variously as [93, 94]

$$\sigma_8 = [0.746 \pm 0.012(\text{stat.}) \pm 0.022(\text{sys.})](\Omega_m/0.3)^{-0.47}; \quad (22.76)$$

$$\sigma_8 = [0.81 \pm 0.03](\Omega_m/0.3)^{-0.17}. \quad (22.77)$$

The higher figure is well consistent with *Planck*, whereas the lower is rather similar to the normalization inferred from weak lensing [95]:

$$\sigma_8 \simeq [0.790_{-0.014}^{+0.018}](\Omega_m/0.3)^{-0.5}. \quad (22.78)$$

This figure is in 1.9σ tension with the *Planck* values of $(\sigma_8, \Omega_m) = (0.811 \pm 0.006, 0.315 \pm 0.007)$. If real, such a discrepancy could indicate interesting new physics; but the current evidence is not strong enough to make such a claim. However, it is worth noting that the CMB requires an almost perfect degeneracy, $\Omega_m h^3 = \text{constant}$ for flat models, so that raising h as far as allowed by the CMB would require a lower density, which would reduce the tension with the amplitude of the lensing measurements.

A direct measure of mass inhomogeneity is valuable, since the galaxies inevitably are biased with respect to the mass. This means that the fractional fluctuations in galaxy number, $\delta n/n$,

may differ from the mass fluctuations, $\delta\rho/\rho$. It is commonly assumed that the two fields obey some proportionality on large scales where the fluctuations are small, $\delta n/n = b\delta\rho/\rho$, but even this is not guaranteed [96].

The main shape of the transfer function is a break around the horizon scale at z_{eq} , which depends just on $\Omega_m h$ when wavenumbers are measured in observable units ($h \text{ Mpc}^{-1}$). For reasonable baryon content, weak oscillations in the transfer function are also expected, and these BAOs (baryon acoustic oscillations) have been clearly detected [97,98]. As well as directly measuring the baryon fraction, the scale of the oscillations directly measures the acoustic horizon at decoupling; this can be used as an additional standard ruler for cosmological tests, and the BAO signature has become one of the most important applications of large galaxy surveys. Overall, current power-spectrum data [86–88] favor $\Omega_m h \simeq 0.20$ and a baryon fraction of about 0.15 for $n_s \simeq 1$ (see Fig. 22.5).

In principle, accurate data over a wide range of k could determine both $\Omega_m h$ and n_s , but in practice there is a strong degeneracy between these. In order to constrain n_s itself, it is necessary to examine data on anisotropies in the CMB.

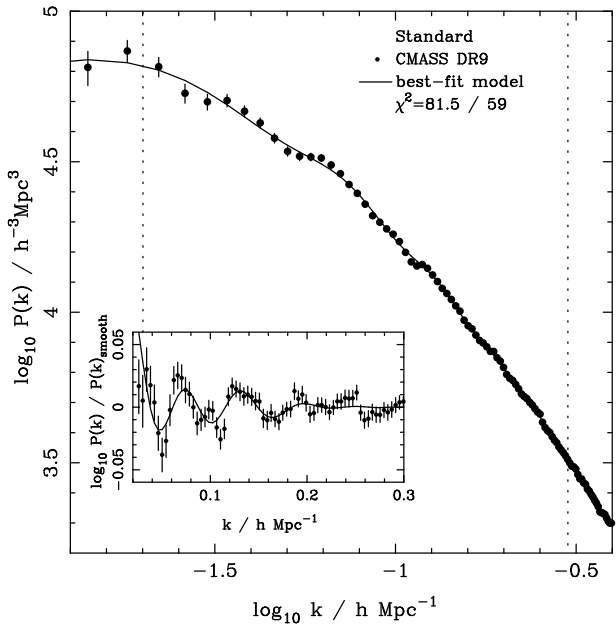


Figure 22.5: The galaxy power spectrum from the SDSS BOSS survey [88]. The solid points with error bars show the power estimate. The solid line shows a standard Λ CDM model with $\Omega_b h^2 \simeq 0.02$ and $\Omega_m h \simeq 0.2$. The inset amplifies the region where BAO features are visible. The fact that these perturb the power by $\sim 20\%$ rather than order unity is direct evidence that the matter content of the Universe is dominated by collisionless dark matter.

22.4.6 CMB anisotropies

The CMB has a clear dipole anisotropy, of magnitude 1.23×10^{-3} . This is interpreted as being due to the Earth’s motion, which is equivalent to a peculiar velocity for the Milky Way of

$$v_{\text{MW}} \simeq 600 \text{ km s}^{-1} \text{ towards } (\ell, b) \simeq (270^\circ, 30^\circ). \quad (22.79)$$

A continuing challenge in cosmology is to demonstrate that this dipole is indeed kinematic, as opposed to representing a violation of large-scale isotropy. Galaxy surveys have attempted to identify the accelerating superclusters responsible for the motion [99], but there are also claims that the observed matter distribution contains an intrinsic dipole, which would be incompatible with the standard interpretation [100], but see also Ref. [101].

All higher-order multipole moments of the CMB are however much smaller than the dipole (of order 10^{-5}), and interpreted as signatures of density fluctuations at last scattering ($\simeq 1100$).

To analyze these, the sky is expanded in spherical harmonics as explained in the review on the CMB – Sec. 29 of this *Review*. The dimensionless power per $\ln k$ or ‘bandpower’ for the CMB is defined as

$$\mathcal{T}^2(\ell) = \frac{\ell(\ell+1)}{2\pi} C_\ell. \quad (22.80)$$

This function encodes information from the three distinct mechanisms that cause CMB anisotropies:

- (1) Gravitational (Sachs – Wolfe) perturbations. Photons from high-density regions at last scattering have to climb out of potential wells, and are thus redshifted.
- (2) Intrinsic (adiabatic) perturbations. In high-density regions, the coupling of matter and radiation can compress the radiation also, giving a higher temperature.
- (3) Velocity (Doppler) perturbations. The plasma has a non-zero velocity at recombination, which leads to Doppler shifts in frequency and hence shifts in brightness temperature.

Because the potential fluctuations obey Poisson’s equation, $\nabla^2\Phi/a^2 = 4\pi G\bar{\rho}\delta$, and the comoving velocity field satisfies the continuity equation $\nabla \cdot \mathbf{u} = -\dot{\delta}$, the resulting different powers of k ensure that the Sachs-Wolfe effect dominates on large scales and adiabatic effects on small scales.

The relation between angle and comoving distance on the last-scattering sphere requires the comoving angular-diameter distance to the last-scattering sphere; because of its high redshift, this is effectively identical to the horizon size at the present epoch, D_H :

$$\begin{aligned} D_H &= \frac{2}{\Omega_m H_0} \quad (\Omega_v = 0); \\ D_H &\simeq \frac{2}{\Omega_m^{0.4} H_0} \quad (\text{flat} : \Omega_m + \Omega_v = 1). \end{aligned} \quad (22.81)$$

These relations show how the CMB is strongly sensitive to curvature: the horizon length at last scattering is $\propto 1/\sqrt{\Omega_m}$, so that this subtends an angle that is virtually independent of Ω_m for a flat model. Observations of a peak in the CMB power spectrum at relatively large scales ($\ell \simeq 221$) are thus strongly inconsistent with zero- Λ models with low density: current CMB + BAO + lensing data require $\Omega_m + \Omega_v = 0.999 \pm 0.004$ (95%) [24]. (See e.g., Fig. 22.2).

In addition to curvature, the CMB encodes information about several other key cosmological parameters. Within the compass of simple adiabatic CDM models, there are nine of these:

$$\omega_c, \omega_b, \Omega_{\text{tot}}, h, \tau, n_s, n_t, r, Q. \quad (22.82)$$

The symbol ω denotes the physical density, Ωh^2 : the transfer function depends only on the densities of CDM (ω_c) and baryons (ω_b). Transcribing the power spectrum at last scattering into an angular power spectrum brings in the total density parameter ($\Omega_{\text{tot}} \equiv \Omega_m + \Omega_v = \Omega_c + \Omega_b + \Omega_v$) and h : there is a near-exact geometrical degeneracy [102] between these that keeps the angular-diameter distance to last scattering invariant, so that models with substantial spatial curvature and large vacuum energy cannot be ruled out without prior knowledge of the Hubble parameter. Alternatively, the CMB alone cannot measure the Hubble parameter without taking into account the line-of-sight information from CMB lensing.

A further possible degeneracy involves the tensor contribution to the CMB anisotropies. These are important at large scales (up to the horizon scales); for smaller scales, only scalar fluctuations (density perturbations) are important. Each of these components is characterized by a spectral index, n , and a ratio between the power spectra of tensors and scalars (r). See Cosmological Parameters – Sec. 25 of this *Review* for a technical definition of the r parameter. Finally, the overall amplitude of the spectrum must be specified (Q), together with the optical depth to Compton scattering owing to recent reionization (τ). Adding a large tensor contribution reduces the contrast between low ℓ and the peak at $\ell \simeq 221$ (because the tensor spectrum has no acoustic component). The previous relative height of the peak can be recovered by increasing n_s to increase the small-scale power in the scalar

component; this in turn over-predicts the power at $\ell \sim 1000$, but this effect can be counteracted by raising the baryon density [103]. This approximate 3-way degeneracy is broken as we increase the range of multipoles sampled.

The reason the tensor component is introduced, and why it is so important, is that it is the only non-generic prediction of inflation. Slow-roll models of inflation involve two dimensionless parameters:

$$\epsilon \equiv \frac{M_{\text{P}}^2}{16\pi} \left(\frac{V'}{V} \right)^2; \quad \eta \equiv \frac{M_{\text{P}}^2}{8\pi} \left(\frac{V''}{V} \right), \quad (22.83)$$

where V is the inflaton potential, and dashes denote derivatives with respect to the inflation field. In terms of these, the tensor-to-scalar ratio is $r \simeq 16\epsilon$, and the spectral indices are $n_s = 1 - 6\epsilon + 2\eta$ and $n_t = -2\epsilon$. The natural expectation of inflation is that the quasi-exponential phase ends once the magnitudes of the slow-roll parameters become of order unity, so that both $n_s \neq 1$ and a significant tensor component are expected. These predictions can be avoided in some models, but it is undeniable that observation of such features would be a great triumph for inflation. Cosmology therefore stands at a fascinating point, given that the most recent CMB data reject the zero-tensor $n_s = 1$ model at more than 8σ : $n_s = 0.965 \pm 0.004$ [24]. This rejection is strong enough that it is also able to break the tensor degeneracy, so that no model with $n_s = 1$ is acceptable, whatever the value of r .

The current limit on r is < 0.036 at 95% confidence [104, 105]. In conjunction with the measured value of n_s , this upper limit sits close to the prediction of a linear potential (i.e. $|\eta| \ll |\epsilon|$). Any further reduction in the limit on r will force η to be negative – i.e. a convex potential at the point where LSS scales were generated (sometimes called a ‘hilltop’), in contrast to simple early models such as $V(\phi) = m^2\phi^2$ or $\lambda\phi^4$, which are now excluded. Examples of models that are currently in excellent agreement with the *Planck* results are the Starobinsky model of $\mathcal{R} + \mathcal{R}^2$ gravity [106], or the Higgs-inflation model where the Higgs field is non-minimally coupled [107]. Assuming 55 e-foldings of inflation, these models predict $n_s = 0.965$ and $r = 0.0035$. Assuming that no systematic error in the CMB data can be identified, cosmology has thus passed a critical hurdle in rejecting scale-invariant fluctuations. The years ahead will be devoted to the task of searching for the tensor fluctuations – for which the main tool will be the polarization of the CMB [14].

22.4.6.1 CMB foregrounds

As the quality of CMB data improves, there is a growing interest in effects that arise along the line of sight. The CMB temperature is perturbed by dark-matter structures and by Compton scattering from ionized gas. In the former case, we have the integrated Sachs-Wolfe effect, which is sensitive to the time derivative of the gravitational potential. In the linear regime, this is damped when the Universe becomes Λ -dominated, and this is an independent way of detecting Λ [108]. The potential also causes gravitational lensing of the CMB: structures at $z \simeq 1-2$ displace features on the CMB sky by about 2 arcmin over coherent degree-scale patches. Detection of these distortions allows a map to be made of overdensity projected from $z = 0$ to 1100 [85]. This is a very powerful calibration for direct studies of gravitational lensing using galaxies. Finally, Comptonization affects the CMB in two ways: the thermal Sunyaev-Zeldovich effect measures the blurring of photon energies by hot gas; and the kinetic Sunyaev-Zeldovich effect is sensitive to the bulk velocity of the gas. Both these effects start to dominate over the intrinsic CMB fluctuations at multipoles $\ell \gtrsim 2000$ [109].

22.4.7 Probing dark energy and the nature of gravity

The most radical element of our current cosmological model is the dark energy that accelerates the expansion. The energy density of this component is approximately $(2.2\text{meV})^4$ (for $w = -1$, $\Omega_v = 0.68$, $h = 0.67$), or roughly $10^{-123} M_{\text{P}}^4$, and such an unnaturally small number is hard to understand. Various quantum effects (most simply, zero-point energy) should make contributions to the vacuum energy density. These may be truncated by new physics at high energy, but this presumably occurs at > 1 TeV scales, not meV; thus the apparent energy scale of the vacuum is at least

10^{15} times smaller than its natural value. A classic review of this situation is given by Weinberg [53], which lists extreme escape routes – especially the multiverse viewpoint, according to which low values of Λ are rare, but high values suppress the formation of structure and observers. It is certainly impressive that Weinberg used such reasoning to predict the value of Λ before any data strongly indicated a non-zero value.

But it may be that the phenomenon of dark energy is entirely illusory. The necessity for this constituent arises from using the Friedmann equation to describe the evolution of the cosmic expansion; if this equation is incorrect, it would require the replacement of Einstein’s relativistic theory of gravity with some new alternative. A frontier of current cosmological research is to distinguish these possibilities [110, 111]. We also note that it has been suggested that dark energy might be an illusion even within general relativity, owing to an incorrect treatment of averaging in an inhomogeneous Universe [112, 113]. Most would argue that a standard Newtonian treatment of such issues should be adequate inside the cosmological horizon, but debate on this issue continues.

Dark energy can differ from a classical cosmological constant in being a dynamical phenomenon [114, 115], e.g., a rolling scalar field (sometimes dubbed ‘quintessence’). Empirically, this means that it is endowed with two thermodynamic properties that astronomers can try to measure: the bulk equation of state, and the sound speed. If the sound speed is close to the speed of light, the effect of this property is confined to very large scales, and mainly manifests itself in the large-angle multipoles of the CMB anisotropies [116]. The equation of state parameter governs the rate of change of the vacuum density: $d \ln \rho_v / d \ln a = -3(1+w)$, so it can be accessed via the evolving expansion rate, $H(a)$. This can be measured most cleanly by using the inbuilt natural ruler of large-scale structure: the BAO horizon scale [117]:

$$D_{\text{BAO}} \simeq 147.0 (\Omega_{\text{m}} h^2 / 0.1424)^{-0.253} (\Omega_{\text{b}} h^2 / 0.0224)^{-0.128} \text{ Mpc}. \quad (22.84)$$

Observing the equivalent acoustic scale at last scattering in the CMB yields the precise geometrical degeneracy $\Omega_{\text{m}} h^3 = 0.09633 \pm 0.00029$ [24].

$H(a)$ is measured by radial clustering, since $dr/dz = c/H$; clustering in the plane of the sky measures the integral of this. The expansion rate is also measured by the growth of density fluctuations, where the pressure-free growth equation for the density perturbation is $\ddot{\delta} + 2H(a)\dot{\delta} = 4\pi G\rho_0\delta$. Thus, both the scale and amplitude of density fluctuations are sensitive to $w(a)$ – but only weakly. These observables typically change by only $\sim 0.2\%$ for a 1% change in w . Current constraints [24] place a constant w to within 5–10% of -1 , depending on the data combination chosen. A substantial improvement in this precision will require us to limit systematics in data to a few parts in 1000.

Testing whether theories of gravity require revision can also be done using data on cosmological inhomogeneities. Two separate issues arise, concerning the metric perturbation potentials Ψ and Φ , which affect respectively the time and space parts of the metric. In Einstein gravity, these potentials are both equal to the Newtonian gravitational potential, which satisfies Poisson’s equation: $\nabla^2\Phi/a^2 = 4\pi G\bar{\rho}\delta$. Empirically, modifications of gravity require us to explore a change with scale and with time of the ‘slip’ (Ψ/Φ) and the effective G on the rhs of the Poisson equation. The former aspect can only be probed via gravitational lensing, whereas the latter can be addressed on 10–100 Mpc scales via the growth of clustering. Various schemes for parameterizing modified gravity exist, but a practical approach is to assume that the growth rate can be tied to the density parameter: $d \ln \delta / d \ln a = \Omega_{\text{m}}^\gamma(a)$ [89, 90]. The parameter γ is close to 0.55 for standard relativistic gravity, but can differ by around 0.1 from this value in many non-standard models. Clearly this parameterization is incomplete, since it explicitly rejects the possibility of early dark energy ($\Omega_{\text{m}}(a) \rightarrow 1$ as $a \rightarrow 0$), but it is a convenient way of capturing the power of various experiments. Current data are consistent with standard Λ CDM [118], and exclude variations in slip or effective G of larger than a few times 10%.

Current planning envisages a set of satellite probes that, a decade hence, will have pursued these fundamental tests via gravitational lensing measurements over thousands of square degrees,

$> 10^8$ redshifts, and photometry of > 1000 supernovae (Euclid in Europe, Roman Space Telescope in the USA) [22, 23]. These experiments will measure both w and the perturbation growth rate to an accuracy of around 1%. The outcome will be either a validation of the standard relativistic vacuum-dominated Big Bang cosmology at a level of precision far beyond anything attempted to date, or the opening of entirely new directions in cosmological models. For a more complete discussion of dark energy and future probes see Dark Energy – Sec. 28 of this *Review*.

References

- [1] V.M. Slipher, *Pop. Astr.* **23**, 21 (1915).
- [2] K. Lundmark, *Mon. Not. R. Astron. Soc* **84**, 747 (1924).
- [3] E. Hubble and M. L. Humason, *Astrophys. J.* **74**, 43 (1931).
- [4] G. Gamow, *Phys. Rev.* **70**, 572 (1946).
- [5] R. A. Alpher, H. Bethe and G. Gamow, *Phys. Rev.* **73**, 803 (1948).
- [6] R.A. Alpher and R.C. Herman, *Phys. Rev.* **74**, 1737 (1948).
- [7] R.A. Alpher and R.C. Herman, *Phys. Rev.* **75**, 1089 (1949).
- [8] A. A. Penzias and R. W. Wilson, *Astrophys. J.* **142**, 419 (1965).
- [9] P.J.E. Peebles, *Principles of Physical Cosmology*, Princeton University Press (1993).
- [10] G. Börner, *The Early Universe: Facts and Fiction*, Springer-Verlag (1988).
- [11] E.W. Kolb and M.S. Turner, *The Early Universe*, Addison-Wesley (1990).
- [12] J.A. Peacock, *Cosmological Physics*, Cambridge Univ. Press (1999).
- [13] A.R. Liddle and D. Lyth, *Cosmological Inflation and Large-Scale Structure*, Cambridge University Press (2000).
- [14] S. Dodelson, *Modern Cosmology*, Academic Press (2003).
- [15] V. Mukhanov, *Physical Foundations of Cosmology*, Cambridge University Press (2005).
- [16] S. Weinberg, *Cosmology*, Oxford Press (2008).
- [17] E.B. Gliner, *Sov. Phys. JETP* **22**, 378 (1966).
- [18] Ya. B. Zeldovich, *Sov. Phys. Usp.* **11**, 381 (1968), [*Usp. Fiz. Nauk*95,209(1968)].
- [19] P.M. Garnavich *et al.*, *Astrophys. J.* **507**, 74 (1998), [arXiv:astro-ph/9806396].
- [20] S. Perlmutter, M. S. Turner and M. J. White, *Phys. Rev. Lett.* **83**, 670 (1999), [arXiv:astro-ph/9901052].
- [21] I. Maor *et al.*, *Phys. Rev.* **D65**, 123003 (2002), [arXiv:astro-ph/0112526].
- [22] A. Albrecht *et al.* (2006), [arXiv:astro-ph/0609591].
- [23] J. A. Peacock *et al.* (2006), [arXiv:astro-ph/0610906].
- [24] N. Aghanim *et al.* (Planck), *Astron. Astrophys.* **641**, A6 (2020), [arXiv:1807.06209].
- [25] A.G. Riess *et al.*, *Astrophys. J.* **116**, 1009 (1998), [arXiv:astro-ph/9805201].
- [26] S. Perlmutter *et al.* (Supernova Cosmology Project), *Astrophys. J.* **517**, 565 (1999), [arXiv:astro-ph/9812133].
- [27] A. G. Riess, *Publ. Astron. Soc. Pac.* **112**, 1284 (2000), [arXiv:astro-ph/0005229].
- [28] J. L. Tonry *et al.* (Supernova Search Team), *Astrophys. J.* **594**, 1 (2003), [arXiv:astro-ph/0305008].
- [29] N. Suzuki *et al.*, *Astrophys. J.* **746**, 85 (2012), [arXiv:1105.3470].
- [30] D. M. Scolnic *et al.*, *Astrophys. J.* **859**, 101 (2018), [arXiv:1710.00845].
- [31] A. G. Riess *et al.*, *Astrophys. J. Lett.* **934**, 1, L7 (2022), [arXiv:2112.04510].
- [32] W. L. Freedman *et al.*, *Astrophys. J.* **882**, 34 (2019), [arXiv:1907.05922].
- [33] W. L. Freedman, *Astrophys. J.* **919**, 1, 16 (2021), [arXiv:2106.15656].
- [34] Planck Collab. 2015 Results XIII, *Astron. & Astrophys.* **594**, A13 (2016), [arXiv:1502.10589].
- [35] P. Astier *et al.*, *Astron. & Astrophys.* **447**, 31 (2006), [arXiv:astro-ph/0510447].
- [36] J. A. Johnson and M. Bolte, *Astrophys. J.* **554**, 888 (2001), [arXiv:astro-ph/0103299].
- [37] R. Cayrel *et al.*, *Nature* **409**, 691 (2001), [arXiv:astro-ph/0104357].
- [38] D. A. Vandenberg *et al.*, *Astrophys. J.* **775**, 134 (2013), [arXiv:1308.2257].
- [39] S. Borsanyi *et al.*, *Nature* **539**, 7627, 69 (2016), [arXiv:1606.07494].
- [40] M. Srednicki, R. Watkins and K. A. Olive, *Nucl. Phys.* **B310**, 693 (1988), [,247(1988)].
- [41] J. J. Bennett *et al.*, *JCAP* **04**, 073 (2021), [arXiv:2012.02726].
- [42] T. M. C. Abbott *et al.* (DES), *Phys. Rev. D* **105**, 2, 023520 (2022), [arXiv:2105.13549].
- [43] A. D. Linde, *Phys. Rev.* **D14**, 3345 (1976).
- [44] A. Linde, *Rept. on Prog. in Phys.* **42**, 389 (1979).
- [45] C.E. Vayonakis, *Surv. High Energy Physics* **5**, 87 (1986).
- [46] S.A. Bonometto and A. Masiero, *Nuovo Cimento* **9N5**, 1 (1986).
- [47] A. Linde, *Particle Physics And Inflationary Cosmology*, Harwood (1990).
- [48] K. A. Olive, *Phys. Rept.* **190**, 307 (1990).
- [49] D. H. Lyth and A. Riotto, *Phys. Rept.* **314**, 1 (1999), [hep-ph/9807278].
- [50] A. H. Guth, *Phys. Rev.* **D23**, 347 (1981), [*Adv. Ser. Astrophys. Cosmol.*3,139(1987)].
- [51] A. D. Linde, *Phys. Lett.* **108B**, 389 (1982), [*Adv. Ser. Astrophys. Cosmol.*3,149(1987)].
- [52] A. Albrecht and P. J. Steinhardt, *Phys. Rev. Lett.* **48**, 1220 (1982), [*Adv. Ser. Astrophys. Cosmol.*3,158(1987)].
- [53] S. Weinberg, *Rev. Mod. Phys.* **61**, 1 (1989).
- [54] L. Susskind 247–266 (2003), [hep-th/0302219].
- [55] B. Carr, *Universe or multiverse?* C.U.P. (2007).
- [56] G. Steigman, *Ann. Rev. Astron. Astrophys.* **14**, 339 (1976).
- [57] A. G. Cohen, A. De Rujula and S. L. Glashow, *Astrophys. J.* **495**, 539 (1998), [arXiv:astro-ph/9707087].
- [58] A. D. Sakharov, *Pisma Zh. Eksp. Teor. Fiz.* **5**, 32 (1967), [*Usp. Fiz. Nauk*161,no.5,61(1991)].
- [59] S. Weinberg, *Phys. Rev. Lett.* **42**, 850 (1979).
- [60] D. Toussaint *et al.*, *Phys. Rev.* **D19**, 1036 (1979).
- [61] I. Affleck and M. Dine, *Nucl. Phys.* **B249**, 361 (1985).
- [62] V. A. Kuzmin, V. A. Rubakov and M. E. Shaposhnikov, *Phys. Lett.* **155B**, 36 (1985).
- [63] M. Fukugita and T. Yanagida, *Phys. Lett.* **B174**, 45 (1986).
- [64] S. Riemer-Sorensen and S. Jenssen, *Universe* **3**, 44 (2017), [arXiv:1502.10589].
- [65] R. J. Cooke, M. Pettini and C. C. Steidel, *Astrophys. J.* **855**, 2, 102 (2018), [arXiv:1710.11129].
- [66] T.-H. Yeh *et al.*, *JCAP* **10**, 046 (2022), [arXiv:2207.13133].
- [67] R. H. Cyburt, B. D. Fields and K. A. Olive, *Phys. Lett.* **B567**, 227 (2003), [arXiv:astro-ph/0302431].
- [68] R. H. Cyburt, B. D. Fields and K. A. Olive, *JCAP* **0811**, 012 (2008), [arXiv:0808.2818].
- [69] B. D. Fields and K. A. Olive, *JCAP* **10**, 078 (2022), [arXiv:2204.03167].
- [70] K. A. Olive, G. Steigman and T. P. Walker, *Phys. Rept.* **333**, 389 (2000), [arXiv:astro-ph/9905320].

- [71] F. Iocco *et al.*, Phys. Rept. **472**, 1 (2009), [arXiv:0809.0631].
- [72] R. H. Cyburt *et al.*, Rev. Mod. Phys. **88**, 015004 (2016), [arXiv:1505.01076].
- [73] C. Pitrou *et al.*, Phys. Rept. **754**, 1 (2018), [arXiv:1801.08023].
- [74] B. D. Fields *et al.*, JCAP **03**, 010 (2020), [Erratum: JCAP **11**, E02 (2020)], [arXiv:1912.01132].
- [75] D. J. Fixsen *et al.*, Astrophys. J. **473**, 576 (1996), [arXiv:astro-ph/9605054].
- [76] J. C. Mather *et al.*, Astrophys. J. **512**, 511 (1999), [arXiv:astro-ph/9810373].
- [77] S. Cole *et al.* (2dFGRS), Mon. Not. Roy. Astron. Soc. **326**, 255 (2001), [arXiv:astro-ph/0012429].
- [78] J. Schroeder, A. Mesinger and Z. Haiman, Mon. Not. Roy. Astron. Soc. **428**, 3058 (2013), [arXiv:1204.2838].
- [79] S. D. M. White *et al.*, Nature **366**, 429 (1993).
- [80] S. W. Allen, R. W. Schmidt and A. C. Fabian, Mon. Not. Roy. Astron. Soc. **334**, L11 (2002), [arXiv:astro-ph/0205007].
- [81] S. W. Allen, Mon. Not. Roy. Astron. Soc. **296**, 392 (1998), [arXiv:astro-ph/9710217].
- [82] G. P. Smith *et al.*, Mon. Not. Roy. Astron. Soc. **456**, 1, L74 (2016), [arXiv:1511.01919].
- [83] H. Hildebrandt *et al.*, Astron. Astrophys. **633**, A69 (2020), [arXiv:1812.06076].
- [84] A. Amon *et al.*, arXiv e-prints (2021), [arXiv:2105.13543].
- [85] Planck Collab. 2015 Results XV, Astron. & Astrophys. **594**, A15 (2016), [arXiv:1502.01591].
- [86] S. Cole *et al.* (2dFGRS), Mon. Not. Roy. Astron. Soc. **362**, 505 (2005), [arXiv:astro-ph/0501174].
- [87] W. J. Percival *et al.*, Astrophys. J. **657**, 645 (2007), [arXiv:astro-ph/0608636].
- [88] L. Anderson *et al.*, Mon. Not. Roy. Astron. Soc. **427**, 4, 3435 (2013), [arXiv:1203.6594].
- [89] E. Linder, Phys. Rev. **D72**, 43529 (2005), [arXiv:astro-ph/0507263].
- [90] D. Polarski and R. Gannouji, Phys. Lett. **B660**, 439 (2008), [arXiv:0710.1510].
- [91] G. Efstathiou and J. R. Bond, Mon. Not. Roy. Astron. Soc. **218**, 1, 103 (1986).
- [92] C. Gordon and A. Lewis, Phys. Rev. **D67**, 123513 (2003), [arXiv:astro-ph/0212248].
- [93] A. Vikhlinin *et al.*, Astrophys. J. **692**, 1060 (2009), [arXiv:0812.2720].
- [94] A. Mantz *et al.*, Mon. Not. Roy. Astron. Soc. **446**, 2205 (2015), [arXiv:1407.4516].
- [95] T. M. C. Abbott *et al.* (Kilo-Degree Survey, DES) (2023), [arXiv:2305.17173].
- [96] A. Dekel and O. Lahav, Astrophys. J. **520**, 24 (1999), [arXiv:astro-ph/9806193].
- [97] W. J. Percival *et al.*, Mon. Not. Roy. Astron. Soc. **381**, 1053 (2007), [arXiv:0705.3323].
- [98] W. J. Percival *et al.* (SDSS), Mon. Not. Roy. Astron. Soc. **401**, 2148 (2010), [arXiv:0907.1660].
- [99] G. Lavaux *et al.*, Astrophys. J. **709**, 483 (2010), [arXiv:0810.3658].
- [100] N. J. Secrest *et al.*, Astrophys. J. **908**, L51 (2021), [arXiv:2009.14826].
- [101] J. Darling, Astrophys. J. Lett. **931**, 2, L14 (2022), [arXiv:2205.06880].
- [102] G. Efstathiou and J. R. Bond, Mon. Not. Roy. Astron. Soc. **304**, 75 (1999), [arXiv:astro-ph/9807103].
- [103] G. Efstathiou *et al.* (2dFGRS), Mon. Not. Roy. Astron. Soc. **330**, L29 (2002), [arXiv:astro-ph/0109152].
- [104] M. Tristram *et al.*, Astron. Astrophys. **647**, A128 (2021), [arXiv:2010.01139].
- [105] P. A. R. Ade *et al.* (BICEP/Keck), Phys. Rev. Lett. **127**, 15, 151301 (2021), [arXiv:2110.00483].
- [106] A. A. Starobinsky, Phys. Lett. **B91**, 99 (1980), [771(1980)].
- [107] F. Bezrukov and M. Shaposhnikov, JHEP **07**, 089 (2009), [arXiv:0904.1537].
- [108] Planck Collab. 2015 Results XXI, Astron. & Astrophys. **594**, A21 (2016), [arXiv:1502.01595].
- [109] Planck Collab. 2015 Results XXII, Astron. & Astrophys. **594**, A22 (2016), [arXiv:1502.01596].
- [110] W. Hu and I. Sawicki, Phys. Rev. **D76**, 4043 (2007), [arXiv:0708.1190].
- [111] B. Jain and P. Zhang, Phys. Rev. **D78**, 3503 (2008), [arXiv:0709.2375].
- [112] D. L. Wiltshire, Phys. Rev. Lett. **99**, 251101 (2007), [arXiv:0709.0732].
- [113] T. Buchert, Gen. Rel. Grav. **40**, 467 (2008), [arXiv:0707.2153].
- [114] I. Zlatev, L.-M. Wang and P. J. Steinhardt, Phys. Rev. Lett. **82**, 896 (1999), [arXiv:astro-ph/9807002].
- [115] C. Armendariz-Picon, V. Mukhanov, and P. J. Steinhardt, Phys. Rev. **D63**, 3510 (2001), [arXiv:astro-ph/0006373].
- [116] S. DeDeo, R. R. Caldwell, and P. J. Steinhardt, Phys. Rev. **D67**, 3509 (2003), [arXiv:astro-ph/0301284].
- [117] É. Aubourg *et al.*, Phys. Rev. **D92**, 123516 (2015), [arXiv:1411.1074].
- [118] S. F. Daniel *et al.*, Phys. Rev. **D81**, 123508 (2010), [arXiv:1002.1962].

23. Inflation

Revised August 2023 by J. Ellis (King's Coll. London; CERN) and D. Wands (Portsmouth U.).

23.1 Motivation and Introduction

The standard Big-Bang model of cosmology provides a successful framework in which to understand the thermal history of our Universe and the growth of cosmic structure, but it is essentially incomplete. As described in Sec. 22.2.4, Big-Bang cosmology requires very specific initial conditions. It postulates a uniform cosmological background, described by a spatially-flat, homogeneous and isotropic Robertson-Walker (RW) metric (Eq. (22.1) in “Big Bang Cosmology” review), with scale factor $R(t)$. Within this setting, it also requires an initial almost scale-invariant distribution of primordial density perturbations as seen, for example, in the cosmic microwave background (CMB) radiation (described in Chap. 29, “Cosmic Microwave Background” review), on scales far larger than the causal horizon at the time the CMB photons last scattered.

The Hubble expansion rate, $H \equiv \dot{R}/R$, in a RW cosmology is given by the Friedmann constraint equation (Eq. (22.8) in “Big Bang Cosmology” review)

$$H^2 = \frac{8\pi\rho}{3M_P^2} + \frac{\Lambda}{3} - \frac{k}{R^2}, \quad (23.1)$$

where k/R^2 is the intrinsic spatial curvature. We use natural units such that the speed of light $c = 1$ and hence we have the Planck mass $M_P = G_N^{-1/2} \simeq 10^{19}$ GeV (see “Astrophysical Constants and Parameters”). A cosmological constant, Λ , of the magnitude required to accelerate the Universe today (see Chap. 28, “Dark Energy” review) would have been completely negligible in the early Universe where the energy density $\rho \gg M_P^2 \Lambda \sim 10^{-12}(\text{eV})^4$. The standard early Universe cosmology, described in Sec. 22.1.5 in “Big Bang Cosmology” review, is thus dominated by non-relativistic matter ($p_m \ll \rho_m$) or radiation ($p_r = \rho_r/3$ for an isotropic distribution). This leads to a decelerating expansion with $\ddot{R} < 0$.

The hypothesis of inflation [1, 2] postulates a period of accelerated expansion, $\ddot{R} > 0$, in the very early Universe, preceding the standard radiation-dominated era, which offers a physical model for the origin of these initial conditions, as reviewed in [3–7]. Such a period of accelerated expansion (i) drives a curved Robertson-Walker spacetime (with spherical or hyperbolic spatial geometry) towards spatial flatness, and (ii) it also expands the causal horizon beyond the present Hubble length, so as to encompass all the scales relevant to describe the large-scale structure observed in our Universe today, via the following two mechanisms.

1. A spatially-flat Universe with vanishing spatial curvature, $k = 0$, has the dimensionless density parameter $\Omega_{tot} = 1$, where we define (Eq. (22.13) in “Big Bang Cosmology” review; see Chap. 25, “Cosmological Parameters” review for more complete definitions)

$$\Omega_{tot} \equiv \frac{8\pi\rho_{tot}}{3M_P^2 H^2}, \quad (23.2)$$

with $\rho_{tot} \equiv \rho + \Lambda M_P^2/8\pi$. If we re-write the Friedmann constraint (Eq. (23.1)) in terms of Ω_{tot} we have

$$1 - \Omega_{tot} = -\frac{k}{R^2}. \quad (23.3)$$

Observations require $|1 - \Omega_{tot,0}| < 0.005$ today [8], where the subscript 0 denotes the present-day value. Taking the time derivative of Eq. (23.3) we obtain

$$\frac{d}{dt}(1 - \Omega_{tot}) = -2\frac{\ddot{R}}{\dot{R}}(1 - \Omega_{tot}). \quad (23.4)$$

Thus in a decelerating expansion, $\dot{R} > 0$ and $\ddot{R} < 0$, any small initial deviation from spatial flatness grows, $(d/dt)|1 - \Omega_{tot}| > 0$. A small value such as $|1 - \Omega_{tot,0}| < 0.005$ today requires an even smaller value at earlier times, e.g., $|1 - \Omega_{tot}| < 10^{-5}$ at

the last scattering of the CMB, which appears unlikely, unless for some reason space is exactly flat. However, an extended period of accelerated expansion in the very early Universe, with $\dot{R} > 0$ and $\ddot{R} > 0$ and hence $(d/dt)|1 - \Omega_{tot}| < 0$, can drive Ω_{tot} sufficiently close to unity, so that $|1 - \Omega_{tot,0}|$ remains unobservable small today, even after the radiation- and matter-dominated eras, for a wide range of initial values of Ω_{tot} .

2. The comoving distance (the present-day proper distance) traversed by light between cosmic time t_1 and t_2 in an expanding Universe can be written, (see Eq. (22.32) in “Big Bang Cosmology” review), as

$$D_0(t_1, t_2) = R_0 \int_{t_1}^{t_2} \frac{dt}{R(t)} = R_0 \int_{\ln R_1}^{\ln R_2} \frac{d(\ln R)}{\dot{R}}. \quad (23.5)$$

In standard decelerated (radiation- or matter-dominated) cosmology the integrand, $1/\dot{R}$, decreases towards the past, and there is a finite comoving distance traversed by light (a particle horizon) since the Big Bang ($R_1 \rightarrow 0$). For example, the comoving size of the particle horizon at the CMB last-scattering surface ($R_2 = R_{lss}$) corresponds to $D_0 \sim 100$ Mpc, or approximately 1° on the CMB sky today (see Sec. 22.2.4 in “Big Bang Cosmology” review). However, during a period of inflation, $1/\dot{R}$ increases towards the past, and hence the integral (Eq. (23.5)) diverges as $R_1 \rightarrow 0$, allowing an arbitrarily large causal horizon, dependent only upon the duration of the accelerated expansion. Assuming that the Universe inflates with a finite Hubble rate H_* at $t_1 = t_*$, ending with $H_{end} < H_*$ at $t_2 = t_{end}$, we have

$$D_0(t_*, t_{end}) > \left(\frac{R_0}{R_{end}}\right) H_*^{-1} (e^{N_*} - 1), \quad (23.6)$$

where $N_* \equiv \ln(R_{end}/R_*)$ describes the duration of inflation, measured in terms of the logarithmic expansion (or “e-folds”) from $t_1 = t_*$ up to the end of inflation at $t_2 = t_{end}$, and R_0/R_{end} is the subsequent expansion from the end of inflation to the present day. If inflation occurs above the TeV scale, the comoving Hubble scale at the end of inflation, $(R_0/R_{end})H_{end}^{-1}$, is less than one astronomical unit ($\sim 10^{11}$ m), and a causally-connected patch can encompass our entire observable Universe today, which has a size $D_0 > 30$ Gpc, if there were more than 40 e-folds of inflation ($N_* > 40$). If inflation occurs at the GUT scale (10^{15} GeV) then we require more than 60 e-folds.

Producing an accelerated expansion in general relativity requires an energy-momentum tensor with negative pressure, $p < -\rho/3$ (see Eq. (22.9) in “Big Bang Cosmology” review and Chap. 28, “Dark Energy” review), quite different from the hot dense plasma of relativistic particles in the hot Big Bang. However a positive vacuum energy $V > 0$ does exert a negative pressure, $p_V = -\rho_V$. The work done by the cosmological expansion must be negative in this case so that the local vacuum energy density remains constant in an expanding Universe, $\dot{\rho}_V = -3H(\rho_V + p_V) = 0$. Therefore, a false vacuum state can drive an exponential expansion, corresponding to a de Sitter spacetime with a constant Hubble rate $H^2 = 8\pi\rho_V/3M_P^2$ on spatially-flat hypersurfaces.

A constant vacuum energy V , equivalent to a cosmological constant Λ in the Friedmann equation Eq. (23.1), cannot provide a complete description of inflation in the early Universe, since inflation must necessarily have come to an end in order for the standard Big-Bang cosmology to follow. A phase transition to the present true vacuum is required to release the false vacuum energy into the energetic plasma of the hot Big Bang and produce the large total entropy of our observed Universe today. Thus, we must necessarily study dynamical models of inflation, where the time-invariance of the false vacuum state is broken by a time-dependent field. A first-order phase transition would produce a very inhomogeneous Universe [9] unless a time-dependent scalar field leads to a rapidly changing percolation rate [10–12]. However,

a second-order phase transition [13, 14], controlled by a slowly-rolling scalar field, can lead to a smooth classical exit from the vacuum-dominated phase.

As a spectacular bonus, quantum fluctuations in that scalar field could provide a source of almost scale-invariant density fluctuations [15, 16], as detected in the CMB (see Chap. 29), which are thought to be the origin of the structures seen in the Universe today.

Accelerated expansion and primordial perturbations can also be produced in some modified gravity theories (e.g., [1, 17]), which introduce additional non-minimally coupled degrees of freedom. Such inflation models can often be conveniently studied by transforming variables to an ‘Einstein frame’ in which Einstein’s equations apply with minimally coupled scalar fields [18–20].

In the following we will review scalar field cosmology in general relativity and the spectra of primordial fluctuations produced during inflation, before studying selected inflation models.

23.2 Scalar Field Cosmology

The energy-momentum tensor for a canonical scalar field ϕ with self-interaction potential $V(\phi)$ is given in Eq. (22.52) in “Big Bang Cosmology” review. In a homogeneous background this corresponds to a perfect fluid with density

$$\rho = \frac{1}{2}\dot{\phi}^2 + V(\phi), \quad (23.7)$$

and isotropic pressure

$$p = \frac{1}{2}\dot{\phi}^2 - V(\phi), \quad (23.8)$$

while the 4-velocity is proportional to the gradient of the field, $u^\mu \propto \nabla^\mu \phi$.

A field with vanishing potential energy acts like a stiff fluid with $p = \rho = \dot{\phi}^2/2$, whereas if the time-dependence vanishes we have $p = -\rho = -V$ and the scalar field is uniform in time and space. Thus a classical, potential-dominated scalar-field cosmology, with $p \simeq -\rho$, can naturally drive a quasi-de Sitter expansion; the slow time-evolution of the energy density weakly breaks the exact $O(1, 3)$ symmetry of four-dimensional de Sitter spacetime down to a Robertson-Walker (RW) spacetime, where the scalar field plays the role of the cosmic time coordinate.

In a scalar-field RW cosmology the Friedmann constraint equation (Eq. (23.1)) reduces to

$$H^2 = \frac{8\pi}{3M_P^2} \left(\frac{1}{2}\dot{\phi}^2 + V \right) - \frac{k}{R^2}, \quad (23.9)$$

while energy conservation (Eq. (22.10) in “Big Bang Cosmology” review) for a homogeneous scalar field reduces to the Klein-Gordon equation of motion (Eq. (22.54) in “Big Bang Cosmology” review)

$$\ddot{\phi} = -3H\dot{\phi} - V'(\phi). \quad (23.10)$$

The evolution of the scalar field is thus driven by the potential gradient $V' = dV/d\phi$, subject to damping by the Hubble expansion $3H\dot{\phi}$.

If we define the Hubble slow-roll parameter

$$\epsilon_H \equiv -\frac{\dot{H}}{H^2}, \quad (23.11)$$

then we see that inflation ($\dot{R} > 0$ and hence $\dot{H} > -H^2$) requires $\epsilon_H < 1$. In this case the spatial curvature decreases relative to the scalar field energy density as the Universe expands. Hence, in the following we drop the spatial curvature and consider a spatially-flat RW cosmology, assuming that inflation has lasted sufficiently long that our observable Universe is very close to spatially flatness. However, we note that bubble nucleation, leading to a first-order phase transition during inflation, can lead to homogeneous hypersurfaces with a hyperbolic (‘open’) geometry, effectively resetting the spatial curvature inside the bubble [21]. This is the basis of so-called open inflation models [22–24], where inflation inside the bubble has a finite duration, leaving a finite negative spatial curvature.

In a scalar field-dominated cosmology (Eq. (23.11)) gives

$$\epsilon_H = \frac{3\dot{\phi}^2}{2V + \dot{\phi}^2}, \quad (23.12)$$

in which case we see that inflation requires a potential-dominated expansion, $\dot{\phi}^2 < V$.

23.2.1 Slow-Roll Inflation

It is commonly assumed that the field acceleration term, $\ddot{\phi}$, in (Eq. (23.10)) can be neglected, in which case one can give an approximate solution for the inflationary attractor [25]. This slow-roll approximation reduces the second-order Klein-Gordon equation (Eq. (23.10)) to a first-order system, which is over-damped, with the potential gradient being approximately balanced against to the Hubble damping:

$$3H\dot{\phi} \simeq -V', \quad (23.13)$$

and at the same time that the Hubble expansion (Eq. (23.9)) is dominated by the potential energy

$$H^2 \simeq \frac{8\pi}{3M_P^2} V(\phi), \quad (23.14)$$

corresponding to $\epsilon_H \ll 1$.

A necessary condition for the validity of the slow-roll approximation is that the potential slow-roll parameters

$$\epsilon \equiv \frac{M_P^2}{16\pi} \left(\frac{V'}{V} \right)^2, \quad \eta \equiv \frac{M_P^2}{8\pi} \left(\frac{V''}{V} \right), \quad (23.15)$$

are small, i.e., $\epsilon \ll 1$ and $|\eta| \ll 1$, requiring the potential to be correspondingly flat. If we identify V'' with the effective mass of the field, we see that the slow-roll approximation requires that the mass of the scalar field must be small compared with the Hubble scale. We note that the Hubble slow-roll parameter (Eq. (23.11)) coincides with the potential slow-roll parameter, $\epsilon_H \simeq \epsilon$, to leading order in the slow-roll approximation.

The slow-roll approximation allows one to determine the Hubble expansion rate as a function of the scalar field value, and vice versa. In particular, we can express, in terms of the scalar field value during inflation, the total logarithmic expansion, or number of “e-folds”:

$$\begin{aligned} N_* &\equiv \ln \left(\frac{R_{end}}{R_*} \right) \\ &= \int_{t_*}^{t_{end}} H dt \simeq - \int_{\phi_*}^{\phi_{end}} \sqrt{\frac{4\pi}{\epsilon}} \frac{d\phi}{M_P} \text{ for } V' > 0. \end{aligned} \quad (23.16)$$

Given that the slow-roll parameters are approximately constant during slow-roll inflation, $d\epsilon/dN \simeq 2\epsilon(\eta - 2\epsilon) = \mathcal{O}(\epsilon^2)$, we have

$$N_* \simeq \frac{4}{\sqrt{\epsilon}} \frac{\Delta\phi}{M_P}. \quad (23.17)$$

Since we require $N > 40$ to solve the flatness, horizon and entropy problems of the standard Big Bang cosmology, we require either very slow roll, $\epsilon < 0.01$, or a large change in the value of the scalar field relative to the Planck scale, $\Delta\phi > M_P$.

23.2.2 Reheating

Slow-roll inflation can lead to an exponentially large Universe, close to spatial flatness and homogeneity, but the energy density is locked in the potential energy of the scalar field, and needs to be converted to particles and thermalised to recover a hot Big Bang cosmology at the end of inflation [26, 27]. This process is usually referred to as reheating, although there was not necessarily any preceding thermal era. Reheating can occur when the scalar field evolves towards the minimum of its potential, converting the potential energy first to kinetic energy. This can occur either through the breakdown of the slow-roll condition in single-field models, or due to an instability triggered by the inflaton reaching

a critical value, in multi-field models known as hybrid inflation models [28].

Close to a simple minimum, the scalar field potential can be described by a quadratic function, $V = m^2\phi^2/2$, where m is the mass of the field. We can obtain slow-roll inflation in such a potential at large field values, $\phi \gg M_P$. However, for $\phi \ll M_P$ the field approaches an oscillatory solution:

$$\phi(t) \simeq \frac{M_P}{\sqrt{3\pi}} \frac{\sin(mt)}{mt}. \quad (23.18)$$

For $|\phi| < M_P$ the Hubble rate drops below the inflaton mass, $H < m$, and the field oscillates many times over a Hubble time. Averaging over several oscillations, $\Delta t \gg m^{-1}$, we find $\langle \dot{\phi}^2/2 \rangle_{\Delta t} \simeq \langle m^2\phi^2/2 \rangle_{\Delta t}$ and hence

$$\langle \rho \rangle_{\Delta t} \simeq \frac{M_P^2}{6\pi t^2}, \quad \langle p \rangle_{\Delta t} \simeq 0. \quad (23.19)$$

This coherent oscillating field corresponds to a condensate of non-relativistic massive inflaton particles, driving a matter-dominated era at the end of inflation, with scale factor $R \propto t^{2/3}$.

The inflaton condensate can lose energy through perturbative decays due to terms in the interaction Lagrangian, such as

$$\mathcal{L}_{int} \subset -\lambda_i \sigma \phi \chi_i^2 - \lambda_j \phi \bar{\psi}_j \psi_j \quad (23.20)$$

that couple the inflation to scalar fields χ_i or fermions ψ_j , where σ has dimensions of mass and the λ_i are dimensionless couplings. When the mass of the inflaton is much larger than the decay products, the decay rate is given by [29]

$$\Gamma_i = \frac{\lambda_i^2 \sigma^2}{8\pi m}, \quad \Gamma_j = \frac{\lambda_j^2 m}{8\pi}. \quad (23.21)$$

These decay products must in turn thermalise with Standard Model particles before we recover conventional hot Big Bang cosmology. An upper limit on the reheating temperature after inflation is given by [27]

$$T_{rh} = 0.2 \left(\frac{100}{g_*} \right)^{1/4} \sqrt{M_P \Gamma_{tot}}, \quad (23.22)$$

where g_* is the effective number of degrees of freedom and Γ_{tot} is the total decay rate for the inflaton, which is required to be less than m for perturbative decay.

The baryon asymmetry of the Universe must be generated after the main release of entropy during inflation, which is an important constraint on possible models. Also, the fact that the inflaton mass is much larger than the mass scale of the Standard Model opens up the possibility that it may decay into massive stable or metastable particles that could be connected with dark matter, constraining possible models. For example, in the context of supergravity models the reheat temperature is constrained by the requirement that gravitinos are not overproduced, potentially destroying the successes of Big Bang nucleosynthesis. For a range of gravitino masses one must require $T_{rh} < 10^9$ GeV [30, 31].

The process of inflaton decay and reheating can be significantly altered by interactions leading to space-time dependences in the effective masses of the fields. In particular, parametric resonance can lead to explosive, non-perturbative decay of the inflaton in some cases, a process often referred to as preheating [26, 32]. For example, an interaction term of the form

$$\mathcal{L}_{int} \subset -\lambda^2 \phi^2 \chi^2, \quad (23.23)$$

leads to a time-dependent effective mass for the χ field as the inflaton ϕ oscillates. This can lead to non-adiabatic particle production if the bare mass of the χ field is small for large couplings or for rapid changes of the inflaton field. The process of preheating is highly model-dependent, but it highlights the possible role of non-thermal particle production after and even during inflation.

23.3 Primordial Perturbations from Inflation

Although inflation was originally discussed as a solution to the problem of initial conditions required for homogeneous and isotropic hot Big Bang cosmology, it was soon realised that inflation also offered a mechanism to generate the inhomogeneous initial conditions required for the formation of large-scale structure [15–17, 33].

23.3.1 Metric Perturbations

In a homogeneous classical inflationary cosmology driven by a scalar field, the inflaton field is uniform on constant-time hypersurfaces, $\phi = \phi_0(t)$. However, quantum fluctuations inevitably break the spatial symmetry leading to an inhomogeneous field:

$$\phi(t, x^i) = \phi_0(t) + \delta\phi(t, x^i). \quad (23.24)$$

At the same time, one should consider inhomogeneous perturbations of the RW spacetime metric (see, e.g., [34–36]):

$$ds^2 = (1 + 2A)dt^2 - 2RB_i dt dx^i - R^2 [(1 + 2C)\delta_{ij} + \partial_i \partial_j E + h_{ij}] dx^i dx^j, \quad (23.25)$$

where A , B , E and C are scalar perturbations while h_{ij} represents transverse and tracefree, tensor metric perturbations. Vector metric perturbations can be eliminated using Einstein constraint equations in a scalar field cosmology.

The tensor perturbations remain invariant under a temporal gauge transformation $t \rightarrow t + \delta t(t, x^i)$, but both the scalar field and the scalar metric perturbations transform. For example, we have

$$\delta\phi \rightarrow \delta\phi - \dot{\phi}_0 \delta t, \quad C \rightarrow C - H \delta t. \quad (23.26)$$

However, there are gauge invariant combinations, such as [37]

$$Q = \delta\phi - \frac{\dot{\phi}_0}{H} C, \quad (23.27)$$

which describes the scalar field perturbations on spatially-flat ($C = 0$) hypersurfaces. This is simply related to the curvature perturbation on uniform-field ($\delta\phi = 0$) hypersurfaces:

$$\mathcal{R} = C - \frac{H}{\dot{\phi}_0} \delta\phi = -\frac{H}{\dot{\phi}_0} Q, \quad (23.28)$$

which coincides in slow-roll inflation, $\rho \simeq \rho(\phi)$, with the curvature perturbation on uniform-density hypersurfaces [16]

$$\zeta = C - \frac{H}{\dot{\rho}_0} \delta\rho. \quad (23.29)$$

Thus scalar field and scalar metric perturbations are coupled by the evolution of the inflaton field.

23.3.2 Gravitational waves from inflation

The tensor metric perturbation, h_{ij} in Eq. (23.25), is gauge-invariant and decoupled from the scalar perturbations at first order. This represents the free excitations of the spacetime, i.e., gravitational waves, which are the simplest metric perturbations to study at linear order.

Each tensor mode, with wavevector \vec{k} , has two linearly-independent transverse and trace-free polarization states:

$$h_{ij}(\vec{k}) = h_{\vec{k}} q_{ij} + \bar{h}_{\vec{k}} \bar{q}_{ij}. \quad (23.30)$$

The linearised Einstein equations then yield the same evolution equation for the amplitude as that for a massless field in RW spacetime:

$$\ddot{h}_{\vec{k}} + 3H\dot{h}_{\vec{k}} + \frac{k^2}{R^2} h_{\vec{k}} = 0, \quad (23.31)$$

(and similarly for $\bar{h}_{\vec{k}}$). This can be re-written in terms of the conformal time, $\eta = \int dt/R$, and the conformally rescaled field:

$$u_{\vec{k}} = \frac{M_P R h_{\vec{k}}}{\sqrt{32\pi}}. \quad (23.32)$$

This conformal field then obeys the wave equation for a canonical scalar field in Minkowski spacetime with a time-dependent mass:

$$u_{\vec{k}}'' + \left(k^2 - \frac{R''}{R}\right) u_{\vec{k}} = 0. \quad (23.33)$$

During slow roll

$$\frac{R''}{R} \simeq (2 - \epsilon)R^2 H^2. \quad (23.34)$$

This makes it possible to quantise the linearised metric fluctuations, $u_{\vec{k}} \rightarrow \hat{u}_{\vec{k}}$, on sub-Hubble scales, $k^2/R^2 \gg H^2$, where the background expansion can be neglected.

Crucially, in an inflationary expansion, where $\dot{R} > 0$, the comoving Hubble length $H^{-1}/R = 1/\dot{R}$ decreases with time. Thus, all modes start inside the Hubble horizon and it is possible to take the initial field fluctuations to be in a vacuum state at early times or on small scales:

$$\langle u_{\vec{k}_1} u_{\vec{k}_2} \rangle = \frac{i}{2} (2\pi)^3 \delta^{(3)}(\vec{k}_1 + \vec{k}_2). \quad (23.35)$$

In terms of the amplitude of the tensor metric perturbations, this corresponds to

$$\langle h_{\vec{k}_1} h_{\vec{k}_2} \rangle = \frac{1}{2} \frac{\mathcal{P}_t(k_1)}{4\pi k_1^3} (2\pi)^3 \delta^{(3)}(\vec{k}_1 + \vec{k}_2), \quad (23.36)$$

where the factor 1/2 appears due to the two polarization states that contribute to the total tensor power spectrum:

$$\mathcal{P}_t(k) = \frac{64\pi}{M_P^2} \left(\frac{k}{2\pi R}\right)^2. \quad (23.37)$$

On super-Hubble scales, $k^2/R^2 \ll H^2$, we have the growing mode solution to Eq. (23.33), $u_{\vec{k}} \propto R$, corresponding to $h_{\vec{k}} \rightarrow \text{constant}$, i.e., tensor modes are frozen-in on super-Hubble scales, both during and after inflation. Thus, connecting the initial vacuum fluctuations on sub-Hubble scales to the late-time power spectrum for tensor modes at Hubble exit during inflation, $k = R_* H_*$, we obtain

$$\mathcal{P}_t(k) \simeq \frac{64\pi}{M_P^2} \left(\frac{H_*}{2\pi}\right)^2. \quad (23.38)$$

In the de Sitter limit, $\epsilon \rightarrow 0$, the Hubble rate becomes time-independent and the tensor spectrum on super-Hubble scales becomes scale-invariant [39]. However slow-roll evolution leads to weak time dependence of H_* and thus a scale-dependent spectrum on large scales, with a spectral tilt

$$n_t \equiv \frac{d \ln \mathcal{P}_t}{d \ln k} \simeq -2\epsilon_*. \quad (23.39)$$

23.3.3 Density Perturbations from single-field inflation

The inflaton field fluctuations on spatially-flat hypersurfaces are coupled to scalar metric perturbations at first order, but these can be eliminated using the Einstein constraint equations to yield an evolution equation

$$\ddot{Q}_{\vec{k}} + 3H\dot{Q}_{\vec{k}} + \left[\frac{k^2}{R^2} + V'' - \frac{8\pi}{M_P^2 R^3} \frac{d}{dt} \left(\frac{R^3 \dot{\phi}^2}{H} \right) \right] Q_{\vec{k}} = 0. \quad (23.40)$$

Terms proportional to M_P^{-2} represent the effect on the field fluctuations of gravity at first order. As can be seen, this vanishes in the limit of a constant background field, and hence is suppressed in the slow-roll limit, but it is of the same order as the effective mass, $V'' = 3\eta H^2$, so must be included if we wish to model deviations from exact de Sitter symmetry.

This wave equation can also be written in the canonical form for a free field in Minkowski spacetime if we define [37]

$$v_{\vec{k}} \equiv RQ_{\vec{k}}, \quad (23.41)$$

to yield

$$v_{\vec{k}}'' + \left(k^2 - \frac{z''}{z}\right) v_{\vec{k}} = 0, \quad (23.42)$$

where we define

$$z \equiv \frac{R\dot{\phi}}{H}, \quad \frac{z''}{z} \simeq (2 + 5\epsilon - 3\eta)R^2 H^2, \quad (23.43)$$

where the last approximate equality holds to leading order in the slow-roll approximation.

As previously done for gravitational waves, we quantise the linearised field fluctuations $v_{\vec{k}} \rightarrow \hat{v}_{\vec{k}}$ on sub-Hubble scales, $k^2/R^2 \gg H^2$, where the background expansion can be neglected. Thus, we impose

$$\langle v_{\vec{k}_1} v_{\vec{k}_2}' \rangle = \frac{i}{2} \delta^{(3)}(\vec{k}_1 + \vec{k}_2). \quad (23.44)$$

In terms of the field perturbations, this corresponds to

$$\langle Q_{\vec{k}_1} Q_{\vec{k}_2} \rangle = \frac{\mathcal{P}_Q(k_1)}{4\pi k_1^3} (2\pi)^3 \delta^{(3)}(\vec{k}_1 + \vec{k}_2), \quad (23.45)$$

where the power spectrum for vacuum field fluctuations on sub-Hubble scales, $k^2/R^2 \gg H^2$, is simply

$$\mathcal{P}_Q(k) = \left(\frac{k}{2\pi R}\right)^2, \quad (23.46)$$

yielding the classic result for the vacuum fluctuations for a massless field in de Sitter at Hubble exit, $k = R_* H_*$:

$$\mathcal{P}_Q(k) \simeq \left(\frac{H}{2\pi}\right)_*^2. \quad (23.47)$$

In practice there are slow-roll corrections due to the small but finite mass (η) and field evolution (ϵ) [40].

Slow-roll corrections to the field fluctuations are small on sub-Hubble scales, but can become significant as the field and its perturbations evolve over time on super-Hubble scales. Thus, it is helpful to work instead with the curvature perturbation, ζ defined in equation (Eq. (23.29)), which remains constant on super-Hubble scales for adiabatic density perturbations both during and after inflation [16,41]. Thus we have an expression for the primordial curvature perturbation on super-Hubble scales produced by single-field slow-roll inflation:

$$\mathcal{P}_\zeta(k) = \left[\left(\frac{H}{\dot{\phi}}\right)^2 \mathcal{P}_Q(k) \right]_* \simeq \frac{4\pi}{M_P^2} \left[\frac{1}{\epsilon} \left(\frac{H}{2\pi}\right)^2 \right]_*. \quad (23.48)$$

Comparing this with the primordial gravitational wave power spectrum (Eq. (23.38)) we obtain the tensor-to-scalar ratio

$$r \equiv \frac{\mathcal{P}_t}{\mathcal{P}_\zeta} \simeq 16\epsilon_*. \quad (23.49)$$

Note that the scalar amplitude is boosted by a factor $1/\epsilon_*$ during slow-roll inflation, because small scalar field fluctuations can lead to relatively large curvature perturbations on hypersurfaces defined with respect to the density if the potential energy is only weakly dependent on the scalar field, as in slow roll. Indeed, the de Sitter limit is singular, since the potential energy becomes independent of the scalar field at first order, $\epsilon \rightarrow 0$, and the curvature perturbation on uniform-density hypersurfaces becomes ill-defined.

We note that in single-field inflation the tensor-to-scalar ratio and the tensor tilt (Eq. (23.39)) at the same scale are both determined by the first slow-roll parameter at Hubble exit, ϵ_* , giving rise to an important consistency test for single-field slow-roll inflation:

$$n_t \simeq -\frac{r}{8}. \quad (23.50)$$

This may be hard to verify if r is small, making any tensor tilt n_t difficult to measure. On the other hand, it does offer a way to rule out single-field slow-roll inflation if either r or n_t is large.

Given the relatively large scalar power spectrum, it has proved easier to measure the scalar tilt, conventionally defined as $n_s - 1$.

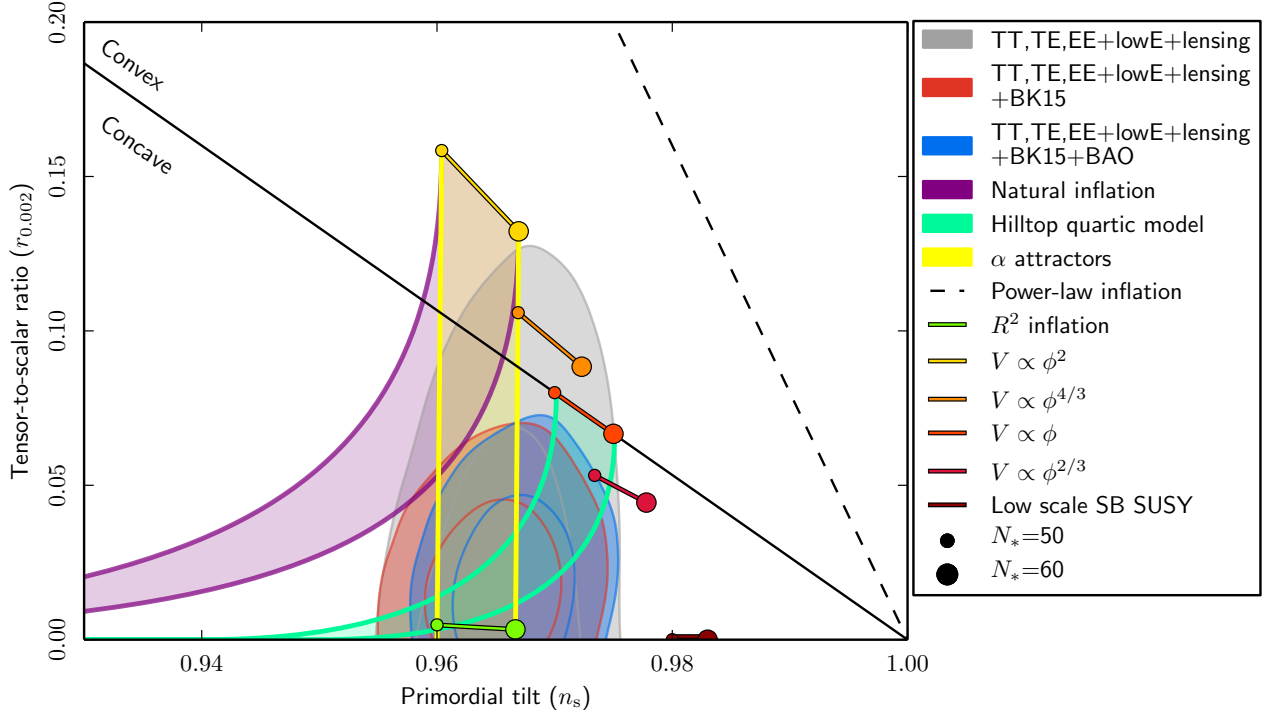


Figure 23.1: The marginalized joint 68 and 95% CL regions for the tilt in the scalar perturbation spectrum, n_s , and the relative magnitude of the tensor perturbations, r , obtained from the *Planck* 2018 and lensing data alone, and their combinations with BICEP2/Keck Array (BK15) and (optionally) BAO data, confronted with the predictions of some of the inflationary models discussed in this review. This figure is taken from [38].

Slow-roll corrections lead to slow time-dependence of both H_* and ϵ_* , giving a weak scale-dependence of the scalar power spectrum:

$$n_s - 1 \equiv \frac{d \ln \mathcal{P}_\zeta}{d \ln k} \simeq -6\epsilon_* + 2\eta_*, \quad (23.51)$$

and a running of this tilt at second-order in slow roll:

$$\frac{dn_s}{d \ln k} \simeq -8\epsilon_*(3\epsilon_* - 2\eta_*) - 2\xi_*^2, \quad (23.52)$$

where the running introduces a new slow-roll parameter at second-order:

$$\xi^2 = \frac{M_P^4}{64\pi^2} \frac{V'V'''}{V^2}. \quad (23.53)$$

23.3.4 Observational Bounds

The observed scale-dependence of the power spectrum makes it necessary to specify the comoving scale, k , at which quantities are constrained and hence the Hubble-exit time, $k = a_* H_*$, when the corresponding theoretical quantities are calculated during inflation. This is usually expressed in terms of the number of e-folds from the end of inflation [42]:

$$N_*(k) \simeq 67 - \ln \left(\frac{k}{a_0 H_0} \right) + \frac{1}{4} \ln \left(\frac{V_*^2}{M_P^4 \rho_{end}} \right) + \frac{1}{12} \ln \left(\frac{\rho_{rh}}{\rho_{end}} \right) - \frac{1}{12} \ln(g_*), \quad (23.54)$$

where H_0^{-1}/a_0 is the present comoving Hubble length. Different models of reheating and and thus different reheat temperatures and densities, ρ_{rh} in Eq. (23.54), lead to a range of possible values for N_* corresponding to a fixed physical scale, and hence we have a range of observational predictions for a given inflation model, as seen in Fig. 23.1.

The *Planck* 2018 temperature and polarization data (see Chap. 29, “Cosmic Microwave Background” review) are consistent with a smooth featureless power spectrum over a range of comoving

wavenumbers, $0.008 h^{-1} \text{ Mpc}^{-1} \leq k \leq 0.1 h \text{ Mpc}^{-1}$. In the absence of running, the data measure the spectral index to be [38]

$$n_s = 0.9649 \pm 0.0042, \quad (23.55)$$

corresponding to a deviation from scale-invariance exceeding the 7σ level. If running of the spectral tilt is included in the model, this is constrained to be [38]

$$\frac{dn_s}{d \ln k} = -0.0045 \pm 0.0067 \quad (23.56)$$

at the 95% CL, assuming no running of the running. The most recent analysis [43] of the BICEP, Keck Array and *Planck* data places an upper bound on the tensor-to-scalar ratio

$$r < 0.036, \quad (23.57)$$

at the 95% CL.

These observational bounds can be converted into bounds on the slow-roll parameters and hence the potential during slow-roll inflation. Setting higher-order slow-roll parameters (beyond second-order in horizon-flow parameters [44]) to zero, the *Planck* collaboration obtain the following 95% CL bounds when lensing and BK15 data are included [38]

$$\epsilon < 0.0044, \quad (23.58)$$

$$\eta = -0.015 \pm 0.006, \quad (23.59)$$

$$\xi^2 = 0.0029_{-0.0069}^{+0.0073}, \quad (23.60)$$

which can be used to constrain models, as discussed in the next Section.

Fig. 23.1, which is taken from [38], compares observational CMB constraints on the tilt, n_s , in the spectrum of scalar perturbations and the ratio, r , between the magnitudes of tensor and scalar perturbations. Important rôles are played by data from the *Planck* satellite and on lensing, the BICEP2/Keck Array (BK15) and measurements of baryon acoustic oscillations (BAO). The reader is referred to [38] for technical details. These experimental constraints are compared with the predictions of some

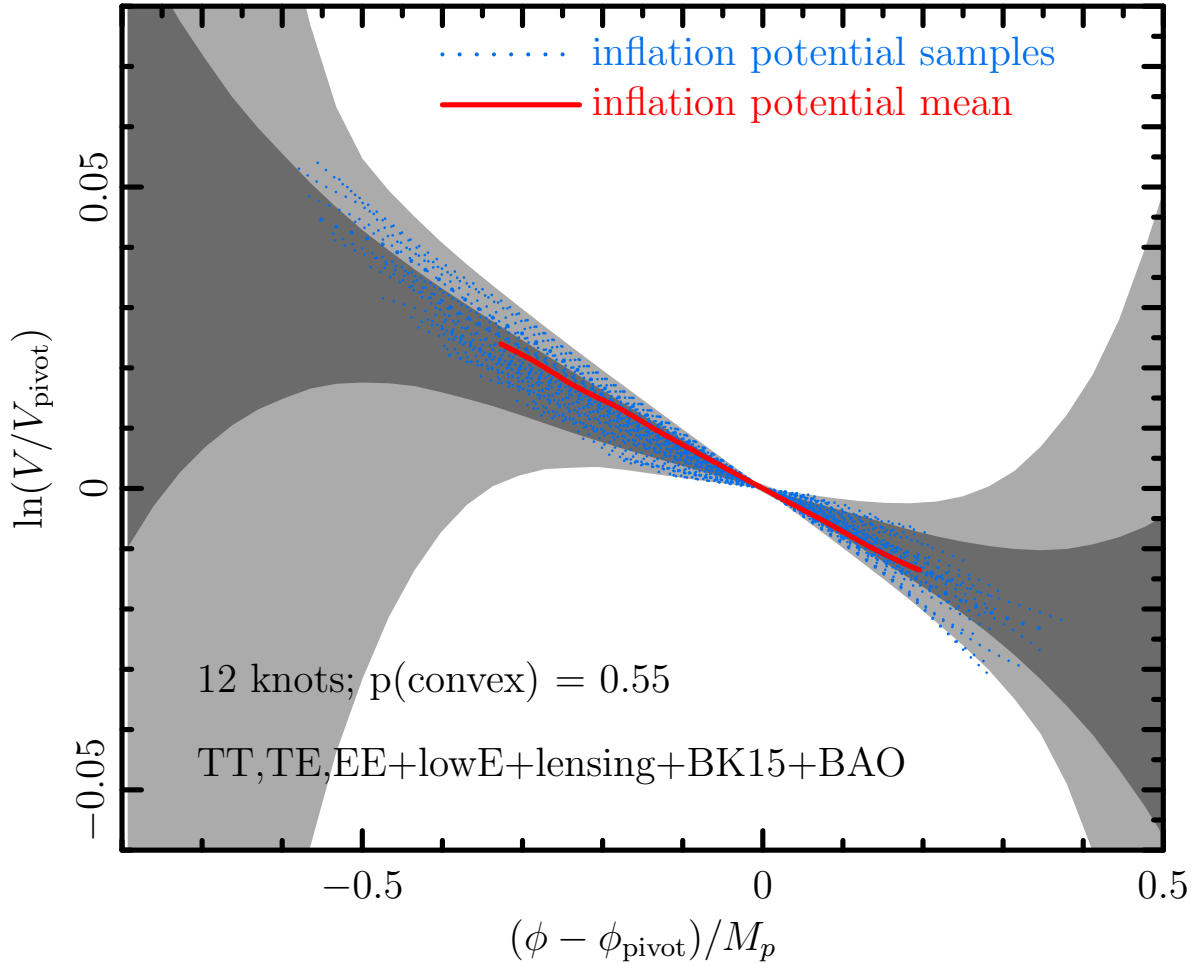


Figure 23.2: The result of reconstructing a single-field inflaton potential using a cubic-spline power-spectrum mode expansion and the full *Planck*, lensing, BK15 and BAO data set. This figure is taken from [38].

of the inflationary models discussed in this review. Generally speaking, models with a concave potential are favored over those with a convex potential, and models with power-law inflation are now excluded, as opposed to models with de Sitter-like (quasi-)exponential expansion.

There is no significant evidence for local features within the range of inflaton field values probed by the data [38]. However, the data may be used to reconstruct partially the effective inflationary potential over a range of inflaton field values, assuming that it is suitably smooth. The result of one such exercise by the *Planck* collaboration [38] in the framework of a generic single-field inflaton potential is shown in Fig. 23.2. This reconstruction assumes a cubic-spline power-spectrum mode expansion and employs the full *Planck*, lensing, BK15 and BAO data set. The reader is again referred to [38] for technical details. We see that the effective inflaton potential is relatively well reconstructed over field values ϕ within ± 0.5 of the chosen pivot value, but the potential is only very weakly constrained for larger values of $|\phi - \phi_{pivot}|$, providing wide scope for inflationary model-builders.

23.4 Models

23.4.1 Pioneering Models

The paradigm of the inflationary Universe was proposed in [2], where it was pointed out that an early period of (near-)exponential expansion, in addition to resolving the horizon and flatness problems of conventional Big-Bang cosmology as discussed above (the possibility of a de Sitter phase in the early history of the Universe was also proposed in the non-minimal gravity model of [1], with the motivation of avoiding an initial singularity), would also dilute the prior abundance of any unseen heavy, (meta-)stable particles, as exemplified by monopoles

in grand unified theories (GUTs; see Chap. 93, “Grand Unified Theories” review). The original proposal was that this inflationary expansion took place while the Universe was in a metastable state (a similar suggestion was made in [45, 46], where in [45] it was also pointed out that such a mechanism could address the horizon problem) and was terminated by a first-order transition due to tunnelling through a potential barrier. However, it was recognized already in [2] that this ‘old inflation’ scenario would need modification if the transition to the post-inflationary Universe were to be completed smoothly without generating unacceptable inhomogeneities.

This ‘graceful exit’ problem was addressed in the ‘new inflation’ model of [13] (see also [14] and footnote [39] of [2]), which studied models based on an $SU(5)$ GUT with an effective potential of the Coleman-Weinberg type (i.e., dominated by radiative corrections), in which inflation could occur during the roll-down from the local maximum of the potential towards a global minimum. However, it was realized that the Universe would evolve to a different minimum from the Standard Model [47], and it was also recognized that density fluctuations would necessarily be too large [15], since they were related to the GUT coupling strength.

These early models of inflation assumed initial conditions enforced by thermal equilibrium in the early Universe. However, this assumption was questionable: indeed, it was not made in the model of [1], in which a higher-order gravitational curvature term was assumed to arise from quantum corrections, and the assumption of initial thermal equilibrium was jettisoned in the ‘chaotic’ inflationary model of [48]. These are the inspirations for much recent inflationary model building, so we now discuss them in more detail, before reviewing contemporary models.

In this section we will work in natural units where we set the reduced Planck mass to unity, i.e., $8\pi/M_P^2 = 1$. All masses are thus relative to the reduced Planck scale.

23.4.2 R^2 Inflation

The first-order Einstein-Hilbert action, $(1/2) \int d^4x \sqrt{-g} R$, where R is the Ricci scalar curvature, is the minimal possible theory consistent with general coordinate invariance. However, it is possible that there might be non-minimal corrections to this action, and the unique second-order possibility is

$$S = \frac{1}{2} \int d^4x \sqrt{-g} \left(R + \frac{R^2}{6M^2} \right). \quad (23.61)$$

It was pointed out in [1] that an R^2 term could be generated by quantum effects, and that (Eq. (23.61)) could lead to de Sitter-like expansion of the Universe. Scalar density perturbations in this model were calculated in [17]. Because the initial phase was (almost) de Sitter, these perturbations were (approximately) scale-invariant, with magnitude $\propto M$. It was pointed out in [17] that requiring the scalar density perturbations to lie in the range 10^{-3} to 10^{-5} , consistent with upper limits at that time, would require $M \sim 10^{-3}$ to 10^{-5} in Planck units, and it was further suggested that these perturbations could lead to the observed large-scale structure of the Universe, including the formation of galaxies.

Although the action (Eq. (23.61)) does not contain an explicit scalar field, [17] reduced the calculation of density perturbations to that of fluctuations in the scalar curvature R , which could be identified (up to a factor) with a scalar field of mass M . The formal equivalence of R^2 gravity (Eq. (23.61)) to a theory of gravity with a massive scalar ϕ had been shown in [18], see also [19]. The effective scalar potential for what we would nowadays call the ‘inflaton’ [49] takes the form

$$S = \frac{1}{2} \int d^4x \sqrt{-g} \left[R + (\partial_\mu \phi)^2 - \frac{3}{2} M^2 (1 - e^{-\sqrt{2/3} \phi})^2 \right] \quad (23.62)$$

when the action is written in the Einstein frame, and the potential is shown as the solid black line in Fig. 23.3. Using (Eq. (23.48)), one finds that the amplitude of the scalar density perturbations in this model is given by

$$\Delta_{\mathcal{R}} = \frac{3M^2}{8\pi^2} \sinh^4 \left(\frac{\phi}{\sqrt{6}} \right), \quad (23.63)$$

The measured magnitude of the density fluctuations in the CMB requires $M \simeq 1.3 \times 10^{-5}$ in Planck units (assuming $N_* \simeq 55$), so one of the open questions in this model is why M is so small. Obtaining $N_* \simeq 55$ also requires an initial value of $\phi \simeq 5.5$, i.e., a super-Planckian initial condition, and another issue for this and many other models is how the form of the effective potential is protected and remains valid at such large field values. Using Eq. (23.51) one finds that $n_s \simeq 0.965$ for $N_* \simeq 55$ and using (Eq. (23.49)) one finds that $r \simeq 0.0035$. These predictions are consistent with the present data from *Planck* and other experiments, as seen in Fig. 23.1.

23.4.3 Chaotic Models with Power-Law Potentials

As has already been mentioned, a key innovation in inflationary model-building was the suggestion to abandon the questionable assumption of a thermal initial state, and consider ‘chaotic’ initial conditions with very general forms of potential [48]. (Indeed, the R^2 model discussed above can be regarded as a prototype of this approach.) The chaotic approach was first proposed in the context of a simple power-law potential of the form $\mu^{4-\alpha} \phi^\alpha$, and the specific example of $\lambda \phi^4$ was studied in [48]. Such models make the following predictions for the slow-roll parameters ϵ and η :

$$\epsilon = \frac{1}{2} \left(\frac{\alpha}{\phi} \right)^2, \quad \eta = \frac{\alpha(\alpha-1)}{\phi^2}, \quad (23.64)$$

leading to the predictions

$$r \approx \frac{4\alpha}{N_*}, \quad n_s - 1 \approx -\frac{\alpha+2}{2N_*}, \quad (23.65)$$

which are shown in Fig. 23.1 for some illustrative values of α . We note that the prediction of the original ϕ^4 model lies out of the frame, with values of r that are too large and values of n_s that are too small. The ϕ^3 model has similar problems, and would in any case require modification in order to have a well-defined minimum. The simplest possibility is ϕ^2 , but this is now also disfavored by the data, at the 95% CL if only the *Planck* data are considered, and more strongly if other data are included, as seen in Fig. 23.1. (For non-minimal models of quadratic inflation that avoid this problem, see, e.g., [51].)

Indeed, as can be seen in Fig. 23.1, all single-field models with a convex potential (i.e., one curving upwards) are disfavored compared to models with a concave potential.

23.4.4 Hilltop Models

This preference for a concave potential motivates interest in ‘hilltop’ models [52], whose starting-point is a potential of the form

$$V(\phi) = \Lambda^4 \left[1 - \left(\frac{\phi}{\mu} \right)^p + \dots \right], \quad (23.66)$$

where the \dots represent extra terms that yield a positive semi-definite potential. To first order in the slow-roll parameters, when $x \equiv \phi/\mu$ is small, one has

$$n_s \simeq 1 - p(p-1)\mu^{-2} \frac{x^{p-2}}{(1-x^p)} - \frac{3}{8}r, \quad r \simeq 8p^2\mu^{-2} \frac{x^{2p-2}}{(1-x^p)^2}. \quad (23.67)$$

As seen in Fig. 23.1, a hilltop model with $p = 4$ can be compatible with the *Planck* and other measurements, if $\mu \gg M_P$.

23.4.5 D-Brane Inflation

Many scenarios for inflation involving extra dimensions have been proposed, e.g., the possibility that observable physics resides on a three-dimensional brane, and that there is an inflationary potential that depends on the distance between our brane and an antibrane, with a potential of the form [53]

$$V(\phi) = \Lambda^4 \left[1 - \left(\frac{\mu}{\phi} \right)^p + \dots \right]. \quad (23.68)$$

In this scenario the effective potential vanishes in the limit $\phi \rightarrow \infty$, corresponding to complete separation between our brane and the antibrane. The predictions for n_s and r in this model can be obtained from (Eq. 23.67) by exchanging $p \leftrightarrow -p$, and are also consistent with the *Planck* and other data.

23.4.6 Natural Inflation

Also seen in Fig. 23.1 are the predictions of ‘natural inflation’ [54], in which one postulates a non-perturbative shift symmetry that suppresses quantum corrections, so that a hierarchically small scale of inflation, $H \ll M_P$, is technically natural. In the simplest models, there is a periodic potential of the form

$$V(\phi) = \Lambda^4 \left[1 + \cos \left(\frac{\phi}{f} \right) \right], \quad (23.69)$$

where f is a dimensional parameter reminiscent of an axion decay constant (see the next subsection) [55], which must have a value $> M_P$. Natural inflation can yield predictions similar to quadratic inflation (which are no longer favored, as already discussed), but can also yield an effective convex potential. Thus, it may lead to values of r that are acceptably small, but for values of n_s that are in tension with the data, as seen in Fig. 23.1.

23.4.7 Axion Monodromy Models

The effective potentials in stringy models [56, 57] motivated by axion monodromy may be of the form

$$V(\phi) = \mu^{4-\alpha} \phi^\alpha + \Lambda^4 e^{-C \left(\frac{\phi}{\phi_0} \right)^{p_\Lambda}} \cos \left[\gamma + \frac{\phi}{f} \left(\frac{\phi}{\phi_0} \right)^{p_f + 1} \right], \quad (23.70)$$

where μ, Λ, f and ϕ_0 are parameters with the dimension of mass, and C, p, p_Λ, p_f and γ are dimensionless constants, generalizing the potential ([54]) in the simplest models of natural inflation. The oscillations in (Eq. 23.70) are associated with the axion field, and powers $p_\Lambda, p_f \neq 0$ may arise from ϕ -dependent evolutions of

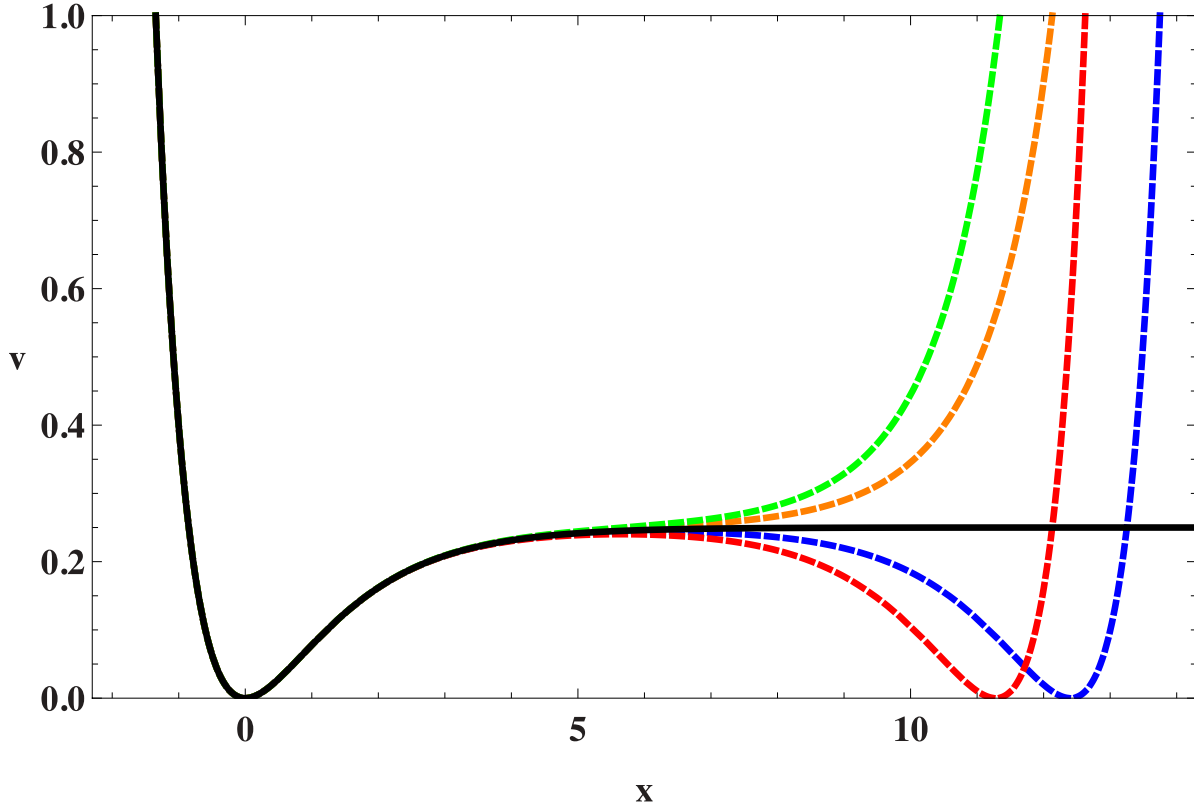


Figure 23.3: The inflationary potential V in the R^2 model (solid black line) compared with its form in various no-scale models discussed in detail in [50] (dashed coloured lines).

string moduli. Since the exponential prefactor in (Eq. 23.70) is due to non-perturbative effects that may be strongly suppressed, the oscillations may be unobservable small. Specific string models having ϕ^α with $\alpha = 4/3, 1$ or $2/3$ have been constructed in [56,57], providing some motivation for the low-power models mentioned above.

As seen in Fig. 23.1, the simple axion monodromy models with the power $\alpha = 4/3$ or 1 are no longer compatible with the current CMB data at the 95% CL, while $\alpha = 2/3$ is only marginally compatible at 95% CL. The *Planck* Collaboration has also searched for characteristic effects associated with the second term in (Eq. (23.70)), such as a possible drift in the modulation amplitude (setting $p_A = C = 0$), and a possible drifting frequency generated by $p_f \neq 0$, without finding any compelling evidence [38].

23.4.8 Higgs Inflation

Since the energy scale during inflation is commonly expected to lie between the Planck and TeV scales, it may serve as a useful bridge with contacts both to string theory or some other quantum theory of gravity, on the one side, and particle physics on the other side. However, as the above discussion shows, much of the activity in building models of inflation has been largely independent of specific connections with these subjects, though some examples of string-motivated models of inflation were mentioned above.

The most economical scenario for inflation might be to use as inflaton the only established scalar field, namely the Higgs field (see Chap.11, “Status of Higgs boson physics” review). A specific model assuming a non-minimal coupling of the Higgs field h to gravity was constructed in [58]. Its starting-point is the action

$$S = \int d^4x \sqrt{-g} \left[\frac{M^2 + \xi h^2}{2} R + \frac{1}{2} \partial_\mu h \partial^\mu h - \frac{\lambda}{4} (h^2 - v^2)^2 \right], \quad (23.71)$$

where v is the Higgs vacuum expectation value. The model requires $\xi \gg 1$, in which case it can be rewritten in the Einstein

frame as

$$S = \int d^4x \sqrt{-g} \left[\frac{1}{2} R + \frac{1}{2} \partial_\mu \chi \partial^\mu \chi - U(\chi) \right], \quad (23.72)$$

where the effective potential for the canonically-normalized inflaton field χ has the form

$$U(\chi) = \frac{\lambda}{4\xi^2} \left[1 + \exp\left(-\frac{2\chi}{\sqrt{6}M_P}\right) \right]^{-2}, \quad (23.73)$$

which is similar to the effective potential of the R^2 model at large field values. As such, the model inflates successfully if $\xi \simeq 5 \times 10^4 m_h / (\sqrt{2}v)$, with predictions for n_s and r that are indistinguishable from the predictions of the R^2 model shown in Fig. 23.1.

This model is very appealing, but must confront several issues. One is to understand the value of ξ , and another is the possibility of unitarity violation. However, a more fundamental issue is whether the effective quartic Higgs coupling is positive at the scale of the Higgs field during inflation. Extrapolations of the effective potential in the Standard Model using the measured values of the masses of the Higgs boson and the top quark indicate that probably $\lambda < 0$ at this scale [59], though there are still significant uncertainties associated with the appropriate input value of the top mass and the extrapolation to high renormalization scales.

23.4.9 Supersymmetric Models of Inflation

Supersymmetry [60] is widely considered to be a well-motivated possible extension of the Standard Model that might become apparent at the TeV scale. It is therefore natural to consider supersymmetric models of inflation. These were originally proposed because of the problems of the new inflationary theory [13,14] based on the one-loop (Coleman-Weinberg) potential for breaking SU(5). Several of these problems are related to the magnitude of the effective potential parameters: in any model of inflation based on an elementary scalar field, some parameter in the effective potential must be small in natural units, e.g., the quartic

coupling λ in a chaotic model with a quartic potential, or the mass parameter μ in a model of chaotic quadratic inflation. These parameters are renormalized multiplicatively in a supersymmetric theory, so that the quantum corrections to small values would be

under control. Hence, it was suggested that inflation cries out for supersymmetry [61], though non-supersymmetric resolutions of the problems of Coleman-Weinberg inflation are also possible: see, e.g., Ref. [62].

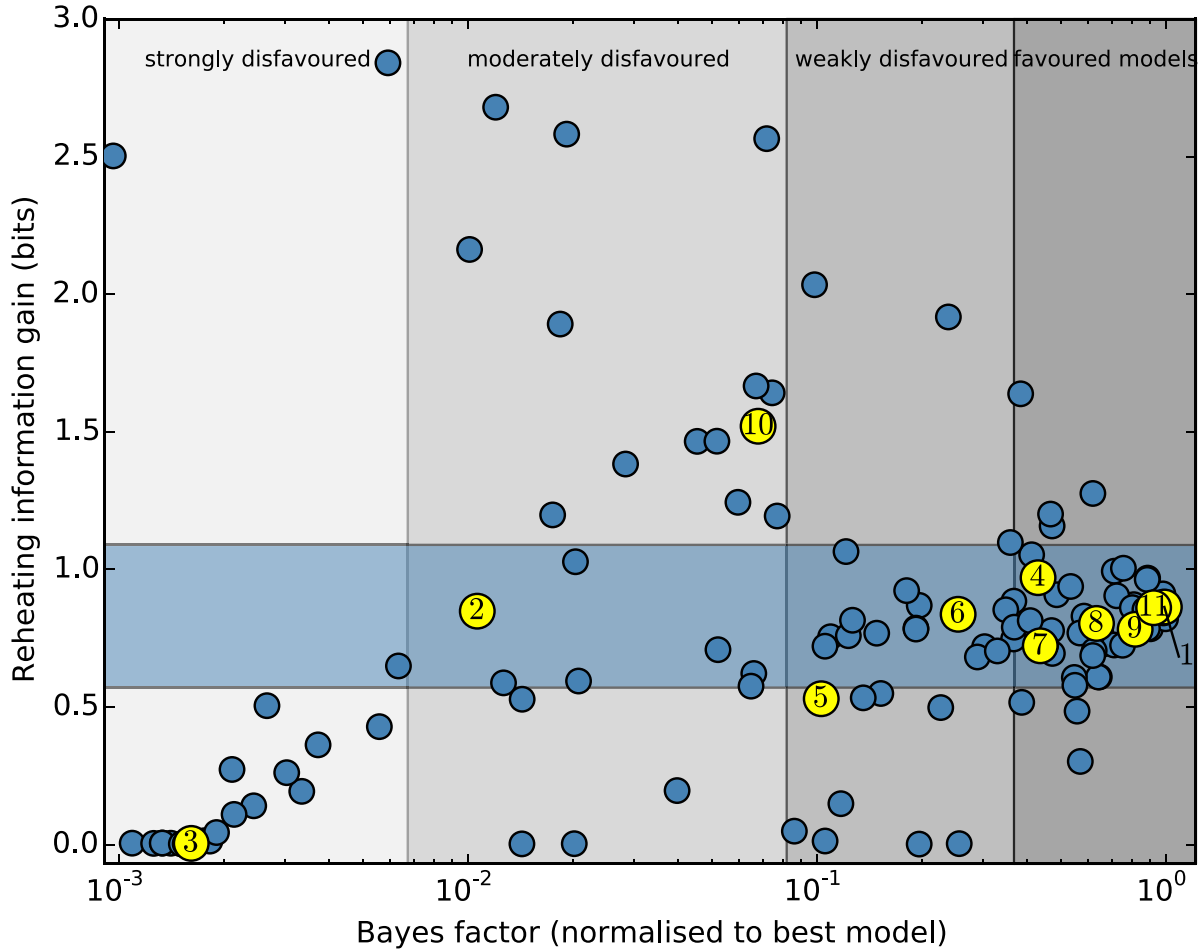


Figure 23.4: The Bayes factors calculated in [63] for a large sample of inflationary models using *Planck* 2015 data [64]. Those highlighted in yellow are featured in this review, according to the numbers listed in the text.

In the Standard Model there is only one scalar field that could be a candidate for the inflaton, namely the Higgs field discussed above, but even the minimal supersymmetric extension of the Standard Model (MSSM) contains many scalar fields. However, none of these is a promising candidate for the inflaton. The minimal extension of the MSSM that may contain a suitable candidate is the supersymmetric version of the minimal seesaw model of neutrino masses, which contains the three supersymmetric partners of the heavy singlet (right-handed) neutrinos. One of these singlet sneutrinos $\tilde{\nu}$ could be the inflaton [65]: it would have a quadratic potential, the mass coefficient required would be $\sim 10^{13}$ GeV, very much in the expected ballpark for singlet (right-handed) neutrino masses, and sneutrino inflaton decays also could give rise to the cosmological baryon asymmetry via leptogenesis. However, as seen in Fig. 23.1 and already discussed, a purely quadratic inflationary potential is no longer favored by the data. This difficulty could in principle be resolved in models with multiple sneutrinos [66], or by postulating a trilinear sneutrino coupling and hence a superpotential of Wess-Zumino type [67], which can yield successful inflation with predictions intermediate between those of natural inflation and hilltop inflation in Fig. 23.1.

Finally, we note that it is also possible to obtain inflation via supersymmetry breaking, as in the model [68] whose predictions are illustrated in Fig. 23.1.

23.4.10 Supergravity Models

Any model of early-Universe cosmology, and specifically inflation, must necessarily incorporate gravity. In the context of supersymmetry this requires an embedding in some supergravity theory [69, 70]. An $\mathcal{N} = 1$ supergravity theory is specified by three functions: a Hermitian function of the matter scalar fields ϕ^i , called the Kähler potential K , that describes its geometry, a holomorphic function of the superfields, called the superpotential W , which describes their interactions, and another holomorphic function $f_{\alpha\beta}$, which describes their couplings to gauge fields V_α [71].

The simplest possibility is that the Kähler metric is flat:

$$K = \phi^i \phi_i^*, \quad (23.74)$$

where the sum is over all scalar fields in the theory, and the simplest inflationary model in minimal supergravity had the superpotential [72]

$$W = m^2(1 - \phi)^2, \quad (23.75)$$

Where ϕ is the inflaton. However, this model predicts a tilted scalar perturbation spectrum, $n_s = 0.933$, which is now in serious disagreement with the data from *Planck* and other experiments shown in Fig. 23.1.

Moreover, there is a general problem that arises in any supergravity theory coupled to matter, namely that, since its ef-

fective scalar potential contains a factor of e^K , scalars typically receive squared masses $\propto H^2 \sim V$, where H is the Hubble parameter [73], an issue called the ‘ η problem’. The theory given by (Eq. (23.75)) avoids this η problem, but a generic supergravity inflationary model encounters this problem of a large inflaton mass. Moreover, there are additional challenges for supergravity inflation associated with the spontaneous breaking of local supersymmetry [74–76].

Various approaches to the η problem in supergravity have been proposed, including the possibility of a shift symmetry [77], and one possibility that has attracted renewed attention recently is no-scale supergravity [78, 79]. This is a form of supergravity with a Kähler potential that can be written in the form [80]

$$K = -3 \ln \left(T + T^* - \frac{\sum_i |\phi^i|^2}{3} \right), \quad (23.76)$$

which has the special property that it naturally has a flat potential, at the classical level and before specifying a non-trivial superpotential. As such, no-scale supergravity is well-suited for constructing models of inflation. Adding to its attraction is the feature that compactifications of string theory to supersymmetric four-dimensional models yield effective supergravity theories of the no-scale type [81]. There are many examples of superpotentials that yield effective inflationary potentials for either the T field (which is akin to a modulus field in some string compactification) or a ϕ field (generically representing matter) that are of the same form as the effective potential of the R^2 model (Eq. (23.62)) when the magnitude of the inflaton field $\gg 1$ in Planck units, as required to obtain sufficiently many e-folds of inflation, N_* [82, 83]. This framework also offers the possibility of using a suitable superpotential to construct models with effective potentials that are similar, but not identical, to the R^2 model, as shown by the dashed coloured lines in Fig. 23.3.

23.4.11 Other Exponential Potential Models

This framework also offers the possibility [82] of constructing models in which the asymptotic constant value of the potential at large inflaton field values is approached via a different exponentially-suppressed term:

$$V(\phi) = A \left[1 - \delta e^{-B\phi} + \mathcal{O}(e^{-2B\phi}) \right], \quad (23.77)$$

where the magnitude of the scalar density perturbations fixes A , but δ and B are regarded as free parameters. In the case of R^2 inflation $\delta = 2$ and $B = \sqrt{2/3}$. In a model such as (Eq. (23.77)), one finds at leading order in the small quantity $e^{-B\phi}$ that

$$\begin{aligned} n_s &= 1 - 2B^2 \delta e^{-B\phi}, \\ r &= 8B^2 \delta^2 e^{-2B\phi}, \\ N_* &= \frac{1}{B^2 \delta} e^{+B\phi}. \end{aligned} \quad (23.78)$$

yielding the relations

$$n_s = 1 - \frac{2}{N_*}, \quad r = \frac{8}{B^2 N_*^2}. \quad (23.79)$$

These relations correspond to the class of models labeled as ‘ α attractors’ [84] in Fig. 23.1. CMB bounds on the tensor-to-scalar ratio translate into an upper bound on the parameter $\alpha = 2/3B^2$ in α -attractor models, which determines the curvature of the Kähler manifold in supergravity models [85]. There are generalizations of the simplest no-scale model (Eq. (23.76)) with prefactors before the $\ln(\dots)$ that are 1 or 2, leading to larger values of $B = \sqrt{2}$ or 1, respectively, and hence smaller values of r than in the R^2 model. CMB constraints on the scalar spectral index can also place a lower bound on the magnitude of α [86], due to the implicit dependence of N_* upon α [87].

23.5 Model Comparison

Given a particular inflationary model, one can obtain constraints on the model parameters, informed by the likelihood, corresponding to the probability of the data given a particular

choice of parameters (see Sec. 40, “Statistics” review). In the light of the detailed constraints on the statistical distribution of primordial perturbations now inferred from high-precision observations of the cosmic microwave background, it is also possible to make quantitative comparison of the statistical evidence for or against different inflationary models. This can be done either by comparing the logarithm of the maximum likelihood that can be obtained for the data using each model, i.e., the minimum χ^2 (with some correction for the number of free parameters in each model), or by a Bayesian model comparison [88] (see also Sec. 40.3.4 in “Statistics” review).

In such a Bayesian model comparison one computes [7] the evidence, $\mathcal{E}(\mathcal{D}|\mathcal{M}_A)$ for a model, \mathcal{M}_A , given the data \mathcal{D} . This corresponds to the likelihood, $\mathcal{L}(\theta_{Aj}) = p(\mathcal{D}|\theta_{Aj}, \mathcal{M}_A)$, integrated over the assumed prior distribution, $\pi(\theta_{Aj}|\mathcal{M}_A)$, for all the model parameters θ_{Aj} :

$$\mathcal{E}(\mathcal{D}|\mathcal{M}_A) = \int \mathcal{L}(\theta_{Aj}) \pi(\theta_{Aj}|\mathcal{M}_A) d\theta_{Aj}. \quad (23.80)$$

The posterior probability of the model given the data follows from Bayes’ theorem

$$p(\mathcal{M}_A|\mathcal{D}) = \frac{\mathcal{E}(\mathcal{D}|\mathcal{M}_A) \pi(\mathcal{M}_A)}{p(\mathcal{D})}, \quad (23.81)$$

where the prior probability of the model is given by $\pi(\mathcal{M}_A)$. Assuming that all models are equally likely a priori, $\pi(\mathcal{M}_A) = \pi(\mathcal{M}_B)$, the relative probability of model A relative to a reference model, in the light of the data, is thus given by the Bayes factor

$$B_{A,ref} = \frac{\mathcal{E}(\mathcal{D}|\mathcal{M}_A)}{\mathcal{E}(\mathcal{D}|\mathcal{M}_{ref})}. \quad (23.82)$$

Computation of the multi-dimensional integral (Eq. (23.80)) is a challenging numerical task. Even using an efficient sampling algorithm requires hundreds of thousands of likelihood computations for each model, though slow-roll approximations can be used to calculate rapidly the primordial power spectrum using the APSIC numerical library [7] for a large number of single-field, slow-roll inflation models.

The change in χ^2 for selected slow-roll models relative to the Starobinsky R^2 inflationary model, used as a reference, is given in Table 23.1 (taken from [38]). All the other inflation models require a substantial amplitude of tensor modes, and so have an increased χ^2 with respect to the Starobinsky and other models with a scalar tilt but small tensor modes. Table 23.1 also shows the Bayesian evidence for ($\ln B_{A,ref} > 0$) or against ($\ln B_{A,ref} < 0$) a selection of inflation models using the *Planck* analysis priors [38]. The Starobinsky R^2 inflationary model may be chosen as a reference [38] that provides a good fit to current data. Higgs inflation [58] is indistinguishable using current data, making the model comparison “inconclusive” on the Jeffrey’s scale ($|\ln B_{A,ref}| < 1$). (Recall, though, that this model is disfavored by the measured values of the Higgs and top quark masses [59].) We note that although α -attractor models can provide a good fit to the data, they are disfavored relative to the Starobinsky model due to their larger prior volume. There is now strong evidence ($|\ln B_{A,ref}| > 5$) against large-field models such as chaotic inflation with a quadratic or a quartic potential. Indeed, over 30% of the slow-roll inflation models considered in Ref. [7] are strongly disfavored by the *Planck* data.

The Bayes factors for a wide selection of slow-roll inflationary models are displayed in Fig. 23.4, which is adapted from Fig. 3 in [63], where more complete descriptions of the models and the calculations of the Bayes factors using *Planck* 2015 data [64] are given. Models discussed in this review are highlighted in yellow, and numbered as follows: (1) R^2 inflation (Sec. 23.4.2) and models with similar predictions, such as Higgs inflation (Sec. 23.4.8) and no-scale supergravity inflation (Sec. 23.4.10); chaotic inflation models (2) with a ϕ^2 potential; (3) with a ϕ^4 potential; (4) with a $\phi^{2/3}$ potential, and (5) with a ϕ^p potential marginalising over $p \in [0.2, 6]$ (Sec. 23.4.3); hilltop inflation models (6) with $p = 2$; (7) with $p = 4$ and (8) marginalising over p (Sec. 23.4.4); (9) brane

Table 23.1: Observational evidence for and against selected inflation models: $\Delta\chi^2$ and the Bayes factors are calculated relative to the Starobinsky R^2 inflationary model, which is treated as a reference. Results from *Planck* 2018 analysis [38].

Model	$\Delta\chi^2$	$\ln B_{A,ref}$
R^2 inflation	0	0
Power-law potential $\phi^{2/3}$	+4.0	-4.6
Power-law potential ϕ^2	+21.6	< -10
Power-law potential ϕ^4	+75.3	< -10
Natural inflation	+9.9	-6.6
Hilltop quartic model	-0.3	-1.4

inflation Sec. 23.4.5); (10) natural inflation (Sec. 23.4.6); (11) exponential potential models such as α -attractors (Sec. 23.4.11). As seen in Fig. 23.4 and discussed in the next Section, constraints on reheating are starting to provide additional information about models of inflation.

23.6 Constraints on Reheating

One connection between inflation and particle physics is provided by inflaton decay, whose products are expected to have thermalized subsequently. As seen in Eq. (23.54), the number of e-folds required during inflation depends on details of this reheating process, including the matter density upon reheating, denoted by ρ_{th} , which depends in turn on the inflaton decay rate Γ_ϕ . We see in Fig. 23.1 that, within any specific inflationary model, both n_s and particularly r are sensitive to the value of N_* . In particular, the uncertainty in the experimental measurement of n_s is comparable to the variation in many model predictions for $N_* \in [50, 60]$. This implies that the data start to constrain scenarios for inflaton decay in many models. For example, it is clear from Fig. 23.1 that $N_* = 60$ would be preferred over $N_* = 50$ in a chaotic inflationary model with a quadratic potential.

As a specific example, let us consider α -attractor models that predict small values of r . As seen in Fig. 23.1, within these models the combination of *Planck*, BICEP2/Keck Array and BAO data would require a limited range of n_s , corresponding to a limited range of N_* , as seen by comparing the left and right vertical axes in Fig. 23.5:

$$N_* \gtrsim 52 \quad (68\% \text{ CL}), \quad N_* \gtrsim 44 \quad (95\% \text{ CL}). \quad (23.83)$$

Within any specific model for inflaton decay, these bounds can be translated into constraints on the effective decay coupling. For example, if one postulates a two-body inflaton decay (Eq. (23.21)), the bounds (Eq. (23.83)) can be translated into bounds on $y^2 \equiv 8\pi\Gamma/m$. This is illustrated in Fig. 23.5 [85], where any value of $N_{0.05}$ (the number of e-folds for a scale 0.05 Mpc $^{-1}$, on the left vertical axis), corresponding to the scalar tilt n_s shown on the right vertical axis, when projected onto the diagonal line representing one of the three illustrated choices of α -attractor models, corresponds to a specific value of y (lower horizontal axis) and T_{reh} (upper horizontal axis). For example, for $\alpha = 1$ one has

$$y \gtrsim 10^{-10} \quad (68\% \text{ CL}), \quad y \gtrsim 10^{-17} \quad (95\% \text{ CL}). \quad (23.84)$$

These bounds are not very constraining, but they can be expected to improve significantly in the coming years and thereby provide significant information on the connections between inflation and particle physics.

23.7 Beyond Single-Field Slow-Roll Inflation

There are numerous possible scenarios beyond the simplest single-field models of slow-roll inflation. These include models with features in the potential leading to deviations from slow roll, as well as theories in which non-canonical fields are considered, such as k-inflation [89] or DBI inflation [90], and multiple-field models, such as the curvaton scenario [91]. As well as altering the single-field slow-roll predictions for the primordial curvature power spectrum (Eq. (23.48)) and the tensor-scalar ratio (Eq. (23.49)), they may introduce new quantities that vanish in

single-field slow-roll models, such as isocurvature matter perturbations, corresponding to entropy fluctuations in the photon-to-matter ratio, at first order:

$$S_m = \frac{\delta n_m}{n_m} - \frac{\delta n_\gamma}{n_\gamma} = \frac{\delta \rho_m}{\rho_m} - \frac{3}{4} \frac{\delta \rho_\gamma}{\rho_\gamma}. \quad (23.85)$$

Another possibility is non-Gaussianity in the distribution of the primordial curvature perturbation (see Chap. 29, ‘‘Cosmic Microwave Background’’ review), encoded in higher-order correlators such as the primordial bispectrum [92]

$$\langle \zeta(\mathbf{k})\zeta(\mathbf{k}')\zeta(\mathbf{k}'') \rangle \equiv (2\pi)^3 \delta(\mathbf{k} + \mathbf{k}' + \mathbf{k}'') B_\zeta(k, k', k''), \quad (23.86)$$

which is often expressed in terms of a dimensionless non-linearity parameter

$$f_{NL} \propto B_\zeta(k, k', k'')/P_\zeta(k)P_\zeta(k').$$

The three-point function (Eq. (23.86)) can be thought of as defined on a triangle whose sides are $\mathbf{k}, \mathbf{k}', \mathbf{k}''$, of which only two are independent, since they sum to zero. Further assuming statistical isotropy ensures that the bispectrum depends only on the magnitudes of the three vectors, k, k' and k'' . The search for f_{NL} and other non-Gaussian effects was a prime objective of the *Planck* data analysis [93, 94].

23.7.1 Enhanced perturbations on small scales

Although the observed primordial power spectrum on CMB scales is constrained to be almost scale invariant, consistent with the simplest slow-roll inflation models, the form of the power spectrum is largely unconstrained on much smaller scales, corresponding to scales that would have left the horizon closer to the end of inflation. Although free-streaming and other damping of perturbations in the primordial plasma are expected to have washed out small-scale fluctuations in the matter sector [95], gravitational relics such as primordial black holes [96, 97] or induced gravitational waves [98–101] produced by sufficiently large primordial density perturbations could have survived and might be detectable in the present day. Rapid growth of the power spectrum on small scales requires violation of slow roll in single-field models [102]. This could arise from features in the scalar field potential, such as an inflection point [103], leading to a transient phase of ultra-slow-roll evolution [104, 105] which can give a k^4 -rise in the scalar power spectrum on small scales [106, 107].

The LIGO-Virgo-KAGRA collaboration has placed an upper limit on such a stochastic gravitational wave background (SGWB), conventionally expressed in terms of the effective density of gravitational waves per logarithmic frequency interval, of $\Omega_{GW} \leq 5.8 \times 10^{-9}$ for a scale-invariant spectrum in the frequency range 20 – 77 Hz [108]. On the other hand, pulsar timing arrays have found growing evidence for a low-frequency SGWB at nano-Hertz frequencies [109–112]. While this could be associated with an astrophysical background due to supermassive black hole binary systems, the NANOGrav collaboration report that a cosmological background provides a better fit to their 15-year dataset [113]. This could be generated by large primordial density fluctuations on the corresponding comoving scales, $k \sim 10^6$ Mpc $^{-1}$, but these are constrained by the production of primordial black holes of approximately solar mass [114] and possible one-loop or higher-order corrections to the primordial power spectrum on CMB scales.

23.7.2 Effective Field Theory of Inflation

Since slow-roll inflation is a phase of accelerated expansion with an almost constant Hubble parameter, one may think of inflation in terms of an effective theory where the de Sitter spacetime symmetry is spontaneously broken down to RW symmetry by the time-evolution of the Hubble rate, $\dot{H} \neq 0$. There is then a Goldstone boson, π , associated with the spontaneous breaking of time-translation invariance, which can be used to study model-independent properties of inflation. The Goldstone boson describes a spacetime-dependent shift of the time coordinate, corresponding to an adiabatic perturbation of the matter fields:

$$\delta\phi_i(t, \vec{x}) = \phi_i(t + \pi(t, \vec{x})) - \phi_i(t). \quad (23.87)$$

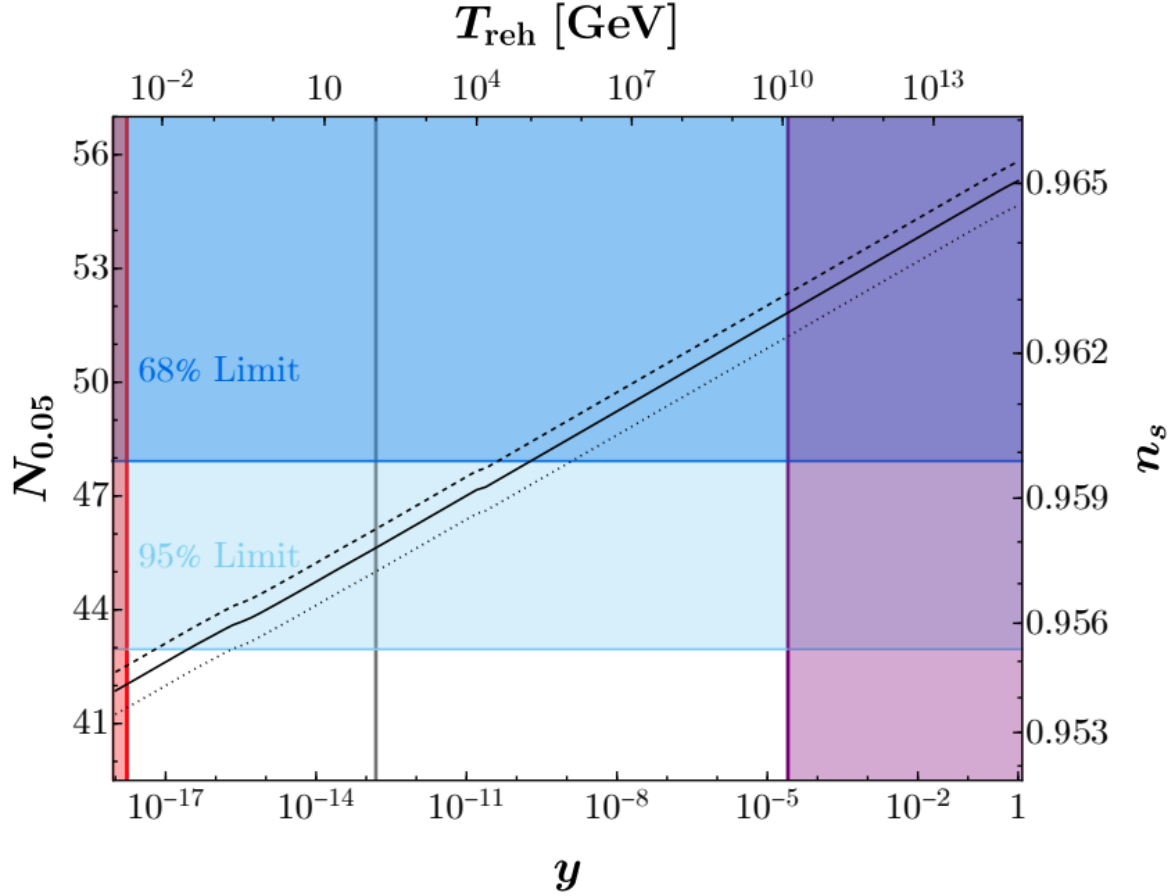


Figure 23.5: Illustration of the impact of the BICEP/Keck [43] and other constraints on the inflaton decay coupling, y , and the number of e-folds at a scale 0.05 Mpc^{-1} , $N_{0.05}$, in α -attractor models of inflation. The horizontal blue lines are 68% and 95% C.L. lower limits on n_s . The left and right axes show the relation between $N_{0.05}$ and n_s and the top and bottom axes show the relation between the inflaton coupling, y , and the reheating temperature, T_{reh} . The diagonal dashed, solid and dotted black lines illustrate the correlations between these quantities for α -attractor models with $\alpha = 0.1, 1, \text{ and } 5$. We also include the lower limit on y from Big Bang Nucleosynthesis (red line), the constraint that T_{reh} be no smaller than the electroweak scale (gray line), and a constraint from gravitino production (purple line) for $\alpha = 1$, which strengthens for smaller α . Plot taken from Ref. [85].

Thus adiabatic field fluctuations can be absorbed into the spatial metric perturbation, \mathcal{R} in Eq. (23.28) at first order, in the comoving gauge:

$$\mathcal{R} = -H\pi, \quad (23.88)$$

where we define π on spatially-flat hypersurfaces. In terms of inflaton field fluctuations, we can identify $\pi \equiv \delta\phi/\dot{\phi}$, but in principle this analysis is not restricted to inflation driven by scalar fields.

The low-energy effective action for π can be obtained by writing down the most general Lorentz-invariant action and expanding in terms of π . The second-order effective action for the free-field wave modes, π_k , to leading order in slow roll is then

$$S_\pi^{(2)} = - \int d^4x \sqrt{-g} \frac{M_P^2 \dot{H}}{c_s^2} \left[\dot{\pi}_k^2 - \frac{c_s^2}{R^2} (\nabla\pi)^2 \right], \quad (23.89)$$

where ϵ_H is the Hubble slow-roll parameter (Eq. (23.11)). We identify c_s^2 with an effective sound speed, generalising canonical slow-roll inflation, which is recovered in the limit $c_s^2 \rightarrow 1$.

The scalar power spectrum on super-Hubble scales (Eq. (23.48)) is enhanced for a reduced sound speed, leading to a reduced tensor-scalar ratio (Eq. (23.49))

$$\mathcal{P}_\zeta(k) \simeq \frac{4\pi}{M_P^2} \frac{1}{c_s^2 \epsilon} \left(\frac{H}{2\pi} \right)_*^2, \quad r \simeq 16(c_s^2 \epsilon)_*. \quad (23.90)$$

At third perturbative order and to lowest order in derivatives, one

obtains [115]

$$S_\pi^{(3)} = \int d^4x \sqrt{-g} \frac{M_P^2 (1 - c_s^2) \dot{H}}{c_s^2} \left[\frac{\dot{\pi} (\nabla\pi)^2}{R^2} - \left(1 + \frac{2}{3} \tilde{c}_3 \right) \dot{\pi}^3 \right]. \quad (23.91)$$

Note that this expression vanishes for canonical fields with $c_s^2 = 1$. For $c_s^2 \neq 1$ the cubic action is determined by the sound speed and an additional parameter \tilde{c}_3 . Both terms in the cubic action give rise to primordial bispectra that are well approximated by equilateral bispectra. However, the shapes are not identical, so one can find a linear combination for which the equilateral bispectra of each term cancel, giving rise to a distinctive orthogonal-type bispectrum [115].

Analysis based on *Planck* 2018 temperature and polarization data has placed bounds on several bispectrum shapes including equilateral and orthogonal shapes [94]:

$$f_{NL}^{equil} = -26 \pm 47, \quad f_{NL}^{orthog} = -38 \pm 24 \quad (68\% \text{ CL}). \quad (23.92)$$

For the simplest case of a constant sound speed, and marginalising over \tilde{c}_3 , this provides a bound on the inflaton sound speed [94]

$$c_s \geq 0.021 \quad (95\% \text{ CL}). \quad (23.93)$$

For a specific model such as DBI inflation [90], corresponding to $\tilde{c}_3 = 3(1 - c_s^2)/2$, one obtains a tighter bound [94]:

$$c_s^{DBI} \geq 0.086 \quad (95\% \text{ CL}). \quad (23.94)$$

The *Planck* team have analysed a wide range of non-Gaussian templates from different inflation models, including tests for deviations from an initial Bunch-Davies vacuum state, direction-dependent non-Gaussianity, and feature models with oscillatory bispectra [94]. No individual feature or resonance is above the three- σ significance level after accounting for the look-elsewhere effect. These results are consistent with the simplest canonical, slow-roll inflation models, but do not rule out most alternative models; rather, bounds on primordial non-Gaussianity place important constraints on the parameter space for non-canonical models.

23.7.3 Multi-Field Fluctuations

There is a very large literature on two- and multi-field models of inflation, most of which lies beyond the scope of this review [116, 117]. However, two important general topics merit being mentioned here, namely residual isocurvature perturbations and the possibility of non-Gaussian effects in the primordial perturbations.

One might expect that other scalar fields besides the inflaton might have non-negligible values that evolve and fluctuate in parallel with the inflaton, without necessarily making the dominant contribution to the energy density during the inflationary epoch. However, the energy density in such a field might persist beyond the end of inflation before decaying, at which point it might come to dominate (or at least make a non-negligible contribution to) the total energy density. In such a case, its perturbations could end up generating the density perturbations detected in the CMB. This could occur due to a late-decaying scalar field [91] or a field fluctuation that modulates the end of inflation [118] or the inflaton decay [119].

23.7.3.1 Isocurvature Perturbations

Primordial perturbations arising in single-field slow-roll inflation are necessarily adiabatic, i.e., they affect the overall density without changing the ratios of different contributions, such as the photon-matter ratio, $\delta(n_\gamma/n_m)/(n_\gamma/n_m)$. This is because inflaton perturbations represent a local shift of the time, as described in section Sec. 23.7.2:

$$\pi = \frac{\delta n_\gamma}{\dot{n}_\gamma} = \frac{\delta n_m}{\dot{n}_m}. \quad (23.95)$$

However, any light scalar field (i.e., one with effective mass less than the Hubble scale) acquires a spectrum of nearly scale-invariant perturbations during inflation. Fluctuations orthogonal to the inflaton in field space are decoupled from the inflaton at Hubble-exit, but can affect the subsequent evolution of the density perturbation. In particular, they can give rise to local variations in the equation of state (non-adiabatic pressure perturbations) that can alter the primordial curvature perturbation ζ on super-Hubble scales. Since these fluctuations are statistically independent of the inflaton perturbations at leading order in slow roll [117], non-adiabatic field fluctuations can only increase the scalar power spectrum with respect to adiabatic perturbations at Hubble exit, while leaving the tensor modes unaffected at first perturbative order. Thus, the single-field result for the tensor-scalar ratio (Eq. (23.49)) becomes an inequality [120]

$$r \leq 16\epsilon_*. \quad (23.96)$$

Hence, an observational upper bound on the tensor-scalar ratio does not bound the slow-roll parameter ϵ in multi-field models.

If all the scalar fields present during inflation eventually decay completely into fully thermalized radiation, these field fluctuations are converted fully into adiabatic perturbations in the primordial plasma [121]. On the other hand, non-adiabatic field fluctuations can also leave behind primordial isocurvature perturbations (Eq. (23.85)) after inflation. In multi-field inflation models it is thus possible for non-adiabatic field fluctuations to generate both curvature and isocurvature perturbations leading to correlated primordial perturbations [122].

The amplitudes of any primordial isocurvature perturbations (Eq. (23.85)) are strongly constrained by the current CMB data,

especially on large angular scales. Using temperature and low- ℓ polarization data yields the following bound on the amplitude of cold dark matter isocurvature perturbations at scale $k = 0.002h^{-1}\text{Mpc}^{-1}$ (marginalising over the correlation angle and in the absence of primordial tensor perturbations) [38]:

$$\frac{\mathcal{P}_{S_m}}{\mathcal{P}_\zeta + \mathcal{P}_{S_m}} < 0.025 \text{ (95\% CL)}. \quad (23.97)$$

For fully (anti-)correlated isocurvature perturbations, corresponding to a single isocurvature field providing a source for both the curvature and residual isocurvature perturbations, the bounds become significantly tighter [38]:

$$\frac{\mathcal{P}_{S_m}}{\mathcal{P}_\zeta + \mathcal{P}_{S_m}} < 0.0002 \text{ (95\% CL), correlated}, \quad (23.98)$$

$$\frac{\mathcal{P}_{S_m}}{\mathcal{P}_\zeta + \mathcal{P}_{S_m}} < 0.003 \text{ (95\% CL), anti-correlated} \quad (23.99)$$

23.7.3.2 Local-Type Non-Gaussianity

Since non-adiabatic field fluctuations in multi-field inflation may lead to the evolution of the primordial curvature perturbation at all orders, it becomes possible to generate significant non-Gaussianity in the primordial curvature perturbation. Non-linear evolution on super-Hubble scales leads to local-type non-Gaussianity, where the local integrated expansion is a non-linear function of the local field values during inflation, $N(\phi_i)$. While the field fluctuations at Hubble exit, $\delta\phi_{i*}$, are Gaussian in the slow-roll limit, the curvature perturbation, $\zeta = \delta N$, becomes a non-Gaussian distribution [123]:

$$\zeta = \sum_i \frac{\partial N}{\partial \phi_i} \delta\phi_i + \frac{1}{2} \sum_{i,j} \frac{\partial^2 N}{\partial \phi_i \partial \phi_j} \delta\phi_i \delta\phi_j + \dots \quad (23.100)$$

with non-vanishing bispectrum in the squeezed limit ($k_1 \approx k_2 \gg k_3$):

$$B_\zeta(k_1, k_2, k_3) \approx \frac{12}{5} f_{NL}^{local} \frac{\mathcal{P}_\zeta(k_1)}{4\pi k_1^3} \frac{\mathcal{P}_\zeta(k_3)}{4\pi k_3^3}, \quad (23.101)$$

where

$$\frac{6}{5} f_{NL}^{local} = \frac{\sum_{i,j} \frac{\partial^2 N}{\partial \phi_i \partial \phi_j}}{\left(\sum_i \frac{\partial N}{\partial \phi_i}\right)^2}. \quad (23.102)$$

Both equilateral and orthogonal bispectra, discussed above in the context of generalised single field inflation, vanish in the squeezed limit, enabling the three types of non-Gaussianity to be distinguished by observations, in principle.

Non-Gaussianity during multi-field inflation is highly model dependent, though f_{NL}^{local} can often be smaller than unity in multi-field slow-roll inflation [124]. Scenarios where a second light field plays a role during or after inflation can make distinctive predictions for f_{NL}^{local} , such as $f_{NL}^{local} = -5/4$ in some curvaton scenarios [123, 125] or $f_{NL}^{local} = 5$ in simple modulated reheating scenarios [119, 126]. By contrast the constancy of ζ on super-Hubble scales in single-field slow-roll inflation leads to a very small non-Gaussianity [127, 128], and in the squeezed limit we have the simple result $f_{NL}^{local} = 5(1 - n_S)/12$ [129, 130].

A combined analysis of the *Planck* 2018 temperature and polarization data [94] yields the following range for f_{NL}^{local} defined in (Eq. (23.102)):

$$f_{NL}^{local} = -1 \pm 5 \text{ (68\% CL)}. \quad (23.103)$$

This sensitivity is sufficient to rule out parameter regimes giving rise to relatively large non-Gaussianity, but insufficient to probe $f_{NL}^{local} = \mathcal{O}(\epsilon)$, as expected in single-field models, or the range $f_{NL}^{local} = \mathcal{O}(1)$ found in the simplest two-field models.

Local-type primordial non-Gaussianity can also give rise to a striking scale-dependent bias in the distribution of collapsed dark matter halos and thus the galaxy distribution [131, 132]. Bounds from high-redshift galaxy surveys are not currently competitive

with the best CMB constraints. An analysis based on the clustering of quasars in the final data release (DR16) of the extended Baryon acoustic Oscillation Spectroscopic Survey (eBOSS) [133] yields

$$f_{NL}^{local} = -12 \pm 21 \quad (68\% \text{ CL}). \quad (23.104)$$

A recent analysis based on the clustering of luminous red galaxies in imaging surveys from the Dark Energy Spectroscopic Instrument (DESI) [134] finds $f_{NL}^{local} = 47_{-11}^{+14}$, suggesting that $f_{NL}^{local} > 0$ at more than 99.9% confidence, although the possibility that this could be due to unforeseen systematics cannot yet be excluded.

23.8 Initial Conditions and Fine-tuning

This review is based on the assumption that the inflationary paradigm is valid. However, it remains the object of many criticisms (see, e.g., [135]), many of them related to the perceived unnaturalness of the required initial conditions.

Most work on inflation is done in the context of RW cosmology, which assumes a high degree of symmetry, or small inhomogeneous perturbations (usually first order) about an RW cosmology. The isotropic RW space-time is an attractor for many homogeneous but anisotropic cosmologies in the presence of a false vacuum energy density [136], or a scalar field with suitable self-interaction potential energy [137, 138]. However it is much harder to establish the range of highly inhomogeneous initial conditions that yield a successful RW Universe, with only limited studies initially (see, e.g., [139, 140]). A related open question is the general nature of the pre-inflationary state of the inflaton and other fields that could have provided initial conditions suitable for inflation [135]. They would need to have satisfied non-trivial homogeneity and isotropy conditions, and one may ask how these could have arisen, whether these are plausible, and whether there may be some observable signature of the pre-inflationary state. These and other criticisms of inflation were addressed in [141], which presented studies of the sensitivity of inflation to the initial conditions. Complementing the studies reported in [141], there have been numerical relativity investigations of highly inhomogeneous initial conditions [142–144]. The general conclusion is that inflation is rather robust with respect to inhomogeneities in the initial conditions in both the scalar field profile and the extrinsic curvature, including large tensor perturbations.

To quantify the fine-tuning of initial conditions requires a measure in the space of possible cosmologies [145], however it has been argued that some of the measures historically used to frame this problem are formally invalid [146]. It is sometimes also objected that inflationary models predict the existence of a multiverse, and potentially a loss of predictive power [147], if it undergoes the process termed eternal inflation [148–150]. However, whether this is actually a bug or a feature remains a topic of debate [151, 152]. The existence of the multiverse is a purely philosophical problem, unless it has observable consequences, e.g., in the CMB.

One might expect signatures of any pre-inflationary state to appear at large angular scales, i.e., low multipoles ℓ . Indeed, various anomalies have been noted in the large-scale CMB anisotropies, as also discussed in Chap. 29, the “Cosmic Microwave Background” review, including a possible suppression of the quadrupole and other very large-scale anisotropies, an apparent feature in the range $\ell \approx 20$ to 30, and a possible hemispheric asymmetry. However, none of these are highly significant statistically, in view of the limitations due to cosmic variance [64]. They cannot yet be regarded as signatures of initial conditions, the multiverse or some pre-inflationary dynamics, such as might emerge from string theory.

A different kind of initial condition problem, called the trans-Planckian problem [153], is that the perturbations now seen in the CMB would have had wavelengths shorter than the Planck length at the onset of inflation. However, under quite general and conservative assumptions the usual inflationary predictions would be quite robust [154], with the possibility of $\mathcal{O}((H/m_P)^n)$ corrections that might have interesting signatures in the CMB [155].

When inflation was first proposed [1] [2] there was no evidence for the existence of scalar fields or the accelerated expansion of the Universe. The situation has changed dramatically in recent

years with the observational evidence that the cosmic expansion is currently accelerating and with the discovery of a scalar particle, namely the Higgs boson (see Chap. 11, “Status of Higgs boson physics” review). Combined with the lack of any widely accepted alternative model for the origin of cosmic structure, these discoveries have lent support to the idea of a primordial accelerated expansion driven by a scalar field, i.e., cosmological inflation. In parallel, successive CMB experiments have been consistent with generic predictions of inflationary models, although without yet providing irrefutable evidence. It was concluded in [141] that the inflationary paradigm is not currently in trouble. However, we note that inflation via a formally elementary scalar inflaton should probably only be regarded as an effective field theory valid at energy densities hierarchically smaller than the Planck scale. It should eventually be embedded in a suitable ultraviolet completion, on which inflationary dynamics may be our clearest window.

23.9 Future Probes of Inflation

Prospective future CMB experiments, both ground- and space-based are reviewed in the separate PDG “Cosmic Microwave Background” review, Chap. 29. The main emphasis in CMB experiments in the coming years will be on ground-based experiments providing improved measurements of B -mode polarization and greater sensitivity to the tensor-to-scalar ratio r , and more precise measurements at higher ℓ that will constrain n_s better. As is apparent from Fig. 23.1 and the discussion of models such as R^2 inflation, there is a strong incentive to reach a 5- σ sensitivity to $r \sim 3$ to 4×10^{-3} . This could be achieved with a moderately-sized space mission with large sky coverage [156], improvements in de-lensing and foreground measurements. The discussion in Sec. 23.3 (see also Fig. 23.5), also brought out the importance of reducing the uncertainty in n_s , as a way to constrain post-inflationary reheating and the connection to particle physics. CMB temperature anisotropies probe primordial density perturbations down to comoving scales of order 50 Mpc, beyond which scale secondary sources of anisotropy dominate. CMB spectral distortions could potentially constrain the amplitude and shape of primordial density perturbations on comoving scales from Mpc to kpc due to distortions caused by the Silk damping of pressure waves in the radiation dominated era, before the last scattering of the CMB photons but after the plasma can be fully thermalised [95].

Improved sensitivity to non-Gaussianities is also a priority. In addition to CMB measurements, future large-scale structure surveys will also have roles to play as probes into models of inflation, for which there are excellent prospects. Current surveys such as DESI may reach $\Delta f_{NL} \sim 4$ [157] comparable with the *Planck* sensitivity. In the future, radio surveys such as SKA will measure large-scale structure out to redshift $z \sim 3$ [158], initially through mapping the intensity of the neutral hydrogen 21-cm line, and eventually through radio galaxy surveys which will probe local-type non-Gaussianity to $f_{NL} \sim 1$.

Galaxy clustering using DESI and *Euclid* satellite data could also constrain the running of the scalar tilt to a precision of $\Delta\alpha_s \approx 0.0028$, a factor of 2 improvement on *Planck* constraints, or a precision of 0.0016 using LSST data [157].

As an example of a proposed future satellite mission, *SPHEREx* [159] will use measurements of the galaxy power spectrum to target a measurement of the running of the scalar spectral index with a sensitivity $\Delta\alpha_s \sim 10^{-3}$ and local-type primordial non-Gaussianity, $\Delta f_{NL} \sim 1$. Including information from the galaxy bispectrum one might reduce the measurement error on non-Gaussianity to $\Delta f_{NL} \sim 0.2$, making it possible to distinguish between single-field slow-roll models and alternatives such as the curvaton scenario for the origin of structure, which generate $f_{NL} \sim 1$.

Finally we note that future gravitational wave experiments such as the Laser Interferometer Space Antenna (LISA) will be sensitive to a stochastic gravitational wave background, including tensor perturbations produced during inflation or induced by large primordial density perturbations on small scales after inflation [160], which could provide constraints on inflationary perturbations on smaller scales.

Acknowledgements

The authors are grateful to Vincent Vennin for preparing

Fig. 23.4 for this review. The work of J.E. was supported in part by the UK STFC research grant ST/T000759/1. The work of D.W. was supported in part by the UK STFC research grant ST/W001225/1.

References

- [1] A. A. Starobinsky, Phys. Lett. **B91**, 99 (1980), [Adv. Ser. Astrophys. Cosmol.3,130(1987)].
- [2] A. H. Guth, Phys. Rev. **D23**, 347 (1981), [Adv. Ser. Astrophys. Cosmol.3,139(1987)].
- [3] K. A. Olive, Phys. Rept. **190**, 307 (1990).
- [4] D. H. Lyth and A. Riotto, Phys. Rept. **314**, 1 (1999), [hep-ph/9807278].
- [5] A.R. Liddle and D.H. Lyth, *Cosmological inflation and large-scale structure* (Cambridge University Press, 2000).
- [6] D. Baumann, in “Physics of the large and the small, TASI 09, proceedings of the Theoretical Advanced Study Institute in Elementary Particle Physics, Boulder, Colorado, USA, 1-26 June 2009,” 523–686 (2011), [arXiv:0907.5424].
- [7] J. Martin, C. Ringeval and V. Vennin, Phys. Dark Univ. **5-6**, 75 (2014), [arXiv:1303.3787]; J. Martin *et al.*, JCAP **1403**, 039 (2014), [arXiv:1312.3529]; J. Martin, Astrophys. Space Sci. Proc. **45**, 41 (2016), [arXiv:1502.05733].
- [8] P. A. R. Ade *et al.* (Planck), Astron. Astrophys. **594**, A13 (2016), [arXiv:1502.01589].
- [9] A. H. Guth and E. J. Weinberg, Nucl. Phys. **B212**, 321 (1983).
- [10] D. La and P. J. Steinhardt, Phys. Rev. Lett. **62**, 376 (1989), [Erratum: Phys. Rev. Lett.62,1066(1989)].
- [11] A. D. Linde, Phys. Lett. **B249**, 18 (1990).
- [12] F. C. Adams and K. Freese, Phys. Rev. **D43**, 353 (1991), [hep-ph/0504135].
- [13] A. D. Linde, Phys. Lett. **108B**, 389 (1982), [Adv. Ser. Astrophys. Cosmol.3,149(1987)].
- [14] A. Albrecht and P. J. Steinhardt, Phys. Rev. Lett. **48**, 1220 (1982), [Adv. Ser. Astrophys. Cosmol.3,158(1987)].
- [15] W. H. Press, Phys. Scripta **21**, 702 (1980); S. W. Hawking, Phys. Lett. **115B**, 295 (1982); A. A. Starobinsky, Phys. Lett. **117B**, 175 (1982); A. H. Guth and S. Y. Pi, Phys. Rev. Lett. **49**, 1110 (1982).
- [16] J. M. Bardeen, P. J. Steinhardt and M. S. Turner, Phys. Rev. **D28**, 679 (1983).
- [17] V. F. Mukhanov and G. V. Chibisov, JETP Lett. **33**, 532 (1981), [Pisma Zh. Eksp. Teor. Fiz.33,549(1981)].
- [18] K. S. Stelle, Gen. Rel. Grav. **9**, 353 (1978).
- [19] B. Whitt, Phys. Lett. **145B**, 176 (1984).
- [20] D. Wands, Class. Quant. Grav. **11**, 269 (1994), [arXiv:gr-qc/9307034].
- [21] S. R. Coleman and F. De Luccia, Phys. Rev. **D21**, 3305 (1980).
- [22] M. Sasaki *et al.*, Phys. Lett. **B317**, 510 (1993).
- [23] M. Bucher, A. S. Goldhaber and N. Turok, Phys. Rev. **D52**, 3314 (1995), [hep-ph/9411206].
- [24] A. D. Linde and A. Mezhlumian, Phys. Rev. **D52**, 6789 (1995), [arXiv:astro-ph/9506017].
- [25] A. R. Liddle, P. Parsons and J. D. Barrow, Phys. Rev. **D50**, 7222 (1994), [arXiv:astro-ph/9408015].
- [26] L. Kofman, A. D. Linde and A. A. Starobinsky, Phys. Rev. **D56**, 3258 (1997), [hep-ph/9704452].
- [27] B. A. Bassett, S. Tsujikawa and D. Wands, Rev. Mod. Phys. **78**, 537 (2006), [arXiv:astro-ph/0507632].
- [28] A. D. Linde, Phys. Rev. **D49**, 748 (1994), [arXiv:astro-ph/9307002].
- [29] A. D. Dolgov and A. D. Linde, Phys. Lett. **116B**, 329 (1982).
- [30] J. R. Ellis *et al.*, Nucl. Phys. **B238**, 453 (1984), [,223(1983)].
- [31] M. Kawasaki and T. Moroi, Prog. Theor. Phys. **93**, 879 (1995), [hep-ph/9403364].
- [32] J. H. Traschen and R. H. Brandenberger, Phys. Rev. **D42**, 2491 (1990).
- [33] G. V. Chibisov and V. F. Mukhanov, Mon. Not. Roy. Astron. Soc. **200**, 535 (1982).
- [34] H. Kodama and M. Sasaki, Prog. Theor. Phys. Suppl. **78**, 1 (1984).
- [35] V.F. Mukhanov, H.A. Feldman and R.H. Brandenberger, Phys. Rept. **215**, 203 (1992).
- [36] K. A. Malik and D. Wands, Phys. Rept. **475**, 1 (2009), [arXiv:0809.4944].
- [37] V. F. Mukhanov, Sov. Phys. JETP **67**, 1297 (1988), [Zh. Eksp. Teor. Fiz.94N7,1(1988)].
- [38] Y. Akrami *et al.* (Planck), Astron. Astrophys. **641**, A10 (2020), [arXiv:1807.06211].
- [39] A. A. Starobinsky, JETP Lett. **30**, 682 (1979), [,767(1979)].
- [40] E. D. Stewart and D. H. Lyth, Phys. Lett. **B302**, 171 (1993), [arXiv:gr-qc/9302019].
- [41] D. Wands *et al.*, Phys. Rev. **D62**, 043527 (2000), [arXiv:astro-ph/0003278].
- [42] A. R. Liddle and S. M. Leach, Phys. Rev. **D68**, 103503 (2003), [arXiv:astro-ph/0305263].
- [43] P. A. R. Ade *et al.* (BICEP/Keck), Phys. Rev. Lett. **127**, 15, 151301 (2021), [arXiv:2110.00483].
- [44] S.M. Leach, A.R. Liddle, J. Martin, and D.J. Schwarz, Phys. Rev. **D66**, 23515 (2002).
- [45] D. Kazanas, Astrophys. J. **241**, L59 (1980).
- [46] K. Sato, Mon. Not. Roy. Astron. Soc. **195**, 467 (1981).
- [47] A. Billoire and K. Tamvakis, Nucl. Phys. **B200**, 329 (1982); J. D. Breit, S. Gupta and A. Zaks, Phys. Rev. Lett. **51**, 1007 (1983).
- [48] A. D. Linde, Phys. Lett. **129B**, 177 (1983).
- [49] D. V. Nanopoulos, K. A. Olive and M. Srednicki, Phys. Lett. **127B**, 30 (1983).
- [50] J. Ellis, D. V. Nanopoulos and K. A. Olive, Phys. Rev. Lett. **111**, 111301 (2013), [Erratum: Phys. Rev. Lett.111,no.12,129902(2013)], [arXiv:1305.1247].
- [51] T. S. Koivisto and F. R. Urban, JCAP **1503**, 03, 003 (2015), [arXiv:1407.3445].
- [52] L. Boubekeur and D. H. Lyth, JCAP **0507**, 010 (2005), [hep-ph/0502047].
- [53] G. R. Dvali, Q. Shafi and S. Solganik, in “4th European Meeting From the Planck Scale to the Electroweak Scale (Planck 2001) La Londe les Maures, Toulon, France, May 11-16, 2001,” (2001), [hep-th/0105203]; J. Garcia-Bellido, R. Rabadan and F. Zamora, JHEP **01**, 036 (2002), [hep-th/0112147]; S. Kachru *et al.*, JCAP **0310**, 013 (2003), [hep-th/0308055].
- [54] F. C. Adams *et al.*, Phys. Rev. **D47**, 426 (1993), [hep-ph/9207245].
- [55] E. Pajer and M. Peloso, Class. Quant. Grav. **30**, 214002 (2013), [arXiv:1305.3557].
- [56] E. Silverstein and A. Westphal, Phys. Rev. **D78**, 106003 (2008), [arXiv:0803.3085].
- [57] L. McAllister, E. Silverstein and A. Westphal, Phys. Rev. **D82**, 046003 (2010), [arXiv:0808.0706].
- [58] F. L. Bezrukov and M. Shaposhnikov, Phys. Lett. **B659**, 703 (2008), [arXiv:0710.3755].
- [59] D. Buttazzo *et al.*, JHEP **12**, 089 (2013), [arXiv:1307.3536].
- [60] H. P. Nilles, Phys. Rept. **110**, 1 (1984); H. E. Haber and G. L. Kane, Phys. Rept. **117**, 75 (1985).
- [61] J.R. Ellis *et al.*, Phys. Lett. **118B**, 335 (1982).

- [62] N. Okada and Q. Shafi (2013), [arXiv:1311.0921].
- [63] J. Martin, C. Ringeval and V. Vennin, *Phys. Rev.* **D93**, 10, 103532 (2016), [arXiv:1603.02606].
- [64] P. A. R. Ade *et al.* (Planck), *Astron. Astrophys.* **594**, A20 (2016), [arXiv:1502.02114].
- [65] H. Murayama *et al.*, *Phys. Rev. Lett.* **70**, 1912 (1993).
- [66] J. Ellis, M. Fairbairn and M. Sueiro, *JCAP* **1402**, 044 (2014), [arXiv:1312.1353].
- [67] D. Croon, J. Ellis and N. E. Mavromatos, *Phys. Lett.* **B724**, 165 (2013), [arXiv:1303.6253].
- [68] G. R. Dvali, Q. Shafi and R. K. Schaefer, *Phys. Rev. Lett.* **73**, 1886 (1994), [hep-ph/9406319].
- [69] D. V. Nanopoulos *et al.*, *Phys. Lett.* **123B**, 41 (1983).
- [70] A. B. Goncharov and A. D. Linde, *Phys. Lett.* **139B**, 27 (1984).
- [71] E. Cremmer *et al.*, *Nucl. Phys.* **B212**, 413 (1983), [413(1982)].
- [72] R. Holman, P. Ramond and G. G. Ross, *Phys. Lett.* **137B**, 343 (1984).
- [73] E. J. Copeland *et al.*, *Phys. Rev.* **D49**, 6410 (1994), [arXiv:astro-ph/9401011]; E. D. Stewart, *Phys. Rev.* **D51**, 6847 (1995), [hep-ph/9405389].
- [74] G. D. Coughlan *et al.*, *Phys. Lett.* **131B**, 59 (1983); A. S. Goncharov, A. D. Linde and M. I. Vysotsky, *Phys. Lett.* **147B**, 279 (1984); T. Banks, D. B. Kaplan and A. E. Nelson, *Phys. Rev.* **D49**, 779 (1994), [hep-ph/9308292]; B. de Carlos *et al.*, *Phys. Lett.* **B318**, 447 (1993), [hep-ph/9308325]; M. Kawasaki, T. Moroi and T. Yanagida, *Phys. Lett.* **B370**, 52 (1996), [hep-ph/9509399].
- [75] J. R. Ellis, D. V. Nanopoulos and M. Quiros, *Phys. Lett.* **B174**, 176 (1986).
- [76] T. Moroi, M. Yamaguchi and T. Yanagida, *Phys. Lett.* **B342**, 105 (1995), [hep-ph/9409367].
- [77] M. Kawasaki, M. Yamaguchi and T. Yanagida, *Phys. Rev. Lett.* **85**, 3572 (2000), [hep-ph/0004243]; K. Nakayama, F. Takahashi and T. T. Yanagida, *JCAP* **1308**, 038 (2013), [arXiv:1305.5099].
- [78] E. Cremmer *et al.*, *Phys. Lett.* **133B**, 61 (1983).
- [79] A. S. Goncharov and A. D. Linde, *Class. Quant. Grav.* **1**, L75 (1984); C. Kounnas and M. Quiros, *Phys. Lett.* **151B**, 189 (1985).
- [80] J. R. Ellis, C. Kounnas and D. V. Nanopoulos, *Nucl. Phys.* **B247**, 373 (1984).
- [81] E. Witten, *Phys. Lett.* **155B**, 151 (1985).
- [82] J. Ellis, D. V. Nanopoulos and K. A. Olive, *JCAP* **1310**, 009 (2013), [arXiv:1307.3537].
- [83] J. Ellis *et al.*, *Class. Quant. Grav.* **33**, 9, 094001 (2016), [arXiv:1507.02308].
- [84] R. Kallosh, A. Linde and D. Roest, *JHEP* **11**, 198 (2013), [arXiv:1311.0472].
- [85] J. Ellis *et al.*, *Phys. Rev. D* **105**, 4, 043504 (2022), [arXiv:2112.04466].
- [86] L. Iacconi *et al.* (2023), [arXiv:2306.00918].
- [87] J. Ellis *et al.*, *JCAP* **1507**, 07, 050 (2015), [arXiv:1505.06986].
- [88] A. R. Liddle, *Mon. Not. Roy. Astron. Soc.* **377**, L74 (2007), [arXiv:astro-ph/0701113].
- [89] C. Armendariz-Picon, T. Damour and V. F. Mukhanov, *Phys. Lett.* **B458**, 209 (1999), [hep-th/9904075].
- [90] M. Alishahiha, E. Silverstein and D. Tong, *Phys. Rev.* **D70**, 123505 (2004), [hep-th/0404084].
- [91] K. Enqvist and M. S. Sloth, *Nucl. Phys.* **B626**, 395 (2002), [hep-ph/0109214]; D. H. Lyth and D. Wands, *Phys. Lett.* **B524**, 5 (2002), [hep-ph/0110002]; T. Moroi and T. Takahashi, *Phys. Lett.* **B522**, 215 (2001), [Erratum: *Phys. Lett.* **B539**, 303(2002)], [hep-ph/0110096].
- [92] N. Bartolo *et al.*, *Phys. Rept.* **402**, 103 (2004), [arXiv:astro-ph/0406398].
- [93] P. A. R. Ade *et al.* (Planck), *Astron. Astrophys.* **594**, A17 (2016), [arXiv:1502.01592].
- [94] Y. Akrami *et al.* (Planck), *Astron. Astrophys.* **641**, A9 (2020), [arXiv:1905.05697].
- [95] J. Chluba, J. Hamann and S. P. Patil, *Int. J. Mod. Phys.* **D24**, 10, 1530023 (2015), [arXiv:1505.01834].
- [96] Y. B. Zel'dovich and I. D. Novikov, *Soviet Astron. AJ (Engl. Transl.)*, **10**, 602 (1967).
- [97] S. W. Hawking, *Nature* **248**, 30 (1974).
- [98] S. Matarrese, O. Pantano and D. Saez, *Phys. Rev. Lett.* **72**, 320 (1994), [arXiv:astro-ph/9310036].
- [99] S. Matarrese, S. Mollerach and M. Bruni, *Phys. Rev. D* **58**, 043504 (1998), [arXiv:astro-ph/9707278].
- [100] K. N. Ananda, C. Clarkson and D. Wands, *Phys. Rev. D* **75**, 123518 (2007), [arXiv:gr-qc/0612013].
- [101] D. Baumann *et al.*, *Phys. Rev. D* **76**, 084019 (2007), [hep-th/0703290].
- [102] H. Motohashi and W. Hu, *Phys. Rev. D* **96**, 6, 063503 (2017), [arXiv:1706.06784].
- [103] J. Garcia-Bellido and E. Ruiz Morales, *Phys. Dark Univ.* **18**, 47 (2017), [arXiv:1702.03901].
- [104] S. Inoue and J. Yokoyama, *Phys. Lett. B* **524**, 15 (2002), [hep-ph/0104083].
- [105] W. H. Kinney, *Phys. Rev. D* **72**, 023515 (2005), [arXiv:gr-qc/0503017].
- [106] S. M. Leach *et al.*, *Phys. Rev. D* **64**, 023512 (2001), [arXiv:astro-ph/0101406].
- [107] C. T. Byrnes, P. S. Cole and S. P. Patil, *JCAP* **06**, 028 (2019), [arXiv:1811.11158].
- [108] R. Abbott *et al.* (KAGRA, Virgo, LIGO Scientific), *Phys. Rev. D* **104**, 2, 022004 (2021), [arXiv:2101.12130].
- [109] G. Agazie *et al.* (NANOGrav), *Astrophys. J. Lett.* **951**, 1, L8 (2023), [arXiv:2306.16213].
- [110] J. Antoniadis *et al.* (EPTA) (2023), [arXiv:2306.16214].
- [111] D. J. Reardon *et al.*, *Astrophys. J. Lett.* **951**, 1, L6 (2023), [arXiv:2306.16215].
- [112] H. Xu *et al.*, *Res. Astron. Astrophys.* **23**, 7, 075024 (2023), [arXiv:2306.16216].
- [113] A. Afzal *et al.* (NANOGrav), *Astrophys. J. Lett.* **951**, 1, L11 (2023), [arXiv:2306.16219].
- [114] B. Carr *et al.*, *Rept. Prog. Phys.* **84**, 11, 116902 (2021), [arXiv:2002.12778].
- [115] L. Senatore, K. M. Smith and M. Zaldarriaga, *JCAP* **1001**, 028 (2010), [arXiv:0905.3746].
- [116] C. Gordon *et al.*, *Phys. Rev.* **D63**, 023506 (2001), [arXiv:astro-ph/0009131]; R. Easther *et al.*, *Phys. Rev. Lett.* **112**, 161302 (2014), [arXiv:1312.4035]; J. Ellis *et al.*, *JCAP* **1501**, 010 (2015), [arXiv:1409.8197]; S. Renaux-Petel and K. Turzyski, *JCAP* **1506**, 06, 010 (2015), [arXiv:1405.6195].
- [117] C. T. Byrnes and D. Wands, *Phys. Rev.* **D74**, 043529 (2006), [arXiv:astro-ph/0605679].
- [118] D. H. Lyth, *JCAP* **0511**, 006 (2005), [arXiv:astro-ph/0510443].
- [119] G. Dvali, A. Gruzinov and M. Zaldarriaga, *Phys. Rev.* **D69**, 023505 (2004), [arXiv:astro-ph/0303591].
- [120] D. Wands *et al.*, *Phys. Rev.* **D66**, 043520 (2002), [arXiv:astro-ph/0205253].
- [121] S. Weinberg, *Phys. Rev.* **D67**, 123504 (2003), [arXiv:astro-ph/0302326].
- [122] D. Langlois, *Phys. Rev.* **D59**, 123512 (1999), [arXiv:astro-ph/9906080].

- [123] D. H. Lyth and Y. Rodriguez, *Phys. Rev. Lett.* **95**, 121302 (2005), [arXiv:astro-ph/0504045].
- [124] F. Vernizzi and D. Wands, *JCAP* **0605**, 019 (2006), [arXiv:astro-ph/0603799].
- [125] M. Sasaki, J. Valiviita and D. Wands, *Phys. Rev.* **D74**, 103003 (2006), [arXiv:astro-ph/0607627].
- [126] G. Dvali, A. Gruzinov and M. Zaldarriaga, *Phys. Rev.* **D69**, 083505 (2004), [arXiv:astro-ph/0305548].
- [127] D. S. Salopek and J. R. Bond, *Phys. Rev.* **D43**, 1005 (1991).
- [128] A. Gangui *et al.*, *Astrophys. J.* **430**, 447 (1994), [arXiv:astro-ph/9312033].
- [129] J. M. Maldacena, *JHEP* **05**, 013 (2003), [arXiv:astro-ph/0210603].
- [130] V. Acquaviva *et al.*, *Nucl. Phys.* **B667**, 119 (2003), [arXiv:astro-ph/0209156].
- [131] N. Dalal *et al.*, *Phys. Rev.* **D77**, 123514 (2008), [arXiv:0710.4560].
- [132] S. Matarrese and L. Verde, *Astrophys. J.* **677**, L77 (2008), [arXiv:0801.4826].
- [133] E.-M. Mueller *et al.* (2021), [arXiv:2106.13725].
- [134] M. Rezaie *et al.* (2023), [arXiv:2307.01753].
- [135] A. Ijjas, P. J. Steinhardt and A. Loeb, *Phys. Lett.* **B723**, 261 (2013), [arXiv:1304.2785].
- [136] R. M. Wald, *Phys. Rev.* **D28**, 2118 (1983).
- [137] M. Heusler, *Phys. Lett.* **B253**, 33 (1991).
- [138] Y. Kitada and K.-i. Maeda, *Phys. Rev.* **D45**, 1416 (1992).
- [139] D. S. Goldwirth and T. Piran, *Phys. Rept.* **214**, 223 (1992).
- [140] T. Vachaspati and M. Trodden, *Phys. Rev.* **D61**, 023502 (1999), [arXiv:gr-qc/9811037].
- [141] D. Chowdhury *et al.*, *Phys. Rev. D* **100**, 8, 083537 (2019), [arXiv:1902.03951].
- [142] W. E. East *et al.*, *JCAP* **1609**, 09, 010 (2016), [arXiv:1511.05143].
- [143] K. Clough *et al.*, *JCAP* **1709**, 09, 025 (2017), [arXiv:1608.04408].
- [144] K. Clough, R. Flauger and E. A. Lim, *JCAP* **1805**, 05, 065 (2018), [arXiv:1712.07352].
- [145] G. W. Gibbons, S. W. Hawking and J. M. Stewart, *Nucl. Phys.* **B281**, 736 (1987).
- [146] J. S. Schiffrin and R. M. Wald, *Phys. Rev.* **D86**, 023521 (2012), [arXiv:1202.1818].
- [147] A. Ijjas, P. J. Steinhardt and A. Loeb, *Phys. Lett.* **B736**, 142 (2014), [arXiv:1402.6980].
- [148] A. Vilenkin, *Phys. Rev.* **D27**, 2848 (1983).
- [149] A. D. Linde, *Phys. Lett.* **B175**, 395 (1986).
- [150] A. S. Goncharov, A. D. Linde and V. F. Mukhanov, *Int. J. Mod. Phys.* **A2**, 561 (1987).
- [151] A. H. Guth, D. I. Kaiser and Y. Nomura, *Phys. Lett.* **B733**, 112 (2014), [arXiv:1312.7619].
- [152] A. Linde, in “Proceedings, 100th Les Houches Summer School: Post-Planck Cosmology: Les Houches, France, July 8 - August 2, 2013,” 231–316 (2015), [arXiv:1402.0526].
- [153] J. Martin and R. H. Brandenberger, *Phys. Rev.* **D63**, 123501 (2001), [hep-th/0005209].
- [154] R. H. Brandenberger and J. Martin, *Mod. Phys. Lett.* **A16**, 999 (2001), [arXiv:astro-ph/0005432].
- [155] J. Martin and R. H. Brandenberger, in “Recent developments in theoretical and experimental general relativity, gravitation and relativistic field theories. Proceedings, 9th Marcel Grossmann Meeting, MG’9, Rome, Italy, July 2-8, 2000. Pts. A-C,” 2001–2002 (2000), [arXiv:astro-ph/0012031].
- [156] A. Kogut *et al.*, *JCAP* **1107**, 025 (2011), [arXiv:1105.2044].
- [157] A. Font-Ribera *et al.*, *JCAP* **1405**, 023 (2014), [arXiv:1308.4164].
- [158] R. Maartens *et al.* (SKA Cosmology SWG), *PoS AASKA14*, 016 (2015), [arXiv:1501.04076].
- [159] O. Doré *et al.* (2014), [arXiv:1412.4872].
- [160] P. Auclair *et al.* (LISA Cosmology Working Group) (2022), [arXiv:2204.05434].

24. Big Bang Nucleosynthesis

Revised August 2023 by B.D. Fields (Astronomy, Illinois U.; Physics, Illinois U.), P. Molaro (INAF-OATS Trieste; IFPU) and S. Sarkar (Rudolf Peierls, Oxford U.).

24.1 Abstract

Big-Bang nucleosynthesis (BBN) offers the deepest reliable probe of the early Universe, being based on well-understood Standard Model physics [1]. Predictions of the abundances of the light elements, D, ^3He , ^4He , and ^7Li , synthesized at the end of the *first three minutes*, are in good overall agreement with the primordial abundances inferred from observational data, thus validating the standard hot Big-Bang cosmology (see [2–5] for reviews). This is particularly impressive given that these abundances span nine orders of magnitude – from $^4\text{He}/\text{H} \sim 0.08$ down to $^7\text{Li}/\text{H} \sim 10^{-10}$ (ratios by number). Thus BBN provides powerful constraints on possible deviations from the standard cosmology, and on new physics beyond the Standard Model [6–9].

24.2 Theory

The synthesis of the light elements is sensitive to physical conditions in the early radiation-dominated era at a temperature $T \sim 1$ MeV, corresponding to an age $t \sim 1$ s. At higher temperatures, weak interactions were in thermal equilibrium, thus fixing the ratio of the neutron and proton number densities to be $n/p = e^{-Q/T}$, where $Q = 1.293$ MeV is the neutron-proton mass difference. As the temperature dropped, the neutron-proton inter-conversion rate per nucleon, $\Gamma_{n \leftrightarrow p} \sim G_F^2 T^5$, fell faster than the Hubble expansion rate, $H \sim \sqrt{g_* G_N} T^2$, where g_* counts the number of relativistic particle species determining the energy density in radiation (see ‘Big Bang Cosmology’ — Sec. 22 of this *Review*). This resulted in departure from chemical equilibrium (freeze-out) at $T_{\text{fr}} \sim (g_* G_N / G_F^4)^{1/6} \simeq 1$ MeV. The neutron fraction at this time, $n/p = e^{-Q/T_{\text{fr}}} \simeq 1/6$, is thus sensitive to every known physical interaction, since Q is determined by both strong and electromagnetic interactions while T_{fr} depends on the weak as well as gravitational interactions. Moreover, the sensitivity to the Hubble expansion rate affords a probe of, *e.g.*, the number of relativistic neutrino species [10]. After freeze-out, the neutrons were free to β -decay, so the neutron fraction dropped to $n/p \simeq 1/7$ by the time nuclear reactions began. A simplified analytic model of freeze-out yields the n/p ratio to an accuracy of $\sim 1\%$ [11, 12].

The rates of these reactions depend on the density of baryons (strictly speaking, nucleons), which is usually expressed normalized to the relic blackbody photon density as $\eta \equiv n_b/n_\gamma$. As we shall see, all the light-element abundances can be explained with $\eta_{10} \equiv \eta \times 10^{10}$ in the range 6.143 ± 0.190 . With n_γ fixed by the present CMB temperature 2.7255 K (see ‘Cosmic Microwave Background’ — Sec. 29 of this *Review*), this can be stated as the allowed range for the baryon mass density today, $\rho_b = (4.2 \pm 0.1) \times 10^{-31}$ g cm $^{-3}$, or as the baryonic fraction of the critical density, $\Omega_b = \rho_b/\rho_{\text{crit}} \simeq \eta_{10} h^{-2}/274 = (0.02244 \pm 0.00069) h^{-2}$, where $h \equiv H_0/100$ km s $^{-1}$ Mpc $^{-1}$ is the present Hubble parameter (see ‘The Cosmological Parameters’ — Sec. 25 of this *Review*).

The nucleosynthesis chain begins with the formation of deuterium in the process $p(n, \gamma)\text{D}$. However, photo-dissociation by the high number density of photons delays production of deuterium (and other complex nuclei) until well after T drops below the binding energy of deuterium, $\Delta_{\text{D}} = 2.23$ MeV. The quantity $\eta^{-1} e^{-\Delta_{\text{D}}/T}$, *i.e.*, the number of photons per baryon above the deuterium photo-dissociation threshold, falls below unity at $T \simeq 0.1$ MeV; nuclei can then begin to form without being immediately photo-dissociated again. Only 2-body reactions, such as $\text{D}(p, \gamma)^3\text{He}$ and $^3\text{He}(\text{D}, p)^4\text{He}$ are important because the density by this time has become rather low – comparable to that of air!

Nearly all neutrons end up bound in the most stable light element ^4He . Heavier nuclei do not form in any significant quantity both because of the absence of stable nuclei with mass number 5 or 8 (which impedes nucleosynthesis via $n^4\text{He}$, $p^4\text{He}$ or $^4\text{He}^4\text{He}$ reactions), and the large Coulomb barriers for reactions such as $^3\text{He}(^4\text{He}, \gamma)^7\text{Li}$ and $^3\text{He}(^4\text{He}, \gamma)^7\text{Be}$. Hence the primordial mass fraction of ^4He , $Y_{\text{p}} \equiv \rho(^4\text{He})/\rho_b$, can be estimated by the simple

counting argument

$$Y_{\text{p}} = \frac{2(n/p)}{1 + n/p} \simeq 0.25 \quad (24.1)$$

where strictly speaking this gives the baryon fraction in ^4He , which is what we will quote throughout. This differs slightly from the mass fraction due to small binding energy corrections.

There is little sensitivity here to the actual nuclear reaction rates for the production of ^4He . Nuclear rates are, however, critically important in determining the other ‘left-over’ abundances: D and ^3He at the level of a few times 10^{-5} by number relative to H, and $^7\text{Li}/\text{H}$ at the level of about 10^{-10} (when η_{10} is in the range 1–10). These values can be understood in terms of approximate analytic arguments [12, 13].

The elemental abundances shown in Fig. 24.1 as a function of η_{10} were calculated using an updated version [14] of the Wagoner code [1]; other versions [15–17] too are publicly available. The ^4He curve includes small corrections due to radiative processes at zero and finite temperatures [18], non-equilibrium neutrino heating during e^\pm annihilation [19], and finite nucleon mass effects [20]; the range primarily reflects the 2σ uncertainty in the neutron lifetime. The spread in the curves for D, ^3He , and ^7Li corresponds to the 2σ uncertainties in nuclear cross sections, as estimated by Monte Carlo methods [21–24]. The input nuclear data have been carefully reassessed [2, 14, 21–31], leading to improved precision for the abundance predictions. In particular, the uncertainty in $^7\text{Li}/\text{H}$ at interesting values of η has been reduced recently by a factor ~ 2 , a consequence of a similar reduction in the error budget [32] for the dominant mass-7 production channel $^3\text{He}(^4\text{He}, \gamma)^7\text{Be}$. Polynomial fits to the predicted abundances and the error correlation matrix have been given in refs. [23, 33]. The boxes in Fig 24.1 show the observationally inferred primordial abundances with their associated uncertainties, as discussed below.

The nuclear reaction cross sections important for BBN have all been measured at the relevant energies. Recently however there have been substantial advances in the precision of light element observations (*e.g.*, D/H) and in the determination of cosmological parameters (*e.g.*, from *Planck*). This motivates corresponding improvement in BBN predictions and thus in the key reaction cross sections. Recent measurements of $\text{D}(p, \gamma)^3\text{He}$ by the LUNA collaboration have significantly improved the precision of D/H predictions [34]. Even so, the nuclear uncertainties still leave D/H prediction errors larger than those of the observations [14, 30, 31]. The $\text{D}(\text{D}, n)^3\text{He}$ and $\text{D}(\text{D}, p)^3\text{H}$ reactions now not only dominate the uncertainty budget, but they can give significantly different D/H predictions depending on whether one uses just the empirical determination of the cross sections, or also uses theory to guide the functional form. Clearly, more experimental data is needed.

An additional experimental parameter important in determining the light element abundances is the neutron lifetime, τ_n , which normalizes (the inverse of) $\Gamma_{n \leftrightarrow p}$. Its value has been revised downwards to $\tau_n = 879.4 \pm 0.6$ s (see *N Baryons Listing*).

24.3 Observations: the Light Element Abundances

BBN theory predicts the universal abundances of D, ^3He , ^4He , and ^7Li which are essentially fixed by $t \sim 180$ s. However, abundances are *derived* at much later epochs, after stellar nucleosynthesis commenced. Stars produce heavy elements such as C, N, O, and Fe (“metals”), while the ejected remains of stellar processing alters the light element abundances from their primordial values. Thus, one seeks astrophysical sites with low metal abundances to measure light element abundances that are closer to primordial.

BBN is the only significant source of deuterium which is entirely destroyed when it is cycled into stars [35]. Thus, any detection provides a lower limit to primordial $\text{D}/\text{H}|_{\text{p}}$, and an upper limit on η_{10} . The best proxy to the primordial value of D is its measure in distant and chemically unprocessed matter, where stellar processing (astration) is minimal [35, 36]. This has become possible with the advent of large telescopes, but after nearly three decades

of observational efforts we have only 11 determinations listed in Table 24.1 [37–43].

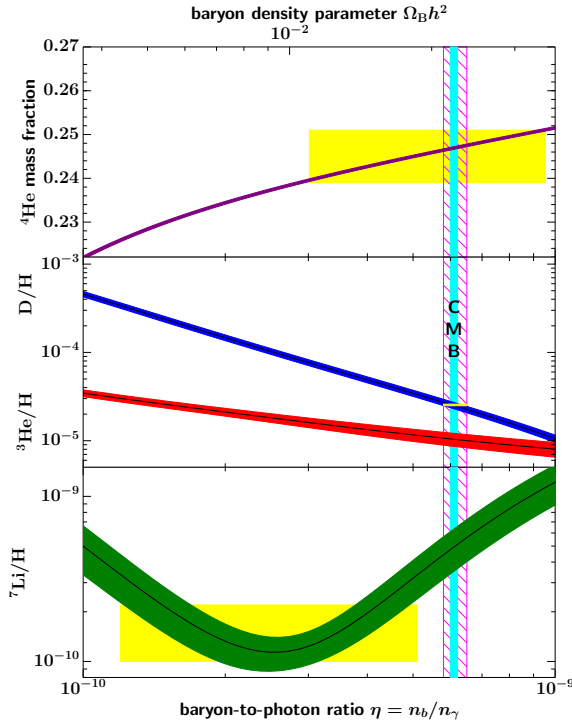


Figure 24.1: The primordial abundances of ${}^4\text{He}$, D, ${}^3\text{He}$, and ${}^7\text{Li}$ as predicted by the standard model of Big-Bang nucleosynthesis — the bands show the 95% CL range [44]. Boxes indicate the observed light element abundances. The narrow vertical band indicates the CMB measure of the cosmic baryon density, while the wider band indicates the BBN $\text{D}+{}^4\text{He}$ concordance range (both at 95% CL).

High-resolution spectra reveal the presence of D in high-redshift, low-metallicity quasar absorption systems via its isotope-shifted Lyman- α absorption features, though, unfortunately, these are often obscured or contaminated by the hydrogen features of the Lyman- α forest. A few DLA systems show D lines resolved up to the higher members of the Lyman series. Recent determinations [38, 40] and re-analyses [41–43] provide strikingly improved precision over earlier work. D/H shows no correlation with metallicity, redshift, or the neutral hydrogen column density $N(\text{HI})$ ($= \int_{\text{los}} n_{\text{HI}} ds$) integrated over the line-of-sight through the absorber. Metallicities of the absorbers are $(0.001 - 0.03) \times \text{Solar}$, and the level astringency is estimated at the 0.1–1 % level [36]. In the Galaxy DI/HI measurements are anti-correlated with metal abundances, which suggests that interstellar D partly resides in dust particles [45]. However, in the absorbers where deuterium is measured, the dust content is small, as implied by Solar proportions of the abundances of refractory and non refractory elements. Thus, the neutral atomic ratio $\text{DI}/\text{HI} \equiv \text{D}/\text{H}$ should match the underlying isotope ratio, and be truly representative of the primordial value $\text{D}/\text{H}|_{\text{p}}$. The weighted mean of the 11 most precise measurements in Table 24.1 is $\text{D}/\text{H}|_{\text{p}} \times 10^6 = (25.47 \pm 0.25)$. However, these measurements provide $\chi^2/(N - 1) = 1.295$, showing that some error is underestimated. We thus increase the uncertainty by a factor $S = \sqrt{\chi^2/(N - 1)} = 1.137$ and the recommended value is:

$$\text{D}/\text{H}|_{\text{p}} \times 10^6 = (25.47 \pm 0.29). \quad (24.2)$$

Considering also the previous determinations of [46–50], the weighted mean of 16 measurements is $\text{D}/\text{H}|_{\text{p}} \times 10^6 = (25.36 \pm 0.26)$, while different selections provide $\text{D}/\text{H}|_{\text{p}} \times 10^6 = (25.27 \pm$

$0.30)$ [43] or $\text{D}/\text{H}|_{\text{p}} \times 10^6 = (25.45 \pm 0.25)$ [42]. These are all consistent with each other, even without the S correction.

The primordial ${}^4\text{He}$ abundance is best determined through recombination emission lines of He and H in the most metal-poor extragalactic HII (ionized) regions, *viz.* blue compact galaxies, generally found at low redshift. There is now a large body of data on ${}^4\text{He}$ and CNO in these galaxies, with over 1000 such systems in the Sloan Digital Sky Survey alone [51]. These data confirm that the stellar contribution to the helium abundance is positively correlated with metal production, so extrapolation to zero metallicity gives the primordial ${}^4\text{He}$ abundance Y_{p} . However, HII regions are complex systems and several physical parameters enter in the He/H determination, notably the electron density and temperature, as well as reddening. Thus, systematic effects dominate the uncertainties in the abundance determination [52, 53]. A major step forward has been the inclusion of the He $\lambda 10830$ infrared emission line which shows a strong dependence on the electron density and is thus useful to break the degeneracy with the temperature, allowing for a more robust helium abundance determination. In recent works the underlying ${}^4\text{He}$ stellar absorption, and/or the newly derived values of the HeI-recombination and H-excitation-collisional coefficients are addressed and the ${}^4\text{He}$ abundances have increased significantly. Some recent results are reported in Table 24.2.

There is a reassuring convergence towards the value of $Y_{\text{p}} = 0.245$ between detailed analyses of specific extragalactic HII regions with other (statistically more significant) analyses of many systems. Thus our recommended ${}^4\text{He}$ abundance is:

$$Y_{\text{p}} = 0.245 \pm 0.003. \quad (24.3)$$

The central value is close to the mean/weighted average of the values in Table 24.2, however we caution that combining these partially overlapping data sets is not straightforward. The uncertainty reflects the combined statistical and systematic errors, with the latter, estimated to be ± 0.002 [59], being dominant.

The best suited objects for the determination of primordial ${}^7\text{Li}$ are metal-poor stars in the Galactic halo, which have metallicities going down to 10^{-6} of the Solar value [61]. Observations have long shown [62–65] that ${}^7\text{Li}$ does not vary significantly in halo dwarfs with metallicities $\lesssim 1/30$ of Solar — the *Spite plateau* [62, 66]. Recent observations show a puzzling drop in the Li/H abundance in metal-poor stars with $[\text{Fe}/\text{H}] < -3.0$ [67–69]. This becomes particularly acute at the very low metallicity end where only one star out of the seven dwarfs with metallicities $[\text{Fe}/\text{H}] \lesssim -4.5$ shows a ${}^7\text{Li}$ abundance close to the Spite Plateau, while in the others where it ought to be present it is either lower or totally absent [61, 70]. The reason for the increase in scatter at low metallicity is unknown and prevents derivation of the primordial ${}^7\text{Li}$ value by extrapolation to zero metallicity [68, 69].

To estimate the primordial ${}^7\text{Li}$ value we consider only stars with metallicity in the range $-2.8 < [\text{Fe}/\text{H}] < -1.5$ [69], where no scatter in excess of the observational errors is observed. This yields:

$$\text{Li}/\text{H}|_{\text{p}} = (1.6 \pm 0.3) \times 10^{-10}. \quad (24.4)$$

Strictly speaking the suggested primordial ${}^7\text{Li}$ abundance should be considered a *lower bound* rather than a measure. In fact, ${}^7\text{Li}$ in Pop II stars may have been partially destroyed due to mixing of the outer layers with the hotter interior [71]. Such processes can be constrained by the absence of significant scatter in ${}^7\text{Li}$ versus T_{eff} [64], but ${}^7\text{Li}$ depletion by a factor as large as ~ 1.8 may have occurred [64, 72]. Stellar determination of Li abundances typically sum over both ${}^6\text{Li}$ and ${}^7\text{Li}$ isotopes. However, high-precision measurements indicate ${}^6\text{Li}/{}^7\text{Li} \leq 0.05$, thus confirming that ${}^7\text{Li}$ is dominant [73].

The primordial abundance of ${}^3\text{He}$ has the poorest observational determination of all of the light nuclides. The only data available come from the Solar system and from solar-metallicity HII regions in the Galaxy [74]. Therefore, inferring the primordial ${}^3\text{He}$ abundance is problematic, compounded by the fact that stellar nucleosynthesis models for ${}^3\text{He}$ are in conflict with observations. Consequently, we consider it inappropriate to use ${}^3\text{He}$ (and also $\text{D}+{}^3\text{He}$) as a cosmological probe.

Table 24.1: D/H measurements. For systems with multiple measurements we used the most recent one which is generally more precise.

QSO	z_{em}	z_{abs}	$\log N(\text{HI})$	[X/H]	(D/H) $\times 10^6$	Ref
SDSS J1419+0829	3.03	3.049	20.392 \pm 0.003	-1.92[O/H]	25.06 \pm 0.52	[37]
HS 0105+1619	2.65	2.536	19.426 \pm 0.006	-1.77[O/H]	25.76 \pm 1.54	[37]
QSO B0913+0715	2.78	2.618	20.312 \pm 0.008	-2.40[O/H]	25.29 \pm 1.05	[37]
SDSS J1358+0349	2.89	2.853	20.524 \pm 0.006	-2.80[O/H]	26.18 \pm 0.72	[38]
SDSS J1358+6522	3.17	3.067	20.495 \pm 0.008	-2.33[O/H]	25.82 \pm 0.71	[37]
SDSS J1558-0031	2.82	2.702	20.75 \pm 0.03	-1.55[O/H]	24.04 \pm 1.44	[37]
PKS 1937-1009	3.78	3.256	18.09 \pm 0.03	-1.87[O/H]	24.49 \pm 2.80	[39]
QSO J1444+2919	2.66	2.437	19.983 \pm 0.010	-2.04[O/H]	19.68 $^{+3.3}_{-2.8}$	[40]
PKS 1937-1009	3.78	3.572	17.925 \pm 0.006	-2.26[O/H]	26.24 \pm 0.48	[41]
QSO 1009+2956	2.63	2.504	17.362 \pm 0.005	-2.50[Si/H]	24.77 $^{+4.1}_{-3.5}$	[42]
QSO 1243+307	2.55	2.525	19.761 \pm 0.026	-2.77[O/H]	23.88 \pm 0.82	[43]
Weighted mean, with $S = 1.137$					25.47 \pm 0.29	

Table 24.2: Recent primordial ^4He measurements in extragalactic HII regions.

$Y_{\text{p}}(^4\text{He})$	$\pm 1\sigma_{\text{stat}}$	$\pm 1\sigma_{\text{sys}}$	$\pm 1\sigma_{\text{tot}}$	# systems	Ref
0.2453	0.0034			16	[54]
0.2451	0.0019	0.0018	0.0026	1	[55]
0.243	0.005			16	[56]
0.2462	0.0022			120	[57]
0.2436	0.0040			54	[58]
0.2448	0.0027	0.0018	0.0033	7	[59]
0.2448			0.0033	17	[60]

24.4 Concordance, Dark Matter, and the CMB

We now use the observed light element abundances to test the theory. We first consider standard BBN, which is based on Standard Model physics alone, so $N_{\nu} = 3$ and the only free parameter is the baryon-to-photon ratio η . (The implications of BBN for physics beyond the Standard Model will be considered below). Thus, any abundance measurement determines η , and additional measurements overconstrain the theory and thereby provide a consistency check.

While the η ranges spanned by the boxes in Fig 24.1 do not all overlap, they are all within a factor ~ 2 of each other. In particular, the lithium abundance corresponds to η values that are inconsistent with that of the (now very precise) D/H abundance as well as the less-constraining ^4He abundance. This discrepancy marks the *lithium problem*. The problem could simply reflect difficulty in determining the primordial lithium abundance, or could hint at a more fundamental omission in the theory. The possibility that lithium reveals new physics is addressed in detail in the next section. If however we exclude the lithium constraint because its inferred abundance suffers from systematic uncertainties, then D/H and ^4He are in agreement. The concordant η range is essentially determined by D/H, and yields [75]

$$\eta_{10} = 6.040 \pm 0.118 \quad (24.5)$$

where the errors are 1σ . Despite the lithium problem, the overall concordance remains remarkable: using only well-established microphysics we can extrapolate back to $t \sim 1$ s to predict light element abundances spanning nine orders of magnitude, in approximate agreement with observation. This is a major success for the standard cosmology, and inspires confidence in extrapolation back to such early times.

This concordance provides a measure of the baryon content:

$$\Omega_{\text{b}}h^2 = 0.02205 \pm 0.00043 \quad (24.6)$$

where again errors are 1σ , a result that plays a key role in our understanding of the matter budget of the Universe. First of all $\Omega_{\text{b}} \ll 1$, *i.e.*, baryons cannot close the Universe [76]. Furthermore, the cosmic density of (optically) luminous matter is $\Omega_{\text{lum}} \simeq 0.0024h^{-1}$ [77], so that $\Omega_{\text{b}} \gg \Omega_{\text{lum}}$: most baryons

are optically dark, probably in the form of a diffuse intergalactic medium [78]. Finally, given that $\Omega_{\text{m}} \sim 0.3$ (see the ‘Dark Matter’ and ‘Cosmological Parameters’ reviews), we infer that most matter in the Universe is not only dark, but also takes some non-baryonic (more precisely, non-nucleonic) form.

The BBN prediction for the cosmic baryon density can be tested through precision measurements of CMB temperature fluctuations (see the ‘Cosmic Microwave Background’ review). One can determine η from the amplitudes of the acoustic peaks in the CMB angular power spectrum [79], making it possible to compare two measures of η using very different physics, at two widely separated epochs. In the standard cosmology, there is no change in η between BBN and CMB decoupling, thus, a comparison of η_{BBN} and η_{CMB} is a key test. Agreement would endorse the standard picture, while disagreement could point to new physics during/between the BBN and CMB epochs.

The analysis described in the Cosmic Microwave Background review (Sec.29), based on *Planck* TT, TE, EE + lowE data and lensing, yields $\Omega_{\text{b}}h^2 = 0.02237 \pm 0.00015$ [80], which corresponds to $\eta_{10} = 6.12 \pm 0.04$ [81]. This result depends weakly on the primordial helium abundance, and the fiducial *Planck* analysis uses BBN theory to fix $Y_{\text{p}}(\eta)$. Without BBN theory, the *Planck* TT, TE, EE + lowE data plus lensing give $\Omega_{\text{b}}h^2 = 0.02230 \pm 0.00021$, corresponding to $\eta_{10} = 6.104 \pm 0.058$. As shown in Fig. 24.1, this CMB estimate of the baryon density (narrow vertical band) is consistent with the BBN range, *i.e.*, in good agreement with the value inferred from high-redshift D/H measurements and local ^4He determinations; together these observations span diverse environments from redshifts $z \sim 1000$ to the present. Combining the CMB and BBN sharpens the baryon measures to $\eta_{10} = 6.115 \pm 0.038$ and $\Omega_{\text{b}}h^2 = 0.02233 \pm 0.00014$ [75].

The ^4He abundance is proportional to the n/p ratio when the weak-interaction rate falls behind the Hubble expansion rate at $T_{\text{fr}} \sim 1$ MeV. The presence of additional neutrino flavors (or of any other relativistic species) at this time increases g_* , hence the expansion rate, leading to a larger value of T_{fr} , n/p , and therefore Y_{p} [10, 82]. In the Standard Model at $T = 1$ MeV, $g_* = 5.5 + \frac{7}{4}N_{\nu}$, where N_{ν} is the *effective* number of (nearly) massless neutrino flavors. The helium curves in 24.1 were computed taking $N_{\nu} = 3$; small corrections for non-equilibrium neu-

trino heating [19] are included in the thermal evolution and lead to an effective $N_\nu = 3.044$ compared to assuming instantaneous neutrino freezeout (see ‘Big Bang Cosmology’ — Sec. 22 of this *Review*). The computed ${}^4\text{He}$ abundance scales as $\Delta Y_p \simeq 0.013 \Delta N_\nu$ [11]. Clearly the central value for N_ν from BBN will depend on η , which is independently determined (with weaker sensitivity to N_ν) by the adopted D or ${}^7\text{Li}$ abundance. For example, if the best value for the observed primordial ${}^4\text{He}$ abundance is 0.249, then, for $\eta_{10} \sim 6$, the central value for N_ν is very close to 3. A maximum likelihood analysis on η and N_ν based on ${}^4\text{He}$ and D abundances nearly identical to those above finds the (correlated) 68% CL ranges to be $\eta_{10} = 6.088 \pm 0.054$ and $N_\nu = 2.898 \pm 0.141$ [44, 75, 83]. Identical results are obtained using a simpler method to extract such bounds based on χ^2 statistics, given a set of input abundances [84].

The CMB damping tail is sensitive to the primordial ${}^4\text{He}$ abundance independently of both BBN and local ${}^4\text{He}$ measurements [85]. The *Planck* analysis using TT, TE, EE+lowE and lensing but not the BBN $Y_p(\eta)$ relation gives a ${}^4\text{He}$ mass fraction $0.239^{+0.024}_{-0.025}$, and nucleon fraction $Y_p = 0.240^{+0.24}_{-0.25}$, both at 95% CL [80]. This is consistent with the HII region helium abundance determination. Moreover, this value is consistent with the Standard ($N_\nu = 3$) BBN prediction for Y_p with the *Planck*-determined baryon density. This concordance represents a successful CMB-only test of BBN.

The precision determination of the baryon density using the CMB motivates using this as an input to BBN calculations. Within the context of the Standard Model, BBN then becomes a zero-parameter theory, and the light element abundances are completely determined to within the uncertainties in η_{CMB} and the BBN theoretical errors. Comparison with the observed abundances then can be used to test the astrophysics of post-BBN light element evolution [86]. Alternatively, one can consider possible physics beyond the Standard Model (*e.g.*, which might change the expansion rate during BBN) and then use all of the abundances to test such models; this is discussed in 24.6 below.

24.5 The Lithium Problem and its Possible Resolution

As Fig. 24.1 shows, stellar Li/H measurements are inconsistent with the D/H (and CMB) measurements, given the error budgets we have quoted. For instance, the value of $\text{Li}/\text{H}|_p = (4.72 \pm 0.7) \times 10^{-10}$ [44] is a factor 3.1 higher than in eq. 24.4 which is a 4.4σ discrepancy.

Stars that have been accreted by the Milky Way Gyrs ago from external galaxies show the same abundances as those in the Milky Way, showing that the Li problem is universal [87–89]. The question then becomes pressing as to whether this mismatch comes from systematic errors in the observed abundances, and/or uncertainties in stellar astrophysics or nuclear inputs, or whether there might be new physics at work [9]. Nuclear inputs (cross sections) for BBN reactions are constrained by extensive laboratory measurements; to increase ${}^7\text{Be}$ destruction requires enhancement of otherwise subdominant processes that can be attained by missed resonances in a few reactions such as ${}^7\text{Be}(d, p)2\alpha$ if the compound nuclear state properties are particularly favorable [29, 90–92]. However, experimental searches have now closed off these possibilities [93–95], making a *nuclear fix* increasingly unlikely.

Another means to solve the lithium problem is by *in situ* destruction over the long lifetimes of the host halo stars. Stellar depletion mechanisms include diffusion, rotationally induced mixing, or pre-main-sequence depletion. These effects certainly occur, but to reduce lithium to the required levels generally requires some *ad hoc* mechanism and fine tuning of the initial stellar parameters [72, 96–98]. General features of diffusive models are a dispersion in the Li abundances and a pronounced downturn in the Li abundances at the hot end of the Li plateau. Some extra turbulence needs to be invoked to limit diffusion in the hotter stars and to restore uniform Li abundance along the Spite plateau [98]. Li abundances for over 100 000 field stars have been obtained in the GALAH (Galactic Archeology with HERMES) survey. Warm stars with $[\text{Fe}/\text{H}]$ in between -1.0 and -0.5 form an elevated plateau

consistent with the BBN prediction and it has been suggested that this could have been also true for the more metal poor stars which have evolved further [99]. Li destruction in the pre-Main sequence phase has been also proposed [97].

Recent ${}^6\text{Li}$ measurements have cast new light on the lithium problem. BBN production of ${}^6\text{Li}$ is negligible [100]; instead it is created much later by energetic cosmic-ray p and ${}^4\text{He}$ interactions with interstellar gas, in fusion reactions such as ${}^4\text{He} + {}^4\text{He} \rightarrow {}^6,{}^7\text{Li} + \dots$ and spallation reactions on interstellar carbon, nitrogen, and oxygen such as $p_{\text{cr}} + {}^{16}\text{O} \rightarrow {}^6,{}^7\text{Li} + {}^9\text{Be} + {}^{10,11}\text{B} + \dots$. Thus ${}^6\text{Li}$, beryllium, and boron are co-produced, and the detection of Be and B in metal-poor stars thus requires cosmic-ray ${}^6\text{Li}$ was present when these stars were formed. ${}^6\text{Li}$ detections were reported for some of these stars [101–103], and because the weakly-bound ${}^6\text{Li}$ nucleus is more easily destroyed than ${}^7\text{Li}$, the survival of ${}^6\text{Li}$ implied that ${}^7\text{Li}$ destruction should be small. But new observations place strong upper limits on ${}^6\text{Li}/\text{H}$ in the plateau stars where this isotope had long been reported to exist [104]. This removes the ${}^6\text{Li}$ argument against stellar depletion. Indeed, detailed models of cosmic-ray lithium production can quantify the ${}^6\text{Li}$ depletion, and may suggest the ${}^7\text{Li}$ destruction could be sufficient to explain the mismatch between the observed Li abundance and the expected BBN ${}^7\text{Li}$ [105]. This line of argument supports the predictions of stellar depletion as the possible resolution of the lithium problem [72, 96–98]. Additional ${}^6\text{Li}$ limits or detections, in concert with model calculations, can firm up this conclusion.

Observations of interstellar lithium in low-metallicity systems probe lithium abundances not subject to stellar depletion. Measurements of interstellar Li/H in the Small Magellanic Cloud lie near the primordial level, but also are consistent with Milky Way stellar abundances at that metallicity ($\sim 1/4$ solar) [106]. Additional such measurements in more metal-poor systems would be of great interest.

It remains possible that the lithium problem points to new physics. Nucleosynthesis models in which the baryon-to-photon ratio is inhomogeneous can alter abundances for a given η_{BBN} , but will overproduce ${}^7\text{Li}$ [107]. Entropy generation by some non-standard process could have decreased η between the BBN era and CMB decoupling, however the lack of spectral distortions in the CMB rules out any significant energy injection up to a redshift $z \sim 10^7$ [108]. The most intriguing resolution of the lithium problem thus involves new physics during BBN [7–9]

We summarize the general features of such solutions here, and later consider examples in the context of specific particle physics models. Many proposed solutions introduce perturbations to light-element formation during BBN; while all element abundances may suffer perturbations, the interplay of ${}^7\text{Li}$ and D is often the most important *i.e.* observations of D often provide the strongest constraints on the allowed perturbations to ${}^7\text{Li}$. In this connection it is important to note that the new, very precise determination of D/H will significantly constrain the ability of such models to ameliorate or solve the lithium problem.

A well studied class of models invokes the injection of suprathermal hadronic or electromagnetic particles due to decays of dark matter particles. The effects are complex and depend on the nature of the decaying particles and their branchings and spectra. However, the models that most successfully solve the lithium problem generally feature non-thermal nucleons, which dissociate all light elements. Dissociation of even a small fraction of ${}^4\text{He}$ introduces a large abundance of free neutrons, which quickly thermalize. The thermal neutrons drive the ${}^7\text{Be}(n, p){}^7\text{Li}$ conversion of ${}^7\text{Be}$. The resulting ${}^7\text{Li}$ has a lower Coulomb barrier relative to ${}^7\text{Be}$ and is readily destroyed via ${}^7\text{Li}(p, \alpha){}^4\text{He}$ [109, 110]. But ${}^4\text{He}$ dissociation also produces D directly as well as via nonthermal neutron $n(p, \gamma)d$ reactions. This introduces a tension between Li/H reduction and D/H enhancement that becomes increasingly restrictive with the increasing precision of deuterium observations. Indeed, this now forces particle injection scenarios to make very small ${}^7\text{Li}$ perturbations — far short of the level needed. An exception is a recent model wherein MeV-scale decays by construction avoid ${}^4\text{He}$ dissociation and associated D/H overproduction, instead *borrowing* neutrons by dissociating only deuterons [111].

Another important class of models retains the standard cosmic

particle content, but changes their interactions via time variations in the fundamental constants [112–118]. Here too, the details are model-dependent, but scenarios that solve or alleviate the lithium problem often feature perturbations to the deuteron binding energy. A weaker D binding leads to the D bottleneck being overcome later, so that element formation commences at a lower temperature and lower density. This leads in turn to slower nuclear rates that freeze out earlier. The net result is a *higher* final D/H, due to less efficient processing into ${}^4\text{He}$, but also *lower* Li, due to suppressed production via ${}^3\text{He}(\alpha, \gamma){}^7\text{Be}$.

The *cosmological lithium problem* remains an unresolved issue in BBN. Nevertheless, the remarkable concordance between the CMB and the D (as well as ${}^4\text{He}$) abundance, is a non-trivial success, and provides important constraints on the early Universe.

24.6 Beyond the Standard Model

Given the simple physics underlying BBN, it is remarkable that it still provides the most effective test for the cosmological viability of ideas concerning physics beyond the Standard Model. Although baryogenesis and inflation must have occurred at higher temperatures in the early Universe, we do not as yet have ‘standard models’ for these, so BBN still marks the boundary between the established and the speculative in Big Bang cosmology. It might appear possible to push the boundary back to the quark-hadron transition at $T \sim \Lambda_{\text{QCD}}$, or electroweak symmetry breaking at $T \sim 1/\sqrt{G_{\text{F}}}$; however, so far no observable relics of these epochs have been identified, either theoretically or observationally. Thus, although the Standard Model provides a precise description of physics up to the Fermi scale, cosmology cannot be traced in detail before the BBN era.

The CMB power spectrum in the damping tail is independently sensitive to N_ν (e.g. [119]). The CMB value N_ν^{CMB} probes the cosmic radiation content at (re)combination, so a discrepancy would imply new physics or astrophysics. Indeed, observations by the South Pole Telescope implied $N_\nu^{\text{CMB}} = 3.85 \pm 0.62$ [120], prompting discussion of *dark radiation* such as sterile neutrinos [121]. However, *Planck* 2018 results give $N_\nu^{\text{CMB}} = 2.92^{+0.36}_{-0.37}$, 95% CL, when using *Planck* TT, TE, EE+lowE, a result quite consistent with 3 Standard Model neutrinos [80] (and adjusting for the CMB’s measurement of $N_{\text{eff}} = 3.044$ due to neutrino heading effects [122–124]). Indeed, the BBN and CMB constraints on N_ν are independent and of similar precision, so that it is now possible to limit any *change* in this parameter (and/or the baryon-to-photon ratio) between nucleosynthesis and recombination [75]. This can, for example, constrain models with late particle decays, or with early dark energy.

Just as one can use the measured helium abundance to place limits on g_* [82, 113, 125–127], any changes in the strong, weak, electromagnetic, or gravitational coupling constants, arising e.g., from the dynamics of new dimensions, can be similarly constrained [128], as can any speed-up of the expansion rate in, e.g., scalar-tensor theories of gravity [129].

The limits on N_ν can be translated into limits on other types of particles or particle masses that would affect the expansion rate of the Universe during nucleosynthesis. For example, consider *sterile* neutrinos with only right-handed interactions of strength $G_{\text{R}} < G_{\text{F}}$. Such particles would decouple at higher temperature than (left-handed) neutrinos, so their number density ($\propto T^3$) relative to neutrinos would be reduced by any subsequent entropy release, e.g., due to annihilations of massive particles that become non-relativistic between the two decoupling temperatures. Thus, (relativistic) particles with less than full strength weak interactions contribute less to the energy density than particles that remain in equilibrium up to the time of nucleosynthesis [130]. If we impose $N_\nu < 4$ as an illustrative constraint, then the three right-handed neutrinos must have a temperature $3(T_{\nu_{\text{R}}}/T_{\nu_{\text{L}}})^4 < 1$. Since the temperature of the decoupled ν_{R} is determined by entropy conservation (see ‘Big Bang Cosmology’ — Sec. 22 of this *Review*), $T_{\nu_{\text{R}}}/T_{\nu_{\text{L}}} = [(43/4)/g_*(T_{\text{d}})]^{1/3} < 0.76$, where T_{d} is the decoupling temperature of the ν_{R} . This requires $g_*(T_{\text{d}}) > 24$, so decoupling must have occurred at $T_{\text{d}} > 140$ MeV. The decoupling temperature is related to G_{R} through $(G_{\text{R}}/G_{\text{F}})^2 \sim (T_{\text{d}}/3\text{ MeV})^{-3}$, where 3 MeV is the decoupling temperature for ν_{L} s. This yields a limit $G_{\text{R}} \lesssim 10^{-2}G_{\text{F}}$. The above argument sets lower limits on the

masses of new Z' gauge bosons to which right-handed neutrinos would be coupled in models of superstrings [131], or extended technicolour [132]. Similarly a Dirac magnetic moment for neutrinos, which would allow the right-handed states to be produced through scattering and thus increase g_* , can be significantly constrained [133], as can any new interactions for neutrinos that have a similar effect [134–136]. Right-handed states can be populated directly by helicity-flip scattering if the neutrino mass is large enough, and this property has been used to infer a bound of $m_{\nu_\tau} \lesssim 1$ MeV (taking $N_\nu < 4$) [137]. If there is mixing between active and sterile neutrinos then the effect on BBN is more complicated [138, 139].

BBN limits on the cosmic expansion rate constrain supersymmetric scenarios in which the neutralino or gravitino are very light, so that they contribute to g_* [140]. A gravitino in the mass range $\sim 10^{-4} - 10$ eV will affect the expansion rate of the Universe similarly to a light neutralino (which is however now probably ruled out by collider data, especially the decays of the Higgs-like boson). The net contribution to N_ν then ranges between 0.74 and 1.69, depending on the gravitino and slepton masses [141].

The limit on the expansion rate during BBN can also be translated into bounds on the mass/lifetime of non-relativistic particles that decay during BBN. This results in an even faster speed-up rate, and typically also changes the entropy [142–144]. If the decays include Standard Model particles, the resulting electromagnetic [145] [86, 131, 146] and/or hadronic [147, 148] cascades can strongly perturb the light elements, which leads to even stronger constraints. Such arguments have been applied to rule out an MeV mass for ν_τ , which decays during nucleosynthesis [149].

Decaying-particle arguments have proved very effective in probing supersymmetry. Light-element abundances generally are complementary to accelerator data in constraining SUSY parameter space, with BBN reaching to values kinematically inaccessible to the LHC. Much recent interest has focused on the case in which the next-to-lightest supersymmetric particle is metastable and decays during or after BBN. The constraints on unstable particles discussed above imply stringent bounds on the allowed abundance of such particles [109]; if the metastable particle is charged (e.g., the stau), then it is possible for it to form atom-like electromagnetic bound states with nuclei, and the resulting impact on light elements can be quite complex [8, 90, 150]. Moreover, SUSY decays can destroy ${}^7\text{Li}$ and/or produce ${}^6\text{Li}$, leading to a possible supersymmetric solution to the lithium problems noted above [151] (see [7] for a review).

These arguments impose powerful constraints on supersymmetric inflationary cosmology [86, 131, 146–148], particularly thermal leptogenesis [152]. These limits can be evaded only if the gravitino is massive enough to decay before BBN, i.e., $m_{3/2} \gtrsim 50$ TeV [153] (which would be unnatural), or if it is in fact the lightest supersymmetric particle and thus stable [131, 146, 154, 155]. Similar constraints apply to moduli – very weakly coupled fields in string theory that obtain an electroweak-scale mass from supersymmetry breaking [156].

Finally, we mention that BBN places powerful constraints on the possibility that there are new large dimensions in nature, perhaps enabling the scale of quantum gravity to be as low as the electroweak scale [157]. Thus, Standard Model fields may be localized on a *brane*, while gravity alone propagates in the *bulk*. It has been further noted that the new dimensions may be non-compact, even infinite [158], and the cosmology of such models has attracted considerable attention. The expansion rate in the early Universe can be significantly modified, so BBN is able to set interesting constraints on such possibilities [159, 160].

References

- [1] R. V. Wagoner, W. A. Fowler and F. Hoyle, *Astrophys. J.* **148**, 3 (1967).
- [2] D. N. Schramm and M. S. Turner, *Rev. Mod. Phys.* **70**, 303 (1998), [arXiv:astro-ph/9706069].
- [3] G. Steigman, *Ann. Rev. Nucl. Part. Sci.* **57**, 463 (2007), [arXiv:0712.1100].
- [4] F. Iocco *et al.*, *Phys. Rept.* **472**, 1 (2009), [arXiv:0809.0631].

- [5] R. H. Cyburt *et al.*, *Rev. Mod. Phys.* **88**, 015004 (2016), [arXiv:1505.01076].
- [6] S. Sarkar, *Rept. on Prog. in Phys.* **59**, 1493 (1996).
- [7] K. Jedamzik and M. Pospelov, *New J. Phys.* **11**, 105028 (2009), [arXiv:0906.2087].
- [8] M. Pospelov and J. Pradler, *Ann. Rev. Nucl. Part. Sci.* **60**, 539 (2010), [arXiv:1011.1054].
- [9] B. D. Fields, *Ann. Rev. Nucl. Part. Sci.* **61**, 47 (2011), [arXiv:1203.3551].
- [10] P.J.E. Peebles, *Phys. Rev. Lett.* **16**, 411 (1966).
- [11] J. Bernstein, L. S. Brown and G. Feinberg, *Rev. Mod. Phys.* **61**, 25 (1989).
- [12] S. Mukhanov, *Int. J. Theor. Phys.* **143**, 669 (2004).
- [13] R. Esmailzadeh, G. D. Starkman and S. Dimopoulos, *Astrophys. J.* **378**, 504 (1991).
- [14] T.-H. Yeh, K. A. Olive and B. D. Fields, *JCAP* **03**, 046 (2021), [arXiv:2011.13874].
- [15] L. Kawano, Technical report (1992), URL <https://ui.adsabs.harvard.edu/abs/1992STIN...9225163K>.
- [16] A. Arbey *et al.*, *Comput. Phys. Commun.* **248**, 106982 (2020), [arXiv:1806.11095].
- [17] R. Consiglio *et al.*, *Computer Physics Communications* **233**, 237 (2018), [arXiv:1712.04378].
- [18] S. Esposito *et al.*, *Nucl. Phys.* **B568**, 421 (2000), [arXiv:astro-ph/9906232].
- [19] S. Dodelson and M. S. Turner, *Phys. Rev.* **D46**, 3372 (1992).
- [20] D. Seckel (1993), [hep-ph/9305311].
- [21] R. H. Cyburt, B. D. Fields and K. A. Olive, *New Astron.* **6**, 215 (2001), [arXiv:astro-ph/0102179].
- [22] M. S. Smith, L. H. Kawano and R. A. Malaney, *Astrophys. J. Suppl.* **85**, 219 (1993).
- [23] G. Fiorentini *et al.*, *Phys. Rev.* **D58**, 063506 (1998), [arXiv:astro-ph/9803177].
- [24] A. Coc *et al.*, *Astrophys. J.* **744**, 158 (2012), [arXiv:1107.1117].
- [25] R. H. Cyburt, B. D. Fields and K. A. Olive, *JCAP* **0811**, 012 (2008), [arXiv:0808.2818].
- [26] K. M. Nollett and S. Burles, *Phys. Rev.* **D61**, 123505 (2000), [arXiv:astro-ph/0001440].
- [27] R. H. Cyburt, *Phys. Rev.* **D70**, 023505 (2004), [arXiv:astro-ph/0401091].
- [28] P. D. Serpico *et al.*, *JCAP* **0412**, 010 (2004), [arXiv:astro-ph/0408076].
- [29] R. N. Boyd *et al.*, *Phys. Rev.* **D82**, 105005 (2010), [arXiv:1008.0848].
- [30] C. Pitrou *et al.*, *Mon. Not. Roy. Astron. Soc.* **502**, 2, 2474 (2021), [arXiv:2011.11320].
- [31] O. Pisanti *et al.*, *JCAP* **04**, 020 (2021), [arXiv:2011.11537].
- [32] R.H. Cyburt and B. Davids, *Phys. Rev.* **C78**, 012 (2008).
- [33] S. Burles, K. M. Nollett and M. S. Turner, *Astrophys. J.* **552**, L1 (2001), [arXiv:astro-ph/0010171].
- [34] V. Mossa *et al.*, *Nature* **587**, 7833, 210 (2020).
- [35] R. I. Epstein, J. M. Lattimer and D. N. Schramm, *Nature* **263**, 198 (1976).
- [36] F. van de Voort *et al.*, *Mon. Not. Roy. Astron. Soc.* **477**, 1, 80 (2018), [arXiv:1704.08254].
- [37] R. Cooke *et al.*, *Astrophys. J.* **781**, 1, 31 (2014), [arXiv:1308.3240].
- [38] R. J. Cooke *et al.*, *Astrophys. J.* **830**, 2, 148 (2016), [arXiv:1607.03900].
- [39] S. Riemer-Sørensen *et al.*, *Mon. Not. Roy. Astron. Soc.* **447**, 3, 2925 (2015), [arXiv:1412.4043].
- [40] S. A. Balashev *et al.*, *Mon. Not. Roy. Astron. Soc.* **458**, 2, 2188 (2016), [arXiv:1511.01797].
- [41] S. Riemer-Sørensen *et al.*, *Mon. Not. Roy. Astron. Soc.* **468**, 3, 3239 (2017), [arXiv:1703.06656].
- [42] E. O. Zavarygin *et al.*, *Mon. Not. Roy. Astron. Soc.* **477**, 4, 5536 (2018), [arXiv:1706.09512].
- [43] R. J. Cooke, M. Pettini and C. C. Steidel, *Astrophys. J.* **855**, 2, 102 (2018), [arXiv:1710.11129].
- [44] B. D. Fields *et al.*, *JCAP* **2020**, 3, 010 (2020), [arXiv:1912.01132].
- [45] J. L. Linsky *et al.*, *Astrophys. J.* **647**, 1106 (2006), [arXiv:astro-ph/0608308].
- [46] M. Pettini and D. V. Bowen, *Astrophys. J.* **560**, 41 (2001), [arXiv:astro-ph/0104474].
- [47] S. D'Odorico, M. Dessauges-Zavadsky and P. Molaro, *Astron. Astrophys.* **368**, L21 (2001), [arXiv:astro-ph/0102162].
- [48] M. Fumagalli, J. M. O'Meara and J. X. Prochaska, *Science* **334**, 1245 (2011), [arXiv:1111.2334].
- [49] P. Noterdaeme *et al.*, *Astron. Astrophys.* **542**, L33 (2012), [arXiv:1205.3777].
- [50] R. Srianand *et al.*, *Mon. Not. Roy. Astron. Soc.* **405**, 3, 1888 (2010), [arXiv:1002.4620].
- [51] Y. I. Izotov, T. X. Thuan and N. G. Guseva, *Mon. Not. Roy. Astron. Soc.* **445**, 1, 778 (2014), [arXiv:1408.6953].
- [52] Y. I. Izotov *et al.*, *Astrophys. J.* **527**, 757 (1999), [arXiv:astro-ph/9907228].
- [53] K. A. Olive and E. D. Skillman, *Astrophys. J.* **617**, 29 (2004), [arXiv:astro-ph/0405588].
- [54] E. Aver *et al.*, *JCAP* **2021**, 3, 027 (2021), [arXiv:2010.04180].
- [55] M. Valerdi *et al.*, *Astrophys. J.* **876**, 2, 98 (2019), [arXiv:1904.01594].
- [56] V. Fernández *et al.*, *Mon. Not. Roy. Astron. Soc.* **487**, 3, 3221 (2019), [arXiv:1905.09215].
- [57] O. A. Kurichin *et al.*, *Mon. Not. Roy. Astron. Soc.* **502**, 2, 3045 (2021), [arXiv:2101.09127].
- [58] T. Hsyu *et al.*, *Astrophys. J.* **896**, 1, 77 (2020), [arXiv:2005.12290].
- [59] M. Valerdi, A. Peimbert and M. Peimbert, *Mon. Not. Roy. Astr. Soc.* **505**, 3, 3624 (2021), [arXiv:2105.12260].
- [60] E. Aver *et al.*, *Mon. Not. Roy. Astr. Soc.* **510**, 1, 373 (2022), [arXiv:2109.00178].
- [61] D. S. Aguado *et al.*, *Astrophys. J. Lett.* **874**, 2, L21 (2019), [arXiv:1904.04892].
- [62] M. Spite and F. Spite, *Nature* **297**, 483 (1982).
- [63] E. Vangioni-Flam *et al.*, *New Astron.* **4**, 245 (1999), [arXiv:astro-ph/9811327].
- [64] S. G. Ryan *et al.*, *Astrophys. J.* **530**, L57 (2000), [arXiv:astro-ph/9905211].
- [65] P. Bonifacio and P. Molaro, *Mon. Not. Roy. Astron. Soc.* **285**, 847 (1997), [arXiv:astro-ph/9611043].
- [66] R. Rebolo, P. Molaro and J. E. Beckman, *Astron. Astrophys.* **192**, 192 (1988).
- [67] P. Bonifacio *et al.*, *Astron. & Astrophys.* **462**, 851 (2007).
- [68] W. Aoki *et al.*, *Astrophys. J.* **698**, 1803 (2009), [arXiv:0904.1448].
- [69] L. Sbordone *et al.*, *Astron. & Astrophys.* **522**, A26 (2010).
- [70] P. Bonifacio *et al.*, *Astron. Astrophys.* **612**, A65 (2018), [arXiv:1801.03935].
- [71] M.H. Pinsonneault *et al.*, *Astrophys. J.* **574**, 389 (2002).
- [72] A. J. Korn *et al.*, *Nature* **442**, 657 (2006), [arXiv:astro-ph/0608201].

- [73] R. Cayrel *et al.*, *Astron. & Astrophys.* **473**, L37 (2007).
- [74] D. S. Baler and T. M. Bania, *Astrophys. J.* **156**, 6, 280 (2018), [arXiv:1810.09422].
- [75] T.-H. Yeh *et al.*, *JCAP* **10**, 046 (2022), [arXiv:2207.13133].
- [76] H. Reeves *et al.*, *Astrophys. J.* **179**, 909 (1973).
- [77] M. Fukugita and P. J. E. Peebles, *Astrophys. J.* **616**, 643 (2004), [arXiv:astro-ph/0406095].
- [78] R. Cen and J. P. Ostriker, *Astrophys. J.* **514**, 1 (1999), [arXiv:astro-ph/9806281].
- [79] G. Jungman *et al.*, *Phys. Rev.* **D54**, 1332 (1996), [arXiv:astro-ph/9512139].
- [80] Planck Collaboration *et al.*, arXiv e-prints arXiv:1807.06209 (2018), [arXiv:1807.06209].
- [81] P.A.R. Ade *et al.*, *Astron. & Astrophys.* **594**, A13 (2016).
- [82] G. Steigman, D. N. Schramm and J. E. Gunn, *Phys. Lett.* **B66**, 202 (1977), [159(1977)].
- [83] B. D. Fields *et al.*, *JCAP* **2020**, 11, E02 (2020).
- [84] E. Lisi, S. Sarkar and F. L. Villante, *Phys. Rev.* **D59**, 123520 (1999), [hep-ph/9901404].
- [85] R. Trotta and S. H. Hansen, *Phys. Rev.* **D69**, 023509 (2004), [arXiv:astro-ph/0306588].
- [86] R. H. Cyburt, B. D. Fields and K. A. Olive, *Phys. Lett.* **B567**, 227 (2003), [arXiv:astro-ph/0302431].
- [87] P. Molaro, G. Cescutti and X. Fu, *Mon. Not. Roy. Astron. Soc.* **496**, 3, 2902 (2020), [arXiv:2006.00787].
- [88] J. D. Simpson *et al.*, *Mon. Not. Roy. Astron. Soc.* (2021).
- [89] D. S. Aguado *et al.*, *Mon. Not. Roy. Astron. Soc.* **500**, 1, 889 (2021), [arXiv:2007.11003].
- [90] R. H. Cyburt *et al.*, *JCAP* **1305**, 014 (2013), [arXiv:1303.0574].
- [91] N. Chakraborty, B. D. Fields and K. A. Olive, *Phys. Rev.* **D83**, 063006 (2011), [arXiv:1011.0722].
- [92] C. Brogini *et al.*, *JCAP* **1206**, 030 (2012), [arXiv:1202.5232].
- [93] P. D. O'Malley *et al.*, *Phys. Rev.* **C84**, 042801 (2011).
- [94] F. Hammache *et al.*, *Phys. Rev.* **C88**, 6, 062802 (2013), [arXiv:1312.0894].
- [95] M. W. Paris *et al.*, *Nucl. Data Sheets* **120**, 184 (2014), [arXiv:1304.3153].
- [96] P. Molaro *et al.*, *Memorie della Soc. Astronomica Italiana Supp.* **22**, 233 (2012).
- [97] X. Fu *et al.*, *Mon. Not. R. Astron. Soc* **452**, 325 (2015).
- [98] O. Richard, G. Michaud and J. Richer, *Astrophys. J.* **619**, 538 (2005), [arXiv:astro-ph/0409672].
- [99] X. Gao *et al.*, *Mon. Not. Roy. Astron. Soc.* **497**, 1, L30 (2020), [arXiv:2006.05173].
- [100] D. Thomas *et al.*, *Astrophys. J.* **406**, 569 (1993), [arXiv:astro-ph/9206002].
- [101] V. V. Smith, D. L. Lambert and P. E. Nissen, *Astrophys. J.* **408**, 262 (1993).
- [102] L. M. Hobbs and J. A. Thorburn, *Astrophys. J. Lett.* **428**, L25 (1994).
- [103] R. Cayrel *et al.*, *Astron. Astrophys.* **343**, 923 (1999), [arXiv:astro-ph/9901205].
- [104] E. X. Wang *et al.*, *Mon. Not. Roy. Astron. Soc.* **509**, 1, 1521 (2021), [arXiv:2110.03822].
- [105] B. D. Fields and K. A. Olive, *JCAP* **10**, 078 (2022), [arXiv:2204.03167].
- [106] J. C. Howk *et al.*, *Nature* **489**, 7414, 121 (2012), [arXiv:1207.3081].
- [107] K. Jedamzik and J. B. Rehm, *Phys. Rev.* **D64**, 023510 (2001), [arXiv:astro-ph/0101292].
- [108] D. J. Fixsen *et al.*, *Astrophys. J.* **473**, 576 (1996), [arXiv:astro-ph/9605054].
- [109] M. Kawasaki, K. Kohri and T. Moroi, *Phys. Rev.* **D71**, 083502 (2005), [arXiv:astro-ph/0408426].
- [110] K. Jedamzik, *Phys. Rev.* **D70**, 063524 (2004), [arXiv:astro-ph/0402344].
- [111] A. Goudelis, M. Pospelov and J. Pradler, *Phys. Rev. Lett.* **116**, 21, 211303 (2016), [arXiv:1510.08858].
- [112] J. D. Barrow, *Phys. Rev.* **D35**, 1805 (1987).
- [113] B. A. Campbell and K. A. Olive, *Phys. Lett.* **B345**, 429 (1995), [hep-ph/9411272].
- [114] L. Bergstrom, S. Iguri and H. Rubinstein, *Phys. Rev.* **D60**, 045005 (1999), [arXiv:astro-ph/9902157].
- [115] V. V. Flambaum and E. V. Shuryak, *Phys. Rev.* **D65**, 103503 (2002), [hep-ph/0201303].
- [116] A. Coc *et al.*, *Phys. Rev.* **D76**, 023511 (2007), [arXiv:astro-ph/0610733].
- [117] J. C. Berengut *et al.*, *Phys. Rev.* **D87**, 8, 085018 (2013), [arXiv:1301.1738].
- [118] C. J. A. P. Martins, *Astron. Astrophys.* **646**, A47 (2021), [arXiv:2012.10505].
- [119] Z. Hou *et al.*, *Phys. Rev.* **D87**, 083008 (2013), [arXiv:1104.2333].
- [120] R. Keisler *et al.*, *Astrophys. J.* **743**, 28 (2011), [arXiv:1105.3182].
- [121] J. Hamann *et al.*, *Phys. Rev. Lett.* **105**, 181301 (2010), [arXiv:1006.5276].
- [122] K. Akita and M. Yamaguchi, *JCAP* **2020**, 8, 012 (2020), [arXiv:2005.07047].
- [123] J. Froustey, C. Pitrou and M. C. Volpe, *JCAP* **2020**, 12, 015 (2020), [arXiv:2008.01074].
- [124] J. J. Bennett *et al.*, *JCAP* **04**, 073 (2021), [arXiv:2012.02726].
- [125] F. S. Accetta, L. M. Krauss and P. Romanelli, *Phys. Lett.* **B248**, 146 (1990).
- [126] K. M. Nollett and R. E. Lopez, *Phys. Rev.* **D66**, 063507 (2002), [arXiv:astro-ph/0204325].
- [127] C. Bambi, M. Giannotti and F. L. Villante, *Phys. Rev.* **D71**, 123524 (2005), [arXiv:astro-ph/0503502].
- [128] E. W. Kolb, M. J. Perry and T. P. Walker, *Phys. Rev.* **D33**, 869 (1986).
- [129] A. Coc *et al.*, *Phys. Rev.* **D73**, 083525 (2006), [arXiv:astro-ph/0601299].
- [130] K. A. Olive, D. N. Schramm and G. Steigman, *Nucl. Phys.* **B180**, 497 (1981).
- [131] J. R. Ellis *et al.*, *Phys. Lett.* **167B**, 457 (1986).
- [132] L. M. Krauss, J. Terning and T. Appelquist, *Phys. Rev. Lett.* **71**, 823 (1993), [hep-ph/9305265].
- [133] J. A. Morgan, *Phys. Lett.* **102B**, 247 (1981).
- [134] E. W. Kolb, M. S. Turner and T. P. Walker, *Phys. Rev.* **D34**, 2197 (1986).
- [135] J. A. Grifols and E. Masso, *Mod. Phys. Lett.* **A2**, 205 (1987).
- [136] K. S. Babu, R. N. Mohapatra and I. Z. Rothstein, *Phys. Rev. Lett.* **67**, 545 (1991).
- [137] A. D. Dolgov, S. H. Hansen and D. V. Semikoz, *Nucl. Phys.* **B524**, 621 (1998), [hep-ph/9712284].
- [138] K. Enqvist, K. Kainulainen and M. J. Thomson, *Nucl. Phys.* **B373**, 498 (1992).
- [139] A. D. Dolgov, *Phys. Rept.* **370**, 333 (2002), [hep-ph/0202122].
- [140] J. A. Grifols, R. N. Mohapatra and A. Riotto, *Phys. Lett.* **B400**, 124 (1997), [hep-ph/9612253].

- [141] H. K. Dreiner *et al.*, Phys. Rev. **D85**, 065027 (2012), [arXiv:1111.5715].
- [142] K. Sato and M. Kobayashi, Prog. Theor. Phys. **58**, 1775 (1977).
- [143] D. A. Dicus *et al.*, Phys. Rev. **D17**, 1529 (1978).
- [144] R. J. Scherrer and M. S. Turner, Astrophys. J. **331**, 19 (1988), [Astrophys. J.331,33(1988)].
- [145] D. Lindley, Mon. Not. R. Astron. Soc **188**, 15 (1979).
- [146] J. R. Ellis *et al.*, Nucl. Phys. **B373**, 399 (1992).
- [147] M. H. Reno and D. Seckel, Phys. Rev. **D37**, 3441 (1988).
- [148] S. Dimopoulos *et al.*, Nucl. Phys. **B311**, 699 (1989).
- [149] S. Sarkar and A. M. Cooper-Sarkar, Phys. Lett. **148B**, 347 (1984).
- [150] M. Kawasaki, K. Kohri and T. Moroi, Phys. Lett. **B649**, 436 (2007), [hep-ph/0703122].
- [151] K. Jedamzik *et al.*, JCAP **0607**, 007 (2006), [hep-ph/0512044].
- [152] S. Davidson *et al.*, Phys. Rev. **466**, 105 (2008).
- [153] S. Weinberg, Phys. Rev. Lett. **48**, 1303 (1982).
- [154] R. H. Cyburt *et al.*, Phys. Rev. **D67**, 103521 (2003), [arXiv:astro-ph/0211258].
- [155] M. Bolz, A. Brandenburg and W. Buchmuller, Nucl. Phys. **B606**, 518 (2001), [Erratum: Nucl. Phys.B790,336(2008)], [hep-ph/0012052].
- [156] G. D. Coughlan *et al.*, Physics Letters B **131**, 1-3, 59 (1983).
- [157] N. Arkani-Hamed, S. Dimopoulos and G. R. Dvali, Phys. Rev. **D59**, 086004 (1999), [hep-ph/9807344].
- [158] L. Randall and R. Sundrum, Phys. Rev. Lett. **83**, 3370 (1999), [hep-ph/9905221].
- [159] J. M. Cline, C. Grojean and G. Servant, Phys. Rev. Lett. **83**, 4245 (1999), [hep-ph/9906523].
- [160] P. Binetruy *et al.*, Phys. Lett. **B477**, 285 (2000), [hep-th/9910219].

25. Cosmological Parameters

Revised August 2023 by O. Lahav (UCL) and A.R. Liddle (ULisboa).

25.1 Parametrizing the Universe

Rapid advances in observational cosmology have led to the establishment of a precision cosmological model, with many of the key cosmological parameters determined to one or two significant figure accuracy. Particularly prominent are measurements of cosmic microwave background (CMB) anisotropies, with the highest precision observations being those of the *Planck* Satellite [1, 2], which supersede the landmark *WMAP* results [3, 4]. However the most accurate model of the Universe requires consideration of a range of observations, with complementary probes providing consistency checks, lifting parameter degeneracies, and enabling the strongest constraints to be placed.

The term ‘cosmological parameters’ now has a wide scope, and may include the parameterization of some functions as well as simple numbers describing properties of the Universe. The original usage referred to the parameters describing the global dynamics of the Universe, such as its expansion rate and curvature. Now we wish to know how the matter budget of the Universe is built up from its constituents: baryons, photons, neutrinos, dark matter, and dark energy. We also need to describe the nature of perturbations in the Universe, through global statistical descriptors such as the matter and radiation power spectra. There may be additional parameters describing the physical state of the Universe, such as the ionization fraction as a function of time during the era since recombination. Typical comparisons of cosmological models with observational data now feature between five and ten parameters.

25.1.1 The global description of the Universe

Ordinarily, the Universe is taken to be a perturbed Robertson–Walker space-time, with dynamics governed by Einstein’s equations. This is described in detail in the Big-Bang Cosmology chapter in this volume. Using the density parameters Ω_i for the various matter species and Ω_Λ for the cosmological constant, the Friedmann equation can be written

$$\sum_i \Omega_i + \Omega_\Lambda - 1 = \frac{k}{R^2 H^2}, \quad (25.1)$$

where the sum is over all the different species of material in the Universe. This equation applies at any epoch, but later in this article we will use the symbols Ω_i and Ω_Λ to refer specifically to the present-epoch values.

The complete present-epoch state of the homogeneous Universe can be described by giving the current-epoch values of all the density parameters and the Hubble constant h (the present-day Hubble parameter being written $H_0 = 100h \text{ km s}^{-1} \text{ Mpc}^{-1}$). A typical collection would be baryons Ω_b , photons Ω_γ , neutrinos Ω_ν , and cold dark matter Ω_c (given charge neutrality, the electron density is guaranteed to be too small to be worth considering separately and is effectively included with the baryons). The spatial curvature can then be determined from the other parameters using Eq. (25.1). The total present matter density $\Omega_m = \Omega_c + \Omega_b$ may be used in place of the cold dark matter density Ω_c .

These parameters also allow us to track the history of the Universe, at least back until an epoch where interactions allow interchanges between the densities of the different species; this is believed to have last happened at neutrino decoupling, shortly before Big-Bang Nucleosynthesis (BBN). To probe further back into the Universe’s history requires assumptions about particle interactions, and perhaps about the nature of physical laws themselves.

The standard neutrino sector has three flavors. For neutrinos of mass in the range $5 \times 10^{-4} \text{ eV}$ to 1 MeV, the density parameter in neutrinos is predicted to be

$$\Omega_\nu h^2 = \frac{\sum m_\nu}{93.12 \text{ eV}}, \quad (25.2)$$

where the sum is over all families with mass in that range (higher masses need a more sophisticated calculation). We use units with $c = 1$ throughout. Results on atmospheric and Solar neutrino oscillations [5] imply non-zero mass-squared differences between the

three neutrino flavors. These oscillation experiments cannot tell us the absolute neutrino masses, but within the normal assumption of a mass hierarchy suggest a lower limit of approximately 0.06 eV for the sum of the neutrino masses (see the Neutrino chapter).

Even a mass this small has a potentially observable effect on the formation of structure, as neutrino free-streaming damps the growth of perturbations. Analyses commonly now either assume a neutrino mass sum fixed at this lower limit, or allow the neutrino mass sum to be a variable parameter. To date there is no decisive evidence of any effects from either neutrino masses or an otherwise non-standard neutrino sector, and observations impose quite stringent limits; see the Neutrinos in Cosmology chapter. However, we note that the inclusion of the neutrino mass sum as a free parameter can affect the derived values of other cosmological parameters.

25.1.2 Inflation and perturbations

A complete model of the Universe must include a description of deviations from homogeneity, at least statistically. Indeed, the most powerful probes of the parameters described above come from the evolution of perturbations, so their study is naturally intertwined with the determination of cosmological parameters.

There are many different notations used to describe the perturbations, both in terms of the quantity used and the definition of the statistical measure. We use the dimensionless power spectrum Δ^2 as defined in the Big Bang Cosmology section (also denoted \mathcal{P} in some of the literature). If the perturbations obey Gaussian statistics, the power spectrum provides a complete description of their properties.

From a theoretical perspective, a useful quantity to describe the perturbations is the curvature perturbation \mathcal{R} , which measures the spatial curvature of a comoving slicing of the space-time. A simple case is the Harrison–Zeldovich spectrum, which corresponds to a constant $\Delta_{\mathcal{R}}^2$. More generally, one can approximate the spectrum by a power law, writing

$$\Delta_{\mathcal{R}}^2(k) = \Delta_{\mathcal{R}}^2(k_*) \left[\frac{k}{k_*} \right]^{n_s - 1}, \quad (25.3)$$

where n_s is known as the spectral index, always defined so that $n_s = 1$ for the Harrison–Zeldovich spectrum, and k_* is an arbitrarily chosen scale. The initial spectrum, defined at some early epoch of the Universe’s history, is usually taken to have a simple form such as this power law, and we will see that observations require n_s close to one. Subsequent evolution will modify the spectrum from its initial form.

The simplest mechanism for generating the observed perturbations is the inflationary cosmology, which posits a period of accelerated expansion in the Universe’s early stages [6, 7]. It is a useful working hypothesis that this is the sole mechanism for generating perturbations, and it may further be assumed to be the simplest class of inflationary model, where the dynamics are equivalent to that of a single scalar field ϕ with canonical kinetic energy slowly rolling on a potential $V(\phi)$. One may seek to verify that this simple picture can match observations and to determine the properties of $V(\phi)$ from the observational data. Alternatively, more complicated models, perhaps motivated by contemporary fundamental physics ideas, may be tested on a model-by-model basis (see more in the Inflation chapter in this volume).

Inflation generates perturbations through the amplification of quantum fluctuations, which are stretched to astrophysical scales by the rapid expansion. The simplest models generate two types, density perturbations that come from fluctuations in the scalar field and its corresponding scalar metric perturbation, and gravitational waves that are tensor metric fluctuations. The former experience gravitational instability and lead to structure formation, while both generate CMB anisotropies. Defining slow-roll parameters (with primes indicating derivatives with respect to the scalar field, and $m_{\text{Pl}} \equiv \sqrt{\hbar c/G}$ the Planck mass) as

$$\epsilon = \frac{m_{\text{Pl}}^2}{16\pi} \left(\frac{V'}{V} \right)^2, \quad \eta = \frac{m_{\text{Pl}}^2}{8\pi} \frac{V''}{V}, \quad (25.4)$$

which should satisfy $\epsilon, |\eta| \ll 1$, the spectra can be computed using the slow-roll approximation as

$$\Delta_{\mathcal{R}}^2(k) \simeq \frac{8}{3m_{\text{Pl}}^4} \frac{V}{\epsilon} \Big|_{k=aH}, \quad \Delta_{\mathcal{T}}^2(k) \simeq \frac{128}{3m_{\text{Pl}}^4} V \Big|_{k=aH}. \quad (25.5)$$

In each case, the expressions on the right-hand side are to be evaluated when the scale k is equal to the Hubble radius during inflation. The symbol ‘ \simeq ’ here indicates use of the slow-roll approximation, which is expected to be accurate to a few percent or better.

From these expressions, we can compute the spectral indices [8]:

$$n_s \simeq 1 - 6\epsilon + 2\eta \quad ; \quad n_t \simeq -2\epsilon. \quad (25.6)$$

Another useful quantity is the ratio of the two spectra, defined by

$$r \equiv \frac{\Delta_{\mathcal{T}}^2(k_*)}{\Delta_{\mathcal{R}}^2(k_*)}. \quad (25.7)$$

We have

$$r \simeq 16\epsilon \simeq -8n_t, \quad (25.8)$$

which is known as the consistency equation.

One could consider corrections to the power-law approximation, which we discuss later. However, for now we make the working assumption that the spectra can be approximated by such power laws. The consistency equation shows that r and n_t are not independent parameters, and so the simplest inflation models give initial conditions described by three parameters, usually taken as $\Delta_{\mathcal{R}}^2$, n_s , and r , all to be evaluated at some scale k_* , usually the ‘statistical center’ of the range explored by the data. Alternatively, one could use the parametrization V , ϵ , and η , all evaluated at a point on the putative inflationary potential.

After the perturbations are created in the early Universe, they undergo a complex evolution up until the time they are observed in the present Universe. When the perturbations are small, this can be accurately followed using a linear theory numerical code such as **CAMB** or **CLASS** [9]. This works right up to the present for the CMB, but for density perturbations on small scales non-linear evolution is important and can be addressed by a variety of semi-analytical and numerical techniques. However the analysis is made, the outcome of the evolution is in principle determined by the cosmological model and by the parameters describing the initial perturbations, and hence can be used to determine them.

Of particular interest are CMB anisotropies. Both the total intensity and two independent polarization modes are predicted to have anisotropies. These can be described by the radiation angular power spectra C_{ℓ} as defined in the CMB article in this volume, and again provide a complete description if the density perturbations are Gaussian.

25.1.3 The standard cosmological model

We now have most of the ingredients in place to describe the cosmological model. Beyond those of the previous subsections, we need a measure of the ionization state of the Universe. The Universe is known to be highly ionized at redshifts below 5 or so (otherwise radiation from distant quasars would be heavily absorbed in the ultra-violet), and the ionized electrons can scatter microwave photons, altering the pattern of observed anisotropies. The most convenient parameter to describe this is the optical depth to scattering τ (*i.e.*, the probability that a given photon scatters once); in the approximation of instantaneous and complete reionization, this could equivalently be described by the redshift of reionization z_1 .

As described in Sec. 25.4, models based on these parameters are able to give a good fit to the complete set of high-quality data available at present, and indeed some simplification is possible. Observations are consistent with spatial flatness, and the inflation models so far described automatically generate negligible spatial curvature, so we can set $k = 0$; the density parameters then must sum to unity, and so one of them can be eliminated. The neutrino energy density is often not taken as an independent parameter; provided that the neutrino sector has the standard interactions, the neutrino energy density, while relativistic, can be

related to the photon density using thermal physics arguments, and a minimal assumption takes the neutrino mass sum to be that of the lowest mass solution to the neutrino oscillation constraints, namely 0.06 eV. In addition, there is no observational evidence for the existence of tensor perturbations (with the upper limits now starting to become constraining on models), and so r could be set to zero. This leaves seven parameters, which is the smallest set that can usefully be compared to the present cosmological data. This model is referred to by various names, including Λ CDM, the concordance cosmology, and the standard cosmological model.

Of these parameters, only Ω_{γ} is accurately measured directly. The radiation density is dominated by the energy in the CMB, and the *COBE* satellite FIRAS experiment determined its temperature to be $T = (2.7255 \pm 0.0006) \text{ K}$ [10],¹ corresponding to $\Omega_{\gamma} = 2.47 \times 10^{-5} h^{-2}$. It typically can be taken as fixed when fitting other data. Hence the minimum number of cosmological parameters varied in fits to data is six, though as described below there may additionally be many ‘nuisance’ parameters necessary to describe astrophysical processes influencing the data.

In addition to this minimal set, there is a range of other parameters that might prove important in future as the datasets further improve, but for which there is so far no direct evidence, allowing them to be set to specific values for now. We discuss various speculative options in the next section. For completeness at this point, we mention one other interesting quantity, the helium fraction, which is a non-zero parameter that can affect the CMB anisotropies at a subtle level. It is usually fixed in microwave anisotropy studies, but the data are approaching a level where allowing its variation may become mandatory.

In conventional parameter estimation, a set of parameters is chosen by hand and the aim is to constrain their values. The higher-level inference problem of model selection instead compares different choices of parameter sets, as is necessary to assess whether observations are pointing towards inclusion of new physical effects. Bayesian inference offers an attractive framework for cosmological model selection, setting a tension between model predictiveness and ability to fit the data [11], and its use is becoming widespread.

25.1.4 Derived parameters

The parameter list of the previous subsection is sufficient to give a complete description of cosmological models that agree with observational data. However, it is not a unique parameterization, and one could instead use parameters derived from that basic set. Parameters that can be obtained from the set given above include the age of the Universe, the present horizon distance, the present neutrino background temperature, the epoch of matter–radiation equality, the epochs of recombination and decoupling, the epoch of transition to an accelerating Universe, the baryon-to-photon ratio, and the baryon-to-dark-matter density ratio. In addition, the physical densities of the matter components, $\Omega_i h^2$, are often more useful than the density parameters. The density perturbation amplitude can be specified in many different ways other than the large-scale primordial amplitude, for instance, in terms of its effect on the CMB, or by specifying a short-scale quantity, a common choice being the present linear-theory mass dispersion in a radius of $8 h^{-1} \text{ Mpc}$, known as σ_8 .

Different types of observation are sensitive to different subsets of the full cosmological parameter set, and some are more naturally interpreted in terms of some of the derived parameters of this subsection than on the original base parameter set. In particular, most types of observation feature degeneracies whereby they are unable to separate the effects of simultaneously varying specific combinations of several of the base parameters.

25.2 Extensions to the standard model

At present, there is no positive evidence in favor of extensions of the standard model. These are becoming increasingly constrained by the data, though there always remains the possibility of trace effects at a level below present observational capability.

¹All quoted uncertainties in this article are $1\sigma/68\%$ confidence and all upper limits are 95% confidence. Cosmological parameters sometimes have significantly non-Gaussian uncertainties. Values from original sources have been rounded according to the conventions of this volume.

25.2.1 More general perturbations

The standard cosmology assumes adiabatic, Gaussian perturbations. Adiabaticity means that all types of material in the Universe share a common perturbation, so that if the space-time is foliated by constant-density hypersurfaces, then all fluids and fields are homogeneous on those slices, with the perturbations completely described by the variation of the spatial curvature of the slices. Gaussianity means that the initial perturbations obey Gaussian statistics, with the amplitudes of waves of different wavenumbers being randomly drawn from a Gaussian distribution of width given by the power spectrum. Note that gravitational instability generates non-Gaussianity; in this context, Gaussianity refers to a property of the initial perturbations, before they evolve.

The simplest inflation models, based on one dynamical field, predict adiabatic perturbations and a level of non-Gaussianity that is too small to be detected by any experiment so far conceived. For present data, the primordial spectra are usually assumed to be power laws.

25.2.1.1 Non-power-law spectra

For typical inflation models, it is an approximation to take the spectra as power laws, albeit usually a good one. As data quality improves, one might expect this approximation to come under pressure, requiring a more accurate description of the initial spectra, particularly for the density perturbations. In general, one can expand $\ln \Delta_{\mathcal{R}}^2$ as

$$\ln \Delta_{\mathcal{R}}^2(k) = \ln \Delta_{\mathcal{R}}^2(k_*) + (n_{s,*} - 1) \ln \frac{k}{k_*} + \frac{1}{2} \left. \frac{dn_s}{d \ln k} \right|_* \ln^2 \frac{k}{k_*} + \dots, \quad (25.9)$$

where the coefficients are all evaluated at some scale k_* . The term $dn_s/d \ln k|_*$ is often called the running of the spectral index [12]. Once non-power-law spectra are allowed, it is necessary to specify the scale k_* at which the spectral index is defined.

25.2.1.2 Isocurvature perturbations

An isocurvature perturbation is one that leaves the total density unperturbed, while perturbing the relative amounts of different materials. If the Universe contains N fluids, there is one growing adiabatic mode and $N - 1$ growing isocurvature modes (for reviews see Ref. [7] and Ref. [13]). These can be excited, for example, in inflationary models where there are two or more fields that acquire dynamically-important perturbations. If one field decays to form normal matter, while the second survives to become the dark matter, this will generate a cold dark matter isocurvature perturbation.

In general, there are also correlations between the different modes, and so the full set of perturbations is described by a matrix giving the spectra and their correlations. Constraining such a general construct is challenging, though constraints on individual modes are beginning to become meaningful, with no evidence that any other than the adiabatic mode must be non-zero.

25.2.1.3 Seeded perturbations

An alternative to laying down perturbations at very early epochs is that they are seeded throughout cosmic history, for instance by topological defects such as cosmic strings. It has long been excluded that these are the sole original of structure, but they could contribute part of the perturbation signal, current limits being just a few percent [14]. In particular, cosmic defects formed in a phase transition ending inflation is a plausible scenario for such a contribution.

25.2.1.4 Non-Gaussianity

Multi-field inflation models can also generate primordial non-Gaussianity (reviewed, *e.g.*, in Ref. [7]). The extra fields can either be in the same sector of the underlying theory as the inflaton, or completely separate, an interesting example of the latter being the curvaton model [15]. Current upper limits on non-Gaussianity are becoming stringent, but there remains strong motivation to push down those limits and perhaps reveal trace non-Gaussianity in the data. If non-Gaussianity is observed, its nature may favor an inflationary origin, or a different one such as topological defects.

25.2.2 Dark matter properties

Dark matter properties are discussed in the Dark Matter chapter in this volume. The simplest assumption concerning the dark matter is that it has no significant interactions with other matter, and that its particles have a negligible velocity as far as structure formation is concerned. Such dark matter is described as ‘cold,’ and candidates include the lightest supersymmetric particle, the axion, and primordial black holes. As far as astrophysicists are concerned, a complete specification of the relevant cold dark matter properties is given by the density parameter Ω_c , though those seeking to detect it directly need also to know its interaction properties.

Cold dark matter is the standard assumption and gives an excellent fit to observations, except possibly on the shortest scales where there remains some controversy concerning the structure of dwarf galaxies and possible substructure in galaxy halos. It has long been excluded for all the dark matter to have a large velocity dispersion, so-called ‘hot’ dark matter, as it does not permit galaxies to form; for thermal relics the mass must be above about 1 keV to satisfy this constraint, though relics produced non-thermally, such as the axion, need not obey this limit. However, in future further parameters might need to be introduced to describe dark matter properties relevant to astrophysical observations. Suggestions that have been made include a modest velocity dispersion (warm dark matter) and dark matter self-interactions. There remains the possibility that the dark matter is comprised of two separate components, *e.g.*, a cold one and a hot one, an example being if massive neutrinos have a non-negligible effect.

25.2.3 Relativistic species

The number of relativistic species in the young Universe (omitting photons) is denoted N_{eff} . In the standard cosmological model only the three neutrino species contribute, and its baseline value is assumed fixed at 3.044 (the small shift from 3 is because of a slight predicted deviation from a thermal distribution [16]). However other species could contribute, for example an extra neutrino, possibly of sterile type, or massless Goldstone bosons or other scalars. It is hence interesting to study the effect of allowing this parameter to vary, and indeed although 3.044 is consistent with the data, most analyses currently suggest a somewhat higher value (*e.g.*, Ref. [17]).

25.2.4 Dark energy and modified gravity

While the standard cosmological model given above features a cosmological constant, in order to explain observations indicating that the Universe is presently accelerating, further possibilities exist under the general headings of ‘dark energy’ and ‘modified gravity’. These topics are described in detail in the Dark Energy chapter in this volume. This article focuses on the case of the cosmological constant, since this simple model is a good match to existing data. We note that more general treatments of dark energy/modified gravity will lead to weaker constraints on other parameters.

25.2.5 Complex ionization history

The full ionization history of the Universe is given by the ionization fraction as a function of redshift z . The simplest scenario takes the ionization to have the small residual value left after recombination up to some redshift z_i , at which point the Universe instantaneously reionizes completely. Then there is a one-to-one correspondence between τ and z_i (that relation, however, also depending on other cosmological parameters). An accurate treatment of this process will track separate histories for hydrogen and helium. While currently rapid ionization appears to be a good approximation, as data improve a more complex ionization history may need to be considered.

25.2.6 Varying ‘constants’

Variation of the fundamental constants of Nature over cosmological times is another possible enhancement of the standard cosmology. There is a long history of study of variation of the gravitational constant G_N , and more recently attention has been drawn to the possibility of small fractional variations in the fine-structure constant. There is presently no observational evidence for the former, which is tightly constrained by a variety of mea-

measurements. Evidence for the latter has been claimed from studies of spectral line shifts in quasar spectra at redshift $z \simeq 2$ [18], but this is presently controversial and in need of further observational study.

25.2.7 Cosmic topology

The usual hypothesis is that the Universe has the simplest topology consistent with its geometry, for example that a flat Universe extends forever. Observations cannot tell us whether that is true, but they can test the possibility of a non-trivial topology on scales up to roughly the present Hubble scale. Extra parameters would be needed to specify both the type and scale of the topology; for example, a cuboidal topology would need specification of the three principal axis lengths and orientation. At present, there is no evidence for non-trivial cosmic topology [19].

25.3 Cosmological Probes

The goal of the observational cosmologist is to utilize astronomical information to derive cosmological parameters. The transformation from the observables to the parameters usually involves many assumptions about the nature of the data, as well as of the dark sector. Below we outline the physical processes involved in each of the major probes, and the main recent results. The first two subsections concern probes of the homogeneous Universe, while the remainder consider constraints from perturbations.

In addition to statistical uncertainties we note three sources of systematic uncertainties that will apply to the cosmological parameters of interest: (i) due to the assumptions on the cosmological model and its priors (*i.e.*, the number of assumed cosmological parameters and their allowed range); (ii) due to the uncertainty in the astrophysics of the objects (*e.g.*, light-curve fitting for supernovae or the mass–temperature relation of galaxy clusters); and (iii) due to instrumental and observational limitations (*e.g.*, the effect of ‘seeing’ on weak gravitational lensing measurements, or beam shape on CMB anisotropy measurements).

These systematics, the last two of which appear as ‘nuisance parameters’, pose a challenging problem to the statistical analysis. We attempt a statistical fit to the whole Universe with 6 to 12 parameters, but we might need to include hundreds of nuisance parameters, some of them highly correlated with the cosmological parameters of interest (for example time-dependent galaxy biasing could mimic the growth of mass fluctuations). Fortunately, there is some astrophysical prior knowledge on these effects, and a small number of physically-motivated free parameters would ideally be preferred in the cosmological parameter analysis.

25.3.1 Measures of the Hubble constant

In 1929, Edwin Hubble discovered the law of expansion of the Universe by measuring distances to nearby galaxies. The slope of the relation between the distance and recession velocity is defined to be the present-epoch Hubble constant, H_0 . Astronomers argued for decades about the systematic uncertainties in various methods and derived values over the wide range $40 \text{ km s}^{-1} \text{ Mpc}^{-1} \lesssim H_0 \lesssim 100 \text{ km s}^{-1} \text{ Mpc}^{-1}$.

One of the most reliable results on the Hubble constant came from the Hubble Space Telescope (*HST*) Key Project [20]. This study used the empirical period–luminosity relation for Cepheid variable stars, and calibrated a number of secondary distance indicators: Type Ia Supernovae (SNe Ia); the Tully–Fisher relation; surface-brightness fluctuations; and Type II Supernovae. Various systematics are under investigation, for example *JWST* is helping understanding of the effect of field crowding. This approach has been further extended, *e.g.* using *HST* observations of Cepheids in the hosts of 42 SNe Ia and exploiting Gaia EDR3 parallaxes, the SH0ES team derived $H_0 = (73.0 \pm 1.0) \text{ km s}^{-1} \text{ Mpc}^{-1}$ [21].

Three other methods have been used recently. One is a calibration of the tip of the red-giant branch applied to Type Ia supernovae, the Carnegie–Chicago Hubble Programme (CCHP), finding $H_0 = (69.8 \pm 0.6 \text{ (stat.)} \pm 1.6 \text{ (sys.)}) \text{ km s}^{-1} \text{ Mpc}^{-1}$ [22]. The second uses the method of time delay in gravitationally-lensed quasars; Birrer et al. [23] find $H_0 = 67.4_{-3.2}^{+4.1} \text{ km s}^{-1} \text{ Mpc}^{-1}$ from a sample of 40 lenses. A third method that came to fruition recently is based on gravitational waves; the ‘bright standard siren’ method applied to the binary neutron star GW170817

yields $H_0 = 70_{-8}^{+12} \text{ km s}^{-1} \text{ Mpc}^{-1}$ [24]. Adding two ‘dark standard siren’ systems shifts this to $H_0 = 73_{-8}^{+11} \text{ km s}^{-1} \text{ Mpc}^{-1}$ [25], still dominated by the single bright siren system. The 47 sources in the third Gravitational-Wave Transient Catalog (GWTC-3), again combined with the bright siren, yield the similar result $H_0 = 68_{-8}^{+12} \text{ km s}^{-1} \text{ Mpc}^{-1}$ [26]. When many more gravitational-wave events have been acquired, the future uncertainties on H_0 from standard sirens will get smaller.

The determination of H_0 by the *Planck* Collaboration [2] gives a lower value than most of the above methods, $H_0 = (67.4 \pm 0.5) \text{ km s}^{-1} \text{ Mpc}^{-1}$. As they discuss, there is a strong degeneracy of H_0 with other parameters, particularly Ω_m and the neutrino mass. It is worth noting that using the ‘inverse distance ladder’ method gives a result $H_0 = (67.8 \pm 1.3) \text{ km s}^{-1} \text{ Mpc}^{-1}$ [27], close to the *Planck* result. The inverse distance ladder relies on absolute-distance measurements from baryon acoustic oscillations (BAOs) to calibrate the intrinsic magnitude of the SNe Ia (rather than nearby Cepheids and parallax). This measurement was derived from 207 spectroscopically-confirmed Type Ia supernovae from the Dark Energy Survey (DES), an additional 122 low-redshift SNe Ia, and measurements of BAOs. A combination of DES Year 3 (Y3) clustering and weak lensing with BAO and BBN (assuming Λ CDM) gives $H_0 = (67.6 \pm 0.9) \text{ km s}^{-1} \text{ Mpc}^{-1}$ [28]. The completed Extended Baryon Oscillation Spectroscopic Survey (eBOSS) [29] inverse distance ladder result, within an assumed extended cosmological model, is $H_0 = (68.2 \pm 0.8) \text{ km s}^{-1} \text{ Mpc}^{-1}$, also close to the *Planck* value.

The tension between the H_0 values from *Planck* and the traditional cosmic distance-ladder methods, with the SH0ES result deviating from *Planck* by about 5σ , is under intense investigation for potential systematic effects. There is possibly a trend for higher H_0 derived from the nearby Universe and a lower H_0 from the early Universe, which has led some researchers to propose a time-variation of the dark energy component or other exotic scenarios. Ongoing studies are addressing the question of whether the Hubble tension is due to systematics in at least one of the probes, or a signature of new physics. Figure 25.1 shows a selection of recent H_0 values, summarizing the current status of the Hubble constant tension. See Ref. [30] for a review.

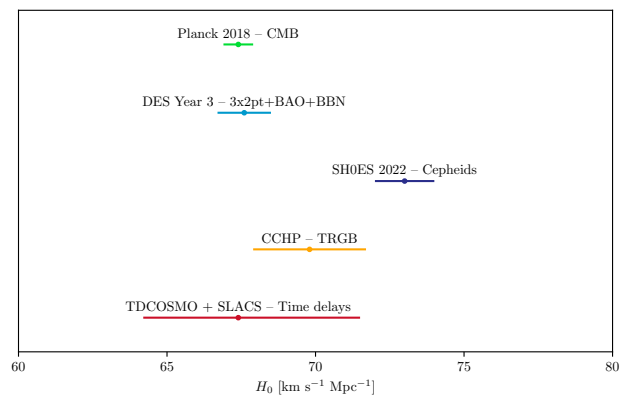


Figure 25.1: A selection of recent H_0 measurements from the various projects as described in the text. The standard-siren determinations are omitted as they are too wide for the plot. Figure courtesy of Pablo Lemos.

25.3.2 Supernovae as cosmological probes

Empirically, the peak luminosity of SNe Ia can be used as an efficient distance indicator (*e.g.*, Ref. [31]), thus allowing cosmology to be constrained via the distance–redshift relation. The favorite theoretical explanation for SNe Ia is the thermonuclear disruption of carbon–oxygen white dwarfs. Although not perfect ‘standard candles,’ it has been demonstrated that by correcting for a relation between the light-curve shape, color, and luminosity at maximum brightness, the dispersion of the measured luminosities can

be greatly reduced. There are several possible systematic effects that may affect the accuracy of the use of SNe Ia as distance indicators, *e.g.*, evolution with redshift and interstellar extinction in the host galaxy and in the Milky Way.

In the late 1990s two major studies, the Supernova Cosmology Project and the High- z Supernova Search Team, found evidence for an accelerating Universe [32], interpreted as due to a cosmological constant or a dark energy component. When combined with the CMB data (which indicate near flatness, *i.e.*, $\Omega_m + \Omega_\Lambda \simeq 1$), the best-fit values were $\Omega_m \simeq 0.3$ and $\Omega_\Lambda \simeq 0.7$. Most results in the literature are consistent with the $w = -1$ cosmological constant case. The leading sample currently is the Pantheon+ compilation [33]. This set of 1550 spectroscopically-confirmed SNe Ia gives $\Omega_m = 0.334 \pm 0.018$ (stat+sym) for an assumed flat Λ CDM model, while in combination with the CMB, for a flat w CDM model these data give $w = -0.98^{+0.2}_{-0.3}$ [34]. Future experiments (*e.g.* DES year 5 SNIa) will refine constraints on the cosmic equation of state $w(z)$.

25.3.3 Cosmic microwave background

The physics of the CMB is described in detail in the CMB chapter in this volume. Before recombination, the baryons and photons are tightly coupled, and the perturbations oscillate in the potential wells generated primarily by the dark matter perturbations. After decoupling, the baryons are free to collapse into those potential wells. The CMB carries a record of conditions at the time of last scattering, often called primary anisotropies. In addition, it is affected by various processes as it propagates towards us, including the effect of a time-varying gravitational potential (the integrated Sachs-Wolfe effect), gravitational lensing, and scattering from ionized gas at low redshift.

The primary anisotropies, the integrated Sachs–Wolfe effect, and the scattering from a homogeneous distribution of ionized gas, can all be calculated using linear perturbation theory. Available codes include **CAMB** and **CLASS** [9], the former widely used embedded within the analysis package **CosmoMC** [35] and in higher-level analysis packages such as **CosmoSIS** [36], **CosmoLike** [37], and **Cobaya** [38]. Gravitational lensing is also calculated in these codes. Secondary effects, such as inhomogeneities in the reionization process, and scattering from gravitationally-collapsed gas (the Sunyaev–Zeldovich or SZ effect), require more complicated, and more uncertain, calculations.

The upshot is that the detailed pattern of anisotropies depends on all of the cosmological parameters. In a typical cosmology, the anisotropy power spectrum [usually plotted as $\ell(\ell+1)C_\ell/2\pi$] features a flat plateau at large angular scales (small ℓ), followed by a series of oscillatory features at higher angular scales, the first and most prominent being at around one degree ($\ell \simeq 200$). These features, known as acoustic peaks, represent the oscillations of the photon–baryon fluid around the time of decoupling. Some features can be closely related to specific parameters—for instance, the location in multipole space of the set of peaks probes the spatial geometry, while the relative heights of the peaks probe the baryon density—but many other parameters combine to determine the overall shape.

The 2018 data release from the *Planck* satellite [1] gives the most powerful results to date on the spectrum of CMB temperature anisotropies, with a precision determination of the temperature power spectrum to beyond $\ell = 2000$. The Atacama Cosmology Telescope (ACT) and South Pole Telescope (SPT) experiments extend these results to higher angular resolution, though without full-sky coverage. *Planck* and the polarization-sensitive versions of ACT and SPT give the current state of the art in measuring the spectrum of E -polarization anisotropies and the correlation spectrum between temperature and polarization. These are consistent with models based on the parameters we have described, and provide accurate determinations of many of those parameters [2]. Primordial B -mode polarization has not been detected (although the gravitational lensing effect on B modes has been measured).

The data provide an exquisite measurement of the location of the set of acoustic peaks, determining the angular-diameter distance of the last-scattering surface. In combination with other data this strongly constrains the spatial geometry, in a manner

consistent with spatial flatness and excluding significantly-curved Universes. CMB data give a precision measurement of the age of the Universe. The CMB also gives a baryon density consistent with, and at higher precision than, that coming from BBN. It affirms the need for both dark matter and dark energy. It shows no evidence for dynamics of the dark energy, being consistent with a pure cosmological constant ($w = -1$). The density perturbations are consistent with a power-law primordial spectrum, and there is no indication yet of tensor perturbations. The current best-fit for the reionization optical depth from CMB data, $\tau = 0.054$, is in line with models of how early structure formation induces reionization.

Planck also made the first all-sky map of the CMB lensing field, which probes the entire matter distribution in the Universe and adds some additional constraining power to the CMB-only datasets. The recent ACT results [39] demonstrate very well the reconstruction of the mass power spectrum at intermediate redshifts from CMB gravitational lensing. These measurements are consistent with *Planck*, supporting Λ CDM (see more in the CMB chapter).

25.3.4 Galaxy clustering

The power spectrum of density perturbations is affected by the nature of the dark matter. Within the Λ CDM model, the power spectrum shape depends primarily on the primordial power spectrum and on the combination $\Omega_m h$, which determines the horizon scale at matter–radiation equality, with a subdominant dependence on the baryon density. The matter distribution is most easily probed by observing the galaxy distribution, but this must be done with care since the galaxies do not perfectly trace the dark matter distribution. Rather, they are a ‘biased’ tracer of the dark matter [40]. The need to allow for such bias is emphasized by the observation that different types of galaxies show bias with respect to each other. In particular, scale-dependent and stochastic biasing may introduce a systematic effect on the determination of cosmological parameters from redshift surveys [41]. Prior knowledge from simulations of galaxy formation or from gravitational lensing data could help to quantify biasing. Furthermore, the observed 3D galaxy distribution is in redshift space, *i.e.*, the observed redshift is the sum of the Hubble expansion and the line-of-sight peculiar velocity, leading to linear and non-linear dynamical effects that also depend on the cosmological parameters. On the largest length scales, the galaxies are expected to trace the location of the dark matter, except for a constant multiplier b to the power spectrum, known as the linear bias parameter. On scales smaller than 20 Mpc or so, the clustering pattern is ‘squashed’ in the radial direction due to coherent infall, which depends approximately on the parameter $\beta \equiv \Omega_m^{0.6}/b$ (on these shorter scales, more complicated forms of biasing are not excluded by the data). On scales of a few Mpc, there is an effect of elongation along the line of sight (colloquially known as the ‘finger of God’ effect) that depends on the galaxy velocity dispersion.

25.3.4.1 Baryon acoustic oscillations

The power spectra of the 2-degree Field (2dF) Galaxy Redshift Survey and the Sloan Digital Sky Survey (SDSS) are well fit by a Λ CDM model and both surveys showed first evidence for baryon acoustic oscillations (BAOs) [42, 43]. When eBOSS is combined with *Planck*, Pantheon Type Ia Supernovae and other probes the result is $w_p = -1.020 \pm 0.032$ at the pivot redshift $z_p = 0.29$ [29]. Similar results for w were obtained *e.g.* by the WiggleZ survey [44]. Preliminary results from the DESI galaxy redshift survey [45] confirm the detection of the BAOs, in agreement with previous surveys.

25.3.4.2 Redshift distortion

There is continuing interest in Kaiser’s ‘redshift distortion’ effect [46]. This distortion depends on cosmological parameters via the perturbation growth rate in linear theory $f(z) = d \ln \delta / d \ln a \simeq \Omega_m^\gamma(z)$, where $\gamma \simeq 0.55$ for the Λ CDM model and may be different for modified gravity models. By measuring $f(z)$ it is feasible to constrain γ and rule out certain modified gravity models [47, 48]. We note the degeneracy of the redshift-distortion pattern and the geometric distortion (the so-called Alcock–Paczynski effect [49]), *e.g.*, as illustrated by the

WiggleZ survey [50] and eBOSS [29].

25.3.4.3 Limits on neutrino mass from galaxy surveys and other probes

Large-scale structure data place constraints on Ω_ν due to the neutrino free-streaming effect [51]. Presently there is no clear detection, and upper limits on neutrino mass are commonly estimated by comparing the observed galaxy power spectrum with a four-component model of baryons, cold dark matter, a cosmological constant, and massive neutrinos. Such analyses also assume that the primordial power spectrum is adiabatic, scale-invariant, and Gaussian. Potential systematic effects include biasing of the galaxy distribution and non-linearities of the power spectrum. An upper limit can also be derived from CMB anisotropies alone, while combination with additional cosmological datasets can improve the results.

The most recent results on neutrino mass upper limits and other neutrino properties are summarized in the Neutrinos in Cosmology chapter in this volume. The latest cosmological data constrain the sum of neutrino masses to be below 0.13 eV [28], consistent with Refs. [2, 29, 39]. Since the lower limit on this sum from oscillation experiments (assuming normal hierarchy) is 0.06 eV it is expected that future cosmological surveys will soon detect effects from neutrino mass. Also, current cosmological datasets are in good agreement with the standard value for the effective number of neutrino species $N_{\text{eff}} = 3.044$.

25.3.5 Clustering in the inter-galactic medium

It is commonly assumed, based on hydrodynamic simulations, that the neutral hydrogen in the inter-galactic medium (IGM) can be related to the underlying mass distribution. It is then possible to estimate the matter power spectrum from the absorption observed in quasar spectra, the so-called Lyman- α forest. The usual procedure is to measure the power spectrum of the transmitted flux, and then to infer the mass power spectrum. Photoionization heating by the ultraviolet background radiation and adiabatic cooling by the expansion of the Universe combine to give a simple power-law relation between the gas temperature and the baryon density. It also follows that there is a power-law relation between the optical depth τ and ρ_b . Therefore, the observed flux $F = \exp(-\tau)$ is strongly correlated with ρ_b , which itself traces the mass density. The matter and flux power spectra can be related by a biasing function that is calibrated from simulations. There are two variants of Lyman-alpha analyses: 1-dimensional power spectra from individual lines-of-sight that probe small (\sim Mpc) scales; and 3-dimensional Lyman-alpha BAO analyses that measure large-scale correlations (over \sim 100 Mpc scales) using neighboring quasar lines-of-sight.

The latest BOSS and eBOSS datasets have provided measurements of the BAO scale both in the Lyman- α absorption and in its cross-correlation with quasars at an effective redshift $z = 2.3$ [29, 52]. The results agree within $1.5\text{-}\sigma$ with the *Planck* CMB flat- Λ estimation for BAO scale. Such measurements will improve with the Dark Energy Spectroscopic Instrument (DESI) and other future spectroscopic surveys. The Lyman- α flux power spectrum has also been used to constrain the nature of dark matter, for example limiting the amount of warm dark matter [53].

25.3.6 Weak gravitational lensing

Images of background galaxies are distorted by the gravitational effect of mass variations along the line of sight. Deep gravitational potential wells, such as galaxy clusters, generate ‘strong lensing’ leading to arcs, arclets, and multiple images, while more moderate perturbations give rise to ‘weak lensing.’ Weak lensing is now widely used to measure the mass power spectrum in selected regions of the sky (see Ref. [54] for reviews). Since the signal is weak, the image of deformed galaxy shapes (the ‘shear map’) must be analyzed statistically to measure the power spectrum, higher moments, and cosmological parameters. There are various systematic effects in the interpretation of weak lensing, *e.g.*, due to atmospheric distortions during observations, the redshift distribution of the background galaxies (usually depending on the accuracy of photometric redshifts), the intrinsic correlation

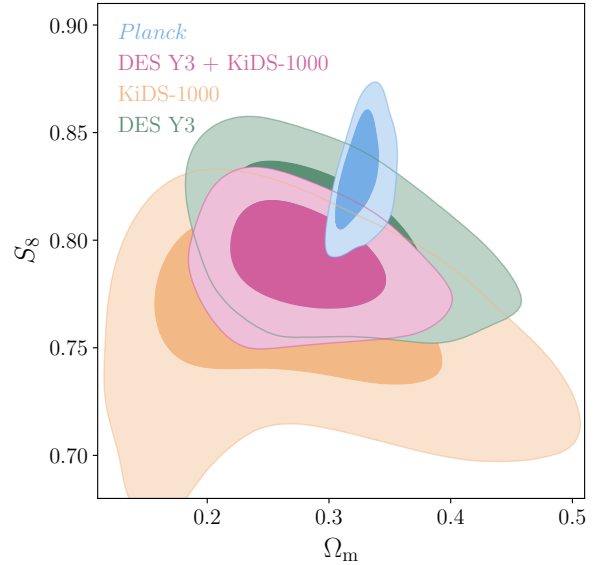


Figure 25.2: Marginalized posterior contours (inner 68% confidence level, outer 95% confidence level) in the Ω_m – S_8 plane. The plot shows KiDS weak lensing alone, DES Y3 weak lensing alone, DES and KiDS combined, and *Planck* CMB. Figure courtesy of Alexandra Amon and the DES and KiDS collaborations.

of galaxy shapes, and non-linear modeling uncertainties.

Weak-lensing measurements from the Kilo-Degree Survey (KiDS) [55], the Subaru Hyper-Suprime-Cam (HSC) [56], and DES [57] have constrained the clumpiness parameter $S_8 \equiv \sigma_8(\Omega_m/0.3)^{0.5}$. Each of these surveys has yielded S_8 lower than that derived from *Planck*. Figure 25.2 shows the Ω_m – S_8 constraints derived from a joint KiDS/DES analysis [58] versus the CMB constraint from *Planck*, where the tension is significantly reduced, to 1.7σ , as compared to previous analyses. Results from weak lensing from DES, combined with other probes, are described in the next section.

25.3.7 Other probes

Other probes that have been used to constrain cosmological parameters, but that are not presently competitive in terms of accuracy, are the integrated Sachs-Wolfe effect [59,60], the number density or composition of galaxy clusters [61], and galaxy peculiar velocities that probe the mass fluctuations in the local Universe [62].

25.4 Bringing probes together

Although it contains two ingredients—dark matter and dark energy—which have not yet been verified by laboratory experiments, the Λ CDM model is almost universally accepted by cosmologists as the best description of the present data. The approximate values of some of the key parameters are $\Omega_b \simeq 0.05$, $\Omega_c \simeq 0.25$, $\Omega_\Lambda \simeq 0.70$, and a Hubble constant $h \simeq 0.70$. The spatial geometry is very close to flat (and usually assumed to be precisely flat), and the initial perturbations Gaussian, adiabatic, and nearly scale-invariant.

The most powerful data source is the CMB, which on its own supports all these main tenets. Values for some parameters, as given in Ref. [2], are reproduced in Table 25.1. These particular results presume a flat Universe. The constraints are somewhat strengthened by adding additional datasets, BAO being shown in the Table as an example, though most of the constraining power resides in the CMB data. Similar constraints at lower precision were previously obtained by the *WMAP* collaboration, and more recently by SPT.

If the assumption of spatial flatness is lifted, it turns out that the primary CMB on its own constrains the spatial curvature fairly weakly, due to a parameter degeneracy in the angular-diameter distance. However, inclusion of other data readily re-

Table 25.1: Parameter constraints reproduced from Ref. [2] (Table 2, column 5), with some additional rounding. Both columns assume the Λ CDM cosmology with a power-law initial spectrum, no tensors, spatial flatness, a cosmological constant as dark energy, and the sum of neutrino masses fixed to 0.06 eV. Above the line are the six parameter combinations actually fit to the data (θ_{MC} is a measure of the sound horizon at last scattering); those below the line are derived from these. The first column uses *Planck* primary CMB data plus the *Planck* measurement of CMB lensing. This column gives our present recommended values. The second column adds in data from a compilation of BAO measurements described in Ref. [2]. The perturbation amplitude $\Delta_{\mathcal{R}}^2$ (denoted A_s in the original paper) is specified at the scale 0.05 Mpc^{-1} . Uncertainties are shown at 68% confidence.

	<i>Planck</i> TT,TE,EE+lowE+lensing	+BAO
$\Omega_b h^2$	0.02237 ± 0.00015	0.02242 ± 0.00014
$\Omega_c h^2$	0.1200 ± 0.0012	0.1193 ± 0.0009
$100 \theta_{\text{MC}}$	1.0409 ± 0.0003	1.0410 ± 0.0003
n_s	0.965 ± 0.004	0.966 ± 0.004
τ	0.054 ± 0.007	0.056 ± 0.007
$\ln(10^{10} \Delta_{\mathcal{R}}^2)$	3.044 ± 0.014	3.047 ± 0.014
h	0.674 ± 0.005	0.677 ± 0.004
σ_8	0.811 ± 0.006	0.810 ± 0.006
Ω_m	0.315 ± 0.007	0.311 ± 0.006
Ω_Λ	0.685 ± 0.007	0.689 ± 0.006

moves this degeneracy. Simply adding the *Planck* lensing measurement, and with the assumption that the dark energy is a cosmological constant, yields a 68% confidence constraint on $\Omega_{\text{tot}} \equiv \sum \Omega_i + \Omega_\Lambda = 1.011 \pm 0.006$ and further adding BAO makes it 0.9993 ± 0.0019 [2]. Results of this type are normally taken as justifying the restriction to flat cosmologies.

One derived parameter that is very robust is the age of the Universe, since there is a useful coincidence that for a flat Universe the position of the first peak is strongly correlated with the age. The CMB data give 13.797 ± 0.023 Gyr (assuming flatness). This is in good agreement with the ages of the oldest globular clusters and with radioactive dating.

The baryon density Ω_b is now measured with high accuracy from CMB data alone, and is consistent with and more precise than the determination from BBN. The value quoted in the Big-Bang Nucleosynthesis chapter in this volume is $\Omega_b h^2 = 0.0220 \pm 0.0004$.

While Ω_Λ is measured to be non-zero with very high confidence, there is no evidence of evolution of the dark energy density. As described in the Dark Energy chapter in this volume a combination of CMB, SN, RSD, and BAO measurements, assuming a flat Universe, yield $w = -1.03 \pm 0.03$ [28], consistent with the cosmological constant case $w = -1$. Allowing more complicated forms of dark energy weakens the limits.

The data provide strong support for the main predictions of the simplest inflation models: spatial flatness and adiabatic, Gaussian, nearly scale-invariant density perturbations. But it is disappointing that there is no sign of primordial gravitational waves; combining *Planck* and *WMAP* with BICEP2/Keck Array BK18 data (plus BAO data to help constrain n_s) gives a 95% confidence upper limit of $r < 0.036$ at the scale 0.05 Mpc^{-1} [63]. The density perturbation spectral index is clearly required to be less than one by current data, though the strength of that conclusion can weaken if additional parameters are included in the model fits.

Tests have been made for various types of non-Gaussianity, a particular example being a parameter f_{NL} that measures a quadratic contribution to the perturbations. Various non-Gaussian shapes are possible (see Ref. [64] for details), and current

constraints on the popular ‘local’, ‘equilateral’, and ‘orthogonal’ types (combining CMB temperature and polarization data) are $f_{\text{NL}}^{\text{local}} = -1 \pm 5$, $f_{\text{NL}}^{\text{equil}} = -26 \pm 47$, and $f_{\text{NL}}^{\text{ortho}} = -38 \pm 24$, respectively (these may appear weak, but prominent non-Gaussianity requires the product $f_{\text{NL}} \Delta_{\mathcal{R}}$ to be large, and $\Delta_{\mathcal{R}}$ is of order 10^{-5}). Clearly none of these give any indication of primordial non-Gaussianity.

While the above results come from the CMB alone, other probes are becoming competitive (especially when considering more complex cosmological models), and so the combination of data from different sources is of growing importance. We note that it has become fashionable to combine probes at the level of power-spectrum data vectors, taking into account nuisance parameters in each type of measurement. Discussions on ‘tension’ in resulting cosmological parameters depend on the statistical approaches used. Commonly the cosmology community works within the Bayesian framework, and assesses agreement amongst data sets with respect to a model via Bayesian evidence, essentially the denominator in Bayes’ theorem.

As an example of results, combining DES Y3 (position–position clustering, galaxy–galaxy lensing, and weak lensing shear) with *Planck*, BAO, and RSD measurements from eBOSS, and Type Ia supernovae from the Pantheon dataset compilation, has shown the datasets to be mutually compatible and yields very tight constraints on cosmological parameters: $S_8 \equiv \sigma_8 (\Omega_m / 0.3)^{0.5} = 0.812 \pm 0.008$ and $\Omega_m = 0.306_{-0.005}^{+0.004}$ in Λ CDM, and $w = -1.03 \pm 0.03$ in w CDM [28] matching the constraint in Ref. [29]. The combined measurement of the Hubble constant within Λ CDM gives $H_0 = 68.0_{-0.3}^{+0.4} \text{ km s}^{-1} \text{ Mpc}^{-1}$, still leaving substantial tension with the SH0ES measurement described earlier. Future analyses and the next generation of surveys will test for deviations from Λ CDM, for example epoch-dependent $w(z)$ and modifications to General Relativity.

25.5 Outlook for the future

The concordance model is now well-established, and there seems little room left for any dramatic revision of this paradigm. A measure of the strength of that statement is how difficult it has proven to formulate convincing alternatives.

Should there indeed be no major revision of the current paradigm, we can expect future developments to take one of two directions. Either the existing parameter set will continue to prove sufficient to explain the data, with the parameters subject to ever-tightening constraints, or it will become necessary to deploy new parameters. The latter outcome would be very much the more interesting, offering a route towards understanding new physical processes relevant to the cosmological evolution. There are many possibilities on offer for striking discoveries, for example:

- the cosmological effects of a neutrino mass may be unambiguously detected, shedding light on fundamental neutrino properties;
- detection of primordial non-Gaussianities would indicate that non-linear processes influence the perturbation generation mechanism;
- detection of variation in the dark energy density (*i.e.*, $w \neq -1$) would provide much-needed experimental input into its nature.

These supply more than enough motivation for continued efforts to test the cosmological model and improve its accuracy. Over the coming years, there are a wide range of new observations that will bring further precision to cosmological studies. Indeed, there are far too many to mention them all here, and so we highlight just a few areas.

The CMB observations will improve in several directions. A current frontier is the study of polarization, for which power spectrum measurements have now been made by several experiments. Detection of primordial B -mode anisotropies is the next major goal and a variety of projects are targeting this, though theory gives little guidance as to the likely signal level. Future CMB projects that are approved include the Simons Observatory and *LiteBIRD*.

An impressive array of cosmology surveys are already operational, under construction, or proposed, including the ground-based Hyper Suprime Camera (HSC) and Rubin-LSSST imaging surveys, spectroscopic surveys such as DESI, and space missions *Euclid* (successfully launched in July 2023) and the *Roman* Space Telescope.

An exciting area for the future is radio surveys of the redshifted 21-cm line of hydrogen. Because of the intrinsic narrowness of this line, by tuning the bandpass the emission from narrow redshift slices of the Universe will be measured to extremely high redshift, probing the details of the reionization process at redshifts up to perhaps 20, as well as measuring large-scale features such as the BAOs. LOFAR and CHIME are the first instruments able to do this and have begun operations. In the longer term, the Square Kilometre Array (SKA) will take these studies to sophisticated levels.

The development of the first precision cosmological model is a major achievement. However, it is important not to lose sight of the motivation for developing such a model, which is to understand the underlying physical processes at work governing the Universe's evolution. From that perspective, progress has been much less dramatic. For instance, there are many proposals for the nature of the dark matter, but no consensus as to which is correct. The nature of the dark energy remains a mystery. Even the baryon density, now measured to an accuracy of a percent, lacks an underlying theory able to predict it within orders of magnitude. Precision cosmology may have arrived, but at present many key questions remain, to motivate and challenge the cosmology community.

References

- [1] Planck Collab. 2018 Results I, *Astron. Astrophys.* **641**, A1 (2020), [arXiv:1807.06205].
- [2] Planck Collab. 2018 Results VI, *Astron. Astrophys.* **641**, A6 (2020), [arXiv:1807.06209].
- [3] C. L. Bennett *et al.* (WMAP), *Astrophys. J. Suppl.* **208**, 20 (2013), [arXiv:1212.5225].
- [4] G. Hinshaw *et al.* (WMAP), *Astrophys. J. Suppl.* **208**, 19 (2013), [arXiv:1212.5226].
- [5] S. Fukuda *et al.* (Super-Kamiokande), *Phys. Rev. Lett.* **85**, 3999 (2000), [hep-ex/0009001]; Q. R. Ahmad *et al.* (SNO), *Phys. Rev. Lett.* **87**, 071301 (2001), [arXiv:nucl-ex/0106015].
- [6] E.W. Kolb and M.S. Turner, *The Early Universe*, Addison-Wesley (Redwood City, 1990).
- [7] D.H. Lyth and A.R. Liddle, *The Primordial Density Perturbation*, Cambridge University Press (2009).
- [8] A. R. Liddle and D. H. Lyth, *Phys. Lett.* **B291**, 391 (1992), [arXiv:astro-ph/9208007].
- [9] A. Lewis, A. Challinor and A. Lasenby, *Astrophys. J.* **538**, 473 (2000), [arXiv:astro-ph/9911177]; D. Blas, J. Lesgourgues and T. Tram, *JCAP* **1107**, 034 (2011), [arXiv:1104.2933].
- [10] D. J. Fixsen, *Astrophys. J.* **707**, 916 (2009), [arXiv:0911.1955].
- [11] M. Hobson *et al.* (eds). *Bayesian Methods in Cosmology*, Cambridge University Press (2009).
- [12] A. Kosowsky and M. S. Turner, *Phys. Rev.* **D52**, R1739 (1995), [arXiv:astro-ph/9504071].
- [13] K. A. Malik and D. Wands, *Phys. Rept.* **475**, 1 (2009), [arXiv:0809.4944].
- [14] Planck Collab. 2013 Results XXV, *Astron. Astrophys.* **571**, A25 (2014), [arXiv:1303.5085].
- [15] D. H. Lyth and D. Wands, *Phys. Lett.* **B524**, 5 (2002), [hep-ph/0110002]; K. Enqvist and M. S. Sloth, *Nucl. Phys.* **B626**, 395 (2002), [hep-ph/0109214]; T. Moroi and T. Takahashi, *Phys. Lett.* **B522**, 215 (2001), [Erratum: *Phys. Lett.* **B539**, 303 (2002)], [hep-ph/0110096].
- [16] J. J. Bennett *et al.*, *JCAP* **04**, 073 (2021), [arXiv:2012.02726].
- [17] S. Riemer-Sorensen, D. Parkinson and T. M. Davis, *Publ. Astron. Soc. Austral.* **30**, e029 (2013), [arXiv:1301.7102].
- [18] J. K. Webb *et al.*, *Phys. Rev. Lett.* **107**, 191101 (2011), [arXiv:1008.3907]; J. A. King *et al.*, *Mon. Not. Roy. Astron. Soc.* **422**, 3370 (2012), [arXiv:1202.4758]; P. Molaro *et al.*, *Astron. & Astrophys.* **555**, 68 (2013).
- [19] Planck Collab. 2015 Results XVIII, *Astron. Astrophys.* **594**, A18 (2016), [arXiv:1502.01593].
- [20] W. L. Freedman *et al.* (HST), *Astrophys. J.* **553**, 47 (2001), [arXiv:astro-ph/0012376].
- [21] A. G. Riess *et al.*, *Astrophys. J. Lett.* **934**, 1, L7 (2022), [arXiv:2112.04510].
- [22] W. L. Freedman, *Astrophys. J.* **919**, 1, 16 (2021), [arXiv:2106.15656].
- [23] S. Birrer *et al.*, *Astron. Astrophys.* **643**, A165 (2020), [arXiv:2007.02941].
- [24] B. P. Abbott *et al.* (LIGO Scientific, Virgo, 1M2H, Dark Energy Camera GW-E, DES, DLT40, Las Cumbres Observatory, VINROUGE, MASTER), *Nature* **551**, 7678, 85 (2017), [arXiv:1710.05835].
- [25] A. Palmese *et al.*, *Astrophys. J.* **943**, 1, 56 (2023), [arXiv:2111.06445].
- [26] R. Abbott *et al.* (LIGO Scientific, Virgo, KAGRA, VIRGO), *Astrophys. J.* **949**, 2, 76 (2023), [arXiv:2111.03604].
- [27] E. Macaulay *et al.* (DES), *Mon. Not. Roy. Astron. Soc.* **486**, 2, 2184 (2019), [arXiv:1811.02376].
- [28] T. M. C. Abbott *et al.* (DES), *Phys. Rev. D* **105**, 2, 023520 (2022), [arXiv:2105.13549].
- [29] S. Alam *et al.* (eBOSS), *Phys. Rev. D* **103**, 8, 083533 (2021), [arXiv:2007.08991].
- [30] P. Shah, P. Lemos and O. Lahav, *Astron. Astrophys. Rev.* **29**, 1, 9 (2021), [arXiv:2109.01161].
- [31] B. Leibundgut, *Ann. Rev. Astron. Astrophys.* **39**, 67 (2001).
- [32] A. G. Riess *et al.* (Supernova Search Team), *Astron. J.* **116**, 1009 (1998), [arXiv:astro-ph/9805201]; P. M. Garnavich *et al.* (Supernova Search Team), *Astrophys. J.* **509**, 74 (1998), [arXiv:astro-ph/9806396]; S. Perlmutter *et al.* (Supernova Cosmology Project), *Astrophys. J.* **517**, 565 (1999), [arXiv:astro-ph/9812133].
- [33] D. Scolnic *et al.*, *Astrophys. J.* **938**, 2, 113 (2022), [arXiv:2112.03863].
- [34] D. Brout *et al.*, *Astrophys. J.* **938**, 2, 110 (2022), [arXiv:2202.04077].
- [35] A. Lewis and S. Bridle, *Phys. Rev.* **D66**, 103511 (2002), [arXiv:astro-ph/0205436].
- [36] J. Zuntz *et al.*, *Astron. Comput.* **12**, 45 (2015), [arXiv:1409.3409].
- [37] E. Krause and T. Eifler, *Mon. Not. Roy. Astron. Soc.* **470**, 2, 2100 (2017), [arXiv:1601.05779].
- [38] J. Torrado and A. Lewis, *JCAP* **05**, 057 (2021), [arXiv:2005.05290].
- [39] M. S. Madhavacheril *et al.* (ACT) (2023), [arXiv:2304.05203].
- [40] N. Kaiser, *Astrophys. J.* **284**, L9 (1984).
- [41] A. Dekel and O. Lahav, *Astrophys. J.* **520**, 24 (1999), [arXiv:astro-ph/9806193].
- [42] D. J. Eisenstein *et al.* (SDSS), *Astrophys. J.* **633**, 560 (2005), [arXiv:astro-ph/0501171].
- [43] S. Cole *et al.* (2dFGRS), *Mon. Not. Roy. Astron. Soc.* **362**, 505 (2005), [arXiv:astro-ph/0501174].
- [44] D. Parkinson *et al.*, *Phys. Rev.* **D86**, 103518 (2012), [arXiv:1210.2130].
- [45] J. Moon *et al.* (DESI) (2023), [arXiv:2304.08427].
- [46] N. Kaiser, *Mon. Not. Roy. Astron. Soc.* **227**, 1 (1987).
- [47] L. Guzzo *et al.*, *Nature* **451**, 541 (2008), [arXiv:0802.1944].

- [48] A. Nusser and M. Davis, *Astrophys. J.* **736**, 93 (2011), [arXiv:1101.1650].
- [49] C. Alcock and B. Paczynski, *Nature* **281**, 358 (1979).
- [50] C. Blake *et al.*, *Mon. Not. Roy. Astron. Soc.* **425**, 405 (2012), [arXiv:1204.3674].
- [51] J. Lesgourgues and S. Pastor, *Phys. Rept.* **429**, 307 (2006), [arXiv:astro-ph/0603494].
- [52] H. du Mas des Bourboux *et al.*, *Astrophys. J.* **901**, 2, 153 (2020), [arXiv:2007.08995].
- [53] M. Viel *et al.*, *Phys. Rev.* **D88**, 043502 (2013), [arXiv:1306.2314].
- [54] A. Refregier, *Ann. Rev. Astron. Astrophys.* **41**, 645 (2003), [arXiv:astro-ph/0307212]; R. Massey *et al.*, *Nature* **445**, 286 (2007), [arXiv:astro-ph/0701594]; H. Hoekstra and B. Jain, *Ann. Rev. Nucl. Part. Sci.* **58**, 99 (2008), [arXiv:0805.0139].
- [55] M. Asgari *et al.* (KiDS), *Astron. Astrophys.* **645**, A104 (2021), [arXiv:2007.15633].
- [56] C. Hikage *et al.* (HSC), *Publ. Astron. Soc. Jap.* **71**, 2, 43 (2019), [arXiv:1809.09148].
- [57] L. F. Secco *et al.* (DES) (2021), [arXiv:2105.13544].
- [58] T. M. C. Abbott *et al.* (Kilo-Degree Survey, DES) (2023), [arXiv:2305.17173].
- [59] R. G. Crittenden and N. Turok, *Phys. Rev. Lett.* **75**, 2642 (1995), [arXiv:astro-ph/9505120].
- [60] Planck Collab. 2015 Results XXI, *Astron. Astrophys.* **594**, A21 (2016), [arXiv:1502.01595].
- [61] Planck Collab. 2015 Results XXIV, *Astron. Astrophys.* **594**, A24 (2016), [arXiv:1502.01597].
- [62] A. Dekel, *Ann. Rev. Astron. Astrophys.* **32**, 371 (1994), [arXiv:astro-ph/9401022].
- [63] P. A. R. Ade *et al.* (BICEP/Keck), *Phys. Rev. Lett.* **127**, 15, 151301 (2021), [arXiv:2110.00483].
- [64] Planck Collab. 2018 Results IX, *Astron. Astrophys.* **641**, A9 (2020), [arXiv:1905.05697].

26. Neutrinos in Cosmology

Revised August 2023 by J. Lesgourgues (TTK, RWTH) and L. Verde (ICC, U. of Barcelona; ICREA, Barcelona).

26.1 Standard neutrino cosmology

Neutrinos leave detectable imprints on cosmological observations that can then be used to constrain neutrino properties. This is a great example of the remarkable interconnection and interplay between nuclear physics, particle physics, astrophysics and cosmology (for general reviews see *e.g.*, [1–4]). Present cosmological data are already providing constraints on neutrino properties not only complementary but also competitive with terrestrial experiments; for instance, upper bounds on the total neutrino mass have shrunk by a factor of about 20 in the past two decades. Forthcoming cosmological data may soon provide key information, not obtainable in other ways like *e.g.*, a measurement of the absolute neutrino mass scale.

A relic neutrino background pervading the Universe (the Cosmic Neutrino background, $C\nu B$) is a generic prediction of the standard hot Big Bang model (see Big Bang Nucleosynthesis – Chap. 24 of this *Review*). While it has not yet been detected directly, it has been indirectly confirmed by the accurate agreement of predictions and observations of: *a*) the primordial abundance of light elements (see Big Bang Nucleosynthesis – Chap. 24) of this *Review*; *b*) the power spectrum of Cosmic Microwave Background (CMB) anisotropies (see Cosmic Microwave Background – Chap. 29 of this *Review*); and *c*) the large-scale clustering of cosmological structures. Within the hot Big Bang model such good agreement would fail dramatically without a $C\nu B$ with properties matching closely those predicted by the standard neutrino decoupling process (*i.e.*, involving only weak interactions).

We will illustrate below that cosmology is sensitive to the following neutrino properties: their density, related to the number of active (*i.e.*, left-handed, see Neutrino Mass, Mixing, and Oscillations – Chap. 14 of this *Review*) neutrino species, and their masses. At first order, cosmology is sensitive to the total neutrino mass, but is blind to the mixing angles and CP violation phase as discussed in Neutrino Mass, Mixing, and Oscillations (Chap. 14 of this *Review*). This makes cosmological constraints nicely complementary to measurements from terrestrial neutrino experiments.

The minimal cosmological model, Λ CDM, currently providing a good fit to most cosmological data sets (with the exception of some data in tension, discussed in The Cosmological Parameters Chap. 25 of this *Review*), assumes that the only massless or light (sub-keV) relic particles since the Big Bang Nucleosynthesis (BBN) epoch are photons and active neutrinos. Extended models with light sterile neutrinos, light thermal axions or other light relics – sometimes referred to as “dark radiation” – would produce effects similar to, and potentially degenerate with, those of active neutrinos. Thus neutrino bounds are often discussed together with limits on such scenarios. In case of anomalies in cosmological data, it might not be obvious to discriminate between interpretation in terms of active neutrinos with non-standard decoupling, additional production mechanisms, non-standard interactions, etc., or in terms of some additional light particles. Such extensions have been explored as a possible way to resolve the H_0 tension between late and early Universe determinations [5–8], but are not widely favoured [9–11].

Hence neutrino density and mass bounds can be derived under the assumption of no additional massless or light relic particles, and the neutrino density measured in that way provides a test of standard (*i.e.*, involving only weak interactions) neutrino decoupling.

In that model, the three active neutrino types thermalize in the early Universe, with a negligible leptonic asymmetry. Then they can be viewed as three propagating mass eigenstates sharing the same temperature and identical Fermi-Dirac distributions, thus with no visible effects of flavour oscillations. Neutrinos decouple gradually from the thermal plasma at temperatures $T \sim 2$ MeV. In the instantaneous neutrino decoupling limit, *i.e.*, assuming that neutrinos were fully decoupled at the time when electron-positrons annihilate and release entropy in the thermal bath, the neutrino-to-photon density ratio between the time of electron-positron an-

ihilation and the non-relativistic transition of neutrinos would be given by

$$\frac{\rho_\nu}{\rho_\gamma} = \frac{7}{8} N_{\text{eff}} \left(\frac{4}{11} \right)^{4/3}, \quad (26.1)$$

with $N_{\text{eff}} = 3$, and the last factor comes from the fourth power of the temperature ratio $T_\nu/T_\gamma = (4/11)^{1/3}$ (see Big Bang Cosmology – Chap. 22 in this *Review*). In the above formula, N_{eff} is called the effective number of neutrino species because it can be viewed as a convenient parametrisation of the relativistic energy density of the Universe beyond that of photons, in units of one neutrino in the instantaneous decoupling limit. Precise simulations of neutrino decoupling and electron-positron annihilation, taking into account flavor oscillations, provide precise predictions for the actual phase-space distribution of relic neutrinos [12–18]. These distributions differ from the instantaneous decoupling approximation through a combination of a small shift in the photon temperature and small flavor-dependent non-thermal distortions, all at the percent level. The final result for the density ratio ρ_ν/ρ_γ in the relativistic regime can always be expressed as in Eq. (26.1), but with a different value of N_{eff} . The most recent analyses, that includes the effect of neutrino oscillations with the present values of the mixing parameters, an improved calculation of the collision terms and the most recent results on plasma thermodynamics QED corrections, give¹ $N_{\text{eff}} = 3.044$ [16, 17]. The precise number density ratio n_ν/n_γ can also be derived from such studies, and is important for computing the ratio $\Omega_\nu h^2 / \sum_i m_i$ (ratio of the physical density of neutrinos in units of the critical density to the sum of neutrino masses) in the non-relativistic regime. Once neutrinos are decoupled, their momentum redshifts like $p \propto 1/a$ but, due to the absence of interactions, their phase-space distributions remain constant when expressed in terms of the comoving momentum $q = pa$, even when they become non-relativistic.

The neutrino temperature today, $T_\nu^0 \simeq 1.7 \times 10^{-4}$ eV $\simeq 1.9$ K, is smaller than at least two of the neutrino masses, since the two squared-mass differences are $|\Delta m_{31}^2|^{1/2} > |\Delta m_{21}^2|^{1/2} > T_\nu^0$ (see Neutrino mass, Mixing, and oscillations – Chap. 14 of this *Review*). Thus at least two neutrino mass eigenstates are non-relativistic today and behave as a small “hot” fraction of the total dark matter (they cannot be all the dark matter, as explained in Chap. 27 in this *Review*). This fraction of hot dark matter can be probed by cosmological experiments, for two related reasons, as we now describe.

First, neutrinos are the only known particles behaving as radiation at early times (during the CMB acoustic oscillations) and dark matter at late times (during structure formation), which has consequences on the background evolution. Neutrinos become non-relativistic when their mass is equal to their average momentum, given for any Fermi-Dirac-distributed particle by $\langle p \rangle = 3.15 T$. Thus the redshift of the non-relativistic transition is given by $z_i^{\text{nr}} = m_i / (3.15 T_\nu^0) - 1 = m_i / [0.53 \text{ meV}] - 1$ for each eigenstate of mass m_i , giving for instance $z_i^{\text{nr}} = 110$ for $m_i = 60$ meV, corresponding to a time deep inside the matter-dominated regime. Second, until the non-relativistic transition, neutrinos travel at the speed of light, and later on they move at a typical velocity $\langle v_i/c \rangle = 3.15 T_\nu(z) / m_i = 0.53(1+z) \text{ meV} / m_i$, which is several orders of magnitude larger than that of the dominant cold (or even of possibly warm) dark matter component(s). This brings their characteristic diffusion scale, called the “free-streaming length”, to cosmological relevant values, with consequences on gravitational clustering and the growth of structure.

Once neutrinos are non-relativistic, their energy density is given by $\rho_\nu \simeq \sum m_i n_i$. Since the number densities n_i are equal to each other (up to negligible corrections coming from flavour effects in the decoupling phase), the total mass $\sum m_\nu = m_1 + m_2 + m_3$ can be factorized out. It is possible that the lightest neutrino is still relativistic today, in which case this relation is slightly incorrect, but given that the total density is always strongly dominated by that of non-relativistic neutrinos, the error made is completely

¹The last effects that potentially require some further checks in order to fully settle the fourth significant digit in N_{eff} are temperature QED corrections; according to [18], the final result might be closer to 3.043 than to 3.044.

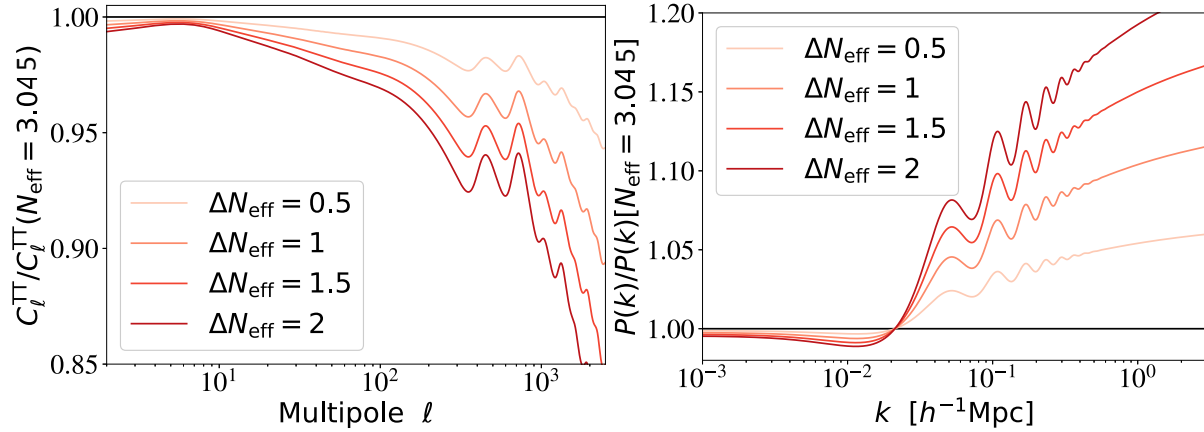


Figure 26.1: Ratio of the CMB C_ℓ^{TT} (left, including lensing effects) and matter power spectrum $P(k)$ (right, computed for each model in units of $(h^{-1}\text{Mpc})^3$) for different values of $\Delta N_{\text{eff}} \equiv N_{\text{eff}} - 3.044$ over those of a reference model with $\Delta N_{\text{eff}} = 0$. In order to minimize and better characterise the effect of N_{eff} on the CMB, the parameters that are kept fixed are $\{z_{\text{eq}}, z_\Lambda, \omega_b, \tau\}$ and the primordial spectrum parameters. Fixing $\{z_{\text{eq}}, z_\Lambda\}$ is equivalent to fixing the fractional density of total radiation, of total matter and of cosmological constant $\{\Omega_r, \Omega_m, \Omega_\Lambda\}$ while increasing the Hubble parameter as a function of N_{eff} . The statistical errors on the C_ℓ are $\sim 1\%$ for a band power of $\Delta\ell = 30$ at $\ell \sim 1000$. The error on $P(k)$ is estimated to be of the order of 5%.

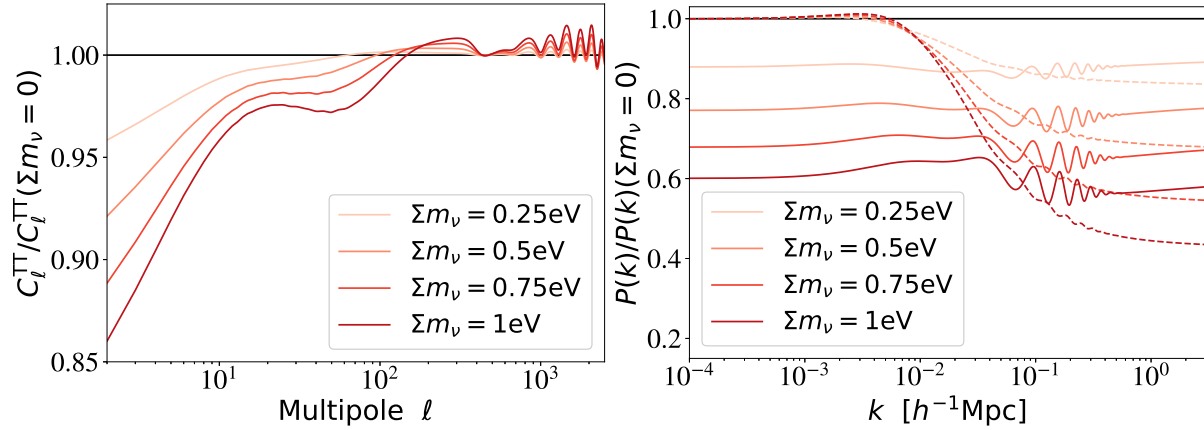


Figure 26.2: Ratio of the CMB C_ℓ^{TT} and matter power spectrum $P(k)$ (computed for each model in units of $(h^{-1}\text{Mpc})^3$) for different values of $\sum m_\nu$ over those of a reference model with massless neutrinos. In order to minimize and better characterise the effect of $\sum m_\nu$ on the CMB, the parameters that are kept fixed are ω_b, ω_c, τ , the angular scale of the sound horizon θ_s and the primordial spectrum parameters (solid lines). This implies that we are increasing the Hubble parameter h as a function of $\sum m_\nu$. For the matter power spectrum, in order to single out the effect of neutrino free-streaming on $P(k)$, the dashed lines show the spectrum ratio when $\{\omega_m, \omega_b, \Omega_\Lambda\}$ are kept fixed. For comparison, the error on $P(k)$ is of the order of 5% with current observations, and the fractional C_ℓ errors are of the order of $1/\sqrt{\ell}$ at low ℓ .

negligible. Using the expression for n_i/n_γ obtained from precise neutrino decoupling studies [16, 17], and knowing n_γ from the measurement of the CMB temperature, one can compute ρ_ν^0 , the total neutrino density today,² in units of the critical density ρ_{crit}^0 :

$$\Omega_\nu = \frac{\rho_\nu^0}{\rho_{\text{crit}}^0} = \frac{\sum m_\nu}{93.12 h^2 \text{ eV}}, \quad (26.2)$$

and the total neutrino average number density today: $n_\nu^0 = 339.5 \text{ cm}^{-3}$ [19]. Here h is the Hubble constant in units of $100 \text{ km s}^{-1} \text{ Mpc}^{-1}$.

26.2 Effects of neutrino properties on cosmological observables

As long as they are relativistic, *i.e.*, until some time deep inside the matter-dominated regime for neutrinos with a mass

²The value 93.12 eV applies to the limit of large masses, in which $\rho_\nu^0 = \sum m_i n_i^0$ and neutrinos are degenerate in mass [19]. This number would be larger by $\sim 0.1\%$ in the limit of minimal normal hierarchy (or smaller by $\sim 0.06\%$ for minimal inverted hierarchy), due the lightest mass state(s) being still relativistic today and to flavor-dependent non-thermal distortions in the neutrino phase-space distributions.

$m_i \ll 3.15 T_\nu^{\text{eq}} \sim 1.5 \text{ eV}$ (see Big Bang Cosmology, Chap. 22 in this *Review*), neutrinos enhance the density of radiation: this effect is parameterised by N_{eff} and can be discussed separately from the effect of the mass that will be described later in this section. Increasing N_{eff} impacts the observable spectra of CMB anisotropies and matter fluctuations through background and perturbation effects.

26.2.1 Effect of N_{eff} on the CMB

The background effects depend on what is kept fixed when increasing N_{eff} . If the densities of other species are kept fixed, a higher N_{eff} implies a smaller redshift of radiation-to-matter equality, with very strong effects on the CMB spectrum: when the amount of expansion between radiation-to-matter equality and photon decoupling is larger, the CMB peaks are suppressed. This effect is not truly characteristic of the neutrino density, since it can be produced by varying several other parameters. Hence, to characterise the effect of N_{eff} , it is more useful and illuminating to enhance the density of total radiation, of total matter and of Λ by exactly the same amount, in order to keep the redshift of radiation-to-matter equality z_{eq} and matter-to- Λ equality z_Λ fixed [20–22]. The primordial spectrum parameters, the baryon

density $\omega_b \equiv \Omega_b h^2$ and the optical depth to reionization τ can be kept fixed at the same time, since we can simply vary N_{eff} together with the Hubble parameter h with fixed $\{\omega_b, \Omega_c, \Omega_\Lambda\}$. The impact of such a transformation is shown in Fig. 26.1 for the CMB temperature spectrum C_ℓ^{TT} (defined in Chap. 29 in this *Review*) and for the matter power spectrum $P(k)$ (defined in Chap. 22 in this *Review*) for several representative values of N_{eff} . These effects are within the reach of cosmological observations given current error bars, as discussed in Section 26.3.1 (for instance, with the *Planck* satellite data, the statistical error on the C_ℓ 's is of the order of one per cent for a band power of $\Delta\ell = 30$ at $\ell \sim 1000$).

With this transformation, the main background effect of N_{eff} is an increase in the diffusion scale (or Silk damping scale, see Cosmic Microwave Background – Chap. 29 in this *Review*) at the time of decoupling, responsible for the decrease in C_ℓ^{TT} at high ℓ , plus smaller effects coming from a slight increase in the redshift of photon decoupling [20–22]. At the level of perturbations, a higher N_{eff} implies that photons feel gravitational forces from a denser neutrino component; this tends to decrease the acoustic peaks (because neutrinos are distributed in a smoother way than photons) and to shift them to larger scales / smaller multipoles (because photon perturbations traveling at the speed of sound in the photon-baryon fluid feel some dragging effect from neutrino perturbations travelling at the speed of light) [20, 22, 23]. The effect of increasing N_{eff} on the polarization spectrum features are the same as on the temperature spectrum: an increased Silk damping, and a shift in the acoustic peak amplitude and location – the latter effect is even more clear in the polarization spectrum, in which the location of acoustic peaks does not get further influenced by a Doppler effect like for temperature. The combination of these effects is truly characteristic of the radiation density parameter N_{eff} and cannot be mimicked by other parameters; thus N_{eff} can be accurately measured from the CMB alone. However, there are correlations between N_{eff} and other parameters. In particular, we have seen (Fig. 26.1) that in order to minimise the effect of N_{eff} on the CMB spectrum, one should vary h at the same time, hence there is a correlation between N_{eff} and h , which implies that independent measurements reducing the error bar on h also reduce that on N_{eff} . Note that this correlation is not equivalent to a perfect degeneracy, so both parameters can be constrained with CMB data alone.

26.2.2 Effect of N_{eff} on the matter spectrum

We have discussed the effect of increasing N_{eff} while keeping z_{eq} and ω_b fixed, because the latter two quantities are very accurately constrained by CMB data. This implies that ω_c increases with N_{eff} , and that the ratio $\omega_b/\omega_c = \Omega_b/\Omega_c$ decreases. However, the ratio of baryonic-to-dark matter has a strong impact on the shape of the matter power spectrum, because until the time of decoupling of the baryons from the photons, CDM experiences gravitational collapse, while baryons are kept smoothly distributed by photon pressure and affected by acoustic oscillations. The decrease of Ω_b/Ω_c following from the increase of N_{eff} gives more weight to the most clustered of the two components, namely the dark matter one, and produces an enhancement of the small-scale matter power spectrum and a damping of the amplitude of baryon acoustic oscillations (BAOs), clearly visible in Fig. 26.1 (right plot). The scale of BAOs is also slightly shifted by the same neutrino dragging effect as for CMB peaks [20, 26].

The increase in the small-scale matter power spectrum is also responsible for a last effect on the CMB spectra: the CMB last scattering surface is slightly more affected by weak lensing from large-scale structures. This tends to smooth the maxima, the minima, and the damping scale of the CMB spectra [27].

26.2.3 Effect of neutrino masses on the CMB

Neutrino eigenstates with a mass $m_i \ll 0.6 \text{ eV}$ become non-relativistic after photon decoupling. They contribute to the non-relativistic matter budget today, but not at the time of equality or recombination. If we increase the neutrino mass while keeping fixed the density of baryons and dark matter (ω_b and ω_c), the early cosmological evolution remains fixed and independent of the neutrino mass, until the time of the non-relativistic tran-

sition. Thus one might expect that the CMB temperature and polarization power spectra are left invariant. This is not true for four reasons.

First, the neutrino density enhances the total non-relativistic density at late times, $\omega_m = \omega_b + \omega_c + \omega_\nu$, where $\omega_\nu \equiv \Omega_\nu h^2$ is given as a function of the total mass $\sum m_\nu$ by Eq. (26.2). The late background evolution impacts the CMB spectrum through the relation between scales on the last scattering surface and angles on the sky, and through the late ISW effect (see Cosmic Microwave Background – Chap. 29 of this *Review*). These two effects depend respectively on the angular diameter distance to recombination, $d_A(z_{\text{rec}})$, and on the redshift of matter-to- Λ equality. Increasing $\sum m_\nu$ tends to modify these two quantities. By playing with h and Ω_Λ , it is possible to keep one of them fixed, but not both at the same time. Since the CMB measures the angular scale of acoustic oscillations with exquisite precision, and is only loosely sensitive to the late ISW effect due to cosmic variance, we choose in Fig. 26.2 to play with the Hubble parameter in order to maintain a fixed scale $d_A(z_{\text{rec}})$. With such a choice, an increase in neutrino mass comes together with a decrease in the late ISW effect explaining the depletion of the CMB spectrum for $l \leq 20$. The fact that both $\sum m_\nu$ and h enter the expression of $d_A(z_{\text{rec}})$ implies that measurements of the neutrino mass from CMB data are strongly correlated with h . Second, the non-relativistic transition of neutrinos affects the total pressure-to-density ratio of the Universe, and causes a small variation of the metric fluctuations. If this transition takes place not too long after photon decoupling, this variation is observable through the early ISW effect [22, 28, 29]. It is responsible for the dip seen in Fig. 26.2 for $20 \leq \ell \leq 200$. Third, when the neutrino mass is higher, the CMB spectrum is less affected by the weak lensing effect induced by the large-scale structure at small redshift. This is due to a decrease in the matter power spectrum described in the next paragraphs. This reduced lensing effect is responsible for most of the oscillatory patterns visible in Fig. 26.2 (left plot) for $\ell \geq 200$. Fourth, the neutrinos with the smallest momenta start to be non-relativistic earlier than the average ones. The photon perturbations feel this through their gravitational coupling with neutrinos. This leads to a small enhancement of C_ℓ^{TT} for $\ell \geq 500$, hardly visible on Fig. 26.2 because it is balanced by the lensing effect.

26.2.4 Effect of neutrino masses on the matter spectrum

The physical effect of neutrinos on the matter power spectrum is related to their velocity dispersion. Neutrinos free-stream over large distances without falling into small potential wells. The free-streaming scale is roughly defined as the distance travel by neutrinos over a Hubble time scale $t_H = (a/\dot{a})$, and approximates the scale below which neutrinos remain very smooth. On larger scales, they cluster in the same way as cold dark matter. The power spectrum of total matter fluctuations, related to the squared fluctuation δ_m^2 with $\delta_m \equiv \delta_b + \delta_c + \delta_\nu$, gets a negligible contribution from the neutrino component on small scales, and is reduced by a factor $(1 - 2f_\nu)$, where $f_\nu = \omega_\nu/\omega_m$. Additionally, on scales below the free-streaming scale, the growth of ordinary cold dark matter and baryon fluctuations is modified by the fact that neutrinos contribute to the background density, but not to the density fluctuations. This changes the balance between the gravitational forces responsible for clustering, and the Hubble friction term slowing it down. Thus the growth rate of CDM and baryon fluctuations is reduced [30]. This results today in an additional suppression of the small-scale linear matter power spectrum by approximately $(1 - 6f_\nu)$. These two effects sum up to a factor $(1 - 8f_\nu)$ [31] (more precise approximations can be found in [2, 22]). The non-linear spectrum is even more suppressed on mildly non-linear scales [3, 32–36].

This effect is often illustrated by plots of the matter power spectrum ratio with fixed parameters $\{\omega_m, \omega_b, \Omega_\Lambda\}$ and varying f_ν , *i.e.*, with the CDM density adjusted to get a fixed total dark matter density [2, 22, 31] (see Fig. 26.2, right plot, dashed lines). This transformation does not leave the redshift of equality z_{eq} invariant, and has very large effects on the CMB spectra. If one follows the logic of minimizing CMB variations and fixing z_{eq} like in the previous paragraphs, the increase in $\sum m_\nu$ must take place together with an increase of h , which tends to suppress the large-

Table 26.1: Summary of N_{eff} constraints.

	Model	N_{eff}	Ref.
CMB alone			
P118[TT,TE,EE+lowE]	$\Lambda\text{CDM}+N_{\text{eff}}$	$2.92^{+0.36}_{-0.37}$ (95%CL)	[24]
CMB + background evolution + LSS			
P118[TT,TE,EE+lowE+lensing] + BAO	$\Lambda\text{CDM}+N_{\text{eff}}$	$2.99^{+0.34}_{-0.33}$ (95%CL)	[24]
"	" +5-params.	$2.85^{+0.23}_{-0.23}$ (68%CL)	[25]

scale power spectrum, by approximately the same amount as the neutrino free-streaming effect [37]. In that case, the impact of neutrino masses on the matter power spectrum appears as an overall amplitude suppression, which can be seen in Fig. 26.2 (right plot, solid lines). The oscillations on intermediate wavenumbers come from a small shift in the BAO scale [37]. This global effect is not degenerate with a variation of the primordial spectrum amplitude A_s , because it only affects the matter power spectrum, and not the CMB spectra. However, the amplitude of the CMB temperature and polarization spectrum is given by the combination $A_s e^{-2\tau}$. Hence a measurement of τ is necessary in order to fix A_s from CMB data, and avoid a parameter degeneracy between $\sum m_\nu$ and A_s [37–39].

A few of the neutrino mass effects described above –free-streaming scale, early ISW– depend on individual masses m_i , but most of them depend only on the total mass through f_ν –suppression of the matter power spectrum, CMB lensing, shift in angular diameter distance–. Because the latter effects are easier to measure, cosmology is primarily sensitive to the total mass $\sum m_\nu$ [40, 41]. The possibility that future data sets might be able to measure individual masses or the mass hierarchy, despite systematic errors and parameter degeneracies, an active area of investigation [42–48].

26.3 Cosmological Constraints on neutrino properties

In this review we focus on cosmological constraints on the abundance and mass of ordinary active neutrinos. Several stringent but model-dependent constraints on non-standard neutrinos (*e.g.*, sterile neutrinos, active neutrinos with interactions beyond the weak force, unstable neutrinos with invisible decay, etc.) can also be found in the literature.

We highlight that cosmological constraints on neutrino properties are always obtained within the framework of a ΛCDM model or simple and popular extensions of this model as spelled out in the following subsections. In light of the emergence of cosmological tensions and especially the so-called Hubble tension which has now reached the $\sim 5\sigma$ level (see Chap. 25 of this *Review*), it is important to bear in mind the following considerations. Inconsistent measurements should not be combined: bounds obtained from combination of discrepant data sets should be considered with extreme caution. Additionally, the constraints reported below assume that the solution of the H_0 tension –whatever that may be– leaves the interpretation of the adopted probes unaffected.

26.3.1 Neutrino abundance

Table 26.1 shows a list of constraints on N_{eff} obtained with several combination of data sets. ‘P118’ denotes the *Planck* 2018 data, composed of a high- ℓ temperature+polarization likelihood (TT,TE,EE), low- ℓ polarization (low E) and CMB lensing spectrum likelihood (lensing) based on lensing extraction from quadratic estimators [24]. ‘BAO’ refers to measurements of the BAO scale (and hence of the angular diameter distance) described in detail in the references given in the table.

Within the framework of a 7-parameter cosmological model ($\Lambda\text{CDM}+N_{\text{eff}}$), the constraint on N_{eff} from the *Planck* 2018 data release [TT,TE,EE+lowE] is $N_{\text{eff}} = 2.92^{+0.36}_{-0.37}$ (95%CL). This number is perfectly compatible with the prediction of the standard neutrino decoupling model, $N_{\text{eff}} = 3.044$, and can be viewed as a proof of self-consistency of the cosmological model.

The bounds can be tightened by adding information on the low-redshift background expansion from BAOs. Finally one may

also add information from large-scale structure (LSS), *i.e.*, on the growth rate and clustering amplitude of matter as a function of scale, although LSS data are not very constraining for the N_{eff} parameter. The second result quoted in Table 26.1 shows that the N_{eff} bound tightens slightly when adding BAO information from the BOSS galaxy survey plus LSS information from the *Planck* CMB lensing spectrum. Adding more recent data on BAOs and redshift-space distortions (RSDs) from the eBOSS galaxy survey [49] only provides a very marginal improvement of the bounds [54]. All combinations of *Planck* 2018 data with BAO and/or LSS data return measurements consistent with the standard expectation.

The situation is different with the inclusion of low-redshift measurements of H_0 with distance ladders (DLs) [55,56], now reaching a 5.7σ tension with *Planck* in the ΛCDM framework. As explained in Section 26.2, the positive correlation between N_{eff} and h means that inclusion of the H_0 measurement would tend to push N_{eff} to higher values. However, the high values of N_{eff} that would potentially reconcile the measured CMB or BAO peak scale with the Hubble parameter suggested by DLs, $H_0 \sim 73$ km/s/Mpc, are excluded by the measurement of the damping tail of the CMB temperature spectrum, either by *Planck* itself (given the previously quoted N_{eff} bounds) or by more recent and independent small-scale CMB data sets (as shown *e.g.* in [57]). Thus, the N_{eff} extension to the ΛCDM model does not reduce the tension significantly, and the combination of *Planck* and DL data does not return any meaningful constraint on N_{eff} in this context. It is currently unclear whether a resolution of the Hubble tension would require a departure from the ΛCDM (or $\Lambda\text{CDM}+N_{\text{eff}}$) model [11, 58–62].

As long as DL data are not included, the error bars on N_{eff} degrade mildly when the data are analysed in the context of more extended cosmological scenarios. Adding only the total neutrino mass as an 8th free parameter has a negligible impact on the bounds. The authors of Ref. [25] take a more extreme point of view and fit a 12-parameter model to P118[TT,TE,EE+lowE+lensing] data; they obtain $N_{\text{eff}} = 2.95 \pm 0.24$ (68% CL), showing that it is very difficult with current cosmological data to accommodate shifts of more than 0.5 from the standard N_{eff} value, and to obtain good fits with, for instance, a fourth (sterile) thermalized neutrino. This is interesting since the anomalies in some oscillation data could be interpreted as evidence for at least one sterile neutrino with a large mixing angle, which would need to be thermalised unless non-standard interactions come into play [5]. In other words, cosmology disfavors the explanation of the oscillations anomalies in terms of extra neutrinos if they are thermalized.

However, if a resolution to the Hubble tension requires a departure from the ΛCDM model or its most simple extensions, the situation is more open. In the presence of new physical ingredients (such as, *e.g.*, non-standard interactions, exotic dark matter candidates, non-minimal dark energy properties or modified gravity), it is in principle conceivable that N_{eff} reaches larger values. However, to date, none of these ingredients has been shown to fully solve the Hubble tension and reconcile CMB, BAO, DL, and supernovae data.

26.3.2 Are they really neutrinos, as expected?

While a value of N_{eff} significantly different from zero (at more than 15σ) and consistent with the expected number 3.044 yields a powerful indirect confirmation of the $C\nu B$, departures from standard N_{eff} could be caused by any ingredient affecting the early-time expansion rate of the Universe. Extra relativistic particles (either decoupled, self-interacting, or interacting with a dark sector), a background of gravitational waves, an oscillating scalar

Table 26.2: Summary of $\sum m_\nu$ constraints.

	Model	95% CL (eV)	Ref.
CMB alone			
P118[TT+lowE]	$\Lambda\text{CDM} + \sum m_\nu$	< 0.54	[24]
P118[TT,TE,EE+lowE]	$\Lambda\text{CDM} + \sum m_\nu$	< 0.26	[24]
CMB + probes of background evolution			
P118[TT,TE,EE+lowE] + BAO	$\Lambda\text{CDM} + \sum m_\nu$	< 0.13	[49]
P118[TT,TE,EE+lowE] + BAO	$\Lambda\text{CDM} + \sum m_\nu + 5 \text{ params.}$	< 0.515	[25]
CMB + LSS			
P118[TT+lowE+lensing]	$\Lambda\text{CDM} + \sum m_\nu$	< 0.44	[24]
P118[TT,TE,EE+lowE+lensing]	$\Lambda\text{CDM} + \sum m_\nu$	< 0.24	[24]
P118[TT,TE,EE+lowE] + ACT[lensing]	$\Lambda\text{CDM} + \sum m_\nu$	< 0.12	[50]
CMB + probes of background evolution + LSS			
P118[TT,TE,EE+lowE] + BAO + RSD	$\Lambda\text{CDM} + \sum m_\nu$	< 0.10	[49]
P118[TT,TE,EE+lowE+lensing] + BAO + RSD + Shape	$\Lambda\text{CDM} + \sum m_\nu$	< 0.082	[51]
P118[TT+lowE+lensing] + BAO + Lyman- α	$\Lambda\text{CDM} + \sum m_\nu$	< 0.087	[52]
P118[TT,TE,EE+lowE] + BAO + RSD + SN + DES-Y1	$\Lambda\text{CDM} + \sum m_\nu$	< 0.12	[49]
P118[TT,TE,EE+lowE] + BAO + RSD + SN + DES-Y3	$\Lambda\text{CDM} + \sum m_\nu$	< 0.13	[53]

field with quartic potential, departures from Einstein gravity, or large extra dimensions are some of the possibilities for such ingredients. In principle one could even assume that the cosmic neutrino background never existed or has decayed (like in the “neutrinoless Universe” model of [63]) while another dark radiation component is responsible for N_{eff} . At least, cosmological data allow to narrow the range of possible interpretations of $N_{\text{eff}} \simeq 3$ to the presence of decoupled relativistic relics like standard neutrinos. Indeed, free-streaming particles leave specific signatures in the CMB and LSS spectra, because their density and pressure perturbations, bulk velocities and anisotropic stress also source the metric perturbations. These signatures can be tested in several ways.

A first approach consists of introducing a self-interaction term in the neutrino equations [6, 7]. Ref. [8] finds that current CMB and BAO data are compatible with no self-interactions. The upper limit to the effective coupling constant G_{eff} for a Fermi-like four-fermions interaction at 95% confidence is $\log_{10}(G_{\text{eff}}\text{MeV}^2) < -1.47$ for P118+BAO [11]. Note however that neutrino self-interactions as strong as $\log_{10}(G_{\text{eff}}\text{MeV}^2) \simeq -1.4$ could reconcile CMB temperature and BAO data with the direct H_0 measurement of Ref [64], but such interactions seem to be hardly compatible with BBN, laboratory constraints [10] and CMB polarization [9, 11].

A second approach consists of introducing two phenomenological parameters, c_{eff} and c_{vis} (see *e.g.*, [65–67]): c_{eff}^2 generalizes the linear relation between isotropic pressure perturbations and density perturbations, while c_{vis}^2 modifies the neutrino anisotropic stress equation. While relativistic free-streaming species have $(c_{\text{eff}}^2, c_{\text{vis}}^2) = (1/3, 1/3)$, a perfect relativistic fluid would have $(c_{\text{eff}}^2, c_{\text{vis}}^2) = (1/3, 0)$. Other values do not necessarily refer to a concrete model, but make it possible to interpolate between these limits. *Planck* data, alone or in combination with galaxy clustering, strongly suggests $(c_{\text{eff}}^2, c_{\text{vis}}^2) = (1/3, 1/3)$ [68–70].

Finally, Ref. [23] (resp. [26]) shows that current data are precise enough to detect the “neutrino drag” effect mentioned in Sec. 26.2 through the measurement of the CMB peak (resp. BAO) scale. These findings show that current cosmological data are able to detect not just the average density of some relativistic relics, but also their anisotropies.

26.3.3 Neutrino masses

Table 26.2 shows a list of constraints on $\sum m_\nu$ obtained with several combinations of data sets. The acronyms ‘P118’ and ‘BAO’ have been described in the previous subsection, while ‘ACT’ refers to CMB observations from the Atacama Cosmology Telescope [50], ‘RSD’ to redshift-space distortions from the eBOSS galaxy survey [49], ‘Shape’ to the shape parameter of the matter power spectrum measured by the BOSS (eBOSS) galaxy redshift survey [51, 71–73], ‘Lyman- α ’ to the one-dimensional flux power spectrum of eBOSS quasars [52], ‘SN’ to the Type Ia supernovae

compilation of [74], ‘DES-Y1’ to the weak lensing and galaxy auto- and cross-correlation measured by the Dark Energy Survey (DES) using Year 1 data [75], and ‘DES-Y3’ for the same quantity estimated from DES Year 3 data [53].

Given that most determinations of N_{eff} are compatible with the standard prediction, $N_{\text{eff}} = 3.044$, it is reasonable to adopt this value as a theoretical prior and to investigate neutrino mass constraints in the context of a minimal 7-parameter model, $\Lambda\text{CDM} + \sum m_\nu$. Under this assumption, the most robust constraints come from *Planck* 2018 temperature and polarization data alone: $\sum m_\nu < 0.26 \text{ eV}$ (95%CL) [24]. Among the four effects of neutrino masses on the CMB spectra described before, current bounds are dominated by the first and the third effects (modified late background evolution, and distortions of the temperature and polarization spectra through weak lensing).

Adding measurements of the BAO scale is crucial, since the determination of the angular diameter distance at small redshift allows us to break parameter degeneracies, for instance between $\sum m_\nu$ and h . The combination of P118[TT,TE,EE+lowE] with the most recent BAO measurements, including the eBOSS Data Release 16 (DR16), gives $\sum m_\nu < 0.13 \text{ eV}$ (95%CL) [49]. Supernovae data are less constraining than BAO data for the neutrino mass determination.

Because the parameter correlation between $\sum m_\nu$ and H_0 is negative, the inclusion of DL data would tend to provide stronger bounds on neutrino masses. However, like for N_{eff} , such bounds would not be meaningful, since they would arise from a combination of discrepant data sets. Thus, to constrain neutrino masses, it is once more crucial to understand whether the Hubble tension arises from unmodeled aspects that have no effect on the current treatment and interpretation of the datasets adopted here or new physical ingredients.

Taking the former point of view, it is interesting to add LSS data sets, sensitive also to the small-scale suppression of the matter power spectrum due to neutrino free-streaming, although most of the constraining power for current data sets comes from the constraints on the expansion history and growth-history signals [76]. The inclusion of CMB lensing data from *Planck* 18 improves the CMB-only bound only by a small amount, but the inclusion of higher resolution CMB lensing maps from ACT [50] brings the limit down to 0.12 eV. To get an even stronger bound, one can add data from the eBOSS survey, which infers the growth rate of structures from RSDs. The addition of BAO and RSD measurements from eBOSS tightens the bound down to $\sum m_\nu < 0.10 \text{ eV}$ (95%CL) [49]. Further including information about the large-scale shape (‘Shape’) of the power spectrum, BOSS+eBOSS data alone give $\sum m_\nu < 0.40 \text{ eV}$ (95%CL) with a BBN prior on ω_b , while *Planck*+BOSS+eBOSS give $\sum m_\nu < 0.082 \text{ eV}$ (95% CL) [51]. A similar bound arises from the most recent Ly α forest data from BOSS combined with *Planck* and BAO data, giving $\sum m_\nu < 0.087 \text{ eV}$ (95% CL). Such bounds already challenge the

inverted hierarchy mass scheme, which predicts $\sum m_\nu \geq 0.11$ eV (e.g., [47] and refs. therein).

It should however be noticed that DES prefers a lower σ_8 value than the *Planck* best fit, relaxing the bound to $\sum m_\nu < 0.12$ eV (95%CL) [49] when using Year 1 data in combination with eBOSS and other datasets (PL18+BAO+RSD+SN+DES). Using Year 3 data and a similar combination, the DES collaboration obtains $\sum m_\nu < 0.13$ eV (95%CL) [53]. Notice however that the DES analysis adopts a theory prior $\sum m_\nu \geq 0.06$ eV while other constraints only assume $\sum m_\nu \geq 0$. For a direct comparison, the combined constraint of reference [49] can be recomputed with the same theory prior and becomes $\sum m_\nu < 0.13$ eV (95%CL).

Leaving aside DL measurements, one finds that upper bounds on neutrino masses become weaker when other data are analysed in the context of extended cosmological models, but only by a small amount. Floating N_{eff} instead of fixing it to 3.044 has no significant impact on the neutrino mass bounds reported in the previous paragraphs. Even in the extreme case considered by Ref. [25], with 12 free cosmological parameters, one can see in Table 26.2 that the bound from *Planck* 2018 (without lensing) + BAO increases from 0.13 eV to 0.52 eV (95% CL) only. This shows that current cosmological data are precise enough to disentangle the effect of several extended cosmological parameters, and that neutrino mass bounds are becoming increasingly robust.

One should stress again that if the explanation of DL measurements requires a cosmological scenario with new – and yet unknown – physical ingredients, the current neutrino mass bounds may in principle be shifted or relaxed. However, in the absence of working scenarios that convincingly explain the Hubble tension without raising other tensions, we do not at the moment have any framework for quoting alternative mass bounds and assessing their model dependence.

26.4 Future prospects and outlook

The cosmic neutrino background has been detected indirectly at very high statistical significance. Direct detection experiments are now being planned, e.g., at the Princeton Tritium Observatory for Light, Early Universe, Massive-neutrino Yield (PTOLEMY) [77]. The detection prospects crucially depend on the exact value of neutrino masses and on the enhancement of their density at the location of the Earth through gravitational clustering in the Milky Way and its sub-halos – an effect however expected to be small [78–81].

Over the past few years the upper limit on the sum of neutrino masses has become increasingly stringent, first indicating that the mass ordering is hierarchical and recently putting the inverted hierarchy under pressure and favouring the normal hierarchy (although quantitative estimates of how disfavoured the inverted hierarchy is vary depending on assumptions, see e.g. [44, 46, 47, 82–84]) which has consequences for planning future double beta-decay experiments. However, these bounds rely on the Λ CDM model or its most simple extensions, and thus, on the assumption that a resolution of the Hubble tension with DL measurements does not affect the modeling and interpretation of the data sets adopted here. If this is not the case, a shift of paradigm might be required, potentially leading to weaker neutrino density and mass bounds.

Neutrino mass and density bounds are expected to keep improving significantly over the next years, thanks to new LSS experiments like DESI [85], Euclid [86], LSST [87], SPHEREx [88] and SKA [89], in combinations with new CMB experiments like Simons Observatory [90], CMB-S4 [91] or LiteBird [92]. If the Λ CDM model is confirmed, and if neutrinos have standard properties, the total neutrino mass should be detected at the level of at least $3-4\sigma$ even at the minimum level allowed by oscillations. This is the conclusion reached by several independent studies, using different dataset combinations (see e.g., [39, 93–98]). One should note that at the minimum level allowed by oscillations $\sum m_\nu \sim 0.06$ eV, neutrinos constitute $\sim 0.5\%$ of the Universe matter density, and their effects on the matter power spectrum is only at the 5% level, implying that exquisite control of systematic errors will be crucial to achieve the required accuracy. At this level, the information coming from the power spectrum

shape is more powerful than that coming from geometrical measurements (e.g., BAO). But exploiting the shape information, especially on small, mildly non-linear or non-linear scales, requires improved understanding of the non-linear regime, and of galaxy bias for galaxy surveys. The fact that different surveys, different probes, and different data set combinations have enough statistical power to reach this level, offers a much needed redundancy and the possibility to perform consistency checks which in turns helps immensely with the control of systematic errors and in making the measurement robust. Using the entire Universe as a particle detector, the on-going and future observational efforts hold the exciting prospect to provide a measurement of the sum of neutrino masses and possibly indication of their mass hierarchy.

References

- [1] A. D. Dolgov, Phys. Rept. **370**, 333 (2002), [hep-ph/0202122].
- [2] J. Lesgourgues and S. Pastor, Phys. Rept. **429**, 307 (2006), [arXiv:astro-ph/0603494].
- [3] S. Hannestad, Prog. Part. Nucl. Phys. **65**, 185 (2010), [arXiv:1007.0658].
- [4] J. Lesgourgues *et al.*, *Neutrino Cosmology*, Cambridge University Press (2013), ISBN 978-1-108-70501-1, 978-1-139-60341-6.
- [5] M. Archidiacono *et al.*, JCAP **1608**, 08, 067 (2016), [arXiv:1606.07673].
- [6] L. Lancaster *et al.*, JCAP **1707**, 07, 033 (2017), [arXiv:1704.06657].
- [7] I. M. Oldengott *et al.*, JCAP **1711**, 11, 027 (2017), [arXiv:1706.02123].
- [8] M. Park *et al.*, Phys. Rev. D **100**, 6, 063524 (2019), [arXiv:1904.02625].
- [9] C. D. Kreisch, F.-Y. Cyr-Racine and O. Doré, Phys. Rev. D **101**, 12, 123505 (2020), [arXiv:1902.00534].
- [10] N. Blinov *et al.*, Phys. Rev. Lett. **123**, 19, 191102 (2019), [arXiv:1905.02727].
- [11] N. Schöneberg *et al.*, Phys. Rept. **984**, 1 (2022), [arXiv:2107.10291].
- [12] J. Birrell, C.-T. Yang and J. Rafelski, Nucl. Phys. **B890**, 481 (2014), [arXiv:1406.1759].
- [13] G. Mangano *et al.*, Nucl. Phys. **B729**, 221 (2005), [hep-ph/0506164].
- [14] E. Grohs *et al.*, Phys. Rev. **D93**, 8, 083522 (2016), [arXiv:1512.02205].
- [15] P. F. de Salas and S. Pastor, JCAP **1607**, 07, 051 (2016), [arXiv:1606.06986].
- [16] J. Froustey, C. Pitrou and M. C. Volpe, JCAP **12**, 015 (2020), [arXiv:2008.01074].
- [17] J. J. Bennett *et al.*, JCAP **04**, 073 (2021), [arXiv:2012.02726].
- [18] M. Cielo *et al.* (2023), [arXiv:2306.05460].
- [19] J. Froustey, *The Universe at the MeV era : neutrino evolution and cosmological observables*, Ph.D. thesis, Institut d’Astrophysique de Paris, France, Paris, Inst. Astrophys. (2022), [arXiv:2209.06672].
- [20] S. Bashinsky and U. Seljak, Phys. Rev. **D69**, 083002 (2004), [arXiv:astro-ph/0310198].
- [21] Z. Hou *et al.*, Phys. Rev. **D87**, 083008 (2013), [arXiv:1104.2333].
- [22] J. Lesgourgues *et al.*, *Neutrino cosmology* (Cambridge University Press, 2013).
- [23] B. Follin *et al.*, Phys. Rev. Lett. **115**, 9, 091301 (2015), [arXiv:1503.07863].
- [24] N. Aghanim *et al.* (Planck), Astron. Astrophys. **641**, A6 (2020), [Erratum: Astron. Astrophys. 652, C4 (2021)], [arXiv:1807.06209].
- [25] E. Di Valentino, A. Melchiorri and J. Silk, JCAP **01**, 013 (2020), [arXiv:1908.01391].

- [26] D. Baumann *et al.*, *Nature Phys.* **15**, 465 (2019), [arXiv:1803.10741].
- [27] A. Lewis and A. Challinor, *Phys. Rept.* **429**, 1 (2006), [arXiv:astro-ph/0601594].
- [28] J. Lesgourgues and S. Pastor, *Adv. High Energy Phys.* **2012**, 608515 (2012), [arXiv:1212.6154].
- [29] Z. Hou *et al.*, *Astrophys. J.* **782**, 74 (2014), [arXiv:1212.6267].
- [30] J. R. Bond, G. Efstathiou and J. Silk, *Phys. Rev. Lett.* **45**, 1980 (1980), [61(1980)].
- [31] W. Hu, D. J. Eisenstein and M. Tegmark, *Phys. Rev. Lett.* **80**, 5255 (1998), [arXiv:astro-ph/9712057].
- [32] S. Bird, M. Viel and M. G. Haehnelt, *Mon. Not. Roy. Astron. Soc.* **420**, 2551 (2012), [arXiv:1109.4416].
- [33] C. Wagner, L. Verde and R. Jimenez, *Astrophys. J.* **752**, L31 (2012), [arXiv:1203.5342].
- [34] C. J. Todero Peixoto, V. de Souza and P. L. Biermann, *JCAP* **1507**, 07, 042 (2015), [arXiv:1502.00305].
- [35] J. Brandbyge and S. Hannestad, *JCAP* **1710**, 10, 015 (2017), [arXiv:1706.00025].
- [36] J. Adamek, R. Durrer and M. Kunz, *JCAP* **1711**, 11, 004 (2017), [arXiv:1707.06938].
- [37] M. Archidiacono *et al.*, *JCAP* **1702**, 02, 052 (2017), [arXiv:1610.09852].
- [38] A. Liu *et al.*, *Phys. Rev.* **D93**, 4, 043013 (2016), [arXiv:1509.08463].
- [39] R. Allison *et al.*, *Phys. Rev.* **D92**, 12, 123535 (2015), [arXiv:1509.07471].
- [40] J. Lesgourgues, S. Pastor and L. Perotto, *Phys. Rev.* **D70**, 045016 (2004), [hep-ph/0403296].
- [41] A. Slosar, *Phys. Rev.* **D73**, 123501 (2006), [arXiv:astro-ph/0602133].
- [42] R. Jimenez *et al.*, *JCAP* **1005**, 035 (2010), [arXiv:1003.5918].
- [43] R. Jimenez, C. P. Garay and L. Verde, *Phys. Dark Univ.* **15**, 31 (2017), [arXiv:1602.08430].
- [44] A. F. Heavens and E. Sellentin, *JCAP* **04**, 047 (2018), [arXiv:1802.09450].
- [45] M. Archidiacono, S. Hannestad and J. Lesgourgues, *JCAP* **09**, 021 (2020), [arXiv:2003.03354].
- [46] F. Capozzi *et al.*, *Phys. Rev. D* **104**, 8, 083031 (2021), [arXiv:2107.00532].
- [47] R. Jimenez *et al.*, *JCAP* **09**, 006 (2022), [arXiv:2203.14247].
- [48] S. Gariazzo, O. Mena and T. Schwetz, *Phys. Dark Univ.* **40**, 101226 (2023), [arXiv:2302.14159].
- [49] S. Alam *et al.* (eBOSS), *Phys. Rev. D* **103**, 8, 083533 (2021), [arXiv:2007.08991].
- [50] M. S. Madhavacheril *et al.* (ACT) (2023), [arXiv:2304.05203].
- [51] S. Brieden, H. Gil-Marín and L. Verde, *JCAP* **08**, 08, 024 (2022), [arXiv:2204.11868].
- [52] N. Palanque-Delabrouille *et al.*, *JCAP* **04**, 038 (2020), [arXiv:1911.09073].
- [53] T. M. C. Abbott *et al.* (DES), *Phys. Rev. D* **105**, 2, 023520 (2022), [arXiv:2105.13549].
- [54] E. di Valentino, S. Gariazzo and O. Mena, *Phys. Rev. D* **106**, 4, 043540 (2022), [arXiv:2207.05167].
- [55] A. G. Riess *et al.*, *Astrophys. J. Lett.* **934**, 1, L7 (2022), [arXiv:2112.04510].
- [56] Y. S. Murakami *et al.* (2023), [arXiv:2306.00070].
- [57] E. Di Valentino *et al.* (2023), [arXiv:2305.12989].
- [58] J. L. Bernal, L. Verde and A. G. Riess, *JCAP* **1610**, 10, 019 (2016), [arXiv:1607.05617].
- [59] L. Verde, T. Treu and A. G. Riess, *Nature Astron.* **3**, 891 (2019), [arXiv:1907.10625].
- [60] J. L. Bernal *et al.*, *Phys. Rev. D* **103**, 10, 103533 (2021), [arXiv:2102.05066].
- [61] E. Di Valentino *et al.*, *Class. Quant. Grav.* **38**, 15, 153001 (2021), [arXiv:2103.01183].
- [62] E. Abdalla *et al.*, *JHEAp* **34**, 49 (2022), [arXiv:2203.06142].
- [63] J. F. Beacom, N. F. Bell and S. Dodelson, *Phys. Rev. Lett.* **93**, 121302 (2004), [arXiv:astro-ph/0404585].
- [64] A. G. Riess *et al.*, *Astrophys. J. Lett.* **908**, 1, L6 (2021), [arXiv:2012.08534].
- [65] W. Hu, *Astrophys. J.* **506**, 485 (1998), [arXiv:astro-ph/9801234].
- [66] W. Hu *et al.*, *Phys. Rev.* **D59**, 023512 (1999), [arXiv:astro-ph/9806362].
- [67] M. Gerbino, E. Di Valentino and N. Said, *Phys. Rev.* **D88**, 6, 063538 (2013), [arXiv:1304.7400].
- [68] B. Audren *et al.*, *JCAP* **1503**, 036 (2015), [arXiv:1412.5948].
- [69] P. A. R. Ade *et al.* (Planck), *Astron. Astrophys.* **594**, A13 (2016), [arXiv:1502.01589].
- [70] S. Kumar, R. C. Nunes and P. Yadav, *JCAP* **09**, 060 (2022), [arXiv:2205.04292].
- [71] T. Simon, P. Zhang and V. Poulin, *JCAP* **07**, 041 (2023), [arXiv:2210.14931].
- [72] A. Semenaite *et al.*, *Mon. Not. Roy. Astron. Soc.* **512**, 4, 5657 (2022), [arXiv:2111.03156].
- [73] C. Moretti *et al.* (2023), [arXiv:2306.09275].
- [74] D. M. Scolnic *et al.*, *Astrophys. J.* **859**, 2, 101 (2018), [arXiv:1710.00845].
- [75] T. M. C. Abbott *et al.* (DES), *Phys. Rev. D* **98**, 4, 043526 (2018), [arXiv:1708.01530].
- [76] A. Boyle and E. Komatsu, *JCAP* **03**, 035 (2018), [arXiv:1712.01857].
- [77] S. Betts *et al.*, in “Proceedings, 2013 Community Summer Study on the Future of U.S. Particle Physics: Snowmass on the Mississippi (CSS2013): Minneapolis, MN, USA, July 29-August 6, 2013,” (2013), [arXiv:1307.4738], URL <http://www.slac.stanford.edu/econf/C1307292/docs/submittedArxivFiles/1307.4738.pdf>.
- [78] A. Ringwald and Y. Y. Y. Wong, *JCAP* **0412**, 005 (2004), [hep-ph/0408241].
- [79] F. Villaescusa-Navarro *et al.*, *JCAP* **1303**, 019 (2013), [arXiv:1212.4855].
- [80] P. F. de Salas *et al.*, *JCAP* **1709**, 09, 034 (2017), [arXiv:1706.09850].
- [81] M. Bauer and J. D. Shergold, *JCAP* **01**, 003 (2023), [arXiv:2207.12413].
- [82] F. Simpson *et al.*, *JCAP* **1706**, 06, 029 (2017), [arXiv:1703.03425].
- [83] S. Hannestad and T. Schwetz, *JCAP* **1611**, 11, 035 (2016), [arXiv:1606.04691].
- [84] S. Roy Choudhury and S. Hannestad, *JCAP* **07**, 037 (2020), [arXiv:1907.12598].
- [85] A. Aghamousa *et al.* (DESI) (2016), [arXiv:1611.00036].
- [86] R. Laureijs *et al.* (EUCLID) (2011), [arXiv:1110.3193].
- [87] Paul A. Abell *et al.*, LSST Science and LSST Project Collaborations, <http://lss.fnal.gov/archive/test-tm/2000/fermilab-tm-2495-a.pdf> (2009) arXiv:0912.0201.
- [88] J. Bock and SPHEREx Science Team, in “American Astronomical Society Meeting Abstracts #231,” volume 231 of *American Astronomical Society Meeting Abstracts*, 354.21 (2018).
- [89] <http://www.skatelescope.org>.
- [90] P. Ade *et al.* (Simons Observatory), *JCAP* **02**, 056 (2019), [arXiv:1808.07445].

- [91] K. N. Abazajian *et al.* (CMB-S4) (2016), [arXiv:1610.02743].
- [92] M. Hazumi *et al.*, J. Low Temp. Phys. **194**, 5-6, 443 (2019).
- [93] C. Carbone *et al.*, JCAP **1103**, 030 (2011), [arXiv:1012.2868].
- [94] J. Hamann, S. Hannestad and Y. Y. Y. Wong, JCAP **1211**, 052 (2012), [arXiv:1209.1043].
- [95] B. Audren *et al.*, JCAP **1301**, 026 (2013), [arXiv:1210.2194].
- [96] R. Pearson and O. Zahn, Phys. Rev. **D89**, 4, 043516 (2014), [arXiv:1311.0905].
- [97] F. Villaescusa-Navarro, P. Bull and M. Viel, Astrophys. J. **814**, 2, 146 (2015), [arXiv:1507.05102].
- [98] T. Brinckmann *et al.*, JCAP **1901**, 059 (2019), [arXiv:1808.05955].

27. Dark Matter

Revised August 2023 by L. Baudis (Zurich U.) and S. Profumo (UC Santa Cruz).

27.1 The case for dark matter

Modern cosmological models invariably include an electromagnetically close-to-neutral, non-baryonic matter species with negligible velocity from the standpoint of structure formation, generically referred to as “cold dark matter” (CDM; see The Big-Bang Cosmology—Sec. 22 of this *Review*). For the benchmark Λ CDM cosmology adopted in the Cosmological Parameters—Sec. 25 of this *Review*, the DM accounts for 26.4% of the critical density in the universe, or 84.4% of the total matter density. The nature of only a small fraction, between at least 0.5% (given neutrino oscillations) and at most 1.6% (from combined cosmological constraints), of the non-baryonic matter content of the universe is known: the three Standard Model neutrinos (see the Neutrino Masses, Mixing, and Oscillations—Sec. 14 of this *Review*). The fundamental makeup of the large majority of the DM is, as of yet, unknown.

Assuming the validity of General Relativity, DM is observed to be ubiquitous in gravitationally collapsed structures of size ranging from the smallest known galaxies [1] to galaxies of size comparable to the Milky Way [2], to groups and clusters of galaxies [3]. The mass-to-light ratio is observed to saturate at the largest collapsed scales to a value indicative, and close to, what inferred from other cosmological observations for the universe as a whole [4]. In such collapsed structures, the existence of DM is inferred directly using tracers of mass enclosed within a certain radius such as stellar velocity dispersion, rotation curves in axisymmetric systems, the virial theorem, gravitational lensing, and measures of the amount of non-dark, i.e. baryonic, mass such as stellar number counts and tracers of gas density such as X-ray emission [5]. The global DM abundance as determined from cosmological probes is discussed in Sec. 22.

The picture of structure formation in modern cosmology heavily relies on, and can be considered an independent and exceptionally strong motivation for, DM. Baryonic density fluctuations at CMB decoupling are observed to be at most on the order of $\delta\rho_b/\rho_b|_{\text{rec}} \approx 10^{-5}$; since density perturbations grow linearly with the scale factor in the linear regime, absent any other matter fluid, one would predict that

$$\delta\rho_b/\rho_b|_{\text{today}} \approx \frac{\delta\rho_b/\rho_b|_{\text{rec}}}{a_{\text{rec}}} \approx 10^{-2}, \quad (27.1)$$

at odds with the observed highly non-linear structures in the universe, $\delta\rho_b/\rho_b|_{\text{obs}} \gg 1$. The presence of a dominant non-relativistic (“cold”) pressure-less matter component decoupled from the thermal bath well before recombination allows instead for the prediction of a matter power spectrum in remarkable agreement with observations [6].

Assuming deviations of gravitational interactions on large scales from general relativity or from its Newtonian limit, certain effects, attributed in the standard scenario to DM, can be explained by modified gravity [7]. Usually such theories mimic the effects otherwise attributed to DM on a limited range of scales, but fail globally, and especially at the largest scales. Key issues that at present appear highly problematic in the framework of theories of modified gravity without DM include (i) predicting the correct spectrum of density perturbations, (ii) predicting the observed anisotropy power spectrum of the CMB, and (iii) explaining weak lensing and X-ray observations of merging clusters such as 1E 0657-558 (the “Bullet” cluster) [8]. The inferred relative speed of gravitational and electromagnetic radiation in GW170817 additionally excludes a significant swath of modified theories of gravity where the two speeds (of gravitational and electromagnetic waves) differ [9].

27.2 Properties of dark matter candidates

Electric charge: The “darkness” of DM can be quantified based on constraints from the CMB and large-scale structure: if the DM is charged, or “milli-charged” (for instance via a kinetic mixing with a dark photon field, producing an effective

suppressed coupling to the visible photon field), it might impact the baryon-photon plasma during recombination; in turn, DM density fluctuations can be suppressed by radiation pressure and photon diffusion, additionally altering the baryon acoustic peak structure. [10] finds that the most stringent constraints stem from the requirement that the DM be completely decoupled from the baryon-photon plasma at recombination, yielding a maximal “milli-electric” charge, in units of the electron charge, of $3.5 \times 10^{-7} (m_{\text{DM}}/1 \text{ GeV})^{0.58}$ for $m_{\text{DM}} > 1 \text{ GeV}$, and of $4.0 \times 10^{-7} (m_{\text{DM}}/1 \text{ GeV})^{0.35}$ for $m_{\text{DM}} < 1 \text{ GeV}$. Limits also exist from structure formation on how optically dark and dissipationless the DM should be.

Self-interactions: Observations of merging clusters [8] and of the ellipticity of certain galaxies as inferred from X-rays [11] constrain the level of DM-DM self interactions. The figure of merit is the ratio of the DM-DM cross section and the DM mass [12] (see Ref. [13] for a review), $\sigma_{\text{DM-DM}}/m_{\text{DM}} < 0.47 \text{ cm}^2/\text{g} \simeq 0.84 \text{ barn}/\text{GeV}$ at 95% C.L.. Assuming a velocity dependence in $\sigma_{\text{DM-DM}}$, “self-interacting DM” has been advocated as a possible solution to certain possible small-scale structure issues in the standard non-collisional ($\sigma_{\text{DM-DM}} \simeq 0$) setup [13, 14] (see Sec. 27.4).

Mass: Lower Limits: Model-independent lower limits for very small DM masses are due to quantum effects: for fermionic DM particles, the phase-space density $f(\vec{x}, \vec{p})$ is bounded from above due to Pauli’s exclusion principle, $f < gh^{-3}$, with g the number of internal degrees of freedom and h Planck’s constant; observations of the velocity dispersion (or, equivalently, measures of the enclosed mass) and physical density in dwarf galaxies, lead to a lower limit on fermionic DM masses, sometimes known as the Tremaine-Gunn limit [15]. Using the Fornax dwarf, Ref. [16] finds $m_F > 70 \text{ eV}$. More stringent limits can be drawn from Lyman- α observations, although such limits depend on the thermal history of the DM. In the case of bosonic DM, the Compton wavelength of an ultra-light species might erase small-scale structure, in conflict with CMB and large-scale structure [17], Lyman- α observations [18, 19], and measurements of high-redshift galaxy luminosity functions and the Milky Way satellite luminosity function [20–22]: these observations indicate that $m_B \gtrsim 10^{-22} \text{ eV}$.

Mass: Upper Limits: General upper limits exist on the mass of the DM constituent from the stability against tidal disruption of structures immersed in DM halos, such as galactic disks and globular clusters, and of individual small galaxies. The most stringent limits can be derived using wide halo binaries [23] and the stability of the star cluster within Eridanus II [24]. Such limits constrain an individual, point-like DM constituent, assuming it makes up 100% of the DM, to be lighter than around $5 M_{\odot}$. (Notice that the mass limits discussed here do not assume any specific production mechanism, and do not depend on the observed cosmological DM density).

Stability: The DM lifetime must be long compared to cosmological timescales [25].

27.3 Genesis of dark matter

The generation of DM in the early universe can proceed via thermal or non-thermal production, or both, or it may result from a particle-antiparticle asymmetry.

Freeze-out: The process of chemical decoupling from the high-temperature, high-density thermal bath (freeze-out) as a paradigm for particle production in the early universe is both a predictive and a successful one. The possibility that just like light elements, neutrinos, and CMB photons, particle DM also originated from a thermal decoupling process has thus garnered significant attention.

A particle species *chemically* decouples when the rate Γ for the species’ number-changing processes drops below the Hubble rate H . Rough estimates for the abundance of relics can be obtained by (i) calculating the freeze-out (i.e. “decoupling”) temperature $T_{\text{f.o.}}$, corresponding to $H(T_{\text{f.o.}}) \sim \Gamma(T_{\text{f.o.}})$, (ii) equating the comoving number density at freeze-out and today, eventually (iii) obtaining the physical density of relic particles today. This procedure assumes that entropy is conserved between $T_{\text{f.o.}}$ and today, an assumption that could well be violated, especially for

heavy relics that decouple early, for instance by entropy injection episodes [26]. Notice also that the freeze-out calculation strongly depends on the assumed background cosmology, and changes e.g. if the early universe is not radiation-dominated around DM decoupling.

The calculation of the freeze-out relic abundance hinges on a Boltzmann equation relating the Liouville operator to the collision operator acting on the phase space density. Under a variety of simplifying assumptions including homogeneity and isotropy, it is possible to reduce the relevant equation for the number density n of a single species pair-annihilating with particles in the thermal bath via 2-to-2 processes to

$$\frac{dn}{dt} - 3Hn = -\langle\sigma v\rangle (n^2 - n_{\text{eq}}^2), \quad (27.2)$$

where $\langle\sigma v\rangle$ is the thermally-averaged pair-annihilation cross section times relative velocity (see Ref. [27]), and n_{eq} is the equilibrium number density. Relics for which the freeze-out temperature is much larger than the particle mass (and thus that freeze-out as ultra-relativistic) are called *hot* relics; if the opposite is true, the relic is instead considered *cold*.

A straightforward calculation shows that to leading order the frozen-out density of *hot* relics is *linearly proportional to the relic particle mass*. The comoving number density $Y = n/s$, where s is the entropy density, for a hot relic is approximately given by its equilibrium value,

$$Y_{\text{f.o.}} \simeq Y_{\text{eq}} \simeq 0.278 \frac{g_{\text{eff}}}{g_{*s}}, \quad (27.3)$$

where g_{eff} is the relic's effective number of degrees of freedom, and g_{*s} is the number of entropic relativistic degrees of freedom, both calculated at $T_{\text{f.o.}}$. The resulting relic abundance, assuming an iso-entropic expansion, is

$$\Omega_{\text{hot}} h^2 = \frac{m Y_{\text{f.o.}} s_0 h^2}{\rho_c} \simeq \frac{m}{93 \text{ eV}}, \quad (27.4)$$

with s_0 the entropy density today, and with the latter equality holding for the case of SM neutrinos, with a freeze-out temperature around 1 MeV (which enters in the final relic abundance through the degrees of freedom dependence on the right-hand-side of Eq. (27.3)).

For *cold* relics, the leading-order dependence of the relic abundance on the DM particle properties is an *inverse proportionality relation to the pair-annihilation cross section*,

$$\Omega_{\text{cold}} h^2 \simeq 0.1 \left(\frac{x_{\text{f.o.}}}{20} \right) \left(\frac{10^{-8} \text{ GeV}^{-2}}{\sigma_{\text{DM+DM} \leftrightarrow \text{anything}}} \right), \quad (27.5)$$

where $x \equiv m_{\text{DM}}/T$. In turn, the freeze-out temperature is approximately given by the solution to the equation

$$\sqrt{x} \cdot e^{-x} = \left(m_{\text{DM}} \cdot M_P \cdot \sigma_{\text{DM+DM} \leftrightarrow \text{anything}} \right)^{-1}, \quad (27.6)$$

where $M_P \simeq 2.435 \times 10^{18}$ GeV is the reduced Planck mass. As a result, $T_{\text{f.o.}} \simeq m_{\text{DM}}/x_{\text{f.o.}}$, with $x_{\text{f.o.}}$ a number between 10 and 50, depending on the cross section, with only a logarithmic dependence on the DM mass. Since for electroweak-scale cross sections and masses $\sigma_{\text{DM+DM}} \simeq 10^{-8} \text{ GeV}^{-2}$, “weakly-interacting massive particles”, or WIMPs have gained exceptional popularity. Notice that Eq. (27.5) bears, however, no connection to the weak scale [28], despite the relation being known as “WIMP miracle”.

Numerous scenarios exist, including notably supersymmetry [29,30] and models with universal extra dimensions [31,32] where the relic abundance of the DM is controlled by processes involving a slightly heavier, unstable, co-annihilating species [33]. In this case the calculation of the abundance of the stable species proceeds similarly to what outlined above, with an effective pair-annihilation cross section that captures the effects of co-annihilation replacing the pair-annihilation cross section [30].

Freeze-in: Collisional processes can lead to the production of out-of-equilibrium particles that progressively accumulate over cosmic time, a process sometimes called *freeze-in*. The abundance

of the frozen-in particles produced at a given redshift depends on the product of the production rate times the Hubble time at that redshift. Freeze-in generally implies that the lightest observable-sector particles decay to the DM with relatively long lifetimes, giving peculiar signals at colliders (see e.g. [34]). Gravitinos are an example of DM candidates possibly produced via a freeze-in type scenario, albeit the portal coupling is in that case via a higher dimensional, Planck-suppressed operator [35].

Cannibalization and other dark-sector number-changing processes: Thermal processes can drive the abundance of the DM beyond simple 2-to-2 number-changing interactions. For instance, DM can “cannibalize” [36,37] itself if $n \rightarrow 2$ processes exist. In this case, a critical aspect is whether or not the DM sector is in thermal contact with the Standard Model thermal bath. If it is, $n \rightarrow 2$ processes can drive the relic abundance, e.g. in the Strongly Interacting Massive Particles (SIMP) scenario [38]. Models exist where the *kinetic decoupling* (i.e. the decoupling from the *thermal equilibrium velocity distribution*) of the two sectors drives the abundance of the DM (elastically decoupling relics, or ELDERS [39]). When the two sectors are not in thermal contact, $n \rightarrow 2$ processes heat the DM sector dramatically, rapidly affecting the temperature ratio between the visible and dark sectors [36,38]. If the relevant cross sections are large enough, and the DM mass light enough, significant effects can arise in structure formation [36].

Non-thermal production: DM production can proceed via processes out of thermal equilibrium (“non-thermal” production). These include DM production via the decay of a “mother” particle [40,41] (or of topological defects [42], moduli [43] etc.) to the DM, or production via gravitational effects.

Asymmetric DM: An enticing alternative possibility for DM production is that of *asymmetric* DM [44,45]: the relic DM abundance arises from an asymmetry between anti-DM and DM. This asymmetry may or may not be related to the baryon-antibaryon asymmetry. If it is, then depending on the model and its thermal history, a relation exists between the mass of the DM and the proton mass. A variety of proposals have been put forward where alternately baryogenesis is explained from a DM sector asymmetry, or vice-versa (see e.g. Ref. [46] for a review).

Primordial Black Holes production: A qualitatively stand-alone class of DM candidates, primordial black holes (PBHs), arises from entirely different mechanisms from what reviewed above. PBHs are thought to originate from gravitational collapse of large density fluctuations in the early universe [47,48]. The over-densities could be produced in a variety of ways, such as topological defects like cosmic strings, necklaces or domain walls, curvature fluctuations from a period of ultra-slow-roll, a sound speed “resonance”, an early phase of matter domination, or sub-horizon phenomena including a phase transition and pre-heating. Albeit the calculation depends on the details of gravitational collapse, the formation time is connected to the PBH mass via $M = \gamma M_{\text{PBH}} \simeq 2 \times 10^5 \gamma \left(\frac{t}{1 \text{ s}} \right) M_{\odot}$, with $\gamma \simeq (1/\sqrt{3})^3$ during radiation domination [49].

27.4 Density and velocity distribution of dark matter

27.4.1 Local density and velocity distribution

The density and distribution of DM in the Milky Way encipher relevant dynamical information about our Galaxy, and are particularly important for direct and indirect detection experiments. The *local density* (ρ_0) is an average over a volume of a few hundred parsecs in the Solar neighbourhood.

To determine the local density from observations, two classes of methods are used [50]. So-called *local measures* rely on the vertical motion of tracer stars in the vicinity of the Sun, while *global measures* extrapolate ρ_0 from the measured rotation curve, with additional assumptions about the Galactic halo shape. Conversely, by comparing the extrapolated local density with the one obtained from local measures, one can constrain the local shape of the Milky Way halo. A major source of uncertainty on ρ_0 is the contribution of baryons (stars, gas, stellar remnants) to the local dynamical mass. For instance, the motion of tracer stars used in local measures is dictated by the total potential generated by

baryons and DM, and a robust baryonic census must be available to infer the additional contribution from DM. Recent determinations from global methods lie in the range $(0.2 - 0.6) \text{ GeV/cm}^3$, while new studies of the local DM density from *Gaia* satellite data yield $(0.3 - 1.5) \text{ GeV/cm}^3$, depending on the type of stars used in the study.

Other observational quantities that enter in the phase space distribution of DM, and provide constraints on mass models of the Milky Way are the local circular speed v_c and the escape velocity v_{esc} . The local circular speed is measured by various methods, roughly divided into measurements of the Sun’s velocity with respect to an object assumed to be at rest with respect to the Galactic centre or direct measurements of the local radial force. These methods yield values of $v_c = (218 - 246) \text{ km/s}$. A recent estimate of the escape velocity, defined as the speed above which objects are not gravitationally bound to our galaxy, is $v_{esc} = 533_{-41}^{+54} \text{ km/s}$ [51] (see also the more recent estimate in [52] of $v_{esc} = 484.6_{-7.4}^{+17.8} \text{ km/s}$, which is not in tension with the value we use).

The local velocity distribution of DM particles can not be measured directly at present, and is mostly derived from simulations. In general, experiments use the simplest, so-called *Standard Halo Model (SHM)* for their data analysis. It assumes an isotropic, isothermal sphere of DM particles with a density profile of $\rho(r) \propto r^{-2}$, for which the velocity distribution is Maxwellian, with a velocity dispersion $\sigma_v = v_c/\sqrt{2}$. This distribution, which formally extends to infinity, is truncated at v_{esc} [53]. Earlier high resolution, dark-matter-only simulations found velocity distributions that markedly deviated from a Maxwell-Boltzmann distribution and in addition revealed components above the dominant smooth distribution, including narrow spikes due to tidal streams. Recent hydrodynamical simulations of Milky Way-like galaxies including baryons, which have a non-negligible effect on the DM distribution in the Solar neighbourhood, find velocity distributions that are indeed close to Maxwellian, arguing that the SHM is a good approximation.

Ultimately the goal is to determine the velocity distribution from observations (for example by studying the motion of stars that share the same kinematics as the DM), and the *Gaia* satellite data offers a unique opportunity to study the various stellar populations. Recently it was revealed that the local stellar halo has two components: a quasi-spherical, weakly rotating structure with metal-poor stars, and a flattened, radially anisotropic structure of metal-rich stars, which arose due to accretion of a large $(10^{11-12} M_\odot)$ dwarf galaxy around $(8-10) \times 10^9$ y ago [54]. The expectation is that the local DM halo shows a similar bimodal structure, and first velocity distributions of the two components - using the stellar populations as tracers - were inferred in [55]. In Ref. [56], an updated halo model is introduced: it includes the anisotropic structure seen in the *Gaia* data and provides an analytic expression for the velocity distribution. The value of the local DM density is updated to $(0.55 \pm 0.17) \text{ GeV/cm}^3$, where the 30% error accounts for the systematics. The circular rotation and the escape speeds are updated to $v_c = (233 \pm 3) \text{ km/s}$ and $v_{esc} = 528_{-25}^{+24} \text{ km/s}$. The former is in agreement with a new Bayesian estimation of the circular velocity using *Gaia* DR3, of $v_c = (233 \pm 7) \text{ km/s}$ [57]. With *Gaia* DR3, new stellar streams are being discovered, some of these likely originating from the disruption and merger of dwarf galaxies. The study of the velocities of such streams will allow for increasingly improved constraints on both the DM subhalo density profiles and the velocity distributions.

27.4.2 Small-scale challenges

The Λ CDM framework is tremendously successful at explaining the observed large-scale structures of the Universe (corresponding to distances $\geq 1 \text{ Mpc}$, the typical inter-galactic distance), as well as the main properties of galaxies that form within DM haloes, see the comprehensive review in Ref. [58]. The observed large-scale structure is consistent with point-like, cold DM particles that interact purely via the gravitational force. However, in the past decades, observations at scales below $\sim 1 \text{ Mpc}$, where structure formation becomes strongly nonlinear, turned out more problematic to be described within the Λ CDM model. The main *small-*

scale challenges are known as: the missing satellites problem, the cusp-core problem and the too-big-to-fail problem. Initially these issues, which are not all independent of one another, arose by comparing theoretical predictions from dark-matter-only simulations to observation. While their most likely solutions are in dissipative, baryonic physics (such gas cooling, star formation, supernovae feedback), see the recent reviews in Ref. [59,60], the small-scale problems could in addition call for a modification or an extension of the Λ CDM paradigm. Most importantly, the ever increasing amount of data on the satellites of the MW and M31 are used to constrain alternative DM models.

The missing satellites problem: High-resolution cosmological simulations of DM haloes the size of the MW predict hundreds or thousands of subhaloes with masses that are in principle large enough to allow for galaxy formation ($> 10^7 M_\odot$). Yet less than ~ 100 satellite galaxies with masses down to $\sim 300 M_\odot$ are known to orbit our galaxy within 300 kpc. Galaxies in the field show a similar under-abundance. One solution could be that galaxy formation becomes increasingly inefficient as the halo mass drops, and thus the smallest DM haloes have naturally failed to form galaxies. Progress in both observations and theoretical modeling of observable properties of dwarf galaxies show that there is very scant evidence for a “missing satellite problem” [60]. Nonetheless, additional, related strong tensions remain, including the *diversity of observed rotation curves* [61] and the *unexpected alignment of satellite planes*, the latter issue possibly solved by high-precision simulations tracking inflow along filaments of the cosmic web [62].

The cusp-core problem: The mass density profiles of DM haloes in Λ CDM simulations rise steeply at small radii, $\rho(r) \propto r^{-\gamma}$, with $\gamma \simeq 0.8 - 1.4$. This is in contrast to the observed density profiles of many low-mass galaxies (albeit not all), the rotation curves of which are best fit with constant-density cores, $\gamma \simeq 0 - 0.5$. A related issue is that simulations predict more DM than measured in the central regions of galaxies (also known as the central density problem). A likely solution is that baryonic feedback modifies the structure of DM haloes. Hydrodynamic simulations which include the effects of baryons on galaxy formation have shown that baryonic feedback (e.g., supernova-driven blowouts) can erase the central cusps and produce core-like density profiles. Surveys of satellites of hundreds of galaxies similar to the Milky Way, such as SAGA [63], will likely provide important observational information.

The too-big-to-fail problem: This problem is related to the fact that the dark matter haloes of the largest observed Milky Way satellites are typically much smaller than those of the most massive subhalos of simulated Milky Way-like haloes. DM haloes of such masses are thought to be too massive to have failed to form stars (hence the name of the problem), especially if lower-mass subhaloes are capable of doing so. A similar issue is present in Andromeda and in field galaxies outside the Local Group. Possible solutions include lowering the mass assumed for the Milky Way host halo, or baryonic effects including tidal stripping and larger-than-expected inner cores [60]. Other issues relate to the origin of ultra-faint galaxies, and the opposite problem of dwarf galaxies with very little dark matter given their stellar mass; there exist proposed solutions to both challenges, including the “bullet dwarf” scenario of Ref. [64].

The solutions that were briefly mentioned above do not require modifications to the Λ CDM framework. Other solutions involve either modifications of linear theory predictions (via the nature of the DM particle, e.g., Warm DM - WDM) or modifications of nonlinear predictions (via DM models that involve a self-interaction of DM particles - SIDM). WDM models postulate particles with masses at the keV-scale, and the observed number of dark-matter-dominated satellites is used to set a lower limit on the number of subhaloes in the MW and thus a lower limit on the particle’s mass [59]. Current constraints are in the range $m_{WDM} > (1.6 - 2.3) \text{ keV}$. Cosmological simulations with SIDM find that $\sigma/m_{SIDM} \simeq (0.5-10) \text{ cm}^2/\text{g}$ can alleviate the cusp-core and too-big-to-fail problems, giving rise to DM cores in dwarf galaxies with sizes of $(0.3-1.5) \text{ kpc}$ [13]. Galaxy clusters provide important constraints, and their large central DM densities pre-

fer models with $\sigma/m_{\text{DM}} \lesssim 0.1 \text{ cm}^2/\text{g}$ [65]. Thus, if SIDM is to solve the small-scale CDM problems and obey the constraints observed on the scales of clusters, σ must depend on the velocity of the particle: it must increase as the rms speed of the particle decreases from the scale of clusters ($v \sim 10^3 \text{ km/s}$) to the scale of dwarf galaxies ($v \sim 10 \text{ km/s}$).

27.5 Dark matter models

Particle DM model building is deeply intertwined with the question of the nature of physics beyond the Standard Model (BSM) of particle physics¹. Directions in this area have followed a few strategies, including, but not limited to

(1) pursuing DM candidates embedded in frameworks that include solutions to other open issues in particle physics, for example WIMPs in connection with electroweak-scale new physics that addresses the hierarchy problem, such as supersymmetry (see the Supersymmetry reviews Sec. 88 and 88); axions in connection with frameworks that address the strong CP problem (see Axions and Other Similar Particles—Sec. 90); sterile neutrinos in connection with the problem of neutrino masses and mixing (see the Neutrino Masses, Mixing, and Oscillations—Sec. 14); or (2) *ad hoc*, or *bottom-up* models built with the intent of addressing or explaining a putative experimental (e.g. particle physical anomalies) or observational (e.g. astronomical) signal.

WIMPs: The WIMP paradigm has been a preferred framework chiefly because it often arises in beyond the Standard Model scenarios that address the hierarchy problem whilst also providing a simple mechanism to explain the observed relic abundance via the “WIMP miracle” described above. Perhaps the most notable example of a framework containing a paradigmatic WIMP is the minimal supersymmetric extension to the Standard Model, if the lightest supersymmetric particle is a neutralino (the mass eigenstate resulting from the mixing of the supersymmetric partners to the Higgses and to the $SU(2)$ and hypercharge gauge bosons, and, possibly, of additional singlet scalars); purely $SU(2)$ sneutrinos have long been ruled out by direct detection, but with suitable mixing with “inert” (gauge-singlet) sneutrinos they can also play the role of WIMP candidates. For more details see the Supersymmetry—Sec. 88 and 89 in this *Review*. Other non-supersymmetric WIMP models include models with a Higgs or Z (or Z') portal, universal extra dimensions [32], and other models with extra (warped or flat) dimensions, little Higgs theories, technicolor and composite Higgs theories, among others (see e.g. the review in [66]).

Axions and axion-like particles: Axions are an especially compelling example of a broad category of DM candidates encompassing very light scalar or pseudoscalar fields. The QCD axion provides a solution to the strong CP problem, and is at present a viable DM candidate (see Sec. 90 for details on motivations, production mechanisms, and detection prospects for the QCD axion). Ultra-light, bosonic DM generally implies the imprint of quantum effects on macroscopic scales (hence the name of *wave* or *fuzzy* DM). Specifically, some of the small-scale issues mentioned in sec. 27.4 can be addressed if the de Broglie wavelength of the DM, of mass m_a and velocity v_a ,

$$\frac{\lambda}{2\pi} = \frac{\hbar}{m_a v_a} \simeq 1.9 \text{ kpc} \left(\frac{10^{-22} \text{ eV}}{m_a} \right) \left(\frac{10 \text{ km/s}}{v_a} \right) \quad (27.7)$$

is comparable to the size of the smallest observed gravitationally collapsed structures, roughly, for a self-gravitating system of mass M , a scale $r \simeq GM/v^2$. The typical expectation is the formation of a soliton-like core in the DM density profile of size λ , thus inversely proportional to the DM mass, with an upper limit on the central density of around

$$\rho_s \lesssim 7 M_\odot/\text{pc}^3 \left(\frac{m_a}{10^{-22} \text{ eV}} \right)^6 \left(\frac{M}{10^9 M_\odot} \right) \quad (27.8)$$

for a halo of virial mass M . Additionally, wave DM predicts that halos lighter than around $10^7 (m_a/10^{-22} \text{ eV})^{-3/2} M_\odot$ should not

exist [67], and that the number of halos in the local universe with a mass at or less $10^9 (m_a/10^{-22} \text{ eV})^{-4/3} M_\odot$ [68] will be significantly depleted, addressing in part the too big to fail and missing satellite problems (see Sec. 27.4 above). Light bosonic DM is necessarily produced non-thermally [69], and the connection with the visible sector need not, but might, exist.

Dark photons: Light *vector* bosons such as a “dark photon” V with a mass below $m_V < 2m_e$, can be cosmologically stable (depending upon its kinetic mixing coupling with the visible photon) and be a viable DM candidate. Light dark photons can be produced in the early universe through scattering or annihilation via processes such as $\gamma e^\pm \rightarrow V e^\pm$ or $e^+ e^- \rightarrow V \gamma$, or via resonant photon-dark photon conversion, or from a condensate seeded by inflationary perturbations [70], or from a misalignment mechanism similar to the one commonly invoked for axion production; constraints on the parameter space stem from a combination of direct detection experiments, where the dark photon is absorbed and leads to a large ionization signal, from stellar cooling constraints from the Sun, horizontal branch stars, and red giants, and from CMB and the diffuse radiation from the $V \rightarrow 3\gamma$ decay mode. More broadly, light dark (pseudo-)scalars and vectors can be best constrained with experiments that rely on their wave-like behaviour and/or on their possible “portal” with the visible sector. A broad assortment of experiments is sensitive to the range of masses between 10^{-22} eV and 10^{-2} eV . Among these experimental efforts, the lowest masses are probed by torsion balance experiments [71, 72], atom interferometry [73], comagnetometers [74, 75], and even gravitational wave detectors [76]; at increasing masses, if the light bosons couple electromagnetically, they can generate effective currents which are detectable with different apparatus depending on the relevant, mass-dependent target frequency. The experimental portfolio includes the broadband axion search ABRACADABRA [77, 78], the LC resonator DM Radio [79], lumped-element LC resonators [80], and cavity resonators such as HAYSTAC [81] and ADMX [82].

Sterile Neutrinos: Sterile (gauge-singlet) neutrinos, assumed to share a Dirac mass term with ordinary, $SU(2)_L$ -active neutrinos, have long been considered viable DM candidates [83]. The mostly-sterile mass eigenstate participates in $SU(2)_L$ interactions via a mixing parameter $\theta \ll 1$ that controls much of the particle’s phenomenology. In particular, the sterile neutrino possesses an inverse-lifetime on the order of $\tau^{-1} \sim G_F^2 m_\nu^5 \theta^2$, forcing the mixing to not exceed

$$\theta < 3.3 \times 10^{-4} \left(\frac{10 \text{ keV}}{m_\nu} \right)^5 \quad (27.9)$$

in order for the lifetime to exceed the age of the universe. While the main decay channel is to three active neutrinos, observationally the radiative decay mode to one neutrino plus a photon is much more relevant, giving rise to a quasi-monochromatic photon line at half the sterile neutrino mass. A recent tentative signal at 3.5 keV was reported from stacked observations of clusters of galaxies, individual clusters [84, 85], and the Galactic center [86] with both the XMM and Chandra X-ray observatories. The signal however was not detected in a large sample of galaxies and groups of galaxies [87] and dwarf galaxies [88], and especially Draco [89], shedding strong doubts on its sterile neutrino decay origin. Future observations with increased energy resolution might conclusively pinpoint the origin of the 3.5 keV emission [90].

Models with rich dark sectors: The absence of any conclusive signals from DM as a particle thus far motivates the hypothesis that the DM be charged under some new “hidden” dark-sector force, an idea that dates back many decades [91], including in the guise of “mirror DM” (more recently in the context of “neutral naturalness”). Top-down motivation for hidden-sector DM comes from string theory [92], although TeV-scale BSM framework such as supersymmetry and composite Higgs models can also naturally accommodate hidden sectors [93]. Although no coupling of the visible sector to the hidden sector need exist in principle, there are a few reasons to expect it [94]. The mass scale for hidden-sector DM is broader than, but overlapping with, that for WIMPs (this latter being limited to roughly between a few GeV and a few TeV). In particular, while some motivation exists for electroweak-scale

¹Notice that this includes the case of PBHs, as successful formation of the correct number density of PBHs involves new ingredients beyond standard cosmology and particle physics

hidden sectors, light, sub-GeV hidden sectors have a strong theoretical underpinning, and offer novel detection avenues and opportunities. The phenomenology of hidden-sector DM depends primarily on the nature of the force and its force carrier. The most-widely considered cases are (pseudo-)scalar and (axial-)vector mediators. Among the structures for the mediators' coupling to the visible sector, renormalizable “portals” include the $H^\dagger H$ operator, through Lagrangian terms of the type $(\mu\phi + \lambda\phi^2)H^\dagger H$, coupling to the hypercharge field strength $B^{\mu\nu}$ via kinetic mixing, $e' B_{\mu\nu} F'^{\mu\nu}$, and the “neutrino” portal, $y_n L H N$, where L is the lepton doublet of any generation, N is a right-handed neutrino, H is the SM Higgs doublet, and y_n the Yukawa coupling. Other possibilities are for instance a vector mediator directly coupled to SM fermions charged under its corresponding symmetry [95], or a Z' associated to $U(1)_{B-L}$. Additional possibilities, arising for instance from vector couplings to anomalous global symmetries of the SM like baryon or lepton number, also exist [94]. The accelerator program necessary to probe hidden-sector DM often involves small-scale colliders and fixed-target experiments, with experiments utilizing missing energy and momentum offering the best sensitivity. Beam-dump experiments can test large ranges of DM-mediator couplings as long as mediators decay or scatter inside the detector (see e.g. the recent review [96]). Such experiments can also probe dark sectors with light vectors coupled to visible matter besides gauge kinetic mixing: an instance are neutrino trident scattering used to place bounds on e.g. $L_\mu - L_\tau$ Z' gauge bosons. Being virtually unconstrained, the phenomenology of dark sectors can be arbitrarily rich, with possibilities ranging from dark non-Abelian gauge interactions creating non-trivial self-interacting and/or particle number-changing dynamics, to models of “dynamical” DM, with multi-component, unstable DM candidates and a time-variable effective total DM abundance and equation of state [97].

27.6 Laboratory detection of dark matter

Laboratory searches for DM particles can be roughly classified in direct detection experiments, axion searches (see Axions and Other Similar Particles—Sec. 90), and searches at accelerators and colliders.

27.6.1 Searches at Accelerators and Colliders

Various searches for dark matter have been carried out by the CMS and ATLAS collaborations at the LHC in pp collisions [98–102]. In general, these assume that dark matter particles escape the detector without interacting leading to significant amounts of missing energy and momentum.

Searches for DM with the LHC and other colliders have targeted DM models that interact with the SM via Higgs or Z boson exchange, effective field theories with heavy mediators, UV-complete models such as supersymmetry, models with long-lived particles, and models with rich dark sectors. The experimental program correspondingly includes searches for invisible-particle production mediated by a SM boson, generic searches for invisible particles produced via new particle mediators, and specific searches for complete models.

There are a variety of types of signals for DM, as noted by Ref. [98]:

- (a) the imbalance in the transverse momentum in an event due to the presence of DM particles, produced together with one Standard Model particle,
- (b) a bump in the di-jet or di-lepton invariant mass distributions, or
- (c) an excess of events in the di-jet angular distribution, produced by a dark matter mediator. No signal for DM has been observed in the LHC experiments so far. Instead, limits are set on masses, couplings, and cross-sections. The latter can be compared, generally in a model-dependent way, with direct detection experiments.

Searches strategies are designed to optimize signal-to-noise by selecting search-specific cuts: a model-independent instance is initial-state electromagnetic or strong-interaction radiation plus missing transverse energy. Collider searches for DM inform, and are informed, by DM searches through direct or indirect detection (see below), and, if possible, by the inferred thermal relic

DM abundance. The collider searches alone cannot prove that a discovery is of dark matter.

In the latter category, searches for DM with the LHC and other colliders have targeted DM models that interact with the SM via Higgs or Z boson exchange, effective field theories with heavy mediators, UV-complete models such as supersymmetry, models with long-lived particles, and models with rich dark sectors. The experimental program correspondingly includes searches for invisible-particle production mediated by a SM boson, generic searches for invisible particles produced via new particle mediators, and specific searches for complete models. Searches strategies are designed to optimize signal-to-noise by selecting specific search-specific cuts: a model-independent instance is initial-state electromagnetic or strong-interaction radiation plus missing transverse energy.

New fixed-target experiments are increasingly probing lighter, sub-GeV dark sectors; thermal, or quasi-thermal relics (such as asymmetric, SIMP, ELDER DM models) provide sharp, largely model-independent experimental targets in the case of direct annihilation to Standard Model particles; even “secluded” annihilation to dark-sector particles can be probed with fixed-target experiments, albeit with some model-dependent caveats. Accelerator searches provide unique ways to test light DM models in that they present a lower dependence on the DM particle nature, that could e.g. drive suppressed velocity-dependent direct detection cross sections, and on kinematic thresholds that can similarly suppress rates with other search strategies; additionally, accelerator searches offer opportunities to explore dark sectors in greater detail than other search strategies [94].

Experimental approaches to explore scenarios with a light DM χ and mediator A' include (i) searches for missing mass in exclusive reactions such as $e^+e^- \rightarrow \gamma(A'\chi\bar{\chi})$ or $e^-p \rightarrow e^-p(A'\chi\bar{\chi})$, (ii) missing momentum/energy, e.g. in fixed-target reactions such as $eZ \rightarrow eZ(A'\chi\bar{\chi})$, (iii) electron and proton beam dump, where the DM particle is detected from scattering in a downstream detector after being produced in the beam dump, (iv) direct dark photon searches, when the mediator cannot decay to the dark matter, $m_{A'} < 2m_\chi$. Current facilities actively probing the methods listed above include APEX and HPS and JLab, MiniBooNE at Fermilab, NA64 at CERN, and TREK at J-PARC. Future experiments that will eventually contribute to covering the mentioned thermal targets include Belle-II at KEK, MAGIX at MESA, PADME at LNF, SHIP at CERN, VEPP3 at BINP, BDX at JLab, COHERENT at ORNL, DarkLight at JLab, LDMX at SLAC or JLab, MMAPS at Cornell, SBN at Fermilab, and SeaQuest [94].

27.6.2 Direct detection formalism

Direct detection experiments mostly aim to observe elastic or inelastic scatters of Galactic DM particles with atomic nuclei, or with electrons in the detector material. Predicted event rates assume a certain mass and scattering cross section, as well as a set of astrophysical parameters: the local density ρ_0 , the velocity distribution $f(\vec{v})$, and the escape velocity v_{esc} (see Sec. 27.4).

Interactions with atomic nuclei: For DM scattering off nuclei, the differential scattering rate R as a function of nuclear recoil energy E_R is

$$\frac{dR(E_R, t)}{dE_R} = N_T \frac{\rho_0}{m_{\text{DM}}} \int_{v > v_{\min}} v f(\vec{v} + \vec{v}_E(t)) \frac{d\sigma(E_R, v)}{dE_R} d^3v, \quad (27.10)$$

where N_T is the number of target nuclei, m_{DM} is the mass of the DM particles, $v = |\vec{v}|$ is the speed of the particle in the experiment's rest frame, $f(\vec{v} + \vec{v}_E(t))$ is the velocity distribution in the Earth's frame, v_{\min} is the minimum speed of the DM particles that can cause a recoil energy E_R and σ is the scattering cross section on the nucleus [29, 120]. For elastic scattering, the minimum velocity is $v_{\min} = (m_N E_R / 2m_r^2)^{1/2}$, with m_N being the mass of the nucleus, and $m_r = (m_N m_{\text{DM}}) / (m_N + m_{\text{DM}})$ the reduced mass of the nucleus-DM system. In case of inelastic scattering, the minimum speed becomes $v_{\min} = (m_N E_R / 2m_r^2)^{1/2} + E^* / (2m_N E_R)^{1/2}$, with the nuclear excitation energy E^* , for part of the kinetic energy of the incoming particle will be spent on exciting the nucleus. The prompt de-excitation energy, if observed

Table 27.1: Best constraints from direct detection experiments on the SI (at high >5 GeV and low < 5 GeV masses) and SD DM-nucleon couplings.

Experiment	Target	Fiducial mass [kg]	Cross section [cm ²]	DM mass [GeV]	Ref.
Spin independent high mass (>5 GeV)					
LUX-ZEPLIN	Xe	5500	9.2×10^{-48}	36	[103]
PandaX-4T	Xe	2670	3.8×10^{-47}	40	[104]
XENONnT	Xe	4180	2.6×10^{-47}	30	[105]
SuperCDMS	Ge	12	1.0×10^{-44}	46	[106]
DarkSide-50	Ar	20	1.9×10^{-43}	10	[107]
DEAP-3600	Ar	2000	3.9×10^{-45}	100	[108]
Spin independent low mass (<5 GeV)					
LUX (Migdal)	Xe	118	6.9×10^{-38}	2	[109]
XENON1T (Migdal)	Xe	1042	3×10^{-40}	2	[110]
XENON1T (ionisation only)	Xe	1042	3.6×10^{-41}	3	[111]
DarkSide-50 (ionisation only)	Ar	20	1.4×10^{-42}	2	[107]
SuperCDMS (CDMSlite)	Ge	0.6	2×10^{-40}	2	[112]
SuperCDMS (CDMSlite, Migdal)	Ge	0.6	6×10^{-38}	2	[113]
CRESST	CaWO ₄ - O	0.024	1×10^{-39}	2	[114]
CRESST	Si	0.0035	4.5×10^{-32}	0.15	[115]
DAMIC	Si	0.3	1×10^{-40}	4	[116]
NEWS-G	Ne	0.3	1×10^{-38}	2	[117]
Spin dependent proton					
PICO60	C ₃ F ₈ - F	49	3.2×10^{-41}	25	[118]
PandaX-4T	Xe	2670	1.7×10^{-40}	40	[119]
LUX-ZEPLIN	Xe	5500	4.2×10^{-41}	32	[103]
XENONnT	Xe	4180	1.4×10^{-40}	30	[105]
Spin dependent neutron					
PandaX-4T	Xe	2670	5.8×10^{-42}	40	[119]
LUX-ZEPLIN	Xe	5500	1.5×10^{-42}	30	[103]
XENONnT	Xe	4180	4.3×10^{-42}	30	[105]

in addition to the nuclear recoil energy, will boost the region-of-interest to higher energies [121].

If one assumes the standard, leading order spin-independent (SI) and spin-dependent (SD) interactions, which couple to the charge/mass and spin of the nucleus, respectively, the differential cross-section is proportional to the inverse squared speed of the DM particle, $d\sigma/dE_R \propto v^{-2}$, and the dependence on the velocity distribution can be expressed as:

$$g(v_{min}, t) = \int_{v > v_{min}} \frac{f(\vec{v} + \vec{v}_E(t))}{v} d^3v. \quad (27.11)$$

This function allows for the comparison of various experimental results independently of the underlying velocity distribution [122], for a given DM mass. The time-integrated differential cross section is the sum of the SI and SD contributions:

$$\frac{d\sigma(E_R, v)}{dE_R} = \frac{m_N}{2m_p^2 v^2} \left(\sigma_0^{SI} F_{SI}^2(E_R) + \sigma_0^{SD} F_{SD}^2(E_R) \right), \quad (27.12)$$

where $F^2(E_R)$ are the nuclear form factors and σ_0 the cross-sections in the limit of zero momentum transfer. Since the incoming particle velocity is $v/c \sim 10^{-3}$, the nuclear recoil energy is at most tens of keV (much smaller than typical nuclear binding energies per nucleon), and the momentum transfer $q = (2m_N E_R)^{1/2} \sim \mathcal{O}(10 - 100)$ MeV. This implies that $1/q$ can be of the same order as nuclear radii $R \sim A^{1/3}$ fm, and that nuclei are not point-like from the perspective of a DM particle. The cross sections will thus involve nuclear form factors. These were calculated in [123] and [124] for the SI and SD case, respectively, for specific target nuclei, while the cross sections are often expressed in terms of single-nucleon cross sections and effective couplings of the DM particle to protons and neutrons. In the SI case, all the nucleons in the nucleus contribute coherently to the cross-section (under the assumption of isospin independence in the DM couplings). Dominant sources of uncertainty are the nucleon sigma terms, especially for Higgs-dominated interactions,

where the couplings are proportional to the quark masses. An overview is presented in Ref. [125]. For SD scattering, the nuclear spin contents due to the protons and neutrons must be considered.

The interactions of DM particles with nuclei can be treated in a non-relativistic effective field theory (NR-EFT) approach, which considers more general DM scenarios based on the lowest-order, four-field operators that describe the couplings to nucleons. These operators, which correspond to different types of interactions between the DM and quark fields, can be momentum- and velocity-dependent, and might be leading when momentum-independent interactions are suppressed, or even vanish in the limit of zero momentum [126, 127]. In Ref. [127, 128] all 15 operators (arising from 20 possible bilinear combinations between the DM and nucleon fields) which obey Galilean-invariance, T -symmetry and are Hermitian are written out up to quadratic order in q , and the nuclear response functions evaluated in shell-model calculations for DM targets made of F, Na, Ge, I and Xe isotopes. The connection to particle physics within the context of *simplified DM models* is made in Ref. [129, 130], where the simplified models assume a single DM particle with one mediator which couples it to quarks. More recently the DM-nucleus scattering was also analysed in the framework of chiral effective field theory (Ch-EFT), a low-energy effective theory of QCD, which allows for a consistent derivation of the nuclear responses beyond the leading-order expressions [131, 132]. Ch-EFT preserves the QCD symmetries, and predicts DM couplings to two nucleons (e.g., when the hypothetical particle couples to a virtual pion exchanged between the nucleons). It also provides a power counting that suggests a hierarchy of the various NR-EFT operators, which is however approximate given that the couplings between the DM and the Standard Model fields are not known. The generalized SI structure factors for spin-1/2 and spin-0 DM particles and various isotopes of F, Si, Ar, Ge and Xe employed in direct detection experiments are provided in Ref. [132].

Scattering off bound electrons and absorption: For DM particle masses below the GeV-scale, most searches for DM-nucleus scattering rapidly lose sensitivity, due to energy thresholds around a few 100 eV - few keV. As an example, a light DM particle

with a mass of 100 MeV and $v \propto 10^{-3}c$ will induce a nuclear recoil energy of about 0.5 eV in a target made of argon. Another strategy is to search for DM scattering off bound electrons, allowing for all of the kinetic energy (50 eV in the above case) to be transferred to the material [133]. The leading possibilities are ionisation, excitation, and molecular dissociation processes, which typically require energies of (1-10) eV, and thus allow to probe scattering of DM particles with masses down to the $\mathcal{O}(\text{MeV})$ range.

For a bound electron with binding energy E_B DM particle masses of $m_{\text{DM}} \geq 250 \text{ keV} \times E_B/1 \text{ eV}$ can in principle be probed. The signal depends on the material, and can consist of one or more electrons (in semiconductors, noble liquids, graphene), one or more photons (in scintillators) or phonons (in superconductors and superfluids) and quasiparticles (in superconductors). As an example, the differential event rate for ionization in atoms is given by:

$$\frac{dR_{\text{ion}}}{d \ln E_R} = N_T \frac{\rho_0}{m_{\text{DM}}} \frac{d\langle\sigma_{\text{ion}}v\rangle}{d \ln E_R}, \quad (27.13)$$

where E_R is the recoil energy transferred to the electron, $\langle\sigma_{\text{ion}}v\rangle$ is the thermally averaged ionization cross section and N_T is the number of target atoms per unit mass. The cross-section is related to the non relativistic DM-electron elastic scattering cross-section (σ_e):

$$\begin{aligned} \frac{dR_{\text{ion}}}{d \ln E_R} &= \frac{6.2}{A} \left(\frac{\rho_0}{0.4 \text{ GeV cm}^{-3}} \right) \left(\frac{\sigma_e}{10^{-40} \text{ cm}^2} \right) \left(\frac{10 \text{ MeV}}{m_{\text{DM}}} \right) \\ &\times \frac{d\langle\sigma_{\text{ion}}v\rangle/d \ln E_R \text{ events}}{10^{-3} \sigma_e \text{ kg d}} \end{aligned} \quad (27.14)$$

Predicted differential rates in various materials (He, Ar, Ge, Xe) and for different particle masses are shown in [133], together with cross section sensitivities as a function of mass and expected background rates from neutrinos. More recently, rates of electronic transitions induced by DM-electron scattering on Xe, Si and Ge for spin 0, spin 1/2, and spin 1 DM models were calculated in [134]. The code EXCEED-DM (extended calculation of electronic excitations for direct detection of dark matter) can compute DM-electron interaction rates with inputs from a variety of *ab initio* electronic structure calculations [135].

Two classes of DM candidates, axion-like-particles (ALPs) and dark (or hidden) photons (see Sec. 27.5), can be absorbed in a target material by interactions with bound electrons via the axioelectric effect, which is analogous to the photoelectric effect: a boson is absorbed by a bound electron, which is then ejected from the atom [70,136,137]. The dark photon arises in extensions of the SM by a new massive or massless U(1)' field, coupled to the SM U(1)_Y via a kinetic mixing term κ , see Sec. 27.5. The absorption cross-section of a massive, NR particle m_V with coupling $e' = e\kappa$ to electrons is (in natural units, and for energies $E_V \ll m_e$)

$$\sigma_{\text{abs}} = \frac{\alpha'}{\alpha} \left(\frac{E_V}{2m_e} \right)^2 \sigma_{\text{pe}}, \quad (27.15)$$

where σ_{pe} is the photoelectric cross-section, and an analogue to the electromagnetic fine structure constant α is introduced, $\alpha' = (e\kappa)^2/4\pi$. The rate per atom is

$$R \simeq \frac{\rho_0}{m_V} \times \kappa^2 \sigma_{\text{pe}}. \quad (27.16)$$

Since the kinetic energy of the dark photon is negligible compared to its rest energy, a mono-energetic peak at its mass is expected in the spectrum of a direct detection experiment. Dark photons with a thermally generated abundance are excluded by direct detection experiments [70], however non-thermal mechanisms (e.g., via perturbations during inflation) could create the relic abundance, see Section 27.3.

Similarly to axions, ALPs arise in the spontaneous breaking of a global symmetry, and are phenomenologically described by a mass m_a and a decay constant f_a . Unlike for QCD axions, however, there is no strict relation between m_a and f_a . The coupling strength to electrons with mass m_e is parameterised by

$g_{ae} = 2m_e/f_a$, and the absorption cross section of a particle with incoming velocity v_a is related to the cross-section for the photoelectric effect as

$$\sigma_{\text{abs}} v_a \simeq \frac{3E_a^2}{4\pi\alpha f_a^2} \sigma_{\text{pe}} = \frac{3g_{ae}^2}{4\pi\alpha} \left(\frac{E_a}{2m_e} \right)^2 \sigma_{\text{pe}}. \quad (27.17)$$

As in the case of the dark photon, the signature is a mono-energetic peak at the mass of the particle, broadened by the energy resolution of the detector. Constraints on the couplings of ALPs and dark photons to electrons from direct detection experiments in m_a and m_V mass ranges from $\sim (1 - 10^4)$ eV were derived in Ref. [138, 139], and compared to indirect limits from anomalous energy losses in the Sun, in red-giant and horizontal-branch stars. For a detailed discussion of axion and ALP searches, we refer to the *Axion* review.

27.6.3 Current and future direct detection technologies

Direct detection experiments aim to observe the small (keV-scale and below) and rare (fewer than ~ 1 event/(kg y)) signals which are induced by DM particle scatters in a detector, mostly in the form of ionisation, scintillation or lattice vibrations. A majority of experiments detects more than one signal, which allows to distinguish between scattering off of electrons (electronic recoils, ER) and off of atomic nuclei (nuclear recoils, NR). A 3D position resolution is required to define central detector regions (or fiducial volumes) with low background rates from surrounding materials, and the distinction between single- versus multiple-scatters rejects a significant fraction of backgrounds, given that DM will scatter at most once. We refer to [140, 141] for recent reviews of the field.

Specific signatures: For NRs, the shape of the differential recoil spectrum is exponentially falling with recoil energy, and depends on the mass of the particle and on the nuclear mass. Unless $m_{\text{DM}} \gg m_N$, m_{DM} can in principle be determined from the measured recoil spectrum, where multiple targets will provide tighter constraints [142]. The Earth's motion through the MW induces a seasonal variation of the total event rate and a forward-backward asymmetry in a directional signal [143, 144]. The annual modulation is due to the Earth's motion in the Galactic rest frame, which is a superposition of the Earth's rotation around the Sun and the Sun's rotation around the Galactic center. Since the Earth's orbital speed is much smaller than the Sun's speed, the expected amplitude of the modulation is $\simeq 5\%$. In the SHM, the period is one year, and the phase is 150 d (June 2), when both speeds add up maximally. This expectation is modified for different DM distributions, e.g. in the case of sub-structures such as clumps and streams [145, 146] and a DM disc [147]. In addition, the modulation changes phase at a specific recoil energy (known as crossing-energy) [148], which depends on the DM and nuclear mass, allowing to in principle determine m_{DM} if low energy thresholds can be achieved. A powerful signature is provided by the ability to detect the axis and direction of the recoiling nucleus. Since the DM flux in the laboratory frame is peaked in the direction of motion of the Sun towards the constellation Cygnus, the recoil spectrum is peaked in the opposite direction. The observation of such a dipole feature would provide a 'smoking-gun' evidence for DM, where the forward-backward rates can differ by a factor of ~ 10 , depending on the energy threshold. Ref. [149] provides a review of the theoretical framework and of the discovery reach of directional detectors.

Backgrounds, including neutrinos: Early direct detection experiments employing low-background Ge spectrometers featured background levels around 2 events/(kg d keV), while the latest generation of liquid Xe experiments reduced this noise by almost five orders of magnitude, to 4×10^{-5} events/(kg d keV). In liquid xenon detectors, the measured ER spectra at low energies are for the first time dominated by solar *pp* neutrino interactions, second-order weak decays, as well as ^{214}Pb β -decays from radon mixed with the xenon. Other backgrounds are due to the radioactivity of detector components, followed by cosmic muons and their secondaries such as fast neutrons. The cosmic and environmental radiation are suppressed by going deep underground and surrounding the experiments with appropriate shielding structures (mainly large water Cherenkov detectors for the current and

next-generation detectors). Activation of materials via cosmic-ray interactions produce long-lived radio-nuclides (e.g., ^{39}Ar , ^{60}Co , ^{68}Ge , ^{32}Si , etc), while long-lived, human-made isotopes (^{85}Kr , ^{137}Cs , etc) can mix with detector materials or generate surface backgrounds. For details, we refer to *Section 36.6* of this *Review*.

The final backgrounds are due to the irreducible neutrino flux from the Sun, the atmosphere and the diffuse supernovae background [150]. Solar pp-neutrinos start dominating the electronic recoil background due to elastic neutrino-electron scatters, at a level of $\sim (10 - 25)$ events/(t y) below energies of ~ 100 keV, while coherent elastic neutrino-nucleus scatters (CE ν NS) from ^8B solar neutrinos will induce up to $\sim 10^3$ events/(t y) for high-A targets, at nuclear recoil energies below \sim few keV. Nuclear recoils from atmospheric neutrinos and the diffuse supernovae neutrino background will yield event rates in the range $(1 - 5)$ events/(100 t y), depending on the detector material. In general, ^8B and atmospheric neutrinos will impact light (≤ 6 GeV) and heavy (100 GeV and above) DM searches for cross sections on nucleons below $\sim 10^{-45}$ cm 2 and $\sim 10^{-49}$ cm 2 , respectively. The precise cross-sections where neutrinos constitute a dominant background strongly depend on the systematic uncertainties on the neutrino flux normalisation for each source [151]. For very low energy thresholds to nuclear recoils, e.g. 10-30 eV in Ge and Si detectors, CE ν NS due to the ^7Be neutrino flux become relevant for exposures of ~ 50 kg y [152]. For DM searches with electron recoils via DM-electron scattering and dark photon or ALP absorption, solar neutrinos will also limit the sensitivity to DM masses in the range $\sim (1-10^3)$ MeV and $\sim (1-10^3)$ eV, respectively, for large exposures ~ 1 t y, as shown in Ref. [153].

Solid-state cryogenic detectors: Current experiments using the bolometric technique (see *Section 36.5* of this *Review*), together with either charge or light readout, are SuperCDMS (Si, Ge) at Soudan (until 2015) and SNOLAB (in construction), EDELWEISS (Ge) at the Laboratoire Souterrain de Modane (LSM) and CRESST (CaWO $_4$, Al $_2$ O $_3$, Si, LiAlO $_2$) at the Laboratori Nazionali del Gran Sasso (LNGS). These experiments are optimised for low-mass DM searches, and can probe WIMP masses down to ~ 0.03 GeV. CRESST operated a 0.35-g thin wafer Si detector and reached a 10-eV energy threshold, probing DM masses in the range (115–500) MeV, improving existing limits by up to a factor 20 for masses below 160 MeV. CDMSlite operated detectors at higher bias voltages to amplify the phonon signals produced by drifting charges and thus have access to light DM around 1.5 GeV. A reanalysis of the CDMSlite data using the Migdal effect allowed to exclude new parameter space for WIMP-nucleon cross-sections down to 30 MeV [113]. The goal at SNOLAB is to probe the (0.05–5) GeV region down to cross sections of $\sim 10^{-44}$ cm 2 . Much smaller, gram-scale versions of cryogenic detectors can have single-charge resolution and thus probe low-mass DM via inelastic electron recoils. A SuperCDMS single-charge sensitive Si detector placed upper limits on DM interacting with electrons for masses between $(0.5-10^4)$ MeV, as well as on dark photon kinetic mixing for dark photon masses in the range (1.5–40) eV. With Ge crystals operated at Soudan, SuperCDMS constrained dark photons and ALPs in the mass range 40 eV to 500 keV.

Germanium ionisation detectors operated at 77 K can reach sub-keV energy thresholds and low backgrounds, but lack the ability to distinguish electronic from nuclear recoils. The CDEX-10 experiment at the China Jinping Underground Laboratory (CJPL) uses p-type, point-contact Ge detectors operated in liquid nitrogen to probe DM masses down to 3 GeV. It also reported constraints on the kinetic mixing of dark photons in the mass range (0.1–4.0) keV. The $0\nu\beta\beta$ -decay experiments Majorana Demonstrator and GERDA have obtained constraints on the couplings of ALPs and dark photons to electrons, with masses between (6–100) keV and (60–1000) keV, respectively. The Majorana Demonstrator improved laboratory constraints on solar axion masses between (1.2–100) eV, setting limits on the axion-photons coupling of $g_{a\gamma} < 1.45 \times 10^{-9}$ GeV $^{-1}$ (95% CL).

Noble liquids: Liquid argon (LAr) and liquid xenon (LXe) are employed as DM targets, while R&D on liquid helium is ongoing. We refer to Ref. [154] for a review of the liquid noble gas detector technology in low-energy physics, as well to *Section 36.4*

of this *Review*. At present the best constraints on DM-nucleus interactions come from multi-tonne experiments using xenon: the LZ experiment at SURF, PandaX-4T at CJPL and XENONnT at LNGS. These experiments probe particle masses down to ~ 6 GeV (when using both light and charge signals) and the SI DM-nucleon cross section down to 9.2×10^{-48} cm 2 (at 36 GeV). LAr experiments employ pulse shape discrimination (PSD) that allows for distinguishing between ER and NR events, at the expense of higher energy thresholds than in LXe. The DarkSide-50 TPC at LNGS (until 2019) sets a minimum upper limit on the SI, DM-nucleon cross-section of 6×10^{-43} cm 2 at 10 GeV, while the single-phase experiment DEAP-3600 at SNOLAB constrains the SI cross-section to values below 3.9×10^{-45} cm 2 at 100 GeV.

In noble liquids, sub-GeV DM particles can be searched for by observing inelastic, ER processes following a low-energy nuclear recoil: excitation and ionisation of the recoiling atom (the hypothetical Migdal effect) and a bremsstrahlung photon [155]. As an example, LUX and XENON1T constrained DM particle masses between (0.3–5) GeV via bremsstrahlung photons and Migdal electrons. Even lower masses are accessible when using the amplified, charge signal only, at the expense of giving up discrimination between ERs and NRs. XENON1T probed particle masses down to 60 MeV, while DarkSide-50 published constraints on WIMP masses as low as 40 MeV. DM masses at the MeV-scale can also be probed by exploiting the scattering off electrons. PandaX-4T presented light DM searches with ionisation signals, with NR and ER energy thresholds of 0.77 keV and 0.07 keV, obtaining leading constraints in the mass range 40 MeV–100 GeV and 100 MeV–10 GeV for a heavy and light mediator, respectively [156]. DarkSide-50 set limits in the mass range (16 – 56) MeV and above 80 MeV for a heavy and light mediator, respectively [157]. Noble liquids TPCs also search for solar axions, galactic ALPs and dark photons. XENONnT set upper limits on the axion-electron coupling of 2×10^{-12} in the mass range $(10^{-6}-1)$ eV for solar axions, and probes couplings between $(1 - 2) \times 10^{-14}$ in the mass range (1–10) keV for galactic ALPs [158]. DarkSide-50 probes ALP masses down to 0.03 keV with couplings in the range $10^{-13} - 10^{-14}$ [157].

The next generation of liquefied noble gas detectors are in construction (DarkSide-20k) or at the design and R&D stage (Argo, DARWIN/XLZD, PandaX-xT). These will increase the sensitivity to various DM candidates by 1-2 orders of magnitude, with the ultimate goal of exploring the experimentally accessible parameter space, until the backgrounds from neutrinos will start dominating the event rates.

Room temperature scintillators: Several large DM experiments using high-purity NaI(Tl) crystals are acquiring data in various underground laboratories. Of these, DAMA/LIBRA at LNGS has the highest mass, 250 kg, and the largest exposure: 1.33 t y with an energy threshold of 1 keV and 2.46 t y with an energy threshold of 2 keV. It is the only experiment in the field that reported an annually modulated event rate with a statistical significance of 12.9σ C.L. (20 annual cycles), with a modulation amplitude around 0.02 events/(kg d keV) in the energy region (1–4) keV. These findings were interpreted as due to DM interactions via nuclear or electronic recoils. The ANAIS experiment at Canfranc operates 112.5 kg of NaI(Tl) scintillators with an energy threshold of 1 keV and a background rate of 3.6 events/(kg d keV) in the (1–6) keV region. A blind analysis of 3 y of data, for an exposure of 314 kg y is consistent with an absence of modulation at 3.3σ . The COSINE-100 experiment, located at the Yangyang Underground Laboratory in Korea, operates 106 kg of NaI(Tl) crystals in a liquid scintillator, with an energy threshold of keV and a background rate of 3.6 events/(kg d keV). Results from a 173 kg y exposure in the (1–6) keV energy range are consistent, at 68.3% C.L., with both the null hypothesis and DAMA/LIBRA's best fit value in the same energy range. A larger exposure and a reduced energy threshold are required to test DAMA/LIBRA for 3σ coverage. COSINE-200, under construction at the new, deeper underground laboratory Yemilab, will be a larger experiment with reduced backgrounds. The SABRE experiment plans to operate a total of 50 kg of NaI(Tl) crystals, focussing on reaching a background level of 0.1 events/(kg d keV), an order of magnitude below DAMA/LIBRA. Twin detectors will be installed at

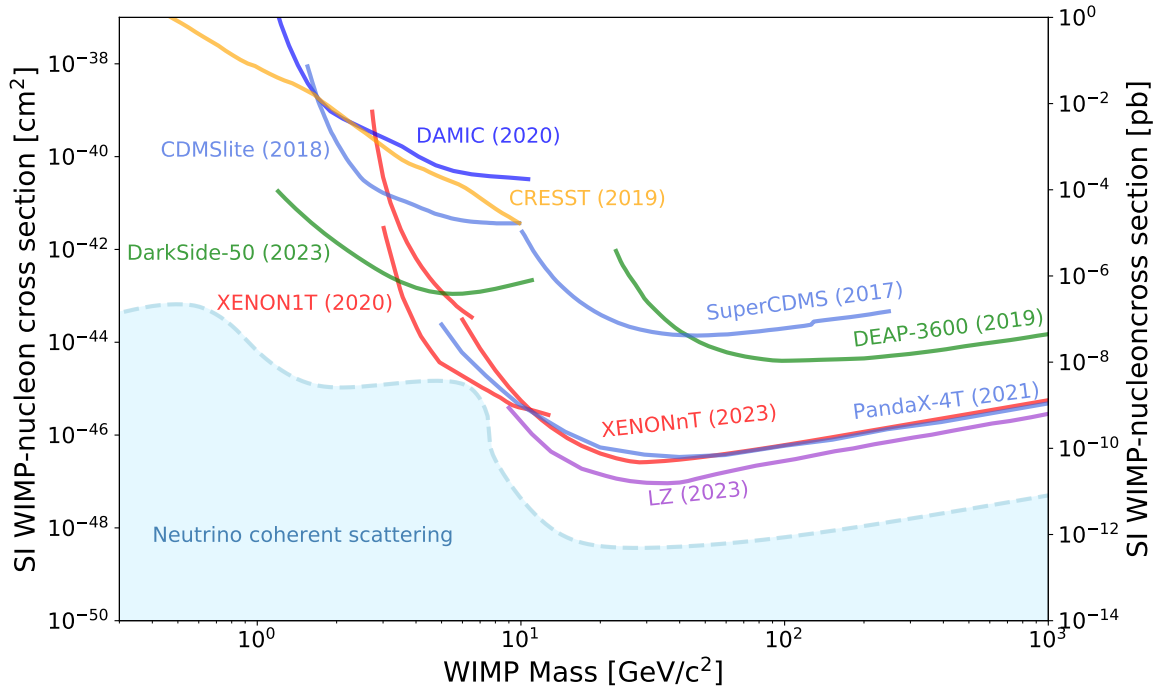


Figure 27.1: Upper limits on the SI DM-nucleon cross section as a function of DM mass.

LNGS and at the Stawell Underground Physics Laboratory in the Southern hemisphere. While a DM-induced signal is expected to have the same phase in both hemispheres, seasonal or site-related effects would show different amplitudes and phases in the twin detectors. The COSINUS experiment, under construction at LNGS, will use NaI crystals operated as cryogenic scintillating calorimeters to differentiate between nuclear and electronic recoils based on the observation of phonon and light signals. The first phase aims for an exposure of 100 kg d, while the second phase aims to achieve, with 1000 kg d, a fully model-independent cross-check of a NR origin of the DAMA/LIBRA signal.

Room temperature ionisation detectors: Silicon charged-coupled devices (CCDs) are employed for low-mass DM searches, as well as for hidden photon searches in the eV-mass range. Ionisation events induced in bulk silicon of high-resistivity, fully depleted CCDs are observed with charge resolutions around $1\text{--}2e^-$ and extremely low leakage currents, at the level of few $e^- \text{mm}^{-2}\text{d}^{-1}$. The position of an energy deposit is reconstructed in 3 dimensions and the particle type (electron, neutron, muon, α -particles, etc) is reconstructed based on the recorded track pattern.

The DAMIC experiment at SNOLAB yielded new constraints on DM-electron scattering, and on the hidden-photon kinetic mixing parameter in the mass range (1-30) eV with an exposure of 7.6 kg d and on low-mass WIMPs with an exposure of 11 kg d. The SENSEI projects employ the skipper technology to achieve single-electron sensitivity. A run with a 2 g detector in the MINOS cavern at Fermilab yielded world-leading constraints on DM-electron scattering for a large range of sub-GeV dark matter masses. The skipper technology is also employed in the next stage of the DAMIC programme, DAMIC-M at LSM, which plans for a kg-size mass. The goal is to achieve thresholds of 2-3 electrons and to probe the DM-nucleon cross-section down to $\text{few} \times 10^{-43} \text{cm}^2$ around 2-3 GeV and the DM-electron cross section down to $2 \times 10^{-41} \text{cm}^2$ at 10 MeV mass. DAMIC-M has operated first CCDs at LSM and achieved constraints on sub-GeV DM particles interacting with electrons in the mass range (0.53-1000) MeV, for an exposure of 85.23 g d.

The NEWS-G collaboration operates spherical proportional counters filled with a noble gas. Advantages of this technology are the low intrinsic electronic noise and a high amplification gain, allowing for low energy thresholds down to single-electron detec-

tion, and the possibility to use different light targets (He, Ne, etc). A 60 cm diameter chamber operated at LSM with a gas mixture of Ne + CH₄ (0.7%) at 3.1 bar, excluded SI, WIMP-nucleon cross sections above $4.4 \times 10^{-37} \text{cm}^2$ at 0.5 GeV after an exposure of 9.6 kg d with an energy threshold ~ 100 eV. The next iteration, a 140-cm sphere detector made of very low radioactivity copper (few $\mu\text{Bq/kg}$ of ²³⁸U and ²³²Th) has been installed at SNOLAB in 2021. The detector has recently started to acquire physics data, with a predicted background level of (5 ± 2) events/(kg keV d) for sub-keV events.

Superheated liquid detectors: Investigation of the spin-dependent interaction channel calls for target nuclei with uneven total angular momentum. A particularly favourable candidate is ¹⁹F, the spin of which is carried mostly by the unpaired proton, yielding a cross-section which is almost a factor of ten higher than of other employed nuclei with spin (e.g., ²³Na, ⁷³Ge, ¹²⁷I, ¹²⁹Xe, ¹³¹Xe). Fluorine is part of the target of experiments using superheated liquids, such as the ones operated by the PICO collaboration. A search in the PICO-60 C₃F₆ bubble chamber at SNOLAB with an exposure of 1404 kg d and an energy threshold of 2.45 keV, yielded the most stringent constraint on the DM-proton SD cross-section at $3.2 \times 10^{-41} \text{cm}^2$ for a 25 GeV particle mass. In construction at SNOLAB is PICO-500, a detector with 250 l of superheated freon (C₃F₈) contained between two quartz jars inside a pressure vessel filled with mineral oil, itself inside a tank of ultra-pure water.

Directional detectors: Detectors capable of measuring the direction of the recoiling nucleus would unequivocally confirm the Galactic origin of a signal and could probe the region below the neutrino floor [159, 160]. Because nuclear recoils have a range which is about 10 times smaller than the one of Compton recoils of the same energy, gaseous detectors have an excellent intrinsic background rejection if they can measure the range of events precisely. Several directional detectors are presently in operation, where a 1 m³ detector has a typical mass of a few 100 g and can measure the sense of an incoming nuclear recoil above a few tens of keV. Cygnus is a proto-collaboration which coordinates the R&D efforts for gas based TPCs with 1 keV threshold. One of these is CYGNO, an experiment that aims to build a 1-m drift length gaseous TPC filled with a He:CF₄ 60:40 gas mixture at atmospheric pressure and room temperature at LNGS.

A new technique is based on fine-grained nuclear emulsions

(solid-state detectors with silver halide crystals uniformly dispersed in a gelatine film, where each crystal works as a sensor for charged particles), as proposed by the NEWSdm collaboration. These act as target and nanometric tracking device, and the expected NR tracks are sub- μm in size. Due to the small crystal size and larger number density, a superior spatial resolution compared to gaseous detectors is obtained. Simulations show that to reach the neutrino floor, exposures of 10 ty and 100 ty are required if a 30 nm and 50 nm threshold for detecting the track length is reached. This requires further R&D, since current emulsions allow for 100 nm tracking and target masses are around 1 kg, with 10 ky exposures planned. A proposed approach for the directional detection of sub-GeV DM is to use two-dimensional materials such as monolayer graphene [161], from which the DM particle can eject electrons. Their energy and direction, correlated with the direction of the incoming DM, can be measured for instance with the proposed PTOLEMY experiment.

New techniques: To probe light (sub-GeV) DM particles, either via scatters off electrons or via couplings to phonons, new techniques beyond the ones discussed above are proposed. The DM particle mass that can be accessed in DM-electron scattering in noble liquids and semiconductors is limited by the minimum ionisation/excitation energy and the size of the band gap, respectively (at the $\sim\text{eV}$ -scale). To reach lower energy thresholds, materials with smaller band gaps for electron excitations ($\sim\text{meV}$), such as superconductors and superfluids, as well as Dirac materials were proposed [162]. These would in principle allow for the detection of keV-scale DM. Other ideas to detect keV-MeV scale DM are to observe NRs in superfluid He, via collective excitation modes in the fluid [163], as realised in HeRALD and DELight, or based on the breaking of chemical bonds between atoms [164].

Even lighter DM, with masses in the meV-eV range, could be detected via absorption on a conduction electron in a superconductor, followed by the emission of an athermal phonon [165]. Another proposed target for light DM are polar materials (for example GaAs, sapphire), which are especially sensitive for scattering through an ultralight dark photon, via excitation of single optical phonons [166]. If an anisotropic crystal such as sapphire is employed, a daily modulation interaction rate could be established [167]. A new class of detectors for bosonic DM, based on resonant absorption onto a gas of small polyatomic molecules, is proposed in [168]. The DM would effectively act as a laser that resonantly excites transitions in molecules when its mass closely matches the transition energy. While DM with SI couplings can efficiently excite phonons, it has been shown in [169] that if DM couples to the electron spin, magnon excitations (quanta of collective spin wave excitations) in materials with magnetic dipole order may also offer a promising detection avenue. Yet another approach for sub-GeV DM is to employ superconducting nanowires as both target and sensor, and first bounds on DM-electron interactions were placed from a 4.3 ng tungsten-silicide prototype with a 0.8 eV energy threshold and an exposure of 8.8×10^{-14} ky [170].

The detection of light DM via collective excitations in condensed matter systems and other methods is a rapidly evolving field, and a growing area of research at the interface of DM physics, condensed matter and materials science. We refer to Ref. [171,172] for discussions of some of these new directions and models. Critical challenges are to detect these very small energy depositions, and to reliably assess the background noise.

Table 27.1 summarises the most stringent constraints on the DM-nucleon SI and SD cross-sections, and Figure 27.1 shows the best constraints for SI couplings in the cross-section versus DM mass parameter space, above masses of 0.3 GeV.

27.7 Astrophysical detection of dark matter

DM as a microscopic constituent can have measurable, macroscopic effects on astrophysical systems. Indirect DM detection refers to the search for the annihilation or decay debris from DM particles, resulting in detectable species, including especially gamma rays, neutrinos, and antimatter particles. The production rate of such particles depends on (i) the annihilation (or decay) rate (ii) the density of pairs (respectively, of individual particles) in the region of interest, and (iii) the number of final-state particles produced in one annihilation (decay) event. In formulae, the

rate for production of a final state particle f per unit volume from DM annihilation can be cast as

$$\Gamma_f^A = c \frac{\rho_{\text{DM}}^2}{m_{\text{DM}}^2} \langle \sigma v \rangle N_f^A, \quad (27.18)$$

where $\langle \sigma v \rangle$ indicates the thermally-averaged cross section for DM annihilation times relative velocity [27], calculated at the appropriate temperature, ρ_{DM} is the physical density of DM, and N_f^A is the number of final state particles f produced in one individual annihilation event. The constant c depends on whether the DM is its own antiparticle, in which case $c = 1/2$, or if there is a mixture of DM particles and antiparticles (in case there is no asymmetry, $c = 1/4$). The analog for decay is

$$\Gamma_f^D = \frac{\rho_{\text{DM}}}{m_{\text{DM}}} \frac{1}{\tau_{\text{DM}}} N_f^D, \quad (27.19)$$

with the same conventions for the symbols, and where τ_{DM} is the DM's lifetime.

Gamma Rays: DM annihilation to virtually any final state produces gamma rays: emission processes include the dominant two-photon decay mode of neutral pions resulting from the hadronization of strongly-interacting final states; final state radiation; and internal bremsstrahlung, the latter two including, possibly, the emission of massive gauge or Higgs bosons subsequently producing photons via their decay products. Similarly, neutrinos are produced from charged pion decay and from radiative processes. The flux of gamma rays and neutrinos is calculated integrating the rate Γ_f per steradian (simply meaning, for isotropic emission, $\Gamma_f/(4\pi)$) along the line of sight within the appropriate angular region (the *differential* flux is obtained in the same way by simply replacing N_f with the differential flux at production, at the appropriate redshift in the case of cosmologically distant sources),

$$\phi_f = \int_{\Delta\Omega} d\Omega \int_{\text{l.o.s.}} dl \frac{\Gamma_f}{4\pi}. \quad (27.20)$$

It is customary to factor out, in the expression for the rate, a *particle physics* factor, depending upon the DM particle mass and its annihilation or decay rate, and an *astrophysical* factor, which only depends on the observational target. The latter is sometimes denoted with $J_{\Delta\Omega}(\psi)$ with ψ indicating the direction of the line of sight. Although different conventions are in use, a common choice is to define

$$J_{\Delta\Omega}(\psi) = \int_{\Delta\Omega} \int_{\text{l.o.s.}(\psi)} \rho_{\text{DM}}^2(l, \Omega) dl d\Omega. \quad (27.21)$$

For a target with uniform density ρ and radius r at a distance $d \gg r$, such that the target is entirely within the solid angle $\Delta\Omega$,

$$J \simeq \frac{4\pi r^3 \rho^2}{3d^2}. \quad (27.22)$$

Searches for gamma-ray emission from DM annihilation have focused on targets chosen based on a variety of considerations, primarily intended to maximize signal to noise. Nearby dwarf spheroidal galaxies contain very small amounts of gas, and do not host any significant astrophysical background at gamma-ray or X-ray frequencies, and are thus an optimal target choice for DM searches. An accurate determination of the DM density profile in these objects results in somewhat large systematics when deriving constraints from the non-observation of emission from DM; future optical surveys will help pinpoint with greater accuracy stellar kinematics and thus reduce such uncertainty; a second target is the inner region of the Milky Way: while nearby and potentially hosting a large density of DM, the Galactic center region is however very bright at almost any wavelength, making the extraction of a signal highly problematic; nearby clusters of galaxies are also known to host significant astrophysical emission, but are potentially ideally suited to constrain DM decay. Finally, putative nearby DM clumps are also a possible source of a bright DM signal (albeit from an unknown direction), as is the annihilation of DM in all halos at all redshifts.

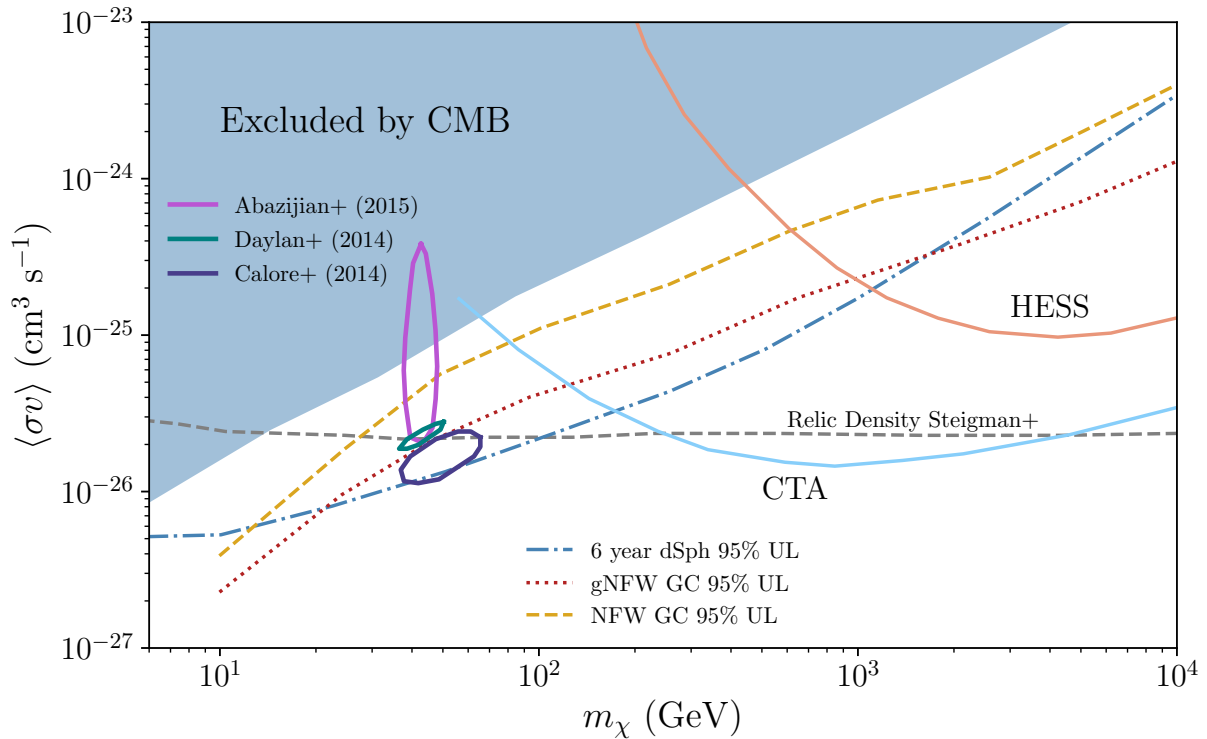


Figure 27.2: Upper limits and projected sensitivity from CTA on the pair-annihilation rate versus the DM mass from gamma-ray and CMB observations (figure courtesy of Logan Morrison).

DM annihilation and decay can lead to striking spectral features. Since the process happens typically at very low particle velocities, if the DM pair-annihilates e.g. to two photons or two neutrinos, the final-state particles will be nearly monoenergetic, with an energy close to the DM particle mass and a width proportional to the DM velocity in units of c (if a $\gamma\gamma$ line is present electroweak symmetry also implies a $Z\gamma$ line, if kinematically allowed). No astrophysical processes are known to produce lines at gamma-ray or neutrino energies in the GeV and above (with, perhaps, the possible exception of cold pulsar winds [173]) making this channel virtually background-free. At lower energy, lines are expected from radiative decay modes of candidates such as sterile neutrinos (see Sec. 27.5). DM annihilation or decay can lead to additional spectral features besides lines. These include (one or more) “boxes” [174], produced by boosted final states decaying to monochromatic photons (such as e.g. neutral pions), or combinations thereof. Processes occurring at higher redshift can distort these spectral features by smearing them to lower energies. Neglecting gamma-ray attenuation, the flux of gamma rays from all redshift can be cast as

$$\frac{dN_\gamma(E_\gamma)}{dE_\gamma} = \frac{c}{8\pi} \int \frac{\langle\sigma v\rangle \rho_{\text{DM}}(z) dz}{H(z)(1+z)^3 m_{\text{DM}}^2} \left(\frac{dN_\gamma}{dE'} \right)_{E'=E_\gamma(1+z)}. \quad (27.23)$$

While the calculation of the differential spectrum of gamma rays from a given final state f , dN_γ^f/dE_γ , is carried out using numerical tools, such as PYTHIA [175] that reproduce hadronization and particle decay for masses well above a few GeV, in the sub-GeV range gamma-ray production follows primarily from meson decay and radiative processes well outside the range of applicability of the Altarelli-Parisi splitting function. The MeV gamma-ray range will soon be probed with forthcoming satellites [176]. Recently a code that provides the expected gamma-ray spectrum for sub-GeV DM, *Hazma*, has become available [177].

Observations with the Fermi Large Area Telescope (LAT) and with ground-based facilities such as HESS, VERITAS, MAGIC, and HAWC have provided an unprecedented picture of the gamma-ray sky ideally suited to look for a signal from DM annihilation or decay for DM particles from a few GeV mass up to several

TeV. The LAT has provided some of the most stringent constraints to-date on DM pair-annihilation for a variety of annihilation final states, chiefly from stacked observations of nearby satellite dwarf spheroidal galaxies [178]. Excesses of gamma rays over the expected diffuse and point-source background have been claimed, most importantly from the direction of the inner Galaxy, where a signal from DM annihilation might be especially bright [179, 180]. The nature of this excess is quite controversial: while the morphology and spectrum fall within what expected for a standard WIMP with a mass of a few tens of GeV [181], unresolved point sources, including especially an (expected) population of millisecond pulsars (MSPs) have been advocated as a possible plausible counterpart [182]. Statistical methods to discriminate between DM and MSPs have been utilized [183, 184], but recent studies indicate that such results might not be conclusive [185]. Large uncertainties in the Galactic diffuse background emission model are additionally known to exist, and possible plague the morphological and spectral information [186, 187]. Other notable potential gamma-ray excesses include a diffuse emission from the Andromeda galaxy (M31) [188–190], possibly in excess of what expected from cosmic-ray models [191]; and a diffuse emission at 511 keV energy in the inner Galaxy from Integral-SPI observations [192]; such emission has known astrophysical counterparts [193], as well as several proposed DM explanations (e.g. [194]).

While DM annihilation and decay typically occurs at low velocities, the possibility of “boosted” DM has also been considered [195]. In this case, the DM particle might dominantly pair-annihilate to a lighter dark species, which does interact with Standard Model particle, and could be detected with neutrino telescopes or direct detection experiments. Future facilities that promise to widen the reach of gamma-ray searches for DM include especially the Cherenkov Telescope Array (CTA), see fig. 27.2.

Neutrinos: DM can be captured in celestial bodies in significant amounts, depending on the DM scattering cross section off of nucleons, the DM mass, and the DM flux incident on the celestial body of interest. For DM masses at or around the GeV scale, evaporation from the celestial body plays an important role [196]. If enough DM accumulates, DM annihilation inside the celestial body can then lead to the production of Standard Model parti-

cles. Such particles can heat up the body, if they lose most of their energy before escaping. Utilizing models for heat production in planets, or stellar interior models in the case of stars, constraints can be put on DM particle properties. Of note are constraints from anomalous warming of cold planets such as Uranus [197], alterations to the stellar structure or the Sun’s seismic activity [198], and anomalous Earth heat flow [199]. Alternately, DM annihilation in celestial bodies can result in the production of particles that can escape the body. Within the Standard Model, the only such instance is annihilation to neutrinos, but, similarly to the boosted DM case the DM can annihilate to a (stable or unstable) dark-sector particles, whose decay or interactions can be detected on Earth [200,201]. For direct annihilation to neutrinos, given the lower limit on the DM mass from evaporation, the typical neutrino energies usually exceed the energy of neutrinos from the Sun, the best target for this type of searches, making this a virtually background-free DM search. Significant neutrino fluxes can only be achieved, however, if near-equilibration is reached between the capture and annihilation rates. In turn, this requires large-enough DM-nucleon scattering cross sections, to-date very close to the limits from direct detection (see sec. 27.6). Only spin-dependent cross section, and capture in the Sun usually provide large-enough neutrino fluxes. IceCube and ANTARES searches for an anomalous flux of high-energy neutrinos from the Sun yielded null results, which can be interpreted as constraints on spin-dependent nucleon-DM interactions under the assumption of equilibration and of specific annihilation final states [202,203]. Lower-threshold detectors, including DeepCore [204] and PINGU [205], can produce interesting limits on lower-mass DM candidates above the evaporation threshold.

Cosmic-ray Antimatter: Stable charged particles produced by decays of products of, or directly from DM annihilation or decay, populate the cosmic radiation and are a prime target for indirect DM searches. To maximize signal to noise, searches focus on relatively rare particle species, such as positrons, antiprotons, and antinuclei. While in certain models the production of particles and antiparticles is not symmetric [206], generally DM annihilation or decay produces as many particles as antiparticles in the final state. Charged particles produced by DM propagate and lose energy prior to reaching detectors. The transport of charged particles is customarily carried out in the context of diffusion models such as the Galactic “leaky box” setup, see e.g. [207]. While progress in constraining the uncertain propagation and energy-loss processes has been steady with improved data from new detectors such as PAMELA [208] and AMS-02 [209], the calculation of the particle flux at Earth from that at production suffers from significant uncertainties [207].

An excess of high-energy positrons over the standard secondary production from inelastic cosmic-ray interactions has been firmly established by several experiments, most recently and with the highest statistics by AMS-02 [210]. The excess has been ascribed to DM annihilation, although strong constraints from the non-observation of corresponding anomalies in other channels, such as antiprotons and gamma rays, and the peculiar spectral shape, force DM models to be quite convoluted (see e.g. [211]). Alternately, excess *primary* positrons can be produced in the magnetosphere of nearby pulsars [212, 213]. This latter explanation was questioned in [214] in connection with the detection of a TeV halo around two candidate pulsars, leading to the determination of a highly suppressed diffusion coefficient within the pulsar nebula; with such low diffusion coefficient, positrons from the pulsars would not contribute significantly to the flux at Earth; Ref. [215], however, showed that likely the diffusion coefficient is not constant, and that if it increases outside the nebula, as expected from other cosmic-ray measurements, pulsars can still be considered as the counterpart to the positron excess. Other explanations for the excess, albeit somewhat controversial, and increasingly constrained by data, also exist [216, 217].

The antiproton spectrum in the cosmic radiation as measured by AMS-02 [209] also exhibits features that might be considered as excess flux between 10 and 20 GeV, and energies above 100 GeV [218], which have been interpreted as possible signal of DM annihilation; more realistically, however, systematic uncertainties

in the antiproton production cross section, in cosmic-ray transport, reacceleration at high energy and, at low energy, solar modulation make it extremely difficult to assess the robustness of the excesses [219, 220].

Antinuclei such as anti-deuterium and anti-helium could also form as a result of DM annihilation or decay. While baryon number conservation forces the typical kinetic energy of antinuclei produced in inelastic cosmic-ray processes to large values, antinuclei arising from hadronization of DM-initiated jets have low energy, offering optimal signal-to-noise when a low-energy cut on the antinucleus kinetic energy is used [221–225]. Specific detector designs have been developed to single out low-energy cosmic-ray antinuclei (e.g. $E < 0.25$ GeV/nucleon in the case of the General Antiparticle Spectrometer, or GAPS [226]). The detection of even a single antinucleus would have considerable importance as a possible sign of new physics [227].

Multi-wavelength studies: Electrons and positrons from DM lose energy quite efficiently, radiating at a variety of wavelengths. This *secondary* radiative emission presents spectral and morphological features that might provide an important additional indirect detection channel. The most efficient energy loss mechanisms for high-energy electrons and positrons are inverse Compton (IC) up-scattering of background photons, and synchrotron radiation in the presence of magnetic fields. Depending on the DM mass, the emitted light from synchrotron peaks at MHz-GHz frequencies, while the IC emission at X-ray to gamma-ray frequencies, depending on the energy of the background radiation, typically ranging from CMB photons up to starlight photons [228–230]. The calculation of the secondary emission from DM entails both solving the transport of the electrons and positrons from DM, and for the radiative emission; codes exist that perform these calculations for certain astrophysical environments [231–233], with diffusion playing an increasingly critical role in smaller and smaller structures such as dwarf galaxies [229]. It has been demonstrated that for large magnetic fields and for certain final states, the synchrotron emission is more constraining than the gamma-ray emission [234].

Stellar Physics: Microscopic properties of the DM can meaningfully alter, and thus be constrained by, several astrophysical environments, from planets and stars, up to the universe as a whole. DM particles light enough to be produced in collisional processes inside stars, with typically temperatures in the keV, or supernovae, with energy scales in the MeV, lead to an additional energy-loss mechanism, if capable of escaping the system. If this is the case, the increased needed energy output would also result in an increased neutrino flux, leading to constraints on the masses and couplings of the DM, see e.g. [235] for a comprehensive review. DM annihilation can even have fueled early stages of stellar evolution, perhaps with measurable consequences [236]. DM capture in neutron stars could lead to the collapse of the star into black holes; the existence of neutron stars in DM-rich environments can thus be used to constrain the mass and interaction cross section of DM with nucleons [237] and even relatively light, but stable, primordial black holes [238].

Cosmology: Energy injection from DM processes in the early universe, as well as the contribution of DM to the effective relativistic degrees of freedom, are severely constrained from data on Big Bang Nucleosynthesis (see Sec. 24 in this *Review*) and on the energy and anisotropy power spectrum of the CMB (see Sec. 29). Codes exist that perform the calculation of the constraints on particle DM models [177, 239].

PBH Detection: Macroscopic DM candidates can gravitationally perturb structure and compromise the stability of, for instance, globular clusters such as Eridanus II [24], and/or disrupt wide binaries [240]. This constrains the maximal mass of a macroscopic DM candidate to not much more than $5 M_{\odot}$ [240] (see also [24]). In the specific case or primordial black holes, strong constraints also stem from the acceleration of charged particles around and after recombination, with significant effects on the CMB [241], albeit a lively debate exists over the accretion efficiency around such objects at high redshift [242, 243]. Whether or not PBH in the solar-mass range can be 100% of the DM is therefore disputed at present. Other effects produced by macroscopic,

massive DM candidates are the microlensing of stars [244, 245] and quasars [246], femtolensing of gamma-ray bursts [247], and neutron star capture [238]. It is important to note that recently constraints from both microlensing and femtolensing have been corrected after the realization of important finite-size source and wave effects [245, 248, 249], leaving a substantial window, at PBH masses $10^{17} \lesssim M_{\text{BH}}/g \lesssim 10^{21}$ where PBH can be 100% of the DM. Light black holes, $M_{\text{BH}} \lesssim 10^{17}$ g, are also constrained by the non-detection of products of evaporation [250]; future MeV gamma-ray detectors are slated to significantly improve such constraints and to enable the direct detection of Hawking radiation [251]. If evaporation shuts down at or near the Planck scale, Planck-scale relic PBH are generally expected to carry electric charge and to be detectable with direct detection and neutrino experiments, or with paleo-detectors [252].

References

- [1] J. D. Simon, arXiv e-prints arXiv:1901.05465 (2019), [arXiv:1901.05465].
- [2] P. Salucci, *Astron. Astrophys. Rev.* **27**, 1, 2 (2019), [arXiv:1811.08843].
- [3] S. W. Allen, A. E. Evrard and A. B. Mantz, *Ann. Rev. Astron. Astrophys.* **49**, 409 (2011), [arXiv:1103.4829].
- [4] N. A. Bahcall *et al.*, *ApJ* **541**, 1 (2000).
- [5] S. D. M. White, G. Efstathiou and C. S. Frenk, *Mon. Not. Roy. Astron. Soc.* **262**, 1023 (1993).
- [6] A. J. S. Hamilton and M. Tegmark, *Mon. Not. Roy. Astron. Soc.* **330**, 506 (2002), [arXiv:astro-ph/0008392].
- [7] B. Famaey and S. McGaugh, *Living Rev. Rel.* **15**, 10 (2012), [arXiv:1112.3960].
- [8] S. W. Randall *et al.*, *Astrophys. J.* **679**, 1173 (2008), [arXiv:0704.0261].
- [9] R. H. Sanders, *Int. J. Mod. Phys. D* **27**, 14, 14 (2018), [arXiv:1805.06804].
- [10] S. D. McDermott, H.-B. Yu and K. M. Zurek, *Phys. Rev. D* **83**, 063509 (2011), [arXiv:1011.2907].
- [11] D. A. Buote *et al.*, *Astrophys. J.* **577**, 183 (2002), [arXiv:astro-ph/0205469].
- [12] D. Harvey *et al.*, *Science* **347**, 1462 (2015), [arXiv:1503.07675].
- [13] S. Tulin and H.-B. Yu, *Phys. Rept.* **730**, 1 (2018), [arXiv:1705.02358].
- [14] D. N. Spergel and P. J. Steinhardt, *Phys. Rev. Lett.* **84**, 3760 (2000), [arXiv:astro-ph/9909386].
- [15] S. Tremaine and J. E. Gunn, *Phys. Rev. Lett.* **42**, 407 (1979), [66(1979)].
- [16] L. Randall, J. Scholtz and J. Unwin, *Mon. Not. Roy. Astron. Soc.* **467**, 2, 1515 (2017), [arXiv:1611.04590].
- [17] R. Hlozek *et al.*, *Phys. Rev. D* **91**, 10, 103512 (2015), [arXiv:1410.2896].
- [18] E. Armengaud *et al.*, *Mon. Not. Roy. Astron. Soc.* **471**, 4, 4606 (2017), [arXiv:1703.09126].
- [19] M. Nori *et al.*, *Mon. Not. Roy. Astron. Soc.* **482**, 3, 3227 (2019), [arXiv:1809.09619].
- [20] B. Bozek *et al.*, *Mon. Not. Roy. Astron. Soc.* **450**, 1, 209 (2015), [arXiv:1409.3544].
- [21] H.-Y. Schive *et al.*, *Astrophys. J.* **818**, 1, 89 (2016), [arXiv:1508.04621].
- [22] E. O. Nadler *et al.*, *Astrophys. J.* **878**, 2, L32 (2019), [*Astrophys. J. Lett.* 878,32(2019)], [arXiv:1904.10000].
- [23] M. A. Monroy-Rodríguez and C. Allen, *ApJ* **790**, 2, 159 (2014), [arXiv:1406.5169].
- [24] T. D. Brandt, *Astrophys. J.* **824**, 2, L31 (2016), [arXiv:1605.03665].
- [25] B. Audren *et al.*, *JCAP* **1412**, 12, 028 (2014), [arXiv:1407.2418].
- [26] M. Dutra *et al.*, *JCAP* **1803**, 037 (2018), [arXiv:1801.05447].
- [27] P. Gondolo and G. Gelmini, *Nucl. Phys.* **B360**, 145 (1991).
- [28] J. L. Feng and J. Kumar, *Phys. Rev. Lett.* **101**, 231301 (2008), [arXiv:0803.4196].
- [29] G. Jungman, M. Kamionkowski and K. Griest, *Phys. Rept.* **267**, 195 (1996), [hep-ph/9506380].
- [30] J. Edsjo *et al.*, *JCAP* **0304**, 001 (2003), [hep-ph/0301106].
- [31] G. Servant and T. M. P. Tait, *Nucl. Phys.* **B650**, 391 (2003), [hep-ph/0206071].
- [32] D. Hooper and S. Profumo, *Phys. Rept.* **453**, 29 (2007), [hep-ph/0701197].
- [33] K. Griest and D. Seckel, *Phys. Rev.* **D43**, 3191 (1991).
- [34] R. T. Co *et al.*, *JCAP* **1512**, 12, 024 (2015), [arXiv:1506.07532].
- [35] V. S. Rychkov and A. Strumia, *Phys. Rev. D* **75**, 075011 (2007), [hep-ph/0701104].
- [36] E. D. Carlson, M. E. Machacek and L. J. Hall, *Astrophys. J.* **398**, 43 (1992).
- [37] D. Pappadopulo, J. T. Ruderman and G. Trevisan, *Phys. Rev. D* **94**, 3, 035005 (2016), [arXiv:1602.04219].
- [38] Y. Hochberg *et al.*, *Phys. Rev. Lett.* **113**, 171301 (2014), [arXiv:1402.5143].
- [39] E. Kuflik *et al.*, *Phys. Rev. Lett.* **116**, 22, 221302 (2016), [arXiv:1512.04545].
- [40] W. B. Lin *et al.*, *Phys. Rev. Lett.* **86**, 954 (2001), [arXiv:astro-ph/0009003].
- [41] G. B. Gelmini and P. Gondolo, *Phys. Rev. D* **74**, 023510 (2006), [hep-ph/0602230].
- [42] M. Hindmarsh, R. Kirk and S. M. West, *JCAP* **1403**, 037 (2014), [arXiv:1311.1637].
- [43] T. Moroi and L. Randall, *Nucl. Phys.* **B570**, 455 (2000), [hep-ph/9906527].
- [44] P. Hut and K. A. Olive, *Phys. Lett.* **87B**, 144 (1979).
- [45] S. Nussinov, *Phys. Lett.* **165B**, 55 (1985).
- [46] K. M. Zurek, *Phys. Rept.* **537**, 91 (2014), [arXiv:1308.0338].
- [47] Y. B. Zel’dovich and I. D. Novikov, *Soviet Ast.* **10**, 602 (1967).
- [48] S. Hawking, *Mon. Not. Roy. Astron. Soc.* **152**, 75 (1971).
- [49] B. J. Carr, *ApJ* **201**, 1 (1975).
- [50] J. I. Read, *J. Phys.* **G41**, 063101 (2014), [arXiv:1404.1938].
- [51] T. Piffi *et al.*, *Astron. Astrophys.* **562**, A91 (2014), [arXiv:1309.4293].
- [52] L. Necib and T. Lin, *Astrophys. J.* **926**, 2, 189 (2022), [arXiv:2102.02211].
- [53] A. M. Green, *J. Phys.* **G44**, 8, 084001 (2017), [arXiv:1703.10102].
- [54] A. Helmi *et al.*, *Nature* **7729**, 985 (2018).
- [55] L. Necib, M. Lisanti and V. Belokurov (2018), [arXiv:1807.02519].
- [56] N. W. Evans, C. A. J. O’Hare and C. McCabe, *Phys. Rev. D* **99**, 2, 023012 (2019), [arXiv:1810.11468].
- [57] S. Pöder *et al.*, *A&A* **676**, A134 (2023).
- [58] J. S. Bullock and M. Boylan-Kolchin, *Ann. Rev. Astron. Astrophys.* **55**, 343 (2017), [arXiv:1707.04256].
- [59] J. Zavala and C. S. Frenk (2019), [arXiv:1907.11775].
- [60] L. V. Sales, A. Wetzel and A. Fattahi, *Nature Astron.* **6**, 8, 897 (2022), [arXiv:2206.05295].
- [61] I. M. E. Santos-Santos *et al.*, *Mon. Not. Roy. Astron. Soc.* **495**, 1, 58 (2020), [arXiv:1911.09116].
- [62] J. Madhani *et al.*, in “American Astronomical Society Meeting Abstracts,” volume 54 of *American Astronomical Society Meeting Abstracts*, 209.08 (2022).

- [63] M. Geha *et al.*, *Astrophys. J.* **847**, 1, 4 (2017), [arXiv:1705.06743].
- [64] P. van Dokkum *et al.*, *Nature* **605**, 7910, 435 (2022), [arXiv:2205.08552].
- [65] K. E. Andrade *et al.* (2019), [arXiv:1901.00507].
- [66] G. Servant, in “Particle dark matter,” 164–189 (2010).
- [67] L. Hui *et al.*, *Phys. Rev.* **D95**, 4, 043541 (2017), [arXiv:1610.08297].
- [68] A. Fattahi *et al.* (2016), [arXiv:1607.06479].
- [69] D. J. E. Marsh, *Phys. Rept.* **643**, 1 (2016), [arXiv:1510.07633].
- [70] H. An *et al.*, *Phys. Lett.* **B747**, 331 (2015), [arXiv:1412.8378].
- [71] P. W. Graham and S. Rajendran, *Phys. Rev.* **D88**, 035023 (2013), [arXiv:1306.6088].
- [72] P. W. Graham *et al.*, *Phys. Rev.* **D93**, 7, 075029 (2016), [arXiv:1512.06165].
- [73] A. Arvanitaki *et al.*, *Phys. Rev.* **D97**, 7, 075020 (2018), [arXiv:1606.04541].
- [74] P. W. Graham *et al.*, *Phys. Rev.* **D97**, 5, 055006 (2018), [arXiv:1709.07852].
- [75] I. M. Bloch *et al.* (2019), [arXiv:1907.03767].
- [76] A. Pierce, K. Riles and Y. Zhao, *Phys. Rev. Lett.* **121**, 6, 061102 (2018), [arXiv:1801.10161].
- [77] Y. Kahn, B. R. Safdi and J. Thaler, *Phys. Rev. Lett.* **117**, 14, 141801 (2016), [arXiv:1602.01086].
- [78] R. Henning *et al.* (ABRACADABRA), in “Proceedings, 13th Patras Workshop on Axions, WIMPs and WISPs, (PATRAS 2017): Thessaloniki, Greece, 15 May 2017 - 19, 2017,” 28–31 (2018).
- [79] S. Chaudhuri *et al.*, *Phys. Rev.* **D92**, 7, 075012 (2015), [arXiv:1411.7382].
- [80] P. Sikivie, N. Sullivan and D. B. Tanner, *Phys. Rev. Lett.* **112**, 13, 131301 (2014), [arXiv:1310.8545].
- [81] B. M. Brubaker *et al.*, *Phys. Rev.* **D96**, 12, 123008 (2017), [arXiv:1706.08388].
- [82] G. Rybka (ADMX), *Phys. Dark Univ.* **4**, 14 (2014).
- [83] S. Dodelson and L. M. Widrow, *Phys. Rev. Lett.* **72**, 17 (1994), [hep-ph/9303287].
- [84] E. Bulbul *et al.*, *Astrophys. J.* **789**, 13 (2014), [arXiv:1402.2301].
- [85] A. Boyarsky *et al.*, *Phys. Rev. Lett.* **113**, 251301 (2014), [arXiv:1402.4119].
- [86] T. E. Jeltema and S. Profumo, *Mon. Not. Roy. Astron. Soc.* **450**, 2, 2143 (2015), [arXiv:1408.1699].
- [87] M. E. Anderson, E. Churazov and J. N. Bregman, *Mon. Not. Roy. Astron. Soc.* **452**, 4, 3905 (2015), [arXiv:1408.4115].
- [88] D. Malyshev, A. Neronov and D. Eckert, *Phys. Rev.* **D90**, 103506 (2014), [arXiv:1408.3531].
- [89] T. E. Jeltema and S. Profumo, *Mon. Not. Roy. Astron. Soc.* **458**, 4, 3592 (2016), [arXiv:1512.01239].
- [90] F. A. Aharonian *et al.* (Hitomi), *Astrophys. J.* **837**, 1, L15 (2017), [arXiv:1607.07420].
- [91] I. Yu. Kobzarev, L. B. Okun and I. Ya. Pomeranchuk, *Sov. J. Nucl. Phys.* **3**, 6, 837 (1966), [*Yad. Fiz.*3,1154(1966)].
- [92] M. J. Strassler and K. M. Zurek, *Phys. Lett.* **B651**, 374 (2007), [hep-ph/0604261].
- [93] M. J. Strassler (2006), [hep-ph/0607160].
- [94] M. Battaglieri *et al.*, in “U.S. Cosmic Visions: New Ideas in Dark Matter,” (2017), [arXiv:1707.04591].
- [95] Y. Kahn *et al.*, *JHEP* **05**, 002 (2017), [arXiv:1609.09072].
- [96] J. Alexander *et al.* (2016), [arXiv:1608.08632], URL <http://lss.fnal.gov/archive/2016/conf/fermilab-conf-16-421.pdf>.
- [97] K. R. Dienes and B. Thomas, *Phys. Rev.* **D85**, 083523 (2012), [arXiv:1106.4546].
- [98] N. Trevisani (ATLAS, CMS), *Universe* **4**, 11, 131 (2018).
- [99] E. Tolley (ATLAS), *PoS ICHEP2018*, 171 (2019).
- [100] W. C. Kalderon (ATLAS), *PoS DIS2018*, 085 (2018).
- [101] D. Vannerom (CMS), *PoS DIS2019*, 111 (2019).
- [102] G. Gómez-Ceballos (CMS), *PoS EDSU2018*, 014 (2018).
- [103] J. Aalbers *et al.* (LUX-ZEPLIN), *Phys. Rev. Lett.* **131**, 4, 041002 (2023), [arXiv:2207.03764].
- [104] Y. Meng *et al.* (PandaX-4T), *Phys. Rev. Lett.* **127**, 26, 261802 (2021), [arXiv:2107.13438].
- [105] E. Aprile *et al.* (XENON), *Phys. Rev. Lett.* **131**, 4, 041003 (2023), [arXiv:2303.14729].
- [106] R. Agnese *et al.* (SuperCDMS), *Phys. Rev. Lett.* **120**, 6, 061802 (2018), [arXiv:1708.08869].
- [107] P. Agnes *et al.* (DarkSide-50), *Phys. Rev. D* **107**, 6, 063001 (2023), [arXiv:2207.11966].
- [108] R. Ajaj *et al.* (DEAP), *Phys. Rev.* **D100**, 022004 (2019), [arXiv:1902.04048].
- [109] D. S. Akerib *et al.* (LUX), *Phys. Rev. Lett.* **122**, 13, 131301 (2019), [arXiv:1811.11241].
- [110] E. Aprile *et al.* (XENON) (2019), [arXiv:1907.12771].
- [111] E. Aprile *et al.* (2019), [arXiv:1907.11485].
- [112] R. Agnese *et al.* (SuperCDMS), *Phys. Rev.* **D99**, 6, 062001 (2019), [arXiv:1808.09098].
- [113] M. F. Albakry *et al.* (SuperCDMS), *Phys. Rev. D* **107**, 11, 112013 (2023), [arXiv:2302.09115].
- [114] A. H. Abdelhameed *et al.* (CRESST) (2019), [arXiv:1904.00498].
- [115] G. Angloher *et al.* (CRESST), *Phys. Rev. D* **107**, 12, 122003 (2023), [arXiv:2212.12513].
- [116] A. Aguilar-Arevalo *et al.* (DAMIC), *Phys. Rev. Lett.* **125**, 241803 (2020), [arXiv:2007.15622].
- [117] Q. Arnaud *et al.* (NEWS-G), *Astropart. Phys.* **97**, 54 (2018), [arXiv:1706.04934].
- [118] C. Amole *et al.* (PICO), *Phys. Rev.* **D100**, 2, 022001 (2019), [arXiv:1902.04031].
- [119] Z. Huang *et al.* (PandaX), *Phys. Lett. B* **834**, 137487 (2022), [arXiv:2208.03626].
- [120] J. D. Lewin and P. F. Smith, *Astropart. Phys.* **6**, 87 (1996).
- [121] J. R. Ellis, R. A. Flores and J. D. Lewin, *Phys. Lett.* **B212**, 375 (1988).
- [122] P. J. Fox, J. Liu and N. Weiner, *Phys. Rev.* **D83**, 103514 (2011), [arXiv:1011.1915].
- [123] L. Vietze *et al.*, *Phys. Rev.* **D91**, 4, 043520 (2015), [arXiv:1412.6091].
- [124] B. S. Hu *et al.*, *Phys. Rev. Lett.* **128**, 7, 072502 (2022), [arXiv:2109.00193].
- [125] J. Ellis, N. Nagata and K. A. Olive, *Eur. Phys. J.* **C78**, 7, 569 (2018), [arXiv:1805.09795].
- [126] J. Fan, M. Reece and L.-T. Wang, *JCAP* **1011**, 042 (2010), [arXiv:1008.1591].
- [127] A. L. Fitzpatrick *et al.*, *JCAP* **1302**, 004 (2013), [arXiv:1203.3542].
- [128] N. Anand, A. L. Fitzpatrick and W. C. Haxton, *Phys. Rev.* **C89**, 6, 065501 (2014), [arXiv:1308.6288].
- [129] M. I. Gresham and K. M. Zurek, *Phys. Rev.* **D89**, 12, 123521 (2014), [arXiv:1401.3739].
- [130] J. B. Dent *et al.*, *Phys. Rev.* **D92**, 6, 063515 (2015), [arXiv:1505.03117].
- [131] D. Gazda, R. Catena and C. Forssén, *Phys. Rev.* **D95**, 10, 103011 (2017), [arXiv:1612.09165].

- [132] M. Hoferichter *et al.*, Phys. Rev. **D99**, 5, 055031 (2019), [arXiv:1812.05617].
- [133] R. Essig, J. Mardon and T. Volansky, Phys. Rev. **D85**, 076007 (2012), [arXiv:1108.5383].
- [134] R. Catena *et al.*, JCAP **03**, 052 (2023), [arXiv:2210.07305].
- [135] T. Trickle, Phys. Rev. D **107**, 3, 035035 (2023), [arXiv:2210.14917].
- [136] F. T. Avignone, III *et al.*, Phys. Rev. **D35**, 2752 (1987).
- [137] M. Pospelov, A. Ritz and M. B. Voloshin, Phys. Rev. **D78**, 115012 (2008), [arXiv:0807.3279].
- [138] I. M. Bloch *et al.*, JHEP **06**, 087 (2017), [arXiv:1608.02123].
- [139] Y. Hochberg, T. Lin and K. M. Zurek, Phys. Rev. **D95**, 2, 023013 (2017), [arXiv:1608.01994].
- [140] M. Schumann, J. Phys. G **46**, 10, 103003 (2019), [arXiv:1903.03026].
- [141] J. Billard *et al.*, Rept. Prog. Phys. **85**, 5, 056201 (2022), [arXiv:2104.07634].
- [142] M. Pato *et al.*, Phys. Rev. **D83**, 083505 (2011), [arXiv:1012.3458].
- [143] A. K. Drukier, K. Freese and D. N. Spergel, Phys. Rev. **D33**, 3495 (1986).
- [144] D. N. Spergel, Phys. Rev. **D37**, 1353 (1988).
- [145] D. Stiff, L. M. Widrow and J. Frieman, Phys. Rev. **D64**, 083516 (2001), [arXiv:astro-ph/0106048].
- [146] K. Freese *et al.*, Phys. Rev. Lett. **92**, 111301 (2004), [arXiv:astro-ph/0310334].
- [147] T. Bruch *et al.*, Astrophys. J. **696**, 920 (2009), [arXiv:0804.2896].
- [148] M. J. Lewis and K. Freese, Phys. Rev. **D70**, 043501 (2004), [arXiv:astro-ph/0307190].
- [149] F. Mayet *et al.*, Phys. Rept. **627**, 1 (2016), [arXiv:1602.03781].
- [150] L. E. Strigari, New J. Phys. **11**, 105011 (2009), [arXiv:0903.3630].
- [151] C. A. J. O'Hare, Phys. Rev. Lett. **127**, 25, 251802 (2021), [arXiv:2109.03116].
- [152] L. E. Strigari, Phys. Rev. **D93**, 10, 103534 (2016), [arXiv:1604.00729].
- [153] R. Essig, M. Sholapurkar and T.-T. Yu, Phys. Rev. **D97**, 9, 095029 (2018), [arXiv:1801.10159].
- [154] V. Chepel and H. Araujo, JINST **8**, R04001 (2013), [arXiv:1207.2292].
- [155] M. J. Dolan, F. Kahlhoefer and C. McCabe, Phys. Rev. Lett. **121**, 10, 101801 (2018), [arXiv:1711.09906].
- [156] S. Li *et al.* (PandaX), Phys. Rev. Lett. **130**, 26, 261001 (2023), [arXiv:2212.10067].
- [157] P. Agnes *et al.* (DarkSide), Phys. Rev. Lett. **130**, 10, 101002 (2023), [arXiv:2207.11968].
- [158] E. Aprile *et al.* (XENON), Phys. Rev. Lett. **129**, 16, 161805 (2022), [arXiv:2207.11330].
- [159] P. Grothaus, M. Fairbairn and J. Monroe, Phys. Rev. **D90**, 5, 055018 (2014), [arXiv:1406.5047].
- [160] C. A. J. O'Hare *et al.*, Phys. Rev. **D92**, 6, 063518 (2015), [arXiv:1505.08061].
- [161] Y. Hochberg *et al.*, Phys. Lett. **B772**, 239 (2017), [arXiv:1606.08849].
- [162] Y. Hochberg *et al.*, Phys. Rev. **D97**, 1, 015004 (2018), [arXiv:1708.08929].
- [163] S. Knapen, T. Lin and K. M. Zurek, Phys. Rev. **D95**, 5, 056019 (2017), [arXiv:1611.06228].
- [164] R. Essig *et al.*, Phys. Rev. **D95**, 5, 056011 (2017), [arXiv:1608.02940].
- [165] Y. Hochberg, T. Lin and K. M. Zurek, Phys. Rev. **D94**, 1, 015019 (2016), [arXiv:1604.06800].
- [166] S. Knapen *et al.*, Phys. Lett. **B785**, 386 (2018), [arXiv:1712.06598].
- [167] S. Griffin *et al.*, Phys. Rev. **D98**, 11, 115034 (2018), [arXiv:1807.10291].
- [168] A. Arvanitaki, S. Dimopoulos and K. Van Tilburg, Phys. Rev. **X8**, 4, 041001 (2018), [arXiv:1709.05354].
- [169] T. Trickle, Z. Zhang and K. M. Zurek (2019), [arXiv:1905.13744].
- [170] Y. Hochberg *et al.*, Phys. Rev. D **106**, 11, 112005 (2022), [arXiv:2110.01586].
- [171] T. Lin, PoS **333**, 009 (2019), [arXiv:1904.07915].
- [172] R. Essig *et al.*, in "Snowmass 2021," (2022), [arXiv:2203.08297].
- [173] F. Aharonian, D. Khangulyan and D. Malyshev, Astron. Astrophys. **547**, A114 (2012), [arXiv:1207.0458].
- [174] K. K. Boddy *et al.*, Phys. Rev. **D94**, 9, 095027 (2016), [arXiv:1606.07440].
- [175] T. Sjöstrand (2019), [arXiv:1907.09874].
- [176] M. Tavani *et al.* (e-ASTROGAM), JHEAp **19**, 1 (2018), [arXiv:1711.01265].
- [177] A. Coogan, L. Morrison and S. Profumo (2019), [arXiv:1907.11846].
- [178] M. Ackermann *et al.* (Fermi-LAT), Phys. Rev. Lett. **115**, 23, 231301 (2015), [arXiv:1503.02641].
- [179] D. Hooper and L. Goodenough, Phys. Lett. **B697**, 412 (2011), [arXiv:1010.2752].
- [180] M. Ackermann *et al.* (Fermi-LAT), Astrophys. J. **840**, 1, 43 (2017), [arXiv:1704.03910].
- [181] F. Calore, I. Cholis and C. Weniger, JCAP **1503**, 038 (2015), [arXiv:1409.0042].
- [182] K. N. Abazajian and M. Kaplinghat, Phys. Rev. **D86**, 083511 (2012), [Erratum: Phys. Rev. **D87**, 129902 (2013)], [arXiv:1207.6047].
- [183] S. K. Lee, M. Lisanti and B. R. Safdi, JCAP **1505**, 05, 056 (2015), [arXiv:1412.6099].
- [184] T. Daylan *et al.*, Phys. Dark Univ. **12**, 1 (2016), [arXiv:1402.6703].
- [185] R. K. Leane and T. R. Slatyer (2019), [arXiv:1904.08430].
- [186] E. Carlson, T. Linden and S. Profumo, Phys. Rev. Lett. **117**, 11, 111101 (2016), [arXiv:1510.04698].
- [187] M. Ajello *et al.* (Fermi-LAT), Astrophys. J. **819**, 1, 44 (2016), [arXiv:1511.02938].
- [188] M. Ackermann *et al.* (Fermi-LAT), Astrophys. J. **836**, 2, 208 (2017), [arXiv:1702.08602].
- [189] A. McDaniel, T. Jeltema and S. Profumo, Phys. Rev. **D97**, 10, 103021 (2018), [arXiv:1802.05258].
- [190] C. Karwin *et al.* (2019), [arXiv:1903.10533].
- [191] A. McDaniel, T. Jeltema and S. Profumo, Phys. Rev. **D100**, 2, 023014 (2019), [arXiv:1903.06833].
- [192] R. L. Kinzer *et al.*, Astrophys. J. **559**, 282 (2001).
- [193] R. M. Bandyopadhyay *et al.*, Mon. Not. Roy. Astron. Soc. **392**, 1115 (2009), [arXiv:0810.3674].
- [194] D. P. Finkbeiner and N. Weiner, Phys. Rev. **D76**, 083519 (2007), [arXiv:astro-ph/0702587].
- [195] K. Agashe *et al.*, JCAP **1410**, 10, 062 (2014), [arXiv:1405.7370].
- [196] T. Damour and L. M. Krauss, Phys. Rev. Lett. **81**, 5726 (1998), [arXiv:astro-ph/9806165].
- [197] S. L. Adler, Phys. Lett. **B671**, 203 (2009), [arXiv:0808.2823].
- [198] J. Casanellas and I. Lopes, Astrophys. J. **765**, L21 (2013), [arXiv:1212.2985].
- [199] G. D. Mack, J. F. Beacom and G. Bertone, Phys. Rev. **D76**, 043523 (2007), [arXiv:0705.4298].

- [200] J. Smolinsky and P. Tanedo, Phys. Rev. **D95**, 7, 075015 (2017), [Erratum: Phys. Rev.D96,no.9,099902(2017)], [arXiv:1701.03168].
- [201] C. Niblaeus, A. Beniwal and J. Edsjo (2019), [arXiv:1903.11363].
- [202] M. G. Aartsen *et al.* (IceCube), JCAP **1604**, 04, 022 (2016), [arXiv:1601.00653].
- [203] S. Adrian-Martinez *et al.* (ANTARES), Phys. Lett. **B759**, 69 (2016), [arXiv:1603.02228].
- [204] C. R. Das *et al.*, Phys. Lett. **B725**, 297 (2013), [arXiv:1110.5095].
- [205] M. G. Aartsen *et al.* (IceCube), J. Phys. **G44**, 5, 054006 (2017), [arXiv:1607.02671].
- [206] Y. Zhao and K. M. Zurek, JHEP **07**, 017 (2014), [arXiv:1401.7664].
- [207] A. W. Strong, I. V. Moskalenko and V. S. Ptuskin, Ann. Rev. Nucl. Part. Sci. **57**, 285 (2007), [arXiv:astro-ph/0701517].
- [208] O. Adriani *et al.* (PAMELA), Phys. Rev. Lett. **111**, 081102 (2013), [arXiv:1308.0133].
- [209] M. Aguilar *et al.* (AMS), Phys. Rev. Lett. **117**, 9, 091103 (2016).
- [210] M. Aguilar *et al.* (AMS), Phys. Rev. Lett. **110**, 141102 (2013).
- [211] S. Profumo, F. Queiroz and C. Siqueira (2019), [arXiv:1903.07638].
- [212] D. Hooper, P. Blasi and P. D. Serpico, JCAP **0901**, 025 (2009), [arXiv:0810.1527].
- [213] S. Profumo, Central Eur. J. Phys. **10**, 1 (2011), [arXiv:0812.4457].
- [214] A. U. Abeysekara *et al.* (HAWC), Science **358**, 6365, 911 (2017), [arXiv:1711.06223].
- [215] S. Profumo *et al.*, Phys. Rev. **D97**, 12, 123008 (2018), [arXiv:1803.09731].
- [216] R. Cowsik, B. Burch and T. Madziwa-Nussinov, Astrophys. J. **786**, 124 (2014), [arXiv:1305.1242].
- [217] K. Blum, B. Katz and E. Waxman, Phys. Rev. Lett. **111**, 21, 211101 (2013), [arXiv:1305.1324].
- [218] M.-Y. Cui *et al.*, Phys. Rev. Lett. **118**, 19, 191101 (2017), [arXiv:1610.03840].
- [219] A. Reinert and M. W. Winkler, JCAP **1801**, 01, 055 (2018), [arXiv:1712.00002].
- [220] M. W. Winkler, JCAP **1702**, 02, 048 (2017), [arXiv:1701.04866].
- [221] F. Donato, N. Fornengo and P. Salati, Phys. Rev. **D62**, 043003 (2000), [hep-ph/9904481].
- [222] K. Mori *et al.*, Astrophys. J. **566**, 604 (2002), [arXiv:astro-ph/0109463].
- [223] H. Baer and S. Profumo, JCAP **0512**, 008 (2005), [arXiv:astro-ph/0510722].
- [224] E. Carlson *et al.*, Phys. Rev. **D89**, 7, 076005 (2014), [arXiv:1401.2461].
- [225] M. Cirelli *et al.*, JHEP **08**, 009 (2014), [arXiv:1401.4017].
- [226] R. Bird *et al.*, in “36th International Cosmic Ray Conference (ICRC 2019) Madison, Wisconsin, USA, July 24-August 1, 2019,” (2019), [arXiv:1908.03154].
- [227] A. Coogan and S. Profumo, Phys. Rev. **D96**, 8, 083020 (2017), [arXiv:1705.09664].
- [228] S. Colafrancesco, S. Profumo and P. Ullio, Astron. Astrophys. **455**, 21 (2006), [arXiv:astro-ph/0507575].
- [229] S. Colafrancesco, S. Profumo and P. Ullio, Phys. Rev. **D75**, 023513 (2007), [arXiv:astro-ph/0607073].
- [230] S. Profumo and P. Ullio (2010), [arXiv:1001.4086].
- [231] T. E. Jeltema and S. Profumo, JCAP **0811**, 003 (2008), [arXiv:0808.2641].
- [232] M. Cirelli *et al.*, JCAP **1103**, 051 (2011), [Erratum: JCAP1210,E01(2012)], [arXiv:1012.4515].
- [233] A. McDaniel *et al.*, JCAP **1709**, 09, 027 (2017), [arXiv:1705.09384].
- [234] E. Storm *et al.*, Astrophys. J. **768**, 106 (2013), [arXiv:1210.0872].
- [235] G. G. Raffelt, *Stars as laboratories for fundamental physics* (1996), ISBN 9780226702728, URL <http://wwwth.mpp.mpg.de/members/raffelt/mypapers/199613.pdf>.
- [236] D. Spolyar, K. Freese and P. Gondolo, Phys. Rev. Lett. **100**, 051101 (2008), [arXiv:0705.0521].
- [237] S. Dimopoulos, J. Preskill and F. Wilczek, Phys. Lett. **119B**, 320 (1982).
- [238] P. Pani and A. Loeb, JCAP **1406**, 026 (2014), [arXiv:1401.3025].
- [239] H. Liu, G. W. Ridgway and T. R. Slatyer (2019), [arXiv:1904.09296].
- [240] M. A. Monroy-Rodríguez and C. Allen, Astrophys. J. **790**, 2, 159 (2014), [arXiv:1406.5169].
- [241] M. Ricotti, J. P. Ostriker and K. J. Mack, Astrophys. J. **680**, 829 (2008), [arXiv:0709.0524].
- [242] S. Bird *et al.*, Phys. Rev. Lett. **116**, 20, 201301 (2016), [arXiv:1603.00464].
- [243] V. Poulin *et al.*, Phys. Rev. **D96**, 8, 083524 (2017), [arXiv:1707.04206].
- [244] P. Tisserand *et al.* (EROS-2), Astron. Astrophys. **469**, 387 (2007), [arXiv:astro-ph/0607207].
- [245] H. Niihara *et al.*, Nat. Astron. **3**, 6, 524 (2019), [arXiv:1701.02151].
- [246] E. Mediavilla *et al.*, Astrophys. J. **706**, 1451 (2009), [arXiv:0910.3645].
- [247] A. Barnacka, J. F. Glicenstein and R. Moderski, Phys. Rev. **D86**, 043001 (2012), [arXiv:1204.2056].
- [248] A. Katz *et al.*, JCAP **1812**, 005 (2018), [arXiv:1807.11495].
- [249] N. Smyth *et al.* (2019), [arXiv:1910.01285].
- [250] B. J. Carr *et al.*, Phys. Rev. **D81**, 104019 (2010), [arXiv:0912.5297].
- [251] A. Coogan, L. Morrison and S. Profumo, Phys. Rev. Lett. **126**, 17, 171101 (2021), [arXiv:2010.04797].
- [252] B. V. Lehmann *et al.*, JCAP **10**, 046 (2019), [arXiv:1906.06348].

28. Dark Energy

Revised August 2023 by D.H. Weinberg (Ohio State U.) and M. White (UC Berkeley; LBNL).

28.1 Repulsive Gravity and Cosmic Acceleration

In the first modern cosmological model, Einstein [1] modified his field equation of General Relativity (GR), introducing a “cosmological term” that enabled a solution with time-independent, spatially homogeneous matter density ρ_m and constant positive space curvature. Although Einstein did not frame it this way, one can view the “cosmological constant” Λ as representing a constant energy density of the vacuum [2], whose repulsive gravitational effect balances the attractive gravity of matter and thereby allows a static solution. After the development of dynamic cosmological models [3,4] and the discovery of cosmic expansion [5], the cosmological term appeared unnecessary, and Einstein and de Sitter [6] advocated adopting an expanding, homogeneous and isotropic, spatially flat, matter-dominated Universe as the default cosmology until observations dictated otherwise. Such a model has matter density equal to the critical density, $\Omega_m \equiv \rho_m/\rho_c = 1$, and negligible contribution from other energy components [7].

By the mid-1990s, the Einstein-de Sitter model was showing numerous cracks, under the combined onslaught of data from the cosmic microwave background (CMB), large-scale galaxy clustering, and estimates of the matter density, the expansion rate (H_0), and the age of the Universe. As noted in a number of papers from this time, introducing a cosmological constant offered a potential resolution of many of these tensions, yielding the most empirically successful version of the inflationary cold dark matter scenario. In the late 1990s, supernova surveys by two independent teams provided direct evidence for accelerating cosmic expansion [8,9], establishing the cosmological constant model (with $\Omega_m \simeq 0.3$, $\Omega_\Lambda \simeq 0.7$) as the preferred alternative to the $\Omega_m = 1$ scenario. Shortly thereafter, CMB evidence for a spatially flat Universe [10,11], and thus for $\Omega_{\text{tot}} \simeq 1$, cemented the case for cosmic acceleration by firmly eliminating the free-expansion alternative with $\Omega_m \ll 1$ and $\Omega_\Lambda = 0$. Today, the accelerating Universe is well established by multiple lines of independent evidence from a tight web of precise cosmological measurements.

As discussed in the Big Bang Cosmology article of this *Review* (Sec. 22), the scale factor $R(t)$ of a homogeneous and isotropic Universe governed by GR grows at an accelerating rate if the pressure $p < -\frac{1}{3}\rho$ (in $c = 1$ units). A cosmological constant has $\rho_\Lambda = \text{constant}$ and pressure $p_\Lambda = -\rho_\Lambda$ (see Eq. 22.10), so it will drive acceleration if it dominates the total energy density. However, acceleration could arise from a more general form of “dark energy” that has negative pressure, typically specified in terms of the equation-of-state-parameter $w = p/\rho$ ($= -1$ for a cosmological constant). Furthermore, the conclusion that acceleration requires a new energy component beyond matter and radiation relies on the assumption that GR is the correct description of gravity on cosmological scales. The title of this article follows the common but inexact usage of “dark energy” as a catch-all term for the origin of cosmic acceleration, regardless of whether it arises from a new form of energy or a modification of GR. Our account here draws on the much longer review of cosmic acceleration in Ref. [12], which provides background explanation and extensive literature references for the discussion in Secs. 28.2 and 28.3.

Below we will use the abbreviation ΛCDM to refer to a model with cold dark matter, a cosmological constant, inflationary initial conditions, standard radiation and neutrino content, and a flat Universe with $\Omega_{\text{tot}} = 1$ (though we will sometimes describe this model as “flat ΛCDM ” to emphasize this last restriction). We will use $w\text{CDM}$ to denote a model with the same assumptions but a free, constant value of w . Models with the prefix “o” (*e.g.*, $o\text{wCDM}$) allow non-zero space curvature.

28.2 Theories of Cosmic Acceleration

28.2.1 Dark Energy or Modified Gravity?

A cosmological constant is the mathematically simplest, and perhaps the physically simplest, theoretical explanation for the accelerating Universe. The problem is explaining its unnaturally small magnitude, as discussed in Sec. 22.4.7 of this *Review*. An alternative (which still requires finding a way to make the cos-

mological constant zero or at least negligibly small) is that the accelerating cosmic expansion is driven by a new form of energy such as a scalar field [13] with potential $V(\phi)$. The energy density and pressure of the field $\phi(\mathbf{x})$ take the same forms as for inflationary scalar fields, given in Eq. (22.52) of the Big Bang Cosmology article. In the limit that $\frac{1}{2}\dot{\phi}^2 \ll |V(\phi)|$, the scalar field acts like a cosmological constant, with $p_\phi \simeq -\rho_\phi$. In this scenario, today’s cosmic acceleration is closely akin to the epoch of inflation, but with radically different energy and timescale.

More generally, the value of $w = p_\phi/\rho_\phi$ in scalar field models evolves with time in a way that depends on $V(\phi)$ and on the initial conditions $(\phi_i, \dot{\phi}_i)$; some forms of $V(\phi)$ have attractor solutions in which the late-time behavior is insensitive to initial values. Many forms of time evolution are possible, including ones where w is approximately constant and broad classes where w “freezes” towards or “thaws” away from $w = -1$, with the transition occurring when the field comes to dominate the total energy budget. If ρ_ϕ is even approximately constant, then it becomes dynamically insignificant at high redshift, because the matter density scales as $\rho_m \propto (1+z)^3$. “Early dark energy” models are ones in which ρ_ϕ is a small but not negligible fraction (*e.g.*, a few percent) of the total energy throughout the matter- and radiation-dominated eras, tracking the dominant component before itself coming to dominate at low redshift.

Instead of introducing a new energy component, one can attempt to modify gravity in a way that leads to accelerated expansion [14]. One option is to replace the Ricci scalar \mathcal{R} with a function $\mathcal{R} + f(\mathcal{R})$ in the gravitational action [15]. Other changes can be more radical, such as introducing extra dimensions and allowing gravitons to “leak” off the brane that represents the observable Universe (the “DGP” model [16]). The DGP example has inspired a more general class of “galileon” and massive gravity models. Constructing viable modified gravity models is challenging, in part because it is easy to introduce theoretical inconsistencies (such as “ghost” fields with negative kinetic energy), but above all because GR is a theory with many high-precision empirical successes on solar system scales [17]. Modified gravity models typically invoke screening mechanisms that force model predictions to approach those of GR in regions of high density or strong gravitational potential. Screening offers potentially distinctive signatures, as the strength of gravity (*i.e.*, the effective value of G_N) can vary by order unity in environments with different gravitational potentials.

More generally, one can search for signatures of modified gravity by comparing the history of cosmic structure growth to the history of cosmic expansion. Within GR, these two are linked by a consistency relation, as described below (Eq. (28.2)). Modifying gravity can change the predicted rate of structure growth, and it can make the growth rate dependent on scale or environment. In some circumstances, modifying gravity alters the combinations of potentials responsible for gravitational lensing and the dynamics of non-relativistic tracers (such as galaxies or stars) in different ways (see Sec. 22.4.7 in this *Review*), leading to order unity mismatches between the masses of objects inferred from lensing and those inferred from dynamics in unscreened environments.

At present there are no fully realized and empirically viable modified gravity theories that explain the observed level of cosmic acceleration. The constraints on $f(\mathcal{R})$ models now force them so close to GR that they cannot produce acceleration without introducing a separate dark energy component [18]. The DGP model is empirically ruled out by several tests, including the expansion history, the integrated Sachs-Wolfe effect, and redshift-space distortion measurements of the structure growth rate [19]. The near-simultaneous arrival of gravitational waves and electromagnetic signals from the neutron star merger event GW170817, which shows that gravitational waves travel at almost exactly the speed of light, is a further strong constraint on modified gravity theories [20]. The elimination of models should be considered an important success of the program to empirically test theories of cosmic acceleration. However, it is worth recalling that there was no fully realized gravitational explanation for the precession of Mercury’s orbit prior to the completion of GR in 1915, and the fact that no complete and viable modified gravity theory exists

today does not mean that one will not arise in the future. In the meantime, we can continue empirical investigations that can tighten restrictions on such theories or perhaps point towards the gravitational sector as the origin of accelerating expansion.

28.2.2 Expansion History and Growth of Structure

The main line of empirical attack on dark energy is to measure the history of cosmic expansion and the history of matter clustering with the greatest achievable precision over a wide range of redshift. Within GR, the expansion rate $H(z)$ is governed by the Friedmann equation (see the articles on Big Bang Cosmology and Cosmological Parameters—Secs. 22 and 25 in this *Review*). For dark energy with an equation of state $w(z)$, the cosmological constant contribution to the expansion, Ω_Λ , is replaced by a redshift-dependent contribution. The evolution of the dark energy density follows from Eq. (22.10),

$$\begin{aligned} \Omega_{\text{de}} \frac{\rho_{\text{de}}(z)}{\rho_{\text{de}}(z=0)} &= \Omega_{\text{de}} \exp \left[3 \int_0^z [1 + w(z')] \frac{dz'}{1+z'} \right] \\ &= \Omega_{\text{de}} (1+z)^{3(1+w)}, \end{aligned} \quad (28.1)$$

where the second equality holds for constant w . If Ω_m , Ω_r , and the present value of Ω_{tot} are known, then measuring $H(z)$ pins down $w(z)$. (Note that Ω_{de} is the same quantity denoted Ω_v in Sec. 22, but we have adopted the ‘de’ subscript to avoid implying that dark energy is necessarily a vacuum effect.)

While some observations can probe $H(z)$ directly, others measure the distance-redshift relation. The basic relations between angular diameter distance or luminosity distance and $H(z)$ are given in Ch. 22—and these are generally unaltered in time-dependent dark energy or modified gravity models. For convenience, in later sections, we will sometimes refer to the comoving angular diameter distance, $D_{A,c}(z) = (1+z)D_A(z)$.

In GR-based linear perturbation theory, the density contrast $\delta(\mathbf{x}, t) \equiv \rho(\mathbf{x}, t)/\bar{\rho}(t) - 1$ of pressureless matter grows in proportion to the linear growth function $G(t)$ (not to be confused with the gravitational constant G_N), which follows the differential equation

$$\ddot{G} + 2H(z)\dot{G} - \frac{3}{2}\Omega_m H_0^2 (1+z)^3 G = 0. \quad (28.2)$$

To a good approximation, the logarithmic derivative of $G(z)$ is

$$f(z) \equiv -\frac{d \ln G}{d \ln(1+z)} \simeq \left[\Omega_m (1+z)^3 \frac{H_0^2}{H^2(z)} \right]^\gamma, \quad (28.3)$$

where $\gamma \simeq 0.55$ for relevant values of cosmological parameters [21]. In an $\Omega_m = 1$ Universe, $G(z) \propto (1+z)^{-1}$, but growth slows when Ω_m drops significantly below unity. One can integrate Eq. (28.3) to get an approximate integral relation between $G(z)$ and $H(z)$, but the full (numerical) solution to Eq. (28.2) should be used for precision calculations. Even in the non-linear regime, the amplitude of clustering is determined mainly by $G(z)$, so observations of non-linear structure can be used to infer the linear $G(z)$, provided one has good theoretical modeling to relate the two.

In modified gravity models the growth rate of gravitational clustering may differ from the GR prediction. A general strategy to test modified gravity, therefore, is to measure both the expansion history and the growth history to see whether they yield consistent results for $H(z)$ or $w(z)$.

28.2.3 Parameters

Constraining a general history of $w(z)$ is nearly impossible, because the dark energy density, which affects $H(z)$, is given by an integral over $w(z)$, and distances and the growth factor involve a further integration over functions of $H(z)$. Oscillations in $w(z)$ over a range $\Delta z/(1+z) \ll 1$ are therefore extremely difficult to constrain. It has become conventional to phrase constraints or projected constraints on $w(z)$ in terms of a linear evolution model,

$$w(a) = w_0 + w_a(1-a) = w_p + w_a(a_p - a), \quad (28.4)$$

where $a \equiv (1+z)^{-1}$, w_0 is the value of w at $z=0$, and w_p is the value of w at a ‘pivot’ redshift $z_p \equiv a_p^{-1} - 1$, where it

is best constrained by a given set of experiments. For typical data combinations, $z_p \simeq 0.5$. This simple parameterization can provide a good approximation to the predictions of many physically motivated models for observables measured with percent-level precision. A widely used ‘Figure of Merit’ (FoM) for dark energy experiments [22] is the projected combination of errors $[\sigma(w_p)\sigma(w_a)]^{-1}$. Ambitious future experiments with 0.1–0.3% precision on observables can constrain richer descriptions of $w(z)$, which can be characterized by principal components.

There has been less convergence on a standard parameterization for describing modified gravity theories. Deviations from the GR-predicted growth rate can be described by a deviation $\Delta\gamma$ in the index of Eq. (28.3), together with an overall multiplicative offset relative to the $G(z)$ expected from extrapolating the CMB-measured fluctuation amplitude to low redshift. However, these two parameters may not accurately capture the growth predictions of all physically interesting models. Another important parameter to constrain is the ratio of the gravitational potentials governing space curvature and the acceleration of non-relativistic test particles. The possible phenomenology of modified gravity models is rich [23], which enables many consistency tests but complicates the task of constructing parameterized descriptions.

The more general set of cosmological parameters is discussed elsewhere in this *Review* (Sec. 25), but here we highlight a few that are particularly important to the dark energy discussion.

- The dimensionless Hubble parameter $h \equiv H_0/100 \text{ km s}^{-1} \text{ Mpc}^{-1}$ determines the present day value of the critical density and the overall scaling of distances inferred from redshifts.
- Ω_m and Ω_{tot} affect the expansion history and the distance-redshift relation.
- The sound horizon $r_s = \int_0^{t_{\text{rec}}} c_s(t) dt/a(t)$, the comoving distance that pressure waves can propagate between $t=0$ and recombination, determines the physical scale of the acoustic peaks in the CMB and the baryon acoustic oscillation (BAO) feature in low-redshift matter clustering [24].
- The amplitude of matter fluctuations, conventionally represented by the quantity $\sigma_8(z)$, scales the overall amplitude of growth measures such as weak lensing or redshift-space distortions (discussed in the next section).

Specifically, $\sigma_8(z)$ refers to the rms fluctuation of the matter overdensity $\rho/\bar{\rho}$ in spheres of radius $8 h^{-1} \text{ Mpc}$, computed from the linear theory matter power spectrum at redshift z , and σ_8 on its own refers to the value at $z=0$ (just like our convention for Ω_m).

While discussions of dark energy are frequently phrased in terms of values and errors on quantities like w_p , w_a , $\Delta\gamma$, and Ω_{tot} , parameter precision is the means to an end, not an end in itself. The underlying goal of empirical studies of cosmic acceleration is to address two physically profound questions:

1. Does acceleration arise from a breakdown of GR on cosmological scales or from a new energy component that exerts repulsive gravity within GR?
2. If acceleration is caused by a new energy component, is its energy density constant in space and time, as expected for a fundamental vacuum energy, or does it show variations that indicate a dynamical field?

Substantial progress towards answering these questions, in particular any definitive rejection of the cosmological constant ‘null hypothesis,’ would be a major breakthrough in cosmology and fundamental physics.

28.3 Observational Probes

We briefly summarize the observational probes that play the greatest role in current constraints on dark energy. Further discussion can be found in other articles of this *Review*, in particular Secs. 25 (Cosmological Parameters) and 29 (The Cosmic Microwave Background), and in Ref. [12], which provides extensive references to background literature. Recent observational results from these methods are discussed in Sec. 28.4.

28.3.1 Methods, Sensitivity, Systematics

Cosmic Microwave Background Anisotropies: Although CMB anisotropies provide limited information about dark energy on their own, CMB constraints on the geometry, matter content, and radiation content of the Universe play a critical role in dark energy studies when combined with low-redshift probes. In particular, CMB data supply measurements of $\theta_s = r_s/D_{A,c}(z_{\text{rec}})$, the angular size of the sound horizon at recombination, from the angular location of the acoustic peaks, measurements of $\Omega_m h^2$ and $\Omega_b h^2$ from the heights of the peaks, and normalization of the amplitude of matter fluctuations at z_{rec} from the amplitude of the CMB fluctuations themselves. The comparison of the acoustic scale to the diffusion damping scale helps to constrain the expansion rate near recombination. *Planck* data yield a 0.18% determination of r_s , which scales as $(\Omega_m h^2)^{-0.25}$ for cosmologies with standard matter and radiation content. The uncertainty in the matter fluctuation amplitude at the epoch of recombination is 0.5%. Secondary anisotropies, including the integrated Sachs-Wolfe effect, the Sunyaev-Zeldovich (SZ, [25]) effect, and weak lensing of primary anisotropies, provide additional information about dark energy by constraining low-redshift structure growth.

Type Ia Supernovae (SN): Type Ia supernovae, produced by the thermonuclear explosions of white dwarfs, exhibit 10–15% scatter in peak luminosity after correction for light curve duration (the time to rise and fall) and color (which is a diagnostic of dust extinction). Since the peak luminosity is not known *a priori*, supernova surveys constrain ratios of luminosity distances $D_L(z)$ at different redshifts. If one is comparing a high-redshift sample to a local calibrator sample measured with much higher precision (and distances inferred from Hubble’s law), then one essentially measures the luminosity distance in $h^{-1}\text{Mpc}$, constraining the combination $hD_L(z)$. With distance uncertainties of 5–8% per well observed supernova, a sample of around 100 SNe is sufficient to achieve sub-percent statistical precision. The percent-level systematic uncertainties in current samples are dominated by uncertainties associated with photometric calibration and dust extinction corrections and modeling the correlations among supernova luminosity, color, light-curve shape, and host galaxy properties. Another potential systematic is redshift evolution of the supernova population itself, which can be tested by analyzing subsamples grouped by spectral properties or host galaxy properties to confirm that they yield consistent results. Recent analyses of large supernova compilations calibrate these systematic uncertainties internally in parallel with cosmological constraints, with an overall error budget that has similar contributions from systematic and statistical uncertainties (e.g., [26]).

Baryon Acoustic Oscillations (BAO): Pressure waves that propagate in the pre-recombination photon-baryon fluid imprint a characteristic scale in the clustering of matter and galaxies, which appears in the galaxy correlation function as a localized peak at the sound horizon scale r_s , or in the power spectrum as a series of oscillations. Since observed galaxy coordinates consist of angles and redshifts, measuring this “standard ruler” scale in a galaxy redshift survey determines the angular diameter distance $D_A(z)$ and the expansion rate $H(z)$, which convert coordinate separations to comoving distances. Errors on the two quantities are correlated, and in existing galaxy surveys the best determined combination is approximately $D_V(z) = [czD_{A,c}^2(z)/H(z)]^{1/3}$. As a useful rule of thumb, a survey that fully samples structures at redshift z over a comoving volume V , and is therefore limited by cosmic variance rather than shot noise, measures $D_{A,c}(z)$ with a fractional error of $0.005(V/10\text{Gpc}^3)^{-1/2}$ and $H(z)$ with a fractional error 1.6–1.8 times higher. The most precise BAO measurements to date come from large galaxy redshift surveys probing $z < 0.8$, and these will be extended to higher redshifts by ongoing and future projects. At redshifts $z > 2$, BAO can also be measured in the Lyman- α forest of intergalactic hydrogen absorption towards background quasars, where the fluctuating absorption pattern provides tens or hundreds of samples of the density field along each quasar sightline. For Lyman- α forest BAO, the best measured parameter combination is more heavily weighted towards $H(z)$ because of strong redshift-space distortions that enhance clustering in the line-of-sight direction. Radio intensity mapping, which maps large-scale

structure in redshifted 21-cm hydrogen emission without resolving individual galaxies, offers a potential route to measuring BAO over large volumes at relatively low cost, but the technique is still under development. Photometric redshifts in optical imaging surveys can be used to measure BAO in the angular direction, though the typical distance precision is a factor of 3–4 lower compared to a well sampled spectroscopic survey of the same area, and angular BAO measurements do not directly constrain $H(z)$. BAO distance measurements complement SN distance measurements by providing absolute rather than relative distances (with precise calibration of r_s from the CMB) and by having greater achievable precision at high redshift thanks to the increasing comoving volume available. Theoretical modeling suggests that BAO measurements from even the largest feasible redshift surveys will be limited by statistical rather than systematic uncertainties.

Weak Gravitational Lensing: Gravitational light bending by a clustered distribution of matter shears the shapes of higher redshift background galaxies in a spatially coherent manner, producing a correlated pattern of apparent ellipticities. By studying the weak lensing signal for source galaxies binned by photometric redshift (estimated from broad-band colors), one can probe the history of structure growth. “Cosmic shear” weak lensing uses the correlation of source ellipticities to deduce the clustering of intervening matter. “Galaxy-galaxy lensing” (GGL) uses the correlation between a shear map and a foreground galaxy sample to measure the average mass profile around the foreground galaxies, which can be combined with galaxy clustering to constrain total matter clustering. For a specified expansion history, the predicted signals scale approximately as $\sigma_8 \Omega_m^\alpha$, with $\alpha \simeq 0.3\text{--}0.5$. The predicted signals also depend on the distance-redshift relation, so weak lensing becomes more powerful in concert with SN or BAO measurements that can pin this relation down independently. The most challenging systematics are shape measurement biases, biases in the distribution of photometric redshifts, and intrinsic alignments of galaxy orientations that could contaminate the lensing-induced signal. Weak lensing of CMB anisotropies is an increasingly powerful tool, in part because it circumvents many of these observational and astrophysical systematics. Predicting the large-scale weak lensing signal is straightforward in principle, but the number of independent modes on large scales is small, and the inferences are therefore dominated by sample variance. Exploiting small-scale measurements, for tighter constraints, requires modeling the effects of complex physical processes such as star formation and feedback on the matter power spectrum. Strong gravitational lensing can also provide constraints on dark energy, either through time delay measurements that probe the absolute distance scale, or through measurements of multiple-redshift lenses that constrain distance ratios. The primary uncertainty for strong lensing constraints is modeling the mass distribution of the lens systems.

Clusters of Galaxies: Like weak lensing, the abundance of massive dark-matter halos probes structure growth by constraining $\sigma_8 \Omega_m^\alpha$, where $\alpha \simeq 0.3\text{--}0.5$. These halos can be identified as dense concentrations of galaxies or through the signatures of hot ($10^7\text{--}10^8\text{K}$) gas in X-ray emission or SZ distortion of the CMB. The critical challenge in cluster cosmology is calibrating the relation $P(M_{\text{halo}}|O)$ between the halo mass as predicted from theory and the observable O used for cluster identification. Measuring the stacked weak lensing signal from clusters has emerged as a promising approach to achieve percent-level accuracy in calibration of the mean relation, which is required for clusters to remain competitive with other growth probes. This method requires accurate modeling of completeness and contamination of cluster catalogs, projection effects on cluster selection and weak lensing measurements, and possible baryonic physics effects on the mass distribution within clusters.

Redshift-Space Distortions (RSD) and the Alcock-Paczynski (AP) Effect: Redshift-space distortions of galaxy clustering, induced by peculiar motions, probe structure growth by constraining the parameter combination $f(z)\sigma_8(z)$, where $f(z)$ is the growth rate defined by Eq. (28.3). Uncertainties in theoretical modeling of non-linear gravitational evolution and the non-linear bias between the galaxy and matter distributions currently limit application of the

Table 28.1: A selection of major dark-energy experiments, based on Ref. [27]. Abbreviations in the “Data” column refer to optical (Opt) or near-infrared (NIR) imaging (I) or spectroscopy (S). For spectroscopic experiments, the “Spec- z ” column lists the primary redshift range for galaxies (gals), quasars (QSOs), or the Lyman- α forest (Ly α F). Abbreviations in the “Methods” column are weak lensing (WL), clusters (CL), supernovae (SN), baryon acoustic oscillations (BAO), and redshift-space distortions (RSD).

Project	Dates	Area/deg ²	Data	Spec- z Range	Methods
BOSS	2008–2014	10,000	Opt-S	0.3–0.7 (gals) 2–3.5 (Ly α F)	BAO/RSD
KiDS	2011–2019	1350	Opt-I	—	WL/CL
DES	2013–2019	5000	Opt-I	—	WL/CL SN/BAO
eBOSS	2014–2018	7500	Opt-S	0.6–2.0 (gal/QSO) 2–3.5 (Ly α F)	BAO/RSD
SuMIRE	2014–2029	1500	Opt-I	—	WL/CL
			Opt/NIR-S	0.8–2.4 (gals)	BAO/RSD
DESI	2021–2026	14,000	Opt-S	0–1.7 (gals) 2–3.5 (Ly α F)	BAO/RSD
VRO/LSST	2025–2035	20,000	Opt-I	—	WL/CL SN/BAO
<i>Euclid</i>	2023–2029	15,000	Opt-I	—	WL/CL
			NIR-S	0.7–2.2 (gals)	BAO/RSD
<i>Roman</i>	2027–2032	2200	NIR-I	—	WL/CL/SN
			NIR-S	1.0–3.0 (gals)	BAO/RSD

method to large scales (comoving separations $r \gtrsim 10 h^{-1} \text{Mpc}$ or wavenumbers $k \lesssim 0.2 h \text{Mpc}^{-1}$). A second source of anisotropy arises if one adopts the wrong cosmological metric to convert angles and redshifts into comoving separations, a phenomenon known as the Alcock-Paczynski effect [28]. Demanding isotropy of clustering at redshift z constrains the parameter combination $H(z)D_A(z)$. The main challenge for the AP method is correcting for the anisotropy induced by peculiar velocity RSD.

Low Redshift Measurement of H_0 : The value of H_0 sets the current value of the critical density $\rho_c = 3H_0^2/8\pi G_N$, and combination with CMB measurements provides a long lever arm for constraining the evolution of dark energy. The challenge in conventional H_0 measurements is establishing distances to galaxies that are “in the Hubble flow,” *i.e.*, far enough away that their peculiar velocities are small compared to the expansion velocity $v = H_0 d$. This can be done by building a ladder of distance indicators tied to stellar parallax on its lowest rung, or by using gravitational-lens time delays or geometrical measurements of maser data to circumvent this ladder.

28.3.2 Dark Energy Experiments

Most observational applications of the above methods now take place in the context of large cosmological surveys, for which constraining dark energy and modified gravity theories is a central objective. Table 28.1 lists a selection of recent, ongoing, and planned dark-energy experiments, taken originally from the Snowmass 2013 Dark Energy Facilities review [27], which focused on projects in which the U.S. has either a leading role or significant participation. References and links to further information about these projects can be found in Ref. [27]. We have adjusted some of the dates in this Table relative to those in Ref. [27] and added the European-led KiloDegree Survey (KiDS). Dates in the Table correspond to the duration of survey observations, and the final cosmological results frequently require 1–3 years of analysis and modeling beyond the end of data taking. We are now at an exciting phase in which most of the “Stage III” experiments (in the parlance of Ref. [29]) have completed observations and in some cases final analysis, and the more powerful “Stage IV” experiments are underway or beginning operations in the near future.

Beginning our discussion with imaging surveys, the Dark Energy Survey (DES) observed 1/8 of the sky to a depth roughly 2 magnitudes deeper than the Sloan Digital Sky Survey (SDSS), enabling weak lensing measurements with much greater statistical precision, cluster measurements calibrated by weak lensing, and angular BAO measurements based on photometric redshifts. With repeated imaging of selected fields, DES identified thou-

sands of Type Ia SNe, which together with spectroscopic follow-up data enabled significant improvements for supernova (SN) cosmology. Cosmological results from weak lensing and galaxy clustering analyses of the 3-year (Y3) DES data set are presented in Ref. [30]. The first cosmological results from the DES supernova survey are presented in Ref. [31], and DES supernovae are incorporated into the Pantheon+ compilation analyzed in Ref. [26]. KiDS carried out an optical imaging survey of about 1000 deg², with cosmology results from weak lensing and galaxy clustering reported in Refs. [32, 33]. The Subaru Hyper-Suprime Camera (HSC) collaboration is surveying about 1500 deg² with greater depth and sharper image quality than DES; cosmology results from the 3-year HSC data set are presented in Refs. [34, 35]. Beginning in the mid-2020s, the Legacy Survey of Space and Time (LSST) of the Vera Rubin Observatory (VRO) will scan the southern sky to SDSS-like depth every four nights. The co-added data from LSST’s decade-long primary survey will provide deep multi-band imaging over a wide area, enabling weak lensing, cluster, and photometric BAO studies from billions of galaxies. Additionally, LSST time-domain monitoring will identify and measure light curves for thousands of Type Ia SNe per year.

Turning to spectroscopic surveys, the Baryon Oscillation Spectroscopic Survey (BOSS) and its successor eBOSS used fiber-fed optical spectrographs to map the redshift-space distributions of millions of galaxies and quasars. These 3-dimensional maps enable BAO and RSD measurements, and Lyman- α forest spectra of high-redshift quasars extend these measurements to redshifts $z > 2$. As discussed below, the eBOSS Collaboration has now published BAO and RSD analyses from the final data sets of the BOSS and eBOSS programs. The Dark Energy Spectroscopic Instrument (DESI) follows a strategy similar to BOSS/eBOSS but on a much grander scale, using a larger telescope (4-m versus 2.5-m) and a much higher fiber multiplex (5000 versus 1000) to survey an order-of-magnitude more galaxies. DESI began full operations in May 2021, and in its first two years it has measured well over 20 million redshifts; at least 40 million redshifts are expected by the survey end. A new Prime Focus Spectrograph (PFS) for the Subaru telescope will enable the spectroscopic component of SuMIRE, starting in 2024, with the large telescope aperture and wavelength sensitivity that extends to the near-infrared (NIR) allowing it to probe a higher redshift galaxy population than DESI, over a smaller area of sky.

Compared to ground-based observations, space observations afford higher angular resolution and a far lower NIR sky background. The *Euclid* mission and the *Nancy Grace Roman Space Telescope* (formerly *WFIRST*) will exploit these advantages, con-

ducting large area imaging surveys for weak lensing and cluster studies and slitless spectroscopic surveys of emission-line galaxies for BAO and RSD studies. *Roman* will also incorporate an imaging and spectrophotometric supernova (SN) survey, extending to redshift $z \simeq 1.7$. One can roughly characterize the difference between the *Euclid* and *Roman* dark-energy experiments as “wide versus deep,” with currently planned survey areas of 15,000 deg² and 2200 deg², respectively. For weak lensing shape measurements, *Euclid* uses a single wide optical filter, while *Roman* will use three NIR filters. The *Euclid* galaxy redshift survey will cover a large volume at relatively low space density, while the *Roman* survey will provide denser sampling of structure in a smaller volume. *Euclid* was launched successfully in July 2023 and has released first light images; it will begin its 6.5-year main mission survey in late 2023. *Roman* is scheduled for launch in late 2026 or early 2027, and details of its cosmology surveys will likely evolve before operations begin. There are numerous synergies among the LSST, *Euclid*, and *Roman* dark energy programs, as discussed in Ref. [36].

28.4 Current Constraints on Expansion, Growth, and Dark Energy

The last decade has seen dramatic progress in measurements of the cosmic expansion history and structure growth, leading to much tighter constraints on the parameters of dark energy models. CMB data from the *WMAP* and *Planck* satellites and from higher resolution ground-based experiments have provided an exquisitely detailed picture of structure at the recombination epoch and CMB-based measures of low-redshift structure through lensing and SZ cluster counts. Cosmological supernova samples have increased in size from tens to thousands, with continuous coverage from $z = 0$ to $z \simeq 1.4$, alongside major improvements in data quality, analysis methods, and detailed understanding of local populations. BAO measurements have advanced from the first detections to 1–2% precision at multiple redshifts, with increasingly sophisticated methods for testing systematics, fitting models, and evaluating statistical errors. Advances in X-ray, SZ, and weak-lensing observations of large samples of galaxy clusters allow a multi-faceted approach to mass calibration, improving statistical precision but also revealing sources of astrophysical uncertainty. Cluster constraints have been joined, and for the present superseded, by precise matter-clustering constraints from cosmic-shear weak lensing and galaxy-galaxy lensing, and by redshift-space distortion measurements that probe different aspects of structure growth at (presently) lower precision. The precision of low-redshift H_0 measurements has sharpened from the roughly 10% error of the *HST* Key Project [37] to claimed precision as high as 1–2% in recent analyses.

As an illustration of current measurements of the cosmic expansion history, Fig. 28.1 compares distance-redshift measurements from SN and BAO data to the predictions for a flat Universe with a cosmological constant. SN cosmology relies on compilation analyses that try to bring data from different surveys probing distinct redshift ranges to a common scale. Here we use the “joint light curve analysis” (JLA) sample of Ref. [39], who carried out a careful intercalibration of the 3-year Supernova Legacy Survey (SNLS3, [41]) and the full SDSS-II Supernova Survey [3] data in combination with several local supernova samples and high-redshift supernovae from *HST*. For illustration purposes, we have binned the JLA data in redshift and plotted the diagonal elements of the covariance matrix as error bars, and we have converted the SN luminosity distances to an equivalent comoving angular diameter distance. Because the peak luminosity of a fiducial SN Ia is an unknown free parameter, the SN distance measurements could all be shifted up and down by a constant multiplicative factor; cosmological information resides in the relative distances as a function of redshift. The normalization used here corresponds to a Hubble parameter $h = 0.674$.

For the BAO data points in Fig. 28.1 we have used the compilation in Table 3 (the “BAO-only” row) from the summary cosmology paper by the eBOSS collaboration [40], where one can find references for the original data sources. The individual BAO measurements come (in order of increasing redshift) from the SDSS-II

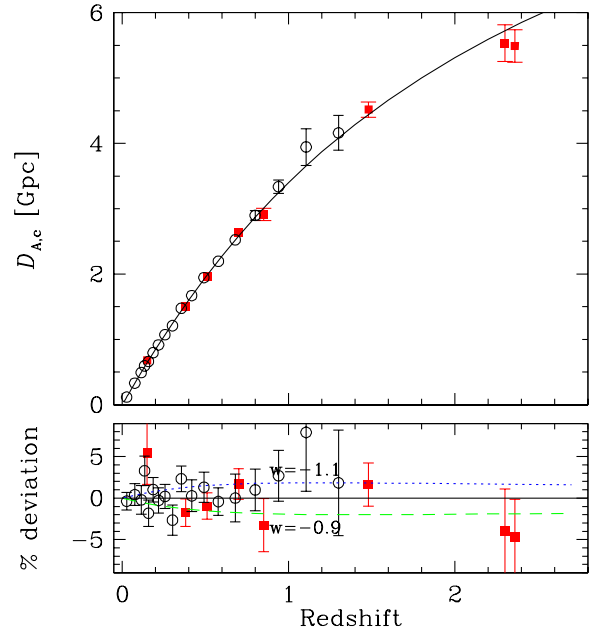


Figure 28.1: Distance-redshift relation measured from Type Ia SNe and BAO compared to the predictions (black curve) of a flat Λ CDM model with $\Omega_m = 0.315$ and $h = 0.674$, the best-fit parameters inferred from *Planck* CMB data [38]. Circles show binned luminosity distances from the JLA SN sample [39], multiplied by $(1+z)^{-1}$ to convert to comoving angular diameter distance. Red squares show BAO distance measurements from the SDSS-II, BOSS, and eBOSS surveys as compiled in Ref. [40]. The lower panel plots residuals from the Λ CDM prediction, with dashed and dotted curves that show the effect of changing w by ± 0.1 while all other parameters are held fixed. Note that the SN data points can be shifted up or down by a constant factor to account for freedom in the peak luminosity, while the BAO points are calibrated to 0.2% precision by the sound horizon scale computed from *Planck* data. The errors on the BAO data points are approximately independent, but not entirely so. In the upper panel, error bars are plotted only at $z > 0.7$ to avoid visual confusion. The two Lyman- α forest data points are slightly offset from their effective redshift of $z = 2.33$ for clarity.

main galaxy sample and from luminous red galaxies, emission line galaxies, and quasars mapped by BOSS and eBOSS. The two highest redshift points, both with an effective $z \approx 2.3$, come from the auto-correlation of the Lyman- α forest in high-redshift ($z > 2$) quasars from BOSS and eBOSS and from the cross-correlation of the Lyman- α forest with the quasars themselves. The BAO measurements are converted to absolute distances using the sound horizon scale $r_s = 147.09$ Mpc from *Planck* 2018 CMB data, whose 0.18% uncertainty is small compared to the current BAO measurement errors. For the $z = 0.15$ and $z = 1.5$ data points we have converted values of D_V to $D_{A,c}$, while for other redshifts we use the $D_{A,c}$ determinations measured directly by the transverse BAO scale. The galaxy and Lyman- α forest analyses also measure $H(z)$ at the same redshifts, providing further leverage on expansion history that is not captured in Fig. 28.1.

The plotted cosmological model has $\Omega_m = 0.315$ and $h = 0.674$, the best-fit values from *Planck* (TT+TE+EE+lowE+lensing) assuming $w = -1$ and $\Omega_{tot} = 1$ [38]. The SN, BAO, and CMB data sets, probing a wide range of redshifts with radically different techniques, are for the most part mutually consistent with the predictions of a flat Λ CDM cosmology. This consistency has held steady or improved as the measurements themselves have improved over the past decade. Dotted and dashed curves in the lower panel of Fig. 28.1 show the effect of changing w by ± 0.1 with all other parameters held fixed, which leads to significantly worse agreement with the data. However, such a single-parameter com-

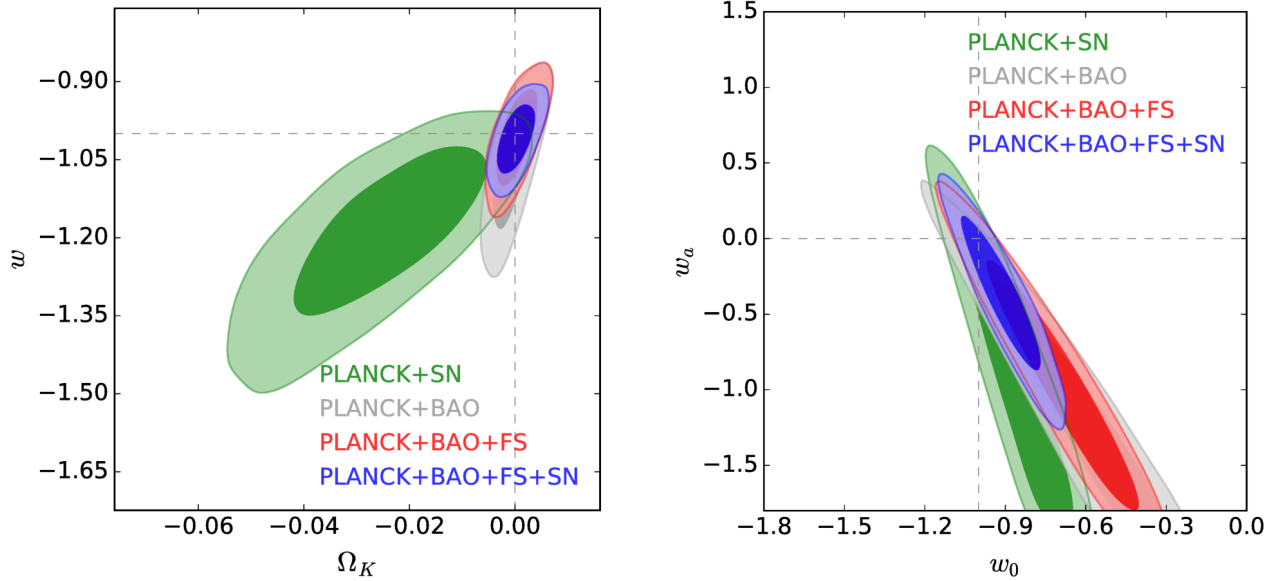


Figure 28.2: Constraints on dark energy model parameters from combinations of CMB, BAO, galaxy clustering, and supernova (SN) data, taken from Ref. [42]. The left panel shows 68% and 95% confidence contours in the ωw CDM model, with constant equation-of-state parameter w and non-zero space curvature $\Omega_K \equiv 1 - \Omega_{\text{tot}}$. Green and gray contours show the combination of *Planck* CMB data with SN or BAO data, respectively. Red contours combine CMB, BAO, and the full shape (FS) of redshift-space galaxy clustering. Blue contours add SN data to this combination. The right panel shows confidence contours for the same data combinations in the $w_0 w_a$ CDM model, which assumes a flat Universe and an evolving equation of state with $w(a) = w_0 + w_a(1 - a)$.

parison does not capture the impact of parameter degeneracies or the ability of complementary data sets to break them, and if one instead forced a match to CMB data by changing h and Ω_m when changing w then the predicted BAO distances would diverge at $z = 0$ rather than converging there. The recent Pantheon+ compilation [43] comprises more than 1500 spectroscopically confirmed Type Ia supernovae from 18 different samples, including those in the JLA. With higher statistical precision and reduced systematic uncertainties, a joint fit of Pantheon+ with CMB and BAO data remains fully compatible with a flat Λ CDM model [26]. Other good representations of recent observational constraints on the cosmic expansion history include Fig. 4 of Ref. [26] for SNIa and Fig. 2 of Ref. [40] for BAO.

Fig. 28.2, taken from Ref. [42], presents constraints on models that allow a free but constant value of w with non-zero space curvature (ωw CDM, left panel) or the evolving equation of state of Eq. (28.4) in a flat Universe ($w_0 w_a$ CDM, right panel). Green contours show constraints from the combination of *Planck* 2015 CMB data and the JLA supernova sample. Gray contours show the combination of *Planck* with BAO measurements from BOSS, 6dFGS [44], and SDSS-II [45]. Red contours adopt a more aggressive analysis of the BOSS galaxy data that uses the full shape (FS) of the redshift-space power spectrum and correlation function, modeled via perturbation theory, in addition to the measurement of the BAO scale itself. The full shape analysis improves the constraining power of the data, primarily because measurement of the Alcock-Paczynski effect on sub-BAO scales helps to break the degeneracy between $D_{A,c}(z)$ and $H(z)$. Blue contours show constraints from the full combination of CMB, BAO+FS, and SN data. Supernovae provide fine-grained relative distance measurements with good bin-by-bin precision at $z < 0.7$ (see Fig. 28.1), which is complementary to BAO for constraining redshift evolution of w . In both classes of model, the flat Λ CDM parameters ($w = w_0 = -1$, $\Omega_K = w_a = 0$) lie within the 68% confidence contour. Many recent papers feature constraint diagrams analogous to Fig. 28.2, and the constraints within this parameter space have tightened moderately with new data while remaining consistent with flat Λ CDM.

The precision on dark energy parameters depends, of course, on both the data being considered and the flexibility of the model being assumed. For w CDM, Ref. [40] find $w = -1.026 \pm 0.033$ using *Planck* CMB data, BAO measurements from SDSS-II and

BOSS/eBOSS, and SN measurements from the Pantheon compilation. With the addition of eBOSS RSD data and DES weak lensing and galaxy clustering measurements, they constrain a more flexible model ($\omega w_0 w_a$ CDM) that allows non-zero curvature and an evolving equation-of-state (Eq. 28.4), finding

$$w_p = -1.020 \pm 0.032 \quad (28.5)$$

at a pivot redshift $z_p = 0.29$, a tight constraint on curvature,

$$1 - \Omega_{\text{tot}} = -0.0023 \pm 0.0022, \quad (28.6)$$

but only a loose constraint on the evolution parameter,

$$w_a = -0.48^{+0.36}_{-0.30}. \quad (28.7)$$

Obtaining a tight constraint on w_p in such a flexible cosmological model requires measurements that have complementary sensitivity to its multiple free parameters, and the precision of Eq. (28.5) is a testament to the remarkable improvements in cosmological measurements over the past decade. BAO and FS measurements from DESI will likely supersede those from BOSS/eBOSS in the near future, enabling substantially sharper parameter constraints.

A flat Λ CDM model fit to *Planck* CMB data alone predicts $H_0 = (67.4 \pm 0.5) \text{ km s}^{-1} \text{ Mpc}^{-1}$ (see Chapter 29 of this *Review*). This prediction and its error bar are sensitive to the assumptions of constant dark energy and a flat Universe. However, by adding BAO and supernova data one can construct an “inverse distance ladder” to measure H_0 precisely, even with a general dark energy model and free curvature [46]. Ref. [40] applies this approach to obtain $H_0 = (68.2 \pm 0.8) \text{ km s}^{-1} \text{ Mpc}^{-1}$. As discussed in Sec. 25.3.1 of this *Review*, some recent measurements from low-redshift data yield higher values of H_0 . For example, Ref. [47] uses a distance ladder based on Cepheid calibration of Type Ia supernova luminosities to find $H_0 = (73.0 \pm 1.0) \text{ km s}^{-1} \text{ Mpc}^{-1}$, in strong tension with cosmologically inferred values. However, calibrations based on tip-of-the-red-giant-branch (TRGB) distances give lower H_0 , consistent with the cosmological values [48].

The tension in H_0 could reflect some combination of statistical flukes and systematic errors in one or more of the data sets employed in these analyses. However, if the resolution lies in new physics rather than measurement errors, then this is probably physics that operates in the *pre-recombination* Universe, rescaling the BAO standard ruler in a way that shifts the Λ CDM and

inverse-distance-ladder values upward. Models with extra relativistic degrees of freedom or dark energy that is dynamically significant in the early Universe can achieve this effect by increasing the early expansion rate, but they are tightly constrained by the damping tail of CMB anisotropies and by the shape of the galaxy power spectrum. These constraints will sharpen significantly with the next generation of CMB experiments, which will improve measurements of polarization anisotropies in the damping tail. A finely tuned model in which early dark energy decays rapidly after recombination can mitigate the tension between CMB data and local H_0 measurements [49], though it still prefers H_0 values below those of Ref. [47]. Numerous theory papers have examined possible physical solutions to the H_0 tension, all of which involve significant modifications to the Λ CDM scenario.

The amplitude of CMB anisotropies is proportional to the amplitude of density fluctuations present at recombination, and by assuming GR and a specified dark energy model one can extrapolate the growth of structure forward to the present day to predict σ_8 . Probes of low-redshift structure yield constraints in the (σ_8, Ω_m) plane, which can be summarized in terms of the parameter combination $S_8 \equiv \sigma_8(\Omega_m/0.3)^{0.5}$. As discussed in earlier editions of this *Review*, many weak-lensing and cluster studies to date yield S_8 values lower than those predicted for *Planck*-normalized Λ CDM.

Fig. 28.3, taken from Ref. [50], illustrates the current state-of-play on S_8 . (Similar figures with different selections of data can be found in many recent papers and in the previous edition of this *Review*.) The topmost point represents the predicted value and 1σ uncertainty, $S_8 = 0.830 \pm 0.014$, based on a flat Λ CDM model normalized to *Planck* CMB anisotropies. The next two points illustrate a different treatment of the *Planck* data or an alternative CMB data combination. The next four points, in red, illustrate values of S_8 measured from weak lensing of the CMB, again assuming flat Λ CDM. Although the background being lensed is the CMB, this is still a measurement of low-redshift clustering; for multipoles $\ell > 100$ roughly half of the expected signal comes from structure at $z < 2$ and nearly all from $z < 10$ [51].

The remaining points, in blue, represent galaxy-based measurements that probe structure at $z \approx 0.2$ – 0.8 , lower than the peak of the CMB-lensing kernel. The first four come from analyses of the DES, KiDS, and HSC weak lensing surveys, using cosmic shear and galaxy-galaxy lensing combined with galaxy clustering. The three points labeled CX come from cross-correlation of galaxies with CMB lensing maps, which measures the galaxy-matter cross-correlation without using optical weak lensing data. The point labeled GC (fourth from bottom) is inferred from RSD analysis of eBOSS galaxies. Details and references can be found in Sec. 3.4 of Ref. [50].

It is evident from Fig. 28.3 that CMB lensing measurements of S_8 (red points) are in good agreement with predictions based on primary CMB anisotropy (green points), but S_8 values measured from weak lensing at lower redshifts are consistently lower than this prediction (blue points, excluding the GC point derived from RSD). The discrepancy with any individual measurement is only 1 – 2σ , but the significance is higher if one treats the points derived from separate surveys as statistically independent. For instance, after averaging the two HSC measurements, an unweighted mean of the six low redshift lensing measurements in Fig. 28.3 yields $S_8 = 0.759 \pm 0.009$, where the 1σ error is simply the dispersion of the measurements divided by $\sqrt{N-1} = \sqrt{5}$. With this estimate, the $+3\sigma$ bound $S_8 = 0.786$ lies just below the -3σ bound of the *Planck* prediction, $S_8 = 0.788$. However, several or all of these measurements could be affected by a common systematic error, such as the modeling of galaxy intrinsic alignments or the modeling of structure on non-linear scales. Furthermore, the RSD measurement, which probes similar redshifts with a physically distinct observable, gives a much higher S_8 value, though with an uncertainty large enough to accommodate both the CMB-based prediction and the low- z weak lensing measurement.

The tension between the Λ CDM prediction of S_8 and low redshift weak lensing measurements has persisted through several cycles of this *Review*, without getting obviously stronger or obviously weaker. The sharpest conflicts arise in analyses that extend

to non-linear scales and thus have the highest statistical precision, but these analyses are also the most susceptible to modeling uncertainties such as the impact of baryonic dissipation and feedback on the mass distribution. If the tension suggested by Fig. 28.3 represents a true deviation between the clustering growth extrapolated forward from the early Universe and the clustering of matter at late times, then it is difficult to explain by changing the dark energy equation of state because the expansion history is already well constrained by BAO and SN data. Instead, such a deviation might point towards modified gravity, decaying dark matter, or coupling between dark matter and dark energy.

Progress in understanding this tension should come from several directions. Unified analyses of multiple weak lensing data sets are now testing consistency and highlighting the influence of analysis choices on cosmological results [52,53]. Final data from DES and HSC will have better statistical power, which improves the internal calibration of systematic nuisance parameters and affords greater precision at the larger scales that are easier to model. Improved CMB lensing maps will allow better cross-correlation measurements (the CX points in Fig. 28.3), which avoid some of the main systematics affecting optical weak lensing. DESI data will soon allow the first RSD-based measurements of structure growth at the 1–2% level, which will show whether the low matter clustering amplitude suggested by weak lensing data is also apparent in galaxy peculiar velocities. In modified gravity models these two methods of constraining structure can yield inconsistent results because they respond to different combinations of metric components, but either consistency or inconsistency would provide valuable guidance. Finally, if there is truly a 5–10% discrepancy between CMB-normalized Λ CDM predictions and low-redshift clustering, it should be measured at high statistical significance in *Euclid* weak lensing data and, subsequently, in LSST and *Roman* data.

28.5 Summary and Outlook

Figure 28.2 focuses on model parameter constraints, but to describe the observational situation it is more useful to characterize the precision, redshift range, and systematic uncertainties of the basic expansion and growth measurements. At present, supernova surveys constrain distance ratios at the 1–2% level in redshift bins of width $\Delta z = 0.1$ out to $z \approx 0.8$, with larger but still interesting error bars out to $z \simeq 1.3$. Estimated systematic uncertainties are comparable to statistical uncertainties and include effects of photometric calibration, dust reddening, host-galaxy correlations, and possible evolution of the SN population. BAO surveys have measured the angular diameter distance $D_{A,c}(z)$ and the expansion rate $H(z)$ over the range $0 < z < 2.5$, calibrated to absolute units using the CMB-based value of the sound horizon r_s . For $D_{A,c}(z)$, the final analyses of BOSS/eBOSS achieve precision of 1.6–1.8% in three overlapping redshift bins from luminous galaxies at $z = 0.2 - 1.0$, 2.6% from quasars at $z \approx 1.5$, and 2.9% from the Lyman- α forest at $z \approx 2.3$. For $H(z)$, the precision at the same redshifts is 2.6–3.0%, 4.1%, and 2.1%, respectively. SDSS, DES, KiDS, and HSC have used combinations of weak lensing and galaxy clustering to measure the parameter combination $S_8 = \sigma_8(\Omega_m/0.3)^{0.5}$ with estimated precision of 2–4%, and the cross-correlation of galaxy distributions with CMB lensing maps achieves comparable precision. These estimates account for identified systematic uncertainties, but the measurements and modeling are challenging, and it is possible that the systematics are underestimated. Our simple average of these measurements, treating them as independent and using their dispersion as an empirical estimate of uncertainty, yields an error on the mean of 1.1%. The statistical power of these weak lensing surveys is concentrated at $z \approx 0.2$ – 0.8 , and they provide useful constraints at lower precision on redshift evolution over this range and on individual values of Ω_m and σ_8 . RSD measurements constrain the similar parameter combination $f(z)\sigma_8(z)$, but they do not yet have precision competitive with that of weak lensing measurements. Distance-ladder estimates of H_0 now span a small range, using overlapping data but distinct treatments of key steps. Individual studies quote uncertainties as small as 1–2%, with similar statistical and systematic contributions.

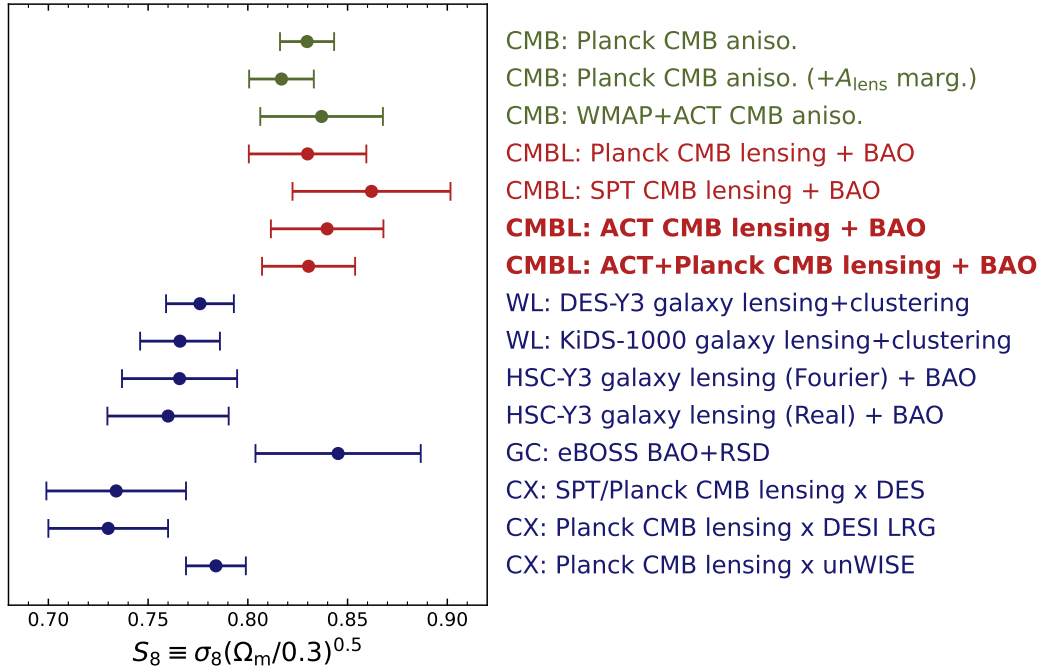


Figure 28.3: Predicted values of $S_8 \equiv \sigma_8(\Omega_m/0.3)^{0.5}$ from a CMB-normalized Λ CDM model (green points), compared to observational estimates from CMB lensing (red points), from optical weak lensing surveys (first four blue points), from galaxy clustering RSD (blue GC point), and from cross-correlation of galaxies with CMB lensing maps (blue CX points). The predictions (green) are extrapolated forward from primary CMB anisotropy measurements that measure structure at $z \approx 1100$. CMB lensing (red) is most sensitive to structure at $z \approx 1 - 2$, while the galaxy-based data (blue) probe structure at $z \approx 0.2-0.8$. Taken from Ref. [50].

Planck data and higher resolution ground-based experiments now measure CMB anisotropies with exquisite precision; for example, CMB measurements now constrain the physical size of the BAO sound horizon to 0.2% and the angular scale of the sound horizon to 0.01%. A flat Λ CDM model with standard radiation and neutrino content can fit the CMB data and the BAO and SN distance measurements to within their estimated uncertainties. The value of H_0 implied by this model disagrees with recent Cepheid+SN Ia distance-ladder measurements of H_0 at a $\sim 5\sigma$ level. This disagreement persists in models that allow non-zero curvature and low redshift evolution of $w(z)$, provided one assumes standard pre-recombination physics to compute the sound horizon r_s . The discrepancy could reflect underestimated systematic uncertainties in the Cepheid-based H_0 estimate, or it could be a sign of new physics in the early Universe that rescales r_s . Improved parallax data from *HST* and *Gaia*, discovery of new SNIa in nearby galaxies, and observing programs on the *James Webb Space Telescope (JWST)* are all allowing improvements and systematic checks in the Cepheid distance ladder. It will be equally important to bring the TRGB calibration method to a comparable level of precision and systematics control, and to understand any differences between the Cepheid and TRGB distance scales. Polarization measurements of the CMB damping tail from ground-based experiments will provide increasingly strong constraints on resolutions of the H_0 -tension that invoke novel pre-recombination physics.

Extrapolating forward from the CMB anisotropies measured by *Planck* predicts a low redshift value of S_8 that is higher than recent estimates from weak gravitational lensing and galaxy clustering. Comparing the *Planck* central value to the simple average of recent experiments discussed in Sec.28.4 implies a difference of 9.3%: $S_8 = 0.830 \pm 0.014$ versus $S_8 = 0.759 \pm 0.009$. This disagreement could reflect a common systematic that biases several of the weak lensing analyses in the same direction, and it would be weakened if the *Planck* S_8 value were high because of an unlucky statistical fluctuation or a residual systematic. If real, this discrepancy could point towards modified gravity, decaying dark matter, or coupling between dark matter and dark energy.

There are numerous directions for progress over the next several years. Analyses of the final weak lensing data sets from KiDS, HSC, and DES will yield tighter statistical constraints and more complete understanding of systematic uncertainties. Cross-correlation of galaxy maps with higher signal-to-noise CMB lensing maps will provide independent clustering measurements that avoid many of the systematics of optical weak lensing. Collectively these efforts could achieve an unambiguous determination of the amplitude of low redshift matter clustering at the 1–2% level.

The DESI redshift survey already exceeds the size of the SDSS and BOSS/eBOSS surveys, with a factor of ~ 10 increase expected by the end of the 5-year program. DESI will enable the first high precision BAO measurements of expansion history at $z \approx 0.7-1.4$, as well as improved BAO measurements at $z < 0.7$ from denser galaxy samples and at $z > 2$ from much larger Lyman- α forest samples. DESI will also enable the first percent-level measurements of structure growth through RSD. The BAO measurements will complement increasingly precise measurements of the relative distance scale at $z < 1$ from supernova compilations that include the final data from DES. Large galaxy samples will also enable more powerful applications of the Alcock-Paczynski effect and parameter measurements based on voids or higher order clustering statistics.

Euclid, LSST, and *Roman* provide another major leap in observational capabilities. LSST will be the ultimate ground-based optical weak-lensing experiment, measuring several billion galaxy shapes over 20,000 deg^2 of the southern hemisphere sky, and it will detect and monitor many thousands of SNe per year. *Euclid* and *Roman* also have weak lensing as a primary science goal, taking advantage of the high angular resolution and extremely stable image quality achievable from space. Both missions plan large spectroscopic galaxy surveys, which will provide better sampling at high redshifts than DESI or Subaru PFS because of the lower infrared sky background above the atmosphere. *Roman* is also designed to carry out what should be the ultimate supernova cosmology experiment, with deep, high resolution, near-IR observations and the stable calibration achievable with a space platform.

The 2020s will also see dramatic advances in CMB lensing from the Simons Observatory and, potentially, CMB-S4 and/or a space-based probe; cross-correlation with galaxy surveys allows precise tomographic studies of clustering as a function of redshift. While the measurement goals of these next generation facilities overlap, the history of precision cosmology demonstrates the crucial importance of pursuing these measurements with multiple experiments that have distinct challenges and complementary strengths, and with analysis teams that develop ideas independently. The ensemble of experiments will produce cosmological constraints that are much tighter and much more robust to systematic uncertainties than any one of them could achieve individually.

If the anomalies suggested in Fig. 28.3 are real, then these experiments will map out their redshift, scale, and environment dependence in great detail, providing detailed empirical constraints on dynamical dark energy or modified gravity models. If these tensions dissipate with improved measurements, then the experiments of the 2020s will achieve much more stringent tests of the Λ CDM paradigm, with the potential to reveal deviations that are still within the statistical uncertainties of current data. The critical clue to the origin of cosmic acceleration could also come from a surprising direction, such as laboratory, solar-system, or gravitational-wave tests that challenge GR, time variation of fundamental “constants,” or anomalous behavior of gravity in some astronomical environments. Experimental advances along these multiple axes could confirm today’s relatively simple, but frustratingly incomplete, “standard model” of cosmology, or they could force yet another radical revision in our understanding of energy, or gravity, or the spacetime structure of the Universe.

References

- [1] A. Einstein, Sitzungsber. Preuss. Akad. Wiss. Berlin (Math. Phys.), 142 (1917).
- [2] Ya. B. Zel’dovich, A. Krasinski and Ya. B. Zeldovich, Sov. Phys. Usp. **11**, 381 (1968), [Gen. Rel. Grav.40,1557(2008); Usp. Fiz. Nauk95,209(1968)].
- [3] A. Friedman, Z. Phys. **10**, 377 (1922), [Gen. Rel. Grav.31,1991(1999)].
- [4] G. Lemaître, Annales de la Societe Scientifique de Bruxelles **47**, 49 (1927).
- [5] E. Hubble, Proc. Nat. Acad. Sci. **15**, 168 (1929).
- [6] A. Einstein and W. de Sitter, Proc. Nat. Acad. Sci. **18**, 213 (1932).
- [7] For background and definitions, see Big-Bang Cosmology – Sec. 22 of this *Review*.
- [8] A. G. Riess *et al.* (Supernova Search Team), Astron. J. **116**, 1009 (1998), [arXiv:astro-ph/9805201].
- [9] S. Perlmutter *et al.* (Supernova Cosmology Project), Astrophys. J. **517**, 565 (1999), [arXiv:astro-ph/9812133].
- [10] P. de Bernardis *et al.* (Boomerang), Nature **404**, 955 (2000), [arXiv:astro-ph/0004404].
- [11] S. Hanany *et al.*, Astrophys. J. **545**, L5 (2000), [arXiv:astro-ph/0005123].
- [12] D. H. Weinberg *et al.*, Phys. Rept. **530**, 87 (2013), [arXiv:1201.2434].
- [13] C. Wetterich, Nucl. Phys. **B302**, 668 (1988), [arXiv:1711.03844].
- [14] A. Joyce *et al.*, Phys. Rept. **568**, 1 (2015), [arXiv:1407.0059].
- [15] S. M. Carroll *et al.*, Phys. Rev. **D70**, 043528 (2004), [arXiv:astro-ph/0306438].
- [16] G. R. Dvali, G. Gabadadze and M. Porrati, Phys. Lett. **B485**, 208 (2000), [hep-th/0005016].
- [17] C.M. Will, Living Reviews in Relativity, **9**, 3 (2006). See also the chapter on Experimental Tests of Gravitational Theory — in this *Review*.
- [18] J. Wang, L. Hui and J. Khoury, Phys. Rev. Lett. **109**, 241301 (2012), [arXiv:1208.4612].
- [19] M. Fairbairn and A. Goobar, Phys. Lett. **B642**, 432 (2006), [arXiv:astro-ph/0511029]; Y.-S. Song, I. Sawicki and W. Hu, Phys. Rev. **D75**, 064003 (2007), [arXiv:astro-ph/0606286]; C. Blake *et al.*, Mon. Not. Roy. Astron. Soc. **415**, 2876 (2011), [arXiv:1104.2948].
- [20] T. Baker *et al.*, Phys. Rev. Lett. **119**, 25, 251301 (2017), [arXiv:1710.06394].
- [21] E. V. Linder, Phys. Rev. **D72**, 043529 (2005), [arXiv:astro-ph/0507263].
- [22] This is essentially the FoM proposed in the Dark Energy Task Force (DETF) report, A. Albrecht *et al.*, astro-ph/0609591, though they based their FoM on the area of the 95% confidence contour in the $w_0 - w_a$ plane.
- [23] T. Baker *et al.*, Rev. Mod. Phys. **93**, 1, 015003 (2021), [arXiv:1908.03430].
- [24] For high accuracy, the impact of acoustic oscillations must be computed with a full Boltzmann code, but the simple integral for r_s captures the essential physics and the scaling with cosmological parameters.
- [25] R. A. Sunyaev and Ya. B. Zeldovich, Astrophys. Space Sci. **7**, 3 (1970).
- [26] D. Brout *et al.*, Astrophys. J. **938**, 2, 110 (2022), [arXiv:2202.04077].
- [27] D. Weinberg *et al.* (2013), [arXiv:1309.5380].
- [28] C. Alcock and B. Paczynski, Nature **281**, 358 (1979).
- [29] A. Albrecht *et al.* (2006), [arXiv:astro-ph/0609591].
- [30] T. M. C. Abbott *et al.* (DES) (2021), [arXiv:2105.13549].
- [31] T. M. C. Abbott *et al.* (DES), Astrophys. J. **872**, 2, L30 (2019), [arXiv:1811.02374].
- [32] M. Asgari *et al.* (KiDS), Astron. Astrophys. **645**, A104 (2021), [arXiv:2007.15633].
- [33] C. Heymans *et al.*, Astron. Astrophys. **646**, A140 (2021), [arXiv:2007.15632].
- [34] R. Dalal *et al.* (2023), [arXiv:2304.00701].
- [35] X. Li *et al.* (2023), [arXiv:2304.00702].
- [36] B. Jain *et al.* (2015), [arXiv:1501.07897].
- [37] W. L. Freedman *et al.* (HST), Astrophys. J. **553**, 47 (2001), [arXiv:astro-ph/0012376].
- [38] N. Aghanim *et al.* (Planck) (2018), [arXiv:1807.06209].
- [39] M. Betoule *et al.*, Astron. & Astrophys. **568**, 22 (2014).
- [40] S. Alam *et al.* (eBOSS), Phys. Rev. D **103**, 8, 083533 (2021), [arXiv:2007.08991].
- [41] M. Sullivan *et al.* (SNLS), Astrophys. J. **737**, 102 (2011), [arXiv:1104.1444].
- [42] S. Alam *et al.* (BOSS), Mon. Not. Roy. Astron. Soc. **470**, 3, 2617 (2017), [arXiv:1607.03155].
- [43] D. Scolnic *et al.*, Astrophys. J. **938**, 2, 113 (2022), [arXiv:2112.03863].
- [44] F. Beutler *et al.*, Mon. Not. Roy. Astron. Soc. **416**, 3017 (2011), [arXiv:1106.3366].
- [45] A. J. Ross *et al.*, Mon. Not. Roy. Astron. Soc. **449**, 1, 835 (2015), [arXiv:1409.3242].
- [46] E. Aubourg *et al.*, Phys. Rev. **D92**, 12, 123516 (2015), [arXiv:1411.1074].
- [47] A. G. Riess *et al.*, Astrophys. J. Lett. **934**, 1, L7 (2022), [arXiv:2112.04510].
- [48] S. A. Uddin *et al.* (2023), [arXiv:2308.01875].
- [49] V. Poulin *et al.*, Phys. Rev. Lett. **122**, 22, 221301 (2019), [arXiv:1811.04083].
- [50] M. S. Madhavacheril *et al.* (ACT) (2023), [arXiv:2304.05203].
- [51] A. Lewis and A. Challinor, Phys. Rept. **429**, 1 (2006), [arXiv:astro-ph/0601594].
- [52] A. Amon *et al.*, Mon. Not. Roy. Astron. Soc. **518**, 1, 477 (2023), [arXiv:2202.07440].
- [53] T. M. C. Abbott *et al.* (Kilo-Degree Survey, DES) (2023), [arXiv:2305.17173].

29. Cosmic Microwave Background

Revised August 2023 by D. Scott (U. of British Columbia) and G.F. Smoot (HKUST; UC Berkeley; LBNL; DIPC; Paris U.).

29.1 Introduction

The energy content in electromagnetic radiation from beyond our Galaxy is dominated by the cosmic microwave background (CMB), discovered in 1965 [1]. Its spectral distribution is well described by a blackbody function with $T = 2.7255$ K, which is a principal pillar of the hot Big Bang model for the Universe, with the lack of any observed deviations from a Planckian spectrum constraining physical processes over cosmic history at redshifts $z \lesssim 10^7$ (see earlier versions of this review).

The key information in the CMB sky is extracted from the observed angular variation of its temperature (or intensity) correlations, and to a growing extent polarization [2]. After the first detection of CMB anisotropies by the Cosmic Background Explorer (*COBE*) satellite in 1992 [3], there has been intense activity to map the sky at increasing levels of sensitivity and angular resolution by ground-based and balloon-borne measurements. These were joined in 2003 by the first results from NASA's Wilkinson Microwave Anisotropy Probe (*WMAP*) [4], which were improved upon by analyses of data added every 2 years, culminating in the 9-year results [5]. In 2013 we had the first results [6] from the third generation CMB satellite, ESA's *Planck* mission [7], which were enhanced by results from the 2015 *Planck* data release [8,9], and then the final 2018 *Planck* data release [10,11]. Additionally, CMB anisotropies have been extended to smaller angular scales by ground-based experiments, particularly the Atacama Cosmology Telescope (ACT) [12] and the South Pole Telescope (SPT) [13]. Together these observations have led to a stunning confirmation of the 'Standard Model of Cosmology.' In combination with other astrophysical data, the CMB anisotropy measurements place quite precise constraints on a number of cosmological parameters, and have launched us into an era of precision cosmology. With more than half a century of study of the CMB, the program to map temperature anisotropies is effectively wrapping up, and attention is increasingly focussing on polarization measurements, which promise further tests of fundamental physics.

29.2 CMB Spectrum

It is well-known that the spectrum of the microwave background is very precisely that of blackbody radiation, whose temperature evolves with redshift as $T(z) = T_0(1+z)$ in an expanding Universe. As a direct confirmation of its cosmological origin, this relationship has been tested by measuring the strengths of emission and absorption lines in high-redshift systems (*e.g.*, Ref. [14]).

Measurements of the spectrum are consistent with a blackbody distribution over more than three decades in frequency (there is a claim by ARCADE [15] of a possible unexpected extragalactic emission signal at low frequency, but the interpretation is debated [16]). All viable cosmological models predict a very nearly Planckian spectrum to within the current observational limits. Because of this, measurements of deviations from a blackbody spectrum have received little attention in recent years, with only a few exceptions. However, that situation will likely change as proposed experiments [17] are built that have the potential to dramatically improve early Universe energy release constraints. It now seems feasible to probe spectral distortion mechanisms that are *required* in the standard picture, such as those arising from the damping and dissipation of relatively small-scale primordial perturbations, or the average effect of inverse Compton scattering. A more ambitious goal would be to reach the precision needed to detect the residual lines from the cosmological recombination of hydrogen and helium and hence to test whether conditions at $z \gtrsim 1000$ accurately follow those in the standard picture [18].

29.3 Description of CMB Anisotropies

Observations show that the CMB contains temperature anisotropies at the 10^{-5} level and polarization anisotropies at the 10^{-6} (and lower) level, over a wide range of angular scales. These anisotropies are usually expressed using a spherical harmonic expansion

of the CMB sky:

$$T(\theta, \phi) = \sum_{\ell m} a_{\ell m} Y_{\ell m}(\theta, \phi) \quad (29.1)$$

(with the linear polarization pattern written in a similar way using the so-called spin-2 spherical harmonics). Increasing angular resolution requires that the expansion goes to higher multipoles. Because only very weak phase correlations are observed in the CMB sky and no preferred direction is seen, the vast majority of the cosmological information is found in the temperature 2-point function, *i.e.*, the variance as a function only of angular separation. Equivalently, the anisotropy power per unit $\ln \ell$ is $\ell \sum_m |a_{\ell m}|^2 / 4\pi$.

29.3.1 The Monopole

The CMB has a mean temperature of $T_\gamma = 2.7255 \pm 0.0006$ K (1σ) [19], which can be considered as the monopole component of CMB maps, a_{00} . Because all mapping experiments involve difference measurements, they are insensitive to this average level; monopole measurements can only be made with absolute temperature devices, such as the FIRAS instrument on the *COBE* satellite [20]. The measured kT_γ is equivalent to 0.234 meV or $4.60 \times 10^{-10} m_e c^2$. A blackbody of the measured temperature has a number density $n_\gamma = (2\zeta(3)/\pi^2) T_\gamma^3 \simeq 411 \text{ cm}^{-3}$, energy density $\rho_\gamma = (\pi^2/15) T_\gamma^4 \simeq 4.64 \times 10^{-34} \text{ g cm}^{-3} \simeq 0.260 \text{ eV cm}^{-3}$, and a fraction of the critical density $\Omega_\gamma \simeq 5.38 \times 10^{-5}$.

29.3.2 The Dipole

The largest anisotropy is in the $\ell = 1$ (dipole) first spherical harmonic, with amplitude 3.3621 ± 0.0010 mK [10]. The dipole is interpreted to be the result of the Doppler boosting of the monopole caused by the Solar System motion relative to the nearly isotropic blackbody field, as broadly confirmed by measurements of the radial velocities of local galaxies (*e.g.*, Ref. [21]); the intrinsic (non-Doppler) part of the signal is expected to be 2 orders of magnitude smaller (and fundamentally difficult to distinguish). The motion of an observer with velocity $\beta \equiv v/c$ relative to an isotropic Planckian radiation field of temperature T_0 produces a Lorentz-boosted temperature pattern

$$T(\theta) = T_0(1 - \beta^2)^{1/2} / (1 - \beta \cos \theta) \\ \simeq T_0 \left[1 + \beta \cos \theta + \left(\beta^2/2 \right) \cos 2\theta + \mathcal{O}(\beta^3) \right]. \quad (29.2)$$

At every point in the sky, one observes a blackbody spectrum, with temperature $T(\theta)$. The spectrum of the dipole has been confirmed to be the differential of a blackbody spectrum [22]. At higher order there are additional effects arising from aberration and from modulation of the anisotropy pattern, which have also been observed [23].

The implied velocity for the Solar System barycenter is $v = 369.82 \pm 0.11 \text{ km s}^{-1}$, assuming a value $T_0 = T_\gamma$, towards $(l, b) = (264.021^\circ \pm 0.011^\circ, 48.253^\circ \pm 0.005^\circ)$ [10]. This Solar System motion implies a velocity for the Galaxy and the Local Group of galaxies relative to the CMB of $v_{\text{LG}} = 620 \pm 15 \text{ km s}^{-1}$ towards $(l, b) = (271.9^\circ \pm 2.0^\circ, 29.6^\circ \pm 1.4^\circ)$ [10]; most of the error comes from uncertainty in the velocity of the Solar System relative to the Local Group.

The dipole is a frame-dependent quantity, and one can thus determine the 'CMB frame' (in some sense this is a special frame) as that in which the CMB dipole would be zero. Any velocity of the receiver relative to the Earth and the Earth around the Sun is removed for the purposes of CMB anisotropy studies, while our velocity relative to the Local Group of galaxies and the Local Group's motion relative to the CMB frame are normally removed for cosmological studies. The dipole is now routinely used as a primary calibrator for mapping experiments, either via the time-varying orbital motion of the Earth, or through the cosmological dipole measured by satellite experiments.

29.3.3 Higher-Order Multipoles

The variations in the CMB temperature maps at higher multipoles ($\ell \geq 2$) are interpreted as being mostly the result of density

perturbations in the early Universe, manifesting themselves at the epoch of the last scattering of the CMB photons. In the hot Big Bang picture, the expansion of the Universe cools the plasma so that by a redshift $z \simeq 1100$ (with little dependence on the details of the model), the hydrogen and helium nuclei can bind electrons into neutral atoms, a process usually referred to as ‘recombination’ [24]. Before this epoch, the CMB photons were tightly coupled to the charged baryons, while afterwards they could freely stream towards us. By measuring the $a_{\ell m}$ s we are thus learning directly about physical conditions in the early Universe.

A statistically-isotropic sky means that all m s are equivalent, *i.e.*, there is no preferred axis, so that the temperature correlation function between two positions on the sky depends only on angular separation and not orientation. Together with the assumption of Gaussian statistics (*i.e.*, no correlations between the modes), the 2-point function of the temperature field (or equivalently the power spectrum in ℓ) then fully characterizes the anisotropies. The power summed over all m s at each ℓ is $(2\ell+1)C_\ell/(4\pi)$, where $C_\ell \equiv \langle |a_{\ell m}|^2 \rangle$. Thus, averages of $a_{\ell m}$ s over m can be used as estimators of the C_ℓ s to constrain their expectation values, which are the quantities predicted by a theoretical model. For an idealized full-sky observation, the variance of each measured C_ℓ (*i.e.*, the variance of the variance) is $[2/(2\ell+1)]C_\ell^2$. This sampling uncertainty (known as ‘cosmic variance’) comes about because each C_ℓ is χ^2 distributed with $(2\ell+1)$ degrees of freedom for our observable volume of the Universe. For fractional sky coverage, f_{sky} , this variance is increased by $1/f_{\text{sky}}$ and the modes become partially correlated.

It is important to understand that theories predict the expectation value of the power spectrum, whereas our sky is a *single* realization. Hence, the cosmic variance is an unavoidable source of uncertainty when constraining models; it dominates the scatter at lower ℓ s, while the effects of instrumental noise and resolution dominate at higher ℓ s [25].

Theoretical models generally predict that the $a_{\ell m}$ modes are Gaussian random fields to high precision, matching the empirical tests, *e.g.*, standard slow-roll inflation’s non-Gaussian contribution is expected to be at least an order of magnitude below current observational limits [26]. Although non-Gaussianity of various forms is possible in early Universe models, tests show that Gaussianity is an extremely good simplifying approximation [27]. The only current indications of any non-Gaussianity or statistical anisotropy are some relatively weak signatures at large scales, seen in both *WMAP* [28] and *Planck* data [29], but not of high enough significance to reject the simplifying assumption. Nevertheless, models that deviate from the inflationary slow-roll conditions can have measurable non-Gaussian signatures. So while the current observational limits make the power spectrum the dominant probe of cosmology, it is worth noting that higher-order correlations are tools for constraining otherwise viable theories.

29.3.4 Angular Resolution and Binning

There is no one-to-one conversion between multipole ℓ and the angle subtended by a particular spatial scale projected onto the sky. However, crudely speaking, a single spherical harmonic $Y_{\ell m}$ corresponds to angular variations of $\theta \sim \pi/\ell$. CMB maps contain anisotropy information from the size of the map (or in practice some fraction of that size) down to the beam-size of the instrument, σ (the standard deviation of the beam, in radians). One can think of the effect of a Gaussian beam as rolling off the power spectrum with the function $e^{-\ell(\ell+1)\sigma^2}$.

For less than full sky coverage, the ℓ modes become correlated. Hence, experimental results are usually quoted as a series of ‘band powers,’ defined as estimators of $\ell(\ell+1)C_\ell/2\pi$ over different ranges of ℓ . Because of the strong foreground signals in the Galactic plane, even ‘all-sky’ surveys, such as *WMAP* and *Planck*, involve a cut sky. The amount of binning required to obtain uncorrelated estimates of power also depends on the map size.

29.4 Cosmological Parameters

The current ‘Standard Model’ of cosmology contains around 10 free parameters, only six of which are required to have non-null values (see The Cosmological Parameters—Sec. 25 of this *Review*).

The basic framework is the Friedmann-Robertson-Walker (FRW) metric (*i.e.*, a Universe that is approximately homogeneous and isotropic on large scales), with density perturbations laid down at early times and evolving into today’s structures (see Big-Bang cosmology—Sec. 22 of this *Review*). The most general possible set of density variations is a linear combination of an adiabatic density perturbation and some isocurvature perturbations. Adiabatic means that there is no change to the entropy per particle for each species, *i.e.*, $\delta\rho/\rho$ for matter is $(3/4)\delta\rho/\rho$ for radiation. Isocurvature means that the set of individual density perturbations adds to zero, for example, matter perturbations compensate radiation perturbations so that the total energy density remains unperturbed, *i.e.*, $\delta\rho$ for matter is $-\delta\rho$ for radiation. These different modes give rise to distinct (temporal) phases during growth, with those of the adiabatic scenario being fully consistent with the data. Models that generate mainly isocurvature type perturbations (such as most topological defect scenarios) are not viable. However, an admixture of the adiabatic mode with up to 1.7% isocurvature contribution (depending on details of the mode) is still allowed [30].

29.4.1 Initial Condition Parameters

Within the adiabatic family of models, there is, in principle, a free function describing the variation of comoving curvature perturbations, $\mathcal{R}(\mathbf{x}, t)$. The great virtue of \mathcal{R} is that it is constant in time on super-horizon scales for a purely adiabatic perturbation. There are physical reasons to anticipate that the variance of these perturbations will be described well by a power law in scale, *i.e.*, in Fourier space $\langle |\mathcal{R}|_k^2 \rangle \propto k^{n_s-4}$, where k is wavenumber and n_s is the spectral index as usually defined. So-called ‘scale-invariant’ initial conditions (meaning gravitational potential fluctuations that are independent of k) correspond to $n_s = 1$. In inflationary models [31] (see Inflation—Sec. 23 of this *Review*), perturbations are generated by quantum fluctuations, which are set by the energy scale of inflation together with the slope and higher derivatives of the inflationary potential. One generally expects that the Taylor series expansion of $\ln \mathcal{R}_k(\ln k)$ has terms of steadily decreasing size. For the simplest models, there are thus two parameters describing the initial conditions for density perturbations, namely the amplitude and slope of the power spectrum. These can be explicitly defined, for example, through

$$\mathcal{P}_{\mathcal{R}}^2 \equiv k^3 \langle |\mathcal{R}|_k^2 \rangle / 2\pi^2 \simeq A_s (k/k_0)^{n_s-1}, \quad (29.3)$$

with $A_s \equiv \mathcal{P}_{\mathcal{R}}^2(k_0)$ and $k_0 = 0.05 \text{ Mpc}^{-1}$, say. There are other equally valid definitions of the amplitude parameter (see also Secs. 22, 23, and 25 of this *Review*), and we caution that the relationships between some of them can be cosmology-dependent. In slow-roll inflationary models, this normalization is proportional to the combination $V^3/(V')^2$, for the inflationary potential $V(\phi)$. The slope n_s also involves V'' , and so the combination of A_s and n_s can constrain potentials.

Inflation generates tensor (gravitational wave) modes, as well as scalar (density perturbation) modes. This property introduces another parameter, measuring the amplitude of a possible tensor component, or equivalently the ratio of the tensor to scalar contributions. The tensor amplitude is $A_t \propto V$, and thus one expects a larger gravitational wave contribution in models where inflation happens at higher energies. The tensor power spectrum also has a slope, often denoted n_t , but since this seems unlikely to be measured in the near future (and there is also a consistency relation with tensor amplitude), it is sufficient for now to focus only on the amplitude of the gravitational wave component. It is most common to define the tensor contribution through r , the ratio of tensor to scalar perturbation spectra at some fixed value of k (*e.g.*, $k = 0.002 \text{ Mpc}^{-1}$ or $k = 0.05 \text{ Mpc}^{-1}$, although it was historically defined in terms of the ratio of contributions at $\ell = 2$). Different inflationary potentials will lead to different predictions, *e.g.*, for 50 e-folds, $\lambda\phi^4$ inflation gives $r = 0.32$ and $m^2\phi^2$ inflation gives $r = 0.16$ (both now strongly disfavored by the data), while other models can have arbitrarily small values of r . In any case, whatever the specific definition, and whether they come from inflation or something else, the ‘initial conditions’ give rise to a minimum of three parameters, A_s , n_s , and r .

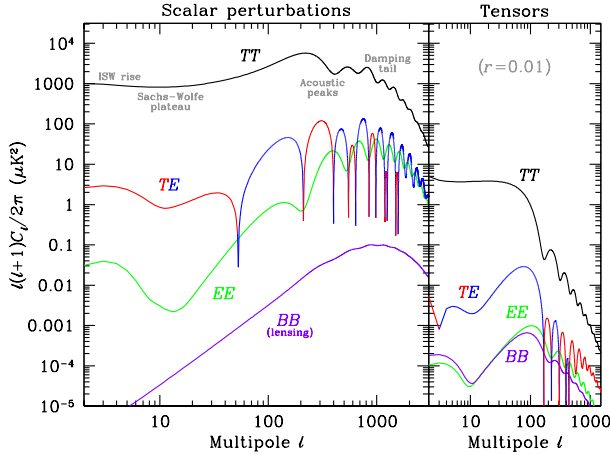


Figure 29.1: Theoretical CMB anisotropy power spectra, using the best-fitting Λ CDM model from *Planck*, calculated using CAMB. The panel on the left shows the theoretical expectation for scalar perturbations, while the panel on the right is for tensor perturbations, with an amplitude set to $r = 0.01$ for illustration. Note that the horizontal axis is logarithmic here. For the well-measured scalar TT spectrum, these regions, each covering roughly a decade in ℓ , are labeled as in the text: the ISW rise; Sachs-Wolfe plateau; acoustic peaks; and damping tail. The TE cross-correlation power spectrum changes sign, indicated here by plotting the absolute value, but switching color for the negative parts.

29.4.2 Background Cosmology Parameters

The FRW cosmology requires an expansion parameter (the Hubble constant, H_0 , often represented through $H_0 = 100 \text{ h km s}^{-1} \text{ Mpc}^{-1}$) and several parameters to describe the matter and energy content of the Universe. These are usually given in terms of the critical density, *i.e.*, for species ‘ x ,’ $\Omega_x \equiv \rho_x / \rho_{\text{crit}}$, where $\rho_{\text{crit}} \equiv 3H_0^2 / 8\pi G$. Since physical densities $\rho_x \propto \Omega_x h^2 \equiv \omega_x$ are what govern the physics of the CMB anisotropies, it is these ω s that are best constrained by CMB data. In particular, CMB observations constrain $\Omega_b h^2$ for baryons and $\Omega_c h^2$ for cold dark matter (with $\rho_m = \rho_c + \rho_b$ for the matter sum).

The contribution of a cosmological constant Λ (or other form of dark energy, see Dark Energy—Sec. 28) is usually included, together with a parameter that quantifies the curvature, $\Omega_K \equiv 1 - \Omega_{\text{tot}}$, where $\Omega_{\text{tot}} = \Omega_m + \Omega_\Lambda$. The radiation content, while in principle a free parameter, is precisely enough determined by the measurement of T_γ that it can be considered fixed, making a $< 10^{-4}$ contribution to Ω_{tot} today.

Astrophysical processes at relatively low redshift can also affect the C_ℓ s, with a particularly significant influence during reionization. The Universe became reionized at some redshift z_i , long after recombination, affecting the CMB when it passed through the integrated Thomson-scattering optical depth:

$$\tau = \int_0^{z_i} \sigma_T n_e(z) \frac{dt}{dz} dz, \quad (29.4)$$

where σ_T is the Thomson cross-section, $n_e(z)$ is the number density of free electrons (which depends on astrophysics), and dt/dz is fixed by the background cosmology. In principle, τ could be determined from the small-scale matter power spectrum, together with the physics of structure formation and radiative feedback processes; however, because this is a sufficiently intractable calculation, in practice τ needs to be considered as a free parameter.

Thus, we have eight basic cosmological parameters, namely A_s , n_s , r , h , $\Omega_b h^2$, $\Omega_c h^2$, Ω_{tot} , and τ . One can add additional parameters to this list, particularly when using the CMB in combination with other data sets. The next most relevant ones might be: $\Omega_\nu h^2$, the massive neutrino contribution; w ($\equiv p/\rho$), the equation of state parameter for the dark energy; and $dn_s/d \ln k$, measuring deviations from a constant spectral index. To these 11 one could

of course add further parameters describing additional physics, such as details of the reionization process, features in the initial power spectrum, a sub-dominant contribution of isocurvature modes, *etc.*

As well as these underlying parameters, there are other (dependent) quantities that can be obtained from them. Such derived parameters include the actual Ω s of the various components (*e.g.*, Ω_m), the variance of density perturbations at particular scales (*e.g.*, σ_8), the angular scale of the sound horizon (θ_*), the age of the Universe today (t_0), the age of the Universe at recombination, reionization, *etc.* (see The Cosmological Parameters—Sec. 25).

29.5 Physics of Anisotropies

The cosmological parameters affect the anisotropies through the well understood physics of the evolution of linear perturbations within a background FRW cosmology. There are very effective, fast, and publicly-available software codes for computing the CMB temperature, polarization, and matter power spectra, *e.g.*, CAMFAST [32], CAMB [33], and CLASS [34]. These have been tested over a wide range of cosmologies and are considered to be accurate to much better than the 1% level [35], so that numerical errors are less than 10% of the parameter uncertainties for *Planck* [6].

For pedagogical purposes, it is easiest to focus on the temperature anisotropies, before moving to the polarization power spectra. A description of the physics underlying the C_ℓ^{TT} s can be separated into four main regions (the first two combined below), as shown in the top left part of Fig. 29.1.

29.5.1 The ISW Rise, $\ell \lesssim 10$, and Sachs-Wolfe Plateau, $10 \lesssim \ell \lesssim 100$

The horizon scale (or more precisely, the angle subtended by the Hubble radius) at last scattering corresponds to $\ell \simeq 100$. Anisotropies at larger scales have not evolved significantly, and hence directly reflect the ‘initial conditions.’ Temperature variations are $\delta T/T = -(1/5)\mathcal{R}(\mathbf{x}_{\text{LSS}}) \simeq (1/3)\delta\phi/c^2$, where $\delta\phi$ is the perturbation to the gravitational potential, evaluated on the last-scattering surface (LSS). This is a result of the combination of gravitational redshift and intrinsic temperature fluctuations, and is usually referred to as the Sachs-Wolfe effect [36].

Assuming that a nearly scale-invariant spectrum of curvature (and corresponding density) perturbations was laid down at early times (*i.e.*, $n_s \simeq 1$, meaning equal power per decade in k), then $\ell(\ell+1)C_\ell \simeq \text{constant}$ at low ℓ s. This predicted near-flatness is hard to see unless the multipole axis is plotted logarithmically (as in Fig. 29.1, and part of Fig. 29.2).

Time variation of the potentials (*i.e.*, time-dependent metric perturbations) at late times leads to an upturn in the C_ℓ s in the lowest several multipoles; any deviation from a total equation of state $w = 0$ has such an effect. So the dominance of the dark energy at low redshift (see Dark Energy—Sec. 28) makes the lowest ℓ s rise above the plateau. This is usually called the integrated Sachs-Wolfe effect (or ISW rise), since it comes from the line integral of $\dot{\phi}$; it has been confirmed through correlations between the large-angle anisotropies and large-scale structure [37]. Specific models can also give additional contributions at low ℓ (*e.g.*, perturbations in the dark-energy component itself [38]), but typically these are buried in the cosmic variance.

In principle, the mechanism that produces primordial perturbations could generate scalar, vector, and tensor modes. However, the vector (vorticity) modes decay with the expansion of the Universe. The tensors (transverse trace-free perturbations to the metric) generate temperature anisotropies through the integrated effect of the locally-anisotropic expansion of space. Since the tensor modes also redshift away after they enter the horizon, they contribute only to angular scales above about 1° (see Fig. 29.1). Hence, some fraction of the low- ℓ signal could be due to a gravitational wave contribution, although small amounts of tensors are essentially impossible to discriminate from other effects that might raise the level of the plateau. Nevertheless, the tensors *can* be distinguished using polarization information (see Sec. 29.7).

29.5.2 The Acoustic Peaks, $100 \lesssim \ell \lesssim 1000$

On sub-degree scales, the rich structure in the anisotropy spectrum is the consequence of gravity-driven acoustic oscillations occurring before the atoms in the Universe became neutral [39]. Perturbations inside the horizon at last scattering were able to evolve causally and produce anisotropy at the last-scattering epoch, which reflects this evolution. The frozen-in phases of these sound waves imprint a dependence on the cosmological parameters, which gives CMB anisotropies their great constraining power.

The underlying physics can be understood as follows. Before the Universe became neutral, the proton-electron plasma was tightly coupled to the photons, and these components behaved as a single ‘photon-baryon fluid.’ Perturbations in the gravitational potential, dominated by the dark-matter component, were steadily evolving. They drove oscillations in the photon-baryon fluid, with photon pressure providing most of the restoring force and baryons giving some additional inertia. The perturbations were quite small in amplitude, $\mathcal{O}(10^{-5})$, and so evolved linearly. That means each Fourier mode developed independently, and hence can be described as a driven harmonic oscillator, with frequency determined by the sound speed in the fluid. Thus, the fluid density underwent oscillations, giving time variations in temperature. These combine with a velocity effect, which is $\pi/2$ out of phase and has its amplitude reduced by the sound speed.

After the Universe recombined, the radiation decoupled from the baryons and could travel freely towards us. At that point, the (temporal) phases of the oscillations were frozen-in, and became projected on the sky as a harmonic series of peaks and troughs in power. The main peak is the mode that went through 1/4 of a period, reaching maximal compression. The even peaks are maximal *under*-densities, which are generally of smaller amplitude because the rebound has to fight against the baryon inertia. The troughs, which do not extend to zero power, are partially filled by the Doppler effect because they are at the velocity maxima.

The physical length scale associated with the peaks is the sound horizon at last scattering, which can be straightforwardly calculated. This length is projected onto the sky, leading to an angular scale that depends on the geometry of space, as well as the distance to last scattering. Hence, the angular position of the peaks is a sensitive probe of a particular combination of cosmological parameters. In fact, this characteristic angular scale, θ_* , is the most precisely measured observable, and hence is usually treated as an element of the cosmological parameter set.

One additional effect arises from reionization at redshift z_i . A fraction of photons (τ) will be isotropically scattered at $z < z_i$, partially erasing the anisotropies at angular scales smaller than those subtended by the Hubble radius at z_i . This corresponds typically to ℓ s above about 10, depending on the specific reionization model. The acoustic peaks are therefore reduced by a factor $e^{-2\tau}$ relative to the plateau.

These acoustic peaks were a clear theoretical prediction going back to about 1970 [40]. One can think of them as a snapshot of stochastic standing waves. Since the physics governing them is simple and their structure rich, one can see how they encode extractable information about the cosmological parameters. Their empirical existence started to become clear around 1994 [41], and the emergence, over the following decade, of a coherent series of acoustic peaks and troughs is a triumph of modern cosmology. This picture has received further confirmation with the detection in the power spectrum of galaxies (at redshifts $z \lesssim 1$) of the imprint of these same acoustic oscillations in the baryon component [42], as well as through detection of the expected oscillations in CMB polarization power spectra (see Sec. 29.7).

29.5.3 The Damping Tail, $\ell \gtrsim 1000$

The recombination process is not instantaneous, and this imparts a thickness to the LSS. This leads to a damping of the anisotropies at the highest ℓ s, corresponding to scales smaller than that subtended by this thickness. One can also think of the photon-baryon fluid as having imperfect coupling, so that there is diffusion between the two components, and hence the amplitudes of the oscillations decrease with time. These effects lead to a damping of the C_ℓ s, sometimes called ‘Silk damping’ [43], which cuts off the anisotropies at multipoles above about 2000. So, although

in principle it is possible to measure to ever smaller scales, this becomes increasingly difficult in practice.

29.5.4 Gravitational Lensing Effects

CMB gravitational lensing is caused by structures at lower redshift along the line of sight to the LSS. Photon paths are deflected by the lensing potential ϕ , such that $T(\hat{n}) \rightarrow T(\hat{n} + \nabla\phi)$. Typical deflections are around 2 arcmin, but coherent over scales of a degree or so. Lensing preserves surface brightness, which means that a uniform temperature field would be unaffected; however, since there are anisotropies, then several distinct effects can be identified. The C_ℓ s are convolved with a smoothing function in a calculable way, partially flattening the peaks and troughs, generating a power-law tail at the highest multipoles, and complicating the polarization signal [44] (see Sec. 29.7.3). Additionally, the effect of lensing on the CMB can be detected through the 4-point function, which correlates temperature gradients and small-scale anisotropies, enabling a map of the lensing potential to be constructed [45].

Lensing is important because it gives an independent estimate of A_s , breaking the parameter combination $A_s e^{-2\tau}$ that is largely degenerate in the temperature anisotropy power spectra. Lensing is an example of a ‘secondary effect,’ *i.e.*, the processing of anisotropies due to relatively nearby structures (see Sec. 29.9.2). Galaxies and clusters of galaxies give several such effects; all are expected to be of low amplitude, but are increasingly important at the highest ℓ s. Such effects carry additional cosmological information (about evolving gravitational potentials in the low-redshift Universe) and are receiving more attention as experiments push to higher sensitivity and angular resolution. The lensing power spectrum (see Sec. 29.8) can potentially constrain dark-energy evolution, while future measurements at high ℓ are a particularly sensitive probe of the sum of the neutrino masses [46].

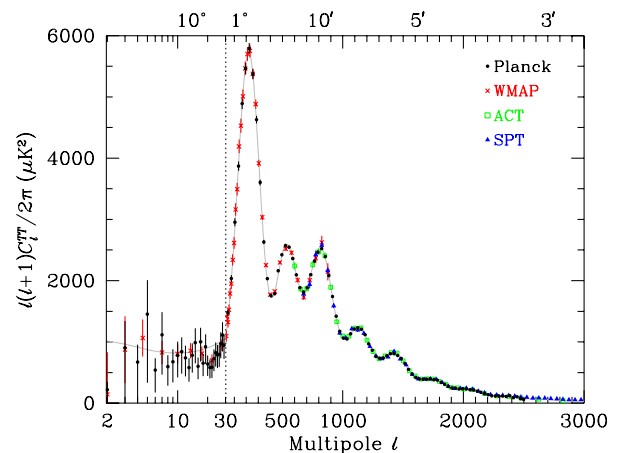


Figure 29.2: CMB temperature anisotropy band-power estimates from the *Planck*, *WMAP*, ACT, and SPT experiments. Note that the widths of the multipole bands vary between experiments and have not been plotted. This figure represents only a selection of the most recent available experimental results, and some points with large error bars have been omitted. At the higher multipoles these band-powers involve subtraction of particular foreground models, and so proper analysis requires simultaneous fitting of CMB and foregrounds over multiple frequencies. The horizontal axis here is logarithmic for the lowest multipoles, to show the Sachs-Wolfe plateau, and linear for the other multipoles. The acoustic peaks and damping region are very clearly observed, with no need for a theoretical line to guide the eye; however, the curve plotted is the best-fit *Planck* Λ CDM model.

29.6 Current Temperature Anisotropy Data

Steady improvement in CMB data quality has led to the present-day cosmological model. The most robust constraints currently available come from *Planck* satellite [47, 48] data (together with constraints from non-CMB cosmological data sets), although

smaller-scale results from the ACT [49] and SPT [50] experiments are beginning to add useful constraining power. We plot power spectrum estimates from these experiments in Fig. 29.2, along with *WMAP* data [5] for comparison (see previous versions of this review for data from earlier experiments). Independent experimental data show consistency, both in maps and in derived power spectra (up to systematic uncertainties in the overall calibration for some experiments). This makes it clear that systematic effects are largely under control.

The band-powers shown in Fig. 29.2 are in very good agreement with a ‘ Λ CDM’ model. As described earlier, several (at least seven) of the peaks and troughs are quite apparent. The original papers present the details on how these estimates were made, on the band-power correlation strengths, and on the information needed for their proper interpretation.

29.7 CMB Polarization

Thomson scattering of an anisotropic radiation field also generates linear polarization and the CMB is predicted to be polarized, at the level of roughly 5% of the temperature anisotropies [51]. Polarization is a spin-2 field on the sky, and the algebra of the modes in multipole space is strongly analogous to spin-orbit coupling in quantum mechanics [52]. The linear polarization pattern can be decomposed in a number of ways, with two quantities required for each pixel in a map, often given as the Q and U Stokes parameters. However, the most intuitive and physical decomposition is a geometrical one, splitting the polarization pattern into a part that comes from a divergence (often referred to as the ‘ E mode’) and a part with a curl (called the ‘ B mode’) [53]. More explicitly, the modes are defined in terms of second derivatives of the polarization amplitude, with the Hessian for the E modes having principal axes in the same sense as the polarization, while the B -mode pattern can be thought of as a 45° rotation of the E -mode pattern. Globally one sees that the E modes have $(-1)^\ell$ parity (like the spherical harmonics), while the B modes have $(-1)^{\ell+1}$ parity.

The existence of this linear polarization allows for six different cross-power spectra to be determined from data that measure the full temperature and polarization anisotropy information. Parity considerations make two of these zero, and we are left with four potential observables, C_ℓ^{TT} , C_ℓ^{TE} , C_ℓ^{EE} , and C_ℓ^{BB} (see Fig. 29.1). Because scalar perturbations have no handedness, the B -mode power spectrum can only be sourced by vectors or tensors. Moreover, inflationary scalar perturbations give only E modes, while tensors generate roughly equal amounts of E and B , therefore the determination of a non-zero B -mode signal is a way to measure the gravitational-wave contribution (and thus potentially derive the energy scale of inflation). However, because the signal is expected to be rather weak, one must first eliminate the foreground contributions and other systematic effects down to very low levels. In addition, CMB lensing creates B modes from E modes, further complicating the extraction of a tensor signal.

As with temperature, the polarization C_ℓ s exhibit a series of acoustic peaks generated by the oscillating photon-baryon fluid. The main ‘ EE ’ power spectrum has peaks that are out of phase with those in the ‘ TT ’ spectrum because the polarization anisotropies are sourced by the fluid velocity. The ‘ TE ’ part of the polarization and temperature patterns comes from correlations between density and velocity perturbations on the last-scattering surface, which can be both positive and negative, and is of larger amplitude than the EE signal. There is no polarization Sachs-Wolfe effect, and hence no large-angle (low- ℓ) plateau. However, scattering during a recent period of reionization can create a polarization ‘bump’ at large angular scales.

Because the polarization anisotropies have only a small fraction of the amplitude of the temperature anisotropies, they took longer to detect. The first measurement of a polarization signal came in 2002 from the DASI experiment [54], which provided a convincing detection, confirming the general paradigm, but of low enough significance that it lent no real constraint to models. Despite dramatic progress since then, it is still the case that polarization data mainly support the basic paradigm, while reducing error bars on parameters by only around 20%. However, there are exceptions to this, specifically in the reionization optical depth, and the po-

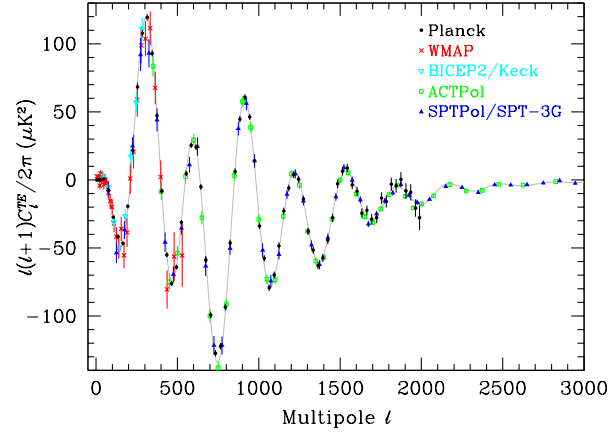


Figure 29.3: Cross-power spectrum band-powers of the temperature anisotropies and E -mode polarization signal from *Planck* (the low multipole data have been binned here), as well as *WMAP*, BICEP2/Keck, ACTPol, and SPTPol/SPT-3G. The curve is the best fit to the *Planck* temperature, polarization, and lensing band-powers. Note that each data point is an average over a band of multipoles, and hence to compare in detail with a model one has to integrate the theoretical curve through the band.

tential to constrain primordial gravitational waves. Moreover, the situation is expected to change dramatically as more of the available polarization modes are measured.

29.7.1 T - E Power Spectrum

Because the T and E skies are correlated, one has to measure the TE power spectrum, as well as TT and EE , in order to extract all the cosmological information. This TE signal has now been mapped out extremely accurately by *Planck* [48], and these band-powers are shown in Fig. 29.3, along with those from *WMAP* [55] and BICEP2/Keck [56], with ACTPol [57] and SPTPol/SPT-3G [58, 59] extending to smaller angular scales. The anti-correlation at $\ell \simeq 150$ and the peak at $\ell \simeq 300$ were the first features to become distinct, but now a whole series of oscillations is clearly seen in this power spectrum (including six or seven peaks and troughs [10]). The measured shape of the cross-correlation power spectrum provides supporting evidence for the general cosmological picture, and also directly constrains the thickness of the last-scattering surface. Because the polarization anisotropies are generated in this scattering surface, the existence of correlations at angles above about a degree demonstrates that there were super-Hubble fluctuations at the recombination epoch. The sign of this correlation also confirms the adiabatic paradigm.

The overall picture of the source of CMB polarization and its oscillations has also been confirmed through tests that average the maps around both temperature hot spots and cold spots [60]. One sees precisely the expected patterns of radial and tangential polarization configurations, as well as the phase shift between polarization and temperature. This leaves no doubt that the oscillation picture is the correct one and that the polarization is coming from Thomson scattering at $z \simeq 1100$.

29.7.2 E - E Power Spectrum

Experimental band-powers for C_ℓ^{EE} from *Planck*, *WMAP*, BICEP2/Keck Array [56], ACTPol [57], and SPTPol/SPT-3G [58, 59] are shown in Fig. 29.4. Without the benefit of correlating with the temperature anisotropies (*i.e.*, measuring C_ℓ^{TE}), the polarization anisotropies are very weak and challenging to measure. Nevertheless, the oscillatory pattern is now well established and the data closely match the TT -derived theoretical prediction. In Fig. 29.4 one can clearly see the ‘shoulder’ expected at $\ell \simeq 140$, the first main peak at $\ell \simeq 400$ (corresponding to the first trough in C_ℓ^{TT}), and the series of oscillations that is out of phase with those of the temperature anisotropy power spectrum (including six or seven peaks and troughs [10]).

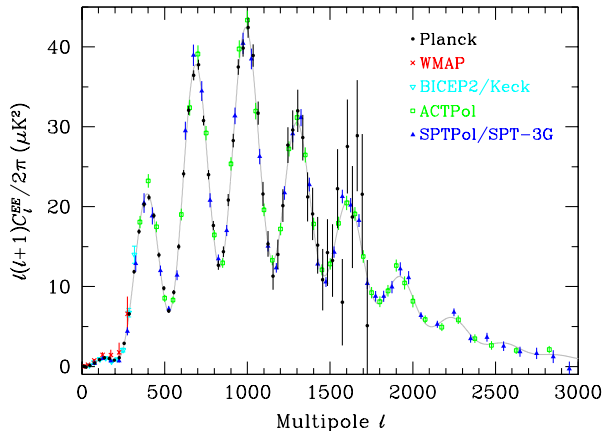


Figure 29.4: Power spectrum of E -mode polarization from *Planck*, together with *WMAP*, BICEP2/Keck, ACTPol, and SPTPol/SPT-3G. Note that some band-powers with larger uncertainties have been omitted and that the unbinned *Planck* low- ℓ data have been binned here. Also plotted is the best-fit theoretical model from *Planck* temperature + polarization + lensing data.

Perhaps the most unique result from the polarization measurements is at the largest angular scales ($\ell < 10$) in C_ℓ^{TE} and C_ℓ^{EE} , where there is evidence for an excess signal (not visible in Fig. 29.4) compared to that expected from the temperature power spectrum alone. This is precisely the signal anticipated from an early period of reionization, arising from Doppler shifts during the partial scattering at $z < z_i$. The amplitude of the signal indicates that the first stars, presumably the source of the ionizing radiation, formed around $z \simeq 8$ (although the uncertainty is still quite large). This corresponds to a scattering optical depth $\tau \simeq 0.06$, so roughly 6% of CMB photons were re-scattered at the reionization epoch, with the other 94% last scattering at $z \simeq 1100$. However, estimates of the amplitude of this reionization excess have come down since the first measurements by *WMAP* (indicating that this is an extremely difficult measurement to make) and the latest *Planck* results have reduced the value further [11, 61].

29.7.3 B - B Power Spectrum

The expected amplitude of C_ℓ^{BB} is very small, so measurements of this polarization curl-mode are extremely challenging. The first indication of the existence of the BB signal came from the detection of the expected conversion of E modes to B modes by gravitational lensing, through a correlation technique using the lensing potential and polarization measurements from SPT [62]. However, the real promise of B modes lies in the detection of primordial gravitational waves at larger scales. This tensor signature could be seen either in the ‘recombination bump’ at around $\ell = 100$ (caused by an ISW effect as gravitational waves redshift away at the last-scattering epoch) or the ‘reionization bump’ at $\ell \lesssim 10$ (from additional scattering at low redshifts).

Results from the BICEP2 experiment [63] in 2014 suggested a detection of the primordial B -mode signature around the recombination peak. BICEP2 mapped a small part of the CMB sky with the best sensitivity level reached at that time (below 100 nK), but at a single frequency. Higher frequency data from *Planck* indicated that much of the BICEP2 signal was due to dust within our Galaxy, and a combined analysis by the BICEP2, Keck Array, and *Planck* teams [64] indicated that the data are consistent with no primordial B modes. The current constraint from *Planck* data alone is $r < 0.069$ (95% at $k = 0.05 \text{ Mpc}^{-1}$ [11, 61]) using all CMB power spectra, and this limit is reduced to $r < 0.044$ with the inclusion of BICEP2/Keck Array data [61, 65]. The most constraining limit is $r < 0.036$ from a combination of BICEP2, Keck Array, and BICEP3 data, using *WMAP* and *Planck* maps to help remove foregrounds [66].

Several experiments are continuing to push down the sensitivity

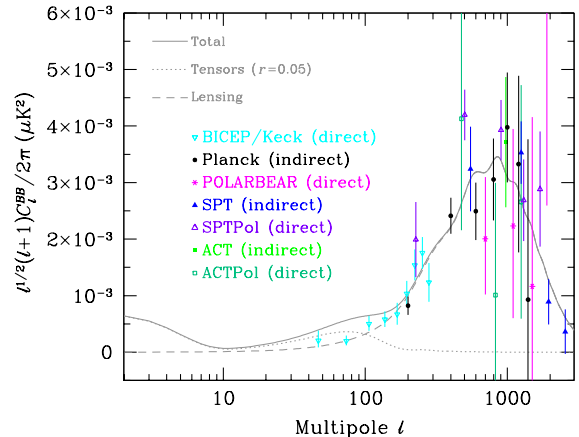


Figure 29.5: Power spectrum of B -mode polarization, including results from the BICEP2/BICEP3/Keck Array combined analysis, *Planck*, POLARBEAR, SPT, and ACT. Note that some of the measurements are direct estimates of B modes on the sky, while others are only sensitive to the lensing signal and come from combining E -mode and lensing potential measurements. Several earlier experiments reported upper limits, which are all off the top of this plot. A logarithmic horizontal axis is adopted here and the y -axis has been divided by a factor of $\sqrt{\ell}$ in order to show all three theoretically expected contributions: the low- ℓ reionization bump; the $\ell \simeq 100$ recombination peak; and the high- ℓ lensing signature. The dotted line is for a tensor (primordial gravitational wave) fraction $r = 0.05$, simply as an example, with all other cosmological parameters set at the best *Planck*-derived values, for which model the expected lensing B modes have also been shown with a dashed line.

of B -mode measurements, motivated by the enormous importance of a future detection of this telltale signature of inflation (or other physics at the highest energies). A compilation of experimental results for C_ℓ^{BB} is shown in Fig. 29.5, coming from a combination of direct estimates of the B modes (BICEP2/BICEP3/Keck Array [66], POLARBEAR [67], SPTPol [68], and ACTPol [57]) and indirect determinations of the lensing B modes based on estimating the effect of measured lensing on measured E modes (*Planck* [69], SPT [62], and ACT [70]). Additional band-power estimates are expected from these and other experiments in the near future, with the Simons Observatory [71], the so-called ‘Stage 4’ CMB project [72] and the *LiteBIRD* satellite [73], holding great promise for pushing down to the $r \sim 0.001$ level.

29.8 CMB Lensing Power Spectrum

One further CMB observable is the gravitational lensing deflection, leading to the construction of a map of the lensing potential. The latest *Planck* results [74] give a map that is detected at the $> 4\sigma$ level using a minimum-variance procedure from the 4-point function of temperature and polarization data. From these maps, estimates can be constructed of $C_\ell^{\phi\phi}$, the lensing-potential power spectrum, which is found to be consistent with predictions from the best-fit temperature and polarization model. Recent results from ACT give a power spectrum that has a similar overall signal-to-noise ratio [75] and there are also interesting measurements from SPT [76]. Figure 29.6 plots the *Planck*, ACT, and SPT estimates of $C_\ell^{\kappa\kappa}$, the lensing convergence power spectrum, which is proportional to $\ell^2(\ell + 1)^2$ times the potential power spectrum $C_\ell^{\phi\phi}$.

We can think of each sky pixel as possessing three independent quantities that can be measured, namely T , E , and ϕ (and potentially B , if that becomes detectable). Determining the constraining power comes down to counting $Y_{\ell m}$ modes [77], as well as appreciating that some modes help to break particular parameter degeneracies. We have only scratched the surface of CMB lensing so far, and it is expected that future small-scale experiments will

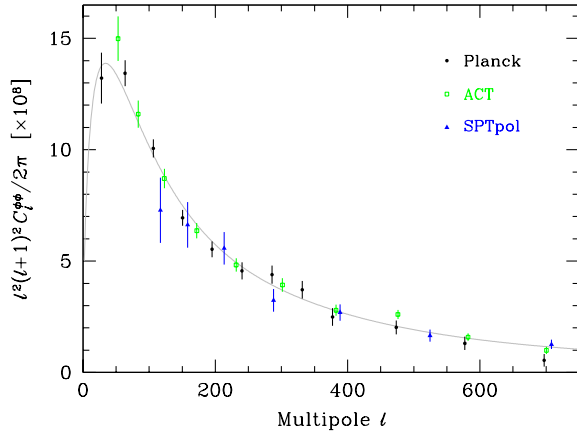


Figure 29.6: Power spectrum measurements for CMB lensing, including selected results from *Planck*, ACT, and SPT. The quantity plotted is the (dimensionless) potential power spectrum, scaled by $l^2(l+1)^2$ and multiplied by a factor of 10^8 to make the numbers more manageable. Some less reliable measurements have not been plotted. The best-fit *Planck* Λ CDM spectrum is plotted as a gray line.

be able to extract more of the cosmological information. Further constraints can also be derived on the lower-redshift Universe by cross-correlating CMB lensing with other cosmological tracers of large-scale structure. Additionally, small-scale lensing, combined with E -mode measurements, can be used to ‘delens’ CMB B -mode data, which will be important for pushing down into the $r \lesssim 0.01$ regime [78].

29.9 Complications

There are a number of issues that complicate the interpretation of CMB anisotropy data (and are considered to be *signal* by many astrophysicists), some of which we sketch out below.

29.9.1 Foregrounds

The microwave sky contains significant emission from our Galaxy and from extragalactic sources [79]. Fortunately, the frequency dependence of these various sources is in general substantially different from that of the CMB anisotropy signals. The combination of Galactic synchrotron, bremsstrahlung, and dust emission reaches a minimum at a frequency of roughly 100 GHz (or wavelength of about 3 mm). As one moves to greater angular resolution, the minimum moves to slightly higher frequencies, but becomes more sensitive to unresolved (point-like) sources.

At frequencies around 100 GHz, and for portions of the sky away from the Galactic plane, the foregrounds are typically 1 to 10% of the CMB anisotropies. By making observations at multiple frequencies, it is relatively straightforward to separate the various components and determine the CMB signal to the few per cent level. For greater sensitivity, it is necessary to use the spatial information and statistical properties of the foregrounds to separate them from the CMB. Furthermore, at higher l s it is essential to carefully model extragalactic foregrounds, particularly the clustering of infrared-emitting galaxies and scattering due to galaxy clusters, which dominate the measured power spectrum as we move into the damping tail.

The foregrounds for CMB polarization follow a similar pattern to those for temperature, but are intrinsically brighter relative to CMB anisotropies. *WMAP* showed that the polarized foregrounds dominate at large angular scales, and that they must be well characterized in order to be discriminated [80]. *Planck* has shown that it is possible to characterize the foreground polarization signals, with synchrotron dominating at low frequencies and dust at high frequencies [81]. On smaller scales there are no strongly-polarized foregrounds, and hence at high multipoles it is in principle easier to measure foreground-free modes in polarization than in temperature. Although foreground contamination will no doubt become

more complicated as we push down in sensitivity, making analysis more difficult, for the time being, foreground contamination is not a fundamental limit for CMB experiments.

29.9.2 Secondary Anisotropies

With increasingly precise measurements of the primary anisotropies, there is growing theoretical and observational interest in ‘secondary anisotropies,’ pushing experiments to higher angular resolution and sensitivity. These secondary effects arise from the processing of the CMB due to ionization history and the evolution of structure, including gravitational lensing (which was already discussed) and patchy reionization effects [82]. Additional information can thus be extracted about the Universe at $z \ll 1000$. This tends to be most effectively done through correlating CMB maps with other cosmological probes of structure. Secondary signals are also typically non-Gaussian, unlike the primary CMB anisotropies.

A secondary signal of great current interest is the Sunyaev-Zeldovich (SZ) effect [83], which is Compton scattering ($\gamma e \rightarrow \gamma' e'$) of the CMB photons by hot electrons in intergalactic plasma. This creates spectral distortions by transferring energy from the electrons to the photons. It is particularly important for clusters of galaxies, through which one observes a partially Comptonized spectrum, resulting in a decrement at radio wavelengths and an increment in the submillimeter.

The imprint on the CMB sky is of the form $\Delta T/T = y f(x)$, with the y parameter being the integral of Thomson optical depth times $kT_e/m_e c^2$ through the cluster, and $f(x)$ describing the frequency dependence. This is simply $x \coth(x/2) - 4$ for a non-relativistic gas (the electron temperature in a cluster is typically a few keV), where the dimensionless frequency $x \equiv h\nu/kT_\gamma$. As well as this ‘thermal’ SZ effect, there is also a smaller ‘kinetic’ effect due to the bulk motion of the cluster gas, giving $\Delta T/T \sim \tau(v/c)$, with either sign, but having the same spectrum as the primary CMB anisotropies.

A significant advantage in finding galaxy clusters via the SZ effect is that the signal is largely independent of redshift, so in principle clusters can be found to arbitrarily large distances. The SZ effect can be used to find and study individual clusters, and to obtain estimates of the Hubble constant. There is also the potential to constrain other cosmological parameters, such as the clustering amplitude σ_8 and the equation of state of the dark energy, through counts of detected clusters as a function of redshift. The promise of the method has been realized through detections of clusters purely through the SZ effect by SPT [84], ACT [85], and *Planck* [86]. Results from *Planck* clusters [87] suggest a somewhat lower value of σ_8 than inferred from CMB anisotropies, but there are still systematic uncertainties that might encompass the difference, and a more recent analysis of SPT-detected clusters shows better agreement [88]. Further analysis of scaling relations among cluster properties should enable more robust cosmological constraints to be placed in future, so that we can understand whether this ‘tension’ might be a sign of new physics.

29.9.3 Higher-order Statistics

Although most of the CMB anisotropy information is contained in the power spectra, there will also be weak signals present in higher-order statistics. These can measure any primordial non-Gaussianity in the perturbations, as well as non-linear growth of the fluctuations on small scales and other secondary effects (plus residual foreground contamination of course). There are an infinite variety of ways in which the CMB could be non-Gaussian [26]; however, there is a generic form to consider for the initial conditions, where a quadratic contribution to the curvature perturbations is parameterized through a dimensionless number f_{NL} . This weakly non-linear component can be constrained in several ways, the most popular being through measurements of the bispectrum (or 3-point function).

The constraints depend on the shape of the triangles in harmonic space, and it has become common to distinguish the ‘local’ or ‘squeezed’ configuration (in which one side is much smaller than the other two) from the ‘equilateral’ configuration. Other configurations are also relevant for specific theories, such as ‘orthogonal’ non-Gaussianity, which has positive correlations for

$k_1 \simeq 2k_2 \simeq 2k_3$, and negative correlations for the equilateral configuration. The constraints from the *Planck* team [89] are $f_{\text{NL}}^{\text{local}} = 1 \pm 5$, $f_{\text{NL}}^{\text{equil}} = -26 \pm 47$, and $f_{\text{NL}}^{\text{ortho}} = -38 \pm 24$.

These results are consistent with zero, but are at a level that is now interesting for model predictions. The amplitude of f_{NL} expected is small, so that a detection of $f_{\text{NL}} \gg 1$ would rule out all single-field, slow-roll inflationary models. It is still possible to improve upon these *Planck* results, and it certainly seems feasible that a measurement of primordial non-Gaussianity may yet be within reach. *Non*-primordial detections of non-Gaussianity from expected signatures have already been made. For example, the bispectrum and trispectrum contain evidence of gravitational lensing, the ISW effect, and Doppler boosting. For now the primordial signal is elusive, but should it be detected, then detailed measurements of non-Gaussianity will become a unique probe of inflationary-era physics. Because of that, much effort continues to be devoted to honing predictions and measurement techniques, with the expectation that we will need to go beyond the CMB (*e.g.*, 3D galaxy surveys) to dramatically improve the constraints.

29.9.4 Anomalies

Several features seen in the *Planck* data [29,60,90] confirm those found earlier with *WMAP* [28], showing mild deviations from a simple description of the sky; these are often referred to as ‘anomalies.’ One such feature is the lack of power in the multipole range $\ell \simeq 20\text{--}30$ [11, 48]. Other examples involve the apparent breaking of statistical anisotropy, caused by alignment of the lowest multipoles, as well as a somewhat excessive cold spot and a power asymmetry between hemispheres. No such feature is significant at more than the roughly 3σ level, and the importance of ‘*a posteriori*’ statistics here has been emphasized by many authors. Since these effects are at large angular scales, where cosmic variance dominates, the results will not increase in significance with more data, although there is the potential for more sensitive polarization measurements to provide independent tests.

29.10 Constraints on Cosmological Parameters

The most striking outcome of the last couple of decades of experimental results is that the standard cosmological paradigm continues to be in very good shape. A large amount of high-precision data on the CMB power spectrum is adequately fit with fewer than 10 free parameters (and only six need non-trivial values). The framework is that of FRW models, which have nearly flat geometry, containing dark matter and dark energy, and with adiabatic perturbations having close to scale-invariant initial conditions.

Within this basic picture, the values of the cosmological parameters can be constrained. Of course, more stringent bounds can be placed on models that cover a restricted parameter space, *e.g.*, assuming that $\Omega_{\text{tot}} = 1$ or $r = 0$. More generally, the constraints depend upon the adopted prior probability distributions, even if they are implicit, for example by restricting the parameter freedom or their ranges (particularly where likelihoods peak near the boundaries), or by using different choices of other data in combination with the CMB. As the data become even more precise, these considerations will be less important, but for now we caution that restrictions on model space and choice of non-CMB data sets and priors need to be kept in mind when adopting specific parameter values and uncertainties.

There are some combinations of parameters that fit the CMB anisotropies almost equivalently. For example, there is a nearly exact geometric degeneracy, where any combination of Ω_{m} and Ω_{Λ} that provides the same angular-diameter distance to last scattering will give nearly identical C_{ℓ} s. There are also other less exact degeneracies among the parameters. Such degeneracies can be broken when using the CMB results in combination with other cosmological data sets. Particularly useful are complementary constraints from baryon acoustic oscillations, galaxy clustering, the abundance of galaxy clusters, weak gravitational lensing measurements, and Type Ia supernova distances. For an overview of some of these other cosmological constraints, see The Cosmological Parameters—Sec. 25 of this *Review*.

Within the context of a 6-parameter family of models (which fixes $\Omega_{\text{tot}} = 1$, $dn_{\text{s}}/d\ln k = 0$, $r = 0$, and $w = -1$) the

Planck results for *TT*, together with *TE*, *EE*, and CMB lensing, yield [11]: $\ln(10^{10} A_{\text{s}}) = 3.044 \pm 0.014$; $n_{\text{s}} = 0.965 \pm 0.004$; $\Omega_{\text{b}} h^2 = 0.02237 \pm 0.00015$; $\Omega_{\text{c}} h^2 = 0.1200 \pm 0.0012$; $100\theta_{*} = 1.04092 \pm 0.00031$; and $\tau = 0.054 \pm 0.007$. Other parameters can be derived from this basic set, including $h = 0.674 \pm 0.005$, $\Omega_{\Lambda} = 0.685 \pm 0.007$ ($= 1 - \Omega_{\text{m}}$) and $\sigma_8 = 0.811 \pm 0.006$ (see also Astrophysical Constants and Parameters—Sec. 2). Somewhat different (although consistent) values are obtained using other data combinations, such as including BAO, supernova, H_0 , or weak-lensing constraints (see Sec. 25 of this *Review*). However, the *Planck* results quoted above are currently the best available from CMB data alone. Results from other CMB experiments (*e.g.*, SPT-3G [59]) are consistent and becoming competitive.

The standard cosmological model still fits the data well, with the error bars on the parameters continuing to shrink. Improved measurement of higher acoustic peaks has dramatically reduced the uncertainty in the θ_{*} parameter, which is now detected at $> 3000\sigma$. The evidence for $n_{\text{s}} < 1$ is now at the 8σ level from *Planck* data alone. The value of the reionization optical depth has decreased compared with earlier estimates; it is convincingly detected, but still not at very high significance.

The inferred value of H_0 is smaller than the most precise values derived from the cosmic distance ladder. This parameter tension is discussed more fully in other sections of this *Review*. The CMB anisotropies also provide the most precise estimate of the age of the Universe, with *Planck* giving the value $t_0 = 13.797 \pm 0.023$ Gyr.

Constraints can also be placed on parameters beyond the basic six, particularly when including other astrophysical data sets. Relaxing the flatness assumption, the constraint on Ω_{tot} is 1.011 ± 0.006 . Note that for h , the CMB data alone provide only a very weak constraint if spatial flatness is not assumed. However, with the addition of other data (particularly powerful in this context being a compilation of BAO measurements; see Sec. 25 of this *Review*), the constraints on the Hubble constant and curvature improve considerably, leading to $\Omega_{\text{tot}} = 0.9993 \pm 0.0019$ [11].

For $\Omega_{\text{b}} h^2$ the CMB-derived value is generally consistent with completely independent constraints from Big Bang nucleosynthesis (see Sec. 24 of this *Review*). Related are constraints on additional neutrino-like relativistic degrees of freedom, which lead to $N_{\text{eff}} = 2.99 \pm 0.17$ (including BAO), *i.e.*, no evidence for extra neutrino species.

The tightest published limit on the tensor-to-scalar ratio is $r < 0.036$ (measured at $k = 0.05 \text{ Mpc}^{-1}$) from BICEP/Keck Array [66]. The detailed limit depends on how other parameters, especially A_{s} , n_{t} , and $dn_{\text{s}}/d\ln k \neq 0$ are restricted. The joint constraints on n_{s} and r allow specific inflationary models to be tested [30,91]. Looking at the (n_{s}, r) plane, this means that $m^2\phi^2$ (mass-term quadratic) inflation is disfavored by the data, as well as $\lambda\phi^4$ (self-coupled) inflation.

The addition of the dark-energy equation of state w adds the partial degeneracy of being able to fit a ridge in (w, h) space, extending to low values of both parameters. This degeneracy is broken when the CMB is used in combination with other data sets, *e.g.*, adding a compilation of BAO and supernova data gives $w = -1.028 \pm 0.031$ [11]. Constraints can also be placed on more general dark energy and modified-gravity models [92]. However, when extending the search space, one needs to be careful not to over-interpret some tensions between data sets as evidence for new physics.

For the reionization optical depth, a reanalysis of *Planck* data in 2016 resulted in a reduction in the value of τ , with the tightest result giving $\tau = 0.055 \pm 0.009$, and the newest analyses giving similar numbers. This corresponds to $z_{\text{i}} = 7.8\text{--}8.8$ (depending on the functional form of the reionization history), with an uncertainty of ± 0.9 [93]. This redshift is only slightly higher than that suggested from studies of absorption lines in high- z quasar spectra [94] and Ly α -emitting galaxies [95], perhaps hinting that the process of reionization was not as complex as previously suspected. The important constraint provided by CMB polarization, in combination with astrophysical measurements, thus allows us to investigate how the first stars formed and brought about the end of the cosmic dark ages.

29.11 Particle Physics Constraints

CMB data place limits on parameters that are directly relevant for particle physics models. For example, there is a limit on the sum of the masses of the neutrinos, $\Sigma m_\nu < 0.12 \text{ eV}$ (95%) [11] coming from *Planck* together with BAO measurements (although limits are weaker when considering both N_{eff} and Σm_ν as free parameters). This assumes the usual number density of fermions, which decoupled when they were relativistic. The limit is tantalizingly only a factor of a few higher than the minimum value coming from neutrino mixing experiments (see Neutrino Mixings—Secs. 14 and 26). As well as being an indirect probe of the neutrino background, *Planck* data also require that the neutrino fluid has perturbations, *i.e.*, that it possesses a sound speed $c_s^2 \simeq 1/3$, as expected [9].

The current suite of data suggests that $n_s < 1$, with a best-fitting value about 0.035 below unity. This is already quite constraining for inflationary models, particularly along with r limits. There is no current evidence for running of the spectral index, with $dn_s/d\ln k = -0.004 \pm 0.007$ from *Planck* alone [11] (with a similar value when BAO data are included), although this is less of a constraint on models. Similarly, primordial non-Gaussianity is being probed to interesting levels, although tests of simple inflationary models will only come with significant reductions in uncertainty.

The large-angle anomalies, such as the hemispheric modulation of power and the dip in power at $\ell \simeq 20\text{--}30$, have the potential to be hints of new physics. Such effects might be expected in a Universe that has a large-scale power cut-off, or anisotropy in the initial power spectrum, or is topologically non-trivial. However, cosmic variance and *a posteriori* statistics limit the significance of these anomalies, absent the existence of a model that naturally yields some of these features (and ideally also predicting other phenomena that can be tested).

Constraints on ‘cosmic birefringence’ (*i.e.*, rotation of the plane of CMB polarization that generates non-zero TB and EB power) can be used to place limits on theories involving parity violation, Lorentz violation, or axion-photon mixing [96].

It is possible to place limits on additional areas of physics [97], for example annihilating dark matter [9, 9], primordial magnetic fields [98], and time variation of the fine-structure constant [99], as well as the neutrino chemical potential, a contribution of warm dark matter, topological defects, or physics beyond general relativity. Further particle physics constraints will follow as the smaller-scale and polarization measurements continue to improve.

The CMB anisotropy measurements precisely pin down physics at the time of last-scattering, and so any change of physics can be constrained if it affects the relevant energies or timescales. Future, higher sensitivity measurements of the CMB frequency spectrum will push the constraints back to cover energy injection at much earlier times (~ 1 year). Comparison of CMB and BBN observables extend these constraints to timescales of order seconds, and energies in the MeV range. And to the extent that inflation provides an effective description of the generation of perturbations, the inflationary observables may constrain physics at GUT-type energy scales.

More generally, careful measurement of the CMB power spectra and non-Gaussianity can in principle put constraints on physics at the highest energies, including ideas of quantum gravity, string theory, extra dimensions, colliding branes, *etc.* At the moment any calculation of predictions appears to be far from definitive. However, there is a great deal of activity on implications of fundamental theories for the early Universe, and hence a chance that there might be observational implications for specific scenarios.

29.12 Fundamental Lessons

More important than the precise values of parameters is what we have learned about the general features that describe our observable Universe. Beyond the basic hot Big Bang picture, the CMB has taught us that:

- the (observable) Universe is very close to isotropic;
- the Universe recombined at $z \sim 1000$ and started to become ionized again at $z \sim 10$;
- the geometry of the Universe is close to flat;

- both dark matter and dark energy are required;
- gravitational instability is sufficient to grow all of the observed large structures in the Universe;
- topological defects were not important for structure formation;
- there were ‘synchronized’ super-Hubble modes generated in the early Universe;
- the initial perturbations were predominantly adiabatic in nature;
- the primordial perturbation spectrum has a slightly red tilt;
- the perturbations had close to Gaussian (*i.e.*, maximally random) initial conditions.

These features form the basis of the cosmological standard model, Λ CDM, for which it is tempting to make an analogy with the Standard Model of particle physics (see earlier Sections of this *Review*). In comparison, the cosmological model is much further from any underlying ‘fundamental theory,’ which might ultimately provide the values of the parameters from first principles. Nevertheless, any genuinely complete ‘theory of everything’ must include an explanation for the values of these cosmological parameters in addition to the parameters of the Standard Model of particle physics.

29.13 Future Directions

Given the significant progress in measuring the CMB sky, which has been instrumental in tying down the cosmological model, what can we anticipate for the future? There will be a steady improvement in the precision and confidence with which we can determine the appropriate cosmological parameters. Ground-based experiments operating at smaller angular scales will continue to place tighter constraints on the damping tail, lensing, and cross-correlations. New polarization experiments at small scales will probe further into the damping tail, without the limitation of extragalactic foregrounds. And polarization experiments at large angular scales will push down the limits on primordial B modes.

Planck, the third generation CMB satellite mission, was launched in May 2009, and produced a large number of papers, including a set of cosmological studies based on the first two full surveys of the sky (accompanied by a public release of data products) in 2013, a further series coming from analysis of the full mission data release in 2015 (eight surveys for the Low Frequency Instrument and five surveys for the High Frequency Instrument), and a third series derived from a final analysis of the 2018 data release, including full constraints from polarization data. *Planck* data currently dominate constraints on models, but that situation will change soon.

A set of cosmological parameters is now known to percent-level accuracy, and that may seem sufficient for many people. However, we should certainly demand more of measurements that describe *the entire observable Universe!* Hence a lot of activity in the coming years will continue to focus on determining those parameters with increasing precision. This necessarily includes testing for consistency among different predictions of the cosmological Standard Model, and searching for signals that might require additional physics.

A second area of focus will be the smaller-scale anisotropies and ‘secondary effects.’ There is a great deal of information about structure formation at $z \ll 1000$ encoded in the CMB sky. This may involve higher-order statistics and cross-correlations with other large-scale structure tracers, as well as spectral signatures, with many experiments targeting the galaxy cluster SZ effect, for example. The current status of CMB lensing is similar (in terms of total signal-to-noise) to the quality of the first CMB anisotropy measurements by *COBE*, and thus we can expect that experimental probes of lensing will improve dramatically in the coming years. All of these investigations can provide constraints on the dark-energy equation of state, for example, which is a major area of focus for several future cosmological surveys at optical wavelengths. CMB lensing also promises to yield a measurement of the sum of the neutrino masses.

A third direction is increasingly sensitive searches for specific signatures of physics at the highest energies. The most promising

of these may be the primordial gravitational wave signals in C_ℓ^{BB} , which could be a probe of the $\sim 10^{16}$ GeV energy range. There are several experiments underway or being developed that are designed to search for the polarization B modes, with the most ambitious being CMB-S4 on the ground and *LiteBIRD* in space. Additionally, non-Gaussianity holds the promise of constraining models beyond single-field slow-roll inflation.

Anisotropies in the CMB have proven to be the premier probe of cosmology and the early Universe. Theoretically the CMB involves well-understood physics in the linear regime, and is under very good calculational control. A substantial and improving set of observational data now exists. Systematics appear to be under control and are not currently a limiting factor. And so for the next several years we can expect an increasing amount of cosmological information to be gleaned from CMB anisotropies, with the prospect also of some genuine surprises.

References

- [1] A. A. Penzias and R. W. Wilson, *Astrophys. J.* **142**, 419 (1965); R. H. Dicke *et al.*, *Astrophys. J.* **142**, 414 (1965).
- [2] M. White, D. Scott and J. Silk, *Ann. Rev. Astron. Astrophys.* **32**, 319 (1994); W. Hu and S. Dodelson, *Ann. Rev. Astron. Astrophys.* **40**, 171 (2002), [arXiv:astro-ph/0110414]; A. Challinor and H. Peiris, in M. Novello and S. Perez, editors, “American Institute of Physics Conference Series,” volume 1132, 86–140 (2009), [arXiv:0903.5158].
- [3] G. F. Smoot *et al.*, *Astrophys. J. Lett.* **396**, L1 (1992).
- [4] C. L. Bennett *et al.*, *Astrophys. J. Supp.* **148**, 1 (2003), [arXiv:astro-ph/0302207].
- [5] G. Hinshaw *et al.*, *Astrophys. J. Supp.* **208**, 19 (2013), [arXiv:1212.5226].
- [6] Planck Collab. 2013 Results XVI, *Astron. Astrophys.* **571**, A16 (2014), [arXiv:1303.5076].
- [7] J. A. Tauber *et al.*, *Astron. Astrophys.* **520**, A1 (2010); Planck Collab. 2013 Results I, *Astron. Astrophys.* **571**, A1 (2014), [arXiv:1303.5062].
- [8] Planck Collab. 2015 Results I, *Astron. Astrophys.* **594**, A1 (2016), [arXiv:1502.01582].
- [9] Planck Collab. 2015 Results XIII, *Astron. Astrophys.* **594**, A13 (2016), [arXiv:1502.01589].
- [10] Planck Collab. 2018 Results I, *Astron. Astrophys.* **641**, A1 (2020), [arXiv:1807.06205].
- [11] Planck Collab. 2018 Results VI, *Astron. Astrophys.* **641**, A6 (2020), [arXiv:1807.06209].
- [12] D. S. Swetz *et al.*, *Astrophys. J. Supp.* **194**, 41 (2011), [arXiv:1007.0290].
- [13] J. E. Carlstrom *et al.*, *Proc. Astron. Soc. Pacific* **123**, 568 (2011), [arXiv:0907.4445].
- [14] V. V. Klimentenko *et al.*, *Astronomy Letters* **46**, 11, 715 (2020), [arXiv:2106.00119]; D. A. Riechers *et al.*, *Nature* **602**, 7895, 58 (2022), [arXiv:2202.00693].
- [15] D. J. Fixsen *et al.*, *Astrophys. J.* **734**, 5 (2011), [arXiv:0901.0555].
- [16] J. Singal *et al.*, *Proc. Astron. Soc. Pacific* **130**, 985, 036001 (2018), [arXiv:1711.09979].
- [17] A. Kogut *et al.*, *J. Cosmology Astropart. Phys.* **2011**, 7, 025 (2011), [arXiv:1105.2044]; P. André *et al.*, *J. Cosmology Astropart. Phys.* **2014**, 2, 006 (2014), [arXiv:1310.1554]; J. Delabrouille *et al.*, *Experimental Astronomy* **51**, 3, 1471 (2021), [arXiv:1909.01591].
- [18] V. Desjacques *et al.*, *Mon. Not. R. Astron. Soc.* **451**, 4460 (2015), [arXiv:1503.05589].
- [19] D. J. Fixsen, *Astrophys. J.* **707**, 916 (2009), [arXiv:0911.1955].
- [20] J. C. Mather *et al.*, *Astrophys. J.* **512**, 511 (1999), [arXiv:astro-ph/9810373].
- [21] Y. Hoffman, H. M. Courtois and R. B. Tully, *Mon. Not. R. Astron. Soc.* **449**, 4494 (2015), [arXiv:1503.05422].
- [22] D. J. Fixsen *et al.*, *Astrophys. J.* **420**, 445 (1994).
- [23] Planck Collab. 2013 Results XXVII, *Astron. Astrophys.* **571**, A27 (2014), [arXiv:1303.5087].
- [24] S. Seager, D. D. Sasselov and D. Scott, *Astrophys. J. Supp.* **128**, 407 (2000), [arXiv:astro-ph/9912182].
- [25] L. Knox, *Phys. Rev.* **D52**, 4307 (1995), [arXiv:astro-ph/9504054].
- [26] N. Bartolo *et al.*, *Phys. Rep.* **402**, 103 (2004), [arXiv:astro-ph/0406398].
- [27] Planck Collab. 2013 Results XXIV, *Astron. Astrophys.* **571**, A24 (2014), [arXiv:1303.5084].
- [28] C. L. Bennett *et al.*, *Astrophys. J. Supp.* **192**, 17 (2011), [arXiv:1001.4758].
- [29] Planck Collab. 2013 Results XXIII, *Astron. Astrophys.* **571**, A23 (2014), [arXiv:1303.5083].
- [30] Planck Collab. 2018 Results X, *Astron. Astrophys.* **641**, A10 (2020), [arXiv:1807.06211].
- [31] A. R. Liddle and D. H. Lyth, *Cosmological Inflation and Large-Scale Structure*, Cambridge University Press, Cambridge (2000).
- [32] U. Seljak and M. Zaldarriaga, *Astrophys. J.* **469**, 437 (1996), [arXiv:astro-ph/9603033].
- [33] A. Lewis, A. Challinor and A. Lasenby, *Astrophys. J.* **538**, 473 (2000), [arXiv:astro-ph/9911177].
- [34] D. Blas, J. Lesgourgues and T. Tram, *J. Cosmology Astropart. Phys.* **7**, 034 (2011), [arXiv:1104.2933].
- [35] U. Seljak *et al.*, *Phys. Rev.* **D68**, 083507 (2003), [arXiv:astro-ph/0306052].
- [36] R. K. Sachs and A. M. Wolfe, *Astrophys. J.* **147**, 73 (1967).
- [37] R. G. Crittenden and N. Turok, *Phys. Rev. Lett.* **76**, 575 (1996), [arXiv:astro-ph/9510072]; Planck Collab. 2015 Results XXI, *Astron. Astrophys.* **594**, A21 (2016), [arXiv:1502.01595].
- [38] W. Hu *et al.*, *Phys. Rev.* **D59**, 2, 023512 (1998), [arXiv:astro-ph/9806362].
- [39] W. Hu, N. Sugiyama and J. Silk, *Nature* **386**, 37 (1997), [arXiv:astro-ph/9604166].
- [40] P. J. E. Peebles and J. T. Yu, *Astrophys. J.* **162**, 815 (1970); Sunyaev, R. A. and Zeldovich, Ya. B., *Astron. Astrophys. Supp.* **7**, 3 (1970).
- [41] D. Scott, J. Silk and M. White, *Science* **268**, 829 (1995), [arXiv:astro-ph/9505015].
- [42] D. J. Eisenstein, *New Astron. Rev.* **49**, 360 (2005).
- [43] J. Silk, *Astrophys. J.* **151**, 459 (1968).
- [44] M. Zaldarriaga and U. Seljak, *Phys. Rev.* **D58**, 023003 (1998), [arXiv:astro-ph/9803150].
- [45] Planck Collab. 2013 Result XVII, *Astron. Astrophys.* **571**, A17 (2014), [arXiv:1303.5077].
- [46] M. Kaplinghat, L. Knox and Y.-S. Song, *Phys. Rev. Lett.* **91**, 24, 241301 (2003), [arXiv:astro-ph/0303344].
- [47] Planck Collab. 2013 Results XV, *Astron. Astrophys.* **571**, A15 (2014), [arXiv:1303.5075].
- [48] Planck Collab. 2018 Results V, *Astron. Astrophys.* **641**, A5 (2020), [arXiv:1907.12875].
- [49] S. Das *et al.*, *J. Cosmology Astropart. Phys.* **4**, 014 (2014), [arXiv:1301.1037].
- [50] K. T. Story *et al.*, *Astrophys. J.* **779**, 86 (2013), [arXiv:1210.7231].
- [51] W. Hu and M. White, *New Astron.* **2**, 323 (1997), [arXiv:astro-ph/9706147].
- [52] W. Hu and M. J. White, *Phys. Rev.* **D56**, 596 (1997), [arXiv:astro-ph/9702170].

- [53] M. Zaldarriaga and U. Seljak, *Phys. Rev.* **D55**, 1830 (1997), [arXiv:astro-ph/9609170]; M. Kamionkowski, A. Kosowsky and A. Stebbins, *Phys. Rev.* **D55**, 7368 (1997), [arXiv:astro-ph/9611125].
- [54] J. M. Kovac *et al.*, *Nature* **420**, 772 (2002), [arXiv:astro-ph/0209478].
- [55] D. Larson *et al.*, *Astrophys. J. Supp.* **192**, 16 (2011), [arXiv:1001.4635].
- [56] Keck Array and BICEP2 Collabs. V, *Astrophys. J.* **811**, 126 (2015), [arXiv:1502.00643].
- [57] S. K. Choi *et al.*, *J. Cosmology Astropart. Phys.* **2020**, 12, 045 (2020), [arXiv:2007.07289].
- [58] A. T. Crites *et al.*, *Astrophys. J.* **805**, 36 (2015), [arXiv:1411.1042].
- [59] L. Balkenhol *et al.*, *Phys. Rev.* **D108**, 2, 023510 (2023), [arXiv:2212.05642].
- [60] Planck Collab. 2018 Results VII, *Astron. Astrophys.* **641**, A7 (2020), [arXiv:1906.02552].
- [61] M. Tristram *et al.*, *Astron. Astrophys.* **647**, A128 (2021), [arXiv:2010.01139].
- [62] D. Hanson *et al.*, *Phys. Rev. Lett.* **111**, 14, 141301 (2013), [arXiv:1307.5830].
- [63] BICEP2 Collab., *Phys. Rev. Lett.* **112**, 24, 241101 (2014), [arXiv:1403.3985].
- [64] BICEP2/Keck and Planck Collabs., *Phys. Rev. Lett.* **114**, 10, 101301 (2015), [arXiv:1502.00612].
- [65] BICEP2 and Keck Array Collab., *Phys. Rev. Lett.* **121**, 22, 221301 (2018), [arXiv:1810.05216].
- [66] BICEP/Keck Collab., *Phys. Rev. Lett.* **127**, 151301 (2021), [arXiv:2110.00483].
- [67] POLARBEAR Collab., *Astrophys. J.* **848**, 121 (2017), [arXiv:1705.02907].
- [68] J. T. Sayre *et al.*, *Phys. Rev.* **D101**, 12, 122003 (2020), [arXiv:1910.05748].
- [69] Planck Collab. 2015 Results XV, *Astron. Astrophys.* **594**, A15 (2016), [arXiv:1502.01591].
- [70] A. van Engelen *et al.*, *Astrophys. J.* **808**, 7 (2015), [arXiv:1412.0626].
- [71] P. Ade *et al.* (Simons Observatory Collab.), *J. Cosmology Astropart. Phys.* **2019**, 2, 056 (2019), [arXiv:1808.07445].
- [72] K. N. Abazajian *et al.*, *ArXiv e-prints* (2016), [arXiv:1610.02743].
- [73] LiteBIRD Collaboration, *Progress of Theoretical and Experimental Physics* **2023**, 4, 042F01 (2023), [arXiv:2202.02773].
- [74] Planck Collab. 2018 Results VIII, *Astron. Astrophys.* **641**, A8 (2020), [arXiv:1807.06210].
- [75] F. J. Qu *et al.*, *arXiv e-prints* arXiv:2304.05202 (2023), [arXiv:2304.05202].
- [76] W. L. K. Wu *et al.*, *Astrophys. J.* **884**, 1, 70 (2019), [arXiv:1905.05777].
- [77] D. Scott *et al.*, *J. Cosmology Astropart. Phys.* **2016**, 6, 046 (2016), [arXiv:1603.03550].
- [78] L. Knox and Y.-S. Song, *Phys. Rev. Lett.* **89**, 1, 011303 (2002), [arXiv:astro-ph/0202286]; M. Kesden, A. Cooray and M. Kamionkowski, *Phys. Rev. Lett.* **89**, 011304 (2002), [arXiv:astro-ph/0202434]; C. M. Hirata and U. Seljak, *Phys. Rev.* **D68**, 8, 083002 (2003), [arXiv:astro-ph/0306354].
- [79] Planck Collab. 2013 Results XII, *Astron. Astrophys.* **571**, A12 (2014), [arXiv:1303.5072]; Planck Collab. 2015 Results X, *Astron. Astrophys.* **594**, A10 (2016), [arXiv:1502.01588]; Planck Collab. 2018 Results IV, *Astron. Astrophys.* **641**, A4 (2020), [arXiv:1807.06208].
- [80] B. Gold *et al.*, *Astrophys. J. Supp.* **192**, 15 (2011), [arXiv:1001.4555].
- [81] Planck Collab. Interm. Results XXX, *Astron. Astrophys.* **586**, A133 (2016), [arXiv:1409.5738].
- [82] M. Millea *et al.*, *Astrophys. J.* **746**, 4 (2012), [arXiv:1102.5195].
- [83] Sunyaev, R. A. and Zeldovich, Ya. B., *Ann. Rev. Astron. Astrophys.* **18**, 537 (1980).
- [84] R. Williamson *et al.*, *Astrophys. J.* **738**, 139 (2011), [arXiv:1101.1290].
- [85] M. Hilton *et al.*, *Astrophys. J. Supp.* **253**, 1, 3 (2021), [arXiv:2009.11043].
- [86] Planck Collab. Early Results VIII, *Astron. Astrophys.* **536**, A8 (2011), [arXiv:1101.2024].
- [87] Planck Collab. 2013 Results XX, *Astron. Astrophys.* **571**, A20 (2014), [arXiv:1303.5080].
- [88] T. de Haan *et al.*, *Astrophys. J.* **832**, 95 (2016), [arXiv:1603.06522].
- [89] Planck Collab. 2018 Results IX, *Astron. Astrophys.* **641**, A9 (2020), [arXiv:1905.05697].
- [90] Planck Collab. 2015 Results XVI, *Astron. Astrophys.* **594**, A16 (2016), [arXiv:1506.07135].
- [91] Planck Collab. 2013 Results XXII, *Astron. Astrophys.* **571**, A22 (2014), [arXiv:1303.5082]; Planck Collab. 2015 Results XX, *Astron. Astrophys.* **594**, A20 (2016), [arXiv:1502.02114].
- [92] Planck Collab. 2015 Results XIV, *Astron. Astrophys.* **594**, A14 (2016), [arXiv:1502.01590].
- [93] Planck Collab. Interm. Results XLVI, *Astron. Astrophys.* **596**, A107 (2016), [arXiv:1605.02985].
- [94] X. Fan, C. L. Carilli and B. Keating, *Ann. Rev. Astron. Astrophys.* **44**, 415 (2006), [arXiv:astro-ph/0602375].
- [95] C. A. Mason *et al.*, *Astrophys. J.* **856**, 1, 2 (2018), [arXiv:1709.05356].
- [96] Planck Collab. Interm. Results XLIX, *Astron. Astrophys.* **596**, A110 (2016), [arXiv:1605.08633]; E. Komatsu, *Nature Reviews Physics* **4**, 7, 452 (2022), [arXiv:2202.13919].
- [97] M. Kamionkowski and A. Kosowsky, *Ann. Rev. Nucl. Part. Sci.* **49**, 77 (1999), [arXiv:astro-ph/9904108].
- [98] Planck Collab. 2015 Results XIX, *Astron. Astrophys.* **594**, A19 (2016), [arXiv:1502.01594].
- [99] Planck Collab. Interm. Results XXIV, *Astron. Astrophys.* **580**, A22 (2015), [arXiv:1406.7482].

30. Cosmic Rays

Revised March 2024 by J. Alvarez-Muñiz (Santiago de Compostela U.), Z. Cao (IHEP Beijing), U.F. Katz (Erlangen U.), P. Mertsch (TTK, RWTH) and C. Spiering (DESY, Zeuthen).

30.1 Theory

Cosmic rays (CRs) are a non-thermal population of particles that pervade the Universe. Their salient characteristics can be inferred from their major observational properties: spectrum, composition and arrival directions. For charged CRs, the energies extend from tens of MeV to close to 1 ZeV, the intensity is $\sim 10^4 \text{ m}^{-2} \text{ s}^{-1} \text{ sr}^{-1}$ above 1 GeV, but the differential spectrum falls steeply with energy E , following a power-law dependence $E^{-\gamma}$. The most striking spectral features are the “knee” at a few PeV where the spectral index γ changes from ~ 2.7 to ~ 3 , the “second knee” at ~ 100 PeV with a change to ~ 3.3 and the “ankle” at a few EeV where γ changes to ~ 2.5 . The flux is largely suppressed above a few tens of EeV. (More detailed discussion of spectral features can be found below in Secs. 30.2.1 and 30.2.2.) Charged CRs are composed mostly of protons, helium, and other nuclei, as well as electrons, positrons and anti-protons. The arrival directions are mostly isotropic, but below and around the knee interesting $\mathcal{O}(10^{-4} \dots 10^{-3})$ anisotropies due to the distribution of sources and properties of the Galactic magnetic fields have been observed, reaching $\sim \mathcal{O}(10^{-1})$ at the highest energies. Gamma-rays can be resolved into those from astrophysical sources (~ 6660 [36] above 50 MeV, ~ 300 [37, 38] at TeV energies), plus diffuse fluxes of galactic and extra-galactic origin, predominantly showing power-law dependence on energy. The observation of high-energy neutrinos has opened a new window; while the distribution is largely isotropic, evidence for two extra-galactic sources as well as for a contribution from the galactic plane has been found. The energy spectra of charged CRs, diffuse gamma-rays and neutrinos are shown in Fig. 30.1. Combined observations of charged CRs, gamma-rays and neutrinos as well as gravitational waves (see Sec. 21.2.3) allow for valuable insights into the most extreme astrophysical environments and is referred to as multi-messenger astrophysics. Adding the contribution from all species results in the all-particle spectrum. While it was believed for a long-time that it was a featureless power law up to the knee at a few PeV, it has now been recognized that it has much more structure, mirroring the features in the individual species. These features carry important information on the acceleration and transport of CRs.

The energy variables used are kinetic energy E , kinetic energy per nucleon, $E_n = E/A$ for a particle of mass number A , or rigidity $\mathcal{R} \equiv pc/(Ze)$ (given in units of volt) for a particle of charge number Z , p being the momentum of the particle; the term rigidity refers to the resistance against deflections in a magnetic field B : particles of low (high) rigidity have small (large) gyroradii $r_g = \mathcal{R}/B$. Kinetic energy is closely related to the experimental signatures of a calorimetric instrument, while rigidity is the most natural one for a spectrometric one. Note also that relativistic nuclei suffer little energy losses and their transport is prescribed by magnetic fields, thus it can only depend on rigidity. The *intensity* J of CRs, also called the diffuse flux, is defined through the differential number dN of particles with energy in the interval $[E, E + dE]$, crossing the area dA from a solid angle $d\Omega$ in the time dt : $dN = J dE dA d\Omega dt$. Its isotropic part is related to the differential density $\psi = (4\pi/v)J$, v being the particle speed and to the phase-space density f as $J = p^2 f$. Note that the intensity can be also defined in reference to particle energy per nucleon or rigidity. To stress this, often the intensity is written as dJ/dE , dJ/dE_n or $dJ/d\mathcal{R}$.

In the detection of CRs, two classes of techniques are distinguished [39]. *Direct observations*, see Sec. 30.2.1, make use of the interactions of CRs in particle physics detectors (e.g. trackers, spectrometers and calorimeters). Given the limited exposures of such instruments and the steeply falling spectra, this is currently only realistic below ~ 100 TeV. In *indirect observations*, see Sec. 30.2.2, showers of secondary particles initiated by charged CR interactions in natural materials (e.g. air, water or ice) are detected through fluorescence, air-Cherenkov, water-Cherenkov or scintillation effects. This allows for large instrumented surfaces or volumes. Historically, the two classes of techniques have been

employed by two separate communities and we structure the review of charged CRs accordingly. For detection of gamma-rays, direct observations are relevant mostly below hundreds of GeV; for gamma-rays of higher energies and neutrinos of essentially all energies, indirect observations are required.

Charged CRs are deflected by magnetic fields and so generally speaking the observed events do not point back to sources. CRs can however reach the earth from galactic and even cosmological distances. Between hundreds of MeV and at least a few PeV, CRs are believed to be of galactic origin; above a few EeV, the sources are most likely extra-galactic. If CRs with energies in excess of ~ 1 EeV came from sources in the Galactic disk, the angular distribution at Earth would be very anisotropic, which is at variance with observations. And if CRs below ~ 1 PeV were dominantly of extra-galactic origin, this would result in a gamma-ray flux from objects like the Large Magellanic Cloud exceeding observations [40]. Direct and indirect observations therefore also largely refer to galactic/extra-galactic sources, respectively. CRs with energies in excess of 1 EeV are referred to as ultra-high energy cosmic rays (UHECRs).

Sources of non-thermal electromagnetic radiation are routinely observed, see Sec. 30.3, yet the dominant source of locally measured CRs have not been unambiguously identified. Source candidates are typically associated with endpoints of stellar evolution or supermassive black holes that release large amounts of gravitational or rotational energy [41]. In the Galaxy, the prime candidates are supernova remnants [42] where particles can be shock-accelerated by their blast waves [43]. Other candidates are star cluster winds [44, 45], stellar wind binaries, micro quasars [46] (a source powered by accretion from a donor star onto a stellar mass black hole) or even the Galactic Center [47]. The candidate sources for extra-galactic CRs are Active Galactic Nuclei (AGN) [48], specifically blazars and radio galaxies, gamma-ray bursts [49], starburst galaxies [50, 51], pulsars [52] and magnetars [53]. These objects exhibit power-law spectra in electromagnetic radiation, albeit in limited wavelength ranges. The acceleration mechanisms considered in the literature are shock acceleration [43], stochastic acceleration [54], and reconnection [55]. A fundamental constraint on the maximum energy, the so-called Hillas criterion [56], follows from the requirement that the gyroradius must be smaller than the source size.

In the Milky Way, the dominant process in CR transport is diffusion as evidenced by the small anisotropies in CR arrival directions and by certain abundance ratios of nuclear species. This diffusive transport bears some resemblance with heat transport in that it smooths the spatial distribution of CRs. However, in contrast to heat transport, CR diffusion is not due to collisions, but interactions with turbulent magnetic fields. Generally, CRs interact “resonantly” with plasma waves, that is they get affected only by waves with a wavelength similar to the gyroradius of the CR particle. If this condition is satisfied, a CR particle will be deflected by the Lorentz force. Many random deflections lead to a random walk in space, that is diffusion [57].

There is a number of other processes contributing to the transport of charged CRs: momentum losses, i.e. radiative losses for electrons and positrons [59], ionization and Coulomb losses for nuclei, electrons and positrons [60]; spallation, that is production of (mostly) lighter nuclei by inelastic collisions of heavier ones; and other inelastic collisions, e.g. the production of light mesons. We note that progress in the study of CR transport is often limited by the nuclear interactions since many cross-sections are poorly known, if at all [61]. The various processes are encoded in the CR transport equation [62], also referred to as the Parker transport equation [63] in the space physics community. This partial differential equation is supplemented by the boundary condition of free escape on the surface of the (often cylindrical) confinement volume. Only in simplified cases can this equation be solved analytically. The most instructive case is the 1D approximation where only the direction perpendicular to the Galactic disk is retained. The solution differs for *primaries*, that is species present and accelerated in the CR sources, and *secondaries*, which are not present in CR sources, but produced by inelastic collisions of primaries in the gaseous disk of

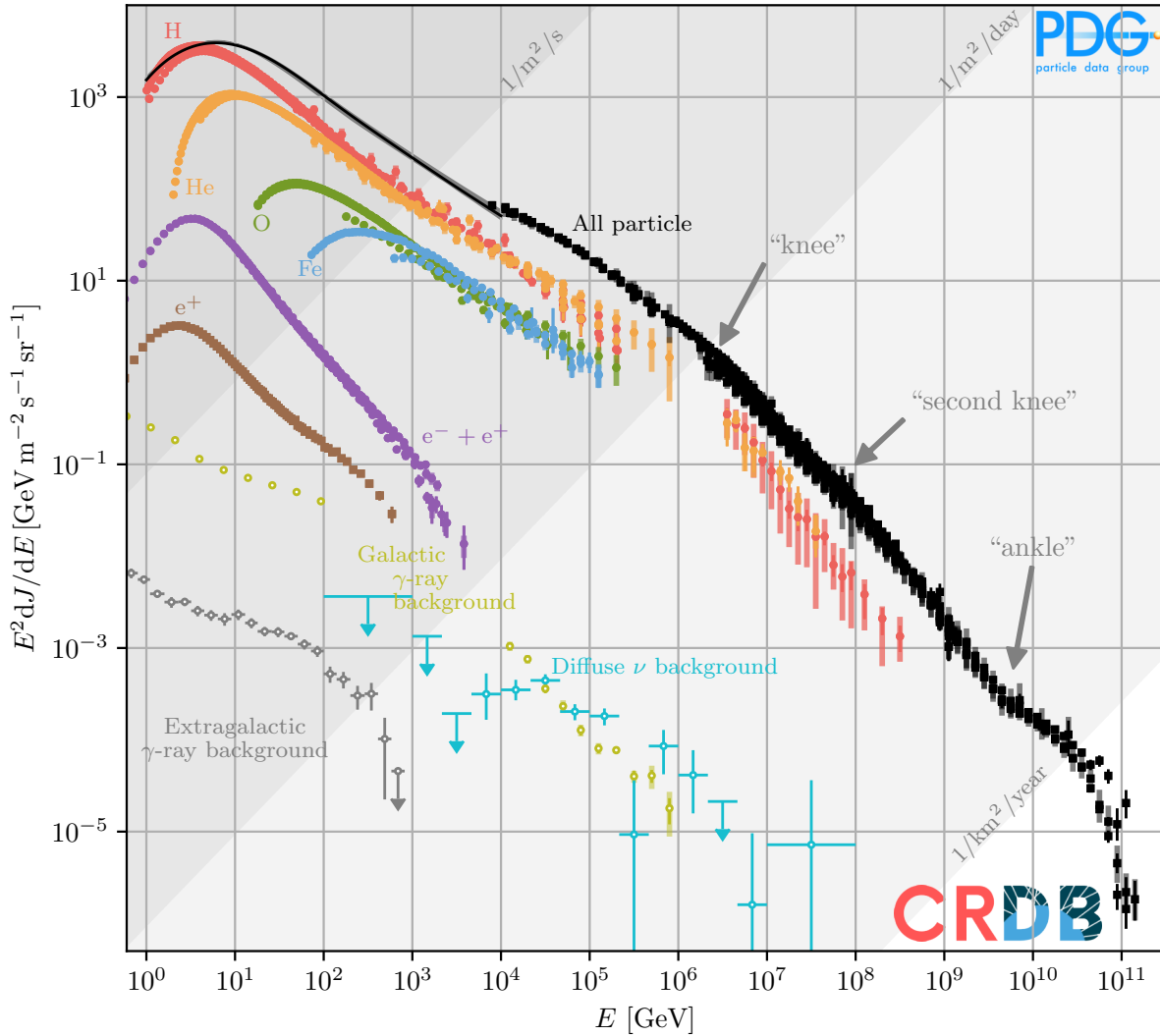


Figure 30.1: The spectrum of cosmic rays (CRs). Shown are measurements of the intensity of charged and neutral CRs, multiplied by kinetic energy squared. The data for the charged CRs [1–30] have been extracted from the Cosmic Ray Database (CRDB) [31]. Below 10^4 GeV, the all-particle spectrum is the sum of spline fits of the most important nuclear species. The diffuse γ -ray fluxes have been extracted from Refs. [32–34], measurements of the diffuse neutrino background from Ref. [35]. Energy-integrated intensities are indicated by the various diagonal lines.

the Galaxy. Diffusion in the Galaxy, characterized by a diffusion coefficient $\kappa(\mathcal{R})$, modifies the source spectrum $q(\mathcal{R})$, resulting in the steady-state spectrum $\psi(\mathcal{R}) \propto q(\mathcal{R})/\kappa(\mathcal{R})$. As the production spectrum of secondaries follows the steady-state spectrum of primaries, $q_2(\mathcal{R}) \propto \psi_1(\mathcal{R})$, the secondary steady-state spectrum is $\psi_2(\mathcal{R}) \propto q_2(\mathcal{R})/\kappa(\mathcal{R}) \propto \psi_1(\mathcal{R})/\kappa(\mathcal{R})$. As $\kappa(\mathcal{R})$ grows with \mathcal{R} , secondary spectra $\psi_2(\mathcal{R})$ fall more quickly with rigidity than primary spectra $\psi_1(\mathcal{R})$. Unstable secondaries provide additional constraints on the gas density and residence time of CRs. The solution of the transport equation in more realistic setups requires numerical codes [64–67].

Protons (iron nuclei) with energies in excess of ~ 1 EeV (~ 26 EeV) in a micro-Gauss magnetic field have gyroradii larger than the typical kiloparsec scales of the Galaxy, thus they cannot be confined. Their directions are however affected by so-called small-angle scattering, both in the Milky Way and possibly outside. As far as their spectrum and composition is concerned, protons and heavier nuclei suffer from inelastic collisions with the CMB and the extra-galactic background light at the highest energies. For protons above 10 EeV, photo-pion production limits the propagation distances to ~ 100 Mpc; for nuclei, heavier ones photo-disintegrate to lighter ones, also limiting their spatial reach. Both processes can lead to a suppression of the flux known as the

GZK effect [68, 69] and produce secondary gamma-rays and neutrinos. Other secondary particles include neutral and charged pions, which ultimately decay to photons, electrons, positrons and neutrinos, and electron-positron pairs which can also initiate a cascade of photons and lower energy electrons and positrons. The stable decay products, in particular gamma-rays and neutrinos can be used as an additional diagnostic tool for the study of the origin and transport of UHECRs.

In many astrophysical environments, the energy density of CRs constitutes a significant fraction of the total or is comparable to that of other ingredients. For instance, on galactic scales, the CR energy density is of the same order as that of magnetic fields, radiation fields or the turbulent gas. Due to their pressure, CRs can be dynamically important and shape their environments: Specifically, CRs contribute to the gravitational support of galaxies and can drive galaxy-scale outflows. They ionize neutral gas, thus determining coupling of gas and magnetic fields. CRs can generate turbulence by a variety of streaming instabilities [70, 71], which play a central role in shock acceleration and galactic transport [72]. Finally, CRs also produce diffuse emission through interactions with gas and radiation fields, an additional handle for CR studies.

CRs are also important probes of fundamental physics. If dark

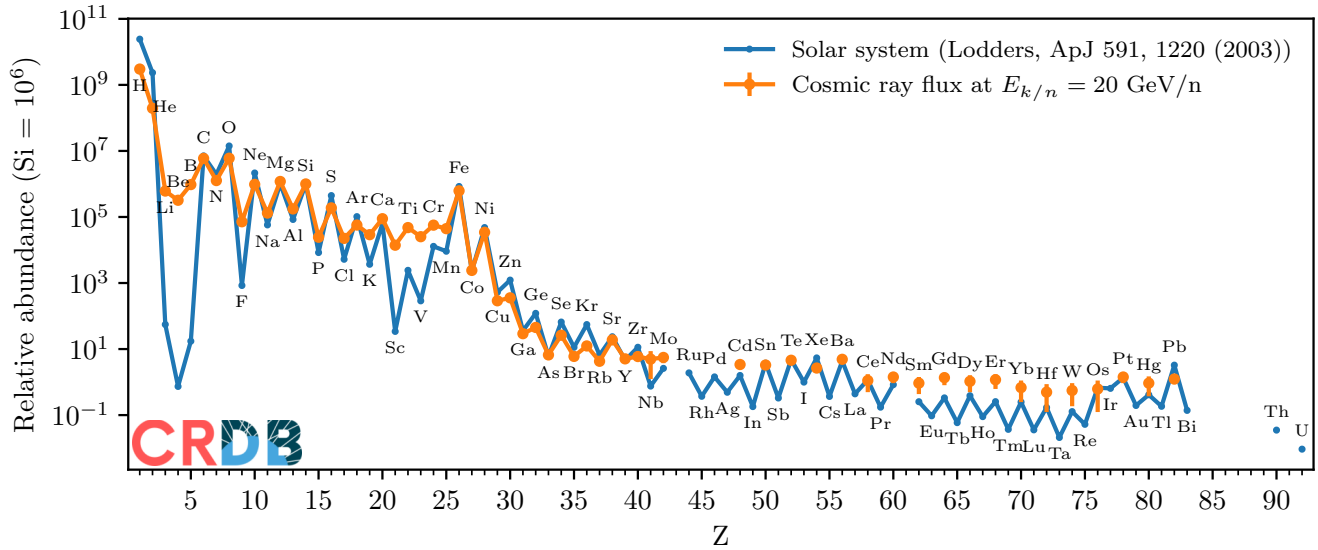


Figure 30.2: CR abundances compared with solar system ones [58]. Modified from [31].

matter has interactions with the Standard Model, the products of self-annihilation or decay of DM particles can potentially be observed (DM, see Sec. 27.7). This is called DM indirect observation. Generically, one would expect similar rates of production of particles and antiparticles whereas astrophysical sources predominantly accelerate matter particles. It is therefore advisable to search for signals in CRs positrons, anti-protons and anti-nuclei [73, 74]. In fact, excesses have been reported of positrons and anti-protons, yet astrophysical pollutions and/or experimental systematic uncertainties can not be excluded. There have also been searches in gamma-rays and neutrinos and a number of studies have identified an excess of gamma-rays from the Galactic Center that is compatible with DM particles of weak-scale mass and weak annihilation cross-section [75]. Another target for exotic searches in CRs is anti-matter of primordial origin [76]. Most interestingly, the AMS-02 collaboration has claimed $\mathcal{O}(10)$ $\bar{\text{He}}$ candidate events, but whether those are of primordial origin as opposed to instrumental effects is at this point not clear.

30.2 Charged cosmic rays

30.2.1 Direct observations

Direct observations [77] cover energies between a few MeV and a few tens of TeV, where CRs must be of Galactic origin. At energies lower than a few MeV, solar energetic particles [78] are dominating the flux; above a few tens of TeV, the fluxes are too low to be observed directly and instead indirect detection techniques [79] need to be used. Besides spectral information, direct observations enable identification of species on an event-by-event basis, certain experiments even provide isotopic discrimination. We present a compilation of direct observations of the most important primary and secondary nuclei in Fig. 30.3. These show broken power-law spectra in rigidity with $J \propto E^{-\gamma}$ in different rigidity ranges. The various changes in spectral slope contain valuable information on the rigidity-dependence of the diffusion coefficient κ and the primary source spectra q_1 .

Protons are dominating the CR flux by number and by energy below ~ 10 TeV and their spectrum has been measured with excellent precision. Measurements of the proton spectrum and other primaries are shown in the left panel of Fig. 30.3. Data from the AMS-02 experiment [8] show a $\mathcal{R}^{-2.8}$ spectrum above ~ 10 GeV with a break to $\mathcal{R}^{-2.7}$ at ~ 300 GV. This feature had been observed by PAMELA earlier [2], and also with CREAM and ATIC for heavier nuclei [80, 81]. As a reminder, at energies above a few GeV, the measured spectrum can be interpreted as the ratio of the source spectrum $q(\mathcal{R}) \propto \mathcal{R}^{-\Gamma}$ divided by the diffusion coefficient $\kappa(\mathcal{R}) \propto \mathcal{R}^{\delta}$. Thus a spectral index of $\gamma = \Gamma + \delta \simeq 2.8$ can describe the data. On the basis of proton data alone, the degen-

eracy between the source spectral index Γ and the spectral index of the diffusion coefficient δ cannot be broken. Also, the break at ~ 300 GV could be a break in the source spectrum or in the diffusion coefficient, but see below. At energies lower than ~ 10 GeV, the spectrum turns over because of energy losses and solar modulation. At energies beyond the reach of AMS-02, both DAMPE and CALET data show a softening at rigidity ~ 10 TV [7, 10], confirming earlier indications [80, 81].

Most of the other primary species, that is helium, carbon, nitrogen, oxygen, neon, magnesium and silicon with the notable exception of iron, also show a spectral break at ~ 300 GV, but their spectra are generally harder than the proton one, e.g. $\gamma_{\text{He}} < \gamma_{\text{p}}$, both below and above the break. Suggested explanations for this difference in spectrum include gradients in the relative circumstellar abundances of protons and heavier nuclei or invoking different source populations for these two groups. At ~ 10 TV a softening break mirrors the feature observed in protons [82]. Above an energy of ~ 100 TeV, elemental information is scarce, but a combined analysis of proton and helium by DAMPE extends to ~ 300 TeV and indicates another spectral hardening [83]. (Note that this data are not included in Fig. 30.3 though.) Such a feature was to be expected to a certain degree in order to connect to the indirect measurements of proton and helium which start at ~ 1 PeV. Note that there exist some 20% discrepancies between the oxygen and carbon data from AMS-02 [8], CALET [13] and PAMELA experiments [84] in normalization, possibly also in spectral shapes.

Iron constitutes an exception to the otherwise rather similar slopes of primary species heavier than proton. As is also the case for other nuclei, AMS-02 [15] and CALET [16] disagree on the normalization by $\sim 20\%$, but both measurements of the iron spectrum exhibit spectral shapes different from the oxygen ones. While the ratio of Fe/O could be accommodated if all nuclei traversed the same amount of matter (grammage) between source and observer (the so-called slab model), more realistic models cannot explain the observations [85]. Also, the AMS-02 data on Fe/O are in tension with earlier measurements [86, 87]. Most interestingly, if extrapolated to lower energies, the Fe/O could only be accommodated if solar modulation was negligible.

Measurements of *stable* secondary nuclei contribute two important pieces of information to the standard scenario of galactic CRs: First, their over-abundance in CRs (with respect to solar system values, see Fig. 30.2) indicates diffusion as the primary transport process; and second, their spectral shapes, or rather the difference in spectral shapes between secondaries and primaries allows inference of the diffusion coefficient. Specifically, at energies where energy losses can be ignored for nuclei, that is above a

few GeV, the propagated spectra of primaries $\psi_1(\mathcal{R})$ are approximately $\propto \mathcal{R}^{-2.8 \dots -2.7}$, which is explained as a softening of the sources spectrum $q_1(\mathcal{R})$. Secondaries, however, are produced with a spectrum proportional to the propagated primary spectrum, $q_2(\mathcal{R}) \propto \psi_1(\mathcal{R})$ which also gets further softened by the diffusion coefficient. The difference in spectral index can be clearly seen when comparing primary with secondary spectra. A compilation of such secondary spectra from AMS-02 [8, 88, 89], CALET [90] and PAMELA [84] is shown in the right panel of Fig. 30.3. Lithium, beryllium, boron and fluorine can be identified as almost pure secondaries by their soft spectra. Aluminium, sodium and neon, however, have harder spectra, somewhere intermediate between primaries and secondaries. This can be understood as being due to mixture of softer secondary contribution from spallation in the interstellar medium (ISM) and a harder primary source component. Secondaries also exhibit a hardening break at ~ 300 GV, but the change in spectral slope is about twice as big [91] when compared to that of the primaries. This fact serves as evidence for the break being due to a change in the rigidity-dependence of the diffusion coefficient, as opposed to a break in the source spectrum [92, 93]. Recently, there have been some claims of excesses in low-energy intensities of Li, F, Al [94], however these claims are somewhat controversial. We note the importance of composition studies for shedding light on cosmic ray origin.

Unstable isotopes with a lifetime similar to the residence time of CRs can be used to study galactic propagation. Among these species, ^{10}Be , ^{26}Al and ^{60}Fe have been studied the most as their rest lifetime is close to the residence time of CRs at GV rigidities. Roughly speaking, the flux ratio of an unstable and a stable secondary that are both produced from similar primary species, reflects the ratio of production cross-section at high energies (where decay is suppressed by time-dilation). On the other hand, at low energies, this ratio is suppressed due to the decay of the unstable species. The transition takes place at energies where the decay time equals the residence time in the Galactic disk. At present, there is limited information on ratios at energies beyond 1 GeV/nucleon where the transition for the ratios of the above mentioned unstable nuclei is expected to take place.

CR electrons are also believed to be accelerated in the preferred candidate sources of nuclei, that is, SNRs. Other source candidates are pulsars and pulsar wind nebulae (PWNe); in the simplest models those also accelerate similar amounts of CR positrons. We show a compilation of the most recent and precise data from AMS-02 [8], CALET [19], DAMPE [17], *Fermi-LAT* [18], H.E.S.S. [95] and PAMELA [96] on CR electrons, positrons and the sum of electrons and positrons in Fig. 30.4. In addition to the processes at work in the propagation of nuclei, electrons suffer significant radiative losses due to synchrotron emission and inverse Compton scattering. In fact, for the parameters determined in the standard scenario, the cooling time is shorter than the residence time above ~ 10 GeV. For the same source spectral index, the spectra are predicted to be softer than those of primary nuclei. Indeed, the observed spectrum is roughly $\propto E^{-3.1}$.

If positrons were only produced by spallation in the interstellar medium, the positron spectrum should be softer than the electron one, however, on the contrary it is markedly harder. Between ~ 10 GeV and ~ 100 GeV its spectral index γ_{e^+} transitions from 3 to 2.7 before a spectral break or cut-off at a few hundred GeV as shown in Fig. 30.4. The fact that the positron spectrum is harder than the electron one above a few GeV had first been detected by PAMELA [97] after earlier indications. AMS-02 has now measured the spectrum with great precision up to ~ 1 TeV [8]. The origin of the harder positron spectrum remains unclear today. After the discovery by PAMELA, there had been hope that this was the long sought for signature of self-annihilation or decay of weakly interacting massive particles (WIMP) dark matter [98]. However, such interpretations are now severely constrained by observations of gamma-rays, anti-protons and the cosmic microwave background (CMB, see Chap. 29). Production of e^+ in pulsars or PWNe is an astrophysical explanation that had been hypothesized long before the PAMELA observations (e.g. [99]). Recently, there have been observations of extended emission of high-energy gamma-rays, so-called gamma-ray halos

around PWNe [100], interpreted as evidence of the presence of high-energy electrons and positrons around these objects. Other astrophysical explanations include the production and subsequent acceleration of secondaries in old SNRs [101, 102].

Measurements of the spectra of electrons and positrons are particularly interesting at high energies. Due to the increasingly important radiative losses, the distance to the sources which could significantly contribute to the total flux decreases with energy. Estimates at 1 TeV of this diffusion-loss length are only $\simeq 0.3$ kpc. The predicted spectrum therefore becomes rather sensitive to the exact distances and ages of young, nearby sources which manifest as individual bumps in the spectrum. Turning this around, observations can be used to search for young, nearby sources of CRs. At energies above ~ 1 TeV, only calorimetric observations are currently available which cannot discriminate between electrons and positrons. Observations of the all-electron flux, that is the sum of electron and positron fluxes, find a break at ~ 1 TeV, displayed in Fig. 30.4. This was first seen by H.E.S.S. [95] and later confirmed by DAMPE [17] and CALET [19]. The break by about one power in energy has been interpreted either as due to a break in the spectrum of a large number of sources, e.g. [104] or as a stochasticity effect from a small population of sources [105].

In the standard scenario of galactic cosmic rays, anti-protons are also produced as secondary particles, but unlike secondary nuclei or electrons and positrons, their production is kinematically suppressed at lower energies. The spectrum of anti-protons observed by PAMELA (Fig. 3 in [106]) and AMS-02 (Fig. 62 in [8]) is close to $E^{-2.8}$, which is somewhat harder than predicted by earlier models. More recent models can accommodate the observations, in part due to a re-evaluation of the production cross-section. Note that there have been claims that the transport parameters obtained when fitting to proton and anti-proton data differ from those obtained by fitting to heavier nuclei [107]. An alternative explanation for the harder anti-proton spectrum is the acceleration of secondaries in old supernova remnants [102, 108]. At energies of a few GeV, there have been claims of an excess in the measured anti-proton spectrum. If interpreted as a sign of dark matter annihilation, such an excess could be explained by a weak-scale particle of mass of a few tens of GeV and annihilation cross-sections close to the thermal relic value. However, the significance of the signal is relatively low if correlations in the cross-section uncertainties and in the measurements are taken into account. Considering the spectra of anti-protons together with protons and positrons, it appears that all three have similar spectral indices between ~ 10 GV and ~ 300 GV. This is rather surprising, given that as secondaries positrons and anti-protons should have spectra softer than the primary protons, due to energy losses and diffusive losses, respectively. In the standard scenario this cannot be explained and thus must be considered a mere coincidence.

The only astrophysical mechanism for production of anti-nuclei like anti-deuterons (\bar{D}) or anti-helium ($^3\bar{\text{He}}$ or $^4\bar{\text{He}}$) is coalescence of anti-nucleons produced in the spallation of primary nuclei in the interstellar medium. Due to kinematics, however, this is significantly suppressed at energies below a few GeV, thus rendering this an interesting channel for searches of dark matter, in particular for relatively light WIMPs with masses of a few GeV or less. The AMS-02 collaboration has reported some ten candidate events of anti-helium, yet the rate of $^3\bar{\text{He}}$ or $^4\bar{\text{He}}$ is incompatible with models of coalescence (e.g. [109]). Currently, the most constraining limits on \bar{D} are from the BESS balloon flights [110]. This should be improved on by the upcoming GAPS experiment, and also an upgrade of the AMS-02 experiment increasing the acceptance by a factor of three could help clarifying the situation.

Another important observable in the study of CRs are anisotropies, most commonly defined as the relative directional deviation of the CR intensity from the angular average. As the typical anisotropies are at the level of one part in 10^3 or 10^4 , high statistics are required. At TeV and PeV energies, only ground-based experiments have enough statistics, yet they cannot constrain the component of the anisotropy that is aligned with the Earth's rotation axis. Traditionally, therefore, only the projection of the true 2D dipole into the equatorial plane has been reported in terms of an amplitude and phase. We show a

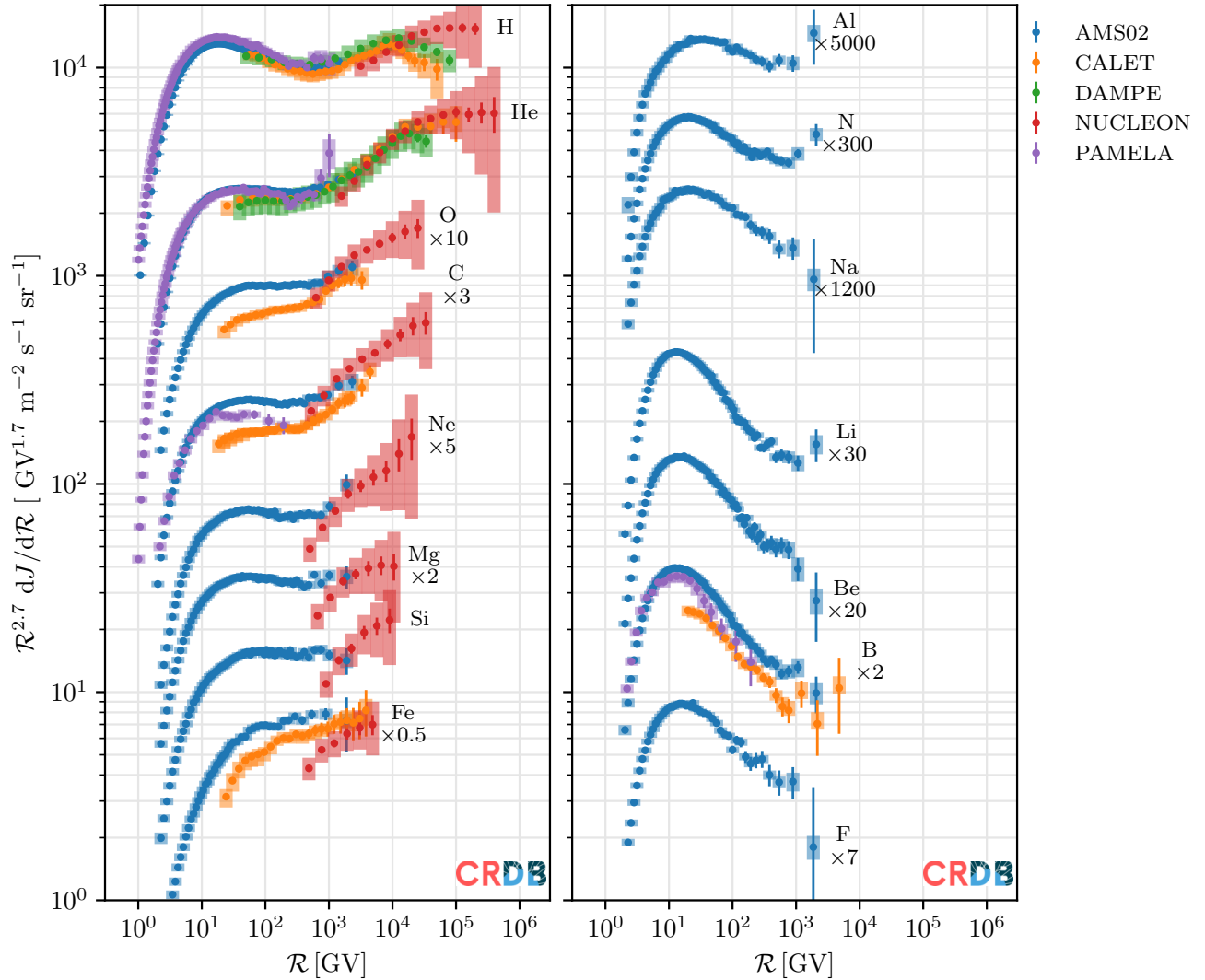


Figure 30.3: Rigidity spectra for a selection of CR nuclei. Primary species are shown in the left panel, (mostly) secondary species in the right panel. The error bars denote the statistical uncertainties, the shaded bars represent the systematic uncertainties. The spectra have been shifted and multiplied by $\mathcal{R}^{2.7}$ to better bring out spectral features. Here, we have constrained ourselves to data from space-borne experiments of the last ten years, that is AMS-02 [8, 15, 88, 89, 103], CALET [10, 16, 82, 90], DAMPE [7, 13], NUCLEON [5] and PAMELA [2, 84]. Data have been extracted from [31].

compilation [31] in Fig. 30.5. The amplitude is at the level of $\approx 10^{-4}$ at energies of hundreds of GeV and increases to $\approx 10^{-3}$ at tens of TeV. At ~ 100 TeV there is a dip before the amplitude rises again. Beyond a few PeV upper limits exist at the level of 10^{-2} . The Compton-Getting effect [111, 112], that is a dipole anisotropy due to the relative motion of the solar system with respect to the Galactic rest frame has been experimentally confirmed [113]. The phase is relatively constant at a direction of 45° and switches to 250° , which is close to the Galactic Center direction, also around 100 TeV. For a description of anisotropies at the highest energies see Section 30.2.2. In addition, observations of anisotropies on scales smaller than the dipole have been reported (see Ref. [114]). These are not expected in standard diffusion theories that only predict a dipole. The leading explanation is the generation due to the specific realization of the turbulent magnetic field in our Galactic neighbourhood.

30.2.2 Indirect observations

In the energy range above ≈ 1 PeV the intensity of cosmic rays is so low that it prevents the collection of a statistically significant sample of these particles in a direct manner with detectors carried on balloons or satellites. Instead, cosmic rays are detected indirectly through the cascade of particles they produce

in the atmosphere, the so-called extensive air showers (EAS). In this way, cosmic rays up to and even above 100 EeV have been observed [115, 116], corresponding to about a hundred million times larger energy than that achieved by particles accelerated in human-made experiments.

Extensive Air Showers. Extensive air showers (EAS) are cascades of millions to billions of secondary particles initiated by a single primary particle (cosmic ray: proton, neutron or heavier nucleus; photon; or neutrino) of energy E in the atmosphere. Due to the small density of air $\rho \lesssim 10^{-3} \text{ g cm}^{-3}$, the shower develops throughout the whole of the atmosphere, and for a primary particle of 10 EeV has a lateral spread of $\sim 10 \text{ km}^2$ at ground level, hence the name EAS.

When an energetic, $E \gtrsim 1 \text{ PeV}$, cosmic proton or nucleus interacts with a nucleus of air, it generates between a few and hundreds of secondary particles depending on its energy. On average $\sim 30\% - 40\%$ of the energy of the primary particle is carried by a leading baryon or nucleus. The remaining energy is employed in the creation of ultra-relativistic secondary particles, most of them charged (π^\pm) and neutral (π^0) pions, with a smaller number of hadrons and heavier mesons such as charged and neutral kaons, ρ -mesons, etc. The energy of the primary particle

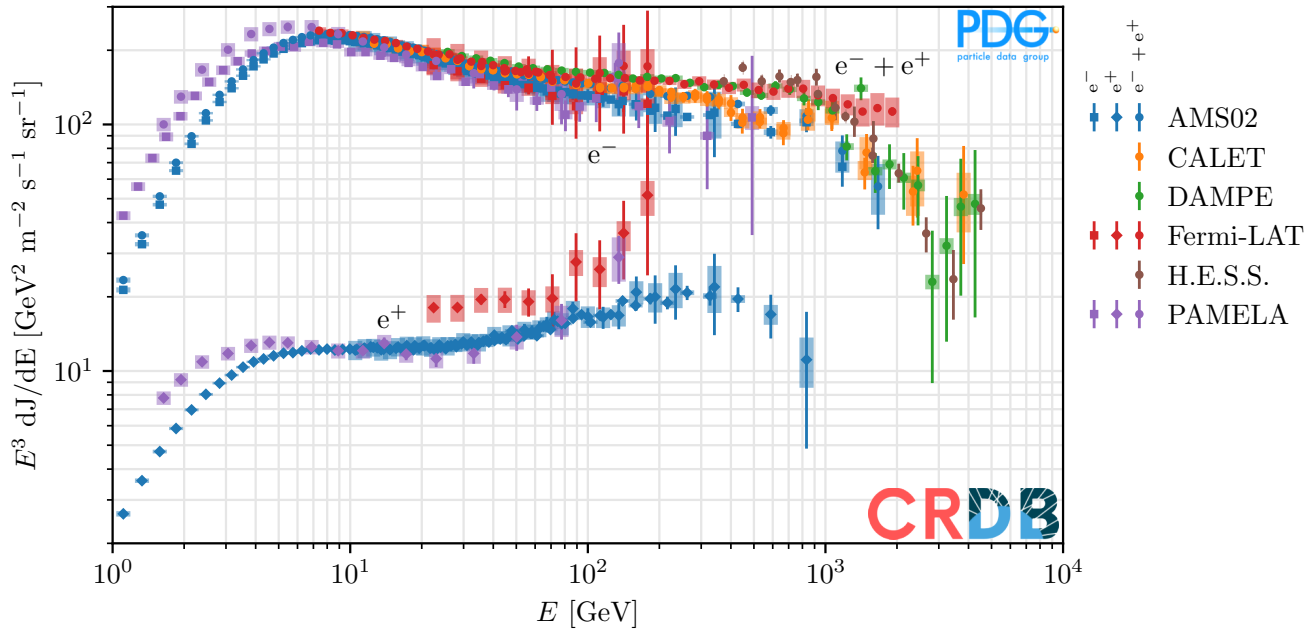


Figure 30.4: Intensities of cosmic ray electrons (squares), positrons (diamonds) and their sum (dots) as a function of kinetic energy E . We have included data from the most recent space experiments AMS-02 [8], CALET [19], DAMPE [17], *Fermi*-LAT [18] and PAMELA [96] as well as from the ground-based H.E.S.S. experiment [95]. The spectra have been multiplied by E^3 to enhance the visibility of the spectral features. Data have been extracted from [31].

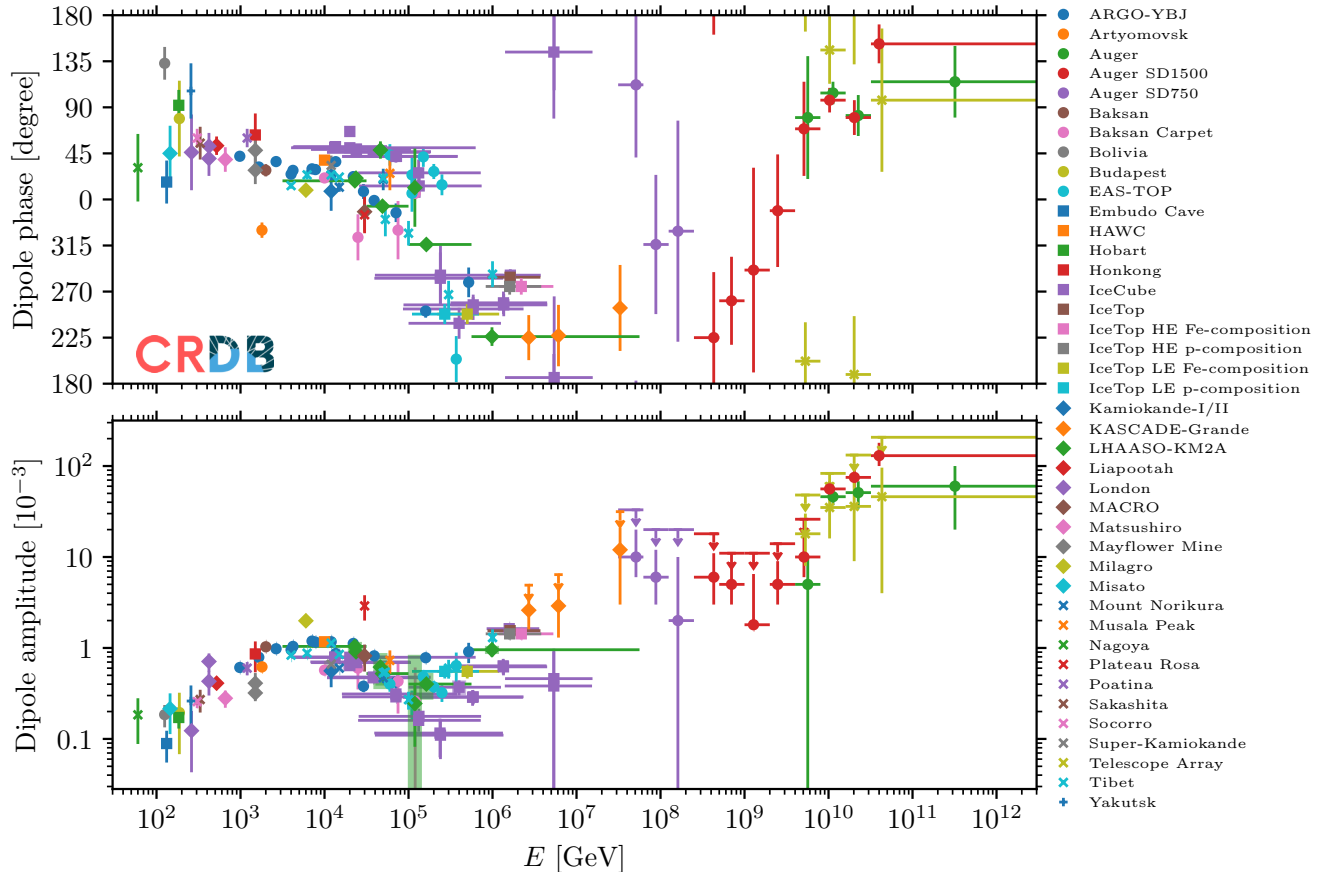


Figure 30.5: Phase and amplitude of the dipole anisotropy in CRs. Modified from Ref. [31].

rapidly degrades into a large number of secondaries that can subsequently interact or decay depending on the nature and energy of the particle and the density of the medium, further contributing to the shower development. If π^\pm live long enough they can interact with an air nucleus before decaying. At altitudes of a few km where the atmosphere is less dense than at sea level, most π^\pm with $E_{\pi^\pm} \gtrsim 100$ GeV interact while lower energy π^\pm decay. Interacting π^\pm along with the leading baryon and other hadrons, form a penetrating core of shower particles constituting the *hadronic component* of the cascade (Fig. 30.6). Charged pions decaying into muons, $\pi^+ \rightarrow \mu^+ + \nu_\mu$ and $\pi^- \rightarrow \mu^- + \bar{\nu}_\mu$, represent the main contribution to the *muonic component* of the shower (Fig. 30.6), being also responsible for the production of the bulk of the so-called atmospheric neutrinos. Most muons of energies above a few GeV travel through the atmosphere without decaying and reach ground, constituting a penetrating component of the shower. On the other hand, most π^0 s, continuously produced in the hadronic core of the shower, do not travel long enough distances to interact with an air nucleus unless their energy is well above 1 EeV. Instead, they decay almost immediately $\pi^0 \rightarrow \gamma\gamma$, initiating electromagnetic showers. Neutral pions play a significant role in generating the *electromagnetic component* that forms the majority of the shower (Fig. 30.6). This is composed of e^- and e^+ with a mean energy of 10 MeV as a result of photon pair production, as well as secondary photons from bremsstrahlung. Decaying muons also contribute to the electromagnetic component of the shower. The longitudinal development of the distinct and intertwined shower components, electromagnetic, muonic, and hadronic, is shown in Fig. 30.6. High-energy primary or secondary photons can occasionally photoproduce π^\pm and initiate a hadronic subcascade resulting in an additional muonic component.

As a cosmic ray shower develops in the atmosphere, the number of particles increases in the longitudinal direction along the shower axis. The amount of matter traversed, X , is measured in units of g cm^{-2} . The shower reaches a maximum size of the electromagnetic component N_{max} at a depth known as X_{max} (Fig. 30.6). The number of electrons and positrons declines rapidly after maximum when their energy reaches the *critical energy* in air, ~ 80 MeV, and they lose their remaining energy dominantly through ionization loss. Since neutrinos do not suffer electromagnetic interactions, and high energy muons reach ground level after releasing only a portion of their energy, a fraction of the energy of the primary initiating the shower is not deposited in the atmosphere. This is the so-called *invisible energy* that amounts to $\approx 10\% - 20\%$ of the shower energy for energies above 0.1 EeV, decreasing with the energy of the primary particle initiating the shower and increasing with its mass number [118]. At the same time the shower develops in the transverse or lateral dimension to the shower axis, as shown in Fig. 30.6, mainly due to the transverse momentum in hadronic interactions and multiple Coulomb scattering of e^- and e^+ .

Shower development is driven by the particles carrying most of the energy in the forward region of the kinematical phase space of the collisions with air nuclei. Particle production is dominated by non-perturbative QCD which is necessarily treated by using phenomenological approaches. Moreover, particle collisions occurring in the atmosphere at 0.1 EeV are equivalent to center-of-mass energies presently achieved at the LHC, and this energy scales up by a factor of approximately 30 at the highest cosmic ray energies observed. These two facts result in the need for extrapolations both in energy and phase space when modeling hadronic interactions. The cosmic-ray community has developed sophisticated simulation packages such as AIRES [117] and CORSIKA [119] to predict EAS observables as a function of primary energy and mass. These programs adopt models of hadronic interactions such as SIBYLL [120], QGSJET [121] and EPOS [122], tuned to a large data set including recent LHC data. Inferring fundamental properties of the primary particle initiating the shower, most notably its mass, requires the use of these air shower simulations. Large uncertainties remain, both due to theoretical limitations and the lack of data from existing collider experiments. A toy model to describe electromagnetic showers is due to Heitler [123], while for hadronic showers a model was developed by Matthews [124]. These oversimplified models shed light on the

relation between the main shower observables and the nature of the primaries and predict that for the electromagnetic component, $N_{\text{max}} \propto E$; $X_{\text{max}} \propto \log E$ and $X_{\text{max}} \propto \log A^{-1}$ with A the mass number of the primary nucleus; while for the muonic component, $N_\mu \propto A^{(1-\beta)} E^\beta$ with $\beta \simeq 0.85 \dots 0.95$. These important features of air showers constitute the basis for the identification of the primary particle with EAS (see next section). Similar features are also obtained in detailed Monte Carlo simulations of EAS development (Fig. 30.6), and have been observed experimentally.

Shower detection and cosmic-ray reconstruction. EAS have been detected with several techniques. Arrays of conventional particle detectors such as scintillators, water-Cherenkov stations or underground muon detectors, measure the lateral distribution of the shower front at ground, i.e., at a fixed depth. Due to the low cosmic-ray intensity especially at EeV energies (Figs. 30.1 and 30.7), the particle detectors are spread over large areas to compensate for the low flux, separated by distances that range from hundreds of meters to above 1 km. From the times at which the shower front hits several of these particle detectors, the arrival direction of the cosmic ray is measured with an accuracy typically better than $\sim 1^\circ$. Shower arrays measure a shower size parameter, proportional to the number of secondary particles, that can be related to the energy E of the primary particle. With several types of detectors working together, it becomes possible to effectively separate the electromagnetic and muonic components of the shower, thereby providing an estimate of the mass of the primary. The main arrays of particle detectors for EAS observation currently in operation are the surface detector of water-Cherenkov stations of the Pierre Auger Observatory in Argentina [125] spread over a total area of $\sim 3000 \text{ km}^2$, and the Telescope Array (TA) of scintillators in USA ($\sim 700 \text{ km}^2$) [126]. They typically work with almost 100% duty cycle and have measured many properties of the cosmic-ray flux (see next section).

Other arrays can measure the radiation emitted when the shower develops in the atmosphere, namely, optical Cherenkov radiation, fluorescence light, or radio emission in the MHz to GHz frequency range. Cherenkov detectors measure the forward-beamed incoherent emission at optical wavelengths. This can be achieved with arrays of individual elements such as at the Yakutsk [127] and Tunka-133 [128] observatories. A fluorescence telescope can monitor a large volume of the atmosphere and detect the isotropic fluorescence radiation emitted by the nitrogen molecules of air excited by the passage of the charged particles of the shower. The fluorescence radiation is produced in proportion to the energy dissipation and the shower size $N(X)$, allowing a reconstruction of the longitudinal profile of the energy deposit dE/dX of the shower as a function of atmospheric depth X and, in particular, providing a measurement of X_{max} . With the fluorescence detection technique, the atmosphere is used as a calorimeter, with the integral $E_{\text{cal}} = \int (dE/dX) dX$ called the calorimetric energy of the shower. An estimation of the primary energy with the fluorescence detection technique is obtained by adding to E_{cal} a correction to account for the invisible energy introduced above. Fluorescence and optical Cherenkov detectors are limited by operation during clear and moonless nights which reduces their duty cycle to $\simeq 15\%$. The main fluorescence detectors currently in operation are those of the Pierre Auger Observatory [125] and TA [126].

Arrays of detectors of radio emission employ cost-effective elements (antennas) to detect the radiation in the 10's of MHz to GHz produced by the charged particles in the EAS. Radio emission is mainly due to two mechanisms: the transverse current induced by the magnetic field of the Earth that travels at the speed of light along shower axis, and the Askaryan effect i.e the radiation emitted by the excess of negative charge (e^-) that develops in the shower through Compton scattering of shower photons on e^- in the medium, as well as Möller and Bhabha scatterings. The measurement of the radiated energy in radio waves at ground also provides an estimate of the primary energy [129]. In a radio-quiet environment, these detectors can operate with a close to 100% duty cycle, only limited by thunderstorms and heavy rain. The principal arrays of radio antennas currently operating include the Auger Engineering Radio Array (AERA) and the ongoing deploy-

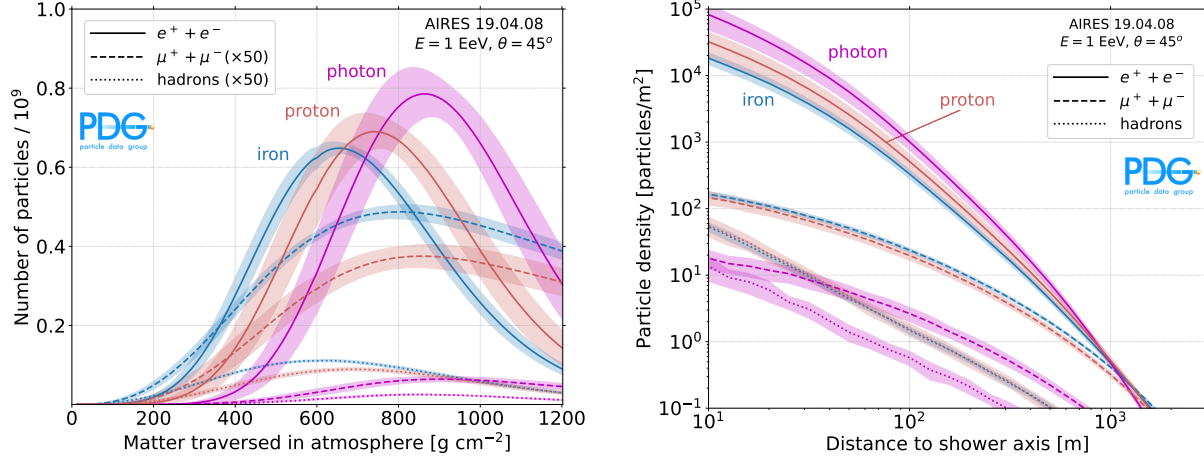


Figure 30.6: Left: Average number of $e^+ + e^-$, $\mu^+ + \mu^-$, and hadrons (lines), and their $\pm 1\sigma$ deviation (bands), as a function of matter (in g cm^{-2}) crossed in the atmosphere along the shower axis. The profiles are obtained with AIRES simulations [117] of proton, iron and photon-induced extensive air showers of energy $E = 1 \text{ EeV} = 10^{18} \text{ eV}$ and zenith angle $\theta = 45^\circ$ w.r.t. the vertical to ground (at depth 870 g cm^{-2}). Right: Lateral development (perpendicular to shower axis) at ground level of the same components as in the left panel as a function of distance to shower axis.

ment of the AugerPrime Radio Detector at the site of the Pierre Auger Observatory in Argentina [130], the Tunka-Rex [131] and Yakutsk [132] radio extensions in Russia, the LOw Frequency ARray (LOFAR) with its core detector in The Netherlands [133], and the Square Kilometer Array (SKA) in Australia [134].

Combining several types of detectors in the same array has proven very fruitful for increasing the accuracy in event reconstruction and energy calibration. Complementary measurements of the same event are expected to improve the determination of mass composition of the primary flux on an event-by-event basis. Projects under construction exploiting the simultaneous use of several detector kinds include, AugerPrime (water-Cherenkov stations, scintillators, underground muon detectors, fluorescence detectors and radio antennas) [135], TAx4 (scintillators and fluorescence detectors) [136], and the IceCube-Gen2 surface array (scintillators and radio antennas) [137]. Other arrays in the planning stages utilizing radio antennas are GRAND [138] and BEACON [139].

Experimental results. Cosmic rays in the PeV to EeV energy range have been regularly detected for decades, with energies up to $> 100 \text{ EeV}$. Despite the progress made in the field in the last 20 years, the nature and identity of their sources as well as the acceleration mechanisms that boost the particles to these extreme energies remain open questions. The understanding of CRs is mainly derived from analyzing their energy spectrum, several observables sensitive to their primary nature, and their arrival direction distribution. This is a challenging task mainly due to the small flux, with less than 1 particle per km^2 per year above 30 EeV (see Fig. 30.1), but also because the properties of CRs in this energy range can only be inferred indirectly from measurements of the EAS whose description relies on extrapolations of particle physics properties at energies several orders of magnitude above those achieved in terrestrial accelerators. Last but not least, since CRs are charged they are deflected by the galactic and intergalactic magnetic fields and their arrival directions at Earth point back only approximately to their actual sources.

Energy spectrum: The cosmic-ray spectrum observed at Earth (Fig. 30.1, with Fig. 30.7 highlighting the highest energies) can be characterized by a series of power-law functions proportional to $E^{-\gamma}$ with $\gamma \in (\simeq 2.5, \simeq 5.0)$ the spectral index that changes with energy. The production mechanism of CRs, mainly the unknown maximum CR energy achievable, CR composition and spectral index at the sources; the source type and distribution in the Universe; and the propagation through the Galaxy and the

intergalactic space, all leave distinct imprints on the spectrum giving rise to several observable features. The differential flux over 5 orders of magnitude in energy is shown in Fig. 30.7. The flux has been multiplied by E^3 to highlight the deviations from a pure power law with a single value of γ . Several features are apparent, namely: a steepening at $\simeq 5 \text{ PeV}$ known as the *knee* (Fig. 30.1); another steepening around 100 PeV dubbed the *second knee*; the *ankle*, a flattening of the spectrum at around 5 EeV ; a recently discovered feature corresponding to a further flattening starting at 10 EeV dubbed the *instep*; and the *suppression* of the spectrum starting around 50 EeV . These features are thought to be correlated with the observed changes on the average CR composition (see *Primary composition* below).

Cosmic-ray experiments have systematic differences in their energy scales and this manifests itself in differences in the measured spectrum, not only on the energy axis but also on the normalization when the flux is scaled with a power of the energy. The diagonal uncertainty bars in Fig. 30.7 serve to visualize the impact of these systematic differences on the spectrum. In the energy range above $\sim 100 \text{ PeV}$ the fluorescence technique is used to determine the primary cosmic-ray energy, with the atmosphere where the EAS develops functioning as a calorimeter. In the two state-of-the-art experiments for UHECRs, the Pierre Auger Observatory and the Telescope Array, a sub-sample of events is recorded simultaneously with the fluorescence (FD) and the surface detector (SD) arrays. With the SD, a shower size parameter is measured and calibrated against the energy measured with the FD. This approach provides a more direct method for determining cosmic-ray energy without relying on simulations. Differences in the energy scale between Auger and TA remain, however, primarily due to the use of different measurements of the amount fluorescence light emitted per unit of energy deposited, and to the different models for the invisible energy in EAS adopted. When these systematic uncertainties are accounted for, the spectra of the Pierre Auger Observatory and TA have been shown to agree within 5%, except in the energy region near the end of the instep feature and at the suppression.

Primary composition: The main observable sensitive to CR composition is the depth in the atmosphere along shower axis (X_{max}) at which the number of particles in the shower is maximum. Observatories capable of detecting Cherenkov and/or fluorescence light induced by the passage of the EAS through the atmosphere, can measure X_{max} on an event-by-event basis. With sufficient statistics, the distributions of X_{max} can be determined from which the average value ($\langle X_{\text{max}} \rangle$) and its fluctuations

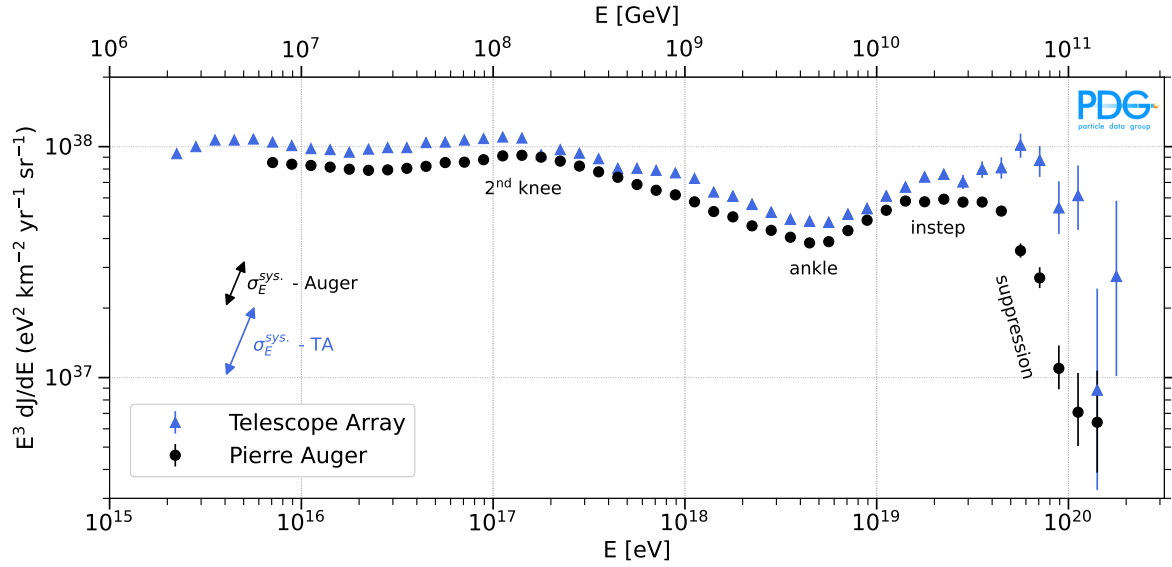


Figure 30.7: Measurements of the all-particle CR flux from Telescope Array (TA) [140] (blue triangles) and the Pierre Auger Observatory [29,141] (black circles). The direction and magnitude of the systematic uncertainty on the flux due to the energy scale (σ_E^{sys}) for TA and Auger is indicated by the corresponding arrows. For a comprehensive compilation of measurements see [142].

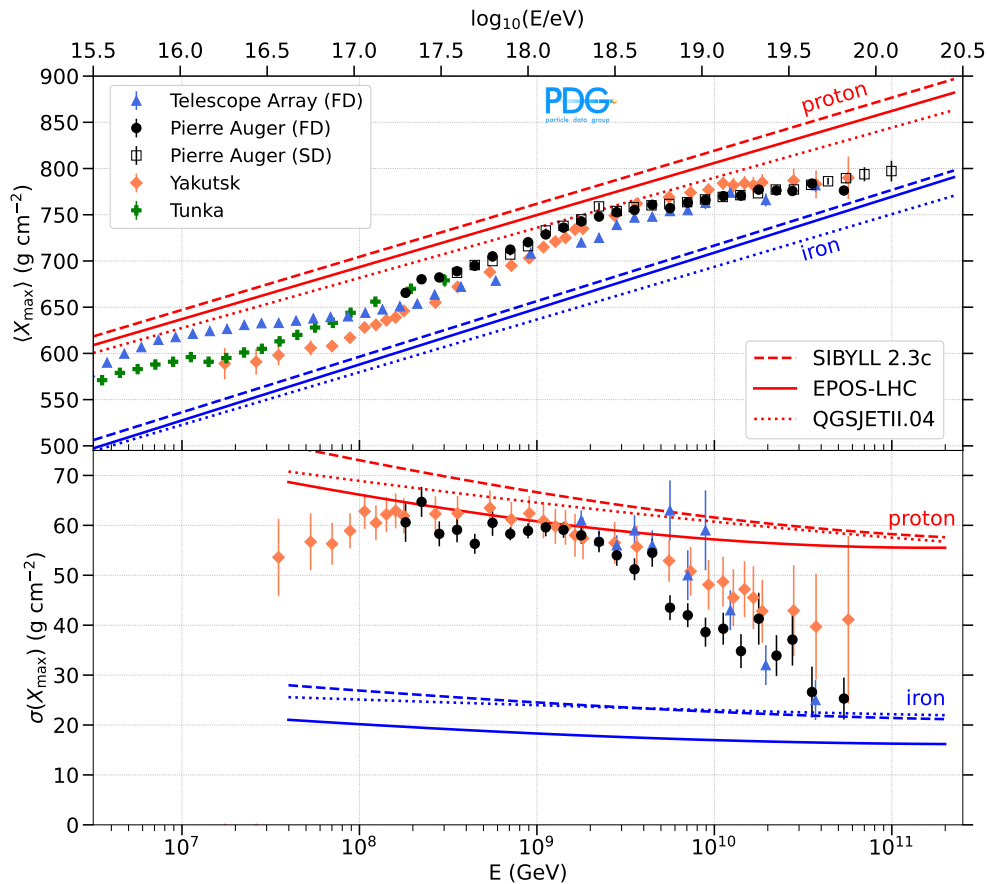


Figure 30.8: Measurements of $\langle X_{\text{max}} \rangle$ (top) and $\sigma(X_{\text{max}})$ (bottom) obtained by the Telescope Array [143,144], Pierre Auger Observatory [145,146], Yakutsk [127] and Tunka [147] UHECR detectors, compared to predictions for proton and iron nuclei using the hadronic models SIBYLL 2.3c [148], EPOS-LHC [122] and QGSJET-II.04 [121]. Detection techniques: fluorescence (FD), Cherenkov (Yakutsk, Tunka, and TA below $\simeq 1$ EeV), and using the surface detector array of the Auger Observatory (SD). For a compilation including experiments using the radio technique see [142] and also [149].

$\sigma(X_{\max})$ are obtained. A comparison with the $\langle X_{\max} \rangle$ and $\sigma(X_{\max})$ as predicted in simulations of EAS for different primaries and energies, as well as fits to the X_{\max} distributions lead to the determination of the mean fractions of primary protons, helium, carbon-nitrogen-oxygen and iron in the cosmic-ray flux at Earth. However, the interpretation of any mass-sensitive observable relies on modeling hadronic interactions up to the highest energies where there are no data from terrestrial accelerators, and this introduces a considerable uncertainty in the determination of the mass. Also, due to intrinsic shower-to-shower fluctuations (see Fig. 30.6), an event-by-event determination of the mass of the primaries is not currently possible. Despite these limitations, the measurements presented in Fig. 30.8 alongside the predictions of EAS simulations for proton and iron primaries, reveal a broad trend toward a lighter composition at the knee, within the energy range of a few PeV. This is followed by a gradual rise in the average logarithm of the primary cosmic-ray mass, eventually leading to a heavier composition at around 100 PeV, although notable differences between experiments exist. As the energy increases from 100 PeV up to ~ 2 EeV the measurements point consistently to a predominantly light composition with a large fraction of primary protons. Above that energy, the data from the largest statistical sample of events collected with the FD of the Pierre Auger Observatory indicate that the composition is mixed with the mean mass steadily growing. This observation is further supported by the shower-to-shower fluctuations of X_{\max} also shown in Fig. 30.8. Though the data of the Telescope Array seem in apparent tension with this picture, they have been shown to be compatible with the results of the Pierre Auger and Yakutsk Observatories [150] within the current levels of statistics and understanding of systematic uncertainties. In particular, TA data are compatible with the mixed composition inferred by the Pierre Auger Collaboration [142].

The small duty cycle of the fluorescence technique combined with the steeply falling spectrum above $\simeq 50$ EeV prevents a statistically significant determination of the composition in this energy range. Information on the distribution of nuclear masses can be obtained with the surface arrays alone that work with a high duty cycle. Exploiting the arrival times of particles in the SD stations, that are known to contain information on the penetration of the shower in the atmosphere, measurements of X_{\max} with the Pierre Auger Observatory were extended up to 100 EeV as shown in Fig. 30.8, after calibration of the mass-sensitivity of the SD with the measurements of X_{\max} with FD at lower energy. Other novel methods such as those based on deep learning analysis techniques are also being explored [151]. Additionally, the arrays of radio detectors are also sensitive to X_{\max} through the measurement of the shape of the radio emission footprint on the ground induced mainly by the electromagnetic component of the EAS. The radio technique demonstrates considerable potential in this respect and scalability, making it a cost-effective possibility for future UHECR detectors [149, 152].

Arrival directions: Anisotropies in the arrival direction of CRs are a key to discovering their sources. This is in principle feasible if the charges of the CRs and the galactic and extragalactic magnetic fields are well-enough determined. UHECRs are subject to the GZK effect, the energy loss of protons and heavier nuclei in interactions with the cosmic background. This imposes a horizon to possible sources of ~ 250 Mpc for protons and Fe nuclei, but shorter for nuclei in between these two, for instance ~ 5 Mpc for He and ~ 100 Mpc for Si at energies above $\simeq 50$ EeV [153]. Having only a limited range of source distances contributing to the signal makes it potentially feasible to identify sources or infer their properties statistically.

The Pierre Auger Collaboration has discovered a large-scale dipolar anisotropy at energies above 8 EeV with 6.9σ significance [154]. The amplitude of the dipolar anisotropy is $d = 0.073_{-0.008}^{+0.010}$ and the dipole points at a direction that is $\sim 115^\circ$ away from the Galactic Center, evidencing the extragalactic origin of UHECRs above this energy threshold. The dipole direction is not aligned with any obvious individual source, or with the expected CMB dipole, and is instead consistent with the local distribution of stellar mass (2MASS Redshift Survey), after accounting for the deflections expected in the Galactic magnetic

field. A compelling feature is the growth of the amplitude of the dipole with energy in agreement with the expectation that particles of higher rigidity are less deflected by magnetic fields. Combining the Pierre Auger Observatory data set in the southern hemisphere and the smaller statistical sample of events from Telescope Array in the north, a full-sky coverage is achieved. The combined results regarding the dipolar anisotropy are compatible with the Pierre Auger Observatory-only results with no evidence of the existence of a quadrupole component. At energies between ~ 10 PeV and ~ 1 EeV the amplitude of the dipole is smaller (Fig. 30.5, bottom panel), but there is a trend for its direction to change from pointing close to the Galactic Center (GC) at low energy towards a direction away from the GC (Fig. 30.5, top panel) in the EeV energy range. This suggests that there is a transition between the galactic and extragalactic origin of UHECRs around the ankle in the spectrum, at a few EeV.

Hints of correlation of arrival direction of UHECRs with potential sources have been confirmed in several analyses [142, 154, 155]. With data from the Pierre Auger Observatory a 4σ excess of events above 38 EeV was found in a region of angular radius $\simeq 27^\circ$ centered on the radio galaxy Centaurus A (CenA) [154]. The Telescope Array Collaboration has also reported an excess of events with energies above 57 EeV (the so-called *hot spot*) in the northern sky in the direction of R.A. = 144.0° , Dec. = 40.5° , with a 2.8σ significance and in an angular window of 25° [155]. Correlations with catalogs of potential UHECR sources have also been found. The sky viewed from the Pierre Auger Observatory is better modeled with a $\simeq 10\%$ flux excess in the directions of nearby starburst galaxies with a significance of 3.8σ and an energy threshold of 38 EeV with the correlation driven by the region of CenA where two prominent starburst galaxies are also located [154].

Despite the comprehensive observations made, it remains challenging to definitively ascertain the origin of UHECRs, primarily due to their deviation caused by the insufficiently constrained galactic and extragalactic magnetic fields. However, the constructed CR observatories designed to detect extensive air showers have the potential to also identify neutral particles of comparable energies. These include neutrinos, neutrons, and photons. Such searches can be made provided that methods are devised to separate photon and neutrino-induced EAS from those produced by the more abundant charged CRs, or in the case of neutrons if excesses in the sky are found. No photon or neutrino candidates have been clearly identified in the energy range around and above 100 PeV and upper limits to their flux have been obtained (see Fig. 30.13). UHECR observatories are thus also multi-messenger observatories of neutral particles [156]. These can be combined with gravitational wave detection and conventional radio, optical, X-ray and gamma-ray astronomy to greatly improve our knowledge about the most powerful objects in the Universe, as happened with the discovery of gravitational and electromagnetic radiation from the binary neutron star merger system in 2017 [157], with no neutrinos identified in temporal and spatial coincidence with it [158].

Astrophysical interpretation. A coherent picture of the nature and sources of CRs is emerging from the observations of the spectrum, composition and arrival directions, with many open questions. Cosmic rays below $\simeq 10$ PeV most likely have a galactic origin. The observed dipolar anisotropy in arrival directions imply that above 8 EeV they have their origin in extragalactic sources. One likely scenario is that the transition takes place at a few EeV, a hypothesis supported by the observed phase of the dipolar anisotropy changing around that energy from pointing to near the Galactic Center towards away from it (Fig. 30.5). Cosmic-ray rigidity Ze determines the maximum energy at which different particle species can be accelerated in the sources $E_{\max}(Z) = Z \times E_{\max}(Z = 1)$. As a consequence, protons would cutoff first in the spectrum, followed by helium, carbon ... up to iron. The observed increase with energy of the mass below the *second knee* could be interpreted as the signature of the end of the Galactic contribution dominating below the *second knee* [159]. As energy increases above a few times 100 PeV, the composition starts to become lighter. This could signify the

emergence of an extragalactic component because no correlation with the densely populated Galactic plane is observed. A combined fit of the Pierre Auger Observatory measurements of the UHECR energy spectrum and composition [160] is compatible with the existence of this extragalactic component along with a second one at higher energy responsible for the sharp change in spectral index at the *ankle* feature in the spectrum at $\simeq 5$ EeV. Observations above the ankle suggest that each accelerated nuclear species from protons to iron, dominates in a narrow energy band of the UHECR spectrum produced through a combination of the individual composition peaks. In particular, the *instep* reflects the interplay between the flux contributions of the helium and carbon-nitrogen-oxygen components injected at the source with their distinct cutoff energies, all shaped by nuclear photo-disintegration on background light during the propagation. This is consistent with the *suppression* above $\simeq 50$ EeV attributable to the E_{\max} reachable at the cosmic accelerators along with the GZK and photodisintegration propagation effects. This comprehensive and unified understanding is continually evolving as additional data accumulates. Multi-messenger observations of the expected secondary neutrino and gamma-ray fluxes, or the lack thereof, will provide valuable constraints.

Hadronic interactions and Extensive Air Showers. EAS detectors probe energy and phase-space regions of hadronic interactions currently not accessible with terrestrial accelerators, although only in a very indirect manner. The tail of the distribution of X_{\max} is sensitive to the attenuation length of primary p in the atmosphere, and the inelastic p -air cross-section can be inferred. In this manner, measurements of the p -air cross-section have been obtained at equivalent center-of-mass pp collision energy, $\sqrt{s_{pp}} > 40$ TeV, and are in agreement with model predictions within systematic uncertainties [142]. The muonic component in the air shower is generally used as a probe of the hadronic interactions during the shower development. Various measurements of muons with energies in the $\simeq 100$ MeV to $\simeq 10$ GeV range produced in EAS, have revealed that hadronic models of multiparticle production fall short in predicting the observed number of muons above cosmic-ray energies of $\simeq 100$ PeV [161]. On the other hand, the simulated shower-to-shower fluctuations in the muon number that are particularly sensitive to the first hadronic interactions in the shower, are in good agreement with the measurements [162]. This indicates that the shortage in the number of simulated muons builds-up in multiple soft-QCD processes throughout the EAS development rather than being driven by only the first few and highest-energy interactions of the EAS. This constrains possible explanations of the so-called *Muon Puzzle* based on new physics beyond the Standard Model.

30.3 Gamma Rays

There is a well-studied flux of cosmic gamma rays (defined here as having energy greater than 1 MeV) present at the top of the atmosphere. Known as the diffuse gamma-ray flux, it has been measured with multiple space and ground-based instruments across a broad range of energy. On top of the diffuse one, many discrete sources have been found with either a steady gamma-ray flux or variability of many types.

30.3.1 Observational Instruments: Space borne and Ground based

Space borne γ -ray detectors, including AGILE [163], DAMPE [164], CALET [165], mainly Fermi-LAT [166], cover the energy range above 10 MeV up to 100 GeV. With the wide Field-of-View (FoV), they effectively survey the whole sky for steady γ -ray sources, and monitor all types of transient phenomena such as flares of Active Galactic Nuclei (AGN) and γ -ray bursts (GRBs). Above 100 GeV, ground-based Imaging Air Cherenkov telescope (IACT) experiments H.E.S.S [167], MAGIC [168], VERITAS [169] and CTA-LST [170] are very effective observational instruments. Using the stereo measurement technique, the IACT arrays achieve the angular resolution of the arrival direction of γ -rays at the level of 3 arc minute which is necessary for the high precision measurements of discrete sources. The small Field-of-View (FoV) of the telescopes and low-operation duty cycle make the all-sky

surveys for new sources difficult. Only H.E.S.S scanned the region along the Galactic plane around the Galactic Center [171], as shown in Figure 30.9. Non-imaging Cherenkov light technique is also developed trying to cover wider FoV, e.g. in the TAIGA experiment [172]. The most suitable detectors for all-sky surveys are extensive air shower detector arrays at high altitudes, such as ARGO-YBJ [173], AS γ [174], HAWC [175] and LHAASO [176]. They are operated with very high duty cycle, typically $> 95\%$, have compatible sensitivity for discrete sources to IACT telescopes in much wider FoV in the same energy band, and higher sensitivity at higher energies above 10 TeV. In Table 30.1, the main features of the major facilities in γ -ray astronomy are listed.

30.3.2 Diffuse Gamma Rays

The majority of photons detected at high energies are characterized as diffuse emission that is not resolved as discrete sources. The observations of the diffuse emission are mainly carried out by wide FoV detectors, including space missions, OSO-3 [180], SAS-2 [181], COS-B [182], CGRO/EGRET [183], and Fermi-LAT [184] at energies below 1 TeV, and ground-based experiments Milagro [185], H.E.S.S [171], ARGO-YBJ [186], AS γ [187] and LHAASO [33] at energies up to 1 PeV. Evident in Figure 30.9, the dominant component comes from the plane of the Galaxy (i.e., $|b| \lesssim 10^\circ$, and is referred as the Galactic Diffuse Emission (GDE). Precise measurement of the GDE flux strongly depends on the subtraction of the contamination from discrete sources most of which are found spatially extended. With significantly improved sensitivity of source detection, Fermi-LAT and LHAASO largely reduce the contamination by removing the regions associated with known sources. In case of LHAASO, the flux in the Galactic plane with longitudes of $15^\circ < l < 235^\circ$ and latitudes of $|b| < 5^\circ$ is well measured [33].

Three components are expected in GDE, namely γ -rays from the decay of neutral pions produced via inelastic collisions between energetic cosmic ray nuclei and the interstellar medium (ISM); bremsstrahlung radiation of electrons and positrons in ISM; and inverse Compton scattering of electrons and positrons off the interstellar radiation field. Possible annihilation or decay of dark matter (DM) particles might also give rise to diffuse γ -rays particularly in the densest region of the Galaxy. Therefore, GDE serves not only as a very important tool to probe the production, propagation, and interaction of cosmic rays, but also as a route to search for DM in any excess over the expectation, which is based on assumptions of the cosmic-ray spatial distribution, composition, energy spectrum and on the ISM column density along the line-of-sight. The search for DM also depends on the fraction of the contribution by the unresolved dim discrete sources in the GDE. Unfortunately, all of the assumptions have their own large uncertainties at present.

Evidence of an isotropic component of diffuse γ -ray emission, presumably of extragalactically originated, was obtained with the measurement of its spectrum by CGRO/EGRET [188] and Fermi-LAT [189]. The Fermi-LAT spectrum covers the energy range from 0.1 GeV to 820 GeV and is well described by a power-law with an exponential cutoff. It is consistent with a scenario of a discrete source population, such as blazars with power-law spectral shape, dominating the emission and experiencing attenuation due to the extragalactic background light (EBL) [189]. Contributions from the cascade of very-high-energy gamma rays and UHECRs are not ruled out as a fraction of the extragalactic diffuse emission.

30.3.3 Discrete Gamma Ray Sources

As a neutral component of cosmic rays, γ -rays directly reach the earth from their sources, thus allowing us to identify the origin of the photons by association with known celestial objects or events. As shown in Figure 30.9, the source-associated contributions are revealed directly by the bright spots whose sizes are due to the point-spread-function (PSF) of the instruments and the intrinsic spatial extensions of the sources. It is also clearly shown that the sources are divided into two groups: *Galactic* and *extragalactic*.

Galactic Sources More than 6600 sources have been found emitting γ -rays in the Milky Way. Most of them have steady photon emissions over a wide energy range above 0.1 GeV up to

Table 30.1: Facilities for γ -ray detection and their specifications in reference a) [166], b) [177], c) [178], d) [179], e) [170], f) [174], g) [173], h) [175], i) [176]. † milli-CU = 10^{-3} Crab Unit.

Instrument	energy range	Effective area (m^2)	sensitivity (milli-CU †)	energy resolution (%)	PSF ($^\circ$)	FoV (sr)	duty cycle (%)
Fermi-LAT ^{a)}	20 MeV - 300 GeV	~ 0.95	10 - 30	8 - 18	0.15 - 3.5	~ 2.4	~ 60
H.E.S.S. ^{b)}	10 GeV - 50 TeV	$\sim 10^5$	~ 5	15	< 0.1	~ 0.03	~ 10
MAGIC ^{c)}	≥ 30 GeV	$\sim 10^5$	~ 7	16	≤ 0.07	0.02	~ 18
VERITAS ^{d)}	50 GeV - 50 TeV	$\sim 10^5$	~ 5	10 - 15	0.08 - 0.13	0.02	10-14
CTA-LST1 ^{e)}	20 GeV - 300 GeV	$\sim 10^4$	~ 10	10 - 30	0.05 - 0.1	0.02	~ 10
AS γ ^{f)}	10 TeV - 1 PeV	$\sim 7 \times 10^4$	~ 200	20 - 40	~ 0.8	~ 2.0	90
ARGO-YBJ ^{g)}	50 GeV - 10 TeV	$\sim 0.8 \times 10^4$	~ 300	> 13	~ 0.5	~ 2.0	86
HAWC ^{h)}	100 GeV - 100 TeV	$\sim 3 \times 10^4$	~ 50	20 - 50	~ 0.69	> 1.5	95
LHAASO-WCDA ⁱ⁾	100 GeV - 20 TeV	$\sim 0.8 \times 10^5$	~ 12	~ 33	0.2 - 0.84	~ 2.0	95
LHAASO-KM2A ⁱ⁾	10 TeV - 4 PeV	$\sim 10^6$	~ 12	15 - 40	0.2 - 0.6	~ 2.0	95

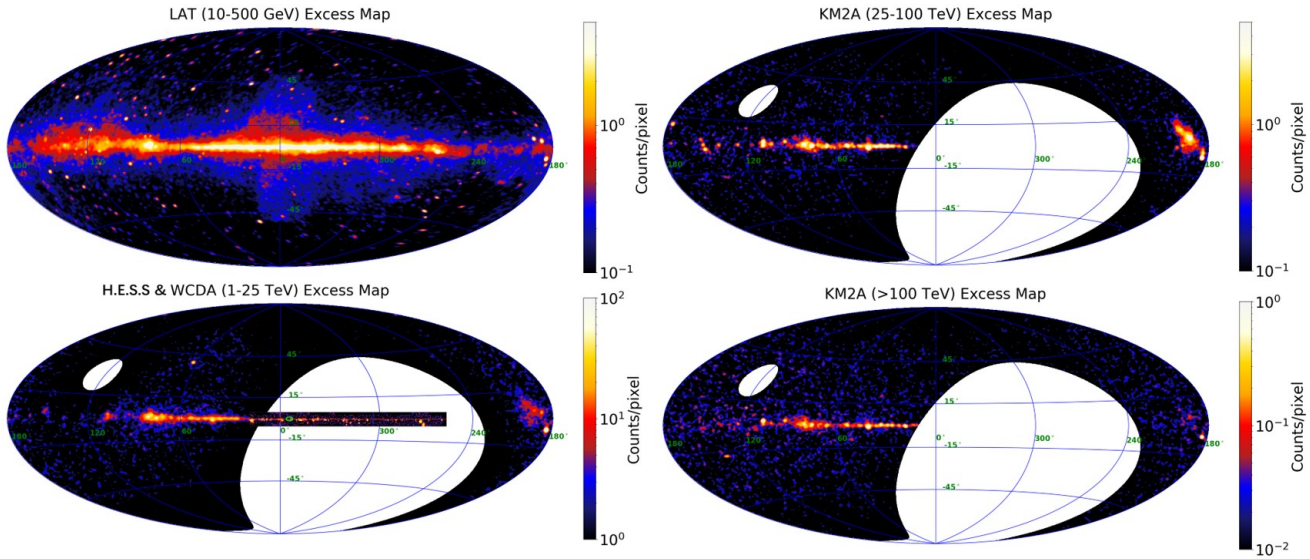


Figure 30.9: The GeV γ -ray sky maps surveyed by Fermi-LAT [184], LHAASO [38] and H.E.S.S. [171] from 1 GeV to 100 TeV and above.

2 PeV. 43 of them have emission of γ -rays above 0.1 PeV referred as *PeVatrons* since the parent particles that emitted the photons must be accelerated above 1 PeV on average in the source regions. Variability of the photon fluxes has also been observed from known objects such as pulsars and binary systems or transient phenomena.

A. Sources with steady emissions are the majority of Galactic γ -ray emitters which are well documented in reviews [190], [191], [192] and in γ -ray source catalogs [193] (for < 100 MeV), 4FLGT (for 0.1-300 GeV) by Fermi-LAT [194], TeV-Catalog available on-line (<http://tevcat.uchicago.edu>) and the newly released 1LHAASO (for 1-2000 TeV) by LHAASO [38]. All associations with known celestial objects, such as SNRs, PWNe, young massive-star clusters (YMC) are discussed in the corresponding catalog papers (e.g. individual catalogs collected in <http://tevcat.uchicago.edu>). Most of the sources, particularly for their high-energy emission above tens of TeV, remain unidentified. Among the identified ones, the Crab [195] and RX J1713-3946 [196] are the most extensively studied objects and constitute paradigmatic examples of PWNe and SNRs.

The Crab has a compact PWN powered by the rotation energy of the pulsar in its heart. Electrons and positrons in the wind are accelerated at the termination shocks and emit γ -rays through synchrotron radiation at energies lower than 0.1 GeV. Simultaneously, accelerated electrons and positrons boost soft background photons, such as those in the cosmic microwave background, to energies well above 1 GeV via inverse Compton scattering. Figure 30.10 shows the spectral energy density (SED) of the Crab

nebula with a fit using a simple one-zone leptonic model. It generally describes the radiation of the nebula over energies up to $E_\gamma \sim 1.1$ PeV, implying that electrons and positrons are confined in a small region of $\simeq 0.2$ pc by a magnetic field of intensity $B \simeq 110 \mu\text{G}$ and are accelerated to energies as high as $\simeq 2.3$ PeV. This requires a surprisingly high acceleration rate, $\eta = \bar{\epsilon}/B = 0.14(B/100\mu\text{G})(E_\gamma/1 \text{ PeV})^{1.54}$ PeV, at the level of 15%, where $\bar{\epsilon}$ is projection of the electric field averaged over the particle trajectory. This rate is 3 orders of magnitude higher than that in the normal shock environment such as in SNRs, revealing the existence of a so-called ‘extreme accelerator’ in the middle of the nebula [195]. The flux of photons above 0.8 PeV indicates some deviation from the pure leptonic scenario implying that a hadronic component might be responsible. It could be a hint of the super PeVatron which may contribute to the Galactic cosmic rays above the knee [195] (see Fig. 30.1).

RX J1713.7-3946 is one of the brightest objects in the TeV sky, and is the first SNR shell to be confirmed as a TeV gamma-ray source [196]. The detailed TeV morphology reveals a shell structure similar to the X-ray observations, indicating that particles are accelerated to very high energy therein. The TeV gamma-ray spectrum extends to nearly 100 TeV. It is not determined yet whether the gamma-rays are produced via Inverse Compton scattering of relativistic electrons (leptonic process), or via neutral pion decay with the pions produced in the inelastic scattering of CR protons with ambient gas (hadronic process) [200]. Nevertheless, the spectral information demonstrates the efficient acceleration of charged particles to energies beyond 100 TeV in this

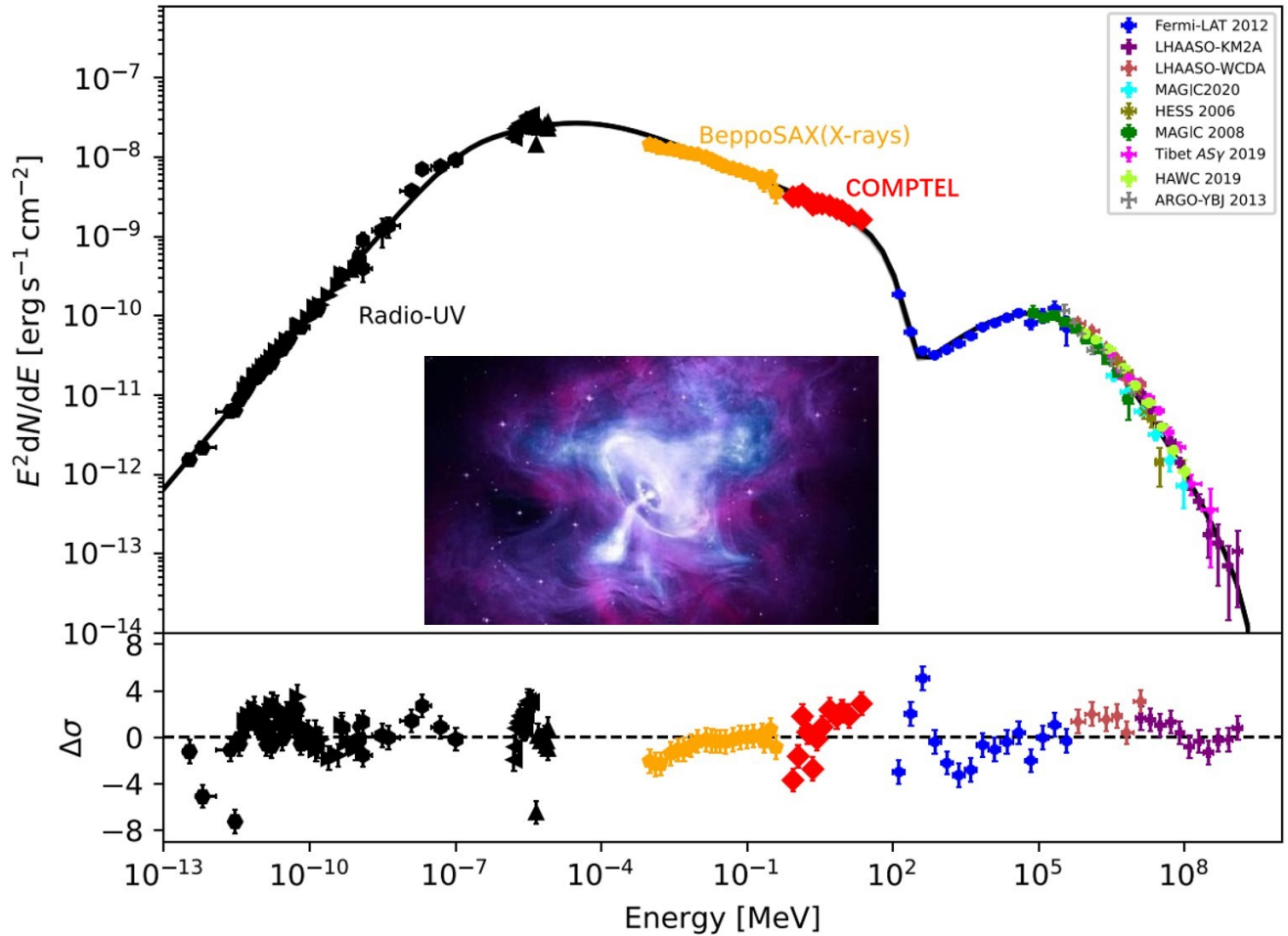


Figure 30.10: Spectral energy density (SED) of photons from the Crab from sub- μeV to 1.1 PeV. Above 1 TeV, data are collected from 7 experiments listed in legend in the upper panel. The lower panel shows the deviation between data and the model based on a widely accepted one-zone leptonic origin in the nebula. Only Fermi-LAT and LHAASO data are shown for simplicity. Inset is the X-ray image of the nebula by Chandra [197].

object. The latest H.E.S.S observations also found that the TeV gamma-ray emission region extends significantly beyond the X-ray emitting shell [201], which may be due to either the escape of particles from the shell or to particle acceleration in the shock precursor region.

B. Variable sources Crab flares, binaries and pulsars are observed in the Galactic γ -ray sky. Their activity varies on timescales from a fraction of one second (pulsars), to days (Crab Nebula, Novae), weeks, months or even years (γ -ray binaries). Various analysis pipelines are developed mainly by the LAT collaboration to search for and monitor γ -ray transients.

The Crab Nebula shows flare activities on a timescale of days [202]. The instability is observed only in GeV band by AGILE and Fermi/LAT. The flaring mechanism is still unclear with a couple of models being under debate.

Each γ -ray binary is composed of a compact object (pulsar or black hole) and a massive star. Their γ -ray emissions characterized by the orbital modulation, with time scales ranging from 3.9 days (LS 5039) to ~ 47 years (PSR J2032+4127). Microquasars are also binary systems that launch powerful jets from the compact objects by accreting matter from their companions. Three microquasars have been detected namely, Cyg X-1, Cyg X-3, and SS 433. They have shown γ -ray activities correlated with orbital motion [203], jet precession [204], X-ray state changes [205], and flares [206]. Eta Carinae is the only colliding wind binary firmly detected, showing orbital modulation in the γ -ray emission in a period of 5.54 years [207].

Pulsars show steady pulsation on their spin periods ranging from several milliseconds to seconds in GeV band [208], thereby

qualifying as γ -ray pulsars. Only the Crab and Vela pulsar are pulsating in TeV [209] [210]. PSR J2021+4026 is observed for the γ -ray flux variability on time scales of several years [211], making it the only variable γ -ray pulsar. Many millisecond pulsars themselves are γ -ray pulsars showing periodic variability in milliseconds [212]. γ -ray eclipses and orbital modulations have been detected in several binaries hosting millisecond pulsars, usually on the time scale of hours to days, arising from the intra binary shock between the pulsar wind and stellar wind [213] [214]. Millisecond pulsars could transit between spin-down-powered state and accretion-powered state. Variability in the γ -ray flux is observed accompanying these changes [215].

Novae outbursts have been detected in γ -rays, arising from the particle acceleration at shocks and last for months [216]. RS Ophiuchi is the first nova with its outburst detected in TeV up to 1 month [217].

Extragalactic Sources The majority of extragalactic γ -ray sources are active galactic nuclei (AGN). The fourth catalog of AGNs (4LAC) by LAT for 8 year observations contains 2863 objects located at high Galactic latitudes ($|b| > 10^\circ$) while 344 others were found at lower latitudes [218]. 98% of them are blazars. The blazar population consists of Flat Spectrum Radio Quasars (FSRQs), BL Lac-type objects and unknown types [218]. The Data Release 3 adds 587 more blazars and 4 radio galaxies to the catalog [219]. More than 70 blazars and a few radio galaxies are detected in the very high-energy (VHE) band, namely photon energy greater than 0.1 TeV, by imaging atmospheric Cherenkov

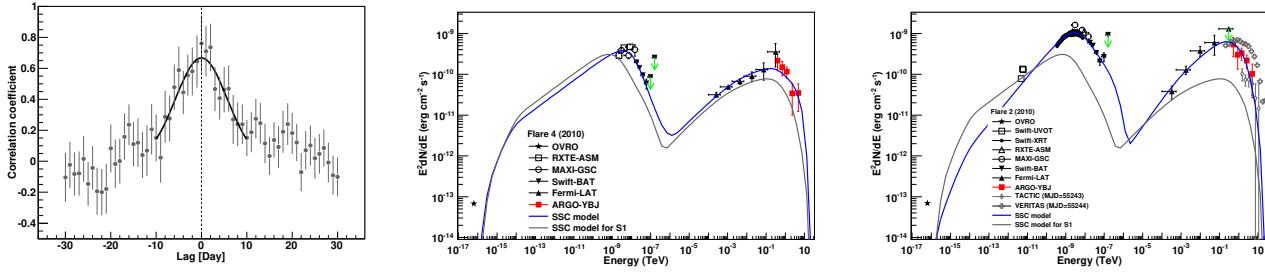


Figure 30.11: The multi wavelength analysis of Mrk 421 involving measurements over wide energy range from radio to TeV γ -ray during 4.5 years when ARGO-YBJ and LAT were operated [198]. The discrete correlation function between the light curves in X-ray band and TeV γ -ray band is calculated and clearly shows no time lag between emissions in the two bands [198] (left panel). The SED significantly changes from steady states (grey solid lines in middle and right panels) to flaring states depending on the strength of flares. Comparing a small flare in the middle panel and a larger one in right panel, the later has harder SED in VHE band [199].

telescopes (IACT) (<http://tevcat.uchicago.edu>).

Blazars belong to a class of AGN where the jets are oriented at a relatively small angle with respect to the line of sight. This specific viewing angle allows us to observe the emission from those jets with significant Doppler boosting. The photon flux in the jets may enhance significantly with respect to that in quiet states, a phenomenon referred to as blazar flares. They are simultaneously observed over a wide energy band from radio to VHE γ -rays with timescales ranging from a few minutes to year [220] [221]. The broad-band SED of blazars typically shows two humps of non-thermal radiation. The one in the lower energy range from radio to X-rays is generally attributed to synchrotron emission from relativistic electrons and positrons in the jet, while the origin of the hump at higher energies is still under debate. Possible emission mechanisms are the IC scattering of accelerated leptons off low energy photons, which are inside jets or from outside regions [222], or decay of neutral pions produced in collisions of accelerated protons against ambient matter [223], or some combination of the two processes.

The ground-based EAS experiments are suitable γ -ray detectors for monitoring the flares of AGNs with the advantages of large FoV and full duty cycle of operation. The ARGO-YBJ collaboration reported a long-term continuous monitoring of Mrk 421 and Mrk 501 [198, 199, 224], the two brightest blazars in the TeV sky. The γ -ray flux shows a good long-term correlation with that in the X-ray band. HAWC detected the persistent emission from those two AGNs [225]. Recently, the LHAASO collaboration reported eight sources detected at Galactic latitude $|b| > 12^\circ$, among which some are AGNs, including well-known emitters, such as the radio galaxy M87, VER J0521+211 and 1ES 1215+303 [38].

Using data for 4.5 years when ARGO-YBJ and Fermi-LAT simultaneously operated from 2008 to 2013, the ARGO-YBJ collaboration realized the long-term multi wavelength observation of Mrk 421 in all bands of radio, optical, X-ray, GeV, and TeV gamma-rays [198]. The well-known correlation [226] between the photon fluxes in X-ray band and TeV γ -ray band is investigated in a quantitative way, namely the discrete correlation function between the light curves in two energy bands being calculated. No time lag in the scale of days is found (see Figure 30.11). This is regarded as evidence of favoring the one-zone Self-Synchrotron Compton scattering scenario [199].

Flares happened in that time window are systematically analyzed and clear correlation between the strength of flares and features of the SEDs are observed as an example shown in Figure 30.11. Detailed investigation of SEDs implies that various particle acceleration mechanisms, such as relativistic diffusive shock acceleration, might be responsible for different flares. A similar analysis is carried out with data during outbursts of Mrk 501. The SEDs in the VHE band are observed to be harder during flares than that in the quiet period. The detection of energetic photons above 10 TeV and the hardness of the SED hint some exceeds over the expectation of one-zone SSC model [224].

Gamma-Ray Bursts (GRBs) GRBs are violent explosions observed in distant galaxies, characterized by a rapid flash of γ -rays lasting from a fraction of a second up to several hundreds of seconds. The emission from GRBs occurs in two stages, namely the prompt emission phase and the afterglow phase, as can be seen in Figure 30.12.

In the second catalog of Fermi/LAT-detected GRBs, covering the first 10 yr of operations, 169 GRBs are detected above 100 MeV [231]. The high-energy emission generally lasts much longer than the prompt keV-MeV emission. The widely discussed scenario for the extended GeV emission is synchrotron radiation by relativistic electrons that are accelerated in shocks resulting from the interaction of the jet with the surrounding medium [232, 233].

VHE emission has been detected from just a few GRBs by IACTs during the afterglow decay phase. MAGIC slewed to the direction of GRB 190114C only $\simeq 60$ seconds after the trigger and detected photons above 300 GeV from the burst for the first 20 minutes [234]. This VHE emission is explained by inverse Compton up-scattering of synchrotron photons by high energy electrons in the external shock [229], as shown in the right-upper panel of Figure 30.12. Two other events, GRB 180720B and GRB 190829A, were also detected during the afterglow decay phase by H.E.S.S. [230, 235], the unexpected SED is shown in the right-lower panel of Figure 30.12.

The brightest-of-all-time GRB 221009A serendipitously occurred within the FoV of LHAASO. More than 64,000 photons (above 0.2 TeV) were detected within the first 3000 seconds by LHAASO-WCDA [228]. The detection covers both the prompt emission phase and the early afterglow in the TeV band, revealing the onset of afterglow emission in the TeV band for the first time, as shown in the left panels of Figure 30.12. In addition, the unprecedented photon statistics of the TeV emission enabled identifying a jet break in the light curve, indicating an opening angle of GRB 221009A of $\sim 0.8^\circ$. This is consistent with the brightest core of a structured jet, explaining the unexpected high isotropic equivalent energy of this GRB. LHAASO-KM2A registered more than 140 photons with energies above 3 TeV from GRB 221009A (to be published). The intrinsic energy spectrum of gamma-rays is well fitted by a power law after correcting for EBL absorption, with the highest energy photon above 13 TeV traveling over a distance with red shift $z \sim 0.152$ (TBP).

Tests on Lorentz Invariance Violation (LIV) Tests on LIV are feasible and thus, limits can be set using the highest energetic photons collected from remote sources. Any tiny violation of the invariance leads the fundamental dissipation relation to be rewritten [236] as $E^2 = m^2c^4 + p^2c^2(1 + A_1pc/M_p c^2 + A_2(pc/M_p c^2)^2 + \dots)$, where E, p are the energy and momentum of a particle with the mass m , the M_p is the Plank scale and A_1, A_2 are theoretic parameters of the violation at the first and second order levels. This must lead instability of photons that may decay on their way to the Earth [237]. The first order violation effect due to the decay channel $\gamma \rightarrow e^+ + e^-$ has not been found at energies ~ 5 orders

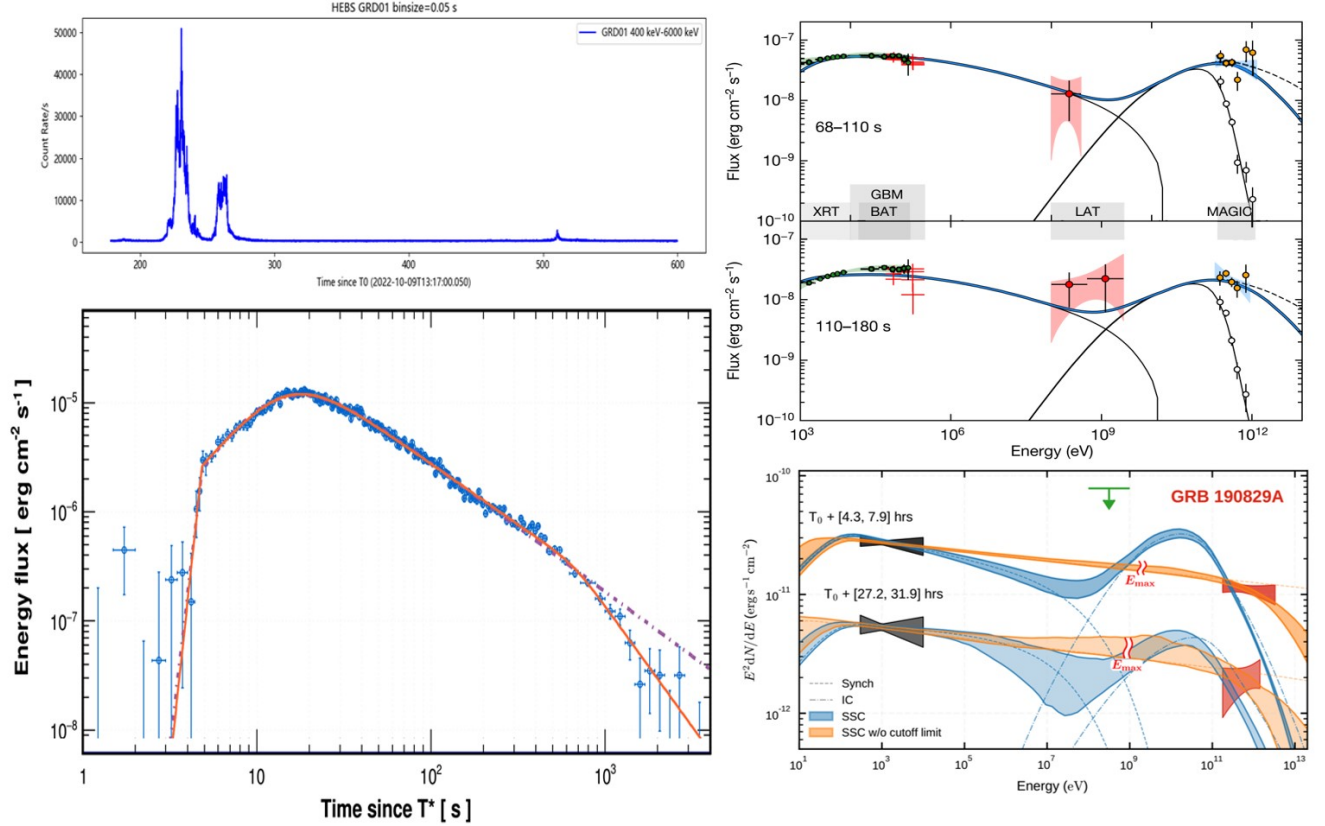


Figure 30.12: The typical multi-wavelength measurement of the light curves of the γ -ray burst GRB 221009A in the GeV band [227] (top left) and in the TeV band [228] (bottom left). The clear different structures of the brightness variation patterns indicate the different origins of the synchrotron radiation and inverse Compton scattering of leptons accelerated by the internal and external shock waves, respectively. The spectral energy distributions of the GRB 190114C and GRB 190829A, respectively measured by MAGIC [229] (top right) and H.E.S.S. [230] (bottom right). The Self-Synchrotron Compton scattering model of the afterglow is marginally supported in the observations covering a wide energy band from X-rays to TeV γ -rays.

of magnitudes higher than the Planck scale, regarded as the null evidence of the quantum gravitational effect. However, the limit due to second-order effect caused by decay channel $\gamma \rightarrow 3\gamma$ is still found still ~ 3 orders of magnitudes below the Planck scale, using the latest observations of photons up to 1.4 PeV from the Cygnus X direction [238].

30.4 Neutrinos

In contrast to charged particles, neutrinos are not deflected by electromagnetic fields and thus point back to their origin, making them appealing messengers for astronomical observations. In addition, neutrinos of cosmic origin, or produced in the atmosphere of the Earth, allow us to study particle physics in a kinematic regime not accessible to date to accelerator experiments. In the following, we will consider neutrinos with energies at the GeV energy scale and above.

30.4.1 Production of high-energy neutrinos

High-energy neutrinos can be produced in hadronic interactions in a variety of astrophysical objects (*astrophysical* or *cosmic* neutrinos), in scattering of extremely energetic protons (p) with the cosmic microwave background (*cosmogenic* neutrinos) and by cosmic-ray interactions in the Earth's atmosphere (*atmospheric* neutrinos). The main production chain is (A denoting atomic nuclei and X a hadronic system)

$$\begin{aligned}
 p(A) + p(A, \gamma) &\rightarrow \pi^\pm + X \\
 &\text{with subsequent decays} \\
 \pi &\rightarrow \mu \nu_\mu \text{ and } \mu \rightarrow e \nu_e \nu_\mu, \quad (30.1)
 \end{aligned}$$

resulting in a ratio $\nu_e : \nu_\mu : \nu_\tau = 1 : 2 : 0$ (not distinguishing here between ν and $\bar{\nu}$). If the source density is high, muons can lose most of their energy before decaying, yielding a ratio $0 : 1 : 0$

in the extreme case. If protons were kept in the source region by magnetic fields without interacting, and only neutrons could escape and then decay via $n \rightarrow p + e^- + \bar{\nu}_e$, the ratio would be $1 : 0 : 0$. Over cosmic distances, flavor mixing turns these ratios to 0.30:0.36:0.34 for the first source scenario (1:2:0), 0.17:0.45:0.37 for the second (0:1:0) and 0.55:0.17:0.28 for the third scenario (1:0:0) [239].

30.4.2 Measurement methods

Most experiments targeting high-energy cosmic neutrinos are based on the detection of Cherenkov light induced by charged secondary particles produced in neutrino interactions. This includes underground detectors like Super-Kamiokande with its fiducial volume of $22.5 \times 10^3 \text{ m}^3$ (see Sect. 36.3.1) and underwater/ice detectors like ANTARES, KM3NeT or IceCube, the latter with a volume of 10^9 m^3 (see Sect. 36.3.2). Neutrinos with energies exceeding some tens of PeV can be also detected via the coherent emission of Cherenkov radiation at radio wavelengths in ice or other radio-transparent media (e.g. ANITA or RNO-G, see Sect. 36.3.3). Neutrinos with EeV energies could be identified via extensive air showers starting too deep in the atmosphere to be due to particles with strong or electromagnetic interaction. Alternatively, they could be detected via slightly upward-directed air showers from the decay of tau leptons generated in interactions of Earth-skimming or mountain-traversing ν_τ [249]. These signatures could be observed by cosmic-ray experiments such as the Pierre Auger Observatory [250].

30.4.3 Diffuse fluxes

Atmospheric neutrinos The flux of atmospheric neutrinos as measured by different experiments is shown in Fig. 30.13. The production chain for *conventional* atmospheric neutrinos follows eq. (30.1), with an observed ratio $\nu_e : \nu_\mu = 1 : 2$ at energies of

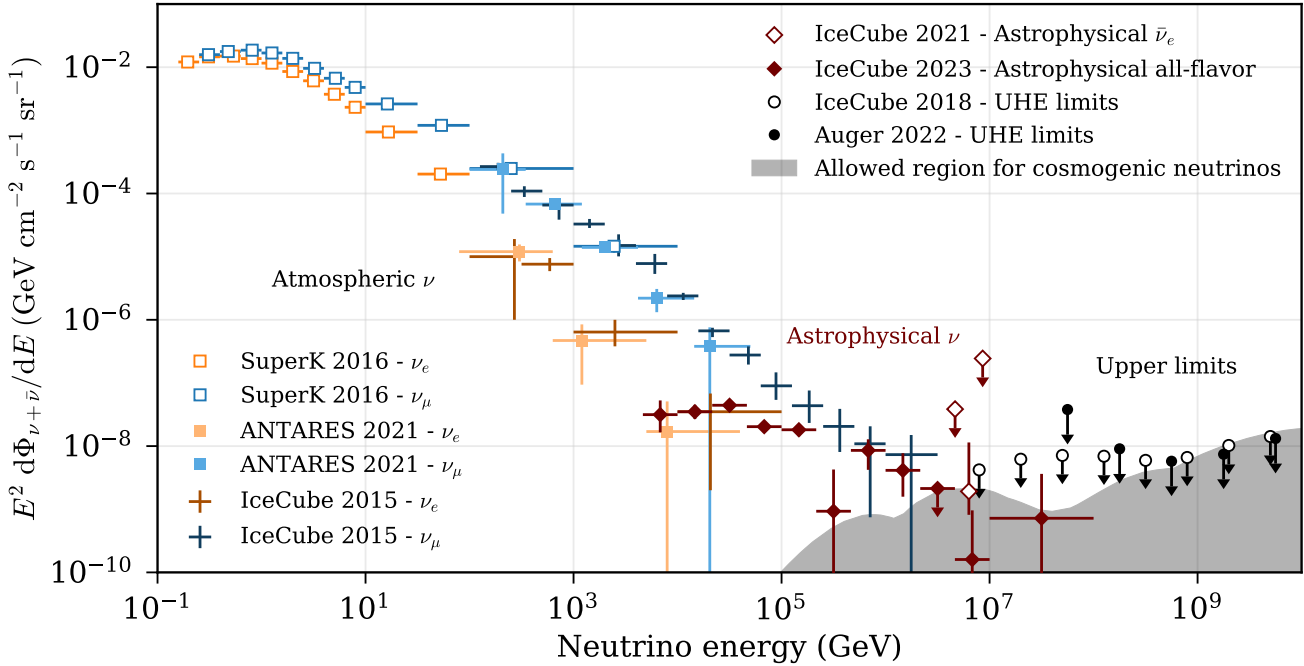


Figure 30.13: Measured energy spectra of atmospheric and cosmic diffuse neutrino fluxes. Experimental limits at highest energy are compared to model predictions for cosmogenic neutrinos [160]. All fluxes are normalized to one flavor ($\nu + \bar{\nu}$), assuming a ratio $\bar{\nu} : \nu = 1$ and, for cosmic neutrinos, a ratio $\nu_e : \nu_\mu : \nu_\tau = 1 : 1 : 1$ at Earth. Data sources: SuperK 2016 [240]; ANTARES 2021 [241]; IceCube 2015 ν_e [242]; IceCube 2015 ν_μ [243]; IceCube 2021 astrophysical $\bar{\nu}_e$ ($\nu + \bar{\nu}$ flux derived from a single candidate event for the Glashow resonance) [244]; IceCube 2023 astrophysical all flavor [35]. The limits at the highest energies are taken from [245] (IceCube) and [246] (Auger). They are shown in the energy bins used for the corresponding analyses and have been adjusted to bin widths of one decade. The region allowed for the expected cosmogenic neutrino fluxes is taken from [247] (see also Fig. 36.10).

a few GeV (where almost all muons decay in the atmosphere), and a ratio below 1 : 10 at TeV energies, where muons reach the ground before decaying. The flux of muon neutrinos with energies below 100 GeV from the lower hemisphere is reduced due to neutrino oscillations, reducing the $\nu_e : \nu_\mu$ ratio at the lowest energies. The flux of ν_e is obtained by subtracting the number of neutral-current muon neutrino interactions (as deduced from the measured charged-current muon neutrino reactions) from the number of contained events without a muon track and converting the resulting E_{ν_e} distribution into the ν_e flux using the differential cross sections for CC and NC ν_e -nucleon scattering. The conventional atmospheric neutrino flux dominates in the GeV to TeV region, following an $E_\nu^{-3.7}$ power law.

Prompt atmospheric neutrinos are produced by the decay of hadrons containing a charm or bottom quark, the production of which is strongly suppressed. Since they are produced early in the air shower and decay before losing energy, however, the energy spectrum of prompt neutrinos is expected to be harder ($E_\nu^{-2.7}$) and to dominate the atmospheric neutrino flux at its highest energies. The corresponding theoretical prediction has large uncertainties related to the cosmic-ray spectrum and mass composition, the model for heavy-flavor production, and the parton distribution functions [251]. At present, experimental measurements only provide upper limits for the prompt flux (see e.g. Fig. 30.14 where the prompt component was fitted to zero).

Diffuse extragalactic neutrino flux In 2013, a diffuse and isotropic flux of neutrinos of astrophysical origin was discovered with the IceCube Neutrino Observatory. The flux was identified with the so-called HESE (high-energy starting events) selection as an excess of neutrino events at high energies over atmospheric neutrinos and a background of misreconstructed atmospheric muons (see Fig. 30.14, for the 7.5-year HESE sample [252]). Similar high-energy excesses were also identified for tracks entering the detector from outside [253], and for fully contained cascade events. Evidence for this flux has meanwhile also been

reported by ANTARES [254] and Baikal-GVD [255], albeit with much lower significance. The measured fluxes are consistent with a parameterization as power-law functions proportional to $E_\nu^{-\gamma}$, with the normalization factor and the spectral index γ as parameters. The resulting γ values vary from 2.2 to 2.5 for different event classes covering different energy ranges.

Different production mechanisms result in different neutrino flavor compositions at sources and, after neutrino oscillations over astrophysical distances, at the Earth. An IceCube study of the event topologies [239] slightly favors $\nu_e : \nu_\mu : \nu_\tau = 1 : 2 : 0$ at the source (pion decay according to eq. (30.1) versus 0 : 1 : 0 (damped muons) and disfavors a 1 : 0 : 0 scenario (neutron decay).

A single event with energy 6.05 ± 0.72 PeV has been detected in IceCube [244]. It is compatible with having been generated by the resonant process $\bar{\nu}_e + e^- \rightarrow W^- \rightarrow \text{hadrons}$ at $E_\nu = 6.3$ PeV (Glashow resonance) [256]. A statistically significant observation of the Glashow resonance would reveal the presence of electron antineutrinos in the astrophysical flux and could provide information about their production process: the expected ratio $\bar{\nu}_e : \nu_e$ depends on the mass composition of cosmic-rays and also on the photon density and the magnetic field strength of the source [257].

Cosmogenic neutrinos Cosmogenic neutrinos stem from the decay of charged pions generated in interactions of ultra-high-energy cosmic rays with cosmic microwave (a) and infrared (b) background radiation ($p + \gamma \rightarrow n + \pi^+$) [258] and from the decays of neutrons produced in photodisintegration processes [259, 260] (c). The neutrino flux at EeV energies is expected to be dominated by (a) and (c).

Measurement methods and experimental data are described in Sect. 36.3.3. and Fig. 36.10. The expected flux can be estimated from the measured spectrum and composition of charged cosmic rays, using the CMB density and the well measured properties of proton and nuclear interactions with photons at a center-of-mass energy in the GeV range. The current uncertainty of these pre-

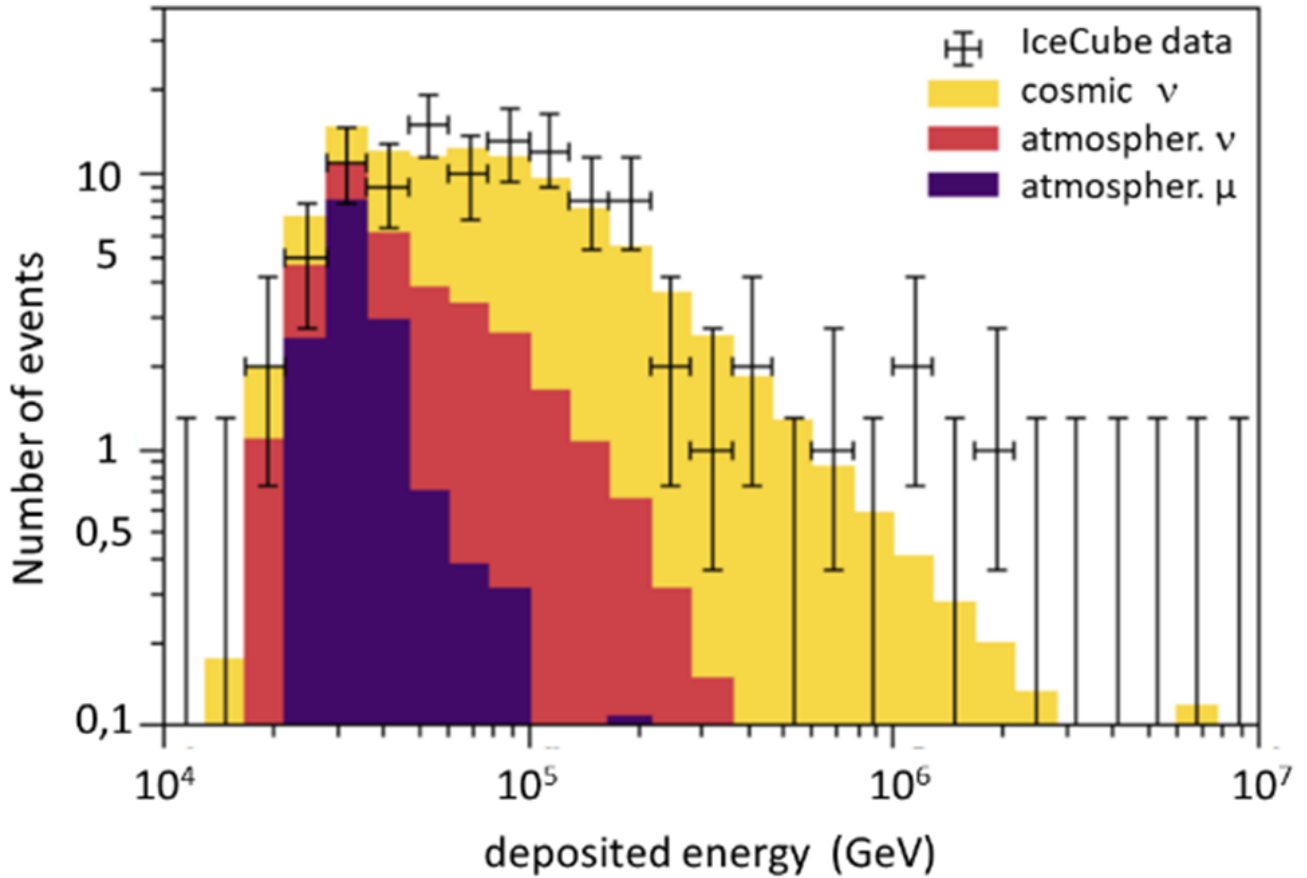


Figure 30.14: Measured (data points) and expected (histograms) distributions of the deposited energy measured in the IceCube detector for events passing the HESE selection, which strongly suppresses down-going atmospheric neutrinos by vetoing accompanying muons. The cosmic neutrino flux has been assumed to follow an unbroken power law in E_ν . Its normalization and spectral index, as well as the normalizations of the conventional and prompt atmospheric neutrino and the atmospheric muon contributions were fitted to the data, where only the region above 60 TeV was used to constrain the cosmic neutrino flux.

dictions exceeds one order of magnitude. Figure 30.13 reproduces the presently tightest limits and compares them to the region for which cosmogenic neutrino fluxes would be consistent with those limits (as of 2019) and cosmic-ray analyses [247].

Neutrinos from the Galactic Plane The Milky Way is an emitter across the electromagnetic spectrum ranging from radio to gamma-rays. A large part of the observed gamma-ray flux is believed to consist of photons from the decays of π^0 s produced by cosmic rays colliding with the interstellar medium. The TeV diffuse neutrino flux from the corresponding π^\pm decays along the Galactic plane has been estimated with different models, ranging from a simple extrapolation of Fermi-LAT gamma-ray data to higher energies, to more sophisticated approaches (see e.g. [261]).

First hints for a TeV neutrino emission from the Galactic Ridge have been reported by the ANTARES collaboration [262]. IceCube has measured the flux of galactic neutrinos with a significance of 4.5σ against the only-background-hypothesis [248]. Figure 30.15 shows a map of the Galactic plane with the point-by-point pre-trial significance of the IceCube neutrino observations. While the overall signal is consistent with the modeled diffuse emission from the Galactic plane, a significant part could also arise from a population of unresolved point sources. All individual "warm spots", however, are statistically consistent with background fluctuations.

30.4.4 Neutrinos from astrophysical point sources

Most point source candidates include Active Galactic Nuclei (AGN). In particular, blazars – AGN that have jets pointing

towards the observer – are thought to be likely sources. In 2017, a spatial and temporal correlation was found between a flare of the electromagnetic emission from blazar TXS 0506+056 and the high-energy neutrino event IC170922A, detected by IceCube. An alert was sent to other observatories and a follow-up campaign in multiple wavelengths was started. At the moment of neutrino detection, the blazar was flaring in gamma rays, with an accidental coincidence excluded at the 3σ level [263]. Subsequent analyses of archival data revealed an excess in neutrino events with a significance of 3.5σ with respect to the expected atmospheric background, coincident with the position of TXS 0506+056, albeit not correlated with an electromagnetic flare [264].

In another analysis, the positions of 110 gamma-ray sources selected a priori were analyzed individually for a possible surplus of neutrinos over atmospheric and cosmic background expectations. An excess of 79^{+22}_{-20} neutrinos was found in the direction of the nearby AGN NGC 1068 (not a blazar, but a Seyfert-2 galaxy), at a significance of 4.2σ (see figure 30.16). The excess is spatially consistent with the direction of the strongest clustering of neutrinos in the Northern sky. The inferred flux exceeds the potential TeV gamma-ray flux by at least an order of magnitude [265], suggesting that the sight to the gamma-ray generation region is obscured, as expected for Seyfert-2 galaxies.

Other potential sources include starburst galaxies, galaxy clusters, supernovae remnants (steady emission) as well as Gamma Ray Bursts (GRBs) and Tidal Disruption Events, TDEs (transient emission). Indeed, using data from IceCube and the Zwicky Transient Facility ZTF, hints for a correlation of high-energy muon neutrinos with TDEs have been reported [266].

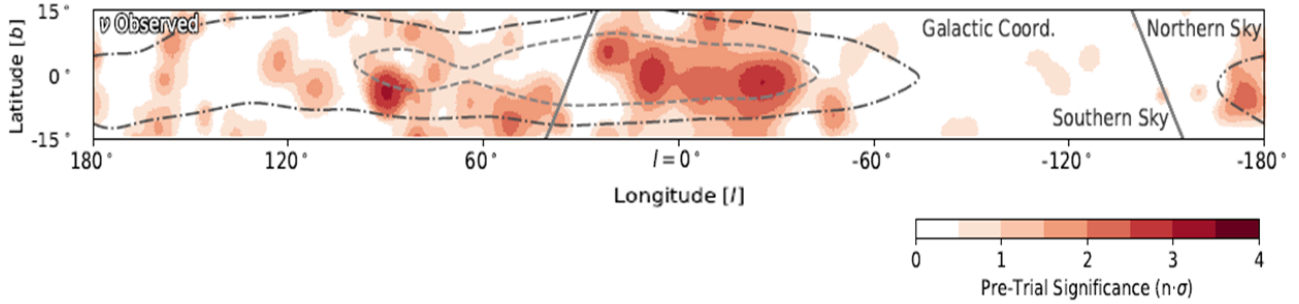


Figure 30.15: The Milky Way plane in neutrinos (Galactic coordinates, with the origin being at the Galactic Center). Shown is the pre-trial significance of the IceCube observations using a cascade neutrino event sample, calculated from an all-sky scan for point-like sources [248]. Contours indicate the regions that contain 20% and 50% of the predicted diffuse neutrino emission according to an extrapolation of Fermi-LAT results. Grey lines indicate the Northern-Southern sky horizon line.

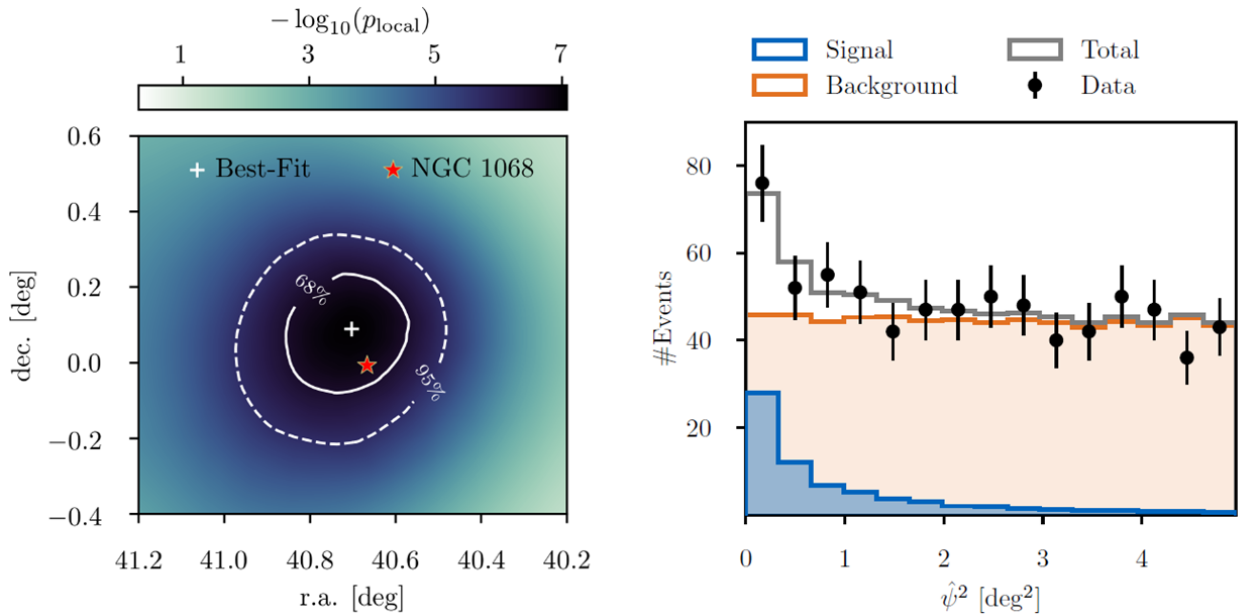


Figure 30.16: Left: The sky region around the most significant spot in the Northern Hemisphere and NGC 1068. Shown is a fine scan of the region around the hottest spot, marked by a white cross. The red circle shows the position of NGC 1068. The solid and dashed contours show the 68% and 95% confidence regions of the hot spot localization. Right: Distribution of the squared angular distance between NGC 1068 and the reconstructed event direction. Figures taken from [265].

30.4.5 Results on particle physics

Investigating the attenuation of high-energy neutrinos as a function of energy and their path length through the Earth, the first measurement of the neutrino-nucleon cross section at energies between a few tens of TeV and ≈ 1 PeV (corresponding to center-of-mass energies between a few 100 GeV and about 1.4 TeV) has been achieved [267], giving access in deep-inelastic scattering in a kinematic region currently not accessible to accelerator-based experiments.

The study of atmospheric high-energy neutrinos allows for the investigation of oscillation physics (see Sect. 14) at higher energies and over longer baselines than Earth-bound experiments. Constraints ($\sin^2 \theta_{23} = 0.51 \pm 0.050$ and $\Delta m_{32}^2 = (2.41 \pm 0.07) \times 10^{-3} \text{ eV}^2$) have been obtained with IceCube and are compatible with corresponding results from accelerator experiments [268]. Both IceCube and KM3NeT/ORCA are also sensitive to ν_τ appearance [269]. The KM3NeT/ORCA detector (under construction, see Sect. 36.3.2) is furthermore expected to provide sensitivity to the neutrino mass hierarchy.

Also, Beyond-Standard-Model (BSM) physics is being tested. For instance, constraints by IceCube on 2/4 mixing (the fourth

state being a sterile neutrino) are comparable to constraints from accelerator experiments [270]. Neutrinos may have BSM interactions, and if the coupling strengths are weak or if heavy mediators are involved, these interactions may only manifest themselves in the HE and UHE neutrino sector. Corresponding constraints from IceCube have been published in [271]. Also, possible oscillation-like effects induced by quantum gravity are investigated [272].

Acknowledgement Many thanks to team members, Prof. Q. Yuan, R.Z. Yang, J. Li, X.Y. Wang, S.Z. Chen and Dr. S.Q. Xi, L. Nie, R.F. Xu, who made substantial contributions to the γ -ray part of this section. We are grateful to C. Haack and L. Schumacher for their invaluable help in producing Fig. 30.13.

References

- [1] Y. S. Yoon *et al.*, *Astrophys. J.* **728**, 122 (2011), [arXiv:1102.2575].
- [2] O. Adriani *et al.* (PAMELA), *Science* **332**, 69 (2011), [arXiv:1103.4055].
- [3] O. Adriani *et al.*, *Adv. Space Res.* **51**, 219 (2013).
- [4] Y. S. Yoon *et al.*, *Astrophys. J.* **839**, 1, 5 (2017), [arXiv:1704.02512].

- [5] N. Gorbunov *et al.*, Adv. Space Res. **64**, 12, 2546 (2019), [arXiv:1809.05333].
- [6] M. G. Aartsen *et al.* (IceCube), Phys. Rev. D **100**, 8, 082002 (2019), [arXiv:1906.04317].
- [7] Q. An *et al.* (DAMPE), Sci. Adv. **5**, 9, eaax3793 (2019), [arXiv:1909.12860].
- [8] M. Aguilar *et al.* (AMS), Phys. Rept. **894**, 1 (2021).
- [9] G. H. Choi *et al.*, Astrophys. J. **940**, 2, 107 (2022).
- [10] O. Adriani *et al.* (CALET), Phys. Rev. Lett. **129**, 10, 101102 (2022), [arXiv:2209.01302].
- [11] F. Alemanno *et al.*, Phys. Rev. Lett. **126**, 201102 (2021), [arXiv:2105.09073].
- [12] H. S. Ahn *et al.*, Astrophys. J. **707**, 593 (2009), [arXiv:0911.1889].
- [13] O. Adriani *et al.*, Phys. Rev. Lett. **125**, 251102 (2020), [arXiv:2012.10319].
- [14] F. Aharonian *et al.* (H.E.S.S.), Phys. Rev. D **75**, 042004 (2007), [arXiv:astro-ph/0701766].
- [15] M. Aguilar *et al.* (AMS), Phys. Rev. Lett. **126**, 4, 041104 (2021).
- [16] O. Adriani *et al.* (CALET), Phys. Rev. Lett. **126**, 24, 241101 (2021), [arXiv:2106.08036].
- [17] G. Ambrosi *et al.* (DAMPE), Nature **552**, 63 (2017), [arXiv:1711.10981].
- [18] S. Abdollahi *et al.* (Fermi-LAT), Phys. Rev. D **95**, 8, 082007 (2017), [arXiv:1704.07195].
- [19] O. Adriani *et al.*, Phys. Rev. Lett. **120**, 26, 261102 (2018), [arXiv:1806.09728].
- [20] T. Antoni *et al.* (KASCADE), Astropart. Phys. **24**, 1 (2005), [arXiv:astro-ph/0505413].
- [21] M. G. Aartsen *et al.* (IceCube), Phys. Rev. D **88**, 4, 042004 (2013), [arXiv:1307.3795].
- [22] V. V. Prosin *et al.*, Nucl. Instrum. Meth. A **756**, 94 (2014).
- [23] S. Schoo *et al.* (KASCADE-Grande), PoS **ICRC2015**, 263 (2016).
- [24] K. Rawlins and T. Feusels (IceCube), PoS **ICRC2015**, 334 (2016).
- [25] D. Ivanov, PoS **ICRC2015**, 349 (2016).
- [26] A. Aab *et al.* (Pierre Auger), in “34th Int. Cosmic Ray Conf.”, (2015), [arXiv:1509.03732].
- [27] R. Alfaro *et al.* (HAWC), Phys. Rev. D **96**, 12, 122001 (2017), [arXiv:1710.00890].
- [28] M. G. Aartsen *et al.* (IceCube), Phys. Rev. D **102**, 122001 (2020), [arXiv:2006.05215].
- [29] P. Abreu *et al.* (Pierre Auger), Eur. Phys. J. C **81**, 11, 966 (2021), [arXiv:2109.13400].
- [30] J. A. Morales-Soto *et al.* (HAWC), PoS **ICRC2021**, 330 (2021), [arXiv:2108.04748].
- [31] D. Maurin *et al.* (2023), [arXiv:2306.08901].
- [32] M. Ackermann *et al.* (Fermi-LAT), Astrophys. J. **750**, 3 (2012), [arXiv:1202.4039].
- [33] Z. Cao *et al.* (LHAASO) (2023), [arXiv:2305.05372].
- [34] M. Ackermann *et al.* (Fermi-LAT), Astrophys. J. **799**, 86 (2015), [arXiv:1410.3696].
- [35] R. Abbasi *et al.* (IceCube), PoS **ICRC2023**, 1064 (2023).
- [36] S. Abdollahi *et al.* (Fermi-LAT), Astrophys. J. Supp. **260**, 2, 53 (2022), [arXiv:2201.11184].
- [37] S. P. Wakely and D. Horan, in “30th Int. Cosmic Ray Conf.”, volume 3, 1341–1344 (2007).
- [38] Z. Cao *et al.* (LHAASO) (2023), [arXiv:2305.17030].
- [39] T. K. Gaisser, R. Engel and E. Resconi, *Cosmic Rays and Particle Physics: 2nd Edition*, Cambridge University Press (2016), ISBN 978-0-521-01646-9.
- [40] P. Sreekumar *et al.*, Phys. Rev. Lett. **70**, 127 (1993).
- [41] W. Baade and F. Zwicky, Proceedings of the National Academy of Science **20**, 259 (1934).
- [42] D. Ter Haar, Reviews of Modern Physics **22**, 119 (1950).
- [43] L. O. Drury, Rept. Prog. Phys. **46**, 973 (1983).
- [44] C. J. Cesarsky and T. Montmerle, Space Sci. Rev. **36**, 2, 173 (1983).
- [45] A. M. Bykov, Astron. Astrophys. Rev. **22**, 1, 77 (2014), [arXiv:1511.04608].
- [46] V. Bosch-Ramon, F. A. Aharonian and J. M. Paredes, Astron. Astrophys. **432**, 609 (2005), [arXiv:astro-ph/0411508].
- [47] V. S. Ptuskin and Y. M. Khazan, Soviet Astronomy **25**, 547 (1981).
- [48] F. M. Rieger, Universe **8**, 11, 607 (2022), [arXiv:2211.12202].
- [49] M. Milgrom and V. Usov, Astrophys. J. Lett. **449**, L37 (1995), [arXiv:astro-ph/9505009].
- [50] L. A. Anchordoqui, G. E. Romero and J. A. Combi, Phys. Rev. D **60**, 103001 (1999), [arXiv:astro-ph/9903145].
- [51] G. E. Romero, A. L. Müller and M. Roth, Astron. Astrophys. **616**, A57 (2018), [arXiv:1801.06483].
- [52] P. Blasi, R. I. Epstein and A. V. Olinto, Astrophys. J. **533**, L123 (2000), [arXiv:astro-ph/9912240].
- [53] J. Arons, Astrophys. J. **589**, 871 (2003), [arXiv:astro-ph/0208444].
- [54] V. Petrosian, Space Sci. Rev. **173**, 535 (2012), [arXiv:1205.2136].
- [55] E. G. Zweibel and M. Yamada, ARA&A **47**, 1, 291 (2009).
- [56] A. M. Hillas, Ann. Rev. Astron. Astrophys. **22**, 425 (1984).
- [57] J. R. Jokipii, Astrophys. J. **146**, 480 (1966).
- [58] K. Lodders, Astrophys. J. **591**, 1220 (2003).
- [59] G. B. Rybicki, *Radiative Processes in Astrophysics*, Wiley-VCH (2004), ISBN 978-0-471-82759-7, 978-3-527-61817-0.
- [60] K. Mannheim and R. Schlickeiser, Astron. Astrophys. **286**, 983 (1994), [arXiv:astro-ph/9402042].
- [61] Y. Genolini *et al.*, Phys. Rev. C **98**, 3, 034611 (2018), [arXiv:1803.04686].
- [62] V. L. Ginzburg and S. I. Syrovatskii, *The Origin of Cosmic Rays*, Pergamon Press (1964).
- [63] E. N. Parker, Planet. Space Sci. **13**, 1, 9 (1965).
- [64] A. E. Vladimirov *et al.*, Comput. Phys. Commun. **182**, 1156 (2011), [arXiv:1008.3642].
- [65] C. Evoli *et al.*, JCAP **10**, 018 (2008), [Erratum: JCAP 04, E01 (2016)], [arXiv:0807.4730].
- [66] R. Kissmann, Astropart. Phys. **55**, 37 (2014), [arXiv:1401.4035].
- [67] D. Maurin, Comput. Phys. Commun. **247**, 106942 (2020), [arXiv:1807.02968].
- [68] K. Greisen, Phys. Rev. Lett. **16**, 748 (1966).
- [69] G. T. Zatsepin and V. A. Kuzmin, JETP Lett. **4**, 78 (1966).
- [70] R. Kulsrud and W. P. Pearce, Astrophys. J. **156**, 445 (1969).
- [71] A. R. Bell and S. G. Lucek, Mon. Not. Roy. Astron. Soc. **321**, 3, 433 (2001).
- [72] C. Evoli *et al.*, Phys. Rev. Lett. **121**, 2, 021102 (2018), [arXiv:1806.04153].
- [73] J. Silk and M. Srednicki, Phys. Rev. Lett. **53**, 624 (1984).
- [74] F. Donato, N. Fornengo and P. Salati, Phys. Rev. D **62**, 043003 (2000), [hep-ph/9904481].
- [75] S. Murgia, Ann. Rev. Nucl. Part. Sci. **70**, 455 (2020).
- [76] G. Steigman, Ann. Rev. Astron. Astrophys. **14**, 339 (1976).
- [77] J. W. Mitchell and T. Hams, *Astrophysics and Space Instrumentation*, 559–592 (2012).

- [78] D. V. Reames, Lect. Notes Phys. **978**, pp. (2021), [arXiv:2010.08517].
- [79] R. Engel, *Indirect Detection of Cosmic Rays*, 593–632 (2012).
- [80] A. D. Panov *et al.*, Bull. Russ. Acad. Sci. Phys. **71**, 494 (2007), [arXiv:astro-ph/0612377].
- [81] H. S. Ahn *et al.*, Astrophys. J. Lett. **714**, L89 (2010), [arXiv:1004.1123].
- [82] O. Adriani *et al.* (CALET), Phys. Rev. Lett. **130**, 17, 171002 (2023), [arXiv:2304.14699].
- [83] F. Alemanno *et al.* (DAMPE) (2023), [arXiv:2304.00137].
- [84] O. Adriani *et al.*, Astrophys. J. **791**, 2, 93 (2014), [arXiv:1407.1657].
- [85] B. Schroer, C. Evoli and P. Blasi, Phys. Rev. D **103**, 123010 (2021), [arXiv:2102.12576].
- [86] K. A. Lave *et al.*, Astrophys. J. **770**, 2, 117 (2013).
- [87] J. J. Engelmann *et al.*, Astron. Astrophys. **233**, 96 (1990).
- [88] M. Aguilar *et al.* (AMS), Phys. Rev. Lett. **126**, 8, 081102 (2021).
- [89] M. Aguilar *et al.* (AMS), Phys. Rev. Lett. **127**, 2, 02101 (2021), [Erratum: Phys.Rev.Lett. 127, 159901 (2021)].
- [90] O. Adriani *et al.* (CALET), Phys. Rev. Lett. **129**, 25, 251103 (2022), [arXiv:2212.07873].
- [91] M. Aguilar *et al.* (AMS), Phys. Rev. Lett. **120**, 2, 021101 (2018).
- [92] A. E. Vladimirov *et al.*, Astrophys. J. **752**, 68 (2012), [arXiv:1108.1023].
- [93] P. Blasi, E. Amato and P. D. Serpico, Phys. Rev. Lett. **109**, 061101 (2012), [arXiv:1207.3706].
- [94] M. J. Boschini *et al.*, Astrophys. J. **889**, 167 (2020), [arXiv:1911.03108].
- [95] F. Aharonian *et al.* (H.E.S.S.), Phys. Rev. Lett. **101**, 261104 (2008), [arXiv:0811.3894].
- [96] O. Adriani *et al.* (PAMELA), Phys. Rev. Lett. **111**, 081102 (2013), [arXiv:1308.0133].
- [97] O. Adriani *et al.* (PAMELA), Nature **458**, 607 (2009), [arXiv:0810.4995].
- [98] M. Klasen, M. Pohl and G. Sigl, Prog. Part. Nucl. Phys. **85**, 1 (2015), [arXiv:1507.03800].
- [99] F. A. Aharonian, A. M. Atoyan and H. J. Volk, Astron. Astrophys. **294**, L41 (1995).
- [100] A. U. Abeysekara *et al.* (HAWC), Science **358**, 6365, 911 (2017), [arXiv:1711.06223].
- [101] P. Blasi, Phys. Rev. Lett. **103**, 051104 (2009), [arXiv:0903.2794].
- [102] P. Mertsch, A. Vittino and S. Sarkar, Phys. Rev. D **104**, 103029 (2021), [arXiv:2012.12853].
- [103] M. Aguilar *et al.* (AMS), Phys. Rev. Lett. **124**, 21, 211102 (2020).
- [104] C. Evoli *et al.*, Phys. Rev. D **103**, 8, 083010 (2021), [arXiv:2010.11955].
- [105] P. Mertsch, JCAP **11**, 045 (2018), [arXiv:1809.05104].
- [106] O. Adriani *et al.*, Pisma Zh. Eksp. Teor. Fiz. **96**, 693 (2012).
- [107] G. Jóhannesson *et al.*, Astrophys. J. **824**, 1, 16 (2016), [arXiv:1602.02243].
- [108] P. Blasi and P. D. Serpico, Phys. Rev. Lett. **103**, 081103 (2009), [arXiv:0904.0871].
- [109] V. Poulin *et al.*, Phys. Rev. D **99**, 2, 023016 (2019), [arXiv:1808.08961].
- [110] H. Fuke *et al.*, Phys. Rev. Lett. **95**, 081101 (2005), [arXiv:astro-ph/0504361].
- [111] A. H. Compton and I. A. Getting, Phys. Rev. **47**, 11, 817 (1935).
- [112] L. J. Gleeson and W. I. Axford, Astrophys. Sp. Sc. **2**, 4, 431 (1968).
- [113] M. Aglietta *et al.* (EAS-TOP), Astrophys. J. **470**, 501 (1996).
- [114] M. Ahlers and P. Mertsch, Prog. Part. Nucl. Phys. **94**, 184 (2017), [arXiv:1612.01873].
- [115] A. Abdul Halim *et al.* (Pierre Auger), Astrophys. J. Suppl. **264**, 2, 50 (2023), [arXiv:2211.16020].
- [116] R. U. Abbasi *et al.* (Telescope Array), Science **382**, 6673, abo5095 (2023), [arXiv:2311.14231].
- [117] S. Sciutto, AIRE User's Manual and Reference Guide; version 19.04.00 <http://aires.fisica.unlp.edu.ar/>.
- [118] A. Aab *et al.* (Pierre Auger), Phys. Rev. D **100**, 8, 082003 (2019), [arXiv:1901.08040].
- [119] D. Heck and T. Pierog, Extensive Air Shower Simulation with CORSIKA: A User's Guide (Version 7.7420) <https://www.iap.kit.edu/corsika/70.php>.
- [120] F. Riehn *et al.*, Phys. Rev. D **102**, 6, 063002 (2020), [arXiv:1912.03300].
- [121] S. Ostapchenko, EPJ Web Conf. **208**, 11001 (2019).
- [122] T. Pierog *et al.*, Phys. Rev. C **92**, 3, 034906 (2015), [arXiv:1306.0121].
- [123] W. Heitler, *The quantum theory of radiation*, volume 5 of *International Series of Monographs on Physics*, Oxford University Press, Oxford (1936).
- [124] J. Matthews, Astropart. Phys. **22**, 387 (2005).
- [125] A. Aab *et al.* (Pierre Auger), Nucl. Instrum. Meth. A **798**, 172 (2015), [arXiv:1502.01323].
- [126] H. Kawai *et al.* (Telescope Array), Nucl. Phys. B Proc. Suppl. **175–176**, 221 (2008).
- [127] S. Knurenko and I. Petrov, Adv. Space Res. **64**, 12, 2570 (2019), [arXiv:1908.01508].
- [128] N. M. Budnev *et al.*, Astropart. Phys. **117**, 102406 (2020), [arXiv:2104.03599].
- [129] A. Aab *et al.* (Pierre Auger), Phys. Rev. Lett. **116**, 24, 241101 (2016), [arXiv:1605.02564].
- [130] J. Pawlowski (Pierre Auger), PoS **ICRC2023**, 016 (2023), [arXiv:2312.14673].
- [131] P. A. Bezyazeev *et al.*, Phys. Rev. D **97**, 12, 122004 (2018), [arXiv:1803.06862].
- [132] I. Petrov and S. Knurenko, PoS **ICRC2019**, 385 (2020).
- [133] P. Schellart *et al.*, Astron. Astrophys. **560**, A98 (2013), [arXiv:1311.1399].
- [134] S. Buitink *et al.*, PoS **ICRC2023**, 503 (2023).
- [135] A. Aab *et al.* (Pierre Auger) (2016), [arXiv:1604.03637].
- [136] E. Kido (Telescope Array), EPJ Web Conf. **210**, 06001 (2019).
- [137] M. G. Aartsen *et al.* (IceCube) (2014), [arXiv:1412.5106].
- [138] J. Álvarez-Muñiz *et al.* (GRAND), Sci. China Phys. Mech. Astron. **63**, 1, 219501 (2020), [arXiv:1810.09994].
- [139] D. Southall *et al.*, Nucl. Instrum. Meth. A **1048**, 167889 (2023), [arXiv:2206.09660].
- [140] D. Ivanov (Telescope Array), PoS **ICRC2019**, 298 (2020).
- [141] A. Aab *et al.* (Pierre Auger), Phys. Rev. D **102**, 6, 062005 (2020), [arXiv:2008.06486].
- [142] A. Coleman *et al.*, Astropart. Phys. **149**, 102819 (2023), [arXiv:2205.05845].
- [143] R. U. Abbasi *et al.* (Telescope Array), Astrophys. J. **858**, 2, 76 (2018), [arXiv:1801.09784].
- [144] R. U. Abbasi *et al.* (Telescope Array), Astrophys. J. **909**, 2, 178 (2021), [arXiv:2012.10372].
- [145] A. Yushkov (Pierre Auger), PoS **ICRC2019**, 482 (2020).

- [146] C. J. Todero Peixoto (Pierre Auger), PoS **ICRC2019**, 440 (2020).
- [147] N. M. Budnev *et al.* (TAIGA), PoS **ICRC2021**, 731 (2021).
- [148] A. Fedynitch *et al.*, Phys. Rev. D **100**, 10, 103018 (2019), [arXiv:1806.04140].
- [149] A. Abdul Halim *et al.* (Pierre Auger), Phys. Rev. Lett. **132**, 2, 021001 (2024), [arXiv:2310.19963].
- [150] A. A. Watson, JHEAp **33**, 14 (2022), [arXiv:2112.06525].
- [151] A. Aab *et al.* (Pierre Auger), JINST **16**, 07, P07019 (2021), [arXiv:2101.02946].
- [152] F. G. Schröder, Prog. Part. Nucl. Phys. **93**, 1 (2017), [arXiv:1607.08781].
- [153] D. Hooper, S. Sarkar and A. M. Taylor, Astropart. Phys. **27**, 199 (2007), [arXiv:astro-ph/0608085].
- [154] G. Golup *et al.* (Pierre Auger), PoS **ICRC2023**, 252 (2023).
- [155] J. Kim *et al.* (Telescope Array), PoS **ICRC2023**, 244 (2023).
- [156] A. Aab *et al.* (Pierre Auger), Front. Astron. Space Sci. **6**, 24 (2019), [arXiv:1904.11918].
- [157] B. P. Abbott *et al.*, Astrophys. J. Lett. **848**, 2, L12 (2017), [arXiv:1710.05833].
- [158] A. Albert *et al.*, Astrophys. J. Lett. **850**, 2, L35 (2017), [arXiv:1710.05839].
- [159] S. Mollerach and E. Roulet, JCAP **03**, 017 (2019), [arXiv:1812.04026].
- [160] A. A. Halim *et al.* (Pierre Auger), JCAP **05**, 024 (2023), [arXiv:2211.02857].
- [161] J. C. Arteaga Velazquez, PoS **ICRC2023**, 466 (2023).
- [162] A. Aab *et al.* (Pierre Auger), Phys. Rev. Lett. **126**, 15, 152002 (2021), [arXiv:2102.07797].
- [163] M. Tavani *et al.* (AGILE), Astron. Astrophys. **502**, 995 (2009), [arXiv:0807.4254].
- [164] J. Chang *et al.* (DAMPE), Astropart. Phys. **95**, 6 (2017).
- [165] S. Torii, C. Collaboration *et al.*, J. Jpn. Soc. Microgravity Appl. **24**, 1, 120 (2007).
- [166] W. B. Atwood *et al.* (Fermi-LAT), Astrophys. J. **697**, 1071 (2009).
- [167] F. Aharonian *et al.* (H.E.S.S.), Astron. Astrophys. **457**, 899 (2006), [arXiv:astro-ph/0607333].
- [168] J. Sitarek *et al.* (MAGIC), in “33rd Int. Cosmic Ray Conf.”, 0074 (2013), [arXiv:1308.0141].
- [169] D. B. Kieda (VERITAS), in “33rd Int. Cosmic Ray Conf.”, 0700 (2013), [arXiv:1308.4849].
- [170] F. Di Piero (CTA LST Project), J. Phys. Conf. Ser. **2429**, 1, 012020 (2023).
- [171] A. Abramowski *et al.* (H.E.S.S.), Phys. Rev. D **90**, 12, 122007 (2014).
- [172] N. Budnev *et al.*, Nucl. Instrum. Meth. A **958**, 162113 (2020).
- [173] G. Aielli *et al.*, Nucl. Instrum. Meth. A **661**, S50 (2012).
- [174] M. Takita *et al.* (TIBET AS γ), in “30th Int. Cosmic Ray Conf.”, volume 2, 575–578 (2007).
- [175] B. M. Baughman, in “32nd Int. Cosmic Ray Conf.”, volume 9, 123 (2011).
- [176] Z. Cao, Nature Astron. **5**, 8, 849 (2021).
- [177] J. A. Hinton (H.E.S.S.), New Astron. Rev. **48**, 331 (2004).
- [178] C. Baixeras, Nuclear Physics B - Proceedings Supplements **114**, 247 (2003), ISSN 0920-5632.
- [179] H. B. T.C Weekes *et al.*, Astroparticle Physics **17**, 2, 221 (2002), ISSN 0927-6505.
- [180] G. W. Clark *et al.*, Astrophysical Journal, Letters **153**, L203 (1968).
- [181] C. E. Fichtel *et al.*, Astrophysical Journal **198**, 163 (1975).
- [182] H. A. Mayer-Hasselwander *et al.*, Astronomy and Astrophysics **105**, 1, 164 (1982).
- [183] S. D. Hunter *et al.*, Astrophys. J. **481**, 205 (1997).
- [184] M. Ackermann *et al.*, The Astrophysical Journal **750**, 1, 3 (2012).
- [185] A. A. Abdo *et al.*, Astrophys. J. **688**, 1078 (2008).
- [186] B. Bartoli *et al.* (ARGO-YBJ), Astrophys. J. **806**, 20 (2015).
- [187] M. Amenomori *et al.* (Tibet ASgamma), Phys. Rev. Lett. **126**, 14, 141101 (2021).
- [188] P. Sreekumar *et al.* (EGRET), Astrophys. J. **494**, 523 (1998).
- [189] M. Ackermann *et al.* (Fermi-LAT), Astrophys. J. **799**, 86 (2015).
- [190] Z. Cao *et al.*, Annual Review of Nuclear and Particle Science **73**, in press, 341 (2023).
- [191] S. Funk, Ann. Rev. Nucl. Part. Sci. **65**, 245 (2015).
- [192] J. A. Hinton and W. Hofmann, Ann. Rev. Astron. Astrophys. **47**, 523 (2009), [arXiv:1006.5210].
- [193] V. Schoenfelder (COMPTEL), Astron. Astrophys. Suppl. Ser. **143**, 145 (2000), [arXiv:astro-ph/0002366].
- [194] S. Abdollahi *et al.* (Fermi-LAT), Astrophys. J. Suppl. **247**, 1, 33 (2020).
- [195] Z. Cao *et al.* (LHAASO), Science **373**, 6553, 425 (2021).
- [196] F. A. Aharonian *et al.* (H.E.S.S.), Nature **432**, 75 (2004).
- [197] M. C. Weisskopf *et al.*, Astrophys. J. Lett. **536**, L81 (2000).
- [198] B. Bartoli *et al.* (ARGO-YBJ), Astrophys. J. Suppl. **222**, 1, 6 (2016).
- [199] B. Bartoli *et al.* (ARGO-YBJ), Astrophys. J. **734**, 110 (2011).
- [200] F. Aharonian (H.E.S.S.), Astron. Astrophys. **464**, 235 (2007).
- [201] H. Abdalla *et al.* (H.E.S.S.), Astron. Astrophys. **612**, A6 (2018).
- [202] R. Bühler and R. Blandford, Rept. Prog. Phys. **77**, 066901 (2014).
- [203] A. A. Abdo *et al.*, Science **326**, 5959, 1512 (2009).
- [204] J. Li *et al.*, Nature Astron. **4**, 12, 1177 (2020).
- [205] R. Zanin *et al.*, Astron. Astrophys. **596**, A55 (2016), [arXiv:1605.05914].
- [206] J. Albert *et al.* (MAGIC), Astrophys. J. Lett. **665**, L51 (2007).
- [207] G. Martí-Devesa and O. Reimer, Astron. Astrophys. **654**, A44 (2021).
- [208] A. A. Abdo *et al.*, VizieR Online Data Catalog J/ApJS/208/17 (2013).
- [209] S. Ansoldi *et al.* (MAGIC), Astron. Astrophys. **585**, A133 (2016), [arXiv:1510.07048].
- [210] A. Djannati-Ataï, in “31st Texas Symposium on Relativistic Astrophysics,” 33 (2022).
- [211] A. Allafort *et al.* (Fermi-LAT), Astrophys. J. Lett. **777**, L2 (2013).
- [212] A. A. Abdo *et al.* (Fermi-LAT), Astrophys. J. Suppl. **208**, 17 (2013).
- [213] H. An, Astrophys. J. **924**, 2, 91 (2022).
- [214] C. J. Clark *et al.*, Nature Astron. **7**, 4, 451 (2023).
- [215] D. F. Torres *et al.*, Astrophys. J. **836**, 1, 68 (2017).
- [216] A. Franckowiak *et al.*, Astron. Astrophys. **609**, A120 (2018).
- [217] S. De Wolf *et al.* (H.E.S.S.), Science **376**, 6588, abn0567 (2022).
- [218] M. Ajello *et al.* (Fermi-LAT), Astrophys. J. **892**, 105 (2020).
- [219] M. Ajello *et al.* (Fermi-LAT), Astrophys. J. Suppl. **263**, 2, 24 (2022).

- [220] M. Hayashida *et al.*, *Astrophys. J.* **807**, 1, 79 (2015).
- [221] V. A. Acciari *et al.*, *Astrophys. J.* **738**, 25 (2011), [arXiv:1106.1210].
- [222] M. Sikora, M. C. Begelman and M. J. Rees, *Astrophys. J.* **421**, 153 (1994).
- [223] F. A. Aharonian, *New Astron.* **5**, 377 (2000).
- [224] B. Bartoli, r. Xu *et al.* (ARGO-YBJ), *Astrophys. J.* **758**, 2 (2012).
- [225] A. Albert *et al.* (HAWC), *Astrophys. J.* **929**, 2, 125 (2022).
- [226] K. Katarzynski *et al.*, *Astron. Astrophys.* **433**, 479 (2005), [arXiv:astro-ph/0412405].
- [227] Z.-H. An *et al.* (Insight-HXMT, GECAM) (2023), [arXiv:2303.01203].
- [228] Z. Cao *et al.* (LHAASO), *Science* **380**, 6652, 9328 (2023).
- [229] V. A. Acciari *et al.* (MAGIC), *Nature* **575**, 7783, 459 (2019).
- [230] H. Abdalla *et al.*, *Nature* **575**, 7783, 464 (2019).
- [231] M. Ajello *et al.*, *Astrophys. J.* **878**, 1, 52 (2019).
- [232] P. Kumar and R. B. Duran, *Mon. Not. Roy. Astron. Soc.* **400**, 75 (2009).
- [233] X.-Y. Wang *et al.*, *Astrophys. J.* **712**, 1232 (2010).
- [234] V. A. Acciari *et al.* (MAGIC), *Nature* **575**, 7783, 455 (2019).
- [235] H. Abdalla *et al.* (H.E.S.S.), *Science* **372**, 6546, 1081 (2021).
- [236] S. R. Coleman and S. L. Glashow, *Phys. Rev. D* **59**, 116008 (1999), [hep-ph/9812418].
- [237] F. W. Stecker and S. L. Glashow, *Astropart. Phys.* **16**, 97 (2001), [arXiv:astro-ph/0102226].
- [238] Z. Cao *et al.* (LHAASO), *Phys. Rev. Lett.* **128**, 5, 051102 (2022).
- [239] R. Abbasi *et al.* (IceCube), *Eur. Phys. J. C* **82**, 11, 1031 (2022), [arXiv:2011.03561].
- [240] E. Richard *et al.* (Super-Kamiokande), *Phys. Rev. D* **94**, 052001 (2016), [arXiv:1510.08127].
- [241] S. Adrian-Martinez *et al.* (ANTARES), *Eur. Phys. J. C* **73**, 2606 (2013), [arXiv:1308.1599].
- [242] M. G. Aartsen *et al.* (IceCube), *Phys. Rev. D* **91**, 122004 (2015), [arXiv:1504.03753].
- [243] M. Börner *et al.* (IceCube), *PoS ICRC2015*, 1098 (2016).
- [244] M. Aartsen *et al.* (IceCube), *Nature* **591**, 220 (2021), [arXiv:2110.15051].
- [245] M. G. Aartsen *et al.* (IceCube), *Phys. Rev. D* **98**, 6, 062003 (2018), [arXiv:1807.01820].
- [246] M. Niechciol *et al.* (Pierre Auger), *PoS ICRC2023*, 1488 (2023).
- [247] A. van Vliet, R. Alves Batista and J. R. Hörandel, *Phys. Rev. D* **100**, 2, 021302 (2019), [arXiv:1901.01899].
- [248] R. Abbasi *et al.* (IceCube), *Science* **380**, 6652 (2023), [arXiv:2307.04427].
- [249] R. Mammen Abraham *et al.*, *J. Phys. G* **49**, 11, 110501 (2022), [arXiv:2203.05591].
- [250] J. Abraham *et al.* (Pierre Auger), *Phys. Rev. Lett.* **100**, 211101 (2008), [arXiv:0712.1909].
- [251] S. Ostapchenko, M. V. Garzelli and G. Sigl, *Phys. Rev. D* **107**, 2, 023014 (2023), [arXiv:2208.12185].
- [252] R. Abbasi *et al.* (IceCube), *Phys. Rev. D* **104**, 02202 (2021), [arXiv:2011.03545].
- [253] R. Abbasi *et al.* (IceCube), *Astrophys. J.* **928**, 50 (2022), [arXiv:2111.10299].
- [254] L. A. Fusco and F. Versari (ANTARES), *PoS ICRC2019*, 891 (2020).
- [255] V. Allakhverdyan *et al.* (Baikal-GVD), *Phys. Rev. D* **107**, 042005 (2023), [arXiv:2211.09447].
- [256] S. L. Glashow, *Phys. Rev.* **118**, 316 (1960).
- [257] D. Biehl *et al.*, *JCAP* **01**, 033 (2017), [arXiv:1611.07983].
- [258] V. Berezhinsky and G. Zatsepin, *Phys. Lett. B* **28**, 423 (1969).
- [259] M. Ave *et al.*, *Phys. Rev. Lett.* **85**, 2244 (2000), [arXiv:astro-ph/0007386].
- [260] D. Hooper, A. Taylor and S. Sarkar, *Astropart. Phys.* **23**, 11 (2005), [arXiv:astro-ph/0407618].
- [261] D. Gaggero *et al.*, *Phys. Rev. D* **91**, 083012 (2014), [arXiv:1411.7623].
- [262] A. Albert *et al.* (ANTARES), *Phys. Lett. B* **481**, 137951 (2023), [arXiv:2212.11876].
- [263] M. Aartsen *et al.* (IceCube, Fermi-LAT, MAGIC, AGILE, ASAS-SN, HAWC, H.E.S.S., INTEGRAL, Kanata, Kiso, Kapteyn, Liverpool Telescope, Subaru, Swift NuSTAR, VERITAS, VLA/17B-403), *Science* **361**, eaat1378 (2018), [arXiv:1807.08816].
- [264] M. Aartsen *et al.* (IceCube), *Science* **361**, 147 (2018), [arXiv:1807.08794].
- [265] R. Abbasi *et al.* (IceCube), *Science* **378**, 538 (2022), [arXiv:2211.09972].
- [266] R. Stein *et al.*, *MNRAS* **521**, 4, 5046 (2023), [arXiv:2203.17135].
- [267] M. G. Aartsen *et al.* (IceCube), *Nature* **551**, 596 (2017), [arXiv:1711.08119].
- [268] R. Abbasi *et al.* (IceCube), *Phys. Rev. D* **108**, 1, 012014 (2023), [arXiv:2304.12236].
- [269] N. Geisselbrecht (KM3NeT), *PoS ICRC2023*, 1107 (2023).
- [270] M. G. Aartsen *et al.* (IceCube), *Phys. Rev. Lett.* **125**, 14, 141801 (2020), [arXiv:2005.12942].
- [271] R. Abbasi *et al.* (IceCube), *Phys. Rev. Lett.* **129**, 1, 011804 (2022), [arXiv:2201.03566].
- [272] A. Addazi *et al.*, *Prog. Part. Nucl. Phys.* **125**, 103948 (2022), [arXiv:2111.05659].

Experimental Methods and Colliders

- 31. Accelerator physics of colliders (rev.) 559
- 32. High-energy collider parameters (rev.) 569
- 33. Neutrino beam lines at high-energy proton synchrotrons (rev.) 574
- 34. Passage of particles through matter (rev.) 575
- 35. Particle detectors at accelerators (rev.) 591
- 36. Particle detectors for non-accelerator phys. (rev.) 649
- 37. Radioactivity and radiation protection (rev.) 679
- 38. Commonly used radioactive sources (rev.) 685





31. Accelerator Physics of Colliders

Revised July 2023 by V. Shiltsev (FNAL) and F. Zimmermann (CERN).

This article provides background for the High-Energy Collider Parameter Tables that follow and some additional information; see in-depth review and a comprehensive list of references in [1]; citations below are limited to widely used textbooks and open access seminal papers and reviews.

31.1 Energy and Luminosity

Collisions of two beams of particles accelerated to high energies $E_{1,2}$ provide access to center-of-mass energies (c.m.e.) $E_{\text{c.m.e.}} \approx 2\sqrt{E_1 E_2}$, assuming a typically small or zero crossing angle. Most of the 31 colliders that have ever reached the operational stage (seven are operational now) used equal masses and energies of colliding particles, with c.m.e. equal to twice the beam energy $E_{\text{c.m.e.}} = 2E_b$. Other machines collide beams of unequal energies, such as electron-proton or electron-ion colliders, or asymmetric B -factories, that produce new short-lived particles, whose decays are more easily detected and analyzed with a Lorentz boost.

In an accelerator, charged particles gain energy from an electric field, which usually varies in time at a high frequency ranging from 100s of kHz to 10s of GHz. With proper phasing to the RF field over distance l , the energy gain of a particle with charge Ze is proportional to the average accelerating gradient G , i.e. $\Delta E_b = ZeGl$. In principle, the highest beam accelerating gradients achieved to date in operational machines or beam test facilities ($G \approx 100$ MV/m in 12 GHz normal-conducting RF cavities and 31.5 MV/m in 1.3 GHz superconducting ones) allow accessing high energies over reasonably long linear accelerators (linacs), but cost considerations often call for minimization of RF acceleration via repeated use of the same RF system which, in that case, would boost the energy in small portions $\Delta E_b = ZeV_{\text{RF}}$ per turn every time a particle passes through the total cavity voltage V_{RF} . Such an arrangement can be realized either in the form of storage-ring circular colliders or also through novel schemes based on, e.g., recirculating linear accelerators (RLAs) with or without energy recovery. Circular colliders are by far the most common; here, the momentum and energy of ultra-relativistic particles are determined by the bending radius inside the dipole magnets, ρ , and by the average magnetic field B of these magnets:

$$p = ZeB\rho \quad \text{or} \quad E_b [\text{GeV}] = 0.3Z(B\rho) [\text{Tm}]. \quad (31.1)$$

Such *synchrotron condition* assures approximately constant radius of the beam orbit during acceleration. Transverse focusing by quadrupole magnets is needed to keep particles inside the rather limited space provided by the accelerator beam pipe passing through the magnet apertures. The maximum field of normal-conducting (NC) magnets is about 2 T, due to the saturation of ferromagnetic materials, and, while this is sufficient for lower energy colliders, such as most e^+e^- storage rings, it is not adequate for frontier-energy hadron (or muon) beams, because of the implied need for excessively long accelerator tunnels and prohibitively high total magnet power consumption. The development of superconducting (SC) magnets that employ high electric current carrying Nb-Ti wires cooled by liquid helium below 5 K, opened up the way towards higher fields and to hadron colliders at record energies [2]. For example, the 14 TeV c.m.e. LHC at CERN, uses double-bore SC magnets with a maximum field of 8.3 T at a temperature of 1.9 K, in a tunnel of $C = 26.7$ km circumference (dipole-magnet bending radius $\rho = 2800$ m). The double-bore design allows acceleration of the same particle type in opposite directions and also the operation with different particle species (e.g., protons and heavy ions) in the two apertures, while a single bore magnet implies the use of particles and antiparticles for the collider application. As the production of anti-particles is energy consuming and therefore limited, this concept opens the door to high-performance hadron colliders.

The exploration of rare nuclear and high energy particle physics phenomena requires not only an appropriately high energy, but also a sufficiently large number of detectable reactions. The number of events of interest N_{exp} is given by the product of the cross section of the reaction under study, σ_{exp} , and the time integral

over the instantaneous *luminosity*, \mathcal{L} :

$$N_{\text{exp}} = \sigma_{\text{exp}} \cdot \int \mathcal{L}(t) dt. \quad (31.2)$$

In the Tables, luminosity is stated in the units of $\text{cm}^{-2}\text{s}^{-1}$. The integral on the right is referred to as integrated luminosity \mathcal{L}_{int} , and, reflecting the smallness of typical particle-interaction cross-sections is often reported in units of inverse femto- or attobarn, e.g., $1 \text{ ab}^{-1} = 10^{42} \text{ cm}^{-2}$. Colliders usually employ bunched beams of particles with approximately Gaussian distributions, and for two bunches containing N_1 and N_2 particles colliding head-on with frequency f_{coll} , a basic expression for the luminosity is

$$\mathcal{L} = f_{\text{coll}} \frac{N_1 N_2}{4\pi\sigma_x^* \sigma_y^*} \mathcal{F} \quad (31.3)$$

where σ_x^* and σ_y^* characterize the rms transverse beam sizes in the horizontal and vertical directions at the interaction point, and \mathcal{F} is a factor of order 1, that takes into account inefficient geometric overlapping of the beams due to a crossing angle and finite bunch length, and dynamic effects, such as the mutual focusing of the two beam during the collision (see below). Having n_b bunches per beam increases the frequency of collisions $f_{\text{coll}} = n_b f_0$ where f_0 is either the revolution frequency of a circular collider or the repetition rate of a linear one. To achieve a high luminosity, one, therefore, has to maximize the population and number of bunches, either producing these narrowly or focusing them tightly, and colliding them at high frequencies at dedicated locations, where products of their reactions can be registered by particle detectors.

Subsequent sections in this report briefly expand on the beam dynamics behind collider design, comment on the realization of collider performance in a selection of today's facilities, and end with some remarks on future possibilities.

31.2 Beam Dynamics

Given the enormous and highly concentrated power carried by modern high energy particle beams, the main concern of beam dynamics in colliders is stability of motion of i) individual particles in accelerators, ii) single high-intensity beams of many particles moving together, and iii) colliding beams [3–5].

31.2.1 Single Particle Dynamics

While a reference particle at the nominal energy proceeds along the design trajectory (reference orbit) mostly determined by transverse magnetic dipole fields, other particles in the bunch are kept close by through the focusing effect of quadrupole fields. Assume that the reference particle carries a right-handed Cartesian coordinate system, with the co-moving z -coordinate pointed in the direction of motion along the reference trajectory, $z = s - vt$ (with v the reference particle velocity, and t time). The independent variable is the distance s of the reference particle along this trajectory, rather than time t , and for simplicity this reference path is taken to be planar. The transverse coordinates are x (horizontal) and y (vertical), where $\{x, z\}$ defines the plane of the reference trajectory.

Several time scales are involved, and this is reflected in the approximations used in formulating the equations of motion. All of today's high-energy colliders are alternating gradient synchrotrons or, respectively, storage rings and the shortest time scale is set by so-called *betatron oscillations*. The linearized equations of motion of a particle displaced from the reference trajectory are:

$$\begin{aligned} x'' + K_x(s)x &= 0, \quad y'' + K_y(s)y = 0, \quad z' = -x/\rho(s), \\ \text{with } K_x &\equiv \frac{Ze}{p} \frac{\partial B_y}{\partial x} + \frac{1}{\rho^2} \quad \text{and} \quad K_y \equiv -\frac{Ze}{p} \frac{\partial B_y}{\partial x} \end{aligned} \quad (31.4)$$

where $\rho = p/ZeB_y$ is the radius of curvature due to the field on the reference orbit. The prime denotes d/ds and the Maxwell equation in vacuum $\nabla \times \mathbf{B} = \mathbf{0}$ helps to eliminate $B_x(s)$ using the relation $\partial B_x/\partial y = \partial B_y/\partial x$. In this linear approximation, the vertical magnetic field $B_y(s)$ in the (x, z) -plane contains only

dipole and quadrupole terms, which are treated as static in time, but s -dependent.

The solutions of the Hill's equations (31.4) for x and y with a restoring force periodic in s are those of quasi-harmonic oscillators:

$$x(s) = \sqrt{2J_x\beta_x} \cos \psi_x, \quad x'(s) = -\sqrt{\frac{2J_x}{\beta_x}} [\alpha_x \cos \psi_x + \sin \psi_x], \quad (31.5)$$

where the action J_x is a constant of integration, $\alpha_x = \alpha_x(s) \equiv -(1/2)d\beta_x(s)/ds$, and the envelope of oscillations is modulated by the *beta-function* $\beta_x(s)$. A solution of the same form describes the motion in y . The betatron oscillation phase advances according to $d\psi_x/ds = 1/\beta_x$; that is, $2\pi\beta_x$ also plays the role of a local wavelength of oscillations along the orbit. An extremely important parameter for circular machines is the *tune*, Q_x , which is the number of such oscillations per turn about the closed path:

$$Q_x = \frac{1}{2\pi} \oint d\psi_x = \frac{1}{2\pi} \oint \frac{ds}{\beta_x(s)}. \quad (31.6)$$

While the integer part of the tune $[Q_{x,y}]$ generally characterizes the extent of the focusing lattice, it is the fractional part of the tune $\{Q_{x,y}\}$ that needs to be well defined and controlled by the machine operators in order to stay away from potentially detrimental resonances, which may occur under conditions of $kQ_x + lQ_y = m$, where k, l , and m are integers. For example, for the LHC a combination of horizontal and vertical tunes — also called the *working point* — equal to $(Q_x, Q_y) = (64.31, 59.32)$ has been selected, such that resonances up to the order of $|k| + |l| = 10$ or 12 are avoided. These resonances are driven by high order multipole components of the fields in the magnets, or by self-fields of the beam, or by the electromagnetic fields of the opposite bunch. Normally, the nonlinear components are very weak compared to linear ones, nevertheless, when the nonlinear resonance condition is encountered, the amplitudes of particle oscillations could grow over the beam lifetime, resulting in the escape of the particles to the machine aperture, in the increase of the average beam size, or in both; either of these is highly undesirable phenomena. Careful analysis of nonlinear beam dynamics is instrumental in determining and optimizing the *dynamic aperture*, which is defined as the maximum amplitude of a bounded particle motion.

Neglecting for now all nonlinear effects and usually small $x-y$ coupling, and considering only the linear dynamics, the beta-function is well defined and satisfies the following equation:

$$2\beta_x\beta_x'' - \beta_x'^2 + 4\beta_x^2 K_x = 4. \quad (31.7)$$

In a region free of magnetic fields, such as in the neighborhood of a collider interaction point (IP), usually occupied by particle detectors, a symmetric solution of Eq. (31.7) is a parabola:

$$\beta_x(s) = \beta_x^* + \frac{s^2}{\beta_x^*}, \quad (31.8)$$

where, in this case, s denotes the longitudinal distance from the IP. The location of the beam waist usually coincides with the IP and corresponds to the minimum value of the beta-function β_x^* ; the asterisk is used to indicate IP parameters.

Note that individual quadrupole magnet focuses particles in one plane and defocuses in another, see Eq.(31.4), and a standard way to provide focusing in both planes is to employ an alternating gradient periodic focusing lattice, consisting of a sequence of equally-spaced quadrupoles with a magnetic field gradient equal in magnitude, but alternating in sign ("focusing quadrupole - drift space - defocusing quadrupole - drift space" — known as a *FODO cell*). Eq. (31.7) has stable periodic solutions $\beta_x(s), \beta_y(s)$ in both planes provided that the focal length of the quadrupoles is longer than half the focusing-lens spacing L , i.e., $f = p/(eB_2l) > L/2$ (where l is the length of a quadrupole magnet, here assumed to be short $l \ll L$, and $B_2 \equiv |\partial B_y/\partial x|$ the quadrupoles' field gradient). In that case, the beta-functions have maxima at the focusing quadrupoles and minima at the defocusing ones, equal to, for example, $\beta_{\max, \min} = (2 \pm \sqrt{2})L$ in the case of $f = L/\sqrt{2}$, which

corresponds to a betatron phase advance $\Delta\psi_{x,y} = 90^\circ$ per FODO cell.

Expressing the invariant J_x in terms of x, x' yields

$$J_x = \frac{1}{2} (\gamma_x x^2 + 2\alpha_x x x' + \beta_x x'^2) = \frac{x^2 + (\alpha_x x + \beta_x x')^2}{2\beta_x} \quad (31.9)$$

with $\gamma_x = \gamma_x(s) \equiv (1 + \alpha_x^2(s))/\beta_x(s)$. In a periodic system, these *Courant-Snyder parameters* [6] (frequently referred to as *Twiss parameters*) $\alpha(s), \beta(s), \gamma(s)$ are usually defined by the focusing lattice; in a single pass system such as a linac, the parameters may be selected to match the $x-x'$ distribution of the input beam. For a given position s in the ring, the transverse particle motion in $\{x, x' \equiv dx/ds\}$ phase space describes an ellipse, the area of which is $2\pi J_x$, where the horizontal action J_x is a constant of motion and independent of s . If the interior of that ellipse is populated by an ensemble of non-interacting and non-radiating particles, that area, given the name *emittance*, is constant over the trajectory as well and would only change with energy. In a typical case of the particle's energy change rate being much slower than betatron motion, and considering a Hamiltonian system (i.e., a hadron collider or a linear collider, either without significant synchrotron radiation), the adiabatic invariant $\int p_x dx$ is conserved, and given that for small angles $p_x = x' \cdot \beta\gamma mc^2$, it is common practice to consider an energy-independent *normalized emittance* that is equal to the product of the emittance and relativistic factor $\beta\gamma/\pi$ and denoted by ε_n . For a beam with a Gaussian distribution in $\{x, x'\}$, average action value $\langle J_x \rangle$ and standard deviations σ_x , and $\sigma_{x'}$, the definition of the normalized rms emittance is

$$\varepsilon_{nx} \equiv \beta\gamma \langle J_x \rangle = \beta\gamma \frac{\sigma_x^2(s)}{\beta_x(s)} = \beta\gamma \frac{\sigma_{x'}^2(s)}{\gamma_x(s)}, \quad (31.10)$$

with a corresponding expression for the other transverse direction, y . The angular brackets denote an average over the beam distribution. For 1D Gaussian beam, 95% of the particles are contained within $\{x, x'\}$ phase space area of $6\pi\varepsilon_n/(\beta\gamma)$. Normalized beam emittances are conserved over the acceleration cycle in linear, static focusing lattices $K_{x,y}(s)$, and consequently, one would expect the same ε_n at the hadron (or linear) collider top energy as the one coming from the very initial low energy particle source. Unfortunately, that is rarely the case as many time-varying or nonlinear phenomena come into play. In an e^-/e^+ storage ring, the normalized emittance is not preserved during acceleration, but at each energy the beam's equilibrium emittance is determined by the effect of synchrotron radiation as a balance between radiation damping and quantum excitation [7]. In such a ring, for a given accelerator optics, the normalized equilibrium emittance increases with the third power of the beam energy [8].

As for the description of a particle's longitudinal motion, one takes the fractional momentum deviation $\Delta p/p$ from that of the reference particle as the variable conjugate to z . The factors $K_{x,y}$ and ρ in Hill's equations (31.4) are dependent on momentum p , leading to a number of effects: first, the trajectory of off-momentum particles deviates by $\Delta x(s) = D_x(s)(\Delta p/p)$, where the *dispersion function* $D_x(s)$ is determined by the magnetic lattice and is usually positive, periodic, and of the order of $\sim \rho/Q_x^2$. Second, the radius of curvature and orbit path-length C vary with the momentum and, to first order, are characterized by the momentum compaction factor α_c ,

$$\alpha_c \equiv \frac{\Delta C/C}{\Delta p/p} = \frac{1}{C} \oint \frac{D_x(s)}{\rho(s)} ds, \quad (31.11)$$

which typically is of order $1/Q_x^2$. Energy deviations also result in changes of machine focusing lattice properties and variations of the particle tunes, characterized by the *chromaticity* $Q'_{x,y} \equiv \Delta Q_{x,y}/(\Delta p/p)$. The natural chromaticity due to momentum dependence of the quadrupole focusing is negative and large $\sim -Q_{x,y}$. Corresponding chromatic tune variations can, therefore, become unacceptably large even for relatively small energy deviations $(\Delta p/p) \sim (0.1 - 1) \cdot 10^{-3}$. To assure transverse particle stability, usually, the chromaticity is partially or fully com-

compensated by additional sextupole magnets placed at locations of non-zero dispersion.

Radiofrequency electric fields in s direction provide a longitudinal focusing effect, allowing a stable increase of particle energy. The frequency f_s of such longitudinal *synchrotron oscillations* is (expressed in units of revolution frequency f_0 , to become the synchrotron tune Q_s)

$$Q_s \equiv \frac{f_s}{f_0} = \sqrt{\frac{(\alpha_c - 1/\gamma^2)hZeV_{\text{RF}} \sin(\phi_s)}{2\pi\beta cp}}, \quad (31.12)$$

where $h = f_{\text{RF}}/f_0$ denotes the RF harmonic number, V_{RF} the RF voltage, and $\phi_s = \cos^{-1}(\Delta E/Z_e V_{\text{RF}})$ the synchronous phase, with ΔE the average energy loss per turn (e.g. due to synchrotron radiation and impedance). The synchrotron tune Q_s determines the amplitude of longitudinal oscillations for a particle with an initial momentum offset, e.g., the rms bunch length σ_z relates to the rms momentum spread $\delta p/p$ as:

$$\sigma_z = \frac{c(\alpha_c - 1/\gamma^2)}{2\pi Q_s f_0} \left(\frac{\delta p}{p} \right). \quad (31.13)$$

Similarly to the case of transverse oscillations, the area of the longitudinal phase space $\{\Delta E, \Delta t\}$, or $\{\gamma\beta\delta p/p = (1/\beta)\Delta\gamma, z = \beta c\Delta t\}$, encircled by a moving particle is an adiabatic invariant, and the corresponding normalized *longitudinal emittance* $\varepsilon_{n,L} = \beta\gamma mc\sigma_z(\delta p/p)$ is a generally conserved quantity in hadron accelerators and also in linear accelerators. In the case of lepton storage rings, synchrotron radiation determines the equilibrium relative momentum spread, which grows linearly with beam energy [7, 8], and the corresponding bunch length follows from Eq. (31.13). In hadron synchrotrons, the longitudinal emittance sometimes is intentionally blown up during acceleration, so as to preserve longitudinal beam stability.

Longitudinal oscillations are the slowest of all the periodic processes which take place in the accelerators. For example, in the LHC, the frequency of synchrotron oscillations at the top energy of 7 TeV is about $f_s = 23$ Hz, the revolution frequency is $f_0 = 11.3$ kHz, the frequency of betatron oscillations is about $Q_{x,y}f_{\text{rev}} \simeq 700$ kHz and the RF frequency is $f_{\text{RF}} = 400.8$ MHz ($h = 35640$). It should be noted that longitudinal motion is practically absent in linacs. In the absence of bending dipoles, dispersion $D_x(s)$ is zero and so are the momentum compaction factor α_c and the synchrotron tune Q_s . As a result, ultrarelativistic particles in a linac barely change their relative positions during acceleration despite significant energy spread.

Highest-energy circular colliders face a serious impediment in the form of synchrotron radiation (SR) that causes an energy loss per turn of

$$\Delta E_{\text{SR}} = \frac{1}{3\varepsilon_0} \frac{Z^2 e^2 \beta^3 \gamma^4}{\rho}, \quad (31.14)$$

here, ε_0 is the permittivity of vacuum. For electrons and positrons it is equal to $\Delta E_{\text{SR}} = 88.5$ [keV/turn] $E_b^4[\text{GeV}]/\rho[\text{m}]$ and requires correspondingly high total RF voltage per turn to replenish the loss. Above a few hundred GeV, the SR energy loss becomes comparable to beam energy $\Delta E_{\text{SR}} \sim E_b$, which makes circular e^+e^- colliders impractical for c.m.e. above ~ 500 GeV.

Dynamics of the particle spin and sophisticated methods to maintain beam polarization along the acceleration chain, from the polarized sources to collisions, dedicated spin matching procedures to enable self polarization in e^+/e^- storage rings and the *resonant depolarization* method of ultra-precise c.m.e. calibration are described in [9].

31.2.2 High Intensity Beams

Ultimate collider luminosity calls for high beam currents $I_b = Ze f_0 n_b N$. Three related major difficulties include growing RF demands to compensate the synchrotron-radiation power loss $P = I_b \Delta E_{\text{SR}}$ in e^+/e^- beams, the advent of so-called *coherent* (or *collective*) *beam instabilities*, and growing demands for minimization of radiation due to inevitable particle losses. Many types of single- and multi-bunch instabilities are caused by beam interactions with electromagnetic fields induced by the beam itself due

to the *impedance* of the vacuum chambers and RF cavities [4], or caused by unstable clouds of secondary particles, like electrons or ions, which are formed around the circulating beams [10]. These instabilities can develop as quickly as within tens to thousands of turns and need to be controlled. Mechanisms that are routinely employed to avoid coherent instabilities include the use of nonlinear magnets to generate sufficient spread of the tunes and therefore, provide *Landau damping*, fast beam-based transverse and longitudinal feedback systems, and electron/ion clearing (either by weak magnetic or electric fields or by modulation of the primary beam current profile rendering secondaries unstable, or by reducing the yield of secondary electrons via either a special coating or extensive *beam scrubbing* of the vacuum chamber walls).

High current beam operation is sensitive to even minuscule fractional intensity losses caused by particles' scattering at a large angle or with a large energy loss, sufficient for either the particle amplitudes $\sqrt{2J_{x,y}\beta_{x,y}(s)}$, or their dispersive position deviations $\Delta x = D_x(s)(\delta p/p)$ to exceed the available transverse aperture, usually set by collimators (otherwise, by the vacuum chamber and magnet apertures). This can be due to residual vacuum molecules near the beam orbit or Compton scattering off thermal photons, due to Coulomb scattering off other particles within the same bunch (*Touschek effect*), or due to collisions with opposite beam particles and fields, such as inelastic interaction of protons, Bhabha scattering $e^+e^- \rightarrow e^+e^-$, or radiative Bhabha scattering $e^+e^- \rightarrow e^+e^-\gamma$ (see corresponding chapters in [11]).

Particles can also get lost on the aperture as a result of much slower mechanisms of diffusion caused either by the above processes with smaller scattering amplitudes, but stochastically repeated many times, such as intensity-dependent multiple Coulomb *intrabeam scattering* [12], by external noises such as ground motion or magnetic field fluctuations, or via chaotic mechanisms like Arnold diffusion, modulational diffusion, or resonance streaming in nonlinear fields, enhanced by minor tune modulations. Diffusion leads to a slow evolution of the beam distribution function and appearance of highly unwanted large-amplitude tails and beam emittance growth. The only way to counteract it is to arrange *beam cooling* (damping of particle oscillations). The cooling requires a reaction force opposite to particle momentum arranged such that, on average, the corresponding dissipative particle energy loss is compensated for by external power [13, 14].

In the case of electron or positron storage rings, such cooling occurs naturally due to synchrotron radiation and provides an automatic route to achieve small equilibrium emittances through a balance between radiation damping and excitation of oscillations by random radiation of individual photons. Fast radiation damping allows *top-up injection* of new particles without removing existing ones, a useful method to maximize the integrated luminosity of circular e^+e^- colliders. Synchrotron radiation damping will also be an important cooling mechanism for future energy-frontier hadron colliders, like the proposed FCC-hh and SppC (see below). Four other methods of beam cooling have been developed and successfully employed to attain low emittances, namely *electron cooling* and *stochastic cooling* of heavy particles (ions and antiprotons), *laser cooling* of ion beams, and the *ionization cooling* of muons.

To avoid damage or excessive irradiation of accelerator components so that these remain accessible for maintenance in the tunnel, sophisticated collimation systems are utilized. These systems usually employ a series of targets or primary collimators which scatter the halo particles, and numerous absorbers (sometimes as many as a hundred, which intercept particles in dedicated locations) [15, Ch.9.7]. In the highest energy modern and future colliders, extreme total beam energies $n_b N E_b$ ranging from MJs to GJs and impacting surface energy densities reaching many GJ/mm² pose one of the biggest challenges for high efficiency and robust particle collimation.

31.2.3 High Luminosity Collisions

Eq. (31.3) for luminosity can be recast in terms of normalized transverse emittances Eq. (31.10) and the beta-functions β^* at

the IP as:

$$\mathcal{L} = f_0 \gamma n_b \frac{N^2}{4\pi \sqrt{\varepsilon_{nx} \beta_x^* \varepsilon_{ny} \beta_y^*}} \mathcal{F}. \quad (31.15)$$

Here, equal bunch populations N are assumed in two Gaussian beams with the same emittances. Naturally, to achieve a high luminosity, one has to maximize the total beam populations $n_b N$ within the lowest possible emittances, and collide the beams at high frequency at locations where the focusing beam optics provides the lowest possible values of the amplitude functions β^* , the so-called *low-beta insertion*. The latter requires sophisticated systems of strong focusing elements, sometimes occupying quite a significant fraction of the collider's total length. The lowest $\beta_{x,y}^*$ is determined by the maximum field gradients and apertures in the interaction region (IR) magnets and the effectiveness of compensation of chromatic and nonlinear aberrations.

The typical geometric reduction factor is $\mathcal{F} \approx 1$, and it rarely drops below 0.5 for the majority of colliders, unless this is specifically required by physics processes under study. The reduction due to the *hourglass effect* is caused by the increase in transverse beam sizes as one proceeds away from the IP, where $\beta(s)$ grows parabolically, as in Eq. (31.8). For long round bunches the effect scales as $\mathcal{F} \approx \sqrt{\pi} A \exp(A^2) \operatorname{erfc}(A)$, where $A = \beta^*/\sigma_z$. Nonzero beam crossing angles θ_c in the horizontal plane and long bunches (rms bunch length σ_z) will reduce the luminosity, too, by a factor $\mathcal{F} \approx 1/(1 + \Phi^2)^{1/2}$, where the parameter $\Phi = \sigma_z \tan(\theta_c/2)/\sigma_x^*$ is known as the *Piwiński angle*.

One of the most common limits to producing high luminosity arises from electric and magnetic forces of the opposite bunch at the IPs, characterized by a dimensionless *beam-beam parameter*:

$$\xi_{x,y} = \frac{r_0 N \beta_{x,y}^*}{2\pi \gamma \sigma_{x,y}^* (\sigma_x^* + \sigma_y^*)}, \quad (31.16)$$

where $r_0 = Z^2 e^2 / (4\pi \varepsilon_0 m c^2)$ is the classical radius of the colliding particle (with charge Ze and mass m). From Eqs. (31.3) or (31.15) and (31.16), one can note that the path to higher luminosity via higher beam intensity and smaller beam sizes almost automatically calls for a higher beam-beam parameter as $\mathcal{L} \propto \xi$. Cited in the Tables, the beam-beam parameter is roughly equal to the betatron tune shift experienced by small-amplitude particles – positive in the case of opposite charge beams, like e^+e^- , and negative for same charge beams as in pp collisions. Beam-beam forces can lead to coherent effects, such as unstable beam oscillations or blow-up of one beam's size while the other beam remains small or even shrinks (*flip-flop effect*). The tune spread arising from ξ and the nonlinear nature of beam-beam interactions results in strong diffusion along high-order transverse resonances $kQ_x + lQ_y = m$ and, ultimately, in beam size growth and beam losses. Operational experience indicates that the aforementioned effects are tolerable below certain *beam-beam limit* of $\xi_{x,y} \approx 0.003 - 0.012$ in hadron colliders [16], and – due to strong synchrotron radiation damping – an order of magnitude higher one in e^+e^- colliders, with maximum $\xi_{x,y} \approx 0.03 - 0.12$ [17, 18]. The accessible beam-beam parameter range can also be restricted by coherent beam-beam instabilities. These various limits translate into a maximum allowed single bunch intensity N and call for an increase of the number of bunches n_b to achieve higher luminosities.

In linear colliders, where each bunch collides only once, with typically much smaller beam size and experiencing much stronger forces, the strength of the collision is measured by the ratio of the rms bunch length σ_z to the beam-beam focal length. This ratio, called *disruption parameter* D_y , is related to ξ_y via $D_y = 4\pi \sigma_z \xi_y / \beta_y^*$. Stronger beam-beam focusing and higher D_y lead to effectively smaller beam sizes and a resulting luminosity enhancement; but it also makes the collisions more sensitive to small offsets, resulting in a *kink instability*. Additional beam-beam effects arising in the collisions at linear colliders are the emission of *beamstrahlung* (synchrotron radiation in the field of the opposing beam), along with e^+e^- pair creation, and depolarization by various mechanisms.

Beamstrahlung is relevant for both linear colliders, where it may significantly degrade the luminosity spectrum, and for future

highest-energy circular colliders, where it may limit the beam lifetime, and also increases the energy spread and bunch length of the stored beam. For both types of colliders, the beamstrahlung is mitigated by making the colliding beams as flat as possible at the interaction point ($\sigma_x^* \gg \sigma_y^*$) to lower the beams' EM fields. The photon energy spectrum of the beamstrahlung is characterized by the parameter $\Upsilon = (2/3)\hbar\omega_c/E_b$ [19], with $\hbar\omega_c$ denoting the critical photon energy. The spectrum strongly deviates from the classical synchrotron radiation spectrum for Υ approaching or exceeding 1.

For hadron colliders, two fundamental luminosity limits are the beam lifetime, determined by burn-off in the collisions due to inelastic pp interaction $dN/dt = -\mathcal{L}\sigma_{in}$, and the radiation from the collision debris, which may induce “quenches” (transitions to the normal-conducting state) of the superconducting final quadrupole magnets, and, in the long term, affect the equipment lifetime. Another limit on the achievable integrated luminosity in circular colliders is set by the minimum or average turnaround time (the time between the beam abort at the end of a physics fill and the start of the next physics collisions). Achieving practical filling times with many bunches in the collider requires either fast cycling injector machines and/or the top-up injection operation. The latter makes the average luminosity of circular electron-positron colliders approximately equal to the peak luminosity.

31.3 Recent High Energy Colliders

In this and the following section, elaboration is made on various issues associated with some of the recently operating colliders, particularly factors which impact integrated luminosity. Only general references are provided, where further information can be obtained. A more complete list of recent colliders and their parameters can be found in the High-Energy Collider Parameters tables.

31.3.1 Tevatron

The first superconducting synchrotron in history, the Tevatron [20] was converted into a proton-antiproton collider in 1985. Its 4.4 T dipole magnets employed Nb-Ti superconducting cable operating at 4.5 K, requiring what was then the world's largest cryogenic system. With \sqrt{s} up to 1.96 TeV it was the highest energy collider for 25 years and delivered more than 12 fb^{-1} of the integrated luminosity to each $p\bar{p}$ detector experiments (CDF and D0) before being shut off in 2011. The route to high integrated luminosity in the Tevatron was governed by the antiproton production rate, the turn-around time to produce another store, and the resulting optimization of store time [21]. The antiproton production complex consisted of three 8 GeV \bar{p} accelerators (the Accumulator, Debuncher, and Recycler – the latter was the first high energy accelerator built with permanent magnets), and employed 25 independent stochastic cooling systems and one pioneering high-energy electron cooling set-up to accumulate up to a record high value of $25 \cdot 10^{10} \bar{p}$ per hour. Despite severe parasitic long-range interactions of the two beams, each consisting of 36 bunches placed on helical orbits by two dozen $\pm 150 \text{ kV}$ high-voltage (HV) separators, a total beam-beam tune shift parameter of $n_{IP}\xi \approx 0.025-0.03$ was achieved, a record for hadron beams, with $n_{IP} = 2$ primary collision points. Other notable advances in the accelerator science and technology included advanced longitudinal beam manipulation techniques of *slip-stacking* and *momentum mining* and the first operational use of *electron lenses* for beam collimation and for compensation of long-range beam-beam effects [22]. The Tevatron ultimately achieved luminosities a factor of 430 higher than the original design specification.

31.3.2 HERA

The first lepton-proton collider, the 6.4 km long Hadron-Elektron-Ring-Anlage (HERA) at DESY in Germany [23], operated between 1992 and 2007 and delivered nearly 1 fb^{-1} of integrated luminosity at \sqrt{s} of about 320 GeV to the electron-proton collider experiments H1 and ZEUS [24, Ch.10.5]. It was the first facility to employ both applications of superconductivity: 5 T magnets in the 920 GeV proton ring and SRF accelerating structures to provide about 12 MW of RF power to compensate for synchrotron radiation losses of 30 GeV lepton beams (positrons or

electrons, in a conventional-magnet ring). With proper orbit and optics control, the HERA lepton beam would naturally become transversely polarized to about 60% (within about 40 minutes) thanks to the *Sokolov-Ternov effect*. Special magnets called *spin rotators* were implemented on either side of the collider IPs to produce 30–45% longitudinal polarization at the experiments.

31.3.3 LEP

Installed in a tunnel of 26.7 km circumference, LEP [25] was the largest circular e^+e^- collider built so far. LEP was operated from 1989 to 2000 with beam energies ranging from 45.6 to 104.5 GeV. The synchrotron radiation loss per turn reached some 3% of beam energy and it was the total available RF voltage and power, respectively, that determined LEP maximum energy and luminosity of $10^{32} \text{ cm}^{-2}\text{s}^{-1}$. At a beam energy of 98 GeV, LEP operated with a beam-beam parameter $\xi \approx 0.083$, i.e., the total beam-beam tune shift for four interaction points was $n_{\text{IP}}\xi \approx 0.33$. In the last year of operation, 288 SRF cavities were powered by 36 klystrons with an average power of 0.6 MW each and provided $V_{\text{RF}} = 3.63 \text{ GV}$. Up to about 60 GeV, LEP used resonant depolarization to measure the beam energy with 0.001% accuracy.

31.3.4 SLC

Based on an existing 3-km long 2.85 GHz warm RF linac, the SLC [26] was the first and only linear collider. It was operated from 1987 to 1998 with a constant beam energy of 45.6 GeV, up to about 80% electron-beam polarization, quasi-flat beams, a final-focus optics with local chromatic correction based on four interleaved sextupoles and $\beta_y^* \approx 1 \text{ mm}$. In its last year, SLC achieved a peak luminosity of about $3 \times 10^{30} \text{ cm}^{-2}\text{s}^{-1}$, roughly half of the design value. The SLC had a high-efficiency positron source providing $5 \times 10^{12} e^+$ per s for 120 Hz injection into the linac. It also employed the *BNS damping* to suppress the single-bunch beam break up instability, and also demonstrated an about 2-fold increase of luminosity from *disruption enhancement* due to the mutual focusing of the colliding electron and positron bunches at the interaction point.

31.4 Presently Operating Colliders

31.4.1 LHC

With a beam energy of 6.8 TeV (to be raised to the design value of 7 TeV through consolidation and magnet training), the superconducting Large Hadron Collider [27] presently is the world's highest energy collider. In the latest runs, peak luminosities of up to $2.1 \times 10^{34} \text{ cm}^{-2}\text{s}^{-1}$ have been achieved at 13 TeV c.m. - more than twice the design value (the current status is best checked at the Web site [28]). To meet its luminosity goals, the LHC operates with a high beam current of approximately 0.5 A, leading to stored energies of about 330 MJ per beam. Controlled energy deposition and component protection are given a high priority and a sophisticated highly efficient system of more than 100 beam collimators is employed [29]. At the energy of about 7 TeV per particle, synchrotron radiation poses a challenge, as the cryogenic system must remove roughly 7 kW due to synchrotron radiation, intercepted with a specially designed *beamscreen* inside the vacuum chamber, at a temperature of about 5–20 K, to be compared with a temperature of 1.9 K for the magnet cold bore. The elevated temperature allows for a more energy-efficient removal of beam-induced heat. The beamscreen also provides an effective cryo-pump for the vacuum system. When synchrotron-radiation photons hit the beamscreen, they can generate photoelectrons. These photoelectrons, and also any other electrons generated in the vacuum system, e.g. by residual-gas ionization, are accelerated in the electric field of the beam and may multiply via secondary-electron emission, with consequent electron cloud development. To mitigate this issue, the beamscreen is regularly subjected to beam-induced surface conditioning (*scrubbing*), thereby lowering the secondary emission yield. The two proton beams of 2556 bunches spaced by 25 ns are contained in separate pipes throughout most of the circumference and are brought together into a single 130 m long beam pipe at the interaction points. To avoid approximately 30 head-on collisions a small crossing angle of about 0.3 mrad is employed, which reduces the luminosity by about 15%. Still, the bunches moving in one direction experience multi-

ple long-range encounters with the counter-rotating bunches and the resulting perturbations of the particle motion substantially contribute to the beam lifetime reduction. The dominant source of approximately 8 hour characteristic luminosity decay time is proton burn-off due to inelastic pp interaction with $\sigma_{\text{in}} \approx 81 \text{ mbarn}$, corresponding to *pile-up* of up to 50 (number of events per individual bunch crossing). In special physics runs with a few bunches and large β^* , the LHC achieved a head-on beam-beam tune shift of $n_{\text{IP}}|\xi| \approx 0.02$ with $n_{\text{IP}} = 2$, about twice as high as in regular operation.

The Tables also show the LHC luminosity performance in Pb-Pb collisions, which for the ATLAS and CMS experiments well exceeded the design value, while for the ALICE experiment, the luminosity is *levelled* near the Pb-Pb design value of $10^{27} \text{ cm}^{-2}\text{s}^{-1}$. The LHC can also provide Pb-p collisions as it did in 2013 and 2016, and other ion-ion or ion-proton collisions, at different energies.

In the coming years, an ambitious upgrade program, HL-LHC [30], with the accompanying LHC Injectors Upgrade [31], has as its target an order-of-magnitude increase in integrated luminosity through doubling the proton beam current, the utilization of new larger aperture Nb₃Sn superconducting final quadrupoles to allow squeezing the β^* to as low as 10 cm, superconducting compact *crab cavities* and luminosity leveling also for ATLAS and CMS as its key ingredients.

31.4.2 Electron-Positron Rings

Asymmetric energies of the two beams allow for the enhancement of *B*-physics research and for interesting interaction region designs. SuperKEKB operates with 7 GeV electron and 4 GeV positron beams since 2018 and is aiming for luminosities of $8 \times 10^{35} \text{ cm}^{-2}\text{s}^{-1}$ [32]. By summer 2022, a world record luminosity of $4.7 \times 10^{34} \text{ cm}^{-2}\text{s}^{-1}$ has been reached, still at rather low beam currents. Vertical beam-beam tune shifts of $\xi_y \approx 0.05$ for the 4 GeV positron beam, and $\xi_y \approx 0.03$ for the 7 GeV electron beam have been achieved. These values are still about a factor of two lower than at the previous KEKB. Since 2020 SuperKEKB operates with a virtual *crab-waist* collision scheme, first developed for the FCC-ee design [33]. The original crab-waist scheme, based on additional sextupole magnets, was earlier implemented at DAΦNE [34]. The general crab-waist concept combines a large Piwinski angle Φ , and an extremely low $\beta_y^* (\ll \sigma_z)$ with the cancellation of the transverse betatron resonances which occur under conditions of $kQ_x + lQ_y = n$, where k, l, n are integers. The latter is achieved by means of existing or additional electromagnetic sextupoles with special betatron phase advances to the collision point [35]. The crab-waist collision scheme has become a design choice for all proposed future e^+e^- circular colliders.

Beside SuperKEKB and DAΦNE, three other e^+e^- ring colliders currently in operation are VEPP-2000 with \sqrt{s} up to 2.0 GeV, BEPC-II with \sqrt{s} up to 4.6 GeV and VEPP-4M with maximum c.m.e. of 12 GeV [1].

31.4.3 RHIC

The Relativistic Heavy Ion Collider [36] employs 3.45 T Nb-Ti superconducting magnets, and collides combinations of fully-stripped ions such as H-H ($p-p$), p -Al, p -Au, d -Au, h -Au, Cu-Cu, Cu-Au, Zr-Zr, Ru-Ru, Au-Au, and U-U over a wide energy range. The high charge per particle (+79 for gold, for instance) makes intra-beam scattering of particles within the bunch a special concern, even for seemingly moderate bunch intensities. In 2012, 3-D stochastic cooling was successfully implemented in RHIC [37] and is now routinely used. With stochastic cooling, steady increases in the bunch intensity, and numerous other upgrades, RHIC now operates at 44 times the Au-Au design average luminosity. Unique among high energy colliders, RHIC heavy ions beams cross the *transition energy* $\gamma_{\text{rmt}} = 1/\sqrt{\alpha_c}$ during acceleration – see Eqs.(31.11, 31.12) – a point where the derivative with respect to momentum of the revolution period is zero. This period of time is kept as short as allowed by the magnet ramp rate and must be dealt with carefully.

RHIC is also unique in its ability to accelerate and collide polarized proton beams. As proton beam polarization must be maintained from its low-energy source, successful acceleration through

the myriad of depolarizing resonance conditions in high energy circular accelerators has taken years to accomplish [38]. An energy of 255 GeV per proton with 60% final polarization per beam has been realized. As part of a scheme to compensate the head-on beam-beam effect, electron lenses operated routinely during the record high beam-beam parameter polarized proton operation at 100 GeV energy in 2015 [39].

31.5 Future High Energy Colliders and Prospects

Modern nuclear physics and high energy particle physics face critical questions which require next-generation high-energy and high-intensity experiments using hadron-hadron, lepton-lepton, and lepton-proton colliding-beam facilities. Understanding the structure of the proton and neutron directly from the dynamics of their quarks and gluons governed by the quantum chromodynamics calls for new ion-ion and electron-ion colliders. Two types of colliders are generally aspired by the HEP community [40, 41]: i) Higgs factories with a c.m.e. of 240–250 GeV in e^+e^- collisions for precision studies of the Higgs boson ($m_H = 125$ GeV) and exploration of the Higgs sector in greater detail, including measurements of Higgs couplings to fermions and vector bosons, self-coupling, rare decays, mass and width, that can also deliver other electroweak precision physics, e.g. on the Z -pole (91 GeV c.m.e.), at the W -pair threshold (about 160 GeV), and when run as a top quark factory (365–380 GeV); and ii) colliders with c.m.e. levels significantly beyond those of the LHC to explore the energy frontier for potential discoveries through direct searches in pp , $\mu\mu$, and e^+e^- interactions. In addition, precision physics at future high-luminosity factories operating at the τ -charm energy also provides sensitivity to new physics at multi-TeV energies and beyond. A comprehensive review of the future colliders' projects, ideas, and R&D activities can be found in Ref. [1]; Ref. [42] presents comparative analysis of implementation challenges of numerous future HEP collider proposals. Below we only briefly summarize leading collider proposals for construction over the next several decades which rely mostly on currently available technologies, such as normal-conducting (NC) or SC RF and/or NC or SC magnets, some of them requiring reasonable scope and duration mission-oriented development programs, as well as advanced schemes based on plasma acceleration and other innovative ideas. Tentative parameters of some of the colliders discussed, or mentioned, in this section are summarized in Table 31.1 and Table 31.2.

31.5.1 Ion-Ion and Electron-Ion Colliders

NICA (Nuclotron-based Ion Collider FAcility) is a new accelerator complex under construction at the Joint Institute for Nuclear Research (JINR, Dubna, Russia) to study properties of hot and dense baryonic matter, strong interactions between quarks and gluons, and spin physics [43]. NICA will provide a variety of beam species, ranging from protons and polarized deuterons to massive gold ions. The 500 m circumference SC magnet based collider is designed for average luminosity in heavy ion and light ion interactions at $\sqrt{s_{NN}}=4\text{--}11$ GeV of $1 \times 10^{27} \text{cm}^{-2} \text{s}^{-1}$ for a variety of nuclei up to $^{197}\text{Au}^{79+}$, and for polarized proton and deuteron collisions at $\sqrt{s}=12\text{--}27$ GeV with $\mathcal{L}=(1\text{--}10) \times 10^{31} \text{cm}^{-2} \text{s}^{-1}$. NICA major accelerator challenges include strong intrabeam scattering and space-charge effects which will be mitigated by extensive use of electron and stochastic cooling systems.

The recently announced Electron-Ion Collider (EIC) for nuclear physics research will be built at Brookhaven National Laboratory in the US and arrange collisions between an the reconfigured RHIC with a 41–275 GeV proton beam and a 5–18 GeV electron beam stored in a new ring (eRHIC) [44]. The EIC physics requirements [45], include highly polarized ($P_{e,n} \sim 70\%$) electron and nucleon beams (as the precision of measurements of interest scales as $\mathcal{L}P_e^2P_n^2$), a spectrum of ion beams from deuterons to the heaviest nuclei (U or Pb), variable c.m.e. values from $\sqrt{s}=20$ GeV to 140 GeV, high luminosities of up to $10^{33\text{--}34} \text{cm}^{-2} \text{s}^{-1}$, as well as possibilities of having more than one interaction region. Main accelerator design challenges on the path to the required energy, luminosity, and polarization, include the development of SRF crab-cavities and advanced SC magnets for interaction re-

gion focusing, energy-recovery linac (ERL) based electron cooling of hadron beams, essential to attain luminosities two orders of magnitude beyond the predecessor HERA ep collider, and high intensity polarized particle sources, augmented by the development of special magnets and operational techniques to preserve the polarization through the acceleration process to the collisions, including swap-out injection.

31.5.2 Higgs/Electroweak Factories

Higgs factory proposals generally aim at improving the precision of coupling measurements of Higgs boson, top quark, W and Z by an order of magnitude or more compared with previous studies. Two proposals for ~ 100 km circumference circular e^+e^- colliders have recently gained momentum: the Future Circular Collider (FCC-ee) at CERN [33] and the Circular Electron-Positron Collider (CEPC) in China [46]. Design philosophy of these machines assumes use of the maximum RF power available to compensate $O(100 \text{ MW})$ synchrotron radiation losses $P_{SR} = 2I \cdot \Delta E_{SR}$ and operation at the beam-beam limit ξ_y that yields peak luminosity:

$$\mathcal{L} = \frac{3}{16\pi r_0^2 (m_e c^2)} \frac{P_{SR} \xi_y \rho}{\beta_y^* \gamma^3}, \quad (31.17)$$

that scales approximately as $1/E_b^{3.5}$ for practical limits on P , ξ_y and β_y^* . The short beam lifetime at the high target luminosity, due to radiative Bhabha scattering, requires these machines to be constructed with a full-energy injector ring installed in the same tunnel to *top off* the electron and positron currents in the collider rings operating at constant energy. Beamstrahlung introduces an additional beam lifetime limitation depending on momentum acceptance (so that achieving sufficient off-momentum dynamic aperture becomes one of the design challenges), as well as some bunch lengthening.

These ambitious, large-scale projects based on well-established technologies are not extendable to TeV or multi-TeV energies, but they offer several important advantages that include the potential for much higher luminosities, and, thus, higher precision, the ability to operate multiple experiments simultaneously, and their ~ 100 km circular tunnels that could later house $O(100 \text{ TeV})$ hadron colliders. The high energy efficiency of circular e^+e^- colliders is further boosted by advances in RF power sources, by improved SC cavities, and by innovative low-power magnet systems including ones based on high-temperature superconductors (HTS) at moderate magnetic field.

For more than four decades, efforts have been devoted to developing high-gradient RF technology linear e^+e^- colliders in order to overcome the synchrotron radiation limitations of circular e^+e^- machines. The International Linear Collider (ILC), with a c.m.e. of 250 GeV in e^+e^- collisions, has been under consideration for more than two decades and could potentially be upgraded to $\sqrt{s}=500$ GeV and further to 1 TeV. CERN's Compact Linear Collider (CLIC) design, developed since the mid-1980s, also includes possible upgrades, from an initial 380 GeV c.m.e. to ultimately 3 TeV, which would enable searches for new particles of significantly higher masses.

The primary challenge confronting a high energy, high luminosity single pass collider design is the beam power requirement, so that measures must be taken to keep the demand within bounds as illustrated in a transformed Eq.(31.15):

$$\mathcal{L} = \frac{1}{8\pi\alpha r_0} \frac{P_{\text{wall}}}{\sqrt{s}} \frac{\eta}{\sigma_y^*} N_\gamma H_D. \quad (31.18)$$

Here, P_{wall} is the total wall-plug power of the collider, to be converted into beam power $P_b = 2f_0 N E_b$ with efficiency η , $N_\gamma \approx 2\alpha r_0 N / \sigma_x^*$ is the number of beamstrahlung photons emitted per e^\pm ($\alpha \approx 1/137$ denotes the fine-structure constant), and the last factor H_D , typically between 1 and 2, represents the enhancement of luminosity due to the *pinch effect*, the additional focusing occurring during the collision of oppositely charged bunches. The management of P_{wall} leads to an upward push on the bunch population N with an attendant rise in the energy radiated due to the electromagnetic field of one bunch acting on the particles of the other (beamstrahlung). Keeping a significant fraction of the

Table 31.1: Tentative parameters of selected future e^+e^- high-energy colliders. Parameters associated with different beam energy scenarios are comma-separated; H and V indicate horizontal and vertical directions.

	FCC-ee	CEPC	ILC	CLIC
Species	e^+e^-	e^+e^-	e^+e^-	e^+e^-
Beam energy E_b (GeV)	46, 120, 183	46, 120, 180	125, 250	190, 1500
Circumference or length (km)	90.66	100	20.5, 31	11, 50
Interaction regions	4	2	1	1
Est. integrated luminosity per experiment ($\text{ab}^{-1}/\text{year}$)	17, 0.6, 0.15	15, 0.65, 0.07	0.2, 0.3	0.1, 0.6
Peak lumi. \mathcal{L}/IP ($10^{34}\text{cm}^{-2}\text{s}^{-1}$)	140, 5.0, 1.25	115, 5.0, 0.5	1.4, 1.8	1.5, 6
Rep.rate (Hz, f_{rev} for rings)	3307	3000	5	50
Polarization (%)	≥ 10 , 0, 0	5–10, 0, 0	80/30 (e^-/e^+)	80/0 (e^-/e^+)
Time between collisions (μs)	0.025, 0.3, 2.5	0.025, 0.68, 2.6	0.55	0.0005
Energy spread (rms, 10^{-3})	1.09, 1.43, 1.92	1.3, 1.7, 2.0	e^- : 1.9, 1.2 e^+ : 1.5, 0.7	3.5
Bunch length σ_z (rms, mm)	15.5, 4.7, 2.2	8.7, 3.9, 2.9	0.3	0.07, 0.044
IP beam size σ^* (rms, μm)	H: 9, 13, 40 V: 0.04, 0.04, 0.05	H: 5.9, 14, 38 V: 0.04, 0.04, 0.11	H: 0.52, 0.47 V: 0.008, 0.006	H: 0.15, 0.04 V: 0.003, 0.001
Emittance, ε_n (rms, μm)	H: 63, 167, 568 V: 0.17, 0.3, 0.6	H: 24, 150, 493 V: 0.12, 0.3, 1.7	H: 5, 10 V: 0.035, 0.035	H: 0.95, 0.66 V: 0.03, 0.02
β^* at interaction point (cm)	H: 11, 24, 100 V: 0.07, 0.1, 0.16	H: 13, 33, 104 V: 0.09, 0.1, 0.27	H: 1.3, 1.1 V: 0.041, 0.048	H: 0.8, 0.69 V: 0.01, 0.0068
Full crossing angle θ_c (mrad)	30	33	14	20
Crossing scheme	crab waist	crab waist	crab crossing	crab crossing
Piwinski angle $\Phi = \sigma_z \theta_c / (2\sigma_x^*)$	26, 5.4, 0.8	24, 4.8, 1.3	0	0
Beam-beam param. ξ_y (10^{-3})	97, 88, 134	110, 127, 100	n/a	n/a
Disruption parameter D_y	1.3, 0.9, 2.0	0.6, 1.3, 0.8	35, 25	13, 8
Average Upsilon Υ (10^{-2})	0.01, 0.04, 0.06	0.02, 0.04, 0.05	3, 6	17, 500
RF frequency f_{RF} (MHz)	400, 400, 800	650	1300	11994
Particles per bunch N (10^{10})	21, 12, 16	14, 13, 20	2	0.52, 0.37
Bunches per beam n_b	11200, 440, 60	11951, 249, 35	1312 (pulse)	352, 312 (trains at 50 Hz)
Average beam current I_b (mA)	1270, 27, 4.9	804, 16.7, 3.3	0.021	0.014, 0.009
Injection energy (GeV)	on E_b (top off)	on E_b (top off)	5.0 (linac)	9.0 (linac)
RF gradient G (MV/m)	5.7, 10.6, 20.1	17.4, 24.9, 27.6	31.5	72, 100
Total SR power loss (MW)	100	60	n/a	n/a
Total beam power (MW)	n/a	n/a	5.3, 10.5	5.6, 28
Key technology	—	—	high grad. SC RF	two-beam accel.

Table 31.2: Tentative parameters of selected future high-energy hadronic and muon colliders. Parameters associated with different particle species for NICA and EIC, and different beam-energy scenarios for a muon collider, are comma-separated. Quantities are, where appropriate, r.m.s.; unless noted otherwise, energies refer to beam energy; H and V indicate horizontal and vertical directions. Parameters of HL-LHC can be found in the High-Energy Collider Parameters review tables.

	NICA	EIC	FCC-hh	SPPC	$\mu\mu$ collider
Species	ion-ion, pp	ep , e -ion	pp	pp	$\mu^+\mu^-$
Beam energy E_b (TeV)	10^{-3} -(4.5/u, 13)	0.01(e),0.275(p)	40-58	62.5	0.063, 5
Circumference C (km)	0.503	3.834	90.66	100	0.3, 10
Interaction regions	2	1(2)	4	2	1, 2
Est. integr. luminosity per exp. ($\text{ab}^{-1}/\text{year}$)	10^{-8} ,-3 (ii , pp)	0.1	0.2–1.0	0.6	0.001, 2.0
Peak luminosity \mathcal{L} ($10^{34}\text{cm}^{-2}\text{s}^{-1}$)	10^{-7} ,-2 (ii , pp)	1.05	5–30	4.3	0.008, 20
Rep.rate (Hz, f_{rev} for rings)	$5.9 \cdot 10^5$	$7.8 \cdot 10^4$	3307	3000	15, 5
Time between collisions (μs)	0.077	0.009	0.025	0.025	1, 33
Energy spread (rms, 10^{-3})	1.6 (Au)	0.6 (e), 0.7 (p)	0.1	0.1	0.04, 1
Bunch length σ_z (rms, mm)	600	7 (e), 60 (p)	80	60	63, 1.5
IP beam size σ^* (H/V rms, μm)	360	95/8.5	6.7-3.5 (init.)	3.0 (init.)	75, 0.9
Emittance ε_n (H/V rms, mm mrad)	1.1	11.3/1.0 (e), 9.2/1.6 (p)	2.2 (init.)	1.2 (init.)	200, 25
Beta function at IP β^* (H/V cm)	60	45/5.6 (e), 80/7.2 (p)	110–30	50	1.7, 0.15
Beam-beam param. ξ (10^{-3} H/V)	25	72/100 (e),12 (p)	5–15	15	22, 78
RF frequency f_{RF} (MHz)	13/39	591	400	400/200	805/1300
Particles per bunch N (10^{10})	0.23	17.2(e), 6.9(p)	10	4	400, 180
Bunches per beam n_b	22	1160	9648	10082	1
Average beam current I_b (mA)	480	2500(e),1000 (p)	500	190	640, 9 (peak)
Injection energy (GeV)	1-3.8	on E_b (e), 25 (p)	≥ 1000	3200	on E_b
Peak magnetic field B (T)	1.8	0.248 (e), 3.80 (p)	14-20	20	10
Polarization (%)	0(i), >50 (p)	> 70 (e), >70 (p)	0	0	0
SR power loss/beam (MW)	10^{-6}	10(e), $< 10^{-6}$ (p)	1.0-4.25	2.2	10^{-3} , 0.16
Key technology	electron and stoch. cooling	strong hadron cooling	Nb ₃ Sn/HTS magnets	HTS magnets	muon prod. & cooling

luminosity close to the nominal energy represents a design goal, which is met if N_γ does not exceed a value of about 1. A consequence is the use of flat beams, where N_γ is managed by the beam width, and luminosity adjusted by the beam height, thus the explicit appearance of the vertical beam size σ_y^* .

The ILC [47, 48] is based on 1.3 GHz standing-wave superconducting accelerating structures operating at 2 K with 31.5 MV/m average gradient, up to 8 nm vertical beam size at the IP, and luminosity comparable to the LHC. Progress toward higher field gradients and Q values continues to be made, with nitrogen-doping techniques being a recent example [49]. CLIC is based on a novel two-beam acceleration scheme [50]. Here, room-temperature NC copper high-gradient 12 GHz accelerating structures are powered by a high-current 1.9 GeV drive beam to efficiently enable accelerating gradients of up to 100 MV/m (though optimal $G=70$ MV/m for the first CLIC stage at $\sqrt{s}=380$ GeV, and for this stage an alternative RF power drive option with 12 GHz klystrons powering is also being considered). To reach their design luminosities, both CLIC and ILC require unprecedented rates of positron production about 40 times the world record set by the SLC positron source, and very tight control of imperfections, such as $O(10 \mu\text{m})$ accuracy of pre-alignment of the main linac and beam delivery system components at the level, suppression of fast vibrations of the quadrupoles due to ground motion to $O(1 \text{ nm})$ level at frequencies above 1 Hz, advanced beam-based trajectory tuning, and mitigation of the effect of wakefields [51].

Recent developments of the RF technologies show promise of more compact linear e^+e^- Higgs/Electroweak factories based on either ~ 70 MV/m travelling-wave 1.3 GHz SRF structures [52] or on 70–120 MV/m high-efficiency, distributed RF coupling, normal-conducting cold copper 5.7 GHz accelerating cavities at liquid nitrogen temperature [53].

There are a number of alternative ideas proposed for studies of the Higgs/Electroweak physics, such as high-energy, high-luminosity e^+e^- collider in a 100 km tunnel using ERLs to accelerate particles to collision energy in 4 to 6 passes and return up to 81% of the energy back into the SRF cavities on deceleration turns, thus, lowering the required facility power several-fold [54]; similar power recovery in one pass can greatly improve efficiency of linear colliders [55–57]; an arrangement of $\gamma\gamma$ collision through near-IP conversion of high energy electron beams into intense photon beams by backward Compton scattering off a high-power laser [58, 59] or off an FEL photon pulse [60, 61]; $\mu\mu$ Higgs factory with unprecedented 0.004% energy resolution [62], and a high-energy lepton-hadron collider bringing into collision a 60-GeV electron beam from an ERL with the 7 TeV protons circulating in the LHC (LHeC) [63]. At lower energies, Super Tau-Charm Factory proposals aim at the production and precise study of charmonium states and of the tau lepton [64, 65].

31.5.3 Energy Frontier Circular Colliders

Several hadron and lepton colliders have been proposed to extend the energy reach beyond the LHC. As noted above, ambitious plans have been proposed to upgrade the FCC and CEPC to hadron colliders – FCC-hh at CERN and Super Proton Proton Collider (SPPC) in China, respectively – by means of next- or next-next generation SC magnets installed in the arc sections of the 100 km rings, so as to enable \sqrt{s} of the order 100 TeV or above [66, 67]. Comparable discovery reach is expected for a circular 10–14 TeV muon collider [68], significantly beyond that of practical e^+e^- linear colliders.

The maximum beam energy Eq.(31.1) is directly proportional to the magnetic field and to the ring circumference, hence, future hadron colliders like FCC-hh and SppC rely on the development of the technology of 14–16 T Nb_3Sn dipole magnets [69] or dipole magnets based on high-temperature superconductors (HTS) with a field of up to 18–20 T, including iron-based HTS [70]. Though higher fields are possible with HTS, more cost-effective might be hybrid magnet designs incorporating Nb-Ti, Nb_3Sn , and an inner layer of HTS and providing fields of about 20 T. Another important technology is the cryogenic beam vacuum system, which has to cope with unusually high levels of synchrotron radiation (up to 15 MW in total, for FCC-hh) in a cold environment. The beam-screen intercepting the radiation inside the cold bore of the

magnets should operate at or above 50 K — significantly higher temperature than in the LHC.

Design luminosities of these hadron colliders $O(10^{35} \text{ cm}^{-2}\text{s}^{-1})$ will result in a pile-up of events per crossing $O(500)$ (from up to 50 in LHC) and fast intensity drop due to burn-off. Significant radiation damping of beam emittances will naturally level luminosity evolution, though the total beam-beam tune shift $n_{\text{IP}}\xi \sim (0.01 - 0.03)$ might need a special control as it will increase during the store [71].

Future hadron colliders are characterized by record high stored beam energy, e.g. 6–9 GJ in FCC-hh, rendering machine protection a paramount concern. A very challenging multi-stage collimation system is needed to avoid local beam loss spikes near cold magnets, which would induce magnet quenches. The primary and secondary collimators of the LHC are based on carbon-carbon composite material. For the future hadron colliders, ever stronger materials are being developed and examined, which also feature higher conductivity and, hence, lower impedance. More advanced options include the use of short bent crystals as primary collimators [72] and the deployment of hollow electron-beam lenses as non-destructible collimators [73].

It is noteworthy that machines like FCC-hh or SPPC can additionally be used for ion-ion/ion-proton collisions; their high-energy proton beams can also be collided with high-intensity $O(60 \text{ GeV})$ electrons from an ERL resulting in c.m.e. of 3.5 TeV.

The lifetime of the muon, $\gamma\tau_0$ where $\tau_0=2.2\mu\text{s}$, is sufficient to allow fast acceleration to high energy before most, or all, of the muons decay, and storage for some 300B turns in a ring with an average bending magnets field of B (in units of Tesla). The muon to electron mass ratio of 210 implies removal of the synchrotron radiation barrier and possibility of a muon collider facility scale to a level compatible with on-site placement at existing accelerator laboratories. High-energy muon colliders, as presently conceived, are predicted to be more compact, more power-efficient and significantly less expensive than the equivalent energy-frontier hadron or e^+e^- machines [74], and a neutrino factory could potentially be realized in the course of their construction [75]. The Higgs production cross-section in the s -channel is enhanced by a factor of $(m_\mu/m_e)^2$ compared to that in e^+e^- collisions.

The average luminosity of a muon collider,

$$\langle \mathcal{L} \rangle = f_0 \gamma^2 \frac{c\tau_0}{2C} \frac{n_b N^2}{4\pi\epsilon_n \beta^*} \mathcal{F} = B P_b \frac{N r_0}{4\pi\epsilon_n \beta^*} \gamma \left(\frac{c\tau_0 \mathcal{F}}{8\pi e} \right), \quad (31.19)$$

scales with B , the total beam power P_b , and the beam brightness – the third factor above is nothing but the muon beam-beam tune shift Eq. (31.16). There is an obvious incentive to have all the particles in just one bunch per beam. The beta-function at the two IPs $\beta^* \approx \sigma_z$ scales as $1/\gamma$ within certain range of energies, giving overall scaling $\langle \mathcal{L} \rangle \propto \gamma^2$ with other limiting parameters fixed. The main challenges to luminosity achievement with decaying particles are related to production and fast cooling and acceleration of $O(10^{12})$ muons per bunch without emittance degradation. A multi-TeV c.m.e. high luminosity $O(10^{34} \text{ cm}^{-2}\text{s}^{-1})$ muon collider would consist of [76]: (i) a high power proton driver (e.g., 8 GeV 2–4 MW H^- SRF linac), (ii) pre-target accumulation and compressor rings, in which high intensity 1–3 ns long proton bunches are formed, (iii) a liquid-mercury or other high-power target for converting the proton beam into a tertiary muon beam with energy of about 200 MeV, (iv) a multi-stage ionization cooling section that reduces transverse and longitudinal emittances by several orders of magnitude and creates a low emittance beam, similarly to that recently demonstrated [77], (v) a multistage acceleration system, possibly employing either rapid cycling synchrotrons or RLAs to accelerate muons in a modest number of turns up to the final energy using superconducting RF technology, and, finally, (vi) a 3–14 km diameter collider ring, where counter-propagating muon beams are stored and collide over the roughly 3000 turns corresponding to the muon lifetime.

The intense neutrino flux originating from the multi-TeV muon beams decaying in the collider poses another challenge — the need to minimize the environmental impact. The collider complex is usually located underground and when the produced neutrinos emerge at the surface, a small fraction interacts with the rock (and

other material) and produces ionizing radiation dose scaling as γ^3 . The impact of this neutrino-induced radiation can be mitigated, for example, by continually adjusting the orbits of the beams to spread them out on a wider area, by deeper collider tunnels or with a further reduced emittance of the muon beam so that the required luminosity could be obtained using a substantially smaller number of muons.

31.5.4 Plasma Acceleration and Other Advanced Concepts

Since about the mid-1950s, it has been understood that collective plasma-based accelerators promise extremely large accelerating gradients, approximately three orders of magnitude greater than ~ 100 MV/m obtained in conventional breakdown limited RF structures [78]. Ionized plasmas can sustain electron plasma density waves with electric fields in excess of $E_0 = cm_e\omega_p/\epsilon$ or

$$E_0 \approx 96 \text{ [V/m]} \sqrt{n_0[\text{cm}^{-3}]}, \quad (31.20)$$

where n_0 denotes the ambient electron number density and $\omega_p = \sqrt{e^2 n_0 / (m_e \epsilon_0)}$ is the electron plasma frequency [79].

Such gradients can be effectively excited by either powerful external pulses of laser light or by electron bunches if they are shorter than the plasma wavelength $\lambda_p = c/\omega_p \approx 1 \text{ mm} \times \sqrt{10^{15} \text{ cm}^{-3}/n_0}$, or by longer beams of protons if their charge density is modulated with the period of λ_p . In the past decade, we have seen impressive progress in the plasma wakefield acceleration of high-quality beams. Laser-driven electron energy gain of about 8 GeV over 20 cm of plasma with density $3 \times 10^{17} \text{ cm}^{-3}$ has been demonstrated at the BELLA facility at the Lawrence Berkeley National Laboratory (LBNL) [80]. Short electron bunches were used to boost the energy of externally injected electron bunches by 9 GeV over 1.3 m of $\sim 10^{17} \text{ cm}^{-3}$ plasma at the FACET facility in SLAC [81]. The AWAKE experiment at CERN used self-modulating long 450 GeV proton bunches to accelerate electrons to 2 GeV over 10 m of 10^{15} cm^{-3} plasma [82].

Whether plasma acceleration will find application in an HEP facility is not yet clear, given the necessity of staging and phase-locking acceleration in multiple plasma chambers [83]. Another critical issue is the power efficiency η for a collider based on plasma acceleration, whose luminosity would still be described by Eq. (31.18). Positrons can be accelerated as well but, contrary to electrons, plasma-wakefields will naturally defocus positively charged particles. Such fundamental deficiency can be addressed, e.g., in more complicated plasma acceleration schemes for e^+ [84]; or by acceleration of electrons in both linacs with conversion into a $\gamma\gamma$ collider at the IP. In addition, many novel approaches have been proposed to extend the energy or physics reach of future particle colliders, reduce their cost, and improve their luminosity or energy efficiency. Those include: i) *dielectric wakefield accelerators* in which resonant dielectric accelerating structures are fed by ultra-short RF pulses of wakefields driven by either collinear or preceding high charge electron bunches and withstand 270 MV/m operational accelerating gradients [85]; ii) *dielectric laser accelerators* – micron-size dielectric accelerating structures driven by a laser and supporting $O(1 \text{ GV/m})$ accelerating fields [86]; iii) compact *linear muon crystal colliders* with ultimate energies $O(1\text{--}10 \text{ PeV})$ [87] based on 1–10 TeV/m wakefield acceleration of muons (instead of electrons or hadrons) channeling between the planes in crystals or inside carbon nanotubes (CNT) with charge carrier density $\sim 10^{20\text{--}22} \text{ cm}^{-3}$ [88]; iv) the *Gamma Factory* concept [89], where frequent bursts of gamma rays are generated by repeatedly colliding a partially stripped heavy-ion beam circulating in the LHC, or in a future higher-energy hadron storage ring like the FCC-hh, with a conventional laser pulse, profiting from two Lorentz boosts. Active R&D programs are presently underway worldwide to determine the suitability of novel technologies for use in future high-energy colliders.

References

[1] V. Shiltsev and F. Zimmermann, *Reviews of Modern Physics* **93**, 1, 015006 (2021).
 [2] A. Tollestrup and E. Todesco, in “Reviews Of Accelerator Science And Technology: Volume 1,” 185–210, World Scientific (2008).

[3] D. A. Edwards and M. J. Syphers, *An introduction to the physics of high energy accelerators*, John Wiley & Sons, New York, NY (2008).
 [4] A. W. Chao, *Physics of collective beam instabilities in high energy accelerators*, Wiley, New York, NY (1993), URL <https://cds.cern.ch/record/246480>.
 [5] S.-Y. Lee, *Accelerator physics*, World Scientific, Singapore (2018).
 [6] E. D. Courant and H. S. Snyder, *Annals of physics* **3**, 1, 1 (1958).
 [7] H. Wiedemann, *Particle accelerator physics*, Springer Nature (2015), URL <https://library.oapen.org/handle/20.500.12657/23641>.
 [8] M. Sands, *Conf. Proc. C* **6906161**, 257 (1969).
 [9] S.-Y. Lee, *Spin dynamics and snakes in synchrotrons*, World Scientific Publishing Company (1997).
 [10] F. Zimmermann, *Physical Review Special Topics-Accelerators and Beams* **7**, 12, 124801 (2004).
 [11] A. W. Chao *et al.*, editors, *Handbook of accelerator physics and engineering*, World Scientific, Hackensack, USA (2013), ISBN 9789814415842, URL <http://www.worldscientific.com/worldscibooks/10.1142/8543>.
 [12] A. Piwinski, J. D. Bjorken and S. K. Mtingwa, *Physical Review Accelerators and Beams* **21**, 11, 114801 (2018).
 [13] V. Parkhomchuk and A. Skrinsky, *Reviews of Accelerator Science and Technology* **1**, 01, 237 (2008).
 [14] M. Minty and F. Zimmermann, *Measurement and control of charged particle beams*, Springer Nature (2003), URL <https://library.oapen.org/handle/20.500.12657/23642>.
 [15] S. Myers, *Particle Physics Reference Library: Volume 3: Accelerators and Colliders*, volume 3, Springer Nature (2020), URL <https://library.oapen.org/handle/20.500.12657/39571>.
 [16] V. Shiltsev *et al.*, *Physical Review Special Topics-Accelerators and Beams* **8**, 10, 101001 (2005).
 [17] J. T. Seeman, *Observations of the beam-beam interaction*, Springer (1986).
 [18] R. Assmann, M. Lamont and S. Myers, *Nucl. Phys. B Proc. Suppl.* **109**, 17 (2002).
 [19] K. Yokoya and P. Chen, *Lect. Notes Phys.* **400**, 415 (1992).
 [20] H. T. Edwards, *Annual Review of Nuclear and Particle Science* **35**, 1, 605 (1985).
 [21] V. Lebedev and V. Shiltsev, *Accelerator physics at the Tevatron collider*, Springer (2014).
 [22] S. D. Holmes and V. D. Shiltsev, *Annual Review of Nuclear and Particle Science* **63**, 435 (2013).
 [23] G. Voss and B. Wiik, *Annual Review of Nuclear and Particle Science* **44**, 1, 413 (1994).
 [24] S. Myers and H. Schopper, *Landolt Börnstein* **21** (2013).
 [25] D. Brandt *et al.*, *Reports on Progress in Physics* **63**, 6, 939 (2000).
 [26] N. Phinney, eConf **C00082**, MO102 (2000), [arXiv:physics/0010008].
 [27] L. Evans, *Annual Review of Nuclear and Particle Science* **61**, 435 (2011).
 [28] CERN, The Large Hadron Collider web site: <http://lhc.web.cern.ch/lhc/>.
 [29] G. Valentino *et al.*, *Physical Review Special Topics-Accelerators and Beams* **15**, 5, 051002 (2012).
 [30] G. Apollinari *et al.*, Technical Report CERN Yellow Report: Monograph 2017-007-M (2017).
 [31] H. Damerou *et al.*, *LHC Injectors Upgrade, Technical Design Report* (2014), URL <https://cds.cern.ch/record/1976692>.
 [32] Y. Ohnishi *et al.*, *Progress of Theoretical and Experimental Physics* **2013(3)**, 3 (2013).

- [33] M. Benedikt *et al.*, The European Physical Journal Special Topics **228**, 2, 261 (2019).
- [34] M. Zobov *et al.*, Physical Review Letters **104**, 17, 174801 (2010).
- [35] P. Raimondi, D. N. Shatilov and M. Zobov (2007), [arXiv:physics/0702033].
- [36] M. Harrison, S. Peggs and T. Roser, Annual Review of Nuclear and Particle Science **52**, 1, 425 (2002).
- [37] M. Blaskiewicz, J. M. Brennan and K. Mernick, Phys. Rev. Lett. **105**, 094801 (2010).
- [38] M. Bai *et al.*, Physical Review Letters **96**, 17, 174801 (2006).
- [39] W. Fischer *et al.*, Phys. Rev. Lett. **115**, 26, 264801 (2015).
- [40] 2020 Update of the European Strategy for Particle Physics by the European Strategy Group, <https://home.cern/sites/home.web.cern.ch/files/2020-06/2020UpdateEuropeanStrategy.pdf> (2020), accessed: June 20, 2020.
- [41] J. N. Butler *et al.*, arXiv preprint arXiv:2301.06581 (2023).
- [42] T. Roser *et al.*, Journal of Instrumentation **18**, 05, P05018 (2023).
- [43] V. Kekelidze *et al.*, The European Physical Journal A **52**, 8, 211 (2016).
- [44] E. Beebe-Wang (ed.) *et al.*, Technical Report BNL Formal Report BNL-211943-2019-FORE, Brookhaven (2019).
- [45] A. Accardi *et al.*, The European Physical Journal A **52**, 9, 268 (2016).
- [46] CEPC Study Group (2018), [arXiv:1809.00285].
- [47] C. Adolphsen *et al.*, Technical Report arXiv:1306.6328. CERN-ATS-2013-037. IHEP-AC-ILC-2013-001. ILC-REPORT-2013-040. INFN-13-04-LNF. JINR-E9-2013-35. JLAB-R-2013-01. LLNL-TR-635539. comments: See also <http://www.linearcollider.org/ILC/TDR>. The full list of signatories is inside the Report, URL <http://cds.cern.ch/record/1601969>.
- [48] L. Evans and S. Michizono (Linear Collider) (2017), [arXiv:1711.00568].
- [49] A. Grassellino *et al.*, Supercond. Sci. Technol. **26**, 102001 (2013), [arXiv:1306.0288].
- [50] T. K. Charles *et al.* (CLICdp, CLIC), CERN Yellow Rep. Monogr. **1802**, 1 (2018), [arXiv:1812.06018].
- [51] T. O. Raubenheimer, Physical Review Special Topics-Accelerators and Beams **3**, 12, 121002 (2000).
- [52] S. Belomestnykh *et al.* (2022), [arXiv:2203.08211].
- [53] C. Vernieri *et al.*, Journal of Instrumentation **18**, 07, P07053 (2023).
- [54] V. N. Litvinenko, T. Roser and M. Chamizo-Llata, Physics Letters B **804**, 135394 (2020), ISSN 0370-2693, URL <http://www.sciencedirect.com/science/article/pii/S0370269320301982>.
- [55] M. Tigner, Il Nuovo Cimento (1955-1965) **37**, 3, 1228 (1965).
- [56] U. Amaldi, Physics Letters B **61**, 3, 313 (1976).
- [57] V. I. Telnov, Journal of Instrumentation **16**, 12, P12025 (2021).
- [58] V. Telnov, Journal of Instrumentation **9**, 09, C09020 (2014).
- [59] S. A. Bogacz *et al.* (2012), [arXiv:1208.2827].
- [60] C. Adolphsen *et al.* (2022), [arXiv:2207.02095].
- [61] T. Barklow *et al.*, Journal of Instrumentation **18**, 07, P07028 (2023).
- [62] Y. Alexahin, E. Gianfelice-Wendt and V. Kapin, Journal of Instrumentation **13**, 11, P11002 (2018).
- [63] P. Agostini *et al.*, Journal of Physics G: Nuclear and Particle Physics **48**, 11, 110501 (2021).
- [64] P. Piminov, Physics of Particles and Nuclei Letters **15**, 7, 732 (2018).
- [65] J. Lan *et al.*, Journal of Instrumentation **16**, 07, T07001 (2021).
- [66] M. Benedikt *et al.*, The European Physical Journal Special Topics **228**, 4, 755 (2019), ISSN 1951-6401, URL <https://doi.org/10.1140/epjst/e2019-900087-0>.
- [67] CEPC Study Group (2018), [arXiv:1809.00285].
- [68] H. Al Ali *et al.*, Reports on Progress in Physics **85**, 8, 084201 (2022).
- [69] D. Schoerling and A. V. Zlobin, *Nb₃Sn Accelerator Magnets: Designs, Technologies and Performance*, Springer Nature (2019).
- [70] E. Kong *et al.*, International Journal of Modern Physics A **34**, 13n14, 1940003 (2019).
- [71] M. Benedikt, D. Schulte and F. Zimmermann, Phys. Rev. ST Accel. Beams **18**, 101002 (2015).
- [72] W. Scandale and A. Taratin, Physics Reports **815**, 1 (2019).
- [73] V. Shiltsev, Journal of Instrumentation **16**, 03, P03039 (2021).
- [74] K. R. Long *et al.*, Nature Physics **17**, 3, 289 (2021).
- [75] S. Geer, Annual Review of Nuclear and Particle Science **59**, 347 (2009).
- [76] C. Ankenbrandt *et al.*, Physical Review Special Topics-Accelerators and Beams **2**, 8, 081001 (1999).
- [77] M. Bogomilov *et al.*, Nature **578**, 53 (2020).
- [78] V. Veksler, The Soviet Journal of Atomic Energy **2**, 5, 525 (1957).
- [79] T. Tajima and J. M. Dawson, Physical Review Letters **43**, 4, 267 (1979).
- [80] A. Gonsalves *et al.*, Physical Review Letters **122**, 8, 084801 (2019).
- [81] M. Litos *et al.*, Plasma Physics and Controlled Fusion **58**, 3, 034017 (2016).
- [82] E. Adli *et al.*, Nature **561**, 7723, 363 (2018).
- [83] D. Schulte, Reviews of Accelerator Science and Technology **9**, 209 (2016).
- [84] Z.Y. Xu *et al.*, Phys. Rev. Accel. Beams **23**, 091301 (2020).
- [85] C. Jing, Reviews of Accelerator Science and Technology **9**, 127 (2016).
- [86] E. Peralta *et al.*, Nature **503**, 7474, 91 (2013).
- [87] V. D. Shiltsev, Physics-Uspekhi **55**, 10, 965 (2012).
- [88] T. Tajima and M. Cavenago, Physical Review Letters **59**, 13, 1440 (1987).
- [89] D. Budker *et al.*, Annalen der Physik **532**, 8, 2000204 (2020).

32. High-Energy Collider Parameters

High-Energy Collider Parameters: e^+e^- Colliders (I)

Table 32.1: Updated in March 2024 with numbers received from representatives of the colliders (contact E. Pianori, LBNL). The table shows the parameter values achieved. Quantities are, where appropriate, r.m.s.; unless noted otherwise, energies refer to beam energy; H and V indicate horizontal and vertical directions; s.c. stands for superconducting. Parameters for the defunct SPEAR, DORIS, PETRA, PEP, TRISTAN, and VEPP-2M colliders may be found in our 1996 edition (Phys. Rev. **D54**, 1 July 1996, Part I).

	VEPP-2000 (Novosibirsk)	VEPP-4M (Novosibirsk)	BEPC (China)	BEPC-II (China)	DAΦNE (Frascati)
Physics start date	2010	1994	1989	2008	1999
Physics end date	—	—	2005	—	—
Maximum beam energy (GeV)	1.0	6	2.5	1.89 (2.474 max)	0.510
Delivered integrated luminosity per exp. (fb^{-1})	0.25	0.05	0.11	48	≈ 4.7 in 2001-2007 ≈ 2.7 w/crab-waist ≈ 6.8 2014-2018* ≈ 0.4 2021-2022† ≈ 1.1 2023-2024‡
Luminosity ($10^{30} \text{ cm}^{-2}\text{s}^{-1}$)	50	20	12.6 at 1.843 GeV 5 at 1.55 GeV	1096	453
Time between collisions (μs)	0.04	0.6	0.8	0.006	0.0027
Full crossing angle (μ rad)	0	0	0	2.2×10^4	5×10^4
Energy spread (units 10^{-3})	0.71	1	0.58 at 2.2 GeV	0.52	0.40
Bunch length (cm)	4	5	≈ 5	1.35	low current: 1 at 15mA: 2
Beam radius (10^{-6} m)	125 (round)	H:1000 V:30	H:890 V:37	H:347 V:4.5	H:260 V:4.8
Free space at interaction point (m)	± 0.5	± 2	± 2.15	± 0.63	± 0.295
Luminosity lifetime (hr)	continuous	2	7–12	1.5	0.2
Turn-around time (min)	continuous	18	32	4 (topping up)	2 (topping up)
Injection energy (GeV)	0.2–1.0	1.8	1.55	on energy	on energy
Transverse emittance (10^{-9} m)	H:150 V:150	H:200 V:20	H:660 V:28	H:121 V:1.56	H:260 V:2.6
β^* , amplitude function at interaction point (m)	H:0.05 - 0.11 V:0.05 - 0.11	H:0.75 V:0.05	H:1.2 V:0.05	H:1.0 V:0.0135	H:0.26 V:0.009
Beam-beam tune shift per crossing (units 10^{-4})	H:850 V:850	500	350	383	440/894 (crab-waist run/test)
RF frequency (MHz)	172	180	199.53	499.8	368.667
Particles per bunch (units 10^{10})	8	15	20 at 2 GeV 11 at 1.55 GeV	3.8	e^- : 3.2 e^+ : 2.1
Bunches per ring per species	1	2	1	119	100 to 110 (120 buckets)
Average beam current per species (mA)	160	80	40 at 2 GeV 22 at 1.55 GeV	910	e^- : 1250 e^+ : 800
Circumference or length (km)	0.024	0.366	0.2404	0.23753	0.098
Interaction regions	2	1	2	1	1
Magnetic length of dipole (m)	1.1	2	1.6	outer ring: 1.6 inner ring: 1.41	outer ring: 1.2 inner ring: 1
Length of standard cell (m)	12	7.2	6.6	outer ring: 6.6 inner ring: 6.2	n/a
Phase advance per cell (deg)	H:745 V:385	65	≈ 60	60–90 non-standard cells	—
Dipoles in ring	8	78	40 + 4 weak	84 + 8 weak	8
Quadrupoles in ring	24 + 4 s.c.	150	68	134+2 s.c.	48
Peak magnetic field (T)	2.4	0.6	0.903 at 2.8 GeV	outer ring: 0.677 inner ring: 0.766	1.2

*KLOE-2

†SIDDHARTINO

‡SIDDHARTA-2

High-Energy Collider Parameters: e^+e^- Colliders (II)

Table 32.2: Updated in March 2020 with numbers received from representatives of the colliders (contact E. Pianori, LBNL). The table shows the parameter values achieved. Quantities are, where appropriate, r.m.s.; unless noted otherwise, energies refer to beam energy; H and V indicate horizontal and vertical directions; s.c. stands for superconducting. ILC and CLIC parameters are documented in the Accelerator physics of colliders review.

	CESR (Cornell)	CESR-C (Cornell)	LEP (CERN)	SLC (SLAC)
Physics start date	1979	2002	1989	1989
Physics end date	2002	2008	2000	1998
Maximum beam energy (GeV)	6	6	100 - 104.6	50
Delivered integrated luminosity per experiment (fb^{-1})	41.5	2.0	0.221 at Z peak 0.501 at 65 – 100 GeV 0.275 at >100 GeV	0.022
Luminosity ($10^{30} \text{ cm}^{-2}\text{s}^{-1}$)	1280 at 5.3 GeV	76 at 2.08 GeV	24 at Z peak 100 at > 90 GeV	2.5
Time between collisions (μs)	0.014 to 0.22	0.014 to 0.22	22	8300
Full crossing angle (μ rad)	± 2000	± 3300	0	0
Energy spread (units 10^{-3})	0.6 at 5.3 GeV	0.82 at 2.08 GeV	0.7→1.5	1.2
Bunch length (cm)	1.8	1.2	1.0	0.1
Beam radius (μm)	H:460 V:4	H:340 V:6.5	H:200→300 V:2.5→8	H:1.5 V:0.5
Free space at interaction point (m)	± 2.2 (± 0.6 to REC quads)	± 2.2 (± 0.3 to PM quads)	± 3.5	± 2.8
Luminosity lifetime (hr)	2–3	2–3	20 at Z peak 10 at > 90 GeV	—
Turn-around time (min)	5 (topping up)	1.5 (topping up)	50	120 Hz (pulsed)
Injection energy (GeV)	1.8–6	1.5–6	22	45.64
Transverse emittance (10^{-9} m)	210 1	120 3.5	H:20–45 V:0.25→1	H:0.5 V:0.05
β^* , amplitude function at interaction point (m)	1.0 0.018	0.94 0.012	1.5 0.05	0.0025 0.0015
Beam-beam tune shift per crossing (10^{-4}) or disruption	250 620	e^- : 420 (H), 280 (V) e^+ : 410 (H), 270 (V)	830	0.75 (H) 2.0 (V)
RF frequency (MHz)	500	500	352.2	2856
Particles per bunch (units 10^{10})	1.15	4.7	45 in collision 60 in single beam	4.0
Bunches per ring per species	9 trains of 5 bunches	8 trains of 3 bunches	4 trains of 1 or 2	1
Average beam current per species (mA)	340	72	4 at Z peak 4→6 at > 90 GeV	0.0008
Beam polarization (%)	—	—	55 at 45 GeV 5 at 61 GeV	e^- : 80
Circumference or length (km)	0.768	0.768	26.66	1.45 +1.47
Interaction regions	1	1	4	1
Magnetic length of dipole (m)	1.6–6.6	1.6–6.6	11.66/pair	2.5
Length of standard cell (m)	16	16	79	5.2
Phase advance per cell (deg)	45–90 (no standard cell)	45–90 (no standard cell)	102/90	108
Dipoles in ring	86	84	3280 + 24 inj. + 64 weak	460+440
Quadrupoles in ring	101 + 4 s.c.	101 + 4 s.c.	520 + 288 + 8 s.c.	—
Peak magnetic field (T)	0.3 / 0.8 at 8 GeV	0.3 / 0.8 at 8 GeV, 2.1 wigglers at 1.9 GeV	0.135	0.597

High-Energy Collider Parameters: ep , e^+e^- Colliders (III)

Table 32.3: Updated in March 2022 with numbers received from representatives of the colliders (contact E. Pianori, LBNL). The table shows the parameter values achieved. Design parameters for SuperKEKEB may be found in our 2018 edition (Phys. Rev. **D98**, 030001 (2018)) Quantities are, where appropriate, r.m.s.; unless noted otherwise, energies refer to beam energy; H and V indicate horizontal and vertical directions; s.c. stands for superconducting.

	HERA (DESY)	KEKB (KEK)	PEP-II (SLAC)	SuperKEKB (KEK)
Physics start date	1992	1999	1999	2018
Physics end date	2007	2010	2008	—
Particles collided	ep	e^+e^-	e^+e^-	e^+e^-
Maximum beam energy (TeV)	e : 0.030 p : 0.92	e^- : 8.33 (8.0 nominal) e^+ : 3.64 (3.5 nominal)	e^- : 7–12 (9.0 nominal) e^+ : 2.5–4 (3.1 nominal)	e^- : 7 e^+ : 4
Delivered integrated luminosity per exp. (fb^{-1})	0.8	1040	557	491
Luminosity ($10^{30} \text{ cm}^{-2}\text{s}^{-1}$)	75	21083	12069 (design: 3000)	4.71×10^4
Time between collisions (ns)	96	5.9 or 7.86	4.2	4.2
Full crossing angle (μ rad)	0	$\pm 11000^*$	0	± 41500
Energy spread (units 10^{-3})	e : 0.91 p : 0.2	e^-/e^+ : 0.67/0.73	e^-/e^+ : 0.61/0.77	e^-/e^+ : 0.64/0.81
Bunch length (cm)	e : 0.83 p : 8.5	0.65	e^-/e^+ : 1.1/1.0	e^-/e^+ : 0.6/0.6
Beam radius (μm)	e : 110 (H), 30 (V) p : 111 (H), 30 (V)	H: 124 (e^-), 117 (e^+) V: 1.9	157 4.7	e^- : 16.6 (H), 0.22 (V) e^+ : 17.9 (H), 0.22 (V)
Free space at interaction point (m)	± 2	+0.75/−0.58 (+300/−500) mrad cone	± 0.2 , ± 300 mrad cone	e^- : +1.20/−1.28 e^+ : +0.78/−0.73 (+300/−500) mrad cone
Initial luminosity decay time, $-L/(dL/dt)$ (hr)	10	continuous	continuous	continuous
Turn-around time (min)	e : 75, p : 135	continuous	continuous	continuous
Injection energy (GeV)	e : 12 p : 40	e^-/e^+ : 8.0/3.5 (nominal)	e^-/e^+ : 9.0/3.1 (nominal)	e^-/e^+ : 7/4
Transverse emittance (10^{-9} m)	e : 20 (H), 3.5 (V) p : 5 (H), 5 (V)	e^- : 24 (57^\dagger) (H), 0.61 (V) e^+ : 18 (55^\dagger) (H), 0.56 (V)	e^- : 48 (H), 1.8 (V) e^+ : 24 (H), 1.8 (V)	e^- : 4.6 (H), 0.05 (V) e^+ : 4.0 (H), 0.05 (V)
β^* , amplitude function at interaction point (m)	e : 0.6 (H), 0.26 (V) p : 2.45 (H), 0.18 (V)	e^- : 1.2 (0.27 †) (H), 0.0059 (V) e^+ : 1.2 (0.23 †) (H), 0.0059 (V)	e^- : 0.50 (H), 0.012 (V) e^+ : 0.50 (H), 0.012 (V)	e^- : 0.060 (H), 1×10^{-3} (V) e^+ : 0.080 (H), 1×10^{-3} (V)
Beam-beam tune shift per crossing (units 10^{-4})	e : 190 (H), 450 (V) p : 12 (H), 9 (V)	e^- : 1020 (H), 900 (V) e^+ : 1270 (H), 1290 (V)	e^- : 703 (H), 498 (V) e^+ : 510 (H), 727 (V)	e^- : 15 (H), 278 (V) e^+ : 27 (H), 398 (V)
RF frequency (MHz)	e : 499.7 p : 208.2/52.05	508.887	476	508.887
Particles per bunch (units 10^{10})	e : 3 p : 7	e^-/e^+ : 4.7/6.4	e^-/e^+ : 5.2/8.0	e^-/e^+ : 3.12/3.81
Bunches per ring per species	e : 189 p : 180	1585	1732	2249
Average beam current per species (mA)	e : 40 p : 90	e^-/e^+ : 1188/1637	e^-/e^+ : 1960/3026	e^-/e^+ : 1118/1393
Beam polarization (%)	—	—	—	—
Circumference or length (km)	6.336	3.016	2.2	3.016
Interaction regions	2 colliding beams 1 fixed target (e beam)	1	1	1
Magnetic length of dipole (m)	e : 9.185; p : 8.82	e^-/e^+ : 5.86/0.915	e^-/e^+ : 5.4/0.45	e^-/e^+ : 5.9/4.0
Length of standard cell (m)	e : 23.5 p : 47	e^-/e^+ : 75.7/76.1	15.2	e^-/e^+ : 75.7/76.1
Phase advance per cell (deg)	e : 60 p : 90	450	e^-/e^+ : 60/90	450
Dipoles in ring	e : 396 p : 416	e^-/e^+ : 116/112	e^-/e^+ : 192/192	e^-/e^+ : 116/112
Quadrupoles in ring	e : 580 p : 280	e^-/e^+ : 452/452	e^-/e^+ : 290/326	e^-/e^+ : 466/460
Peak magnetic field (T)	e : 0.274; p : 5	e^-/e^+ : 0.25/0.72	e^-/e^+ : 0.18/0.75	e^-/e^+ : 0.22/0.19

* KEKB was operated with crab crossing from 2007 to 2010.

 † With dynamic beam-beam effect.

High-Energy Collider Parameters: $\bar{p}p$, pp Colliders

Table 32.4: Updated in March 2024 with numbers received from representatives of the colliders (contact E. Pianori, LBNL). The table shows the parameter values achieved. Parameters for the defunct $Spp\bar{p}S$ collider may be found in our 2002 edition (Phys. Rev. D66, 010001 (2002)). Quantities are, where appropriate, r.m.s.; unless noted otherwise, energies refer to beam energy; H and V indicate horizontal and vertical directions; s.c. stands for superconducting.

	TEVATRON*	RHIC	LHC			
	(Fermilab)	Brookhaven	(CERN)			
Physics start date	1987	2001	2009 (Run 1)	2015 (Run 2)	2022 (Run 3)	2029 (HL-LHC)
Physics end date	2011	—	—			
Particles collided	$p\bar{p}$	pp (polarized)	pp			
Maximum beam energy (TeV)	0.980	0.255 55% polarization	4.0	6.5	6.8	7.0
Max. delivered integrated luminosity per exp. (fb^{-1})	12	0.38 at 100 GeV 1.3 at 250/255 GeV	23.3 at 4.0 TeV 6.1 at 3.5 TeV	160	70	250/y
Luminosity ($10^{30} \text{ cm}^{-2}\text{s}^{-1}$)	431	245 (pk) 160 (avg)	7.7×10^3	2.1×10^4	2×10^4 (leveled)	5.0×10^4 (leveled)
Time between collisions (ns)	396	107	49.90	24.95	24.95	24.95
Full crossing angle (μ rad)	0	0	290	$320 \rightarrow 260^\dagger$	$320 \rightarrow 270^\dagger$	500
Energy spread (units 10^{-3})	0.14	0.15	0.1445	0.11	0.11	0.11
Bunch length (cm)	p : 50 \bar{p} : 45	60	9.4	8	9.7	7.6
Beam radius (10^{-6} m)	p : 28 \bar{p} : 16	85	18.8	8.5^\ddagger	9.3^\ddagger	7^\ddagger
Free space at interaction point (m)	± 6.5	16	38	38	38	38
Initial luminosity decay time, $-L/(dL/dt)$ (hr)	6 (avg)	7.5	≈ 6	8.4	12^\S	≈ 7.5 (leveled)
Turn-around time (min)	90	25	180	150	180^\P	150
Injection energy (TeV)	0.15	0.023	0.450	0.450	0.450	0.450
Transverse emittance (10^{-9} m)	p : 3 \bar{p} : 1	11	0.59	0.29	0.29	0.33
β^* , ampl. function at interaction point (m)	0.28	0.65	0.6	$0.3 \rightarrow 0.25^\parallel$	$1.2 \rightarrow 0.3^\parallel$	$1 \rightarrow 0.15^\parallel$
Beam-beam tune shift per crossing (units 10^{-4})	p : 120 \bar{p} : 120	73	72	45	57^\S	104
RF frequency (MHz)	53	accel: 9 store: 28	400.8	400.8	400.8	400.8
Particles per bunch (units 10^{10})	p :26 \bar{p} :9	18.5	16	11	16	22
Bunches per ring per species	36	111	1380	2556 2544 (i.r. 1/5**)	2464 2452 (i.r. 1/5**)	2760 2748 (i.r. 1/5**)
Average beam current per species (mA)	p :70 \bar{p} :24	257	400	510	710	1094
Circumference (km)	6.28	3.834	26.659			
Interaction regions	2 high \mathcal{L}	6 total, 2 high \mathcal{L}	4 total, 2 high \mathcal{L}			
Magnetic length of dipole (m)	6.12	9.45	14.3			
Length of standard cell (m)	59.5	29.7	106.90			
Phase advance per cell (deg)	67.8	84	90			
Dipoles in ring	774	192 per ring + 12 common	1232 main dipoles			
Quadrupoles in ring	216	246 per ring	482 2-in-1 24 1-in-1			
Magnet types	s.c., $\cos\theta$ warm iron	s.c., $\cos\theta$ cold iron	s.c., 2-in-1 cold iron			
Peak magnetic field (T)	4.4	3.5	$8.3^{\ddagger\ddagger}$			

*Other TEVATRON parameters: \bar{p} source accum. rate: $25 \times 10^{10} \text{ hr}^{-1}$; max. no. of \bar{p} stored: 3.4×10^{12} (Accumulator), 6.1×10^{12} (Recycler).

† Variable crossing angle decreasing during the fill with the reduction in bunch population

‡ Minimum beam radius during levelling

§ Value at start of levelling

¶ Most likely value as observed in 2023

$^\parallel$ β^* levelling

** Number of bunches colliding at the interaction regions (i.r.) 1 (ATLAS) and 5 (CMS).

‡‡ Value for design beam energy of 7 TeV.

High-Energy Collider Parameters: Heavy Ion Colliders

Table 32.5: Updated in March 2024 with numbers received from representatives of the collider (contact E. Pianori, LBNL) The table shows the parameter values achieved. For the LHC, only maximum values for the ATLAS and CMS experiments are provided (ALICE and LHCb have different requirements for energy and luminosity). Design values for a high-luminosity upgrade are also given. Quantities are, where appropriate, r.m.s.; unless noted otherwise, energies refer to beam energy; s.c. stands for superconducting. pk and avg denote peak and average values.

	RHIC (Brookhaven)				LHC (CERN)			
	2000	2012 / 2018 / 2018 / 2012 / 2004 2021 / 2014 / 2002 / 2015 / 2015	2010	2012	2017	≥ 2029 (high lum.)*		
Physics start date	2000		2010	2012	2017	≥ 2029 (high lum.)*		
Physics end date		—		—				
Particles collided	Au Au	U U / Zr Zr / Ru Ru / Cu Au / Cu Cu O O / h Au / d Au / p Au / p Al	Pb Pb	p Pb	Xe Xe	Pb Pb		
Max. beam energy (TeV/n)	0.1	0.1	2.68	p:6.5 Pb:2.56	2.72	2.76		
$\sqrt{s_{NN}}$ (TeV)	0.2	0.2	5.36	8.16	5.44	5.5		
Max. delivered int. nucleon-pair lumin. per exp. (pb^{-1})	2639 (at 100 GeV/n)	21 / 36 / 36.9 / 167 / 60 8.2 / 43 / 169 / 124 / 63 (all at 100 GeV/n)	84.8	194	0.05	$\approx 121/y$		
Luminosity ($10^{27} \text{ cm}^{-2} \text{ s}^{-1}$)	pk: 15.5 avg: 8.7	pk: 0.4 / 4.8 / 3.8 / 12 / 21 450 / 170 / 850 / 880 / 7600 avg: 0.6 / 2.2 / 2.1 / 10 / 8 230 / 100 / 500 / 450 / 3800	6.4 [†]	900	0.4	6.4 (leveled)		
Time between collisions (ns)	107	107 / 107 / 107 / 107 / 321 107 / 107 / 107 / 107 / 107	49.9	99.8 / 149.7	≈ 5500	49.9		
Full crossing angle (μ rad)	0	0	200	280	300	340		
Energy spread (units 10^{-3})	0.75	0.75	0.13	0.11	0.11	0.11		
Bunch length (cm)	30	30	9.1	p / Pb: 9 / 11.5	11	7.9		
Beam radius (10^{-6} m)	114 [‡]	123 [‡] / 87 [‡] / 88 [‡] / 163 [‡] / 145 [‡] 100 [‡] / 136 [‡] / 124 [‡] / 147 [‡] / 128 [‡]	20	19	12	17		
Free space at inter. point (m)	16	16	38	38	38	38		
Initial luminosity decay time, $-L/(dL/dt)$ (hr)	1	-0.35 [§] / ∞ [¶] / ∞ [¶] / ∞ [§] / 1.8 ∞ / 0.6 / ∞ [§] / 0.5 / 0.25	2.8	≈ 2	≈ 6	∞		
Turn-around time (min)	30	60** / 40** / 40** / 160** / 90** 45** / 45** / 90** / 60** / 50**	144	150	180	≈ 200		
Injection energy (TeV/n)	0.011	0.011	0.177	p / Pb: 0.45 / 0.177	0.188	0.177		
Transverse emittance (10^{-9} m)	19 [‡]	22 [‡] / 10.7 [‡] / 11.2 [‡] / 38 [‡] / 23 [‡] 12 [‡] / 19 [‡] / 22 [‡] / 26 [‡] / 21 [‡]	0.80	0.29	0.3	0.5		
β^* , ampl. function at interaction point (m)	0.7	0.7 / 0.7 / 0.7 / 0.7 / 0.9 0.7 / 1.0 / 0.7 / 0.8 / 0.8	0.5	0.5	0.4	0.5		
Beam-beam tune shift per crossing (units 10^{-4})	39 [‡]	6 [‡] / 18 [‡] / 21 [‡] / 14 [‡] , 14 [‡] / 30 [‡] / 34 [‡] 42 [‡] , 22 [‡] / 40 [‡] , 27 [‡] / 53 [‡] , 41 [‡] / 80 [‡] , 59 [‡]	3.1	15	≈ 10	4.3		
RF frequency (MHz)		accel: 28, store: 197	400.8	400.8	400.8	400.8		
Particles per bunch (units 10^{10})	0.20	0.03 / 0.1 / 0.1 / 0.4, 0.13 / 0.45 / 0.85 4.5, 0.13 / 13, 0.20 / 22.5, 0.16 / 24, 1.1	0.018 (r.m.s.)	p:2.6 Pb:0.022	0.027	0.018		
Bunches per ring per species	111	111 / 111 / 111 / 111 / 37 106 / 111 / 111 / 111 / 111	960 ^{††}	p:540 Pb:684	16	1240		
Average beam current per species (mA)	224	38 / 56 / 61 / 160,138 / 60 / 95 125,143 / 181,213 / 313,176 / 334,199	25.5	p:16 Pb:15	0.54	33		
Circumference (km)		3.834		26.659				
Interaction regions		6 total, 2 high \mathcal{L}		4 total, 3 high \mathcal{L}				
Magnetic length of dipole (m)		9.45		14.3				
Length of standard cell (m)		29.7		106.90				
Phase advance per cell (deg)	93	84 / 84 / 84 / 84 / 84 / 84 93 / 84(d), 93 / 84(p), 93 / 84(p), 93		90				
Dipoles in ring		192 per ring, + 12 common		1232, main dipoles				
Quadrupoles in ring		246 per ring		482 2-in-1, 24 1-in-1				
Magnet Type		s.c. $\cos \theta$, cold iron		s.c., 2 in 1, cold iron				
Peak magnetic field (T)		3.5		8.3				

* For HL-LHC. Conservative estimates.

[†]Highest value achieved in ALICE.[‡]Initial value, increases (decreases) without (with) cooling.[§]Negative or infinite decay time is effect of cooling.[¶]luminosity leveled to flat after set to target value, with cooling.^{||}for a typical good fill without luminosity levelling.

**measured minimum, not theoretical.

^{††}1240 bunches per ring were also used, but with lower peak performance due to lower bunch intensity.

33. Neutrino Beam Lines at High-Energy Proton Synchrotrons

Revised August 2023 with numbers verified by representatives of the synchrotrons (contact C.-J. Lin, LBNL). For existing (future) neutrino beam lines the latest achieved (design) values are given.

The main source of neutrinos at proton synchrotrons is from the decay of pions and kaons produced by protons striking a nuclear target. There are different schemes to focus the secondary particles to enhance neutrino flux and/or tune the neutrino energy profile. In wide-band beams (WBB), the neutrino parent mesons are focused over a wide momentum range to obtain maximum neutrino intensity. In narrow-band beams (NBB), the secondary particles are first momentum-selected to produce a monochromatic parent beam. Another approach to generate a narrow-band neutrino spectrum is to select neutrinos that are emitted off-axis relative to the momentum of the parent mesons. For a comprehensive review of the topic, including other historical neutrino beam lines, see the article by S. E. Kopp, “Accelerator-based neutrino beams,” Phys. Rept. **439**, 101 (2007).

	PS (CERN)				SPS (CERN)			PS (KEK)	Main Ring (JPARC)	
Date	1963	1969	1972	1983	1977	1995	2006	1999	2023	(2028)
Proton Kinetic Energy (GeV)	20.6	20.6	26	19	350	450	400	12	30	(30)
Protons per Cycle (10^{12})	0.7	0.6	5	5	10	36	48	6	153	(330)
Cycle Time (s)	3	2.3	-	-	-	14.4	6	2.2	1.36	(1.16)
Beam Power (kW)	0.8	0.9	-	-	-	180	510	5	540	(1300)
Target	-	-	-	-	-	Be	Graphite	Al	Graphite	(Graphite)
Target Length (cm)	-	-	-	-	-	290	130	66	91	(91)
Secondary Focussing	1-horn WBB	3-horn WBB	2-horn WBB	bare target	2-horn WBB	2-horn WBB	2-horn WBB	2-horn WBB	3-horn off-axis	(3-horn off-axis)
Decay Pipe Length (m)	-	-	-	-	-	110	1090	200	96	(96)
$\langle E_\nu \rangle$ (GeV)	1.5	1.5	1.5	1	20	24.3	17	1.3	0.6	(0.6)
Experiments	HLBC, Spark Ch.	HLBC, Spark Ch.	GGM, Aachen-Padova	CDHS, CHARM	GGM, CDHS, CHARM, BEBC	NOMAD, CHORUS	OPERA, ICARUS	K2K	T2K	Hyper-K

	Main Ring (Fermilab)					Booster (Fermilab)	Main Injector (Fermilab)			
Date	1974	1979	1976	1991	1998	2002, (2022)	2005	2017	2021	(2031)
Proton Kinetic Energy (GeV)	300	400	350	800	800	8	120	120	120	(60 – 120)
Protons per Cycle (10^{12})	10	10	13	10	12	4.5	37	54	55	(75)
Cycle Time (s)	-	-	-	60	60	0.2	2	1.333	1.2	(1.2)
Beam Power (kW)	-	-	-	20	25	29	350	720	840	(1200)
Target	-	-	-	-	BeO	Be	Graphite	Graphite	Graphite	(Graphite)
Target Length (cm)	-	-	-	-	31	71	95	120	120	(150-180)
Secondary Focussing	dichromatic NBB	2-horn WBB	1-horn WBB	quad trip.	SSQT WBB	1-horn WBB	2-horn WBB	2-horn off-axis	2-horn off-axis	(3-horn WBB)
Decay Pipe Length (m)	400	400	400	400	400	50	675	675	675	(220)
$\langle E_\nu \rangle$ (GeV)	50,180 [†]	25	100	90,260	70,180	1	3-20 [‡]	2	2	(2.5)
Experiments	CITF, HPWF, 15' BC	15' BC	HPWF 15' BC	15' BC, CCFRR	NuTeV	MiniBooNE, SciBooNE, MicroBooNE, (SBND, ICARUS)	MINOS, MINER ν A	NO ν A, MINER ν A, MINOS+	NO ν A	DUNE

[†]Pion and kaon peaks in the momentum-selected channel.

[‡]Tunable WBB energy spectrum.

34. Passage of Particles Through Matter

Revised August 2023 by D.E. Groom (LBNL) and S.R. Klein (NSD LBNL; UC Berkeley).

34.1	Notation	575
34.2	Electronic energy loss by heavy particles	575
34.2.1	Moments and cross sections	575
34.2.2	Maximum energy transfer to an electron in a single collision	576
34.2.3	Stopping power at intermediate energies	576
34.2.4	Mean excitation energy	576
34.2.5	Density effect	576
34.2.6	Energy loss at low energies	577
34.2.7	Energetic knock-on electrons (δ rays)	579
34.2.8	Restricted energy loss rates for relativistic ionizing particles	579
34.2.9	Fluctuations in energy loss	579
34.2.10	Energy loss in mixtures and compounds	580
34.2.11	Ionization yields	580
34.3	Multiple scattering through small angles	580
34.4	Photon and electron interactions in matter	581
34.4.1	Collision energy losses by e^\pm	581
34.4.2	Radiation length	582
34.4.3	Bremsstrahlung energy loss by e^\pm	582
34.4.4	Critical energy	583
34.4.5	Energy loss by photons	583
34.4.6	Bremsstrahlung and pair production at very high energies	584
34.4.7	Photonuclear and electronuclear interactions at still higher energies	585
34.5	Electromagnetic cascades	585
34.6	Muon energy loss at high energy	586
34.7	Cherenkov and transition radiation	587
34.7.1	Optical Cherenkov radiation	587
34.7.2	Coherent radio Cherenkov radiation	588
34.7.3	Transition radiation	588

This review covers the interactions of photons and electrically charged particles in matter, concentrating on energies of interest for high-energy physics and astrophysics and processes of interest for particle detectors (ionization, Cherenkov radiation, transition radiation). Much of the focus is on particles heavier than electrons (π^\pm , p , etc.). Although the charge number z of the projectile is included in the equations, only $z = 1$ is discussed in detail. Muon radiative losses are discussed, as are photon/electron interactions at high to ultrahigh energies. Neutrons are not discussed.

34.1 Notation

The notation and important numerical values are shown in Table 34.1.

34.2 Electronic energy loss by heavy particles

34.2.1 Moments and cross sections

The electronic interactions of fast charged particles with speed $v = \beta c$ occur in *single collisions with energy losses* W [1], leading to ionization, atomic, or collective excitation. Most frequently the energy losses are small (for 90% of all collisions the energy losses are less than 100 eV). In thin absorbers few collisions will take place and the total energy loss will show a large variance [1]; also see Sec. 34.2.9 below. For particles with charge ze more massive than electrons (“heavy” particles), scattering from free electrons is adequately described by the Rutherford differential cross section [2, 3].

$$\frac{d\sigma_R(W; \beta)}{dW} = \frac{2\pi r_e^2 m_e c^2 z^2 (1 - \beta^2 W/W_{\max})}{\beta^2 W^2}, \quad (34.1)$$

where W_{\max} , the maximum energy transfer possible in a single collision, is discussed below. It differs from the classical cross section by the factor $(1 - \beta^2 W/W_{\max})$, which arises when the spin of the target electrons is taken into account.

Table 34.1: Summary of variables used in this section. The kinematic variables β and γ have their usual relativistic meanings.

Symb.	Definition	Value or (usual) units
$m_e c^2$	electron mass $\times c^2$	0.510 998 950 00(15) MeV
r_e	classical electron radius $e^2/4\pi\epsilon_0 m_e c^2$	2.817 940 3227(19) fm
α	fine structure constant $e^2/4\pi\epsilon_0 \hbar c$	1/137.035 999 139(31)
N_A	Avogadro’s number	$6.022 140 76 \times 10^{23}$ mol $^{-1}$
ρ	density	g cm $^{-3}$
x	mass per unit area	g cm $^{-2}$
M	incident particle mass	MeV/ c^2
E	incident part. energy $\gamma M c^2$	MeV
T	kinetic energy, $(\gamma - 1) M c^2$	MeV
W	energy transfer to an electron in a single collision	MeV
W_{\max}	Maximum possible energy transfer to an electron in a single collision	MeV
k	bremsstrahlung photon energy	MeV
z	charge number of incident particle	
Z	atomic number of absorber	
A	atomic mass of absorber	g mol $^{-1}$
K	$4\pi N_A r_e^2 m_e c^2$ (Coefficient for dE/dx)	0.307 075 MeV mol $^{-1}$ cm 2
I	mean excitation energy	eV (<i>Nota bene!</i>)
$\delta(\beta\gamma)$	density effect correction to ionization energy loss	
$\hbar\omega_p$	plasma energy $\sqrt{4\pi N_e r_e^3 m_e c^2 / \alpha}$	$\sqrt{\rho (Z/A)} \times 28.816$ eV ↳ ρ in g cm $^{-3}$
N_e	electron density	(units of r_e) $^{-3}$
w_j	weight fraction of the j th element in a compound or mixt.	
n_j	\times number of j th kind of atoms in a compound or mixture	
X_0	radiation length	g cm $^{-2}$
E_c	critical energy for electrons	MeV
$E_{\mu c}$	critical energy for muons	GeV
E_s	scale energy $\sqrt{4\pi/\alpha} m_e c^2$	21.2052 MeV
R_M	Molière radius	g cm $^{-2}$

Bethe’s original theory applied only to energies above which atomic effects are not important. The free-electron cross section (Eq. (34.1)) was used to extend the cross section to W_{\max} . This free-electron approximation is not valid if W is not large compared to electron binding energies. For this energy regime Bethe [4, 5] used “Born Theorie” to obtain the differential cross section

$$\frac{d\sigma_B(W; \beta)}{dW} = \frac{d\sigma_R(W; \beta)}{dW} B(W). \quad (34.2)$$

Electronic binding is accounted for by the correction factor $B(W)$. Examples of $B(W)$ and $d\sigma_B/dW$ can be seen in Figs. 5 and 6 of Ref. [1]. For a given material, the correction results in introducing an *effective ionization energy* I “which is a geometric average of the excitation energies of the medium weighed by the corresponding oscillator strength.” [6]. The nontrivial task of finding these values is discussed in Sec. 34.2.4.

At high energies the stopping power is further modified by polarization of the medium, and this “density effect,” discussed in Sec. 34.2.5, must also be included.

The mean number of collisions with energy loss between W and $W + dW$ occurring in a distance δx is $N_e \delta x (d\sigma/dW) dW$, where $d\sigma(W; \beta)/dW$, where the cross section is the Rutherford formula if free electrons can be assumed and the Bethe form where binding energy is important. It is convenient to define the moments

$$M_j(\beta) = N_e \delta x \int W^j \frac{d\sigma(W; \beta)}{dW} dW, \quad (34.3)$$

so that M_0 is the mean number of collisions in δx , M_1 is the

mean energy loss in δx , $(M_2 - M_1)^2$ is the variance, *etc.* The number of collisions is Poisson-distributed with mean M_0 . N_e is either measured in electrons/g ($N_e = N_A Z/A$) or electrons/cm³ ($N_e = N_A \rho Z/A$). The former is used throughout this chapter, since quantities of interest (dE/dx , X_0 , *etc.*) vary smoothly with composition when there is no density dependence.

34.2.2 Maximum energy transfer to an electron in a single collision

For a point-like particle with mass $M \gg m_e$,

$$W_{\max} = \frac{2m_e c^2 \beta^2 \gamma^2}{1 + 2\gamma m_e/M + (m_e/M)^2}. \quad (34.4)$$

In older references [2, 9] the “low-energy” approximation $W_{\max} = 2m_e c^2 \beta^2 \gamma^2$, valid for $2\gamma m_e \ll M$, is often implicit. For a pion in copper, the error thus introduced into dE/dx is greater than 6% at 100 GeV. For $2\gamma m_e \gg M$, $W_{\max} = M c^2 \beta^2 \gamma$.

At energies of order 100 GeV, the maximum 4-momentum transfer to the electron can exceed 1 GeV/c, where hadronic structure effects modify the cross sections. This problem has been investigated by J.D. Jackson [10], who concluded that for incident hadrons (but not for large nuclei) corrections to dE/dx are negligible below energies where radiative effects dominate. While the cross section for rare hard collisions is modified, the average stopping power, dominated by many softer collisions, is almost unchanged.

34.2.3 Stopping power at intermediate energies

The mean rate of energy loss by moderately relativistic charged heavy particles is well described by the “Bethe equation” [2,4,5,9],

$$\left\langle -\frac{dE}{dx} \right\rangle = K z^2 \frac{Z}{A} \frac{1}{\beta^2} \left[\frac{1}{2} \ln \frac{2m_e c^2 \beta^2 \gamma^2 W_{\max}}{I^2} - \beta^2 - \frac{\delta(\beta\gamma)}{2} \right]. \quad (34.5)$$

Eq. (34.5) is valid in the region $0.1 \lesssim \beta\gamma \lesssim 1000$ with an accuracy of a few percent. At $\beta\gamma \sim 0.1$ the projectile speed is comparable to a atomic electron “speed,” and at $\beta\gamma \sim 1000$ radiative effects begin to be important (Sec. 34.6). Both limits are Z dependent. A minor dependence on M at high energies is introduced through W_{\max} , but for all practical purposes the stopping power in a given material is a function of β alone. Small corrections are discussed in Sec. 34.2.6.^{1,2}

This is the *mass stopping power*; with the symbol definitions and values given in Table 34.1, the units are MeV g⁻¹cm². As can be seen from Fig. 34.2, dE/dx defined in this way is about the same for most materials, decreasing slowly with Z . The *linear stopping power*, in MeV/cm, is $\rho dE/dx$, where ρ is the density in g/cm³.

The stopping power at first falls as $1/\beta^\alpha$ where $\alpha \approx 1.7$ – 1.5 , decreasing with increasing Z , and reaches a broad minimum at $\beta\gamma = 3.8$ – 3.0 as Z rises from 6 to 82. It then inexorably rises as the argument of the logarithmic term increases. Two independent mechanisms contribute. Two thirds of the rise is produced by the explicit $\beta^2 \gamma^2$ dependence through the relativistic flattening and extension of the particle’s electric field. Rather than producing ionization at greater and greater distances, the field polarizes the medium, cancelling the increase in the logarithmic term at high energies. This is taken into account by the density-effect correction $\delta(\beta\gamma)$. The other third is introduced by the $\beta^2 \gamma$ dependence of W_{\max} , the maximum possible energy transfer to a recoil electron. “Hard collision” events increasingly extend the tail of the energy loss distribution, increasing the mean but with little effect on the position of the maximum, the most probable energy loss.

Few concepts in high-energy physics are as misused as dE/dx , since the mean is weighted by rare events with large single-collision energy losses. Even with samples of hundreds of events in a typical detector, the mean energy loss cannot be obtained

¹For incident spin 1/2 particles, $(W_{\max}/E)^2/4$ is included in the square brackets. Although this correction is within the uncertainties in the total stopping power, its inclusion avoids a systematic bias.

²In this section, “ dE/dx ” will be understood to mean the mass stopping power “ $\langle -dE/dx \rangle$ ”.

dependably. Far better and more easily measured is the most probable energy loss, discussed in Sec. 34.2.9. The most probable energy loss in a typical detector is considerably smaller than the mean given by the Bethe equation. It does not continue to rise with the mean stopping power, but approaches a “Fermi plateau.”

In analysing TPC data (Sec. 35.6.5), the same end is often accomplished by using a restricted energy loss, the mean of 50%–70% of the samples with the smallest signals as the estimator.

Although it must be used with cautions and caveats, dE/dx as described in Eq. (34.5) still forms the basis of much of our understanding of energy loss by charged particles. Extensive tables are available [6, 7] and pdg.lbl.gov/current/AtomicNuclearProperties/.

For heavy projectiles, like ions, additional terms are required to account for higher-order photon coupling to the target, and to account for the finite target radius. These can change dE/dx by a factor of two or more for the heaviest nuclei in certain kinematic regimes [11].

The function as computed for muons on copper is shown as the “Bethe” region of Fig. 34.1. Mean energy loss behavior below this region is discussed in Sec. 34.2.6, and the radiative effects at high energy are discussed in Sec. 34.6. Only in the Bethe region is it a function of β alone; the mass dependence is more complicated elsewhere. The stopping power in several other materials is shown in Fig. 34.2. Except in hydrogen, particles with the same speed have similar rates of energy loss in different materials, although there is a slow decrease in the rate of energy loss with increasing Z . The qualitative behavior difference at high energies between a gas (He in the figure) and the other materials shown in the figure is due to the density-effect correction, $\delta(\beta\gamma)$, discussed in Sec. 34.2.5. The stopping power functions are characterized by broad minima whose position drops from $\beta\gamma = 3.5$ to 3.0 as Z goes from 7 to 100. The values of minimum ionization as a function of atomic number are shown in Fig. 34.3.

In practical cases, most relativistic particles (*e.g.*, cosmic-ray muons) have mean energy loss rates close to the minimum; they are “minimum-ionizing particles,” or mip’s.

Eq. (34.5) may be integrated to find the total (or partial) “continuous slowing-down approximation” (CSDA) range R for a particle which loses energy only through ionization and atomic excitation. Since dE/dx depends only on β , R/M is a function of E/M or pc/M . In practice, range is a useful concept only for low-energy hadrons ($R \lesssim \lambda_I$, where λ_I is the nuclear interaction length), and for muons below a few hundred GeV (above which radiative effects dominate). Fig. 34.4 shows R/M as a function of $\beta\gamma$ ($= p/Mc$) for a variety of materials.

The mass scaling of dE/dx and range is valid for the electronic losses described by the Bethe equation, but not for radiative losses.

34.2.4 Mean excitation energy

“The determination of the mean excitation energy is the principal non-trivial task in the evaluation of the Bethe stopping-power formula” [15]. Recommended values have varied substantially with time. Estimates based on experimental stopping-power measurements for protons, deuterons, and alpha particles and on oscillator-strength distributions and dielectric-response functions were given in ICRU 49 [6]. See also ICRU 37 [12]. These values, shown in Fig. 34.5, have since been widely used. Machine-readable versions can also be found [16].

34.2.5 Density effect

As the particle energy increases, its electric field flattens and extends, so that the distant-collision contribution to the logarithmic term in Eq. (34.5) increases as $\beta^2 \gamma^2$. However, real media become polarized, limiting the field extension and effectively truncating this part of the logarithmic rise [2,3,6,17,18]. At very high energies,

$$\delta(\beta\gamma)/2 \rightarrow \ln(\hbar\omega_p/I) + \ln \beta\gamma - 1/2, \quad (34.6)$$

where $\delta(\beta\gamma)/2$ is the density effect correction introduced in Eq. (34.5) and $\hbar\omega_p$ is the plasma energy defined in Table 34.1. A comparison with Eq. (34.5) shows that dE/dx then grows as $\ln T_{\max}$ rather than $\ln \beta^2 \gamma^2 T_{\max}$, and that the mean excitation

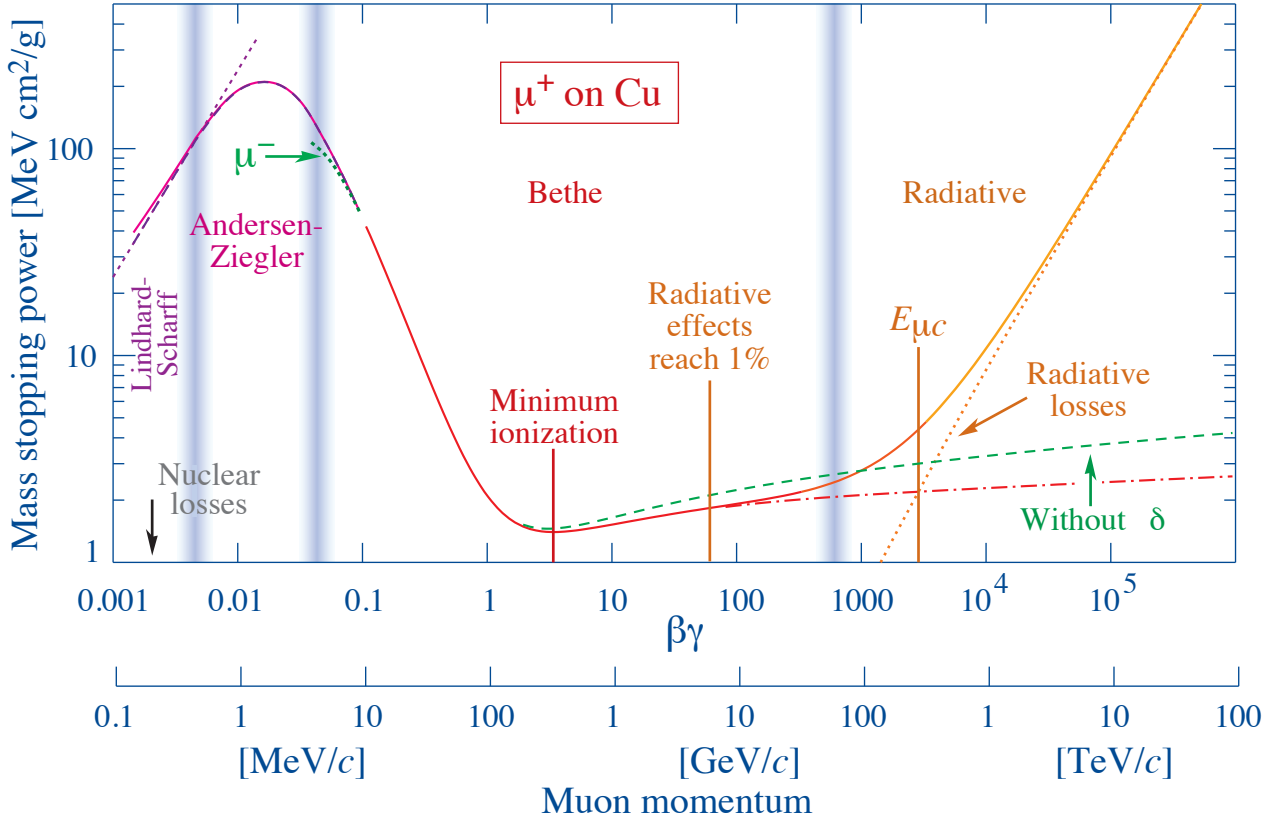


Figure 34.1: Mass stopping power (dE/dx) for positive muons in copper as a function of $\beta\gamma = p/Mc$ over nine orders of magnitude in momentum (12 orders of magnitude in kinetic energy). Solid curves indicate the total stopping power. Data below the break at $\beta\gamma \approx 0.1$ are taken from ICRU 49 [6] assuming only β dependence, and data at higher energies are from [7]. Vertical bands indicate boundaries between different approximations discussed in the text. The short dotted lines labeled “ μ^- ” illustrate the “Barkas effect,” the dependence of stopping power on projectile charge at very low energies [8]. dE/dx in the radiative region is not simply a function of β .

energy I is replaced by the plasma energy $\hbar\omega_p$. An example of the ionization stopping power as calculated with and without the density effect correction is shown in Fig. 34.1. Since the plasma frequency scales as the square root of the electron density, the correction is much larger for a liquid or solid than for a gas, as is illustrated in Fig. 34.2.

The density effect correction is usually computed using Sternheimer’s parameterization [17]:

$$\delta(\beta\gamma) = \begin{cases} 2(\ln 10)x - \bar{C} & \text{if } x \geq x_1; \\ 2(\ln 10)x - \bar{C} + a(x_1 - x)^k & \text{if } x_0 \leq x < x_1; \\ 0 & \text{if } x < x_0 \text{ (nonconductors);} \\ \delta_0 10^{2(x-x_0)} & \text{if } x < x_0 \text{ (conductors)} \end{cases} \quad (34.7)$$

Here $x = \log_{10} \beta\gamma = \log_{10}(p/Mc)$. \bar{C} (the negative of the C used in Ref. [17]) is obtained by equating the high-energy case of Eq. (34.7) with the limit given in Eq. (34.6). The other parameters are adjusted to give a best fit to the results of detailed calculations for momenta below $Mc \exp(x_1)$. For nonconductors the correction is 0 below $\beta\gamma = 10^{x_0}$, corresponding to 100–200 MeV for pions and 1–2 GeV for protons. For conductors it decreases rapidly below this point. Parameters for the elements and nearly 200 compounds and mixtures of interest are published in a variety of places, notably in Ref. [18]. A recipe for finding the coefficients for nontabulated materials is given by Sternheimer and Peierls [19] and is summarized in Ref. [7].

The remaining relativistic rise comes from the $\beta^2\gamma$ growth of W_{\max} , which in turn is due to (rare) large energy transfers to a few electrons. When these events are excluded, the energy deposit in an absorbing layer approaches a constant value, the Fermi plateau (see Sec. 34.2.8 below). At even higher energies (*e.g.*, > 332 GeV for muons in iron, and at a considerably higher energy for pro-

tons in iron), radiative effects are more important than ionization losses. These are especially relevant for high-energy muons, as discussed in Sec. 34.6.

34.2.6 Energy loss at low energies

The theory of energy loss by ionization and excitation as given by Bethe is based on a first-order Born approximation. It assumes free electrons, and should be valid when the projectile’s speed is large compared to that of the atomic electrons. This presents a problem at low energies, where W_{\max} is less than the K shell binding energy. However, Mott showed that the Born approximation can be applied at energies much smaller than atomic binding energies [20]; the incident particle can be treated by classical mechanics since its wavelength is shorter than atomic dimensions. The Born method is actually better justified when its speed is not large compared to the K electron speed [5].

Higher-order corrections must still be made to extend the Bethe equation (Eq. (34.5)) to low energies. An improved approximation for the terms in the square brackets of Eq. (34.5) at low energies is obtained with

$$L(\beta) = L_a(\beta) - \frac{C(\beta)}{Z} + zL_1(\beta) + z^2L_2(\beta). \quad (34.8)$$

Here L_a is the square-bracketed terms of Eq. (34.5), C/Z is the sum of shell corrections and zL_1 and z^2L_2 are Barkas and Bloch correction terms [6, 21]. With these corrections, the Bethe treatment is accurate to about 1% down to $\beta \approx 0.05$, or about 1 MeV for protons (0.13 MeV for muons). Values of L_a , C/Z , L_1 , and L_2 in the range $T = 0.3$ –30 MeV for a proton traversing aluminum can be found in Table I of Ref. [21].

Shell correction $-C/Z$. As the speed of the projectile decreases, the contribution to the stopping power from K shell electrons decreases, and at even lower velocities contributions from L and

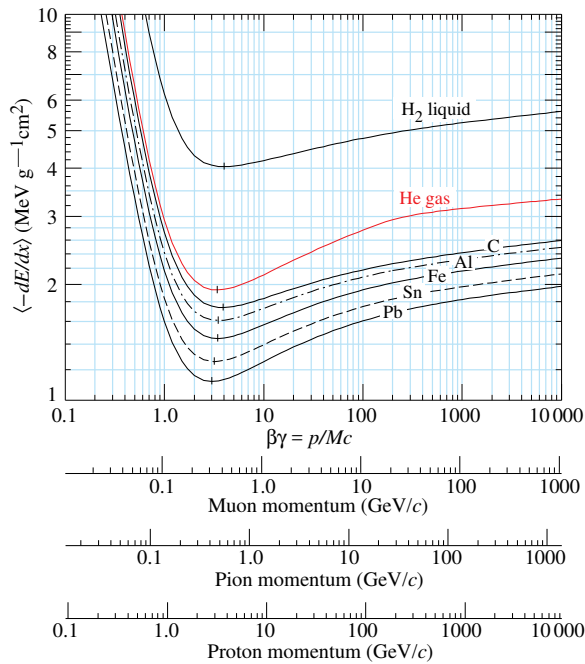


Figure 34.2: Mean energy loss rate in liquid (bubble chamber) hydrogen, gaseous helium, carbon, aluminum, iron, tin, and lead. Radiative effects, relevant for muons and pions, are not included. These become significant for muons in iron for $\beta\gamma \gtrsim 1000$, and at lower momenta for muons in higher- Z absorbers. See Fig. 34.23.

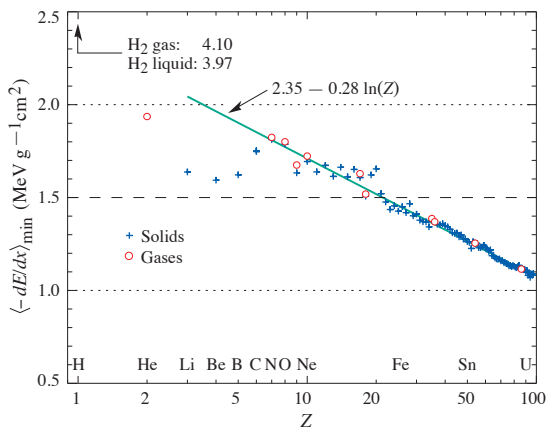


Figure 34.3: Mass stopping power at minimum ionization for the chemical elements. The straight line is fitted for $Z > 6$. A simple functional dependence on Z is not to be expected, since dE/dx also depends on other variables.

higher shells further reduce it. The correction $(C_K + C_L + \dots)/Z$ is should be included in the square brackets of Eq. (34.5). It is calculated and tabulated (for a few common materials) in a number of places; Refs. [6, 12, 21] are especially useful. As an example, the shell correction for a 30 MeV proton traversing aluminum is 0.6%, increasing to 9.9% as the proton's energy decreases to 0.3 MeV.

Barkas correction zL_1 . Qualitatively, one might imagine an atom's electron cloud slightly recoiling at the approach of a negative projectile and being attracted toward an approaching positive projectile. Hence the stopping power for negative particles should be slightly smaller than the stopping power for positive particles. In a 1956 paper, Barkas *et al.* noted that negative pions possibly had a longer range than positive pions [8]. The effect has been measured for a number of negative/positive particle pairs, and more recently in detailed studies with antiprotons at the CERN LEAR facility [22]. Since no complete theory exists, an empirical approach is necessary. A 1972 harmonic-oscillator model by Ash-

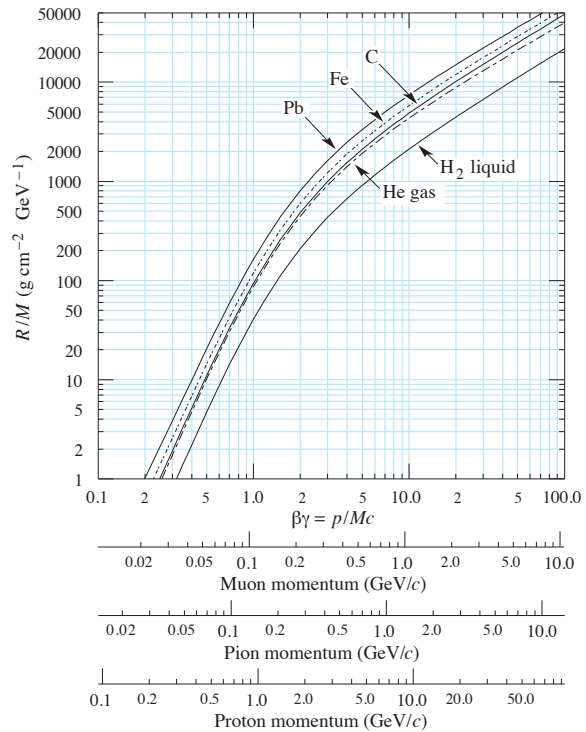


Figure 34.4: Range of heavy charged particles in liquid (bubble chamber) hydrogen, helium gas, carbon, iron, and lead. For example: For a K^+ whose momentum is 700 MeV/c, $\beta\gamma = 1.42$. For lead we read $R/M \approx 396$, and so the range is 195 g cm $^{-2}$ (17 cm).

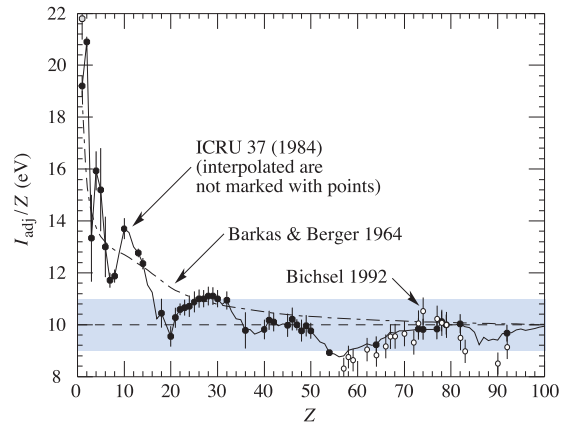


Figure 34.5: Mean excitation energies (divided by Z) as adopted by the ICRU [12]. Those based on experimental measurements are shown by symbols with error flags; the interpolated values are simply joined. The grey point is for liquid H $_2$; the black point at 19.2 eV is for H $_2$ gas. The open circles show more recent determinations by Bichsel [13]. The dash-dotted curve is from the approximate formula of Barkas [14] used in early editions of this *Review*.

ley *et al.* [23] is often used; it has two parameters determined by experimental data. For protons in aluminum, L_1/L_a is less than 0.1% at 30 MeV, but increases to 17% as T decreases to 0.3 MeV. This correction is indicated in Fig. 34.1.

Bloch correction z^2L_2 . Bloch's extension of Bethe's theory introduced a low-energy correction that takes account of perturbations of the atomic wave functions. The form obtained by Lindhard and Sørensen [11] is used *e.g.* in Refs. [6, 21]. For protons in aluminum, $-L_2/L_1$ is less than 0.3% at 3.0 MeV, but rises to 7% when the energy has fallen to 0.3 MeV.

For the interval $0.01 < \beta < 0.05$ there is no satisfactory theory. For protons, one usually relies on the phenomenological fitting formulae developed by Andersen and Ziegler [6,24]. As tabulated in ICRU 49 [6], the nuclear plus electronic proton stopping power in copper is $113 \text{ MeV cm}^2 \text{ g}^{-1}$ at $T = 10 \text{ keV}$ ($\beta\gamma = 0.005$), rises to a maximum of $210 \text{ MeV cm}^2 \text{ g}^{-1}$ at $T \approx 120 \text{ keV}$ ($\beta\gamma = 0.016$), then falls to $118 \text{ MeV cm}^2 \text{ g}^{-1}$ at $T = 1 \text{ MeV}$ ($\beta\gamma = 0.046$). Above $0.5\text{--}1.0 \text{ MeV}$ the corrected Bethe theory is adequate.

For particles moving more slowly than $\approx 0.01c$ (more or less the speed of the outer atomic electrons), Lindhard has been quite successful in describing electronic stopping power, which is proportional to β [25]. Finally, we note that at even lower energies, *e.g.*, for protons of less than several hundred eV, non-ionizing nuclear recoil energy loss dominates the total energy loss [6, 25, 26].

34.2.7 Energetic knock-on electrons (δ rays)

The distribution of secondary electrons with kinetic energies $T \gg I$ is [2]

$$\frac{d^2 N}{dT dx} = \frac{1}{2} K z^2 \frac{Z}{A} \frac{1}{\beta^2} \frac{F(T)}{T^2} \quad (34.9)$$

for $I \ll T \leq W_{\max}$, where W_{\max} is given by Eq. (34.4). Here β is the speed of the primary particle. The factor F is spin-dependent, but is about unity for $T \ll W_{\max}$. For spin-0 particles $F(T) = (1 - \beta^2 T/W_{\max})$; forms for spins $1/2$ and 1 are also given by Rossi [2] (Sec. 2.3, Eqs. 7 and 8). Additional formulae are given in [27]. Equation Eq. (34.9) is inaccurate for T close to I [28].

δ rays of even modest energy are rare. For a $\beta \approx 1$ particle, for example, on average only one collision with $T_e > 10 \text{ keV}$ will occur along a path length of 90 cm of argon gas [1].

A δ ray with kinetic energy T_e and corresponding momentum p_e is produced at an angle θ given by

$$\cos \theta = (T_e/p_e)(p_{\max}/W_{\max}), \quad (34.10)$$

where p_{\max} is the momentum of an electron with the maximum possible energy transfer W_{\max} .

34.2.8 Restricted energy loss rates for relativistic ionizing particles

Further insight can be obtained by examining the mean energy deposit by an ionizing particle when energy transfers are restricted to $T \leq W_{\text{cut}} \leq W_{\max}$. The restricted energy loss rate is

$$\left. \frac{dE}{dx} \right|_{T < W_{\text{cut}}} = K z^2 \frac{Z}{A} \frac{1}{\beta^2} \left[\frac{1}{2} \ln \frac{2m_e c^2 \beta^2 \gamma^2 W_{\text{cut}}}{I^2} - \frac{\beta^2}{2} \left(1 + \frac{W_{\text{cut}}}{W_{\max}} \right) - \frac{\delta}{2} \right]. \quad (34.11)$$

This form approaches the normal Bethe function (Eq. (34.5)) as $W_{\text{cut}} \rightarrow W_{\max}$. It can be verified that the difference between Eq. (34.5) and Eq. (34.11) is equal to $\int_{W_{\text{cut}}}^{W_{\max}} T(d^2 N/dT dx) dT$, where $d^2 N/dT dx$ is given by Eq. (34.9).

Since W_{cut} replaces W_{\max} in the argument of the logarithmic term of Eq. (34.5), the $\beta\gamma$ term producing the relativistic rise in the close-collision part of dE/dx is replaced by a constant, and $|dE/dx|_{T < W_{\text{cut}}}$ approaches the constant “Fermi plateau.” (The density effect correction δ eliminates the explicit $\beta\gamma$ dependence produced by the distant-collision contribution.) This behavior is illustrated in Fig. 34.6, where restricted loss rates for two examples of W_{cut} are shown in comparison with the full Bethe dE/dx and the Landau-Vavilov most probable energy loss (to be discussed in Sec. 34.2.9 below).

“Restricted energy loss” is cut at the total mean energy, not the single-collision energy above W_{cut} . It is of limited use. The most probable energy loss, discussed in the next Section, is far more useful in situations where single-particle energy loss is observed.

34.2.9 Fluctuations in energy loss

For detectors of moderate thickness x (*e.g.* scintillators or LAr cells),³ the energy loss probability distribution $f(\Delta; \beta\gamma, x)$ is ad-

³“Moderate thickness” means $G \lesssim 0.05\text{--}0.1$, where G is given by Rossi Ref. [2], Eq. 2.7(10). It is Vavilov’s κ [29]. G is proportional to the ab-

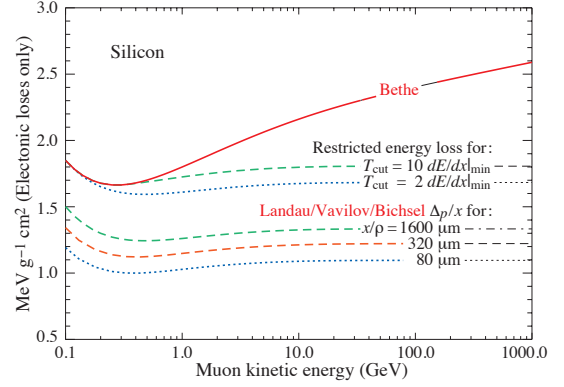


Figure 34.6: Bethe dE/dx , two examples of restricted energy loss, and the Landau most probable energy per unit thickness in silicon. The change of Δ_p/x with thickness x illustrates its $a \ln x + b$ dependence. Minimum ionization $(dE/dx)_{\min}$ is $1.664 \text{ MeV g}^{-1} \text{ cm}^2$. Radiative losses are excluded. The incident particles are muons.

equately described by the highly-skewed Landau (or Landau-Vavilov) distribution [29,30].

The most probable energy loss is [31]⁴

$$\Delta_p = \xi \left[\ln \frac{2m_e c^2 \beta^2 \gamma^2}{I} + \ln \frac{\xi}{I} + j - \beta^2 - \delta(\beta\gamma) \right], \quad (34.12)$$

where $\xi = (K/2) \langle Z/A \rangle z^2 (x/\beta^2) \text{ MeV}$ for a detector with a thickness x in g cm^{-2} , and $j = 0.200$ [31].⁵ While dE/dx is independent of thickness, Δ_p/x scales as $a \ln x + b$. The density correction $\delta(\beta\gamma)$ was not included in Landau’s or Vavilov’s work, but it was later included by Bichsel [31]. The high-energy behavior of $\delta(\beta\gamma)$ (Eq. (34.6)) is such that

$$\Delta_p \xrightarrow{\beta\gamma \gtrsim 100} \xi \left[\ln \frac{2m_e c^2 \xi}{(h\omega_p)^2} + j \right]. \quad (34.13)$$

Thus the Landau-Vavilov most probable energy loss, like the restricted energy loss, reaches a Fermi plateau. The Bethe dE/dx and Landau-Vavilov-Bichsel Δ_p/x in silicon are shown as a function of muon energy in Fig. 34.6. The energy deposit in the $1600 \mu\text{m}$ case is roughly the same as in a 3 mm thick plastic scintillator.

The distribution function for the energy deposit by a 10 GeV muon going through a detector of about this thickness is shown in Fig. 34.7. In this case the most probable energy loss is 62% of the mean ($M_1(\langle \Delta \rangle)/M_1(\infty)$). Folding in experimental resolution displaces the peak of the distribution, usually toward a higher value. 90% of the collisions ($M_1(\langle \Delta \rangle)/M_1(\infty)$) contribute to energy deposits below the mean. It is the very rare high-energy-transfer collisions, extending to W_{\max} at several GeV, that drives the mean into the tail of the distribution. The large weight of these rare events makes the mean of an experimental distribution consisting of a few hundred events subject to large fluctuations and sensitive to cuts. *The mean of the energy loss given by the Bethe equation, Eq. (34.5), is thus ill-defined experimentally and is not useful for describing energy loss by single particles.*⁶ It rises as $\ln \gamma$ because W_{\max} increases as γ at high energies. *The most probable energy loss should be used.*

A practical example: For muons traversing 0.25 inches (0.64 cm) of PVT (polyvinyltolulene) based plastic scintillator,

sorber’s thickness, and as such parameterizes the constants describing the Landau distribution. These are fairly insensitive to thickness for $G \lesssim 0.1$, the case for most detectors.

⁴Practical calculations can be expedited by using the tables of δ and β from the text versions of the muon energy loss tables to be found at pdg.lbl.gov/current/AtomicNuclearProperties.

⁵Rossi [2], Talman [32], and others give somewhat different values for j . The most probable loss is not sensitive to its value.

⁶It does find application in dosimetry, where only bulk deposit is relevant.

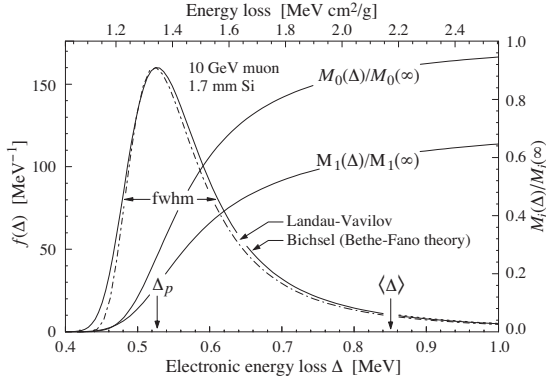


Figure 34.7: Electronic energy deposit distribution for a 10 GeV muon traversing 1.7 mm of silicon, the stopping power equivalent of about 0.3 cm of PVT-based scintillator [1, 13, 33]. The Landau-Vavilov function (dot-dashed) uses a Rutherford cross section without atomic binding corrections but with a kinetic energy transfer limit of W_{\max} . The solid curve was calculated using Bethe-Fano theory. $M_0(\Delta)$ and $M_1(\Delta)$ are the cumulative 0th moment (mean number of collisions) and 1st moment (mean energy loss) in crossing the silicon. (See Sec. 34.2.1). The fwhm of the Landau-Vavilov function is about 4ξ for detectors of moderate thickness. Δ_p is the most probable energy loss, and $\langle\Delta\rangle$ divided by the thickness is the Bethe dE/dx .

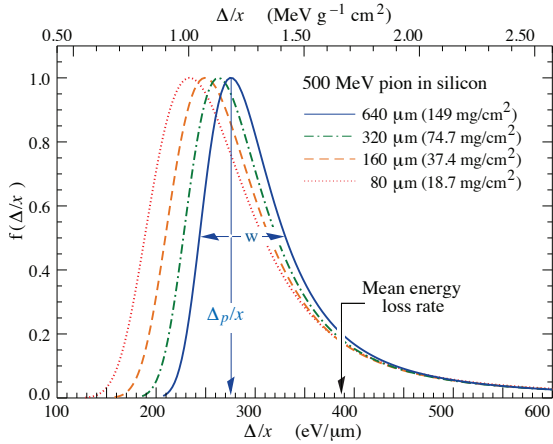


Figure 34.8: Straggling functions in silicon for 500 MeV pions, normalized to unity at the most probable value Δ_p/x . The width w is the full width at half maximum.

the ratio of the most probable E loss rate to the mean loss rate via the Bethe equation is $[0.69, 0.57, 0.49, 0.42, 0.38]$ for $T_\mu = [0.01, 0.1, 1, 10, 100]$ GeV. Radiative losses add less than 0.5% to the total mean energy deposit at 10 GeV, but add 7% at 100 GeV. The most probable E loss rate rises slightly beyond the minimum ionization energy, then is essentially constant.

The Landau distribution fails to describe energy loss in thin absorbers such as gas TPC cells [1] and Si detectors [31], as can be seen *e.g.* in Fig. 1 of Ref. [1] for an argon-filled TPC cell. Also see Talman [32]. While Δ_p/x may be calculated adequately with Eq. (34.12), the distributions are significantly wider than the Landau width $w = 4\xi$ Ref. [31], Fig. 15. Examples for 500 MeV pions incident on thin silicon detectors are shown in Fig. 34.8. For very thick absorbers the distribution is less skewed but never approaches a Gaussian.

The most probable energy loss, scaled to the mean loss at minimum ionization, is shown in Fig. 34.9 for several silicon detector thicknesses.

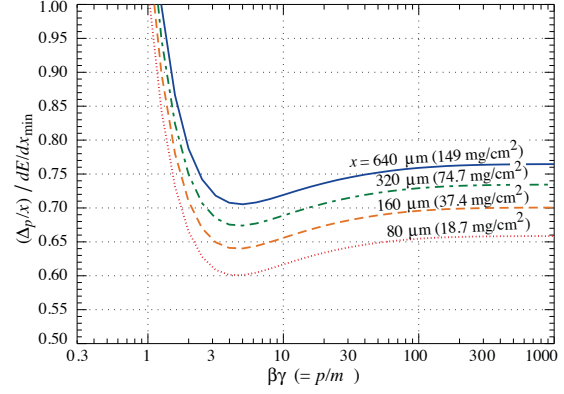


Figure 34.9: Most probable energy loss in silicon, scaled to the mean loss of a minimum ionizing particle, $388 \text{ eV}/\mu\text{m}$ ($1.66 \text{ MeV g}^{-1} \text{ cm}^2$).

34.2.10 Energy loss in mixtures and compounds

A mixture or compound can be thought of as made up of thin layers of pure elements in the right proportion (Bragg additivity). In this case,

$$\left\langle \frac{dE}{dx} \right\rangle = \sum w_j \left\langle \frac{dE}{dx} \right\rangle_j, \quad (34.14)$$

where $dE/dx|_j$ is the mean rate of energy loss (in MeV g cm^{-2}) in the j th element. Eq. (34.5) can be inserted into Eq. (34.14) to find expressions for $\langle Z/A \rangle$, $\langle I \rangle$, and $\langle \delta \rangle$; for example, $\langle Z/A \rangle = \sum w_j Z_j/A_j = \sum n_j Z_j / \sum n_j A_j$. However, $\langle I \rangle$ as defined this way is an underestimate, because in a compound electrons are more tightly bound than in the free elements, and $\langle \delta \rangle$ as calculated this way has little relevance, because it is the electron density that matters. If possible, one uses the tables given in Refs. [18, 34], or the recipes given in [19] (repeated in Ref. [7]), that include effective excitation energies and interpolation coefficients for calculating the density effect correction for the chemical elements and nearly 200 mixtures and compounds. Otherwise, use the recipe for δ given in Refs. [7, 19], and calculate $\langle I \rangle$ following the discussion in Ref. [15]. (Note the “13%” rule!)

34.2.11 Ionization yields

The Bethe equation describes energy loss via excitation and ionization. Many gaseous detectors (proportional counters or TPCs) or liquid ionization detectors count the number of electrons or positive ions from ionization, rather than the ionization energy. As a further complication, the electron liberated in the initial ionization often has enough energy to ionize other atoms or molecules; this process can happen several times. The number of electron-ion pairs per unit length is typically three or more times the original number. Ion or electron counting is a proxy for a direct dE/dx measurement. Calibrations link the number of observed ions to the traversing particle’s dE/dx .

The details depend on the gases (or liquids) and the particular detector involved. A useful discussion of the physics is provided in Sec. 35.6 of this Review.

34.3 Multiple scattering through small angles

A charged particle traversing a medium is deflected by many small-angle scatters. Most of this deflection is due to Coulomb scattering from nuclei as described by the Rutherford cross section. (However, for hadronic projectiles, the strong interactions also contribute to multiple scattering.) For many small-angle scatters the net scattering and displacement distributions are Gaussian via the central limit theorem. Less frequent “hard” scatters produce non-Gaussian tails. These Coulomb scattering distributions are well-represented by the theory of Molière [35]. Accessible discussions are given by Rossi [2] and Jackson [3], and exhaustive reviews have been published by Scott [36] and Motz *et al.* [37]. Experimental measurements have been published by Bichsel [38] (low energy protons) and by Shen *et al.* [39] (relativistic pions,

kaons, and protons).⁷

If we define

$$\theta_0 = \theta_{\text{plane}}^{\text{rms}} = \frac{1}{\sqrt{2}} \theta_{\text{space}}^{\text{rms}}, \quad (34.15)$$

then it is sufficient for many applications to use a Gaussian approximation for the central 98% of the projected angular distribution, with an rms width given by Lynch & Dahl [40]:

$$\begin{aligned} \theta_0 &= \frac{13.6 \text{ MeV}}{\beta c p} \approx \sqrt{\frac{x}{X_0}} \left[1 + 0.088 \log_{10} \left(\frac{x z^2}{X_0 \beta^2} \right) \right] \\ &= \frac{13.6 \text{ MeV}}{\beta c p} \approx \sqrt{\frac{x}{X_0}} \left[1 + 0.038 \ln \left(\frac{x z^2}{X_0 \beta^2} \right) \right] \end{aligned} \quad (34.16)$$

Here p , βc , and z are the momentum, speed, and charge number of the incident particle, and x/X_0 is the thickness of the scattering medium in radiation lengths (defined below). This takes into account the p and z dependence quite well at small Z , but for large Z and small x the β -dependence is not well represented. Further improvements are discussed in Ref. [40].

Eq. (34.16) describes scattering from a single material, while the usual problem involves the multiple scattering of a particle traversing many different layers and mixtures. Since it is from a fit to a Molière distribution, it is incorrect to add the individual θ_0 contributions in quadrature; the result is systematically too small. It is much more accurate to apply Eq. (34.16) once, after finding x and X_0 for the combined scatterer.

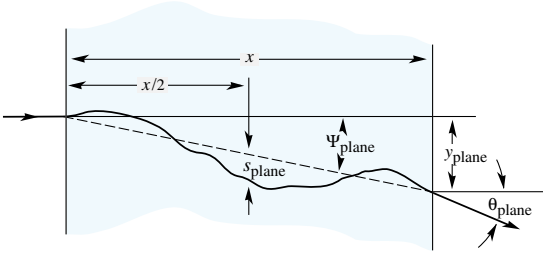


Figure 34.10: Quantities used to describe multiple Coulomb scattering. The particle is incident in the plane of the figure.

The nonprojected (space) and projected (plane) angular distributions are given approximately by [35]

$$\frac{1}{2\pi \theta_0^2} \exp \left(-\frac{\theta_{\text{space}}^2}{2\theta_0^2} \right) d\Omega, \quad (34.17)$$

$$\frac{1}{\sqrt{2\pi} \theta_0} \exp \left(-\frac{\theta_{\text{plane}}^2}{2\theta_0^2} \right) d\theta_{\text{plane}}, \quad (34.18)$$

where θ is the deflection angle. In this approximation, $\theta_{\text{space}}^2 \approx (\theta_{\text{plane},x}^2 + \theta_{\text{plane},y}^2)$, where the x and y axes are orthogonal to the direction of motion, and $d\Omega \approx d\theta_{\text{plane},x} d\theta_{\text{plane},y}$. Deflections into $\theta_{\text{plane},x}$ and $\theta_{\text{plane},y}$ are independent and identically distributed. Fig. 34.10 shows these and other quantities sometimes used to describe multiple Coulomb scattering. They are

$$\psi_{\text{plane}}^{\text{rms}} = \frac{1}{\sqrt{3}} \theta_{\text{plane}}^{\text{rms}} = \frac{1}{\sqrt{3}} \theta_0, \quad (34.19)$$

$$y_{\text{plane}}^{\text{rms}} = \frac{1}{\sqrt{3}} x \theta_{\text{plane}}^{\text{rms}} = \frac{1}{\sqrt{3}} x \theta_0, \quad (34.20)$$

$$s_{\text{plane}}^{\text{rms}} = \frac{1}{4\sqrt{3}} x \theta_{\text{plane}}^{\text{rms}} = \frac{1}{4\sqrt{3}} x \theta_0. \quad (34.21)$$

All the quantitative estimates in this section apply only in the limit of small $\theta_{\text{plane}}^{\text{rms}}$ and in the absence of large-angle scatters. The random variables s , ψ , y , and θ in a given plane are correlated.

⁷Shen *et al.*'s measurements show that Bethe's simpler methods of including atomic electron effects agrees better with experiment than does Scott's treatment.

Obviously, $y \approx x\psi$. In addition, y and θ have the correlation coefficient $\rho_{y\theta} = \sqrt{3}/2 \approx 0.87$. For Monte Carlo generation of a joint $(y_{\text{plane}}, \theta_{\text{plane}})$ distribution, or for other calculations, it may be most convenient to work with independent Gaussian random variables (z_1, z_2) with mean zero and variance one, and then set

$$y_{\text{plane}} = z_1 x \theta_0 (1 - \rho_{y\theta}^2)^{1/2} / \sqrt{3} + z_2 \rho_{y\theta} x \theta_0 / \sqrt{3} \quad (34.22a)$$

$$= z_1 x \theta_0 / \sqrt{12} + z_2 x \theta_0 / 2; \quad (34.22b)$$

$$\theta_{\text{plane}} = z_2 \theta_0. \quad (34.22c)$$

Note that the second term for y_{plane} equals $x \theta_{\text{plane}}/2$ and represents the displacement that would have occurred had the deflection θ_{plane} all occurred at the single point $x/2$.

For heavy ions the multiple Coulomb scattering has been measured and compared with various theoretical distributions [41].

34.4 Photon and electron interactions in matter

At low energies electrons and positrons primarily lose energy by ionization, although other processes (Møller scattering, Bhabha scattering, e^+ annihilation) contribute, as shown in Fig. 34.11. While ionization loss rates rise logarithmically with energy, bremsstrahlung losses rise nearly linearly (fractional loss is nearly independent of energy), and dominates above the critical energy (Sec. 34.4.4 below), a few tens of MeV in most materials.

34.4.1 Collision energy losses by e^\pm

Stopping power differs somewhat for electrons and positrons, and both differ from stopping power for heavy particles because of the kinematics, spin, charge, and the identity of the incident electron with the electrons that it ionizes. Complete discussions and tables can be found in Refs. [12, 15, 34].

For electrons, large energy transfers to atomic electrons (taken as free) are described by the Møller cross section. From Eq. (34.4), the maximum energy transfer in a single collision should be the entire kinetic energy, $W_{\text{max}} = m_e c^2 (\gamma - 1)$, but because the particles are identical, the maximum is half this, $W_{\text{max}}/2$. (The results are the same if the transferred energy is ϵ or if the transferred energy is $W_{\text{max}} - \epsilon$. The stopping power is by convention calculated for the faster of the two emerging electrons.) The first moment of the Møller cross section [27] (divided by dx) is the stopping power:

$$\begin{aligned} \left\langle -\frac{dE}{dx} \right\rangle &= \frac{1}{2} K \frac{Z}{A} \frac{1}{\beta^2} \left[\ln \frac{m_e c^2 \beta^2 \gamma^2 \{m_e c^2 (\gamma - 1)/2\}}{I^2} + (1 - \beta^2) \right. \\ &\quad \left. - \frac{2\gamma - 1}{\gamma^2} \ln 2 + \frac{1}{8} \left(\frac{\gamma - 1}{\gamma} \right)^2 - \delta \right] \end{aligned} \quad (34.23)$$

The logarithmic term can be compared with the logarithmic term in the Bethe equation (Eq. (34.2)) by substituting $W_{\text{max}} = m_e c^2 (\gamma - 1)/2$. Electron-positron scattering is described by the fairly complicated Bhabha cross section [27]. There is no identical particle problem, so $W_{\text{max}} = m_e c^2 (\gamma - 1)$. The first moment of the Bhabha equation yields

$$\begin{aligned} \left\langle -\frac{dE}{dx} \right\rangle &= \frac{1}{2} K \frac{Z}{A} \frac{1}{\beta^2} \left[\ln \frac{m_e c^2 \beta^2 \gamma^2 \{m_e c^2 (\gamma - 1)\}}{2I^2} + 2 \ln 2 \right. \\ &\quad \left. - \frac{\beta^2}{12} \left(23 + \frac{14}{\gamma + 1} + \frac{10}{(\gamma + 1)^2} + \frac{4}{(\gamma + 1)^3} \right) - \delta \right]. \end{aligned} \quad (34.24)$$

Following ICRU 37 [12], the density effect correction δ has been added to Uehling's equations [27] in both cases.

For heavy particles, shell corrections were developed assuming that the projectile is equivalent to a perturbing potential whose center moves with constant speed. This assumption has no sound theoretical basis for electrons. The authors of ICRU 37 [12] estimated the possible error in omitting it by assuming the correction was twice as great as for a proton of the same speed. At $T = 10$ keV, the error was estimated to be $\approx 2\%$ for water, $\approx 9\%$ for Cu, and $\approx 21\%$ for Au.

As shown in Fig. 34.11, stopping powers for e^- , e^+ , and heavy particles are not dramatically different. In silicon, the minimum value for electrons is $1.50 \text{ MeV cm}^2/\text{g}$ (at $\gamma = 3.3$); for positrons, $1.46 \text{ MeV cm}^2/\text{g}$ (at $\gamma = 3.7$), and for muons, $1.66 \text{ MeV cm}^2/\text{g}$ (at $\gamma = 3.58$).

34.4.2 Radiation length

High-energy electrons predominantly lose energy in matter by bremsstrahlung, and high-energy photons by e^+e^- pair production. The characteristic amount of matter traversed for these related interactions is called the radiation length X_0 , usually measured in g cm^{-2} . It is the mean distance over which a high-energy electron loses all but $1/e$ of its energy by bremsstrahlung. It is also the appropriate scale length for describing high-energy electromagnetic cascades. X_0 has been calculated and tabulated by Y.S. Tsai [42]:

$$\frac{1}{X_0} = 4\alpha r_e^2 \frac{N_A}{A} \left\{ Z^2 [L_{\text{rad}} - f(Z)] + Z L'_{\text{rad}} \right\}. \quad (34.25)$$

For $A = 1 \text{ g mol}^{-1}$, $4\alpha r_e^2 N_A/A = (716.408 \text{ g cm}^{-2})^{-1}$. L_{rad} and L'_{rad} are given in Table 34.2. The function $f(Z)$ is an infinite sum, but for elements up to uranium can be represented to 4-place accuracy by

$$f(Z) = a^2 \left[(1 + a^2)^{-1} + 0.20206 - 0.0369 a^2 + 0.0083 a^4 - 0.002 a^6 \right], \quad (34.26)$$

where $a = \alpha Z$ [43].

Table 34.2: Tsai's L_{rad} and L'_{rad} , for use in calculating the radiation length in an element using Eq. (34.25).

Element	Z	L_{rad}	L'_{rad}
H	1	5.31	6.144
He	2	4.79	5.621
Li	3	4.74	5.805
Be	4	4.71	5.924
Others	> 4	$\ln(184.15 Z^{-1/3})$	$\ln(1194 Z^{-2/3})$

The radiation length in a mixture or compound may be approximated by

$$1/X_0 = \sum w_j/X_j, \quad (34.27)$$

where w_j and X_j are the fraction by weight and the radiation length for the j th element.

34.4.3 Bremsstrahlung energy loss by e^\pm

At very high energies and except at the high-energy tip of the bremsstrahlung spectrum, the cross section can be approximated in the “complete screening case” as [42]

$$d\sigma/dk = (1/k)4\alpha r_e^2 \left\{ \left(\frac{4}{3} - \frac{4}{3}y + y^2 \right) [Z^2(L_{\text{rad}} - f(Z)) + Z L'_{\text{rad}}] + \frac{1}{9}(1-y)(Z^2 + Z) \right\}, \quad (34.28)$$

where $y = k/E$ is the fraction of the electron's energy transferred to the radiated photon. At small y (the “infrared limit”) the term on the second line ranges from 1.7% (low Z) to 2.5% (high Z) of the total. If it is ignored and the first line simplified with the definition of X_0 given in Eq. (34.25), we have

$$\frac{d\sigma}{dk} = \frac{A}{X_0 N_A k} \left(\frac{4}{3} - \frac{4}{3}y + y^2 \right). \quad (34.29)$$

This cross section (times k) is shown by the top curve in Fig. 34.12.

This formula is accurate except near $y = 1$, where screening may become incomplete, and near $y = 0$, where the infrared divergence is removed by the interference of bremsstrahlung amplitudes from

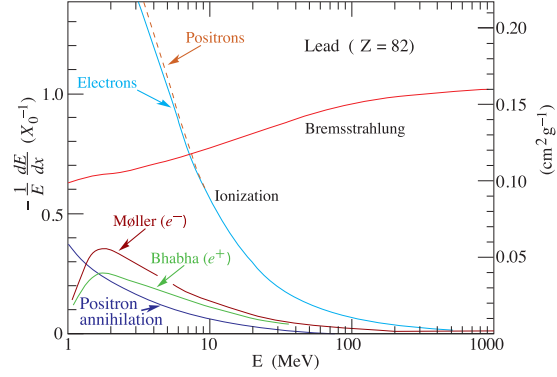


Figure 34.11: Fractional energy loss per radiation length in lead as a function of electron or positron energy. Electron (positron) scattering is considered as ionization when the energy loss per collision is below 0.255 MeV , and as Møller (Bhabha) scattering when it is above. Adapted from Fig. 3.2 from Messel and Crawford, *Electron-Photon Shower Distribution Function Tables for Lead, Copper, and Air Absorbers*, Pergamon Press, 1970. Messel and Crawford use $X_0(\text{Pb}) = 5.82 \text{ g/cm}^2$, but we have modified the figures to reflect the value given in the Table of Atomic and Nuclear Properties of Materials ($X_0(\text{Pb}) = 6.37 \text{ g/cm}^2$).

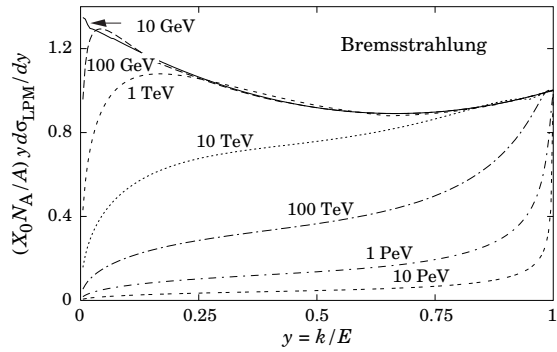


Figure 34.12: The normalized bremsstrahlung cross section $k d\sigma_{\text{LPM}}/dk$ in lead versus the fractional photon energy $y = k/E$. The vertical axis has units of photons per radiation length.

nearby scattering centers (the LPM effect) [44, 45] and dielectric suppression [46, 47]. These and other suppression effects in bulk media are discussed in Sec. 34.4.6.

With decreasing energy ($E \lesssim 10 \text{ GeV}$) the high- y cross section drops and the curves become rounded as $y \rightarrow 1$. Curves of this familiar shape can be seen in Rossi [2] (Figs. 2.11.2,3); see also the review by Koch & Motz [48].

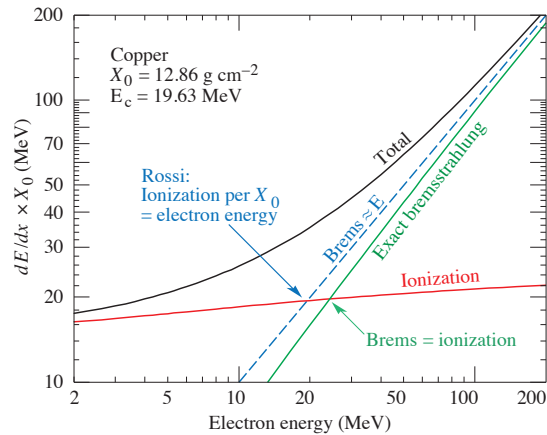


Figure 34.13: Two definitions of the critical energy E_c .

Except at these extremes, and still in the complete-screening approximation, the number of photons with energies between k_{\min} and k_{\max} emitted by an electron travelling a distance $d \ll X_0$ is

$$N_\gamma = \frac{d}{X_0} \left[\frac{4}{3} \ln \left(\frac{k_{\max}}{k_{\min}} \right) - \frac{4(k_{\max} - k_{\min})}{3E} + \frac{k_{\max}^2 - k_{\min}^2}{2E^2} \right] \quad (34.30)$$

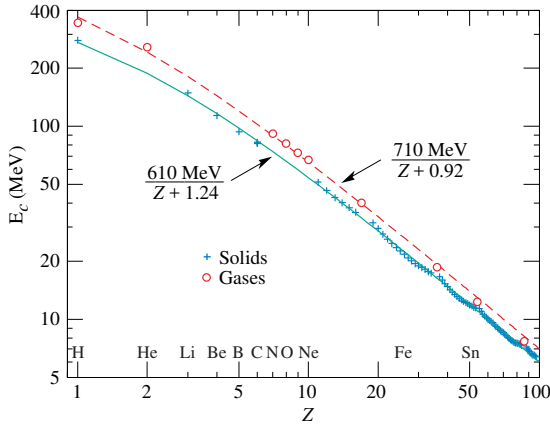


Figure 34.14: Electron critical energy for the chemical elements, using Rossi’s definition [2]. The fits shown are for solids and liquids (solid line) and gases (dashed line). The rms deviation is 2.2% for the solids and 4.0% for the gases.

34.4.4 Critical energy

An electron loses energy by bremsstrahlung at a rate nearly proportional to its energy, while the ionization loss rate varies only logarithmically with the electron energy. The *critical energy* E_c is sometimes defined as the energy at which the two loss rates are equal [49]. Among alternate definitions is that of Rossi [2], who defines the critical energy as the energy at which the ionization loss per radiation length is equal to the electron energy. Equivalently, it is the same as the first definition with the approximation $|dE/dx|_{\text{brems}} \approx E/X_0$. This form has been found to describe transverse electromagnetic shower development more accurately (see below). These definitions are illustrated in the case of copper in Fig. 34.13.

The accuracy of approximate forms for E_c has been limited by the failure to distinguish between gases and solid or liquids, where there is a substantial difference in ionization at the relevant energy because of the density effect. We distinguish these two cases in Fig. 34.14. Fits were also made with functions of the form $a/(Z + b)^\alpha$, but α was found to be essentially unity. Since E_c also depends on A , I , and other factors, such forms are at best approximate.

Values of E_c for both electrons and positrons in more than 300 materials at pdg.lbl.gov/current/AtomicNuclearProperties.

34.4.5 Energy loss by photons

Contributions to the photon cross section in a light element (carbon) and a heavy element (lead) are shown in Fig. 34.15. At low energies it is seen that the photoelectric effect dominates, although Compton scattering, Rayleigh scattering, and photonuclear absorption also contribute. The photoelectric cross section is characterized by discontinuities (absorption edges) as thresholds for photoionization of various atomic levels are reached. Photon attenuation lengths for a variety of elements are shown in Fig. 34.16, and data for $30 \text{ eV} < k < 100 \text{ GeV}$ for all elements are available from the web pages given in the caption. Here k is the photon energy.

The increasing domination of pair production as the energy increases is shown in Fig. 34.17. Using approximations similar to those used to obtain Eq. (34.29), Tsai’s formula for the differential

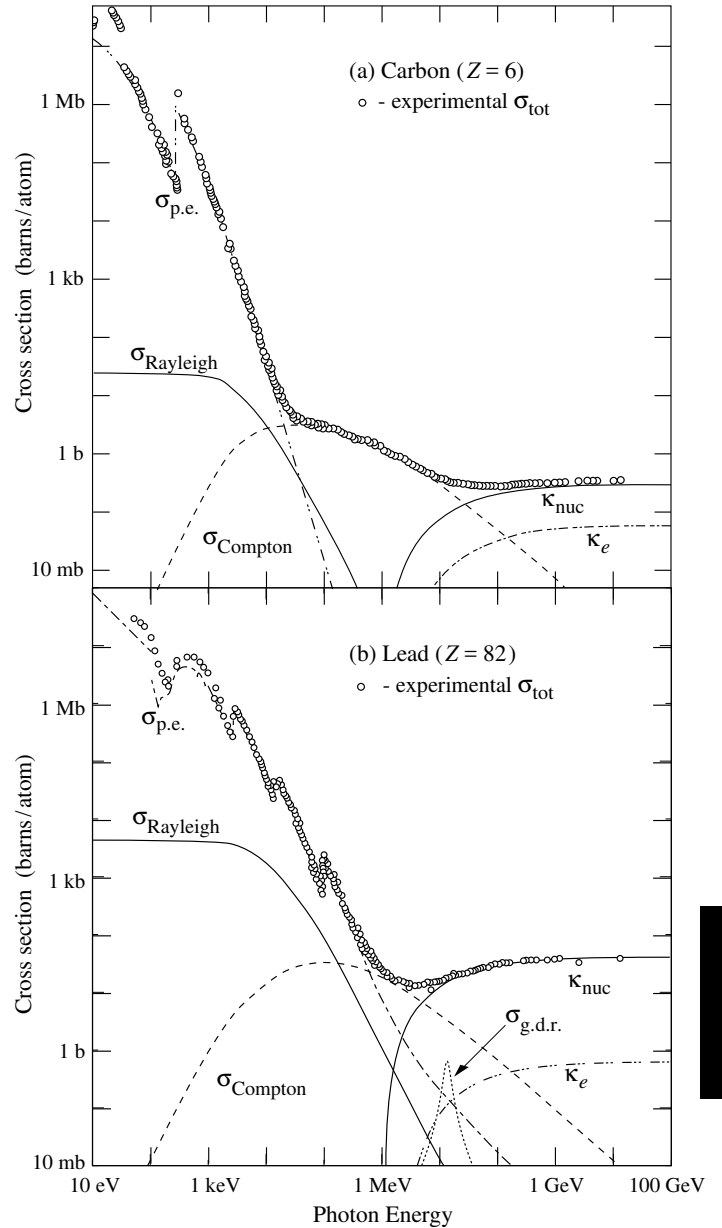


Figure 34.15: Photon total cross sections as a function of energy in carbon and lead, showing the contributions of different processes [50]:

- $\sigma_{\text{p.e.}}$ = Atomic photoelectric effect (electron ejection, photon absorption)
- σ_{Rayleigh} = Rayleigh (coherent) scattering—atom neither ionized nor excited
- σ_{Compton} = Incoherent scattering (Compton scattering off an electron)
- κ_{nuc} = Pair production, nuclear field
- κ_e = Pair production, electron field
- $\sigma_{\text{g.d.r.}}$ = Photonuclear interactions, most notably the Giant Dipole Resonance [51]. In these interactions, the target nucleus is usually broken up.

Original figures through the courtesy of John H. Hubbell (NIST).

cross section [42] reduces to

$$\frac{d\sigma}{dx} = \frac{A}{X_0 N_A} \left[1 - \frac{4}{3}x(1-x) \right] \quad (34.31)$$

in the complete-screening limit valid at high energies. Here $x = E/k$ is the fractional energy transfer to the pair-produced electron (or positron), and k is the incident photon energy. The cross

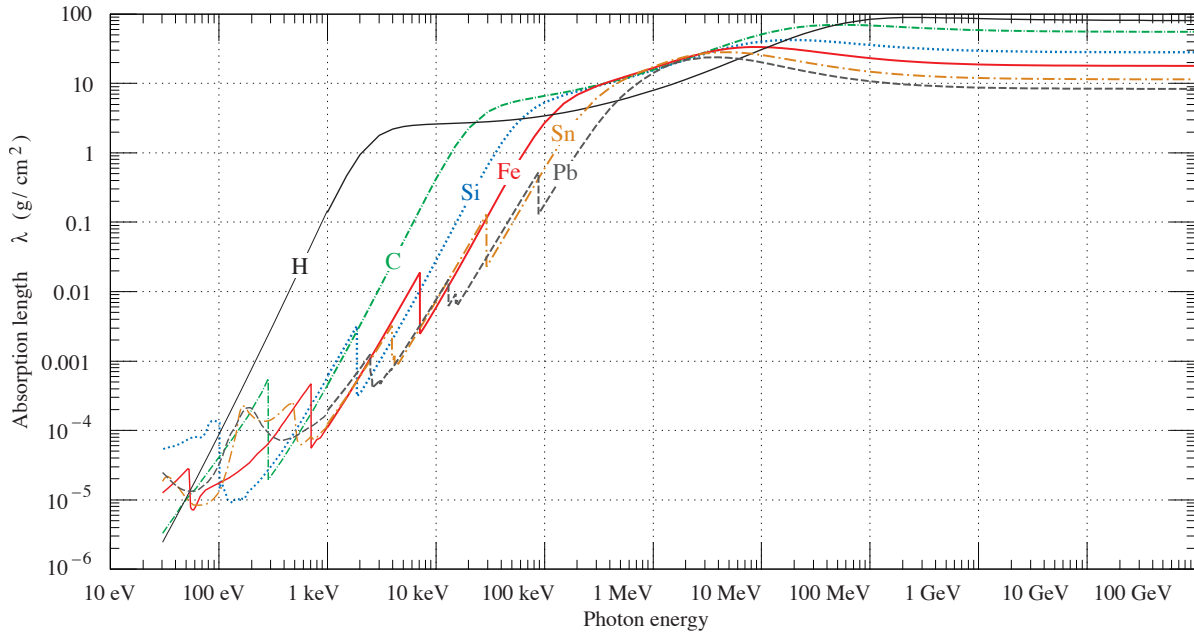


Figure 34.16: The photon mass attenuation length (or mean free path) $\lambda = 1/(\mu/\rho)$ for various elemental absorbers as a function of photon energy. The mass attenuation coefficient is μ/ρ , where ρ is the density. The intensity I remaining after traversal of thickness t (in mass/unit area) is given by $I = I_0 \exp(-t/\lambda)$. The accuracy is a few percent. For a chemical compound or mixture, $1/\lambda_{\text{eff}} \approx \sum_{\text{elements}} w_Z/\lambda_Z$, where w_Z is the proportion by weight of the element with atomic number Z . The processes responsible for attenuation are given in Fig. 34.11. Since coherent processes are included, not all these processes result in energy deposition. The data for $30 \text{ eV} < E < 1 \text{ keV}$ are from Ref. [52], those for $1 \text{ keV} < E < 100 \text{ GeV}$ from Ref. [53].

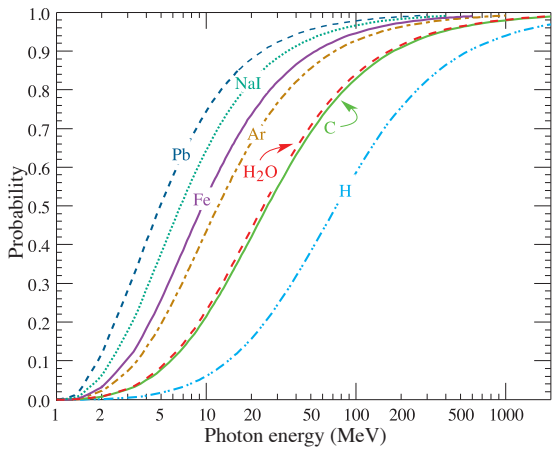


Figure 34.17: Probability P that a photon interaction will result in conversion to an e^+e^- pair. Except for a few-percent contribution from photonuclear absorption around 10 or 20 MeV, essentially all other interactions in this energy range result in Compton scattering off an atomic electron. For a photon attenuation length λ (Fig. 34.16), the probability that a given photon will produce an electron pair (without first Compton scattering) in thickness t of absorber is $P[1 - \exp(-t/\lambda)]$.

section is very closely related to that for bremsstrahlung, since the Feynman diagrams are variants of one another. The cross section is of necessity symmetric between x and $1 - x$, as can be seen by the solid curve in Fig. 34.18. See the review by Motz, Olsen, & Koch for a more detailed treatment [54]. Eq. (34.31) may be integrated to find the high-energy limit for the total e^+e^- pair-production cross section:

$$\sigma = \frac{7}{9}(A/X_0N_A). \tag{34.32}$$

Equation Eq. (34.32) is accurate to within a few percent down to energies as low as 1 GeV, particularly for high- Z materials.

34.4.6 Bremsstrahlung and pair production at very high energies

At ultrahigh energies, Eqns. 34.28–34.32 will fail because of quantum mechanical interference between amplitudes from different scattering centers. Since the longitudinal momentum transfer to a given center is small ($\propto k/E(E - k)$, in the case of bremsstrahlung), the interaction is spread over a comparatively long distance called the formation length ($\propto E(E - k)/k$) via the uncertainty principle. In alternate language, the formation length is the distance over which the highly relativistic electron and the photon “split apart.” The interference is usually destructive. Calculations of the “Landau-Pomeranchuk-Migdal” (LPM) effect may be made semi-classically based on the average multiple scattering, or more rigorously using a quantum transport approach [44, 45].

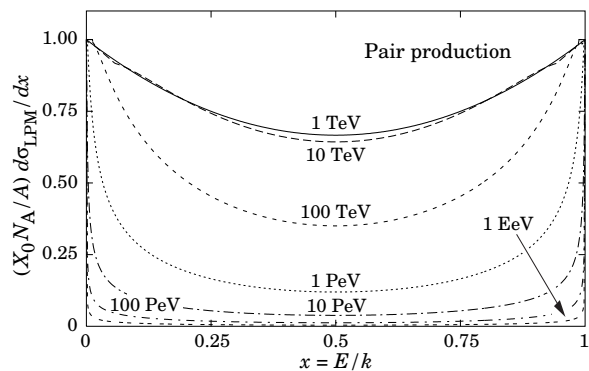


Figure 34.18: The normalized pair production cross section $d\sigma_{LPM}/dx$, versus fractional electron energy $x = E/k$.

In amorphous media, bremsstrahlung is suppressed if the pho-

ton energy k is less than $E^2/(E + E_{LPM})$ [45], where⁸

$$E_{LPM} = (m_e c^2)^2 \alpha \frac{X_0}{4\pi\hbar c \rho} = (7.7 \text{ TeV/cm}) \times \frac{X_0}{\rho}. \quad (34.33)$$

Since physical distances are involved, X_0/ρ , in cm, appears. The energy-weighted bremsstrahlung spectrum for lead, $k d\sigma_{LPM}/dk$, is shown in Fig. 34.12. With appropriate scaling by X_0/ρ , other materials behave similarly.

For photons, pair production is reduced for $E(k - E) > k E_{LPM}$. The pair-production cross sections for different photon energies are shown in Fig. 34.18.

If $k \ll E$, several additional mechanisms can also produce suppression. When the formation length is long, even weak factors can perturb the interaction. For example, the emitted photon can coherently forward scatter off of the electrons in the media. Because of this, for $k < \omega_p E/m_e \sim 10^{-4}$, bremsstrahlung is suppressed by a factor $(k m_e / \omega_p E)^2$ [47]. Magnetic fields can also suppress bremsstrahlung.

In crystalline media, the situation is more complicated, with coherent enhancement or suppression possible. The cross section depends on the electron and photon energies and the angles between the particle direction and the crystalline axes [56].

34.4.7 Photonuclear and electronuclear interactions at still higher energies

At still higher photon and electron energies, where the bremsstrahlung and pair production cross-sections are heavily suppressed by the LPM effect, photonuclear and electronuclear interactions predominate over electromagnetic interactions.

At photon energies above about 10^{20} eV, for example, photons usually interact hadronically. The exact cross-over energy depends on the model used for the photonuclear interactions. These processes are illustrated in Fig. 34.19. At still higher energies ($\gtrsim 10^{23}$ eV), photonuclear interactions can become coherent, with the photon interaction spread over multiple nuclei. Essentially, the photon coherently converts to a ρ^0 , in a process that is somewhat similar to kaon regeneration [57].

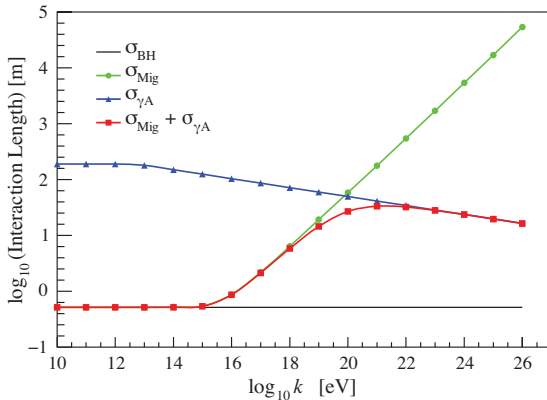


Figure 34.19: Interaction length for a photon in ice as a function of photon energy for the Bethe-Heitler (BH), LPM (Mig) and photonuclear (γA) cross sections [57]. The Bethe-Heitler interaction length is $9X_0/7$, and X_0 is 0.393 m in ice.

Similar processes occur for electrons. As electron energies increase and the LPM effect suppresses bremsstrahlung, electronuclear interactions become more important. At energies above 10^{21} eV, these electronuclear interactions dominate electron energy loss [57].

34.5 Electromagnetic cascades

When a high-energy electron or photon is incident on a thick absorber, it initiates an electromagnetic cascade as pair production and bremsstrahlung generate more electrons and photons with

⁸This definition differs from that of Ref. [55] by a factor of two. E_{LPM} scales as the 4th power of the mass of the incident particle, so that $E_{LPM} = (1.4 \times 10^{10} \text{ TeV/cm}) \times X_0/\rho$ for a muon.

lower energy. The longitudinal development is governed by the high-energy part of the cascade, and therefore scales as the radiation length in the material. Electron energies eventually fall below the critical energy, and then dissipate their energy by ionization and excitation rather than by the generation of more shower particles. In describing shower behavior, it is therefore convenient to introduce the scale variables

$$t = x/X_0, \quad y = E/E_c, \quad (34.34)$$

so that distance is measured in units of radiation length and energy in units of critical energy.

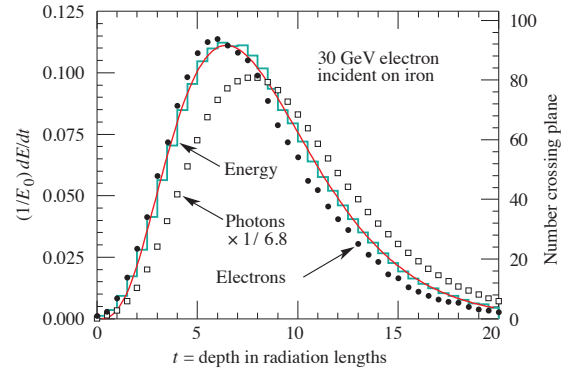


Figure 34.20: An EGS4 simulation of a 30 GeV electron-induced cascade in iron. The histogram shows fractional energy deposition per radiation length, and the curve is a gamma-function fit to the distribution. Circles indicate the number of electrons with total energy greater than 1.5 MeV crossing planes at $X_0/2$ intervals (scale on right) and the squares the number of photons with $E \geq 1.5$ MeV crossing the planes (scaled down to have same area as the electron distribution).

Longitudinal profiles from an EGS4 [58] simulation of a 30 GeV electron-induced cascade in iron are shown in Fig. 34.20. The number of particles crossing a plane (very close to Rossi's Π function [2]) is sensitive to the cutoff energy, here chosen as a total energy of 1.5 MeV for both electrons and photons. The electron number falls off more quickly than energy deposition. This is because, with increasing depth, a larger fraction of the cascade energy is carried by photons. Exactly what a calorimeter measures depends on the device, but it is not likely to be exactly any of the profiles shown. In gas counters it may be very close to the electron number, but in glass Cherenkov detectors and other devices with “thick” sensitive regions it is closer to the energy deposition (total track length). In such detectors the signal is proportional to the “detectable” track length T_d , which is in general less than the total track length T . Practical devices are sensitive to electrons with energy above some detection threshold E_d , and $T_d = T F(E_d/E_c)$. An analytic form for $F(E_d/E_c)$ obtained by Rossi [2] is given by Fabjan in Ref. [59]; see also Amaldi [60].

The mean longitudinal profile of the energy deposition in an electromagnetic cascade is reasonably well described by a gamma distribution [61]:

$$\frac{dE}{dt} = E_0 b \frac{(bt)^{a-1} e^{-bt}}{\Gamma(a)} \quad (34.35)$$

The maximum t_{\max} occurs at $(a - 1)/b$. We have made fits to shower profiles in elements ranging from carbon to uranium, at energies from 1 GeV to 100 GeV. The energy deposition profiles are well described by Eq. (34.35) with

$$t_{\max} = (a - 1)/b = 1.0 \times (\ln y + C_j), \quad j = e, \gamma, \quad (34.36)$$

where $C_e = -0.5$ for electron-induced cascades and $C_\gamma = +0.5$ for photon-induced cascades. To use Eq. (34.35), one finds $(a - 1)/b$ from Eq. (34.36) and Eq. (34.34), then finds a either by assuming $b \approx 0.5$ or by finding a more accurate value from Fig. 34.21. The results are very similar for the electron number profiles, but there

is some dependence on the atomic number of the medium. A similar form for the electron number maximum was obtained by Rossi in the context of his “Approximation B,” [2] (see Fabjan’s review in Ref. [59]), but with $C_e = -1.0$ and $C_\gamma = -0.5$; we regard this as superseded by the EGS4 result.

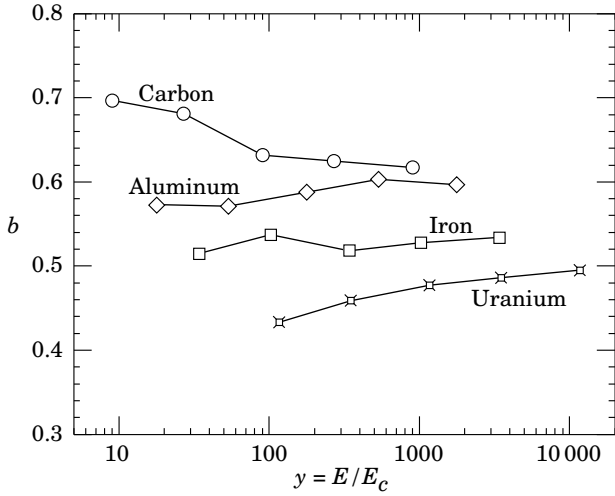


Figure 34.21: Fitted values of the scale factor b for energy deposition profiles obtained with EGS4 for a variety of elements for incident electrons with $1 \leq E_0 \leq 100$ GeV. Values obtained for incident photons are essentially the same.

The “shower length” $X_s = X_0/b$ is less conveniently parameterized, since b depends upon both Z and incident energy, as shown in Fig. 34.21. As a corollary of this Z dependence, the number of electrons crossing a plane near shower maximum is underestimated using Rossi’s approximation for carbon and seriously overestimated for uranium. Essentially the same b values are obtained for incident electrons and photons. For many purposes it is sufficient to take $b \approx 0.5$.

The length of showers initiated by ultra-high energy photons and electrons is somewhat greater than at lower energies since the first or first few interaction lengths are increased via the mechanisms discussed above.

The gamma function distribution is very flat near the origin, while the EGS4 cascade (or a real cascade) increases more rapidly. As a result Eq. (34.35) fails badly for about the first two radiation lengths; it was necessary to exclude this region in making fits.

Because fluctuations are important, Eq. (34.35) should be used only in applications where average behavior is adequate. Grindhammer *et al.* have developed fast simulation algorithms in which the variance and correlation of a and b are obtained by fitting Eq. (34.35) to individually simulated cascades, then generating profiles for cascades using a and b chosen from the correlated distributions [62].

The transverse development of electromagnetic showers in different materials scales fairly accurately with the *Molière radius* R_M , given by [63, 64]

$$R_M = X_0 E_s/E_c, \quad (34.37)$$

where $E_s \approx 21$ MeV (Table 34.1), and the Rossi definition of E_c is used.

In a material containing a weight fraction w_j of the element with critical energy E_{cj} and radiation length X_j , the Molière radius is given by

$$\frac{1}{R_M} = \frac{1}{E_s} \sum \frac{w_j E_{cj}}{X_j}. \quad (34.38)$$

Measurements of the lateral distribution in electromagnetic cascades are shown in Refs. [63, 64]. On the average, only 10% of the energy lies outside the cylinder with radius R_M . About 99% is contained inside of $3.5R_M$, but at this radius and beyond composition effects become important and the scaling with R_M fails. The distributions are characterized by a narrow core, and broaden

as the shower develops. They are often represented as the sum of two Gaussians.

At high enough energies, the LPM effect (Sec. 34.4.6) reduces the cross sections for bremsstrahlung and pair production, and hence can cause significant elongation of electromagnetic cascades [45].

34.6 Muon energy loss at high energy

At sufficiently high energies, radiative processes become more important than ionization for all charged particles. For muons and pions in materials such as iron, this “critical energy” occurs at several hundred GeV. (There is no simple scaling with particle mass, but for protons the “critical energy” is much, much higher.) Radiative effects dominate the energy loss of energetic muons found in cosmic rays or produced at the newest accelerators. These processes are characterized by small cross sections, hard spectra, large energy fluctuations, and the associated generation of electromagnetic and (in the case of photonuclear interactions) hadronic showers [65–73]. As a consequence, at these energies the treatment of energy loss as a uniform and continuous process is for many purposes inadequate.

It is convenient to write the average rate of muon energy loss as [74]

$$\langle -dE/dx \rangle = a(E) + b(E)E. \quad (34.39)$$

Here $a(E)$ is the ionization energy loss given by Eq. (34.5), and $b(E)$ is the sum of e^+e^- pair production, bremsstrahlung, and photonuclear contributions. To the approximation that these slowly-varying functions are constant, the mean range x_0 of a muon with initial energy E_0 is given by

$$x_0 \approx (1/b) \ln(1 + E_0/E_{\mu c}), \quad (34.40)$$

where $E_{\mu c} = a/b$.

Fig. 34.22 shows contributions to $b(E)$ for iron. Since $a(E) \approx 0.002$ GeV $g^{-1} \text{ cm}^2$, $b(E)E$ dominates the energy loss above several hundred GeV, where $b(E)$ is nearly constant. The rates of energy loss for muons in hydrogen, uranium, and iron are shown in Fig. 34.23 [7].

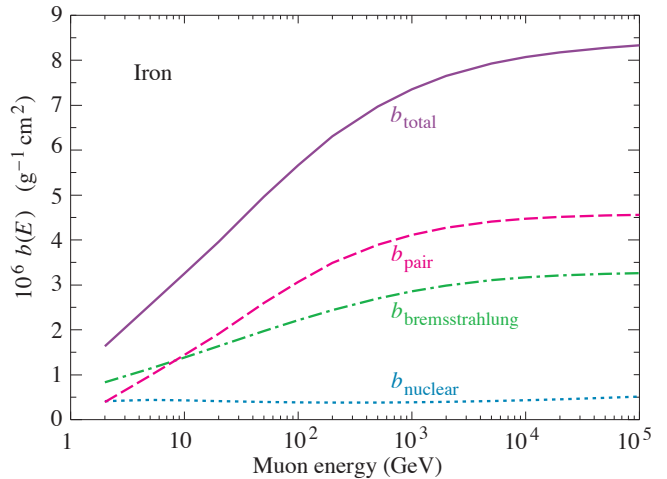


Figure 34.22: Contributions to the fractional energy loss by muons in iron due to e^+e^- pair production, bremsstrahlung, and photonuclear interactions, as obtained from Groom *et al.* [7] except for post-Born corrections to the cross section for direct pair production from atomic electrons.

The “muon critical energy” $E_{\mu c}$ can be defined more exactly as the energy at which radiative and ionization losses are equal, and can be found by solving $E_{\mu c} = a(E_{\mu c})/b(E_{\mu c})$. This definition corresponds to the solid-line intersection in Fig. 34.13, and is different from the Rossi definition we used for electrons. It serves the same function: below $E_{\mu c}$ ionization losses dominate, and above $E_{\mu c}$ radiative effects dominate. The dependence of $E_{\mu c}$ on atomic number Z is shown in Fig. 34.24.

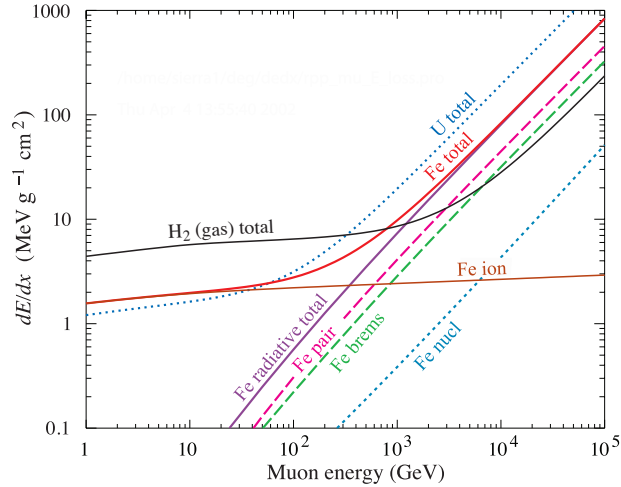


Figure 34.23: The average energy loss of a muon in hydrogen, iron, and uranium as a function of muon energy. Contributions to dE/dx in iron from ionization and pair production, bremsstrahlung and photonuclear interactions are also shown.

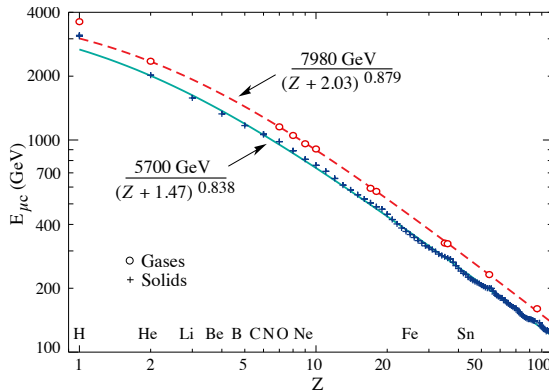


Figure 34.24: Muon critical energy for the chemical elements, defined as the energy at which radiative and ionization energy loss rates are equal [7]. The equality comes at a higher energy for gases than for solids or liquids with the same atomic number because of a smaller density effect reduction of the ionization losses. The fits shown in the figure exclude hydrogen. Alkali metals fall 3–4% above the fitted function, while most other solids are within 2% of the function. Among the gases the worst fit is for radon (2.7% high).

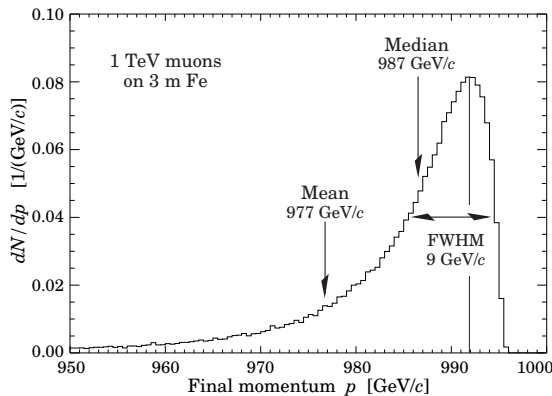


Figure 34.25: The momentum distribution of 1 TeV/c muons after traversing 3 m of iron as calculated by S.I. Striganov [7].

The radiative cross sections are expressed as functions of the fractional energy loss ν . The bremsstrahlung cross section goes

roughly as $1/\nu$ over most of the range, while for the pair production case the distribution goes as ν^{-3} to ν^{-2} [75]. “Hard” losses are therefore more probable in bremsstrahlung, and in fact energy losses due to pair production may very nearly be treated as continuous. The simulated momentum distribution of an incident 1 TeV/c muon beam after it crosses 3 m of iron is shown in Fig. 34.25 [7]. The most probable loss is 8 GeV, or 3.4 MeV $g^{-1}cm^2$. The full width at half maximum is 9 GeV/c, or 0.9%. The radiative tail is almost entirely due to bremsstrahlung, although most of the events in which more than 10% of the incident energy lost experienced relatively hard photonuclear interactions. The latter can exceed detector resolution [76], necessitating the reconstruction of lost energy. Tables in Ref. [7] list the stopping power as 9.82 MeV $g^{-1}cm^2$ for a 1 TeV muon, so that the mean loss should be 23 GeV (≈ 23 GeV/c), for a final momentum of 977 GeV/c, far below the peak. This agrees with the indicated mean calculated from the simulation. Electromagnetic and hadronic cascades in detector materials can obscure muon tracks in detector planes and reduce tracking efficiency [77].

34.7 Cherenkov and transition radiation [3, 78, 79]

A charged particle radiates if its speed is greater than the local phase speed of light (Cherenkov radiation) or if it crosses suddenly from one medium to another with different optical properties (transition radiation). Neither process is important for energy loss, but both are used in high-energy and cosmic-ray physics detectors.

34.7.1 Optical Cherenkov radiation

The angle θ_c of Cherenkov radiation, relative to the particle’s direction, for a particle with speed βc in a medium with index of refraction n is

$$\begin{aligned} \cos \theta_c &= (1/n\beta) \\ \text{or } \tan \theta_c &= \sqrt{\beta^2 n^2 - 1} \\ &\approx \sqrt{2(1 - 1/n\beta)} \quad \text{for small } \theta_c, \text{ e.g. in gases. (34.41)} \end{aligned}$$

The threshold speed β_t is $1/n$, and $\gamma_t = 1/(1 - \beta_t^2)^{1/2}$. Therefore, $\beta_t \gamma_t = 1/(2\delta + \delta^2)^{1/2}$, where $\delta = n - 1$. Values of δ for various commonly used gases are given as a function of pressure and wavelength in Ref. [80]. See its Table 6.1 for values at atmospheric pressure. Data for other commonly used materials are given in Ref. [81].

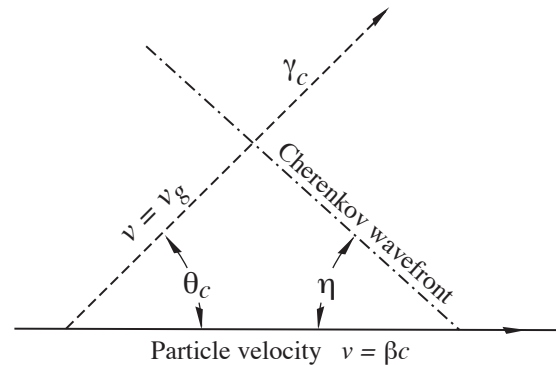


Figure 34.26: Cherenkov light emission and wavefront angles. In a dispersive medium, $\theta_c + \eta \neq 90^\circ$.

Practical Cherenkov radiator materials are dispersive. Let ω be the photon’s frequency, and let $k = 2\pi/\lambda$ be its wavenumber. The photons propagate at the group speed $v_g = d\omega/dk = c/[n(\omega) + \omega(dn/d\omega)]$. In a non-dispersive medium, this simplifies to $v_g = c/n$.

In his classical paper, Tamm [82] showed that for dispersive media the radiation is concentrated in a thin conical shell whose

vertex is at the moving charge, and whose opening half-angle η is

$$\begin{aligned} \cot \eta &= \left[\frac{d}{d\omega} (\omega \tan \theta_c) \right]_{\omega_0} \\ &= \left[\tan \theta_c + \beta^2 \omega n(\omega) \frac{dn}{d\omega} \cot \theta_c \right]_{\omega_0}, \end{aligned} \quad (34.42)$$

where ω_0 is the central value of the small frequency range under consideration. (See Fig. 34.26.) This cone has a opening half-angle η , and, unless the medium is non-dispersive ($dn/d\omega = 0$), $\theta_c + \eta \neq 90^\circ$. The Cherenkov wavefront ‘sideslips’ along with the particle [83]. This effect has timing implications for ring imaging Cherenkov counters [84], but it is probably unimportant for most applications.

The number of photons produced per unit path length of a particle with charge ze and per unit energy interval of the photons is

$$\begin{aligned} \frac{d^2 N}{dE dx} &= \frac{\alpha z^2}{\hbar c} \sin^2 \theta_c = \frac{\alpha^2 z^2}{r_e m_e c^2} \left(1 - \frac{1}{\beta^2 n^2(E)} \right) \\ &\approx 370 \sin^2 \theta_c(E) \text{ eV}^{-1} \text{ cm}^{-1} \quad (z = 1), \end{aligned} \quad (34.43)$$

or, equivalently,

$$\frac{d^2 N}{dx d\lambda} = \frac{2\pi\alpha z^2}{\lambda^2} \left(1 - \frac{1}{\beta^2 n^2(\lambda)} \right). \quad (34.44)$$

The index of refraction n is a function of photon energy $E = \hbar\omega$, as is the sensitivity of the transducer used to detect the light. For practical use, Eq. (34.43) must be multiplied by the the transducer response function and integrated over the region for which $\beta n(\omega) > 1$. Further details are given in the discussion of Cherenkov detectors in the Particle Detectors section (Sec. 35.5 of this Review).

When two particles are close together (lateral separation $\lesssim 1$ wavelength), the electromagnetic fields from the particles may add coherently, affecting the Cherenkov radiation. Because of their opposite charges, the radiation from an e^+e^- pair at close separation is suppressed compared to two independent leptons [85].

34.7.2 Coherent radio Cherenkov radiation

Coherent Cherenkov radiation is produced by many charged particles with a non-zero net charge moving through matter on an approximately common “wavefront”—for example, the electrons and positrons in a high-energy electromagnetic cascade. The signals can be visible for energies above 10^{16} eV; see Sec. 36.3.3 for more details. The phenomenon is called the Askaryan effect [86]. Near the end of a shower, when typical particle energies are below E_c (but still relativistic), a charge imbalance develops. Photons can Compton-scatter atomic electrons, and positrons can annihilate with atomic electrons to contribute even more photons which can in turn Compton scatter. These processes result in a roughly 20% excess of electrons over positrons in a shower. The net negative charge leads to coherent radio Cherenkov emission. The radiation includes a component from the decelerating charges (as in bremsstrahlung). Because the emission is coherent, the electric field strength is proportional to the shower energy, and the signal power increases as its square. The electric field strength also increases linearly with frequency, up to a maximum frequency determined by the lateral spread of the shower. This cutoff occurs at about 1 GHz in ice, and scales inversely with the Moliere radius. At low frequencies, the radiation is roughly isotropic, but, as the frequency rises toward the cutoff frequency, the radiation becomes increasingly peaked around the Cherenkov angle. The radiation is linearly polarized in the plane containing the shower axis and the photon direction. A measurement of the signal polarization can be used to help determine the shower direction. The characteristics of this radiation have been nicely demonstrated in a series of experiments at SLAC [87]. A detailed discussion of the radiation can be found in Ref. [88].

34.7.3 Transition radiation

The energy radiated when a particle with charge ze crosses the boundary between vacuum and a medium with plasma frequency ω_p is

$$I = \alpha z^2 \gamma \hbar \omega_p / 3, \quad (34.45)$$

where

$$\hbar \omega_p = \sqrt{4\pi N_e r_e^3} m_e c^2 / \alpha = \sqrt{\rho \text{ (in g/cm}^3\text{)} \langle Z/A \rangle} \times 28.81 \text{ eV}. \quad (34.46)$$

For styrene and similar materials, $\hbar \omega_p \approx 20$ eV; for air it is 0.7 eV.

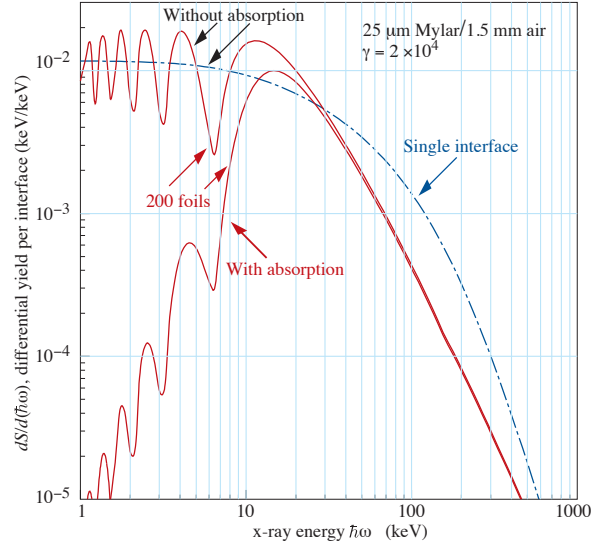


Figure 34.27: X-ray photon energy spectra for a radiator consisting of 200 25 μm thick foils of Mylar with 1.5 mm spacing in air (solid lines) and for a single surface (dashed line). Curves are shown with and without absorption. Adapted from Ref. [89].

The number spectrum $dN_\gamma/d(\hbar\omega)$ diverges logarithmically at low energies and decreases rapidly for $\hbar\omega/\gamma\hbar\omega_p > 1$. About half the energy is emitted in the range $0.1 \leq \hbar\omega/\gamma\hbar\omega_p \leq 1$. Inevitable absorption in a practical detector removes the divergence. For a particle with $\gamma = 10^3$, the radiated photons are in the soft x-ray range 2 to 40 keV. The γ dependence of the emitted energy thus comes from the hardening of the spectrum rather than from an increased quantum yield.

The number of photons with energy $\hbar\omega > \hbar\omega_0$ is given by the answer to problem 13.15 in Ref. [3],

$$N_\gamma(\hbar\omega > \hbar\omega_0) = \frac{\alpha z^2}{\pi} \left[\left(\ln \frac{\gamma \hbar \omega_p}{\hbar \omega_0} - 1 \right)^2 + \frac{\pi^2}{12} \right], \quad (34.47)$$

within corrections of order $(\hbar\omega_0/\gamma\hbar\omega_p)^2$. The number of photons above a fixed energy $\hbar\omega_0 \ll \gamma\hbar\omega_p$ thus grows as $(\ln \gamma)^2$, but the number above a fixed fraction of $\gamma\hbar\omega_p$ (as in the example above) is constant. For example, for $\hbar\omega > \gamma\hbar\omega_p/10$, $N_\gamma = 2.519 \alpha z^2 / \pi = 0.59\% \times z^2$.

The particle stays “in phase” with the x ray over a distance called the formation length, $d(\omega) = (2c/\omega)(1/\gamma^2 + \omega_p^2/\omega^2)^{-1}$. Most of the radiation is produced in this distance. Here θ is the x-ray emission angle, characteristically $1/\gamma$. For $\theta = 1/\gamma$ the formation length has a maximum at $d(\gamma\omega_p/\sqrt{2}) = \gamma c/\sqrt{2}\omega_p$. In practical situations it is tens of μm .

Since the useful x-ray yield from a single interface is low, in practical detectors it is enhanced by using a stack of N foil radiators—foils L thick, where L is typically several formation lengths—separated by gas-filled gaps. The amplitudes at successive interfaces interfere to cause oscillations about the single-interface spectrum. At increasing frequencies above the position of the last interference maximum ($L/d(\omega) = \pi/2$), the formation zones, which have opposite phase, overlap more and more and the

spectrum saturates, $dI/d\omega$ approaching zero as $L/d(\omega) \rightarrow 0$. This is illustrated in Fig. 34.27 for a realistic detector configuration.

For regular spacing of the layers fairly complicated analytic solutions for the intensity have been obtained [89,90]. Although one might expect the intensity of coherent radiation from the stack of foils to be proportional to N^2 , the angular dependence of the formation length conspires to make the intensity $\propto N$.

References

- [1] H. Bichsel, Nucl. Instrum. Meth. **A562**, 154 (2006).
- [2] B. Rossi, *High Energy Particles*, Prentice-Hall, Inc., Englewood Cliffs, NJ, 1952.
- [3] J.D. Jackson, *Classical Electrodynamics*, 3rd edition, (John Wiley and Sons, New York, 1998).
- [4] H.A. Bethe, *Zur Theorie des Durchgangs schneller Korpuskularstrahlen durch Materie*, H. Bethe, Ann. Phys. **5**, 325 (1930).
- [5] M. S. Livingston and H. A. Bethe, Rev. Mod. Phys. **9**, 245 (1937).
- [6] "Stopping Powers and Ranges for Protons and Alpha Particles," ICRU Report No. 49 (1993); Tables and graphs are available at physics.nist.gov/PhysRefData/Star/Text/PSTAR.html and physics.nist.gov/PhysRefData/Star/Text/ASTAR.html.
- [7] D.E. Groom, N.V. Mokhov, and S.I. Striganov, "Muon stopping-power and range tables: 10 MeV–100 TeV," Atomic Data and Nuclear Data Tables **78**, 183–356 (2001). Since submission of this paper it has become likely that post-Born corrections to the direct pair production cross section should be made. Code used to make Figs. 34.22–34.24 included these corrections [D.Yu. Ivanov *et al.*, Phys. Lett. **B442**, 453 (1998)]. The effect is negligible except at high Z . (It is less than 1% for iron.); The introductory text of the paper can be found at pdg.lbl.gov/current/AtomicNuclearProperties/adndt.pdf

Extensive printable and machine-readable tables for muons are given at pdg.lbl.gov/current/AtomicNuclearProperties/.
- [8] W. H. Barkas, W. Birnbaum and F. M. Smith, Phys. Rev. **101**, 778 (1956).
- [9] U. Fano, Ann. Rev. Nucl. Part. Sci. **13**, 1 (1963).
- [10] J. D. Jackson, Phys. Rev. **D59**, 017301 (1999).
- [11] J. Lindhard and A. H. Sørensen, Phys. Rev. **A53**, 2443 (1996).
- [12] "Stopping Powers for Electrons and Positrons," ICRU Report No. 37 (1984); Tables and graphs are available at physics.nist.gov/PhysRefData/Star/Text/ESTAR.html.
- [13] H. Bichsel, Phys. Rev. **A46**, 5761 (1992).
- [14] W.H. Barkas and M.J. Berger, *Tables of Energy Losses and Ranges of Heavy Charged Particles*, NASA-SP-3013 (1964).
- [15] S.M. Seltzer and M.J. Berger, Int. J. of Applied Rad. **33**, 1189 (1982).
- [16] physics.nist.gov/PhysRefData/XrayMassCoef/tab1.html.
- [17] R. M. Sternheimer, Phys. Rev. **88**, 851 (1952).
- [18] R. M. Sternheimer, M. J. Berger and S. M. Seltzer, Atom. Data Nucl. Data Tabl. **30**, 261 (1984); Minor errors are corrected in Ref. 5. Chemical composition for the tabulated materials is given in Ref. 10.
- [19] R. M. Sternheimer and R. F. Peierls, Phys. Rev. **B3**, 3681 (1971).
- [20] N. F. Mott, Proceedings of the Cambridge Philosophical Society **27**, 553 (1931).
- [21] H. Bichsel, Phys. Rev. **A65**, 5, 052709 (2002).
- [22] S. P. Møller *et al.*, Phys. Rev. **A56**, 4, 2930 (1997).
- [23] J. C. Ashley, R. H. Ritchie and W. Brandt, Phys. Rev. B **5**, 2393 (1972).
- [24] H.H. Andersen and J.F. Ziegler, *Hydrogen: Stopping Powers and Ranges in All Elements*. Vol. 3 of *The Stopping and Ranges of Ions in Matter* (Pergamon Press 1977).
- [25] J. Lindhard, Kgl. Danske Videnskab. Selskab, Mat.-Fys. Medd. **28**, No. 8 (1954); J. Lindhard, M. Scharff, and H.E. Schiøtt, Kgl. Danske Videnskab. Selskab, Mat.-Fys. Medd. **33**, No. 14 (1963).
- [26] J.F. Ziegler, J.F. Biersac, and U. Littmark, *The Stopping and Range of Ions in Solids*, Pergamon Press 1985.
- [27] E.A. Uehling, Ann. Rev. Nucl. Sci. **4**, 315 (1954) (For heavy particles with unit charge, but e^\pm cross sections and stopping powers are also given).
- [28] N.F. Mott and H.S.W. Massey, *The Theory of Atomic Collisions*, Oxford Press, London, 1965.
- [29] P. V. Vavilov, Sov. Phys. JETP **5**, 749 (1957), [Zh. Eksp. Teor. Fiz.32,920(1957)].
- [30] L.D. Landau, J. Exp. Phys. (USSR) **8**, 201 (1944).
- [31] H. Bichsel, Rev. Mod. Phys. **60**, 663 (1988).
- [32] R. Talman, Nucl. Instrum. Meth. **159**, 189 (1979).
- [33] H. Bichsel, Ch. 87 in the Atomic, Molecular and Optical Physics Handbook, G.W.F. Drake, editor (Am. Inst. Phys. Press, Woodbury NY, 1996).
- [34] S.M. Seltzer and M.J. Berger, Int. J. of Applied Rad. **35**, 665 (1984). This paper corrects and extends the results of Ref. [15].
- [35] H. A. Bethe, Phys. Rev. **89**, 1256 (1953).
- [36] W. T. Scott, Rev. Mod. Phys. **35**, 231 (1963).
- [37] J. W. Motz, H. Olsen and H. W. Koch, Rev. Mod. Phys. **36**, 881 (1964).
- [38] H. Bichsel, Phys. Rev. **112**, 182 (1958).
- [39] G. Shen *et al.*, Phys. Rev. **D20**, 1584 (1979).
- [40] G. R. Lynch and O. I. Dahl, Nucl. Instrum. Meth. **B58**, 6 (1991).
- [41] M. Wong *et al.*, Med. Phys. **17**, 163 (1990).
- [42] Y.-S. Tsai, Rev. Mod. Phys. **46**, 815 (1974), [Erratum: Rev. Mod. Phys.49,521(1977)].
- [43] H. Davies, H. A. Bethe and L. C. Maximon, Phys. Rev. **93**, 788 (1954).
- [44] L. D. Landau and I. Pomeranchuk, Dokl. Akad. Nauk Ser. Fiz. **92**, 535 (1953); **92**, 735 (1953). These papers are available in English in L. Landau, *The Collected Papers of L.D. Landau*, Pergamon Press, 1965; A. B. Migdal, Phys. Rev. **103**, 1811 (1956).
- [45] S. Klein, Rev. Mod. Phys. **71**, 1501 (1999).
- [46] M.L. Ter-Mikaelian, SSSR **94**, 1033 (1954); M.L. Ter-Mikaelian, *High Energy Electromagnetic Processes in Condensed Media* (John Wiley and Sons, New York, 1972).
- [47] P. L. Anthony *et al.*, Phys. Rev. Lett. **76**, 3550 (1996).
- [48] H. W. Koch and J. W. Motz, Rev. Mod. Phys. **31**, 920 (1959).
- [49] M.J. Berger and S.M. Seltzer, "Tables of Energy Losses and Ranges of Electrons and Positrons," National Aeronautics and Space Administration Report NASA-SP-3012 (Washington DC 1964).
- [50] Curves for these and other elements, compounds, and mixtures may be obtained from nist.gov/pml/xcom-photon-cross-sections-database. The photon total cross section is approximately flat for at least two decades beyond the energy range shown.
- [51] B. L. Berman and S. C. Fultz, Rev. Mod. Phys. **47**, 713 (1975).
- [52] www.cxro.lbl.gov/optical_constants/pert_form.html.
- [53] physics.nist.gov/PhysRefData/XrayMassCoef/tab3.html.
- [54] J. W. Motz, H. A. Olsen and H. W. Koch, Rev. Mod. Phys. **41**, 581 (1969).

- [55] P. L. Anthony *et al.*, Phys. Rev. Lett. **75**, 1949 (1995).
- [56] U. I. Uggerhøj, Rev. Mod. Phys. **77**, 1131 (2005).
- [57] L. Gerhardt and S. R. Klein, Phys. Rev. **D82**, 074017 (2010).
- [58] W.R. Nelson, H. Hirayama, and D.W.O. Rogers, “The EGS4 Code System,” SLAC-265, Stanford Linear Accelerator Center (Dec. 1985).
- [59] *Experimental Techniques in High Energy Physics*, ed. T. Ferbel (Addison-Wesley, Menlo Park CA 1987).
- [60] U. Amaldi, Phys. Scripta **23**, 409 (1981).
- [61] E. Longo and I. Sestili, Nucl. Instrum. Meth. **128**, 283 (1975), [Erratum: Nucl. Instrum. Meth.135,587(1976)].
- [62] G. Grindhammer *et al.*, in *Proceedings of the 1988 Summer Study on High Energy Physics in the 1990’s*, Snowmass, CO, June 27 – July 15, 1990, edited by F.J. Gilman and S. Jensen, (World Scientific, Teaneck, NJ, 1989) p. 151.
- [63] W. R. Nelson *et al.*, Phys. Rev. **149**, 201 (1966).
- [64] G. Bathow *et al.*, Nucl. Phys. **B20**, 592 (1970).
- [65] H. Bethe and W. Heitler, Proc. Roy. Soc. Lond. **A146**, 83 (1934); H.A. Bethe, *Proc. Cambridge Phil. Soc.* **30**, 542 (1934).
- [66] A.A. Petrukhin and V.V. Shestakov, Can. J. Phys. **46**, S377 (1968).
- [67] V.M. Galitskii and S.R. Kel’ner, Sov. Phys. JETP **25**, 948 (1967).
- [68] S.R. Kel’ner and Yu.D. Kotov, Sov. J. Nucl. Phys. **7**, 237 (1968).
- [69] R.P. Kokoulin and A.A. Petrukhin, in *Proceedings of the International Conference on Cosmic Rays*, Hobart, Australia, August 16–25, 1971, Vol. **4**, p. 2436 .
- [70] A. I. Nikishov, Sov. J. Nucl. Phys. **27**, 677 (1978), [Yad. Fiz.27,1281(1978)].
- [71] Yu. M. Andreev, L. B. Bezrukov and E. V. Bugaev, Phys. Atom. Nucl. **57**, 2066 (1994), [Yad. Fiz.57,2146(1994)].
- [72] L. B. Bezrukov and E. V. Bugaev, Yad. Fiz. **33**, 1195 (1981), [Sov. J. Nucl. Phys.33,635(1981)].
- [73] N.V. Mokhov and C.C. James, The MARS Code System User’s Guide, Fermilab-FN-1058-APC (2018), mars.fnal.gov/; N. Mokhov *et al.*, Prog. Nucl. Sci. Tech. **4**, 496 (2014).
- [74] P. H. Barrett *et al.*, Rev. Mod. Phys. **24**, 3, 133 (1952).
- [75] A. Van Ginneken, Nucl. Instrum. Meth. **A251**, 21 (1986).
- [76] U. Becker *et al.*, Nucl. Instrum. Meth. **A253**, 15 (1986).
- [77] J.J. Eastman and S.C. Loken, in *Proceedings of the Workshop on Experiments, Detectors, and Experimental Areas for the Supercollider*, Berkeley, CA, July 7–17, 1987, edited by R. Donaldson and M.G.D. Gilchriese (World Scientific, Singapore, 1988), p. 542.
- [78] *Methods of Experimental Physics*, L.C.L. Yuan and C.-S. Wu, editors, Academic Press, 1961, Vol. 5A, p. 163.
- [79] W.W.M. Allison and P.R.S. Wright, “The Physics of Charged Particle Identification: dE/dx , Cherenkov Radiation, and Transition Radiation,” p. 371 in *Experimental Techniques in High Energy Physics*, T. Ferbel, editor, (Addison-Wesley 1987).
- [80] E.R. Hayes, R.A. Schluter, and A. Tamosaitis, “Index and Dispersion of Some Cherenkov Counter Gases,” ANL-6916 (1964).
- [81] T. Ypsilantis, in “Proceedings of the Symposium on Particle Identification at High Luminosity Hadron Colliders, Apr 5-7, 1989 Batavia, Ill.”, 0661–676 (1989).
- [82] I. Tamm, J. Phys. U.S.S.R., **1**, 439 (1939).
- [83] H. Motz and L.I. Schiff, Am. J. Phys. **21**, 258 (1953).
- [84] B. N. Ratcliff, Nucl. Instrum. Meth. **A502**, 211 (2003).
- [85] S. K. Mandal, S. R. Klein and J. D. Jackson, Phys. Rev. **D72**, 093003 (2005).
- [86] G. A. Askar’yan, Sov. Phys. JETP **14**, 2, 441 (1962), [Zh. Eksp. Teor. Fiz.41,616(1961)].
- [87] P. W. Gorham *et al.*, Phys. Rev. **D72**, 023002 (2005).
- [88] E. Zas, F. Halzen and T. Stanev, Phys. Rev. **D45**, 362 (1992).
- [89] M. L. Cherry *et al.*, Phys. Rev. **D10**, 3594 (1974); M. L. Cherry, Phys. Rev. **D17**, 2245 (1978).
- [90] B. Dolgoshein, Nucl. Instrum. Meth. **A326**, 434 (1993).

35. Particle Detectors at Accelerators

Revised 2024. See the various sections for authors.

35.1	Introduction	591
35.2	Photon detectors	591
35.2.1	Vacuum photodetectors	592
35.2.2	Gaseous photon detectors	593
35.2.3	Solid-state photon detectors	593
35.2.4	Superconducting photon detectors	594
35.3	Organic scintillators	594
35.3.1	Scintillation mechanism	594
35.3.2	Plastic scintillator practicalities	595
35.3.3	Organic glass scintillators	596
35.3.4	Liquid scintillator practicalities	596
35.4	Inorganic scintillators	596
35.5	Cherenkov detectors	598
35.6	Gaseous detectors	601
35.6.1	Energy loss and charge transport in gases	601
35.6.2	Multi-Wire Proportional and Drift Chambers	603
35.6.3	High Rate Effects	604
35.6.4	Micro-Pattern Gas Detectors	605
35.6.5	Time-projection chambers	607
35.6.6	Transition radiation detectors (TRD's)	609
35.6.7	Resistive-plate chambers	611
35.7	LAr Time Projection Chamber	613
35.7.1	Introduction	613
35.7.2	A Mass of ultra-pure Liquid Argon	614
35.7.3	Charge and Light Signals	614
35.7.4	LAr TPC topologies	615
35.7.5	Data Acquisition and event reconstruction	615
35.7.6	Developments	617
35.8	Semiconductor detectors	617
35.8.1	Signal generation in semiconductors	617
35.8.2	Junction detectors	618
35.8.3	Detectors with structured electrodes	619
35.8.4	Precise timing with silicon detectors	620
35.8.5	Radiation damage in silicon detectors	621
35.9	Low-noise detector readout	623
35.9.1	Principal noise origins	623
35.9.2	Equivalent noise analysis	623
35.9.3	Timing measurements	626
35.9.4	Digital signal processing	626
35.9.5	What to use when?	626
35.10	Calorimeters	626
35.10.1	Introduction	626
35.10.2	Electromagnetic calorimeters	629
35.10.3	Hadronic calorimeters	630
35.10.4	Free electron drift velocities in liquid ionization chambers	634
35.11	Accelerator-based neutrino detectors	634
35.11.1	Introduction	635
35.11.2	Signals and Backgrounds	635
35.11.3	Instances of Neutrino Detector Technology	635
35.11.4	Outlook	638
35.12	Superconducting magnets for collider detectors	639
35.12.1	Solenoid Magnets	639
35.12.2	Properties of collider detector magnets	639
35.12.3	Toroidal magnets	640
35.13	Measurement of particle momenta in a uniform magnetic field	640

35.1 Introduction

This review summarizes the detector technologies employed at accelerator particle physics experiments. Several of these detectors are also used in a non-accelerator context and examples of such applications will be provided. The detector techniques which are specific to non-accelerator particle physics experiments are the subject of Chap. 36. More detailed discussions of detectors and their underlying physics can be found in books by Kolanoski & Vermes [1], Ferbel [2], Kleinknecht [3], Knoll [4], Green [5], Leroy & Rancoita [6], and Grupen [7].

In Table 35.1 are given typical resolutions and deadtimes of common charged particle detectors. The quoted numbers are usually based on typical devices, and should be regarded only as rough approximations for new designs. The spatial resolution refers to the intrinsic detector resolution, i.e. without multiple scattering. We note that analog detector readout can provide better spatial resolution than digital readout by measuring and averaging the deposited charge in neighboring channels. Quoted ranges attempt to be representative of both possibilities. The time resolution is defined by how accurately the time at which a particle crossed the detector can be determined. The deadtime is the minimum separation in time between two resolved hits on the same channel. Typical performance of calorimetry and particle identification are provided in the relevant sections below.

Table 35.1: Typical resolutions and deadtimes of common charged particle detectors. Revised September 2023.

Detector Type	Intrinsic Spatial Resolution (rms)	Time Resolution	Dead Time
Resistive plate chamber	50 μm	50–1000 ps*	10 ns [†]
Liquid argon TPC	0.5–1 mm [‡]	0.01–1 μs [§]	— [¶]
Scintillation tracker	\sim 100 μm	100 ps/n	10 ns
Bubble chamber	10–150 μm	1 ms	50 ms**
Wire chambers (proportional and drift chambers)	50–100 μm	5–10 ns ^{††}	20–200 ns ^{‡‡}
Micro-pattern gas detector	30–40 μm	5–10 ns ^{††}	20–200 ns ^{‡‡}
Silicon strips/pixels	\lesssim 10 μm ^{§§}	few ns ^{¶¶} ^{‡‡}	\lesssim 50 ns ^{‡‡}

*LHC: \sim 2 mm gap, \sim 1 ns. HL-LHC: \sim 1 mm gap, \sim 350 ps. Timing RPC: \sim 50 ps

[†]Limited by amplifier and discriminator bandwidth, usually around 100 MHz

[‡]Detector geometry dependent

[§]Using the scintillation signal

[¶]No deadtime for medium

^{||} n = index of refraction.

**Multiple pulsing time.

^{††}For fast particles

^{‡‡}Depending/limited by the amplifying electronics [8]

^{§§}Depending on electrode pitch, best values around 2–4 μm have been achieved

^{¶¶}Resolutions $<$ 100 ps are reached in dedicated pixel developments

35.2 Photon detectors

Revised August 2023 by P. Križan (Ljubljana U; Jozef Stefan Inst.).

Most detectors in high-energy, nuclear, and astrophysics rely on the detection of photons in or near the visible range, 100 nm \lesssim λ \lesssim 1000 nm, or 1 eV \lesssim E \lesssim 10 eV. This range covers scintillation and Cherenkov radiation as well as the light detected in many astronomical observations.

Generally, photodetection involves generating a detectable electrical signal proportional to the (usually very small) number of incident photons. The process involves three distinct steps:

1. generation of a primary photoelectron or electron-hole (e - h) pair by an incident photon by the photoelectric or photoconductive effect,
2. multiplication of the photoelectron or electron-hole pair signal to detectable levels, usually by one or more multiplicative bombardment steps and/or an avalanche process, and,
3. detection of charges induced by secondary electrons.

The important characteristics of a photodetector include the following:

1. quantum efficiency (QE or ϵ_Q): the average number of primary photoelectrons generated per incident photon ($0 \leq \epsilon_Q \leq 1$; in silicon more than one $e-h$ pair per incident photon can be generated for $\lambda \lesssim 165$ nm),
2. collection efficiency (CE or ϵ_C): the overall acceptance factor other than the generation of photoelectrons ($0 \leq \epsilon_C \leq 1$),
3. gain (G): the number of electrons collected for each photoelectron generated,
4. dark current or dark noise: the electrical signal when there is no incident photon,
5. precision of measuring the intensity I of the incoming light: electronic noise (ENC or N_e) and statistical fluctuations in the amplification process compound the Poisson distribution of n_γ photons from a given source:

$$\frac{\sigma(I)}{\langle I \rangle} = \sqrt{\frac{f_N}{n_\gamma \epsilon_Q \epsilon_C} + \left(\frac{N_e}{G n_\gamma \epsilon_Q \epsilon_C} \right)^2}, \quad (35.1)$$

where f_N , or the excess noise factor (ENF), is the contribution to the intensity distribution variance due to multiplication statistics [9],

6. dynamic range, linearity and saturation: relation between the number of incident photons and the sensor output in the pulsed mode,
7. time dependence of the response: this includes the transit time, which is the time between the arrival of the photon and the electrical pulse, and the transit time spread, and
8. rate capability: maximal rate of light pulses at which detection is still possible.

The QE is a strong function of the photon wavelength (λ), and is usually quoted at maximum, together with a range of λ where the QE is comparable to its maximum. Spatial uniformity and linearity with respect to the number of photons are highly desirable in a photodetector response.

Optimization of these factors involves many trade-offs and varies widely between applications. For example, while a large gain is desirable, attempts to increase the gain for a given device also increases the ENF and after-pulsing ("echos" of the main pulse). In solid-state devices, a higher QE often requires a compromise in the timing properties. In other types, coverage of large areas by focusing photoelectrons increases the transit time spread.

Other important considerations also are highly application-specific. These include the photon flux and wavelength range, the total area to be covered, and the efficiency required, the volume available to accommodate the detectors, characteristics of the environment such as chemical composition, temperature, magnetic field, ambient background, as well as ambient radiation of different types, mode of operation (continuous or triggered), bias (high-voltage) requirements, power consumption, calibration needs, aging, cost, and so on. Several technologies employing different phenomena for the three steps described above, and many variants within each, offer a wide range of solutions to choose from. The salient features of the main technologies and the common variants are described below. Some key characteristics are summarized in Table 35.2.

35.2.1 Vacuum photodetectors

Vacuum photodetectors can be broadly subdivided into three types: photomultiplier tubes, microchannel plate photomultiplier tubes, and hybrid photodetectors.

35.2.1.1 Photomultiplier tubes

A versatile class of photon detectors, vacuum photomultiplier tube (PMT) has been employed by a vast majority of all particle physics experiments to date [9]. Both "transmission-" and "reflection-type" PMTs are widely used. In the former, the photocathode material is deposited on the inside of a transparent window through which the photons enter, while in the latter, the photocathode material rests on a separate surface that the incident photons strike. The cathode material has a low work function, chosen for the wavelength band of interest. When a photon hits

the cathode and liberates an electron (the photoelectric effect), the latter is accelerated and guided by electric fields to impinge on a secondary-emission electrode, or dynode, which then emits several (~ 5) secondary electrons. The multiplication process is repeated typically about 10 times in series to generate a sufficient number of electrons, which are collected at the anode for delivery to the external circuit. The total gain of a PMT depends on the applied high voltage V as $G = AV^{kn}$, where $k \approx 0.7-0.8$ (depending on the dynode material), n is the number of dynodes in the chain, and A a constant (which also depends on n). Typically, G is in the range of 10^5-10^7 ; time resolution is $O(1ns)$ but can be as good as ≈ 100 ps for certain PMT types.

A large variety of PMTs covers a wide span of wavelength ranges from infrared (IR) to extreme ultraviolet (XUV) [10]. They are categorized by the window materials, photocathode materials, dynode structures, and anode configurations. Common window materials are borosilicate glass for IR to near-UV, fused quartz and sapphire (Al_2O_3) for UV, and MgF_2 or LiF for XUV. The choice of photocathode materials include a variety of mostly Cs- and/or Sb-based compounds such as CsI, CsTe, bi-alkali (SbR-bCs, SbKCs), multi-alkali (SbNaKCs), GaAs(Cs), GaAsP(Cs), etc. Sensitive wavelengths and peak quantum efficiencies for these materials are summarized in Table-35.3. Typical dynode structures used in PMTs are circular cage, line focusing, box-and-grid, venetian blind, and fine mesh.

Multianode PMTs (MaPMTs) of up to 5×5 cm² in size are based on the parallel (side-by-side) arrangement of several dynode channels and anodes in the same tube, requiring advanced micro-machining and processing techniques. Fast PMTs with very large windows—measuring up to 508 mm across—have been developed for detection of Cherenkov radiation in neutrino experiments such as Super-Kamiokande and KamLAND among many others. Specially prepared low-radioactivity glass is used to make these PMTs, and they are also able to withstand the high pressure of the surrounding liquid.

PMTs are vulnerable to magnetic fields—sometimes even the geomagnetic field causes large orientation-dependent gain changes. A high-permeability metal shield is often necessary. However, proximity-focused PMTs, e.g. the fine-mesh types, can be used even in a high magnetic field (≥ 1 T) if the direction of electric field of the tube is close to the direction of the external magnetic field. CMS uses custom-made vacuum phototriodes (VPT) mounted on the back face of projective lead tungstate crystals to detect scintillation light in the endcap sections of its electromagnetic calorimeters, which are inside a 3.8 T superconducting solenoid. A VPT employs a single dynode (thus, $G \approx 10$) placed close to the photocathode, and a mesh anode plane between the two, to help it cope with the strong magnetic field, which is not too unfavorably oriented with respect to the photodetector axis in the endcaps (within 25°), but where the radiation level is too high for Avalanche Photodiodes (APDs) like those used in the barrel section.

35.2.1.2 Microchannel plate photomultiplier tubes

A typical microchannel plate photomultiplier tube (MCP-PMT) consists of two or more ~ 1 mm thick glass plates with densely packed $O(10 \mu m)$ -diameter cylindrical holes, or "microchannels", sitting between the transmission-type photocathode and anode planes, separated by $O(1$ mm) gaps. Instead of discrete dynodes, the inner surface of each cylindrical hole with a length-to-diameter ratio of 40-100 serves as a continuous dynode for the entire cascade of multiplicative bombardments initiated by a photoelectron. Gain fluctuations are reduced by operating each of the MCPs in the saturation mode. MCPs are stacked in a "chevron" configuration that alternates their bias angle; this reduces ion and photon feed-back effects and optimizes the overall amplification gain.

MCP-PMTs are thin, offer good spatial resolution, have excellent time resolution (~ 20 ps), and can tolerate magnetic fields up to 0.1 T and axial fields up to 1–2 T. The technology has significantly evolved over the past 10 years [11]. A main breakthrough was the introduction of the atomic layer deposition (ALD) coatings on the MCP surfaces to increase the lifetime (>20 C/cm² of charge accumulated on the anode) and gain. The Large Area Pi-

Table 35.2: Representative characteristics of some photodetectors commonly used in particle physics.

Type	λ (nm)	$\epsilon_Q \epsilon_C$	Gain	Risetime (ns)	Single photon time resol. (ps)	Area (mm ²)	1-p.e noise * (Hz/mm ²)	HV (V)
PMT †	115–1700	0.15–0.25	10 ⁵ –10 ⁷	0.7–10	~200	10–10 ⁵	10 ⁻² –10 ²	500–3000
MCP-PMT†	115–650	0.01–0.10	10 ³ –10 ⁷	0.15–0.3	~20	1–10 ⁴	1–10	500–3500
HPD†	115–850	0.1–0.3	10 ³ –10 ⁴	$O(1)$	~1000	10–10 ⁵	10–100	~2 × 10 ⁴
HAPD†	115–850	0.1–0.3	10 ⁴ –10 ⁵	$O(1)$	~30	10–10 ⁵	~1	~1 × 10 ⁴
GPD†	115–500	0.15–0.3	10 ³ –10 ⁶	$O(0.1)$	~100	$O(10)$	~1	300–2000
APD	300–1700	~0.7	10–10 ⁸	$O(1)$	- ‡	1–10 ³	$O(10^7)$ §	400–1400
SiPM	125–1000	0.15–0.4	10 ⁵ –10 ⁶	~1	~50	1–36	10 ⁴ –10 ⁵	30–60

*Normalized to photocathode/sensor area; room temperature operation assumed.

†These devices often come in multi-anode configurations. In such cases, the area is to be considered on a “per readout-channel” basis.

‡No single photon detection possible.

§Since in an APD no single photon detection is possible, dark current is usually quoted instead of the dark count rate; here we assumed a gain of 50 to convert from the dark current to the dark count rate.

cosecond Photo-Detector (LAPPD) project [12] is an important attempt to produce at a reasonable cost large (20 by 20 cm²) sensors with a transit time spread of 50-70 ps.

35.2.1.3 Hybrid photon detectors

Hybrid photon detectors (HPD) combine the sensitivity of a vacuum PMT with the excellent spatial and energy resolutions of a silicon sensor [13]. A single photoelectron ejected from the photocathode is accelerated through a large potential difference of ~20 kV before it impinges on the silicon sensor/anode. The gain nearly equals the maximum number of e - h pairs that could be created from the entire kinetic energy of the accelerated electron: $G \approx eV/w$, where e is the electronic charge, V is the applied potential difference, and $w \approx 3.7$ eV is the mean energy required to create an e - h pair in Si at room temperature. Since the gain is achieved in a single step, one can expect to have the excellent resolution of a simple Poisson statistic with large mean, but in fact it is even better, thanks to the Fano effect discussed in Sec. 35.8.

Low-noise electronics must be used to read out HPDs if one intends to take advantage of the low fluctuations in gain, *e.g.* when counting small numbers of photons. HPDs can have the same $\epsilon_Q \epsilon_C$ and window geometries as PMTs and can be segmented down to ~50 μ m. However, they require rather high biases and will not function in a magnetic field. The exception is proximity-focused devices (\Rightarrow no (de)magnification) in an axial field. With time resolutions of ~10 ps and superior rate capability, proximity-focused HPDs can be an alternative to MCP-PMTs. Applications of HPDs include the CMS hadronic calorimeter and the RICH detector in LHCb. Large-size HPDs with sophisticated focusing may be suitable for future water Cherenkov experiments.

Hybrid APDs (HAPDs) add an avalanche multiplication step following the electron bombardment to boost the gain by a factor of ~50. This affords a higher gain and/or a lower bias voltage, but also increases the detector capacitance and fluctuations in multiplication. The forward RICH detector of Belle II uses a 144-channel device of this type [14].

Table 35.3: Properties of photocathode and window materials commonly used in vacuum photodetectors. [10]

Photocathode material	λ (nm)	Window material	Peak ϵ_Q (λ /nm)
CsI	115–200	MgF ₂	0.13 (130)
CsTe	115–320	MgF ₂	0.17 (200)
Bi-alkali	300–650	Borosilicate	0.27 (390)
	160–650	Synthetic Silica	0.27 (390)
"Ultra Bi-alkali"	300–650	Borosilicate	0.43 (350)
	160–650	Synthetic Silica	0.43 (350)
Multi-alkali	300–850	Borosilicate	0.20 (375)
	160–850	Synthetic Silica	0.25 (380)
GaAsP(Cs)	280–720	Borosilicate	0.40 (480-530)

35.2.2 Gaseous photon detectors

In a gaseous photon detector (GPD) a photoelectron in a suitable gas mixture initiates an avalanche in a high-field region, producing a large number of secondary impact-ionization electrons. In principle the charge multiplication and collection processes are identical to those employed in gaseous tracking detectors such as multiwire proportional chambers (MWPC), micromesh gaseous detectors (Micromegas), or gas electron multipliers (GEM). These are discussed in Sec. 35.6.4.

The devices can be divided into two types depending on the photosensitive material. One type uses solid photocathode materials much in the same way as PMTs. Since it is resistant to gas mixtures typically used in tracking chambers, CsI is a common choice. In the other type, photoionization occurs on suitable molecules vaporized and mixed in the drift volume. Most gases have photoionization work functions in excess of 10 eV, which would limit their sensitivity to wavelengths far too short. However, vapors of tetrakis dimethyl-amine ethylene (TMAE) or triethyl-amine (TEA), which have smaller work functions (5.3 eV for TMAE and 7.5 eV for TEA), are suited for XUV photon detection [15]. Since devices like GEMs offer sub-mm spatial resolution, GPDs are often used as position-sensitive photon detectors. They can be made into flat panels to cover large areas ($O(1$ m²)), can operate in high magnetic fields, and are relatively inexpensive. Many of the ring imaging Cherenkov (RICH) detectors have used GPDs for the detection of Cherenkov light [16–19]. Special care must be taken to suppress the ion-feedback and photon-feedback processes in GPDs. It is also important to maintain high purity of the gas as minute traces of O₂ or H₂O can significantly degrade the detection efficiency.

35.2.3 Solid-state photon detectors

In a phase of rapid development, solid-state photodetectors are competing with vacuum- or gas-based devices for many existing applications and making way for a multitude of new ones. Compared to traditional vacuum- and gaseous photodetectors, solid-state devices are more compact, lightweight, rugged, tolerant to magnetic fields, and often cheaper. They also allow fine pixelization, are easy to integrate into large systems, and can operate at low electric potentials, while matching or exceeding most performance criteria.

Silicon photodiodes (PD) are widely used in high-energy physics as particle detectors and in a large number of applications as photon detectors. The structure is discussed in some detail in Sec. 35.8. In its simplest form, the PD is a reverse-biased p - n junction. Photons with energies above the indirect bandgap energy (wavelengths shorter than about 1050 nm, depending on the temperature) can create e - h pairs (the photoconductive effect), which are collected on the p and n sides, respectively. Often, as in the PDs used for crystal scintillator readout in CLEO, L3, Belle, BaBar, and GLAST, intrinsic silicon is doped to create a p - i - n structure. The reverse bias increases the thickness of the depleted region; in the case of these particular detectors, to full

depletion at a depth of about 100 μm . Increasing the depletion depth decreases the capacitance (and hence electronic noise) and extends the red response. Quantum efficiency can exceed 90%, but falls toward the red because of the decrease of the light absorption probability in silicon; the absorption length reaches 100 μm at 985 nm. However, since $G = 1$, electronic signal amplification is necessary. Optimal low-noise amplifiers are slow, but, even so, noise limits the minimum detectable signal in room-temperature devices to several hundred photons.

In APDs, an exponential cascade of impact ionizations initiated by the original photogenerated e - h pair under a large reverse-bias voltage leads to an avalanche multiplication [20–23], and eventually to breakdown in Geiger-mode APDs. As a result, detectable electrical response can be obtained from low-intensity optical signals down to single photons. Excellent junction uniformity is critical, and a guard ring is generally used as a protection against edge breakdown. Well-designed APDs, such as those used in CMS crystal-based electromagnetic calorimeter, have achieved $\epsilon_Q \epsilon_C \approx 0.7$ with sub-ns response time. The sensitive wavelength window and gain depend on the semiconductor used. The gain is typically 10–200 in linear and up to 10^8 in Geiger mode of operation. Stability and close monitoring of the operating temperature are important for linear-mode operation, and substantial cooling is often necessary.

One of the most promising recent developments in the field is SiPMs ("Silicon Photomultiplier"), a device consisting of large arrays ($O(10^3)$) of tiny APDs packed over a small area ($O(1 \text{ mm}^2)$) and operated in a limited Geiger mode [24–26]. Although each cell only offers a binary output, linearity with respect to the number of photons is achieved by summing the cell outputs. The sum of all cells is proportional to the number of photons received so long as the probability of an individual cell receiving multiple photons during a single time gate is negligible. SiPMs are being adopted as the preferred solution for various purposes including medical imaging, *e.g.* positron emission tomography (PET). These compact, rugged, and economical devices allow auto-calibration through decent separation of photoelectron peaks and offer gains of $O(10^6)$ at a moderate bias voltage ($\sim 30 \text{ V}$). However, the single-photoelectron noise of a SiPM, being the logical "or" of $O(10^3)$ Geiger APDs, is rather large: $O(10\text{--}100 \text{ kHz/mm}^2)$ at room temperature. Intensive R&D in recent years [27] led to a substantial reduction in dark count rates and in correlated noise levels, resulting in coverage of larger areas and in a wider range of applications. One way to further improve the signal-to-noise ratio in SiPMs is by using dedicated light collectors, either as quartz Winston cone like arrays [28] or suitably designed meta-materials [29]. In this way, photons propagate from a larger entry window to a considerably smaller semiconductor sensor, resulting in an improved signal photon to dark-count ratio. Intense R&D is expected to improve radiation hardness of these sensors. The fabrication of the sensors and the front-end electronics combined in the same process with the goal of making SiPMs extremely easy to use has already been successful (digital SiPMs) [30], and remains a topic of intense R&D.

More solid-state light sensors have either been developed or are potentially interesting for use in HEP experiments. The Run 2 DØ detector used 86000 Visible-light photon counters (VLPC) to read the optical signal from its scintillating-fiber tracker and scintillator-strip preshower detectors. These light sensors utilize the formation of an impurity band only 50 meV below the conduction band in As-doped Si to generate strong ($G \approx 5 \times 10^4$) yet sharp response to single photons with $\epsilon_Q \approx 0.9$ [31–33]. Only a very small bias ($\sim 7 \text{ V}$) is needed, but high sensitivity to infrared photons requires cooling below 10 K. Another interesting light sensor that has not yet found its use in HEP instrumentation are quantum dots, realized by nanometer-sized semiconductor 'particles' embedded in a semiconductor bulk.

35.2.4 Superconducting photon detectors

In this rapidly developing technology field, three most established technologies are the superconducting nano-wire single photon detector (SNSPD), the transition edge sensor (TES), and the microwave kinetic inductance detector (MKID). An SNSPD consists of a thin (4 nm) and narrow (100–250 nm) superconducting

nanostructure that is current-biased just below its critical current. Absorption of a photon generates a resistive domain in the superconducting nanostructure, which leads to a transient voltage signal that can be detected. SNSPDs offer a unique combination of speed, both in terms of count rate ($\sim \text{GHz}$) and low timing jitter ($< 3 \text{ ps}$ [34]), large range of wavelength sensitivity from VUV (120 nm) to mid-IR (10 μm), high detection efficiencies (approaching 100% for UV to near-IR), and low dark count rates ($\sim 5\text{--}10 \text{ Hz}$), making them appealing for a wide variety of demanding applications.

Examples of present use in particle physics are small nanowire detectors for dark matter and dark photons. Work is in progress that could make these sensors relevant to HEP applications by increasing the area (using 300 mm wafers and larger) and pixel size, coupling via windows to cryogenic stages, and readout of arrays (superconducting electronics for data processing). While the performance of these sensors is impressive, an application in large accelerator-based detectors would require an extensive R&D program because of the severe cryogenic requirements.

35.3 Organic scintillators

Revised August 2023 by S. C. Eno (U. Maryland) and Matthieu Hamel (Paris-Saclay U. CEA, LIST).

Organic scintillators produce light when transversely by a charged particle. They can be broadly categorized into four types: single crystal, liquid, plastic, and a recently emerged glass [35]. The most useful scintillators produce photons with wavelengths between 370–750 nm (ultraviolet to red), typically peaking at 425 nm [36] via a series of processes that are initialized when charged particles interact with the material via both excitation and ionization/recombination (see Sec. 34.2 of this *Review*). Typical photon yields are about 1 photon per 100 eV of energy deposit [37], although the collected and transduced signal can be much lower. Methods to guide the light towards the photon-electron converter, such as diffusive paint, reflectors, photonic crystals, or light guides, may be required to optimize light yield.

Organic scintillators have found use in a wide variety of detectors [38]. Plastics are mostly used in collider detectors, and liquids in neutrino experiments. Ease of fabrication into desired shapes and low cost has made plastic scintillator ideal for large detectors. In the form of scintillating fiber, it has found widespread use in tracking and calorimetry. Demand for large volume detectors (*e.g.* neutrino detectors: MiniBooNE, NOvA) has led to increased use of liquid scintillator, which can be very low cost.

35.3.1 Scintillation mechanism

Plastic and liquid scintillators are based on an aromatic "matrix" such as benzene. The p electrons form both "pi" and "sigma" bonds between the atoms; the pi bonds are responsible for scintillation. Scintillation is produced via standard photophysical interactions, shown schematically in Fig. 35.1. While there have been claims of delayed light production on long time scales (labeled "phosphorescence" in the figure), this is still a subject of active debate in the community. As aromatic molecules scintillate in the ultraviolet (UV), useful scintillators have one or several fluorophores dissolved into the matrix as dopants. Common fluorophores include 2,5-diphenyloxazole, *p*-terphenyl, 9,10-diphenylanthracene (9,10-DPA), 1,4-bis(2-methylstyryl)benzene (bis-MSB) and 1,4-bis(5-phenyl-2-oxazolyl)benzene (POPOP). Each molecule has its own role: the matrix (whether liquid or plastic) is where most of the radiation/matter interaction occurs. After radiation interaction, ions may recombine giving birth to excited molecules (excitons). Excitons in the matrix are transferred to a "primary fluorophore", whose concentration is typically 1–3 weight % in commercial plastic and liquid scintillators. This concentration is large enough to ensure exciton transfer – primarily via the Förster mechanism, a resonant dipole-dipole interaction which decreases at sixth the power of the distance between molecules. The concentration, however, can be up to the solubility limit. Transfer via the Förster mechanism increases both speed and light output

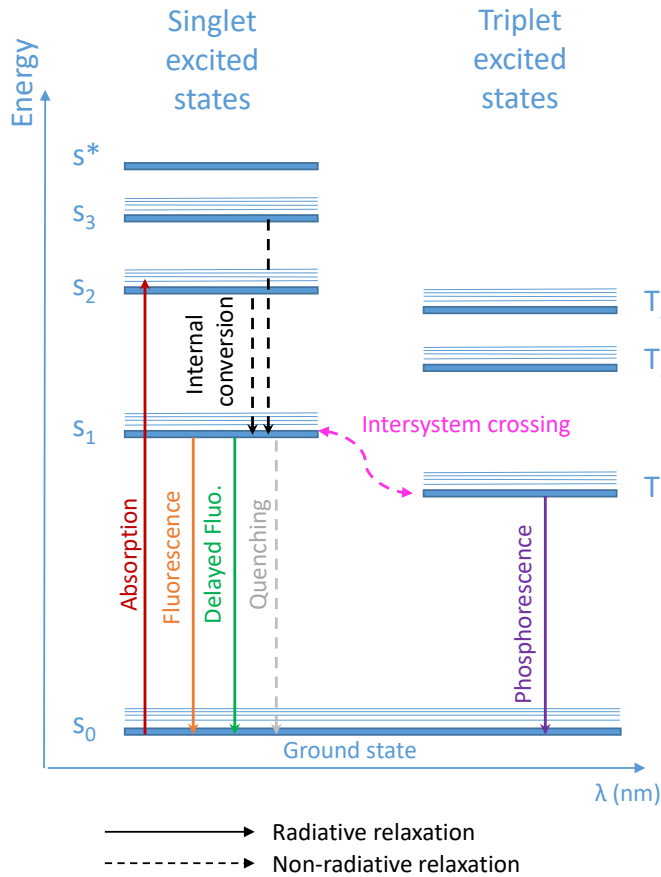


Figure 35.1: Schematic of scintillation mechanism. Schematic of typical excitation and de-excitation of matrix modules.

of the organic scintillator. To reduce reabsorption of the emitted light by the matrix or the primary fluorophore, and the resulting shortened attenuation length, a “secondary fluorophore” is also used to shift the light to longer wavelengths. Transfer from the primary to the secondary is generally radiative. Typical secondary concentrations in plastic and liquids are 0.01-0.2 weight %. The chain of emission and absorption from the matrix to the subsequent fluorophores is shown in Fig. 35.2. Scintillators with

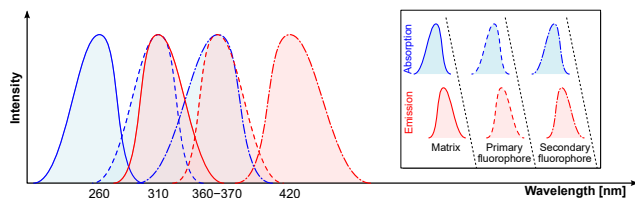


Figure 35.2: Schematic of scintillation mechanism. Typical emission and absorption spectra for the matrix, the primary, and the secondary fluorophore.

two fluorophores typically have absorption lengths of several meters. The longest attenuation lengths require a third fluorophore: when the matrix is transparent up to 1 cm, adding a primary fluorophore increases the light transmission up to ≈ 10 cm, whereas the ternary cocktail is transparent up to 2 m and longer [39].

For most scintillators, decay times are in the ns range; rise times are much faster. Sub-ns timing resolutions have been achieved [40].

Organic scintillators do not respond linearly to the ionization density. Very dense ionization tracks, with large dE/dx , emit less light than expected compared to minimum-ionizing particles. A widely used semi-empirical model by Birks posits that recombination and quenching effects between the excited molecules reduce

the light yield [41]. These effects are more pronounced the greater the density of the excited molecules. Birks’ formula is

$$\frac{d\mathcal{L}}{dx} = \mathcal{L}_0 \frac{dE/dx}{1 + kB dE/dx}, \quad (35.2)$$

where \mathcal{L} is the luminescence, \mathcal{L}_0 is the luminescence at low specific ionization density, and the product kB is known as Birks’ constant, which must be determined for each scintillator by measurement. The value of kB for polystyrene is 0.126 mm/MeV, which is large enough to play an important role in compensation in scintillator-based calorimetry. The high hydrogen content of plastic, which enhances the neutron interaction cross section, as well as its large mass stopping power, also contributes to calorimetry compensation. In the case of large dE/dx values (e.g. with alpha particles), ion recombination may lead to the creation of triplet excited states instead of singlet excited states. If two triplet states are close enough (typically in the order of 10\AA), then triplet-triplet annihilation may occur following the Dexter process [42], leading to delayed fluorescence. This phenomenon is useful for α/β or neutron/ γ discrimination and is more efficient in liquid scintillators than in plastics due to the molecular motion.

Extensive research searching for new efficient molecules that can act as matrix, primary, or secondary fluorophores, is ongoing [43]. Other chemical modifications can affect the scintillator emission wavelength and decay time, or be used e.g. as stabilizers or to enhance thermal neutron sensitivity. Other parameters that can be modified are the density and the effective atomic number.

35.3.2 Plastic scintillator practicalities

Most commercial plastic scintillators use either polystyrene (PS) or poly(vinyltoluene) (PVT) as matrix. A variety of manufacturing techniques [43] are used in the production of plastic scintillator. Cast plastic has the highest light yield, while extruded scintillator is less expensive and allows creation of the scintillator and coating with a diffusive reflector in a single process. In the last couple of years, 3D printing of plastic scintillator has emerged as a reliable production method. The technique has been applied towards plastics for pulse-shape discrimination (PSD) [44]. However, large-scale production (10+ liters) has not yet been achieved. Plastic scintillator is also used to produce scintillating, wavelength-shifting, and clear fibers. These fibers can be useful to guide light to photodetectors, and as the active element in the type of calorimeter pioneered by the RD52/DREAM collaboration [45]. They have even been used in the construction of trackers [46, 47].

Plastic scintillators are reliable, robust, and convenient. However, exposure to solvent vapors, high temperatures, mechanical flexing, irradiation, or rough handling will cause degradation. The surface is a particularly fragile region and can “craze” – develop microcracks which degrade transmission of light by total internal reflection. Crazing is particularly likely where oils, solvents, or fingerprints have contacted the surface or when mechanical stresses are present. The light yield is influenced by several environmental factors: it decreases with the partial pressure of oxygen [48] and increases with increasing magnetic field. In particular, the combination of elevated temperature with relative humidity accelerates aging. This apparent fogging is typically observed in radiation portal monitors, which are exposed to harsh environmental conditions. The aging can become irreversible after multiple cycles. Recently the T2K collaboration reported a 10-year light-yield measurement showing damage due to aging [49].

Plastics are susceptible to radiation damage [50]. At high enough dose, the visible color of the plastic can change to yellow or (at high enough dose) even brown. During irradiation, broken atomic bonds (“radicals”) absorb light, generally strongly in the UV, with tails to longer wavelengths. Because of this, shifting the light to longer wavelengths reduces the decrease in light output and in attenuation length due to radiation effects. Radicals produce mostly temporary damage that “anneals” when the irradiation ends, as the bonds can reform. Radicals can also polymerize via cross linking, and this leads to a permanent reduction in light yield [51]. In an inert atmosphere at room temperature, the bond reformation timescale is on the order of a month. Oxygen, which

diffuses into the plastic during radiation to a depth that scales as the inverse square root of dose rate, can quickly bind to the radicals, reducing but not eliminating temporary damage at the price of a small increased permanent damage [52–54]. After irradiation, oxygen, if present, will diffuse through the entire sample, leading to oxide formation and speeding the annealing process. The decrease in light output due to permanent damage depends on the dose rate. Lower dose rates show large light losses for the same dose. The ratio of the light output to the unirradiated light output can roughly be parameterized as an exponential. For dose rates typical of current collider detectors at the Large Hadron Collider (from a few 10^{-3} to 10 Gy/hr), an exponential dose constant of tens of kGy is observed.

35.3.3 Organic glass scintillators

Starting in 2016, extensive research by Sandia National Laboratories lead to a new organic scintillator family: organic glasses (OGSs) [55]. Whereas polymers are long-chain molecules built from a standard unit called a monomer, OGSs consist of small organic molecules. In addition, polymers such as PS or PVT require dopants, when OGSs are intrinsically good scintillators. This new material has the useful properties present in inorganic single crystals (light yield, PSD properties, along with fast-timing properties), without the poor mechanical characteristics seen in single crystals. The maintenance of the amorphous state of these bulk optical materials was achieved mainly either by using molecules with high configurational disorder or by introducing compositional disorder. OGSs can be prepared in medium to large scales when they are blended with polymers, or pixelated for neutron detection systems, and they can eventually be loaded with heavy elements.

35.3.4 Liquid scintillator practicalities

Liquid scintillators have been used in large scale neutrino experiments 36.3.1.1 due to their low cost. They can hermetically fill any vessel shape. Liquid scintillators are also, due to the mobility of the molecules, much less susceptible to radiation damage.

Care must be taken to avoid dissolved water, solvents such as isopropyl alcohol, and oxygen, which reduce light yield. As they can dissolve many materials (e.g. plastics, adhesives, paints...) care must be taken in their handling. Flammability concerns limit their use in practical experiments in intense radiation fields.

35.4 Inorganic scintillators

Revised August 2023 by C.L. Woody (BNL) and R.-Y. Zhu (HEP California Inst. of Technology).

Inorganic crystals form a class of scintillating materials with much higher densities than organic plastic scintillators (typically $\sim 4\text{--}8\text{ g/cm}^3$) with a variety of different properties for use as scintillation detectors. Due to their high density and high effective atomic number, they can be used in applications where high stopping power or a high conversion efficiency for electrons or photons is required. These include total absorption electromagnetic calorimeters (see Sec. 35.10.2), which consist of a totally active absorber (as opposed to a sampling calorimeter), as well as serving as gamma ray detectors over a wide range of energies. Many of these crystals also have very high light output, and can therefore provide excellent energy resolution down to very low energies (\sim few hundred keV).

Some crystals are intrinsic scintillators in which the luminescence is produced by a part of the crystal lattice itself. However, other crystals require the addition of a dopant, typically fluorescent ions such as thallium (Tl) or cerium (Ce) which is responsible for producing the scintillation light. However, in both cases, the scintillation mechanism is the same. Energy is deposited in the crystal by ionization, either directly by charged particles, or by the conversion of photons into electrons or positrons which subsequently produce ionization. This energy is transferred to the luminescent centers which then radiate scintillation photons. The light yield LY in terms of the number of scintillation photons produced per MeV of energy deposit in the crystal can be expressed as [56]

$$LY = 10^6 S \cdot Q / (\beta \cdot E_g), \quad (35.3)$$

where $\beta \cdot E_g$ is the energy required to create an e-h pair expressed as a multiple of the band gap energy E_g (eV), S is the efficiency of energy transfer to the luminescent center and Q is the quantum efficiency of the luminescent center. The values of β , S and Q are crystal dependent and are the main factors in determining the intrinsic light yield of the scintillator. The decay time of the scintillator is mainly dominated by the decay time of the luminescent center.

Table-35.4 lists the basic properties of some commonly used inorganic crystals. NaI(Tl) is one of the most common and widely used scintillators, with an emission that is well matched to a bialkali photomultiplier tube, but it is highly hygroscopic and difficult to work with, and has a rather low density. CsI(Tl) and CsI(Na) have high light yield, low cost, and are mechanically robust (high plasticity and resistance to cracking). However, they need careful surface treatment and are slightly and highly hygroscopic respectively. Pure CsI has identical mechanical properties as CsI(Tl), but a faster emission at shorter wavelength and a much lower light yield.

Undoped BaF₂ has a fast component with a less than 0.6 ns decay time, and is the fastest known scintillator. However, it also has a slow component with a much longer decay time (~ 630 ns). Bismuth germanate (Bi₄Ge₃O₁₂ or BGO) has a high density, and consequently a short radiation length X_0 and Molière radius R_M . Similar to CsI(Tl), BGO's emission is well-matched to the spectral sensitivity of silicon photodiodes, and it is easy to handle and not hygroscopic. Lead tungstate (PbWO₄ or PWO) has a very high density, with a very short X_0 and R_M , but its intrinsic light yield is rather low.

Cerium doped lutetium oxyorthosilicate (Lu₂SiO₅:Ce, or LSO:Ce) [57] and cerium doped lutetium-yttrium oxyorthosilicate (Lu_{2(1-x)}Y_{2x}SiO₅, LYSO:Ce) [58] are dense crystal scintillators which have a high light yield and a fast decay time. Only the properties of LSO:Ce are listed in Table-35.4 since the properties of LYSO:Ce are similar to that of LSO:Ce except a slightly lower density than LSO:Ce depending on the yttrium fraction (typically 5 to 10%) in LYSO:Ce. This material is also featured with excellent radiation hardness [59,60], so is expected to be used where extraordinary radiation hardness is required.

Also listed in Table-35.4 are other fluoride crystals such as PbF₂ as a Cherenkov material and CeF₃, which have been shown to provide excellent energy resolution in calorimeter applications. Table-35.4 also includes cerium doped lanthanum tri-halides, such as LaBr₃ [61] and CeBr₃ [62], which are brighter and faster than LSO:Ce, but they are highly hygroscopic and have a lower density. The FWHM energy resolution measured for these materials coupled to a PMT with bi-alkali photocathode for 0.662 MeV γ -rays from a ¹³⁷Cs source is about 3%, and has recently been improved to 2% by co-doping with cerium and strontium [63], which is the best among all inorganic crystal scintillators. For this reason, LaBr₃ and CeBr₃ are expected to be used in applications where a good energy resolution for low energy photons are required, such as homeland security.

Beside the crystals listed in Table-35.4, a number of new crystals are being developed that may have potential applications in high energy or nuclear physics. Of particular interest is the family of yttrium and lutetium perovskites and garnet, which include YAP (YAIO₃:Ce), LuAP (LuAlO₃:Ce), YAG (Y₃Al₅O₁₂:Ce) and LuAG (Lu₃Al₅O₁₂:Ce) and their mixed compositions. These have been shown to be linear over a large energy range [64], and have the potential for providing good intrinsic energy resolution.

Aiming at the best jet-mass resolution inorganic scintillators are being investigated for HEP calorimeters with dual readout for both Cherenkov and scintillation light to be used at future lepton colliders. These materials may be used for an electromagnetic calorimeter [65] or a homogeneous hadronic calorimetry (HHCAL) detector concept, including both electromagnetic and hadronic parts [66,67]. Because of the unprecedented volume (70 to 100 m³) foreseen for the HHCAL detector concept the materials must be (1) dense (to minimize the leakage) and (2) cost-effective. It should also be UV transparent (for effective collection of the Cherenkov light) and allow for a clear discrimination between the Cherenkov and scintillation light. The preferred scintillation light

Table 35.4: Properties of several inorganic crystals. Most of the notation is defined in Sec. 6 of this Review.

Parameter:	ρ	MP	X_0^*	R_M^*	dE/dx^*	λ_I^*	τ_{decay}	λ_{max}	n^\dagger	Relative yield [‡]	Hygro-scopic?	$d(LY)/dT$ [§]
Units:	g/cm^3	$^\circ\text{C}$	cm	cm	MeV/cm	cm	ns	nm				$\%/^\circ\text{C}^\S$
NaI(Tl)	3.67	651	2.59	4.13	4.8	42.9	245	410	1.85	100	yes	-0.2
BGO	7.13	1050	1.12	2.23	9.0	22.8	300	480	2.15	21	no	-0.9
BaF ₂	4.89	1280	2.03	3.10	6.5	30.7	650 ^s	300 ^s	1.50	36 ^s	no	-1.9 ^s
							<0.6 ^f	220 ^f		4.1 ^f		0.1 ^f
CsI(Tl)	4.51	621	1.86	3.57	5.6	39.3	1220	550	1.79	165	slight	0.4
CsI(Na)	4.51	621	1.86	3.57	5.6	39.3	690	420	1.84	88	yes	0.4
CsI(pure)	4.51	621	1.86	3.57	5.6	39.3	30 ^s	310	1.95	3.6 ^s	slight	-1.4
							6 ^f			1.1 ^f		
PbWO ₄	8.30	1123	0.89	2.00	10.1	20.7	30 ^s	425 ^s	2.20	0.3 ^s	no	-2.5
							10 ^f	420 ^f		0.077 ^f		
LSO(Ce)	7.40	2050	1.14	2.07	9.6	20.9	40	402	1.82	85	no	-0.2
PbF ₂	7.77	824	0.93	2.21	9.4	21.0	-	-	-	Cherenkov	no	-
CeF ₃	6.16	1460	1.70	2.41	8.42	23.2	30	340	1.62	7.3	no	0
LaBr ₃ (Ce)	5.29	783	1.88	2.85	6.90	30.4	20	356	1.9	180	yes	0.2
CeBr ₃	5.23	722	1.96	2.97	6.65	31.5	17	371	1.9	165	yes	-0.1

* Numerical values calculated using formulae in this review.

[†] Refractive index at the wavelength of the emission maximum.

[‡] Relative light yield measured for samples of 1.5 X_0 cube with a Tyvek paper wrapping and a full end face coupled to a photodetector. The quantum efficiencies of the photodetector are taken out.

[§] Variation of light yield with temperature evaluated at the room temperature.

f = fast component, s = slow component

is thus at a longer wavelength, and not necessarily bright or fast. Dense crystals, scintillating glasses and ceramics offer a very attractive implementation for this detector concept [68].

The fast scintillation light provides timing information about electromagnetic interactions and showers, which may be used to mitigate pile-up effects and/or for particle identification since the time development of electromagnetic and hadronic showers, as well as minimum ionizing particles, are different. The timing information is primarily determined by the scintillator rise time and decay time, and the number of photons produced. For fast timing, it is important to have a large number of photons emitted in the initial part of the scintillation pulse, e.g. in the first ns, since one is often measuring the arrival time of the particle in the crystal using the leading edge of the light pulse. A good example of this is BaF₂, which has $\sim 10\%$ of its light in its fast component with a decay time of less than 0.6 ns. Recent investigation shows that doping with yttrium in BaF₂ reduces its slow component significantly, while keeping its ultrafast scintillation component unchanged [69, 70]. The light propagation can spread out the arrival time of the scintillation photons at the photodetector due to time dispersion [71]. The time response of the photodetector also plays a major role in achieving good time resolution with fast scintillating crystals.

Table-35.4 gives the light yield of other crystals relative to NaI(Tl) and their dependence to the temperature variations. The light output was measured for 1.5 X_0 cube crystal samples with a Tyvek paper wrapping and a full end face coupled to a photodetector [72]. The quantum efficiency of the photodetector is taken out to facilitate a direct comparison of crystal's light yield. However, the measured light output produced by a scintillator is usually quoted in terms of the number of photoelectrons per MeV produced by a given photodetector. The relationship between the light yield (LY) in number of photons/MeV produced ($N_{\text{photons}}/\text{MeV}$) and the light output (LO) in number of photoelectrons/MeV detected involves the factors for the light collection efficiency (LCE) and the quantum efficiency (QE) of the photodetector:

$$LO = LY \cdot LCE \cdot QE. \quad (35.4)$$

LCE depends on the size and shape of the crystal sample, and includes effects such as the transmission of scintillation light within the crystal (i.e., the bulk attenuation length of the material), scattering from within the crystal, reflections and scattering from the crystal surfaces, and re-bouncing back into the crystal by wrapping materials. These factors can vary considerably depending on the sample, but can be in the range of $\sim 10\text{--}60\%$. The inter-

nal light transmission depends on the intrinsic properties of the material, e.g. the density and type of the scattering centers and defects that can produce internal absorption within the crystal, and can be highly affected by factors such as radiation damage, as discussed below.

The quantum efficiency depends on the type of photodetector used to detect the scintillation light, which is typically $\sim 15\text{--}30\%$ for photomultiplier tubes and higher for silicon photodetectors for visible wavelengths. The response of the detector is usually highly wavelength dependent and should be matched to the particular crystal of interest to give the highest quantum yield at the wavelength corresponding to the peak of the scintillation emission. Fig. 35.3 shows the quantum efficiency for a Hamamatsu R2059 PMT with bi-alkali cathode and quartz window, and the particle detection efficiency (PDE) for a Hamamatsu S14160-3015ps multi-pixel photon counter (MPPC), which is also called silicon photomultiplier (SiPM), as a function of wavelength. Also shown in the figure are emission spectra of three crystal scintillators, BGO, LSO:Ce/LYSO:Ce and CsI(Tl), and the numerical values of the emission weighted quantum efficiency. The area under each emission spectrum is proportional to crystal's light yield, as shown in Table-35.4, where the quantum efficiencies of the photodetector has been taken out. Results with different photodetectors can be significantly different. For example, the response of CsI(Tl) relative to NaI(Tl) with a standard photomultiplier tube with a bi-alkali photo-cathode, e.g. Hamamatsu R2059, would be 45 rather than 165 because of the photomultiplier's low quantum efficiency at longer wavelengths. For scintillators which emit in the UV, a detector with a quartz window should be used.

For very low energy applications (typically below 1 MeV), non-proportionality of the scintillation light yield may be important. It has been known for a long time that the conversion factor between the energy deposited in a crystal scintillator and the number of photons produced is not constant. It is also known that the energy resolution measured by all crystal scintillators for low energy γ -rays is significantly worse than the contribution from photo-electron statistics alone, indicating an intrinsic contribution from the scintillator itself. Precision measurement using low energy electron beam shows that this non-proportionality is crystal dependent [73]. Recent study on this issue also shows that this effect is also sample dependent even for the same crystal [74]. Further work is therefore needed to fully understand this subject.

One important issue related to the application of a crystal scintillator is its radiation hardness. Stability of its light output, or the ability to track and monitor the variation of its light output

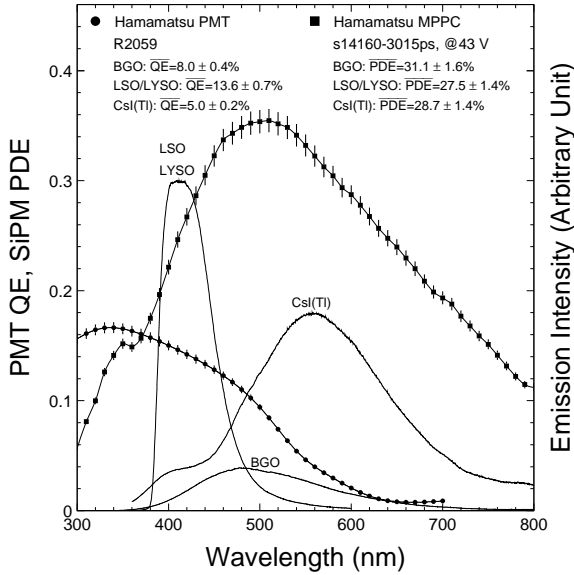


Figure 35.3: The quantum efficiency for a Hamamatsu R2059 PMT with bi-alkali cathode and quartz window and the particle detection efficiency (PDE) for a Hamamatsu S14160-3015ps multi-pixel photon counter (MPPC), which is also called silicon photomultiplier (SiPM), are shown as a function of wavelength. Also shown in the figure are emission spectra of three crystal scintillators, BGO, LSO and CsI(Tl), and the numerical values of the emission weighted quantum efficiencies. The area under each emission spectrum is proportional to crystal's light yield.

in a radiation environment, is required for high resolution and precision calibration [75]. All known crystal scintillators suffer from ionization dose induced radiation damage [76], where a common damage phenomenon is the appearance of radiation induced absorption caused by the formation of color centers originated from the impurities or point defects in the crystal. This radiation induced absorption reduces the light attenuation length in the crystal, and hence its light output. For crystals with high defect density, a severe reduction of light attenuation length may cause a distortion of the light response uniformity, leading to a degradation of the energy resolution. Additional radiation damage effects may include a reduced intrinsic scintillation light yield (damage to the luminescent centers) and an increased phosphorescence (afterglow). For crystals to be used in a high precision calorimeter in a radiation environment, its scintillation mechanism must not be damaged and its light attenuation length in the expected radiation environment must be long enough so that its light response uniformity, and thus its energy resolution, does not change.

While radiation damage induced by ionization dose is well understood [77], investigation is on-going to understand radiation damage caused by hadrons, including both charged hadrons [78] and neutrons [79]. Two additional fundamental processes may cause defects by hadrons: displacement damage and nuclear breakup. While charged hadrons can produce all three types of damage (and it's often difficult to separate them), neutrons can produce only the last two, and electrons and photons only produce ionization damage. Studies on hadron induced radiation damage to lead tungstate [80] show a proton-specific damage component caused by fragments from fission induced in lead and tungsten by particles in the hadronic shower. The fragments cause a severe, local damage to the crystalline lattice due to their extremely high energy loss over a short distance [80]. Recent investigation also sees evidence of neutron-specific damage in various crystals [79].

Most of the crystals listed in Table-35.4 have been used in high energy or nuclear physics experiments when the ultimate energy resolution for electrons and photons is desired. Examples are the Crystal Ball NaI(Tl) calorimeter at SPEAR, the L3 BGO calorimeter at LEP, the CLEO CsI(Tl) calorimeter at CESR, the KTeV CsI calorimeter at the Tevatron, and the BaBar, BELLE

and BES III CsI(Tl) calorimeters at PEP-II, KEK and BEPC II, respectively. Because of their high density and relative low cost, PWO calorimeters are used by CMS and ALICE at LHC, by CLAS and PrimEx at CEBAF and by PANDA at GSI, and is planned to be used for the Backward Endcap Calorimeter for the ePIC experiment at the EIC. Similarly, PbF₂ calorimeters are used by the A4 experiment at MAINZ and by the g-2 experiment at Fermilab. A CsI calorimeter is being built for the Mu2e experiment at Fermilab. An LYSO:Ce calorimeter is being built for the COMET experiment at J-PARC, and an LYSO:Ce crystal-based precision timing layer is being built for the CMS experiment for the HL-LHC.

35.5 Cherenkov detectors

Revised August 2023 by J. Schwieng (GSI Darmstadt).

Although devices using Cherenkov radiation are often thought of as only particle identification (PID) detectors, in practice they are used over a much broader range of applications including; (1) fast particle counters; (2) hadronic PID; (3) electromagnetic calorimeters (EMC); and (4) tracking detectors performing complete event reconstruction. Examples of applications from each category include; (1) the BaBar luminosity detector [81] and the Quartic fast timing counter for the ATLAS Forward Proton Detector, designed to measure small angle scatters at the LHC [82]; (2) the hadronic PID detectors at the B factory detectors—DIRC in BaBar [83], and the modern Imaging Aerogel and TOP counters at Belle II [84]; (3) the CMS Hadron Forward calorimeter based on Cherenkov light emitted in quartz fibers embedded in a steel absorber [85]; and (4) large water Cherenkov counters such as Super-Kamiokande [86].

Cherenkov counters contain two main elements; (1) a radiator through which the charged particle passes, and (2) a photodetector. As Cherenkov radiation is a weak source of photons, light collection and detection must be as efficient as possible. The refractive index n and the particle's path length through the radiator L appear in the Cherenkov relations allowing the tuning of these quantities for particular applications. One or more of the properties of Cherenkov radiation discussed in the Passages of Particles through Matter section (Sec. 34 of this *Review*) are utilized in Cherenkov detectors: the prompt emission of a light pulse; the existence of a velocity threshold for radiation; and the dependence of the Cherenkov cone half-angle θ_c and the number of emitted photons on the velocity of the particle v_p and the refractive index n of the medium. The Cherenkov angle can be calculated as

$$\cos \theta_c = \frac{1}{n(E)\beta}, \quad (35.5)$$

where $\beta = v_p/c$ with c being the speed of light, and E the photon energy. The number of photoelectrons ($N_{p.e.}$) detected in a given device with radiator of length L is

$$N_{p.e.} = L \frac{\alpha^2 z^2}{r_e m_e c^2} \int \epsilon(E) \sin^2 \theta_c(E) dE, \quad (35.6)$$

where $\epsilon(E)$ is the efficiency for collecting the Cherenkov light and transducing it into photoelectrons, and $\alpha^2/(r_e m_e c^2) = 370 \text{ cm}^{-1} \text{ eV}^{-1}$. The quantities ϵ and θ_c are functions of the photon energy. As the typical energy dependent variation of the index of refraction is modest, a quantity called the *Cherenkov detector quality factor* N_0 can be defined as

$$N_0 = \frac{\alpha^2 z^2}{r_e m_e c^2} \int \epsilon dE, \quad (35.7)$$

so that, taking the charge number $z = 1$ (the usual case in high-energy physics),

$$N_{p.e.} \approx LN_0 \langle \sin^2 \theta_c \rangle. \quad (35.8)$$

This definition of the quality factor N_0 is not universal, nor, indeed, very useful for those common situations where ϵ factorizes as $\epsilon = \epsilon_{\text{coll}} \epsilon_{\text{det}}$ with the geometrical photon collection efficiency

(ϵ_{coll}) varying substantially for different tracks while the photon detector efficiency (ϵ_{det}) remains nearly track independent. In this case, it can be useful to explicitly remove (ϵ_{coll}) from the definition of N_0 . A typical value of N_0 for a photomultiplier (PMT) detection system working in the visible and near UV, and collecting most of the Cherenkov light, is about 100 cm^{-1} . Practical counters, utilizing a variety of different photodetectors, have values ranging between about 30 and 180 cm^{-1} . Radiators can be chosen from a variety of transparent materials (Sec. 34 of this *Review* and Table 6). In addition to refractive index, the choice requires consideration of factors such as material density, radiation length and radiation hardness, transmission bandwidth, absorption length, chromatic dispersion, optical workability (for solids), availability, environmental impact, and cost. When the momenta of particles to be identified is high, the refractive index must be set close to one, so that the photon yield per unit length is low and a long particle path in the radiator is required. In recent years, the gap in refractive index that has traditionally existed between gases and liquid or solid materials has been partially closed with transparent *silica aerogels* with indices that range between about 1.003 and 1.26. Due to the potential ability to tune the refractive index to the exact requirements of an experiment, metamaterials, including photonic crystals, are being investigated as radiators for future Cherenkov counters [87].

Cherenkov counters may be classified as either *imaging* or *threshold* types, depending on whether they do or do not make use of Cherenkov angle (θ_c) information. Imaging counters may be used to track particles as well as identify them. The recent development of very fast photodetectors such as micro-channel plate PMTs (MCP-PMT) (see 35.2 of this *Review*) also potentially allows very fast Cherenkov based time of flight (TOF) detectors of either class [87]. The track timing resolution of imaging detectors can be extremely good as it scales approximately as $\frac{1}{\sqrt{N_{\text{p.e.}}}}$.

Threshold Cherenkov detectors [88], in their simplest form, make a yes/no decision based on whether the particle is above or below the Cherenkov threshold velocity $\beta_t = 1/n$. A straightforward enhancement of such detectors uses the number of observed photoelectrons (or a calibrated pulse height) to discriminate between species or to set probabilities for each particle species [89]. This strategy can increase the momentum range of particle separation by a modest amount (to a momentum some 20% above the threshold momentum of the heavier particle in a typical case).

Careful designs give $\langle \epsilon_{\text{coll}} \rangle \gtrsim 90\%$. For a photomultiplier with a typical alkali cathode, $\int \epsilon_{\text{det}} dE \approx 0.27 \text{ eV}$, so that

$$N_{\text{p.e.}}/L \approx 90 \text{ cm}^{-1} \langle \sin^2 \theta_c \rangle \quad (\text{i.e., } N_0 = 90 \text{ cm}^{-1}). \quad (35.9)$$

Suppose, for example, that n is chosen so that the threshold for species a is p_t ; that is, at this momentum species a has velocity $\beta_a = 1/n$. A second, lighter, species b with the same momentum has velocity β_b , so $\cos \theta_c = \beta_a/\beta_b$, and

$$N_{\text{p.e.}}/L \approx 90 \text{ cm}^{-1} \frac{m_a^2 - m_b^2}{p_t^2 + m_a^2}. \quad (35.10)$$

For K/π separation at $p = p_t = 1(5) \text{ GeV}/c$, $N_{\text{p.e.}}/L \approx 16(0.8) \text{ cm}^{-1}$ for π 's and (by design) 0 for K 's.

For limited path lengths $N_{\text{p.e.}}$ will usually be small. The overall efficiency of the device is controlled by Poisson fluctuations, which can be especially critical for separation of species where one particle type is dominant. Moreover, the effective number of photoelectrons is often less than the average number calculated above due to additional equivalent noise from the photodetector (see the discussion of the excess noise factor in 35.2 of this *Review*). It is common to design for at least 10 photoelectrons for the high velocity particle in order to obtain a robust counter. As rejection of the particle that is below threshold depends on *not* seeing a signal, electronic and other background noise, especially overlapping tracks, can be important. Physics sources of light production for the below threshold particle, such as decay to an above threshold particle, scintillation light, or the production of delta rays in the radiator, often limit the separation attainable, and need to be

carefully considered. Well designed, modern multi-channel counters, such as the ACC at Belle [90], can attain adequate particle separation performance over a substantial momentum range.

Imaging counters make the most powerful use of the information available by measuring the ring-correlated angles of emission of the individual Cherenkov photons. They typically provide positive ID information both for the “wanted” and the “unwanted” particles, thus reducing mis-identification substantially. Since low-energy photon detectors can measure only the position (and, perhaps, a precise detection time) of the individual Cherenkov photons (not the angles directly), the photons must be “imaged” onto a detector so that their angles can be derived [91]. Typically the optics map the Cherenkov cone onto (a portion of) a distorted “circle” at the photodetector. Though the imaging process is directly analogous to familiar imaging techniques used in telescopes and other optical instruments, there is a somewhat bewildering variety of methods used in a wide variety of counter types with different names. Some of the imaging methods used include (1) focusing by a lens or mirror; (2) proximity focusing (i.e., focusing by limiting the emission region of the radiation); and (3) focusing through an aperture (a pinhole). In addition, the prompt Cherenkov emission coupled with the speed of some modern photon detectors allows the use of (4) time imaging, a method which is little used in conventional imaging technology, and may allow some separation with particle TOF. Finally, (5) correlated tracking (and event reconstruction) can be performed in large water counters by combining the individual space position and time of each photon together with the constraint that Cherenkov photons are emitted from each track at the same polar angle (Sec. 36.3.1 of this *Review*).

In a simple model of an imaging PID counter, the fractional error on the particle velocity (δ_β) is given by

$$\delta_\beta = \frac{\sigma_\beta}{\beta} = \tan \theta_c \sigma(\theta_c), \quad (35.11)$$

where

$$\sigma(\theta_c) = \frac{\langle \sigma(\theta_i) \rangle}{\sqrt{N_{\text{p.e.}}}} \oplus C, \quad (35.12)$$

and $\langle \sigma(\theta_i) \rangle$ is the average single photoelectron resolution, as defined by the optics, detector resolution and the intrinsic chromaticity spread of the radiator index of refraction averaged over the photon detection bandwidth. C combines a number of other contributions to resolution including, (1) correlated terms such as tracking, alignment, and multiple scattering, (2) hit ambiguities, (3) background hits from random sources, and (4) hits coming from other tracks. The actual separation performance is also limited by physics effects such as decays in flight and particle interactions in the material of the detector. In many practical cases, the performance is limited by these effects.

For a $\beta \approx 1$ particle of momentum (p) well above threshold entering a radiator with index of refraction (n), the number of σ separation (N_σ) between particles of mass m_1 and m_2 is approximately

$$N_\sigma \approx \frac{|m_1^2 - m_2^2|}{2p^2 \sigma(\theta_c) \sqrt{n^2 - 1}}. \quad (35.13)$$

In practical counters, the angular resolution term $\sigma(\theta_c)$ varies between about 0.1 and 5 mrad depending on the size, radiator, and photodetector type of the particular counter. The range of momenta over which a particular counter can separate particle species extends from the point at which the number of photons emitted becomes sufficient for the counter to operate efficiently as a threshold device ($\sim 20\%$ above the threshold for the lighter species) to the value in the imaging region given by the equation above. For example, for $\sigma(\theta_c) = 2 \text{ mrad}$, a fused silica radiator ($n = 1.474$), or a fluorocarbon gas radiator (C_5F_{12} , $n = 1.0017$), would separate π/K 's from the threshold region starting around $0.15(3) \text{ GeV}/c$ through the imaging region up to about $4.2(18) \text{ GeV}/c$ at better than 3σ .

Many different imaging counters have been built during the last several decades [87]. Among the earliest examples of this class of counters are the very limited acceptance *Differential Cherenkov*

detectors, designed for particle selection in high momentum beam lines. These devices use optical focusing and/or geometrical masking to select particles having velocities in a specified region. With careful design, a velocity resolution of $\sigma_\beta/\beta \approx 10^{-4}$ – 10^{-5} can be obtained [88].

Practical multi-track *Ring-Imaging Cherenkov detectors* (generically called RICH counters) are a more recent development. RICH counters are sometimes further classified by ‘generations’ that differ based on historical timing, performance, design, and photodetection techniques. Prototypical examples of first generation RICH counters are those used in the DELPHI and SLD detectors at the LEP and SLC Z factory e^+e^- colliders [87]. They have both liquid (C_6F_{14} , $n = 1.276$) and gas (C_5F_{12} , $n = 1.0017$) radiators, the former being proximity imaged with the latter using mirrors. The phototransducers are a TPC/wire-chamber combination. They are made sensitive to photons by doping the TPC gas (usually, ethane/methane) with $\sim 0.05\%$ TMAE (tetrakis(dimethylamino)ethylene). Great attention to detail is required, (1) to avoid absorbing the UV photons to which TMAE is sensitive, (2) to avoid absorbing the single photoelectrons as they drift in the long TPC, and (3) to keep the chemically active TMAE vapor from interacting with materials in the system. In spite of their unforgiving operational characteristics, these counters attained good $e/\pi/K/p$ separation over wide momentum ranges (from about 0.25 to 20 GeV/c) during several years of operation at LEP and SLC. Related but smaller acceptance devices include the OMEGA RICH at the CERN SPS, and the RICH in the balloon-borne CAPRICE detector [87]. Despite their excellent match to the radiator requirement for gaseous RICHes, saturated fluorocarbons may soon need to be replaced due to their high global warming impact. Possible alternatives for a similar refractive index include hydrofluoroolefins or Argon, pressurized at a few bar [87].

Later generation counters [87] generally operate at much higher rates, with more detection channels, than the first generation detectors just described. They also utilize faster, more forgiving photon detectors, covering different photon detection bandwidths. Radiator choices have broadened to include materials such as lithium fluoride, fused silica, and aerogel.

Vacuum-based photodetection systems (*e.g.*, single or multi anode PMTs, MCP-PMTs, or hybrid photodiodes (HPD)) have become increasingly common (see 35.2 of this *Review*). They handle high rates, and can be used with a wide choice of radiators. Examples include (1) the SELEX RICH at Fermilab, which mirror focuses the Cherenkov photons from a neon radiator onto a camera array made of ~ 2000 PMTs to separate hadrons over a wide momentum range (to well above 200 GeV/c for heavy hadrons); (2) the NA62 RICH at CERN, which uses a 17 m long tank filled with neon gas as radiator and spherical mirrors to focus the photons on two arrays of 2000 PMTs to separate pions from muons for momenta between 15 and 35 GeV/c; (3) the CBM RICH under construction at FAIR where the Cherenkov photons, produced in about 30 m³ of CO₂ radiator gas, are mirror-focused on arrays of multi-anode PMTs (MaPMTs) with a total of about 55,000 pixels, to identify electrons with momenta up to 10 GeV/c; and (4) the LHCb detector now running at the LHC. It uses two separate counters. One volume contains C₄F₁₀ (originally in combination with aerogel, which was removed in 2015) while the second volume contains CF₄. Photons are mirror-focused onto arrays of photon detectors to cover a π/K separation momentum range between 1 and 150 GeV/c. Additional upgrades, including the replacement of the HPDs by MaPMTs and improved readout electronics, were performed to deal with increases in luminosity.

Other fast detection systems that use solid cesium iodide (CsI) photocathodes or triethylamine (TEA) doping in proportional chambers are useful with certain radiator types and geometries. Examples include (1) the CLEO-III RICH at CESR that uses a LiF radiator with TEA doped proportional chambers; (2) the ALICE detector at the LHC that uses proximity focused liquid (C_6F_{14} radiators and solid CsI photocathodes (similar photodetectors have been used for several years by the HADES and COMPASS detectors), and the hadron blind detector (HBD) in the PHENIX detector at RHIC that couples a low index CF₄ radiator

to a photodetector based on electron multiplier (GEM) chambers with reflective CsI photocathodes [87].

Recent technological advances in the production of aerogel with improved transparency in the UV range and finely tuned refractive indices enable several new RICH designs. The innovative hybrid geometry of the CLAS12 RICH, with complex photon paths that feature multiple passes through the aerogel tiles, is only possible due to the improved scattering length of the aerogel. It minimizes the material inside of the detector acceptance as well as the size and cost of the photon sensor array. Beam tests have demonstrated that the counter will be able to provide clean π/K separation up to 8 GeV/c. The forward endcap Aerogel RICH (ARICH) for the Belle II upgrade at KEKB, designed to provide clean π/K separation for momenta up to 3.5 GeV/c, is an example of the so-called focusing aerogel approach [92]. The radiator is a dual-layer aerogel, with a thickness of 20 mm for each layer and increasing refractive indices of $n = 1.045$ and $n = 1.055$ along the particle path. The Cherenkov ring images from the two layers overlap on the array of Hybrid Avalanche Photo Detectors (HAPDs), which provide efficient single photon detection in the 1.5 T magnetic field.

A DIRC (Detection [of] Internally Reflected Cherenkov [light]) is a distinctive, compact RICH subtype first used in the BaBar detector [83]. A DIRC “inverts” the usual RICH principle for use of light from the radiator by collecting and imaging the total internally reflected light rather than the transmitted light. It utilizes the optical material of the radiator in two ways, simultaneously: as a Cherenkov radiator and as a light pipe. The magnitudes of the photon angles are preserved during transport by the flat, rectangular cross section radiators, allowing the photons to be efficiently transported to a detector outside the path of the particle where they may be imaged in up to three independent dimensions (the usual two in space and, due to the long photon paths lengths, one in time). Because the index of refraction in the radiator is large ($n \sim 1.47$ for fused silica), the momentum range with good π/K separation goes up to 4–5 GeV/c. It is plausible, but difficult, to extend it up to about 10 GeV/c with an improved design.

The BaBar experiment at the asymmetric PEP-II e^+e^- collider studied CP violation in $\Upsilon(4S)$ decays. Excellent pion/kaon separation for particle momenta up to 4 GeV/c was required. The BaBar DIRC used 4.9 m long, rectangular bars made from synthetic fused silica as radiator and light guide. The photons were imaged via a “pin-hole” through an expansion region filled with 6000 liters of purified water onto an array of 10752 densely packed photomultiplier tubes placed at a distance of about 1.2 m from the bar end. During more than 8 years of operation, the BaBar DIRC achieved π/K separation of 2.5 standard deviations or more up to 4 GeV/c momentum. For a pion identification rate around 85% the DIRC provided a kaon misidentification rate well below 1% up to 3 GeV/c.

The next generation of DIRC detectors [93] takes advantage of the new, very fast, pixelated photodetectors becoming available, such as MaPMTs and MCP-PMTs. They typically utilize either time imaging or lens/mirror-focused optics, or both, leading not only to a precision measurement of the Cherenkov angle, but in some cases, to a precise measurement of the particle time of flight, and/or to correction of the chromatic dispersion in the radiator. Examples [87] include (1) the Belle II Time of Propagation (TOP) counter that emphasizes precision timing for both Cherenkov imaging and TOF to perform π/K separation of at least 3 standard deviations up to 4 GeV/c; (2) the DIRC upgrade of the GlueX experiment at Jefferson Lab that places four decommissioned BaBar DIRC modules, coupled to upgraded optics and readout, perpendicular to the beamline, the first application of a DIRC in a detector endcap; (3) the high-performance DIRC for the ePIC detector at the EIC, to be installed in 2030, that will combine lens focusing with fast photon time imaging and is expected to provide more than 3 standard deviations π/K separation up to 6 GeV/c; and (4) the TORCH counter being developed for an LHCb upgrade in 2033 which uses DIRC imaging for individual photons with fast photon detectors to provide π/K separation up to 10 GeV/c via particle TOF with a precision of

10-15 ps per track over a flight path length of 9.5 m.

35.6 Gaseous detectors

35.6.1 Energy loss and charge transport in gases

Revised November 2021 by F. Sauli (CERN) and M. Titov (IRFU, CEA, Université Paris-Saclay).

Gas-filled detectors use the localized ionization produced by charged particles, generally after charge multiplication. The statistics of ionization processes, having asymmetries in the ionization trails, affect the coordinate determination deduced from the measurement of drift time, or of the center of gravity of the collected charge. For thin gas layers, the width of the energy loss distribution can be larger than its average, requiring multi-sampling devices or truncated mean analysis to achieve good particle identification. In the truncated mean method for calculating $\langle dE/dx \rangle$, the ionization measurements along the track length are broken into many samples and then a fixed fraction of high-side (and sometimes also low-side) values are rejected [94].

Table 35.5: Properties of noble and molecular gases at normal temperature and pressure (NTP: 20° C, one atm). E_X , E_I : first excitation, ionization energy; W_I : average energy for creation of ion pair; $dE/dx|_{\min}$, N_P , N_T : differential energy loss, primary and total number of electron-ion pairs per cm, for unit charge minimum ionizing particles. Values often differ, depending on the source, and those in the table should be taken only as approximate.

Gas	Density, mg cm ⁻³	E_x eV	E_I eV	W_I eV	$dE/dx _{\min}$ keV cm ⁻¹	N_P cm ⁻¹	N_T cm ⁻¹
H ₂	0.084	10.8	13.6	37	0.34	5.2	9.2
He	0.179	19.8	24.6	41.3	0.32	3.5	8
Ne	0.839	16.7	21.6	37	1.45	13	40
Ar	1.66	11.6	15.7	26	2.53	25	97
Xe	5.495	8.4	12.1	22	6.87	41	312
CH ₄	0.667	8.8	12.6	30	1.61	28	54
C ₂ H ₆	1.26	8.2	11.5	26	2.91	48	112
iC ₄ H ₁₀	2.49	6.5	10.6	26	5.67	90	220
CO ₂	1.84	7.0	13.8	34	3.35	35	100
CF ₄	3.78	10.0	16.0	35-52	6.38	52-63	120

The energy loss of charged particles and photons in matter is discussed in Sec. 34. Every ionization process is a quantum mechanical transition initiated by the Coulomb field of the particle and the field created by neighbouring polarizable atoms; the average energy losses are described by the Bethe-Bloch formula with Sternheimer's density effect corrections. The fluctuations caused by Rutherford scattering on quasi-free electrons follow a Landau distribution and the influence of atomic shells is described by the photoabsorption ionization (PAI) model, which allows simulation of each energy transfer [95], with relaxation cascades and simulation of delta-electrons [96]. Table 35.5 provides values of relevant parameters in some commonly used gases at NTP for unit-charge minimum-ionizing particles (MIPs) [97] [98]. When an ionizing particle passes through the gas it creates electron-ion pairs; often the ejected electrons have sufficient energy to further ionize the medium. The number of pairs is known as cluster-size distribution, because the secondary electrons are created in the immediate vicinity of the primary encounter and, together with the primary electrons, form clusters of one, several, or sometimes many, electron-ion pairs. As shown in Table 35.5, the total number of pairs (N_T) is a few times larger than the number of primaries (N_P). For different conditions and for mixtures, and neglecting energy transfer processes (*e.g.* Penning effect), one can scale the density, N_P , and N_T with temperature and pressure assuming a perfect gas law.

The probability for a released electron to have an energy E or larger follows an approximate $1/E^2$ dependence (Rutherford law),

shown in Fig. 35.4 for Ar at NTP (dotted line, left scale). More detailed estimates taking into account the electronic structure of the medium are shown in the figure, for three values of the particle velocity factor $\beta\gamma$ [99]. The dot-dashed line provides, on the right scale, the practical range of electrons (including scattering) of energy E . As an example, about 0.6% of released electrons have 1 keV or more energy, substantially increasing the total ionization loss. The practical range of 1 keV electrons in argon (dot-dashed line, right scale) is 70 μm and this can contribute to the error in the coordinate determination.

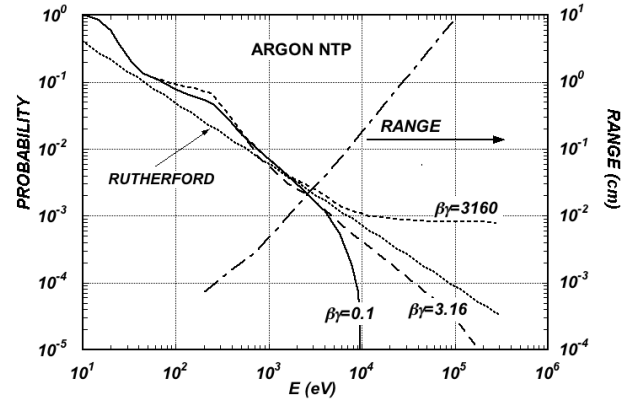


Figure 35.4: Probability of single collisions in which released electrons have an energy E or larger (left scale) and practical range of electrons in Ar at NTP (dot-dashed curve, right scale) [99].

Garfield⁺⁺ [100], together with HEED [96], Degrad [101], Magboltz [102, 103], SRIM, ANSYS, COMSOL, and neBEM [104] software packages represent the core simulation tools for microscopic modelling of gaseous detector response. The number of electron-ion pairs per primary ionization, or cluster size depends little on the medium; it can be computed with the programs mentioned above or experimentally measured. For example, there is about 1% probability for primary clusters to contain ten or more electron-ion pairs in argon [105].

Once released in the gas, and under the influence of an applied electric field, electrons and ions drift in opposite directions and diffuse towards the electrodes. The electron-molecule collision cross sections are determined by the details of atomic and molecular structure and depends strongly on the electron energy and therefore on the electric field \mathbf{E} for most gases. High values of the total electron scattering cross section reduce the electron diffusion and increase the drift velocity; a large inelasticity implies that high fields are required to raise the electron energy. For noble gases, the inelastic cross section is zero until the electrons reach the first excitation and ionization energies $\mathcal{O}(10 \text{ eV})$; on the contrary, for molecular gases, like CH_4 , inelastic channels, involving rotational and vibrational levels, open up at energies above $\sim 0.1 \text{ eV}$. Large drift velocities are achieved by adding polyatomic gases (usually hydrocarbons C_xH_y , CO_2 , CF_4) having large inelastic component at moderate energies of a few eV; this results in the electron "cooling" into the energy range of the Ramsauer-Townsend minimum (at $\sim 0.5 \text{ eV}$) of the elastic ("momentum-transfer") cross-section in Ar [98]. Under these circumstances, it is not surprising that the addition of very small quantities of one gas to another can dramatically modify the average electron energy and alter the dependence of the drift velocity (v_d) on \mathbf{E}/P and temperature; this has a particularly strong effect for noble gases, as illustrated in Fig. 35.5 for Ar. Carbon tetrafluoride (CF_4) has the largest drift velocity and the lowest electron diffusion among known gases due to the sizeable Ramsauer-Townsend dip in the elastic cross-section which coincides with a very large vibrational modes. Another principal role of the polyatomic gas is to absorb the ultraviolet photons emitted by the excited noble gas atoms. Addition of molecular gases (hydrocarbons or CO_2 are widely used in the proportional counters as a quencher) to noble gas allows to dissipate a good fraction of energy through rotational and vibrational radiationless transitions without the creation of photons or ions. On the

contrary, CF_4 has a small quenching cross-section of excited Ar states and light emission in CF_4 (from the far UV to the visible light) is a complex process, involving the creation of CF_3^+ excited states [106].

Extensive collections of experimental data [107] and theoretical calculations based on transport theory permit evaluation of drift and diffusion properties in pure gases and their mixtures; modern compilations of the electron-molecule cross sections are available at the open-access website LXCAT [108]. Fig. 35.5 and Fig. 35.6 show drift velocity and transverse diffusion for some commonly used gases at NTP, computed with the Magboltz program [102, 103]. For different conditions, the horizontal axis must be scaled inversely with the gas density. Standard deviations for longitudinal (σ_L) and transverse diffusion (σ_T) are given for one cm of drift, and scale with the the square root of the drift distance.

In a simple approximation, gas kinetic theory provides the drift velocity v_d as a function of the mean collision time τ and the electric field \mathbf{E} : $v_d = eE\tau/m_e$ (Townsend's expression). In the presence of an external magnetic field, the Lorentz force acting on electrons between collisions deflects the drifting electrons and modifies the drift properties. The electron trajectories, velocities and diffusion parameters can be computed with Magboltz. The friction force model provides an approximate expression for the vector drift velocity \mathbf{v} as a function of electric and magnetic field vectors \mathbf{E} and \mathbf{B} , of the Larmor frequency $\omega = eB/m_e$, and of the mean collision time τ (more precise calculation is available in Magboltz, which computes drift velocity by tracing electrons at the microscopic level through numerous collisions with gas molecules):

$$\mathbf{v} = \frac{e}{m_e} \frac{\tau}{1 + \omega^2\tau^2} \left(\mathbf{E} + \frac{\omega\tau}{B} (\mathbf{E} \times \mathbf{B}) + \frac{\omega^2\tau^2}{B^2} (\mathbf{E} \cdot \mathbf{B}) \mathbf{B} \right) \quad (35.14)$$

To a good approximation, and for moderate fields, one can assume that the energy of the electrons is not affected by B , and use for τ the values deduced from the drift velocity at $B = 0$ (the Townsend expression). For \mathbf{E} perpendicular to \mathbf{B} , the drift angle relative to the electric field vector is $\tan\theta_B = \omega\tau$ and $v = (E/B)(\omega\tau/\sqrt{1 + \omega^2\tau^2})$. For parallel electric and magnetic fields, drift velocity and longitudinal diffusion are not affected, while the transverse diffusion can be strongly reduced: $\sigma_T(B) = \sigma_T(B=0)/\sqrt{1 + \omega^2\tau^2}$. As an example, the dotted line in Fig. 35.6 represents σ_T for the classic Ar/ CH_4 (90:10) mixture at 4 T. Large values of $\omega\tau \sim 20$ at 5 T are consistent with the measurement of diffusion coefficient in Ar/ CF_4 / iC_4H_{10} (95:3:2). This reduction is exploited to substantially improve spatial resolution in the Drift (Sec. 35.6.2) and Time Projection Chambers (Sec. 35.6.5).

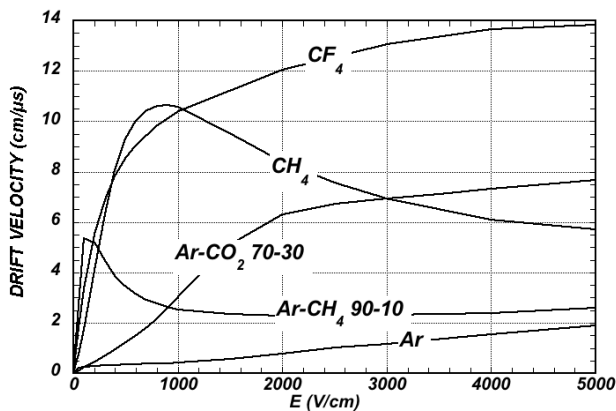


Figure 35.5: Computed electron drift velocity as a function of electric field in several gases at NTP and $B = 0$ [102, 103].

In some mixtures containing molecules with electronic affinity, electrons can be captured to form negative ions. Capture cross sections vary considerably with an energy and, hence, the electric field; as a consequence, the three-body electron attachment coefficients may differ significantly for the same additive in different mixtures. As an example, at moderate fields (up to 1 kV/cm)

the addition of 0.1% of oxygen to an Ar/ CO_2 mixture results in an electron capture probability about twenty times larger than in Ar/ CH_4 . Among common molecules, the largest electron affinities are found for the halogenides, O_2 and H_2O . The attachment probability in O_2 or H_2O is large at low fields and electron energies close to thermal, but decreases at increasing fields. On the contrary, CF_4 is not electronegative at low and moderate fields, but has a large electron capture cross section at fields above ~ 8 kV/cm, before reaching the avalanche field strengths. Depending on the mixture and detector geometry, some signal reduction and energy resolution loss is expected in this gas.

If the electric field is increased sufficiently, electrons gain enough energy between collisions to excite and ionize molecules. Above a gas-dependent threshold, the mean free path for ionization, λ_i , decreases exponentially with the field; its inverse, $\alpha = 1/\lambda_i$, is named the first Townsend coefficient. In wire chambers, most of the increase of avalanche particle density occurs very close to the anode wires, and a simple electrostatic consideration shows that the largest fraction of the detected signal is due to the motion of positive ions receding from the wires. The electron component, although very fast, contributes very little to the signal. This determines the characteristic shape of the detected signals in the proportional mode: a fast rise followed by a gradual increase. The slow component, the so-called "ion tail" that limits the time resolution of the detector, is usually removed by differentiation of the signal. In uniform fields, N_0 initial electrons multiply over a length x forming an electron avalanche of size $N = N_0 e^{\alpha x}$; N/N_0 is the gain of the detector. Fig. 35.7 shows examples of Townsend coefficients for several gas mixtures, computed with Magboltz [102, 103].

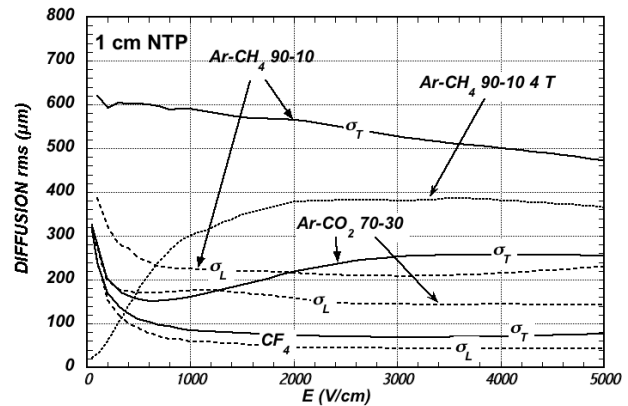


Figure 35.6: Electron longitudinal diffusion (σ_L) (dashed lines) and transverse diffusion (σ_T) (full lines) for 1 cm of drift at NTP and $B = 0$. The dotted line shows σ_T for the P10 mixture at 4 T [102, 103].

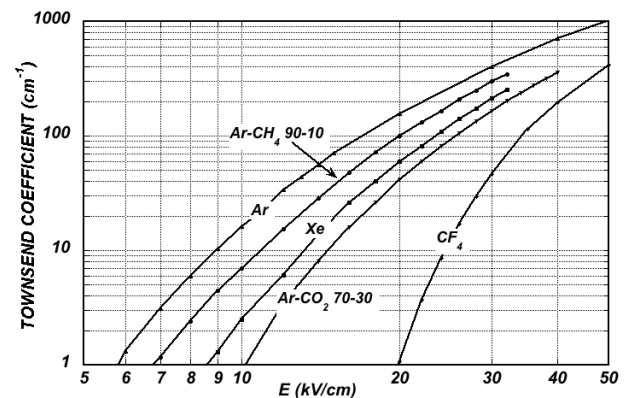


Figure 35.7: Computed first Townsend coefficient α as a function of electric field in several gases at NTP [102, 103].

Additional ionizing energy transfer mechanisms due to the excited noble gas atoms, called collisional Penning energy transfers, occur when the excitation energy of a noble gas is higher than the ionization potential of an admixture gas. The energy transfer rate, probability that an excited atom ionizes a quenching agent, is a priori not known for a mixture but can be extracted from the fits of the experimental gas gain data [109] using the Magboltz simulations [102, 103]. In the gain calculations, the Penning adjusted Townsend coefficient is defined in terms of the total production frequencies of the noble gas excitations and direct ionizations of the mixture. Systematic gas gain measurements for varying mixing ratios and pressures are critical for determining the efficiency of the different mechanisms involved in the transfers. Collisional energy transfer mostly scales linearly with the gas pressure and the fraction of quenching gas in the mixture, while ionization by photons emitted from excitations is independent of the medium [110]. In addition, collisional Penning transfers of some higher excited states can occur before they decay at atmospheric pressure and are not restricted to metastable states of the excited noble gas. For example, the impact of the Penning effect on gas gain is roughly a factor 10 in Ar-CO₂ mixtures and exceeding a factor of 100 in Ar-C₂H₂ mixtures [110].

Positive ions released by the primary ionization or produced in the avalanches drift and diffuse under the influence of the electric field. Negative ions may also be produced by electron attachment to gas molecules. The drift velocity of ions in the fields encountered in gaseous detectors (up to few kV/cm) is typically about three orders of magnitude smaller than for electrons. The ion mobility μ , the ratio of drift velocity to electric field, is constant for a given ion type up to very high fields. Values of ions mobility at NTP are given in Table 35.6 [111]. For different temperatures and pressures, the mobility can be scaled inversely with the density assuming an ideal gas law. Both the longitudinal and transverse diffusion of ions are proportional to the square root of the drift time, with a coefficient that depends on temperature but not on the ion mass. It has been historically assumed that, due to a very effective charge transfer mechanism, only ions with the lowest ionization potential survive after a short path in the mixture. However, recent experimental data suggests that the signal ions, in e.g. CO₂-quenched mixtures of Ar and Ne are CO₂⁺·(CO₂)_n cluster ions, and not CO₂⁺ or noble gas ions [112]. Since the cluster ions are slower than the initial ions, the signals induced by ion motion are altered. The effect can be present in constant-field detectors and TPCs (see Sec. 35.6.5), and might affect devices such as Micromegas (see Sec. 35.6.4) and drift tubes. A negative-ion TPC can be used to expand the reach of directional dark matters searches [113].

Table 35.6: Mobility of ions in gases and mixtures at NTP [111].

Gas	Mobility μ (cm ² V ⁻¹ s ⁻¹)
He	10.4
Ne	4.7
Ar	1.54
Ar/CH ₄	1.87
Ar/CO ₂	1.72
CH ₄	2.26
CO ₂	1.09

35.6.2 Multi-Wire Proportional and Drift Chambers

Revised November 2021 by F. Sauli (CERN) and M. Titov (IRFU, CEA, Université Paris-Saclay).

Single-wire counters that detect the ionization produced in a gas by a charged particle, followed by charge multiplication and collection around a thin (typically 20 – 50 μm diameter) wire, have been used for decades. Good energy resolution is obtained in the proportional amplification mode, while very large saturated pulses can be detected in the streamer and Geiger modes [114].

Modern fully electronic devices, multiwire proportional chambers (MWPCs) [115, 116] introduced in the late 1960's, detect, localize and measure energy deposit by charged particles over large areas. A mesh of parallel anode wires at a suitable potential, inserted between two cathodes, acts almost as a set of independent proportional counters (see Fig. 35.8a). Electrons released in the gas volume drift towards the anodes and produce avalanches in the increasing field. Analytic expressions for the electric field can be found in many textbooks. The fields close to the wires $E(r)$, in the drift region E_D , and the capacitance C per unit length of anode wire are approximately given by

$$E(r) = \frac{CV_0}{2\pi\epsilon_0} \frac{1}{r} \quad E_D = \frac{CV_0}{2\epsilon_0 s} \quad C = \frac{2\pi\epsilon_0}{\pi(\ell/s) - \ln(2\pi a/s)}, \quad (35.15)$$

where r is the distance from the center of the anode, s the wire spacing, ℓ and V_0 the distance and potential difference between anode and cathode, and a the anode wire radius.

Because of electrostatic forces, anode wires are in equilibrium only for a perfect geometry. Small deviations result in forces displacing the wires alternatively below and above the symmetry plane, sometimes with catastrophic results [117]. These displacement forces are countered by the mechanical tension of the wire, up to a maximum unsupported stable length, L_M [118], above which the wire displaces:

$$L_M = \frac{s}{CV_0} \sqrt{4\pi\epsilon_0 T_M} \quad (35.16)$$

The maximum tension T_M depends on the wire diameter and modulus of elasticity. Table 35.7 gives approximate values for tungsten and the corresponding maximum stable wire length under reasonable assumptions for the operating voltage ($V_0 = 5$ kV) [119]. Internal supports and spacers can be used in the construction of longer detectors to overcome limits on the wire length imposed by Eq. (35.16).

Table 35.7: Maximum tension T_M and stable unsupported length L_M for tungsten wires with spacing s , operated at $V_0 = 5$ kV. No safety factor is included.

Wire diameter (μm)	T_M (newton)	s (mm)	L_M (cm)
10	0.16	1	25
20	0.65	2	85

Traditionally, several simplifying assumptions are made in such analytical calculations: electrostatic force acting on the wire does not change during wire movements, or varies linearly with the displacement, the wire shape is parabolic; only one wire moves at a time. Therefore, for complicated electrode geometries the approximations listed above are not applicable. The advantage of numerical integrations using Garfield⁺⁺ program is to simulate the collective movement of all wires, which are difficult analytically, and to consider all forces acting on a wire: forces between anode wire and other electrodes (wires, cathode) and a gravitational force [120].

Detection of charge on the wires over a predefined threshold provides the transverse coordinate to the wire with an accuracy comparable to that of the wire spacing. The coordinate along each wire can be obtained by measuring the ratio of collected charge at the two ends of resistive wires. The cathode planes can be fabricated in the form of group of wires or isolated strips, which are often patterned in orthogonal directions. Making use of the charge profile induced by avalanches on segmented cathodes, the so-called electronic center-of-gravity (COG) method allows localization of tracks to sub-mm accuracy. Due to the statistics of energy loss and asymmetric ionization clusters, the position accuracy is ~ 50 μm rms for fast particles perpendicular to the wire plane, but degrades to ~ 250 μm at 30° to the normal [121].

Drift chambers, developed in the early '70's, can be used to estimate the space coordinate perpendicular to the wires by exploiting the arrival time of electrons at the anodes if the time of interaction is known [122]. The distance between anode wires (e.g.

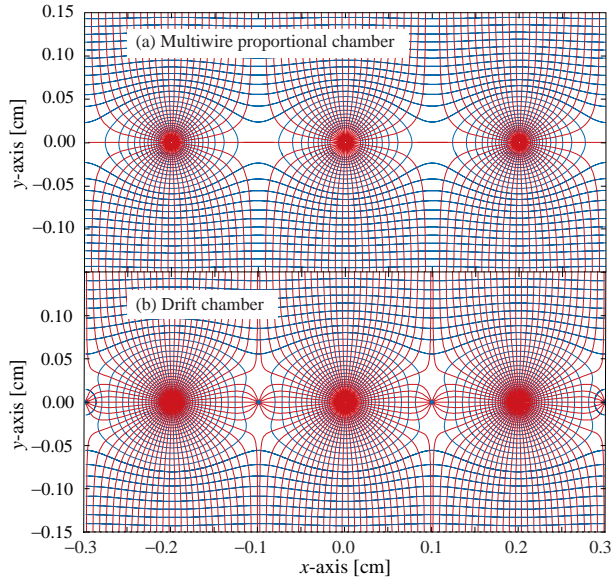


Figure 35.8: Electric field lines and equipotentials in (a) a multiwire proportional chamber and (b) a drift chamber.

Au-plated W) is usually several cm, allowing coverage of large areas at reduced cost. In the original design, a thicker wire (the field wire, often from Cu-Be or Al) at the proper voltage, placed between the anode wires, removes the low-field region at the midpoint between anodes and improves charge collection (Fig. 35.8b). In some drift chamber designs, and with the help of suitable voltages applied to field-shaping electrodes, the electric field structure is adjusted to improve the linearity of space-to-drift-time relation, resulting in better spatial resolution [123].

Drift chambers can reach a longitudinal spatial resolution from timing measurement of order $100 \mu\text{m}$ (rms) or better for minimum ionizing particles, depending on the geometry and operating conditions. However, a degradation of resolution is observed [124] due to primary ionization statistics for tracks close to the anode wires, caused by the spread in arrival time of the nearest ionization clusters. The effect can be reduced by operating the detector at higher pressures. Sampling the drift time on rows of anodes led to the concept of multiple arrays such as the multi-drift module [125] and the JET chamber [126]. A measurement of drift time, together with the recording of charge sharing from the two ends of the anode wires provides the coordinates of segments of tracks. An ultimate drift chamber design is the Time Projection Chamber (TPC) concept [127], which provides 3D precision tracking with low material budget and enables particle identification through differential energy loss dE/dx measurement or cluster counting dN_{cl}/dx techniques. In all cases, a good knowledge of electron drift velocity and diffusion properties is required. This has to be combined with the knowledge of the electric fields in the structures [103]. Accumulation of ions in the gas volume may induce gain reduction and field distortions, especially for long drift distances in TPC (see Sec. 35.6.5). An important major innovation is related to the replacement of MWPC with Micro-Pattern Gaseous Detectors (MPGD) (see Sec. 35.6.4) for the TPC endplate readout, which offers many advantages: reduced track-angle, and negligible $E \times B$ track distortion effects, narrower pad response function (PRF), and intrinsic suppression of Ion Back Flow (IBF). For an overview of detectors exploiting the drift time for coordinate measurement see Refs. [118, 128].

Multiwire and drift chambers have been operated with a variety of gas fillings and operating modes, depending on experimental requirements. The so-called “Magic Gas,” a mixture of argon, isobutane and Freon [116], permits very high and saturated gains ($\sim 10^6$). This gas mixture was used in early wire chambers, but was found to be susceptible to severe aging processes. DAFNE’s KLOE Drift Chamber and the recent version of it developed for

the MEG2 experiment [129] are the precursors of the next generation of ultralight central trackers for future colliders. Since the main contribution in terms of radiation length is related to tungsten wires, high transparency can be achieved thanks to the development of new wire materials (e.g. carbon monofilaments) and novel approaches for the wiring and assembly procedures. Drift chambers have been operated with a light helium/hydrocarbon mixtures, which are not reliable for long-term, high-rate operation [130]. Dedicated R&D is necessary to find an alternative hydrocarbon-free mixture adapted to the desired performance at future colliders.

Although very powerful in terms of performance, multi-wire structures have reliability problems when used in harsh or hard-to-access environments, since a single broken wire can disable the entire detector. Introduced in the 1980s, straw and drift tube systems make use of large arrays of proportional counters encased in individual enclosures, each acting as an independent wire counter [131]. Techniques for low-cost mass production of these detectors have been developed for large experiments, such as the Transition Radiation Tracker and the Drift Tubes arrays for CERN’s LHC experiments [132]. The state-of-the-art NA62 straw tracker utilizes new construction techniques of ultrasonic welding to close the straw and to keep them straight and withstand the vacuum pressure without breaking [133]. Future efforts for straw detectors, e.g. COMET Phase-II at JPARC or Mu2e-II at Fermilab, will focus on ultra-thin wall development, long and thin wire handling, precise mechanics and innovative designs.

35.6.3 High Rate Effects

Revised November 2021 by F. Sauli (CERN) and M. Titov (IRFU, CEA, Université Paris-Saclay).

The production of positive ions in the avalanches and their slow drift before neutralization result in a rate-dependent accumulation of positive charge in the detector. This may result in significant field distortion, gain reduction and degradation of spatial resolution. As shown in Fig. 35.9 [134], the proportional gain drops above a charge production rate around 10^9 electrons per second and mm of wire, independently of the avalanche size. For a proportional gain of 10^4 and 100 electrons per track, this corresponds to a particle flux of $10^3 \text{ s}^{-1} \text{ mm}^{-1}$ (1 kHz/mm² for 1 mm wire spacing). For the description of rate effects in MPGD, see Sec. 35.6.4.

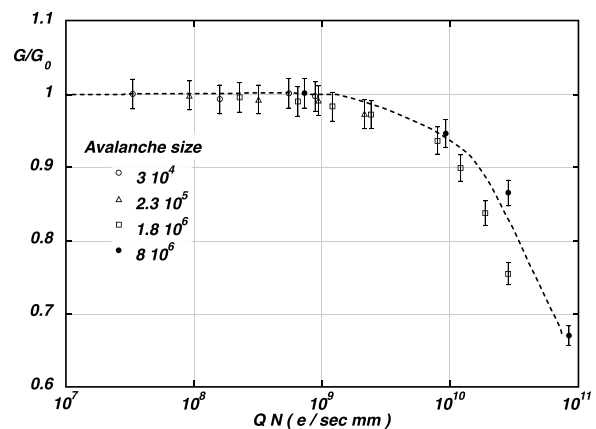


Figure 35.9: Charge rate dependence of normalized gas gain G/G_0 (relative to zero counting rate) in proportional thin-wire detectors [134]. Q is the total charge in single avalanche; N is the particle rate per wire length.

Although almost any gas can be used to operate wire chambers, CF_4 -based mixtures have been preferred due to their properties. Their main advantage for the use in large volume detectors are high drift velocity, low diffusion, non-flammability and low sensitivity to neutrons; also they do not form polymers in avalanches.

However, the problem of greenhouse gases, such as CF_4 , could become a fundamental limitation for their future applications in

gaseous detectors; due to the EU regulations their prices might go up and future availability is unknown. Performance studies of several eco-friendly mixtures have been initiated, together with a better understanding of their long-term ageing effects [135] (see also Sec. 35.6.4).

Ageing phenomena (formation of polymer deposits on the electrodes) constitute one of the most complex and serious potential problems which could limit or severely impair the use of gaseous detectors in unprecedented harsh radiation environments and lead to operational instabilities [136] [130]. The process has been extensively investigated, often with conflicting results. Several causes have been identified, including organic pollutants and silicone oils. Addition of small amounts of water in many (but not all) cases has been shown to extend the lifetime of the detectors. Addition of fluorinated gases (*e.g.*, CF_4) or oxygen may result in an etching action that can overcome polymer formation, or even eliminate already existing deposits. However, the issue of long-term survival of gas detectors with these gases is controversial. Under optimum operating conditions, a total collected charge of a few coulombs per cm of wire can usually be reached before noticeable degradation occurs. This corresponds, for one mm spacing and at a gain of 10^4 , to a total particle flux of $\sim 10^{14}$ MIPS/cm².

35.6.4 Micro-Pattern Gas Detectors

Revised November 2021 by F. Sauli (CERN) and M. Titov (IRFU, CEA, Université Paris-Saclay).

Despite various improvements, position-sensitive detectors based on wire structures are limited by basic diffusion processes and space charge effects to localization accuracies of 50–100 μm [137]. Industrial advances in microelectronics and photolithographic technology on flexible and standard PCB substrates has favored the invention, in the last years of the 20th century, of novel Micro-Pattern Gaseous Detectors (MPGD) [138–140]. Since the very beginning, the goal was the development of novel devices with high rate capability (up to 10^6 Hz/mm²) and excellent spatial resolution (down to 30 μm), single photo-electron time resolution in the ns-range, large sensitive area and dynamic range, superior radiation hardness and low-cost for large area coverage. Nowadays, a broad family of MPGD technologies are being developed and optimized for numerous applications, such as [141,142]: Micro-Strip Gas Chamber (MSGC), Gas Electron Multiplier (GEM), Micro-Mesh Gaseous Structure (Micromegas), THick GEMs (THGEM), also referred to in the literature as Large Electron Multipliers (LEM), Resistive Plate WELL (RPWELL), GEM-derived architecture (μ -RWELL), Micro-Pixel Gas Chamber (μ -PIC), and an integrated readout of gaseous detectors (Gridpix) using solid-state pixel chips (*e.g.* Medipix or Timepix).

The MSGC concept, invented in 1988, was the first of the micro-structure gas chambers [138]. It consists of a set of tiny parallel metal strips laid on a thin resistive support, alternatively connected as anodes and cathodes and resembles a multi-anode proportional counter. Through an accurate and simple photolithography process, the anode strips can be made very narrow (~ 10 μm) with a typical pitch (distance between strips) of ~ 100 μm . When appropriate potentials are applied to the electrodes, electrons released in the drift volume move toward the strips and multiply in the high-field region. Owing to the small anode-to-cathode distance, the fast removal of positive ions by nearby cathode strips reduces space charge build-up, and improves significantly the rate capability, compared to wire counter. Despite their promising performance, experience with MSGCs has raised serious concerns about their long-term behavior. There are several major processes, particularly at high rates, leading to the MSGC operational instabilities: substrate charging-up and time-dependent distortions of the electric field, surface deposition of polymers (“aging”) during sustained irradiation, and destructive micro-discharges under exposure to heavily ionizing particles [143]. The physical parameters used to manufacture and operate these detectors (substrate material, metal of strips, type and purity of the gas mixture) appeared to play dominant roles in determining the medium- and long-term stability. The problems encountered inspired the development of novel structures, using modern photolithographic

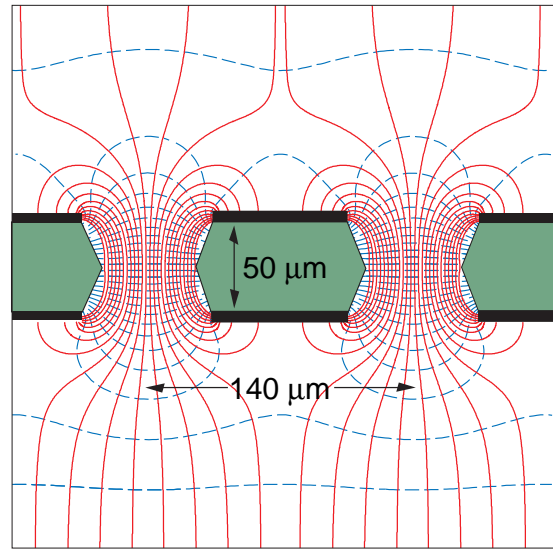


Figure 35.10: Schematic view and typical dimensions of the hole structure in the GEM amplification cell. Electric field lines (solid) and equipotentials (dashed) are shown. Electron trajectories do not strictly follow the field lines as drifting electrons scatter isotropically with gas molecules and diffuse transversally.

processes: GEM, Micromegas and others, having increased reliability and radiation hardness.

A GEM detector consists of a thin-foil copper-insulator-copper sandwich chemically perforated to obtain a high density of holes in which avalanches occur [139,144]. The hole diameter is typically between 25 μm and 150 μm , while the corresponding distance between holes varies between 50 μm and 200 μm . The central insulator is usually (in the original design) a polyimide foil, with a thickness of 50 μm . Application of a potential difference between the two metal sides of the GEM generates the electric fields indicated in Fig. 35.10. Each hole acts as an independent proportional counter. Electrons released by the primary ionization particle in the upper conversion region (above the GEM foil) drift into the holes, where charge multiplication occurs in the high electric field (50–70 kV/cm), and are transferred into the gap below the GEM. Systematic measurements with cascaded multi-GEM structures confirm that the gains and charge transfer processes are predictable from electrostatic considerations and avalanche development models; an overall gas gain well above 10^4 can be reached in the presence of highly ionizing particles, while strongly reducing the risk of discharges [145]. Other important parameters such as attachment, diffusion depend on the gas mixture composition and E/P . The majority of the charges created in the avalanche process follow the field lines and are collected by the metallic electrodes; owing however to diffusion, some may deposit on the dielectric surfaces, modifying the field and affecting gain and transparency of the structures [146]. This effect is known as “charging-up” effect; its time constant and amplitude depend largely on the shape of the holes.

The micro-mesh gaseous structure (Micromegas) is a thin parallel-plate avalanche counter, as shown in Fig. 35.11 [140]. It consists of a drift region and a narrow multiplication gap (25–150 μm) between a thin metal grid (micromesh) and the read-out electrode (strips or pads of conductor printed on an insulator board). Electrons from the primary ionization drift through the mesh into the narrow multiplication gap, where they are amplified. The electric field is mostly homogeneous in both the drift (electric field ~ 1 kV/cm) and amplification (50–70 kV/cm) regions and exhibits a funnel-like shape close to the openings of the micromesh: field lines are compressed into a small diameter of the order of a few microns, depending on the electric field ratio between the two gaps. In the narrow multiplication region, small variations of the amplification gap are approximately compensated by an inverse variation of the Townsend coefficient from

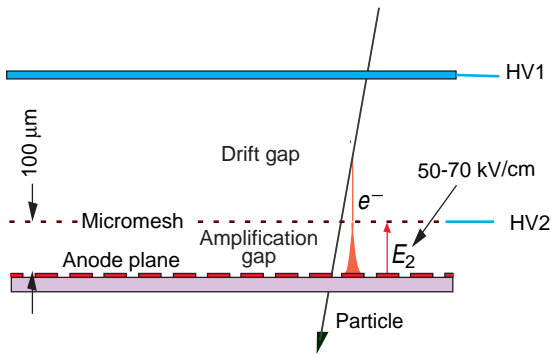


Figure 35.11: Schematic drawing of the Micromegas detector.

the electric field, resulting in a more uniform gain. The transverse size of the electron avalanche due to diffusion is of the order of 10–15 μm , depending on the gas mixture, the electric field, and the gap width, giving rise to excellent spatial resolution (12 μm for MIPs) [147]. Most positive ions are quickly removed by the micromesh; this prevents space-charge accumulation and induces very fast signals (~ 100 ns length) due to electrons with a (fast) tail due to ions. Efforts have been also focused on producing Micromegas detector using innovative manufacturing techniques - the “Bulk” and “MicroBulk” technologies [148].

The absence of space-charge effects in GEMs at the highest rates reached so far, thanks to its fine-pitch structure of a few hundred microns, improves the maximum rate capability by more than two orders of magnitude compared to MWPC (see Fig.35.12) [149] [150]. Even larger rate capability has been reported for Micromegas [151].

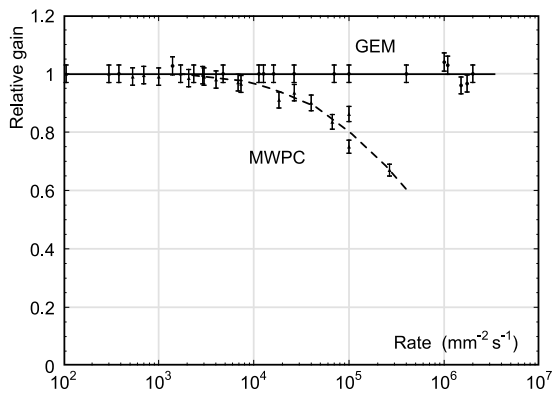


Figure 35.12: Normalized gas gain as a function of particle rate for MWPC [149] and GEM [150].

The fine granularity and high-rate capability of GEM and Micromegas can be fully exploited by using high-density pixel readout with a size corresponding to the intrinsic width of the detected avalanche charge. An elegant solution is the use of a CMOS pixel ASIC, assembled directly below the GEM or Micromegas amplification structure. Modern wafer post-processing technology allows an integration of a small-scale micromesh grid directly on top of a Timepix chip, thus forming an integrated MPGD readout, called GridPix concept (see Fig.35.13) [152]. With this arrangement, avalanche electrons are collected on the metalized input pads, exposed to the gas and signals are induced at the input gate of a charge-sensitive preamplifier. Every pixel is then directly connected to the amplification and digitization circuits, integrated in the underlying CMOS layers. A thin insulating layer, e.g. a few μm of silicon nitride, is usually deposited on top of CMOS ASIC to protect against destructive discharges across the $\mathcal{O}(50 \mu\text{m})$ amplification gap. The GridPix concept provides the high granularity needed to resolve individual electron clusters (separated by an average distance of a few hundred microns) and to determine energy loss by the cluster counting technique, rather

than by the charge measurement, with a precision of better than 3%. Despite the enormous challenges, real breakthrough was the development of the TPC readout endplate with a 160 GridPix ASICs, each 2 cm^2 , corresponding to 10.5 million pixels, demonstrating for the first time the feasibility of large-area MPGD with CMOS pixel readout [153]. New structures, where a GEM foil is facing the Medipix chip, forming the GEMpix detector, are in use for medical applications [154] as well as for monitoring the radioactive waste [155].

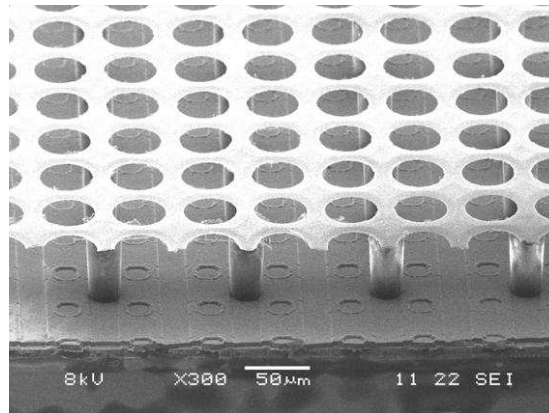


Figure 35.13: Photo of the Micromegas (“GridPix”) detector. The grid holes can be accurately aligned with readout pixels of Timepix CMOS chip. The insulating pillars are centered between the grid holes, thus avoiding dead regions.

Gaseous detectors represent the most cost-effective solution to cover very large areas with photosensitive elements. MPGD-based gaseous photomultipliers, conceived with the aim to overcome the limitations of MWPCs, with semi-transparent or reflective photocathodes (PC), allow to minimize PC aging due to the ion and photon feedback and to avoid secondary effects causing electrical instability. For RICH applications requiring large-area coverage and moderate spatial resolution, coarser macro-patterned structures (e.g. THGEM with typical thickness of 0.4–1 mm and hole spacing of 0.7–1.2 mm) offer an interesting cheaper solution [156]. These are derived from the GEM design, scaling up ~ 10 -fold geometrical parameters, and can be mass-produced with standard PCB technology and mechanical drilling of large number of holes: some millions per square meter. Systematic studies to find the optimal electrostatic configuration revealed that the presence of a rim, a circular region around the holes where metal is etched away, plays a major role in THGEM performance. A small or zero rim allows to achieve better gain stability in time and under irradiation, while large rims permit to attain larger maximum gain and to reduce discharges, at the cost of significant charging up of the insulating surface, which modify the electric field. Therefore, in spite of the enhanced gain performance, the use of large rim THGEMs must be avoided to guarantee stable detector performance [157]. MPGDs are now in operation for single photon detection in the COMPASS RICH where a hybrid architecture formed by two THGEM layers (one covered by CsI-PC) and a Micromegas, acting as a third amplification stage, has been adopted.

Lately, closed geometry THGEM-based structures (RPWELL) [158], in common with some MPGDs invented at the end of the last century – C.A.T. and WELL, with resistive anodes have been developed, combining THGEM and RPC properties. This concept consists of a single-faced THGEM, copper-clad on its top side only, mounted directly on top of a resistive film deposited on a thin insulating sheet. Compared to THGEM with an induction gap, higher gains could be achieved in RPWELL for lower applied voltage across the THGEM electrode, due to the larger electric field within the closed holes. Another promising GEM-derived architecture is that of the μ -RWELL [159], with its \sim seven-fold smaller pitch with respect to the RPWELL. Two different layouts for resistive stage have been studied: the simplest one is based on

a single-resistive Diamond-Like Carbon (DLC) layer, and grounded by edges (2D charge evacuation for low-rates $\mathcal{O}(\text{kHz}/\text{cm}^2)$) and a more sophisticated scheme using double-resistive layer with a through-vias between them and the grounding done by means of the readout electrodes (3D charge evacuation for high-rate $\mathcal{O}(\text{MHz}/\text{cm}^2)$ applications) [160]. The μ -PIC structure is an industrially produced PCB including anode strips on one side and orthogonal cathode strips on the other one. A regular pattern of uncoated regions is present along the cathode strips; an electric conductor buried in the thin PCB substrate transfers the anode voltage to a "dot" at the center of each of the uncoated cathode zones. Electron avalanches occur under the high-electric field around the point-like anodes; the electric field near cathode edges is weaker than in MSGCs, resulting in a lower discharge probability. A resistive coating of the cathode strips (e.g. using DLC layers) ensures tolerance to occasional discharges [161].

A big step in the direction of large-size applications has been obtained both with conceptual consolidation and industrial and cost-effective manufacturing of MPGDs by developing new fabrication techniques: resistive Micromegas (to suppress destructive sparks in hadron environments) [162] and single-mask and self-stretching GEM techniques (to enable production of large-size foils and significantly reduce detector assembly time) [163]. Scaling up of MPGDs to very large single unit detectors of $\mathcal{O}(\text{m}^2)$, has facilitated their use in the High Luminosity LHC upgrades: Micromegas will instrument an area of $\mathcal{O}(1000 \text{ m}^2)$ in the New Small Wheel of the ATLAS Muon endcaps, while GEMs be used in the CMS Muon system and for the ALICE TPC readout. Exploiting the Micromegas, GEM, and μ -RWELL ability to measure both position and arrival time of the charge released in the drift gap, a novel μ -TPC concept has been developed; it permits achieving nearly constant spatial resolution over a wide range of particle incident angles and allows 3D track reconstruction with a single MPGD layer [164]. Although normally used as planar detectors, GEM, Micromegas, and μ -RWELL can be bent to form cylindrically curved ultra-light inner tracking systems, without support and cooling structures [165].

The consolidation of the better-established technologies has been accompanied with flourishing of novel ones, often specific to well-defined applications. Modern technologies have been also derived from Micromegas and GEM concepts, hybrid approaches combining different elements in a single device, gaseous with non-gaseous detectors, as is the case for optical read-out. MPGD hybridization, a strategy aiming to strengthen the detector performance, remains a valid asset for addressing future experimental challenges such as high granularity and picosecond-precision timing (e.g. PICOSEC-Micromegas concept [166]). A clear direction for future developments is that of resistive materials and related detector architectures. Their usage improves detector stability, making possible a higher gain in a single multiplication layer. Recent DLC resistive layers studies are the key ingredients for increasing the rate capability of MPGDs [167]. Future developments call for novel materials as well as for new fabrication techniques. Contributions to the detector concepts are required in several domains: resistive materials, solid-state photon and neutron converters, innovative nanotechnology components. Material studies can contribute to requirements related to low out-gassing, radiation hardness, radio-purity, converter robustness, and eco-friendly gases. The development of the next generation of MPGDs can largely profit from emerging technologies as those related to MicroElectroMechanical Systems (MEMS), sputtering, novel photoconverters, 3D printing of amplifying structures and cooling circuits, etc. Nowadays, many intensive MPGD R&D activities and their diversified applications are pursued within the world-wide CERN-RD51 collaboration [168].

35.6.5 Time-projection chambers

Revised August 2023 by C. Lippmann (GSI Darmstadt).

The Time Projection Chamber (TPC) concept was invented by David Nygren in the 1970's [169]. It consists of a cylindrical or square field cage that is filled with a gaseous (or liquid) detection medium. Charged particles produce tracks of ionization electrons

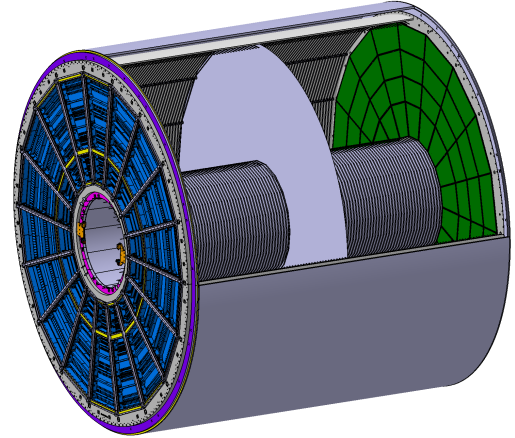


Figure 35.14: Schematic view of the ALICE TPC [170, 171]. The drift volume with 5 m diameter is divided into two halves, each providing 2.5 m drift length. The amplification stage has recently been upgraded from wire planes to GEMs.

that drift in a uniform electric field towards a position-sensitive amplification stage which provides a 2D projection of the particle trajectories. The third coordinate can be calculated from the arrival times of the drifted electrons. The start for this drift time measurement is usually derived from an external detector, e.g. a fast interaction trigger detector.

This section focuses on the gas-filled TPCs that are often used in particle or nuclear physics experiments at accelerators on account of their low material budget. For neutrino physics (Sec. 35.11) or for detecting rare events (Sec. 36.4), on the contrary, usually high density and large active mass are required, and a liquid detection medium is favored.

The TPC enables full 3D measurements of charged particle tracks, which gives it a distinct advantage over other tracking detector designs which record information only in two-dimensional detector planes and have less overall segmentation. The track points recorded in a TPC are basically adjacent, which facilitates the track finding enormously. This advantage is often exploited for pattern recognition in events with large numbers of particles, e.g. heavy-ion collisions. Two examples of modern large-volume gaseous TPCs are shown in (Figure 35.14) and (Figure 35.15).

Identification of the charged particles crossing the TPC is possible by simultaneously measuring their momentum and specific energy deposit through ionisation (dE/dx). The momentum, as well as the charge sign, are calculated from a helix fit to the particle trajectory in the presence of a magnetic field (typically parallel to the drift field). For this application, precise spatial measurements in the plane transverse to the magnetic field are most important. The specific energy deposit is estimated from many charge measurements along the particle trajectory (e.g. one measurement per anode wire or per row of readout pads). As the charge collected per readout segment depends on the track angle and on the ambient conditions, the measured values are corrected for the effective length of the track segments and for variations of the gas temperature and pressure. The most probable value of the corrected signal amplitudes for a given track provides the best estimator for the specific energy deposit (see Sec. 34.2.3); it is usually approximated by the truncated mean, i.e. the average of the 50%–70% smallest values. The resulting particle identification performance is illustrated in (Figure 35.16), for the ALICE TPC.

The dependence of the achievable energy resolution on the number of measurements N , on the thickness of the sampling layers t , and on the gas pressure P can be estimated using an empirical formula [173]:

$$\sigma_{dE/dx} = 0.41 N^{-0.43} (tP)^{-0.32}. \quad (35.17)$$

Typical values at nominal pressure are $\sigma_{dE/dx} = 4.5$ to 7.5%, with $t = 0.4$ to 1.5 cm and $N = 40$ up to more than 300. The

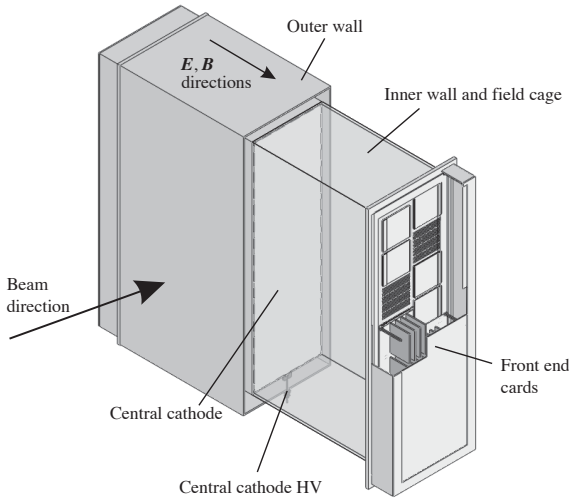


Figure 35.15: One of the 3 TPC modules for the near detector of the T2K experiment [172]. The size is $2 \times 2 \times 0.8 \text{ m}^3$. Micromegas devices are used for gas amplification and readout.

record, with an unprecedented energy resolution of 3%, is held by the PEP-4/9 TPC [174], due to the high gas pressure of 8.5 bar.

The greatest challenges for a large TPC are due to the length of the drift of up to a few meters. In particular, it can make the device sensitive to small distortions in the electric field. Such distortions can arise from a number of sources, e.g. imperfections in the field cage construction or the presence of ions in the drift volume. The electron drift in a TPC in the presence of a magnetic field is defined by Eq. (35.14). The $E \times B$ term of Eq. (35.14) vanishes for perfectly aligned electric and magnetic fields, which can however be difficult to achieve in practice. Furthermore, the electron drift depends on the $\omega\tau$ factor, which is defined by the gas mixture and the magnetic field strength. The electrons will tend to follow the magnetic field lines for $\omega\tau > 1$, or the electric field lines for $\omega\tau < 1$. The former mode of operation makes the TPC less sensitive to non-uniformities of the electric field, which is usually desirable.

The drift of the ionization electrons is superposed with a random diffusion motion which degrades their position information. The ultimate resolution of a single position measurement is limited to around

$$\sigma_x = \frac{\sigma_D \sqrt{L}}{\sqrt{n}}, \quad (35.18)$$

where σ_D is the transverse diffusion coefficient for 1 cm drift, L is the drift length in cm and n is the effective number of electrons collected. Without a magnetic field, $\sigma_{D,B=0} \sqrt{L}$ is typically a few mm after a drift of $L = 100 \text{ cm}$. However, in a strong magnetic field parallel to the drift field, a large value of $\omega\tau$ can significantly reduce diffusion:

$$\frac{\sigma_{D,B>0}}{\sigma_{D,B=0}} = \frac{1}{\sqrt{1 + \omega^2 \tau^2}}. \quad (35.19)$$

This factor can reach values of up to 10. In practice, the final resolution limit due to diffusion typically lies around $\sigma_x = 100 \mu\text{m}$.

The drift and diffusion of electrons depend strongly on the gas mixture. The optimal gas mixture varies according to the environment in which the TPC operates. In all cases, the oxygen concentration must be kept very low (few ten parts per million in a large TPC) in order to avoid electron loss through attachment.

Ideally, the drift velocity should depend only weakly on the electric field at the nominal operating condition. The classic Ar/CH₄ (90:10) mixture, known as P10, has a drift velocity maximum of

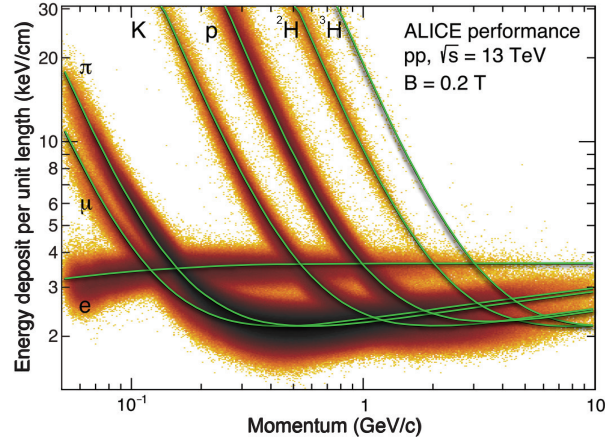


Figure 35.16: Energy deposit versus momentum measured in the ALICE TPC.

5 cm/ μs at an electric field of only 125 V/cm (Figure 35.5). In this regime, the electron arrival time is not affected by small variations in the ambient conditions. Moreover, low electric fields simplify the design and operation of the field cage. The mixture has a large transverse diffusion at $B = 0$, but this can be reduced significantly in a strong magnetic field due to the relatively large value of $\omega\tau$.

For some applications organic gases like CH₄ are not desirable since they may cause aging. An alternative is to replace CH₄ with CO₂. An Ar/CO₂ (90:10) mixture has a low transverse diffusion at all magnetic field strengths, but does not provide a saturated drift velocity for the typical electric fields used in TPCs (up to a few 100 V/cm). As a consequence, it is quite sensitive to the ambient conditions. Freon admixtures like CF₄ can be an attractive option for a TPC as well, since the resulting gas mixtures provide high drift velocities at low electric fields. However, the use of CF₄ always needs to be thoroughly validated for compatibility with all materials of the detector and the gas system.

Historically, the amplification stages used in gaseous TPCs have been planes of anode wires operated in proportional mode. The performance is limited by effects related to the feature size (wire spacing) of a few mm. Since near the wires the electric and magnetic fields are not parallel, the incoming ionisation electrons are displaced in the direction of the wires (“wire $E \times B$ effect”), which degrades the resolution. The smaller feature sizes of Micro-Pattern Gas Detectors (MPGDs) like GEMs and Micromegas lead to many advantages as compared to wire planes (see Sec. 35.6.4). In particular, $E \times B$ effects in the amplification stage are much smaller. Moreover, the signal induction process in MPGDs leads to a very narrow pad response, allowing for a much finer segmentation, which improves the separation for two very close tracks. Combinations of MPGDs with silicon sensors have resulted in the highest granularity readout systems so far (see Sec. 35.6.4). These devices make it possible to count the number of ionization clusters along the length of a track, which can, in principle, improve the particle identification capability. However, the big challenge for such a system is the huge number of readout channels for a TPC of a typical size.

The accumulation of the positive ions created by the ionization from the particle tracks can lead to time-dependent distortions of the drift field. Due to their low drift velocity, ions from many events may coexist in the drift volume. To reduce the effect of such a build-up of space charge, Argon can be replaced by Neon as the main component of the gas mixture. Neon features a lower number of ionisation electrons per unit of track length (see 35.5) and a higher ion mobility (see 35.6).

Of greater concern are the ions produced in the gas amplification stage. In order to prevent them from entering the drift volume, large TPCs built until now have a gating grid. The gating

grid can be switched to transparent mode (usually in the presence of an interaction trigger) to allow the ionization electrons to pass into the amplification region. After all electrons have reached the amplification region, it is usually closed such that it is rendered opaque to electrons and ions. For triggered operation, a combination of a MPGD and a gating structure may be an attractive solution. However, a gating grid implies a principal rate limitation to a few kHz.

A next generation of TPCs (e.g. ALICE [171], sPHENIX [175]) has been developed for applications where a triggered operation would lead to unacceptable data loss. The employed readout schemes are based on MPGDs, as these can be optimised in order to drastically reduce the ion back-flow. Extensive work has been carried out during the 2010's to design such readout structures. In ALICE and sPHENIX ion back-flow values below 1% are achieved with a thorough adjustment of the various fields in a quadruple GEM system. Similar levels of ion back-flow can be reached with Micromegas detectors [176].

35.6.6 Transition radiation detectors (TRD's)

Revised July 2021 by P. Nevski (BNL) and A. Romaniouk (Innsbruck U.; MEPHI Moscow).

Transition radiation (TR) x-rays are produced when a highly relativistic particle ($\gamma \gtrsim 10^3$) crosses a refractive index interface, as discussed in Sec. 34.7. Since the TR yield is about a few % per boundary crossing, radiation from multiple surface crossings (e.g., a stack of foils) is used in practical detectors. The x-rays, ranging from a few keV to a few dozen keV or more, are emitted in a forward direction at small angles (within few mrad) to the particle trajectory. The TR intensity for a single boundary crossing always increases with γ , but, for multiple boundary crossings, interference leads to saturation above a Lorentz factor $\gamma_{\text{sat}} = 0.6 \omega_1 \sqrt{\ell_1 \ell_2} / c$ [177], where ω_1 is the radiator material plasma frequency, ℓ_1 is its thickness, and ℓ_2 the spacing between material elements. The probability density function of TR is a fairly complex function of γ , radiator parameters, photon energy (ω) and its emission angle (θ). For well defined radiator parameters a measured two-dimensional distribution of photon energy vs its reconstructed emission angle is in very good agreement with the theory predictions [178].

Integration over the angle yields the TR spectrum, which typically features many maxima (see Sec. 34.7). Most of the TR energy is emitted near the last maximum of the spectra determined by radiator material parameters at $\omega_{\text{max}} = \ell_1 \omega_1^2 / 2\pi c$. The effective TR photon emission starts at about $\gamma_{\text{thr}} = \ell_1 \omega_1 / c$. By varying radiator parameters one may optimize the particle separation for a given range of the γ -factor. The angular distribution of TR photons has a few maxima and extends up to $\theta_{\text{max}} = (1/\gamma^2 + \omega_1^2/\omega^2)^{1/2}$ [179]. For a single foil the largest part of the TR energy is emitted around the most probable angle $\theta = (1/\gamma^2 + \omega_2^2/\omega^2)^{1/2}$, where ω_2 is the plasma frequency of the gas surrounding the radiator material elements. However, in case of multiple interfaces, interference effects may significantly change this angle and more realistic expression for the angle which corresponds to the last interference maximum of the energy spectra is $\theta \approx \sqrt{1.4\pi^2/\gamma_{\text{sat}}^2 - 1/\gamma^2}$ [178]. The higher is the gamma-factor, the larger is the angle of the first interference maximum. It reaches almost its asymptotic limit at $\gamma = \gamma_{\text{sat}}$. This effect is illustrated in Fig. 35.17 [178] which shows two-dimensional distribution of the TR photon energy versus the reconstructed production angle obtained in 20 GeV electron beam with the radiator containing a stack of foils of 15.5 μm thickness spaced by 210 μm (the left plot) using a Si-pixel detector. TR produced by 20 GeV electrons is emitted mostly around $\theta \sim 0.9$ mrad. All features of this distribution are well reproduced with MC simulations (the right plot).

The simplified numerical expressions can be used for practical estimation of the main TR production parameters [178]: $\theta \sim 1.2/\omega_1 \sqrt{\ell_1 \ell_2}$, $\gamma_{\text{thr}} \sim 3 \times 10^3 \omega_1 \ell_1$, $\gamma_{\text{sat}} \sim 3 \times 10^3 \omega_1 \sqrt{\ell_1 \ell_2}$ and $\omega_{\text{max}} = 0.65 \ell_1 \omega_1^2$, where θ in mrad, ω_1 in eV, ω_{max} in keV and ℓ_1 and ℓ_2 in mm.

In the simplest concept, a detector module might consist of a

low-Z TR radiator followed by a high-Z active layer made of proportional counters filled with a Xe-rich gas mixture. The atomic number considerations follow from the dominant photoelectric absorption cross section per atom going roughly as Z^n/ω^3 , where n varies between 4 and 5 over the region of interest.¹ To minimize self-absorption, materials such as polypropylene, Mylar, carbon, and (rarely) lithium in the form of foils, fibers or foams are used as radiators. The TR signal in the active regions is in most cases superimposed upon the particle ionization losses, which are proportional to Z. In most of the detectors used in particle physics the radiator parameters are chosen to provide $\gamma_{\text{sat}} \approx 3000$. Those detectors normally work as threshold devices, ensuring the best electron/pion separation in the momentum range $1 \text{ GeV}/c \lesssim p \lesssim 150 \text{ GeV}/c$.

One can distinguish two design concepts—“thick” and “thin” detectors. In “thick” detectors the radiator, optimized for a fixed total radiation length at maximum TR yield and maximum TR absorption in the detector, consists of few hundred foils (for instance 300 20 μm thick polypropylene foils). Most of the TR photons are absorbed in the radiator itself. To maximise the number of TR photons reaching the detector, part of the radiator far from the active layers is often made of thicker foils, which shifts the x-ray spectrum to higher energies. The detector thickness, about 2-4 cm for Xe-filled gas chambers, is optimized to absorb most of the incoming x-ray spectrum. A classical detector is composed of several similar modules which respond nearly independently. Such detectors were used in the UA2, NA34 and other experiments [180], are being used in the ALICE experiment [181, 182] and are built for the CBM experiment [183]. In another TRD concept a fine granular radiator/detector structure exploits the soft part of the TR spectrum more efficiently. This can be achieved, for instance, by distributing small-diameter straw-tube detectors uniformly or in thin layers throughout the radiator material. This approach allows to realise a TRD as an integral part of a tracking detector providing many points of measurements on the particle track. Even with a relatively thin radiator stack, radiation below 4 keV is mostly lost in the radiators themselves. However, for photon energies above this value, the absorption is reduced and the radiation can be registered by several consecutive detector layers, thus creating a strong TR build-up effect. Descriptions of detectors using this approach in both accelerator and space experiments can be found in [181, 184–187]. For example, in the ATLAS TR tracker (TRT), charged particles on average cross about 35 straw tube layers embedded in the radiator material [184]. The effective thickness of the Xe gas per straw is about 2.5 mm and the average number of foils per straw is about 40 with an effective foil thickness of about 18 μm . In this approach straw walls also act as radiator and make some contribution to the TR spectrum.

Although the values mentioned above are typical for most of the plastic radiators used with Xe-based detectors, they vary significantly depending on the detector requirements. Careful simulations are usually needed to build a detector optimized for a particular application. For TRD simulations the codes are based on well understood TR emission formulas (see for instance [179] for regular radiators and [188] for irregular radiators). They are realised as the stand-alone simulation programs [178, 189, 190] or GEANT4 based ones [191] and give both a good agreement of the TR energy spectra and of the angular distributions with data [178, 192, 193].

The discrimination between electrons and pions can be based on the charge deposition measured in each detection module, on the number of clusters – energy depositions observed above an optimal threshold (usually it is 5–7 keV), or on more sophisticated methods such as analyzing the pulse shape as a function of time. The total energy measurement technique is more suitable for thick gas volumes, which absorb most of the TR radiation and where the ionization loss fluctuations are relatively small. The cluster-counting method works better for detectors with thin gas layers, where the fluctuations of the ionization losses are bigger. Cluster-counting replaces the Landau-Vavilov distribution of background ionization energy losses with the Poisson statistics of

¹Photon absorption coefficients for the elements (via a NIST link), and $dE/dx|_{\text{min}}$ and plasma energies for many materials are given in <https://pdg.lbl.gov/current/AtomicNuclearProperties>.

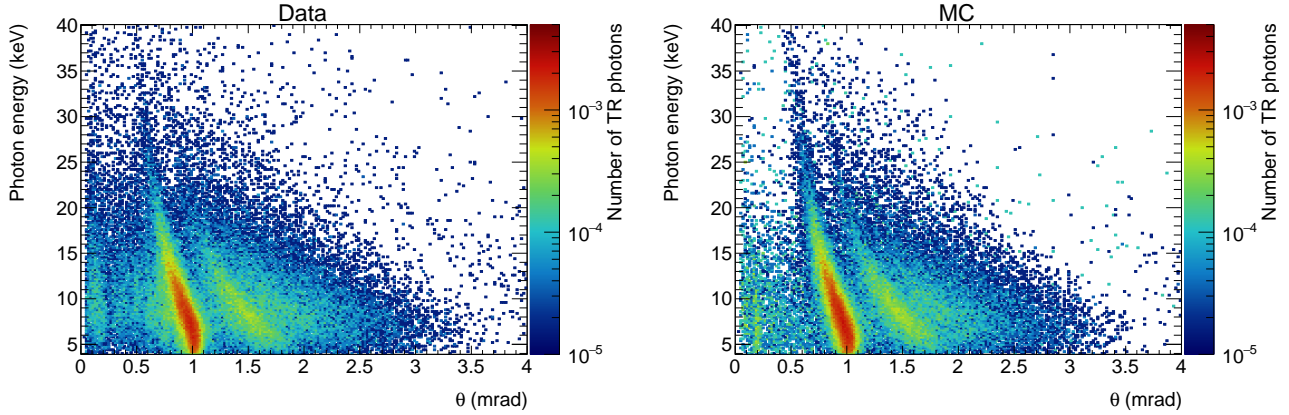


Figure 35.17: Two dimensional distributions of photon energy versus reconstructed production angle obtained with the polypropylene radiator with 20 GeV/c electron beam. Data - the left plot, MC - the right plot. Z-axis is a number of photons per particle [178]

δ -electrons, responsible for the distribution tails. The latter distribution is narrower than the Landau-Vavilov distribution. In practice, most of the experiments use a likelihood method, which exploits detailed knowledge of the detector response for different particles and gives the best separation. The more parameters are considered, the better achievable separation power. The neural network method is the most powerful tool. When it used by the ALICE TRD (ALICE point in Fig. 35.18) it lead to an increase of the rejection power by another factor of 2–3 with respect to the likelihood method [181].

The major factor in the performance of any TRD is its overall length. This is illustrated in Fig. 35.18, which shows, for a variety of detectors, the pion efficiency at a fixed electron efficiency of 90% as a function of the overall detector length. As TRD performance depends on particle energy, the experimental data in this figure covering a range of particle energies from 1 GeV to 40 GeV, are rescaled to an energy of 10 GeV when possible. Phenomenologically, the rejection power against pions increases as $5 \cdot 10^{L/38}$, where the range of validity is $L \approx 20\text{--}100$ cm. Apart from the beam energy variations, the observed scattering of the points in the plot reflects how effectively the detector space is used and how well the exact response to different particles is taken into account in the analysis. For instance, the ATLAS TRT was built as a compromise between TR and tracking requirements; that is why the test-beam prototype result (lower point) is better than the real End-Cap TRT performance at the LHC shown in Fig. 35.18 for different regions in the detector (in agreement with MC).

In most cases, recent TRDs combine particle identification with charged-track measurement in the same detector [181, 183, 186]. This is particularly important for collider experiments, where the available space for the inner detector is very limited. For a modest increase of the radiation length due to the radiator ($\sim 4\%$ X0), a significant enhancement of the electron identification was obtained in the case of the ATLAS TRT. Here, the combination of the two detector functions provides a powerful tool for electron identification even at very high particle densities.

In addition to the enhancement of the electron identification during offline data analysis, TRD signatures are often used in the trigger algorithms at collider experiments. The ALICE experiment [182] is a good example for the use of the TRD in a First Level Trigger. In the ATLAS experiment, the TRT information is used in the High Level Trigger (HLT) algorithms. At increasing luminosities, the electron trigger output rate becomes so high, that a significant increase of the calorimeter energy threshold is required to keep it at an acceptable level. This may affect the trigger efficiency of very important physics channels (e.g. $W \rightarrow e\nu$ inclusive decay). Even a very soft TR cut at the HLT level, which preserves high electron efficiency (98%), allows to suppress a significant part of fake triggers and enhance the purity for physics events with electrons in a final state. The TRT also plays a crucial role in the studies where an electron suppression is required (e.g.

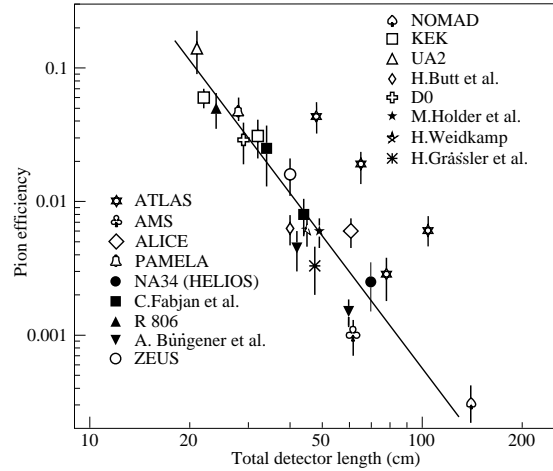


Figure 35.18: Pion efficiency measured (or predicted) for different TRDs as a function of the detector length for a fixed electron efficiency of 90%. The plot is based on the table given in [180]. Results from more recent detectors are added from [181, 185–187, 194].

hadronic mode of τ -decays). TR information is a completely independent tool for electron identification and allows to study systematic uncertainties of other electron reconstruction methods.

Electron identification is not the only TRD application. Some TRDs for particle astrophysics are designed to directly measure the Lorentz factor of high-energy nuclei by using the quadratic dependence of the TR yield on nuclear charge; see, for instance, in [195]. The radiator configuration (ℓ_1, ℓ_2) is tuned to extend the TR yield rise up to $\gamma \approx 10^5$ using the more energetic part of the TR spectrum (up to 100 keV). High density radiator materials (such as Al) are the best for this purpose. Direct absorption of the TR-photons of these energies with thin detectors becomes problematic and TR detection methods based on Compton scattering have been proposed, see in [196].

The high granularity of the semiconductor pixel or microstrip detectors provides spatial separation of the TR photons and dE/dx losses at relatively modest distances between radiator and detector. These detectors may be the basis for novel devices which combine precise tracking and PID properties [178, 190, 197]. Use of the TR production angle in addition to its energy can help to improve PID properties of the TRD. The presence of a magnetic field could enhance the separation between TR photons and dE/dx losses [198]. New detector techniques for TRDs are also under consideration. GasPixel detectors allow to reconstruct a track segment with a space point accuracy of $< 30 \mu\text{m}$ and ex-

exploit all details of the particle tracks to highlight individual TR clusters in the gas, see in [199]. Thin films of heavy scintillators might be a very attractive option for non-gas based TRD [200].

35.6.7 Resistive-plate chambers

Revised August 2023 by G. Aielli (Rome U. Tor Vergata).

The resistive-plate chamber (RPC) is a gaseous detector working at atmospheric pressure developed by R. Santonico and R. Cardarelli in the early 1980's [201]. A precursor of the RPC was the Pestov spark chamber [202] [203], which had a metallic plate cathode and a thick glass plate anode, designed to work at 12 bar to obtain an outstanding 0.1 ns time resolution. Although the original purpose of RPCs was to provide a competitive alternative to large scintillator counters, the RPC's potential for timing tracker systems was quickly recognized given its high detection efficiency (>95%), excellent temporal and spatial resolutions and ease of constructing large-format single frame detectors. The RPC, as sketched in Fig. 35.19, is a large planar capacitor with two parallel high bulk resistivity electrode plates (10^9 – 10^{13} Ω -cm) separated by a set of insulating spacers. The spacers define a gap in the range from a few millimeters down to 0.1 mm with a precision of a few μ m. The gap is filled with a suitable atmospheric-pressure gas mixture which serves as a target for ionizing radiation. The gas gap thickness practically determines the time resolution of the RPC. On the other hand, the limit for reaching full detection efficiency at atmospheric pressure is typically 1 mm (also influenced by the gas molecular weight). Since the primary ionization released in sub-millimeter gas gaps is limited, multiple gaps can be combined to effectively obtain a very high detection efficiency [204]. The electrodes are most commonly made of high pressure phenolic-melaminic laminate (HPL), commonly referred to as "bakelite", or soda-lime glass (glass from

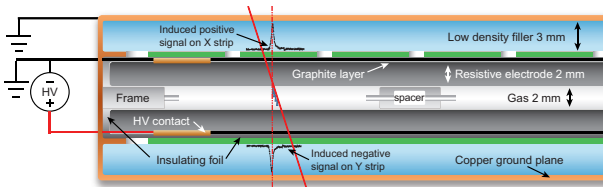


Figure 35.19: Schematic cross section of a generic single gap RPC.

now on), having a lower resistivity than borosilicate glass. A uniform electric field of several kV/mm is established on the gas gap, sufficient to promptly start an avalanche multiplication of the primary electrons. The electric field is typically applied through a moderately conductive ($\sim 10^9$ to 10^8 Ω/\square) graphite varnish, forming an ohmic contact with the external faces of the electrodes. Its conductivity is sufficiently low to be transparent to the fast avalanche signal transients, and high enough to suppress surface voltage gradients arising from the working current flowing in it. Due to the high electrode resistivity in RPCs, the time constant of the equivalent RC circuit ($\tau = \rho \epsilon_r$ being ρ the electrode resistivity and ϵ_r its dielectric constant) is much longer than the discharge processes duration. Therefore only the locally-stored electrostatic energy contributes to the discharge, preventing the formation of sparks and leaving the rest of the detector field unaffected. The gas-facing surface of HPL electrodes are commonly coated with a few μ m-thick layer of polymerized linseed oil [205] with the function of smoothing the electrode surface, improving the electric field uniformity. Glass-based RPCs don't require such treatment. It also has the function of protecting the electrode from the being eventually etched by free radicals generated in the discharge e.g. in presence of fluorocarbons. In RPCs the gaseous target and the multiplication region coincide. In the early stage of the avalanche multiplication the uniform electric field exponentially amplifies each primary ionization cluster, as the avalanche progresses away from the location of the primary ionization. Since the ionization clusters generated by the incident MIP are randomly distributed along the ionizing particle track, for low gains

the observed RPC charge spectrum is broad and approximately exponentially distributed² with the mode close to zero. Because of this, it is difficult to separate noise from signals using a discrimination threshold. This is not the case in gaseous detectors where ionization and amplification occur in separate regions.

For increasingly larger avalanches, the space-charge progressively saturates the avalanche growth from exponential to almost linear, producing a peaked charge spectrum, essential to efficiently separate the signal from the noise [207]. For large gains³ the avalanche, with increasing probability, onsets a transition to "streamer" [208], a plasma filament connecting the electrodes, depleting all the locally-available energy [209], and generating an almost fixed amplitude signal. This prevents any further evolution of the discharge. This streamer mode was the first ever used by RPCs, until the introduction of very electronegative gases and more sensitive front end electronics made it possible to detect the precursor avalanche independently on the streamer [210,211] Any of this operating regimes can be used in RPC detectors, depending on the application.

As with other gaseous detectors, the gas mixture is optimized for each specific application. In general it needs to contain a UV photons quencher suppressing the photon-mediated feedback that can lead to self generated after-pulse discharges, and one or more electronegative components, to extend the avalanche growth, free from streamers, to as high as possible electric fields [212]. The addition of small fractions of electronegative molecules with a very high capture cross section for slow electrons, such as SF₆, was proven to inhibit the transition to streamer over a wide electric field range. Even though there is not yet an accepted and robust avalanche-to-streamer-transition model, this effect is commonly explained as a delay in the growth of the electron density of the avalanche front, which perturbs the electric field driving the transition to streamer. As a reference, the mixture for stable avalanche operation in ATLAS and CMS is C₂H₂F₄/i-C₄H₁₀/SF₆=94.5%/5%/0.3%.

The avalanche induces a fast electron signal on a set of metallic readout electrodes (e.g. pads or strips) commonly placed externally and insulated from the resistive electrodes. The signal is isotropically distributed with respect to the field direction and present with equal but opposite amplitude on both electrodes. Thanks to these features, performances of the readout electrodes on both RPC sides are equivalent. The induced charge density distribution can be ideally calculated for a simplified RPC model [213] [214] as: $\sigma(x) = A / \cosh[(r)/\delta]$ where A is a normalization constant, r is the distance from the center of the avalanche axis and $\delta = (g+2d)/\pi$ depends on the gap and electrode width (g and d , respectively). Depending on the specific RPC layout and geometry, the interplay between conductive coating and pick-up electrodes typically broadens, by means of a diffusion-like process (see [214] [215]). This effect mostly preserves the information on the avalanche position, which can be obtained using the charge centroid method, with the drawback of increasing the signal space occupancy. Sensitivity to the high-frequency spectrum of electron avalanche signals over large RPC areas requires a correspondingly adequate Faraday cage and readout design. At the same time, to preserve the excellent timing features of the RPC signal, the front end electronics should have a short rise time (ideally \ll than the signal rise time) and low noise, although these requirements could be in competition [216].

35.6.7.1 RPC types and applications

RPCs are generally classified in two categories depending on the gas gap structure: single gap RPCs (described above) and multiple gap RPCs [204] (typically referred as MRPCs). While they are both based on the same principle they have different construction techniques, performance and limitations, making them suitable for different applications. Due to its simplicity and robustness, the single gap RPC is ideal for covering very large surfaces. Typical detector systems can have sensitive surface areas

²An analytic treatment of the low gain avalanche process shows that the charge distribution is well described by the Γ function [206]

³A multiplicity of the order of 10^8 electrons is classically referred as Raether/Meek limit for on-setting a streamer

up to $\sim 10^4$ m², with single module areas of a few m², and a space-time resolution down to ~ 0.4 ns \times 100 μ m [217] [218]. Representative examples are the muon systems of ATLAS [219] and CMS [220] or ground and underground based cosmic rays [221] and neutrino arrays [222]. It is interesting to note that CMS implemented a bi-gap structure, i.e. the pickup signal is sandwiched by 2 single gas gaps, both contributing to the signal induction, improving efficiency and time resolution with respect to the single gas gap. Relevant new trends for single gap RPC applications are represented by new Dark Matter search experiments such as CODEX-B [223] and ANUBIS [224], in both cases exploiting RPCs to enclose and instrument large detection volumes with a good space-time tracker. Single gap RPCs have also recently demonstrated good candidates for application in tracking calorimetry [225].

The MRPC [226], as sketched in Fig. 35.20, segments the gaseous target by means of a stack of floating glass electrodes separated by a monofilament (i.e. fishing line) sandwiched between two external electrodes providing the high-voltage bias. Since the current flowing in between the gas gaps must be in average equal, the difference of potential between each couple of adjacent floating electrodes will tend to be the same. An extensive description can be found in [227]. It has been observed that higher time resolution is inversely correlated to the gas gap size, so this configuration allows for smaller gas thicknesses while maintaining a sufficient total gas thickness. This tends to separate primary clusters avalanches in different gas gaps, treating them independently, and determines a shorter avalanche growth time, increasing time resolution by one order of magnitude with respect to the classic RPCs [228]. The mechanical fragility of sub-mm-gap structures makes this technique less suitable for very large detector areas. Moreover the only material nowadays practically suitable for building such structures is soda-lime glass with resistivity above 10^{12} Ω -cm, limiting the rate capability to about 500 Hz/cm² [229].

MRPCs have been largely used in Time Of Flight systems such as ALICE [230], HADES [231], FOPI [232] and BESSIII [233], and in applications such as timing PET [234]. In perspective MRPC will be used for upgraded and new nuclear physics experiments such as CBM@FAIR [235] and SoLID [236].

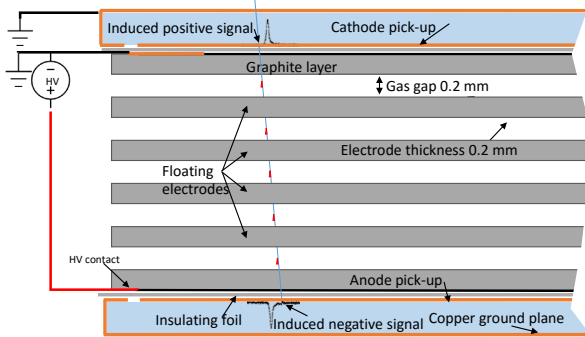


Figure 35.20: Schematic cross section of a generic multi gap RPC.

35.6.7.2 Time and space resolution

Space-time uncertainties in RPCs are determined by the statistical fluctuations of the primary and secondary ionization, the avalanche multiplication rate, which is a function of the electric field, and on the Signal/Noise ratio of the front end electronics. The intrinsic signal latency is commonly in a few ns range (avalanche growth time to produce a detectable signal), making the RPC suitable for applications where a low latency is essential.

The gas gap size is a crucial feature for the RPC timing performance: producing the same total charge (for a detectable signal) in a smaller gas gap implies the necessity of increasing the first Townsend coefficient by increasing the electric field, reducing at the same time the total signal duration and the related time fluctuations; moreover the chance of having multiple clusters in the

same gas gap decreases with the gap size, suppressing the charge collection fluctuations [237], due to the unknown distance in between the clusters. This chance becomes necessarily higher along with the intrinsic efficiency of the single gas gap. Typical timing performances range from around 1 ns with a 2 mm gas gap, down to 20 ps for a stack of several 0.1 mm gaps [238].

The intrinsic position sensitivity of an RPC is in the range of tens of μ m depending on the lateral spread of the avalanche induced charge distribution, influenced also by the gap size. In typical RPC applications the pick up electrodes pitch L (~ 1 cm) is much broader than the intrinsic resolution, and being readout via a discriminator, the spatial resolution is geometrically limited in the range of $L/\sqrt{12}$. A much better result is obtained by using a finer electrodes granularity and measuring the charge in each strip collecting the avalanche charge, so to reconstruct the charge centroid. It has been demonstrated, through charge centroid techniques, that the RPC avalanche space-time localization can be as good as ~ 50 ps \times 40 μ m [239] [240].

35.6.7.3 Rate capability and ageing

RPC rate capability is limited by the voltage drop on resistive electrodes, $\Delta V = V_a - V_{\text{gas}} = I \cdot R$ [241]. Here V_a is the applied voltage, V_{gas} is the effective voltage on the gas, $R = \rho \cdot d/S$ is the total electrode resistance, ρ being the resistivity and d , S the sample thickness and surface respectively, and I is the working current. Assuming uniform irradiation we can express $I = \phi \cdot S \cdot \langle Q \rangle$ where ϕ is the particle fluence and $\langle Q \rangle$ is average charge per avalanche. So we obtain a state equation for the RPC rate capability:

$$\Delta V/\phi = \rho \cdot d \cdot \langle Q \rangle$$

A large I not only limits the rate capability but also affects the long term performance of the detector since the working current, associated to discharges, depletes the conductive properties of HPL electrodes [242]. In presence of fluorocarbons and water, discharges generate hydrofluoric acid (HF) and other fluorinated compounds, which damage internal detector surfaces, especially if made of glass, known to be not resistant to HF [243]. The practical way to suppress HF formation in glass RPCs is preventing water vapor contamination. Conversely, HPL electrodes, coated with linseed oil, are relatively resistant to HF, but the presence of water can not be avoided since it mediates the HPL conduction. In this case the HF damage is mitigated by removing it with a forced flow of gas through the gas gap.

Operating in the streamer regime places low requirements on the front end electronics sensitivity, but generally limits the counting rate capability to ~ 100 Hz/cm². Higher-rate operation can be achieved by reducing gas gain in favor of electronic amplification, operating the detector in avalanche mode. Increasing concentrations of electronegative gases, such as C₂H₂F₄ and SF₆ [212], shifts the streamer transition to higher gains, thus the avalanche signal can access a higher dynamic range, which puts further stress on the performance request on the front end electronics. By further lowering the avalanche mode gas gain compatibly with the front end performance, efficient and stable performance at high rates (e.g. 10 kHz/cm²) has been achieved for large area single gap RPCs [216]. Two complementary strategies rely either on the natural redundancy and higher signal yield of multiple micro gap structures [244] or on electrodes made with lower resistivity materials [245]. Lowering the electrode resistivity in presence of high uniform field is increasingly difficult, since high resistivity limits the appearance of larger discharge events and increase of spurious counts, favoured by the effect of local electrode defects on the field gradient. In this case, to safely lower the electrode resistivity, a safety margin would be given by operating with a lower electric field, and a correspondingly lower average charge per count.

35.6.7.4 Alternative gas mixtures

The standard gas mixture mentioned above is based on Hydrofluorocarbon (HFC), specifically the R134A, extensively used in the refrigeration industry. R134A features matches very well the RPCs performance requirements. It has high density that results in high primary ionization. It is electronegative, which limits secondary discharge phenomena. It is not flammable, and it has a

limited degradation if exposed to UV photons due to the absence of saturated bonds. This last feature permits high rate operation, limiting the ageing effects due to the byproducts of the avalanche discharges. However, this gas has a Global Warming Potential (GWP) of 1450 thus it is not considered anymore a viable option for future industrial applications. Therefore, since a few years the RPC community is researching alternative gases [246,247] to replace R134A, focusing on the Hydro-Fluoro-Olefins, a category of gases recently proposed for industrial applications. HFOs exhibit important limitations with respect to HFCs, if used in high concentrations. In particular its much higher electronegativity implies an impractically high applied electric field for the existing RPC systems, and a much higher charge per count due to a large fraction of negative ions produced by electron capture, which do not contribute to the prompt signal. A further side effect is a larger production of fluoride ions by UV decomposition of the gas. To contrast the ageing acceleration drive represented by the phenomena stated above, the proposed strategy was to largely dilute HFO with a neutral gas, such as CO₂, compatibly with keeping an enough dense gaseous target, and whenever possible, operate at a lower gain by using very performing front end electronics. A representative example of the several variants tested [248] is CO₂/C₃H₂F₄/i-C₄H₁₀/SF₆=59%/35%/5%/1%. This mixture with a large fraction of CO₂ is suitable for thicker (2mm) gas gap. The presence of CO₂ in 1 mm gas gaps lower the amount of primary electrons thus practically limiting its fraction to no more than 30%. Thus for a safe operation a reduction of the charge per count by an order of magnitude is necessary to compensate the stronger ageing phenomena. It has to be noted that the research in this field is recent and very intensive [249,250], so relevant updates are expected in future.

35.6.7.5 A new detector: the Resistive Cylindrical Counter

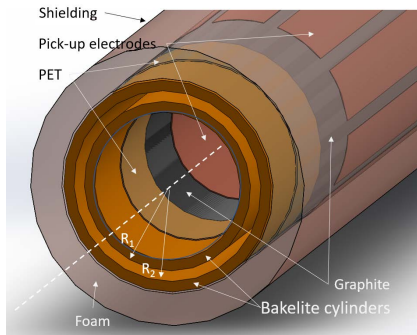


Figure 35.21: Schematic drawing of an RCC.

The RCC, illustrated in fig. 35.20, has been recently proposed as an evolution of the RPC [251] and is essentially an RPC warped to a cylindrical shape. The idea is to combine the advantages of parallel plate geometry and high pressure drift tubes in a single detector. The electric field $E(r)$, which is uniform in RPCs, here depends instead on the distance from the axis r , according to $E(r) = -\frac{V}{r \ln(R_1/R_2)}$. By choosing appropriate values for R_1 , R_2 , V and its polarization (the innermost cylinder is the cathode), it is possible to virtually segment the cylindrical gap in an innermost sensitive layer, where the field is sufficiently high to start the avalanche multiplication, and an outermost layer where the drift happens, increasing the induced signal with lower or no multiplication at all. This effect is called geometrical quenching and limits the avalanche growth without the necessity of electronegative gases. Moreover a geometrically quenched avalanche would have a much better prompt to total charge ratio, lowering the total operative current, hence increasing the rate capability. The cylindrical structure has a further major advantage with respect to the planar one, it can be easily pressurized overcoming the RPC limitation of working at atmospheric pressure only. Pressurization on one side increases the gaseous target density, thus increasing the efficiency of narrow gaps, on the other, it could largely improve RPC time resolution since the Townsend coef-

ficient $\alpha = A p \cdot \exp(-Bp/E)$ (where p is the pressure, E the electric field and A, B are constants), as we learn from the RPC precursor, the Pestov spark chamber [203]. The performance of the RCC concept in terms of time resolution and counting rates are yet to be demonstrated. On the other side, being insensitive to the environmental pressure, potentially extends its range to space and under water applications.

35.7 LAr Time Projection Chamber

Written in October 2021 by F. Pietropaolo (CERN; INFN, Padova) and S. Pordes (FNAL). Revised in August 2023 by A. Fava (FNAL) and F. Pietropaolo (CERN; INFN, Padova).

35.7.1 Introduction

Liquid argon is an attractive material for particle detection. Some properties of argon are given in table 35.8; for many more see [252]. Energy deposition in the argon produces scintillation light

Table 35.8: Some physical properties of liquid argon from [253].

Property	Unit	Value
Boiling Point (BP) at 1013 hPa	K	87.3
Density (ρ) at 1013 hPa	kg m ⁻³	1395
$d(BP)/dP$	K hPa ⁻¹	9×10^{-3}
$d\rho/dT$	kg m ⁻³ K ⁻¹	-6.2
Latent Heat of Evaporation	kJ kg ⁻¹	161
Freezing Point (1013 hPa)	K	83.8

and ionization electrons; in the presence of a moderate electric field, a significant fraction of the electrons escape recombination, making them available for detection as a charge signal. Typical values for a minimum ionizing particle are $\sim 40,000$ photons/MeV at zero field (lower at finite fields) and $\sim 30,000$ electrons/MeV at a field of 500 V/cm. That the liquid has a relative density of 1.4, that the free electrons can be drifted many meters with minimal dispersion and that it is abundant in the atmosphere and commercially available as a by-product in the distillation of air to produce nitrogen and oxygen, makes it particularly attractive for use in massive time-projection chambers (TPC) to study rare processes, as realized in [254] and [255]. Since that time, the liquid argon TPC (LAr TPC) has been developed into a detector that combines mm³ resolution with particle identification, calorimetry, and 100% live time. Detectors with masses up to 600 tons have been built and operated and detectors of 10's of kilotons are being planned.

The operation of a liquid argon time projection chamber requires

1. a cryostat and cryogenic system to maintain ultra-pure liquid argon clean and stable,
2. an electric field that permeates the liquid argon volume and allows ionization electrons to escape recombination, and drifts them to the charge sensors,
3. an array of charge sensors and associated electronics to amplify and digitize the charge signals,
4. sensors to detect the scintillation light and associated electronics,
5. a data-acquisition system to read out and record the data,
6. software to reconstruct and interpret the data.

Surveys of previous, present and proposed detectors are described in the literature [271] [272] and in detailed descriptions of detectors which have operated in experiments [273–279]. This article provides a description of the challenges in achieving items 1 to 4 with some of the solutions presently adopted. Topics 5 and 6, crucial to the successful exploitation of the LAr TPC technology and subject of intense activity, are also introduced [280–282]. References are also given for a number of ancillary devices - cameras that can operate in the liquid argon [279], monitors to provide a rapid measurement of the purity of the argon [283,284], ionization lasers to measure distortions of the drift field due to space charge

Table 35.9: Some Detector Relevant Properties of liquid argon.

Property	Unit	Value
Stopping Power (m.i.p.)	MeV g ⁻¹ cm ²	1.51
Radiation Length	g cm ⁻²	19.6
Nuclear Interaction / Collision Length	g cm ⁻²	120 / 76
W _{el} , Energy to form one electron-ion pair	eV	23.6 (±0.3) [256,257]
Ion mobility	cm ² V ⁻¹ s ⁻¹	1.6 × 10 ⁻³ [258]
Temperature dependence of drift velocity	% K ⁻¹	-1.7 [259]
Longitudinal diffusion coefficient, D _L	mm ² ms ⁻¹	0.4 (see text)
W _{ph} , Energy to produce one scint. photon	eV	25 [260,261]
Scintillation photon wavelength (vacuum)	nm	128 ± 8 (FWHM) [262]
Scintillation light inverse velocity	ns m ⁻¹	7.46 (±0.08) [263]
Rayleigh scattering length (predicted)	m	0.9 (±0.2) [263–265]
Scintillation Decay times fast/slow	ns	6 (±1)/1500 (±100) [266–268]
Dielectric strength	kV cm ⁻¹	>40 [269,270]

or electrical problems [285] - that have been developed to improve performance. A list of experiments with their masses is also given in 35.14.

35.7.2 A Mass of ultra-pure Liquid Argon

Argon is commercially available in large quantities as a by-product in the distillation of air to produce liquid nitrogen and oxygen. Critical to any LAr TPC are the cryostat and the cryogenic and purification system to maintain the argon liquid, ultra-clean and stable in temperature and pressure. Evacuatable double-walled vacuum cryostats are practical for detectors with a mass of O(100) t. Based on the demonstration that ultra-clean argon can be achieved without initial evacuation [284], current and proposed larger detectors are hosted in foam-insulated non-evacuatable cryostats based on a technology used in liquefied natural gas transport [279]. A convenient feature of these cryostats is that their components (inner walls, insulation, outer structures) are modular and of a size suited to assembly in underground environment. In addition, passive insulation is intrinsically safer than vacuum insulation because the heat input cannot rapidly increase as in the case of vacuum degradation.

The absence of electronegative contaminants, mainly environmental oxygen and water, from the liquid argon is crucial to ensure the ionization electrons drift from their point of production to the charge sensors without being captured (the drift motion of the produced negative ions is too slow to be detectable). The ‘electron lifetime’, τ , is the parameter describing the purity level of argon. To set a scale, the electron capture time in liquid argon with a concentration of oxygen of 0.1 ppb (part per billion by volume - all concentrations here are by volume) is ~ 3 ms [286,287], largely independent of electric field in our range of interest. For detectors with electron drift times in the milliseconds, the oxygen level must be well below 0.1 ppb to avoid losing most of the signal. In order to achieve this goal, first the air is removed from the cryostat volume mostly by controlled purging with argon [288], allowing to reach ppm purity levels; a purification system is then required during filling, to purify the commercial argon delivered from its typical ppm oxygen and water levels. Molecular sieve and activated copper on alumina [289] are commonly used to remove water and oxygen, respectively. This purification is performed in the liquid phase and the discovery that purification with standard materials is effective at cryogenic temperatures [290] allowed for an enormous gain in throughput compared to purification in the gas phase. The purification system delivers essentially pure argon - which then mixes with contaminants from outgassing or residual leaks. To avoid the build-up of contaminants, both the boil-off gas and the liquid are continuously recirculated through the purification system. Schematics of experiment cryogenics systems are shown in [274, 276, 279]. While reconstructed tracks eventually determine the argon quality, so-called ‘purity monitors’, double-gridded ionization chambers, are often installed to give rapid feedback on the purity of the liquid [279].

Another potential contaminant is environmental nitrogen. This does not affect the free electron lifetime at levels up to many ppm but it does affect light production [267] and transmission [291] at

the few ppm level.

35.7.3 Charge and Light Signals

Figure 35.22 (left) shows how the electron and scintillation yields for a minimum ionizing particle (m.i.p.) change with electric field. The free electron yield from the passage of a charged particle can be calculated from ‘W_{el}’ = 23.6 eV [256], the energy deposit that generates one ion-electron pair, the dE/dx of the particle, and ‘R’ the (unfortunately labeled) fraction of electrons that escape recombination - see figure 35.22 (left). Measurements of electron yield have been made at various electric fields and at different ionization densities [292–296] and show good consistency. Of the models proposed to predict recombination [297,298], none is fully successful; the so-called ‘box model’ [299] which considers the situation of mobile electrons and stationary ions makes more realistic assumptions than other models and it is commonly used [300]. The data from [295] which are some of the most comprehensive are described by the form $R = \frac{0.8}{(1+0.049(dE/dx)/\mathcal{E})}$ where dE/dx is in MeV/cm and \mathcal{E} in kV/cm. At a drift field of 500 V/cm, The recombination factor R for a minimum ionizing particle is 70%. A comprehensive summary and analysis of charge yield is given in [301].

The movement of the free electron charge towards the charge sensors is characterized by the drift velocity, the charge loss due to impurities, and the diffusion. The drift velocity depends on the strength of the electric field and slightly on the argon temperature (see table 35.9); a measurement of drift velocity vs electric field from [302] with a fit from [259] is shown in 35.22 (right). At an electric field of 500 V/cm, the drift velocity is 1.55 m/ms at 89 K. The charge loss depends on the purity of the liquid. For a drift of duration, t , the fraction of charge that survives to the sense electrodes is $e^{-t/\tau}$ where τ is the electron lifetime. Values of τ exceeding tens of ms have been achieved [303–305]. Diffusion broadens the charge distribution as it travels to the sensor. The diffusion coefficient, D, defines the contribution to the spatial distribution of the charge at the sensor from diffusion after a drift of time, t , via $\sigma_D^2 = 2Dt$. Several measurements of the longitudinal diffusion component, D_L , have been made with a typical value around 0.4 mm²/ms [294,306–308]. For a 3 ms drift, this gives a contribution of $(0.4 \cdot 6)^{1/2}$ mm, ~ 1.5 mm, to the spread of the charge.

The scintillation light comes from the decay of excited argon dimers, Ar₂^{*}, (excimers) produced through direct excitation and through recombination of ionized argon ions and electrons [309]. The contribution of the latter process is reduced in the presence of an electric field as shown in figure 35.22, (left). The excimer is produced either in a singlet (‘allowed’ decay) or in a triplet spin state (‘forbidden’ (spin-flip) decay), with lifetimes of 6 ns and 1.5 μ s respectively. The states are almost degenerate and photons are emitted, somewhat inconveniently [310], in the VUV with a spectrum peaked at 128 nm with a ± 8 nm (FWHM) spread [262]. The relative populations of the two states depends on the ionization density; typically 1:3 (singlet:triplet) for minimum ionizing and 3:1 for highly ionizing nuclear fragments [266]. The long life-

time of the triplet state makes it sensitive to quenching impurities such as nitrogen or oxygen to which the excitation energy of the dimer can be transferred without the subsequent emission of a visible photon [267, 311].

The propagation of the scintillation is affected by two processes: absorption and Rayleigh scattering. While the large Stokes shift [312] makes pure LAr transparent to its own scintillation light, methane at the few ppb level [313] and nitrogen at the few ppm [291] level lead to light absorption. Rayleigh scattering increases the effective travel distance of photons between their production point and their detection and for detectors where the distance between origin and detection covers a range of many meters, the short Rayleigh scattering length for argon scintillation has a serious effect on the uniformity of detection. In this situation, the long lifetime of the triplet state can be exploited by the use of dopants to which the argon dimers can transfer their excitation energy with subsequent photon emission. Xenon, where almost complete transfer of the long-lived state energy is achieved at a concentration of 10's of ppm (mass), is a leading candidate. [314, 315].

35.7.4 LAr TPC topologies

Currently operating LAr-TPC detectors come in a range of sizes but the basic form of a cathode and field cage generating a field which drives the ionization electrons to planes of charge sensors at ground potential is universal. A standard criterion is to make the TPC drift as long as considered possible to maximize the detector mass for a given channel count; this can result in a single drift volume; two drift volumes with a common cathode, or multiple drift volumes with multiple common cathodes. An exception is the DUNE near detector TPC; it is segmented into many small TPCs to help resolve the large interaction rate [316].

The drift field is produced by a planar cathode at -HV, a graded field-cage surrounding the active volume, and the sensing electrodes at a potential near ground which form the anode. The field cage is designed to produce a uniform electric field throughout the drift region although for detectors at surface, the slow-moving positive ions generated by the flux of cosmic rays distort the field, particularly for TPCs with long drift [301, 305, 317–319]. Particular challenges in the drift field system are the feed-through [274, 320] that brings the voltage from the HV supply outside the cryostat to the cathode (the cathode can sit at negative voltages up to 300 kV), avoiding damage to the electronics from a potential cathode discharge [279], and ensuring the integrity of the field-cage resistor chain [321]. Avoiding discharge and current draw in a medium chosen because it allows electron flow is possibly the hardest challenge in the technology.

The schematics in figure 35.23 shows the sensor arrangement using vertical planes of wires as sense electrodes and a horizontal electric field.

The sense planes are perpendicular to the drift direction and can be arranged in a stack with the wires in each plane oriented at a different angle. While the schematic shows three planes, in principle only two are needed; however three views are useful in the 3D reconstruction procedures to remove ambiguities in the hit associations and in case of dead or noisy channels. The wire-pitch, p , is a few mm and the plane spacing is similar. As indicated in figure 35.23, the planes are biased such that all field lines from the drift region pass through the intermediate planes and terminate on the final plane as shown in 35.23. (The condition for transparency across one plane is derived in [322].) The drift electrons follow the field lines, inducing bi-polar current pulses on the first two planes, and terminate on the last one, the collection plane, producing a unipolar signal [323].

The raw signal rise and fall times are a few μs as determined by the electron drift velocity and the plane spacing, and any geometric effects from the track angles. The signals from each wire are recorded as wave-forms spanning the maximum drift time at typically 2 or 2.5 MHz sampling rate. The intersection of wires on different planes which record signals at the same time, and the drift time converted to a distance knowing the drift velocity give the position of the charge source.

The design of large (> kiloton) detectors faces an intrinsic electrical challenge in that long (> few m) cables from the sense elec-

trodes to the first-stage amplifier will introduce an unacceptable amount of noise through their capacitance, and attempts to avoid such cables leads to impractical constraints on the charge sensor geometry; both of these are emphasized in [323]. To address this problem, CMOS based ASIC amplifiers that operate in the cold and can be placed next to the charge sensor (wire or strip or pixel) have been developed, their design rules and robustness validated, and successfully deployed [324, 325]. The subsequent problem that individual feed-throughs for each signal in a detector with hundreds of thousands of channels complicate the cryostat structure and raise the specter of leaks has been resolved by the development of flash-ADC and signal multiplexers [326] that also operate in the liquid. These implementations have resulted in equivalent noise charge levels of a few hundred electrons [305, 327] to be compared with a charge yield for a m.i.p of 30000 e/MeV or, equivalently, 60000 e/cm. With such low noise, energy depositions well below 1 MeV on wires/pixels with 0.5 cm pitch or less are quite accessible.

Large LAr detectors usually contain a system to detect the primary scintillation light. These provide an event time for drift time measurement [328], a trigger [329, 330], calorimetry that can be independent of and complementary to the charge [305], and event position information [280]. Given the VUV nature of the scintillation, a wavelength shifter is typically used to move the light into the visible [310]. Photo-multiplier tubes that operate in liquid argon were developed under the ICARUS program [331], while some recent systems are based on Silicon Photo-Multipliers. This latter approach separates the light collection from the light-to-electrical signal transducer, and many designs for the first task are being pursued [279, 332, 333].

35.7.5 Data Acquisition and event reconstruction

For the operation of large mass LAr-TPCs, the recording and storage of large volumes of data from the digitised charge waveforms and scintillation light channels is a critical issue. For instance, in the DUNE experiment, the throughput will amount to 1.5 TB/s per detector module (10 kt fiducial mass). To cope with, data reduction strategies are typically applied [334], [335]: (1) channel by channel zero suppression applied to the digitised wave forms, (2) fast signals from photon detectors or from external sources (for instance a neutrino beam), to trigger the readout of the TPC over a limited, predefined time window. The trigger rate is tuned to match the throughput capabilities of the Data Acquisition (DAQ). Recent advances in communication and computing technologies have reshaped the approach to DAQ for LAr-TPCs. It is now possible to readout the complete digitised data and process them online [336], [337], allowing to identify space-time Regions of Interest (RoI) where charge or light activity is detected. For the DUNE experiment, the data reduction could be in the order of 10^5 . With this architecture, charge and photon detectors become truly complementary and their information can be combined online for high efficiency data filtering even for energy depositions at a few MeV scale.

The goals of LArTPC event reconstruction are to provide the building blocks necessary to perform physics analyses: reconstruct the event topology, particle identification and calorimetry. Generally, this proceeds in subsequent stages. (1) Signal Processing: the waveforms providing a measure of the charge deposited in the TPC as a function of time are conditioned to mitigate detector issues, suppress noise, deconvolve the detector/electronic response; this allows to produce hit objects - measurements of the drift time and charge deposited by tracks in the LAr active volume on any readout channel [338] [339] [340]. (2) Wire readout LArTPCs produce 2D images in drift time and coordinate transverse to the wire direction with, generally, 3 planes allowing for stereo imaging for 3D reconstruction. Pattern Recognition (PR) approaches are distinguished between those acting of the 2D images with matching of objects to build the 3D picture and those working in the 3D space directly. The common goal is to find and reconstruct tracks and showers, their common vertices and identify the event topology. An example of 2D to 3D PR is the Pandora package [341]. An example of a pure 3D approach is the WireCell package [342]. Recent efforts in PR aim at employing sophisticated machine learning (ML) techniques. In

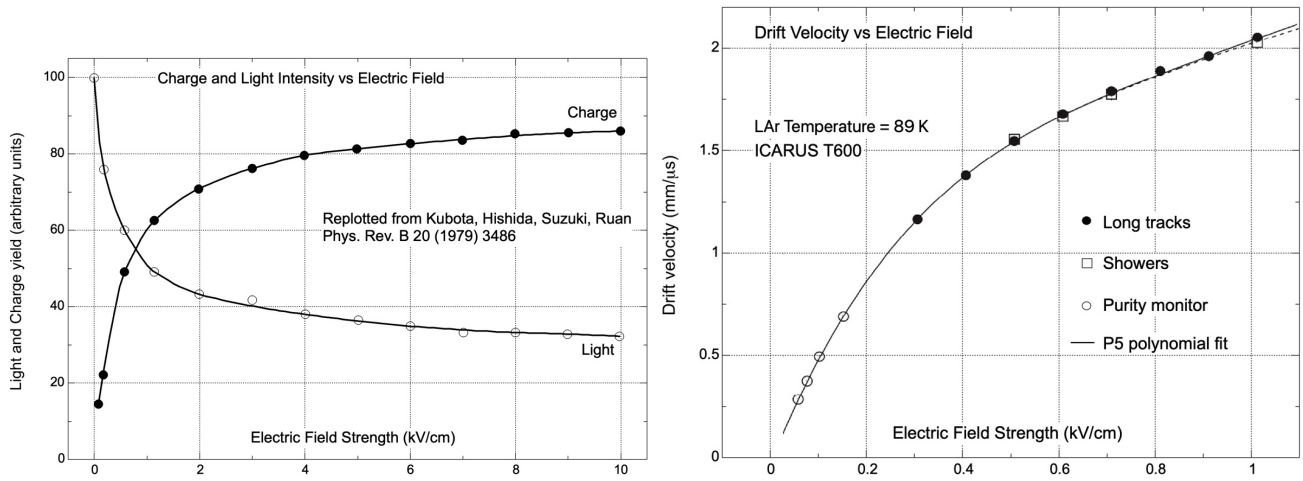


Figure 35.22: (left) the form of the light yield and the charge yield vs electric field redrawn from [309]; (right) electron drift velocity vs electric field redrawn from [302].

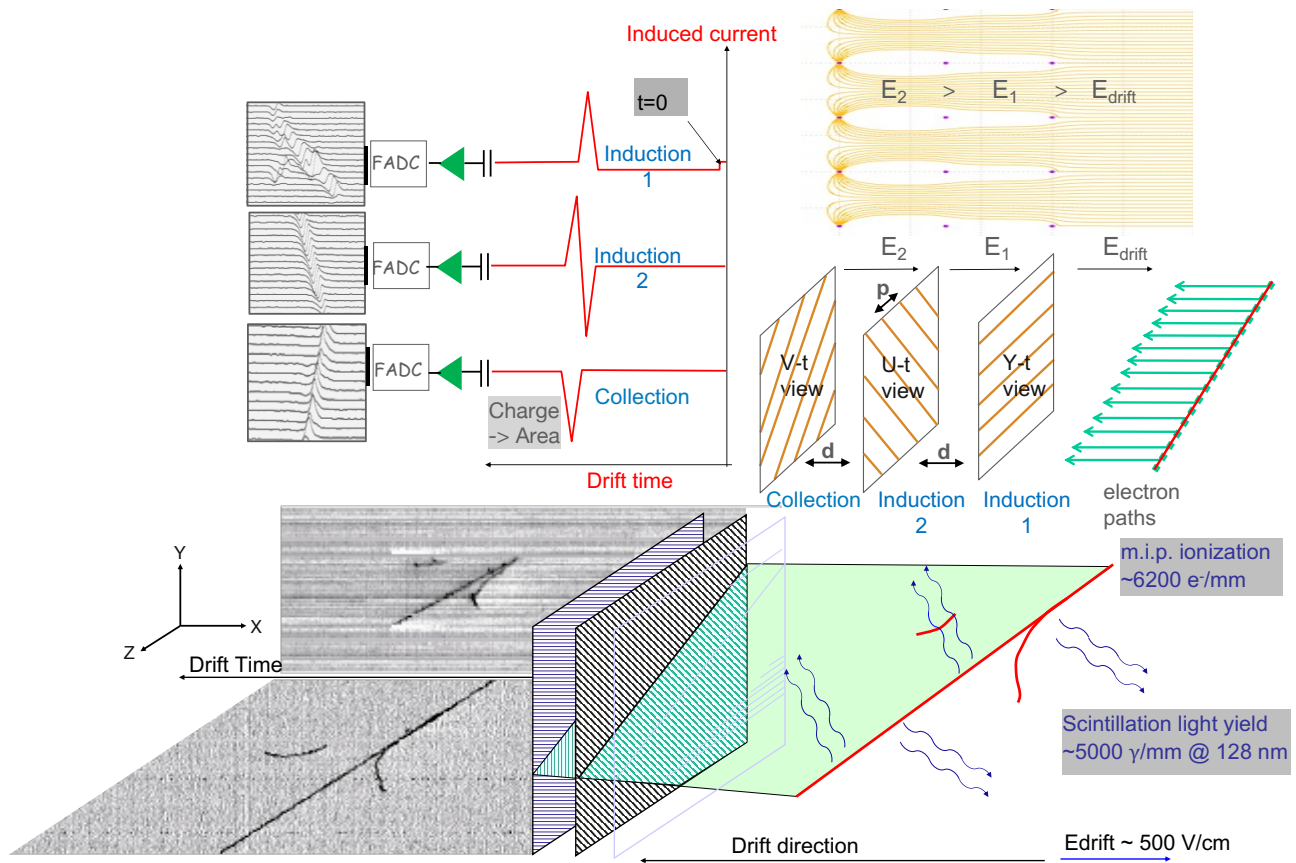


Figure 35.23: Schematic of an event in the ICARUS 3 t LAr TPC; *Top* (from right to left): field lines from drift region to collection wires, electron flow & arrangement of wire-planes, signal shapes on the wires, and wave-forms from the continuous readout and digitization; *Bottom*: the passage of a muon. The gray scale on the track indicates the ionization density.

the 2D-to-3D approach convolution neural networks (CNNs) are applied on 2D images to identify objects which can be matched across planes [343] [344]. In the 3D approach CNNs, graph neural networks (GNNs), etc., are used in several steps to de-ghost the original 3D image and perform full event reconstruction including calorimetry, particle ID, etc. [345]. (3) The reconstructed tracks and showers are then passed to the calorimetry and particle ID modules. These modules utilize the charge deposition per unit length, after calibrations, to compute track and/or shower energy and particle identification [346].

35.7.6 Developments

The successful operation [347] of the ICARUS T600 TPC served as clear demonstration of the feasibility of the liquid argon TPC technology on a massive scale. Since this milestone, the liquid argon TPC community has expanded and the technology has continued to evolve. Notable developments include in-liquid electronics, the adoption of Silicon Photo-Multipliers and new light collection technologies, the use of dopants in the argon to improve the light performance, improved techniques for wavelength shifting, the adoption of a cryostat technology which permits detector masses of tens of kilotons and, in a major change to the standard single-phase topology, the implementation of pixelated readout to replace projective geometry in busy environments [348]. Technical R&D is continuing; as examples, the vertical-drift single-phase design for the second DUNE far-detector that uses strips on perforated printed circuit boards as charge sensors [349], a dual-phase TPC readout [350] using fast cameras to read out the scintillation light produced in the gas region in place of a charge readout; a light detection system powered and readout using optical fiber allowing the readout to operate at any potential and therefore anywhere in the TPC, and efforts to build up the HV directly in the liquid argon with a voltage multiplier (Greiner design) [351].

An abundance of data from recent experiments is encouraging insights into the liquid argon medium as in [301,352] and revealing new phenomena. For a taste, see [353]. The ground is fertile, busy, and full of opportunity.

35.8 Semiconductor detectors

Revised August 2023 by N. Wermes (Bonn U.).

Semiconductor detectors provide outstanding detection opportunities in terms of position, energy and also time resolution, often in combination. In accelerator experiments, they are most widely used as position-sensing devices, *e.g.* in tracking detectors, or as photodetectors (Sec. 35.2), for example in calorimeters (Sec. 35.10) or in imaging Cherenkov detectors (Sec. 35.5). In recent years also precise time measurement ($\mathcal{O}(10\text{--}30\text{ ps})$) with silicon detectors has come into the focus of development. When comparing semiconductor detectors particularly with gaseous detectors, the main features are high density and low ionisation threshold, providing in high resistivity substrates comparatively large signals even without intrinsic amplification. Silicon detectors with active layers only 100–300 μm thick provide adequately large and fast signals on a typical time scale⁴ of 10–50 ns. Challenges are the purity of the semiconductor material, characterised by its mobility-lifetime ($\mu\tau$) product, and its radiation resistance. The development of modern semiconductor detectors is strongly interconnected with integrated circuit technology. Micro-processing and micro-electronics technologies enable fabrication of high-density micron-scale electrodes on large wafers (6–8 in \approx 15–20 cm diameter for sensor wafers) and allow for high-density amplification and readout circuits connected to them (chip wafer sizes are up to 12 in \approx 30 cm with typical reticles of $26\times 33\text{ mm}^2$).

Some important material properties of common semiconductors used as detectors are summarised in Tab. 35.10. While for particle tracking the excellent position resolution is the main (but not the only) interest, high stopping power and high energy resolution are key parameters in X-ray, gamma-ray, and β spectroscopy, for example in neutrinoless double-beta decay searches. Due to its small

bandgap, germanium excels in energy resolution but needs to be operated at very low temperatures (liq. N₂) to reduce thermally generated reverse bias current. Besides Ge, also GaAs, CdTe and CdZnTe (CZT) feature high atomic numbers and hence much higher stopping power and shorter absorption length which is important, especially for X-ray detection. Diamond, fabricated by chemical vapour deposition (CVD) and strictly speaking classified as an insulator with a large bandgap (Tab. 35.10), features low Z and large radiation length X_0 . Thanks to its radiation hardness (Sec. 35.8.5) it is used for particle detection in dedicated applications, especially in zones with high particle flux (see *e.g.* [354] and references therein).

Materials R&D for radiation sensors extends to other bulk semiconductors as well, for example, ZnS, SiC, GaN or InP, and also to new material structures and metamaterials. Examples are semiconductor Quantum Dots, realised by nanometer-sized semiconductor “particles” embedded in a semiconductor bulk, or graphene, which – as a zero bandgap 2D material – features extraordinarily high conductivity (electrical and thermal) as well as outstanding photonic properties. A bandgap can be introduced by employing doped bi- or multi-layer graphene structures, thus rendering transistor and sensor realisations possible. The interested reader is referred to references [355] or [356], for example.

Operating usually without intrinsic amplification, semiconductor detectors crucially depend on low-noise electronics (see Sec. 35.9), so the detection sensitivity is determined largely by signal charge and input capacitance. Reviews of semiconductor detectors and electronics can be found for example in Refs. [1, 8, 357–359]

35.8.1 Signal generation in semiconductors

35.8.1.1 Creation of charges

Semiconductor detectors are solid-state ionisation chambers. Absorbed energy forms electron-hole ($e-h$) pairs, *i.e.* negative and positive charge carriers which—when moving in an applied electric field—generate a signal current on the electrodes by electrostatic induction (see Sec. 35.8.1.2). For the signal charge carriers to (freely) drift in the electric field and to become detectable, semiconductors must feature small intrinsic charge-carrier densities (as existing for example in diamond and to some extent also in GaAs and CZT) or they must be depleted by reverse-bias junction configurations (as for Si, Ge or CdTe). In addition, they should feature low intrinsic density of defects which can act as trapping or generation/recombination centers (see Sec. 35.8.5).

The minimum energy required to form an $e-h$ pair is the bandgap energy (1.12 eV in Si, 0.66 eV in Ge, 5.5 eV in diamond). However, impinging radiation or particles also release energy to lattice vibrations (phonons) such that the average energy for $e-h$ pair creation is higher. In an “indirect” semiconductor like Si, the valence-band maximum is not at the same position in k -space (crystal-momentum space) as the conduction-band minimum and additional momentum transfer is required for a band transition to occur. Since the “direct” bandgap energy without k -transfer in Si is 3.4 eV, fewer-eV photons must receive momentum from lattice phonons. Because phonons are Bose-Einstein distributed the needed momentum kick causes a steep rise in photon absorption probability between 1.12 eV and about 3.4 eV. For larger energy deposits the average energy w_i needed to produce an $e-h$ pair assumes a constant value of 3.65 eV at room temperature. For other semiconductors consult Tab. 35.10.

For minimum-ionising particles, the most probable charge deposition in a 300 μm thick silicon detector is about 3.7 fC (\sim 23 000 electrons). In tracking detectors, a particle’s energy loss and scattering in the detector material should be minimal (large X_0), whereas, for energy spectroscopy, *e.g.* of X-ray photons, the stopping power should be maximised by choosing high- Z semiconductors⁵. A smaller bandgap (in fact a smaller w_i) leads to a larger signal per deposited energy and improves the energy resolution, but also (exponentially) increases thermally excited carrier generation. To cope with excessive leakage currents at room temperature, Ge diodes are typically operated at liquid nitrogen temperature (77 K). In pure Si at 300 K, the intrinsic carrier concentration

⁴Characterised here by the peaking time of the signal pulse.

⁵The cross section for photo effect scales as Z^5 .

Table 35.10: Properties of some detector-relevant semiconductors; temperature- μ -dependent quantities given at 300 K (from [1] and references therein).

Property	Si	Ge	GaAs	CdTe (CZT*)	Diamond
atomic number (Z)	14	32	31/33	48/(30)/52	6
density ρ (g/cm ³)	2.328	5.327	5.32	5.85	3.51
dielectric constant ϵ	11.9	16.0	13.1	10.2	5.7
semiconductor type	indirect	indirect	direct	direct	indirect
bandgap E_G (eV)	1.12	0.66	1.424	1.44(1.44–2.2)	5.5
intr. carrier density (cm ⁻³)	1.09×10^{10}	2.4×10^{13}	2.1×10^6	10^7	≈ 0
radiation length X_0 (cm)	9.36	2.30	2.29	1.52	12.15
average energy w_i for (e/h) creation (eV)	3.65	2.96	4.35	4.43	13.1
mobility (cm ² /Vs)					
electrons μ_n	1450	3900	8500	1050	$\approx 1800^\dagger$
holes μ_h	500	1800	400	90	$\approx 2300^\dagger$
lifetime					
electrons τ_e	$>100 \mu\text{s}$	$\sim\text{ms}$	1–10 ns	0.1–2 μs	$\approx 100 \text{ ns}$
holes τ_h	$>100 \mu\text{s}$	$\sim\text{ms}$	20 ns	0.1–1 μs	$\approx 50 \text{ ns}$

* CZT = CdZnTe with the bandgap depending on the Cd to Zn ratio.

[†] Approximate averages. Values quoted in the literature for the mobility in diamond vary strongly.

is $n_i \simeq 10^{10} \text{ cm}^{-3}$ (Tab. 35.10), corresponding to a resistivity in the order of $\rho \simeq (e\mu n)^{-1} \approx 400 \text{ k}\Omega \text{ cm}$. In reality, crystal imperfections and minute impurity concentrations limit Si carrier concentrations to about 10^{11} cm^{-3} at 300 K ($\rho \approx 40 \text{ k}\Omega \text{ cm}$). In practice, wafer resistivities up to $20 \text{ k}\Omega \text{ cm}$ are available, with mass production ranging from 1 to $10 \text{ k}\Omega \text{ cm}$.

The energy released in a semiconductor is absorbed by electronic excitations (e/h) and lattice excitations (phonons) in an anti-correlated way. Therefore, for a fixed released energy E (for example of an X-ray photon), the variance in the number of charge carriers $N = E/w_i$ follows binomial statistics. Due to the energy constraint, this variance is reduced by the Fano factor F relative to Poisson statistics ($F \approx 0.1$ in Si and Ge). Thus, $\sigma_N = \sqrt{FN}$ and the energy resolution is $\sigma_E/E = \sqrt{Fw_i/E}$. However, for semiconductors the measured fluctuations of a detected energy signal are usually dominated by electronic noise rather than by signal fluctuations. The electronic noise contribution depends much on the detector leakage current and the electrode capacitance as well as on pulse shaping (*i.e.* the shaping time) in the signal processing electronics (see Sec. 35.9).

For X-ray detection, a major effort is made to find high- Z materials with a bandgap that is sufficiently large to allow for room-temperature operation while still providing good energy resolution. Compound semiconductors, *e.g.* CZT, can allow this but typically suffer from charge collection problems, which are characterised by the product $\mu\tau$ of mobility and carrier lifetime; this is the depth per field strength that generated carriers can drift before being trapped, *i.e.* in this context the distance over which photon absorption can still be detected.

In Si and Ge $\mu\tau$ is orders of magnitude larger than in compound semiconductors for both electrons and holes (see Tab. 35.10). Since for holes $\mu\tau$ is typically much smaller than for electrons, detector configurations where the electron contribution to the charge signal near the readout electrode dominates—*e.g.* strip or pixel structures with electron collection—usually provide better performance (see also next section).

35.8.1.2 Signal formation

The signal and its pulse shape depend on the instantaneous carrier velocity $\vec{v}(\vec{x}) = \mu\vec{E}(\vec{x})$, μ = mobility, and the electrode configuration and its geometry which determine the distribution of induced current according to the Shockley-Ramo theorem

$$i_S(t) = Ne\vec{E}_w(\vec{x})\vec{v}(\vec{x}(t)), \quad (35.20)$$

where Ne represents a drifting charge cloud of N elementary charges, $\vec{E}_w(\vec{x})$ is the “weighting field”, which accounts for the

coupling of the charge to a specific electrode and depends on the electrode configuration; \vec{v} is the drift velocity. Note the difference between the electric field \vec{E} and the weighting field \vec{E}_w and take account of the fact that the mobility is, in general, field-dependent, $\mu = \mu(E)$, with $v \approx \text{const}$ at high fields (velocity saturation, for electrons in Si approaching 10^7 cm/s at $E > 10^4 \text{ V/cm}$). Both, electron and hole movements contribute to an electrode’s signal. Hence, if the carrier mobility is very different for electrons and holes, like *e.g.* in CdTe where $\mu_h \ll \mu_e$ (Tab. 35.10), a photon signal, for example, becomes absorption-point dependent.

Integration of the induced current signal on an electrode yields the “collected charge”. The average time to collect the created charge decreases with increasing bias voltage (*i.e.* field strength) until velocity saturation occurs at field strengths of about 10^4 V/cm in Si.

For a simple parallel-plate geometry with two electrodes the weighting field is constant, whereas for structured electrode geometries, like for example strips or pixels, E_w is position dependent which for small electrodes (compared to the sensor dimensions) strongly enhances the contribution of the movement close to the electrode (“small-pixel effect”). More details and practical accounts of the Shockley-Ramo theorem and its usage can be found in [1, 8] and references therein.

Position resolution is ultimately limited by transverse diffusion of the moving charge cloud (typically 3–5 μm for 200–300 μm thickness) and by the emission of δ electrons. The performance then depends on optimal usage of charge sharing between neighbouring electrodes and on noise. In magnetic fields, Lorentz drift deflects the electron and hole trajectories thus increasing the spatial spreading. The total spreading and hence charge sharing between electrodes can be tuned (increased or decreased) by tilting the detector relative to the incoming (average) particle direction. Overall spatial resolutions of 2–4 μm (rms) have been obtained.

35.8.2 Junction detectors

Si and Ge detector substrates must be—others like CdTe, GaAs should be and CZT can be—depleted from free charge carriers by operating them as reverse-bias junctions (p - n or Schottky) to be sensitive to the charge created by impinging particles. A typical cross-section of a junction detector is shown in Fig. 35.24, here with structured electrodes at the top. A p - n junction—even without external voltage—forms a sensitive space-charge region across itself depleted of mobile charges, hence also called “depletion region”. The space charge establishes an electric field corresponding to a “built-in” voltage V_{bi} . Additional reverse-bias voltage V applied externally increases the space-charge region such that in-

jected charge liberated by radiation is swept to the electrodes by the existing field. Detectors typically use an asymmetric structure, for example, a thin and highly doped p^+ electrode⁶ region and a lightly doped n^- substrate region – or vice versa, so that the depletion region extends predominantly into the more lightly doped bulk volume.

In such planar Si (or Ge) devices, the thickness of the depleted region is

$$\begin{aligned} d &= \sqrt{2\epsilon(V + V_{bi})/Ne} = \sqrt{2\rho\mu\epsilon(V + V_{bi})} & (35.21) \\ &\approx \frac{0.5}{\mu\text{m}} \times \sqrt{\frac{\rho V}{\Omega\text{cm} \cdot V}} & \text{for } n\text{-type Si bulk} \\ &\approx \frac{0.3}{\mu\text{m}} \times \sqrt{\frac{\rho V}{\Omega\text{cm} \cdot V}} & \text{for } p\text{-type Si bulk} \end{aligned}$$

with (values for Si)

$$\begin{aligned} V &= \text{external bias voltage} \\ V_{bi} &= \text{“built-in” voltage } (\approx 0.5\text{ V for typ. used resistivities}) \\ N &= \text{doping concentration} \\ e &= \text{elementary charge} \\ \epsilon &= \text{dielectric constant} = 11.9\epsilon_0 \approx 1\text{ pF/cm} \\ \rho &= \text{resistivity (typically } 1\text{--}10\text{ k}\Omega\text{ cm)} \\ \mu &= \text{charge carrier mobility} \\ &\quad (\sim 1450\text{ cm}^2/\text{Vs (electrons)}, \sim 500\text{ cm}^2/\text{Vs (holes)}) [360] \end{aligned}$$

The conductive p and n regions together with the depleted volume form a capacitor with capacitance per unit area

$$C' = \frac{\epsilon}{d} \approx \frac{1\text{ pF/cm}}{d} \quad \text{in Si.} \quad (35.22)$$

The depletion depth d becomes as large as the sensor’s thickness at the “full depletion voltage” $V = V_{fd}$ for which the sensor capacitance reaches a minimum (about 35 pF/cm² for $d = 300\ \mu\text{m}$). In strip and pixel detectors (see next section) the capacitance is dominated by the fringing capacitance to neighbouring electrodes as the electrode pitch is typically much smaller than the sensor thickness. For example, the strip-to-strip Si fringing capacitance is about 1–1.5 pF per cm of strip length at a strip pitch of 25–50 μm .

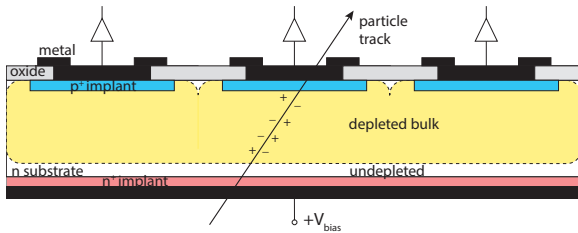


Figure 35.24: Reverse-biased junction detector with planar readout electrodes at the top in a standard sensor configuration (p^+ -in- n): lightly doped n -type substrate with p^+ implants forming the diode junction at the top side. Electrons move to the bottom electrode and holes to the top. Both movements contribute to the (induced) signal at the top electrodes with amounts as specified by the weighting field (see Sec. 35.8.1.2). The n^+ implant at the bottom side forms an ohmic contact between bulk and metal.

The electric field strength and shape inside the semiconductor bulk are important for efficient signal charge collection. Governed not only by the applied external voltage but also by the space charge inside the semiconductor bulk, leads (for constant space charge) to a linear field-strength decrease from its maximum at the junction’s boundary into the depleted semiconductor bulk. Space charge can also occur from ionised lattice defects

⁶ $n^{+/++}$, $p^{+/++}$ as well as n^- , p^- qualitatively denote relative doping-concentration levels.

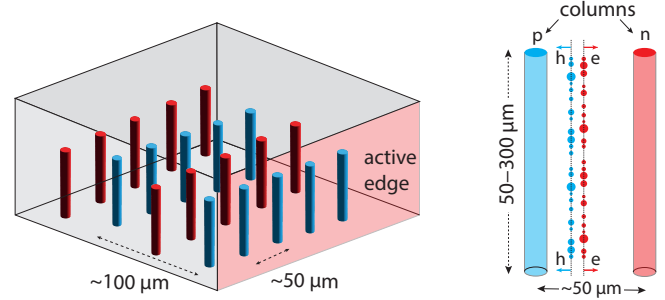


Figure 35.25: Junction detector with vertical electrodes, n (red) and p (blue), and “active” edges called 3D-Si. Dimensions given are typical. This electrode configuration provides short drift paths for moving charges while keeping a large sensing thickness. An active edge minimises dead areas at the sensor boundaries. This geometry has also been employed in CVD diamond substrates.

which either naturally exist for example in GaAs or can be created by irradiation in any semiconductor material. This can lead to low-field regions as well as to changes in the field’s shape (deviating from linear), both of which usually deteriorate the charge collection properties of a detector.

In partial depletion (*i.e.* $V < V_{fd}$) the field decreases to zero at the end of the depletion zone. Overbias ($V > V_{fd}$) adds a constant electric field component which avoids a vanishing field region and also provides faster charge collection as long as the carrier drift velocity has not yet saturated. At an average field of $E = 10^4\text{ V/cm}$, the onset of velocity saturation, where $\mu_e \approx 7 \times 10^3\text{ cm}^2/\text{Vs}$, $\mu_h \approx 3.5 \times 10^3\text{ cm}^2/\text{Vs}$, the collection times for Si are about 15 ps/ μm for electrons and 30 ps/ μm for holes. In typical fully-depleted detectors, 100–300 μm thick, electrons are collected within less than about 5 ns, and holes within less than about 10 ns.

Large volume ($\sim 10^2 - 10^3\text{ cm}^3$) germanium detectors, especially for γ -ray detection, are commonly configured in cylindrical or hexagonal rod shapes, for example, a 10 cm long cylindrical n -type crystal with 5–10 cm diameter with an inner 5–10 mm diameter n^+ electrode and an outer p^+ layer forming the diode junction. Germanium can be grown with fairly low impurity levels, $10^9\text{--}10^{10}\text{ cm}^{-3}$ (HPGe, high-purity germanium), so these large volumes can be depleted with several kilovolts.

Diamond, featuring free charge carrier densities close to zero, needs no further depletion and is operated as a parallel plate capacitor with an insulator dielectric inside. Still, a substantial bias voltage is required to overcome charge trapping.

35.8.3 Detectors with structured electrodes

35.8.3.1 Microstrip-, Si-drift- and hybrid-pixel detectors

In HEP experiments semiconductor detectors usually aim at good position resolution achieved with electrodes patterned in “strips” or “pixels” with typical dimension scales (electrode pitch) of 50–100 μm , or in “pads” ($\text{mm}^2\text{--cm}^2$) if coarser granularity is affordable for the benefit of fewer channels.

Electrodes are usually placed “planar”, *i.e.*, at the surface of the sensing Si bulk (Fig. 35.24). In an alternative, but more elaborate way, electrodes can be shaped as columns or trenches running orthogonally to the surface and hence parallel to the average direction of impinging particles (Fig. 35.25) [361]. This geometry (termed “3D-Si”, but is also exercised with diamond) enhances the radiation tolerance due to shorter drift distances of charges at the same thickness (see also Sec. 35.8.5).

In strip detectors, the strip ends are connected to dedicated readout ICs where the signals are amplified and processed. Two-dimensional readout is realised either by angled double-layers of strip detectors or by “double-sided” strip sensors structured by readout strips on either side (see *e.g.* [1, 358] and references therein). For the latter, one electrode surface features n^+n or p^+p strip junctions (rather than pn), respectively, which require dedicated measures, *e.g.* intermediate strips or special doping profiles to break the electron accumulation layer that occurs at an

n^+n interface. For p^+p , intermediate n strips or similar are not necessary, thanks to positive oxide charges residing at the Si/SiO₂ interface.

As for gaseous driftchambers, silicon driftchambers provide the position of a hit orthogonal to a strip's coordinate from a measurement of the charge cloud's drift time, drifting over centimeter-long paths inside the silicon bulk. For this to work the bulk is "sideways depleted" by using junction strip implants of the same polarity on both sides of the sensor (p in n or n in p , respectively), different to standard double-sided strip detectors (see *e.g.* [1]). This way a quadratic potential minimum for electrons is created, confining them amid the sensor bulk, on which a linear electric potential in drift direction is superimposed; holes, instead, drift to the sides. In comparison to strip detectors, much fewer electrodes are necessary for the same active area coverage. Low rate capability is a drawback caused by the long drift path of created charges. Arranged with only one small electrode with low capacitance in the center of a cylindrical disk, so-called silicon-drift diodes (SDD) are low-noise single-channel devices with large area coverage, used for example in X-ray fluorescence analysis and electron microscopy.

Very small pixel structures for particle detection were first realised with CCDs [362]. Most current applications, particularly those for high-rate applications such as at the LHC, employ the "hybrid-pixel" concept in which both, the sensing diode structure as well as the readout IC, have equal electrode structures and patterns (pixels). The connection is made by two-dimensional arrays of solder or indium bumps that mate the two parts by employing flip-chip technology (Fig. 35.26, usually chip-to-chip or chip-to-sensor; more details *e.g.* in [358,363]). Further advancements in bonding techniques especially address chip-to-wafer or even wafer-to-wafer placements, such as SLID (Solid Liquid Interface Diffusion) employing a very thin liquid metal layer (Sn) in between metals with higher melting points (*e.g.* Cu). Also, Cu-Cu, Cu-Sn, or oxide-oxide (SiO₂) diffusion bonding without solder is feasible.

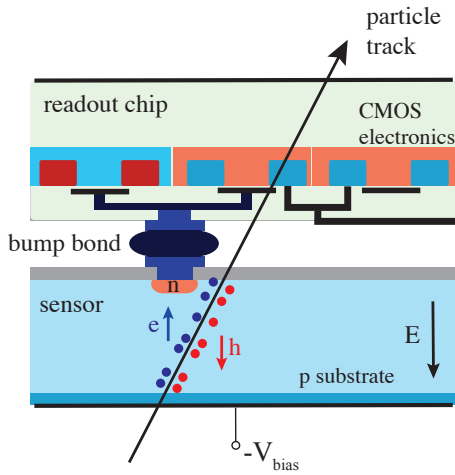


Figure 35.26: Cross-sectional view of a hybrid-pixel detector cell (one pixel) consisting of sensor (bottom) and readout chip (top) with CMOS circuitry illustrated by three transistors (red and blue implant areas plus metal lines). The sensor is a depleted diode structure (here p substrate with n electrode). Both parts are mated by a microbond (bump bond), typically solder or indium.

The hybrid approach excels in optimally utilising chip and sensor technologies for radiation hardness and rate capability (see *e.g.* [364]). It is, therefore, the technology of choice for pixel trackers in high-rate, high-radiation environments optimised for the purpose by employing very thin modules ($\mathcal{O}(300\ \mu\text{m})$ total). A disadvantage is the complex and cost-intensive module assembly.

35.8.3.2 Monolithic pixels

Partially or fully monolithic pixel detectors directly connect the generated signal charge with an embedded active electronics de-

vice (*i.e.* one or several transistors). An example of a partially monolithic device is the DEPFET (depleted p -channel FET) pixel sensor (see *e.g.* [365]), employed, for example, in the pixel tracker of the Belle-II detector. A single transistor (pMOSFET) is implemented in every pixel (Fig. 35.27(a)). The sensor substrate is "sideways depleted", as similarly done in Si driftchambers (Sec. 35.8.3.1), by means of the backside p -contact and several p regions near the transistor. Depletion is provided by the n^+ *clear* contact (see below) plus a bulk n -implant outside the matrix. In addition, the structure features a deep n -implant located a few micrometers underneath the transistor channel on floating potential. This implant becomes the most positive point of the structure, hence being an electron accumulation point, which acts as an "internal gate" of the transistor. The gate voltage changes by an amount $\alpha q_S/C$, with q_S = signal charge, gate-oxide capacitance $C = C_{ox} WL$ with $W \times L$ = gate area, and $\alpha \lesssim 1$ accounting for stray capacitance. The gate voltage changes due to an accumulated signal charge q_S and leads to a detectable change in drain current (in saturation):

$$I_D = \frac{W}{2L} \mu C_{ox} \left(V_G + \frac{\alpha q_S}{C} - V_{th} \right)^2. \quad (35.23)$$

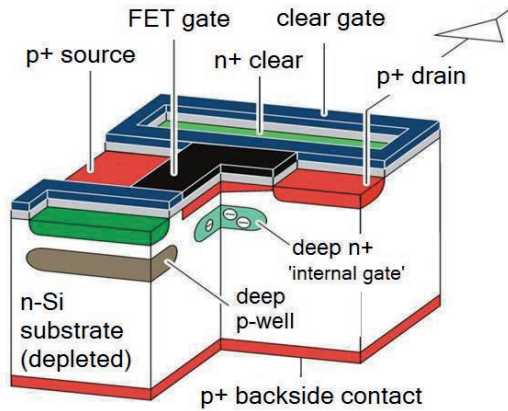
Other elements in Fig. 35.27(a) like the external FET gate and the *clear* implant provide control and reset of the structure. The device gain $g_q = dI_D/dq_S \approx \alpha g_m/C$, with transconductance $g_m = \mu C_{ox} \frac{W}{L} (V_G - V_{th})$, is of order $500\ \text{pA}/e^-$. The small capacitance of the internal gate (few fF) enables very low noise operation ($\lesssim 2e^-$) when operating with long shaping times (see Sec. 35.9).

Fully monolithic pixels combine the sensing task and the complete readout circuitry, *i.e.* the two separated parts of hybrid pixels, in one chip. Both functions must be properly shielded against each other, which is achieved by exploiting multi-well IC technology. Realised as MAPS (monolithic active pixel sensors) standard CMOS wafers can be used for pixel detector fabrication. CMOS wafers often feature a Si epitaxial layer where the transistors are implanted. It is possible to use this epi-layer as a sensitive detection volume for particle detection. However, in such detectors, only the immediate regions near the collection nodes (see Fig. 35.27(b)) are depleted. Outside these confined regions there is no or little electric field and charge collection is dominantly governed by slow and non-directional charge diffusion, a problem for high-rate applications. Depleted MAPS (DMAPS) exploit non-standard high resistivity wafers or high-ohmic epilayers, typically with resistivities $>1\ \text{k}\Omega\ \text{cm}$, as well as high bias voltage (up to $\gtrsim 300\ \text{V}$) resulting in charge collection by directed drift motion. Charge collecting electrodes are deep wells (n -wells in Fig. 35.27(b)), either formed as large (typ. $50 \times 100\ \mu\text{m}^2$) structures to fully contain the CMOS circuitry (Fig. 35.27(b), top) or as small nodes, set aside the electronics (Fig. 35.27(b), bottom), with obvious pros and cons resulting from shorter average drift distance (large electrode) versus much smaller capacitance (small electrode). The former benefits radiation tolerance, whereas the latter allows for smaller pixels and benefits from small sensor capacitance in noise and rise time. However, in both approaches radiation tolerance levels of $\gtrsim 10^{15}\ n_{\text{eq}}/\text{cm}^2$ (fluence) and $1\ \text{MGy}$ (ion. dose) have been demonstrated.

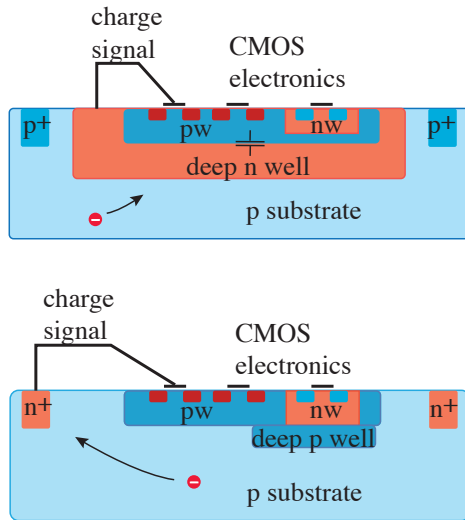
A variant of the monolithic approach are SOI (silicon on insulator) pixels providing high spatial resolution, but less radiation tolerance: A high-resistivity supporting wafer, employed for particle sensing, connects through an embedded insulator (a buried oxide layer, BOX) to the CMOS readout circuitry. The BOX separates the sensing volume from the electronics layer and provides shielding. Because the area between BOX and the transistor layer acts as a "back-gate", transistor operation can be affected requiring dedicated cures (see *e.g.* [366]).

35.8.4 Precise timing with silicon detectors

Typical time scales for silicon detector output signals are several tens of nanoseconds (*e.g.* rise times, shaping times, etc.) accompanied by a typical time mark precision in the order of nanoseconds. Essential for achieving precision timing ($< 100\ \text{ps}$) are steep signal rise and low noise according to eq. (35.38) in Sec. 35.9. This,



(a) DEPFET pixel structure.



(b) DMAPS pixel structures.

Figure 35.27: Partially (a) and fully (b) monolithic pixels: (a) DEPFET pixel structure with an embedded pMOSFET transistor; source and drain are p implants (red), gate metal (black), oxide (grey), deep- n internal gate (light green), other metal (blue), clear contact (green), and deep p -well (brown). (b) Depleted MAPS with joint sensing and electronics volumes: (top) charge collection by a *large-electrode* housing the electronics in a deep- n well; (bottom) charge collection by a *small electrode* set aside from the electronics area.

in turn, requires fast charge collection, *e.g.* in thin planar or 3D-Si detectors with high E -fields, as well as fast and strong amplification, both together yielding large slew rates (dS/dt , with S = “signal”, *e.g.* an induced current or a voltage). Important parameters that influence timing precision are the detector capacitance (including stray contributions) and the amplification gain.

Detectors that have achieved precise time measurement are so-called LGADs (low gain avalanche diodes, Fig. 35.28). They have planar electrode geometry that includes an implanted low-gain ($g = 10$ – 50) amplification structure on either the top or bottom electrode side to maximise the slew rate. Electrons created from ionising traversing particles are accelerated towards a very high field created by an amplification layer near the (here) top electrode, where impact ionisation creates a multitude of e - h pairs. They induce a very fast and large signal rise, mainly governed

by the holes’ movement away from the amplification layer. Sufficiently low amplification gain minimises excess noise contributions and avoids the creation of hole-induced avalanches moving in the opposite direction to electron avalanches.

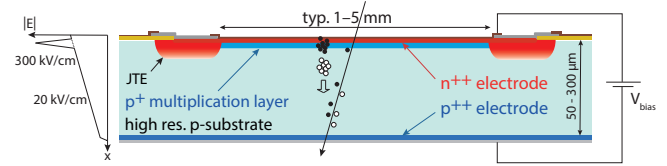


Figure 35.28: LGAD amplification structure for precision timing. Amplification (typ. $\times 20$ – 50) occurs at the structure boundary in a highly doped p - n junction near the (here: top) surface (JTE = Junction Termination Extension, deep n -well).

The achievable time resolution has several contributions:

$$\sigma_t^2 \approx \left(\frac{\sigma_S^{thr}}{dS/dt} \right)^2 + \left(\frac{\sigma_n}{dS/dt} \right)^2 + \sigma_{arrival}^2 + \sigma_{dist}^2 + \sigma_{TDC}^2. \quad (35.24)$$

The first term represents “time walk” coming from Landau fluctuations, defined as originating from number and energy-transfer fluctuations in the energy-loss process with σ_S^{thr} being the signal-height variations at discriminator threshold. This term can be kept minimal, *e.g.*, by employing constant fraction discrimination or by applying corrections using amplitude information. The second term is the contribution of noise to the time jitter, which can be approximated by $(t_r/SNR)^2$ with t_r = rise time, SNR = signal-to-noise ratio. Both first terms are kept small by large signal slew rates. An irreducible contribution comes from fluctuations in non-uniform depositions of charge along the particle path (including fluctuations in the amplification process) which causes an intrinsic jitter in the arrival time (third term)⁷. The thinner the detector the less disturbing is this effect. The fourth contribution is signal distortion due to non-uniform weighting field regions and variations in (non-saturated) drift velocities. “Junction Termination Extensions” (JTE, see Fig. 35.28) serve to lower this term. The final term denotes time fluctuations due to uncertainties in digitization, which can, however, be made negligible with GHz TDCs. Timing precision of order 30 ps has been reached. Structural and operational variants to improve charge collection and position resolution are “resistive AC-coupled LGADs”, “deep junction LGADs”, “trench-isolated LGADs” and others. More details on LGADs are given in [367] and [368].

Columnar electrode geometries such as shown in Fig. 35.25 with small diameter and small pitch are by design a very suitable choice for precision timing due to short collection paths and strong fields. Employing an optimised trench-like column shape field- and weighting-field distortions are minimised and time resolutions in the order of 10 ps have been achieved in prototypes [369].

High precision timing can also be approached by exploiting the benefits of SiGe BiCMOS technology: strain mismatch of Si-Ge alloy layers results in a smaller bandgap as well as higher mobility and hence larger transconductance. This benefits the speed in hetero-junction bipolar transistors (HBTs) which also feature less $1/f$ noise than MOS transistors. Resolutions of order 20 ps have been reached in a monolithic pixel matrix using this technology [370]. More elaborate discussions on timing in silicon detectors can be found *e.g.* in [371].

35.8.5 Radiation damage in silicon detectors

High channel density and response times in the nanosecond range render micro-patterned semiconductor detectors particularly suited for high particle rates. This is usually accompanied by high radiation causing damage of sensors and front-end electronics. We restrict ourselves here to damage in Si detectors and their electronics. Radiation damage occurs in semiconductor detectors through two basic mechanisms:

⁷In LGAD literature these fluctuations are sometimes also referred to as “Landau fluctuations”.

1. *Bulk damage* due to displacement of atoms from their lattice sites resulting in defect energy levels inside the band gap. This leads to increased leakage current, carrier trapping, and build-up of space charge that changes the required operating voltage. Displacement damage results from non-ionizing energy loss (NIEL). The energy imparted to the recoil atoms can initiate a chain of subsequent displacements including “damage clusters”. For a description, it is critical to consider both, particle type and energy. Conventionally, for silicon, the received NIEL is normalised to the damage level caused by 1 MeV neutrons and specified in units of neutron-equivalent fluence Φ_{eq} with units n_{eq}/cm^2 .
2. *Surface damage* due to charge build-up in surface layers and formation of interface traps at *e.g.* Si–SiO₂ boundaries. These influence transistor currents and thresholds or cause thin charge carrier layers at a silicon surface, leading to increased surface leakage currents in sensors or circuits and affecting electrodes’ isolation and/or transistor characteristics. The effects of charge build-up are strongly dependent on the device structure and on fabrication details. The damage is dominantly due to ionising energy loss (IEL) and hence proportional to the absorbed total ionisation dose (TID) measured in Gy (or rad), independent of the particle type.

The increase in reverse bias generation current (leakage current) due to bulk damage is $\Delta I_L = \alpha \Phi_{eq} V$, where V is the volume under an electrode and $\alpha \approx 4 \times 10^{-17}$ A/cm, a universal constant when normalised to temperature (conventionally 20°C), and measured after annealing for 80 min at 60°C. Note that for devices with intrinsic amplification, generation current is amplified accordingly. Reverse bias leakage current depends strongly on temperature

$$I_L(T) \propto T^2 \exp\left(-\frac{E_a}{2kT}\right), \quad (35.25)$$

where $E_a \approx 1.2$ eV (activation energy), so rather modest cooling can reduce the current substantially (~ 6 -fold reduction in cooling from room temperature to 0°C).

For bulk damage in silicon, the *NIEL hypothesis* is a good first-order description of the observed damage (especially regarding I_L). It states that all lattice radiation damage in silicon linearly scales with NIEL and can be traced back to the abundance of primary defects (point defects and clusters), irrespective of their initial distribution over energy and space, that is, regardless of the damage’s topology and origin. Under the NIEL hypothesis, the observed differences in damage caused by neutrons, protons, pions and electrons are hence usually scaled to each other.

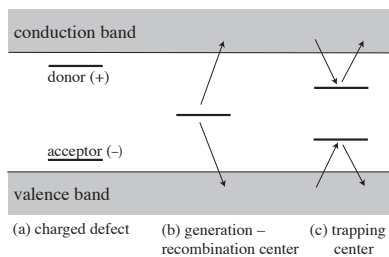


Figure 35.29: Characteristic locations of energy levels caused by bulk radiation damage and their main action effects.

Three main bulk displacement damage effects are sketched in Fig. 35.29: (a) defects acting as charged donors/acceptors, (b) deep defects (near the middle of the bandgap) causing increased leakage current, and (c) carrier trapping centers. Damage effects are not constant with time; for example in *n*-type bulk, radiation-induced negative space charge anneals at first, reaching a stable damage minimum (beneficial annealing), but later electrically active defects (negative space charge from acceptor-type damage) build up over the time scale of months (reverse annealing).

Acceptor- (usually dominant) or donor-like (deep) defect states, when ionised, build up space charge (dominantly negative), which in turn normally requires an increase in the applied voltage to

sweep signal charge through the detector thickness. For *n*-type bulk starting material, however, donor (*e.g.* phosphorous) removal by forming electrically inactive vacancy-phosphor (V-P) complexes induced by the incipient radiation, leads to a faster decrease in depletion voltage (faster than only by the compensation of donors through generated deep acceptors) until positive and negative space charges effectively balance; only little bias voltage then is required for operation (point of effective space charge inversion, also called “type inversion” (Fig. 35.30)). At larger fluences the negative space charge dominates, and the required operating voltage increases proportional to the increasing effective space charge density N_{eff} , also called effective doping concentration. Also the space-charge distribution can no longer be regarded as constant and homogeneous over the detector volume, thus destroying the linear slope of the electric field from the junction to the backside as was introduced in Sec. 35.8.2; instead “double-junction”-like field distributions typically occur.

Today, *p*-type silicon with n^+ electrode-implants is the preferred choice for sensors operating in high-radiation environments for reasons of cost-effectiveness in production as well as high radiation hardness due to fast (high mobility) electron collection in high electric- and high weighting-field regions at small segmented n^+ electrodes. Space charge inversion is usually not observed since the initial space charge is negative already (Fig. 35.30).

Removal of acceptors (*i.e.* substitution of electrically active boron at its lattice site) in *p* material is found to be dominantly caused by interstitial silicon replacing boron on its lattice position. The highly active interstitial boron then can cause the formation of other defects such as interstitial oxygen-boron complexes (B_iO_i , subscript *i* for “interstitial”) which absorb boron atoms into electrically active defects, dominantly as donors, that means that space charge is changed twice.

Various techniques have been explored to neutralise radiation damage effects by defect engineering. For *n*-type material, oxygen enrichment with a larger abundance than phosphorus, introduced during the Si growth, successfully reduces the formation of multi-vacancy, acceptor-like complexes which are dominantly produced by charged hadrons, because it enhances instead the formation of electrically neutral V-O complexes. Carbon enrichment, on the other hand, reduces acceptor removal in *p*-type Si by building stable C_i-S_i complexes, thus trapping the Si interstitials which could else remove boron as described above.

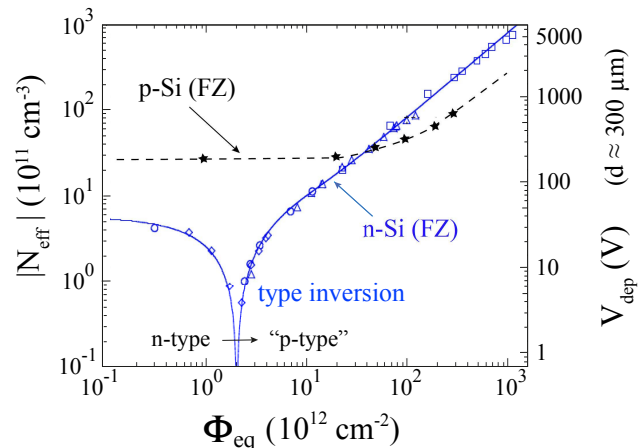


Figure 35.30: Effective space charge concentration N_{eff} (left axis) and required voltage for full depletion V_{dep} (right axis) of approximately 300 μm thick Si sensors as a function of neutron-equivalent radiation fluence for typical *n*-type (blue) and *p*-type (black) silicon float zone (FZ) material before annealing. While initial *n*-type Si inverts to effectively *p*-type Si, this is not observed for initial *p*-type silicon. Bias voltage supply for large systems is usually limited to less than 600–1000 V. Figure adapted using [372, 373] and [374].

Dopant removal plays a particularly important role in more

complex sensor structures such as, for example, DMAPS or LGADs. In particular, the high p -doping concentration in LGAD's gain layer is vulnerable to acceptor removal causing a drastic gain decrease with increasing fluence.

Deep level defects (Fig. 35.29(b)) typically are the origin of leakage current increase, whereas trapping centers (Fig. 35.29(c)) dominate carrier lifetime and signal loss at high fluences beyond $10^{15} \text{ n}_{\text{eq}}/\text{cm}^2$. The safe limit on the operating voltage ultimately limits the detector lifetime. Strip and pixel detectors, specifically designed for high voltages, have been extensively operated at bias voltages of 500–600 V. Sensors with columnar electrodes normal to the surface (3D-Si, Fig. 35.25) need significantly lower voltages for full depletion and are prime contenders for radiation-hard sensors.

Synthetic CVD diamond has proven strong against radiation damage due to its large bandgap (see Tab. 35.10) and strong lattice binding with a roughly twice higher threshold ($\sim 40 \text{ eV}$) for a displacement of lattice atoms than silicon (see *e.g.* [354]). Even for polycrystalline material, charge collection distances (CCD = sum of the mean free paths $\mu\tau E$ of e and h over which charges reach the electrodes) of 300–400 μm have been achieved. Diamond wafer cost, however, is comparatively very high. Smaller scale trackers acting *e.g.* as beam monitors have been built.

GaAs has received interest as a potentially radiation-hard material in the 1990ies. For particle detection it must still be depleted from charge carriers despite comparatively small intrinsic carrier densities (see Tab. 35.10). It suffers from a strong loss in charge collection efficiency when irradiated, dominantly because of electron trapping. Other semiconductor materials such as SiC or GaN feature wider bandgaps (3.26 eV and 3.39 eV, respectively) than Si (but smaller than diamond) and possess other suitable properties relevant to high-fluence operation, such as density, e - h ionisation energy, and displacement energies. They have regained attention after the material quality has improved much due to an industrial push coming from power devices and LEDs. So far, charge collection degrades faster with radiation fluence than for Si and diamond, however.

Strip and pixel detectors have remained functional in large detectors even at particle fluences well beyond $10^{15} \text{ n}_{\text{eq}}/\text{cm}^2$ where charge loss due to recombination and trapping becomes significant. Thin planar ($\sim 100 \mu\text{m}$) and 3D silicon detectors have been successfully operated at fluences of 2 and $3 \times 10^{16} \text{ n}_{\text{eq}}/\text{cm}^2$, respectively, and measurements indicate that operation above $10^{17} \text{ n}_{\text{eq}}/\text{cm}^2$ does not seem impossible. The large SNR obtainable with low capacitance pixel structures extends the detector lifetime. The higher mobility of electrons makes them less sensitive to carrier lifetime than holes, so detector configurations that emphasize the electron contribution to the charge signal are advantageous, *i.e.* n^+ strips or pixels on p - or n -substrates. The occupancy of the defect charge states is strongly temperature dependent; competing processes can increase or decrease space charge and the required operating voltage. It is critical to choose the operating temperature judiciously (-30°C to 0°C in typical collider detectors) and to limit warm-up periods during maintenance. Detailed discussions of radiation damage and its effects on semiconductor detectors can be found *e.g.* in [373, 375]; an introduction to the subject can be found in [1].

Tolerance against surface damage, especially in SiO_2 layers as in gates and in oxide trenches of CMOS transistor structures, largely depends on the feature size of a technology and on appropriately designed circuitry. Deep submicron technology nodes of 130 nm and 65 nm sustain total ionisation doses of up to 5 MGy (500 Mrad), corresponding to fluences of up to $5 \times 10^{15} \text{ cm}^{-2}$ of minimum ionising pions or protons.

35.9 Low-noise detector readout

Revised November 2021 by N. Wermes (Bonn U.), revised November 2013 by H. Spieler (LBNL).

Many detectors rely critically on low-noise readout electronics, for best energy resolution or to allow low thresholds for high detection efficiencies. A typical detector front-end is shown in Fig. 35.31.

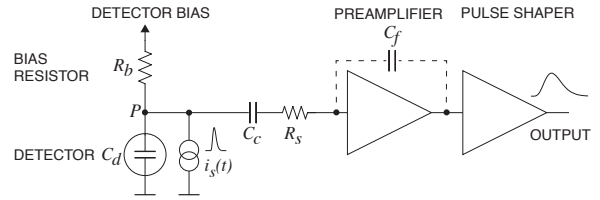


Figure 35.31: Typical detector front-end. The dashed circuit part is a charge-sensitive amplifier (CSA) realization.

In a model relevant to most readout applications, the detector, represented by a capacitance C_d , delivers a delta-function-shaped current signal, represented by a current source in parallel. Bias voltage is applied through resistor R_b and the signal is (often) coupled to the amplifier through a blocking capacitor C_c . The series resistance R_s represents the sum of all resistances present in the input signal path, *e.g.* the electrode resistance, any input protection network, and parasitic resistances in the input transistor. The amplification stage contains the preamplifier providing gain and a pulse shaper (characterized by a shaping time τ), which tailors the overall frequency response to optimize the signal-to-noise ratio (SNR) while limiting the duration of the signal pulse to accommodate the signal-pulse rate. For a given input signal, purely random noise leads to a gaussianly smeared signal distribution behind the shaper. Even if not explicitly stated, all amplifiers provide some form of pulse shaping due to their limited frequency response.

It is useful to distinguish between noise inherent to a detector's signal amplification and processing circuitry (per channel) on the one hand, depending on the detector specifics and the experimental environment (*e.g.* the data rate), and — on the other hand — external noise sources introduced *e.g.* by systems external to a specific readout circuit often resulting in “common-mode” noise, *i.e.* common to all channels. External noise can be introduced from power supplies, digital signal switching, RF pick-up, or from effects due to “common grounding” allowing noise to couple to the current loop connecting the detector to the preamplifier. These noise sources differ from setup to setup and must be dealt with — and should at best be eliminated — individually. In the following, therefore, only the noise inherent to typical detector signal processing is discussed.

35.9.1 Principal noise origins

As principal noise origins in circuit elements we mainly distinguish *thermal noise* resulting from velocity fluctuations of charge carriers (Brownian motion), as well as *shot noise* and $1/f$ noise, both resulting from charge carrier number fluctuations. Shot noise is due to emission statistics of electrons crossing a barrier, $1/f$ noise is often — especially in MOSFETs — due to charge trapping–detrapping processes leading to a spectral behaviour as $1/f^\alpha$ with $\alpha = 0.5 \dots 2$. Further noise nomenclature, like for example RTS (random telegraph signal) noise, also called “burst noise” or “popcorn noise”, is in its origin usually related to trapping/detrapping processes, like $1/f$ noise. The popping-up nature of individual RTS bursts eventually leads to the $1/f$ noise spectral density when the noise of several traps with (very) different trapping times are superimposed. RTS noise is omitted in the following for simplicity reasons.

35.9.2 Equivalent noise analysis

The equivalent circuit for noise analysis (Fig. 35.32) shows contributions of the mentioned noise sources at several circuit points. Originating from fluctuations, noise is expressed as the variance $\langle i^2 \rangle$ or $\langle v^2 \rangle$ of a noise current or voltage distribution. Shot noise, such as that produced in a semiconductor detector by leakage current fluctuations, is represented by a current noise generator in parallel with the detector and the amplifier input. The statistical fluctuations in a charge measurement will scale with the square root of the total number of recorded charges, so this noise contribution increases with the measurement (shaping) time. Thermal noise in resistors produces a white noise, *i.e.* a noise power density independent of frequency. Hence limiting the bandwidth by

a shaper, *i.e.* increasing the shaping time, will decrease the noise at the expense of slowing down the detector response. Usually, resistors shunting the input act as noise current sources and resistors in series with the amplifier input act as noise voltage sources, so that they are often referred to as “parallel” and “series” noise. Thermal fluctuations in the bias resistor result in fluctuations of the voltage at point P in Fig. 35.31 and its noise current source $\langle i_b^2 \rangle$ has the same effect as the shot noise current $\langle i_d^2 \rangle$ from the detector. Conversely, the series resistor R_s acts as a voltage noise generator $\langle v_s^2 \rangle$ for the amplifier input.

Shot noise and thermal noise have a “white” frequency distribution, *i.e.* the (power) spectral densities (f = frequency) $d\langle i^2 \rangle/df$ and $d\langle v^2 \rangle/df$ are constant with magnitudes

$$\begin{aligned} d\langle i_d^2 \rangle &= 2eI_d df, \\ d\langle i_b^2 \rangle &= \frac{4kT}{R_b} df, \\ d\langle v_s^2 \rangle &= 4kTR_s df, \end{aligned} \quad (35.26)$$

where e is the elementary charge, I_d the detector leakage current, and k, T Boltzmann constant and temperature. Hence, in a 1 k Ω resistor at room temperature, for example, one finds a current-independent thermal noise of $\sqrt{d\langle i^2 \rangle/df} = 4 \text{ pA}/\sqrt{\text{Hz}}$ or $\sqrt{d\langle v^2 \rangle/df} = 4 \text{ nV}/\sqrt{\text{Hz}}$, respectively. For $1/f$ noise, by contrast, the spectral power density is proportional to $1/f^\alpha$ ($\alpha = 0.5-2$) with a device specific proportionality constant. In what follows, we will assume $\alpha = 1$ for simplicity reasons, noting though that more complex models exist.

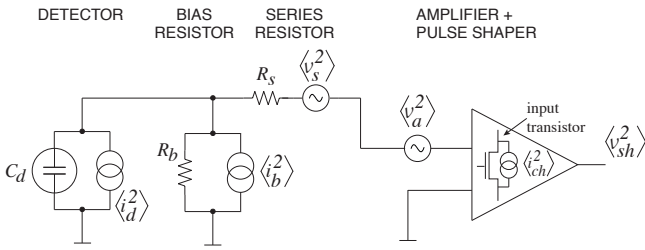


Figure 35.32: Equivalent circuit diagram for noise analysis.

An important noise source is the preamplifier input stage, very often dominated by the first amplification transistor. In what follows we assume a MOSFET at this point, as the large majority of amplification circuits is based on MOS transistors. Noise sources in bipolar amplification is shortly mentioned at the end of this section. A MOS transistor’s channel features thermal noise with “resistance” $1/g_m$, where $g_m = \partial I/\partial V$ is the transconductance. Correction factor(s) for parametrization depend on the transistor operation point. Conventionally, a factor γ is applied varying between 0.5 and 1 when temperature dependence is implicit, but is commonly taken as $\gamma \approx 2/3$ for operation in strong inversion and 0.5 in weak inversion.

In addition, especially in MOSFETs, there is $1/f$ noise originating from trapping/detrapping processes of charge carriers at the channel’s Si-SiO₂ interface. The channel’s current noise is equivalent to a voltage noise at the transistor input (the gate) via

$$\langle i_{ch}^2 \rangle = \langle (g_m v_a)^2 \rangle \quad (35.27)$$

leading to respective noise power spectral densities of

$$\frac{d\langle v_a^2 \rangle}{df} = 4kT\gamma \frac{1}{g_m} + K_f \frac{1}{C'_{ox} WL} \frac{1}{f}, \quad (35.28)$$

where the individual (uncorrelated) noise contributions add in quadrature. The “ $1/f$ noise constant” K_f has magnitude in the order of $10^{-24} - 10^{-26} \text{ J}$ depending on the device type and the technology⁸. C'_{ox} is the oxide capacitance per unit area, and W, L are width and length of the gate.

⁸Other $1/f$ noise parametrizations also exist with correspondingly different numerical values for K_f .

Particle and radiation detectors typically convert the deposited energy into charge (usually e -ion or e -h pairs) which can be measured by integrating the current induced on an electrode by the drifting charge pairs (see *e.g.* Sec. 35.8) employing a “charge-sensitive (pre)amplifier” (CSA), realized by feeding back the preamp’s output to the input through capacitor C_f (dashed circuit part of Fig. 35.31). The feedback capacitance must be discharged for the next pulse to appear, for example by a resistor, a (constant) current source or a switch. Noise contributions from such components can usually be kept small in comparison.

For a CSA the noise output voltage after the preamplifier (v_{pa}^2) relates to the input (current or voltage) noise sources via the transimpedance $1/\omega C_f$ as

$$\langle v_{pa}^2 \rangle = \langle i_{in}^2 \rangle \left(\frac{1}{\omega C_f} \right)^2 \quad \text{or} \quad \langle v_{pa}^2 \rangle = \langle v_{in}^2 \rangle \left(\frac{\omega C_D}{\omega C_f} \right)^2 \quad (35.29)$$

with $\omega = 2\pi f$. The capacitance C_D includes the detector capacitance C_d plus all capacitances shunting the input. Considering only the (usually) dominant noise sources, being the detector shot noise as well as the transistor channel noise, and neglecting the resistor parallel and serial noise sources of (35.26) by choosing R_b large and keeping R_s small, one obtains

$$\frac{d\langle v_{pa}^2 \rangle}{d\omega} = \sum_{k=-2}^0 c_k \omega^k \quad (35.30)$$

with

$$c_{-2} = \frac{e}{\pi} I_d \frac{1}{C_f^2}, \quad c_{-1} = K_f \frac{1}{C'_{ox} WL} \frac{C_D^2}{C_f^2}, \quad c_0 = \frac{2\gamma}{\pi} kT \frac{1}{g_m} \frac{C_D^2}{C_f^2}, \quad (35.31)$$

which correspond to the discussed main noise components, c_{-2} : shot noise, c_{-1} : $1/f$ noise, c_0 : thermal noise, respectively.

The filtering effect of the shaper limits the bandwidth of the system and is generally described by a transfer function $H(\omega)$ for $\langle v_{pa}^2 \rangle$ integrated over the full bandwidth

$$\langle v_{sh}^2 \rangle = \int_0^\infty \frac{d\langle v_{pa}^2 \rangle}{d\omega} |H(\omega)|^2 d\omega \quad (35.32)$$

with $\langle v_{sh}^2 \rangle$ being the shaper output voltage noise. $H(\omega)$ depends on the filter circuit, *i.e.* the shape of the pulse formed by the shaper, and is characterized by a characteristic time τ , the shaping time, which can, for example, be the peaking time of a semi-gaussian pulse or the sampling interval in a correlated double-sampler (see *e.g.* [8]). The peaking time is an important quantity for readout systems since for peaking times large compared to the duration of the input signal the amplitude at peaking time corresponds to the total input charge.

For a simple time-invariant CR-RC filter, consisting of a high-pass followed by a low-pass filter with equal time constants, the transfer function is

$$|H(\omega)|^2 = A^2 \left(\frac{\omega\tau}{1 + \omega^2\tau^2} \right)^2 \quad (35.33)$$

and (35.30) becomes

$$\langle v_{sh}^2 \rangle = \frac{\pi}{4} A^2 \left(c_{-2} \tau + \frac{2}{\pi} c_{-1} + c_0 \frac{1}{\tau} \right) \quad (35.34)$$

with A being an overall gain factor.

The system noise for a charge measurement is conveniently expressed as an equivalent noise charge (ENC) referring the noise to the equivalent signal of one electron at the input:

$$\text{ENC}^2 = \frac{\langle v_{sh}^2 \rangle}{v_{\text{signal}}^2 (1e^-)}. \quad (35.35)$$

While being dimensionless by definition, ENC is commonly expressed as an equivalent number of electrons (e^-) at the input or alternatively as equivalent Coulombs (C) when multiplying by the

elementary charge or as equivalent deposited energy (eV), where $1e^-$ equivalent charge corresponds to 3.65 eV of equivalent deposited energy in Si (see Tab. 35.10 in Sec. 35.8).

A charge of one electron at the input yields a voltage signal (peak) behind the shaper of $v_{\text{signal}} = \frac{A}{2.71} \frac{e}{C_f}$. Hence with (35.35) and (35.34) one obtains:

$$\begin{aligned} \text{ENC}^2 (e^{-2}) &= \frac{(2.71)^2}{4e^2} \left(eI_d\tau + 2C_D^2 K_f \frac{1}{C'_{ox}WL} + \gamma \frac{2kT}{g_m} \frac{C_D^2}{\tau} \right) \\ &= a_{\text{shot}} \tau + a_{1/f} C_D^2 + a_{\text{therm}} \frac{C_D^2}{\tau}, \end{aligned} \quad (35.36)$$

where 2.71 is Euler's number resulting from the amplitude peak value behind the (CR-RC) shaper (for $t = \tau$), while e is the elementary charge and (e^-) explicitly denotes the equivalent number of electrons at the input.

Equation (35.36) accentuates the main noise dependencies of the system. The contribution from parallel current shot noise (*i.e.* detector leakage) increases with shaping time, *i.e.* with pulse duration, whereas thermal noise (here serial voltage noise at the gate, originating from transistor channel noise) decreases with increasing shaping time, *i.e.* with reduced bandwidth. Noise with a $1/f$ spectrum depends only on the ratio of upper to lower cutoff frequencies (low pass to high pass time constants) and is hence independent of τ for a given shaper topology. Furthermore, the contribution of serial noise voltage ($1/f$ and thermal noise) to ENC increases with input (detector) capacitance C_D . Pulse shapers can be designed to optimize the noise performance of a system or to mitigate operation variations with time (*e.g.* due to radiation damage) deteriorating the performance, at the expense of loss of simplicity. For example, a shaper with one high-pass filter followed by four cascaded low-pass filters, increases the pulse symmetry and tends to decrease the current noise, but increases the voltage noise contributions for the circuit of Fig. 35.32, if the same peaking time is assured by adjusting the individual time constants of the filter stages. If instead the low-pass filters cause the peaking time of the pulse to increase, the opposite can be true. More details about shaping filters can be found *e.g.* in [8, 376–378].

Figure 35.33 shows a typical example of eq. (35.36) displaying ENC as a function of shaping time τ for a system. At short shaping times, thermal noise dominates, whereas for longer shaping times the shot noise contribution takes over. The total noise has a minimum at a shaping time where shot and thermal noise contributions are equal. The minimum is flattened by the presence of $1/f$ noise. Increasing the detector capacitance increases the thermal and $1/f$ contributions and shifts the noise minimum to larger shaping times. One can hence exploit the shaping time dependence of the total noise to determine the individual noise contributions of a system.

For quick estimates (35.36) is cast into a useful equation for a typical CSA-shaper system [1]:

$$\begin{aligned} \text{ENC}^2 (e^{-2}) &= 11 \frac{I_d}{\text{nA}} \frac{\tau}{\text{ns}} + 740 \frac{1}{WL/(\mu\text{m}^2)} \frac{C_D^2}{(100 \text{ fF})^2} \\ &+ 4000 \frac{1}{g_m/\text{mS}} \frac{C_D^2/(100 \text{ fF})^2}{\tau/\text{ns}}, \end{aligned} \quad (35.37)$$

where $\gamma = 2/3$, $K_f = 33 \times 10^{-25} \text{ J}$, and $C'_{ox} = 6 \text{ fF}/\mu\text{m}^2$ has been used, the latter being typical for CMOS technologies as employed for example for the detector readout chips of the LHC experiments and their upgrades. Generally, noise performance is improved by reducing the detector capacitance and the leakage current, judiciously selecting all resistances in the input circuit, and by choosing the optimum shaping time constant τ . Another noise contribution to consider is the fact that noise can cross-couple from the neighbouring front-ends in detectors with structured electrodes through the inter-electrode capacitance.

As mentioned, the noise parameters of the amplifier depend primarily on the input device (input transistor(s)). In field-effect transistors, the input noise current contribution of the transistor itself is very small. Hence, if the experiment's time structure permits, reducing the detector leakage current and increasing the

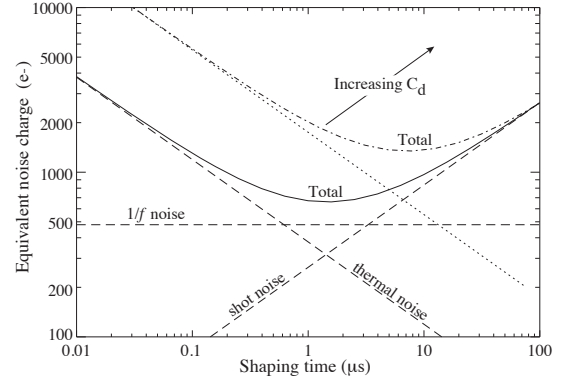


Figure 35.33: Equivalent noise charge *vs* shaping time. Changing the detector capacitance C_D affects thermal and $1/f$ noise contributions and moves the noise minimum as indicated by the dotted and dash-dotted lines. The $1/f$ noise contribution is small for the chosen parameters ($C_D = 20 \text{ pF}$, $I_d = 10 \text{ nA}$, $g_m = 1 \text{ mS}$) in this example.

bias resistance will allow long shaping times with correspondingly lower noise. For amplifiers employing bipolar transistors, shot noise sources originate from both, base-emitter and collector-base, junctions and from the series resistance at the base which is especially important for small structures optimized for radiation hardness. For the shot-noise contribution, the input base current I_B sets a lower bound on the noise current, such that these devices are best at short shaping times.

35.9.2.0.1 Examples Using (35.37) one finds for a typical pixel detector (before heavy irradiation) with $C_D = 200 \text{ fF}$, $I_d = 1 \text{ nA}$, $\tau = 50 \text{ ns}$, $W = 20 \mu\text{m}$, $L = 0.5 \mu\text{m}$, $g_m = 0.5 \text{ mS}$:

$$\text{ENC}^2 \approx (24 e^-)^2 \Big|_{\text{shot}} + (17 e^-)^2 \Big|_{1/f} + (25 e^-)^2 \Big|_{\text{therm}} \approx (40 e^-)^2.$$

For a typical silicon microstrip detector after radiation damage (fluence $\gtrsim 10^{14} \text{ neq}/\text{cm}^2$, assuming no degradation of the front-end electronics due to radiation) one obtains for $C_D = 20 \text{ pF}$, $I_d = 1 \mu\text{A}$, $\tau = 50 \text{ ns}$, $W = 2000 \mu\text{m}$, $L = 0.4 \mu\text{m}$, $g_m = 5 \text{ mS}$:

$$\text{ENC}^2 \approx (750 e^-)^2 \Big|_{\text{shot}} + (200 e^-)^2 \Big|_{1/f} + (800 e^-)^2 \Big|_{\text{therm}} \approx (1100 e^-)^2.$$

Apart from the larger leakage current, the larger capacitance of strips compared to pixels leads to a much worse noise performance which can only be partially compensated by allowing more power in the amplification transistor, *i.e.* by increasing g_m .

A liquid argon calorimeter cell is a suitable example of a detector with a large electrode capacitance with typical parameters (similar to the ATLAS central electromagnetic calorimeter, see Sec. 35.10). Using $C_D = 1.5 \text{ nF}$, $I_d = < 2 \mu\text{A}$, $\tau = 50 \text{ ns}$, $W = 3000 \mu\text{m}$, $L = 0.25 \mu\text{m}$, $g_m = 100 \text{ mS}$, one obtains:

$$\begin{aligned} \text{ENC}^2 &\approx (1000 e^-)^2 \Big|_{\text{shot}} + (15000 e^-)^2 \Big|_{1/f} + (13500 e^-)^2 \Big|_{\text{therm}} \\ &\approx (20200 e^-)^2. \end{aligned}$$

Here only a small (negligible) parallel shot noise (leakage current) contribution is assumed, which is typical for liquid argon calorimeters.

Practical noise levels range from $\sim 1e^-$ for CCD's at long shaping times to $\sim 10^4 e^-$ in high-capacitance liquid argon calorimeters. Gaseous micropattern detectors like GEMs or MicroMegas (see Sec. 35.6.4) typically feature noise levels between $1000 e^-$ and $1500 e^-$, depending on the ability to correct for common-mode noise. Silicon strip detectors typically operate at levels of $\sim 10^3 e^-$, whereas pixel detectors with fast readout typically have noise levels below about 100 electrons.

35.9.3 Timing measurements

In timing measurements, the slope-to-noise ratio must be optimized, rather than the signal-to-noise ratio alone, so the rise time t_r of the pulse is important. The “jitter” σ_t of the timing distribution is

$$\sigma_t = \frac{\sigma_n}{(dS/dt)_{\text{trig}}} \approx \frac{t_r}{\text{SNR}}, \quad (35.38)$$

where σ_n is the rms noise, SNR the signal-to-noise ratio and the “slew rate” dS/dt , *i.e.* the derivative of the signal, is evaluated at the trigger level. The rise-time of a CSA again depends on the detector and feedback capacitances and on the amplifier transconductance

$$t_r \propto \frac{C_D}{C_f \cdot g_m}. \quad (35.39)$$

To increase dS/dt without incurring excessive noise, the amplifier bandwidth should match the rise time of the detector signal. The 10% to 90% rise time of an amplifier with bandwidth f_U is $0.35/f_U$. For example, an oscilloscope with 350 MHz bandwidth has a 1 ns rise time. For cascaded amplifiers, the individual rise times add in quadrature to first order.

As increasing SNR also improves the time resolution, minimizing the total input capacitance is extremely important for timing measurements (see also Sec. 35.8). At high signal-to-noise ratios, the time jitter can be much smaller than the rise time. The time-mark distribution of pulses may shift with the signal level (“time walk”), but this can be corrected by various means, either in hardware or in software.

For applications aiming at extreme time resolution charge-sensitive (integrating) amplification can be less optimal. Transimpedance or voltage amplifiers converting current/voltage to voltage are usually preferred. Also, when aiming for picosecond timing using voltage amplifiers, *e.g.*, with LGAD detectors having C_D of $\mathcal{O}(\text{pF})$ (see Sec. 35.8), not only the preamplifier rise time t_r but also the signal pulse duration t_d at the preamplifier input is important, *i.e.*, the preamplifier must react draining the charge from C_D before the input voltage $v_{in} = Q_S/C_D$ (Q_S = signal charge) reaches its peak. Both times must reasonably match, $t_r \approx t_d$, resulting in a time jitter of [379]

$$\sigma_t^2 \approx \frac{C_D^2}{Q_S^2} \frac{d\langle v_n^2 \rangle}{df} t_d, \quad (35.40)$$

where $d\langle v_n^2 \rangle/df$ is the voltage noise spectral density.

35.9.4 Digital signal processing

The filtering principles apply to both analog and digital signal processing. In digital signal processing the pulse shaper shown in Fig. 35.31 is replaced by an analog to digital converter (ADC) followed by a digital processor that determines the pulse shape. Digital signal processing allows great flexibility in implementing filtering functions. The software can be changed readily to adapt to a wide variety of operating conditions and it is possible to implement filters that are impractical or even impossible using analog circuitry. However, this comes at the expense of increased circuit complexity and increased demands on the ADC compared to analog shaping.

If the sampling rate of the ADC is too low, high frequency components will be transferred to lower frequencies (“aliasing”). The sampling rate of the ADC must be high enough to capture the maximum frequency component of the input signal. Apart from missing information on the fast components of the pulse, under-sampling introduces spurious artifacts. If the frequency range of the input signal is much larger than the sampling rate, the noise at the higher frequencies will be transferred to lower frequencies and will increase the noise level in the frequency range of pulses formed in the subsequent digital shaper. The Nyquist criterion states that the sampling frequency must be at least twice the maximum relevant input frequency. This requires that the bandwidth of the circuitry preceding the ADC must be limited. The most reliable technique is to insert a low-pass filter.

The digitization process also introduces inherent noise, since the voltage range ΔV corresponding to a minimum bit step introduces

quasi-random fluctuations relative to the exact amplitude

$$\sigma_n = \frac{\Delta V}{\sqrt{12}}. \quad (35.41)$$

When the Nyquist condition is fulfilled the noise bandwidth Δf_n is spread nearly uniformly and extends to 1/2 the sampling frequency f_S , so the spectral noise density is

$$\frac{\sigma_n}{\sqrt{\Delta f_n}} = \frac{\Delta V}{\sqrt{12}} \cdot \frac{1}{\sqrt{f_S/2}} = \frac{\Delta V}{\sqrt{6f_S}}. \quad (35.42)$$

Sampling at a higher frequency spreads the total noise over a larger frequency range, so oversampling can be used to increase the effective resolution. In practice, this quantization noise is increased by the ADC’s differential non-linearity (DNL). Furthermore, the equivalent input noise of ADCs is often rather high, so the overall gain of the stages preceding the ADC must be sufficiently large for the preamplifier to override the ADC input noise.

35.9.5 What to use when?

When implemented properly, digital signal processing provides significant advantages in systems where the shape of detector signal pulses changes greatly, for example in large semiconductor detectors for gamma rays or in gaseous detectors (*e.g.* TPCs) where the duration of the current pulse varies with drift time, which can range over orders of magnitude. Analog signal processing is best or most efficient in systems that require fast time response, but the high power requirements of high-speed ADCs are prohibitive. Systems that are not sensitive to pulse shape can use fixed shaping time constants and rather simple filters (like CR–RC), which can be either continuous or sampled. In high-density systems that require small circuit area and low power (*e.g.*, in strip and pixel detectors), analog filtering often yields the required response and tends to be most efficient.

As stressed already in the introduction, it is important to consider that additional noise is often introduced externally. Recognizing additional noise sources and minimizing cross-coupling to the detector current loop is often essential to obtain the best overall noise performance. Understanding basic physics and its practical effects is important in forming a broad view of the detector system and recognizing potential problems (*e.g.* modified data), rather than merely following standard recipes.

More comprehensive treatments of low noise detector readout and signal processing can be found, for example, in [8, 376, 378] and in [1, 363].

35.10 Calorimeters

35.10.1 Introduction

Revised August 2023 by F. Sefkow (DESY, Hamburg) and F. Simon (KIT).

A calorimeter measures the energy and direction of particles by absorption in the detector material and registration of the energy deposited in an (ideally) contained electromagnetic (EM) or hadronic shower. Calorimeters are central components of modern high energy physics experiments, due to their ability to measure not only the energy of charged particles (with the exception of muons), but also of photons and neutral hadrons, thus enabling the reconstruction of π^0 and η decays and of exclusive final states involving long-lived neutral kaons, or neutrons. They are indispensable for the measurement of particle jets and for the reconstruction of total event properties, which, via the measurement of missing energy (or missing transverse energy in hadron colliders), enable the detection of the presence of “invisible” particles such as neutrinos and hypothetical particles such as dark-matter candidates. Calorimeters are also important for the identification of particle species, using information on the longitudinal and transverse shape of the energy deposition to separate electrons, photons, hadrons and muons. While the performance of calorimeters is typically assessed by the quality of their energy measurements, position resolution, both for EM and hadronic showers, is also

highly relevant, for example for the reconstruction of effective jet masses. The capability to measure high-level observables that serve to classify events, such as particle and jet energies, missing energy and isolated leptons, makes calorimeters central components of the trigger systems in high-energy physics experiments.

In collider experiments, the importance of calorimeters tends to increase with increasing collision energies since the relative energy resolution improves with increasing particle energy while the depth required for full containment of the showers shows only logarithmic growth with energy. This is in contrast to the precision of track-based measurements, which is decreasing with increasing momentum. With recent advances in timing capabilities calorimeters are also contributing to the rejection of pile-up from multiple interactions within the same bunch crossings at colliders.

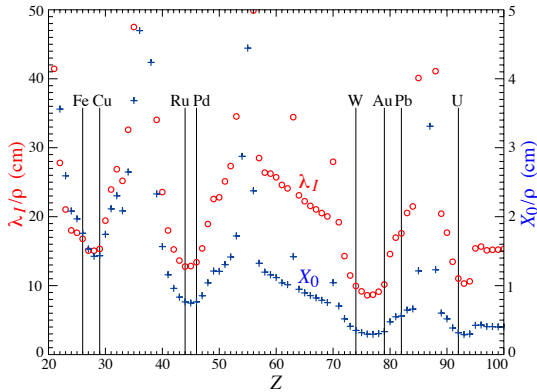


Figure 35.34: Nuclear interaction length λ_I/ρ (circles) and radiation length X_0/ρ (+'s) in cm for the chemical elements with $Z > 20$ and $\lambda_I < 50$ cm.

The characteristic length scale for EM showers is the radiation length X_0 , which ranges from 1.8 cm (13.8 g cm^{-2}) in iron to 3.2 mm (6.0 g cm^{-2}) in uranium for materials used to generate showers in calorimeters.⁹ Similarly, the characteristic nuclear interaction length λ_I varies from 16.8 cm (132.1 g cm^{-2}) (Fe) to 11.0 cm (209 g cm^{-2}) (U).¹⁰ There is a premium on small λ_I/ρ and X_0/ρ (both with units of length). These quantities are shown for elements with $Z > 20$ in Fig. 35.34. The minima for both X_0 and λ_I correspond to elements between W and Au. Some of these elements are very difficult to work with (e.g. W) or expensive (e.g. Au), so, depending on the application (size of the required calorimeter) other materials, such as Fe, Cu, Pb, and different alloys like brass and CuW are often chosen. For EM calorimeters high Z is preferred; here Pb is a popular choice, while W provides even higher density and is generally affordable due to the limited volume of EM systems.

Most existing calorimeters are subdivided into a front EM section (ECAL) and a hadronic part (HCAL) behind; electrons and photons are measured in the ECAL, while hadrons and jets are measured in the combined ECAL and HCAL system. The detailed design depends on energy range and performance requirements as well as on size and cost constraints for the entire system. EM calorimeters tend to be $15\text{--}30 X_0$ deep, while hadronic calorimeters are usually optimised for cost and performance at $5\text{--}8 \lambda_I$. The depth of the ECAL typically corresponds to approximately $1 \lambda_I$, with the exact value depending on the material. This means that approximately 70% of all hadronic showers will already begin in the electromagnetic calorimeter, making its response to a hadronic cascade highly relevant for the overall performance of the system. The choice of the calorimeter technology for the ECAL is thus a result of simultaneous optimisation for EM and hadronic performance of the overall system.

Sampling calorimeters consist of a high-density, normally metallic absorber sandwiched (or threaded) with an active ma-

terial which generates a signal in response to shower particles. The active medium may be a scintillator, a noble liquid, a gas, silicon, or a Cherenkov radiator. These active media all have a relatively low Z , a significantly lower density, and larger X_0 and λ_I values than typical absorber materials. The average radiation and interaction lengths in the full detector are thus larger than those of the absorber alone.

There are also *homogeneous calorimeters*, in which the entire volume contributes to the signal. Homogeneous calorimeters may be built with inorganic heavy scintillating crystals or non-scintillating Cherenkov radiators such as lead glass and lead fluoride. Nuclear interaction lengths in inorganic crystals range from 17.8 cm (LuAlO_3) to 42.2 cm (NaI). Materials with low X_0 used in large systems are for example BGO with $\lambda_I = 22.3$ cm and $X_0 = 1.12$ cm, and PbWO_4 (20.3 cm and 0.89 cm). Properties of these and other commonly used inorganic crystal scintillators can be found in Table 35.4. Cryogenic noble liquids, where scintillation light and/or ionization can be detected, are also suitable materials for homogeneous detectors.

Homogeneous calorimeters at colliders are usually only used for the EM section. For the use of homogeneous calorimeters for hadron energy measurement, the large differences in the response to EM and hadronic parts of the shower are a significant challenge, as is the three-dimensional segmentation. This is still requiring substantial R&D, including the search for affordable materials. In non-accelerator physics experiments or at neutrino beams, homogeneous calorimeters, where the sensitive medium can be water or ice, scintillator, a noble liquid or the atmosphere itself, are used to detect both EM and hadronic showers.

Comprehensive tables of particle-physics calorimeters are given as Appendix C in Ref. [380].

35.10.1.1 Energy Resolution and System Performance

The energy resolution of calorimeters is a complex observable, due to the variety of contributing processes with different energy dependencies, and response functions often not perfectly Gaussian. Nevertheless, a simplified picture is useful in practice, and in particular for EM calorimeters also numerically accurate. For hadronic calorimeters additional complications must be taken into account. In such a simplified picture, due to the stochastic nature of shower evolution, the intrinsic calorimeter energy resolution, σ , is proportional to \sqrt{E} , as the number of charged particles, or the total ionising track length in a shower are on average proportional to the incident particle energy E . The relative resolution σ/E therefore improves with A/\sqrt{E} , where A denotes the so-called *stochastic term*. The readout system of the active medium will contribute noise to the resolution, $\sigma_N = B$, which in general is not energy-dependent. Effects that are proportional to the total deposited energy result in a *constant term*, $\sigma_C = C \cdot E$. Different sources contribute to this term, depending on the type of calorimeter. For both EM and hadronic calorimeters, imperfections of the detector, inhomogeneities such as density variations or those introduced by the detector mechanics, instabilities in time, imperfections of the readout or incorrect calibration of channels contribute. Shower leakage, which depends on particle energy, also contributes to the resolution with approximately linear dependence on energy. In non-compensating hadronic calorimeters, fluctuations of the EM fraction f_{em} from shower to shower, together with the energy dependence of the average f_{em} value, can lead to a significant constant term that often dominates over the instrumental effects. Adding up all contributions in quadrature yields the standard parameterisation of the relative energy resolution of a calorimeter:

$$\frac{\sigma}{E} = \frac{A}{\sqrt{E}} \oplus \frac{B}{E} \oplus C. \quad (35.43)$$

In particular the effects specific to hadronic showers give rise to non-Gaussian distributions of the energy response. Therefore care must be used in performance comparisons, as different parameterisations of the line shape and different definitions of the resolution are in use. In some cases, a linear rather than a quadratic addition of the stochastic and constant term may provide a better description of the energy resolution as a function of energy. It should be noted that the individual terms then lose the simplified

⁹ $X_0 = 120 \text{ g cm}^{-2} Z^{-2/3}$ to better than 5% for $Z > 23$.

¹⁰ $\lambda_I = 37.8 \text{ g cm}^{-2} A^{0.312}$ to within 0.8% for $Z > 15$.

See <https://pdg.lbl.gov/current/AtomicNuclearProperties> for actual values.

interpretation discussed above, and care has to be taken when comparing performance based on fits to the energy dependence of the resolution.

Typically, primarily the stochastic term — which is determined by the calorimeter design in terms of material and geometry — is considered in order to describe the overall properties of a calorimeter. For the calorimeters of the multi-purpose experiments at the LHC, the stochastic terms are 3 – 10% for electromagnetic and 50 – 80% for hadronic calorimeters. In practice, the energy resolution of a calorimeter at high energies is limited by the constant term C , which in the EM case mainly reflects the precision and stability of the mechanical construction, electronic readout system and calibration. Typical constant terms are a few per-mil for EM and a few percent for hadronic calorimeters. For concrete examples and references see Tables 35.11 and 35.13.

For sampling calorimeters, the stochastic term depends on the *sampling fraction* f_{samp} , i.e. the ratio of energies deposited in the active and passive material. Also the *sampling frequency* enters, which is determined by the number N of different sampling elements present in the region in which the shower develops. The stochastic term A scales approximately with $1/\sqrt{f_{\text{samp}}}$, and for given f_{samp} and total depth, with $1/\sqrt{N}$.

While the energy resolution for single hadrons (most commonly pions) is often used as the key performance criterion for a hadronic calorimeter, it has to be noted that this value is only of limited relevance in high-energy physics experiments. In most experiments, the calorimetric measurement of hadrons is based on the combined system consisting of ECAL and HCAL. Moreover, for the physics capabilities of a detector at a high-energy particle collider, also the combined calorimetric resolution for single hadrons is not a sufficient criterion to fully characterise hadronic performance, but rather the jet energy resolution, the resolution for missing (transverse) energy, and the capability to cope with high background and pile-up levels. These quantities cannot be measured directly with prototypes in beam tests, and strongly depend on overall system aspects and reconstruction tools. However, the performance in these observables can be reliably inferred from system simulations once the simulated response to single particles and the simulated topology of showers has been validated in detail by beam tests.

Besides energy resolution, response linearity is an important factor in the design of calorimeters. While a non-linear response for single particles can be corrected for if appropriate calibration measurements exist, such corrections deteriorate the energy resolution, in particular in the case of superposition of several showers, as it often occurs in jets. Sources for non-linearities can be intrinsic to the design, for example due to saturation effects in the active medium with increasing energy density, due to leakage, or connected to shower physics as discussed in section 35.10.3.

The energy resolution for hadrons is intrinsically limited by large event-to-event fluctuations of the shower evolution and of "invisible" components not contributing to the detector signal. It remains the limiting factor for single particles and for the high-level performance for jets and total event properties. This has motivated intense research in the past decades. One direction aims at improving the hadronic resolution by extracting additional signals to disentangle the shower composition, e.g. with so-called dual read-out methods, and is explained in the hadron calorimeter section 35.10.3. Another, so-called "particle flow" approach described below optimises the combination of measurements of individual particles in different detector components. Ideally, both methods can be combined.

35.10.1.2 Role of Simulations

Simulations have become indispensable for the design of detectors and the development of reconstruction algorithms. Since event-to-event fluctuations drive calorimeter performance, Monte Carlo techniques that accurately model the evolution of particle cascades in material are required. By far the most common computer code in use today is the *GEANT4* toolkit [381, 382], which provides a step-based simulation of the passage of particles through matter. Thanks to the relative simplicity of EM cascades, simulations of EM showers are typically highly accurate.

The modelling of hadronic showers is more complex, and suffers from larger uncertainties. Significant improvement has been achieved in this area, moving from simpler parameterised models to physics-driven interaction models. From early on, detailed codes and data describing nuclear break-up and neutron transport like *CALOR* [383] or *FLUKA* [384, 385] contributed crucially to the understanding of hadron calorimetry. The simulations reproduce the general features of the substructure of hadronic showers, characterised by dense shower activity and sparser ionising track segments, and their accuracy is adequate for most purposes of quantitative design optimisations. Details of the implementation of physics models in *GEANT4* are discussed in [386].

35.10.1.3 Particle flow approach

In a typical collider experiment, the EM and hadronic calorimeter system surrounds a charged-particle tracking volume devised for momentum measurement in a magnetic field. Matching tracks to calorimetric energy deposits provides corrections for the magnetic deflection of the charged particles, necessary for the reconstruction of invariant masses in multi-jet final states, or of the total momentum imbalance. Furthermore, for charged particles the track-based measurements are far more precise for particles in jets with energies of up to several hundred GeV, so using these instead of calorimeter energies may optimise the jet energy resolution. This so-called "particle flow" approach aims at reconstructing each particle individually, using a combination of the best measurements from the detector.

About 60% of the energy in a typical jet is carried by charged particles, predominantly hadrons, 30% by photons and only 10% by long-lived neutral hadrons (K_L^0 and n), for which hadronic calorimetry is unavoidable. Assuming, as motivated by detector designs proposed for a future Higgs factory, $15\%/\sqrt{E(\text{GeV})}$ for photons and $55\%/\sqrt{E(\text{GeV})}$ for hadrons, then, in the ideal case, where each particle is resolved, a jet energy resolution of $19\%/\sqrt{E(\text{GeV})}$ could be obtained. Here the dominant part ($18\%/\sqrt{E(\text{GeV})}$) is still due to the calorimeter resolution for neutral hadrons.

The particle flow method places high demands on the imaging capabilities of the calorimeters, and on the pattern recognition performance of the reconstruction algorithms. Only energy deposits not associated with charged particles and not identified as photons, will be interpreted as neutral hadrons. In practice, this cannot always be done unambiguously, and mis-assignments give rise to an additional measurement uncertainty, which is called *confusion*. For simulated detectors at proposed future Higgs factories jet energy resolutions of 3-4% have been demonstrated, significantly larger than in the ideal case, but sufficient for the required efficient separation of W and Z hadronic final states.

Particle flow-like techniques were first applied in the ALEPH detector [387], which achieved a jet energy resolution of $60\%/\sqrt{E}$, or 6.2 GeV for hadronic Z decays. More recently, particle flow techniques are successfully used in the CMS experiment [388], for example improving the missing energy resolution by one third over a wide range.

The Pandora particle flow algorithm (PFA) [389] is the most developed and best performing today in the context of future lepton colliders. The algorithms make use of topological information, including the sub-structure of showers, as well as the compatibility of calorimetric and track-based measurements. In this way the purely calorimetric performance for the jet is either retained or improved. In the framework of studies for CLIC [390], it was shown that the required jet energy resolution of 3.5% can be achieved with the PF technique for jet energies up to 1500 GeV.

For the use of energy-momentum matching in the assignment of energy depositions, and for energy flow treatment of dense jets, particle flow calorimeters with their emphasis on imaging must still feature a good energy resolution. Furthermore, the neutral hadron energy uncertainty is the dominant contribution to the jet resolution for low energy jets, where particles are well separated, while at higher energies the confusion effects take over.

High granularity in all three space dimensions comparable to or smaller than the length scales of particle showers given by X_0

and ρ_M for both ECAL and HCAL brings additional advantages; for example it offers ideal conditions for the application of software compensation methods, which improves the intrinsic resolution and also reduces "confusion" [391]. A particular strength is the possibility to use topological information such as the reconstructed starting point of the shower for the estimation of leakage. Moreover, the combination of fine-grained topological reconstruction and cuts on cluster-wise timing with a precision of few tens of pico-seconds allows for powerful pile-up rejection. This extends the application range of particle flow methods towards collider environments with less benign background conditions, like multi-TeV e^+e^- collisions, and it is an asset on its own for high-intensity hadron colliders, even if particle flow methods are difficult to apply.

The performance of highly granular calorimeters depends, among others, on the particle separation and pattern recognition capabilities and on the single particle energy and timing resolution. They are thus not only optimised for energy measurement, but also for multi-dimensional shower reconstruction and particle separation in space and time. The potential of such calorimeters can be further enhanced by combining a fine spatial segmentation with maximised information on energy, time, and possibly the nature of the energy deposition, for example by using dual-readout methods. This may be achieved, for example, by combining multiple optical materials sensitive to different components in the shower in finely segmented sandwich calorimeters, or by using timing information to extract the position of the energy deposition along a fibre. For future collider experiments, different approaches based on silicon, scintillator, noble liquid, fibre and crystal readout are being pursued [392]. They all foresee, with different level of emphasis, high granularity to enable the application of particle flow methods, and in some cases to further enhance their performance by additional information not exploited in current algorithms. One such example is the proposal [393] to benefit from the superior electromagnetic energy performance of crystals to pair photons from π^0 decays and thereby resolve jet finding ambiguities to improve the jet energy resolution.

35.10.2 Electromagnetic calorimeters

Revised August 2023 by C.L. Woody (BNL) and R.-Y. Zhu (HEP California Inst. of Technology).

The development of electromagnetic showers is discussed in the section on "Passage of Particles Through Matter" (Sec. 34 of this *Review*). Formulae are given which approximately describe average showers, but since the physics of electromagnetic showers is well understood, a detailed and reliable Monte Carlo simulation is possible. EGS4 [394] and GEANT [381] have emerged as the standards.

Electromagnetic calorimeters are devices that are designed to measure the total energy of electrons and photons by total absorption. They come in two general categories: homogeneous and sampling. In a homogeneous calorimeter, all of the particle's energy is deposited in the active detector volume and is used to produce a measurable signal (either scintillation light, Cherenkov light or charge). Homogeneous electromagnetic calorimeters are typically constructed using high density, high Z inorganic scintillating crystals such as BaF₂, BGO, CsI, CsI(Tl), LYSO, NaI(Tl) and PWO, non-scintillating Cherenkov radiators such as lead glass and lead fluoride (PbF₂), or ionizing noble liquids such as liquid argon, liquid krypton or liquid xenon. The properties of some commonly used inorganic crystal scintillators can be found in Table 35.4. Total absorption homogeneous calorimeters such as those built with heavy crystal scintillators provide the best energy resolution for measuring electromagnetic showers and are generally used when the best possible performance is required, particularly at lower energies. Attention, however, needs to be paid to radiation damage in inorganic scintillators when exposed to the typical environment of high luminosity proton colliders, as discussed below and in Section 35.4.

A sampling calorimeter consists of an active medium which generates a signal and a passive medium which functions as an absorber. In this case, most of the particle's energy is deposited in

the absorber and only a fraction of the energy is detected in the active medium. The ratio of energy in the sampling medium to the total energy in calorimeter is called the sampling fraction. The active medium may be a scintillator, an ionizing noble liquid, a semiconductor, or a gas ionization detector. The absorber is typically a heavy metal with a high Z such as lead, tungsten, iron, copper, or depleted uranium. The active material is interspersed with the passive absorber in a variety of ways, e.g. by using alternating plates of active material and absorber or embedding the active material, such as scintillating fibers, into the absorber. The main difficulty in this approach is extracting the signal from the active material. One possibility is a simple stack of alternating absorber and active material, which, however, usually leads to gaps for services and hence non-uniformities. This can be improved by using a so-called "spaghetti" design, where scintillating fibers are brought to the front or back of the detector and read out. This can also be done with either wavelength shifting plates or fibers, such as in a so-called "shashlik" design where wavelength shifting fibers run through the stack of alternating scintillator and absorber plates and are read out at end, or embedding wavelength shifting fibers in the scintillating plates which are then brought out to the edges or back of the detector and read out. For ionization detectors, there is also an "accordion" design which avoids all gaps for services and where the absorber plates are folded into an accordion shape along with interspersed electrodes to collect the ionization charge [395]. While these readout schemes are generally more complicated than those for homogeneous calorimeters, the sampling calorimeter design allows the construction of large calorimeters at much lower cost than homogeneous calorimeters.

The energy resolution σ_E/E of a calorimeter can be parameterized as $a/\sqrt{E} \oplus b \oplus c/E$, where \oplus represents addition in quadrature and E and σ_E are in GeV. The stochastic term a represents statistics-related fluctuations such as intrinsic shower fluctuations, photoelectron statistics, dead material at the front of the calorimeter, and sampling fluctuations for minimum ionizing particles. For a fixed number of radiation lengths, the stochastic term a for a sampling calorimeter is expected to be proportional to $\sqrt{t/f}$, where t is plate thickness and f is sampling fraction [396–398]. The stochastic term a is typically of the order of a few percent for a homogeneous calorimeter, and is generally in the range of 8 to 20% for sampling calorimeters, depending on the sampling fraction.

The main contributions to the systematic, or constant, term b are detector non-uniformity and calibration uncertainties. In the case of hadronic cascades discussed below, non-compensation also contributes deviations from \sqrt{E} scaling. Another important contribution to the energy resolution of calorimeters that are used in high radiation environments such as high luminosity colliders is radiation damage of the active medium. Radiation damage can induce optical absorption in scintillating materials which reduces the measured light output and produces non-uniformities in light collection. This can be mitigated by developing radiation-hard active media [399], by reducing the signal path length [400] and by frequent *in situ* calibration and monitoring [75, 398]. With effort, the constant term b can be reduced to below one percent. The term c is due mainly to electronic noise summed over the readout channels required to measure the shower energy (typically a few Molière radii).

The position resolution depends on the effective Molière radius and the transverse granularity of the calorimeter. Like the energy resolution, it can be factored as $a/\sqrt{E} \oplus b$, where a is the stochastic term, typically of the order of a few mm to 20 mm, and b can be as small as a fraction of mm for a dense calorimeter with fine granularity. Fine granularity also helps particle flow analysis discussed in the hadron calorimeters section below.

Electromagnetic calorimeters may also provide angular measurements for electrons and photons. This is particularly important for photon-related physics to identify the correct primary vertex, since photons are not detected by the tracking system of the overall experiment. The typical photon angular resolution is about 45 mrad/ \sqrt{E} , which can be achieved by implementing longitudinal segmentation [395] for a sampling calorimeter or by adding a preshower detector [401] for a homogeneous calorimeter

Table 35.11: Resolution of typical electromagnetic calorimeters. E is in GeV.

Technology (Experiment)	Depth	Energy resolution	Date
NaI(Tl) (Crystal Ball)	$20X_0$	$2.7\%/E^{1/4}$	1983
$\text{Bi}_4\text{Ge}_3\text{O}_{12}$ (BGO) (L3)	$22X_0$	$2\%/ \sqrt{E} \oplus 0.7\%$	1993
CsI (KTeV)	$27X_0$	$2\%/ \sqrt{E} \oplus 0.45\%$	1996
CsI(Tl) (BaBar)	$16\text{--}18X_0$	$2.3\%/E^{1/4} \oplus 1.4\%$	1999
CsI(Tl) (BELLE)	$16X_0$	1.7% for $E_\gamma > 3.5$ GeV	1998
CsI(Tl) (BES III)	$15X_0$	2.5% for $E_\gamma = 1$ GeV	2010
PbWO_4 (PWO) (CMS)	$25X_0$	$3\%/ \sqrt{E} \oplus 0.5\% \oplus 0.2/E$	1997
PbWO_4 (PWO) (ALICE)	$19X_0$	$3.6\%/ \sqrt{E} \oplus 1.2\%$	2008
Lead glass (OPAL)	$20.5X_0$	$5\%/ \sqrt{E}$	1990
Liquid Kr (NA48)	$27X_0$	$3.2\%/ \sqrt{E} \oplus 0.42\% \oplus 0.09/E$	1998
Scintillator/depleted U (ZEUS)	$20\text{--}30X_0$	$18\%/ \sqrt{E}$	1988
Scintillator/Pb (CDF)	$18X_0$	$13.5\%/ \sqrt{E}$	1988
SciFi/Pb spaghetti (KLOE)	$15X_0$	$5.7\%/ \sqrt{E} \oplus 0.6\%$	1995
SciFi/W (sPHENIX)	$20X_0$	$13\%/ \sqrt{E}$	2022
Liquid Ar/Pb (NA31)	$27X_0$	$7.5\%/ \sqrt{E} \oplus 0.5\% \oplus 0.1/E$	1988
Liquid Ar/Pb (SLD)	$21X_0$	$8\%/ \sqrt{E}$	1993
Liquid Ar/Pb (H1)	$20\text{--}30X_0$	$12\%/ \sqrt{E} \oplus 1\%$	1998
Liquid Ar/depl. U (DØ)	$20.5X_0$	$16\%/ \sqrt{E} \oplus 0.3\% \oplus 0.3/E$	1993
Liquid Ar/Pb accordion (ATLAS)	$25X_0$	$10\%/ \sqrt{E} \oplus 0.4\% \oplus 0.3/E$	1996

without longitudinal segmentation.

There have been many electromagnetic calorimeters built and used in particle physics experiments for a variety of applications. Table 35.11 provides a short list of the major ones used in some of the larger experiments. Also listed are calorimeter depths in radiation lengths (X_0) and the achieved energy resolution. Whenever possible, the performance of the calorimeters *in situ* is quoted, which is usually in good agreement with prototype test beam results as well as EGS or GEANT simulations, provided that all systematic effects are properly included. Details about detector design and performance can be found in Appendix C of reference [398] and Proceedings of the International Conference series on Calorimetry in High Energy Physics.

35.10.3 Hadronic calorimeters

Revised August 2021 by F. Sefkow (DESY, Hamburg) and F. Simon (KIT).

Hadronic calorimetry [380, 402, 403] is considerably more complex than electromagnetic (EM) calorimetry due to the wider range and different nature of physical processes contributing to shower development and energy deposition, which in turn are characterised by different length and time scales. Hadronic showers are initiated by inelastic strong interactions of highly-energetic charged and neutral hadrons with atomic nuclei. These interactions result in the production of secondary particles, which drive the development of the shower. Among these are energetic hadrons, as well as lower-energy nucleons, photons and nuclear fragments. Energy transferred to nuclear break-up, excitation or recoil does not, in general, produce a signal, but remains *invisible*, and event-to-event fluctuations of this invisible energy deposit ultimately limit the resolution of hadronic calorimeters (HCALs).

The length scale of the interaction of relativistic hadrons is given by the nuclear interaction length λ_I . As discussed in Section 35.10.1, λ_I is a factor 10 to 30 larger than X_0 for common materials used in the construction of calorimeters. HCALs thus require a significantly larger geometrical depth for full containment than electromagnetic calorimeters (ECALs), albeit not by the factor suggested by the ratio of λ_I/X_0 due to the different nature of the showers. A key role is played by the production of π^0 s and their subsequent decay into two photons. These result in the formation of electromagnetic sub-showers which evolve on the scale given by the radiation length X_0 , and thus require sufficiently fine sampling of the shower activity to capture also this electromagnetic component. The two different length scales occurring in hadronic

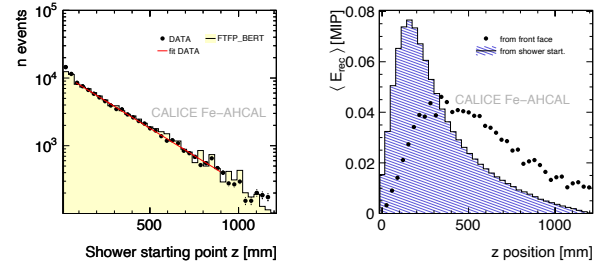


Figure 35.35: Longitudinal profile of hadronic showers induced by 45 GeV negative pions measured in the CALICE highly-granular steel-scintillator sampling calorimeter [404]. Left: Reconstructed position of the first inelastic interaction, compared to simulations (GEANT4 9.4p03, FTFP_BERT), and an exponential fit yielding a slope consistent with the expected pion interaction length. Right: Longitudinal shower profile measured from the front face of the calorimeter (dots, without corrections for dead cells) and relative to the position of the shower start given by the first inelastic interaction (filled histogram). The visible energy is given in units of the most probable energy loss of a minimum-ionizing particle (MIP). The integrals of the distributions are normalized to unity.

showers, and the large fluctuations of hadronic, electromagnetic and invisible activity, result in significant event-to-event variations of the energy response and of the shower topology. This topology is characterized by a lumpy structure, with compact regions of high local energy density originating from electromagnetic sub-showers, and sparser hadronic activity with minimum-ionizing hadrons.

Figure 35.35 (left) shows the distribution of the longitudinal position of the first inelastic interaction measured for pion-induced hadronic showers with the highly-granular scintillator-steel HCAL of the CALICE collaboration [404]. The figure illustrates the exponential distribution, with a slope consistent with the pion interaction length expected from the geometry and material composition of the calorimeter. This distribution is well reproduced by simulations using GEANT4 [381, 386]. Figure 35.35 (right) shows the mean longitudinal shower profile, given by the mean energy deposition in each calorimeter layer, both relative to the front face of the calorimeter (dots, without corrections for dead

cells) and relative to the measured shower starting point given by the first inelastic interaction (filled histogram). The latter is much more compact than the former, which is a convolution of the latter with the distribution of shower starting point shown in the left panel of the figure. This shows that the detector depth required for adequate shower containment is significantly influenced by the fluctuations of the position of the first hadronic interaction. Detection of this position allows for an estimate of leakage from a finite calorimeter volume, and it enables stringent tests of shower evolution models. In the past years, motivated by precision needs at the next generation of e^+e^- colliders, the CALICE collaboration has constructed a number of prototypes with high 3-dimensional spatial granularity and recorded large sets of data at test beams, allowing for studies of shower evolution processes in unprecedented detail. The refined simulations support the trend to proceed from research focused on understanding the global intrinsic properties of showers, e.g. for the purpose of compensation, towards the study of detailed information, in space, time, and energy deposition type, through many and multiple readout channels.

In an inelastic hadronic collision a significant fraction f_{em} of the energy is removed from further hadronic interaction by the production of secondary π^0/η 's, whose decay photons generate high-energy electromagnetic showers. Charged secondaries (π^\pm, p, \dots) deposit energy via ionization and excitation, but also interact with nuclei, producing evaporation neutrons, spallation protons and neutrons, and heavier spallation fragments. The charged collision products produce detectable ionization, as do the showering γ -rays from the prompt de-excitation of highly excited nuclei. The recoiling nuclei generate little or no detectable signal, as mentioned previously. The neutrons lose kinetic energy in elastic collisions which generate ionization signals via recoiling protons, thermalize on a time scale of several μs , and are finally captured, with the production of more γ -rays—usually outside the acceptance gate of the electronics. Between endothermic spallation losses, nuclear recoils, and late neutron capture, a significant fraction of the hadronic energy (20%–40%, depending on the absorber and energy of the incident particle) is used to overcome nuclear binding energies and is therefore lost or “invisible.”

In a hadron-nucleus collision a large fraction of the incident energy is carried by a “leading particle” with the same quark content as the incident hadron. If the projectile is a charged pion, the leading particle is usually a pion, which can be neutral and hence contributes to the EM sector. This is not true for incident protons. The result is an increased mean hadronic fraction for incident protons.

The complexity of hadronic showers also has a significant impact on the energy measurement. In contrast to EM showers, hadronic cascade processes are characterised by the production of relatively few high-energy particles. The number multiplicity of these particles produced in hadronic interactions increases only logarithmically with energy. The lost energy and f_{em} are highly variable from event to event, and on average increase with increasing energy [405]. Electromagnetic sub-showers typically result in a higher response than the hadronic parts of the cascade, where undetectable energy loss due to nuclear dissociation, the long time scales and the material dependence of neutron signals, as well as other effects reduce the measured signal. This difference in response is often expressed by the $\langle h/e \rangle$ ratio, a calorimeter-dependent quantity which is smaller than unity for many, but not all, HCALS. The increase of the electromagnetic fraction with energy thus introduces a non-linear contribution to the response. Combined with the significant event-by-event fluctuations between electromagnetic and hadronic fractions of the showers and between different hadronic processes the non-equality of h and e deteriorates the energy resolution of HCALS. Different strategies to address this exist, as discussed further below.

Most large HCALS are parts of complex 4π detectors at colliding beam facilities. To date, all these HCALS are sampling calorimeters. This choice is imposed by the physics of hadronic showers, both by the required depth for containment which favours high-density materials with short λ_I , and by the differences in response to electromagnetic and hadronic parts of the cascade, which are

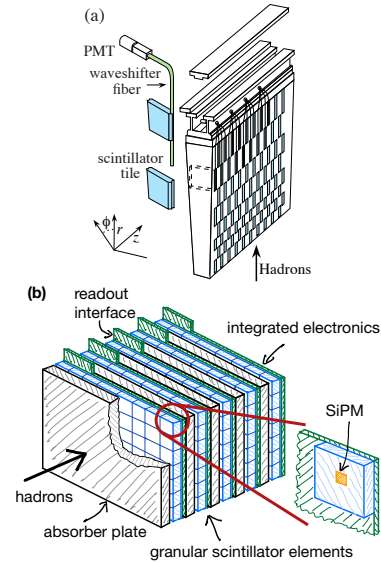


Figure 35.36: Two examples of geometrical structures of scintillator-based HCALS. (a) A wedge of the ATLAS central tile calorimeter consisting of scintillator tiles in iron, read out via wavelength-shifting fibers and PMTs [406]. The coordinate system is that of the ATLAS calorimeter within the experiment, with the z axis along the beam direction, r pointing radially outward, and ϕ being the azimuthal angle. (b) An illustration of the “SiPM-on-tile” structure used in the CALICE analogue HCAL prototype, and in the CMS High-Granularity Calorimeter (HG-CAL), highly granular calorimeters with steel absorbers and small scintillator tiles directly read out via SiPMs with embedded electronics [403, 407–409].

particularly severe for homogeneous calorimeters. Common absorber materials are Fe, Cu, Pb, and U, with W also used occasionally. A large variety of different active materials are used, depending on application and optimisation, from plastic scintillators (plates, tiles, bars, fibers), crystals and Cherenkov media, silicon, liquid argon (LAr), to gaseous detectors. The energy loss of particles in the active medium is either detected directly by collecting charge, or via scintillation or Cherenkov light observed with conventional photomultipliers (PMTs), photodiodes or silicon photomultipliers (SiPMs). The choice of both active and passive materials is driven by different, sometimes conflicting, constraints, including performance requirements, space and other mechanical boundary conditions, radiation tolerance, and cost considerations.

A wide range of different geometries of absorbers and sensors is used, with design choices depending on the chosen priorities of addressing these constraints, also considering the need to bring the signals to the outside of the detector while achieving a hermetic coverage and other constraints. In this context it is important to note that a classic sandwich structure with absorber plates and active elements approximately perpendicular to the particle incidence is not required, and arbitrary orientations are viable for good calorimetric measurements, as long as channelling, meaning the extended passage of primary particles through low-density active regions, is excluded. Figure 35.36 shows two examples of plastic scintillator-based calorimeters to illustrate differences in design between coarsely-segmented and highly-granular calorimeters. The ATLAS tile calorimeter [406] uses scintillator tiles coupled to wavelength-shifting fibers which collect the light from the tiles and guide them to PMTs outside of the active region of the calorimeter. The calorimeter is segmented in ϕ (azimuthal angle) and η (pseudorapidity, defined as $\eta = -\ln \tan(\theta/2)$, where θ is the angle relative to the beam axis), with coarse longitudinal segmentation. The technological prototype of the CALICE analogue HCAL, a highly granular SiPM-on-tile calorimeter is based on scintillator tiles directly coupled to SiPMs, which, together with

the front-end electronics, are embedded inside of the the active volume of the calorimeter. The CMS HGICAL [409] uses the same concept in part of the detector, and in addition embeds elements for digital data concentration and power distribution in the active volume. Other detector solutions include scintillating fibres threading an absorber [410], liquid-argon-filled tubes [411] and the “accordion” LAr detector [412]. The latter has zig-zag absorber plates to minimize channeling effects; the calorimeter is hermetic (no cracks), and plates are oriented so that cascades cross the same plate repeatedly.

In particular, but not exclusively, the combination of heavy absorber materials (Pb, U) with plastic scintillators allows the construction of HCALS that have a near-equal response to electromagnetic and hadronic parts of the cascade, so-called compensating calorimeters [413]. In this first study, it was recognized that nuclear fission can amplify the hadronic signal when using uranium absorbers. However, the key drivers of compensation are the reduction of the electromagnetic response with high-Z absorbers and an increased sensitivity to neutrons, which are strongly correlated to otherwise invisible energy loss due to nuclear dissociation, with a homogeneous active medium [414–418]. Since the electromagnetic cross section increases, and the critical energy decreases with Z, and since most of the energy of an electromagnetic shower is deposited by low-energy, short-range electrons, a disproportionate fraction of the total electromagnetic energy is deposited in the absorber in the high-Z case. Hydrogenous active media, such as organic scintillators, have a high sensitivity to spallation neutrons via elastic $n - p$ scattering. The number of produced neutrons is highly correlated with the invisible energy of the hadronic cascade. Increasing the sensitivity to these particles can thus boost the visible hadronic signal. Achieving compensation requires carefully-chosen sampling fractions and frequencies, with the response to the hadronic parts of the shower also sensitive to the integration time of the electronics due to the time structure of the neutron component of the signal.

Since Cherenkov light, for example in quartz plates or fibers, or in crystals, is produced only by relativistic particles in the cascade and thus predominantly by the electromagnetic component of the shower, such media are less common in hadronic than in ECALS. Notable exceptions are applications that require high radiation tolerance, and dual-readout calorimeters which specifically exploit this feature, as discussed below.

Silicon offers high compactness, high granularity, high radiation tolerance, long-term stability and fast charge collection, and is thus an interesting active material for sampling calorimeters. A thorough overview of the development and of the features of this technology can be found in a recent review paper [419]. The first silicon-based calorimeter in a collider experiment was a HCAL, the H1 PLUG calorimeter [420] covering the very forward region of the H1 experiment at HERA. The SICAPO collaboration has demonstrated the conceptual possibility of constructing compensating HCALS using silicon sensors [421]. Silicon is currently the technology of choice for several ECALS for future Higgs factories [422–424]. It is also being used extensively in the CMS HGICAL [409] in both electromagnetic and hadronic sections, complemented by scintillator tiles with on-tile SiPM readout where the radiation levels allow.

More generally, high-granularity calorimeters play an increasingly important role, in particular motivated by the use of particle-flow algorithms for global event reconstruction (see Section 35.10.1). The associated technologies for both electromagnetic and HCALS have been pioneered by the CALICE collaboration, which has built and tested an increasingly sophisticated series of “imaging” calorimeters with a highly granular readout [425]. In the area of HCALS, this includes the scintillator-based analog HCAL [426] with the latest SiPM-on-tile technological prototype with fully-integrated electronics having approximately 22,000 channels [407, 408], as well as digital [427] and semidigital [428] calorimeters using gas detectors, such as RPCs (Sec. 35.6.7) and micropattern gas detectors (Sec. 35.6.4), with channel counts of up to 500,000. The large numbers of channels of high-granularity calorimeters presents a significant integration challenge for full detector systems, and requires the full integra-

tion of the front-end electronics inside of the active volume of the detector, as well as very compact data concentration and interface units. The first such detector in construction for a collider experiment is the CMS HGICAL [409]. Beam tests with a combined prototype using both silicon and scintillator-SiPM instrumented active layers have confirmed simulation-based expectations [429]. The total silicon area of the full HGICAL amounts to about 600 m², and about 240,000 SiPMs are foreseen. The calibration of such calorimeters requires the monitoring of a large number of cells, which is achieved in-situ using reconstructed track segments within hadronic showers [409, 430] or externally identified muons. For this method, the capability to detect the most probable energy loss of a minimum-ionizing particle in a single cell is essential. This is required over the full lifetime of the detector, also after the active elements have received significant radiation damage, resulting in increased noise and reduced charge or signal collection efficiency. Due to the large number of cells contributing to the measurement of one shower, the requirements on the precision of the calibration of individual cells is relaxed relative to the global energy calibration of the calorimeter.

The energy resolution of HCALS is severely affected by fluctuations between different components of the cascade, exacerbated by differences in response to purely hadronic and to electromagnetic sub-showers. In many detectors, fluctuations in the electromagnetic energy fraction, f_{em} , and the related, consequential variations in nuclear energy dissociation losses, represent the biggest single contribution to the hadron energy resolution. One strategy to address this problem is the construction of intrinsically-compensating calorimeters, which imposes stringent constraints on materials and geometries as discussed above. Compensating calorimeters are not used in current large collider experiments, and are at the moment not considered for future collider detectors. Two different strategies are presently followed to improve the energy resolution in non-compensating calorimeters: Offline weighting or software compensation in longitudinally-segmented or in highly-granular calorimeters; and dual-readout calorimetry.

Software compensation techniques exploit the fact that electromagnetic sub-showers typically have a higher spatial density than the purely hadronic parts of the cascade. Amplitude (or energy-density) dependent weights are applied in the reconstruction to reduce the effects of shower-to-shower fluctuations. These techniques were pioneered by the CDHS collaboration for a longitudinally segmented steel-plastic scintillator calorimeter [431], where an improvement of the energy resolution of 10% (at 10 GeV) to 30% (at 140 GeV) for charged pion showers was achieved. Similar techniques were successfully applied in the H1 [432] liquid argon calorimeter system resulting in a stochastic term of $51\%/\sqrt{E}$, and in the ATLAS [433] endcap calorimeters, also based on liquid argon, with an energy resolution of $84\%/\sqrt{E}$. Inspired by these approaches, a software compensation technique using the detailed spatial information provided by highly-granular calorimeters of the CALICE collaboration has been developed, achieving up to 25% improvement of the energy resolution compared to the resolution without software compensation, resulting in a stochastic term of $45\%/\sqrt{E}$ [434] in a scintillator tile calorimeter with steel absorbers. This technique has also been successfully transferred to particle-flow reconstruction [435], resulting in an improvement of the jet-energy resolution in simulated events by 8% - 15%, depending on jet energy. Highly-granular calorimeters with software compensation and particle-flow reconstruction are currently studied as the baseline configuration for several Higgs-factory detectors.

The *dual-readout method*, originally proposed by Mockett in 1983 [436], measures f_{em} event by event in parallel to the total deposited energy. It uses the fact that most of the relativistic particles in the shower originate from the electromagnetic part, and that only those produce Cherenkov light, while the signal of the hadronic part is mostly due to non-relativistic protons. In practice either two different active media, e.g. scintillator and quartz, are used to register scintillation and Cherenkov light, respectively, or the optical signals from the two processes occurring in heavy crystals are disentangled, using their different spectral, directional or timing properties.

The Cherenkov and scintillation signals, normalised to the response for electrons, are given by

$$C = [f_{em} + (h/e)_C(1 - f_{em})]E, \quad (35.44)$$

$$S = [f_{em} + (h/e)_S(1 - f_{em})]E, \quad (35.45)$$

respectively, which can be solved for the fraction f_{em} and the energy

$$E = (\xi S - C)/(\xi - 1), \quad (35.46)$$

where $\xi = [1 - (h/e)_C]/[1 - (h/e)_S]$ and $(h/e)_{C,S}$ denote the average ratios of hadronic to electromagnetic response in the Cherenkov and scintillator parts, respectively. This is illustrated in Figure 35.37, which shows their correlation for a set of simulated negative pion events [437] using FLUKA [385].

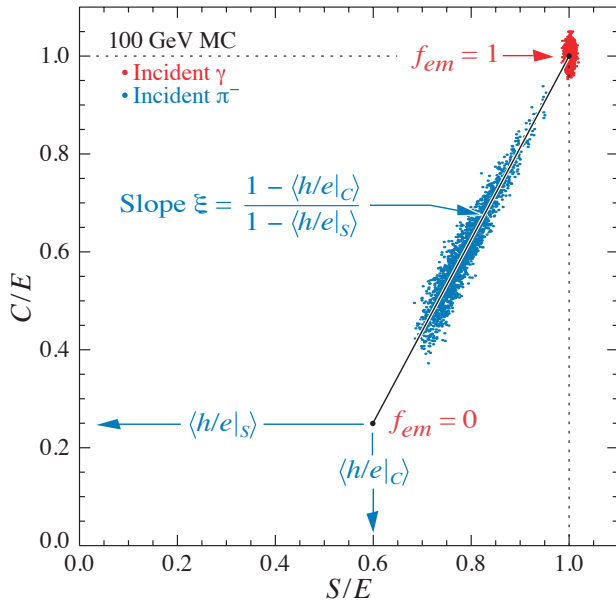


Figure 35.37: Scatter plot of Monte Carlo C/E (Cherenkov) vs S/E (scintillator) signals for individual events in a dual-readout calorimeter for 100 GeV negative pions and photons. Hadronic events are shown in blue, and scatter about the indicated event locus. Electromagnetic events cluster about $(C/E, S/E) = (1,1)$. In this case worse resolution (fewer p.e.'s) was assumed for the Cherenkov events, leading to the “elliptical” distribution.

It was noted that the method demands a steep slope ξ , which implies that the scintillator read-out should be as compensating as possible, which however reduces the room for improvement by adding Cherenkov information.

The method was tested by the DREAM/RD52 collaboration [438,439], using a 1 ton copper matrix with embedded quartz and scintillating fibers. The value of ξ was about 3 in this detector. With this detector, a resolution of $70\%/\sqrt{E(\text{GeV})}$ was obtained for single hadrons [440]. Due to the small size of the module, this includes contributions from transverse leakage which prevent the full exploitation of key features of dual readout, and thus underestimates the potential of the method.

The separate Cherenkov read-out evidently provides excellent pion-electron separation for particle identification. In another RD52 prototype, each fiber is read out individually by SiPMs, giving also a superior transverse granularity. A fiber-based calorimeter with full solid-angle coverage requires a pointing geometry due to the limited or missing longitudinal segmentation. The resulting challenges for a mechanical design are studied in the framework of the IDEA detector concept [441].

Table 35.12 shows selected examples of the energy resolution of HCALs for single charged pions achieved in beam tests. The examples are selected to illustrate the performance achieved with different designs ranging from intrinsic compensation to software compensation and dual readout, with a focus on results by R&D

projects. It should be noted that the exact values of the different resolution terms depend on the functional form used in the fit, here the addition in quadrature is used for the cases where more than just the stochastic term is quoted. The results shown in the table illustrate that (close to) compensating calorimeters with optimized sampling fraction and frequency, such as HELIOS (U-plastic scintillator) and SPACAL (Pb-plastic scintillator), achieve a very good energy resolution. The comparison with Bernardi *et al.*, which has the same Pb/scintillator ratio by volume as SPACAL, but coarser sampling in a sandwich structure, illustrates the importance of the geometrical details. Beyond the examples shown in the table, liquid argon has also been explored as an active medium, for example in the context of the SLD detector with different absorber options [446]. Due to the reduced sensitivity to neutrons in the shower, not the same resolution as for plastic-scintillator-based systems is achieved. This technology has also been used in the D0 experiment, as discussed below. The dual-readout method has the potential to reach or surpass this performance, but would require a prototype sufficiently large for full longitudinal and transverse shower containment for an experimental demonstration. The two CALICE calorimeters shown, which use the same active elements (5 mm thick scintillator tiles) but different absorbers (21.4 mm Fe vs 10 mm W + 4 mm Fe) per layer, illustrate the impact of the absorber choice on energy resolution and reconstruction possibilities. While the tungsten-based W-AHCAL setup is very close to compensating, the steel-based AHCAL achieves a better energy resolution when software compensation is applied, profiting from the finer sampling of the electromagnetic parts of the cascade and the correction for shower-to-shower fluctuations of the electromagnetic fraction in the reconstruction. In the case of tungsten, software compensation does not significantly improve the energy resolution, as expected. The comparison of the CALICE AHCAL performance with the one of CDHS illustrates the benefits of higher granularity for software compensation techniques, but it should be noted that the absorber thickness of the latter is 25 mm, with the same scintillator thickness as in the case of CALICE.

As explained in the introduction, in most high-energy physics experiments, the HCAL follows after an ECAL, making the response of the latter to hadronic cascades highly relevant for the overall performance of the combined ECAL and HCAL system. For scenarios where the electromagnetic and the HCAL have very different $\langle h/e \rangle$, as is typically the case for crystal-based ECALs, the fluctuations of the fraction of the hadronic shower contained within the ECAL result in a significant deterioration of the energy resolution for hadrons. A deterioration of the hadronic performance also results from larger amounts of not-instrumented material, e.g. supports and services, between electromagnetic and hadronic sections. In particle-flow calorimeters, a large value of the λ_T/X_0 ratio of the absorber material, like in tungsten, maximises the longitudinal separation of electromagnetic and hadronic showers. This is reflected in the design of particle-flow-based detector concepts for future Higgs Factories.

Table 35.13 summarizes the single hadron energy resolution obtained from test beams of the combined ECAL and HCAL systems of the large multi-purpose experiments at HERA, the Tevatron and at the LHC. These systems are examples of different optimization strategies. D0 and ZEUS are near-compensating systems with the same technology in ECAL and HCAL emphasizing hadronic performance. ATLAS and H1 use sampling ECALs with good electromagnetic resolution and weighting techniques exploiting longitudinal and transverse shower information for hadronic energy reconstruction. CMS, with a crystal ECAL and a scintillator-brass HCAL, prioritizes electromagnetic performance, with very different $\langle h/e \rangle$ in the electromagnetic and hadronic system. Of the detectors shown in the table, CMS has the best electromagnetic resolution by a comfortable margin, but consequently the weakest hadronic resolution. The best hadronic performance is achieved with the compensating calorimeter of ZEUS, which however has a weaker electromagnetic performance than the other calorimeter systems shown here. It should be noted that an excellent single-hadron resolution in general does not fully propagate into the jet-energy performance. Inactive material in

Table 35.12: Energy resolution of selected hadron calorimeters for single charged hadrons obtained in beam tests.

Calorimeter	Passive	Active	Resolution	Ref.
Bernardi <i>et al.</i>	Pb	Scintillator layers	$44.2\%/\sqrt{E}$ §	[442]
CALICE AHCAL	Fe	Scintillator tiles	$44.3\%/\sqrt{E} \oplus 1.8\%$ †	[434]
CALICE W-AHCAL	W	Scintillator tiles	$57.9\%/\sqrt{E} \oplus 4.6\% \oplus 0.065/E$ §	[443]
CDHS	Fe	Scintillator layers	$58\%/\sqrt{E}$ ‡	[431]
DREAM/RD52	Pb	Scint.+ Quartz fibers	$70\%/\sqrt{E}$ *	[440]
HELIOS	U	Scintillator layers	$34\%/\sqrt{E}$ §	[444]
SPACAL	Pb	Scintillating fibers	$33.3\%/\sqrt{E} \oplus 2.2\%$ §	[445]

§ Bernardi *et al.*, CALICE W-AHCAL, HELIOS, SPACAL: (near-)compensating calorimeters.
† CALICE AHCAL: Local software compensation exploiting the high granularity of the calorimeter.
‡ CDHS: Offline weighting using longitudinal information.
* DREAM/RD52: Due to the relatively small transverse size of the detector lateral leakage was significant, deteriorating the energy resolution with respect to the full potential of the dual readout method.

Table 35.13: Energy resolution of selected combined electromagnetic and hadronic calorimeter systems in past and present high-energy collider experiments for single hadrons. The results are taken from beam tests of prototypes with the electromagnetic calorimeter upstream of the hadronic calorimeter.

Experiment	technology (ECAL, HCAL)	Combined hadronic resolution	Reference
H1	Pb/LAr, Steel / LAr	$46\%/\sqrt{E} \oplus 2.6\% \oplus 0.73/E$	[447]
ZEUS	depleted U / plastic scintillator	$35\%/\sqrt{E}$	[448]
CDF	Pb/plastic scint., Steel/plastic scint.	$68\%/\sqrt{E} \oplus 4.1\%$	[449]
D0	depleted U / LAr	$44.6\%/\sqrt{E} \oplus 3.9\%$	[450]
ATLAS	Pb/LAr, Steel/plastic scintillator	$52\%/\sqrt{E} \oplus 3.0\% \oplus 1.6/E$	[451]
CMS	PbWO ₄ , brass/plastic scintillator	$84.7\%/\sqrt{E} \oplus 7.4\%$	[452]

front of the calorimeter can significantly worsen the energy resolution for jets, with an impact in particular on lower-energy particles. For example, the core of the invariant mass distribution of hadronically-decaying Z^0 bosons measured in ZEUS, which had a superconducting coil in front of the calorimeter, is well described by a Gaussian with a σ of 6 GeV [453], approximately 40% wider than would be expected for a jet-energy resolution that is identical to the single-hadron performance.

35.10.4 Free electron drift velocities in liquid ionization chambers

Revised August 2009 by W. Walkowiak (Siegen U.).

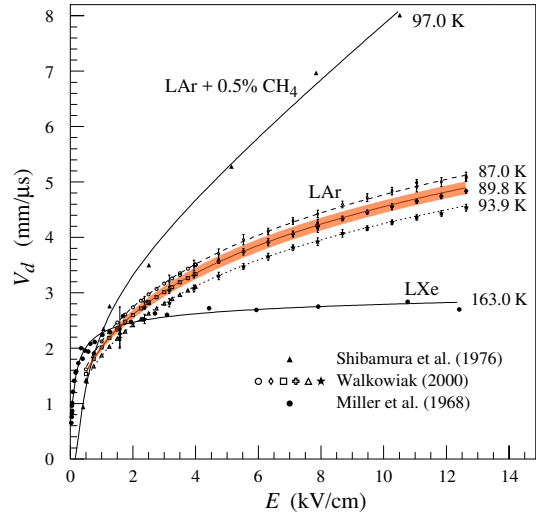
Drift velocities of free electrons in LAr [259] are given as a function of electric field strength for different temperatures of the medium in Fig. 35.38. The drift velocities in LAr have been measured using a double-gridded drift chamber with electrons produced by a laser pulse on a gold-plated cathode. The average temperature gradient of the drift velocity of the free electrons in LAr is described [259] by

$$\frac{\Delta v_d}{\Delta T v_d} = (-1.72 \pm 0.08) \%/\text{K}. \quad (35.47)$$

Previous measurements [454, 455, 457, 458] range from 13% higher [455] to 18% lower [457] than these measurements. They used different techniques and show drift velocities for free electrons which cannot be explained by the temperature dependence mentioned above.

Drift velocities of free electrons in LXe [454] as a function of electric field strength are also displayed in Fig. 35.38. The drift velocity saturates for $|E| > 3$ kV/cm, and decreases with increasing temperature for LXe as well as measured e.g. by [459].

The addition of small concentrations of other molecules like N₂, H₂ and CH₄ in solution to the liquid typically increases the drift velocities of free electrons above the saturation value [454, 457], see example for CH₄ admixture to LAr in Fig. 35.38. Therefore, actual drift velocities are critically dependent on even small additions or contaminations.

**Figure 35.38:** Drift velocity of free electrons as a function of electric field strength for LAr [259], LAr + 0.5% CH₄ [454] and LXe [455]. The average temperatures of the liquids are indicated. Results of a fit to an empirical function [456] are superimposed. In case of LAr at 91 K the error band for the global fit [259] including statistical and systematic errors as well as correlations of the data points is given. Only statistical errors are shown for the individual LAr data points.

35.11 Accelerator-based neutrino detectors

Written by M.O. Wascko (Imperial Coll. London). Minor revision in August 2023 by A. Fava (FNAL) and F. Pietropaolo (CERN);

INFN, Padova).

35.11.1 Introduction

Accelerator-based neutrino experiments span many orders of magnitude in neutrino energy, from a few MeV to hundreds of GeV. This wide range of neutrino energy is driven by the many physics applications of accelerator-based neutrino beams. Foremost among them is neutrino oscillation, which varies as the ratio L/E_ν , where L is the neutrino baseline (distance traveled), and E_ν is the neutrino energy. But accelerator-based neutrino beams have also been used to study the nature of the weak interaction, to probe nucleon form factors and structure functions, and to study nuclear structure.

The first accelerator-based neutrino experiment used neutrinos from the decays of high energy pions in flight to show that the neutrinos emitted from pion decay are different from the neutrinos emitted by beta decay [460]. The field of accelerator-based neutrino experiments would likely not have expanded beyond this without Simon van der Meer's invention of the magnetic focusing horn [461], which significantly increased the flux of neutrinos aimed toward the detector. In this mini-review, we focus on experiments employing decay-in-flight beams—pions, kaons, charmed mesons, and taus—producing fluxes of neutrinos and antineutrinos from ~ 10 MeV to ~ 100 GeV.

Neutrino interactions with matter proceed only through the weak interaction, making the cross section extremely small and requiring high fluxes of neutrinos and large detector masses in order to achieve satisfactory event rates. Therefore, neutrino detector design is a balancing act taking into account sufficient numbers of nuclear targets (often achieved with inactive detector materials), adequate sampling/segmentation to ensure accurate reconstruction of the tracks and showers produced by neutrino-interaction secondary particles, and practical readout systems to allow timely analysis of data.

35.11.2 Signals and Backgrounds

The neutrino interaction processes available increase with increasing neutrino energy as interaction thresholds are crossed; in general neutrino-interaction cross sections grow with energy; for a detailed discussion of neutrino interactions see [462]. The multiplicity of secondary particles from each interaction process grows in complexity with neutrino energy, while the forward-boost due to increasing E_ν compresses the occupied phase space in the lab frame, impacting detector designs. Because decay-in-flight beams produce neutrinos at well-defined times, leading to very small duty factors, the predominant backgrounds usually stem from unwanted beam-induced neutrino interactions, i.e. neutrinos interacting via other processes than the one being studied. A noteworthy exception is time projection chambers, wherein the long drift times can admit substantially more cosmic backgrounds than most other detection methods. Cosmic backgrounds are more rare at higher energies because the secondary particles produced by neutrino interactions yield detector signals that resemble cosmic backgrounds less and less.

Below, we describe a few of the dominant neutrino interaction processes, with a focus on the final state particle content and topologies.

35.11.2.1 Charged-Current Quasi-Elastic Scattering and Pion Production

Below ~ 2 GeV neutrino energy, the dominant neutrino-nucleus interaction process is quasi-elastic (QE) scattering. In the charged current (CC) mode, the CCQE base neutrino reaction is $\nu_\ell n \rightarrow \ell^- p$, where $\ell = e, \mu, \tau$, and similarly for antineutrinos, $\bar{\nu}_\ell p \rightarrow \ell^+ n$. The final state particles are a charged lepton, and perhaps a recoiling nucleon if it is given enough energy to escape the nucleus. Detectors designed to observe this process should have good single-particle track resolution for muon neutrino interactions, but should have good μ/e separation for electron neutrino interactions. Because the interaction cross section falls sharply with Q^2 , the lepton typically carries away more of the neutrino's kinetic energy than the recoiling nucleon. The fraction of backward-scattered leptons is large, however, so detectors with 4π coverage are desirable. The dominant backgrounds in this channel tend to

come from single pion production events in which the pion is not detected.

Near 1 GeV, the quasi-elastic cross section is eclipsed by pion production processes. A typical single pion production ($CC1\pi$) reaction is $\nu_\ell n \rightarrow \ell^- \pi^+ n$, but many more final state particle combinations are possible. Single pion production proceeds through the coherent channel and many incoherent processes, dominated by resonance production. With increasing neutrino energy, higher-order resonances can be excited, leading to multiple pions in the final state. Separating these processes from quasi-elastic scattering, and indeed from each other, requires tagging, and ideally reconstructing, the pions. Since these processes can produce neutral pions, electromagnetic (EM) shower reconstruction is more important here than it is for the quasi-elastic channel. The predominant backgrounds for pion production change with increasing neutrino energy. Detection of pion processes is also complicated because near threshold the quasi-elastic channel creates pion backgrounds through final state interactions of the recoiling nucleon, and at higher energies backgrounds come from migration of multiple pion events in which one or more pions is not detected.

35.11.2.2 Deep Inelastic Scattering

Beyond a few GeV, the neutrino has enough energy to probe the nucleon at the parton scale, leading to deep inelastic scattering (DIS). In the charged-current channel, the DIS neutrino reaction is $\nu_\ell N \rightarrow \ell^- X$, where N is a nucleon and X encompasses the entire recoiling hadronic system. The final state particle reconstruction revolves around accurate reconstruction of the lepton momentum and containment and reconstruction of the hadronic shower energy. Because of the high neutrino energies involved, DIS events are very forward boosted, and can have extremely long particle tracks. For this reason, detectors measuring DIS interactions must be large to contain the hadronic showers in the detector volume.

35.11.2.3 Neutral Currents

Neutrino interactions proceeding through the neutral current (NC) channel are identified by the lack of a charged lepton in the final state. For example, the NC elastic reaction is $\nu_\ell N \rightarrow \nu_\ell N$, and the NC DIS reaction is $\nu_\ell N \rightarrow \nu_\ell X$. NC interactions are suppressed relative to CC interactions by a factor involving the weak mixing angle; the primary backgrounds for NC interactions come from CC interactions in which the charged lepton is misidentified.

35.11.3 Instances of Neutrino Detector Technology

Below we describe many of the actual detectors that have been built and operated for use in accelerator-based neutrino beams.

35.11.3.1 Spark Chambers

In the first accelerator-based neutrino beam experiment, Lederman, Schwartz, and Steinberger [460] used an internally-triggered spark chamber detector, filled with 10 tons of Al planes and surrounded by external scintillator veto planes, to distinguish muon tracks from electron showers, and hence muon neutrinos from electron neutrinos. The inactive Al planes served as the neutrino interaction target and as radiators for EM shower development. The detector successfully showed the presence of muon tracks from neutrino interactions. It was also sensitive to the hadronic showers induced by NC interactions, which were unknown at the time. In 1963, CERN also built and ran a large (20 ton) Al plane spark chamber in a wideband beam based on the PS accelerator [463]. More than a decade later, the Aachen-Padova [464] experiment at CERN employed a 40 ton Al spark chamber in the PS-WBB.

35.11.3.2 Bubble Chambers

Several large bubble chamber detectors were employed as accelerator neutrino detectors in the 1970s and 80s, performing many of the first studies of the properties of the weak interaction. Bubble chambers provide exquisite granularity in the reconstruction of secondary particles, allowing very accurate separation of interaction processes. However, the extremely slow and labor-intensive acquisition and analysis of the data from photographic film led to them being phased out in favor of electronically read out detectors.

Table 35.14: Properties of detectors for accelerator-based neutrino beams. Revised in August 2023 by A. Fava (FNAL) and F. Pietropaolo (CERN; INFN, Padova).

Name	Type	Target	Total Mass (fiducial) [t]	$\langle E_\nu \rangle$ [GeV]	Location	Dates
Lederman et al.	Spark	Al	10	[0.2-3]	BNL	1962
CERN-spark.	Spark	Al	20	1.5	CERN	1963
Serpukhov	Spark	Al	20	[3-30]	IHEP	1974-82
Aachen-Padova	Spark	Al	40(20)	1.4	CERN	1976-77
Gargamelle	Bubble	Freon	12	[1-10]	CERN	1970-79
BEBC	Bubble	H,D,Ne-H	2-42	[50-150],20	CERN	1977-84
SKAT	Bubble	Freon	8	7	IHEP	1976-1987
ANL-12ft	Bubble	H,D	1-2	0.5	ANL	1970
BNL-7ft	Bubble	HD	0.4-0.9	1.3,3	BNL	1976-82
Fermilab-15ft	Bubble	D, Ne	1,20	[50-180],[25-100]	FNAL	1973-92
CITF	Iron	Fe	92	[50-180]	FNAL	1974-83
CDHS	Iron	Fe	1250(520)	10-200	CERN	1976-84
MINOS	Iron	Fe	980(23.7), 5.5k (4.2k)	3	FNAL, SUL	2005-2012
MINOS+	Iron	Fe	980, 5.5k	4-10	FNAL, SUL	2013-2016
INGRID	Iron	Fe	160	0.6-3	J-PARC	2010-
SuperKamiokande	Cherenkov	H ₂ O	50k (22.5k)	0.6	Kamioka	1996-2018
SuperK-Gd	Cherenkov	H ₂ O doped with Gd	50k (22.5k)	0.6	Kamioka	2020-
HyperK	Cherenkov	H ₂ O	260k(190k)	0.6	Kamioka	2027-
K2K-1kt	Cherenkov	H ₂ O	25	0.8	KEK	1998-2004
MiniBooNE	Cherenkov	CH ₂	818(440)	0.5	FNAL	2002-19
ANNIE	Cherenkov	H ₂ O with GD sulfate	26	0.8	FNAL	2021-
HWPf	Scintillation	CH ₂ , Fe	160	[50-180]	FNAL	1974-78
LSND	Scintillation	CH ₂	167	0.003-0.06	LANL	1993-1998
NOvA	Scintillation	CH ₂	300, 14k	2	FNAL,Ash River	2014-
SciBar	Scintillation	CH	15(9.5)	0.6	KEK	2003-2004
SciBooNE,	Scintillation	CH	15(9.5)	0.8	FNAL	2007-08
Captain Mills	Scintillation	Ar	10	0.003-0.06	LANL	2022-2024
ICARUS	LArTPC	Ar	760(476)	17	LNGS	2006-12
ICARUS	LArTPC	Ar	760(476)	0.8	FNAL	2020-
Argoneut	LArTPC	Ar	0.025	3	FNAL	2009-10
MicroBooNE	LArTPC	Ar	170(85)	0.8	FNAL	2014-21
SBND	LArTPC	Ar	220(112)	0.8	FNAL	2024-
DUNE	LArTPC	Ar	70(40)	3	FNAL,SURF	2027-
FNAL-E-531	Emulsion	Ag, Br	0.009	22	FNAL	1984
CHORUS	Emulsion	Ag, Br	0.8	27	CERN	1994-97
DONuT	Emulsion	Fe	0.26	53	FNAL	1997
OPERA	Emulsion	Pb	1.25k	17	LNGS	2008-12
NINJA	Emulsion	Fe	0.002(0.001)	0.6	J-PARC	2015-
FASEr ν	Emulsion	W	1.2	[360-6300]	CERN (LHC)	2022-
CHARM	Hybrid	CaCO ₃	(27),156(122)	20	CERN	1978-84
CHARM-II	Hybrid	glass	692	20	CERN	1984-91
BNL-E-734	Hybrid	CH ₂	172	1.3	BNL	1981-86
BNL-E-776	Hybrid	concrete	240	1.4	BNL	1986
NOMAD	Hybrid	CH	2.9(2.7)	27	CERN	1995-98
CCFR	Hybrid	Fe	690	[30-260]	FNAL	1985-88
NuTeV	Hybrid	Fe	690	[70-180]	FNAL	1996-97
MINERvA	Hybrid	CH,H ₂ O,Fe,Pb,C,He	8	3.8	FNAL	2010-19
T2K-ND280	Hybrid	CH,H ₂ O	2	0.6	J-PARC	2010-
COHERENT	Hybrid	several	between 0.01 and 1.3	0.03	ORNL	2015-
SND@LHC	Hybrid	Emulsions & SciFi	0.81	[100-1000]	CERN (LHC)	2022-

The Gargamelle [465] detector at CERN used Freon and propane gas targets to make the first observation of neutrino-induced NC interactions and more. The BEBC [466] detector at CERN was a bubble chamber that was alternately filled with liquid hydrogen, deuterium, and a neon-hydrogen mixture; BEBC was also outfitted with a track-sensitive detector to improve event tagging, and sometimes used with a small emulsion chamber. The SKAT [467] Freon bubble chamber was exposed to wideband neutrino and antineutrino beams at the Serpukhov laboratory in the former Soviet Union. A series of American bubble chambers in the 1970's and 1980's made measurements on free nucleons that are still crucial inputs for neutrino-nucleus scattering predictions. The 12-foot bubble chamber at ANL [468] in the USA used both deuterium and hydrogen targets, as did the 7-foot bubble cham-

ber at BNL [469]. Fermilab's 15 foot bubble chamber [470] used deuterium and neon targets.

35.11.3.3 Iron Tracking Calorimeters

Because of the forward boost of high energy interactions, long detectors made of magnetized iron interspersed with active detector layers have been very successfully employed. The long magnetized detectors allow measurements of the momentum of penetrating muons. The iron planes also act as shower-inducing layers, allowing separation of EM and hadronic showers; the large number of iron planes provide enough mass for high statistics and/or shower containment. Magnetized iron spectrometers have been used for studies of the weak interaction, measurements of structure functions, and searches for neutrino oscillation. Non-

magnetized iron detectors have also been successfully employed as neutrino monitors for oscillation experiments and also for neutrino-nucleus interaction studies.

The Caltech-Fermilab counter (CITF) [468] combined a 92 ton iron-scintillator target-calorimeter detector with a downstream toroidal magnet to perform early studies of weak interactions—including observations of neutral currents. The CDHS [471] detector used layers of magnetized iron modules interspersed with wire drift chambers, with a fiducial mass of 1250 t, to detect neutrinos in the range 10–200 GeV. Within each iron module, 5 cm (or 15 cm) iron plates were interspersed with scintillation counters. The MINOS [472] detectors, a near detector of 980 t at FNAL and a far detector of 5500 t in the Soudan Underground Laboratory (SUL), were functionally identical magnetized iron calorimeters, comprised of iron plates interleaved with layers of 4 cm wide plastic scintillator strips in alternating orientations. The T2K [473] on-axis detector, INGRID, consists of 16 non-magnetized iron scintillator sandwich detectors, each with nine 6.5 cm iron plane (7.1 t total) interspersed between layers of 5 cm wide plastic scintillator strips readout out by multi-pixel photon counters (MPPCs) coupled to WLS fibers. Fourteen of the INGRID modules are arranged in a cross-hair configuration centered on the neutrino beam axis.

35.11.3.4 Cherenkov Detectors

Open volume water Cherenkov detectors were originally built to search for proton decay. Large volumes of ultra-pure water were lined with photomultipliers to collect Cherenkov light emitted by the passage of relativistic charged particles. See Sec. 36.3.1 for a detailed discussion of deep liquid detectors for rare processes. The Cherenkov light, which has significant production in the visible range, appears on the walls of the detectors in distinctive ring patterns, and topological characteristics of the rings are employed to separate muon-induced rings from electron-induced with very high accuracy. As neutrino detectors, Cherenkov detectors optimize the design balance since the entire neutrino target is also active detector medium.

When used to detect \sim GeV neutrinos, the detector medium acts as a natural filter for final state particles below the Cherenkov threshold; this feature has been exploited successfully by the K2K, MiniBooNE (using mineral oil instead of water), and T2K neutrino oscillation experiments. This makes event reconstruction simple and robust since electrons and muons have very different signatures, but does require making assumptions when inferring neutrino energy since not all final state particles are observed. At higher energies Cherenkov detectors become less accurate because the overlapping rings from many final state particles become increasingly difficult to resolve.

The second-generation Cherenkov detector in Japan, Super-Kamiokande [86] (Super-K), comprises 22.5 kt of water viewed by 50 cm photomultiplier tubes with 40% photocathode coverage; it is surrounded by an outer detector region viewed by 20 cm photomultipliers. Super-K is the far detector for K2K and T2K, and is described in greater detail elsewhere in this review. The K2K experiment also employed a 1 kt water Cherenkov detector in the suite of near detectors [474], with 40% photocathode coverage. The MiniBooNE detector at FNAL was a 0.8 kt [475] mineral oil Cherenkov detector, with 20 cm photomultipliers giving 10% photocathode coverage, surrounded by a veto detector also with 20 cm photomultipliers. The ANNIE detector also at FNAL consists of a 26-ton water Cherenkov detector loaded with gadolinium sulfate (Gd₂O₁₂S₃), complemented by a muon range detector and a veto wall. In addition to traditional PMTs, it exploits novel Large Area Picosecond Photodetectors (LAPPDs) for the detection of the Cherenkov light.

35.11.3.5 Scintillation Detectors

Liquid and solid scintillator detectors also employ fully (or nearly fully) active detector media. Typically organic scintillators, which emit into the ultraviolet range, are dissolved in mineral oil or plastic and read out by photomultipliers coupled to wavelength shifters (WLS). Open volume scintillation detectors lined with photomultipliers are conceptually similar to Cherenkov detectors, although energy reconstruction is calorimetric in nature

as opposed to kinematic (see also Sec. 36.3.1). For higher energies and higher particle multiplicities, it becomes beneficial to use segmented detectors to help distinguish particle tracks and showers from each other.

The HWPf collaboration [476] employed a 2 t liquid scintillator total-absorption hadron calorimeter followed by a magnetic spectrometer to observe neutral current events in the early days of Fermilab. The LSND [477] detector at LANL was a 130 t open volume liquid scintillator detector employed to detect relatively low energy (<300 MeV) neutrinos. The NOvA [478] detectors use segmented volumes of liquid scintillator in which the scintillation light is collected by WLS fibers in the segments that are coupled to avalanche photodiodes (APDs) at the ends of the volumes. The NOvA far detector, located in Ash River, MN, is comprised of 896 layers of 15.6 m long extruded PVC scintillator cells for a total mass of 14 kt; the NOvA near detector is comprised of 214 layers of 4.1 m scintillator volumes for a total mass of 300 t. Both are placed in the NuMI beamline at 0.8° off-axis. The SciBar (Scintillation Bar) detector was originally built for K2K at KEK in Japan and then re-used for SciBooNE [479] at FNAL. SciBar used plastic scintillator strips with 1.5 cm×2.5 cm rectangular cross section, read out by multianode photomultipliers (MAPMTs) coupled to WLS fibers, arranged in alternating horizontal and vertical layers. Both SciBooNE and K2K employed an EM calorimeter downstream of SciBar and a muon range detector (MRD) downstream of that.

The Coherent Captain Mills (CCM) detector is an upright cylindrical cryostat 2.58 m in diameter and 2.25 m high that holds 10 tons of LAr and is designed to be movable for distances between 20 m to 40 m from the neutrino source. It is instrumented with 120 8-inch PMTs, out of which 96 are coated with Tetraphenyl Butadiene (TPB) wavelength shifter.

35.11.3.6 Liquid Argon Time Projection Chambers

Liquid argon time projection chambers (LAr-TPCs) were conceived in the 1970s as a way to achieve a fully active detector with sub-centimeter track reconstruction [480]. A massive volume of purified liquid argon is put under a strong electric field (hundreds of V/cm), so that the liberated electrons from the paths of ionizing particles can be drifted to the edge of the volume and read out, directly by collecting charge from wire planes or non-destructively through charge induction in the wire planes. Dual-phase readout methods have also been developed, in which the charge is drifted vertically and then passed through an amplification region inside a gas volume above the liquid volume; the bottom of the liquid volume is equipped with a PMT array for detecting scintillation photons from the liquid argon. The first large scale LAr-TPC was the ICARUS T-600 module [481], comprising 760 t of liquid argon with a charge drift length of 1.5 m read out by wires with 3 mm pitch, which operated in LNGS, both standalone and also exposed to the CNGS high energy neutrino beam. The ICARUS detector has been transported to Fermilab and installed and presently operated in an on-axis position in the Booster Neutrino Beamline at 600 m from target, where it is also exposed to off-axis neutrinos from the NuMI beamline. It will be complemented by the SBND detector (100 m from BNB target, 112 t fiducial mass), currently in the final phases of installation to search for possible anomalies in short baseline neutrino oscillation in the context of the SBN Program.

The ArgoNeuT [482] detector at FNAL, with fiducial mass 25 kg of argon read out with 4 mm pitch wires, was exposed to the NuMI neutrino and antineutrino beams. The MicroBooN [483] detector at FNAL comprises 170 t (85t active) of liquid Ar, read out with 3 mm wire pitch, which began collecting data in the Booster Neutrino Beam Oct 2015. A LAr-TPC has also been chosen as the multi-kton detector design for the future DUNE [484] neutrino oscillation experiment, from FNAL to Sanford Underground Research Facility. The design choices for the first two DUNE far detector modules (each with a total LAr mass of 17 kt) are being validated in the NP04 (horizontal drift) and the NP02 (vertical drift) experiments at the CERN Neutrino Platform facility [485, 486].

35.11.3.7 Emulsion Detectors

Photographic film emulsions have been employed in particle physics experiments since the 1940s [487]. Thanks to advances in scanning technology and automation [488], they have been successfully employed as neutrino detectors. Emulsions are used for experiments observing CC tau neutrino interactions, where the short lifetime of the tau, $\tau_\tau = 2.90 \times 10^{-13}$ s, leading to the short mean path length, $c \times \tau = 87 \mu\text{m}$, requires extremely precise track resolution. They are employed in hybrid detectors in which the emulsion bricks are embedded inside fine-grained tracker detectors. In the data analysis, the tracker data are used to select events with characteristics typical of a tau decay in the final state, such as missing energy and unbalanced transverse momentum. The reconstructed tracks are projected back into an emulsion brick and used as the search seed for a neutrino interaction vertex.

E531 [489] at Fermilab tested many of the emulsion-tracker hybrid techniques employed by later neutrino experiments, in a detector with approximately 9 kg of emulsion target. The CHORUS [488] experiment at CERN used 1,600 kg of emulsion, in a hybrid detector with a fiber tracker, high resolution calorimeter, and muon spectrometer, to search for $\nu_\mu \rightarrow \nu_\tau$ oscillation. The DONuT [490] experiment at FNAL used a hybrid detector, with 260 kg of emulsion bricks interspersed with fiber trackers, followed by a magnetic spectrometer, and calorimeter, to make the first direct observation of tau neutrino CC interactions. The OPERA [491] [492] [493] experiment used an automated hybrid emulsion detector, with 1,25x0 t of emulsion, to make the first direct observation of the appearance of ν_τ in a ν_μ beam. Recently, the NINJA collaboration has developed an emulsion cloud chamber detector to observe neutrinos in the J-PARC neutrino beam [494].

FASER ν [495] (a sub-detector of the FASER [496] experiment) is designed to detect and study all neutrino flavors produced at the LHC in the far-forward region of the ATLAS interaction point at the TeV energies scale. It consists of emulsion films interleaved with tungsten plates with a total target mass of 1.2 tons, enabling the identification of the leptons in charged current ν interactions. Placed 480m downstream of ATLAS, FASER ν will measure neutrino cross sections at energies where they are currently unconstrained and will bound models of forward particle production.

35.11.3.8 Hybrid Detectors

In the previous neutrino detector examples, one can point to a specific detection technology or configuration that defines a category of detectors. In this section we look at detectors that combine multiple elements or techniques, without one facet being specifically dominant or crucial; we call these detectors hybrids.

The CHARM detector [497] at CERN was built to study neutral-current interactions and search for muon neutrino oscillation. It was a fine-grained ionization calorimeter tracker with approximately 150 t of marble as neutrino target, surrounded by a magnetized iron muon system for tagging high angle muons, and followed downstream by a muon spectrometer. The CHARM II detector [498] at CERN comprised a target calorimeter followed by a downstream muon spectrometer. Each target calorimeter module consists of a 4.8 cm thick glass plate followed by a layer of plastic streamer tubes, with spacing 1 cm, instrumented with 2 cm wide pickup strips. Every fifth module is followed by a 3 cm thick scintillator layer. The total mass of the target calorimeter was 692 t.

The Brookhaven E-734 [499] detector was a tracking calorimeter made up of 172 t liquid scintillator modules interspersed with proportional drift tubes, followed by a dense EM calorimeter and a muon spectrometer downstream of that. The detector was exposed to a wideband horn-focused beam with peak neutrino energy near 1 GeV. The Brookhaven E-776 [500] experiment comprised a finely segmented EM calorimeter, with 2.54 cm concrete absorbers interspersed with planes of drift tubes and acrylic scintillation counters, with total mass 240 t, followed by a muon spectrometer.

The FNAL Lab-E neutrino detector was used by the CCFR [501] and NuTeV [502] collaborations to perform a series of experiments in the Fermilab high energy neutrino beam ($50 \text{ GeV} < E_\nu < 300 \text{ GeV}$). The detector was comprised of six iron target

calorimeter modules, with 690 t total target mass, followed by three muon spectrometer modules, followed by two drift chambers. Each iron target calorimeter module comprised 5.2 cm thick steel plates interspersed with liquid scintillation counters and drift chambers.

The NOMAD [503] detector at CERN consisted of central tracker detector inside a 0.4 T dipole magnet (the magnet was originally used by the UA1 experiment at CERN) followed by a hadronic calorimeter and muon detectors downstream of the magnet. The main neutrino target is 3 t of drift chambers followed downstream by transition radiation detectors which are followed by an EM calorimeter. NOMAD was exposed to the same wide-band neutrino beam as was CHORUS.

MINERvA [504] is a hybrid detector based around a central plastic scintillator tracker: 8.3 t of plastic scintillator strips with triangular cross section read out by MAPMTs coupled to WLS fibers. The scintillator tracker is surrounded by electromagnetic and hadronic calorimetry, which is achieved by interleaving thin lead (steel) layers between the scintillator layers for the ECAL (HCAL). MINERvA is situated upstream of the MINOS near detector which acts as a muon spectrometer. Upstream of the scintillator tracker is a nuclear target region containing inactive layers of C (graphite), Pb, Fe (steel), and O (water). MINERvA's physics goals span a wide range of neutrino-nucleus interaction studies, from form factors to nuclear effects.

T2K [473] in Japan employs two near detectors at 280 m from the neutrino beam target, one centered on the axis of the horn-focused J-PARC neutrino beam and one placed 2.5° off-axis. The on-axis detector, INGRID, is described above. The 2.5° off-axis detector, ND280, employs the UA1 magnet (at 0.2 T) previously used by NOMAD. Inside the magnet volume are three separate detector systems: the trackers, the Pi0 Detector (P0D), and several ECAL modules. The tracker detectors comprise two fine-grained scintillator detectors (FGDs), read out by MPPCs coupled to WLS fibers, interleaved between three gas TPCs read out by micro-megas planes. The downstream FGD contains inactive water layers in addition to the scintillators. Upstream of the tracker is the P0D, a sampling tracker calorimeter with active detector materials comprising plastic scintillator read out by MPPCs and WLS fibers, and inactive sheets of brass radiators and refillable water modules. Surrounding the tracker and P0D, but still inside the magnet, are lead-scintillator EM sampling calorimeters.

The COHERENT collaboration aims to measure CEvNS (Coherent Elastic Neutrino-Nucleus Scattering) using the high-quality pion-decay-at-rest neutrino source at the Spallation Neutron Source in Oak Ridge, Tennessee. For doing so, it is deploying a suite of detector systems in a hallway in the basement of the SNS target hall with a phased approach. This includes CsI[Na] crystal, LAr scintillation detector, NaI[Tl], interwoven EJ200 scintillator and gadolinium-doped Mylar, thorium-232 metal plates and Germanium detectors.

The SND@LHC experiment [505] will perform measurements with high-energy neutrinos (100 GeV–1 TeV) produced at the LHC in the pseudo-rapidity region $7.2 < \eta < 8.6$. It allows the identification of all neutrino flavours with high efficiency. It is located 480 m downstream and off-axis with respect to the ATLAS interaction point and consists of a target region followed by a muon identification system. The target (810 kg) is instrumented with nuclear emulsions and Scintillating Fibre (SciFi) planes. The muon identification system is made of iron slabs interleaved with scintillating bars planes. SND@LHC is complementary to FASER ν as it intercepts different components of the neutrino flux from LHC collisions, mainly those produced in heavy flavour decays, mostly charm.

35.11.4 Outlook

Detectors for accelerator-based neutrino beams have been in use, and constantly evolving, for six decades now. The rich program of neutrino oscillation physics and attendant need for newer and better neutrino-nucleus scattering measurements means that more neutrino detectors with broader capabilities will be needed in the coming decades.

One of the most intriguing prospects is a large volume, high pressure gas time projection chamber (HPTPC). With the

prospect of megawatt power accelerator-based neutrino beams, it is entirely feasible to collect high statistics data sets with a gas target. The low momentum thresholds for particle detection, and excellent momentum resolution and particle identification capabilities, of an HPTPC would open a new window into the physics of neutrino-nucleus scattering. Moreover, the ability to change the gas mixtures in the HPTPC would allow measurements in the same detector on multiple nuclear targets, which would, in turn, allow unprecedentedly accurate constraints and tuning of neutrino-nucleus interaction models.

35.12 Superconducting magnets for collider detectors

Revised March 2024 by Y. Makida (KEK).

35.12.1 Solenoid Magnets

In all cases SI unit are assumed, so that the magnetic field, B , is in Tesla, the stored energy, E , is in joules, the dimensions are in meters, and vacuum permeability of $\mu_0 = 4\pi \times 10^{-7}$.

The magnetic field (B) in an simple solenoid with a flux return iron yoke, in which the magnetic field is lower than magnetic saturation of < 2 T, is given by

$$B = \frac{\mu_0 n I}{L} \quad (35.48)$$

where n is the number of turns, I is the current and L is the coil length.

In an air-core solenoid case, the central field is given by

$$B(0,0) = \mu_0 n I \frac{1}{\sqrt{L^2 + 4R^2}}, \quad (35.49)$$

where R is the coil radius.

In most cases, momentum analysis is made by measuring the circular trajectory of the passing particles according to $p = mv = qrB$, where p is the momentum, m the mass, q the charge, r the bending radius. The sagitta, s , of the trajectory is given by

$$s = qB \ell^2 / 8p, \quad (35.50)$$

where ℓ is the path length in the magnetic field as shown in Fig. 35.39.

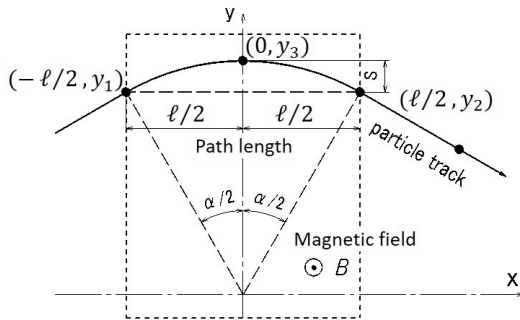


Figure 35.39: Geometric relation of sagitta between path length.

In a practical momentum measurement in colliding beam detectors, it is more effective to increase the magnetic volume than the field strength, since

$$dp/p \propto p/B \ell^2, \quad (35.51)$$

where ℓ corresponds to the solenoid coil radius R . The energy stored in the magnetic field of any magnet is calculated by integrating B^2 over all space:

$$E = \frac{1}{2\mu_0} \int B^2 dV \quad (35.52)$$

If the coil thin and inside an iron return yoke, (which is the case if it is to superconducting coil), then

$$E \approx (B^2/2\mu_0)\pi R^2 L. \quad (35.53)$$

For a detector in which the calorimetry is outside the aperture of the solenoid, the coil must be transparent in terms of radiation and absorption lengths. This usually means that the superconducting solenoid and its cryostat is of minimum real thickness and is made of a material with long radiation length. There are two major contributors to the thickness of a thin solenoid:

1. The conductor consisting of the current-carrying superconducting material (usually Nb-Ti/Cu) and the quench protecting stabilizer (usually aluminum) are wound on the inside of a structural support cylinder (usually aluminum alloy). The coil thickness scales as $B^2 R$, so the thickness in radiation lengths (X_0) is

$$t_{\text{coil}}/X_0 = (R/\sigma_h X_0)(B^2/2\mu_0), \quad (35.54)$$

where t_{coil} is the physical thickness of the coil, X_0 the average radiation length of the coil/stabilizer material, and σ_h is the hoop stress in the coil [506]. $B^2/2\mu_0$ is the magnetic pressure. In large detector solenoids, the aluminum stabilizer and support cylinders dominate the thickness; the superconductor (Nb-Ti/Cu) contributes a smaller fraction. The main coil and support cylinder components typically contribute about 2/3 of the total thickness in radiation lengths.

2. Another contribution to the material comes from the outer cylindrical shell of the vacuum vessel. Since this shell is susceptible to buckling collapse, its thickness is determined by the diameter, length and the modulus of the material of which it is fabricated. The outer vacuum shell represents about 1/3 of the total thickness in radiation length.

35.12.2 Properties of collider detector magnets

The physical dimensions, central field stored energy and thickness in radiation lengths normal to the beam line of the superconducting solenoids associated with the major collider are given in Table 35.15 [507]. Fig. 35.40 shows thickness in radiation lengths as a function of $B^2 R$ in various collider detector solenoids.

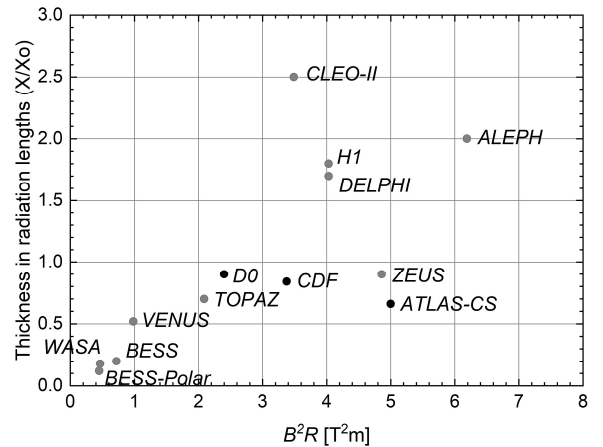


Figure 35.40: Magnet wall thickness in radiation length as a function of $B^2 R$ for various detector solenoids. Gray entries are for magnets no longer in use.

The ratio of stored energy to cold mass (E/M) is a useful performance measure. It can also be expressed as the ratio of the stress, σ_h , to twice the equivalent density, ρ , in the coil [506]:

$$\frac{E}{M} = \frac{E}{\rho 2\pi t_{\text{coil}} R L} \approx \frac{\sigma_h}{2\rho} \quad (35.55)$$

The E/M ratio in the coil is approximately equivalent to H ,^{¶¶}

^{¶¶}The enthalpy, or heat content, is called H in the thermodynamics literature. It is not to be confused with the magnetic field intensity B/μ .

Table 35.15: Progress of superconducting magnets for particle physics detectors.

Experiment	Laboratory	B [T]	Radius [m]	Length [m]	Energy [MJ]	X/X_0	E/M [kJ/kg]
TOPAZ*	KEK	1.2	1.45	5.4	20	0.70	4.3
CDF*	Tsukuba/Fermi	1.5	1.5	5.07	30	0.84	5.4
VENUS*	KEK	0.75	1.75	5.64	12	0.52	2.8
AMY*	KEK	3	1.29	3	40	†	
CLEO-II*	Cornell	1.5	1.55	3.8	25	2.5	3.7
ALEPH*	Saclay/CERN	1.5	2.75	7.0	130	2.0	5.5
DELPHI*	RAL/CERN	1.2	2.8	7.4	109	1.7	4.2
ZEUS*	INFN/DESY	1.8	1.5	2.85	11	0.9	5.5
H1*	RAL/DESY	1.2	2.8	5.75	120	1.8	4.8
BaBar*	INFN/SLAC	1.5	1.5	3.46	27	†	3.6
D0*	Fermi	2.0	0.6	2.73	5.6	0.9	3.7
BELLE*	KEK	1.5	1.8	4	42	†	5.3
BES-III	IHEP	1.0	1.475	3.5	9.5	†	2.6
ATLAS-CS	ATLAS/CERN	2.0	1.25	5.3	38	0.66	7.0
ATLAS-BT	ATLAS/CERN	1	4.7–9.75	26	1080	(Toroid)†	
ATLAS-ET	ATLAS/CERN	1	0.825–5.35	5	2 × 250	(Toroid)†	
CMS	CMS/CERN	4	6	12.5	2600	†	12
SiD**	ILC	5	2.9	5.6	1560	†	12
ILD**	ILC	4	3.8	7.5	2300	†	13
SiD**	CLIC	5	2.8	6.2	2300	†	14
ILD**	CLIC	4	3.8	7.9	2300	†	13
FCC**		6	6	23	54000	†	12

* No longer in service
** Conceptual design in future
† EM calorimeter is inside solenoid, so small X/X_0 is not a goal

the enthalpy of the coil, and it determines the average coil temperature rise after energy absorption in a quench:

$$E/M = H(T_2) - H(T_1) \approx H(T_2) \quad (35.56)$$

where T_2 is the average coil temperature after the full energy absorption in a quench, and T_1 is the initial temperature. E/M ratios of 5, 10, and 20 kJ/kg correspond to ~ 65 , ~ 80 , and ~ 100 K, respectively. The E/M ratios of various detector magnets are shown in Fig. 35.41 as a function of total stored energy. One would like the cold mass to be as small as possible to minimize the thickness, but temperature rise during a quench must also be minimized. An E/M ratio as large as 12 kJ/kg is designed into the CMS solenoid, with the possibility that about half of the stored energy can go to an external dump resistor. Thus the coil temperature can be kept below 80 K if the energy extraction system works well. The limit is set by the maximum temperature that the coil design can tolerate during a quench. This maximum local temperature should be < 130 K (50 K + 80 K), so that thermal expansion effects, which are remarkable beyond 80 K, in the coil are manageable less than 50 K.

35.12.3 Toroidal magnets

Toroidal coils uniquely provide a closed magnetic field without the necessity of an iron flux-return yoke. Because no field exists at the collision point and along the beam line, there is, in principle, no effect on the beam. On the other hand, the field profile generally has $1/r$ dependence. The particle momentum may be determined by measurements of the deflection angle combined with the sagitta. The deflection (bending) power BL is

$$BL \approx \int_{R_i}^{R_0} \frac{B_i R_i dR}{R \sin \theta} = \frac{B_i R_i}{\sin \theta} \ln(R_0/R_i), \quad (35.57)$$

where R_i is the inner coil radius, R_0 is the outer coil radius, and θ is the angle between the particle trajectory and the beam line axis. The momentum resolution given by the deflection may be expressed as

$$\frac{\Delta p}{p} \propto \frac{p}{BL} \approx \frac{p \sin \theta}{B_i R_i \ln(R_0/R_i)}. \quad (35.58)$$

The momentum resolution is better in the forward/backward (smaller θ) direction. The geometry has been found to be optimal

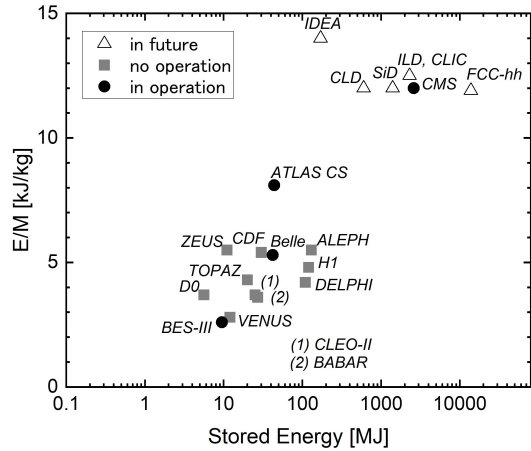


Figure 35.41: Ratio of stored energy to cold mass for major detector solenoids. Gray indicates magnets no longer in operation.

when $R_0/R_i \approx 3-4$. In practical designs, the coil is divided into 6–12 lumped coils in order to have reasonable acceptance and accessibility. This causes the coil design to be much more complex. The mechanical structure needs to sustain the decentering force between adjacent coils, and the peak field in the coil is 3–5 times higher than the useful magnetic field for the momentum analysis [508].

35.13 Measurement of particle momenta in a uniform magnetic field

The trajectory of a particle with momentum p (in GeV/c) and charge ze in a constant magnetic field \vec{B} is a helix, with radius of curvature R and pitch angle λ . The radius of curvature and momentum component perpendicular to \vec{B} are related by

$$p \cos \lambda = 0.3 z B R, \quad (35.59)$$

where B is in tesla and R is in meters.

The distribution of measurements of the curvature $k \equiv 1/R$ is approximately Gaussian. The curvature error for a large number

of uniformly spaced measurements on the trajectory of a charged particle in a uniform magnetic field can be approximated by

$$(\delta k)^2 = (\delta k_{\text{res}})^2 + (\delta k_{\text{ms}})^2, \quad (35.60)$$

where δk = curvature error

δk_{res} = curvature error due to finite measurement resolution

δk_{ms} = curvature error due to multiple scattering.

If many (≥ 10) uniformly spaced position measurements are made along a trajectory in a uniform medium,

$$\delta k_{\text{res}} = \frac{\epsilon}{L'^2} \sqrt{\frac{720}{N+4}}, \quad (35.61)$$

where N = number of points measured along track
 L' = the projected length of the track onto the bending plane
 ϵ = measurement error for each point, perpendicular to the trajectory.

If a vertex constraint is applied at the origin of the track, the coefficient under the radical becomes 320.

For arbitrary spacing of coordinates s_i measured along the projected trajectory and with variable measurement errors ϵ_i the curvature error δk_{res} is calculated from:

$$(\delta k_{\text{res}})^2 = \frac{4}{w} \frac{V_{ss}}{V_{ss}V_{s^2s^2} - (V_{ss^2})^2}, \quad (35.62)$$

where V are covariances defined as $V_{s^m s^n} = \langle s^m s^n \rangle - s^m \langle s^n \rangle$ with $\langle s^m \rangle = w^{-1} \sum (s_i^m / \epsilon_i^2)$ and $w = \sum \epsilon_i^{-2}$.

The contribution due to multiple Coulomb scattering is approximately

$$\delta k_{\text{ms}} \approx \frac{(0.016)(\text{GeV}/c)z}{Lp\beta \cos^2 \lambda} \sqrt{\frac{L}{X_0}}, \quad (35.63)$$

where p = momentum (GeV/ c)
 z = charge of incident particle in units of e
 L = the total track length
 X_0 = radiation length of the scattering medium (in units of length; the X_0 defined elsewhere must be multiplied by density)
 β = the kinematic variable v/c .

More accurate approximations for multiple scattering may be found in the section on Passage of Particles Through Matter (Sec. 34 of this *Review*). The contribution to the curvature error is given approximately by $\delta k_{\text{ms}} \approx 8s_{\text{plane}}^{\text{rms}}/L^2$, where $s_{\text{plane}}^{\text{rms}}$ is defined there.

References

- [1] H. Kolanoski and N. Wermes, *Particle Detectors - Fundamentals and Applications*, Oxford University Press (2020), ISBN 978-0-19-885836-2.
- [2] T. Ferbel, *Experimental techniques in high energy physics; 1st ed.*, Frontiers in physics, Addison-Wesley, Menlo Park, CA (1987), URL <https://cds.cern.ch/record/110951>.
- [3] K. Kleinknecht, *Detectors for particle radiation* (1998), ISBN 978-0-521-64854-7.
- [4] G. Knoll, *Radiation Detection and Measurement (4th ed.)*, John Wiley, Hoboken, NJ (2010), ISBN 978-0-470-13148-0.
- [5] D. Green, *The physics of particle detectors*, Cambridge University Press, Cambridge, UK (2000), ISBN 9780521675680.
- [6] C. Leroy and P.-G. Rancoita, *Principles of radiation interaction in matter and detection*, World Scientific, Singapore (2011), ISBN 978-981-238-909-1.
- [7] C. Grupen and B. Schwartz, *Particle detectors*, Cambridge University Press, Cambridge, UK (2008), ISBN 9780521187954.
- [8] H. Spieler, *Semiconductor Detector Systems*, Oxford University Press, Oxford (2005), ISBN 978-0-19-852784-8.
- [9] K. Arisaka, Nucl. Instrum. Meth. **A442**, 80 (2000).
- [10] N. Matsunaga (ed.), *Photomultiplier Tubes: Basics and Applications*, 4th edition, Hamamatsu Photonics K.K., Hamamatsu (2017), https://www.hamamatsu.com/resources/pdf/etd/PMT_handbook_v4E.pdf.
- [11] M. Böhm *et al.*, JINST **15**, 11, C11015 (2020).
- [12] M. J. Minot *et al.*, Nuovo Cim. C **43**, 1, 11 (2020).
- [13] A. Braem *et al.*, Nucl. Instrum. Meth. **A518**, 574 (2004).
- [14] S. Korpar *et al.*, Nucl. Instrum. Meth. A **766**, 145 (2014).
- [15] R. Arnold *et al.*, Nucl. Instrum. Meth. **A314**, 465 (1992).
- [16] P. Mangeot *et al.*, Nucl. Instrum. Methods **A216**, 79 (1983).
- [17] R. Apsimon *et al.*, IEEE Trans. **NS33**, 112 (1986).
- [18] R. Arnold *et al.*, Nucl. Instrum. Meth. **A270**, 255 (1988).
- [19] D. Aston *et al.*, Nucl. Instrum. Meth. **A283**, 582 (1989).
- [20] R. Haitz *et al.*, J. Appl. Phys. **36**, 3123 (1965).
- [21] R. McIntyre, IEEE Trans. Electron Devices **13**, 164 (1966).
- [22] H. Dautet *et al.*, Applied Optics, **32**, 3894 (1993).
- [23] Perkin-Elmer Optoelectronics, *Avalanche Photodiodes: A User's Guide*, (2003).
- [24] P. Buzhan *et al.*, Nucl. Instrum. Meth. **A504**, 48 (2003).
- [25] Z. Sadygov *et al.*, Nucl. Instrum. Methods **A504**, 301 (2003).
- [26] V. Golovin and V. Savelev, Nucl. Instrum. Meth. **A518**, 560 (2004).
- [27] F. Simon, Nuclear Instruments and Methods in Physics Research Section A: Accelerators, Spectrometers, Detectors and Associated Equipment **926**, 85–100 (2019), ISSN 0168-9002, URL <http://dx.doi.org/10.1016/j.nima.2018.11.042>.
- [28] S. Korpar *et al.*, Nucl. Instrum. Meth. **A766**, 107 (2014).
- [29] R. H. Pots *et al.*, Nucl. Instrum. Meth. **A940**, 254 (2019).
- [30] D. R. Schaart *et al.*, Nuclear Instruments and Methods in Physics Research Section A: Accelerators, Spectrometers, Detectors and Associated Equipment **809**, 31 (2016).
- [31] M. Petrov, M. Stapelbroek, and W. Kleinhans, Appl. Phys. Lett. **51**, 406 (1987).
- [32] M. Atac and M. Petrov, IEEE Trans. **NS36**, 163 (1989).
- [33] M. Atac *et al.*, Nucl. Instrum. Meth. **A314**, 56 (1992).
- [34] B. Korzh *et al.*, Nature Photonics **14**, 250 (2020).
- [35] J. S. Carlson *et al.*, J. Am. Chem. Soc. **139**, 28, 9621 (2017).
- [36] J.B. Birks, *The Theory and Practice of Scintillation Counting*, Pergamon, London (1964).
- [37] D. Clark, Nucl. Instrum. Meth. **117**, 1, 295 (1974).
- [38] Y. Khazdhev, Ann. Rev. Nucl. Part. **4**, 1 (2017).
- [39] S. Moser *et al.*, Rad. Phys. and Chem. **41**, 1, 31 (1993), ISSN 0969-806X.
- [40] M. Moszyński and B. Bengtson, Nucl. Instrum. Methods **158**, 1 (1979).
- [41] J. B. Birks, Proc. Phys. Soc. **A64**, 874 (1951).
- [42] D. Dexter, J. Chem. Phys. **21**, 836 (1953).
- [43] C. Dujardin and M. Hamel, *Introduction—Overview on Plastic and Inorganic Scintillators*, 3–33, Springer International Publishing, Cham (2021).
- [44] C. Chandler and et al., Additive Manufacturing **73**, 103688 (2023).
- [45] S. Lee, M. Livan and R. Wigmans, Rev. Mod. Phys. **90**, 025002 (2018).
- [46] R. C. Ruchti, Ann. Rev. Nucl. Part. **46**, 281 (1996).
- [47] C. Joram, G. Haefeli and B. Leverington, JINST **10**, 08, C08005 (2015).
- [48] D. Horstmann and U. Holm, Radiat. Phys. Chem. **41**, 1, 395 (1993), ISSN 0969-806X.
- [49] K. Abe and et al. (T2K), JINST **17**, P10028 (2022).

- [50] Y. Khazdhev, *Phys. Part. Nucl.* **50**, 1, 42 (2019).
- [51] C. Zorn, in F. Sauli, editor, "Instrumentation in high-energy physics, Advanced Series on Directions in High Energy Physics," volume 9, 218, World Scientific (1992).
- [52] CMS Collaboration, *J. Instrum.* **15**, 06, P06009 (2020).
- [53] K. Gillen and R. Clough, *Polymer* **38**, 1929 (1992).
- [54] T. Seguchi *et al.*, *Radiat. Phys. Chem.* **17**, 195 (1981), ISSN 0146-5724.
- [55] P. Feng and *et al.*, *Organic glass scintillators*, 243–283, Springer International Publishing, Cham (2021).
- [56] S.E. Derenzo, W.-S. Choong and W.W. Moses, *Phys. Med. Biol.* **59**, 3261 (2014).
- [57] C. Melcher and J. Schweitzer, *Nucl. Instrum. Methods* **A314**, 212 (1992).
- [58] D.W. Cooke *et al.*, *J. Appl. Phys.* **88**, 7360 (2000).
- [59] J.M. Chen *et al.*, *IEEE Trans.* **NS54**, 718 (2007).
- [60] J.M. Chen *et al.*, *IEEE Trans.* **NS54**, 1319 (2007).
- [61] E.V.D. van Loef *et al.*, *Nucl. Instrum. Methods* **A486**, 254 (2002).
- [62] W. Drozdowski *et al.*, *IEEE Trans.* **NS55**, 1391 (2008).
- [63] M.S. Alekhin *et al.*, *Appl. Phys. Lett.* **102**, 161915 (2013).
- [64] C. Kuntner *et al.* (Crystal Clear), *Nucl. Instrum. Meth.* **A493**, 131 (2002).
- [65] N. Akchurin *et al.*, *Nucl. Instrum. Meth.* **A595**, 359 (2008).
- [66] H. Wenzel, *Journal of Physics: Conference Series* **404**, 012049 (2012).
- [67] A. Benaglia *et al.*, *IEEE Transactions on Nuclear Science* **63**, 2, 574 (2016).
- [68] R.H. Mao, L.Y. Zhang and R.Y. Zhu, *IEEE Trans.* **NS59**, 2229 (2012).
- [69] R. Y. Zhu, TIPP 2017, SPPHY 213, 70 (2018).
- [70] C. Hu *et al.*, *IEEE Transactions on Nuclear Science* **66**, 7, 1854 (2019).
- [71] W.W. Moses, W.-S. Choong and S.E. Derenzo, *Acta Physica Polonica* **B7**, 725 (2014).
- [72] R.H. Mao, L.Y. Zhang and R.Y. Zhu, *IEEE Trans.* **NS55**, 2425 (2008).
- [73] B.D. Rooney and J.D. Valentine, *IEEE Trans.* **NS44**, 509 (1997).
- [74] W.W. Moses *et al.*, *IEEE Trans.* **NS55**, 1049 (2008).
- [75] G. Gratta, H. Newman and R. Y. Zhu, *Ann. Rev. Nucl. Part. Sci.* **44**, 453 (1994).
- [76] R.-Y. Zhu, in "Handbook of Particle Detection and Imaging," 1–25, Springer International Publishing (2020).
- [77] F. Yang *et al.*, *IEEE Trans.* **NS63**, 612 (2016).
- [78] F. Yang *et al.*, *IEEE Trans.* **NS64**, 665 (2017).
- [79] C. Hu *et al.*, *IEEE Transactions on Nuclear Science* **67**, 6, 1086 (2020).
- [80] G. Dissertori *et al.*, *Nucl. Instrum. Methods* **745**, 1 (2014), and references therein.
- [81] S. Ecklund, C. Field and G. Mazaheri, *Nucl. Instr. and Meth. Res. Sect.* **A463**, 68 (2001).
- [82] M. G. Albrow *et al.*, *JINST* **7**, P10027 (2012), [arXiv:1207.7248].
- [83] B. Aubert *et al.* (BaBar), *Nucl. Instr. and Meth. Res. Sect.* **A479**, 1 (2002), [hep-ex/0105044].
- [84] E. Torassa (Belle-II PID Group), *Nucl. Instr. and Meth. Res. Sect.* **A824**, 152 (2016).
- [85] G. Bayatian *et al.* (CMS), *Eur. Phys. J.* **C53**, 139 (2008).
- [86] Y. Fukuda *et al.* (Super-Kamiokande), *Nucl. Instrum. Meth.* **A501**, 418 (2003).
- [87] Proceedings of the International Workshops on Ring Imaging Cherenkov Detectors, *Nucl. Instr. and Meth. Res. Sect.* **A343**, 1 (1993); *Nucl. Instr. and Meth. Res. Sect.* **A371**, 1 (1996); *Nucl. Instr. and Meth. Res. Sect.* **A433**, 1 (1999); *Nucl. Instr. and Meth. Res. Sect.* **A502**, 1 (2003); *Nucl. Instr. and Meth. Res. Sect.* **A553**, 1 (2005); *Nucl. Instr. and Meth. Res. Sect.* **A595**, 1 (2008); *Nucl. Instr. and Meth. Res. Sect.* **A639**, 1 (2011); *Nucl. Instr. and Meth. Res. Sect.* **A766**, 1 (2014); *Nucl. Instr. and Meth. Res. Sect.* **A876**, 1 (2017); *Nucl. Instr. and Meth. Res. Sect.* **A 952**, 1 (2019).
- [88] J. Litt and R. Meunier, *Ann. Rev. Nucl. Part. Sci.* **23**, 1 (1973).
- [89] D. Bartlett *et al.*, *Nucl. Instr. and Meth. Res. Sect.* **A260**, 55 (1987).
- [90] A. Abashian *et al.*, *Nucl. Instr. and Meth. Res. Sect.* **A479**, 117 (2002).
- [91] B. N. Ratcliff, *Nucl. Instr. and Meth. Res. Sect.* **A502**, 211 (2003).
- [92] T. Iijima *et al.*, *Nucl. Instr. and Meth. Res. Sect.* **A548**, 383 (2005), [arXiv:physics/0504220].
- [93] B. Ratcliff and J. Va'vra, *Nucl. Instrum. Meth.* **A**, 163442 (2020).
- [94] W. Blum, W. Riegler, and L. Rolandi, *Particle Detection with Drift Chambers*, Springer-Verlag, Berlin (2008).
- [95] R. M. Sternheimer and R. F. Peierls, *Phys. Rev. B* **3**, 3681 (1971); L. Landau, *J. Phys. (USSR)* **8**, 201 (1944); W. W. M. Allison and J. H. Cobb, *Ann. Rev. Nucl. Part. Sci.* **30**, 253 (1980).
- [96] I. Smirnov, *Nucl. Instrum. Meth.* **A554**, 474 (2005); I. Smirnov, HEED - High Energy Electro Dynamics, <http://ismirnov.web.cern.ch/ismirnov/heed>.
- [97] L.G. Christophorou, *Atomic and Molecular Radiation Physics*, John Wiley & Sons, Hoboken (1971); J. Berkowitz, *Atomic and Molecular Photoabsorption*, Academic Press, Cambridge (2015).
- [98] F. Sauli, *Gaseous Radiation Detectors: Fundamentals and Applications*, Cambridge University Press (2014).
- [99] H. Bichsel, *Nucl. Instrum. Meth.* **A562**, 154 (2006).
- [100] R. Veenhof, Garfield - Simulation of Gaseous Detectors, <http://garfield.web.cern.ch/garfield/>.
- [101] Degrad - cluster size distribution and primary cluster distribution in gas mixtures for minimum ionising particles and X-rays, <http://magboltz.web.cern.ch/magboltz/>.
- [102] S. F. Biagi, *Nucl. Instrum. Meth.* **A421**, 1-2, 234 (1999).
- [103] S. Biagi, R. Veenhof, Magboltz - Boltzmann transport equations for electrons in gas mixtures under the influence of electric and magnetic fields, <http://magboltz.web.cern.ch/magboltz/>.
- [104] S. Mukhopadhyay and N. Majumdar, in "17th DAE-BRNS High Energy Physics Symposium," (2007), [arXiv:physics/0703009].
- [105] H. Fischle, J. Heintze and B. Schmidt, *Nucl. Instrum. Meth.* **A301**, 202 (1991).
- [106] M. M. F. R. Fraga *et al.*, *Nucl. Instrum. Meth. A* **504**, 88 (2003).
- [107] A. Peisert and F. Sauli, Drift and Diffusion of Electrons in Gases: A Compilation (With an Introduction to the Use of Computing Program) CERN-84-08, CERN-YELLOW-84-08 (1984).
- [108] <https://fr.lxcat.net/instructions/categories.php>.
- [109] O. Şahin, T. Z. Kowalski and R. Veenhof, *Nucl. Instrum. Meth. A* **768**, 104 (2014).
- [110] O. Şahin *et al.*, *JINST* **5**, 05, P05002 (2010); O. Şahin, *JINST* **16**, 03, P03026 (2021).

- [111] E. McDaniel and E. Mason, *The Mobility and Diffusion of Ions in Gases*, John Wiley & Sons, Hoboken (1973); G. Schultz, G. Charpak and F. Sauli, *Rev. Phys. Appl.* **12**, 1, 67 (1977).
- [112] Y. Kalkan *et al.*, *JINST* **10**, 07, P07004 (2015).
- [113] T. Ikeda *et al.*, *JINST* **15**, 07, P07015 (2020), [arXiv:2004.09706].
- [114] G.F. Knoll, *Radiation Detection and Measurement*, 3rd edition, John Wiley & Sons, New York (1999).
- [115] G. Charpak *et al.*, *Nucl. Instrum. Methods* **A62**, 262 (1968).
- [116] G. Charpak and F. Sauli, *Ann. Rev. Nucl. Sci.* **34**, 285 (1984).
- [117] G. Charpak *et al.*, *Nucl. Instrum. Methods* **A97**, 377 (1971).
- [118] W. Blum, W. Riegler, and L. Rolandi, *Particle Detection with Drift Chambers*, Springer-Verlag, Berlin (2008).
- [119] T. Ferbel (ed.), *Experimental Techniques in High Energy Physics*, Addison-Wesley, Menlo Park, CA (1987), see “Principles of Operation of Multiwire Proportional and Drift Chambers”.
- [120] R. Veenhof, *Nucl. Instrum. Meth. A* **419**, 726 (1998).
- [121] G. Charpak *et al.*, *Nucl. Instrum. Methods* **A167**, 455 (1979).
- [122] A.H. Walenta *et al.*, *Nucl. Instrum. Methods* **A92**, 373 (1971).
- [123] A. Breskin *et al.*, *Nucl. Instrum. Methods* **A124**, 189 (1975).
- [124] A. Breskin *et al.*, *Nucl. Instrum. Methods* **A156**, 147 (1978).
- [125] R. Bouclier *et al.*, *Nucl. Instrum. Meth.* **A265**, 78 (1988), [556(1987)].
- [126] H. Drumm *et al.*, *Nucl. Instrum. Methods* **A176**, 333 (1980).
- [127] D.R. Nygren and J.N. Marx, *Phys. Today* **31N10**, 46 (1978).
- [128] C. Grupen, *Particle Detectors*, Cambridge Monographs on Particle Physics, Nuclear Physics and Cosmology, Cambridge University Press (2008).
- [129] G. F. Tassielli *et al.*, *JINST* **15**, 09, C09051 (2020), [arXiv:2006.02378].
- [130] M. Titov, *ICFA Instrum. Bull.* **26**, 002 (2004), [arXiv:physics/0403055]; M. Titov *et al.*, *ICFA Instrum. Bull.* **24**, 22 (2002), [hep-ex/0204005].
- [131] P. S. Baringer *et al.*, *Nucl. Instrum. Meth.* **A254**, 542 (1987).
- [132] J. Virdee, *Phys. Reports* **403**, 401 (2004).
- [133] A. Sergi, *Phys. Procedia* **37**, 530 (2012).
- [134] A. H. Walenta, *Phys. Scripta* **23**, 354 (1981).
- [135] <https://indico.cern.ch/event/1022051/>.
- [136] J. A. Kadyk, *Nucl. Instrum. Meth. A* **300**, 436 (1991); J. Va’vra, *ICFA Instrum. Bull.* **24**, 1 (2002).
- [137] M. Aleksa *et al.*, *Nucl. Instrum. Meth.* **A446**, 435 (2000).
- [138] A. Oed, *Nucl. Instrum. Meth.* **A263**, 351 (1988).
- [139] F. Sauli, *Nucl. Instrum. Meth.* **A386**, 531 (1997).
- [140] Y. Giomataris *et al.*, *Nucl. Instrum. Meth.* **A376**, 29 (1996).
- [141] Input to the European Particle Physics Strategy no. 87 (2019), S. Dalla Torre, E. Oliveri, L. Ropelewski, M. Titov, Development of the Micro-Pattern Gaseous Detector Technologies: an overview of the CERN-RD51 Collaboration, <https://indico.cern.ch/event/765096/contributions/3295721>.
- [142] F. Sauli, *Micro-pattern gaseous detectors principles of operation and applications*, World Scientific, Singapore (2020).
- [143] R. Bouclier *et al.*, *Nucl. Instrum. Meth. A* **381**, 289 (1996); Y. Bagaturia *et al.*, *Nucl. Instrum. Meth. A* **490**, 223 (2002).
- [144] A. Bressan *et al.*, *Nucl. Instrum. Meth.* **A425**, 262 (1999).
- [145] S. Bachmann *et al.*, *Nucl. Instrum. Meth.* **A479**, 294 (2002); A. Bressan *et al.*, *Nucl. Instrum. Meth.* **A424**, 321 (1999).
- [146] M. Alfonsi *et al.*, *Nucl. Instrum. Meth. A* **671**, 6 (2012).
- [147] J. Derre *et al.*, *Nucl. Instrum. Meth. A* **459**, 523 (2001).
- [148] I. Giomataris *et al.*, *Nucl. Instrum. Meth. A* **560**, 405 (2006); S. Andriamonje *et al.*, *JINST* **5**, P02001 (2010).
- [149] A. Breskin *et al.*, *Nucl. Instrum. Meth.* **124**, 189 (1975).
- [150] J. Benlloch *et al.*, *IEEE Trans. Nucl. Sci.* **45**, 234 (1998).
- [151] Y. Giomataris, *Nucl. Instrum. Meth.* **A419**, 239 (1998).
- [152] M. Chefdeville *et al.*, *Nucl. Instrum. Meth. A* **556**, 490 (2006).
- [153] M. Lupberger *et al.*, *IEEE Trans. Nucl. Sci.* **64**, 5, 1159 (2017).
- [154] J. Leidner, F. Murtas and M. Silari, *Applied Sciences* **11**, 1 (2021).
- [155] A. Curioni *et al.*, *Nucl. Instrum. Meth. A* **849**, 60 (2017).
- [156] R. Chechik *et al.*, *Nucl. Instrum. Meth. A* **535**, 303 (2004); M. Alexeev *et al.*, *JINST* **8**, C12005 (2013).
- [157] S. Dalla Torre, *Nucl. Instrum. Meth. A* **639**, 111 (2011).
- [158] L. Moleri *et al.*, *JINST* **12**, 10, P10017 (2017), [arXiv:1707.00125].
- [159] G. Bencivenni *et al.*, *JINST* **10**, 02, P02008 (2015), [arXiv:1411.2466].
- [160] G. Bencivenni *et al.*, *JINST* **15**, 09, C09034 (2020).
- [161] F. Yamane *et al.*, *Nucl. Instrum. Meth. A* **951**, 162938 (2020), [arXiv:1901.03836].
- [162] T. Alexopoulos *et al.*, *Nucl. Instrum. Meth. A* **640**, 110 (2011).
- [163] D. Abbaneo *et al.*, *Nucl. Instrum. Meth. A* **718**, 383 (2013).
- [164] T. Alexopoulos *et al.*, *Nucl. Instrum. Meth. A* **617**, 161 (2010); L. Lavezzi *et al.*, in “2017 IEEE Nuclear Science Symposium and Medical Imaging Conference,” (2017), [arXiv:1803.07266].
- [165] A. Balla *et al.*, *Nucl. Instrum. Meth. A* **732**, 221 (2013).
- [166] J. Bortfeldt *et al.*, *Nucl. Instrum. Meth. A* **903**, 317 (2018), [arXiv:1712.05256].
- [167] RD51 DLC Workshop Report, RD51-NOTE-2021-002 (2021).
- [168] RD51 Collaboration: <https://rd51-public.web.cern.ch/>; S. Dalla Torre *et al.* (2018), [arXiv:1806.09955].
- [169] D.R. Nygren and J.N. Marx, *Phys. Today* **31N10**, 46 (1978).
- [170] J. Alme *et al.*, *Nucl. Instrum. Meth.* **A622**, 316 (2010), [arXiv:1001.1950].
- [171] J. Adolffson *et al.*, *Journal of Instrumentation* **16**, 03, P03022 (2021), URL <https://doi.org/10.1088/1748-0221/16/03/p03022>.
- [172] N. Abgrall *et al.* (T2K ND280 TPC), *Nucl. Instrum. Meth. A* **637**, 25 (2011), [arXiv:1012.0865].
- [173] A. H. Walenta *et al.*, *Nucl. Instrum. Meth.* **161**, 45 (1979).
- [174] H. Aihara *et al.*, *IEEE Trans.* **NS30**, 63 (1983).
- [175] K. Dehmelt (sPHENIX), *PoS MPGD2017*, 044 (2019).
- [176] P. Colas, I. Giomataris and V. Lepeltier, *Nucl. Instrum. Meth.* **A535**, 226 (2004).
- [177] X. Artru, G. B. Yodh and G. Mennessier, *Phys. Rev.* **D12**, 1289 (1975).
- [178] J. Alozy *et al.*, *Nucl. Instrum. Meth.* **A961**, 163681 (2020).
- [179] M. L. Cherry *et al.*, *Phys. Rev.* **D10**, 3594 (1974).
- [180] B. Dolgoshein, *Nucl. Instrum. Meth.* **A326**, 434 (1993).

- [181] A. Andronic and J. P. Wessels, Nucl. Instrum. Meth. **A666**, 130 (2012).
- [182] S. Acharya *et al.* (ALICE), Nucl. Instrum. Meth. **A881**, 88 (2018), [arXiv:1709.02743].
- [183] M. Petris *et al.*, Nucl. Instrum. Meth. **A714**, 17 (2013).
- [184] T. Akesson *et al.* (ATLAS TRT), Nucl. Instrum. Meth. **A522**, 131 (2004).
- [185] M. Ambriola *et al.*, Nucl. Instrum. Meth. **A522**, 77 (2004).
- [186] J. Adelman (ATLAS), Nucl. Instrum. Meth. **A706**, 33 (2013).
- [187] T. Kirn (AMS 02 TRD), Nucl. Instrum. Meth. **A706**, 43 (2013).
- [188] G. M. Garibian, L. A. Gevorgian and C. Yang, Nucl. Instrum. Meth. **125**, 133 (1975).
- [189] P. Nevski, Nucl. Instrum. Meth. **A522**, 116 (2004).
- [190] J. Alozy *et al.*, Nucl. Instrum. Meth. **A927**, 1 (2019), [arXiv:1901.11265].
- [191] V. M. Grishin and S. S. Sadilov, Nucl. Instrum. Meth. **A522**, 122 (2004).
- [192] B. Beischer *et al.*, Nucl. Instrum. Meth. **A583**, 485 (2007).
- [193] A. A. Savchenko *et al.*, JINST **15**, 06, C06024 (2020).
- [194] T. Akesson *et al.* (ATLAS TRT), Nucl. Instrum. Meth. **A412**, 200 (1998).
- [195] M. Ave *et al.*, Nucl. Instrum. Meth. **A654**, 140 (2011).
- [196] M. L. Cherry, Nucl. Instrum. Meth. **A706**, 39 (2013).
- [197] J. Alozy *et al.*, J. Phys. Conf. Ser. **1690**, 1, 012041 (2020).
- [198] M. Brigida *et al.*, Nucl. Instrum. Meth. **A706**, 69 (2013).
- [199] F. Hartjes *et al.*, Nucl. Instrum. Meth. **A706**, 59 (2013).
- [200] V. V. Berdnikov *et al.*, Nucl. Instrum. Meth. **A706**, 65 (2013).
- [201] R. Santonico and R. Cardarelli, Nucl. Instrum. Meth. **187**, 377 (1981).
- [202] V. Parkhomchuck, Y. Pestov and N. Petrovykh, Nuclear Instruments and Methods **93**, 2, 269 (1971).
- [203] G. V. Fedotov, Y. N. Pestov and K. N. Putilin, in "International Conference on Instrumentation for Colliding Beam Physics," 127–131 (1982).
- [204] E. Cerron Zeballos *et al.*, Nucl. Instrum. Meth. **A374**, 132 (1996).
- [205] J. Juita *et al.*, Fire Science Reviews **1** (2012).
- [206] P. Fonte, Journal of Instrumentation **8**, 04, P04017 (2013), URL <https://dx.doi.org/10.1088/1748-0221/8/04/P04017>.
- [207] G. Aielli *et al.*, Nucl. Instrum. Meth. **A508**, 6 (2003).
- [208] J. M. Meek, Phys. Rev. **57**, 722 (1940), URL <https://link.aps.org/doi/10.1103/PhysRev.57.722>.
- [209] R. Cardarelli, R. Santonico and V. Makeev, Nucl. Instrum. Meth. **A382**, 470 (1996).
- [210] R. Cardarelli, A. Di Ciaccio and R. Santonico, Nucl. Instrum. Meth. **A333**, 399 (1993).
- [211] R. Cardarelli, Sci Acta **8**, 159 (1993).
- [212] P. Camarri *et al.*, Nucl. Instrum. Meth. **A414**, 317 (1998).
- [213] L. Pontecorvo, ATLAS Muon Internal note **20** (1993).
- [214] W. Riegler, JINST **11**, 11, P11002 (2016).
- [215] R. Santonico, Nucl. Instrum. Meth. **A456**, 1 (2000).
- [216] R. Cardarelli *et al.*, JINST **8**, P01003 (2013).
- [217] G. Aielli *et al.*, JINST **9**, 09, C09030 (2014).
- [218] R. Santonico, JINST **9**, 11, C11007 (2014).
- [219] G. Aad *et al.* (ATLAS), JINST **3**, S08003 (2008).
- [220] S. Chatrchyan *et al.* (CMS), JINST **3**, S08004 (2008).
- [221] G. Aielli *et al.*, Nucl. Instrum. Meth. A **562**, 92 (2006).
- [222] A. Bertolin *et al.*, Nucl. Instrum. Meth. A **602**, 631 (2009).
- [223] Aielli, Giulio *et al.*, Eur. Phys. J. C **80**, 12, 1177 (2020).
- [224] M. Bauer *et al.*, ANUBIS: Proposal to search for long-lived neutral particles in CERN service shafts (2019), [arXiv:1909.13022].
- [225] M. Bedjidian *et al.*, JINST **6**, P02001 (2011), [arXiv:1011.5969].
- [226] P. Fonte, A. Smirnitsky and M. C. S. Williams (ALICE), Nucl. Instrum. Meth. **A443**, 201 (2000).
- [227] M. Abbrescia, V. Peskov and P. Fonte, *Resistive Gaseous Detectors: Designs, Performance, and Perspectives*, Wiley (2018), ISBN 9783527340767.
- [228] W. Riegler and C. Lippmann, Nucl. Instrum. Meth **A508**, 14 (2003).
- [229] P. Fonte (AIDA2020), Validation of new resistive materials for RPCs .
- [230] A. Akindinov *et al.*, Eur. Phys. J. Plus **128**, 44 (2013).
- [231] D. Belver *et al.*, Nucl. Instrum. Meth. A **602**, 687 (2009).
- [232] A. Schuttauf (FOPI), Nucl. Instrum. Meth. A **533**, 65 (2004).
- [233] M. Ablikim *et al.*, Nucl. Instrum. Meth. A **614**, 3, 345 (2010), ISSN 0168-9002.
- [234] e. a. P. Fonte, Nucl.Instrum.Meth.A **1051** (2023).
- [235] I. Deppner and N. Herrmann, JINST **15**, 10, C10030 (2020).
- [236] J. P. Chen *et al.*, A White Paper on SoLID (Solenoidal Large Intensity Device) (2014), [arXiv:1409.7741].
- [237] M. Benoit *et al.*, Journal of Instrumentation **11** (2015).
- [238] S. An *et al.*, Nucl. Instrum. Meth. **A594**, 39 (2008).
- [239] A. Blanco *et al.*, JINST **7**, P11012 (2012).
- [240] C. Iacobaeus *et al.*, Nucl. Instrum. Meth. **A513**, 244 (2003), [arXiv:physics/0210006].
- [241] G. Aielli *et al.*, Nucl. Instrum. Meth. **A456**, 82 (2000).
- [242] G. Aielli *et al.*, Nucl. Instrum. Meth. **533**, 1, 86 (2004), ISSN 0168-9002, proceedings of the Seventh International Workshop on Resistive Plate Chambers and Related Detectors.
- [243] H. Sakai *et al.*, Nucl. Instrum. Meth. **A484**, 153 (2002).
- [244] R. Santonico, JINST **8**, P04023 (2013).
- [245] L. Lopes *et al.*, Nucl. Instrum. Meth. **A533**, 69 (2004).
- [246] B. Liberti *et al.*, Journal of Instrumentation **11**, 09, C09012 (2016), URL <https://dx.doi.org/10.1088/1748-0221/11/09/C09012>.
- [247] S. Pisano *et al.*, Journal of Instrumentation **14**, 08, C08008 (2019), URL <https://dx.doi.org/10.1088/1748-0221/14/08/C08008>.
- [248] G. Rigoletti, B. Mandelli and R. Guida, Journal of Instrumentation **15**, 11, C11003 (2020), URL <https://dx.doi.org/10.1088/1748-0221/15/11/C11003>.
- [249] R. Guida, B. Mandelli and G. Rigoletti, Nuclear Instruments and Methods in Physics Research Section A: Accelerators, Spectrometers, Detectors and Associated Equipment **1039**, 167045 (2022), ISSN 0168-9002, URL <https://www.sciencedirect.com/science/article/pii/S0168900222004685>.
- [250] G. Proto *et al.*, Journal of Instrumentation **17**, 05, P05005 (2022), URL <https://dx.doi.org/10.1088/1748-0221/17/05/P05005>.
- [251] R. Cardarelli, JINST **16**, 05, C05004 (2021).
- [252] Summary of Liquid Argon Properties Accessed August 2021, URL <https://lar.bnl.gov/properties/>.
- [253] E. W. Lemmon *et al.*, NIST Standard Reference Database 23: Reference Fluid Thermodynamic and Transport Properties-REFPROP, Version 10.0, National Institute of Standards and Technology (2018), URL <https://www.nist.gov/srd/refprop>.

- [254] C. Rubbia, “The liquid-argon time projection chamber: a new concept for neutrino detectors: CERN-EP-INT-77-8,” (1977), URL <https://cds.cern.ch/record/117852>.
- [255] H. H. Chen and J. F. Lathrop, *Nucl. Instrum. Meth.* **150**, 585 (1978).
- [256] M. Miyajima *et al.*, *Phys. Rev. A* **9**, 1438 (1974).
- [257] M. Miyajima *et al.*, *Phys. Rev. A* **10**, 1452 (1974).
- [258] N. Gee *et al.*, *Journal of Applied Physics* **57**, 4, 1097 (1985).
- [259] W. Walkowiak, *Nucl. Instrum. Meth. A* **449**, 288 (2000).
- [260] T. Doke *et al.*, *Nucl. Instrum. Meth. A* **269**, 291 (1988).
- [261] T. Doke, K. Masuda and E. Shibamura, *Nucl. Instrum. Meth. A* **291**, 617 (1990).
- [262] T. Heindl *et al.*, *EPL* **91**, 6, 62002 (2010), [arXiv:1511.07718].
- [263] M. Babicz *et al.*, *JINST* **15**, 09, P09009 (2020), [arXiv:2002.09346].
- [264] G. M. Seidel, R. E. Lanou and W. Yao, *Nucl. Instrum. Meth. A* **489**, 189 (2002), [hep-ex/0111054].
- [265] E. Grace and J. A. Nikkel, *Nucl. Instrum. Meth. A* **867**, 204 (2017), [arXiv:1502.04213].
- [266] A. Hitachi *et al.*, *Phys. Rev. B* **27**, 5279 (1983).
- [267] R. Acciarri *et al.* (WArP), *JINST* **5**, P06003 (2010), [arXiv:0804.1217].
- [268] P. Adhikari *et al.* (DEAP), *Eur. Phys. J. C* **80**, 4, 303 (2020), [arXiv:2001.09855].
- [269] B. Abi *et al.* (DUNE), *JINST* **15**, 08, T08010 (2020), [arXiv:2002.03010].
- [270] M. Auger *et al.*, *JINST* **11**, 03, P03017 (2016), [arXiv:1512.05968].
- [271] A. Marchionni, *Ann. Rev. Nucl. Part. Sci.* **63**, 269 (2013), [arXiv:1307.6918].
- [272] K. Majumdar and K. Mavrokoridis, *Appl. Sciences* **11**, 6, 2455 (2021), [arXiv:2103.06395].
- [273] F. Arneodo *et al.* (The ICARUS-Milano Collaboration), *Phys. Rev. D* **74**, 112001 (2006).
- [274] S. Amerio *et al.* (ICARUS), *Nucl. Instrum. Meth. A* **527**, 329 (2004).
- [275] C. Anderson *et al.* (ArgoNeuT), *JINST* **7**, P10019 (2012), [arXiv:1205.6747].
- [276] R. Acciarri *et al.* (MicroBooNE), *JINST* **12**, 02, P02017 (2017), [arXiv:1612.05824].
- [277] R. Acciarri *et al.* (LArIAT), *JINST* **15**, 04, P04026 (2020), [arXiv:1911.10379].
- [278] C. E. Taylor *et al.* (CAPTAIN), *Nucl. Instrum. Meth. A* **1001**, 165131 (2021), [arXiv:2008.11422].
- [279] A. A. Abud *et al.* (DUNE (protoDUNE-SP)) (2021), [arXiv:2108.01902].
- [280] P. Abratenko *et al.* (MicroBooNE), *JINST* **16**, 06, P06043 (2021), [arXiv:2011.01375].
- [281] M. Wang *et al.* (2020), [arXiv:2009.04509].
- [282] B. Abi *et al.* (DUNE), *Phys. Rev. D* **102**, 9, 092003 (2020), [arXiv:2006.15052].
- [283] G. Carugno *et al.* (ICARUS), *Nucl. Instrum. Meth. A* **292**, 580 (1990).
- [284] M. Adamowski *et al.*, *JINST* **9**, P07005 (2014), [arXiv:1403.7236].
- [285] C. Adams *et al.* (MicroBooNE), *JINST* **15**, 07, P07010 (2020), [arXiv:1910.01430].
- [286] G. Bakale, U. Sowada and W. F. Schmidt, *The Journal of Physical Chemistry* **80**, 23, 2556 (1976).
- [287] A. Bettini *et al.* (ICARUS), *Nucl. Instrum. Meth. A* **305**, 177 (1991).
- [288] W. Jaskierny *et al.* (Fermilab-TM-2384-E), Technical report (2006), URL <https://lss.fnal.gov/archive/test-tm/2000/fermilab-tm-2384-e.pdf>.
- [289] Sigma-Aldrich 4A, BASF Copper Getter CU-0226S.
- [290] P. Cennini *et al.*, *Nucl. Instrum. Meth. A* **333**, 567 (1993).
- [291] B. J. P. Jones *et al.*, *JINST* **8**, P07011 (2013), [Erratum: *JINST* **8**, E09001 (2013)], [arXiv:1306.4605].
- [292] R. T. Scalettar *et al.*, *Phys. Rev. A* **25**, 2419 (1982).
- [293] E. Aprile *et al.*, *Nucl. Instrum. Meth. A* **261**, 519 (1987).
- [294] P. Cennini *et al.* (ICARUS), *Nucl. Instrum. Meth. A* **345**, 230 (1994).
- [295] S. Amoroso *et al.* (ICARUS), *Nucl. Instrum. Meth. A* **523**, 275 (2004).
- [296] R. Acciarri *et al.* (ArgoNeuT), *JINST* **8**, P08005 (2013), [arXiv:1306.1712].
- [297] G. Jaffe, *Annalen der Physik* **42**, 12, 303 (1913).
- [298] L. Onsager, *Phys. Rev.* **54**, 554 (1938).
- [299] J. Thomas and D. A. Imel, *Phys. Rev. A* **36**, 614 (1987).
- [300] C. Adams *et al.* (MicroBooNE), *JINST* **15**, 03, P03022 (2020), [arXiv:1907.11736].
- [301] T. Yang, *Instruments* **5**, 1, 2 (2020), [arXiv:2012.01319].
- [302] S. Amoroso *et al.* (ICARUS), *Nucl. Instrum. Meth. A* **516**, 68 (2004).
- [303] M. Antonello *et al.* (ICARUS), *JINST* **9**, 12, P12006 (2014), [arXiv:1409.5592].
- [304] V. Meddage (MicroBooNE), in “Meeting of the APS Division of Particles and Fields,” (2017), [arXiv:1710.00396].
- [305] B. Abi *et al.* (DUNE), *JINST* **15**, 12, P12004 (2020), [arXiv:2007.06722].
- [306] Y. Li *et al.*, *Nucl. Instrum. Meth. A* **816**, 160 (2016), [arXiv:1508.07059].
- [307] P. Agnes *et al.* (DarkSide), *Nucl. Instrum. Meth. A* **904**, 23 (2018), [arXiv:1802.01427].
- [308] P. Abratenko *et al.* (MicroBooNE), *JINST* **16**, 09, P09025 (2021), [arXiv:2104.06551].
- [309] S. Kubota *et al.*, *Phys. Rev. B* **20**, 8, 3486 (1979).
- [310] M. Kuźniak and A. M. Szelc, *Instruments* **5**, 1, 4 (2020), [arXiv:2012.15626].
- [311] R. Acciarri *et al.* (WArP), *JINST* **5**, P05003 (2010), [arXiv:0804.1222].
- [312] F. Spiegelmann and J.-P. Malrieu, *Chemical Physics Letters* **57**, 2, 214 (1978), ISSN 0009-2614.
- [313] B. Jones *et al.*, *JINST* **8**, P12015 (2013), [arXiv:1308.3658].
- [314] A. Buzulutskov, *EPL* **117**, 3, 39002 (2017), [arXiv:1702.03612].
- [315] J. Soto-Oton (DUNE), in “International Conference on Technology and Instrumentation in Particle Physics,” (2021), [arXiv:2109.05858].
- [316] A. Abed Abud *et al.* (DUNE) (2021), [arXiv:2103.13910].
- [317] P. Abratenko *et al.* (MicroBooNE), *JINST* **15**, 12, P12037 (2020), [arXiv:2008.09765].
- [318] M. Antonello *et al.* (ICARUS), *JINST* **15**, 07, P07001 (2020), [arXiv:2001.08934].
- [319] S. Palestini, *Instruments* **5**, 1, 9 (2021), [arXiv:2102.06082].
- [320] C. Cantini *et al.*, *JINST* **12**, 03, P03021 (2017), [arXiv:1611.02085].
- [321] J. Asaadi *et al.*, *JINST* **9**, P09002 (2014), [arXiv:1406.5216].
- [322] O. Bunemann, T. E. Cranshaw and J. A. Harvey, *Canadian Journal of Research* **27a**, 5, 191 (1949).
- [323] V. Radeka *et al.*, *J. Phys. Conf. Ser.* **308**, 012021 (2011).
- [324] H. Chen *et al.*, *Phys. Procedia* **37**, 1287 (2012).
- [325] S. Li *et al.*, *IEEE Transactions on Nuclear Science* **60**, 6, 4737 (2013).

- [326] H. Chen *et al.*, Nucl. Instrum. Meth. A **936**, 271 (2019).
- [327] R. Acciarri *et al.* (MicroBooNE), JINST **12**, 08, P08003 (2017), [arXiv:1705.07341].
- [328] P. Cennini *et al.* (ICARUS), Nucl. Instrum. Meth. A **432**, 240 (1999).
- [329] D. Caratelli (MicroBooNE), JINST **15**, 03, C03023 (2020).
- [330] B. Ali-Mohammadzadeh *et al.* (ICARUS), JINST **15**, 10, T10007 (2020), [arXiv:2006.05261].
- [331] A. Ankowski *et al.* (ICARUS), Nucl. Instrum. Meth. A **556**, 146 (2006).
- [332] N. Anfimov *et al.*, JINST **15**, 07, C07022 (2020).
- [333] E. Segreto *et al.*, JINST **15**, 05, C05045 (2020).
- [334] M. Antonello *et al.*, JINST **9** (2014), URL <https://iopscience.iop.org/article/10.1088/1748-0221/9/08/P08003/pdf>.
- [335] H. Chen *et al.*, 16th IEEE-NPSS Real Time Conference 159–162 (2009), URL <https://ieeexplore.ieee.org/document/5322032>.
- [336] B. Abi *et al.* (DUNE) (2018), [arXiv:1807.10327].
- [337] B. Abi *et al.* (DUNE) (2018), [arXiv:1807.10340].
- [338] R. Acciarri *et al.*, JINST **12**, 08, P08003 (2017), [arXiv:1705.07341].
- [339] C. Adams *et al.*, JINST **13**, 07, P07006 (2018), [arXiv:1802.08709].
- [340] B. Abi *et al.*, JINST **15**, 12, P12004 (2020), [arXiv:2007.06722].
- [341] R. Acciarri *et al.* (MicroBooNE), Eur. Phys. J. C **78**, 1, 82 (2018), [arXiv:1708.03135].
- [342] X. Qian *et al.*, JINST **13**, 05, P05032 (2018), [arXiv:1803.04850].
- [343] R. Acciarri *et al.* (MicroBooNE), JINST **12**, 03, P03011 (2017), [arXiv:1611.05531].
- [344] A. Abed Abud *et al.* (DUNE), Eur. Phys. J. C **82**, 10, 903 (2022), [arXiv:2203.17053].
- [345] F. Drielsma *et al.* [arXiv:2102.01033].
- [346] P. Abratenko *et al.* (MicroBooNE), JHEP **2021**, 153 (2021), [arXiv:2109.02460].
- [347] C. Rubbia *et al.* (ICARUS), JINST **6**, P07011 (2011), [arXiv:1106.0975].
- [348] D. A. Dwyer *et al.*, JINST **13**, 10, P10007 (2018), [arXiv:1808.02969].
- [349] B. Baibussinov *et al.* (ICARUS), JINST **13**, 03, T03001 (2018), [arXiv:1711.06781].
- [350] A. Lowe *et al.*, Instruments **4**, 4, 35 (2020), [arXiv:2011.02292].
- [351] A. Ereditato *et al.*, JINST **8**, 07, P07002 (2013), [arXiv:1304.6961].
- [352] E. Segreto, Phys. Rev. D **103**, 4, 043001 (2021), [arXiv:2012.06527].
- [353] LIDINE 2021 Accessed October 2021, URL <https://indico.physics.ucsd.edu/event/1/book-of-abstracts.pdf>.
- [354] L. Bäni *et al.* (RD42), J. Phys. Conf. Ser. **2374**, 1, 012172 (2022).
- [355] A. Rogalski, Adv. Opt. Photon. **11**, 2, 314 (2019).
- [356] V. Saraswat, R. Jacobberger and M. Arnold, ACS Nano **15**:3, 3674–3708 (2021).
- [357] G. Lutz, *Semiconductor Radiation Detectors*, Springer (1999), ISBN 978-3-540-64859-8.
- [358] F. Hartmann, *Evolution of Silicon Sensor Technology in Particle Physics*, volume 275 of *Springer Tracts in Modern Physics*, Springer (2017), ISBN 978-3-319-64434-9, 978-3-319-64436-3.
- [359] G. Lutz and R. Klanner, *Particle Physics Reference Library (Vol. 2, Ch. 5., Solid State Detectors)*, Eds. Fabjan, C. W. and Schopper, H., Springer Nature (2020), ISBN 978-3-030-35317-9, 978-3-030-35318-6.
- [360] Landolt-Börnstein, Springer (Berlin), 2002, https://doi.org/10.1007/10832182_456 and https://doi.org/10.1007/10832182_458.
- [361] C. Da Via *et al.*, Nucl. Instrum. Meth. **587**, 243 (2008).
- [362] C. Damerell, Nucl. Instrum. Meth. A **342**, 78 (1994).
- [363] L. Rossi *et al.*, *Pixel Detectors – From Fundamentals to Applications*, Springer, Berlin (2006), ISBN 978-3-540-28332-4, 978-3-540-28333-1.
- [364] M. Garcia-Sciveres and N. Wermes, Rept. Prog. Phys. **81**, 6, 066101 (2018).
- [365] H.-G. Moser *et al.*, PoS **VERTEX2007**, 022 (2007).
- [366] Y. Arai *et al.*, Nucl. Instrum. Meth. A **623**, 186 (2010).
- [367] H. Sadrozinski, A. Seiden and N. Cartiglia, Rept. Prog. Phys. **81**, 2, 026101 (2018).
- [368] M. Ferrero *et al.*, *Ultra-Fast Silicon Detectors*, CRC Press, Open Access, Creative Commons (2021), ISBN 978-1-003-13194-6.
- [369] A. Lampis *et al.*, JINST **18**, 01, C01051 (2023).
- [370] S. Zambito *et al.*, JINST **18**, 03, P03047 (2023).
- [371] W. Riegler and G. Aglieri Rinella, JINST **12**, 11, P11017 (2017).
- [372] R. Wunstorff, *Systematische Untersuchungen zur Strahlenresistenz von Silizium-Detektoren für die Verwendung in Hochenergiephysikexperimenten*, Ph.D. thesis, Universität Hamburg (1992), URL https://www-library.desy.de/preparch/desy/int_rep/fh1k-92-01.pdf.
- [373] M. Moll, IEEE Trans. Nucl. Sci. **65**, 8, 1561 (2018).
- [374] G. Kramberger, Initial acceptor removal in p-type silicon-Talk at 26th CERN-RD50 Workshop, Santander (2015), <https://indico.cern.ch/event/381195/contributions/905665/>.
- [375] G. Kramberger, *Particle Physics Reference Library (Vol. 2, Ch. 21., Solid State Detectors for High Radiation Environments)*, Eds. Fabjan, C. W. and Schopper, H., Springer Nature (2020), ISBN 978-3-030-35317-9, 978-3-030-35318-6.
- [376] W. Blum, L. Rolandi and W. Riegler, *Particle detection with drift chambers*, Particle Acceleration and Detection, Springer (2008), ISBN 978-3-540-76683-4, 978-3-540-76684-1.
- [377] F. S. Goulding, Nucl. Instrum. Meth. **100**, 493 (1972).
- [378] V. Radeka, Ann. Rev. Nucl. Part. Sci. **38**, 217 (1988).
- [379] C. Agapopoulou *et al.*, JINST **15**, 07, P07007 (2020).
- [380] R. Wigmans, *Calorimetry*, International Series of Monographs on Physics, Oxford University Press (2017).
- [381] S. Agostinelli *et al.* (GEANT4), Nucl. Instrum. Meth. A **506**, 250 (2003).
- [382] J. Allison *et al.*, IEEE Trans. Nucl. Sci. **53**, 270 (2006).
- [383] T. Gabriel and L. Charlton (1997).
- [384] T. T. Böhlen *et al.*, Nucl. Data Sheets **120**, 211 (2014).
- [385] A. Ferrari *et al.* (2005).
- [386] J. Allison *et al.*, Nucl. Instrum. Meth. A **835**, 186 (2016).
- [387] D. Buskulic *et al.* (ALEPH), Nucl. Instrum. Meth. A **360**, 481 (1995).
- [388] A. M. Sirunyan *et al.* (CMS), JINST **12**, 10, P10003 (2017), [arXiv:1706.04965].
- [389] M. A. Thomson, Nucl. Instrum. Meth. A **611**, 25 (2009), [arXiv:0907.3577].
- [390] L. Linssen *et al.* (2012), [arXiv:1202.5940].
- [391] H. L. Tran *et al.*, Eur. Phys. J. C **77**, 10, 698 (2017), [arXiv:1705.10363].

- [392] M. Aleksa *et al.*, Eur. Phys. J. Plus **136**, 10, 1066 (2021), [arXiv:2109.00391].
- [393] M. T. Lucchini *et al.*, JINST **15**, 11, P11005 (2020), [arXiv:2008.00338].
- [394] W.R. Nelson, H. Hirayama, and D.W.O. Rogers, SLAC-265 (1985).
- [395] ATLAS Collab., CERN/LHCC 96-41 (1996).
- [396] D. Hitlin *et al.*, Nucl. Instrum. Meth. **137**, 225 (1976).
- [397] W. J. Willis and V. Radeka, Nucl. Instrum. Meth. **120**, 221 (1974).
- [398] R. Wigmans, *Calorimetry: Energy Measurement in Particle Physics*, Inter. Series of Monographs on Phys. **107**, Second Edition, Oxford Scholarship Online (2017).
- [399] R. Y. Zhu, Nucl. Instrum. Meth. **A413**, 297 (1998).
- [400] R.Y. Zhu, Journal of Physics: Conference Series **587**, 012055 (2015).
- [401] CMS Collab., CERN/LHCC 97-33 (1997).
- [402] C. Leroy and P. Rancoita, Rept. Prog. Phys. **63**, 505 (2000).
- [403] F. Sefkow and F. Simon, *Calorimeters*, in Fleck I., Titov M., Grupen C., Buvat I. (eds) Handbook of Particle Detection and Imaging, Springer (2021), ISBN 978-3-319-47999-6.
- [404] C. Adloff *et al.* (CALICE), JINST **8**, 07005 (2013).
- [405] T. A. Gabriel *et al.*, Nucl. Instrum. Meth. **A338**, 336 (1994).
- [406] F. Ariztizabal *et al.* (RD-34), Nucl. Instrum. Meth. **A349**, 384 (1994).
- [407] F. Sefkow and F. Simon (CALICE), J. Phys. Conf. Ser. **1162**, 1, 012012 (2019), [arXiv:1808.09281].
- [408] A. White *et al.* (CALICE), JINST **18**, 11, P11018 (2023), [arXiv:2209.15327].
- [409] CMS, CERN-LHCC-2017-023, CMS-TDR-019 (2017).
- [410] N. Akchurin *et al.*, Nucl. Instrum. Meth. **A399**, 202 (1997).
- [411] A. Artamonov *et al.*, JINST **3**, P02010 (2008).
- [412] B. Aubert *et al.*, Nucl. Instrum. Meth. **A321**, 467 (1992).
- [413] C. W. Fabjan *et al.*, Nucl. Instrum. Meth. **141**, 61 (1977).
- [414] J. Brau *et al.*, Nucl. Instrum. Meth. **A238**, 489 (1985).
- [415] H. Brückmann and H. Kowalski, ZEUS Int. Note 86/026 DESY, Hamburg (1986).
- [416] R. Wigmans, Nucl. Instrum. Meth. **A259**, 389 (1987).
- [417] R. Wigmans, Nucl. Instrum. Meth. **A265**, 273 (1988).
- [418] J. E. Brau and T. A. Gabriel, Nucl. Instrum. Meth. A **275**, 190 (1989).
- [419] J. C. Brient, R. Rusack and F. Sefkow, Ann. Rev. Nucl. Part. Sci. **68**, 271 (2018).
- [420] E. Fretwurst *et al.* (1989), URL <http://cds.cern.ch/record/368113>.
- [421] E. Borchi *et al.* (SICAPO), Nucl. Instrum. Meth. **A279**, 57 (1989).
- [422] H. Abramowicz *et al.* (2013), [arXiv:1306.6329].
- [423] N. Alipour Tehrani *et al.* (CLICdp) (2017), CLICdp-Note-2017-001.
- [424] N. Bacchetta *et al.* (2019), [arXiv:1911.12230].
- [425] <https://twiki.cern.ch/twiki/bin/view/CALICE/CaliceDetectors>.
- [426] C. Adloff *et al.* (CALICE), JINST **5**, P05004 (2010), [arXiv:1003.2662].
- [427] M. Chefdeville *et al.* (CALICE), Nucl. Instrum. Meth. A **939**, 89 (2019), [arXiv:1901.08818].
- [428] G. Baulieu *et al.*, JINST **10**, 10, P10039 (2015), [arXiv:1506.05316].
- [429] B. Acar *et al.* (CMS, CALICE), JINST **18**, 08, P08014 (2023), [arXiv:2211.04740].
- [430] C. Adloff *et al.* (CALICE), JINST **8**, P09001 (2013), [arXiv:1305.7027].
- [431] H. Abramowicz *et al.*, Nucl. Instrum. Meth. **180**, 429 (1981).
- [432] B. Andrieu *et al.* (H1 Calorimeter Group), Nucl. Instrum. Meth. A **336**, 499 (1993).
- [433] C. Cojocar *et al.* (ATLAS Liquid Argon EMEC/HEC), Nucl. Instrum. Meth. A **531**, 481 (2004), [arXiv:physics/0407009].
- [434] C. Adloff *et al.* (CALICE), J. Instr. **7**, 09, P09017 (2012).
- [435] H. L. Tran *et al.*, The European Physical Journal C **77**, 10, 698 (2017).
- [436] P. Mockett, SLAC-267, 335 (1983).
- [437] D. E. Groom, Nucl. Instrum. Meth. **A572**, 633 (2007), erratum: Nucl. Instrum. Meth. **A593**, 628 (2008).
- [438] R. Wigmans, *Proc. 7th Inter. Conf. on Calorimetry in High Energy Physics*, 182 World Scientific, River Edge, NJ, (1998);.
- [439] S. Lee, M. Livan and R. Wigmans, Rev. Mod. Phys. **90**, 2, 025002 (2018).
- [440] S. Lee *et al.*, Nucl. Instrum. Meth. A **866**, 76 (2017), [arXiv:1703.09120].
- [441] M. Antonello *et al.*, JINST **15**, 06, C06015 (2020).
- [442] E. Bernardi *et al.*, Nucl. Instrum. Meth. **A262**, 229 (1987).
- [443] M. Chefdeville *et al.* (CALICE), JINST **10**, 12, P12006 (2015), [arXiv:1509.00617].
- [444] T. Akesson *et al.*, Nucl. Instrum. Meth. **A262**, 243 (1987).
- [445] D. Acosta *et al.*, Nucl. Instrum. Meth. **A308**, 481 (1991).
- [446] R. Dubois *et al.*, IEEE Trans. Nucl. Sci. **33**, 194 (1986).
- [447] B. Andrieu *et al.* (H1 Calorimeter Group), Nucl. Instrum. Meth. A **336**, 460 (1993).
- [448] A. Bernstein *et al.* (ZEUS Barrel Calorimeter Group), Nucl. Instrum. Meth. A **336**, 23 (1993).
- [449] J.-b. Liu (CDF), in “7th International Conference on Calorimetry in High-Energy Physics (ICCHEP 97),” 237–240 (1997).
- [450] S. Abachi *et al.* (D0), Nucl. Instrum. Meth. A **324**, 53 (1993).
- [451] G. Aad *et al.* (ATLAS), JINST **3**, S08003 (2008).
- [452] S. Abdullin *et al.* (USCMS, ECAL/HCAL), Eur. Phys. J. C **60**, 359 (2009), [Erratum: Eur.Phys.J.C 61, 353–356 (2009)].
- [453] H. Abramowicz *et al.* (ZEUS), Phys. Lett. B **718**, 915 (2013), [arXiv:1210.5511].
- [454] E. Shibamura *et al.*, Nucl. Instrum. Methods **A316**, 184 (1975).
- [455] L. S. Miller, S. Howe and W. E. Spear, Phys. Rev. **166**, 871 (1968).
- [456] A.M. Kalinin *et al.*, ATLAS-LARG-NO-058 (1996).
- [457] K. Yoshino, U. Sowada and W. F. Schmidt, Phys. Rev. **A14**, 438 (1976).
- [458] A.O. Allen *et al.*, NSRDS-NBS-58 (1976).
- [459] P. Benetti *et al.*, Nucl. Instrum. Methods **A32**, 361 (1993).
- [460] G. Danby *et al.*, Phys. Rev. Lett. **9**, 36 (1962).
- [461] S. van der Meer (1961).
- [462] J. A. Formaggio and G. P. Zeller, Rev. Mod. Phys. **84**, 1307 (2012), [arXiv:1305.7513].
- [463] H. Faissner, “CERN Spark Chamber Neutrino Experiment”, INSPIRE-1377455.
- [464] H. Faissner *et al.*, Phys. Lett. **68B**, 377 (1977).
- [465] F. J. Hasert *et al.* (Gargamelle Neutrino), Nucl. Phys. **B73**, 1 (1974).

- [466] N. Armenise *et al.* (BEBC TST Neutrino), *Phys. Lett.* **81B**, 385 (1979).
- [467] A.E. Asratien *et al.*, *Phys. Lett.* **79**, 497 (1978).
- [468] S. J. Barish *et al.*, *Phys. Rev.* **D16**, 3103 (1977).
- [469] N. J. Baker *et al.*, *Phys. Rev.* **D23**, 2499 (1981).
- [470] J. W. Chapman *et al.*, *Phys. Rev.* **D14**, 5 (1976).
- [471] M. Holder *et al.*, *Nucl. Instrum. Meth.* **148**, 235 (1978).
- [472] I. Ambats *et al.* (MINOS) (1998).
- [473] K. Abe *et al.* (T2K), *Nucl. Instrum. Meth.* **A659**, 106 (2011), [arXiv:1106.1238].
- [474] M. H. Ahn *et al.* (K2K), *Phys. Rev.* **D74**, 072003 (2006), [hep-ex/0606032].
- [475] A. A. Aguilar-Arevalo *et al.* (MiniBooNE), *Nucl. Instrum. Meth.* **A599**, 28 (2009), [arXiv:0806.4201].
- [476] A. C. Benvenuti *et al.*, *Nucl. Instrum. Meth.* **125**, 447 (1975).
- [477] C. Athanassopoulos *et al.* (LSND), *Nucl. Instrum. Meth.* **A388**, 149 (1997), [arXiv:nucl-ex/9605002].
- [478] D. S. Ayres *et al.* (NOvA) (2007).
- [479] K. Hiraide *et al.* (SciBooNE), *Phys. Rev.* **D78**, 112004 (2008), [arXiv:0811.0369].
- [480] C. Rubbia, CERN-EP-INT-77-08 (1977).
- [481] S. Amerio *et al.* (ICARUS), *Nucl. Instrum. Meth.* **A527**, 329 (2004).
- [482] C. Anderson *et al.*, *JINST* **7**, 10020 (2012).
- [483] H. Chen *et al.*, FERMILAB-PROPOSAL-0974 (2007).
- [484] B. Abi *et al.*, Deep Underground Neutrino Experiment (DUNE), Far Detector Technical Design Report, Volume I: Introduction to DUNE (2020), [arXiv:2002.02967].
- [485] T. D. Collaboration, A. A. Abud *et al.*, *Journal of Instrumentation* **17**, 01, P01005 (2022), URL <https://dx.doi.org/10.1088/1748-0221/17/01/P01005>.
- [486] B. Abi *et al.*, *Journal of Instrumentation* **15**, 12, P12004 (2020), URL <https://dx.doi.org/10.1088/1748-0221/15/12/P12004>.
- [487] D. H. Perkins, *Nature* **159**, 126 (1947).
- [488] S. Aoki *et al.*, *Nucl. Instrum. Meth.* **A447**, 361 (2000).
- [489] N. Uhida *et al.*, *Nucl. Instrum. Methods* **224**, 50 (1984).
- [490] K. Kodama *et al.*, *Nucl. Instrum. Meth.* **B93**, 340 (1994).
- [491] T. Adam *et al.*, *Nucl. Instrum. Meth.* **A577**, 523 (2007), [arXiv:physics/0701153].
- [492] D. Di Ferdinando (OPERA), *Radiat. Meas.* **44**, 840 (2009), [arXiv:0812.0451].
- [493] R. Acquafredda *et al.* (OPERA), *New J. Phys.* **8**, 303 (2006), [hep-ex/0611023].
- [494] T. Fukuda *et al.*, *PTEP* **2017**, no. 6, 063C02 (2017).
- [495] H. Abreu *et al.*, *The European Physical Journal C* **80**, 1 (2020), URL <https://doi.org/10.1140%2Fepjc%2Fs10052-020-7631-5>.
- [496] F. Collaboration, H. Abreu *et al.*, *The FASER Detector* (2022), [arXiv:2207.11427].
- [497] A. N. Diddens *et al.* (CERN-Hamburg-Amsterdam-Rome-Moscow), *Nucl. Instrum. Meth.* **178**, 27 (1980).
- [498] D. Geiregat *et al.* (CHARM-II), *Nucl. Instrum. Meth.* **A325**, 92 (1993).
- [499] L. A. Ahrens *et al.*, *Nucl. Instrum. Meth.* **A254**, 515 (1987).
- [500] G. Gidal, LBL-91 Suppl., *Rev.* (1985).
- [501] W. K. Sakumoto *et al.*, *Nucl. Instrum. Meth.* **A294**, 179 (1990).
- [502] D. A. Harris *et al.* (NuTeV), *Nucl. Instrum. Meth.* **A447**, 377 (2000), [hep-ex/9908056].
- [503] J. Altegoer *et al.* (NOMAD), *Nucl. Instrum. Meth.* **A404**, 96 (1998).
- [504] L. Aliaga *et al.* (MINERvA), *Nucl. Instrum. Meth.* **A743**, 130 (2014), [arXiv:1305.5199].
- [505] R. Albanese *et al.* (SND@LHC Collaboration), *Phys. Rev. Lett.* **131**, 031802 (2023), URL <https://link.aps.org/doi/10.1103/PhysRevLett.131.031802>.
- [506] A. Yamamoto, *Nucl. Instrum. Meth.* **A453**, 445 (2000).
- [507] A. Yamamoto and Y. Makida, *Nucl. Instrum. Meth.* **A494**, 255 (2002).
- [508] T. M. Taylor, *Phys. Scripta* **23**, 459 (1981).
- [509] R. L. Gluckstern, *Nucl. Instrum. Meth.* **24**, 381 (1963).
- [510] V. Karimaki, *Nucl. Instrum. Meth.* **A410**, 284 (1998).

36. Particle Detectors for Non-Accelerator Physics

Revised 2024. See the various sections for authors.

36.1	Introduction	649
36.2	High-energy cosmic-ray hadron and gamma-ray detectors	649
36.2.1	Atmospheric fluorescence detectors	649
36.2.2	Atmospheric Cherenkov telescopes for high-energy gamma ray astronomy	651
36.3	Large neutrino detectors	652
36.3.1	Deep liquid detectors for rare processes	652
36.3.2	Neutrino telescopes	654
36.3.3	Radio emission from (ultra-)high energy particle showers	657
36.4	Large time-projection chambers for rare event detection	661
36.4.1	Dark matter and other low energy signals	663
36.4.2	$0\nu\beta\beta$ Decay	664
36.5	Sub-kelvin detectors	665
36.5.1	Motivation for Sub-kelvin Detectors	665
36.5.2	Detector Types	666
36.5.3	Experimental Applications	668
36.6	Low-radioactivity background techniques	670
36.6.1	Introduction	670
36.6.2	Radio-purity assay	671
36.6.3	Radon and its progeny	671
36.6.4	Surface backgrounds	672
36.6.5	Mitigation of backgrounds and active background discrimination	672

36.1 Introduction

Non-accelerator experiments have become increasingly important in particle physics and astrophysics. From them comes the evidence of physics beyond the SM, with the discovery of neutrino oscillations and adiabatic flavor conversion. Explored energies range from the meV scale to above the EeV, some 24 orders of magnitude. The physics and the design of the detectors vary as a consequence. Some experiments look at astrophysical high-energy phenomena using the atmosphere as a detector in the fluorescence and Cherenkov observatories or the polar ice and the ocean water in neutrino telescopes. Experiments on extremely rare events, such as neutrino-less double beta decay, solar neutrinos and dark matter induced scattering, need dedicated fully equipped deep underground laboratories, existing in different countries. Critical is the research to push back the ultra-low radioactive background frontier, with dedicated facilities in these laboratories. Detectors range from hyper-pure liquid scintillators, both organic and not, to thermalized and ballistic phonon detectors at the sub-Kelvin temperature, to dual phase noble fluid TPCs, etc. Space-based detectors also use some unique instrumentation, but these are beyond the present scope of this review. Gravitational wave detectors are not included as well.

36.2 High-energy cosmic-ray hadron and gamma-ray detectors

36.2.1 Atmospheric fluorescence detectors

Revised March 2024 by L.R. Wiencke (Colorado School of Mines).

Cosmic-ray fluorescence detectors (FDs) use the atmosphere as a giant calorimeter to measure isotropic scintillation light that traces the development profiles of extensive air showers. An extensive air shower (EAS) is produced by the interactions of ultra high-energy ($E > 10^{17}$ eV) subatomic particles in the stratosphere and upper troposphere. The amount of scintillation light generated by an EAS is proportional to the energy deposited in the atmosphere and nearly independent of the primary species. With energies extending beyond 10^{20} eV, ultra high energy cosmic rays (UHECRs) are the highest energy subatomic particles

known to exist. In addition to particle arrival directions, energy spectra and primary composition, the astroparticle science investigated with FDs also includes multi-messenger studies, searches for high energy photons, neutrinos, monopoles and deeply penetrating forms of dark matter. The Pierre Auger Observatory FD also measures UV scintillation that traces the development of ring-shaped atmospheric transient luminous events, called Elves, in the ionosphere that are initiated by strong lightning [1].

Previous experiments with FDs included the pioneering Fly’s Eye [2, 3], and the High Resolution Fly’s Eye (HiRes and HiRes prototype) [4]. The history of the fluorescence technique includes earlier studies in the 1950’s and 1960’s [5, 6]. The current generation of experiments include the Telescope Array (TA) [7] in the northern hemisphere, and the larger Pierre Auger Observatory (Auger) [8] in the southern hemisphere. (Discussion, with extensive references, of current and possible future UHECR experiments can be found in [9].) Auger and TA are hybrid observatories. Their FD telescopes overlook sparse arrays of particle detectors on the ground. Select parameters are listed in Table 36.1. TA and Auger have each one FD site populated with additional telescopes that view up to 60° in elevation to measure lower EASs using a combination of scintillation and direct Cherenkov light. As part of a fourfold coverage upgrade of TA (TAx4), 12 HiRes refurbished telescopes have been installed at the north and south-east sites of TA. A set of prototype FD telescopes, dubbed FAST [10], have observed EASs at the TA site using design that features wide field of view PMTs, fast timing and economical optics for a next-generation ground-based observatory. A second prototype has been installed at the Pierre Auger Observatory.

The fluorescence light is emitted primarily between 290 and 430 nm (Figure 36.1) with major lines at 337, 357, and 391 nm, when relativistic charged particles, primarily electrons and positrons, excite nitrogen molecules in air, resulting in transitions of the 1P and 2P systems. Reviews and references for the pioneering and recent laboratory measurements of fluorescence yield, $Y(\lambda, P, T, u)$, including dependence on wavelength (λ), temperature (T), pressure (p), and humidity (u) may be found in Refs. [11–13]. The results of various laboratory experiments have been combined (Figure 36.2) to obtain an absolute average and uncertainty for $Y(337 \text{ nm}, 800 \text{ hPa}, 293 \text{ K}, \text{ dry air})$ of $7.04 \pm 0.24 \text{ ph/MeV}$ after corrections for different electron beam energies and other factors. The units of ph/MeV correspond to the number of fluorescence photons produced per MeV of energy deposited in the atmosphere by the electromagnetic component of an EAS.

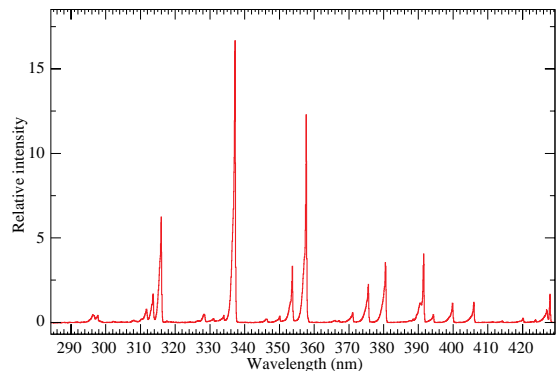


Figure 36.1: Measured fluorescence spectrum excited by 3 MeV electrons in dry air at 800 hPa and 293 K. Airfly experiment. Figure from Ref [14].

An FD element (telescope) consists of a non-tracking spherical mirror of less than astronomical quality, a “camera” of photomultiplier tubes (PMTs) near the focal plane, and a flash ADC readout system with a pulse and track-finding trigger scheme [8, 16]. The major experiments listed in Table 36.1 all use conventional PMTs (for example, Hamamatsu R9508 or Photonis XP3062) with

Table 36.1: Parameters of major fluorescence detectors. Note 1: Year when all FD sites were operational. Note 2: At TA 1 of the 3 FD sites features 24 telescopes from the HiRes experiment. Note 3: A-C for one telescope where A is the full area and C the area obscured by the camera and support structures. Thus A-C is the effective light collecting area. For the modified Schmidt design at Auger, the area of the entrance pupil, A, is listed because the pupil is smaller than the mirror and thus defines the entrance aperture. For the other experiments, the area of the mirror, A, is listed

Observatory	Fly's Eye	HiRes	Telescope Array	Pierre Auger
Location	Dugway UT US	Dugway UT US	Delta UT US	Malargüe AR
Start-End	1981-1992	1996-2006	2008-present	2005-present
Sites (note 1)	2 (1986)	2 (1999)	3 (2008)	4 (2008)
Separation	3.3 km	12.6 km	31-40 km	39-62 km
Telescopes/site	67,18	21,42	12+8,12,14+10+4	6, 6, 6, 6+3
Pixel FOV	5.5°	1°	1°	1.5°
Telescope FOV	≈18°×≈18°	16°×13.5°	18°×15° (note 2)	30°×28.1°
Azi×Elv				
Light collection area (note 3)	1.95 m ² - 0.25 m ²	3.72 m ² - 0.5 m ²	6.8 m ² - 0.85 m ² (for 2 sites)	3.80 m ² - 0.80 m ² (modified schmidt)
Energy Scale	≤40%	≈20%	≈20%	14%
Uncertainty				

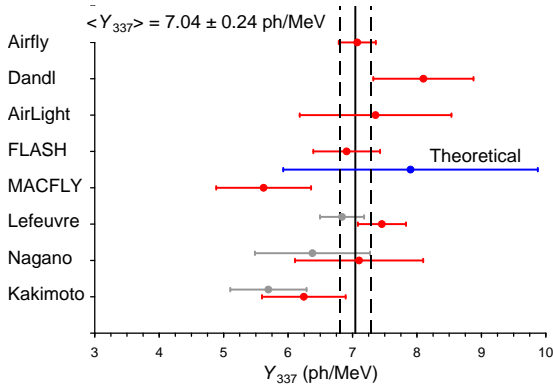


Figure 36.2: Fluorescence yield values and associated uncertainties at 337 nm (Y_{337}) in dry air at 800 hPa and 293 K. The methodology and corrections that were applied to obtain the average and the uncertainty are discussed extensively in this reference. The vertical axis denotes different laboratory experiments that measured FY. The gray bars show three of the original measurements to illustrate the scale of the corrections applied. Figure from Ref [15].

grounded cathodes and AC coupled readout. Segmented mirrors have been fabricated from slumped or slumped/polished glass with an anodized aluminum coating or fabricated using shaped aluminum that was then chemically anodized with AlMgSiO₅. A broadband UV filter (custom fabricated, BG-3, or Schott MUG-6) reduces background light such as starlight, airglow, man-made light pollution, and airplane strobe-lights.

At 10²⁰ eV, where the flux drops below 1 EAS/km²century, the aperture for an eye of adjacent FD telescopes that span the horizon can reach 10⁴ km² sr. FD operation requires (nearly) moonless nights and clear atmospheric conditions, which typically imposes a duty cycle of about 10%. Arrangements of LEDs, calibrated diffuse sources [17], pulsed UV lasers [18], LIDARs¹ and IR detectors that are sensitive to clouds are used for photometric calibration, atmospheric calibration [19], and determination of exposure [20]. For purposes of optical transmission, the atmosphere is treated as having a dominant molecular component and a secondary aerosol component. The latter is well described [21] by molecular scattering theory and models derived from radiosonde measurements. The aerosol component can include dust, haze and pollution and the aerosol optical depth profile must be measured on site in the UV during FD data taking.

The EAS generates a track consistent with a light source mov-

ing at $v = c$ across the FOV. The number of photons (N_γ) as a function of atmospheric depth (X) can be expressed as [12]

$$\frac{dN_\gamma}{dX} = \frac{dE_{\text{dep}}^{\text{tot}}}{dX} \int Y(\lambda, P, T, u) \cdot \tau_{\text{atm}}(\lambda, X) \cdot \varepsilon_{\text{FD}}(\lambda) d\lambda, \quad (36.1)$$

where $\tau_{\text{atm}}(\lambda, X)$ is the atmospheric transmission, including wavelength (λ) dependence, and $\varepsilon_{\text{FD}}(\lambda)$ is the FD efficiency. $\varepsilon_{\text{FD}}(\lambda)$ includes geometric factors and collection efficiency of the optics, quantum efficiency of the PMTs, and other throughput factors. The typical systematic uncertainties, τ_{atm} (10%) and ε_{FD} (photometric calibration 10%), currently dominate the systematic uncertainty the absolute EAS energy scale. FD energy resolution, defined as event-to-event statistical uncertainty, is typically less than 10% for final data samples used for science analysis.

Analysis methods to reconstruct the EAS profile and deconvolve the contributions of re-scattered scintillation light, and direct and scattered Cherenkov light are described in [2] and more recently in [23]. The EAS energy is typically obtained by integrating over the Gaisser-Hillas function [24]

$$E_{\text{cal}} = \int_0^\infty [w_{\text{max}} \left(\frac{X - X_0}{X_{\text{max}} - X_0} \right)^{(X_{\text{max}} - X_0)/\lambda} e^{(X_{\text{max}} - X)/\lambda}] dX, \quad (36.2)$$

where E_{cal} is the energy of electromagnetic energy component of the EAS and X_{max} is the atmospheric slant depth at which the shower reaches its maximum energy deposit rate. This maximum dE/dX is denoted as w_{max} . X_0 and λ are two shape parameters. The energy of the primary cosmic ray is obtained by correcting E_{cal} upward by about 10% to account for the invisible energy carried by particles that do not interact in the atmosphere. Auger reported a data-driven method to estimate the invisible energy from the muon number at ground level and X_{max} to reduce systematic uncertainties [25]. Energy resolution, $\Delta E/E$, of 15-20% is achievable, provided the geometric fit of the EAS axis is constrained, typically by multi-eye stereo projection or hybrid observations, and the profile fit of EAS development along the track is constrained by the observed rise and fall about X_{max} . An example of a recorded EAS light profile and its corresponding dE/dX development profile are shown in Fig. 36.3. The EAS generates a track consistent with a light source moving at $v = c$ across the FOV. The number of photons (N_γ) as a function of atmospheric depth (X) can be expressed as [12]. In 2023 the Pierre Auger Collaboration published a public data release [26] of the 100 highest energy cosmic ray events collected over a 17-year span through 2020 with an additional 9 energetic hybrid events used in the calibration procedure. In 2024 the collaboration reported the first comparison of X_{max} measurements [27] between fluorescence and radio detectors at the same location. This comparison includes a subset of 53 airshowers that were observed by the two detectors simultaneously.

¹LIDAR stands for "Light Detection and Ranging" and refers here to systems that measure atmospheric properties from the light scattered backwards from laser pulses directed into the sky.

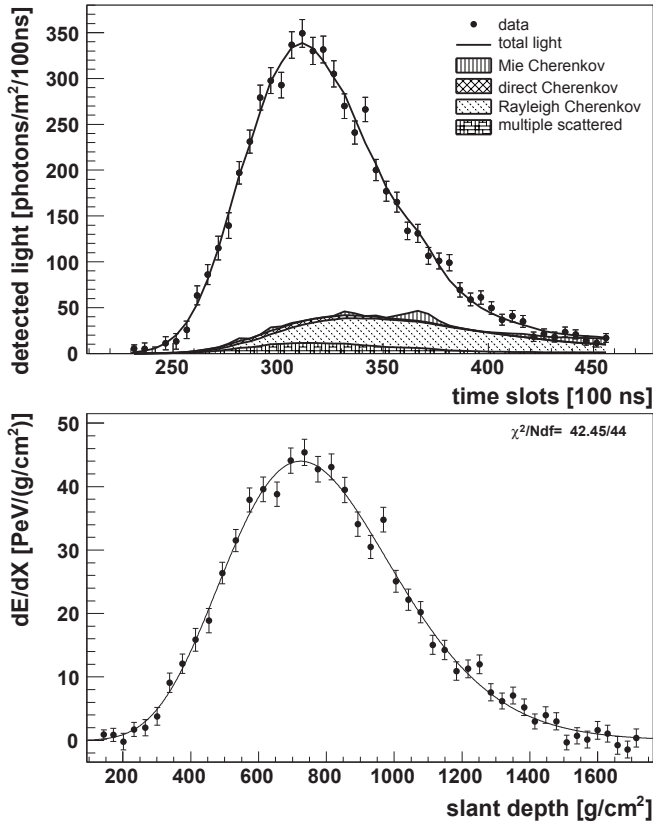


Figure 36.3: Example light profile (left) of one EAS recorded by the Pierre Auger FD and the corresponding profile (right) of energy deposited in the atmosphere vs atmospheric slant depth. The light profiles include the estimated components of Cherenkov light that have been scattered out of the forward beam by the molecular and aerosol (Mie) components of the atmosphere. The reconstructed energy of this EAS was $3.0 \pm 0.2 \times 10^{19}$ eV. Figure from Ref [22].

An FD that would look down on the earth’s atmosphere from space orbit to view a much larger area than ground based instruments is an active area of R&D. Prototypes that have been built and flown in orbit include the pioneering TUS instrument [28], [29] operated 2016-2018 onboard the Lomonosov satellite. The JEM-EUSO collaboration has flown prototype FD telescopes on stratospheric balloon flights in 2014 (EUSO-Balloon) [30], 2017 (EUSO-SPB1) [31] and 2023 (EUSO-SPB2) [32]. The Mini-EUSO [33] FD continues recording terrestrial UV emission by looking down through a 25 cm diameter UV-transmitting window inside the International Space Station since 2019. The Probe of Extreme Multimessenger Astrophysics (POEMMA) project has completed a detailed conceptual design study for a twin-satellite mission [34] that would observe UHECRs and PeV scale cosmogenic tau neutrinos.

36.2.2 Atmospheric Cherenkov telescopes for high-energy gamma ray astronomy

Revised October 2023 by J. Holder (Delaware U.; Delaware U., Bartol Inst.).

A wide variety of astrophysical objects are now known to produce high-energy γ -ray photons. Leptonic or hadronic particles, accelerated to relativistic energies in the source, produce γ -rays typically through inverse Compton boosting of ambient photons or through the decay of neutral pions produced in hadronic interactions. At energies below ~ 30 GeV, γ -ray emission can be efficiently detected using satellite or balloon-borne instrumentation, with an effective area approximately equal to the size of the detector (typically < 1 m²). At higher energies, a technique with

much larger effective collection area is desirable to measure astrophysical γ -ray fluxes, which decrease rapidly with increasing energy. Atmospheric Cherenkov detectors achieve effective collection areas of $> 10^5$ m² by employing the Earth’s atmosphere as an intrinsic part of the detection technique.

As described in Chapter 30, a hadronic cosmic ray or high energy γ -ray incident on the Earth’s atmosphere triggers a particle cascade, or air shower. Relativistic charged particles in the cascade generate Cherenkov radiation, which is emitted along the shower direction, resulting in a light pool on the ground with a radius of ~ 130 m. Cherenkov light is produced throughout the cascade development, with the maximum emission occurring when the number of particles in the cascade is largest, at an altitude of ~ 10 km for primary energies of 100 GeV–1 TeV. Following absorption and scattering in the atmosphere, the Cherenkov light at ground level peaks at a wavelength, $\lambda \approx 300$ –350 nm. The photon density is typically ~ 100 photons/m² for a 1 TeV primary, arriving in a brief flash of a few nanoseconds duration. This Cherenkov pulse can be detected from any point within the light pool radius by using large reflecting surfaces to focus the Cherenkov light on to fast photon detectors (Fig. 36.4).

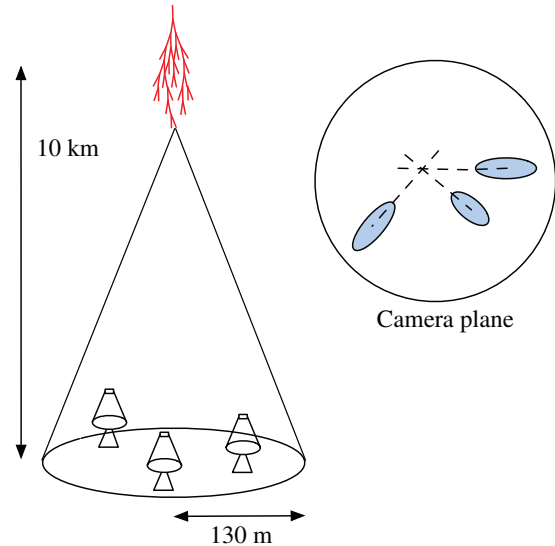


Figure 36.4: A schematic illustration of an imaging atmospheric Cherenkov telescope array. The primary particle initiates an air shower, resulting in a cone of Cherenkov radiation. Telescopes within the Cherenkov light pool record elliptical images; the intersection of the long axes of these images indicates the arrival direction of the primary, and hence the location of a γ -ray source in the sky

Modern atmospheric Cherenkov telescopes, such as those built and operated by the VERITAS [35], H.E.S.S. [36] and MAGIC [37] collaborations, consist of large (> 100 m²) segmented mirrors on steerable altitude-azimuth mounts. A camera made from an array of photosensors is placed at the focus of each mirror and used to record a Cherenkov image of each air shower. In these imaging atmospheric Cherenkov telescopes, single-anode photomultiplier tubes (PMTs) have traditionally been used (2048, in the case of H.E.S.S. II), but silicon devices now feature in more modern designs. The telescope cameras typically cover a field-of-view of $3 - 10^\circ$ in diameter. Images are recorded at kHz rates, the vast majority of which are due to showers with hadronic cosmic-ray primaries. The shape and orientation of the Cherenkov images are used to discriminate γ -ray photon events from this cosmic-ray background, and to reconstruct the photon energy and arrival direction. γ -ray images result from purely electromagnetic cascades and appear as narrow, elongated ellipses in the camera plane. The long axis of the ellipse corresponds to the vertical extension of the air shower, and points back towards the source position in the field-of-view. If multiple telescopes are used to view the same shower (“stereoscopy”), the source position is simply the in-

tersection point of the various image axes. Cosmic-ray primaries produce secondaries with large transverse momenta, which initiate sub-showers. Their images are consequently wider and less regular than those with γ -ray primaries and, since the original charged particle has been deflected by Galactic magnetic fields before reaching the Earth, the images have no preferred orientation.

The measurable differences in Cherenkov image orientation and morphology provide the background discrimination which makes ground-based γ -ray astronomy possible. For point-like sources, such as distant active galactic nuclei, modern instruments can reject over 99.999% of the triggered cosmic-ray events, while retaining up to 50% of the γ -ray population. In the case of spatially extended sources, such as Galactic supernova remnants, the background rejection is less efficient, but the technique can be used to produce γ -ray maps of the emission from the source. The angular resolution depends upon the number of telescopes which view the image and the energy of the primary γ -ray, but is typically less than 0.1° per event (68% containment radius) at energies above a few hundred GeV.

The total Cherenkov yield from the air shower is proportional to the energy of the primary particle. The image intensity, combined with the reconstructed distance of the shower core from each telescope, can therefore be used to estimate the primary energy. The energy resolution of this technique, also energy-dependent, is typically 15–20% at energies above a few hundred GeV. Energy spectra of γ -ray sources can be measured over a wide range, depending upon the instrument characteristics, source properties (flux, spectral slope, elevation angle, *etc.*), and exposure time. The effective energy range is typically from 30 GeV to 100 TeV and peak sensitivity lies in the range from 100 GeV to a few TeV.

The first astrophysical source to be convincingly detected using the imaging atmospheric Cherenkov technique was the Crab Nebula [38], with an integral flux of 2.1×10^{-11} photons $\text{cm}^{-2} \text{s}^{-1}$ above 1 TeV [39]. Modern imaging atmospheric Cherenkov telescopes have sensitivity sufficient to detect sources with less than 1% of the Crab Nebula flux in a few tens of hours. The TeV source catalog now consists of over 200 sources (see e.g. Ref. [40]). A large fraction of these were detected by scanning the Galactic plane from the southern hemisphere with the H.E.S.S. telescope array [41]. Recent reviews of the field include [42] and [43], and a historical overview can be found in [44].

Major upgrades of the existing telescope arrays include the 2012 addition of a 28 m diameter central telescope to H.E.S.S. (H.E.S.S. II). Cherenkov telescopes also play an important role in hybrid air-shower detector systems such as TAIGA [45] and LHAASO [46]. Development for the next generation instrument, the Cherenkov Telescope Array Observatory (CTAO), is now at an advanced stage. CTAO will consist of a northern and a southern hemisphere observatory, with a combined total of more than 60 telescopes [47]. Telescopes of three different sizes are planned, spread over an area of $> 1 \text{ km}^2$, providing wider energy coverage, improved angular and energy resolutions, and an order of magnitude improvement in sensitivity relative to existing imaging atmospheric Cherenkov telescopes. A number of prototype telescopes are already operating, exploiting technological developments in telescope structural design and high-speed data acquisition. Novel features of some designs include dual mirror optics and silicon photo-detectors. In particular, the first 23 m diameter “Large Size Telescope” is now operating regularly on La Palma, and is producing scientific results [48]. The wide range of physics questions that CTAO will address is summarized in [49].

36.3 Large neutrino detectors

36.3.1 Deep liquid detectors for rare processes

Revised October 2023 by K. Scholberg (Duke U.) and C.W. Walter (Duke U.).

Deep, large detectors for rare processes tend to be multi-purpose with physics reach that includes not only solar, reactor, supernova and atmospheric neutrinos, but also searches for baryon

number violation and lepton number violation, searches for exotic particles and beyond-the-standard-model physics, and neutrino and cosmic-ray astrophysics in different energy regimes. The detectors may also serve as targets for long-baseline neutrino beams for neutrino oscillation physics studies. In general, detector design considerations can be divided into high- and low-energy regimes, for which background and event reconstruction issues differ. The high-energy regime, from about 100 MeV to a few hundred GeV, is relevant for proton decay searches, atmospheric neutrinos and high-energy astrophysical neutrinos. The low-energy regime (a few tens of MeV or less) is relevant for supernova, solar, reactor and geological neutrinos.

Large water Cherenkov and scintillator detectors (see Table 36.2) usually consist of a volume of transparent liquid viewed by photomultiplier tubes (PMTs) (see Sec 35.2); the liquid serves as active target. PMT hit charges and times are recorded and digitized, and triggering is usually based on coincidence of PMT hits within a time window comparable to the detector’s light-crossing time. Because photosensors lining an inner surface represent a driving cost that scales as surface area, very large volumes can be used for comparatively reasonable cost. Some detectors are segmented into subvolumes individually viewed by PMTs, and may include other detector elements (*e.g.*, tracking detectors). Devices to increase light collection, *e.g.*, reflectors or waveshifter plates, may be employed. A common configuration is to have at least one concentric outer layer of liquid material separated from the inner part of the detector to serve as shielding against ambient background. If optically separated and instrumented with PMTs, an outer layer may also serve as an active veto against entering cosmic rays and other background events. The PMTs for large detectors typically range in size from 20 cm to 51 cm diameter, and typical quantum efficiencies are in the 20–25% range for scintillation and water-Cherenkov photons. PMTs with higher quantum efficiencies, 35% or higher, are now available. The active liquid volume requires purification and there may be continuous recirculation of liquid. For large homogeneous detectors, the event interaction vertex is determined using relative timing of PMT hits, and energy deposition is determined from the number of recorded photoelectrons. A “fiducial volume” is usually defined within the full detector volume, some distance away from the PMT array. Inside the fiducial volume, enough PMTs are illuminated per event that reconstruction is considered reliable, and furthermore, entering background from the enclosing walls is suppressed by a buffer of self-shielding. PMT and detector optical parameters are calibrated using laser, LED, or other light sources. Quality of event reconstruction typically depends on photoelectron yield, pixelization and timing.

Because in most cases one is searching for rare events, large detectors are usually sited underground to reduce cosmic-ray-related background (see Chapter 30). The minimum depth required varies according to the physics goals [50].

36.3.1.1 Liquid scintillator detectors

Past and current large underground detectors based on hydrocarbon scintillators include LVD, MACRO, BUST (Baksan), Borexino, KamLAND and SNO+; JUNO is a future detector. Experiments at nuclear reactors include CHOOZ, Double CHOOZ, Daya Bay, and RENO. Organic liquid scintillators (see Section 35.3) for large detectors are chosen for high light yield and attenuation length, good stability, compatibility with other detector materials, high flash point, low toxicity, appropriate density for mechanical stability, and low cost. They may be doped with waveshifters and stabilizing agents. Popular choices are pseudocumene (1,2,4-trimethylbenzene) with a few g/L of the PPO (2,5-diphenyloxazole) fluor, and linear alkylbenzene (LAB), with light yield $\sim 10^4$ photons/MeV. In a typical detector configuration there will be active or passive regions of undoped scintillator, non-scintillating mineral oil or water surrounding the inner neutrino target volume. A thin vessel or balloon made of nylon, acrylic or other material transparent to scintillation light may contain the inner target; if the scintillator is buoyant with respect to its buffer, ropes may hold the balloon in place. For phototube surface coverages in the 20–40% range, yields in the few hundreds of photoelectrons per MeV of energy deposition can be obtained.

Table 36.2: Properties of large detectors for rare processes. If total target mass is divided into large submodules, the number of subdetectors is indicated in parentheses. Projects with first data expected in 2024 or later are indicated in italics.

Detector	Mass, kton (modules)	PMTs (diameter, cm)	ξ	p.e./MeV	Dates
BUST	0.33, scint (3150)	1/module (15)	segmented	40	1980–
MACRO	0.56, scint (476)	2-4/module (20)	segmented	18	1989–2000
LVD	1, scint. (840)	3/module (15)	segmented	15	1992–
KamLAND	0.41*, scint	1325(43)+554(51) [†]	34%	460	2002–
Borexino	0.1*, scint	2212 (20)	30%	500	2007–2021
SNO+	0.78, scint [‡]	9394 (20)	47%	400–600	2021–
CHOOZ	0.005, scint (Gd)	192 (20)	15%	130	1997–1998
Double Chooz	0.017, scint (Gd)(2)	534/module (20)	13%	180	2011–2017
Daya Bay	0.160, scint (Gd)(8)	192/module (20)	5.6% [§]	100	2011–2020
RENO	0.032, scint (Gd)(2)	342/module (25)	12.6%	100	2011–
<i>JUNO</i>	20.0*, scint	17612 (51)/25600 (8)	77.9%	1200	2024 (exp.)
IMB-1	3.3*, H ₂ O	2048 (12.5)	1%	0.25	1982–1985
IMB-2	3.3*, H ₂ O	2048 (20)	4.5%	1.1	1987–1990
Kam I	0.88/0.78*, H ₂ O	1000/948 (51)	20%	3.4	1983–1985
Kam II	1.04*, H ₂ O	948 (51)	20%	3.4	1986–1990
Kam III	1.04*, H ₂ O	948 (51)	20% [¶]	4.3	1990–1995
SK I	22.5*, H ₂ O	11146 (51)	40%	6	1996–2001
SK II	22.5*, H ₂ O	5182 (51)	19%	3	2002–2005
SK III-V	22.5*, H ₂ O	11129 (51)	40%	6	2006–2020
SK-Gd	22.5*, H ₂ O (Gd)	11129 (51)	40%	6	2020–
<i>Hyper-K</i>	187*, H ₂ O	>20000 (51)**	>20%	>6	2027 (exp.)
SNO	1, D ₂ O/1.7, H ₂ O	9438 (20)	31% ^{††}	9	1999–2006
<i>DUNE</i>	40*, Ar (4)	TBD ^{‡‡}	TBD ^{‡‡}	TBD ^{‡‡}	2028 (exp.) ^{§§}

*Indicates typical fiducial mass used for data analysis; this may vary by physics topic.

[†]Measurements made before 2003 only considered data from the 43 cm PMTs.

[‡]SNO+ ran with water fill from May 2017 to July 2019.

[§]The effective Daya Bay coverage is 12% with top and bottom reflectors.

[¶]The effective Kamiokande III coverage was 25% with light collectors.

^{||}A second staged module is being investigated.

**Additional photosensor modules and PMTs are planned.

^{††}The effective SNO coverage was 54% with light collectors.

^{‡‡}Photodetector technology and coverage varies according to TPC type and is not yet fully determined.

^{§§}Modules will be constructed in a phased approach.

Typical energy resolution is about $5-7\%/\sqrt{E(\text{MeV})}$ [51,52], and typical position reconstruction resolution is a few tens of cm at ~ 1 MeV, scaling as $\sim N^{-1/2}$, where N is the number of photoelectrons detected.

Shallow detectors for reactor neutrino oscillation experiments require excellent muon veto capabilities. For $\bar{\nu}_e$ detection via inverse beta decay on free protons, $\bar{\nu}_e + p \rightarrow n + e^+$, the neutron is captured by a proton on a $\sim 180 \mu\text{s}$ timescale, resulting in a 2.2 MeV γ ray, observable by Compton scattering and which can be used as a tag in coincidence with the positron signal. The positron annihilation γ rays may also contribute. Inverse beta decay tagging may be improved by addition of Gd at $\sim 0.1\%$ by mass, which for natural isotope abundance has a $\sim 49,000$ barn cross-section for neutron capture (in contrast to the 0.3 barn cross-section for capture on free protons). Gd capture takes $\sim 30 \mu\text{s}$, and is followed by a cascade of γ rays adding up to about 8 MeV. Gadolinium doping of scintillator requires specialized formulation to ensure adequate attenuation length and stability.

Scintillation detectors have an advantage over water Cherenkov detectors in the lack of Cherenkov threshold and the high light yield. However, scintillation light emission is nearly isotropic, and therefore directional capabilities are relatively weak. Liquid scintillator is especially suitable for detection of low-energy events. Radioactive backgrounds are a serious issue, and include long-lived cosmogenics such as ^{14}C . To go below a few MeV, very careful selection of materials and purification of the scintillator is required (see Section 36.6). Fiducialization and tagging can reduce background. One can also dissolve neutrinoless double beta decay ($0\nu\beta\beta$) isotopes in scintillator. This has been realized by KamLAND-Zen, which deployed a 1.5 m-radius balloon containing enriched Xe dissolved in scintillator inside KamLAND, and ^{130}Te is planned for SNO+.

36.3.1.2 Water Cherenkov detectors

Very large imaging water detectors reconstruct ten-meter-scale Cherenkov rings produced by charged particles (see Section 35.5). The first such large detectors were IMB and Kamiokande. The only currently existing instance of this class of detector, with fiducial mass of 22.5 kton and total mass of 50 kton, is Super-Kamiokande (Super-K, SK). Hyper-Kamiokande (Hyper-K) plans at least one, and possibly two, detectors with 187-kton fiducial mass. For volumes of this scale, absorption and scattering of Cherenkov light are non-negligible, and a wavelength-dependent factor $\exp(-d/L(\lambda))$ (where d is the distance from emission to the sensor and $L(\lambda)$ is the attenuation length of the medium) must be included in the integral of Eq. (35.6) for the photoelectron yield. Attenuation lengths on the order of 100 meters have been achieved.

Cherenkov detectors are excellent electromagnetic calorimeters, and the number of Cherenkov photons produced by an e/γ is nearly proportional to its kinetic energy. For massive particles, the number of photons produced is also related to the energy, but not linearly. For any type of particle, the *visible energy* E_{vis} is defined as the energy of an electron which would produce the same number of Cherenkov photons. The number of collected photoelectrons depends on the scattering and attenuation in the water along with the photo-cathode coverage, quantum efficiency and the optical parameters of any external light collection systems or protective material surrounding them. Event-by-event corrections are made for geometry and attenuation. For a typical case, in water $N_{\text{p.e.}} \sim 15 \xi E_{\text{vis}}(\text{MeV})$, where ξ is the effective fractional photosensor coverage. Cherenkov photoelectron yield per MeV of energy is relatively small compared to that for scintillator, *e.g.*, ~ 6 pe/MeV for Super-K with a PMT surface coverage of $\sim 40\%$. In spite of light yield and Cherenkov threshold issues, the intrinsic directionality of Cherenkov light allows individual particle tracks

to be reconstructed. Vertex and direction fits are performed using PMT hit charges and times, requiring that the hit pattern be consistent with a Cherenkov ring.

High-energy (~ 100 MeV or more) neutrinos from the atmosphere or beams interact with nucleons; for the nucleons bound inside the ^{16}O nucleus, nuclear effects must be considered both at the interaction and as the particles leave the nucleus. Various event topologies, with final-state particles contained, exiting, or entering the detector, can be distinguished by their timing and fit patterns, and by presence or absence of light in a veto. At high energies, multi-photoelectron hits are likely and the charge collected by each PMT (rather than the number of PMTs firing) must be used; the energy resolution in this case is approximately $2\%/\sqrt{\xi E_{\text{vis}}(\text{GeV})}$. The absolute energy scale in this regime can be known to $\sim 2\text{--}3\%$ using cosmic-ray muon energy deposition, Michel electrons and π^0 from atmospheric neutrino interactions. Typical vertex resolutions for GeV energies are a few tens of cm [53]. Angular resolution for determination of the direction of a charged particle track is a few degrees. For a neutrino interaction, because some final-state particles are usually below Cherenkov threshold, knowledge of direction of the incoming neutrino direction itself is generally worse than that of the lepton direction, and dependent on neutrino energy.

Multiple particles in an interaction (so long as they are above Cherenkov threshold) may be reconstructed, allowing for the exclusive reconstruction of final states. In searches for proton decay, multiple particles can be kinematically reconstructed to form a decaying nucleon. High-quality particle identification is also possible: γ rays and electrons shower, and electrons scatter, which results in fuzzy rings, whereas muons, pions and protons make sharp rings. These patterns can be quantitatively separated with high reliability using maximum likelihood methods [54]. Sources of background for high energy interactions include misidentified cosmic muons and anomalous light patterns when the PMTs sometimes “flash” and emit photons themselves. The latter class of events can be removed using its distinctive PMT signal patterns, which may be repeated. More information about high energy event selection and reconstruction may be found in reference [55].

In spite of the fairly low light yield, large water Cherenkov detectors may be employed for reconstructing low-energy events, down to *e.g.* $\sim 4\text{--}5$ MeV for Super-K [56]. Low-energy neutrino interactions of solar neutrinos in water are predominantly elastic scattering off atomic electrons; single electron events are then reconstructed. At solar neutrino energies, the visible energy resolution ($\sim 30\%/\sqrt{\xi E_{\text{vis}}(\text{MeV})}$) is about 20% worse than photoelectron counting statistics would imply. Using an electron LINAC and/or nuclear sources, approximately 0.5% determination of the absolute energy scale has been achieved at solar neutrino energies. Angular resolution is limited by multiple scattering in this energy regime ($25\text{--}30^\circ$). At these energies, radioactive backgrounds become a dominant issue. These backgrounds include radon in the water itself or emanated from detector materials, and γ rays from the rock and detector materials. In the few to few tens of MeV range, radioactive products of cosmic-ray-muon-induced spallation are troublesome, and are removed by proximity in time and space to preceding muons, at some cost in dead time. Gadolinium doping using 0.2% $\text{Gd}_2(\text{SO}_4)_3$ has now been initiated for Super-K to improve selection of low-energy $\bar{\nu}_e$ and other events with accompanying neutrons [57].

The Sudbury Neutrino Observatory (SNO) detector [58] was the only instance of a large heavy water detector. In addition to an outer 1.7 kton of light water, SNO contained 1 kton of D_2O , giving it unique sensitivity to neutrino neutral current ($\nu_x + d \rightarrow \nu_x + p + n$), and charged current ($\nu_e + d \rightarrow p + p + e^-$) deuteron breakup reactions. The neutrons were detected in three ways: via capture on deuterons, via capture on dissolved ^{35}Cl , and via specialized ^3He counters.

36.3.1.3 Noble liquid detectors

Noble liquids scintillate and can be used as the active medium for particle detection. Detectors employing argon and xenon are also used as time-projection chambers (TPCs), either as dual-phase low-energy recoil detectors, or as track-imaging detectors.

Noble-liquid detectors with low energy (few to few tens of keV) capability for detecting electronic and nuclear recoils are employed for dark matter and other rare event searches and are described in Sec. 36.4. These detectors can also be employed for some of the same physics (baryon number violation, astrophysical neutrino transient searches, etc.) as for the other large detectors described here, especially as they approach tens of ton scale and higher (*e.g.*, DARWIN, DarkSide-20, ARGO). Track-imaging time-projection chambers, which are described in detail Section 36.4, have a dynamic range reaching down to the few to few tens of MeV scale, enabling sensitivity to *e.g.*, solar and supernova burst neutrinos. Surface LArTPCs have significant cosmic backgrounds, but may still have sensitivity to astrophysical transients such as supernova burst neutrinos. DUNE will be sufficiently deep to have sensitivity to steady-state low-energy neutrino sources such as solar neutrinos.

36.3.2 Neutrino telescopes

Revised February 2024 by U.F. Katz (Erlangen U.) and C. Spiering (DESY, Zeuthen).

The primary goal of neutrino telescopes (NTs) is the detection of astrophysical neutrinos, in particular those which are expected to accompany the production of high-energy cosmic rays in astrophysical accelerators. NTs in addition address a variety of other fundamental physics issues like the indirect search for dark matter, studies of neutrino oscillations, searches for exotic particles like magnetic monopoles or study of cosmic rays and their interactions [59–61]. Electromagnetic radio frequency detectors for high energy neutrinos are discussed in “Radio emission from (ultra-) high energy particle showers” section 36.3.3.

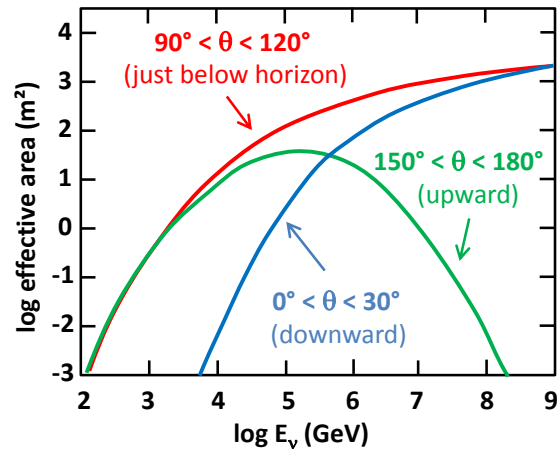


Figure 36.5: Average over the effective ν_μ and $\bar{\nu}_\mu$ areas for IceCube as an example of a cubic-kilometre NT, as a function of neutrino energy for three intervals of the zenith angle θ . The values shown here correspond to a specific event selection for point source searches.

NTs are large-volume arrays of “optical modules” (OMs) installed in open transparent media like water or ice, at depths that completely block the daylight. The OMs are sensitive to individual photons of the Cherenkov light induced by charged secondary particles produced in reactions of high-energy neutrinos in or around the instrumented volume. The time of photon-induced signals (“hits”) is registered with a precision of a few nanoseconds. The neutrino energy, E_ν , and direction can be reconstructed from the hit pattern recorded. NTs typically target an energy range $E_\nu \gtrsim 100$ GeV; sensitivity to lower energies is achieved in dedicated setups with denser instrumentation.

In detecting cosmic neutrinos, three sources of backgrounds have to be considered: (i) *atmospheric neutrinos* from cosmic-ray interactions in the atmosphere, which can be separated from cosmic neutrinos on a statistical basis, or, for down-going neutrinos, by vetoing accompanying muons; (ii) down-going punch-through *atmospheric muons* from cosmic-ray interactions, which are sup-

pressed by several orders of magnitude with respect to the ground level due to the large detector depths and can be further reduced by selecting upward-going or high-energy neutrinos or by self-veto methods; (iii) random backgrounds due to photomultiplier (PMT) dark counts, ^{40}K decays (mainly in sea water) or bioluminescence (only water). Atmospheric neutrinos and muons allow for investigating neutrino oscillations and cosmic ray anisotropies, respectively. Since 2012, it has become obvious that a precise measurement of the energy-zenith-distribution of atmospheric neutrinos in the energy range from a few to about 100 GeV may allow for determining the neutrino mass hierarchy by exploiting matter-induced oscillation effects in the Earth [62,63].

Neutrinos can interact with target nucleons N through charged current ($\bar{\nu}_\ell N \rightarrow \ell^\mp X$, CC) or neutral current ($\bar{\nu}_\ell N \rightarrow \bar{\nu}_\ell X$, NC) processes. A CC reaction of a $\bar{\nu}_\mu$ produces a muon track and a hadronic particle cascade, whereas all NC reactions and CC reactions of $\bar{\nu}_e$ produce particle cascades only. CC interactions of $\bar{\nu}_\tau$ can have either signature, depending on the τ decay mode. Of particular interest is the so-called double-bang signature, where the τ decays sufficiently far away from the primary interaction to create a second, distinguishable cascade (typically at PeV energies and above). In most astrophysical models, neutrinos are expected to be produced through the $\pi/K \rightarrow \mu \rightarrow e$ decay chain, *i.e.*, with a flavour ratio $\nu_e : \nu_\mu : \nu_\tau \approx 1 : 2 : 0$. For sources outside the solar system, neutrino oscillations turn this ratio to $\nu_e : \nu_\mu : \nu_\tau \approx 1 : 1 : 1$ upon arrival on Earth.

The total neutrino-nucleon cross section is about 10^{-34} cm^2 at $E_\nu = 20 \text{ TeV}$ and rises roughly linearly with E_ν below this energy and as $E_\nu^{0.3-0.5}$ above, flattening out towards high energies. The CC:NC cross-section ratio is about 2:1. At energies above several TeV, neutrino absorption in the Earth becomes noticeable; for vertically upward-moving neutrinos (zenith angle $\theta = 180^\circ$), the survival probability is 74 (27, < 2)% for 10 (100, 1000) TeV. The energy transferred to the final-state lepton varies between 0 and 100% of E_ν , with a mean of 50% (65%) for neutrinos (antineutrinos) at 100 GeV and 75% for both neutrinos and antineutrinos at 10 PeV.

The final-state lepton follows the initial (anti)neutrino direction with an average mismatch angle of about $\langle \phi_{\nu\ell} \rangle \approx 1^\circ / (E_\nu / \text{TeV})^{0.55}$, with a steeper decrease beyond 10 TeV, reaching 0.005° at 1 PeV [64]. These values indicate the intrinsic kinematic limit to the angular resolution of NTs. For CC $\bar{\nu}_\mu$ reactions at energies above about 10 TeV, the angular resolution is dominated by the muon reconstruction accuracy of a few times 0.1° at most. For muon energies $E_\mu \gtrsim 1 \text{ TeV}$, the increasing light emission due to radiative processes allows for reconstructing E_μ from the measured Cherenkov light intensity with an accuracy of $\sigma(\log E_\mu) \approx 0.3$; at lower energies, E_μ can be estimated from the length of the muon track if it is contained in the detector. These properties make CC $\bar{\nu}_\mu$ reactions the prime channel for the identification of individual astrophysical neutrino sources.

Hadronic and electromagnetic particle cascades at the relevant energies are 5–20 m long, *i.e.*, short compared to typical OM spacings. The total amount of Cherenkov light provides a direct measurement of the cascade energy with an accuracy of about 20% at energies above 10 TeV and 10% beyond 100 TeV for events contained in the instrumented volume. Except for double-bang events, the neutrino flavour and reaction mechanism can, however, be determined on a statistical basis at best, and neutrinos from NC reactions or τ decays may carry away significant “invisible” energy. Above 100 TeV, the average directional reconstruction accuracy of cascades is better than 10 (2) degrees in polar ice (sea water), the difference being due to the inhomogeneity of the ice and stronger light scattering in ice. These features, together with the small background of atmospheric $\bar{\nu}_e$ and $\bar{\nu}_\tau$ events, makes the cascade channel particularly interesting for searches for a diffuse, high-energy excess of extraterrestrial over atmospheric neutrinos. Cascade events can also be used to complement the muon channel in searches for point sources or transient signals, albeit with inferior angular accuracy compared to muon tracks.

The detection efficiency of a NT is quantified by its effective area, *e.g.*, the fictitious area for which the full incoming neutrino

flux would be recorded (see Figure 36.5). The increase with E_ν is due to the rise of neutrino cross section and muon range, while neutrino absorption in the Earth causes the decrease at large θ for large E_ν . Identification of downward-going neutrinos requires stringent event selection to suppress atmospheric muons, hence the cut-off towards low E_ν at low θ . Due to the small cross section, the effective area is many orders of magnitude smaller than the geometrical dimension of the detector; a $\bar{\nu}_\mu$ with 1 TeV can, *e.g.*, be detected with a probability of the order 10^{-6} if the NT is on its path.

Due to the long muon range, CC interactions of up-going $\bar{\nu}_\mu$ can be detected from far outside the instrumented volume. This method also works for horizontal neutrinos up to about 10° above the horizon (depth dependent), where the background from atmospheric muons become prohibitive. Alternatively, one can select events that start inside the instrumented volume and thus remove incoming muons that generate early hits in the outer layers of the detector. Such a veto-based event selection is sensitive to neutrinos of all flavours from all directions, albeit with a reduced efficiency since a part of the instrumented volume is sacrificed for the veto. Such a muon veto, or vetoing events with a coincident signal in the surface array, also rejects down-going atmospheric neutrinos that are accompanied by muons from the same air shower and thus reduces the atmospheric-neutrino background. Actually, the breakthrough in detecting high-energy cosmic neutrinos was first achieved with this technique.

Note that the fields of view of NTs at the South Pole and in the Northern hemisphere are complementary for each reaction channel and neutrino energy.

36.3.2.1 The Projects

Table 36.3 lists past, present and future neutrino telescope projects and their main parameters.

36.3.2.2 Properties of media

The efficiency and quality of event reconstruction depend strongly on the optical properties (absorption and scattering length, intrinsic optical activity) of the medium in the spectral range of alkali photocathodes (300–550 nm). Large absorption lengths result in a better light collection, large scattering lengths in superior angular resolution. Deep-sea sites typically have effective scattering lengths of $> 100 \text{ m}$ and, at their peak transparency around 450 nm, absorption lengths of 50–65 m. The absorption length for Lake Baikal is 22–24 m. The properties of South Polar ice vary strongly with depth; at the peak transparency wave length (400 nm), the scattering length is between 5 and 75 m and the absorption length between 15 and 250 m, with the best values in the depth region 2200–2450 m and the worst ones in the layer 1950–2100 m.

Noise rates measured by PMTs with a diameter of 25 cm in deep polar ice are about 0.5 kHz per PMT and almost entirely due to radioactivity in the OM components. The corresponding rates in sea water are typically 60 kHz, mostly due to ^{40}K decays. Bioluminescence activity can locally cause rates on the MHz scale for seconds; the frequency and intensity of such “bursts” depends strongly on the sea current, the season, the geographic location, and the geometry of the detector elements. Experience from ANTARES shows that these backgrounds are manageable without a major loss of efficiency or experimental resolution.

36.3.2.3 Technical realisation

Optical modules (OMs) and PMTs: An OM is a pressure-tight glass sphere housing one or several PMTs with a time resolution in the nanosecond range, and in most cases also electronics for control, high-voltage generation, operation of calibration LEDs, time synchronisation and signal digitisation.

Hybrid PMTs with 37 cm diameter have been used for NT-200, conventional hemispheric PMTs with 20 cm diameter for AMANDA and with 25 cm diameter for ANTARES, IceCube and Baikal-GVD. A novel concept has been chosen for KM3NeT. Each OM (43 cm) is equipped with 31 PMTs (7.5 cm), plus control, calibration and digitisation electronics. Advantages are that (i) the overall photocathode area exceeds that of a 25 cm PMT by more than a factor of 3; (ii) the individual readout of the PMTs results in a very good separation between one- and two-photoelectron

Table 36.3: Past, present and future NT projects and their main parameters. The milestone years give the times of project start, of first data taking with partial configurations, of detector completion, and of project termination. Projects with first data expected past 2024 are indicated in italics. The size refers to the largest instrumented volume reached during the project development. The status of projects under construction is reported as of February 2024. See [61] for references to the different projects where unspecified.

Experiment	Milestones	Location	Size (km ³)	Remarks
DUMAND	1978/-/-/1995	Pacific Ocean		Terminated due to technical/funding problems
NT-200	1980/1993/1998/2015	Lake Baikal	10 ⁻⁴	First proof of principle
GVD [65]	2012/2015/-/-	Lake Baikal	ca. 1	High-energy ν astronomy first 12 clusters installed
AMANDA	1990/1996/2000/2009	South Pole	0.015	First deep-ice NT
IceCube [66]	2001/2005/2010/-	South Pole	1.0	First km ³ -sized detector
<i>IceCube-Gen2</i> [67, 68]	2014/-/-/-	South Pole	5–10	Planned future extension of IceCube covering low and high energies, a surface array and radio detection
NESTOR	1991/-/-/-	Med. Sea		2004 data taking with prototype
NEMO	1998/-/-/-	Med. Sea		R&D project, prototype tests
ANTARES	1997/2006/2008/2022	Med. Sea	0.010	First deep-sea NT
KM3NeT/ARCA [63]	2013/2021/-/-	Med. Sea	ca. 1	High-energy configuration for neutrino astronomy. Under construction, data taking with 28 strings
KM3NeT/ORCA [63]	2014/2020/-/-	Med. Sea	0.007	Low-energy configuration for neutrino mass hierarchy. Under construction, data taking with 18 strings
<i>KM3NeT Phase 3</i>	2013/-/-/-	Med. Sea	ca. 3	Possible future extension, 6 ARCA blocks + ORCA
<i>P-ONE</i> [69]	2018/-/-/-	Pacific Ocean	$\mathcal{O}(1)$	Planned future NT, R&D phase
<i>TRIDENT</i> [70]	2021/-/-/-	South China Sea	$\mathcal{O}(10)$	Planned future NT, R&D phase

signals which is essential for online data filtering and random background suppression; (iii) the hit pattern on an OM provides directional information; (iv) no mu-metal shielding against the Earth magnetic field is required. Figure 36.6 shows the OM designs of IceCube and KM3NeT.

Readout and data filtering: In current NTs the PMT data are digitised in situ: for ANTARES and Baikal-GVD in special electronics containers close to the OMs, for IceCube and KM3NeT inside the OMs. For IceCube, data are transmitted via electrical cables of up to 3.3 km length, depending on the location of the strings and the depth of the OMs; for ANTARES, KM3NeT and Baikal-GVD optical fibre connections have been chosen (several 10 km for the first two and 4 km for GVD).

The full digitised waveforms of the IceCube OMs are transmitted to the surface for pulses appearing in local coincidences on a string; for other pulses, only time and charge information is provided. For ANTARES (time and charge) and KM3NeT (time and time over threshold), all PMT signals above an adjustable threshold are sent to shore.

The data are subsequently processed on online computer farms, where multiplicity- and topology-driven filter algorithms are applied to select event candidates. The filter output data rate is about 10 GByte/day for ANTARES and of the order 1 TByte/day for IceCube (100 GByte/day transferred via satellite) and KM3NeT.

Calibration: For efficient event recognition and reconstruction, the OM timing must be synchronised at the few-nanosecond level and the OM positions and orientations must be known to a few 10 cm and a few degrees, respectively. Time calibration is achieved by sending synchronisation signals to the OM electronics and also by light calibration signals emitted in situ at known times by LED or laser flashers (ANTARES, KM3NeT). Precise position calibration is achieved by measuring the travel time of light calibration signals sent from OM to OM (IceCube) or acoustic signals sent from transducers at the sea floor to receivers on the detector strings (ANTARES, KM3NeT, Baikal-GVD). Absolute pointing and an-

gular resolution can be determined by measuring the “shadow of the moon” (*i.e.*, the directional depletion of muons generated in cosmic-ray interactions). IceCube and ANTARES have both shown that they have angular resolution below 1°, confirming MC calculations which indicate a precision of $\approx 0.5^\circ$ for energies above 10 TeV. For KM3NeT, simulations indicate that sub-degree precision in the absolute pointing can be reached within a few weeks of operation.

Detector configurations: IceCube [66] (see Figure 36.7) consists of 5160 Digital OMs (DOMs) installed on 86 strings at depths of 1450 to 2450 m in the Antarctic ice; except for the DeepCore region, string distances are 125 m and vertical distances between OMs 17 m. 324 further DOMs are installed in IceTop, an array of detector stations on the ice surface above the strings. DeepCore is a high-density sub-array at large depths (*i.e.*, in the best ice layer) at the centre of IceCube.

The NT200 detector in Lake Baikal at a depth of 1100 m consisted of 8 strings attached to an umbrella-like frame, with 12 pairs of OMs per string. The diameter of the instrumented volume was 42 m, its height 70 m. Meanwhile (February 2024), the Baikal collaboration has installed the first 12 clusters of a future cubic-kilometre array, GVD [65]. It will consist of 18 clusters, each with 288 OMs at 8 strings, plus several single strings between the clusters; its completion is scheduled for 2027.

The operation of ANTARES (see [61] and references therein) was terminated in 2022. It comprised 12 strings with lateral distances of 60–70 m, each carrying 25 triplets of OMs at vertical distances of 14.5 m, located at depths of 2.1–2.4 km, starting 100 m above the sea floor. An additional string held devices for calibration and environmental monitoring. A system to investigate the feasibility of acoustic neutrino detection was also implemented.

KM3NeT will consist of building blocks of 115 strings each, with 18 OMs per string. Operation of the first strings deployed has successfully verified the KM3NeT technology and sensitivity. In the upcoming phase of its staged implementation, KM3NeT

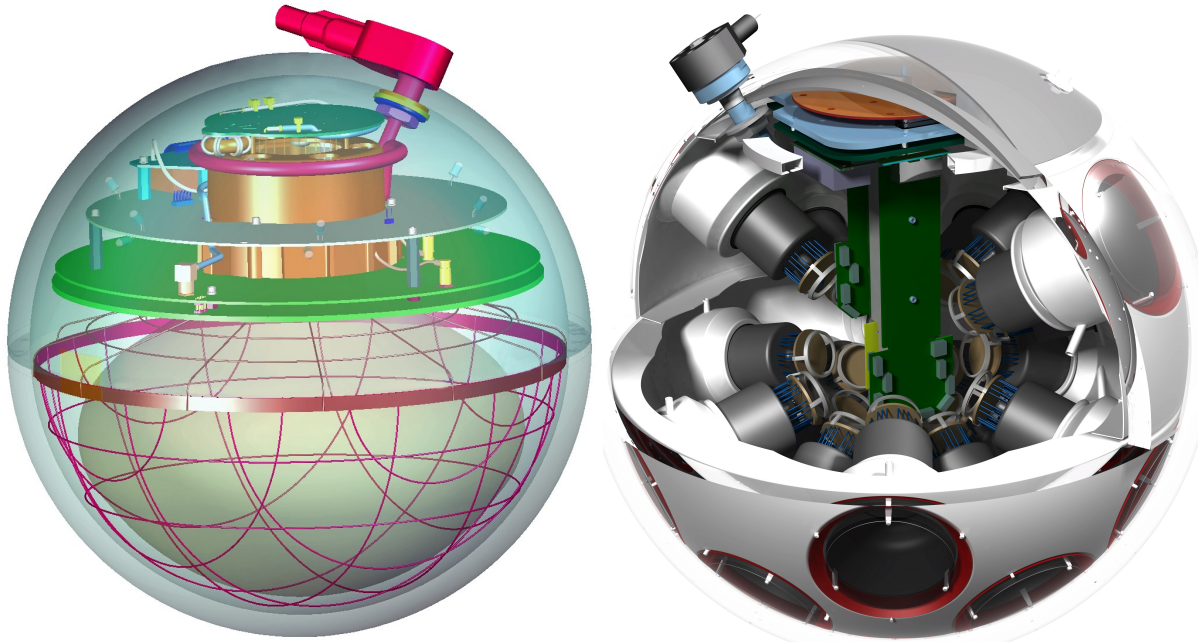


Figure 36.6: Schematic views of the digital OMs of IceCube (left) and KM3NeT (right).

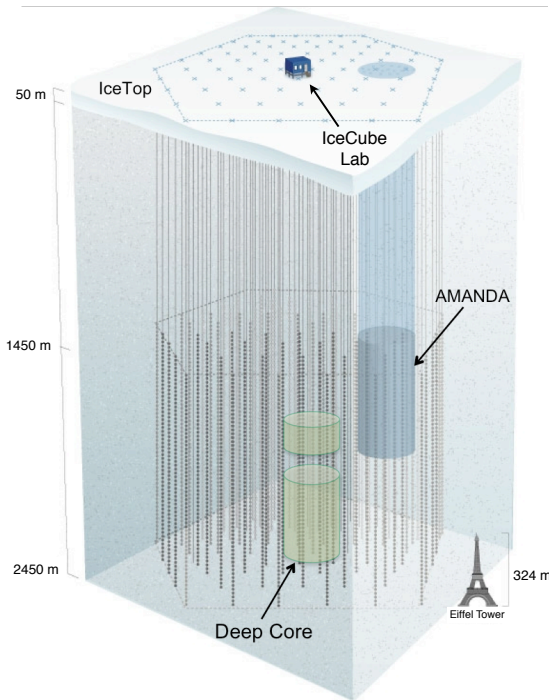


Figure 36.7: Schematic view of the IceCube neutrino observatory comprising the deep-ice detector including its nested dense part DeepCore, and the surface air shower array IceTop. The IceCube Lab houses data acquisition electronics and the computer farm for online processing. Operation of AMANDA was terminated in 2009.

aims at two building blocks for neutrino astronomy, with vertical distances between OMs of 36 m and a lateral distance between adjacent strings of 90 m (ARCA, for *Astroparticle Research with Cosmics in the Abyss*) and at one block for the measurement of the neutrino mass hierarchy, with vertical distances between OMs of 9 m and a lateral distance between adjacent strings of about 20 m (ORCA, for *Oscillation Research with Cosmics in the Abyss*) [63]. The installation of ARCA near Capo Passero, East of Sicily (depth

3440 m) and of ORCA near Toulon (depth 2450 m) is ongoing and as of now (February 2024) 28/18 strings have been deployed for ARCA/ORCA and are continuously operated. Completion of the full ARCA and ORCA arrays is planned for 2028.

P-ONE (*Pacific Ocean Neutrino Experiment*) [69] is a new initiative in its R&D phase, envisaging a large NT in the Pacific Ocean off the Canadian coast. It is intended to use an existing deep-sea cable infrastructure and to optimise the sensitivity for horizontal neutrinos with energies of about 100 TeV and beyond.

TRIDENT (Tropical Deep-Sea Neutrino Telescope) is a proposed future neutrino telescope in the South China Sea with an instrumented volume of 7.5 km³. R&D and site exploration efforts are ongoing and a pathfinder (TRIDENT Phase-1) is planned to be commissioned around 2026 [71].

36.3.2.4 Results

See Sect. 30.4 for a summary of the results from neutrino telescopes.

36.3.2.5 Plans beyond 2023

Within the future IceCube-Gen2 project, it is planned to extend the sensitivity of IceCube towards both higher and lower energies. To increase the detector sensitivity at high energies, a large-volume extension is envisaged, combined with a radio array for highest-energy neutrinos and a surface array providing also a powerful veto against atmospheric events [67, 68]. A substantially denser instrumentation of a sub-volume of DeepCore will be achieved with 7 closely spaced strings to be deployed in 2025/26 (the IceCube Upgrade), aiming to cover a low-energy program, to better calibrate the existing IceCube detector and the archival data, and to test new technologies. More information on the future extensions of GVD and KM3NeT and on P-ONE and TRIDENT are given above and in Table 36.3.

36.3.3 Radio emission from (ultra-)high energy particle showers

Revised August 2023 by S.R. Klein (NSD LBNL; UC Berkeley) and A. Nelles (DESY, Zeuthen; Erlangen U.).

Coherent radio-frequency (RF) electromagnetic radiation is an attractive signature to search for particle cascades produced by interactions of high-energy particles. RF signatures have been used to study both cosmic-ray air showers and to search for neutrino-induced showers. This article will discuss the radio signal generation, the relevant energy regime and the application in de-

tectors. Air showers are discussed in more detail in two recent reviews [72, 73]. At lower energies, incoherent optical Cherenkov radiation is frequently used, as discussed in "Neutrino telescopes" section 36.3.2. This article uses the general definitions and properties of neutrino telescopes as described in 36.3.2.

36.3.3.1 Signal generation and its characteristics

As discussed in the "Passage of Particles Through Matter" review Sec. 34 the electromagnetic component of a high energy shower gives rise to radio emission. For the signal generation itself the type of primary particle is irrelevant. However, the signal medium is important. It must be non-conducting (and non-absorptive at RF frequencies). The different shower length scales (radiation length, X_0) between air and the solid materials used for neutrino searches leads to surprisingly large differences in shower development. Due to the interaction with the medium the shower contains more electrons than positrons, which results in a net charge excess and leads to coherent Cherenkov emission, also known as Askaryan effect [74–76]. In air, during propagation through the geomagnetic field, the relative motion of electrons and positrons is affected, which leads to a varying transverse current, usually referred to as the geomagnetic effect [72]. Both effects may be described more generally as being due to radiation from a time-varying net charge [77]. Their relative importance is governed by the density of the medium, as the electric field scales as the net charge excess, and a lower density allows the geomagnetic effect to gain importance. Thus, in solid materials the emission from the Askaryan effect dominates, but it is a $< 20\%$ correction in air showers.

Coherent radiation is possible at wavelengths longer than the instantaneous thickness of the shower along an observer's line of sight. Since air showers have a larger extent than showers in solid media, their coherent radiation appears at lower frequencies [78].

High-frequency radiation is concentrated around the Cherenkov angle θ_C . Viewed directly on the Cherenkov cone, the electric field strength, ϵ_{Ch} at a frequency f from an electromagnetic shower from a ν_e with energy E_ν in ice may be roughly parameterized as [79, 80]

$$\epsilon_{Ch}(\text{V/mMHz}) = 2.53 \times 10^{-7} \frac{E_\nu}{1\text{TeV}} \frac{f}{f_c} \left[\frac{1}{1 + (f/f_c)^{1.44}} \right]. \quad (36.3)$$

The electric field strength increases linearly with frequency, up to a cut-off frequency f_c , which is set by the transverse size of the shower [81, 82]. The maximum wavelength c/f_c is roughly the Moliere radius divided by $\cos(\theta_C)$ where θ_C is the Cherenkov angle. The cutoff frequencies depend on the density (which affects the Moliere radius). They are about 1 GHz in ice, about 3 GHz in the lunar regolith, and below 100 MHz in air.

Near f_c , radiation is narrowly concentrated around θ_C [81, 82]. At lower frequencies, the limited length of the emitting region leads to a broadening in emission angle around the Cherenkov cone. Away from θ_C , the electric field from Eq. (36.3) is reduced by [79],

$$\frac{\epsilon}{\epsilon_{Ch}} = \exp\left(-\frac{1}{2} \frac{(\theta - \theta_C)^2}{(2.2^\circ \times [1\text{GHz}/f])^2}\right). \quad (36.4)$$

The angular distribution of the signal around θ_C can be parameterized by a Gaussian peak modulated by a $\sin\theta$. In both ice and the lunar regolith, θ_C is about 56° , in air only 1° . Close to θ_C , the 1 GHz maximum frequency in ice/regolith leads to a generated pulse width of ≈ 1 nsec.

These equations are appropriate for ice. More general parameterizations can be found in [80, 83].

More accurate calculations of the predicted radio signal, in particular air showers are not easily parameterized, but require detailed Monte Carlo simulations. For air showers, these are built on microscopic air shower simulations, calculate the emission from all individual particles in the shower development and add them for different observer positions [72]. For neutrinos, most approaches calculate (directly or from a parameterization) the Askaryan signal from a shower profile. The signal is then propagated through the medium and into an antenna model [80].

At energies above 10^{16} eV in ice, the Landau-Pomeranchuk-Migdal effect lengthens electromagnetic showers, by reducing the cross-sections for bremsstrahlung and pair production [84]. The lengthening of the shower leads to a narrowing of the radio emission around the Cherenkov cone, and a reduction in high-frequency emission away from the cone [80]. At higher energies, this leads to two separate components of the Askaryan radiation from a neutrino interaction: an un-altered component from the hadronic portion of the shower and an angularly narrowed component from the LPM-lengthened electromagnetic shower. The width of the narrowed component scales as $E_\nu^{1/3}$. If these two components can be observed separately, they could, in principle, be combined to determine the inelasticity of the neutrino interaction [85], allowing for improved measurements of low- x parton distributions and searches for beyond-standard-model interactions.

Similarly, energetic outgoing μ^\pm and τ^\pm from neutrino interactions will dominantly lose energy via stochastic pair production and photonuclear interactions. These secondary particles will produce electromagnetic showers that can be detected by radio detectors, if they are above threshold energy. This will enable multiple detections of the same particle track and thus present interesting reconstruction opportunities [86].

At still higher energies, above 10^{20} eV, the LPM effect strengthens, and the electromagnetic shower splits into multiple subshowers with significant separation. When these separations become large enough, the subshowers will effectively become independent radiators, with the total emission showing substantial event-by-event variation, depending on the division into subshowers [84]. Because of this, many experiments that study higher energy (well above 10^{20} eV) neutrinos focus on the hadronic shower from the struck nucleus. This contains an average of only about 20% of the energy, but with fewer large fluctuations.

36.3.3.2 Energy regime of radio detectors

The electric field amplitude is linearly proportional to the shower energy. Since the signal is a radio wave, the field amplitude decreases as $1/R$, plus potential absorption in the intervening medium, while the energy fluence decreases as $1/R^2$, again, plus potential absorption. The detection threshold depends on the distance to the antenna and the bandwidth and noise characteristics of the antenna and detector. For an antenna located in the detection medium, at a distance of 1 km the typical threshold is around 10^{17} eV. For stand-off (remote sensing) detectors, the threshold rises roughly linearly with the distance. These thresholds can be reduced by using directional antennas and/or combining the signals from multiple antennas using beam-forming techniques.

RF detectors are used to search for energetic neutrinos from three types of sources: astrophysical objects (*i.e.* extending measurements of the neutrino energy spectrum observed at TeV to PeV energies upward in energy), cosmogenic neutrinos associated with cosmic-ray-cosmic microwave background radiation (CMBR) interactions, and neutrinos from beyond-standard-model physics. These types are very roughly associated with energies below 10^{18} eV, the energy range 10^{18} to 10^{20} eV, and above 10^{20} eV.

Cosmogenic neutrinos are produced when ultra-high energy (UHE) protons with energy $E > 5 \times 10^{19}$ eV interact with photons from the CMBR, infrared light from old stars, and other extragalactic background light. These protons are excited to a Δ^+ resonance which may decay via $\Delta^+ \rightarrow n\pi^+$, leading to neutrinos with energies above 10^{18} eV [87, 88]. The cosmogenic neutrino signal depends heavily on the fraction of UHE cosmic-rays that are protons. For a 100% proton composition (disfavored by most data [89]), observing a cosmogenic neutrino signal of at least a few events per year requires a solid or liquid detector with an active volume of about 100 km^3 .

To reach the effective volumes necessary to observe the expected low fluxes of UHE neutrinos, common, naturally occurring, non-conducting solid (or potentially liquid) media, with a long absorption length for radio waves are needed. Optical Cherenkov and acoustical detectors are limited by short (< 100 m) attenuation lengths [90] so would require a prohibitively expensive number of sensors. The radio detection technique has been used to detect air

showers, targeting neutrinos as well as cosmic rays, and to search for neutrino showers in ice, salt domes and the lunar regolith.

36.3.3.3 Reconstruction of particle energy and direction and background suppression

Since radio detectors view the interaction from afar, the reconstruction techniques differ from optical neutrino telescopes.

Radio detection is a calorimetric measurement, thus provides good energy estimates of the shower energy. The energy fluence (integrated pulse power) of the signal scales quadratically with shower energy. It also depends on the distance to the shower, through potential attenuation losses and the usual $1/R$ loss in electric field amplitude. The arrival times in antennas and a spherical wave approximation can be used to determine the interaction vertex, although some uncertainty due to the viewing angle with respect to the Cherenkov angle may remain, if not corrected for by using the frequency information. If the radio signal travels through media where the index of refraction varies (like the firn of glacial ice), then ray-tracing techniques may be required to follow the signal back to the interaction point. For buried antennas, the bending of the signal trajectories due to the index of refraction creates an opportunity. For some geometries, there may be two paths to the detector: a 'direct' path, with minor bending, and a second where the signal is bent beyond horizontal, bouncing off the surface before reaching the antenna. By measuring the time difference between the two paths, the distance to the interaction vertex may be determined; this greatly simplifies the energy determination [91,92]. For most neutrino interactions (except for ν_e charged-current interactions), the shower energy is less than the neutrino energy. The uncertainty on the interaction inelasticity is a major contributor to the uncertainty in the neutrino energy, along with uncertainties on the distance between the antenna(s) and the interaction vertex [93].

Reconstruction of the neutrino arrival direction depends on several aspects of the signal. First, the direction from the antenna to the interaction site must be determined. This can be done by using the relative timing from separated antennas, or using beam-forming techniques with multi-element arrays. For air showers, the signal arrival direction is (almost) equal to the particle arrival direction, with corrections being obtainable by fitting a hyperbolic wavefront [72,73].

For showers in solid/liquid media, the arrival direction with respect to the interaction point - antenna vector is determined from two additional angles. The frequency spectrum can be used to determine the angle between signal arrival direction and Cherenkov cone according to Eq. (36.4) [94]. The second angle can be determined from the polarization of the signal. The radio signal is produced with a linear polarization in the plane containing both the particle direction and the radio wave direction. These two angles can be combined to determine the direction, subject to a (usually) four-fold ambiguity, due to uncertainty as to whether the antenna is inside or outside the Cherenkov cone, and because the particle direction can be flipped 180° without affecting the observed signal. Often, some of these solutions can be rejected because they correspond to long path lengths through the Moon or the Earth, where the neutrino would be absorbed.

Spectral information is crucial for the reconstruction and background rejection. However, large bandwidth antennas typically disperse (i.e. broaden) the pulses. As long as the dispersion can be compensated for and backgrounds controlled, a large bandwidth detector is the most sensitive.

All radio experiments must contend with background. Common sources are anthropogenic noise, antenna/preamp noise, charge generated by blowing snow, lightning, and, at low frequencies, radiation from the Milky Way. While narrowband noise impacts triggering and contaminates signal quality, impulsive backgrounds could mimic a signal. One of the major issues for radio-detection experiments is anthropogenic noise. Most anthropogenic noise has distinctive characteristics (such as being narrow-band, and coming from near the horizon) which makes it relatively easy to reject during data analysis, via narrow-band filters and other techniques [72]. However, these factors complicate triggering and reduce data purity. This is even an issue in Antarctica, where communication radios and passing satellites can mimic showers,

at least at the trigger level. The need to limit anthropogenic noise has led most experimental groups to select remote locations for their detectors. Still, experiments have used approaches to reduce trigger-level noise, and/or to reject background at the analysis level. For example, for multi-element arrays, the threshold drops as the square root of number of antennas, since the signal adds in-phase while the backgrounds add with random phases [95]. It seems, however, that triboelectric signals recorded in periods with winds exceeding 10 m/s are a problematic trigger-level background, for experiments in polar regions [96] and will require removal during analysis.

Most dedicated air shower experiments have used radio antennas in combination with at least one other detector technology, such as scintillation counters, if the site quality is not sufficient and/or computing power on autonomous stations is limited. One exception is ARIANNA, which is located in an uninhabited part of Antarctica, enabling them to efficiently self-trigger on air showers [97].

Lunar experiments (discussed below) use different techniques to reduce the anthropogenic background. Some experiments use multiple antennas, separated by at least hundreds of meters; by requiring a coincidence within a small time window, anthropogenic noise can be rejected. With good enough timing, beam-forming techniques can be used to further reduce the background. An alternative approach is to use beam forming with multiple feed antennas viewing a single reflector, to ensure that the signal points back to the moon.

Due to the similarity in the radio emission of air showers and neutrino showers, the more abundant cosmic rays can act as background to neutrino searches. In-ice detectors need to suppress in-air emission that is refracted into the ice, emission that is created from developing air showers continuing in the ice, as well as from stochastic energy-losses of atmospheric muons. Lunar experiments may face challenges in separating neutrino interactions from cosmic ray interactions.

36.3.3.4 Recent experiments

Figure 36.8 shows some current limits from neutrino searches, including from prototype arrays. Except for LOFAR, which is fully operational, projected limits from future experiments are not shown in the figure.

i. Ice

The most common dense medium transparent to radio waves is ice. Natural ice is an attractive medium for neutrino detection with radio attenuation lengths from over 300 m to 1 km [108]. The attenuation length varies with frequency and ice temperature, with higher attenuation in warmer ice. Although glacial ice is mostly uniform, the top ≈ 100 m of ice, the 'firn,' exhibits a gradual transition from packed snow at the surface (typically $\rho = 0.35$ g/cm³) to solid ice ($\rho = 0.92$ g/cm³) below [109]. The thickness of the firn varies with location; it is thicker in central Antarctica than in the coastal ice sheets or in Greenland. The varying density has several implications.

The index of refraction depends linearly on the density, so radio waves curve downward in the firn. This bending reduces the effective volume of surface or aerial antennas. A surface antenna cannot see near-surface interactions at large horizontal distances. There are also indications that the increase in firn density is non-monotonic [110,111]. This leads to non-monotonic changes in index of refraction which may create waveguides that trap a small fraction of the radio energy and propagate it horizontally.

In one type of experiment, antennas mounted on high-altitude balloons observe the ice from above. Radio signals from in-ice neutrino interactions propagate to the surface, traverse the ice-air interface, and then travel to the balloon. The surface roughness of the ice can affect signals as they transition from the ice to the atmosphere. The best known example, ANITA, has made four flights around Antarctica, floating at an altitude around 35 km [112]. Its 32/40/48 (depending on the flight) dual-polarization horn antennas scanned the surrounding ice, out to the horizon (650 km away). Because of the small angle of incidence, ANITA could use polarization information to separate signals from back-

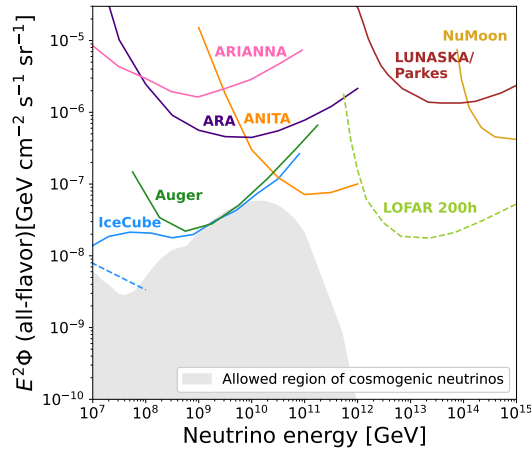


Figure 36.8: Representative 3-flavor (summed, assuming equal fluxes of each flavor) differential (over one decade in energy) limits from different experiments and prototype experiments. Shown are limits from the IceCube ultra-high energy ν search [98], the Auger search for earth-skimming ν_τ [99], the LUNASKA/Parkes [100] and NuMoon lunar searches [101], the ANITA balloon experiment [102], ARA [103] and ARIANNA prototypes [104], along with projections for the LOFAR array [105]. The dashed blue line is the extrapolation of the IceCube through-going ν_μ flux measured at lower energies (few 10s of TeV to 10 PeV), with spectral index $\alpha = -2.37$ [106]. Because of the long extrapolation, this should only be treated as a rough reference. The ARA and ARIANNA limits are from prototype arrays, and indicate the energy range that might be covered, with far higher sensitivity by larger arrays. The shaded area is the allowed region for cosmogenic neutrinos, from a recent global analysis that included the measured cosmic-ray spectrum and composition [107].

ground; ν signals should be vertically polarized, while most background from cosmic-ray air showers should be horizontally polarized.

As with all radio-detection experiments, ANITA had to contend with anthropogenic backgrounds. The ANITA collaboration uses their multiple antennas as a phased array to achieve good pointing accuracy, with a resolution of $0.2\text{--}0.4^\circ$ in elevation, and $0.5\text{--}1.1^\circ$ in azimuth. They rejected all events that pointed toward known or suspected areas of human activity. ANITA has set the most stringent flux limits yet on neutrinos with energies above 10^{20} eV [102]. The ANITA experiment has also reported several anomalous events, matching cosmic ray signals, but with unexpected polarization signature, which the collaboration has indicated might be from Earth-skimming ν_τ [113, 114]. However, this interpretation is controversial.

Because of the significant source-detector separation, ANITA is most sensitive at energies above 10^{19} eV. A lower energy threshold requires a smaller antenna-target separation.

Other ice based experiments use antennas located within the active volume, allowing them to reach thresholds around 10^{17} eV, or lower with phased array antennas. This approach was pioneered by the RICE experiment [115] which buried 18 half-wave dipole antennas in holes drilled for AMANDA at the South Pole, at depths from 100 to 300 m. The hardware was sensitive from 200 MHz to 1 GHz. Each antenna fed an in-situ preamplifier which transmitted the signals to surface digitizing electronics.

More recently, two groups have deployed prototype arrays which have explored different detector concepts. The Askaryan Radio Array (ARA) deployed surface and buried antennas at the South Pole [116], while the Antarctic Ross Iceshelf Antenna Neutrino Array (ARIANNA) installed surface antennas on the Ross Ice Shelf [104], about 110 km north of McMurdo station. ARIANNA offered the possibility of detecting downward-going ν , from the radio waves reflected off the ice-sea water interface on the bottom of the Ross Ice Shelf, while ARA took advantage of the colder,

deeper ice at the South Pole, with its longer radio attenuation length. ARA buried antennas up to 200 m deep to be able to observe a larger portion of ice, due to the refraction of the signal in the firn. In contrast, ARIANNA deployed antennas just below the surface, allowing them to use high-gain, but large log periodic dipole antennas. Recently, phased-array trigger techniques have been demonstrated that can reduce the energy threshold by a factor of several [95, 117].

Both experiments use stations which operate independently, spaced far enough to maximize sensitivity, but where only a small fraction of neutrino events will be visible in multiple stations. Each station includes multiple antennas, which will be sensitive to both horizontal and vertical polarization. The expected angular resolution is a few degrees [94].

In 2021, the Radio Neutrino Observatory Greenland (RNO-G) started deploying stations at Summit Station. RNO-G is planned to consist of 35 stations, which employ ARIANNA-style surface antennas, an ARA-style phased array and deep antennas, and draw heavily on ANITA's electronics heritage [118].

ii. The Moon

Because of its large size and non-conducting regolith, and the availability of large radio-telescopes, the Moon is an attractive target [119]. Conventional radio-telescopes are quite well suited to lunar neutrino searches, with natural beam widths not too dissimilar from the size of the Moon. Still, there are experimental challenges. The attenuation length is typically estimated to be $9\text{m}/f(\text{GHz})$ [120], so only near-surface interactions can be studied. The composition of the lunar regolith is not well known, and there are significant uncertainties due to this uncertainty. One big limitation of lunar experiments is that the 385,000 km target-antenna separation leads to energy thresholds above 10^{20} eV.

The effective volume probed by experiments depends on the geometry, which itself depends on the frequency range used. At high frequencies f , the electric field strength is high, leading to a lower energy threshold, but the sensitive volume is limited because the Cherenkov cone only points toward the Earth for a narrow range of geometries. Lower frequency radiation is more isotropic, so the effective volume is larger, but, because the electric field is weaker, the energy threshold is higher. The $1/f$ dependence of the attenuation length in the lunar regolith further increases the effective volume at low frequencies. The frequency range affects the energy dependence of the sensitivity. As can be seen in Fig. 36.8, a low-frequency experiment like NuMoon (which covered 115–180 MHz) has good sensitivity, but only above about 10^{14} GeV, while Lunaska/Parkes, which observed in the range 1200–1500 MHz, has a higher flux limit, but is sensitive above about $10^{12.5}$ GeV.

Current limits and projected sensitivities are sensitive to many details. A recent review [121] compared different radio-detection experiments using a common framework, and found some significant shifts in sensitivities due to, e.g. different assumptions about lunar composition and inelasticities.

With modern technology, it is increasingly viable to search over very broad frequency ranges [122]. One technical challenge is due to dispersion (frequency dependent time delays) in the ionosphere. Dispersion can be largely removed with a de-dispersion filter, using either analog circuitry or post-collection digital processing.

iii. Air

Radio detection in air is sensitive to all particles inducing air showers. Radio-detection can be used to determine the energy of cosmic rays, as done by e.g. the Auger and Tunka-Rex experiments [123, 124]. Radio signals can also be used to infer the altitude for shower-maximum, where the shower contains the most particles, as done by e.g. the LOFAR and Tunka-Rex collaborations [124, 125]. This altitude is sensitive to the cosmic-ray composition. Reconstructing the particle arrival direction is much easier in air since the Cherenkov angle, and thus the radio wavefront, aligns with the axis to 1° . Radio-detection is also useful for energy cross-calibrations between different experiments and may

be able to provide an independent energy scale calibration for air shower arrays [126].

One variation on the radio-detection approach is to look for radio emission from Earth-skimming ν_τ [127, 128]. Although ν_τ are much less commonly produced than ν_μ and ν_e , over astrophysical distances, oscillations lead to a $\nu_e : \nu_\mu : \nu_\tau$ ratio near 1 : 1 : 1, for almost all non-exotic acceleration and propagation mechanisms.

If the ν_τ traverse the Earth and interact while traveling upward, the resulting τ^\pm may exit the Earth before decaying. 83% of the time, the decay produces a hadronic or electromagnetic shower in the atmosphere [129]. Experiments have searched for these upgoing showers, and for the resulting optical Cherenkov and coherent RF radiation. The threshold energy dependence for these searches depends on several factors, notably including the average τ^\pm decay length, which increases linearly with energy. For somewhat lower energy ν_τ , with shorter decay lengths, a mountain may serve as a target, with τ^\pm expected to emerge from the other side. The Pierre Auger observatory sets stringent limits on this neutrino flux at energies above 10^{17} eV [99].

36.3.3.5 Future experiments

Looking ahead, RNO-G [118] will continue deployment until 2026 and reach the largest yearly sensitivity of any radio array thus far. Further out, the proposed IceCube-Gen2 expansion includes a substantial radio array component [68], which will be sensitive to both neutrinos from the ice and air showers from cosmic rays. PUEO, a successor of ANITA has been funded and is scheduled for its first flight in 2025 [130].

In the near future, several large radio detector arrays should reach significantly lower energies for lunar neutrino detection. The LOFAR array is taking data with 36 detector clusters spread over Northern Europe [105]. In the longer term, the Square Kilometer Array (SKA) with its 1 km² effective area will push thresholds down to near 10^{20} eV [122]. The SKA will also study air showers.

A number of dedicated prototype ν_τ radio-detection experiments exist. The GRAND Collaboration, e.g., is proposing to deploy a large array of simple autonomous radio stations optimized for near-horizontal signals [131]. The Pierre Auger Collaboration is currently upgrading their surface array to include radio antennas at all water Cherenkov detectors. This array will improve the sensitivity of the instrument to horizontal showers, both for composition sensitivity for cosmic rays and for the detection of Earth skimming neutrinos [132].

36.4 Large time-projection chambers for rare event detection

Written August 2023 by L. Baudis (Zurich U.).

Initially developed for particle physics experiments at accelerators (see *Section 35.6.5*), the concept of a Time Projection Chamber (TPC) [133] evolved and is now tailored to a large range of applications, most notably to experiments in astroparticle physics searching for rare interactions deep underground. Present and proposed experiments designed to observe interactions of dark matter and other exotic particles, second order weak nuclear decays, as well as neutrinos from a variety of sources are based on TPCs operated with pure noble elements, either in gaseous or liquid form. The detectors aim for large target masses, low energy thresholds (keV-scale) and ultra-low levels of backgrounds from radioactivity and cosmic rays. Historical introductions, reviews of the operation principles, instrumentation and technological aspects, as well as applications, are found in Refs. [134–138].

The two most common noble fluids employed as detector media in present TPCs for rare event searches are argon and xenon, either as a high-pressure gas, or in liquid phase, or in liquid and gas phase (dual-phase). An interaction within the active volume of a TPC will create ionisation electrons and scintillation photons. The prompt scintillation signal is detected with one or two arrays of photosensors, while the ionisation electrons, which drift in the pure medium under the influence of an external, uniform electric field, are observed either directly with charge sensors, or via proportional scintillation, or electroluminescence. Since transverse electron diffusion is small, albeit non-negligible, the ionisation

signal provides the $x - y$ information of the interaction site, with the z -information coming from the drift time measurement. The TPC thus yields a three-dimensional event localisation, enabling fiducial volume selections and differentiation between single- and multiple-scatters in the active volume. These features are crucial for filtering out rare events from the much higher backgrounds due to residual radioactivity of detector components. The specific energy loss (dE/dx) depends on the primary interacting particle, and leads to a distinct ratio of scintillation to ionisation for gammas/electrons, alphas and fast neutrons, allowing for further background discrimination. Two examples for the operation principle of TPCs for rare event detection are shown in Fig. 36.9.

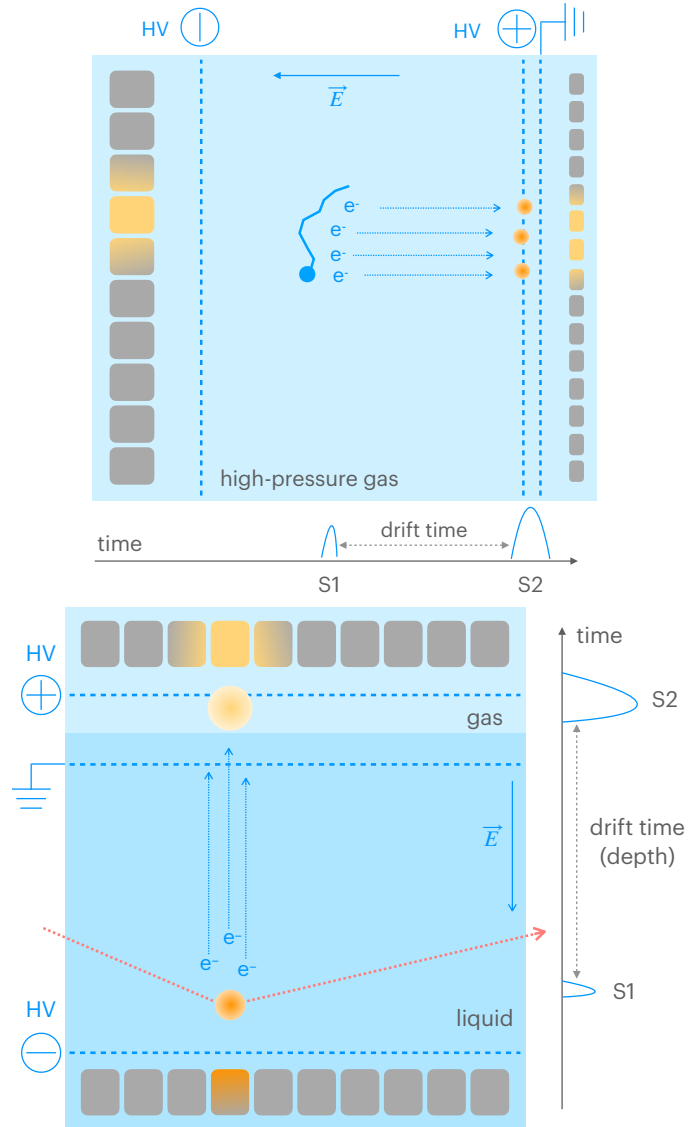


Figure 36.9: Operation principle of TPCs for rare event detection: a high-pressure gas (left) and a dual (liquid/gas) phase (right) TPC. A particle interaction yields a prompt scintillation signal (S1) and a delayed, amplified proportional scintillation signal (S2). The latter is caused by ionisation electrons drifted in a homogeneous electric field (and, for dual phase TPCs, extracted into the gas phase above the liquid). In these examples, both S1 and S2 signals are observed with photosensor arrays placed behind the anode and cathode (left), or at the top and bottom (right) of the TPC. The position information along the drift field is inferred from the time difference between the two light signals, while the position in the transverse plane to the field is derived from the S2 light pattern in the photosensor plane close to the electroluminescent light production site.

The properties of liquid argon as detection medium in a TPC are reviewed in *Section 35.7*. Here some properties for xenon are given in Tab. 36.4. In the liquid phase, the high xenon density allows for compact, large and homogeneous detector geometries with efficient self-shielding against external radiation, given that the cross sections for the photoelectric effect, Compton scattering and pair production scale as $Z^5/E_\gamma^{7/2}$, Z/E_γ and $Z^2 \ln(2E_\gamma)$, respectively, for incoming X-rays and gammas with energy E_γ . The radioactive isotopes ^{124}Xe , ^{126}Xe , ^{134}Xe and ^{136}Xe have very long half-lives, and their second-order weak decay modes are subject to investigation (see *Section 36.4.2*).

In an argon or xenon detector, the energy loss of an incident particle is shared between ionisation, excitation and sub-excitation electrons liberated in the ionisation process. The average energy loss in ionisation is slightly larger than the ionisation potential, as it includes multiple ionisation processes. In their condensed phases, argon and xenon exhibit a band structure of electronic states, with the band gap energy being around 14.3 eV and 9.3 eV for liquid argon and xenon, respectively. In gaseous xenon, the ionisation potential is about 12.1 eV. Scintillation arises from excited atoms (excitons) and from ions, via recombination, with the emitted vacuum-ultraviolet (VUV) photons in single bands centred at $\lambda = 128$ nm for argon and $\lambda = 175$ nm for xenon. The excited dimers (or excimers), at their lowest excited level, de-excite to the dissociative ground state by the emission of a single VUV photon. This comes from the large energy gap between the lowest excitation and the ground levels, forbidding other decay channels such as non-radiative transitions. The scintillation light has two decay components due to de-excitation of spin singlet and spin triplet states of the excited dimers to the ground state. The singlet and triplet states refer to the total spin quantum number ($s=0$ or $s=1$) of the excited Rydberg electron and the angular momentum due to the molecular orbit, with the shorter and longer decay shapes being produced by the de-excitation of $s=0$ states and $s=1$ states, respectively. The different pulse decay time for different type of particle interactions, and thus ionisation densities, is employed to discriminate electronic from nuclear recoils in dark matter detectors. While this is very effective in liquid argon, due to the large time separation of (6 ± 1) ns versus (1500 ± 100) ns, it is difficult to put in practice for xenon [139], considering the much smaller separation, (2.2 ± 0.3) ns versus (27 ± 1) ns, of the two components.

The recombination-independent, mean energy required to produce a single detectable quantum (photon or electrons), called the W-value, assumes that each recombining electron-ion pair produces an exciton, which leads to a photon. In liquid argon, the W-value is (19.5 ± 1.0) eV [148]. In liquid xenon, the widely-adopted W-value is (13.7 ± 0.2) eV, measured with 122 keV γ -rays from an external ^{57}Co source [149]. Recently, a lower value of $11.5^{+0.2}_{-0.3}$ (syst.) eV was obtained in a small TPC with internal sources at energies between 2.8 keV and 42 keV [150], consistent with the value measured at the MeV-scale, 11.5 ± 0.5 (syst.) ± 0.1 (stat.) eV with the EXO-200 detector [151]. The ionisation and scintillation W-values in gaseous xenon are 24.8 eV and (76 ± 6) eV, respectively [152].

The partition between excitation and ionisation depends on the density of the electron-ion pairs produced along the track of a particle, and the recombination fraction depends on the applied electric field, as well as on the ionisation density in the track. While several phenomenological models exist to describe electron-ion recombination as a function of stopping power and electric drift field (see [134] and discussions therein), a solid theory of energy loss of low-energy ions in noble fluids is still missing. For nuclear recoils as generated by interactions of neutrons, neutrinos or hypothetical WIMPs, an energy-dependent quenching is introduced via the Lindhard factor \mathcal{L} [153], with \mathcal{L} being around 0.2 – 0.25 and 0.15 – 0.2 in liquid argon [154] and xenon [155], respectively, at nuclear recoil energies in the range 3-100 keV. A comprehensive framework to simulate scintillation and ionisation yields in argon and xenon as a function of interaction type, energy and electric field in a TPC is the Noble Element Simulation Technique (NEST) [156].

To calibrate the energy scale and determine the energy reso-

lution of low-background TPCs, mono-energetic lines from external (e.g., ^{57}Co , ^{60}Co , ^{137}Cs , ^{228}Th , etc) and internal (^{83m}Kr , ^{37}Ar) calibration sources, as well as from neutron activation lines (e.g., ^{129m}Xe , ^{131m}Xe in xenon) are used. Relative energy resolutions (σ/μ) at the level of 4-6% at energies of a few tens of keV and 2-3% at energies of a few 100 keV were reached in argon and xenon TPCs, respectively. At higher energies, relevant for the neutrinoless double beta decay of ^{136}Xe , relative resolutions of 0.67%, 0.8% and 1.2% around 2.5 MeV were obtained by LZ [157], XENON1T [158] and EXO-200 [159], respectively. Superior energy resolutions are attained in high-pressure gas TPCs with electroluminescent amplification [160], with a relative resolution of 0.4% obtained in the NEXT-White detector [161]. This is due to the fact that the Fano factor in pure gaseous xenon, $F_{\text{GXe}} = 0.15 \pm 0.02$, is about two orders of magnitude smaller than in the liquid phase.

To achieve a high collection efficiency for both ionisation and scintillation signals, the concentration of impurities is reduced and maintained at a level below one part per 10^9 (ppb) oxygen equivalent. While the light can be strongly reduced by the presence of water vapour, the ionisation signal also requires high purity in terms of molecules with high electronegative affinity. The purity is commonly expressed via the electron drift lifetime, τ_e , which is the time over which the number of drifting electrons, n_e , is reduced by a factor e: $n_e(t) = n_e(t_0) \exp(-t/\tau_e)$. Ideally, τ_e should be a few times larger than the total drift time in a TPC, to prevent charge losses. Lifetimes > 10 ms were achieved both in argon and xenon (corresponding to impurity concentrations $\ll 1$ ppb O_2 equivalent) via continuous recirculation and purification in the liquid or gas phase.

The drift velocity of electrons, which depends on the drift field E_d and the electron mobility μ as $v_d = \mu \cdot E_d$, has been measured for drift fields between $\sim (10 - 10^4)$ V/cm. It also depends on the temperature in the medium and the impurity concentration, often making the comparison between different measurements difficult. In general, the drift velocity raises from about 0.25 mm/ μs at low fields to 2 mm/ μs at high fields in both argon and xenon. As electrons drift in the electric field, the initial electron cloud spreads both in longitudinal and transversal direction to the field, expressed in terms of longitudinal D_L and transversal D_T diffusion coefficients, with $D_L < D_T$ and $D_L/D_T \approx 1$ for fields approaching zero. In argon, D_L was measured as ~ 4.2 cm²/s at 200 V/cm [162], ~ 3.7 cm²/s at 274 V/cm [163], ~ 7.2 cm²/s at 500 V/cm and D_T as ~ 12 cm²/s [164]. In xenon, D_L is around 100 cm²/s at low fields, reaching ~ 25 cm²/s at higher drift fields [142], while D_T has been measured to be ~ 55 cm²/s at fields between (20-600) V/cm [165]. As an example, the spatial distribution of an initially point-like electron cloud, after a drift time t , is $\sigma_D = \sqrt{2Dt}$, resulting in a value of ~ 20 mm for 1 ms drift and a 25 cm²/s diffusion coefficient.

The scintillation light can be attenuated by absorption on impurities or due to Rayleigh scattering, the latter depending strongly on the wavelengths of the photons and the optical properties of the materials. Since only the combined effect is observed, it is non-trivial to disentangle the two contributions. A combination of measurements and theoretical calculations yield total attenuation and Rayleigh scattering lengths between 55-110 cm and 60-99 cm for argon and 30-50 cm and 30-50 cm for xenon detectors, with refractive indexes between 1.34 and 1.57-1.72, respectively, and absorption lengths > 100 cm [134, 166].

Background sources for rare-event searches, their mitigation techniques and radio-purity assays are discussed in *Section 36.6* of this *Review*. The main backgrounds in large TPCs are due to decays of other noble isotopes mixed with the argon and xenon (^{39}Ar , ^{85}Kr , ^{222}Rn), from natural, anthropogenic or cosmogenic radioactivity of detector materials in close proximity to the target (^{238}U , ^{232}Th , ^{40}K , ^{60}Co), and from muons and their secondary particles, including *in situ* production of isotopes which are sufficiently long-lived to render their vetoing difficult (e.g., ^{137}Xe in xenon TPCs). Astrophysical neutrinos cause largely irreducible backgrounds in dark matter detectors, but deliver exciting physics signatures in their own right. To mitigate the ^{39}Ar background, argon is extracted from underground sources (CO_2 wells), ^{85}Kr

Table 36.4: Physical properties, volume fraction in the atmosphere, radioactive isotopes of the noble element xenon.

Property [unit]	Xe
Atomic number, mean atomic mass [g/mol]	54, 131.29
Boiling T_b and melting T_m point at 1 atm [K]	165.0, 161.4
Gas density at 1 atm and 298 K (T_b) [g/l]	5.40 (9.99)
Liquid density at T_b [g/cm ³]	2.94
Volume ratio ($\rho_{\text{liquid}}/\rho_{\text{gas}}$)	526
Dielectric constant of liquid	1.95
Scintillation light yield (in liquid, at 122 keV) [140]	63 photons/keV
Wavelength (peak centred at)	175 nm
Decay time constants (s=0, s=1)	2.2 ns, 27 ns
Refractive index	1.69
Electron mobility* [142]	0.29 mm ² /($\mu\text{s V}$) ($\lesssim 100$ V/cm) 0.01 mm ² /($\mu\text{s V}$) ($\gtrsim 100$ V/cm)
Volume fraction in Earth's atmosphere [ppm]	0.087
Isotopes with spin, abundance [%]	¹²⁹ Xe, 26.44; ¹³¹ Xe, 21.18
Radioactive isotopes, abundance [%] and $T_{1/2}$ [y]	¹³⁶ Xe, 8.87; 2.2×10^{21} [143, 144] ¹²⁴ Xe, 0.095; 1.1×10^{22} [145] ¹³⁴ Xe, 10.4; $> 8.7 \times 10^{20}$ (90% C.L.) [146] ¹²⁶ Xe, 0.089; $> 1.9 \times 10^{22}$ (90% C.L.) [147]

*Measured values in two benchmark regimes, so-called "cold" and "hot" electrons [141]. In the first case, the electron energies are due to thermal bath of the xenon fluid and they rapidly gain energy with increasing field; in the second case, the electrons have gained most of their energy through acceleration in the field and experience increased energy loss on their path due to collisions with Xe atoms.

and ²²²Rn are reduced by cryogenic distillation, exploiting the different vapour pressures of the different noble gases, or with gas chromatography using synthetic charcoal. In xenon detectors, ^{nat}Kr concentrations of < 50 ppq [167] and ²²²Rn concentrations of $0.8 \mu\text{Bq/kg}$ were achieved by cryogenic distillation. In argon TPCs, ³⁹Ar concentrations of $(0.73 \pm 0.11) \text{ mBq/kg}$ were demonstrated [168].

An overview of large TPCs for rare event searches is given in Table 36.5.

36.4.1 Dark matter and other low energy signals

TPCs built to search for particle dark matter are based on the two-phase principle. Starting with total masses of a few kilogram the detectors evolved and reached active target masses at the tonne- and more recently multi-tonne scale. Concomitantly, the background levels in the most inner regions constantly decreased, with current electronic recoil rates of 15 events/(t y keV) in the energy region below 100 keV for xenon detectors [169]. Typically, the TPCs contain two arrays of photosensors, one immersed in the liquid, and one in the gas phase above the liquid at similar low temperature. The xenon scintillation light can be observed directly by PMTs with synthetic silica (quartz) windows or with VUV-sensitive SiPMs, while for argon detectors, tetraphenyl butadiene (TPB) is used to shift the 128 nm light to 420 nm, given that it is absorbed by quartz windows.

The DarkSide-50 experiment [168] operated a 50 kg TPC with liquid argon depleted in ³⁹Ar until 2019. DarkSide-20k [170], to operate 51.1 t of underground LAr in an octagonal TPC, the walls made of gadolinium-loaded acrylic panels, with two arrays of SiPMs, is under construction in Hall C of the Laboratori Nazionali del Gran Sasso (LNGS) in Italy. A larger, 400 t LAr detector, Argo, has been proposed for SNOLAB in Canada. After the successful operation of TPCs for LUX, PandaX-II and XENON1T, the current generation of xenon detectors, LUX-ZEPLIN (LZ) [171] at the Sanford Underground Facility (SURF) in USA, PandaX-4T [172] at the China Jinping Laboratory (CJPL) and XENONnT [173] at LNGS, employ several tons of LXe as active target mass. Their overall TPC design is rather similar, with cylindrical, polytetrafluoroethylene (PTFE) enclosed target regions viewed by two arrays of low-radioactivity, 3-inch diameter Hamamatsu R11410 PMTs. The PTFE has a high reflectivity for the Xe scintillation light [174]. Next-generation detectors, at the 50 t LXe scale or beyond, have been proposed with DARWIN/XLZD [175, 176] and PandaX-xT [177]. Recent constraints on various dark matter candidates are presented in

Section 27.6. The search for WIMP dark matter is ongoing, with the sensitivity goal of current experiments to the spin-independent WIMP-nucleon cross section around $1.5 \times 10^{-48} \text{ cm}^2$ at 40-50 GeV/ c^2 mass [171, 173].

Owing to low electronic recoil backgrounds and low energy thresholds in noble liquid TPCs, high-sensitivity searches for dark matter electron scattering with particle candidates from a hidden sector, for keV-scale axion-like-particles (ALPs) and dark photons via absorption in LXe, as well as searches for solar axions, became feasible (see Section 27.6). Looking at ionisation-only signals allows for a further reduction of the energy threshold, given the much higher efficiency to detect an ionisation electron compared to a primary scintillation photon (typically 90% versus 10%). While this gain comes at the expense of higher backgrounds, it allows nonetheless to set stringent limits on light dark matter electron interactions at masses from a few tens of MeV to a few GeV, as shown by DarkSide-50 [178], PandaX-4T [179], XENONnT [180] and LZ [181]. Further, current-generation dual-phase TPCs have reached target masses which will allow for the first time the detection of solar pp neutrinos via elastic neutrino-electron scattering at energies down to 1 keV and of ⁸B neutrinos via coherent elastic neutrino-nucleus scattering (CE ν NS).

Dual-phase TPCs were successful in gradually scaling up their target mass and in reducing the background levels for each iteration, while maintaining a low-energy threshold of ~ 1 keV for electronic recoils. Notwithstanding, the construction of next-generation detectors at the multi-ten-tons scale poses multiple technological challenges. The background goals are such that electronic and nuclear recoil rates are below the ones from irreducible astrophysical neutrino interactions. This requirement sets the goals for the intrinsic ²²²Rn and ⁸⁵Kr concentrations: the background from the decay of these isotopes should be significantly lower than the solar pp -neutrino elastic scattering rate. This translates into $0.1 \mu\text{Bq/kg}$ for ²²²Rn and 0.1 ppt for ^{nat}Kr, assuming a ⁸⁵Kr/^{nat}Kr ratio of 2×10^{-11} mol/mol. While ^{nat}Kr concentrations of < 50 ppq were already achieved, for ²²²Rn a factor of about 10 reduction compared to the current values is needed. This calls for a high liquid throughput (close to 1 t/hour) with efficient cooling power based on cryogenic heat pumps and radon-free heat exchangers. Cryogenic distillation or charcoal chromatography must go hand in hand with selection of low radon

²A ²²²Rn concentration of $0.1 \mu\text{Bq/kg}$ corresponds to less than one radon atom per 100 mol of xenon. The main background is due to ²¹⁴Bi β -decays which are not accompanied by an α -decay and thus cannot be tagged in the TPC.

Table 36.5: Selected experiments using large TPCs for rare event searches. Shown are experiments that operated until recently, as well as current, soon-to-be-operating and proposed experiments. UAr stands for underground argon; HP-GXe stands for high-pressure gaseous xenon. For some of the proposed experiments, the location or the readout scheme is not yet decided (marked as "TBD").

Experiment	Location	TPC type	Total (active) mass	Readout
Dark matter				
DarkSide-50	LNGS	Dual-phase, UAr	51.1 kg (46.4 kg)	3" PMTs, TPB
DarkSide-20k	LNGS	Dual-phase, UAr	50 t (50 t)	SiPMs, TPB
Argo	SNOLAB	Dual-phase*, UAr	~400 t (~400 t)	SiPMs, TPB
LUX-ZEPLIN	SURF	Dual-phase, Xe	10 t (7 t)	3" PMTs
PandaX-4T	CJPL	Dual-phase, Xe	5.6 t (3.7 t)	3" PMTs
PandaX-xT	CJPL	Dual-phase, Xe	47 t (43 t)	2" PMTs
XENONnT	LNGS	Dual-phase, Xe	8.6 (5.9 t)	3" PMTs
DARWIN/XLZD	TBD	Dual-phase, Xe	50-100 t (40-80 t)	3" PMTs
$0\nu\beta\beta$ decay				
EXO-200	WIPP	LXe, ^{136}Xe 81%	175 kg (110 kg)	LAAPDs, wires
nEXO	SNOLAB	LXe, ^{136}Xe 90%	4.8 t (3.65 t)	SiPMs, charge pads
NEXT-White	LSC	HP-GXe, ^{136}Xe 91%	5 kg (4.3 kg)	3" PMTs, SiPMs, TPB
NEXT-100	LSC	HP-GXe, ^{136}Xe 90%	100 kg (80 kg)	3" PMTs, SiPMs, TPB
NEXT-HD	TBD	HP-GXe, ^{136}Xe 90%	1.2 t (1 t)	Fibres + SiPMs, TPB
PandaX-III [†]	CJPL	HP-GXe, ^{136}Xe 90%	140 kg (100 kg)	Micromegas

*The option to build Argo as a single-phase detector is also under consideration.

[†]This is an R&D program for a future larger, enriched PandaX-xT detector.

emanation materials and new coating techniques to prevent radon emanation from surfaces.

Other challenges related to the liquid target are the continuous purification for electronegative impurities and water, to maintain high charge and light yields, while not introducing radon into the TPCs, as well as new solutions for reliable storage and recuperation at large scales. A dedicated single-closed-loop cryogenic system capable of handling 100 t of underground argon was designed and constructed for DarkSide-20k [182]. Liquid phase purification powered by a liquid xenon pump, as demonstrated in [183], was employed to achieve an electron drift lifetime above 15 ms in about 8.6 t of xenon in XENONnT. A system capable of handling 30 t of xenon in liquid phase, including long-term storage and transfer of the cryogenic liquid between storage module and detectors was constructed for PandaX-xT [177, 184].

Regarding the detector design, electrodes with large (>2.5 m) diameters, with high transparency, minimal sagging and low spurious electron emission, as well as high-voltage feed-throughs that can safely deliver 50 kV or more to the cathode must be employed. DarkSide-20k will use for the first time anode and cathode plates made out of acrylic coated with a commercial conductive polymer and with TPB. LZ successfully built custom-woven wire-mesh grids with 1.5 m diameter, produced with an in-house built loom to weave the wire meshes [185]. Finally the cryostat design must ensure stability, while reducing as much as possible the amount of material, and thus gamma and neutron emitters in proximity to the TPCs.

Besides Ar and Xe TPCs, detectors using superfluid ^4He , targeted at low-mass dark matter, are under development within the HeRALD [186] and DELight [187] programs, based on the basic principles demonstrated by the HERON solar neutrino project [188]. The detectors will be instrumented with transition edge sensors or magnetic micro-calorimeters to observe both atomic signals, such as scintillation light, and quasiparticle (phonon and roton) excitations. As in other noble elements, the He_2^* dimers appear in a short-lived (<10 ns) singlet and long-lived (13 s) triplet state. The former decay promptly, emitting photons with energies peaked around 16 eV, while the triplet states can propagate through the fluid and de-excite at surfaces. Liquid helium is transparent to its VUV photons, since the first excited state of atomic helium is at 20 eV. Quasiparticles will propagate ballistically through the liquid without decaying, and can also be detected via the evaporation of ^4He atoms from the surface of the liquid, with the helium binding energy being ~ 0.7 meV.

Large volume, low-background TPCs are also developed for directional dark matter searches. An example is CYGNO [189] which aims to build a TPC with 50 cm drift, filled with a He:CF₄ gas mixture at room temperature and atmospheric pressure at LNGS. The liberated charge in a particle interaction is drifted towards an amplification stage consisting of a triple GEM structure, where the charge is multiplied and also light is produced. The readout will consist of light detectors, PMTs and scientific CMOS cameras, yielding the energy and z-position of events and the 2D track projections, respectively. The combined information thus allows for a 3D track reconstruction, with the goal being to achieve energy thresholds for electronic recoils around 1 keV.

36.4.2 $0\nu\beta\beta$ Decay

Experiments built to search for the $0\nu\beta\beta$ -decay of ^{136}Xe , at a Q-values of 2457.8 keV, are based on single-phase TPCs, filled either with liquid or gas xenon at high pressure. The drift region is horizontal (EXO-200, NEXT-100) or vertical (nEXO, NEXT-HD, PandaX-xT-enriched). For EXO-200 and nEXO, the TPCs are enclosed by radio-pure, thin-walled Cu vessels in cryofluid, hydro-fluoro ether, acting thermal bath and radiation shield. In EXO-200, which took data at the Waste Isolation Pilot Plant (WIPP) until 2018, the charge drifted to crossed-wire planes at each anode, while the light was collected by arrays of large area avalanche photodiodes placed behind the wire planes at both ends. In nEXO, the TPC vessel will be a vertical Cu cylinder with 130 cm height and diameter (for 118.3 cm drift), with the charge collected at the anode by 0.6 cm pitch and 9.6 m long electrode strips, and the scintillation light observed by SiPMs arranged in a barrel configuration. Unlike for dark matter TPCs, there are no reflector panels and the field rings and cathode are coated with reflective aluminium deposition. The design drift field is 400 V/cm and the goal for the relative energy resolution is 0.8%. EXO-200 set a lower limit on the half-life of $0\nu\beta\beta$ -decay of 3.5×10^{25} y with a total exposure of 231.4 kg y [190]. The future nEXO aims for a sensitivity of 1.35×10^{28} y with 5 t of enriched xenon and ten years of data taking [191].

TPCs using high-pressure xenon gas aim to reconstruct the tracks from the two electrons emitted in double beta decays, and the decay vertex, thus providing also a topological signature. In the NEXT project at the Laboratorio Subterráneo de Canfranc (LSC), the horizontal TPC, to be operated at 10-15 bar, features a single drift region. The primary (S1) and secondary (S2) scintillation light, the latter due to electroluminescence when the ion-

isation electrons cross a high-field region close to the anode, are collected by arrays of PMTs and SiPMs placed behind the cathode and anode, respectively, for energy measurements and tracking. The surfaces facing the active volume are coated with TPB to shift the VUV light to the visible spectrum. An inner Cu shield absorbs radiation from the high-pressure vessel of the cryostat.

The NEXT-White experiment, a prototype for NEXT-100 and for the proposed tonne-scale NEXT-HD, has been operating a TPC with 20.8 cm radius and 53 cm drift, with 4.3 kg of xenon at 10 bar. It has shown excellent energy resolution ($< 1\%$ FWHM [161]) and demonstrated background rejection using the capability to reconstruct the trajectories of ionising charges in the gas, thus separating the two-electron signature of $\beta\beta$ -decay from single electrons due to background sources [192, 193]. Using data collected with xenon enriched and depleted in ^{136}Xe , it measured the half-life of the $2\nu\beta\beta$ -decay and demonstrated clear Bragg peaks for the 2 electrons emitted in the decay [194]. NEXT-HD will operate a vertical-drift TPC, 2.6 m in diameter and height, to accommodate ~ 1.1 t of enriched xenon at 15 bar [195]. An intense R&D programme for the *in situ* identification of the barium ions ($^{136}\text{Ba}^{2+}$, $^{136}\text{Ba}^+$) produced in the $0\nu\beta\beta$ -decay (called Ba-tagging) is ongoing [196–198]. PandaX-III, an R&D program for a future, enriched PandaX-xT detector, operates a high-pressure Xe gas TPC, where the xenon is mixed with 1% trimethylamine (TMA) to ensure stable operation of the Micromegas employed in the readout planes, and to minimise electron diffusion [199]. Experimental searches for $0\nu\beta\beta$ -decay are discussed in more detail in Section 14.9.

Apart from enriched xenon detectors, large TPCs using xenon in its natural isotopic abundance are also sensitive to second-order weak decays, such as the double beta decay of ^{134}Xe and ^{136}Xe , and the double electron capture process in ^{124}Xe and ^{126}Xe . In its electronic recoil channel, XENON1T observed for the first time the $2\nu\text{ECEC}$ process in ^{124}Xe by detecting the simultaneously emitted K-shell X-rays/Auger electrons of the daughter atom ^{124}Te with a combined energy of 64.33 keV, which is twice the K-shell binding energy. With a half-life of $(1.1 \pm 0.2_{\text{stat}} \pm 0.1_{\text{sys}}) \times 10^{22}$ y, this is the slowest process ever measured directly [145, 200]. The double electron capture in ^{124}Xe can also be studied with high-pressure xenon gas TPCs, as demonstrated by NEXT [201]. LZ, PandaX-4T and XENONnT will improve upon existing results and will also search for the $2\nu\beta^+\text{EC}$ decay. This channel has a distinct signature due to the two 511 keV gammas emitted after the positron annihilates with an electron in the medium. With a predicted half-life around 1.6×10^{23} y [202] its first observation is within reach of these running experiments, which will also measure the half-life and in particular also the shape of the $2\nu\beta\beta$ -decay of ^{136}Xe with high statistics and at low energies not previously accessed. The current generation of dark matter detectors will also set constraints on the $0\nu\beta\beta$ -decays of ^{136}Xe and ^{134}Xe , as predicted or shown in [145, 203–205], delivering proof-of-principle methods towards higher sensitivity searches in DARWIN/XLZD and PandaX-xT. As an example, with 40 t of natural xenon in a TPC, a ^{136}Xe half-life sensitivity of 3×10^{27} y (90% C.L.) after ten years of operation can be reached [206], a number which increases by about a factor of 1.7 for an enlarged xenon mass of 60 t.

36.5 Sub-kelvin detectors

Revised August 2023 by O. Cremonesi (INFN, Milano-Bicocca), L. Hsu (FNAL) and G. Signorelli (Pisa U.; INFN, Pisa).

36.5.1 Motivation for Sub-kelvin Detectors

Detectors operating below 1 K are referred to as low-temperature detectors (LTDs). The advantage of using LTDs over conventional detectors resides in their better energy resolutions, lower noise, and improved energy thresholds, which can all be achieved with a versatile choice in materials. In certain applications, these advantages outweigh the potential drawbacks of cooling and reading out a detector payload at sub-kelvin temperatures, and thus enable exploration of new frontiers in fundamental physics, astrophysics and cosmology. Among the endeavors enabled by LTDs are direct searches for dark matter over

a wide mass range, precision experiments to measure the electron neutrino mass, searches for neutrinoless double-beta decay, and X-ray observation of the Universe. Large arrays of LTDs are also employed to measure the properties of the cosmic microwave background (CMB) spectrum whose parameters are determined by fundamental physics. These include dark matter and dark energy densities, the sum of neutrino masses and the number of light relativistic species, as well as probing the physics of inflation at energy scales of $\sim 10^{16}$ GeV. This article presents a brief overview of LTDs, their features, and several applications. More detailed treatment of this subject is available in the literature [207–210].

The advantages of LTDs are enabled by the detection of very low energy excitations (e.g. phonons and quasiparticles). In a typical interaction, energy from an incident particle is dissipated through excitation of secondary particles such as electrons, ions, holes, photons, phonons etc. These particles will in turn produce their own secondaries. Thus there is a cascade down in energy until the original energy deposit is converted entirely into heat and the detector reaches thermal equilibrium. Prior to the equilibrium phase, the energy at any given moment is partitioned among multiple excitation modes. Conventional particle detectors work by sensing the higher energy excitation modes, such as ionization and scintillation, which require an average minimum energy of few eV to 10's of eV to produce. For such detectors, a large fraction of the deposited energy remains undetected in the form of heat. Furthermore, the measurements are subject to the fluctuations inherent in the partition of energy across different excitation modes. Secondaries that don't eventually escape the detector, will de-excite or recombine to dissipate their energy in the form of phonons and quasiparticles, which are characterized by energies in the range of meV down to μeV . These can be detected by LTDs at various stages of their final degradation towards thermal equilibrium. Thus LTDs allow for energy resolutions and operational thresholds much lower than detectors that only sense scintillation and ionization. Furthermore, LTDs provide a precise energy measurement owing to the relatively large number of excitation quanta that can be detected. In fact, LTDs designed to measure thermal phonons achieve the highest possible energy resolutions with optimal noise performance.

At thermal equilibrium, energy E deposited in an LTD causes a temperature rise $\Delta T = E/C$ where C is the heat capacity. Thermal equilibrium is characterized by the condition where the average heat flowing to an LTD equals the average heat flowing from the LTD (into a proper heat sink or bath). In this state, the ideal intrinsic energy resolution is determined by the statistical fluctuations in the phonon system. Fluctuations in the total number of phonons in the LTD absorber have variance C/k_B , which yields a minimum resolution of $\Delta E^2 = k_B T^2 C$ to the device energy resolution, where k_B is Boltzmann's constant. Thus, the smaller the heat capacity, the more sensitive the response of the calorimeter and the better the energy resolution. The most relevant feature of this result is that the latter is independent of the energy deposition. The heat capacity itself is the product of the detector volume (V) and the specific heat (c_p). Optimization of LTD response can be achieved by using small detector volumes and materials with low specific heat. Noise contributions from additional sources will increase the variance and are generally parameterized as a multiplicative factor ($\xi \gtrsim 1$) to the variance expression above.

Similarly, the power P from incident particles or radiation can be measured through a temperature rise given by $\Delta T = P/G$, where G is the thermal conductance to a weakly linked bath held at constant temperature. Power fluctuations are limited by G and have a spectral density of $S_P = NE P^2 = 4k_B T^2 G$, where $NE P$ is the noise equivalent power, defined as the power in a 1 Hz bandwidth that gives a response signal with an equal amplitude to the noise. Hence lower conductance yields better sensitivities. To minimize thermal conductance in precise power measurements, weak thermal links can be realized by using thin membranes or by decoupling the electron and phonon systems. However, a compromise must be made. While lower G yields better noise metrics, conversely, larger G is needed to dissipate all incident power (which can be large in the case of CMB detectors) or to have a

faster detector response (the characteristic response time being $\tau = C/G$).

LTDs that measure power are sometimes referred to as *bolometers* in literature, as opposed to *calorimeters* that measure energy, generating some confusion. In principle, there is no clear distinction between a calorimeter and a bolometer. The operation mode is generally determined by the ratio of the characteristic time constant and the average time between the arrival of incident particles or quanta [211]. Yet another convention is to refer to *non-equilibrium* LTDs as those detectors that measure incident energy or power by counting excitations that have energy $\gg k_B T$. In such detectors, energy resolution is determined by the statistical fluctuations of the energy partition, similar to conventional ionization detectors but with a much lower average excitation energy and hence a larger number of excitation quanta.

Table 36.6: Low temperature dependence on temperature (T) for specific heat, based on different material classes. In the table below Θ_D is the Debye temperature and T_C is the transition temperature of the superconductor.

Heat Capacity	Material
$\propto \left(\frac{T}{\Theta_D}\right)^3$	Dielectric and diamagnetic
$\propto T$	Conductor
$\propto \exp\left(-\frac{2T_C}{T}\right)$	Superconductor
$\propto \left(\frac{\mu_B B}{k_B T}\right)^2 \text{sech}^2\left(\frac{\mu_B B}{k_B T}\right)$	Paramagnet (in magnetic field \mathbf{B})

A variety of possible detector materials and sensor technologies makes LTDs very versatile and highly customizable. Dielectric, superconducting and paramagnetic materials are often used owing to the fact that at very low temperatures, the specific heat decreases strongly as a function of T (see table 36.6). Superconductors offer additional advantages: the abrupt change in resistance when a material transitions from its normal to superconducting state enables highly sensitive measures of temperature changes. Additionally, the existence of a small (less than a meV) but distinct energy gap that is required to break a Cooper pair, provides a means to measure energy deposits by counting the resulting quasiparticles (QP). QP relaxation processes are typically faster than thermal processes making these detectors suitable for high-rate photo-counting. In summary, both the sensitivity and energy resolution of an LTD benefit greatly from low temperature operation.

36.5.2 Detector Types

A generalized LTD calorimeter consists of an absorber in thermal contact with a phonon or quasiparticle sensor, and a thermal link to a heat bath at a constant temperature (see figure 36.10). The absorber provides the mass necessary for the interaction of the particle and a fast and complete thermalization of the deposited energy. The sensor accomplishes the task of translating the particle interaction into measurable parameters. It is generally sensitive to equilibrium phonons (e.g. thermistors and MMCs) and thus provides a precise measurement of the temperature. However, non-equilibrium (e.g. STJs) and mixed (e.g. TES) phonon sensors have been devised and implemented in many applications as well. The goal of the thermal link is to cool the absorber down to its equilibrium temperature after the absorption of a particle. In monolithic detectors the thermometer and absorber are identical, while in composite detectors the thermometer is attached to a separate absorber. This basic design applies to single-event particle detection as well as for continuous radiation measurement devices. In the case of the latter, a suitable absorber whose mass is irrelevant, e.g. an antenna at the end of a waveguide, collects the incident power and dissipates it onto a resistive (e.g. Au) film, which is put in contact with a sensor capable of detecting tiny temperature changes (e.g. semiconduc-

tor thermistors, transition-edge sensors, and kinetic inductance detectors, to name a few).

Superconducting Tunnel Junctions (STJs) and Kinetic Inductance Detectors (KIDs) are examples of non-equilibrium detectors. STJs exploit Josephson tunnelling of particles and QPs between two superconductors. The superconductors act as radiation absorbers, and are separated by a thin insulating layer. When such a junction is DC biased at a voltage just below the gap voltage, the excess quasiparticles generated by the incoming radiation are detected as a tunneling-current proportional to the incoming energy. Statistical fluctuations in the tunnelling process limit the energy resolution which is given by:

$$\sigma_E = \sqrt{\varepsilon(F+G)E_0}, \quad (36.5)$$

where $\varepsilon \sim \Delta$, the band-gap, while $F \sim 0.2$ and $G > 1$ are the Fano factor and tunnelling fluctuation respectively. STJs have been proven to be excellent single photon and UV-VIS spectroscopic detectors with near theoretical energy resolutions, high detection efficiencies and excellent time resolution. In astrophysics they are used as mixers to detect radiation in the 100 GHz to 1 THz range by exploiting the non-linear behaviour of their current versus voltage characteristic curve. STJs share similar design elements to charge qubits, which are being used for the development of quantum computers. Such qubits have also recently been used in dark matter searches as single photon detectors to evade the standard quantum limit in measurement noise [212]. Despite their extremely good energy resolutions, STJs cannot be scaled-up to produce sensors with large observing volumes due to readout complexity and the difficulty in uniformly suppressing the superconducting Josephson current, which is superimposed on the QP current.

KIDs exploit the variation of the kinetic energy T stored in a superconductor by Cooper pairs whose inertia acts as an effective inductance, given by:

$$T = \frac{1}{2}nm^*v^2 = \frac{1}{2}LI^2 \quad (36.6)$$

where n is the number density of Cooper pairs, $m^* = 2m_e$ is the Cooper pair mass and $I = 2nev$ is the Cooper pair current. $L = m_e/2ne$ is defined as Kinetic Inductance and is inversely proportional to the number of Cooper pairs [213]. When a KID is placed in series with a superconducting capacitor, the resonance frequency of the circuit will be temporarily shifted by incident radiation, which converts Cooper pairs to QPs, thus changing the effective inductance. The presence and amount of radiation is observed as a change in amplitude or phase of a tuned sinusoidal signal that is sent through the circuit. In practice the change in L is small, and very high Q microwave resonance circuits are needed to sense this variation (hence the name MKIDs, for Microwave-KIDs). Furthermore, only areas of the film where large currents are flowing will be sensitive to pair breaking, thus making the response of a distributed KID position dependent. To overcome this issue, QP trapping (by coupling two superconductors with different band-gaps) is used for absorbing optical photons and X-rays. To detect lower frequencies (e.g. in the 100-1000 GHz range for CMB) a lumped element resonator (LEKID), with little current variation across the device, is used. The device itself, based on a series LC circuit inductively coupled to a microstrip feed line, can act as the absorber as well as the sensing element in a detector system. Macroscopic devices (few mm²) can be fabricated by shaping the inductor in the form of a meander coupled to an inter-digitated capacitor [214]. The theoretical noise limit of these devices is governed by generation-recombination noise and takes the form:

$$NEP_{QP} = 2\Delta \sqrt{\frac{n_{QP}}{\tau_{QP}}}, \quad (36.7)$$

where n_{QP} and τ_{QP} are the QP number and lifetime respectively. KIDs are easy to fabricate, very sensitive, broad band and easily multiplexable: they can be coupled with a single microstrip that simultaneously reads 1000s of detectors resonating at different frequencies. They provide therefore a promising solution

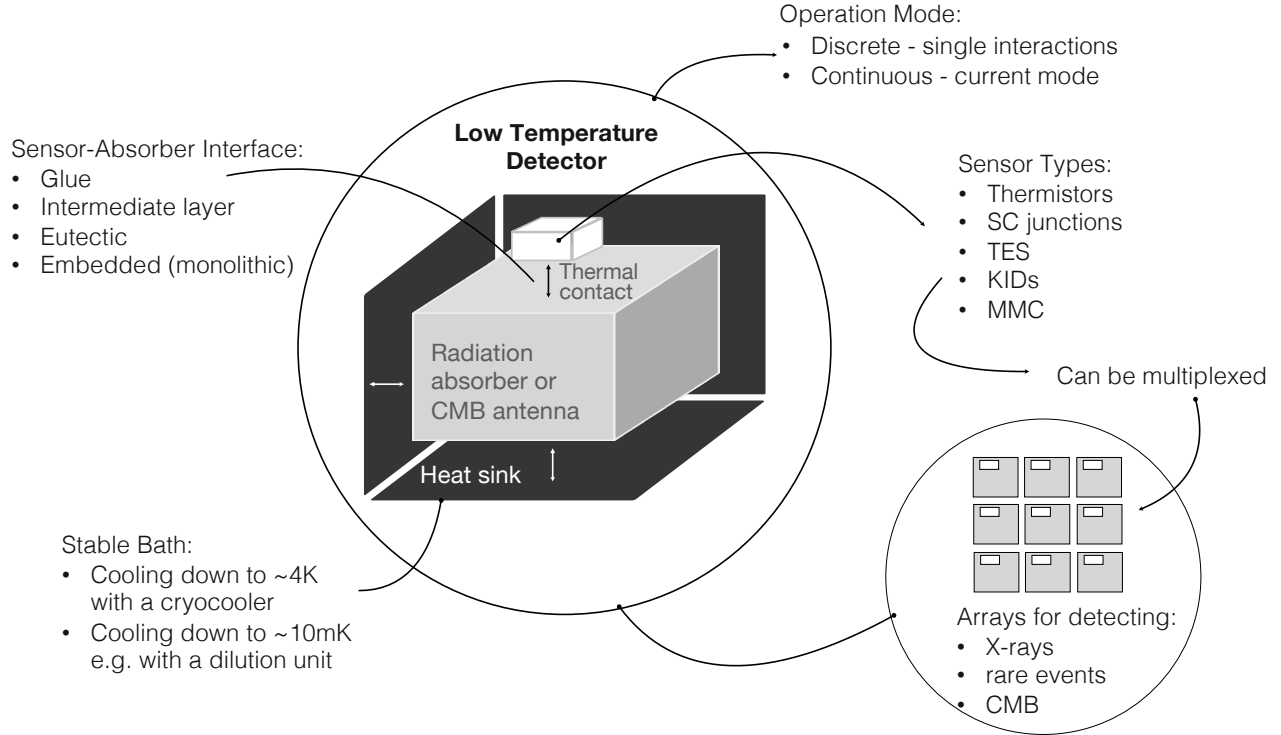


Figure 36.10: A generalized LTD consists of an absorber, a sensor and a thermal link to a stable-temperature bath. Biasing schemes and readout is described in detail in the text for individual sensor types.

for deploying large arrays of detectors with applications to high-energy physics, astronomy or CMB measurements, although there are still some challenges, especially at frequencies below 100 GHz, related to their worse noise performance when compared to other LTDs, and to the choice of materials with a sufficiently small energy-gap.

Semiconductor thermistors are resistive elements characterised by a strong dependence of the resistance on the temperature. Usually, they consist of small crystals of germanium or silicon with a dopant concentration slightly below the metal-to-insulator transition. However, they can also be realized in the form of amorphous films such as NbSi. At low temperatures, their resistivity (ρ) is governed by variable range hopping (VRH) conduction and is described by the expression $\rho(T) = \rho_0 \exp((T_0/T)^\gamma)$, where T_0 and ρ_0 are parameters controlled by the doping level, while γ depends on the compensation level K (ratio of acceptor to donor concentrations). For low values of K , γ is well approximated by $1/4$ while it converges to $1/2$ as K increases.

Semiconductor thermistors are high impedance devices (1–100 M Ω) whose performance is usually parameterized in terms of the logarithmic sensitivity $\alpha = d \log R / d \log T$, typically in the range of 1–10. Silicon thermistors are fabricated using a multiple ion implantation process in high purity silicon wafers to produce a thin and uniformly doped box-like volume. The best germanium thermistors are fabricated starting from bulk, high-purity germanium crystals doped by means of neutron irradiation in the core of a nuclear reactor, referred to as nuclear transmutation doping (NTD). Individual sensors are then produced by dicing the irradiated samples and finishing them by hand. The great advantage of NTDs is the highly uniform doping level over large volumes which results in a better signal to noise ratio with respect to other doping techniques. The doping level depends on the isotopic composition of the starting material and the irradiation time.

The weak coupling to the heat sink can be provided by the electrical leads used for the read-out. However, nowadays microelectronic planar technologies and silicon micromachining are

more commonly preferred, and sensors are suspended on thin silicon nitride membranes or thin silicon beams. Thermistors are read-out in an approximately constant current biasing configuration obtained by inserting large load resistors in the bias circuit, which allows for direct conversion of the thermal signal (ΔT) into a voltage signal (ΔV).

Semiconductor thermistors are very practical to use with some drawbacks. One of these is related to their high impedance which requires a JFET front-end placed as close as possible to the device in order to minimize the signal integration on parasitic electrical capacitances. This can represent a technical challenge, because JFETs must be maintained at significantly higher temperatures ($\gtrsim 100$ K). Furthermore, deviations from the exponential behaviour of the conductivity have been observed at low temperatures. They are usually described in terms of a finite thermal coupling between electrons and phonons which results in an intrinsic limit to the signal rise times, which is of the order of hundreds of milliseconds at temperatures below 100 mK. Nevertheless, semiconductor thermistors are an established and robust technology, and arrays of detectors based on these devices have been widely used for neutrinoless double beta decay searches, neutrino mass measurements and X-ray spectroscopy. Energy resolutions lower than 5 eV have been achieved with Sn or HgTe absorbers.

Superconducting Transition Edge Sensors (TESs) exploit the sharp transition between superconducting and normal conducting phases, yielding a high sensitivity to temperature variations. Temperature perturbations, and hence resistance changes, are sensed as modulations in the current through the TES. TESs are operated in a constant voltage biasing configuration where Joule heating, arising from the current flowing in the TES, decreases with a rise in resistance, which then brings the TES back to its nominal operating temperature. This electrothermal feedback (ETF) is achieved by providing a TES with a voltage bias whose power, $P_J = V_{\text{bias}}^2 / R(T)$, heats the TES to its nominal operation point, the superconducting transition temperature. Operation in ETF mode improves linearity, speeds up response (to

faster than $\tau = C/G$), and in some cases it provides tolerance for T_C (critical temperature) variation between multiple TESs in a large array. The low impedance in this configuration makes them well-suited for readout by SQUID (Superconducting QUantum Interference Device) based amplifiers. Logarithmic sensitivities $\alpha = d \log R/d \log T$ of the order of several hundreds can be achieved. By using different superconductors, or superconductor-metal pairs patterned in suitable shapes, a wide range of resistances, transition temperatures and time constants are obtainable to meet the requirements of the desired application [215].

Nano-TESs are fabricated by lithographic techniques in the form of long (few μm) and narrow (nm) wires that exhibit extremely small NEPs due to their reduced C and G , enabling single-photon sensing. Superconducting Nanowire Single-Photon Detectors (SNSPDs) are similarly patterned superconductors or superconducting bilayers maintained at a temperature well below their T_C . When a DC current just below the critical current is driven through the nanowire, the absorption of a single photon causes the formation of a hot spot that drives the superconductor to a normal conducting state, resulting in a very fast (tens of picoseconds) current pulse through a shunt resistor. For this reason, nano-TESs and SNSPDs are used as single photon detectors for light dark matter and axion searches in applications where large detecting mass is not critical [216].

Magnetic Metallic Calorimeters (MMC) exploit paramagnetic sensors exposed to a weak magnetic field with a weak thermal link to a heat bath. A temperature rise causes a change in the sensor magnetization, which is sensed by a SQUID magnetometer. A common material is an Au:Er mixture, with the addition of a few hundred ppm of enriched ^{166}Er , which is needed to reduce the unwanted contribution of nuclear magnetic moments of other Er isotopes. The read-out is non-dissipative and avoids the noise sources common to the dissipative devices. The use of a metallic host ensures relatively fast time response, since the typical spin-electron relaxation times are of the order of 0.1 microseconds at ~ 50 mK [217]. For an optimized MMC, the energy resolution is given by $\Delta_E = \sqrt{2k_B T^2 C (\tau_0/\tau_1)^{1/4}}$, where τ_0 (order of micro second) and τ_1 (order of milli second) denote the signal rising and decay times respectively [207]. In order to obtain a fast and efficient energy thermalization, MMC are typically fabricated from gold. The intrinsically large heat capacity of the paramagnet does not spoil the temperature sensitivity and allows the use of relatively large gold absorbers without degrading the device performance. Furthermore, thermal isolation from the heat sink is not generally an issue. Owing to the simple concept of these devices, MMC can be precisely customized and fabricated by employing standard microtechnology. Planar MMC arrays characterized by an excellent energy resolution, large dynamic range and good linearity have been successfully used for the detection of soft X-rays.

Performance and technological constraints limit the maximum size of LTDs. To improve overall experimental sensitivities, a large number of sensors must be deployed, typically at temperatures of a few tens of mK, where cooling power is limited to a few μW . To reduce the readout complexity and the heat load at the colder stages, multiplexing (MUX) techniques are often employed. Multiplexing consists of reading multiple detectors out through a limited number of lines that traverse room temperature to cryogenic temperatures [218]. In frequency-domain multiplexing (FDM), a tuned superconducting LC circuit is placed in series with each sensor, and a frequency comb of AC biases (usually in the MHz range) is sent to a group of sensors in parallel. A synchronous demodulation of the amplified current signal allows the recovery of the resistance variation of each detector. Microwave-multiplexing (μMUX) represents a variation of this concept, based on the usage of rf-SQUIDS, where the frequency comb is in the GHz range. Alternatively, the signal from a single detector can be recovered by readout of one detector at a time (time-domain multiplexing, TDM). KIDs have been gaining popularity owing to the fact that they naturally form resonant circuits, hence multiplexing in the frequency domain is readily achieved by adjusting their capacitance.

36.5.3 Experimental Applications

LTDs are sensitive over a wide range of energy, from centimetre wavelength ($\sim \text{meV}$) through the visible spectrum ($\sim \text{eV}$) up to the X-ray domain ($\sim \text{keV}$) and beyond. Several broad categories of LTD applications towards measurements of fundamental physics are described in more detail in the text below and summarized in tables 36.7 and 36.8.

Bolometric detectors are favored as microwave detectors owing to their nearly constant response over frequency, playing an important role in far-infrared astronomy and in the survey of the cosmic background radiation. The high-frequency instrument of the Planck satellite (HFI) used spiderweb bolometers read by NTD-Ge thermistors, but current experiments use mainly TESs or, more recently, KIDs. Depending on the objective of the experiment, antenna coupling or absorber coupling is used. In the former case, the bolometer detects one polarization and one (or a few) modes of the radiation, while absorber-coupled bolometers do not distinguish between polarizations. In order to avoid the absorption or emission from Earth's atmosphere, many (CMB) instruments are operated by observatories located at high altitude, dry places (such as the Atacama desert or Antarctica), balloon-borne platforms, or from space. In Table 36.7, we list a subset of the ongoing or planned CMB experiments (see Section 29 of this Review for the details on present challenges). In the Atacama desert in Chile, CLASS is taking data, POLARBEAR is being upgraded to Simons Array and ACTPol is being upgraded to AdvancedACT-Pol, the next big step being the deployment of the Simons Observatory. At the South Pole, SPTPol has been upgraded to SPT-3G, while BICEP3 and BICEP array will constitute the South Pole Observatory. The most powerful upgrade in terms of both size and sensitivity will be CMB-S4, a consortium of telescopes both at the Pole and in Chile. In the Canary islands, QUIJOTE and GroundBIRD are operating and LSPE/STRIP is in preparation. QUBIC has recently started operations in Argentina and AliCPT is in preparation in Tibet. Regarding balloon projects, SPIDER and EBEX were already launched while LSPE/SWIPE and PIPER will be in the near future. Finally from space, after the success of Planck, LiteBIRD has been selected by the Japan Aerospace Exploration Agency (JAXA) as the next strategic large mission to be launched in the 2020s.

The incoming radiation couples directly to the antenna probes (as in BICEP/Keck) or through micro-machined horn waveguides (AdvancedACT-Pol, CLASS) or lenslets (Simons Array, SPT-3G), depending on the frequency range. All of these experiments have focal planes with hundreds to hundreds of thousands of sensors. To optimize focal plane occupancy, multi-mode or multi-choic, dual polarization sensitive detectors are used. In the former case, the sensitivity is enhanced by collecting power from a larger number of modes at the expense of angular resolution. In the latter, one single mode of the radiation is focused on a broad band antenna, and on-chip polarization separation and band-pass filters split the signal in different frequency bands directing the power to different absorbers and sensors.

Experimental design is driven by a trade-off between the sensitivity and the complexity of the production processes and readout. On the one front, single-sensor NEP at the level of $10^{-21} \text{ W}/\sqrt{\text{Hz}}$ has been achieved in laboratories and research centers. Meanwhile, efforts are in place for the industrialization of the fabrication processes, which is essential for scaling up production for the large number of detectors needed for future experiments.

Massive cryogenic calorimeters have been proposed since the 1980's as particle detectors for the search of rare processes (e.g. dark matter, neutrinoless double beta decay) [219]. Almost simultaneously, the use of arrays of small mass calorimeters was suggested for X-ray astrophysics [220] and precision measurements of the neutrino mass [221, 222]. Although essential to understanding the nature of neutrinos, neutrinoless double beta decay (NDBD) has eluded discovery (or definitive exclusion) for over 50 years. Calorimetric techniques provide the best sensitivities to NDBD. However, before the advent of low temperature calorimeters (LTC), only a few isotopes (^{48}Ca , ^{136}Xe and ^{76}Ge) could be utilized for NDBD studies with the calorimetric approach. This limitation was removed by the advancement of LTC's, and in par-

Table 36.7: Some selected experiments using LTDs to measure the CMB. These experiments constrain the physics of inflation and the absolute mass, hierarchy, and number of neutrino species. The experiment location determines the part of the sky that is observed. The size of the aperture determines the angular resolution. The table also indicates the type of sensor used, the number of sensors, the frequency range, and the number of frequency bands. Data for planned upgrades or future experiments are provided in parentheses.

Sub-K CMB Experiment	Location	Aperture	Sensor type	# Sensors (planned)	Frequency (planned)	Bands (planned)
Ground-based						
Atacama Cosmology Telescope (2007–)	Chile	6 m	TES	5,614	30–230 GHz	5
BICEP/Keck (2006–)	South Pole	26/68 cm	TES	2,500	95–270 GHz	6
CLASS (2015–)	Chile	60 cm	TES	3,488	40–220 GHz	4
GroundBIRD (2021–)	Canary Island	30 cm	MKID	322	145–220 GHz	2
POLARBEAR / Simons Array (2012–)	Chile	3.5 m	TES	1,274 (22,764)	150 GHz (90–280 GHz)	1 (4)
South Pole Telescope (2007–)	South Pole	10 m	TES	16,260	90–220 GHz	3
Simons Observatory (2022–)	Chile	6 m/0.5 m	TES	(60,000)	(27–280 GHz)	(6)
CMB-S4 (2024–)	Chile + South Pole	21 telescopes	TES	(500,000)	(20–280 GHz)	(11)
Balloon						
EBEX (2013–)	McMurdo	1.5 m	TES	~1,000	150–410 GHz	3
PIPER (2016–)	New Mexico	2 m	TES	5,120	200–600 GHz	4
SPIDER (2014–)	McMurdo	30 cm	TES	1,959	90–280 GHz	3
LSPE (2022–)	Longyearbyen	60 cm	TES	(326)	(140–270 GHz)	(3)
Satellite						
Planck HFI (2003–2013)	L2	1.5 m	NTD	52	100–857 GHz	9
LiteBIRD (2028–)	L2	20–40 cm	TES	(4,508)	(34–448 GHz)	(15)

ticular by CUORE, which takes advantage of the naturally high abundance of ^{130}Te in TeO_2 crystals. Additionally, the operation of CUORE at LNGS [223] has demonstrated that the technical challenges of operating ton-sized LTD detectors in a deep, underground location are surmountable. Currently, the most promising future approach is based on the hybrid approach of scintillating LTCs, which unfortunately cannot be used for ^{130}Te . Now, new projects are being proposed based on different scintillating compounds. In particular ^{100}Mo is the choice of CUPID [224] (NTD thermistors glued to $\text{Li}_2^{100}\text{MoO}_4$ crystals), which will use the same infrastructure of CUORE and follows from the successful operation of several demonstrators (CUPID-0 [225] and CUPID-Mo [226]), and AMORE (MMC sensors on $\text{Ca}^{100}\text{MoO}_4$ or $\text{Li}_2^{100}\text{MoO}_4$ crystals) [227]. With an energy resolution comparable to germanium diodes and a mass of the order of a ton, these experiments aim to probe the inverted hierarchy of neutrino masses. The slow response of these detectors is still a dominant limitation because pile-up may prove to be a serious background. Extremely pure materials, careful assembly procedures, and deep underground laboratories are therefore necessary.

In the 1980's, the calorimetric technique was recognized as a feasible approach to make a direct measurement of the neutrino mass from the end-point of a beta spectrum. Thus, LTCs were proposed as a possible alternative to the standard spectrometric measurements [228]. Calorimetric measurements offer a number of advantages: i) a weak dependence on the final excited states, ii) no source effects (e.g. self-absorption), and iii) lack of back-scattering from the detector. Therefore LTCs provide a faithful reconstruction of the beta spectral shape over a broad energy range below the end-point. However, the difficulty in resolving a small fraction of the spectrum near the end-point is a serious limitation that strongly constrains the source strength and the statistics that need to be accumulated. Such an inconvenience can be mitigated by selecting beta emitters with a small Q value, owing to the fact that the fraction of counts in an interval, δ close to Q, scales as $(\delta/Q)^3$. However, this is generally at the cost of choosing decays with more complex nuclear transitions. In addition, LTCs may be affected by specific systematics (e.g. solid state effects). Ultimately it is recognized that spectrometers and

calorimeters have complicated but different systematic effects. It is therefore critical to develop complementary experiments exploiting both techniques.

LTCs were initially proposed as perfect calorimeters to measure the energy spectrum of a low Q beta emitter embedded in an absorber. However, the requirements of excellent energy resolution and a low rate (to avoid pileup) requires a very large number, $O(10^4 - 10^6)$, of small mass devices (micro-calorimeters). Early experiments used ^{187}Re , which is a long-lived beta emitter that is naturally abundant in rhenium samples and is characterised by a very low Q value (2.4709 keV [229]). A large number of ^{187}Re based experiments have been developed over the years (MANU [230], MIBETA [231], MARE [232]). Nowadays a different approach is preferred and is based on the measurement of the atomic radiation following electron capture, typically in ^{163}Ho which is also characterized by a very low Q (2.837 keV [233]). Different experiments have been proposed to face the challenge: ECHO in Germany [234] (using MMC sensors), HOLMES in Italy [235] and NUMECS [236] in the US (using TESs). The very large number of microcalorimeters needed to obtain sensitivities comparable to spectrometric measurements is a serious challenge, both for the readout and the thermal heat load. An alternative readout based on the use of KIDs, for their multiplexing capability, has been proposed and is presently under development.

Traditional searches for WIMP-like dark matter aim to measure the scatter of a massive dark matter particle off of a target nucleus. Similar to detectors employed for neutrinoless double beta decay, these searches benefit from large-mass absorbers for the target because the dark matter interaction rate scales directly with the number of nuclei in the target and hence its mass. Among the most successful experiments to date, are those that combine the detection of phonons with another channel such as ionization energy (EDELWEISS and SuperCDMS) or scintillation light (CRESST). This simultaneous, dual measurement takes advantage of the fact that the energy deposited in the absorber is partitioned into these channels differently depending on whether the initial particle interaction produces electron or nuclear recoils (or both). This particle identification allows for the rejection of background from natural sources of radiation, which most commonly

Table 36.8: Selected experiments using low temperature calorimeters. The table shows currently or soon-to-be operating experiments that will search for dark matter or neutrino properties. The dates refer to the start of the program.

Sub-K Experiment	Location	Detection mode	Absorber (Total mass)	Sensor type	# Sensor # Crystal
WIMPs					
CRESST III (2016)	LNGS Italy	Athermal phonon and scint.	CaWO ₄ /Al ₂ O ₃	TES	10
EDELWEISS † ($_SubGeV$)	LSM Modane France	Thermal phonon and ion.	Ge	NTD Ge	-
SuperCDMS (2023)	SNOLAB Canada	Athermal phonon and ion.	Ge/Si	TES	24
Neutrino mass					
ECHO [234] (2012)	Heidelberg Germany	Thermal phonon	Au: ¹⁶³ Ho (0.2 μ g)	MMC	16
HOLMES [235] (2015)	Milan Italy	Thermal phonon	implanted ¹⁶³ Ho (18 μ g)	TES	1000
NUMECS† [236] (2015)	LANL USA	Thermal phonon	implanted ¹⁶³ Ho	TES	4096
$0\nu\beta\beta$ decay					
CUORE [223, 237] (2015)	LNGS Italy	Thermal phonon	^{nat} TeO ₂ (741 kg)	NTD Ge	988
CUPID [224] (2015)	LNGS Italy	Phonon and scint.	Li ₂ ¹⁰⁰ MoO ₄ (450 kg)	NTD Ge	1596
AMoRe-I [227] (2018)	Y2L South Korea	Phonon and scint.	Ca ¹⁰⁰ MoO ₄ /Li ₂ ¹⁰⁰ MoO ₄ (6 kg)	MMC	13/5

†No payload size quoted for experiments that are primarily in R&D phase.

manifest themselves as electron recoils in the detector.

In recent years, multi-ton liquid noble detectors have outclassed LTD-based technologies in searches for heavy (>10 GeV/ c^2) dark matter owing to their ability to more easily and cheaply scale to large target masses. However, the lower thresholds achieved by LTDs continue to make them the technology of choice for low-mass dark matter searches. New advances have enabled these detectors to reach much lower energy thresholds than previously obtained, albeit sometimes at the cost of being able to detect energy in more than one channel as described above. For example, the use of an electric field to generate Neganov-Trofimov-Luke [238, 239] phonons in proportion to the applied voltage, has enabled the detection of single electron hole pairs in Si detectors with thresholds as low as a few eV (SuperCDMS HVEV). This and similar advances in Ge LTDs (EDELWEISS_SubGeV) have enabled sensitive searches for dark photons and dark matter that scatters off electrons [240, 241]. Next generation experiments such as SPICE/HERALD aim to further optimize the intrinsic energy resolution of TES detectors, coupled with a strategic choice of target materials (superfluid He and polar crystals) to enable sensitivities to dark matter with masses below an MeV/ c^2 [242]. Current state-of-the-art axion searches use SQUID based quantum amplifiers such as Josephson Parametric Amplifiers along with resonant cavities operating below 100 mK to look for a signal above fluctuations in the thermal noise [243]. Future axion experiments are also working to close the sensitivity gap between particle and wave-like dark matter with the help of LTDs. Broad-band axion searches in the THz range are being proposed, which will make use of TES, SNSPDs or KIDs for single photon detection [244]. Finally, LTD-based dark matter detectors are also actively employed to study coherent neutrino scattering, owing to the fact that the hypothesized signal from dark matter-nucleus scattering is nearly identical to that from neutrino-nucleus scattering, with both inducing nuclear recoils in a similar energy range [245, 246].

36.6 Low-radioactivity background techniques

Revised October 2023 by Al. Ianni (INFN, LNGS) and S. Schönert (Munich Tech. U.).

36.6.1 Introduction

The study of rare phenomena in fundamental physics, such as proton decay, neutrinoless double beta decay, dark matter,

and MeV-scale neutrino interactions, requires extremely low levels of background radiation. Experiments searching for these rare events record electron recoils or nuclear recoils in the energy scale from a few eV to several MeV. The detector technologies used are multiple from organic and cryogenic liquid scintillators, to bolometers, solid state calorimeters, gaseous detectors, and crystal scintillators. As far as the background contamination is concerned at some extent the application defines the requirements, although the common denominator is that an extreme reduction of all background sources is essential. Leading experiments in rare events search have obtained in the region-of-interest (ROI) a background as low as $\sim 10^{-4}$ cts/kg/y/keV. As a first and crucial step, a dedicated radio-purity assay of the detector set-up components has to be carried out. Over the last fifty years, special screening and cleaning techniques have been developed to measure and mitigate ultra-low levels of background. In order to characterize the background sources we refer to Heusser [247] and identify the following five main categories:

- environmental radioactivity in the location where the detector is installed;
- radioimpurities in the detector and shielding;
- radon and its progenies;
- cosmic rays and induced radioactivity;
- neutrons from natural fission, (α, n) reactions, and from cosmic-ray muons interactions.

The energy range affected by these background sources is mainly <10 MeV. All materials contain traces of long-lived primordial radioimpurities, such as ²³⁸U, ²³²Th, ²³⁵U (²³⁸U/²³⁵U ~ 138), and ⁴⁰K (⁴⁰K/ K^{nat} $\sim 1.17 \times 10^{-4}$). We recall that 1 ppt of ²³⁸U and ²³²Th corresponds to 12.36 and 4.06 μ Bq/kg, respectively; 1 ppb of K^{nat} corresponds to 30.25 μ Bq/kg. In the Earth's crust the abundance of uranium and thorium is of the order of 1 – 10 ppm which corresponds to about 10 – 100 Bq/kg. Taking into account these contamination levels and the low background requirements, a fundamental background reduction and mitigation is essential to carry out rare phenomena research.

Besides primordial radionuclides other radioactive elements are produced through interactions with matter of secondary cosmic ray particles. Among these so-called cosmogenic radionuclides we recall, in particular, ³H, ¹⁴C, ⁷Be, ³⁹Ar, ⁴²Ar, and, in copper, steel and iron often used as shielding materials, ^{57,60}Co.

A third category of background source in our environment consists of anthropogenic radionuclides. These are artificially produced mainly through nuclear reactions in nuclear power plants, nuclear fuel reprocessing plants, and nuclear weapons testing. Anthropogenic background elements of concern for rare phenomena are ^{85}Kr , ^{137}Cs , ^{241}Am , ^{60}Co , and ^{90}Sr . The concentration of ^{85}Kr ($T_{1/2}=10.76\text{ y}$, $Q_{\beta}=687\text{ keV}$) in air has been slowly increasing since World War Two with a present activity of order 1 Bq/m^3 . As a consequence ^{85}Kr is a crucial background in experiments making use of nitrogen, xenon, and argon from air.

Once detector components radioactive backgrounds have been assayed and reduced by a careful selection campaign, which can last several years, a further step to push the background level beyond the screening possibilities is needed to reach the required sensitivity. For this purpose special active vetos, purification methods, and offline analyses have been developed. A meticulous background understanding and mitigation is crucial to explain any possible signal excess which may be detected. Background mitigation techniques are based on:

- use of radio-pure materials that absorb ionizing radiation;
- identify radio-pure material for detector construction;
- perform advanced surface and sub-surface cleaning treatment;
- reduce muon flux with underground detector deployment and using active vetos;
- exploit advanced detection and tagging techniques to discriminate signal from background.

In the following we describe radio-assay and background mitigation techniques developed and exploited in the framework of rare phenomena searches in deep underground laboratories.

36.6.2 Radio-purity assay

The radio-purity assay of detector components is a basic prerequisite to be carried out in low counting experiments. Several techniques are exploited for radio-purity assay. They are complementary to characterise the radio-purity of materials for shielding or core detector components. Next generation experiments radioassay campaign requires a considerable effort and organization for several years [248–251].

Gamma spectroscopy (GS) via high purity germanium (HPGe) detectors is a powerful and crucial technique [247]. It is non-destructive and thanks to the energy resolution allows to distinguish various radionuclides elements. Radiation from ^{238}U and ^{232}Th comes with all decay products in the radioactive chains. However, if secular equilibrium is broken, this crucial information can be addressed by separating different gamma-ray lines characterizing elements in the decay chains. In the ^{238}U chain one can have three sub-chains out of equilibrium. The first sub-chain can be assessed through ^{234}Th direct progeny of ^{238}U . The second sub-chain, which originates from ^{226}Ra , can be probed by ^{214}Pb and ^{214}Bi . A third sub-chain, which starts from ^{210}Pb , cannot be efficiently probed by GS, yet is of crucial importance and alternative methods must be used. In the ^{232}Th chain again one can probe two sub-chains which can be out of secular equilibrium: the first one through ^{228}Ac from ^{228}Ra ; the second from ^{228}Th can be measured through ^{212}Pb , ^{212}Bi and ^{208}Tl . The technology for HPGe operated in deep underground counting facilities [252, 253] or in shallow laboratories with an efficient active veto shielding [254] has been boosted to sensitivities of the order of $10\text{--}100\ \mu\text{Bq/kg}$ by carefully selecting detector components, electronics and sample handling systems. The HPGe screening method requires order of $\sim 0.1\text{--}a\text{ few kg}$ of material, and weeks of acquisition to produce a reliable measurement.

A second crucial technique is based on inductively coupled plasma mass spectrometry (ICP-MS) [255]. This technique can probe primordial parent activities at the level of $1\ \mu\text{Bq/kg}$. It is a destructive method and often needs special sample preparation on a small quantity of material. The ICP-MS does not measure the radioactive decay of isotopes but determines their concentration. At present, it is the most sensitive and rapid screening technique which allows to select materials at sub-ppt level of impurities. The drawback is that ICP-MS cannot assess whether the uranium and

thorium chains are out of equilibrium and to reach ultra-high sensitivities one needs to carefully prepare and handle the samples in a cleanroom environment. ICP-MS screening must be coupled with other methods to properly assess the radio-purity of materials in the context of rare events searches. The Glow Discharge Mass Spectroscopy (GDMS) is a trace element analysis technique somehow alternative to ICP-MS. An advantage of GDMS is the possibility to determine the bulk composition of the sample, assuming homogeneity. Sensitivities of the order of 10 ppt can be achieved.

A third screening technique is based on neutron activation analysis (NAA) [256]. A sample exposed to a neutrons flux can be activated to form radioactive isotopes which can be detected using HPGe detectors or ICP-MS. Considering the difficulties to irradiate samples, this method is less often used. NAA can probe sensitivities at the level of $0.01\ \mu\text{Bq/kg}$.

In case out of secular equilibrium conditions are measured for uranium and thorium from GS screening, a rigorous assessment cannot avoid radon emanation measurements. This matter is discussed in Section 36.6.3.

Complementarity between radio-purity assay techniques is a crucial parameter to design detectors for rare phenomena searches. As it has been pointed out above, requirements can be more stringent than the best sensitivity which can be obtained with the current radioassay techniques. In these cases, a number of prototype detectors have been built and operated to prove the feasibility to reach ultra-low backgrounds.

36.6.3 Radon and its progeny

Radon is considered to be rare in nature because most of its isotopes are short-lived. However, ^{222}Rn ($T_{1/2}=3.82\text{ d}$) is of particular concern in our context. ^{222}Rn is produced by ^{226}Ra and is a radioactive noble gas which can move within active detector components. ^{222}Rn daughters are heavy metals which can deposit on surfaces. Diffusive ^{222}Rn , supported by ^{226}Ra , can deposit on surfaces the long-lived ^{210}Pb , which is a major concern for low counting experiments. In addition, due to $\sim 100\text{ keV}$ nuclear recoil energies from alpha decays in the ^{226}Ra sub-chain, eventually ^{210}Pb can be implanted into a sub-surface layer of a material exposed to radon. This sub-surface contamination can remain even after surface cleaning. Surface contamination of ^{210}Pb is a serious background for direct dark matter experiments through alpha decay of ^{210}Po , which can generate neutrons by (α, n) reactions. Low energy beta/gamma emissions from ^{210}Pb are also a concern. Therefore, radon-free cleanrooms are essential for the assembly of the detector components. Effective radon abatement systems are available for this purpose.

In assembling and commissioning rare events experiments, special care must be dedicated to the estimate of radon emanation of the materials and continuous radon monitoring. For this purpose different methods for radon assay have been developed and exploited since the beginning of solar neutrino observations. ^{222}Rn atoms are collected inside an exhalation chamber for several half-lives before adsorption and counting. Detection limits of the order of $100\ \mu\text{Bq}$ (about $50\ ^{222}\text{Rn}$ atoms) can be obtained with $\sim 50\text{ l}$ stainless steel electro-polished chambers [257]. This limit can be pushed down to $30\ \mu\text{Bq}$ for 1-liter scale chamber. Emanation of large vessels (cryostats, storage tanks, purification columns) can be determined by collecting exhaled radon into transportable charcoal traps [258]. The same method can be used for liquid samples. In this case instead of evacuating the exhalation chamber into a charcoal trap, He is flushed through a sparger tube for about 10 times the volume of the liquid used. Sensitivities of the order of $10\ \mu\text{Bq/kg}$ have been reached.

Nitrogen or synthetic air is often used in rare events experiments for purging, stripping, and assembling the experimental apparatus. These gases might contain radon. In gases ^{222}Rn can also be detected using electrostatic collection of ^{218}Po and ^{214}Po [259, 260]. Sensitivities of the order of mBq/m^3 can be obtained. In Borexino three grades of nitrogen purity were used: regular purity, high purity, and low argon and krypton purity. The regular purity is obtained from boil-off gas and has radon, measured with the method reported above, at the level of $< 100\ \mu\text{Bq/m}^3$. For stripping the purified liquid scintillator a higher purity is needed.

To remove radon from regular purity nitrogen a dedicated absorber plant has been built. This system can reduce radon by a factor of 100. Finally, we mention that not only radon is found in nitrogen. For specific applications the long-lived ^{39}Ar and ^{85}Kr in nitrogen are an important source of background.

36.6.4 Surface backgrounds

Surface contamination of long-lived ^{222}Rn daughters can be challenging in low-counting experiments. Considering required sensitivities of the next generation experiments, this source of background has to be properly quantified and mitigated. Therefore, exposure to ^{222}Rn should be monitored and limited to reduce build-up of ^{210}Pb on surfaces. In addition, ^{222}Rn exposure could also produce sub-surface contamination as discussed in Section 36.6.3. For one cannot avoid radon contamination in many circumstances during production of detector components, it is crucial to quantify the effectiveness of cleaning aiming at removing surface contamination of ^{210}Pb , ^{210}Bi , and ^{210}Po . A simple cleaning procedure, which implies degreasing, wiping, and rinsing the material surfaces is not effective in removing these surface contaminants. Studies of cleaning procedures have been carried out exposing stainless steel, copper and other materials to a strong radon source. Etching and electropolishing with subsequent passivation and rinsing have been investigated in great details. Several recipes for etching and electropolishing have been proposed [261]. Electropolishing has been shown to be very effective in reducing ^{210}Pb , ^{210}Bi , and ^{210}Po from both copper and stainless steel by a factor greater than 100. Etching, which is easier to perform than electropolishing, followed by passivation and rinsing with deionized water is effective in reducing ^{210}Pb and ^{210}Bi by a factor between 50 and 100. However, it is less effective for ^{210}Po , which in copper is very poorly reduced. Removing ^{210}Po from surfaces is crucial, therefore, naturally ^{210}Po contaminated copper and stainless steel surfaces have been deeply investigated with a high sensitivity (1 mBq/m^2) alpha spectrometer [262]. After multi-etching steps (≥ 3), followed by a passivation, a reduction of order 100 has been obtained. On the contrary, static etching (single step) is poorly effective. Electropolishing, or multi-etching are recommended in case copper is in direct contact with the active core of the detector and ultra-high radio-purity is essential or when copper electroforming cannot be used. Electroplating of a thin layer of high radio-pure copper onto the surface of less radio-pure copper has also been investigated to mitigate surface background [262]. This technique is shown to be efficient in reducing surface activity of ^{210}Po when electroformed copper is used [262].

Besides copper and steel other materials often used, such as polyethylene and teflon, have been investigated to understand how to reduce radon plate-out contaminations [263].

As far as surface contamination is concerned particulate fallout in cleanroom environments could be of concern. In general, chemical composition of dust reflects local composition of soil and dust. This is not necessarily true in cleanroom spaces, where the composition of dust depends on ongoing activities and handled materials [264]. The rate of fallout is an important information in the framework of rare events experiments, where assembling is performed in cleanrooms. The ^{210}Pb contamination, inferred from stable lead measured by ICP-MS, due to dust fallout has been investigated [264]. This contamination has a different origin with respect to ^{210}Pb from radon progeny implantation. Ultimately, one can conclude that radon exposure is more crucial than dust fallout. Therefore, the best practice for rare events experiments to face surface background contamination is to perform cleaning and assembling in a radon-free cleanroom environment.

36.6.5 Mitigation of backgrounds and active background discrimination

In this Section we discuss a selection of different background mitigation techniques used in experiments to search for rare events in deep underground laboratories. This includes both the avoidance or reduction of specific radioactive contamination, as well as active background suppression techniques based on specific event features and topologies.

- *Mitigation of ^{222}Rn daughters deposition.* In dark matter

direct search radiogenic (α, n) reactions due to radioactive decays are of great concern. The emitted neutron can mimic a nuclear recoil induced by a dark matter particle interaction. In the DarkSide-50 and LUX-ZEPLIN (LZ) experiments to mitigate this background, cleaning of parts and assembling of the dual-phase Time Projection Chamber have been carried out in a radon-free cleanroom with ^{222}Rn activity of the order of $\lesssim 50\text{ mBq/m}^3$.

- *Underground argon.* Liquid argon is an excellent scintillator to search for dark matter interactions due to the high electron-recoils rejection power through pulse shape discrimination. Events from $\beta-\gamma$ background can be rejected at the level of 10^7 or better with respect to nuclear-recoils. Liquid argon is very effective as active shield and has been used in experiments for neutrinoless double beta decay. However, a major drawback for dark matter search using argon as a target is due to the fact that atmospheric argon contains about 1 Bq/kg of cosmogenic ^{39}Ar ($T_{1/2}=269\text{ y}$, $Q_{\beta}=565\text{ keV}$) [265]. For neutrinoless double beta decay search using argon as an active veto, ^{42}Ar ($T_{1/2}=32.9\text{ y}$, $Q_{\beta}=599\text{ keV}$) with its short lived progeny ^{42}K ($T_{1/2}=12\text{ h}$, $Q_{\beta}=3525\text{ keV}$) is a major source of background. ^{39}Ar limits significantly the dark matter and ^{42}Ar the neutrinoless double beta decay sensitivity search. Therefore, a source of argon with reduced ^{39}Ar and ^{42}Ar is crucial. Centrifugation or differential thermal diffusion are established methods to separate $^{39/42}\text{Ar}$ and ^{40}Ar . However, this is an expensive method for a large fiducial mass. Argon from underground natural gas reservoirs is shown to contain low ^{39}Ar [266], and it is expected that ^{42}Ar is similar or even strongly reduced. Therefore, the use of underground argon mitigates the $^{39/42}\text{Ar}$ backgrounds. DarkSide-50, with a mass of 150 kg of underground argon, has shown that this source of argon contains ^{39}Ar at a level reduced by a factor of $(1.4 \pm 0.3) \times 10^3$ with respect to atmospheric argon [267]. DarkSide-20k and LEGEND-1000 are planning to exploit underground argon from the Urania facility with a production capacity of 330 kg/day [268]. The former to reduce ^{39}Ar and the latter ^{42}Ar .
- *Electro-formed copper.* High radio-purity copper is often used as shielding and as core detectors components. The radioimpurities in the copper can be a dominant source of external background. Copper electro-forming is a technique used to reduce this background component in rare events experiments. Copper electro-forming is a well known process to obtain ultra-high radio-purity copper. This technique has been used in the framework of the Majorana experiment to search for neutrinoless double beta decay and in ANAIS to search for dark matter annual modulation. Sub-ppt levels in uranium and thorium have been achieved with electro-formed copper [269].
- *Background suppression using topological event information.* In addition to rigorous selection of high-purity target and shielding materials from external radiation, additional active suppression techniques must usually be employed in low background experiments to achieve the appropriate experimental sensitivities. While signal and background events may be indistinguishable if only their energy deposition is measured, their event features may differ significantly in time and space. Liquid scintillators use the characteristic photon emission time distributions to distinguish between electron- and alpha-like signals [270] and nuclear recoils [271], respectively. High-purity germanium detectors use the time evolution of the induced charges to separate point-like signal candidates for neutrinoless double-beta decay events from background signals induced, for example, by gamma interactions with multiple interactions within a crystal, or from β or α events on the n+ or p+ electrodes [272]. The operation of bare high-purity germanium detectors in an instrumented liquid argon shield enabled the GERDA and LEGEND experiments to identify backgrounds with signal-like event topology within the HPGe detectors, but with characteristic energy deposition in the surrounding liquid argon. These synergistic back-

ground suppression techniques enabled for a first time ever a quasi background-free search for neutrinoless double beta decays with GERDA [273].

EXO-200 [190] exploited topological event information distinguishing single-site against multi-site events with a liquid xenon TPC for neutrinoless double beta decay in ^{136}Xe to reject background and thereby enhancing signal discovery sensitivity. With a gas xenon TPC the NEXT experiment will fully exploit the differences in the spatial ionization patterns of double beta decay and single electron events [274]. The former is characterized by two Bragg peaks at opposite ends of the tracks, the latter on the contrary displays only one peak. The combination of topology information and good energy resolution offer a powerful tool for background rejection. In general, the 3D reconstruction of detected events in a multivariate fit, which accounts for spacial surface and bulk distributions of signal and background together with other properties, such as pulse shape and topological features, is a powerful tool for background mitigation.

- *Signal selection in direct Dark Matter experiments.* In direct dark matter experiments electron recoil events have to be mitigated with respect to nuclear recoil events. In semiconductor bolometers, operating at a few tens of mK under a bias electric field and used as calorimeters, drifting charges produce a large phonon signal proportional to the ionization, which allows to discriminate electron recoils by the combination of charge and phonon signals [275]. In scintillating bolometers the phonon and light signals are used for the same purpose [276]. Cryogenic scintillators, such as xenon and argon, in time projection chambers offer a strong electron recoils background mitigation through the detection of a primary scintillation signal in liquid and a secondary signal in gas from the drift and extraction of ionization electrons. This background mitigation technique is also being used for neutrinoless double beta decay with ^{136}Xe . The accurate fiducialization and good rejection of multiple-scattering events allow dark matter optimized experiments to attempt a search for this very rare phenomenon.
- *Neutron tagging.* Present and next generation experiments need large neutron tagging detectors. In DarkSide-50 a dedicated active veto has been developed to both suppress and measure *in situ* the rate of neutron-induced background events [277]. The detector consisted of a boron-loaded liquid scintillator, which served both as shielding against γ -rays and as a tag for neutrons. Neutrons are thermalised and captured on ^{10}B . Experimental data has shown a neutron rejection power greater than 99.1% with 5% concentration of TMB in 30 tonnes pseudocumene-based liquid scintillator. The LZ direct dark matter detector with a central TPC of 7 tonnes of liquid xenon makes use of an outer Gd-loaded liquid scintillator neutron tagging veto, which works similarly to the DarkSide-50 veto, replacing boron with gadolinium. The 22 tonnes liquid scintillator is based on linear alkyl benzene (LAB) as solvent. This detector has been designed to operate with a neutron tagging efficiency greater than 95%. The nuclear-recoil background is reduced by a factor of 10. The XENONnT detector is making use of a cylindrical stainless steel tank filled with Gd-loaded water, which surrounds the cryostat with a TPC of 5.9 tonnes of active liquid xenon. The Gd concentration in water is 0.2% in mass. Neutrons leaving the TPC volume will be moderated and captured by the Gd with a probability of 91%. The gamma-rays emitted after the capture are detected from Cherenkov photons, providing a neutron tagging [278]. Neutron tagging techniques are also crucial for coherent neutrino-nucleus elastic scattering detection from pion-decay-at-rest neutrino source at spallation sources [279, 280]. Neutrons can be produced in the Pb shielding from CC and NC interactions and propagate into the nuclear recoil sensitive volume, generating a beam-related background. Careful shielding design and implementation of neutron tagging is crucial.

- *Mitigation of cosmogenic background.* In recent years the required sensitivity to search for dark matter and neutrinoless double beta decay asks for a strong reduction of cosmogenic background. Muons can produce neutrons that can enter the active volume of the detector from the surrounding rock or from external detector components. The yield of these so-called *cosmogenic neutrons* depend on the muon energies and the material properties of the medium the muon passes through. In addition, muons can produce by spallation radioisotopes inside the detector active volume. Cosmogenic backgrounds are a function of depth and experimental design, and can limit the sensitivity to search for rare events. Most of these radioisotopes are short-lived and their effect can be easily removed by an active veto based on the time correlation with a crossing muon. However, a number of cosmogenic radioisotopes are long-lived and they require an important consideration. Mitigation of these cosmogenic backgrounds produced in-situ deep underground are a major challenge for upcoming and future experiments. Optimizing the detector design and analysis strategies at a given depth equals an effective muon flux reduction. In particular, we mention two discrimination techniques for muon-induced isotopes: 1) ^{11}C tagging by a three-fold coincidence between the crossing muon, the capture of the ejected neutron from ^{12}C , and the ^{11}C decay [281]; 2) similar delayed coincidence tagging can be exploited to mitigate the background due to ^{77}Ge and its metastable state ^{77m}Ge , which have been identified as dominant cosmogenic background in the search for neutrinoless double beta decay of ^{76}Ge [282].
- *Purification.* A number of high efficiency specific purification methods have been developed for different detectors in order to remove long-lived radio-isotopes, ^{39}K , ^{85}Kr , and ^{210}Pb progeny. For organic liquid scintillators, distillation and water extraction have been shown to be very effective to reach radiopurity levels of the order of $10^{-5}\mu\text{Bq/kg}$ or better in uranium and thorium, and $10^{-3}\mu\text{Bq/kg}$ in ^{210}Pb [283]. Distillation has been used to reduce ^{85}Kr in xenon by a factor of 10^3 [284]. Cryogenic distillation can be used to reduce the isotopic abundance of ^{39}Ar in argon extracted from underground with a 350 m column in the ARIA project [285]. For semiconductors [286] and scintillating crystals [287] zone-refining followed by single-crystal growth has been exploited to remove impurities at the cost of a small fraction of material kept after the purification.
- *Direct isotope tagging.* In neutrinoless double beta decay in order to explore half-lives greater than 10^{28} y one needs an almost background-free detector. The most robust signature is the identification of the daughter atom in the decay: for example, for ^{136}Xe , the $^{136}\text{Ba}^{2+}$. Important step forwards to establish a valid and promising method for this tagging have been recently made [288, 289].

References

- [1] A. Aab *et al.* (Pierre Auger), *Earth and Space Science* **7**, 4, e2019EA000582 (2020), URL <https://agupubs.onlinelibrary.wiley.com/doi/abs/10.1029/2019EA000582>.
- [2] R. M. Baltrusaitis *et al.*, *Nucl. Instrum. Meth.* **A240**, 410 (1985).
- [3] D. J. Bird *et al.* (HiRes), *Astrophys. J.* **424**, 491 (1994).
- [4] T. Abu-Zayyad *et al.*, *Nucl. Instrum. Meth.* **A450**, 253 (2000).
- [5] A. Watson, *European Phys. J. Web of Confs.* **210**, 00001 (2019), [arXiv:1901.06676].
- [6] P. Sokolsky, *European Phys. J. Web of Confs.* **283**, 01003 (2023).
- [7] H. Tokuno *et al.*, *Nucl. Instrum. Meth.* **A676**, 54 (2012), [arXiv:1201.0002].
- [8] J. Abraham *et al.* (Pierre Auger), *Nucl. Instrum. Meth.* **A620**, 227 (2010), [arXiv:0907.4282].

- [9] A. C. *et al.*, *Astroparticle Physics* **149**, 102819 (2023), ISSN 0927-6505, URL <https://www.sciencedirect.com/science/article/pii/S0927650523000051>.
- [10] M. M. Malacari *et al.* (FAST), *Astroparticle Physics* **119**, 102430 (2020), ISSN 0927-6505, URL <https://www.sciencedirect.com/science/article/pii/S0927650520300037>.
- [11] F. Arqueros, J. R. Hoerandel and B. Keilhauer, *Nucl. Instrum. Meth.* **A597**, 23 (2008), [arXiv:0807.3844].
- [12] F. Arqueros, J. R. Hoerandel and B. Keilhauer, *Nucl. Instrum. Meth.* **A597**, 1 (2008), [arXiv:0807.3760].
- [13] J. Rosado, F. Blanco and F. Arqueros, *Astropart. Phys.* **34**, 164 (2010), [arXiv:1004.3971].
- [14] M. Ave *et al.* (AIRFLY), *Astropart. Phys.* **28**, 41 (2007), [arXiv:astro-ph/0703132].
- [15] J. Rosado, F. Blanco and F. Arqueros, *Astropart. Phys.* **55**, 51 (2014), [arXiv:1401.4310].
- [16] J. H. Boyer *et al.*, *Nucl. Instrum. Meth.* **A482**, 457 (2002).
- [17] J. T. Brack *et al.*, *Astropart. Phys.* **20**, 653 (2004).
- [18] B. Fick *et al.*, *JINST* **1**, 11, P11003 (2006).
- [19] J. Abraham *et al.* (Pierre Auger), *Astropart. Phys.* **33**, 108 (2010), [arXiv:1002.0366].
- [20] P. Abreu *et al.* (Pierre Auger), *Astropart. Phys.* **34**, 368 (2011), [arXiv:1010.6162].
- [21] R. Thalman *et al.* *Journal of Quantitative Spectroscopy and Radiative Transfer*, **147**, 171 (2014), Erratum-ibid. **189**, 281 (2017).
- [22] J. Abraham *et al.* [Pierre Auger Collab.], *Nucl. Instrum. Methods* **A789**, 172 (2015).
- [23] M. Unger *et al.*, *Nucl. Instrum. Meth.* **A588**, 433 (2008), [arXiv:0801.4309].
- [24] T.K. Gaisser and A.M. Hillas, *Proc. 15th Int. Cosmic Ray Conf. Bulgarska Akademiia na Naukite, Conf. Papers* **8**, 353 (1978), (archived at <http://adsabs.harvard.edu/abs/1977ICRC....8..353G>).
- [25] A. e. a. T. P. A. C. Aab (The Pierre Auger Collaboration), *Phys. Rev. D* **100**, 082003 (2019), URL <https://link.aps.org/doi/10.1103/PhysRevD.100.082003>.
- [26] A. Abdul Halim *et al.* (Pierre Auger), "*Astrophys. J. Suppl.*" **264**, 2, 50 (2023).
- [27] A. H. *et al.* (Pierre Auger Collaboration), *Phys. Rev. Lett.* **132**, 021001 (2024), URL <https://link.aps.org/doi/10.1103/PhysRevLett.132.021001>.
- [28] P. A. Klimov *et al.*, *Space Sci. Rev.* **212**, 3-4, 1687 (2017), [arXiv:1706.04976].
- [29] B. A. e. a. Khrenov, *Cosmic Research* **58**, 5, 317 (2020).
- [30] G. Abdellaoui *et al.* (JEM-EUSO), *Journal of Instrumentation* **13**, 5 (2018), ISSN 17480221.
- [31] G. Abdellaoui *et al.* (The JEM-EUSO Collaboration), *Astroparticle Physics* **154**, 102891 (2024).
- [32] J. Eser *et al.* (The JEM-EUSO Collaboration), *Proceedings of Science* **444**, 397 (2023).
- [33] F. Capel *et al.*, *Advances in Space Research* **62**, 2954 (2018).
- [34] A. O. *et al.*, *Journal of Cosmology and Astroparticle Physics* **2021**, 06, 007 (2021), URL <https://doi.org/10.1088/1475-7516/2021/06/007>.
- [35] J. Holder *et al.*, *AIP Conf. Proc.* **1085**, 657 (2009), [arXiv:0810.0474].
- [36] F. Aharonian *et al.* (H.E.S.S.), *Astron. Astrophys.* **457**, 899 (2006), [arXiv:astro-ph/0607333].
- [37] J. Albert *et al.* (MAGIC), *Astrophys. J.* **674**, 1037 (2008), [arXiv:0705.3244].
- [38] T. C. Weekes *et al.*, *Astrophys. J.* **342**, 379 (1989).
- [39] A. M. Hillas *et al.*, *Astrophys. J.* **503**, 744 (1998).
- [40] <http://tevcat.uchicago.edu/>.
- [41] F. Aharonian *et al.* (H.E.S.S.), *Astrophys. J.* **636**, 777 (2006), [arXiv:astro-ph/0510397].
- [42] M. de Naurois and D. Mazin, *Comptes Rendus Physique* **16**, 610 (2015), [arXiv:1511.00463].
- [43] A. Mitchell, in "37th International Cosmic Ray Conference," 46 (2022), [arXiv:2109.13753].
- [44] A. M. Hillas, *Astropart. Phys.* **43**, 19 (2013).
- [45] M. Thuczykont *et al.*, in "The Sixteenth Marcel Grossmann Meeting. On Recent Developments in Theoretical and Experimental General Relativity," 3324–3342 (2023).
- [46] Z. Cao *et al.*, *ChA&A* **43**, 4, 457 (2019).
- [47] B. S. Acharya *et al.* (CTA Consortium), *Astropart. Phys.* **43**, 3 (2013).
- [48] C.-L. Project *et al.*, arXiv e-prints arXiv:2306.12960 (2023), [arXiv:2306.12960].
- [49] Cherenkov Telescope Array Consortium *et al.*, *Science with the Cherenkov Telescope Array* (2019).
- [50] A. Bernstein *et al.*, *Report on the Depth Requirements for a Massive Detector at Homestake* (2009), [arXiv:0907.4183].
- [51] A. Suzuki, *Eur. Phys. J. C* **74**, 10, 3094 (2014), [arXiv:1409.4515].
- [52] G. Alimonti *et al.* (Borexino), *Nucl. Instrum. Meth. A* **600**, 568 (2009), [arXiv:0806.2400].
- [53] Y. Ashie *et al.* (Super-Kamiokande), *Phys. Rev.* **D71**, 112005 (2005), [hep-ex/0501064].
- [54] S. Kasuga *et al.*, *Phys. Lett.* **B374**, 238 (1996).
- [55] M. Shiozawa (Super-Kamiokande), *Nucl. Instrum. Meth.* **A433**, 240 (1999).
- [56] K. Abe *et al.* (Super-Kamiokande), *Phys. Rev.* **D83**, 052010 (2011), [arXiv:1010.0118].
- [57] J. F. Beacom and M. R. Vagins, *Phys. Rev. Lett.* **93**, 171101 (2004), [hep-ph/0309300].
- [58] J. Boger *et al.* (SNO), *Nucl. Instrum. Meth.* **A449**, 172 (2000), [arXiv:nucl-ex/9910016].
- [59] T. K. Gaisser, F. Halzen and T. Stanev, *Phys. Rept.* **258**, 173 (1995), [Erratum: *Phys. Rept.* 271,355(1996)], [hep-ph/9410384].
- [60] J.G. Learned and K. Mannheim, *Ann. Rev. Nucl. and Part. Sci.* **50**, 679 (2000).
- [61] U. F. Katz and C. Spiering, *Prog. Part. Nucl. Phys.* **67**, 651 (2012), [arXiv:1111.0507].
- [62] M. G. Aartsen *et al.* (IceCube), *J. Phys.* **G44**, 5, 054006 (2017), [arXiv:1607.02671].
- [63] S. Adrián-Martínez *et al.* (KM3NeT), *J. Phys.* **G43**, 8, 084001 (2016), [arXiv:1601.07459].
- [64] A. Gazizov and M. P. Kowalski, *Comput. Phys. Commun.* **172**, 203 (2005), [arXiv:astro-ph/0406439].
- [65] A. D. Avrorin *et al.*, *Phys. Part. Nucl.* **46**, 2, 211 (2015).
- [66] M. G. Aartsen *et al.* (IceCube), *JINST* **12**, 03, P03012 (2017), [arXiv:1612.05093].
- [67] M. G. Aartsen *et al.* (IceCube) (2014), [arXiv:1412.5106].
- [68] M. G. Aartsen *et al.* (IceCube-Gen2), *J. Phys. G* **48**, 6, 060501 (2021), [arXiv:2008.04323].
- [69] M. Agostini *et al.* (P-ONE), *Nature Astron.* **4**, 10, 913 (2020), [arXiv:2005.09493].
- [70] Z. P. Ye *et al.* (2022), [arXiv:2207.04519].
- [71] F. Hu, *PoS ICRC2023*, 1203 (2023).
- [72] T. Huege, *Phys. Rept.* **620**, 1 (2016), [arXiv:1601.07426].
- [73] F. G. Schroder, *Prog. Part. Nucl. Phys.* **93**, 1 (2017), [arXiv:1607.08781].
- [74] G. A. Askar'yan, *Sov. Phys. JETP* **14**, 2, 441 (1962), [*Zh. Eksp. Teor. Fiz.* 41,616(1961)].

- [75] G.A. Askaryan, *Sov. Phys. JETP* **21**, 658 (1965).
- [76] E. Zas, F. Halzen and T. Stanev, *Phys. Rev. D* **45**, 362 (1992).
- [77] C. W. James *et al.*, *Phys. Rev.* **E84**, 056602 (2011), [arXiv:1007.4146].
- [78] C. W. James, *Phys. Rev. D* **105**, 2, 023014 (2022), [arXiv:2201.01298].
- [79] J. Alvarez-Muniz, R. A. Vazquez and E. Zas, *Phys. Rev.* **D62**, 063001 (2000), [arXiv:astro-ph/0003315].
- [80] C. Glaser *et al.*, *Eur. Phys. J. C* **80**, 77 (2020), [arXiv:1906.01670].
- [81] D. Saltzberg *et al.*, *Phys. Rev. Lett.* **86**, 2802 (2001), [hep-ex/0011001].
- [82] O. Scholten *et al.*, *J. Phys. Conf. Ser.* **81**, 012004 (2007).
- [83] J. Alvarez-Muñiz *et al.*, *Phys. Rev. D* **74**, 023007 (2006), URL <https://link.aps.org/doi/10.1103/PhysRevD.74.023007>.
- [84] L. Gerhardt and S. R. Klein, *Phys. Rev.* **D82**, 074017 (2010), [arXiv:1007.0039].
- [85] J. Alvarez-Muniz, R. A. Vazquez and E. Zas, *Phys. Rev.* **D61**, 023001 (2000), [arXiv:astro-ph/9901278].
- [86] D. García-Fernández, A. Nelles and C. Glaser, *Phys. Rev. D* **102**, 8, 083011 (2020), [arXiv:2003.13442].
- [87] K. Greisen, *Phys. Rev. Lett.* **16**, 748 (1966).
- [88] G. T. Zatsepin and V. A. Kuzmin, *JETP Lett.* **4**, 78 (1966), [*Pisma Zh. Eksp. Teor. Fiz.*4,114(1966)].
- [89] V. de Souza (Pierre Auger, Telescope Array), *PoS ICRC2017*, 522 (2018).
- [90] R. Abbasi *et al.* (IceCube), *Astropart. Phys.* **34**, 382 (2011), [arXiv:1004.1694].
- [91] P. Allison *et al.* (ARA), *Astropart. Phys.* **108**, 63 (2019), [arXiv:1712.03301].
- [92] A. Anker *et al.* (ARIANNA), *JCAP* **1911**, 030 (2019), [arXiv:1909.02677].
- [93] J. A. Aguilar *et al.*, *Eur. Phys. J. C* **82**, 2, 147 (2022), [arXiv:2107.02604].
- [94] I. Plaisier, S. Bouma and A. Nelles, *Eur. Phys. J. C* **83**, 5, 443 (2023), [arXiv:2302.00054].
- [95] A. G. Vieregge, K. Bechtol and A. Romero-Wolf, *JCAP* **1602**, 02, 005 (2016), [arXiv:1504.08006].
- [96] J. A. Aguilar *et al.*, *Astropart. Phys.* **145**, 102790 (2023), [arXiv:2103.06079].
- [97] S. W. Barwick *et al.* (ARIANNA), *Astropart. Phys.* **90**, 50 (2017), [arXiv:1612.04473].
- [98] M. G. Aartsen *et al.* (IceCube), *Phys. Rev.* **D98**, 6, 062003 (2018), [arXiv:1807.01820].
- [99] A. Aab *et al.* (Pierre Auger), *JCAP* **1910**, 10, 022 (2019), [arXiv:1906.07422].
- [100] J. D. Bray *et al.*, *Phys. Rev.* **D91**, 6, 063002 (2015), [arXiv:1502.03313].
- [101] O. Scholten *et al.*, *Phys. Rev. Lett.* **103**, 191301 (2009), [arXiv:0910.4745].
- [102] P. W. Gorham *et al.* (ANITA), *Phys. Rev.* **D99**, 12, 122001 (2019), [arXiv:1902.04005].
- [103] P. Allison *et al.* (ARA), *Phys. Rev. D* **102**, 4, 043021 (2020), [arXiv:1912.00987].
- [104] A. Anker *et al.* (ARIANNA), *JCAP* **03**, 053 (2020), [arXiv:1909.00840].
- [105] T. Winchen *et al.*, *J. Phys. Conf. Ser.* **1181**, 1, 012077 (2019), [arXiv:1903.08472].
- [106] R. Abbasi *et al.* (IceCube), *Astrophys. J.* **928**, 1, 50 (2022), [arXiv:2111.10299].
- [107] A. van Vliet, R. Alves Batista and J. R. Hörandel, *Phys. Rev. D* **100**, 2, 021302 (2019), [arXiv:1901.01899].
- [108] S. Barwick *et al.*, *Journal of Glaciology* **51**, 173, 231–238 (2005).
- [109] J.A. Dowdeswell and S. Evans, *Rept. on Prog. in Phys.* **67**, 1821 (2004).
- [110] S. W. Barwick *et al.*, *JCAP* **1807**, 07, 055 (2018), [arXiv:1804.10430].
- [111] C. Deaconu *et al.*, *Phys. Rev.* **D98**, 4, 043010 (2018), [arXiv:1805.12576].
- [112] P. W. Gorham *et al.* (ANITA), *Phys. Rev. Lett.* **103**, 051103 (2009), [arXiv:0812.2715].
- [113] P. W. Gorham *et al.* (ANITA), *Phys. Rev. Lett.* **121**, 16, 161102 (2018), [arXiv:1803.05088].
- [114] P. W. Gorham *et al.* (ANITA), *Phys. Rev. Lett.* **126**, 7, 071103 (2021), [arXiv:2008.05690].
- [115] I. Kravchenko *et al.* (RICE), *Phys. Rev.* **D73**, 082002 (2006), [arXiv:astro-ph/0601148].
- [116] P. Allison *et al.* (ARA), *Phys. Rev.* **D93**, 8, 082003 (2016), [arXiv:1507.08991].
- [117] J. Avva *et al.*, *Nucl. Instrum. Meth.* **A869**, 46 (2017), [arXiv:1605.03525].
- [118] J. A. Aguilar *et al.* (RNO-G), *JINST* **16**, 03, P03025 (2021), [arXiv:2010.12279].
- [119] R.D. Dagkesamanskii and I.M. Zheleznykh, *Sov. Phys. JETP Lett.* **50**, 233 (1989).
- [120] G. R. Olhoeft and D. W. Strangway, *Earth and Planetary Science Letters* **24**, 3, 394 (1975).
- [121] J. D. Bray, *Astropart. Phys.* **77**, 1 (2016), [arXiv:1601.02980].
- [122] C. W. James *et al.*, *EPJ Web Conf.* **135**, 04001 (2017), [arXiv:1704.05336].
- [123] A. Aab *et al.* (Pierre Auger), *Phys. Rev. Lett.* **116**, 24, 241101 (2016), [arXiv:1605.02564].
- [124] P. A. Bezyazeev *et al.* (Tunka-Rex), *Phys. Rev.* **D97**, 12, 122004 (2018), [arXiv:1803.06862].
- [125] S. Buitink *et al.* (LOFAR), *Phys. Rev.* **D90**, 8, 082003 (2014), [arXiv:1408.7001].
- [126] K. Mulrey *et al.* (LOFAR), *JCAP* **11**, 017 (2020), [arXiv:2005.13441].
- [127] D. Fargion, *Astrophys. J.* **570**, 909 (2002), [arXiv:astro-ph/0002453].
- [128] X. Bertou *et al.*, *Astropart. Phys.* **17**, 183 (2002), [arXiv:astro-ph/0104452].
- [129] J. L. Feng *et al.*, *Phys. Rev. Lett.* **88**, 161102 (2002), [hep-ph/0105067].
- [130] Q. Abarr *et al.* (PUEO), *JINST* **16**, 08, P08035 (2021), [arXiv:2010.02892].
- [131] J. Álvarez Muñoz *et al.* (GRAND), *Sci. China Phys. Mech. Astron.* **63**, 1, 219501 (2020), [arXiv:1810.09994].
- [132] P. Abreu *et al.* (Pierre Auger), *PoS ICRC2021*, 262 (2021).
- [133] D. Nygren, *eConf C740805*, 58 (1974).
- [134] V. Chepel and H. Araujo, *JINST* **8**, R04001 (2013), [arXiv:1207.2292].
- [135] E. Aprile and T. Doke, *Rev. Mod. Phys.* **82**, 2053 (2010), [arXiv:0910.4956].
- [136] D. Gonzalez-Diaz, F. Monrabal and S. Murphy, *Nucl. Instrum. Meth. A* **878**, 200 (2018), [arXiv:1710.01018].
- [137] E. Aprile *et al.*, *Noble Gas Detectors*, Wiley (2008), ISBN 978-3-527-40597-8, 978-3-527-61002-0.
- [138] A. I. Bolozdynya, *Emission detectors*, World Scientific (2010).
- [139] D. S. Akerib *et al.* (LUX), *Phys. Rev. D* **97**, 11, 112002 (2018), [arXiv:1802.06162].
- [140] B. Lenardo *et al.*, *IEEE Trans. Nucl. Sci.* **62**, 6, 3387 (2015), [arXiv:1412.4417].

- [141] W. F. Schmidt, IEEE Trans. Electric. Insul. **19**, 389 (1984).
- [142] L. Baudis *et al.*, Eur. Phys. J. C **83**, 8, 717 (2023), [arXiv:2303.13963].
- [143] J. Albert *et al.* (EXO-200), Phys. Rev. C **89**, 1, 015502 (2014), [arXiv:1306.6106].
- [144] A. Gando *et al.* (KamLAND-Zen), Phys. Rev. Lett. **122**, 19, 192501 (2019), [arXiv:1901.03871].
- [145] E. Aprile *et al.* (XENON), Phys. Rev. C **106**, 2, 024328 (2022), [arXiv:2205.04158].
- [146] J. B. Albert *et al.* (EXO-200), Phys. Rev. D **96**, 9, 092001 (2017), [arXiv:1704.05042].
- [147] K. Abe *et al.* (XMASS), PTEP **2018**, 5, 053D03 (2018), [arXiv:1801.03251].
- [148] T. Doke *et al.*, Jap. J. Appl. Phys. **41**, 1538 (2002).
- [149] C. E. Dahl, *The Physics of Background Discrimination in Liquid Xenon, and First Results from XENON10 in the Hunt for WIMP Dark Matter*, Ph.D. thesis, Princeton University (2009).
- [150] L. Baudis, P. Sanchez-Lucas and K. Thieme, Eur. Phys. J. C **81**, 12, 1060 (2021), [arXiv:2109.07151].
- [151] G. Anton *et al.* (EXO-200), Phys. Rev. C **101**, 6, 065501 (2020), [arXiv:1908.04128].
- [152] J. J. Gomez-Cadenas, F. Monrabal Capilla and P. Ferrario, Front. in Phys. **7**, 51 (2019), [arXiv:1903.02435].
- [153] M. S. J. Lindhard, V. Nielsen and P. Thomsen, Kgl. Danske Videnskab., Selskab. Mat. Fys. Medd **33**, 1 (1963).
- [154] A. Hitachi and A. Mozumder (2019), [arXiv:1903.05815].
- [155] P. Sorensen and C. E. Dahl, Phys. Rev. D **83**, 063501 (2011), [arXiv:1101.6080].
- [156] M. Szydagis *et al.*, JINST **6**, P10002 (2011), [arXiv:1106.1613].
- [157] G. Pereira, C. Silva and V. N. Solovov (LZ), JINST **18**, 04, C04007 (2023).
- [158] E. Aprile *et al.* (XENON), Eur. Phys. J. C **80**, 8, 785 (2020), [arXiv:2003.03825].
- [159] G. Anton *et al.* (EXO-200), Phys. Rev. Lett. **123**, 16, 161802 (2019), [arXiv:1906.02723].
- [160] D. Nygren, Nucl. Instrum. Meth. A **603**, 337 (2009).
- [161] J. Renner *et al.* (NEXT), JHEP **10**, 230 (2019), [arXiv:1905.13110].
- [162] P. Agnes *et al.* (DarkSide), Nucl. Instrum. Meth. A **904**, 23 (2018), [arXiv:1802.01427].
- [163] P. Abratenko *et al.* (MicroBooNE), JINST **16**, 09, P09025 (2021), [arXiv:2104.06551].
- [164] Y. Li *et al.*, Nucl. Instrum. Meth. A **816**, 160 (2016), [arXiv:1508.07059].
- [165] J. B. Albert *et al.* (EXO-200), Phys. Rev. C **95**, 2, 025502 (2017), [arXiv:1609.04467].
- [166] M. Babicz *et al.*, JINST **15**, 09, P09009 (2020), [arXiv:2002.09346].
- [167] E. Aprile *et al.* (XENON), PTEP **2022**, 5, 053H01 (2022), [arXiv:2112.12231].
- [168] P. Agnes *et al.* (DarkSide), Phys. Rev. D **98**, 10, 102006 (2018), [arXiv:1802.07198].
- [169] E. Aprile *et al.* (XENON), Phys. Rev. Lett. **129**, 16, 161805 (2022), [arXiv:2207.11330].
- [170] P. Agnes (DarkSide), EPJ Web Conf. **280**, 06003 (2023).
- [171] D. S. Akerib *et al.* (LZ), Nucl. Instrum. Meth. A **953**, 163047 (2020), [arXiv:1910.09124].
- [172] Y. Meng *et al.* (PandaX-4T), Phys. Rev. Lett. **127**, 26, 261802 (2021), [arXiv:2107.13438].
- [173] E. Aprile *et al.* (XENON), JCAP **11**, 031 (2020), [arXiv:2007.08796].
- [174] S. Kravitz *et al.*, Eur. Phys. J. C **80**, 3, 262 (2020), [arXiv:1909.08730].
- [175] J. Aalbers *et al.* (DARWIN), JCAP **1611**, 11, 017 (2016), [arXiv:1606.07001].
- [176] J. Aalbers *et al.*, J. Phys. G **50**, 1, 013001 (2023), [arXiv:2203.02309].
- [177] X. Wang *et al.*, JINST **18**, 05, P05028 (2023), [arXiv:2301.06044].
- [178] P. Agnes *et al.* (DarkSide), Phys. Rev. Lett. **130**, 10, 101002 (2023), [arXiv:2207.11968].
- [179] S. Li *et al.* (PandaX), Phys. Rev. Lett. **130**, 26, 261001 (2023), [arXiv:2212.10067].
- [180] E. Aprile *et al.* (XENON), Phys. Rev. Lett. **129**, 16, 161805 (2022), [arXiv:2207.11330].
- [181] J. Aalbers *et al.* (LZ) (2023), [arXiv:2307.15753].
- [182] T. N. Thorpe (DarkSide-20k), SciPost Phys. Proc. **12**, 069 (2023), [arXiv:2210.00322].
- [183] G. Plante *et al.*, Eur. Phys. J. C **82**, 10, 860 (2022), [arXiv:2205.07336].
- [184] A. Abdurkerim *et al.* (PandaX) (2024), [arXiv:2402.03596].
- [185] K. Stifter (LZ), J. Phys. Conf. Ser. **1468**, 1, 012016 (2020).
- [186] R. Anthony-Petersen *et al.* (2023), [arXiv:2307.11877].
- [187] B. von Krosigk *et al.*, SciPost Phys. Proc. **12**, 016 (2023), [arXiv:2209.10950].
- [188] R. E. Lanou, H. J. Maris and G. M. Seidel, Phys. Rev. Lett. **58**, 2498 (1987).
- [189] F. D. Amaro *et al.*, Nucl. Instrum. Meth. A **1054**, 168325 (2023), [arXiv:2306.04568].
- [190] G. Anton *et al.* (EXO-200), Phys. Rev. Lett. **123**, 16, 161802 (2019), [arXiv:1906.02723].
- [191] G. Adhikari *et al.* (nEXO), J. Phys. G **49**, 1, 015104 (2022), [arXiv:2106.16243].
- [192] A. Simón *et al.* (NEXT), JHEP **07**, 146 (2021), [arXiv:2102.11931].
- [193] P. Ferrario *et al.* (NEXT), JHEP **10**, 052 (2019), [arXiv:1905.13141].
- [194] P. Novella *et al.* (NEXT), Phys. Rev. C **105**, 5, 055501 (2022), [arXiv:2111.11091].
- [195] C. Adams *et al.* (NEXT), JHEP **2021**, 08, 164 (2021), [arXiv:2005.06467].
- [196] A. D. McDonald *et al.*, Phys. Rev. Lett. **120**, 13, 132504 (2018), [arXiv:1711.04782].
- [197] P. Herrero-Gómez *et al.* (NEXT), Nature Commun. **13**, 1, 7741 (2022), [arXiv:2201.09099].
- [198] H. Rasiwala *et al.* (nEXO Ba-tagging group), Nucl. Instrum. Meth. B **541**, 298 (2023), [arXiv:2303.04698].
- [199] T. Li *et al.*, JHEP **05**, 200 (2023), [arXiv:2211.14992].
- [200] E. Aprile *et al.* (XENON), Nature **568**, 7753, 532 (2019), [arXiv:1904.11002].
- [201] G. Martínez-Lema *et al.* (NEXT), JHEP **21**, 203 (2020), [arXiv:2006.07320].
- [202] C. Wittweg *et al.*, Eur. Phys. J. C **80**, 12, 1161 (2020), [arXiv:2002.04239].
- [203] L. Si *et al.* (PandaX), Research **2022**, 9798721 (2022), [arXiv:2205.12809].
- [204] D. S. Akerib *et al.* (LZ), Phys. Rev. C **102**, 1, 014602 (2020), [arXiv:1912.04248].
- [205] D. S. Akerib *et al.* (LZ), Phys. Rev. C **104**, 6, 065501 (2021), [arXiv:2104.13374].
- [206] F. Agostini *et al.* (DARWIN), Eur. Phys. J. C **80**, 9, 808 (2020), [arXiv:2003.13407].
- [207] C. Enss, editor, *Cryogenic particle detection*, volume 99 of *Topics in applied physics*, Springer, Berlin, Germany (2005).

- [208] K. Pretzl, *Cryogenic Detectors* (2020).
- [209] *Proc. of the Low Temperature Detectors for Neutrinos and Dark Matter*, Low Temperature Detectors for Neutrinos and Dark Matter (start 1987).
- [210] G. H. Rieke, *Detection of Light*, Cambridge University Press, 3rd edition (2021).
- [211] H. Kraus, *Superconductor Science and Technology* **9**, 10, 827 (1996), URL <https://doi.org/10.1088/0953-2048/9/10/001>.
- [212] A. V. Dixit *et al.*, *Phys. Rev. Lett.* **126**, 14, 141302 (2021), [arXiv:2008.12231].
- [213] J. Zmuidzinas, *Annual Review of Condensed Matter Physics* **3**, 1, 169 (2012), URL <https://doi.org/10.1146/annurev-conmatphys-020911-125022>.
- [214] S. Doyle *et al.*, *Journal of Low Temperature Physics* **151**, 1, 530 (2008), URL <https://doi.org/10.1007/s10909-007-9685-2>.
- [215] K. Irwin and G. Hilton, *Transition-Edge Sensors*, 63–150, Springer Berlin Heidelberg, Berlin, Heidelberg (2005), ISBN 978-3-540-31478-3, URL https://doi.org/10.1007/10933596_3.
- [216] F. Paolucci and F. Giazotto, *Instruments* **5**, 2 (2021), ISSN 2410-390X, URL <https://www.mdpi.com/2410-390X/5/2/14>.
- [217] S. B. Bandler *et al.*, *J. Low Temp. Phys.* **93**, 709 (1993).
- [218] D. Prele, *Journal of Instrumentation* **10**, 08, C08015 (2015), URL <https://doi.org/10.1088/1748-0221/10/08/c08015>.
- [219] E. Fiorini and T. Niinikoski, *Nucl. Instrum. Meth. A* **224**, 83 (1984).
- [220] S. H. Moseley, J. C. Mather and D. McCammon, *Thermal detectors as x-ray spectrometers* (1984).
- [221] V. Barger and D. Cline (1985), telemark, 1984.
- [222] A. Blasi *et al.* (1985), I.N.F.N./BE-85/2, internal report.
- [223] D. Q. Adams *et al.* (CUORE) (2021), [arXiv:2104.06906].
- [224] W. R. Armstrong *et al.* (CUPID) (2019), [arXiv:1907.09376].
- [225] O. Azzolini *et al.* (CUPID), *Phys. Rev. Lett.* **123**, 3, 032501 (2019), [arXiv:1906.05001].
- [226] E. Armengaud *et al.* (CUPID), *Phys. Rev. Lett.* **126**, 18, 181802 (2021), [arXiv:2011.13243].
- [227] V. Alenkov *et al.*, *Eur. Phys. J. C* **79**, 9, 791 (2019), [arXiv:1903.09483].
- [228] D. Mccammon *et al.* (1984).
- [229] P. Filianin *et al.*, *Phys. Rev. Lett.* **127**, 7, 072502 (2021), [arXiv:2108.07039].
- [230] D. Pergolesi *et al.*, *Nucl. Instrum. Meth. A* **559**, 349 (2006).
- [231] M. Sisti *et al.*, *Nuclear Instruments and Methods in Physics Research Section A: Accelerators, Spectrometers, Detectors and Associated Equipment* **520**, 1, 125 (2004), ISSN 0168-9002, proceedings of the 10th International Workshop on Low Temperature Detectors, URL <https://www.sciencedirect.com/science/article/pii/S0168900203031814>.
- [232] E. Ferri *et al.*, *Phys. Procedia* **61**, 227 (2015).
- [233] C. Velte, *Measurement of a high energy resolution and high-statistics ^{163}Ho electron capture spectrum for the ECHO experiment.*, Ph.D. thesis, U. Heidelberg (main) (2020).
- [234] L. Gastaldo *et al.*, *Eur. Phys. J. ST* **226**, 8, 1623 (2017).
- [235] B. Alpert *et al.*, *Eur. Phys. J. C* **75**, 3, 112 (2015), [arXiv:1412.5060].
- [236] M. P. Croce *et al.*, *J. Low Temp. Phys.* **184**, 3-4, 958 (2016), [arXiv:1510.03874].
- [237] R. Ardito *et al.* (2005), [hep-ex/0501010].
- [238] P. Luke *et al.*, *Nucl. Instrum. Meth. A* **289**, 406 (1990).
- [239] B. Neganov *et al.*, *J Low Temp Phys* **93**, 417–422 (1993), URL <https://doi.org/10.1007/BF00693454>.
- [240] I. Alkhatib *et al.* (SuperCDMS), *Phys. Rev. Lett.* **127**, 8, 081802 (2021), [arXiv:2011.09183].
- [241] Q. Arnaud *et al.* (EDELWEISS), *Phys. Rev. Lett.* **125**, 14, 141301 (2020), [arXiv:2003.01046].
- [242] *Snowmass2021-Letter of Interest The TESSERACT Dark Matter Project* (2020).
- [243] T. Braine *et al.* (ADMX), *Phys. Rev. Lett.* **124**, 10, 101303 (2020), [arXiv:1910.08638].
- [244] *Snowmass2021-Letter of Interest Opening the Terahertz Axion Window* (2020).
- [245] C. Bellenghi *et al.*, *Eur. Phys. J. C* **79**, 9, 727 (2019), [arXiv:1905.10611].
- [246] I. Colantoni *et al.*, *J. Low Temp. Phys.* **199**, 3-4, 593 (2020).
- [247] G. Heusser, *Ann. Rev. Nucl. Part. Sci.* **45**, 543 (1995).
- [248] D. S. Akerib *et al.*, *The European Physical Journal C* **80**, 11 (2020), URL <https://doi.org/10.1140/epjlc/2Fs10052-020-8420-x>.
- [249] D. S. Leonard *et al.*, *Nucl. Instrum. Meth. A* **871**, 169 (2017), [arXiv:1703.10799].
- [250] N. Abgrall *et al.* (Majorana), *Nucl. Instrum. Meth. A* **823**, 83 (2016), [arXiv:1603.08483].
- [251] E. Aprile *et al.* (XENON), *Eur. Phys. J. C* **82**, 7, 599 (2022), [arXiv:2112.05629].
- [252] M. Laubenstein, *International Journal of Modern Physics A* **32**, 30, 1743002 (2017), URL <https://doi.org/10.1142/s0217751x17430023>.
- [253] P. Scovell *et al.*, *Astroparticle Physics* **97**, 160 (2018), URL <https://doi.org/10.1016/j.astropartphys.2017.11.006>.
- [254] G. Heusser *et al.*, *The European Physical Journal C* **75**, 11 (2015), URL <https://doi.org/10.1140/epjlc/2Fs10052-015-3704-2>.
- [255] N. Jakubowski, *Analytical and Bioanalytical Chemistry* **392**, 5, 775 (2008), URL <https://doi.org/10.1007/s00216-008-2374-4>.
- [256] M. Clemenza, *J. Radioanal. Nucl. Chem.* **318**, 3, 1765 (2018).
- [257] G. Heusser *et al.*, *Applied Radiation and Isotopes* **52**, 3, 691 (2000), URL [https://doi.org/10.1016/S0969-8043\(2899\)2900231-6](https://doi.org/10.1016/S0969-8043(2899)2900231-6).
- [258] M. Wojcik, G. Zuzel and H. Simgen, *International Journal of Modern Physics A* **32**, 30, 1743004 (2017), URL <https://doi.org/10.1142/2Fs0217751x17430047>.
- [259] Y. Takeuchi *et al.*, *Nuclear Instruments and Methods in Physics Research Section A: Accelerators, Spectrometers, Detectors and Associated Equipment* **421**, 1-2, 334 (1999), URL [https://doi.org/10.1016/0168-9002\(2898\)2901204-2](https://doi.org/10.1016/0168-9002(2898)2901204-2).
- [260] J. Kiko, *Nuclear Instruments and Methods in Physics Research Section A: Accelerators, Spectrometers, Detectors and Associated Equipment* **460**, 2-3, 272 (2001), URL [https://doi.org/10.1016/0168-9002\(2800\)2901082-2](https://doi.org/10.1016/0168-9002(2800)2901082-2).
- [261] E. Hoppe *et al.*, *Nuclear Instruments and Methods in Physics Research Section A: Accelerators, Spectrometers, Detectors and Associated Equipment* **579**, 1, 486 (2007), URL [https://doi.org/10.1016/0168-9002\(2007\)04.101](https://doi.org/10.1016/0168-9002(2007)04.101).
- [262] R. Bunker *et al.*, *Nuclear Instruments and Methods in Physics Research Section A: Accelerators, Spectrometers, Detectors and Associated Equipment* **967**, 163870 (2020), URL <https://doi.org/10.1016/j.nima.2020.163870>.
- [263] S. Bruenner *et al.*, *The European Physical Journal C* **81**, 4 (2021), URL <https://doi.org/10.1140/epjlc/s10052-021-09047-2>.

- [264] M. L. di Vacri *et al.*, Nucl. Instrum. Meth. A **994**, 165051 (2021), [arXiv:2006.12746].
- [265] H. Loosli, Earth and Planetary Science Letters **63**, 1, 51 (1983), URL <https://doi.org/10.1016%2F0012-821x%2883%2990021-3>.
- [266] D. Acosta-Kane *et al.*, Nuclear Instruments and Methods in Physics Research Section A: Accelerators, Spectrometers, Detectors and Associated Equipment **587**, 1, 46 (2008), URL <https://doi.org/10.1016%2Fj.nima.2007.12.032>.
- [267] P. Agnes *et al.* (DarkSide), Phys. Rev. D **93**, 8, 081101 (2016), [Addendum: Phys.Rev.D 95, 069901 (2017)], [arXiv:1510.00702].
- [268] H. O. Back *et al.*, in “Snowmass 2021,” (2022), [arXiv:2203.09734].
- [269] I. Bandac *et al.*, Appl. Radiat. Isot. **126**, 127 (2017).
- [270] G. Ranucci, in “IEEE Symposium Conference Record Nuclear Science 2004.”, volume 2, 804–809 Vol. 2 (2004).
- [271] P. Adhikari *et al.*, The European Physical Journal C **80**, 4 (2020), URL <https://doi.org/10.1140%2Fepjc%2Fs10052-020-7789-x>.
- [272] D. Budjáš *et al.*, Journal of Instrumentation **4**, 10, P10007 (2009), URL <https://doi.org/10.1088/1748-0221/4/10/p10007>.
- [273] M. Agostini *et al.* (GERDA), Phys. Rev. Lett. **125**, 25, 252502 (2020), [arXiv:2009.06079].
- [274] A. Simón *et al.* (NEXT), JHEP **21**, 146 (2020), [arXiv:2102.11931].
- [275] R. Agnese *et al.* (SuperCDMS Collaboration), Phys. Rev. Lett. **120**, 061802 (2018), URL <https://link.aps.org/doi/10.1103/PhysRevLett.120.061802>.
- [276] W. Westphal *et al.*, Nucl. Instrum. Meth. A **559**, 372 (2006).
- [277] S. Westerdale, E. Shields and F. Calaprice, Astroparticle Physics **79**, 10 (2016), URL <https://doi.org/10.1016%2Fj.astropartphys.2016.01.005>.
- [278] Marco Selvi, The XENONnT Neutron Veto (2023), URL <https://indico.cern.ch/event/1188759/>.
- [279] D. Akimov *et al.* (COHERENT), Science **357**, 6356, 1123 (2017), [arXiv:1708.01294].
- [280] D. Akimov *et al.*, in “Snowmass 2021,” (2022), [arXiv:2204.04575].
- [281] H. Back *et al.* (Borexino Collaboration), Phys. Rev. C **74**, 045805 (2006), URL <https://link.aps.org/doi/10.1103/PhysRevC.74.045805>.
- [282] C. Wiesinger, L. Pandola and S. Schönert, Eur. Phys. J. C **78**, 7, 597 (2018), [arXiv:1802.05040].
- [283] J. Benziger *et al.*, Nuclear Instruments and Methods in Physics Research Section A: Accelerators, Spectrometers, Detectors and Associated Equipment **587**, 2-3, 277 (2008), URL <https://doi.org/10.1016/j.nima.2007.12.043>.
- [284] K. Abe *et al.*, Nucl. Instrum. Meth. A **716**, 78 (2013), [arXiv:1301.2815].
- [285] E. Aaron *et al.* (DarkSide-20k), Eur. Phys. J. C **83**, 5, 453 (2023), [arXiv:2301.09639].
- [286] K.-P. Gradwohl *et al.*, Journal of Instrumentation **15**, 12, P12010 (2020), URL <https://doi.org/10.1088/1748-0221/15/12/p12010>.
- [287] B. Suerfu, F. Calaprice and M. Souza, Physical Review Applied **16**, 1 (2021), URL <https://doi.org/10.1103/physrevapplied.16.014060>.
- [288] I. Rivilla *et al.*, Nature **583**, 7814, 48 (2020), URL <https://doi.org/10.1038/s41586-020-2431-5>.
- [289] A. McDonald *et al.*, Physical Review Letters **120**, 13 (2018), URL <https://doi.org/10.1103/physrevlett.120.132504>.

37. Radioactivity and Radiation Protection

Revised July 2023 by S. Roesler (CERN) and M. Silari.

37.1 Definitions [1–3]

It would be desirable if legal protection limits could be expressed in directly measurable *physical quantities*. However, this does not allow quantifying biological effects of the exposure of the human body and its detriment to ionizing radiation.

For this reason, dose limits are expressed in terms of so-called *protection quantities* which, although calculable, are not measurable. Protection quantities are used to quantify the extent of exposure of the human body to ionizing radiation from both whole and partial body external irradiation and from intakes of radionuclides.

In order to demonstrate compliance with dose limits, so-called *operational quantities* are typically used, which aim at providing conservative estimates of protection quantities. Often radiation protection detectors used for individual and area monitoring are calibrated in terms of operational quantities and, thus, these quantities become “measurable”.

37.1.1 Physical quantities

• **Fluence, Φ** (unit: $1/\text{m}^2$): The fluence is the quotient of the sum of the particle track lengths dl in the volume dV

$$\Phi = dl/dV .$$

It can also be expressed in terms of number of particles dN incident upon a small sphere of cross-sectional area da

$$\Phi = dN/da .$$

• **Absorbed dose, D** (unit: gray, $1 \text{ Gy}=1 \text{ J/kg}=100 \text{ rad}$): The absorbed dose is the energy imparted by ionizing radiation in a volume element of a specified material divided by the mass of this volume element.

• **Kerma, K** (unit: gray): Kerma is the sum of the initial kinetic energies of all charged particles set in motion by indirectly ionizing radiation in a volume element of the specified material divided by the mass of this volume element.

• **Linear energy transfer, L or LET** (unit: J/m , often given in $\text{keV}/\mu\text{m}$, $1 \text{ keV}/\mu\text{m} \approx 1.602 \times 10^{-10} \text{ J/m}$): The linear energy transfer is the mean energy, dE , lost by a charged particle owing to collisions with electrons in traversing a distance dl in matter. *Low-LET radiation*: X rays and gamma rays (accompanied by charged particles due to interactions with the surrounding medium) or light charged particles such as electrons that produce sparse ionizing events far apart at a molecular scale ($L < 10 \text{ keV}/\mu\text{m}$). *High-LET radiation*: neutrons and heavy charged particles that produce ionizing events densely spaced at a molecular scale ($L > 10 \text{ keV}/\mu\text{m}$). While the above LET definition refers to electronic stopping power only, at low energy nuclear stopping power could be a significant fraction of the total stopping power.

• **Activity, A** (unit: Becquerel, $1 \text{ Bq}=1/\text{s}=27 \text{ pCi}$): Activity is the expectation value of the number of nuclear decays occurring in a given quantity of material per unit time.

37.1.2 Protection quantities

• **Organ absorbed dose, D_T** (unit: gray): The mean absorbed dose in an organ or tissue T of mass m_T is defined as

$$D_T = \frac{1}{m_T} \int_{m_T} D dm .$$

• **Equivalent dose, H_T** (unit: sievert, $1 \text{ Sv}=1 \text{ J/kg}=100 \text{ rem}$):

The equivalent dose H_T in an organ or tissue T is equal to the sum of the absorbed doses $D_{T,R}$ in the organ or tissue caused by different radiation types R weighted with so-called radiation weighting factors w_R :

$$H_T = \sum_R w_R \times D_{T,R} .$$

It expresses long-term risks (primarily cancer and leukemia) from low-level chronic exposure. The values for w_R recommended by ICRP [2] are given in Table 37.1.

Table 37.1: Radiation weighting factors, w_R .

Radiation type	w_R
Photons, electrons and muons	1
Neutrons, $E_n < 1 \text{ MeV}$	$2.5 + 18.2 \times \exp[-(\ln E_n)^2/6]$
$1 \text{ MeV} \leq E_n \leq 50 \text{ MeV}$	$5.0 + 17.0 \times \exp[-(\ln(2E_n))^2/6]$
$E_n > 50 \text{ MeV}$	$2.5 + 3.25 \times \exp[-(\ln(0.04E_n))^2/6]$
Protons and charged pions	2
Alpha particles, fission fragments, heavy ions	20

• **Effective dose, E** (unit: sievert): The sum of the equivalent doses, weighted by the tissue weighting factors w_T ($\sum_T w_T = 1$) of several organs and tissues T of the body that are considered to be most sensitive [2], is called “effective dose”:

$$E = \sum_T w_T \times H_T . \quad (37.1)$$

37.1.3 Operational quantities

• **Dose equivalent, H** (unit: sievert): The dose equivalent at a point in tissue is given by:

$$H = D \times Q \quad (37.2)$$

where D is the absorbed dose and Q is the quality factor at that point. The quality factor at a point in tissue, is given by:

$$Q = \frac{1}{D} \int_{L=0}^{\infty} Q(L) D_L dL$$

where D_L is the distribution of D in unrestricted linear energy transfer L at the point of interest, and $Q(L)$ is the quality factor as a function of L . The integration is to be performed over D_L , due to all charged particles, excluding their secondary electrons.

• **Ambient dose equivalent, $H^*(10)$** (unit: sievert): The dose equivalent at a point in a radiation field that would be produced by the corresponding expanded and aligned field in a 30 cm diameter sphere of unit density tissue (so-called ICRU sphere/tissue with a mass composition of 76.2% oxygen, 11.1% carbon, 10.1% hydrogen and 2.6% nitrogen) at a depth of 10 mm on the radius vector opposing the direction of the aligned field. Ambient dose equivalent is the operational quantity for *area monitoring*.

• **Personal dose equivalent, $H_p(d)$** (unit: sievert): The dose equivalent in ICRU tissue at an appropriate depth, d , below a specified point on the human body. The specified point is normally taken to be where the individual dosimeter is worn. For the assessment of effective dose, $H_p(10)$ with a depth $d = 10 \text{ mm}$ is chosen, and for the assessment of the dose to the skin and to the hands and feet the personal dose equivalent, $H_p(0.07)$, with a depth $d = 0.07 \text{ mm}$, is used. Personal dose equivalent is the operational quantity for *individual monitoring*.

37.1.4 Dose conversion coefficients

Dose conversion coefficients allow direct calculation of protection or operational quantities from particle fluence and are functions of particle type, energy and irradiation configuration. The most common coefficients are those for effective dose and ambient dose equivalent. The former are based on simulations in which the dose to organs of anthropomorphic phantoms is calculated for approximate actual conditions of exposure, such as irradiation of the front of the body (antero-posterior irradiation) or isotropic irradiation.

Conversion coefficients from fluence to effective dose are given for anterior-posterior irradiation and various particle types in Fig. 37.1 [4]. For example, the effective dose from an anterior-posterior irradiation in a field of 1-MeV neutrons with a fluence of 1 neutron per cm^2 is about 290 pSv. In Monte Carlo simulations such coefficients allow multiplication with fluence at scoring time such that effective dose to a human body at the considered location is directly obtained.

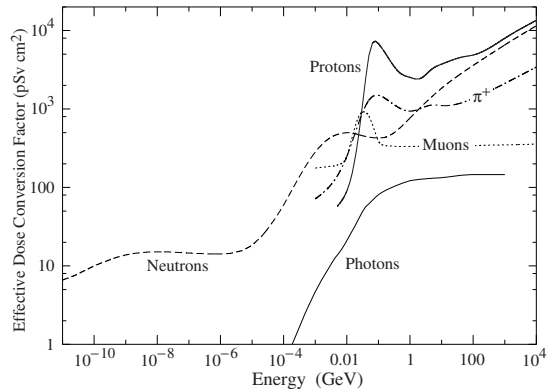


Figure 37.1: Fluence to effective dose conversion coefficients for anterior-posterior irradiation and various particle types [4].

37.2 Radiation levels [5]

• Natural background radiation:

On a worldwide average, the annual whole-body dose equivalent due to all sources of natural background radiation ranges from 1.0 to 13 mSv (0.1–1.3 rem) with an annual average of 2.4 mSv [6]. In certain areas values up to 50 mSv (5 rem) have been measured. A large fraction (typically more than 50%) originates from inhaled natural radioactivity, mostly radon and radon daughters [7]. The latter can vary by more than one order of magnitude: it is 0.1–0.2 mSv in open areas, 2 mSv on average in a house and more than 20 mSv in poorly ventilated mines.

• **Cosmic ray background radiation:** At sea level, the whole-body dose equivalent due to cosmic ray background radiation is dominated by muons; at higher altitudes also nucleons contribute. Dose equivalent rates range from less than 0.1 μ Sv/h at sea level to a few μ Sv/h at aircraft altitudes. Details on cosmic ray fluence levels are given in the Cosmic Rays section (Sec. 30 of this Review).

37.3 Health effects of ionizing radiation

Radiation can cause two types of health effects, deterministic and stochastic:

• **Deterministic effects** are tissue reactions which cause injury to a population of cells if a given threshold of absorbed dose is exceeded. The severity of the reaction increases with dose. The quantity in use for tissue reactions is the absorbed dose, D . When particles other than photons and electrons (low-LET radiation) are involved, a Relative Biological Effectiveness (RBE)-weighted dose may be used. The RBE of a given radiation is the reciprocal of the ratio of the absorbed dose of that radiation to the absorbed dose of a reference radiation (usually X rays) required to produce the same degree of biological effect. It is a complex quantity that depends on many factors such as cell type, dose rate, fractionation, etc.

• **Stochastic effects** are malignant diseases and heritable effects for which the probability of an effect occurring, but not its severity, is a function of dose without threshold.

• **Lethal dose:** The whole-body dose from penetrating ionizing radiation resulting in 50% mortality in 30 days (assuming no medical treatment) is 2.5–4.5 Gy (250–450 rad)¹, as measured internally on the body longitudinal center line. The surface dose varies due to variable body attenuation and may be a strong function of energy.

• Cancer induction:

The cancer induction probability is about 5% per Sv on average for the entire population [3].

• **Recommended effective dose limits:** The International Commission on Radiological Protection (ICRP) recommends a limit for radiation workers of 20 mSv effective dose per year averaged over 5 years, with the provision that the dose should not exceed 50 mSv in any single year [3]. The limit in the EU-countries

¹ RBE -weighted when necessary

and Switzerland is 20 mSv per year, in the U.S. it is 50 mSv per year (5 rem per year). Many physics laboratories in the U.S. and elsewhere set lower limits. The effective dose limit for the general public is typically 1 mSv per year.

37.4 Prompt neutrons at accelerators

Neutrons dominate the radiation environment outside thick shielding (*e.g.*, > 1 m of concrete) for high energy (> a few hundred MeV) electron and hadron accelerators. In addition, for accelerators with energies above about 10 GeV, muons contribute significantly at small angles with regard to the beam, even behind several meters of shielding. Another special case are synchrotron light sources where particular care has to be taken to shield the very intense low-energy photons extracted from the electron synchrotron into the experimental areas. Due to its importance at high energy accelerators this section focuses on prompt neutrons.

37.4.1 Electron accelerators

At electron accelerators, neutrons are generated via photonuclear reactions from bremsstrahlung photons. Neutron production takes place above a threshold value which varies from 10 to 19 MeV for light nuclei (with important exceptions, such as 2.23 MeV for deuterium and 1.67 MeV for beryllium) and from 4 to 6 MeV for heavy nuclei. It is commonly described by different mechanisms depending on the photon energy: the giant dipole resonance interactions (from threshold up to about 30 MeV, often the dominant process), the quasi-deuteron effect (between 30 MeV and a few hundred MeV), the delta resonance mechanism (between 200 MeV and a few GeV) and the vector meson dominance model at higher energies.

The giant dipole resonance reaction consists in a collective excitation of the nucleus, in which neutrons and protons oscillate in the direction of the photon electric field. The oscillation is damped by friction in a few cycles, with the photon energy being transferred to the nucleus in a process similar to evaporation. Nucleons emitted in the dipolar interaction have an anisotropic angular distribution, with a maximum at 90°, while those leaving the nucleus as a result of evaporation are emitted isotropically with a Maxwellian energy distribution described as [8]:

$$\frac{dN}{dE_n} = \frac{E_n}{T^2} e^{-E_n/T}, \quad (37.3)$$

where T is a nuclear ‘temperature’ (in units of MeV) characteristic of the particular target nucleus and its excitation energy. For heavy nuclei the ‘temperature’ generally lies in the range of $T = 0.5$ –1.0 MeV. Neutron yields from semi-infinite targets per kW of electron beam power are plotted in Fig. 37.2 as a function of the electron beam energy [8].

While for thick targets neutron production is mainly due to photonuclear interactions, for thin targets (thickness of fractions of the radiation length) electronuclear interactions are the dominating process.

Typical neutron energy spectra outside of concrete (80 cm thick, 2.35 g/cm³) and iron (40 cm thick) shields are shown in Fig. 37.3. In order to compare these spectra to those caused by proton beams (see below) the spectra are scaled by a factor of 100, which roughly corresponds to the difference in the high energy hadronic cross sections for photons and hadrons (*e.g.*, the fine structure constant). The shape of these spectra are generally characterized by a low-energy peak at around 1 MeV (evaporation neutrons) and a high-energy shoulder at around 70–80 MeV. In case of concrete shielding, the spectrum also shows a pronounced peak at thermal neutron energies.

37.4.2 Proton accelerators

At proton accelerators, neutron yields emitted per incident proton by different target materials are roughly independent of proton energy between 20 MeV and 1 GeV, and are given by the ratio C : Al : Cu-Fe : Sn : Ta-Pb = 0.3 : 0.6 : 1.0 : 1.5 : 1.7 [11]. Above about 1 GeV, the neutron yield is proportional to E^m , where $0.80 \leq m \leq 0.85$ [12].

Typical neutron energy spectra outside of concrete and iron shielding are shown in Fig. 37.3. Here, the radiation fields are

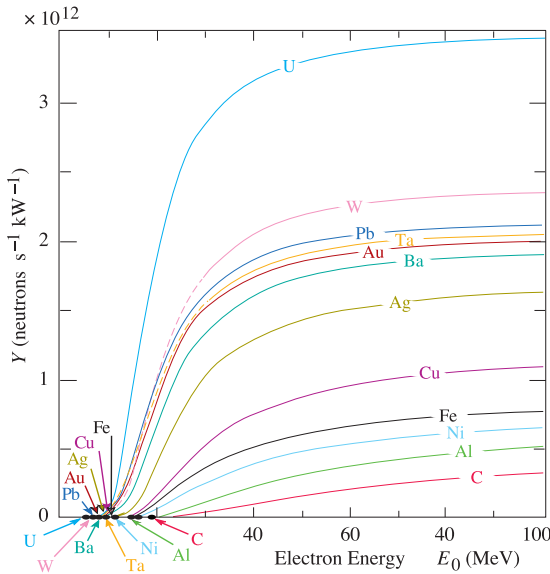


Figure 37.2: Neutron yields from semi-infinite targets per kW of electron beam power, as a function of the electron beam energy, disregarding target self-shielding [8].

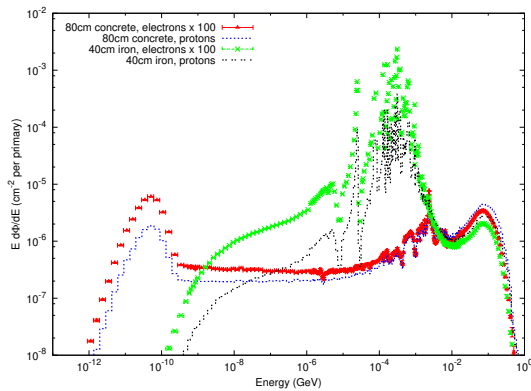


Figure 37.3: Neutron energy spectra calculated with the FLUKA code [9,10] from 25 GeV proton and electron beams on a thick copper target. Spectra are evaluated at 90° to the beam direction behind 80 cm of concrete or 40 cm of iron. All spectra are normalized per beam particle. For better visualization, spectra for electron beam are multiplied by a factor of 100.

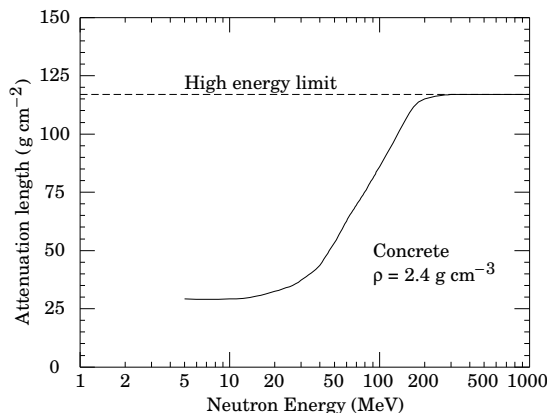


Figure 37.4: The variation of the attenuation length for mono-energetic neutrons in concrete as a function of neutron energy [11].

caused by a 25 GeV proton beam interacting with a thick copper target. The comparison of these spectra with those for an electron beam of the same energy reflects the difference in the hadronic cross sections between photons and hadrons above a few 100 MeV. Differences are increasing towards lower energies because of different interaction mechanisms. Furthermore, the slight shift in energy above about 100 MeV follows from the fact that the energies of the interacting photons are lower than 25 GeV. Apart from this the shapes of the two spectra are similar.

The neutron-attenuation length is shown in Fig. 37.4 for concrete and mono-energetic broad-beam conditions. It reaches an asymptotic value of about 117 g/cm² above 200 MeV. As the cascade through thick shielding is carried by particles with energies between about 100 MeV and 300 MeV (in this energy range non-elastic cross sections are at minimum and are dominated by quasi-elastic processes leading to low attenuation) this value is equal to the equilibrium attenuation length for particles emitted at 90° in concrete.

37.5 Photon sources

The dose equivalent rate in tissue (in mSv/h) from a gamma point source emitting one photon of energy E (in MeV) per second at a distance of 1 m is $4.6 \times 10^{-9} \mu_{en}/\rho E$, where μ_{en}/ρ is the mass energy absorption coefficient. The latter has a value of $0.029 \pm 0.004 \text{ cm}^2/\text{g}$ for photons in tissue over an energy range between 60 keV and 2 MeV (see Ref. [13] for tabulated values).

Similarly, the dose equivalent rate in tissue (in mSv/h) at the surface of a semi-infinite slab of uniformly activated material containing 1 Bq/g of a gamma emitter of energy E (in MeV) is $2.9 \times 10^{-4} R_{\mu} E$, where R_{μ} is the ratio of the mass energy absorption coefficients of the photons in tissue and in the material.

37.6 Accelerator-induced radioactivity

Typical medium- and long-lived activation products in metallic components of accelerators are ²²Na, ⁴⁶Sc, ⁴⁸V, ⁵¹Cr, ⁵⁴Mn, ⁵⁵Fe, ⁵⁹Fe, ⁵⁶Co, ⁵⁷Co, ⁵⁸Co, ⁶⁰Co, ⁶³Ni and ⁶⁵Zn. Gamma-emitting nuclides dominate doses from external irradiation at longer decay times (more than one day) while at short decay times β^+ emitters are also important (through photons produced by β^+ annihilation). Due to their short range, β^- emitters are relevant, for example, only for dose to the skin and eyes or for doses due to inhalation or ingestion. Fig. 37.5 and Fig. 37.6 illustrate the contributions of gamma and β^+ emitters to the total dose rate at 12.4 cm distance to a copper sample [14]. The sample was activated by the stray radiation field created by a 120 GeV mixed hadron beam dumped in a copper target during about 8 hours at intensities between $10^7 - 10^8$ hadrons per second. Here, the contributions by individual nuclides were calculated analytically assuming exponential decay of the nuclide inventory present at 20 minute cooling time. The total dose rate, however, also includes decay chains and as such also contributions from daughter nuclides.

Typically, dose rates at a certain decay time are mainly determined by radionuclides having a half-life of the order of the decay time. Extended irradiation periods might be an exception to this general rule as in this case the activity of long-lived nuclides can build up sufficiently so that it dominates that one of short-lived even at short cooling times.

Activation in concrete is dominated by ²⁴Na (short decay time) and ²²Na (long decay time). Both nuclides can be produced either by low-energy neutron reactions on the sodium-component in the concrete or by spallation reactions on silicon, calcium and other constituents such as aluminum. At long decay times nuclides of radiological interest in activated concrete can also be ⁶⁰Co, ¹⁵²Eu, ¹⁵⁴Eu and ¹³⁴Cs, all of which produced by (n, γ)-reactions with traces of natural cobalt, europium and cesium. Thus, such trace elements might be important even if their content in concrete is only a few parts per million or less by weight.

The explicit simulation of radionuclide production with general-purpose Monte Carlo codes has become the most commonly applied method to calculate induced radioactivity and its radiological consequences [14] (see also Sec. 37.8). They are complemented by analytical codes based on folding particle fluence spectra with nuclide production cross sections. ActiWiz [15, 16] is an example

with energy.

- **Proportional counters:** Proportional counters are another type of gas-filled detector, operated in pulse mode. They are normally of cylindrical geometry, with a thin central wire (the anode) on the axis of a hollow tube (the cathode). The initial electron charge created by the interaction of the radiation with the gas is amplified by the multiplication process (Townsend avalanche) produced by the strong electric field in a narrow volume around the anode. The generated pulses are still proportional to the original number of ion pairs but are much larger than in an ionization chamber, yielding a much improved signal-to-noise ratio. Proportional counters are also used for neutron detection: the rem counter and BSS discussed in the previous sections typically employ ^3He or BF_3 filled tubes with a large sensitivity to thermal neutrons.

- **Scintillators:** Scintillation-based detectors are used in radiation protection as hand-held probes and in fixed installations, e.g., portal monitors. A scintillation detector or counter is obtained coupling a scintillator to an electronic light sensor such as a photomultiplier tube (PMT), a photodiode or a silicon photomultiplier (SiPM). There is a wide range of scintillating materials, inorganic (such as CsI and BGO), organic or plastic; they find application in both photon dosimetry and spectrometry.

37.7.3 Operation in pulsed radiation fields

There are many practical situations with particle accelerators used for scientific, industrial and medical applications where the time structure of the stray radiation limits the use of active monitors or requires specifically designed electronics. Pulsed neutron and gamma fields may be present because of beam losses at, e.g., targets, collimators and beam dumps. The time duration of a single burst can range from a few ns to about 1 ms with a typical repetition rate in the range 0.1–100 Hz. Conventional detectors generally suffer from dead time effects and have strong limitations in the measurements of pulsed fields. Severe under response has been observed, e.g., in commercial rem counters, with tremendous underestimation of the ambient dose equivalent, $H^*(10)$, up to three orders of magnitude [25]. The common techniques used to correct the response of radiation detectors which include dead-time corrections operate properly in a steady-state radiation field, whereas it is much more difficult to cope with dead time losses in a pulsed radiation field of unknown time structure and burst dose. Generally speaking the monitoring instrumentation must be chosen on the basis of the knowledge of the radiation field. Detectors with specifically designed electronics must be employed in pulsed field conditions in place of conventional rem counters for neutrons, such as the LUPIN detector [26]. If real-time monitoring is not required, passive detectors or dosimeters such as TEDs mentioned in Sec. 37.7.1 or LiF mentioned in Sec. 37.7.5 can be employed, as they are insensitive to the time structure of the radiation.

37.7.4 Operation in presence of magnetic fields

There may be circumstances in which a radiation survey needs to be performed in the presence of a magnetic field. This may be the case for example for measurements on activated detector components in the underground experimental areas of CERN LHC experiments without switching off the intense magnetic field of the detectors; or measurements of the residual radioactivity of permanent magnets sometimes used in particle accelerators. In hospitals, one of most advanced diagnostic modalities is PET-MRI, in which PET imaging uses radioactive substances (radio-pharmaceuticals) in proximity of the strong magnetic field of the MRI scanner. Most of the commercial survey meters do not operate correctly or do not function at all in the presence of even comparatively weak magnetic fields below 0.3 T, and often already at 0.1 T. This is either because of the presence of components in their electronics sensitive to magnetic field (e.g. inductive elements), ferromagnetic materials in general (such as shells, screws and frames), battery drain/heating or LCD screen failure. An instrument called B-RAD has recently been developed [27] that overcomes the above limitations and is now commercially available. It is a hand-held instrument for gamma dose rate and gamma spectrometry measurements, consisting of a central unit (housing a microcontroller, magnetic field insensitive electronic

circuitry, the battery and two displays) and a probe connected through a cable, certified to operate up to 3 T fields. The probe uses a $\text{LaBr}_3(\text{Ce})$ crystal coupled to an array of silicon photomultipliers. The excellent scintillation properties and the high photon resolution of the scintillator (3.3% FWHM at 662 keV) make the device capable of operating in the energy range from 30 keV to 2 MeV photons with a very fast response.

37.7.5 Personal dosimeters

Personal dosimeters, calibrated in $H_p(10)$, are worn by persons exposed to ionizing radiation for professional reasons to record the dose received. They are typically passive detectors, either film, track etched detectors, $^6\text{Li}/^7\text{Li}$ -based dosimeters (e.g. LiF), optically stimulated luminescence (OSL) or radiophotoluminescence detectors (RPL) but semi-active dosimeters using miniaturized ion-chambers also exist, like the Direct Ion Storage (DIS) dosimeters in use at CERN.

Electronic personal dosimeters are small active units for on-line monitoring of individual exposure, designed to be worn on the body. They can give an alarm on both the integral dose received or dose rate once a pre-set threshold is exceeded.

37.8 Monte Carlo codes for radiation protection studies

The use of general-purpose particle interaction and transport Monte Carlo codes is often the most accurate and efficient choice for assessing radiation protection quantities at accelerators. Due to the vast spread of such codes to all areas of particle physics and the associated extensive benchmarking with experimental data, the modeling has reached an unprecedented accuracy. Furthermore, most codes allow the user to simulate all aspects of a high energy particle cascade in one and the same run: from the first interaction of a TeV nucleus over the transport and re-interactions (hadronic and electromagnetic) of the produced secondaries, to detailed nuclear fragmentation, the calculation of radioactive decays and even of the electromagnetic shower caused by the radiation from such decays. A brief account of the codes most widely used for radiation protection studies at high energy accelerators is given in the following.

- **FLUKA [9, 10, 28, 29]:** FLUKA is a general-purpose particle interaction and transport code. It comprises all features needed for radiation protection, such as detailed hadronic and nuclear interaction models up to 10 PeV, full coupling between hadronic and electromagnetic processes and numerous variance reduction options. The latter include weight windows, region importance biasing, and leading particle, interaction, and decay length biasing (among others). The capabilities of FLUKA are unique for studies of induced radioactivity, especially with regard to nuclide production, decay, and transport of residual radiation. In particular, particle cascades by prompt and residual radiation are simulated in parallel based on the microscopic models for nuclide production and a solution of the Bateman equations for activity build-up and decay.

- **GEANT4 [30–32]:** GEANT4 is an object-oriented toolkit consisting of a kernel that provides the framework for particle transport, including tracking, geometry description, material specifications, management of events and interfaces to external graphics systems. The kernel also provides interfaces to physics processes. It allows the user to freely select the physics models that best serve the particular application needs. Implementations of interaction models exist over an extended range of energies, from optical photons and thermal neutrons to high-energy interactions required for the simulation of accelerator and cosmic ray experiments. To facilitate the use of variance reduction techniques, general-purpose biasing methods such as importance biasing, weight windows, and a weight cut-off method have been introduced directly into the toolkit. Other variance reduction methods, such as leading particle biasing for hadronic processes, come with the respective physics packages.

- **MARS15 [33, 34]:** The MARS15 code system is a set of Monte Carlo programs for the simulation of hadronic and electromagnetic cascades. It covers a wide energy range: 1 keV to 100 TeV for muons, charged hadrons, heavy ions and electromagnetic showers; and 0.00215 eV to 100 TeV for neutrons. Hadron-nucleus inter-

actions as well as practically all other strong, weak and electromagnetic interactions in the entire energy range can be simulated either inclusively or exclusively. MARS15 uses ENDFB-VII nuclear data to handle interactions of neutrons with energies below 14 MeV. Several variance reduction techniques, such as weight windows, particle splitting, and Russian roulette, are available. A tagging module allows tagging the origin of a given signal for source term or sensitivity analyses. The geometry module allows either a basic solid body representation option or a ROOT-based powerful engine. Further features of MARS15 include a MAD-MARS merge for a convenient creation of accelerator models and multi-turn tracking and cascade simulation in accelerator and beamline lattices.

• **MCNP6 [35, 36]:** MCNP6 is the latest version of the Monte Carlo N-Particle transport (MCNP) family of neutron interaction and transport codes and, therefore, features one of the most comprehensive and detailed descriptions of the related physical processes. It transports 37 different particle types, including ions and electromagnetic particles. The neutron interaction and transport modules use standard evaluated data libraries mixed with physics models where such libraries are not available. The transport is continuous in energy. MCNP6 contains one of the most powerful implementations of variance reduction techniques. Spherical mesh weight windows can be created by a generator in order to focus the simulation time on certain spatial regions of interest. In addition, a more generalized phase space biasing is also possible through energy- and time-dependent weight windows. Other biasing options include pulse-height tallies with variance reduction and criticality source convergence acceleration.

• **PHITS [37, 38]:** The Particle and Heavy-Ion Transport code System PHITS was among the first general-purpose codes to simulate the transport and interactions of heavy ions in a wide energy range, from 10 MeV/nucleon to 100 GeV/nucleon. It is based on the high-energy hadron transport code NMTC/JAM that was extended to heavy ions. The transport of low-energy neutrons employs cross sections from evaluated nuclear data libraries such as ENDF and JENDL below 20 MeV. Electromagnetic interactions are simulated based on the ITS code in the energy range between 1 keV and 100 MeV for electrons and positrons and between 1 keV and 100 GeV for photons. Several variance reduction techniques, including weight windows and region importance biasing, are available.

References

- [1] International Commission on Radiation Units and Measurements, *Fundamental Quantities and Units for Ionizing Radiation*, ICRU Report 60 (1998).
- [2] ICRP, 2010. *Conversion Coefficients for Radiological Protection Quantities for External Radiation Exposures*, ICRP Publication 116, Annals of the ICRP 40(2-5).
- [3] ICRP Publication 103, *The 2007 Recommendations of the International Commission on Radiological Protection*, Annals of the ICRP, Elsevier (2007).
- [4] M. Pelliccioni, *Radiation Protection Dosimetry* **88**, 279 (2000).
- [5] E. Pochin, *Nuclear Radiation: Risks and Benefits*, Clarendon Press, Oxford, 1983.
- [6] United Nations, *Report of the United Nations Scientific Committee on the Effect of Atomic Radiation*, General Assembly, Official Records A/63/46 (2008).
- [7] G. Cinelli *et al.*, *European Atlas of Natural Radiation*, G. Cinelli, M. De Cort, and T. Tollefsen, editor(s), Publications Office of the European Union, Luxembourg, 2019, ISBN 978-92-76-08259-0, JRC116795.
- [8] W. P. Swanson, *Radiological Safety Aspects of the Operation of Electron Linear Accelerators*, IAEA Technical Reports Series No. 188 (1979) (1979).
- [9] A. Ferrari, *et al.*, FLUKA: A Multi-particle Transport Code, CERN-2005-010 (2005), SLAC-R-773, INFN-TC-05-11, <http://www.fluka.org>.
- [10] G. Battistoni *et al.*, *Annals of Nuclear Energy* **82**, 10 (2015).
- [11] R.H. Thomas and G.R. Stevenson, *Radiological Safety Aspects of the Operation of Proton Accelerators*, SSC-N-354 (1986), IAEA Technical Report Series No. 283 (1988).
- [12] T. Gabriel *et al.*, *Nucl. Instrum. Meth. A* **338**, 336 (1994).
- [13] <http://physics.nist.gov/PhysRefData/XrayMassCoef/cover.html>.
- [14] S. Roesler, *et al.*, "Simulation of Remanent Dose Rates and Benchmark Measurements at the CERN-EU High Energy Reference Field Facility," in *Proceedings of the Sixth International Meeting on Nuclear Applications of Accelerator Technology*, San Diego, CA, 1-5 June 2003, 655-662 (2003).
- [15] C. Theis and H. Vincke, "The use of ActiWiz in operational radiation protection," in *Proceedings of the Twelfth Meeting of Task-Force on Shielding Aspects of Accelerators, Targets and Irradiation Facilities of Accelerator Technology, SATIF12* FNAL, 28-30 April 2014, Nuclear Science Report NEA/NSC/R 3, (2015).
- [16] C. Theis and H. Vincke, "ActiWiz3 an overview of the concepts, architecture and new features," CERN Technical Note CERN-RP-2016-117-REPORTS-TN (2016), <http://actiwiz.web.cern.ch>.
- [17] I.O. Andersson and J. Braun, "A neutron rem counter with uniform sensitivity from 0.025 eV to 10 MeV" in *Proceedings of the IAEA Symposium on Neutron dosimetry*, IAEA, Vienna, Vol. II, 87-95, (1963).
- [18] C. Birattari, *et al.*, *Radiation Protection Dosimetry* **76**, 135 (1998).
- [19] R.L. Bramblett, R.I. Ewing and T.W. Bonner, *Nucl. Instrum. Methods* **9**, 1 (1960).
- [20] M. Matzke, PTB, Braunschweig PTBN-19, (1994).
- [21] M. Reginatto and P. Goldhagen, *Health Physics* **77**, 579 (1999).
- [22] F. d'Errico, *Nucl. Instrum. Methods* **B184**, 229 (2001).
- [23] K. Becker, *Dosimetric applications of track etching*, in *Topics in Radiation Dosimetry* Ed. F.H. Attix, Academic Press, London, 79-143, (1972).
- [24] G.F. Knoll, *Radiation detection and measurements*, Wiley (2010).
- [25] M. Caresana *et al.*, *Nucl. Instrum. Meth. A* **737**, 203 (2014).
- [26] M. Caresana, *et al.*, A new version of the LUPIN detector: Improvements and latest experimental verification, *Review of Scientific Instruments* **85**, 065102 (2014).
- [27] D. Celeste, A. Curioni, A. Fazzi, M. Silari and V. Varoli, B-RAD: a radiation survey meter for operation in intense magnetic fields *Journal of Instrumentation* **14**, T05007 (2019).
- [28] C. Ahdida, *et al.*, New Capabilities of the FLUKA Multi-Purpose Code, *Frontiers in Physics* **9**, 788253 (2022) <http://fluka.cern>.
- [29] T. T. Böhlen *et al.*, *Nucl. Data Sheets* **120**, 211 (2014).
- [30] S. Agostinelli *et al.* (GEANT4), *Nucl. Instrum. Meth. A* **506**, 250 (2003).
- [31] J. Allison *et al.*, *IEEE Trans. Nucl. Sci.* **53**, 270 (2006).
- [32] J. Allison *et al.*, *Nucl. Instrum. Meth. A* **835**, 186 (2016), <http://geant4.cern.ch>.
- [33] N.V. Mokhov and C.C. James, The MARS Code System User's Guide, Fermilab-FN-1058-APC (2018), <https://mars.fnal.gov>.
- [34] N. Mokhov *et al.*, *Prog. Nucl. Sci. Tech.* **4**, 496 (2014), [arXiv:1409.0033].
- [35] J.T. Goorley, *et al.*, *Nuclear Technology* **180**, 298 (2012).
- [36] J.A. Kulesza *et al.*, MCNP Code Version 6.3.0 Theory and User Manual, Los Alamos National Laboratory report, LA-UR-22-30006 (2022), <https://mcnp.lanl.gov>.
- [37] T. Sato, *et al.*, *Journal of Nuclear Science and Technology* **55**, 684 (2018).
- [38] T. Sato, *et al.*, PHITS Particle and Heavy Ion Transport code System, Version 3.31 (2023), <https://phits.jaea.go.jp>.

38. Commonly Used Radioactive Sources

Revised September 2023 by D.E. Groom (LBNL).

Table 38.1: Radioactive sources

Nuclide	Half-life	Type of Decay	Particle		Photon	
			Energy (MeV)	Emission prob.	Energy (MeV)	Emission prob.
²² ₁₁ Na	2.603 y	β^+ , EC	0.546	90%	0.511 1.275	Annih. 100%
⁵¹ ₂₄ Cr	27.70 d	EC			0.320 V K x rays	10% 100%
Neutrino calibration source						
⁵⁴ ₂₅ Mn	0.855 y	EC			0.835 Cr K x rays	100% 26%
⁵⁵ ₂₆ Fe	2.747 y	EC			Mn K x rays: 0.00590 0.00649	24.4% 2.86%
⁵⁷ ₂₇ Co	271.8 d	EC			0.014 0.122 0.136	9% 86% 11%
⁶⁰ ₂₇ Co	5.271 y	β^-	0.317	99.9%	Fe K x rays 1.173 1.333	99.9% 99.9%
⁶⁸ ₃₂ Ge → ⁶⁸ ₃₁ Ga	271.0 d	EC			Ga K x rays	42%
	67.8 m	β^+ , EC	1.899	90%	0.511 1.077	Annih. 3%
⁹⁰ ₃₈ Sr → ⁹⁰ ₃₉ Y	28.8 y 2.67 d	β^- β^-	0.546 2.279	100%		
¹⁰⁶ ₄₄ Ru → ¹⁰⁶ ₄₅ Rh	371.5 d 30.1 s	β^- β^-	0.039 3.546	100%		
					0.512 0.622	21% 10%
¹⁰⁹ ₄₈ Cd	1.265 y	EC	0.063 e^- 0.084 e^-	42% 44%	0.088 Ag K x rays	3.7% 100%
¹¹³ ₅₀ Sn	115.1 d	EC	0.364 e^- 0.388 e^-	28% 6%	0.392 In K x rays	65% 97
¹³⁷ ₅₅ Cs	30.0 y	β^-	0.514 1.176	94% 6%	0.662	85%
¹³³ ₅₆ Ba	10.55 y	EC	0.045 e^- 0.075 e^-	50% 6%	0.081 0.356	33% 62%
					Cs K x rays	121%
¹⁵² ₆₃ Eu	13.537 y	EC		72.1%	Many γ 's	
		β^-		27.9%	0.1218–1.408 MeV	
²⁰⁷ ₈₃ Bi	32.9 y	EC	0.481 e^- 0.975 e^- 1.047 e^-	2% 7% 2%	0.569 1.063 1.770	98% 75% 7%
					Pb K x rays	78%
²²⁸ ₉₀ Th	1.912 y	6 α : 3 β^- :	5.341 – 8.785 0.334 – 2.246		0.239 0.583 2.614	44% 31% 36%
$\left(\begin{array}{cccccc} \rightarrow & \rightarrow & \rightarrow & \rightarrow & \rightarrow & \rightarrow \\ \text{}^{224}\text{Ra} & \text{}^{220}\text{Rn} & \text{}^{216}\text{Po} & \text{}^{212}\text{Pb} & \text{}^{212}\text{Bi} & \text{}^{212}\text{Po} \\ \text{}_{88} & \text{}_{86} & \text{}_{84} & \text{}_{82} & \text{}_{83} & \text{}_{84} \\ 361 \text{ d} & 55.8 \text{ s} & 0.148 \text{ s} & 10.64 \text{ h} & 60.54 \text{ m} & 300 \text{ ns} \end{array} \right)$						
²⁴¹ ₉₅ Am	432.6 y	α	5.433 5.486	13% 85%	0.0595409 Np L x rays	36% 38%
²⁴¹ ₉₅ Am/Be	432.6 y	neutrons ($E = 4$ MeV) and γ 's (4.43 MeV from ${}^9\text{Be}(\alpha, n)$)				
²⁴⁴ ₉₆ Cm	18.11 y	α	5.763 5.805	24% 76%	Pu L x rays	$\sim 9\%$
²⁵² ₉₈ Cf	2.645 y	α (97%)	6.076 6.118	15% 82%		
Fission (3.1%): Average 7.8 γ 's/fission; $\langle E_\gamma \rangle = 0.88$ MeV ≈ 4 neutrons/fission; $\langle E_n \rangle = 2.14$ MeV						

“Emission probability” is the probability per decay of a given emission; because of cascades these may total more than 100%. Only principal emissions are listed. EC means electron capture, and e^- means monoenergetic internal conversion (Auger) electron. The intensity of 0.511 MeV e^+e^- annihilation photons depends upon the number of stopped positrons. Endpoint β^\pm energies are listed. In some cases when energies are closely spaced, the γ -ray values are approximate weighted averages. Radiation from short-lived daughter isotopes is included where relevant.

Isotopic data may be found at https://physics.nist.gov/cgi-bin/Compositions/stand_alone.pl.

Neutron sources: See *e.g.* J. Liu *et al.*, “Neutron Calibration Sources in the Daya Bay Experiment” [1]. ⁵¹₂₄Cr calibration of neutrino detectors is discussed in *e.g.* J.N. Abdurashitov *et al.*, “Measurement of the response of a gallium metal solar neutrino experiment to neutrinos from a ⁵¹Cr source” [2]. The use of ⁷⁵₃₄Se and other isotopes has also been proposed.

References

- [1] J. Liu *et al.*, Nucl. Instrum. Meth. A **797**, 260 (2015), [arXiv:1504.07911].
- [2] J. N. Abdurashitov *et al.* (SAGE), Phys. Rev. C **59**, 2246 (1999), [hep-ph/9803418].



Mathematical Tools or Statistics, Monte Carlo, Group Theory

39. Probability	689
40. Statistics (rev.)	694
41. Machine Learning	711
42. Monte Carlo techniques	748
43. Monte Carlo event generators (rev.)	752
44. Monte Carlo neutrino event generators	764
45. Monte Carlo particle numbering scheme (rev.)	768
46. Clebsch-Gordan coefficients, spherical harmonics, and d functions	772
47. SU(3) isoscalar factors and representation matrices	773
48. SU(n) multiplets and Young diagrams	774





39. Probability

Revised August 2021 by G. Cowan (RHUL).

39.1 General

Further discussion of probability can be found, *e.g.*, in Refs. [1–8].

An abstract definition of probability can be given by considering a set S , called the sample space, and possible subsets A, B, \dots , the interpretation of which is left open. The probability P is a real-valued function defined by the following axioms due to Kolmogorov [9]:

1. For every subset A in S , $P(A) \geq 0$;
2. For disjoint subsets (*i.e.*, $A \cap B = \emptyset$), $P(A \cup B) = P(A) + P(B)$;
3. $P(S) = 1$.

In addition, one defines the conditional probability $P(A|B)$ (read as P of A given B) as

$$P(A|B) = \frac{P(A \cap B)}{P(B)}. \quad (39.1)$$

From this definition and using the fact that $A \cap B$ and $B \cap A$ are the same, one obtains *Bayes' theorem*,

$$P(A|B) = \frac{P(B|A)P(A)}{P(B)}. \quad (39.2)$$

From the three axioms of probability and the definition of conditional probability, one obtains the *law of total probability*,

$$P(B) = \sum_i P(B|A_i)P(A_i), \quad (39.3)$$

for any subset B and for disjoint A_i with $\cup_i A_i = S$. This can be combined with Bayes' theorem (Eq. (39.2)) to give

$$P(A|B) = \frac{P(B|A)P(A)}{\sum_i P(B|A_i)P(A_i)}, \quad (39.4)$$

where the subset A could, for example, be one of the A_i .

The most commonly used interpretation of the elements of the sample space are outcomes of a repeatable experiment. The probability $P(A)$ is assigned a value equal to the limiting frequency of occurrence of A . This interpretation forms the basis of *frequentist statistics*.

The elements of the sample space might also be interpreted as *hypotheses*, *i.e.*, statements that are either true or false, such as ‘The mass of the W boson lies between 80.3 and 80.5 GeV.’ Upon repetition of a measurement, however, such statements are either always true or always false, *i.e.*, the corresponding probabilities in the frequentist interpretation are either 0 or 1. Using *subjective probability*, however, $P(A)$ is interpreted as the degree of belief that the hypothesis A is true. Subjective probability is used in *Bayesian* (as opposed to frequentist) statistics. Bayes' theorem can be written

$$P(\text{theory}|\text{data}) \propto P(\text{data}|\text{theory})P(\text{theory}), \quad (39.5)$$

where ‘theory’ represents some hypothesis and ‘data’ is the outcome of the experiment. Here $P(\text{theory})$ is the *prior* probability for the theory, which reflects the experimenter’s degree of belief before carrying out the measurement, and $P(\text{data}|\text{theory})$ is the probability to have gotten the data actually obtained, given the theory, which is also called the *likelihood*.

Bayesian statistics provides no fundamental rule for obtaining the prior probability, which may depend on previous measurements, theoretical prejudices, *etc.* Once this has been specified, however, Eq. (39.5) tells how the probability for the theory must be modified in the light of the new data to give the *posterior* probability, $P(\text{theory}|\text{data})$. As Eq. (39.5) is stated as a proportionality, the probability must be normalized by summing (or integrating) over all possible hypotheses.

39.2 Random variables

A *random variable* is a numerical characteristic assigned to an element of the sample space. In the frequency interpretation of probability, it corresponds to an outcome of a repeatable experiment. Let x be a possible outcome of an observation. If x can take on any value from a continuous range, we write $f(x; \theta)dx$ as the probability that the measurement’s outcome lies between x and $x + dx$. The function $f(x; \theta)$ is called the *probability density function* (p.d.f.), which may depend on one or more parameters θ . If x can take on only discrete values (*e.g.*, the non-negative integers), then we use $f(x; \theta)$ to denote the probability to find the value x . In the following the term p.d.f. is often taken to cover both the continuous and discrete cases, although technically the term density should only be used in the continuous case.

The p.d.f. is always normalized to unity. Both x and θ may have multiple components and are then often written as vectors. If θ is unknown, we may wish to estimate its value from a given set of measurements of x ; this is a central topic of *statistics* (see Sec. 40).

The *cumulative distribution function* $F(a)$ is the probability that $x \leq a$:

$$F(a) = \int_{-\infty}^a f(x) dx. \quad (39.6)$$

Here and below, if x is discrete-valued, the integral is replaced by a sum. The endpoint a is expressly included in the integral or sum. Then $0 \leq F(x) \leq 1$, $F(x)$ is nondecreasing, and $P(a < x \leq b) = F(b) - F(a)$. If x is discrete, $F(x)$ is flat except at allowed values of x , where it has discontinuous jumps equal to $f(x)$.

Any function of random variables is itself a random variable, with (in general) a different p.d.f. The *expectation value* of any function $u(x)$ is

$$E[u(x)] = \int_{-\infty}^{\infty} u(x) f(x) dx, \quad (39.7)$$

assuming the integral is finite. The expectation value is linear, *i.e.*, for any two functions u and v of x and constants c_1 and c_2 , $E[c_1 u + c_2 v] = c_1 E[u] + c_2 E[v]$.

The n^{th} moment of a random variable x is

$$\alpha_n \equiv E[x^n] = \int_{-\infty}^{\infty} x^n f(x) dx, \quad (39.8a)$$

and the n^{th} central moment of x (or moment about the mean, α_1) is

$$m_n \equiv E[(x - \alpha_1)^n] = \int_{-\infty}^{\infty} (x - \alpha_1)^n f(x) dx. \quad (39.8b)$$

The most commonly used moments are the mean μ and variance σ^2 :

$$\mu \equiv \alpha_1, \quad (39.9a)$$

$$\sigma^2 \equiv V[x] \equiv m_2 = \alpha_2 - \mu^2. \quad (39.9b)$$

The mean is the location of the ‘center of mass’ of the p.d.f., and the variance is a measure of the square of its width. Note that $V[cx + k] = c^2 V[x]$. It is often convenient to use the *standard deviation* of x , σ , defined as the square root of the variance.

Any odd moment about the mean is a measure of the skewness of the p.d.f. The simplest of these is the dimensionless coefficient of skewness $\gamma_1 = m_3/\sigma^3$.

The fourth central moment m_4 provides a convenient measure of the tails of a distribution. For the Gaussian distribution (see Sec. 39.4), one has $m_4 = 3\sigma^4$. The *kurtosis* is defined as $\gamma_2 = m_4/\sigma^4 - 3$, *i.e.*, it is zero for a Gaussian, positive for a *leptokurtic* distribution with longer tails, and negative for a *platykurtic* distribution with tails that die off more quickly than those of a Gaussian.

The *quantile* x_α is the value of the random variable x at which the cumulative distribution is equal to α . That is, the quantile

is the inverse of the cumulative distribution function, *i.e.*, $x_\alpha = F^{-1}(\alpha)$. An important special case is the *median*, x_{med} , defined by $F(x_{\text{med}}) = 1/2$, *i.e.*, half the probability lies above and half lies below x_{med} . (More rigorously, x_{med} is a median if $P(x \geq x_{\text{med}}) \geq 1/2$ and $P(x \leq x_{\text{med}}) \geq 1/2$. If only one value exists, it is called ‘*the median*.’)

Under a monotonic change of variable $x \rightarrow y(x)$, the quantiles of a distribution (and hence also the median) obey $y_\alpha = y(x_\alpha)$. In general the expectation value and *mode* (most probable value) of a distribution do not, however, transform in this way.

Let x and y be two random variables with a *joint* p.d.f. $f(x, y)$. The *marginal* p.d.f. of x (the distribution of x with y unobserved) is

$$f_1(x) = \int_{-\infty}^{\infty} f(x, y) dy, \tag{39.10}$$

and similarly for the marginal p.d.f. $f_2(y)$. The *conditional* p.d.f. of y given fixed x (with $f_1(x) \neq 0$) is defined by $f_3(y|x) = f(x, y)/f_1(x)$, and similarly $f_4(x|y) = f(x, y)/f_2(y)$. From these, we immediately obtain Bayes’ theorem (see Eqs. (39.2) and (39.4)),

$$f_4(x|y) = \frac{f_3(y|x)f_1(x)}{f_2(y)} = \frac{f_3(y|x)f_1(x)}{\int f_3(y|x')f_1(x') dx'}. \tag{39.11}$$

The mean of x is

$$\mu_x = \int_{-\infty}^{\infty} \int_{-\infty}^{\infty} x f(x, y) dx dy = \int_{-\infty}^{\infty} x f_1(x) dx, \tag{39.12}$$

and similarly for y . The *covariance* of x and y is

$$\text{cov}[x, y] = E[(x - \mu_x)(y - \mu_y)] = E[xy] - \mu_x\mu_y. \tag{39.13}$$

A dimensionless measure of the covariance of x and y is given by the *correlation coefficient*,

$$\rho_{xy} = \text{cov}[x, y]/\sigma_x\sigma_y, \tag{39.14}$$

where σ_x and σ_y are the standard deviations of x and y . It can be shown that $-1 \leq \rho_{xy} \leq 1$.

Two random variables x and y are *independent* if and only if

$$f(x, y) = f_1(x)f_2(y). \tag{39.15}$$

If x and y are independent, then $\rho_{xy} = 0$; the converse is not necessarily true. If x and y are independent, $E[u(x)v(y)] = E[u(x)]E[v(y)]$, and $V[x+y] = V[x] + V[y]$; otherwise, $V[x+y] = V[x] + V[y] + 2\text{cov}[x, y]$, and $E[uv]$ does not necessarily factorize.

Consider a set of n continuous random variables $\mathbf{x} = (x_1, \dots, x_n)$ with joint p.d.f. $f(\mathbf{x})$, and a set of n new variables $\mathbf{y} = (y_1, \dots, y_n)$, related to \mathbf{x} by means of a function $\mathbf{y}(\mathbf{x})$ that is one-to-one, *i.e.*, the inverse $\mathbf{x}(\mathbf{y})$ exists. The joint p.d.f. for \mathbf{y} is given by

$$g(\mathbf{y}) = f(\mathbf{x}(\mathbf{y}))|J|, \tag{39.16}$$

where $|J|$ is the absolute value of the determinant of the square matrix $J_{ij} = \partial x_i / \partial y_j$ (the Jacobian determinant). If the transformation from \mathbf{x} to \mathbf{y} is not one-to-one, the \mathbf{x} -space must be broken into regions where the function $\mathbf{y}(\mathbf{x})$ can be inverted, and the contributions to $g(\mathbf{y})$ from each region summed.

Given a set of functions $\mathbf{y} = (y_1, \dots, y_m)$ with $m < n$, one can construct $n - m$ additional independent functions, apply the procedure above, then integrate the resulting $g(\mathbf{y})$ over the unwanted y_i to find the marginal distribution of those of interest.

For a one-to-one transformation of discrete random variables, the probability is obtained by simple substitution; no Jacobian is necessary because in this case f is a probability rather than a probability density. If the transformation is not one-to-one, then one must sum the probabilities for all values of the original variable that contribute to a given value of the transformed variable. If f depends on a set of parameters θ , a change to a different parameter set $\eta(\theta)$ is made by simple substitution; no Jacobian is used.

39.2.1 Propagation of errors

Consider n random variables $\mathbf{x} = (x_1, \dots, x_n)$ and m functions $\mathbf{y}(\mathbf{x}) = (y_1(\mathbf{x}), \dots, y_m(\mathbf{x}))$. Suppose here that the mean values $\boldsymbol{\mu} = (\mu_1, \dots, \mu_n) = E[\mathbf{x}]$ are known, although in practice they will only be estimated, and suppose we also know or have estimated the covariance matrix $V_{ij} = \text{cov}[x_i, x_j]$. The goal of *error propagation* is to determine the covariance matrix for the functions, $U_{ij} = \text{cov}[y_i, y_j]$. In particular, the diagonal elements $U_{ii} = V[y_i]$ give the variances. The new covariance matrix can be found by expanding the functions $\mathbf{y}(\mathbf{x})$ about the means $\boldsymbol{\mu}$ to first order in a Taylor series. Using this one finds

$$U_{ij} \approx \sum_{k,l} \left. \frac{\partial y_i}{\partial x_k} \frac{\partial y_j}{\partial x_l} \right|_{\boldsymbol{\mu}} V_{kl}. \tag{39.17}$$

This can be written in matrix notation as $U \approx AVA^T$ where the matrix of derivatives A is

$$A_{ij} = \left. \frac{\partial y_i}{\partial x_j} \right|_{\boldsymbol{\mu}}, \tag{39.18}$$

and A^T is its transpose. The approximation is exact if $\mathbf{y}(\mathbf{x})$ is linear. If this is not the case, the approximation can break down if, for example, $\mathbf{y}(\mathbf{x})$ is significantly nonlinear close to $\boldsymbol{\mu}$ in a region of a size comparable to the standard deviations of \mathbf{x} .

39.3 Characteristic functions

The characteristic function $\phi(u)$ associated with the p.d.f. $f(x)$ is essentially its Fourier transform, or the expectation value of e^{iux} :

$$\phi(u) = E[e^{iux}] = \int_{-\infty}^{\infty} e^{iux} f(x) dx. \tag{39.19}$$

Once $\phi(u)$ is specified, the p.d.f. $f(x)$ is uniquely determined and vice versa; knowing one is equivalent to the other. Characteristic functions are useful in deriving a number of important results about moments and sums of random variables.

It follows from Eqs. (39.8) and (39.19) that the n^{th} moment of a random variable x that follows $f(x)$ is given by

$$i^{-n} \left. \frac{d^n \phi}{du^n} \right|_{u=0} = \int_{-\infty}^{\infty} x^n f(x) dx = \alpha_n. \tag{39.20}$$

Thus it is often easy to calculate all the moments of a distribution defined by $\phi(u)$, even when $f(x)$ cannot be written down explicitly.

If the p.d.f.s $f_1(x)$ and $f_2(y)$ for independent random variables x and y have characteristic functions $\phi_1(u)$ and $\phi_2(u)$, then the characteristic function of the weighted sum $ax + by$ is $\phi_1(au)\phi_2(bu)$. The rules of addition for several important distributions (*e.g.*, that the sum of two Gaussian distributed variables also follows a Gaussian distribution) easily follow from this observation.

Let the (partial) characteristic function corresponding to the conditional p.d.f. $f_2(x|z)$ be $\phi_2(u|z)$, and the p.d.f. of z be $f_1(z)$. The characteristic function after integration over the conditional value is

$$\phi(u) = \int \phi_2(u|z)f_1(z) dz. \tag{39.21}$$

Suppose we can write ϕ_2 in the form

$$\phi_2(u|z) = A(u)e^{ig(u)z}. \tag{39.22}$$

Then

$$\phi(u) = A(u)\phi_1(g(u)). \tag{39.23}$$

The cumulants (semi-invariants) κ_n of a distribution with characteristic function $\phi(u)$ are defined by the relation

$$\phi(u) = \exp \left[\sum_{n=1}^{\infty} \frac{\kappa_n}{n!} (iu)^n \right] = \exp \left(i\kappa_1 u - \frac{1}{2} \kappa_2 u^2 + \dots \right). \tag{39.24}$$

The values κ_n are related to the moments α_n and m_n . The first few relations are

$$\begin{aligned}\kappa_1 &= \alpha_1 (= \mu, \text{ the mean}) \\ \kappa_2 &= m_2 = \alpha_2 - \alpha_1^2 (= \sigma^2, \text{ the variance}) \\ \kappa_3 &= m_3 = \alpha_3 - 3\alpha_1\alpha_2 + 2\alpha_1^3.\end{aligned}\quad (39.25)$$

39.4 Commonly used probability distributions

Table 39.1 gives a number of common probability density functions and corresponding characteristic functions, means, and variances. Further information may be found in Refs. [1–8] [10], and [11], which has particularly detailed tables. Monte Carlo techniques for generating each of them may be found in our Sec. 42.4 and in Ref. [10]. We comment below on all except the trivial uniform distribution.

39.4.1 Binomial and multinomial distributions

A random process with exactly two possible outcomes which occur with fixed probabilities is called a *Bernoulli* process. If the probability of obtaining a certain outcome (a “success”) in an individual trial is p , then the probability of obtaining exactly r successes ($r = 0, 1, 2, \dots, N$) in N independent trials, without regard to the order of the successes and failures, is given by the binomial distribution $f(r; N, p)$ in Table 39.1. If r and s are binomially distributed with parameters (N_r, p) and (N_s, p) , then $t = r + s$ follows a binomial distribution with parameters $(N_r + N_s, p)$. If there are m possible outcomes for each trial having probabilities p_1, p_2, \dots, p_m , then the joint probability to find r_1, r_2, \dots, r_m of each outcome after a total of N independent trials is given by the multinomial distribution as shown in Table 39.1. We can regard outcome i as “success” and all the rest as “failure”, so individually, any of the r_i follow a binomial distribution for N trials and a success probability p_i .

39.4.2 Poisson distribution

The Poisson distribution $f(n; \nu)$ gives the probability of finding exactly n events in a given interval of x (e.g., space or time) when the events occur independently of one another and of x at an average rate of ν per the given interval. The variance σ^2 equals ν . It is the limiting case $p \rightarrow 0$, $N \rightarrow \infty$, $Np = \nu$ of the binomial distribution. The Poisson distribution approaches the Gaussian distribution for large ν .

For example, a large number of radioactive nuclei of a given type will result in a certain number of decays in a fixed time interval. If this interval is small compared to the mean lifetime, then the probability for a given nucleus to decay is small, and thus the number of decays in the time interval is well modeled as a Poisson variable.

39.4.3 Normal or Gaussian distribution

The normal (or Gaussian) probability density function $f(x; \mu, \sigma^2)$ given in Table 39.1 has mean $E[x] = \mu$ and variance $V[x] = \sigma^2$. Comparison of the characteristic function $\phi(u)$ given in Table 39.1 with Eq. (39.24) shows that all cumulants κ_n beyond κ_2 vanish; this is a unique property of the Gaussian distribution. Some other properties are:

$$\begin{aligned}P(x \text{ in range } \mu \pm \sigma) &= 0.6827, \\ P(x \text{ in range } \mu \pm 0.6745\sigma) &= 0.5, \\ E[|x - \mu|] &= \sqrt{2/\pi}\sigma = 0.7979\sigma, \\ \text{half-width at half maximum} &= \sqrt{2 \ln 2}\sigma = 1.177\sigma.\end{aligned}$$

For a Gaussian with $\mu = 0$ and $\sigma^2 = 1$ (the *standard normal*) the cumulative distribution, often written $\Phi(x)$, is related to the error function erf by

$$F(x; 0, 1) \equiv \Phi(x) = \frac{1}{2} [1 + \operatorname{erf}(x/\sqrt{2})]. \quad (39.26)$$

The error function and standard Gaussian are tabulated in many references (e.g., Ref. [11, 12]) and are available in software packages such as ROOT [13]. For a mean μ and variance σ^2 , replace x by $(x - \mu)/\sigma$. The probability of x in a given range can be calculated with Eq. (40.76).

For x and y independent and normally distributed, $z = ax + by$ follows a normal p.d.f. $f(z; a\mu_x + b\mu_y, a^2\sigma_x^2 + b^2\sigma_y^2)$; that is, the weighted means and variances add.

The Gaussian derives its importance in large part from the *central limit theorem*:

If independent random variables x_1, \dots, x_n are distributed according to any p.d.f. with finite mean and variance, then the sum $y = \sum_{i=1}^n x_i$ will have a p.d.f. that approaches a Gaussian for large n . If the p.d.f.s of the x_i are not identical, the theorem still holds under somewhat more restrictive conditions. The mean and variance are given by the sums of corresponding terms from the individual x_i . Therefore, the sum of a large number of fluctuations x_i will be distributed as a Gaussian, even if the x_i themselves are not.

For a set of n Gaussian random variables \mathbf{x} with means $\boldsymbol{\mu}$ and covariances $V_{ij} = \operatorname{cov}[x_i, x_j]$, the p.d.f. for the one-dimensional Gaussian is generalized to

$$f(\mathbf{x}; \boldsymbol{\mu}, V) = \frac{1}{(2\pi)^{n/2} \sqrt{|V|}} \exp \left[-\frac{1}{2} (\mathbf{x} - \boldsymbol{\mu})^T V^{-1} (\mathbf{x} - \boldsymbol{\mu}) \right], \quad (39.27)$$

where the determinant $|V|$ must be greater than 0. For diagonal V (independent variables), $f(\mathbf{x}; \boldsymbol{\mu}, V)$ is the product of the p.d.f.s of n Gaussian distributions.

For $n = 2$, $f(\mathbf{x}; \boldsymbol{\mu}, V)$ is

$$\begin{aligned}f(x_1, x_2; \mu_1, \mu_2, \sigma_1, \sigma_2, \rho) &= \frac{1}{2\pi\sigma_1\sigma_2\sqrt{1-\rho^2}} \\ &\times \exp \left\{ \frac{-1}{2(1-\rho^2)} \left[\frac{(x_1 - \mu_1)^2}{\sigma_1^2} - \frac{2\rho(x_1 - \mu_1)(x_2 - \mu_2)}{\sigma_1\sigma_2} \right. \right. \\ &\quad \left. \left. + \frac{(x_2 - \mu_2)^2}{\sigma_2^2} \right] \right\}.\end{aligned}\quad (39.28)$$

The characteristic function for the multivariate Gaussian is

$$\phi(\mathbf{u}; \boldsymbol{\mu}, V) = \exp \left[i\boldsymbol{\mu} \cdot \mathbf{u} - \frac{1}{2} \mathbf{u}^T V \mathbf{u} \right]. \quad (39.29)$$

If the components of \mathbf{x} are independent, then Eq. (39.29) is the product of the characteristic functions of n Gaussians.

For an n -dimensional Gaussian distribution for \mathbf{x} with mean $\boldsymbol{\mu}$ and covariance matrix V , the marginal distribution for any single x_i is a one-dimensional Gaussian with mean μ_i and variance V_{ii} . The equation $(\mathbf{x} - \mathbf{a})^T V^{-1} (\mathbf{x} - \mathbf{a}) = C$, where C is any positive number, defines an n -dimensional ellipsoid centered about \mathbf{a} . If \mathbf{a} is equal to the mean $\boldsymbol{\mu}$, then C is a random variable obeying the χ^2 distribution for n degrees of freedom, which is discussed in the following section. The probability that \mathbf{x} lies outside the ellipsoid for a given value of C is given by $1 - F_{\chi^2}(C; n)$, where F_{χ^2} is the cumulative χ^2 distribution. This may be read from Fig. 40.1. For example, the “ s -standard-deviation ellipsoid” occurs at $C = s^2$. For the two-variable case ($n = 2$), the point \mathbf{x} lies outside the one-standard-deviation ellipsoid with 61% probability. The use of these ellipsoids as indicators of probable error is described in Sec. 40.4.2.2; the validity of those indicators assumes that $\boldsymbol{\mu}$ and V are correct.

39.4.4 Log-normal distribution

If a random variable y follows a Gaussian distribution with mean μ and variance σ^2 , then $x = e^y$ follows a log-normal distribution, as given in Table 39.1. As a consequence of the central limit theorem described in Sec. 39.4.3, the distribution of the product of a large number of positive random variables approaches a log-normal. It is bounded below by zero and is thus well suited for modeling quantities that are intrinsically non-negative such as an efficiency. One can implement a log-normal model for a random variable x by defining $y = \ln x$ so that y follows a Gaussian distribution.

39.4.5 χ^2 distribution

If x_1, \dots, x_n are independent Gaussian random variables, the sum $z = \sum_{i=1}^n (x_i - \mu_i)^2 / \sigma_i^2$ follows the χ^2 p.d.f. with n degrees

Table 39.1: Some common probability density functions, with corresponding characteristic functions and means and variances. In the Table, $\Gamma(k)$ is the gamma function, equal to $(k - 1)!$ when k is an integer; ${}_1F_1$ is the confluent hypergeometric function of the 1st kind [11].

Distribution	Probability density function f (variable; parameters)	Characteristic function $\phi(u)$	Mean	Variance
Uniform	$f(x; a, b) = \begin{cases} 1/(b-a) & a \leq x \leq b \\ 0 & \text{otherwise} \end{cases}$	$\frac{e^{ibu} - e^{iau}}{(b-a)iu}$	$\frac{a+b}{2}$	$\frac{(b-a)^2}{12}$
Binomial	$f(r; N, p) = \frac{N!}{r!(N-r)!} p^r q^{N-r}$ $r = 0, 1, 2, \dots, N; \quad 0 \leq p \leq 1; \quad q = 1 - p$	$(q + pe^{iu})^N$	Np	Npq
Multinomial	$f(r_1, \dots, r_m; N, p_1, \dots, p_m) = \frac{N!}{r_1! \dots r_m!} p_1^{r_1} \dots p_m^{r_m}$	$(\sum_{k=1}^m p_k e^{iu_k})^N$	$E[r_i] = Np_i$	$\text{cov}[r_i, r_j] = Np_i(\delta_{ij} - p_j)$
Poisson	$f(n; \nu) = \frac{\nu^n e^{-\nu}}{n!}; \quad n = 0, 1, 2, \dots; \quad \nu > 0$	$\exp[\nu(e^{iu} - 1)]$	ν	ν
Normal (Gaussian)	$f(x; \mu, \sigma^2) = \frac{1}{\sigma\sqrt{2\pi}} \exp(-(x - \mu)^2/2\sigma^2)$	$\exp(i\mu u - \frac{1}{2}\sigma^2 u^2)$	μ	σ^2
Multivariate Gaussian	$f(\mathbf{x}; \boldsymbol{\mu}, \mathbf{V}) = \frac{1}{(2\pi)^{n/2} \sqrt{ \mathbf{V} }} \times \exp[-\frac{1}{2}(\mathbf{x} - \boldsymbol{\mu})^T \mathbf{V}^{-1}(\mathbf{x} - \boldsymbol{\mu})]$ $-\infty < x_j < \infty; \quad -\infty < \mu_j < \infty; \quad \mathbf{V} > 0$	$\exp[i\boldsymbol{\mu} \cdot \mathbf{u} - \frac{1}{2}\mathbf{u}^T \mathbf{V} \mathbf{u}]$	\mathbf{u}	V_{jk}
Log-normal	$f(x; \mu, \sigma^2) = \frac{1}{\sigma\sqrt{2\pi}} \frac{1}{x} \exp(-(\ln x - \mu)^2/2\sigma^2)$ $0 < x < \infty; \quad -\infty < \mu < \infty; \quad \sigma > 0$	—	$\exp(\mu + \sigma^2/2)$	$\exp(2\mu + \sigma^2) \times [\exp(\sigma^2) - 1]$
χ^2	$f(z; n) = \frac{z^{n/2-1} e^{-z/2}}{2^{n/2} \Gamma(n/2)}; \quad z \geq 0$	$(1 - 2iu)^{-n/2}$	n	$2n$
Student's t	$f(t; n) = \frac{1}{\sqrt{n\pi}} \frac{\Gamma[(n+1)/2]}{\Gamma(n/2)} \left(1 + \frac{t^2}{n}\right)^{-(n+1)/2}$ $-\infty < t < \infty; \quad n \text{ not required to be integer}$	—	0 for $n > 1$	$n/(n-2)$ for $n > 2$
Gamma	$f(x; \lambda, k) = \frac{x^{k-1} \lambda^k e^{-\lambda x}}{\Gamma(k)}; \quad 0 \leq x < \infty; \quad k \text{ not required to be integer}$	$(1 - iu/\lambda)^{-k}$	k/λ	k/λ^2
Beta	$f(x; \alpha, \beta) = \frac{\Gamma(\alpha+\beta)}{\Gamma(\alpha)\Gamma(\beta)} x^{\alpha-1} (1-x)^{\beta-1}$ $0 \leq x \leq 1$	${}_1F_1(\alpha; \alpha + \beta; iu)$	$\frac{\alpha}{\alpha+\beta}$	$\frac{\alpha\beta}{(\alpha+\beta)^2(\alpha+\beta+1)}$

of freedom, which we denote by $\chi^2(n)$. More generally, for n correlated Gaussian variables as components of a vector \mathbf{X} with covariance matrix V , $z = \mathbf{X}^T V^{-1} \mathbf{X}$ follows $\chi^2(n)$ as in the previous section. For a set of z_i , each of which follows $\chi^2(n_i)$, $\sum z_i$ follows $\chi^2(\sum n_i)$. For large n , the χ^2 p.d.f. approaches a Gaussian with a mean and variance given by $\mu = n$ and $\sigma^2 = 2n$, respectively (here the formulae for μ and σ^2 are valid for all n).

The χ^2 p.d.f. is often used in evaluating the level of compatibility between observed data and a hypothesis for the p.d.f. that the data might follow. This is discussed further in Sec. 40.3.2 on significance tests.

39.4.6 Student's t distribution

Suppose that y and x_1, \dots, x_n are independent and Gaussian distributed with mean 0 and variance 1. We then define

$$z = \sum_{i=1}^n x_i^2 \quad \text{and} \quad t = \frac{y}{\sqrt{z/n}}. \tag{39.30}$$

The variable z thus follows a $\chi^2(n)$ distribution. Then t is distributed according to Student's t distribution with n degrees of freedom, $f(t; n)$, given in Table 39.1.

If defined through gamma functions as in Table 39.1, the parameter n is not required to be an integer. As $n \rightarrow \infty$, the distribution approaches a Gaussian, and for $n = 1$ it is a *Cauchy* or *Breit-Wigner* distribution.

As an example, consider the *sample mean* $\bar{x} = \sum x_i/n$ and the *sample variance* $s^2 = \sum (x_i - \bar{x})^2/(n-1)$ for normally distributed x_i with unknown mean μ and variance σ^2 . The sample mean has a Gaussian distribution with a variance σ^2/n , so the variable $(\bar{x} - \mu)/\sqrt{\sigma^2/n}$ is normal with mean 0 and variance 1. The quantity $(n-1)s^2/\sigma^2$ is independent of this and follows $\chi^2(n-1)$.

The ratio

$$t = \frac{(\bar{x} - \mu)/\sqrt{\sigma^2/n}}{\sqrt{(n-1)s^2/\sigma^2}} = \frac{\bar{x} - \mu}{\sqrt{s^2/n}} \tag{39.31}$$

is distributed as $f(t; n-1)$. The unknown variance σ^2 cancels, and t can be used to test the hypothesis that the true mean is some particular value μ .

39.4.7 Gamma distribution

For a process that generates events as a function of x (e.g., space or time) according to a Poisson distribution, the distance in x from an arbitrary starting point (which may be some particular event) to the k^{th} event follows a *gamma* distribution, $f(x; \lambda, k)$. The Poisson parameter μ is λ per unit x . The special case $k = 1$ (i.e., $f(x; \lambda, 1) = \lambda e^{-\lambda x}$) is called the *exponential* distribution. A sum of k' exponential random variables x_i is distributed as $f(\sum x_i; \lambda, k')$.

The parameter k is not required to be an integer. For $\lambda = 1/2$ and $k = n/2$, the gamma distribution reduces to the $\chi^2(n)$ distribution.

39.4.8 Beta distribution

The beta distribution describes a continuous random variable x in the interval $[0, 1]$. By scaling and translation one can easily generalize it to have arbitrary endpoints. In Bayesian inference about the parameter p of a binomial process, if the prior p.d.f. is a beta distribution $f(p; \alpha, \beta)$ then the observation of r successes out of N trials gives a posterior beta distribution $f(p; r + \alpha, N - r + \beta)$ (Bayesian methods are discussed further in Sec. 40). The uniform distribution is a beta distribution with $\alpha = \beta = 1$.

References

[1] H. Cramér, *Mathematical Methods of Statistics*, (Princeton Univ. Press, New Jersey, 1958).

-
- [2] A. Stuart and J.K. Ord, *Kendall's Advanced Theory of Statistics*, Vol. 1 *Distribution Theory* 6th Ed., (Halsted Press, New York, 1994), and earlier editions by Kendall and Stuart.
- [3] F.E. James, *Statistical Methods in Experimental Physics*, 2nd Ed., (World Scientific, Singapore, 2006).
- [4] L. Lyons, *Statistics for Nuclear and Particle Physicists*, (Cambridge University Press, New York, 1986).
- [5] B.R. Roe, *Probability and Statistics in Experimental Physics*, 2nd Ed., (Springer, New York, 2001).
- [6] R.J. Barlow, *Statistics: A Guide to the Use of Statistical Methods in the Physical Sciences*, (John Wiley, New York, 1989).
- [7] S. Brandt, *Data Analysis*, 3rd Ed., (Springer, New York, 1999).
- [8] G. Cowan, *Statistical Data Analysis*, (Oxford University Press, Oxford, 1998).
- [9] A.N. Kolmogorov, *Grundbegriffe der Wahrscheinlichkeitsrechnung*, (Springer, Berlin, 1933); *Foundations of the Theory of Probability*, 2nd Ed., (Chelsea, New York 1956).
- [10] Ch. Walck, *Hand-book on Statistical Distributions for Experimentalists*, University of Stockholm Internal Report SUF-PFY/96-01, available from www.physto.se-walck.
- [11] M. Abramowitz and I. Stegun, eds., *Handbook of Mathematical Functions*, (Dover, New York, 1972).
- [12] F.W.J. Olver *et al.*, eds., NIST Handbook of Mathematical Functions, (Cambridge University Press, 2010); A companion Digital Library of Mathematical Functions is available at dlmf.nist.gov.
- [13] R. Brun and F. Rademakers, Nucl. Instrum. Meth. **A389**, 81 (1997); See also root.cern.ch.

40. Statistics

Revised August 2023 by G. Cowan (RHUL).

This chapter gives an overview of statistical methods used in high-energy physics. In statistics, we are interested in using a given sample of data to make inferences about a probabilistic model, *e.g.*, to assess the model's validity or to determine the values of its parameters. There are two main approaches to statistical inference, which we may call frequentist and Bayesian.

In frequentist statistics, probability is interpreted as the limiting frequency of the outcome of a repeatable experiment. The most important tools in this framework are parameter estimation, covered in Section 40.2, statistical tests, discussed in Section 40.3, and confidence intervals, which are constructed so as to cover the true value of a parameter with a specified probability, as described in Section 40.4.2. Note that in frequentist statistics one does not define a probability for a hypothesis or for the value of a parameter.

In Bayesian statistics, the subjective interpretation of probability is used to quantify one's *degree of belief* in a hypothesis. This allows one to define a probability density function (p.d.f.) for a parameter, which reflects one's knowledge about where its true value lies.

Bayesian methods provide a natural means to include additional information, which in general may be subjective; in fact they *require* prior probabilities for the hypotheses (or parameters) in question, *i.e.*, the degree of belief about the parameters' values, before carrying out the measurement. Using Bayes' theorem (Eq. (39.4)), the prior degree of belief is updated by the data from the experiment. Bayesian methods for interval estimation are discussed in Sections 40.4.1 and 40.4.2.4.

For many inference problems, the frequentist and Bayesian approaches give similar numerical values, even though they answer different questions and are based on fundamentally different interpretations of probability. In some important cases, however, the two approaches may yield very different results. For a discussion of Bayesian vs. non-Bayesian methods, see references written by a statistician [1], by a physicist [2], or the detailed comparison in Ref. [3].

40.1 Fundamental concepts

Consider an experiment whose outcome is characterized by one or more data values, which we can write as a vector \mathbf{x} . A *hypothesis* H is a statement about the probability for the data, often written $P(\mathbf{x}|H)$. (We will usually use a capital letter for a probability and lower case for a probability density. Often the term p.d.f. is used loosely to refer to either a probability or a probability density.) This could, for example, define completely the p.d.f. for the data (a *simple* hypothesis), or it could specify only the functional form of the p.d.f., with the values of one or more parameters not determined (a *composite* hypothesis).

If the probability $P(\mathbf{x}|H)$ for data \mathbf{x} is regarded as a function of the hypothesis H , then it is called the *likelihood* of H , usually written $L(H)$. Often the hypothesis is characterized by one or more parameters θ , in which case $L(\theta) = P(\mathbf{x}|\theta)$ is called the likelihood function.

In some cases one can obtain at least approximate frequentist results using the likelihood evaluated only with the data obtained, for example, when determining confidence regions with Eq. (40.79). In general, however, the frequentist approach requires a full specification of the probability model $P(\mathbf{x}|H)$ both as a function of the data \mathbf{x} and hypothesis H .

In the Bayesian approach, inference is based on the posterior probability for H given the data \mathbf{x} , which represents one's degree of belief that H is true given the data. This is obtained from Bayes' theorem (39.4), which can be written

$$P(H|\mathbf{x}) = \frac{P(\mathbf{x}|H)\pi(H)}{\int P(\mathbf{x}|H')\pi(H') dH'}. \quad (40.1)$$

Here $P(\mathbf{x}|H)$ is the likelihood for H , which depends only on the data actually obtained. The quantity $\pi(H)$ is the prior probability for H , which represents one's degree of belief for H before carrying out the measurement. The integral in the denominator (or sum, for discrete hypotheses) serves as a normalization factor. If H

is characterized by a continuous parameter θ then the posterior probability is a p.d.f. $p(\theta|\mathbf{x})$. Note that the likelihood function itself is not a p.d.f. for θ .

40.2 Parameter estimation

Here we review *point estimation* of parameters, first with an overview of the frequentist approach and its two most important methods, maximum likelihood and least squares, treated in Sections 40.2.2 and 40.2.3. The Bayesian approach is outlined in Sec. 40.2.6.

An *estimator* $\hat{\theta}$ (written with a hat) is a function of the data used to estimate the value of the parameter θ . Sometimes the word 'estimate' is used to denote the value of the estimator when evaluated with given data. There is no fundamental rule dictating how an estimator must be constructed. One tries, therefore, to choose that estimator which has the best properties. The most important of these are (a) *consistency*, (b) *bias*, (c) *efficiency*, and (d) *robustness*.

(a) An estimator is said to be *consistent* if the estimate $\hat{\theta}$ converges in probability (see Ref. [3]) to the true value θ as the amount of data increases. This property is so important that it is possessed by all commonly used estimators.

(b) The *bias*, $b = E[\hat{\theta}] - \theta$, is the difference between the expectation value of the estimator and the true value of the parameter. The expectation value is taken over a hypothetical set of similar experiments in which $\hat{\theta}$ is constructed in the same way. When $b = 0$, the estimator is said to be unbiased. The bias depends on the chosen metric, *i.e.*, if $\hat{\theta}$ is an unbiased estimator of θ , then $\hat{\theta}^2$ is not in general an unbiased estimator for θ^2 .

(c) *Efficiency* is the ratio of the minimum possible variance for any estimator of θ to the variance $V[\hat{\theta}]$ of the estimator $\hat{\theta}$. For the case of a single parameter, under rather general conditions the minimum variance is given by the Rao-Cramér-Fréchet bound,

$$\sigma_{\min}^2 = \left(1 + \frac{\partial b}{\partial \theta}\right)^2 / I(\theta), \quad (40.2)$$

where

$$I(\theta) = E \left[\left(\frac{\partial \ln L}{\partial \theta} \right)^2 \right] = -E \left[\frac{\partial^2 \ln L}{\partial \theta^2} \right] \quad (40.3)$$

is the *Fisher information*, L is the likelihood, and the operator $E[\]$ in (40.3) is the expectation value with respect to the data. For the final equality to hold, the range of allowed data values must not depend on θ .

The *mean-squared error*,

$$\text{MSE} = E[(\hat{\theta} - \theta)^2] = V[\hat{\theta}] + b^2, \quad (40.4)$$

is a measure of an estimator's quality which combines bias and variance.

(d) *Robustness* is the property of being insensitive to departures from assumptions about the p.d.f., *e.g.*, owing to uncertainties in the distribution's tails.

It is not in general possible to optimize simultaneously for all the measures of estimator quality described above. For some common estimators, the properties above are known exactly. More generally, it is possible to evaluate them by Monte Carlo simulation. Note that they will in general depend on the unknown θ .

40.2.1 Estimators for mean, variance, and median

Suppose we have a set of n independent measurements, x_1, \dots, x_n , each assumed to follow a p.d.f. with unknown mean μ and unknown variance σ^2 (the measurements do not necessarily have to follow a Gaussian distribution). Then

$$\hat{\mu} = \frac{1}{n} \sum_{i=1}^n x_i \quad (40.5)$$

$$\hat{\sigma}^2 = \frac{1}{n-1} \sum_{i=1}^n (x_i - \hat{\mu})^2 \quad (40.6)$$

are unbiased estimators of μ and σ^2 . The variance of $\widehat{\mu}$ is σ^2/n and the variance of $\widehat{\sigma^2}$ is

$$V\left[\widehat{\sigma^2}\right] = \frac{1}{n} \left(m_4 - \frac{n-3}{n-1} \sigma^4 \right), \quad (40.7)$$

where m_4 is the 4th central moment of x (see Eq. (39.8)). For Gaussian distributed x_i , this becomes $2\sigma^4/(n-1)$ for any $n \geq 2$, and for large n the standard deviation of $\widehat{\sigma}$ is $\sigma/\sqrt{2n}$. For any n and Gaussian x_i , $\widehat{\mu}$ is an efficient estimator for μ , and the estimators $\widehat{\mu}$ and $\widehat{\sigma^2}$ are uncorrelated. Otherwise the arithmetic mean (40.5) is not necessarily the most efficient estimator; this is discussed further in Sec. 8.7 of Ref. [4].

If σ^2 is known, it does not improve the estimate $\widehat{\mu}$, as can be seen from Eq. (40.5); however, if μ is known, one can substitute it for $\widehat{\mu}$ in Eq. (40.6) and replace $n-1$ by n to obtain an estimator of σ^2 still with zero bias but smaller variance. If the x_i have different, known variances σ_i^2 , then the weighted average

$$\widehat{\mu} = \frac{1}{w} \sum_{i=1}^n w_i x_i, \quad (40.8)$$

where $w_i = 1/\sigma_i^2$ and $w = \sum_i w_i$, is an unbiased estimator for μ with a smaller variance than an unweighted average. The standard deviation of $\widehat{\mu}$ is $1/\sqrt{w}$.

As an estimator for the median x_{med} , one can use the value \widehat{x}_{med} such that half the x_i are below and half above (the sample median). If there are an even number of observations and the sample median lies between two observed values, the estimator is set by convention to their arithmetic average. If the p.d.f. of x has the form $f(x-\mu)$ and μ is both mean and median, then for large n the variance of the sample median approaches $1/[4nf^2(0)]$, provided $f(0) > 0$ [5]. Although estimating the median can often be more difficult computationally than the mean, the resulting estimator is generally more robust, as it is insensitive to the exact shape of the tails of a distribution.

40.2.2 The method of maximum likelihood

Suppose we have a set of measured quantities \mathbf{x} and the likelihood $L(\boldsymbol{\theta}) = P(\mathbf{x}|\boldsymbol{\theta})$ for a set of parameters $\boldsymbol{\theta} = (\theta_1, \dots, \theta_M)$. The *maximum likelihood estimators* (MLEs) for $\boldsymbol{\theta}$ are defined as the values that give the maximum of L . Because of the properties of the logarithm, it is usually easier to work with $\ln L$, and since both are maximized for the same parameter values $\boldsymbol{\theta}$, the MLEs can be found by solving the *likelihood equations*,

$$\frac{\partial \ln L}{\partial \theta_i} = 0, \quad i = 1, \dots, M. \quad (40.9)$$

Often the solution must be found numerically. Maximum likelihood estimators are important because they are asymptotically (*i.e.*, for large data samples) unbiased, efficient and have a Gaussian sampling distribution under quite general conditions, and the method has a wide range of applicability.

In general the likelihood function is obtained from the probability of the data under assumption of the parameters. An important special case is when the data consist of *i.i.d.* (independent and identically distributed) values. Here one has a set of n statistically independent quantities $x = (x_1, \dots, x_n)$, where each component follows the same p.d.f. $f(x; \boldsymbol{\theta})$. In this case the joint p.d.f. of the data sample factorizes and the likelihood function is

$$L(\boldsymbol{\theta}) = \prod_{i=1}^n f(x_i; \boldsymbol{\theta}). \quad (40.10)$$

Here the number n of observations (usually individual “events” in particle physics) is regarded as fixed. If, however, the probability to observe n events itself depends on the parameters $\boldsymbol{\theta}$, then this dependence should be included in the likelihood. For example, if n follows a Poisson distribution with mean μ and the independent x values all follow $f(x; \boldsymbol{\theta})$, then the likelihood becomes

$$L(\boldsymbol{\theta}) = \frac{\mu^n}{n!} e^{-\mu} \prod_{i=1}^n f(x_i; \boldsymbol{\theta}). \quad (40.11)$$

Equation (40.11) is often called the *extended likelihood* (see, *e.g.*, Refs. [6–8]). If μ is given as a function of $\boldsymbol{\theta}$, then including the probability for n given $\boldsymbol{\theta}$ in the likelihood provides additional information about the parameters. This therefore leads to a reduction in their statistical uncertainties and in general changes their estimated values.

In evaluating the likelihood function, it is important that any normalization factors in the p.d.f. that involve $\boldsymbol{\theta}$ be included. However, we will only be interested in the maximum of L and in ratios of L at different values of the parameters; hence any multiplicative factors that do not involve the parameters that we want to estimate may be dropped, including factors that depend on the data but not on $\boldsymbol{\theta}$.

Under a one-to-one change of parameters from $\boldsymbol{\theta}$ to $\boldsymbol{\eta}$, the MLEs $\widehat{\boldsymbol{\theta}}$ transform to $\boldsymbol{\eta}(\widehat{\boldsymbol{\theta}})$. That is, the maximum-likelihood solution is invariant under change of parameter. However, other properties of MLEs, in particular the bias, are not invariant under change of parameter.

The inverse V^{-1} of the covariance matrix $V_{ij} = \text{cov}[\widehat{\theta}_i, \widehat{\theta}_j]$ for a set of MLEs can be estimated by using

$$(\widehat{V}^{-1})_{ij} = - \left. \frac{\partial^2 \ln L}{\partial \theta_i \partial \theta_j} \right|_{\widehat{\boldsymbol{\theta}}}. \quad (40.12)$$

Equation (40.12) holds for a sufficiently large data sample (or for a small sample only in special cases, *e.g.*, where the means of Gaussian distributed data are linear functions of the parameters); otherwise it can result in a misestimation of the variances. Under the conditions where the equation is valid, L has a Gaussian form and $\ln L$ is (hyper)parabolic. In this case, s times the standard deviations σ_i of the estimators for the parameters can be obtained from the hypersurface defined by the $\boldsymbol{\theta}$ such that

$$\ln L(\boldsymbol{\theta}) = \ln L_{\text{max}} - s^2/2, \quad (40.13)$$

where $\ln L_{\text{max}}$ is the value of $\ln L$ at the solution point (compare with Eq. (40.79)). The minimum and maximum values of θ_i on the hypersurface then give an approximate s -standard deviation confidence interval for θ_i (see Section 40.4.2.2).

40.2.2.1 Maximum likelihood with binned data

If the total number of data values x_i , ($i = 1, \dots, n_{\text{tot}}$), is small, the unbinned maximum-likelihood method, *i.e.*, use of Equation (40.10) (or (40.11) for extended maximum likelihood), is preferred since binning can only result in a loss of information, and hence larger statistical errors for the parameter estimates. If the sample is large, it can be convenient to bin the values in a histogram with N bins, so that one obtains a vector of data $\mathbf{n} = (n_1, \dots, n_N)$ with expectation values $\boldsymbol{\mu} = E[\mathbf{n}]$ and probabilities $f(\mathbf{n}; \boldsymbol{\mu})$. Suppose the mean values $\boldsymbol{\mu}$ can be determined as a function of a set of parameters $\boldsymbol{\theta}$. Then one may maximize the likelihood function based on the contents of the bins.

As mentioned in Sec. 40.2.2, the total number of events $n_{\text{tot}} = \sum_i n_i$ can be regarded either as fixed or as a random variable. If it is fixed, the histogram follows a multinomial distribution,

$$f_M(\mathbf{n}; \boldsymbol{\theta}) = \frac{n_{\text{tot}}!}{n_1! \dots n_N!} p_1^{n_1} \dots p_N^{n_N}, \quad (40.14)$$

where we assume the probabilities p_i are given functions of the parameters $\boldsymbol{\theta}$. The distribution can be written equivalently in terms of the expected number of events in each bin, $\mu_i = n_{\text{tot}} p_i$. If the n_i are regarded as independent and Poisson distributed, then the data are instead described by a product of Poisson probabilities,

$$f_P(\mathbf{n}; \boldsymbol{\theta}) = \prod_{i=1}^N \frac{\mu_i^{n_i}}{n_i!} e^{-\mu_i}, \quad (40.15)$$

where the mean values μ_i are given functions of $\boldsymbol{\theta}$. The total number of events n_{tot} thus follows a Poisson distribution with mean $\mu_{\text{tot}} = \sum_i \mu_i$.

When using maximum likelihood with binned data, one can find the estimators and at the same time obtain a statistic usable for a test of goodness of fit (see Sec. 40.3.3.1). For independent Poisson distributed data, maximizing the likelihood

$L(\theta) = f_P(\mathbf{n}; \theta)$ is equivalent to maximizing the likelihood ratio $\lambda(\theta) = f_P(\mathbf{n}; \theta)/f_{\text{sat}}(\mathbf{n}; \hat{\boldsymbol{\mu}})$, where in the denominator $f_{\text{sat}}(\mathbf{n}; \hat{\boldsymbol{\mu}})$ is the corresponding model with an adjustable parameter for each bin, $\boldsymbol{\mu} = (\mu_1, \dots, \mu_N)$, with estimators $\hat{\boldsymbol{\mu}} = (n_1, \dots, n_N)$ (called the “saturated model”). Equivalently one often minimizes the quantity $-2 \ln \lambda(\theta)$. For independent Poisson distributed n_i this is [9]

$$-2 \ln \lambda(\theta) = 2 \sum_{i=1}^N \left[\mu_i(\theta) - n_i + n_i \ln \frac{n_i}{\mu_i(\theta)} \right], \quad (40.16)$$

where for bins with $n_i = 0$, the last term in (40.16) is zero. The expression (40.16) without the terms $\mu_i - n_i$ also gives $-2 \ln \lambda(\theta)$ for multinomially distributed n_i , *i.e.*, when the total number of entries is regarded as fixed. In the limit of zero bin width, minimizing (40.16) is equivalent to maximizing the unbinned extended likelihood function (40.11); in the corresponding multinomial case without the $\mu_i - n_i$ terms one obtains Eq. (40.10).

A smaller value of $-2 \ln \lambda(\hat{\theta})$ corresponds to better agreement between the data and the hypothesized form of $\boldsymbol{\mu}(\theta)$. The value of $-2 \ln \lambda(\hat{\theta})$ can thus be translated into a p -value as a measure of goodness-of-fit, as described in Sec. 40.3.3.1. Assuming the model is correct, then according to Wilks’ theorem [10], for sufficiently large μ_i and provided certain regularity conditions are met, the minimum of $-2 \ln \lambda$ as defined by Eq. (40.16) follows a χ^2 distribution (see, *e.g.*, Ref. [9]). If there are N bins and M fitted parameters, then the number of degrees of freedom for the χ^2 distribution is $N - M$ if the data are treated as Poisson-distributed, and $N - M - 1$ if the n_i are multinomially distributed.

Suppose the n_i are Poisson-distributed and the overall normalization $\mu_{\text{tot}} = \sum_i \mu_i$ is taken as an adjustable parameter, so that $\mu_i = \mu_{\text{tot}} p_i(\theta)$, where the probability to be in the i th bin, $p_i(\theta)$, does not depend on μ_{tot} . Then by minimizing Eq. (40.16), one obtains that the area under the fitted function is equal to the sum of the histogram contents, *i.e.*, $\sum_i \hat{\mu}_i = \sum_i n_i$. This is a property not possessed by the estimators from the method of least squares (see, *e.g.*, Sec. 40.2.3 and Ref. [8]).

40.2.2.2 Frequentist treatment of nuisance parameters

Suppose we want to determine the values of parameters θ using a set of measurements \mathbf{x} described by a probability model $P(\mathbf{x}|\theta)$. In general the model is not perfect, which is to say it cannot provide an accurate description of the data even at the most optimal point of its parameter space. As a result, the estimated parameters can have a systematic bias.

One can improve the model by including in it additional parameters. That is, $P(\mathbf{x}|\theta)$ is replaced by a more general model $P(\mathbf{x}|\theta, \boldsymbol{\nu})$, which depends on parameters of interest θ and *nuisance parameters* $\boldsymbol{\nu}$. The additional parameters are not of intrinsic interest but must be included for the model to be sufficiently accurate for some point in the enlarged parameter space.

Although including additional parameters may eliminate or at least reduce the effect of systematic uncertainties, their presence will result in increased statistical uncertainties for the parameters of interest. This occurs because the estimators for the nuisance parameters and those of interest will in general be correlated, which results in an enlargement of the contour defined by Eq. (40.13).

To reduce the impact of the nuisance parameters one often tries to constrain their values by means of control or calibration measurements, say, having data \mathbf{y} . For example, some components of \mathbf{y} could represent estimates of the nuisance parameters, often from separate experiments. Suppose the measurements \mathbf{y} are statistically independent from \mathbf{x} and are described by a model $P(\mathbf{y}|\boldsymbol{\nu})$. The joint model for both \mathbf{x} and \mathbf{y} is in this case therefore the product of the probabilities for \mathbf{x} and \mathbf{y} , and thus the likelihood function for the full set of parameters is

$$L(\theta, \boldsymbol{\nu}) = P(\mathbf{x}|\theta, \boldsymbol{\nu})P(\mathbf{y}|\boldsymbol{\nu}). \quad (40.17)$$

Note that in this case if one wants to simulate the experiment by means of Monte Carlo, both the primary and control mea-

surements, \mathbf{x} and \mathbf{y} , must be generated for each repetition under assumption of fixed values for the parameters θ and $\boldsymbol{\nu}$.

Using all of the parameters $(\theta, \boldsymbol{\nu})$ in Eq. (40.13) to find the statistical errors in the parameters of interest θ is equivalent to using the *profile likelihood*, which depends only on θ . It is defined as

$$L_p(\theta) = L(\theta, \hat{\boldsymbol{\nu}}(\theta)), \quad (40.18)$$

where the double-hat notation indicates the profiled values of the parameters $\boldsymbol{\nu}$, defined as the values that maximize L for the specified θ . The profile likelihood is discussed further in Section 40.3.2.1 in connection with hypothesis tests.

40.2.3 The method of least squares

The *method of least squares* (LS) coincides with the method of maximum likelihood in the following special case. Consider a set of N independent measurements y_i at known points x_i . The measurement y_i is assumed to be Gaussian distributed with mean $\mu(x_i; \theta)$ and known variance σ_i^2 . The goal is to construct estimators for the unknown parameters θ . The log-likelihood function contains the sum of squares

$$\chi^2(\theta) = -2 \ln L(\theta) + \text{constant} = \sum_{i=1}^N \frac{(y_i - \mu(x_i; \theta))^2}{\sigma_i^2}. \quad (40.19)$$

The parameter values that maximize L are the same as those which minimize χ^2 .

The minimum of the chi-square function in Equation (40.19) defines the least-squares estimators $\hat{\theta}$ for the more general case where the y_i are not Gaussian distributed as long as they are independent. If they are not independent but rather have a covariance matrix $V_{ij} = \text{cov}[y_i, y_j]$, then the LS estimators are determined by the minimum of

$$\chi^2(\theta) = (\mathbf{y} - \boldsymbol{\mu}(\theta))^T V^{-1} (\mathbf{y} - \boldsymbol{\mu}(\theta)), \quad (40.20)$$

where $\mathbf{y} = (y_1, \dots, y_N)$ is the (column) vector of measurements, $\boldsymbol{\mu}(\theta)$ is the corresponding vector of predicted values, and the superscript T denotes the transpose. If the y_i are not Gaussian distributed, then the least-squares and maximum-likelihood estimators will not in general coincide.

Often one further restricts the problem to the case where $\mu(x_i; \theta)$ is a linear function of the parameters, *i.e.*,

$$\mu(x_i; \theta) = \sum_{j=1}^m \theta_j h_j(x_i). \quad (40.21)$$

Here the $h_j(x)$ are m linearly independent functions, *e.g.*, $1, x, x^2, \dots, x^{m-1}$ or Legendre polynomials. We require $m < N$ and at least m of the x_i must be distinct.

Minimizing χ^2 in this case with m parameters reduces to solving a system of m linear equations. Defining $H_{ij} = h_j(x_i)$ and minimizing χ^2 by setting its derivatives with respect to the θ_i equal to zero gives the LS estimators,

$$\hat{\boldsymbol{\theta}} = (H^T V^{-1} H)^{-1} H^T V^{-1} \mathbf{y} \equiv D \mathbf{y}. \quad (40.22)$$

The covariance matrix for the estimators $U_{ij} = \text{cov}[\hat{\theta}_i, \hat{\theta}_j]$ is given by

$$U = D V D^T = (H^T V^{-1} H)^{-1}, \quad (40.23)$$

or equivalently, its inverse U^{-1} can be found from

$$(U^{-1})_{ij} = \frac{1}{2} \frac{\partial^2 \chi^2}{\partial \theta_i \partial \theta_j} \Big|_{\boldsymbol{\theta}=\hat{\boldsymbol{\theta}}} = \sum_{k,l=1}^m h_i(x_k) (V^{-1})_{kl} h_j(x_l). \quad (40.24)$$

The LS estimators can also be found from the expression

$$\hat{\boldsymbol{\theta}} = U \mathbf{g}, \quad (40.25)$$

where the vector \mathbf{g} is defined by

$$\mathbf{g}_i = \sum_{j,k=1}^m y_j h_i(x_k) (V^{-1})_{jk}. \quad (40.26)$$

For the case of uncorrelated y_i , for example, one can use (40.25) with

$$(U^{-1})_{ij} = \sum_{k=1}^N \frac{h_i(x_k)h_j(x_k)}{\sigma_k^2}, \quad (40.27)$$

$$g_i = \sum_{k=1}^N \frac{y_k h_i(x_k)}{\sigma_k^2}. \quad (40.28)$$

Expanding $\chi^2(\theta)$ about $\hat{\theta}$, one finds that the contour in parameter space defined by

$$\chi^2(\theta) = \chi^2(\hat{\theta}) + 1 = \chi_{\min}^2 + 1 \quad (40.29)$$

has tangent planes located at plus-or-minus-one standard deviation $\sigma_{\hat{\theta}}$ from the LS estimates $\hat{\theta}$ (the relation is approximate if the fit function $\mu(x; \theta)$ is nonlinear in the parameters).

In constructing the quantity $\chi^2(\theta)$ one requires the variances or, in the case of correlated measurements, the covariance matrix. Often these quantities are not known *a priori* and must be estimated from the data. In this case the least-squares and maximum-likelihood methods are no longer exactly equivalent even for Gaussian distributed measurements. An important example is where the measured value y_i represents the event count in a histogram bin. If, for example, y_i represents a Poisson variable, for which the variance is equal to the mean, then one can either estimate the variance from the predicted value, $\mu(x_i; \theta)$, or from the observed number itself, y_i . In the first option, the variances become functions of the parameters, and as a result the estimators may need to be found numerically. The second option can be undefined if y_i is zero, and for small y_i , the variance will be poorly estimated. In either case, one should constrain the normalization of the fitted curve to the correct value, *i.e.*, one should determine the area under the fitted curve directly from the number of entries in the histogram (see Ref. [8], Section 7.4). As noted in Sec. 40.2.2.1, this issue is avoided when using the method of extended maximum likelihood with binned data by minimizing Eq. (40.16). In that case if the expected number of events μ_{tot} does not depend on the other fitted parameters θ , then its extended MLE is equal to the observed total number of events.

As the minimum value of the χ^2 represents the level of agreement between the measurements and the fitted function, it can be used for assessing the goodness-of-fit; this is discussed further in Section 40.3.3.1.

40.2.4 Parameter estimation with constraints

In some applications one is interested in using a set of measured quantities $\mathbf{y} = (y_1, \dots, y_N)$ to estimate parameters $\theta = (\theta_1, \dots, \theta_M)$ subject to a number of constraints. For example, one may have measured coordinates from two tracks, and the goal is to estimate their momentum vectors subject to the constraint that the tracks have a common vertex. The parameters can also include momenta of undetected particles such as neutrinos, as long as the constraints from conservation of energy and momentum and from known masses of particles involved in the reaction chain provide enough information for these quantities to be inferred.

A set of K constraints can be given in the form of equations

$$c_k(\theta) = 0, \quad k = 1, \dots, K. \quad (40.30)$$

In some problems it may be possible to define a new set of parameters $\eta = (\eta_1, \dots, \eta_L)$ with $L = M - K$ such that every point in η -space automatically satisfies the constraints. If this is possible then the problem reduces to one of estimating η with, *e.g.*, maximum likelihood or least squares and then transforming the estimators back into θ -space.

In many cases it may be difficult or impossible to find an appropriate transformation $\eta(\theta)$. Suppose that the parameters are determined by minimizing an objective function such as $\chi^2(\theta)$ in the method of least squares. Here one may enforce the constraints

by finding the stationary points of the *Lagrange function*

$$\mathcal{L}(\theta, \lambda, \mathbf{y}) = \chi^2(\theta, \mathbf{y}) + \sum_{k=1}^K \lambda_k c_k(\theta) \quad (40.31)$$

with respect to both the parameters θ and a set of *Lagrange multipliers* $\lambda = (\lambda_1, \dots, \lambda_K)$. Combining the parameters and Lagrange multipliers into an $(M + K)$ -component vector $\gamma = (\theta_1, \dots, \theta_M, \lambda_1, \dots, \lambda_K)$, the solutions for γ , *i.e.*, the estimators $\hat{\gamma}$, are found (*e.g.*, numerically) from the system of equations

$$F_i(\gamma, \mathbf{y}) \equiv \frac{\partial \mathcal{L}}{\partial \gamma_i} = 0, \quad i = 1, \dots, M + K. \quad (40.32)$$

To obtain the covariance matrix of the estimated parameters one can find solutions $\tilde{\gamma}$ corresponding to the expectation values of the data $\langle \mathbf{y} \rangle$ and expand $F_i(\tilde{\gamma}, \mathbf{y})$ to first order about these values. This gives (see, *e.g.*, Sec. 11.6 of Ref. [8]) linearized approximations for the estimators, $\hat{\gamma}(\mathbf{y}) \approx \tilde{\gamma} + C(\mathbf{y} - \langle \mathbf{y} \rangle)$, where the matrix $C = -A^{-1}B$, and A and B are given by

$$A_{ij} = \left[\frac{\partial F_i}{\partial \gamma_j} \right]_{\tilde{\gamma}, \langle \mathbf{y} \rangle} \quad \text{and} \quad B_{ij} = \left[\frac{\partial F_i}{\partial y_j} \right]_{\tilde{\gamma}, \langle \mathbf{y} \rangle}. \quad (40.33)$$

In practice the values $\langle \mathbf{y} \rangle$ and corresponding solutions $\tilde{\gamma}$ are estimated using the data from the actual measurement. Using this approximation for $\hat{\gamma}(\mathbf{y})$, one can find the covariance matrix $U_{ij} = \text{cov}[\hat{\gamma}_i, \hat{\gamma}_j]$ of the estimators for the γ_i in terms of that of the data $V_{ij} = \text{cov}[y_i, y_j]$ using error propagation (cf. Eqs. (39.17) and (39.18)),

$$U = CVC^T. \quad (40.34)$$

The upper-left $M \times M$ block of the matrix U gives the covariance matrix for the estimated parameters $\text{cov}[\hat{\theta}_i, \hat{\theta}_j]$. One can show for linear constraints that $\text{cov}[\hat{\theta}_i, \hat{\theta}_j]$ is also given by the upper-left $M \times M$ block of $2A^{-1}$. If the parameters are estimated using the method of least squares, then the number of degrees of freedom for the distribution of the minimized χ^2 is increased by the number of constraints, *i.e.*, it becomes $N - M + K$. Further details can be found in, *e.g.*, Ch. 8 of Ref. [4] and Ch. 7 of Ref. [11].

40.2.5 Unfolding

An important class of parameter estimation problem involves measurement of the differential distribution of a kinematic variable in the form of a histogram with N bins. The data thus consist of the vector of measured data values $\mathbf{n} = (n_1, \dots, n_N)$, with expectation values $\nu_i = E[n_i]$. The n_i are usually independent and often modeled as Poisson distributed, from which it follows that the maximum-likelihood estimators are $\hat{\nu}_i = n_i$ for all i .

Because of the limited acceptance and resolution of the experiment, however, the measured values of the kinematic variable in question differ in general from their true values, and as a consequence the form of the data histogram is distorted relative to what would be obtained with perfect resolution. The desired parameters are not, therefore, the ν_i but rather one wants to estimate the expected number of entries in a given bin that would be found with a perfect detector. We call this the “true histogram” and denote it with $\boldsymbol{\mu} = (\mu_1, \dots, \mu_M)$, where the number of bins M is not required to equal that of the observed histogram. The μ_i are related to the expected numbers of events in the observed histogram by

$$\nu_i = \sum_{j=1}^M R_{ij} \mu_j + \beta_i, \quad (40.35)$$

where β_i here represents the expected number of events in bin i due to background processes and the $N \times M$ *response matrix* R_{ij} gives the probability for an event to be observed in bin i of $\boldsymbol{\nu}$ given that the true value of the variable was in bin j of $\boldsymbol{\mu}$. For purposes of this discussion let us suppose that the response matrix and expected background values are known. There are two main approaches to this type of problem, which we can call *unfolding* and *folding*.

In unfolding, one treats the true histogram μ as the parameters of interest. The result is thus given by estimators $\hat{\mu}$ and the corresponding covariance matrix $U_{ij} = \text{cov}[\hat{\mu}_i, \hat{\mu}_j]$. Provided the response matrix can be inverted, the maximum-likelihood solution is easily found as $\hat{\mu} = R^{-1}(\mathbf{n} - \beta)$. If the response matrix allows for significant migration of events between bins, then the variances of these estimators can be very large, sometimes to the point where the $\hat{\mu}$ bear essentially no resemblance to the true μ . In such cases the estimators can be found by maximizing a linear combination of the log-likelihood and a regularization function that imposes some degree of smoothness on the unfolded distribution. In achieving a reduction in variance one inevitably introduces some bias into the estimators.

In the approach of folding, by contrast, to test a given model prediction for the true histogram μ it is first “folded” with the response matrix and corrected for expected background to give the corresponding ν according to Eq. (40.35), and these are compared to the corresponding \mathbf{n} using, e.g., a likelihood ratio as shown in Sec. 40.2.2.1. In this way, one avoids any bias due to regularization.

To account for systematic uncertainties, the response matrix and background values may not be expressed as constants but rather as functions of nuisance parameters θ . These may be constrained by auxiliary measurements \mathbf{u} with p.d.f. $p(\mathbf{u}|\theta)$ so that the full likelihood becomes (as in Eq. (40.17) but with different notation)

$$L(\mu, \theta) = P(\mathbf{n}|\nu(\mu, \theta))p(\mathbf{u}|\theta). \quad (40.36)$$

Here the mean values $\nu = R(\theta)\mu + \beta(\theta)$ now depend on both the true histogram parameters μ as well as the nuisance parameters θ . Thus to record enough information for a future analysis using folding one must provide all of the ingredients used above: the primary data \mathbf{n} , the auxiliary measurements \mathbf{u} , and also the response matrix $R(\theta)$ and expected backgrounds $\beta(\theta)$ as functions of the nuisance parameters. If unfolding is used, then future model tests or comparisons with other experiments can be carried out directly using the estimators $\hat{\mu}$ and their covariance matrix.

If several distributions are unfolded, then to combine these in a test of a given model one should know how estimators for bins of different distributions are correlated, as can arise, e.g., through common systematic effects. If only the unfolded distributions and their separate covariance matrices are reported, however, then information on such correlations is not retained. In folding, one can include information on correlated systematic effects if the ingredients (R and β) are known in terms of nuisance parameters that are common to different distributions.

In unfolding, the estimators for μ can be constructed either by maximizing the log-likelihood using Eq. (40.36) or in the case where regularization is required one can maximize $\varphi(\mu, \theta) = \ln L(\mu, \theta) + \tau S(\mu)$, where the *regularization function* $S(\mu)$ reflects the smoothness of the true histogram and serves to reduce the variances of the estimators. Possible functions are based on the mean squared second derivative (a commonly used type of Tikhonov regularization) or the entropy of the true histogram. The parameter τ fixes the relative weighting of the log-likelihood and the regularization function and thus determines the balance between the bias and variance of the resulting estimators. Further discussion of the unfolding problem including methods for choosing the regularization function and parameter, as well as techniques that employ other types of regularization such as the iterative Bayes (Richardson-Lucy) method, can be found in Refs. [8, 11–13] and references therein.

40.2.6 The Bayesian approach

In the frequentist methods discussed above, probability is associated only with data, not with the value of a parameter. This is no longer the case in Bayesian statistics, however, which we introduce in this section. For general introductions to Bayesian statistics see, e.g., Refs. [14–17].

Suppose the outcome of an experiment is characterized by a vector of data \mathbf{x} , whose probability distribution depends on an unknown parameter (or parameters) θ that we wish to determine. In Bayesian statistics, all knowledge about θ is summarized by

the posterior p.d.f. $p(\theta|\mathbf{x})$, whose integral over any given region gives the degree of belief for θ to take on values in that region, given the data \mathbf{x} . It is obtained by using Bayes’ theorem,

$$p(\theta|\mathbf{x}) = \frac{P(\mathbf{x}|\theta)\pi(\theta)}{\int P(\mathbf{x}|\theta')\pi(\theta') d\theta'}, \quad (40.37)$$

where $P(\mathbf{x}|\theta)$ is the likelihood function, i.e., the joint p.d.f. for the data viewed as a function of θ , evaluated with the data actually obtained in the experiment, and $\pi(\theta)$ is the prior p.d.f. for θ . Note that the denominator in Eq. (40.37) serves to normalize the posterior p.d.f. to unity.

As it can be difficult to report the full posterior p.d.f. $p(\theta|\mathbf{x})$, one would usually summarize it with statistics such as the mean, mode or median value and covariance matrix. In addition one may construct intervals with a given probability content, as is discussed in Sec. 40.4.1 on Bayesian interval estimation.

40.2.6.1 Priors

Bayesian statistics supplies no unique rule for determining the prior $\pi(\theta)$; this reflects the analyst’s subjective degree of belief (or state of knowledge) about θ before the measurement was carried out. For the result to be of value to the broader community, whose members may not share these beliefs, it is important to carry out a *sensitivity analysis*, that is, to show how the result changes under a reasonable variation of the prior probabilities.

One might like to construct $\pi(\theta)$ to represent complete ignorance about the parameters by setting it equal to a constant. A problem here is that if the prior p.d.f. is flat in θ , then it is not flat for a nonlinear function of θ , and so a different parametrization of the problem would lead in general to a non-equivalent posterior p.d.f.

For the special case of a constant prior, one can see from Bayes’ theorem (40.37) that the posterior is proportional to the likelihood, and therefore the mode (peak position) of the posterior is equal to the maximum-likelihood estimator. The posterior mode, however, will change in general upon a transformation of parameter. One may use as the Bayesian estimator a summary statistic other than the mode, such as the median, which is invariant under parameter transformation. But this will not in general coincide with the MLE.

The difficult and subjective nature of encoding personal knowledge into priors has led to what is called *objective Bayesian statistics*, where prior probabilities are based not on an actual degree of belief but rather derived from formal rules. These give, for example, priors which are invariant under a transformation of parameters, or ones which result in a maximum gain in information for a given set of measurements. For an extensive review see, e.g., Ref. [18].

Objective priors do not in general reflect degree of belief, but they could in some cases be taken as possible, although perhaps extreme, subjective priors. The posterior probabilities as well therefore do not necessarily reflect a degree of belief. However one may regard investigating a variety of objective priors to be an important part of the sensitivity analysis. Furthermore, use of objective priors with Bayes’ theorem can be viewed as a recipe for producing estimators or intervals which have desirable frequentist properties.

An important procedure for deriving objective priors is due to Jeffreys. According to *Jeffreys’ rule* one takes the prior as

$$\pi(\theta) \propto \sqrt{\det(I(\theta))}, \quad (40.38)$$

where

$$I_{ij}(\theta) = -E \left[\frac{\partial^2 \ln P(\mathbf{x}|\theta)}{\partial \theta_i \partial \theta_j} \right] \quad (40.39)$$

is the *Fisher information matrix*. One can show that the Jeffreys prior leads to inference that is invariant under a transformation of parameters. One should note that the Jeffreys prior does not in general correspond to one’s degree of belief about the value of a parameter. As examples, the Jeffreys prior for the mean μ of a Gaussian distribution is a constant, and for the mean of a Poisson distribution one finds $\pi(\mu) \propto 1/\sqrt{\mu}$.

Neither the constant nor $1/\sqrt{\mu}$ priors can be normalized to unit area and are therefore said to be *improper*. This can be allowed because the prior always appears multiplied by the likelihood function, and if the likelihood falls to zero sufficiently quickly then one may have a normalizable posterior density.

An important type of objective prior is the reference prior due to Bernardo and Berger [19]. To find the reference prior for a given problem one considers the Kullback-Leibler divergence $D_n[\pi, p]$ of the posterior $p(\theta|\mathbf{x})$ relative to a prior $\pi(\theta)$, obtained from a set of i.i.d. data $\mathbf{x} = (x_1, \dots, x_n)$:

$$D_n[\pi, p] = \int p(\theta|\mathbf{x}) \ln \frac{p(\theta|\mathbf{x})}{\pi(\theta)} d\theta. \quad (40.40)$$

This is effectively a measure of the gain in information provided by the data. The reference prior is chosen so that the expectation value of this information gain is maximized for the limiting case of $n \rightarrow \infty$, where the expectation is computed with respect to the marginal distribution of the data,

$$p(\mathbf{x}) = \int p(\mathbf{x}|\theta)\pi(\theta) d\theta. \quad (40.41)$$

For a single, continuous parameter the reference prior is usually identical to the Jeffreys prior. In the multiparameter case an iterative algorithm exists, which requires sorting the parameters by order of inferential importance. Often the result does not depend on this order, but when it does, this can be part of a sensitivity analysis. Further discussion and applications to particle physics problems can be found in Ref. [20].

40.2.6.2 Bayesian treatment of nuisance parameters

As discussed in Sec. 40.2.2, a model may depend on parameters of interest θ as well as on nuisance parameters ν , which must be included for an accurate description of the data. Knowledge about the values of ν may be supplied by control measurements, theoretical insights, physical constraints, etc. Suppose, for example, one has data \mathbf{y} from a control measurement which is characterized by a probability $p(\mathbf{y}|\nu)$. Suppose further that before carrying out the control measurement one's state of knowledge about ν is described by an initial prior $\pi_0(\nu)$, which in practice is often taken to be a constant or in any case very broad. By using Bayes' theorem (40.1) one obtains the updated prior $\pi(\nu)$ (*i.e.*, now $\pi(\nu) = \pi(\nu|\mathbf{y})$, the probability for ν given \mathbf{y}),

$$\pi(\nu|\mathbf{y}) \propto p(\mathbf{y}|\nu)\pi_0(\nu). \quad (40.42)$$

In the absence of a model for $P(\mathbf{y}|\nu)$ one may make some reasonable but *ad hoc* choices in order to approximate $\pi(\nu)$. For a single nuisance parameter ν , for example, one might characterize the uncertainty by a p.d.f. $\pi(\nu)$ centered about its nominal value with a certain standard deviation σ_ν . Often a Gaussian p.d.f. provides a reasonable model for one's degree of belief about a nuisance parameter; in other cases, more complicated shapes may be appropriate. If, for example, the parameter represents a non-negative quantity then a log-normal or gamma p.d.f. can be a more natural choice than a Gaussian truncated at zero. Note also that truncation of the prior of a nuisance parameter ν at zero will in general make $\pi(\nu)$ nonzero at $\nu = 0$, which can lead to an unnormalizable posterior for a parameter of interest that appears multiplied by ν .

The likelihood function, prior, and posterior p.d.f.s all depend on both θ and ν , and are related by Bayes' theorem, as usual. Note that the likelihood here only refers to the primary measurement \mathbf{x} . Once any control measurements \mathbf{y} are used to find the updated prior $\pi(\nu)$ for the nuisance parameters, this information is fully encapsulated in $\pi(\nu)$ and the control measurements do not appear further.

One can obtain the posterior p.d.f. for θ alone by integrating over the nuisance parameters, *i.e.*,

$$p(\theta|\mathbf{x}) = \int p(\theta, \nu|\mathbf{x}) d\nu. \quad (40.43)$$

Such integrals can often not be carried out in closed form, and if the number of nuisance parameters is large, then they can be difficult to compute with standard Monte Carlo methods. *Markov Chain Monte Carlo* (MCMC) techniques are often used for computing integrals of this type (see Sec. 42.6).

40.3 Statistical tests

In addition to estimating parameters, one often wants to assess the validity of certain statements concerning the data's underlying distribution. Frequentist *hypothesis tests*, described in Sec. 40.3.1, provide a rule for accepting or rejecting hypotheses depending on the outcome of a measurement. In *significance tests*, covered in Sec. 40.3.2, one gives the probability to obtain a level of incompatibility with a certain hypothesis that is greater than or equal to the level observed with the actual data. Goodness-of-fit tests that quantify the general level of compatibility between data and a hypothesis are described in Sec. 40.3.3. In the Bayesian approach, the corresponding procedure is based fundamentally on the posterior probabilities of the competing hypotheses. In Sec. 40.3.4 we describe a related construct called the Bayes factor, which can be used to quantify the degree to which the data prefer one or another hypothesis.

40.3.1 Hypothesis tests

A frequentist *test* of a hypothesis (often called the null hypothesis, H_0) is a rule that states for which data values \mathbf{x} the hypothesis is rejected. A region of \mathbf{x} -space called the critical region, w , is specified such that there is no more than a given probability under H_0 , α , called the *size* or *significance level* of the test, to find $\mathbf{x} \in w$. If the data are discrete, it may not be possible to find a critical region with exact probability content α , and thus we require $P(\mathbf{x} \in w|H_0) \leq \alpha$. If the data are observed in the critical region, H_0 is rejected.

The data \mathbf{x} used to construct a test could be, for example, a set of values that characterizes an individual event. In this case the test corresponds to classification as, *e.g.*, signal or background. Alternatively the data could represent a set of values from a collection of events. Often one is interested in knowing whether all of the events are of a certain type (background), or whether the sample contains at least some events of a new type (signal). Here the background-only hypothesis plays the role of H_0 , and in the alternative H_1 both signal and background are present. Rejecting H_0 is, from the standpoint of frequentist statistics, the required step to establish discovery of the signal process.

The critical region is not unique. Its choice should take into account the probabilities for the data predicted by some alternative hypothesis (or set of alternatives) H_1 . Rejecting H_0 if it is true is called a *type-I error*, and occurs by construction with probability no greater than α . Not rejecting H_0 if an alternative H_1 is true is called a *type-II error*, and for a given test this will have a certain probability $\beta = P(\mathbf{x} \notin w|H_1)$. The quantity $1 - \beta$ is called the *power* of the test of H_0 with respect to the alternative H_1 . A strategy for defining the critical region can therefore be to maximize the power with respect to some alternative (or alternatives) given a fixed size α .

To maximize the power of a test of H_0 with respect to the alternative H_1 , the *Neyman-Pearson lemma* states that the critical region w should be chosen such that for all data values \mathbf{x} inside w , the likelihood ratio

$$\lambda(\mathbf{x}) = \frac{f(\mathbf{x}|H_1)}{f(\mathbf{x}|H_0)} \quad (40.44)$$

is greater than or equal to a given constant c_α , and everywhere outside the critical region one has $\lambda(\mathbf{x}) < c_\alpha$, where the value of c_α is determined by the size of the test α . The hypotheses H_0 and H_1 must be simple, *i.e.*, they should not contain undetermined parameters.

It is convenient to define the test using a scalar function of the data \mathbf{x} called a *test statistic*, $t(\mathbf{x})$, such that the boundary of the critical region is given by a surface of constant $t(\mathbf{x})$. The Neyman-Pearson lemma is equivalent to the statement that the likelihood ratio (40.44) represents the optimal test statistic. It can be difficult in practice, however, to determine $\lambda(\mathbf{x})$, since this requires knowledge of the joint p.d.f.s $f(\mathbf{x}|H_0)$ and $f(\mathbf{x}|H_1)$.

Often one does not have explicit formulae for these, but rather Monte Carlo models that allow one to generate instances of \mathbf{x} that follow the p.d.f.s.

In the case where the likelihood ratio (40.44) cannot be used explicitly, there exist a variety of other multivariate methods for constructing a test statistic that may approach its performance. These are based on machine-learning algorithms that use samples of *training data* corresponding to the hypotheses in question, often generated from Monte Carlo models. Further information on Machine Learning can be found in Sec. 41 of this Review.

The multivariate algorithms designed to classify events into signal and background types also form the basis of tests of the hypothesis that a sample of events consists of background only. Such a test can be constructed using the distributions of the test statistic $t(\mathbf{x})$ for event classification obtained from a multivariate algorithm such as a Neural Network output. The distributions $p(t|s)$ and $p(t|b)$ for signal and background events, respectively, are used to construct the likelihood ratio of the signal-plus-background hypothesis relative to that of background only. To the extent that the test statistic $t(\mathbf{x})$ approximates the likelihood ratio (or a monotonic function thereof) for individual events given by (40.44), the resulting test of the background-only hypothesis for the event sample will have maximum power with respect to the signal-plus-background alternative (see Ref. [21]).

40.3.2 Tests of significance, p -values

A frequentist *significance test* allows one to assign a numerical value, called the p -value, that reflects the level of agreement between a hypothesis H_0 and the observed data \mathbf{x} . To carry out a significance test one must specify a subset of the data space, whose boundary includes the observed data point \mathbf{x}_{obs} , that is deemed to have equal or lesser compatibility with H_0 relative to \mathbf{x}_{obs} . The p -value of H_0 is the probability, assuming data distributed according to H_0 , to find \mathbf{x} in the region of equal or lesser compatibility.

For continuous data, one can show that the p -value of H_0 , here called p_0 , follows a uniform distribution for data generated under H_0 . Therefore one has $P(p_0 \leq \alpha|H_0) = \alpha$ for any constant α in $[0, 1]$. In this way the region of data space where $p_0 \leq \alpha$ gives a critical region w of a test of size α , as it satisfies $P(\mathbf{x} \in w|H_0) \leq \alpha$. Thus rejecting H_0 if $p_0 \leq \alpha$ is equivalent to the hypothesis test of Sec. 40.3.1 above. For the critical region w defined by $p_0 \leq \alpha$ one can find the power $P(\mathbf{x} \in w|H_1)$ with respect to an alternative hypothesis H_1 , as defined in Sec. 40.3.1. In general the region of low compatibility with H_0 is defined so as to have a high probability for data generated under H_1 , so that the distribution of p_0 , assuming data \mathbf{x} that follows H_1 , will be concentrated at low values, and the critical region w derived from $p_0 \leq \alpha$ will have a high power with respect to H_1 .

Similar to construction of a test's critical region in Sec. 40.3.1, finding the p -value is generally done by defining a statistic $t(\mathbf{x})$ whose value corresponds to better or worse levels of agreement with the hypothesis. The hypothesis being tested, H_0 , will determine the p.d.f. $f(t|H_0)$ for the statistic. If, for example, t is defined such that large values correspond to poor agreement with the hypothesis, then the p -value is

$$p = \int_{t_{\text{obs}}}^{\infty} f(t|H_0) dt, \quad (40.45)$$

where $t_{\text{obs}} = t(\mathbf{x}_{\text{obs}})$ is the value of the statistic obtained in the actual experiment.

Note that the p -value is not the probability of the hypothesis, which in frequentist statistics is not defined. The p -value should also not be confused with the size (significance level) of a test, or the confidence level of a confidence interval (Section 40.4), both of which are pre-specified constants.

When searching for a new phenomenon, one tries to reject the hypothesis H_0 that the data are consistent with known (*e.g.*, Standard Model) processes. If the p -value of H_0 is sufficiently low, then one is willing to accept that some alternative hypothesis is true. Often one converts the p -value into an effective significance Z , defined as an equivalent number of standard deviations of a

Gaussian distributed random variable. In a search for an intrinsically positive signal, *i.e.*, where only upward fluctuations of the estimated rate appear signal like, this is defined as

$$Z = \Phi^{-1}(1 - p). \quad (40.46)$$

Here Φ is the cumulative distribution of the standard Gaussian, and Φ^{-1} is its inverse (quantile) function. In this way, a p -value of 1/2 gives $Z = 0$, *i.e.*, having an estimated signal rate of zero corresponds to zero significance. If either positive or negative data fluctuations would indicate evidence of the signal, then one defines

$$Z = \Phi^{-1}(1 - p/2). \quad (40.47)$$

In this case an estimated signal rate of zero gives $p = 1$ and $Z = 0$.

Often in particle physics the level of significance where an effect is said to qualify as a discovery is $Z = 5$, *i.e.*, a 5σ effect, corresponding to a p -value of 2.87×10^{-7} . One's actual degree of belief that a new process is present, however, will depend in general on other factors as well, such as the plausibility of the new signal hypothesis and the degree to which it can describe the data, one's confidence in the model that led to the observed p -value, and possible corrections for multiple observations out of which one focuses on the smallest p -value obtained (the "look-elsewhere effect", discussed in Section 40.3.2.2).

40.3.2.1 Frequentist treatment of nuisance parameters and asymptotic methods for tests

Suppose one wants to test hypothetical values of parameters θ , but the model also contains nuisance parameters ν . To find a p -value for θ we can construct a test statistic q_θ such that larger values constitute increasing incompatibility between the data and the hypothesis. Then for an observed value of the statistic $q_{\theta, \text{obs}}$, the p -value of θ is

$$p_\theta(\nu) = \int_{q_{\theta, \text{obs}}}^{\infty} f(q_\theta|\theta, \nu) dq_\theta, \quad (40.48)$$

which depends in general on the nuisance parameters ν . In the strict frequentist approach, θ is rejected only if the p -value is less than α for all possible values of the nuisance parameters.

The difficulty described above is effectively solved if we can define the test statistic q_θ in such a way that its distribution $f(q_\theta|\theta)$ is independent of the nuisance parameters. Although exact independence is only found in special cases, it can be achieved approximately by use of the *profile likelihood ratio*. This is given by the profile likelihood from Eq.(40.18) divided by the value of the likelihood at its maximum, *i.e.*, when evaluated with the maximum-likelihood estimators $\hat{\theta}$ and $\hat{\nu}$:

$$\lambda_p(\theta) = \frac{L(\theta, \hat{\nu}(\theta))}{L(\hat{\theta}, \hat{\nu})}. \quad (40.49)$$

Wilks' theorem [10] states that, providing certain general conditions are satisfied, the distribution of $-2 \ln \lambda_p(\theta)$, under assumption of θ , approaches a χ^2 distribution in the limit where the data sample is very large, independent of the values of the nuisance parameters ν . Here the number of degrees of freedom is equal to the number of components of θ . More details on use of the profile likelihood are given in Refs. [22, 23] and in contributions to the PHYSTAT conferences [24]; explicit formulae for special cases can be found in Ref. [25]. Further discussion on how to incorporate systematic uncertainties into p -values can be found in Ref. [26].

Even with use of the profile likelihood ratio, for a finite data sample the p -value of hypothesized parameters θ will retain in general some dependence on the nuisance parameters ν . Ideally one would find the the maximum of $p_\theta(\nu)$ from Eq. (40.48) explicitly, but that is often impractical. An approximate and computationally feasible technique is to use $p_\theta(\hat{\nu}(\theta))$, where $\hat{\nu}(\theta)$ are the profiled values of the nuisance parameters as defined in Section 40.2.2.2. The resulting p -value is correct if the true values of the nuisance parameters are equal to the profiled values used; otherwise it could be either too high or too low. This is discussed further in Section 40.4.2 on confidence intervals.

The methods above based on the profile likelihood ratio are useful in practice because, provided one has a sufficiently large data sample, the distributions of the test statistics are related through Wilks' theorem to the chi-square p.d.f. If the data sample is not large enough to justify use of the asymptotic formulae, then some adjustments can be made to the test statistics so that their distributions are better approximated by the asymptotic ones; these improvements go under the general name of "higher-order asymptotics". Using these methods one may obtain p -values using the asymptotic formulae even for smaller data samples, avoiding costly Monte Carlo simulation to find distributions of test statistics.

Roughly speaking, the chi-square distribution for the profile likelihood ratio relies on having a Gaussian distribution for estimators of the model's parameters. An important type of corrected statistic relies on an improved distribution for the maximum-likelihood estimator due to Barndorff-Nielsen [27] (the p^* approximation). Another class of improved statistic due to Bartlett [28, 29] starts with a statistic t which, asymptotically, should be chi-square distributed with n_d degrees of freedom. A new statistic is defined as $t' = tn_d/E[t]$, which by construction has mean $E[t'] = n_d$, as for the chi-square distribution. Further details and applications of these methods are described in Refs. [30, 31].

One may also treat model uncertainties in a Bayesian manner but then use the resulting model in a frequentist test. Suppose the uncertainty in a set of nuisance parameters ν is characterized by a Bayesian prior p.d.f. $\pi(\nu)$. This can be used to construct the marginal (also called the prior predictive) model for the data \mathbf{x} and parameters of interest θ ,

$$P_m(\mathbf{x}|\theta) = \int P(\mathbf{x}|\theta, \nu)\pi(\nu) d\nu. \quad (40.50)$$

The marginal model does not represent the probability of data that would be generated if one were really to repeat the experiment, as in that case one would assume that the nuisance parameters do not vary. Rather, the marginal model represents a situation in which every repetition of the experiment is carried out with new values of ν , randomly sampled from $\pi(\nu)$. It is in effect an average of models each with a given ν , where the average is carried out with respect to the prior p.d.f. $\pi(\nu)$.

The marginal model for the data \mathbf{x} can be used to determine the distribution of a test statistic Q , which can be written

$$P_m(Q|\theta) = \int P(Q|\theta, \nu)\pi(\nu) d\nu. \quad (40.51)$$

In a search for a new signal process, the test statistic can be based on the ratio of likelihoods corresponding to the experiments where signal and background events are both present, L_{s+b} , to that of background only, L_b . Often the likelihoods are evaluated with the profiled values of the nuisance parameters, which may give improved performance. It is important to note, however, that it is through use of the marginal model for the distribution of Q that the uncertainties related to the nuisance parameters are incorporated into the result of the test. Different choices for the test statistic itself only result in variations of the power of the test with respect to different alternatives. Studies of marginalization versus profiling of nuisance parameters for specific problems, e.g., related to a Poisson counting experiment, can be found in Refs. [32, 33].

40.3.2.2 The look-elsewhere effect

The "look-elsewhere effect" relates to multiple measurements used to test a single hypothesis. The classic example is when one searches in a distribution for a peak whose position is not predicted in advance. Here the no-peak hypothesis is tested using data in a given range of the distribution. In the frequentist approach the correct p -value of the no-peak hypothesis is the probability, assuming background only, to find a signal as significant as the one found or more so anywhere in the search region. This can be substantially higher than the probability to find a peak of equal or greater significance in the particular place where it

appeared. There is in general some ambiguity as to what constitutes the relevant search region or even the broader set of relevant measurements. Although the desired p -value is well defined once the search region has been fixed, an exact treatment can require extensive computation.

The "brute-force" solution to this problem by Monte Carlo involves generating data under the background-only hypothesis and for each data set, fitting a peak of unknown position and recording a measure of its significance. To establish a discovery one often requires a p -value smaller than 2.87×10^{-7} , corresponding to a 5σ or larger effect. Determining this with Monte Carlo thus requires generating and fitting a very large number of experiments, perhaps several times 10^7 . In contrast, if the position of the peak is fixed, then the fit to the distribution is much easier, and furthermore one can in many cases use formulae valid for sufficiently large samples that bypass completely the need for Monte Carlo (see, e.g., Ref. [25]). However, this fixed-position or "local" p -value would not be correct in general, as it assumes the position of the peak was known in advance.

A method that allows one to modify the local p -value computed under assumption of a fixed position to obtain an approximation to the correct "global" value using a relatively simple calculation is described in Ref. [34]. Suppose a model contains a nuisance parameter such as the peak position that is only defined under the signal model (there is no peak in the background-only model). Furthermore, suppose a test statistic q_0 is defined using the profile likelihood ratio, so that by Wilk's theorem it would be asymptotically chi-square distributed if the peak position were to be fixed. The asymptotic distribution no longer holds if the peak position is adjustable, however, as this violates the regularity conditions of Wilks' theorem. If the statistic has an observed value u , then an approximation for the global p -value is found to be

$$p_{\text{global}} \approx p_{\text{local}} + \langle N_u \rangle, \quad (40.52)$$

where $\langle N_u \rangle$, which is much smaller than one in cases of interest, is the mean number of "upcrossings" (as defined in Ref. [34]) of the statistic q_0 above the level u in the range of the nuisance parameter considered (e.g., the mass range). The value of $\langle N_u \rangle$ can be estimated from the number of upcrossings $\langle N_{u_0} \rangle$ above some much lower value, u_0 , by using a relation due to Davis [35],

$$\langle N_u \rangle \approx \langle N_{u_0} \rangle e^{-(u-u_0)/2}. \quad (40.53)$$

By choosing u_0 sufficiently low, the value of $\langle N_u \rangle$ can be estimated by simulating only a very small number of experiments, or even from the observed data, rather than of the order 10^7 needed if one is dealing with a 5σ effect.

40.3.3 Goodness of fit

At times one wants to quantify the level of agreement between the data \mathbf{x} and a hypothesis H_0 without explicit reference to alternative hypotheses. In the frequentist approach this is done using a *goodness-of-fit test*. The result is quantified with a p -value, in general obtained from a statistic $t(\mathbf{x})$ as done in Sec. 40.3.2 with a significance test. Here, however, the *goodness-of-fit statistic* is defined using general considerations of what constitutes greater or lesser compatibility between data and hypothesis and not with reference to alternative hypotheses or power. Nevertheless, for a given statistic $t(\mathbf{x})$, the power of the resulting test with respect to an alternative can be found, so that types of alternatives to which one is sensitive (i.e., to which the test has high power) can be investigated.

The Neyman-Pearson lemma (see Sec. 40.3.1) states that a test of H_0 that has maximum power with respect to an alternative H_1 should be based on a statistic that is monotonic in the likelihood ratio $P(\mathbf{x}|H_1)/P(\mathbf{x}|H_0)$. Therefore a goodness-of-fit statistic derived without reference to a specific H_1 will not in general attain this maximum power. And even if a given $t(\mathbf{x})$ happens to be optimal or nearly so for some alternative H_1 , there may be other relevant alternatives for which its power is lower. In practice, goodness-of-fit statistics are defined so as to provide sensitivity to a broad class of alternatives, e.g., those that differ in the location of the bulk of the distribution's probability or the distribution's width or the nature of the tails. It may therefore be useful to use

several goodness-of-fit tests that are sensitive to different aspects of the data distribution in question.

The most important application of goodness-of-fit tests is no doubt in conjunction with the method of least squares, which we describe in Sec. 40.3.3.1 below. Other types of tests, particularly those based on the *empirical distribution function* are described in Sec. 40.3.3.2. Further discussion of goodness of fit can be found in Refs. [4,36] and references therein.

40.3.3.1 *Goodness-of-fit with chi-square or likelihood ratio*

An important type of goodness-of-fit test arises when a set of measurements $\mathbf{y} = (y_1, \dots, y_N)$ are used to test the hypothesis that the values are Gaussian distributed with given mean values $E[y_i] = \mu_i$ and variances $V[y_i] = \sigma_i^2$ (or covariance $V_{ij} = \text{cov}[y_i, y_j]$ if the values are correlated). The general procedures also hold when the data are Poisson or multinomially distributed with sufficiently large mean values so that the Gaussian represents an adequate approximation. The Gaussian hypothesis may be simple (all parameters fully specified), or the mean values μ_i may be given as functions of some other parameters $\boldsymbol{\theta} = (\theta_1, \dots, \theta_M)$, with $M < N$. The (co)variances are treated as fixed.

The test statistic derived from the likelihood ratio has already been introduced in Sec. 40.2.3 in connection with the method of least squares, and is given by the minimum of the function $\chi^2(\boldsymbol{\theta})$ with respect to $\boldsymbol{\theta}$, i.e., $t = \chi^2_{\min} = \chi^2(\hat{\boldsymbol{\theta}})$, e.g., in the case of uncorrelated measurements

$$t = \sum_{i=1}^N \frac{(y_i - \mu_i(\hat{\boldsymbol{\theta}}))^2}{\sigma_i^2}. \tag{40.54}$$

For Gaussian distributed \mathbf{y} , the statistic t follows a chi-square distribution for $N - M$ degrees of freedom. From Eq. (40.54) one sees that greater t corresponds to increasing incompatibility between the measured y_i and predicted μ_i . The p -value of the Gaussian hypothesis is therefore taken to be

$$p = \int_{\chi^2_{\min}}^{\infty} f(t; n_d) dt, \tag{40.55}$$

where $f(t; n_d)$ is the χ^2 p.d.f. and $n_d = N - M$ is the appropriate number of degrees of freedom. Values are shown in Fig. 40.1 or obtained from standard computer libraries. If the asymptotic conditions for using the χ^2 p.d.f. do not hold, the statistic can still be defined as before, but its p.d.f. must be determined by other means in order to obtain the p -value, e.g., using a Monte Carlo calculation.

Often the data represent numbers of events in N bins of a histogram, i.e., $\mathbf{n} = (n_1, \dots, n_N)$. An important case is when \mathbf{n} follows a multinomial distribution with $n_{\text{tot}} = \sum_{i=1}^N n_i$ total entries and mean values μ_i , or equivalently bin probabilities $p_i = \mu_i/n_{\text{tot}}$. Alternatively one may model the n_i as independent and Poisson distributed with means μ_i . If there are no adjustable parameters in the hypotheses, then the goodness-of-fit can be quantified with *Pearson's χ^2 statistic*, defined for multinomial data as

$$t_M = \sum_{i=1}^N \frac{(n_i - n_{\text{tot}}p_i)^2}{n_{\text{tot}}p_i}, \tag{40.56}$$

or for the independent Poisson data as

$$t_P = \sum_{i=1}^N \frac{(n_i - \mu_i)^2}{\mu_i}. \tag{40.57}$$

In the limit where the means μ_i are large, the statistics t_M and t_P are found to follow chi-square distributions for $N - 1$ and N degrees of freedom, respectively. Having one fewer degrees of freedom in the multinomial case is related to the fact that n_{tot} is fixed and thus the n_i are correlated.

Alternatively one can use the test statistic based on the likelihood ratio $t = -2 \ln \lambda(\hat{\boldsymbol{\theta}})$ given previously in Eq. (40.16). Here

the likelihood ratio λ is chosen to correspond to the multinomial or Poisson model as appropriate, as described in Sec. 40.2.2.1. One finds that the distribution of the likelihood-ratio statistic approaches the asymptotic limit faster than does Pearson's chi-square and thus when using the chi-square p.d.f. to compute a p -value one obtains in general a more accurate result from $-2 \ln \lambda$ (see [9]).

Since the mean of the chi-square distribution is equal to n_d , one expects in a "reasonable" experiment to obtain $\chi^2 \approx n_d$ (here χ^2 refers to the minimized value). Hence the quantity χ^2/n_d is sometimes reported. Since the p.d.f. of χ^2/n_d depends on n_d , however, one must report n_d as well if one wishes to determine the p -value. The p -values obtained for different values of χ^2/n_d are shown in Fig. 40.2.

If the minimized χ^2 value indicates a low level of agreement between data and hypothesis, one may be tempted to expect a high degree of uncertainty for any fitted parameters. Poor goodness-of-fit, however, does not mean that one will have large statistical errors for parameter estimates. If, for example, the error bars (or covariance matrix) used in constructing the χ^2 are underestimated, then this will lead to underestimated statistical errors for the fitted parameters and an increased value of the minimized χ^2 . The standard deviations of estimators that one finds from, say, Eq. (40.13) reflect how widely the estimates would be distributed if one were to repeat the measurement many times, assuming that the hypothesis and measurement errors used in the χ^2 are also correct. They do not include the systematic error which may result from an incorrect hypothesis or incorrectly estimated measurement errors in the χ^2 .

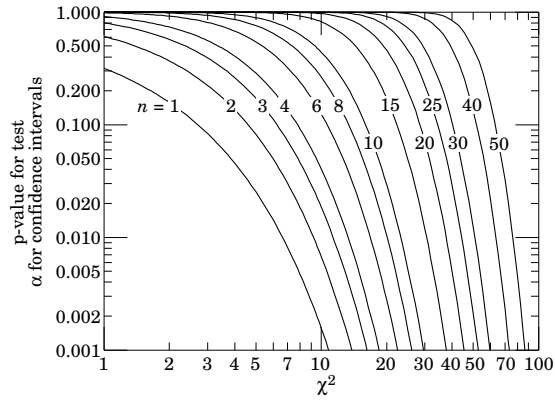


Figure 40.1: One minus the χ^2 cumulative distribution, $1 - F(\chi^2; n)$, for n degrees of freedom. This gives the p -value for the χ^2 goodness-of-fit test as well as one minus the coverage probability for confidence regions (see Sec. 40.4.2.2).

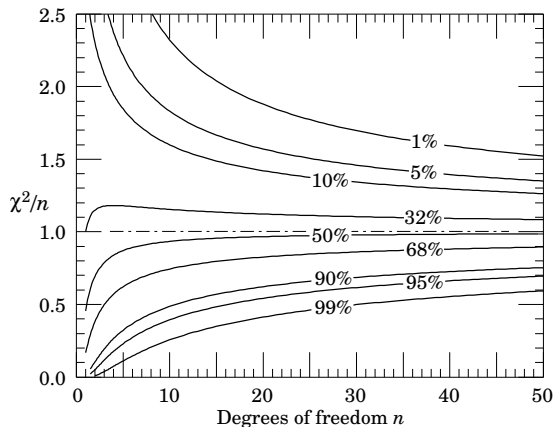


Figure 40.2: The 'reduced' χ^2 , equal to χ^2/n , for n degrees of freedom. The curves show as a function of n the χ^2/n that corresponds to a given p -value.

40.3.3.2 Goodness-of-fit with the empirical distribution function

Suppose a measurement yields a sample of independent and identically distributed (i.i.d.) values $\mathbf{x} = (x_1, \dots, x_n)$. Often the values may be summarized by creating a histogram, but this inevitably results in a loss of information, since the position of the x values within each bin is not retained. Particularly with small numbers of observations n one therefore may prefer to keep the values of each of the x_i (i.e., “unbinned”). The sample may be displayed graphically using the *empirical distribution function* (e.d.f.)

$$F_n(x) = \frac{\text{number of elements in sample with value } \leq x}{n} \quad (40.58)$$

The e.d.f. $F_n(x)$ begins at zero for x less than the lowest observed value, increases by $1/n$ at each observed x_i , and saturates at unity for x equal to the highest value in the sample.

Given an i.i.d. data sample $\mathbf{x} = (x_1, \dots, x_n)$, suppose one wants to test the hypothesis H_0 that x follows the p.d.f. $f(x)$ using a goodness-of-fit test, i.e., without reference to a specific alternative. The hypothesis of the p.d.f. $f(x)$ is equivalent to saying the cumulative distribution function (c.d.f.) is $F(x) = \int_{-\infty}^x f(x') dx'$. As the e.d.f. $F_n(x)$ can be viewed as an estimator for the c.d.f. $F(x)$, we can derive a goodness-of-fit statistic by some appropriately defined measure of the “distance” between the two.

A widely used example is the Kolmogorov-Smirnov (K-S) test, based on

$$D_n = \sup_x |F_n(x) - F(x)|, \quad (40.59)$$

where \sup denotes the supremum. That is, D_n is the greatest vertical distance between $F_n(x)$ and $F(x)$ for any x . In the limit of large sample size n , one can show that the distribution of D_n , assuming the data follows the c.d.f. $F(x)$, approaches the Kolmogorov distribution, which is independent of the specific form of $F(x)$ and is provided in many software packages. A larger value of D_n corresponds to greater incompatibility between data and hypothesis, so the p -value is the probability $P(D_n \geq D_{n,\text{obs}} | H_0)$. The K-S test is sensitive in particular to differences in location (i.e., in the mean of x), as this corresponds to a horizontal shift between $F_n(x)$ and $F(x)$, giving a large maximum vertical distance D_n .

The Cramér-von Mises family of tests is based on the squared difference between $F_n(x)$ and $F(x)$ through an integral of the form

$$W^2 = \int_{-\infty}^{\infty} (F(x) - F_n(x))^2 w(x) f(x) dx, \quad (40.60)$$

where $f(x) = dF/dx$ is the p.d.f. of x and $w(x)$ is a weight function that must be specified. Two important choices are the classic Cramér-von Mises test with $w(x) = 1$, and the Anderson-Darling test with $w(x) = [F(x)(1 - F(x))]^{-1}$, which gives increased sensitivity to departures in the tails of the distribution. For cases such as these where the weight function depends on x only through the cumulative distribution $F(x)$, one can show (see, e.g., Refs. [4,36]) that the distribution of W^2 , assuming data that follows $F(x)$, is independent of the form of $F(x)$. The distributions of the Smirnov-Cramér-von Mises and Anderson-Darling statistics are available in standard computer libraries.

40.3.4 Bayes factors

In Bayesian statistics, all of one’s knowledge about a model is contained in its posterior probability, which one obtains using Bayes’ theorem (Eq. (40.37)). Thus one could reject a hypothesis H if its posterior probability $P(H|\mathbf{x})$ is sufficiently small. The difficulty here is that $P(H|\mathbf{x})$ is proportional to the prior probability $P(H)$, and there will not be a consensus about the prior probabilities for the existence of new phenomena. Nevertheless one can construct a quantity called the Bayes factor (described below), which can be used to quantify the degree to which the data prefer one hypothesis over another, and is independent of their prior probabilities.

Consider two models (hypotheses), H_i and H_j , described by vectors of parameters θ_i and θ_j , respectively. Some of the components will be common to both models and others may be distinct. The full prior probability for each model can be written in the form

$$\pi(H_i, \theta_i) = P(H_i)\pi(\theta_i|H_i). \quad (40.61)$$

Here $P(H_i)$ is the overall prior probability for H_i , and $\pi(\theta_i|H_i)$ is the normalized p.d.f. of its parameters. For each model, the posterior probability is found using Bayes’ theorem,

$$P(H_i|\mathbf{x}) = \frac{\int P(\mathbf{x}|\theta_i, H_i)P(H_i)\pi(\theta_i|H_i) d\theta_i}{P(\mathbf{x})}, \quad (40.62)$$

where the integration is carried out over the internal parameters θ_i of the model. The ratio of posterior probabilities for the models is therefore

$$\frac{P(H_i|\mathbf{x})}{P(H_j|\mathbf{x})} = \frac{\int P(\mathbf{x}|\theta_i, H_i)\pi(\theta_i|H_i) d\theta_i}{\int P(\mathbf{x}|\theta_j, H_j)\pi(\theta_j|H_j) d\theta_j} \frac{P(H_i)}{P(H_j)}. \quad (40.63)$$

The *Bayes factor* is defined as

$$B_{ij} = \frac{\int P(\mathbf{x}|\theta_i, H_i)\pi(\theta_i|H_i) d\theta_i}{\int P(\mathbf{x}|\theta_j, H_j)\pi(\theta_j|H_j) d\theta_j}. \quad (40.64)$$

This gives what the ratio of posterior probabilities for models i and j would be if the overall prior probabilities for the two models were equal. If the models have no nuisance parameters, i.e., no internal parameters described by priors, then the Bayes factor is simply the likelihood ratio. The Bayes factor therefore shows by how much the probability ratio of model i to model j changes in the light of the data, and thus can be viewed as a numerical measure of evidence supplied by the data in favor of one hypothesis over the other.

Although the Bayes factor is by construction independent of the overall prior probabilities $P(H_i)$ and $P(H_j)$, it does require priors for all internal parameters of a model, i.e., one needs the functions $\pi(\theta_i|H_i)$ and $\pi(\theta_j|H_j)$. In a Bayesian analysis where one is only interested in the posterior p.d.f. of a parameter, it may be acceptable to take an unnormalizable function for the prior (an improper prior) as long as the product of likelihood and prior can be normalized. Improper priors are, however, only defined up to an arbitrary multiplicative constant, and so the Bayes factor would depend on this constant. Furthermore, although the range of a constant normalized prior is unimportant for parameter determination (provided it is wider than the likelihood), this is not so for the Bayes factor when such a prior is used for only one of the hypotheses. So to compute a Bayes factor, all internal parameters must be described by normalized priors that represent meaningful probabilities over the entire range where they are defined.

An exception to this rule may be considered when the identical parameter appears in the models for both numerator and denominator of the Bayes factor. In this case one can argue that the arbitrary constants would cancel. One must exercise some caution, however, as parameters with the same name and physical meaning may still play different roles in the two models.

Both integrals in Equation (40.64) are of the form

$$m = \int P(\mathbf{x}|\theta)\pi(\theta) d\theta, \quad (40.65)$$

which is similar to the marginal likelihood seen previously in Eq. (40.50) (in some fields this quantity is called the *evidence*). Computing marginal likelihoods can be difficult; in many cases it can be done with the nested sampling algorithm [37] as implemented, e.g., in the program `MultiNest` [38]. A review of Bayes factors can be found in Ref. [39].

40.4 Intervals and limits

When the goal of an experiment is to determine a parameter θ , the result is usually expressed by quoting, in addition to the point estimate, some sort of interval which reflects the statistical precision of the measurement. In the simplest case, this can be

given by the parameter's estimated value $\hat{\theta}$ plus or minus an estimate of the standard deviation of $\hat{\theta}$, $\hat{\sigma}_{\hat{\theta}}$. If, however, the p.d.f. of the estimator is not Gaussian or if there are physical boundaries on the possible values of the parameter, then one usually quotes instead an interval according to one of the procedures described below.

In reporting an interval or limit, the experimenter may wish to

- communicate as objectively as possible the result of the experiment;
- provide an interval that is constructed to cover on average the true value of the parameter with a specified probability;
- provide the information needed by the consumer of the result to draw conclusions about the parameter or to make a particular decision;
- draw conclusions about the parameter that incorporate stated prior beliefs.

With a sufficiently large data sample, the point estimate and standard deviation (or for the multiparameter case, the parameter estimates and covariance matrix) satisfy essentially all of these goals. For small data samples, no single method for quoting an interval will achieve all of them.

In addition to the goals listed above, the choice of method may be influenced by practical considerations such as ease of producing an interval from the results of several measurements. Of course the experimenter is not restricted to quoting a single interval or limit; one may choose, for example, first to communicate the result with a confidence interval having certain frequentist properties, and then in addition to draw conclusions about a parameter using a judiciously chosen subjective Bayesian prior. It is recommended, however, that there be a clear separation between these two aspects of reporting a result. In the remainder of this section, we assess the extent to which various types of intervals achieve the goals stated here.

40.4.1 Bayesian intervals

As described in Sec. 40.2.6, a Bayesian posterior probability may be used to determine regions that will have a given probability of containing the true value of a parameter. In the single parameter case, for example, an interval (called a Bayesian or credible interval) $[\theta_{lo}, \theta_{up}]$ can be determined which contains a given fraction $1 - \alpha$ of the posterior probability, *i.e.*,

$$1 - \alpha = \int_{\theta_{lo}}^{\theta_{up}} p(\theta|x) d\theta . \tag{40.66}$$

Sometimes an upper or lower limit is desired, *i.e.*, θ_{lo} or θ_{up} can be set to a physical boundary or to plus or minus infinity. In other cases, one might be interested in the set of θ values for which $p(\theta|x)$ is higher than for any θ not belonging to the set, which may constitute a single interval or a set of disjoint regions; these are called highest posterior density (HPD) intervals. Note that HPD intervals are not invariant under a nonlinear transformation of the parameter.

If a parameter is constrained to be non-negative, then the prior p.d.f. can simply be set to zero for negative values. An important example is the case of a Poisson variable n , which counts signal events with unknown mean s , as well as background with mean b , assumed known. For the signal mean s , one often uses the prior

$$\pi(s) = \begin{cases} 0 & s < 0 \\ 1 & s \geq 0 \end{cases} . \tag{40.67}$$

This prior may be regarded as providing an interval whose frequentist properties can be studied, rather than as representing a degree of belief. For example, to obtain an upper limit on s , one may proceed as follows. The likelihood for s is given by the Poisson distribution for n with mean $s + b$,

$$P(n|s) = \frac{(s + b)^n}{n!} e^{-(s+b)} , \tag{40.68}$$

along with the prior (40.67) in (40.37) gives the posterior density for s . An upper limit s_{up} at confidence level (or here, rather,

credibility level) $1 - \alpha$ can be obtained by requiring

$$1 - \alpha = \int_{-\infty}^{s_{up}} p(s|n) ds = \frac{\int_{-\infty}^{s_{up}} P(n|s) \pi(s) ds}{\int_{-\infty}^{\infty} P(n|s) \pi(s) ds} , \tag{40.69}$$

where the lower limit of integration is effectively zero because of the cut-off in $\pi(s)$. By relating the integrals in Eq. (40.69) to incomplete gamma functions, the solution for the upper limit is found to be

$$s_{up} = \frac{1}{2} F_{\chi^2}^{-1} [p, 2(n + 1)] - b , \tag{40.70}$$

where $F_{\chi^2}^{-1}$ is the quantile of the χ^2 distribution (inverse of the cumulative distribution). Here the quantity p is

$$p = 1 - \alpha (1 - F_{\chi^2} [2b, 2(n + 1)]) , \tag{40.71}$$

where F_{χ^2} is the cumulative χ^2 distribution. For both F_{χ^2} and $F_{\chi^2}^{-1}$ above, the argument $2(n + 1)$ gives the number of degrees of freedom. For the special case of $b = 0$, the limit reduces to

$$s_{up} = \frac{1}{2} F_{\chi^2}^{-1} (1 - \alpha; 2(n + 1)) . \tag{40.72}$$

It happens that for the case of $b = 0$, the upper limit from Eq. (40.72) coincides numerically with the frequentist upper limit discussed in Section 40.4.2.3. Values for $1 - \alpha = 0.9$ and 0.95 are given by the values μ_{up} in Table 40.3. The frequentist properties of confidence intervals for the Poisson mean found in this way are discussed in Refs. [2] and [40].

As in any Bayesian analysis, it is important to show how the result changes under assumption of different prior probabilities. For example, one could consider the Jeffreys prior as described in Sec. 40.2.6. For this problem one finds the Jeffreys prior $\pi(s) \propto 1/\sqrt{s + b}$ for $s \geq 0$ and zero otherwise. As with the constant prior, one would not regard this as representing one's prior beliefs about s , both because it is improper and also as it depends on b . Rather it is used with Bayes' theorem to produce an interval whose frequentist properties can be studied.

If the model contains nuisance parameters then these are eliminated by marginalizing, as in Eq. (40.43), to obtain the p.d.f. for the parameters of interest. For example, if the parameter b in the Poisson counting problem above were to be characterized by a prior p.d.f. $\pi(b)$, then one would first use Bayes' theorem to find $p(s, b|n)$. This is then marginalized to find $p(s|n) = \int p(s, b|n) \pi(b) db$, from which one may determine an interval for s . One may not be certain whether to extend a model by including more nuisance parameters. In this case, a Bayes factor may be used to determine to what extent the data prefer a model with additional parameters, as described in Section 40.3.4.

40.4.2 Frequentist confidence intervals

The unqualified phrase "confidence intervals" refers to frequentist intervals obtained with a procedure due to Neyman [41], described below. The boundary of the interval (or in the multiparameter case, region) is given by a specific function of the data, which would fluctuate if one were to repeat the experiment many times. The *coverage probability* refers to the fraction of intervals in such an ensemble that contain the true parameter value. Confidence intervals are constructed so as to have a coverage probability greater than or equal to a given *confidence level*, regardless of the true parameter's value. It is important to note that in the frequentist approach, such a probability is not meaningful for a fixed interval. In this section we discuss several techniques for producing intervals that have, at least approximately, this property of coverage.

40.4.2.1 The Neyman construction for confidence intervals

Consider a p.d.f. $f(x; \theta)$ where x represents the outcome of the experiment and θ is the unknown parameter for which we want to construct a confidence interval. The variable x could (and often does) represent an estimator for θ . Using $f(x; \theta)$, we can find using a pre-defined rule and probability $1 - \alpha$ for every value of

θ , a set of values $x_1(\theta, \alpha)$ and $x_2(\theta, \alpha)$ such that

$$P(x_1 < x < x_2; \theta) = \int_{x_1}^{x_2} f(x; \theta) dx \geq 1 - \alpha. \quad (40.73)$$

If x is discrete, the integral is replaced by the corresponding sum. In that case there may not exist a range of x values whose summed probability is exactly equal to a given value of $1 - \alpha$, and one requires by convention $P(x_1 < x < x_2; \theta) \geq 1 - \alpha$.

This is illustrated for continuous x in Fig. 40.3: a horizontal line segment $[x_1(\theta, \alpha), x_2(\theta, \alpha)]$ is drawn for representative values of θ . The union of such intervals for all values of θ , designated in the figure as $D(\alpha)$, is known as a *confidence belt*. Typically the curves $x_1(\theta, \alpha)$ and $x_2(\theta, \alpha)$ are monotonic functions of θ , which we assume for this discussion.

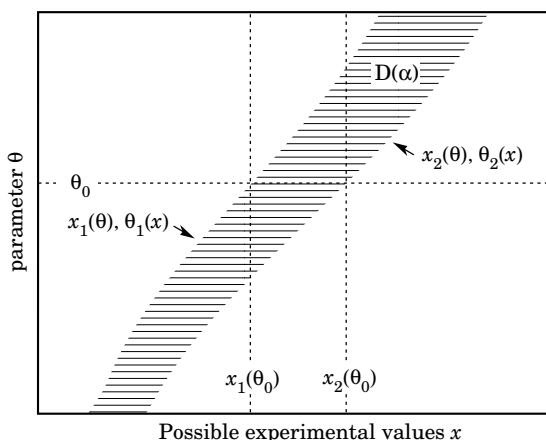


Figure 40.3: Construction of the confidence belt (see text).

Upon performing an experiment to measure x and obtaining a value x_0 , one draws a vertical line through x_0 . The confidence interval for θ is the set of all values of θ for which the corresponding line segment $[x_1(\theta, \alpha), x_2(\theta, \alpha)]$ is intercepted by this vertical line. Such confidence intervals are said to have a *confidence level* (CL) equal to $1 - \alpha$.

Now suppose that the true value of θ is θ_0 , indicated in the figure. We see from the figure that θ_0 lies between $\theta_1(x)$ and $\theta_2(x)$ if and only if x lies between $x_1(\theta_0)$ and $x_2(\theta_0)$. The two events thus have the same probability, and since this is true for any value θ_0 , we can drop the subscript 0 and obtain

$$1 - \alpha = P(x_1(\theta) < x < x_2(\theta)) = P(\theta_2(x) < \theta < \theta_1(x)). \quad (40.74)$$

In this probability statement, $\theta_1(x)$ and $\theta_2(x)$, *i.e.*, the endpoints of the interval, are the random variables and θ is an unknown constant. If the experiment were to be repeated a large number of times, the interval $[\theta_1, \theta_2]$ would vary, covering the fixed value θ in a fraction $1 - \alpha$ of the experiments.

The condition of coverage in Eq. (40.73) does not determine x_1 and x_2 uniquely, and additional criteria are needed. One possibility is to choose *central intervals* such that the probabilities to find x below x_1 and above x_2 are each $\alpha/2$. In other cases, one may want to report only an upper or lower limit, in which case one of $P(x \leq x_1)$ or $P(x \geq x_2)$ can be set to α and the other to zero. Another principle based on *likelihood ratio ordering* for determining which values of x should be included in the confidence belt is discussed below.

When the observed random variable x is continuous, the coverage probability obtained with the Neyman construction is $1 - \alpha$, regardless of the true value of the parameter. Because of the requirement $P(x_1 < x < x_2) \geq 1 - \alpha$ when x is discrete, one obtains in that case confidence intervals that include the true parameter with a probability greater than or equal to $1 - \alpha$.

An equivalent method of constructing confidence intervals is to consider a test (see Sec. 40.3) of the hypothesis that the parameter's true value is θ (assume one constructs a test for all physical

values of θ). One then excludes all values of θ where the hypothesis would be rejected in a test of size α or less. The remaining values constitute the confidence interval at confidence level $1 - \alpha$. If the critical region of the test is characterized by having a p -value $p_\theta \leq \alpha$, then the endpoints of the confidence interval are found in practice by solving $p_\theta = \alpha$ for θ .

In the procedure outlined above, one is still free to choose the test to be used; this corresponds to the freedom in the Neyman construction as to which values of the data are included in the confidence belt. One possibility is to use a test statistic based on the *likelihood ratio*,

$$\lambda(\theta) = \frac{f(x; \theta)}{f(x; \hat{\theta})}, \quad (40.75)$$

where $\hat{\theta}$ is the value of the parameter which, out of all allowed values, maximizes $f(x; \theta)$. The confidence belt is taken to contain the values of x that give the greatest values of $\lambda(\theta)$. This results in the intervals described in Ref. [42] by Feldman and Cousins.

If the model contains nuisance parameters ν , then these can be incorporated into the test (or the p -values) used to determine the limit by profiling as discussed in Section 40.3.2.1. As mentioned there, the strict frequentist approach is to regard the parameter of interest θ as excluded only if it is rejected for all possible values of ν . The resulting interval for θ will then cover the true value with a probability greater than or equal to the nominal confidence level for all points in ν -space.

If the p -value is based on the profiled values of the nuisance parameters, *i.e.*, with $\nu = \hat{\nu}(\theta)$ used in Eq. (40.48), then the resulting interval for the parameter of interest will have the correct coverage if the true values of ν are equal to the profiled values. Otherwise the coverage probability may be too high or too low. This procedure has been called *profile construction* in particle physics [32] (see also Ref. [26]).

40.4.2.2 Gaussian distributed measurements

An important example of constructing a confidence interval is when the data consists of a single random variable x that follows a Gaussian distribution; this is often the case when x represents an estimator for a parameter and one has a sufficiently large data sample. If there is more than one parameter being estimated, the multivariate Gaussian is used. For the univariate case with known σ , the probability that the measured value x will fall within $\pm\delta$ of the true value μ is

$$\begin{aligned} 1 - \alpha &= \frac{1}{\sqrt{2\pi}\sigma} \int_{\mu-\delta}^{\mu+\delta} e^{-(x-\mu)^2/2\sigma^2} dx \\ &= \text{erf}\left(\frac{\delta}{\sqrt{2}\sigma}\right) = 2\Phi\left(\frac{\delta}{\sigma}\right) - 1, \end{aligned} \quad (40.76)$$

where erf is the Gaussian error function, which is rewritten in the final equality using Φ , the Gaussian cumulative distribution. Fig. 40.4 shows a $\delta = 1.64\sigma$ confidence interval unshaded. The choice $\delta = \sigma$ gives an interval called the *standard error* which has $1 - \alpha = 68.27\%$ if σ is known. Values of α for other frequently used choices of δ are given in Table 40.1.

Table 40.1: Area of the tails α outside $\pm\delta$ from the mean of a Gaussian distribution.

α	δ	α	δ
0.3173	1σ	0.2	1.28σ
4.55×10^{-2}	2σ	0.1	1.64σ
2.7×10^{-3}	3σ	0.05	1.96σ
6.3×10^{-5}	4σ	0.01	2.58σ
5.7×10^{-7}	5σ	0.001	3.29σ
2.0×10^{-9}	6σ	10^{-4}	3.89σ

We can set a one-sided (upper or lower) limit by excluding above $x + \delta$ (or below $x - \delta$). The values of α for such limits are half the values in Table 40.1.

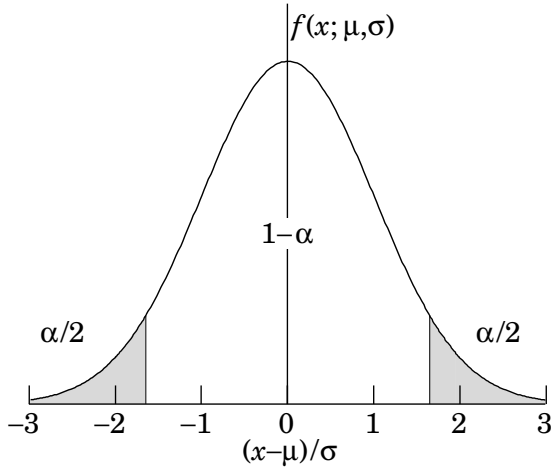


Figure 40.4: Illustration of a symmetric 90% confidence interval (unshaded) for a Gaussian-distributed measurement of a single quantity. Integrated probabilities, defined by $\alpha = 0.1$, are as shown.

The relation (40.76) can be re-expressed using the cumulative distribution function for the χ^2 distribution as

$$\alpha = 1 - F(\chi^2; n), \tag{40.77}$$

for $\chi^2 = (\delta/\sigma)^2$ and $n = 1$ degree of freedom. This can be seen as the $n = 1$ curve in Fig. 40.1 or obtained using standard computer libraries. For multivariate measurements of, say, M parameter estimates $\hat{\theta} = (\hat{\theta}_1, \dots, \hat{\theta}_M)$, construction of the confidence region requires the full covariance matrix $V_{ij} = \text{cov}[\hat{\theta}_i, \hat{\theta}_j]$, which can be estimated as described in Sections 40.2.2 and 40.2.3. Under fairly general conditions with the methods of maximum-likelihood or least-squares in the large sample limit, the estimators will be distributed according to a multivariate Gaussian centered about the true (unknown) values θ , and furthermore, the likelihood function itself will take on a Gaussian shape.

The standard error ellipse for the pair $(\hat{\theta}_i, \hat{\theta}_j)$ is shown in Fig. 40.5, corresponding to a contour $\chi^2 = \chi_{\text{min}}^2 + 1$ or $\ln L = \ln L_{\text{max}} - 1/2$. The ellipse is centered about the estimated values $\hat{\theta}$, and the tangents to the ellipse give the standard deviations of the estimators, σ_i and σ_j . The angle of the major axis of the ellipse is given by

$$\tan 2\phi = \frac{2\rho_{ij}\sigma_i\sigma_j}{\sigma_j^2 - \sigma_i^2}, \tag{40.78}$$

where $\rho_{ij} = \text{cov}[\hat{\theta}_i, \hat{\theta}_j]/\sigma_i\sigma_j$ is the correlation coefficient.

The correlation coefficient can be visualized as the fraction of the distance σ_i from the ellipse's horizontal center-line at which the ellipse becomes tangent to vertical, *i.e.*, at the distance $\rho_{ij}\sigma_i$ below the center-line as shown. As ρ_{ij} goes to $+1$ or -1 , the ellipse thins to a diagonal line.

It could happen that one of the parameters, say, θ_j , is known from previous measurements to a precision much better than σ_j , so that the current measurement contributes almost nothing to the knowledge of θ_j . However, the current measurement of θ_i and its dependence on θ_j may still be important. In this case, instead of quoting both parameter estimates and their correlation, one sometimes reports the value of θ_i , which minimizes χ^2 at a fixed value of θ_j , such as the PDG best value. This θ_i value lies along the dotted line between the points where the ellipse becomes tangent to vertical, and has statistical error σ_{inner} as shown on the figure, where $\sigma_{\text{inner}} = (1 - \rho_{ij}^2)^{1/2}\sigma_i$. Instead of the correlation ρ_{ij} , one reports the dependency $d\hat{\theta}_i/d\theta_j$, which is the slope of the dotted line. This slope is related to the correlation coefficient by $d\hat{\theta}_i/d\theta_j = \rho_{ij} \times \frac{\sigma_i}{\sigma_j}$.

As in the single-variable case, because of the symmetry of the Gaussian function between θ and $\hat{\theta}$, one finds that contours of

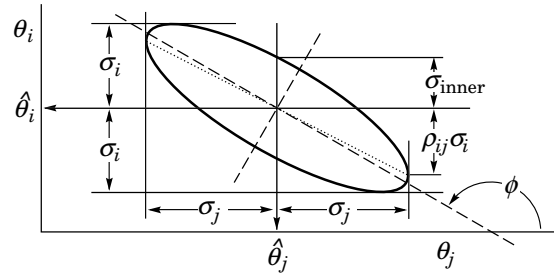


Figure 40.5: Standard error ellipse for the estimators $\hat{\theta}_i$ and $\hat{\theta}_j$. In the case shown the correlation is negative.

constant $\ln L$ or χ^2 cover the true values with a certain, fixed probability. That is, the confidence region is determined by

$$\ln L(\theta) \geq \ln L_{\text{max}} - \Delta \ln L, \tag{40.79}$$

or where a χ^2 has been defined for use with the method of least-squares,

$$\chi^2(\theta) \leq \chi_{\text{min}}^2 + \Delta \chi^2. \tag{40.80}$$

Values of $\Delta \chi^2$ or $2\Delta \ln L$ are given in Table 40.2 for several values of the coverage probability $1 - \alpha$ and number of fitted parameters M . For Gaussian distributed data, these are related by $\Delta \chi^2 = 2\Delta \ln L = F_{\chi^2_M}^{-1}(1 - \alpha)$, where $F_{\chi^2_M}^{-1}$ is the chi-square quantile (inverse of the cumulative distribution) for M degrees of freedom.

Table 40.2: Values of $\Delta \chi^2$ or $2\Delta \ln L$ corresponding to a coverage probability $1 - \alpha$ in the large data sample limit, for joint estimation of M parameters.

$(1 - \alpha)$ (%)	$M = 1$	$M = 2$	$M = 3$
68.27	1.00	2.30	3.53
90.	2.71	4.61	6.25
95.	3.84	5.99	7.82
95.45	4.00	6.18	8.03
99.	6.63	9.21	11.34
99.73	9.00	11.83	14.16

For non-Gaussian data samples, the probability for the regions determined by Equations (40.79) or (40.80) to cover the true value of θ becomes independent of θ only in the large-sample limit. So for a finite data sample these are not exact confidence regions according to our previous definition. Nevertheless, they can still have a coverage probability only weakly dependent on the true parameter, and approximately as given in Table 40.2. In any case, the coverage probability of the intervals or regions obtained according to this procedure can in principle be determined as a function of the true parameter(s), for example, using a Monte Carlo calculation.

One of the practical advantages of intervals that can be constructed from the log-likelihood function or χ^2 is that it is relatively simple to produce the interval for the combination of several experiments. If N independent measurements result in log-likelihood functions $\ln L_i(\theta)$, then the combined log-likelihood function is simply the sum,

$$\ln L(\theta) = \sum_{i=1}^N \ln L_i(\theta). \tag{40.81}$$

This can then be used to determine an approximate confidence interval or region with Eq. (40.79), just as with a single experiment.

40.4.2.3 Poisson or binomial data

Another important class of measurements consists of counting a certain number of events, n . In this section, we will assume these are all events of the desired type, *i.e.*, there is no background. If n

represents the number of events produced in a reaction with cross section σ and selection efficiency ε in a fixed integrated luminosity \mathcal{L} , then it follows a Poisson distribution with mean $\mu = \sigma\varepsilon\mathcal{L}$. If, on the other hand, one has selected a larger sample of N events and found n of them to have a particular property, then n follows a binomial distribution where the parameter p gives the probability for the event to possess the property in question. This is appropriate, *e.g.*, for estimates of branching ratios or selection efficiencies based on a given total number of events.

For the case of Poisson distributed n , limits on the mean value μ can be found from the Neyman procedure as discussed in Section 40.4.2.1 with n used directly as the statistic x . The upper and lower limits are found to be

$$\mu_{\text{lo}} = \frac{1}{2} F_{\chi^2}^{-1}(\alpha_{\text{lo}}; 2n), \quad (40.82a)$$

$$\mu_{\text{up}} = \frac{1}{2} F_{\chi^2}^{-1}(1 - \alpha_{\text{up}}; 2(n+1)), \quad (40.82b)$$

where confidence levels of $1 - \alpha_{\text{lo}}$ and $1 - \alpha_{\text{up}}$ refer separately to the corresponding intervals $\mu \geq \mu_{\text{lo}}$ and $\mu \leq \mu_{\text{up}}$, and $F_{\chi^2}^{-1}$ is the quantile of the χ^2 distribution (inverse of the cumulative distribution). For central confidence intervals at confidence level $1 - \alpha$, set $\alpha_{\text{lo}} = \alpha_{\text{up}} = \alpha/2$.

Table 40.3: Lower and upper (one-sided) limits for the mean μ of a Poisson variable given n observed events in the absence of background, for confidence levels of 90% and 95%.

n	$1 - \alpha = 90\%$		$1 - \alpha = 95\%$	
	μ_{lo}	μ_{up}	μ_{lo}	μ_{up}
0	–	2.30	–	3.00
1	0.105	3.89	0.051	4.74
2	0.532	5.32	0.355	6.30
3	1.10	6.68	0.818	7.75
4	1.74	7.99	1.37	9.15
5	2.43	9.27	1.97	10.51
6	3.15	10.53	2.61	11.84
7	3.89	11.77	3.29	13.15
8	4.66	12.99	3.98	14.43
9	5.43	14.21	4.70	15.71
10	6.22	15.41	5.43	16.96

It happens that the upper limit from Eq. (40.82b) coincides numerically with the Bayesian upper limit for a Poisson parameter, using a uniform prior p.d.f. for μ . Values for confidence levels of 90% and 95% are shown in Table 40.3. For the case of binomially distributed n successes out of N trials with probability of success p , the upper and lower limits on p are found to be

$$p_{\text{lo}} = \frac{n F_F^{-1}[\alpha_{\text{lo}}; 2n, 2(N-n+1)]}{N-n+1 + n F_F^{-1}[\alpha_{\text{lo}}; 2n, 2(N-n+1)]}, \quad (40.83a)$$

$$p_{\text{up}} = \frac{(n+1) F_F^{-1}[1 - \alpha_{\text{up}}; 2(n+1), 2(N-n)]}{(N-n) + (n+1) F_F^{-1}[1 - \alpha_{\text{up}}; 2(n+1), 2(N-n)]}. \quad (40.83b)$$

Here F_F^{-1} is the quantile of the F distribution (also called the Fisher–Snedecor distribution; see Ref. [4]).

40.4.2.4 Parameter exclusion in cases of low sensitivity

An important example of a statistical test arises in the search for a new signal process. Suppose the parameter μ is defined such that it is proportional to the signal cross section. A statistical test may be carried out for hypothesized values of μ , which may be done by computing a p -value, p_μ , for all μ . Those values not rejected in a test of size α , *i.e.*, for which one does not find $p_\mu \leq \alpha$, constitute a confidence interval with confidence level $1 - \alpha$.

In general one will find that for some regions in the parameter space of the signal model, the predictions for data are almost indistinguishable from those of the background-only model. This corresponds to the case where μ is very small, as would occur,

e.g., in a search for a new particle with a mass so high that its production rate in a given experiment is negligible. That is, one has essentially no experimental sensitivity to such a model.

One would prefer that if the sensitivity to a model (or a point in a model's parameter space) is very low, then it should not be excluded. Even if the outcomes predicted with or without signal are identical, however, the probability to reject the signal model will equal α , the type-I error rate. As one often takes α to be 5%, this would mean that in a large number of searches covering a broad range of a signal model's parameter space, there would inevitably be excluded regions in which the experimental sensitivity is very small, and thus one may question whether it is justified to regard such parameter values as disfavored.

Exclusion of models to which one has little or no sensitivity occurs, for example, if the data fluctuate very low relative to the expectation of the background-only hypothesis. In this case the resulting upper limit on μ may be anomalously low. As a means of controlling this effect one often determines the mean or median limit under assumption of the background-only hypothesis, as discussed in Sec. 40.5.

One way to mitigate the problem of excluding models to which one is not sensitive is the CL_s method, where the measure used to test a parameter is increased for decreasing sensitivity [43, 44]. The procedure is based on a statistic called CL_s , which is defined as

$$\text{CL}_s = \frac{p_\mu}{1 - p_b}, \quad (40.84)$$

where p_b is the p -value of the background-only hypothesis. In the usual formulation of the method, both p_μ and p_b are defined using a single test statistic, and the definition of CL_s above assumes this statistic is continuous; more details can be found in Refs. [43, 44].

A point in a model's parameter space is regarded as excluded if one finds $\text{CL}_s \leq \alpha$. As the denominator in Eq. (40.84) is always less than or equal to unity, the exclusion criterion based on CL_s is more stringent than the usual requirement $p_\mu \leq \alpha$. In this sense the CL_s procedure is conservative, and the coverage probability of the corresponding intervals will exceed the nominal confidence level $1 - \alpha$. If the experimental sensitivity to a given value of μ is very low, then one finds that as p_μ decreases, so does the denominator $1 - p_b$, and thus the condition $\text{CL}_s \leq \alpha$ is effectively prevented from being satisfied. In this way the exclusion of parameters in the case of low sensitivity is suppressed.

The CL_s procedure has the attractive feature that the resulting intervals coincide with those obtained from the Bayesian method in two important cases: the mean value of a Poisson or Gaussian distributed measurement with a constant prior. The CL_s intervals overcover for all values of the parameter μ , however, by an amount that depends on μ .

The problem of excluding parameter values to which one has little sensitivity is particularly acute when one wants to set a one-sided limit, *e.g.*, an upper limit on a cross section. Here one tests a value of a rate parameter μ against the alternative of a lower rate, and therefore the critical region of the test is taken to correspond to data outcomes with a low event yield. If the number of events found in the search region fluctuates low enough, however, it can happen that all physically meaningful signal parameter values, including those to which one has very little sensitivity, are rejected by the test.

Another solution to this problem, therefore, is to replace the one-sided test by one based on the likelihood ratio, where the critical region is not restricted to low rates. This is the approach followed in the Feldman-Cousins procedure described in Section 40.4.2.1. The critical region for the test of a given value of μ contains data values characteristic of both higher and lower rates. As a result, for a given observed rate one can in general obtain a two-sided interval. If, however, the parameter estimate $\hat{\mu}$ is sufficiently close to the lower limit of zero, then only high values of μ are rejected, and the lower edge of the confidence interval is at zero. Note, however, that the coverage property of $1 - \alpha$ pertains to the entire interval, not to the probability for the upper edge μ_{up} to be greater than the true value μ . For parameter estimates increasingly far away from the boundary, *i.e.*, for increasing signal significance, the point $\mu = 0$ is excluded and the interval has nonzero upper and lower edges.

An additional difficulty arises when a parameter estimate is not significantly far away from the boundary, in which case it is natural to report a one-sided confidence interval (often an upper limit). It is straightforward to force the Neyman prescription to produce only an upper limit by setting $x_2 = \infty$ in Eq. (40.73). Then x_1 is uniquely determined and the upper limit can be obtained. If, however, the data come out such that the parameter estimate is not so close to the boundary, one might wish to report a central confidence interval (*i.e.*, an interval based on a two-sided test with equal upper and lower tail areas). As pointed out by Feldman and Cousins [42], if the decision to report an upper limit or two-sided interval is made by looking at the data (“flip-flopping”), then in general there will be parameter values for which the resulting intervals have a coverage probability less than $1 - \alpha$. With the confidence intervals suggested in Ref. [42], the prescription determines whether the interval is one- or two-sided in a way which preserves the coverage probability (and are thus said to be *unified*).

The intervals according to this method for the mean of Poisson variable in the absence of background are given in Table 40.4. (Note that α in Ref. [42] is defined following Neyman [41] as the coverage probability; this is opposite the modern convention used here in which the coverage probability is $1 - \alpha$.) The values of $1 - \alpha$ given here refer to the coverage of the true parameter by the whole interval $[\mu_1, \mu_2]$. In Table 40.3 for the one-sided upper limit, however, $1 - \alpha$ refers to the probability to have $\mu_{\text{up}} \geq \mu$ (or $\mu_{\text{lo}} \leq \mu$ for lower limits).

Table 40.4: Unified confidence intervals $[\mu_1, \mu_2]$ for a the mean of a Poisson variable given n observed events in the absence of background, for confidence levels of 90% and 95%.

n	$1 - \alpha = 90\%$		$1 - \alpha = 95\%$	
	μ_1	μ_2	μ_1	μ_2
0	0.00	2.44	0.00	3.09
1	0.11	4.36	0.05	5.14
2	0.53	5.91	0.36	6.72
3	1.10	7.42	0.82	8.25
4	1.47	8.60	1.37	9.76
5	1.84	9.99	1.84	11.26
6	2.21	11.47	2.21	12.75
7	3.56	12.53	2.58	13.81
8	3.96	13.99	2.94	15.29
9	4.36	15.30	4.36	16.77
10	5.50	16.50	4.75	17.82

A potential difficulty with unified intervals arises if, for example, one constructs such an interval for a Poisson parameter s of some yet to be discovered signal process with, say, $1 - \alpha = 0.9$. If the true signal parameter is zero, or in any case much less than the expected background, one will usually obtain a one-sided upper limit on s . In a certain fraction of the experiments, however, a two-sided interval for s will result. Since, however, one typically chooses $1 - \alpha$ to be only 0.9 or 0.95 when setting limits, the value $s = 0$ may be found below the lower edge of the interval before the existence of the effect is well established. It must then be communicated carefully that in excluding $s = 0$ at, say, 90% or 95% confidence level from the interval, one is not necessarily claiming to have discovered the effect, for which one would usually require a higher level of significance (*e.g.*, 5σ).

Another possibility is to construct a Bayesian interval as described in Section 40.4.1. The presence of the boundary can be incorporated simply by setting the prior density to zero in the unphysical region. More specifically, the prior may be chosen using formal rules such as the reference prior or Jeffreys prior mentioned in Sec. 40.2.6.

In particle physics a widely used prior for the mean μ of a Poisson distributed measurement has been the uniform distribution for $\mu \geq 0$. This prior does not follow from any fundamental rule nor can it be regarded as reflecting a reasonable degree of belief, since the prior probability for μ to lie between any two finite values is zero. The procedure above can be more appropriately regarded

as a way for obtaining intervals with frequentist properties that can be investigated. The resulting upper limits have a coverage probability that depends on the true value of the Poisson parameter, and is nowhere smaller than the stated probability content. Lower limits and two-sided intervals for the Poisson mean based on uniform priors undercover, however, for some values of the parameter, although to an extent that in practical cases may not be too severe [2, 40].

In any case, it is important to always report sufficient information so that the result can be combined with other measurements. Often this means giving an unbiased estimator and its standard deviation, even if the estimated value is in the unphysical region.

It can also be useful with a frequentist interval to calculate its subjective probability content using the posterior p.d.f. based on one or several reasonable guesses for the prior p.d.f. If it turns out to be significantly less than the stated confidence level, this warns that it would be particularly misleading to draw conclusions about the parameter’s value from the interval alone.

40.5 Experimental sensitivity

In this section we describe methods for characterizing the sensitivity of a search for a new physics signal. As discussed in Sec. 40.3, an experimental analysis can often be formulated as a test of hypothetical model parameters. Therefore we may quantify the sensitivity by giving the results that we expect from such a test under specific assumptions about the signal process.

Here to be concrete we will consider a parameter μ proportional to the rate of a signal process, although the concepts described in this section may be easily generalized to other parameters. One may wish to establish discovery of the signal process by testing and rejecting the hypothesis that $\mu = 0$, and in addition one often wants to test nonzero values of μ to construct a confidence interval (*e.g.*, limits) as described in Sec. 40.4. In the frequentist framework, the result of each tested value of μ is the p -value p_μ or equivalently the significance $Z_\mu = \Phi^{-1}(1 - p_\mu)$, where as usual Φ is the standard Gaussian cumulative distribution and its inverse Φ^{-1} is the standard Gaussian quantile.

Prior to carrying out the experiment, one generally wants to quantify what significance Z_μ is expected under given assumptions for the presence or absence of the signal process. Specifically, for the significance of a test of $\mu = 0$ (the discovery significance) one usually quotes the Z_0 one would expect if the signal is present at a given nominal rate, which we can define in general to correspond to $\mu = 1$. For limits, one often gives the expected limit under assumption of the background-only ($\mu = 0$) model. These quantities are used to optimize the analysis and to quantify the experimental sensitivity, that is, to characterize how likely it is to make a discovery if the signal is present, and to say what values of μ one may be able to exclude if the signal is in fact absent.

First we clarify the notion of *expected significance*. Because the significance Z_μ is a function of the data, it is itself a random quantity characterized by a certain sampling distribution. This distribution depends on the assumed value of μ , which is not necessarily the same as the hypothesized value of μ being tested. We may therefore consider the distribution $f(Z_\mu|\mu')$, *i.e.*, the distribution of Z_μ that would be obtained by considering data samples generated under assumption of μ' . In a similar way one can talk about the sampling distribution of an upper limit for μ , $f(\mu_{\text{up}}|\mu')$.

One can identify the expected significance or limit with either the mean or median of these distributions, but the median may be preferred since it is invariant under monotonic transformations. For example, the monotonic relation between p -value and significance, $p = 1 - \Phi(Z)$, then gives $\text{med}[p_\mu|\mu'] = 1 - \Phi(\text{med}[Z_\mu|\mu'])$, whereas the corresponding relation does not hold in general for the mean.

In some cases one may be able to write down approximate formulae for the distributions of Z_μ and for limits, but more generally they must be determined from Monte Carlo calculations. In many cases of interest, the significance Z_μ and the limits on μ will have approximate Gaussian distributions.

As an example, consider a Poisson counting experiment, where the result consists of an observed number n of events, modeled as a Poisson distributed variable with a mean of $\mu s + b$. Here s and b ,

the expected numbers of events from signal and background processes, are taken to be known. If we are interested in discovering the signal process we test and try to reject the hypothesis $\mu = 0$. To characterize the experimental sensitivity, we want to give the discovery significance expected under the assumption of $\mu = 1$.

In the limit where its mean value is large, the Poisson variable n can be approximated as an almost continuous Gaussian variable with mean $\mu s + b$ and standard deviation $\sigma = \sqrt{\mu s + b}$. In the usual case where a physical signal model corresponds to $\mu > 0$, the p -value of $\mu = 0$ is the probability to find n greater than or equal to the value observed,

$$p_0 = \Phi\left(\frac{n-b}{\sqrt{b}}\right), \quad (40.85)$$

and the corresponding significance is $Z_0 = \Phi^{-1}(1 - p_0) = (n - b)/\sqrt{b}$. The median (here equal to the mean) of n assuming $\mu = 1$ is $s + b$, and therefore the median discovery significance is

$$\text{med}[Z_0|\mu = 1] = \frac{s}{\sqrt{b}}. \quad (40.86)$$

The figure of merit “ s/\sqrt{b} ” has been widely used in particle physics as a measure of expected discovery significance. A better approximation for the Poisson counting experiment, however, may be obtained by testing $\mu = 0$ using the likelihood ratio (40.49) $\lambda(0) = L(0)/L(\hat{\mu})$, where

$$L(\mu) = \frac{(\mu s + b)^n}{n!} e^{-(\mu s + b)} \quad (40.87)$$

is the likelihood function, and $\hat{\mu} = (n - b)/s$ is the estimator of μ . In this example there are no nuisance parameters, as s and b are taken to be known. For the case where the relevant signal models correspond to positive μ , one may test the $\mu = 0$ hypothesis with the statistic $q_0 = -2 \ln \lambda(0)$ when $\hat{\mu} > 0$, *i.e.*, an excess is observed, and $q_0 = 0$ otherwise. One can show (see, *e.g.*, Ref. [25]) that in the large-sample limit, the discovery significance is then $Z_0 = \sqrt{q_0}$, for which one finds

$$Z_0 = \sqrt{2 \left(n \ln \frac{n}{b} + b - n \right)} \quad (40.88)$$

for $n > b$ and $Z_0 = 0$ otherwise. To approximate the expected discovery significance assuming $\mu = 1$, one may simply replace n with the expected value $E[n|\mu = 1] = s + b$ (the so-called “Asimov data set”), giving

$$\text{med}[Z_0|\mu = 1] = \sqrt{2 \left((s + b) \ln \left(1 + \frac{s}{b} \right) - s \right)}. \quad (40.89)$$

This has been shown in Ref. [25] to provide a good approximation to the median discovery significance for values of s of several and for b well below unity. The right-hand side of Eq. (40.89) reduces to s/\sqrt{b} in the limit $s \ll b$.

Beyond the simple Poisson counting experiment, in general one may test values of a parameter μ with more complicated functions of the measured data to obtain a p -value p_μ , and from this one can quote the equivalent significance Z_μ or find, *e.g.*, an upper limit μ_{up} . In this case as well one may quantify the experimental sensitivity by giving the significance Z_μ expected if the data are generated with a different value of the parameter μ' . In some problems, finding the sampling distribution of the significance or limits may be possible using large-sample formulae as described, *e.g.*, in Ref. [25]. In other cases a Monte Carlo study may be needed. Using whatever method of calculation is most appropriate, one usually quotes the expected (mean or, preferably, median) discovery significance or exclusion limit as the primary measure of experimental sensitivity.

Even if the true signal is present at its nominal rate, the actual discovery significance Z_0 obtained from the real data is subject to statistical fluctuations and will not in general be equal to its expected value. In an analogous way, the observed limit will differ

from the expected limit even if the signal is absent. Upon observing such a difference one would like to know how large this is compared to expected statistical fluctuations. Therefore, in addition to the observed significance and limits it is useful to communicate not only their expected values but also a measure of the width of their distributions.

As the distributions of significance and limits are often well approximated by a Gaussian, one may indicate the intervals corresponding to plus-or-minus one and/or two standard deviations. If the distributions are significantly non-Gaussian, one may use instead the quantiles that give the same probability content, *i.e.*, [0.1587, 0.8413] for $\pm 1\sigma$, [0.02275, 0.97725] for $\pm 2\sigma$. An upper limit found significantly below the background-only expectation may indicate a strong downward fluctuation of the data, or perhaps as well an incorrect estimate of the background rate.

The procedures described above pertain to frequentist hypothesis tests and limits. Bayesian limits, just like those found from a frequentist procedure, are functions of the data and one may therefore find, usually with approximations or Monte Carlo studies, their sampling distribution and corresponding mean (or, preferably, median) and standard deviation.

When trying to establish discovery of a signal process, the Bayesian approach may employ a Bayes factor as described in Sec. 40.3.4. In the case of the Poisson counting experiment with the likelihood from Eq. (40.87), the log of the Bayes factor that compares $\mu = 1$ to $\mu = 0$ is $\ln B_{10} = \ln(L(1)/L(0)) = n \ln(1 + s/b) - s$. That is, the expectation value, assuming $\mu = 1$, of $\ln B_{10}$ for this problem is

$$E[\ln B_{10}|\mu = 1] = (s + b) \ln \left(1 + \frac{s}{b} \right) - s. \quad (40.90)$$

Comparing this to Eq. (40.89), one finds $\text{med}[Z_0|1] = \sqrt{2E[\ln B_{10}|1]}$. Thus for this particular problem the frequentist median discovery significance can be related to the corresponding Bayes factor in a simple way.

In some analyses, the goal may not be to establish discovery of a signal process but rather to measure, as accurately as possible, the signal rate. If we consider again the Poisson counting experiment described by the likelihood function of Eq. (40.87), the maximum-likelihood estimator $\hat{\mu} = (n - b)/s$ has a variance, assuming $\mu = 1$, of

$$V[\hat{\mu}] = V \left[\frac{n - b}{s} \right] = \frac{1}{s^2} V[n] = \frac{s + b}{s^2}, \quad (40.91)$$

so that the standard deviation of $\hat{\mu}$ is $\sigma_{\hat{\mu}} = \sqrt{s + b}/s$. One may therefore use $s/\sqrt{s + b}$ as a figure of merit to be maximized in order to obtain the best measurement accuracy of a rate parameter. The quantity $s/\sqrt{s + b}$ is also the expected significance with which one rejects s assuming the signal is absent, and thus can be used to optimize the expected upper limit on s .

References

- [1] B. Efron, *Am. Stat.* **40**, 11 (1986).
- [2] R. D. Cousins, *Am. J. Phys.* **63**, 398 (1995).
- [3] A. Stuart, J.K. Ord, and S. Arnold, *Kendall's Advanced Theory of Statistics*, Vol. 2A: *Classical Inference and the Linear Model*, 6th ed., Oxford Univ. Press (1999), and earlier editions by Kendall and Stuart. The likelihood-ratio ordering principle is described at the beginning of Ch. 23. Chapter 26 compares different schools of statistical inference.
- [4] F. James, *Statistical methods in experimental physics* (2006), ISBN 9789812567956.
- [5] P. R. Rider, *Journal of the American Statistical Association* **55**, 289, 148 (1960).
- [6] L. Lyons, *Statistics for Nuclear and Particle Physicists* (1986), ISBN 9780521379342.
- [7] R. J. Barlow, *Nucl. Instrum. Meth.* **A297**, 496 (1990).
- [8] G. Cowan, *Statistical data analysis* (1998), ISBN 9780198501565.
- [9] S. Baker and R. D. Cousins, *Nucl. Instrum. Meth.* **221**, 437 (1984).

- [10] S. S. Wilks, *Annals Math. Statist.* **9**, 1, 60 (1938).
- [11] O. Behnke *et al.*, editors, *Data analysis in high energy physics*, Wiley-VCH, Weinheim, Germany (2013), ISBN 9783527410583, 9783527653447, 9783527653430, URL <http://www.wiley-vch.de/publish/dt/books/ISBN3-527-41058-9>.
- [12] S. Schmitt, *EPJ Web of Conferences* **137**, 11008 (2017), ISSN 2100-014X, URL <http://dx.doi.org/10.1051/epjconf/201713711008>.
- [13] L. Brenner *et al.*, *Int. J. Mod. Phys. A* **35**, 24, 2050145 (2020), [arXiv:1910.14654].
- [14] A. O'Hagan and J.J. Forster, *Bayesian Inference*, (2nd edition, volume 2B of *Kendall's Advanced Theory of Statistics*, Arnold, London, 2004).
- [15] D. Sivia and J. Skilling, *Data Analysis: A Bayesian Tutorial*, (Oxford University Press, 2006).
- [16] P.C. Gregory, *Bayesian Logical Data Analysis for the Physical Sciences*, (Cambridge University Press, 2005).
- [17] J.M. Bernardo and A.F.M. Smith, *Bayesian Theory*, (Wiley, 2000).
- [18] Robert E. Kass and Larry Wasserman, *J. Am. Stat. Assoc.* **91**, 1343 (1996).
- [19] J.M. Bernardo, *J. R. Statist. Soc.* **B41**, 113 (1979); J.M. Bernardo and J.O. Berger, *J. Am. Stat. Assoc.* **84**, 200 (1989). See also J.M. Bernardo, *Reference Analysis*, in *Handbook of Statistics*, 25 (D.K. Dey and C.R. Rao, eds.), 17-90, Elsevier (2005) and references therein.
- [20] L. Demortier, S. Jain and H. B. Prosper, *Phys. Rev.* **D82**, 034002 (2010), [arXiv:1002.1111].
- [21] K. Cranmer, J. Pavez and G. Louppe (2015), [arXiv:1506.02169].
- [22] N. Reid, *Likelihood Inference in the Presence of Nuisance Parameters*, *Proceedings of PHYSTAT2003*, L. Lyons, R. Mount, and R. Reitmeyer, eds., eConf C030908, Stanford, 2003.
- [23] W. A. Rolke, A. M. Lopez and J. Conrad, *Nucl. Instrum. Meth.* **A551**, 493 (2005), [arXiv:physics/0403059].
- [24] Links to the *Proceedings of the PHYSTAT* conference series (Durham 2002, Stanford 2003, Oxford 2005, and Geneva 2007, 2011) can be found at <https://espace.cern.ch/phystat>.
- [25] G. Cowan *et al.*, *Eur. Phys. J.* **C71**, 1554 (2011), [arXiv:1007.1727]; G. Cowan *et al.*, *Eur. Phys. J.* **C73**, 1434 (2013).
- [26] L. Demortier, *P-Values and Nuisance Parameters*, *Proceedings of PHYSTAT 2007*, CERN-2008-001, p. 23.
- [27] O. Barndorff-Nielsen, *Biometrika* **67**, 2, 293 (1980), ISSN 00063444, URL <http://www.jstor.org/stable/2335474>.
- [28] M. S. Bartlett, *Proceedings of the Royal Society of London. Series A - Mathematical and Physical Sciences* **160**, 901, 268 (1937), URL <https://royalsocietypublishing.org/doi/abs/10.1098/rspa.1937.0109>.
- [29] D. N. Lawley, *Biometrika* **43**, 3-4, 295 (1956), ISSN 0006-3444, URL <https://doi.org/10.1093/biomet/43.3-4.295>.
- [30] A. R. Brazzale, A. C. Davison and N. Reid, *Applied Asymptotics: Case Studies in Small-Sample Statistics*, Cambridge University Press, Cambridge (2007), URL <http://infoscience.epfl.ch/record/104219>.
- [31] G. Cordeiro and F. Cribari-Neto, *An Introduction to Bartlett Correction and Bias Reduction*, SpringerBriefs in Statistics, Springer Berlin Heidelberg (2014), ISBN 9783642552557, URL <https://books.google.co.uk/books?id=MJyKAwAAQBAJ>.
- [32] K. Cranmer, in "Statistical Problems in Particle Physics, Astrophysics and Cosmology (PHYSTAT 05): Proceedings, Oxford, UK, September 12-15, 2005," 112-123 (2005), [arXiv:physics/0511028].
- [33] R. D. Cousins, J. T. Linnemann and J. Tucker, *Nucl. Instrum. Meth. A* **595**, 2, 480 (2008), URL <https://doi.org/10.1016%2Fj.nima.2008.07.086>.
- [34] E. Gross and O. Vitells, *Eur. Phys. J.* **C70**, 525 (2010), [arXiv:1005.1891].
- [35] R. B. Davies, *Biometrika* **74**, 33 (1987).
- [36] R. D. Cousins, *Lectures on Statistics in Theory: Prelude to Statistics in Practice* (2023), [arXiv:1807.05996].
- [37] J. Skilling, *Nested Sampling*, *AIP Conference Proceedings*, **735**, 395-405 (2004).
- [38] F. Feroz, M. P. Hobson and M. Bridges, *Mon. Not. Roy. Astron. Soc.* **398**, 1601 (2009), [arXiv:0809.3437].
- [39] R. E. Kass and A. E. Raftery, *J. Am. Statist. Assoc.* **90**, 430, 773 (1995).
- [40] B. P. Roe and M. B. Woodroffe, *Phys. Rev.* **D63**, 013009 (2001), [hep-ex/0007048].
- [41] J. Neyman, *Phil. Trans. Roy. Soc. Lond.* **A236**, 767, 333 (1937); Reprinted in *A Selection of Early Statistical Papers on J. Neyman*, (University of California Press, Berkeley, 1967).
- [42] G. J. Feldman and R. D. Cousins, *Phys. Rev.* **D57**, 3873 (1998), [arXiv:physics/9711021]; This paper does not specify what to do if the ordering principle gives equal rank to some values of x . Eq. 21.6 of Ref. [3] gives the rule: all such points are included in the acceptance region (the domain $D(\alpha)$). Some authors have assumed the contrary, and shown that one can then obtain null intervals.
- [43] A. L. Read, in "Workshop on confidence limits, CERN, Geneva, Switzerland, 17-18 Jan 2000: Proceedings," 81-101 (2000), URL <http://weblib.cern.ch/record/451614>.
- [44] T. Junk, *Nucl. Instrum. Meth.* **A434**, 435 (1999), [hep-ex/9902006].

41. Machine Learning

Written November 2021 by K. Cranmer (Wisconsin U.), U. Seljak (UC Berkeley; LBNL) and K. Terao (SLAC; Stanford U.).

41.1	Introduction	711			
41.1.1	A gentle introduction with a representative example	712			
41.2	Fundamental concepts	712			
41.2.1	Loss, risk, empirical risk	712			
41.2.2	Generalization	713			
41.3	Common tasks and their associated loss functions	713			
41.3.1	Supervised learning	713			
41.3.1.1	Regression	713			
41.3.1.2	A note on regularization	714			
41.3.1.3	Classification	714			
41.3.2	Unsupervised learning	715			
41.3.2.1	Density estimation	715			
41.3.2.2	Representation learning, compression, and auto-encoders	716			
41.3.2.3	Clustering	716			
41.3.3	Optimal control, reinforcement learning, and active learning	717			
	Reinforcement learning	717			
	Multi-arm bandits	717			
	Bayesian optimization	717			
	Connection to experimental design	718			
	Active learning	718			
41.3.4	Anomaly detection and out-of-distribution detection	718			
41.3.5	Simulation-based inference	719			
41.3.5.1	Differentiable simulations	719			
41.3.5.2	Unfolding as an inverse problem	719			
41.4	Data representations, inductive bias, and example applications	720			
41.5	Flavors of ML models	721			
41.5.1	Support vector machines and kernel machines	721			
	Maximum-margin classifiers	721			
	Soft margins and slack variables	721			
	The dual problem	721			
	The kernel trick	721			
	Support vector regression	722			
	Kernel ridge regression	722			
	Gaussian Process Regression (kriging)	722			
41.5.2	Decision trees	722			
	Tree-based models	722			
	Ensemble methods	723			
	Bagging	723			
	Random forests	723			
	AdaBoost	724			
	Gradient boosting	724			
41.5.3	Neural networks	724			
41.5.3.1	Feed-forward multi-layer perceptron	724			
41.5.3.2	Activation functions	724			
41.5.3.3	Softmax	725			
41.5.3.4	The rise of deep learning	725			
41.5.3.5	Convolutional neural networks	725			
41.5.3.6	Pooling	725			
41.5.3.7	CNN architectures for image analysis	726			
	Region Convolutional Neural Network	726			
	U-Net	726			
41.5.3.8	Residual networks and skip connections	727			
41.5.3.9	Recurrent neural networks	727			
41.5.3.10	LSTM and GRU	729			
41.5.3.11	Attention	729			
41.5.3.12	Scaled dot-product attention	730			
41.5.3.13	Transformer and multi-head attention	731			
41.5.3.14	Graph networks and geometric deep learning	731			
41.5.4	Deep generative models	732			
41.5.4.1	Variational auto-encoders	733			
41.5.4.2	Generative adversarial networks	733			
41.5.4.3	Normalizing flows, autoregressive models, and score based models	734			
41.6	Learning algorithms	735			
41.6.1	Gradient-based optimization	735			
41.6.2	Stochastic gradient descent	735			
41.6.3	Optimization algorithms	735			
41.6.4	Automatic differentiation and back propagation	735			
41.6.5	The vanishing and exploding gradient problems	736			
41.6.6	Early stopping	736			
41.6.7	Initialization of model parameters	736			
41.6.8	Input normalization	736			
41.6.9	Batch normalization	736			
41.6.10	Transfer learning: pre-training and fine-tuning	737			
41.6.11	Zero, one, and a few shot learning	737			
41.7	Incorporating uncertainty	737			
41.7.1	Propagation of errors	738			
41.7.2	Domain adaptation	738			
41.7.3	Parameterized models	739			
41.7.4	Data augmentation	739			
41.7.5	Aleatoric and epistemic uncertainty	739			
41.7.6	Model averaging and Bayesian machine learning	740			
41.7.7	Connection to probabilistic machine learning	740			
41.8	Infrastructure for deployment in experiments	741			
41.1 Introduction					
<p>This chapter gives an overview of the core concepts of machine learning that are relevant to particle physics with some examples of applications to the energy, intensity, cosmic, and accelerator frontiers. Machine learning (ML) is an enormous field that has grown substantially in the last decade, propelled largely by the emergence of so-called deep learning (DL) [1, 2]. ML has a long history in particle physics going back to the late 1980s and early 1990s, see Refs. [3–5] for recent reviews.</p> <p>Physicists are exploring and contributing to machine learning at an unprecedented rate, which poses a challenge for those that wish to have an up-to-date view of the field. This motivated an effort to create <i>A Living Review of Machine Learning for Particle and Nuclear Physics</i> [6], which can be downloaded here: https://github.com/iml-wg/HEPML-LivingReview. As of the time of this writing, the Living Review includes over 500 references organized hierarchically by topic. While we make references to some of these papers, this chapter focuses on the methodology and does not attempt to give a comprehensive review of the applications.</p> <p>Despite the connotations of machine learning and artificial intelligence as a mysterious and radical departure from traditional approaches, we stress that machine learning has a mathematical formulation that is closely tied to statistics, the calculus of variations, approximation theory, and optimal control theory.</p> <p>The topic can be organized along a few axes, which we use to organize this section. First, there are different learning paradigms, for example supervised learning, unsupervised learning, and reinforcement learning. We focus on the first two in this review, since reinforcement learning is less commonly used in particle physics. Within these paradigms there are various tasks; for example, classification and regression – which have been the primary use of ML in particle physics – are examples of supervised learning. In addition to the learning paradigm and tasks, there are various types of machine learning models that generically process some input and produce some output. The types of models vary based on what it is they are modelling (<i>e.g.</i> so-called discriminative vs. generative</p>					

models), as well as the way that they are implemented (e.g. neural networks, decision trees, and kernel machines). Next, there are the issues around training or learning within the context of a given task and model class, which connects to optimization and regularization. We will briefly discuss the various considerations that emerge in the application of machine learning methods to physics, such as the treatment of systematic uncertainty, the interpretability of the models, the incorporation of symmetry, etc..

41.1.1 A gentle introduction with a representative example

We will use a specific, familiar example to introduce the various ingredients in context before factorizing and abstracting them. Consider the task of *classifying* energy deposits in a particle detector as electrons or protons. For this example, let the detector data consist of energy deposits in d sensors so that the data can be represented as *feature vector* $x \in \mathbb{R}^d$. Different components of x may have different units (e.g. units of energy, momentum, position etc.). Due to the complex interactions of particles in the detector, we do not have an explicit probability model for the high-dimensional data for the electron and proton scenarios, but we do have a simulator that allows us to generate Monte Carlo samples for each. This allows us to assemble a *training dataset* $\{x_i, y_i\}_{i=1, \dots, n}$, where y is used as a *label* to identify how the example was generated (e.g. $y = 0$ for electrons and $y = 1$ for protons). We would like to find a function $f : x \rightarrow y$ that is able to accurately *predict* the label on new data. Because we have feature-label pairs, this is considered a *supervised learning* problem. We can use a *neural network* to provide a flexible family of functions $f_\phi : \mathbb{R}^d \rightarrow \mathbb{R}$, where ϕ denotes the internal parameters of the neural network (i.e. the weights and biases that we will discuss in Sec.41.5.3). The goal of the *training procedure* is to find the value of the parameters ϕ that provide the ‘best’ predictions, but since no model is perfect, we must be explicit about the trade-offs. This is made concrete through a *loss function* $\mathcal{L}(f_\phi(x), y)$. For this example, instead of the obvious zero-one loss (which is 0 if $f_\phi(x)$ equals y and 1 if they are not), we choose to use the squared-loss $\mathcal{L}_{\text{sq}}(f_\phi(x), y) = (y - f_\phi(x))^2$ (which may seem *ad hoc* now, but will be motivated in Sec. 41.3.1.3). We can evaluate the average of the loss on the training set of size n , which is referred to as the *empirical risk* $\mathcal{R}_{\text{emp}}(f_\phi) = \sum_{i=1}^n \mathcal{L}(f_\phi(x), y)/n$. *Training* refers to numerically minimizing the empirical risk (often referred to as the *training loss* through some abuse of terminology). We can numerically optimize the model through *gradient descent*, which iteratively adjusts the parameters of the network according to $\phi^{t+1} = \phi^t - \lambda \nabla_\phi \mathcal{R}_{\text{emp}}(f_\phi)$, where λ is referred to as the *learning rate*. Once the optimization is complete and we obtain the solution $\hat{\phi}$, it is natural to assess the quality of the trained model $f_{\hat{\phi}}$ on an independent *testing dataset*. The empirical risk evaluated on the testing set is often larger than on the training set, and large differences indicate *overfitting*, which indicates that the model does not generalize well to the unseen data. The ability to accurately predict on unseen data is referred to as *generalization* and the empirical risk on the test data provides a measure of the *generalization error*. In order to reduce the *generalization error* one might explore different model choices (e.g. neural network architectures), additional regularization terms in the loss function, different learning rates, optimization algorithms, or early stopping criterion in the optimization. Once trained, the model can be applied to data. In order to produce a binary electron vs. proton decision from the continuous output of the neural network, we must threshold (i.e. classify as proton if $f_{\hat{\phi}}(x) > k$). The choice of the threshold k is often referred to as a working point and it sets the tradeoff between electron and proton efficiency, fake-rates, purity, etc. These familiar concepts in particle physics are usually referred to in different terms in machine learning and a *receiver operating characteristic curve*, or ROC curve, is used to summarize the tradeoff between true positive rate (TPR) and false positive rate (FPR). Importantly, the characterization of the efficiency / rejection (or equivalently the ROC curve) requires labeled data. In a particle physics context, it is recognized that the simulation is not perfect and the mismodelling is associated to the presence of systematic uncertainty. In machine learning, the discrepancy between the distribution of the training dataset

and the distribution of the data that the model will be applied to in practice is referred to as *domain shift* or *distribution shift*. While mismodelling in the training dataset might lead to a less-than-optimal classifier in practice, the real source of systematic uncertainty comes from mismatch between the data used to characterize the performance of the classifier and the unlabeled data that the classifier is applied to. This motivates the use of data-driven methods to calibrate the resulting model.

This example provides a vertical slice through the various aspects of supervised machine learning in particle physics. Now we factorize and abstract the various ingredients in order to provide a more general treatment with a broader scope.

41.2 Fundamental concepts

41.2.1 Loss, risk, empirical risk

The term *learning* in machine learning generally refers to optimization of some objective, which can be thought of as maximizing utility or minimizing *risk*. The risk brings together three main ingredients. The first is the *model family* \mathcal{F} (where $f \in \mathcal{F}$ is the quantity that we vary during optimization), the second is the *loss function* \mathcal{L} , and the third is a data distribution $p(u)$. The *risk* for a model $f \in \mathcal{F}$ is defined as its expected loss

$$\mathcal{R}[f] := \mathbb{E}_{p(u)}[\mathcal{L}(u, f(u))] \equiv \int \mathcal{L}(u, f(u)) p(u) du, \quad (41.1)$$

where $\mathbb{E}_p[\cdot]$ refers to the expectation with respect to the distribution p . In the context of supervised learning, the distribution $p(u)$ describes a joint distribution over the features x and the labels y (i.e. $p(u) = p(x, y)$), the model only depends on the features $f(u) = f(x)$, and the loss function takes on the special form $\mathcal{L}(u, f(u)) = \mathcal{L}(y, f(x))$. In the context of unsupervised learning there are no labels, and $u = x$. Written this way, the risk is a functional, and the idealized goal for machine learning is to solve the optimization problem

$$f^* = \arg \min_{f \in \mathcal{F}} \mathcal{R}[f], \quad (41.2)$$

where \mathcal{F} would include all possible functions.

One of the defining characteristics of machine learning in practice is that one does not know the data distribution $p(u)$, but does have access to samples from that distribution, i.e. $\{u_i\}_{i=1, \dots, n}$ with $u_i \stackrel{i.i.d.}{\sim} p(u)$. This leads to the corresponding *empirical risk*

$$\mathcal{R}_{\text{emp}}[f] := \mathbb{E}_{\hat{p}(u)}[\mathcal{L}(u, f(u))] \equiv \frac{1}{n} \sum_{i=1}^n \mathcal{L}(u_i, f(u_i)), \quad (41.3)$$

where $\hat{p}(u) = \frac{1}{n} \sum_{i=1}^n \delta(u - u_i)$ is referred to as the empirical distribution of the dataset $\{u_i\}_{i=1, \dots, n}$. The *empirical risk minimization* principle is a core idea in statistical learning theory [7], which approximates f^* with its empirical analogue

$$\hat{f} = \arg \min_{f \in \hat{\mathcal{F}}} \mathcal{R}_{\text{emp}}[f], \quad (41.4)$$

where $\hat{\mathcal{F}}$ are all possible functions parametrized by the model parameters ϕ . In an idealized infinite parameter limit machine learning functions, such as neural networks, are universal approximators, such that they cover all functions and $\mathcal{F} = \hat{\mathcal{F}}$. For finite size networks this may or may not be a valid assumption. Expressivity of the network characterizes this universality property and is a function of the network architecture and its parameters such as width and depth of neural network layers. If the expressivity is too small it leads to underfitting. However, an equally important consideration is the risk of overfitting if we optimize equation 41.4 for too long.

While the loss function may quantify some well-motivated notion of (negative) utility, it is also common to design loss functions so that f^* has some desired property. While in practice one does not know the data distribution $p(u)$, it is constructive to imagine that one does and analyze Eq. 41.2 with the calculus of variations. In Secs. 41.3 we will consider several such loss functions where one can show that the corresponding f^* has the desired property even

if the form of the loss is not obvious from the point of view of utility. Furthermore, there are often multiple loss functions that can lead to the same f^* . Then one can think of machine learning as applied calculus of variations where one solves Eq. 41.4 with a sufficiently flexible model, powerful optimization algorithms, and practical considerations to break the degeneracy between different loss functions that lead to the same f^* .

41.2.2 Generalization

With a sufficiently flexible model, it is possible to fit the training dataset very well, though the model might not *generalize* well to unseen data due to overfitting. More concretely, for a non-negative loss function one might have $\mathcal{R}_{\text{emp}}[\hat{f}] \rightarrow 0$, while the true risk might be large ($\mathcal{R}[\hat{f}] \gg 0$). The gap between the $\mathcal{R}[\hat{f}] - \mathcal{R}_{\text{emp}}[\hat{f}]$ is typically referred to as the *excess risk*¹. While it is generally not possible to evaluate $\mathcal{R}[\hat{f}]$ exactly because we do not know $p(u)$, we can use an independent testing dataset (also called validation dataset) to obtain an unbiased estimate of it. This *cross-validation* method motivates the test – train split of the data.

Intuitively, a model with many parameters has more flexibility and is more prone to overfitting. A common and intuitive heuristic is that one should not fit a model with more parameters than there are data points. However, a more careful treatment reveals that this heuristic can be both pessimistic and optimistic. For example, the single-parameter model $f_\phi(x) = \text{sign}(\sin(\phi x))$ can perfectly classify any assignment of labels on data (x_i, y_i) with $x \in \mathbb{R}$ and $y \in \{-1, 1\}$ and generalize poorly. Conversely, sometimes highly over-parameterized models (that have large subspaces of their parameters where $\mathcal{R}_{\text{emp}}[\hat{f}_\phi] \rightarrow 0$) might generalize well [8,9]. Often this is achieved through *regularization*, both explicit and implicit (section 41.3.1.2).

Structural risk minimization is a modification to the empirical risk minimization principle that was introduced by Vapnik and Chervonenkis to account for the potential for overfitting [7]. However, the bounds are based on a worst-case type analysis and are often very weak. Recall that while one cannot calculate the true risk, one can obtain an unbiased estimate of it with a held-out, independent testing sample. Thus one can empirically compare the generalization error of two models and find that one generalizes better than the other even if the bounds might suggest the opposite. One of the major conceptual shifts that happened with the rise of deep learning was to more fully appreciate that these bounds and structural risk minimization were not a good learning principle in practice and that more theoretical work is needed to close the gap between formal bounds and empirical estimates of generalization error.

41.3 Common tasks and their associated loss functions

We now move to common tasks encountered in machine learning and their associated loss functions.

41.3.1 Supervised learning

Supervised learning generally refers to the class of problems where the training dataset are presented as input-output pairs $\{x_i, y_i\}_{i=1, \dots, n}$, where $x_i \in \mathcal{X}$ are the input features and $y_i \in \mathcal{Y}$ are the corresponding target labels. Furthermore, it is typically assumed that $(x_i, y_i) \stackrel{i.i.d.}{\sim} p(x, y)$, though $p(x, y)$ is usually not known explicitly. Finally, the loss function in supervised learning takes on the special form $\mathcal{L}(y, f(x))$. The resulting trained model is then used to predict the labels for dataset where labels are not available.

In what follows we will make use of the equalities $p(x, y) = p(x|y)p(y) = p(y|x)p(x)$ and Bayes theorem, which is discussed in Sec. 39.1. We will also use the notation $x \sim p(x)$ to indicate that the random variable x is being drawn, sampled, or generated from the distribution $p(x)$.

¹Similarly, the gap between the true risk of the learned model and the true risk of the optimal model (i.e. $\mathcal{R}[\hat{f}] - \mathcal{R}[f^*]$) is referred to as the *regret*. This quantity is mainly of interest for theoretical analysis of machine learning algorithms, and not of practical concern since usually neither term is tractable.

41.3.1.1 Regression

The goal of regression is to predict a label $y \in \mathcal{Y}$ given an input feature vector $x \in \mathcal{X}$. Typically, the label is a real-valued scalar, but \mathcal{X} can be \mathbb{R}^d or some more structured target (e.g. an image, sequence, graph, quantile, or distribution). When \mathcal{Y} is discrete, the task is usually referred to as classification; however, the two are closely related and *logistic regression* is an example where the model predicts a continuous probability associated to the possible label values. In elementary statistical language, the target label y is often called a dependent variable, while the feature x is called the independent variable. In classical statistics, one often assumes a model for the data such as

$$y_i = f_\phi(x_i) + e_i, \quad (41.5)$$

where e_i is an additive error term that is often assumed to be independent of x and often assumed to be normally distributed. This leads to classic approaches like least-squares (see Sec. 40.2.3), and when the model f_ϕ is linear in ϕ (not in x !) one has linear regression that has a closed-form solution. However, we can relax these assumptions and consider the general case of an arbitrary joint distribution $p(x, y)$, which can be written as $p(y|x)p(x)$ without loss of generality. Consider the *squared error* as a loss function, which leads to the mean-squared error (MSE) for the empirical risk:

$$\mathcal{L}_{\text{MSE}}(y, f(x)) = (y - f(x))^2. \quad (41.6)$$

One might expect that the squared error would only be appropriate in the case that the conditional distribution $p(y|x)$ is normally distributed, but one can use the calculus of variations to show that in general

$$f_{\text{MSE}}^*(x) = \mathbb{E}_{p(y|x)}[y], \quad (41.7)$$

that is the optimal regressor for the MSE is the conditional expectation of y given x .

One issue with the squared-error as a loss function is that it is sensitive to outliers. Alternatively, one can use the absolute error $|y - f(x)|$ as a loss function². However, the discontinuous derivative of the absolute (L1) error leads to challenges in optimization. As a result there are various other loss functions, such as the Huber loss, that aim to be both robust and more amenable to optimization that we do not discuss here.

Note that these this framing of regression yields a function $f(x)$ that only provides a point estimate for y . An alternative approach to regression is to model the full conditional distribution $p(y|x)$. One such example is Gaussian Process regression, which is discussed in Sec. 41.5.1. In that probabilistic approach, one can still obtain a point estimator, such as the conditional expectation or the maximum a posteriori (MAP) estimator

$$f^*(x) = \arg \max_y p(y|x), \quad (41.8)$$

and one can also derive uncertainty estimates on the predicted value y . In this setting, the prior distribution on the model family is closely related to the concept of regularization, which we touch on in Sec. in Sec. 41.3.1.2 and in Sec. 41.5.1.

When one directly models $p(y|x)$, or goes further to model the joint distribution $p(x, y) = p(y|x)p(x)$, then one can use maximum likelihood for the loss function. In that approach, the problem is really one of density estimation, which is a type of unsupervised learning that we discuss in Sec. 41.3.2.1. These two approaches are a classic examples of two different approaches to modelling. Regression with $f_{\text{MSE}}^*(x)$ is the prototypical example of *discriminative* modelling, while modelling the joint distribution is a prototypical example of *generative* modelling. Generally, discriminative approaches with supervised learning out perform generative approaches when there is sufficient data, but generative approaches can be beneficial in data-starved settings [10].

²The absolute error and squared error are often denoted as L1 and L2 errors, respectively, in reference to the corresponding norms.

41.3.1.2 A note on regularization

The trained model \hat{f} , or equivalently, the parameters of the trained model $\hat{\phi}$ can be thought of as point estimates of f^* , and there is a correspondence to the issues of bias and variance discussed in Sec. 40.2 on parameter estimation. Generically, there is a bias–variance tradeoff, and when the number of parameters is large and the number of data points is not much larger, introducing a small bias can often lead to a significant reduction in variance. This motivates the explicit addition of a *regularization* term to the loss function, which will introduce some bias $f_{\text{reg}}^* \neq f^*$. A common form for regularization is to penalize by the L2 norm of the parameters (*i.e.* $\|\phi\|^2$), which is referred to as *Tikhonov regularization*. This appears in the form of penalized maximum likelihood, and it is also commonly used in unfolding [11]. One can also interpret the regularization term as an explicit prior on the parameters, and the resulting model as the Bayesian maximum a posteriori (MAP) estimator. When paired with linear regression this is known as *ridge regression*, and when paired with kernel machines (see Sec. 41.5.1) this gives rise to kernel ridge regression or Gaussian process regression.

Another form of regularization is to restrict the model class $\hat{\mathcal{F}}$. For example, a neural network and a sequence of narrow step functions (delta functions) can both be shown to be universal approximators in infinite parameter size limit, but on real world examples the former generalizes much better than the latter. Within the class of neural network models, convolutional neural networks are a subset of generic feedforward neural networks that enforce translational symmetry (see Sec. 41.5.3.5 for more discussion). Similarly, one might restrict to Lipschitz continuous functions. These types of choices are often encoded in the architecture of a neural network and are broadly referred to as *inductive bias* in the model.

In addition to explicit regularization terms in the loss function or through restrictions to the model class, it is also possible to regularize implicitly. One implicit regularization is through early stopping [11, 12], where we monitor the loss on training dataset and the loss on test dataset. While the training dataset loss continues to decrease with more gradient descent cycles, the test loss may not, and early stopping stops the training when test loss flattens out or begins to increase. Another powerful form of regularization used in deep learning models is known as *dropout* [13], which randomly removes some parts of the model during training and can be thought of as implementing a type of model averaging [14]. What is more surprising is that in the case of highly over-parameterized models where there is a large degenerate parameter space that achieves zero loss, $\Phi_0 = \{\phi | \mathcal{R}_{\text{emp}}[f_\phi] = 0\}$, that the dynamics of the optimization algorithm that is used will break the degeneracy and favor some particular $\hat{\phi} \in \Phi_0$ as if an additional regularization term was secretly included. Despite zero loss and over-parametrization, the corresponding generalization error may be small, a phenomenon called *benign overfitting* [15]. Importantly, the dynamics of different optimization algorithms will have different implicit regularization effects, and thus favor different parameter points in Φ_0 that will have different generalization error [16]. Understanding this interaction is a topic of contemporary research in machine learning [17].

41.3.1.3 Classification

The goal of classification is to predict one of a finite number of class labels $y \in \mathcal{Y}$ given an input feature vector $x \in \mathbb{X}$. It is similar to regression in this way, but the focus is on discrete target space \mathcal{Y} . An important special case is when the label can only take on one of two values (*e.g.* “signal” or “background”), which is referred to as binary classification and is equivalent to simple hypothesis testing in statistics. It is common for a classifier to be the composition of a model $g : \mathcal{X} \rightarrow \mathbb{R}^{|\mathcal{Y}|}$ that predicts continuous probabilities for each class (*i.e.* $g(x) \approx p(y|x)$) followed by an operation that then chooses the discrete label $y \in \mathcal{Y}$, such as a fixed threshold or $f(x) = \arg \max g(x) \approx \arg \max_y p(y|x)$. This is the case for both classical methods like logistic regression and modern, deep learning approaches to classification; therefore, we will use the term probabilistic classifier for $g(x)$ or just classifier

when it is clear in context.

An intuitive loss function for classification is the zero-one loss, which simply counts the number of mis-classifications:

$$\mathcal{L}_{0/1}(y, f(x)) = \begin{cases} 0, & \text{if } f(x) = y \\ 1, & \text{otherwise.} \end{cases} \quad (41.9)$$

The zero-one loss can also be written as $\mathcal{L}_{0/1}(y, f(x)) = \mathbf{1}(y \neq f(x))$, where $\mathbf{1}(\cdot)$ is the indicator function. The zero-one loss is non-differentiable, so it does not pair well with gradient-based optimization.

For binary classification, one can use $y = \{0, 1\}$ as numerical values for the class labels and the mean-squared error $\mathcal{L}_{\text{MSE}}(y, f(x))$ in Eq. 41.6 for the loss function. The resulting model will approximate f_{MSE}^* , the conditional expectation of Eq. 41.7 takes on the form

$$f_{\text{MSE}}^*(x) = \mathbb{E}_{p(y|x)}[y] \rightarrow p(y=1|x) \\ = \frac{p(x|y=1)p(y=1)}{p(x|y=0)p(y=0) + p(x|y=1)p(y=1)}. \quad (41.10)$$

That is the MSE loss for binary classification leads to the Bayesian posterior probability that the label $y = 1$ given the feature vector x .

Equation 41.10 highlights an important general feature of supervised learning relevant for particle physics, which is that the joint distribution $p(x, y)$ of the training dataset implies a prior distribution $p(y)$ on the labels or classes. This prior distribution need not reflect a degree of belief or the frequency in real data, it represents the frequency in the training dataset. However, it is important to keep in mind that when applying the resulting model to a different dataset with the same conditional distribution (data likelihood) $p(x|y)$ for the features and a different prior $p'(y)$ for the labels that the probabilistic interpretation of the result will not be properly calibrated. A common choice for binary classification is to use a balanced training dataset with $p(y=0) = p(y=1) = \frac{1}{2}$, while in many cases the true $p'(y=1)$ in the experimental data might be very small (*i.e.* low signal-to-background), unknown, or zero (*i.e.* a hypothetical particle that does not exist).

If $p'(y)$ and $p(y)$ are known then the Bayes theorem can be used to re-calibrate the posterior $p(y|x)$ from one prior to another. One example of such re-calibration is the correspondence of binary classification to simple hypothesis tests in frequentist statistics discussed in Sec. 40.3.1 of the Statistics chapter. In that setting, the Neyman-Pearson lemma states that the optimal classifier is given by the likelihood-ratio. Adapting to the notation of this chapter, we have

$$f_{\text{N.P.}}^*(x) = \frac{p(x|y=1)}{p(x|y=0)}, \quad (41.11)$$

which does not depend on the prior probabilities $p'(y=0)$ or $p'(y=1)$ as in Eq. 41.10, or, equivalently, assumes equal priors $p'(y=0) = p'(y=1)$. From Bayes theorem, we have the identity $p(y=1|x)/p(y=0|x) = [p(x|y=1)p(y=1)]/[p(x|y=0)p(y=0)]$, which can be used to show that the two functions are related by a one-to-one, monotonic transformation

$$f_{\text{N.P.}}^*(x) = \frac{p(y=0)}{p(y=1)} \frac{f_{\text{MSE}}^*(x)}{1 - f_{\text{MSE}}^*(x)}, \quad (41.12)$$

which is referred to as the *likelihood-ratio trick*, which plays an important role in simulation-based inference (see Sec. 41.3.5). Importantly, the monotonic transformation does not impact the tradeoff of type-I and type-II error (or, equivalently, the FPR and TPR), therefore the ROC curve for $f_{\text{N.P.}}^*(x)$ and $f_{\text{MSE}}^*(x)$ are identical and do not depend on the prior probabilities $p(y)$. This property has been leveraged in the context of *weakly supervised* approaches [18] and enables one to train a classifier on data without access to labels as long as one has two datasets with different ratios $p(y=1)/p(y=0)$ and the same conditional distribution $p(x|y)$ of the features given the labels.

A generalization of the binary loss function for classification of Eq. 41.10, which applies to multiple classes, is the *cross-entropy* loss

$$\mathcal{L}_{\text{xe}}(y, f(x)) = - \sum_{c \in |\mathcal{Y}|} \mathbf{1}(y = c) \log(f_c(x)), \quad (41.13)$$

where $f: \mathcal{X} \rightarrow \mathbb{R}^{|\mathcal{Y}|}$ and the indicator function picks out the term in the sum for the corresponding class label y . This loss can be derived from maximizing the posterior of Eq. 41.57 using a discrete set of class labels y , which identifies $f_c(x) = \tilde{f}(y = c|x) = p(y = c|x)$ and thus enforces the constraint $\sum_c f_c(x) = 1$ and $f_c(x) \geq 0$ (for all $x \in \mathcal{X}$, e.g. by using the *softmax* function). The notation is aligned with the interpretation of $\tilde{f}(y|x)$ as a conditional distribution, i.e. an approximation to the true posterior $p(y|x)$. The risk associated to the cross entropy loss function is

$$\begin{aligned} \mathcal{R}_{\text{xe}}[f] &= \mathbb{E}_{p(x,y)} \left[- \sum_{c \in |\mathcal{Y}|} \mathbf{1}(y = c) \log f_c(x) \right] \\ &= - \sum_{c \in |\mathcal{Y}|} p(y = c) \mathbb{E}_{p(x|y)} [\log \tilde{f}(y = c|x)]. \end{aligned} \quad (41.14)$$

This is equivalent to $\mathcal{R}_{\text{xe}}[f] = \mathbb{E}_{p(x)} [H[p(y|x), \tilde{f}(y|x)]]$, where $H[p, f] = \mathbb{E}_p[-\log f]$ is the cross-entropy between the two distributions. One can use a Lagrange multiplier λ to enforce the normalization constraint (e.g. equation 41.10) and the calculus of variations to show that

$$f_{\text{x.e.,c}}^*(x) = \lambda p(x, y = c) = \lambda p(y = c|x)p(x) = p(y = c|x). \quad (41.15)$$

This approach is closely related to the loss functions that are used for density estimation, the forward Kullback–Leibler (KL) divergence, and the maximum likelihood estimation. Minimizing cross entropy $H[p, f_\phi]$ with respect to ϕ is equivalent to minimizing the forward KL divergence

$$KL(p||f_\phi) := \mathbb{E}_p[\log p(x)] - \log f_\phi = H[p, f_\phi] - H[p], \quad (41.16)$$

where $H[p] := \int p(x) \log p(x) dx$ is the entropy and independent of f_ϕ . The KL divergence $KL(p||f) \geq 0$, and equal if and only if $p = f$.

One can also consider the reverse KL divergence $KL[f_\phi||p]$, which is also minimized by $f_\phi = p$; however, this requires one to be able to generate samples $x_i \sim f_\phi(x)$ and be able to evaluate the probability density $p(x_i)$. Often this is not the case for real world data, but this approach is useful in the context of variational inference, where $f_\phi(x)$ is an approximation to the posterior of x , and $p(x)$ is the likelihood times the prior, which can be evaluated on samples x_i drawn from f_ϕ . Because likelihood times prior is not normalized this KL divergence optimizes the lower bound to the normalization (Evidence Lower Bound Objective or ELBO).

The forward KL is also closely related to the variational free energy principle in statistical mechanics where $H[f_\phi]$ represents the entropy of the variational distribution, $p(x) \propto \exp(-E(x)/kT)$ is the Boltzman factor for the state x with energy $E(x)$, and $H[f_\phi, p] = \mathbb{E}_{f_\phi}[E(x)]$ represents the expected energy for the variational distribution. As is well known to physicists, minimizing the free energy involves a balance between minimizing the energy and maximizing the entropy.

In some cases it is possible to augment the training dataset with an unbiased, stochastic estimate of $p(y = c|x)$ that we denote $s_c(x, z)$. For example, when the simulation involves latent variables z (i.e. Monte Carlo truth quantities), then the simulation encodes $p(x, z|y)$, the joint distribution over the observed features x and the latent variables z conditioned on the class y . In many cases the simulation evolves through a Markov process (e.g. the detector response only depends on the momenta of the incoming particles z , not the details of the hard scattering y). In that case, it is often possible to calculate $s_c(x, z) = p(y = c|x, z)$ for each training sample [19]. Using the identity, $\mathbb{E}_{p(z|x)}[p(y|x, z)] = p(y|x)$, we see that $s_c(x, z)$ is an unbiased estimator of $p(y = c|x)$.

In this case, one can use $s_c(x, z)$ in place of the indicator function in Eq. 41.13 to construct an improved (lower-variance) loss function that reproduces the same cross-entropy risk function^{3,4}

$$\begin{aligned} \mathcal{R}'_{\text{xe}}[f] &= \mathbb{E}_{p(x,y,z)} \left[- \sum_{c \in |\mathcal{Y}|} s_c(x, z) \log f_c(x) \right] \\ &= - \sum_{c \in |\mathcal{Y}|} \mathbb{E}_{p(x)} [p(y = c|x) \log f_c(x)], \end{aligned} \quad (41.17)$$

which yields the same optimal classifier $f_{\text{x.e.,c}}^*(x) = p(y = c|x)$ [20, 21].

We note that unlike in the binary classification case, the multi-class classifier is sensitive to the priors $p(y)$ used in training. This leads to complications as often the class proportions are unknown. For example, one might be interested in classifying a signal when multiple backgrounds are present and the relative proportion of those different background components is uncertain. Ideally one would like the class proportions for the background components used in training to match those in the data, which presents an additional training challenge if those proportions are heavily unbalanced.

41.3.2 Unsupervised learning

Unsupervised learning generally refers to the class of problems that use unlabeled training dataset $\{x_i\}_{i=1,\dots,n}$, where $x_i \in \mathcal{X}$ are the input features. Furthermore, it is typically assumed that $(x_i) \stackrel{i.i.d.}{\sim} p(x)$, though $p(x)$ is usually not known explicitly. Finally, the loss function in supervised learning takes on the special form $\mathcal{L}(x, f(x))$.

A related concept is that of self-supervised learning, which also aims to distill useful features in the data without requiring supervision labels for every sample in the input data. Self-supervised methods can make use of large unsupervised datasets and build meaningful representations by performing data augmentation, and learning the latent space mapping that is insensitive to it. For example, in the case of galaxy images one may augment the data by performing image rotations, adding noise, size scaling, adding point spread function smoothing etc., all of which are realistic transformations expected in a real galaxy image survey [22]. Self-supervised learning then learns the latent space representation where all of these augmentations of the same training sample result in the same latent space position. This training is augmented with contrastive learning, which ensures that different training samples do not all collapse to the same latent space position. When this latent space representation is used for downstream tasks such as classification it outperforms other forms of supervised learning [23].

41.3.2.1 Density estimation

The goal of density estimation is to estimate a distribution $p(x)$ based on samples $\{x_i\}_{i=1,\dots,n}$ with $x_i \stackrel{i.i.d.}{\sim} p(x)$. Conceptually, this is the same goal as when fitting a parameterized distribution $f(x; \theta)$ to data using the method of maximum likelihood as described in Sec. 40.2.2 of the chapter on statistics. In practice, the difference in the machine learning context has to do with the flexibility of the model and the dimensionality of the data. A highly-flexible model, which can effectively approximate any distribution, is referred to as a non-parametric model (though, ironically, usually this means the model has many parameters). In contrast, typical maximum likelihood fits in particle physics are based on restricted families of distributions with relatively few parameters and the data is typically one- or two-dimensional, though occasionally five- or six-dimensional.

Maximizing the likelihood function in Eq. 40.10 $\mathcal{L}(\theta) =$

³A similar approach can also be used for the squared-error, see Ref. [20].

⁴The right hand side of Eqs. 41.14 and 41.17 are written in a different form, but are equivalent.

$\prod_{i=1}^n f(x_i; \theta)$ is equivalent to minimizing the empirical risk:

$$\mathcal{R}_{\text{emp,xe}}[f_\phi] = -\frac{1}{n} \sum_{i=1}^n \log f_\phi(x), \quad (41.18)$$

where we adopt the notion used in this chapter. The loss is simply $\mathcal{L}(x, f_\phi(x)) = -\log f_\phi(x)$, and the corresponding risk is

$$\mathcal{R}_{\text{xe}}[f_\phi] = \mathbb{E}_{p(x)}[-\log f_\phi(x)], \quad (41.19)$$

which is the cross entropy $H[p, f_\phi]$. For density estimation, the model is usually constructed to enforce $\int f_\phi(x) dx = 1$ and $f_\phi(x) \geq 0$ so that it can be interpreted as a distribution. With this constraint, one can show that $f_{\text{xe}}^*(x) = p(x)$.

The concepts of generalization and overfitting are particularly acute in unsupervised learning, where the likelihood maximization of equation 41.18, combined with universal approximator assumption, must converge onto $\hat{p}(x) = \frac{1}{n} \sum_{i=1}^n \delta(x - x_i)$, the empirical distribution of the dataset $\{x_i\}_{i=1, \dots, n}$. This distribution has the highest likelihood on the training dataset and the lowest likelihood on the test data where it gives $\hat{p}(x) = 0$. as long as the test dataset are not identical to the training dataset. So the empirical distribution of the training dataset has the worst possible generalization property, yet it is the solution we converge to for sufficiently expressive architectures in the absence of any regularization. In contrast, in supervised learning we often observe the phenomenon of benign overfitting, where even zero loss can generalize well.

In addition to approaches to density estimation that involve learning in the sense of minimizing a loss or risk function, we note that there are also classical density estimation techniques such as histogramming and kernel density estimation [24–26].

41.3.2.2 Representation learning, compression, and auto-encoders

A recurring topic in machine learning and statistics is how to represent the data. Much of classical statistics involves constructing a low-dimensional summary statistic that extracts the relevant information from the data for a particular task (a sufficient statistic in language of classical statistics). There is a spectrum of representations with trade-offs. At one end of this spectrum is lossless compression that allows you to encode the data into a smaller, intermediate representation that carries all the information since it can be decoded back into the original data. At the other end of the spectrum is something like the likelihood-ratio, which is a single scalar that carries the relevant information needed for hypothesis testing for a single hypothesis, but it discards all the other information that might be needed for other tasks (such as testing other hypotheses). An intermediate point in this spectrum is the process of feature engineering, which refers to the creation of new features \mathcal{X}' from the original features \mathcal{X} in hopes that the down-stream task will be easier with the new features. For example, instead of working directly with the energy and momentum of particles, one might compute invariant masses, angles between particles, etc. This type of feature engineering generally improved performance for shallow neural networks, decision trees, etc.; however, with the rise of deep learning this is often no longer necessary and often limits performance compared to working with the original features. One can think of the intermediate layers of a neural network between the input and the output a representation of the data that is good for the task at hand, and by training all the layers of the network simultaneously (or “end-to-end”) one can see the intermediate layers as a learned representations. For a review see Ref. [27].

An example of a linear dimensionality reduction representation and data compression is principal component analysis (PCA) of data $x \in \mathbb{R}^d$ at fixed latent space dimensionality k ($k < d$), which finds the orthogonal linear transformation, O ,

$$O : \mathbb{R}^k \rightarrow \mathbb{R}^d, z \mapsto Oz, OO^T = I_d \quad (41.20)$$

that maximizes the data variance in the latent space. Maximizing the variance of the transformed data is equivalent to minimizing

the average reconstruction error (the residual variance in data space),

$$\mathcal{L}_{a.e.}(x, f(x)) = \|x - f(x)\|^2. \quad (41.21)$$

A PCA can thus be interpreted as a linear, orthogonal model that is trained to minimize the L_2 -distance between the input data and the reconstructed data given the fixed dimensionality k . In practice, the PCA problem can be solved analytically without the use of optimization algorithms or the loss function: the principal components are given by the eigenvectors of the data covariance matrix.

A suitable latent space dimensionality, k , is chosen by ordering the eigenvalues, λ_i , of the data covariance in descending order, and keeping only the first few eigenvectors that correspond to the largest eigenvalues. The cut is often made at dimensionalities that capture around 90% of the data variance. For many data sets this results in $k \ll d$. The average reconstruction error that originates from the discarded eigenvalues is $\sigma_{\text{recon}}^2 = \sum_{i=k+1}^d \lambda_i$.

Another common type of representation learning and nonlinear dimensionality reduction is based on the *auto-encoder* $f = g \circ e : \mathcal{X} \rightarrow \mathcal{X}$, where $e : \mathcal{X} \rightarrow \mathcal{Z}$ is referred to as the *encoder* and $g : \mathcal{Z} \rightarrow \mathcal{X}$ is referred to as the *generator* or *decoder*. Typically the dimensionality of \mathcal{Z} is much less than \mathcal{X} , and $z = e(x)$ can be thought of as a compressed representation of the input. The intermediate space \mathcal{Z} is sometimes referred to as the *bottleneck* or the *latent space* of the auto-encoder. If the bottleneck is sufficiently large and the encoder and decoder are sufficiently flexible, then the function f could just be the identity (*i.e.* lossless compression). However, if the encoder and decoder are not sufficiently flexible or the dimensionality of the latent space is not large enough there will be some reconstruction error. Therefore the reconstruction error of Eq. 41.21 serves as a natural loss function of an auto-encoder.

Once trained, the encoder $e(x)$ can be used independently of the decoder to provide a generic low-dimensional representation of the data. The flexibility of this approach is attractive; however, there are no guarantees that this representation will be optimal for the other task. Indeed, the transition from pre-trained auto-encoders to end-to-end learning is one of the important trends that characterized the onset of the deep learning era.

While achieving zero reconstruction error may seem good as it would imply lossless compression, it often performs poorly in practice. First, the encoder may be overfit to the training dataset and not generalize well to held out data. Secondly, it may not be robust to domain shift (see Sec. 41.7.2). One approach to address these issues is the *denoising auto-encoder*, which uses a form of regularization that corrupts the input with noise $x' \sim q(x|x)$ while still targeting reconstruction of the uncorrupted input x .

$$\mathcal{L}_{d.a.e.}(x, f(x)) = \|x - f(x')\|^2 \quad \text{with} \quad x' \sim q(x'|x), \quad (41.22)$$

where $q(x'|x)$ is some probability distribution such as a multivariate normal.

41.3.2.3 Clustering

The goal of clustering is to group the data $\{x_i\}_{i=1, \dots, n}$ into k groups, or *clusters*, usually with $k \ll n$. Intuitively, if two data points belong to the same cluster, then they should be similar in some sense. Conversely, if two data points are very different, then they should be assigned to different clusters. The notion of similarity usually is based on some heuristic, and there are a variety of algorithmic and probabilistic clustering algorithms. In some cases k is specified, while in others it is determined by the clustering algorithm. There is also a distinction between flat clustering that directly partitions the data into k clusters and hierarchical clustering where clusters are nested hierarchically as the name suggests. In many cases clustering uses some notion of distance $d(x_i, x_j)$, which may be the L_p norm $\|x_i - x_j\|_p$.

One of the most common clustering algorithms is known as *k*-means, where k is specified by the user and results in sets $S = \{S_1, \dots, S_k\}$ that minimize the variance of each cluster. Thus,

the objective is

$$\begin{aligned} \arg \min_{\mathbf{S}} \sum_{i=1}^k \sum_{\mathbf{x} \in S_i} \|\mathbf{x} - \boldsymbol{\mu}_i\|^2 &= \arg \min_{\mathbf{S}} \sum_{i=1}^k |S_i| \text{Var } S_i \\ &= \arg \min_{\mathbf{S}} \sum_{i=1}^k \frac{1}{2|S_i|} \sum_{\mathbf{x}, \mathbf{y} \in S_i} \|\mathbf{x} - \mathbf{y}\|^2 \end{aligned} \quad (41.23)$$

where $\boldsymbol{\mu}_i$ is the mean of points in S_i .

While k -means and many other clustering algorithms are defined in terms of an optimization problem, the optimization objective is often not representative of the actual notions of performance in a given context. As a result, there are a number of quantities used for the evaluation and assessment of the resulting clustering. These include Davies–Bouldin index, Dunn index, Rand index, Jaccard index, purity, F-measure, Hopkins statistic, *etc.* [28].

41.3.3 Optimal control, reinforcement learning, and active learning

Many problems in science and engineering can be cast as a control problem, which comprises a cost functional that is a function of state and some control variables that specify some underlying dynamical system. This is relevant for the control of accelerators where the dynamical system is physical. This formalism can also be used to describe the design of experiments, planning of an observational survey, and other decision making processes relevant to the scientific method. There is a tremendous amount of literature on the subject, and it is closely connected to planning, dynamic programming, and reinforcement learning. Optimal control can be seen as an extension of the calculus of variations, and thus generalizes the framing of learning presented in Sec. 41.2.

Optimal control theory deals with finding a control for a dynamical system over a period of time such that the objective function is optimized. The underlying system can be discrete or continuous and may be deterministic or stochastic. The commonalities and differences between optimal control and reinforcement learning can be best understood through the formalism of a Markov decision process (MDP), which is a discrete-time stochastic control process. We follow common notation, such as that found in Wikipedia.

A Markov decision process comprises four components often organized as a 4-tuple (S, A, P_a, R_a) , where: S is a set of states called the state space, A is a set of actions called the action space, $P_a(s, s') = \Pr(s_{t+1} = s' \mid s_t = s, a_t = a)$ is the probability that action a in state s at time t will lead to state s' at time $t + 1$, $R_a(s, s')$ is the immediate reward (or expected immediate reward) received after transitioning from state s to state s' , due to action a .

The policy function π is a mapping from state space to action space that can be either deterministic or probabilistic. For examples, the policy that drives a computer chess playing system, decides which move to make given the current state of the board. Similarly, policies dictate which experiment should be built next, which field of the sky should be observed, or how to adjust the operational parameters of an accelerator. The dynamics of the resulting system are then fixed by combining the policy with the underlying MDP. The evolution of the resulting dynamical system behaves like a Markov chain since the action chosen in state s is completely determined by $\pi(s)$ and $\Pr(s_{t+1} = s' \mid s_t = s, a_t = a)$ implies the Markov transition matrix $\Pr(s_{t+1} = s' \mid s_t = s)$.

The objective optimal control is to choose a policy π that will maximize a cumulative function of the instantaneous rewards R_a . A common choice is the expected discounted sum:

$$\mathbb{E} \left[\sum_{t=0}^{\infty} \gamma^t R_{a_t}(s_t, s_{t+1}) \right], \quad (41.24)$$

where $a_t \sim \pi(s_t)$ are the actions given by the policy, the expectation computed with respect to the distribution $s_{t+1} \sim P_{a_t}(s_t, s_{t+1})$, and γ is the discount factor satisfying

$0 \leq \gamma \leq 1$. The discount factor is usually close to 1 and sometimes reparameterized as $\gamma = 1/(1+r)$, where r is called the discount rate. A lower discount factor motivates the decision maker to favor taking actions early, rather than postpone them indefinitely.

A policy that maximizes the objective function is called an optimal policy and denoted π^* , though the optimal policy need not be unique. Importantly, the Markov property implies that the optimal policy is only a function of the current state. Dynamic programming can be used to find the optimal policy for MDPs with finite state and action spaces. For instance, in value iteration (a.k.a. backward induction) can be used to solve the ‘‘Bellman equation’’ [29]. For continuous-time systems, the optimal policy is defined by the Hamilton–Jacobi–Bellman equation [30].

In many settings, it is assumed that the state s is fully known when action is to be taken and there are no latent variables. When this assumption is not true, the problem is called a partially observable MDP. These problems are generally more difficult and the dynamic programming algorithms do not directly apply [31].

Reinforcement learning The main difference between the classical dynamic programming methods and reinforcement learning (RL) algorithms is that the latter do not assume knowledge of an exact mathematical model of the MDP and they target large MDPs where exact methods become infeasible. For example, RL was used in the context of jet physics to search for the most likely jet clustering when the number of constituents was too large for the exact dynamic programming algorithm to be used [32]. In addition, RL can be used when the probabilities or rewards are unknown. Instead, the transition probabilities are often accessed indirectly through interaction with a real or simulated environment. For example, in Q-learning one uses experience to estimate the array $Q(s, a)$ defined as

$$Q(s, a) = \sum_{s'} P_a(s, s') (R_a(s, s') + \gamma V(s')). \quad (41.25)$$

While this function is also unknown, it can be estimated during learning based on (s, a) pairs together with the outcome s' .

Numerous variations to RL exist, which include so-called model-based and model-free approaches (referring to models of the instantaneous rewards and the state transitions) and on-policy and off-policy (which describes how the actions taken during learning are related to the current policy). See Ref. [33] for an introduction and Ref. [34] for a recent review.

Multi-arm bandits Multi-arm bandit problems are a classic reinforcement learning problem where one tries to maximize the expected gain by allocating a limited set of resources to various alternatives. The name is a reference to a gambler with a fixed amount of money that must choose between multiple slot machines (or ‘‘one-armed’’ bandits) when the payoff for the individual machines is unknown. A hallmark of multi-arm bandit problems is that they involve a trade-off between exploration (playing machines to estimate their payoff) and exploitation (playing machines with the highest estimated payoff). Multi-armed bandits are used to manage large projects, organizations, and scheduling problems. The theory has a long history going back to Robbins in 1952 that used it to study the sequential design of experiments [35] and Gittins who derived an optimal policy under some conditions [36].

Bayesian optimization A closely related set of techniques involve optimizing some expensive black box function $f(x)$. For instance, the function may be computationally expensive to evaluate or low-latency, *e.g.* it may involve manually re-configuring a system. This is particularly relevant for analysis optimization in particle physics where evaluating $f(x)$ involves processing large numbers of simulated collisions. Another common use case involves optimizing the hyperparameters of a learning algorithm.

Without any assumptions about the function $f(x)$ this is hopeless; however, if one assumes something about the functions (*e.g.*

some notion of smoothness) then one can leverage function evaluations $\{f(x_t)\}_{t=1,\dots,T}$ to say something about what value the function might take on at other values of x . This is usually cast in Bayesian terms, and Gaussian processes (Section 41.5.1) are often used to model the distribution over $f(x)$. The optimization techniques that use this framing are generically referred to as Bayesian Optimization [37].

Optimization in this context is usually characterized by an *exploration-exploitation* trade-off, similar to what is found in multi-arm bandits. Here, exploration refers to function evaluations that characterize the function in regions that haven't been evaluated, while exploitation refers to evaluations near what is predicted to be its maximum. This setting is similar to reinforcement learning in that it involves sequential decisions (*i.e.* where to evaluate the function next), but usually the target function $f(x)$ is assumed to be static. In that sense, the state referred to in the language of an MDP is the state of knowledge about the function after sequential evaluations $\{f(x_t)\}_{t=1,\dots,T}$. The reward at time t is not the value of the function $f(x_t)$, but some quantity that characterizes what was learned about the function's maximum. In this literature, one often refers to the *acquisition function*, which plays a similar role as the expected value of the reward in RL. Common acquisition functions include the probability of improvement, the expected improvement, and an upper-confidence bound [38].

Connection to experimental design In the context of physics experiments we often want to build the next generation experiment which can reach certain target precision on parameters of interest that the experiment can measure. To achieve this precision we may deploy the concept of *experimental design*, where the objective is to optimize some objective that quantifies the expected performance of an experiment. Moreover, we would like to achieve this within some constraints such as a minimal cost. Such problems are often solved using the Fisher matrix optimization, where Fisher matrix can be viewed as the expectation of the inverse covariance matrix. We can define

$$t(x|\theta_0) := \nabla_{\theta} \log p(x|\theta)|_{\theta_0}, \quad (41.26)$$

where $t(x|\theta_0)$ is referred to by statisticians as the score [20]. The score plays an important role in the classical statistics as it is a sufficient statistic when $p(x|\theta)$ is in the exponential family, and through the Rao-Cramér-Fréchet bound on the variance of an estimator for θ , and is used to define the Fisher information matrix $I_{ij}(\theta) := \mathbb{E}_{p(x|\theta)}[t_i(x|\theta)t_j(x|\theta)]$. The Fisher information, in turn is an important object in experimental design. In particle physics, the score is closely related to the concept of optimal observables. The corresponding diagonal element of the inverse of the Fisher matrix thus provides expected uncertainty estimation of a given parameter, and is a lower bound to the error of an unbiased estimator (Cramér-Rao bound). In experimental design we vary the experiment parameters within the constraints such as the total cost to minimize this uncertainty. This framework has been widely used in cosmology, where Fisher analysis is the foundation of any experiment proposal.

Active learning Active learning is closely related to Bayesian optimization, described above. In Bayesian optimization one estimates the function $f(x)$ from some set of evaluations $\{y_t = f(x_t)\}_{t=1,\dots,T}$; however, the goal is to find the maximum $x^* = \arg \max_x f(x)$. In active learning, the goal is not to find the maximum of $f(x)$, but to approximate the function as one does in supervised learning. The main difference compared to vanilla supervised learning is that the labeled training dataset isn't provided a priori in a passive way, but the learning algorithm actively decides where to generate $(x_t, y_t = f(x_t))$ pairs. The function $f(x)$ is sometimes referred to as an *oracle*. Active learning is particularly attractive when obtaining labelled data is a costly process.

More broadly, a challenge of many machine learning applications is obtaining labeled data, which can be a costly process. If a system could learn from small amounts of data, and choose by itself what data it would like the user to label via an external process called oracle, it would make machine learning more

powerful. Such frameworks are also called Experiment Design or Active Learning. In Active Learning, a model is trained on a small amount of data (the initial training dataset), and an acquisition function (often based on the model's uncertainty) decides on which data points to ask for a label. The acquisition function selects one or more points from a pool of unlabelled data points, with the pool points lying outside of the training dataset. Once we label the selected data points, these are added to the training dataset, and a new model is trained on the updated training dataset. This process is then repeated, with the training dataset increasing in size over time. The advantage of such systems is that they often result in dramatic reductions in the amount of labelling required to train an ML system (and therefore cost and time).

41.3.4 Anomaly detection and out-of-distribution detection

Unsupervised anomaly detection techniques detect anomalies in an unlabeled test data set under the assumption that the majority of the in-distribution data are normal under some measure, while out-of-distribution (OOD) data are not. In the context of auto-encoders a popular technique is to use the reconstruction error of Eq. 41.21 to identify an outlier as one with a large reconstruction error [39,40]. One issue with this method is that for higher dimensional latent space and flexible neural network architectures the encoder-decoder map become identity for any input data, $f(x) = x$, regardless of whether input x is from the in-distribution training dataset or from the out-of-distribution data. The choice of auto-encoder latent space dimensionality is thus an important hyperparameter that must be tuned.

Another set of anomaly detection techniques construct a model representing normal behavior from a given In Distribution training dataset, and then test the likelihood of a test instance to be generated by the utilized model. For instance, one can use density estimation methods such as normalizing flows (section 41.5.4.3) to learn the density (likelihood) of the In Distribution training dataset $p(x)$, and apply it to the test data. The expectation is that out-of-distribution data will have a lower density (likelihood) under the in-distribution density model. This expectation is however not always met in high dimensions and the method suffers because likelihood based training is sensitive to the smallest variance directions [41]: for example, a zero variance pixels leads to an infinite $p(x)$, and noise must be added to regularize it. But low variance directions may contain little or no information on the global structure of the image, so there is a mismatch between the training objective and outlier detection objective. A related issue is that of typicality: an in-distribution likelihood will typically be lower than the maximum value. For a Gaussian likelihood the typical set is on average be $n/2$ in log likelihood below the peak value, where n is the dimensionality of the data. So an out-of-distribution dataset that is closer to the peak would be preferred in terms of likelihood even though its distribution does not match the in-distribution data. If this happens by chance on low variance directions which dominate the likelihood, normalizing flows can assign higher likelihoods to out-of-distribution data than to in-distribution training dataset [42]. A number of techniques have been proposed to circumvent these limitations, such as likelihood regret [43], likelihood-ratio [41], likelihood in auto-encoder latent space [44], and Wasserstein distance training of the likelihood $p(x)$ [45]. These methods can achieve better anomaly detection performance than the auto-encoder reconstruction error [44,46].

Supervised anomaly detection techniques require a data set that has been labeled as in-distribution and out-of-distribution and involves training a classifier (the key difference to many other statistical classification problems is the inherent unbalanced nature of outlier detection). These methods assume some form for what out-of-distribution data may look like, and their success relies on whether the assumed form is a realistic representation of actual out-of-distribution data. When this assumption is valid these methods can be more powerful than unsupervised methods, but the reverse is also true. A hybrid between the two approaches is to train a classifier without labels [47]. All these approaches are largely complementary to each other [48]. An example of different anomaly detection methods applied to HEP is LHC Olympics

2020 and Dark Machines challenges [49, 50].

41.3.5 Simulation-based inference

The goal of simulation-based inference (related to, but distinct from, likelihood-free inference) is to extend the statistical procedures described in the Chapter on Statistics (*e.g.* parameter estimation, hypothesis tests, confidence intervals, and Bayesian posterior distributions) to the situation where one does not know the explicit likelihood $p(x|\theta)$, the probability of the data given the parameters θ , but has access to a simulator that defines the likelihood $p(x|\theta)$ implicitly [51, 52]. In a typical setup we would like to solve the so called inverse problem of getting the posterior of the parameters given the data, $p(\theta|x)$, but we cannot use Bayes theorem directly because we do not have explicit $p(x|\theta)$.

In particle physics, the simulators usually use Monte Carlo event generators (see Sec. 43) to sample unobserved latent variables z , such as the z_p phase space of the hard scattering (see Sec. 49.4), z_s associated to showering and hadronization, and z_d associated to the interaction of particles with the detector (see Sec. 34). As such, the full simulation chain can be expressed symbolically as

$$\begin{aligned} p(x|\theta) &= \int dz_p p(x, z|\theta) \\ &= \int dz_d \int dz_s \int dz_p p(x|z_d) p(z_d|z_s) p(z_s|z_p) p(z_p|\theta), \end{aligned} \quad (41.27)$$

where θ are the Lagrangian parameters that dictate the hard scattering. Evaluating the likelihood is intractable as it would require evaluating the integral above for each event.

While the likelihood is intractable, simulators provide the ability to generate synthetic data $x_i \stackrel{i.i.d.}{\sim} p(x|\theta)$ for any value of the parameters θ . One can use a suitable proposal distribution $\tilde{p}(\theta)$, sample $\theta_i \stackrel{i.i.d.}{\sim} \tilde{p}(\theta)$, generate synthetic data $x_i \sim p(x|\theta_i)$, and then assemble a training dataset $\{x_i, \theta_i\}_{i=1, \dots, n}$ that can be used to train various machine learning models.

There is thus a close analogy between Simulation-based Inference and data driven machine learning tasks discussed so far, replacing θ with y . One difference is that in simulation-based inference we can always generate new samples by running additional simulations, while we typically view training dataset in machine learning as fixed. This property of Simulation-based Inference enables Active Learning, where the additional simulations are chosen such as to minimize the error on the desired statistical inference task. Another difference is that we often have access to the joint likelihood $p(x, z|\theta)$, where z are unobserved latent variables⁵.

Typically in particle physics, one uses histograms or kernel density estimation to model the distribution of observables (low-dimensional summary statistics such as the invariant mass) of simulated data [53]. Alternatively, one can use an explicit parametric family (such as a falling exponential, a Gaussian distribution, *etc.*) to model $\hat{f}(x|\theta) \approx p(x|\theta)$. That model is then used as a surrogate for the unknown density implicitly defined by the simulator. A related approach is known as Approximate Bayesian Computation (ABC), which approximates the likelihood through an acceptance probability that synthetic data is sufficiently close to the observed data [54, 55]. In practice, these techniques are limited to low-dimensional representations of the data. Thus the potential of recent machine learning approaches to simulation-based inference is to extend this approach to higher-dimensional data, while maintaining the already well-established statistical procedures.

For instance, one can use normalizing flows (see Sec. 41.5.4.3) and the loss functions for density estimation (see Sec. 41.3.2.1) to learn a surrogate model for the likelihood $\hat{f}(x|\theta) \approx p(x|\theta)$ [56]. Similarly, one can use conditional density estimation to learn a surrogate model for the posterior $\hat{f}(\theta|x) \approx p(\theta|x)$, which may involve including the prior-to-proposal ratio $\tilde{p}(\theta)/p(\theta)$ [57]. In addition to the unsupervised learning

techniques, one can also use supervised learning to learn the likelihood-ratio $r(x|\theta_0, \theta_1) = p(x|\theta_0)/p(x|\theta_1)$ by leveraging the *likelihood-ratio trick* of Eq. 41.12 [20, 58].

In some cases one can also augment the training dataset to include the joint likelihood-ratio

$$r(x_i, z_i|\theta_0, \theta_1) := p(x_i, z_i|\theta_0)/p(x_i, z_i|\theta_1), \quad (41.28)$$

which can be used to reduce the variance for the squared-error loss or the improved cross-entropy estimator of Eq. 41.17 [20, 21]. While the marginal likelihood $p(x|\theta)$ is intractable due to the high-dimensional integral over the latent space, the joint likelihood is often tractable since no integration is necessary. In addition, one can often augment the training dataset with the joint score

$$t(x_i, z_i|\theta_0) := \nabla_{\theta} \log p(x_i, z_i|\theta)|_{\theta_0}. \quad (41.29)$$

Regressing on the joint score with the squared loss function $\mathcal{L}(t(x, z|\theta_0), f(x)) = (t(x, z|\theta_0) - f(x))^2$ corresponds to risk functional

$$\mathcal{R}_{\text{score}}[f] := \mathbb{E}_{p(x, z|\theta_0)} [(\nabla_{\theta} \log p(x_i, z_i|\theta)|_{\theta_0} - f(x))^2]. \quad (41.30)$$

One can show with the calculus of variations that the risk is minimized by the score of equation 41.26.

41.3.5.1 Differentiable simulations

One of the approaches to make inference feasible in high dimensional latent space is to make simulations differentiable with respect to all of its parameters, global variables θ and latent variables z . Latent variable models are known in Machine Learning as generative models and are discussed below, but latent variable models are also common in scientific applications. As an example, in cosmology one can view the initial conditions of the large scale structure or cosmic microwave background as Gaussian distributed latent variables.

While differentiable simulations have traditionally not been developed for scientific applications, the success of Machine Learning, where backpropagation algorithm combined with gradient descent optimization (see Sec. 41.6.1) is the basis of its recent advances, has inspired a new look at this. One recent example is FlowPM cosmological N-body simulation, which takes advantage of Mesh-Tensorflow to achieve a GPU-accelerated, distributed, and differentiable simulation [59].

One broad class of inference problems where gradients make the problem simpler are the so called inverse problems. As a simple example let's assume the data x are observed with some Gaussian noise with known variance σ^2 , equal for all data points. The likelihood of the data can be written as

$$\log p(x|z, \theta) = -\frac{N}{2} \log[2\pi\sigma^2] - \frac{\|x - g(z, \theta)\|^2}{2\sigma^2}. \quad (41.31)$$

Here $g(z, \theta)$ is the forward model (generator or decoder), *i.e.* the simulation output in the absence of noise. The joint distribution is $p(x, z|\theta) = p(x|z, \theta)p(z|\theta)$, where $p(z|\theta)$ is the prior of latent space variables, assumed to be known, with a known gradient with respect to θ and z . In this case the gradients $\nabla_{\theta} \log p(x, z|\theta)$ and $\nabla_z \log p(x, z|\theta)$ are available when the simulation forward model gradients $\nabla_{\theta} g(z, \theta)$ and $\nabla_z g(z, \theta)$ are available.

Availability of simulation gradients in turn enables gradient based optimization or sampling. In sampling approach one can use Monte Carlo Markov Chains to obtain the posterior samples of latent space z and parameter space θ [60]. In optimization approach one can find the best-fit point \hat{z} , which is the MAP estimate of the latent space variables z given x and fixed θ [61]. Another optimization approach is Variational Inference, which attempts to model the posterior probability distribution using optimization. This is discussed further in Section 41.5.4.

41.3.5.2 Unfolding as an inverse problem

While much of the work on simulation-based inference described above is aimed at inferring the parameters θ of the simulator, there is also work that aims to infer the latent variables z . Here it is useful to think of the parameters θ as parameters of a theory, such as masses, coupling constants, or Lagrangian parameters, while z

⁵For this reason we prefer to use simulation-based inference instead of likelihood-free inference: joint likelihood $p(x, z|\theta)$ is often available, it is the marginal integral over latent space z that is assumed to be intractable.

might describe the kinematics of a collision before the detector response.

Inferring the distribution $p(z|\{x_1, \dots, x_n\})$ from a dataset of multiple observations is commonly referred to as unfolding in particle physics, and deconvolution in other contexts. Unfolding is a classic inverse problem, and the collection of ideas being used for machine-learning based simulation-based inference are also being applied in this setting. Examples of recent work exploring these approaches are Refs. [62–73]. In addition, there has been work to infer the posterior distribution for an individual event $p(z|x_i)$ using probabilistic programming techniques [74–76].

41.4 Data representations, inductive bias, and example applications

In Sec. 41.3 we describe the input data as living in an abstract space $x_i \in \mathcal{X}$. In this section, we briefly describe some of the common types of structured data that are encountered in physics and refer to the corresponding model classes that have been developed to work with them. We will describe the model classes in more detail in the following section.

The most basic and common type of data structure is when $\mathcal{X} = \mathbb{R}^d$. This is often referred to as *tabular data* since the entire data set $\{x_i\}_{i=1, \dots, n}$ can be thought of as a table with n rows and d columns. It is common to think of an individual entry x_i as a vector in d -dimensional Euclidean space, where the coordinates correspond to the columns of this table. In some cases individual components of x_i might be integers or take on only discrete values, in which case describing the space of the data as real-valued is a slight abuse of notation and representation. For many years this was the dominant type of data in high energy physics as it is a natural input type for shallow neural networks, multi-layer perceptrons, support vector machines, and tree-based methods found in popular tools such as TMVA [77].

For categorical data, one typically uses a numerical representation such as *integer encoding* where different categories are mapped to integers with a corresponding dictionary. Another common representation of categorical data is based on the so-called *one-hot encoding* (aka ‘one-of-K’ or ‘dummy’), in which case the category is mapped to a k -dimensional binary vector where k is the number of categories and each component of this vector corresponds to a particular category. In the one-hot encoding, only one of the components is non-zero. Finally, there are approaches in one learns an *embedding* that maps discrete categories into \mathbb{R}^d ; an example of this is *Word2Vec* [78]. Interestingly, such embeddings can preserve various types of semantics; for instance, the vector *walking-walk* is similar to the vector *swimming-swam* as are the vectors connecting countries and their capital cities. This allows for a loose sense of algebra on the word embeddings such as *walking-swimming+swam = walk*. Similar types of embeddings have also been used in a number of scientific use-cases including biological sequences (e.g. DNA, RNA, and Proteins) for bioinformatics applications [79].

Particle physics data often is represented with an extension of the simple tabular data structure where the number of columns is not fixed. For instance, if the rows correspond to data for individual collisions, the number of electrons (and positrons) reconstructed in the event is variable. Thus the number of columns needed to represent the energy, momentum, and charge of these particles is also variable. A common solution to this problem is to fix a maximum number of particles and then *truncate* and *zero-pad* to fit the data into a fixed tabular representation, though this is not the natural representation of the data and it leads to a loss of information.

Sequential data is also commonly encountered in physics (e.g. in time series). Here an individual entry $x_i = (x_i^1, \dots, x_i^t, \dots, x_i^{T_i})$ where t is index for the ordered sequence, T_i is the length of the sequence (which might be variable), and the data associated to each ‘time’ $x_i^t \in \mathbb{R}^d$. This is similar to the previous example where the energy, momentum, and charge of the t -th electron in the i -th event would be x_i^t and the electrons might be sorted according to their energy or transverse momentum. Sequential data is also encountered in natural language processing, where x_i^t correspond to individual words in a sentence. Recurrent neural networks (see

Sec. 41.5.3.9) are particularly well suited to sequential data. Examples applications from the Living Review include [80–85].

Image-like data is one of the most dominant forms of data in industrial applications of deep learning, is very relevant for astronomy and cosmology, and also appears in particle physics in various forms. Image-like data typically involves d -dimensional features associated to a regular grid or lattice that does not vary across the individual instances x_i . The canonical example is a standard image from a camera with $W \times H$ pixels where the p -th pixel has data $x_i^p \in \mathbb{R}^3$ corresponding to the three *channels* in the RGB color model. It is important to recognize that the data corresponding to the 2-dimensional image is not 2-dimensional; instead, it is $(W \times H \times c)$ -dimensional, where c is the number of channels. In astronomy, an image may be grey scale ($c = 1$) or there may be more *channels* ($c > 3$) corresponding to different color filters. In other applications, the grid or lattice might be 3- or 4-dimensional. For example, the data associated to a regularly segmented calorimeter can be thought of as a 3-dimensional image and the data associated to a lattice simulation of a classical or quantum system can be thought of as a 4-dimensional image. Convolutional neural networks, described in Sec. 41.5.3.5, are particularly well suited to image-like data. Example applications from the Living Review include [81, 86–108].

It is also possible that the the data (or features) associated to one ‘pixel’ or lattice site may itself be structured. For example, the single read-out plane of a Liquid Argon time projection chamber (LArTPC) may involve a 1-dimensional or 2-dimensional grid, but the data associated to each ‘pixel’ is itself a sequence or waveform. Example applications in Neutrino Physics from the Living Review include [109–139]. Similarly, in lattice quantum chromodynamics, the data associate to a particular site (or link) would be group valued (e.g. $x_i^p \in SU(3)$ as in Refs. [140, 141]).

Both sequential and image-like data have a notion of temporal or spatial structure. While it is possible to unroll an image into a $(W \times H \times c)$ -dimensional vector, that would erase the spatial structure and obfuscate the fact that nearby pixels are highly correlated. Similarly, one could permute the time index for sequential data, but that would destroy the temporal structure of the data. The complementary point of view is that the model class should also be aware of the structure of the data. Recurrent neural networks and convolutional neural networks are good examples of what is called *inductive bias* as the models do incorporate something about the structure of the data that they are expected to be used with. In some cases this can be formalized in terms of symmetry. For example, if we train model to classify images of cats and dogs, we would like it’s prediction to be invariant to where in the image the cat is. This type of translational invariance can be enforced in the design of the model class.

While permuting the elements of a sequence destroys the temporal structure of a time series, attaching a temporal index t to a set of objects with features x_i^t can also be problematic. If the data corresponding to x_i really are a set $\{x_i^1, \dots, x_i^{T_i}\}$ (e.g. a point cloud), then we would like the output of the model to be *permutation invariance*. A standard sequential or convolutional model will not generally be permutation invariant, but recently models such as Deep Sets, various types of graph neural networks, and transformers can be made to enforce permutation symmetry. Example applications from the Living Review include [100, 142–152].

The temporal and spatial structure of sequences and image like data can also be generalized. For instance, a 1-dimensional sequence can be generalized to a tree structured data like one finds in the hierarchical clustering of jets or as in a directed-acyclic graph (DAG). Generalizations of recurrent neural networks have been constructed that can operate over these more complex data structures [153, 154]. More generally, one can considered graph-structured data composed of nodes and edges or multi-graphs that group together three nodes into faces or k nodes into k -edges. Graph neural networks are a class of models that work with this type of data. The emerging subfield of geometric deep learning aims to unify the notation, terminology, and theory that connect these considerations of the structure of the data and the corresponding model architecture. Example applications in the Living Review include [121, 128, 131, 132, 134, 155–181].

If the data are expected to have a symmetry associated to them but one is working with a model class that does not enforce this symmetry, then *data augmentation* is a common procedure used to improve generalization performance. Here one starts with an initial dataset $\{x_i\}_{i=1,\dots,n}$ and produces an augmented dataset $\{x'_i\}_{i'=1,\dots,n'}$ through some data augmentation strategy. For example, one might apply a random rotation $R_{i'}$ to an image to produce $x'_{i'} = R_{i'}(x_i)$ if one assumes rotational invariance in the underlying problem.

In some cases some of the individual features (components) of x are functions of other features. For instance, one may include components of a four-vector (E, p_x, p_y, p_z) as well as redundant information such as transverse momentum, azimuthal angles, rapidity, etc. In this case, the data is restricted to a lower-dimensional surface embedded in \mathcal{X} . Even if the features aren't redundant, statistically the data are often effectively restricted to a small subspace of statistically likely samples and those that are exceedingly unlikely. For instance, the space of natural images is a small and highly structured subspace of all possible images, which are dominated by what we would perceive visually as noise. The term *data manifold* is used to describe this restricted subspace where the data are to be found, even though it does not necessarily satisfy the formal requirements of a manifold in the mathematical sense.

These considerations on the structure of the data not only apply not to the input data $x_i \in \mathcal{X}$, but also to the output data $y_i \in \mathcal{Y}$. For instance, one might want a sequence-to-sequence model as in machine translation of written text [182] or to learn a function that takes sets as input and produces graphs as output as in the Set2Graph mode [183]. One might also want the input and output of the model to be different in representations of an underlying symmetry group and for the model to enforce group-equivariance [140, 141]. The development of the necessary modelling components to enable practitioners to compose and train these types of models is a significant development for the field of physics.

41.5 Flavors of ML models

41.5.1 Support vector machines and kernel machines

Support Vector Machines (SVM) are a class of supervised learning models used for classification and regression. The learning algorithm involves a convex optimization problem that has a unique solution and can be solved with quadratic programming techniques. In this sense, they are robust and easier to characterize than neural networks that involve non-convex optimization. While their history goes back to Vapnik and Chervonenkis in the 1960s, they gained popularity after Bernhard Boser, Isabelle Guyon and Vladimir Vapnik suggested a way to create nonlinear classifiers by applying the kernel trick in 1992 [184]. Originally they were developed for binary classification and only supported the restricted case where the training dataset can be separated without errors, but in 1995 Cortes and Vapnik extended the technique to non-separable training dataset [185]. A variant targeting regression, known as support vector regression (SVR), was developed in 1997 [186]. The theory around support vector machines was well developed, and they dominated machine learning research for roughly a decade before the rise of deep learning (see Sec. 41.5.3.4).

Maximum-margin classifiers Linear support vector machines are used for binary classification, where $\mathcal{X} = \mathbb{R}^d$ and the target labels are conventionally defined as $\mathcal{Y} = \{-1, 1\}$. The classification is simply based on which side of a hyperplane the data lie. Any hyperplane can be written as the set of points x satisfying $w^T x - b = 0$, where $w, b \in \mathbb{R}^d$ are the parameters of the model. The vector w is normal to the hyperplane, but not necessarily normalized. The quantity $\frac{b}{\|w\|}$ quantifies the offset of the hyperplane from the origin along the normal vector w .

If the training dataset is linearly separable, then there is a region bounded by two parallel hyperplanes, called the *margin*, that separate the two classes of data. The maximum margin classifier is uniquely defined by making the distance between these two hyperplanes as large as possible. The boundaries of the margin

can be defined by $w^T x_i - b = \pm 1$, and the width of the margin is given by $\frac{2}{\|w\|}$. Figure 41.1 illustrates this for $x \in \mathbb{R}^2$.

Since the width of the margin is maximized when $\|w\|$ is minimized, we can state the goal of the (hard) maximum-margin classifier in the linear separable case as the following constrained optimization problem: Minimize $\|w\|^2$ subject to the constraint $y_i(w^T x_i - b) \geq 1$ for $i = 1, \dots, n$. The w and b that solve this problem uniquely determine the resulting classifier, $\hat{y}(x) = \text{sgn}(w^T x - b)$.

This geometric description makes it clear that the maximum-margin hyperplane is completely determined by those x_i that lie nearest to it: the eponymous *support vectors*.

Soft margins and slack variables Often the data will not be linearly separable and thus the hard-margin optimization problem described above has no solution. Such a non-separable case can be accommodated with the use of so-called *slack variables*. One slack variable $\xi_i > 0$ is introduced for each data point. As shown in Figure 41.1 (right), if a data point x_i is outside the margin and correctly classified as in the separable case, then $\xi_i = 0$. If it is within the margin but still correctly classified, then $0 < \xi_i < 1$. If it is misclassified, then $\xi_i > 1$. The new constrained optimization problem is to minimize

$$\sum_i \xi_i + \lambda \|w\|^2 \quad (41.32)$$

subject to the constraints $y_i(w^T x_i - b) \geq 1 - \xi_i$ and $\xi_i > 0$ for $i = 1, \dots, n$. Effectively, this corresponds to minimizing $\sum_i \max(0, 1 - y_i(w^T x_i - b)) + \lambda \|w\|^2$, where the first term is called the *hinge loss*.

The dual problem In the language of convex optimization, linear programming, and quadratic programming the optimization problems stated above for the hard and soft maximum-margin classifiers define the *primal* objective to be minimized. There is a *Lagrange dual* problem where the solution corresponds to maximization with $\min_{\phi} L(\phi) = \sup_{\alpha > 0} \bar{L}(\phi, \alpha)$, where α are Lagrange multipliers. While it is not apparent in the primal formulation of the constrained optimization problems, the solution to the dual problem takes on the form

$$\hat{y}(x) = \text{sgn}\left(\sum_i y_i \alpha_i x_i^T x - b\right), \quad (41.33)$$

where the $\alpha_i > 0$ for the support vectors and otherwise zero. This reformulation is plausible since the orientation of the maximum-margin hyperplanes defined by w is completely specified by the support vectors. The crucial observation for the kernel trick described below is that the final model is defined in terms of coefficients and the inner product $\langle x_i, x \rangle_{\mathcal{X}} = x_i^T x$.

The kernel trick One approach to obtain non-linear decision boundaries is introduce a non-linear mapping $\varphi: \mathcal{X} \rightarrow \mathcal{V}$ that embeds the data in some higher-dimensional space \mathcal{V} . One can then use the linear SVM described above in the space \mathcal{V} . This is not unlike the many neural network models where the first layers use a non-linear activation function while the last layer is linear.

The *kernel trick* avoids the explicit mapping φ that is needed to get linear learning algorithms to learn a nonlinear function or decision boundary. This is possible because the solution to the dual problem in Eq. 41.33 is represented in terms of inner products $\langle \varphi(x_i), \varphi(x) \rangle_{\mathcal{V}} = \varphi(x_i)^T \varphi(x)$ corresponding to the candidate point x and the support vectors x_i . Thus all that is needed is a way to evaluate the inner products. A *kernel* or a kernel function $k: \mathcal{X} \times \mathcal{X} \rightarrow \mathbb{R}$ is a function that can be expressed as an inner product in another space \mathcal{V} via $k(x, x') = \langle \varphi(x), \varphi(x') \rangle_{\mathcal{V}}$. Critically, one does not need to ever evaluate the map $\varphi(x')$, which is implicitly defined by the kernel. In some cases the kernel is straight forward to evaluate, even though the target space \mathcal{V} is implicitly defined by the kernel would be infinite dimensional.

The choice of the kernel is roughly the analog of the architecture of a neural network. It dictates the types of non-linearities the

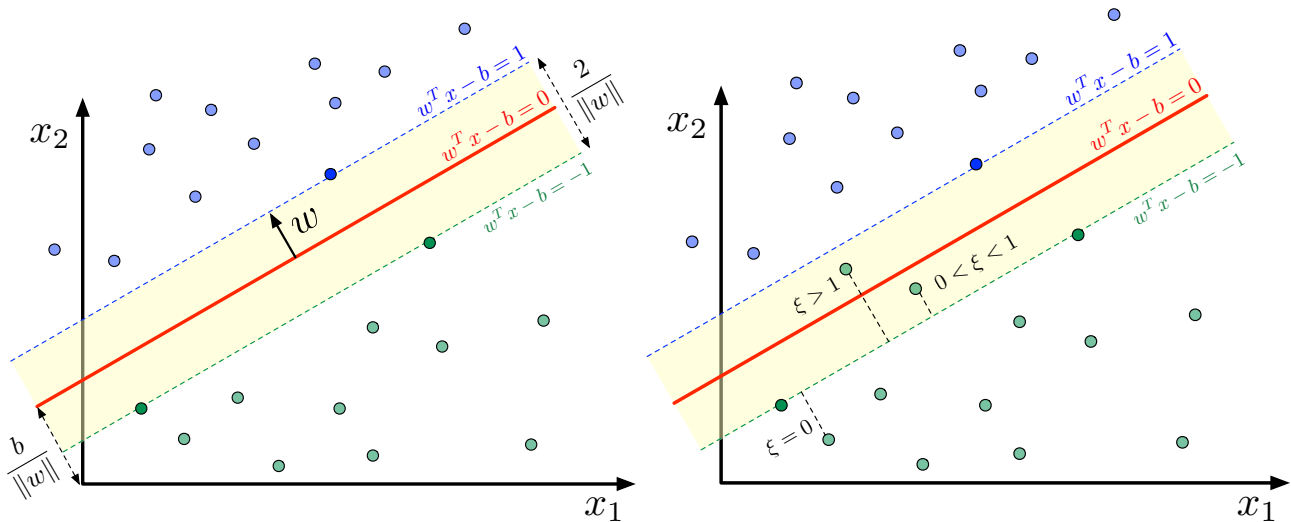


Figure 41.1: Illustration of a maximum margin classifier for a linear support vector machine in the separable case (left) and with the soft-margin and slack variables ξ (right).

SVM can implement in the input space. It also provides an opportunity to encode prior knowledge from physics such as symmetries, length scales, *etc.* There are also connections between very wide neural networks with random weights and biases and the kernel of a Gaussian process [187–189], which, when applied to deep networks, lead to the concept of neural tangent kernel [190]. While it is beyond the scope of this chapter, the interested reader may also be curious to understand the connections as formalized in the language of Reproducing kernel Hilbert spaces (RKHS) [191].

Support vector regression There are a few flavors of SVR. In Vapnik’s ϵ -SVR formulation is similar to the picture for classification, but the boundary hyperplane serves as the prediction and the width of the margin for which there is no penalty is ϵ . Again, one can introduce a non-linear map $\phi(x)$ explicitly or implicitly via the corresponding kernel $k(x, x')$. One can view the predictive model as $\hat{y}(x) = w^T \phi(x) - b$ and the goal of the optimization problem is to minimize

$$\|w\|^2 + C \sum_i (\xi_i + \xi_i^*) \quad (41.34)$$

where ξ_i and ξ_i^* are slack variables associated to the model over or under-estimating $y_i \in \mathbb{R}$. The constrained optimization is subject to $w^T x_i - b - y_i \leq \epsilon + \xi_i$, $y_i - w^T x_i + b \leq \epsilon + \xi_i^*$, $\xi_i, \xi_i^* \geq 0$ for $i = 1, \dots, n$. The solution to the dual problem leads to a kernelized representation of the solution

$$\hat{y}(x) = \sum_i (\alpha_i^* - \alpha_i) K(x, x_i) - b, \quad (41.35)$$

where the α_i, α_i^* are the parameters of the dual problem. In libraries like `LibSVM` the output of the algorithm is just $\alpha_i^* - \alpha_i$ for $i = 1, \dots, n$.

Kernel ridge regression Kernel Ridge Regression (KRR) uses the same model as in SVR; however, it uses a different loss function. KRR uses the squared error loss while support vector regression uses the ϵ -insensitive loss function (*i.e.* no penalty is incurred if the prediction is within ϵ). Both are combined with l2 regularization (the $\|w\|^2$ term). While SVR leads to a sparse solution that only depends on the support vectors, it can be slow to solve the constrained convex optimization problem. In contrast, KRR can be done in closed-form and is typically faster to train for medium-sized datasets. The consequence is that the learned model is non-sparse and thus slower than SVR to evaluate at prediction-time.

Gaussian Process Regression (kriging) Another variation on kernel-based regression is Gaussian process regression (GPR), also referred to as *kriging*. Again the model is based on the kernel trick. While KRR aims to minimize the mean-squared error loss $(y_i - \hat{y}(x_i))^2$ along with an l2 regularization term proportional to $\|w\|^2$, GPR elevates these terms to a probabilistic interpretation where the first is proportional to a log-likelihood for Gaussian $N(y_i | \hat{y}(x_i), \sigma)$ likelihood and the second corresponds to the log of a Gaussian prior on w_i . This is related to the discussion on Tikhonov regularization found in Sec. 41.3.1.2. GPR goes further and uses a mean function $m(x)$ and kernel $k(x, x')$ to define a probabilistic model for $y(x)$ and $y(x')$ that includes correlations. For any finite number of points $\{x_j\}_{j=1, \dots, m}$, the Gaussian process defines the joint distribution for the values that $f(x_i)$ might take. Typically, one specifies the prior mean $m(x)$ and prior covariance function $k(x, x')$ and then conditions on the training dataset $\{x_i, y_i\}_{i=1, \dots, n}$. The posterior can then be evaluated for an independent set of points $\{x_j\}_{j=1, \dots, m}$. The posterior mean is typically used as the prediction equivalent to SVR and KRR, but GPR also gives a meaningful notion of uncertainty in the predictions, and can be viewed as a realization of kernel Bayesian regression [192].

One advantage of GPR is that one can work with a family of kernel functions parameterized by some hyperparameters η . One can then optimize the hyperparameters via gradient-ascent on the marginal likelihood function. In contrast, hyperparameter tuning in SVR and KRR typically requires a grid search or some other black-box optimization procedure evaluated on held out data or some form of cross-validation.

Rasmussen and Williams provides an excellent review of Gaussian processes [193]. Numerically, Gaussian Process libraries are confronted with computing the log determinant of the covariance kernel, which naively scales like $\mathcal{O}(n^3)$ in computational complexity. However, recently there have been a number of numerical advances that make these methods fast and scalable to large datasets [194, 195]. While Gaussian Processes are used more widely in cosmology, they are not widely used in particle physics or astro-particle physics. Recent works explore the design of physics-inspired kernels and use Gaussian Processes to model the intensity for a Poisson point process like those found in experimental particle physics and γ -ray and X-ray astronomy [196–198]. Gaussian Processes are also extensively used in Bayesian Optimization (Section 41.3.3).

41.5.2 Decision trees

Tree-based models Classification and Regression Trees (CART) typically partition the input space into J disjoint regions $\mathcal{X} = \mathcal{X}^1 \cup \dots \cup \mathcal{X}^J$ through a sequence of $J-1$ binary splits based

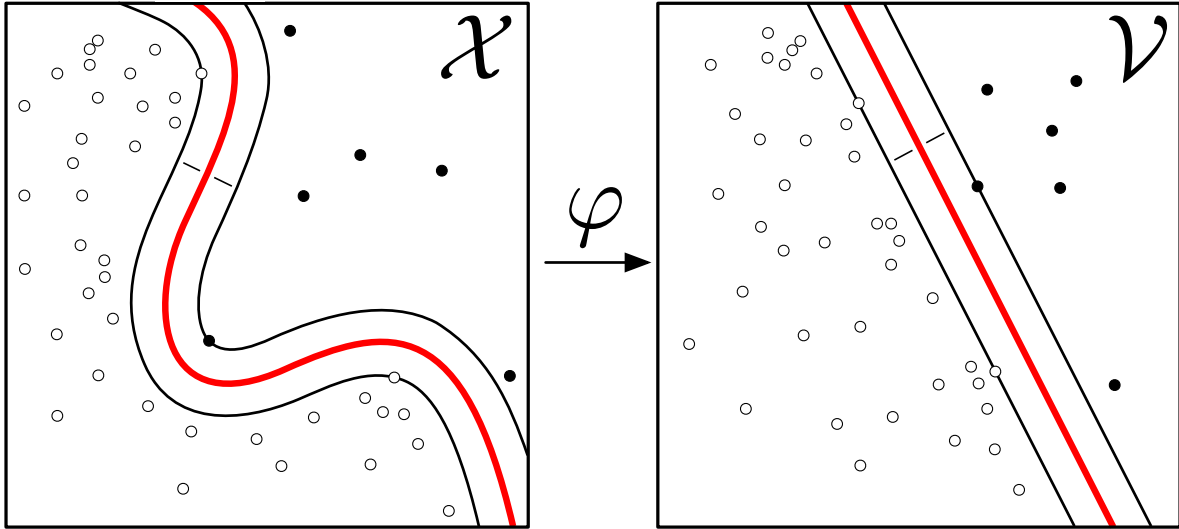


Figure 41.2: Figure depicting the nonlinear SVM decision boundary in \mathcal{X} (left) and the corresponding linear maximum margin classifier in \mathcal{V} (right). Figure adapted from Kernel_Macine.svg Wikimedia Commons (CC BY-SA 4.0) by Cranmer.

on an individual components of $x \in \mathcal{X}$ (e.g. $x_4 < 0.7$) [199]. The model is piecewise constant and assigns the value $b_j \in \mathcal{V}$ to the j -th terminal region \mathcal{X}^j . The model can be written

$$\hat{y}(x) = f_\phi(x) = \sum_j b_j \mathbf{1}(x \in \mathcal{X}^j). \quad (41.36)$$

The parameters ϕ of the model comprise the components index and thresholds for the successive splittings and the coefficients b_j .

Tree learning refers to the algorithm used to choosing the tree structure and determining the predictions at leaf nodes. Optimization of the tree structure involves a difficult discrete optimization since the change in the loss with respect to the tree structure is non-differentiable and it is intractable to explore the combinatorially large space of possible trees with brute force. Therefore, the discrete optimization component of tree learning typically involves some approximate algorithm based on heuristics. In contrast, optimization of the b_j for a given tree structure can exploit gradient-based optimization algorithms.

Common approaches to building the decision tree start with a root node and grow with splits based on individual attributes (components of x). These are referred to as top-down induction strategies. There are various impurity heuristics used for choosing the best attribute to split on such as the Gini index, cross-entropy and mis-classification error. Generally they aim to find a split that will refine the the terminal nodes such that they have higher purity than the parent node.

Because most tree learning algorithms consider splits aligned with individual feature components, there are some failure modes for tree-based models. However, tree-based models work well with tabular data that is composed of a mix of continuous and discrete features. Tools such as `XGBoost` [200] are widely used in data science competitions such as Kaggle and the boosted decision trees (BDTs) implemented in `StatPatternRecognition` [201] and `TMVA` [77] have been one of the most used techniques in particle physics [3].

Individual trees are often referred to as weak-learners and they can be combined in various ways described below. Regularization is also an important consideration with tree-based models as one can always learn a tree that assigns exactly one training dataset point per terminal node and memorize the training dataset exactly. One approach to this is called *pre-pruning*, which simply terminates the growing of the trees if the number of training samples reaching the terminal node drops below some threshold, the purity of a terminal nodes is below some threshold, or if the improvement in purity due to a proposed split is not above a

threshold. Another regularization approach is called *post-pruning*, which uses a validation data set that is disjoint from the training dataset to probe generalization performance. In this approach, after initially growing a tree with the training dataset, one considers a sequences of pruned trees where splits are removed based on some heuristic. One finds the tree in this sequence of pruned trees that minimizes the generalization error on the validation set. Alternatively, in tools such as `XGBoost` there is an explicit regularization term included in the loss function (see Eq. 41.43).

Ensemble methods The idea of ensemble methods is to combine multiple models into a more performant one by exploiting the bias-variance tradeoff [202]. This is most commonly achieved through averaging (e.g. bagging and random forests), which primarily reduces variance, or boosting (e.g. AdaBoost and gradient boosting), which primarily reduces bias. Here bias refers to the difference between the Bayes optimal model and the average model produced by the learning procedure with different training sets and variance quantifies how much the learned model varies from one training set to another.

The motivation of boosting is to combine the outputs of many “weak” models to produce a more expressive model. Compared to averaging techniques like bagging and random forests, the model is built sequentially on modified versions of the data and the final predictions are combined through a weighted sum

$$\hat{y}(x) = \sum_{t=1}^T \beta_t \hat{y}_t(x), \quad (41.37)$$

where β_t expand the parameters of the model ϕ .

Bagging The idea behind bagging (bootstrap aggregating) is to create T bootstrap training datasets B_1, \dots, B_T drawn from the training dataset $\{x_i, y_i\}_{i=1, \dots, n}$, then learn a model \hat{y}_t for each, and finally construct an average model $\hat{y}(x) = (1/T) \sum_t \hat{y}_t(x)$. If one had T independent training datasets each of size n , then the bias of the average model would be the same as the original model, but the variance would be reduced by a factor of T . By using bootstrap resampling, the bias may increase but the reduction in variance often dominates, which leads to improved performance.

Random forests Random forests refers to a type of “perturb and combine algorithm” that combines bagging and random attribute subset selection. Again one builds trees $\hat{y}_t(x)$ from bootstrap training datasets B_t , but instead of choosing the best split

among all attributes, one select the best split among a random subset of k attributes. If k includes all attributes, then it is equivalent to bagging.

AdaBoost In AdaBoost (adaptive boost) the sequence of trees $\hat{y}_1, \dots, \hat{y}_T$ are trained with reweighted versions of the original training dataset such that the weight of individual training sample is based on the prediction error in the previous iteration [203]. This requires working with a loss function that and learning procedure for the individual iterations that is amenable to weighted training dataset $\{x_i, y_i, w_i\}_{i=1, \dots, n}$. Incorporating the weights w_i is straight forward when the risk is expressed as an expectation, since the empirical risk of Eq. 41.3 is just replaced with the weighted average. Similarly, the heuristic for many of the tree-based learning algorithms (e.g. the Gini index) also have natural generalizations with weighted events.

In the context of classification, the weighted error of the model $\hat{y}_t(x)$ is

$$\text{err}_t = \frac{\sum_i w_i^{(t)} \mathbf{1}[y_i \neq \hat{y}_t(x_i)]}{\sum_i w_i^{(t)}}. \quad (41.38)$$

Based on this weighted error, the coefficient β_t of the component $\hat{y}_t(x)$ in Eq. 41.37 is given by

$$\beta_t = \log\left(\frac{1 - \text{err}_t}{\text{err}_t}\right). \quad (41.39)$$

Then for the next iteration the weights of the misclassified events are updated as $w^{(t+1)} = w^{(t)} \exp(\beta_t)$ and then renormalized so that the sum of all weights is 1. This reweighted dataset is then used to train the next model $\hat{y}_{t+1}(x)$ and the entire procedure is initialized with uniform weights $w_i^{t=0} = 1/n$.

There is an analogous procedure for regression with the squared loss function based on the residuals $r_i = y_i - \hat{y}_t(x_i)$ (see for example Ref. [77] for details).

Gradient boosting One of the most powerful forms of tree based models, which is implemented in the tool **XGBoost** is referred to as *gradient boosting* [204]. In this setup, the model is purely additive as in the case of random forests, so the model is Eq. 41.37 with all $\beta_t = 1$. Note this is without loss of generality since the β_t can be absorbed into the b_j of Eq. 41.36. As with AdaBoost, the model is built sequentially through the sequence $\hat{y}_1, \dots, \hat{y}_T$.

At each iteration, a new term f_t will be added to the sum in Eq. 41.37. For a given decision tree defined by splits on attributes, one can approximate the objective function (the loss function \mathcal{L} plus a regularization term Ω) as a function of b_j in a second order Taylor series:

$$\begin{aligned} \text{obj}^{(t)} = \sum_{i=1}^n [\mathcal{L}(y_i, \hat{y}_i^{(t-1)}) + g_i f_t(x_i) + \frac{1}{2} h_i f_t^2(x_i)] + \Omega(f_t) + \\ + \text{constant}, \end{aligned} \quad (41.40)$$

where

$$g_i = \partial_{\hat{y}_i^{(t-1)}} \mathcal{L}(y_i, \hat{y}_i^{(t-1)}) \quad (41.41)$$

and

$$h_i = \partial_{\hat{y}_i^{(t-1)}}^2 \mathcal{L}(y_i, \hat{y}_i^{(t-1)}) \quad (41.42)$$

In **XGBoost**, the regularization term is taken to be

$$\Omega(f) = \gamma J + \frac{1}{2} \lambda \sum_{j=1}^J b_j^2, \quad (41.43)$$

where J is the number of terminal nodes in the tree. With the second-order approximation of the objective, one can directly solve for the optimal b_j for the next tree and the corresponding value of the optimized objective function. The improvement in the objective function can then be used as a heuristic for choosing the best split. Specifically, define $G_j = \sum_{i \in I_j} g_i$ and

$H_j = \sum_{i \in I_j} h_i$, where I_j is the set of indices of data points assigned to the j -th leaf. The heuristic used in **XGBoost** for splitting a node is

$$\text{Gain} = \frac{1}{2} \left[\frac{G_L^2}{H_L + \lambda} + \frac{G_R^2}{H_R + \lambda} - \frac{(G_L + G_R)^2}{H_L + H_R + \lambda} \right] - \gamma. \quad (41.44)$$

This formula can be interpreted as the score on the new left leaf plus the score on the new right leaf minus the score on the original leaf minus a regularization penalty on the additional leaf. If the gain from splitting a leaf is smaller than γ , then the total Gain is negative and the split will not be added, which can be seen as implementing a form of pruning.

41.5.3 Neural networks

In this section we focus on the different types of components used in modern neural network architectures. Gradient-based optimization techniques are most commonly used for training neural networks, and they are described in Sec. 41.6.1. Similarly, other important aspects to effectively training neural network models such as parameter initialization, early stopping, etc. are discussed in Sec. 41.6.

The vanishing and exploding gradient problem is a common challenge for gradient-based optimization of neural networks and is described in Sec. 41.6.5. That problem is referred to repeatedly in this section because it has motivated the development of numerous architectural components described below.

41.5.3.1 Feed-forward multi-layer perceptron

One of the core components in neural networks is the fully-connected, feedforward network or *multi-layer perceptron* (MLP), which is composed of L layers: $f = f^{(L)} \circ \dots \circ f^{(1)}$. The l^{th} layer defines a function that maps a d_{l-1} -dimensional input vector, called *features*, to an d_l -dimensional output $f^{(l)} : \mathbb{R}^{d_{l-1}} \rightarrow \mathbb{R}^{d_l}$. A unit responsible for producing an individual output in d_l -dimensional output is called a *neuron* or a *filter* interchangeably. For $l < L$, the functions f_l are called hidden layers, and the number of neurons (d_l) is referred to as the width of the hidden layers. The layers in an MLP take on the form:

$$f^{(l)}(u) = \sigma^{(l)}(W^{(l)}u + b^{(l)}), \quad (41.45)$$

where $W^{(l)} \in \mathbb{R}^{d_l \times d_{l-1}}$ is called the *weight matrix*, the components of the vector $b^{(l)} \in \mathbb{R}^{d_l}$ are referred to as the *biases*, $u \in \mathbb{R}^{d_{l-1}}$ is the input from the previous layer, $W^{(l)}u$ denotes a matrix-vector product, and $\sigma^{(l)}$ is a non-linear *activation function* that is usually applied element-wise. The parameters of the network comprise the full collection of weights and biases, $\phi = (W^{(1)}, \dots, W^{(L)}, b^{(1)}, \dots, b^{(L)})$.

41.5.3.2 Activation functions

The activation functions σ in neural networks are nonlinear functions and key to the expressiveness of the resulting family of functions. Two traditionally used functions are *logistic* and *hyperbolic tangent* functions. These functions are bounded to be $(0, 1)$ and $(-1, 1)$ respectively, and are symmetric about the input value of zero. On the other hand, away from the zero input value, a gradient of both functions quickly vanishes and this poses a challenge in using gradient-based optimization method (see Sec. 41.6.1). This can be avoided, to some extent, by normalizing the input values and carefully initializing the values of $W^{(l)}$ and $b^{(l)}$. These are discussed in Sec. 41.6.7, 41.6.8 and 41.6.9. Yet, it becomes difficult to maintain a null input value for a *deep* neural network, a model with many layers. Instead, a popular choice for a deep neural network is *Rectified Linear Unit* (ReLU):

$$\sigma(x) = \begin{cases} x & \text{if } x > 0 \\ 0 & \text{otherwise} \end{cases} \quad (41.46)$$

which computational cost is small and provides the gradient does not vanish for $x \in (0, +\infty)$ [205,206]. An alternative to preserve a non-zero gradient in negative input values are called *Leaky ReLU* and modifies the output to $0.01x$ for $x \in (-\infty, 0)$ [207]. Another variant, called *Parametric ReLU* (PReLU), turns the coefficient

0.01 into a variable that is optimized as a part of the model during optimization [208].

The choice of activation functions depends on the model architecture and applications. As described, while the use of ReLU types are a typical choice for a deep neural network, a logistic function is a popular choice at the final layer for classification tasks. Recently, in the area of neural scene representation, sinusoidal activation functions have been found to be surprisingly effective [209].

41.5.3.3 Softmax

A softmax function is often used to normalize elements of a discrete vector u , or to interpret the output as a probability over a set of n discrete categories. Given a real-valued input vector $u \in \mathbb{R}^n$, the softmax function computes the output vector $v \in \mathbb{R}^n$ the i -th component is given by:

$$v_i = \frac{\exp(u_i)}{\sum_{j=1}^n \exp(u_j)}. \quad (41.47)$$

The result has the property that $v_i \in (0, 1)$ and $\sum v_i = 1$. The components of the input vector u are often referred to as *logits* in reference to their connection to the logistic function used in logistic regression. The softmax function is commonly used as the last layer in multi-class classifier. The softmax is also used in the context of attention (see Sec. 41.5.3.11).

41.5.3.4 The rise of deep learning

There are a number of universal approximation theorems in the theory of neural networks. One of the first was that even with one hidden layer ($L = 2$), an MLP can approximate any continuous function if the non-linear activation function σ not a polynomial and the width d_1 is large enough [210]. However, it is often more efficient (in terms of the number of parameters) to increase the *depth* of the network L [211].

Training a deep network (*i.e.* $L > 2$) that generalizes well can be more difficult, requiring large training datasets, many gradient updates, and suitable regularization. The introduction of large labeled training sets, advances in computing (*e.g.* graphic processing units or GPUs which enabled orders of magnitude acceleration in parallel computation including matrix multiplies [212]), development of ReLU, research progress in initialization and optimization algorithms for model parameters, and regularization techniques like *dropout* [13] all played an important role in the rise of *deep learning* [2, 213]. Though the name deep learning was originally a reference to the depth L of such networks, modern deep learning is characterized more by the composition of various types of modules that are trained through gradient-based optimization. Below we introduce some other common network architectures.

41.5.3.5 Convolutional neural networks

Convolutional Neural Networks (CNNs) are widely used for image-like data. They implement the convolution of the input image u and a *filter* W (also referred to as a kernel). The parameters of the filter are learnable and the convolution involves traversing over input and calculating the inner product of the filter W with the part of the input in the *receptive field*, which has the same spatial shape as the filter and is centered at the target pixel. At each location – indexed by i and j below – there is a pixel that may have a vector of features associated with it. In the context of CNNs, these components of these features – indexed by c and c' below – are often referred to as *channels* in reference to the red, green, and blue color channels in a traditional image. The convolution operation is often denoted with a $*$, and the result can be expressed as

$$v_c(j) = (W * u_c)(j) = \sum_{c'} \sum_i W_{c,c'}(i) u_{c'}(“j - i”), \quad (41.48)$$

where “ $j - i$ ” is shorthand for the pixel index corresponding to the translation from pixel j to i . By repeating the operation over all pixels, the result of a kernel convolution is also an image as

illustrated in Figure 41.3. Note that the the number of channels in the output v does not need to be the same as in the input, and the collection of filters $W_{c,c'}$ is often referred to as a filter bank. The entire image for a fixed channel index is often referred to as a *feature map*.

A key feature of the CNN architecture is that it is *equivariant* to translations, meaning that if the input image is shifted (*e.g.* $u(i) \rightarrow u'(i) = u(i - k)$), then the output is also shifted by the same amount (*e.g.* $v(j) \rightarrow v'(j) = v(j - k)$). This equivariance property is a natural consequence of using convolutions. A fully connected MLP would not generally have this symmetry; however, it is enlightening to imagine transferring the computation performed by a CNN to the weights and biases of a fully connected MLP, which would result in duplicating the weights of the filters multiple times. In this view, the CNN can be interpreted as a fully connected MLP with *shared weights*, which would maintain the equivariance property. This view is helpful for gaining intuition about the inductive bias of models and makes clear that a CNN is a subset of the fully connected MLPs that satisfy the translation equivariance property.

The discussion above makes it clear that CNNs will have fewer parameters than the corresponding fully connected MLP, which can alleviate the optimization challenge. In addition, the convolutional structure allows for data to be reused effectively as patterns in one part of an image in the training dataset effectively contribute to learning that pattern anywhere in the image. Larger kernel sizes allow for the filters to learn more complicated patterns, but at the expense of having more parameters and needing more data to train (the extreme case being a kernel size that is the size of the entire image, which would be equivalent to a fully connected MLP). In practice, kernel sizes of 3 are popular, 5 is sometimes used, and larger kernels are rarely used.

A kernel convolution involves three hyperparameters, the size of kernel (typically an odd number so that the filter has an unambiguous center), *stride*, and *padding*. The stride is the number of pixels between each target pixel (*i.e.* the center of the filter). The stride size of 1 implies the target pixels are adjacent, and a stride of 2 implies skipping 1 pixel in between (along each spatial axis). Padding is an operation to expand the input image by a specified number of pixels (*i.e.* “padding size”) for when the target pixel is near the edge and the filter would extend beyond the input image. In Figure 41.3, the input image is 4×4 pixels, the kernel is of size 3, and no (zero) padding is applied. The result is a smaller image. Alternatively, With the padding of size 1, the output would retain the 4×4 shape of the input image.

A kernel size of 1 is also frequently used and is referred to as a 1×1 *convolution*. While it cannot capture a geometrical features, it can perform linear operations on the input features, including increasing or decreasing the number of features. When combined with a non-linearity and stacked repeatedly this can be seen as a small MLP attached to an individual pixel, and for this reason the 1×1 convolution is sometimes referred to as a *network-in-network* [214]. This is often used to extract more powerful features to be used by the latter layers, and also to compress features when the next layers may be computationally demanding such as a block of many convolution layers with a large kernel size [215, 216].

One may wonder how CNNs identify features with a spatial size larger than a typical kernel size. One mechanism for this is by stacking multiple convolutional layers – *e.g.* the composition of two 3×3 kernels will lead to an effective 4×4 kernel. In addition, a typical CNN architecture uses pooling (described below), which effectively down-samples the image so that it can be processed at different resolutions. The effective receptive field in the input image may be much larger than the kernel size in this case. An alternative approach is to use an *inception module* which is designed to extract features simultaneously using kernels of different size [215].

41.5.3.6 Pooling

Pooling plays an important role in convolutional neural networks both practically and in terms of their mathematical properties. A pooling operation is a type of aggregation or down-sampling that takes many pixels as input and produce one pixel for output. Typically, the pooling operation is applied indepen-

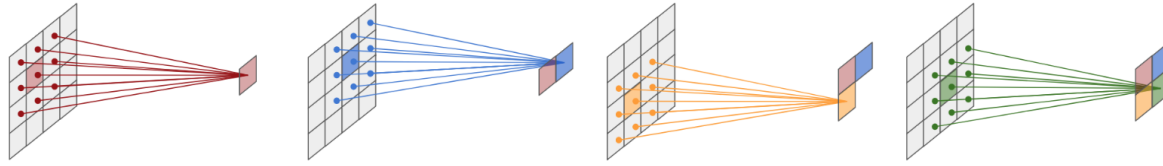


Figure 41.3: A pictorial description of a kernel convolution over four input pixels. It takes a product of the weight matrix (kernel) and the local input matrix centered at a target pixel. The operation is repeated over the input image using the same kernel. The size of the output image depends on the size of the kernel, stride, and padding. In this figure, the kernel size of 3, stride of 1, and padding of 0 is used.

dently for each channel or feature component. The most popular pooling operations are *max* and *average* pooling. Max-pooling picks the highest activation pixel value within the specified receptive field, while the average pooling computes the average pixel value in the receptive field. The idea of pooling generalizes to other architectures, including graph neural networks where the receptive field includes the neighbors of a particular node in the graph (see Sec. 41.5.3.14). The pooling operation gives rise to robustness of the model to small, local deformations in the input, a property called *geometric stability* [217–219]. This type of local deformation is important and distinct from the equivariance to rigid translations provided by the convolutional structure. Repeated pooling operations that eventually lead to a single feature vector with no spatial index is what gives rise to the invariance of common CNN architectures to translations (*i.e.* an image with a dog will be labeled ‘dog’ even independent of where the dog is in the image).

On the practical side, it is also beneficial to reduce the dimensionality of the input to a smaller hidden state representation. This can be done either a convolution operation with the stride size larger than 1, or employing a *pooling*.

A typical CNN for extracting a 1-dimensional array of features is designed with repeating blocks of convolution layers and pooling operations [220]. Figure 41.4 shows an example evolution of a data tensor through the succession of a convolution and pooling operations in order to extract a 1-dimensional array of features, which then can be fed into a block of MLP for an image classification (or a regression) task. This type of an architecture is referred to as an *encoder* or *feature extractor*.

The reduction in the spatial size of an image is performed *slowly*, typically by a factor of 2, which is the minimum possible reduction factor. After the reduction of the spatial extent, the number of channels is typically increased (also by a factor of 2 in most cases), converging one set of feature maps into a larger number of down-sampled feature maps. There may be more than one convolution layer within each spatial resolution (*i.e.* in between pooling operations). Following these design principles, CNN encoders typically become *deep*, consisting of dozens or sometimes hundreds of convolution layers, and face challenges of vanishing gradients problem (see Sec. 41.6.5). A standard practice to mitigate this issue is explicitly *normalize* the input tensor input at each convolution layer using algorithms like *Batch Normalization*. This will be discussed in Sec. 41.6.9.

41.5.3.7 CNN architectures for image analysis

There are three major categories of computer vision tasks where CNNs are often used:

- *Image classification or regression* requires a prediction of single value for the whole image (*i.e.* a category or target value)
- *Object detection* produces a list location information for arbitrary number of objects in the input image
- *Semantic segmentation* outputs an image of the same spatial dimension as the input, in which every pixel is segmented by a predicted value for a target task (classification or regression).

As discussed previously, a CNN feature extractor followed by MLP is often used for image classification and regression tasks in wide range of applications including particle physics. Many successful

CNN architectures for object detection and semantic segmentation applications share key designs which we briefly discuss below.

Region Convolutional Neural Network (R-CNN) is one of the most successful design for object detection [221]. R-CNN is explored in HEP experiments where the number and location of signal (e.g. neutrino interactions) are not known a priori in large image data such as neutrino detectors [3, 116, 222].

R-CNN consists of multiple CNNs. The first is a feature extractor which produces a spatially compressed feature tensor. The second CNN applies 1×1 convolution to predict two information: an *object score* which indicates whether there is an object in this (spatially compressed) pixel or not, and prediction of the location and size of a rectangular, axis-aligned bounding box that contains the object (if exists). This second CNN is called *Region Proposal Network* (RPN), and the bounding box is called *Region of Interest* (ROI). The size of a bounding box is not directly solved by a regression. Instead, the model requires a set of pre-defined *anchor* boxes, which sizes and aspect ratios are hyperparameters, and predict the object score, location, and size (as a multiplicative factor to the defined anchor box) for each anchor box. This allows RPN to detect multiple objects with different aspect ratios even if they are within the same receptive field in the original input image. For each ROI with an object score above threshold (hyperparameter), the third CNN operates in the corresponding sub-field of an already-compressed tensor (*i.e.* by the first CNN) to perform a classification for an object inside the ROI.

This approach can produce multiple ROIs for the same object with a high overlap. Those predictions are reduced using Non-Maximum Suppression (NMS) algorithm. Given a list of bounding boxes with confidence scores, NMS takes the box with the highest score, and computes the Intersection-over-Union (IoU) of this box and all the rest of boxes. Boxes with the IoU higher than a threshold (hyperparameter) are eliminated as they are likely to represent the same object. Then NMS repeats the same operation for the box with the second highest score among the remaining boxes. This is repeated till the list is exhausted.

U-Net is one of the of most successful models used for semantic segmentation [223]. As the output of U-Net is also an image, it gives some interpretability compared to models for an image-level classification or regression tasks. The model is used widely in HEP experiments in both 2D and 3D image data [112, 113, 118, 125, 127].

The architecture of U-Net consists of a CNN encoder and *decoder*. A decoder consists of convolution and *convolution-transpose* layer (also called strided transpose-convolution, or rarely deconvolution). The operation of a convolution transpose can be seen an opposite of a convolution: for every pixel in an input image, its value is multiplied to the kernel and copied to the output. 3×3 kernel in transpose-convolution layer fills 3×3 pixels in the output tensor. The concept of padding and the stride are also applied to the output tensor. For instance, the stride 2 transpose-convolution fills 3×3 fields centered at every other pixel (*i.e.* stride 2) for every input pixel. The spatial size of an output tensor is therefore determined by the spatial size of an input tensor, stride, and padding. In the decoder of U-Net, convolution-transpose layers are used to up-sample spatially compressed feature tensors back to the original image resolution. The

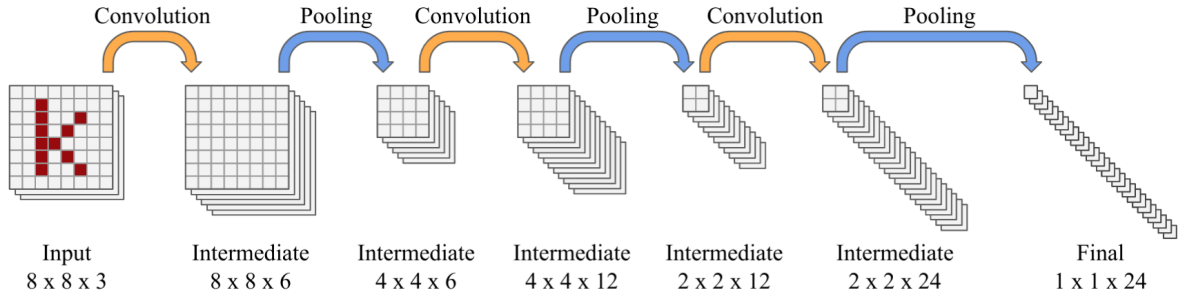


Figure 41.4: An example CNN architecture to extract a 1-dimensional array of features from an image via succession of convolution layers and pooling operations. The (square) kernel, stride, and padding size of a convolution operation are 3, 1, and 1 in respective order. The pooling operation uses a square kernel size of 2. The number of filters at the first convolution layer is 6, and is increased by a factor of 2 at subsequent convolution layers.

stride size of a convolution-transpose layer is almost always 2 in order to *slowly* transform the spatial size, and standard convolution layers (with stride 1) are placed in-between up-sampling operations. Because the output of the decoder has the same size as the input image, features for every pixel can be used for either a classification or a regression task at the pixel-level.

The idea behind encoder-decoder architecture is to extract features in the encoder, and the decoder interpolates those features back to the original spatial resolution. The down-sampling operation (e.g. max-pooling) in the encoder is, however, a lossy process where spatial information is permanently lost. This prevents a simple encoder-decoder architecture to perform a semantic segmentation task at the level of precision required for science research and industrial use. Interesting observation made by the U-Net authors is a symmetry in the encoder-decoder architecture in which there are tensors of corresponding (i.e. the same) spatial size between two parts of the model. This observation inspired them to concatenate the intermediate tensors in the encoder block to the intermediate tensors of the corresponding size in the decoder block before convolution layers are applied in the decoder, which dramatically improved the performance of semantic segmentation. This is a type of a *skip connection* discussed below.

41.5.3.8 Residual networks and skip connections

The representation power of a neural network increases as more hidden layers are added, but gradient-based optimization of deep models can be notoriously difficult due to vanishing gradients (see Sec. 41.6.5). One of powerful techniques to address this challenge is a *residual network* (ResNet), which is a modular architecture design that can be applied to neural network models [216]. Suppose a $f^*(x)$ as the target transformation to be learned by a few stacked layers where x is the input to the first layer. The authors of ResNet hypothesized that it may be easier for a model to learn a residual transformation $\tilde{f}(x) := f^*(x) - x$, thus the objective to learn is $\tilde{f}(x) + x$ where $\tilde{f}(x)$ denotes the output of stacked layers. This form assumes $\tilde{f}(x)$ and x share the same tensor dimension and size. If they differ in the feature dimension, equivalently the count of channels in an image tensor, one could use 1×1 convolutions to transform and match the dimension. The design is modular as it can be applied per a stack of convolution layers (e.g. U-ResNet introduced for LArTPC detectors uses ResNet modules within a U-Net architecture [112, 113]) widely in the present applications.

The authors of ResNet successfully demonstrated an improved performance of some models at the depth exceeding 1000 layers where the non-residual counter part could not improve the accuracy beyond a few dozens of layers. This remarkable success was due to the *skip connections* in ResNet, namely the element-wise addition of the input to the output at each block of convolution layers as shown in Figure 41.5. Without the presence of the skip connections, the gradients from the loss function is forced to go through all convolution layers (i.e. the reverse direction of orange allows in Figure 41.5), which results in the gradient being altered at every convolution layer. The layers closer to the input receive

altered gradients by the continuously updated weights of deeper layers, making conversion difficult and slow. The skip connections provides the path for the gradient to flow directly to the preceding layers. As a result, the gradient can flow more directly to preceding layers and allows simultaneous optimization across layers. It is possible, however, that some convolution layers in ResNet may learn an identity mapping, thus contributing no effect to solving a given task despite consuming computing power.

Another type of skip connections is a concatenation of feature maps, in which case the input and the output of a block of convolution layers do not necessarily have to have the same number of features. This is shown to be very powerful in number of popular model architectures including U-Net [223] and DenseNet [224]. In this case, the input features are re-used: the next block of hidden layers can learn an optimal way to combine the input and the output of the preceding block (i.e. it could learn a simple addition operation, which makes it identical to ResNet). In DenseNet, input to a convolution layer is concatenated with the output of all preceding convolution layers of the same spatial dimension, thus $x_l = f_l([x_1, x_2, \dots, x_{l-1}])$ where x_l is the output of l -th layer f_l and $[x_1, \dots, x_{l-1}]$ denotes a concatenation of the inputs. In U-Net, tensors from the encoder block are concatenated with the tensors in the decoder block where they have the same size in spatial dimensions. This was critical for achieving a high spatial resolution for *semantic segmentation*, a class of tasks in Computer Vision to classify every pixel in an image among the predefined set of types (semantics), because the geometrical features at each spatial resolution is otherwise lost via pooling operation in the encoder block [223].

41.5.3.9 Recurrent neural networks

Recurrent Neural Networks (RNNs) [225] are a family of neural networks designed for sequential data (e.g. time series). Consider sequential data where x_t represents each step in a sequence with $t \in [1, n]$. A typical RNN takes the following form:

$$h_t = g_h(h_{t-1}, x_t, \theta) \quad (41.49)$$

where h_t and θ denote the *hidden state* of the system and parameters of g_h , the RNN model. The term *recurrent* refers the nature of the model operating on the previous state of the system (and hence the whole history). RNNs operate on three types of tasks:

- *One-to-many* takes a single input and generates a sequence (e.g. generates a sequence data, such as a sentence or waveform, given a category).
- *Many-to-one* takes a sequence and generates an output (e.g. sequence-labeling).
- *Many-to-many* takes a sequence and generates a sequence where the length of input and output sequence may be same (e.g. classification of individual element in a sequence) or different (e.g. sequence to sequence mapping).

Figure 41.6 shows an example for a many-to-many task, where $\{x_t\}_{t=1:n}$, $\{y_t\}_{t=1:n}$, and $\{h_t\}_{t=0:n}$ denote the inputs, outputs,

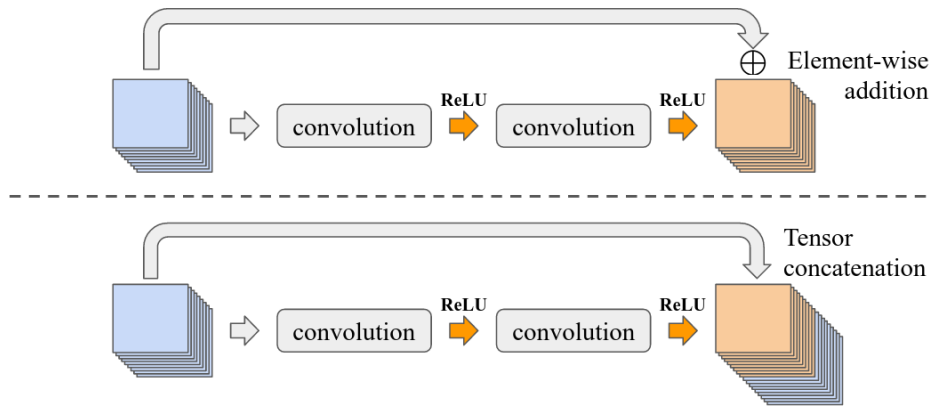


Figure 41.5: Two types of skip connections: the top is from ResNet where the input is element-wise added to the output tensor of a block of convolution layers while the bottom shows a concatenation of the input to the output tensor as employed in other models including U-Net and DenseNet.

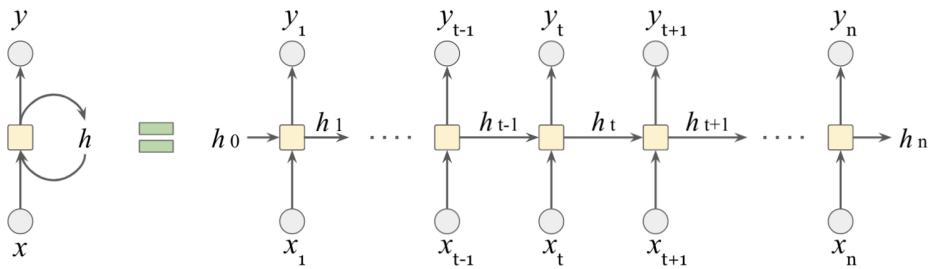


Figure 41.6: Pictorial description of a RNN (on the left) which takes an input and produces an output at every step with a hidden-to-hidden connection. The right diagram is unrolled over discrete steps. The yellow box represents a cell: a set of operations unique to each architecture.

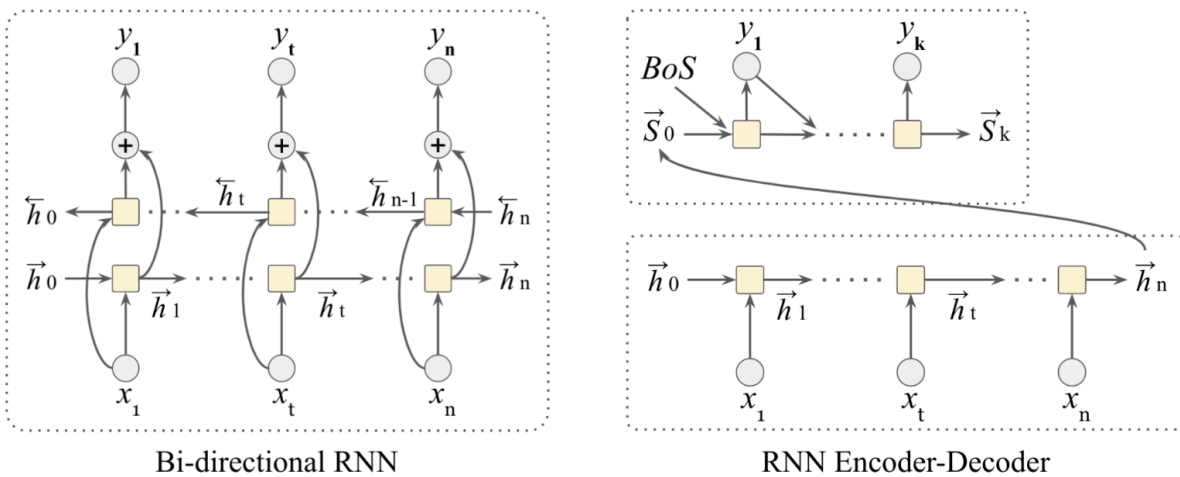


Figure 41.7: Bi-directional RNN (left) provides contexts in the preceding and subsequent parts of the input sequence. RNN encoder-decoder (right) can generate an output with a different sequence length from an input. Each cell in the decoder may take a previously generated element, starting from a special marker that signals the beginning of the sequence (BoS) and ending when the end of sequence is generated.

and hidden states respectively. A set of operations at each time step is called a *cell*. A simple RNN cell may look like:

$$\begin{aligned} h_t &= g_h(Wx_t + Vh_{t-1} + b) \\ y_t &= g_o(Uh_t) \end{aligned} \quad (41.50)$$

where $W \in \mathbb{R}^{d_h \times d_i}$, $V \in \mathbb{R}^{d_h \times d_h}$, $U \in \mathbb{R}^{d_o \times d_h}$ are matrices g_h and g_o represent functions. d_i , d_h , and d_o are the dimension of input, hidden state, and output. $b \in \mathbb{R}^{d_h}$ is a bias term. An example application is sequence-labeling where the goal is for y_t to classify each input x_t in the sequence. In that case, one might use $g_h = \tanh$ and $g_o = \text{softmax}$ and use a loss function that averages classification accuracy over the sequence.

Variations in RNN architectures result from the design of cells (described below) and flow of information across the cells. For instance, a bi-directional RNN (Figure 41.7 left) employs two set of RNNs, one processing the sequence in the forward direction and the other in the backward direction, and the hidden states from both directions are then combined to capture the context from both parts of the sequence. An RNN encoder-decoder (Figure 41.7 right) use one RNN to generate a context vector that encodes the whole input sequence, and use a separate RNN to generate

another sequence from the encoded context. This can be used for machine translation.

41.5.3.10 LSTM and GRU

An RNN applies the same functions g_h and g_o in Eq. 41.50 repeatedly for each element of the sequence. This repeated component is similar to the shared weights for a convolutional filter in a CNN.

A hyperbolic tangent (\tanh) is traditionally a popular choice for g_h as it regulates the magnitude of the hidden states and prevents it from diverging. Yet, this simple model is challenging to train for a long sequence of data [226, 227]. This is partially due to the fact that \tanh contributes to the vanishing gradient problem and because repeated multiplication of the same weight matrices (i.e. V and W in Eq. 41.50) can lead to gradients that can either explode or vanish (see Sec. 41.6.5). Additionally, the way the signal accumulates means that changes early in the sequence have different impact from changes late in the sequence.

Long Short-Term Memory (LSTM) [228] is a model designed to address the issue of vanishing gradient for RNNs. In this model, a *context* is introduced as a way to enable the model to hold long-term memory while the hidden states remain to hold short-term memory. The context c_t and hidden state h_t at step t are computed as follows:

$$\begin{aligned} c_t &= f_t \odot c_{t-1} + i_t \odot \tilde{c}_t \\ h_t &= o_t \odot c_t \end{aligned} \quad \text{where} \quad \begin{aligned} f_t &= \sigma(W^f x_t + V^f h_{t-1} + b^f) \\ i_t &= \sigma(W^i x_t + V^i h_{t-1} + b^i) \\ o_t &= \sigma(W^o x_t + V^o h_{t-1} + b^o) \\ \tilde{c}_t &= \tanh(W^c x_t + V^c h_{t-1} + b^c) \end{aligned} \quad (41.51)$$

where σ and \odot denote logistic function and an element-wise (i.e. Hadamard) product and f_t , i_t , and o_t are referred to as *gates*. Each gate outputs a value between 0 and 1, and is associated with unique weights, W and V , and a bias b . One can see c_t is a combination of the previous context vector c_{t-1} and a new context vector \tilde{c}_t . The *forget* gate f_t controls which and how much of the past context should be kept or forgotten. The *input* gate i_t controls how much of the present context \tilde{c}_t should propagate to the current state c_t . The output gate o_t controls which and how much of the context vector should represent the present hidden state h_t . From Figure 41.8, one can see that the context vector c_t

evolves with a gated addition operation. As such, it can be seen as an uninterrupted path for gradients to flow. This is similar to a residual connection (see ResNet in Sec. 41.5.3.8), which enabled training of CNNs with thousands of layers.

Another gated model to solve a vanishing gradient problem is the *Gated Recurrent Unit* (GRU) [182]. The GRU is similar to the LSTM with a few simplifications: the GRU merges the context vector and the hidden states and combines three gates into two. As a result, it requires less computational resources while retaining a similar level of performance for long sequences. The GRU operations are defined as follows:

$$\begin{aligned} h_t &= z_t \odot h_{t-1} + (1 - z_t) \tilde{h}_t \quad \text{where} \\ r_t &= \sigma(W^r x_t + V^r h_{t-1} + b^r) \\ z_t &= \sigma(W^z x_t + V^z h_{t-1} + b^z) \\ \tilde{h}_t &= \tanh(W^h x_t + V^h (r_t \odot h_{t-1}) + b^h) \end{aligned} \quad (41.52)$$

where r_t and z_t are referred to as *reset* and *update* gate. As one can see in Figure 41.6, the reset gate in GRU performs the same task as the forget gate in LSTM by removing or reducing the elements of its memory (i.e. the hidden state). The update gate z_t determines the relative proportion of the previous hidden state h_{t-1} and the new context \tilde{h}_t to be mixed in producing the new hidden state.

In addition to sequential data, the LSTM and GRU units can be used for data that has a tree-like structure. In this setting, the networks are often referred to as recursive neural networks or TreeRNN and they have found applications in natural language processing and jet physics [153, 154, 229–231].

41.5.3.11 Attention

Many tasks encountered in machine learning can be divided into subtasks. For example, classifying each pixel of an image or element of a sequence, predicting a target for each node in a graph, etc.. For each subtask the model may need to draw upon information from the entire input, but some parts of the input will be more relevant than others. At some point, the model will

need to form a representation for the input as context for the subtask at hand. A fixed length vector c as a global context for this subtask is possible, but this approach scales poorly as the size of the input and number of subtasks grow. Either the size of the global context must grow or it will not have the capacity to represent all the relevant information, which would lead to a degradation in performance.

The idea behind *attention* is intuitive: one still forms a representation for the entire input, but different parts of the input are weighted differently according to the task at hand. By making the weights a learnable component, the network can learn to attend to the relevant parts of the input. A softmax function is a natural way to represent attention as it assigns a positive value to each component of the input and sums to one. Then for the i -th task, one can simply form a task-specific context c_i by computing the weighted average of the hidden state representations h_j for each component of the input. Let α_{ij} be the weights assigned to the j -th input for the i -th task, such that $\sum_j \alpha_{ij} = 1$. We can satisfy this naturally if for each i the α_{ij} are computed from the logits β_{ij} using a softmax function that normalizes by summing over j .

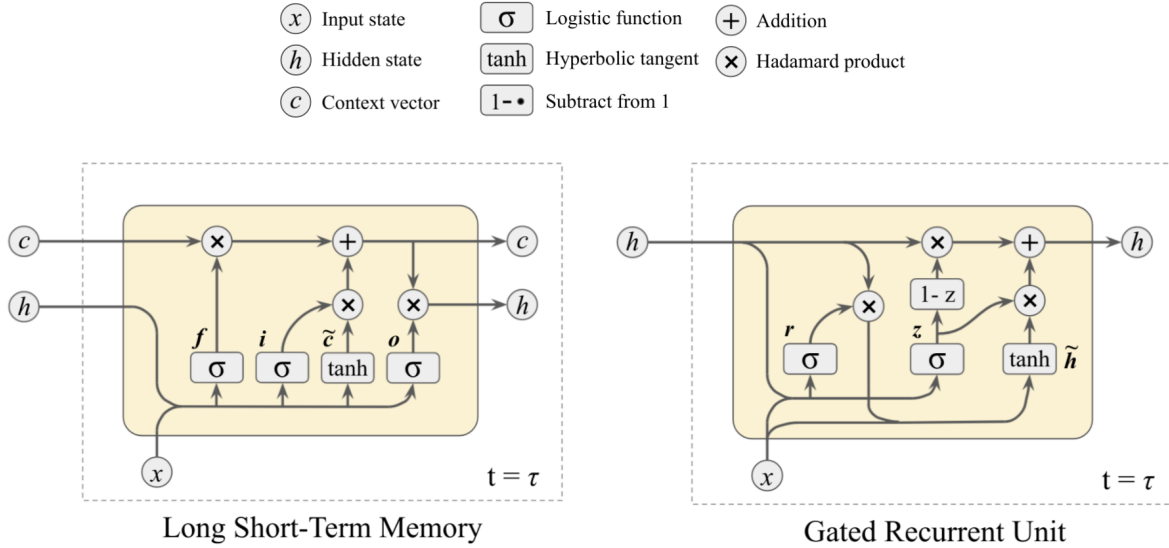


Figure 41.8: LSTM (left) and GRU (right) are both gated neural network designed to address a vanishing gradient problem for RNNs.

Putting these ingredients together, we have the *additive attention mechanism*

$$c_i = \sum_{j=1}^n \alpha_{ij} h_j \quad \text{where} \quad \alpha_{ij} = \text{softmax}(\beta_{ij}) \text{ over } j. \tag{41.53}$$

As in the case of a multi-class classifier, the logits β_{ij} can be computed from a network component with learnable parameters. For instance, in the case of a cell of an RNN encoder-decoder network (see Fig. 41.7) that is decoding element i with an incoming input state s_{i-1} , the logits for the attention mechanism could be computed as follows

$$\beta_{ij} = U \tanh(W s_{i-1} + \tilde{W} h_j + b_i), \tag{41.54}$$

where U, W, \tilde{W} are the weights and b is the bias term of the model. Fig. 41.9 from Ref. [232] illustrates the full attention mechanism. The idea was implemented by a model called *RNNSearch* which made a breakthrough in machine translation by combining a bi-directional RNN with an additive attention mechanism [233].

We end this section by noting that the softmax α_{ij} can be used to visualize the influence of the j -th input element on the i -th output element, which improves interpretability of the model. An example of this from Ref. [232] is shown in Fig. 41.10.

41.5.3.12 Scaled dot-product attention

Shortly after the introduction of RNNSearch, the attention mechanism has been recognized as a powerful tool. One such variant is *scaled dot-product attention*, which is most widely recognized as the foundation of the *Transformer* architecture [234], which is described in more detail below.

In additive attention (Eq. 41.53) the hidden representations h_j were combined through a weighted average based on the coefficients α_{ij} , resulting in a task-specific context vector c_i . In the literature around scaled dot-product attention, multi-head attention, and transformers, the hidden states that will be combined are referred to as *values*, and they are often arranged in a matrix labeled $V \in \mathbb{R}^{m \times d_v}$, where the m rows of the matrix correspond to individual hidden state vectors of length d_v . The α_{ij} can also be represented as a $n \times m$ matrix α resulting from applying the softmax function to the $n \times m$ matrix β , normalized independently for each row. With this notation, Eq. 41.53 could be rewritten as $c = \text{softmax}(\beta)V$, where the softmax is normalized per row.

In scaled dot-product attention, the basic structure will be different, but instead of using a non-linear network component to compute the logits β as in Eq. 41.54, the logits will be computed

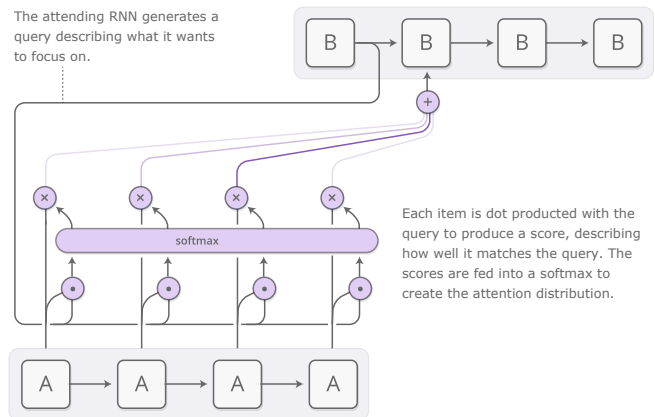


Figure 41.9: An illustration of the attention mechanism From Olah and Carter, “Attention and Augmented Recurrent Neural Networks”.

by forming a dot product between a in incoming *query* and a *key*. The set of n query vectors can be arranged into the matrix $Q \in \mathbb{R}^{n \times d}$ and the set of d key vectors can be arranged into the matrix (transpose) $K^T \in \mathbb{R}^{d \times m}$. When the dot product between a particular query vector $q_i \in \mathbb{R}^d$ and key vector $k_j \in \mathbb{R}^d$ is large, then the resulting logit β_{ij} and attention weight α_{ij} will be large. One can interpret the keys as trying to detect certain types of queries and routing the attention to the relevant value. Typically, the dot-product is scaled by a factor of $1/\sqrt{d}$. The resulting task-dependent context is $c_i = \text{softmax}_j(q_i \cdot k_j / \sqrt{d})v_j$, where softmax_j indicates that normalizing sum runs over the index j . A common, though sometimes confusing, notation is simply

$$c = \text{Attention}(Q, K, V) = \text{softmax}\left(\frac{QK^T}{\sqrt{d}}\right)V, \tag{41.55}$$

where c is a $n \times d_v$ matrix organizing the n context vectors of length d_v that are taylored summaries of the input vector for each of the n tasks.

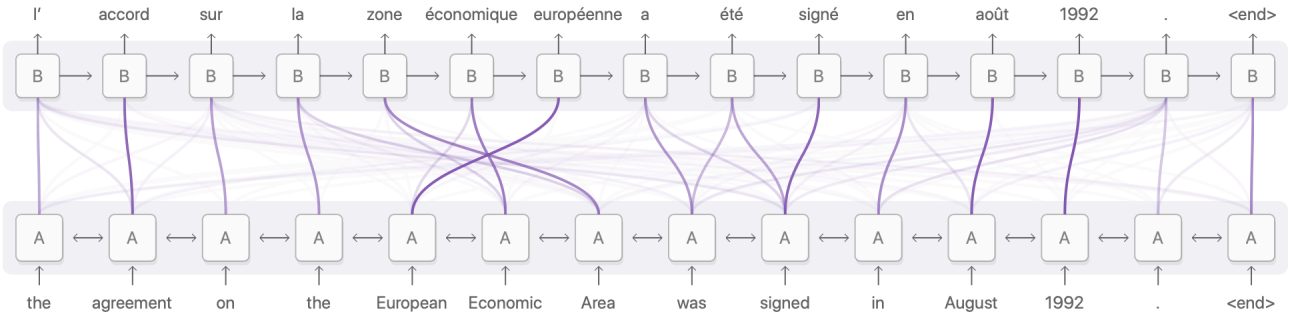


Figure 41.10: Visualization of the attention weights in a sequence-to-sequence problem taken from Olah & Carter, "Attention and Augmented Recurrent Neural Networks". The thickness of the lines is proportional to the attention weights α_{ij} .

41.5.3.13 Transformer and multi-head attention

The Transformer architecture is a powerful encoder-decoder model based on the scaled-dot product attention mechanism. It was originally designed for sequential data like RNNSearch, and subsequently used in other areas of research including computer vision. One advantage of scaled-dot product attention compared to the approach used in RNNSearch (Eq. 41.54) is that computing the logits β_{ij} (and thus the attention weights) does not involve any sequential processing. This allows the models to better leverage parallelism of the hardware to train much more expressive models than before. In place of the gated units of an RNN that are key to avoiding the vanishing gradient problem, the Transformer architecture employs a residual connections at every attention module (*i.e.* the input tensor is added to the output as in Fig 41.5).

The second major ingredient in the Transformer architecture is the *multi-head attention* mechanism. A multi-head attention module executes multiple scaled dot-product attention in parallel. The query Q , key K , and value V matrices in each scaled dot-product attention module is obtained by applying a linear transformation (with learnable weights) to the common Q , K , and V input matrices. Each of them can be considered as a different (albeit rotated) *perspective* to derive attention.

For a sequence-to-sequence mapping task, the output of encoder is used to derive key K and value V matrices for the multi-head attention module in the decoder. The decoder is then responsible for mapping between the key-value features derived from the input (the encoder) and the queries from the decoder (which is still executed sequentially) in order to produce the final decoded output.

$$\begin{aligned} \mathbf{e}'_k &= \phi^e(\mathbf{e}_k, \mathbf{v}_{r_k}, \mathbf{v}_{s_k}, \mathbf{u}) & \mathbf{e}'_i &= \rho^{e \rightarrow v}(E'_i) \\ \mathbf{v}'_i &= \phi^v(\bar{\mathbf{e}}_i, \mathbf{v}_i, \mathbf{u}) & \bar{\mathbf{e}}' &= \rho^{e \rightarrow u}(E') \\ \mathbf{u}' &= \phi^u(\bar{\mathbf{e}}', \bar{\mathbf{v}}', \mathbf{u}) & \bar{\mathbf{v}}' &= \rho^{v \rightarrow u}(V') \end{aligned}$$

where \mathbf{e}' , \mathbf{v}' , and \mathbf{u}' denote the updated node, edge, and graph features. In Graph Networks, three types of information are updated in the following order. The first step is ϕ^e to update every edge. The second step updates every node: for i -th node, compute $\rho^{e \rightarrow v}$ to aggregate updated attributes from the edges with $r_k = i$ then compute ϕ^v to update the node attributes. The third step updates the graph attributes through ϕ^u which takes the original state \mathbf{u} , aggregated node and edge attributes by $\rho^{v \rightarrow u}$ and $\rho^{e \rightarrow u}$ respectively.

Graph Neural Networks [237] (GNNs) are the class of neural networks that work on graph-structured data. A direct analog in Computer Vision and physics is the *point cloud* data type, which is an unordered set of points. Operations on point cloud need to be permutation invariant (e.g. \min , \max , $+$, \cdot), and analysis of 3-dimensional physical object represented by point cloud need to be rotation and translation invariant as in the case for an image. PointNet [238, 239], a GNN that performs an object classification

Finally, we note that the Transformer architecture does not just employ an attention mechanism in the decoder. By employing attention in the encoder as well the model has more capacity to "interpret" the input – a concept referred to as *self-attention*.

Models such as these have made breakthroughs in many areas of scientific and industrial research [235].

41.5.3.14 Graph networks and geometric deep learning

Graphs are a powerful data structure for representing structure data. A graph consists of *nodes* as elements and *edges* between them. Graphs are sufficiently flexible to describe many types of structured data including images and sequences. Graph-based neural networks can also be seen as a generalization of many common types of machine learning models such as recurrent networks, convolutional neural networks, *etc.* [219]. The term *geometric deep learning* refers to this recent formulation that focuses largely on the symmetries of the data.

An earlier attempt to organize the variations on different flavors of graph-based neural networks can be found in Ref. [236]. In their formalism a Graph Network may be represented as $G(\mathbf{u}, V, E)$ where \mathbf{u} represents an array of global features, $V = \{\mathbf{v}_i\}_{i=1:N^v}$ represents a set of N^v nodes with \mathbf{v}_i as features for the i -th node (e.g. such as RGB channels if a node represents a pixel in image data), and $E = \{(\mathbf{e}_k, r_k, s_k)\}_{k=1:N^e}$ represents a set of N^e edges with \mathbf{e}_k as features for the k -th edge. An edge may be (bi-)directional where r_k and s_k denotes the destination and origin nodes respectively. The features of a graph may evolve with three *update* functions ϕ and and three *aggregate* functions ρ :

$$\begin{aligned} \text{where } E'_i &= \{(\mathbf{e}'_k, r_k, s_k)\}_{r_k=i, k=1:N^e} \\ \text{where } E' &= \cup_i E'_i = \{(\mathbf{e}'_k, r_k, s_k)\}_{k=1:N^e} \\ \text{where } V' &= \{\mathbf{v}'_i\}_{i=1:N^v} \end{aligned} \quad (41.56)$$

on point cloud of 3-dimensional positions, treats each point as a node, applies MLPs as ϕ^v to update node features, and global max-pooling operation as $\rho^{v \rightarrow u}$. There is no explicit edge definition in PointNet (though the model applies affine transformation to all points using Spatial Transformer Network [240], which could be considered as a separate graph operation, to introduce rotation and translation invariance and to capture topological features). Deep Sets [241] follows the same manner except ϕ^v takes the global entities \mathbf{u} . This is same for PointNet when performing point cloud segmentation: ϕ^v takes a step of simply concatenating \mathbf{u} to node entities to combine a local and global features. Dynamic Graph CNN [242] is a variant that (re)define edges dynamically using attention mechanism: $\rho^{e \rightarrow v}$ aggregates k neighbor nodes where the inter-node distance is defined as a Cartesian distance in the feature space. ϕ^v remains a MLP and, while edges are defined, there is no associated entity. A similar technique is used in Non-Local Neural Network [243] to efficiently propagate local

feature information to points that may be far in the 3D cartesian coordinate. Message Passing Neural Network [244] (MPNN) explicitly defines a feature vector as edge entities. In MPNN, $\rho^{e \rightarrow v}$ performs element-wise sum of features and feed into ϕ^e , explicitly passing features across nodes as the name suggests. While these are representative models that are frequently used in particle physics applications [117, 121, 132, 142, 156, 183, 245, 246], it is only a tiny fraction of GNN models developed over the past decade.

Graph-based models are particularly interesting for science applications because they often offer a natural way to organize the entities in the data and encode how those components should interact each other. This particular type of inductive bias is referred to as *relational inductive bias* in Ref. [237]. The structure of the graph is both an opportunity and a responsibility as one needs to define the graph structure including the edges to define the mode. A naive approach may be defining a fully-connected graph. However, for applications on hundreds of thousands of nodes (e.g. high resolution 3D point cloud), this may require a prohibitive amount of memory and computation. On the other hand, if the graph is too sparse, it may negatively impact the performance. One may need to compare the model performance among differently constructed graphs and balance against computational burden. Ideally the graph would be based on some knowledge of the interactions, but in the absence of such knowledge, popular graph construction methods include fully-connected, k -Nearest Neighbors, a Delaunay graph, and Minimum Spanning Tree.

Classification and regression tasks for graphs can be formulated such that the prediction is made for the entire graph or its individual nodes or edges. Graph-level prediction is like classifying an entire image, while node-level prediction is like semantic segmentation where individual pixels are classified. For clustering of points, GNNs can approximate a transformation function for nodes into the latent space where an optimal clustering of points can be performed. Alternatively, one can formulate clustering as an edge classification task. A comprehensive review on particle physics applications have been made available recently [247].

41.5.4 Deep generative models

Deep generative models are powerful machine learning models that can learn complex, high-dimensional distributions and generate samples from them. Because of their inherently probabilistic formulation, generative models are rapidly becoming an indispensable tool for scientific data analysis in a range of domains. Generative models can be contrasted against discriminative models that are primarily used for supervised learning tasks. Roughly, discriminative models are used for prediction and $f(x)$ provides a point estimate of the target y , and they are more closely connected to function approximation. In contrast, generative models describe the data distribution $p(x)$ (or the joint data distribution $p(x, y)$ in a supervised setting). An enlightening discussion of these two approaches can be found in Ref. [10].

There are a number of different types of deep generative models that have various pros and cons as they do not all have the same capabilities. We will focus on Variational Auto-Encoders (VAEs) [248, 249], Generative Adversarial Networks (GANs) [250, 251], and Normalizing Flows (NFs) [252–256], though there other approaches have been explored in this quickly developing area of research. Consider these three distinct types of functionality:

- **generation:** ability to sample or “generate” a data point $x_i \sim p(x)$.
- **likelihood for generated data:** ability to evaluate the probability density (likelihood) $p(x_i)$ for a data point x_i sampled from the model $x_i \sim p(x)$.
- **likelihood for arbitrary data:** ability to evaluate the probability density $p(x_i)$ for an arbitrary data point $x_i \in \mathcal{X}$.

Each of the models above can be used for generation; however, only normalizing flows provide all three capabilities. For reasons that we will describe below, GANs and VAEs do not provide a tractable likelihood function, and they are sometimes referred to as *implicit models*. This establishes a connection to simulation-based inference where most scientific simulators are also implicit

models with an intractable likelihood. Because normalizing flows have a tractable likelihood, they can be trained via maximum likelihood (Eq. 41.18) as described in Sec. 41.3.2.1. GANs and VAEs, on the other hand, need to employ some other loss function to be trained. In the case of VAEs, training is based on the ELBO used in variational inference (see Sec. 41.3.1.3 and the discussion around the reverse KL divergence below Eq. 41.16). While GANs are also implicit models they data they can generate is typically restricted to a lower-dimensional manifold $\mathcal{M} \subset \mathcal{X}$, meaning that almost all real training dataset doesn’t “live on” the subspace of possibilities that the model can produce. In this case, the likelihood is for almost all data is zero, and so even ELBO-based training will not work. The breakthrough idea introduced in Ref. [250] was to use adversarial training where a classifier would be used to quantify how different the data generated from the model is from the data from the target distribution.

VAEs, GANs, and normalizing flows introduce a mapping $g(z, \theta)$ from a base random variable z to the space of the data \mathcal{X} . The map $g(z, \theta)$ is typically implemented with a neural network. The random variable z is sampled from some known base distribution $p(z)$ that is both easy to sample and has a density that is easy to evaluate. Typically, the base distribution is a multivariate normal.

In the literature on GANs and normalizing flows, this base random variable is often referred to as a latent variable and $p(z)$ is often referred to as a prior distribution, but this may cause confusion as the relationship between z and the observed x is deterministic. Typically, one would reserve the term latent variable for situations where one must marginalize (integrate) over z to obtain the marginal likelihood as in $p(x) = \int p(x, z) dz$. In this integral would involve a delta function imposing the deterministic relationship $x = g(z, \theta)$. A more natural interpretation of the relationship between x and z is through the change of variables formula, which is the essence of normalizing flows.

In the case of VAEs, the one additionally adds some normally-distributed (Gaussian) random noise ϵ to the output so that $x = g(z, \theta) + \epsilon$. In this case, x and z are not deterministically related and z is a legitimate latent variable in the model and $p(z)$ can be interpreted as the prior on that latent variable. In this case, the model can populate the full space of the data. Unfortunately, the marginal likelihood $p(x) = \int p(x, z) dz$ involves an intractable integral, thus maximum likelihood training is infeasible. However, the likelihood term $p(x|z)$ is tractable (*i.e.* the Gaussian noise), so training with the ELBO is possible.

Note that the dimensionality of z need not be the same as that of x . If $z \in \mathbb{R}^q$ and $\mathcal{X} = \mathbb{R}^d$ with $q < d$, then all points $g(z, \theta)$ will lie on a d -dimensional surface in \mathbb{R}^d . In the case of a VAE, the Gaussian noise ϵ means that the generated data x will be distributed in a thin region around the surface defined by $g(z, \theta)$. The presence of a bottleneck (*i.e.* $q < d$) leads to advantages and disadvantages. The disadvantages for GANs is that the likelihood assigned to almost all real world data (*i.e.* data not generated by the model) will be zero, so training is more difficult and many tasks in probabilistic inference won’t be applicable. However, often real world data is also effectively described by a low-dimensional subspace in the full space of the data – random images look like noise, while natural images are in some sense special. For this reason, images produced by GANs for instance often have better visual quality than those produced by other techniques. This points to the ambiguity encountered in quantifying how close two distributions are, and also motivates the use of distance measures such as the Earth Movers distance or Wasserstein distance [257, 258]. Conversely, the lack of a bottleneck (*i.e.* $q = d$) leads to very large models and scalability issues when the data is high dimensional.

Recent work has also focused on combining ideas from VAEs, GANs, and normalizing flows so that the generative model does involve a bottleneck but can still provide tractable likelihoods for density estimation restricted to that manifold [44, 46, 252, 259, 260]. Some of these models can also be used in the context of anomaly detection and out of distribution detection by identifying data that is off the manifold.

The parametrization of the mapping (the architecture of the neural network) should match the structure of the data and be

expressive enough. For problems with explicit symmetries it is beneficial to include them into the architecture of the network explicitly, which restricts the allowed space of the models and matches their inductive bias (implicit regularization inherently built into the choice of architecture of the network) to the data. Different architectures have been proposed [255, 261–263], and to achieve the best performance on a new dataset one needs extensive hyperparameter explorations [264].

41.5.4.1 Variational auto-encoders

The auto-encoder was described in Sec. 41.3.2.2 as model for compression and representation learning. The model is $f = g \circ e : \mathcal{X} \rightarrow \mathcal{X}$, where $e : \mathcal{X} \rightarrow \mathcal{Z}$ is referred to as the *encoder* and $g : \mathcal{Z} \rightarrow \mathcal{X}$ is referred to as the *generator* or *decoder*. The standard auto-encoder is not a probabilistic model, but additional probabilistic structure can be added.

One approach is VAE mentioned above [248, 249]. By equipping the latent space with a prior distribution $p(z)$, the decoder of the auto-encoder $g(z, \theta)$ implies a distribution on a manifold in the output space \mathcal{X} . VAEs additionally add some normally-distributed (Gaussian) random noise ϵ to the output so that $x = g(z, \theta) + \epsilon$. This implies that $p_\theta(x|z)$ is a tractable quantity, and it is interpreted as the likelihood in this context.

In a VAE one also elevates the encoder to have a probabilistic form. Instead of encoding $z = e(x)$ in a deterministic way, one seeks a distribution over z given x . A natural target for the probabilistic encoder would be to probabilistically invert the decoder. This inverse problem is solved by the posterior distribution $p(z|x)$ via Bayes theorem

$$p(z|x) = \frac{p(x|z)p(z)}{p(x)}. \quad (41.57)$$

While the likelihood and the prior may both be tractable, the normalizing constant $p(x) = \int p(x, z) dz$ involves an intractable integral (the same intractable integral that makes maximum likelihood training of the VAE infeasible).

One approach to Bayesian inference in these settings is variational inference (VI). In VI one approximates the posterior with some parametric family $q_\phi(z|x)$ in a parametric form, and then uses optimization to optimize the ELBO with respect to its parameters ϕ .

$$\begin{aligned} \text{ELBO} &= \mathbb{E}_{q(z)} \log p(x|z) - D_{KL}[q(z)||p(z)] \\ &\leq \log \mathbb{E}_{q(z)} \left[\frac{p(x, z)}{q(z)} \right] = \log p(x), \end{aligned} \quad (41.58)$$

where we used Jensen's inequality for concave functions (\log) and the reverse Kullback-Leibler (KL) divergence term is

$$D_{KL}[q(z)||p(z)] = \mathbb{E}_{q(z)} [\log q(z) - \log p(z)] \geq 0. \quad (41.59)$$

In a VAE, the variational model for the posterior $q_\phi(z|x)$ is often assumed to be an uncorrelated Gaussian (this is often called mean field approximation) defined by the mean μ and variance Σ . Instead of optimizing the mean and variance independently for each x , VAEs use neural networks to predict the mean $\mu_\phi(x)$ and the variance $\Sigma_\phi(x)$. This is called *amortized inference*, since after an up-front training cost the approximate posterior $q_\phi(z|x)$ can be evaluated efficiently with a single forward pass of the neural network. Note the standard auto-encoder is recovered if one only used the mean $\mu_\phi(x)$ for the encoder and did not add noise ϵ to the decoder.

Both the probabilistic encoder $q_\phi(z|x)$ and the probabilistic decoder $p_\theta(x|z)$ are trained jointly by optimizing the ELBO. Unlike the standard auto-encoder, which only minimizes the reconstruction error, ELBO optimization of Eq. 41.58 has a trade-off between minimizing the reconstruction error in the first term (averaged over the approximate posterior $q(z)$), which encourages high quality reconstructions, and minimizing the KL divergence term, which forces the posterior $q(z)$ to be as close to the chosen prior $p(z)$, and thus controls the sample quality by matching the aggregate posterior with a chosen prior distribution [265]. This term regularizes the VAE latent space, such that every sample drawn

from the prior $p(z)$ correspond to a valid sample. Successful VAE training requires to find a delicate balance between the two contributing terms to the ELBO. Whether the VAE training process succeeds in striking this balance depends on a number of factors, including the network architectures, the chosen prior and the class of allowed posterior distributions. Once trained, the VAE can be used as a generative model by sampling from the prior $z_i \sim p(z)$ and then decoding according to $p_\theta(x|z) = g(z, \theta) + \epsilon$.

VAEs allow for expressive architectures, enjoy the benefits of regularization through data compression and have a firm theoretical foundation. Compared to GANs [250], VAEs are of particular interest to the scientific community as they provide a lower bound to the marginal likelihood (albeit potentially with a large gap) and a posterior distribution for the latent variables.

It is also interesting to consider a special case of the auto-encoder and VAE where the encoder and decoder are restricted to be linear transformations, which is effectively PCA. In PCA the (linear) decoder can be written $g(z) = Oz$, where O is a matrix. As in the case of the auto-encoder, PCA is not a probabilistic model, but probabilistic structure can be added. Probabilistic PCA [266] assumes that the latent variables follow a Gaussian distribution with mean zero and covariance Λ , where Λ is a diagonal matrix with the rank-ordered eigenvalues λ_i along its diagonal. The true distribution of the PCA components may be non-Gaussian, but a Gaussian is the maximum entropy approximation given their first two moments. Note that in Probabilistic PCA these moments are measured on training dataset (when finding the principal components).

One can generalize Probabilistic PCA to use non-linear encoder and decoder as in an auto-encoder. A Gaussian prior is a poor ansatz for the latent space distribution of data proceed by an auto-encoder. Instead one can learn the density of the training samples in latent space using a normalizing flow. This model was introduced in \mathcal{M} -flows [46] and in Probabilistic Auto-Encoder (PAE) [44], which achieves similar performance to a VAE in terms of sample quality without explicit ELBO optimization. In all these cases the dimensionality of the latent space is a hyperparameter to be chosen or optimized by the user. Unlike a standard VAE, these models do not add noise to the decoded output, thus the data is strictly restricted to the manifold defined by the decoder $g(z, \theta)$. However, unlike a GAN there is a well defined way to take an arbitrary data point x , project it onto the manifold, and calculate the density of the data point projected onto the manifold. Thus these models can also be used in the context of anomaly detection and out of distribution detection by identifying data that is off the manifold.

41.5.4.2 Generative adversarial networks

GANs [250] also typically choose a low dimensional latent space z with a known prior distribution $p(z)$, typically a normal (Gaussian) distribution with zero mean and unit variance. GANs do not add noise to the output $g(z, \theta)$, so the likelihood $p(x|z)$ (and marginal likelihood $p(x)$) for almost all of the data space is 0, which precludes training by maximum likelihood and the ELBO. Instead of training on ELBO, GANs train on a dissimilarity measure defined implicitly by a discriminator $D(x)$ (also referred to as the critic). Calculating the dissimilarity often involves it's own learning problem (*i.e.* adversarial training of the discriminator).

The training is usually framed as a mini-max game

$$\begin{aligned} \min_g \max_D \mathcal{L}_{\text{GAN}} &= \\ \min_g \max_D \{ \mathbb{E}_{x \sim p(x)} \log D(x) + \mathbb{E}_{z \sim p(z)} \log [1 - D[g(z)]] \}. \end{aligned} \quad (41.60)$$

The goal of the discriminator is to distinguish between true and generated data, hence we want to maximize this loss with respect to D , assigning 1 to true data and 0 to generated data. The goal of generator is to fool the discriminator such that it cannot distinguish between true and generated data, hence we want to minimize this loss with respect to g at fixed D . This can be viewed as a game theoretical setup in a zero sum game between generator and discriminator.

Instead of this game theory interpretation we can view the internal objective $\max_D \mathcal{L}_{\text{GAN}}$ as an implicit loss function that mea-

sures the dissimilarity between the target and generated distributions. The loss of Eq. 41.60 corresponds to the Jensen-Shannon (JS) divergence, which is a symmetrized form of KL divergence. However, JS divergence is hard to directly work with, and the adversarial training could bring many problems such as vanishing gradient, mode collapse (tendency of generator to cluster the samples around the training samples, with holes between them) and non-convergence [257, 258]. One of the core issues is that the distribution generated by the GAN is restricted to a manifold and the KL divergence isn't well defined in this case (because p is not absolutely continuous with respect to q). To address these issues Wasserstein GANs train on

$$\min_g \max_D \mathcal{L}_{WGAN} = \min_g \max_D \{ \mathbb{E}_{x \sim p(x)} D(x) - \mathbb{E}_{z \sim p(z)} D(g(z)) \}. \quad (41.61)$$

Here again the goal of discriminator is to make the loss as large as possible between the true data and the generated data, while the goal of generator is to make it as small as possible, so that the discriminator cannot distinguish between the two. There is no requirement for $D(x)$ to be between 0 and 1, which helps with the above mentioned problems of JS divergence. Instead, this is replaced with a requirement that $D(x)$ is 1-Lipshitz, i.e. the absolute value of the norm of the gradient of the discriminator output with respect to the input has to be less or equal to 1.

Eq. 41.61 can be interpreted as the dual form of the 1-Wasserstein distance between the true and generated distribution [267]. Wasserstein distances are a measure of dissimilarity between two distributions used in the context of Optimal Transport, mathematical theory of how to optimally transport one distribution to another. Since the transport distance increases with the separation between the two distributions when they are non-overlapping, there is no gradient collapse that plagues other measures. In its primal form p-Wasserstein distance, $p \in [1, \infty)$, between two probability distributions p_1 and p_2 , is defined as $W_p(p_1, p_2) = \inf_{\gamma \in \Pi(p_1, p_2)} \left(\mathbb{E}_{(x, y) \sim \gamma} [|x - y|^p] \right)^{\frac{1}{p}}$, where $\Pi(p_1, p_2)$ is the set of all possible joint distributions $\gamma(x, y)$ with marginalized distributions p_1 and p_2 . In 1D the Wasserstein distance has a closed form solution via Cumulative Distribution Functions (CDFs), but this evaluation is intractable in high dimensions.

In the dual form of 1-Wasserstein distance, one instead maximizes Eq. 41.61 over all possible functions $D(x)$ that are 1-Lipshitz. One way to implement this is through weight clipping of the parameters of discriminator network, but a simpler solution is to add a gradient norm penalty term explicitly to the loss function [268].

Because of the discriminative nature of the dissimilarity measure defined in data space, GANs often generate more realistic samples than VAE or normalizing flows in high dimensions such as natural images. However, GANs do not provide an encoder from data to latent space, do not provide a tractable likelihood $p(x)$.

41.5.4.3 Normalizing flows, autoregressive models, and score based models

Normalizing Flows (NF) provide a powerful framework for density estimation and sampling [252–256, 269]. These models map the data x to latent variables z through a sequence of invertible transformations $f = f_1 \circ f_2 \circ \dots \circ f_n$, such that $z = f(x)$ or $x = g(z) = f^{-1}(x)$. As in the VAE and GAN, z is modelled as a random number with a simple base distribution $p_Z(z)$, which is typically chosen to be a standard normal (Gaussian) distribution. The probability density of the model be evaluated using the change of variables formula:

$$p_X(x) = p_Z(f(x)) \left| \det \left(\frac{\partial f(x)}{\partial x} \right) \right| = p_Z(f(x)) \prod_{l=1}^n \left| \det \left(\frac{\partial f_l(x)}{\partial x} \right) \right|, \quad (41.62)$$

where we have added subscripts to $p_X(x)$ and $p_Z(z)$ for clarity. The Jacobian determinant $\det(\frac{\partial f_l(x)}{\partial x})$ must be efficient to compute for density estimation to be practical, and the transformation f_l should be easy to invert for sampling. In contrast to VAE and

GANs, standard normalizing flows preserve the dimensionality of the data space as they are invertible (though there are normalizing flows that are defined on lower dimensional manifolds embedded in the data space [44, 46, 252, 259, 260]). As such, they do not have the problems of GANs and VAEs they can be trained via maximum likelihood (Eq. 41.18) as described in Sec. 41.3.2.1.

There are several popular architectures of NFs. A method used by NICE, RealNVP and Glow [253–255] is to split the space into two disjoint sets z_1 and z_2 , and then use an identity forward map $z \rightarrow x$ for x_1 , $x_1 = z_1$, and an affine transformation for x_2 of the form

$$x_2 = \exp(s(z_1)) \odot z_2 + m(z_1), \quad (41.63)$$

where \odot is elementwise product and $m(z_1)$, $s(z_1)$ are neural networks. The Jacobian of this map is lower triangular, and its determinant is simply the product of elements along the diagonal, which is tractable, as is the inverse of the transformation. At the next layer one then performs a different split of dimensions into z_1 and z_2 . The affine transformation can be further generalized to a nonlinear form using rational splines [270].

One can interpret the sequence of invertible transformations $f_1 \circ f_2 \circ \dots \circ f_n$ as n discrete time steps in a continuous flow. In particular, one can think of a continuous-time flow described by an ordinary differential equation (ODE) and then interpret the discrete time steps as the result of a numerical integration of that ODE. This is the approach taken by the Fjord algorithm [271] and other variants.

A different approach creating a deep generative model with a tractable likelihood is to model $p(x)$ autoregressively as

$$p(x) = \prod_{i=1}^n p(x_i | x_1, x_2, \dots, x_{i-1}). \quad (41.64)$$

This form describes each new dimension conditionally on all previous dimensions. It can model a general likelihood $p(x)$ as a sequence of conditional 1d distributions, whose conditional dependence on the parameters x_1, x_2, \dots, x_{i-1} can be modeled with neural networks. If x is a time series this form imposes a causal structure where x_i depends on all previous times x_j , $j < i$. WaveNet [272] and PixelCNN [273]) are two well known examples. Sampling from an autoregressive model is sequential, and can be slow in high dimensions. Inverse autoregressive flow reverses this process and makes sampling fast, but the likelihood evaluation is slow. Some normalizing flows have autoregressive coupling layers, such as Masked Autoregressive Flow (MAF) [269].

All of the methods above use maximum likelihood training of likelihood $p(x)$ against network parameters, so the training is to minimize KL divergence between the data distribution and a Gaussian in latent space. This can be overly sensitive to small variance directions that dominate the likelihood, without being sensitive to the global structure of the data. An alternative is to use Optimal Transport Wasserstein distance between the density of the generated samples and the data, which can be evaluated either in data space or in latent space. As Wasserstein distance is difficult to evaluate in high dimensions, one can instead use slices, 1d projections of the data along different directions in high dimensional space, to build the flow [45]. Along each slice direction one obtains the 1d marginal distribution that can be mapped to a Normal distribution using a cumulative distribution function method. In 1d the Jacobian and the inverse transformation are tractable. The projection directions are chosen to maximize the sliced 1d Wasserstein distance between the data and the distribution generated by the samples, or between the inverse flow from the data to the latent space and the target distribution (typically chosen as the Normal distribution). Because this training is less sensitive to small variance directions than maximum likelihood training it achieves better results on anomaly detection tasks [45].

One can reduce the architectural restrictions imposed by normalizing flows or autoregressive models by modeling the “score” $\nabla_x \log p(x)$ instead of $p(x)$. Note this usage of the term “score” is non-standard and goes back to Ref. [274]; the standard use of the term score is theta of Eq. 41.26. Score-based training avoids the normalization requirement. Score based models learn gradients of log probability density functions on a large number of

noise-perturbed data distributions, and then generate samples by Langevin-type sampling. The resulting generative models, called score-based generative models [275] or diffusion probabilistic models [276], have several advantages over existing model families. They achieve GAN-level sample quality without adversarial training, and enable exact log-likelihood computation through their connection to continuous-time flows, which can be represented as a probability flow ordinary differential equation [276]. The main advantage is that the distribution $p(x)$ can be specified solely by its gradient, which can subsequently be sampled from using Langevin dynamics. This is similar to the gradient based Monte Carlo Markov Chain methods (such as Langevin or Hamiltonian Monte Carlo) that sample from Bayesian posteriors without directly estimating the normalizing constant. This in turn enables more flexible model architectures than what can be used in normalizing flows or autoregressive models.

We end by noting that normalizing flows, autoregressive models, and other deep generative models that provide a tractable likelihood are incredibly powerful tools for simulation-based inference. They can provide surrogate models trained from large simulated datasets when the simulators have intractable likelihood functions, which is usually the case. As described in Sec. 41.3.5, one would like to work with models that can provide conditional density estimation in order to model either the likelihood $p(x|\theta)$ or the posterior $p(\theta|x)$ [56, 57]. These techniques are being actively explored and applied to a number of scientific problems.

41.6 Learning algorithms

41.6.1 Gradient-based optimization

Given a parameterized model $f(x, \theta)$ and a loss function $\mathcal{L}(x, \theta)$, where x and θ denotes data and model parameters, one way to optimize θ is to first apply an appropriate initialization, $\theta_{t=0}$ (e.g. Sec. 41.6.7 for neural networks), and perform an iterative update:

$$\theta_t = \theta_{t-1} - \lambda \nabla_{\theta} \mathcal{L}(x, \theta), \quad (41.65)$$

where λ is a small, real valued hyperparameter called *learning rate*. To see how this works, define $\delta\theta \equiv \theta_t - \theta_{t-1}$ and consider $\delta(\nabla_{\theta} \mathcal{L}(x, \theta))$:

$$\delta(\nabla_{\theta} \mathcal{L}(x, \theta)) \approx \delta\theta \cdot \nabla_{\theta} \mathcal{L}(x, \theta) = -\lambda |\nabla_{\theta} \mathcal{L}(x, \theta)|^2 \quad (41.66)$$

which would monotonically decrease the loss function, and locally move the parameter values in the desired direction of loss function minimization. This algorithm is called *Gradient Descent*. We note that λ needs to be sufficiently small for the approximation to hold. When λ is too large, this can be a cause of a gradient explosion discussed in Sec. 41.6.7.

41.6.2 Stochastic gradient descent

Stochastic Gradient Descent (SGD) follows GD but replaces the exact gradient term $\nabla_{\theta} \mathcal{L}(x, \theta)$ with a stochastic approximation, where we subsample the data in the loss function using N samples, where $N < n$,

$$\nabla_{\theta} \mathbb{E}_{\hat{p}(x)} \mathcal{L} \approx \frac{1}{N} \sum_i^N \nabla_{\theta} \mathcal{L}_i, \quad (41.67)$$

where \mathcal{L}_i is the loss function for data sample i . It should be noted that N needs to be randomly and independently sampled for the approximation to hold. Implementation of SGD follows three steps: take new samples of size N , approximate the gradient, then update the parameters θ .

In the case of optimizing the loss using a static database (*i.e.* one cannot take new N samples for every update), *mini-batch learning* is often employed. This replaces the first step with a randomly sampled *batch* of data, which is a subset of all the samples in the database. In this case, however, since a batch of data used for each parameter update is not entirely independent, a model may overfit. In practice, a part of the whole dataset is reserved as a *validation* sample, and the model performance is carefully monitored during the optimization process to avoid overfitting via an early stopping criterion (see Sec. 41.6.6 and Fig. 41.11).

SGD with slowly decreasing learning rate can be shown to converge to a local minimum almost surely under mild conditions,

and to a global minimum for unimodal loss functions. SGD may also prevent getting stuck in shallow local minima of the loss function, thereby reaching a better local minimum for multi-modal loss functions. The noise in SGD with a constant learning rate can be viewed as a form of Langevin dynamics, which under proper conditions on the learning rate and mini-batch size converges to the stationary posterior distribution of the weights [277]. Thus SGD at a constant learning rate can be viewed as a sampler bouncing around and exploring the posterior surface for better solutions, descending onto the best found solution as the learning rate is decreased, a process related to temperature annealing in global optimization.

Another advantage of SGD is simply the computational cost: rather than evaluating the loss over all the data samples at each update, we use a small subset of data instead at each update. Furthermore, mini-batching can take advantage of vectorization libraries and GPU architectures. Large batch training requires specialized methods of training, such as Layer-wise Adaptive Rate Scaling (LARS).

41.6.3 Optimization algorithms

GD and SGD are the basic building blocks for more advanced optimization algorithms. One can improve the convergence rate of gradient based optimization by considering the learning rate λ to depend on individual θ_i . Second order algorithms such as Newton's method take into account second order derivatives (Hessian) to find the minimum, and give an exact solution in a single update when the loss is quadratic around the peak. However, this requires a matrix inversion of the Hessian, which is exceedingly expensive in ML applications, where the number of network parameters is very large. As a consequence, second order optimization is rarely used in ML.

There are several improvements to the basic SGD even in the absence of Hessian information. Momentum based optimization takes a physics perspective of a viscous fluid in an external potential, where one updates current velocity with the potential gradient (force), followed by an update in position based on velocity. This approach therefore uses previous gradients in addition to the current one to compute a running average of the gradient, with a forgetting factor that controls how far back the averaging goes. This helps move faster towards the minimum in ravines, where gradient descent is usually inefficient due to the high condition number of the Hessian.

One way to make the learning rate dependent on θ_i is to consider the gradient norm squared $(\nabla_{\theta_i} \mathcal{L})^2$. RMSprop learns its running average and then reduces the learning rate in directions with a large average gradient norm squared, thereby reducing the oscillations along that direction. ADAM (Adaptive Moment Estimation) combines the momentum and gradient norm ideas, computing running averages of both the gradient and the gradient norm squared, each with its own forgetting factor [278].

41.6.4 Automatic differentiation and back propagation

In practice, $f(x, \theta)$ might take a complex form and may include a large set of parameters. The term $\nabla_{\theta} \mathcal{L} = \nabla_{\theta} \mathcal{L}(f(x, \theta))$ requires computing partial derivatives with respect to individual parameter θ_i . If f is a composite model (*i.e.* $f = f_n(f_{n-1}(\dots, \theta_{n-1}), \theta_n)$), and if all of $f_{i:1,n}$ are differentiable, a chain rule can be applied:

$$\nabla_{\theta_i} \mathcal{L} = \frac{\partial \mathcal{L}(f(x, \theta))}{\partial \theta_i} = \frac{\partial \mathcal{L}}{\partial x_n} \cdot \frac{\partial x_n}{\partial x_{n-1}} \dots \frac{\partial x_i}{\partial \theta_i} \quad (41.68)$$

where x_n denotes the output of n -th composite function f_n . In order to compute $\nabla_{\theta_i} \mathcal{L}$ for f_i , it needs computation of a gradient at all preceding (or subsequent if seen in the forward context) functions. As the gradients accumulate across differentiable functions in the reverse order of the model composition, this technique is called *back propagation* [225]. An example of f that satisfies conditions to apply back propagation is a neural network, which consists of repeating blocks of a (differentiable) activation function and an affine transformation.

When the model $f(x, \theta)$ is implemented as a computer program in practice, *automatic differentiation* (AD), also called *algorithmic differentiation*, is used to compute the derivatives. AD ex-

exploits the fact that any computer program consists of a sequence of elementary arithmetic operations (i.e. addition, subtraction, multiplication, division) and functions (e.g. log, exp, sin, cos) and apply chain rules to compute the target derivative. AD has advantages over traditional approaches including symbolic and numerical differentiation. The symbolic differentiation faces a serious difficulty of converting a program into a single expression, and the numerical differentiation suffers from round-off errors. Finally, both methods scale poorly in speed of computation for calculating partial derivatives with a large number of inputs. AD delivers much faster speed and does not suffer from increasing errors for calculating higher derivatives.

There are two modes of AD: the *forward* and *backward* mode. Consider a composite function $f(x, \theta) = f_n(f_{n-1}(\dots f_1(x, \theta_1) \dots), \theta_{n-1}), \theta_n$. The forward mode applies the chain rule in the same order of the forward evaluation of f by computing $\partial f_1/\partial x$ first, then $\partial f_2/\partial f_1$, and continue to $\partial f_n/\partial f_{n-1}$. The backward mode traverses the reverse direction: starting from the last (outer-most) function $\partial f_n/\partial f_{n-1}$, next $\partial f_{n-1}/\partial f_{n-2}$, and continue to $\partial f_1/\partial x$. Therefore, the back propagation of gradients can be implemented using the backward AD, in which the target variable to be differentiated is fixed and the derivative is computed with respect to each sub-expression recursively as shown in Eq. 41.68. The forward mode is simpler to implement as the order of gradient calculation follows the order of composite functions to be executed. The reverse mode typically requires less amount of computation than the forward mode, but more memory is required to store intermediate function output values to calculate derivatives efficiently. Another consideration is the mapping of dimensionality $f: \mathbb{R}^k \rightarrow \mathbb{R}^\ell$ as it concerns the number of variables to sweep from each end. The forward mode is efficient when $k \ll \ell$ while the reverse mode takes an advantage if $\ell \ll k$. For instance, in the case of an image classification where $(k, \ell) = (\text{pixel count}, 1)$, the reverse AD is more efficient.

41.6.5 The vanishing and exploding gradient problems

Gradient based optimization crucially depends on the size of gradient with respect to each model parameter. If the magnitude of gradient is too large with respect to the distance to an optimal parameter value, it may repeatedly overshoot the target and cause an oscillation preventing convergence. If the gradient is too small, it may take an impractically long time to converge. As shown in Eq. 41.68, the gradient of i -th function f_i is a product of gradients from the subsequent functions. If those gradients are too large or too small, the magnitude can either increase or decrease exponentially in the number of layers. These are called *exploding* and *vanishing* gradient problem respectively.

Modern deep neural networks consist with many composite functions (i.e. layers) and are particularly prone to this effect. Let us consider a simple RNN. From Eq. 41.50, we can write the back-propagating gradient:

$$\frac{\partial h_t}{\partial h_{t-1}} = \text{diagonal}(f'(Wx_t + Vh_{t-1} + b1))W \quad (41.69)$$

where f' denotes the derivative of an activation function. The gradient of the contribution to the loss \mathcal{L}_i from the i -th element in the sequence with respect to the j -th hidden state h_j is therefore:

$$\frac{\partial \mathcal{L}_i}{\partial h_j} = \frac{\partial \mathcal{L}_i}{\partial h_i} V^{i-j} \prod_{j < t \leq i} \text{diagonal}(f'(Wx_t + Vh_{t-1} + b1)) \quad (41.70)$$

where we can see that V contributes multiplicatively with $i - j$ powers when $i - j > 1$. This example is explored in depth for recurrent models [226, 227] but is common for all types of deep neural networks.

In practice, one may explicitly inspect the magnitude of gradients propagating across layers to ensure an effective optimization. One way to mitigate an exploding gradient is to set the maximum gradient value δ_{\max} as a model hyperparameter and *clip* any larger gradients δ where it appears in the back propagation:

$$\delta = \frac{\delta_{\max}}{\|\delta\|} \delta \text{ if } \|\delta\| > \delta_{\max}. \quad (41.71)$$

This is called *gradient clipping* [227].

Alternatively, there are many architecture designs that are motivated by the vanishing and exploding gradient problem or which aim to help propagate gradients across many layers. These considerations drove the design of gated models like the LSTM and GRU for sequential data and also motivated the ReLU non-linearity. Other example architectural designs or components motivated by these considerations include identity mapping and skip connections used in ResNet, U-Net, and DenseNet, which allow gradients to flow across many layers.

Other factors contributing to vanishing and exploding gradient include initialization of model parameters and normalization of input data. These factors contribute in keeping the magnitude of activation, which also concerns the magnitude of gradient, within a reasonable range. A recommended practice for a gradient-based optimization of a neural network is to maintain the input values centered around zero and a similar level of covariance across the inputs (and the outputs that are the inputs to the next layer) [279]. These factors are discussed in the following.

41.6.6 Early stopping

Early stopping is a form of regularization used to avoid overfitting when an iterative method, such as gradient descent, is used as a learning algorithm. Imagine a plot of the training loss and test loss as a function of iterations (i.e. parameter updates). As learning proceeds, the training loss will generally decrease. However, the test loss will often decrease initially and then start to increase, which is the classic sign of overfitting as shown in Fig. 41.11. The basic idea of early stopping is simply to stop training before overfitting takes place. In some approaches to early stopping theoretical analysis of the learning problem provides a prescription for when to stop the training [280]; however, the most straight forward approaches use a held-out validation dataset to monitor the generalization performance [281].

41.6.7 Initialization of model parameters

An improper initialization can slow down the optimization process or even result in a loss of convergence. While $b^{(l)}$ is typically initialized to zero, $W^{(l)}$ values need to be stochastic to avoid identical updates during optimization. One way is to sample $W^{(l)}$ from a zero-centered Gaussian distribution with a small variance (e.g. 0.01) [282]. However, this method does not guarantee the same variance in the input to each layer, which depends on the size of the input layer, and makes it difficult to train a deep neural network [220]. The *Xavier* initialization takes this into account and sets the variance of a Gaussian distribution to be $\sigma^2 = 1/d^{(l-1)}$ assuming a symmetric activation function around zero, such as a logistic function or hyperbolic tangent [283]. The *He* initialization uses the variance $\sigma^2 = 0.5/d^{(l-1)}$, and is a simple extension of Xavier initialization for leaky, parametric, and standard ReLU activation [208].

41.6.8 Input normalization

Input data to a neural network is often pre-processed for the same goals discussed previously: values are shift to have the mean of zero and scaled to keep a similar covariance across features. Furthermore, a data may be transformed using techniques including PCA and whitening (sphering) to keep input features independent and uncorrelated from each other [279].

41.6.9 Batch normalization

Even with careful normalization of the input data and initialization of model parameters, the mean and covariance of the data representations in hidden layers will evolve during training and may pose challenges for learning for downstream layers. This is called an *internal covariate shift* [284] and may cause negative effects to an optimization process. Accordingly, techniques to explicitly normalize features in between hidden layers are often employed for a deep neural network. One of them is *Batch Normalization*, which shifts and scales the input to a hidden layer:

$$\tilde{u}^{(l)} = \gamma \frac{u^{(l)} - \mu_B}{\sqrt{\sigma_B^2 + \epsilon}} + \beta \quad (41.72)$$

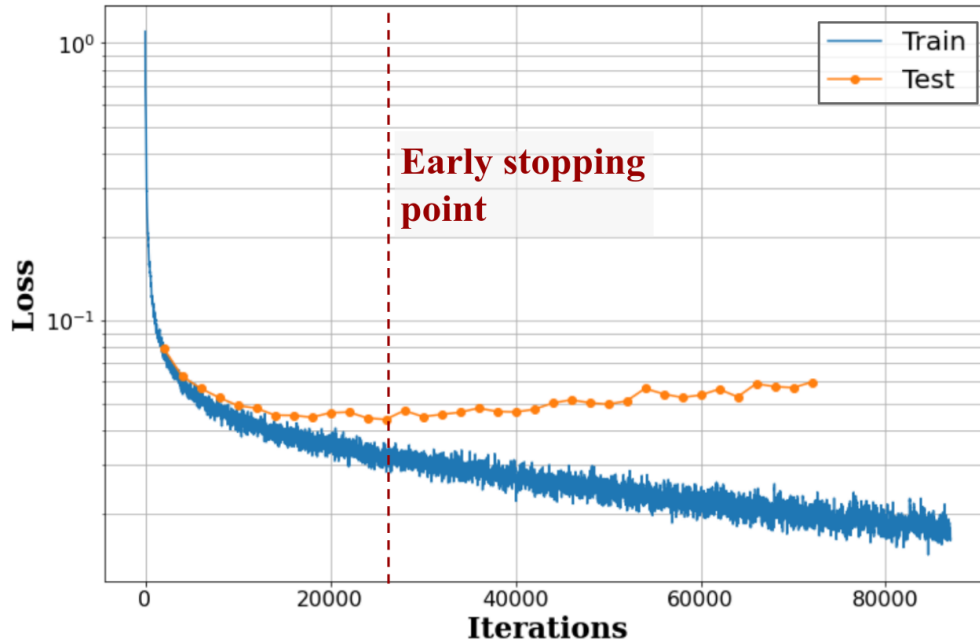


Figure 41.11: An example instance of overfitting. The training loss (vertical axis) shown in blue decreasing over iterations (horizontal axis) while the loss values evaluated on test samples shown in orange start to increase at around 26,000 iterations as indicated by the vertical line.

where $u^{(l)}$ and $\tilde{u}^{(l)}$ refer to the raw and normalized input to the l -th layer, μ_B and σ_B represent the mean and mean-squared-error of $u^{(l)}$ calculated using a *batch* of input data used to update the network parameters. γ and β are part of model parameters that are updated during the optimization. After optimization is complete, these parameters are fixed for model evaluation during production. ϵ is a small, fixed constant value to ensure numerical stability. While it is popular (especially in Computer Vision), a downside of BN is its dependency on the batch size. In situations where the batch size is limited to be a small number (e.g. memory limitation for a large data or a model), the performance using BN could degrade since β and γ values may not be generalized for the dataset during training.

There are several variants to batch normalization with considerations on how to group a subset of values in u^l . For instance, an image naturally has three groupings: a set of pixels across spatial axis, features within one pixel (i.e. image *channels*), alongside with a grouping across multiple images (i.e. *batch*). Different groupings have been studied and found and some are found effective to particular type of applications: Layer Normalization groups values along the channel and spatial dimensions [285], Instance Normalization groups along the spatial dimension but not along the batch nor channel [286], and Group Normalization is similar to Layer Normalization but forms multiple sub-groups of channels [287]. These variants does not apply normalization across samples within a batch, and thus agnostic to the batch size.

41.6.10 Transfer learning: pre-training and fine-tuning

Transfer learning is a technique to improve performance and accelerate optimization process by reusing a pre-trained machine learning model for a new task. Two tasks and data sets for each task may be different: the idea is that fundamental features may be reusable across different data and tasks. Transfer learning typically takes two steps: the first is to alter the model or data if necessary, then train (*fine-tuning*) the model. The first step is required, for example, when solving a different task that requires a different architecture (e.g. regression v.s. classification), or when input data format requires a change (e.g. original model trained on three channel image, such as RGB images, while new data has a single channel). Transfer learning has been widely practiced in the field of Computer Vision where large, labeled data sets

are available [288–291]: a CNN trained for classifying images of an animal can be largely reused for object detection, or even for analyzing image data in science (e.g. particle trajectories recorded by an imaging detector). It is a critical aspect for the development of generic AI as well as interdisciplinary sharing of models across research fields.

For sequential models, transfer learning had been challenging before the appearance of Transformer. While Transformer was initially introduced for machine translation, Generative Pre-trained Transformer (GPT-1) showed that the model can be generalized to multiple NLP tasks by achieving the state-of-the-art in several seemingly different tasks including a sentence classification, semantic similarity, question answering and commonsense reasoning [292].

41.6.11 Zero, one, and a few shot learning

Fine-tuning (and thus transfer learning) may not be necessary if model is well generalized: humans can picture an imaginary animal in mind just from descriptions, or perform a task that he or she has never done before. One-shot learning is an extreme case of transfer learning where only one example is presented at the fine-tuning stage [293]. A similar variant is called a few-shot learning (fine-tuning using a few examples). This is possible only if the model has already learned the solution during the pre-training and the example is used to map the solution to the task. Zero-shot [294–296] learning is even more extreme where the model is given a new task without any example. This is only possible if the task is already learned during the pre-training in an implicit or unsupervised manner since zero-shot training implies that the model was never trained for the task.

41.7 Incorporating uncertainty

A fundamental aspect of data analysis is the quantification of uncertainty. This broad topic includes the traditional distinction between statistical and systematic uncertainty, procedures for propagation of errors, and the incorporation of uncertainty in to the statistical models (e.g. with nuisance parameters) that are used in Bayesian or frequentist statistical procedures (see Sec. 40). Accounting for systematic uncertainty can be seen as a requirement, but ideally systematic uncertainties are also taken into account in the design of the analysis so as to mitigate their effect. The introduction of machine learning into the analysis pipeline

requires revisiting the techniques used for uncertainty quantification and exposes many fundamental issues that have nothing to do with the use of machine learning per se. See Ref. [297] for a recent review on this topic.

In machine learning research and industrial settings, the mismatch between the data distribution $p_{\text{train}}(x, y)$ used for training and the data distribution $p_{\text{prod}}(x, y)$ that the model will be applied to in production is referred to as *covariate shift* or *domain shift*. For example, one might train a classifier to identify cats and dogs with images taken in doors with poor lighting conditions and a scratched lens. Not surprisingly, the mis-classification rate of the classifier will be different between the two settings.

Physicists are keenly aware that the simulations that we use to describe the data are not perfect, and this mismodelling corresponds to a large fraction of the of systematic uncertainties accounted for in published works. Since simulated data is often used to train machine learning models (*i.e.* $p_{\text{train}}(x, y)$), it is important to understand and account for how this mismodelling will influence results when applied to real data (*i.e.* $p_{\text{prod}}(x, y)$).

One of the primary approaches to incorporating this type uncertainty is to introduce nuisance parameters ν corresponding to the uncertain inputs to the simulation and to parameterize various types of perturbations (*e.g.* corrections to efficiencies, energy scales, *etc.*) in hopes that the resulting family of distributions $p(x|y, \nu)$ is flexible enough to encompass the true data distribution for class y . In this approach one does not have just two “domains” for the data (*i.e.* p_{train} and p_{prod}), but a continuous family of domains parameterized by the nuisance parameters ν .

With this framing in mind, there are several approaches to incorporating uncertainty into an analysis that includes ML-based components:

- **propagation of errors:** one works with a model $f(x)$ and simply characterizes how uncertainty in the data distribution propagate through the function to the down-stream task irrespective of how it was trained.
- **domain adaptation:** one incorporates knowledge of the distribution for domains (or the parameterized family of distributions $p(x|y, \nu)$) into the training procedure so that the performance of $f(x)$ for the down-stream task is robust or insensitive to the uncertainty in ν .
- **parameterized models:** instead of learning a single function of the data $f(x)$, one learns a family of functions $f(x; \nu)$ that is explicitly parameterized in terms of nuisance parameters and then accounts for the dependence on the nuisance parameters in the down-stream task.
- **data augmentation:** one trains a model $f(x)$ in the usual way using training dataset from multiple domains by sampling from some distribution over ν .

In this setting it is best to consider the trained model $f(x)$ or $f(x; \nu)$ to be a fixed function and decouple the variability associated to training or the choice of architecture. The fact that one could have chosen a different architecture or learning algorithm should be treated in the same way as other choices that are made in the data analysis pipeline. While it is reasonable to want downstream inference and decisions to be robust to these choices, they are of a different nature than the uncertainty in the modelling of the data distribution. We return to this point in Sections 41.7.5 and 41.7.6.

41.7.1 Propagation of errors

In this Section we consider the common scenario in which one has used some machine learning technique to train a model $f(x)$ for classification or regression and wants to assess the sensitivity of the output of $f(x)$ to uncertainty in the input x . We regard the function $f(x)$ as fixed and we are not concerned with how the model was trained.

Propagating uncertainty through a ML-based model $f(x)$ is not fundamentally different than for any other function, and one can use the standard propagation of errors formula of Sec. 39.2.1. As always, it is important to recognize the limitations of the propagation of errors formula, which is accurate when the uncertainty

on x is Gaussian and the function $f(x)$ is approximately linear within the region set by the uncertainty on x .

Similarly, classifiers are often used for particle identification or event selection. In that case, one is primarily interested in the efficiency ϵ to satisfy a cut on the classifier output. The efficiency depends on the distribution $p(x|y)$ through the equation $\epsilon_y = P(f(x) > f_{\text{cut}}|y) = \int H(f(x) - f_{\text{cut}})p(x|y)dx$, where H is the Heaviside step function and y is an index or label for the category of data that is being considered (*e.g.* signal or background, electron or jet, *etc.*). Thus, the question in this context is what is the uncertainty on the efficiency ϵ_y due to uncertainty in the distribution $p(x|y)$. In practice, the quantification of the uncertainty in the efficiency ϵ_y is usually based on either a calibration measurement on real data or estimated with simulated data. These procedures typically treat the classifier as a black-box, and thus nothing precludes using those procedures on a ML-based classifier. An early example of this approach for b-tagging can be found in Ref. [298].

In the case where simulation is used to estimate the efficiency ϵ_y and its uncertainty, one usually varies nuisance parameters ν associated to the simulation. One then uses simulated samples to approximate $\epsilon_y(\nu) = P(f(x) > f_{\text{cut}}|y, \nu) = \int H(f(x) - f_{\text{cut}})p(x|y, \nu)dx$. Again, the procedure for incorporating uncertainty isn’t fundamentally different if the classifier $f(x)$ is based on machine learning or a hand-crafted observable.

41.7.2 Domain adaptation

While estimating the uncertainty for a ML-based model is not fundamentally different than any other hand-crafted observable used for regression or classification, the worry of many physicists is that by working with a high-dimensional set of features x that one is more susceptible to mismodelling of subtle correlations. This is a valid concern, and it should be appreciated that a great deal of prior knowledge and physical insight goes into the construction of hand-crafted observables so that they will be robust to the most uncertain aspects of data. However, much of this craft is based on heuristics that are difficult to systematize. Furthermore, one can only validate that such an observable is robust if one can explicitly evaluate the performance for a perturbed distribution. Thus in the settings where one can validate the robustness to a perturbed scenario ν_0 , one must have access to $p(x|y, \nu_0)$.

One approach to formalize this type of robustness is to consider the dependence on the distribution of the output of the model $f(x)$ to the nuisance parameters. In statistics, if the distribution of f is independent of the nuisance parameters, then f is referred to as a *pivotal quantity*. This is a property that we can incorporate directly into the training procedure to target a particular notion of robustness. The authors of Ref. [299] introduced an adversarial approach (similar to what is used in the generative adversarial network of Sec. 41.5.4.2) to penalize a model during training if the distribution of the output varies with the nuisance parameters. To construct the training dataset $\{x_i, y_i, \nu_i\}_{i=1, \dots, n}$, one must sample y and ν according to some proposal distribution (similar to a prior, but only used for the creation of training dataset, not necessarily for statistical inference), corresponding to a joint distribution $p(x, y, \nu)$. Instead of minimizing the target loss \mathcal{L}_f (*e.g.* cross-entropy, squared-error, *etc.*) with respect to the parameters ϕ_f that parameterize the model f , one trains with a minimax strategy that also includes an adversary q with parameters ϕ_r . The trained model is characterized by the saddle point

$$\hat{\phi}_f, \hat{\phi}_r = \arg \min_{\phi_f} \arg \max_{\phi_r} E_{\lambda}(\phi_f, \phi_r), \quad (41.73)$$

where the value function E_{λ} includes the target loss as well as a regularization term associated to the adversary

$$E_{\lambda}(\phi_f, \phi_r) = \mathcal{L}_f(\phi_f) - \lambda \mathcal{L}_r(\phi_f, \phi_r). \quad (41.74)$$

The constant λ is a hyperparameter, since generially there is a tradeoff between the two terms and only in special cases can the model that minimizes \mathcal{L}_f also be a pivotal quantity. The regularization term

$$\mathcal{L}_r(\phi_f, \phi_r) = \mathbb{E}_{p(x, y, \nu)}[-\log q_{\phi_r}(\nu|f_{\phi_f}(x))] \quad (41.75)$$

is an example of conditional density estimation (see Sec. 41.3.2.1), where the model $q_{\phi_r}(\nu|f)$ is trying to predict the distribution of the nuisance parameter ν given the output of the model $f(x)$. This term is maximized when f is independent of ν . Earlier work had also used an adversarial technique for domain adaptation, but was limited to just two domains [300–302], while here ν parameterizes a continuous family of distributions and can have multiple components corresponding to different sources of uncertainty. Furthermore, the previous work aimed to make the distribution for a high-dimensional, intermediate representation of the data be invariant to the domain shift as opposed to just the final output $f(x)$.

One way of interpreting Eq. 41.73 is that the goal is to minimize a regularized loss function $\mathcal{L}(\phi_f) = \arg \max_{\phi_r} E_{\lambda}(\phi_f, \phi_r)$, where the optimization with respect to ϕ_r is not exposed. This motivates another approach in which the regularization is not achieved through a learned adversary, but by a measure of discrepancy between distributions that can be computed directly from samples. In particular, the authors of Ref. [303] proposed the use of *distance correlation* to avoid what can be a challenging min-max optimization problem.

In either case, the optimization of the hyperparameter λ is based on the downstream task. For example, in Ref. [299] considered the case where f was a signal vs. background binary classifier where the nuisance parameter ν was associated to uncertainty in the background model. The hyperparameter λ was then optimized to maximize the approximate median significance (AMS). Similarly, the authors of Refs. [304] and [303] considered new physics searches in the context of boosted jet tagging, where the hyperparameter controls the sculpting of the side-bands used for background estimation.

While these strategies modify the training procedure so that the sensitivity to the nuisance parameters is reduced, it does not typically eliminate it. As a result, one still needs to propagate the uncertainty in the data distribution through the learned model as described in the preceding section.

Note, this adversarial technique has also been employed in other settings where one would like to decorrelate the output of the classifier with an observed quantity so that it can be used for background estimation [304]. Widely used alternative approaches to decorrelation include boost [305] and DDT [306]. Other examples of the domain adaptation and decorrelation use cases from the Living Review include [299, 303–318].

41.7.3 Parameterized models

An alternative to learning a model $f(x)$ that is pivotal — *i.e.* whose distribution is independent of the nuisance parameter ν — is to learn a family of models $f(x; \nu)$ that is parameterized in terms of the nuisance parameters. In general, there is a tradeoff between the two terms of Eq. 41.74 for a single model $f(x)$. In a parameterized model, $f(x; \nu)$ optimizes the performance of the model for every value of ν . Parameterized classifiers were first advocated in Ref. [58] in the context of simulation-based inference (see Sec. 41.7.7) and in Ref. [319] for new physics searches. It has also been applied to simulation-based inference for effective field theory parameters in Ref. [19] and Ref. [320] provides additional pedagogical examples.

The training of a parameterized model is similar to the standard procedure. For example, if one originally wanted to minimize the squared loss function $\mathcal{L}(y, f(x)) = (y - f(x))^2$ with training dataset $\{x_i, y_i\}_{i=1, \dots, n}$, then the corresponding training procedure for the parameterized model would be as follows. One would need to construct a training set $\{x_i, y_i, \nu_i\}_{i=1, \dots, n}$ as described in the preceding section, construct a parameterized model $f(x; \nu)$ that takes as input the original feature vector x as well as the nuisance parameters ν , and then train using the same loss $\mathcal{L}(y, f(x; \nu)) = (y - f(x; \nu))^2$.

One complication of the parameterized approach is that it is no longer possible to evaluate the model on a dataset $\{x_i\}$ and pass on only $\{f_i\}$ for downstream analysis tasks since $f(x_i; \nu)$ still depends on ν . Instead, one delays evaluating the model to some downstream stage when the dependence on ν would be accounted for. For example, in the context of a likelihood based analysis where one is testing a hypothesis where the nuisance parameters

take on a particular value ν_{est} , then one will consider the data distribution $p(x|\nu_{\text{est}})$, and at that point one would evaluate the model at the corresponding nuisance parameter value, *i.e.* $f(x; \nu_{\text{est}})$. Explicit examples are given in Refs. [19, 58, 297, 320]. While this may seem complicated, it actually corresponds to what is done in a typical likelihood-based fit when the statistical model has nuisance parameters; *i.e.* the likelihood-ratio corresponds to the model $f(x; \nu)$ as in Eq. 41.12.

41.7.4 Data augmentation

An intuitive approach to building in robustness to systematic effects that can lead to domain shift, is simply to augment the training dataset so that it includes examples corresponding to several values of the nuisance parameter or systematic variations. As before one can construct a dataset $\{x_i, y_i, \nu_i\}_{i=1, \dots, n}$, but instead of leveraging the information about ν_i , one simply discards this information. This corresponds to sampling from the marginal distribution $x_i, y_i \sim p(x, y) = \int d\nu p(x, y|\nu)p(\nu)$, and is often referred to as *smearing*. One can then use this smeared dataset for supervised learning in the traditional way. While it is possible that this approach will lead to improved robustness to systematic variations (*i.e.* generalization for ν other than the nominal value) than if systematic uncertainty weren't considered at all, this intuitive approach has several shortcomings. The approach does not yield a pivotal quantity as in the adversarial approach, so propagation of uncertainty through the network is still required. Moreover, there is no direct way to control the trade-off between independence from the nuisance parameter and the original target loss as in the adversarial approach. Finally, it can lead to significant performance loss compared to what is possible with the parameterized approach. These trade-offs were studied in Refs. [319, 320] with both pedagogical and physically-motivated examples.

41.7.5 Aleatoric and epistemic uncertainty

In the machine learning and risk assessment literature, uncertainty is often characterized in terms of *aleatoric* and *epistemic* uncertainty [321–324]. Familiarity with these terms is useful, but the distinction between the two can be ambiguous, the terms are not always consistently used, and they do not clearly map onto the concepts used in physics.

For example, Ref. [323], states that “roughly speaking, aleatoric (aka statistical) uncertainty refers to the notion of randomness, that is, the variability in the outcome of an experiment which is due to inherently random effects”, while “epistemic (aka systematic) uncertainty refers to uncertainty caused by a lack of knowledge (about the best model)”. This seems clear enough, but in that same reference (and in Ref. [325]) the aleatoric uncertainty is considered irreducible, while the epistemic uncertainty could be reduced with additional information. This may seem backwards for many physicists since often in particle physics, we think of how uncertainties scale as we collect more data but keep the experimental design fixed. In that case, the statistical uncertainty will be reduced with time while the systematic uncertainty will remain constant⁶. There is no paradox here, it is simply a different point of view. The emphasis of the risk assessment community is not on collecting more data with the same experimental design, but collecting different types of data that will inform the models themselves. Clearly even for physicists, data from new experiments or calibration measurements could also reduce our systematic uncertainties. While there are exceptions in the literature, the bulk of it associates aleatoric uncertainty with the randomness of classical probability (*i.e.* the statistical uncertainty associated to repeating the same experiment many times) and epistemic uncertainty with our state of knowledge.

Perhaps a more important distinction between the perspective of physicists and machine learning researchers has to do with the use of the term “model” and what exactly is uncertain. In physics, the systematic and epistemic uncertainty is typically associated to our understanding of the underlying physics and “the model” usually refers to the physics model, detector model encapsulated

⁶Further complicating the relationship between the terms is that many experimental uncertainties that are characterized as systematic are actually statistical in nature as auxiliary measurements and control regions are used to constrain the corresponding nuisance parameters.

in a simulation. In contrast, for machine learning research, “the model” usually refers to the trained model $\hat{f} \in \mathcal{F}$ used as described in Section 41.2.1 (or the class of functions \mathcal{F} itself). This makes sense if we recall that in the bulk of machine learning research, one has little insight into the process that generated the data (*e.g.* images of cats and dogs, natural language, *etc.*). In that sense, the epistemic uncertainty in machine learning is usually associated to uncertainty in the model parameters ϕ after training, which would be reduced if one could collect more training dataset (see Ref. [324] for this point of view).

In the literature on Uncertainty Quantification (UQ), which is more closely connected to physics given the role of computer simulations, the terminology is more fine grained and less ambiguous. That community uses the terms parameter uncertainty (*i.e.* nuisance parameters), structural uncertainty (*i.e.* mismodelling), algorithmic uncertainty (*i.e.* numerical uncertainty), experimental uncertainty (*i.e.* uncertainty from experimental resolution and statistical fluctuations), and interpolation uncertainty (*i.e.* uncertainty due to interpolating between different parameter values due to lack of computational resources).

41.7.6 Model averaging and Bayesian machine learning

The core of Bayesian machine learning is the model averaging view. Here one often takes a more ambitious view of learning than described in Sec. 41.2.1, which is framed mainly as function approximation. While in Sec. 41.2.1, the goal is to find a function that minimizes the risk, in Bayesian machine learning one explicitly builds a probability model $q_\phi(x, y)$ for the training dataset $\mathcal{D} = \{x_i, y_i\}_{i=1, \dots, n}$. It is the same change in perspective that one has when one views the squared error loss function $\mathcal{L}_{MSE} = (y - f_\phi(x))^2$ as the log-likelihood for a probability model $y \sim N(f(x), \sigma)$. In addition, one assumes some prior on the model parameters $p(\phi)$, which is often a Gaussian distribution, and is analogous to Tikhonov regularization (see Sec. 41.3.1.2). With this view in mind, a single trained model $\hat{f} = f_\phi$ is the MAP point estimate and the more complete Bayesian solution is the entire posterior distribution over the model parameters $p(\phi|\mathcal{D})$. With this view, it is clear how increasing the number of training examples n will lead to a reduction in uncertainty on ϕ . However, this notion of epistemic uncertainty has little to do with the notion of systematic uncertainty as the term is used by particle physicists.

Bayesian methods can be applied to non-probabilistic regression problems, in which case they can provide uncertainty quantification. Consider the case of regression in traditional (non-Bayesian) machine learning. The trained model $f_\phi(x)$ is used to predict the target label y . For a fixed x , the model does not provide any notion of uncertainty on the prediction. One could propagate uncertainty on x through $f(x)$, but that is also not the desired quantity to characterize the intrinsic spread $p(y|x)$ in the data, which may exist even if x has negligible uncertainty. In contrast, Gaussian process regression (a Bayesian method) does provide a natural way to communicate the uncertainty on the prediction, which is possible because one first had to specify a prior on the mean and covariance of the Gaussian process.

In the context of Bayesian deep learning and Bayesian Neural Networks, one would place a prior on the weights and biases of the neural network $p(\phi)$ and then use one of the many emerging techniques to calculate the approximate posterior $p(\phi|\mathcal{D})$. However, we should recognize that we have little-to-no insight into the parameters of a deep neural network, so the prior on ϕ is hardly well-justified. Furthermore, just as in all Bayesian approaches, the prior is not invariant to reparametrizing the model: $\phi \rightarrow \eta(\phi)$. While it is difficult to justify the choice of the prior on the parameters (and, thus, the resulting posterior), the resulting model may perform well empirically. In such high-dimensional parameter spaces, the bias-variance tradeoff can be dramatic.

Bayesian model averaging (BMA) performs Bayesian average over the posterior $p(\phi|\mathcal{D})$. This can be applied to any quantity f_ϕ , such as a regression or classification prediction y . Suppose we can draw from the posterior $\phi \sim p(\phi|\mathcal{D})$. For each draw we can evaluate the predicted regression variable $y = f_\phi(x) + \epsilon$, where ϵ is some noise to account for uncertainty in the predictions. We

can denote this process as a draw from $p(y|x, \phi)$, $y \sim p(y|x, \phi) = N(f_\phi(x), \sigma_\epsilon^2)$, where σ_ϵ^2 is the noise variance. The BMA then performs

$$p(y|x, \mathcal{D}) = \int d\phi p(\phi|\mathcal{D})p(y|x, \phi). \quad (41.76)$$

In practice $p(y|x, \phi)$ is evaluated by drawing samples of y and ϕ , so the posterior is defined implicitly by the samples. For example, the mean prediction is obtained by averaging $f_\phi(x)$ over the samples of ϕ , and the covariance matrix is similarly evaluated by averaging the second moments over the samples of ϕ .

Ref. [326] provides a different perspective on BMA analyzed in what are referred to as the \mathcal{M} -open and \mathcal{M} -closed settings [326]. The \mathcal{M} -closed setting refers to the situation where the true data generating process is in the space of models, even if it is unknown to us. In contrast, the \mathcal{M} -open setting refers to when the true data generating process is not in model space (*i.e.* the model is mis-specified). Interestingly, in the \mathcal{M} -open case one can potentially do better than any one model in the model class by considering an average over the models, since averaging can create a new model that is not in the model class. BMA provides one such averaging, but other averages, which are not weighted by $p(\phi|\mathcal{D})$, can be a better choice. When the weights of each model are optimized against appropriate loss the resulting procedure is called stacking, which has been shown to be superior to BMA in the \mathcal{M} -open setting [326]. Ref. [327] performed experiments indicating that in some cases model averaging can also improve predictive uncertainty estimates under domain shifts.

Neural network model averaging beyond BMA comes in several different flavors. Two successful model averaging procedures are Monte Carlo dropout [328], which uses dropout ensembling, and deep ensembles [329], which use random initialization ensembling. These methods may not only be superior to BMA, they are also often significantly faster than BMA. Whether these model averages are an approximation to BMA, or an alternative to it, remains a debated topic, and both views have been advocated. BMA itself can be accelerated using approximate methods, such as stochastic Variational Inference with reparametrization trick [330].

41.7.7 Connection to probabilistic machine learning

We end this Section by reinforcing the connection between uncertainty quantification in traditional machine learning and the more probabilistic approaches to machine learning exemplified by simulation-based inference (see Sec 41.3.5) and deep generative models (see Sec. 41.5.4). In the standard approach to supervised learning (*e.g.* classification and regression) the model $f(x)$ provides a point estimate for y . Estimating an uncertainty on y goes a step further, but the complete picture would be to model the posterior distribution $p(y|x)$. Gaussian processes (see Sec. 41.5.1) are an example, but the form of the models is limited to Gaussian posteriors. In Sec 41.3.5 we discussed approaches to model $p(y|x)$ using conditional density estimation [51, 56, 57]. If we extend this task to include a family of distributions parameterized by some nuisance parameters ν , then the task is to model $p(y|x, \nu)$, which is structurally similar.

In the context of classification, the output is already probabilistic, and the interpretation of the resulting classifier is $\hat{f}_{MSE}(x) \approx p(y = 1|x)$ (see Eq. 41.10). Incorporating the dependence on the nuisance parameter, then connects to the likelihood-ratio trick (see Eq. 41.12), approaches to simulation-based inference that involve learning the likelihood-ratio, and the parameterized approaches described in Sec. 41.7.3.

If one pairs the training procedure for classification, regression, or density estimation used in the approaches above with model averaging techniques such as BMA, then it would be possible to incorporate both uncertainty associated to finite training dataset and the uncertainty associated to systematic uncertainties. However, as described in Sec. 41.7.5 and Sec. 41.7.1, it is not clear that in physics applications it is desirable to account for the variability associated to training when the more common practice is to regard the trained model $\hat{f}(x)$ as fixed.

While these probabilistic approaches to machine learning are attractive conceptually, it is known in the machine learning community that classifiers often are poorly calibrated and often overly

confident in their predictions. This is a problem even if one regards the trained model $\hat{f}(x)$ as fixed. Various approaches, including model averaging, are being pursued to improve the calibration of trained models, but the problem is unlikely to be eliminated entirely. Miscalibration can be verified by evaluating the true positive and false positive rates on held out data. This is common practice in experimental particle physics, where the output of a binary classifier is rarely taken at face value. Instead, the true and false positive rates are estimated with simulated data or control samples as described in Sec. 41.7.1. Furthermore, the true and false positives can be characterized as a function of the nuisance parameters. These procedures can be used to help calibrate parameterized models based on the likelihood-ratio trick (see Refs. [58, 320]). Unfortunately, calibration in the context of density estimation is more challenging. This connects to topics and challenges in anomaly detection (see Sec. 41.3.4).

41.8 Infrastructure for deployment in experiments

The software and computing needs of training a machine learning model are different than those encountered when it deployed for use. In machine learning jargon, the two stages are often referred to as *training* and *inference*, where inference might refer to making a prediction for y given x in a classification or regression problem. Sometimes this transition also involves using different programming languages for implementing the trained model from the ones used for training them. Modern machine learning frameworks support various serialization formats to exchange trained models. For instance, **ONNX** provides an open source format for many types of models and is widely supported and can be found in many frameworks, tools, and hardware. This is important when integrating a trained model into the large software frameworks used by the large experiments.

While hardware acceleration with GPUs is important for efficiently training modern machine learning techniques, there are also advantages of hardware acceleration at inference time. This may include GPUs or Field Programmable Gate Arrays (FPGAs), and the Living Review includes many example works focusing on efficient inference for a given hardware architecture [81, 108, 331–340]. For applications where latency is a key concern (eg triggering at collider experiments), various accelerators have been investigated [167, 171, 341–355]. In addition, some solutions for deployment of ML models involve deployment in the cloud [356, 357].

References

- [1] Y. Lecun, Y. Bengio and G. Hinton, *Nature* **521**, 7553, 436 (2015), ISSN 14764687.
- [2] J. Schmidhuber, *Neural Networks* **61**, 85 (2015).
- [3] A. Radovic *et al.*, *Nature* **560**, 7716, 41 (2018).
- [4] D. Guest, K. Cranmer and D. Whiteson, *Ann. Rev. Nucl. Part. Sci.* **68**, 161 (2018), [arXiv:1806.11484].
- [5] G. Carleo *et al.*, *Rev. Mod. Phys.* **91**, 4, 045002 (2019), [arXiv:1903.10563].
- [6] M. Feickert and B. Nachman (2021), [arXiv:2102.02770].
- [7] V. Vapnik, *The nature of statistical learning theory*, Springer science & business media (2013).
- [8] C. Zhang *et al.*, *Communications of the ACM* **64**, 3, 107 (2021).
- [9] P. Nakkiran *et al.*, arXiv preprint arXiv:1912.02292 (2019).
- [10] A. Y. Ng and M. I. Jordan, in T. G. Dietterich, S. Becker and Z. Ghahramani, editors, “Advances in Neural Information Processing Systems 14 [Neural Information Processing Systems: Natural and Synthetic, NIPS 2001, December 3–8, 2001, Vancouver, British Columbia, Canada],” 841–848, MIT Press (2001), URL <https://proceedings.neurips.cc/paper/2001/hash/7b7a53e239400a13bd6be6c91c4f6c4e-Abstract.html>.
- [11] M. Kuusela and V. M. Panaretos, *Ann. Appl. Stat.* **9**, 1671 (2015), [arXiv:1505.04768].
- [12] L. Rosasco, A. Tacchetti and S. Villa, CoRR **abs/1405.0042** (2014), URL <http://arxiv.org/abs/1405.0042>.
- [13] G. E. Hinton *et al.*, CoRR **abs/1207.0580** (2012), [arXiv:1207.0580], URL <http://arxiv.org/abs/1207.0580>.
- [14] P. Baldi and P. J. Sadowski, *Advances in neural information processing systems* **26**, 2814 (2013).
- [15] M. Belkin, S. Ma and S. Mandal, in J. G. Dy and A. Krause, editors, “Proceedings of the 35th International Conference on Machine Learning, ICML 2018, Stockholm, Sweden, July 10–15, 2018,” volume 80 of *Proceedings of Machine Learning Research*, 540–548, PMLR (2018), URL <http://proceedings.mlr.press/v80/belkin18a.html>.
- [16] S. Gunasekar *et al.*, in J. Dy and A. Krause, editors, “Proceedings of the 35th International Conference on Machine Learning,” volume 80 of *Proceedings of Machine Learning Research*, 1832–1841, PMLR (2018), URL <http://proceedings.mlr.press/v80/gunasekar18a.html>.
- [17] L. Zdeborová, *Nature Physics* **16**, 6, 602 (2020).
- [18] E. M. Metodiev, B. Nachman and J. Thaler, *JHEP* **10**, 174 (2017), [arXiv:1708.02949].
- [19] J. Brehmer *et al.*, *Phys. Rev.* **D98**, 5, 052004 (2018), [arXiv:1805.00020].
- [20] J. Brehmer *et al.*, *Proc. Nat. Acad. Sci.* 201915980 (2020), [arXiv:1805.12244].
- [21] M. Stoye *et al.* (2018), [arXiv:1808.00973].
- [22] M. A. Hayat *et al.*, *ApJ Letters* **911**, 2, L33 (2021).
- [23] T. Chen *et al.*, in “Proceedings of the 37th International Conference on Machine Learning, ICML 2020, 13–18 July 2020, Virtual Event,” volume 119 of *Proceedings of Machine Learning Research*, 1597–1607, PMLR (2020), URL <http://proceedings.mlr.press/v119/chen20j.html>.
- [24] E. Parzen, *The annals of mathematical statistics* **33**, 3, 1065 (1962).
- [25] R. A. Davis, K.-S. Lii and D. N. Politis, in “Selected Works of Murray Rosenblatt,” 95–100, Springer (2011).
- [26] K. S. Cranmer, *Comput. Phys. Commun.* **136**, 198 (2001), [hep-ex/0011057].
- [27] Y. Bengio, A. Courville and P. Vincent, *IEEE transactions on pattern analysis and machine intelligence* **35**, 8, 1798 (2013).
- [28] https://en.wikipedia.org/wiki/Cluster_analysis.
- [29] R. E. Bellman, *Dynamic Programming*, Princeton University Press, USA (1957), ISBN 069107951X.
- [30] D. E. Kirk, *Optimal control theory: an introduction*, Courier Corporation (2004).
- [31] K. J. Åström, *Journal of Mathematical Analysis and Applications* **10**, 174 (1965).
- [32] J. Brehmer *et al.*, in “34th Conference on Neural Information Processing Systems,” (2020), [arXiv:2011.08191].
- [33] R. S. Sutton and A. G. Barto, Cambridge, MA **22447** (1998).
- [34] K. Arulkumaran *et al.*, *IEEE Signal Processing Magazine* **34**, 6, 26 (2017).
- [35] H. Robbins, *Bulletin of the American Mathematical Society* **58**, 5, 527 (1952).
- [36] J. C. Gittins, *Journal of the Royal Statistical Society: Series B (Methodological)* **41**, 2, 148 (1979).
- [37] J. Mockus, *Bayesian approach to global optimization: theory and applications*, volume 37, Springer Science & Business Media (2012).
- [38] E. Brochu, V. M. Cora and N. De Freitas, arXiv preprint arXiv:1012.2599 (2010).

- [39] M. Farina, Y. Nakai and D. Shih, *Physical Review D* **101**, 7 (2020), ISSN 2470-0029, URL <http://dx.doi.org/10.1103/PhysRevD.101.075021>.
- [40] T. Heimel *et al.*, *SciPost Physics* **6**, 3 (2019), ISSN 2542-4653, URL <http://dx.doi.org/10.21468/SciPostPhys.6.3.030>.
- [41] J. Ren *et al.*, in H. M. Wallach *et al.*, editors, “Advances in Neural Information Processing Systems 32: Annual Conference on Neural Information Processing Systems 2019, NeurIPS 2019, December 8-14, 2019, Vancouver, BC, Canada,” 14680–14691 (2019).
- [42] E. T. Nalisnick *et al.*, in “7th International Conference on Learning Representations, ICLR 2019, New Orleans, LA, USA, May 6-9, 2019,” OpenReview.net (2019), URL <https://openreview.net/forum?id=H1xwNhCcYm>.
- [43] Z. Xiao, Q. Yan and Y. Amit, arXiv preprint arXiv:2003.02977 (2020).
- [44] V. Böhm and U. Seljak, arXiv preprint arXiv:2006.05479 (2020).
- [45] B. Dai and U. Seljak, in M. Meila and T. Zhang, editors, “Proceedings of the 38th International Conference on Machine Learning, ICML 2021, 18-24 July 2021, Virtual Event,” volume 139 of *Proceedings of Machine Learning Research*, 2352–2364, PMLR (2021), URL <http://proceedings.mlr.press/v139/dai21a.html>.
- [46] J. Brehmer and K. Cranmer (2020), [arXiv:2003.13913].
- [47] E. M. Metodiev, B. Nachman and J. Thaler, *Journal of High Energy Physics* **2017**, 10 (2017), ISSN 1029-8479, URL [http://dx.doi.org/10.1007/JHEP10\(2017\)174](http://dx.doi.org/10.1007/JHEP10(2017)174).
- [48] J. H. Collins *et al.*, *The European Physical Journal C* **81**, 7 (2021), ISSN 1434-6052, URL <http://dx.doi.org/10.1140/epjc/s10052-021-09389-x>.
- [49] G. Kasieczka *et al.* (2021), [arXiv:2101.08320].
- [50] T. Aarrestad *et al.* (2021), [arXiv:2105.14027].
- [51] K. Cranmer, J. Brehmer and G. Louppe, *Proc. Nat. Acad. Sci.* **117**, 48, 30055 (2020), [arXiv:1911.01429].
- [52] J. Brehmer and K. Cranmer, *Artificial Intelligence for Particle Physics*, chapter Simulation-based inference methods for particle physics, World Scientific Publishing Co (2021).
- [53] P. J. Diggle and R. J. Gratton, in “Journal of the Royal Statistical Society: Series B (Methodological),” volume 46, 193–212 (1984), ISSN 0035-9246.
- [54] D. B. Rubin, *The Annals of Statistics* **12**, 4, 1151 (1984), ISSN 0090-5364, URL <https://doi.org/10.1214/aos/1176346785>.
- [55] M. A. Beaumont, W. Zhang and D. J. Balding, *Genetics* **162**, 4, 2025 (2002), ISSN 00166731.
- [56] K. Cranmer and G. Louppe, *J. Brief Ideas* (2016), 10.5281/zenodo.198541.
- [57] G. Papamakarios and I. Murray, in “Advances in Neural Information Processing Systems,” 1036–1044 (2016), ISSN 10495258, [arXiv:1605.06376].
- [58] K. Cranmer, J. Pavez and G. Louppe, arXiv:1506.02169 (2015), [arXiv:1506.02169], URL <http://arxiv.org/abs/1506.02169>.
- [59] C. Modi, F. Lanusse and U. Seljak, FlowPM: Distributed TensorFlow Implementation of the FastPM Cosmological N-body Solver (2020), [arXiv:2010.11847].
- [60] J. Jasche and B. D. Wandelt, *Mon. Not. Roy. Astron. Soc.* **432**, 894 (2013), [arXiv:1203.3639].
- [61] U. Seljak *et al.*, *JCAP* **12**, 009 (2017), [arXiv:1706.06645].
- [62] A. Andreassen *et al.*, *Phys. Rev. Lett.* **124**, 18, 182001 (2020), [arXiv:1911.09107].
- [63] K. Datta, D. Kar and D. Roy (2018), [arXiv:1806.00433].
- [64] M. Bellagente *et al.* (2019), [arXiv:1912.00477].
- [65] N. D. Gagunashvili (2010), [arXiv:1004.2006].
- [66] A. Glazov (2017), [arXiv:1712.01814].
- [67] M. Bellagente *et al.* (2020), [arXiv:2006.06685].
- [68] M. Vandegar *et al.*, in A. Banerjee and K. Fukumizu, editors, “Proceedings of The 24th International Conference on Artificial Intelligence and Statistics,” volume 130 of *Proceedings of Machine Learning Research*, 2107–2115, PMLR (2021), [arXiv:2011.05836], URL <https://proceedings.mlr.press/v130/vandegar21a.html>.
- [69] P. Baroň (2021), [arXiv:2104.03036].
- [70] A. Andreassen *et al.* (2021), [arXiv:2105.04448].
- [71] P. Komiske, W. P. McCormack and B. Nachman (2021), [arXiv:2105.09923].
- [72] V. Andreev *et al.* (H1) (2021), [arXiv:2108.12376].
- [73] M. Arratia *et al.* (2021), [arXiv:2109.13243].
- [74] T. A. Le, A. G. Baydin and F. Wood, in “Proceedings of the 20th International Conference on Artificial Intelligence and Statistics, AISTATS 2017,” volume 54 of *Proceedings of Machine Learning Research*, 1338–1348, PMLR, Fort Lauderdale, FL, USA (2017), [arXiv:1610.09900].
- [75] A. G. Baydin *et al.* (2018), [arXiv:1807.07706].
- [76] A. G. Baydin *et al.*, International Conference for High Performance Computing, Networking, Storage and Analysis, SC arXiv:1907.03382 (2019), ISSN 21674337, [arXiv:1907.03382].
- [77] A. Hocker *et al.*, *PoS ACAT*, 040 (2007), [arXiv:physics/0703039].
- [78] T. Mikolov *et al.*, arXiv preprint arXiv:1301.3781 (2013).
- [79] E. Asgari and M. R. Mofrad, *PloS one* **10**, 11, e0141287 (2015).
- [80] D. Guest *et al.*, *Phys. Rev.* **D94**, 11, 112002 (2016), [arXiv:1607.08633].
- [81] T. Q. Nguyen *et al.*, *Comput. Softw. Big Sci.* **3**, 1, 12 (2019), [arXiv:1807.00083].
- [82] E. Bols *et al.* (2020), [arXiv:2008.10519].
- [83] K. Goto *et al.*, Development of a Vertex Finding Algorithm using Recurrent Neural Network (2021), [arXiv:2101.11906].
- [84] R. T. de Lima (2021), [arXiv:2102.06128].
- [85] Technical Report ATL-PHYS-PUB-2017-003, CERN, Geneva (2017), URL <http://cdsweb.cern.ch/record/2255226>.
- [86] J. Pumplin, *Phys. Rev. D* **44**, 2025 (1991).
- [87] J. Cogan *et al.*, *JHEP* **02**, 118 (2015), [arXiv:1407.5675].
- [88] L. G. Almeida *et al.*, *JHEP* **07**, 086 (2015), [arXiv:1501.05968].
- [89] L. de Oliveira *et al.*, *JHEP* **07**, 069 (2016), [arXiv:1511.05190].
- [90] Technical Report ATL-PHYS-PUB-2017-017, CERN, Geneva (2017), URL <http://cds.cern.ch/record/2275641>.
- [91] J. Lin *et al.*, *JHEP* **10**, 101 (2018), [arXiv:1807.10768].
- [92] P. T. Komiske *et al.*, *Phys. Rev.* **D98**, 1, 011502 (2018), [arXiv:1801.10158].
- [93] J. Barnard *et al.*, *Phys. Rev.* **D95**, 1, 014018 (2017), [arXiv:1609.00607].
- [94] P. T. Komiske, E. M. Metodiev and M. D. Schwartz, *JHEP* **01**, 110 (2017), [arXiv:1612.01551].
- [95] G. Kasieczka *et al.*, *JHEP* **05**, 006 (2017), [arXiv:1701.08784].
- [96] S. Macaluso and D. Shih, *JHEP* **10**, 121 (2018), [arXiv:1803.00107].
- [97] J. Li, T. Li and F.-Z. Xu (2020), [arXiv:2008.13529].
- [98] J. Li and H. Sun (2020), [arXiv:2009.00170].
- [99] J. S. H. Lee *et al.*, *J. Korean Phys. Soc.* **74**, 3, 219 (2019), [arXiv:2012.02531].

- [100] J. Collado *et al.*, Learning to Isolate Muons (2021), [arXiv:2102.02278].
- [101] Y.-L. Du, D. Pablos and K. Tywoniuk (2020), [arXiv:2012.07797].
- [102] J. Filipek *et al.* (2021), [arXiv:2105.04582].
- [103] Technical Report ATL-PHYS-PUB-2019-028, CERN, Geneva (2019), URL <http://cds.cern.ch/record/2684070>.
- [104] M. Andrews *et al.* (2018), [arXiv:1807.11916].
- [105] Y.-L. Chung, S.-C. Hsu and B. Nachman (2020), [arXiv:2009.05930].
- [106] Y.-L. Du *et al.*, Eur. Phys. J. C **80**, 6, 516 (2020), [arXiv:1910.11530].
- [107] M. Andrews *et al.* (2021), [arXiv:2104.14659].
- [108] A. A. Pol *et al.* (2021), [arXiv:2105.05785].
- [109] A. Aurisano *et al.*, JINST **11**, 09, P09001 (2016), [arXiv:1604.01444].
- [110] R. Acciarri *et al.* (MicroBooNE), JINST **12**, 03, P03011 (2017), [arXiv:1611.05531].
- [111] L. Hertel *et al.* (2017), URL https://dl4physicalsciences.github.io/files/nips_dlps_2017_7.pdf.
- [112] C. Adams *et al.* (MicroBooNE), Phys. Rev. D **99**, 9, 092001 (2019), [arXiv:1808.07269].
- [113] L. Dominé and K. Terao (DeepLearnPhysics), Phys. Rev. D **102**, 1, 012005 (2020), [arXiv:1903.05663].
- [114] S. Aiello *et al.* (KM3NeT) (2020), [arXiv:2004.08254].
- [115] C. Adams, K. Terao and T. Wongjirad (2020), [arXiv:2006.01993].
- [116] L. Dominé *et al.* (DeepLearnPhysics), Phys. Rev. D **104**, 3, 032004 (2021), [arXiv:2006.14745].
- [117] F. Drielsma *et al.* (DeepLearnPhysics), Phys. Rev. D **104**, 7, 072004 (2021), [arXiv:2007.01335].
- [118] D. H. Koh *et al.* (DeepLearnPhysics) (2020), [arXiv:2007.03083].
- [119] H. Yu *et al.*, JINST **16**, 01, P01036 (2021), [arXiv:2007.12743].
- [120] F. Psihas *et al.* (2020), [arXiv:2008.01242].
- [121] S. Alonso-Monsalve *et al.*, Phys. Rev. D **103**, 3, 032005 (2021), [arXiv:2009.00688].
- [122] P. Abratenko *et al.* (MicroBooNE) (2020), [arXiv:2010.08653].
- [123] B. Clerbaux *et al.* (2020), [arXiv:2011.08847].
- [124] J. Liu *et al.* (2020), [arXiv:2012.06181].
- [125] P. Abratenko *et al.* (MicroBooNE) (2020), [arXiv:2012.08513].
- [126] S. Y.-C. Chen *et al.* (2020), [arXiv:2012.12177].
- [127] R. Acciarri *et al.* (SBND) (2020), [arXiv:2012.01301].
- [128] Z. Qian *et al.* (2021), [arXiv:2101.04839].
- [129] R. Abbasi *et al.* (IceCube), A Convolutional Neural Network based Cascade Reconstruction for the IceCube Neutrino Observatory (2021), [arXiv:2101.11589].
- [130] F. Drielsma *et al.*, in “34th Conference on Neural Information Processing Systems,” (2021), [arXiv:2102.01033].
- [131] M. Rossi and S. Vallecorsa, in “25th International Conference on Computing in High-Energy and Nuclear Physics,” (2021), [arXiv:2103.01596].
- [132] J. Hewes *et al.* (2021), [arXiv:2103.06233].
- [133] R. Acciarri *et al.* (ArgoNeuT) (2021), [arXiv:2103.06391].
- [134] V. Belavin, E. Trofimova and A. Ustyuzhanin (2021), [arXiv:2104.02040].
- [135] D. Maksimović, M. Nieslony and M. Wurm (2021), [arXiv:2104.13426].
- [136] A. Gavrikov and F. Ratnikov, in “25th International Conference on Computing in High-Energy and Nuclear Physics,” (2021), [arXiv:2106.02907].
- [137] J. García-Méndez *et al.* (2021), [arXiv:2107.13654].
- [138] K. Carloni *et al.* (2021), [arXiv:2110.10766].
- [139] P. Abratenko *et al.* (MicroBooNE) (2021), [arXiv:2110.11874].
- [140] D. Boyda *et al.*, Phys. Rev. D **103**, 7, 074504 (2021), [arXiv:2008.05456].
- [141] G. Kanwar *et al.*, Phys. Rev. Lett. **125**, 12, 121601 (2020), [arXiv:2003.06413].
- [142] P. T. Komiske, E. M. Metodiev and J. Thaler, JHEP **01**, 121 (2019), [arXiv:1810.05165].
- [143] H. Qu and L. Gouskos, Phys. Rev. D **101**, 5, 056019 (2020), [arXiv:1902.08570].
- [144] V. Mikuni and F. Canelli, Eur. Phys. J. Plus **135**, 6, 463 (2020), [arXiv:2001.05311].
- [145] J. Shlomi *et al.* (2020), [arXiv:2008.02831].
- [146] M. J. Dolan and A. Ore (2020), [arXiv:2012.00964].
- [147] M. J. Fenton *et al.* (2020), [arXiv:2010.09206].
- [148] J. S. H. Lee *et al.* (2020), [arXiv:2012.03542].
- [149] V. Mikuni and F. Canelli (2021), [arXiv:2102.05073].
- [150] A. Shmakov *et al.* (2021), [arXiv:2106.03898].
- [151] C. Shimmin (2021), [arXiv:2107.02908].
- [152] Technical Report ATL-PHYS-PUB-2020-014, CERN, Geneva (2020), URL <https://cds.cern.ch/record/2718948>.
- [153] G. Louppe *et al.*, Journal of High Energy Physics **2019**, 1, 57 (2019), ISSN 10298479, [arXiv:1702.00748].
- [154] T. Cheng (2017), [arXiv:1711.02633].
- [155] I. Henrion *et al.* (2017), URL https://dl4physicalsciences.github.io/files/nips_dlps_2017_29.pdf.
- [156] X. Ju *et al.*, 33rd Annual Conference on Neural Information Processing Systems (2020), [arXiv:2003.11603].
- [157] M. Abdughani *et al.*, JHEP **08**, 055 (2019), [arXiv:1807.09088].
- [158] J. Arjona Martínez *et al.*, Eur. Phys. J. Plus **134**, 7, 333 (2019), [arXiv:1810.07988].
- [159] J. Ren, L. Wu and J. M. Yang, Phys. Lett. B **802**, 135198 (2020), [arXiv:1901.05627].
- [160] E. A. Moreno *et al.*, Eur. Phys. J. C **80**, 1, 58 (2020), [arXiv:1908.05318].
- [161] S. R. Qasim *et al.*, Eur. Phys. J. C **79**, 7, 608 (2019), [arXiv:1902.07987].
- [162] A. Chakraborty, S. H. Lim and M. M. Nojiri, JHEP **19**, 135 (2020), [arXiv:1904.02092].
- [163] A. Chakraborty *et al.* (2020), [arXiv:2003.11787].
- [164] M. Abdughani *et al.* (2020), [arXiv:2005.11086].
- [165] E. Bernreuther *et al.* (2020), [arXiv:2006.08639].
- [166] J. Shlomi, P. Battaglia and J.-R. Vlimant, Machine Learning: Science and Technology **2**, 2, 021001 (2021), ISSN 2632-2153, URL <http://dx.doi.org/10.1088/2632-2153/abbf9a>.
- [167] Y. Iiyama *et al.*, Front. Big Data **3**, 598927 (2020), [arXiv:2008.03601].
- [168] X. Ju and B. Nachman, Phys. Rev. D **102**, 075014 (2020), [arXiv:2008.06064].
- [169] N. Choma *et al.* (2020), [arXiv:2007.00149].
- [170] Jun Guo and Jinmian Li and Tianjun Li (2020), [arXiv:2010.05464].
- [171] A. Heintz *et al.*, 34th Conference on Neural Information Processing Systems (2020), [arXiv:2012.01563].

- [172] Y. Verma and S. Jena (2020), [arXiv:2012.08515].
- [173] F. A. Dreyer and H. Qu (2020), [arXiv:2012.08526].
- [174] J. Pata *et al.* (2021), [arXiv:2101.08578].
- [175] C. Biscarat *et al.*, in “25th International Conference on Computing in High-Energy and Nuclear Physics,” (2021), [arXiv:2103.00916].
- [176] S. Thais and G. DeZoort (2021), [arXiv:2103.06509].
- [177] G. Dezoort *et al.* (2021), [arXiv:2103.16701].
- [178] Y. Verma and S. Jena (2021), [arXiv:2103.14906].
- [179] A. Hariri, D. Dyachkova and S. Gleyzer (2021), [arXiv:2104.01725].
- [180] O. Atkinson *et al.* (2021), [arXiv:2105.07988].
- [181] P. Konar, V. S. Ngairangbam and M. Spannowsky (2021), [arXiv:2109.14636].
- [182] K. Cho *et al.*, in “Conference on Empirical Methods in Natural Language Processing (EMNLP 2014),” (2014).
- [183] H. Serviansky *et al.*, in H. Larochelle *et al.*, editors, “Advances in Neural Information Processing Systems,” volume 33, 22080–22091, Curran Associates, Inc. (2020), URL <https://proceedings.neurips.cc/paper/2020/file/fb4ab556bc42d6f0ee0f9e24ec4d1af0-Paper.pdf>.
- [184] B. E. Boser, I. M. Guyon and V. N. Vapnik, in “Proceedings of the fifth annual workshop on Computational learning theory,” 144–152 (1992).
- [185] C. Cortes and V. Vapnik, *Machine learning* **20**, 3, 273 (1995).
- [186] H. Drucker *et al.*, *Advances in neural information processing systems* **9**, 155 (1997).
- [187] R. M. Neal, University of Toronto (1994).
- [188] C. K. Williams, *Advances in neural information processing systems* 295–301 (1997).
- [189] J. Lee *et al.*, in “6th International Conference on Learning Representations, ICLR 2018, Vancouver, BC, Canada, April 30 - May 3, 2018, Conference Track Proceedings,” OpenReview.net (2018), URL <https://openreview.net/forum?id=B1EA-M-OZ>.
- [190] A. Jacot, C. Hongler and F. Gabriel, in S. Bengio *et al.*, editors, “Advances in Neural Information Processing Systems 31: Annual Conference on Neural Information Processing Systems 2018, NeurIPS 2018, December 3-8, 2018, Montréal, Canada,” 8580–8589 (2018), URL <https://proceedings.neurips.cc/paper/2018/hash/5a4be1fa34e62bb8a6ec6b91d2462f5a-Abstract.html>.
- [191] T. Hofmann, B. Schölkopf and A. J. Smola, *The Annals of Statistics* 1171–1220 (2008).
- [192] C. M. Bishop, *Pattern recognition and machine learning*, Springer (2006).
- [193] C. K. Williams and C. E. Rasmussen, *Gaussian processes for machine learning*, volume 2, MIT press Cambridge, MA (2006).
- [194] S. Ambikasaran *et al.*, *IEEE transactions on pattern analysis and machine intelligence* **38**, 2, 252 (2015).
- [195] J. R. Gardner *et al.*, arXiv preprint arXiv:1809.11165 (2018).
- [196] M. Frate *et al.* (2017), [arXiv:1709.05681].
- [197] S. Mishra-Sharma and K. Cranmer, in “34th Conference on Neural Information Processing Systems,” (2020), [arXiv:2010.10450].
- [198] J. W. Foster *et al.*, *Phys. Rev. Lett.* **127**, 5, 051101 (2021), [arXiv:2102.02207].
- [199] L. Breiman *et al.* (1984).
- [200] XGBoost <https://xgboost.readthedocs.io/>.
- [201] I. Narsky (2005), [arXiv:physics/0507143].
- [202] G. Louppe, arXiv preprint arXiv:1407.7502 (2014).
- [203] Y. Freund and R. E. Schapire, *Journal of computer and system sciences* **55**, 1, 119 (1997).
- [204] J. H. Friedman, *Annals of statistics* 1189–1232 (2001).
- [205] K. Fukushima, *Biological Cybernetics* **36**, 193 (1980).
- [206] V. Nair and G. E. Hinton, in “ICML,” (2010).
- [207] A. L. Maas, A. Y. Hannun and A. Y. Ng, in “in ICML Workshop on Deep Learning for Audio, Speech and Language Processing,” (2013).
- [208] K. He *et al.*, *IEEE International Conference on Computer Vision (ICCV 2015)* **1502** (2015).
- [209] V. Sitzmann *et al.*, in “Proc. NeurIPS,” (2020).
- [210] G. Cybenko, *Mathematics of control, signals and systems* **2**, 4, 303 (1989).
- [211] O. Delalleau and Y. Bengio, in J. Shawe-Taylor *et al.*, editors, “Advances in Neural Information Processing Systems,” volume 24, Curran Associates, Inc. (2011), URL <https://proceedings.neurips.cc/paper/2011/file/8e6b42f1644ecb1327dc03ab345e618b-Paper.pdf>.
- [212] R. Raina, A. Madhavan and A. Y. Ng, in “Proceedings of the 26th Annual International Conference on Machine Learning,” ICML ’09, 873–880, Association for Computing Machinery, New York, NY, USA (2009), ISBN 9781605585161, URL <https://doi.org/10.1145/1553374.1553486>.
- [213] Y. LeCun, *Deep Learning est mort. Vive Differentiable Programming!* <https://www.facebook.com/yann.lecun/posts/10155003011462143> (2018), URL <https://www.facebook.com/yann.lecun/posts/10155003011462143andhttps://techburst.io/deep-learning-est-mort-vive-differentiable-programming-5060d3c55074>.
- [214] M. Lin, Q. Chen and S. Yan, arXiv preprint arXiv:1312.4400 (2013).
- [215] C. Szegedy *et al.*, in “2015 IEEE Conference on Computer Vision and Pattern Recognition (CVPR),” 1–9 (2015).
- [216] K. He *et al.*, in “2016 IEEE Conference on Computer Vision and Pattern Recognition (CVPR),” 770–778 (2016).
- [217] N. Cohen and A. Shashua, *CoRR abs/1605.06743* (2016), URL <http://arxiv.org/abs/1605.06743>.
- [218] A. Bietti, L. Venturi and J. Bruna, arXiv preprint arXiv:2106.07148 (2021).
- [219] M. M. Bronstein *et al.*, arXiv preprint arXiv:2104.13478 (2021).
- [220] K. Simonyan and A. Zisserman, *CoRR abs/1409.1556* (2015).
- [221] S. Ren *et al.*, in C. Cortes *et al.*, editors, “Advances in Neural Information Processing Systems,” volume 28, Curran Associates, Inc. (2015), URL <https://proceedings.neurips.cc/paper/2015/file/14bfa6bb14875e45bba028a21ed38046-Paper.pdf>.
- [222] M. collaboration, *Journal of Instrumentation* **12**, 03, P03011 (2017), URL <https://doi.org/10.1088/1748-0221/12/03/p03011>.
- [223] O. Ronneberger, P. Fischer and T. Brox, in N. Navab *et al.*, editors, “Medical Image Computing and Computer-Assisted Intervention – MICCAI 2015,” 234–241, Springer International Publishing, Cham (2015), ISBN 978-3-319-24574-4.
- [224] G. Huang *et al.*, in “2017 IEEE Conference on Computer Vision and Pattern Recognition (CVPR),” 2261–2269 (2017).
- [225] D. Rumelhart, G. Hinton and R. Williams .
- [226] Y. Bengio, P. Simard and P. Frasconi, *Neural Networks, IEEE Transactions on* **5**, 2, 157 (1994).
- [227] R. Pascanu, T. Mikolov and Y. Bengio, in S. Dasgupta and D. McAllester, editors, “Proceedings of the 30th International Conference on Machine Learning,” volume 28 of *Proceedings of Machine Learning Research*, 1310–1318, PMLR, Atlanta, Georgia, USA (2013), URL <https://proceedings.mlr.press/v28/pascanu13.html>.

- [228] S. Hochreiter and J. Schmidhuber, *Neural Computation* **9**, 8, 1735 (1997).
- [229] R. Socher *et al.*, in “ICML,” (2011).
- [230] R. Socher *et al.*, in “Proceedings of the 2011 conference on empirical methods in natural language processing,” 151–161 (2011).
- [231] X. Chen *et al.*, in “Proceedings of the 2015 conference on empirical methods in natural language processing,” 793–798 (2015).
- [232] C. Olah and S. Carter, *Distill* (2016), URL <http://distill.pub/2016/augmented-rnns>.
- [233] D. Bahdanau, K. Cho and Y. Bengio (2015), 3rd International Conference on Learning Representations, ICLR 2015 ; Conference date: 07-05-2015 Through 09-05-2015.
- [234] A. Vaswani *et al.*, in I. Guyon *et al.*, editors, “Advances in Neural Information Processing Systems,” volume 30, Curran Associates, Inc. (2017), URL <https://proceedings.neurips.cc/paper/2017/file/3f5ee243547dee91fbd053c1c4a845aa-Paper.pdf>.
- [235] R. Bommasani *et al.*, arXiv preprint arXiv:2108.07258 (2021).
- [236] P. Battaglia *et al.*, arXiv (2018), URL <https://arxiv.org/pdf/1806.01261.pdf>.
- [237] M. Gori, G. Monfardini and F. Scarselli, in “Proceedings. 2005 IEEE International Joint Conference on Neural Networks, 2005.”, volume 2, 729–734 vol. 2 (2005).
- [238] C. R. Qi *et al.*, in “Proceedings of the IEEE Conference on Computer Vision and Pattern Recognition (CVPR),” (2017).
- [239] C. Qi *et al.*, in “NIPS,” (2017).
- [240] M. Jaderberg *et al.*, in C. Cortes *et al.*, editors, “Advances in Neural Information Processing Systems,” volume 28, Curran Associates, Inc. (2015), URL <https://proceedings.neurips.cc/paper/2015/file/33ceb07bf4eeb3da587e268d663aba1a-Paper.pdf>.
- [241] M. Zaheer *et al.*, in I. Guyon *et al.*, editors, “Advances in Neural Information Processing Systems,” volume 30, Curran Associates, Inc. (2017), URL <https://proceedings.neurips.cc/paper/2017/file/f22e4747da1aa27e363d86d40ff442fe-Paper.pdf>.
- [242] Y. Wang *et al.*, *ACM Transactions on Graphics* **38** (2018).
- [243] X. Wang *et al.*, in “2018 IEEE/CVF Conference on Computer Vision and Pattern Recognition (CVPR),” 7794–7803, IEEE Computer Society, Los Alamitos, CA, USA (2018), URL <https://doi.ieeecomputersociety.org/10.1109/CVPR.2018.00813>.
- [244] J. Gilmer *et al.*, in D. Precup and Y. W. Teh, editors, “Proceedings of the 34th International Conference on Machine Learning,” volume 70 of *Proceedings of Machine Learning Research*, 1263–1272, PMLR (2017), URL <https://proceedings.mlr.press/v70/gilmer17a.html>.
- [245] N. Choma *et al.* (IceCube) (2018), [arXiv:1809.06166].
- [246] S. R. Qasim *et al.*, *The European Physical Journal C* **79**, 7 (2019), ISSN 1434-6052, URL <http://dx.doi.org/10.1140/epjc/s10052-019-7113-9>.
- [247] J. Shlomi, P. Battaglia and J.-R. Vlimant, *Machine Learning: Science and Technology* **2**, 2, 021001 (2021), URL <https://doi.org/10.1088/2632-2153/abbf9a>.
- [248] D. P. Kingma and M. Welling, arXiv preprint arXiv:1312.6114 (2013).
- [249] D. J. Rezende, S. Mohamed and D. Wierstra, in “Proceedings of the 31th International Conference on Machine Learning, ICML 2014, Beijing, China, 21–26 June 2014,” volume 32 of *JMLR Workshop and Conference Proceedings*, 1278–1286, JMLR.org (2014), URL <http://proceedings.mlr.press/v32/rezende14.html>.
- [250] I. J. Goodfellow *et al.*, in Z. Ghahramani *et al.*, editors, “Advances in Neural Information Processing Systems 27: Annual Conference on Neural Information Processing Systems 2014, December 8–13 2014, Montreal, Quebec, Canada,” 2672–2680 (2014), URL <http://papers.nips.cc/paper/5423-generative-adversarial-nets>.
- [251] A. Radford, L. Metz and S. Chintala, in Y. Bengio and Y. LeCun, editors, “4th International Conference on Learning Representations, ICLR 2016, San Juan, Puerto Rico, May 2–4, 2016, Conference Track Proceedings,” (2016), URL <http://arxiv.org/abs/1511.06434>.
- [252] D. Rezende and S. Mohamed, *Proceedings of the 32nd International Conference on Machine Learning* **37**, 1530 (2015), URL <http://proceedings.mlr.press/v37/rezende15.html>.
- [253] L. Dinh, D. Krueger and Y. Bengio, 3rd International Conference on Learning Representations, ICLR 2015 - Workshop Track Proceedings (2015), [arXiv:1410.8516].
- [254] L. Dinh, J. Sohl-Dickstein and S. Bengio, in “5th International Conference on Learning Representations, ICLR 2017, Toulon, France, April 24–26, 2017, Conference Track Proceedings,” OpenReview.net (2017), URL <https://openreview.net/forum?id=HkpbmH91x>.
- [255] D. P. Kingma and P. Dhariwal, in S. Bengio *et al.*, editors, “Advances in Neural Information Processing Systems 31: Annual Conference on Neural Information Processing Systems 2018, NeurIPS 2018, December 3–8, 2018, Montréal, Canada,” 10236–10245 (2018).
- [256] I. Kobyzev, S. Prince and M. Brubaker, *IEEE Transactions on Pattern Analysis and Machine Intelligence* (2020).
- [257] M. Arjovsky and L. Bottou, in “5th International Conference on Learning Representations, ICLR 2017, Toulon, France, April 24–26, 2017, Conference Track Proceedings,” OpenReview.net (2017), URL https://openreview.net/forum?id=Hk4_qw5xe.
- [258] M. Wiatrak and S. V. Albrecht, arXiv preprint arXiv:1910.00927 (2019).
- [259] D. J. Rezende *et al.*, in “International Conference on Machine Learning,” 8083–8092, PMLR (2020).
- [260] M. C. Gemici, D. Rezende and S. Mohamed, arXiv preprint arXiv:1611.02304 (2016).
- [261] A. van den Oord, O. Vinyals and K. Kavukcuoglu, in I. Guyon *et al.*, editors, “Advances in Neural Information Processing Systems 30: Annual Conference on Neural Information Processing Systems 2017, December 4–9, 2017, Long Beach, CA, USA,” 6306–6315 (2017).
- [262] T. Karras *et al.*, in “6th International Conference on Learning Representations, ICLR 2018, Vancouver, BC, Canada, April 30 – May 3, 2018, Conference Track Proceedings,” OpenReview.net (2018), URL <https://openreview.net/forum?id=Hk99zCeAb>.
- [263] T. Karras, S. Laine and T. Aila, in “IEEE Conference on Computer Vision and Pattern Recognition, CVPR 2019, Long Beach, CA, USA, June 16–20, 2019,” 4401–4410, Computer Vision Foundation / IEEE (2019), URL http://openaccess.thecvf.com/content_CVPR_2019/html/Karras_A_Style-Based_Generator_Architecture_for_Generative_Adversarial_Networks_CVPR_2019_paper.html.
- [264] M. Lucic *et al.*, in S. Bengio *et al.*, editors, “Advances in Neural Information Processing Systems 31: Annual Conference on Neural Information Processing Systems 2018, NeurIPS 2018, December 3–8, 2018, Montréal, Canada,” 698–707 (2018).
- [265] A. A. Alemi *et al.*, in J. G. Dy and A. Krause, editors, “Proceedings of the 35th International Conference on Machine Learning, ICML 2018, Stockholm, Sweden, July 10–15, 2018,” volume 80 of *Proceedings of Machine Learning Research*, 159–168, PMLR (2018), URL <http://proceedings.mlr.press/v80/alemi18a.html>.

- [266] M. E. Tipping and C. M. Bishop, Journal of the Royal Statistical Society: Series B (Statistical Methodology) **61**, 3, 611 (1999), URL <https://rss.onlinelibrary.wiley.com/doi/abs/10.1111/1467-9868.00196>.
- [267] M. Arjovsky, S. Chintala and L. Bottou, arXiv preprint arXiv:1701.07875 (2017).
- [268] L. Mescheder, S. Nowozin and A. Geiger, in I. Guyon *et al.*, editors, “Advances in Neural Information Processing Systems,” volume 30, Curran Associates, Inc. (2017), URL <https://proceedings.neurips.cc/paper/2017/file/4588e674d3f0faf985047d4c3f13ed0d-Paper.pdf>.
- [269] G. Papamakarios, I. Murray and T. Pavlakou, in “Advances in Neural Information Processing Systems,” 2335–2344 (2017).
- [270] C. Durkan *et al.*, in H. M. Wallach *et al.*, editors, “Advances in Neural Information Processing Systems 32: Annual Conference on Neural Information Processing Systems 2019, NeurIPS 2019, December 8-14, 2019, Vancouver, BC, Canada,” 7509–7520 (2019).
- [271] W. Grathwohl *et al.*, in “7th International Conference on Learning Representations, ICLR 2019, New Orleans, LA, USA, May 6-9, 2019,” OpenReview.net (2019), URL <https://openreview.net/forum?id=rJxgkCck7>.
- [272] A. van den Oord *et al.*, arXiv:1609.03499 (2016), [arXiv:1609.03499], URL <http://arxiv.org/abs/1609.03499>.
- [273] A. van den Oord *et al.*, in D. D. Lee *et al.*, editors, “Advances in Neural Information Processing Systems 29: Annual Conference on Neural Information Processing Systems 2016, December 5-10, 2016, Barcelona, Spain,” 4790–4798 (2016), URL <https://proceedings.neurips.cc/paper/2016/hash/b1301141feffabac455e1f90a7de2054-Abstract.html>.
- [274] A. Hyvärinen and P. Dayan, Journal of Machine Learning Research **6**, 4 (2005).
- [275] Y. Song and S. Ermon, in Wallach *et al.* [358], 11895–11907, URL <https://proceedings.neurips.cc/paper/2019/hash/3001ef257407d5a371a96dcd947c7d93-Abstract.html>.
- [276] Y. Song *et al.*, CoRR **abs/2011.13456** (2020), [arXiv:2011.13456], URL <https://arxiv.org/abs/2011.13456>.
- [277] S. Mandt, M. D. Hoffman and D. M. Blei, J. Mach. Learn. Res. **18**, 134:1 (2017), URL <http://jmlr.org/papers/v18/17-214.html>.
- [278] D. P. Kingma and J. Ba, arXiv e-prints arXiv:1412.6980 (2014), [arXiv:1412.6980].
- [279] Y. LeCun *et al.*, *Efficient backprop*, 9–48, Lecture Notes in Computer Science (including subseries Lecture Notes in Artificial Intelligence and Lecture Notes in Bioinformatics), Springer Verlag (2012), ISBN 9783642352881, copyright: Copyright 2021 Elsevier B.V., All rights reserved.
- [280] Y. Yao, L. Rosasco and A. Caponnetto, Constructive Approximation **26**, 2, 289 (2007).
- [281] L. Prechelt, in “Neural Networks: Tricks of the trade,” 55–69, Springer (1998).
- [282] A. Krizhevsky, I. Sutskever and G. Hinton, Neural Information Processing Systems **25** (2012).
- [283] X. Glorot and Y. Bengio, in Y. W. Teh and M. Titterton, editors, “Proceedings of the Thirteenth International Conference on Artificial Intelligence and Statistics,” volume 9 of *Proceedings of Machine Learning Research*, 249–256, PMLR, Chia Laguna Resort, Sardinia, Italy (2010), URL <http://proceedings.mlr.press/v9/glorot10a.html>.
- [284] S. Ioffe and C. Szegedy, CoRR **abs/1502.03167** (2015), [arXiv:1502.03167], URL <http://arxiv.org/abs/1502.03167>.
- [285] J. L. Ba, J. R. Kiros and G. E. Hinton, Layer Normalization (2016), [arXiv:1607.06450].
- [286] D. Ulyanov, A. Vedaldi and V. Lempitsky, Instance Normalization: The Missing Ingredient for Fast Stylization (2017), [arXiv:1607.08022].
- [287] Y. Wu and K. He, Group Normalization (2018), [arXiv:1803.08494].
- [288] T.-Y. Lin *et al.*, in D. Fleet *et al.*, editors, “Computer Vision – ECCV 2014,” 740–755, Springer International Publishing, Cham (2014), ISBN 978-3-319-10602-1.
- [289] O. Russakovsky *et al.*, International Journal of Computer Vision (IJCV) **115**, 3, 211 (2015).
- [290] M. Cordts *et al.*, in “Proc. of the IEEE Conference on Computer Vision and Pattern Recognition (CVPR),” (2016).
- [291] L. Yi *et al.*, SIGGRAPH Asia (2016).
- [292] A. Radford *et al.* (2018), URL https://s3-us-west-2.amazonaws.com/openai-assets/research-covers/language-unsupervised/language_understanding_paper.pdf.
- [293] L. Fei-Fei, R. Fergus and P. Perona, IEEE Transactions on Pattern Analysis and Machine Intelligence **28**, 4, 594 (2006).
- [294] H. Larochelle, D. Erhan and Y. Bengio, in “Proceedings of the 23rd National Conference on Artificial Intelligence – Volume 2,” AAAI’08, 646–651, AAAI Press (2008), ISBN 9781577353683.
- [295] M. Palatucci *et al.*, in Y. Bengio *et al.*, editors, “Advances in Neural Information Processing Systems,” volume 22, Curran Associates, Inc. (2009), URL <https://proceedings.neurips.cc/paper/2009/file/1543843a4723ed2ab08e18053ae6dc5b-Paper.pdf>.
- [296] R. Socher *et al.*, in “Proceedings of the 26th International Conference on Neural Information Processing Systems - Volume 1,” NIPS’13, 935–943, Curran Associates Inc., Red Hook, NY, USA (2013).
- [297] T. Dorigo and P. De Castro Manzano (2020), [arXiv:2007.09121].
- [298] R. Barate *et al.* (ALEPH), Phys. Lett. B **412**, 173 (1997).
- [299] G. Louppe, M. Kagan and K. Cranmer, in I. Guyon *et al.*, editors, “Advances in Neural Information Processing Systems,” volume 30, Curran Associates, Inc. (2017), [arXiv:1611.01046], URL <https://papers.nips.cc/paper/2017/hash/48ab2f9b45957ab574cf005eb8a76760-Abstract.html>.
- [300] H. Edwards and A. Storkey, arXiv preprint arXiv:1511.05897 (2015).
- [301] Y. Ganin and V. Lempitsky, in “International conference on machine learning,” 1180–1189, PMLR (2015).
- [302] H. Ajakan *et al.*, ArXiv e-prints (2014), [arXiv:1412.4446].
- [303] G. Kasieczka and D. Shih, Phys. Rev. Lett. **125**, 12, 122001 (2020), [arXiv:2001.05310].
- [304] C. Shimmin *et al.*, Phys. Rev. **D96**, 7, 074034 (2017), [arXiv:1703.03507].
- [305] J. Stevens and M. Williams, JINST **8**, P12013 (2013), [arXiv:1305.7248].
- [306] J. Dolen *et al.*, JHEP **05**, 156 (2016), [arXiv:1603.00027].
- [307] I. Moutl, B. Nachman and D. Neill, JHEP **05**, 002 (2018), [arXiv:1710.06859].
- [308] L. Bradshaw *et al.* (2019), [arXiv:1908.08959].
- [309] ATL-PHYS-PUB-2018-014 (2018), URL <http://cds.cern.ch/record/2630973>.
- [310] L.-G. Xia, Nucl. Instrum. Meth. **A930**, 15 (2019), [arXiv:1810.08387].
- [311] C. Englert *et al.*, Eur. Phys. J. **C79**, 1, 4 (2019), [arXiv:1807.08763].
- [312] S. Wunsch *et al.* (2019), [arXiv:1907.11674].
- [313] A. Rogozhnikov *et al.*, JINST **10**, 03, T03002 (2015), [arXiv:1410.4140].

- [314] C. Collaboration, *Machine Learning: Science and Technology* (2020).
- [315] J. M. Clavijo, P. Glaysher and J. M. Katzy (2020), [arXiv:2005.00568].
- [316] G. Kasieczka *et al.* (2020), [arXiv:2007.14400].
- [317] O. Kitouni *et al.* (2020), [arXiv:2010.09745].
- [318] A. Ghosh and B. Nachman (2021), [arXiv:2109.08159].
- [319] P. Baldi *et al.*, *Eur. Phys. J.* **C76**, 5, 235 (2016), [arXiv:1601.07913].
- [320] A. Ghosh, B. Nachman and D. Whiteson (2021), [arXiv:2105.08742].
- [321] W. L. Oberkampf *et al.*, *Reliability Engineering & System Safety* **85**, 1, 11 (2004), ISSN 0951-8320, alternative Representations of Epistemic Uncertainty, URL <https://www.sciencedirect.com/science/article/pii/S0951832004000493>.
- [322] A. O'Hagan and J. E. Oakley, *Reliability Engineering & System Safety* **85**, 1, 239 (2004), ISSN 0951-8320, alternative Representations of Epistemic Uncertainty, URL <https://www.sciencedirect.com/science/article/pii/S0951832004000638>.
- [323] E. Hüllermeier and W. Waegeman, *CoRR* **abs/1910.09457** (2019), URL <http://arxiv.org/abs/1910.09457>.
- [324] A. Kendall and Y. Gal, in I. Guyon *et al.*, editors, "Advances in Neural Information Processing Systems," volume 30, Curran Associates, Inc. (2017), URL <https://proceedings.neurips.cc/paper/2017/file/2650d6089a6d640c5e85b2b88265dc2b-Paper.pdf>.
- [325] A. D. Kiureghian and O. Ditlevsen, *Structural Safety* **31**, 2, 105 (2009), ISSN 0167-4730, risk Acceptance and Risk Communication, URL <https://www.sciencedirect.com/science/article/pii/S0167473008000556>.
- [326] Y. Yao *et al.*, *Bayesian Analysis* **13**, 3 (2018), ISSN 1936-0975, URL <http://dx.doi.org/10.1214/17-BA1091>.
- [327] J. Snoek *et al.*, in Wallach *et al.* [358], 13969–13980, URL <https://proceedings.neurips.cc/paper/2019/hash/8558cb408c1d76621371888657d2eb1d-Abstract.html>.
- [328] Y. Gal and Z. Ghahramani, in M. Balcan and K. Q. Weinberger, editors, "Proceedings of the 33rd International Conference on Machine Learning, ICML 2016, New York City, NY, USA, June 19–24, 2016," volume 48 of *JMLR Workshop and Conference Proceedings*, 1050–1059, JMLR.org (2016), URL <http://proceedings.mlr.press/v48/gal16.html>.
- [329] B. Lakshminarayanan, A. Pritzel and C. Blundell, in I. Guyon *et al.*, editors, "Advances in Neural Information Processing Systems 30: Annual Conference on Neural Information Processing Systems 2017, December 4–9, 2017, Long Beach, CA, USA," 6402–6413 (2017), URL <https://proceedings.neurips.cc/paper/2017/hash/9ef2ed4b7fd2c810847ffa5fa85bce38-Abstract.html>.
- [330] D. P. Kingma, T. Salimans and M. Welling, *CoRR* **abs/1506.02557** (2015), URL <http://arxiv.org/abs/1506.02557>.
- [331] G. C. Strong (2020), [arXiv:2002.01427].
- [332] V. V. Gligorov and M. Williams, *JINST* **8**, P02013 (2013), [arXiv:1210.6861].
- [333] D. W. III *et al.* (2017), URL https://d14physicalsciences.github.io/files/nips_dlps_2017_3.pdf.
- [334] D. Bourgeois, C. Fitzpatrick and S. Stahl (2018), [arXiv:1808.00711].
- [335] J. Alimena, Y. Iiyama and J. Kieseler (2020), [arXiv:2004.10744].
- [336] C. Balázs *et al.* (DarkMachines High Dimensional Sampling Group) (2021), [arXiv:2101.04525].
- [337] F. Rehm *et al.* (2021), [arXiv:2103.10142].
- [338] C. Mahesh *et al.*, in "34th Conference on Neural Information Processing Systems," (2021), [arXiv:2104.06622].
- [339] S. Amrouche *et al.* (2021), [arXiv:2105.01160].
- [340] P. Goncharov *et al.*, in "24th International Scientific Conference of Young Scientists and Specialists," (2021), [arXiv:2109.08982].
- [341] J. Duarte *et al.*, *JINST* **13**, 07, P07027 (2018), [arXiv:1804.06913].
- [342] J. Ngadiuba *et al.*, *Mach. Learn.: Sci. Tech.* **2**, 1, 015001 (2020), [arXiv:2003.06308].
- [343] S. Summers *et al.*, *JINST* **15**, 05, P05026 (2020), [arXiv:2002.02534].
- [344] J. Krupa *et al.* (2020), [arXiv:2007.10359].
- [345] L. R. M. Mohan *et al.* (2020), [arXiv:2008.09210].
- [346] S. Carrazza, J. M. Cruz-Martinez and M. Rossi (2020), [arXiv:2009.06635].
- [347] D. S. Rankin *et al.*, 2020 IEEE/ACM International Workshop on Heterogeneous High-performance Reconfigurable Computing (H2RC) 38 (2020), [arXiv:2010.08556].
- [348] M. Rossi, S. Carrazza and J. M. Cruz-Martinez (2020), [arXiv:2012.08221].
- [349] T. Aarrestad *et al.* (2021), [arXiv:2101.05108].
- [350] B. Hawks *et al.* (2021), [arXiv:2102.11289].
- [351] T. Teixeira, L. Andrade and J. M. de Seixas (2021), [arXiv:2103.12467].
- [352] T. M. Hong *et al.* (2021), [arXiv:2104.03408].
- [353] G. Di Guglielmo *et al.* (2021), [arXiv:2105.01683].
- [354] M. Migliorini *et al.* (2021), [arXiv:2105.04428].
- [355] E. Govorkova *et al.* (2021), [arXiv:2108.03986].
- [356] V. Kuznetsov, L. Giommi and D. Bonacorsi (2020), [arXiv:2007.14781].
- [357] O. Sunneborn Gudnadottir *et al.*, *EPJ Web Conf.* **251**, 02054 (2021), [arXiv:2109.00264].
- [358] H. M. Wallach *et al.*, editors, *Advances in Neural Information Processing Systems 32: Annual Conference on Neural Information Processing Systems 2019, NeurIPS 2019, December 8–14, 2019, Vancouver, BC, Canada* (2019), URL <https://proceedings.neurips.cc/paper/2019>.

42. Monte Carlo Techniques

Revised September 2021 by G. Cowan (RHUL).

Monte Carlo techniques are often the only practical way to evaluate difficult integrals or to sample random variables governed by complicated probability density functions. Here we describe an assortment of methods for sampling some commonly occurring probability density functions.

42.1 Sampling the uniform distribution

Most Monte Carlo sampling or integration techniques assume a “random number generator,” which generates uniform statistically independent values on the half open interval $[0, 1)$; for reviews see, *e.g.*, Refs. [1, 2].

Uniform random number generators are available in software libraries such as CLHEP [3], and ROOT [4]. For example, in addition to a basic congruential generator TRandom (see below), ROOT provides three more sophisticated routines: TRandom1 implements the RANLUX generator [5] based on the method by Lüscher, and allows the user to select different quality levels, trading off quality with speed; TRandom2 is based on the maximally equidistributed combined Tausworthe generator by L’Ecuyer [6]; the TRandom3 generator implements the Mersenne twister algorithm of Matsumoto and Nishimura [7]. All of the algorithms produce a periodic sequence of numbers, and to obtain effectively random values, one must not use more than a small subset of a single period. The Mersenne twister algorithm has an extremely long period of $2^{19937} - 1$. A recent review of high-quality random number generators can be found in Ref. [8].

The performance of the generators can be investigated with tests such as DIEHARD [9] or TestU01 [10]. Many commonly available congruential generators fail these tests and often have sequences (typically with periods less than 2^{32}), which can be easily exhausted on modern computers. A short period is a problem for the TRandom generator in ROOT, which, however, has the advantage that its state is stored in a single 32-bit word. The generators TRandom1, TRandom2, or TRandom3 have much longer periods, with TRandom3 being recommended by the ROOT authors as providing the best combination of speed and good random properties. For further information see, *e.g.*, Ref. [11].

42.2 Inverse transform method

If the desired probability density function is $f(x)$ on the range $-\infty < x < \infty$, its cumulative distribution function (expressing the probability that $x \leq a$) is given by Eq. (39.6). If a is chosen with probability density $f(a)$, then the integrated probability up to point a , $F(a)$, is itself a random variable which will occur with uniform probability density on $[0, 1]$. Suppose u is generated according to a uniformly distributed in $(0, 1)$. If x can take on any value, and ignoring the endpoints, we can then find a unique x chosen from the p.d.f. $f(x)$ for a given u if we set

$$u = F(x), \tag{42.1}$$

provided we can find an inverse of F , defined by

$$x = F^{-1}(u). \tag{42.2}$$

This method is shown in Fig. 42.1a. It is most convenient when one can calculate by hand the inverse function of the indefinite integral of f . This is the case for some common functions $f(x)$ such as $\exp(x)$, $(1 - x)^n$, and $1/(1 + x^2)$ (Cauchy or Breit-Wigner), although it does not necessarily produce the fastest generator. Standard libraries contain software to implement this method numerically, working from functions or histograms in one or more dimensions, *e.g.*, the UNU.RAN package [12], available in ROOT. For a discrete distribution, $F(x)$ will have a discontinuous jump of size $f(x_k)$ at each allowed $x_k, k = 1, 2, \dots$. Choose u from a uniform distribution on $(0, 1)$ as before. Find x_k such that

$$F(x_{k-1}) < u \leq F(x_k) \equiv \text{Prob}(x \leq x_k) = \sum_{i=1}^k f(x_i); \tag{42.3}$$

then x_k is the value we seek (note: $F(x_0) \equiv 0$). This algorithm is illustrated in Fig. 42.1b.

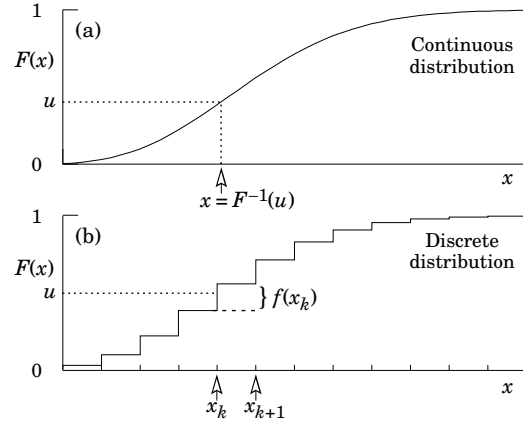


Figure 42.1: Use of a random number u chosen from a uniform distribution $(0,1)$ to find a random number x from a distribution with cumulative distribution function $F(x)$.

42.3 Acceptance-rejection method (Von Neumann)

Very commonly an analytic form for $F(x)$ is unknown or too complex to work with, so that obtaining an inverse as in Eq. (42.2) is impractical. We suppose that for any given value of x , the probability density function $f(x)$ can be computed, and further that enough is known about $f(x)$ that we can enclose it entirely inside a shape which is C times an easily generated distribution $h(x)$, as illustrated in Fig. 42.2. That is, $Ch(x) \geq f(x)$ must hold for all x . Frequently $h(x)$ is uniform or is a normalized

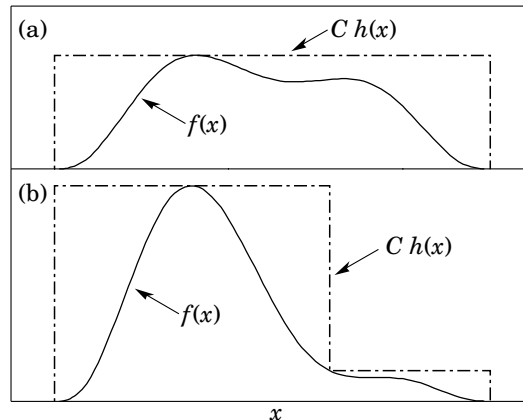


Figure 42.2: Illustration of the acceptance-rejection method. Random points are chosen inside the upper bounding figure, and rejected if the ordinate exceeds $f(x)$. The lower figure illustrates a method to increase the efficiency (see text).

sum of uniform distributions. Note that both $f(x)$ and $h(x)$ must be normalized to unit area, and therefore, the proportionality constant $C > 1$. To generate $f(x)$, first generate a candidate x according to $h(x)$. Calculate $f(x)$ and the height of the envelope $Ch(x)$; generate u and test if $uCh(x) \leq f(x)$. If so, accept x ; if not reject x and try again. If we regard x and $uCh(x)$ as the abscissa and ordinate of a point in a two-dimensional plot, these points will populate the entire area $Ch(x)$ in a smooth manner; then we accept those which fall under $f(x)$. The efficiency is the ratio of areas, which must equal $1/C$; therefore we must keep C as close as possible to 1.0. Therefore, we try to choose $Ch(x)$ to be as close to $f(x)$ as convenience dictates, as in the lower part of Fig. 42.2.

42.4 Algorithms

Algorithms for generating random numbers belonging to many different distributions are given for example by Press [13], Ahrens and Dieter [14], Rubinstein [15], Devroye [16], Walck [17] and Gentle [18]. For many distributions, alternative algorithms exist, varying in complexity, speed, and accuracy. For time-critical applications, these algorithms may be coded in-line to remove the significant overhead often encountered in making function calls.

In the examples given below, we use the notation for the variables and parameters given in Table 39.1. Variables named “ u ” are assumed to be independent and uniform on $[0,1]$. Denominators must be verified to be non-zero where relevant.

42.4.1 Exponential decay

This is a common application of the inverse transform method, and uses the fact that if u is uniformly distributed in $[0,1]$, then $(1-u)$ is as well. Consider an exponential p.d.f. $f(t) = (1/\tau)\exp(-t/\tau)$ that is truncated so as to lie between two values, a and b , and renormalized to unit area. To generate decay times t according to this p.d.f., first let $\alpha = \exp(-a/\tau)$ and $\beta = \exp(-b/\tau)$; then generate u and let

$$t = -\tau \ln(\beta + u(\alpha - \beta)). \quad (42.4)$$

For $(a,b) = (0,\infty)$, we have simply $t = -\tau \ln u$. (See also Sec. 42.4.6.)

42.4.2 Isotropic direction in 3D

Isotropy means the density is proportional to solid angle, the differential element of which is $d\Omega = d(\cos\theta)d\phi$. Hence $\cos\theta$ is uniform $(2u_1 - 1)$ and ϕ is uniform $(2\pi u_2)$. For alternative generation of $\sin\phi$ and $\cos\phi$, see the next subsection.

42.4.3 Sine and cosine of random angle in 2D

Generate u_1 and u_2 . Then $v_1 = 2u_1 - 1$ is uniform on $(-1,1)$, and $v_2 = u_2$ is uniform on $(0,1)$. Calculate $r^2 = v_1^2 + v_2^2$. If $r^2 > 1$, start over. Otherwise, the sine (S) and cosine (C) of a random angle (*i.e.*, uniformly distributed between zero and 2π) are given by

$$S = 2v_1v_2/r^2 \quad \text{and} \quad C = (v_1^2 - v_2^2)/r^2. \quad (42.5)$$

42.4.4 Gaussian distribution

If u_1 and u_2 are uniform on $(0,1)$, then

$$z_1 = \sin(2\pi u_1)\sqrt{-2\ln u_2} \quad \text{and} \quad z_2 = \cos(2\pi u_1)\sqrt{-2\ln u_2} \quad (42.6)$$

are independent and Gaussian distributed with mean 0 and $\sigma = 1$.

There are many variants of this basic algorithm, which may be faster. For example, construct $v_1 = 2u_1 - 1$ and $v_2 = 2u_2 - 1$, which are uniform on $(-1,1)$. Calculate $r^2 = v_1^2 + v_2^2$, and if $r^2 > 1$ start over. If $r^2 < 1$, it is uniform on $(0,1)$. Then

$$z_1 = v_1\sqrt{\frac{-2\ln r^2}{r^2}} \quad \text{and} \quad z_2 = v_2\sqrt{\frac{-2\ln r^2}{r^2}} \quad (42.7)$$

are independent numbers chosen from a normal distribution with mean 0 and variance 1. $z'_i = \mu + \sigma z_i$ distributes with mean μ and variance σ^2 .

For a multivariate Gaussian with an $n \times n$ covariance matrix V , one can start by generating n independent Gaussian variables, $\{\eta_j\}$, with mean 0 and variance 1 as above. Then the new set $\{x_i\}$ is obtained as $x_i = \mu_i + \sum_j L_{ij}\eta_j$, where μ_i is the mean of x_i , and L_{ij} are the components of L , the unique lower triangular matrix that fulfils $V = LL^T$. The matrix L can be easily computed by the following recursive relation (Cholesky's method):

$$L_{jj} = \left(V_{jj} - \sum_{k=1}^{j-1} L_{jk}^2 \right)^{1/2}, \quad (42.8a)$$

$$L_{ij} = \frac{V_{ij} - \sum_{k=1}^{j-1} L_{ik}L_{jk}}{L_{jj}}, \quad j = 1, \dots, n; \quad i = j + 1, \dots, n, \quad (42.8b)$$

where $V_{ij} = \rho_{ij}\sigma_i\sigma_j$ are the components of V . For $n = 2$ one has

$$L = \begin{pmatrix} \sigma_1 & 0 \\ \rho\sigma_2 & \sqrt{1 - \rho^2}\sigma_2 \end{pmatrix}, \quad (42.9)$$

and therefore the correlated Gaussian variables are generated as $x_1 = \mu_1 + \sigma_1\eta_1$, $x_2 = \mu_2 + \rho\sigma_2\eta_1 + \sqrt{1 - \rho^2}\sigma_2\eta_2$.

42.4.5 $\chi^2(n)$ distribution

To generate a variable following the χ^2 distribution for n degrees of freedom, use the Gamma distribution with $k = n/2$ and $\lambda = 1/2$ using the method of Sec. 42.4.6.

42.4.6 Gamma distribution

All of the following algorithms are given for $\lambda = 1$. For $\lambda \neq 1$, divide the resulting random number x by λ .

- If $k = 1$ (the *exponential* distribution), accept $x = -\ln u$. (See also Sec. 42.4.1.)
- If $0 < k < 1$, initialize with $v_1 = (e+k)/e$ (with $e = 2.71828\dots$ being the natural log base). Generate u_1, u_2 . Define $v_2 = v_1 u_1$.

Case 1: $v_2 \leq 1$. Define $x = v_2^{1/k}$. If $u_2 \leq e^{-x}$, accept x and stop, else restart by generating new u_1, u_2 .

Case 2: $v_2 > 1$. Define $x = -\ln([v_1 - v_2]/k)$. If $u_2 \leq x^{k-1}$, accept x and stop, else restart by generating new u_1, u_2 . Note that, for $k < 1$, the probability density has a pole at $x = 0$, so that return values of zero due to underflow must be accepted or otherwise dealt with.

- Otherwise, if $k > 1$, initialize with $c = 3k - 0.75$. Generate u_1 and compute $v_1 = u_1(1 - u_1)$ and $v_2 = (u_1 - 0.5)\sqrt{c/v_1}$. If $x = k + v_2 - 1 \leq 0$, go back and generate new u_1 ; otherwise generate u_2 and compute $v_3 = 64v_1^3u_2^2$. If $v_3 \leq 1 - 2v_2^2/x$ or if $\ln v_3 \leq 2\{[k-1]\ln[x/(k-1)] - v_2\}$, accept x and stop; otherwise go back and generate new u_1 .

42.4.7 Binomial distribution

Begin with $k = 0$ and generate u uniform in $[0,1)$. Compute $P_k = (1-p)^n$ and store P_k into B . If $u \leq B$ accept $r_k = k$ and stop. Otherwise, increment k by one; compute the next P_k as $P_k \cdot (p/(1-p)) \cdot (n-k)/(k+1)$; add this to B . Again, if $u \leq B$, accept $r_k = k$ and stop, otherwise iterate until a value is accepted. If $p > 1/2$, it will be more efficient to generate r from $f(r; n, q)$, *i.e.*, with p and q interchanged, and then set $r_k = n - r$.

42.4.8 Poisson distribution

Iterate until a successful choice is made: Begin with $k = 1$ and set $A = 1$ to start. Generate u . Replace A with uA ; if now $A < \exp(-\mu)$, where μ is the Poisson parameter, accept $n_k = k - 1$ and stop. Otherwise increment k by 1, generate a new u and repeat, always starting with the value of A left from the previous try.

Note that the Poisson generator used in ROOT's `TRandom` classes before version 5.12 (including the derived classes `TRandom1`, `TRandom2`, `TRandom3`) uses a Gaussian approximation when μ exceeds a given threshold. This may be satisfactory (and much faster) for some applications. To do this, generate z from a Gaussian with zero mean and unit standard deviation; then use $x = \max(0, [\mu + z\sqrt{\mu} + 0.5])$ where $[\]$ signifies the greatest integer \leq the expression. The routines from Numerical Recipes [13] and CLHEP's routine `RandPoisson` do not make this approximation (see, *e.g.*, Ref. [11]).

42.4.9 Student's t distribution

Generate u_1 and u_2 uniform in $(0,1)$; then $t = \sin(2\pi u_1)[n(u_2^{-2/n} - 1)]^{1/2}$ follows the Student's t distribution for $n > 0$ degrees of freedom (n not necessarily an integer).

Alternatively, generate x from a Gaussian with mean 0 and $\sigma^2 = 1$ according to the method of 42.4.4. Next generate y ,

an independent gamma random variate, according to 42.4.6 with $\lambda = 1/2$ and $k = n/2$. Then $z = x/\sqrt{y/n}$ is distributed as a t with n degrees of freedom.

For the special case $n = 1$, the Breit-Wigner distribution, generate u_1 and u_2 ; set $v_1 = 2u_1 - 1$ and $v_2 = 2u_2 - 1$. If $v_1^2 + v_2^2 \leq 1$ accept $z = v_1/v_2$ as a Breit-Wigner distribution with unit area, center at 0.0, and FWHM 2.0. Otherwise start over. For center M_0 and FWHM Γ , use $W = z\Gamma/2 + M_0$.

42.4.10 Beta distribution

The choice of an appropriate algorithm for generation of beta distributed random numbers depends on the values of the parameters α and β . For, e.g., $\alpha = 1$, one can use the transformation method to find $x = 1 - u^{1/\beta}$, and similarly if $\beta = 1$ one has $x = u^{1/\alpha}$. For more general cases see, e.g., Refs. [17, 18] and references therein.

42.5 Importance sampling and weighted Monte Carlo

Often the goal of a Monte Carlo calculation is to determine an expectation value of a function $h(x)$, where x is a (single or vector) random variable that follows a pdf $f(x)$,

$$E_f[h(x)] = \int h(x)f(x) dx \equiv \mu. \quad (42.10)$$

A Monte-Carlo estimator $\hat{\mu}_{MC}$ for μ is the average of N values of $h(x)$ where x is sampled (generated) from $f(x)$, i.e., $\hat{\mu}_{MC} = \frac{1}{N} \sum_{i=1}^N h(x_i)$. This has a variance

$$V[\hat{\mu}_{MC}] = \frac{1}{N} V_f[h(x)] = \frac{1}{N} (E_f[h^2(x)] - \mu^2). \quad (42.11)$$

By using the method of *importance sampling*, one can achieve a reduction in this variance and thus a more accurate determination of the expectation value for a given number of random values generated. The key idea is to rewrite the expectation value in Eq. (42.10) as

$$\mu = \int h(x)f(x) dx = \int \frac{h(x)f(x)}{g(x)} g(x) dx = E_g \left[\frac{h(x)f(x)}{g(x)} \right], \quad (42.12)$$

where $g(x)$ is any other pdf of x with the same support as $f(x)$ (i.e., nonzero for the same region of x). Thus the desired quantity μ is the expectation value with respect to g of $h(x)f(x)/g(x)$. It can be estimated by generating N values of x sampled from g and computing

$$\hat{\mu}_{IS} = \frac{1}{N} \sum_{i=1}^N \frac{h(x_i)f(x_i)}{g(x_i)}. \quad (42.13)$$

The variance of $\hat{\mu}_{IS}$ is given by

$$V[\hat{\mu}_{IS}] = \frac{1}{N} V_g \left[\frac{h(x)f(x)}{g(x)} \right] = \frac{1}{N} \left(E_g \left[\frac{h^2(x)f^2(x)}{g^2(x)} \right] - \mu^2 \right), \quad (42.14)$$

By choosing $g(x)$ such that $h(x)f(x)/g(x)$ is as constant as possible, the variance of $\hat{\mu}_{IS}$ can be substantially reduced. One can show (see, e.g., Refs. [19, 20]) that the variance is minimized when $g(x) \propto |h(x)|f(x)$.

An alternative importance sampling estimator can be constructed by replacing the number of generated values N in Eq. (42.13) by the sum $\sum_{i=1}^N f(x_i)/g(x_i)$. This can give an even smaller variance at the price of a small bias. It can be of further advantage in problems where the pdf $f(x)$ is known only up to a normalization constant, which then cancels (see Refs. [19, 20]).

A closely related application of importance sampling is the use of weighted Monte Carlo to compute the probability $P_f(x \in A)$ for x to be in a specified region A :

$$P_f(x \in A) = \int_A f(x) dx. \quad (42.15)$$

It may be, however, that one does not have an MC model capable of generating $x \sim f(x)$, but rather one can generate x according to a different density $g(x)$. The probability $P_f(x \in A)$ can be written

$$\begin{aligned} P_f(x \in A) &= \frac{\int_A \frac{f(x)}{g(x)} g(x) dx}{\int_A g(x) dx} \int_A g(x) dx \\ &= E_g[w(x)|x \in A] P_g(x \in A), \end{aligned} \quad (42.16)$$

where $w(x) = f(x)/g(x)$ is the *weight function* and $P_g(x \in A) = \int_A g(x) dx$ is the probability to find $x \in A$ assuming $x \sim g(x)$. That is, $P_f(x \in A)$ is the conditional expectation value of $w(x)$ with respect to $g(x)$ given $x \in A$ multiplied by the probability to find $x \in A$ under assumption of $g(x)$.

Suppose N values of x are generated according to $g(x)$ and m of them are found in the region A . Then the probability to be in A for $x \sim g(x)$ can be estimated by m/N , and the expectation value above can be obtained from the average of the weights in A . Therefore the desired probability $P_f(x \in A)$ can be estimated using

$$\hat{P}_f(x \in A) = \frac{1}{m} \sum_{i=1}^m w_i \times \frac{m}{N} = \frac{1}{N} \sum_{i=1}^m w_i, \quad (42.17)$$

where $w_i = w(x_i)$ and the sum includes only the m values of x found in A . That is, when generating the x values according to $g(x)$ instead of $f(x)$, the number of events m found in A is replaced by the corresponding sum of weights. The variance of $\hat{P}_f(x \in A)$ can be found from

$$\widehat{V}[\hat{P}_f(x \in A)] = \frac{1}{N^2} \sum_{i=1}^m w_i^2. \quad (42.18)$$

By choosing $g(x)$ so that a larger fraction of x values are sampled in the “important” region A , one can reduce the variance of the estimated probability for a given total number of generated values.

42.6 Markov Chain Monte Carlo

In applications involving generation of random numbers following a multivariate distribution with a high number of dimensions, the transformation method may not be possible and the acceptance-rejection technique may have too low of an efficiency to be practical. If it is not required to have independent random values, but only that they follow a certain distribution, then Markov Chain Monte Carlo (MCMC) methods can be used. In depth treatments of MCMC can be found, e.g., in the texts by Robert and Casella [19], Liu [20], and the review by Neal [21]. HEP-oriented software for MCMC is available from the Bayesian Analysis Toolkit (BAT) [22, 23].

MCMC is particularly useful in connection with Bayesian statistics, where a p.d.f. $p(\theta)$ for an n -dimensional vector of parameters $\theta = (\theta_1, \dots, \theta_n)$ is obtained, and one needs the marginal distribution of a subset of the components. Here one samples θ from $p(\theta)$ and simply records the marginal distribution for the components of interest.

A simple and broadly applicable MCMC method is the Metropolis-Hastings algorithm, which allows one to generate multidimensional points θ distributed according to a target p.d.f. that is proportional to a given function $p(\theta)$. It is not necessary to have

$p(\theta)$ normalized to unit area, which is useful in Bayesian statistics, as posterior probability densities are often determined only up to an unknown normalization constant.

To generate points that follow $p(\theta)$, one first needs a proposal p.d.f. $q(\theta; \theta_0)$, which can be (almost) any p.d.f. from which independent random values θ can be generated, and which contains as a parameter another point in the same space θ_0 . For example, a multivariate Gaussian centered about θ_0 can be used. Beginning at an arbitrary starting point θ_0 , the Hastings algorithm iterates the following steps:

1. Generate a value θ using the proposal density $q(\theta; \theta_0)$;
2. Form the Hastings test ratio, $\alpha = \min \left[1, \frac{p(\theta)q(\theta_0; \theta)}{p(\theta_0)q(\theta; \theta_0)} \right]$;
3. Generate a value u uniformly distributed in $[0, 1]$;
4. If $u \leq \alpha$, take $\theta_1 = \theta$. Otherwise, repeat the old point, *i.e.*, $\theta_1 = \theta_0$.
5. Set $\theta_0 = \theta_1$ and return to step 1.

If one takes the proposal density to be symmetric in θ and θ_0 , then this is the *Metropolis-Hastings* algorithm, and the test ratio becomes $\alpha = \min[1, p(\theta)/p(\theta_0)]$. That is, if the proposed θ is at a value of probability higher than θ_0 , the step is taken. If the proposed step is rejected, the old point is repeated.

Methods for assessing and optimizing the performance of the algorithm are discussed in, *e.g.*, Refs. [19–21]. One can, for example, examine the autocorrelation as a function of the lag k , *i.e.*, the correlation of a sampled point with that k steps removed. This should decrease as quickly as possible for increasing k .

Generally one chooses the proposal density so as to optimize some quality measure such as the autocorrelation. For certain problems it has been shown that one achieves optimal performance when the acceptance fraction, that is, the fraction of points with $u \leq \alpha$, is around 40%. This can be adjusted by varying the width of the proposal density. For example, one can use for the proposal p.d.f. a multivariate Gaussian with the same covariance matrix as that of the target p.d.f., but scaled by a constant.

References

- [1] F. James, *Comput. Phys. Commun.* **60**, 329 (1990).
- [2] P. L'Ecuyer, *Proc. 1997 Winter Simulation Conference*, IEEE Press, Dec. 1997, 127–134.
- [3] L. Lonnblad, *Comput. Phys. Commun.* **84**, 307 (1994).
- [4] R. Brun and F. Rademakers, *Nucl. Instrum. Meth.* **A389**, 81 (1997); See also root.cern.ch.
- [5] F. James, *Comput. Phys. Commun.* **79**, 111 (1994), [Erratum: *Comput. Phys. Commun.* **97**, 357 (1996)]; M. Luscher, *Comput. Phys. Commun.* **79**, 100 (1994), [hep-lat/9309020].
- [6] P. L'Ecuyer, *Mathematics of Computation*, **65**, 213 (1996) and **65**, 225 (1999).
- [7] M. Matsumoto and T. Nishimura, *ACM Transactions on Modeling and Computer Simulation*, Vol. 8, No. 1, January 1998, 3–30.
- [8] F. James and L. Moneta, *Comput. Softw. Big Sci.* **4**, 2, 12 p (2019), 4 figures, [[arXiv:1903.01247](https://arxiv.org/abs/1903.01247)], URL <http://cds.cern.ch/record/2678858>.
- [9] Much of DIEHARD is described in: G. Marsaglia, *A Current View of Random Number Generators*, keynote address, *Computer Science and Statistics: 16th Symposium on the Interface*, Elsevier (1985).
- [10] P. L'Ecuyer and R. Simard, *ACM Transactions on Mathematical Software* **33**, 4, Article 1, December 2007.
- [11] J. Heinrich, CDF Note CDF/MEMO/STATISTICS/PUBLIC/8032, 2006.
- [12] UNU.RAN is described at statmath.wu.ac.at/software/unuran; See also W. Hörmann, J. Leydold, and G. Derflinger, *Automatic Nonuniform Random Variate Generation*, (Springer, New York, 2004).
- [13] W.H. Press *et al.*, *Numerical Recipes*, 3rd edition, (Cambridge University Press, New York, 2007).
- [14] J.H. Ahrens and U. Dieter, *Computing* **12**, 223 (1974).
- [15] R.Y. Rubinstein, *Simulation and the Monte Carlo Method*, (John Wiley and Sons, Inc., New York, 1981).
- [16] L. Devroye, *Non-Uniform Random Variate Generation*, (Springer-Verlag, New York, 1986); Available online at luc.devroye.org/rnbookindex.html.
- [17] C. Walck, *Handbook on Statistical Distributions for Experimentalists*, University of Stockholm Report SUF-PFY/96-01, available from www.fysik.su.se/~walck.
- [18] J.E. Gentle, *Random Number Generation and Monte Carlo Methods*, 2nd ed., (Springer, New York, 2003).
- [19] C.P. Robert and G. Casella, *Monte Carlo Statistical Methods*, 2nd ed., (Springer, New York, 2004).
- [20] J.S. Liu, *Monte Carlo Strategies in Scientific Computing*, (Springer, New York, 2001).
- [21] R.M. Neal, *Probabilistic Inference Using Markov Chain Monte Carlo Methods*, Technical Report CRG-TR-93-1, Dept. of Computer Science, University of Toronto, available from www.cs.toronto.edu/~radford/res-mcmc.html.
- [22] A. Caldwell, D. Kollar, K. Kröninger, *Comput. Phys. Commun.* **180** (2009) pages 2197–2209.
- [23] Schulz, O., Beaujean, F., Caldwell, A. *et al.*, *SN Computer Science* **2**, 210 (2021).

43. Monte Carlo Event Generators

Revised Oct 2023 by P. Nason (INFN, Milano-Bicocca; Milano-Bicocca U.) and P. Skands (Monash U.).

General-purpose Monte Carlo (GPMC) generators like HERWIG [1–3], PYTHIA [4,5], and SHERPA [6], provide detailed simulations of high-energy collisions. They play an essential role in QCD modeling (in particular for aspects beyond fixed-order perturbative QCD) and in data analysis and the planning of new experiments, where they are used together with detector simulation to estimate signals and backgrounds in high-energy processes. They are built from several components, that describe the physics starting from very short distance scales, up to the typical scale of hadron formation and decay. Since QCD is weakly interacting at short distances (below a femtometer), the components of the GPMC dealing with short-distance physics are based upon perturbation theory. At larger distances, all soft hadronic phenomena, like hadronization and the formation of the underlying event in hadron collisions, cannot be computed from first principles at present, and one must rely upon QCD-inspired models.

The purpose of this review is to illustrate the main components of these generators. It is divided into four sections. The first one deals with short-distance, perturbative phenomena. The basic concepts leading to the simulations of the dominant QCD processes are illustrated here. In the second section, the nonperturbative transition from partons to hadrons (“hadronization”) is treated. The two most popular hadronization models, the string and cluster models, are illustrated. The basics of the implementation of decay chains of unstable “primary” hadrons into stable “secondaries” is also illustrated here. In the third section, models for soft hadron physics are discussed. These include models for the underlying event and for low- p_{\perp} (“minimum-bias”) interactions. Aspects of collective effects, such as Bose-Einstein and color-reconnection effects, are also discussed here. The fourth section briefly introduces the challenges of MC uncertainty estimates and tuning.

We use natural units throughout, such that $c = 1$ and $\hbar = 1$, with energies, momenta and masses measured in GeV, and times and distances measured in GeV^{-1} .

43.1 Short-distance physics in GPMC generators

The short-distance components of a GPMC generator deal with the computation of the primary process at hand, with decays of short-lived particles, and with the generation of QCD and QED radiation. QCD radiation is computable in perturbation theory as long as the time scales involved are well below $1/\Lambda$, where Λ is a typical hadronic scale of few hundred MeV. Because of the presence of logarithmic enhancements due to both collinear and soft emissions, this description involves an indefinite number of final-state particles that are emitted at time scales below $1/\Lambda$. In e^+e^- annihilation into hadrons, for example, the time scale of the primary process is of the order of the inverse of the annihilation energy Q . Collinear and soft emissions take place at all time scales between $1/Q$ and $1/\Lambda$. Technically, the computation of the dominant collinear and soft radiation is carried out by the so called shower algorithms. Historically, “Parton Shower” algorithms were first developed for resummation of collinear singularities. We will briefly describe this approach in this section. We stress, however, that many modern generators adopt approaches that focus initially upon soft singularities, leading to “Dipole Showers”, discussed in Sec. 43.1.3.

Collinear singularities arise when the angle between two emitted light partons becomes small. For example, in a process in which a quark and a gluon are emitted, if the angle θ among them is very small (and is smaller than the angles among all other pairs of light partons in the process) the squared amplitude factorizes as follows

$$|M_{qg}|^2 d\Phi_{qg} \approx |M_q|^2 d\Phi_q \frac{\alpha_s}{2\pi} P_{q,gg}(z) dz \frac{d\phi}{2\pi} \frac{d\theta^2}{\theta^2} \quad (43.1)$$

where M_{qg} , $d\Phi_{qg}$ are the amplitude and phase space describing the emission of both the gluon and the quark; M_q , $d\Phi_q$ are the amplitude and phase space when only the quark is emit-

ted; $z = E_q/(E_q + E_g)$ is the fraction of energy carried by the quark; ϕ is the azimuth of the splitting plane, and $P_{q,gg}(z) = C_F(1+z^2)/(1-z)$ is the Altarelli-Parisi splitting kernel for gluon emission from a quark line, with color factor $C_F = 4/3$. The factorized form of Eq. (43.1) is due to the fact that for small angle the process is dominated by a single amplitude in which the splitting quark is almost on shell and hence propagates for long distances. We define the energy scale corresponding to the inverse of this distance as the *hardness* of the splitting process, so that larger hardness corresponds to shorter distance. We can define the hardness t as the product $E^2\theta^2$, or as the virtuality of the splitting parton p^2 , or as a measure of the relative transverse momentum in the splitting such as the k_t of an emitted parton relative to its parent, defined by

$$p^2 = 2E^2z(1-z)(1-\cos\theta) \approx z(1-z)E^2\theta^2, \\ k_t^2 = z^2(1-z)^2E^2\theta^2. \quad (43.2)$$

If the region of small values of z and $1-z$ was not important, these definitions would be equivalent. In QCD we also have soft divergences, arising when soft gluons are emitted. In Eq. (43.1) they appear as $z \rightarrow 1$, because of the $1/(1-z)$ singularity of $P_{q,gg}(z)$. Thus, we expect that the choice of the appropriate ordering variable will be relevant when dealing with soft divergences (see Sec. 43.3). The $d\theta^2/\theta^2$ factor in Eq. (43.1) can be equivalently written in terms of the hardness dt/t . After integration, it gives rise to a logarithmic factor $\log(Q^2/\Lambda^2)$. We can have many subsequent splittings, that we can describe by applying Eq. (43.1) recursively, as long as the splittings are strongly ordered in decreasing hardness. This means that, from a typical final-state configuration, by clustering together final-state parton pairs with the smallest hardness recursively, we can reconstruct a branching tree, that may be viewed as the splitting history of the event. We stress that all hardness values between the hardness of the primary process and the cutoff scale Λ are equally involved here. The collinear approximation is applied recursively to splitting processes that have much smaller hardness with respect to all previous ones.

By integrating over the phase space (and neglecting for the moment soft divergences), a process with n collinear splittings will be of order $(\alpha_S(Q^2) \log(Q^2/\Lambda^2))^n$ with respect to the primary process. Since $\alpha_S(Q^2) \propto 1/\log(Q^2/\Lambda^2)$ [7], these corrections are not small. The so-called KLN theorem [8,9] guarantees that large logarithmic enhancements arising from final-state collinear splitting cancel against the virtual corrections in inclusive cross sections, order by order in perturbation theory. Furthermore, the factorization theorem guarantees that initial-state collinear singularities can be factorized into the parton density functions (PDFs) [7]. Therefore, the cross section for the basic process remains accurate up to corrections of higher orders in $\alpha_S(Q)$, provided it is interpreted as an inclusive cross section, rather than as a bare partonic cross section. For example, the leading order (LO) cross section for $e^+e^- \rightarrow q\bar{q}$ is a good estimate of the e^+e^- cross section for the production of a pair of quarks accompanied by an arbitrary number of collinear and soft gluons, but is not a good estimate of the cross section for the production of a $q\bar{q}$ pair with a veto on extra radiation. In summary, perturbation theory at fixed order can yield increasingly accurate predictions for inclusive observables, but cannot be used to describe the indefinite sequence of collinear and soft radiations that accompany the hard partons.

Parton-Shower algorithms are used to compute the cross section for generic hard processes including all dominant collinear radiation. These algorithms begin with the generation of the kinematics of the basic process, performed with a probability proportional to its LO partonic cross section. This is interpreted physically as the inclusive cross section for the basic process, followed by an arbitrary sequence of shower splittings. The algorithm then assigns a probability to each splitting sequence, so that the initial LO cross section is partitioned into the cross sections for a multitude of final states of arbitrary multiplicity, with their sum being equal to the cross section of the primary process. This property of the GPMCs reflects the KLN cancellation mentioned earlier, and it is often called “unitarity of the shower process”, a name

that reminds us that the KLN cancellation itself is a consequence of unitarity. The fact that a quantum mechanical process can be described in terms of composition of probabilities, rather than amplitudes, follows from the collinear approximation. In fact, because of strong ordering, a radiated parton cannot be collinear to more than one parton in the amplitude, and this suppresses interference effects.

We now illustrate the basic parton-shower algorithm, as first introduced in Ref. [10]. (For more pedagogical introductions see Ref. [11] and references therein.) For simplicity, we consider the example of e^+e^- annihilation into $q\bar{q}$ pairs, where we only have to deal with final state radiation (FSR). We consider all final states that can be built by dressing the q and \bar{q} partons with an indefinite number of splitting processes. By recursively clustering together final state parton pairs with the smallest relative hardness, from each final state configuration we can construct two trees rooted at the q and \bar{q} partons. The momenta of all intermediate lines of the tree diagrams are then uniquely determined from the final-state momenta. Hardnesses in the trees are ordered. One assigns to each splitting vertex the hardness t , the energy fractions z and $1-z$ of the two generated partons, and the azimuth ϕ of the splitting process with respect to the momentum of the incoming parton. For definiteness, we assume that z and ϕ are defined in the center-of-mass (CM) frame of the e^+e^- collision. The differential cross section for a given final state is given by the product of the differential cross section for the initial $e^+e^- \rightarrow q\bar{q}$ process, multiplied by a factor

$$\Delta_i(t_m, t_n) \frac{\alpha_S(t)}{2\pi} P_{i,jk}(z) \frac{dt_m}{t_m} dz \frac{d\phi}{2\pi} \quad (43.3)$$

for each intermediate line arising from the n^{th} and ending in the m^{th} splitting vertex. $\Delta(t_m, t_n)$ is the so-called Sudakov form factor

$$\Delta_i(t_m, t_n) = \exp \left[- \int_{t_m}^{t_n} \frac{dq^2}{q^2} \frac{\alpha_S(q^2)}{2\pi} \int dz \frac{d\phi}{2\pi} \sum_{jk} P_{i,jk}(z) \right]. \quad (43.4)$$

The suffixes i and jk represent the parton species of the incoming and final partons, respectively, and $P_{i,jk}(z)$ are the Altarelli-Parisi [12] splitting kernels. Notice that the endpoints on the z integration depend upon the definition of hardness. For example, in case of virtuality or transverse momentum ordering, the z integration is automatically cut-off near the extremes, see eq. (1.2). When this is not the case (as, for example, for angular ordering) an explicit cut-off on z must be introduced, corresponding to the requirement that an emission must have some minimum energy to be distinguishable from no emission. For lines originating at the primary vertex, the scale t_n is replaced by the typical scale of the primary process and for lines ending without any further splitting the scale t_m is replaced by t_0 , an infrared cutoff defined by the shower hadronization scale (at which the charges are screened by hadronization) or, for an unstable particle, its width (a source cannot emit radiation with a period exceeding its lifetime).

Eq. (43.3) can be obtained by iterating formula Eq. (43.1) recursively, with two important corrections: a) the strong coupling is evaluated at a scale corresponding to the hardness of the splitting process; b) the presence of the Sudakov form factor. Both these modifications arise from the inclusion of all collinear-dominant virtual corrections.

Notice that the Sudakov form factor for a small hardness interval $\Delta_i(t, t + \delta t)$ is equal to one minus the integrated emission probability of Eq. (43.3), i.e. it can be interpreted as the probability of no emission in the interval $t, t + \delta t$. From this, it immediately follows that $\Delta_i(t_m, t_n)$ can be interpreted as the no-emission probability in the full t_m, t_n interval. This interpretation allows one to formulate the shower process as a probabilistic algorithm. We first notice that $0 < \Delta_i(t_m, t_n) \leq 1$, where the upper extreme is reached for $t_m = t_n$, and the lower extreme is approached for $t_m = t_0$. Starting from each of the partons in the primary process (e.g., $e^+e^- \rightarrow q\bar{q}$), event generation then proceeds recursively as follows. Given a parton exiting a vertex with hardness t_n , (taken to be of order the annihilation scale Q^2 for the first branching)

one seeks a solution of the equation $r = \Delta_i(t_m, t_n)$, with $r \in [0, 1]$ a uniform random number, and solves it for the hardness of the next branching t_m . If $t_m \leq t_0$, no splitting is generated and the line is interpreted as a final parton. If $t_m > t_0$, a branching is generated at the scale t_m . Its z value and the final parton species jk are generated with a probability proportional to $P_{i,jk}(z)$. If angular correlations are neglected (see Sec. 43.1.1) the azimuth can be generated uniformly. This procedure is started with each of the primary process partons, and is applied recursively to all generated partons. It may generate an arbitrary number of partons, and it stops when no final-state partons undergo further splitting.

The four-momenta of the final-state partons are reconstructed from the momenta of the initial ones, and from the whole sequence of splitting variables, subject to overall momentum conservation. Different algorithms employ different strategies to treat recoil effects due to momentum conservation, which may be applied either locally for each splitting, or globally for the entire set of partons (a procedure called *momentum reshuffling*).

We emphasize that the shower cross sections described above can be derived from perturbative QCD by keeping only the collinear-dominant real and virtual contributions to the cross section. As such it is unproductive for large-angle radiation. It is thus unsafe to rely upon Parton Shower Monte Carlo alone to compute backgrounds to new physics signals that are characterized by several widely separated jets.

A Shower Monte Carlo builds its final state as if it developed from an iterative process, often with each intermediate stage made available to the user. It should be remarked that the meaning of these intermediate stages is only relevant within the approximation adopted by the generator, and could also differ in different implementations.

43.1.1 Angular correlations

In gluon-splitting processes ($g \rightarrow q\bar{q}$, $g \rightarrow gg$) in the collinear approximation, the distribution of the split pair is not uniform in azimuth, and the Altarelli-Parisi splitting functions are recovered only after azimuthal averaging. This dependence is due to the interference of positive and negative helicity states for the gluon that undergoes splitting. Spin correlations propagate through the splitting process, and determine acausal correlations of the EPR kind [13]. A method to partially account for these effects was introduced in Ref. [14], in which the azimuthal correlation between two successive splittings is computed by averaging over polarizations. This can then be applied at each branching step. Acausal correlations are argued to be small, and are discarded with this method, that is still used in PYTHIA [4]. A method that fully includes spin correlation effects was later proposed [15], and has been implemented in HERWIG [3, 16]. For more recent developments, see refs. [17] and references therein.

43.1.2 Initial-state radiation

Initial-state radiation (ISR) arises because incoming particles may undergo collinear radiation before entering the hard-scattering process. In doing so, they acquire a non-vanishing transverse momentum, and their virtuality becomes negative (spacelike). In order to efficiently sample the hard collision, it turns out to be convenient to develop the ISR shower starting with the highest hardness (i.e. with the hard process) and ending with the smallest (i.e. with the incoming parton in the hadron). Unlike the case of FSR, however, hardness ordering is opposite to time ordering in the ISR case. A corresponding backwards-evolution algorithm was formulated by Sjöstrand [18], and was basically adopted in all shower models. It can be illustrated by considering a primary interaction initiated by a quark where no collinear emissions of hardness $\geq t$ have taken place, and the same process where the quark also emits a collinear gluon of hardness t . The respective cross sections are proportional to

$$|M_q(x)|^2 dx f_q(x, t), \quad \text{and} \quad |M_q(x)|^2 dx \frac{\alpha_S(t)}{2\pi} f_q(x/z, t) P_{q,qg}(z) dz \frac{d\phi}{2\pi} \frac{dt}{t}. \quad (43.5)$$

Here f_q is the quark PDF in the incoming hadron, x is the fraction of momentum of the incoming quark that enters the basic

process, while x/z is the fraction of momentum of the incoming quark before it emits the collinear gluon. The elementary *emission probability* is the ratio of the second over the first expression in Eq. (43.5). In analogy with the final state radiation case, this ratio will appear in the exponent of the Sudakov form factor, that (after the inclusion of all splitting subprocesses) is given by

$$\Delta_i^{\text{ISR}}(t, t') = \exp \left[- \int_{t'}^t \frac{dt''}{t''} \frac{\alpha_S(t'')}{2\pi} \int_x^1 \frac{dz}{z} \sum_{jk} P_{j,ik}(z) \frac{f_j(t'', x/z)}{f_i(t'', x)} \right]. \quad (43.6)$$

Notice that there are two uses of the PDFs: they are used to compute the cross section for the basic hard process, and they control ISR via backward evolution. Since the evolution is generated with leading-logarithmic accuracy, it is acceptable to use two different PDF sets for these two tasks, provided they agree at the LO level.

In the context of GPMC evolution, each ISR emission generates a finite amount of transverse momentum. Details on how the recoils generated by these transverse “kicks” are distributed among other partons in the event, in particular the ones involved in the hard process, constitute one of the main areas of difference between existing algorithms, see Ref. [11]. An additional $\mathcal{O}(1 \text{ GeV})$ of “primordial k_T ” is typically added, to represent the sum of unresolved and/or non-perturbative motion below the shower cutoff scale.

43.1.3 Soft emissions and QCD coherence

Soft singularities arise in QCD due to the real or virtual emission of soft gluons. For example, the cross section for the emission of a soft gluon in e^+e^- annihilation into hadrons is given by

$$\begin{aligned} d\sigma_{q\bar{q}g} &\approx d\sigma_{q\bar{q}} C_F (4\pi\alpha_S) \left[\frac{2 p_q \cdot p_{\bar{q}}}{p_q \cdot l p_{\bar{q}} \cdot l} \right] \frac{d^3l}{2l^0 (2\pi)^3} \\ &= d\sigma_{q\bar{q}} \frac{\alpha_S}{2\pi} C_F \frac{d^0}{l^0} \frac{d\phi}{2\pi} \frac{d \cos \theta}{1 - \cos^2 \theta}, \end{aligned} \quad (43.7)$$

where p_q , $p_{\bar{q}}$ and l are the quark, antiquark and gluon momentum, and θ and ϕ are the polar and azimuthal angle of the gluon momentum with respect to the quark direction. Since the gluon is soft, we may assume that p_q and $p_{\bar{q}}$ are unaffected by the gluon emission. The soft singularity is manifest in the d^0/l^0 factor. Notice that also collinear singularities are present at the same time when $\theta \rightarrow 0$ and $\theta \rightarrow \pi$, corresponding to the gluon becoming collinear to either the quark or the antiquark. It is easy to check that in the collinear limits Eq. (43.7) becomes equivalent to Eq. (43.1) with $P_{q,qq}(z) = C_F 2/(1-z)$, i.e. the limiting form of $P_{q,qq}(z)$ when z approaches 1. Thus, soft singularities coexist with collinear ones, so that two potentially large logarithms can arise simultaneously due to gluon emission.

Unlike the case of collinear emission, soft emission is not tied to a single emitting particle. The amplitude for the emission of a soft gluon from an external (incoming or outgoing) line with momentum p is proportional to $p \cdot \epsilon / p \cdot l$. When squaring the amplitude, products like the one appearing in the square bracket of Eq. (43.1) arise for all pairs of external particles, with the product of a single emission amplitude with itself appearing only if $p^2 > 0$, i.e. for massive colored particles. Thus, interference plays here a crucial role. This is unlike the case of collinear singularities, where because of strong ordering a radiated parton cannot be collinear to more than one other parton.

It was shown in a set of publications (see Ref. [19]) that, within the conventional parton-shower formalism based on collinear factorization, the region of collinear and soft emissions can be correctly described by using the angle of the emissions as the ordering variable, rather than the virtuality, and by setting the argument of α_S at the splitting vertex equal to the relative parton transverse momentum after the splitting. Physically, the ordering in angle approximates the coherent interference arising from large-angle soft emission from a bunch of collinear partons. Without this effect, the particle multiplicity would grow too rapidly with energy, in conflict with e^+e^- data. For this reason, angular ordering is

used as the default evolution variable in all versions of HERWIG (see Ref. [20]). To partially account for soft interference effects, an angular veto is imposed on the virtuality-ordered evolution in PYTHIA 6 [21]. In modern designs this type of fix is avoided, the soft problem being addressed from the start.

A radical alternative formulation of QCD cascades first proposed in Ref. [22] focuses upon soft emission, rather than collinear emission, as the basic splitting mechanism. It then becomes natural to consider a branching process where it is a parton pair (i.e. a dipole) rather than a single parton, that emits a soft parton. Adding a suitable correction for non-soft, collinear partons, one can simultaneously achieve the correct logarithmic structure for both the collinear and soft emissions in the so called leading color approximation, i.e. when terms suppressed by a power of the number of colors are neglected. The ARIADNE [23] and VINCIA [24] programs are based on this approach. Dipole-type showers [25] are also used by default in SHERPA [26] and exist as an option in HERWIG [27]. An alternative dipole-based model is available in PYTHIA and SHERPA via the DIRE [28] plugin. The p_\perp -ordered showers in PYTHIA 6 and 8 represent a hybrid, combining collinear splitting kernels with dipole kinematics [29].

43.1.4 Resummation

Shower Monte Carlo generators perform resummation of all-order collinear- and/or soft-enhanced perturbative contributions, and it is thus natural to compare them to QCD resummation calculations [7]. The latter start from the definition of specific infrared-safe observables, that develop towers of large logarithms in certain regions of phase space, typically organized as

$$A(\alpha_S) \exp[Lg_0(\alpha_S L) + g_1(\alpha_S L) + \alpha_S g_2(\alpha_S L) + \dots] \quad (43.8)$$

where L is the large logarithm, α_S is the strong coupling constant evaluated at some hard scale. The functions A has a power expansion in α_S starting with a constant, and the functions g_i have a power series expansion in their argument starting with the linear term. We talk about N^n LL accuracy if all g_i functions for $i \leq n$ are fully included in the resummation formula, and the A function is given up to the order $n-1$ in α_S . In particular we talk about LL accuracy if the function g_0 is included, NLL accuracy if also g_1 is included. In both cases only the constant term in A is needed, while for N^2 LL (or NNLL) g_0 , g_1 and g_2 are included and A is given up to order α_S .

In general, a dedicated resummation calculation must be performed for each new observable. The predictions of shower MCs, on the other hand, are cast in terms of complete sets of final-state momenta, on which one can evaluate any observable; i.e., the shower algorithm itself is normally independent of the specific observable(s) under study. Because of this, it is not easy to qualifying the accuracy of a shower MC using the same criteria adopted in resummation calculation. In spite of this fact, shower MCs perform generally quite well in the description of observables that require resummation. This is related to their inclusion of several universal but formally subleading aspects. There is no guarantee, however, that the shower MC should perform to a certain level of accuracy for all distributions that require resummation. Thus, a more systematic treatment of subleading effects is quite desirable.

Several studies have appeared in the literature, aiming at either improving the current shower algorithms or formulate totally new ones, in such a way that the theoretical accuracy can be discussed in more precise terms [17, 30–35]. In particular, in refs [17, 30, 31] (the PanScales collaboration), it was shown that criteria for defining the accuracy of Shower Generators can indeed be given on a quite general ground. They identified two such criteria: the first one regards the approximations to multi-parton real matrix elements generated by the shower algorithm, that are required to be accurate in the region of phase space that are relevant for N^n LL accuracy. The second one regards the implementation of the virtual corrections, and it requires that for a large class of shape variables the shower MC must agree with the resummed calculation at the N^n LL level. The PanScales collaboration has constructed shower algorithms that are (with some restrictions) NLL accurate according to these criteria for e^+e^- annihilation,

hadronic collisions, Deep Inelastic Scattering and Vector Boson fusion processes (see [36] and references therein). Other NLL accurate (according to the same criteria) shower algorithms have been proposed in refs. [32] and [35].

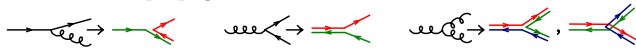
43.1.5 Massive quarks

Quark masses act as a cut-off on collinear singularities. If the mass of a quark is below, or of the order of Λ , its effect in the shower is small. For larger quark masses, like in c , b , or t production, it is the mass, rather than the typical hadronic scale, that cuts off collinear radiation. For a quark with energy E and mass m_Q , the divergent behavior $d\theta/\theta$ of the collinear splitting process is regulated for $\theta \leq \theta_0 = m_Q/E$. We thus expect less collinear activity for heavy quarks than for light ones, which in turn is the reason why heavy quarks carry a larger fraction of the momentum acquired in the hard production process.

This feature can be implemented with different levels of sophistication. Using the fact that soft radiation is strongly suppressed at zero emission angle, older parton shower algorithms simply limited the shower emission to be not smaller than the angle θ_0 . More modern approaches are used in both PYTHIA, where mass effects are included using a kind of matrix-element correction method [37], and in HERWIG and SHERPA, where a generalization of the Altarelli-Parisi splitting kernel is used for massive quarks [38]. For newer approaches for QCD evolution in processes with massive partons see ref. [39] and references therein.

43.1.6 Color information

In event generators, quarks and antiquarks are represented by color lines, with arrows indicating the direction of color flow. In the limit of infinitely many colors (called the leading color approximation), each such line can be associated with a unique label; the probability for two quarks (or antiquarks) to have the same color (anticolor) vanishes. Moreover, in the same limit gluons can be represented by a pair of color lines with opposite arrows, as can be realized e.g. from the SU(3) group relation $8 = 3 \otimes \bar{3} \ominus 1$. The rules for color propagation are:



During the shower development, partons are connected by color lines. We can have a quark directly connected by a color line to an antiquark, or via an arbitrary number of intermediate gluons, as shown in Fig. 43.1. It is also possible for a set of gluons to be connected cyclically in color, as e.g. in the decay $\Upsilon \rightarrow ggg$. The color information is used in angular-ordered showers, where

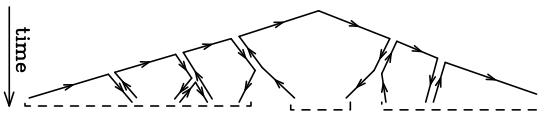


Figure 43.1: Color development of a shower in e^+e^- annihilation. Color-neutral clusters of partons are indicated by the dashed under-brackets.

the angle of color-connected partons (i.e. partons connected by the same color line) determines the initial angle for the shower development, and in dipole showers, where dipoles are formed by color-connected partons. It is also used in hadronization models, where the initial strings or clusters used for hadronization are formed by color-neutral clusters of partons.

43.1.7 Electromagnetic (and weak) corrections

The physics of photon emission from charged particles, and of photon splittings to pairs of charged fermions, can also be treated with a shower MC algorithm. High-energy electrons and quarks, for example, are accompanied by bremsstrahlung photons. Also here, similarly to the QCD case, electromagnetic corrections are of order $\alpha_{em} \ln(Q/m)$, where m is the mass of the radiating particle, or even of order $\alpha_{em} \ln(Q/m) \ln(E_\gamma/E)$ for soft γ emissions, so that, especially for the case of electrons, their inclusion in the simulation process is mandatory. This is done in most GPMC (for a comparative study see [40]), which typically agree in collinear (DGLAP) limits but differ in whether and how soft (multipole)

QED interference effects are handled. The specialized generator PHOTOS [41] is sometimes used as an afterburner for an improved treatment of QED radiation in non-hadronic resonance decays.

For photon emissions off leptons, the shower can be continued down to virtualities arbitrarily close to the lepton mass shell (unlike the case in QCD). In practice, an infrared cutoff is still required for the shower algorithm to terminate. Therefore, there is always an energy cut-off for emitted photons that depends upon the implementations [40]. In the case of electrons, this energy is typically of the order of its mass. Electromagnetic radiation below this scale is not enhanced by collinear singularities, and is thus bound to be soft, so that the electron momentum is not affected by it.

For photons emitted from quarks, there is instead the obvious limitation that the photon wavelength cannot exceed the typical hadronic size. Longer-wavelength photons are in fact emitted by hadrons, rather than quarks. This last effect is in practice never modeled by existing shower MC implementations. Thus, electromagnetic radiation from quarks is cut off at a typical hadronic scale. Finally, hadron (and τ) decays involving charged particles can produce additional soft bremsstrahlung. In PYTHIA, this is done via interfacing with PHOTOS, while HERWIG and SHERPA contain their own dedicated implementations [42, 43] based upon the YFS formalism [44], which is also adopted in the KKMC-hh Monte Carlo [45].

At energies significantly above the electroweak (EW) scale, showers involving emissions (and splittings) of weak gauge and Higgs bosons can also be relevant, with recent implementations based on collinear limits ranging from weak-boson emissions from fermions in PYTHIA 8 [46], to triple-boson couplings in HERWIG 7 [47], to the full set of EW branching processes in VINCIA [48].

43.1.8 Beyond-the-Standard-Model Physics

The inclusion of processes for physics beyond the Standard Model (BSM) in event generators is to some extent only a matter of implementing the relevant hard processes and (chains of) decays, with the level of difficulty depending on the complexity of the model and the degree of automation [49, 50]. Notable exceptions are long-lived colored particles [51], particles in exotic color representations, and particles showering under new gauge symmetries, with a growing set of implementations documented in the individual GPMC manuals. Further complications that may be relevant are finite-width effects (discussed in Sec. 43.1.9) and the assumed threshold behavior.

In addition to code-specific implementations [11], there are a few commonly adopted standards that are useful for transferring information and events between codes. Currently, the most important of these is the Les Houches Event File (LHEF) standard [52], normally used to transfer parton-level events from a hard-process generator to a shower generator. Another important standard is the Supersymmetry Les Houches Accord (SLHA) format [53], originally used to transfer information on supersymmetric particle spectra and couplings, but by now extended to apply also to more general BSM frameworks and incorporated within the LHEF standard [54]. Unfortunately, at present no standard method for handling multiple shower starting scales has been defined in the LHEF, so that further code, specific to the given GPMC, needs to be added to the interface in this case.

43.1.9 Decay Chains and Particle Widths

In most BSM processes and some SM ones, an important aspect of the event simulation is how decays of short-lived particles, such as top quarks, EW and Higgs bosons, and new BSM resonances, are handled. We here briefly summarize the spectrum of possibilities, but emphasize that there is no universal standard. Users are advised to check whether the treatment of a given code is adequate for the physics study at hand.

The appearance of an unstable resonance as a physical particle at an intermediate stage of the event generation implies that its production and decay processes are treated as being factorized. This is valid up to corrections of order Γ/m_0 , with Γ the width and m_0 the pole mass. States whose widths are a substantial fraction of their mass should instead be treated as intrinsically off-shell internal propagator lines.

For states treated as physical particles, two aspects are relevant: the mass distribution of the decaying particle itself and the distributions of its decay products. For the former, matrix-element generators often use a simple δ function at m_0 . The next level up, typically used in GPMCs, is to use a Breit-Wigner distribution, which formally resums higher-order virtual corrections to the mass distribution. Note, however, that this still only generates an improved picture for *moderate* fluctuations away from m_0 . Similarly to above, particles that are significantly off-shell (in units of Γ) should not be treated as resonant, but rather as internal off-shell propagator lines. In most GPMCs, further refinements are included, for instance by letting Γ be a function of m (“running widths”) and by limiting the magnitude of the allowed fluctuations away from m_0 . We finally point out that NLO+PS generators have appeared that can deal with resonances including off-shell effects, non-resonance contributions and interference of radiation generated in resonance decay and production, see [55] and references therein. A new “interleaved” shower treatment also allows for interference between production and decay in the VINCIA model [48].

For the distributions of the decay products, the simplest treatment is again to assign them their respective m_0 values, with a uniform phase-space distribution. A more sophisticated treatment distributes the decay products according to the differential decay matrix elements, capturing at least the internal dynamics and helicity structure of the decay process, including EPR-like correlations. Further refinements include polarizations of the external states [56] and assigning the decay products their own Breit-Wigner distributions, the latter of which opens the possibility to include also intrinsically off-shell decay channels, like $H \rightarrow WW^*$.

GPMC manuals often give instructions on how to include new decay modes, at varying levels of sophistications ranging from simple uniform phase-space sampling (which the user can reweight a posteriori) and step-function thresholds, to fully matrix-element weighted decay implementations including potential off-shell / threshold effects.

During subsequent showering of the decay products, most parton-shower models will preserve the total invariant mass of the decayed resonance, so as not to skew the original resonance shape. In the context of passing externally generated LHEF files [52] to a GPMC for showering, note that this is only possible if the intermediate resonances are present (with status code 2) in the LHEF event record [57].

43.1.10 Matching and Merging with Fixed-Order Matrix Elements

Shower algorithms are based upon a combination of the collinear (small-angle) and soft (small-energy) approximations and are thus normally inaccurate for hard, wide-angle emissions (i.e., additional well-resolved jets). They also contain only the leading singular pieces of next-to-leading order (NLO) and higher corrections to the basic process.

Traditional GPMCs, like HERWIG and PYTHIA, have included for a long time the so called Matrix-Element Corrections (MEC), first formulated in Ref. [58] with later developments summarized in Ref. [11]. They are typically available for $2 \rightarrow 1$ or $1 \rightarrow 2$ processes, like DIS, vector boson and Higgs production and decays, and top decays. The MEC corrects the emission of the hardest jet at large angles, so that it becomes exact at LO. A generalization of the method to multiple emissions was formulated in [59].

Aside from MECs implemented directly in the GPMCs, the improvements on the parton-shower description of hard collisions have been made in two main directions: the so called Matrix Elements and Parton Shower matching (ME+PS from now on), and the matching of NLO calculations and Parton Showers (NLO+PS). We now discuss each of these, and then briefly summarize techniques becoming available for combining them.

The ME+PS method allows one to use tree-level matrix elements for hard, large-angle emissions. It was first formulated in the so-called CKKW paper [60], and several variants have appeared, including the CKKW-L, MLM, pseudoshower and MESS methods, see Refs. [11, 61, 62] and references therein. So called “Truncated Showers” are required [63] to maintain color coher-

ence when interfacing to angular-ordered parton showers, and care must be taken to use consistent α_S choices for the real (ME-driven) and virtual (PS-driven) corrections [64].

In the ME+PS method one typically starts by generating LO matrix elements for the production of the basic process plus a certain number $\leq n$ of other partons. A minimum separation is imposed on the produced partons, requiring, for example, that the relative transverse momentum in any pair of partons is above a given cut Q_{cut} . One then reweights these amplitudes in such a way that, in the strongly ordered region, the virtual effects that are included in the shower algorithm (i.e. running couplings and Sudakov form factors) are also accounted for. At this stage, before parton showers are added, the generated configurations are tree-level accurate at large angle, and at small angle they match the results of the shower algorithm, except that there are no emissions below the scale Q_{cut} , and no final states with more than n partons. These kinematic configurations are thus fed into a GPMC, that must generate all splittings with relative transverse momentum below the scale Q_{cut} , for initial events with less than n partons, or below the scale of the smallest pair transverse momentum, for events with n partons. The matching parameter Q_{cut} must be chosen to be large enough for fixed-order perturbation theory to hold, but small enough so that the shower is accurate for emissions below it. Notice that the accuracy achieved with MEC is equivalent to that of ME+PS with $n = 1$, where MEC has the advantage of not having a matching parameter Q_{cut} .

The popularity of the ME+PS method is due to the fact that processes with many jets often appear as backgrounds to new-physics searches. These jets are typically required to be well separated, and to have large transverse momenta. These kinematic configurations are exactly those for which pure shower algorithms are unreliable, hence it is mandatory to describe them using at least LO matrix elements.

Several ME+PS implementations use existing LO generators, like ALPGEN [65], MADGRAPH [66], and others summarized in Ref. [61], for the calculation of the matrix elements, and feed the partonic events to a GPMC like PYTHIA or HERWIG using the Les Houches Interface for User Processes (LHI/LHEF) [52, 57]. SHERPA and HERWIG also include their own matrix-element generators.

The NLO+PS methods promote the accuracy of the generation of the basic process from LO to NLO in QCD. They must thus include the radiation of one extra parton with tree-level accuracy, since this radiation constitutes a NLO correction to the basic process. They must also include NLO virtual corrections. They can be viewed as an extension of the MEC methods with the inclusion of NLO virtual corrections. They are however more general, since they are applicable to processes of arbitrary complexity. Two of these methods are now widely used: MC@NLO [67] and POWHEG [63, 68], with several alternative methods now also being pursued, see [69] and references therein, and the recent method presented in [70].

NLO+PS generators produce NLO accurate distributions for inclusive quantities, and generate the hardest jet with tree-level accuracy. Note also that the optimal tuning of an NLO+PS generator may well be different from that of the pure PS.

Several NLO+PS processes are implemented in the MC@NLO program [67], together with the AMC@NLO development [71], and in the POWHEG-BOX framework [68]. HERWIG supports its own variants of POWHEG and MC@NLO for several processes. SHERPA instead implements a variant of the MC@NLO method.

For applications that require an accurate description of more than one hard, large-angle jet associated with the primary process, ME+PS schemes are still superior to NLO+PS ones. Ideally, one would like to improve NLO generators in such a way that also the production of associated jets achieves NLO accuracy. The FFX [72], UNLOPS [73], MiNLO [74] and MEPS@NLO [75] methods address this problem. The solution of this problem is also a prerequisite for the construction of NNLO+PS generators, i.e. generators that, besides being NLO accurate for the production of an associated jet, are also NNLO accurate for fully inclusive observables. Three different approaches have appeared in the literature for dealing with this problem: the UN²NLOPS, based upon UNLOPS method [76]; methods extending the MiNLO ap-

proach by reweighting [77] and by the so called MiNNLO_{PS} technique [78]; and the GENEVA method [79]. Several processes have been implemented with the MiNLO related and GENEVA methods, mostly for the production of color singlet systems, with the exception of the recent MiNNLO_{PS} implementation of $t\bar{t}$ production (see refs. [69, 80, 81] for an extensive list of references).

43.2 Hadronization Models

In the context of GPMCs, *hadronization* denotes the process by which a set of colored partons (*after showering*) is transformed into a set of “primary hadrons”, which may then subsequently decay further (to “secondary hadrons”). This non-perturbative transition takes place at the *hadronization scale* Q_{had} , which by construction is equal to the infrared cutoff of the parton shower. In the absence of a first-principles solution to the relevant dynamics, GPMCs use QCD-inspired phenomenological models to describe this transition.

An important result in “quenched” lattice QCD (see Chap. 17 of PDG book) is that the potential energy between two partons with opposite color charges grows linearly with their separation, at distances greater than about a femtometer. This is known as “linear confinement”, and it forms the starting point for the *string model of hadronization*, discussed below in Sec. 43.2.1. Alternatively, a property of perturbative QCD called “preconfinement” is the basis of the *cluster model of hadronization*, discussed in Sec. 43.2.2.

A key difference between MC hadronization models and the fragmentation-function (FF) formalism used to describe inclusive hadron spectra in perturbative QCD (see Chap. 9 and Chap. 19 of PDG book) is that FFs can be defined at an arbitrary perturbative scale Q while MC hadronization models are intrinsically defined at the scale Q_{had} . Direct comparisons are therefore only meaningful if the perturbative evolution between Q and Q_{had} is taken into account. FFs are calculable in pQCD, given a non-perturbative initial condition obtained by fits to hadron spectra. In the MC context, one can prove that the correct QCD evolution of the FFs arises from the shower formalism, with the hadronization model providing an explicit parameterization of the non-perturbative component. However, the MC modeling of shower and hadronization includes much more information on the final state since it is fully exclusive (i.e., it addresses all particles in the final state explicitly), while FFs only describe inclusive spectra. This exclusivity also enables MC models to make use of the color-flow information coming from the perturbative shower evolution (see Sec. 43.1.6) to determine between which partons confining potentials should arise. E.g., in the string picture, the nonperturbative limit of a QCD dipole is a string piece [82].

Given an ideal, exact hadronization model, its dependence on the scale Q_{had} should in principle be compensated by the corresponding scale dependence of the shower algorithm, which stops generating branchings at the scale Q_{had} . However, due to their complicated and fully exclusive nature, it is generally not possible to enforce this compensation automatically in MC models. One must therefore be aware that the nonperturbative model parameters must be “retuned” by hand if the infrared cutoff is modified. Any other changes to the perturbative part of the calculation, such as matching to further (fixed-order or resummed) coefficients, may also necessitate a retuning. Tuning is discussed briefly in Sec. 43.4.

The impact of hadronization corrections in a GPMC can be estimated by switching off hadronization. It should be emphasized, however, that the so-called “parton level” obtained this way is not a fully universal concept. This is because Q_{had} is typically defined in a model-dependent way, via a cutoff in the respective shower model’s evolution variable, sometimes with supplementary cutoffs, e.g., in invariant mass, p_T , or the like and different tunes possibly using different numerical values for the cutoff(s). Variations of the main shower cutoff scale (e.g., by a factor of 2) may give an indication of the level of model dependence, which may be mild for sufficiently inclusive observables. Nevertheless our recommendation is to avoid correcting experimental measurements to “parton level” as the intrinsic model dependence will always imply a loss of accuracy.

43.2.1 The String Model

Starting from early concepts [83], several hadronization models based on strings have been proposed [11]. Of these, the most widely used today is the so-called Lund model [84, 85], implemented in PYTHIA [4, 5]. We concentrate on that particular model here, though many of the overall concepts would be shared by any string-inspired method.

Consider a quark and an antiquark that have a large relative momentum and which are in an overall color-singlet state, such as the $\bar{q}q$ pair produced at the end of the shower in the center of Fig. 43.1. As the charges move apart, linear confinement implies that a potential $V(r) = \kappa r$ is reached for large distances r . (At short distances, there is a Coulomb term $\propto 1/r$ as well, but this is neglected in the Lund string.) This potential describes a string with tension $\kappa \sim 1 \text{ GeV/fm} \sim 0.2 \text{ GeV}^2$. The physical picture is that of a color flux tube being stretched between the q and the \bar{q} . As the string grows, the nonperturbative creation

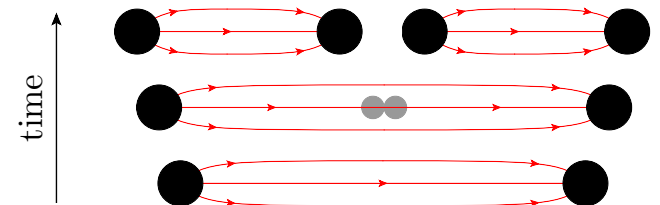


Figure 43.2: Illustration of string breaking by quark pair creation in the string field.

of quark-antiquark pairs can break the string, via the process illustrated in Fig. 43.2. If either of the resulting string pieces after the break still has a large invariant mass, new breaks will then continue to occur until every piece has a mass of the order of that of a typical hadron. In nature, quantum mechanics ensures that these masses are (Breit-Wigner-distributed around) those of the physical hadron states in QCD, while in an algorithmic implementation, this is less trivial to impose. Within the Lund model, the constraint that each final string piece must have a mass consistent with that of physical hadron is addressed by first noting that each breakup vertex is spacelike separated from all others (the string cannot break again in the forward lightcone of a point where it has already broken); since the breakups are therefore causally disconnected, they do not have to be considered in any particular order. The Lund model exploits this to perform the fragmentation in an outwards-in manner [85], splitting off one physical hadron at a time from either the left or right endpoint (chosen randomly in each step).

The first hadron to be generated (starting either from the left or right) is thus the “outermost” one (sometimes called the “first-rank” hadron), formed by combining the original hadronizing endpoint quark (or antiquark) q_0 with an antiquark (or quark) \bar{q}_1 produced by the first breakup. The new leftover quark (or antiquark) q_1 becomes the string endpoint for the next iteration, in a Markov chain which continues, alternating randomly between the left and right ends of the string, until finally a small last bit of string is decayed directly to two hadrons, with no energy left over.

Not only does this allow for the hadron that is split off in each step to be assigned a physical mass, the fact that the fragmentation spectrum should be independent of whether one performs the fragmentation from left to right or vice versa places a strong constraint on the form of the nonperturbative *string fragmentation function*¹, $f(z)$, which governs the probability for the hadron produced in a given step to take a fraction $z \in [0, 1]$ of the remaining energy. Thus, in the Lund model, causality dictates that the

¹Note that the string fragmentation function differs from the parton-to-hadron fragmentation functions discussed earlier. In principle, the two kinds should be related (with the latter evolved to a low scale of the order of the hadronization scale), but the relationship is not trivial and goes beyond the scope of this review.

fragmentation function should be of the form,

$$f(z) \propto \frac{1}{z}(1-z)^a \exp\left(-\frac{b(m_h^2 + p_{T,h}^2)}{z}\right). \quad (43.9)$$

This is known as the Lund symmetric fragmentation function (normalized to unit integral). The dimensionless parameter a dampens the hard tail of the fragmentation function, towards $z \rightarrow 1$, and may in principle be flavor-dependent, while b , with dimension GeV^{-2} , is a universal constant related to the string tension [85] which determines the behavior in the soft limit, $z \rightarrow 0$. Note that the dependence on the hadron mass, m_h , in $f(z)$ implies that heavier hadrons have higher $\langle z \rangle$. We return to the transverse momentum $p_{T,h}$ below.

The model is Lorentz invariant, so considerations involving boosted string systems are straightforward, involving the usual Lorentz effects.

As a by-product, the probability distribution in invariant time τ of $q\bar{q}$ breakup vertices, or equivalently $\Gamma = (\kappa\tau)^2$, is also obtained, with $dP/d\Gamma \propto \Gamma^a \exp(-b\Gamma)$ implying an area law for the color flux, and the average breakup time lying along a hyperbola of constant invariant time $\tau_0 \sim 10^{-23}\text{s}$ [85].

For massive endpoints (e.g. c and b quarks), which do not move along straight lightcone sections, the exponential suppression with string area leads to modifications of the form $f(z) \rightarrow f(z)/z^{b m_Q^2}$, with m_Q the mass of the heavy quark [86]. Although different forms, such as the Peterson formula [87], can also be used to describe inclusive heavy-meson spectra (see Sec 19.8 of PDG book), such choices are not strictly consistent with causality in the string framework.

43.2.1.1 Strings with Gluons

In the string model, energetic gluons lead to transverse “kinks” on strings, illustrated in Fig. 43.3. The order of these kinks follows from the color ordering produced by the parton shower, cf. the $\bar{q}gggq$ and $\bar{q}qg$ systems on the left and right part of Fig. 43.1. (Modifications to this order, by possible color reconnection/rearrangement effects, are discussed in Sec. 43.3.2.) Thus gluons

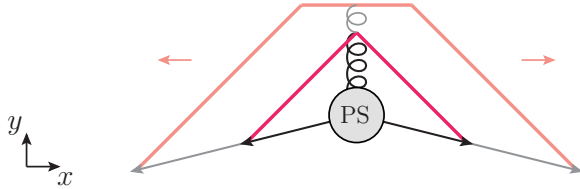


Figure 43.3: Schematic illustration of an $e^+e^- \rightarrow q\bar{q}$ configuration emerging from the parton shower (PS). Snapshots of string positions are shown at two different times (full and shaded lines respectively). The gluon forms a transverse kink which grows in the y direction until all the gluon’s kinetic energy has been used up.

effectively build up a transverse structure in the originally one-dimensional object, with infinitely soft ones smoothly absorbed into the string. Note: cyclic topologies made entirely of gluons (closed strings) are also possible, e.g. in decays such as $H \rightarrow gg$ or $\Upsilon \rightarrow ggg$. The space-time evolution is more involved when kinks are taken into account [85], but no additional free parameters need to be introduced. The main difference between quark and gluon hadronization stems from the fact that gluons are connected to two string pieces (one on either side), while quarks are only connected to a single string piece. Hence, the relative rate of energy loss per unit invariant time — and consequently also the rate of hadron production — is larger by a factor of 2 for gluons (analogously to the ratio of gluon to quark color charges $C_A/C_F = 2.25$).

43.2.1.2 Transverse Momentum and Flavors

For each breakup vertex, quantum mechanical tunneling is assumed to control the masses and p_T kicks (transverse to the string

axis, in a frame in which the string itself has no transverse motion) that can be produced, leading to a Gaussian suppression

$$\text{Prob}(m_q^2, p_{T,q}^2) \propto \exp\left(\frac{-\pi m_q^2}{\kappa}\right) \exp\left(\frac{-\pi p_{T,q}^2}{\kappa}\right), \quad (43.10)$$

where m_q is the mass of the produced quark flavor and p_T is the nonperturbative transverse momentum imparted to it by the breakup process, with a universal average value of $\langle p_{T,q}^2 \rangle = \kappa/\pi \sim (250 \text{ MeV})^2$. The antiquark has the same mass and opposite p_T .

In an MC model with a fixed shower cutoff t_0 , the effective amount of p_T in string breaks may be larger than the purely nonperturbative κ/π above, to account for effects of additional (unresolved) radiation below t_0 .

From the mass term in Eq. (43.10), one concludes that charm and bottom quarks are too heavy to be produced in string breaks, while strange quarks will be suppressed relative to up and down ones. Lacking unambiguous and precise mass definitions for light quarks, however, the effective amount of strangeness suppression is normally extracted from experimental data, using observables such as K/π , K^*/ρ , and ϕ/K^* ratios.

Baryon production can also be incorporated, at various levels of sophistication. The simplest option is to allow string breaks to produce a diquark-antidiquark pair, where a diquark is a loosely bound state of two quarks in an overall $\bar{3}$ representation. Again, the relative rate of such pairs is extracted from data, e.g. using p/π or Λ/K ratios. Since the perturbative shower splittings do not produce diquarks, the optimal value for this parameter is mildly correlated with the amount of $g \rightarrow q\bar{q}$ splittings in the shower. More sophisticated options, including the so-called “popcorn” mechanism, are discussed in Ref. [85]. Finally, the PYTHIA framework also allows for baryon string junctions [88], in which three string pieces (which can be thought of as red, green, and blue, respectively) join together. These are used, e.g., to model the fragmentation of baryon beam remnants, and can also be created (in pairs of junctions and antijunctions) in some color-reconnection scenarios [89], making the effective baryon-to-meson ratios in such models dependent on the amount and type of color reconnections that occur in each event.

The next step of the algorithm is the assignment of the produced quarks within hadron multiplets. Using a nonrelativistic classification of spin states, the hadronizing q may combine with the \bar{q}' from a newly created breakup to produce a hadron of a given spin S and angular momentum L . The lowest-lying pseudoscalar and vector meson multiplets, and spin-1/2 and -3/2 baryons, are assumed to dominate in a string framework², but individual rates are not predicted by the model, and hence the ratios of spin-1 to spin-0 mesons and diquarks are free parameters (modulo a factor 3 from spin counting) which must be constrained by data. In that context, it is often advisable to begin with the heaviest states, since so-called feed-down from the decays of higher-lying hadron states complicates the extraction for lighter particles, see Sec. 43.2.3.

43.2.2 The Cluster Model

The cluster hadronization model is based on *preconfinement*, i.e., on the observation [90,91] that the color structure of a perturbative QCD shower evolution at any scale Q_0 is such that color-singlet subsystems of partons (labeled “clusters”) occur with a universal invariant mass distribution which is power suppressed at large masses. For any starting scale $Q \gg Q_0 \gg \Lambda_{\text{QCD}}$, only the number of such clusters depends on Q , while the shape of their mass distribution only depends on Q_0 and on Λ_{QCD} .

Following early models based on this universality [10,92], the cluster model developed by Webber [93] has for many years been a hallmark of the HERWIG generators, with an alternative implementation [94] now available in the SHERPA generator. The key idea, in addition to preconfinement, is to force “by hand” all gluons to split into quark-antiquark pairs at the end of the parton shower.

²In PYTHIA, the four $L = 1$ meson multiplets (scalar, tensor, and 2 pseudovectors) are also available but are disabled by default, since many states (and their decays) are poorly known.

Compared with the string description, this effectively amounts to viewing gluons as “seeds” for string breaks, rather than as kinks in a continuous object. After the splittings, a new set of low-mass color-singlet clusters is obtained, formed only by quark-antiquark pairs. These can be decayed to on-shell hadrons in a simple manner, with the relative yields of different hadron species mainly governed by their masses and the size of the phase space.

The algorithm starts by generating the forced $g \rightarrow q\bar{q}$ breakups, and by assigning flavors and momenta to the produced quark pairs. For a typical shower cutoff corresponding to a gluon virtuality of $Q_{\text{had}} \sim 1$ GeV, the p_T generated by the splittings can be neglected. The constituent light-quark masses, $m_{u,d} \sim 300$ MeV and $m_s \sim 450$ MeV, imply a suppression (typically even an absence) of strangeness production. In principle, the model also allows for diquarks to be produced at this stage, but due to the larger constituent masses this would only become relevant for shower cutoffs larger than 1 GeV.

If a cluster formed in this way has an invariant mass above some cutoff value, typically 3–4 GeV, it is forced to undergo sequential $1 \rightarrow 2$ cluster breakups, along an axis defined by the constituent partons of the original cluster, until all sub-cluster masses fall below the cutoff value. Due to the preservation of the original axis in these breakups, this treatment has some resemblance to the string-like picture, though the nonperturbative p_\perp kicks generated in this way are generally larger, up to half the allowed cluster mass.

Next, on the low-mass side of the spectrum, some clusters are allowed to decay directly to a single hadron, with nearby clusters absorbing any excess momentum. This improves the description of the high- z part of the spectrum — where the hadron carries almost all the momentum of its parent jet — at the cost of introducing one additional parameter, controlling the probability for single-hadron cluster decay.

Having obtained a final distribution of small-mass clusters, now with a strict cutoff at 3–4 GeV and with the component destined to decay to single hadrons already removed, the remaining clusters are interpreted as a smoothed-out spectrum of excited mesons, each of which decays isotropically to two hadrons, with relative probabilities proportional to the available phase space for each possible two-hadron combination that is consistent with the cluster’s internal flavors, including spin degeneracy. It is important that all the light members (containing only uds) of each hadron multiplet be included, as the absence of members can lead to unphysical isospin or SU(3) flavor violation. Typically, the lightest pseudoscalar, vector, scalar, even and odd charge conjugation pseudovector, and tensor multiplets of light mesons are included. In addition, some excited vector multiplets of light mesons may be available. For baryons, usually only the lightest flavor-octet, -decuplet and -singlet baryons are present, although both the HERWIG and SHERPA implementations now include some heavier baryon multiplets as well.

Differently from the string model, the mechanism of phase-space suppression employed here leads to a natural enhancement of the lighter pseudoscalars, and no parameters beyond the spectrum of hadron masses need to be introduced at this point. The phase space also limits the transverse momenta of the produced hadrons relative to the jet axis.

Note that, since the masses and decays of excited heavy-flavor hadrons in particular are not well known, there is some freedom in the model to adjust these, which in turn will affect their relative phase-space populations.

43.2.3 Hadron and τ Decays

Of the so-called primary hadrons, originating directly from string breaks and/or cluster decays (see above), many are unstable and so decay further, until a set of particles is obtained that can be considered stable on time scales relevant to the given measurement. (A typical hadron-collider definition of a “stable particle” $c\tau \geq 10$ mm includes weakly-decaying strange hadrons $K, \Lambda, \Sigma^\pm, \bar{\Sigma}^\pm, \Xi, \Omega$.) The decay modeling can therefore have a significant impact on final particle yields and spectra, especially for the lowest-lying hadronic states, which receive the largest relative contributions from decays (feed-down). This interplay also implies that hadronization parameters may need to be retuned if

significant changes to the decay treatment are made.

Particle summary tables, such as those given elsewhere in this *Review*, represent a condensed summary of the available experimental measurements and hence may be incomplete and/or exhibit inconsistencies within the experimental precision. In an MC decay package, on the other hand, all information must be quantified and consistent, with all branching ratios summing to unity. When adapting particle summary information for use in a decay package, a number of choices must therefore be made. The amount of ambiguity increases as more excited hadron multiplets are added to the simulation, about which less and less is known from experiment, with each GPMC making its own choices.

A related choice is how to distribute the decay products differentially in phase space, in particular which matrix elements to use. Historically, MC generators contained matrix elements only for selected (generator-specific) classes of hadron and τ decays, coupled with a Breit-Wigner smearing of the masses, truncated at the edges of the physical decay phase space (the treatment of decay thresholds can be important for certain modes [11]). A more sophisticated treatment can then be obtained by reweighting the generated events using the obtained particle four-momenta and/or by using specialized external packages such as EVTGEN [95] for hadron decays and TAUOLA [96] for τ decays.

More recently, HERWIG and SHERPA include helicity-dependence in τ decays [6, 97], with a more limited treatment available in PYTHIA 8 [5]. The HERWIG and SHERPA generators have also included significantly improved internal simulations of hadronic decays, which include spin correlations between those decays for which matrix elements are used. Photon-bremsstrahlung effects are discussed in Sec. 43.1.7.

HERWIG and PYTHIA include the probability for B mesons to oscillate into \bar{B} ones before decay. SHERPA and EVTGEN also include CP -violating effects and, for common decay modes of the neutral meson and its antiparticle, the interference between the direct decay and oscillation followed by decay.

We end on a note of warning on double counting. This may occur if a particle can decay via an intermediate on-shell resonance. An example is $a_1 \rightarrow \pi\pi\pi$ which may proceed via $a_1 \rightarrow \rho\pi$, $\rho \rightarrow \pi\pi$. If these decay channels of the a_1 are both included, each with their full partial width, a double counting of the on-shell $a_1 \rightarrow \rho\pi$ contribution would result. Such cases are normally dealt with consistently in the default MC generator packages, so this warning is mostly for users that wish to edit decay tables on their own.

43.3 Models for Soft Hadron-Hadron Physics

43.3.1 Underlying Event

In the GPMC context, “underlying event” (UE) denotes any additional activity *beyond* the basic process and its associated ISR and FSR activity. The UE is thus only defined in the context of events selected with a “hard” (i.e., high- p_\perp) trigger which defines the basic process at hand. The dominant contribution to the UE is believed to come from additional color exchanges between the colliding hadronic states. These multiple exchanges can be modeled either as additional perturbative (mainly t -channel gluon) exchanges, called multiple parton-parton interactions (MPI), or nonperturbatively using so-called cut pomerons (roughly equivalent to exchange of gluons with $p_\perp \rightarrow 0$). The experimental observation that events with a hard trigger are accompanied by a higher-than-average level of associated activity is called the “jet pedestal” effect.

The most clearly identifiable consequence of MPI is arguably the possibility of observing several hard parton-parton interactions in one and the same hadron-hadron event. Typically, these are QCD $2 \rightarrow 2$ interactions, which produce additional back-to-back jet pairs, with each pair having a small value of $\text{sum}(p_\perp)$. The fraction of MPI that give rise to additional reconstructible jets is, however, small. Soft interactions, that exchange color and a small amount of momentum without giving rise to observable jets, are much more plentiful, and can give significant corrections to the color flow and total scattered energy of the event. This affects the final-state activity in a more global way, increasing hadron-multiplicity and summed E_T distributions, and contribut-

ing to the break-up of the beam remnants in the forward direction.

The first detailed Monte Carlo model for perturbative MPI was proposed in Ref. [98], and with some variation this still forms the basis for most modern implementations. Some useful additional references can be found in Ref. [11]. The first crucial observation is that the t -channel propagators appearing in perturbative QCD $2 \rightarrow 2$ scattering almost go on shell at low p_T , causing the differential cross sections to behave roughly as

$$d\sigma_{2 \rightarrow 2} \propto \frac{dt}{t^2} \sim \frac{dp_T^2}{p_T^4}. \quad (43.11)$$

This cross section represents the inclusive scattering of partons against partons in perturbative QCD, summed over all partons. Thus, if a single hadron-hadron scattering contains *two* parton-parton interactions, that event will contribute twice to the parton-parton cross section $\sigma_{2 \rightarrow 2}$ but only once to the hadron-hadron one σ_{tot} , and so on. In the limit that all the parton-parton interactions are independent and equivalent, one has

$$\sigma_{2 \rightarrow 2} = \langle n \rangle \sigma_{\text{tot}}, \quad (43.12)$$

with $\langle n \rangle$ the average number of parton-parton interactions, typically defined with some minimal $p_T > p_{\perp \text{min}}$ to render the parton-parton cross section finite. The probability for n parton-parton scatterings then follows a Poisson distribution,

$$\mathcal{P}_n = \langle n \rangle^n \frac{\exp(-\langle n \rangle)}{n!}. \quad (43.13)$$

This simple argument expresses unitarity; instead of the total hadron-hadron interaction cross section diverging as the parton-parton $p_T \rightarrow 0$ (which would violate unitarity), we have restated the problem so that it is now the *number of parton-parton interactions per hadron-hadron collision* that diverges, with the total hadron-hadron cross section remaining finite. At LHC energies, the parton-parton scattering cross sections computed using the LO QCD cross section folded with modern PDFs become larger than the total pp one for $p_{\perp \text{min}}$ values of order 4–5 GeV (see e.g. [99, 100]). One therefore expects the average number of perturbative MPI to exceed unity at around that scale.

Two ingredients remain to fully regulate the remaining divergence. Firstly, the interactions cannot use up more momentum than is available in the parent hadron. This suppresses the large- n tail of the estimate above. In PYTHIA-based models, the MPI are ordered in p_T , and the parton densities for each successive interaction are explicitly constructed so that the sum of x fractions can never be greater than unity. In the HERWIG models, the Poisson estimate of $\langle n \rangle$ above is used as an initial guess, but the generation of actual MPI is stopped once the energy-momentum conservation limit is reached. Both of these approaches generate momentum (conservation) correlations among the MPI.

The second ingredient invoked to suppress the number of interactions, at low p_T and x , is color screening; if the wavelength $\sim 1/p_T$ of an exchanged colored parton becomes larger than a typical color-anticolor separation distance, it will only see an *average* color charge that vanishes in the limit $p_T \rightarrow 0$. This provides an infrared cutoff for MPI similar to that provided by the hadronization scale for parton showers. A first estimate of the color-screening cutoff would be the proton size, $p_{\perp \text{min}} \approx \hbar/r_p \approx 0.3 \text{ GeV} \approx \Lambda_{\text{QCD}}$, but empirically this appears to be far too low. In current models, one replaces the proton radius r_p in the above formula by a “typical color screening distance,” i.e., an average size of a region within which the net compensation of a given color charge occurs. This number is not known from first principles [101] and is perceived of simply as an effective cutoff parameter. The simplest choice is to introduce a step function $\Theta(p_T - p_{\perp \text{min}})$. Alternatively, one may note that the jet cross section is divergent like $\alpha_S^2(p_T^2)/p_T^4$, cf. Eq. (43.11), and that therefore a factor

$$\frac{\alpha_S^2(p_{T,0}^2 + p_T^2)}{\alpha_S^2(p_T^2)} \frac{p_T^4}{(p_{T,0}^2 + p_T^2)^2} \quad (43.14)$$

would smoothly regulate the divergences, now with $p_{T,0}$ as the free parameter. Regardless of whether it is imposed as a smooth

(PYTHIA and SHERPA) or step (HERWIG) function, this is effectively the main “tuning” parameter in such models.

Note that the numerical value obtained for the cross section depends upon the PDF set used, and therefore the optimal value to use for the cutoff will also depend on this choice. Note also that the cutoff does not have to be energy-independent. Higher energies imply that parton densities can be probed at smaller x values, where the number of partons rapidly increases. Partons then become closer packed and the color screening distance d decreases. The uncertainty on the energy and/or x scaling of the cutoff is a major concern when extrapolating between different collider energies [102].

We now turn to the origin of the observational fact that hard jets appear to sit on top of a higher “pedestal” of underlying activity than events with no hard jets. This is interpreted as a consequence of impact-parameter-dependence: in peripheral collisions, only a small fraction of events contain any high- p_T activity, whereas central collisions are more likely to contain at least one hard scattering; a high- p_T triggered sample will therefore be biased towards small impact parameters, b . The ability of a model to describe both the UE in events with a hard trigger as well as the activity in inclusive “minimum-bias” (MB) samples (see below) therefore depends upon its modeling of the b -dependence, and correspondingly the impact-parameter shape constitutes another main tuning parameter.

For each impact parameter b , the number of interactions $\tilde{n}(b)$ can still be assumed to be distributed according to Eq. (43.13), again modulo momentum conservation, but now with the mean value of the Poisson distribution depending on impact parameter, $\langle \tilde{n}(b) \rangle$. This causes the final n -distribution (integrated over b) to be wider than a Poissonian.

Finally, there are two perturbative modeling aspects which go beyond the introduction of MPI themselves: 1) parton showers off the MPI, and 2) perturbative parton-rescattering effects. Without showers, MPI models would generate very sharp peaks for back-to-back MPI jets, caused by unshowered partons passed directly to the hadronization model. However, with the exception of the oldest PYTHIA6 model, all GPMC models do include such showers [11], and hence should exhibit more realistic (i.e., broader and more decorrelated) MPI jets. On the initial-state side, the main questions are whether and how correlated multi-parton densities are taken into account and, as discussed previously, how the showers are regulated at low p_T and/or low x . Although none of the general purpose MC models currently impose a rigorous correlated multi-parton evolution, all of them include some elementary aspects. The most significant for parton-level results is arguably momentum conservation, which is enforced explicitly in all the models. The so-called “interleaved” models [29] attempt to go a step further, generating an explicitly correlated multi-parton evolution in which flavor sum rules are imposed to conserve, e.g. the total numbers of valence and sea quarks [88]. Fully correlated double-parton evolution is so far only available in the more specialised code dShower [103]; see [104] for comparisons between this and Pythia’s interleaved model.

Perturbative rescattering in the final state can occur if partons are allowed to undergo several distinct interactions, with showering activity possibly taking place in-between. This has so far not been studied extensively, but a first exploratory model is available [105]. In the initial state, parton rescattering/recombination effects have so far not been included in any of the GPMC models.

43.3.2 Bose-Einstein and Color-Reconnection Effects

In the context of e^+e^- collisions, Bose-Einstein (BE) correlations have mostly been discussed as a source of uncertainty on high-precision W mass determinations at LEP [106]. In hadron-hadron (and nucleus-nucleus) collisions, however, BE correlations are used extensively to study the space-time structure of hadronizing matter (“femtoscropy”).

In MC models of hadronization, each string break or particle-/cluster decay is normally factorized from all other ones. This reduces the number of variables that must be considered in each step, but also makes it intrinsically difficult to introduce correlations among particles from different breaks/decays. In GPMCs, a few semi-classical models are available within the PYTHIA 6 and

8 generators [107], in which the BE effect is mimicked by an attractive interaction between pairs of identical particles in the final state, with no higher correlations included. Variants of this model differ mainly by the assumed shape of the correlation function and how overall momentum conservation is handled.

As discussed in Sec. 43.2, leading-color (“planar”) color flows are used to set up the hadronizing systems (clusters or strings) at the hadronization stage. If the systems do not overlap significantly in space and time, subleading-color ambiguities and/or nonperturbative reconnections are expected to be small. However, if the density of displaced color charges is sufficiently high that several systems can overlap significantly, full-color and/or reconnection effects should become progressively larger.

In the specific context of MPI, a crucial question is how color is neutralized *between* different MPI systems, including the remnants. The large rapidity differences involved imply large invariant masses (though normally low p_T), and hence large amounts of (soft) particle production. Indeed, in the context of soft-inclusive physics, it is these “inter-system” strings/clusters that furnish the dominant particle-production mechanism, and hence their modeling is an essential part of the soft-physics description, affecting topics such as MB/UE multiplicity and p_T distributions, rapidity gaps, and precision mass measurements. Reviews of color-reconnection effects can be found in [11, 89].

43.3.3 Minimum-Bias Events and Diffraction

The term “minimum bias” (MB) originates from the experimental requirement of a minimal number of tracks (or hits) in a given instrumented region. In order to make MC predictions for such observables, all possible contributions to the relevant phase-space region must be accounted for. There are essentially four types of physics processes, which together make up the total hadron-hadron (hh) cross section: 1) elastic scattering³: $hh \rightarrow hh$, 2) single diffractive dissociation: $hh \rightarrow h + \text{gap} + X$, with X denoting anything that is not the original beam particle, and “gap” denoting a rapidity region devoid of observed activity; 3) double diffractive dissociation: $hh \rightarrow X + \text{gap} + X$, and 4) inelastic non-diffractive scattering: everything else. A fifth class may also be defined, called central diffraction ($hh \rightarrow h + \text{gap} + X + \text{gap} + h$). Note that different terminologies exist [108]: in experimental settings, diffraction is typically defined by an observable gap, of some minimal size in rapidity, while in the MC context, each diffractive physics process produces a whole spectrum of gaps, with small ones suppressed but not excluded.

The inelastic non-diffractive part of the cross section is typically modeled either by smoothly regulating and extending the perturbative QCD scattering cross sections all the way to zero p_\perp [98] (PYTHIA and SHERPA), or by regulating the QCD cross sections with a sharp cutoff [109] and adding a separate class of nonperturbative scatterings below that scale [110] (HERWIG). See also Sec. 43.3.1. In all cases, the most important ingredients are: 1) the IR regularization of the perturbative scattering cross sections, including their PDF dependence, 2) the assumed matter distribution of the colliding hadrons, possibly including multi-parton correlations [88] and/or x dependence [111], and 3) additional soft-QCD effects such as color reconnections, discussed in Sec. 43.3.2.

Currently, there are essentially three methods for simulating diffraction in the main MC models: 1) in PYTHIA 6, one picks a diffractive mass according to parameterized cross sections $\propto dM^2/M^2$ [112]. This mass is represented as a string, which is hadronized as described in Sec. 43.2.1, though differences in the effective scale of the hadronization may necessitate a (re)tuning of the hadronization parameters for diffraction; 2) in PYTHIA 8, the high-mass tail beyond $M \sim 10$ GeV is augmented by a partonic description in terms of pomeron PDFs [113], allowing diffractive jet production including showers and underlying event [114]; 3) the PHOJET and DPMJET programs also include central diffraction and rely directly on a formulation in terms of pomerons (color-singlet multi-gluon states) [115–117]. Cut pomerons correspond to exchanges of soft gluons while uncut ones give elastic and diffractive topologies as well as virtual corrections that help preserve unitar-

ity. So-called “hard pomerons” provide a transition to the perturbative regime. Hadronization is still handled using the Lund string model, so there is some overlap with the above models at the hadronization stage. In addition, a pomeron-based package exists for HERWIG [118], and an effort is underway to construct an MC implementation of the “KMR” model [101] within the SHERPA generator. Color reconnections (Sec. 43.3.2) may also play a role in creating rapidity gaps and the underlying event (Sec. 43.3.1) in filling them.

43.4 Uncertainties and Tuning

The accuracy that can be achieved by a GPMC model depends on the sophistication of the theory models it incorporates, on the available constraints on its free parameters, and on the nature of the observable(s) under study. Using existing data to constrain the model parameters is referred to as generator tuning. Although tuned models do tend to yield improved results also for observables that they have not been tuned to, the question of evaluating the remaining uncertainties reliably is still far from solved. It is worth noting, however, that all of the GPMCs now provide options for automatic evaluation of perturbative shower uncertainties (e.g., via renormalization-scale variations), in the form of vectors of alternative event weights [119–121]. One must be aware that these variations are not necessarily exhaustive and significant weight fluctuations can be a problem for processes with large shower phase spaces. Nonperturbative uncertainties are normally still evaluated by varying salient model parameters by hand, though this looks set to change with a new method based on reweighting [122]. A general method called eigentunes [123] is also available, based on global fits to data.

Typically, the overall event properties are determined by only a few, very important parameters, such as the effective value of α_s , for perturbative corrections, and the shape of the fragmentation functions, for nonperturbative ones. More parameters may then be introduced to describe successively more detailed aspects (e.g., the rates and decays of individual hadron species), but these should have progressively less impact on the overall modeling. One may therefore take a factorized approach, first constraining the perturbative parameters and thereafter the nonperturbative ones, in order of decreasing significance to the overall modeling. Furthermore, by identifying which measurements are most sensitive to each parameter, this ordering can be reflected in the way that data is selected and applied to constrain the models. Thus, measurements sensitive to global event properties would typically be applied first, to constrain the most inclusive parameters, and so on for progressively more exclusive aspects. For high- p_T processes, one should be aware that if the perturbative modelling is not adequate, there is a risk that one may end up effectively mistuning nonperturbative parameters to compensate for perturbative deficiencies. This is obviously wrong and care must be taken to avoid it. E.g., it would not make sense to tune to get the right total number of hadrons unless one also gets the right total number of jets. In this context, it may be more desirable to use ratios like the number of hadrons *per jet*.

Note also that the unitarity of shower and hadronization models implies that the Born-level cross-section normalization is not tunable, hence in tuning contexts one tends to focus on the shapes of distributions rather than their normalizations.

At LO \times (N)LL, perturbation theory is doing well if it agrees with an IR safe shape measurement within $\sim 10\%$. It would therefore not make much sense to tune a GPMC to agree with individual data points beyond this level. To reflect this, and to protect against overfitting, a 5% sanity limit has sometimes been enforced in tuning studies [99, 124]. The advent of NLO Monte Carlos may reduce this number slightly, but only for quantities for which one expects NLO precision. For quantities governed by nonperturbative physics, uncertainties are larger. For some quantities, e.g. ones for which the underlying modeling is known to be poor, an order-of-magnitude agreement or worse may have to be accepted.

In the context of LO \times LL GPMC tuning, subleading aspects of coupling-constant and PDF choices are relevant. In particular, one should be aware that the choice of QCD A parameter $A_{\text{MC}} = 1.569 A_{\overline{\text{MS}}}$ (for 5 active flavors) improves the predictions

³The QED elastic cross section diverges and is normally a non-default option.

of coherent shower algorithms at the NLL level for a class of relevant observables [125]. The question of LO vs. NLO PDFs is more involved [11], but it should be emphasized that the gluon PDF at (very) low x is important for determining the level of the underlying event in MPI models (Sec. 43.3.1), and hence the MB/UE tuning (and energy scaling [102]) is linked to the choice of PDF in such models. Further issues and an example of a specific recipe that could be followed in a realistic set-up can be found in Ref. [99]. A useful online resource can be found at the mcplots.cern.ch website [126], based on the RIVET tool [127].

Recent years have seen the emergence of automated tools to reduce the amount of both computer and manpower required for tuning [123,128,129]. Automating the human expert input is more difficult. In the tools currently on the market, this is addressed by a combination of input solicited from the GPMC authors (e.g., which parameters and ranges to consider, which observables constitute a complete set, etc) and a set of weights determining the relative priority given to each bin in each distribution. The final result is therefore still subjective but at least reproducible. Backed by careful demonstrations of sensitivities, correlations, and uncertainties, competitive tunes can be produced. The field is still burgeoning, with future sophistications to be expected.

References

- [1] G. Corcella *et al.*, JHEP **01**, 010 (2001), [hep-ph/0011363].
- [2] M. Bahr *et al.*, Eur. Phys. J. C **58**, 639 (2008), [arXiv:0803.0883].
- [3] J. Bellm *et al.*, Eur. Phys. J. C **76**, 4, 196 (2016), [arXiv:1512.01178].
- [4] T. Sjostrand, S. Mrenna and P. Z. Skands, JHEP **05**, 026 (2006), [hep-ph/0603175].
- [5] C. Bierlich *et al.*, SciPost Phys. Codebases **8** (2022), [arXiv:2203.11601].
- [6] T. Gleisberg *et al.*, JHEP **02**, 007 (2009), [arXiv:0811.4622].
- [7] QCD summary, PDG.
- [8] T. Kinoshita, J. Math. Phys. **3**, 650 (1962).
- [9] T. Lee and M. Nauenberg, Phys. Rev. **133**, B1549 (1964).
- [10] G. C. Fox and S. Wolfram, Nucl. Phys. B **168**, 285 (1980).
- [11] A. Buckley *et al.*, Phys. Rept. **504**, 145 (2011), [arXiv:1101.2599].
- [12] G. Altarelli and G. Parisi, Nucl. Phys. B **126**, 298 (1977).
- [13] A. Einstein, B. Podolsky and N. Rosen, Phys. Rev. **47**, 777 (1935).
- [14] B. Webber, Phys. Lett. B **193**, 91 (1987).
- [15] J. C. Collins, Nucl. Phys. B **304**, 794 (1988).
- [16] I. Knowles, Comput. Phys. Commun. **58**, 271 (1990).
- [17] A. Karlberg *et al.*, Eur. Phys. J. C **81**, 8, 681 (2021), [arXiv:2103.16526].
- [18] T. Sjostrand, Phys. Lett. B **157**, 321 (1985).
- [19] G. Marchesini and B. Webber, Nucl. Phys. B **310**, 461 (1988).
- [20] S. Gieseke, P. Stephens and B. Webber, JHEP **12**, 045 (2003), [hep-ph/0310083].
- [21] M. Bengtsson and T. Sjostrand, Nucl. Phys. B **289**, 810 (1987).
- [22] G. Gustafson and U. Pettersson, Nucl. Phys. B **306**, 746 (1988).
- [23] L. Lonnblad, Comput. Phys. Commun. **71**, 15 (1992).
- [24] W. T. Giele, D. A. Kosower and P. Z. Skands, Phys. Rev. D **78**, 014026 (2008), [arXiv:0707.3652].
- [25] Z. Nagy and D. E. Soper, JHEP **10**, 024 (2005), [hep-ph/0503053].
- [26] S. Schumann and F. Krauss, JHEP **03**, 038 (2008), [arXiv:0709.1027].
- [27] S. Platzer and S. Gieseke, Eur. Phys. J. C **72**, 2187 (2012), [arXiv:1109.6256].
- [28] S. Höche and S. Prestel, Eur. Phys. J. C **75**, 9, 461 (2015), [arXiv:1506.05057].
- [29] T. Sjostrand and P. Z. Skands, Eur. Phys. J. C **39**, 129 (2005), [hep-ph/0408302].
- [30] M. Dasgupta *et al.*, JHEP **09**, 033 (2018), [Erratum: JHEP **03**, 083 (2020)], [arXiv:1805.09327].
- [31] M. Dasgupta *et al.*, Phys. Rev. Lett. **125**, 5, 052002 (2020), [arXiv:2002.11114].
- [32] J. R. Forshaw, J. Holguin and S. Plätzer, JHEP **09**, 014 (2020), [arXiv:2003.06400].
- [33] J. R. Forshaw, J. Holguin and S. Plätzer, JHEP **08**, 145 (2019), [arXiv:1905.08686].
- [34] Z. Nagy and D. E. Soper, Phys. Rev. D **99**, 5, 054009 (2019), [arXiv:1902.02105].
- [35] F. Herren *et al.* (2022), [arXiv:2208.06057].
- [36] M. van Beekveld and S. Ferrario Ravasio (2023), [arXiv:2305.08645].
- [37] E. Norrbin and T. Sjostrand, Nucl. Phys. B **603**, 297 (2001), [hep-ph/0010012].
- [38] S. Catani *et al.*, Nucl. Phys. B **627**, 189 (2002), [hep-ph/0201036].
- [39] B. Assi and S. Höche (2023), [arXiv:2307.00728].
- [40] J. Cembranos *et al.*, JHEP **09**, 077 (2013), [arXiv:1305.2124].
- [41] N. Davidson, T. Przedzinski and Z. Was, Comput. Phys. Commun. **199**, 86 (2016), [arXiv:1011.0937].
- [42] K. Hamilton and P. Richardson, JHEP **07**, 010 (2006), [hep-ph/0603034].
- [43] M. Schonherr and F. Krauss, JHEP **12**, 018 (2008), [arXiv:0810.5071].
- [44] D. R. Yennie, S. C. Frautschi and H. Suura, Annals Phys. **13**, 379 (1961).
- [45] S. Jadach *et al.*, Phys. Rev. D **94**, 7, 074006 (2016), [arXiv:1608.01260].
- [46] J. R. Christiansen and T. Sjöstrand, JHEP **04**, 115 (2014), [arXiv:1401.5238].
- [47] M. R. Masouminia and P. Richardson (2021), [arXiv:2108.10817].
- [48] H. Brooks, P. Skands and R. Verheyen (2021), [arXiv:2108.10786].
- [49] A. Semenov, Comput. Phys. Commun. **180**, 431 (2009), [arXiv:0805.0555].
- [50] N. D. Christensen and C. Duhr, Comput. Phys. Commun. **180**, 1614 (2009), [arXiv:0806.4194].
- [51] M. Fairbairn *et al.*, Phys. Rept. **438**, 1 (2007), [hep-ph/0611040].
- [52] J. Alwall *et al.*, Comput. Phys. Commun. **176**, 300 (2007), [hep-ph/0609017].
- [53] P. Z. Skands *et al.*, JHEP **07**, 036 (2004), [hep-ph/0311123].
- [54] J. Alwall *et al.* (2007), [arXiv:0712.3311].
- [55] T. Ježo *et al.*, Eur. Phys. J. C **76**, 12, 691 (2016), [arXiv:1607.04538].
- [56] P. Richardson, JHEP **11**, 029 (2001), [hep-ph/0110108].
- [57] E. Boos *et al.*, in “2nd Les Houches Workshop on Physics at TeV Colliders,” (2001), [hep-ph/0109068].
- [58] M. Bengtsson and T. Sjostrand, Phys. Lett. B **185**, 435 (1987).
- [59] W. Giele, D. Kosower and P. Skands, Phys. Rev. D **84**, 054003 (2011), [arXiv:1102.2126].
- [60] S. Catani *et al.*, JHEP **11**, 063 (2001), [hep-ph/0109231].
- [61] J. Alwall *et al.*, Eur. Phys. J. C **53**, 473 (2008), [arXiv:0706.2569].

- [62] H. Brooks and C. T. Preuss, *Comput. Phys. Commun.* **264**, 107985 (2021), [arXiv:2008.09468].
- [63] P. Nason, *JHEP* **11**, 040 (2004), [hep-ph/0409146].
- [64] B. Cooper *et al.*, *Eur. Phys. J. C* **72**, 2078 (2012), [arXiv:1109.5295].
- [65] M. L. Mangano *et al.*, *JHEP* **07**, 001 (2003), [hep-ph/0206293].
- [66] J. Alwall *et al.*, *JHEP* **06**, 128 (2011), [arXiv:1106.0522].
- [67] S. Frixione and B. R. Webber, *JHEP* **06**, 029 (2002), [hep-ph/0204244].
- [68] S. Alioli *et al.*, *JHEP* **06**, 043 (2010), [arXiv:1002.2581].
- [69] J. M. Campbell *et al.*, in “Snowmass 2021,” (2022), [arXiv:2203.11110].
- [70] P. Nason and G. P. Salam, *JHEP* **01**, 067 (2022), [arXiv:2111.03553].
- [71] J. Alwall *et al.*, *JHEP* **07**, 079 (2014), [arXiv:1405.0301].
- [72] R. Frederix and S. Frixione, *JHEP* **12**, 061 (2012), [arXiv:1209.6215].
- [73] L. Lönnblad and S. Prestel, *JHEP* **03**, 166 (2013), [arXiv:1211.7278].
- [74] K. Hamilton, P. Nason and G. Zanderighi, *JHEP* **10**, 155 (2012), [arXiv:1206.3572].
- [75] S. Hoeche *et al.*, *JHEP* **04**, 027 (2013), [arXiv:1207.5030].
- [76] S. Höche, Y. Li and S. Prestel, *Phys. Rev. D* **91**, 7, 074015 (2015), [arXiv:1405.3607].
- [77] K. Hamilton *et al.*, *JHEP* **05**, 082 (2013), [arXiv:1212.4504].
- [78] P. F. Monni *et al.*, *JHEP* **05**, 143 (2020), [arXiv:1908.06987].
- [79] S. Alioli *et al.*, *JHEP* **06**, 089 (2014), [arXiv:1311.0286].
- [80] L. Buonocore *et al.* (2022), [arXiv:2203.07240].
- [81] S. Alioli *et al.*, *JHEP* **05**, 128 (2023), [arXiv:2301.11875].
- [82] G. Gustafson 193–198 (1986).
- [83] X. Artru and G. Mennessier, *Nucl. Phys. B* **70**, 93 (1974).
- [84] B. Andersson *et al.*, *Phys. Rept.* **97**, 31 (1983).
- [85] B. Andersson, *The Lund model*, volume 7, Cambridge University Press (2005), ISBN 978-0-521-01734-3, 978-0-521-42094-5, 978-0-511-88149-7.
- [86] M. Bowler, *Z. Phys. C* **11**, 169 (1981).
- [87] C. Peterson *et al.*, *Phys. Rev. D* **27**, 105 (1983).
- [88] T. Sjostrand and P. Z. Skands, *JHEP* **03**, 053 (2004), [hep-ph/0402078].
- [89] J. R. Christiansen and P. Z. Skands, *JHEP* **08**, 003 (2015), [arXiv:1505.01681].
- [90] D. Amati and G. Veneziano, *Phys. Lett. B* **83**, 87 (1979).
- [91] A. Bassetto, M. Ciafaloni and G. Marchesini, *Phys. Lett. B* **83**, 207 (1979).
- [92] R. D. Field and S. Wolfram, *Nucl. Phys. B* **213**, 65 (1983).
- [93] B. Webber, *Nucl. Phys. B* **238**, 492 (1984).
- [94] J.-C. Winter, F. Krauss and G. Soff, *Eur. Phys. J. C* **36**, 381 (2004), [hep-ph/0311085].
- [95] D. Lange, *Nucl. Instrum. Meth. A* **462**, 152 (2001).
- [96] S. Jadach *et al.*, *Comput. Phys. Commun.* **76**, 361 (1993).
- [97] D. Grellscheid and P. Richardson (2007), [arXiv:0710.1951].
- [98] T. Sjostrand and M. van Zijl, *Phys. Rev. D* **36**, 2019 (1987).
- [99] P. Skands, S. Carrazza and J. Rojo, *Eur. Phys. J. C* **74**, 8, 3024 (2014), [arXiv:1404.5630].
- [100] M. Bahr, J. M. Butterworth and M. H. Seymour, *JHEP* **01**, 065 (2009), [arXiv:0806.2949].
- [101] M. Ryskin, A. Martin and V. Khoze, *Eur. Phys. J. C* **71**, 1617 (2011), [arXiv:1102.2844].
- [102] H. Schulz and P. Skands, *Eur. Phys. J. C* **71**, 1644 (2011), [arXiv:1103.3649].
- [103] B. Cabouat and J. R. Gaunt, *JHEP* **10**, 012 (2020), [arXiv:2008.01442].
- [104] O. Fedkevych and J. R. Gaunt, *JHEP* **02**, 090 (2023), [arXiv:2208.08197].
- [105] R. Casalbuoni *et al.*, *JHEP* **01**, 035 (2009), [arXiv:0812.1982].
- [106] (2005), [hep-ex/0511027].
- [107] L. Lonnblad and T. Sjostrand, *Eur. Phys. J. C* **2**, 165 (1998), [hep-ph/9711460].
- [108] V. Khoze *et al.*, *Eur. Phys. J. C* **69**, 85 (2010), [arXiv:1005.4839].
- [109] J. Butterworth, J. R. Forshaw and M. Seymour, *Z. Phys. C* **72**, 637 (1996), [hep-ph/9601371].
- [110] M. Bahr *et al.*, in “1st International Workshop on Multiple Partonic Interactions at the LHC,” 239–248 (2009), [arXiv:0905.4671].
- [111] R. Corke and T. Sjostrand, *JHEP* **05**, 009 (2011), [arXiv:1101.5953].
- [112] G. A. Schuler and T. Sjostrand, *Phys. Rev. D* **49**, 2257 (1994).
- [113] G. Ingelman and P. Schlein, *Phys. Lett. B* **152**, 256 (1985).
- [114] S. Navin (2010), [arXiv:1005.3894].
- [115] P. Aurenche *et al.*, *Comput. Phys. Commun.* **83**, 107 (1994), [hep-ph/9402351].
- [116] F. W. Bopp, R. Engel and J. Ranft, in “LAFEX International School on High-Energy Physics (LISHEP 98) Session A: Particle Physics for High School Teachers - Session B: Advanced School in HEP - Session C: Workshop on Diffractive Physics,” 729–741 (1998), [hep-ph/9803437].
- [117] S. Roesler, R. Engel and J. Ranft, in “International Conference on Advanced Monte Carlo for Radiation Physics, Particle Transport Simulation and Applications (MC 2000),” 1033–1038 (2000), [hep-ph/0012252].
- [118] B. E. Cox and J. R. Forshaw, *Comput. Phys. Commun.* **144**, 104 (2002), [hep-ph/0010303].
- [119] J. Bellm *et al.*, *Phys. Rev. D* **94**, 3, 034028 (2016), [arXiv:1605.08256].
- [120] S. Mrenna and P. Skands, *Phys. Rev. D* **94**, 7, 074005 (2016), [arXiv:1605.08352].
- [121] E. Bothmann, M. Schönherr and S. Schumann, *Eur. Phys. J. C* **76**, 11, 590 (2016), [arXiv:1606.08753].
- [122] C. Bierlich *et al.* (2023), [arXiv:2308.13459].
- [123] A. Buckley *et al.*, *Eur. Phys. J. C* **65**, 331 (2010), [arXiv:0907.2973].
- [124] S. Amoroso *et al.*, *JCAP* **05**, 007 (2019), [arXiv:1812.07424].
- [125] S. Catani, B. Webber and G. Marchesini, *Nucl. Phys. B* **349**, 635 (1991).
- [126] A. Karneyeu *et al.*, *Eur. Phys. J. C* **74**, 2714 (2014), [arXiv:1306.3436].
- [127] A. Buckley *et al.*, *Comput. Phys. Commun.* **184**, 2803 (2013), [arXiv:1003.0694].
- [128] J. Bellm and L. Gellersen, *Eur. Phys. J. C* **80**, 1, 54 (2020), [arXiv:1908.10811].
- [129] M. Krishnamoorthy *et al.*, *EPJ Web Conf.* **251**, 03060 (2021), [arXiv:2103.05748].

44. Monte Carlo Neutrino Generators

Revised September 2021 by H. Gallagher (Tufts U.) and Y. Hayato (Kamioka Observatory, ICRR, UTokyo; Kavli IPMU (WPI), UTokyo).

Monte Carlo neutrino generators are programs or libraries which simulate neutrino interactions with electrons, nucleons and nuclei. In this capacity their usual task is to take an input neutrino and nucleus and produce a set of 4-vectors for particles emerging from the interaction, which are then input to full detector simulations. Since these generators have to simulate not only the initial interaction of neutrinos with target particles, but re-interactions of the generated particles in the nucleus, they contain a wide range of elementary particle and nuclear physics. Viewed more broadly, they are the access point for neutrino experimentalists to the theory inputs needed for analysis. Examples include cross section libraries for event rate calculations and parameter uncertainties and reweighting tools for systematic error evaluation.

Neutrino experiments typically operate in neutrino beams that are neither completely pure nor mono-energetic. Generators are a crucial component in the convolution of beam flux, neutrino interaction physics, and detector response that is necessary to make predictions about observable quantities. Generated events are used to define experimental analyses, like event selection criteria, for efficiency determination and background subtraction. Similarly they are used to relate reconstructed quantities back to true quantities. In these various capacities they are used from the detector design stage through the extraction of physics measurements from reconstructed observable. Monte Carlo neutrino generators play unique and important roles in the experimental study of neutrino interactions and oscillations.

There are several neutrino event generators available, such as ANIS [1], GENIE [2, 3], GiBUU [4, 5], MARLEY [6], NEGN [7], NEUT [8], NUANCE [9], the FLUKA routines NUNDIS/NUNRES [10, 11], and NuWro [12], as well as tools to facilitate cross-generator comparisons, such as NUISANCE [13]. Historically, experiments would develop their own generators. This was often because they were focused on a particular measurement, energy range, or target, and wanted to ensure that the best physics was included for them. These ‘home-grown’ generators were often tuned primarily or exclusively to the neutrino data most similar to the data that the experiment would be collecting. A major advance in the field was the introduction of conference series devoted to the topic of neutrino interaction physics, NuINT (<https://indico.cern.ch/event/703880/>) and NuFACT (<https://indico.cern.ch/event/855372/>) in particular. Event generator comparisons have been a regular staple of the NuINT conference series from its inception, and a great deal of information on this topic can be found in the Proceedings of these meetings. These meetings have facilitated experiment-theory discussions leading to the first generator developed by a theory group (NuWro) [12], the extension of established nuclear interaction codes (FLUKA and GiBUU) to include neutrino-nuclear processes [4, 5, 10, 11], and inclusion of theorists in existing generator development teams.

These activities have led to more careful scrutiny of the crucial hadron and nuclear theory inputs to these generators, which is evaluated in particular through comparisons to electron-scattering data. At this point in time all simulation codes face challenges in describing the full extent of the lepton scattering data, and the tension between incorporating the best available theory versus obtaining the best agreement with the data plays out in a variety of ways within the field. For the field to make progress, inclusion of state of the art theory needs to be coupled to global analyses that correctly incorporate correlations between measurements. Given the rapid pace of new data and the complexity of analyses, this is a significant challenge for the field in the coming years.

There are many neutrino experiments which use various sources of neutrinos, from reactors, accelerators, the atmosphere, and astrophysical sources, thereby covering a range of energies from MeV to TeV. Much of the emphasis has been on the few-GeV region in the generators, as this is the relevant energy range for short- and long-baseline neutrino oscillation experiments. These gen-

erators use the impulse approximation, which treats the nucleus as a collection of independent nucleons and the primary interaction occurs between the probe and a single nucleon, for most of the initial interaction, and subsequently simulates the interactions of secondary particles in the nucleus in semi-classical ways. Semi-classical hadron transport approaches are commonly used as they are able to simulate a variety of nuclei in a single model, fully describe complex multi-particle final states, and for practical considerations as these approaches are fast. However, there are several challenges facing these simulations coming mainly from the complexity of the nuclear physics, and the need to avoid double counting in combining perturbative and non-perturbative models for the neutrino-nucleon scattering processes. The overall validity of this impulse approximation-based scheme, and in particular the importance of scattering channels that involve more than one nucleon, is a crucial question that is the topic of much current work. While generators share many common ingredients, differences in implementation, parameter values, and approaches to avoid double counting can yield dramatically different predictions [14]. In the following sections, interaction models and their implementations, including final-state interactions of hadrons produced in the nuclei, are described.

In order to assure their validity, neutrino event generators are tuned and validated against a wide variety of data. This means that the quality of the outputs from generators is limited by the quality of experimental data. The existing neutrino-nucleon and neutrino-nucleus scattering data sets are not restrictive enough to eliminate many approaches. On the other hand, there are various precise data sets, which use photon, charged lepton, and hadron probes. These data sets are extensively used to validate the generators. The results from these external data tuning exercises are important for experiments as they quantify the uncertainty on model parameters, needed by experiments in the evaluation of generator-related systematic errors. Electron scattering data plays an important role in determining the vector contribution to the form-factors and structure functions, as well as in evaluating specific aspects of the nuclear model [15, 16]. Hadron scattering data is used in validating the nuclear model, in particular of interactions between hadrons produced in the primary interaction and the residual target nucleus (final state interactions). As mentioned, tuning of neutrino-nucleon scattering and hadronization models relies heavily on the previous generation of high energy neutrino scattering and hydrogen and deuterium bubble chamber experiments. More recent data from the K2K, MiniBooNE, NOMAD, SciBooNE, MINOS, T2K, ArgoNEUT, MINERvA, NOvA, MicroBooNE, ICARUS, SBND and Ninja experiments has been, or will be, used for this purpose, although caution is advisable due to possible biases that mismodeled nuclear effects might introduce. In practice, there are often choices to be made about which models to include in an overall simulation, and which data sets to use for tuning. The process of developing a comprehensive tune in GENIE is discussed in Ref. [3].

However, all the recent experiments use nuclear targets and it is challenging to disentangle the neutrino-nucleon interaction from the effects of the nuclear environment. For example, it is difficult to separate charged current quasi-elastic scattering from the multi-nucleon quasi-elastic like scattering or single pion production, in which a pion is absorbed in the nucleus. Sometimes, there are tensions between the data sets from different experiments. Data on multi-pion and meson production are limited, but are anticipated to be measured in the near future experiments. Next generation experiments are expected to provide better detection capabilities with higher statistics and these data will help in evaluating and validating the models implemented in the generators.

44.1 Neutrino-Nucleon Scattering

Event generators typically begin with free-nucleon cross sections which are then embedded into a nuclear physics model. The most important processes are quasi-elastic (elastic for neutral current (NC)) scattering, resonance production, and non-resonant inelastic scattering, which make comparable contributions for few-GeV interactions. The neutrino cross sections in this energy range can be seen in Figure 52.1 of this *Review*.

44.1.1 Quasi-Elastic Scattering

The cross section for the neutrino nucleon charged current quasi-elastic scattering is described in terms of the leptonic and hadronic weak currents, where dominant contributions to the hadronic current come from the vector (V) and axial-vector (A) form factors. Contributions from the pseudo-scalar form factor (P) are typically small for muon and electron neutrinos and are related to the axial form factor (A) assuming partially conserved axial currents (PCAC). Owing to isospin symmetry, the vector form factors are related to those measured by precise electron scattering experiments [17]. Therefore, most of the generators use parametrizations of these form factors taken directly from the data. For the axial form factor there is no such precise experiment, and most of the generators use a dipole form [18]. Generally, the value of axial form factor at $q^2 = 0$ (q is the four-momentum transfer) is extracted from the polarized nucleon beta decay experiment. However, the selection of the axial vector mass parameter depends on each generator, with values typically around 1.00 GeV/c². Recently, there are several attempts to use the other functions for the axial form factors [19, 20] and some generators have already implemented these form factors [8, 21].

44.1.2 Inelastic Production

Most generators use the prescriptions of Rein-Sehgal [22] to simulate neutrino-induced single pion production, or updated versions that incorporate lepton mass terms and pion pole contributions [23, 24]. To obtain the cross section for a particular channel, they calculate the amplitude for the production of each resonance multiplied by the probability for the decay of that resonance into that particular channel. Implementation differences include the number of resonances included, whether the amplitudes are added coherently or incoherently, the invariant mass range over which the model is used, how non-resonant backgrounds are included, inclusion of lepton mass terms, and the model parameter values (in particular the axial mass). In this model it is also possible to calculate the cross-sections of single photon, and η production by changing the decay probability of the resonances, which are included in some of the programs. However, it is known that discrepancies exist between the recent pion electro/photo-production data and the results from the simulation data with the same framework, i.e. vector part of this model. There are several attempts to overcome this issue [25] and some of the generators started using more appropriate form factors. Recently, there are approaches that improve the theoretical description of non-resonant contributions in the resonance region, [26–28], and which account for interference between resonant and non-resonant amplitudes. This work is expected to be implemented in the generators soon. GiBUU and NuWro generators do not use the Rein-Sehgal model, and instead rely directly on electro-production data for the vector contribution and fit bubble chamber data to determine the remaining parameters for the axial contribution [29–32]. The dynamical coupled-channel model, which has been developed to simulate various electro- and photo-meson productions, was extended to simulate the neutrino single pion production [33]. In this approach pion-nucleon scattering is used to fix the form of the axial current at $q^2 = 0$. This model is also being implemented and expected to be available in some of the generators in future.

44.1.3 Deep and Shallow Inelastic Scattering

For this process the fundamental target shifts from the nucleon to its quark constituents. Therefore, the generators construct the nucleon structure functions F_2 and xF_3 from parton distributions for high Q^2 (the DIS regime: $W \gtrsim 2$ GeV/c² and $Q^2 \gtrsim 1$ GeV²) to calculate the direction and momentum of the lepton. The first challenge is in extending this picture to the lower values of Q^2 and W that dominate the available phase space for few-GeV interactions (the so-called ‘shallow inelastic scattering’, or SIS regime). GRV98LO parton distribution functions [34] with the corrections proposed in [35, 36] are widely used, while others [10] implement their own modifications to the parton distributions at low Q^2 . Both DIS and SIS generate hadrons but their production depends on each generator’s implementation of a hadronization model as described in the next section. There are various difficulties not only in the actual hadronization but the relation with the single

meson production. It is necessary to avoid double counting between the resonance and SIS/DIS models, and all generators are different in this regard. The scheme chosen can have a significant impact on the results of simulations at a few-GeV neutrino energies. For simulating ultra-high energy interactions currently being studied with neutrino telescopes, fully partonic descriptions, which utilize beyond-leading-order pQCD calculations [37, 38] are the norm [39].

44.2 Hadronization Models

For hadrons produced via baryonic resonances, the underlying model amplitudes and resonance branching fractions can be used to fully characterize the hadronic system. For shallow- and deep-inelastic scattering, a hadronization model is required. Most generators use PYTHIA [40] for this purpose, although some with modified parameters. In addition some implement their own models to handle invariant masses that are too low for PYTHIA, typically somewhere around 2.0 GeV/c². Such models rely heavily on measurements of neutrino hadro-production in high-resolution devices, such as bubble chambers and the CHORUS [41] and NOMAD experiments [42], to construct empirical parametrizations that reproduce the key features of the data [43, 44]. The basic ingredients are the empirical observations that average charged particle multiplicities increase logarithmically with the invariant mass of the hadronic system, and that the distribution of charged particle multiplicities about this average are described by a single function (an observation known as KNO scaling [45]). The multiplicity of the neutral particles are usually obtained by scaling the charged particle multiplicity. Simple parametrizations to more accurately reproduce differences observed in the forward/backward hemispheres of hadronic systems are included in GENIE, NEUT, and NuWro.

44.3 Nuclear Physics

The nuclear physics relevant to neutrino-nucleus scattering at few-GeV energies is complicated, involving Fermi motion, nuclear binding, Pauli blocking, in-medium modifications of form factors and hadronization, intranuclear rescattering of hadrons, and many-body scattering mechanisms including long- and short-range nucleon-nucleon correlations.

44.3.1 Treatment of nuclear effects

In order to obtain the cross-section off nucleons in the nucleus, it is necessary to take into account various in-medium effects. Most of the models used for neutrino-nuclear scattering kinematics were developed in the context of few-GeV inclusive electron scattering, by experiments going back nearly 50 years. The basic models employed in event generators rely on impulse approximation schemes, the most simple of which is the Relativistic Fermi Gas Model. The most common implementations have been the Smith-Moniz [46] and Bodek-Ritchie [47] models. However, the results from neutrino-nucleus scattering experiments in 2000 and afterwards, beginning with K2K, MiniBooNE have shown large discrepancies from the naive expectation from the models. Most striking differences are a suppression of forward going muons (low Q^2), a high Q^2 enhancement in the event rate, and an overall larger than expected number of observed events. In order to reproduce the data, the quasi-elastic axial mass was used as the effective parameter and increased by roughly 20% from the nominal values obtained by an earlier generation of bubble chamber experiments using hydrogen or deuterium [18]. This inconsistency between nucleon and nucleus targets suggests that the simple nuclear model is not appropriate in describing the data. Moreover, these simple Fermi-Gas models are not expected to describe the kinematical distributions of final state nucleons. Therefore, several generators have to implement better models, such as local Fermi-Gas model or more sophisticated models. Within the electron scattering community, the analogous calculations have for decades relied on spectral functions, which incorporate information about nucleon momenta and binding energies in the impulse approximation scheme [15]. Therefore, most of the generators have implemented the realistic spectral functions in their latest releases.

Actually, the discrepancies in small q^2 could not be solved alone

by just introducing the local Fermi-gas model nor spectral function models. This implies that the additional medium correction effects are needed to be taken into account. One of the implemented solutions is the local Fermi-Gas model with medium correction calculated using the random phase approximation, which is known to give large suppression in small q^2 [48, 49]. Although, the fundamental parts of the models are same, actual implementations are quite different between the generators. Especially, the constructions of the final state hadron kinematics are quite different. Especially for the quasi-elastic scattering case, treatment of the nucleon masses in the nucleus, the binding and the separation energies are sometimes quite different [50]. Recently, Super-Scaling model with relativistic mean field theory effects (SuSAv2) [51, 52] is implemented in some of the generators. Indications of the suppression in small q^2 in the single pion productions were also observed in K2K and MiniBooNE and it is clearly observed at the MINERvA and NOvA experiments. However, the models to explain the suppression have not been implemented, other than the phenomenological ones. Also, q^2 dependence of the cross-section is largely model and parameter dependent. Further studies of newly implemented single pion models may give new insights. The cause of the discrepancy of small q^2 seems to be identified but the issue of the observed interaction rates are not solved. This implies that there must be some interaction channels which are missing and not considered in the generators.

These led to a revisit of the role played by excitation of multiple particle-hole states in the nucleus, and the experimental study of these scattering channels is an area of intense experimental interest [53]. The contribution of these scattering processes is an extremely active area of theoretical research as well, with significant implications for generators and analyses [54]. Several approaches, ranging from strictly phenomenological descriptions to full theoretical calculations, have recently been incorporated into generators [55–57]. One example of a phenomenological approach utilizes an Effective Spectral Function [58] and a Transverse Enhancement Model [59], which together encapsulate information derived from electron scattering experiments at relevant kinematics. The microscopic model of Nieves and collaborators is now available in GENIE and NEUT [60, 61]. SuSAv2 model [52] also has capability to simulate this multi-nucleon quasi-elastic like interaction and is also implemented in GENIE.

One of the challenges in incorporating full theoretical models of these processes is that they are typically slow, so generators have developed new approaches whereby much of the computation is done offline, and the generators simply read in the hadronic tensor components. This allows for a full prediction of the lepton kinematics, however the ability to simulate the hadronic component of these multinucleon states then relies on separate models. The other challenge is that the theoretical models are not designed to describe exclusive final states. These approaches, while making simulations computationally tractable, neglect correlations between the lepton and hadron kinematics. Also, there are limitations of the model itself to describe some of the kinematic regions. However, the generators need to simulate final all the state particles and thus, several assumptions are made by authors of the generators from time to time.

Also, it is known from photo and electro-nuclear scattering that the Delta width is affected by Pauli blocking and collisional broadening. These effects are included in some, but not all generators.

The remnant nucleus after the scattering is usually in an excited state. Therefore, the remnant may emit gamma-rays, additional nucleons or an alpha particle during the de-excitation process. This de-excitation gamma-ray is used in searching for proton decay in water Cherenkov detectors. Some generators have implemented this process. NEUT implemented the de-excitation process but only for Oxygen. Recently, GENIE has de-excitation processes for various nuclei.

When scattering from a nucleus, coherent scattering of various kinds is possible. Most simulations incorporate, at least, coherent neutral and charged single pion production. While the interaction rate for these interactions is typically around a percent of the total yield, the unique kinematic features of these events can make them potential backgrounds for oscillation searches. Imple-

mented in Monte Carlo are several PCAC-based methods [62, 63]. Microscopic models, valid at lower neutrino energies [64–67], have also been implemented in several generators. One commonly used model by Rein and Sehgal [62] predicts a cross section for charged-current coherent pion production that is much larger than what is observed by K2K, MINERvA and T2K. However, the cross-section is sensitive to the pion cross-section used in the model as parameters and improved models with lepton mass correction [63] give better agreement with the recent data. This improved model is implemented in most of the generators. In addition to coherent pion production, some generators can simulate coherent single photon production [68] and coherent elastic neutrino-nucleus scattering.

44.3.2 Hadron Production in Nuclei

Neutrino pion production is one of the dominant neutrino scattering mechanisms in the few-GeV region and the pions produced in the nucleus have quite large interaction cross sections. Therefore, pion intranuclear scattering can have sizable effects on the results of simulations at these energies. Also, recent neutrino oscillation experiments use the observed information of protons and pions more extensively, in addition to the charged leptons. Therefore, most generators implement this physics through an intranuclear cascade simulation. In generators which utilize cascade models, a hadron, which has been formed in the nucleus, is moved step by step until it interacts with a nucleon or escapes from the nucleus. The probabilities of each interaction in nucleus are usually given as the mean free paths and used to determine whether the hadron has interacted or not. If the hadron is found to have interacted, appropriate final states are selected. Usually, absorption, elastic, charge exchange, and inelastic scatterings including particle productions are simulated as intranuclear interactions. The determination method of the kinematics for the final state particles heavily depends on the generators but most of them use experimentally validated models to simulate hadron interactions in nucleus. No two intranuclear cascade simulations implemented in neutrino event generators are the same [69]. In all cases hadrons propagate from an interaction vertex chosen based on the density distribution of the target nucleus. In determining the generated position of the hadrons in nucleus, the concept of the formation length is sometimes employed. Based on this idea, the hadronization process is not instantaneous and it takes some time before generating the hadrons [12]. The basis for formation times are measurements at relatively high energy and Q^2 , and most generators that employ the concept do not apply them to resonance interactions.

GiBUU does not employ an intranuclear cascade simulation, instead, it utilizes a semi-classical transport model in coupled channels that describes the space-time evolution of a many body system in the presence of potentials and a collision term [4]. This approach assures consistency between nuclear effects in the initial state, such as Fermi motion, Pauli blocking, hadron self-energies [70], and modified cross sections, and the final state, such as particle re-interactions, since the two are derived from the same model. This model has been previously used to describe a wide variety of nuclear interaction data. Similarly, the hadronic simulation of the NUNDIS/NUNRES programs are handled by the well-established FLUKA hadronic simulation package [10]. Recently, GENIE included the interface to the external hadronic simulation package INCL++ [71].

References

- [1] A. Gazizov and M. P. Kowalski, *Comput. Phys. Commun.* **172**, 203 (2005), [arXiv:astro-ph/0406439].
- [2] C. Andreopoulos *et al.*, *Nucl. Instrum. Meth.* **A614**, 87 (2010), [arXiv:0905.2517].
- [3] J. Tena-Vidal *et al.* (GENIE) (2021), [arXiv:2104.09179].
- [4] O. Buss *et al.*, *Phys. Rept.* **512**, 1 (2012), [arXiv:1106.1344].
- [5] K. Gallmeister, U. Mosel and J. Weil, *Phys. Rev.* **C94**, 3, 035502 (2016), [arXiv:1605.09391].
- [6] S. Gardiner, C. Grant, E. Panic, and R. Svoboda, <http://www.marleygen.org>.
- [7] D. Autiero, *Nucl. Phys. Proc. Suppl.* **139**, 253 (2005).

- [8] Y. Hayato and L. Pickering, *Eur. Phys. J. Spec. Top.* (2021), [arXiv:2106.15809].
- [9] D. Casper, *Nucl. Phys. Proc. Suppl.* **112**, 161 (2002), [hep-ph/0208030].
- [10] G. Battistoni *et al.*, *Acta Phys. Polon.* **B40**, 2491 (2009).
- [11] T. T. Böhlen *et al.*, *Nucl. Data Sheets* **120**, 211 (2014).
- [12] T. Golan, C. Juszczak and J. T. Sobczyk, *Phys. Rev.* **C86**, 015505 (2012), [arXiv:1202.4197].
- [13] P. Stowell *et al.*, *JINST* **12**, 01, P01016 (2017), [arXiv:1612.07393].
- [14] M. Betancourt *et al.*, *Phys. Rept.* **773-774**, 1 (2018), [arXiv:1805.07378].
- [15] O. Benhar, D. day and I. Sick, *Rev. Mod. Phys.* **80**, 189 (2008), [arXiv:nucl-ex/0603029].
- [16] B. Schmookler *et al.* (CLAS), *Nature* **566**, 7744, 354 (2019), [arXiv:2004.12065].
- [17] A. Bodek *et al.*, *Eur. Phys. J.* **C53**, 349 (2008), [arXiv:0708.1946].
- [18] H. Gallagher, G. Garvey and G. P. Zeller, *Ann. Rev. Nucl. Part. Sci.* **61**, 355 (2011).
- [19] E. Tomasi-Gustafsson, G. I. Gakh and C. Adamuscin, *Phys. Rev.* **C73**, 045204 (2006), [arXiv:nucl-th/0512039].
- [20] B. Bhattacharya, R. J. Hill and G. Paz, *Phys. Rev.* **D84**, 073006 (2011), [arXiv:1108.0423].
- [21] A. S. Meyer *et al.*, *Phys. Rev.* **D93**, 11, 113015 (2016), [arXiv:1603.03048].
- [22] D. Rein and L. M. Sehgal, *Annals Phys.* **133**, 79 (1981).
- [23] K. S. Kuzmin, V. V. Lyubushkin and V. A. Naumov, *Mod. Phys. Lett. A* **19**, 2815 (2004), [hep-ph/0312107].
- [24] C. Berger and L. M. Sehgal, *Phys. Rev. D* **76**, 113004 (2007), [arXiv:0709.4378].
- [25] K. M. Graczyk and J. T. Sobczyk, *Phys. Rev.* **D77**, 053001 (2008), [Erratum: *Phys. Rev.D79,079903(2009)*], [arXiv:0707.3561].
- [26] M. Kabirnezhad, *Phys. Rev.* **D97**, 1, 013002 (2018), [arXiv:1711.02403].
- [27] M. Kabirnezhad, *Phys. Rev. D* **102**, 5, 053009 (2020), [arXiv:2006.13765].
- [28] E. Hernandez, J. Nieves and M. Valverde, *Phys. Rev. D* **76**, 033005 (2007), [hep-ph/0701149].
- [29] O. Lalakulich and E. A. Paschos, *Phys. Rev.* **D71**, 074003 (2005), [hep-ph/0501109].
- [30] J. A. Nowak, *Phys. Scripta* **T127**, 70 (2006), [hep-ph/0607081].
- [31] T. Leitner *et al.*, *Phys. Rev. C* **79**, 034601 (2009), [arXiv:0812.0587].
- [32] L. Alvarez-Ruso, S. K. Singh and M. J. Vicente Vacas, *Phys. Rev.* **C57**, 2693 (1998), [arXiv:nucl-th/9712058].
- [33] S. X. Nakamura, H. Kamano and T. Sato, *Phys. Rev.* **D92**, 7, 074024 (2015), [arXiv:1506.03403].
- [34] M. Glück, E. Reya and A. Vogt, *Eur. Phys. J.* **C5**, 461 (1998), [hep-ph/9806404].
- [35] A. Bodek and U. K. Yang, *J. Phys.* **G29**, 1899 (2003), [hep-ex/0210024].
- [36] A. Bodek, U. K. Yang and Y. Xu (2021), [arXiv:2108.09240].
- [37] A. Cooper-Sarkar, P. Mertsch and S. Sarkar, *JHEP* **08**, 042 (2011), [arXiv:1106.3723].
- [38] V. Bertone, R. Gauld and J. Rojo, *JHEP* **01**, 217 (2019), [arXiv:1808.02034].
- [39] A. Garcia and A. Heijboer (KM3NeT), *PoS ICRC2019*, 895 (2020), [arXiv:1908.10077].
- [40] T. Sjostrand, S. Mrenna and P. Z. Skands, *JHEP* **05**, 026 (2006), [hep-ph/0603175].
- [41] A. Kayis-Topaksu *et al.* (CHORUS), *Eur. Phys. J.* **C51**, 775 (2007), [arXiv:0707.1586].
- [42] J. Altegoer *et al.* (NOMAD), *Phys. Lett.* **B445**, 439 (1999).
- [43] T. Yang *et al.*, *Eur. Phys. J.* **C63**, 1 (2009), [arXiv:0904.4043].
- [44] J. A. Nowak and J. T. Sobczyk, *Acta Phys. Polon.* **B37**, 2371 (2006), [hep-ph/0608108].
- [45] Z. Koba, H. B. Nielsen and P. Olesen, *Nucl. Phys.* **B40**, 317 (1972).
- [46] R. A. Smith and E. J. Moniz, *Nucl. Phys.* **B43**, 605 (1972), [Erratum: *Nucl. Phys.B101,547(1975)*].
- [47] A. Bodek and J. L. Ritchie, *Phys. Rev.* **D24**, 1400 (1981).
- [48] M. C. Martinez *et al.*, *Phys. Rev. C* **73**, 024607 (2006), [arXiv:nucl-th/0505008].
- [49] J. Nieves, J. E. Amaro and M. Valverde, *Phys. Rev. C* **70**, 055503 (2004), [Erratum: *Phys.Rev.C 72, 019902 (2005)*], [arXiv:nucl-th/0408005].
- [50] A. Bodek and T. Cai, *Eur. Phys. J. C* **79**, 4, 293 (2019), [arXiv:1801.07975].
- [51] J. A. Caballero *et al.*, *Phys. Lett.* **B653**, 366 (2007), [arXiv:0705.1429].
- [52] R. González-Jiménez *et al.*, *Phys. Rev. C* **90**, 3, 035501 (2014), [arXiv:1407.8346].
- [53] X. G. Lu *et al.* (MINERvA) (2021), [arXiv:2107.02064].
- [54] L. Alvarez-Ruso *et al.*, *Prog. Part. Nucl. Phys.* **100**, 1 (2018), [arXiv:1706.03621].
- [55] T. Katori, *AIP Conf. Proc.* **1663**, 1, 030001 (2015), [arXiv:1304.6014].
- [56] M. Alam *et al.* (2015), [arXiv:1512.06882].
- [57] C. Wilkinson *et al.*, *Phys. Rev.* **D93**, 7, 072010 (2016), [arXiv:1601.05592].
- [58] A. Bodek, M. E. Christy and B. Coopersmith, *Eur. Phys. J.* **C74**, 10, 3091 (2014), [arXiv:1405.0583].
- [59] A. Bodek, H. S. Budd and M. E. Christy, *Eur. Phys. J.* **C71**, 1726 (2011), [arXiv:1106.0340].
- [60] J. Nieves, I. Ruiz Simo and M. J. Vicente Vacas, *Phys. Rev.* **C83**, 045501 (2011), [arXiv:1102.2777].
- [61] R. Gran *et al.*, *Phys. Rev.* **D88**, 11, 113007 (2013), [arXiv:1307.8105].
- [62] D. Rein and L. M. Sehgal, *Nucl. Phys.* **B223**, 29 (1983).
- [63] C. Berger and L. M. Sehgal, *Phys. Rev.* **D79**, 053003 (2009), [arXiv:0812.2653].
- [64] L. Alvarez-Ruso *et al.*, *Phys. Rev.* **C75**, 055501 (2007), [Erratum: *Phys. Rev.C80,019906(2009)*], [arXiv:nucl-th/0701098].
- [65] L. Alvarez-Ruso, L. S. Geng and M. J. Vicente Vacas, *Phys. Rev.* **C76**, 068501 (2007), [Erratum: *Phys. Rev.C80,029904(2009)*], [arXiv:0707.2172].
- [66] J. E. Amaro *et al.*, *Phys. Rev. D* **79**, 013002 (2009), [arXiv:0811.1421].
- [67] S. X. Nakamura *et al.*, *Phys. Rev. C* **81**, 035502 (2010), [arXiv:0910.1057].
- [68] E. Wang, L. Alvarez-Ruso and J. Nieves, *Phys. Rev. C* **89**, 1, 015503 (2014), [arXiv:1311.2151].
- [69] S. Dytman *et al.*, *Phys. Rev. D* **104**, 5, 053006 (2021), [arXiv:2103.07535].
- [70] S. K. Singh, M. J. Vicente-Vacas and E. Oset, *Phys. Lett. B* **416**, 23 (1998), [Erratum: *Phys.Lett.B 423, 428 (1998)*].
- [71] A. Boudard *et al.*, *Phys. Rev. C* **87**, 014606 (2013), URL <https://link.aps.org/doi/10.1103/PhysRevC.87.014606>.

45. Monte Carlo Particle Numbering Scheme

Revised August 2023 by A. Buckley (Glasgow U.), F. Krauss (Durham U.), S. Navas (Granada U.) and P. Richardson (Durham U.).

The Monte Carlo particle numbering scheme presented here is intended to facilitate interfacing between matrix-element generators, event generators, detector simulators, and analysis packages used in particle physics, and is widely accepted as the “industry standard”. The numbering scheme was introduced in 1988 [1], and has since been revised and expanded in the light of new information on hadronic resonances, and to encompass as yet undiscovered and hypothetical particles.¹

The general form is a 7–digit number:

$$\pm n \ n_r \ n_L \ n_{q_1} \ n_{q_2} \ n_{q_3} \ n_J .$$

This encodes information about the particle’s spin, flavor content, and internal quantum numbers. A 9–digit extension is used specifically for tetra- and penta-quark states, and a distinct 10–digit scheme is used for encoding (hyper)nuclear states. The details are as follows:

1. Particles are given positive numbers, antiparticles negative numbers. The PDG convention for mesons is used, so that K^+ and B^+ are particles.
2. Quarks and leptons are numbered consecutively starting from 1 and 11 respectively; to do this they are first ordered by family and within families by weak isospin.
3. In composite quark systems (diquarks, mesons, and baryons) $n_{q_{1-3}}$ are quark numbers used to specify the quark content, while the rightmost digit $n_J = 2J + 1$ gives the system’s spin (except for the K_S^0 and K_L^0). The scheme does not cover particles of spin $J > 4$.
4. Diquarks have 4–digit numbers with $n_{q_1} \geq n_{q_2}$ and $n_{q_3} = 0$.
5. The numbering of mesons is guided by the nonrelativistic (L – S decoupled) quark model, as listed in Tables 15.2, 15.3, and 15.4.
 - (a) The numbers specifying the meson’s quark content conform to the convention $n_{q_1} = 0$ and $n_{q_2} \geq n_{q_3}$. The special case K_L^0 is the sole exception to this rule.
 - (b) The quark numbers of flavorless, light (u, d, s) mesons are: 11 for the member of the isotriplet (π^0, ρ^0, \dots), 22 for the lighter isosinglet (η, ω, \dots), and 33 for the heavier isosinglet (η', ϕ, \dots). Since isosinglet mesons are often large mixtures of $u\bar{u} + d\bar{d}$ and $s\bar{s}$ states, 22 and 33 are assigned by mass and do not necessarily specify the dominant quark composition.
 - (c) The special numbers 310 and 130 are given to the K_S^0 and K_L^0 respectively.
 - (d) The fifth digit n_L is reserved to distinguish mesons of the same total (J) but different spin (S) and orbital (L) angular momentum quantum numbers. For $J > 0$ the numbers are: $(L, S) = (J - 1, 1)$ $n_L = 0$, $(J, 0)$ $n_L = 1$, $(J, 1)$ $n_L = 2$ and $(J + 1, 1)$ $n_L = 3$. For the exceptional case $J = 0$ the numbers are $(0, 0)$ $n_L = 0$ and $(1, 1)$ $n_L = 1$ (*i.e.* $n_L = L$). See Table 45.1.
 - (e) If a set of physical mesons correspond to a (non-negligible) mixture of basis states, differing in their internal quantum numbers, then the lightest physical state gets the smallest basis state number. For example the $K_1(1270)$ is numbered 10313 ($1^1P_1 K_{1B}$) and the $K_1(1400)$ is numbered 20313 ($1^3P_1 K_{1A}$).
 - (f) The sixth digit n_r is used to label mesons radially excited above the ground state.
 - (g) Numbers have been assigned for complete $n_r = 0$ S - and P -wave multiplets, even where states remain to be identified.

¹The scheme was substantially updated and extended in 2012. Certain excited baryons follow the pre-2012 scheme. A further revision and/or extension of the numbering scheme is anticipated in the near future.

Table 45.1: Meson numbering logic. Here qq stands for $n_{q_2} n_{q_3}$.

J	$L = J - 1, S = 1$			$L = J, S = 0$			$L = J, S = 1$			$L = J + 1, S = 1$		
	code	J^{PC}	L	code	J^{PC}	L	code	J^{PC}	L	code	J^{PC}	L
0	—	—	—	00qq1	0 ⁺⁺	0	—	—	—	10qq1	0 ⁺⁺	1
1	00qq3	1 ⁻⁻	0	10qq3	1 ⁺⁻	1	20qq3	1 ⁺⁺	1	30qq3	1 ⁻⁻	2
2	00qq5	2 ⁺⁺	1	10qq5	2 ⁺⁻	2	20qq5	2 ⁻⁻	2	30qq5	2 ⁺⁺	3
3	00qq7	3 ⁻⁻	2	10qq7	3 ⁺⁻	3	20qq7	3 ⁺⁺	3	30qq7	3 ⁻⁻	4
4	00qq9	4 ⁺⁺	3	10qq9	4 ⁺⁻	4	20qq9	4 ⁻⁻	4	30qq9	4 ⁺⁺	5

- (h) In some instances assignments within the $q\bar{q}$ meson model are only tentative; here best guess assignments are made.
 - (i) Many states appearing in the Meson Listings are not yet assigned within the $q\bar{q}$ model. Here $n_{q_{2-3}}$ and n_J are assigned according to the state’s likely flavors and spin; all such unassigned light isoscalar states are given the flavor code 22. Within these groups $n_L = 0, 1, 2, \dots$ is used to distinguish states of increasing mass. These states are flagged using $n = 9$. It is to be expected that these numbers will evolve as the nature of the states are elucidated. Codes are assigned to most mesons that are listed in the one-page table at the end of the Meson Summary Table as long as they have a preferred or established spin. Additional heavy meson states expected from heavy quark spectroscopy are also assigned codes.
6. The numbering of baryons is again guided by the nonrelativistic quark model, see Table 15.6. This numbering scheme is illustrated through a few examples in Table 45.2.
 - (a) The numbers specifying a baryon’s quark content are such that in general $n_{q_1} \geq n_{q_2} \geq n_{q_3}$.
 - (b) Two states exist for $J = 1/2$ baryons containing 3 different types of quarks. In the lighter baryon ($\Lambda, \Xi, \Omega, \dots$) the light quarks are in an antisymmetric ($J = 0$) state while for the heavier baryon ($\Sigma^0, \Xi', \Omega', \dots$) they are in a symmetric ($J = 1$) state. In this situation n_{q_2} and n_{q_3} are reversed for the lighter state, so that the smaller number corresponds to the lighter baryon.
 - (c) For excited baryons a scheme is adopted, where the n_r label is used to denote the excitation bands in the harmonic oscillator model, see Sec. 15.5. Using the notation employed there, n_r is given by the N -index of the D_N band identifier.
 - (d) Further degeneracies of excited hadron multiplets with the same excitation number n_r and spin J are lifted by labelling such multiplets with the n_L index according to their mass, as given by its N or Δ -equivalent.
 - (e) In such excited multiplets extra singlets may occur, the $\Lambda(1520)$ being a prominent example. In such cases the ordering is reversed such that the heaviest quark label is pushed to the last position: $n_{q_3} > n_{q_1} > n_{q_2}$.
 7. The gluon, when considered as a gauge boson, has official number 21. In codes for glueballs, however, 9 is used to allow a notation in close analogy with that of hadrons.
 8. The pomeron and odderon trajectories and a generic reggeon trajectory of states in QCD are assigned codes 990, 9990, and 110 respectively, where the final 0 indicates the indeterminate nature of the spin, and the other digits reflect the expected “valence” flavor content. We do not attempt a complete classification of all reggeon trajectories, since there is currently no need to distinguish a specific such trajectory from its lowest-lying member.
 9. Two-digit numbers in the range 21–30 are provided for the Standard Model gauge and Higgs bosons.
 10. Codes 81–100 are reserved for generator-specific pseudoparticles and concepts. Codes 901–930, 1901–1930, 2901–2930, and 3901–3930 are for additional components of Standard Model parton distribution functions: the latter three ranges

Table 45.2: Some examples of octet (top) and decuplet (bottom) members for the numbering scheme for excited baryons. Here qqq stands for $n_{q_1}n_{q_2}n_{q_3}$. See the text for the definition of the notation. The numbers in parenthesis correspond to the mass of the baryons. The states marked as (?) are not experimentally confirmed.

J^P	(D, L_N^P)	$n_r n_L n_{q_1} n_{q_2} n_{q_3} n_J$	N	Λ_8	Σ	Ξ	Λ_1
Octet							
1/2 ⁺	(56, 0 ₀ ⁺)	00qqq2	(939)	(1116)	(1193)	(1318)	—
1/2 ⁺	(56, 0 ₂ ⁺)	20qqq2	(1440)	(1600)	(1660)	(1690)	—
1/2 ⁺	(70, 0 ₁ ⁺)	21qqq2	(1710)	(1810)	(1880)	(?)	(?)
1/2 ⁻	(70, 1 ₁ ⁻)	10qqq2	(1535)	(1670)	(1620)	(1750)	(1405)
Decuplet							
3/2 ⁺	(56, 0 ₀ ⁺)	00qqq4	(1232)	(1385)	(1530)	(1672)	—
3/2 ⁺	(56, 0 ₂ ⁺)	20qqq4	(1600)	(1690)	(?)	(?)	—
1/2 ⁻	(70, 1 ₁ ⁻)	11qqq2	(1620)	(1750)	(?)	(?)	—
3/2 ⁻	(70, 1 ₁ ⁻)	12qqq4	(1700)	(?)	(?)	(?)	—

are intended to distinguish left/ right/ longitudinal components. Codes 998 and 999 are reserved for GEANT tracking purposes.

11. The search for physics beyond the Standard Model is an active area, so these codes are also standardized as far as possible.
 - (a) A standard fourth generation of fermions is included by analogy with the first three.
 - (b) The graviton and the boson content of a two-Higgs-doublet scenario and of additional $SU(2) \times U(1)$ groups are found in the range 31–40.
 - (c) “One-of-a-kind” exotic particles are assigned numbers in the range 41–80. The subrange 61–80 can be used for new heavier fermions in generic models, where partners to the SM fermions would have codes offset by 60. If required, however, other assignments could be made.
 - (d) Fundamental supersymmetric particles are identified by adding a nonzero n to the particle number. The superpartner of a boson or a left-handed fermion has $n = 1$ while the superpartner of a right-handed fermion has $n = 2$. When mixing occurs, such as between the winos and charged Higgsinos to give charginos, or between left and right sfermions, the lighter physical state is given the smaller basis state number.
 - (e) Technicolor states have $n = 3$, with technifermions treated like ordinary fermions. States which are ordinary color singlets have $n_r = 0$. Color octets have $n_r = 1$. If a state has non-trivial quantum numbers under the topcolor groups $SU(3)_1 \times SU(3)_2$, the quantum numbers are specified by $tech, ij$, where i and j are 1 or 2. n_L is then $2i + j$. The coloron, V_8 , is a heavy gluon color octet and thus is 3100021.
 - (f) Excited (composite) quarks and leptons are identified by setting $n = 4$ and $n_r = 0$.
 - (g) Within several scenarios of new physics, it is possible to have colored particles sufficiently long-lived for color-singlet hadronic states to form around them. In the context of supersymmetric scenarios, these states are called R -hadrons, since they carry odd R -parity. R -hadron codes, defined here, should be viewed as templates for corresponding codes also in other scenarios, for any long-lived particle that is either an unflavored color octet or a flavored color triplet. The R -hadron code is obtained by combining the SUSY particle code with a code for the light degrees of freedom, with as many intermediate zeros removed from the former as required to make place for the latter at the end. (To exemplify, a sparticle $n00000n_{\bar{q}}$ combined with quarks q_1 and q_2 obtains code $n00n_{\bar{q}}n_{q_1}n_{q_2}n_J$.) Specifically, the new-particle spin decouples in the limit of large masses, so that the final n_J digit is defined by the spin state of the light-quark system alone. An appropriate number of n_q digits is used to define the ordinary-quark content. As usual, 9

rather than 21 is used to denote a gluon/gluino in composite states. The sign of the hadron agrees with that of the constituent new particle (a color triplet) where there is a distinct new antiparticle, and else is defined as for normal hadrons. Particle names are R with the flavor content as lower index.

- (h) A black hole in models with extra dimensions has code 5000040. Kaluza-Klein excitations in models with extra dimensions have $n = 5$ or $n = 6$, to distinguish excitations of left- or right-handed fermions or, in case of mixing, the lighter or heavier state (cf. 11d). The nonzero n_r digit gives the radial excitation number, in scenarios where the level spacing allow these to be distinguished. Should the model also contain supersymmetry, excited SUSY states would be denoted by an $n_r > 0$, with $n = 1$ or 2 as usual. Should some colored states be long-lived enough that hadrons would form around them, the coding strategy of 11g applies, with the initial two nn_r digits preserved in the combined code.
 - (i) Magnetic monopoles and dyons are assumed to have one unit of Dirac monopole charge and a variable integer number $n_{q_1}n_{q_2}n_{q_3}$ units of electric charge. Codes $411n_{q_1}n_{q_2}n_{q_3}0$ are then used when the magnetic and electrical charge sign agree and $412n_{q_1}n_{q_2}n_{q_3}0$ when they disagree, with the overall sign of the particle set by the magnetic charge. For now no spin information is provided.
 - (j) The nature of Dark Matter (DM) is not known, and therefore a definitive classification is too early. Candidates within specific scenarios are classified therein, such as 1000022 for the lightest neutralino. Generic fundamental states can be given temporary codes in the range 51 - 60, with 51, 52 and 53 reserved for spin 0, 1/2 and 1 ones (this could also be an axion state). Generic mediators of s-channel DM pair creation or annihilation can be given codes 54 and 55 for spin 0 or 1 ones. Separate antiparticles, with negative codes, may or may not exist. More elaborate new scenarios should be constructed with $n = 5$ and $n_r = 9$.
 - (k) Hidden Valley particles have $n = 4$ and $n_r = 9$, and trailing numbers in agreement with their nearest-analog standard particles, as far as possible. Thus 4900021 is the gauge boson g_v of a confining gauge field, 490000 n_{q_v} and 490001 n_{ℓ_v} fundamental constituents charged or not under this, 4900022 is the γ_v of a non-confining field, and 4900 $n_{q_{v1}}n_{q_{v2}}n_J$ a Hidden Valley meson.
12. Occasionally program authors add their own states. To avoid confusion, these should be flagged by setting $nn_r = 99$.
 13. Concerning the non-99 numbers, it may be noted that only quarks, excited quarks, squarks, and diquarks have $n_{q_3} = 0$; only diquarks, baryons, and the odderon have $n_{q_1} \neq 0$; and only mesons, the reggeon, and the pomeron have $n_{q_1} = 0$ and $n_{q_2} \neq 0$. Concerning mesons (not antimessons), if n_{q_1} is odd

CHARMED MESONS		B_c^{*+}	10541	$\Upsilon(11020)$	9010553	CHARMED BARYONS		BOTTOM BARYONS	
D^+	411	B_c^{*0}	543	$\chi_{b2}(1P)$	555	Λ_c^+	4122	Λ_b^0	5122
D^0	421	$B_{c1}(L)^+$	10543	$\eta_{b2}(1D)$	10555	Σ_c^{*+}	4222	Σ_b^-	5112
$D_0^*(2400)^+$	10411	$B_{c1}(H)^+$	20543	$\Upsilon_2(1D)$	20555	Σ_c^+	4212	Σ_b^0	5212
$D_0^*(2400)^0$	10421	B_{c2}^{*+}	545	$\chi_{b2}(2P)$	100555	Σ_c^0	4112	Σ_b^+	5222
$D^*(2010)^+$	413	<hr/>		$\eta_{b2}(2D)$	110555	Σ_c^{*+}	4224	Σ_b^{*-}	5114
$D^*(2007)^0$	423	<hr/>		$\Upsilon_2(2D)$	120555	Σ_c^+	4214	Σ_b^0	5214
$D_1(2420)^+$	10413	<hr/>		$\chi_{b2}(3P)$	200555	Σ_c^{*0}	4114	Σ_b^+	5224
$D_1(2420)^0$	10423	<hr/>		$\Upsilon_3(1D)$	557	Ξ_c^+	4232	Ξ_b^-	5132
$D_1(H)^+$	20413	<hr/>		$\Upsilon_3(2D)$	100557	Ξ_c^0	4132	Ξ_b^0	5232
$D_1(2430)^0$	20423	<hr/>		<hr/>		Ξ_c^{*+}	4322	Ξ_b^+	5312
$D_2^*(2460)^+$	415	<hr/>		<hr/>		Ξ_c^{*0}	4312	Ξ_b^0	5322
$D_2^*(2460)^0$	425	<hr/>		<hr/>		Ξ_c^+	4324	Ξ_b^-	5314
D_s^+	431	<hr/>		<hr/>		Ξ_c^{*0}	4314	Ξ_b^0	5324
$D_{s0}^*(2317)^+$	10431	<hr/>		<hr/>		Ω_c^0	4332	Ω_b^-	5332
D_s^{*+}	433	<hr/>		<hr/>		Ω_c^{*0}	4334	Ω_b^+	5334
$D_{s1}(2536)^+$	10433	<hr/>		<hr/>		Ξ_{cc}^+	4412	Ξ_{bc}^0	5142
$D_{s1}(2460)^+$	20433	<hr/>		<hr/>		Ξ_{cc}^{*+}	4422	Ξ_{bc}^+	5242
$D_{s2}^*(2573)^+$	435	<hr/>		<hr/>		Ξ_{cc}^{*0}	4414	Ξ_{bc}^0	5412
<hr/>		<hr/>		<hr/>		Ξ_{cc}^+	4424	Ξ_{bc}^+	5422
<hr/>		<hr/>		<hr/>		Ξ_{cc}^{*0}	4432	Ξ_{bc}^0	5414
<hr/>		<hr/>		<hr/>		Ω_{cc}^+	4434	Ξ_{bc}^+	5424
<hr/>		<hr/>		<hr/>		Ω_{cc}^{*+}	4444	Ξ_{bc}^0	5342
<hr/>		<hr/>		<hr/>		Ω_{cc}^0		Ω_{bc}^0	5432
<hr/>		<hr/>		<hr/>		Ω_{cc}^{*0}		Ω_{bc}^+	5434
<hr/>		<hr/>		<hr/>		Ω_{cc}^+		Ω_{bc}^0	5442
<hr/>		<hr/>		<hr/>		Ω_{cc}^{*+}		Ω_{bc}^+	5444
<hr/>		<hr/>		<hr/>		Ω_{cc}^0		Ξ_{bb}^-	5512
<hr/>		<hr/>		<hr/>		Ω_{cc}^{*0}		Ξ_{bb}^0	5522
<hr/>		<hr/>		<hr/>		Ω_{cc}^+		Ξ_{bb}^+	5514
<hr/>		<hr/>		<hr/>		Ω_{cc}^{*+}		Ξ_{bb}^0	5524
<hr/>		<hr/>		<hr/>		Ω_{cc}^0		Ω_{bb}^-	5532
<hr/>		<hr/>		<hr/>		Ω_{cc}^{*0}		Ω_{bb}^+	5534
<hr/>		<hr/>		<hr/>		Ω_{cc}^+		Ω_{bbc}^0	5542
<hr/>		<hr/>		<hr/>		Ω_{cc}^{*+}		Ω_{bbc}^+	5544
<hr/>		<hr/>		<hr/>		Ω_{cc}^0		Ω_{bbb}^0	5554
<hr/>		<hr/>		<hr/>		Ω_{cc}^{*0}			
<hr/>		<hr/>		<hr/>		Ω_{cc}^+			
<hr/>		<hr/>		<hr/>		Ω_{cc}^{*+}			
<hr/>		<hr/>		<hr/>		Ω_{cc}^0			
<hr/>		<hr/>		<hr/>		Ω_{cc}^{*0}			
<hr/>		<hr/>		<hr/>		Ω_{cc}^+			
<hr/>		<hr/>		<hr/>		Ω_{cc}^{*+}			
<hr/>		<hr/>		<hr/>		Ω_{cc}^0			
<hr/>		<hr/>		<hr/>		Ω_{cc}^{*0}			
<hr/>		<hr/>		<hr/>		Ω_{cc}^+			
<hr/>		<hr/>		<hr/>		Ω_{cc}^{*+}			
<hr/>		<hr/>		<hr/>		Ω_{cc}^0			
<hr/>		<hr/>		<hr/>		Ω_{cc}^{*0}			
<hr/>		<hr/>		<hr/>		Ω_{cc}^+			
<hr/>		<hr/>		<hr/>		Ω_{cc}^{*+}			
<hr/>		<hr/>		<hr/>		Ω_{cc}^0			
<hr/>		<hr/>		<hr/>		Ω_{cc}^{*0}			
<hr/>		<hr/>		<hr/>		Ω_{cc}^+			
<hr/>		<hr/>		<hr/>		Ω_{cc}^{*+}			
<hr/>		<hr/>		<hr/>		Ω_{cc}^0			
<hr/>		<hr/>		<hr/>		Ω_{cc}^{*0}			
<hr/>		<hr/>		<hr/>		Ω_{cc}^+			
<hr/>		<hr/>		<hr/>		Ω_{cc}^{*+}			
<hr/>		<hr/>		<hr/>		Ω_{cc}^0			
<hr/>		<hr/>		<hr/>		Ω_{cc}^{*0}			
<hr/>		<hr/>		<hr/>		Ω_{cc}^+			
<hr/>		<hr/>		<hr/>		Ω_{cc}^{*+}			
<hr/>		<hr/>		<hr/>		Ω_{cc}^0			
<hr/>		<hr/>		<hr/>		Ω_{cc}^{*0}			
<hr/>		<hr/>		<hr/>		Ω_{cc}^+			
<hr/>		<hr/>		<hr/>		Ω_{cc}^{*+}			
<hr/>		<hr/>		<hr/>		Ω_{cc}^0			
<hr/>		<hr/>		<hr/>		Ω_{cc}^{*0}			
<hr/>		<hr/>		<hr/>		Ω_{cc}^+			
<hr/>		<hr/>		<hr/>		Ω_{cc}^{*+}			
<hr/>		<hr/>		<hr/>		Ω_{cc}^0			
<hr/>		<hr/>		<hr/>		Ω_{cc}^{*0}			
<hr/>		<hr/>		<hr/>		Ω_{cc}^+			
<hr/>		<hr/>		<hr/>		Ω_{cc}^{*+}			
<hr/>		<hr/>		<hr/>		Ω_{cc}^0			
<hr/>		<hr/>		<hr/>		Ω_{cc}^{*0}			
<hr/>		<hr/>		<hr/>		Ω_{cc}^+			
<hr/>		<hr/>		<hr/>		Ω_{cc}^{*+}			
<hr/>		<hr/>		<hr/>		Ω_{cc}^0			
<hr/>		<hr/>		<hr/>		Ω_{cc}^{*0}			
<hr/>		<hr/>		<hr/>		Ω_{cc}^+			
<hr/>		<hr/>		<hr/>		Ω_{cc}^{*+}			
<hr/>		<hr/>		<hr/>		Ω_{cc}^0			
<hr/>		<hr/>		<hr/>		Ω_{cc}^{*0}			
<hr/>		<hr/>		<hr/>		Ω_{cc}^+			
<hr/>		<hr/>		<hr/>		Ω_{cc}^{*+}			
<hr/>		<hr/>		<hr/>		Ω_{cc}^0			
<hr/>		<hr/>		<hr/>		Ω_{cc}^{*0}			
<hr/>		<hr/>		<hr/>		Ω_{cc}^+			
<hr/>		<hr/>		<hr/>		Ω_{cc}^{*+}			
<hr/>		<hr/>		<hr/>		Ω_{cc}^0			
<hr/>		<hr/>		<hr/>		Ω_{cc}^{*0}			
<hr/>		<hr/>		<hr/>		Ω_{cc}^+			
<hr/>		<hr/>		<hr/>		Ω_{cc}^{*+}			
<hr/>		<hr/>		<hr/>		Ω_{cc}^0			
<hr/>		<hr/>		<hr/>		Ω_{cc}^{*0}			
<hr/>		<hr/>		<hr/>		Ω_{cc}^+			
<hr/>		<hr/>		<hr/>		Ω_{cc}^{*+}			
<hr/>		<hr/>		<hr/>		Ω_{cc}^0			
<hr/>		<hr/>		<hr/>		Ω_{cc}^{*0}			
<hr/>		<hr/>		<hr/>		Ω_{cc}^+			
<hr/>		<hr/>		<hr/>		Ω_{cc}^{*+}			
<hr/>		<hr/>		<hr/>		Ω_{cc}^0			
<hr/>		<hr/>		<hr/>		Ω_{cc}^{*0}			
<hr/>		<hr/>		<hr/>		Ω_{cc}^+			
<hr/>		<hr/>		<hr/>		Ω_{cc}^{*+}			
<hr/>		<hr/>		<hr/>		Ω_{cc}^0			
<hr/>		<hr/>		<hr/>		Ω_{cc}^{*0}			
<hr/>		<hr/>		<hr/>		Ω_{cc}^+			
<hr/>		<hr/>		<hr/>		Ω_{cc}^{*+}			
<hr/>		<hr/>		<hr/>		Ω_{cc}^0			
<hr/>		<hr/>		<hr/>		Ω_{cc}^{*0}			
<hr/>		<hr/>		<hr/>		Ω_{cc}^+			
<hr/>		<hr/>		<hr/>		Ω_{cc}^{*+}			
<hr/>		<hr/>		<hr/>		Ω_{cc}^0			
<hr/>		<hr/>		<hr/>		Ω_{cc}^{*0}			
<hr/>		<hr/>		<hr/>		Ω_{cc}^+			
<hr/>		<hr/>		<hr/>		Ω_{cc}^{*+}			
<hr/>		<hr/>		<hr/>		Ω_{cc}^0			
<hr/>		<hr/>		<hr/>		Ω_{cc}^{*0}			
<hr/>		<hr/>		<hr/>		Ω_{cc}^+			
<hr/>		<hr/>		<hr/>		Ω_{cc}^{*+}			
<hr/>		<hr/>		<hr/>		Ω_{cc}^0			
<hr/>		<hr/>		<hr/>		Ω_{cc}^{*0}			
<hr/>		<hr/>		<hr/>		Ω_{cc}^+			
<hr/>		<hr/>		<hr/>		Ω_{cc}^{*+}			
<hr/>		<hr/>		<hr/>		Ω_{cc}^0			
<hr/>		<hr/>		<hr/>		Ω_{cc}^{*0}			
<hr/>		<hr/>		<hr/>		Ω_{cc}^+			
<hr/>		<hr/>		<hr/>		Ω_{cc}^{*+}			
<hr/>		<hr/>		<hr/>		Ω_{cc}^0			
<hr/>		<hr/>		<hr/>		Ω_{cc}^{*0}			
<hr/>		<hr/>		<hr/>		Ω_{cc}^+			
<hr/>		<hr/>		<hr/>		Ω_{cc}^{*+}			
<hr/>		<hr/>		<hr/>		Ω_{cc}^0			
<hr/>		<hr/>		<hr/>		Ω_{cc}^{*0}			
<hr/>		<hr/>		<hr/>		Ω_{cc}^+			
<hr/>		<hr/>		<hr/>		Ω_{cc}^{*+}			
<hr/>		<hr/>		<hr/>		Ω_{cc}^0			
<hr/>		<hr/>		<hr/>		Ω_{cc}^{*0}			
<hr/>		<hr/>		<hr/>		Ω_{cc}^+			
<hr/>		<hr/>		<hr/>		Ω_{cc}^{*+}			
<hr/>		<hr/>		<hr/>		Ω_{cc}^0			
<hr/>		<hr/>		<hr/>		Ω_{cc}^{*0}			
<hr/>		<hr/>		<hr/>		Ω_{cc}^+			
<hr/>		<hr/>		<hr/>		Ω_{cc}^{*+}			
<hr/>		<hr/>		<hr/>		Ω_{cc}^0			
<hr/>		<hr/>		<hr/>		Ω_{cc}^{*0}			
<hr/>		<hr/>		<hr/>		Ω_{cc}^+			
<hr/>		<hr/>		<hr/>		Ω_{cc}^{*+}			
<hr/>		<hr/>		<hr/>		Ω_{cc}^0			
<hr/>		<hr/>		<hr/>		Ω_{cc}^{*0}			
<hr/>		<hr/>		<hr/>		Ω_{cc}^+			
<hr/>		<hr/>		<hr/>		Ω_{cc}^{*+}			
<hr/>		<hr/>		<hr/>		Ω_{cc}^0			
<hr/>		<hr/>		<hr/>		Ω_{cc}^{*0}			
<hr/>		<hr/>		<hr/>		Ω_{cc}^+			
<hr/>		<hr/>		<hr/>		Ω_{cc}^{*+}			
<hr/>		<hr/>		<hr/>		Ω_{cc}^0			
<hr/>		<hr/>		<hr/>		Ω_{cc}^{*0}			
<hr/>		<hr/>		<hr/>		Ω_{cc}^+			
<hr/>		<hr/>		<hr/>		Ω_{cc}^{*+}			

47. SU(3) Isoscalar Factors and Representation Matrices

Revised August 2019 by R. Kelly (LBNL).

The most commonly used SU(3) isoscalar factors, corresponding to the singlet, octet, and decuplet content of $8 \otimes 8$ and $10 \otimes 8$, are shown at the right. The notation uses particle names to identify the coefficients, so that the pattern of relative couplings may be seen at a glance. We illustrate the use of the coefficients below. See J.J de Swart, Rev. Mod. Phys. **35**, 916 (1963) for detailed explanations and phase conventions.

A $\sqrt{\quad}$ is to be understood over every integer in the matrices; the exponent 1/2 on each matrix is a reminder of this. For example, the $\Xi \rightarrow \Omega K$ element of the $10 \rightarrow 10 \otimes 8$ matrix is $-\sqrt{6}/\sqrt{24} = -1/2$.

Intramultiplet relative decay strengths may be read directly from the matrices. For example, in decuplet \rightarrow octet + octet decays, the ratio of $\Omega^* \rightarrow \Xi \bar{K}$ and $\Delta \rightarrow N\pi$ partial widths is, from the $10 \rightarrow 8 \times 8$ matrix,

$$\frac{\Gamma(\Omega^* \rightarrow \Xi \bar{K})}{\Gamma(\Delta \rightarrow N\pi)} = \frac{12}{6} \times (\text{phase space factors}). \quad (47.1)$$

Including isospin Clebsch-Gordan coefficients, we obtain, e.g.,

$$\frac{\Gamma(\Omega^{*-} \rightarrow \Xi^0 K^-)}{\Gamma(\Delta^+ \rightarrow p\pi^0)} = \frac{1/2}{2/3} \times \frac{12}{6} \times p.s.f. = \frac{3}{2} \times p.s.f. \quad (47.2)$$

Partial widths for $8 \rightarrow 8 \otimes 8$ involve a linear superposition of 8_1 (symmetric) and 8_2 (antisymmetric) couplings. For example,

$$\Gamma(\Xi^* \rightarrow \Xi\pi) \sim \left(-\sqrt{\frac{9}{20}} g_1 + \sqrt{\frac{3}{12}} g_2 \right)^2. \quad (47.3)$$

The relations between g_1 and g_2 (with de Swart's normalization) and the standard D and F couplings that appear in the interaction Lagrangian,

$$\mathcal{L} = -\sqrt{2} D \text{Tr}(\{\bar{B}, B\}M) + \sqrt{2} F \text{Tr}([\bar{B}, B]M), \quad (47.4)$$

where $[\bar{B}, B] \equiv \bar{B}B - B\bar{B}$ and $\{\bar{B}, B\} \equiv \bar{B}B + B\bar{B}$, are

$$D = \frac{\sqrt{30}}{40} g_1, \quad F = \frac{\sqrt{6}}{24} g_2. \quad (47.5)$$

Thus, for example,

$$\Gamma(\Xi^* \rightarrow \Xi\pi) \sim (F - D)^2 \sim (1 - 2\alpha)^2, \quad (47.6)$$

where $\alpha \equiv F/(D + F)$. (This definition of α is de Swart's. The alternative $D/(D + F)$, due to Gell-Mann, is also used.)

The generators of SU(3) transformations, λ_a ($a = 1, 8$), are 3×3 matrices that obey the following commutation and anticommutation relationships:

$$[\lambda_a, \lambda_b] \equiv \lambda_a \lambda_b - \lambda_b \lambda_a = 2if_{abc}\lambda_c \quad (47.7)$$

$$\{\lambda_a, \lambda_b\} \equiv \lambda_a \lambda_b + \lambda_b \lambda_a = \frac{4}{3}\delta_{ab}I + 2d_{abc}\lambda_c, \quad (47.8)$$

where I is the 3×3 identity matrix, and δ_{ab} is the Kronecker delta symbol. The f_{abc} are odd under the permutation of any pair of indices, while the d_{abc} are even. The nonzero values are:

$1 \rightarrow 8 \otimes 8$

$$(\Lambda) \rightarrow \begin{pmatrix} N\bar{K} & \Sigma\pi & \Lambda\eta & \Xi K \end{pmatrix} = \frac{1}{\sqrt{8}} \begin{pmatrix} 2 & 3 & -1 & -2 \end{pmatrix}^{1/2}$$

$8_1 \rightarrow 8 \otimes 8$

$$\begin{pmatrix} N \\ \Sigma \\ \Lambda \\ \Xi \end{pmatrix} \rightarrow \begin{pmatrix} N\pi & N\eta & \Sigma K & \Lambda K \\ N\bar{K} & \Sigma\pi & \Lambda\pi & \Sigma\eta & \Xi K \\ N\bar{K} & \Sigma\pi & \Lambda\eta & \Xi K \\ \Sigma\bar{K} & \Lambda\bar{K} & \Xi\pi & \Xi\eta \end{pmatrix} = \frac{1}{\sqrt{20}} \begin{pmatrix} 9 & -1 & -9 & -1 \\ -6 & 0 & 4 & 4 \\ 2 & -12 & -4 & -2 \\ 9 & -1 & -9 & -1 \end{pmatrix}^{1/2}$$

$8_2 \rightarrow 8 \otimes 8$

$$\begin{pmatrix} N \\ \Sigma \\ \Lambda \\ \Xi \end{pmatrix} \rightarrow \begin{pmatrix} N\pi & N\eta & \Sigma K & \Lambda K \\ N\bar{K} & \Sigma\pi & \Lambda\pi & \Sigma\eta & \Xi K \\ N\bar{K} & \Sigma\pi & \Lambda\eta & \Xi K \\ \Sigma\bar{K} & \Lambda\bar{K} & \Xi\pi & \Xi\eta \end{pmatrix} = \frac{1}{\sqrt{12}} \begin{pmatrix} 3 & 3 & 3 & -3 \\ 2 & 8 & 0 & 0 \\ 6 & 0 & 0 & 6 \\ 3 & 3 & 3 & -3 \end{pmatrix}^{1/2}$$

$10 \rightarrow 8 \otimes 8$

$$\begin{pmatrix} \Delta \\ \Sigma \\ \Xi \\ \Omega \end{pmatrix} \rightarrow \begin{pmatrix} N\pi & \Sigma K \\ N\bar{K} & \Sigma\pi & \Lambda\pi & \Sigma\eta & \Xi K \\ \Sigma\bar{K} & \Lambda\bar{K} & \Xi\pi & \Xi\eta \\ \Xi\bar{K} \end{pmatrix} = \frac{1}{\sqrt{12}} \begin{pmatrix} -6 & 6 \\ -2 & 2 & -3 & 3 & 2 \\ 3 & -3 & 3 & 3 \\ 12 \end{pmatrix}^{1/2}$$

$8 \rightarrow 10 \otimes 8$

$$\begin{pmatrix} N \\ \Sigma \\ \Lambda \\ \Xi \end{pmatrix} \rightarrow \begin{pmatrix} \Delta\pi & \Sigma K \\ \Delta\bar{K} & \Sigma\pi & \Sigma\eta & \Xi K \\ \Sigma\pi & \Xi K \\ \Sigma\bar{K} & \Xi\pi & \Xi\eta & \Omega K \end{pmatrix} = \frac{1}{\sqrt{15}} \begin{pmatrix} -12 & 3 \\ 8 & -2 & -3 & 2 \\ -9 & 6 \\ 3 & -3 & -3 & 6 \end{pmatrix}^{1/2}$$

$10 \rightarrow 10 \otimes 8$

$$\begin{pmatrix} \Delta \\ \Sigma \\ \Xi \\ \Omega \end{pmatrix} \rightarrow \begin{pmatrix} \Delta\pi & \Delta\eta & \Sigma K \\ \Delta\bar{K} & \Sigma\pi & \Sigma\eta & \Xi K \\ \Sigma\bar{K} & \Xi\pi & \Xi\eta & \Omega K \\ \Xi\bar{K} & \Omega\eta \end{pmatrix} = \frac{1}{\sqrt{24}} \begin{pmatrix} 15 & 3 & -6 \\ 8 & 8 & 0 & -8 \\ 12 & 3 & -3 & 6 \\ 12 & -12 \end{pmatrix}^{1/2}$$

abc	f_{abc}	abc	d_{abc}	abc	d_{abc}
123	1	118	$1/\sqrt{3}$	355	1/2
147	1/2	146	1/2	366	-1/2
156	-1/2	157	1/2	377	-1/2
246	1/2	228	$1/\sqrt{3}$	448	$-1/(2\sqrt{3})$
257	1/2	247	-1/2	558	$-1/(2\sqrt{3})$
345	1/2	256	1/2	668	$-1/(2\sqrt{3})$
367	-1/2	338	$1/\sqrt{3}$	778	$-1/(2\sqrt{3})$
458	$\sqrt{3}/2$	344	1/2	888	$-1/\sqrt{3}$
678	$\sqrt{3}/2$				

The λ_a 's are

$$\lambda_1 = \begin{pmatrix} 0 & 1 & 0 \\ 1 & 0 & 0 \\ 0 & 0 & 0 \end{pmatrix} \quad \lambda_2 = \begin{pmatrix} 0 & -i & 0 \\ i & 0 & 0 \\ 0 & 0 & 0 \end{pmatrix} \quad \lambda_3 = \begin{pmatrix} 1 & 0 & 0 \\ 0 & -1 & 0 \\ 0 & 0 & 0 \end{pmatrix}$$

$$\lambda_4 = \begin{pmatrix} 0 & 0 & 1 \\ 0 & 0 & 0 \\ 1 & 0 & 0 \end{pmatrix} \quad \lambda_5 = \begin{pmatrix} 0 & 0 & -i \\ 0 & 0 & 0 \\ i & 0 & 0 \end{pmatrix} \quad \lambda_6 = \begin{pmatrix} 0 & 0 & 0 \\ 0 & 0 & 1 \\ 0 & 1 & 0 \end{pmatrix}$$

$$\lambda_7 = \begin{pmatrix} 0 & 0 & 0 \\ 0 & 0 & -i \\ 0 & i & 0 \end{pmatrix} \quad \lambda_8 = \frac{1}{\sqrt{3}} \begin{pmatrix} 1 & 0 & 0 \\ 0 & 1 & 0 \\ 0 & 0 & -2 \end{pmatrix}$$

Equation (47.7) defines the Lie algebra of SU(3). A general d -dimensional representation is given by a set of $d \times d$ matrices satisfying Eq. (47.7) with the f_{abc} given above. Equation (47.8) is specific to the defining 3-dimensional representation.

48. SU(n) Multiplets and Young Diagrams

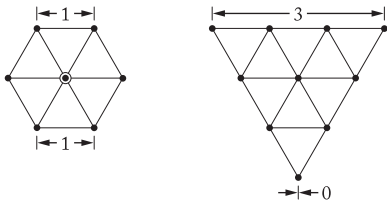
Revised August 2019 by C.G. Wohl (LBNL).

This note tells (1) how SU(n) particle multiplets are identified or labeled, (2) how to find the number of particles in a multiplet from its label, (3) how to draw the Young diagram for a multiplet, and (4) how to use Young diagrams to determine the overall multiplet structure of a composite system, such as a 3-quark or a meson-baryon system.

In much of the literature, the word “representation” is used where we use “multiplet,” and “tableau” is used where we use “diagram.”

48.1 Multiplet labels

An SU(n) multiplet is uniquely identified by a string of (n-1) nonnegative integers: (α, β, γ, ...). Any such set of integers specifies a multiplet. For an SU(2) multiplet such as an isospin multiplet, the single integer α is the number of steps from one end of the multiplet to the other (i.e., it is one fewer than the number of particles in the multiplet). In SU(3), the two integers α and β are the numbers of steps across the top and bottom levels of the multiplet diagram. Thus the labels for the SU(3) octet and decuplet



are (1,1) and (3,0). For larger n, the interpretation of the integers in terms of the geometry of the multiplets, which exist in an (n-1)-dimensional space, is not so readily apparent.

The label for the SU(n) singlet is (0, 0, ..., 0). In a flavor SU(n), the n quarks together form a (1, 0, ..., 0) multiplet, and the n antiquarks belong to a (0, ..., 0, 1) multiplet. These two multiplets are conjugate to one another, which means their labels are related by (α, β, ...) ↔ (... , β, α).

48.2 Number of particles

The number of particles in a multiplet, N = N(α, β, ...), is given as follows (note the pattern of the equations). In SU(2), N = N(α) is

$$N = \frac{(\alpha + 1)}{1} \tag{48.1}$$

In SU(3), N = N(α, β) is

$$N = \frac{(\alpha + 1)}{1} \cdot \frac{(\beta + 1)}{1} \cdot \frac{(\alpha + \beta + 2)}{2} \tag{48.2}$$

In SU(4), N = N(α, β, γ) is

$$N = \frac{(\alpha + 1)}{1} \cdot \frac{(\beta + 1)}{1} \cdot \frac{(\gamma + 1)}{1} \cdot \frac{(\alpha + \beta + 2)}{2} \cdot \frac{(\beta + \gamma + 2)}{2} \cdot \frac{(\alpha + \beta + \gamma + 3)}{3} \tag{48.3}$$

Note that in Eq. (48.3) there is no factor with (α + γ + 2): only a consecutive sequence of the label integers appears in any factor. One more example should make the pattern clear for any SU(n). In SU(5), N = N(α, β, γ, δ) is

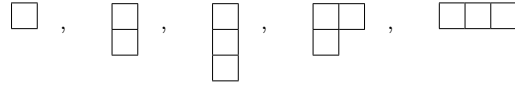
$$N = \frac{(\alpha + 1)}{1} \cdot \frac{(\beta + 1)}{1} \cdot \frac{(\gamma + 1)}{1} \cdot \frac{(\delta + 1)}{1} \cdot \frac{(\alpha + \beta + 2)}{2} \cdot \frac{(\beta + \gamma + 2)}{2} \cdot \frac{(\gamma + \delta + 2)}{2} \cdot \frac{(\alpha + \beta + \gamma + 3)}{3} \cdot \frac{(\beta + \gamma + \delta + 3)}{3} \cdot \frac{(\alpha + \beta + \gamma + \delta + 4)}{4} \tag{48.4}$$

From the symmetry of these equations, it is clear that multiplets that are conjugate to one another have the same number of particles, but so can other multiplets. For example, the SU(4) multi-

plets (3,0,0) and (1,1,0) each have 20 particles. Try the equations and see.

48.3 Young diagrams

A Young diagram consists of an array of boxes (or some other symbol) arranged in one or more left-justified rows, with each row being at least as long as the row beneath. The correspondence between a diagram and a multiplet label is: The top row juts out α boxes to the right past the end of the second row, the second row juts out β boxes to the right past the end of the third row, etc. A diagram in SU(n) has at most n rows. There can be any number of “completed” columns of n boxes buttressing the left of a diagram; these don’t affect the label. Thus in SU(3) the diagrams



represent the multiplets (1,0), (0,1), (0,0), (1,1), and (3,0). In any SU(n), the quark multiplet is represented by a single box, the antiquark multiplet by a column of (n-1) boxes, and a singlet by a completed column of n boxes.

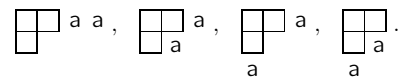
48.4 Coupling multiplets together

The following recipe tells how to find the multiplets that occur in coupling two multiplets together. To couple together more than two multiplets, first couple two, then couple a third with each of the multiplets obtained from the first two, etc.

First a definition: A sequence of the letters a, b, c, ... is admissible if at any point in the sequence at least as many a’s have occurred as b’s, at least as many b’s have occurred as c’s, etc. Thus abcd and aabcb are admissible sequences and abb and acb are not. Now the recipe:

(a) Draw the Young diagrams for the two multiplets, but in one of the diagrams replace the boxes in the first row with a’s, the boxes in the second row with b’s, etc. Thus, to couple two SU(3) octets (such as the π-meson octet and the baryon octet), we start with and . The unlettered diagram forms the upper left-hand corner of all the enlarged diagrams constructed below.

(b) Add the a’s from the lettered diagram to the right-hand ends of the rows of the unlettered diagram to form all possible legitimate Young diagrams that have no more than one a per column. In general, there will be several distinct diagrams, and all the a’s appear in each diagram. At this stage, for the coupling of the two SU(3) octets, we have:



(c) Use the b’s to further enlarge the diagrams already obtained, subject to the same rules. Then throw away any diagram in which the full sequence of letters formed by reading right to left in the first row, then the second row, etc., is not admissible.

(d) Proceed as in (c) with the c’s (if any), etc.

The final result of the coupling of the two SU(3) octets is:

$$\begin{matrix} \square & \square \\ \square & \square \end{matrix} \otimes \begin{matrix} a & a \\ b & \end{matrix} =$$

$$\begin{matrix} \square & \square \\ \square & \square \end{matrix} a a \oplus \begin{matrix} \square & \square \\ \square & \square \end{matrix} a a \oplus \begin{matrix} \square & \square \\ \square & \square \end{matrix} a \oplus \begin{matrix} \square & \square \\ \square & \square \end{matrix} a \oplus \begin{matrix} \square & \square \\ \square & \square \end{matrix} a \oplus \begin{matrix} \square & \square \\ \square & \square \end{matrix} a$$

Here only the diagrams with admissible sequences of a’s and b’s and with fewer than four rows (since n = 3) have been kept. In terms of multiplet labels, the above may be written

$$(1, 1) \otimes (1, 1) = (2, 2) \oplus (3, 0) \oplus (0, 3) \oplus (1, 1) \oplus (1, 1) \oplus (0, 0)$$

In terms of numbers of particles, it may be written

$$8 \otimes 8 = 27 \oplus 10 \oplus \overline{10} \oplus 8 \oplus 8 \oplus 1$$

The product of the numbers on the left here is equal to the sum on the right, a useful check. (See also Sec. 15 on the Quark Model.)

Kinematics, Cross-Section Formulae, and Plots

49. Kinematics	777
50. Resonances (rev.)	781
51. Cross-section formulae for specific processes	792
52. Neutrino cross section measurements (rev.)	801
53. Plots of cross sections and related quantities (rev.)	807





49. Kinematics

Reviewed August 2021 by D. Miller (Glasgow), D.R. Tovey (Sheffield), written January 2000 by J.D. Jackson (LBNL).

Throughout this section units are used in which $\hbar = c = 1$. The following conversions are useful: $\hbar c = 197.3$ MeV fm, $(\hbar c)^2 = 0.3894$ (GeV)² mb.

49.1 Lorentz transformations

The energy E and 3-momentum \mathbf{p} of a particle of mass m form a 4-vector $p = (E, \mathbf{p})$ whose square $p^2 \equiv E^2 - |\mathbf{p}|^2 = m^2$. The velocity of the particle is $\boldsymbol{\beta} = \mathbf{p}/E$. The energy and momentum (E^*, \mathbf{p}^*) viewed from a frame moving with velocity $\boldsymbol{\beta}_f$ are given by

$$\begin{pmatrix} E^* \\ \mathbf{p}_{\parallel}^* \end{pmatrix} = \begin{pmatrix} \gamma_f & -\gamma_f \boldsymbol{\beta}_f \\ -\gamma_f \boldsymbol{\beta}_f & \gamma_f \end{pmatrix} \begin{pmatrix} E \\ \mathbf{p}_{\parallel} \end{pmatrix}, \quad p_T^* = p_T, \quad (49.1)$$

where $\gamma_f = (1 - \beta_f^2)^{-1/2}$ and p_T (p_{\parallel}) are the components of \mathbf{p} perpendicular (parallel) to $\boldsymbol{\beta}_f$. Other 4-vectors, such as the space-time coordinates of events, of course transform in the same way. The scalar product of two 4-momenta $p_1 \cdot p_2 = E_1 E_2 - \mathbf{p}_1 \cdot \mathbf{p}_2$ is invariant (frame independent).

49.2 Center-of-mass energy and momentum

In the collision of two particles of masses m_1 and m_2 the total center-of-mass energy can be expressed in the Lorentz-invariant form

$$\begin{aligned} E_{\text{cm}} &= [(E_1 + E_2)^2 - (\mathbf{p}_1 + \mathbf{p}_2)^2]^{1/2}, \\ &= [m_1^2 + m_2^2 + 2E_1 E_2 (1 - \beta_1 \beta_2 \cos \theta)]^{1/2}, \end{aligned} \quad (49.2)$$

where θ is the angle between the particles. In the frame where one particle (of mass m_2) is at rest (lab frame),

$$E_{\text{cm}} = (m_1^2 + m_2^2 + 2E_{1 \text{ lab}} m_2)^{1/2}. \quad (49.3)$$

The velocity of the center-of-mass in the lab frame is

$$\boldsymbol{\beta}_{\text{cm}} = \mathbf{p}_{\text{lab}} / (E_{1 \text{ lab}} + m_2), \quad (49.4)$$

where $\mathbf{p}_{\text{lab}} \equiv \mathbf{p}_{1 \text{ lab}}$ and

$$\gamma_{\text{cm}} = (E_{1 \text{ lab}} + m_2) / E_{\text{cm}}. \quad (49.5)$$

The c.m. momenta of particles 1 and 2 are of magnitude

$$p_{\text{cm}} = p_{\text{lab}} \frac{m_2}{E_{\text{cm}}}. \quad (49.6)$$

For example, if a 0.80 GeV/c kaon beam is incident on a proton target, the center of mass energy is 1.699 GeV and the center of mass momentum of either particle is 0.442 GeV/c. It is also useful to note that

$$E_{\text{cm}} dE_{\text{cm}} = m_2 dE_{1 \text{ lab}} = m_2 \beta_{1 \text{ lab}} dp_{1 \text{ lab}}. \quad (49.7)$$

49.3 Lorentz-invariant amplitudes

The matrix elements for a scattering or decay process are written in terms of an invariant amplitude $-i\mathcal{M}$. As an example, the S -matrix for $2 \rightarrow 2$ scattering is related to \mathcal{M} by

$$\langle p'_1 p'_2 | S - 1 | p_1 p_2 \rangle = i(2\pi)^4 \delta^4(p_1 + p_2 - p'_1 - p'_2) \mathcal{M}(p_1, p_2; p'_1, p'_2). \quad (49.8)$$

The state normalization is such that

$$\langle p' | p \rangle = (2\pi)^3 2E_p \delta^3(\mathbf{p}' - \mathbf{p}), \quad (49.9)$$

with $E_p = \sqrt{\mathbf{p}^2 + m^2}$.

For a $2 \rightarrow 2$ scattering process producing unstable particles $1'$ and $2'$ decaying via $1' \rightarrow 3'4'$ and $2' \rightarrow 5'6'$ the matrix element for the complete process can be written in the narrow width

approximation as:

$$\begin{aligned} \mathcal{M}(12 \rightarrow 3'4'5'6') &= \\ &= \sum_{h_{1'}, h_{2'}} \frac{\mathcal{M}(12 \rightarrow 1'2') \mathcal{M}(1' \rightarrow 3'4') \mathcal{M}(2' \rightarrow 5'6')}{(m_{3'4'}^2 - m_{1'}^2 + im_{1'}\Gamma_{1'})(m_{5'6'}^2 - m_{2'}^2 + im_{2'}\Gamma_{2'})}. \end{aligned} \quad (49.10)$$

Here, m_{ij} is the invariant mass of particles i and j , m_k and Γ_k are the mass and total width of particle k , and the sum runs over the helicities of the intermediate particles. This enables the cross section for such a process to be written as the product of the cross section for the initial $2 \rightarrow 2$ scattering process with the branching ratios (relative partial decay rates) of the subsequent decays. A more sophisticated treatment, beyond the narrow width approximation, can be found in the review on "Resonances".

49.4 Particle decays

The partial decay rate of a particle of mass M into n bodies in its rest frame is given in terms of the Lorentz-invariant matrix element \mathcal{M} by

$$d\Gamma = \frac{(2\pi)^4}{2M} |\mathcal{M}|^2 d\Phi_n(P; p_1, \dots, p_n), \quad (49.11)$$

where $d\Phi_n$ is an element of n -body phase space given by

$$d\Phi_n(P; p_1, \dots, p_n) = \delta^4(P - \sum_{i=1}^n p_i) \prod_{i=1}^n \frac{d^3 p_i}{(2\pi)^3 2E_i}. \quad (49.12)$$

This phase space is reduced by combinatoric factors whenever there are identical particles in the final state. The phase space can be generated recursively, viz.

$$\begin{aligned} d\Phi_n(P; p_1, \dots, p_n) &= d\Phi_j(q; p_1, \dots, p_j) \\ &\times d\Phi_{n-j+1}(P; q, p_{j+1}, \dots, p_n) (2\pi)^3 dq^2, \end{aligned} \quad (49.13)$$

where $q^2 = (\sum_{i=1}^j E_i)^2 - |\sum_{i=1}^j \mathbf{p}_i|^2$. This form is particularly useful in the case where a particle decays into another particle that subsequently decays.

49.4.1 Survival probability

If a particle of mass M has mean proper lifetime τ ($= 1/\Gamma$) and has momentum (E, \mathbf{p}) , then the probability that it lives for a time t_0 or greater before decaying is given by

$$P(t_0) = e^{-t_0 \Gamma/\gamma} = e^{-Mt_0 \Gamma/E}, \quad (49.14)$$

and the probability that it travels a distance x_0 or greater is

$$P(x_0) = e^{-Mx_0 \Gamma/|\mathbf{p}|}. \quad (49.15)$$

49.4.2 Two-body decays

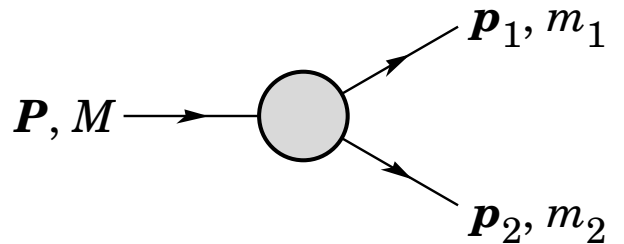


Figure 49.1: Definitions of variables for two-body decays.

In the rest frame of a particle of mass M , decaying into 2 particles labeled 1 and 2,

$$E_1 = \frac{M^2 - m_2^2 + m_1^2}{2M}, \quad (49.16)$$

$$|\mathbf{p}_1| = |\mathbf{p}_2| = \frac{1}{2M} \sqrt{\lambda(M^2, m_1^2, m_2^2)}, \quad (49.17)$$

and

$$d\Gamma = \frac{1}{32\pi^2} |\mathcal{M}|^2 \frac{|\mathbf{p}_1|}{M^2} d\Omega, \quad (49.18)$$

where $\lambda(\alpha, \beta, \gamma) = \alpha^2 + \beta^2 + \gamma^2 - 2\alpha\beta - 2\alpha\gamma - 2\beta\gamma$ is the Källén function and $d\Omega = d\phi_1 d(\cos\theta_1)$ is the solid angle of particle 1. The invariant mass M can be determined from the energies and momenta using Eq. (49.2) with $M = E_{\text{cm}}$.

49.4.3 Three-body decays

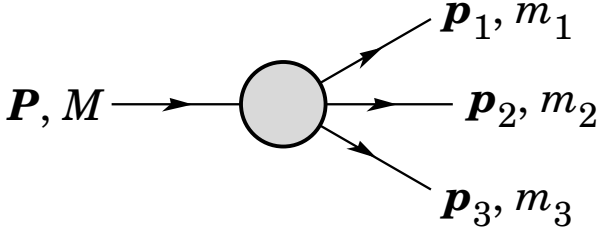


Figure 49.2: Definitions of variables for three-body decays.

Defining $p_{ij} = p_i + p_j$ and $m_{ij}^2 = p_{ij}^2$, then $m_{12}^2 + m_{23}^2 + m_{13}^2 = M^2 + m_1^2 + m_2^2 + m_3^2$ and $m_{12}^2 = (P - p_3)^2 = M^2 + m_3^2 - 2ME_3$, where E_3 is the energy of particle 3 in the rest frame of M . In that frame, the momenta of the three decay particles lie in a plane. The relative orientation of these three momenta is fixed if their energies are known. The momenta can therefore be specified in space by giving three Euler angles (α, β, γ) that specify the orientation of the final system relative to the initial particle. The direction of any one of the particles relative to the frame in which the initial particle is described can be specified in space by two angles (α, β) while a third angle, γ , can be set as the azimuthal angle of a second particle around the first [1]. Then

$$d\Gamma = \frac{1}{(2\pi)^5} \frac{1}{16M} |\mathcal{M}|^2 dE_1 dE_3 d\alpha d(\cos\beta) d\gamma. \quad (49.19)$$

Alternatively

$$d\Gamma = \frac{1}{(2\pi)^5} \frac{1}{16M^2} |\mathcal{M}|^2 |\mathbf{p}_1^*| |\mathbf{p}_3| dm_{12} d\Omega_1^* d\Omega_3, \quad (49.20)$$

where $(|\mathbf{p}_1^*|, \Omega_1^*)$ is the momentum of particle 1 in the rest frame of 1 and 2, and Ω_3 is the angle of particle 3 in the rest frame of the decaying particle. $|\mathbf{p}_1^*|$ and $|\mathbf{p}_3|$ are given by

$$|\mathbf{p}_1^*| = \frac{1}{2m_{12}} \sqrt{\lambda(m_{12}^2, m_1^2, m_2^2)}, \quad (49.21a)$$

and

$$|\mathbf{p}_3| = \frac{1}{2M} \sqrt{\lambda(M^2, m_{12}^2, m_3^2)}. \quad (49.21b)$$

[Compare with Eq. (49.17).]

If the decaying particle is a scalar, or we average over its spin states, then integration over the angles in Eq. (49.19) gives

$$\begin{aligned} d\Gamma &= \frac{1}{(2\pi)^3} \frac{1}{8M} |\overline{\mathcal{M}}|^2 dE_1 dE_3 \\ &= \frac{1}{(2\pi)^3} \frac{1}{32M^3} |\overline{\mathcal{M}}|^2 dm_{12}^2 dm_{23}^2. \end{aligned} \quad (49.22)$$

This is the standard form for the Dalitz plot.

49.4.3.1 Dalitz plot

For a given value of m_{12}^2 , the range of m_{23}^2 is determined by its values when \mathbf{p}_2 is parallel or antiparallel to \mathbf{p}_3 :

$$(m_{23}^2)_{\text{max}} = (E_2^* + E_3^*)^2 - \left(\sqrt{E_2^{*2} - m_2^2} - \sqrt{E_3^{*2} - m_3^2} \right)^2, \quad (49.23a)$$

$$(m_{23}^2)_{\text{min}} = (E_2^* + E_3^*)^2 - \left(\sqrt{E_2^{*2} - m_2^2} + \sqrt{E_3^{*2} - m_3^2} \right)^2. \quad (49.23b)$$

Here $E_2^* = (m_{12}^2 - m_1^2 + m_2^2)/2m_{12}$ and $E_3^* = (M^2 - m_{12}^2 - m_3^2)/2m_{12}$ are the energies of particles 2 and 3 in the m_{12} rest frame. The scatter plot in m_{12}^2 and m_{23}^2 is called a Dalitz plot. If $|\overline{\mathcal{M}}|^2$ is constant, the allowed region of the plot will be uniformly populated with events [see Eq. (49.22)]. A nonuniformity in the plot gives immediate information on $|\mathcal{M}|^2$. For example, in the case of $D \rightarrow K\pi\pi$, bands appear when $m_{(K\pi)} = m_{K^*(892)}$, reflecting the appearance of the decay chain $D \rightarrow K^*(892)\pi \rightarrow K\pi\pi$.

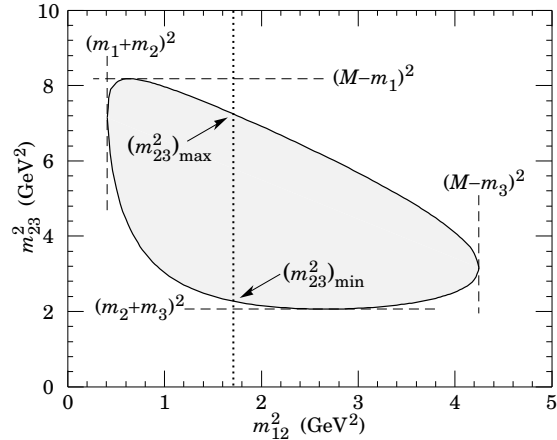


Figure 49.3: Dalitz plot for a three-body final state. In this example, the state is $\pi^+ K^0 p$ at 3 GeV. Four-momentum conservation restricts events to the shaded region.

49.4.4 Kinematic limits

49.4.4.1 Three-body decays

In a three-body decay (Fig. 49.2) the maximum of $|\mathbf{p}_3|$, [given by Eq. (49.21)], is achieved when $m_{12} = m_1 + m_2$, *i.e.*, particles 1 and 2 have the same vector velocity in the rest frame of the decaying particle. If, in addition, $m_3 > m_1, m_2$, then $|\mathbf{p}_3|_{\text{max}} > |\mathbf{p}_1|_{\text{max}}, |\mathbf{p}_2|_{\text{max}}$. The distribution of m_{12} values possesses an end-point or maximum value at $m_{12} = M - m_3$. This can be used to constrain the mass difference of a parent particle and one invisible decay product.

49.4.4.2 Sequential two-body decays

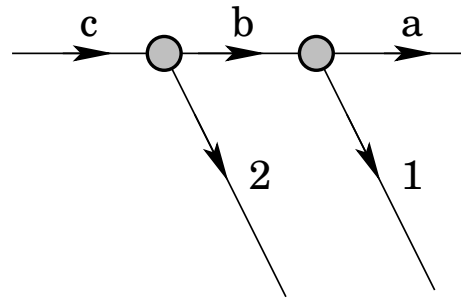


Figure 49.4: Particles participating in sequential two-body decay chain. Particles labeled 1 and 2 are visible while the particle terminating the chain (a) is invisible.

When a heavy particle initiates a sequential chain of two-body decays terminating in an invisible particle, constraints on the masses of the states participating in the chain can be obtained from end-points and thresholds in invariant mass distributions of the aggregated decay products. For the two-step decay chain depicted in Fig. 49.4 the invariant mass distribution of the two visible particles possesses an end-point given by:

$$(m_{12}^{\text{max}})^2 = \frac{(m_c^2 - m_b^2)(m_b^2 - m_a^2)}{m_b^2}, \quad (49.24)$$

provided particles 1 and 2 are massless. If visible particle 1 has non-zero mass m_1 then Eq. (49.24) is replaced by

$$(m_{12}^{\max})^2 = m_1^2 + \frac{(m_c^2 - m_b^2)}{2m_b^2} \times \left(m_1^2 + m_b^2 - m_a^2 + \sqrt{(-m_1^2 + m_b^2 - m_a^2)^2 - 4m_1^2 m_a^2} \right) \quad (49.25)$$

See Refs. [2] and [3] for other cases.

49.4.5 Multibody decays

The above results may be generalized to final states containing any number of particles by combining some of the particles into “effective particles” and treating the final states as 2 or 3 “effective particle” states. Thus, if $p_{ijk\dots} = p_i + p_j + p_k + \dots$, then

$$m_{ijk\dots} = \sqrt{p_{ijk\dots}^2}, \quad (49.26)$$

and $m_{ijk\dots}$ may be used in place of *e.g.*, m_{12} in the relations in Sec. 49.4.3 or Sec. 49.4.4 above.

49.5 Cross sections

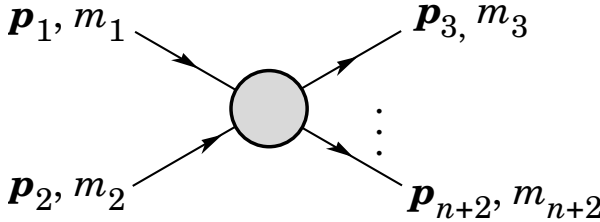


Figure 49.5: Definitions of variables for production of an n -body final state.

The differential cross section is given by

$$d\sigma = \frac{(2\pi)^4 |\mathcal{M}|^2}{4\sqrt{(p_1 \cdot p_2)^2 - m_1^2 m_2^2}} \times d\Phi_n(p_1 + p_2; p_3, \dots, p_{n+2}). \quad (49.27)$$

[See Eq. (49.12).] In the rest frame of m_2 (lab),

$$\sqrt{(p_1 \cdot p_2)^2 - m_1^2 m_2^2} = m_2 p_{1\text{lab}}; \quad (49.28a)$$

while in the center-of-mass frame

$$\sqrt{(p_1 \cdot p_2)^2 - m_1^2 m_2^2} = p_{1\text{cm}} \sqrt{s}. \quad (49.28b)$$

49.5.1 Two-body reactions

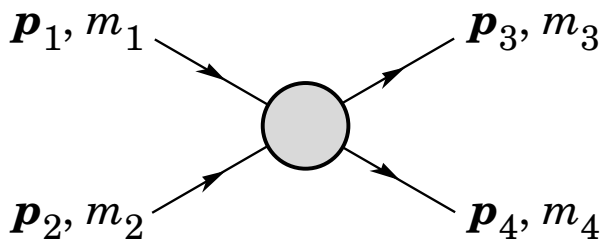


Figure 49.6: Definitions of variables for a two-body final state.

Two particles of momenta p_1 and p_2 and masses m_1 and m_2 scatter to particles of momenta p_3 and p_4 and masses m_3 and m_4 ;

the Lorentz-invariant Mandelstam variables are defined by

$$s = (p_1 + p_2)^2 = (p_3 + p_4)^2 = m_1^2 + 2E_1 E_2 - 2\mathbf{p}_1 \cdot \mathbf{p}_2 + m_2^2, \quad (49.29)$$

$$t = (p_1 - p_3)^2 = (p_2 - p_4)^2 = m_1^2 - 2E_1 E_3 + 2\mathbf{p}_1 \cdot \mathbf{p}_3 + m_3^2, \quad (49.30)$$

$$u = (p_1 - p_4)^2 = (p_2 - p_3)^2 = m_1^2 - 2E_1 E_4 + 2\mathbf{p}_1 \cdot \mathbf{p}_4 + m_4^2, \quad (49.31)$$

and they satisfy

$$s + t + u = m_1^2 + m_2^2 + m_3^2 + m_4^2. \quad (49.32)$$

The two-body cross section may be written as

$$\frac{d\sigma}{dt} = \frac{1}{64\pi s} \frac{1}{|\mathbf{p}_{1\text{cm}}|^2} |\mathcal{M}|^2. \quad (49.33)$$

In the center-of-mass frame

$$t = (E_{1\text{cm}} - E_{3\text{cm}})^2 - (p_{1\text{cm}} - p_{3\text{cm}})^2 - 4p_{1\text{cm}} p_{3\text{cm}} \sin^2(\theta_{\text{cm}}/2) = t_0 - 4p_{1\text{cm}} p_{3\text{cm}} \sin^2(\theta_{\text{cm}}/2), \quad (49.34)$$

where θ_{cm} is the angle between particle 1 and 3. The limiting values t_0 ($\theta_{\text{cm}} = 0$) and t_1 ($\theta_{\text{cm}} = \pi$) for $2 \rightarrow 2$ scattering are

$$t_0(t_1) = \left[\frac{m_1^2 - m_3^2 - m_2^2 + m_4^2}{2\sqrt{s}} \right]^2 - (p_{1\text{cm}} \mp p_{3\text{cm}})^2. \quad (49.35)$$

In the literature the notation t_{\min} (t_{\max}) for t_0 (t_1) is sometimes used, which should be discouraged since $t_0 > t_1$. The center-of-mass energies and momenta of the incoming particles are

$$E_{1\text{cm}} = \frac{s + m_1^2 - m_2^2}{2\sqrt{s}}, \quad E_{2\text{cm}} = \frac{s + m_2^2 - m_1^2}{2\sqrt{s}}, \quad (49.36)$$

For $E_{3\text{cm}}$ and $E_{4\text{cm}}$, change m_1 to m_3 and m_2 to m_4 . Then

$$p_{i\text{cm}} = \sqrt{E_{i\text{cm}}^2 - m_i^2} \text{ and } p_{1\text{cm}} = \frac{p_{1\text{lab}} m_2}{\sqrt{s}}. \quad (49.37)$$

Here the subscript lab refers to the frame where particle 2 is at rest. [For other relations see Eqs. (49.2)–(49.4).]

49.5.2 Inclusive reactions

Choose some direction (usually the beam direction) for the z -axis; then the energy and momentum of a particle can be written as

$$E = m_T \cosh y, \quad p_x, p_y, p_z = m_T \sinh y, \quad (49.38)$$

where m_T , conventionally called the ‘transverse mass’, is given by

$$m_T^2 = m^2 + p_x^2 + p_y^2. \quad (49.39)$$

and the rapidity y is defined by

$$y = \frac{1}{2} \ln \left(\frac{E + p_z}{E - p_z} \right) = \ln \left(\frac{E + p_z}{m_T} \right) = \tanh^{-1} \left(\frac{p_z}{E} \right). \quad (49.40)$$

Note that the definition of the transverse mass in Eq. (49.39) differs from that used by experimentalists at hadron colliders (see Sec. 49.6.1 below). Under a boost in the z -direction to a frame with velocity β , $y \rightarrow y - \tanh^{-1} \beta$. Hence, the shape of the rapidity distribution dN/dy is invariant, as are differences in rapidity. The invariant cross section may also be rewritten

$$E \frac{d^3\sigma}{d^3p} = \frac{d^3\sigma}{d\phi dy p_T dp_T} \implies \frac{d^2\sigma}{\pi dy d(p_T^2)}. \quad (49.41)$$

The second form is obtained using the identity $dy/dp_z = 1/E$, and the third form represents the average over ϕ .

Feynman's x variable is given by

$$x = \frac{p_z}{p_{z \max}} \approx \frac{E + p_z}{(E + p_z)_{\max}} \quad (p_T \ll |p_z|) . \quad (49.42)$$

In the c.m. frame,

$$x \approx \frac{2p_{z \text{ cm}}}{\sqrt{s}} = \frac{2m_T \sinh y_{\text{cm}}}{\sqrt{s}} \quad (49.43)$$

and

$$= (y_{\text{cm}})_{\max} = \ln(\sqrt{s}/m) . \quad (49.44)$$

The invariant mass M of the two-particle system described in Sec. 49.4.2 can be written in terms of these variables as

$$M^2 = m_1^2 + m_2^2 + 2[E_T(1)E_T(2) \cosh \Delta y - \mathbf{p}_T(1) \cdot \mathbf{p}_T(2)] , \quad (49.45)$$

where

$$E_T(i) = \sqrt{|\mathbf{p}_T(i)|^2 + m_i^2} , \quad (49.46)$$

and $\mathbf{p}_T(i)$ denotes the transverse momentum vector of particle i .

For $p \gg m$, the rapidity [Eq. (49.40)] may be expanded to obtain

$$y = \frac{1}{2} \ln \frac{\cos^2(\theta/2) + m^2/4p^2 + \dots}{\sin^2(\theta/2) + m^2/4p^2 + \dots} \approx -\ln \tan(\theta/2) \equiv \eta \quad (49.47)$$

where $\cos \theta = p_z/p$. The pseudorapidity η defined by the second line is approximately equal to the rapidity y for $p \gg m$ and $\theta \gg 1/\gamma$, and in any case can be measured when the mass and momentum of the particle are unknown. From the definition one can obtain the identities

$$\sinh \eta = \cot \theta , \quad \cosh \eta = 1/\sin \theta , \quad \tanh \eta = \cos \theta . \quad (49.48)$$

49.6 Transverse variables

At hadron colliders, a significant and unknown proportion of the energy of the incoming hadrons in each event escapes down the beam-pipe. Consequently, if invisible particles are created in the final state, their net momentum can only be constrained in the plane transverse to the beam direction. Defining the z -axis as the beam direction, this net momentum is equal to the missing transverse energy vector

$$\mathbf{E}_T^{\text{miss}} = - \sum_i \mathbf{p}_T(i) , \quad (49.49)$$

where the sum runs over the transverse momenta of all visible final state particles.

49.6.1 Single production with semi-invisible final state

Consider a single heavy particle of mass M produced in association with visible particles which decays as in Fig. 49.1 to two particles, of which one (labeled particle 1) is invisible. The mass

of the parent particle can be constrained with the quantity M_T defined by

$$M_T^2 \equiv [E_T(1) + E_T(2)]^2 - [\mathbf{p}_T(1) + \mathbf{p}_T(2)]^2 = m_1^2 + m_2^2 + 2[E_T(1)E_T(2) - \mathbf{p}_T(1) \cdot \mathbf{p}_T(2)] , \quad (49.50)$$

where

$$\mathbf{p}_T(1) = \mathbf{E}_T^{\text{miss}} . \quad (49.51)$$

This quantity is called the 'transverse mass' by hadron collider experimentalists but it should be noted that it is quite different from that used in the description of inclusive reactions [Eq. (49.39)]. The distribution of event M_T values possesses an end-point at $M_T^{\text{max}} = M$. If $m_1 = m_2 = 0$ then

$$M_T^2 = 2|\mathbf{p}_T(1)||\mathbf{p}_T(2)|(1 - \cos \phi_{12}) , \quad (49.52)$$

where ϕ_{ij} is defined as the angle between particles i and j in the transverse plane.

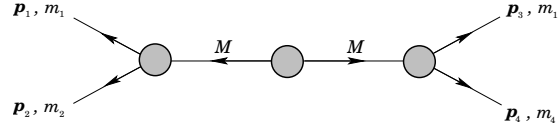


Figure 49.7: Definitions of variables for pair production of semi-invisible final states. Particles 1 and 3 are invisible while particles 2 and 4 are visible.

49.6.2 Pair production with semi-invisible final states

Consider two identical heavy particles of mass M produced such that their combined center-of-mass is at rest in the transverse plane (Fig. 49.7). Each particle decays to a final state consisting of an invisible particle of fixed mass m_1 together with an additional visible particle. M and m_1 can be constrained with the variables M_{T2} and M_{CT} which are defined in Refs. [4] and [5].

References

- [1] J.D. Jackson in *High Energy Physics, Les Houches 1965 Summer School*, GORDON AND BREACH Science Publishers (1965), p. 348.
- [2] I. Hinchliffe *et al.*, Phys. Rev. **D55**, 5520 (1997), [hep-ph/9610544].
- [3] B. C. Allanach *et al.*, JHEP **09**, 004 (2000), [hep-ph/0007009].
- [4] C. G. Lester and D. J. Summers, Phys. Lett. **B463**, 99 (1999), [hep-ph/9906349].
- [5] D. R. Tovey, JHEP **04**, 034 (2008), [arXiv:0802.2879].

50. Resonances

Revised August 2023 by D.M. Asner (BNL), C. Hanhart (FZ Jülich) and M. Mikhasenko (Ruhr U. Bochum).

50.1 General Considerations

Perturbative methods can be applied to systems of quarks and gluons only for large momentum transfers (see review on ‘Quantum Chromodynamics’) and, under certain conditions, to some properties of systems that contain heavy quarks or very large momentum scales (see review on ‘Heavy-quark and soft-collinear effective theory’). Dealing with Quantum Chromodynamics (QCD) in the low momentum transfer region is a very complicated, non-perturbative problem. Most hadrons are resonances, which means that they appear as poles of the \mathcal{S} -matrix in the complex plane on unphysical sheets, a notion further detailed in Sec. 50.2. These resonances can show up either in so-called formation experiments,

$$A + B \rightarrow \mathbf{R} \rightarrow C_1 + \dots + C_n ,$$

where they become visible in an energy scan (for example, the R -function measured in e^+e^- annihilation, *cf.* the corresponding plots in the review on ‘Plots of Cross Sections and Related Quantities’), or together with a spectator particle S in production experiments of the kind

$$\begin{aligned} A + B \rightarrow \mathbf{R} + S &\rightarrow [C_1 + \dots + C_n] + S , \\ Z \rightarrow \mathbf{R} + S &\rightarrow [C_1 + \dots + C_n] + S , \end{aligned}$$

where the first reaction corresponds to an associated production, the second is a decay (see ‘Review of Multibody Charm Analyses’). In the latter case, the resonance properties are commonly extracted from a Dalitz-plot analysis (see review on ‘Kinematics’) or projections thereof.

Resonance phenomena are very rich: while typical hadronic widths are of the order of 100 MeV (*e.g.*, for the meson resonances $\rho(770)$ or $\psi(4040)$ or the baryon resonance $\Delta(1232)$) corresponding to a lifetime of 10^{-23} s, the widths can also be as small as a few MeV (*e.g.* of $\phi(1020)$ or J/ψ) or as large as several hundred MeV (*e.g.* of the meson resonances $f_0(500)$ or $D_1(2430)$ or the baryon resonance $N(2190)$).

Typically, a resonance appears as a peak in the total cross section. If the structure is narrow and if there are no relevant thresholds or other resonances nearby, the resonance properties may be extracted employing a Breit–Wigner parameterization, if necessary improved by using an energy-dependent width (*cf.* Sec. 50.3.1 of this review). However, in general, unitarity and analyticity call for the use of more refined tools as outlined here as well as in recent review articles [1, 2]. When there are overlapping resonances with the same quantum numbers, the resonance terms should not simply be added but combined in a non-trivial way either in a K -matrix approach (*cf.* Sec. 50.3.2 of this review) or using other advanced methods (*cf.* Sec. 50.3.5 of this review). Additional constraints from the \mathcal{S} -matrix allow one to build more reliable amplitudes and, in turn, to reduce the systematic uncertainties of the resonance parameters: pole locations and residues. In addition, for broad resonances there is no direct relation between pole location and the total width/lifetime — then, the pole residues need to be used in order to quantify the decay properties.

For simplicity, throughout this review the formulas are given for resonances in a system of distinguishable, scalar particles. The additional complications that appear in the presence of spins can be controlled in the helicity framework developed by Jacob and Wick [3], or in a non-covariant [4] or covariant [5] tensor-operator formalisms. Within these approaches, sequential (cascade) decays are commonly treated as a coherent sum of two-body interactions. Most of the expressions below are given for two-body kinematics.

50.1.1 Properties of the \mathcal{S} -matrix

The unitary operator that connects asymptotic *in* and *out* states is called the \mathcal{S} -matrix. The scattering amplitude is defined as the interacting part of the \mathcal{S} -matrix. For a two-particles scattering process, it reads:

$$\begin{aligned} i(2\pi)^4 \delta^4(p_1 + p_2 - p_{1'} - p_{2'}) \mathcal{M}(p_1, p_2; p_{1'}, p_{2'})_{ba} \\ = {}_{\text{out}} \langle p_{1'}, p_{2'}, b | \mathcal{S} - 1 | p_1 p_2, a \rangle_{\text{in}} \end{aligned} \quad (50.1)$$

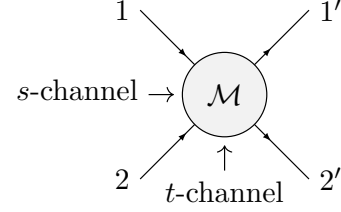


Figure 50.1: Illustration of the relation between s - and t -channel.

where $|p_1 p_2, a\rangle$ and $|p_{1'} p_{2'}, b\rangle$ are asymptotic states that can be treated as non-interacting particles in the spirit of the LSZ-reduction [6]. They carry the momenta p_1, p_2 and $p_{1'}, p_{2'}$, respectively.

The labels a and b are used to specify the *reaction channels*. In general terms, a reaction channel describes the possible outcome of a scattering event, characterized by the quantum numbers of the particles involved. Note, that in general \mathcal{M} operates as a matrix in channel space, connecting the different asymptotic multi-particle states. For a single-particle state, we employ the relativistic normalization,

$$\langle p' | p \rangle = (2\pi)^3 2E_p \delta^3(\vec{p}' - \vec{p}), \quad (50.2)$$

with $E_p = \sqrt{\vec{p}^2 + m^2}$.

Mandelstam variables are defined as $s = (p_1 + p_2)^2$, $t = (p_1 - p_{1'})^2$, and $u = (p_1 - p_{2'})^2$. One finds that the variables s, t , and u are not independent, since

$$s + t + u = m_1^2 + m_2^2 + m_{1'}^2 + m_{2'}^2$$

holds, where m_i with $i \in 1, 1', 2, 2'$ represents the masses of the involved particles. As a result, the reaction amplitude can be expressed as a function of two variables, $\mathcal{M}(s, t)$.

The Mandelstam variables play a crucial role in characterizing particle scattering. Specifically, the process described in Eq. (50.1) is known as *s-channel*, referring to a reaction, $1, 2 \rightarrow 1', 2'$. Here, \sqrt{s} represents the total energy of the interacting system in the center-of-momentum frame. The variable t corresponds to the *momentum transfer*, which is related to the scattering angle, the angle between the momenta of particles 1 and $1'$ in the center-of-momentum frame (see also the review on ‘Kinematics’ in this Review of Particle Physics). The scattering process with particles 1 and the antiparticle of $1'$, denoted by $\bar{1}'$, incoming to the antiparticle of 2, denoted by $\bar{2}$, and $2'$ outgoing represent a different reaction, it is referred to as the *t-channel* reaction. The scattering amplitudes of s - and t -channel are related via the so-called *crossing symmetry*. The *u-channel* is introduced analogously as a reaction with the initial state of particles 1 and $\bar{2}'$ and the final state of particles $1'$ and $\bar{2}$. The t -channel and the u -channel are referred to as the *crossed channels* relative to the reaction in Eq. (50.1). This relationship is illustrated in Fig. 50.1.

The analysis of resonance phenomena requires delving deeper into the complex analysis of the amplitude: $\mathcal{M}(s, t)$ is a multi-valued function due to the complex *branch points* associated with the Mandelstam variables. These branch points emerge whenever a new channel becomes accessible, that is, whenever s exceeds $s_{\text{thr}, a} = (m_{1, a} + m_{2, a})^2$, where $m_{i, a}$ denotes the masses of the two particles in channel a . Every two-particle threshold introduces a square-root singularity. The square-root function is inherently double-valued; for instance, the equation $x = y^2$ has two solutions: \sqrt{x} and $-\sqrt{x}$. In the complex plane, these two solutions are represented as separate layers or surfaces, known as *Riemann sheets* or Riemann surfaces. Consequently, each square-root singularity causes the number of Riemann sheets of the scattering amplitude to double. If a channel opens that has an odd number of particles, the branch point at the threshold exhibits a logarithmic singularity [7]. Such a branch point gives rise to an infinite

number of sheets. The branch points come with their associated branch cuts — by convention those are taken from the threshold to infinity along the real axis and accordingly called *right-hand cuts*. To explore a reaction amplitude in the complex energy plane, one can introduce a complex component to the Mandelstam variable s . The section of the complex plane that relates to a positive imaginary component of the relative momentum can be directly accessed from the physical region and is called the first Riemann sheet or the *physical sheet*. The other sheets are called *unphysical sheets*. The *physical axis* of an s -channel scattering amplitude represents a line for real values of the variable s larger than the lowest threshold to be evaluated on the physical sheet.

While the physical Riemann sheet is free of singularities off the real axis, the unphysical sheets may contain resonance poles and branch points. Branch points appear in the complex plane of an unphysical sheet when there is a resonance in a subsystem of involved particles [7, 8]. The branch points related to thresholds in the crossed channels are located in the portion of the complex plane where the real part is negative and, therefore, are referred to as the *left-hand cuts*. An illustrative example for a left-hand cut is the one-pion exchange in nucleon-nucleon scattering that is located in the unphysical domain at $s = 4m_N^2 - m_\pi^2$. Triangle topologies, which are Feynman diagrams characterized by a triangular loop of three propagators, can lead to logarithmic singularities in the scattering amplitude. These singularities, appearing on the unphysical sheets, are often termed *triangle singularities* (TS) [7, 9, 10].

The reaction amplitude has poles that can be categorized as bound states, virtual states, or resonances. Poles corresponding to bound and virtual states manifest at real values of s . Specifically, *bound state* poles are found on the physical sheet, while *virtual state* poles are situated on an unphysical sheet, both being below the threshold. Resonance poles, on the other hand, emerge inside the complex plane of the unphysical sheets. Notably, those resonance poles that are on the unphysical sheet nearest to the physical region exert the most significant influence on experimental observables. Analyticity dictates that for every pole at a specific complex value of s_p , there must be a corresponding pole at its complex conjugate value s_p^* . This relationship is a direct consequence of the *Schwarz reflection principle*, a mathematical technique utilized for analytic continuation within scattering theory. For a single-channel case, the complex structure of an amplitude with a single resonance is illustrated in Fig. 50.2(a)-(c). Among the two poles, symmetrically positioned relative to the real axis on the second sheet, the one exhibiting a negative imaginary part seamlessly connects to the physical axis, which becomes especially clear in panel (c) of the figure where the physical axis is shown as the blue line. It therefore has a more pronounced effect on observables in the vicinity of the resonance region compared to its conjugate counterpart. The shortest continuous path from the physical region to the second sheet pole with the positive imaginary part is via a line that goes around the threshold. However, as the extra path around the threshold diminishes in the near-threshold region, the effective distance to both poles becomes comparable for near threshold kinematics, thereby rendering the influence of both poles on observables similarly significant.

An alternative way to depict the complex structure is through the k -plane, where k denotes the relative momentum of the two scattering particles in their center-of-momentum frame. For particles of equal mass, denoted as m (expression for unequal masses is given in Eq. (50.7)), one finds

$$k = \frac{1}{2} \sqrt{s - 4m}. \quad (50.3)$$

Unlike the complex s -plane, the k -plane does not have a two-body threshold cut. Consequently, both the physical and unphysical Riemann sheets, which are linked to the branch point in s are mapped onto the upper and lower half of the complex k -plane, respectively. The k -plane is sketched in Fig. 50.2(d), including possible locations of resonance poles. In this representation it becomes especially clear that only one resonance pole drives the dynamics on the physical axis in the resonance region, while at the threshold, where $k = 0$, both poles are of equal significance.

In situations involving two relevant channels, we encounter four Riemann sheets. These are illustrated in the left panel of Fig. 50.3. For a non-relativistic system with two channels, this four-sheeted Riemann surface can be transformed into a plane represented by a new variable, ω . This variable is defined in relation to the channel-momenta, as detailed in references [11, 12] (for a recent application see Ref. [13])

$$k_1 = \sqrt{\frac{\mu_1 \Delta}{2}} \left(\omega + \frac{1}{\omega} \right), \quad k_2 = \sqrt{\frac{\mu_2 \Delta}{2}} \left(\omega - \frac{1}{\omega} \right), \quad (50.4)$$

where Δ denotes the energy difference between the two thresholds and the μ_a the reduced mass of the particles in channel a , $\mu_a = m_{1,a} m_{2,a} / (m_{1,a} + m_{2,a})$. The lower threshold is located at $\omega = i$, the higher at $\omega = 1$. The mapping of the Riemann sheets and the different areas in the ω -plane is shown in the right panel of Fig. 50.3. The ω -plane nicely shows how the different sheets connect to each other.¹ The solid green line shows the physical axis in the physical regime. The thick black line its analytic continuation below the lowest threshold. The pronounced kinks in this line for the ω plane show the thresholds. Please observe that for $\omega \approx i$ the sheet structure agrees to panel (d) of Fig. 50.2, since in this kinematic regime the second channel does not matter.

In the context of a two-channel scenario, the proximity of a sheet to the physical axis varies with increasing energy. Specifically, for energies that exceed the first threshold, but remain below the second, sheet (21) is the one that smoothly connects to the upper half-plane of the physical sheet (11). Once the energy surpasses the second threshold, sheet (22) assumes this role. As a result, any pole on sheet (21) that lies above the second threshold will manifest in the data solely as a cusp right at the second threshold. Sheet (12), on the other hand, is remote for almost all energies.

Singularities, poles and branch points determine the visible structures in observables. However, it is crucial to note that not every observable bump is indicative of a resonance as discussed in [14]. Under certain kinematic conditions, Triangle Singularities, in particular, can either mimic resonance signals, as suggested in Refs. [15–20], or significantly alter resonance signals [21]. Conversely, not all resonances produce a noticeable bump across all observables. For example, in the baryon sector, there is no clear trace of the $N(1440)1/2^+$, the so called Roper resonance, in the πN observables or phase shifts, although careful analyses reveal a pole [22]. In the meson sector, the $f_0(500)$, also known as σ meson, was firmly established only after the application of very sophisticated theoretical analysis tools (see, e.g., Ref. [23] for a review). This complexity arises because the scalar-isoscalar $\pi\pi$ phase shifts reach 90 degrees near 800 MeV, which is approximately 400 MeV above the resonance mass. At this energy, the onset of the next resonance, the $f_0(980)$, is already observable. The analyticity principle of the \mathcal{S} -matrix germane to quantum scattering theories, dictates that only poles and branch points can exist on the real axis of the first Riemann sheet, excluding any singularities in the complex plane. This principle is closely linked to causality, ensuring that effects follow their causes in a chronological order. In non-relativistic scattering, the analyticity finds a solid mathematical base [24]. Similarly, perturbative relativistic theory maintains this analyticity through a series expansion of the \mathcal{S} -matrix, each term depicted by a Feynman diagram, representing processes with distinct analytical expressions. A deeper level of analyticity is proposed by the Mandelstam hypothesis, suggesting not only the analytic properties of the scattering amplitude within the complex plane of the first Riemann sheet but also a nuanced interconnection between crossed scattering processes through analytic continuation [25].

Unitarity further constrains the imaginary part of the amplitude on this real axis, a topic we will explore in the subsequent section. Additional constraints are introduced by principles such as crossing symmetry, duality [26] and positivity [27]. Approaches based on analyticity and crossing symmetry have been implemented through dispersion theory. Among the most notable are

¹An alternative illustration for this two-channel case as well as an extension to three channels can be found in Ref. [2].

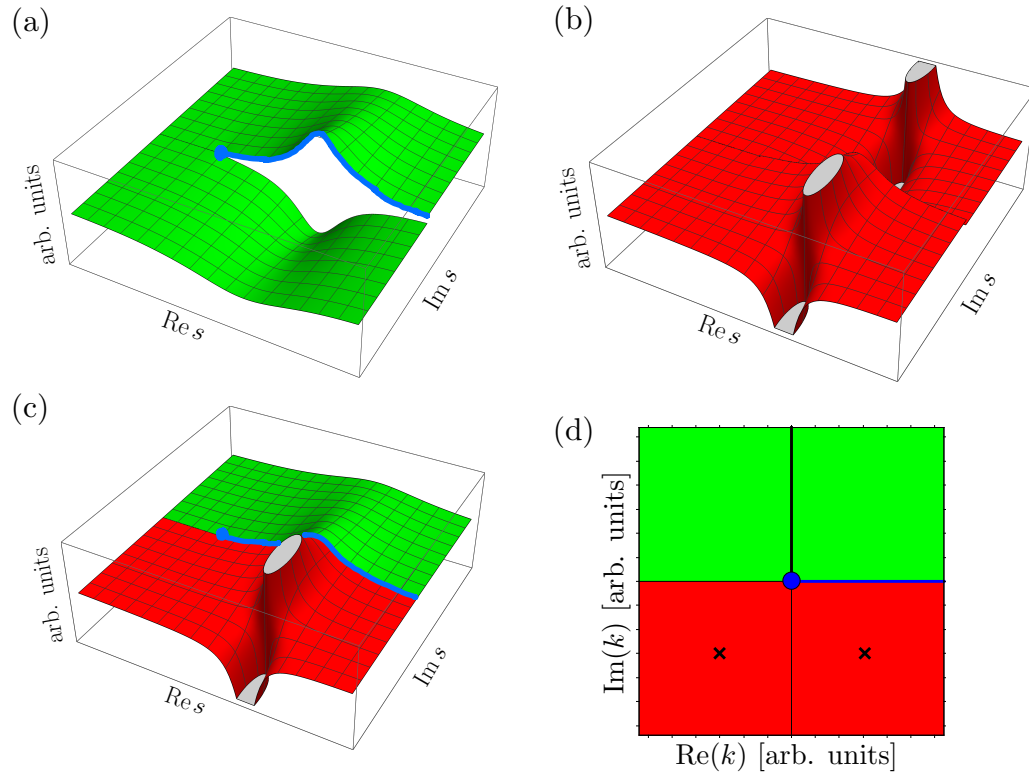


Figure 50.2: (a)-(c): Imaginary part of a typical scattering amplitude with an isolated resonance. The blue line shows the physical range of the Mandelstam variable s : it is real and starts from the threshold shown by the blue dot. Plot (a) shows the imaginary part of the amplitude in the complex s -plane that corresponds to the first or physical sheet (green surface), plot (b) shows the related unphysical or the second sheet (red surface) which contains the resonance poles, and plot (c) shows the analytic continuation of the same amplitude from the upper half plane of the physical sheet to the lower half plane of the unphysical sheet. The two sheets are connected smoothly along the real axis above the threshold. Panel (d) shows the k -plane, which is free of cuts. The upper (lower) half plane maps onto the physical (unphysical) sheet. Also here the blue line corresponds to the physically accessible values of the momentum k , which starts at threshold, where $k = 0$. The thick black line shows the analytic continuation of the on-shell momentum in the below threshold regime. The locations of the resonance poles are indicated by the black crosses.

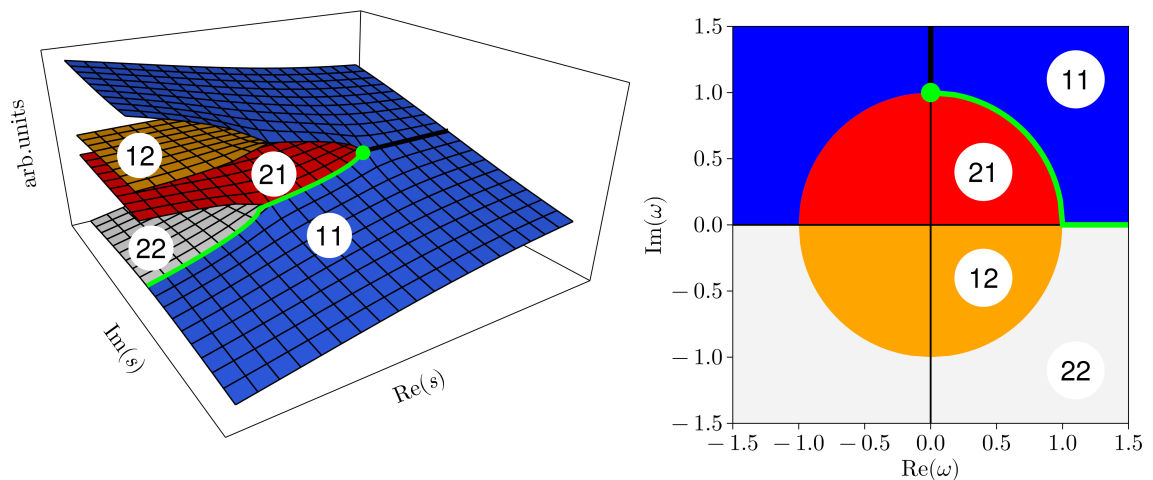


Figure 50.3: Cut structure of the \mathcal{S} -matrix with two channels present. The diagrams feature four sheets, labeled (ij) , where both i and j can be 1 or 2. These labels indicate the doubling of the sheets at the first and second thresholds. The left panel displays the complex s plane, while the right panel represents the ω plane. The physical axis, along with its analytic continuation below the threshold, is highlighted with a thick solid line, green in the physical regime, black for the analytic continuation below the lowest threshold.

the Roy equations and their variants [28]. These have been applied to a range of processes, including $\pi\pi \rightarrow \pi\pi$ [29–31], πK scattering [32], $\gamma\gamma \rightarrow \pi\pi$ interactions [33], and pion-nucleon scattering [34, 35].

50.1.2 Consequences from unitarity

Scattering amplitudes, denoted as \mathcal{M} , and production amplitudes, represented by \mathcal{A} , have distinct characteristics due to the different constraints imposed by unitarity. When considering the scattering amplitude, it is assumed that all channels hold similar significance. In contrast, for production amplitudes, it is assumed that for the dynamics of the particles in the final state the initial state does not play a role. Accordingly, the interactions in the final state among the produced particles are described by relevant scattering amplitudes of those particles only. Scattering processes are for example $\pi^+\pi^- \rightarrow K\bar{K}$ and $D^0\bar{D}^0 \rightarrow D^0\bar{D}^0$. Examples for production processes are $e^+e^- \rightarrow \gamma^* \rightarrow \pi^+\pi^-$, which provides access to the pion vector form factor, $\tau^- \rightarrow K^-\pi^0\nu_\tau$, and $B^0 \rightarrow J/\psi\pi^+\pi^-$.

The unitarity of the \mathcal{S} -matrix, represented by the equation $S^\dagger S = 1$, ensures the conservation of probability. This principle imposes a specific constraint on the imaginary part of the reaction amplitude. Below the lowest threshold, the amplitude remains real. However, once the energy is higher than the threshold, there is a discontinuity associated with the threshold branch point. The \mathcal{S} -matrix unitarity relates the value of the discontinuity, to the amplitude itself [6]:

$$\begin{aligned} \text{Disc } \mathcal{M}_{ba} &= \mathcal{M}_{ba} - \mathcal{M}_{ba}^* , \\ &= i(2\pi)^4 \sum_c \int d\Phi_c \mathcal{M}_{cb}^* \mathcal{M}_{ca} , \end{aligned} \quad (50.5)$$

where $d\Phi_c$ denotes the invariant phase space for a given channel, labeled as c . The factor $(2\pi)^4$ aligns with the definition of the phase space expression (see Eq. (12) in the review on “Kinematics”). It is essential to note that the summation only considers open channels, meaning those with a production threshold below the scattered system’s energy. In the evaluation of an actual Feynman diagram the discontinuity can be extracted by employing the Cutkosky rule, which comprises replacing the propagators in the pertinent intermediate state by delta-distributions. Eq. (50.5) is illustrated graphically in Fig. 50.4. The left part of the expression yields $2i \text{Im} \mathcal{M}_{ba}$ in accordance to analytic properties of reaction amplitude [36]. For the forward scattering, $t = 0$, the right part of Eq. (50.5) resembles the total cross section up to a kinematic factor, a relationship known as the optical theorem:

$$\text{Im } \mathcal{M}_{aa}(s, 0) = 2q_a \sqrt{s} \sigma_{\text{tot}}(a \rightarrow \text{anything}) . \quad (50.6)$$

In this equation, q_a represents the break-up momentum of the particles in the center-of-momentum frame,

$$q_a = \frac{\lambda^{1/2}(s, m_{1,a}^2, m_{2,a}^2)}{2\sqrt{s}} , \quad (50.7)$$

where $\lambda(x, y, z) = x^2 + y^2 + z^2 - 2xy - 2yz - 2zx$ is the Källén function, and the masses of the two particles in the channel a , $m_{1,a}$ and $m_{2,a}$, cf. Eq. (17) of the review on “Kinematics”.

The unitarity relation for a production amplitude in channel a is represented by:

$$\begin{aligned} \text{Disc } \mathcal{A}_a &= \mathcal{A}_a - \mathcal{A}_a^* , \\ &= i(2\pi)^4 \sum_c \int d\Phi_c \mathcal{M}_{ca}^* \mathcal{A}_c . \end{aligned} \quad (50.8)$$

Equation (50.8) is illustrated graphically in Fig. 50.4. A direct consequence of this equation is that the production amplitude shares its poles with the scattering amplitude. A common method to model the production amplitude that adheres to this unitary relation is to express it as a linear combination of the scattering amplitudes. This approach, known as the \mathcal{Q} -vector method (see Sec 50.3.4), has its limitations. Specifically, production amplitude inherits the left-hand singularities of the scattering amplitude,

while, in general, it has a different cut structure. To address this drawback, a more sophisticated method, known as *unitarization* is employed. This method, rooted in dispersion theory, offers a more refined approach to the problem and is detailed in [37]. A notable application of this method is the Khuri-Treiman framework [38, 39], which is frequently used to study three-body decays. This framework has been successfully applied to a range of decays, from light mesons [40–52] to heavy-flavour decays [53–55].

50.1.3 Partial-wave decomposition

It is often convenient to expand a two-body scattering amplitude of a two-body subsystem of a production amplitude in partial waves. Since resonances have a well-defined spin, they appear only in a specific partial wave of the reaction amplitude. For scalar particles, the expansion reads:

$$\mathcal{M}_{ba}(s, t) = \sum_{j=0}^{\infty} (2j+1) \mathcal{M}_{ba}^j(s) P_j(\cos(\theta)) , \quad (50.9)$$

where j denotes the total angular momentum and the $P_j(\cos(\theta))$ denotes the Legendre polynomials. In the presence of spins an expansion more complicated than Eq. (50.9) is necessary — for a general discussion on how to handle spins see *e.g.* Ref. [56]. In the absence of spins the parameter j coincides with the orbital angular momentum of the particle pairs in the initial and the final state. To simplify notation and since all amplitudes from here on are understood to be partial wave projected, we drop the label j for the single-argument function $\mathcal{M}_{ba}(s)$. Plugging Eq. (50.9) into Eq. (50.5) one finds the unitarity relation for the partial-wave amplitude $\mathcal{M}_{ba}(s)$, namely

$$\text{Im } \mathcal{M}_{ba}(s) = \sum_c \mathcal{M}_{cb}(s)^* \rho_c(s) \mathcal{M}_{ca}(s) \quad (50.10)$$

with $\rho_c(s)$ being a factor that is related to the two-body phase space in Eq. (12) of the review on “Kinematics”,

$$\rho_c(s) = \frac{(2\pi)^4}{2} \int d\Phi_2 = \frac{1}{16\pi} \frac{2|\vec{q}_c|}{\sqrt{s}} , \quad (50.11)$$

with the momentum q_c being defined in Eq. (50.7). Note that in case of the two particles being identical the inclusion of symmetry factors becomes necessary. The partial-wave amplitude $f_{ba}(s)$ is introduced by normalizing scattering amplitude with the phase spaces factors,

$$f_{ba}(s) = \sqrt{\rho_b} \mathcal{M}_{ba}(s) \sqrt{\rho_a} . \quad (50.12)$$

The unitarity condition for f_{ba} follows from Eq. (50.10):

$$\text{Im } f_{ba}(s) = \sum_c f_{cb}^*(s) f_{ca}(s) . \quad (50.13)$$

It leads us to deduce that the inverse of the imaginary part of f_{ba} is equal to $-\delta_{ba}$. Moreover, $\mathcal{S} = \mathbb{I} + 2if$ is a unitary matrix. Hence, the diagonal elements of f can be parameterized as

$$f_{bb} = (\eta_b \exp(2i\delta_b) - 1)/2i , \quad (50.14)$$

where δ_b denotes the phase shift for the scattering from channel b to channel b and η_b is the elasticity parameter, also known as inelasticity. Building upon Eq. (50.13), we can further deduce that,

$$\text{Im } f_{bb}(s) = (1 - \eta_b \cos(2\delta_b))/2 = \sum_c |f_{cb}(s)|^2 . \quad (50.15)$$

Using Eq. (50.14) for the last term in the sum, we obtain a relation highlighting the meaning of the inelasticity,

$$\frac{1}{4}(1 - \eta_b^2) = \sum_{c \neq b} |f_{cb}(s)|^2 . \quad (50.16)$$

It is important to note that the parameter η_b is confined within the range $[0, 1]$, where the case, $\eta_b = 1$ is referred to as a purely elastic

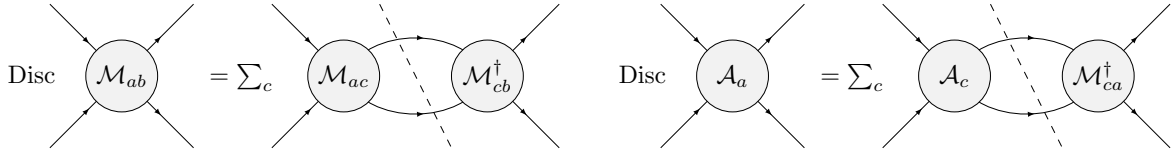


Figure 50.4: Graphical illustration of the discontinuity equations for the scattering and the production amplitude, respectively. The dashed line indicates that the intermediate state is to be put on-shell to find the discontinuity.

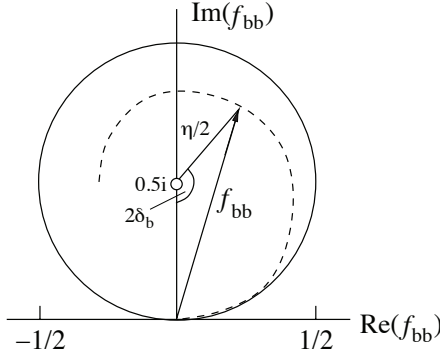


Figure 50.5: Argand plot showing a trajectory of the diagonal element of a partial-wave amplitude, f_{bb} , as a function of energy in the complex plane. As the energy increases the amplitude follows the line counter clockwise. The amplitude leaves the unitary circle (solid line) as soon as inelasticity sets in, $\eta < 1$ (dashed line).

scattering. Thus, the function $\eta_b(s)$ is a direct measure of the contribution of the inelastic channels on the scattering amplitude in a given channel.

The evolution of the partial-wave amplitude f_{bb} with energy can be displayed as a trajectory in the Argand plot, as shown in Fig. 50.5. In case of a two-channel problem, $\eta_1 = \eta_2 = \eta$, and the off-diagonal element is $f_{12} = \sqrt{1 - \eta^2}/2 \exp(i(\delta_1 + \delta_2))$. The unitarity condition Eq. (50.14) sets the limit to the squared amplitude f_{bb} :

$$|f_{bb}|^2 = \frac{1}{4}(\eta_b^2 - 2\eta_b \cos(2\delta_b) + 1) \leq \frac{1}{4}(\eta_b + 1)^2, \quad (50.17)$$

where the maximum value is reached for $\delta_b = \pi/2$. For the absolute square of the partial-wave-projected scattering amplitude the unitarity bound thus reads:

$$|\mathcal{M}_{bb}| \leq \frac{1}{2\rho_b}(\eta_b + 1) \leq \frac{8\pi}{q_b} \sqrt{s}, \quad (50.18)$$

where the second inequality comes from $\eta_b \leq 1$. For energies much larger than the masses of the scattering particles the upper bound for $|\mathcal{M}_{bb}|$ tends to 16π for large s .

The partial-wave projected production amplitude $\mathcal{A}(s)$ (note that the label j has been omitted for consistency) is also constrained by unitarity. As derived from Eq. (50.8):

$$\text{Im } \mathcal{A}_a = \sum_b \mathcal{M}_{ba}^* \rho_b \mathcal{A}_b, \quad (50.19)$$

where the summation encompasses all open channels. In the realm of elastic scattering, solely one channel, denoted by a , contributes to the sum. Consequently, the phase of \mathcal{A}_a must align with the phase of \mathcal{M}_{aa} , given that the left-hand side of Eq. (50.19) represents a real value. This principle is recognized as the *Watson theorem* [57]. To illustrate, consider the phase of the pion vector form factor: it agrees to that of $\pi\pi$ scattering in the vector isovector channel (aside from effects of the isospin-violating $\rho - \omega$ mixing) up to about 1 GeV, where inelastic contributions start gaining significance.

50.2 Properties of resonances

A resonance is defined by its *pole position* in the complex s -plane, denoted as s_R , and by the strength parameters of its couplings to various decay channels evaluated at this pole, known as the *pole residues*. The pole mass M_R and pole width Γ_R are defined via the pole parameters

$$\sqrt{s_R} = M_R - i\Gamma_R/2. \quad (50.20)$$

For states where the relevant thresholds are situated significantly below the resonance location, the lifetime τ_R of the resonance is given by $\tau_R = 1/\Gamma_R$ (refer to the review on “Kinematics” and for a recent discussion, see Ref. [58]). It is important to note that the conventional Breit–Wigner parameters M_{BW} and Γ_{BW} , introduced in Eq. (50.30), differ from the pole parameters due to finite width effects and the influence of thresholds and background terms. It should be stressed that pole location s_R and pole residues are the only resonance properties that are model and parameterization independent.

When a resonance interacts with multiple channels, each channel contributes to the imaginary part of the pole position. However, these individual imaginary contributions do not necessarily simply sum up, leading to the need for redefining the partial widths. This behavior is discussed on the example of the $f_0(980)$ in Refs. [59,60].

In the close vicinity of the resonance pole one defines the residues via

$$\lim_{s \rightarrow s_R} (s - s_R) \mathcal{M}_{ba} = -\mathcal{R}_{ba}. \quad (50.21)$$

Those can be conveniently calculated via an integration along a closed contour around the pole using

$$\mathcal{R}_{ba} = -\frac{1}{2\pi i} \oint ds \mathcal{M}_{ba}. \quad (50.22)$$

The residue adheres to the factorization relation, $(\mathcal{R}_{ba})^2 = \mathcal{R}_{aa} \times \mathcal{R}_{bb}$. This factorization emerges as a universal property stemming from the unitarity of scattering processes [7]. Building on this relation, one can define *pole couplings* as follows:

$$\tilde{g}_a = \mathcal{R}_{ba} / \sqrt{\mathcal{R}_{bb}}. \quad (50.23)$$

The pole couplings characterize the transition strength of a given resonance to some channel a independently of how the particular resonance was produced. They are in general complex valued.

In the baryon sector, it is customary to define the residue of the pole for the f_{ba} amplitude (as described in Eq. (50.13)) in terms of the variable \sqrt{s} rather than s . This residue can be related to the residues mentioned earlier by:

$$r_{ba} = \frac{1}{2} \sqrt{\frac{\rho_a(s_R) \rho_b(s_R)}{s_R}} \mathcal{R}_{ba}, \quad (50.24)$$

where the phase-space factors are to be continued analytically to the pole location s_R . The residues quoted in the baryon listings are those for πN scattering ($a = b = \pi N$).

The branching ratio of a resonance decay to a specific channel represents the fraction of the decay probability directed to that channel.

$$\text{Br}_a = N_a / N_{\text{tot}}. \quad (50.25)$$

Here, N_a is the experimental count of events for the decay channel $R \rightarrow a$, while N_{tot} represents the total number of events produced

in the decay of the resonance. Since the amplitudes of decays to different final states add incoherently, we have $N_{\text{tot}} = \sum_b N_b$. We note, however, that both N_a and N_{tot} may exhibit a dependence on the reaction through which the resonance is produced, due to the resonance's finite width. For a narrow resonance, the experimental count is determined by integrating the squared production amplitude over the decay channel's phase space:

$$N_a = N_0 \int |\mathcal{A}_a|^2 d\Phi_a, \quad (50.26)$$

where N_0 is a normalization constant associated with the integrated luminosity, and \mathcal{A}_a represents the amplitude of the resonance decay to channel a . When the decay rate's variation across the resonance width becomes significant, the resonance's lineshape must be considered:

$$N_a = N_0 \int_{s_{\text{thr},a}}^{\infty} ds \sigma_R(s) \int |\mathcal{A}_a(s)|^2 d\Phi_a(s). \quad (50.27)$$

Here, $\sigma_R(s)$ denotes a proper weight function of the resonance and $s_{\text{thr},a}$ is the threshold value for the channel a . Additionally, the phase space integral, $\Phi_a(s)$, puts the integrand to zero below the energy threshold of the decay channel a . This aspect is particularly crucial for the decays of broad resonances into channels with energy thresholds exceeding the resonance's nominal mass. This methodology is frequently employed in light-meson studies, as demonstrated in Ref. [61], and is also prevalent in light baryon research, as referenced in Ref. [60].

In case of the decay of some heavy state into multi-body final states, the transition amplitude can include resonances within subsystems of particles. When the total amplitude is decomposed as $\mathcal{A}_a = \sum_R \mathcal{A}_{a(R)}$, the relative branching fraction for the decay of the given heavy state into final state a via resonance R in some subsystem, denoted as $\text{Br}_{a(R)} / \text{Br}_a$, is given by:

$$\text{Br}_{a(R)} / \text{Br}_a = \int |\mathcal{A}_{a(R)}|^2 d\Phi_a / \int |\mathcal{A}_a|^2 d\Phi_a \quad (50.28)$$

It is crucial to recognize that the decomposition of the total amplitude, \mathcal{A}_a , into resonance amplitudes, $\mathcal{A}_{a(R)}$, is not a straightforward process. Beyond the differentiation of components based on distinct quantum numbers, this separation is inherently model-dependent. Furthermore, it is essential to be aware that the amplitudes $\mathcal{A}_{a(R)}$ can interfere with one another. As a result, their individual probabilities might not sum up to the total branching fraction of channel a . Nonetheless, in many scenarios, the interference contributions are small, making the fractions $\text{Br}_{a(R)} / \text{Br}_a$ indicative. For recent applications of these formulas in the context of B -decays see Refs. [62–65].

Lastly, an expression analogous to the branching fraction can be formulated using the pole parameters. For two-particle decays in the S -wave, one writes:

$$\text{Br}_a = \frac{|\tilde{g}_a|^2}{M_R \Gamma_R} \rho_a(M_R^2), \quad (50.29)$$

where M_R and Γ_R have been previously defined in Eq. (50.20). This approach was utilized to define a two-photon width for the broad $f_0(500)$ resonance [66, 67]. Similarly, one should use residues to quantify the coupling of resonances to certain production channels [68]. For an application of this approach to the coupling of the $K_0^*(1430)$ resonance to a leptonic current see Ref. [69]. Equation (50.29) provides a definition of branching fraction that remains independent of the reaction used to derive the quantity. For narrow resonances, this definition aligns well with Eq. (50.25) and Eq. (50.26). However, for broad, overlapping resonances, it is essential to recognize that Eq. (50.29) is primarily used to convert residues into metrics that facilitate a more straightforward comparison of resonance transitions across different channels. For resonances with a coupling to a channel that remains closed at the resonance mass, Eq. (50.29) is not applicable due to the phase-space factor. In such scenarios, modification of the expression is required as elaborated upon in Ref. [60], and at the conclusion of Sec. 50.3.5.

50.3 Common parameterizations

In general, there is no universal, model-independent recipe to build scattering amplitudes. However, a few approaches presented in this section are practical to extract resonance properties in experimental analyses. The systematic theory uncertainties need to be assessed from a range of model variations that provide a sufficient quality of description of the available data and are permitted by general \mathcal{S} -matrix principles and the symmetries controlling the system at hand.

50.3.1 The Breit–Wigner parameterization

The relativistic Breit–Wigner parameterization represents a dressed propagator for an isolated resonance. The production amplitude for a resonance observed in a channel a , is given by

$$\mathcal{A}_a(s) = \frac{\mathcal{N}_a(s)}{M_{\text{BW}}^2 - s - iM_{\text{BW}}\Gamma(s)} \quad (50.30)$$

where M_{BW} represents the Breit–Wigner mass, and $\Gamma_{\text{BW}} = \Gamma(M_{\text{BW}}^2)$ denotes the Breit–Wigner width. The function $\Gamma(s)$ is defined by the channels to which the resonance can decay. The numerator function $\mathcal{N}_a(s)$ is tailored to the production process, encompassing kinematic factors and couplings pertinent to both the production and decay processes.

$$\mathcal{N}_a(s) = \alpha g_a n_a(s) \quad (50.31)$$

$$\Gamma(s) = \frac{1}{M_{\text{BW}}} \sum_b g_b^2 \rho_b(s) n_b^2(s), \quad (50.32)$$

Here the index $b = 1, 2, \dots$ runs over all decay channels of the resonance. The coupling constants are represented by g_b , and ρ_b is the phase-space factor as defined in Eq. (50.11). The expression for $n_a(s)$ is:

$$n_a = (q_a/q_0)^{l_a} F_{l_a}(q_a/q_0), \quad (50.33)$$

where l_a indicates the orbital angular momentum in channel a , $q_a(s)$ is the break-up momentum as defined in Eq. (50.7), and q_0 is a suitably selected momentum scale. The term $(q_a)^{l_a}$ ensures the amplitude's appropriate threshold behavior. The rapid growth of this factor for angular momenta $l_a > 0$ is offset at specific s values by a phenomenological form factor, represented here by $F_{l_a}(q_a, q_0)$ — the presence of these suppression factors is also a requirement from positivity which demands that the dressed propagator, the denominator of Eq. (50.30) and similar equations below, is not allowed to drop faster than $1/s$ [27]. The Blatt-Weisskopf form factors are frequently employed in the literature [70–72] to model F_j :

$$F_0^2(z) = 1, \quad (50.34)$$

$$F_1^2(z) = 1/(1+z^2),$$

$$F_2^2(z) = 1/(9+3z^2+z^4),$$

where $z = q/q_0$, the scale parameter $1/q_0$ typically falls within the range of 1 GeV^{-1} to 5 GeV^{-1} . Rather than employing coupling constants as in Eq. (50.32), channel partial widths can be used,

$$\Gamma(s) = \sum_b \Gamma_{\text{BW},b} \frac{\rho_b(s)}{\rho_b(M_{\text{BW}}^2)} \left(\frac{q_b}{q_{bR}} \right)^{2l_b} \frac{F_{l_b}^2(q_b, q_0)}{F_{l_b}^2(q_{bR}, q_0)}. \quad (50.35)$$

Here q_{bR} is the values of the break-up momenta evaluated at $s = M_{\text{BW}}^2$. It is essential to note that this substitution is valid only for channels where the decay channel's threshold is positioned below the nominal resonance mass. In other scenarios, Eq. (50.32) should be applied.

Equation (50.32) incorporates a threshold for each of the coupled channels. The expression is straightforward to use in the physical region above all the thresholds. Its evaluation elsewhere requires a careful analytic continuation. As outlined in Refs. [73, 74], the choice

$$q_c = i\sqrt{-q_c^2} \quad \text{for} \quad q_c^2 < 0, \quad (50.36)$$

leads to an evaluation of the amplitude on the physical sheet below threshold. The *Flatté parameterization* [73] refers to the two

S-wave channels' amplitude near a threshold of a heavier channel in the physical region of the lighter channel computed with Eq. (50.36). When a resonance's coupling to the channel with a higher threshold is notably strong, the parameterization displays scaling invariance. This implies that it is not possible to extract individual partial decay widths; only their ratios can be determined [75].

The Breit–Wigner parameterization is an accurate representation of resonance phenomena strictly in the $\Gamma/\Delta \rightarrow 0$ limit, where Γ is the resonance width and Δ is the distance to the closest unaccounted singularity, be it a pole of a higher resonance or a kinematic threshold related to a coupled channel. However, the situation is often more complex due to multiple singularities in the complex plane around the resonance with different importance. For instance, in P-wave $\pi\pi$ scattering, the Breit–Wigner parameterization aptly describes the ρ -meson resonance over an extensive range. Although the closest singularity to the ρ -meson pole is the ω -pole ($\Gamma_\rho/\Delta_\omega \gg 1$), this isospin breaking effect is typically insignificant except few special cases [76, 77]. Subsequent singularities, namely the 3π , 4π , and 6π thresholds, are also generally disregarded. The two-pion threshold is incorporated in the Breit–Wigner parameterization through an energy-dependent width. Finally, the parameterization's efficacy diminishes around 1.2 GeV due to the ρ' resonance, situated approximately at 1.45 GeV.

Once the applicability of the Breit–Wigner parameterization is established, it is crucial to recognize that its parameters will only align with the pole parameters if the width is small. Yet, extracting the pole position from the Breit–Wigner amplitude is a straightforward technical task, achieved through analytic continuation. However, neither the Breit–Wigner parameters nor the corresponding pole parameters should be deemed reliable without justifying the parameterization's applicability. If there is more than one resonance in one partial wave that significantly couples to the same channel, it is generally inappropriate to employ a sum of Breit–Wigner functions. Such an approach often results in a breach of unitarity constraints, potentially introducing an indeterminate bias to the inferred resonance properties from the reaction amplitude. For overlapping resonances in the same partial wave, more sophisticated methods, such as the \mathcal{K} -matrix approach detailed in the subsequent section, are recommended.

50.3.2 \mathcal{K} -matrix approach

The \mathcal{K} -matrix method offers a comprehensive framework for modelling coupled-channel amplitudes [78]. This method ensures two-particle unitarity. However, it traditionally omits the left-hand cuts. The scattering amplitude $\mathcal{M}_{ba}(s)$ can be derived from the equation:

$$n_b \mathcal{M}_{ba}^{-1} n_a = \mathcal{K}_{ba}^{-1} - i\delta_{ba}\rho_a n_a^2. \quad (50.37)$$

Here, \mathcal{K}_{ba} represents a real function and is subject to modeling. The factor n_a is elaborated upon in Eq. (50.33). Since there is no unique recipe to build \mathcal{K} , it is essential to explore various parameterizations to gauge the theoretical systematic uncertainty. A commonly adopted choice for the \mathcal{K} -matrix is given by:

$$\mathcal{K}_{ba}(s) = \sum_R \frac{g_b^R g_a^R}{m_R^2 - s} + b_{ba}, \quad (50.38)$$

where m_R is referred to as the bare mass of the resonance R (not to be confused with the physical mass), and the g_a^R represents the bare couplings of the resonance R to the channel a (not to be confused with the residues). The b_{ba} is a matrix that parameterizes the non-pole components of the \mathcal{K} -matrix. Provided all parameters in Eq. (50.38) are real, the amplitude $\mathcal{M}_{ba}(s)$ remains unitary. From Eq. (50.37), the scattering amplitude \mathcal{M} can be directly computed using its matrix form:

$$\mathcal{M} = n[1 - \mathcal{K}i\rho n^2]^{-1}\mathcal{K}n, \quad (50.39)$$

where n and ρ are diagonal matrices, $n = \text{diag}(n_a, n_b, \dots)$, and $\rho = \text{diag}(\rho_a, \rho_b, \dots)$. As an alternative to Eq. (50.38), the same

functional structure on the right side of Eq. (50.38) can be employed to parameterize the inverse \mathcal{K} -matrix, termed the \mathcal{M} -matrix, by the authors of Ref. [79]. Numerous alternative formulations within the \mathcal{K} -matrix framework are utilized for amplitude studies related to lattice-QCD calculations [80–82].

A prevalent method to construct the production amplitude within the \mathcal{K} -matrix framework is the \mathcal{P} -vector parameterization [72, 78, 83]. The method utilizes the \mathcal{K} -matrix poles and bare couplings from Eq. (50.38):

$$\mathcal{A}_a(s) = n_a \sum_c \left[1 - \mathcal{K}i\rho n^2\right]_{ac}^{-1} \mathcal{P}_c, \quad (50.40)$$

$$\mathcal{P}_c = \sum_R \frac{\alpha^R g_c^R}{m_R^2 - s} + \mathcal{B}_c. \quad (50.41)$$

The production vector, denoted as \mathcal{P}_c , comprises two main components. The first component represents a transition driven by the coupling of the bare resonance, R , to the source. This coupling is characterized by a strength parameter, α^R . The second component, \mathcal{B}_c , signifies the direct transition from the source to the channel c . The formalism ensures that the complete production vector gets dressed via the final state interaction.

The \mathcal{Q} -vector, as discussed in Ref. [72, 79, 84], offers an alternative methodology for constructing a production amplitude:

$$\mathcal{A}_a(s) = \sum_c \mathcal{M}_{ac}(s)\mathcal{Q}_c(s)/n_c. \quad (50.42)$$

Here, $\mathcal{Q}_c(s)$ represents a smooth function of s and can be parameterized using a polynomial series. The unitarity condition of Eq. (50.19) is satisfied when $\mathcal{Q}_c(s)$ is a real function and in particular does not have singularities above the lowest threshold for all channels c . Besides these conditions $\mathcal{Q}_c(s)$ is arbitrary. In a study of $\gamma\gamma \rightarrow \pi\pi$, cf. Ref. [66, 67] a low-order polynomial is claimed to be sufficient to parameterize the energy dependence of the function $\mathcal{Q}_c(s)$. The \mathcal{Q} -vector method is convenient, if the full matrix \mathcal{M} is known, cf. Ref. [79]. An important distinction between the \mathcal{P} -vector and the \mathcal{Q} -vector methods is highlighted in [83]. When the two-particle scattering amplitude approaches zero, the production amplitude in the \mathcal{Q} -vector construction unavoidably vanishes for finite values of \mathcal{Q}_c , whereas it remains non-zero in the \mathcal{P} -vector approach.

Traditionally, amplitudes constructed using the \mathcal{K} -matrix technique exclude the left-hand cuts. Nevertheless, these can be customarily incorporated into the function b_{ba} from Eq. (50.38) for the scattering amplitude [85, 86]. Similarly, for the production amplitude, the functions \mathcal{B}_c and \mathcal{Q}_c from Eq. (50.40) and Eq. (50.42), respectively, might also encompass the left-hand cuts. Those can often be parameterized by low order polynomials [66, 67, 87].

The position of the resonance poles can be determined by examining the zeros of the analytic function $\det[1 - \mathcal{K}i\rho n^2]$. Owing to the ρ factor, this determinant exhibits a complex multisheet structure. Nonetheless, the nearest unphysical sheet usually has the highest influence to the physical region. It is always the one which is determined by the heaviest threshold below the studied point in s (cf. Fig. 50.3). If for a given resonance the pole closest to the physical axis is not located on a sheet that connects directly to the physical axis, it is possible that \mathcal{K} -matrix fits do not allow one to fix the pole parameters, since a larger distance of the pole to the physical axis can be balanced by increased residues — for a detailed discussion see Ref. [88].

50.3.3 Further improvements: Chew–Mandelstam function

The \mathcal{K} -matrix framework often enables an accurate fit of physical amplitudes and is straightforward to handle. However, it does present a significant drawback: it breaches constraints imposed by analyticity. For instance, ρ_a , as defined in Eq. (50.11), is not well-defined at $s = 0$. Moreover, in cases of unequal masses, it manifests an unphysical cut, as depicted in the left panel of Fig. 50.6.

A method to improve the analytic properties has been suggested in Refs. [89–93]. This approach replaces the term $i\rho_a(s)n_a^2$ from

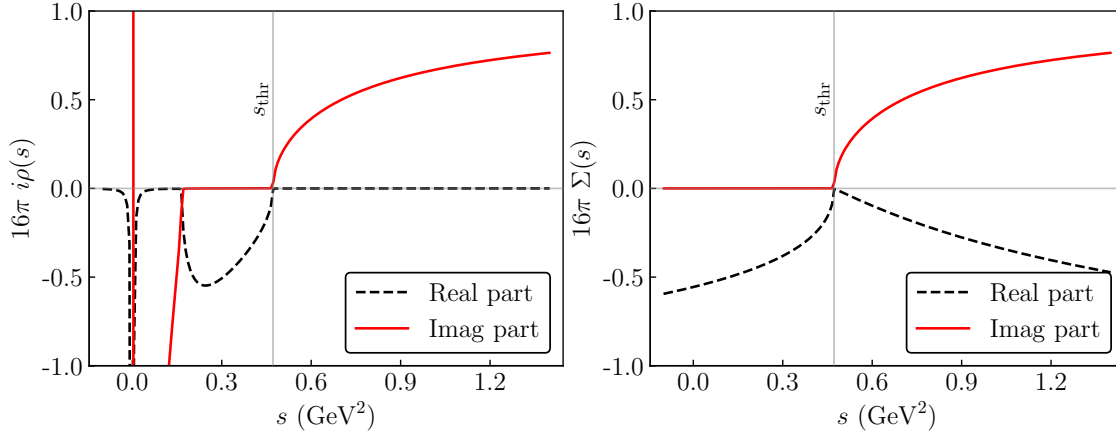


Figure 50.6: Comparison of the $i\rho$ function (left plot) to the *Chew-Mandelstam* function from Eq. (50.44) (right plot), evaluated for the case of S-wave $\eta\pi$ scattering. The values of s are taken slightly above the real axis, $s + i0$. The solid red line shows the imaginary part that is the same for both functions above threshold. The dashed black line presents the real part. One finds indications of the unphysical left-hand singularities of the function $i\rho$ on the left plot, while the Chew-Mandelstam function in analytic below the two-particle threshold.

Eq. (50.37) with the analytic function $\Sigma_a(s)$, known as the *Chew-Mandelstam* function. This function produces the imaginary part $i\rho_a(s)n_a^2$ on the right-hand cut, while maintaining analyticity on the left-hand side, as represented by the once subtracted dispersion integral:

$$\Sigma_a(s + i0) = \frac{s - s_{\text{thr}_a}}{\pi} \int_{s_{\text{thr}_a}}^{\infty} \frac{\rho_a(s')n_a^2(s')}{(s' - s_{\text{thr}_a})(s' - s - i0)} ds'. \quad (50.43)$$

Here, we chose the channel threshold, s_{thr_a} , as the subtraction point, and assumed that the subtraction constant is absorbed into the other parameters used for the amplitude. For an S-wave where $n_a = 1$, the integral has a closed form [37, 91]:

$$\Sigma_a(s) = \frac{1}{16\pi^2} \left[\frac{2q_a}{\sqrt{s}} \log \frac{m_1^2 + m_2^2 - s + 2\sqrt{s}q_a}{2m_1m_2} - (m_1^2 - m_2^2) \left(\frac{1}{s} - \frac{1}{(m_1 + m_2)^2} \right) \log \frac{m_1}{m_2} \right], \quad (50.44)$$

where m_1 and m_2 are masses of the final-state particles in channel a , with $s_{\text{thr}_a} = (m_1 + m_2)^2$. The function's behavior along the real axis is illustrated in the right panel of Fig. 50.6. A further discussion of the calculation of the Chew-Mandelstam function can be found in Refs. [94, 95].

If there is only a single resonance in a given channel, it is possible to feed the imaginary part of the Breit-Wigner function, Eq. (50.30) with an energy-dependent width, directly into a dispersion integral to get a resonance propagator with the correct analytic structure [96, 97].

50.3.4 Effective-range expansion and scattering-length approximation

For elastic scattering, $\eta_b = 1$, Eq. (50.14) simplifies to

$$f_{bb} = e^{i\delta} \sin(\delta) = \frac{q}{q \cot(\delta) - iq}, \quad (50.45)$$

where q is the relative momentum of the scattering particles. For S-waves one may then employ the *effective-range expansion* [98, 99] (ERE)

$$q \cot \delta = \frac{1}{a} + \frac{1}{2}r q^2 + O(r^3 q^4), \quad (50.46)$$

whose radius of convergence is set by the closest non-analyticity, which may be the next threshold, a left-hand cut or a zero in the amplitude which is equivalent to a pole in $q \cot \delta$. The ERE is understood to be an expansion in $R_f q$, where R_f denotes the range of forces provided by the inverse of the lightest exchange particle allowed. The *scattering length*, a , is then defined as the

first term in an expansion of the real part of the inverse scattering amplitude. The sign convention used in Eq. (50.46) is the one commonly employed in particle physics. In this convention a positive scattering length indicates attraction; if, however, the attraction is strong enough to generate a bound state, the scattering length changes sign and turns negative. A negative scattering length also occurs for repulsive interactions. Note that in nuclear physics the leading term in the expansion of Eq. (50.46) is usually defined as $-1/a$ such that *e.g.* a bound state would be related to a positive scattering length. The parameter r is called the *effective range*. Especially in cases where the scattering length is large the ERE not only describes the low energy scattering well but also allows for an analytic continuation to find bound states below threshold by proper analytic continuation. This method was, *e.g.*, employed recently to analyze near threshold scattering phase shifts for $D^{*+}D^0$ scattering found in lattice analyses to extract properties of the $T_{cc}(3875)^+$ [100–102] at unphysical pion masses. It should be stressed that the analyses of the lattice data might call for a modification to account for the nearby left-hand cut which sets the radius of convergence of the ERE [103].

When considering only the scattering length within the ERE, the scattering amplitude is represented as:

$$\mathcal{M}(s) = \frac{8\pi\sqrt{s}}{1/a - iq(s)}. \quad (50.47)$$

The scattering length is thus proportional to the value of the amplitude at threshold. It is worth noting that the scattering length approximation is applicable only in a very limited energy range, however, might well be appropriate to analyze the recently discovered narrow near-threshold states [104, 105]. Examples of such analyses can be found in Refs. [106–108]. Moreover, it is possible to introduce the effect of a weakly coupled lower channel [109, 110]. Such coupling results in a positive imaginary part of the scattering length. It is also crucial to highlight that for large a values, the amplitude of Eq. (50.47) develops a near-threshold pole located on the physical or unphysical sheet for negative or positive values of a , respectively. For readers interested in a exploration of how close-to-threshold poles interact with remote thresholds, we refer to Ref. [111].

While easy to use, it is important to stress, however, that the approximation in Eq. (50.47) is a specific choice of the dynamic function. This choice results in a single pole close to the physical region, suggesting that the state under study has the characteristics of a hadronic molecule, as discussed in references such as [108, 112–114]. Virtual states are discussed in this context in Ref. [115].

50.3.5 Two-potential decomposition

Another advanced technique to construct the scattering amplitude, which is widely used in the literature [69,116–121], is based on the two-potential formalism [122]. While it is possible to formulate this method for the full unprojected amplitude $\mathcal{M}_{ba}(s, t)$, for clarity, we focus on presenting the equations in their partial-wave-projected form.

The scattering amplitude, $\mathcal{M}(s)$, can be broken down into two components: a background part and a pole part. This can be represented as:

$$\mathcal{M}(s) = \mathcal{M}^{\text{b.g.}}(s) + \mathcal{M}^{\text{pole}}(s). \quad (50.48)$$

It is important to note that the division presented in Eq. (50.48) is not unique and model-dependent. This is further discussed in references such as [123,124]. The background scattering matrix is assumed to be unitary by itself. One approach to parameterize it, especially at lower energies, is by using phase shifts and inelasticities, as seen in [69,120,121]. Alternatively, it can be computed based on some potential, $V^{\text{b.g.}}$, fed into a proper scattering equation [118,119].

The complete amplitude, \mathcal{M} , from Eq. (50.48) is unitary, if the pole part follows a specific construction. Namely,

$$\mathcal{M}_{ab}^{\text{pole}}(s) = \Omega_{ac}(s) [1 - V^{\text{R}}(s)\Sigma^u(s)]_{cd}^{-1} V_{de}^{\text{R}}(s) \Omega_{cb}^T(s). \quad (50.49)$$

In this context, we introduce the vertex functions, denoted as $\Omega_{ab}(s)$, and the resonance potential, represented as $V^{\text{R}}(s)$. This potential operates as a matrix in the channel space and can be expressed as:

$$V_{ab}^{\text{R}}(s) = \sum_{\text{R}} \frac{g_a^{\text{R}} g_b^{\text{R}}}{m_{\text{R}}^2 - s}. \quad (50.50)$$

The term Σ_{ab}^u represents the self-energy matrix. Additionally, g_a^{R} denotes the bare coupling of the resonance, labeled as R, to the channel a , and m_{R} is its bare mass. The vertex functions obey a unitarity relation similar to the production amplitude in Eq. (50.8). However, in this case, the final state interaction is determined by $\mathcal{M}^{\text{b.g.}}$. This can be represented as:

$$\text{Disc } \Omega_{ab}(s) = 2i \sum_c \mathcal{M}_{ca}^{\text{b.g.*}}(s) \rho_c(s) \Omega_{cb}(s). \quad (50.51)$$

When using low-energy phase shifts for the background term, it is practical to express the vertex functions in terms of an Omnès matrix, as discussed in [121]. The matrix reduces to the well-known Omnès function

$$\Omega(s) = \exp\left(\frac{s}{\pi} \int_{s_{\text{thr}}}^{\infty} ds' \frac{\delta^{\text{b.g.}}(s')}{s'(s' - s - i\epsilon)}\right) \quad (50.52)$$

in the single-channel case [125], where $\delta^{\text{b.g.}}(s)$ denotes the phase of the background scattering matrix $\mathcal{M}^{\text{b.g.}}(s)$. The discontinuity associated with the self-energy matrix, $\Sigma^u(s)$, is given by:

$$\text{Disc } \Omega_{ab}^u(s) = 2i \sum_c \Omega_{ca}^*(s) \rho_c(s) \Omega_{cb}(s). \quad (50.53)$$

To determine the real part of Σ^u , one can use Eq. (50.53) with a properly subtracted dispersion integral — cf. Eq. (50.43).

When $\mathcal{M}^{\text{b.g.}}$ is unitary, the full amplitude is unitary given Eq. (50.49). However, it is essential to note that the pole term alone is not unitary unless the background amplitude vanishes. Under such conditions, the described amplitude simplifies to the \mathcal{K} -matrix construction with improved analytic behavior as detailed in Sec. 50.3.3. Neglecting non-pole terms is not a good approximation for certain interactions, such as the scalar-isoscalar $\pi\pi$ at low energies, as discussed in [126]. However, for higher partial waves, this approximation is generally effective.

A production amplitude consistent with Eq. (50.49) reads [120,121]:

$$\mathcal{A}_a^{\text{pole}}(s) = \Omega_{ac}(s) [1 - V^{\text{R}}(s)\Sigma^u(s)]_{cd}^{-1} \mathcal{P}_d, \quad (50.54)$$

with function \mathcal{P}_d given in Eq. (50.40). This form was employed in Refs. [120,121] to treat the pion vector and scalar form factor, respectively, and in Ref. [69] for the scalar πK form factor.

There has been considerable interest in the $3 \rightarrow 3$ scattering recently, particularly in light of new data on three-hadron interaction [127] and advancements in lattice calculations [128]. One finds that the methodologies devised for accounting for one-pion exchange bear a resemblance to the two-potential decomposition. For details see Ref. [129], also Eq. (93) in Ref. [130].

References

- [1] M. Albaladejo *et al.* (JPAC), Prog. Part. Nucl. Phys. **127**, 103981 (2022), [arXiv:2112.13436].
- [2] M. Mai, U.-G. Meißner and C. Urbach, Phys. Rept. **1001**, 1 (2023), [arXiv:2206.01477].
- [3] M. Jacob and G. C. Wick, Annals Phys. **7**, 404 (1959), [Annals Phys.281,774(2000)].
- [4] C. Zemach, Phys. Rev. **140B**, 97, 109 (1965).
- [5] A. V. Anisovich *et al.*, J. Phys. **G28**, 15 (2002), [hep-ph/0105330].
- [6] M. E. Peskin and D. V. Schroeder, *An Introduction to quantum field theory*, Addison-Wesley, Reading, USA (1995), ISBN 978-0-201-50397-5.
- [7] V. N. Gribov, Y. L. Dokshitzer and J. Nyiri, *Strong Interactions of Hadrons at High Energies – Gribov Lectures on Theoretical Physics*, Cambridge University Press, Cambridge (2009).
- [8] M. Doring *et al.*, Nucl. Phys. A **829**, 170 (2009), [arXiv:0903.4337].
- [9] L. Landau, Nucl. Phys. **13**, 181 (1959).
- [10] R. Cutkosky, J. Math. Phys. **1**, 429 (1960).
- [11] M. Kato, Annals Phys. **31**, 1, 130 (1965).
- [12] A. M. Badalian *et al.*, Phys. Rept. **82**, 31 (1982).
- [13] V. Baru *et al.*, Phys. Rev. D **99**, 9, 094013 (2019), [arXiv:1901.10319].
- [14] G. Calucci, L. Fonda and G. C. Ghirardi, Phys. Rev. **166**, 1719 (1968).
- [15] S. Coleman and R. E. Norton, Nuovo Cim. **38**, 438 (1965).
- [16] C. Schmid, Phys. Rev. **154**, 5, 1363 (1967).
- [17] I. J. R. Aitchison and C. Kacser, Nuovo Cim. A **40**, 2, 576 (1965).
- [18] M. Mikhasenko, B. Ketzer and A. Sarantsev, Phys. Rev. D **91**, 9, 094015 (2015), [arXiv:1501.07023].
- [19] M. Bayar *et al.*, Phys. Rev. **D94**, 7, 074039 (2016), [arXiv:1609.04133].
- [20] F. Aceti, L. R. Dai and E. Oset, Phys. Rev. **D94**, 9, 096015 (2016), [arXiv:1606.06893].
- [21] J.-J. Wu *et al.*, Phys. Rev. Lett. **108**, 081803 (2012), [arXiv:1108.3772].
- [22] L. D. Roper, Phys. Rev. Lett. **12**, 340 (1964).
- [23] J. R. Pelaez, Phys. Rept. **658**, 1 (2016), [arXiv:1510.00653].
- [24] R. Omnès, *Introduction to Particle Physics*, Frontiers in physics, Wiley-Interscience (1971), ISBN 9780471653721.
- [25] R. Omnès and M. Froissart, *Mandelstam Theory and Regge Poles: An Introduction for Experimentalists*, Frontiers in physics, W.A. Benjamin (1963), URL <https://books.google.fr/books?id=08pEAAAIAAJ>.
- [26] M. Fukugita and K. Igi, Phys. Rept. **31**, 237 (1977).
- [27] S. Weinberg, *The Quantum theory of fields. Vol. 1: Foundations*, Cambridge University Press (2005), ISBN 978-0-521-67053-1, 978-0-511-25204-4.
- [28] S. M. Roy, Phys. Lett. **36B**, 353 (1971).
- [29] B. Ananthanarayan *et al.*, Phys. Rept. **353**, 207 (2001), [hep-ph/0005297].

- [30] G. Colangelo, J. Gasser and H. Leutwyler, Nucl. Phys. **B603**, 125 (2001), [hep-ph/0103088].
- [31] R. Garcia-Martin *et al.*, Phys. Rev. D **83**, 074004 (2011), [arXiv:1102.2183].
- [32] P. Buettiker, S. Descotes-Genon and B. Moussallam, Eur. Phys. J. **C33**, 409 (2004), [hep-ph/0310283].
- [33] M. Hoferichter, D. R. Phillips and C. Schat, Eur. Phys. J. **C71**, 1743 (2011), [arXiv:1106.4147].
- [34] G. E. Hite and F. Steiner, Nuovo Cim. A **18**, 237 (1973).
- [35] M. Hoferichter *et al.*, Phys. Rept. **625**, 1 (2016), [arXiv:1510.06039].
- [36] D. I. Olive, Il Nuovo Cimento (1955-1965) **73**, 1, 73 (1962), ISSN 1827-6121, URL <https://doi.org/10.1007/BF02754344>.
- [37] J. L. Basdevant and E. L. Berger, Phys. Rev. **D16**, 657 (1977).
- [38] N. N. Khuri and S. B. Treiman, Phys. Rev. **119**, 1115 (1960).
- [39] I. J. R. Aitchison and R. Pasquier, Phys. Rev. **152**, 4, 1274 (1966).
- [40] J. Kambor, C. Wiesendanger and D. Wyler, Nucl. Phys. B **465**, 215 (1996), [hep-ph/9509374].
- [41] A. V. Anisovich and H. Leutwyler, Phys. Lett. B **375**, 335 (1996), [hep-ph/9601237].
- [42] P. Guo *et al.*, Phys. Lett. **B771**, 497 (2017), [arXiv:1608.01447].
- [43] M. Albaladejo and B. Moussallam, Eur. Phys. J. **C77**, 8, 508 (2017), [arXiv:1702.04931].
- [44] G. Colangelo *et al.*, Eur. Phys. J. **C78**, 11, 947 (2018), [arXiv:1807.11937].
- [45] K. Kampf *et al.*, Phys. Rev. D **101**, 7, 074043 (2020), [arXiv:1911.11762].
- [46] T. Isken *et al.*, Eur. Phys. J. **C77**, 7, 489 (2017), [arXiv:1705.04339].
- [47] F. Niecknig, B. Kubis and S. P. Schneider, Eur. Phys. J. **C72**, 2014 (2012), [arXiv:1203.2501].
- [48] I. V. Danilkin *et al.*, Phys. Rev. **D91**, 9, 094029 (2015), [arXiv:1409.7708].
- [49] M. Dax, T. Isken and B. Kubis, Eur. Phys. J. C **78**, 10, 859 (2018), [arXiv:1808.08957].
- [50] M. Albaladejo *et al.* (JPAC), Eur. Phys. J. C **80**, 12, 1107 (2020), [arXiv:2006.01058].
- [51] M. Albaladejo *et al.* (JPAC), Phys. Rev. D **101**, 5, 054018 (2020), [arXiv:1910.03107].
- [52] D. Stamen *et al.*, Eur. Phys. J. C **83**, 6, 510 (2023), [Erratum: Eur.Phys.J.C 83, 586 (2023)], [arXiv:2212.11767].
- [53] F. Niecknig and B. Kubis, JHEP **10**, 142 (2015), [arXiv:1509.03188].
- [54] F. Niecknig and B. Kubis, Phys. Lett. **B780**, 471 (2018), [arXiv:1708.00446].
- [55] M. Albaladejo *et al.* (JPAC), Phys. Rev. D **108**, 1, 014035 (2023), [arXiv:2304.09736].
- [56] M. Mikhasenko *et al.* (JPAC), Phys. Rev. D **101**, 3, 034033 (2020), [arXiv:1910.04566].
- [57] K. M. Watson, Phys. Rev. **95**, 228 (1954).
- [58] S. Willenbrock (2022), [arXiv:2203.11056].
- [59] Z.-Q. Wang *et al.*, Phys. Rev. D **105**, 7, 074016 (2022), [arXiv:2201.00492].
- [60] V. Burkert *et al.*, Phys. Lett. B **844**, 138070 (2023), [arXiv:2207.08472].
- [61] M. Aghasyan *et al.* (COMPASS), Phys. Rev. D **98**, 9, 092003 (2018), [arXiv:1802.05913].
- [62] R. Aaij *et al.* (LHCb), Phys. Rev. D **94**, 7, 072001 (2016), [arXiv:1608.01289].
- [63] R. Aaij *et al.* (LHCb), Phys. Rev. D **92**, 1, 012012 (2015), [arXiv:1505.01505].
- [64] R. Aaij *et al.* (LHCb), Phys. Rev. D **91**, 9, 092002 (2015), [Erratum: Phys.Rev.D 93, 119901 (2016)], [arXiv:1503.02995].
- [65] R. Aaij *et al.* (LHCb), Phys. Rev. D **102**, 112003 (2020), [arXiv:2009.00026].
- [66] D. Morgan and M. R. Pennington, Z. Phys. **C37**, 431 (1988), [Erratum: Z. Phys.C39,590(1988)].
- [67] D. Morgan and M. R. Pennington, Z. Phys. **C48**, 623 (1990).
- [68] B. Moussallam, Eur. Phys. J. C **71**, 1814 (2011), [arXiv:1110.6074].
- [69] L. Von Detten *et al.*, Eur. Phys. J. C **81**, 5, 420 (2021), [arXiv:2103.01966].
- [70] J. M. Blatt and V. F. Weisskopf, *Theoretical nuclear physics*, Springer, New York (1952), ISBN 9780471080190.
- [71] F. Von Hippel and C. Quigg, Phys. Rev. **D5**, 624 (1972).
- [72] S. U. Chung *et al.*, Annalen Phys. **4**, 404 (1995).
- [73] S. M. Flatte, Phys. Lett. **63B**, 224 (1976).
- [74] V. V. Anisovich and A. V. Sarantsev, Eur. Phys. J. **A16**, 229 (2003), [hep-ph/0204328].
- [75] V. Baru *et al.*, Eur. Phys. J. **A23**, 523 (2005), [arXiv:nucl-th/0410099].
- [76] R. Aaij *et al.* (LHCb), Phys. Rev. D **108**, 1, L011103 (2023), [arXiv:2204.12597].
- [77] J. P. Lees *et al.* (BaBar), Phys. Rev. D **86**, 032013 (2012), [arXiv:1205.2228].
- [78] I. J. R. Aitchison, Nucl. Phys. **A189**, 417 (1972).
- [79] K. L. Au, D. Morgan and M. R. Pennington, Phys. Rev. D **35**, 1633 (1987).
- [80] J. J. Dudek, R. G. Edwards and D. J. Wilson (Hadron Spectrum), Phys. Rev. **D93**, 9, 094506 (2016), [arXiv:1602.05122].
- [81] R. A. Briceno *et al.*, Phys. Rev. **D97**, 5, 054513 (2018), [arXiv:1708.06667].
- [82] A. J. Woss *et al.*, Phys. Rev. D **100**, 5, 054506 (2019), [arXiv:1904.04136].
- [83] I. J. R. Aitchison (2015), [arXiv:1507.02697].
- [84] R. N. Cahn and P. V. Landshoff, Nucl. Phys. **B266**, 451 (1986).
- [85] J. R. Pelaez, A. Rodas and J. Ruiz De Elvira, Eur. Phys. J. C **79**, 12, 1008 (2019), [arXiv:1907.13162].
- [86] I. Danilkin *et al.*, Phys. Rev. D **107**, 7, 074021 (2023), [arXiv:2206.15223].
- [87] B. Kubis and J. Plenter, Eur. Phys. J. C **75**, 6, 283 (2015), [arXiv:1504.02588].
- [88] A. Asokan *et al.* (2022), [arXiv:2212.07856].
- [89] G. J. Gounaris and J. J. Sakurai, Phys. Rev. Lett. **21**, 244 (1968).
- [90] M. R. Pennington *et al.*, Eur. Phys. J. **C56**, 1 (2008), [arXiv:0803.3389].
- [91] J. A. Oller and E. Oset, Phys. Rev. **D60**, 074023 (1999), [hep-ph/9809337].
- [92] N. N. Achasov and A. V. Kiselev, Phys. Rev. **D83**, 054008 (2011), [arXiv:1011.4446].
- [93] A. V. Anisovich *et al.*, Phys. Rev. **D84**, 076001 (2011).
- [94] J. H. Reid and N. N. Trofimenkoff, J. Math. Phys. **25**, 3540 (1984).
- [95] J. A. Oller and U. G. Meissner, Phys. Lett. B **500**, 263 (2001), [hep-ph/0011146].
- [96] E. L. Lomon and S. Pacetti, Phys. Rev. **D85**, 113004 (2012), [Erratum: Phys. Rev.D86,039901(2012)], [arXiv:1201.6126].

- [97] B. Moussallam, *Eur. Phys. J.* **C73**, 2539 (2013), [arXiv:1305.3143].
- [98] J. M. Blatt and J. D. Jackson, *Phys. Rev.* **76**, 18 (1949).
- [99] H. A. Bethe, *Phys. Rev.* **76**, 38 (1949).
- [100] M. Padmanath and S. Prelovsek, *Phys. Rev. Lett.* **129**, 3, 032002 (2022), [arXiv:2202.10110].
- [101] S. Chen *et al.*, *Phys. Lett. B* **833**, 137391 (2022), [arXiv:2206.06185].
- [102] Y. Lyu *et al.* (2023), [arXiv:2302.04505].
- [103] M.-L. Du *et al.*, *Phys. Rev. Lett.* **131**, 13, 131903 (2023), [arXiv:2303.09441].
- [104] S. K. Choi *et al.* (Belle), *Phys. Rev. Lett.* **91**, 262001 (2003), [hep-ex/0309032].
- [105] R. Aaij *et al.* (LHCb), *Phys. Rev. Lett.* **122**, 22, 222001 (2019), [arXiv:1904.03947].
- [106] E. Braaten and J. Stapleton, *Phys. Rev. D* **81**, 014019 (2010), [arXiv:0907.3167].
- [107] V. Baru *et al.*, *Eur. Phys. J.* **A44**, 93 (2010), [arXiv:1001.0369].
- [108] C. Fernández-Ramírez *et al.* (JPAC), *Phys. Rev. Lett.* **123**, 9, 092001 (2019), [arXiv:1904.10021].
- [109] C. Hanhart *et al.*, *Phys. Rev. Lett.* **115**, 20, 202001 (2015), [arXiv:1507.00382].
- [110] F. K. Guo *et al.*, *Phys. Rev. D* **93**, 7, 074031 (2016), [arXiv:1602.00940].
- [111] X.-K. Dong, F.-K. Guo and B.-S. Zou, *Phys. Rev. Lett.* **126**, 15, 152001 (2021), [arXiv:2011.14517].
- [112] D. Morgan, *Nucl. Phys.* **A543**, 632 (1992).
- [113] V. Baru *et al.*, *Phys. Lett.* **B586**, 53 (2004), [hep-ph/0308129].
- [114] F.-K. Guo *et al.*, *Rev. Mod. Phys.* **90**, 1, 015004 (2018), [arXiv:1705.00141].
- [115] I. Matuschek *et al.*, *Eur. Phys. J. A* **57**, 3, 101 (2021), [arXiv:2007.05329].
- [116] I. R. Afnan and B. Blankleider, *Phys. Rev.* **C22**, 1638 (1980).
- [117] A. D. Lahiff and I. R. Afnan, *Phys. Rev.* **C60**, 024608 (1999), [arXiv:nucl-th/9903058].
- [118] A. Matsuyama, T. Sato and T. S. H. Lee, *Phys. Rept.* **439**, 193 (2007), [arXiv:nucl-th/0608051].
- [119] D. Ronchen *et al.*, *Eur. Phys. J.* **A49**, 44 (2013), [arXiv:1211.6998].
- [120] C. Hanhart, *Phys. Lett.* **B715**, 170 (2012), [arXiv:1203.6839].
- [121] S. Ropertz, C. Hanhart and B. Kubis, *Eur. Phys. J.* **C78**, 12, 1000 (2018), [arXiv:1809.06867].
- [122] K. Nakano, *Phys. Rev.* **C26**, 1123 (1982).
- [123] D. Djukanovic, J. Gegelia and S. Scherer, *Phys. Rev.* **D76**, 037501 (2007), [arXiv:0707.2030].
- [124] M. Doring *et al.*, *Phys. Lett.* **B681**, 26 (2009), [arXiv:0903.1781].
- [125] R. Omnes, *Nuovo Cim.* **8**, 316 (1958).
- [126] J. Gasser and U. G. Meissner, *Nucl. Phys.* **B357**, 90 (1991).
- [127] B. Ketzer, B. Grube and D. Ryabchikov, *Prog. Part. Nucl. Phys.* **113**, 103755 (2020), [arXiv:1909.06366].
- [128] B. Hörz and A. Hanlon, *Phys. Rev. Lett.* **123**, 14, 142002 (2019), [arXiv:1905.04277].
- [129] M. Mikhasenko *et al.*, *JHEP* **08**, 080 (2019), [arXiv:1904.11894].
- [130] M. T. Hansen and S. R. Sharpe, *Phys. Rev. D* **92**, 11, 114509 (2015), [arXiv:1504.04248].

51. Cross-Section Formulae for Specific Processes

Revised August 2019 by H. Baer (Oklahoma U.) and R.N. Cahn (LBNL).

PART I: STANDARD MODEL PROCESSES

Setting aside leptonproduction (for which, see Sec. 16 of this *Review*), the cross sections of primary interest are those with light incident particles, e^+e^- , $\gamma\gamma$, $q\bar{q}$, gq , gg , etc., where g and q represent gluons and light quarks. The produced particles include both light particles and heavy ones - t , W , Z , and the Higgs boson H . We provide the production cross sections calculated within the Standard Model for several such processes.

51.1 Resonance Formation

Resonant cross sections are generally described by the Breit-Wigner formula (Sec. 50.3 of this *Review*).

$$\sigma(E) = \frac{2J+1}{(2S_1+1)(2S_2+1)} \frac{4\pi}{k^2} \left[\frac{\Gamma^2/4}{(E-E_0)^2 + \Gamma^2/4} \right] B_{in} B_{out}, \quad (51.1)$$

where E is the c.m. energy, J is the spin of the resonance, and the number of polarization states of the two incident particles are $2S_1+1$ and $2S_2+1$. The c.m. momentum in the initial state is k , E_0 is the c.m. energy at the resonance, and Γ is the full width at half maximum height of the resonance. The branching fraction for the resonance into the initial-state channel is B_{in} and into the final-state channel is B_{out} . For a narrow resonance, the factor in square brackets may be replaced by $\pi\Gamma\delta(E-E_0)/2$.

51.2 Production of light particles

The production of point-like, spin-1/2 fermions in e^+e^- annihilation through a virtual photon, $e^+e^- \rightarrow \gamma^* \rightarrow f\bar{f}$, at c.m. energy squared s is given by

$$\frac{d\sigma}{d\Omega} = N_c \frac{\alpha^2}{4s} \beta [1 + \cos^2\theta + (1-\beta^2)\sin^2\theta] Q_f^2, \quad (51.2)$$

where β is v/c for the produced fermions in the c.m., θ is the c.m. scattering angle, and Q_f is the charge of the fermion. The factor N_c is 1 for charged leptons and 3 for quarks. In the ultrarelativistic limit, $\beta \rightarrow 1$,

$$\sigma = N_c Q_f^2 \frac{4\pi\alpha^2}{3s} = N_c Q_f^2 \frac{86.8 \text{ nb}}{s(\text{GeV}^2)}. \quad (51.3)$$

The cross section for the annihilation of a $q\bar{q}$ pair into a distinct pair $q'\bar{q}'$ through a gluon is completely analogous up to color factors, with the replacement $\alpha \rightarrow \alpha_s$. Treating all quarks as massless, averaging over the colors of the initial quarks and defining $t = -s \sin^2(\theta/2)$, $u = -s \cos^2(\theta/2)$, one finds [1]

$$\frac{d\sigma}{d\Omega}(q\bar{q} \rightarrow q'\bar{q}') = \frac{\alpha_s^2}{9s} \frac{t^2 + u^2}{s^2}. \quad (51.4)$$

Crossing symmetry gives

$$\frac{d\sigma}{d\Omega}(qq' \rightarrow qq') = \frac{\alpha_s^2}{9s} \frac{s^2 + u^2}{t^2}. \quad (51.5)$$

If the quarks q and q' are identical, we have

$$\frac{d\sigma}{d\Omega}(q\bar{q} \rightarrow q\bar{q}) = \frac{\alpha_s^2}{9s} \left[\frac{t^2 + u^2}{s^2} + \frac{s^2 + u^2}{t^2} - \frac{2u^2}{3st} \right], \quad (51.6)$$

and by crossing

$$\frac{d\sigma}{d\Omega}(qq \rightarrow qq) = \frac{\alpha_s^2}{9s} \left[\frac{t^2 + s^2}{u^2} + \frac{s^2 + u^2}{t^2} - \frac{2s^2}{3ut} \right]. \quad (51.7)$$

Annihilation of e^+e^- into $\gamma\gamma$ has the cross section

$$\frac{d\sigma}{d\Omega}(e^+e^- \rightarrow \gamma\gamma) = \frac{\alpha^2}{2s} \frac{u^2 + t^2}{tu}. \quad (51.8)$$

The related QCD process also has a triple-gluon coupling. The cross section is

$$\frac{d\sigma}{d\Omega}(q\bar{q} \rightarrow gg) = \frac{8\alpha_s^2}{27s} (t^2 + u^2) \left(\frac{1}{tu} - \frac{9}{4s^2} \right). \quad (51.9)$$

The crossed reactions are

$$\frac{d\sigma}{d\Omega}(qg \rightarrow qg) = \frac{\alpha_s^2}{9s} (s^2 + u^2) \left(-\frac{1}{su} + \frac{9}{4t^2} \right) \quad (51.10)$$

and

$$\frac{d\sigma}{d\Omega}(gg \rightarrow q\bar{q}) = \frac{\alpha_s^2}{24s} (t^2 + u^2) \left(\frac{1}{tu} - \frac{9}{4s^2} \right). \quad (51.11)$$

Finally,

$$\frac{d\sigma}{d\Omega}(gg \rightarrow gg) = \frac{9\alpha_s^2}{8s} \left(3 - \frac{ut}{s^2} - \frac{su}{t^2} - \frac{st}{u^2} \right). \quad (51.12)$$

Lepton-quark scattering is analogous (neglecting Z exchange)

$$\frac{d\sigma}{d\Omega}(eq \rightarrow eq) = \frac{\alpha^2}{2s} e_q^2 \frac{s^2 + u^2}{t^2}. \quad (51.13)$$

where e_q is the charge of the quark. For neutrino scattering with the four-Fermi interaction

$$\frac{d\sigma}{d\Omega}(\nu d \rightarrow \ell^- u) = \frac{G_F^2 s}{4\pi^2}, \quad (51.14)$$

where the Cabibbo angle suppression is ignored. Similarly

$$\frac{d\sigma}{d\Omega}(\nu \bar{u} \rightarrow \ell^- \bar{d}) = \frac{G_F^2 s}{4\pi^2} \frac{(1 + \cos\theta)^2}{4}. \quad (51.15)$$

To obtain the formulae for deep inelastic scattering (presented in more detail in Section 18) we consider quarks of type i carrying a fraction $x = Q^2/(2M\nu)$ of the nucleon's energy, where $\nu = E - E'$ is the energy lost by the lepton in the nucleon rest frame. With $y = \nu/E$ we have the correspondences

$$1 + \cos\theta \rightarrow 2(1-y),$$

$$d\Omega_{cm} \rightarrow 4\pi f_i(x) dx dy, \quad (51.16)$$

where the latter incorporates the quark distribution, $f_i(x)$. In this way we find

$$\begin{aligned} \frac{d\sigma}{dx dy}(eN \rightarrow eX) &= \frac{4\pi\alpha^2 x s}{Q^4} \frac{1}{2} [1 + (1-y)^2] \\ &\times \left[\frac{4}{9}(u(x) + \bar{u}(x) + \dots) + \frac{1}{9}(d(x) + \bar{d}(x) + \dots) \right] \end{aligned} \quad (51.17)$$

where now $s = 2ME$ is the cm energy squared for the electron-nucleon collision, and we have suppressed contributions from higher mass quarks.

Similarly,

$$\frac{d\sigma}{dx dy}(\nu N \rightarrow \ell^- X) = \frac{G_F^2 x s}{\pi} [(d(x) + \dots) + (1-y)^2(\bar{u}(x) + \dots)] \quad (51.18)$$

and

$$\frac{d\sigma}{dx dy}(\bar{\nu} N \rightarrow \ell^+ X) = \frac{G_F^2 x s}{\pi} [(\bar{d}(x) + \dots) + (1-y)^2(u(x) + \dots)]. \quad (51.19)$$

Quasi-elastic neutrino scattering ($\nu\mu n \rightarrow \mu^- p$, $\bar{\nu}\mu p \rightarrow \mu^+ n$) is directly related to the crossed reaction, neutron decay. The formula for the differential cross section is presented, for example, in N.J. Baker *et al.*, Phys. Rev. **D23**, 2499 (1981).

51.3 Hadroproduction of heavy quarks

For hadroproduction of heavy quarks $Q = c, b, t$, it is important to include mass effects in the formulae. For $q\bar{q} \rightarrow Q\bar{Q}$, one has

$$\frac{d\sigma}{d\Omega}(q\bar{q} \rightarrow Q\bar{Q}) = \frac{\alpha_s^2}{9s^3} \sqrt{1 - \frac{4m_Q^2}{s}} \left[(m_Q^2 - t)^2 + (m_Q^2 - u)^2 + 2m_Q^2 s \right], \quad (51.20)$$

while for $gg \rightarrow Q\bar{Q}$ one has

$$\begin{aligned} \frac{d\sigma}{d\Omega}(gg \rightarrow Q\bar{Q}) = & \frac{\alpha_s^2}{32s} \sqrt{1 - \frac{4m_Q^2}{s}} \left[\frac{6}{s^2} (m_Q^2 - t)(m_Q^2 - u) - \right. \\ & \left. - \frac{m_Q^2 (s - 4m_Q^2)}{3(m_Q^2 - t)(m_Q^2 - u)} + \frac{4}{3} \frac{(m_Q^2 - t)(m_Q^2 - u) - 2m_Q^2 (m_Q^2 + t)}{(m_Q^2 - t)^2} \right. \\ & \left. + \frac{4}{3} \frac{(m_Q^2 - t)(m_Q^2 - u) - 2m_Q^2 (m_Q^2 + u)}{(m_Q^2 - u)^2} - 3 \frac{(m_Q^2 - t)(m_Q^2 - u) + m_Q^2 (u - t)}{s(m_Q^2 - t)} \right. \\ & \left. - 3 \frac{(m_Q^2 - t)(m_Q^2 - u) + m_Q^2 (t - u)}{s(m_Q^2 - u)} \right]. \quad (51.21) \end{aligned}$$

51.4 Production of Weak Gauge Bosons

51.4.1 W and Z resonant production

Resonant production of a single W or Z is governed by the partial widths

$$\Gamma(W \rightarrow \ell_i \bar{\nu}_i) = \frac{\sqrt{2} G_F m_W^3}{12\pi} \quad (51.22)$$

$$\Gamma(W \rightarrow q_i \bar{q}_j) = 3 \frac{\sqrt{2} G_F |V_{ij}|^2 m_W^3}{12\pi} \quad (51.23)$$

$$\begin{aligned} \Gamma(Z \rightarrow f\bar{f}) = & N_c \frac{\sqrt{2} G_F m_Z^3}{6\pi} \\ & \times \left[(T_3 - Q_f \sin^2 \theta_W)^2 + (Q_f \sin^2 \theta_W)^2 \right] \quad (51.24) \end{aligned}$$

The weak mixing angle is θ_W . The CKM matrix elements are indicated by V_{ij} and N_c is 3 for $q\bar{q}$ final states and 1 for leptonic final states.

The full differential cross section for $f_i \bar{f}_j \rightarrow (W, Z) \rightarrow f_i' \bar{f}_j'$ is given by

$$\begin{aligned} \frac{d\sigma}{d\Omega} = & \frac{N_c^f}{N_c^i} \cdot \frac{1}{256\pi^2 s} \cdot \frac{s^2}{(s - M^2)^2 + s\Gamma^2} \\ & \times \left[(L^2 + R^2)(L'^2 + R'^2)(1 + \cos^2 \theta) \right. \\ & \left. + (L^2 - R^2)(L'^2 - R'^2)2 \cos \theta \right] \quad (51.25) \end{aligned}$$

where M is the mass of the W or Z . The couplings for the W are $L = (8G_F m_W^2 / \sqrt{2})^{1/2} V_{ij} / \sqrt{2}$; $R = 0$ where V_{ij} is the corresponding CKM matrix element, with an analogous expression for L' and R' . For Z , the couplings are $L = (8G_F m_Z^2 / \sqrt{2})^{1/2} (T_3 - \sin^2 \theta_W Q)$; $R = -(8G_F m_Z^2 / \sqrt{2})^{1/2} \sin^2 \theta_W Q$, where T_3 is the weak isospin of the initial left-handed fermion and Q is the initial fermion's electric charge. The expressions for L' and R' are analogous. The color factors $N_c^{i,f}$ are 3 for initial or final quarks and 1 for initial or final leptons.

51.4.2 Production of pairs of weak gauge bosons

The cross section for $f\bar{f} \rightarrow W^+ W^-$ is given in term of the couplings of the left-handed and right-handed fermion f , $\ell = 2(T_3 - Qx_W)$, $r = -2Qx_W$, where T_3 is the third component of weak isospin for the left-handed f , Q is its electric charge (in units of the proton charge), and $x_W = \sin^2 \theta_W$:

$$\begin{aligned} \frac{d\sigma}{dt} = & \frac{2\pi\alpha^2}{N_c s^2} \left\{ \left[\left(Q + \frac{\ell + r}{4x_W} \frac{s}{s - m_Z^2} \right)^2 \right. \right. \\ & \left. \left. + \left(\frac{\ell - r}{4x_W} \frac{s}{s - m_Z^2} \right)^2 \right] A(s, t, u) \right. \\ & \left. + \frac{1}{2x_W} \left(Q + \frac{\ell}{2x_W} \frac{s}{s - m_Z^2} \right) \right. \\ & \left. (\Theta(-Q)I(s, t, u) - \Theta(Q)I(s, u, t)) \right. \\ & \left. + \frac{1}{8x_W^2} (\Theta(-Q)E(s, t, u) + \Theta(Q)E(s, u, t)) \right\}, \quad (51.26) \end{aligned}$$

where $\Theta(x)$ is 1 for $x > 0$ and 0 for $x < 0$, and where

$$\begin{aligned} A(s, t, u) = & \left(\frac{tu}{m_W^4} - 1 \right) \left(\frac{1}{4} - \frac{m_W^2}{s} + 3 \frac{m_W^4}{s^2} \right) + \frac{s}{m_W^2} - 4, \\ I(s, t, u) = & \left(\frac{tu}{m_W^4} - 1 \right) \left(\frac{1}{4} - \frac{m_W^2}{2s} - \frac{m_W^4}{st} \right) + \frac{s}{m_W^2} - 2 + 2 \frac{m_W^2}{t}, \\ E(s, t, u) = & \left(\frac{tu}{m_W^4} - 1 \right) \left(\frac{1}{4} + \frac{m_W^4}{t^2} \right) + \frac{s}{m_W^2}, \quad (51.27) \end{aligned}$$

and s, t, u are the usual Mandelstam variables with $s = (p_f + p_{\bar{f}})^2$, $t = (p_f - p_{W^-})^2$, $u = (p_f - p_{W^+})^2$. The factor N_c is 3 for quarks and 1 for leptons.

The analogous cross-section for $q_i \bar{q}_j \rightarrow W^\pm Z^0$ is

$$\begin{aligned} \frac{d\sigma}{dt} = & \frac{\pi\alpha^2 |V_{ij}|^2}{6s^2 x_W^2} \left\{ \left(\frac{1}{s - m_W^2} \right)^2 \left[\left(\frac{9 - 8x_W}{4} \right) (ut - m_W^2 m_Z^2) \right. \right. \\ & \left. \left. + (8x_W - 6) s (m_W^2 + m_Z^2) \right] \right. \\ & \left. + \left[\frac{ut - m_W^2 m_Z^2 - s(m_W^2 + m_Z^2)}{s - m_W^2} \right] \left[\frac{\ell_j}{t} - \frac{\ell_i}{u} \right] \right. \\ & \left. + \frac{ut - m_W^2 m_Z^2}{4(1 - x_W)} \left[\frac{\ell_j^2}{t^2} + \frac{\ell_i^2}{u^2} \right] + \frac{s(m_W^2 + m_Z^2)}{2(1 - x_W)} \frac{\ell_i \ell_j}{tu} \right\}, \quad (51.28) \end{aligned}$$

where ℓ_i and ℓ_j are the couplings of the left-handed q_i and q_j as defined above. The CKM matrix element between q_i and q_j is V_{ij} .

The cross section for $q_i \bar{q}_i \rightarrow Z^0 Z^0$ is

$$\frac{d\sigma}{dt} = \frac{\pi\alpha^2}{96} \frac{\ell_i^4 + r_i^4}{x_W^2 (1 - x_W^2)^2 s^2} \left[\frac{t}{u} + \frac{u}{t} + \frac{4m_Z^2 s}{tu} - m_Z^4 \left(\frac{1}{t^2} + \frac{1}{u^2} \right) \right]. \quad (51.29)$$

51.5 Production of Higgs Bosons

51.5.1 Resonant Production

The Higgs boson of the Standard Model can be produced resonantly in the collisions of quarks, leptons, W or Z bosons, gluons, or photons. The production cross section is thus controlled by the partial width of the Higgs boson into the entrance channel and its total width. The branching fractions for the Standard Model Higgs boson are shown in Fig. 1 of the "Searches for Higgs bosons" review in the Particle Listings section, as a function of the Higgs boson mass. The partial widths are given by the relations

$$\Gamma(H \rightarrow f\bar{f}) = \frac{G_F m_f^2 m_H N_c}{4\pi\sqrt{2}} \left(1 - 4m_f^2/m_H^2\right)^{3/2}, \quad (51.30)$$

$$\Gamma(H \rightarrow W^+W^-) = \frac{G_F m_H^3 \beta_W}{32\pi\sqrt{2}} \left(4 - 4a_W + 3a_W^2\right), \quad (51.31)$$

$$\Gamma(H \rightarrow ZZ) = \frac{G_F m_H^3 \beta_Z}{64\pi\sqrt{2}} \left(4 - 4a_Z + 3a_Z^2\right), \quad (51.32)$$

where N_c is 3 for quarks and 1 for leptons and where $a_W = 1 - \beta_W^2 = 4m_W^2/m_H^2$ and $a_Z = 1 - \beta_Z^2 = 4m_Z^2/m_H^2$. The decay to two gluons proceeds through quark loops, with the t quark dominating [2]. Explicitly,

$$\Gamma(H \rightarrow gg) = \frac{\alpha_s^2 G_F m_H^3}{36\pi^3 \sqrt{2}} \left| \sum_q I(m_q^2/m_H^2) \right|^2, \quad (51.33)$$

where $I(z)$ is complex for $z < 1/4$. For $z < 2 \times 10^{-3}$, $|I(z)|$ is small so the light quarks contribute negligibly. For $m_H < 2m_t$, $z > 1/4$ and

$$I(z) = 3 \left[2z + 2z(1-4z) \left(\sin^{-1} \frac{1}{2\sqrt{z}} \right)^2 \right], \quad (51.34)$$

which has the limit $I(z) \rightarrow 1$ as $z \rightarrow \infty$.

51.5.2 Higgs Boson Production in W^* and Z^* decay

The Standard Model Higgs boson can be produced in the decay of a virtual W or Z ("Higgstrahlung") [3,4]: In particular, if k is the c.m. momentum of the Higgs boson,

$$\sigma(q_i \bar{q}_j \rightarrow WH) = \frac{\pi \alpha^2 |V_{ij}|^2}{36 \sin^4 \theta_W} \frac{2k}{\sqrt{s}} \frac{k^2 + 3m_W^2}{(s - m_W^2)^2} \quad (51.35)$$

$$\sigma(f\bar{f} \rightarrow ZH) = \frac{2\pi \alpha^2 (\ell_f^2 + r_f^2)}{48 N_c \sin^4 \theta_W \cos^4 \theta_W} \frac{2k}{\sqrt{s}} \frac{k^2 + 3m_Z^2}{(s - m_Z^2)^2}, \quad (51.36)$$

where ℓ and r are defined as above.

51.5.3 W and Z Fusion

Just as high-energy electrons can be regarded as sources of virtual photon beams, at very high energies they are sources of virtual W and Z beams. For Higgs boson production, it is the longitudinal components of the W s and Z s that are important [5]. The distribution of longitudinal W s carrying a fraction y of the electron's energy is [6]

$$f(y) = \frac{g^2}{16\pi^2} \frac{1-y}{y}, \quad (51.37)$$

where $g = e/\sin\theta_W$. In the limit $s \gg m_H \gg m_W$, the partial decay rate is $\Gamma(H \rightarrow W_L W_L) = (g^2/64\pi)(m_H^3/m_W^2)$ and in the equivalent W approximation [7]

$$\begin{aligned} \sigma(e^+e^- \rightarrow \bar{\nu}_e \nu_e H) &= \frac{1}{16m_W^2} \left(\frac{\alpha}{\sin^2 \theta_W} \right)^3 \\ &\times \left[\left(1 + \frac{m_H^2}{s} \right) \log \frac{s}{m_H^2} - 2 + 2 \frac{m_H^2}{s} \right]. \end{aligned} \quad (51.38)$$

There are significant corrections to this relation when m_H is not large compared to m_W [8]. For $m_H = 150$ GeV, the estimate is too high by 51% for $\sqrt{s} = 1000$ GeV, 32% too high at $\sqrt{s} = 2000$ GeV, and 22% too high at $\sqrt{s} = 4000$ GeV. Fusion of ZZ to make a Higgs boson can be treated similarly. Identical formulae apply for Higgs production in the collisions of quarks whose charges permit the emission of a W^+ and a W^- , except that QCD corrections and CKM matrix elements are required. Even in the absence of QCD

corrections, the fine-structure constant ought to be evaluated at the scale of the collision, say m_W . All quarks contribute to the ZZ fusion process.

51.6 Inclusive hadronic reactions

One-particle inclusive cross sections $E d^3\sigma/d^3p$ for the production of a particle of momentum p are conveniently expressed in terms of rapidity y (see above) and the momentum p_T transverse to the beam direction (in the c.m.):

$$E \frac{d^3\sigma}{d^3p} = \frac{d^3\sigma}{d\phi dy p_T dp_T}. \quad (51.39)$$

In appropriate circumstances, the cross section may be decomposed as a partonic cross section multiplied by the probabilities of finding partons of the prescribed momenta:

$$\sigma_{\text{hadronic}} = \sum_{ij} \int dx_1 dx_2 f_i(x_1) f_j(x_2) d\hat{\sigma}_{\text{partonic}}, \quad (51.40)$$

The probability that a parton of type i carries a fraction of the incident particle's that lies between x_1 and $x_1 + dx_1$ is $f_i(x_1)dx_1$ and similarly for partons in the other incident particle. The partonic collision is specified by its c.m. energy squared $\hat{s} = x_1 x_2 s$ and the momentum transfer squared \hat{t} . The final hadronic state is more conveniently specified by the rapidities y_1, y_2 of the two jets resulting from the collision and the transverse momentum p_T . The connection between the differentials is

$$dx_1 dx_2 d\hat{t} = dy_1 dy_2 \frac{\hat{s}}{s} dp_T^2, \quad (51.41)$$

so that

$$\frac{d^3\sigma}{dy_1 dy_2 dp_T^2} = \frac{\hat{s}}{s} \left[f_i(x_1) f_j(x_2) \frac{d\hat{\sigma}}{d\hat{t}}(\hat{s}, \hat{t}, \hat{u}) + f_i(x_2) f_j(x_1) \frac{d\hat{\sigma}}{d\hat{t}}(\hat{s}, \hat{u}, \hat{t}) \right], \quad (51.42)$$

where we have taken into account the possibility that the incident parton types might arise from either incident particle. The second term should be dropped if the types are identical: $i = j$.

51.7 Two-photon processes

In the Weizsäcker-Williams picture, a high-energy electron beam is accompanied by a spectrum of virtual photons of energies ω and invariant-mass squared $q^2 = -Q^2$, for which the photon number density is

$$dn = \frac{\alpha}{\pi} \left[1 - \frac{\omega}{E} + \frac{\omega^2}{E^2} - \frac{m_e^2 \omega^2}{Q^2 E^2} \right] \frac{d\omega dQ^2}{\omega Q^2}, \quad (51.43)$$

where E is the energy of the electron beam. The cross section for $e^+e^- \rightarrow e^+e^-X$ is then [9]

$$d\sigma_{e^+e^- \rightarrow e^+e^-X}(s) = dn_1 dn_2 d\sigma_{\gamma\gamma \rightarrow X}(W^2), \quad (51.44)$$

where $W^2 = m_X^2$. Integrating from the lower limit $Q^2 = m_e^2 \frac{\omega_i^2}{E_i(E_i - \omega_i)}$ to a maximum Q^2 gives

$$\begin{aligned} \sigma_{e^+e^- \rightarrow e^+e^-X}(s) &= \frac{\alpha^2}{\pi^2} \int_{z_{th}}^1 \frac{dz}{z} \\ &\times \left[\left(\ln \frac{Q_{max}^2}{zm_e^2} - 1 \right)^2 f(z) + \frac{1}{3} (\ln z)^3 \right] \sigma_{\gamma\gamma \rightarrow X}(zs), \end{aligned} \quad (51.45)$$

where

$$f(z) = \left(1 + \frac{1}{2}z \right)^2 \ln(1/z) - \frac{1}{2}(1-z)(3+z). \quad (51.46)$$

The appropriate value of Q_{max}^2 depends on the properties of the produced system X . For production of hadronic systems,

$Q_{max}^2 \approx m_\rho^2$, while for lepton-pair production, $Q^2 \approx W^2$. For production of a resonance with spin $J \neq 1$, we have

$$\sigma_{e^+e^- \rightarrow e^+e^-R}(s) = (2J+1) \frac{8\alpha^2 \Gamma_{R \rightarrow \gamma\gamma}}{m_R^3} \times \left[f(m_R^2/s) \left(\ln \frac{m_V^2 s}{m_R^2 m_R^2} - 1 \right)^2 - \frac{1}{3} \left(\ln \frac{s}{M_R^2} \right)^3 \right], \quad (51.47)$$

where m_V is the mass that enters into the form factor for the $\gamma\gamma \rightarrow R$ transition, typically m_ρ .

PART II: PROCESSES BEYOND THE STANDARD MODEL

51.8 Production of supersymmetric particles

In supersymmetric (SUSY) theories (see Supersymmetric Particle Searches in this *Review*), every boson has a fermionic superpartner, and every fermion has a bosonic superpartner. The minimal supersymmetric Standard Model (MSSM) is a direct supersymmetrization of the Standard Model (SM), although a second Higgs doublet is needed to avoid triangle anomalies [10]. Under soft SUSY breaking, superpartner masses are lifted above the SM particle masses. In weak scale SUSY, the superpartners are invoked to stabilize the weak scale under radiative corrections, so the superpartners are expected to have masses of order the TeV scale.

51.8.1 Gluino and squark production

The superpartners of gluons are the color octet, spin- $\frac{1}{2}$ gluinos (\tilde{g}), while each helicity component of quark flavor has a spin-0 squark partner, *e.g.* \tilde{q}_L and \tilde{q}_R . Third generation left- and right- squarks are expected to have large mixing, resulting in mass eigenstates \tilde{q}_1 and \tilde{q}_2 , with $m_{\tilde{q}_1} < m_{\tilde{q}_2}$ (here, q denotes any of the SM flavors of quarks and \tilde{q}_i the corresponding flavor and type ($i = L, R$ or 1, 2) of squark). Gluino pair production ($\tilde{g}\tilde{g}$) takes place via either glue-gluon or quark-antiquark annihilation [11].

The subprocess cross sections are usually presented as differential distributions in the Mandelstam variables s , t and u . Note that for a $2 \rightarrow 2$ scattering subprocess $ab \rightarrow cd$, the Mandelstam variable $s = (p_a + p_b)^2 = (p_c + p_d)^2$, where p_a is the 4-momentum of particle a , and so forth. The variable $t = (p_c - p_a)^2$, where c and a are taken conventionally to be the most similar particles in the subprocess. The variable u would then be equal to $(p_d - p_a)^2$. Note that since s , t and u are squares of 4-vectors, they are invariants in any inertial reference frame.

Gluino pair production at hadron colliders is described by:

$$\begin{aligned} \frac{d\sigma}{dt}(gg \rightarrow \tilde{g}\tilde{g}) &= \frac{9\pi\alpha_s^2}{4s^2} \left\{ \frac{2(m_{\tilde{g}}^2 - t)(m_{\tilde{g}}^2 - u)}{s^2} \right. \\ &+ \frac{(m_{\tilde{g}}^2 - t)(m_{\tilde{g}}^2 - u) - 2m_{\tilde{g}}^2(m_{\tilde{g}}^2 + t)}{(m_{\tilde{g}}^2 - t)^2} \\ &+ \frac{(m_{\tilde{g}}^2 - t)(m_{\tilde{g}}^2 - u) - 2m_{\tilde{g}}^2(m_{\tilde{g}}^2 + u)}{(m_{\tilde{g}}^2 - u)^2} + \frac{m_{\tilde{g}}^2(s - 4m_{\tilde{g}}^2)}{(m_{\tilde{g}}^2 - t)(m_{\tilde{g}}^2 - u)} \\ &- \frac{(m_{\tilde{g}}^2 - t)(m_{\tilde{g}}^2 - u) + m_{\tilde{g}}^2(u - t)}{s(m_{\tilde{g}}^2 - t)} \\ &\left. - \frac{(m_{\tilde{g}}^2 - t)(m_{\tilde{g}}^2 - u) + m_{\tilde{g}}^2(t - u)}{s(m_{\tilde{g}}^2 - u)} \right\}, \quad (51.48) \end{aligned}$$

where α_s is the strong fine structure constant. Also,

$$\begin{aligned} \frac{d\sigma}{dt}(q\bar{q} \rightarrow \tilde{g}\tilde{g}) &= \frac{8\pi\alpha_s^2}{9s^2} \left\{ \frac{4}{3} \left(\frac{m_{\tilde{g}}^2 - t}{m_{\tilde{q}}^2 - t} \right)^2 + \frac{4}{3} \left(\frac{m_{\tilde{g}}^2 - u}{m_{\tilde{q}}^2 - u} \right)^2 \right. \\ &+ \frac{3}{s^2} [(m_{\tilde{g}}^2 - t)^2 + (m_{\tilde{g}}^2 - u)^2 + 2m_{\tilde{g}}^2 s] \\ &- 3 \frac{[(m_{\tilde{g}}^2 - t)^2 + m_{\tilde{g}}^2 s]}{s(m_{\tilde{q}}^2 - t)} \\ &\left. - 3 \frac{[(m_{\tilde{g}}^2 - u)^2 + m_{\tilde{g}}^2 s]}{s(m_{\tilde{q}}^2 - u)} + \frac{1}{3} \frac{m_{\tilde{g}}^2 s}{(m_{\tilde{q}}^2 - t)(m_{\tilde{q}}^2 - u)} \right\}. \quad (51.49) \end{aligned}$$

Gluinos can also be produced in association with squarks: $\tilde{g}\tilde{q}_i$ production, where \tilde{q}_i represents any of the various types (left, right- or mixed) and flavors of squarks. The subprocess cross section is independent of whether the squark is the right-, left- or mixed type:

$$\begin{aligned} \frac{d\sigma}{dt}(gq \rightarrow \tilde{g}\tilde{q}_i) &= \frac{\pi\alpha_s^2}{24s^2} \frac{[\frac{16}{3}(s^2 + (m_{\tilde{q}_i}^2 - u)^2) + \frac{4}{3}s(m_{\tilde{q}_i}^2 - u)]}{s(m_{\tilde{g}}^2 - t)(m_{\tilde{q}_i}^2 - u)^2} \\ &\times \left((m_{\tilde{g}}^2 - u)^2 + (m_{\tilde{q}_i}^2 - m_{\tilde{g}}^2)^2 + \frac{2sm_{\tilde{g}}^2(m_{\tilde{q}_i}^2 - m_{\tilde{g}}^2)}{(m_{\tilde{g}}^2 - t)} \right). \quad (51.50) \end{aligned}$$

There are many different subprocesses for production of squark pairs. Since left- and right- squarks generally have different masses and different decay patterns, we present the differential cross section for each subprocess of \tilde{q}_i ($i = L, R$ or 1, 2) separately. (In early literature, the following formulae were often combined into a single equation which didn't differentiate the various squark types.) The result for $gg \rightarrow \tilde{q}_i\tilde{q}_i$ is:

$$\begin{aligned} \frac{d\sigma}{dt}(gg \rightarrow \tilde{q}_i\tilde{q}_i) &= \frac{\pi\alpha_s^2}{4s^2} \left\{ \frac{1}{3} \left(\frac{m_{\tilde{q}_i}^2 + t}{m_{\tilde{q}_i}^2 - t} \right)^2 + \frac{1}{3} \left(\frac{m_{\tilde{q}_i}^2 + u}{m_{\tilde{q}_i}^2 - u} \right)^2 \right. \\ &+ \frac{3}{32s^2} (8s(4m_{\tilde{q}_i}^2 - s) + 4(u - t)^2) + \frac{7}{12} \\ &- \frac{1}{48} \frac{(4m_{\tilde{q}_i}^2 - s)^2}{(m_{\tilde{q}_i}^2 - t)(m_{\tilde{q}_i}^2 - u)} \\ &+ \frac{3}{32} \frac{[(t - u)(4m_{\tilde{q}_i}^2 + 4t - s) - 2(m_{\tilde{q}_i}^2 - u)(6m_{\tilde{q}_i}^2 + 2t - s)]}{s(m_{\tilde{q}_i}^2 - t)} \\ &+ \frac{3}{32} \frac{[(u - t)(4m_{\tilde{q}_i}^2 + 4u - s) - 2(m_{\tilde{q}_i}^2 - t)(6m_{\tilde{q}_i}^2 + 2u - s)]}{s(m_{\tilde{q}_i}^2 - u)} \\ &\left. + \frac{7}{96} \frac{[4m_{\tilde{q}_i}^2 + 4t - s]}{m_{\tilde{q}_i}^2 - t} + \frac{7}{96} \frac{[4m_{\tilde{q}_i}^2 + 4u - s]}{m_{\tilde{q}_i}^2 - u} \right\}, \quad (51.51) \end{aligned}$$

which has an obvious $u \leftrightarrow t$ symmetry.

For $q\bar{q} \rightarrow \tilde{q}_i\tilde{q}_i$ with the same initial and final state flavors, we have

$$\begin{aligned} \frac{d\sigma}{dt}(q\bar{q} \rightarrow \tilde{q}_i\tilde{q}_i) &= \frac{2\pi\alpha_s^2}{9s^2} \left\{ \frac{1}{(t - m_{\tilde{q}_i}^2)^2} + \frac{2}{s^2} - \frac{2/3}{s(t - m_{\tilde{q}_i}^2)} \right\} \\ &\times [-st - (t - m_{\tilde{q}_i}^2)^2], \quad (51.52) \end{aligned}$$

while if initial and final state flavors are different ($q\bar{q} \rightarrow \tilde{q}_i'\tilde{q}_i'$) we instead have

$$\frac{d\sigma}{dt}(q\bar{q} \rightarrow \tilde{q}_i'\tilde{q}_i') = \frac{4\pi\alpha_s^2}{9s^4} [-st - (t - m_{\tilde{q}_i}^2)^2]. \quad (51.53)$$

If the two initial state quarks are of different flavors, then we have

$$\frac{d\sigma}{dt}(q\bar{q}' \rightarrow \tilde{q}_i\bar{\tilde{q}}'_i) = \frac{2\pi\alpha_s^2}{9s^2} \frac{-st - (t - m_{\tilde{q}_i}^2)^2}{(t - m_{\tilde{g}}^2)^2}. \quad (51.54)$$

If the initial quarks are of different flavor and final state squarks are of different type ($i \neq j$) then

$$\frac{d\sigma}{dt}(q\bar{q}' \rightarrow \tilde{q}_i\bar{\tilde{q}}'_j) = \frac{2\pi\alpha_s^2}{9s^2} \frac{m_{\tilde{g}}^2 s}{(t - m_{\tilde{g}}^2)^2}. \quad (51.55)$$

For same-flavor initial state quarks, but final state unlike-type squarks, we also have

$$\frac{d\sigma}{dt}(q\bar{q} \rightarrow \tilde{q}_i\bar{\tilde{q}}_j) = \frac{2\pi\alpha_s^2}{9s^2} \frac{m_{\tilde{g}}^2 s}{(t - m_{\tilde{g}}^2)^2}. \quad (51.56)$$

There also exist cross sections for quark-quark annihilation to squark pairs. For same flavor quark-quark annihilation to same flavor/same type final state squarks,

$$\begin{aligned} \frac{d\sigma}{dt}(qq \rightarrow \tilde{q}_i\tilde{q}_i) &= \\ &= \frac{\pi\alpha_s^2}{9s^2} m_{\tilde{g}}^2 s \left\{ \frac{1}{(t - m_{\tilde{g}}^2)^2} + \frac{1}{(u - m_{\tilde{g}}^2)^2} - \frac{2/3}{(t - m_{\tilde{g}}^2)(u - m_{\tilde{g}}^2)} \right\}, \end{aligned} \quad (51.57)$$

while if the final type squarks are different ($i \neq j$), we have

$$\begin{aligned} \frac{d\sigma}{dt}(qq \rightarrow \tilde{q}_i\tilde{q}_j) &= \frac{2\pi\alpha_s^2}{9s^2} \times \left\{ \frac{[-st - (t - m_{\tilde{q}_i}^2)(t - m_{\tilde{q}_j}^2)]}{(t - m_{\tilde{g}}^2)} \right. \\ &\quad \left. + \frac{[-su - (u - m_{\tilde{q}_i}^2)(u - m_{\tilde{q}_j}^2)]}{(u - m_{\tilde{g}}^2)} \right\}. \end{aligned} \quad (51.58)$$

If initial/final state flavors are different, but final state squark types are the same, then

$$\frac{d\sigma}{dt}(q\bar{q}' \rightarrow \tilde{q}_i\bar{\tilde{q}}'_i) = \frac{2\pi\alpha_s^2}{9s^2} \frac{m_{\tilde{g}}^2 s}{(t - m_{\tilde{g}}^2)^2}. \quad (51.59)$$

If initial quark flavors are different and final squark types are different, then

$$\frac{d\sigma}{dt}(q\bar{q}' \rightarrow \tilde{q}_i\bar{\tilde{q}}'_j) = \frac{2\pi\alpha_s^2}{9s^2} \frac{-st - (t - m_{\tilde{q}_i}^2)(t - m_{\tilde{q}_j}^2)}{(t - m_{\tilde{g}}^2)^2}. \quad (51.60)$$

51.8.2 Gluino and squark associated production

In the MSSM, the charged spin- $\frac{1}{2}$ winos and higgsinos mix to make chargino states $\chi_{1,2}^{\pm}$ and $\chi_{2,1}^{\pm}$, with $m_{\chi_{1,2}^{\pm}} < m_{\chi_{2,1}^{\pm}}$. The spin- $\frac{1}{2}$ neutral bino, wino and higgsino fields mix to give four neutralino mass eigenstates $\chi_{1,2,3,4}^0$ ordered according to mass. We sometimes denote the charginos and neutralinos collectively as -inos for notational simplicity

For gluino and squark production in association with charginos and neutralinos [12], the quark-squark-neutralino couplings¹ are defined by the interaction Lagrangian terms

$$\mathcal{L}_{f\tilde{f}\tilde{\chi}_i^0} = \left[iA_{\tilde{\chi}_i^0}^f \tilde{f}_L^{\dagger} \tilde{\chi}_i^0 P_L f + iB_{\tilde{\chi}_i^0}^f \tilde{f}_R^{\dagger} \tilde{\chi}_i^0 P_R f + \text{h.c.} \right],$$

where $A_{\tilde{\chi}_i^0}^f$ and $B_{\tilde{\chi}_i^0}^f$ are coupling constants involving gauge couplings, neutralino mixing elements and in the case of third generation fermions, Yukawa couplings. Their form depends on the conventions used for setting up the MSSM Lagrangian, and can

¹The couplings $A_{\tilde{\chi}_i^0}^f$ and $B_{\tilde{\chi}_i^0}^f$ are given explicitly in Ref. [13] in Eq. (8.87). Also, the couplings $A_{\tilde{\chi}_i^{\pm}}^d$ and $A_{\tilde{\chi}_i^{\pm}}^u$ are given in Eq. (8.93). The couplings X_i^j and Y_i^j are given by Eq. (8.103), while the x_i and y_i couplings are given in Eq. (8.100). Finally, the couplings W_{ij} are given in Eq. (8.101).

be found in various reviews [14] and textbooks [13, 15]. P_L and P_R are the usual left- and right- spinor projection operators and f denotes any of the SM fermions u, d, e, ν_e, \dots . The fermion-fermion- chargino couplings have the form $\mathcal{L} = \left[iA_{\tilde{\chi}_i^{\pm}}^d \tilde{u}_L^{\dagger} \tilde{\chi}_i^{\pm} P_L d + iA_{\tilde{\chi}_i^{\pm}}^u \tilde{d}_L^{\dagger} \tilde{\chi}_i^{\pm} P_L u + \text{h.c.} \right]$ for u and d quarks, where the $A_{\tilde{\chi}_i^{\pm}}^d$ and $A_{\tilde{\chi}_i^{\pm}}^u$ couplings are again convention-dependent, and can be found in textbooks. The superscript c denotes ‘‘charge conjugate spinor’’, defined by $\psi^c \equiv C\bar{\psi}^T$.

The subprocess cross sections for chargino-squark associated production occur via squark exchange and are given by

$$\frac{d\sigma}{dt}(\bar{u}g \rightarrow \tilde{\chi}_i^{\pm} \bar{d}_L) = \frac{\alpha_s}{24s^2} |A_{\tilde{\chi}_i^{\pm}}^u|^2 \psi(m_{\tilde{d}_L}, m_{\tilde{\chi}_i^{\pm}}, t), \quad (51.61)$$

$$\frac{d\sigma}{dt}(dg \rightarrow \tilde{\chi}_i^{\pm} \bar{u}_L) = \frac{\alpha_s}{24s^2} |A_{\tilde{\chi}_i^{\pm}}^d|^2 \psi(m_{\tilde{u}_L}, m_{\tilde{\chi}_i^{\pm}}, t), \quad (51.62)$$

while neutralino-squark production is given by

$$\frac{d\sigma}{dt}(qg \rightarrow \tilde{\chi}_i^0 \tilde{q}) = \frac{\alpha_s}{24s^2} \left(|A_{\tilde{\chi}_i^0}^q|^2 + |B_{\tilde{\chi}_i^0}^q|^2 \right) \psi(m_{\tilde{q}}, m_{\tilde{\chi}_i^0}, t), \quad (51.63)$$

where

$$\begin{aligned} \psi(m_1, m_2, t) &= \frac{s + t - m_1^2}{2s} - \frac{m_1^2(m_2^2 - t)}{(m_1^2 - t)^2} \\ &\quad + \frac{t(m_2^2 - m_1^2) + m_2^2(s - m_2^2 + m_1^2)}{s(m_1^2 - t)}. \end{aligned} \quad (51.64)$$

Here, the variable t is given by the square of ‘‘squark-minus-quark’’ four-momentum. The neutralino-gluino associated production cross section also occurs via squark exchange and is given by

$$\begin{aligned} \frac{d\sigma}{dt}(q\bar{q} \rightarrow \tilde{\chi}_i^0 \tilde{g}) &= \frac{\alpha_s}{18s^2} \left(|A_{\tilde{\chi}_i^0}^q|^2 + |B_{\tilde{\chi}_i^0}^q|^2 \right) \left[\frac{(m_{\tilde{\chi}_i^0}^2 - t)(m_{\tilde{g}}^2 - t)}{(m_{\tilde{q}}^2 - t)^2} \right. \\ &\quad \left. + \frac{(m_{\tilde{\chi}_i^0}^2 - u)(m_{\tilde{g}}^2 - u)}{(m_{\tilde{q}}^2 - u)^2} - \frac{2\eta_i \eta_{\tilde{g}} m_{\tilde{g}} m_{\tilde{\chi}_i^0} s}{(m_{\tilde{q}}^2 - t)(m_{\tilde{q}}^2 - u)} \right], \end{aligned} \quad (51.65)$$

where η_i is the sign of the neutralino mass eigenvalue and $\eta_{\tilde{g}}$ is the sign of the gluino mass eigenvalue. We also have chargino-gluino associated production:

$$\begin{aligned} \frac{d\sigma}{dt}(\bar{u}d \rightarrow \tilde{\chi}_i^{\pm} \tilde{g}) &= \frac{\alpha_s}{18s^2} \left[|A_{\tilde{\chi}_i^{\pm}}^u|^2 \frac{(m_{\tilde{\chi}_i^{\pm}}^2 - t)(m_{\tilde{g}}^2 - t)}{(m_{\tilde{d}_L}^2 - t)^2} \right. \\ &\quad \left. + |A_{\tilde{\chi}_i^{\pm}}^d|^2 \frac{(m_{\tilde{\chi}_i^{\pm}}^2 - u)(m_{\tilde{g}}^2 - u)}{(m_{\tilde{u}_L}^2 - u)^2} + \frac{2\eta_i \text{Re}(A_{\tilde{\chi}_i^{\pm}}^u A_{\tilde{\chi}_i^{\pm}}^d)}{(m_{\tilde{d}_L}^2 - t)(m_{\tilde{u}_L}^2 - u)} \right], \end{aligned} \quad (51.66)$$

where $\hat{t} = (\tilde{g} - d)^2$ and in the third term one must take the real part of the in general complex coupling constant product.

51.8.3 Slepton and sneutrino production

The subprocess cross section for $\tilde{\ell}_L \tilde{\nu}_{\ell L}$ production ($\ell = e$ or μ) occurs via s -channel W exchange and is given by

$$\frac{d\sigma}{dt}(d\bar{u} \rightarrow \tilde{\ell}_L \tilde{\nu}_{\ell L}) = \frac{g^4 |D_W(s)|^2}{192\pi s^2} \left(tu - m_{\tilde{\ell}_L}^2 m_{\tilde{\nu}_{\ell L}}^2 \right), \quad (51.67)$$

where $D_W(s) = 1/(s - M_W^2 + iM_W \Gamma_W)$ is the W -boson propagator denominator. The production of $\tilde{\tau}_1 \tilde{\nu}_{\tau}$ is given as above, but replacing $m_{\tilde{\ell}_L} \rightarrow m_{\tilde{\tau}_1}$, $m_{\tilde{\nu}_{\ell L}} \rightarrow m_{\tilde{\nu}_{\tau}}$ and multiplying by an overall factor of $\cos^2 \theta_{\tau}$ (where θ_{τ} is the tau-slepton mixing angle). Similar substitutions hold for $\tilde{\tau}_2 \tilde{\nu}_{\tau}$ production, except the overall factor is $\sin^2 \theta_{\tau}$.

Table 51.1: The constants α_f and β_f that appear in the SM neutral current Lagrangian. Here $t \equiv \tan \theta_W$ and $c \equiv \cot \theta_W$.

f	q_f	α_f	β_f
ℓ	-1	$\frac{1}{4}(3t - c)$	$\frac{1}{4}(t + c)$
ν_ℓ	0	$\frac{1}{4}(t + c)$	$-\frac{1}{4}(t + c)$
u	$\frac{2}{3}$	$-\frac{5}{12}t + \frac{1}{4}c$	$-\frac{1}{4}(t + c)$
d	$-\frac{1}{3}$	$\frac{1}{12}t - \frac{1}{4}c$	$\frac{1}{4}(t + c)$

The subprocess cross section for $\tilde{\ell}_L \bar{\tilde{\ell}}_L$ production occurs via s -channel γ and Z exchange, and depends on the neutral current interaction, with fermion couplings to γ and Z^0 given by $\mathcal{L}_{\text{neutral}} = -eq_f \bar{f} \gamma^\mu f A_\mu + e \bar{f} \gamma^\mu (\alpha_f + \beta_f \gamma_5) f Z_\mu$ (with values of q_f , α_f , and β_f given in Table-51.1).

The subprocess cross section is given by

$$\frac{d\sigma}{dt}(q\bar{q} \rightarrow \tilde{\ell}_L \bar{\tilde{\ell}}_L) = \frac{e^4}{24\pi s^2} \left(tu - m_{\tilde{\ell}_L}^4 \right) \times \left\{ \frac{q_\ell^2 q_q^2}{s^2} + (\alpha_\ell - \beta_\ell)^2 (\alpha_q^2 + \beta_q^2) |D_Z(s)|^2 + \frac{2q_\ell q_q \alpha_q (\alpha_\ell - \beta_\ell) (s - M_Z^2)}{s} |D_Z(s)|^2 \right\}, \quad (51.68)$$

where $D_Z(s) = 1/(s - M_Z^2 + iM_Z \Gamma_Z)$. The cross section for sneutrino production is given by the same formula, but with α_ℓ , β_ℓ , q_ℓ and $m_{\tilde{\ell}_L}$ replaced by α_ν , β_ν , 0 and $m_{\tilde{\nu}_L}$, respectively. The cross section for $\tilde{\tau}_1 \bar{\tilde{\tau}}_1$ production is obtained by replacing $m_{\tilde{\ell}_L} \rightarrow m_{\tilde{\tau}_1}$ and $\beta_\ell \rightarrow \beta_\ell \cos 2\theta_\tau$. The cross section for $\tilde{\ell}_R \bar{\tilde{\ell}}_R$ production is given by substituting $\alpha_\ell - \beta_\ell \rightarrow \alpha_\ell + \beta_\ell$ and $m_{\tilde{\ell}_L} \rightarrow m_{\tilde{\ell}_R}$ in the equation above. The cross section for $\tilde{\tau}_2 \bar{\tilde{\tau}}_2$ production is obtained from the formula for $\tilde{\ell}_R \bar{\tilde{\ell}}_R$ production by replacing $m_{\tilde{\ell}_R} \rightarrow m_{\tilde{\tau}_2}$ and $\beta_\ell \rightarrow \beta_\ell \cos 2\theta_\tau$.

Finally, the cross section for $\tilde{\tau}_1 \bar{\tilde{\tau}}_2$ production occurs only via Z exchange, and is given by

$$\frac{d\sigma}{dt}(q\bar{q} \rightarrow \tilde{\tau}_1 \bar{\tilde{\tau}}_2) = \frac{d\sigma}{dt}(q\bar{q} \rightarrow \tilde{\tau}_1 \tilde{\tau}_2) = \frac{e^4}{24\pi s^2} (\alpha_q^2 + \beta_q^2) \beta_\ell^2 \sin^2 2\theta_\tau |D_Z(s)|^2 (ut - m_{\tilde{\tau}_1}^2 m_{\tilde{\tau}_2}^2). \quad (51.69)$$

51.8.4 Chargino and neutralino pair production

51.8.4.1 $\tilde{\chi}_i^- \tilde{\chi}_j^0$ production

The subprocess cross section for $d\bar{u} \rightarrow \tilde{\chi}_i^- \tilde{\chi}_j^0$ depends on Lagrangian couplings

$$\begin{aligned} \mathcal{L}_{W\bar{u}d} &= -\frac{g}{\sqrt{2}} \bar{u} \gamma_\mu P_L d W^{+\mu} + \text{h.c.}, \\ \mathcal{L}_{W\tilde{\chi}_i^- \tilde{\chi}_j^0} &= -g(-i)^{\theta_j} \bar{\tilde{\chi}}_i^- [X_i^j + Y_i^j \gamma_5] \gamma_\mu \tilde{\chi}_j^0 W^{-\mu} + \text{h.c.}, \\ \mathcal{L}_{q\bar{q}\tilde{\chi}_i^-} &= iA_{\tilde{\chi}_i^-}^d \bar{u} \tilde{\chi}_i^- P_L d + iA_{\tilde{\chi}_i^-}^u \bar{d} \tilde{\chi}_i^- P_L u + \text{h.c.} \end{aligned}$$

and

$$\mathcal{L}_{q\bar{q}\tilde{\chi}_j^0} = iA_{\tilde{\chi}_j^0}^q \bar{q} \tilde{\chi}_j^0 P_L q + \text{h.c.}$$

Contributing diagrams include W exchange and also \tilde{d}_L and \tilde{u}_L squark exchange. The X_i^j and Y_i^j couplings are new, and again convention-dependent: the cross section formulae works if the interaction Lagrangian is written in the above form, so that the couplings can be suitably extracted. The term $\theta_j = 0$ (1) if $m_{\tilde{\chi}_j^0} > 0$ (< 0); it comes about because the neutralino field must be re-defined by a $-i\gamma_5$ transformation if its mass eigenvalue is negative [13]. The subprocess cross section is given in terms of dot products of four momenta, where particle labels are used to

denote their four-momenta; note that all mass terms in the cross section formulae are positive definite, so that the signs of mass eigenstates have been absorbed into the Lagrangian couplings, as for instance in Ref. [13]. We then have

$$\frac{d\sigma}{dt}(d\bar{u} \rightarrow \tilde{\chi}_i^- \tilde{\chi}_j^0) = \frac{1}{192\pi s^2}$$

$$\left[T_W + T_{\tilde{d}_L} + T_{\tilde{u}_L} + T_{W\tilde{d}_L} + T_{W\tilde{u}_L} + T_{\tilde{d}_L\tilde{u}_L} \right] \quad (51.70)$$

where

$$\begin{aligned} T_W &= 8g^4 |D_W(s)|^2 \left\{ [X_i^j + Y_i^j] (\tilde{\chi}_j^0 \cdot d \tilde{\chi}_i^- \cdot \bar{u} + \tilde{\chi}_j^0 \cdot \bar{u} \tilde{\chi}_i^- \cdot d) \right. \\ &\quad + 2(X_i^j Y_i^j) (\tilde{\chi}_j^0 \cdot d \tilde{\chi}_i^- \cdot \bar{u} - \tilde{\chi}_j^0 \cdot \bar{u} \tilde{\chi}_i^- \cdot d) \\ &\quad \left. + [X_i^j - Y_i^j] m_{\tilde{\chi}_i^-} m_{\tilde{\chi}_j^0} d \cdot \bar{u} \right\}, \end{aligned} \quad (51.71)$$

$$T_{\tilde{d}_L} = \frac{4|A_{\tilde{\chi}_i^-}^u|^2 |A_{\tilde{\chi}_j^0}^d|^2}{[(\tilde{\chi}_i^- - \bar{u})^2 - m_{\tilde{d}_L}^2]^2} d \cdot \tilde{\chi}_j^0 \tilde{\chi}_i^- \cdot \bar{u}, \quad (51.72)$$

$$T_{\tilde{u}_L} = \frac{4|A_{\tilde{\chi}_i^-}^d|^2 |A_{\tilde{\chi}_j^0}^u|^2}{[(\tilde{\chi}_j^0 - \bar{u})^2 - m_{\tilde{u}_L}^2]^2} \bar{u} \cdot \tilde{\chi}_j^0 \tilde{\chi}_i^- \cdot d \quad (51.73)$$

$$\begin{aligned} T_{W\tilde{d}_L} &= \frac{-\sqrt{2}g^2 \text{Re}[A_{\tilde{\chi}_j^0}^{d*} A_{\tilde{\chi}_i^-}^u (-i)^{\theta_j}] (s - M_W^2) |D_W(s)|^2}{(\tilde{\chi}_i^- - \bar{u})^2 - m_{\tilde{d}_L}^2} \\ &\times \left\{ 8(X_i^j + Y_i^j) \tilde{\chi}_j^0 \cdot d \bar{u} \cdot \tilde{\chi}_i^- + 4(X_i^j - Y_i^j) m_{\tilde{\chi}_i^-} m_{\tilde{\chi}_j^0} d \cdot \bar{u} \right\} \end{aligned} \quad (51.74)$$

$$\begin{aligned} T_{W\tilde{u}_L} &= \frac{\sqrt{2}g^2 \text{Re}[A_{\tilde{\chi}_i^-}^{d*} A_{\tilde{\chi}_j^0}^u (-i)^{\theta_j}] (s - M_W^2) |D_W(s)|^2}{(\tilde{\chi}_j^0 - \bar{u})^2 - m_{\tilde{u}_L}^2} \\ &\times \left\{ 8(X_i^j - Y_i^j) \tilde{\chi}_j^0 \cdot \bar{u} d \cdot \tilde{\chi}_i^- + 4(X_i^j + Y_i^j) m_{\tilde{\chi}_i^-} m_{\tilde{\chi}_j^0} d \cdot \bar{u} \right\} \end{aligned} \quad (51.75)$$

and

$$T_{\tilde{d}_L\tilde{u}_L} = -\frac{4\text{Re}[A_{\tilde{\chi}_j^0}^d A_{\tilde{\chi}_i^-}^{u*} A_{\tilde{\chi}_i^-}^{d*} A_{\tilde{\chi}_j^0}^u] m_{\tilde{\chi}_i^-} m_{\tilde{\chi}_j^0} d \cdot \bar{u}}{[(\tilde{\chi}_i^- - \bar{u})^2 - m_{\tilde{d}_L}^2][(\tilde{\chi}_j^0 - \bar{u})^2 - m_{\tilde{u}_L}^2]}. \quad (51.76)$$

51.8.4.2 Chargino pair production

The subprocess cross section for $d\bar{d} \rightarrow \tilde{\chi}_i^- \tilde{\chi}_i^+$ ($i = 1, 2$) depends on Lagrangian couplings $\mathcal{L} = e\bar{\tilde{\chi}}_i^- \gamma_\mu \tilde{\chi}_i^- A^\mu - e \cot \theta_W \bar{\tilde{\chi}}_i^- \gamma_\mu (x_i - y_i \gamma_5) \tilde{\chi}_i^- Z^\mu$ and also $\mathcal{L} \ni iA_{\tilde{\chi}_i^-}^d \bar{u} \tilde{\chi}_i^- P_L d + iA_{\tilde{\chi}_i^-}^u \bar{d} \tilde{\chi}_i^- P_L u + \text{h.c.}$. Contributing diagrams include s -channel γ , Z^0 exchange and t -channel \tilde{u}_L exchange [16, 17]. The couplings x_i and y_i are again new and as usual convention-dependent.

The subprocess cross section is given by

$$\frac{d\sigma}{dt}(d\bar{d} \rightarrow \tilde{\chi}_i^- \tilde{\chi}_i^+) = \frac{1}{192\pi s^2} [T_\gamma + T_Z + T_{\tilde{u}_L} + T_{\gamma Z} + T_{\gamma\tilde{u}_L} + T_{Z\tilde{u}_L}] \quad (51.77)$$

where

$$T_\gamma = \frac{32e^4 q_d^2}{s^2} \left[d \cdot \tilde{\chi}_i^+ \bar{d} \cdot \tilde{\chi}_i^- + d \cdot \tilde{\chi}_i^- \bar{d} \cdot \tilde{\chi}_i^+ + m_{\tilde{\chi}_i^-}^2 d \cdot \bar{d} \right] \quad (51.78)$$

$$T_Z = 32e^4 \cot^2 \theta_W |D_Z(s)|^2$$

$$\left\{ (\alpha_d^2 + \beta_d^2) (x_i^2 + y_i^2) \left[d \cdot \tilde{\chi}_i^+ \bar{d} \cdot \tilde{\chi}_i^- + d \cdot \tilde{\chi}_i^- \bar{d} \cdot \tilde{\chi}_i^+ + m_{\tilde{\chi}_i^-}^2 d \cdot \bar{d} \right] \right.$$

$$\mp 4\alpha_d\beta_d x_i y_i \left[d \cdot \tilde{\chi}_i^+ \bar{d} \cdot \tilde{\chi}_i^- - d \cdot \tilde{\chi}_i^- \bar{d} \cdot \tilde{\chi}_i^+ \right] - 2y_i^2 (\alpha_d^2 + \beta_d^2) m_{\tilde{\chi}_i^-}^2 d \cdot \bar{d} \right\}, \quad (51.79)$$

$$T_{\tilde{u}L} = \frac{4|A_{\tilde{\chi}_i^-}^d|^4}{[(d - \tilde{\chi}_i^-)^2 - m_{\tilde{u}L}^2]^2} d \cdot \tilde{\chi}_i^- \bar{d} \cdot \tilde{\chi}_i^+ \quad (51.80)$$

$$T_{\gamma Z} = \frac{64e^4 \cot \theta_W q_d (s - M_Z^2) |D_Z(s)|^2}{s} \times$$

$$\left\{ \alpha_d x_i \left(d \cdot \tilde{\chi}_i^+ \bar{d} \cdot \tilde{\chi}_i^- + d \cdot \tilde{\chi}_i^- \bar{d} \cdot \tilde{\chi}_i^+ + m_{\tilde{\chi}_i^-}^2 d \cdot \bar{d} \right) \right. \\ \left. \pm \beta_d y_i \left(d \cdot \tilde{\chi}_i^- \bar{d} \cdot \tilde{\chi}_i^+ - d \cdot \tilde{\chi}_i^+ \bar{d} \cdot \tilde{\chi}_i^- \right) \right\} \quad (51.81)$$

$$T_{\gamma \tilde{u}L} = \mp \frac{8e^2 q_d}{s} \frac{|A_{\tilde{\chi}_i^-}^d|^2}{[(d - \tilde{\chi}_i^-)^2 - m_{\tilde{u}L}^2]} \left\{ 2\bar{d} \cdot \tilde{\chi}_i^+ d \cdot \tilde{\chi}_i^- + m_{\tilde{\chi}_i^-}^2 d \cdot \bar{d} \right\} \quad (51.82)$$

and

$$T_{Z\tilde{u}L} = \mp 8e^2 \cot \theta_W |D_Z(s)|^2 \frac{|A_{\tilde{\chi}_i^-}^d|^2 (s - M_Z^2)}{[(d - \tilde{\chi}_i^-)^2 - m_{\tilde{u}L}^2]} (\alpha_d - \beta_d) \\ \times \left\{ 2(x_i \mp y_i) d \cdot \tilde{\chi}_i^- \bar{d} \cdot \tilde{\chi}_i^+ + m_{\tilde{\chi}_i^-}^2 (x_i \pm y_i) d \cdot \bar{d} \right\} \quad (51.83)$$

using the upper of the sign choices.

The cross section for $u\bar{u} \rightarrow \tilde{\chi}_i^+ \tilde{\chi}_i^-$ can be obtained from the above by replacing $\alpha_d \rightarrow \alpha_u$, $\beta_d \rightarrow \beta_u$, $q_d \rightarrow q_u$, $\tilde{u}_L \rightarrow \bar{d}_L$, $A_{\tilde{\chi}_i^-}^d \rightarrow A_{\tilde{\chi}_i^-}^u$, $d \rightarrow \bar{u}$, $\bar{d} \rightarrow u$ and adopting the lower of the sign choices everywhere.

The cross section for $q\bar{q} \rightarrow \tilde{\chi}_1^- \tilde{\chi}_2^+$, $\tilde{\chi}_1^+ \tilde{\chi}_2^-$ can occur via Z and \tilde{q}_L exchange. It is usually much smaller than $\tilde{\chi}_{1,2}^- \tilde{\chi}_{1,2}^+$ production, so the cross section will not be presented here. It can be found in Appendix A of Ref. [13].

51.8.4.3 Neutralino pair production

Neutralino pair production via $q\bar{q}$ fusion takes place via s -channel Z exchange plus t - and u -channel left- and right- squark exchange (5 diagrams) [17, 18]. The Lagrangian couplings (see previous footnote*) needed include terms given above plus terms of the form $\mathcal{L} = W_{ij} \bar{\tilde{\chi}}_i^0 \gamma_\mu (\gamma_5)^{\theta_i + \theta_j + 1} \tilde{\chi}_j^0 Z^\mu$. The couplings W_{ij} depend only on the *higgsino* components of the neutralinos i and j . The subprocess cross section is given by:

$$\frac{d\sigma}{dt}(q\bar{q} \rightarrow \tilde{\chi}_i^0 \tilde{\chi}_j^0) = \frac{1}{192\pi s^2} [T_Z + T_{\tilde{q}L} + T_{\tilde{q}R} + T_{Z\tilde{q}L} + T_{Z\tilde{q}R}] \quad (51.84)$$

where

$$T_Z = 128e^2 |W_{ij}|^2 (\alpha_q^2 + \beta_q^2) |D_Z(s)|^2$$

$$\left[q \cdot \tilde{\chi}_i^0 \bar{q} \cdot \tilde{\chi}_j^0 + q \cdot \tilde{\chi}_j^0 \bar{q} \cdot \tilde{\chi}_i^0 - \eta_i \eta_j m_{\tilde{\chi}_i^0} m_{\tilde{\chi}_j^0} q \cdot \bar{q} \right], \quad (51.85)$$

$$T_{\tilde{q}L} = 4|A_{\tilde{\chi}_i^0}^q|^2 |A_{\tilde{\chi}_j^0}^q|^2 \left\{ \frac{q \cdot \tilde{\chi}_i^0 \bar{q} \cdot \tilde{\chi}_j^0}{[(\tilde{\chi}_i^0 - q)^2 - m_{\tilde{q}L}^2]^2} + \frac{q \cdot \tilde{\chi}_j^0 \bar{q} \cdot \tilde{\chi}_i^0}{[(\tilde{\chi}_j^0 - q)^2 - m_{\tilde{q}L}^2]^2} \right. \\ \left. - \eta_i \eta_j \frac{m_{\tilde{\chi}_i^0} m_{\tilde{\chi}_j^0} q \cdot \bar{q}}{[(\tilde{\chi}_i^0 - q)^2 - m_{\tilde{q}L}^2][(\tilde{\chi}_j^0 - q)^2 - m_{\tilde{q}L}^2]} \right\} \quad (51.86)$$

$$T_{\tilde{q}R} = 4|B_{\tilde{\chi}_i^0}^q|^2 |B_{\tilde{\chi}_j^0}^q|^2 \left\{ \frac{q \cdot \tilde{\chi}_i^0 \bar{q} \cdot \tilde{\chi}_j^0}{[(\tilde{\chi}_i^0 - q)^2 - m_{\tilde{q}R}^2]^2} + \frac{q \cdot \tilde{\chi}_j^0 \bar{q} \cdot \tilde{\chi}_i^0}{[(\tilde{\chi}_j^0 - q)^2 - m_{\tilde{q}R}^2]^2} \right. \\ \left. - \eta_i \eta_j \frac{m_{\tilde{\chi}_i^0} m_{\tilde{\chi}_j^0} q \cdot \bar{q}}{[(\tilde{\chi}_i^0 - q)^2 - m_{\tilde{q}R}^2][(\tilde{\chi}_j^0 - q)^2 - m_{\tilde{q}R}^2]} \right\} \quad (51.87)$$

$$T_{Z\tilde{q}L} = 16e(\alpha_q - \beta_q)(s - M_Z^2) |D_Z(s)|^2$$

$$\left\{ \frac{Re(W_{ij} A_{\tilde{\chi}_i^0}^{q*} A_{\tilde{\chi}_j^0}^q)}{[(\tilde{\chi}_i^0 - q)^2 - m_{\tilde{q}L}^2]} \left[2q \cdot \tilde{\chi}_i^0 \bar{q} \cdot \tilde{\chi}_j^0 - \eta_i \eta_j m_{\tilde{\chi}_i^0} m_{\tilde{\chi}_j^0} q \cdot \bar{q} \right] \right. \\ \left. + \eta_i \eta_j \frac{Re(W_{ij} A_{\tilde{\chi}_i^0}^q A_{\tilde{\chi}_j^0}^{q*})}{[(\tilde{\chi}_j^0 - q)^2 - m_{\tilde{q}L}^2]} \left[2q \cdot \tilde{\chi}_j^0 \bar{q} \cdot \tilde{\chi}_i^0 - \eta_i \eta_j m_{\tilde{\chi}_i^0} m_{\tilde{\chi}_j^0} q \cdot \bar{q} \right] \right\} \quad (51.88)$$

$$T_{Z\tilde{q}R} = 16e(\alpha_q + \beta_q)(s - M_Z^2) |D_Z(s)|^2$$

$$\left\{ \frac{Re(W_{ij} B_{\tilde{\chi}_i^0}^{q*} B_{\tilde{\chi}_j^0}^q)}{[(\tilde{\chi}_i^0 - q)^2 - m_{\tilde{q}R}^2]} \left[2q \cdot \tilde{\chi}_i^0 \bar{q} \cdot \tilde{\chi}_j^0 - \eta_i \eta_j m_{\tilde{\chi}_i^0} m_{\tilde{\chi}_j^0} q \cdot \bar{q} \right] \right. \\ \left. - \frac{Re(W_{ij} B_{\tilde{\chi}_i^0}^q B_{\tilde{\chi}_j^0}^{q*})}{[(\tilde{\chi}_j^0 - q)^2 - m_{\tilde{q}R}^2]} \left[2q \cdot \tilde{\chi}_j^0 \bar{q} \cdot \tilde{\chi}_i^0 - \eta_i \eta_j m_{\tilde{\chi}_i^0} m_{\tilde{\chi}_j^0} q \cdot \bar{q} \right] \right\}. \quad (51.89)$$

As before, $\eta_i = \pm 1$ corresponding to whether the neutralino mass eigenvalue is positive or negative. When $i = j$ in the above formula, one must remember to integrate over just 2π steradians of solid angle to avoid double counting in the total cross section.

51.9 Universal extra dimensions

In the Universal Extra Dimension (UED) model of Ref. [19] (see Ref. [20] for a review of models with extra spacetime dimensions), the Standard Model is embedded in a five dimensional theory, where the fifth dimension is compactified on an S_1/Z_2 orbifold. Each SM chirality state is then the zero mode of an infinite tower of Kaluza-Klein excitations labeled by $n = 0 - \infty$. A KK parity is usually assumed to hold, where each state is assigned KK-parity $P = (-1)^n$. If the compactification scale is around a TeV, then the $n = 1$ (or even higher) KK modes may be accessible to collider searches.

Of interest for hadron colliders are the production of massive $n \geq 1$ quark or gluon pairs. These production cross sections have been calculated in Ref. [21, 22]. We list here results for the $n = 1$ case only with $M_1 = 1/R$ (R is the compactification radius) and s , t and u are the usual Mandelstam variables; more general formulae can be found in Ref. [22]. The superscript * stands for any KK excited state, while \bullet stands for left chirality states and \circ stands for right chirality states.

$$\frac{d\sigma}{dt} = \frac{1}{16\pi s^2} T \quad (51.90)$$

where

$$T(q\bar{q} \rightarrow g^* g^*) = \frac{2g_s^4}{27} \left[M_1^2 \left(-\frac{4s^3}{t'^2 u'^2} + \frac{57s}{t' u'} - \frac{108}{s} \right) \right. \\ \left. + \frac{20s^2}{t' u'} - 93 + \frac{108t' u'}{s^2} \right] \quad (51.91)$$

and

$$T(gg \rightarrow g^* g^*) = \frac{9g_s^4}{27} \left[3M_1^4 \frac{s^2 + t'^2 + u'^2}{t'^2 u'^2} - 3M_1^2 \frac{s^2 + t'^2 + u'^2}{st' u'} + 1 \right. \\ \left. + \frac{(s^2 + t'^2 + u'^2)^3}{4s^2 t'^2 u'^2} - \frac{t' u'}{s^2} \right] \quad (51.92)$$

where $t' = t - M_1^2$ and $u' = u - M_1^2$.

Also,

$$T(q\bar{q} \rightarrow q_1^* \bar{q}_1^*) = \frac{4g_s^4}{9} \left[\frac{2M_1^2}{s} + \frac{t'^2 + u'^2}{s^2} \right], \\ T(q\bar{q} \rightarrow q_1^* \bar{q}_1^*) = \frac{g_2^4}{9} \left[2M_1^2 \left(\frac{4}{s} + \frac{s}{t'^2} - \frac{1}{t'} \right) \right. \\ \left. + \frac{23}{6} + \frac{2s^2}{t'^2} + \frac{8s}{3t'} + \frac{6t'}{s} + \frac{8t'^2}{s^2} \right],$$

$$\begin{aligned}
T(qq \rightarrow q_1^* q_1^*) &= \frac{g_s^4}{27} \left[M_1^2 \left(6 \frac{t'}{u'^2} + 6 \frac{u'}{t'^2} - \frac{s}{t'u'} \right) \right. \\
&\quad \left. + 2 \left(3 \frac{t'^2}{u'^2} + 3 \frac{u'^2}{t'^2} + 4 \frac{s^2}{t'u'} - 5 \right) \right], \\
T(gg \rightarrow q_1^* \bar{q}_1^*) &= g_s^4 \left[M_1^4 \frac{-4}{t'u'} \left(\frac{s^2}{6t'u'} - \frac{3}{8} \right) \right. \\
&\quad \left. + M_1^2 \frac{4}{s} \left(\frac{s^2}{6t'u'} - \frac{3}{8} \right) + \frac{s^2}{6t'u'} - \frac{17}{24} + \frac{3t'u'}{4s^2} \right], \\
T(gq \rightarrow g^* q_1^*) &= \frac{-g_s^4}{3} \left[\frac{5s^2}{12t'^2} + \frac{s^3}{t'^2 u'} + \frac{11su'}{6t'^2} + \frac{5u'^2}{12t'^2} + \frac{u'^3}{st'^2} \right], \\
T(q\bar{q}' \rightarrow q_1^* \bar{q}_1^*) &= \frac{g_s^4}{18} \left[4M_1^4 \frac{s}{t'^2} + 5 + 4 \frac{s^2}{t'^2} + 8 \frac{s}{t'} \right], \\
T(qq' \rightarrow q_1^* q_1^*) &= \frac{2g_s^4}{9} \left[-M_1^2 \frac{s}{t'^2} + \frac{1}{4} + \frac{s^2}{t'^2} \right], \\
T(qq \rightarrow q_1^* q_1^{\circ}) &= \\
&\quad \frac{g_s^4}{9} \left[M_1^2 \left(\frac{2s^3}{t'^2 u'^2} - \frac{4s}{t'u'} \right) + 2 \frac{s^4}{t'^2 u'^2} - 8 \frac{s^2}{t'u'} + 5 \right], \\
T(q\bar{q}' \rightarrow q_1^* \bar{q}_1^{\circ}) &= \frac{g_s^4}{9} \left[2M_1^2 \left(\frac{1}{t'} + \frac{u'}{t'^2} \right) + \frac{5}{2} + \frac{4u'}{t'} + \frac{2u'^2}{t'^2} \right],
\end{aligned}$$

and

$$T(qq' \rightarrow q_1^* q_1^{\circ}) = \frac{g_s^4}{9} \left[-2M_1^2 \left(\frac{1}{t'} + \frac{u'}{t'^2} \right) + \frac{1}{2} + \frac{2u'^2}{t'^2} \right].$$

51.10 Large extra dimensions

In the ADD theory [23] with large extra dimensions (LED), the SM particles are confined to a 3-brane, while gravity propagates in the bulk. It is assumed that the n extra dimensions are compactified on an n -dimensional torus of volume $(2\pi r)^n$, so that the fundamental $4+n$ dimensional Planck scale M_* is related to the usual 4-dimensional Planck scale M_{Pl} by $M_{Pl}^2 = M_*^{n+2} (2\pi r)^n$. If $M_* \sim 1$ TeV, then the $M_W - M_{Pl}$ hierarchy problem is just due to gravity propagating in the large extra dimensions.

In these theories, the KK-excited graviton states $G_{\mu\nu}^n$ for $n = 1 - \infty$ can be produced at collider experiments. The graviton couplings to matter are suppressed by $1/M_{Pl}$, so that graviton emission cross sections $d\sigma/dt \sim 1/M_{Pl}^2$. However, the mass splittings between the excited graviton states can be tiny, so the graviton eigenstates are usually approximated by a continuum distribution. A summation (integration) over all allowed graviton emissions ends up cancelling the $1/M_{Pl}^2$ factor, so that observable cross section rates can be attained. Some fundamental production formulae for a KK graviton (denoted G) of mass m at hadron colliders include the subprocesses

$$\frac{d\sigma_m}{dt}(f\bar{f} \rightarrow \gamma G) = \frac{\alpha Q_f^2}{16N_f s M_{Pl}^2} F_1\left(\frac{t}{s}, \frac{m^2}{s}\right), \quad (51.93)$$

where Q_f is the charge of fermion f and N_f is the number of QCD colors of f . Also,

$$\frac{d\sigma_m}{dt}(q\bar{q} \rightarrow gG) = \frac{\alpha_s}{36 s M_{Pl}^2} F_1\left(\frac{t}{s}, \frac{m^2}{s}\right), \quad (51.94)$$

$$\frac{d\sigma_m}{dt}(qg \rightarrow qG) = \frac{\alpha_s}{96 s M_{Pl}^2} F_2\left(\frac{t}{s}, \frac{m^2}{s}\right), \quad (51.95)$$

$$\frac{d\sigma_m}{dt}(gg \rightarrow gG) = \frac{3\alpha_s}{16 s M_{Pl}^2} F_3\left(\frac{t}{s}, \frac{m^2}{s}\right), \quad (51.96)$$

where

$$\begin{aligned}
F_1(x, y) &= \frac{1}{x(y-1-x)} \left[-4x(1+x)(1+2x+2x^2) + \right. \\
&\quad \left. y(1+6x+18x^2+16x^3) - 6y^2x(1+2x) + y^3(1+4x) \right] \quad (51.97)
\end{aligned}$$

$$F_2(x, y) = -(y-1-x)F_1\left(\frac{x}{y-1-x}, \frac{y}{y-1-x}\right) \quad (51.98)$$

and

$$\begin{aligned}
F_3(x, y) &= \frac{1}{x(y-1-x)} \left[1 + 2x + 3x^2 + 2x^3 + x^4 \right. \\
&\quad \left. - 2y(1+x^3) + 3y^2(1+x^2) - 2y^3(1+x) + y^4 \right]. \quad (51.99)
\end{aligned}$$

These formulae must then be multiplied by the graviton density of states formula $dN = S_{n-1} \frac{M_{Pl}^2}{M_*^{n+2}} m^{n-1} dm$ to gain the cross section

$$\frac{d^2\sigma}{dt dm} = S_{n-1} \frac{M_{Pl}^2}{M_*^{n+2}} m^{n-1} \frac{d\sigma_m}{dt} \quad (51.100)$$

where $S_n = \frac{(2\pi)^{n/2}}{\Gamma(n/2)}$ is the surface area of an n -dimensional sphere of unit radius.

Virtual graviton processes can also be searched for at colliders. For instance, in Ref. [24] the cross section for Drell-Yan production of lepton pairs via gluon fusion was calculated, where it is found that, in the center-of-mass system

$$\frac{d\sigma}{dz}(gg \rightarrow \ell^+ \ell^-) = \frac{\lambda^2 s^3}{64\pi M_*^8} (1-z^2)(1+z^2) \quad (51.101)$$

where $z = \cos\theta$ and λ is a model-dependent coupling constant ~ 1 . Formulae for Drell-Yan production via $q\bar{q}$ fusion can also be found in Refs. [24, 25].

51.11 Warped extra dimensions

In the Randall-Sundrum model [26] of warped extra dimensions, the arena for physics is a 5-d anti-deSitter (AdS_5) spacetime, for which a non-factorizable metric exists with a metric warp factor $e^{-2\sigma(\phi)}$. It is assumed that two opposite tension 3-branes exist within AdS_5 at the two ends of an S_1/Z_2 orbifold parameterized by co-ordinate ϕ which runs from $0 - \pi$. The 4-D solution of the Einstein equations yields $\sigma(\phi) = kr_c|\phi|$, where r_c is the compactification radius of the extra dimension and $k \sim M_{Pl}$. The 4-D effective action allows one to identify $\bar{M}_{Pl}^2 = \frac{M^3}{k} (1 - e^{-2kr_c\pi})$, where M is the 5-D Planck scale. Physical particles on the TeV scale (SM) brane have mass $m = e^{-kr_c\pi} m_0$, where m_0 is a fundamental mass of order the Planck scale. Thus, the weak scale-Planck scale hierarchy occurs due to the existence of the exponential warp factor if $kr_c \sim 12$.

In the simplest versions of the RS model, the TeV-scale brane contains only SM particles plus a tower of KK gravitons. The RS gravitons have mass $m_n = kx_n e^{-kr_c\pi}$, where the x_i are roots of Bessel functions $J_1(x_n) = 0$, with $x_1 \simeq 3.83$, $x_2 \simeq 7.02$ etc. While the RS zero-mode graviton couplings suppressed by $1/\bar{M}_{Pl}$ and are thus inconsequential for collider searches, the $n = 1$ and higher modes have couplings suppressed instead by $\Lambda_\pi = e^{-kr_c\pi} \bar{M}_{Pl} \sim TeV$. The $n = 1$ RS graviton should have width $\Gamma_1 = \rho m_1 x_1^2 (k/\bar{M}_{Pl})^2$, where ρ is a constant depending on how many decay modes are open. The formulae for dilepton production via virtual RS graviton exchange can be gained from the above formulae for the ADD scenario via the replacement [27]

$$\frac{\lambda}{M_*^4} \rightarrow \frac{i^2}{8\Lambda_\pi^2} \sum_{n=1}^{\infty} \frac{1}{s - m_n^2 + im_n \Gamma_n}. \quad (51.102)$$

References

- [1] J. F. Owens, E. Reya and M. Gluck, Phys. Rev. **D18**, 1501 (1978).
- [2] F. Wilczek, Phys. Rev. Lett. **39**, 1304 (1977).
- [3] B. L. Ioffe and V. A. Khoze, Sov. J. Part. Nucl. **9**, 50 (1978), [Fiz. Elem. Chast. Atom. Yadra, 9, 118(1978)].
- [4] J. R. Ellis, M. K. Gaillard and D. V. Nanopoulos, Nucl. Phys. **B106**, 292 (1976).
- [5] R. N. Cahn and S. Dawson, Phys. Lett. **136B**, 196 (1984), [Erratum: Phys. Lett. 138B, 464(1984)].
- [6] S. Dawson, Nucl. Phys. **B249**, 42 (1985).

- [7] M. S. Chanowitz and M. K. Gaillard, Phys. Lett. **142B**, 85 (1984).
- [8] R. N. Cahn, Nucl. Phys. **B255**, 341 (1985), [Erratum: Nucl. Phys. B262,744(1985)].
- [9] V. M. Budnev *et al.*, Phys. Rept. **15**, 181 (1975), see for an exhaustive treatment.
- [10] See *e.g.* H.Haber, *Supersymmetry, Part I (Theory), this Review*.
- [11] P. R. Harrison and C. H. Llewellyn Smith, Nucl. Phys. **B213**, 223 (1983), [Erratum: Nucl. Phys. B223,542(1983)]; S. Dawson, E. Eichten and C. Quigg, Phys. Rev. **D31**, 1581 (1985); V. D. Barger *et al.*, Phys. Rev. **D31**, 528 (1985); H. Baer and X. Tata, Phys. Lett. **160B**, 159 (1985).
- [12] H. Baer, D. D. Karatas and X. Tata, Phys. Rev. **D42**, 2259 (1990).
- [13] Weak Scale Supersymmetry: From Superfields to Scattering Events, H. Baer and X. Tata (Cambridge University Press) 2006.
- [14] H. E. Haber and G. L. Kane, Phys. Rept. **117**, 75 (1985).
- [15] Theory and Phenomenology of Sparticles, M. Drees, R. Godbole, and P. Roy (World Scientific) 2005.
- [16] A. Bartl, H. Fraas and W. Majerotto, Z. Phys. **C30**, 441 (1986).
- [17] H. Baer *et al.*, Int. J. Mod. Phys. **A4**, 4111 (1989).
- [18] A. Bartl, H. Fraas and W. Majerotto, Nucl. Phys. **B278**, 1 (1986).
- [19] T. Appelquist, H.-C. Cheng and B. A. Dobrescu, Phys. Rev. **D64**, 035002 (2001), [hep-ph/0012100].
- [20] For a review of models with extra spacetime dimensions, see G. Giudice and J. Wells, *Extra Dimensions, this Review*.
- [21] J. M. Smillie and B. R. Webber, JHEP **10**, 069 (2005), [hep-ph/0507170].
- [22] C. Macesanu, C. D. McMullen and S. Nandi, Phys. Rev. **D66**, 015009 (2002), [hep-ph/0201300].
- [23] N. Arkani-Hamed, S. Dimopoulos and G. R. Dvali, Phys. Lett. **B429**, 263 (1998), [hep-ph/9803315]; N. Arkani-Hamed, S. Dimopoulos and G. R. Dvali, Phys. Rev. **D59**, 086004 (1999), [hep-ph/9807344].
- [24] J. L. Hewett, Phys. Rev. Lett. **82**, 4765 (1999), [hep-ph/9811356].
- [25] G. F. Giudice, R. Rattazzi and J. D. Wells, Nucl. Phys. **B544**, 3 (1999), [hep-ph/9811291]; E. A. Mirabelli, M. Perelstein and M. E. Peskin, Phys. Rev. Lett. **82**, 2236 (1999), [hep-ph/9811337]; T. Han, J. D. Lykken and R.-J. Zhang, Phys. Rev. **D59**, 105006 (1999), [hep-ph/9811350].
- [26] L. Randall and R. Sundrum, Phys. Rev. Lett. **83**, 3370 (1999), [hep-ph/9905221].
- [27] H. Davoudiasl, J. L. Hewett and T. G. Rizzo, Phys. Rev. Lett. **84**, 2080 (2000), [hep-ph/9909255].

52. Neutrino Cross Section Measurements

Revised August 2023 by G.P. Zeller (FNAL).

Neutrino cross sections are an essential ingredient in all neutrino experiments. Interest in neutrino scattering has increased due to the need for such information in the interpretation of neutrino oscillation data [1, 2] and given that uncertainties in neutrino-nucleus scattering remain a dominant source of systematic uncertainty in many neutrino oscillation measurements. Historically, neutrino scattering results on both charged current (CC) and neutral current (NC) channels have been collected over many decades using a variety of targets, analysis techniques, and detector technologies. With the advent of intense neutrino sources constructed for neutrino oscillation investigations, experiments are now remeasuring such interaction cross sections with a renewed appreciation for nuclear effects¹ and the need for more precise neutrino flux estimations [3, 4]. This work summarizes accelerator-based neutrino cross section measurements performed in the $\sim 0.1 - 300$ GeV range with an emphasis on inclusive, quasi-elastic, and pion production processes, areas where we have the most experimental input at present (Table 52.1). For a more comprehensive discussion of neutrino cross sections, including neutrino-electron elastic scattering and lower energy neutrino measurements, the reader is directed to a review of this subject [5]. Here, we survey existing experimental data on neutrino interactions and do not attempt to provide a census of the associated theoretical calculations [6], which are both critical and plentiful. Companion electron-nucleus scattering data [7] are additionally playing an increased role in neutrino interaction predictions through such efforts as the $e4\nu$ collaboration [8].

Table 52.1: List of beam properties, targets, and run durations for modern accelerator-based neutrino experiments studying neutrino scattering.

Experiment	beam	$\langle E_\nu \rangle, \langle E_{\bar{\nu}} \rangle$ (GeV)	neutrino target(s)	run period
ArgoNeuT	$\nu, \bar{\nu}$	4.3, 3.6	Ar	2009 – 2010
FASER ν	$\nu, \bar{\nu}$	> 200	W, emulsion	2021 –
ICARUS (at CNGS)	ν	20	Ar	2010 – 2012
ICARUS (at FNAL)	ν	0.8	Ar	2021 –
K2K	ν	1.3	CH, H ₂ O	2003 – 2004
MicroBooNE	ν	0.8	Ar	2015 – 2020
MINER ν A	$\nu, \bar{\nu}$	3.5 (LE), 5.5 (ME)	He, C, CH, H ₂ O, Fe, Pb	2009 – 2019
MiniBooNE	$\nu, \bar{\nu}$	0.8, 0.7	CH ₂	2002 – 2019
MINOS	$\nu, \bar{\nu}$	3.5, 6.1	Fe	2004 – 2016
NINJA	$\nu, \bar{\nu}$	0.6, 0.6	Fe, emulsion	2015 –
NOMAD	$\nu, \bar{\nu}$	23.4, 19.7	C	1995 – 1998
NO ν A	$\nu, \bar{\nu}$	2.0, 2.0	CH ₂	2010 –
SBND	ν	0.8	Ar	2024 –
SciBooNE	$\nu, \bar{\nu}$	0.8, 0.7	CH	2007 – 2008
T2K	$\nu, \bar{\nu}$	0.6, 0.6	CH, H ₂ O, Fe	2010 –

52.1 Inclusive Scattering

Over the years, many experiments have measured the total inclusive charged current cross section for neutrino ($\nu_\mu N \rightarrow \mu^- X$) and antineutrino ($\bar{\nu}_\mu N \rightarrow \mu^+ X$) scattering covering a broad range of neutrino energies. As can be seen in Fig. 52.1, which shows this data over decades of time and energy, the inclusive cross section approaches a linear dependence on neutrino energy. This behavior is expected for point-like scattering of neutrinos from quarks, an assumption which breaks down at lower energies. Modern measurements of such inclusive neutrino scattering cross sections and their target nuclei are summarized in Table 52.2. The reader is also referred to a recent review of the status of measurements and calculations in the shallow and deep inelastic scattering regions [9].

¹Nuclear effects refer to kinematic and final state effects which impact neutrino scattering off nuclei. Such effects can be significant and are particularly relevant given that modern neutrino experiments make use of nuclear targets to increase their event yields.

To provide a more complete picture, differential cross sections for such inclusive scattering processes have also been reported. These include historical measurements on iron from NuTeV [10] and modern measurements on a variety of nuclear targets from ArgoNeuT [11, 12], MicroBooNE [13, 14], MINER ν A [15–18], NINJA [19, 20], NO ν A [21], and T2K [22, 23]. More recently, MINER ν A has provided measurements in terms of longitudinal and transverse muon momenta [16, 17], MicroBooNE has measured the first triple differential cross sections in argon [24], and T2K has provided the first measurement of the antineutrino inclusive cross section at low energy [25] (Fig. 52.1).

At high energy, the inclusive cross section is dominated by deep inelastic scattering (DIS). Several neutrino experiments have measured DIS cross sections for specific targets and final states, for example, MINER ν A has measured ratios of neutrino DIS cross sections on a variety of nuclear targets including lead, iron, and carbon [26, 27]. Other experiments have measured opposite-sign dimuon production, the most recent being from CHORUS [28], NOMAD [29], and NuTeV [30]. Multiple efforts are also now underway to measure inclusive neutrino scattering cross sections at significantly higher neutrino energies, including at the LHC in FASER ν [31] and using atmospheric neutrinos in IceCube [32].

Table 52.2: Published measurements of muon neutrino and antineutrino CC inclusive cross sections from modern accelerator-based neutrino experiments.

experiment	measurement	target
ArgoNeuT	ν_μ [11, 12], $\bar{\nu}_\mu$ [12]	Ar
MicroBooNE	ν_μ [13, 24, 33]	Ar
MINER ν A	ν_μ [15–18, 26, 27, 34], $\bar{\nu}_\mu$ [34], $\bar{\nu}_\mu/\nu_\mu$ [35]	C, CH, Fe, Pb
MINOS	ν_μ [36], $\bar{\nu}_\mu$ [36]	Fe
NINJA	ν_μ [19, 20], $\bar{\nu}_\mu$ [19]	H ₂ O, Fe
NOMAD	ν_μ [37]	C
NO ν A	ν_μ [21]	CH ₂
SciBooNE	ν_μ [38]	CH
T2K	ν_μ [22, 23, 39–41], $\bar{\nu}_\mu/\nu_\mu$ [25]	CH, H ₂ O, Fe

At lower neutrino energies, the inclusive cross section is an additionally complex combination of quasi-elastic scattering and pion production processes, two areas we discuss next.

52.2 Quasi-elastic scattering

Quasi-elastic (QE) scattering is the dominant neutrino interaction for neutrino energies less than ~ 1 GeV and represents a large fraction of the signal samples in many neutrino oscillation experiments, which is why this process has received considerable attention in recent years. Historically, neutrino (antineutrino) quasi-elastic scattering refers to the process, $\nu_\mu n \rightarrow \mu^- p$ ($\bar{\nu}_\mu p \rightarrow \mu^+ n$), where a charged lepton and single nucleon are ejected in the elastic interaction of a neutrino (or antineutrino) with a nucleon in the target material. This is the final state one would strictly observe, for example, in scattering off of a *free* nucleon target. There were many early measurements of neutrino QE scattering that span back to the 1970's [5]. In many of these initial measurements, bubble chamber experiments employed light targets (hydrogen or deuterium) and required both the detection of the final state muon and single nucleon²; thus the final state was clear and elastic kinematic conditions could be verified. The situation is more complicated, of course, for heavier nuclear targets used in modern neutrino experiments. In this case, nuclear effects can impact the size and shape of the cross section as well as the final state composition, kinematics, and topology. Due to intranuclear hadron rescattering and the effects of correlations between target nucleons, additional particles may be ejected in the final state; hence, a QE interaction on a nuclear target does not necessarily imply the ejection of a lepton and a *single* nucleon. One therefore needs to take care in defining what one means by

²In the case of deuterium, many experiments additionally observed the spectator proton.

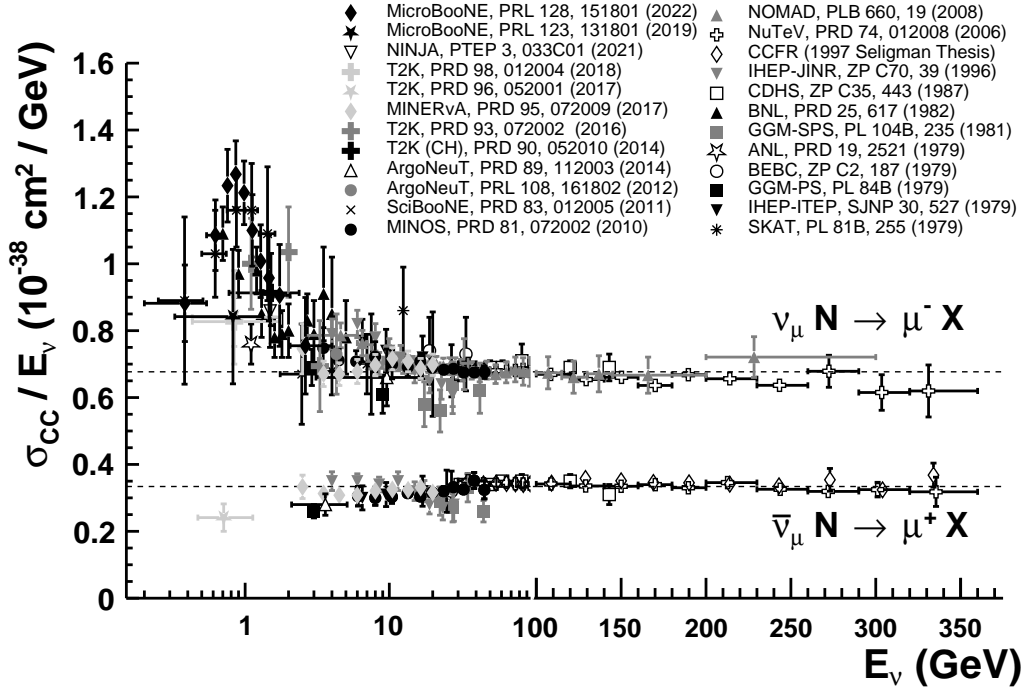


Figure 52.1: Measurements of per nucleon ν_μ and $\bar{\nu}_\mu$ CC inclusive scattering cross sections divided by neutrino energy as a function of neutrino energy. Note the transition between logarithmic and linear scales occurring at 100 GeV. Neutrino cross sections are typically twice as large as their corresponding antineutrino counterparts, although this difference can be larger at lower energies. NC cross sections (not shown) are generally smaller compared to their CC counterparts.

neutrino QE scattering when scattering off targets heavier than hydrogen or deuterium. Because of this, modern experiments tend to instead report cross sections for processes involving pionless (e.g., nucleon-only) final states, often referred to as CC 0π or QE-like reactions in recent literature. Such measurements are summarized in Table 52.3. Many modern experiments have also recently opted to report QE-like cross sections as a function of observed final state particle kinematics. Such measurements can be more difficult to directly compare between experiments but have the advantage of being much less model-dependent and provide more stringent tests of the theory than historical cross sections as a function of derived quantities such as neutrino energy (E_ν) or 4-momentum transfer (Q^2). More recently, new thought has been given to the means for directly comparing experimental measurements produced in these less model-dependent forms [42].

The topic of neutrino QE scattering began drawing considerable attention following the first double differential cross section measurements of this process that revealed a significantly larger cross section than originally anticipated, predominantly in the backwards muon scattering region [64, 65]. Such an enhancement was observed many years prior in transverse electron-nucleus scattering [83] and was attributed to the presence of correlations between nucleons in the target nucleus. As a result, the impact of such nuclear effects on neutrino QE scattering has recently become the subject of intense experimental and theoretical scrutiny with implications on event rates, nucleon emission, neutrino energy reconstruction, and neutrino versus antineutrino cross sections. The reader is referred to reviews of the situation in [6, 84, 85]. To help drive further progress in understanding the underlying nuclear contributions, pionless (e.g., nucleon-only) cross sections have been reported for the first time in the form of double-differential distributions by MiniBooNE [64, 65], MINERvA [51–55, 61], and T2K [73–78]. Such double-differential cross sections in terms of final state particle kinematics reduce the model-dependence of the reported data, provide the most robust measurements available, and allow a more rigorous two-dimensional test of the underlying nuclear theory. MicroBooNE, MINERvA, and T2K have been especially prolific in recent years in probing this interaction process

(Table 52.3). Neutrino experiments have also launched dedicated studies of the hadronic side of these interactions, including ArgoNeuT [43, 86], MicroBooNE [45, 46], MINERvA [60, 87], and T2K [82]. MINERvA has been the first modern experiment to measure neutron emission in antineutrino interactions [88] and has simultaneously measured neutrino QE cross sections on a variety of nuclear targets ranging from carbon to lead [55]. ArgoNeuT [43], MicroBooNE [49], and NINJA [70] have explored two-proton final states. T2K has probed ratios of oxygen to carbon [76, 89], asymmetries between neutrino and antineutrino scattering [77], and simultaneous measurements both on and off axis to the neutrino beam [78]. In addition, the exploration of transverse kinematic variables and momentum imbalances in pionless neutrino scattering is allowing better constraints on the various nuclear contributions to the cross section. Such scrutiny includes important evaluations from MicroBooNE [47, 48], MINERvA [51, 52, 56, 57] and T2K [82]. With the MiniBooNE results having first revealed these additional complexities in neutrino-nucleus QE scattering, measurements from multiple neutrino experiments, on multiple targets, and using a variety of kinematic information have been crucial in gaining a better handle on the underlying nuclear physics impacting neutrino-nucleus interactions. What we once thought was “simple” QE scattering is in fact not so simple.

Equally important, neutrino experiments such as MINERvA have revisited the extraction of the axial form factor from light target data using modern higher statistics data sets [63]. In addition to such charged current investigations, measurements of the neutral current counterpart of this channel have also been performed. The most recent NC elastic scattering cross section measurements include those from BNL E734 [90], MiniBooNE [67, 68], Super-K [72], and T2K [81]. A number of measurements of the Cabibbo-suppressed antineutrino QE hyperon production cross section have additionally been reported [91, 92], most recently by MicroBooNE [50]. As an exciting new addition, there have also been the first observations of the very challenging-to-detect coherent elastic neutrino-nucleus scattering ($\text{CE}\nu\text{NS}$) process now in multiple nuclei by COHERENT [93, 93, 94].

Table 52.3: Published modern measurements of muon neutrino QE and NC elastic scattering cross sections with pionless final states.

experiment	measurement	target
ArgoNeuT	2p [43]	Ar
K2K	M_A [44]	H ₂ O
MicroBooNE	$\frac{d\sigma}{dp_\mu} \frac{d\sigma}{dp_p} \frac{d\sigma}{d\cos\theta_\mu} \frac{d\sigma}{d\cos\theta_p}$ [45, 46], $\frac{d^2\sigma}{d\delta\alpha_T d\delta p_T}$ [47, 48], $\frac{d^2\sigma}{d\delta p_{Tx} d\delta p_{Ty}}$ [47], 2p [49], Λ [50]	Ar
MINERvA	$\frac{d^2\sigma}{dp_T dp_{ }}$ [51–55], $\frac{d\sigma}{d\delta p_{Tx}} \frac{d\sigma}{d\delta p_{Ty}}$ [56], $\frac{d\sigma}{dp_n} \frac{d\sigma}{d\delta\alpha_T}$ [57], $\frac{d\sigma}{dQ^2}$ [58, 59], 1p [60], $\frac{d^2\sigma}{dE_{\nu\alpha ii} dq_3}$ [61], $\frac{d\sigma}{dQ^2}$ [62], $F_A(Q^2)$ [63]	CH, Fe, Pb
MiniBooNE	$\frac{d^2\sigma}{dT_\mu d\theta_\mu}$ [64, 65], M_A [66], NC [67, 68]	CH ₂
MINOS	M_A [69]	Fe
NINJA	2p [70]	Fe
NOMAD	$M_A, \sigma(E_\nu)$ [71]	C
Super-K	NC [72]	H ₂ O
T2K	$\frac{d^2\sigma}{dT_\mu d\theta_\mu}$ [73–78], $\sigma(E_\nu)$ [79], M_A [80], NC [81], $\frac{d\sigma}{d\delta p_T} \frac{d\sigma}{d\delta\alpha_T}$ [82], O/C [76]	CH, H ₂ O

52.3 Pion Production

In addition to such elastic scattering processes, neutrinos can also inelastically scatter producing a nucleon excited state (Δ, N^*). Such baryonic resonances quickly decay, most often to a nucleon and single-pion final state. Historically, experiments have measured various exclusive final states associated with these reactions, the majority of which have been on hydrogen and deuterium targets [5]. There have been several recent re-analyses of this data to better understand the consistency between data sets [95], nucleon form factors [96], and non-resonant contributions [97]. Also, modern measurements of neutrino-induced pion production have since been performed on a variety of nuclear targets (Table 52.4).

Table 52.4: Summary of modern measurements of NC and CC scattering cross sections involving a single pion or multiple pions in the final state.

experiment	π^\pm	π^0	target
ArgoNeuT	CC [98, 99]	NC [100]	Ar
K2K	CC [101, 102]	CC [103], NC [104]	CH, H ₂ O
MicroBooNE	–	CC [105], NC [106]	Ar
MINERvA	CC [107–114]	CC [108, 115–117], NC [118]	C, CH, H ₂ O, Fe, Pb
MiniBooNE	CC [119, 120]	CC [121], NC [122, 123]	CH ₂
MINOS	–	NC [124]	Fe
NOMAD	–	NC [125]	C
NOvA	–	NC [126, 127]	C
SciBooNE	CC [128]	NC [129, 130]	CH
T2K	CC [131–134]	–	CH, H ₂ O

In addition to resonance production processes, neutrinos can also coherently scatter off of the entire nucleus and produce a distinctly forward-scattered single pion final state. Both CC ($\nu_\mu A \rightarrow \mu^- A \pi^+, \bar{\nu}_\mu A \rightarrow \mu^+ A \pi^-$) and NC ($\nu_\mu A \rightarrow \nu_\mu A \pi^0, \bar{\nu}_\mu A \rightarrow \bar{\nu}_\mu A \pi^0$) processes are possible in this case. Even though the level of coherent pion production is small compared to their resonant counterpart, observations exist across a broad energy range and on multiple nuclear targets [135]. More recently, several modern neutrino experiments have either measured or set limits on coherent pion production cross sections including ArgoNeuT [98], K2K [102], MINERvA [109, 111, 113], MiniBooNE [123], MINOS [124], NOMAD [125], NOvA [126], SciBooNE [128, 130], and T2K [102].

As with inclusive and quasi-elastic scattering, a new appreciation for the significance of nuclear effects has also surfaced in pion production physics, again due to the use of heavy nuclear targets in modern neutrino experiments. Many experiments have been careful to report cross sections for various detected final

states, thereby not correcting for large and uncertain nuclear effects (e.g., pion rescattering, charge exchange, and absorption) which can introduce significant sources of uncertainty and model dependence. Providing the most comprehensive survey of neutrino single-pion production to date, MiniBooNE has published a total of 16 single- and double-differential cross sections for both the final state muon (in the case of CC scattering) and pions in these interactions; thus, providing the first measurements of such final state kinematic distributions [119–122]. At similar neutrino energies, T2K has provided new data [131] including the first measurement of the Adler angles in neutrino-nucleus scattering [133] and the first exploration of transverse kinematic imbalances in pion production processes [134]. MINERvA has produced a similar accompaniment of measurements at higher neutrino energies [108, 110, 112, 116] and uniquely on multiple nuclear targets [114]. Importantly, MINERvA has been working towards an improved nuclear model [117] that can potentially describe all of the pion reaction channels simultaneously, an issue that many experiments have struggled with up until now [108]. ArgoNeuT [99, 100] and MicroBooNE [105, 106] have since been adding new information on single pion production in argon. Regardless of the interaction channel or target material, differential cross section measurements in terms of observed final state particle kinematics are preferred for their reduced model dependence and for the additional kinematic information they provide. Such a new direction has been the focus of modern measurements as opposed to the reporting of more model-dependent, historical cross sections as a function of E_ν or Q^2 . Together with similar results for other interaction channels, a better understanding and modeling of nuclear effects will be possible moving forward. MINERvA [136] has already taken a large step in this direction by explicitly tuning the physics in existing neutrino event generators to best fit the experimental data on pion production.

It should be noted that baryonic resonances can also decay to multi-pion, other mesonic (K, η, ρ , etc.), and even photon final states. Experimental results for these channels are typically sparse or non-existent. More recently, MicroBooNE has produced the first measurement of neutrino-induced η production on argon [137]. Photon production processes can comprise an important background for $\nu_\mu \rightarrow \nu_e$ appearance searches in some detectors and thus have become the focus of recent experimental investigations, most notably in NOMAD [138] and T2K [139, 140]. There have also been several recent measurements of kaon final states produced in neutrino NC and CC scattering in MINERvA [141–143] that are providing needed background constraints for certain nucleon decay searches.

52.4 Electron Neutrino Scattering

The aforementioned cross section measurements are all for either muon neutrino or muon antineutrino scattering. With the production of predominantly muon neutrino beams for neutrino oscillation studies, the availability of electron neutrino scattering data is by construction limited. However, for the first time, measurements of electron neutrino scattering cross sections are being produced by a variety of modern neutrino experiments (Table 52.5). Such measurements are important as they verify our assumptions about lepton universality and validate the use of muon neutrino data to constrain electron neutrino interaction predictions. For lower energy and historical electron neutrino cross section measurements, the reader is directed to reference [5].

Table 52.5: Published measurements of electron neutrino and antineutrino cross sections from modern accelerator-based neutrino experiments.

experiment	CC inclusive	QE-like	π production	target
ArgoNeuT	[144]	-	-	Ar
COHERENT	[145]	-	-	I
MicroBooNE	[146, 147]	[148]	-	Ar
MINER ν A	-	[149]	-	CH
NO ν A	[150]	-	-	CH ₂
T2K	[151–153]	-	-	CH, H ₂ O

52.5 Outlook

Neutrino experiments continue to produce critical neutrino scattering measurements on nuclei as they accumulate increased statistics and pursue new ways of reporting their measurements. Analysis of a broad energy range of data from MINER ν A is providing some of the most detailed analysis of nuclear effects in neutrino interactions by examining multiple nuclei in a single experiment. Data from ArgoNeuT, MicroBooNE, ICARUS and soon also SBND are probing deeper into complex neutrino final states using the superior capabilities of liquid argon time projection chambers, while the T2K and NO ν A near detectors continue to collect high statistics samples in intense neutrino beams. Together with dedicated discussions between experiments on how best to report neutrino cross section measurements [154] and with accompanying work being advanced by theorists to further improve nuclear model calculations [6], we are starting to significantly advance our understanding of neutrino-nucleus scattering.

52.6 Acknowledgments

The author thanks Anne Schukraft (Fermilab) for help in preparing the plots and content of this review.

References

- [1] O. Benhar *et al.*, Phys. Rept. **700**, 1 (2017), [arXiv:1501.06448].
- [2] L. Alvarez-Ruso *et al.* (NuSTEC), Prog. Part. Nucl. Phys. **100**, 1 (2018), [arXiv:1706.03621].
- [3] L. Zazueta *et al.* (MINER ν A), Phys. Rev. D **107**, 1, 012001 (2023), [arXiv:2209.05540].
- [4] D. Ruterbories *et al.* (MINER ν A), Phys. Rev. D **104**, 9, 092010 (2021), [arXiv:2107.01059].
- [5] J. A. Formaggio and G. P. Zeller, Rev. Mod. Phys. **84**, 1307 (2012), [arXiv:1305.7513].
- [6] L. Alvarez-Ruso *et al.*, Prog. Part. Nucl. Phys. **100**, 1 (2018), [arXiv:1706.03621].
- [7] D. Drechsel and M. M. Giannini, Rept. Prog. Phys. **52**, 1083 (1989).
- [8] M. Khachatryan *et al.* (CLAS, e4 ν), Nature **599**, 7886, 565 (2021).
- [9] M. Sajjad Athar and J. G. Morfin, J. Phys. G **48**, 3, 034001 (2021), [arXiv:2006.08603].
- [10] M. Tzanov *et al.* (NuTeV), Phys. Rev. **D74**, 012008 (2006), [hep-ex/0509010].
- [11] C. Anderson *et al.* (ArgoNeuT), Phys. Rev. Lett. **108**, 161802 (2012), [arXiv:1111.0103].
- [12] R. Acciarri *et al.* (ArgoNeuT), Phys. Rev. **D89**, 11, 112003 (2014), [arXiv:1404.4809].
- [13] P. Abratenko *et al.* (MicroBooNE), Phys. Rev. Lett. **123**, 13, 131801 (2019), [arXiv:1905.09694].
- [14] P. Abratenko *et al.* (MicroBooNE), Phys. Rev. Lett. **128**, 15, 151801 (2022), [arXiv:2110.14023].
- [15] P. A. Rodrigues *et al.* (MINER ν A), Phys. Rev. Lett. **116**, 071802 (2016), [Addendum: Phys. Rev. Lett. **121**, no. 20, 209902 (2018)], [arXiv:1511.05944].
- [16] A. Filkins *et al.* (MINER ν A), Phys. Rev. D **101**, 11, 112007 (2020), [arXiv:2002.12496].
- [17] D. Ruterbories *et al.* (MINER ν A) (2021), [arXiv:2106.16210].
- [18] M. V. Ascencio *et al.* (MINER ν A), Phys. Rev. D **106**, 3, 032001 (2022), [arXiv:2110.13372].
- [19] A. Hiramoto *et al.* (NINJA), Phys. Rev. D **102**, 7, 072006 (2020), [arXiv:2008.03895].
- [20] H. Oshima *et al.* (NINJA), PTEP **2021**, 3, 033C01 (2021), [arXiv:2012.05221].
- [21] M. A. Acero *et al.* (NO ν A), Phys. Rev. D **107**, 5, 052011 (2023), [arXiv:2109.12220].
- [22] K. Abe *et al.* (T2K), Phys. Rev. **D87**, 9, 092003 (2013), [arXiv:1302.4908].
- [23] K. Abe *et al.* (T2K), Phys. Rev. **D98**, 012004 (2018), [arXiv:1801.05148].
- [24] P. Abratenko *et al.* (MicroBooNE) (2023), [arXiv:2307.06413].
- [25] K. Abe *et al.* (T2K), Phys. Rev. **D96**, 5, 052001 (2017), [arXiv:1706.04257].
- [26] B. G. Tice *et al.* (MINER ν A), Phys. Rev. Lett. **112**, 23, 231801 (2014), [arXiv:1403.2103].
- [27] J. Mousseau *et al.* (MINER ν A), Phys. Rev. **D93**, 7, 071101 (2016), [arXiv:1601.06313].
- [28] A. Kayis-Topaksu *et al.* (CHORUS), Nucl. Phys. **B798**, 1 (2008), [arXiv:0804.1869].
- [29] O. Samoylov *et al.* (NOMAD), Nucl. Phys. **B876**, 339 (2013), [arXiv:1308.4750].
- [30] D. Mason *et al.* (NuTeV), Phys. Rev. Lett. **99**, 192001 (2007).
- [31] H. Abreu *et al.* (FASER), Phys. Rev. Lett. **131**, 3, 031801 (2023), [arXiv:2303.14185].
- [32] R. Abbasi *et al.* (IceCube), Phys. Rev. D. **104**, 022001 (2021), [arXiv:2011.03560].
- [33] C. Adams *et al.* (MicroBooNE), Eur. Phys. J. **C79**, 3, 248 (2019), [arXiv:1805.06887].
- [34] J. Devan *et al.* (MINER ν A), Phys. Rev. **D94**, 11, 112007 (2016), [arXiv:1610.04746].
- [35] L. Ren *et al.* (MINER ν A), Phys. Rev. **D95**, 7, 072009 (2017), [Addendum: Phys. Rev. **D97**, no. 1, 019902 (2018)], [arXiv:1701.04857].
- [36] P. Adamson *et al.* (MINOS), Phys. Rev. **D81**, 072002 (2010), [arXiv:0910.2201].
- [37] Q. Wu *et al.* (NOMAD), Phys. Lett. **B660**, 19 (2008), [arXiv:0711.1183].
- [38] Y. Nakajima *et al.* (SciBooNE), Phys. Rev. **D83**, 012005 (2011), [arXiv:1011.2131].
- [39] K. Abe *et al.* (T2K), Phys. Rev. **D90**, 5, 052010 (2014), [arXiv:1407.4256].
- [40] K. Abe *et al.* (T2K), Phys. Rev. **D93**, 7, 072002 (2016), [arXiv:1509.06940].
- [41] K. Abe *et al.* (T2K), PTEP **2019**, 9, 093C02 (2019), [arXiv:1904.09611].

- [42] K. Mahn, C. Marshall and C. Wilkinson, *Ann. Rev. Nucl. Part. Sci.* **68**, 105 (2018), [arXiv:1803.08848].
- [43] R. Acciarri *et al.* (ArgoNeuT), *Phys. Rev.* **D90**, 1, 012008 (2014), [arXiv:1405.4261].
- [44] R. Gran *et al.* (K2K), *Phys. Rev.* **D74**, 052002 (2006), [hep-ex/0603034].
- [45] P. Abratenko *et al.* (MicroBooNE), *Phys. Rev. D* **102**, 11, 112013 (2020), [arXiv:2010.02390].
- [46] P. Abratenko *et al.* (MicroBooNE), *Phys. Rev. Lett.* **125**, 20, 201803 (2020), [arXiv:2006.00108].
- [47] P. Abratenko *et al.* (MicroBooNE) (2023), [arXiv:2301.03706].
- [48] P. Abratenko *et al.* (MicroBooNE) (2023), [arXiv:2301.03700].
- [49] P. Abratenko *et al.* (MicroBooNE) (2022), [arXiv:2211.03734].
- [50] P. Abratenko *et al.* (MicroBooNE), *Phys. Rev. Lett.* **130**, 23, 231802 (2023), [arXiv:2212.07888].
- [51] D. Ruterbories *et al.* (MINERvA), *Phys. Rev.* **D99**, 1, 012004 (2019), [arXiv:1811.02774].
- [52] C. E. Patrick *et al.* (MINERvA), *Phys. Rev.* **D97**, 5, 052002 (2018), [arXiv:1801.01197].
- [53] M. F. Carneiro *et al.* (MINERvA), *Phys. Rev. Lett.* **124**, 12, 121801 (2020), [arXiv:1912.09890].
- [54] A. Bashyal *et al.* (MINERvA), *Phys. Rev. D* **108**, 3, 032018 (2023).
- [55] J. Kleykamp *et al.* (MINERvA), *Phys. Rev. Lett.* **130**, 16, 161801 (2023), [arXiv:2301.02272].
- [56] T. Cai *et al.* (MINERvA), *Phys. Rev. D* **101**, 9, 092001 (2020), [arXiv:1910.08658].
- [57] X. G. Lu *et al.* (MINERvA), *Phys. Rev. Lett.* **121**, 2, 022504 (2018), [arXiv:1805.05486].
- [58] G. A. Fiorentini *et al.* (MINERvA), *Phys. Rev. Lett.* **111**, 022502 (2013), [arXiv:1305.2243].
- [59] L. Fields *et al.* (MINERvA), *Phys. Rev. Lett.* **111**, 2, 022501 (2013), [arXiv:1305.2234].
- [60] T. Walton *et al.* (MINERvA), *Phys. Rev.* **D91**, 7, 071301 (2015), [arXiv:1409.4497].
- [61] R. Gran *et al.* (MINERvA), *Phys. Rev. Lett.* **120**, 22, 221805 (2018), [arXiv:1803.09377].
- [62] M. Betancourt *et al.* (MINERvA), *Phys. Rev. Lett.* **119**, 8, 082001 (2017), [arXiv:1705.03791].
- [63] T. Cai *et al.* (MINERvA), *Nature* **614**, 7946, 48 (2023).
- [64] A. A. Aguilar-Arevalo *et al.* (MiniBooNE), *Phys. Rev.* **D81**, 092005 (2010), [arXiv:1002.2680].
- [65] A. A. Aguilar-Arevalo *et al.* (MiniBooNE), *Phys. Rev.* **D88**, 3, 032001 (2013), [arXiv:1301.7067].
- [66] A. A. Aguilar-Arevalo *et al.* (MiniBooNE), *Phys. Rev. Lett.* **100**, 032301 (2008), [arXiv:0706.0926].
- [67] A. A. Aguilar-Arevalo *et al.* (MiniBooNE), *Phys. Rev.* **D82**, 092005 (2010), [arXiv:1007.4730].
- [68] A. A. Aguilar-Arevalo *et al.* (MiniBooNE), *Phys. Rev.* **D91**, 1, 012004 (2015), [arXiv:1309.7257].
- [69] P. Adamson *et al.* (MINOS), *Phys. Rev.* **D91**, 1, 012005 (2015), [arXiv:1410.8613].
- [70] H. Oshima *et al.* (NINJA), *Phys. Rev. D* **106**, 3, 032016 (2022), [arXiv:2203.08367].
- [71] V. Lyubushkin *et al.* (NOMAD), *Eur. Phys. J.* **C63**, 355 (2009), [arXiv:0812.4543].
- [72] L. Wan *et al.* (Super-Kamiokande), *Phys. Rev.* **D99**, 3, 032005 (2019), [arXiv:1901.05281].
- [73] K. Abe *et al.* (T2K), *Phys. Rev.* **D93**, 11, 112012 (2016), [arXiv:1602.03652].
- [74] K. Abe *et al.* (T2K), *Phys. Rev.* **D97**, 1, 012001 (2018), [arXiv:1708.06771].
- [75] K. Abe *et al.* (T2K), *Phys. Rev. D* **102**, 1, 012007 (2020), [arXiv:1908.10249].
- [76] K. Abe *et al.* (T2K), *Phys. Rev. D* **101**, 11, 112004 (2020), [arXiv:2004.05434].
- [77] K. Abe *et al.* (T2K), *Phys. Rev. D* **101**, 11, 112001 (2020), [arXiv:2002.09323].
- [78] K. Abe *et al.* (T2K) (2023), [arXiv:2303.14228].
- [79] K. Abe *et al.* (T2K), *Phys. Rev.* **D91**, 11, 112002 (2015), [arXiv:1503.07452].
- [80] K. Abe *et al.* (T2K), *Phys. Rev.* **D92**, 11, 112003 (2015), [arXiv:1411.6264].
- [81] K. Abe *et al.* (T2K), *Phys. Rev.* **D90**, 7, 072012 (2014), [arXiv:1403.3140].
- [82] K. Abe *et al.* (T2K), *Phys. Rev.* **D98**, 3, 032003 (2018), [arXiv:1802.05078].
- [83] J. Carlson *et al.*, *Phys. Rev.* **C65**, 024002 (2002), [arXiv:nucl-th/0106047].
- [84] H. Gallagher, G. Garvey and G. P. Zeller, *Ann. Rev. Nucl. Part. Sci.* **61**, 355 (2011).
- [85] G. T. Garvey *et al.*, *Phys. Rept.* **580**, 1 (2015), [arXiv:1412.4294].
- [86] O. Palamara (ArgoNeuT), *JPS Conf. Proc.* **12**, 010017 (2016).
- [87] D. Ruterbories *et al.* (MINERvA), *Phys. Rev. Lett.* **129**, 2, 021803 (2022), [arXiv:2203.08022].
- [88] M. Elkins *et al.* (MINERvA), *Phys. Rev.* **D100**, 5, 052002 (2019), [arXiv:1901.04892].
- [89] K. Abe *et al.* (T2K), *PTEP* **2021**, 4, 043C01 (2021), [arXiv:2004.13989].
- [90] L. A. Ahrens *et al.*, *Phys. Rev.* **D35**, 785 (1987).
- [91] J. Brunner *et al.* (SKAT), *Z. Phys.* **C45**, 551 (1990).
- [92] V. V. Ammosov *et al.*, *Z. Phys.* **C36**, 377 (1987); O. Enriquez *et al.*, *Phys. Lett.* **70B**, 383 (1977); T. Eichten *et al.*, *Phys. Lett.* **40B**, 593 (1972).
- [93] D. Akimov *et al.* (COHERENT), *Phys. Rev. Lett.* **126**, 1, 012002 (2021), [arXiv:2003.10630].
- [94] D. Akimov *et al.* (COHERENT), *Phys. Rev. Lett.* **129**, 8, 081801 (2022), [arXiv:2110.07730].
- [95] C. Wilkinson *et al.*, *Phys. Rev.* **D90**, 11, 112017 (2014), [arXiv:1411.4482].
- [96] A. S. Meyer *et al.*, *Phys. Rev.* **D93**, 11, 113015 (2016), [arXiv:1603.03048].
- [97] P. Rodrigues, C. Wilkinson and K. McFarland, *Eur. Phys. J.* **C76**, 8, 474 (2016), [arXiv:1601.01888].
- [98] R. Acciarri *et al.* (ArgoNeuT), *Phys. Rev. Lett.* **113**, 26, 261801 (2014), [erratum: *Phys. Rev. Lett.* 114, no. 3, 039901 (2015)], [arXiv:1408.0598].
- [99] R. Acciarri *et al.* (ArgoNeuT), *Phys. Rev. D* **98**, 5, 052002 (2018), [arXiv:1804.10294].
- [100] R. Acciarri *et al.* (ArgoNeuT), *Phys. Rev.* **D96**, 1, 012006 (2017), [arXiv:1511.00941].
- [101] A. Rodriguez *et al.* (K2K), *Phys. Rev.* **D78**, 032003 (2008), [arXiv:0805.0186].
- [102] M. Hasegawa *et al.* (K2K), *Phys. Rev. Lett.* **95**, 252301 (2005), [hep-ex/0506008].
- [103] C. Mariani *et al.* (K2K), *Phys. Rev.* **D83**, 054023 (2011), [arXiv:1012.1794].
- [104] S. Nakayama *et al.* (K2K), *Phys. Lett.* **B619**, 255 (2005), [hep-ex/0408134].
- [105] C. Adams *et al.* (MicroBooNE), *Phys. Rev.* **D99**, 9, 091102 (2019), [arXiv:1811.02700].

- [106] P. Abratenko *et al.* (MicroBooNE), Phys. Rev. D **107**, 1, 012004 (2023), [arXiv:2205.07943].
- [107] B. Eberly *et al.* (MINERvA), Phys. Rev. **D92**, 9, 092008 (2015), [arXiv:1406.6415].
- [108] C. L. McGivern *et al.* (MINERvA), Phys. Rev. **D94**, 5, 052005 (2016), [arXiv:1606.07127].
- [109] A. Higuera *et al.* (MINERvA), Phys. Rev. Lett. **113**, 26, 261802 (2014), [arXiv:1409.3835].
- [110] T. Le *et al.* (MINERvA), Phys. Rev. **D100**, 5, 052008 (2019), [arXiv:1906.08300].
- [111] A. Mislivec *et al.* (MINERvA), Phys. Rev. **D97**, 3, 032014 (2018), [arXiv:1711.01178].
- [112] T. Le *et al.* (MINERvA), Phys. Rev. D **100**, 5, 052008 (2019), [arXiv:1906.08300].
- [113] M. A. Ramírez *et al.* (MINERvA), Phys. Rev. Lett. **131**, 5, 051801 (2023), [arXiv:2210.01285].
- [114] A. Bercellie *et al.* (MINERvA), Phys. Rev. Lett. **131**, 1, 011801 (2023), [arXiv:2209.07852].
- [115] T. Le *et al.* (MINERvA), Phys. Lett. **B749**, 130 (2015), [arXiv:1503.02107].
- [116] O. Altinok *et al.* (MINERvA), Phys. Rev. **D96**, 7, 072003 (2017), [arXiv:1708.03723].
- [117] D. Coplowe *et al.* (MINERvA), Phys. Rev. D **102**, 7, 072007 (2020), [arXiv:2002.05812].
- [118] J. Wolcott *et al.* (MINERvA), Phys. Rev. Lett. **117**, 11, 111801 (2016), [arXiv:1604.01728].
- [119] A. A. Aguilar-Arevalo *et al.* (MiniBooNE), Phys. Rev. **D83**, 052007 (2011), [arXiv:1011.3572].
- [120] A. A. Aguilar-Arevalo *et al.* (MiniBooNE), Phys. Rev. Lett. **103**, 081801 (2009), [arXiv:0904.3159].
- [121] A. A. Aguilar-Arevalo *et al.* (MiniBooNE), Phys. Rev. **D83**, 052009 (2011), [arXiv:1010.3264].
- [122] A. A. Aguilar-Arevalo *et al.* (MiniBooNE), Phys. Rev. **D81**, 013005 (2010), [arXiv:0911.2063].
- [123] A. A. Aguilar-Arevalo *et al.* (MiniBooNE), Phys. Lett. **B664**, 41 (2008), [arXiv:0803.3423].
- [124] P. Adamson *et al.* (MINOS), Phys. Rev. **D94**, 7, 072006 (2016), [arXiv:1608.05702].
- [125] C. T. Kullenberg *et al.* (NOMAD), Phys. Lett. **B682**, 177 (2009), [arXiv:0910.0062].
- [126] M. A. Acero *et al.* (NOvA), Phys. Rev. D **102**, 1, 012004 (2020), [arXiv:1902.00558].
- [127] M. A. Acero *et al.* (NOvA), Phys. Rev. D **107**, 11, 112008 (2023), [arXiv:2306.04028].
- [128] K. Hiraide *et al.* (SciBooNE), Phys. Rev. **D78**, 112004 (2008), [arXiv:0811.0369].
- [129] Y. Kurimoto *et al.* (SciBooNE), Phys. Rev. **D81**, 033004 (2010), [arXiv:0910.5768].
- [130] Y. Kurimoto *et al.* (SciBooNE), Phys. Rev. **D81**, 111102 (2010), [arXiv:1005.0059].
- [131] K. Abe *et al.* (T2K), Phys. Rev. **D95**, 1, 012010 (2017), [arXiv:1605.07964].
- [132] K. Abe *et al.* (T2K), Phys. Rev. Lett. **117**, 19, 192501 (2016), [arXiv:1604.04406].
- [133] K. Abe *et al.* (T2K), Phys. Rev. D **101**, 1, 012007 (2020), [arXiv:1909.03936].
- [134] K. Abe *et al.* (T2K), Phys. Rev. D **103**, 11, 112009 (2021), [arXiv:2102.03346].
- [135] P. Vilain *et al.* (CHARM-II), Phys. Lett. **B313**, 267 (1993); A compilation of historical coherent pion production data.
- [136] P. Stowell *et al.* (MINERvA), Phys. Rev. **D100**, 7, 072005 (2019), [arXiv:1903.01558].
- [137] P. Abratenko *et al.* (MicroBooNE) (2023), [arXiv:2305.16249].
- [138] C. T. Kullenberg *et al.* (NOMAD), Phys. Lett. **B706**, 268 (2012), [arXiv:1111.3713].
- [139] K. Abe *et al.* (T2K), J. Phys. **G46**, 8, 08LT01 (2019), [arXiv:1902.03848].
- [140] K. Abe *et al.* (T2K), Phys. Rev. D **100**, 11, 112009 (2019), [arXiv:1910.09439].
- [141] C. M. Marshall *et al.* (MINERvA), Phys. Rev. **D94**, 1, 012002 (2016), [arXiv:1604.03920].
- [142] C. M. Marshall *et al.* (MINERvA), Phys. Rev. Lett. **119**, 1, 011802 (2017), [arXiv:1611.02224].
- [143] Z. Wang *et al.* (MINERvA), Phys. Rev. Lett. **117**, 6, 061802 (2016), [arXiv:1606.08890].
- [144] R. Acciarri *et al.* (ArgoNeuT), Phys. Rev. D **102**, 1, 011101 (2020), [arXiv:2004.01956].
- [145] P. An *et al.* (COHERENT) (2023), [arXiv:2305.19594].
- [146] P. Abratenko *et al.* (MicroBooNE), Phys. Rev. D **104**, 5, 052002 (2021), [arXiv:2101.04228].
- [147] P. Abratenko *et al.* (MicroBooNE), Phys. Rev. D **105**, 5, L051102 (2022), [arXiv:2109.06832].
- [148] P. Abratenko *et al.* (MicroBooNE), Phys. Rev. D **106**, 5, L051102 (2022), [arXiv:2208.02348].
- [149] J. Wolcott *et al.* (MINERvA), Phys. Rev. Lett. **116**, 8, 081802 (2016), [arXiv:1509.05729].
- [150] M. A. Acero *et al.* (NOvA), Phys. Rev. Lett. **130**, 5, 051802 (2023), [arXiv:2206.10585].
- [151] K. Abe *et al.* (T2K), Phys. Rev. Lett. **113**, 24, 241803 (2014), [arXiv:1407.7389].
- [152] K. Abe *et al.* (T2K), Phys. Rev. **D91**, 112010 (2015), [arXiv:1503.08815].
- [153] K. Abe *et al.* (T2K), JHEP **10**, 114 (2020), [arXiv:2002.11986].
- [154] M. Betancourt *et al.*, Phys. Rept. **773-774**, 1 (2018), [arXiv:1805.07378].

53. Plots of Cross Sections and Related Quantities

Updated in 2023. See various sections for details. For additional cross section results, please see earlier editions of the *Review of Particle Physics* (<https://pdg.lbl.gov/rpp-archive/>).

53.1	Pseudorapidity Distributions in pp and $p\bar{p}$ Interactions	807
53.2	Average Hadron Multiplicities in Hadronic e^+e^- Annihilation Events	808
53.3	Annihilation Cross Section Near M_Z	810

53.1 Pseudorapidity Distributions in pp and $p\bar{p}$ Interactions

Revised August 2013 by D.R. Ward (Cavendish Lab.).

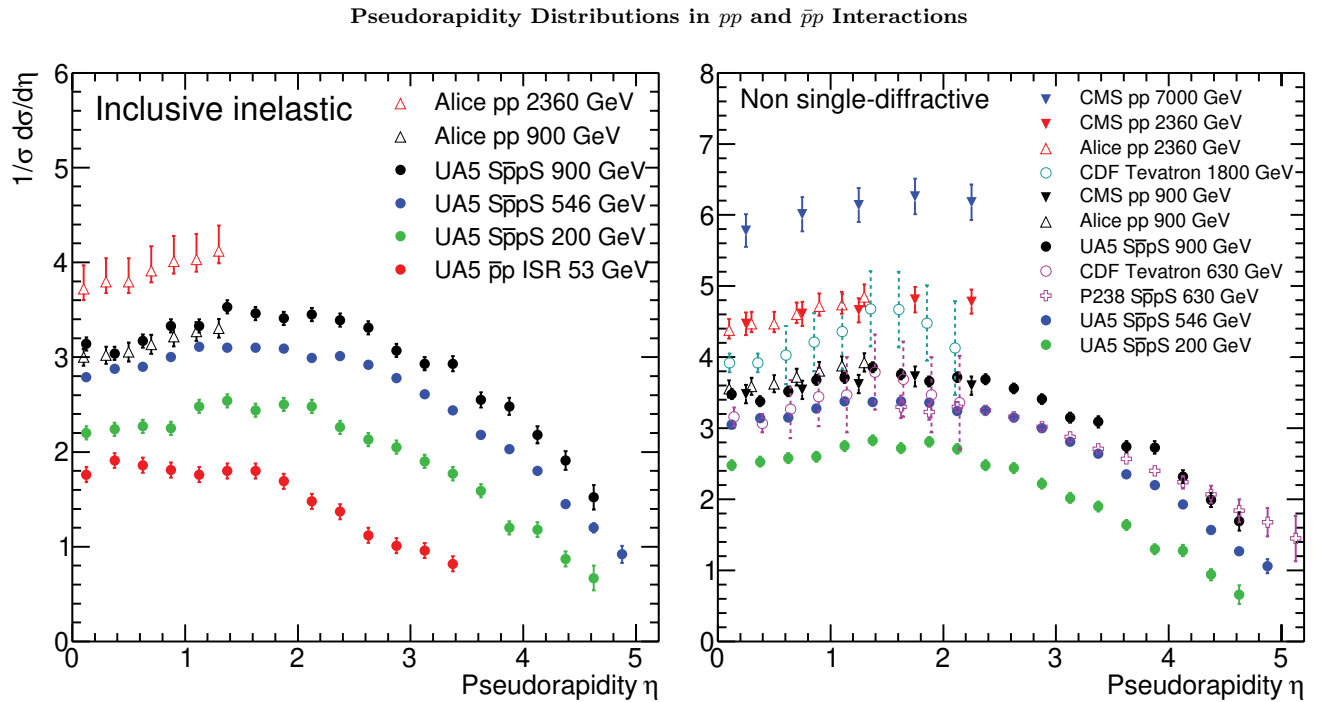


Figure 53.1: Charged particle pseudorapidity distributions in pp collisions for $53 \text{ GeV} \leq \sqrt{s} \leq 1800 \text{ GeV}$. UA5 data from the $S\bar{p}pS$ are taken from [1], and from the ISR from [2]. The UA5 data are shown for both the full inelastic cross-section and with singly diffractive events excluded. Additional non single-diffractive measurements are available from CDF at the Tevatron [3] and from P238 at the $S\bar{p}pS$ [4]. These may be compared with both inclusive and non single-diffractive measurements in pp collisions at the LHC from ALICE [5] and for non single-diffractive interactions from CMS [6, 7]. (Courtesy of D.R. Ward, Cambridge Univ., 2013)

53.2 Average Hadron Multiplicities in Hadronic e^+e^- Annihilation Events

Revised August 2023 by O. Biebel (Ludwig-Maximilians U.).

Table 53.1: Average hadron multiplicities per hadronic e^+e^- annihilation event at $\sqrt{s} \approx 10, 29\text{--}35, 91,$ and $130\text{--}200$ GeV. The rates given include decay products from resonances with $c\tau < 10$ cm, and include the corresponding anti-particle state. Correlations of the systematic uncertainties were considered for the calculation of the averages. Quoted errors are not increased by scale factor S .

Particle	$\sqrt{s} \approx 10$ GeV	$\sqrt{s} = 29\text{--}35$ GeV	$\sqrt{s} = 91$ GeV	$\sqrt{s} = 130\text{--}200$ GeV	References
Pseudoscalar mesons:					
π^+	6.52 ± 0.11	0.3 ± 0.4	17.02 ± 0.19	21.24 ± 0.39	[8–17]
π^0	3.2 ± 0.3	5.83 ± 0.28	9.42 ± 0.32		[12, 18–23]
K^+	0.953 ± 0.018	1.48 ± 0.09	2.228 ± 0.059	2.82 ± 0.19	[9–17, 24, 25]
K^0	0.91 ± 0.05	1.48 ± 0.07	2.049 ± 0.026	2.10 ± 0.12	[12, 17, 20, 26–36]
η	0.20 ± 0.04	0.61 ± 0.07	1.049 ± 0.080		[12, 18, 19, 22, 23, 37–40]
$\eta'(958)$	0.03 ± 0.01	0.26 ± 0.10	0.152 ± 0.020		[20, 39, 41–43]
D^+	$0.194 \pm 0.019^{(a)}$	0.17 ± 0.03	0.175 ± 0.016		[12, 44–47]
D^0	$0.446 \pm 0.032^{(a)}$	0.45 ± 0.07	0.454 ± 0.030		[12, 44–47]
D_s^+	$0.063 \pm 0.014^{(a)}$	$0.45 \pm 0.20^{(b)}$	0.131 ± 0.021		[8, 39, 44, 47–49]
$B^{(c)}$	—	—	$0.134 \pm 0.016^{(d)}$		[46, 50]
B^+	—	—	$0.141 \pm 0.004^{(d)}$		[51]
B_s^0	—	—	$0.054 \pm 0.011^{(d)}$		[52, 53]
Scalar mesons:					
$f_0(980)$	0.024 ± 0.006	$0.05 \pm 0.02^{(e)}$	0.146 ± 0.012		[41, 54–56]
$a_0(980)^\pm$	—	—	$0.27 \pm 0.11^{(f)}$		[43]
Vector mesons:					
$\rho(770)^0$	0.35 ± 0.04	0.81 ± 0.08	1.231 ± 0.098		[9, 12, 55, 57, 58]
$\rho(770)^\pm$	—	—	$2.40 \pm 0.43^{(f)}$		[43]
$\omega(782)$	0.30 ± 0.08	—	1.016 ± 0.065		[40, 42, 43, 57]
$K^*(892)^+$	0.27 ± 0.03	0.64 ± 0.05	0.714 ± 0.055		[9, 12, 33, 57, 59, 60]
$K^*(892)^0$	0.29 ± 0.03	0.56 ± 0.06	0.738 ± 0.024		[9, 12, 36, 57, 58, 61, 62]
$\phi(1020)$	0.044 ± 0.003	0.085 ± 0.011	0.0963 ± 0.0032		[12, 36, 56–58, 61]
$D^*(2010)^+$	$0.177 \pm 0.022^{(a)}$	0.43 ± 0.07	$0.1937 \pm 0.0057^{(g)}$		[12, 44–46, 63, 64]
$D^*(2007)^0$	$0.168 \pm 0.019^{(a)}$	0.27 ± 0.11	—		[12, 44, 45]
$D_s^*(2112)^+$	$0.048 \pm 0.014^{(a)}$	—	$0.101 \pm 0.048^{(h)}$		[48, 65]
$B^*^{(i)}$	—	—	0.288 ± 0.026		[66, 67]
$J/\psi(1S)$	$0.00050 \pm 0.00005^{(a)}$	—	$0.0052 \pm 0.0004^{(j)}$		[68–73]
$\psi(2S)$	—	—	$0.0023 \pm 0.0004^{(j)}$		[71, 73, 74]
$\Upsilon(1S)$	—	—	$0.00014 \pm 0.00007^{(j)}$		[75]
Pseudovector mesons:					
$f_1(1285)$	—	—	0.165 ± 0.051		[76]
$f_1(1420)$	—	—	0.056 ± 0.012		[76]
$\chi_{c1}(3510)$	—	—	$0.0041 \pm 0.0011^{(j)}$		[71, 74]
Tensor mesons:					
$f_2(1270)$	0.09 ± 0.02	0.14 ± 0.04	0.166 ± 0.020		[54–56, 77]
$f_2'(1525)$	—	—	0.012 ± 0.006		[55]
$K_2^*(1430)^+$	—	0.09 ± 0.03	—		[55, 78]
$K_2^*(1430)^0$	—	0.12 ± 0.06	0.084 ± 0.022		[54, 55, 79]
$B^{** (k)}$	—	—	0.118 ± 0.024		[80]
D_{s1}^\pm	—	—	$0.0052 \pm 0.0011^{(l)}$		[81]
$D_{s2}^{*\pm}$	—	—	$0.0083 \pm 0.0031^{(l)}$		[81]
Baryons:					
p	0.266 ± 0.008	0.640 ± 0.050	1.050 ± 0.032	1.41 ± 0.18	[10, 13–17, 24, 25, 77]
Λ	$0.093 \pm 0.006^{(a)}$	0.205 ± 0.010	0.3915 ± 0.0065	0.39 ± 0.03	[17, 20, 34, 36, 77, 82–85]
Σ^0	$0.0221 \pm 0.0018^{(a)}$	—	0.078 ± 0.010		[10, 59, 82, 86–88]
Σ^-	—	—	0.081 ± 0.010		[88, 89]
Σ^+	—	—	0.107 ± 0.011		[87, 88]
Σ^\pm	—	—	0.174 ± 0.009		[84, 88]
Ξ^-	$0.0055 \pm 0.0004^{(a)}$	0.0176 ± 0.0027	0.0262 ± 0.0009		[9, 59, 77, 82–85]
$\Delta(1232)^{++}$	0.040 ± 0.010	—	0.085 ± 0.014		[90–92]
$\Sigma(1385)^-$	0.006 ± 0.002	0.017 ± 0.004	0.0240 ± 0.0017		[59, 82, 84, 85, 93]
$\Sigma(1385)^+$	$0.0062 \pm 0.0011^{(a)}$	0.017 ± 0.004	0.0239 ± 0.0015		[59, 82–85, 93]
$\Sigma(1385)^\pm$	0.0106 ± 0.0020	0.033 ± 0.008	0.0472 ± 0.0027		[59, 82, 84, 85, 93]
$\Xi(1530)^0$	$0.00130 \pm 0.00010^{(a)}$	—	0.00694 ± 0.00049		[59, 82, 83, 85, 94]
Ω^-	$0.00060 \pm 0.00033^{(a)}$	0.014 ± 0.007	0.00124 ± 0.00018		[59, 77, 82, 83, 85, 86]
Λ_c^+	$0.0480 \pm 0.0036^{(a,m)}$	0.110 ± 0.050	$0.0591 \pm 0.0047^{(n)}$		[47, 49, 77, 83, 95, 96]
Λ_b^0	—	—	0.031 ± 0.016		[97]
Σ_c^0	$0.0025 \pm 0.0004^{(a)}$	—	—		[83]
$\Lambda(1520)$	$0.0046 \pm 0.0004^{(a)}$	—	0.0222 ± 0.0027		[83, 85, 89, 98]

(a) $\sigma_{\text{had}} = 3.33 \pm 0.05 \pm 0.21$ nb (CLEO: [99]) has been used in converting the measured cross sections to average hadron multiplicities.(b) $B(D_s \rightarrow \eta\pi, \eta'\pi)$ was used (RPP 1994).

- (c) Comprises both charged and neutral B meson states.
- (d) The Standard Model $B(Z \rightarrow b\bar{b}) = 0.217$ was used.
- (e) $x_p = p/p_{\text{beam}} > 0.1$ only.
- (f) Both charge states.
- (g) $B(D^*(2010)^+ \rightarrow D^0\pi^+) \times B(D^0 \rightarrow K^-\pi^+)$ has been used (RPP 2000).
- (h) $B(D_s^* \rightarrow D_S^+\gamma)$, $B(D_s^+ \rightarrow \phi\pi^+)$, $B(\phi \rightarrow K^+K^-)$ have been used (RPP 1998).
- (i) Any charge state (*i.e.*, B_d^* , B_u^* , or B_s^*).
- (j) $B(Z \rightarrow \text{hadrons}) = 0.699$ was used (RPP 1994).
- (k) Any charge state (*i.e.*, B_d^{*+} , B_u^{*+} , or B_s^{*+}).
- (l) Assumes $B(D_{s1}^+ \rightarrow D^{*+}K^0 + D^{*0}K^+) = 100\%$ and $B(D_{s2}^+ \rightarrow D^0K^+) = 45\%$.
- (m) Derived from the production cross section of $\Lambda_c^+ \rightarrow p\pi K$ using (a) and using $B(\Lambda_c^+ \rightarrow p\pi K) = (6.26 \pm 0.29)\%$ (RPP 2022).
- (n) Derived from [96], updated with $B(\Lambda_c^+ \rightarrow p\pi K) = (6.26 \pm 0.29)\%$ (RPP 2022), and complemented by the Λ_c^+ contribution from $g \rightarrow c\bar{c}$ of [47].

References grouped by collaboration for Table-53.1:

- **RPP:** [12]
- **ALEPH:** [13, 20, 40, 58, 59, 63, 70, 81],
- **ARGUS:** [8, 24, 37, 41, 57, 82, 90, 98],
- **BaBar:** [10, 48, 68, 95],
- **Belle:** [44, 69, 83],
- **CELLO:** [19, 26],
- **CLEO:** [9, 45, 49, 99],
- **Crystal Ball:** [38],
- **DELPHI:** [14, 17, 21, 25, 33, 46, 50–52, 55, 61, 66, 71, 76, 80, 84, 86, 89, 91, 94],
- **HRS:** [27, 54, 78, 93],
- **L3:** [22, 34, 42, 67, 72, 74, 87]
- **MARK II:** [29, 39],
- **JADE:** [18, 28],
- **OPAL:** [15, 23, 35, 43, 47, 53, 56, 60, 62, 64, 65, 73, 75, 79, 85, 88, 92, 97],
- **PLUTO:** [30]
- **SLD:** [16, 36],
- **TASSO:** [31]
- **TPC:** [32].

53.3 Annihilation Cross Section Near M_Z

Courtesy of M. Grünewald and the LEP Electroweak Working Group, 2007.

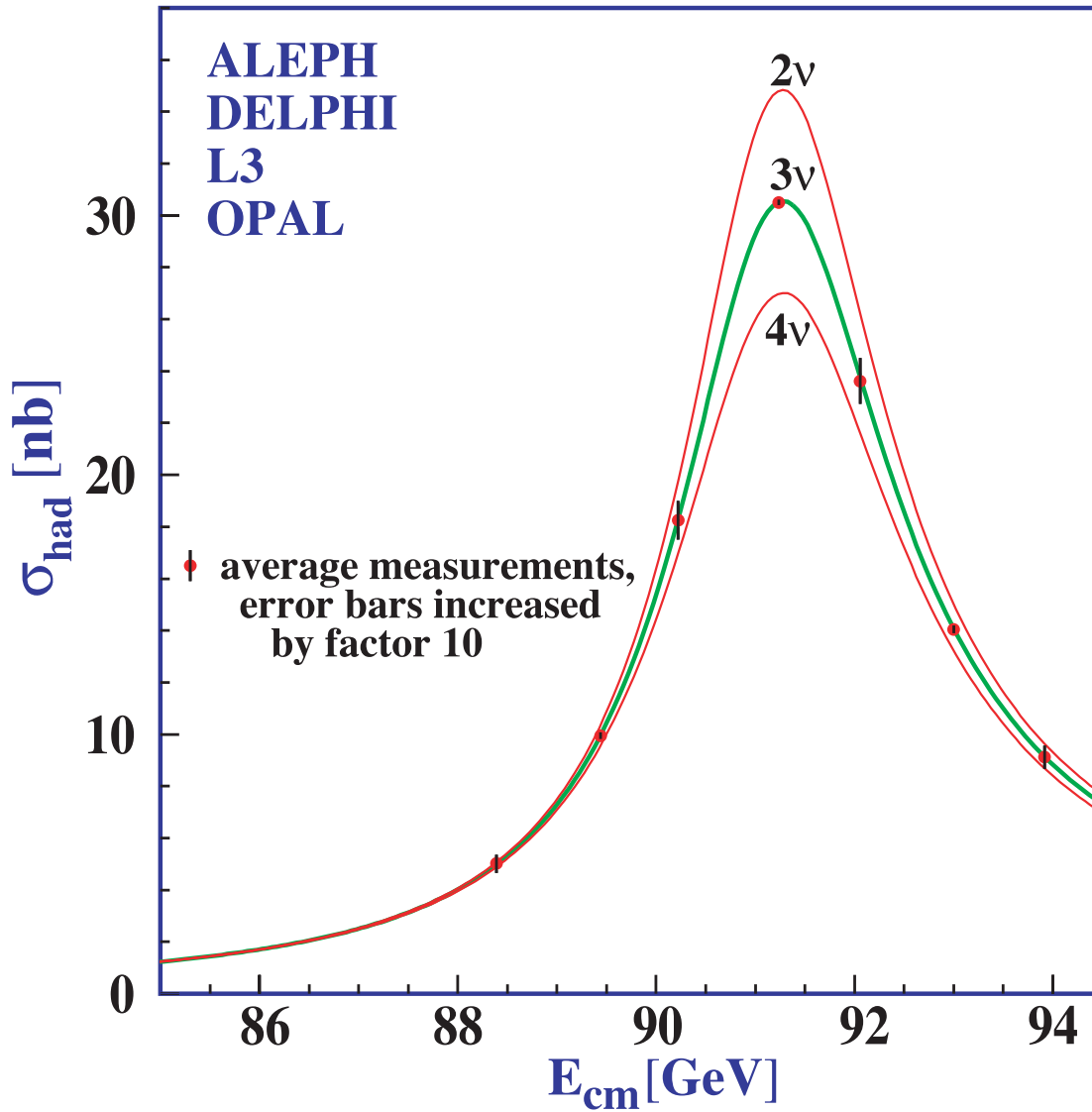


Figure 53.2: Combined data from the ALEPH, DELPHI, L3, and OPAL Collaborations for the cross section in e^+e^- annihilation into hadronic final states as a function of the center-of-mass energy near the Z pole. The curves show the predictions of the Standard Model with two, three, and four species of light neutrinos. The asymmetry of the curve is produced by initial-state radiation. Note that the error bars have been increased by a factor ten for display purposes. References: ALEPH [100], DELPHI [101], L3 [102], OPAL [103], Combination [104],

References

- [1] G. J. Alner *et al.* (UA5), *Z. Phys.* **C33**, 1 (1986).
- [2] K. Alpgard *et al.* (UA5), *Phys. Lett.* **112B**, 183 (1982).
- [3] F. Abe *et al.* (CDF), *Phys. Rev.* **D41**, 2330 (1990), [119(1989)].
- [4] R. Harr *et al.*, *Phys. Lett.* **B401**, 176 (1997), [hep-ex/9703002].
- [5] K. Aamodt *et al.* (ALICE), *Eur. Phys. J.* **C68**, 89 (2010), [arXiv:1004.3034].
- [6] V. Khachatryan *et al.* (CMS), *JHEP* **02**, 041 (2010), [arXiv:1002.0621].
- [7] V. Khachatryan *et al.* (CMS), *Phys. Rev. Lett.* **105**, 022002 (2010), [arXiv:1005.3299].
- [8] H. Albrecht *et al.* (ARGUS), *Z. Phys.* **C54**, 1 (1992).
- [9] S. Behrends *et al.* (CLEO), *Phys. Rev.* **D31**, 2161 (1985).
- [10] J. P. Lees *et al.* (BaBar), *Phys. Rev.* **D88**, 032011 (2013), [arXiv:1306.2895].
- [11] H. Albrecht *et al.*, *Phys. Lett.* **102B**, 291 (1981).
- [12] K. Hikasa *et al.* (Particle Data Group), *Phys. Rev.* **D45**, S1 (1992), [Erratum: *Phys. Rev.*D46,5210(1992)].
- [13] R. Barate *et al.* (ALEPH), *Eur. Phys. J.* **C5**, 205 (1998).
- [14] P. Abreu *et al.* (DELPHI), *Eur. Phys. J.* **C5**, 585 (1998).
- [15] R. Akers *et al.* (OPAL), *Z. Phys.* **C63**, 181 (1994).
- [16] K. Abe *et al.* (SLD), *Phys. Rev.* **D69**, 072003 (2004), [hep-ex/0310017].
- [17] P. Abreu *et al.* (DELPHI), *Eur. Phys. J.* **C18**, 203 (2000), [Erratum: *Eur. Phys. J.*C25,493(2002)], [hep-ex/0103031].
- [18] D. D. Pitzl *et al.* (JADE), *Z. Phys.* **C46**, 1 (1990), [Erratum: *Z. Phys.*C47,676(1990)].
- [19] H. J. Behrend *et al.* (CELLO), *Z. Phys.* **C47**, 1 (1990).
- [20] R. Barate *et al.* (ALEPH), *Eur. Phys. J.* **C16**, 613 (2000).
- [21] W. Adam *et al.* (DELPHI), *Z. Phys.* **C69**, 561 (1996).
- [22] M. Acciarri *et al.* (L3), *Phys. Lett.* **B371**, 126 (1996).
- [23] G. Abbiendi *et al.* (OPAL), *Eur. Phys. J.* **C17**, 373 (2000), [hep-ex/0007017].
- [24] H. Albrecht *et al.* (ARGUS), *Z. Phys.* **C44**, 547 (1989).
- [25] P. Abreu *et al.* (DELPHI), *Nucl. Phys.* **B444**, 3 (1995).
- [26] H. J. Behrend *et al.* (CELLO), *Z. Phys.* **C46**, 397 (1990).
- [27] M. Derrick *et al.*, *Phys. Rev.* **D35**, 2639 (1987).
- [28] W. Bartel *et al.* (JADE), *Z. Phys.* **C20**, 187 (1983).
- [29] H. Schellman *et al.*, *Phys. Rev.* **D31**, 3013 (1985).
- [30] C. Berger *et al.* (PLUTO), *Phys. Lett.* **104B**, 79 (1981).
- [31] M. Althoff *et al.* (TASSO), *Z. Phys.* **C27**, 27 (1985).
- [32] H. Aihara *et al.* (TPC/Two Gamma), *Phys. Rev. Lett.* **53**, 2378 (1984).
- [33] P. Abreu *et al.* (DELPHI), *Z. Phys.* **C65**, 587 (1995).
- [34] M. Acciarri *et al.* (L3), *Phys. Lett.* **B407**, 389 (1997), [Erratum: *Phys. Lett.*B427,409(1998)].
- [35] R. Akers *et al.* (OPAL), *Z. Phys.* **C67**, 389 (1995).
- [36] K. Abe *et al.* (SLD), *Phys. Rev.* **D59**, 052001 (1999), [hep-ex/9805029].
- [37] H. Albrecht *et al.* (ARGUS), *Z. Phys.* **C46**, 15 (1990).
- [38] C. Bieler *et al.* (Crystal Ball), *Z. Phys.* **C49**, 225 (1991).
- [39] G. Wormser *et al.*, *Phys. Rev. Lett.* **61**, 1057 (1988).
- [40] A. Heister *et al.* (ALEPH), *Phys. Lett.* **B528**, 19 (2002), [hep-ex/0201012].
- [41] H. Albrecht *et al.* (ARGUS), *Z. Phys.* **C58**, 199 (1993).
- [42] M. Acciarri *et al.* (L3), *Phys. Lett.* **B393**, 465 (1997).
- [43] K. Ackerstaff *et al.* (OPAL), *Eur. Phys. J.* **C5**, 411 (1998), [hep-ex/9805011].
- [44] R. Seuster *et al.* (Belle), *Phys. Rev.* **D73**, 032002 (2006), [hep-ex/0506068].
- [45] M. Artuso *et al.* (CLEO), *Phys. Rev.* **D70**, 112001 (2004), [hep-ex/0402040].
- [46] P. Abreu *et al.* (DELPHI), *Z. Phys.* **C59**, 533 (1993), [Erratum: *Z. Phys.*C65,709(1995)].
- [47] G. Alexander *et al.* (OPAL), *Z. Phys.* **C72**, 1 (1996).
- [48] B. Aubert *et al.* (BaBar), *Phys. Rev.* **D65**, 091104 (2002), [hep-ex/0201041].
- [49] D. Bortoletto *et al.* (CLEO), *Phys. Rev.* **D37**, 1719 (1988), [Erratum: *Phys. Rev.*D39,1471(1989)].
- [50] P. Abreu *et al.* (DELPHI), *Z. Phys.* **C57**, 181 (1993).
- [51] J. Abdallah *et al.* (DELPHI), *Phys. Lett.* **B576**, 29 (2003), [hep-ex/0311005].
- [52] P. Abreu *et al.* (DELPHI), *Z. Phys.* **C61**, 407 (1994).
- [53] R. Akers *et al.* (OPAL), *Z. Phys.* **C66**, 555 (1995).
- [54] S. Abachi *et al.*, *Phys. Rev. Lett.* **57**, 1990 (1986).
- [55] P. Abreu *et al.* (DELPHI), *Phys. Lett.* **B449**, 364 (1999).
- [56] K. Ackerstaff *et al.* (OPAL), *Eur. Phys. J.* **C4**, 19 (1998), [hep-ex/9802013].
- [57] H. Albrecht *et al.* (ARGUS), *Z. Phys.* **C61**, 1 (1994).
- [58] D. Buskulic *et al.* (ALEPH), *Z. Phys.* **C69**, 379 (1996).
- [59] R. Barate *et al.* (ALEPH), *Phys. Rept.* **294**, 1 (1998).
- [60] P. D. Acton *et al.* (OPAL), *Phys. Lett.* **B305**, 407 (1993).
- [61] P. Abreu *et al.* (DELPHI), *Z. Phys.* **C73**, 61 (1996).
- [62] K. Ackerstaff *et al.* (OPAL), *Phys. Lett.* **B412**, 210 (1997), [hep-ex/9708022].
- [63] R. Barate *et al.* (ALEPH), *Eur. Phys. J.* **C16**, 597 (2000), [hep-ex/9909032].
- [64] K. Ackerstaff *et al.* (OPAL), *Eur. Phys. J.* **C1**, 439 (1998), [hep-ex/9708021].
- [65] K. Ackerstaff *et al.* (OPAL), *Eur. Phys. J.* **C5**, 1 (1998), [hep-ex/9802008].
- [66] P. Abreu *et al.* (DELPHI), *Z. Phys.* **C68**, 353 (1995).
- [67] M. Acciarri *et al.* (L3), *Phys. Lett.* **B345**, 589 (1995).
- [68] B. Aubert *et al.* (BaBar), *Phys. Rev. Lett.* **87**, 162002 (2001), [hep-ex/0106044].
- [69] K. Abe *et al.* (Belle), *Phys. Rev. Lett.* **88**, 052001 (2002), [hep-ex/0110012].
- [70] D. Buskulic *et al.* (ALEPH), *Phys. Lett.* **B295**, 396 (1992).
- [71] P. Abreu *et al.* (DELPHI), *Phys. Lett.* **B341**, 109 (1994).
- [72] M. Acciarri *et al.* (L3), *Phys. Lett.* **B453**, 94 (1999).
- [73] G. Alexander *et al.* (OPAL), *Z. Phys.* **C70**, 197 (1996).
- [74] M. Acciarri *et al.* (L3), *Phys. Lett.* **B407**, 351 (1997).
- [75] G. Alexander *et al.* (OPAL), *Phys. Lett.* **B370**, 185 (1996).
- [76] J. Abdallah *et al.* (DELPHI), *Phys. Lett.* **B569**, 129 (2003), [hep-ex/0309057].
- [77] A. De Angelis, *J. Phys.* **G19**, 1233 (1993).
- [78] S. Abachi *et al.*, *Phys. Lett.* **B199**, 151 (1987).
- [79] R. Akers *et al.* (OPAL), *Z. Phys.* **C68**, 1 (1995).
- [80] P. Abreu *et al.* (DELPHI), *Phys. Lett.* **B345**, 598 (1995).
- [81] A. Heister *et al.* (ALEPH), *Phys. Lett.* **B526**, 34 (2002), [hep-ex/0112010].
- [82] H. Albrecht *et al.* (ARGUS), *Z. Phys.* **C39**, 177 (1988).
- [83] M. Niiyama *et al.* (Belle), *Phys. Rev.* **D97**, 7, 072005 (2018), [arXiv:1706.06791].
- [84] P. Abreu *et al.* (DELPHI), *Z. Phys.* **C67**, 543 (1995).
- [85] G. Alexander *et al.* (OPAL), *Z. Phys.* **C73**, 569 (1997).
- [86] W. Adam *et al.* (DELPHI), *Z. Phys.* **C70**, 371 (1996).
- [87] M. Acciarri *et al.* (L3), *Phys. Lett.* **B479**, 79 (2000), [hep-ex/0002066].

- [88] G. Alexander *et al.* (OPAL), *Z. Phys.* **C73**, 587 (1997).
- [89] P. Abreu *et al.* (DELPHI), *Phys. Lett.* **B475**, 429 (2000), [hep-ex/0103020].
- [90] H. Albrecht *et al.* (ARGUS), *Phys. Lett.* **B230**, 169 (1989).
- [91] P. Abreu *et al.* (DELPHI), *Phys. Lett.* **B361**, 207 (1995).
- [92] G. Alexander *et al.* (OPAL), *Phys. Lett.* **B358**, 162 (1995).
- [93] S. Abachi *et al.*, *Phys. Rev. Lett.* **58**, 2627 (1987), [Erratum: *Phys. Rev. Lett.* 59, 2388 (1987)].
- [94] J. Abdallah *et al.* (DELPHI), *Eur. Phys. J.* **C44**, 299 (2005), [hep-ex/0510023].
- [95] B. Aubert *et al.* (BaBar), *Phys. Rev.* **D75**, 012003 (2007), [hep-ex/0609004].
- [96] L. Gladilin, *Eur. Phys. J. C* **75**, 1, 19 (2015), [arXiv:1404.3888].
- [97] P. D. Acton *et al.* (OPAL), *Phys. Lett.* **B281**, 394 (1992).
- [98] H. Albrecht *et al.* (ARGUS), *Phys. Rept.* **276**, 223 (1996).
- [99] R. Giles *et al.* (CLEO), *Phys. Rev.* **D29**, 1285 (1984).
- [100] R. Barate *et al.* (ALEPH), *Eur. Phys. J.* **C14**, 1 (2000).
- [101] P. Abreu *et al.* (DELPHI), *Eur. Phys. J.* **C16**, 371 (2000).
- [102] M. Acciarri *et al.* (L3), *Eur. Phys. J.* **C16**, 1 (2000), [hep-ex/0002046].
- [103] G. Abbiendi *et al.* (OPAL), *Eur. Phys. J.* **C19**, 587 (2001), [hep-ex/0012018].
- [104] S. Schael *et al.* (ALEPH, DELPHI, L3, OPAL, SLD, LEP Electroweak Working Group, SLD Electroweak Group, SLD Heavy Flavour Group), *Phys. Rept.* **427**, 257 (2006), [hep-ex/0509008].

Particle Properties

Gauge Bosons

54. Mass and width of the W boson (rev.)	815
55. Z boson	817

Charged Leptons

56. Muon anomalous magnetic moment (rev.)	822
57. Muon decay parameters (rev.)	826
58. τ branching fractions (rev.)	829
59. τ -lepton decay parameters (rev.)	832

Quarks

60. Quark masses (rev.)	834
61. Top quark (rev.)	844

Mesons

62. Form factors for semileptonic kaon ($K_{\ell 3}$), radiative pion ($\pi_{\ell 2\gamma}$) & kaon ($K_{\ell 2\gamma}$) decays (rev.)	871
63. Spectroscopy of light meson resonances (rev.)	874
64. Scalar mesons below 1 GeV (rev.)	888
65. Rare kaon decays (rev.)	896
66. CPT invariance tests in neutral kaon decay (rev.)	902
67. V_{ud} , V_{us} , Cabibbo angle, and CKM unitarity (rev.)	904
68. CP -violation in K_L decays (rev.)	908
69. Review of multibody charm analyses (rev.)	911
70. $D^0-\bar{D}^0$ mixing (rev.)	917
71. D_s^+ branching fractions	927
72. Leptonic decays of charged pseudoscalar mesons (rev.)	929
73. Production and decay of b -flavored hadrons (rev.)	940
74. Polarization in B decays (rev.)	951
75. $B^0-\bar{B}^0$ mixing (rev.)	955
76. Semileptonic B decays, V_{cb} and V_{ub} (rev.)	962
77. CKM angles from B hadrons, determination of (rev.)	980
78. Spectroscopy of mesons containing two heavy quarks (rev.)	985
79. Heavy non- $q\bar{q}$ mesons (rev.)	994

Baryons

80. Baryon decay parameters	1001
81. N and Δ resonances	1002
82. Λ and Σ resonances	1007
83. Pole structure of the $\Lambda(1405)$ region	1010
84. Pentaquarks (rev.)	1012

Notes in Volume 2

Triple gauge couplings (TGC's)	1190
Anomalous $ZZ\gamma$, $Z\gamma\gamma$, and ZZV couplings	1216
Anomalous W/Z quartic couplings (rev.)	1217
Neutrino properties (rev.)	1332
Sum of neutrino masses (rev.)	1335
Number of light neutrino types from collider experiments	1341
Neutrinoless double- β decay	1343
Charged kaon mass	1538
Dalitz plot parameters for $K \rightarrow 3\pi$ decays	1547
CP -violation in $K_S \rightarrow 3\pi$	1557
Heavy Flavor Averaging Group (rev.)	1681
Charmonium system (rev.)	1898
Branching ratios of $\psi(2S)$ and $\chi_{c0,1,2}$ (rev.)	1934
Bottomonium system (rev.)	2023
Width determination of the Υ states	2023
Radiative hyperon decays	2219
Ξ resonances (rev.)	2223



54. Mass and Width of the W Boson

Revised April 2024 by M. Grünewald (University Coll. Dublin) and A. Gurtu (CERN; TIFR Mumbai).

Precision determination of the W mass is of great importance in testing the internal consistency of the Standard Model. From the time of its discovery in 1983, the W boson has been studied and its mass determined in $p\bar{p}$ and e^+e^- interactions; it is currently studied in pp interactions at the LHC. The mass and width definition used here corresponds to a Breit-Wigner with mass-dependent width.

Production of on-shell W bosons at hadron colliders is tagged by the high p_T charged lepton from its leptonic decay modes. Owing to the unknown parton-parton effective energy and missing energy in the longitudinal direction, the hadron collider experiments reconstruct the transverse mass of the W boson, and derive the W mass from comparing the transverse mass distribution with Monte Carlo predictions as a function of the mass m_W . The transverse momentum of the charged lepton itself and the transverse missing energy (arising from the neutrino in W decay) are also sensitive to the W mass and used in its determination. These analyses use the electron and muon decay modes of the W boson.

At the e^+e^- collider LEP, a precise knowledge of the beam energy enables one to determine the $e^+e^- \rightarrow W^+W^-$ cross section as a function of center of mass energy, as well as to reconstruct the W mass precisely from its decay products, even if one of them decays leptonically. Close to the W^+W^- production threshold ($\sqrt{s} = 161$ GeV), the dependence of the W -pair production cross section on m_W is large, and this was used to determine m_W . At higher centre-of-mass energies (172 to 209 GeV) this dependence is much weaker, thus W bosons were directly reconstructed and the mass determined as the invariant mass of the decay products, improving the resolution with a kinematic fit.

To compute the LEP average W mass, each experiment provided its measured W mass for the $q\bar{q}q\bar{q}$ and $q\bar{q}\ell\nu$, $\ell = e, \mu, \tau$ channels at each center-of-mass energy, along with a detailed decomposition of uncertainty contributions: statistical, uncorrelated, partially correlated and fully correlated systematics [1]. This yielded a combined LEP average W mass of $m_W = 80.376 \pm 0.033$ GeV. Errors on m_W due to uncertainties in the LEP beam energy (9 MeV), and possible effect of color reconnection (CR) and Bose-Einstein correlations (BEC) between quarks from different W bosons (8 MeV) are included. Similarly the combined LEP average of the W boson total width is determined to be $\Gamma_W = 2.195 \pm 0.083$ GeV [1].

In the past a similar procedure was followed for the measurements at hadron colliders. The two Tevatron experiments CDF [2] and D0 [3] identified common systematic errors: uncertainties due to the parton distribution functions (PDF), radiative corrections, and choice of mass (width) in the width (mass) measurements were treated as correlated and the resultant mass [4] and width [5] of the W were determined. The W boson total width obtained is $\Gamma_W = 2.046 \pm 0.049$ GeV. Similarly the mass results from the two LHC experiments, ATLAS [6] and LHCb [7] were combined to obtain an LHC average mass of the W , and an overall hadron collider average of the W mass was obtained as well [8].

The results on mass and width published by the experiments are shown in Figures 54.1 and 54.2, respectively. Until 2022, all measurements were in good agreement with each other and with the world average [8]. In April 2022 the CDF collaboration published a result $m_W = 80.4335 \pm 0.0094$ GeV [10], based upon their full Run-II dataset of 8.8 fb^{-1} . The result is of higher precision than the 2022 world average, but the two results disagree significantly.¹

The LHC-TeV W -mass Working Group, including W -mass experts from all hadron collider experiments, CDF, D0, ATLAS, CMS, LHCb, has been working to understand better the nature of this disagreement and suggest a way forward to obtain a world average value of the W mass. Corrections, uncertainties and their correlations have been evaluated to a greater detail and used in the

¹The 2022 CDF result includes the 2.2 fb^{-1} of data used for the previous CDF Run-II result of 80.387 ± 0.019 GeV [2]. Incorporating the improved understanding of PDFs and track reconstruction, the central value of the 2.2 fb^{-1} result is increased by 13.5 MeV to $80,400.5$ MeV [10].

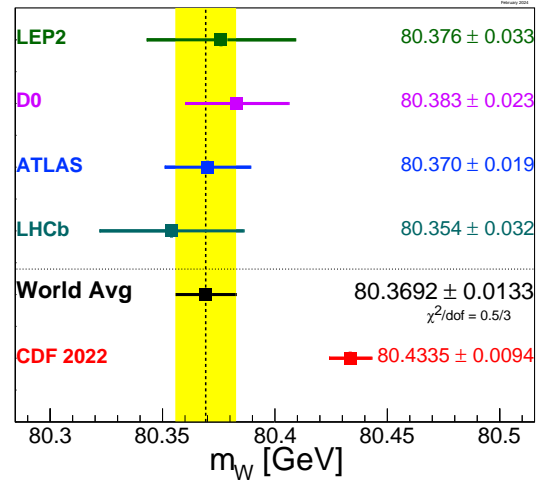


Figure 54.1: Measurements of the W -boson mass by the LEP, Tevatron and LHC experiments. The CDF 2022 result is not used in the world average. In March 2024, after the cut-off of results for this review, the ATLAS Collaboration has submitted for publication a refined analysis of their data used in [6] and obtained a more precise mass value of 80.3665 ± 0.0159 GeV [9].

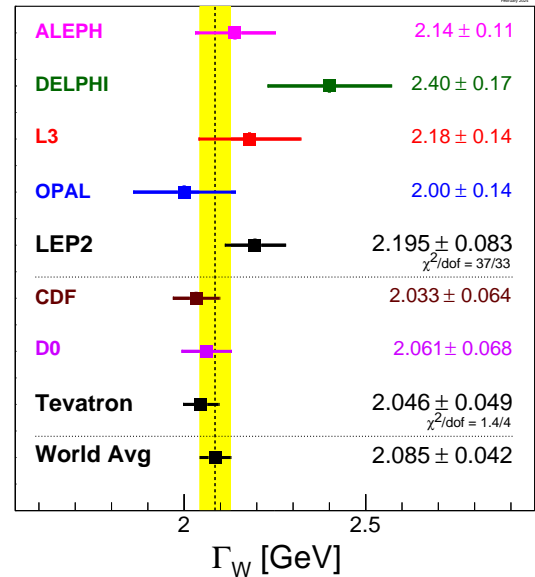


Figure 54.2: Measurements of the W -boson width by the LEP and Tevatron experiments. In March 2024, after the cut-off of results for this review, the ATLAS Collaboration has submitted for publication a refined analysis of their data used in [6] and obtained a width value of 2.202 ± 0.047 GeV [9].

combination: the central values are corrected to a common theory description and PDF, and the uncertainties, especially due to PDFs, have been re-evaluated to account for correlations properly. The group reports [11] that a combination of all W -mass measurements has a probability of compatibility of 0.5% only, and is therefore disfavoured. A 91% probability of compatibility is obtained when the CDF-II measurement is removed. The corresponding value of the W boson mass is $m_W = 80369.2 \pm 13.3$ MeV, which we quote as the World Average. More details are given in [11].

The Standard Model prediction from an electroweak fit, including Z -pole data and the measured masses of the top quark and of the Higgs boson but excluding results on m_W and Γ_W , implies a W -boson mass of $m_W = 80.353 \pm 0.006$ GeV and a W -boson

width of $\Gamma_W = 2.089 \pm 0.001$ GeV; see Section 10, Electroweak Model and Constraints on New Physics, J.Erler and A.Freitas, 2024, this review. Note that the electroweak fit of Section 10 to all measurements uses slightly different measurements of the W boson mass and width as explained there.

References

- [1] S. Schael *et al.* (ALEPH, DELPHI, L3, OPAL, LEP Electroweak Working Group), Phys. Rept. **532**, 119 (2013), [arXiv:1302.3415].
- [2] T. Aaltonen *et al.* (CDF), Phys. Rev. Lett. **108**, 151803 (2012), [arXiv:1203.0275].
- [3] V. M. Abazov *et al.* (D0), Phys. Rev. Lett. **108**, 151804 (2012), [arXiv:1203.0293].
- [4] T. A. Aaltonen *et al.* (CDF, D0), Phys. Rev. D **88**, 5, 052018 (2013), [arXiv:1307.7627].
- [5] The Tevatron Electroweak Working Group, for the CDF and D0 Collaborations, March 2010, [arXiv:1003.2826].
- [6] M. Aaboud *et al.* (ATLAS), Eur. Phys. J. C **78**, 2, 110 (2018), [Erratum: Eur.Phys.J.C 78, 898 (2018)], [arXiv:1701.07240].
- [7] R. Aaij *et al.* (LHCb), JHEP **01**, 166 (2022), [arXiv:2107.10090].
- [8] R. L. Workman *et al.* (Particle Data Group), PTEP **2022**, 083C01 (2022).
- [9] G. Aad *et al.* (ATLAS) (2024), [arXiv:2403.15085].
- [10] T. Aaltonen *et al.* (CDF), Science **376**, 6589, 170 (2022).
- [11] S. Amoroso *et al.* (LHC-TeV MW Working Group), Eur. Phys. J. C **84**, 5, 451 (2024), [arXiv:2308.09417].

55. Z Boson

Revised August 2018 by M. Grünewald (University Coll. Dublin) and A. Gurtu (CERN; TIFR Mumbai).

Precision measurements at the Z -boson resonance using electron–positron colliding beams began in 1989 at the SLC and at LEP. During 1989–95, the four LEP experiments (ALEPH, DELPHI, L3, OPAL) made high-statistics studies of the production and decay properties of the Z . Although the SLD experiment at the SLC collected much lower statistics, it was able to match the precision of LEP experiments in determining the effective electroweak mixing angle $\sin^2\theta_W$ and the rates of Z decay to b - and c -quarks, owing to availability of polarized electron beams, small beam size, and stable beam spot.

The Z -boson properties reported in this section may broadly be categorized as:

- The standard ‘lineshape’ parameters of the Z consisting of its mass, M_Z , its total width, Γ_Z , and its partial decay widths, $\Gamma(\text{hadrons})$, and $\Gamma(\ell\bar{\ell})$ where $\ell = e, \mu, \tau, \nu$;
- Z asymmetries in leptonic decays and extraction of Z couplings to charged and neutral leptons;
- The b - and c -quark-related partial widths and charge asymmetries which require special techniques;
- Determination of Z decay modes and the search for modes that violate known conservation laws;
- Average particle multiplicities in hadronic Z decay;
- Z anomalous couplings.

The effective vector and axial-vector coupling constants describing the Z -to-fermion coupling are also measured in $p\bar{p}$ and ep collisions at the Tevatron and at HERA. The corresponding cross-section formulae are given in Section 39 (Cross-section formulae for specific processes) and Section 16 (Structure Functions) in this *Review*. In this minireview, we concentrate on the measurements in e^+e^- collisions at LEP and SLC.

The standard ‘lineshape’ parameters of the Z are determined from an analysis of the production cross sections of these final states in e^+e^- collisions. The $Z \rightarrow \nu\bar{\nu}(\gamma)$ state is identified directly by detecting single photon production and indirectly by subtracting the visible partial widths from the total width. Inclusion in this analysis of the forward-backward asymmetry of charged leptons, $A_{FB}^{(0,\ell)}$, of the τ polarization, $P(\tau)$, and its forward-backward asymmetry, $P(\tau)^{fb}$, enables the separate determination of the effective vector (\bar{g}_V) and axial vector (\bar{g}_A) couplings of the Z to these leptons and the ratio (\bar{g}_V/\bar{g}_A), which is related to the effective electroweak mixing angle $\sin^2\theta_W$ (see the ‘Electroweak Model and Constraints on New Physics’ review).

Determination of the b - and c -quark-related partial widths and charge asymmetries involves tagging the b and c quarks for which various methods are employed: requiring the presence of a high momentum prompt lepton in the event with high transverse momentum with respect to the accompanying jet; impact parameter and lifetime tagging using precision vertex measurement with high-resolution detectors; application of neural-network techniques to classify events as b or non- b on a statistical basis using event–shape variables; and using the presence of a charmed meson (D/D^*) or a kaon as a tag.

55.1 Z -parameter determination

LEP was run at energy points on and around the Z mass (88–94 GeV) constituting an energy ‘scan’. The shape of the cross-section variation around the Z peak can be described by a Breit-Wigner *ansatz* with an energy-dependent total width [1–3]. The **three** main properties of this distribution, viz., the **position** of the peak, the **width** of the distribution, and the **height** of the peak, determine respectively the values of M_Z , Γ_Z , and $\Gamma(e^+e^-) \times \Gamma(f\bar{f})$, where $\Gamma(e^+e^-)$ and $\Gamma(f\bar{f})$ are the electron and fermion partial widths of the Z . The quantitative determination of these parameters is done by writing analytic expressions for these cross sections in terms of the parameters, and fitting the calculated cross sections to the measured ones by varying these parameters, taking properly into account all the errors.

Single-photon exchange (σ_γ^0) and γ - Z interference ($\sigma_{\gamma Z}^0$) are included, and the large ($\sim 25\%$) initial-state radiation (ISR) effects are taken into account by convoluting the analytic expressions over a ‘Radiator Function’ [1–5] $H(s, s')$. Thus for the process $e^+e^- \rightarrow f\bar{f}$:

$$\sigma_f(s) = \int H(s, s') \sigma_f^0(s') ds' \quad (55.1)$$

$$\sigma_f^0(s) = \sigma_Z^0 + \sigma_\gamma^0 + \sigma_{\gamma Z}^0 \quad (55.2)$$

$$\sigma_Z^0 = \frac{12\pi}{M_Z^2} \frac{\Gamma(e^+e^-)\Gamma(f\bar{f})}{\Gamma_Z^2} \frac{s \Gamma_Z^2}{(s - M_Z^2)^2 + s^2 \Gamma_Z^2/M_Z^2} \quad (55.3)$$

$$\sigma_\gamma^0 = \frac{4\pi\alpha^2(s)}{3s} Q_f^2 N_c^f \quad (55.4)$$

$$\sigma_{\gamma Z}^0 = -\frac{2\sqrt{2}\alpha(s)}{3} (Q_f G_F N_c^f \mathcal{G}_V^e \mathcal{G}_V^f) \times \frac{(s - M_Z^2) M_Z^2}{(s - M_Z^2)^2 + s^2 \Gamma_Z^2/M_Z^2} \quad (55.5)$$

where Q_f is the charge of the fermion, $N_c^f = 3$ for quarks and 1 for leptons, and \mathcal{G}_V^f is the vector coupling of the Z to the fermion-antifermion pair $f\bar{f}$.

Since $\sigma_{\gamma Z}^0$ is expected to be much less than σ_Z^0 , the LEP Collaborations have generally calculated the interference term in the framework of the Standard Model. This fixing of $\sigma_{\gamma Z}^0$ leads to a tighter constraint on M_Z , and consequently a smaller error on its fitted value. It is possible to relax this constraint and carry out the fit within the S-matrix framework, which is briefly described in the next section.

In the above framework, the QED radiative corrections have been explicitly taken into account by convoluting over the ISR and allowing the electromagnetic coupling constant to run [6]: $\alpha(s) = \alpha/(1 - \Delta\alpha)$. On the other hand, weak radiative corrections that depend upon the assumptions of the electroweak theory and on the values of M_{top} and M_{Higgs} are accounted for by **absorbing them into the couplings**, which are then called the *effective* couplings \mathcal{G}_V and \mathcal{G}_A (or alternatively the effective parameters of the \star scheme of Kennedy and Lynn [7].)

\mathcal{G}_V^f and \mathcal{G}_A^f are complex numbers with small imaginary parts. As experimental data does not allow simultaneous extraction of both real and imaginary parts of the effective couplings, the convention $g_A^f = \text{Re}(\mathcal{G}_A^f)$ and $g_V^f = \text{Re}(\mathcal{G}_V^f)$ is used and the imaginary parts are added in the fitting code [4].

Defining

$$A_f = 2 \frac{g_V^f \cdot g_A^f}{(g_V^f)^2 + (g_A^f)^2} \quad (55.6)$$

the lowest-order expressions for the various lepton-related asymmetries on the Z pole are [8–10] $A_{FB}^{(0,\ell)} = (3/4)A_e A_f$, $P(\tau) = -A_\tau$, $P(\tau)^{fb} = -(3/4)A_e$, $A_{LR} = A_e$. The full analysis takes into account the energy-dependence of the asymmetries. Experimentally A_{LR} is defined as $(\sigma_L - \sigma_R)/(\sigma_L + \sigma_R)$, where $\sigma_{L(R)}$ are the $e^+e^- \rightarrow Z$ production cross sections with left- (right)-handed electrons.

The definition of the partial decay width of the Z to $f\bar{f}$ includes the effects of QED and QCD final-state corrections, as well as the contribution due to the imaginary parts of the couplings:

$$\Gamma(f\bar{f}) = \frac{G_F M_Z^3}{6\sqrt{2}\pi} N_c^f (|\mathcal{G}_A^f|^2 R_A^f + |\mathcal{G}_V^f|^2 R_V^f) + \Delta_{ew/QCD} \quad (55.7)$$

where R_V^f and R_A^f are radiator factors to account for final state QED and QCD corrections, as well as effects due to nonzero fermion masses, and $\Delta_{ew/QCD}$ represents the non-factorizable electroweak/QCD corrections.

55.2 S-matrix approach to the Z

While most experimental analyses of LEP/SLC data have followed the ‘Breit-Wigner’ approach, an alternative S-matrix-based

analysis is also possible. The Z , like all unstable particles, is associated with a complex pole in the S matrix. The pole position is process-independent and gauge-invariant. The mass, \overline{M}_Z , and width, $\overline{\Gamma}_Z$, can be defined in terms of the pole in the energy plane via [11–14]

$$\overline{s} = \overline{M}_Z^2 - i\overline{M}_Z\overline{\Gamma}_Z \quad (55.8)$$

leading to the relations

$$\begin{aligned} \overline{M}_Z &= M_Z / \sqrt{1 + \Gamma_Z^2 / M_Z^2} \\ &\approx M_Z - 34.1 \text{ MeV} \end{aligned} \quad (55.9)$$

$$\begin{aligned} \overline{\Gamma}_Z &= \Gamma_Z / \sqrt{1 + \Gamma_Z^2 / M_Z^2} \\ &\approx \Gamma_Z - 0.9 \text{ MeV} . \end{aligned} \quad (55.10)$$

The LEP collaborations [15] have analyzed their data using the S -matrix approach as defined in Eq. (55.8), in addition to the conventional one. They observe a downward shift in the Z mass as expected.

55.3 Handling the large-angle e^+e^- final state

Unlike other $f\bar{f}$ decay final states of the Z , the e^+e^- final state has a contribution not only from the s -channel but also from the t -channel and s - t interference. The full amplitude is not amenable to fast calculation, which is essential if one has to carry out minimization fits within reasonable computer time. The usual procedure is to calculate the non- s channel part of the cross section separately using the Standard Model programs ALIBABA [16] or TOPAZ0 [17], with the measured value of M_{top} , and $M_{\text{Higgs}} = 150 \text{ GeV}$, and add it to the s -channel cross section calculated as for other channels. This leads to two additional sources of error in the analysis: firstly, the theoretical calculation in ALIBABA itself is known to be accurate to $\sim 0.5\%$, and secondly, there is uncertainty due to the error on M_{top} and the unknown value of M_{Higgs} (100–1000 GeV). These errors are propagated into the analysis by including them in the systematic error on the e^+e^- final state. As these errors are common to the four LEP experiments, this is taken into account when performing the LEP average.

55.4 Errors due to uncertainty in LEP energy determination

The systematic errors related to the LEP energy measurement, see [18–23], can be classified as:

- The absolute energy scale error;
- Energy-point-to-energy-point errors due to the nonlinear response of the magnets to the exciting currents;
- Energy-point-to-energy-point errors due to possible higher-order effects in the relationship between the dipole field and beam energy;
- Energy reproducibility errors due to various unknown uncertainties in temperatures, tidal effects, corrector settings, RF status, *etc.*

Precise energy calibration was done outside normal data-taking using the resonant depolarization technique. Run-time energies were determined every 10 minutes by measuring the relevant machine parameters and using a model which takes into account all the known effects, including leakage currents produced by trains in the Geneva area and the tidal effects due to gravitational forces of the Sun and the Moon. The LEP Energy Working Group has provided a covariance matrix from the determination of LEP energies for the different running periods during 1993–1995 [18].

55.5 Choice of fit parameters

The LEP Collaborations have chosen the following primary set of parameters for fitting:

$$M_Z, \Gamma_Z, \sigma_{\text{hadron}}^0, R(\text{lepton}), A_{FB}^{(0,\ell)},$$

where

$$\begin{aligned} R(\text{lepton}) &= \Gamma(\text{hadrons}) / \Gamma(\text{lepton}), \sigma_{\text{hadron}}^0 \\ &= 12\pi\Gamma(e^+e^-)\Gamma(\text{hadrons}) / M_Z^2\Gamma_Z^2. \end{aligned}$$

With a knowledge of these fitted parameters and their covariance matrix, any other parameter can be derived. The main advantage of these parameters is that they form a physics motivated set of parameters with much reduced correlations.

Thus, the most general fit carried out to cross section and asymmetry data determines the **nine parameters**: $M_Z, \Gamma_Z, \sigma_{\text{hadron}}^0, R(e), R(\mu), R(\tau), A_{FB}^{(0,e)}, A_{FB}^{(0,\mu)}, A_{FB}^{(0,\tau)}$. Assumption of lepton universality leads to a **five-parameter fit** determining $M_Z, \Gamma_Z, \sigma_{\text{hadron}}^0, R(\text{lepton}), A_{FB}^{(0,\ell)}$.

55.6 Combining results from LEP and SLC experiments

With a steady increase in statistics over the years and improved understanding of the common systematic errors between LEP experiments, the procedures for combining results have evolved continuously [24]. The Line Shape Sub-group of the LEP Electroweak Working Group investigated the effects of these common errors, and devised a combination procedure for the precise determination of the Z parameters from LEP experiments. Using these procedures, this note also gives the results after combining the final parameter sets from the four experiments, and these are the results quoted as the fit results in the Z listings below. Transformation of variables leads to values of derived parameters like partial decay widths and branching ratios to hadrons and leptons. Finally, transforming the LEP combined nine parameter set to $(M_Z, \Gamma_Z, \sigma_{\text{hadron}}^0, g_A^f, g_V^f, f = e, \mu, \tau)$ using the average values of lepton asymmetry parameters (A_e, A_μ, A_τ) as constraints, leads to the best fitted values of the vector and axial-vector couplings (g_V, g_A) of the charged leptons to the Z .

Brief remarks on the handling of common errors and their magnitudes are given below. The identified common errors are those coming from

- (a) LEP energy-calibration uncertainties, and
- (b) the theoretical uncertainties in (i) the luminosity determination using small angle Bhabha scattering, (ii) estimating the non- s channel contribution to large angle Bhabha scattering, (iii) the calculation of QED radiative effects, and (iv) the parameterization of the cross section in terms of the parameter set used.

55.7 Common LEP energy errors

All the collaborations incorporate in their fit the full LEP energy error matrix as provided by the LEP energy group for their intersection region [18]. The effect of these errors is separated out from that of other errors by carrying out fits with energy errors scaled up and down by $\sim 10\%$ and redoing the fits. From the observed changes in the overall error matrix, the covariance matrix of the common energy errors is determined. Common LEP energy errors lead to uncertainties on M_Z, Γ_Z , and σ_{hadron}^0 of 1.7, 1.2 MeV, and 0.011 nb, respectively.

55.8 Common luminosity errors

BHLUMI 4.04 [25] is used by all LEP collaborations for small-angle Bhabha scattering leading to a common uncertainty in their measured cross sections of 0.061% [26]. BHLUMI does not include a correction for production of light fermion pairs. OPAL explicitly corrects for this effect and reduces their luminosity uncertainty to 0.054%, which is taken fully correlated with the other experiments. The other three experiments among themselves have a common uncertainty of 0.061%.

55.9 Common non- s channel uncertainties

The same standard model programs ALIBABA [16] and TOPAZ0 [17] are used to calculate the non- s channel contribution to the large angle Bhabha scattering [27]. As this contribution is a function of the Z mass, which itself is a variable in the fit, it is parameterized as a function of M_Z by each collaboration to properly track this contribution as M_Z varies in the fit. The common errors on R_e and $A_{FB}^{(0,e)}$ are 0.024 and 0.0014 respectively, and are correlated between them.

55.10 Common theoretical uncertainties: QED

There are large initial-state photon and fermion pair radiation effects near the Z resonance, for which the best currently available evaluations include contributions up to $\mathcal{O}(\alpha^3)$. To estimate the

remaining uncertainties, different schemes are incorporated in the standard model programs ZFITTER [5], TOPAZ0 [17], and MIZA [28]. Comparing the different options leads to error estimates of 0.3 and 0.2 MeV on M_Z and Γ_Z respectively, and of 0.02% on $\sigma_{\text{hadron}}^{\circ}$.

55.11 Common theoretical uncertainties: parametrization of lineshape and asymmetries

To estimate uncertainties arising from ambiguities in the model-independent parametrization of the differential cross-section near the Z resonance, results from TOPAZ0 and ZFITTER were compared by using ZFITTER to fit the cross sections and asymmetries calculated using TOPAZ0. The resulting uncertainties on M_Z , Γ_Z , $\sigma_{\text{hadron}}^{\circ}$, $R(\text{lepton})$, and $A_{FB}^{(0,\ell)}$ are 0.1 MeV, 0.1 MeV, 0.001 nb, 0.004, and 0.0001 respectively.

Thus, the overall theoretical errors on M_Z , Γ_Z , $\sigma_{\text{hadron}}^{\circ}$ are 0.3 MeV, 0.2 MeV, and 0.008 nb respectively; on each $R(\text{lepton})$ is 0.004 and on each $A_{FB}^{(0,\ell)}$ is 0.0001. Within the set of three $R(\text{lepton})$'s and the set of three $A_{FB}^{(0,\ell)}$'s, the respective errors are fully correlated.

All the theory-related errors mentioned above utilize Standard Model programs which need the Higgs mass and running electromagnetic coupling constant as inputs; uncertainties on these inputs will also lead to common errors. All LEP collaborations used the same set of inputs for Standard Model calculations: $M_Z = 91.187$ GeV, the Fermi constant $G_F = (1.16637 \pm 0.00001) \times 10^{-5}$ GeV $^{-2}$ [29], $\alpha^{(5)}(M_Z) = 1/128.877 \pm 0.090$ [30], $\alpha_s(M_Z) = 0.119$ [31], $M_{\text{top}} = 174.3 \pm 5.1$ GeV [31] and $M_{\text{Higgs}} = 150$ GeV. The only observable effect, on M_Z , is due to the variation of M_{Higgs} between 100–1000 GeV (due to the variation of the γ/Z interference term which is taken from the Standard Model): M_Z changes by +0.23 MeV per unit change in $\log_{10} M_{\text{Higgs}}/\text{GeV}$, which is not an error but a correction to be applied once M_{Higgs} is determined. The effect is much smaller than the error on M_Z (± 2.1 MeV).

55.12 Methodology of combining the LEP experimental results

The LEP experimental results actually used for combination are slightly modified from those published by the experiments (which are given in the Listings below). This has been done in order to facilitate the procedure by making the inputs more consistent. These modified results are given explicitly in [24]. The main differences compared to the published results are (a) consistent use of ZFITTER 6.23 and TOPAZ0 (the published ALEPH results used ZFITTER 6.10); (b) use of the combined energy-error matrix, which makes a difference of 0.1 MeV on the M_Z and Γ_Z for L3 only as at that intersection the RF modeling uncertainties are the largest.

Thus, nine-parameter sets from all four experiments with their covariance matrices are used together with all the common errors correlations. A grand covariance matrix, V , is constructed and a combined nine-parameter set is obtained by minimizing $\chi^2 = \Delta^T V^{-1} \Delta$, where Δ is the vector of residuals of the combined parameter set to the results of individual experiments. Imposing lepton universality in the combination results in the combined five-parameter set.

55.13 Study of $Z \rightarrow b\bar{b}$ and $Z \rightarrow c\bar{c}$

In the sector of c - and b -physics, the LEP experiments have measured the ratios of partial widths $R_b = \Gamma(Z \rightarrow b\bar{b})/\Gamma(Z \rightarrow \text{hadrons})$, and $R_c = \Gamma(Z \rightarrow c\bar{c})/\Gamma(Z \rightarrow \text{hadrons})$, and the forward-backward (charge) asymmetries $A_{FB}^{b\bar{b}}$ and $A_{FB}^{c\bar{c}}$. The SLD experiment at SLC has measured the ratios R_c and R_b and, utilizing the polarization of the electron beam, was able to obtain the final state coupling parameters A_b and A_c from a measurement of the left-right forward-backward asymmetry of b - and c -quarks. The high precision measurement of R_c at SLD was made possible owing to the small beam size and very stable beam spot at SLC, coupled with a highly precise CCD pixel detector. Several of the analyses have also determined other quantities, in particular the semileptonic branching ratios, $B(b \rightarrow \ell^-)$, $B(b \rightarrow c \rightarrow \ell^+)$, and $B(c \rightarrow \ell^+)$, the average time-integrated $B^0\bar{B}^0$ mixing parameter

$\bar{\chi}$ and the probabilities for a c -quark to fragment into a D^+ , a D_s , a D^{*+} , or a charmed baryon. The latter measurements do not concern properties of the Z boson, and hence they do not appear in the Listing below. However, for completeness, we will report at the end of this minireview their values as obtained fitting the data contained in the Z section. All these quantities are correlated with the electroweak parameters, and since the mixture of b hadrons is different from the one at the $\Upsilon(4S)$, their values might differ from those measured at the $\Upsilon(4S)$.

All the above quantities are correlated to each other since:

- Several analyses (for example the lepton fits) determine more than one parameter simultaneously;
- Some of the electroweak parameters depend explicitly on the values of other parameters (for example R_b depends on R_c);
- Common tagging and analysis techniques produce common systematic uncertainties.

The LEP Electroweak Heavy Flavour Working Group has developed [32] a procedure for combining the measurements taking into account known sources of correlation. The combining procedure determines fourteen parameters: the six parameters of interest in the electroweak sector, R_b , R_c , $A_{FB}^{b\bar{b}}$, $A_{FB}^{c\bar{c}}$, A_b and A_c and, in addition, $B(b \rightarrow \ell^-)$, $B(b \rightarrow c \rightarrow \ell^+)$, $B(c \rightarrow \ell^+)$, $\bar{\chi}$, $f(D^+)$, $f(D_s)$, $f(c_{\text{baryon}})$ and $P(c \rightarrow D^{*+}) \times B(D^{*+} \rightarrow \pi^+ D^0)$, to take into account their correlations with the electroweak parameters. Before the fit both the peak and off-peak asymmetries are translated to the common energy $\sqrt{s} = 91.26$ GeV using the predicted energy-dependence from ZFITTER [5].

55.14 Summary of the measurements and of the various kinds of analysis

The measurements of R_b and R_c fall into two classes. In the first, named single-tag measurement, a method for selecting b and c events is applied and the number of tagged events is counted. A second technique, named double-tag measurement, has the advantage that the tagging efficiency is directly derived from the data thereby reducing the systematic error on the measurement.

The measurements in the b - and c -sector can be essentially grouped in the following categories:

- Lifetime (and lepton) double-tagging measurements of R_b . These are the most precise measurements of R_b and obviously dominate the combined result. The main sources of systematics come from the charm contamination and from estimating the hemisphere b -tagging efficiency correlation;
- Analyses with $D/D^{*\pm}$ to measure R_c . These measurements make use of several different tagging techniques (inclusive/exclusive double tag, exclusive double tag, reconstruction of all weakly decaying charmed states) and no assumptions are made on the energy-dependence of charm fragmentation;
- A measurement of R_c using single leptons and assuming $B(b \rightarrow c \rightarrow \ell^+)$;
- Lepton fits which use hadronic events with one or more leptons in the final state to measure the asymmetries $A_{FB}^{b\bar{b}}$ and $A_{FB}^{c\bar{c}}$. Each analysis usually gives several other electroweak parameters. The dominant sources of systematics are due to lepton identification, to other semileptonic branching ratios and to the modeling of the semileptonic decay;
- Measurements of $A_{FB}^{b\bar{b}}$ using lifetime tagged events with a hemisphere charge measurement. These measurements dominate the combined result;
- Analyses with $D/D^{*\pm}$ to measure $A_{FB}^{c\bar{c}}$ or simultaneously $A_{FB}^{b\bar{b}}$ and $A_{FB}^{c\bar{c}}$;
- Measurements of A_b and A_c from SLD, using several tagging methods (lepton, kaon, D/D^* , and vertex mass). These quantities are directly extracted from a measurement of the left-right forward-backward asymmetry in $c\bar{c}$ and $b\bar{b}$ production using a polarized electron beam.

55.15 Averaging procedure

All the measurements are provided by the LEP and SLD Collaborations in the form of tables with a detailed breakdown of

the systematic errors of each measurement and its dependence on other electroweak parameters.

The averaging proceeds via the following steps:

- Define and propagate a consistent set of external inputs such as branching ratios, hadron lifetimes, fragmentation models *etc.* All the measurements are checked to ensure that all use a common set of assumptions (for instance, since the QCD corrections for the forward–backward asymmetries are strongly dependent on the experimental conditions, the data are corrected before combining);
- Form the full (statistical and systematic) covariance matrix of the measurements. The systematic correlations between different analyses are calculated from the detailed error breakdown in the measurement tables. The correlations relating several measurements made by the same analysis are also used;
- Take into account any explicit dependence of a measurement on the other electroweak parameters. As an example of this dependence, we illustrate the case of the double-tag measurement of R_b , where c -quarks constitute the main background. The normalization of the charm contribution is not usually fixed by the data and the measurement of R_b depends on the assumed value of R_c , which can be written as:

$$R_b = R_b^{\text{meas}} + a(R_c) \frac{(R_c - R_c^{\text{used}})}{R_c}, \quad (55.11)$$

where R_b^{meas} is the result of the analysis which assumed a value of $R_c = R_c^{\text{used}}$ and $a(R_c)$ is the constant which gives the dependence on R_c ;

- Perform a χ^2 minimization with respect to the combined electroweak parameters.

After the fit the average peak asymmetries $A_{FB}^{c\bar{c}}$ and $A_{FB}^{b\bar{b}}$ are corrected for the energy shift from 91.26 GeV to M_Z and for QED (initial state radiation), γ exchange, and γZ interference effects, to obtain the corresponding pole asymmetries $A_{FB}^{0,c}$ and $A_{FB}^{0,b}$.

This averaging procedure, using the fourteen parameters described above, and applied to the data contained in the Z particle listing below, gives the following results (where the last 8 parameters do not depend directly on the Z):

$$\begin{aligned} R_b^0 &= 0.21629 \pm 0.00066 \\ R_c^0 &= 0.1721 \pm 0.0030 \\ A_{FB}^{0,b} &= 0.0992 \pm 0.0016 \\ A_{FB}^{0,c} &= 0.0707 \pm 0.0035 \\ A_b &= 0.923 \pm 0.020 \\ A_c &= 0.670 \pm 0.027 \end{aligned}$$

$$\begin{aligned} B(b \rightarrow \ell^-) &= 0.1071 \pm 0.0022 \\ B(b \rightarrow c \rightarrow \ell^+) &= 0.0801 \pm 0.0018 \\ B(c \rightarrow \ell^+) &= 0.0969 \pm 0.0031 \\ \bar{\chi} &= 0.1250 \pm 0.0039 \\ f(D^+) &= 0.235 \pm 0.016 \\ f(D_s) &= 0.126 \pm 0.026 \\ f(c_{\text{baryon}}) &= 0.093 \pm 0.022 \end{aligned}$$

$$P(c \rightarrow D^{*+}) \times B(D^{*+} \rightarrow \pi^+ D^0) = 0.1622 \pm 0.0048 \quad (55.12)$$

Among the non-electroweak observables, the B semileptonic branching fraction $B(b \rightarrow \ell^-)$ is of special interest, since the dominant error source on this quantity is the dependence on the semileptonic decay model for $b \rightarrow \ell^-$, with $\Delta B(b \rightarrow \ell^-)_{b \rightarrow \ell^- \text{ model}} = 0.0012$. Extensive studies have been made to understand the size of this error. Among the electroweak quantities, the quark asymmetries with leptons depend also on the semileptonic decay model, while the asymmetries using other

methods usually do not. The fit implicitly requires that the different methods give consistent results and this effectively constrains the decay model, and thus reduces in principle the error from this source in the fit result.

To obtain a conservative estimate of the modelling error, the above fit has been repeated removing all asymmetry measurements. The results of the fit on B -decay related observables are [24]: $B(b \rightarrow \ell^-) = 0.1069 \pm 0.0022$, with $\Delta B(b \rightarrow \ell^-)_{b \rightarrow \ell^- \text{ model}} = 0.0013$, $B(b \rightarrow c \rightarrow \ell^+) = 0.0802 \pm 0.0019$ and $\bar{\chi} = 0.1259 \pm 0.0042$.

References

- [1] R. N. Cahn, Phys. Rev. D **36**, 2666 (1987), [Erratum: Phys.Rev.D 40, 922 (1989)].
- [2] D. Y. Bardin *et al.*, in “LEP Physics Workshop,” 89–127 (1989).
- [3] A. Borrelli *et al.*, Nucl. Phys. B **333**, 357 (1990).
- [4] D. Y. Bardin and G. Passarino (1998), [hep-ph/9803425]; D. Y. Bardin, M. Grunewald and G. Passarino (1999), [hep-ph/9902452].
- [5] D. Bardin *et al.*, Z. Phys. C **44**, 493 (1989); D. Bardin *et al.*, Comput. Phys. Commun. **59**, 303 (1990); D. Y. Bardin *et al.*, Nucl. Phys. B **351**, 1 (1991), [hep-ph/9801208]; D. Y. Bardin *et al.*, Phys. Lett. B **255**, 290 (1991), [hep-ph/9801209]; D. Y. Bardin *et al.* (1992), [hep-ph/9412201]; D. Y. Bardin *et al.*, Comput. Phys. Commun. **133**, 229 (2001), [hep-ph/9908433].
- [6] G. Burgers and F. Jegerlehner, Conf. Proc. C **8902201**, 55 (1989).
- [7] D. Kennedy and B. Lynn, Nucl. Phys. B **322**, 1 (1989).
- [8] M. Consoli, W. Hollik and F. Jegerlehner, in “LEP Physics Workshop,” 7–54 (1989).
- [9] M. Bohm *et al.*, in “LEP Physics Workshop,” 203–234 (1989).
- [10] P. Eberhard *et al.*, in “LEP Physics Workshop,” 235–266 (1989).
- [11] R. G. Stuart, Phys. Lett. B **262**, 113 (1991).
- [12] A. Sirlin, Phys. Rev. Lett. **67**, 2127 (1991).
- [13] A. Leike, T. Riemann and J. Rose, Phys. Lett. B **273**, 513 (1991), [hep-ph/9508390].
- [14] D. Bardin *et al.*, Phys. Lett. B **206**, 539 (1988).
- [15] S. Schael *et al.* (ALEPH, DELPHI, L3, OPAL, LEP Electroweak), Phys. Rept. **532**, 119 (2013), [arXiv:1302.3415].
- [16] W. Beenakker, F. A. Berends and S. van der Marck, Nucl. Phys. B **349**, 323 (1991).
- [17] G. Montagna *et al.*, Nucl. Phys. B **401**, 3 (1993); G. Montagna *et al.*, Comput. Phys. Commun. **76**, 328 (1993); G. Montagna *et al.*, Comput. Phys. Commun. **93**, 120 (1996), [hep-ph/9506329]; G. Montagna *et al.*, Comput. Phys. Commun. **117**, 278 (1999), [hep-ph/9804211].
- [18] R. Assmann *et al.*, Eur. Phys. J. C **6**, 187 (1999).
- [19] R. Assmann *et al.* (Working Group on LEP Energy), Z. Phys. C **66**, 567 (1995).
- [20] L. Arnaudon *et al.* (Working Group on LEP Energy, ALEPH, DELPHI, L3, OPAL), Phys. Lett. B **307**, 187 (1993).
- [21] L. Arnaudon *et al.* (Working Group on LEP energy), in “26th International Conference on High-energy Physics,” (1992).
- [22] L. Arnaudon *et al.* (LEP Polarization), Phys. Lett. B **284**, 431 (1992).
- [23] R. Bailey *et al.*, Conf. Proc. C **900612**, 1765 (1990).
- [24] S. Schael *et al.* (ALEPH, DELPHI, L3, OPAL, SLD, LEP Electroweak Working Group, SLD Electroweak Group, SLD Heavy Flavour Group), Phys. Rept. **427**, 257 (2006), [hep-ex/0509008].
- [25] S. Jadach *et al.*, Comput. Phys. Commun. **102**, 229 (1997); S. Jadach and O. Nicrosini, Event generators for Bhabha scattering, in Physics at LEP2, CERN-96-01 Vol. 2, February 1996.

- [26] B. Ward *et al.*, Phys. Lett. B **450**, 262 (1999), [hep-ph/9811245].
- [27] W. Beenakker and G. Passarino, Phys. Lett. B **425**, 199 (1998), [hep-ph/9710376].
- [28] M. Martinez *et al.*, Z. Phys. C **49**, 645 (1991); M. Martinez and F. Teubert, Z. Phys. **C65**, 267 (1995), updated with results summarized in S. Jadach, B. Pietrzyk, and M. Skrzypek, Phys. Lett. **B456**, 77 (1999) and Reports of the working group on precision calculations for the Z resonance, CERN 95-03, ed. D. Bardin, W. Hollik, and G. Passarino, and references therein.
- [29] T. van Ritbergen and R. G. Stuart, Phys. Lett. B **437**, 201 (1998), [hep-ph/9802341]; T. van Ritbergen and R. G. Stuart, Phys. Rev. Lett. **82**, 488 (1999), [hep-ph/9808283].
- [30] S. Eidelman and F. Jegerlehner, Z. Phys. C **67**, 585 (1995), [hep-ph/9502298]; M. Steinhauser, Phys. Lett. B **429**, 158 (1998), [hep-ph/9803313].
- [31] D. E. Groom *et al.* (Particle Data Group), Eur. Phys. J. C **15**, 1 (2000).
- [32] Nucl. Instrum. Meth. A **378**, 101 (1996).

56. Muon Anomalous Magnetic Moment

Revised August 2023 by A. Höcker (CERN) and W.J. Marciano (BNL).

The Dirac equation predicts a muon magnetic moment, $\vec{M} = g_\mu \frac{e}{2m_\mu} \vec{S}$, with gyromagnetic ratio $g_\mu = 2$. Quantum loop effects lead to a small calculable deviation from $g_\mu = 2$, parameterized by the magnetic anomaly¹

$$a_\mu \equiv \frac{g_\mu - 2}{2}. \quad (56.1)$$

That quantity can be accurately measured and, within the Standard Model (SM) framework, precisely predicted. Hence, comparison of experiment and theory tests the SM at its quantum loop level. A deviation in a_μ^{exp} from the SM expectation would signal effects of new physics, with current sensitivity reaching up to mass scales of $\mathcal{O}(\text{TeV})$ [1]. For recent thorough muon $g-2$ reviews, see e.g. Refs. [2–4].

The E821 experiment at Brookhaven National Lab (BNL) studied during the years 1997–2001 the precession of μ^+ and μ^- in a constant external magnetic field as they circulated in a confining storage ring. It found² [6]

$$\begin{aligned} a_{\mu^+}^{\text{exp,BNL}} &= 116\,592\,040(60)(50) \times 10^{-11}, \\ a_{\mu^-}^{\text{exp,BNL}} &= 116\,592\,150(80)(30) \times 10^{-11}, \end{aligned} \quad (56.2)$$

where the first errors are statistical and the second systematic. Assuming CPT invariance and taking into account correlations between systematic uncertainties, one finds for their average [5,6]

$$a_\mu^{\text{exp,BNL}} = 116\,592\,089(54)(33) \times 10^{-11}. \quad (56.3)$$

These results represent about a factor of 14 improvement over the classic CERN experiments of the 1970s [7].

Further improvement of the measurement by a factor of four by setting up the E821 storage ring at the Fermilab National Accelerator Laboratory (FNAL), and utilizing a cleaner and more intense muon beam and improved detectors [8] is in progress. After six runs, the experiment has completed data taking in 2023. A first analysis with positive muons based on a fraction of the data collected in 2018 was released in 2021 confirming the BNL result with similar precision [9]. A second analysis released in 2023 was based on a four times larger positive muon data sample collected in 2019 and 2020, and benefitted from instrumental improvements and reduced systematic uncertainties [10]. The result is dominated by statistical uncertainty and consistent with but more precise than the previous one. Their combination yields [10]

$$a_{\mu^+}^{\text{exp,FNAL}} = 116\,592\,055(24) \times 10^{-11}. \quad (56.4)$$

The ongoing analysis of the remaining 2021–2023 dataset is expected to further reduce the uncertainty by a factor of two.

The FNAL result agrees with the BNL measurement and has improved precision. Their average assuming CPT invariance reads [10]

$$a_\mu^{\text{exp}} = 116\,592\,059(22) \times 10^{-11}, \quad (56.5)$$

providing a relative precision of 0.19 parts per million.

Another muon $g-2$ experiment with similar sensitivity but using an alternative zero-electric-field technique with a low-emittance and low-momentum muon beam is currently under construction at J-PARC in Japan [11].

The SM prediction a_μ^{SM} is generally divided into three parts (see Fig. 56.1 for representative Feynman diagrams)

$$a_\mu^{\text{SM}} = a_\mu^{\text{QED}} + a_\mu^{\text{EW}} + a_\mu^{\text{Had}}. \quad (56.6)$$

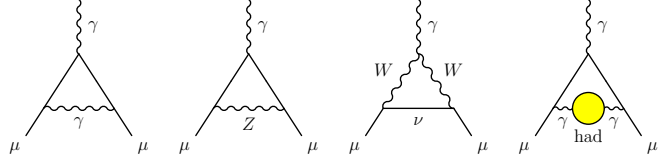


Figure 56.1: Representative diagrams contributing to a_μ^{SM} . From left to right: first order QED (Schwinger term), lowest-order weak, lowest-order hadronic.

In the following discussion we use the numerical estimates provided by the Muon $g-2$ Theory Initiative White Paper [4].

The QED part includes all photonic and leptonic (e, μ, τ) loops starting with the classic $\alpha/2\pi$ Schwinger contribution [12]. It has been computed through five loops [4, 13, 14]

$$\begin{aligned} a_\mu^{\text{QED}} &= \frac{\alpha}{2\pi} + 0.765\,857\,420(13) \left(\frac{\alpha}{\pi}\right)^2 + 24.050\,509\,85(23) \left(\frac{\alpha}{\pi}\right)^3 \\ &\quad + 130.8782(60) \left(\frac{\alpha}{\pi}\right)^4 + 751.0(9) \left(\frac{\alpha}{\pi}\right)^5 + \dots \end{aligned} \quad (56.7)$$

with little change in the coefficients since our last update of this review. Employing $\alpha^{-1} = 137.035\,999\,046(27)$, obtained from the precise measurements of h/m_{Cs} [15], the Rydberg constant, and m_{Cs}/m_e leads to³ [13]

$$a_\mu^{\text{QED}} = 116\,584\,718.93(0.10) \times 10^{-11}, \quad (56.8)$$

where the small error results mainly from the uncertainties in the estimate of the six loop contribution and in α .

Loop contributions involving heavy W^\pm, Z or Higgs particles are collectively labeled as a_μ^{EW} . They are suppressed by at least a factor of $(\alpha/\pi) \cdot (m_\mu^2/m_W^2) \simeq 4 \times 10^{-9}$. At 1-loop order [19]

$$\begin{aligned} a_\mu^{\text{EW}}[1\text{-loop}] &= \\ &= \frac{G_\mu m_\mu^2}{8\sqrt{2}\pi^2} \left[\frac{5}{3} + \frac{1}{3} (1 - 4\sin^2\theta_W)^2 + \mathcal{O}\left(\frac{m_\mu^2}{M_W^2}\right) + \mathcal{O}\left(\frac{m_\mu^2}{M_H^2}\right) \right] \\ &= 194.8 \times 10^{-11}, \end{aligned} \quad (56.9)$$

for $\sin^2\theta_W \equiv 1 - M_W^2/M_Z^2 \simeq 0.223$, and where $G_\mu \simeq 1.166 \times 10^{-5} \text{ GeV}^{-2}$ is the Fermi coupling constant. Two-loop corrections are relatively large and negative [20]. For a Higgs boson mass of 125 GeV it amounts to $a_\mu^{\text{EW}}[2\text{-loop}] = -41.2(1.0) \times 10^{-11}$ [20], where the uncertainty stems from quark triangle loops. The 3-loop leading logarithms are negligible, $\mathcal{O}(10^{-12})$ [20, 21]. Overall one finds

$$a_\mu^{\text{EW}} = 153.6(1.0) \times 10^{-11}. \quad (56.10)$$

A recent complete 2-loop numerical evaluation of the electroweak correction [22] when adjusted for appropriate light quark masses confirmed the result in Eq. (56.10).

Hadronic (quark and gluon) loop contributions to a_μ^{SM} give rise to its main uncertainty. One traditionally relies on a data-driven dispersion relation approach to evaluate the lowest-order $\mathcal{O}(\alpha^2)$ hadronic vacuum polarization contribution $a_\mu^{\text{Had}}[\text{LO}]$ from corresponding cross section measurements [23]

$$a_\mu^{\text{Had}}[\text{LO}] = \frac{1}{3} \left(\frac{\alpha}{\pi}\right)^2 \int_{m_\pi^2}^{\infty} ds \frac{K(s)}{s} R^{(0)}(s), \quad (56.11)$$

¹Also referred to as *anomalous magnetic moment* despite being dimensionless.

²The results reported by the experiment have been updated in Eqs. (56.2) and (56.3) to the newest value for the absolute muon-to-proton magnetic ratio $\lambda = 3.183\,345\,142(71)$ [5]. The change induced in a_μ^{exp} with respect to the value of $\lambda = 3.183\,345\,39(10)$ used in Ref. [6] amounts to $+10 \times 10^{-11}$.

³A recent measurement using Rb-87 atoms [16] resulted in $\alpha^{-1} = 137.035\,999\,206(11)$, which exhibits a larger than 5σ discrepancy with the Cs-133 based result. Using this value in Eq. (56.7) leads to a reduction of a_μ^{QED} by 0.14×10^{-11} , which is larger than the quoted uncertainty in Eq. (56.8), but still negligible compared to other uncertainties affecting a_μ^{SM} . This discrepancy impacts, however, the SM prediction of the magnetic moment of the electron [14, 17], which differs by respectively -3.9σ and $+2.1\sigma$ from the most recent experimental value [18], depending on whether the Cs-133 or Rb-87 based α value is used.

where $K(s)$ is a QED kernel function [24], and where $R^{(0)}(s)$ denotes the ratio of the bare⁴ cross section for e^+e^- annihilation into hadrons to the pointlike muon-pair cross section at center-of-mass energy \sqrt{s} . The function $K(s) \sim 1/s$ in Eq. (56.11) emphasizes the low-energy part of the integral so that $a_\mu^{\text{Had}}[\text{LO}]$ is dominated by the $\rho(770) \rightarrow \pi^+\pi^-$ resonance.

The analysis of Eq. (56.11) results in the representative value [4, 25–30]

$$a_\mu^{\text{Had}}[\text{LO}] = 6931(40) \times 10^{-11}, \quad (56.12)$$

whose error is dominated by systematic uncertainties in the $e^+e^- \rightarrow$ hadrons cross-section data, and also includes a small uncertainty due to perturbative QCD, which is used at intermediate and large energies in the dispersion integral to predict the contribution from the quark-antiquark continuum. The experimental precision of Eq. (56.12) is limited by a discrepancy between the most precise $\pi^+\pi^-$ data from the BABAR and KLOE experiments [27, 29]. Recent preliminary $\pi^+\pi^-$ data from the CMD-3 experiment [31] give a significantly larger contribution to $a_\mu^{\text{Had}}[\text{LO}]$ but disagree with essentially all other datasets. New or updated measurements are expected from several experiments during the next years.

Alternatively, one can use precise vector spectral functions from $\tau \rightarrow \nu_\tau +$ hadrons decays [32] that can be related to isovector $e^+e^- \rightarrow$ hadrons cross sections by isospin symmetry. Analyses replaced e^+e^- data in the two-pion and four-pion channels by the corresponding isospin-transformed τ data, and applied isospin-violating corrections [33]. Owing to the progress in the precision of the e^+e^- data, the τ data are now less precise and less reliable due to additional theoretical uncertainties, so that recent $a_\mu^{\text{Had}}[\text{LO}]$ evaluations ignored them.

Progress has been achieved on the evaluation of $a_\mu^{\text{Had}}[\text{LO}]$ using lattice QCD, which allows to directly compute the real part of the two-point correlation function without invoking the resonances occurring on the imaginary axis [34–36]. The required sub-percent precision represents a challenge requiring to master systematic and extrapolation uncertainties. A combination of recent lattice QCD evaluations [37, 38] gives [4]

$$a_\mu^{\text{Had}}[\text{LO}] = 7116(184) \times 10^{-11}, \quad (56.13)$$

with an uncertainty that is not yet competitive with the data-driven approach. Another recent lattice QCD calculation with much reduced uncertainty found [39]

$$a_\mu^{\text{Had}}[\text{LO}] = 7075(55) \times 10^{-11}, \quad (56.14)$$

whose error is dominated by systematic uncertainties. It exhibits a 2.1σ tension with the data-driven result, growing up to 3.7σ for the modified observable $a_{\mu,\text{win}}$ that has favourable properties for computation on the lattice⁵ [38, 39, 41]. Because of the complexity and challenges of such a calculation, it is critical that it is confronted with independent lattice results of comparable precision [38, 41, 42].

Higher order hadronic loop contributions are also obtained from dispersion relations using the same $e^+e^- \rightarrow$ hadrons data but with different integration kernels [43]. Recent evaluations found $a_\mu^{\text{Had,Disp}}[\text{NLO}] = (-98.3 \pm 0.7) \times 10^{-11}$ [4, 30] and $a_\mu^{\text{Had,Disp}}[\text{NNLO}] = (12.4 \pm 0.1) \times 10^{-11}$ [44]. In the case of hadronic light-by-light scattering contributions, which enter at NLO, recent studies [3, 4, 45, 46] based on short-distance QCD,

⁴The bare cross section is defined as the measured cross section corrected for initial-state radiation, electron-vertex loop contributions and vacuum-polarization effects in the photon propagator. However, QED effects in the hadron vertex and final state, as photon radiation, are included.

⁵A dispersive approach similar to that for $a_\mu^{\text{Had}}[\text{LO}]$ is used to determine the hadronic contribution to the running of the electromagnetic fine structure constant at the Z -boson mass $\Delta\alpha_{\text{had}}(m_Z)$, which is a critical ingredient of the global electroweak fit. One may therefore ask if the goodness of that fit would break down were $a_\mu^{\text{Had}}[\text{LO}]$ in Eq. (56.12) be brought in compatibility with the result (56.14). However, the difference in the relevant integration kernels (whereas 73% of the contribution to $a_\mu^{\text{Had}}[\text{LO}]$ stems from the $\pi^+\pi^-$ channel, it is only 13% in the case of $\Delta\alpha_{\text{had}}(m_Z)$) allows to absorb large effects in $a_\mu^{\text{Had}}[\text{LO}]$ without creating a significant tension in the electroweak fit. Detailed discussions are available in the literature [40].

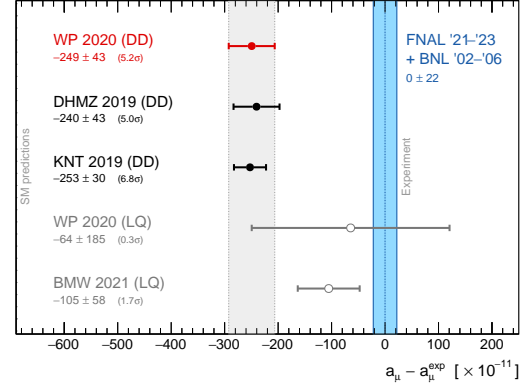


Figure 56.2: Compilation of recent results for a_μ (in units of 10^{-11}), subtracted by the central value of the experimental average (56.3). The light blue vertical band indicates the total experimental uncertainty. The SM predictions shown differ only in the value used for the $a_\mu^{\text{Had}}[\text{LO}]$ contribution. They are taken from: WP 2020 [4] (Eq. (56.16), also indicated by the light grey vertical band), DHMZ 2019 [29], KNT 2019 [30], all three based on the data-driven $a_\mu^{\text{Had}}[\text{LO}]$ evaluation, and the lattice QCD (LQ) based evaluations WP 2020 [4, 37, 38] and BMW 2021 [39]. Note that the quoted errors in the figure do not include the uncertainty on the subtracted experimental value. To obtain for each theory calculation a result equivalent to Eq. (56.17), the errors from theory and experiment must be added in quadrature.

dispersion relations and lattice QCD calculations lead to the improved prediction $a_\mu^{\text{Had,LBL}}[\text{NLO}] = 92(18) \times 10^{-11}$ [4].⁶ One thus finds for the sum of the three higher order hadronic terms

$$a_\mu^{\text{Had}}[\text{N(N)LO}] = 6(18) \times 10^{-11}, \quad (56.15)$$

where the error is dominated by the hadronic light-by-light scattering uncertainty.

Adding Eqs. (56.8), (56.10), (56.12) and (56.15) gives the representative SM prediction

$$a_\mu^{\text{SM}} = 116\,591\,810(1)(40)(18) \times 10^{-11}, \quad (56.16)$$

whose errors are due to the electroweak, lowest-order hadronic, and higher-order hadronic contributions, respectively. The difference between experiment and theory

$$\Delta a_\mu = a_\mu^{\text{exp}} - a_\mu^{\text{SM}} = 249(22)(43) \times 10^{-11}, \quad (56.17)$$

where the errors are from experiment and theory prediction (with all errors combined in quadrature, taking into account a small anticorrelation [4] between the data-driven lowest and higher order contributions), exhibits a discrepancy of 5.2σ .⁷ The new FNAL measurement has increased the discrepancy with the SM prediction from previously 3.7σ (BNL only) and 4.2σ (including the first FNAL result), respectively. Despite the large significance, the situation remains inconclusive due to the discrepancies in the hadronic cross section data underlying the dispersive $a_\mu^{\text{Had}}[\text{LO}]$ determination.

Figure 56.2 represents the difference between experimental and predicted a_μ values based on the most recent data-driven and lattice QCD based evaluations of $a_\mu^{\text{Had}}[\text{LO}]$.

A leading candidate explanation for the deviation observed in Δa_μ has been supersymmetry particle loop contributions. Such a scenario is quite natural, since generically, supersymmetric models predict [1] an additional contribution to a_μ^{SM}

$$a_\mu^{\text{SUSY}} \simeq \pm 130 \times 10^{-11} \cdot \left(\frac{100 \text{ GeV}}{m_{\text{SUSY}}} \right)^2 \tan\beta, \quad (56.18)$$

⁶A very recent lattice QCD based calculation of $a_\mu^{\text{Had,LBL}}[\text{NLO}]$ [47], not included in [4], gives a consistent result with [4, 46] using a different approach.

⁷The probabilistic interpretation of the discrepancy requires caution due to the systematic nature of the a_μ^{SM} uncertainty.

where m_{SUSY} is a representative supersymmetric mass scale, $\tan\beta \simeq 3\text{--}40$ a potential enhancement factor, and ± 1 corresponds to the sign of the μ term in the supersymmetric Lagrangian. Supersymmetric particles in the mass range 100–500 GeV could be the source of the deviation Δa_μ . If so, those particles should be directly observable at the Large Hadron Collider at CERN. So far, there is however no direct evidence in support of the supersymmetry interpretation.

New physics effects [1] other than supersymmetry could also explain a non-vanishing Δa_μ . A popular scenario involves the “dark photon”, a relatively light hypothetical vector boson from the dark matter sector that couples to our world of particle physics through mixing with the ordinary photon [48–50]. As a result, it couples to ordinary charged particles with strength $\varepsilon \cdot e$ and gives rise to an additional muon magnetic anomaly contribution

$$a_\mu^{\text{dark photon}} = \frac{\alpha}{2\pi} \varepsilon^2 F(m_V/m_\mu), \quad (56.19)$$

where $F(x) = \int_0^1 2z(1-z)^2/[(1-z)^2 + x^2z] dz$. For values of $\varepsilon \sim 1\text{--}2 \times 10^{-3}$ and $m_V \sim 10\text{--}100$ MeV, the dark photon, which was originally motivated by cosmology, can provide a viable solution to the muon $g\text{--}2$ discrepancy. However, experimental constraints appear to rule out the simplest model in which the dark photon has equal couplings to electrons and muons and decays primarily to e^+e^- pairs [51] or invisible dark particles [52] that give rise to missing event energy. One can expand the dark photon scenario into a more complete theory in which several new particles contribute to the muon $g\text{--}2$. Direct searches for a dark photon, therefore, continue to be well motivated, but with primary guidance coming from astrophysics [53].

Recent popular solutions to the muon anomaly discrepancy have also focused on loop contributions induced by relatively light scalar or pseudo scalar particle appendages from physics beyond the SM [54, 55].

References

- [1] A. Czarnecki and W. J. Marciano, Phys. Rev. D **64**, 013014 (2001), [hep-ph/0102122]; M. Davier and W. Marciano, Ann. Rev. Nucl. Part. Sci. **54**, 115 (2004).
- [2] J. P. Miller, E. de Rafael and B. Roberts, Rept. Prog. Phys. **70**, 795 (2007), [hep-ph/0703049]; F. Jegerlehner and A. Nyfeler, Phys. Rept. **477**, 1 (2009), [arXiv:0902.3360]; J. P. Miller *et al.*, Ann. Rev. Nucl. Part. Sci. **62**, 237 (2012).
- [3] F. Jegerlehner, Springer Tracts Mod. Phys. **274**, 1 (2017).
- [4] T. Aoyama *et al.*, Phys. Rept. **887**, 1 (2020), [arXiv:2006.04822].
- [5] P. J. Mohr, D. B. Newell and B. N. Taylor, Rev. Mod. Phys. **88**, 3, 035009 (2016), [arXiv:1507.07956].
- [6] G. Bennett *et al.* (Muon $g\text{--}2$), Phys. Rev. Lett. **89**, 101804 (2002), [Erratum: Phys.Rev.Lett. 89, 129903 (2002)], [hep-ex/0208001]; G. Bennett *et al.* (Muon $g\text{--}2$), Phys. Rev. Lett. **92**, 161802 (2004), [hep-ex/0401008]; G. Bennett *et al.* (Muon $g\text{--}2$), Phys. Rev. D **73**, 072003 (2006), [hep-ex/0602035].
- [7] J. Bailey *et al.* (CERN-Mainz-Daresbury), Nucl. Phys. B **150**, 1 (1979).
- [8] J. Grange *et al.* (Muon $g\text{--}2$) (2015), [arXiv:1501.06858].
- [9] B. Abi *et al.* (Muon $g\text{--}2$), Phys. Rev. Lett. **126**, 14, 141801 (2021), [arXiv:2104.03281].
- [10] D. P. Aguillard *et al.* (Muon $g\text{--}2$) (2023), [arXiv:2308.06230].
- [11] M. Abe *et al.*, PTEP **2019**, 5, 053C02 (2019), [arXiv:1901.03047].
- [12] J. S. Schwinger, Phys. Rev. **73**, 416 (1948).
- [13] T. Aoyama *et al.*, Phys. Rev. Lett. **109**, 111808 (2012), [arXiv:1205.5370]; T. Aoyama *et al.*, Phys. Rev. Lett. **109**, 111807 (2012), [arXiv:1205.5368]; T. Kinoshita and M. Nio, Phys. Rev. D **73**, 013003 (2006), [hep-ph/0507249]; T. Aoyama *et al.*, Phys. Rev. Lett. **99**, 110406 (2007), [arXiv:0706.3496]; T. Kinoshita and M. Nio, Phys. Rev. D **70**, 113001 (2004), [hep-ph/0402206]; T. Kinoshita, Nucl. Phys. B Proc. Suppl. **144**, 206 (2005); T. Kinoshita and M. Nio, Phys. Rev. D **73**, 053007 (2006), [hep-ph/0512330]; S. Laporta, Phys. Lett. B **772**, 232 (2017), [arXiv:1704.06996]; A. Kurz *et al.*, Phys. Rev. D **93**, 5, 053017 (2016), [arXiv:1602.02785]; A. Kataev, in “12th Lomonosov Conference on Elementary Particle Physics,” 345–349 (2006), [hep-ph/0602098]; M. Passera, J. Phys. G **31**, R75 (2005), [hep-ph/0411168].
- [14] T. Aoyama, T. Kinoshita and M. Nio, Atoms **7**, 1, 28 (2019).
- [15] R. H. Parker *et al.*, Science **360**, 191 (2018), [arXiv:1812.04130].
- [16] L. Morel *et al.*, Nature **588**, 7836, 61 (2020).
- [17] T. Aoyama *et al.*, Phys. Rev. D **91**, 3, 033006 (2015), [Erratum: Phys.Rev.D 96, 019901 (2017)], [arXiv:1412.8284].
- [18] X. Fan *et al.*, Phys. Rev. Lett. **130**, 7, 071801 (2023), [arXiv:2209.13084].
- [19] R. Jackiw and S. Weinberg, Phys. Rev. D **5**, 2396 (1972); G. Altarelli, N. Cabibbo and L. Maiani, Phys. Lett. B **40**, 415 (1972); I. Bars and M. Yoshimura, Phys. Rev. D **6**, 374 (1972); K. Fujikawa, B. Lee and A. Sanda, Phys. Rev. D **6**, 2923 (1972).
- [20] C. Gnendiger, D. Stöckinger and H. Stöckinger-Kim, Phys. Rev. D **88**, 053005 (2013), [arXiv:1306.5546]; A. Czarnecki, W. J. Marciano and A. Vainshtein, Phys. Rev. D **67**, 073006 (2003), [Erratum: Phys.Rev.D 73, 119901 (2006)], [hep-ph/0212229]; S. Heinemeyer, D. Stockinger and G. Weiglein, Nucl. Phys. B **699**, 103 (2004), [hep-ph/0405255]; T. Gribov and A. Czarnecki, Phys. Rev. D **72**, 053016 (2005), [hep-ph/0509205]; A. Czarnecki, B. Krause and W. J. Marciano, Phys. Rev. Lett. **76**, 3267 (1996), [hep-ph/9512369]; A. Czarnecki, B. Krause and W. J. Marciano, Phys. Rev. D **52**, 2619 (1995), [hep-ph/9506256]; S. Peris, M. Perrotet and E. de Rafael, Phys. Lett. B **355**, 523 (1995), [hep-ph/9505405]; T. Kukhto *et al.*, Nucl. Phys. B **371**, 567 (1992).
- [21] G. Degrossi and G. Giudice, Phys. Rev. D **58**, 053007 (1998), [hep-ph/9803384].
- [22] T. Ishikawa, N. Nakazawa and Y. Yasui, Phys. Rev. D **99**, 7, 073004 (2019), [arXiv:1810.13445].
- [23] C. Bouchiat and L. Michel, J. Phys. Radium **22**, 2, 121 (1961); M. Gourdin and E. De Rafael, Nucl. Phys. B **10**, 667 (1969).
- [24] S. J. Brodsky and E. De Rafael, Phys. Rev. **168**, 1620 (1968).
- [25] M. Davier *et al.*, Eur. Phys. J. C **77**, 12, 827 (2017), [arXiv:1706.09436].
- [26] A. Keshavarzi, D. Nomura and T. Teubner, Phys. Rev. D **97**, 11, 114025 (2018), [arXiv:1802.02995].
- [27] G. Colangelo, M. Hoferichter and P. Stoffer, JHEP **02**, 006 (2019), [arXiv:1810.00007].
- [28] M. Hoferichter, B.-L. Hoid and B. Kubis, JHEP **08**, 137 (2019), [arXiv:1907.01556].
- [29] M. Davier *et al.*, Eur. Phys. J. C **80**, 3, 241 (2020), [Erratum: Eur.Phys.J.C 80, 410 (2020)], [arXiv:1908.00921].
- [30] A. Keshavarzi, D. Nomura and T. Teubner, Phys. Rev. D **101**, 1, 014029 (2020), [arXiv:1911.00367].
- [31] F. V. Ignatov *et al.* (CMD-3) (2023), [arXiv:2302.08834].
- [32] R. Alemany, M. Davier and A. Hocker, Eur. Phys. J. C **2**, 123 (1998), [hep-ph/9703220].
- [33] M. Davier *et al.*, Eur. Phys. J. C **71**, 1515 (2011), [Erratum: Eur.Phys.J.C 72, 1874 (2012)], [arXiv:1010.4180].
- [34] T. Blum, Phys. Rev. Lett. **91**, 052001 (2003), [hep-lat/0212018].
- [35] D. Bernecker and H. B. Meyer, Eur. Phys. J. A **47**, 148 (2011), [arXiv:1107.4388].
- [36] W. A. Bardeen, R. Gastmans and B. E. Lautrup, Nucl. Phys. B **46**, 319 (1972).

- [37] B. Chakraborty *et al.* (Fermilab Lattice, LATTICE-HPQCD, MILC), Phys. Rev. Lett. **120**, 15, 152001 (2018), [arXiv:1710.11212]; S. Borsanyi *et al.* (Budapest-Marseille-Wuppertal), Phys. Rev. Lett. **121**, 2, 022002 (2018), [arXiv:1711.04980]; T. Blum *et al.* (RBC, UKQCD), Phys. Rev. Lett. **121**, 2, 022003 (2018), [arXiv:1801.07224]; D. Giusti *et al.* (ETM), Phys. Rev. **D99**, 11, 114502 (2019), [arXiv:1901.10462]; E. Shintani and Y. Kuramashi, Phys. Rev. **D100**, 3, 034517 (2019), [arXiv:1902.00885]; C. T. H. Davies *et al.* (Fermilab Lattice, LATTICE-HPQCD, MILC), Phys. Rev. **D101**, 3, 034512 (2020), [arXiv:1902.04223]; A. Gérardin *et al.*, Phys. Rev. **D100**, 1, 014510 (2019), [arXiv:1904.03120].
- [38] C. Aubin *et al.*, Phys. Rev. **D101**, 1, 014503 (2020), [arXiv:1905.09307]; D. Giusti and S. Simula, PoS **LATTICE2019**, 104 (2019), [arXiv:1910.03874].
- [39] S. Borsanyi *et al.*, Nature **593**, 7857, 51 (2021), [arXiv:2002.12347].
- [40] A. Crivellin *et al.*, Phys. Rev. Lett. **125**, 9, 091801 (2020), [arXiv:2003.04886]; A. Keshavarzi *et al.*, Phys. Rev. D **102**, 3, 033002 (2020), [arXiv:2006.12666]; E. de Rafael, Phys. Rev. D **102**, 5, 056025 (2020), [arXiv:2006.13880]; B. Malaescu and M. Schott, Eur. Phys. J. C **81**, 1, 46 (2021), [arXiv:2008.08107]; G. Colangelo, M. Hoferichter and P. Stoffer, Phys. Lett. B **814**, 136073 (2021), [arXiv:2010.07943].
- [41] T. Blum *et al.* (RBC, UKQCD), Phys. Rev. Lett. **121**, 2, 022003 (2018), [arXiv:1801.07224].
- [42] C. Lehner and A. S. Meyer, Phys. Rev. D **101**, 074515 (2020), [arXiv:2003.04177].
- [43] B. Krause, Phys. Lett. B **390**, 392 (1997), [hep-ph/9607259].
- [44] A. Kurz *et al.*, Phys. Lett. B **734**, 144 (2014), [arXiv:1403.6400].
- [45] K. Melnikov and A. Vainshtein, Phys. Rev. **D70**, 113006 (2004), [hep-ph/0312226]; P. Masjuan and P. Sánchez-Puertas, Phys. Rev. **D95**, 5, 054026 (2017), [arXiv:1701.05829]; G. Colangelo *et al.*, JHEP **04**, 161 (2017), [arXiv:1702.07347]; M. Hoferichter *et al.*, JHEP **10**, 141 (2018), [arXiv:1808.04823]; A. Gérardin, H. B. Meyer and A. Nyffeler, Phys. Rev. **D100**, 3, 034520 (2019), [arXiv:1903.09471]; J. Bijnens, N. Hermansson-Truedsson and A. Rodríguez-Sánchez, Phys. Lett. **B798**, 134994 (2019), [arXiv:1908.03331]; G. Colangelo *et al.*, JHEP **03**, 101 (2020), [arXiv:1910.13432]; V. Pauk and M. Vanderhaeghen, Eur. Phys. J. **C74**, 8, 3008 (2014), [arXiv:1401.0832]; I. Danilkin and M. Vanderhaeghen, Phys. Rev. **D95**, 1, 014019 (2017), [arXiv:1611.04646]; M. Knecht *et al.*, Phys. Lett. **B787**, 111 (2018), [arXiv:1808.03848]; G. Eichmann, C. S. Fischer and R. Williams, Phys. Rev. **D101**, 5, 054015 (2020), [arXiv:1910.06795]; P. Roig and P. Sánchez-Puertas, Phys. Rev. **D101**, 7, 074019 (2020), [arXiv:1910.02881]; G. Colangelo *et al.*, Phys. Lett. **B735**, 90 (2014), [arXiv:1403.7512].
- [46] T. Blum *et al.*, Phys. Rev. Lett. **124**, 13, 132002 (2020), [arXiv:1911.08123].
- [47] E.-H. Chao *et al.*, Eur. Phys. J. C **81**, 7, 651 (2021), [arXiv:2104.02632].
- [48] P. Fayet, Phys. Rev. D **75**, 115017 (2007), [hep-ph/0702176].
- [49] M. Pospelov, Phys. Rev. D **80**, 095002 (2009), [arXiv:0811.1030].
- [50] D. Tucker-Smith and I. Yavin, Phys. Rev. D **83**, 101702 (2011), [arXiv:1011.4922].
- [51] J. Batley *et al.* (NA48/2), Phys. Lett. B **746**, 178 (2015), [arXiv:1504.00607].
- [52] Y. M. Andreev *et al.* (NA64), Phys. Rev. Lett. **126**, 21, 211802 (2021), [arXiv:2102.01885]; J. P. Lees *et al.* (BaBar), Phys. Rev. Lett. **119**, 13, 131804 (2017), [arXiv:1702.03327].
- [53] J. Alexander *et al.* (2016), [arXiv:1608.08632].
- [54] K.-m. Cheung, C.-H. Chou and O. C. W. Kong, Phys. Rev. D **64**, 111301 (2001), [hep-ph/0103183].
- [55] D. Chang *et al.*, Phys. Rev. D **63**, 091301 (2001), [hep-ph/0009292].

57. Muon Decay Parameters

Revised August 2023 by W. Fetscher (ETH Zurich) and H.-J. Gerber (ETH Zurich).

57.1 Introduction:

All measurements in direct muon decay, $\mu^- \rightarrow e^- + 2$ neutrals, and its inverse, $\nu_\mu + e^- \rightarrow \mu^- + \text{neutral}$, are successfully described by the “ V - A interaction,” which is a particular case of a local, derivative-free, lepton-number-conserving, four-fermion interaction [1]. As shown below, within this framework, the Standard Model assumptions, such as the V - A form and the nature of the neutrals (ν_μ and $\bar{\nu}_e$), and hence the doublet assignments $(\nu_e e^-)_L$ and $(\nu_\mu \mu^-)_L$, have been determined from experiments [2, 3]. All considerations on muon decay are valid for the leptonic tau decays $\tau^- \rightarrow \ell^- + \nu_\tau + \bar{\nu}_\ell$ with the replacements $m_\mu \rightarrow m_\tau$, $m_e \rightarrow m_{e\ell}$, $\ell^- = e^-, \mu^-$.

57.2 Parameters:

The differential decay probability to obtain an e^\pm with (reduced) energy between x and $x + dx$, emitted in the direction $\hat{\mathbf{x}}_3$ at an angle between ϑ and $\vartheta + d\vartheta$ with respect to the muon polarization vector \mathbf{P}_μ , and with its spin parallel to the arbitrary direction $\hat{\boldsymbol{\zeta}}$, neglecting radiative corrections, is given by

$$\begin{aligned} \frac{d^2\Gamma}{dx d\cos\vartheta} &= \frac{m_\mu}{4\pi^3} W_{e\mu}^4 G_F^2 \sqrt{x^2 - x_0^2} \\ &\times (F_{\text{IS}}(x) \pm P_\mu \cos\vartheta F_{\text{AS}}(x)) \\ &\times [1 + \hat{\boldsymbol{\zeta}} \cdot \mathbf{P}_e(x, \vartheta)]. \end{aligned} \quad (57.1)$$

Here, $W_{e\mu} = \max(E_e) = (m_\mu^2 + m_e^2)/2m_\mu$ is the maximum e^\pm energy, $x = E_e/W_{e\mu}$ is the reduced energy, $x_0 = m_e/W_{e\mu} = 9.67 \times 10^{-3}$, and $P_\mu = |\mathbf{P}_\mu|$ is the degree of muon polarization. $\hat{\boldsymbol{\zeta}}$ is the direction in which a perfect polarization-sensitive electron detector is most sensitive. The isotropic part of the spectrum, $F_{\text{IS}}(x)$, the anisotropic part $F_{\text{AS}}(x)$, and the electron polarization, $\mathbf{P}_e(x, \vartheta)$, may be parametrized by the Michel parameter ρ [1], by η [4], by ξ and δ [5, 6], *etc.* These are bilinear combinations of the coupling constants $g_{\varepsilon\mu}^\gamma$, which occur in the matrix element (given below).

If the masses of the neutrinos as well as x_0^2 are neglected, the energy and angular distribution of the electron in the rest frame of a muon (μ^\pm) measured by a polarization insensitive detector, is given by

$$\begin{aligned} \frac{d^2\Gamma}{dx d\cos\vartheta} &\sim x^2 \cdot \left\{ 3(1-x) + \frac{2\rho}{3}(4x-3) + 3\eta x_0(1-x)/x \right. \\ &\quad \left. \pm P_\mu \cdot \xi \cdot \cos\vartheta \left[1 - x + \frac{2\delta}{3}(4x-3) \right] \right\}. \end{aligned} \quad (57.2)$$

Here, ϑ is the angle between the electron momentum and the muon spin, and $x \equiv 2E_e/m_\mu$. For the Standard Model coupling, we obtain $\rho = \xi\delta = 3/4$, $\xi = 1$, $\eta = 0$ and the differential decay rate is

$$\frac{d^2\Gamma}{dx d\cos\vartheta} = \frac{G_F^2 m_\mu^5}{192\pi^3} [3 - 2x \pm P_\mu \cos\vartheta(2x - 1)] \cdot x^2. \quad (57.3)$$

The coefficient in front of the square bracket is the total decay rate.

If only the neutrino masses are neglected, and if the e^\pm polarization is detected, then the functions in Eq. (57.1) become

$$F_{\text{IS}}(x) = x(1-x) + \frac{2}{9}\rho(4x^2 - 3x - x_0^2) + \eta \cdot x_0(1-x) \quad (57.4a)$$

$$\begin{aligned} F_{\text{AS}}(x) &= \frac{1}{3}\xi \sqrt{x^2 - x_0^2} \\ &\times \left[(1-x) + \frac{2}{3}\delta \left\{ (4x-3) + \left(\sqrt{1-x_0^2} - 1 \right) \right\} \right] \end{aligned} \quad (57.4b)$$

$$\mathbf{P}_e(x, \vartheta) = P_{T_1} \cdot \hat{\mathbf{x}}_1 + P_{T_2} \cdot \hat{\mathbf{x}}_2 + P_L \cdot \hat{\mathbf{x}}_3 \quad (57.4c)$$

Here $\hat{\mathbf{x}}_1$, $\hat{\mathbf{x}}_2$, and $\hat{\mathbf{x}}_3$ are orthogonal unit vectors defined as follows:

$$\begin{aligned} \hat{\mathbf{x}}_3 &\text{ is along the } e \text{ momentum } \mathbf{p}_e \\ \frac{\hat{\mathbf{x}}_3 \times \mathbf{P}_\mu}{|\hat{\mathbf{x}}_3 \times \mathbf{P}_\mu|} &= \hat{\mathbf{x}}_2 \text{ is transverse to } \mathbf{p}_e \text{ and perpendicular to} \\ &\text{“the decay plane”} \\ \hat{\mathbf{x}}_2 \times \hat{\mathbf{x}}_3 &= \hat{\mathbf{x}}_1 \text{ is transverse to } \mathbf{p}_e \text{ and in the decay plane} \end{aligned}$$

The components of \mathbf{P}_e then are given by

$$P_{T_1}(x, \vartheta) = P_\mu \sin\vartheta \cdot F_{T_1}(x) / \{F_{\text{IS}}(x) \pm P_\mu \cos\vartheta \cdot F_{\text{AS}}(x)\} \quad (57.5a)$$

$$P_{T_2}(x, \vartheta) = P_\mu \sin\vartheta \cdot F_{T_2}(x) / \{F_{\text{IS}}(x) \pm P_\mu \cos\vartheta \cdot F_{\text{AS}}(x)\} \quad (57.5b)$$

$$P_L(x, \vartheta) = \frac{\pm F_{\text{IP}}(x) + P_\mu \cos\vartheta \cdot F_{\text{AP}}(x)}{F_{\text{IS}}(x) \pm P_\mu \cos\vartheta \cdot F_{\text{AS}}(x)}, \quad (57.5c)$$

where

$$\begin{aligned} F_{T_1}(x) &= \frac{1}{12} \left\{ -2 \left[\xi'' + 12 \left(\rho - \frac{3}{4} \right) \right] (1-x)x_0 \right. \\ &\quad \left. - 3\eta(x^2 - x_0^2) + \eta''(-3x^2 + 4x - x_0^2) \right\} \end{aligned} \quad (57.6a)$$

$$F_{T_2}(x) = \frac{1}{3} \sqrt{x^2 - x_0^2} \cdot \left\{ 3 \frac{\alpha'}{A} (1-x) + 2 \frac{\beta'}{A} \sqrt{1-x_0^2} \right\} \quad (57.6b)$$

$$\begin{aligned} F_{\text{IP}}(x) &= \frac{1}{54} \sqrt{x^2 - x_0^2} \cdot \left\{ 9\xi' \left(-2x + 2 + \sqrt{1-x_0^2} \right) \right. \\ &\quad \left. + 4\xi \left(\delta - \frac{3}{4} \right) \left(4x - 4 + \sqrt{1-x_0^2} \right) \right\} \end{aligned} \quad (57.6c)$$

$$\begin{aligned} F_{\text{AP}}(x) &= \frac{1}{6} \left\{ \xi''(2x^2 - x - x_0^2) + 4 \left(\rho - \frac{3}{4} \right) (4x^2 - 3x - x_0^2) \right. \\ &\quad \left. + 2\eta''(1-x)x_0 \right\}. \end{aligned} \quad (57.6d)$$

For the experimental values of the parameters ρ , ξ , ξ' , ξ'' , δ , η , η'' , α/A , β/A , α'/A , β'/A , which are not all independent, see the Data Listings below. Experiments in the past have also been analyzed using the parameters a , b , c , a' , b' , c' , α/A , β/A , α'/A , β'/A (and $\eta = (\alpha - 2\beta)/2A$), as defined by Kinoshita and Sirlin [5, 6]. They serve as a model-independent summary of all possible measurements on the decay electron (see Listings below). The relations between the two sets of parameters are

$$\rho - \frac{3}{4} = \frac{3}{4}(-a + 2c)/A \quad (57.7a)$$

$$\eta = (\alpha - 2\beta)/A \quad (57.7b)$$

$$\eta'' = (3\alpha + 2\beta)/A \quad (57.7c)$$

$$\delta - \frac{3}{4} = \frac{9}{4} \cdot \frac{(a' - 2c')/A}{1 - [a + 3a' + 4(b + b') + 6c - 14c']/A} \quad (57.7d)$$

$$1 - \xi \frac{\delta}{\rho} = 4 \frac{[(b + b') + 2(c - c')]/A}{1 - (a - 2c)/A} \quad (57.7e)$$

$$1 - \xi = [(a + a') + 4(b + b') + 6(c + c')]/A \quad (57.7f)$$

$$1 - \xi'' = (-2a + 20c)/A \quad (57.7g)$$

$$\text{with } A = a + 4b + 6c \quad (57.7h)$$

The differential decay probability to obtain a *left-handed* ν_e with (reduced) energy between y and $y + dy$, neglecting radiative corrections as well as the masses of the electron and of the neutrinos, is given by [7]

$$\frac{d\Gamma}{dy} = \frac{m_\mu^5 G_F^2}{16\pi^3} \cdot Q_L^{\nu_e} \cdot y^2 \left\{ (1-y) - \omega_L \cdot \left(y - \frac{3}{4} \right) \right\}. \quad (57.8)$$

Here, $y = 2 E_{\nu_e}/m_\mu$. $Q_L^{\nu_e}$ and ω_L are parameters. ω_L is the neutrino analog of the spectral shape parameter ρ of Michel. Since in the Standard Model, $Q_L^{\nu_e} = 1$, $\omega_L = 0$, the measurement of $d\Gamma/dy$ has allowed a null-test of the Standard Model (see Listings below).

Table 57.1: Coupling constants $g_{\varepsilon\mu}^\gamma$ and some combinations of them. Ninety-percent confidence level experimental limits. The limits on $|g_{LL}^S|$ and $|g_{LL}^V|$ are from [8–10], and the others from a general analysis of muon decay measurements. Top three rows: [11], fourth row: [12], next three rows: [13], last row: [14]. The experimental uncertainty on the muon polarization in pion decay is included. Note that, by definition, $|g_{\varepsilon\mu}^S| \leq 2$, $|g_{\varepsilon\mu}^V| \leq 1$ and $|g_{\varepsilon\mu}^T| \leq 1/\sqrt{3}$.

$ g_{RR}^S < 0.035$	$ g_{RR}^V < 0.017$	$ g_{RR}^T \equiv 0$
$ g_{LR}^S < 0.050$	$ g_{LR}^V < 0.023$	$ g_{LR}^T < 0.015$
$ g_{RL}^S < 0.420$	$ g_{RL}^V < 0.105$	$ g_{RL}^T < 0.105$
$ g_{LL}^S < 0.550$	$ g_{LL}^V > 0.960$	$ g_{LL}^T \equiv 0$
$ g_{LR}^S + 6g_{LR}^T < 0.143$	$ g_{RL}^S + 6g_{RL}^T < 0.418$	
$ g_{LR}^S + 2g_{LR}^T < 0.108$	$ g_{RL}^S + 2g_{RL}^T < 0.417$	
$ g_{LR}^S - 2g_{LR}^T < 0.070$	$ g_{RL}^S - 2g_{RL}^T < 0.418$	
$Q_{RR} + Q_{LR} < 8.2 \times 10^{-4}$		

57.3 Matrix element:

All results in direct muon decay (energy spectra of the electron and of the neutrinos, polarizations, and angular distributions), and in inverse muon decay (the reaction cross section) at energies well below $m_W c^2$, may be parametrized in terms of amplitudes $g_{\varepsilon\mu}^\gamma$ and the Fermi coupling constant G_F , using the matrix element

$$\frac{4G_F}{\sqrt{2}} \sum_{\substack{\gamma=S,V,T \\ \varepsilon,\mu=R,L}} g_{\varepsilon\mu}^\gamma \langle \bar{\varepsilon} | \Gamma^\gamma | (\nu_e)_n \rangle \langle \bar{\nu}_\mu | \Gamma_\gamma | \mu_\mu \rangle \quad (57.9)$$

We use the notation of Fetscher *et al.* [2], who in turn use the sign conventions and definitions of Scheck [15]. Here, $\gamma = S, V, T$ indicates a scalar, vector, or tensor interaction; and $\varepsilon, \mu = R, L$ indicate a right- or left-handed chirality of the electron or muon. The chiralities n and m of the ν_e and $\bar{\nu}_\mu$ are then determined by the values of γ, ε , and μ . The particles are represented by fields of definite chirality [16].

As shown by Langacker and London [17], explicit lepton-number nonconservation still leads to a matrix element equivalent to Eq. (57.9). They conclude that it is not possible, even in principle, to test lepton-number conservation in (leptonic) muon decay if the final neutrinos are massless and are not observed.

The ten complex amplitudes $g_{\varepsilon\mu}^\gamma$ (g_{RR}^T and g_{LL}^T are identically zero) and G_F constitute 19 independent (real) parameters to be determined by experiment. The Standard Model interaction corresponds to one single amplitude g_{LL}^V being unity and all the others being zero.

The (direct) muon decay experiments are compatible with an arbitrary mix of the scalar and vector amplitudes g_{LL}^S and g_{LL}^V – in the extreme even with purely scalar $g_{LL}^S = 2$, $g_{LL}^V = 0$. The decision in favour of the Standard Model comes from the quantitative observation of inverse muon decay, which would be forbidden for pure g_{LL}^S [2].

57.4 Experimental determination of $V-A$:

In order to determine the amplitudes $g_{\varepsilon\mu}^\gamma$ uniquely from experiment, the following set of equations, where the left-hand sides

represent experimental results, has to be solved.

$$a = 16 \left(|g_{RL}^V|^2 + |g_{LR}^V|^2 \right) + \left| g_{RL}^S + 6g_{RL}^T \right|^2 + \left| g_{LR}^S + 6g_{LR}^T \right|^2 \quad (57.10a)$$

$$a' = 16 \left(|g_{RL}^V|^2 - |g_{LR}^V|^2 \right) + \left| g_{RL}^S + 6g_{RL}^T \right|^2 - \left| g_{LR}^S + 6g_{LR}^T \right|^2 \quad (57.10b)$$

$$\alpha = 8 \operatorname{Re} \left\{ g_{RL}^V \left(g_{RL}^{S*} + 6g_{LR}^{T*} \right) + g_{LR}^V \left(g_{RL}^{S*} + 6g_{LR}^{T*} \right) \right\} \quad (57.10c)$$

$$\alpha' = 8 \operatorname{Im} \left\{ -g_{RL}^V \left(g_{LR}^{S*} + 6g_{LR}^{T*} \right) + g_{LR}^V \left(g_{RL}^{S*} + 6g_{RL}^{T*} \right) \right\} \quad (57.10d)$$

$$b = 4 \left(|g_{RR}^V|^2 + |g_{LL}^V|^2 \right) + |g_{RR}^S|^2 + |g_{LL}^S|^2 \quad (57.10e)$$

$$b' = 4 \left(|g_{RR}^V|^2 - |g_{LL}^V|^2 \right) + |g_{RR}^S|^2 - |g_{LL}^S|^2 \quad (57.10f)$$

$$c = \frac{1}{2} \left\{ |g_{RL}^S - 2g_{RL}^T|^2 + |g_{LR}^S - 2g_{LR}^T|^2 \right\} \quad (57.10g)$$

$$c' = \frac{1}{2} \left\{ |g_{RL}^S - 2g_{RL}^T|^2 - |g_{LR}^S - 2g_{LR}^T|^2 \right\} \quad (57.10h)$$

and

$$Q_L^{\nu_e} = 1 - \left\{ \frac{1}{4} |g_{LR}^S|^2 + \frac{1}{4} |g_{LL}^S|^2 + |g_{RR}^V|^2 + |g_{RL}^V|^2 + 3 |g_{LR}^T|^2 \right\}$$

$$\omega_L = \frac{3}{4} \frac{|g_{RR}^S|^2 + 4 |g_{LR}^V|^2 + |g_{RL}^S|^2 + 2 |g_{LR}^T|^2}{|g_{RL}^S|^2 + |g_{RR}^S|^2 + 4 |g_{LL}^V|^2 + 4 |g_{LR}^V|^2 + 12 |g_{RL}^T|^2}. \quad (57.10i)$$

It has been noted earlier by C. Jarlskog [18], that certain experiments observing the decay electron are especially informative if they yield the $V-A$ values. The complete solution is now found as follows. Fetscher *et al.* [2] introduced four probabilities $Q_{\varepsilon\mu}(\varepsilon, \mu = R, L)$ for the decay of a μ -handed muon into an ε -handed electron, and showed that there exist upper bounds on Q_{RR} , Q_{LR} , and Q_{RL} , and a lower bound on Q_{LL} . These probabilities are given in terms of the $g_{\varepsilon\mu}^\gamma$'s by

$$Q_{\varepsilon\mu} = \frac{1}{4} |g_{\varepsilon\mu}^S|^2 + |g_{\varepsilon\mu}^V|^2 + 3(1 - \delta_{\varepsilon\mu}) |g_{\varepsilon\mu}^T|^2 \quad (57.11)$$

where $\delta_{\varepsilon\mu} = 1$ for $\varepsilon = \mu$, and $\delta_{\varepsilon\mu} = 0$ for $\varepsilon \neq \mu$. They are related to the parameters a, b, c, a', b' , and c' by

$$Q_{RR} = 2(b + b')/A \quad (57.12a)$$

$$Q_{LR} = [(a - a') + 6(c - c')]/2A \quad (57.12b)$$

$$Q_{RL} = [(a + a') + 6(c + c')]/2A \quad (57.12c)$$

$$Q_{LL} = 2(b - b')/A \quad (57.12d)$$

with $A = 16$. In the Standard Model, $Q_{LL} = 1$ and the others are zero.

Since the upper bounds on Q_{RR} , Q_{LR} , and Q_{RL} are found to be small, and since the helicity of the ν_μ in pion decay is known from experiment [19, 20] to very high precision to be -1 [21], the cross section S of *inverse* muon decay, normalized to the $V-A$ value, yields [2]

$$|g_{LL}^S|^2 \leq 4(1 - S) \quad (57.13a)$$

and

$$|g_{LL}^V|^2 = S. \quad (57.13b)$$

Thus the Standard Model assumption of a pure $V-A$ leptonic charged weak interaction of e and μ is derived (within errors) from experiments at energies far below the mass of the W^\pm : Eq. (57.13 b) gives a lower limit for $V-A$, and Eqs. (57.12 a, b, c)

and (57.13 a) give upper limits for the other four-fermion interactions. The existence of such upper limits may also be seen from $Q_{RR} + Q_{RL} = (1 - \xi^+)/2$ (e^+ longitudinal polarization) and $Q_{RR} + Q_{LR} = \frac{1}{2}(1 + \xi/3 - 16\xi\delta/9)$ (decay asymmetry). Table 57.1 gives the current experimental limits on the magnitudes of the $g_{\varepsilon\mu}^\gamma$'s. More stringent limits on the six coupling constants g_{LR}^S , g_{LR}^V , g_{LR}^T , g_{RL}^S , g_{RL}^V , and g_{RL}^T have been derived from upper limits on the neutrino mass [22]. Limits on the "charge retention" coordinates, as used in the older literature (*e.g.*, Ref. [23]), are given by Burkard *et al.* [24].

References

- [1] L. Michel, Proc. Phys. Soc. **A63**, 514 (1950).
- [2] W. Fetscher, H. J. Gerber and K. F. Johnson, Phys. Lett. **B173**, 102 (1986).
- [3] P. Langacker, Comments Nucl. Part. Phys. **19**, 1, 1 (1989).
- [4] C. Bouchiat and L. Michel, Phys. Rev. **106**, 170 (1957).
- [5] T. Kinoshita and A. Sirlin, Phys. Rev. **107**, 593 (1957).
- [6] T. Kinoshita and A. Sirlin, Phys. Rev. **108**, 844 (1957).
- [7] W. Fetscher, Phys. Rev. **D49**, 5945 (1994).
- [8] S. R. Mishra *et al.*, Phys. Lett. **B252**, 170 (1990).
- [9] S. R. Mishra, private communication.
- [10] P. Vilain *et al.* (CHARM-II), Phys. Lett. **B364**, 121 (1995).
- [11] A. Hillairet *et al.* (TWIST), Phys. Rev. **D85**, 092013 (2012), [arXiv:1112.3606].
- [12] R. P. MacDonald *et al.* (TWIST), Phys. Rev. **D78**, 032010 (2008), [arXiv:0807.1125].
- [13] C. A. Gagliardi, R. E. Tribble and N. J. Williams, Phys. Rev. **D72**, 073002 (2005), [hep-ph/0509069].
- [14] R. Bayes *et al.* (TWIST), Phys. Rev. Lett. **106**, 041804 (2011).
- [15] F. Scheck, in *Electroweak and Strong Interactions* (Springer Verlag, 1996).
- [16] K. Mursula and F. Scheck, Nucl. Phys. **B253**, 189 (1985).
- [17] P. Langacker and D. London, Phys. Rev. **D39**, 266 (1989).
- [18] C. Jarlskog, Nucl. Phys. **75**, 659 (1966).
- [19] A. Jodidio *et al.*, Phys. Rev. **D34**, 1967 (1986), [Erratum: Phys. Rev. **D37**, 237 (1988)].
- [20] L. P. Roesch *et al.*, Helv. Phys. Acta **55**, 74 (1982).
- [21] W. Fetscher, Phys. Lett. **140B**, 117 (1984).
- [22] G. Prezeau and A. Kurylov, Phys. Rev. Lett. **95**, 101802 (2005), [hep-ph/0409193].
- [23] S. E. Derenzo, Phys. Rev. **181**, 1854 (1969).
- [24] H. Burkard *et al.*, Phys. Lett. **160B**, 343 (1985).

58. τ Branching Fractions

Revised April 2024 by Sw. Banerjee (Louisville U.) and A. Lusiani (SNS, Pisa; INFN, Pisa).

58.1 τ Branching Fractions

The τ Listings contain 252 entries that correspond to either a τ partial decay fraction into a specific decay mode (branching fraction) or a ratio of two τ partial decay fractions (branching ratio). Experimental measurements provide values for 148 of these quantities, upper limits for 67 branching fractions to Lepton Family number, Lepton number, or Baryon number violating modes, and 37 additional upper limits for other modes. A total of 129 τ branching fractions and branching ratios are determined with a fit of 170 measurements. 85 quantities have at least one measurement in the fit.

58.2 The constrained fit to τ branching fractions

The τ branching fractions fit uses the reported values, uncertainties and statistical correlations of the τ branching fractions and branching ratios measurements. Asymmetric uncertainties are symmetrized as $\sigma_{\text{symm}}^2 = (\sigma_+^2 + \sigma_-^2)/2$. If only a few measurements are correlated, the correlation coefficients are listed in the footnote for each measurement (see for example $\Gamma(\text{particle}^- \geq 0 \text{ neutrals} \geq 0 K^0 \nu_\tau)$ (“1-prong”)/ Γ_{total}). If a large number of measurements are correlated, then the full correlation matrix is listed in the footnote to the measurement that first appears in the τ Listings. Footnotes to the other measurements refer to the first one. For example, the large correlation matrices for the branching fraction or ratio measurements contained in Refs. [1] [2] are listed in Footnotes to the $\Gamma(e^- \bar{\nu}_e \nu_\tau)/\Gamma_{\text{total}}$ and $\Gamma(h^- \nu_\tau)/\Gamma_{\text{total}}$ measurements respectively. Additionally, the most precise experimental inputs are treated according to how they depend on external parameters on the basis of their documentation [3]. The τ measurements may depend on parameters such as the τ pair production cross-section in e^+e^- annihilations at the $\Upsilon(4S)$ peak. In some cases, measurements reported in different papers by the same collaboration may depend on common parameters like the estimate of the integrated luminosity or of particle identification efficiencies. For all the significant detected dependencies, the τ measurements and their uncertainties are updated to account for the updated values of the external parameters. The dependencies on common systematic effects are also determined in size and sign, and all the common systematic dependencies of different measurements are used together with the published statistical and systematic uncertainties and correlations in order to compute an updated all-inclusive variance and covariance matrix of the experimental inputs of the fit.

The fit procedure parameters correspond to all measured τ branching fractions and ratios, to some non-measured branching fractions and ratios like for instance $\mathcal{B}(\tau^- \rightarrow \pi^- K_L^0 K_L^0 \nu_\tau)$ and to one nuisance variable. When discussing the fit results in the following, the fit χ^2 , the number of degrees of freedom, the residuals and pulls all refer to the subset of fit parameters that correspond to τ branching fractions and ratios, excluding nuisance variables. The fit parameters are optimized while respecting relations described by a series of constraint equations. All the experimental inputs and all the constraint equations are reported in the τ Listings section that follows this review. In some cases, constraints describe approximate relations that nevertheless hold within the present experimental precision. For instance, the constraint $\mathcal{B}(\tau^- \rightarrow K^- K^- K^+ \nu_\tau) = \mathcal{B}(\tau^- \rightarrow K^- \phi \nu_\tau) \times \mathcal{B}(\phi \rightarrow K^+ K^-)$ is justified within the current experimental evidence. The constraint equations between the τ branching fractions and ratios include quantities other than τ branching fractions and branching ratios, like for instance the branching fractions of the η and ω mesons. We neglect the uncertainties on these values for all quantities except $\mathcal{B}(a_1^- \rightarrow \pi^- \gamma)$, whose value and uncertainty were estimated by ALEPH [1] to be $(0.21 \pm 0.08) \cdot 10^{-2}$, relying on a measurement of $\Gamma(a_1^- \rightarrow \pi^- \gamma)$ [4]. This quantity is included in the fit parameters as nuisance variable, with a χ^2 term corresponding to its estimate. We assume that $\mathcal{B}(\tau^- \rightarrow a_1^- \nu_\tau) = \mathcal{B}(\tau^- \rightarrow \pi^- \pi^+ \pi^- \nu_\tau \text{ (ex. } K^0, \omega)) + \mathcal{B}(\tau^- \rightarrow \pi^- 2\pi^0 \nu_\tau \text{ (ex. } K^0)) + \mathcal{B}(\tau^- \rightarrow a_1^- (\pi^- \gamma) \nu_\tau)$, neglecting the observed but negligible branching fractions to other modes, and that

$\mathcal{B}(\tau^- \rightarrow a_1^- (\pi^- \gamma) \nu_\tau) = \mathcal{B}(\tau^- \rightarrow a_1^- \nu_\tau) \cdot \mathcal{B}(a_1^- \rightarrow \pi^- \gamma)$. The values of all other quantities in the constraint equations are taken from the 2023 edition of the Review of Particle Physics.

In the fit, uncertainty scale factors are applied to the published uncertainties of measurements only if significant inconsistency between different measurements remain after accounting for all relevant uncertainties and correlations. When performing the fit with no scale factors, the two measurements of $\mathcal{B}(\tau^- \rightarrow K^- K^- K^+ \nu_\tau)$ have pulls exceeding 5σ from the fit values. There are 170 pulls, one per measurement. They are partially correlated, and the effective number of independent pulls is equal to the number of degrees of freedom of the fit, 125. The probability of getting pulls equal or larger than either one of the two very large pulls in a sample of 125 is smaller than the probability of a 3σ deviation for a Normal variable. Therefore, it has been decided to apply an uncertainty scale factor of 5.4 on all measurements of $\mathcal{B}(\tau^- \rightarrow K^- K^- K^+ \nu_\tau)$ (one by BaBar and one by Belle). The scale factor has been computed according to the standard PDG procedure. After applying the scale factor, the pull distribution of the measurements in figure 58.1 is reasonably Normal and the pull probability distribution in figure 58.2 is reasonably flat.

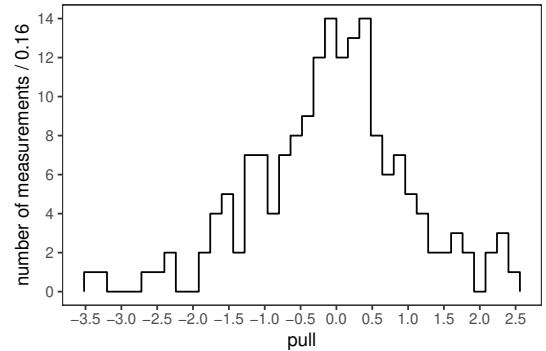


Figure 58.1: Pulls of individual measurements against the respective fitted quantity.

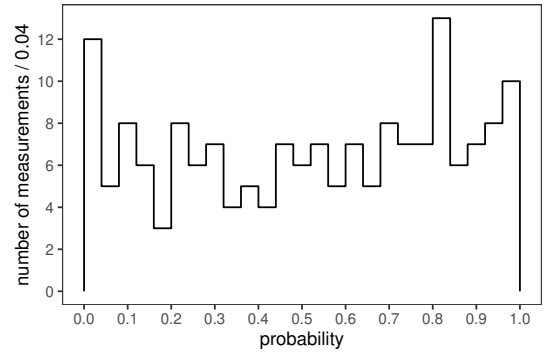


Figure 58.2: Probability of individual measurement pulls against the respective fitted quantity.

Considering only the residuals with respect to τ branching fractions and ratios measurements, the constrained fit has a χ^2 of 135 for 125 degrees of freedom, corresponding to a χ^2 probability of 26.0%. We use 170 measurements and 84 constraints on the branching fractions and ratios to determine 129 quantities, consisting of 112 branching fractions and 17 branching ratios. The constraints include the unitarity constraint on the sum of all the exclusive τ decay modes, $\mathcal{B}_{\text{all}} = 1$. If the unitarity constraint is released, the fit result for \mathcal{B}_{all} is consistent with unitarity with $1 - \mathcal{B}_{\text{all}} = (0.07 \pm 0.11)\%$.

For the convenience of summarizing the fit results, we list in the following the values and uncertainties for a set of 46 “basis” decay modes, from which all remaining branching fractions and ratios

can be obtained using the constraints. The basis decay modes are not intended to sum up to 1. Since some basis quantities represent multiple branching fractions that are related by constraint equations, the unitarity constraint corresponds to a linear combination of branching fractions, with the coefficients listed in the following. The coefficients of $\mathcal{B}(\tau^- \rightarrow \pi^- 2\pi^0 \nu_\tau \text{ (ex. } K^0))$ and $\mathcal{B}(\tau^- \rightarrow \pi^- \pi^+ \pi^- \nu_\tau \text{ (ex. } K^0, \omega))$ depend on the fitted value of the nuisance variable, $\mathcal{B}(a_1^- \rightarrow \pi^- \gamma) = 0.0022 \pm 0.0008$. The correlation matrix between the basis modes is reported in the τ Listings.

decay mode	fit result	coeff.
$\mathcal{B}(\tau^- \rightarrow \mu^- \bar{\nu}_\mu \nu_\tau)$	0.1739 ± 0.0004	1.0000
$\mathcal{B}(\tau^- \rightarrow e^- \bar{\nu}_e \nu_\tau)$	0.1782 ± 0.0004	1.0000
$\mathcal{B}(\tau^- \rightarrow \pi^- \nu_\tau)$	0.1082 ± 0.0005	1.0000
$\mathcal{B}(\tau^- \rightarrow K^- \nu_\tau)$	0.00696 ± 0.00010	1.0000
$\mathcal{B}(\tau^- \rightarrow \pi^- \pi^0 \nu_\tau)$	0.2549 ± 0.0009	1.0000
$\mathcal{B}(\tau^- \rightarrow K^- \pi^0 \nu_\tau)$	0.00433 ± 0.00015	1.0000
$\mathcal{B}(\tau^- \rightarrow \pi^- 2\pi^0 \nu_\tau \text{ (ex. } K^0))$	0.0926 ± 0.0010	1.0022
$\mathcal{B}(\tau^- \rightarrow K^- 2\pi^0 \nu_\tau \text{ (ex. } K^0))$	$(0.65 \pm 0.22) \cdot 10^{-3}$	1.0000
$\mathcal{B}(\tau^- \rightarrow \pi^- 3\pi^0 \nu_\tau \text{ (ex. } K^0))$	0.0104 ± 0.0007	1.0000
$\mathcal{B}(\tau^- \rightarrow K^- 3\pi^0 \nu_\tau \text{ (ex. } K^0, \eta))$	$(0.48 \pm 0.21) \cdot 10^{-3}$	1.0000
$\mathcal{B}(\tau^- \rightarrow h^- 4\pi^0 \nu_\tau \text{ (ex. } K^0, \eta))$	0.0011 ± 0.0004	1.0000
$\mathcal{B}(\tau^- \rightarrow \pi^- \bar{K}^0 \nu_\tau)$	0.00838 ± 0.00014	1.0000
$\mathcal{B}(\tau^- \rightarrow K^- K^0 \nu_\tau)$	0.001486 ± 0.000034	1.0000
$\mathcal{B}(\tau^- \rightarrow \pi^- \bar{K}^0 \pi^0 \nu_\tau)$	0.00382 ± 0.00013	1.0000
$\mathcal{B}(\tau^- \rightarrow K^- K^0 \pi^0 \nu_\tau)$	0.00150 ± 0.00007	1.0000
$\mathcal{B}(\tau^- \rightarrow \pi^- \bar{K}^0 2\pi^0 \nu_\tau \text{ (ex. } K^0))$	$(0.26 \pm 0.23) \cdot 10^{-3}$	1.0000
$\mathcal{B}(\tau^- \rightarrow \pi^- K_S^0 K_S^0 \nu_\tau)$	$(235 \pm 6) \cdot 10^{-6}$	2.0000
$\mathcal{B}(\tau^- \rightarrow \pi^- K_S^0 K_L^0 \nu_\tau)$	0.00108 ± 0.00024	1.0000
$\mathcal{B}(\tau^- \rightarrow \pi^- K_S^0 K_S^0 \pi^0 \nu_\tau)$	$(18.2 \pm 2.1) \cdot 10^{-6}$	2.0000
$\mathcal{B}(\tau^- \rightarrow \pi^- K_S^0 K_L^0 \pi^0 \nu_\tau)$	$(0.32 \pm 0.12) \cdot 10^{-3}$	1.0000
$\mathcal{B}(\tau^- \rightarrow \bar{K}^0 h^- h^- h^+ \nu_\tau)$	$(0.25 \pm 0.20) \cdot 10^{-3}$	1.0000
$\mathcal{B}(\tau^- \rightarrow \pi^- \pi^+ \pi^- \nu_\tau \text{ (ex. } K^0, \omega))$	0.0899 ± 0.0005	1.0022
$\mathcal{B}(\tau^- \rightarrow \pi^- \pi^+ \pi^- \pi^0 \nu_\tau \text{ (ex. } K^0, \omega))$	0.0274 ± 0.0007	1.0000
$\mathcal{B}(\tau^- \rightarrow h^- h^- h^+ 2\pi^0 \nu_\tau \text{ (ex. } K^0, \omega, \eta))$	0.0010 ± 0.0004	1.0000
$\mathcal{B}(\tau^- \rightarrow \pi^- K^- K^+ \nu_\tau)$	0.001435 ± 0.000027	1.0000
$\mathcal{B}(\tau^- \rightarrow \pi^- K^- K^+ \pi^0 \nu_\tau)$	$(61 \pm 18) \cdot 10^{-6}$	1.0000
$\mathcal{B}(\tau^- \rightarrow \pi^- \pi^0 \eta \nu_\tau)$	0.00139 ± 0.00007	1.0000
$\mathcal{B}(\tau^- \rightarrow K^- \eta \nu_\tau)$	$(155 \pm 8) \cdot 10^{-6}$	1.0000
$\mathcal{B}(\tau^- \rightarrow K^- \pi^0 \eta \nu_\tau)$	$(48 \pm 12) \cdot 10^{-6}$	1.0000
$\mathcal{B}(\tau^- \rightarrow \pi^- \bar{K}^0 \eta \nu_\tau)$	$(94 \pm 15) \cdot 10^{-6}$	1.0000
$\mathcal{B}(\tau^- \rightarrow \pi^- \pi^+ \pi^- \eta \nu_\tau \text{ (ex. } K^0))$	$(220 \pm 13) \cdot 10^{-6}$	1.0000
$\mathcal{B}(\tau^- \rightarrow K^- \omega \nu_\tau)$	$(0.41 \pm 0.09) \cdot 10^{-3}$	1.0000
$\mathcal{B}(\tau^- \rightarrow h^- \pi^0 \omega \nu_\tau)$	0.0041 ± 0.0004	1.0000
$\mathcal{B}(\tau^- \rightarrow K^- \phi \nu_\tau)$	$(44 \pm 16) \cdot 10^{-6}$	0.8300
$\mathcal{B}(\tau^- \rightarrow \pi^- \omega \nu_\tau)$	0.0195 ± 0.0006	1.0000
$\mathcal{B}(\tau^- \rightarrow K^- \pi^- \pi^+ \nu_\tau \text{ (ex. } K^0, \omega))$	0.00293 ± 0.00007	1.0000
$\mathcal{B}(\tau^- \rightarrow K^- \pi^- \pi^+ \pi^0 \nu_\tau \text{ (ex. } K^0, \omega, \eta))$	$(0.39 \pm 0.14) \cdot 10^{-3}$	1.0000
$\mathcal{B}(\tau^- \rightarrow \pi^- 2\pi^0 \omega \nu_\tau)$	$(72 \pm 16) \cdot 10^{-6}$	1.0000
$\mathcal{B}(\tau^- \rightarrow 2\pi^- \pi^+ 3\pi^0 \nu_\tau \text{ (ex. } K^0, \eta, \omega, f_1))$	$(14 \pm 27) \cdot 10^{-6}$	1.0000
$\mathcal{B}(\tau^- \rightarrow 3\pi^- 2\pi^+ \nu_\tau \text{ (ex. } K^0, \omega, f_1))$	$(775 \pm 30) \cdot 10^{-6}$	1.0000
$\mathcal{B}(\tau^- \rightarrow K^- 2\pi^- 2\pi^+ \nu_\tau \text{ (ex. } K^0))$	$(0.6 \pm 1.2) \cdot 10^{-6}$	1.0000
$\mathcal{B}(\tau^- \rightarrow 2\pi^- \pi^+ \omega \nu_\tau \text{ (ex. } K^0))$	$(84 \pm 6) \cdot 10^{-6}$	1.0000
$\mathcal{B}(\tau^- \rightarrow 3\pi^- 2\pi^+ \pi^0 \nu_\tau \text{ (ex. } K^0, \eta, \omega, f_1))$	$(38 \pm 9) \cdot 10^{-6}$	1.0000
$\mathcal{B}(\tau^- \rightarrow K^- 2\pi^- 2\pi^+ \pi^0 \nu_\tau \text{ (ex. } K^0))$	$(1.1 \pm 0.6) \cdot 10^{-6}$	1.0000
$\mathcal{B}(\tau^- \rightarrow \pi^- f_1(2\pi^- 2\pi^+) \nu_\tau)$	$(52 \pm 4) \cdot 10^{-6}$	1.0000
$\mathcal{B}(\tau^- \rightarrow \pi^- 2\pi^0 \eta \nu_\tau \text{ (ex. } K^0))$	$(0.19 \pm 0.04) \cdot 10^{-3}$	1.0000

In defining the fit constraints and in selecting the modes that sum up to one we made some assumptions and choices. We assume that some channels, like $\tau^- \rightarrow \pi^- K^+ \pi^- \geq 0\pi^0 \nu_\tau$ and $\tau^- \rightarrow \pi^+ K^- K^- \geq 0\pi^0 \nu_\tau$, have negligible branching fractions as expected from the Standard Model, even if the experimental limits for these branching fractions are not very stringent. The 95% confidence level upper limits are $\mathcal{B}(\tau^- \rightarrow \pi^- K^+ \pi^- \geq 0\pi^0 \nu_\tau) < 0.25\%$ and $\mathcal{B}(\tau^- \rightarrow \pi^+ K^- K^- \geq 0\pi^0 \nu_\tau) < 0.09\%$, values not so different from measured branching fractions for allowed 3-prong modes containing charged kaons. For decays to final states containing one neutral kaon we assume that the branching fraction with the K_L^0 are the same as the corresponding one with a K_S^0 . On decays with two neutral kaons we assume that the branching fractions with $K_L^0 K_L^0$ are the same as the ones with $K_S^0 K_S^0$.

58.3 BaBar and Belle measure on average lower branching fractions and ratios.

We compare the BaBar and Belle measurements with the results of a fit where all the B -factories measurements have been excluded. We restrict the comparison to the measurements that are used in the fit, omitting two measurements that are superseeded with other results, and one measurement that is fully correlated with other measurements. We find that BaBar and Belle measure on average lower τ branching fractions and ratios than the other experiments. Figures 58.3 and 58.4 show histograms of the 25 pulls of the differences between B -factory measurements and the respective non- B -factory fit results. The average pull between the two sets of measurements is -0.8σ (-0.7σ for the 14 Belle measurements and -0.9σ for the 11 BaBar measurements).

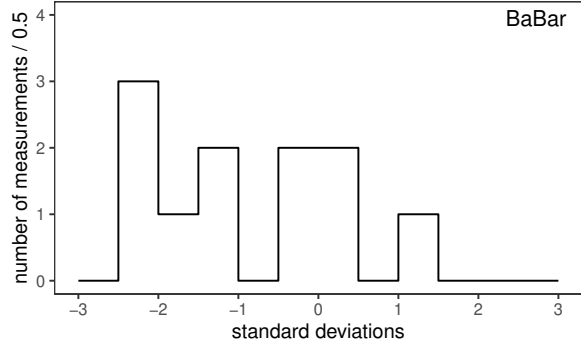


Figure 58.3: Distribution of the normalized difference between 11 measurements of branching fractions and ratios published by the BaBar collaboration and the respective averages computed using only non- B -factory measurements.

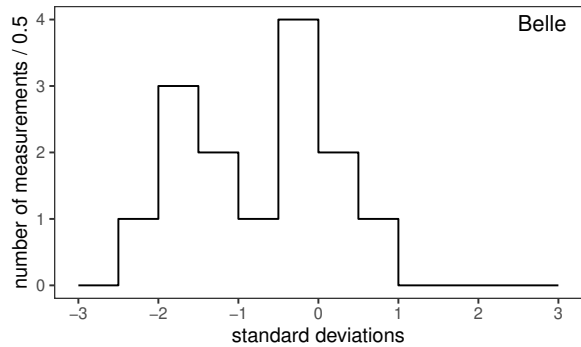


Figure 58.4: Distribution of the normalized difference between 14 measurements of branching fractions and ratios published by the Belle collaboration and the respective averages computed using only non- B -factory measurements.

58.4 Overconsistency of Leptonic Branching Fraction Measurements.

As observed in the previous editions of this review, measurements of the leptonic branching fractions are more consistent with each other than expected from the quoted uncertainties on the individual measurements. The $\chi^2/\text{n.d.o.f.}$ are $0.34/4$ for \mathcal{B}_e and $0.08/4$ for \mathcal{B}_μ . The probability of getting a smaller χ^2 is 1.3% for \mathcal{B}_e and 0.08% for \mathcal{B}_μ .

58.5 Technical implementation of the fit

The fit computes a set of quantities denoted with q_i by minimizing a χ^2 while respecting a series of equality constraints on the q_i . The quantities q_i represent τ branching fractions and branching ratios, and nuisance variables. The fit minimization procedure is equivalent to choosing a set of basis fit variables, using functions of these basis variables to predict measurements, and determining these basis variables by minimizing the measurements' χ^2 . The χ^2 is computed using the measurements m_i and their covariance matrix E_{ij} as $\chi^2 = (m_i - A_{ik} q_k)^t E_{ij}^{-1} (m_j - A_{jl} q_l)$, where the model

matrix A_{ij} is used to get the vector of the predicted measurements m'_i from the vector of the fit parameters q_j as $m'_i = A_{ij}q_j$. There is one fit variable for each of the modes that have measurements, therefore $A_{ij} = 1$ when q_j corresponds to the τ branching fraction or branching ratio of the measurement m_i , and $A_{ij} = 0$ otherwise. The constraints are equations involving the fit parameters. The fit does not impose limitations on the functional form of the constraints. In summary, the fit requires:

$$\min [\chi^2(q_k)] = \min [(m_i - A_{ik}q_k)^t E_{ij}^{-1} (m_j - A_{jl}q_l)] , \quad (58.1)$$

subjected to $f_r(q_s) - c_r = 0$, (58.2)

where the left term of Eq. 58.2 defines the constraint expressions. Using the method of Lagrange multipliers, a set of equations is obtained by taking the derivatives with respect to the fitted quantities q_k and the Lagrange multipliers λ_r of the sum of the χ^2 and the constraint expressions multiplied by the Lagrange multipliers λ_r , one for each constraint:

$$\begin{aligned} \min [(A_{ik}q_k - m_i)^t E_{ij}^{-1} (A_{jl}q_l - m_j) + 2\lambda_r(f_r(q_s) - c_r)] = \\ = \min [\tilde{\chi}^2(q_k, \lambda_r)] , \\ (\partial/\partial q_k, \partial/\partial \lambda_r) [\tilde{\chi}^2(q_k, \lambda_r)] = 0 . \end{aligned} \quad (58.3)$$

Eq. 58.3 defines a set of equations for the vector of the unknowns (q_k, λ_r) , some of which may be non-linear, in case of non-linear constraints. An iterative minimization procedure approximates at each step the non-linear constraint expressions by their first order Taylor expansion around the current values of the fitted quantities, \bar{q}_s :

$$f_r(q_s) - c_r = f_r(\bar{q}_s) + \left. \frac{\partial f_r(q_s)}{\partial q_s} \right|_{\bar{q}_s} (q_s - \bar{q}_s) - c_r ,$$

which can be written as

$$B_{rs}q_s - c'_r ,$$

where c'_r are the resulting constant known terms, independent of q_s at first order. After linearization, the differentiation by q_k and λ_r is trivial and leads to a set of linear equations

$$A_{ki}^t E_{ij}^{-1} A_{jl}q_l + B_{kr}^t \lambda_r = A_{ki}^t E_{ij}^{-1} m_j , \quad (58.4)$$

$$B_{rs}q_s = c'_r , \quad (58.5)$$

which can be expressed as

$$F_{ij}u_j = v_i , \quad (58.6)$$

where $u_j = (q_k, \lambda_r)$ and v_i is the vector of the known constant terms running over the index k and then r in the right terms of Eq. 58.4 and Eq. 58.5, respectively. Solving the equation set in Eq. 58.6 by matrix inversion gives the the fitted quantities and their variance and covariance matrix, using the measurements and their variance and covariance matrix. The fit procedure starts by computing the linear approximation of the non-linear constraint expressions around the quantities seed values. With an iterative procedure, the unknowns are updated at each step by solving the equations and the equations are then linearized around the updated values, until the variation of the fitted unknowns is reduced below a numerically small threshold.

References

- [1] S. Schael *et al.* (ALEPH), Phys. Rept. **421**, 191 (2005), [hep-ex/0506072].
- [2] J. Abdallah *et al.* (DELPHI), Eur. Phys. J. **C46**, 1 (2006), [hep-ex/0603044].
- [3] D. Asner *et al.* (Heavy Flavor Averaging Group) (2010), [arXiv:1010.1589].
- [4] M. Zielinski *et al.*, Phys. Rev. Lett. **52**, 1195 (1984).

59. τ -Lepton Decay Parameters

Revised February 2024 by A. Stahl (RWTH Aachen U.).

The purpose of the measurements of the decay parameters (also known as Michel parameters) of the τ is to determine the structure (spin and chirality) of the current mediating its decays.

59.1 Leptonic Decays:

The Michel parameters are extracted from the energy spectrum of the charged daughter lepton $\ell = e, \mu$ in the decays $\tau \rightarrow \ell \nu_\ell \nu_\tau$. Ignoring radiative corrections, neglecting terms of order $(m_\ell/m_\tau)^2$ and $(m_\tau/\sqrt{s})^2$, and setting the neutrino masses to zero, the spectrum in the laboratory frame reads

$$\frac{d\Gamma}{dx} = \frac{G_{\tau\ell}^2 m_\tau^5}{192 \pi^3} \times \left\{ f_0(x) + \rho f_1(x) + \eta \frac{m_\ell}{m_\tau} f_2(x) - P_\tau [\xi g_1(x) + \xi \delta g_2(x)] \right\} \quad (59.1)$$

with

$$\begin{aligned} f_0(x) &= 2 - 6x^2 + 4x^3 & (59.2) \\ f_1(x) &= -\frac{4}{9} + 4x^2 - \frac{32}{9}x^3 & g_1(x) = -\frac{2}{3} + 4x - 6x^2 + \frac{8}{3}x^3 \\ f_2(x) &= 12(1-x)^2 & g_2(x) = \frac{4}{9} - \frac{16}{3}x + 12x^2 - \frac{64}{9}x^3. \end{aligned}$$

The quantity x is the fractional energy of the daughter lepton ℓ , i.e., $x = E_\ell/E_{\ell, \max} \approx E_\ell/(\sqrt{s}/2)$ and P_τ is the polarization of the tau leptons. The integrated decay width is given by

$$\Gamma = \frac{G_{\tau\ell}^2 m_\tau^5}{192 \pi^3} \left(1 + 4\eta \frac{m_\ell}{m_\tau} \right). \quad (59.3)$$

The situation is similar to muon decays $\mu \rightarrow e \nu_e \nu_\mu$. The generalized matrix element with the couplings $g_{\varepsilon\mu}^\gamma$ and their relations to the Michel parameters ρ , η , ξ , and δ have been described in the ‘‘Note on Muon Decay Parameters’’. The Standard Model expectations are 3/4, 0, 1, and 3/4, respectively. For more details, see [1].

More information can be extracted from the decays, if the polarization of the daughter lepton is measured. Belle presented a first result (see [2]). A new parameter ξ' is introduced. Its relation to the couplings is given by (see [3]):

$$\xi' = 1 - 2 \sum_{\omega=L,R} \left(\frac{1}{4} |g_{R\omega}^S|^2 + |g_{R\omega}^V|^2 \right) + 3 |g_{RL}^T|^2. \quad (59.4)$$

The new measurement improves the limit on g_{RL}^T by about a factor of two.

Additional Michel parameters can be defined in radiative decays $\tau \rightarrow \ell \nu_\ell \nu_\tau \gamma$, see [4]. A first measurement is presented in [5]. The experimental precision does not provide a significant impact on the knowledge about the couplings, yet.

59.2 Hadronic Decays:

In the case of hadronic decays $\tau \rightarrow h \nu_\tau$, with $h = \pi, \rho$, or a_1 , the ansatz is restricted to purely vectorial currents. The matrix element is

$$\frac{G_{\tau h}}{\sqrt{2}} \sum_{\lambda=R,L} g_\lambda \langle \bar{\Psi}_\omega(\nu_\tau) | \gamma^\mu | \Psi_\lambda(\tau) \rangle J_\mu^h \quad (59.5)$$

with the hadronic current J_μ^h . The neutrino chirality ω is uniquely determined from λ . The spectrum depends only on a single parameter ξ_h

$$\frac{d^n \Gamma}{dx_1 dx_2 \dots dx_n} = f(\vec{x}) + \xi_h P_\tau g(\vec{x}), \quad (59.6)$$

with f and g being channel-dependent functions of the n observables $\vec{x} = (x_1, x_2, \dots, x_n)$ (see [6]). The parameter ξ_h is related to the couplings through

$$\xi_h = |g_L|^2 - |g_R|^2. \quad (59.7)$$

ξ_h is the negative of the chirality of the τ neutrino in these decays. In the Standard Model, $\xi_h = 1$. Also included in the Data Listings for ξ_h are measurements of the neutrino helicity which coincide with ξ_h , if the neutrino is massless (ASNER 00 [7], ACKERSTAFF 97R [8], AKERS 95P [9], ALBRECHT 93C [10], and ALBRECHT 90I [11]).

59.3 Combination of Measurements:

The individual measurements are combined, taking into account the correlations between the parameters. In a first fit, universality between the two leptonic decays, and between all hadronic decays, is assumed. A second fit is made without these assumptions. The results of the two fits are provided as OUR FIT in the Data Listings below in the tables whose title includes ‘‘(e or mu)’’ or ‘‘(all hadronic modes)’’, and ‘‘(e)’’, ‘‘(mu)’’ etc., respectively. The measurements show good agreement with the Standard Model. The χ^2 values with respect to the Standard model predictions are 24.1 for 41 degrees of freedom and 26.8 for 56 degrees of freedom, respectively. The correlations are reduced through this combination to less than 20%, with the exception of ρ and η which are correlated by +23%, for the fit with universality and by +70% for $\tau \rightarrow \mu \nu_\mu \nu_\tau$.

59.4 Model-independent Analysis:

From the Michel parameters, limits can be derived on the couplings $g_{\varepsilon\lambda}^\kappa$ without further model assumptions. In the Standard model $g_{LL}^V = 1$ (leptonic decays), and $g_L = 1$ (hadronic decays) and all other couplings vanish. First, the partial decay widths have to be compared to the Standard Model predictions to derive limits on the normalization of the couplings $A_x = G_{\tau x}^2/G_F^2$ with Fermi’s constant G_F :

$$\begin{aligned} A_e &= 1.0022 \pm 0.0041, \\ A_\mu &= 0.983 \pm 0.017, \\ A_\pi &= 0.9957 \pm 0.0049. \end{aligned} \quad (59.8)$$

Then limits on the couplings (95% CL) can be extracted (see [12] and [13]). Without the assumption of universality, the limits given in Table 59.1 are derived.

Table 59.1: Coupling constants $g_{\varepsilon\mu}^\gamma$. 95% confidence level experimental limits. The limits include the quoted values of A_e , A_μ , and A_π and assume $A_\rho = A_{a_1} = 1$.

$\tau \rightarrow e \nu_e \nu_\tau$		
$ g_{RR}^S < 0.70$	$ g_{RR}^V < 0.17$	$ g_{RR}^T \equiv 0$
$ g_{LR}^S < 0.99$	$ g_{LR}^V < 0.13$	$ g_{LR}^T < 0.082$
$ g_{RL}^S < 2.01$	$ g_{RL}^V < 0.52$	$ g_{RL}^T < 0.51$
$ g_{LL}^S < 2.01$	$ g_{LL}^V < 1.004$	$ g_{LL}^T \equiv 0$
$\tau \rightarrow \mu \nu_\mu \nu_\tau$		
$ g_{RR}^S < 0.72$	$ g_{RR}^V < 0.18$	$ g_{RR}^T \equiv 0$
$ g_{LR}^S < 0.95$	$ g_{LR}^V < 0.12$	$ g_{LR}^T < 0.079$
$ g_{RL}^S < 2.01$	$ g_{RL}^V < 0.52$	$ g_{RL}^T < 0.27$
$ g_{LL}^S < 2.01$	$ g_{LL}^V < 1.006$	$ g_{LL}^T \equiv 0$
$\tau \rightarrow \pi \nu_\tau$		
$ g_R^V < 0.15$	$ g_L^V > 0.984$	
$\tau \rightarrow \rho \nu_\tau$		
$ g_R^V < 0.10$	$ g_L^V > 0.995$	
$\tau \rightarrow a_1 \nu_\tau$		
$ g_R^V < 0.16$	$ g_L^V > 0.987$	

59.5 Model-dependent Interpretation:

More stringent limits can be derived assuming specific models. For example, in the framework of a two Higgs doublet model, the measurements correspond to a limit of $m_{H^\pm} > 2.0 \text{ GeV} \times \tan\beta$ on the mass of the charged Higgs boson, or a limit of 500 GeV on the mass of the second W boson in left-right symmetric models for arbitrary mixing (both 95% CL). See [13] and [14].

References

- [1] F. Scheck, Phys. Rept. **44**, 187 (1978); W. Fetscher and H.J. Gerber in *Precision Tests of the Standard Model*, edited by P. Langacker, World Scientific, 1993; A. Stahl, *Physics with τ Leptons*, Springer Tracts in Modern Physics, **160**, 1, (2000).
- [2] D. Bodrov *et al.* (Belle), Phys. Rev. D **108**, 1, 012003 (2023), [arXiv:2303.10574].
- [3] D. Bodrov and P. Pakhlov, JHEP **10**, 035 (2022), [arXiv:2203.12743].
- [4] A. Arbuzov and T. Kopylova, JHEP 109 (2016).
- [5] N. Shimizu *et al.* (Belle), Prog. Theo. Exp. Phys. **2**, 023C01 (2018).
- [6] M. Davier *et al.*, Phys. Lett. B **306**, 411 (1993).
- [7] D. Asner *et al.* (CLEO), Phys. Rev. D **61**, 012002 (2000), [hep-ex/9902022].
- [8] K. Ackerstaff *et al.* (OPAL), Z. Phys. C **75**, 593 (1997).
- [9] R. Akers *et al.* (OPAL), Z. Phys. C **67**, 45 (1995).
- [10] H. Albrecht *et al.* (ARGUS), Z. Phys. C **58**, 61 (1993).
- [11] H. Albrecht *et al.* (ARGUS), Phys. Lett. B **250**, 164 (1990).
- [12] K. Ackerstaff *et al.* (OPAL), Eur. Phys. J. C **8**, 3 (1999), [hep-ex/9808016].
- [13] A. Stahl, Nucl. Phys. B Proc. Suppl. **76**, 173 (1999).
- [14] M.-T. Dova, J. Swain and L. Taylor, Phys. Rev. D **58**, 015005 (1998), [hep-ph/9712384]; T. Hebbeker and W. Lohmann, Z. Phys. C **74**, 399 (1997); A. Pich and J. P. Silva, Phys. Rev. D **52**, 4006 (1995), [hep-ph/9505327].

60. Quark Masses

Revised August 2023 by R.M. Barnett (LBNL), L.P. Lellouch (CNRS & Aix-Marseille U.) and A.V. Manohar (UC San Diego).

60.1 Introduction

This note discusses some of the theoretical issues relevant for the determination of quark masses, which are fundamental parameters of the Standard Model of particle physics. Unlike the leptons, quarks are confined inside hadrons and are not observed as physical particles. Quark masses therefore cannot be measured directly, but must be determined indirectly through their influence on hadronic properties. Although one often speaks loosely of quark masses as one would of the mass of the electron or muon, any quantitative statement about the value of a quark mass must make careful reference to the particular theoretical framework that is used to define it. It is important to keep this *scheme dependence* in mind when using the quark mass values tabulated in the data listings.

Historically, the first determinations of quark masses were performed using quark models. These are usually called constituent quark masses and are of order 350 MeV for the u and d quarks. Constituent quark masses model the effects of dynamical chiral symmetry breaking discussed below, and are not directly related to the quark mass parameters m_q of the QCD Lagrangian of Eq. (60.1). The resulting masses only make sense in the limited context of a particular quark model, and cannot be related to the quark mass parameters, m_q , of the Standard Model. In order to discuss quark masses at a fundamental level, definitions based on quantum field theory must be used, and the purpose of this note is to discuss these definitions and the corresponding determinations of the values of the masses.

60.2 Mass parameters and the QCD Lagrangian

The QCD [1] Lagrangian is

$$\mathcal{L} = \sum_{q=u,d,s,\dots,t} \bar{q}(i\not{D} - m_q)q - \frac{1}{2}\text{tr} G_{\mu\nu}G^{\mu\nu}, \quad (60.1)$$

where the sum runs over the quark flavors u, d, s, c, b and t . $\not{D} = (\partial_\mu - igA_\mu)\gamma^\mu$ is the gauge covariant derivative, A_μ is the SU(3)-valued gluon field, $G_{\mu\nu} = \frac{i}{g}[D_\mu, D_\nu]$ is the gluon field strength, m_q is the mass parameter of quark flavor q , and q is the quark Dirac field. After renormalization, the QCD Lagrangian Eq. (60.1) gives finite values for physical quantities, such as scattering amplitudes. Renormalization is a procedure that invokes a subtraction scheme to render the amplitudes finite, and requires the introduction of a dimensionful scale parameter μ . The mass parameters in the QCD Lagrangian Eq. (60.1) depend on the renormalization scheme used to define the theory, and also on the scale parameter μ . The most commonly used renormalization scheme for QCD perturbation theory is the $\overline{\text{MS}}$ scheme.

The QCD Lagrangian has a chiral symmetry in the limit that the quark masses vanish. This symmetry is spontaneously broken by dynamical chiral symmetry breaking, and explicitly broken by the quark masses. The nonperturbative scale of dynamical chiral symmetry breaking, Λ_χ , is around 1 GeV [2]. It is conventional to call quarks heavy if $m_q > \Lambda_\chi$, so that explicit chiral symmetry breaking dominates (c, b , and t quarks are heavy), and light if $m_q < \Lambda_\chi$, so that spontaneous chiral symmetry breaking dominates (the u and d are light and the s is considered to be light when using SU(3) $_L$ × SU(3) $_R$ chiral perturbation theory). The determination of light- and heavy-quark masses is considered separately in Sec. 60.5 and Sec. 60.6 below.

At high energies or short distances, nonperturbative effects, such as chiral symmetry breaking, become small and one can, in principle, determine quark masses by analyzing mass-dependent effects using QCD perturbation theory. Such computations are conventionally performed using the $\overline{\text{MS}}$ scheme at a scale $\mu \gg \Lambda_\chi$, and give the $\overline{\text{MS}}$ “running” mass $\overline{m}(\mu)$. We use the $\overline{\text{MS}}$ scheme when reporting quark masses; one can readily convert these values into other schemes using perturbation theory.

The μ dependence of $\overline{m}(\mu)$ at short distances can be calculated

using the renormalization group (RG) equation,

$$\mu^2 \frac{d\overline{m}(\mu)}{d\mu^2} = -\gamma(\overline{\alpha}_s(\mu)) \overline{m}(\mu), \quad (60.2)$$

where γ is the anomalous dimension which is now known to four-loop order in perturbation theory [3] [4]. $\overline{\alpha}_s$ is the coupling constant [1] in the $\overline{\text{MS}}$ scheme. Defining the expansion coefficients γ_r by

$$\gamma(\overline{\alpha}_s) \equiv \sum_{r=1}^{\infty} \gamma_r \left(\frac{\overline{\alpha}_s}{4\pi}\right)^r, \quad (60.3)$$

the first four coefficients are given by

$$\begin{aligned} \gamma_1 &= 4, \\ \gamma_2 &= \frac{202}{3} - \frac{20N_L}{9}, \\ \gamma_3 &= 1249 + \left(-\frac{2216}{27} - \frac{160}{3}\zeta(3)\right)N_L - \frac{140}{81}N_L^2, \\ \gamma_4 &= \frac{4603055}{162} + \frac{135680}{27}\zeta(3) - 8800\zeta(5) \\ &\quad + \left(-\frac{91723}{27} - \frac{34192}{9}\zeta(3) + 880\zeta(4) + \frac{18400}{9}\zeta(5)\right)N_L \\ &\quad + \left(\frac{5242}{243} + \frac{800}{9}\zeta(3) - \frac{160}{3}\zeta(4)\right)N_L^2 \\ &\quad + \left(-\frac{332}{243} + \frac{64}{27}\zeta(3)\right)N_L^3, \end{aligned}$$

where N_L is the number of active light quark flavors at the scale μ , i.e. flavors with masses $\leq \mu$, and ζ is the Riemann zeta function ($\zeta(3) \simeq 1.2020569$, $\zeta(4) \simeq 1.0823232$, and $\zeta(5) \simeq 1.0369278$). Eq. (60.2) must be solved in conjunction with the RG equation for $\overline{\alpha}_s(\mu)$ given in [1]. In addition, as the renormalization scale crosses quark mass thresholds one needs to match the scale dependence of \overline{m} below and above the threshold. There are finite threshold corrections; the necessary formulae can be found in Ref. [5].

60.3 Lattice QCD

Ab initio lattice QCD calculations of the fundamental parameters of QCD, i.e. the coupling constant and quark masses (except for the top-quark mass), has become a precision science (see also the sections on Lattice Quantum Chromodynamics and on Quantum Chromodynamics in this *Review*). Here we only briefly recall those features which are required for the determination of quark masses. For more details on lattice QCD, please see the section on Lattice Quantum Chromodynamics.

The inputs into lattice calculations are bare, dimensionless versions of the fundamental parameters of QCD: the bare strong coupling and the bare quark masses in lattice units, i.e. multiplied by the lattice spacing a , the distance between neighboring points of the lattice. The physical values of the quark masses are determined by computing as many physical quantities as there are parameters, including one for the gauge coupling. In practice, the computations are performed for multiple lattice spacings, determined by the bare coupling via dimensional transmutation, and a number of bare quark masses. After renormalizing these masses and converting them to physical units, the resulting renormalized masses are interpolated to their physical values. This is achieved by requiring that the computed physical quantities reproduce their measured values as the $a \rightarrow 0$ limit to our continuum world is taken. Such a tuning of fundamental parameters is required in any regularization of QCD: lattice QCD is simply a tool to perform QCD calculations in the low-energy, nonperturbative domain.

As discussed in the previous paragraph, one must renormalize the bare quark masses of lattice QCD simulations. The values of these bare masses refer to a particular discretization of QCD with the lattice spacing as the ultraviolet cut-off. In order for the resulting physical masses to be useful in phenomenological applications, it is necessary to give their values in some standard

renormalization scheme such as $\overline{\text{MS}}$. Provided that both the ultraviolet cut-off a^{-1} and the renormalization scale μ are much greater than Λ_{QCD} , the bare masses can be renormalized in perturbation theory. However, in order to avoid uncertainties due to the unknown higher-order coefficients in lattice perturbation theory, most results obtained recently use *nonperturbative renormalization*. This procedure relates the bare masses to those defined in renormalization schemes which can be realized directly in lattice and continuum QCD, e.g. those obtained from quark and gluon Green functions at specified momenta in the Landau gauge [6] or those defined using finite-volume techniques and the Schrödinger functional [7], but not $\overline{\text{MS}}$ that is only defined for dimensional regularization. These methods require $\mu \gg \Lambda_{\text{QCD}}$ so that unwanted (nonperturbative) corrections proportional to inverse powers of μ , which appear in some approaches, remain small corrections that can be identified and removed. This condition is also necessary so that matching to other schemes can be performed reliably in perturbation theory. Moreover these methods require $a^{-1} \gg \mu$ so that cutoff effects are small enough to be extrapolated away when the continuum limit is taken. The conversion to the $\overline{\text{MS}}$ scheme is then performed using continuum perturbation theory, which is more readily obtained to higher orders and is usually better behaved than its lattice counterpart.

It is important to note that the final renormalized values for the quark masses must be the same in the continuum limit for any valid discretization of QCD and for any sensible choice of the physical quantities used for calibration, as long as the calculation is performed with a sufficient number of sea-quark flavors and with the relevant electromagnetic and strong-isospin breaking corrections for the claimed precision. It is also worth noting that issues surrounding the renormalization of quark masses disappear when considering pairwise ratios of these masses in QCD alone. Indeed, if the same renormalization scheme and scale are implemented, also for the definition of QCD in the absence or electromagnetism,¹ QCD renormalization factors are identical for all quark flavors, and these factors therefore cancel exactly in quark-mass ratio². In particular, this means that these ratios are scheme and scale independent up to possible QED corrections. Moreover these ratios may suffer less from the uncertainties in the determination of the lattice scale, in particular in cases where the quantities used to fix the two quark masses depend on these masses in a similar way, because these ratios are dimensionless. Thus, quark-mass ratios are often determined with significantly higher precision using lattice QCD than are the individual masses.

The determination of quark masses using lattice simulations is well established and the current emphasis is on the reduction and control of uncertainties. With better methods, improved algorithms and access to more powerful computing resources, the precision of the results has improved significantly in recent years. Vacuum polarization effects are included with $N_f = 2$, $2 + 1$ or $N_f = 2 + 1 + 1$ flavors of sea quarks. The number 2 here indicates that the up and down quarks are degenerate. The first +1 corresponds to the inclusion of strange sea-quark effects and the second +1 to those of the charm. Simulations with $2 + 1$ and $2 + 1 + 1$ flavors represent controlled approximations to physical QCD at the low energies considered for quark mass determinations, up to corrections of $O((\Lambda_{\text{QCD}}/m_c)^2/N_c)$ and $O((\Lambda_{\text{QCD}}/m_b)^2/N_c)$, respectively. This is not the case for simulations with $N_f = 2$ or in which vacuum polarization effects are treated as a mean field (this is the so-called *quenched* approximation) and results obtained in those frameworks will not enter the discussion here.

Particularly pleasing is the observation that different formulations of lattice QCD and different approaches, with different systematic uncertainties, yield results which are largely consistent with each other. This gives us broad confidence in the estimates of the systematic errors. As the precision of the results approaches (or even exceeds in some cases) 1%, isospin breaking effects, including electromagnetic corrections need to be considered and this

is beginning to be done as will be discussed below. In particular, a reliable estimate of these effects is required for determining the individual u and d quark masses.

Members of the lattice QCD community have organized a Flavour Lattice Averaging Group (FLAG) which, against stated quality criteria, critically reviews quantities computed in lattice QCD that are relevant to flavor physics and presents its view of the current status of the results. This includes the determination of quark masses. The latest edition reviews lattice results that appeared in print before April 30th 2021 [8]. Since that deadline and the writing of the previous edition of the present review, the only new results on quark masses that have been published are those of Ref. [9].

60.4 Averaging procedure for lattice QCD results

In this review we present summary numbers for each quark mass which are solely based on averages of lattice results. Those summary numbers differ from those presented in the particle listings, for three reasons. The first is that they do not include non-lattice estimates of the quark masses. The second is that they may differ slightly in the lattice results retained, as made explicit here and in the listings. The third difference comes from the averaging procedures, which are described in the listings and below. In the listings, summary numbers are obtained from averages of the individual quark-mass estimates, weighted by their total errors. Moreover, the resulting one-standard-deviation errors are rescaled by the usual $\sqrt{\chi^2/\text{dof}}$ factor, which is further multiplied by 1.645 to obtain the uncertainty corresponding to a 90% confidence interval. Nevertheless, the averages presented here and in the listings are fully consistent, with comparable uncertainties, signalling the robustness of the two combination procedure.

The results on which the lattice summary numbers presented here are those used in the FLAG reviews, supplemented by any new calculations that satisfy their selection criteria. The methodology that we use is also close to that of FLAG, but here we make an attempt to separate uncertainties into their statistical and systematic components, to provide some idea of what the relative weight of each is for different quark masses. In some cases, also, slightly different choices are also made. Thus, agreement between the results obtained is a further sign of the robustness of the combination procedures used here, as well as in FLAG.

We now lay out our averaging procedure. For each of m_{ud} , m_s or m_s/m_{ud} , and for each of $N_f = 2 + 1$ or $N_f = 2 + 1 + 1$, we perform averages of the relevant, individual lattice results with weights that include the sum in quadrature of the statistical and systematic uncertainties. The weights also account for correlations by assuming that they are 100% on any uncertainty components that may be correlated. This procedure yields a central value and a total error for each of the quantities of interest. The total uncertainty is rescaled by the usual factor of $\sqrt{\chi^2/\text{dof}}$ if that factor is larger than 1, where χ^2 is the one corresponding to the weighted average procedure. To isolate the statistical component of the uncertainty on any given average, like for the total uncertainty we use the standard error formula for correlated data, this time only taking into account the statistical uncertainties on the different collaborations' results. If the total error has been rescaled, this statistical uncertainty is multiplied by the same factor. The candidate systematic error on an average is then obtained by subtracting in quadrature the statistical uncertainty from the total one. For each quantity, the final systematic error on the average is the largest of two uncertainties: the candidate systematic error and the minimum of the systematic uncertainties on the individual lattice determinations. This guarantees that the final systematic error is no smaller than the one of any given calculation. We then repeat this whole procedure to average the $N_f = 2 + 1$ and $N_f = 2 + 1 + 1$ averages, for reasons discussed below. In cases where the error separation is not explicit in a particular collaboration's result, we assume that the quoted error is statistical and take, as the minimum of systematic error, the smallest non-vanishing one among those of the other individual results. While this procedure may change the balance between statistical and systematic errors, it does change the average (which

¹Since QCD without QED is not the real world, it makes a difference, for example, which hadron mass is used to tune a quark mass and the QED correction will differ for different choices.

²The same remains true in the presence of QED if the two quarks in the ratio have the same charge.

is weighted by the total errors of the individual entries and the correlations between them) and does not decrease the total error. When quantities involving m_c or m_b are averaged, we consider only the averages of $N_f = 2 + 1 + 1$ calculations, for reasons also explained below.

The values of the individual results used in the averages obtained below can be found in the quark properties listings of this *Review*.

60.5 Light quarks

In this section we review the determination of the masses of the light quarks u , d and s from lattice simulations and then discuss the consequences of the approximate chiral symmetry.

60.5.1 Lattice QCD results

The most reliable determinations of the strange quark mass, m_s , and of the up and down quark masses, m_u and m_d , are obtained from lattice simulations. This is reflected in part by the uncertainties of individual determinations of these masses given in this *Review's* listings of quark properties: lattice results typically have smaller error bars than phenomenological extractions. As explained in the previous section, the simulations are generally performed in the isospin-symmetric limit of QCD, i.e. with degenerate up and down quarks ($m_u = m_d$) and the electromagnetic coupling α set to zero. Thus, it is initially $m_{ud} = (m_u + m_d)/2$ which is obtained from the computations. The numerical values of these masses depend on the choice of renormalization scale and scheme.³

Below we discuss the derivation of m_u and m_d separately, but we start by briefly presenting our estimates for m_{ud} , m_s and their ratio, using the latest lattice results. FLAG [8] bases its summary numbers on references that the authors consider to have the most reliable estimates of systematic uncertainties, i.e. [12–18] for $N_f = 2 + 1$ and [19–24] for $N_f = 2 + 1 + 1$ flavors of sea quarks. Note that the $N_f = 2 + 1 + 1$ results of Ref. [9] did not make the FLAG deadline. In the estimates given below, we use the fact that Ref. [9] supersedes Ref. [22].

Applying the averaging procedure described in the previous section and the results of Refs. [12–18], for $N_f = 2 + 1$ we obtain $\overline{m}_{ud} = (3.382 \pm 0.026 \pm 0.040[\pm 0.050])$ MeV, $\overline{m}_s = (92.24 \pm 0.24 \pm 1.00[\pm 1.03])$ MeV and $(\overline{m}_s/\overline{m}_{ud}) = 27.42 \pm 0.05 \pm 0.12[\pm 0.12]$. These numbers are $\overline{m}_{ud} = (3.421 \pm 0.035 \pm 0.049[\pm 0.060])$ MeV, $\overline{m}_s = (92.93 \pm 0.51 \pm 0.37[\pm 0.063])$ MeV and $(\overline{m}_s/\overline{m}_{ud}) = 27.25 \pm 0.03 \pm 0.07[\pm 0.08]$ using the latest $N_f = 2 + 1 + 1$ calculations [9, 19–21, 23, 24]. The masses are given in the $\overline{\text{MS}}$ scheme at a renormalization scale of 2 GeV. In these averages, the first error is statistical, the second systematic and the third one in brackets is the sum in quadrature of the first two. Also, QED corrections have been accounted for only to the extent that they have been removed from the hadron mass inputs phenomenologically.

A few comments are in order concerning the compatibility of the results which enter these averages. We begin with the case of $N_f = 2 + 1$. For m_{ud} the results show a good degree of compatibility with a $\chi^2/\text{dof} = 5.7/4$ and the final systematic uncertainty is given by the one of Ref. [17]. The level of compatibility is similar in the case of m_s and the final systematic uncertainty is also given by the one of Ref. [17]. For m_s/m_{ud} the results are even more compatible and here the final systematic error is derived from the averaging procedure. In the case of $N_f = 2 + 1 + 1$, there are only two results for m_{ud} [9, 20] and their level of compatibility is poor, with $\chi^2/\text{dof} = 6.4/1$. This is due to the value of Ref. [9], $m_{ud} = (3.636 \pm 0.066 \pm 0.059)$ MeV, which is significantly larger than all other determinations, including those ob-

tained in $N_f = 2 + 1$ determinations. The scenario repeats for m_s , but is diluted by the fact that there are four results [9, 19–21] which enter the average. However, compatibility is recovered for m_s/m_{ud} , suggesting a problem in the determination of the renormalization constants or the lattice spacing in at least one of the calculations. Since the different collaborations use different formulations of lattice QCD, the (relatively) small variations of the results between the groups provides important information about the reliability of the estimates. Furthermore, the conservative nature of our method for estimating uncertainties is confirmed by the excellent agreement of the averages obtained for $N_f = 2 + 1$ and $N_f = 2 + 1 + 1$ calculations.

Despite being reported in the $\overline{\text{MS}}$ scheme at a renormalization scale of 2 GeV, the schemes in simulations with $2 + 1$ and $2 + 1 + 1$ sea-quark flavors actually differ. This is because the former are renormalized with $N_L = 3$ and the latter with $N_L = 4$. Thus for a comparison one should convert the results to the same scheme. That is not the case for (m_s/m_{ud}) , where renormalization factors cancel in the absence of electromagnetic corrections. The conversion of the $N_f = 2 + 1$ results to the $N_L = 4$ scheme can be performed, for instance, by running them down to the charm threshold in the $N_L = 3$ theory, matching the results to the $N_L = 4$ theory at that scale, and running them back up to 2 GeV with four active flavors. Such a conversion leads to an upward shift in the values of the quark masses of only around 0.3%, well within the quoted uncertainties on the quark masses themselves. Quark-mass ratios are not concerned by this upward shift, because it is identical for the numerator and denominator. There are also nonperturbative contributions to this procedure, of $O((\Lambda_{\text{QCD}}/m_c)^2/N_c) \sim 2\%$. However lattice QCD studies of these effects have shown that they are typically an order of magnitude smaller on hadronic quantities or on Λ_{QCD} [25, 26]. Given that the total errors on the $N_f = 2 + 1$ results for \overline{m}_{ud} and \overline{m}_s are larger than 1%, we consider these matching effects negligible. In addition, for m_{ud} in particular there are six $N_f = 2 + 1$ calculations in which all sources of uncertainty have been accounted for, while there are only two for $N_f = 2 + 1 + 1$. Thus, we average the averages from the two frameworks in the same way as above (see Sec. 60.4), yielding as a final lattice QCD estimate in the $\overline{\text{MS}}$ scheme at $\mu = 2$ GeV in the $N_L = 4$ theory:

$$\overline{m}_{ud} = (3.397 \pm 0.021 \pm 0.040[\pm 0.045]) \text{ MeV}, \quad (60.4)$$

$$\overline{m}_s = (92.74 \pm 0.22 \pm 0.49[\pm 0.54]) \text{ MeV}, \quad (60.5)$$

and

$$r_s \equiv \frac{\overline{m}_s}{\overline{m}_{ud}} = 27.30 \pm 0.03 \pm 0.07[\pm 0.08]. \quad (60.6)$$

In these averages, the first error is statistical, the second systematic and the third one in brackets is the sum in quadrature of the first two. QED corrections have been accounted for only to the extent that they have been removed from the hadron mass inputs phenomenologically. It is worth noting that the result for r_s in Eq. (60.6) is identical to the ratio of m_s and m_{ud} from Eqs. (60.4) and (60.5), within the four digits for r_s given in Eq. (60.6), albeit with a significantly smaller total uncertainty.

To obtain the individual values of \overline{m}_u and \overline{m}_d requires the introduction of isospin breaking effects, including electromagnetism. This is now being done completely using lattice field theory, albeit neglecting electromagnetic effects in the sea in most cases (for an exception, see Ref. [27] which includes a calculation of the valence and sea QED contributions to $\Delta M_K^2 = M_{K^0}^2 - M_{K^+}^2$ that is critical for determining $\overline{m}_d - \overline{m}_u$). The effect of neglecting QED contributions from the sea on the u and d quark masses has been estimated in Ref. [28] to induce a contribution to the uncertainty that ranges from about 3% in $\overline{m}_u/\overline{m}_d$ to less than 1% in \overline{m}_d . FLAG has also reviewed results for these masses [8]. Again, they separate results obtained from $N_f = 2 + 1$ and $N_f = 2 + 1 + 1$ simulations. For the former, they use the results of Ref. [28] and for the latter, those of Refs. [20, 29, 30].

To obtain our estimates, we proceed as for the light quark masses above. For $N_f = 2 + 1$, our estimates are the results

³ If QED is not included, then quark masses also depend on the conditions used to match isospin-symmetric QCD to the low energy effective theory of the Standard Model, which includes QCD and QED with $m_u \neq m_d$. Those matching conditions, which define a matching scheme, are quite similar in the calculations reported on below. Moreover, they have been designed to minimize the impact of isospin-breaking effects on isospin-symmetric combinations of quark masses, such m_{ud} and m_s here, and m_c and m_b below. Thus, as does FLAG [8], we generally assume that any remaining differences between schemes are within the quoted errors. Such an assumption is certainly true for $\overline{m}_c(\overline{m}_c)$ [10], where QED effects have been studied explicitly. On the other hand, in the case of m_b/m_c , where the effects of QED have also been studied explicitly [11] and where uncertainties are less than 0.3%, these effects are no longer negligible.

of the only calculation in which all sources of uncertainty are accounted for [28]. These are $\overline{m}_u = (2.27 \pm 0.06 \pm 0.06[\pm 0.09])$ MeV, $\overline{m}_d = (4.67 \pm 0.06 \pm 0.06[\pm 0.09])$ MeV and $\overline{m}_u/\overline{m}_d = (0.485 \pm 0.011 \pm 0.016[\pm 0.020])$. For $N_f = 2 + 1 + 1$, they rely on Refs. [20, 29, 30]. Our estimates are $\overline{m}_u = (2.14 \pm 0.04 \pm 0.07[\pm 0.08])$ MeV, $\overline{m}_d = (4.70 \pm 0.03 \pm 0.04[\pm 0.05])$ MeV and $\overline{m}_u/\overline{m}_d = (0.460 \pm 0.008 \pm 0.018[\pm 0.020])$. These masses are given in the $\overline{\text{MS}}$ scheme at 2 GeV in the $N_L = 3$ and 4 theories, respectively. Given the size of the uncertainties on these averages, tiny corrections due to QED effects in the renormalization constants have been neglected.

In obtaining the $N_f = 2 + 1 + 1$ averages, there is a significant $\chi^2/1 = 4.7$ tension between the two results for m_u [20, 29] and a $\chi^2/1 = 3.4$ one between those for m_u/m_d [29, 30]. These tensions are accounted for by the usual rescaling of uncertainties. However, agreement is found between the two results for m_d [20, 29]. Moreover, at the level of our conservative uncertainties, agreement is found with the $N_f = 2 + 1$ results.

Again, given the small number of results and the few percent uncertainties, we average the $N_f = 2 + 1$ and $N_f = 2 + 1 + 1$ results, as explained in Sec. 60.4, to obtain our final estimates:

$$\overline{m}_u = (2.20 \pm 0.04 \pm 0.06[\pm 0.07]) \text{ MeV}, \quad (60.7)$$

$$\overline{m}_d = (4.69 \pm 0.03 \pm 0.04[\pm 0.05]) \text{ MeV}, \quad (60.8)$$

$$r \equiv \frac{\overline{m}_u}{\overline{m}_d} = (0.473 \pm 0.007 \pm 0.016[\pm 0.017]), \quad (60.9)$$

where the three uncertainties have the same meaning as described after Eq. 60.6. r in Eq. (60.9) is the combination of direct lattice computations of that ratio in which some systematics cancel. The averages are given in the $\overline{\text{MS}}$ scheme at 2 GeV in the $N_L = 4$ theory and, as above, tiny corrections due to QED effects in the renormalization constants have been neglected. Within one standard deviation it agrees with the ratio of \overline{m}_u over \overline{m}_d from Eqs. (60.7) and (60.8).

It is also worth noting that m_u differs from zero by more than 30 times the quoted error, making a scenario in which $m_u = 0$ very unlikely. This is important because there would be no strong CP problem if m_u were to vanish.

60.5.2 Chiral Perturbation Theory

For light quarks, one can use the techniques of chiral perturbation theory [31–33] to extract quark mass ratios. The mass term for light quarks in the QCD Lagrangian is

$$\overline{\Psi} M \Psi = \overline{\Psi}_L M \Psi_R + \overline{\Psi}_R M^\dagger \Psi_L, \quad (60.10)$$

where M is the light quark mass matrix,

$$M = \begin{pmatrix} m_u & 0 & 0 \\ 0 & m_d & 0 \\ 0 & 0 & m_s \end{pmatrix}, \quad (60.11)$$

$\Psi = (u, d, s)$, and L and R are the left- and right-chiral components of Ψ given by $\Psi_{L,R} = P_{L,R} \Psi$, $P_L = (1 - \gamma_5)/2$, $P_R = (1 + \gamma_5)/2$. The mass term is the only term in the QCD Lagrangian that mixes left- and right-handed quarks. In the limit $M \rightarrow 0$, there is an independent $\text{SU}(3) \times \text{U}(1)$ flavor symmetry for the left- and right-handed quarks. The vector $\text{U}(1)$ symmetry is baryon number; the axial $\text{U}(1)$ symmetry of the classical theory is broken in the quantum theory due to the anomaly. The remaining $G_\chi = \text{SU}(3)_L \times \text{SU}(3)_R$ chiral symmetry of the QCD Lagrangian is spontaneously broken to $\text{SU}(3)_V$, which, in the limit $M \rightarrow 0$, leads to eight massless Goldstone bosons, the π 's, K 's, and η .

The symmetry G_χ is only an approximate symmetry, since it is explicitly broken by the quark mass matrix M . The Goldstone bosons acquire masses which can be computed in a systematic expansion in M , in terms of low-energy constants, which are unknown nonperturbative parameters of the effective theory, and are not fixed by the symmetries. One treats the quark mass matrix M as a uniform, external field that transforms under G_χ as $M \rightarrow L M R^\dagger$, where $\Psi_L \rightarrow L \Psi_L$ and $\Psi_R \rightarrow R \Psi_R$ are the $\text{SU}(3)_L$ and $\text{SU}(3)_R$ transformations, and writes down the most general

Lagrangian invariant under G_χ . Then one sets M to its given constant value Eq. (60.11), which implements the symmetry breaking. To first order in M one finds that [34]

$$\begin{aligned} m_{\pi^0}^2 &= B(m_u + m_d), \\ m_{\pi^\pm}^2 &= B(m_u + m_d) + \Delta_{\text{em}}, \\ m_{K^0}^2 &= m_{K^0}^2 = B(m_d + m_s), \\ m_{K^\pm}^2 &= B(m_u + m_s) + \Delta_{\text{em}}, \\ m_\eta^2 &= \frac{1}{3} B(m_u + m_d + 4m_s), \end{aligned} \quad (60.12)$$

with two unknown constants B , related to the light quark condensate, and Δ_{em} , the electromagnetic mass difference. From Eq. (60.12), one can determine the quark mass ratios [34]

$$\begin{aligned} \frac{m_u}{m_d} &= \frac{2m_{\pi^0}^2 - m_{\pi^+}^2 + m_{K^+}^2 - m_{K^0}^2}{m_{K^0}^2 - m_{K^+}^2 + m_{\pi^+}^2} = 0.56, \\ \frac{m_s}{m_d} &= \frac{m_{K^0}^2 + m_{K^+}^2 - m_{\pi^+}^2}{m_{K^0}^2 + m_{\pi^+}^2 - m_{K^+}^2} = 20.2, \end{aligned} \quad (60.13)$$

to lowest order in chiral perturbation theory, with an error which will be estimated below. Since the mass ratios extracted using chiral perturbation theory use the symmetry transformation property of M under the chiral symmetry G_χ , it is important to use a renormalization scheme for QCD that does not change this transformation law. Any mass-independent subtraction scheme such as $\overline{\text{MS}}$ is suitable. The ratios of quark masses are scale independent in such a scheme (up to electromagnetic corrections), and Eq. (60.13) can be taken to be the ratio of $\overline{\text{MS}}$ masses. Chiral perturbation theory cannot determine the overall scale of the quark masses, since it uses only the symmetry properties of M , and any multiple of M has the same G_χ transformation law as M .

Chiral perturbation theory is a systematic expansion in powers of the light quark masses. The typical expansion parameter is $m_K^2/\Lambda_\chi^2 \sim 0.25$ if one uses $\text{SU}(3)$ chiral symmetry, and $m_\pi^2/\Lambda_\chi^2 \sim 0.02$ if instead one uses $\text{SU}(2)$ chiral symmetry. Electromagnetic effects at the few percent level also break $\text{SU}(2)$ and $\text{SU}(3)$ symmetry. The mass formulae Eq. (60.12) were derived using $\text{SU}(3)$ chiral symmetry, and are expected to have approximately a 25% uncertainty due to second order corrections. This estimate of the uncertainty yields results consistent with the lattice results summarized in Eq. (60.5)–(60.6).

There is a subtlety which arises when one tries to determine quark mass ratios at second order in chiral perturbation theory. The second order quark mass term [35]

$$(M^\dagger)^{-1} \det M^\dagger \quad (60.14)$$

(which can be generated by instantons) transforms in the same way under G_χ as M . Chiral perturbation theory cannot distinguish between M and $(M^\dagger)^{-1} \det M^\dagger$; one can make the replacement $M \rightarrow M(\lambda) = M + \lambda M (M^\dagger M)^{-1} \det M^\dagger$ in the chiral Lagrangian,

$$\begin{aligned} M(\lambda) &= \text{diag}(m_u(\lambda), m_d(\lambda), m_s(\lambda)) \\ &= \text{diag}(m_u + \lambda m_d m_s, m_d + \lambda m_u m_s, m_s + \lambda m_u m_d), \end{aligned} \quad (60.15)$$

and leave all observables unchanged.

The combination

$$\left(\frac{m_u}{m_d}\right)^2 + \frac{1}{Q^2} \left(\frac{m_s}{m_d}\right)^2 = 1 \quad (60.16)$$

where

$$Q^2 = \frac{m_s^2 - m_{ud}^2}{m_d^2 - m_u^2}, \quad m_{ud} = \frac{1}{2}(m_u + m_d),$$

is insensitive to the transformation in Eq. (60.15). Eq. (60.16) gives an ellipse in the m_u/m_d - m_s/m_d plane. The ellipse is well-determined by chiral perturbation theory, but the location on the

ellipse, and the absolute normalization of the quark masses, have larger uncertainties.

A leading-order result for Q in SU(3) chiral perturbation theory can be derived using Eq. (60.12) and the values for the relevant meson masses. This result actually holds to next-to-leading order, yielding $Q^{\text{NLO}} = 24.3$. Phenomenologically, the preferred way to determine Q is from $\eta \rightarrow 3\pi$ decay, giving the smaller value $Q = 22.1(7)$ [36]. Lattice QCD collaborations have also reported determinations of Q . Using $N_f = 2 + 1$ simulations, Ref. [28] obtains $Q = 23.4 \pm 0.6$ and Ref. [29] determines $Q = 23.8 \pm 1.1$ with $N_f = 2 + 1 + 1$ simulations, results which are fully compatible. These results are also compatible with $Q = 23.4 \pm 0.5$, obtained from $Q^2 = (r_s^2 - 1)(1 + r)/[4(1 - r)]$ and from our lattice averages for r_s and r from Eqs. (60.6) and (60.9), respectively. Given the size of the uncertainties on the lattice results for Q , it is safe to neglect effects due to the definition of isosymmetric QCD (see footnote 3). On the whole, the lattice results are larger than the one from phenomenology [36]. This difference could be due to surprisingly large corrections to the NLO substitution of meson masses by Q in the phenomenological determination, as suggested by the authors of [36].

The absolute normalization of the quark masses cannot be determined using chiral perturbation theory. Other methods, such as lattice simulations discussed above, or spectral function sum rules [37, 38] for hadronic correlation functions reviewed next, are necessary.

60.5.3 Sum rules

Sum rule methods have been used extensively to determine quark masses and for illustration we briefly discuss here their application to hadronic τ decays [39]. Other applications involve very similar techniques.

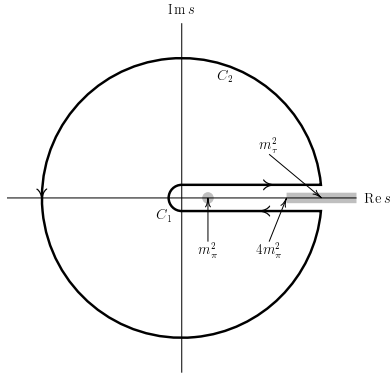


Figure 60.1: The analytic structure of $\Pi(s)$ in the complex s -plane. The contours C_1 and C_2 are the integration contours discussed in the text, and the integral over the closed contour $C_1 + C_2$ vanishes. m_τ^2 has not been drawn to scale; $m_\tau^2 \sim 40(4m_\pi^2)$.

The experimentally measured quantity is R_τ ,

$$\frac{dR_\tau}{ds} = \frac{d\Gamma/ds(\tau^- \rightarrow \text{hadrons} + \nu_\tau(\gamma))}{\Gamma(\tau^- \rightarrow e^- \bar{\nu}_e \nu_\tau(\gamma))} \quad (60.17)$$

the hadronic invariant mass spectrum in semihadronic τ decay, normalized to the leptonic τ decay rate. It is useful to define q as the total momentum of the hadronic final state, so $s = q^2$ is the hadronic invariant mass. The total hadronic τ decay rate R_τ is then given by integrating dR_τ/ds over the kinematically allowed range $0 \leq s \leq M_\tau^2$.

R_τ can be written as

$$R_\tau = 12\pi \int_0^{M_\tau^2} \frac{ds}{M_\tau^2} \left(1 - \frac{s}{M_\tau^2}\right)^2 \times \left[\left(1 + 2\frac{s}{M_\tau^2}\right) \text{Im} \Pi^T(s) + \text{Im} \Pi^L(s) \right] \quad (60.18)$$

where the hadronic spectral functions $\Pi^{L,T}$ are defined from the time-ordered correlation function of two weak currents ($j^\mu(x)$ and

$j^\nu(0)$) by

$$\Pi^{\mu\nu}(q) = i \int d^4x e^{iq \cdot x} \langle 0 | T(j^\mu(x) j^\nu(0)^\dagger) | 0 \rangle, \quad (60.19)$$

$$\Pi^{\mu\nu}(q) = (-g^{\mu\nu} + q^\mu q^\nu) \Pi^T(s) + q^\mu q^\nu \Pi^L(s), \quad (60.20)$$

and the decomposition Eq. (60.19) is the most general possible structure consistent with Lorentz invariance.

By the optical theorem, the imaginary part of $\Pi^{\mu\nu}$ is proportional to the total cross-section for the current to produce all possible states. A detailed analysis including the phase space factors leads to Eq. (60.18). The spectral functions $\Pi^{L,T}(s)$ are analytic in the complex s plane, with singularities along the real axis. There is an isolated pole at $s = m_\pi^2$, and single- and multi-particle singularities for $s \geq 4m_\pi^2$, the two-particle threshold. The discontinuity along the real axis is $\Pi^{L,T}(s + i0^+) - \Pi^{L,T}(s - i0^+) = 2i \text{Im} \Pi^{L,T}(s)$. As a result, Eq. (60.18) can be rewritten with the replacement $\text{Im} \Pi^{L,T}(s) \rightarrow -i \Pi^{L,T}(s)/2$, and the integration being over the contour C_1 . Finally, the contour C_1 can be deformed to $-C_2$ without crossing any singularities, and so leaving the integral unchanged, i.e. the integral over the closed contour $C_1 + C_2$ vanishes. One can derive a series of sum rules analogous to Eq. (60.18) by weighting the differential τ hadronic decay rate by different powers of the hadronic invariant mass [40],

$$R_\tau^{kl} = \int_0^{M_\tau^2} ds \left(1 - \frac{s}{M_\tau^2}\right)^k \left(\frac{s}{M_\tau^2}\right)^l \frac{dR_\tau}{ds}. \quad (60.21)$$

This leads to the final form of the sum rule(s),

$$R_\tau^{kl} = -6\pi i \int_{C_2} \frac{ds}{M_\tau^2} \left(1 - \frac{s}{M_\tau^2}\right)^{2+k} \left(\frac{s}{M_\tau^2}\right)^l \times \left[\left(1 + 2\frac{s}{M_\tau^2}\right) \Pi^T(s) + \Pi^L(s) \right]. \quad (60.22)$$

The manipulations so far are completely rigorous and exact, relying only on the general analytic structure of quantum field theory. The left-hand side of the sum rule Eq. (60.22) is obtained from experiment. The right hand-side can be computed for s far away from any physical cuts using the operator product expansion (OPE) for the time-ordered product of currents in Eq. (60.18), and QCD perturbation theory. The OPE is an expansion in a series of local operators, and is an expansion about the $q \rightarrow \infty$ limit. It gives $\Pi^{L,T}(s)$ as an expansion in powers of $\alpha_s(s)$ and Λ_{QCD}^2/s , and is valid when s is far (in units of Λ_{QCD}^2) from any singularities in the complex s -plane.

The OPE gives $\Pi^{L,T}(s)$ as a series in α_s , quark masses, and various nonperturbative vacuum matrix elements. By computing $\Pi^{L,T}(s)$ theoretically, and comparing with the experimental values of R_τ^{kl} , one determines various parameters such as α_s and the quark masses. The theoretical uncertainties in using Eq. (60.22) arise from neglected higher order corrections (both perturbative and nonperturbative), and because the OPE is no longer valid near the real axis, where $\Pi^{L,T}$ have singularities. The contribution of neglected higher order corrections can be estimated as for any other perturbative computation. The error due to the failure of the OPE is more difficult to estimate. In Eq. (60.22), the OPE fails on the endpoints of C_2 that touch the real axis at $s = M_\tau^2$. The weight factor $(1 - s/M_\tau^2)$ in Eq. (60.22) vanishes at this point, so the importance of the endpoint can be reduced by choosing larger values of k .

Light quark masses are often determined using QCD sum rules [38], which are similar to the τ sum rules. One takes the correlator of two light-quark-bilinear operators (e.g. an axial vector current), as in Eq. (60.18), and computes their Laplace transforms or moments

$$\mathcal{L}_n(\tau) = \int_0^\infty ds s^n e^{-\tau s} \text{Im} \Pi(s),$$

$$\mathcal{M}_n(Q^2) = \int_0^\infty \frac{ds}{(s + Q^2)^n} \text{Im} \Pi(s)$$

to get Laplace or moment sum rules, respectively. The quark masses are extracted by comparing the theoretical and experimental values of $\mathcal{L}_n(\tau)$ and $\mathcal{M}_n(Q^2)$. Considerable theoretical effort has gone into optimizing n and Q^2 to improve the precision of the resulting light quark masses.

60.6 Heavy quarks

60.6.1 Continuum approaches and results

For heavy quark physics one can exploit the fact that $m_Q \gg \Lambda_{\text{QCD}}$ to construct effective theories (m_Q is the mass of the heavy quark Q). The masses and decay rates of hadrons containing a single heavy quark, such as the B and D mesons can be determined using the heavy quark effective theory (HQET) [41]. The theoretical calculations involve radiative corrections computed in perturbation theory with an expansion in $\alpha_s(m_Q)$ and nonperturbative corrections with an expansion in powers of Λ_{QCD}/m_Q . Due to the asymptotic nature of the QCD perturbation series, the two kinds of corrections are intimately related; an example of this are renormalon effects in the perturbative expansion which are associated with nonperturbative corrections.

Systems containing two heavy quarks such as the Υ or J/Ψ are treated using non-relativistic QCD (NRQCD) [42]. The typical momentum and energy transfers in these systems are $\alpha_s m_Q$, and $\alpha_s^2 m_Q$, respectively, so these bound states are sensitive to scales much smaller than m_Q . However, smeared observables, such as the cross-section for $e^+e^- \rightarrow \bar{b}b$ averaged over some range of s that includes several bound state energy levels, are better behaved and only sensitive to scales near m_Q . For this reason, most determinations of the c, b quark masses using perturbative calculations compare smeared observables with experiment [43–45]. The method is similar to that outlined for τ decays. The current correlator in Eq. (60.18) is the electromagnetic current, and the experimental data is the value of $R(s)$ in the threshold region for $e^+e^- \rightarrow Q\bar{Q}$. The theoretical values for the moments are computed using renormalization group improved calculations in non-relativistic QCD.

There are many continuum extractions of the c and b quark masses, some with quoted errors of 10 MeV or smaller. There are systematic effects of comparable size, which are typically not included in these error estimates. Reference [46], for example, shows that even though the error estimate of m_c using the rapid convergence of the α_s perturbation series is only a few MeV, the central value of m_c can differ by a much larger amount depending on which algorithm (all of which are formally equally good) is used to determine m_c from the data. This leads to a systematic error from perturbation theory of around 20 MeV for the c quark and 25 MeV for the b quark. Electromagnetic effects, which also are important at this precision, are often not included. For this reason, we inflate the errors on the continuum extractions of m_c and m_b . The average values of m_c and m_b from continuum determinations are (see Sec. 60.7 for the 1S scheme)

$$\overline{m}_c(\overline{m}_c) = (1.280 \pm 0.025)\text{GeV},$$

$$\overline{m}_b(\overline{m}_b) = (4.18 \pm 0.03)\text{GeV}, \quad m_b^{1\text{S}} = (4.65 \pm 0.03)\text{GeV}.$$

60.6.2 Lattice approaches and results

Lattice QCD simulations of a heavy quark Q , described in a relativistic fermion formulation, lead to potentially large discretization errors which are powers of am_Q (modulated by logarithms); the leading power depends on the formulation of lattice QCD being used and in most cases is quadratic. Clearly those errors can be reduced by performing simulations at smaller lattice spacings a , but also by using *improved* discretizations of the theory, in which the leading discretization errors are systematically eliminated. Recently, with more powerful computing resources, better algorithms and improved discretizations of QCD, it has become possible to perform simulations with quarks more massive than the charm and even up to the b [11], decreasing or eliminating the extrapolation which has to be performed to reach the m_b . It is worth noting that computations using a relativistic fermion formulation for the valence charm with $N_f = 2 + 1$ sea-quark flavors, or with $N_f = 2 + 1 + 1$ flavors and a relativistic b , suffer from partial-quenching effects. This is because the heavy valence

quarks are absent from the sea. While these effects are not expected to be large in $N_f = 2 + 1 + 1$ computations, they should be investigated when quoting results below the percent level in the case of $N_f = 2 + 1$ sea-quark flavors. For that reason we will omit heavy-quark results obtained with $N_f = 2 + 1$ sea-quark flavors from our averages and, more generally focus on $N_f = 2 + 1 + 1$ results. Note that these partial-quenching effects are accounted for systematically in lattice calculations in which the heavy valence quarks are described by HQET or NRQCD.

Traditionally the charm quark mass is obtained by tuning its bare, simulation input value to reproduce the physical mass of charmonium mesons or of the D, D_s mesons (requiring a more precise tuning of the light quark masses and the computation of larger QED effects in some cases). This mass can then be renormalized and matched to the $\overline{\text{MS}}$ scheme using the methods discussed for the light quarks.

An alternative approach for obtaining the $\overline{\text{MS}}$ mass was proposed in [47]. Euclidean-time moments of pseudoscalar, two-point functions of $c\bar{c}$ quark-bilinear operators can readily be computed on the lattice and extrapolated to the continuum limit where they can be compared to perturbative calculations of the same quantities at 4-loop order. In this way, both the strong coupling constant and the charm quark mass can be determined with remarkably small errors. As this approach uses the same perturbative expressions for two-point correlators as the continuum determinations discussed in Sec. 60.6.1, it suffers from similar perturbation-theory, systematic errors. FLAG [8] has reviewed lattice determinations of the charm-quark mass obtained using both approaches. For their $N_f = 2 + 1$ average they retain the results [13, 48–50], with [51] being published after their deadline. As stated above, we focus here on $N_f = 2 + 1 + 1$ results. For these, FLAG uses the results of Refs. [10, 19, 20, 22, 52].

Since the FLAG review, Refs. [22, 52] have been superseded by Ref. [9]. In that reference, only $\overline{m}_c(3\text{GeV})$ is given and we multiply by the running factor 0.7739 ± 0.0060 from $\mu = 3\text{GeV}$ to \overline{m}_c [8]. With this substitution and using the combination method described in Sec. 60.4, we obtain:

$$\overline{m}_c(\overline{m}_c) = (1.275 \pm 0.004 \pm 0.008[\pm 0.009])\text{GeV} \quad (60.23)$$

where the three uncertainties have the same meaning as described after Eq. (60.6). This result is in good agreement with the continuum result given above, but with a smaller error.

It is worth noting that three [10, 19, 20] of the four results entering this average agree, while the other [9] is over 2 standard deviations larger than the average. This is taken into account by stretching errors in the usual way, but the total uncertainty on the lattice average of \overline{m}_c will not significantly be reduced until this discrepancy is resolved. It should also be noted that [10] includes QED directly in the lattice calculation, albeit only for valence quarks, while some of the other computations account for these effects using phenomenology. For $\overline{m}_c(\overline{m}_c)$ considered above, these effects are below the permil [10] and are therefore neglected here.

Historically, the main approach to controlling the discretization errors in lattice studies of b -quark physics was to perform simulations of effective theories such as HQET and NRQCD. This remains an important technique, both in its own right and in providing additional information for extrapolations from lower masses to the bottom region. Using effective theories, m_b is obtained from what is essentially a computation of the difference of $M_{H_b} - m_b$, where M_{H_b} is the mass of a hadron H_b containing a b quark. The relative error on m_b is therefore much smaller than that for $M_{H_b} - m_b$. The principal systematic errors are the matching of the effective theories to QCD and the presence of power divergences in a^{-1} in the $1/m_b$ corrections which have to be subtracted numerically. A procedure for performing these subtractions fully nonperturbatively was proposed and implemented for the first time in [53].

The most recent $N_f = 2 + 1 + 1$ lattice QCD determinations of the b quark mass rely on a variety of approaches, including Euclidean-time moments of correlation functions with [54] or without NRQCD [19] and interpolations [55, 56] (using results from HQET simulations) or extrapolations [11, 20] from above the

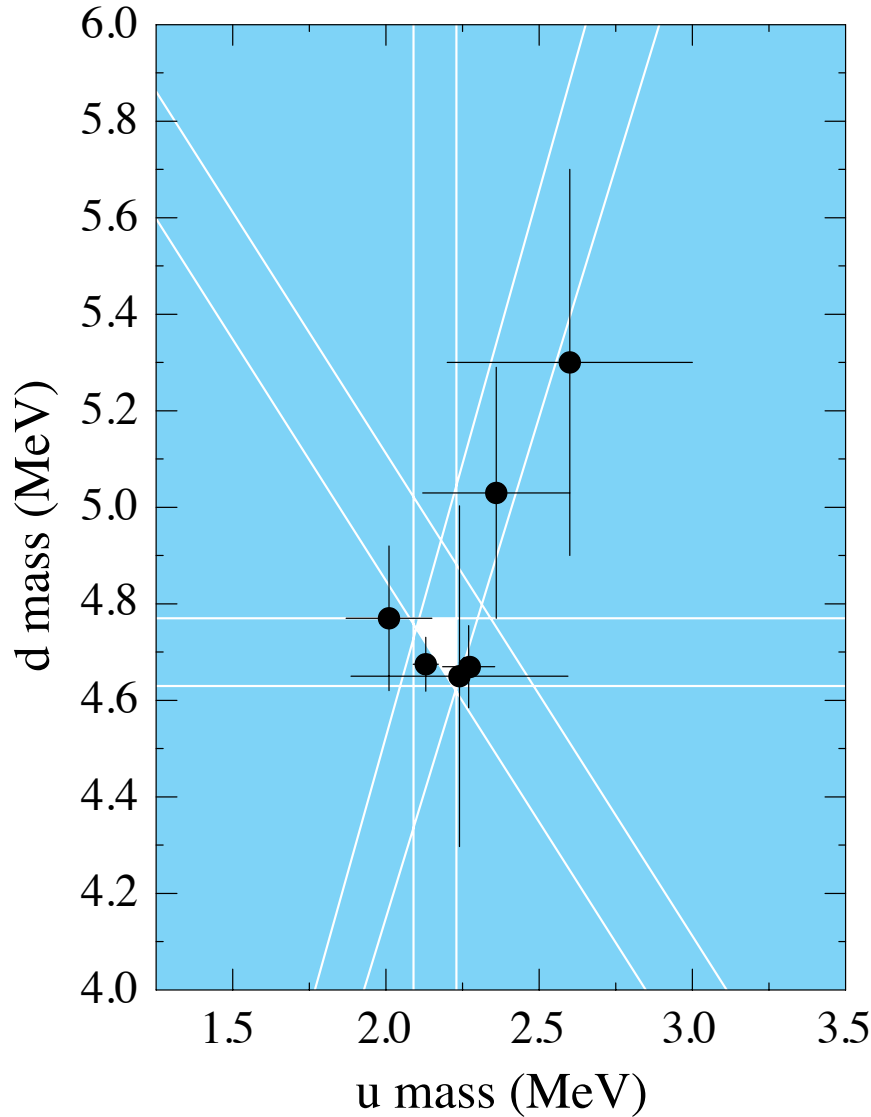


Figure 60.2: The allowed region (shown in white) for up quark and down quark masses renormalized in the $\overline{\text{MS}}$ scheme at 2 GeV, determined from the allowed ranges of mass parameters (see Fig. 60.3). The parameter $(m_u + m_d)/2$ yields the two downward-sloping white lines, while m_u/m_d yields the two rising white lines originating at $(0,0)$. The white region is the remaining allowed parameter space after applying the limits on m_u , m_d , $(m_u + m_d)/2$ and m_u/m_d , where those limits are 90% confidence levels including the scale factors shown in the ideograms in the Data Listings.

charm mass to that of the b . One calculation [11] even includes simulations performed with a heavy quark whose mass is very near that of the b quark. The overall agreement of the results obtained using these very different approaches, which have different systematic errors, is a confirmation that the various groups control these uncertainties. As the range of heavy-quark masses which can be used in numerical simulations increases, the extrapolation or interpolation of results to the physical b mass, possibly including some obtained directly at that mass, are becoming ever more reliable (see e.g. Refs. [11, 20]).

Using the results from Refs. [11, 19, 20, 55, 56], converting those given in the $N_L = 4$ theory to the $N_L = 5$ one and applying the averaging method described in Sec. 60.4, we obtained the estimate:

$$\overline{m}_b(\overline{m}_b) = (4.196 \pm 0.009 \pm 0.009[\pm 0.012]) \text{ GeV} , \quad (60.24)$$

where the three uncertainties have the same meaning as in the estimates given above for light-quark masses.

Among the results entering this average, only one [11] accounts for electromagnetic effects. Using Refs. [10, 11], it is straightforward to show that QED effects on the value of \overline{m}_b at $\mu = 3 \text{ GeV}$,

and thus at $\mu = \overline{m}_b$, are smaller than one permil in the separation scheme of those two references. Assuming that the same is true for the other results, we neglect these corrections here.

The lattice result of Eq. (60.24) is compatible with the average value of continuum results, but with a significantly smaller uncertainty. Note that FLAG [8] also provides an average of $N_f = 2+1$ results, taken from [13, 50]. It is about one combined, standard deviations lower than the result quoted above.

As explained in Sec. 60.3, ratios of quark masses can have significantly smaller errors than the individual masses if they are determined within the same lattice QCD framework. This led HPQCD to leverage their precise determination of m_c [47] to determine m_s and m_{ud} [57], through a precise computation of m_c/m_s [57] and of m_s/m_{ud} [58]. The $N_f = 2+1$ calculation [57] was updated using $N_f = 2+1+1$ simulations in [19]. The ratio m_c/m_s was also computed in Refs [48, 59] with $N_f = 2+1$ simulations and in Refs. [20, 22] with $N_f = 2+1+1$ ones. On the basis of those references, FLAG [8] gives average results from $N_f = 2+1$ and $N_f = 2+1+1$ simulations. Here we focus on $N_f = 2+1+1$ results and we replace the results of Ref. [22] by the collaboration's update [9]. Applying to the modern $N_f = 2+1+1$ computations of

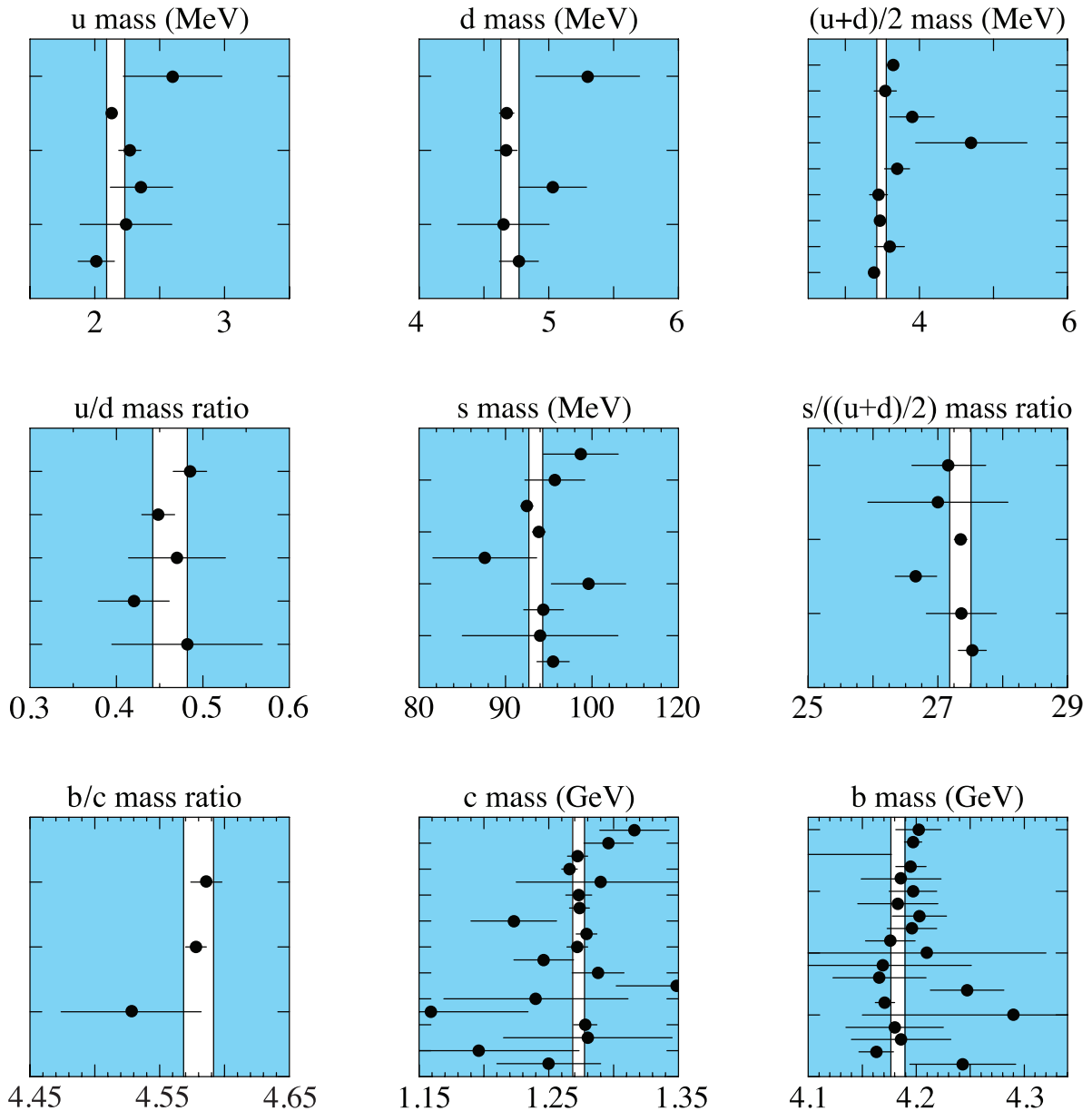


Figure 60.3: The allowed regions (shown in white) for quark masses renormalized in the $\overline{\text{MS}}$ scheme at 2 GeV. The points (taken from the Data Listings) are in chronological order with the more recent measurements shown at the top. The white regions indicate values allowed at the 90% confidence level including the scale factors shown in the ideograms in the Data Listings.

Refs. [9, 19, 20] the combination procedure described in Sec. 60.4, we obtain the following lattice average:

$$\overline{m}_c/\overline{m}_s = 11.769 \pm 0.021 \pm 0.028[\pm 0.035],$$

where the three uncertainties have the same meaning as described after Eq. 60.6. The average is dominated by Ref. [20] that has a substantially smaller error than the other results. The result of Ref. [9] is a little more than 1 standard deviation below that average and the one of Ref. [19] close to 2σ above, for a total $\chi^2/\text{dof} = 5.0/2$ and a rescaling factor of ~ 1.6 in the statistical and systematic errors.

The above ratio is renormalization scheme and scale independent, in the absence of electromagnetic corrections. None of the calculations above estimates the size of those corrections. Nevertheless, they are expected to still be smaller than the total uncertainty quoted above in a standard scheme for defining QCD in the isospin limit.

The ratio m_b/m_c has also been computed on the lattice. The two $N_f = 2 + 1$ results which satisfy FLAG's criteria are [13, 50].

As explained above, we focus on $N_f = 2 + 1 + 1$ calculations [11, 20, 55]. Ref. [11] is the only calculation which accounts for QED directly in the lattice simulations, albeit only for valence quarks, and thus must specify the renormalization scheme and scale of its result, which it chooses to be $\overline{\text{MS}}$ at 3 GeV. Here we correct the results of Refs. [20, 55] by the QED factor 1.0017 obtained in Ref. [11], and ascribe to it a 100% systematic uncertainty with 100% correlation. This means that we assume that the differences due to the separation schemes used in each calculation lies within that error. Averaging the resulting numbers, as prescribed in Sec. 60.4, yields

$$\overline{m}_b/\overline{m}_c = 4.584 \pm 0.006 \pm 0.010[\pm 0.012],$$

where exceptionally the bar indicates that the masses are renormalized in the $\overline{\text{MS}}$ at 3 GeV in the four-flavor theory. Here a scale factor of $\sqrt{\chi^2/\text{dof}} = 1.30$ has been applied to the error bar. Indeed, [55] contributes 3.3 to the total χ^2 .

60.6.3 Warnings concerning the use of the pole mass

For an observable particle such as the electron, the position of the pole in the propagator is the definition of its mass. In QCD this definition of the quark mass is known as the pole mass. It is known that the on-shell quark propagator has no infrared divergences in perturbation theory [60,61], so this provides a perturbative definition of the quark mass. However, the pole mass cannot be used to arbitrarily high accuracy because of nonperturbative infrared effects in QCD. In fact the full quark propagator has no pole because the quarks are confined, so that the pole mass cannot be defined outside of perturbation theory. The relation between the pole mass m_Q and the $\overline{\text{MS}}$ mass \overline{m}_Q , used throughout this review, is known to three loops [62–65]

$$m_Q = \overline{m}_Q(\overline{m}_Q) \left\{ 1 + \frac{4\overline{\alpha}_s(\overline{m}_Q)}{3\pi} \right. \quad (60.25)$$

$$+ \left[-1.0414 \sum_q \left(1 - \frac{4}{3} \frac{\overline{m}_q}{\overline{m}_Q} \right) + 13.4434 \right] \left[\frac{\overline{\alpha}_s(\overline{m}_Q)}{\pi} \right]^2$$

$$\left. + [0.6527N_L^2 - 26.655N_L + 190.595] \left[\frac{\overline{\alpha}_s(\overline{m}_Q)}{\pi} \right]^3 \right\},$$

where $\overline{\alpha}_s(\mu)$ is the strong interaction coupling constants in the $\overline{\text{MS}}$ scheme, and the sum over q extends over the N_L flavors lighter than Q . The complete mass dependence of the α_s^2 term can be found in [62]; the mass dependence of the α_s^3 term is not known. For the b -quark, Eq. (60.25) reads

$$m_b = \overline{m}_b(\overline{m}_b) [1 + 0.10 + 0.05 + 0.03], \quad (60.26)$$

where the contributions from the different orders in α_s are shown explicitly. The two and three loop corrections are comparable in size and have the same sign as the one loop term. This is a signal of the asymptotic nature of the perturbation series (there is a renormalon in the pole mass [66]). Such a badly behaved perturbation expansion can be avoided by directly extracting, from data, the mass defined in the $\overline{\text{MS}}$ (used in this review) or other short-distance schemes (see below), without invoking the pole mass as an intermediate step.

60.7 Numerical values and caveats

The quark masses in the particle data listings have been obtained by using a wide variety of methods. Each method involves its own set of approximations and uncertainties. In most cases, the errors are an estimate of the size of neglected higher-order corrections or other uncertainties. The expansion parameters for some of the approximations are not very small (for example, they are $m_K^2/\Lambda_\chi^2 \sim 0.25$ for the SU(3) chiral expansion and $\Lambda_{\text{QCD}}/m_b \sim 0.1$ for the heavy-quark expansion), so an unexpectedly large coefficient in a neglected higher-order term could significantly alter the results. Thus, before using a particular result, it is important to understand the possible limitations of the approach used to obtain it. It is also important to note that the quark mass values can be significantly different in the different schemes.

We have specified all masses in the $\overline{\text{MS}}$ scheme. For light quarks, the renormalization scale has been chosen to be $\mu = 2 \text{ GeV}$. Quoting these masses at smaller values of μ , where perturbative corrections become significantly larger, would introduce unnecessary uncertainties in the results. In fact, as lattice calculations, performed on finer and finer lattices, allow to determine quark masses, fully nonperturbatively, at larger and larger values of μ , it may become advantageous to quote quark mass results at renormalization scales above 2 GeV, where perturbative uncertainties are smaller.

The heavy quark masses obtained using HQET, QCD sum rules, or lattice gauge theory are consistent with each other if they are all converted into the same scheme and scale. For these quarks it is conventional to choose the renormalization scale equal to the quark mass, so we have quoted $\overline{m}_Q(\mu)$ at $\mu = \overline{m}_Q$ for the c and b quarks. Given the small size of the charm quark mass, in the future it may become advantageous to quote its value at larger values of μ so as not to introduce unnecessary perturbative uncertainties (see discussion above). Analyses of inclusive

B meson decays have shown that other mass definitions lead to a better behaved perturbation series than for the $\overline{\text{MS}}$ mass, and hence to more accurate mass values [67–70]. Thus, we have chosen to also give values for one of these, the b quark mass in the 1S scheme [67,68]. Other schemes that have been proposed are the PS-scheme [69], the kinetic scheme [71] and, most recently, the minimal renormalon-subtracted mass (MRS) [70] used in the lattice calculation [20].

If necessary, we have converted values in the original papers to our chosen scheme using two-loop formulae. It is important to realize that our conversions introduce significant additional errors. In converting to the $\overline{\text{MS}}$ b -quark mass, for example, the three-loop conversions from the 1S and pole masses give values about 35 MeV and 135 MeV lower than the two-loop conversions. The uncertainty in $\alpha_s(M_Z) = 0.1179 \pm 0.0010$ [1] gives an uncertainty of $\pm 9 \text{ MeV}$ and $\pm 21 \text{ MeV}$ respectively in the same conversions. We have not added these additional errors when we do our conversions. The α_s value in the conversion is correlated with the α_s value used in determining the quark mass, so the conversion error is not a simple additional error on the quark mass.

References

- [1] See the review of QCD in this volume.
- [2] A. Manohar and H. Georgi, Nucl. Phys. B **234**, 189 (1984).
- [3] K. Chetyrkin, Phys. Lett. B **404**, 161 (1997), [hep-ph/9703278].
- [4] J. Vermaseren, S. Larin and T. van Ritbergen, Phys. Lett. B **405**, 327 (1997), [hep-ph/9703284].
- [5] K. Chetyrkin, B. A. Kniehl and M. Steinhauser, Nucl. Phys. B **510**, 61 (1998), [hep-ph/9708255].
- [6] G. Martinelli *et al.*, Nucl. Phys. B **445**, 81 (1995), [hep-lat/9411010].
- [7] K. Jansen *et al.*, Phys. Lett. B **372**, 275 (1996), [hep-lat/9512009].
- [8] Y. Aoki *et al.* (Flavour Lattice Averaging Group (FLAG)), Eur. Phys. J. C **82**, 10, 869 (2022), [arXiv:2111.09849].
- [9] C. Alexandrou *et al.* (Extended Twisted Mass), Phys. Rev. D **104**, 7, 074515 (2021), [arXiv:2104.13408].
- [10] D. Hatton *et al.* (HPQCD), Phys. Rev. D **102**, 5, 054511 (2020), [arXiv:2005.01845].
- [11] D. Hatton *et al.*, Phys. Rev. D **103**, 11, 114508 (2021), [arXiv:2102.09609].
- [12] A. Bazavov *et al.* (MILC), PoS **CD09**, 007 (2009), [arXiv:0910.2966].
- [13] C. McNeile *et al.*, Phys. Rev. D **82**, 034512 (2010), [arXiv:1004.4285].
- [14] A. Bazavov *et al.*, PoS **LATTICE2010**, 083 (2010), [arXiv:1011.1792].
- [15] S. Durr *et al.*, Phys. Lett. B **701**, 265 (2011), [arXiv:1011.2403].
- [16] S. Durr *et al.*, JHEP **08**, 148 (2011), [arXiv:1011.2711].
- [17] T. Blum *et al.* (RBC, UKQCD), Phys. Rev. D **93**, 7, 074505 (2016), [arXiv:1411.7017].
- [18] M. Bruno *et al.* (ALPHA), Eur. Phys. J. C **80**, 2, 169 (2020), [arXiv:1911.08025].
- [19] B. Chakraborty *et al.*, Phys. Rev. D **91**, 5, 054508 (2015), [arXiv:1408.4169].
- [20] A. Bazavov *et al.* (Fermilab Lattice, MILC, TUMQCD), Phys. Rev. D **98**, 5, 054517 (2018), [arXiv:1802.04248].
- [21] A. Lytle *et al.* (HPQCD), Phys. Rev. D **98**, 1, 014513 (2018), [arXiv:1805.06225].
- [22] N. Carrasco *et al.* (European Twisted Mass), Nucl. Phys. B **887**, 19 (2014), [arXiv:1403.4504].
- [23] A. Bazavov *et al.* (Fermilab Lattice, MILC), Phys. Rev. D **90**, 7, 074509 (2014), [arXiv:1407.3772].
- [24] A. Bazavov *et al.*, Phys. Rev. D **98**, 7, 074512 (2018), [arXiv:1712.09262].

- [25] M. Bruno *et al.* (ALPHA), Phys. Rev. Lett. **114**, 10, 102001 (2015), [arXiv:1410.8374].
- [26] A. Athenodorou *et al.* (ALPHA), Nucl. Phys. B **943**, 114612 (2019), [arXiv:1809.03383].
- [27] S. Borsanyi *et al.*, Science **347**, 1452 (2015), [arXiv:1406.4088].
- [28] Z. Fodor *et al.*, Phys. Rev. Lett. **117**, 8, 082001 (2016), [arXiv:1604.07112].
- [29] D. Giusti *et al.*, Phys. Rev. D **95**, 11, 114504 (2017), [arXiv:1704.06561].
- [30] S. Basak *et al.* (MILC), Phys. Rev. D **99**, 3, 034503 (2019), [arXiv:1807.05556].
- [31] S. Weinberg, Physica A **96**, 1-2, 327 (1979).
- [32] J. Gasser and H. Leutwyler, Annals Phys. **158**, 142 (1984).
- [33] A. Pich, Rept. Prog. Phys. **58**, 563 (1995), [hep-ph/9502366].
- [34] S. Weinberg, Trans. New York Acad. Sci. **38**, 185 (1977).
- [35] D. B. Kaplan and A. V. Manohar, Phys. Rev. Lett. **56**, 2004 (1986).
- [36] G. Colangelo *et al.*, Eur. Phys. J. C **78**, 11, 947 (2018), [arXiv:1807.11937].
- [37] S. Weinberg, Phys. Rev. Lett. **18**, 507 (1967).
- [38] M. A. Shifman, A. Vainshtein and V. I. Zakharov, Nucl. Phys. B **147**, 385 (1979).
- [39] E. Braaten, S. Narison and A. Pich, Nucl. Phys. B **373**, 581 (1992).
- [40] F. Le Diberder and A. Pich, Phys. Lett. B **286**, 147 (1992).
- [41] N. Isgur and M. B. Wise, Phys. Lett. B **237**, 527 (1990).
- [42] G. T. Bodwin, E. Braaten and G. Lepage, Phys. Rev. D **51**, 1125 (1995), [Erratum: Phys.Rev.D 55, 5853 (1997)], [hep-ph/9407339].
- [43] A. Hoang, Phys. Rev. D **61**, 034005 (2000), [hep-ph/9905550].
- [44] K. Melnikov and A. Yelkhovsky, Phys. Rev. D **59**, 114009 (1999), [hep-ph/9805270].
- [45] M. Beneke and A. Signer, Phys. Lett. B **471**, 233 (1999), [hep-ph/9906475].
- [46] B. Dehnadi *et al.*, JHEP **09**, 103 (2013), [arXiv:1102.2264].
- [47] I. Allison *et al.* (HPQCD), Phys. Rev. D **78**, 054513 (2008), [arXiv:0805.2999].
- [48] Y.-B. Yang *et al.*, Phys. Rev. D **92**, 3, 034517 (2015), [arXiv:1410.3343].
- [49] K. Nakayama, B. Fahy and S. Hashimoto, Phys. Rev. D **94**, 5, 054507 (2016), [arXiv:1606.01002].
- [50] P. Petreczky and J. Weber, Phys. Rev. D **100**, 3, 034519 (2019), [arXiv:1901.06424].
- [51] J. Heitger, F. Joswig and S. Kuberski (ALPHA), JHEP **05**, 288 (2021), [arXiv:2101.02694].
- [52] C. Alexandrou *et al.*, Phys. Rev. D **90**, 7, 074501 (2014), [arXiv:1406.4310].
- [53] J. Heitger and R. Sommer (ALPHA), JHEP **02**, 022 (2004), [hep-lat/0310035].
- [54] B. Colquhoun *et al.*, Phys. Rev. D **91**, 7, 074514 (2015), [arXiv:1408.5768].
- [55] A. Bussone *et al.* (ETM), Phys. Rev. D **93**, 11, 114505 (2016), [arXiv:1603.04306].
- [56] P. Gambino, A. Melis and S. Simula, Phys. Rev. D **96**, 1, 014511 (2017), [arXiv:1704.06105].
- [57] C. Davies *et al.*, Phys. Rev. Lett. **104**, 132003 (2010), [arXiv:0910.3102].
- [58] A. Bazavov *et al.* (MILC), Rev. Mod. Phys. **82**, 1349 (2010), [arXiv:0903.3598].
- [59] Y. Maezawa and P. Petreczky, Phys. Rev. D **94**, 3, 034507 (2016), [arXiv:1606.08798].
- [60] R. Tarrach, Nucl. Phys. B **183**, 384 (1981).
- [61] A. S. Kronfeld, Phys. Rev. D **58**, 051501 (1998), [hep-ph/9805215].
- [62] N. Gray *et al.*, Z. Phys. C **48**, 673 (1990).
- [63] D. J. Broadhurst, N. Gray and K. Schilcher, Z. Phys. C **52**, 111 (1991).
- [64] K. Chetyrkin and M. Steinhauser, Phys. Rev. Lett. **83**, 4001 (1999), [hep-ph/9907509].
- [65] K. Melnikov and T. v. Ritbergen, Phys. Lett. B **482**, 99 (2000), [hep-ph/9912391].
- [66] M. Beneke and V. M. Braun, Nucl. Phys. B **426**, 301 (1994), [hep-ph/9402364].
- [67] A. H. Hoang, Z. Ligeti and A. V. Manohar, Phys. Rev. Lett. **82**, 277 (1999), [hep-ph/9809423].
- [68] A. H. Hoang, Z. Ligeti and A. V. Manohar, Phys. Rev. D **59**, 074017 (1999), [hep-ph/9811239].
- [69] M. Beneke, Phys. Lett. B **434**, 115 (1998), [hep-ph/9804241].
- [70] N. Brambilla *et al.* (TUMQCD), Phys. Rev. D **97**, 3, 034503 (2018), [arXiv:1712.04983].
- [71] P. Gambino and N. Uraltsev, Eur. Phys. J. C **34**, 181 (2004), [hep-ph/0401063].

61. Top Quark

Revised September 2023 by T.M. Liss (City Coll. of New York), F. Maltoni (CP3 U. catholique de Louvain; Bologna U.) and A. Quadt (Göttingen U.).

61.1 Introduction and SM theory overview

In the Standard Model (SM), the left-handed top quark is the $Q = 2/3$, $T_3 = +1/2$ member of the weak-isospin doublet containing the bottom quark, while the right-handed top is an $SU(2)_L$ singlet (see, e.g., the review “Electroweak Model and Constraints on New Physics” here). Its phenomenology is driven by its large mass, $m_t \simeq \frac{v}{\sqrt{2}}$, where $v = 246$ GeV is the vacuum expectation value of the Higgs field, i.e., it is the only quark whose Yukawa coupling to the Higgs boson is of order unity. As it is heavier than the W boson, it is the only quark that decays semi-weakly into a real W boson and a b quark. This results in a lifetime that is shorter than the time that is needed for strong interactions to modify its properties or to bind it into a hadron. In this respect, the top is the only quark that, in its brief life, behaves as a free one. Because of its large mass and Yukawa coupling to the Higgs boson, it also gives important contributions (via loops) to Standard Model precision observables measured at lower scales.

For these reasons, the top quark provides a unique laboratory to test our understanding of matter and fundamental interactions at the ElectroWeak (EW) symmetry-breaking scale and beyond. In addition, since it is abundantly produced at the Large Hadron Collider (LHC), a precise knowledge of its properties (mass, couplings, production cross sections, decay branching ratios, *etc.*) can be achieved. This review provides a concise discussion of the experimental and theoretical issues involved in the determination of the top-quark properties.

61.1.1 Properties

61.1.1.1 Mass

The top quark mass determines to a large extent the unique phenomenology of this quark. In the SM quark masses are derived parameters from the Yukawa coupling and the vacuum expectation value. At the loop level, with the Higgs boson discovery and per mil measurement of its mass, the values of the W -boson and top quark mass are correlated, so that their precise determinations provides a strong test of the SM (see Section 10 “Electroweak Model and constraints on new physics” of this *Review*). At present there is some tension at the 1.7σ level, between the indirect top quark (pole) mass determination from electroweak precision data (176.12 ± 1.9 GeV) and the combination of direct measurements at the LHC that yields $172.52 \pm 0.14(\text{stat.}) \pm 0.30(\text{syst.})$ GeV [1].

The top mass value is also critical in the issue of vacuum stability in the SM [2–4]. At high scales, the Higgs quartic coupling λ evolves to increasingly small values as m_t grows. Above $m_t = 171$ GeV, i.e., very close to the most precise measurements, λ becomes negative at the Planck scale leading to a meta-stable electroweak vacuum, while for slightly larger values, $m_t > 176$ GeV the electroweak vacuum would become unstable. Current top-quark measurements therefore point to a Higgs quartic coupling which is nearly vanishing at the Planck scale. While being quite suggestive, in absence of a clear UV picture this argument allows only to conclude that comparison between our best SM predictions and the data does not imply new physics below the Planck scale (see Section 11.2.3 of “Status of Higgs Boson Physics” in this *Review*).

Given its importance and the large samples of top quarks produced at the LHC, the top mass determination has been one of the most important goals in the precision measurement campaign of the ATLAS and CMS collaborations. The basic methodology rests on the idea of fitting m_t -dependent kinematic distributions to fully-exclusive (Monte Carlo) predictions, via the full or partial reconstruction of the system of the t and \bar{t} decay products. These are called “direct measurements” and aim at a target accuracy in the permil range. With an absolute uncertainty of order or better than Λ_{QCD} , however, a clear relation between the extracted mass and a well defined quantum field theory parameter of the underlying theory has become necessary.

Several mass parameter definitions exist with a precise field-

theoretical meaning, that can be organised in two broad classes, the long-distance ones, such as the “pole mass”, and short-distance masses, such as the $\overline{\text{MS}}$ mass. A mass definition, the MSR mass [5], exists that interpolates between the two. The one measured through direct measurements is sometimes referred to as “Monte Carlo” mass. Several other observables have been put forward that could be expressed in terms of well-defined masses and then overcome the problems of the direct measurements, yet with a target accuracy not quite competitive with the direct determination.

A top mass cannot be defined solely in terms of the mass of the system of its decay products: the top quark is a colored object, therefore it cannot be an asymptotic state of the theory and no final-state hadronic system can be unambiguously associated with it. On the other hand, final state observables such as those arising from its decay, can be related to the top mass through computations, which have perturbative as well as non-perturbative components, as Monte Carlo generators.

From a purely theoretical (calculational) point of view, the top mass parameter is defined within a given renormalization scheme, since divergent perturbative corrections arise order by order in perturbation theory, and need to be subtracted. The pole mass scheme prescribes to subtract the divergent mass corrections so that the pole in the quark propagator remains fixed order by order in perturbation theory. The $\overline{\text{MS}}$ scheme prescribes to employ dimensional regularization and subtract the pure $1/\epsilon$ pole in the divergent mass correction. In doing so, the corresponding mass becomes scale dependent. In this scheme the pole in the top propagator receives corrections at all orders in perturbation theory. This scheme has the advantage that it makes the relation between the mass and the Yukawa coupling straightforward in the SM and is independent from non-perturbative corrections.

The relation between the top pole mass m_t^{pole} and $m_t^{\overline{\text{MS}}}$ up to four loops reads [6]

$$m_t^{\text{pole}} = m_t^{\overline{\text{MS}}}(m_t) [1 + 0.4244 \alpha_s + 0.8345 \alpha_s^2 + 2.375 \alpha_s^3 + (8.49 \pm 0.25) \alpha_s^4], \quad (61.1)$$

which for $\alpha_s = \alpha_s^{(6)}(m) = 0.1088$ and $m_t^{\text{pole}} = 172.5$ GeV gives $m_t^{\overline{\text{MS}}}(m_t) = 162.69 \pm 0.006$ GeV. The two definitions lead to perturbatively equivalent theories: a perturbative expression of the pole mass in terms of the $\overline{m}^{\overline{\text{MS}}}$ mass can be translated to a physical result in the pole mass scheme into the corresponding physical result in the $\overline{\text{MS}}$ scheme. However, the relation above has only a perturbative meaning, as the two masses differ by non-perturbative, long-distance effects. The difference between the top pole mass and the mass extracted in direct measurements, Δm_{MC} , arises due to non-perturbative effects, that are currently modelled by shower Monte Carlo programs. It is expected to be of order $Q_0 \cdot \alpha_s(Q_0)$ with $Q_0 \sim 1$ GeV and estimated of order 0.5 GeV. An overview on the on-going efforts to precisely define and to estimate the uncertainties of the top mass can be found in Refs. [7, 8].

61.1.1.2 Couplings

The SM couplings involving top quarks are of two types: gauge couplings, which are universal, and Yukawa couplings, which instead depend on the generation. Following the notation of Sections 9 and 10 of this *Review*, after EWSB and in the mass eigenstate basis, top quark interactions read

$$\begin{aligned} \mathcal{L}_t^{\text{SM}} = & \bar{\psi}_t [i\not{\partial} - m_t] \psi_t - g_s \bar{\psi}_t \gamma^\mu t^C \psi_t A_\mu^C - e Q_t \bar{\psi}_t \gamma^\mu \psi_t A_\mu \\ & - \frac{g}{2\sqrt{2}} \bar{\psi}_t \gamma^\mu (1 - \gamma^5) (T^+ W_\mu^+ + T^- W_\mu^-) \Psi \\ & - \frac{g}{2 \cos \theta_W} \bar{\psi}_t \gamma^\mu (g_V^t - g_A^t \gamma^5) \psi_t Z_\mu - \frac{m_t}{v} H \bar{\psi}_t \psi_t, \end{aligned} \quad (61.2)$$

where in the first line we include the coupling to the $SU(3)$ field A_μ , and $\Psi = (t, b')$ with $b' = V_{tb} b + V_{ts} s + V_{td} d$. There are no neutral flavor changing interactions in the SM at tree level.

In absence of evidence for physics beyond the SM at the weak scale or below, the Standard Model Effective Field Theory (SMEFT) [9–11] provides a simple and consistent framework

Table 61.1: List of SMEFT operators at dimension six, assuming $U(2)_q \times U(2)_u \times U(2)_d$ flavor symmetry. For more details on notation and conventions, see reference in the text.

Operator	Field content	Operator	Field content
Four-quark		Two-quark-two-lepton	
$O_{qq}^{1(ijkl)}$	$(\bar{q}_i \gamma^\mu q_j)(\bar{q}_k \gamma_\mu q_l)$	$O_{lq}^{1(ijkl)}$	$(\bar{l}_i \gamma^\mu l_j)(\bar{q}_k \gamma^\mu q_l)$
$O_{qq}^{3(ijkl)}$	$(\bar{q}_i \gamma^\mu \tau^I q_j)(\bar{q}_k \gamma_\mu \tau^I q_l)$	$O_{lq}^{3(ijkl)}$	$(\bar{l}_i \gamma^\mu \tau^I l_j)(\bar{q}_k \gamma^\mu \tau^I q_l)$
$O_{qu}^{1(ijkl)}$	$(\bar{q}_i \gamma^\mu q_j)(\bar{u}_k \gamma_\mu u_l)$	$O_{lu}^{(ijkl)}$	$(\bar{l}_i \gamma^\mu l_j)(\bar{u}_k \gamma^\mu u_l)$
$O_{qu}^{8(ijkl)}$	$(\bar{q}_i \gamma^\mu T^A q_j)(\bar{u}_k \gamma_\mu T^A u_l)$	$O_{eq}^{(ijkl)}$	$(\bar{e}_i \gamma^\mu e_j)(\bar{q}_k \gamma^\mu q_l)$
$O_{qd}^{1(ijkl)}$	$(\bar{q}_i \gamma^\mu q_j)(\bar{d}_k \gamma_\mu d_l)$	$O_{eu}^{(ijkl)}$	$(\bar{e}_i \gamma^\mu e_j)(\bar{u}_k \gamma^\mu u_l)$
$O_{qd}^{8(ijkl)}$	$(\bar{q}_i \gamma^\mu T^A q_j)(\bar{d}_k \gamma_\mu T^A d_l)$	$\ddagger O_{lequ}^{1(ijkl)}$	$(\bar{l}_i e_j) \varepsilon (\bar{q}_k u_l)$
$O_{uu}^{(ijkl)}$	$(\bar{u}_i \gamma^\mu u_j)(\bar{u}_k \gamma_\mu u_l)$	$\ddagger O_{lequ}^{3(ijkl)}$	$(\bar{l}_i \sigma^{\mu\nu} e_j) \varepsilon (\bar{q}_k \sigma_{\mu\nu} u_l)$
$O_{ud}^{1(ijkl)}$	$(\bar{u}_i \gamma^\mu u_j)(\bar{d}_k \gamma_\mu d_l)$	$\ddagger O_{ledq}^{(ijkl)}$	$(\bar{l}_i e_j)(\bar{d}_k q_l)$
$O_{ud}^{8(ijkl)}$	$(\bar{u}_i \gamma^\mu T^A u_j)(\bar{d}_k \gamma_\mu T^A d_l)$		
$\ddagger O_{quqd}^{1(ijkl)}$	$(\bar{q}_i u_j) \varepsilon (\bar{q}_k d_l)$		
$\ddagger O_{quqd}^{8(ijkl)}$	$(\bar{q}_i T^A u_j) \varepsilon (\bar{q}_k T^A d_l)$		
Two-quark operators		Baryon- and lepton-number-violating	
$\ddagger O_{u\varphi}^{(ij)}$	$\bar{q}_i u_j \tilde{\varphi} (\varphi^\dagger \varphi)$	$\ddagger O_{quq}^{(ijkl)}$	$(\bar{q}^c_{i\alpha} \varepsilon q_{j\beta})(\bar{u}^c_{k\gamma} e_l) \varepsilon^{\alpha\beta\gamma}$
$O_{\varphi q}^{1(ij)}$	$(\varphi^\dagger \overleftrightarrow{D}_\mu \varphi)(\bar{q}_i \gamma^\mu q_j)$	$\ddagger O_{qqq}^{1(ijkl)}$	$(\bar{q}^c_{i\alpha} \varepsilon q_{j\beta})(\bar{q}^c_{k\gamma} e_l) \varepsilon^{\alpha\beta\gamma}$
$O_{\varphi q}^{3(ij)}$	$(\varphi^\dagger \overleftrightarrow{D}_\mu \varphi)(\bar{q}_i \gamma^\mu \tau^I q_j)$	$\ddagger O_{qqq}^{3(ijkl)}$	$(\bar{q}^c_{i\alpha} \tau^I \varepsilon q_{j\beta})(\bar{q}^c_{k\gamma} \tau^I e_l) \varepsilon^{\alpha\beta\gamma}$
$O_{\varphi u}^{(ij)}$	$(\varphi^\dagger \overleftrightarrow{D}_\mu \varphi)(\bar{u}_i \gamma^\mu u_j)$	$\ddagger O_{duu}^{(ijkl)}$	$(\bar{d}^c_{i\alpha} u_{j\beta})(\bar{u}^c_{k\gamma} e_l) \varepsilon^{\alpha\beta\gamma}$
$\ddagger O_{\varphi ud}^{(ij)}$	$(\varphi^\dagger i D_\mu \varphi)(\bar{u}_i \gamma^\mu d_j)$		
$\ddagger O_{uW}^{(ij)}$	$(\bar{q}_i \sigma^{\mu\nu} \tau^I u_j) \tilde{\varphi} W_{\mu\nu}^I$		
$\ddagger O_{dW}^{(ij)}$	$(\bar{q}_i \sigma^{\mu\nu} \tau^I d_j) \varphi W_{\mu\nu}^I$		
$\ddagger O_{uB}^{(ij)}$	$(\bar{q}_i \sigma^{\mu\nu} u_j) \tilde{\varphi} B_{\mu\nu}$		
$\ddagger O_{uG}^{(ij)}$	$(\bar{q}_i \sigma^{\mu\nu} T^A u_j) \tilde{\varphi} G_{\mu\nu}^A$		

to systematically parameterise possible deviations from the SM predictions in the interactions among the known particles, using minimal theoretical assumptions. It amounts to extend the Lagrangian of the SM, by all higher-dimensional operators that respect the gauge symmetry

$$\mathcal{L}^{\text{SMEFT}} = \mathcal{L}^{\text{SM}} + \sum_{D>4} \sum_i^{N_D} \frac{C_i^{(D)} O_i^{(D)}}{\Lambda^{D-4}}, \quad (61.3)$$

where D is the dimension of the operator $O_i^{(D)}$ and Λ provides an upper bound for the scale of new physics. An EFT model is generally characterised by power counting rules that identify a hierarchy among operators. In the case of the SMEFT, a minimal approach is considered where the large scale Λ provides a universal suppression factor for the higher dimensional operators.

The currently adopted parametrization for SMEFT interpretations of top quark measurements relies on the Warsaw basis of gauge-invariant dimension-six operators [11] and it is presented in Tab. 61.1 as detailed in Ref. [12] (see [13, 14] for early discussions of top-quark related operators). For convenience, often specific degrees of freedom are identified from combinations of Warsaw-basis operator coefficients aligned with the directions of the EFT parameter space which appear in given processes, in interferences with SM amplitudes, and in top-quark interactions with some of the gauge boson mass eigenstates. Model implementations are available for tree-level and even one-loop Monte Carlo simulations.

The definitions of the SMEFT operators can be organised in four categories: Four-quark, two-quark, two-quark-two-lepton, and baryon-lepton-number violating operators. The overwhelming number of four-fermion operators is tamed by adopting simplifying assumptions about beyond-the-standard-model flavor structures. A baseline flavor scenario in the quark sector and motivated by the minimal flavor violation (MFV) ansatz [15–17] corresponds to imposing a $U(2)_q \times U(2)_u \times U(2)_d$ symmetry among the first two generations. In this case the following numbers of degrees of freedom are produced for the operators of each category of field content:

four heavy quarks	11 + 2 CPV
two light and two heavy quarks	14
two heavy quarks and bosons	9 + 6 CPV
two heavy quarks and two leptons	(8 + 3 CPV) \times 3 lepton flavors

where we counted separately CP-conserving and CP-violating (CPV) parameters. They are collected in Table 61.1. Other less restricted scenarios, such as that obtained by imposing $U(2)_{q+u+d}$ symmetry featuring additional 10 + 10 CPV degrees of freedom, or more restricted ones, such as *top-philic* scenario where it is assumed that new physics couples dominantly to the left-handed doublet and right-handed up-type quark singlet of the third generation as well as to bosons, featuring only 19+6 (CPV) degrees of freedom, are often considered. It is also customary to analyse top-quark flavor-changing neutral currents (FCNCs) separately as, at the tree level, they enter only quadratically. More details can be found in Ref. [12].

61.1.2 Decay

As other unstable elementary particles, the lifetime of the top quark, and therefore its width, is perturbatively calculable within the SM. With a mass above the Wb threshold, and $|V_{tb}| \gg |V_{td}|$, $|V_{ts}|$, the decay width of the top quark is expected to be dominated by the two-body channel $t \rightarrow Wb$. Neglecting terms of order m_b^2/m_t^2 , α_s^2 , and $(\alpha_s/\pi)M_W^2/m_t^2$, the width predicted in the SM at NLO is [18]:

$$\Gamma_t = \frac{G_F m_t^3}{8\pi\sqrt{2}} \left(1 - \frac{M_W^2}{m_t^2}\right)^2 \left(1 + 2 \frac{M_W^2}{m_t^2}\right) \left[1 - \frac{2\alpha_s}{3\pi} \left(\frac{2\pi^2}{3} - \frac{5}{2}\right)\right], \quad (61.4)$$

where m_t refers to the top-quark pole mass. The order α_s^2 QCD corrections to Γ_t as well as the EW NLO corrections are known [19, 20], thereby improving the overall theoretical accuracy to better than 1%. As a result, between $m_t = 170$ GeV and 175 GeV the width changes from 1.258 GeV to 1.394 GeV, with a linear dependence ($\alpha_s(M_Z) = 0.1179$ and $m_W = 80.377$ GeV). At the reference value of $m_t = 172.5$ GeV, $\Gamma_t = 1.326$ GeV.

With its correspondingly short lifetime of about 0.5×10^{-24} s, the top quark is expected to decay before top-flavored hadrons

or $t\bar{t}$ -quarkonium-bound states can form [21]. In fact, since the decay time is close to the would-be-resonance binding time, a peak will be visible in e^+e^- scattering at the $t\bar{t}$ threshold [22] and it is in principle present (yet very difficult to measure) in hadron collisions too [23, 24].

As mentioned above, flavor changing neutral interactions are allowed starting at one loop. The branching ratios to charm final state are estimated to be [25, 26]:

$$\begin{aligned} \text{Br}^{\text{SM}}(t \rightarrow gc) &= 5 \cdot 10^{-12}, \text{Br}^{\text{SM}}(t \rightarrow gu) = 4 \cdot 10^{-14}, \\ \text{Br}^{\text{SM}}(t \rightarrow \gamma c) &= 5 \cdot 10^{-14}, \text{Br}^{\text{SM}}(t \rightarrow \gamma u) = 4 \cdot 10^{-16}, \\ \text{Br}^{\text{SM}}(t \rightarrow Zc) &= 1 \cdot 10^{-14}, \text{Br}^{\text{SM}}(t \rightarrow Zu) = 7 \cdot 10^{-17}, \\ \text{Br}^{\text{SM}}(t \rightarrow Hc) &= 3 \cdot 10^{-15}, \text{Br}^{\text{SM}}(t \rightarrow Hu) = 2 \cdot 10^{-17}. \end{aligned}$$

61.1.3 Production

61.1.3.1 Pair production

In hadron collisions, top quarks are produced dominantly in pairs through the processes $q\bar{q} \rightarrow t\bar{t}$ and $gg \rightarrow t\bar{t}$, at leading order in QCD. At the Tevatron ($p\bar{p}$ at 1.96 TeV) approximately 85% of the production cross section is from $q\bar{q}$ annihilation, with the remainder from gluon-gluon fusion. Conversely, at the LHC about 90% (80%) of $t\bar{t}$ production is from gluon-gluon fusion at $\sqrt{s} = 13$ TeV ($\sqrt{s} = 7$ TeV).

Predictions for the top-quark production total cross sections are available at next-to-next-to leading order (NNLO) [27, 28], also including next-to-next-to-leading-log (NNLL) soft gluon resummation. Assuming a top-quark mass of 173.3 GeV, close to the Tevatron + LHC combination [29], the resulting theoretical prediction of the top-quark pair cross-section at NNLO+NNLL accuracy at the Tevatron at $\sqrt{s} = 1.96$ TeV is $\sigma_{t\bar{t}} = 7.16^{+0.11+0.17}_{-0.20-0.12}$ pb where the first uncertainty is from scale dependence and the second from parton distribution functions. At the LHC, assuming a top-quark mass of 172.5 GeV the cross sections are: $\sigma_{t\bar{t}} = 179.6^{+4.8+6.1}_{-6.2-6.1}$ pb at $\sqrt{s} = 7$ TeV, $\sigma_{t\bar{t}} = 256.0^{+6.7+8.0}_{-8.9-8.0}$ pb at $\sqrt{s} = 8$ TeV, $\sigma_{t\bar{t}} = 833.9^{+20.5+21.0}_{-30.0-21.0}$ pb at $\sqrt{s} = 13$ TeV, $\sigma_{t\bar{t}} = 923.6^{+22.6+22.8}_{-33.4-22.8}$ pb at $\sqrt{s} = 13.6$ TeV, and $\sigma_{t\bar{t}} = 985.7^{+24.1+24.1}_{-35.7-24.1}$ pb at $\sqrt{s} = 14$ TeV [27], where the first uncertainty is from scale dependence and the second from parton distribution functions and α_s .

The identification of $t\bar{t}$ events at a collider has to take into account that top quarks decay at microscopic scales and only their decay products can be detected. The final states for the leading pair-production process can be divided into three classes:

- A. $t\bar{t} \rightarrow W^+ b W^- \bar{b} \rightarrow q\bar{q}' b q'' \bar{q}''' \bar{b}$, (45.7%)
- B. $t\bar{t} \rightarrow W^+ b W^- \bar{b} \rightarrow q\bar{q}' b \ell^- \bar{\nu}_\ell \bar{b} + \ell'^+ \nu_\ell b q'' \bar{q}''' \bar{b}$, (43.8%)
- C. $t\bar{t} \rightarrow W^+ b W^- \bar{b} \rightarrow \ell'^+ \nu_\ell b \ell'^- \bar{\nu}_\ell \bar{b}$. (10.5%)

The quarks in the final state evolve into jets of hadrons. A, B, and C are referred to as the all-hadronic, lepton+jets (ℓ +jets), and dilepton ($\ell\ell$) channels, respectively. Their relative contributions, including hadronic corrections, are given in parentheses assuming lepton universality. While ℓ in the above processes refers to e , μ , or τ , most of the analyses distinguish the e and μ from the τ channel, which is more difficult to reconstruct. Therefore, in what follows, we will use ℓ to refer to e or μ , unless otherwise noted. Here, typically leptonic decays of τ are included. In addition to the quarks resulting from the top-quark decays, extra QCD radiation (quarks and gluons) from the colored particles in the event can lead to extra jets.

The number of jets reconstructed in the detectors depends on the decay kinematics, as well as on the algorithm for reconstructing jets used by the analysis. Information on the transverse momenta, p_T of the neutrinos is obtained from the imbalance in transverse momentum measured in each event, the missing p_T , whose magnitude is also called missing transverse energy, E_T .

61.1.3.2 Single top production

Electroweak single top-quark production mechanisms, namely from $q\bar{q}' \rightarrow t\bar{b}$ [30], $qb \rightarrow q't$ [31], mediated by virtual s -channel and t -channel W -bosons, and Wt -associated production, through $bg \rightarrow W^- t$, lead to somewhat smaller cross sections. For example, t -channel production, while suppressed by the weak coupling with respect to the strong pair production, is kinematically

enhanced, resulting in a sizeable cross section both at Tevatron and LHC energies. At the Tevatron, the t - and s -channel cross sections for top quarks are identical to those for antitop quarks, while at the LHC they are not, due to the charge-asymmetric initial state. NNLO cross sections for t -channel single top-quark production ($t + \bar{t}$) are calculated for $m_t = 173.2$ GeV to be $2.08^{+0.04+0.08}_{-0.03-0.10}$ pb in $p\bar{p}$ collisions at $\sqrt{s} = 1.96$ TeV, where the first uncertainty is from scale dependence and the second from parton distribution functions. [32]. A calculation at NNLO accuracy for the t -channel cross section at the LHC has first appeared in [33], superseded by more recent calculations [32, 34] which predict ($m_t = 172.5$ GeV): $\sigma_{t+\bar{t}} = 30.3^{+0.4+0.6}_{-0.3-0.4}$ pb at $\sqrt{s} = 5.02$ TeV, $\sigma_{t+\bar{t}} = 63.7^{+0.9+1.1}_{-0.5-0.7}$ pb at $\sqrt{s} = 7$ TeV, $\sigma_{t+\bar{t}} = 84.3^{+1.1+1.4}_{-0.7-0.9}$ pb at $\sqrt{s} = 8$ TeV, $\sigma_{t+\bar{t}} = 214.2^{+2.4+3.3}_{-1.7-2.0}$ pb at $\sqrt{s} = 13$ TeV, $\sigma_{t+\bar{t}} = 232.2^{+2.6+3.4}_{-1.7-2.2}$ pb at $\sqrt{s} = 13.6$ TeV, and $\sigma_{t+\bar{t}} = 244.5^{+2.7+3.5}_{-2.0-2.5}$ pb at $\sqrt{s} = 14$ TeV, where the first uncertainty is from scale dependence and the second from parton distribution functions and α_s . The corresponding fraction of top quarks are 67%, 65%, 65%, 63%, 62%, and 62%. For the s -channel, NNLO approximated calculations yield $1.03^{+0.05}_{-0.05}$ pb for the Tevatron [35]. An NNLO calculation gives ($t + \bar{t}$), $3.00^{+0.03}_{-0.03}$ pb, $3.61^{+0.03}_{-0.03}$ pb, $6.84^{+0.06}_{-0.06}$ pb, and $7.25^{+0.06}_{-0.04}$ pb, for $\sqrt{s} = 7, 8, 13, 13.6$ TeV at the LHC, respectively, where the uncertainty is from scale dependence only. While negligible at the Tevatron, at LHC energies Wt -associated production becomes relevant. At $\sqrt{s} = 7, 8, 13, 13.6, 14$ TeV, an NLO+NNLL calculation gives ($t + \bar{t}$), $17.1^{+0.4+0.7}_{-0.3-0.7}$ pb, $24.4^{+0.6+0.9}_{-0.5-0.9}$ pb, $79.3^{+1.9+2.2}_{-1.8-2.2}$ pb, $87.9^{+2.0+2.3}_{-1.9-2.4}$ pb, and $93.8^{+2.2+2.5}_{-2.1-2.5}$ pb, respectively, where the first uncertainty is from scale dependence and the second from parton distribution functions and α_s . In this process, an equal proportion of top and anti-top quarks is foreseen. [36].

Assuming $|V_{tb}| \gg |V_{td}|, |V_{ts}|$ (see the Section “The CKM Quark-Mixing Matrix” in this Review for more information), the cross sections for single top production are proportional to $|V_{tb}|^2$, and no extra hypothesis is needed on the number of quark families or on the unitarity of the CKM matrix in extracting $|V_{tb}|$. Separate measurements of the s - and t -channel processes provide sensitivity to physics beyond the Standard Model [37].

The identification of top quarks in the electroweak single top channel is much more difficult than in the QCD $t\bar{t}$ channel, due to a less distinctive signature and significantly larger backgrounds, mostly due to $t\bar{t}$ and W +jets production.

61.1.3.3 Monte Carlo predictions

Fully exclusive predictions via Monte Carlo generators for the $t\bar{t}$ and single top production processes at NLO accuracy in QCD, including top-quark decays and possibly off-shell effects are available [38, 39] through the MC@NLO [40] and POWHEG [41] methods. Recently, the first Monte Carlo implementation of the NNLO QCD computation has become available [42].

61.1.3.4 Associated production

Besides fully inclusive QCD or EW top-quark production, more exclusive final states can be accessed at hadron colliders, whose cross sections are typically much smaller, yet can provide key information on the properties of the top quark. For all relevant final states (*e.g.*, $t\bar{t}V$, $t\bar{t}VV$ with $V = \gamma, W, Z$, $t\bar{t}H$, $t\bar{t}$ +jets, $t\bar{t}b\bar{b}$, $t\bar{t}t\bar{t}$) automatic or semi-automatic predictions at NLO accuracy both in QCD and EW expansions, also in the form of event generators are available (see the review “Monte Carlo event generators” for more information). Results for total cross sections at NLO+NNLL in QCD and NLO EW, are available for $t\bar{t}Z$, $t\bar{t}W$, $t\bar{t}H$ [43] and for $t\bar{t}t\bar{t}$ [44]. Recently, approximate NNLO QCD predictions for and $t\bar{t}H$ and $t\bar{t}W$ have become available [45, 46].

61.2 Top-quark and precision SM tests

Since the discovery of the top quark, direct measurements of $t\bar{t}$ production have been made at seven center-of-mass energies in pp or $p\bar{p}$ and in pPb or $PbPb$ collisions, providing stringent tests of QCD and electroweak theory including parton distribution functions, the strong coupling α_s and the dependence on the top-quark mass m_{top} . The first measurements were made in Run I at the Tevatron at $\sqrt{s} = 1.8$ TeV. In Run II at the Tevatron

relatively precise measurements were made at $\sqrt{s} = 1.96$ TeV. Finally, beginning in 2010, measurements have been made at the LHC at $\sqrt{s} = 7$ TeV, $\sqrt{s} = 8$ TeV, and $\sqrt{s} = 13$ TeV, later also in dedicated low energy runs at $\sqrt{s} = 5.02$ TeV in pp and at $\sqrt{s} = 5.02$ TeV in $PbPb$ collisions and at 8.16 TeV in pPb collisions and recently at $\sqrt{s} = 13.6$ TeV in pp . With the enormous number of over 120 million top quark pairs produced at the LHC, we are entering the era of high precision measurements in the top quark sector.

Production of single top quarks through electroweak interactions has now been measured with good precision at the Tevatron at $\sqrt{s} = 1.96$ TeV, and at the LHC at $\sqrt{s} = 5$ TeV, $\sqrt{s} = 7$ TeV, $\sqrt{s} = 8$ TeV, and also at $\sqrt{s} = 13$ TeV. Measurements at the Tevatron have managed to separate the s - and t -channel production cross sections, and at the LHC, the tW mechanism as well, though the t -channel is measured with best precision to date. The measurements allow an extraction of the CKM matrix element V_{tb} . Also more exclusive production modes and top-quark properties have been measured in single-top production.

With approximately 10 fb^{-1} of Tevatron data, and 255 pb^{-1} at 5 TeV, almost 5 fb^{-1} at 7 TeV, 20 fb^{-1} at 8 TeV, 139 fb^{-1} at 13 TeV and 29 fb^{-1} at 13.6 TeV at the LHC, many properties of the top quark have been measured with high precision. These include properties related to the production mechanism, such as $t\bar{t}$ spin correlations, forward-backward or charge asymmetries, and differential production cross sections, as well as properties related to the tWb decay vertex, such as the helicity of the W -bosons from the top-quark decay. Also studies of the $t\bar{t}b\bar{b}$, $t\bar{t}t\bar{t}$, $t\bar{t}\gamma$, $t\bar{t}Z$, $t\bar{t}h$, th , tZq , $t\gamma q$ or tWZ processes and the corresponding vertices as well as contact interactions have been made, most yielding observations, while first evidence for tWZ has been found and th is still far from evidence. Those processes probe genuinely new aspects of the top-quark such as electroweak couplings to neutral gauge bosons or possibly four-top-quark production via contact interactions. Recently, also first studies for the very fundamental concept of quantum entanglement in top-quark production were pursued. In addition, many searches for physics beyond the Standard Model are being performed with increasing reach in both production and decay channels.

In the following sections we review the current status of measurements of the characteristics of the top quark.

61.2.1 Top-quark production

61.2.1.1 $t\bar{t}$ production

Fig. 61.1 summarizes the $t\bar{t}$ production cross-section measurements from both, the Tevatron and LHC. Please note that some cross section measurements at the LHC have luminosity-related uncertainties which have improved in the meantime [47]. The latest measurement from DØ [48] ($p\bar{p}$ at $\sqrt{s} = 1.96$ TeV), combining the measurements from the dilepton and lepton plus jets final states in 9.7 fb^{-1} , is 7.26 ± 0.13 (stat.) $^{+0.57}_{-0.50}$ (syst.) pb (7.5%). From CDF the most precise measurement made [49] is in 8.8 fb^{-1} in the dilepton channel requiring at least one b -tag, yielding 7.09 ± 0.84 pb. Both of these measurements assume a top-quark mass of $172.5 \text{ GeV}/c^2$. The dependence of the cross-section measurements on the value chosen for the mass is less than that of the theory calculations because it only affects the determination of the acceptance. In some analyses also the shape of topological variables might be modified.

Combining the recent cross section measurements with older ones in other channels yields $\sigma_{t\bar{t}} = 7.63 \pm 0.50$ pb (6.6%) for CDF, $\sigma_{t\bar{t}} = 7.56 \pm 0.59$ pb (7.8%) for DØ and $\sigma_{t\bar{t}} = 7.60 \pm 0.41$ pb (5.4%) for the Tevatron combination [50]. The contributions to the uncertainty are 0.20 pb from statistical sources, 0.29 pb from systematic sources, and 0.21 pb from the uncertainty on the integrated luminosity. The combined result is in good agreement with the SM expectation of $7.35^{+0.28}_{-0.33}$ pb at NNLO+NNLL in perturbative QCD [27] for a top mass of $172.5 \text{ GeV}/c^2$.

CDF has measured the $t\bar{t}$ production cross section in the dilepton channel with one hadronically decaying tau in 9.0 fb^{-1} , yielding $\sigma_{t\bar{t}} = 8.1 \pm 2.1$ pb. By separately identifying the single-tau and the ditau components, they measure the branching fraction of the top quark into the tau lepton, tau neutrino, and bottom quark

to be $(9.6 \pm 2.8)\%$ [51]. CDF has also performed measurements of the $t\bar{t}$ production cross section normalized to the Z production cross section in order to reduce the impact of the luminosity uncertainty [52].

DØ has performed a measurement of differential $t\bar{t}$ cross sections in 9.7 fb^{-1} of lepton+jets data as a function of the transverse momentum, and absolute value of the rapidity of the top quarks as well as of the invariant mass of the $t\bar{t}$ pair [53]. Observed differential cross sections are consistent with SM predictions.

The LHC experiments ATLAS and CMS use similar techniques to measure the $t\bar{t}$ cross section in pp collisions. The most precise measurements typically come from the dilepton channel, and in particular the $e\mu$ channel. In order to test consistency of the cross-section measurements with some systematic uncertainties cancelling out while testing pQCD and PDFs, cross-section ratios between measurements at 7 TeV and at 8 TeV are performed and quoted in several cases. In other cases, the cross-section ratio between $t\bar{t}$ - and Z -production is determined as that is independent of luminosity uncertainties, but keeps its sensitivity to the ratio of gluon versus quark PDFs. These experimental results should be compared to the theoretical calculations at NNLO+NNLL that yield $7.16^{+0.20}_{-0.23}$ pb for top-quark mass of $173.3 \text{ GeV}/c^2$ at $\sqrt{s} = 1.96$ TeV [27], for top-quark mass of $172.5 \text{ GeV}/c^2$ $\sigma_{t\bar{t}} = 68.2^{+5.2}_{-15.4}$ pb at $\sqrt{s} = 5$ TeV [54], $\sigma_{t\bar{t}} = 158^{+23}_{-24}$ pb at $\sqrt{s} = 7$ TeV [55, 56], $\sigma_{t\bar{t}} = 253^{+13}_{-15}$ pb at $\sqrt{s} = 8$ TeV [27, 54, 57–60], $\sigma_{t\bar{t}} = 832.0^{+46}_{-51}$ pb at $\sqrt{s} = 13$ TeV [27, 54, 58–60], $\sigma_{t\bar{t}} = 924^{+32}_{-40}$ pb at $\sqrt{s} = 13.6$ TeV [27, 57–61]. Unless noted otherwise, the theoretical prediction is in agreement with the measurements. Both are aiming for further improvements in precision. The exact details of the measurements such as the top-quark mass assumption at which the cross section values are quoted can be found in the original publications.

$\sqrt{s} = 5.02$ TeV measurements: In a special run, ATLAS recorded 257 pb^{-1} . The $t\bar{t}$ cross-section is measured in both the dilepton and single-lepton final states of the $t\bar{t}$ system and then combined. The combination of the two measurements yields $\sigma_{t\bar{t}} = 67.5 \pm 0.9$ (stat.) ± 2.3 (syst.) ± 1.1 (lumi.) ± 0.2 (beam) pb [62], giving a total uncertainty of 3.9%. The result is in agreement with theoretical QCD calculations at NLO in the strong coupling constant, including the resummation of NNLL soft-gluon terms, and constrains the parton distribution functions of the proton at large Bjorken- x . CMS has measured the $t\bar{t}$ production cross section, accumulating 27.4 pb^{-1} of data. The measurement is performed by analyzing events with at least one charged lepton. The measured cross section is $\sigma_{t\bar{t}} = 69.5 \pm 8.4$ pb [63], with a relative precision of 12%, in agreement with the expectation from the Standard Model. The impact of the presented measurement on the determination of the gluon distribution function is also investigated. In addition, they performed a measurement in opposite-sign $e\mu$ dilepton events with at least two jets using 302 pb^{-1} . They obtain a Drell-Yan scale factor under the Z -boson mass to estimate the background and extract a cross section using a counting technique of $\sigma_{t\bar{t}} = 60.7 \pm 5.0$ (stat.) ± 2.8 (syst.) ± 1.1 (lumi) pb. A combination with the result in the single lepton + jets channel is performed, yielding $\sigma_{t\bar{t}} = 63.0 \pm 4.1$ (stat.) ± 3.0 (syst + lumi) pb [64].

$\sqrt{s} = 7$ TeV measurements: At $\sqrt{s} = 7$ TeV, ATLAS uses the full dataset of 4.6 fb^{-1} of $e\mu$ events, yielding $\sigma_{t\bar{t}} = 182.9 \pm 7.1$ pb, corresponding to 3.9% precision [65]. Other measurements by ATLAS include a measurement in 0.7 fb^{-1} in the lepton+jets channel [66], in the dilepton channel [67], and in 1.02 fb^{-1} in the all-hadronic channel [68], which together yield a combined value of $\sigma_{t\bar{t}} = 177 \pm 3$ (stat.) $^{+3}_{-2}$ (syst.) ± 7 (lumi.) pb (6.2%) [69]. Further analyses in the hadronic τ plus jets channel in 1.67 fb^{-1} [70] and the hadronic $\tau +$ lepton channel in 2.05 fb^{-1} [71], and the all-hadronic channel in 4.7 fb^{-1} [72] yield consistent albeit less precise results. Recently, ATLAS performed a cross section measurement in the lepton+jets channel using 4.6 fb^{-1} using a three-class, multidimensional event classifier based on support vector machines to differentiate $t\bar{t}$ events from $W/Z + b\bar{b}$ and other background processes, yielding $\sigma_{t\bar{t}} = 168.5 \pm 0.7$ (stat.) $^{+6.2}_{-5.9}$ (syst.) $^{+3.4}_{-3.2}$ (lumi.) pb [73].

CMS measures the $t\bar{t}$ cross section in the dilepton channel us-

ing 2.3 fb^{-1} to $\sigma_{t\bar{t}} = 161.9 \pm 2.5(\text{stat.})_{-5.0}^{+5.1}(\text{syst.}) \pm 3.6(\text{lumi.})$ pb, corresponding to a 4.2% precision [74]. The most precise measurement from CMS is also obtained in the dilepton channel using 5 fb^{-1} , where they measure $\sigma_{t\bar{t}} = 173.6 \pm 2.1(\text{stat.})_{-4.0}^{+4.5}(\text{syst.}) \pm 3.8(\text{lumi.})$ pb, corresponding to a 3.6% precision [75]. Other measurements use 2.3 fb^{-1} in the e/μ +jets channel [76], with 3.5 fb^{-1} in the all-hadronic channel [77], with 2.2 fb^{-1} in the lepton+ τ channel [78], and with 3.9 fb^{-1} in the τ +jets channel [79]. ATLAS and CMS also provide a legacy combined cross section of $\sigma_{t\bar{t}} = 178.5 \pm 4.7$ pb using 5 fb^{-1} , yielding a precision of 2.6% [80].

$\sqrt{s} = 8 \text{ TeV}$ measurements: At $\sqrt{s} = 8 \text{ TeV}$, ATLAS measures the $t\bar{t}$ cross section with 20.3 fb^{-1} using $e\mu$ dilepton events, with a simultaneous measurement of the b -tagging efficiency, yielding $\sigma_{t\bar{t}} = 242.9 \pm 1.7(\text{stat.}) \pm 5.5(\text{syst.}) \pm 5.1(\text{lumi.}) \pm 4.2(\text{beam energy})$ pb [81] (3.6% precision). In the $\ell + \text{jets}$ channel, they measure $\sigma_{t\bar{t}} = 260 \pm 1(\text{stat.})_{-23}^{+20}(\text{syst.}) \pm 8(\text{lumi.}) \pm 4(\text{beam energy})$ pb [82] in 20.3 fb^{-1} using a likelihood discriminant fit and b -jet identification. Subsequently, ATLAS performed a new analysis in 20.2 fb^{-1} using $\ell + \text{jets}$ events. They model the W +jets background using Z +jets data and employ neural networks in three jet-multiplicity and b -jet multiplicity regions for the signal and background separation, yielding $\sigma_{t\bar{t}} = 248.3 \pm 0.7(\text{stat.}) \pm 13.4(\text{syst.}) \pm 4.7(\text{lumi.})$ pb [83]. ATLAS also performed a cross section measurement in the hadronic τ +jets channel yielding consistent, albeit less precise results [84].

CMS performs a template fit to the M_{lb} mass distribution using 19.6 fb^{-1} in the lepton+jets channel yielding $\sigma_{t\bar{t}} = 228.5 \pm 3.8(\text{stat.}) \pm 13.7(\text{syst.}) \pm 6.0(\text{lumi.})$ pb [85] (6.7% precision). In the $e\mu$ channel, initially using 5.3 fb^{-1} [86] the cross sections are extracted using a binned likelihood fit to multi-differential final state distributions related to identified b quark and other jets in the event, yielding $\sigma_{t\bar{t}} = 239 \pm 2(\text{stat.}) \pm 11(\text{syst.}) \pm 6(\text{lumi.})$ pb (5.3% precision). Later, they also use the full dataset of 19.7 fb^{-1} , yielding $\sigma_{t\bar{t}} = 244.9 \pm 1.4(\text{stat.})_{-5.5}^{+6.3}(\text{syst.}) \pm 6.4(\text{lumi.})$ pb (3.7% precision) [75]. This most precise CMS measurement at 8 TeV is also used to determine the top pole mass and set SUSY limits. The cross section is also measured in the hadronic τ +jets channel, yielding $\sigma_{t\bar{t}} = 257 \pm 3(\text{stat.}) \pm 24(\text{syst.}) \pm 7(\text{lumi.})$ pb [87] and in the all-hadronic final state giving $\sigma_{t\bar{t}} = 275.6 \pm 6.1(\text{stat.}) \pm 37.8(\text{syst.}) \pm 7.2(\text{lumi.})$ pb [88]. In combination of the most precise $e\mu$ measurements in $5.3 - 20.3 \text{ fb}^{-1}$, ATLAS and CMS together yield $\sigma_{t\bar{t}} = 241.5 \pm 1.4(\text{stat.}) \pm 5.7(\text{syst.}) \pm 6.2(\text{lumi.})$ pb [89] (3.5% precision), challenging the precision of the corresponding theoretical predictions. ATLAS and CMS also provide a legacy combined cross section of $\sigma_{t\bar{t}} = 243.3_{-5.9}^{+6.0}$ pb using 20 fb^{-1} (2.5% precision) [80]. The combinations also provide the ratio between cross sections at 8 and 7 TeV, the top quark pole mass, and the strong coupling.

The LHCb collaboration presented the first observation of top-quark production in the forward region in pp -collisions in the e +jets or μ +jets channel. The results are based on data corresponding to integrated luminosities of 1.0 and 2.0 fb^{-1} collected at center-of-mass energies of 7 and 8 TeV by LHCb. The inclusive top quark production cross sections in the fiducial region are $\sigma_{t\bar{t}} = 239 \pm 53(\text{stat.}) \pm 38(\text{syst.})$ pb at 7 TeV, and $\sigma_{t\bar{t}} = 289 \pm 43(\text{stat.}) \pm 46(\text{syst.})$ pb at 8 TeV [90].

$\sqrt{s} = 13 \text{ TeV}$ measurements: In 36.1 fb^{-1} of $e\mu$ data with one or two b -tags, ATLAS measures $\sigma_{t\bar{t}} = 826.4 \pm 3.6(\text{stat.}) \pm 11.5(\text{syst.}) \pm 15.7(\text{lumi.}) \pm 1.9(\text{beam})$ pb (2.4% precision). This measurement is also used to determine the top quark pole mass and to derive ratios and double ratios of $t\bar{t}$ and Z cross-sections at different energies as well as absolute and normalised differential cross-sections as functions of single lepton and dilepton kinematic variables [91]. In the $\ell + \text{jets}$ channel, using 85 pb^{-1} , the cross-section is extracted by counting the number of events with exactly one e or μ and at least four jets, at least one of which is identified as originating from a b -quark, yielding $\sigma_{t\bar{t}} = 817 \pm 13(\text{stat.}) \pm 103(\text{syst.}) \pm 88(\text{lumi.})$ pb [92]. Later, ATLAS measures the inclusive $t\bar{t}$ cross section in 139 fb^{-1} in the $\ell + \text{jets}$ through a profile-likelihood fit to be $\sigma_{t\bar{t}} = 830.4 \pm 0.4(\text{stat.}) \pm 36(\text{syst.}) \pm 14(\text{lumi.})$ pb (4.6% precision) [93].

Recently, using the complete Run-2 dataset of 140 fb^{-1} in events containing an oppositely charged $e\mu$ pair and b -tagged

jets, ATLAS has presented their legacy measurement of $\sigma_{t\bar{t}} = 829 \pm 1(\text{stat.}) \pm 13(\text{syst.}) \pm 8(\text{lumi.}) \pm 2(\text{beam})$ pb [94], corresponding to a precision of 1.8%. They also measure differential and double-differential distributions of kinematic variables of leptons from decays of top-quark pairs. The results are compared with predictions from several Monte Carlo generators. While no prediction is found to be consistent with all distributions, a better agreement with measurements of the lepton p_T distributions is obtained by reweighting the $t\bar{t}$ sample so as to reproduce the top-quark p_T distribution from an NNLO calculation.

Using 35.9 fb^{-1} of dilepton data, they use a likelihood fit and yield $\sigma_{t\bar{t}} = 803 \pm 2(\text{stat.}) \pm 25(\text{syst.}) \pm 20(\text{lumi.})$ pb (4.0%). This result is also used to extract the top quark mass in both the pole and the $\overline{\text{MS}}$ schemes at NNLO and the strong coupling constant [95]. Using the same dataset in the dilepton channel with a hadronically decaying τ , they measure $\sigma_{t\bar{t}} = 781 \pm 7(\text{stat.}) \pm 62(\text{syst.}) \pm 20(\text{lumi.})$ pb (8.3%) [96]. A first measurement of the total inclusive and the normalized differential cross section in the $\ell + \text{jets}$ channel is made in 42 pb^{-1} yielding $\sigma_{t\bar{t}} = 836 \pm 27(\text{stat.}) \pm 88(\text{syst.}) \pm 100(\text{lumi.})$ pb [97]. Using 2.2 fb^{-1} of data, $\ell + \text{jets}$ events are categorized according to the accompanying jet multiplicity. From a likelihood fit to the invariant mass distribution of the isolated lepton and a b -jet, the cross section is measured to be $\sigma_{t\bar{t}} = 888 \pm 2(\text{stat.})_{-28}^{+26}(\text{syst.}) \pm 20(\text{lumi.})$ pb [98]. This result is also used to extract the top-quark mass. Using the full Run-2 dataset of 137 pb^{-1} , CMS measures the $t\bar{t}$ cross section in four regions determined by top p_T and b -tag score in the $\ell + \text{jets}$ channel. They employ a combined χ^2 fit considering the migration matrices. Most of the measured differential cross sections are well described by standard model predictions with the exception of some double-differential distributions. They obtain $\sigma_{t\bar{t}} = 791 \pm 1(\text{stat.}) \pm 21(\text{syst.}) \pm 14(\text{lumi.})$ pb (3.2%) [99]. In the all-hadronic channel, CMS uses 2.53 fb^{-1} of data, yielding a cross section of $\sigma_{t\bar{t}} = 834 \pm 25(\text{stat.})_{-104}^{+118}(\text{syst.}) \pm 23(\text{lumi.})$ pb [100]. Also differential cross sections as a function of the leading top quark transverse momentum are measured. Very recently, CMS presents a first search for the central exclusive production of $t\bar{t}$ pairs using proton-tagged events, using 29.4 fb^{-1} . The $t\bar{t}$ decay products are reconstructed using the central CMS detector, while forward protons are measured in the CMS-TOTEM precision proton spectrometer. An observed (expected) upper bound on the production cross section of 0.59 (1.14) pb [101] is set at 95% confidence level, for collisions of protons with fractional momentum losses between 2 and 20%.

Using 1.93 fb^{-1} , LHCb studies forward top quark pair production in pp collisions in the $\mu e b$ final state. The cross-section is measured in a fiducial region defined by both leptons transverse momenta and pseudorapidities as well as their angular separation, the b -jet transverse momentum and its angular separation from the leptons, yielding $\sigma_{t\bar{t}} = 126 \pm 19(\text{stat.}) \pm 16(\text{syst.}) \pm 5(\text{lumi.})$ fb [102].

$\sqrt{s} = 13.6 \text{ TeV}$ measurements: Being one year into the Run-3 data taking at $\sqrt{s} = 13.6 \text{ TeV}$ with an expected increase in the $t\bar{t}$ cross section by approximately 10%, both experiments, ATLAS and CMS, present the first $t\bar{t}$ cross section measurements already.

ATLAS uses 29 fb^{-1} of data in events with an opposite-charge $e\mu$ pair and b -tagged jets to obtain $\sigma_{t\bar{t}} = 850 \pm 3(\text{stat.}) \pm 18(\text{syst.}) \pm 20(\text{lumi.})$ pb. Simultaneously, the Z -boson cross section is determined for inclusive e^+e^- and $\mu^+\mu^-$ events in a fiducial phase space, taking cancellation of several systematic uncertainties into account yielding for the ratio $R_{t\bar{t}/Z} = 1.145 \pm 0.003(\text{stat.}) \pm 0.021(\text{syst.}) \pm 0.002(\text{lumi.})$ [103].

CMS presents the first measurement at this energy using 1.21 fb^{-1} in events with one or two charged leptons (e or μ) and additional jets. A maximum likelihood fit is performed in event categories defined by the number and flavors of the leptons, the number of jets, and the number of jets identified as originating from b quarks. An inclusive $t\bar{t}$ production cross section of $881 \pm 23(\text{stat.}) \pm 20(\text{lumi.})$ pb is measured [104].

proton-lead pPb and lead-lead $PbPb$ heavy ion collision measurements: CMS establishes first evidence for the production of top-quark pairs in $PbPb$ collision data at a nucleon-nucleon

center-of-mass energy of 5.02 TeV using events with charged leptons (electrons or muons) and bottom quarks. They obtain $\sigma_{t\bar{t}} = 2.54^{+0.84}_{-0.74} \mu\text{b}$ [105]. CMS also performed a measurement of top-quark pair production in proton-lead pPb heavy ion collisions at $\sqrt{s} = 8.16$ TeV in 174 nb^{-1} of lepton+jets events. They measure a cross section of $\sigma_{t\bar{t}} = 45 \pm 8$ nb [106]. Recently, also ATLAS presents a $t\bar{t}$ cross section measurement in 165 nb^{-1} of pPb collisions at $\sqrt{s} = 8.16$ TeV in the lepton+jets and the dilepton channels, with a significance well over 5 standard deviations in both channels separately, yielding a combination of $\sigma_{t\bar{t}} = 57.9 \pm 2.0(\text{stat.})^{+4.9}_{-4.5}(\text{syst.})$ nb (9%) [107]. Both measurements are consistent with pQCD calculations and with the scaled pp data.

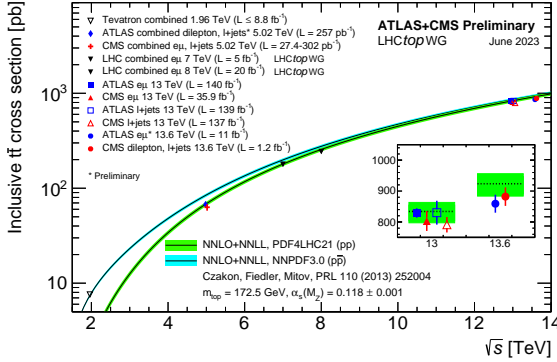


Figure 61.1: Measured and predicted $t\bar{t}$ production cross sections from Tevatron energies in $p\bar{p}$ collisions to LHC energies in pp collisions. The plot is kindly provided by the LHCTopWG working group, status as of June 2023, see <https://twiki.cern.ch/twiki/bin/view/LHCPhysics/LHCTopWGSummaryPlots>.

In Fig. 61.1, one sees the importance of $p\bar{p}$ at Tevatron energies where the valence antiquarks in the antiprotons contribute to the dominant $q\bar{q}$ production mechanism. At LHC energies, the dominant production mode is gluon-gluon fusion and the pp - $p\bar{p}$ difference nearly disappears. The excellent agreement of these measurements with the theory calculations is a strong validation of QCD and the soft-gluon resummation techniques employed in the calculations. The measurements reach high precision and provide stringent tests of pQCD calculations at NNLO+NNLL level including their respective PDF uncertainties.

Most of these measurements assume a $t \rightarrow Wb$ branching ratio of 100%. CDF and DØ have made direct measurements of the $t \rightarrow Wb$ branching ratio [108, 109]. Comparing the number of events with 0, 1 and 2 tagged b jets in the lepton+jets channel, and also in the dilepton channel, using the known b -tagging efficiency, the ratio $R = B(t \rightarrow Wb) / \sum_{q=d,s,b} B(t \rightarrow Wq)$ can be extracted. In 5.4 fb^{-1} of data, DØ measures $R = 0.90 \pm 0.04$, which is 2.5 standard deviations from unity. The currently most precise measurement was made by CMS in 19.7 fb^{-1} at $\sqrt{s} = 8$ TeV. They find $R = 1.014 \pm 0.003(\text{stat.}) \pm 0.032(\text{syst.})$ and $R > 0.955$ at 95% C.L. [110]. A significant deviation of R from unity would imply either non-SM top-quark decay (for example a flavor-changing neutral-current decay), or a fourth generation of quarks. The latter is excluded by other measurements.

61.2.1.2 Differential $t\bar{t}$ cross sections

Thanks to the large available event samples, the Tevatron and the LHC experiments also performed single-, double- or recently even triple-differential cross-section measurements in $t\bar{t}$ production. Such measurements are crucial, as they allow even more stringent tests of perturbative QCD as description of the production mechanism, and allow along with other data the extraction of PDFs in PDF fits. In addition, they enhance the sensitivity to possible new physics contributions, especially now that NNLO predictions for the main differential observables in $t\bar{t}$ prediction have become available [111] and later confirmed [28]. Furthermore, such measurements reduce the uncertainty in the descrip-

tion of $t\bar{t}$ production as background in Higgs physics and searches for rare processes or beyond Standard Model physics.

Differential cross sections are typically measured by a selection of candidate events, their kinematic reconstruction and subsequent unfolding of the obtained event counts in bins of kinematic distributions in order to correct for detector resolution effects, acceptance and migration effects. In some cases a bin-by-bin unfolding is used, while other analyses use more sophisticated techniques. Most commonly used unfolding techniques are the iterative Bayesian unfolding (IBU) [112] as implemented in the **RoUnfold** package [113] and the profile-likelihood unfolding [114] [115], but also a singular value composition approach [116] or maximum likelihood fit methods [117] are used. As general feature across channels, it is found that the measured top quark p_T spectrum is significantly softer than the NLO+PS theory predictions considered in the corresponding publications.

$\sqrt{s} = 7$ TeV measurements: At $\sqrt{s} = 7$ TeV, ATLAS and CMS measure single-differential $t\bar{t}$ cross sections with respect to jet multiplicity, the top-quark transverse momentum, and of the mass, transverse momentum and rapidity of the top quark, the antitop quark as well as the $t\bar{t}$ system or kinematic properties of the final-state charged leptons and jets associated to b -quarks. While CMS finds in general good agreement with the pQCD calculations [118–120], ATLAS finds the data to be softer, in particular in the $t\bar{t}$ mass and the top-quark p_T than the **Alpgen+Herwig** generator. Also some disagreement in the rapidity spectrum is observed indicating a preference for the HERAPDF1.5 pdf set over CT10 [121–123].

$\sqrt{s} = 8$ TeV measurements: At $\sqrt{s} = 8$ TeV, ATLAS measures single-differential cross sections in the dilepton and lepton+jets channel with respect to the mass, the transverse momentum and the rapidity of the $t\bar{t}$ system and event-level kinematic observables [124] [125]. The results are consistent or in fair agreement with the predictions over a wide kinematic range. Predictions beyond NLO accuracy improve the agreement with data at high top-quark transverse momenta. Using the current settings in the Monte Carlo programs and parton distribution functions, improve the agreement with the rapidity distributions. ATLAS also performs a dedicated differential $t\bar{t}$ cross-section measurement of highly boosted top quarks in the lepton+jets channel, where the hadronically decaying top quark has a transverse momentum above 300 GeV [126]. Jet substructure techniques are employed to identify top quarks, which are reconstructed with an anti- k_t jet with a radius parameters $R = 1.0$. The predictions of NLO and LO matrix element plus parton shower Monte Carlo generators are found to generally overestimate the measured cross sections.

CMS measures normalized differential cross sections for $t\bar{t}$ production in lepton+jets events with respect to four kinematic event variables: the missing transverse energy; the scalar sum of the jet transverse momentum (p_T); the scalar sum of the p_T of all objects in the event; and the p_T of leptonically decaying W bosons from top quark decays [119]. Using 19.7 fb^{-1} , they measure the normalized differential cross section in the lepton+jets (e/μ +jets) and in the dilepton (e^+e^- , $\mu^+\mu^-$, and $e^\pm\mu^\pm$) decay channels as a function of the kinematic properties of the charged leptons, the jets associated to b quarks, the top quarks, and the $t\bar{t}$ system. The data are compared with several predictions from perturbative QCD up to approximate next-to-next-to-leading-order precision [127]. Using the same dataset, in the dilepton $e\mu$ channel, they measure normalized double-differential cross sections for $t\bar{t}$ production as a function of various pairs of observables characterizing the kinematics of the top quark and $t\bar{t}$ system [128]. This result has a significant impact on the gluon distribution when included in PDF fits. Overall agreement is observed with the predictions, which is improved when the latest parton distribution functions are used [128]. They also perform a dedicated boosted-top analysis in the e or μ +jets channel where the hadronically decaying top quark is reconstructed as a single large-radius jet and identified as a top candidate using jet substructure techniques [129].

$\sqrt{s} = 13$ TeV measurements: At $\sqrt{s} = 13$ TeV, ATLAS measures the differential $t\bar{t}$ cross section in the lepton+jets and the dilepton channel as a function of the transverse momentum

and absolute rapidity of the top quark, and of the transverse momentum, absolute rapidity and invariant mass of the $t\bar{t}$ system [130] [131] [91]. They find in general good agreement with the theory models with the exception of the Powheg-Box+ Herwig++ predictions, which differ significantly from the data in both the transverse momentum of the top quark and the mass of the $t\bar{t}$ system. ATLAS measures the single- and double-differential $t\bar{t}$ cross-section in the lepton + jets channel at particle and parton level. Two topologies, resolved and boosted, are considered [132]. In the all-hadronic channel, measurements are presented in the boosted regime [133] as well as in the resolved regime with six separately resolved jets [134].

Using the full Run-2 dataset of 140 fb⁻¹, ATLAS measures differential cross sections in the $\ell + jets$ channel and fully hadronic channels in a boosted topology with at least one large- R “top-jet” from a hadronic decay with high- p_T , also as a function of variables that characterise the additional radiation in the events [135]. The measured distribution of the top-quark p_T is used to set limits on the Wilson coefficients describing physics beyond the standard model. The modelling of the additional radiation events show some mild disagreements to the data. Further differential cross-section measurements were made that are specifically useful for MC generator tuning. This includes the ATLAS measurement of the one- and two-dimensional differential cross-sections for eight substructure variables, defined using only the charged components of the jets, in a particle-level phase space by correcting for the smearing and acceptance effects induced by the detector [136] [94]. The QCD predictions for measures of energy-flow are found to be in good agreement with the measurements while variables sensitive to the three-body structure of the top-quark jets exhibit some tensions with the measured distributions. In another example, a measurement of observables sensitive to effects of color reconnection in top-quark pair-production events is presented, in particular for the charged-particle multiplicity, the scalar sum of the transverse momenta of the charged particles, and the same scalar sum in bins of charged-particle multiplicity. These observables are unfolded to the stable-particle level. The particle-level measurements are compared with different color reconnection models in Monte Carlo generators. These measurements disfavour some of the color reconnection models and provide inputs to future optimisation of the parameters in Monte Carlo generators [137]. Furthermore, several observables sensitive to the fragmentation of b-quarks into b-hadrons are measured. Jets containing b-hadrons are used to construct observables that characterize the longitudinal and transverse momentum distributions of the b-hadron within the jet. The measurements have been corrected for detector effects and provide a test of heavy-quark-fragmentation modeling at the LHC in a system where the top-quark decay products are color-connected to the proton beam remnants. The unfolded distributions are compared with the predictions of several modern Monte Carlo parton-shower generators and generator tunes, and a wide range of agreement with the data is observed. These measurements complement similar measurements from e^+e^- collider experiments in which the b-quarks originate from a color-singlet Z/γ^* [138].

CMS measures single- and double-differential $t\bar{t}$ cross sections in the dilepton and the lepton+jets channel as a function of the kinematic properties of the leptons, jets from bottom quark hadronization, top quarks, and top quark pairs and jet multiplicity [139–144]. While in general good agreement is observed, in a dilepton analysis, significant disagreement is observed between data and all predictions for several observables. The measurements are used to constrain the top quark chromomagnetic dipole moment in an effective field theory framework at NLO in QCD and to extract $t\bar{t}$ and leptonic charge asymmetries [145]. In a later dilepton channel analysis, even a triple-differential measurement is performed as a function of the invariant mass and rapidity of the $t\bar{t}$ system and the multiplicity of additional jets at particle level. The measurement is used to extract the strong coupling constant and the top-quark pole mass and parton distribution functions [146]. In the all-hadronic and $\ell + jets$ events in a boosted topology with at least two large- R jets with a b -tag inside and $p_T > 400$ GeV or one large- R jet, respectively, CMS

measures the differential cross section as a function of kinematic variables of individual top quarks or of the $t\bar{t}$ system [147]. The observed absolute cross sections are significantly lower than the predictions from theory. Using the full Run-2 dataset of 137 fb⁻¹ in $\ell + jets$ data, arranged in four regions according to the top p_T , boosted vs. resolved, and the b -tagging score, CMS measures the single- and double-differential $t\bar{t}$ cross sections [99]. Here also the longitudinal momentum is measured well into the TeV range in one measurement starting in the resolved regime.

61.2.1.3 $t\bar{t}$ plus heavy flavor production processes

Further cross-section measurements are performed by ATLAS and CMS for $t\bar{t}$ +heavy flavor. The measurement of the cross section for $t\bar{t}$ +heavy flavour [148] and $t\bar{t}$ +jets production as well as the differential measurement of the jet multiplicity in $t\bar{t}$ events is presented by ATLAS [149] and by CMS [120]. In addition, both experiments measure the production cross section of the $t\bar{t}b\bar{b}$ process as it is an interesting test of QCD due to the different mass scales involved. Furthermore, this process is of high relevance for top quark production as background to searches, for example for measurements of $t\bar{t}h$ production and measurements of 4-top quark production. At $\sqrt{s} = 8$ TeV, CMS measured the cross-section ratio $\sigma_{t\bar{t}b\bar{b}}/\sigma_{t\bar{t}jj}$ using 19.6 fb⁻¹ [150]. ATLAS also measured the $t\bar{t}$ production cross section along with the branching ratios into channels with leptons and quarks using 4.6 fb⁻¹ of 7 TeV data [151]. They find agreement with the standard model at the level of a few percent.

Using 19.7 fb⁻¹ of data recorded at 8 TeV, CMS measures the absolute and normalized differential cross section with respect to the jet multiplicity in $t\bar{t}$ +jets events in the dilepton channel. The differential $t\bar{t}b$ and $t\bar{t}b\bar{b}$ cross sections are presented for the first time as a function of the kinematic properties of the leading additional b jets [152].

Using 139 fb⁻¹ of $t\bar{t} \rightarrow$ dilepton events, ATLAS distinguishes in a dedicated analysis muons originating from $W \rightarrow \mu\nu$ decays and those from $W \rightarrow \tau\nu \rightarrow \mu\nu\nu$ decays via their transverse momentum spectrum and the impact parameter of the muon track, that reflects the tau lifetime, yielding high sensitivity. The measured ratio of $R(\tau/\mu) = 0.992 \pm 0.013$ is in agreement with the hypothesis of universal lepton couplings [153].

Using 36 fb⁻¹ of dilepton events at 13 TeV, ATLAS also measures differential cross sections with respect to high-resolution variables, constructed to characterize the longitudinal and transverse momentum distributions of the b -hadron within the b -jets [138]. They are used to test the heavy-quark-fragmentation modelling.

Using 137 fb⁻¹ of dilepton events at 13 TeV, CMS measures differential cross sections with respect to the mass of the $t\bar{t}$ system and the rapidity difference of the top-quark and antiquark [154]. Exploiting their sensitivity to the top-quark Yukawa coupling yields a best fit value of $Y_t = 1.16_{-0.35}^{+0.24}$, bounding $Y_t < 1.54$ at a 95% confidence level.

At $\sqrt{s} = 13$ TeV, ATLAS measures the $t\bar{t}b\bar{b}$ cross section and cross section ratios in the dilepton and the $\ell + jets$ channels as inclusive and differential cross sections [155]. The measured inclusive fiducial cross-sections generally exceed the $t\bar{t}b\bar{b}$ predictions from various NLO matrix element calculations matched to a parton shower. CMS measures the $t\bar{t}b\bar{b}$ cross section and cross section ratios in the dilepton channel [156], in the dilepton and the lepton+jets channel [157], in the all-jet channel by selecting events containing at least eight jets, of which at least two are identified as b -jets [158]. In the latter, a combination of multivariate analysis techniques is used to reduce the large background from multijet events not containing a top quark pair, and to help discriminate between jets originating from top quark decays and other additional jets. In the all-hadronic channel, they later measured the $t\bar{t} + b\bar{b}$ cross section to $\approx 25\%$ precision employing a multivariate analysis technique and a 2-dimensional likelihood fit [159]. Using the full Run-2 dataset of 138 fb⁻¹, they measure the inclusive and normalized differential $t\bar{t}b\bar{b}$ cross sections in the lepton+jets decay channel of the top quark [160]. Measurements are made in four fiducial phase space regions, targeting different aspects of the process. Distributions are unfolded to the particle level through

maximum likelihood fits, and compared with predictions from several event generators. In most cases, the measured inclusive cross sections exceed the predictions with the chosen generator settings. The differential cross sections show varying degrees of compatibility with the theoretical predictions.

CMS also measured the $t\bar{t} + c\bar{c}$ cross section using 41.5 fb^{-1} of events with dileptonic final states [161]. A multi-class neural network is employed to separate $t\bar{t} + b\bar{b}$, $t\bar{t} + c\bar{c}$ and $t\bar{t} + ll$. The results are compatible with the prediction within $1 - 2 \sigma$.

The production of four top-quarks is an interesting test of QCD in a very rare process and at the same time sensitive to the top quark Yukawa coupling and to production mechanisms with new mediators with strong couplings to top quarks. The latest cross section calculation yields $\sigma_{t\bar{t}\bar{t}\bar{t}} = 13.32^{+1.04}_{-1.78} \text{ fb}$ [44]. Using the full Run-II data set of 139 fb^{-1} , ATLAS measures the four-tops cross section in the two-lepton same sign or three-lepton channel with 13% branching ratio and dominant $t\bar{t}V$ background as $\sigma_{t\bar{t}\bar{t}\bar{t}} = 24^{+7}_{-6} \text{ fb}$ [162]. Using the same data set in the one-lepton or two-lepton opposite-sign channel with 57% branching ratio and dominant $t\bar{t} + \text{heavy flavor}$ background, they measure $\sigma_{t\bar{t}\bar{t}\bar{t}} = 26^{+17}_{-15} \text{ fb}$ [163]. The combination yields $\sigma_{t\bar{t}\bar{t}\bar{t}} = 24^{+7}_{-6} \text{ fb}$ [163], corresponding to an observed (expected) significance of 4.7 (2.6) σ significance. Using the full Run-2 dataset of 140 fb^{-1} , ATLAS presents the observation of the $t\bar{t}\bar{t}\bar{t}$ production process in events containing two leptons with the same electric charge or at least three leptons (e or μ). Event kinematics are used to separate signal from background through a multivariate discriminant based on graph neural networks, and dedicated control regions are used to constrain the dominant backgrounds. The cross section is measured to be $\sigma(t\bar{t}\bar{t}\bar{t}) = 22.5^{+6.6}_{-5.6} \text{ fb}$ [164], almost twice the Standard Model prediction and compatible with it within 2 standard deviations. The observed (expected) significance of the measured signal with respect to the standard model (SM) background-only hypothesis is 6.1 (4.3) standard deviations. Data are also used to constrain the top-Higgs Yukawa coupling and effective field theory operator coefficients.

After a search for four-top production in 35.8 fb^{-1} , in the one-lepton or two-lepton opposite-sign channel [165], CMS uses the full Run-2 dataset of 137 fb^{-1} to measure the four-top cross section in the two-lepton same sign or three-lepton channel, yielding $\sigma_{t\bar{t}\bar{t}\bar{t}} = 12.6^{+5.8}_{-5.2} \text{ fb}$ [166], corresponding to an observed (expected) significance of 2.6 (2.7) σ significance. In the full Run-2 dataset, they manage to achieve evidence for the four-top production in events that have no leptons (all-hadronic), one lepton, or two opposite-sign leptons, yielding $\sigma(t\bar{t}\bar{t}\bar{t}) = 36^{+12}_{-11} \text{ fb}$ [167], corresponding to an observed significance of 3.9 standard deviations (1.5 expected). The combination with earlier CMS results in other final states yields $\sigma(t\bar{t}\bar{t}\bar{t}) = 17 \pm 4(\text{stat.}) \pm 3(\text{syst.}) \text{ fb}$, corresponding to a significance of 4.0 standard deviations (3.2 expected).

Finally, CMS reports the observation of the four-tops production process based on events with two same-sign, three, or four charged leptons (e and μ) and additional jets. Updated identification techniques for charged leptons and jets originating from the hadronization of b quarks, as well as a revised multivariate analysis strategy via a multi-class boosted decision tree to distinguish the signal process from the main backgrounds, lead to an improved signal detection, yielding $\sigma(t\bar{t}\bar{t}\bar{t}) = 17.7^{+3.7}_{-3.5}(\text{stat.})^{+2.3}_{-1.9}(\text{syst.}) \text{ fb}$, corresponding to an observed significance of 5.6 standard deviations (4.9 expected) [168].

61.2.1.4 Single-top production

Top-quarks cannot only be produced in pairs via the strong interaction, but also individually via the electroweak interaction. This interaction is sensitive to the tWb coupling as well as to the CKM-Matrix Element V_{tb} . The single-top quark production process was first observed in 2009 by $D\bar{O}$ [169] and CDF [170, 171] at the Tevatron. The production cross section at the Tevatron is roughly half that of the $t\bar{t}$ cross section, but the final state with a single W -boson and typically two jets, which tend to be emitted more in the forward direction, is less distinct than that for $t\bar{t}$ and much more difficult to distinguish from the background of W +jets and other sources. A comprehensive review of the first

observation and the techniques used to extract the signal from the backgrounds can be found in [172]. A more recent one can be found in [173].

The dominant production at the Tevatron is through s -channel and t -channel W -boson exchange. Associated production with a W -boson (tW production) has a cross section that is too small to observe at the Tevatron. The t -channel process is $qb \rightarrow q't$, while the s -channel process is $qq' \rightarrow t\bar{b}$. The s - and t -channel productions can be separated kinematically. This is of particular interest because potential physics beyond the Standard Model, such as fourth-generation quarks, heavy W and Z bosons, flavor-changing-neutral-currents [37], or a charged Higgs boson, would affect the s - and t -channels differently. However, the separation is difficult and initial observations and measurements at the Tevatron by both experiments were of combined $s + t$ -channel production. The two experiments combined their measurements for maximum precision with a resulting $s + t$ -channel production cross section of $2.76^{+0.58}_{-0.47} \text{ pb}$ [174], which agrees well with the theoretical calculation at $m_t = 173 \text{ GeV}/c^2$ of $\sigma_{s+t} = 3.12^{+0.00}_{-0.04}(\text{scale}) \pm 0.18(\text{pdf}) \text{ pb}$ (including both top and anti-top production) [35, 175].

Using the full Run-II data set of up to 9.7 fb^{-1} , CDF and $D\bar{O}$ have measured the t -channel single-top quark production to be $\sigma_{t+\bar{t}} = 2.25^{+0.29}_{-0.31} \text{ pb}$ [176, 177]. In the same publication, they also present the simultaneously measured s - and t -channel cross sections and the $s + t$ combined cross section measurement resulting in $\sigma_{s+t} = 3.30^{+0.52}_{-0.40} \text{ pb}$, without assuming the SM ratio of σ_s/σ_t . The modulus of the CKM matrix element obtained from the $s + t$ -channel measurement is $|V_{tb}| = 1.02^{+0.06}_{-0.05}$ and its value is used to set a lower limit of $|V_{tb}| > 0.92$ at 95% C.L. Those results are in good agreement with the theoretical value at the mass $172.5 \text{ GeV}/c^2$ of $\sigma_t = 2.08 \pm 0.13 \text{ pb}$ [175]. It should be noted that the theory citations here list cross sections for t or \bar{t} alone, whereas the experiments measure the sum. At the Tevatron, these cross sections are equal. The theory values quoted here already include this factor of two.

Using datasets of 9.7 fb^{-1} each, CDF and $D\bar{O}$ combine their analyses and report the first observation of single-top-quark production in the s -channel, yielding $\sigma_s = 1.29^{+0.26}_{-0.24} \text{ pb}$ [178]. The probability of observing a statistical fluctuation of the background of the given size is 1.8×10^{-10} , corresponding to a significance of 6.3 standard deviations.

t -channel at the LHC:

At the LHC, the t -channel cross section is expected to be more than three times as large as s -channel and tW production, combined.

At $\sqrt{s} = 5.02 \text{ TeV}$, very recently, ATLAS measures the t -channel single-top quark production in a dedicated run using 255 pb^{-1} , yielding $\sigma(tq + \bar{t}q) = 27.1^{+4.4}_{-4.1}(\text{stat.})^{+4.4}_{-3.7}(\text{syst.}) \text{ pb}$ and a cross section ratio between top and antitop production $R_t = 2.73^{+1.43}_{-0.82}(\text{stat.})^{+1.01}_{-0.29}(\text{syst.})$ [179]. This result implies for the CKM-matrix element $f_{LV} \cdot |V_{tb}| = 0.94^{+0.11}_{-0.10}$ with f_{LV} being a left-handed form factor.

At $\sqrt{s} = 7 \text{ TeV}$, using 4.59 fb^{-1} of data, ATLAS measures the t -channel single-top quark cross section in the lepton plus 2 or 3 jets channel with one b -tag by fitting the distribution of a multivariate discriminant constructed with a neural network, yielding $\sigma_t = 46 \pm 6 \text{ pb}$, $\sigma_{\bar{t}} = 23 \pm 4 \text{ pb}$ with a ratio $R_t = \sigma_t/\sigma_{\bar{t}} = 2.04 \pm 0.18$ and $\sigma_{t+\bar{t}} = 68 \pm 8 \text{ pb}$, consistent with SM expectations [180, 181]. CMS follows two approaches in 1.6 fb^{-1} of lepton plus jets events. The first approach exploits the distributions of the pseudorapidity of the recoil jet and reconstructed top-quark mass using background estimates determined from control samples in data. The second approach is based on multivariate analysis techniques that probe the compatibility of the candidate events with the signal. They find $\sigma_{t+\bar{t}}^{\text{chan.}} = 67.2 \pm 6.1 \text{ pb}$, and $|V_{tb}| = 1.020 \pm 0.046(\text{exp.}) \pm 0.017(\text{th.})$ [182]. All combined measurements are consistent with their corresponding SM predictions and yield $67.5 \pm 5.7 \text{ pb}$ [183].

At $\sqrt{s} = 8 \text{ TeV}$, both experiments repeat and refine their measurements. ATLAS uses 20.2 fb^{-1} of data. Total, fiducial and differential cross-sections are measured for both top-quark and top-antiquark production [184]. An artificial neural network is

employed to separate signal from background. The fiducial cross-section is measured with a precision of 5.8% (top quark) and 7.8% (top antiquark), respectively. The total cross-sections are measured to be $\sigma_t^{t\text{-chan.}}(tq) = 56.7_{-3.8}^{+4.3}$ pb for top-quark production and $\sigma_{\bar{t}}^{t\text{-chan.}}(\bar{t}q) = 32.9_{-2.7}^{+3.0}$ pb for top-antiquark production, in agreement with the SM prediction. In addition, the ratio of top-quark to top-antiquark production cross-sections is determined to be $R_t = 1.72 \pm 0.09$. The total cross-section is used to extract the Wtb coupling: $f_{LV} \cdot |V_{tb}| = 1.029 \pm 0.048$, which corresponds to $|V_{tb}| > 0.92$ at the 95% confidence level, when assuming $f_{LV} = 1$ and restricting the range of $|V_{tb}|$ to the interval $[0, 1]$. The differential cross-sections as a function of the transverse momentum and rapidity of both, top and antitop, are measured at both the parton and particle levels. The transverse momentum and rapidity differential cross-sections of the accompanying jet from the t -channel scattering are measured at particle level. All measurements are compared to various Monte Carlo predictions as well as to fixed-order QCD calculations where available. The SM predictions provide good descriptions of the data. Using the same dataset, ATLAS probes the Wtb vertex structure from polarization observables in t -channel single-top quark events. The observables are extracted from asymmetries in angular distributions measured with respect to spin quantisation axes appropriately chosen for the top quark and the W -boson and found to be in agreement with the Standard Model predictions [185]. CMS uses 19.7 fb^{-1} in the e or μ plus jets channel, exploiting the pseudorapidity distribution of the recoil jet. They find $\sigma_t = 53.8 \pm 1.5(\text{stat.}) \pm 4.4(\text{syst.})$ pb and $\sigma_{\bar{t}} = 27.6 \pm 1.3(\text{stat.}) \pm 3.7(\text{syst.})$ pb, resulting in an inclusive t -channel cross section of $\sigma_{t+\bar{t}} = 83.6 \pm 2.3(\text{stat.}) \pm 7.4(\text{syst.})$ [186]. They measure a cross section ratio of $R_t = \sigma_t/\sigma_{\bar{t}} = 1.95 \pm 0.10(\text{stat.}) \pm 0.19(\text{syst.})$, in agreement with the SM. The CKM matrix element V_{tb} is extracted to be $|V_{tb}| = 0.998 \pm 0.038(\text{exp.}) \pm 0.016(\text{th.})$. Later, CMS also provided a fiducial cross section measurement for t -channel single top in the same dataset in events with exactly one μ or e and two jets, one of which is associated with a b -hadron [187]. The total fiducial cross section is measured using different generators at NLO plus parton-shower accuracy. Using as reference the `aMC@NLO` MC predictions in the four-flavor scheme, $\sigma_t^{\text{fid}} = 3.38 \pm 0.25(\text{exp.}) \pm 0.20(\text{th.})$ pb is obtained, in good agreement with the theory predictions. All combined measurements are consistent with their corresponding SM predictions and yield 87.7 ± 5.8 pb [183].

At $\sqrt{s} = 13$ TeV, ATLAS uses 3.2 fb^{-1} to measure the t -channel cross section. Using a binned maximum-likelihood fit to the discriminant distribution of a neural network, the cross-sections are determined to be $\sigma_t(tq) = 156 \pm 5(\text{stat.}) \pm 27(\text{syst.}) \pm 3(\text{lumi.})$ pb and $\sigma(\bar{t}q) = 91 \pm 4(\text{stat.}) \pm 18(\text{syst.}) \pm 2(\text{lumi.})$ pb [188]. The cross-section ratio is measured to be $R_t = \sigma_t/\sigma_{\bar{t}} = 1.72 \pm 0.09(\text{stat.}) \pm 0.18(\text{syst.})$. All results are in agreement with SM predictions. Using the full Run-2 dataset of 140 fb^{-1} , ATLAS measures the t -channel cross sections to be $\sigma(tq) = 137 \pm 8$ pb and $\sigma(\bar{t}q) = 84_{-5}^{+6}$ pb for top-quark and top-antiquark production, respectively [189]. The combined cross-section is found to be $\sigma(tq + \bar{t}q) = 221 \pm 13$ pb and the cross-section ratio is $R_t = \sigma(tq)/\sigma(\bar{t}q) = 1.636_{-0.034}^{+0.036}$, in good agreement with predictions made at NNLO in perturbation theory. The results are also used to demonstrate the potential to constrain parton distribution functions and interpreted in terms of effective field theory operators $-0.25 < C_{qQ}^{(1,3)} < 0.12$, and to derive the constraint $|V_{tb}| > 0.95$ at the 95% confidence level CMS uses 2.2 fb^{-1} for a first measurement. Fits to the transverse W -mass and the output of an artificial neural network allow the determination of the background and the signal contribution. The measured cross-section is $\sigma_t = 238 \pm 13(\text{stat.}) \pm 29(\text{syst.})$ pb [190]. The CKM matrix element is determined to $|V_{tb}| = 1.05 \pm 0.07(\text{exp.}) \pm 0.02(\text{th.})$. Using 35.9 fb^{-1} of data, CMS refines their measurement. Events with one μ or e are selected, and different categories of jet and b -jet multiplicity and multivariate discriminators are applied to separate the signal from the background, resulting in $\sigma_t(tq) = 130 \pm 1(\text{stat}) \pm 19(\text{syst})$ pb and $\sigma_{\bar{t}}(\bar{t}q) = 77 \pm 1(\text{stat}) \pm 12(\text{syst})$ pb, respectively, and their ratio is $1.68 \pm 0.02(\text{stat}) \pm 0.05(\text{syst})$ [191].

The results are in agreement with the predictions from the Standard Model. This dataset is also used to measure differential cross sections in this channel [192]. CMS used the same dataset to measure the CKM matrix elements from their t -channel single-top quark production cross section. In the standard model hypothesis of CKM unitarity, a lower limit of $|V_{tb}| > 0.970$ is measured at the 95% confidence level. Several theories beyond the standard model are considered, and by releasing all constraints among the involved parameters, the values $|V_{tb}| = 0.988 \pm 0.024$, and $|V_{td}|^2 + |V_{ts}|^2 = 0.06 \pm 0.06$ are measured [193].

tW -channel at the LHC:

The predicted cross section for the associated tW process at the LHC at $\sqrt{s} = 7$ TeV is 15.6 ± 1.2 pb [36]. This is of interest because it probes the Wtb vertex in a different kinematic region than s - and t -channel production, and because of its similarity to the associated production of a charged-Higgs boson and a top quark. The signal is difficult to extract because of its similarity to the $t\bar{t}$ signature. Furthermore, it is difficult to uniquely define because at NLO a subset of diagrams has the same final state as $t\bar{t}$ and the two interfere [194]. The cross section is calculated using the *diagram removal* technique [195] to define the signal process. In the diagram removal technique the interfering diagrams are removed, at the amplitude level, from the signal definition (an alternative technique, *diagram subtraction* removes these diagrams at the cross-section level and yields similar results [195]). These techniques work provided the selection cuts are defined such that the interference effects are small, which is usually the case.

At $\sqrt{s} = 7$ TeV, both, ATLAS and CMS, provide evidence for the associated tW production [196, 197]. ATLAS uses 2.05 fb^{-1} in the dilepton plus missing E_T plus jets channel, where a template fit to the final classifier distributions resulting from boosted decision trees as signal to background separation is performed. The result is incompatible with the background-only hypothesis at the 3.3σ (3.4σ expected) level, yielding $\sigma_{tW} = 16.8 \pm 2.9(\text{stat.}) \pm 4.9(\text{syst.})$ pb and $|V_{tb}| = 1.03_{-0.19}^{+0.16}$ [196]. CMS uses 4.9 fb^{-1} in the dilepton plus jets channel with at least one b -tag. A multivariate analysis based on kinematic properties is utilized to separate the $t\bar{t}$ background from the signal. The observed signal has a significance of 4.0σ and corresponds to a cross section of $\sigma_{tW} = 16_{-4}^{+5}$ pb [197]. All combined measurements are consistent with their corresponding SM predictions and yield 16.3 ± 4.1 pb [183].

At $\sqrt{s} = 8$ TeV, both experiments repeated their tW -analyses. ATLAS uses 20.3 fb^{-1} to select events with two leptons and one central b -jet. The tW signal is separated from the backgrounds using boosted decision trees, each of which combines a number of discriminating variables into one classifier. Production of tW events is observed with a significance of 7.7σ . The cross section is extracted in a profile likelihood fit to the classifier output distributions. The tW cross section, inclusive of decay modes, is measured to be $\sigma_{tW} = 23.0 \pm 1.3(\text{stat.})_{-3.5}^{+3.2}(\text{syst.}) \pm 1.1(\text{lumi.})$ pb, yielding a value for the CKM matrix element $|V_{tb}| = 1.01 \pm 0.10$ and a lower limit of 0.80 at the 95% C.L. [198]. A fiducial cross section is also measured. ATLAS and CMS also combine their early measurements and obtain $\sigma_{tW} = 16.3 \pm 4.1$ pb [199], in agreement with the NLO+NNLL expectation. Later, ATLAS used 20.2 fb^{-1} in the single-lepton channel with at least three jets to measure the Wt production cross section. A neural network is trained to separate the tW signal from the dominant $t\bar{t}$ background. The cross-section is extracted from a binned profile maximum-likelihood fit to a two-dimensional discriminant built from the neural-network output and the invariant mass of the hadronically decaying W boson. The measured cross section is $\sigma_{tW} = 26 \pm 7$ pb [200], in good agreement with the Standard Model expectation. CMS uses 12.2 fb^{-1} in events with two leptons and a jet originating from a b -quark. A multivariate analysis based on kinematic properties is utilized to separate the signal and background. The tW associate production signal is observed at the level of 6.1σ , yielding $\sigma_{tW} = 23.4 \pm 5.4$ pb and $|V_{tb}| = 1.03 \pm 0.12(\text{exp.}) \pm 0.04(\text{th.})$ [201].

ATLAS and CMS also combine their early measurements and obtain $\sigma_{tW} = 23.1 \pm 3.6$ pb [183], in agreement with the NLO+NNLL expectation. The product of a form factor with the CKM matrix element V_{tb} is determined to be $|V_{tb}| = 1.02 \pm$

$0.04(\text{meas.}) \pm 0.02(\text{theo.}) > 0.79$.

At $\sqrt{s} = 13$ TeV, ATLAS uses 3.2 fb^{-1} of events with two opposite sign isolated leptons and at least one jet. They are separated into signal and control regions based on their jet multiplicity and the number of jets with b -tags. Signal is separated from background in two regions using boosted decision trees. The cross section is extracted by fitting templates to the data distributions, and is measured to be $\sigma_{tW} = 94 \pm 10(\text{stat.})_{-22}^{+28}(\text{syst.}) \pm 2(\text{lumi.}) \text{ pb}$ [202]. The measurement is in agreement with the SM prediction. CMS uses 36 fb^{-1} of events with two opposite sign isolated leptons, one tight and one loose jet and one b -tag. Signal and background is separated in categories depending on the number of jets and the subset of b -tagged jets using a boosted decision tree. A maximum likelihood fit yields $\sigma_{tW} = 63.1 \pm 1.8(\text{stat.}) \pm 6.4(\text{syst.}) \pm 2.1(\text{lumi.}) \text{ pb}$ [203]. In this dataset, CMS also analyses the single-lepton channel, where a boosted decision tree is used to separate the tW signal from the dominant $t\bar{t}$ background, whilst the subleading W +jets and multi-jet backgrounds are constrained using data-driven estimates. This result is the first observation of the tW process in final states containing a single μ or single e and several jets, with a significance exceeding 5 standard deviations. The cross section is determined to be $\sigma_{tW} = 89 \pm 4(\text{stat.}) \pm 12(\text{syst.}) \pm 1.2(\text{lumi.}) \text{ pb}$ [204], consistent with the Standard Model. Using the full Run-2 dataset of 138 fb^{-1} , CMS measures the inclusive and normalised differential cross sections. Events containing one e and one μ in the final state are analysed. For the inclusive measurement, a multivariate discriminant, exploiting the kinematic properties of the events is used to separate the signal from the dominant $t\bar{t}$ background. A cross section of $79.2 \pm 0.9(\text{stat.})_{-8.0}^{+7.7}(\text{syst.}) \pm 1.2(\text{lumi.}) \text{ pb}$ [205] is obtained, consistent with the predictions of the standard model. For the differential measurements, a fiducial region is defined according to the detector acceptance, and the requirement of exactly one jet coming from the fragmentation of a bottom quark. The resulting distributions are unfolded to particle level and agree with the predictions at NLO in perturbative QCD.

s -channel at the LHC:

At $\sqrt{s} = 7$ TeV, the s -channel production cross section is expected to be $4.6 \pm 0.3 \text{ pb}$ for $m_t = 173 \text{ GeV}/c^2$ [35]. At ATLAS, a search for s -channel single top quark production is performed in 0.7 fb^{-1} using events containing one lepton, missing transverse energy and two b -jets. Using a cut-based analysis, an observed (expected) upper limit at 95% C.L. on the s -channel cross-section of $\sigma_s < 26.5$ (20.5) pb is obtained [206].

At $\sqrt{s} = 8$ TeV, ATLAS uses 20.3 fb^{-1} of data with one lepton, large missing transverse momentum and exactly two b -tagged jets. They perform a maximum-likelihood fit of a discriminant based on a Matrix Element Method and optimized in order to separate single top-quark s -channel events from the main background contributions which are $t\bar{t}$ and W +jets production. They find $\sigma_s = 4.8 \pm 0.8(\text{stat.})_{-1.3}^{+1.6}(\text{syst.}) \text{ pb}$ with a signal significance of 3.2 standard deviations [207], which provides first evidence for s -channel single-top production. The signal is extracted through a maximum-likelihood fit to the distribution of a multivariate discriminant defined using boosted decision trees to separate the expected signal contribution from background processes. At 7 TeV and 8 TeV, CMS uses 5.1 fb^{-1} and 19.3 fb^{-1} , respectively, and analyses leptonic decay modes by performing a maximum likelihood fit to a multivariate discriminant defined using a Boosted Decision Tree, yielding cross sections of $\sigma_s = 7.1 \pm 8.1 \text{ pb}$ and $\sigma_s = 13.4 \pm 7.3 \text{ pb}$, respectively, and a best fit value of 2.0 ± 0.9 for the combined ratio of the measured σ_s values and the ones expected in the Standard Model [208]. The signal significance is 2.5 standard deviations.

ATLAS and CMS present the combinations of their single-top-quark production cross-section measurements, using Run-1 data. For the s -channel cross-section, the combination yields $4.9 \pm 1.4 \text{ pb}$ at $\sqrt{s} = 8$ TeV. All combined measurements are consistent with their corresponding SM predictions [183].

At $\sqrt{s} = 13$ TeV, ATLAS uses 139 fb^{-1} to measure the s -channel cross section on events with an e or μ , missing transverse momentum and exactly two b -tagged jets in the final state. A discriminant based on matrix element calculations is used to

separate single-top-quark s -channel events from the main background contributions, which are top-quark pair production and W -boson production in association with jets. The observed (expected) signal significance over the background-only hypothesis is 3.3 (3.9) standard deviations, and the measured cross-section is $\sigma = 8.2_{-2.9}^{+3.5} \text{ pb}$, consistent with the Standard Model prediction of $\sigma_{SM} = 10.32_{-0.36}^{+0.40} \text{ pb}$ [209].

Both, ATLAS and CMS, also measured the electroweak production of single top-quarks in association with a Z -boson, see section 61.2.5.4 of this review.

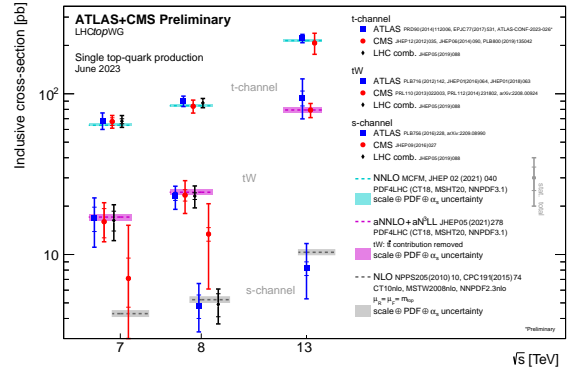


Figure 61.2: Measured and predicted single top production cross sections at LHC energies in pp collisions. The plot is kindly provided by the LHCtopWG working group, status as of June 2023, see <https://twiki.cern.ch/twiki/bin/view/LHCPhysics/LHCtopWGSUMMARYPLOTS>.

Fig. 61.2 provides a summary of all single top cross-section measurements at the LHC as a function of the center-of-mass energy. All cross-section measurements are very well described by the theory calculation within their uncertainty.

Thanks to the large statistics now available at the LHC, both CMS and ATLAS experiments also performed differential cross-section measurements in single-top t -channel production [180], [210]. Such measurements are extremely useful as they test our understanding of both QCD and EW top-quark interactions. Using the full Run-2 dataset of 139 fb^{-1} , ATLAS measures the three components of the top-quark and top-antiquark polarisation vectors in t -channel single-top-quark production simultaneously from the distributions of the direction cosines of the charged-lepton momentum in the top-quark rest frame in single-lepton plus jets events. The three components of the polarisation vector for the selected top-quark event sample are $P_{x'} = 0.01 \pm 0.18$, $P_{y'} = -0.029 \pm 0.027$, $P_{z'} = 0.91 \pm 0.10$ and for the top-antiquark event sample they are $P_{x'} = -0.02 \pm 0.20$, $P_{y'} = -0.007 \pm 0.051$, $P_{z'} = -0.79 \pm 0.16$ [211]. They also present normalised differential cross-sections corrected to a fiducial region at the stable-particle level as a function of the charged-lepton angles for top-quark and top-antiquark events inclusively and separately, which are also used to derive bounds on the complex Wilson coefficient of the dimension-six O_{tW} operator.

The CMS collaboration has measured differential single top quark t -channel production cross sections as functions of the transverse momentum and the absolute value of the rapidity of the top quark. The analysis is performed in the leptonic decay channels of the top quark, with either a muon or an electron in the final state, using data collected with the CMS experiment at the LHC at $\sqrt{s} = 8$ TeV and corresponding to an integrated luminosity of 19.7 fb^{-1} . Neural networks are used to discriminate the signal process from the various background contributions. The results are found to agree with predictions from Monte Carlo generators [210]. Using the same data set and under the assumption that the spin analyzing power of a charged lepton is 100% as predicted in the SM, they are also able to measure the spin asymmetry, sensitive to the top quark polarization of the top quark $A_\mu = 0.26 \pm 0.03(\text{stat}) \pm 0.10(\text{syst})$ [212], which is compatible with a p -value of 4.6%, equivalent to 2.0 standard deviation. At 13 TeV, using 35.9 fb^{-1} , CMS measures the differential t -channel cross

sections, for the first time in single-top production, and charge ratios for t -channel single top quark production [192]. The results are found to be in agreement with SM predictions using various NLO event generators and sets of parton distribution functions. Additionally, the spin asymmetry, sensitive to the top quark polarization, is determined from the differential distribution of the polarization angle at parton level to be 0.440 ± 0.070 , in agreement with the SM prediction. This disfavors the results obtained at 8 TeV. ATLAS has measured the differential tW cross section in 36.1 fb^{-1} at 13 TeV with respect to the energy of the b -jet, the energy of the system of the two leptons and b -jet, and the transverse mass or mass of combinations of leptons, the b -jet and neutrinos [213]. Using 35.9 fb^{-1} of $e\mu$ events, CMS measures the differential tW cross section. A fiducial region is defined according to the detector acceptance, and the requirement of exactly one b -tagged jet. The resulting distributions are unfolded to particle-level and compared with predictions calculated at next-to-leading order in perturbative QCD. Within current uncertainties, all the predictions agree with the data [214].

Further measurements of electroweak single-top quark production in association with addition electroweak gauge bosons such as tZq or $t\gamma q$ production are covered in the section **Top-Quark Electroweak Charges and Couplings**, Sec 61.2.5.4.

61.2.2 Top-Quark Asymmetries

A forward-backward asymmetry in $t\bar{t}$ production at a $p\bar{p}$ collider arises starting at order α_S^3 in QCD from the interference between the Born amplitude $q\bar{q} \rightarrow t\bar{t}$ with 1-loop box production diagrams and between diagrams with initial- and final-state gluon radiation. The asymmetry, A_{FB} , is defined by

$$A_{FB} = \frac{N(\Delta y > 0) - N(\Delta y < 0)}{N(\Delta y > 0) + N(\Delta y < 0)}, \quad (61.5)$$

where $\Delta y = y_t - y_{\bar{t}}$ is the rapidity difference between the top and the anti-top quark. Calculations at α_S^3 predict a measurable A_{FB} at the Tevatron. The most recent calculations up to order α_S^4 , including electromagnetic and electroweak corrections, yield a predicted asymmetry of $\approx (9.5 \pm 0.7)\%$ [215]. This is about 10% higher than the previous calculation at NLO [216, 217], and improves the agreement with experiment.

Contrary to most measurements in the top sector, many measurements in this section are statistically limited. This is true - by construction - in the measurements in extreme corners of phase space (i.e. boosted measurements) and in rare production processes like $t\bar{t}W$ and $t\bar{t}\gamma$. The progress in these measurements is expected to be achieved quite rapidly, as Run-3 at the LHC and subsequent runs deliver more data.

Both CDF and DØ measured asymmetry values in excess of the SM prediction, fueling speculation about exotic production mechanisms (see, for example, [218] and references therein). The first measurement of this asymmetry by DØ in 0.9 fb^{-1} [219] found an asymmetry at the detector level of $(12 \pm 8)\%$. The first CDF measurement in 1.9 fb^{-1} [220] yielded $(24 \pm 14)\%$ at parton level. Both values were higher, though statistically consistent with the SM expectation. With the addition of more data, the uncertainties have been reduced, and the central values, if somewhat smaller, have remained consistent with the first measurements. At the same time, the improved calculations from theory have increased the predicted asymmetry values, improving the agreement between theory and experiment.

CDF and DØ have combined results using the full Tevatron dataset at $\sqrt{s} = 1.96 \text{ TeV}$ [221]. Three combined asymmetries are reported: $A_{FB}^{t\bar{t}}$ as defined in Eq. 61.5 for fully-reconstructed $t\bar{t}$ events, a single-lepton asymmetry, A_{FB}^ℓ defined as in Eq. 61.5 but with Δy replaced by the product of the lepton charge and pseudo-rapidity, and a dilepton asymmetry, $A_{FB}^{\ell\ell}$, defined as in Eq. 61.5 but with Δy replaced by $\Delta\eta$ between the two leptons. The combined results are $A_{FB}^{t\bar{t}} = 0.128 \pm 0.021 \pm 0.014$, $A_{FB}^\ell = 0.073 \pm 0.016 \pm 0.012$, and $A_{FB}^{\ell\ell} = 0.108 \pm 0.043 \pm 0.016$, where the first uncertainty is statistical and the second systematic. These are to be compared to SM predictions at NNLO QCD and NLO electroweak of $A_{FB}^{t\bar{t}} = 0.095 \pm 0.007$ [215], $A_{FB}^\ell = 0.038 \pm 0.003$,

and $A_{FB}^{\ell\ell} = 0.048 \pm 0.004$ [217], respectively. Both experiments have also measured differential asymmetries, in bins of $M_{t\bar{t}}$, Δy , $q_\ell \times \eta_\ell$, and $\Delta\eta_{\ell\ell}$, with consistent results, though the growth of $A_{FB}^{t\bar{t}}$ with increasing $M_{t\bar{t}}$ and Δy appears somewhat more rapid than the SM prediction [221].

At the LHC, where the dominant $t\bar{t}$ production mechanism is the charge-symmetric gluon-gluon fusion, the measurement is more difficult. For the sub-dominant $q\bar{q}$ production mechanism, the symmetric pp collision does not define a forward and backward direction. Instead, the charge asymmetry, A_C , is defined in terms of a positive versus a negative $t - \bar{t}$ rapidity difference, Δy

$$A_C^{t\bar{t}} = \frac{N(\Delta|y| > 0) - N(\Delta|y| < 0)}{N(\Delta|y| > 0) + N(\Delta|y| < 0)}. \quad (61.6)$$

Both CMS and ATLAS have measured A_C in the LHC dataset. Using lepton+jets events in 4.7 fb^{-1} of data at $\sqrt{s} = 7 \text{ TeV}$, ATLAS measures $A_C^{t\bar{t}} = (0.6 \pm 1.0)\%$ [222]. ATLAS has reported on the same measurement performed at $\sqrt{s} = 8 \text{ TeV}$ with 20.3 fb^{-1} of data, with a result of $A_C^{t\bar{t}} = (0.9 \pm 0.5)\%$ [223]. In the dilepton channel at $\sqrt{s} = 8 \text{ TeV}$, ATLAS measures [224] $A_C^{t\bar{t}} = (2.1 \pm 1.6)\%$, and $A_C^{\ell\ell} = (0.8 \pm 0.6)\%$ (defined in terms of the $\Delta\eta$ of the two leptons) in agreement with the SM predictions of $(1.11 \pm 0.04)\%$ and $(0.64 \pm 0.03)\%$, respectively [217]. Using lepton+jets events CMS has measured A_C at both $\sqrt{s} = 7$ and 8 TeV . They measure $A_C^{t\bar{t}} = (0.4 \pm 1.5)\%$ and $A_C^{t\bar{t}} = (0.33 \pm 0.26(\text{stat.}) \pm 0.33(\text{syst.}))\%$ in 5.0 fb^{-1} at $\sqrt{s} = 7 \text{ TeV}$ and in 19.7 fb^{-1} at $\sqrt{s} = 8 \text{ TeV}$, respectively [225, 226]. Both measurements are consistent with the SM expectations of $A_C^{t\bar{t}} = (1.23 \pm 0.05)\%$ at $\sqrt{s} = 7 \text{ TeV}$ and $(1.11 \pm 0.04)\%$ at $\sqrt{s} = 8 \text{ TeV}$ [217], although the uncertainties are still too large for a precision test. In 19.5 fb^{-1} of dilepton events at $\sqrt{s} = 8 \text{ TeV}$, CMS measures $A_C^{t\bar{t}} = (1.1 \pm 1.3)\%$ and $A_C^{\ell\ell} = (0.3 \pm 0.7)\%$ [227], consistent with SM expectations [228].

In their 7 and 8 TeV analyses, ATLAS and CMS also provide differential measurements as a function of $M_{t\bar{t}}$ and the transverse momentum p_T and rapidity y of the $t\bar{t}$ system. To reduce model-dependence, the CMS collaboration has performed a measurement in a reduced fiducial phase space [229], with a result of $A_C = (-0.35 \pm 0.72(\text{stat.}) \pm 0.31(\text{syst.}))\%$, in agreement with SM expectations.

To specifically address the dependence of the asymmetry on $M_{t\bar{t}}$, ATLAS has performed a measurement in boosted $t\bar{t}$ events [230]. In 20.3 fb^{-1} of data at $\sqrt{s} = 8 \text{ TeV}$, in events with $M_{t\bar{t}} > 0.75 \text{ TeV}$, and $|\Delta|y| < 2$, ATLAS measures $A_C^{t\bar{t}} = (4.2 \pm 3.2)\%$ compared to a NLO SM prediction of $(1.60 \pm 0.04)\%$. The measurement is also presented in three bins of $M_{t\bar{t}}$, each in agreement, though with large uncertainties, with the SM expectations.

Both ATLAS and CMS have measured asymmetries in the distribution of leptons from $t\bar{t}$ decays. ATLAS, in 4.6 fb^{-1} of $\sqrt{s} = 7 \text{ TeV}$ data, has measured $A^{\ell\ell} = (2.4 \pm 1.5(\text{stat.}) \pm 0.9(\text{sys.}))\%$ in dilepton events [231]. Using a neutrino weighting technique in the same dataset to reconstruct the top quarks, ATLAS measures $A_C = (2.1 \pm 2.5(\text{stat.}) \pm 1.7(\text{sys.}))\%$. CMS, in 5.0 fb^{-1} of $\sqrt{s} = 7 \text{ TeV}$ data, uses dilepton events to measure $A_C = (1.0 \pm 1.5(\text{stat.}) \pm 0.6(\text{sys.}))\%$, where a matrix weighting technique is used to reconstruct the top quarks, and $A^{\ell\ell} = (0.9 \pm 1.0(\text{stat.}) \pm 0.6(\text{sys.}))\%$ [232]. An earlier result using lepton+jets events from the same CMS dataset found $A_C = (0.4 \pm 1.0 \pm 1.1)\%$ [225]. Combined results from ATLAS and CMS have now been released [233]. At $\sqrt{s} = 7 \text{ TeV}$ the combined result is $A_C = (0.5 \pm 0.7(\text{stat.}) \pm 0.6(\text{sys.}))\%$, and at $\sqrt{s} = 8 \text{ TeV}$ it is $A_C = (0.55 \pm 0.23 \pm 0.25)\%$. These results are all consistent, within their large uncertainties, with the SM expectations of $A^{\ell\ell} = (0.70 \pm 0.03)\%$ and $A_C = (1.23 \pm 0.05)\%$ [217].

ATLAS has released a charge asymmetry measurement at $\sqrt{s} = 13 \text{ TeV}$ using the full 139 fb^{-1} dataset, which combines data in the single-lepton and dilepton channels, and employs reconstruction techniques adapted to both the resolved and boosted topologies. A Bayesian unfolding procedure is performed to correct for detector resolution and acceptance effects. The combined inclusive $t\bar{t}$ charge asymmetry is measured to be $A_C^{t\bar{t}} = 0.0068 \pm 0.0015$,

which differs from zero by 4.7 standard deviations. Differential measurements are performed as a function of the invariant mass, transverse momentum and longitudinal boost of the $t\bar{t}$ system. Both the inclusive and differential measurements are found to be compatible with the Standard Model predictions, at NLO in QCD with NLO electroweak corrections [234]. The measurements are interpreted in the framework of the Standard Model effective field theory, placing competitive bounds on several Wilson coefficients.

A model-independent comparison of the Tevatron and LHC results is made difficult by the differing $t\bar{t}$ production mechanisms at work at the two accelerators and by the symmetric nature of the pp collisions at the LHC. A recent result from the CMS Collaboration [235] in 35.9 fb^{-1} of lepton plus jets events at $\sqrt{s} = 13 \text{ TeV}$, uses a likelihood analysis to separate the $q\bar{q}$ process from production via gluon-gluon and gluon-quark interactions and extract $A_{FB} = (4.8^{+8.8}_{-8.4} \text{ (stat.)} \pm 2.8 \text{ (sys.)})\%$. In addition, given a particular model of BSM physics, a comparison can be obtained through the resulting asymmetry predicted by the model at the two machines, see for example [230].

Using 139 fb^{-1} of data at 13 TeV in the lepton plus jets channel, ATLAS presents a measurement of the charge asymmetry in $t\bar{t}$ production in association with a photon. While the $t\bar{t}$ asymmetry is diluted in inclusive measurements at the LHC owing to the large fraction of gluon-gluon-initiated $t\bar{t}$ events, it is enhanced in other topologies such as $t\bar{t}\gamma$ due to an increased fraction of the quark initiated production mode. The charge asymmetry is obtained from the distribution of the difference of the absolute rapidities of the top quark and antiquark using a profile likelihood unfolding approach. It is measured to be $A_C = -0.003 \pm 0.029$ in agreement with the Standard Model expectation [236], where the precision is limited by the presently available statistics.

In a similar fashion and using the same dataset, ATLAS also searches for the leptonic charge asymmetry (A_C^L) of $t\bar{t}$ pair production in association with a W boson ($t\bar{t}W$) in event final states with exactly three charged light leptons (electrons or muons). Here, the events are also enhanced in quark-initiated production processes. Additionally, the W boson in the initial state causes polarisation of the $t\bar{t}$ pair, which further leads to a sizeable asymmetry. A profile-likelihood fit to the event yields in multiple regions corresponding to positive and negative differences between the pseudorapidities of the charged leptons from top-quark and top-antiquark decays is used to extract the charge asymmetry. At reconstruction level, the asymmetry is found to be $-0.12 \pm 0.14 \text{ (stat.)} \pm 0.05 \text{ (syst.)}$. An unfolding procedure is applied to convert the result at reconstruction level into a charge-asymmetry value in a fiducial volume at particle level with the result of $-0.11 \pm 0.17 \text{ (stat.)} \pm 0.05 \text{ (syst.)}$. The Standard Model expectations for these two observables are calculated using Monte Carlo simulations with NLO plus parton shower precision in QCD and including NLO electroweak corrections. They are $0.084^{+0.005}_{-0.003} \text{ (scale)} \pm 0.006 \text{ (MC stat.)}$ and $0.063^{+0.007}_{-0.004} \text{ (scale)} \pm 0.004 \text{ (MC stat.)}$, respectively, and in agreement with the measurements [237].

ATLAS explores a so-called ‘energy asymmetry’ in $t\bar{t}$ production in association with a high- p_T jet ($t\bar{t}j$ production). The energy asymmetry is defined as a difference between the top and anti-top quarks’ energies, and is measured in ATLAS in three bins of the associated high- p_T jet angle, θ_j . Both, the energies and jet angle, are measured in the $t\bar{t}j$ rest frame. A Bayesian unfolding method corrects for resolution and acceptance effects. The measurement is in agreement with the Standard Model at NLO accuracy [238].

In an early analysis of the Run-2 data, CMS analyzed 35.9 fb^{-1} of 13 TeV data, in particular using $t\bar{t}$ events decaying to muon or electron and jets in final states with low and high Lorentz boosts. Events are reconstructed using a fit of the kinematic distributions of the decay products to those expected for $t\bar{t}$ final states. The values found for the asymmetry parameters are $A_{FB} = 0.048^{+0.095}_{-0.087} \text{ (stat.)}^{+0.020}_{-0.029} \text{ (syst)}$, for the anomalous chromomagnetic dipole moment $\mu^t = -0.024^{+0.013}_{-0.009} \text{ (stat.)}^{+0.016}_{-0.011} \text{ (syst)}$, and a limit is placed on the magnitude of a possible anomalous chromoelectric dipole moment $|d^t| < 0.03$ at 95% confidence level [239].

The measurement of the charge asymmetry in $t\bar{t}$ events with

highly Lorentz-boosted top quarks decaying to a single, nonisolated lepton and overlapping jets is presented by CMS using the complete Run-2 dataset of 138 fb^{-1} of 13 TeV data. The top quark charge asymmetry is measured for events with a $t\bar{t}$ invariant mass larger than 750 GeV, most relevant for BSM searches, and corrected for detector and acceptance effects using a binned maximum likelihood fit. The measured top quark charge asymmetry of $(0.69^{+0.65}_{-0.69})\%$ is in good agreement with the standard model prediction at NNLO in QCD with NLO electroweak corrections. The result is also presented for two invariant mass ranges, 750 – 900 and $> 900 \text{ GeV}$ [240].

61.2.3 Top Quark Spin Correlations, Polarization, and Entanglement

One of the unique features of the top quark is that it decays before its spin can be flipped by chromomagnetic interactions. Thus the top quark polarization is directly observable via the angular distribution of its decay products and it is possible to define and measure observables sensitive to the top quark spin and its production mechanism. Although the top- and antitop-quarks produced by strong interactions in hadron collisions are essentially unpolarized, the spins of t and \bar{t} are correlated. For QCD production at threshold, the $t\bar{t}$ system is produced in a 3S_1 state with parallel spins for $q\bar{q}$ annihilation or in a 1S_0 state with antiparallel spins for gluon-gluon fusion. The situations at the Tevatron, where the production is primarily from $q\bar{q}$ annihilation, and at the LHC, where the production is primarily from gluon-gluon fusion, are therefore somewhat complementary. However, at the LHC production of $t\bar{t}$ pairs at large invariant mass occurs primarily via fusion of gluons with opposite helicities, and the $t\bar{t}$ pairs so produced have parallel spins as in production at the Tevatron via $q\bar{q}$ annihilation. The direction of the top quark spin is 100% correlated to the angular distributions of the down-type fermion (charged leptons or d -type quarks) in the decay. The joint angular distribution [241–243]

$$\frac{1}{\sigma} \frac{d^2\sigma}{d(\cos\theta_+)d(\cos\theta_-)} = \frac{1}{4}(1 + B_+ \cos\theta_+ + B_- \cos\theta_- + \kappa \cdot \cos\theta_+ \cdot \cos\theta_-), \quad (61.7)$$

where θ_+ and θ_- are the angles of the daughters in the top-quark rest frame with respect to a particular spin quantization axis (assumed here to be the same for θ_+ and θ_-), is a very sensitive observable. The maximum value for κ , 0.782 at NLO at the Tevatron [244], is found in the off-diagonal basis [241], while at the LHC the value at NLO is 0.326 in the helicity basis [244]. The coefficients B_+ and B_- are near zero in the SM because the top quarks are unpolarized in $t\bar{t}$ production. In place of κ , $A\alpha_+\alpha_-$ is often used, where α_i is the spin analyzing power, and A is the spin correlation coefficient, defined as

$$A = \frac{N(\uparrow\uparrow) + N(\downarrow\downarrow) - N(\uparrow\downarrow) - N(\downarrow\uparrow)}{N(\uparrow\uparrow) + N(\downarrow\downarrow) + N(\uparrow\downarrow) + N(\downarrow\uparrow)}, \quad (61.8)$$

where the first arrow represents the direction of the top quark spin along a chosen quantization axis, and the second arrow represents the same for the antitop-quark. The spin analyzing power α_i is $+0.998$ for positively charged leptons, -0.966 for down-type quarks from W decays, and -0.393 for bottom quarks [245]. The sign of α flips for the respective antiparticles. The spin correlation could be modified by a new $t\bar{t}$ production mechanism such as through a Z' boson, Kaluza-Klein gluons, a dark-matter mediator, or a Higgs boson.

The experiments typically use a Monte Carlo to provide templates for the measured distributions, or alternatively a matrix-element technique, and fit a parameter f , representing the fraction of events with the expected Standard Model correlation, with $(1-f)$ the fraction with no correlation. The correlation coefficient is extracted via $A_{\text{meas}} = f \cdot A_{\text{SM}}$. A ‘fraction’ $f > 1$ means that the measured correlation coefficient is larger than the Standard Model expectation.

For a more complete introduction and discussion of the spin density matrix, see reference [246].

CDF and DØ have studied spin correlations in $t\bar{t}$ production in the dilepton and lepton+jets channel with limited sensitivity, showing first evidence (see the PDG listings for details).

Spin correlations have been conclusively measured at the LHC by both the ATLAS and CMS collaborations. In the dominant gluon fusion production mode for $t\bar{t}$ pairs at the LHC, the angular distribution between the two leptons in $t\bar{t}$ decays to dileptons is sensitive to the degree of spin correlation [247].

Measurements have been made at 7, 8, and now 13 TeV. While there is some interest in the \sqrt{s} dependence of the correlations as a test of the production mechanism ($q\bar{q}$ vs gluon-gluon and possible sensitivity to new physics) the earlier measurements at 7 and 8 TeV [248–253] had relatively large uncertainties and have now been overtaken by the high-statistics 13 TeV measurements, which we review here.

In an ATLAS measurement at $\sqrt{s} = 8$ TeV [254], the spin-correlation coefficient κ is measured in the helicity basis to be $\kappa = 0.296 \pm 0.093$ in good agreement with the SM expectation of 0.318 (corresponding to a central value of f of 0.931). The polarization coefficients, B , in Eq. 61.7 are measured, also in the helicity basis, to be $B_+ = -0.044 \pm 0.038$ and $B_- = -0.064 \pm 0.040$, consistent with the SM predictions of 0.0030 ± 0.0010 and 0.0034 ± 0.00104 , respectively.

The most recent result from ATLAS, in 36.1 fb^{-1} at $\sqrt{s} = 13$ TeV, uses $\Delta\phi$, the azimuthal angle between the two charged leptons in $e\mu$ events in an analysis that also measures the differential cross sections in $\Delta\phi$ and $\Delta\eta$ between the two leptons [255]. The result, measured by comparison with NLO Monte Carlo generators, is $f = 1.249 \pm 0.024 \pm 0.061^{+0.067}_{-0.090}$, where the uncertainties are statistical, systematic, and theoretical, is again greater than 1.0. Whereas the previous results were statistically consistent with the Standard Model expectation of 1.0, this result is slightly higher than the expectation and hence inconsistent at the level of 2.2σ . The NLO generators are NLO in QCD only (and only at the production level). Including electroweak couplings produces an expected Standard Model distribution consistent with the data, but results in a large scale uncertainty, giving $f = 1.03 \pm 0.13$.

In 35.9 fb^{-1} of data at $\sqrt{s} = 13$ TeV, CMS has studied spin correlations in dilepton events via the measurement of parton-level normalized differential cross sections, sensitive to each of the independent coefficients of the spin-dependent parts of the $t\bar{t}$ production density matrix. The measured distributions and extracted coefficients are compared with standard model predictions from simulations at NLO accuracy in QCD, and from NLO QCD calculations including electroweak corrections. The normalized differential cross sections are used in fits to constrain the anomalous chromomagnetic and chromoelectric dipole moments of the top $-0.24 < C_{tG}/\Lambda^2 < 0.07 \text{ TeV}^{-2}$ and $-0.33 < C_{tG}^I/\Lambda^2 < 0.20 \text{ TeV}^{-2}$, respectively, at 95% confidence level [256]. These results are part of a complete study of the top quark spin density matrix at $\sqrt{s} = 13$ TeV, through the measurement of the coefficients of Eq. 61.7.

Entanglement is a striking feature of quantum mechanics [257–259]. If two particles are entangled, the state of one particle cannot be described independently from the other. More precisely, an entangled state is one that cannot be written as a convex combination of product states of density matrices [260, 261]. It has been observed in a wide variety of systems, ranging from the microscopic to the macroscopic scale. However, up to now entanglement has remained largely unexplored at high-energy colliders, except for flavor entanglement in $\Upsilon(4S) \rightarrow B_0\bar{B}_0$ decays [262] and a study of Bell inequality violation in $B_0 \rightarrow J/\psi K^*$ (892)⁰ decays [263]. Entanglement in top quark pairs has now been proposed to be studied for the first time via their spin correlation [264–271].

At the LHC, $t\bar{t}$ pairs are produced mainly via gluon-gluon fusion. When they are produced close to their production threshold, that is, when their invariant mass ($m_{t\bar{t}}$) is close to twice the mass of the top quark ($m_{t\bar{t}} \approx 2 \cdot m_t \approx 350 \text{ GeV}$), they exist nearly in a spin singlet state, which is therefore expected to be maximally entangled. After averaging over all possible top-quark directions, entanglement only survives at threshold because there the $t\bar{t}$ pairs are produced in a spin singlet, which is rotationally invariant. The

rotational invariance of a spin singlet implies that the trace of the spin correlation matrix C is a good entanglement witness. It is an observable that can signal the presence of entanglement without any assumption on the particular form of the quantum state, with $\text{tr}[C] + 1 < 0$ as a sufficient condition for entanglement. It is more convenient to define an entanglement witness using

$$D = \text{tr}[C]/3, \quad (61.9)$$

which can be experimentally measured as:

$$D = -3 \cdot \langle \cos \phi \rangle, \quad (61.10)$$

where $\langle \cos \phi \rangle$ is the average of the angle between the charged lepton directions in each one of the parent top quark and antitop quark rest frames which can be experimentally measured from an ensemble dataset. The existence of an entangled state is demonstrated if the measurement satisfies $D < -1/3$.

Using 139 fb^{-1} of Run-2 data, recorded at 13 TeV, ATLAS reports the highest-energy observation of entanglement so far in top-antitop quark events produced at the Large Hadron Collider. Spin entanglement is now detected from the measurement of a single observable D , inferred by the angle between the charged leptons in their parent top- and antitop-quark rest frames. The observable is measured on a narrow interval around the $t\bar{t}$ production threshold, where the entanglement detection is expected to be significant. The entanglement observable is measured in a fiducial phase-space with stable particles. The entanglement witness is measured to be $D = -0.547 \pm 0.002(\text{stat.}) \pm 0.021(\text{syst.})$ for $340 < m_{t\bar{t}} < 380 \text{ GeV}$ [272]. The large spread in predictions from several mainstream event generators indicates that modelling this property is challenging. The predictions depend in particular on the parton-shower algorithm used. The observed result is more than five standard deviations from a scenario without entanglement and hence constitutes the first observation of entanglement in a pair of quarks, and the observation of entanglement at the highest energy to date.

61.2.4 *W-Boson Helicity in Top-Quark Decay*

The Standard Model dictates that the top quark has the same vector-minus-axial-vector ($V - A$) charged-current weak interactions $\left(-i \frac{g}{\sqrt{2}} V_{tb} \gamma^\mu \frac{1}{2}(1 - \gamma_5)\right)$ as all the other fermions. In the SM, the fraction of top-quark decays to longitudinally polarized W bosons is proportional to its Yukawa coupling and hence enhanced with respect to the weak coupling. It is expected to be [273] $\mathcal{F}_0^{\text{SM}} \approx x/(1+x)$, $x = m_t^2/2M_W^2$ ($\mathcal{F}_0^{\text{SM}} \sim 70\%$ for $m_t = 173 \text{ GeV}/c^2$). Fractions of left-handed, right-handed, or longitudinal W bosons are denoted as \mathcal{F}_- , \mathcal{F}_+ , and \mathcal{F}_0 respectively. In the SM, \mathcal{F}_- is expected to be $\approx 30\%$ and $\mathcal{F}_+ \approx 0\%$. Predictions for the W polarization fractions at NNLO in QCD are available [274].

The Tevatron and the LHC experiments use various techniques to measure the helicity of the W boson in top-quark decays, in both the lepton+jets and in dilepton channels in $t\bar{t}$ production.

The first method uses a kinematic fit, similar to that used in the lepton+jets mass analyses, but with the top-quark mass constrained to a fixed value, to improve the reconstruction of final-state observables, and render the under-constrained dilepton channel solvable. Alternatively, in the dilepton channel the final-state momenta can also be obtained through an algebraic solution of the kinematics. The distribution of the helicity angle ($\cos \theta^*$) between the lepton and the b quark in the W rest frame provides the most direct measure of the W helicity. In a simplified version of this approach, the $\cos \theta^*$ distribution is reduced to a forward-backward asymmetry.

The second method (p_T^ℓ) uses the different lepton p_T spectra from longitudinally or transversely polarized W -decays to determine the relative contributions.

A third method uses the invariant mass of the lepton and the b -quark in top-quark decays ($M_{\ell b}^2$) as an observable, which is directly related to $\cos \theta^*$.

At the LHC, top-quark pairs in the dilepton channels are reconstructed using the neutrino weighting technique, see section 61.2.5.1.

Finally, the Matrix Element Method (MEM) has also been used [275], in which a likelihood is formed from a product of event probabilities calculated from the MEM for a given set of measured kinematic variables and assumed W -helicity fractions.

The results of recent CDF, $D\bar{O}$, ATLAS, and CMS analyses are summarized in Table 61.2. The datasets are now large enough to allow for a simultaneous fit of \mathcal{F}_0 , \mathcal{F}_- and \mathcal{F}_+ , which we denote by ‘3-param’ or \mathcal{F}_0 and \mathcal{F}_+ , which we denote by ‘2-param’ in the table. Results with either \mathcal{F}_0 or \mathcal{F}_+ fixed at its SM value are denoted ‘1-param’. For the simultaneous fits, the correlation coefficient between the two values is about -0.8 . A complete set of published results can be found in the Listings. All results are in agreement with the SM expectation.

CDF and $D\bar{O}$ combined their results based on $2.7 - 5.4 \text{ fb}^{-1}$ [276] for a top-quark mass of $172.5 \text{ GeV}/c^2$. ATLAS presents results from 1.04 fb^{-1} of $\sqrt{s} = 7 \text{ TeV}$ data using a template method for the $\cos\theta^*$ distribution and angular asymmetries from the unfolded $\cos\theta^*$ distribution in the lepton+jets and the dilepton channel [277]. CMS performs a similar measurement based on template fits to the $\cos\theta^*$ distribution with 5.0 fb^{-1} of 7 TeV data in the lepton+jets final state [278]. As the polarization of the W bosons in top-quark decays is sensitive to the Wtb vertex Lorentz structure and anomalous couplings, both experiments also derive limits on anomalous contributions to the Wtb couplings. CMS and ATLAS collaborations have also combined their results from 7 TeV data to obtain values on the helicity fractions as well as limits on anomalous couplings [279].

At 8 TeV , ATLAS came out with a measurement of the W -helicity fractions in 20.2 fb^{-1} in lepton+jets events with at least one b -tag [280]. Using 19.8 fb^{-1} of 8 TeV data, CMS measured the W -helicity in lepton + 4 jet events with two b -tags [281] as well as in events with two opposite-sign leptons (electron or muon) in the final state, applying six kinematic constraints on the kinematics of the produced particles [282]. Also, using the same dataset, a first measurement of the W -boson helicity in top-quark decays was made in electroweak single top production [283], yielding similarly precise and consistent results. The 8 TeV results obtained in $t\bar{t}$ and single-top events by ATLAS and CMS have also been combined recently [284]. These results are in agreement with the standard model predictions at next-to-next-to-leading order in perturbative QCD and represent an improvement in precision of 25 (29)% for F_0 (F_L) with respect to the most precise single measurement. A limit on anomalous right-handed vector (V_R), and left- and right-handed tensor (g_L, g_R) tWb couplings and on corresponding Wilson coefficients is set.

Recently, ATLAS used 139 fb^{-1} of data recorded at 13 TeV in dilepton events with at least two b -tags to measure the normalised differential $t\bar{t}$ cross section with respect to $\cos\theta^*$ at parton level and from that, based on template fits, extract the helicity fractions. The results are complementary to previous results and compatible with Standard Model expectations [285].

61.2.5 Top-Quark Properties

61.2.5.1 Top-Quark Mass Measurements

The most precisely studied property of the top quark is its mass. The top-quark mass has been measured in the lepton+jets, the dilepton, and the all-jets channel by all four Tevatron and LHC experiments, and now in single-top events at the LHC. The latest and/or most precise results are summarized in Table 61.3. The lepton+jets channel yields the most precise single measurements because of good signal to background ratio (in particular after b -tagging) and the presence of only a single neutrino in the final state. The momentum of a single neutrino can be reconstructed (up to a quadratic ambiguity) via the missing E_T measurement and the constraint that the lepton and neutrino momenta reconstruct to the known W boson mass. In the large data samples available at the LHC, measurements in the dilepton channel can be competitive and certainly complementary to those in the lepton+jets final state.

A large number of techniques have now been applied to measuring the top-quark mass. The original ‘template method’ [286], in which Monte Carlo templates of reconstructed mass distributions are fit to data, has evolved into a precision tool in the lepton+jets channel, where the systematic uncertainty due to the jet energy

scale (JES) uncertainty is controlled by a simultaneous, *in situ* fit to the $W \rightarrow jj$ hypothesis [287]. All the latest measurements in the lepton+jets and the all-jets channels use this technique in one way or another. In 20.2 fb^{-1} of data at $\sqrt{s} = 8 \text{ TeV}$ in the lepton+jets channel, ATLAS achieves a total uncertainty of 0.53% with a statistical component of 0.23% [288]. The measurement is based on a 3-dimensional template fit, determining the top-quark mass, the global jet energy scale and a b -to-light jet energy scale factor. The most precise CMS result in the lepton+jets channel uses an ideogram method and comes from a so-called ‘hybrid’ approach in which the prior knowledge about the jet energy scale is incorporated as a Gaussian constraint, with a width determined by the uncertainty on the jet energy corrections. In 19.7 fb^{-1} of $\sqrt{s} = 8 \text{ TeV}$ data, CMS achieves a total uncertainty of 0.30% with a statistical component of 0.09% with the hybrid approach [289]. Using this same method, CMS has released a top-mass measurement from $\sqrt{s} = 13 \text{ TeV}$ data. Using 35.9 fb^{-1} of lepton+jets events they measure the top mass with a precision of 0.36%, with a statistical component of 0.05% [290]. The measurements at $\sqrt{s} = 13 \text{ TeV}$ include, for the first time, an uncertainty due to ‘color reconnection’ [291, 292]. In this same dataset, CMS has extracted a top mass from highly boosted top-quark decays by selecting events in which the hadronic-side top decay is reconstructed as a single jet with $P_T > 400 \text{ GeV}$. The cross section as a function of jet mass is unfolded at the particle level to extract a top mass with a precision of 1.4% [293].

The template method is complemented by the ‘matrix element’ method. This method was first applied by the $D\bar{O}$ Collaboration [294], and is similar to a technique originally suggested by Kondo *et al.* [275] and Dalitz and Goldstein [295]. In the matrix element method a probability for each event is calculated as a function of the top-quark mass, using a LO matrix element for the production and decay of $t\bar{t}$ pairs. The *in situ* calibration of dijet pairs to the $W \rightarrow jj$ hypothesis is now also used with the matrix element technique to constrain the jet energy scale uncertainty. In the lepton+jets channel, $D\bar{O}$ uses the full Tevatron dataset of 9.7 fb^{-1} and yields an uncertainty of about 0.43% [296].

In the dilepton channel, the signal to background is typically very good, but reconstruction of the mass is non-trivial because there are two neutrinos in the final state, yielding a kinematically unconstrained system. A variety of techniques have been developed to handle this. An analytic solution to the problem has been proposed [297], but this has not yet been used in the mass measurement. One of the most precise measurements in the dilepton channel comes from using the invariant mass of the charged lepton and b -quark system ($M_{\ell b}$), which is sensitive to the top-quark mass and avoids the kinematic difficulties of the two-neutrino final state. In 4.6 fb^{-1} of $\sqrt{s} = 7 \text{ TeV}$ data, ATLAS has measured the top-quark mass in the dilepton channel to a precision of 0.53% using a template fit to the $M_{\ell b}$ distribution [298]. Using 19.7 fb^{-1} of data at $\sqrt{s} = 8 \text{ TeV}$, CMS has released [299] a mass measurement in the dilepton channel based on a simultaneous fit to $M_{\ell b}$ and a transverse-mass-like variable M_{T2} [300]. The most precise result in this analysis, which comes from a linear combination of fits with the jet energy scale fixed at its nominal value and one that simultaneously determines the top mass and jet energy scale, has a total uncertainty of 0.54%. At the LHC, because of their precision, these techniques have largely displaced a number of earlier techniques in the dilepton channel, though these techniques are still included, and described, in the combined results from CMS, reported in Ref. [289].

In the neutrino weighting technique, used by CDF to analyze the full Run 2 dilepton dataset of 9.1 fb^{-1} , a weight is assigned by assuming a top-quark mass value and applying energy-momentum conservation to the top-quark decay, resulting in up to four possible pairs of solutions for the neutrino and anti-neutrino momenta. The missing E_T calculated in this way is then compared to the observed missing E_T to assign a weight [305]. The CDF result achieves a precision of 1.8% using a combination of neutrino weighting and an ‘alternative mass’, which is insensitive to the jet energy scale [306]. The alternative mass depends on the angles between the leptons and the leading jets and the lepton four-momenta.

Table 61.2: Measurement and 95% C.L. upper limits of the W helicity in top-quark decays. The table includes both preliminary, as of September 2023, and published results. A full set of published results, including the results obtained at the Tevatron, is given in the Listings.

W Helicity	Source	$\int \mathcal{L} dt$ (fb^{-1})	Ref.	Method
$\mathcal{F}_0 = 0.67 \pm 0.07$	ATLAS (7 TeV)	1.0	[277]	$\cos \theta^*$ 3-param
$\mathcal{F}_0 = 0.682 \pm 0.045$	CMS (7 TeV)	5.0	[278]	$\cos \theta^*$ 3-param
$\mathcal{F}_0 = 0.626 \pm 0.059$	ATLAS+CMS (7 TeV)	2.2	[279]	$\cos \theta^*$ 3-param
$\mathcal{F}_0 = 0.709 \pm 0.019$	ATLAS (8 TeV)	20.2	[280]	$\cos \theta^*$ 3-param
$\mathcal{F}_0 = 0.681 \pm 0.026$	CMS (8 TeV)	19.8	[281]	$\cos \theta^*$ 3-param
$\mathcal{F}_0 = 0.653 \pm 0.029$	CMS (8 TeV)	19.7	[282]	$\cos \theta^*$ 3-param
$\mathcal{F}_0 = 0.720 \pm 0.054$	CMS (8 TeV)	19.7	[283]	$\cos \theta^*$ 3-param
$\mathcal{F}_0 = 0.693 \pm 0.014$	ATLAS+CMS (8 TeV)	20	[284]	$\cos \theta^*$ 3-param
$\mathcal{F}_0 = 0.684 \pm 0.015$	ATLAS (13 TeV)	139	[285]	$\cos \theta^*$ 3-param
$\mathcal{F}_+ = 0.01 \pm 0.05$	ATLAS (7 TeV)	1.0	[277]	$\cos \theta^*$ 3-param
$\mathcal{F}_+ = 0.008 \pm 0.018$	CMS (7 TeV)	5.0	[278]	$\cos \theta^*$ 3-param
$\mathcal{F}_+ = 0.015 \pm 0.034$	ATLAS+CMS (7 TeV)	2.2	[279]	$\cos \theta^*$ 3-param
$\mathcal{F}_+ = -0.008 \pm 0.014$	ATLAS (8 TeV)	20.2	[280]	$\cos \theta^*$ 3-param
$\mathcal{F}_+ = -0.004 \pm 0.015$	CMS (8 TeV)	19.8	[281]	$\cos \theta^*$ 3-param
$\mathcal{F}_+ = 0.018 \pm 0.027$	CMS (8 TeV)	19.7	[282]	$\cos \theta^*$ 3-param
$\mathcal{F}_+ = -0.018 \pm 0.022$	CMS (8 TeV)	19.7	[283]	$\cos \theta^*$ 3-param
$\mathcal{F}_+ = -0.008 \pm 0.007$	ATLAS+CMS (8 TeV)	20	[284]	$\cos \theta^*$ 3-param
$\mathcal{F}_+ = -0.002 \pm 0.014$	ATLAS (13 TeV)	139	[285]	$\cos \theta^*$ 3-param

Table 61.3: Measurements of top-quark mass from Tevatron and LHC. The results are a selection of both published and preliminary (not yet submitted for publication as of September 2023) measurements. For a complete set of published results see the Listings. Statistical uncertainties are listed first, followed by systematic uncertainties.

m_t (GeV/ c^2)	Source	$\int \mathcal{L} dt$ fb^{-1}	Ref.	Channel
$172.08 \pm 0.25 \pm 0.41$	ATLAS	20.2	[288]	ℓ +jets+ $\ell\ell$ +All jets
$172.44 \pm 0.13 \pm 0.47$	CMS	19.7	[289]	ℓ +jets+ $\ell\ell$ +All jets
$172.35 \pm 0.16 \pm 0.48$	CMS	19.7	[289]	ℓ +jets
$172.34 \pm 0.20 \pm 0.70$	CMS	35.9	[301]	$\ell\ell$
$173.72 \pm 0.55 \pm 1.01$	ATLAS	20.2	[302]	All jets
$172.25 \pm 0.08 \pm 0.62$	CMS	35.9	[290]	ℓ +jets
$172.6 \pm 0.4 \pm 2.4$	CMS	35.9	[293]	Boosted jets
$172.13 \pm 0.32^{+0.69}_{-0.70}$	CMS	35.9	[303]	Single top
$174.30 \pm 0.35 \pm 0.54$	CDF,D0 (I+II)	≤ 9.7	[304]	publ. or prelim.
$173.34 \pm 0.27 \pm 0.71$	Tevatron+LHC	$\leq 8.7 + \leq 4.9$	[29]	publ. or prelim.
$172.52 \pm 0.14 \pm 0.30$	ATLAS+CMS	$\leq 5 + \leq 20$	[1]	prelim.

In the all-jets channel there is no ambiguity due to neutrino momenta, but the signal to background is significantly poorer due to the severe QCD multijets background. The emphasis therefore has been on background modeling, and reduction through event selection. The most recent measurement in the all-jets channel, by CMS in 35.9 fb^{-1} of $\sqrt{s} = 13 \text{ TeV}$ data [301], uses an ideogram method and a 2-dimensional simultaneous fit for m_t and the jet energy scale to extract the top-quark mass and achieves a precision of 0.36%. A measurement from ATLAS [302] uses a template fit to the ratio of three-jet (m_t) to two-jet (M_W) mass in the all-hadronic channel, the two-jet denominator provides an *in situ*, fit to the $W \rightarrow jj$ hypothesis. In 20.2 fb^{-1} of data at $\sqrt{s} = 8 \text{ TeV}$, the result has a precision of 0.65%. A measurement from CDF in 9.3 fb^{-1} uses a two-dimensional template fit and achieves a precision of 1.1% [307].

The CMS Collaboration extracted a top-quark mass measurement from single-top events, something not previously done because of the poor signal to background ratio. The mass is extracted from the invariant mass of the muon, bottom quark, and missing transverse energy. The first measurement with 19.7 fb^{-1} of data at $\sqrt{s} = 8 \text{ TeV}$, achieved a precision of 0.71% [308]. A more recent measurement in 35.9 fb^{-1} of data at $\sqrt{s} = 13 \text{ TeV}$ achieves 0.44% precision [303].

A dominant systematic uncertainty in these methods is the understanding of the jet energy scale, and so several techniques have been developed that have little sensitivity to the jet energy scale uncertainty. In addition to Reference [306] mentioned above, these include the measurement of the top-quark mass using the following techniques: Fitting of the lepton p_T spectrum of can-

didate events [309]; fitting of the transverse decay length of the b -jet (L_{xy}) [310]; fitting the invariant mass of a lepton from the W -decay and a muon from the semileptonic b decay [311, 312], kinematic properties of secondary vertices from b -quark fragmentation [313], the invariant mass of the $J/\psi + \ell$ system in events in which a b -quark fragments to a J/ψ particle [314], fitting the b -jet energy peak [315], and dilepton kinematics in $e\mu$ events [316].

Several measurements have now been made in which the top-quark mass is extracted from the measured $t\bar{t}$ cross section using the theoretical relationship between the mass and the production cross section. These determinations make use of predictions calculated at higher orders, where the top mass enters as an input parameter defined in a given scheme. At variance with the usual methods, which involve the kinematic properties of the final states and therefore the pole mass, this approach can also directly determine a short-distance mass, such as the $\overline{\text{MS}}$ mass [317]. With an alternative method ATLAS extracted the top-quark pole mass using $t\bar{t}$ events with at least one additional jet, basing the measurement on the relationship between the differential rate of gluon radiation and the mass of the quark [318]. A similar analysis by CMS used the differential cross section as a function of the invariant mass of the $t\bar{t}$ system and the leading jet not associated with the top decays [319].

Each of the experiments has produced a measurement combining its various results. The combined measurement from CMS with up to 19.7 fb^{-1} of data achieves statistical and systematic uncertainties of 0.08% and 0.27%, respectively [289]. The combined measurement from ATLAS, with up to 20.3 fb^{-1} yields statistical and systematic uncertainties of 0.14% and 0.24%, re-

spectively [288]. CDF has combined measurements with up to 9.3 fb^{-1} [320] and achieves a statistical precision of 0.33% and a systematic uncertainty of 0.43%. DØ achieves a 0.33% statistical+JES and a 0.28% systematic uncertainty by combining results in 9.7 fb^{-1} [321].

Combined measurements from the Tevatron experiments and from the LHC experiments take into account the correlations between different measurements from a single experiment and between measurements from different experiments. The Tevatron average [304], using up to 9.7 fb^{-1} of data, now has a precision of 0.37%. The LHC combination, using up to 4.9 fb^{-1} of data, has a precision of 0.56% [322], where more work on systematic uncertainties is required. A Tevatron-LHC combination has been released, combining the results of all four experiments, using the full Tevatron dataset and the $\sqrt{s} = 7 \text{ TeV}$ LHC data, with a resulting precision of 0.44% [29]. Recently, ATLAS and CMS have released a combinations of fifteen individual top quark mass measurements in semi-leptonic and hadronic decays of the top quark, and a measurement using events enriched in single top quark production via the electroweak t -channel. The data sets used correspond to an integrated luminosity of up to 5 and 20 fb^{-1} , recorded at 7 and 8 TeV, respectively, yielding a precision of 0.33 GeV (0.2%) [1].

The direct measurements of the top-quark mass, such as those shown in Table 61.3, correspond to the parameter used in the Monte Carlo generators, which is closely related to the pole mass [8]. The relation between the pole mass and short-distance masses, such as \overline{MS} , is affected by non-perturbative effects. Recent calculations evaluate the size of this ambiguity to be below 250 MeV and therefore still smaller than the current measurement uncertainty [323, 324]. ATLAS has recently performed a ‘calibration’ of the top mass parameter in POWHEG + PYTHIA 8 with respect to the so-called ‘MSR’ mass scheme [325]. Using simulated lepton+jets events and the mass distribution of large-radius jets containing the three quarks from the hadronically decaying top quark, they find a mass difference between the Monte Carlo mass and the MSR mass of 80 MeV with large uncertainties [326].

As a result of renormalization at higher-orders in perturbation theory, the top quark mass depends on the scale at which it is evaluated. The CMS collaboration has made the first measurement of the so-called running of the top-quark mass in the \overline{MS} scheme [327]. The running mass is extracted from a measurement of the differential cross section as a function of the $t\bar{t}$ invariant mass, unfolded back to the parton level, in $e\mu$ final states. The running mass varies by about 15% from $M_{t\bar{t}} = 400 \text{ GeV}$ to $M_{t\bar{t}} \approx 1 \text{ TeV}$, in good agreement with the renormalization group calculation at one-loop level. Compared to the hypothesis of no running, the significance of the measured running is 2.6σ . However, caveats of such an interpretation have been raised as a result of the large theoretical uncertainties [328].

With the discovery of a Higgs boson at the LHC with a mass of about $125 \text{ GeV}/c^2$ [329, 330], the precision measurement of the top-quark mass takes a central role in the question of the stability of the electroweak vacuum because top-quark radiative corrections tend to drive the Higgs quartic coupling, λ , negative, potentially leading to an unstable vacuum. A calculation at NNLO [2] leads to the conclusion of vacuum stability for a Higgs mass satisfying $M_H \geq 129.4 \pm 5.6 \text{ GeV}/c^2$ [331]. Given the uncertainty, a Higgs mass of $125 \text{ GeV}/c^2$ satisfies the limit, but the central values of the Higgs and top-quark masses put the electroweak vacuum squarely in the metastable region. The uncertainty is dominated by the precision of the top-quark mass measurement and its interpretation as the pole mass. For more details, see the Higgs boson review in this volume.

As a test of the CPT -symmetry, the mass difference of top- and antitop-quarks $\Delta m_t = m_t - m_{\bar{t}}$, which is expected to be zero, can be measured. CDF measures the mass difference in 8.7 fb^{-1} of 1.96 TeV data in the lepton+jets channel using a template method to find $\Delta m_t = -1.95 \pm 1.11(\text{stat.}) \pm 0.59(\text{syst.}) \text{ GeV}/c^2$ [332] while DØ uses 3.6 fb^{-1} of lepton+jets events and the matrix element method with at least one b -tag. They find $\Delta m_t = 0.8 \pm 1.8(\text{stat.}) \pm 0.5(\text{syst.}) \text{ GeV}/c^2$ [333]. In 4.7 fb^{-1} of 7 TeV data, ATLAS measures the mass difference in lepton+jets events with a double b -tag requirement and hence very low back-

ground to find $\Delta m_t = 0.67 \pm 0.61(\text{stat.}) \pm 0.41(\text{syst.}) \text{ GeV}/c^2$ [334]. CMS measures the top-quark mass difference in 5 fb^{-1} of 7 TeV data in the lepton+jets channel and finds $\Delta m_t = -0.44 \pm 0.46(\text{stat.}) \pm 0.27(\text{syst.}) \text{ GeV}/c^2$ [335]. They repeat this measurement with 19.6 fb^{-1} of 8 TeV data to find $\Delta m_t = -0.15 \pm 0.19(\text{stat.}) \pm 0.09(\text{syst.}) \text{ GeV}/c^2$ [336]. Now that the top mass has been measured in single-top events, the mass difference can be measured by tagging the top- or anti-top quark with the lepton charge. In 35.9 fb^{-1} of 13 TeV single-top candidate events CMS measures the mass ratio and difference to be $0.995_{-0.006}^{+0.005}$ and $0.83_{-1.01}^{+0.77} \text{ GeV}$, respectively [303]. All measurements are consistent with the SM expectation.

61.2.5.2 Width

Observation of top-quark spin correlations requires a top-quark lifetime less than the spin decorrelation timescale [337]. The top-quark width, inversely proportional to its lifetime, is expected to be of order $1 \text{ GeV}/c^2$ (Eq. 1). Early measurements made at CDF [338] and CMS [339] established confidence-level intervals for the width, but did not have the sensitivity to make a direct measurement.

The first direct measurement comes from an ATLAS analysis that directly fits reconstructed lepton+jets events in 20.2 fb^{-1} of data at $\sqrt{s} = 8 \text{ TeV}$. They find $\Gamma_t = 1.76 \pm 0.33_{-0.68}^{+0.79} \text{ GeV}/c^2$ [340]. A more recent measurement from ATLAS with 139 fb^{-1} of data at $\sqrt{s} = 13 \text{ TeV}$ [341], uses a template fit to the lepton- b -quark invariant mass in dilepton final states. The result, $\Gamma_t = (1.9 \pm 0.5) \text{ GeV}/c^2$, is the most precise measurement to date.

The total width of the top-quark can also be determined from the partial decay width $\Gamma(t \rightarrow Wb)$ and the branching fraction $B(t \rightarrow Wb)$. DØ obtains $\Gamma(t \rightarrow Wb)$ from the measured t -channel cross section for single top-quark production in 5.4 fb^{-1} , and $B(t \rightarrow Wb)$ is extracted from a measurement of the ratio $R = B(t \rightarrow Wb)/B(t \rightarrow Wq)$ in $t\bar{t}$ events in lepton+jets channels with 0, 1 and 2 b -tags. Assuming $B(t \rightarrow Wq) = 1$, where q includes any kinematically accessible quark, the result is: $\Gamma_t = 2.00_{-0.43}^{+0.47} \text{ GeV}/c^2$ which translates to a top-quark lifetime of $\tau_t = (3.29_{-0.63}^{+0.90}) \times 10^{-25} \text{ s}$. Assuming a high mass fourth generation b' quark and unitarity of the four-generation quark-mixing matrix, they set the first upper limit on $|V_{tb'}| < 0.59$ at 95% C.L. [342]. A similar analysis has performed by CMS in 19.7 fb^{-1} of $\sqrt{s} = 8 \text{ TeV}$ data. It provides a better determination of the total width with respect to the measurement by DØ giving $\Gamma_t = 1.36 \pm 0.02(\text{stat.})_{-0.11}^{+0.14}(\text{syst.}) \text{ GeV}/c^2$ [110].

61.2.5.3 Yukawa coupling

The top-Higgs Yukawa coupling is expected to be the largest among all Yukawa couplings. It can be accessed directly by measurements of the $t\bar{t}$ cross section in association with a Higgs boson, $t\bar{t}h$, or indirectly via loop processes in $h \rightarrow \gamma\gamma$ or $h \rightarrow WW$ decays or in the rare process of $t\bar{t}t\bar{t}$ production. A discussion of the former can be found in this review, See Sec. 11.3.3 of "Status of Higgs Boson Physics", in this Review. Searches for and recently the observation of $t\bar{t}t\bar{t}$ production is discussed in 61.2.1.3.

61.2.5.4 Top-Quark Electroweak Charges and Couplings

The top quark is the only quark whose electric charge has not been measured through production at threshold in e^+e^- collisions. Furthermore, it is the only quark whose electromagnetic coupling has not been observed and studied until recently. Since the CDF and DØ analyses on top-quark production did not associate the b , \bar{b} , and W^\pm uniquely to the top or antitop, decays such as $t \rightarrow W^+ \bar{b}$, $\bar{t} \rightarrow W^- b$ were not excluded. A charge $4/3$ quark of this kind is consistent with current electroweak precision data. The $Z \rightarrow \ell^+ \ell^-$ and $Z \rightarrow b\bar{b}$ data, in particular the discrepancy between A_{LR} from SLC at SLAC and $A_{FB}^{0,b}$ of b -quarks and $A_{FB}^{0,\ell}$ of leptons from LEP at CERN, can be fitted with a top quark of mass $m_t = 270 \text{ GeV}/c^2$, provided that the right-handed b quark mixes with the isospin $+1/2$ component of an exotic doublet of charge $-1/3$ and $-4/3$ quarks, $(Q_1, Q_4)_R$ [343, 344]. Also the third component of the top quark's weak isospin has not been measured so far.

DØ studied the top-quark charge in double-tagged lepton+jets

events, CDF did it in single tagged lepton+jets and dilepton events. Assuming the top- and antitop-quarks have equal but opposite electric charge, then reconstructing the charge of the b -quark through jet charge discrimination techniques, the $|Q_{top}| = 4/3$ and $|Q_{top}| = 2/3$ scenarios can be differentiated. For the exotic model of Chang *et al.* [344] with a top-quark charge $|Q_{top}| = 4/3$, CDF excluded the model at 99% C.L. [345] in 5.6 fb^{-1} , while $D\bar{O}$ excluded the model at a significance greater than 5 standard deviations using 5.3 fb^{-1} and set an upper limit of 0.46 on the fraction of such quarks in the selected sample [346]. These results indicate that the observed particle is indeed consistent with being a SM $|Q| = 2/3$ quark.

In 2.05 fb^{-1} at $\sqrt{s} = 7 \text{ TeV}$, ATLAS performed a similar analysis, reconstructing the b -quark charge either via a jet-charge technique or via the lepton charge in soft muon decays in combination with a kinematic likelihood fit. They measure the top-quark charge to be $0.64 \pm 0.02(\text{stat.}) \pm 0.08(\text{syst.})$ from the charges of the top-quark decay products in single lepton $t\bar{t}$ events, and hence exclude the exotic scenario with charge $-4/3$ at more than 8σ [347].

In 4.6 fb^{-1} at $\sqrt{s} = 7 \text{ TeV}$, CMS discriminates between the SM and the exotic top-quark charge scenario in the muon+jets final states in $t\bar{t}$ events. They exploit the charge correlation between high- p_t muons from W -boson decays and soft muons from B -hadron decays in b -jets. Using an asymmetry technique, where $A = -1$ represents the exotic $Q = -4/3$ scenario and $A = +1$ the SM $Q = +2/3$ scenario, they find $A_{meas} = 0.97 \pm 0.12(\text{stat.}) \pm 0.31(\text{syst.})$, which agrees with the Standard Model expectation and excludes the exotic scenario at 99.9% C.L. [348].

$t\bar{t}\gamma$ production:

The electromagnetic or the weak coupling of the top quark can be probed directly by investigating $t\bar{t}$ events with an additional gauge boson, such as $t\bar{t}\gamma$, $t\bar{t}W$, and $t\bar{t}Z$ events. The corresponding coupling can be extracted from the corresponding cross section, cross section ratios with respect to the $t\bar{t}$ cross section or extracted from effective field theory (EFT) fits to various measured distributions and differential cross sections.

CDF performed a first search for $t\bar{t}\gamma$ production in events containing a lepton, a photon, significant missing transverse momentum, and a jet identified as containing a b -quark and at least three jets and large total transverse energy in 6.0 fb^{-1} . They reported evidence for the observation of $t\bar{t}\gamma$ production with a cross section $\sigma_{t\bar{t}\gamma} = 0.18 \pm 0.08 \text{ pb}$ and a ratio of $\sigma_{t\bar{t}\gamma}/\sigma_{t\bar{t}} = 0.024 \pm 0.009$ [349].

ATLAS performed a first measurement of the $t\bar{t}\gamma$ cross section in pp collisions at $\sqrt{s} = 7 \text{ TeV}$ using 4.6 fb^{-1} of data. Events are selected that contain a large transverse momentum electron or muon and a large transverse momentum photon. The production of $t\bar{t}\gamma$ events was observed with a significance of 5.3 standard deviations. The resulting cross section times branching ratio into the single lepton channel for $t\bar{t}\gamma$ production with a photon with transverse momentum above 20 GeV is $\sigma^{fid.}(t\bar{t}\gamma) \times BR = 63 \pm 8(\text{stat.})_{-13}^{+17}(\text{syst.}) \pm 1(\text{lumi.}) \text{ pb}$ per lepton flavor [350], which is consistent with leading-order theoretical calculations.

At 8 TeV, ATLAS has used 20.2 fb^{-1} of data to measure the $t\bar{t}\gamma$ cross section with a photon above 15 GeV and $|\eta| < 2.37$. The fiducial cross section is measured to be $139 \pm 18 \text{ fb}$ [351], in good agreement with the NLO prediction [352]. Using 19.7 fb^{-1} of data at 8 TeV, CMS performed a similar measurement of the $t\bar{t}\gamma$ production cross section in the lepton+jets decay mode with a photon transverse momentum above 25 GeV and $|\eta| < 1.44$. They obtain a normalized cross section $\mathcal{R} = \sigma_{t\bar{t}+\gamma}/\sigma_{t\bar{t}} = (5.7 \pm 1.8) \times 10^{-4}$ in e -jets and $(4.7 \pm 1.3) \times 10^{-4}$ in μ -jets. The fiducial $t\bar{t}\gamma$ cross section is obtained by multiplying by the measured $t\bar{t}$ fiducial cross section of $244.9 \pm 1.4(\text{stat.})_{-5.5}^{+6.3}(\text{syst.}) \pm 6.4(\text{lumi.}) \text{ pb}$. Extrapolating to the full phase space, the result is $\sigma_{t\bar{t}\gamma} \times BR = (515 \pm 108) \text{ fb}$, per lepton+jets final state [353], in good agreement with the theoretical prediction.

At $\sqrt{s} = 13 \text{ TeV}$, using 36.1 fb^{-1} of single-lepton and dilepton events with exactly one photon, ATLAS measures the $t\bar{t}\gamma$ cross section. They employ neural network algorithms to separate the signal from the backgrounds. The fiducial cross-sections are measured to be $521 \pm 9(\text{stat.}) \pm 41(\text{syst.}) \text{ fb}$ and $69 \pm 3(\text{stat.}) \pm 4(\text{syst.}) \text{ fb}$ for the single-lepton and dilepton channels, respectively. The differential cross-sections are measured as a function of photon trans-

verse momentum, photon absolute pseudorapidity, and angular distance between the photon and its closest lepton in both channels, as well as azimuthal opening angle and absolute pseudorapidity difference between the two leptons in the dilepton channel. All measurements are in agreement with the theoretical predictions [354].

ATLAS uses 139 fb^{-1} of $\sqrt{s} = 13 \text{ TeV}$ $e\mu + \gamma$ events with at least two jets, out of which at least one is b -tagged, to measure the inclusive and differential cross-sections for the production of a top-quark pair in association with a photon. This analysis is sensitive to both processes, $t\bar{t}\gamma + tW\gamma$. The fiducial cross-section is measured to be $39.6_{-2.3}^{+2.7} \text{ fb}$ in good agreement with the dedicated theoretical calculation provided by the authors of refs. [355,356], which predicts a value of $\sigma_{fid} = 38.50_{-2.18}^{+0.56}(\text{scale})_{-1.18}^{+1.04}(\text{PDF}) \text{ fb}$ for the chosen fiducial phase space. Differential cross-sections as functions of several observables are compared to state-of-the-art Monte Carlo simulations and NLO theoretical calculations. These include cross-sections as functions of the photon transverse momentum and absolute pseudorapidity and angular variables related to the photon and the leptons and between the two leptons in the event. All measurements are in agreement with the predictions [357].

Recently, CMS used 137 fb^{-1} of data to measure the $t\bar{t}\gamma$ cross section. In the lepton-plus-jets channel, they perform measurements in a fiducial volume defined at the particle level. Events with an isolated, highly energetic lepton, at least three jets from the hadronization of quarks, among which at least one is b -tagged, and one isolated photon are selected. The inclusive fiducial $t\bar{t}\gamma$ cross section, for a photon with transverse momentum greater than 20 GeV and pseudorapidity $|\eta| < 1.4442$, is measured to be $\sigma_{t\bar{t}\gamma} = 798 \pm 7(\text{stat}) \pm 48(\text{syst}) \text{ fb}$, in good agreement with the prediction from the standard model at NLO in QCD [358]. The differential cross sections are also measured as a function of several kinematic observables such as the transverse momentum of the photon, its rapidity, or the opening angle between the photon and the lepton. The measurements on detector-level are also interpreted in terms of limits on the Wilson coefficients in the context of the standard model effective field theory. The confidence intervals for the Wilson coefficients c_{tZ} and c_{tZ}^I are the most stringent to date. Using the same dataset, in the dilepton channel, an inclusive cross section of $174.4 \pm 2.5(\text{stat}) \pm 6.1(\text{syst}) \text{ fb}$ is measured in a signal region with at least one b -tagged jet and exactly one photon with transverse momentum above 20 GeV [359]. In the same analysis, differential cross sections are measured as a function of several kinematic observables of the photon, leptons, and jet, and compared to standard model predictions. Combinations of the measurements in the l+jets and the dilepton channels are also interpreted in the standard model effective field theory framework, yielding the most stringent limits for the Wilson coefficients c_{tZ} and c_{tZ}^I to date.

$tq\gamma$ production:

Using the full Run-2 data set of 139 fb^{-1} at 13 TeV, ATLAS observes the production of single top quark together with a photon. The analysis uses the presence of a forward jet, characteristic of t-channel production, and separates the signal from the background with neural networks. Requiring a photon with transverse momentum larger than 20 GeV and within the detector acceptance, the fiducial cross section is measured to be $688 \pm 23(\text{stat.})_{-71}^{+75}(\text{syst.}) \text{ fb}$, to be compared with the Standard Model prediction of $515_{-42}^{+36} \text{ fb}$ at NLO in QCD [360]. In 35.9 fb^{-1} of lepton-plus-photon-plus-jets events, CMS manages to establish the first evidence for the associated production of a single-top quark and a photon at $\sqrt{s} = 13 \text{ TeV}$. They employ a multivariate discriminant based on topological and kinematic event properties to separate signal from background processes. An excess above the background-only hypothesis is observed, with a significance of 4.4 standard deviations. A fiducial cross section is measured for isolated photons with transverse momentum greater than 25 GeV in the central region of the detector. The measured product of the cross section and branching fraction is $\sigma(pp \rightarrow tq\gamma)B(t \rightarrow \mu\gamma b) = 115 \pm 17(\text{stat}) \pm 30(\text{syst}) \text{ fb}$, which is consistent with the SM prediction [361]. A precision test of the vector and axial vector couplings in $t\bar{t}\gamma$ events or searches for

possible tensor couplings of top-quarks to photons will only be feasible with an integrated luminosity of several hundred fb^{-1} in the future [362].

$t\bar{t}Z$ and $t\bar{t}W$ production:

ATLAS and CMS have also studied the associate production of top-antitop quark pairs along with an electroweak gauge boson, $t\bar{t}W$ or $t\bar{t}Z$, where in the Standard Model the W -boson is expected to be produced via initial state radiation, while the Z -boson can also be radiated from a final-state top-quark and hence provides sensitivity to the top-quark neutral current weak gauge coupling, which implies a sensitivity to the third component of the top-quark's weak isospin, which has not been measured so far.

CMS performed measurements of the $t\bar{t}W$ and $t\bar{t}Z$ cross section at $\sqrt{s} = 7$ TeV with 5 fb^{-1} , yielding $\sigma_{t\bar{t}V} = 0.43^{+0.17}_{-0.15}(\text{stat.})^{+0.09}_{-0.07}(\text{syst.})$ pb ($V = Z, W$) and $\sigma_{t\bar{t}Z} = 0.28^{+0.14}_{-0.11}(\text{stat.})^{+0.06}_{-0.03}(\text{syst.})$ fb, at about 3 standard deviations significance [363] and compatible with the SM expectations of $0.306^{+0.031}_{-0.053}$ pb and $0.137^{+0.012}_{-0.016}$ pb, respectively [364, 365]. ATLAS performed a similar analysis with 4.7 fb^{-1} in the three-lepton channel and set an upper limit of 0.71 pb at 95% C.L. [366].

Using 20.3 fb^{-1} of 8 TeV data, ATLAS performs a simultaneous measurement of the $t\bar{t}W$ and $t\bar{t}Z$ cross section. They observe the $t\bar{t}W$ and $t\bar{t}Z$ production at the 5.0σ and 4.2σ level, respectively, yielding $\sigma_{t\bar{t}W} = 369^{+100}_{-91}$ fb and $\sigma_{t\bar{t}Z} = 176^{+58}_{-52}$ fb [367]. CMS performs an analysis where signal events are identified by matching reconstructed objects in the detector to specific final state particles from $t\bar{t}W$ and $t\bar{t}Z$ decays using 19.5 fb^{-1} of 8 TeV data. They obtain $\sigma_{t\bar{t}W} = 382^{+117}_{-102}$ fb and $\sigma_{t\bar{t}Z} = 242^{+65}_{-55}$ fb, yielding a significance of 4.8 and 6.4 standard deviation, respectively [368]. These measurements are used to set bounds on five anomalous dimension-six operators that would affect the $t\bar{t}W$ and $t\bar{t}Z$ cross sections.

The most recent measurements in these channels are made at 13 TeV from ATLAS and CMS in multilepton final states. ATLAS made a measurement using 36.1 fb^{-1} of events with two, three or four leptons. In multiple regions, the $t\bar{t}Z$ and $t\bar{t}W$ cross sections are simultaneously measured using a combined fit to all regions, yielding $\sigma_{t\bar{t}Z} = 0.95 \pm 0.08(\text{stat}) \pm 0.10(\text{syst})$ pb and $\sigma_{t\bar{t}W} = 0.87 \pm 0.13(\text{stat}) \pm 0.14(\text{syst})$ pb [369] to be compared with the NLO+NNLL (QCD) and NLO (EW) SM predictions, $\sigma_{t\bar{t}W} = 579^{+14\%}_{-9\%}$ fb and $\sigma_{t\bar{t}Z} = 811^{+11\%}_{-10\%}$ fb [43]. Recently, ATLAS uses 139 fb^{-1} in three and four lepton events to measure the inclusive and differential $t\bar{t}Z$ cross section. The inclusive cross section is measured to be $\sigma_{t\bar{t}Z} = 0.99 \pm 0.05(\text{stat.}) \pm 0.08(\text{syst.})$ pb [370], in agreement with the most precise theoretical predictions. The differential measurements are presented as a function of a number of kinematic variables which probe the kinematics of the $t\bar{t}Z$ system. Overall, good agreement is observed between the unfolded data and the predictions. Using the same dataset of 140 fb^{-1} , ATLAS performs an improved measurement in both, the inclusive and differential $t\bar{t}Z$ production cross sections. Final states with two, three and four isolated leptons (electrons or muons) are targeted. The inclusive cross section is measured to be $\sigma_{t\bar{t}Z} = 0.86 \pm 0.04(\text{stat.}) \pm 0.04(\text{syst.})$ pb and found to be in agreement with the most advanced Standard Model predictions [371]. The improvement with respect to the previous measurement using the same dataset is mainly in a better machine learning-based separation of signal and background, the addition of a 2-lepton signal region, and better modelling. The differential measurements are presented as a function of a number of observables that probe the kinematics of the $t\bar{t}Z$ system. Both absolute and normalised differential cross section measurements are performed at particle- and parton-level for specific fiducial volumes, and are compared with theoretical predictions at NLO+NNLL. The results are interpreted in the framework of the Standard Model Effective Field Theory and used to set limits on a large number of dimension-6 operators involving the top quark. CMS uses 35.9 fb^{-1} of $\sqrt{s} = 13$ TeV data to measure $\sigma_{t\bar{t}W} = 0.77^{+0.12}_{-0.11}(\text{stat.})^{+0.13}_{-0.12}(\text{syst.})$ pb and $\sigma_{t\bar{t}Z} = 0.99^{+0.09}_{-0.08}(\text{stat.})^{+0.12}_{-0.10}(\text{syst.})$ pb production cross sections, and significances over the background-only hypotheses of 5.5σ and 9.5σ , respectively [372], firmly establishing the observation of these processes. CMS measured the inclusive $t\bar{t}Z$ cross

section in 77.5 fb^{-1} of events with three or four charged leptons, and the Z boson is detected through its decay to an oppositely charged lepton pair. The production cross section is measured to be $\sigma(t\bar{t}Z) = 0.95 \pm 0.05(\text{stat}) \pm 0.06(\text{syst})$ pb. This measurement includes differential cross sections as functions of the transverse momentum of the Z boson and the angular distribution of the negatively charged lepton from the Z boson decay, which characterise the $t\bar{t}Z$ process in detail for the first time, as well as stringent direct limits on the anomalous tZ couplings [373]. Very recently, using the complete Run-2 dataset of 138 fb^{-1} , CMS searches for signs of new physics, interpreted in effective field theory, in $t\bar{t}$ events produced in association with a Lorentz-boosted Z or Higgs boson [374]. Selected events contain a single lepton and hadronic jets, including two identified with the decay of bottom quarks, plus an additional large-radius jet with high transverse momentum identified as a Z or Higgs boson decaying to a bottom quark pair. Machine learning techniques are employed to discriminate between $t\bar{t}Z$ or $t\bar{t}H$ events and events from background processes, which are dominated by $t\bar{t}$ -jets production. No indications of new physics are observed. The signal strengths of boosted $t\bar{t}Z$ and $t\bar{t}H$ production are measured, and upper limits are placed on the $t\bar{t}Z$ and $t\bar{t}H$ differential cross sections as functions of the Z or Higgs boson transverse momentum, expressed as limits on eight possible dimension-six operators.

Recently, CMS measured the $t\bar{t}W$ cross section in 138 fb^{-1} at 13 TeV in events with two or three leptons (electrons and muons) and additional jets. In events with two leptons, a multiclass neural network is used to distinguish between the signal and background processes. Events with three leptons are categorized based on the number of jets and of jets originating from b quark hadronization, and the lepton charges. The inclusive $t\bar{t}W$ production cross section in the full phase space is measured to be $868 \pm 40(\text{stat}) \pm 51(\text{syst})$ fb. The $t\bar{t}W^+$ and $t\bar{t}W^-$ cross sections are also measured as $553 \pm 30(\text{stat}) \pm 30(\text{syst})$ fb and $343 \pm 26(\text{stat}) \pm 25(\text{syst})$ fb, respectively, and the corresponding ratio of the two cross sections is found to be $1.61 \pm 0.15(\text{stat})^{+0.07}_{-0.05}(\text{syst})$ [375]. The measured cross sections are larger than but consistent with the standard model predictions within two standard deviations. Also ATLAS presents both, the inclusive and differential cross-sections of $t\bar{t}W$ production in 140 fb^{-1} of 13 TeV data using final states with two same-sign or three isolated leptons (electrons or muons). The inclusive production cross-section is measured to be 890 ± 80 fb, which turns out a bit high compared to the new reference theoretical prediction at NNLO in QCD of $745.3 \pm 49.9(\text{scale}) \pm 13.4(\text{PDF})$ fb [46]. Differential cross-section measurements characterise this process in detail for the first time. Several particle-level observables are compared to a variety of theoretical predictions which are generally in good agreement with the normalised differential cross-section results [376]. They also measure the $t\bar{t}W^+$ and $t\bar{t}W^-$ cross section individually, yielding a ratio of $R = 1.95^{+0.21}_{-0.18}(\text{stat.})^{+0.16}_{-0.13}(\text{syst.})$.

single-top + W/Z production:

The electroweak couplings can also be probed in single-top production in association with a Z boson. The $pp \rightarrow tZq$ process at the LHC probes both the WWZ coupling in the case where the Z emerges from the t -channel W in single-top production and, in the case where the Z is radiated from the top quark, the tZ coupling. A CMS search at 8 TeV using 19.7 fb^{-1} produced a hint of a tZq signal in tri-lepton events, with a significance compared to the background-only hypothesis of 2.4σ [377]. Very recently, CMS and ATLAS collaborations used 139 fb^{-1} at 13 TeV in three-lepton events to measure $tZ(\rightarrow \ell^+\ell^-)q$. CMS obtains $\sigma_{tZq} = 87.9^{+7.5}_{-7.3}(\text{stat.})^{+7.3}_{-6.0}(\text{syst.})$ fb for $m(\ell\ell) > 30$ GeV [378], following the evidence [361] of the observation of the process [379]. The ratio between the cross sections for the top quark and the top antiquark production in association with a Z boson is measured as $2.37^{+0.56}_{-0.42}(\text{stat.})^{+0.27}_{-0.13}(\text{syst.})$. Differential measurements at parton and particle levels are performed for the first time. Additionally, the spin asymmetry, which is sensitive to the top quark polarization, is determined from the differential distribution of the polarization angle at parton level to be $0.58^{+0.15}_{-0.16}(\text{stat}) \pm 0.06(\text{syst.})$, in agreement with SM predictions at next-to-leading order. Using neural networks, ATLAS improves the background rejection and extracts the signal. The measured cross-section for

$m(\ell\ell) > 30$ GeV is $97 \pm 13(\text{stat.}) \pm 7(\text{syst.})$ fb, consistent with the Standard Model prediction [380].

tWZ production:

Using 138 fb^{-1} at 13 TeV, CMS presents the first evidence for the standard model production of a top quark in association with a W and a Z boson in multilepton final states. The Z boson is reconstructed via its decays to electron or muon pairs. The measured cross section amounts to $0.37 \pm 0.05(\text{stat}) \pm 0.10(\text{syst})$ pb, and corresponds to an observed (expected) significance of 3.5 (1.4) standard deviations [381].

Searches for and now also measurements of the associate production of a top-antitop quark pair along with a Higgs boson, $t\bar{t}h$, with various subsequent decays provide sensitivity to the top-Higgs Yukawa coupling. For further details, see the review on “Status of Higgs boson physics”.

61.2.6 New Physics

The top quark plays a special role in the SM. Being the only quark with a coupling to the Higgs boson of order one, it provides the most important contributions to the quadratic radiative corrections to the Higgs mass exposing the issue of the naturalness of the SM. It is therefore very common for models where the naturalness problem is addressed to have new physics associated with the top quark. In SUSY, for instance, naturalness predicts the scalar top partners to be the lightest among the squarks and to be accessible at the LHC energies (see the review “Supersymmetry: Theory”). In models where the Higgs is a pseudo-Goldstone boson, such as Little Higgs models, naturalness predicts the existence of partners of the top quarks with the same spin and color, but with different electroweak couplings, the so-called vectorial t' . Stops and t' 's are expected to have sizeable branching ratios to top quarks. Another intriguing prediction of SUSY models with universal couplings at the unification scale is that for a top-quark mass close to the measured value, the running of the Yukawa coupling down to 1 TeV naturally leads to the radiative breaking of the electroweak symmetry [382]. In fact, the top quark plays a role in the dynamics of electroweak symmetry breaking in many models [383]. One example is topcolor [384], where a large top-quark mass can be generated through the formation of a dynamic $t\bar{t}$ condensate, X , which is formed by a new strong gauge force coupling preferentially to the third generation. Another example is topcolor-assisted technicolor [385], predicting the existence of a heavy Z' boson that couples preferentially to the third generation of quarks. If light enough such a state might be directly accessible at the present hadron collider energies, or if too heavy, lead to four-top interactions possibly visible in the $t\bar{t}t\bar{t}$ final state. This final state has been observed by CMS [168] and by ATLAS [164].

Table 61.4: 95% C.L. limits on branching ratios (BR) of the top quark for FCNC and other rare non-SM interactions.

Process	BR limit	Reference
$t \rightarrow cH$	9.4×10^{-4}	[386]
	4.3×10^{-4}	[387]
$t \rightarrow cH$ Combined	3.7×10^{-4}	[387]
$t \rightarrow uH$	6.9×10^{-4}	[386]
	7.2×10^{-4}	[387]
$t \rightarrow uH$ Combined	1.9×10^{-4}	[387]
$t \rightarrow Zu$ LH	6.2×10^{-5}	[388]
$t \rightarrow Zc$ LH	1.3×10^{-4}	[388]
$t \rightarrow u\gamma$ LH	0.85×10^{-5}	[389]
$t \rightarrow c\gamma$ LH	4.2×10^{-5}	[389]
$t \rightarrow ug$	0.61×10^{-4}	[390]
$t \rightarrow cg$	3.7×10^{-4}	[390]
$t \rightarrow e\mu\mu$ (Scalar)	0.07×10^{-6}	[391]
$t \rightarrow e\mu\mu$ (Vector)	0.13×10^{-6}	[391]
$t \rightarrow e\mu\mu$ (Tensor)	0.25×10^{-6}	[391]
$t \rightarrow e\mu c$ (Scalar)	0.89×10^{-6}	[391]
$t \rightarrow e\mu c$ (Vector)	1.31×10^{-6}	[391]
$t \rightarrow e\mu c$ (Tensor)	2.59×10^{-6}	[391]
$t \rightarrow \mu\tau q$	11×10^{-7}	[392]

61.2.6.1 Direct Searches for Physics Beyond the Standard Model

In this section we review the latest direct searches for Physics Beyond the Standard Model (PBSM) in top-quark production and decay. These direct search come in two categories: $t\bar{t}$ resonance searches and searches for rare non-SM interactions involving top quarks, including Flavor-Changing-Neutral-Current (FCNC) searches. Top-sector resonance searches come in two categories, $t\bar{t}$ resonances in which a presumed heavy particle X decays into a $t\bar{t}$ pair, and searches in which a non-SM decay product of the top quark is observed via its resonant decay. The most recent results are of the latter category. We refer the reader to Refs. [393–395] for $X \rightarrow t\bar{t}$ searches. Searches for rare non-SM interactions and FCNC final states are interpreted using the EFT approach described in Section 61.1.1.2. In this section we focus on the branching-ratio limits from these searches, while the EFT interpretations are cited in Section 61.2.6.4.

61.2.6.2 FCNC and Rare non-SM Interaction Searches

The most recent FCNC searches target a $t \rightarrow qH$ decay in $t\bar{t}$ production, or an FCNC vertex in single-top production together with a Higgs boson. The ATLAS search in Ref. [386] looks for $H \rightarrow \tau\tau$ in both cases. A small, 2.3σ excess of events is observed and limits on $t \rightarrow qH$ branching ratios are set. The most recent CMS result uses Higgs decays to vector bosons in addition to $\tau\tau$. That result is combined with results from Refs. [396] and [397] that use the $b\bar{b}$ and $\gamma\gamma$ decay channels of the Higgs [387]. Table 61.4 shows the most recent independent limits for $q = u$ or $q = c$ and assume the other branching ratio is zero. Other results can be found in the Listings.

Searches targeting tZq couplings use leptonic decays of the Z -boson and a trilepton final state. In $t\bar{t}$ events, the signal occurs through the FCNC decay $t \rightarrow Zq$, in single-top the signal occurs through the associated production of a top quark and a Z -boson. The branching-ratio limits shown in Table 61.4 are for tZu and tZc left-handed couplings and assume, for tZu , that the tZc coupling is zero and vice versa. Reference [388] also presents limits for right-handed couplings, which are close to the values quoted in Table 61.4 for left-handed couplings

Searches targeting $t\gamma q$ couplings focus on a high- P_T photon in the final state. As with tZq couplings, signal events occur through top-quark decay in $t\bar{t}$ and through associated production of a top quark and a photon in single-top events. In Ref. [389] limits are found for the EFT couplings shown in Table 61.7, and the limits shown in Table 61.4 are derived from the limits on the WCs. The table shows the limits assuming a left-handed coupling. Limits on right-handed couplings are also give in Ref. [389] and are only slightly weaker than those determined for left-handed couplings.

Table 61.5: Wilson coefficients (WC) corresponding to boson operators and related PBSM search references.

WC	Process	Citations
C_{tW}	Single-top polarization	[211]
	$t\bar{t}Z, tZ$	[398]
	Boosted $t\bar{t}Z, t\bar{t}H$	[374]
	$t+$ additional leptons	[399]
	$t\bar{t}Z$	[371]
C_{tZ}	$t\bar{t}Z, tZ$	[398]
	$t\bar{t}Z, t\bar{t}H$	[374]
	$t+$ additional leptons	[399]
C_{bW}	Boosted $t\bar{t}Z, t\bar{t}H$	[374]
C_{tG}	Boosted $t\bar{t}$	[400]
	$t\bar{t}$ charge asymmetry	[234]
	$t\bar{t}Z$	[371]
C_{tB}	$t\bar{t}Z$	[371]
C_{Ht}	$t\bar{t}Z$	[371]
C_{HQ}^1	$t\bar{t}Z$	[371]
C_{HQ}^3	$t\bar{t}Z$	[371]

In Ref. [390] FCNC couplings tgq between a top quark, a gluon, and an up or charm quark are looked for in single-top produc-

Table 61.6: Wilson coefficients (WC) corresponding to four-fermion operators and related PBSM search references.

WC	Process	Citations
C_{Qq}^{11}	$t\bar{t}$ charge asymmetry	[234]
	$t\bar{t}$ energy asymmetry in $t\bar{t}j$	[238]
	$t\bar{t}Z$	[371]
C_{Qq}^{18}	$t\bar{t}$ charge asymmetry	[234]
	$t\bar{t}$ energy asymmetry in $t\bar{t}j$	[238]
	Boosted all-hadronic $t\bar{t}$	[401]
	$t\bar{t}Z$	[371]
C_{tq}^1	$t\bar{t}$ charge asymmetry	[234]
	$t\bar{t}$ energy asymmetry in $t\bar{t}j$	[238]
	$t\bar{t}Z$	[371]
C_{tq}^8	$t\bar{t}$ charge asymmetry	[234]
	$t\bar{t}$ energy asymmetry in $t\bar{t}j$	[238]
	Boosted all-hadronic $t\bar{t}$	[401]
	Boosted $t\bar{t}$	[400]
	$t\bar{t}Z$	[371]
C_{tu}^1	$t\bar{t}$ charge asymmetry	[234]
	$t\bar{t}$ energy asymmetry in $t\bar{t}j$	[238]
	$t\bar{t}Z$	[371]
C_{td}^1	$t\bar{t}$ charge asymmetry	[234]
	$t\bar{t}Z$	[371]
C_{tu}^8	$t\bar{t}$ charge asymmetry	[234]
	$t\bar{t}$ energy asymmetry in $t\bar{t}j$	[238]
	Boosted all-hadronic $t\bar{t}$	[401]
	$t\bar{t}Z$	[371]
C_{td}^8	$t\bar{t}$ charge asymmetry	[234]
	Boosted all-hadronic $t\bar{t}$	[401]
	$t\bar{t}Z$	[371]
C_{Qd}^8	$t\bar{t}$ charge asymmetry	[234]
	Boosted all-hadronic $t\bar{t}$	[401]
	$t\bar{t}Z$	[371]
C_{Qu}^8	$t\bar{t}$ charge asymmetry	[234]
	Boosted all-hadronic $t\bar{t}$	[401]
	$t\bar{t}Z$	[371]
C_{Qu}^1	$t\bar{t}$ charge asymmetry	[234]
	$t\bar{t}Z$	[371]
C_{Qd}^1	$t\bar{t}$ charge asymmetry	[234]
	$t\bar{t}Z$	[371]
C_{Qq}^{31}	$t\bar{t}Z$	[371]
C_{Qq}^{38}	$t\bar{t}$ charge asymmetry	[234]
	Boosted all-hadronic $t\bar{t}$	[401]
	$t\bar{t}Z$	[371]
$C_{lequ}^{3(2313)}$	$t \rightarrow \mu\tau u$	[392]
$C_{lequ}^{1(2323)}$	$t \rightarrow \mu\tau c$	[392]
$C_{e\mu tu}$	top production & decay	[391]
$C_{e\mu tc}$	top production & decay	[391]

tion. The couplings increase the single-top production cross section and, in the case of the tgc coupling, also affect the rapidity distribution of the produced top quark because of the different PDFs for valence and sea quarks.

CMS searches for charged-lepton-flavor-violating interactions in both production, $q \rightarrow e\mu t$, and decay, $t \rightarrow e\mu q$, with $q = u$ or c [391]. The branching ratio limits set are included in Table 61.4 and the Wilson coefficients constrained are listed in Table 61.6.

ATLAS has searched for charged-lepton-flavor-violating $\mu\tau$ qt interactions which are sensitive to the two-quark-two-lepton operators of Table 61.1 [392]. The branching ratio limit set is included in Table 61.4 and the Wilson coefficients constrained are listed in Table 61.6.

61.2.6.3 Resonance Searches

While technically an FCNC search, a decay of the type $t \rightarrow qX$ where $q = u$ or c , could be missed when X is not the expected quark or boson. ATLAS has searched for $t \rightarrow qX$ where X is

Table 61.7: Wilson coefficients (WC) corresponding to flavor-changing-neutral-current (FCNC) operators and related PBSM search references.

WC	Process	Citations
$C_{uW}^{32} + C_{uB}^{32}$	$tq\gamma$	[389]
$C_{uW}^{(23)*} + C_{uB}^{(23)*}$	$tq\gamma$	[389]
$C_{uW}^{31} + C_{uB}^{31}$	$tq\gamma$	[389]
$C_{uW}^{(13)*} + C_{uB}^{(13)*}$	$tq\gamma$	[389]
C_{uW}^{32}, C_{uB}^{32}	tZc	[388]
$C_{uW}^{(23)*}, C_{uB}^{(23)*}$	tZc	[388]
C_{uW}^{31}, C_{uB}^{31}	tZu	[388]
$C_{uW}^{(13)*}, C_{uB}^{(13)*}$	tZu	[388]
C_{uG}	tgu	[390]
C_{cG}	tgc	[390]
$C_{u\phi}$	tHu	[386]
$C_{c\phi}$	tHc	[386]

a light scalar with a mass below the top quark that decays to $b\bar{b}$ [402]. Such phenomena exist in composite Higgs models [403]. The ATLAS search used $t\bar{t}$ events and separated signal from background by categorizing events according to the number of jets and the number of jets tagged as originating from b -quarks. The observed limits correspond to the product of the BR $t \rightarrow qX$ and $X \rightarrow b\bar{b}$. The limit in the $t \rightarrow uX$ ($t \rightarrow cX$) channel is 0.019% (0.018%) for $M_X = 20$ GeV and 0.062% (0.078%) for $M_X = 160$ GeV.

61.2.6.4 Effective Field Theory Results

As described in Section 61.1.1.2, EFTs have become a primary tool for evaluating the outcome of top PBSM searches. EFT provides both model-independent limits, a straightforward way to compare and contrast search results from different processes and different experiments, and a guide to the full space of possible top-quark-related PBSM. In a nice pedagogical paper [404], Zhang and Willenbrock elucidate the advantages of the EFT approach compared to the vertex-function approach for searching for PBSM in top-quark interactions, including the fact that the EFT approach incorporates the SM gauge symmetry and contact interactions that are neglected in the vertex-function approach. As a result of these advantages, EFTs have become the dominant technique for evaluating search limits, and we review the most recent results in this section.

As ATLAS and CMS do, we categorize the top-EFT operators as follows: four-fermion operators, vector-boson operators and scalar-boson operators. Operators can change the overall rate of top-quark production, modify the kinematics of production and/or decay, or produce new interactions, such as flavor-changing neutral currents (FCNC). To date, all results are consistent with the SM expectation of zero for each Wilson coefficient. The numerical values of the limits are not intuitively meaningful, especially given that they correspond to an arbitrarily chosen mass scale of $\Lambda = 1$ TeV. Therefore, rather than providing a table of confidence intervals, we refer the interested reader to the LHC Top Working Group page of summary plots where the limits on the Wilson coefficients are presented graphically [405], and to the references given below. Instead, the tables below provide the most recent relevant references (i.e. those using the full LHC dataset of 139 fb^{-1}) for limits on each coefficient wherein measurement, fitting, and limit derivation techniques can be found. Additional limits and references can be found in the listings and in references [359, 374, 391, 398, 399, 406–408].

61.3 Outlook

Top quark physics at hadron colliders has developed into precision physics. Various properties of the top quark have been measured with high precision, where the LHC has by now surpassed the Tevatron precision and reach in the majority of relevant observables. Several \sqrt{s} -dependent physics quantities, such as the production cross-section, have been measured at several energies

at the Tevatron and the LHC. Up to now, all measurements are consistent with the SM predictions and allow stringent tests of the underlying production mechanisms by strong and weak interactions. Given the very large event samples available at the LHC, top-quark properties will be further determined in $t\bar{t}$ as well as in electroweak single top-quark production. At the Tevatron, the t - and s -channels for electroweak single top-quark production have been established separately. At the LHC, quick progress has been achieved in the last years yielding more than 3 sigma significance of the s -channel and more than 5 sigma significance for the t -channel and Wt -production. Furthermore, $t\bar{t}\gamma$, $t\bar{t}Z$, and $t\bar{t}W$ together with $t\bar{t}H$ associated production have started to provide key information on the top-quark electroweak couplings. Corresponding effective field theory (EFT) fits for the coupling extraction are being developed. At the same time various models of physics beyond the SM involving top-quark production are being constrained. While a majority of the Run-II data recorded at 13 TeV has been analysed or is in an advanced stage, the beginning of the Run-III at $\sqrt{s} = 13.6$ to 14 TeV and an expected integrated luminosity of 160–200 fb⁻¹, doubling the Run-I plus Run-II data set, is immanent. With the first results being released, top-quark physics has the potential to shed light on open questions and new aspects of physics at the TeV scale.

CDF and DØ notes can be retrieved from

<https://inspirehep.net>

with the search command "find CDF-NOTE-XXXXX" or "find D0 Note XXXX",

and ATLAS note references from

<https://twiki.cern.ch/twiki/bin/view/AtlasPublic/TopPublicResults>,

and CMS note references from

<https://twiki.cern.ch/twiki/bin/view/CMSPublic/PhysicsResultsTOP>,

and plots provided by the LHC Top Working Group from

<https://twiki.cern.ch/twiki/bin/view/LHCPhysics/LHCTopWGSummaryPlots>.

References

- [1] ATLAS Collab. and CMS Collab., ATLAS-CONF-2023-066, CMS-PAS-TOP-22-001.
- [2] G. Degrandi *et al.*, JHEP **08**, 098 (2012), [arXiv:1205.6497].
- [3] D. Buttazzo *et al.*, JHEP **12**, 089 (2013), [arXiv:1307.3536].
- [4] A. Andreassen, W. Frost and M. D. Schwartz, Phys. Rev. D **97**, 5, 056006 (2018), [arXiv:1707.08124].
- [5] A. H. Hoang *et al.*, JHEP **04**, 003 (2018), [arXiv:1704.01580].
- [6] P. Marquard *et al.*, Phys. Rev. Lett. **114**, 14, 142002 (2015), [arXiv:1502.01030].
- [7] P. Nason, *The Top Mass in Hadronic Collisions*, 123–151 (2019), [arXiv:1712.02796].
- [8] A. H. Hoang, Ann. Rev. Nucl. Part. Sci. **70**, 225 (2020), [arXiv:2004.12915].
- [9] S. Weinberg, Phys. Rev. Lett. **43**, 1566 (1979).
- [10] W. Buchmuller and D. Wyler, Nucl. Phys. B **268**, 621 (1986).
- [11] B. Grzadkowski *et al.*, JHEP **10**, 085 (2010), [arXiv:1008.4884].
- [12] D. Barducci *et al.* (2018), [arXiv:1802.07237].
- [13] J. A. Aguilar-Saavedra, Nucl. Phys. B **812**, 181 (2009), [arXiv:0811.3842].
- [14] C. Zhang and S. Willenbrock, Phys. Rev. D **83**, 034006 (2011), [arXiv:1008.3869].
- [15] R. S. Chivukula and H. Georgi, Phys. Lett. B **188**, 99 (1987).
- [16] L. J. Hall and L. Randall, Phys. Rev. Lett. **65**, 2939 (1990).
- [17] G. D'Ambrosio *et al.*, Nucl. Phys. B **645**, 155 (2002), [hep-ph/0207036].
- [18] M. Jezabek and J. H. Kuhn, Nucl. Phys. B **314**, 1 (1989).
- [19] A. Czarnecki and K. Melnikov, Nucl. Phys. B **544**, 520 (1999), [hep-ph/9806244]; K. G. Chetyrkin *et al.*, Phys. Rev. D **60**, 114015 (1999), [hep-ph/9906273].
- [20] L.-B. Chen *et al.*, Phys. Rev. D **108**, 5, 054003 (2023), [arXiv:2212.06341].
- [21] I. I. Y. Bigi *et al.*, Phys. Lett. B **181**, 157 (1986).
- [22] A. H. Hoang *et al.*, Phys. Rev. D **65**, 014014 (2002), [hep-ph/0107144].
- [23] K. Hagiwara, Y. Sumino and H. Yokoya, Phys. Lett. B **666**, 71 (2008), [arXiv:0804.1014].
- [24] B. Fuks *et al.*, Phys. Rev. D **104**, 3, 034023 (2021), [arXiv:2102.11281].
- [25] G. Eilam, J. L. Hewett and A. Soni, Phys. Rev. D **44**, 1473 (1991), [Erratum: Phys.Rev.D 59, 039901 (1999)].
- [26] J. A. Aguilar-Saavedra, Acta Phys. Polon. B **35**, 2695 (2004), [hep-ph/0409342].
- [27] M. Czakon, P. Fiedler and A. Mitov, Phys. Rev. Lett. **110**, 252004 (2013), [arXiv:1303.6254].
- [28] S. Catani *et al.*, JHEP **07**, 100 (2019), [arXiv:1906.06535].
- [29] ATLAS, CMS, CDF, & D0 Collab, [arXiv:1403.4427].
- [30] S. Cortese and R. Petronzio, Phys. Lett. B **253**, 494 (1991).
- [31] S. S. D. Willenbrock and D. A. Dicus, Phys. Rev. D **34**, 155 (1986).
- [32] J. Campbell, T. Neumann and Z. Sullivan, JHEP **02**, 040 (2021), [arXiv:2012.01574].
- [33] M. Brucherseifer, F. Caola and K. Melnikov, Phys. Lett. B **736**, 58 (2014), [arXiv:1404.7116].
- [34] E. L. Berger, J. Gao and H. X. Zhu, JHEP **11**, 158 (2017), [arXiv:1708.09405].
- [35] N. Kidonakis, Phys. Rev. D **81**, 054028 (2010), [arXiv:1001.5034].
- [36] N. Kidonakis, Phys. Rev. D **82**, 054018 (2010), [arXiv:1005.4451].
- [37] T. M. P. Tait and C. P. Yuan, Phys. Rev. D **63**, 014018 (2000), [hep-ph/0007298].
- [38] S. Frixione, P. Nason and B. R. Webber, JHEP **08**, 007 (2003), [hep-ph/0305252]; W. Kim and H. Shin, JHEP **07**, 070 (2007), [arXiv:0706.3563]; S. Frixione, P. Nason and G. Ridolfi, JHEP **09**, 126 (2007), [arXiv:0707.3088]; J. M. Campbell *et al.*, JHEP **04**, 114 (2015), [arXiv:1412.1828]; T. Ježo *et al.*, Eur. Phys. J. C **76**, 12, 691 (2016), [arXiv:1607.04538].
- [39] S. Frixione *et al.*, JHEP **03**, 092 (2006), [hep-ph/0512250]; V. Marotta and A. Naddeo, JHEP **08**, 029 (2008), [arXiv:0810.4759]; S. Alioli *et al.*, JHEP **09**, 111 (2009), [Erratum: JHEP02,011(2010)], [arXiv:0907.4076]; E. Re, Eur. Phys. J. C **71**, 1547 (2011), [arXiv:1009.2450]; R. Frederix, E. Re and P. Torrielli, JHEP **09**, 130 (2012), [arXiv:1207.5391]; R. Frederix *et al.*, JHEP **06**, 027 (2016), [arXiv:1603.01178].
- [40] S. Frixione and B. R. Webber, JHEP **06**, 029 (2002), [hep-ph/0204244].
- [41] P. Nason, JHEP **11**, 040 (2004), [hep-ph/0409146].
- [42] J. Mazzitelli *et al.*, Phys. Rev. Lett. **127**, 6, 062001 (2021), [arXiv:2012.14267].
- [43] A. Broggio *et al.*, JHEP **08**, 039 (2019), [arXiv:1907.04343].
- [44] M. van Beekveld, A. Kulesza and L. M. Valero (2022), [arXiv:2212.03259].
- [45] S. Catani *et al.*, Phys. Rev. Lett. **130**, 11, 111902 (2023), [arXiv:2210.07846].
- [46] L. Buonocore *et al.* (2023), [arXiv:2306.16311].
- [47] E. Todesco and J. Wenninger, Phys. Rev. Accel. Beams **20**, 8, 081003 (2017).
- [48] V. M. Abazov *et al.* (D0), Phys. Rev. D **94**, 092004 (2016), [arXiv:1605.06168].

- [49] T. Aaltonen *et al.* (CDF), Phys. Rev. **D88**, 091103 (2013), [arXiv:1304.7961].
- [50] T. A. Aaltonen *et al.* (CDF, D0), Phys. Rev. **D89**, 7, 072001 (2014), [arXiv:1309.7570].
- [51] T. A. Aaltonen *et al.* (CDF), Phys. Rev. **D89**, 9, 091101 (2014), [arXiv:1402.6728].
- [52] T. Aaltonen *et al.* (CDF), Phys. Rev. Lett. **105**, 012001 (2010), [arXiv:1004.3224].
- [53] V. M. Abazov *et al.* (D0), Phys. Rev. **D90**, 9, 092006 (2014), [arXiv:1401.5785].
- [54] M. Czakon and A. Mitov, Comput. Phys. Commun. **185**, 2930 (2014), [arXiv:1112.5675].
- [55] J. M. Campbell and R. K. Ellis, Nucl. Phys. Proc. Suppl. **205-206**, 10 (2010), [arXiv:1007.3492].
- [56] R. Kleiss and W. J. Stirling, Z. Phys. C **40**, 419 (1988).
- [57] M. Cacciari *et al.*, Phys. Lett. B **710**, 612 (2012), [arXiv:1111.5869].
- [58] P. Bärnreuther, M. Czakon and A. Mitov, Phys. Rev. Lett. **109**, 132001 (2012), [arXiv:1204.5201].
- [59] M. Czakon and A. Mitov, JHEP **12**, 054 (2012), [arXiv:1207.0236].
- [60] M. Czakon and A. Mitov, JHEP **01**, 080 (2013), [arXiv:1210.6832].
- [61] S. Catani *et al.*, Phys. Rev. D **99**, 5, 051501 (2019), [arXiv:1901.04005].
- [62] G. Aad *et al.* (ATLAS), JHEP **06**, 138 (2023), [arXiv:2207.01354].
- [63] A. M. Sirunyan *et al.* (CMS), JHEP **03**, 115 (2018), [arXiv:1711.03143].
- [64] A. Tumasyan *et al.* (CMS), JHEP **04**, 144 (2022), [arXiv:2112.09114].
- [65] G. Aad *et al.* (ATLAS), Eur. Phys. J. **C74**, 10, 3109 (2014), [Addendum: Eur. Phys. J.C76,no.11,642(2016)], [arXiv:1406.5375].
- [66] ATLAS Collab., ATLAS-CONF-2011-121 (2011).
- [67] G. Aad *et al.* (ATLAS), JHEP **05**, 059 (2012), [arXiv:1202.4892].
- [68] ATLAS Collab., ATLAS-CONF-2011-140.
- [69] ATLAS Collab., ATLAS-CONF-2012-024.
- [70] G. Aad *et al.* (ATLAS), Eur. Phys. J. **C73**, 3, 2328 (2013), [arXiv:1211.7205].
- [71] G. Aad *et al.* (ATLAS), Phys. Lett. **B717**, 89 (2012), [arXiv:1205.2067].
- [72] ATLAS Collab., ATLAS-CONF-2012-031.
- [73] M. Aaboud *et al.* (ATLAS), Phys. Rev. D **108**, 3, 032014 (2023), [arXiv:2212.00571].
- [74] S. Chatrchyan *et al.* (CMS), JHEP **11**, 067 (2012), [arXiv:1208.2671].
- [75] V. Khachatryan *et al.* (CMS), JHEP **08**, 029 (2016), [arXiv:1603.02303].
- [76] S. Chatrchyan *et al.* (CMS), Phys. Lett. **B720**, 83 (2013), [arXiv:1212.6682].
- [77] S. Chatrchyan *et al.* (CMS), JHEP **05**, 065 (2013), [arXiv:1302.0508].
- [78] S. Chatrchyan *et al.* (CMS), Phys. Rev. **D85**, 112007 (2012), [arXiv:1203.6810].
- [79] S. Chatrchyan *et al.* (CMS), Eur. Phys. J. **C73**, 4, 2386 (2013), [arXiv:1301.5755].
- [80] G. Aad *et al.* (ATLAS, CMS), JHEP **07**, 213 (2023), [arXiv:2205.13830].
- [81] G. Aad *et al.* (ATLAS), Eur. Phys. J. **C74**, 10, 3109 (2014), [Addendum: Eur. Phys. J.C76,no.11,642(2016)], [arXiv:1406.5375].
- [82] G. Aad *et al.* (ATLAS), Phys. Rev. **D91**, 11, 112013 (2015), [arXiv:1504.04251].
- [83] M. Aaboud *et al.* (ATLAS), Eur. Phys. J. **C78**, 487 (2018), [arXiv:1712.06857].
- [84] M. Aaboud *et al.* (ATLAS), Phys. Rev. **D95**, 7, 072003 (2017), [arXiv:1702.08839].
- [85] V. Khachatryan *et al.* (CMS), Eur. Phys. J. **C77**, 1, 15 (2017), [arXiv:1602.09024].
- [86] S. Chatrchyan *et al.* (CMS), JHEP **02**, 024 (2014), [Erratum: JHEP02,102(2014)], [arXiv:1312.7582].
- [87] V. Khachatryan *et al.* (CMS), Phys. Lett. **B739**, 23 (2014), [arXiv:1407.6643].
- [88] V. Khachatryan *et al.* (CMS), Eur. Phys. J. **C76**, 3, 128 (2016), [arXiv:1509.06076].
- [89] ATLAS Collab., ATLAS-CONF-2014-054, CMS Collab., CMS-PAS-TOP-14-016.
- [90] R. Aaij *et al.* (LHCb), Phys. Rev. Lett. **115**, 11, 112001 (2015), [arXiv:1506.00903].
- [91] G. Aad *et al.* (ATLAS), Eur. Phys. J. C **80**, 6, 528 (2020), [arXiv:1910.08819].
- [92] ATLAS collab., ATLAS-CONF-2015-049.
- [93] G. Aad *et al.* (ATLAS), Phys. Lett. B **810**, 135797 (2020), [arXiv:2006.13076].
- [94] G. Aad *et al.* (ATLAS), JHEP **07**, 141 (2023), [arXiv:2303.15340].
- [95] A. M. Sirunyan *et al.* (CMS), Eur. Phys. J. **C79**, 5, 368 (2019), [arXiv:1812.10505].
- [96] A. M. Sirunyan *et al.* (CMS), JHEP **02**, 191 (2020), [arXiv:1911.13204].
- [97] CMS Collab., CMS-PAS-TOP-15-005.
- [98] A. M. Sirunyan *et al.* (CMS), JHEP **09**, 051 (2017), [arXiv:1701.06228].
- [99] A. Tumasyan *et al.* (CMS) (2021), [arXiv:2108.02803].
- [100] CMS Collab., CMS-PAS-TOP-16-013.
- [101] A. Tumasyan *et al.* (CMS, TOTEM) (2023), [arXiv:2310.11231].
- [102] R. Aaij *et al.* (LHCb), JHEP **08**, 174 (2018), [arXiv:1803.05188].
- [103] G. Aad *et al.* (ATLAS) (2023), [arXiv:2308.09529].
- [104] A. Tumasyan *et al.* (CMS), JHEP **08**, 204 (2023), [arXiv:2303.10680].
- [105] A. M. Sirunyan *et al.* (CMS), Phys. Rev. Lett. **125**, 22, 222001 (2020), [arXiv:2006.11110].
- [106] A. M. Sirunyan *et al.* (CMS), Phys. Rev. Lett. **119**, 24, 242001 (2017), [arXiv:1709.07411].
- [107] ATLAS Collab., ATLAS-CONF-2023-063.
- [108] V. M. Abazov *et al.* (D0), Phys. Rev. Lett. **107**, 121802 (2011), [arXiv:1106.5436].
- [109] D. Acosta *et al.* (CDF), Phys. Rev. Lett. **95**, 102002 (2005), [hep-ex/0505091].
- [110] V. Khachatryan *et al.* (CMS), Phys. Lett. **B736**, 33 (2014), [arXiv:1404.2292].
- [111] M. Czakon, D. Heymes and A. Mitov, Phys. Rev. Lett. **116**, 8, 082003 (2016), [arXiv:1511.00549].
- [112] G. D'Agostini, Nucl. Instrum. Meth. A **362**, 487 (1995).
- [113] T. Auye, in "PHYSTAT 2011," 313–318, CERN, Geneva (2011), [arXiv:1105.1160].
- [114] G. Aad *et al.* (ATLAS), Eur. Phys. J. C **80**, 10, 957 (2020), [Erratum: Eur.Phys.J.C 81, 29 (2021), Erratum: Eur.Phys.J.C 81, 398 (2021)], [arXiv:2004.03447].
- [115] A. M. Sirunyan *et al.* (CMS), JHEP **01**, 183 (2019), [arXiv:1807.03825].

- [116] A. Hocker and V. Kartvelishvili, Nucl. Instrum. Meth. A **372**, 469 (1996), [hep-ph/9509307].
- [117] V. Blobel, in “Conference on Advanced Statistical Techniques in Particle Physics,” 258–267 (2002), [hep-ex/0208022].
- [118] S. Chatrchyan *et al.* (CMS), Eur. Phys. J. **C73**, 3, 2339 (2013), [arXiv:1211.2220].
- [119] V. Khachatryan *et al.* (CMS), Phys. Rev. **D94**, 5, 052006 (2016), [arXiv:1607.00837].
- [120] S. Chatrchyan *et al.* (CMS), Eur. Phys. J. **C74**, 3014 (2015), [Erratum: Eur. Phys. J. **C75**, no.5, 216(2015)], [arXiv:1404.3171].
- [121] G. Aad *et al.* (ATLAS), Eur. Phys. J. **C73**, 1, 2261 (2013), [arXiv:1207.5644].
- [122] G. Aad *et al.* (ATLAS), Phys. Rev. **D90**, 7, 072004 (2014), [arXiv:1407.0371].
- [123] G. Aad *et al.* (ATLAS), JHEP **06**, 100 (2015), [arXiv:1502.05923].
- [124] M. Aaboud *et al.* (ATLAS), Phys. Rev. **D94**, 9, 092003 (2016), [arXiv:1607.07281].
- [125] G. Aad *et al.* (ATLAS), Eur. Phys. J. **C76**, 10, 538 (2016), [arXiv:1511.04716].
- [126] G. Aad *et al.* (ATLAS), Phys. Rev. **D93**, 3, 032009 (2016), [arXiv:1510.03818].
- [127] V. Khachatryan *et al.* (CMS), Eur. Phys. J. **C75**, 11, 542 (2015), [arXiv:1505.04480].
- [128] A. M. Sirunyan *et al.* (CMS), Eur. Phys. J. **C77**, 7, 459 (2017), [arXiv:1703.01630].
- [129] V. Khachatryan *et al.* (CMS), Phys. Rev. **D94**, 7, 072002 (2016), [arXiv:1605.00116].
- [130] M. Aaboud *et al.* (ATLAS), Eur. Phys. J. **C77**, 5, 292 (2017), [arXiv:1612.05220].
- [131] M. Aaboud *et al.* (ATLAS), JHEP **11**, 191 (2017), [arXiv:1708.00727].
- [132] G. Aad *et al.* (ATLAS), Eur. Phys. J. **C79**, 12, 1028 (2019), [Erratum: Eur. Phys. J. **C80**, 1092 (2020)], [arXiv:1908.07305].
- [133] M. Aaboud *et al.* (ATLAS), Phys. Rev. **D98**, 1, 012003 (2018), [arXiv:1801.02052].
- [134] G. Aad *et al.* (ATLAS), JHEP **01**, 033 (2021), [arXiv:2006.09274].
- [135] ATLAS Collab., ATLAS-CONF-2021-031.
- [136] ATLAS Collab., ATLAS-CONF-2023-027.
- [137] G. Aad *et al.* (ATLAS), Eur. Phys. J. **C83**, 6, 518 (2023), [arXiv:2209.07874].
- [138] G. Aad *et al.* (ATLAS), Phys. Rev. **D106**, 3, 032008 (2022), [arXiv:2202.13901].
- [139] CMS Collab., CMS-PAS-TOP-15-010.
- [140] A. M. Sirunyan *et al.* (CMS), JHEP **04**, 060 (2018), [arXiv:1708.07638].
- [141] V. Khachatryan *et al.* (CMS), Phys. Rev. **D95**, 9, 092001 (2017), [arXiv:1610.04191].
- [142] A. M. Sirunyan *et al.* (CMS), JHEP **06**, 002 (2018), [arXiv:1803.03991].
- [143] A. M. Sirunyan *et al.* (CMS), Phys. Rev. **D97**, 11, 112003 (2018), [arXiv:1803.08856].
- [144] CMS Collab., CMS-PAS-TOP-2020-006.
- [145] A. M. Sirunyan *et al.* (CMS), JHEP **02**, 149 (2019), [arXiv:1811.06625].
- [146] A. M. Sirunyan *et al.* (CMS), Eur. Phys. J. **C80**, 7, 658 (2020), [arXiv:1904.05237].
- [147] A. M. Sirunyan *et al.* (CMS), Phys. Rev. **D103**, 5, 052008 (2021), [arXiv:2008.07860].
- [148] G. Aad *et al.* (ATLAS), Eur. Phys. J. **C76**, 1, 11 (2016), [arXiv:1508.06868].
- [149] G. Aad *et al.* (ATLAS), JHEP **01**, 020 (2015), [arXiv:1407.0891].
- [150] V. Khachatryan *et al.* (CMS), Phys. Lett. **B746**, 132 (2015), [arXiv:1411.5621].
- [151] G. Aad *et al.* (ATLAS), Phys. Rev. **D92**, 7, 072005 (2015), [arXiv:1506.05074].
- [152] V. Khachatryan *et al.* (CMS), Eur. Phys. J. **C76**, 7, 379 (2016), [arXiv:1510.03072].
- [153] G. Aad *et al.* (ATLAS), Nature Phys. **17**, 7, 813 (2021).
- [154] A. M. Sirunyan *et al.* (CMS), Phys. Rev. **D102**, 9, 092013 (2020), [arXiv:2009.07123].
- [155] M. Aaboud *et al.* (ATLAS), JHEP **04**, 046 (2019), [arXiv:1811.12113].
- [156] A. M. Sirunyan *et al.* (CMS), Phys. Lett. **B776**, 355 (2018), [arXiv:1705.10141].
- [157] A. M. Sirunyan *et al.* (CMS), JHEP **07**, 125 (2020), [arXiv:2003.06467].
- [158] A. M. Sirunyan *et al.* (CMS) (2019), [arXiv:1909.05306].
- [159] A. M. Sirunyan *et al.* (CMS), Phys. Lett. **B803**, 135285 (2020), [arXiv:1909.05306].
- [160] A. Hayrapetyan *et al.* (CMS) (2023), [arXiv:2309.14442].
- [161] A. M. Sirunyan *et al.* (CMS), Phys. Lett. **B820**, 136565 (2021), [arXiv:2012.09225].
- [162] G. Aad *et al.* (ATLAS), Eur. Phys. J. **C80**, 11, 1085 (2020), [arXiv:2007.14858].
- [163] G. Aad *et al.* (ATLAS), JHEP **11**, 118 (2021), [arXiv:2106.11683].
- [164] G. Aad *et al.* (ATLAS), Eur. Phys. J. **C83**, 6, 496 (2023), [arXiv:2303.15061].
- [165] A. M. Sirunyan *et al.* (CMS), JHEP **11**, 082 (2019), [arXiv:1906.02805].
- [166] A. M. Sirunyan *et al.* (CMS), Eur. Phys. J. **C80**, 2, 75 (2020), [arXiv:1908.06463].
- [167] A. Tumasyan *et al.* (CMS), Phys. Lett. **B844**, 138076 (2023), [arXiv:2303.03864].
- [168] A. Hayrapetyan *et al.* (CMS) (2023), [arXiv:2305.13439].
- [169] V. M. Abazov *et al.* (D0), Phys. Rev. Lett. **103**, 092001 (2009), [arXiv:0903.0850]; V. M. Abazov *et al.* (D0), Phys. Rev. **D78**, 012005 (2008), [arXiv:0803.0739]; V. M. Abazov *et al.* (D0), Phys. Rev. Lett. **98**, 181802 (2007), [hep-ex/0612052].
- [170] T. Aaltonen *et al.* (CDF), Phys. Rev. Lett. **103**, 092002 (2009), [arXiv:0903.0885]; T. Aaltonen *et al.* (CDF), Phys. Rev. **D81**, 072003 (2010), [arXiv:1001.4577].
- [171] T. Aaltonen *et al.* (CDF), Phys. Rev. **D82**, 112005 (2010), [arXiv:1004.1181].
- [172] A. Heinson and T. R. Junk, Ann. Rev. Nucl. Part. Sci. **61**, 171 (2011), [arXiv:1101.1275].
- [173] A. Giammanco and R. Schwienhorst, Rev. Mod. Phys. **90**, 3, 035001 (2018), [arXiv:1710.10699].
- [174] Tevatron Electroweak Working Group, (2009), [arXiv:0908.2171].
- [175] N. Kidonakis, Phys. Rev. **D83**, 091503 (2011), [arXiv:1103.2792].
- [176] CDF Collab., CDF conference note 11113 (2014), DØ Collab., DØ conference note 6448 (2014).
- [177] T. A. Aaltonen *et al.* (CDF, D0), Phys. Rev. Lett. **115**, 15, 152003 (2015), [arXiv:1503.05027].
- [178] T. A. Aaltonen *et al.* (CDF, D0), Phys. Rev. Lett. **112**, 231803 (2014), [arXiv:1402.5126].
- [179] G. Aad *et al.* (ATLAS) (2023), [arXiv:2310.01518].

- [180] G. Aad *et al.* (ATLAS), Phys. Rev. **D90**, 11, 112006 (2014), [arXiv:1406.7844].
- [181] G. Aad *et al.* (ATLAS), Phys. Lett. **B717**, 330 (2012), [arXiv:1205.3130].
- [182] S. Chatrchyan *et al.* (CMS), JHEP **12**, 035 (2012), [arXiv:1209.4533].
- [183] M. Aaboud *et al.* (ATLAS, CMS), JHEP **05**, 088 (2019), [arXiv:1902.07158].
- [184] M. Aaboud *et al.* (ATLAS), Eur. Phys. J. **C77**, 8, 531 (2017), [arXiv:1702.02859].
- [185] M. Aaboud *et al.* (ATLAS), JHEP **04**, 124 (2017), [arXiv:1702.08309].
- [186] V. Khachatryan *et al.* (CMS), JHEP **06**, 090 (2014), [arXiv:1403.7366].
- [187] CMS Collab., CMS-PAS-TOP-15-007.
- [188] M. Aaboud *et al.* (ATLAS), JHEP **04**, 086 (2017), [arXiv:1609.03920].
- [189] ATLAS Collab., ATLAS-CONF-2023-026.
- [190] A. M. Sirunyan *et al.* (CMS), Phys. Lett. **B772**, 752 (2017), [arXiv:1610.00678].
- [191] A. M. Sirunyan *et al.* (CMS), Phys. Lett. B **800**, 135042 (2020), [arXiv:1812.10514].
- [192] A. M. Sirunyan *et al.* (CMS), Eur. Phys. J. C **80**, 5, 370 (2020), [arXiv:1907.08330].
- [193] A. M. Sirunyan *et al.* (CMS), Phys. Lett. B **808**, 135609 (2020), [arXiv:2004.12181].
- [194] C. D. White *et al.*, JHEP **11**, 074 (2009), [arXiv:0908.0631].
- [195] S. Frixione *et al.*, JHEP **07**, 029 (2008), [arXiv:0805.3067].
- [196] G. Aad *et al.* (ATLAS), Phys. Lett. **B716**, 142 (2012), [arXiv:1205.5764].
- [197] S. Chatrchyan *et al.* (CMS), Phys. Rev. Lett. **110**, 022003 (2013), [arXiv:1209.3489].
- [198] G. Aad *et al.* (ATLAS), JHEP **01**, 064 (2016), [arXiv:1510.03752].
- [199] M. Aaboud *et al.* (ATLAS, CMS), JHEP **05**, 088 (2019), [arXiv:1902.07158].
- [200] G. Aad *et al.* (ATLAS), Eur. Phys. J. C **81**, 8, 720 (2021), [arXiv:2007.01554].
- [201] S. Chatrchyan *et al.* (CMS), Phys. Rev. Lett. **112**, 23, 231802 (2014), [arXiv:1401.2942].
- [202] M. Aaboud *et al.* (ATLAS), JHEP **01**, 063 (2018), [arXiv:1612.07231].
- [203] A. M. Sirunyan *et al.* (CMS), JHEP **10**, 117 (2018), [arXiv:1805.07399].
- [204] A. Tumasyan *et al.* (CMS) (2021), [arXiv:2109.01706].
- [205] A. Tumasyan *et al.* (CMS), JHEP **07**, 046 (2023), [arXiv:2208.00924].
- [206] ATLAS Collab., ATLAS-CONF-2011-118.
- [207] G. Aad *et al.* (ATLAS), Phys. Lett. **B756**, 228 (2016), [arXiv:1511.05980].
- [208] V. Khachatryan *et al.* (CMS), JHEP **09**, 027 (2016), [arXiv:1603.02555].
- [209] G. Aad *et al.* (ATLAS), JHEP **06**, 191 (2023), [arXiv:2209.08990].
- [210] CMS Collab., CMS-PAS-TOP-14-004.
- [211] G. Aad *et al.* (ATLAS), JHEP **11**, 040 (2022), [arXiv:2202.11382].
- [212] V. Khachatryan *et al.* (CMS), JHEP **04**, 073 (2016), [arXiv:1511.02138].
- [213] M. Aaboud *et al.* (ATLAS), Eur. Phys. J. C **78**, 3, 186 (2018), [arXiv:1712.01602].
- [214] CMS Collab., CMS-PAS-TOP-19-003.
- [215] M. Czakon, P. Fiedler and A. Mitov, Phys. Rev. Lett. **115**, 5, 052001 (2015), [arXiv:1411.3007].
- [216] W. Hollik and D. Pagani, Phys. Rev. **D84**, 093003 (2011), [arXiv:1107.2606].
- [217] W. Bernreuther and Z.-G. Si, Phys. Rev. **D86**, 034026 (2012), [arXiv:1205.6580].
- [218] S. Jung *et al.*, Phys. Rev. **D81**, 015004 (2010), [arXiv:0907.4112].
- [219] V. M. Abazov *et al.* (D0), Phys. Rev. Lett. **100**, 142002 (2008), [arXiv:0712.0851].
- [220] T. Aaltonen *et al.* (CDF), Phys. Rev. Lett. **101**, 202001 (2008), [arXiv:0806.2472].
- [221] T. A. Aaltonen *et al.* (CDF, D0), Phys. Rev. Lett. **120**, 4, 042001 (2018), [arXiv:1709.04894].
- [222] G. Aad *et al.* (ATLAS), JHEP **02**, 107 (2014), [arXiv:1311.6724].
- [223] G. Aad *et al.* (ATLAS), Eur. Phys. J. **C76**, 2, 87 (2016), [Erratum: Eur. Phys. J. **C77**, 564 (2017)], [arXiv:1509.02358].
- [224] G. Aad *et al.* (ATLAS), Phys. Rev. **D94**, 3, 032006 (2016), [arXiv:1604.05538].
- [225] S. Chatrchyan *et al.* (CMS), Phys. Lett. **B717**, 129 (2012), [arXiv:1207.0065].
- [226] V. Khachatryan *et al.* (CMS), Phys. Rev. **D93**, 3, 034014 (2016), [arXiv:1508.03862].
- [227] V. Khachatryan *et al.* (CMS), Phys. Lett. **B760**, 365 (2016), [arXiv:1603.06221].
- [228] M. Czakon *et al.*, Phys. Rev. **D98**, 1, 014003 (2018), [arXiv:1711.03945].
- [229] V. Khachatryan *et al.* (CMS), Phys. Lett. **B757**, 154 (2016), [arXiv:1507.03119].
- [230] G. Aad *et al.* (ATLAS), Phys. Lett. **B756**, 52 (2016), [arXiv:1512.06092].
- [231] G. Aad *et al.* (ATLAS), JHEP **05**, 061 (2015), [arXiv:1501.07383].
- [232] S. Chatrchyan *et al.* (CMS), JHEP **04**, 191 (2014), [arXiv:1402.3803].
- [233] M. Aaboud *et al.* (ATLAS, CMS), JHEP **04**, 033 (2018), [arXiv:1709.05327].
- [234] G. Aad *et al.* (ATLAS), JHEP **08**, 077 (2023), [arXiv:2208.12095].
- [235] CMS Collab., CMS-PAS-TOP-15-018.
- [236] G. Aad *et al.* (ATLAS), Phys. Lett. B **843**, 137848 (2023), [arXiv:2212.10552].
- [237] G. Aad *et al.* (ATLAS), JHEP **07**, 033 (2023), [arXiv:2301.04245].
- [238] G. Aad *et al.* (ATLAS), Eur. Phys. J. C **82**, 4, 374 (2022), [arXiv:2110.05453].
- [239] A. M. Sirunyan *et al.* (CMS), JHEP **06**, 146 (2020), [arXiv:1912.09540].
- [240] A. Tumasyan *et al.* (CMS), Phys. Lett. B **846**, 137703 (2023), [arXiv:2208.02751].
- [241] G. Mahlon and S. J. Parke, Phys. Rev. **D53**, 4886 (1996), [hep-ph/9512264]; G. Mahlon and S. J. Parke, Phys. Lett. **B411**, 173 (1997), [hep-ph/9706304].
- [242] G.R. Goldstein, in *Spin 96: Proceedings of the 12th International Symposium on High Energy Spin Physics*, Amsterdam, 1996, ed. C.W. Jager (World Scientific, Singapore, 1997), p. 328.
- [243] T. Stelzer and S. Willenbrock, Phys. Lett. **B374**, 169 (1996), [hep-ph/9512292].
- [244] W. Bernreuther *et al.*, Nucl. Phys. **B690**, 81 (2004), [hep-ph/0403035].
- [245] A. Brandenburg, Z. G. Si and P. Uwer, Phys. Lett. **B539**, 235 (2002), [hep-ph/0205023].

- [246] W. Bernreuther, D. Heisler and Z.-G. Si, JHEP **12**, 026 (2015), [arXiv:1508.05271].
- [247] G. Mahlon and S. J. Parke, Phys. Rev. **D81**, 074024 (2010), [arXiv:1001.3422].
- [248] G. Aad *et al.* (ATLAS), Phys. Rev. **D90**, 11, 112016 (2014), [arXiv:1407.4314].
- [249] G. Aad *et al.* (ATLAS), Phys. Rev. Lett. **114**, 14, 142001 (2015), [arXiv:1412.4742].
- [250] G. Aad *et al.* (ATLAS), Phys. Rev. **D93**, 1, 012002 (2016), [arXiv:1510.07478].
- [251] S. Chatrchyan *et al.* (CMS), Phys. Rev. Lett. **112**, 18, 182001 (2014), [arXiv:1311.3924].
- [252] V. Khachatryan *et al.* (CMS), Phys. Lett. **B758**, 321 (2016), [arXiv:1511.06170].
- [253] V. Khachatryan *et al.* (CMS), Phys. Rev. **D93**, 5, 052007 (2016), [arXiv:1601.01107].
- [254] M. Aaboud *et al.* (ATLAS), JHEP **03**, 113 (2017), [arXiv:1612.07004].
- [255] M. Aaboud *et al.* (ATLAS), Eur. Phys. J. C **80**, 8, 754 (2020), [arXiv:1903.07570].
- [256] A. M. Sirunyan *et al.* (CMS), Phys. Rev. **D100**, 7, 072002 (2019), [arXiv:1907.03729].
- [257] A. Einstein, B. Podolsky and N. Rosen, Phys. Rev. **47**, 777 (1935).
- [258] E. Schrödinger, Mathematical Proceedings of the Cambridge Philosophical Society **31**, 4, 555–563 (1935).
- [259] J. S. Bell, Physics Physique Fizika **1**, 195 (1964).
- [260] R. Horodecki *et al.*, Rev. Mod. Phys. **81**, 865 (2009), [arXiv:quant-ph/0702225].
- [261] H. Casini and M. Huerta, PoS **TASI2021**, 002 (2023), [arXiv:2201.13310].
- [262] A. Go *et al.* (Belle), Phys. Rev. Lett. **99**, 131802 (2007), [arXiv:quant-ph/0702267].
- [263] M. Fabbrichesi *et al.* (2023), [arXiv:2305.04982].
- [264] Y. Afik and J. R. M. n. de Nova, Eur. Phys. J. Plus **136**, 9, 907 (2021), [arXiv:2003.02280].
- [265] M. Fabbrichesi, R. Floreanini and G. Panizzo, Phys. Rev. Lett. **127**, 16, 161801 (2021), [arXiv:2102.11883].
- [266] C. Severi *et al.*, Eur. Phys. J. C **82**, 4, 285 (2022), [arXiv:2110.10112].
- [267] Y. Afik and J. R. M. n. de Nova, Quantum **6**, 820 (2022), [arXiv:2203.05582].
- [268] J. A. Aguilar-Saavedra and J. A. Casas, Eur. Phys. J. C **82**, 8, 666 (2022), [arXiv:2205.00542].
- [269] Y. Afik and J. R. M. n. de Nova, Phys. Rev. Lett. **130**, 22, 221801 (2023), [arXiv:2209.03969].
- [270] R. Ashby-Pickering, A. J. Barr and A. Wierzychucka, JHEP **05**, 020 (2023), [arXiv:2209.13990].
- [271] J. A. Aguilar-Saavedra (2023), [arXiv:2307.06991].
- [272] ATLAS Collab., ATLAS-CONF-2023-069.
- [273] G. L. Kane, G. A. Ladinsky and C. P. Yuan, Phys. Rev. **D45**, 124 (1992).
- [274] A. Czarnecki, J. G. Korner and J. H. Piclum, Phys. Rev. **D81**, 111503 (2010), [arXiv:1005.2625].
- [275] K. Kondo, T. Chikamatsu and S. H. Kim, J. Phys. Soc. Jap. **62**, 1177 (1993).
- [276] T. Aaltonen *et al.* (CDF, D0), Phys. Rev. **D85**, 071106 (2012), [arXiv:1202.5272].
- [277] G. Aad *et al.* (ATLAS), JHEP **06**, 088 (2012), [arXiv:1205.2484].
- [278] S. Chatrchyan *et al.* (CMS), JHEP **10**, 167 (2013), [arXiv:1308.3879].
- [279] ATLAS and CMS Collab., ATLAS-CONF-2013-033, CMS-PAS-TOP-12-025.
- [280] M. Aaboud *et al.* (ATLAS), Eur. Phys. J. **C77**, 4, 264 (2017), [Erratum: Eur. Phys. J.C79,no.1,19(2019)], [arXiv:1612.02577].
- [281] V. Khachatryan *et al.* (CMS), Phys. Lett. **B762**, 512 (2016), [arXiv:1605.09047].
- [282] CMS Collab., CMS-PAS-TOP-14-017.
- [283] V. Khachatryan *et al.* (CMS), JHEP **01**, 053 (2015), [arXiv:1410.1154].
- [284] G. Aad *et al.* (CMS, ATLAS), JHEP **08**, 08, 051 (2020), [arXiv:2005.03799].
- [285] G. Aad *et al.* (ATLAS), Phys. Lett. B **843**, 137829 (2023), [arXiv:2209.14903].
- [286] F. Abe *et al.* (CDF), Phys. Rev. **D50**, 2966 (1994).
- [287] A. Abulencia *et al.* (CDF), Phys. Rev. **D73**, 032003 (2006), [hep-ex/0510048].
- [288] M. Aaboud *et al.* (ATLAS), Eur. Phys. J. **C79**, 4, 290 (2019), [arXiv:1810.01772].
- [289] V. Khachatryan *et al.* (CMS), Phys. Rev. **D93**, 7, 072004 (2016), [arXiv:1509.04044].
- [290] A. M. Sirunyan *et al.* (CMS), Eur. Phys. J. **C78**, 11, 891 (2018), [arXiv:1805.01428].
- [291] S. Argyropoulos and T. Sjöstrand, JHEP **11**, 043 (2014), [arXiv:1407.6653].
- [292] J. R. Christiansen and P. Z. Skands, JHEP **08**, 003 (2015), [arXiv:1505.01681].
- [293] A. M. Sirunyan *et al.* (CMS), Phys. Rev. Lett. **124**, 20, 202001 (2020), [arXiv:1911.03800].
- [294] V. M. Abazov *et al.* (D0), Nature **429**, 638 (2004), [hep-ex/0406031].
- [295] R. H. Dalitz and G. R. Goldstein, Phys. Rev. **D45**, 1531 (1992); R. H. Dalitz and G. R. Goldstein, Phys. Lett. **B287**, 225 (1992).
- [296] V. M. Abazov *et al.* (D0), Phys. Rev. Lett. **113**, 032002 (2014), [arXiv:1405.1756].
- [297] L. Sonnenschein, Phys. Rev. **D73**, 054015 (2006), [Erratum: Phys. Rev.D78,079902(2008)], [hep-ph/0603011].
- [298] G. Aad *et al.* (ATLAS), Eur. Phys. J. **C75**, 7, 330 (2015), [arXiv:1503.05427].
- [299] A. M. Sirunyan *et al.* (CMS), Phys. Rev. **D96**, 3, 032002 (2017), [arXiv:1704.06142].
- [300] C. G. Lester and D. J. Summers, Phys. Lett. **B463**, 99 (1999), [hep-ph/9906349].
- [301] A. M. Sirunyan *et al.* (CMS), Eur. Phys. J. **C79**, 4, 313 (2019), [arXiv:1812.10534].
- [302] M. Aaboud *et al.* (ATLAS), JHEP **09**, 118 (2017), [arXiv:1702.07546].
- [303] CMS Collab., CMS-PAS-TOP-19-009.
- [304] The Tevatron Electroweak Working Group and Aaltonen, T., For the CDF and D0 Collab., arXiv:1608.01881, FERMILAB-CONF-16-298-E.
- [305] B. Abbott *et al.* (D0), Phys. Rev. **D60**, 052001 (1999), [hep-ex/9808029]; F. Abe *et al.* (CDF), Phys. Rev. Lett. **82**, 271 (1999), [Erratum: Phys. Rev. Lett.82,2808(1999)], [hep-ex/9810029].
- [306] T. Aaltonen *et al.* (CDF), Phys. Rev. **D92**, 3, 032003 (2015), [arXiv:1505.00500].
- [307] T. A. Aaltonen *et al.* (CDF), Phys. Rev. **D90**, 9, 091101 (2014), [arXiv:1409.4906].
- [308] A. M. Sirunyan *et al.* (CMS), Eur. Phys. J. **C77**, 5, 354 (2017), [arXiv:1703.02530].
- [309] T. Aaltonen *et al.* (CDF), Phys. Lett. **B698**, 371 (2011), [arXiv:1101.4926].
- [310] CMS Collab., CMS-PAS-TOP-12-030.

- [311] T. Aaltonen *et al.* (CDF), Phys. Rev. **D80**, 051104 (2009), [arXiv:0906.5371].
- [312] ATLAS Collab., ATLAS-CONF-2019-046.
- [313] V. Khachatryan *et al.* (CMS), Phys. Rev. **D93**, 9, 092006 (2016), [arXiv:1603.06536].
- [314] V. Khachatryan *et al.* (CMS), JHEP **12**, 123 (2016), [arXiv:1608.03560].
- [315] CMS Collab., CMS-PAS-TOP-15-002.
- [316] CMS Collab., CMS-PAS-TOP-16-002.
- [317] V. M. Abazov *et al.* (D0), Phys. Rev. Lett. **100**, 192004 (2008), [arXiv:0803.2779]; S. Chatrchyan *et al.* (CMS), Phys. Lett. **B728**, 496 (2014), [Erratum: Phys. Lett. B738,526(2014)], [arXiv:1307.1907]; V. M. Abazov *et al.* (D0), Phys. Lett. **B703**, 422 (2011), [arXiv:1104.2887]; ATLAS Collab., ATLAS-CONF-2019-041; U. Langenfeld, S. Moch and P. Uwer, Phys. Rev. **D80**, 054009 (2009), [arXiv:0906.5273]; J. Fuster *et al.*, Eur. Phys. J. C **77**, 11, 794 (2017), [arXiv:1704.00540].
- [318] G. Aad *et al.* (ATLAS), JHEP **11**, 150 (2019), [arXiv:1905.02302].
- [319] CMS Collab., CMS-PAS-TOP-13-006 (2016).
- [320] CDF Collab., CDF conference note 11080 (2014).
- [321] V. M. Abazov *et al.* (D0), Phys. Rev. **D91**, 11, 112003 (2015), [arXiv:1501.07912].
- [322] CMS Collab., CMS-PAS-TOP-13-005.
- [323] M. Beneke *et al.*, Phys. Lett. **B775**, 63 (2017), [arXiv:1605.03609].
- [324] A. H. Hoang, C. Lepenik and M. Preisser, JHEP **09**, 099 (2017), [arXiv:1706.08526].
- [325] A. H. Hoang *et al.*, Phys. Rev. Lett. **101**, 151602 (2008), [arXiv:0803.4214].
- [326] ATLAS Collab., ATLAS-PHYS-PUB-2021-034.
- [327] A. M. Sirunyan *et al.*, Physics Letters B **803**, 135263 (2020), [arXiv:1909.09193].
- [328] S. Catani *et al.*, JHEP **08**, 08, 027 (2020), [arXiv:2005.00557].
- [329] G. Aad *et al.* (ATLAS), Phys. Lett. **B716**, 1 (2012), [arXiv:1207.7214].
- [330] S. Chatrchyan *et al.* (CMS), Phys. Lett. **B716**, 30 (2012), [arXiv:1207.7235].
- [331] S. Alekhin, A. Djouadi and S. Moch, Phys. Lett. **B716**, 214 (2012), [arXiv:1207.0980].
- [332] T. Aaltonen *et al.* (CDF), Phys. Rev. **D87**, 5, 052013 (2013), [arXiv:1210.6131].
- [333] V. M. Abazov *et al.* (D0), Phys. Rev. **D84**, 052005 (2011), [arXiv:1106.2063].
- [334] G. Aad *et al.* (ATLAS), Phys. Lett. **B728**, 363 (2014), [arXiv:1310.6527].
- [335] S. Chatrchyan *et al.* (CMS), JHEP **06**, 109 (2012), [arXiv:1204.2807].
- [336] S. Chatrchyan *et al.* (CMS), Phys. Lett. **B770**, 50 (2017), [arXiv:1610.09551].
- [337] A. F. Falk and M. E. Peskin, Phys. Rev. **D49**, 3320 (1994), [hep-ph/9308241].
- [338] T. A. Aaltonen *et al.* (CDF), Phys. Rev. Lett. **111**, 20, 202001 (2013), [arXiv:1308.4050].
- [339] CMS Collab., CMS-PAS-TOP-16-019.
- [340] M. Aaboud *et al.* (ATLAS), Eur. Phys. J. **C78**, 2, 129 (2018), [arXiv:1709.04207].
- [341] ATLAS Collab., ATLAS-CONF-2019-038.
- [342] V. M. Abazov *et al.* (D0), Phys. Rev. **D85**, 091104 (2012), [arXiv:1201.4156].
- [343] D. Choudhury, T. M. P. Tait and C. E. M. Wagner, Phys. Rev. **D65**, 053002 (2002), [hep-ph/0109097].
- [344] D. Chang, W.-F. Chang and E. Ma, Phys. Rev. **D59**, 091503 (1999), [hep-ph/9810531]; D. Chang, W.-F. Chang and E. Ma, Phys. Rev. **D61**, 037301 (2000), [hep-ph/9909537].
- [345] T. Aaltonen *et al.* (CDF), Phys. Rev. **D88**, 3, 032003 (2013), [arXiv:1304.4141].
- [346] V. M. Abazov *et al.* (D0), Phys. Rev. **D90**, 5, 051101 (2014), [Erratum: Phys. Rev. D90,no.7,079904(2014)], [arXiv:1407.4837].
- [347] G. Aad *et al.* (ATLAS), JHEP **11**, 031 (2013), [arXiv:1307.4568].
- [348] CMS Collab., CMS-PAS-TOP-11-031.
- [349] T. Aaltonen *et al.* (CDF), Phys. Rev. **D84**, 031104 (2011), [arXiv:1106.3970].
- [350] G. Aad *et al.* (ATLAS), Phys. Rev. **D91**, 7, 072007 (2015), [arXiv:1502.00586].
- [351] M. Aaboud *et al.* (ATLAS), JHEP **11**, 086 (2017), [arXiv:1706.03046].
- [352] K. Melnikov, M. Schulze and A. Scharf, Phys. Rev. **D83**, 074013 (2011), [arXiv:1102.1967].
- [353] A. M. Sirunyan *et al.* (CMS), JHEP **10**, 006 (2017), [arXiv:1706.08128].
- [354] M. Aaboud *et al.* (ATLAS), Eur. Phys. J. **C79**, 5, 382 (2019), [arXiv:1812.01697].
- [355] G. Bevilacqua *et al.*, JHEP **10**, 158 (2018), [arXiv:1803.09916].
- [356] G. Bevilacqua *et al.*, JHEP **01**, 188 (2019), [arXiv:1809.08562].
- [357] G. Aad *et al.* (ATLAS), JHEP **09**, 049 (2020), [arXiv:2007.06946].
- [358] A. Tumasyan *et al.* (CMS), JHEP **12**, 180 (2021), [arXiv:2107.01508].
- [359] A. Tumasyan *et al.* (CMS), JHEP **05**, 091 (2022), [arXiv:2201.07301].
- [360] G. Aad *et al.* (ATLAS) (2023), [arXiv:2302.01283].
- [361] A. M. Sirunyan *et al.* (CMS), Phys. Rev. Lett. **121**, 22, 221802 (2018), [arXiv:1808.02913].
- [362] M. Cepeda *et al.* (HL/HE WG2 group) (2019), [arXiv:1902.00134].
- [363] S. Chatrchyan *et al.* (CMS), Phys. Rev. Lett. **110**, 172002 (2013), [arXiv:1303.3239].
- [364] J. M. Campbell and R. K. Ellis, JHEP **07**, 052 (2012), [arXiv:1204.5678].
- [365] M. V. Garzelli *et al.*, JHEP **11**, 056 (2012), [arXiv:1208.2665].
- [366] ATLAS Collab., ATLAS-CONF-2012-126.
- [367] G. Aad *et al.* (ATLAS), JHEP **11**, 172 (2015), [arXiv:1509.05276].
- [368] V. Khachatryan *et al.* (CMS), JHEP **01**, 096 (2016), [arXiv:1510.01131].
- [369] M. Aaboud *et al.* (ATLAS), Phys. Rev. **D99**, 7, 072009 (2019), [arXiv:1901.03584].
- [370] G. Aad *et al.* (ATLAS), Eur. Phys. J. C **81**, 737 (2021), [arXiv:2103.12603].
- [371] ATLAS Collab., ATLAS-CONF-2023-065.
- [372] A. M. Sirunyan *et al.* (CMS), JHEP **08**, 011 (2018), [arXiv:1711.02547].
- [373] A. M. Sirunyan *et al.* (CMS), JHEP **03**, 056 (2020), [arXiv:1907.11270].
- [374] A. Tumasyan *et al.* (CMS), Phys. Rev. D **108**, 032008 (2023), [arXiv:2208.12837].
- [375] A. Tumasyan *et al.* (CMS), JHEP **07**, 219 (2023), [arXiv:2208.06485].
- [376] ATLAS Collab., ATLAS-CONF-2023-019.

- [377] A. M. Sirunyan *et al.* (CMS), JHEP **07**, 003 (2017), [arXiv:1702.01404].
- [378] A. Tumasyan *et al.* (CMS), JHEP **02**, 107 (2022), [arXiv:2111.02860].
- [379] A. M. Sirunyan *et al.* (CMS), Phys. Rev. Lett. **122**, 13, 132003 (2019), [arXiv:1812.05900].
- [380] G. Aad *et al.* (ATLAS), JHEP **07**, 124 (2020), [arXiv:2002.07546].
- [381] CMS Collab., CMS-PAS-TOP-22-008.
- [382] S. P. Martin 1–98 (1997), [Adv. Ser. Direct. High Energy Phys.18,1(1998)], [hep-ph/9709356].
- [383] C. T. Hill and E. H. Simmons, Phys. Rept. **381**, 235 (2003), [Erratum: Phys. Rept.390,553(2004)], [hep-ph/0203079].
- [384] C. T. Hill, Phys. Lett. **B266**, 419 (1991).
- [385] C. T. Hill, Phys. Lett. **B345**, 483 (1995), [hep-ph/9411426].
- [386] G. Aad *et al.* (ATLAS), JHEP **2306**, 155 (2023), [arXiv:2208.11415].
- [387] CMS Collab., CMS-PAS-TOP-22-002.
- [388] ATLAS Collab., CERN-EP-2022-044, [arXiv:2301.11605].
- [389] G. Aad *et al.* (ATLAS), Phys. Lett. B **842**, 137379 (2023), [arXiv:2205.02537].
- [390] G. Aad *et al.* (ATLAS), Eur. Phys. J. C **82**, 4, 334 (2022), [arXiv:2112.01302].
- [391] A. Tumasyan *et al.* (CMS), JHEP **06**, 082 (2022), [arXiv:2201.07859].
- [392] ATLAS Collab., ATLAS-CONF-2023-001.
- [393] S. Chatrchyan *et al.* (CMS), Phys. Rev. D **87**, 072002 (2013), URL <https://link.aps.org/doi/10.1103/PhysRevD.87.072002>.
- [394] S. Chatrchyan *et al.* (CMS), JHEP **12**, 015 (2012), [arXiv:1209.4397].
- [395] G. Aad *et al.* (ATLAS), JHEP **10**, 061 (2020), [arXiv:2005.05138].
- [396] A. Tumasyan *et al.* (CMS), JHEP **02**, 169 (2022), [arXiv:2112.09734].
- [397] A. Tumasyan *et al.* (CMS), Phys. Rev. Lett. **129**, 032001 (2022), URL <https://link.aps.org/doi/10.1103/PhysRevLett.129.032001>.
- [398] A. Tumasyan *et al.* (CMS) (2021), [arXiv:2107.13896].
- [399] CMS Collab., CMS-PAS-TOP-22-006.
- [400] G. Aad *et al.* (ATLAS), JHEP **06**, 063 (2022), [arXiv:2202.12134].
- [401] G. Aad *et al.* (ATLAS), JHEP **04**, 080 (2023), [arXiv:2205.02817].
- [402] G. Aad *et al.* (ATLAS), JHEP **07**, 199 (2023), [arXiv:2301.03902].
- [403] S. Banerjee, M. Chala and M. Spannowsky, Eur. Phys. J. C **78**, 8, 683 (2018), [arXiv:1806.02836].
- [404] C. Zhang and S. Willenbrock, Nuovo Cim. C **033**, 4, 285 (2010), [arXiv:1008.3155].
- [405] LHC Top Working Group Summary Plots <https://twiki.cern.ch/twiki/bin/view/LHCPhysics/LHCTopWGSummaryPlots>.
- [406] A. M. Sirunyan *et al.* (CMS), JHEP **03**, 095 (2021), [arXiv:2012.04120].
- [407] CMS Collab., CMS-PAS-TOP-21-013.
- [408] CMS Collab., CMS-PAS-TOP-22-005.

62. Form Factors for Semileptonic Kaon ($K_{\ell 3}$), Radiative Pion ($\pi_{\ell 2\gamma}$) and Kaon ($K_{\ell 2\gamma}$) Decays

Revised August 2023 by M.A. Bychkov (Virginia U.) and G. D'Ambrosio (INFN, Napoli).

62.1 $\pi_{\ell 2\gamma}^{\pm}$ and $K_{\ell 2\gamma}^{\pm}$ Form Factors

The radiative decays, $\pi^{\pm} \rightarrow l^{\pm}\nu\gamma$ and $K^{\pm} \rightarrow l^{\pm}\nu\gamma$, with l standing for an e or a μ , and γ for a real or virtual photon ($e^{+}e^{-}$ pair), provide a powerful tool to investigate the hadronic structure of pions and kaons. The structure-dependent part SD_i of the amplitude describes the emission of photons from virtual hadronic states, and is parametrized in terms of form factors V, A , (vector, axial vector), in the standard description [1–4]. Note that in the Listings and some literature, equivalent nomenclature F_V and F_A for the vector and axial form factors is often used. Exotic, non-standard contributions like $i = T, S$ (tensor, scalar) have also been considered. Apart from the SD terms, there is also the Inner Bremsstrahlung amplitude, IB, corresponding to photon radiation from external charged particles and described by Low theorem in terms of the physical decay $\pi^{\pm}(K^{\pm}) \rightarrow l^{\pm}\nu$. Experiments try to optimize their kinematics so as to minimize the IB part of the amplitude.

The SD amplitude in its standard form is given as

$$M(SD_V) = \frac{-eG_F U_{qq'}}{\sqrt{2}m_P} \epsilon^{\mu\nu} V^P \epsilon_{\mu\nu\sigma\tau} k^{\sigma} q^{\tau} \quad (62.1)$$

$$M(SD_A) = \frac{-ieG_F U_{qq'}}{\sqrt{2}m_P} \epsilon^{\mu\nu} \{A^P [(qk - k^2)g_{\mu\nu} - q_{\mu}k_{\nu}] + R^P k^2 g_{\mu\nu}\}, \quad (62.2)$$

which contains an additional axial form factor R^P which only can be accessed if the photon remains virtual. $U_{qq'}$ is the Cabibbo-Kobayashi-Maskawa mixing-matrix element; ϵ^{μ} is the polarization vector of the photon (or the effective vertex, $\epsilon^{\mu} = (e/k^2)\bar{u}(p_-)\gamma^{\mu}v(p_+)$, of the $e^{+}e^{-}$ pair); $\ell^{\nu} = \bar{u}(p_{\nu})\gamma^{\nu}(1 - \gamma_5)v(p_{\ell})$ is the lepton-neutrino current; q and k are the meson and photon four-momenta ($k = p_+ + p_-$ for virtual photons); and P stands for π or K .

For decay processes where the photon is real, the partial decay width can be written in analytical form as a sum of IB, SD, and IB/SD interference terms INT [1, 4]:

$$\begin{aligned} \frac{d^2\Gamma_{P \rightarrow \ell\nu\gamma}}{dxdy} &= \frac{d^2(\Gamma_{IB} + \Gamma_{SD} + \Gamma_{INT})}{dxdy} \\ &= \frac{\alpha}{2\pi} \Gamma_{P \rightarrow \ell\nu} \frac{1}{(1-r)^2} \left\{ \text{IB}(x, y) \right. \\ &+ \frac{1}{r} \left(\frac{m_P}{2f_P} \right)^2 \left[(V+A)^2 \text{SD}^+(x, y) + (V-A)^2 \text{SD}^-(x, y) \right] \\ &\left. + \epsilon_P \frac{m_P}{f_P} \left[(V+A) S_{INT}^+(x, y) + (V-A) S_{INT}^-(x, y) \right] \right\}. \quad (62.3) \end{aligned}$$

Here

$$\begin{aligned} \text{IB}(x, y) &= \left[\frac{1-y+r}{x^2(x+y-1-r)} \right] \\ &\left[x^2 + 2(1-x)(1-r) - \frac{2xr(1-r)}{x+y-1-r} \right] \\ \text{SD}^+(x, y) &= (x+y-1-r) \left[(x+y-1)(1-x) - r \right] \\ \text{SD}^-(x, y) &= (1-y+r) \left[(1-x)(1-y) + r \right] \\ S_{INT}^+(x, y) &= \left[\frac{1-y+r}{x(x+y-1-r)} \right] \left[(1-x)(1-x-y) + r \right] \\ S_{INT}^-(x, y) &= \left[\frac{1-y+r}{x(x+y-1-r)} \right] \left[x^2 - (1-x)(1-x-y) - r \right] \quad (62.4) \end{aligned}$$

where $x = 2E_{\gamma}/m_P$, $y = 2E_{\ell}/m_P$, $r = (m_{\ell}/m_P)^2$, f_P is the meson decay constant, and ϵ_P is +1 for pions and -1 for kaons. The structure dependent terms SD^+ and SD^- are shown in Fig. 1. The SD^- term is maximized in the same kinematic region where overwhelming IB term dominates (along $x+y=1$ diagonal). Thus experimental yields with less background are dominated by SD^+ contribution and proportional to $A^P + V^P$ making simultaneous precise determination of the form factors difficult.

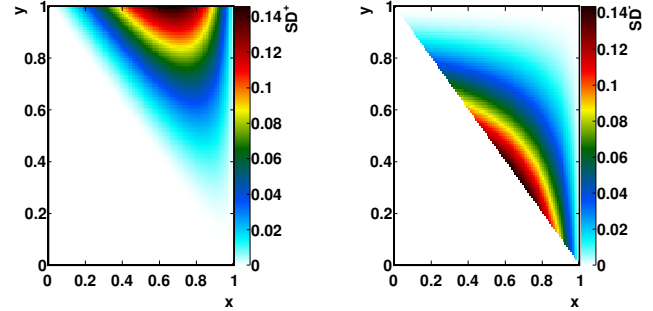


Figure 62.1: Components of the structure dependent terms of the decay width. Left: SD^+ , right: SD^-

Recently, formulas 62.3 and 62.4 have been extended to describe polarized distributions in radiative meson and muon decays [5].

The ‘‘helicity’’ factor r is responsible for the enhancement of the SD over the IB amplitude in the decays $\pi^{\pm} \rightarrow e^{\pm}\nu\gamma$, while $\pi^{\pm} \rightarrow \mu^{\pm}\nu\gamma$ is dominated by IB. Interference terms are important for the decay $K^{\pm} \rightarrow \mu^{\pm}\nu\gamma$ [6], but contribute only a few percent correction to pion decays. However, they provide the basis for determining the signs of V and A . Radiative corrections to the decay $\pi^+ \rightarrow e^+\nu\gamma$ have to be taken into account in the analysis of the precision experiments. They make up to 4% corrections in the total decay rate [7]. In $\pi^{\pm} \rightarrow e^{\pm}\nu e^+e^-$ and $K^{\pm} \rightarrow l^{\pm}\nu e^+e^-$ decays, all three form factors, V^P , A^P , and R^P , can be determined [8, 9].

Theoretically, the first non-trivial χPT contributions to A^P and V^P appear at $\mathcal{O}(p^4)$ [4], respectively from Gasser-Leutwyler coefficients, L_i 's, and the anomalous lagrangian:

$$A^P = \frac{4\sqrt{2}M_P}{F_{\pi}} (L_9^r + L_{10}^r), \quad V^P = \frac{\sqrt{2}M_P}{8\pi^2 F_{\pi}}. \quad (62.5)$$

In case of the kaon $A^K = 0.042$ and $V^K = 0.096$. $\mathcal{O}(p^6)$ contributions to A^K can be predicted accurately: they are flat in the momentum dependence and shift the $\mathcal{O}(p^4)$ value to 0.034. $\mathcal{O}(p^6)$ contributions to V^K are model dependent and can be approximated by a form factor linearly dependent on momentum. For example, when looking at the spread of results obtained within two different models, the constant piece of this linear form factor is shifted to 0.078 ± 0.005 [1, 2, 4].

We give the experimental π^{\pm} form factors V^{π} , A^{π} , and R^{π} in the Listings. In the K^{\pm} Listings, we give the extracted sum $A^K + V^K$ and difference $A^K - V^K$, as well as V^K , A^K and R^K . In particular KLOE has measured for the constant piece of the form factor $A^K + V^K = 0.125 \pm 0.007 \pm 0.001$ [10] while ISTRA+, $V^K - A^K = 0.21 \pm 0.04 \pm 0.04$ [11].

The pion vector form factor, V^{π} , is related via CVC (Conserved Vector Current) to the $\pi^0 \rightarrow \gamma\gamma$ decay width. The constant term is given by $|V^{\pi}(0)| = (1/\alpha)\sqrt{2\Gamma_{\pi^0 \rightarrow \gamma\gamma}/\pi m_{\pi^0}}$ [3]. The resulting value, $V^{\pi}(0) = 0.0259(9)$, has been confirmed by calculations based on chiral perturbation theory (χPT) [4], and by two experiments given in the Listings.

A recent experiment by the PIBETA collaboration [12] obtained a $V^{\pi}(0)$ that is in excellent agreement with the CVC hypothesis. It also measured the slope parameter a in $V^{\pi}(s) = V^{\pi}(0)(1+a \cdot s)$, where $s = (1-2E_{\gamma}/m_{\pi})$, and E_{γ} is the gamma energy in the pion rest frame: $a = 0.095 \pm 0.058$. A functional dependence on s is expected for all form factors. It becomes non-negligible in the

case of $V^\pi(s)$ when a wide range of photon momenta is recorded; proper treatment in the analysis of K decays is mandatory.

The form factor, R^P , can be related to the electromagnetic radius, r_P , of the meson [2]: $R^P = \frac{1}{3}m_P f_P \langle r_P^2 \rangle$ using PCAC (Partial Conserved Axial vector Current).

In lowest order χPT , the ratio A^π/V^π is related to the pion electric polarizability $\alpha_E = [\alpha/(8\pi^2 m_\pi f_\pi^2)] \times A^\pi/V^\pi$ [13]. Direct experimental and theoretical status of pion polarizability studies currently is not settled. Most recent theoretical predictions from χPT at $\mathcal{O}(p^6)$ [14] and experimental results from COM-PASS collaboration [15] favor a small value of pion polarizability $\alpha_\pi \sim (2 \div 3) \times 10^{-4} \text{ fm}^3$. Dispersive analysis of $\gamma\gamma \rightarrow \pi^+\pi^-$ cross-section [16] and experimental results from MAMI collaboration [17] report a much larger value of $\alpha_\pi \sim 6 \times 10^{-4} \text{ fm}^3$. Precise measurement of the pion form factors by PIBETA collaboration favors smaller values of polarizability $\alpha_\pi = 2.7_{-0.5}^{+0.6} \times 10^{-4} \text{ fm}^3$.

Several searches for the exotic form factors F_T^π , F_T^K (tensor), and F_S^K (scalar) have been pursued in the past. In particular, F_T^π has been brought into focus by experimental as well as theoretical work [18]. New high-statistics data from the PIBETA collaboration have been re-analyzed together with an additional data set optimized for low backgrounds in the radiative pion decay. In particular, lower beam rates have been used in order to reduce the accidental background, thereby making the treatment of systematic uncertainties easier and more reliable. The PIBETA analysis now restricts F_T^π to the range $-5.2 \times 10^{-4} < F_T^\pi < 4.0 \times 10^{-4}$ at a 90% confidence limit [12]. This result is in excellent agreement with the most recent theoretical work [4].

Precision measurements of radiative pion and kaon decays are effective tools to study QCD in the non-perturbative region and are of interest beyond the scope of radiative decays. Meanwhile other processes such as $\pi^+ \rightarrow e^+\nu$ that seem to be better suited to search for new physics at the precision frontier are currently studied. The advantages of such process are the very accurate and reliable theoretical predictions and the more straightforward experimental analysis.

62.2 $K_{\ell 3}^\pm$ and $K_{\ell 3}^0$ Form Factors

Assuming that only the vector current contributes to $K \rightarrow \pi \ell \nu$ decays, we write the matrix element as

$$M \propto f_+(t) [(P_K + P_\pi)_\mu \bar{\ell} \gamma_\mu (1 + \gamma_5) \nu] + f_-(t) [m_\ell \bar{\ell} (1 + \gamma_5) \nu], \quad (62.6)$$

where P_K and P_π are the four-momenta of the K and π mesons, m_ℓ is the lepton mass, and f_+ and f_- are dimensionless form factors which can depend only on $t = (P_K - P_\pi)^2$, the square of the four-momentum transfer to the leptons. If time-reversal invariance holds, f_+ and f_- are relatively real. $K_{\mu 3}$ experiments, discussed immediately below, measure f_+ and f_- , while K_{e3} experiments, discussed further below, are sensitive only to f_+ because the small electron mass makes the f_- term negligible.

62.2.1 $K_{\mu 3}$ Decays

Analyses of $K_{\mu 3}$ data frequently assume a linear dependence of f_+ and f_- on t , *i.e.*,

$$f_\pm(t) = f_\pm(0) [1 + \lambda_\pm(t/m_{\pi^\pm}^2)]. \quad (62.7)$$

Most $K_{\mu 3}$ data are adequately described by formula 62.7 for f_+ and a constant f_- (*i.e.*, $\lambda_- = 0$).

There are two equivalent parametrizations commonly used in these analyses: $\lambda_+, \xi(0)$ parametrization and λ_+, λ_0 parametrization.

Older analyses of $K_{\mu 3}$ data often introduce the ratio of the two form factors

$$\xi(t) = f_-(t)/f_+(t). \quad (62.8)$$

The $K_{\mu 3}$ decay distribution is then described by the two parameters λ_+ and $\xi(0)$ (assuming time reversal invariance and $\lambda_- = 0$).

More recent $K_{\mu 3}$ analyses have parametrized in terms of the form factors f_+ and f_0 , which are associated with vector and

scalar exchange, respectively, to the lepton pair. f_0 is related to f_+ and f_- by

$$f_0(t) = f_+(t) + [t/(m_K^2 - m_\pi^2)] f_-(t). \quad (62.9)$$

Here $f_0(0)$ must equal $f_+(0)$. The earlier assumption that f_+ is linear in t and f_- is constant leads to f_0 linear in t :

$$f_0(t) = f_0(0) [1 + \lambda_0(t/m_{\pi^\pm}^2)]. \quad (62.10)$$

With the assumption that $f_0(0) = f_+(0)$, the two parametrizations, $(\lambda_+, \xi(0))$ and (λ_+, λ_0) are equivalent as long as correlation information is retained. (λ_+, λ_0) correlations tend to be less strong than $(\lambda_+, \xi(0))$ correlations.

Since the 2006 edition of the *Review* [19], we no longer quote results in the $(\lambda_+, \xi(0))$ parametrization. We have removed many older low statistics results from the Listings. See the 2004 version of this note [20] for these older results, and the 1982 version [21] for additional discussion of the $K_{\mu 3}^0$ parameters, correlations, and conversion between parametrizations.

More recent high-statistics experiments have included a quadratic term in the expansion of $f_+(t)$,

$$f_+(t) = f_+(0) \left[1 + \lambda'_+(t/m_{\pi^\pm}^2) + \frac{\lambda''_+}{2}(t/m_{\pi^\pm}^2)^2 \right]. \quad (62.11)$$

If there is a non-vanishing quadratic term, then λ_+ of formula 62.7 represents the average slope, which is then different from λ'_+ . Our convention is to include the factor $\frac{1}{2}$ in the quadratic term, and to use m_{π^\pm} even for K_{e3}^+ and $K_{\mu 3}^+$ decays. We have converted other's parametrizations to match our conventions, as noted in the beginning of the " $K_{\ell 3}^\pm$ and $K_{\ell 3}^0$ Form Factors" sections of the Listings.

There are two alternatives to the Taylor parametrization: The Pole Parametrization and Dispersive Parametrization.

The pole model describes the t -dependence of $f_+(t)$ and $f_0(t)$ in terms of the exchange of the lightest vector and scalar K^* mesons with masses M_V and M_S , respectively:

$$f_+(t) = f_+(0) \left[\frac{M_V^2}{M_V^2 - t} \right], \quad f_0(t) = f_0(0) \left[\frac{M_S^2}{M_S^2 - t} \right]. \quad (62.12)$$

The Dispersive Parametrization approach, valid in a much wider kinematic range and able to describe at the same time τ -decay data, [22] uses dispersive techniques and the known low-energy K - π phases to parametrize the vector and scalar form factors:

$$f_+(t) = f_+(0) \exp \left[\frac{t}{m_\pi^2} (\Lambda_+ + H(t)) \right]; \quad (62.13)$$

$$f_0(t) = f_+(0) \exp \left[\frac{t}{(m_K^2 - m_\pi^2)} (\ln[C] - G(t)) \right], \quad (62.14)$$

where Λ_+ is the slope of the vector form factor, and $\ln C = \ln [f_0(m_K^2 - m_\pi^2)]$ is the logarithm of the scalar form factor at the Callan-Treiman point. The functions $H(t)$ and $G(t)$ are dispersive integrals.

62.2.2 K_{e3} Decays

Analysis of K_{e3} data is simpler than that of $K_{\mu 3}$ because the second term of the matrix element assuming a pure vector current [formula 62.6 above] can be neglected. Here f_+ can be assumed to be linear in t , in which case the linear coefficient λ_+ of formula 62.7 is determined, or quadratic, in which case the linear coefficient λ'_+ and quadratic coefficient λ''_+ of formula 62.11 are determined.

If we remove the assumption of a pure vector current, then the matrix element for the decay, in addition to the terms in formula 62.6, would contain

$$+2m_K f_S \bar{\ell} (1 + \gamma_5) \nu + (2f_T/m_K) (P_K)_\lambda (P_\pi)_\mu \bar{\ell} \sigma_{\lambda\mu} (1 + \gamma_5) \nu, \quad (62.15)$$

where f_S is the scalar form factor, and f_T is the tensor form factor. In the case of the K_{e3} decays where the f_- term can be neglected, experiments have yielded limits on $|f_S/f_+|$ and $|f_T/f_+|$.

For K_{e3} data, we determine best values for the three parametrizations: linear (λ_+), quadratic (λ'_+, λ''_+) and pole (M_V). For $K_{\mu 3}$ data, we determine best values for the three parametrizations: linear (λ_+, λ_0), quadratic ($\lambda'_+, \lambda''_+, \lambda_0$) and pole (M_V, M_S). We then assume $\mu-e$ universality so that we can combine K_{e3} and $K_{\mu 3}$ data, and again determine best values for the three parametrizations: linear (λ_+, λ_0), quadratic ($\lambda'_+, \lambda''_+, \lambda_0$), and pole (M_V, M_S). When there is more than one parameter, fits are done including input correlations. Simple averages suffice in the two K_{e3} cases where there is only one parameter: linear (λ_+) and pole (M_V).

A comprehensive global analysis of the semileptonic kaon decay data and its effect on the CKM unitarity debate can be found in [23, 24]. An update on experimental data including NA48/2 newest results can be found in [25].

Both KTeV and KLOE see an improvement in the quality of their fits relative to linear fits when a quadratic term is introduced, as well as when the pole parametrization is used. The quadratic parametrization has the disadvantage that the quadratic parameter λ''_+ is highly correlated with the linear parameter λ'_+ , in the neighborhood of 95%, and that neither parameter is very well determined. The pole fit has the same number of parameters as the linear fit, but yields slightly better fit probabilities, so that it would be advisable for all experiments to include the pole parametrization as one of their choices.

The ‘‘Kaon Particle Listings’’ show the results with and without assuming $\mu-e$ universality. The ‘‘Meson Summary Tables’’ show all of the results assuming $\mu-e$ universality, but most results not assuming $\mu-e$ universality are given only in the Listings.

References

- [1] D. A. Bryman, P. Depommier and C. Leroy, Phys. Rept. **88**, 151 (1982), see our note on ‘‘Decay Constants of Charged Pseudoscalar Mesons’’ elsewhere in this *Review*; S. G. Brown and S. A. Bludman, Phys. Rev. **136**, B1160 (1964); P. DeBaenst and J. Pestieau, Nuovo Cimento **A53**, 137 (1968).
- [2] W. T. Chu, T. Ebata and D. M. Scott, Phys. Rev. **166**, 1577 (1968); D. Yu. Bardin and E. A. Ivanov, Sov. J. Part. Nucl. **7**, 286 (1976), [Fiz. Elem. Chast. Atom. Yadra7,726(1976)]; A. Kersch and F. Scheck, Nucl. Phys. **B263**, 475 (1986).
- [3] V.G. Vaks and B.L. Ioffe, Nuovo Cimento **10**, 342 (1958); V.F. Muller, Z. Phys. **173**, 438 (1963).
- [4] C. Q. Geng, I.-L. Ho and T. H. Wu, Nucl. Phys. **B684**, 281 (2004), [hep-ph/0306165]; J. Bijnens and P. Talavera, Nucl. Phys. **B489**, 387 (1997), [hep-ph/9610269]; V. Mateu and J. Portoles, Eur. Phys. J. **C52**, 325 (2007), [arXiv:0706.1039]; R. Unterdorfer and H. Pichl, Eur. Phys. J. **C55**, 273 (2008), [arXiv:0801.2482]; V. Cirigliano *et al.*, Rev. Mod. Phys. **84**, 399 (2012), [arXiv:1107.6001].
- [5] E. Gabrielli and L. Trentadue, Nucl. Phys. **B792**, 48 (2008), [hep-ph/0507191].
- [6] S. Adler *et al.* (E787), Phys. Rev. Lett. **85**, 2256 (2000), [hep-ex/0003019].
- [7] E. A. Kuraev, Yu. M. Bystritsky and E. P. Velicheva, Phys. Rev. **D69**, 114004 (2004), [hep-ph/0310275]; R. Unterdorfer and H. Pichl have treated radiative corrections of the structure terms to lowest order within χPT for the first time. See the reference under [4].
- [8] S. Egli *et al.* (SINDRUM), Phys. Lett. **B175**, 97 (1986).
- [9] A. A. Poblaguev *et al.*, Phys. Rev. Lett. **89**, 061803 (2002), [hep-ex/0204006].
- [10] F. Ambrosino *et al.* (KLOE), Eur. Phys. J. **C64**, 627 (2009), [Erratum: Eur. Phys. J.65,703(2010)], [arXiv:0907.3594].
- [11] V. A. Duk *et al.* (ISTRA+), Phys. Lett. **B695**, 59 (2011), [arXiv:1005.3517].
- [12] D. Pocanic *et al.*, Phys. Rev. Lett. **93**, 181803 (2004), [hep-ex/0312030]; E. Frlez *et al.*, Phys. Rev. Lett. **93**, 181804 (2004), [hep-ex/0312029]; M. Bychkov *et al.*, Phys. Rev. Lett. **103**, 051802 (2009), [arXiv:0804.1815].
- [13] J. F. Donoghue and B. R. Holstein, Phys. Rev. **D40**, 2378 (1989).
- [14] J. Gasser, M. A. Ivanov and M. E. Sainio, Nucl. Phys. **B745**, 84 (2006), [hep-ph/0602234].
- [15] C. Adolph *et al.* (COMPASS), Phys. Rev. Lett. **114**, 062002 (2015), [arXiv:1405.6377].
- [16] L. V. Fil’kov and V. L. Kashevarov, Phys. Rev. **C73**, 035210 (2006), [arXiv:nucl-th/0512047].
- [17] J. Ahrens *et al.*, Eur. Phys. J. **A23**, 113 (2005), [arXiv:nucl-ex/0407011].
- [18] A. A. Poblaguev, Phys. Lett. **B238**, 108 (1990); V. N. Bolotov *et al.*, Phys. Lett. **B243**, 308 (1990); V. M. Belyaev and I. I. Kogan, Phys. Lett. **B280**, 238 (1992); A. V. Chernyshev *et al.*, Mod. Phys. Lett. **A12**, 1669 (1997); A. A. Poblaguev, Phys. Rev. **D68**, 054020 (2003), [hep-ph/0307166]; M. V. Chizhov, Phys. Part. Nucl. Lett. **2**, 193 (2005), [Pisma Fiz. Elem. Chast. Atom. Yadra2005,no.4,7(2005)], [hep-ph/0402105].
- [19] W. Yao *et al.*, Journal of Physics G: Nuclear and Particle Physics **33**, 1 (2006), ISSN 0954-3899.
- [20] S. Eidelman *et al.*, Physics Letters B **592**, 1, 1 (2004), ISSN 0370-2693, review of Particle Physics, URL <https://www.sciencedirect.com/science/article/pii/S0370269304007579>.
- [21] M. Roos *et al.*, Physics Letters B **111**, i (1982), ISSN 0370-2693, URL <https://www.sciencedirect.com/science/article/pii/0370269382912862>.
- [22] V. Bernard *et al.*, Physics Letters B **638**, 5, 480 (2006), ISSN 0370-2693, URL <https://www.sciencedirect.com/science/article/pii/S0370269306006812>; A. Lai *et al.*, Physics Letters B **647**, 5, 341 (2007), ISSN 0370-2693, URL <https://www.sciencedirect.com/science/article/pii/S0370269307002432>.
- [23] M. Antonelli *et al.* (FlaviaNet Working Group on Kaon Decays), Eur. Phys. J. **C 69**, 399 (2010), [arXiv:1005.2323].
- [24] C.-Y. Seng *et al.* (2021), [arXiv:2107.14708].
- [25] J. R. Batley *et al.* (NA48/2), JHEP **10**, 150 (2018), [arXiv:1808.09041].
- [26] L.-M. Chounet, J.-M. Gaillard and M. Gaillard, Physics Reports **4**, 5, 199 (1972), ISSN 0370-1573, URL <https://www.sciencedirect.com/science/article/pii/037015737290018X>.
- [27] H. W. Fearing, E. Fischbach and J. Smith, Phys. Rev. **D 2**, 542 (1970), URL <https://link.aps.org/doi/10.1103/PhysRevD.2.542>.
- [28] N. Cabibbo and A. Maksymowicz, Phys. Lett. **9**, 352 (1964).

63. Spectroscopy of Light Meson Resonances

Revised March 2024 by C. Amsler (Stefan Meyer Inst.), A. Masoni (INFN, Cagliari) and G. Venanzoni (Liverpool U.; INFN, Pisa).

63.1	Introduction	874
63.2	Scalar mesons	874
63.3	Glueballs	875
63.3.1	Scalar glueballs	876
63.3.2	Tensor glueballs	877
63.4	Pseudoscalar mesons	877
63.5	Vector mesons	878
63.5.1	The $\rho(770)$ meson	878
63.5.2	The $\rho(770)$ excitations	878
63.6	Axial-vector mesons	879
63.7	Hybrid mesons	880
63.8	Tetraquark states	880
63.9	Baryonia	881
63.10	Conclusions	881

63.1 Introduction

According to the constituent quark model, a light meson consists of a color singlet quark-antiquark pair made of the u , d , or s quarks and the \bar{u} , \bar{d} , or \bar{s} antiquarks, grouped into a flavor multiplet of SU(3). However, additional mesons made of bound gluons (glueballs) could exist in the same mass range, suggested by the self coupling of gluons in QCD. Multi-quark structures are also possible, such as quark-antiquark pairs with an excited gluon (hybrid mesons). Tetraquarks are compact color singlets of diquark-antidiquark pairs ($qq\bar{q}\bar{q}$) or ‘molecular’ bound states of two mesons ($q\bar{q}q\bar{q}$). More complex systems such as $qq\bar{q}\bar{q}\bar{q}$ (baryonia) are also predicted.

Fundamentals on the constituent quark model on light and heavy mesons and baryons (including hadrons with charm and bottom quarks), and on predictions from lattice gauge theories, are described in ‘Quark Model’ in this issue of the *Review of Particle Physics*, henceforth called the *Review*. In the present text we describe the experimental spectrum of light mesons and their classifications within the constituent quark model, with emphasis on states exhibiting properties incompatible with $q\bar{q}$ structures. The discussion is driven by the results entered in the database of the *Review*. The spectrum of kaon excitations is much less clear cut and therefore deferred to a future edition, when further data might become available. More detailed discussions on exotic mesons – including those involving the c and b quarks – can be found in Refs. [1–7] and in ‘Heavy Non- $q\bar{q}$ Mesons’ of the *Review*. For more information on the meson (and baryon) spectrum of light (and heavy) quarks we refer to one of the textbooks [8].

Figure 63.1 shows the mass spectrum of $q\bar{q}$ mesons. The mass (vertical axis) increases with orbital excitations ℓ (horizontal axis) and radial excitation n . In the quark model one uses the notation nS , nP , $nD\dots$ for the radial excitations ($n = 1$ for the ground states), in contrast to the usual $1s$, $2p$, $3d\dots$ notation in atomic physics. Each box represents an SU(3) nonet containing multiplets of the isospin i , three isovectors, two strange isodoublets, and two isosinglets (one SU(3) singlet and one SU(3) octet). The spin, parity [$P = -(-1)^\ell$] and C -parity [$C = (-1)^{\ell+s}$] take the possible values $J^{PC} = 0^{++}$ (scalar), 0^{-+} (pseudoscalar), 1^{--} (vector), $1^{\pm\pm}$ (axial- or pseudovector), 2^{++} (tensor), etc. There are mesons with the *exotic* quantum numbers 0^{-+} , 0^{+-} , 1^{-+} , 2^{+-} , 3^{-+} , etc. cannot be $q\bar{q}$ states. Note that the C -parity is defined only for the electrically neutral non-strange nonet members.

The two isosinglets in each nonet mix with an angle θ close to the *ideal* value of 35.3° for the 1^{--} , $1^{\pm\pm}$, 2^{++} and 3^{--} nonets, in which case the isosinglets decouple to $u\bar{u} + d\bar{d}$ and $s\bar{s}$. The orbital excitations $\ell \geq 1$ consist of four nonets for each value of n , since $j = \ell$ for antiparallel quark spins and $j = \ell - 1, \ell$ or $\ell + 1$ for parallel spins. Since the C -parity is not defined for strange mesons, the K_{1A} and K_{1B} in the axial vector 1^{++} and 1^{+-} nonets of fig. 63.1 are mathematical constructs which mix to give the observed

$K_1(1270)$ and $K_1(1400)$ mesons. A similar scenario occurs for the observed 2^{-+} $K_2(1770)$ and 2^{--} $K_2(1820)$ mesons.

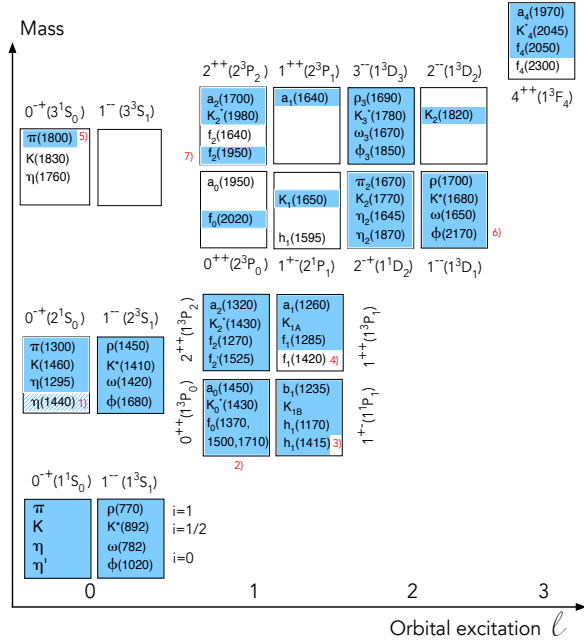


Figure 63.1: The mesons made of the u , d , and s light quarks are organised in $J^{PC}(n^{2s+1}\ell_j)$ nonets with isospin i . The established mesons (which appear in the *Summary Table* of the *Review*) are shown in the dark (blue) areas. The white areas contain those omitted in the *Summary Table* but reported in the *Listings*. States with the same J^{PC} mix, such as the 2^3S_1 and 1^3D_1 mesons. The states become broad and overlap with increasing masses, which complicates the determination of the resonance parameters *e.g.* mass, width and spin. For a complete list of mesons see the *Listings*.

1 The $\eta(1440)$ stands for the $\eta(1405)$ and the $\eta(1475)$, section 63.4.

2 The classification of the scalar nonet is controversial. In alternative schemes the 1^3P_0 nonet contains the light scalars below 1 GeV, section 63.2.

3 Considered established, but more data would be desirable.

4 An alternative to the $f_1(1420)$ is the $f_1(1510)$, section 63.6.

5 The $\pi(1800)$ has also been proposed as a hybrid meson, section 63.7.

6 The $\phi(2170)$ has also been proposed as a tetraquark state, section 63.8.

7 The $f_2(1950)$ has also been proposed as a tensor glueball, section 63.3.2.

As described in more detail below (section 63.2), it is hard to accommodate all the known scalar mesons in the lower $q\bar{q}$ nonets: The light scalar mesons $a_0(980)$, $K_0^*(700)$ (also known as κ), the $f_0(500)$ (also known as σ), and the $f_0(980)$, not shown in the figure, could build the lightest nonet, but could also be two-meson resonances or tetraquarks (section 63.8). Three isoscalars are known in the 1500 MeV region, the $f_0(1500)$ or $f_0(1710)$ being proposed as gluonic states mixing with the $f_0(1370)$ (section 63.3.1). The pseudoscalar labeled $\eta(1440)$ may consist of two states (section 63.4). The status of vector meson excitations is described in section 63.5. The axial-vector meson $f_1(1420)$ could be replaced in the 1^{++} nonet by the $f_1(1510)$ which, however, needs confirmation (see the *Listings* and section 63.6). Mesons with exotic quantum numbers are discussed in section 63.7.

63.2 Scalar mesons

Scalar mesons decay dominantly into pairs of pseudoscalar mesons ($\pi\pi$, $K\bar{K}$, $\pi\eta$, $\eta\eta$ or $\eta\eta'$). The widths tend to be large for those decaying into $\pi\pi$, due to the absence of angular momentum barrier and the large available phase space. Broad overlapping

states decaying into the same final state interfere, which complicates the determination of their masses and widths. Furthermore, the ground state glueball, a 0^{++} expected below 2 GeV, will mix with the isoscalar 0^{++} $q\bar{q}$ states. The onset of the $K\bar{K}$, $\eta\eta$ or $\eta\eta'$ thresholds also distorts the line shapes and produces cusps. This requires high statistics data and the use of coupled channel analyses taking into account unitarity and analyticity (see ‘Resonances’ in the *Review*).

Two isovector scalars are established, the $a_0(980)$ and the $a_0(1450)$, together with five isoscalars: the very broad $f_0(500)$, the $f_0(980)$, the broad $f_0(1370)$, and the comparatively narrow $f_0(1500)$ and $f_0(1710)$. The strange partners are the $K_0^*(700)$ and the $K_0^*(1430)$. The $f_0(500)$ and $K_0^*(700)$ deserve a separate treatment and can be found in ‘Scalar Mesons below 1 GeV’, which contains more details on the $a_0(980)$ and $f_0(980)$, briefly reviewed in section 63.8.

The $a_0(1450)$ was first reported by the Crystal Barrel experiment in $\bar{p}p$ annihilation with stopped antiprotons [9, 10] (see [11] for a review of Crystal Barrel results). An isovector scalar, possibly the $a_0(1450)$ (albeit at a lower mass of 1317 MeV) is observed by Belle in $\gamma\gamma$ collisions leading to $\eta\pi^0$ [12]. The state interferes destructively with the non-resonant background. Its $\gamma\gamma$ coupling is comparable to that of the $a_2(1320)$, in accord with simple predictions (see *e.g.* [13]). A contribution from $a_0(1450) \rightarrow K\bar{K}$ is also found in the CLEO-c analysis of $D^\pm \rightarrow K^+K^-\pi^\pm$ [14] and $D^0 \rightarrow K_S^0K^\pm\pi^\mp$ from LHCb [15]. The $a_0(1450)$ is reported at a lower mass in $\bar{p}p$ annihilation in flight, overlapping with the $a_2(1320)$ [16, 17].

The $f_0(1370)$ and $f_0(1500)$ were observed by Crystal Barrel [18–20] and by WA102 in central production with 450 GeV protons [21, 22]. They decay mostly into 2π and 4π . The $f_0(1500)$ was also observed to decay into $\eta\eta$ [23–25] and $\eta\eta'$ [26]. All data agree that the 4π decay mode represents about half of the $f_0(1500)$ decay width, but is dominant for $f_0(1370)$.

The determination of the $\pi\pi$ coupling of the very broad $f_0(1370)$ is complicated by its interference with the $f_0(500)$. The existence of the $f_0(1370)$ was questioned by COMPASS from $\pi^-p \rightarrow \pi^-\pi^-\pi^+p$ data [27] and by LHCb in $\bar{B}_s^0 \rightarrow J/\psi(1S)\pi^+\pi^-$ [28]. In $\bar{B}^0 \rightarrow J/\psi(1S)\pi^+\pi^-$ the $\pi\pi$ mass spectrum does not show any significant scalar component above ~ 1.2 GeV [29] (an analysis that is challenged in [30]). The existence of the $f_0(1370)$ has been disputed by a reassessment of various production modes [31] (the $K_0^*(700)$ is also not needed in $K\pi$ scattering). This contrasts with its $\pi\pi$ decay analyzed in Ref. [32]). However, data from CLEO-c in $D^0 \rightarrow \pi^+\pi^-\pi^+\pi^-$ require a contribution from $f_0(500)f_0(1370) \rightarrow 4\pi$ [33]. A broad 2π signal is also observed by BaBar around 1400 MeV in the decay $B^\pm \rightarrow \pi^\pm\pi^\pm\pi^\mp$ [34] which is attributed to the $f_0(1370)$ (but could also be due to the $f_0(1500)$). The existence of the $f_0(1370)$ is confirmed by a recent dispersive analysis of $\pi\pi$ scattering data, which leads to a complex pole around 1245 MeV with a very large width of about 600 MeV [35].

In Refs. [36, 37] the $f_0(1370)$ and $f_0(1710)$ (together with the $f_2(1270)$ and $f_2'(1525)$) are interpreted as bound systems of two vector mesons. This view is challenged in Ref. [38] where in a covariant formalism, *e.g.* the $f_2(1270)$ does not appear as a $\rho\rho$ bound state. Photoproduction data of the $f_2(1270)$ in $\gamma p \rightarrow \pi^0\pi^0p$ from CLAS [39], as a function of momentum transfer, also disagree with predictions [40] for the $f_2(1270)$ to be a $\rho\rho$ bound state.

While the $K\bar{K}$ decay branching ratio of the $f_0(1500)$ is small [21] [41], the $f_0(1710)$ decays dominantly into $K\bar{K}$. The $f_0(1710)$ is not observed in $\bar{p}p$ annihilation at rest [41] and only weakly produced in $\bar{p}p$ annihilation in flight [42], with a rate strongly suppressed compared to that of the $f_0(1500)$ ($\sim 7\%$). For comparison, the rate for the ($s\bar{s}$) $f_2'(1525)$ production is about 9% that of the ($u\bar{u} + d\bar{d}$) $f_2(1270)$, as expected from the OZI rule [42]. On the other hand the $f_0(1370)$ does not couple strongly to $K\bar{K}$ [21]. This suggests an $n\bar{n}$ structure ($u\bar{u} + d\bar{d}$) for the $f_0(1370)$ and $s\bar{s}$ for the $f_0(1710)$. The $f_0(1500)$ would also qualify as an $n\bar{n}$ state, although it is very narrow compared to the other states. Occam’s razor principle therefore suggests that the $f_0(1370)$, $a_0(1450)$, and the $f_0(1710)$ are in the 1^3P_0 $q\bar{q}$ SU(3) flavor nonet, the $f_0(1370)$

and $a_0(1450)$ being the two (mostly) $n\bar{n}$ states, and the $f_0(1710)$ the (dominantly) $s\bar{s}$ one. The nature of the $f_0(1500)$ is discussed along this scheme in section 63.3.1.

There is long-time evidence for the existence of two scalar nonets and one glueball below 2 GeV [43]. The ground state 1^3P_0 $q\bar{q}$ nonet and a lighter one made of four-quark states which recombine at large distances to become meson-meson resonances, the $a_0(980)$, $a_0(980)$, $f_0(500)$ and $K_0^*(700)$, see section 63.8. For a review see Ref. [1] and for the $f_0(500)$ Ref. [44].

Other schemes have been proposed, for example a tetraquark for the $f_0(1500)$ [45] or flavor octets for the $f_0(1500)$ and $f_0(1710)$ [3]. In Ref. [46] the $a_0(1450)$, $f_0(1370)$, $f_0(1500)$ and $K_0^*(1430)$ are radial excitations of the scalar nonet below 1 GeV. In Ref. [47] the light and 1^3P_0 scalar nonets are interpreted as mixing of two tetraquark nonets. In the unitarized quark model with coupled $q\bar{q}$ and meson-meson channels, the scalars below 1 GeV are manifestations of bare $q\bar{q}$ confinement states, mass shifted from the 1.4 GeV region and distorted by the strong 3P_0 coupling to S -wave two-meson decay channels [48, 49]. Thus, in these models the light scalar nonet comprising the light and 1^3P_0 scalar nonets are manifestations of the same bare input states (see also [50]). Surprisingly for a state decaying strongly into 2π and 4π , the $f_0(1370)$ is assumed to be an $s\bar{s}$ state in Ref. [51]. The $f_0(1500)$ is then a radial excitation.

There is evidence for the existence of two further 0^{++} mesons in the 1700 – 1800 MeV range, one isoscalar ($f_0(1770)$) and one isovector ($a_0(1710)$), which could be the isovector partner of the $f_0(1710)$. The $f_0(1770)$, claimed by BESII/III [52–54], and also observed in $\pi^-p \rightarrow n\omega\phi$ [55], has been interpreted as a radial excitation [56]. Two isoscalars are also reported by a re-analysis of BESIII radiative $J/\psi(1S)$ decay data [57, 58]. Evidence for the $a_0(1710)$ is inferred from the interference of the K^+K^- and $K_S^0K_S^0$ decays of the $f_0(1710)$ in $D_s^+ \rightarrow f_0(1710)\pi^+$, leading to a relative branching ratio an order of magnitude larger than expected from isospin symmetry [59, 60]. A signal for $a_0(1710) \rightarrow K_S^0K^+$ is indeed reported by BESIII [61], albeit at 1817 MeV, in contrast to the state observed by BaBar in $\eta\pi$ at 1704 MeV [62].

From a study of the vector-vector interaction the authors of Ref. [63], predict an isovector pole at 1780 MeV, while the $f_0(1710)$ is a $K^*\bar{K}^*$ molecule, a view also supported by Refs. [64–67]. Thus the $f_0(1710)$ and $a_0(1710)$ might be $K^*\bar{K}^*$ molecules, similar to the $f_0(980)$ and $a_0(980)$ which have been interpreted as $K\bar{K}$ molecules. Scalar resonances near the D_0 mass such as the $f_0(1710)$ and the $f_0(1770)$ are also suggested to produce CP violation enhancements in the charm system [68]. Unfortunately, the spectrum of scalar mesons above the $f_0(1710)$ is not well established experimentally and more data are needed to confirm the $f_0(1770)$ and $a_0(1710)$.

63.3 Glueballs

Lattice calculations, QCD sum rules, flux tube, and constituent glue models agree that the lightest glueball has quantum numbers $J^{PC} = 0^{++}$ and the first excited state 2^{++} . Lattice calculations predict for the ground state (0^{++}) a mass around 1600 – 1700 MeV [69–72], while the 2^{++} state lies around 2300 MeV. For more information on lattice calculations see ‘Quark Model’ in the *Review* and fig. 15.3 therein for an example of mass spectrum. These predictions were made in the quenched approximation, neglecting $q\bar{q}$ loops. However quenched predictions and full QCD calculations lead to small mass shifts (see ‘Quark Model’ and fig. 15.15 therein).

Heavier glueballs with quantum numbers 0^{-+} , 2^{-+} , 1^{+-} , etc. are predicted above 2500 MeV and the lowest exotic ones (with exotic quantum numbers such as 0^{+-} and 2^{+-}) are expected above 4000 MeV [72]. In holographic QCD the 0^{-+} is predicted to be very broad [73] and the 1^{+-} is at least as broad as its width [74]. Calculations of the three lowest scalar and pseudoscalar glueball masses in pure Yang-Mills theory are in quantitative agreement with lattice results [75]. The lightest glueballs lie in the same mass region as ordinary isoscalar $q\bar{q}$ states, in the mass range of the $1^3P_0(0^{++})$, $2^3P_2(2^{++})$, $3^3P_2(2^{++})$, and $1^3F_2(2^{++})$ $q\bar{q}$ states. Therefore, mixing of glueballs with nearby $q\bar{q}$ states of the same quantum numbers leads to supernumerary isoscalar state in the $q\bar{q}$ nonets (however, see Ref. [57] discussed in section

63.3.1).

Among the signatures naively expected for glueballs are (i) isoscalar states that do not fit into $q\bar{q}$ nonets, (ii) enhanced production in gluon-rich channels such as central production and radiative $J/\psi(1S)$ decay, (iii) decay branching fractions incompatible with SU(3) predictions for $q\bar{q}$ states, and (iv) reduced $\gamma\gamma$ couplings (see however [76, 77]). Mixing effects with isoscalar $q\bar{q}$ mesons [31, 69, 76, 78–84] and decay form factors [85] can also obscure these simple signatures.

According to SU(3) the decay branching ratios for $q\bar{q}$ mesons and pure glueballs are different, and therefore useful to determine the internal structures of mesons. For pure glueballs with flavor symmetric couplings the decay ratios are $\pi\pi : K\bar{K} : \eta\eta : \eta\eta' = 3 : 4 : 1 : 0$, apart from phase space factors. The partial widths for the decay of a scalar (or a tensor) meson into a pair of pseudoscalar mesons are given in fig. 63.2 (for a derivation see e.g. [8]). The decay of a $q\bar{q}$ meson into a pair of mesons involves the creation of a $q\bar{q}$ pair, and SU(3) symmetry assumes that the matrix elements for the creation of $s\bar{s}$, $u\bar{u}$, and $d\bar{d}$ pairs are equal. (The generalization to unequal $s\bar{s}$, $u\bar{u}$, and $d\bar{d}$ couplings is given in Ref. [78].) An excellent fit to the tensor meson decay widths is obtained with $\beta \simeq 0.5$ GeV/c, $\theta_V \simeq 26^\circ$ and $\theta_P \simeq -17^\circ$ [78].

Note that the assumption of flavor symmetric couplings may not apply in models describing the scalar glueball by a dilaton field, which lead to mass dependent couplings [86, 87] (see Ref. [88] which predicts that a scalar glueball above 1 GeV would be unobservably wide).

Another way to determine the flavor contents of neutral mesons is the decay $B \rightarrow J/\psi(1S)X$ which filters out the $d\bar{d}$ content of X , while $B_s^0 \rightarrow J/\psi(1S)X$ selects its $s\bar{s}$ component [89]. More precise data on $B_{(s)}^0 \rightarrow J/\psi(1S)[f_0(1370), f_0(1500), f_0(1710)]$ would help to pin down the nature of these scalar mesons [90].

63.3.1 Scalar glueballs

One of the three isoscalars, the $f_0(1370)$, $f_0(1500)$ or $f_0(1710)$, appears to be supernumerary. The branching ratios in fig. 63.2 can be used to deduce the structures of these states, assuming that they are $q\bar{q}$. The comparison of decay branching ratios from Crystal Barrel annihilation and WA102 central collision data shows that the $f_0(1500)$ is compatible with an $n\bar{n}$ structure, while the $f_0(1710)$ is mostly $s\bar{s}$ [13]. However, the close vicinity of the very broad $n\bar{n}$ $f_0(1370)$, its narrow width, enhanced production at low transverse momentum transfer in central collisions [91–93] favor the $f_0(1500)$ to be the supernumerary non- $q\bar{q}$ state. According to [78, 83] the $f_0(1370)$ and $f_0(1710)$ would be dominantly $q\bar{q}$ states mixing with glue, while the $f_0(1500)$ would be dominantly a glueball mixing with $q\bar{q}$ states. Its suppressed $K\bar{K}$ decay would be due to interferences with the $f_0(1370)$ and $f_0(1710)$. In the analogous mixing scheme of Ref. [56], which uses central production data from WA102 and the hadronic $J/\psi(1S)$ decay data from BES [94, 95], glue is shared between the $f_0(1370)$ (mainly $n\bar{n}$), $f_0(1500)$ (mainly glue) and $f_0(1710)$ (dominantly $s\bar{s}$). This agrees with the analyses [78, 83]. In the mixing scheme of Ref. [96] the QCD spectral sum rule also leads to a large gluonic component in the $f_0(1500)$ (satisfying the observed strong $\pi\pi$ and $f_0(500)f_0(500) \rightarrow 4\pi$ decays).

However, not everybody agrees that the strong $K\bar{K}$ signal is indicative of an $s\bar{s}$ structure for the $f_0(1710)$. The $f_0(1710)$ could still be the glueball, since the two-gluon coupling to $n\bar{n}$ appears to be suppressed by chiral symmetry [97], thus $K\bar{K}$ would be enhanced compared to $\pi\pi$. It was argued that chiral symmetry constraints in a multichannel analysis imply that the $f_0(1710)$ is an unmixed scalar glueball [98]. However, this view is challenged in [63].

The $K\bar{K}$ decay is also naturally enhanced in the extended linear sigma model with a dilaton as glueball [86] and in the holographic model of [87, 99] which both prefer the $f_0(1710)$ as the glueball. For a scalar glueball Ref. [87] finds a strong enhancement of the decays into $K\bar{K}$ and $\eta\eta$, in fairly close agreement with the measured branching ratios of the $f_0(1710)$, while Ref. [99] predicts the (so far not measured) rate into $\eta\eta'$ to be very small.

In $\gamma\gamma$ collisions leading to $K_S K_S$ [100] and $K^+ K^-$ [101] a spin-0 signal is observed at the $f_0(1710)$ mass (together with a

dominant spin-2 component), while the $f_0(1500)$ is not observed in $\gamma\gamma \rightarrow K\bar{K}$ nor $\pi^+\pi^-$ [102]. The $f_0(1500)$ is also not observed by Belle in $\gamma\gamma \rightarrow \pi^0\pi^0$, although a shoulder is seen which could also be due to the $f_0(1370)$ [103]. The absence of $f_0(1500)$ signal in the $\pi\pi$ channel in $\gamma\gamma$ collisions does not favor an $n\bar{n}$ interpretation for the $f_0(1500)$. The upper limit for $\Gamma_{2\gamma} (< 1.4$ keV) in $\pi^+\pi^-$ [13] excludes a large $n\bar{n}$ content, and hence points to a mainly $s\bar{s}$ content [13], which contradicts the small $K\bar{K}$ decay branching ratio of the $f_0(1500)$ [10, 21, 41]. Belle finds that in $\gamma\gamma \rightarrow K_S K_S$ collisions the 1500 MeV region is dominated by the $f_2'(1525)$. The $f_0(1710)$ is also observed with a production rate \times branching ratio compatible with an $s\bar{s}$ state [104]. Note, however, that the $\gamma\gamma$ couplings of glueballs are sensitive to glue mixing with $q\bar{q}$ [56]. Ref. [76] predict the glueball $\gamma\gamma$ partial width in the few keV range (comparable to that of $q\bar{q}$ mesons) due to couplings of vector mesons to γ via VDM, in agreement with holographic models [77].

Alternative assignments for the scalar glueball have been proposed: In Ref. [80] the gluonic signal is distributed over $f_0(1370)$, $f_0(1500)$ and another broad isoscalar around 1530 MeV, while the gluonic contribution to the $f_0(1710)$ is small. As mentioned already, in Ref. [69, 86, 87] the $f_0(1710)$ is the glueball state, as in Ref. [84], where the $f_0(1500)$ is the $q\bar{q}$ octet state degenerate with the $a_0(1450)$. In the generalized linear sigma model [105] the $a_0(980)$ is dominantly a tetraquark and $a_0(1450)$ a $q\bar{q}$ state. The $f_0(980)$, $f_0(1370)$ and $f_0(1500)$ (or $f_0(1710)$) are dominantly tetraquark, $q\bar{q}$ and glue.

In Ref. [82] the $f_0(500)$ and $f_0(1370)$ are signals from a single broad resonance proposed as the scalar glueball. The ground state scalar nonet then consists of the $f_0(980)$, $a_0(980)$, $K_0^*(1430)$, $f_0(1500)$ and $f_0(1710)$ [31]. The $f_0(980)$ and $f_0(1500)$ mix (similarly to the η and η' in the pseudoscalar nonet), while the $f_0(1500)$ mixes with a glueball in the 500 – 1000 MeV mass range, which is identified as the $f_0(500)$.

In Ref. [106], a large $K^+ K^-$ scalar signal reported by Belle in B decays into $K K \bar{K}$ [107], compatible with the $f_0(1500)$, is explained as due to constructive interference of a flavor octet with a broad glueball background. However, the Belle data are inconsistent with the BaBar measurements which show instead a broad scalar at this mass for B decays into both $K^\pm K^\pm K^\mp$ [108] and $K^+ K^- \pi^0$ [109].

The $f_0(1500)$ is observed by BESII in $J/\psi(1S) \rightarrow \gamma\pi\pi$ [110] and by BESIII in $J/\psi(1S) \rightarrow \gamma\eta\eta$ [111] with a much smaller rate than for the $f_0(1710)$, which would speak against a glueball interpretation of the former, although the systematic errors are large. Also, the $f_0(1500)$ appears at a lower mass and the $f_0(1710)$ at a higher mass than the accepted values. However, the coupled channel analysis of more data on radiative $J/\psi(1S)$ decay from BESIII [57] (described in the next paragraph) finds comparable contributions from $f_0(1500)$ and $f_0(1710)$ with a preference for $\pi\pi$ decay over $K\bar{K}$ for the former and $K\bar{K}$ over $\pi\pi$ for the latter.

The authors of Ref. [57] have analyzed the high statistics data from $J/\psi(1S)$ radiative decays into $\pi^0\pi^0$, $K_S^0 K_S^0$, $\eta\eta$ and $\omega\phi$ from BESIII, including data on $\pi\pi$, $\eta\eta$ and $\eta\eta'$ from the CERN SPS, BNL data on $\pi\pi \rightarrow K_S^0 K_S^0$ and $p\bar{p}$ annihilation data from LEAR into various final states. The coupled channel analysis requires ten scalar mesons, the established ones in the *Review* and the $f_0(2020)$, as well as the isoscalars $f_0(2100)$, 2200 , 2330 so far omitted from the *Summary Table*. As a new feature, the $f_0(1710)$ splits into two states, one at about 1700 MeV, the former $f_0(1710)$, and the new $f_0(1770)$ discussed above, being mandatory to obtain a good fit. A broad (~ 370 MeV) enhancement is observed in $J/\psi(1S)$ radiative decays around 1865 MeV, attributed to the contribution of glue distributed among the scalar mesons, with a very strong contribution from the 1770 MeV state [58]. In this model there are no supplementary states as the glue ‘fragments’ between the various isoscalars.

Ref. [112] reports on a very recent re-analysis of the BESIII $J/\psi(1S)$ radiative decay data into $\pi^0\pi^0$ and $K_S^0 K_S^0$. A good fit is obtained with only two scalar resonances below 2 GeV, the $f_0(1500)$ and $f_0(1710)$. The latter is more strongly produced, which points to a sizeable glueball component.

Isospin	Decay channel	γ^2
0	$\pi\pi$	$3 \cos^2 \alpha$
	$K\bar{K}$	$(\cos \alpha - \sqrt{2} \sin \alpha)^2$
	$\eta\eta$	$(\cos \alpha \cos^2 \phi - \sqrt{2} \sin \alpha \sin^2 \phi)^2$
	$\eta\eta'$	$\frac{1}{2} \sin^2 2\phi (\cos \alpha + \sqrt{2} \sin \alpha)^2$
1	$\eta\pi$	$2 \cos^2 \phi$
	$\eta'\pi$	$2 \sin^2 \phi$
	$K\bar{K}$	1
$\frac{1}{2}$	$K\pi$	$\frac{3}{2}$
	$K\eta$	$(\sin \phi - \frac{\cos \phi}{\sqrt{2}})^2$
	$K\eta'$	$(\cos \phi + \frac{\sin \phi}{\sqrt{2}})^2$

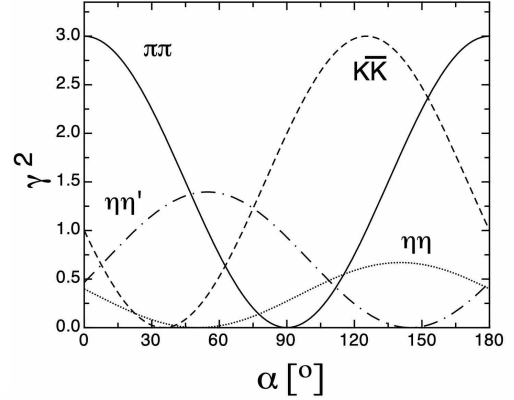


Figure 63.2: Left: SU(3) couplings γ^2 for scalar (or tensor) $q\bar{q}$ meson decays. The angles α and ϕ are defined as $\alpha = 54.7^\circ + \theta$ and $\phi = 54.7^\circ + \theta_P$, where θ is the mixing angle of the decaying isoscalars and θ_P the mixing angle in the 0^{-+} nonet. The partial decay width is given by $\Gamma = C \times \gamma^2 \times |F(q)|^2 \times q$, where C is a nonet constant, q the momentum of the decay products and $F(q)$ a form factor which may be taken as $|F(q)|^2 = q^{2\ell} \times \exp(-q^2/8\beta^2)$ with $\beta = 0.5$ GeV/c, and where ℓ is the relative angular momentum between the decay products ($\ell = 0$ for scalars and $\ell = 2$ for tensors). Right: SU(3) couplings as a function of mixing angle α for isoscalar decays for $\theta_P = -17.3^\circ$ (from [78]).

63.3.2 Tensor glueballs

Above the well known $f_2(1270)$ and $f_2'(1525)$ $q\bar{q}$ mesons, the $f_2(1640)$ and $f_2(1950)$ are tentatively assigned to the 2^3P_2 nonet (see fig. 63.1). The broad $f_2(1950)$ has been observed by several experiments, *e.g.* in central production [22] and in $\bar{p}p$ annihilation in flight [17] and is often identified as a glueball [113], the ground state of the pomeron [114, 115]. Three further isoscalar tensors are established, the $f_2(2010)$, $f_2(2300)$ and $f_2(2340)$, which are in the range of the 1^3F_2 and 3^3P_2 nonets. The large $\phi\phi$ cross section in $\bar{p}p$ just above threshold [116] could be due to the production of the 2^{++} glueball, in accord with earlier observations in $\pi^-N \rightarrow \phi\phi n$ reactions [117, 118] and in central collisions [119].

The $f_2(2010)$, $f_2(2300)$ and $f_2(2340)$ have been observed by BESIII in $J/\psi(1S) \rightarrow \gamma\phi\phi$ [120]. The production rate of a tensor glueball in $J/\psi(1S)$ radiative decay has been calculated in quenched lattice QCD to be large (around 1%) [121] and is claimed by BESIII [120] to be compatible with their rates measured in $J/\psi(1S) \rightarrow f_2(2340)$, $f_2(2340) \rightarrow \eta\eta$ [111], and $f_2(2340) \rightarrow \phi\phi$ [120]. The authors of Ref. [122] have re-analyzed the $J/\psi(1S)$ radiative decay into $\pi^0\pi^0$ and $K_S K_S$ from BESIII and found an enhancement described by a 360 MeV broad pole around 2210 MeV, possibly composed of the resonances observed earlier in $\phi\phi$.

The relatively narrow $f_2(2300)$ with a measured width of 149 MeV [118] is preferred by the holographic QCD model of Ref. [123]. However, the tensor glueball is predicted to be much broader (600–900 MeV) by the holographic model of Ref. [124].

There is no evidence for a narrow meson, $f_J(2220)$ (a tensor candidate) in $\bar{p}p$ annihilation (see the note under the $f_J(2220)$ in the 2004 issue of the *Review*). The measured partial width to $\bar{p}p$ in radiative $J/\psi(1S)$ decay [125] is too large and inconsistent with the upper limit from $\bar{p}p$ annihilation into $\pi\pi$ [126].

63.4 Pseudoscalar mesons

We now deal with the first radial excitations of the 0^{-+} nonet (fig. 63.1). The $\pi(1300)$ is a very broad resonance (200–600 MeV) decaying into 3π . The $K(1460)$ was recently confirmed with high statistics data from LHCb in $D^0 \rightarrow K3\pi$ decays [127] and has become an established kaon excitation. The first observation of an isoscalar resonance around 1425 MeV – the E -meson – was made in $\bar{p}p$ annihilation at rest into $E\pi^+\pi^-$, $E \rightarrow K\bar{K}\pi$ [128]. This state was reported to decay into $a_0(980)\pi$ and $K^*(892)\bar{K}$ with roughly equal contributions. An isoscalar state, the ι meson, was observed in radiative $J/\psi(1S)$ decay into $K\bar{K}\pi$ [129–131] and $\gamma\rho$ [132], and was considered at that time as a glueball candidate, owing to its strong signal in radiative $J/\psi(1S)$ decay. The E and ι were later assumed to be the same state, called $\eta(1440)$.

The $\eta(1295)$ has been observed in various production mechanisms, in π^-p experiments [133–136], and possibly in $\bar{p}p$ anni-

hilation [137, 138]. In $J/\psi(1S)$ radiative decay, the $\eta(1295)$ signal is also evident in the 0^{-+} $\eta\pi\pi$ wave of the DM2 data [139]. Also BaBar reports a signal around 1295 MeV in B decays into $\eta\pi\pi K$ [140]. We therefore assume that the $\eta(1295)$ is one of the isoscalars in this nonet.

However, two isoscalars were later observed in this mass region, the $\eta(1405)$ and $\eta(1475)$. The former decays mainly into $a_0(980)\pi$ (or direct $K\bar{K}\pi$) and the latter mainly into $K^*(892)\bar{K}$. The simultaneous observation of two pseudoscalars is reported in three production mechanisms: π^-p [133, 141], radiative $J/\psi(1S)$ decay [139, 142], and $\bar{p}p$ annihilation at rest [143–146]. All of them give values for the masses, widths, and decay modes that are in reasonable agreement. (However, Ref. [139] favors a state decaying into $K^*(892)\bar{K}$ at a lower mass than the state decaying into $a_0(980)\pi$.) In $J/\psi(1S)$ radiative decay, the $\eta(1405)$ decays into $K\bar{K}\pi$ through $a_0(980)\pi$, and hence a signal is also expected in the $\eta\pi\pi$ mass spectrum. This was indeed observed by MARK III in $\eta\pi^+\pi^-$ [147], which reported a mass of 1400 MeV, in line with the existence of the $\eta(1405)$ decaying into $a_0(980)\pi$. The $\eta(1405)$ decaying into $\eta\pi\pi$ is also observed by Crystal Barrel [138]. Two states were also reported by BES: Around 1452 MeV BESII observed a $K\bar{K}\pi$ enhancement in $J/\psi(1S) \rightarrow \omega K\bar{K}\pi$ but not in $J/\psi(1S) \rightarrow \phi K\bar{K}\pi$ [148], while BESIII reported a 52 MeV broad state in $\psi(2S) \rightarrow \omega K^*K$ [149], both left without J^{PC} determination.

The $K\bar{K}\pi$ and $\eta\pi\pi$ channels were studied in $\gamma\gamma$ collisions by L3 [150]. (For the 2γ couplings of glueballs and $q\bar{q}$ mesons see [76, 77, 151, 152].) The analysis led to a clear $\eta(1475)$ signal in $K\bar{K}\pi$, decaying into $K^*\bar{K}$, well identified in the untagged data sample, where spin 1 resonances are not allowed. At the same time, L3 did not observe the $\eta(1405)$, neither in $K\bar{K}\pi$ nor in $\eta\pi\pi$ [150]. On the other hand, CLEO-II did not observe any pseudoscalar signal with tagged γ 's in $\gamma\gamma \rightarrow \eta(1475) \rightarrow K_S^0 K^\pm \pi^\mp$ [153], with an upper limit slightly smaller than the signal observed by L3. After the CLEO-II result, L3 performed a further analysis with full statistics [154], confirming their previous evidence for the $\eta(1475)$. The CLEO upper limit [153] for $\Gamma_{\gamma\gamma}$, and the L3 results [154], are consistent with the world average for the $\eta(1475)$ width. BaBar [140] also reported the $\eta(1475)$ in B decays into $K\bar{K}^*$ recoiling against a K , while upper limits only were given for the $\eta(1405)$.

Hence, in radiative $J/\psi(1S)$ decay, π^-p and $\bar{p}p$ annihilation at rest two isoscalar signals are observed in the 1400 – 1500 MeV mass region, while the $\eta(1405)$ is not seen in $\gamma\gamma$ interactions nor in B decays. The $\eta(1475)$ could be the first radial excitation of the η , with the $\eta(1295)$ being the first radial excitation of the η' . Ideal mixing, suggested by the $\eta(1295)$ and $\pi(1300)$ mass degeneracy, would then imply that the second isoscalar in the nonet is mainly

$s\bar{s}$, and hence couples to $K^*\bar{K}$, in agreement with properties of the $\eta(1475)$. Also, its width agrees with the expected one for the radially excited $s\bar{s}$ state [85, 91]. A study of radial excitations of pseudoscalar mesons [155] also favors the $s\bar{s}$ interpretation of the $\eta(1475)$. However, due to the strong kinematical suppression in $\eta(1405) \rightarrow K^*\bar{K}$ the data are not sufficient to exclude a sizeable $s\bar{s}$ admixture also in the $\eta(1405)$.

The supernumerary isoscalar $\eta(1405)$ would be a candidate for the 0^{-+} glueball in the fluxtube model [156], in which the 0^{++} glueball is also naturally related to a 0^{-+} glueball with mass degeneracy broken in QCD. However, this scenario is not favored by lattice gauge theories which predict the 0^{-+} state above 2 GeV [70, 157] (see ‘Quark model’ in this issue of the *Review*). Nevertheless, the pseudoscalar glueball could lie at a lower mass than predicted from lattice calculation [158], see also Refs. [159–161]. The holographic model of Ref. [77] predicts the pseudoscalar glueball below 2600 MeV, decaying dominantly into two vector mesons. A detailed review of the experimental situation on the pseudoscalar glueball is available in Ref. [162].

Here also, there are alternative explanations. The mere existence of the $\eta(1295)$ is questioned in Refs. [3, 163], in which the authors also propose a single pseudoscalar meson at 1440 MeV, the first radial excitation of the η . According to Ref. [3] the splitting of the 1440 MeV state into $\eta(1405)$ and $\eta(1475)$ is due to nodes in the decay amplitudes, which differ in $\eta\pi\pi$ and $K^*(892)\bar{K}$. The splitting could also be due to a triangle singularity, hence the manifestation of one state only (fig. 63.3) [164–166]. The importance of the triangle singularity for the $\eta(1295)$ and $\eta(1405/1475)$ in the $\eta\pi\pi$ and $K\bar{K}\pi$ channels is stressed in Ref. [167].

In Ref. [168], using the triangle singularity approach of [164], the authors conclude that the BESIII results can be reproduced either with the $\eta(1405)$ or the $\eta(1475)$, or by a mixture of these two states. From a high statistics data sample in $J/\psi(1S) \rightarrow \gamma K_S K_S \pi^0$ BESIII reports the observation of both $\eta(1405)$ and $\eta(1475)$ [169]. A one resonance parametrization is ruled out and triangle singularity models do not describe the data satisfactorily. This radiative decay channel has been studied in a three-body unitary coupled-channel analysis and compared to the BESIII data, including ratios of radiative branching ratios into $\eta\pi^+\pi^-$ and $K\bar{K}\pi$ through the $\eta(1405/1475)$ intermediate states [170]. Two poles emerge for $K^*\bar{K}$ in different Riemann sheets around 1400 MeV and only one pole around 1500 MeV.

To summarise this section, the experimental data on the 1400 – 1500 MeV region span several decades, various production mechanisms and decay modes, with models for data analysis evolving with time. A comprehensive coherent picture of all available data is therefore difficult. We believe that there is sufficient evidence to consider the 0^{-+} nonet with the $\eta(1440)$ in fig. 63.1 as established. Whether one or two different states – $\eta(1405)$ and $\eta(1475)$ – exist is an open question, in which case the $\eta(1405)$ would be supernumerary. The most recent high statistics data and their theoretical interpretation seem to favor the two-resonance scenario.

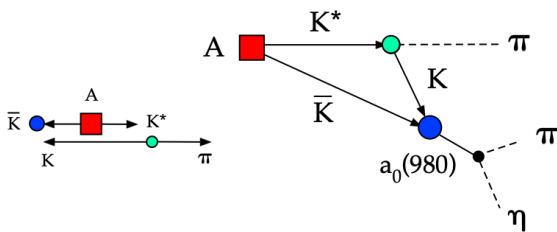


Figure 63.3: Triangle singularity: a state A decays into $K^*\bar{K}$. The K from K^* decay catches up with the \bar{K} and excites the $a_0(980)$ resonance which in turn decays into $\eta\pi$. This mechanism can lead to two distinct peaks (depending on the width of A), one in $K^*\bar{K}$ and the other via rescattering in $\eta\pi\pi$. Similarly, the virtual $K^*\bar{K}$ loop can couple to $f_0(980)$ which, decaying into $\pi\pi$, leads to a peak in the 3π final state.

63.5 Vector mesons

In this section we restrict ourselves to the more interesting isovector spectrum which contains broad and overlapping states.

63.5.1 The $\rho(770)$ meson

The determination of the parameters of the $\rho(770)$ is beset with many difficulties because of its large width. The line shape depends on the production process and is not described by a relativistic Breit-Wigner function with a P -wave width, but requires some additional shape parameter. This dependence on parameterization was demonstrated long ago [171]. Bose-Einstein correlations are another source of shifts in the $\rho(770)$ line shape, particularly in multiparticle final-state systems [172].

The same model dependence afflicts any other source of resonance parameters, such as the energy dependence of the phase shift δ_1^+ , or the pole position. It is, therefore, not surprising that a study of $\rho(770)$ dominance in the decays of the η and η' reveals the need for specific dynamical effects, in addition to the $\rho(770)$ pole [173, 174].

The cleanest determination of the $\rho(770)$ mass and width comes from e^+e^- annihilation and τ -lepton decays. ALEPH data [175] showed that the charged $\rho(770)$ parameters measured from τ -lepton decays are consistent with those of the neutral one determined from e^+e^- data [176]. This conclusion is qualitatively supported by the later studies of CLEO [177] and Belle [178]. However, a comparison of the two-pion mass spectrum in τ decays from OPAL [179], CLEO [177], and ALEPH [180, 181], and the $e^+e^- \rightarrow \pi^+\pi^-$ cross section from CMD-2 [182, 183], showed significant discrepancies between the two shapes which can be as high as 10% above the ρ meson mass [184, 185]. This discrepancy remains after measurements of the two-pion cross section in e^+e^- annihilation at KLOE [186–189], SND [190, 191], BaBar [192] and, more recently BESIII [193]. The effect is not accounted for by isospin breaking [194–197], but the accuracy of its calculation may be overestimated [198, 199].

Two recent measurements of the $e^+e^- \rightarrow \pi^+\pi^-$ cross section by SND [200] and CMD-3 [201, 202] show discrepancies in the ρ region: while SND is consistent with previous e^+e^- experiments, CMD-3 finds differences as high as 5% around the ρ meson mass. In addition, in the fit of the $e^+e^- \rightarrow \pi^+\pi^-$ cross section CMD-3 reports values for the mass of the ω and the mass and width of the ϕ , which differ slightly from the PDG values, showing for the first time the effect of the $\phi \rightarrow \pi^+\pi^-$ interference.

The problem of the difference in the $\pi^+\pi^-$ shapes between e^+e^- and τ decays seems to be solved after a recent analysis by [203], which showed that, after correcting the τ data for the missing $\rho-\gamma$ mixing contribution, besides the other known isospin symmetry violating corrections, the $\pi\pi$ isospin 1 part of the hadronic vacuum polarization contribution to the muon $g-2$ is fully compatible between τ -based and e^+e^- -based evaluations. The global fit of the whole set of the ρ , ω , and ϕ decays, taking into account mixing effects in the hidden local symmetry model, also showed consistency of the two-pion data in τ decay and e^+e^- annihilation [204, 205]. However, because of the progress in e^+e^- data, the τ input is now less precise and less reliable due to additional theoretical uncertainties [206] decreasing the importance of τ decay for the determination of the $\rho(770)$ parameters.

63.5.2 The $\rho(770)$ excitations

In our 1988 edition, we replaced the $\rho(1600)$ entry with two new ones, the $\rho(1450)$ and the $\rho(1700)$, because there was emerging evidence that the 1600-MeV region actually contains two ρ -like resonances. This possibility was pointed out by a theoretical analysis [207] on the consistency of the 2π and 4π electromagnetic form factors and the $\pi\pi$ scattering length. A consistent picture of $e^+e^- \rightarrow 2\pi, 4\pi$ and diffractive photoproduction is obtained with two resonances [208]. The existence of the $\rho(1450)$ was supported by the analysis of $\eta\rho^0$ mass spectra obtained in photoproduction and e^+e^- annihilation [209], as well as that of $e^+e^- \rightarrow \omega\pi$ [210].

The analysis of [208] was further extended by [211, 212] to include new data on 4π -systems produced in e^+e^- annihilation, and in τ decays ($\tau \rightarrow 4\pi$ and $e^+e^- \rightarrow 4\pi$ are related by the Conserved Vector Current hypothesis). These systems were successfully analyzed using interfering contributions from two ρ -like

states, and from the tail of the $\rho(770)$ two-body decay. While specific conclusions on $\rho(1450) \rightarrow 4\pi$ were obtained, little could be said about the $\rho(1700)$. Independent evidence for two 1^- states is provided by [213] in 4π electroproduction at $(Q^2) = 1$ (GeV/c)², and by [214] in a high-statistics sample of the $\eta\pi\pi$ system in π^-p charge exchange.

This scenario with two overlapping resonances is supported by other data. DM2 [215] measured the pion form factor in the interval 1.35–2.4 GeV, and observed a deep minimum around 1.6 GeV. The best fit was obtained with the hypothesis of ρ -like resonances at 1420 and 1770 MeV, with widths of about 250 MeV. DM2 [216] found that the $e^+e^- \rightarrow \eta\pi^+\pi^-$ cross section is better fitted with two fully interfering Breit-Wigners, with parameters in fair agreement with those of [208] and [215]. These results can be considered as a confirmation of the $\rho(1450)$.

Decisive evidence for the $\pi\pi$ decay mode of both $\rho(1450)$ and $\rho(1700)$ comes from $\bar{p}p$ annihilation at rest [217]. It has been shown that these resonances possess a $K\bar{K}$ decay mode [10, 218, 219]. This decay mode has also been studied in three-body hadronic B decays [220]. High-statistics studies of the decays $\tau \rightarrow \pi\pi\nu_\tau$ [175, 177], and $\tau \rightarrow 4\pi\nu_\tau$ [221] also require the $\rho(1450)$, but are not sensitive to the $\rho(1700)$, being too close to the τ mass. A recent very-high-statistics study of the $\tau \rightarrow \pi\pi\nu_\tau$ from Belle [178] reports the first observation of both $\rho(1450)$ and $\rho(1700)$ in τ decays. A clear picture of the two $\pi^+\pi^-$ resonances interfering with the $\rho(770)$ in e^+e^- annihilation was also reported by BaBar using the ISR (Initial State Radiation) method [222], and more recently by CMD-3 [201].

The structure of these ρ states is not yet completely clear. The authors of Refs. [85, 223] claim that $\rho(1450)$ has a mass consistent with radial $2S$, but its decays show characteristics of hybrids, and suggest that this state may be a $2S$ -hybrid mixture. Hybrid states could have a 4π decay mode dominated by the $a_1\pi$ [224]. Such behavior has been observed by [225] in $e^+e^- \rightarrow 4\pi$ in the energy range 1.05–1.38 GeV, and by [221] in $\tau \rightarrow 4\pi$ decays. CLEO [226] and Belle [227] observe the $\rho(1450) \rightarrow \omega\pi$ decay mode in B -meson decays, however, do not find $\rho(1700) \rightarrow \omega\pi^0$. A similar conclusion is made in Refs. [228, 229], which studied the process $e^+e^- \rightarrow \omega\pi^0$ and do not observe a statistically significant signal of the $\rho(1700)$. Various decay modes of the $\rho(1450)$ and $\rho(1700)$ are observed in $\bar{p}n$ and $\bar{p}p$ annihilation [230, 231], but no definite conclusions can be drawn. More data should be collected to clarify the nature of the ρ states, particularly in the energy range above 1.6 GeV.

We now list under a separate entry the $\rho(1570)$, the $\phi\pi$ state with $J^{PC} = 1^{--}$ earlier observed in [232] – referred to as $C(1480)$ – also reported in [233] and possibly seen in [234]. While this may be due to a threshold effect [235], Refs. [211] and [236] suggest two independent vector states with this decay mode. The $C(1480)$ has not been seen in $\bar{p}p$ [237] nor in other e^+e^- [238, 239] experiments. However, the sensitivity of the two latter is an order of magnitude lower than that of Ref. [234] which cannot exclude that the observation is due to an OZI-suppressed decay mode of the $\rho(1700)$.

Several observations on the $\omega\pi$ system in the 1200 MeV region [240–246] may be interpreted in terms of either $J^P = 1^-$ $\rho(770) \rightarrow \omega\pi$ production [247], or $J^P = 1^+$ $b_1(1235)$ production [245, 246]. The LASS amplitude analysis [248] showing evidence for $\rho(1270)$ is preliminary and needs confirmation. Evidence for a $\rho(1250)$ from a reanalysis of elastic scattering data is claimed in Ref. [249].

Ref. [250] reported a very broad 1^{--} resonance-like K^+K^- state in $J/\psi \rightarrow K^+K^-\pi^0$ decays. Its pole position corresponds to mass of 1576 MeV and width of 818 MeV. Its exotic structure (molecular or multiquark) is suggested [251–253], while in Refs. [254] and [255] this is explained by the interference between the $\rho(1450)$ and $\rho(1700)$. The latter statement is qualitatively supported by BaBar [256] and SND [257]. We quote the state reported by [250] as $X(1575)$ in the section “Further States.” Another state observed in $J/\psi \rightarrow K^+K^-\pi^0$ is the $\phi(2170)$ [258] which has been interpreted as exotic, e.g. as tetraquark, see section 63.8.

Evidence for ρ -like mesons decaying into 6π was first noted by [259] in the analysis of $e^+e^- \rightarrow 6\pi$ [260, 261] and diffractive photoproduction [262]. The authors of Ref. [259] argued that two states at about 2.1 and 1.8 GeV exist: while the former is

a candidate for the $\rho(2150)$, the latter could be a manifestation of the $\rho(1700)$ distorted by threshold effects. BaBar reported observations of the new decay modes of the $\rho(2150)$ in the channels $\eta'(958)\pi^+\pi^-$, $f_1(1285)\pi^+\pi^-$ [263] and $\pi^+\pi^-$ [264]. The decay of the $\rho(2150)$ into K^+K^- has been observed by BESIII [265] and confirmed by BaBar [266]. The relativistic quark model [267] predicts the 2^3D_1 state with $J^{PC} = 1^{--}$ at 2.15 GeV which can be identified with the $\rho(2150)$.

Under $\rho(1900)$ we list various observations of irregular behavior of the cross sections near the $N\bar{N}$ threshold. Dips of various width around 1.9 GeV were reported by the E687 Collaboration (a narrow one in the $3\pi^+3\pi^-$ diffractive photoproduction [268, 269]), by the FENICE experiment reporting a narrow dip [270], by BaBar in ISR (a narrow structure in $e^+e^- \rightarrow \phi\pi$ final state [234], but much broader in $e^+e^- \rightarrow 3\pi^+3\pi^-$ and $e^+e^- \rightarrow 2(\pi^+\pi^-\pi^0)$ [271]), by CMD-3 (also a rather broad dip in $e^+e^- \rightarrow 3\pi^+3\pi^-$ [272]). A dedicated scan of the $N\bar{N}$ -threshold region by CMD-3 confirms this effect in the $e^+e^- \rightarrow 3\pi^+3\pi^-$ and $e^+e^- \rightarrow K^+K^-\pi^+\pi^-$ final states, but does not see it in the cross section of $e^+e^- \rightarrow 2\pi^+2\pi^-$ [273]. Most probably, these structures emerge as a threshold effect due to the opening of the $N\bar{N}$ channel [274–276]. A similar enhancement is observed by BESIII in $e^+e^- \rightarrow \Lambda\bar{\Lambda}$ near the $\Lambda\bar{\Lambda}$ threshold [277, 278] which can be described as $\Lambda\bar{\Lambda}$ final state interaction [279].

63.6 Axial-vector mesons

The $J^{PC} = 1^{++}$ nonet consists of the isovector $a_1(1260)$, the isoscalars $f_1(1285)$ and $f_1(1420)$, and the K_{1A} , which is a superposition of the physical states $K_1(1270)$ and $K_1(1400)$ with a mixing angle of about 35° [280]. The nonet mixing angle $\theta_{1^{++}}$ is around 23° . The orthogonal combination – the K_{1B} – belongs to the 1^{+-} nonet with a mixing angle $\theta_{1^{+-}}$ of about 28° [280]. $f_1(1510)$. However, a two-pole structure for the $K_1(1270)$ emerges when using the unitary extension of chiral perturbation theory [281].

The mass region above 1400 MeV is rather complex [282–284]. The $f_1(1420)$ was first reported in π^-p reactions at 4 GeV/c, decaying into $K^*\bar{K}$ [285]. The $f_1(1420) \rightarrow K\bar{K}\pi$ was also observed in a reanalysis of the MARK III data [142], and a $C=+1$ state seen in tagged $\gamma\gamma$ collisions [286]. Axial-vector mesons are not observed in $\bar{p}p$ annihilation at rest in liquid hydrogen, which proceeds dominantly through S -wave annihilation. However, in gaseous hydrogen, P -wave annihilation is enhanced and the $f_1(1420)$ is indeed observed, decaying into $K^*\bar{K}$ [144]. The $f_1(1420)$, decaying into $K\bar{K}\pi$, is also seen in pp central production, together with the $f_1(1285)$. The latter decays via $a_0(980)\pi$, and the former only via $K^*\bar{K}$. The $K_S^0 K_S^0 \pi^0$ decay mode of the $f_1(1420)$ establishes unambiguously $C=+1$. Neither central production [287] nor π^-p interactions at 100 GeV [135] find any evidence for a $\eta\pi\pi$ decay mode of the $f_1(1420)$.

The $f_1(1285)$ has been suggested to be a $K^*\bar{K}$ molecule [288]. However, LHCb has determined the 1^{++} nonet mixing angle to be consistent with a mostly $n\bar{n}$ structure for the $f_1(1285)$ from $\bar{B}^0/\bar{B}^0 \rightarrow J/\psi(1S)f_1(1285)$, independent of the identity of its isoscalar partner [289]. The mixing angle $\theta_{1^{++}} = 24^\circ$ agrees with that of Ref. [280] quoted above. The ratio of \bar{B}^0/\bar{B}_s^0 decay rates also excludes the tetraquark interpretation of the $f_1(1285)$ [289]. This is consistent with earlier determinations assuming that the $f_1(1420)$ is the other isoscalar in the nonet [290].

The resonance candidate $a_1(1420)$ decaying into 3π , reported earlier by COMPASS at 1420 MeV in $\pi^-p \rightarrow \pi^-\pi^+\pi^0$ [291, 292], appears to originate from a triangle singularity: the decay of the $a_1(1260)$ into $K^*(\rightarrow K\pi)\bar{K}$ is followed by rescattering into the $f_0(980)\pi$ channel, $f_0(980) \rightarrow \pi\pi$ [293] (see the caption of fig. 63.3). A similar triangle singularity is proposed for the $f_1(1420)$, resulting from the $K^*\bar{K}$ and $a_0(980)\pi$ decay modes of the $f_1(1285)$ [294]. The $f_1(1420)$ was also suggested to be a hybrid $q\bar{q}g$ meson [295] or a $K^*\bar{K}$ molecule, due to the proximity of the $K^*\bar{K}$ threshold [296]. The $f_1(1420)$ is not seen in the K^-p data [297], which would argue against this state being the $s\bar{s}$ member of the 1^{++} nonet. Note, however, that Ref. [298] reports a signal from $f_1(1420)$ in K^-p , but not in π^-p .

The $s\bar{s}$ partner of the $f_1(1285)$ could also be the (not well

established) $f_1(1510)$ [299]. This state was seen to decay into $K\bar{K}\pi$ in K^-p interactions at 4 and 11 GeV/c, recoiling against a A [297, 300], which indeed points to an $s\bar{s}$ state. Evidence was reported in π^-p interactions, based on the phase motion of the $1^{++} K^*\bar{K}$ wave [284]. The $f_1(1510)$ is also needed by CMD-3 in $e^+e^- \rightarrow f_1\rho(770)$, together with the $f_1(1285)$ and $f_1(1420)$ peaks, to describe the shoulder in the $K_S K^\pm \pi^\mp$ mass around 1500 MeV [301]. A somewhat broader 1^{++} signal is observed in $J/\psi(1S) \rightarrow \gamma\eta\pi^+\pi^-$ [302] and a small signal in $J/\psi(1S) \rightarrow \gamma\eta'\pi^+\pi^-$ [303].

However, there is no evidence for the $f_1(1510)$ in other K^-p experiments [298, 304]. The $f_1(1510)$ is not seen in central collisions [305], nor in $\gamma\gamma$ collisions [306], although surprisingly for an assumed $s\bar{s}$ meson, a signal is reported in 4π decays [307]. Given this confusing experimental situation, the meson classification in the 1^{++} nonet is not entirely settled.

63.7 Hybrid mesons

Hybrids may be viewed as $q\bar{q}$ mesons with a vibrating gluon flux tube. In contrast to glueballs, they can have isospin 0 or 1 and be electrically charged. The mass spectrum of hybrids with exotic (non- $q\bar{q}$) quantum numbers was predicted in Ref. [308], while Ref. [309] also deals with non-exotic quantum numbers. The ground-state hybrids with quantum numbers (0^{-+} , 1^{-+} , 1^{--} , and 2^{-+}) are expected around 1.7 to 1.9 GeV. Lattice calculations predict that the hybrid with exotic quantum numbers 1^{-+} lies at a mass of 1.9 ± 0.2 GeV [310, 311]. Most hybrids are expected to be rather broad, but some can be as narrow as 100 MeV [312]. They prefer to decay into a pair of S - and P -wave mesons. The lattice study in [313, 314], based on full QCD with pion masses around 400 MeV, finds that several of the high-lying states observed in their spectrum show significant overlap with gluon rich source terms interpreted as hybrid states. A very broad 1^{-+} structure is predicted by a recent lattice calculation [315]. The main decay mode is $b_1(1235)\pi$ (a pair of S - and P -wave mesons), while other modes, such as $\rho\pi$, $\eta\pi$ and $\eta'\pi$, are suppressed by at least an order of magnitude. For an experimental and theoretical review on hybrid mesons see [4, 316].

Two isovector 1^{-+} candidates have been reported, one around 1400 MeV (the $\pi_1(1400)$ in previous versions on this *Review*) and the $\pi_1(1600)$. The ~ 350 –400 MeV broad $\pi_1(1400)$, was reported in $\pi^-p \rightarrow \eta\pi^-p$ [317, 318] and in $\pi^-p \rightarrow \eta\pi^0n$ [319]. It was observed as an interference between the angular momentum $L = 1$ and $L = 2$ $\eta\pi$ amplitudes, leading to a forward/backward asymmetry in the $\eta\pi$ angular distribution. This state had been reported earlier in π^-p reactions [320], but ambiguous solutions in the partial wave analysis were pointed out [321, 322]. A resonating 1^{-+} contribution to the $\eta\pi$ P -wave is also required in the Dalitz plot analysis of $\bar{p}n$ annihilation into $\pi^-\pi^0\eta$ [323], and in $\bar{p}p$ annihilation into $\pi^0\pi^0\eta$ [324]. Mass and width are consistent with the results of Ref. [317]. A coupled channel re-analysis of the $\pi^0\pi^0\eta$, $\pi^0\eta\eta$ and $K^+K^-\pi^0$ Crystal Barrel data at 900 MeV/c, supplemented with data from other collaboration in $\pi\pi \rightarrow \pi\pi, K\bar{K}, \eta\eta$ and $\eta\eta'$, leads to a single $1^{-+} \sim 600$ MeV broad state with a pole around 1400 MeV, decaying into $\eta\pi^0$ [16]. Ref. [325] suggested for the production in π^-p that a Deck-generated $\eta\pi$ background from final state rescattering in $\pi_1(1600)$ decay could mimic $\pi_1(1400)$, a mechanism that is, however, absent in $\bar{p}p$ annihilation.

The $\pi_1(1600)$, decaying into $\rho\pi$, was reported by COMPASS with 190 GeV pions hitting a lead target [326, 327]. It had already been observed in π^-p interactions in the decay modes $\eta'\pi$ [328], $f_1(1285)\pi$ [329], and $\omega\pi\pi$ [330], $b_1(1235)\pi$, but not $\eta\pi$ [331]. A strong enhancement in the $1^{-+} \eta'\pi$ wave, compared to $\eta\pi$, was reported at this mass in [332]. The enhancement is also observed by COMPASS in $\pi^-p \rightarrow \eta'\pi$ but in $\eta\pi$ a peak appears at 1400 MeV and in $\eta'\pi$ at 1600 MeV [333]. A coupled channel analysis of the $\eta\pi$ and $\eta'\pi$ COMPASS data leads to a single pole at 1564 ± 89 MeV, with a width of 492 ± 115 MeV [334]. The predicted width from the lattice calculation [315] is compatible with the COMPASS result. Furthermore, a combined analysis of the COMPASS and Crystal Barrel data at 900 MeV/c leads to similar results, a single pole around 1623 MeV, with a width of about 455 MeV, although a two-pole scenario cannot be completely excluded [335]. Accordingly, in the current review we have moved

the former $\pi_1(1400)$ data into the $\pi_1(1600)$ section.

Very recently, BESIII reported a 188 MeV broad enhancement at 1855 MeV in $J/\psi(1S)$ radiative decay into the $\eta\eta'$ P -wave [336], hence with exotic quantum numbers 1^{-+} . This isoscalar resonance is needed with very high significance, albeit the contribution to $\gamma\eta\eta'$ is weak and several other isoscalars expected to contribute are absent [337]. Hence this state needs confirmation. In the past there had been claims for such a state decaying into $\eta\eta'$ in this mass range, which we have listed under the $f_2(1910)$ (see e.g. Ref. [26] from WA102 central production, suggesting 1^{-+} as an alternative to 2^{++}). If confirmed, the $\eta(1855)$ could be one of the isospin 0 partners of the $\pi_1(1600)$, a member of the 1^{-+} hybrid nonet [338–340] or a $K\bar{K}_1(1400)$ molecule [341].

Hybrid candidates with the non-exotic quantum numbers 0^{-+} , 1^{--} , and 2^{-+} have also been reported: the $\pi(1800)$ is somewhat narrow if interpreted as the second radial excitation of the pion. It decays mostly into a pair of S - and P -wave mesons [342, 343], in line with expectations for 0^{-+} hybrid mesons. The evidence for 1^{--} hybrids in e^+e^- annihilation and in τ decays has been discussed in [224]. The near degeneracy of the $\eta_2(1645)$ and $\pi_2(1670)$ suggests ideal mixing in the $2^{-+} q\bar{q}$ nonet, and hence, the second isoscalar, presumably the $\eta_2(1870)$, should be mainly $s\bar{s}$ (fig. 63.1). However, the $\eta_2(1870)$ is also observed in $\bar{p}p$ annihilation and decays mainly into $a_2(1320)\pi$ and $f_2(1270)\pi$ [344], with a relative rate compatible with a hybrid state [309].

Evidence for another exotic $\pi_1(2015)$ has been claimed in π^-p interactions [329, 330]. A flavor multiplet of vector hybrids between 2200 and 2300 MeV is predicted by the constituent gluon model [340].

Summarizing, there is evidence for a very broad 1^{-+} enhancement in the 1400–1600 MeV region, which consists in one (or possibly two) exotic states, the lowest mass one favored by $\bar{p}p$ annihilation data, the highest one by high energy π^-p data. As isovectors, these states cannot be glueballs. The coupling to $\eta\pi$ of the lighter one points to a four-quark state [345], while the $\eta'\pi$ coupling of the heavier one is favored for hybrid states [346, 347]. The mass of the latter, the $\pi_1(1600)$, is not far below the lattice and flux tube model predictions. The $\eta_1(1855)$ is an isoscalar candidate for the ground state 1^{-+} hybrid nonet.

63.8 Tetraquark states

The existence of multi-quark states was suggested a long time ago, based on duality arguments [348, 349]. The most prominent light tetraquark candidates are the $a_0(980)$ and $f_0(980)$ [350–352]. A remarkable prediction for the existence of low-lying four quarks states is based on color hyperfine splitting. The lowest ground state ($L = 0$) tetraquark multiplet is predicted to be a scalar nonet. The scalar nonet lies just below 1 GeV when one assumes as mass scale the hyperfine color splitting between the ρ and the π (for a simple derivation see [8]). One then gets the nonet structures

$$\begin{aligned} |a_0(980)\rangle &= |us\bar{d}\bar{s}\rangle, \frac{1}{\sqrt{2}}|(u\bar{u} - d\bar{d})s\bar{s}\rangle, |\bar{u}\bar{s}ds\rangle, \\ |f_0(980)\rangle &= \frac{1}{\sqrt{2}}|(u\bar{u} + d\bar{d})s\bar{s}\rangle, \\ |f_0(500)\rangle &= |\bar{u}\bar{d}ud\rangle, \\ |K_0^*(700)\rangle &= |\bar{s}\bar{d}ud\rangle, |\bar{s}\bar{u}ud\rangle \text{ and } |\bar{u}\bar{d}us\rangle, |\bar{u}\bar{d}ds\rangle. \end{aligned} \quad (63.1)$$

The two isoscalars are expected to mix with the angle φ :

$$\begin{aligned} |f_0(980)\rangle &= \cos\varphi|s\bar{s}\rangle + \sin\varphi|n\bar{n}\rangle, \\ |f_0(500)\rangle &= -\sin\varphi|s\bar{s}\rangle + \cos\varphi|n\bar{n}\rangle. \end{aligned} \quad (63.2)$$

Whether these mesons are really tetraquark states or $q\bar{q}$ mesons, is still an open issue. The $f_0(980)$ is strongly produced in D_s^+ decay [354], which suggests a large $s\bar{s}$ component, due to the Cabibbo-favored $c \rightarrow s$ coupling. However, the mainly $n\bar{n}$ $f_0(1370)$ is also strongly produced in D_s^+ decay, hence additional graphs must contribute [355].

The relative branching ratios for \bar{B}^0 and $\bar{B}_s^0 \rightarrow J/\psi(1S)f_0(500)$ and $J/\psi(1S)f_0(980)$ can be used to probe the $q\bar{q}$ or tetraquark natures of the $f_0(500)$ and $f_0(980)$, as proposed in Refs. [353, 356].

Table 63.1: Coupling amplitudes for \bar{B}^0 and \bar{B}_s^0 decays into $J/\psi(1S)f_0(500)/f_0(980)$, depending on the $q\bar{q}$ or tetraquark structures of the $f_0(500)$ and $f_0(980)$ (from [353] where illustrative decay diagrams can be found). The angle φ is defined in Eq. 63.2.

		\bar{B}^0		\bar{B}_s^0	
		$f_0(980)$	$f_0(500)$	$f_0(980)$	$f_0(500)$
$q\bar{q}$	$\sin \varphi/\sqrt{2}$	$\cos \varphi/\sqrt{2}$		$\cos \varphi$	$\sin \varphi$
$qq\bar{q}\bar{q}$	$1/\sqrt{2}$	1		$\sqrt{2}$	0

LHCb observes the $f_0(980)$ in \bar{B}_s^0 decays, but not the $f_0(500)$ [28], as would be expected for tetraquarks (see Table 63.1). In contrast, LHCb also observes the $f_0(500)$ in \bar{B}^0 decays, but not the $f_0(980)$ with an upper limit eight standard deviations below the predicted value for a tetraquark state [29]. However, these contradicting findings have been challenged by a dispersive analysis [357], using a model independent inclusion of hadronic final state interactions, in which a substantial $f_0(980)$ contribution is nevertheless found in \bar{B}^0 -decays, thus still leaving the tetraquark structure as an open possibility. The ALICE collaboration reports a much stronger $K_S K_S$ femtoscopic correlation than for $K_S K^\pm$ in high energy pp collisions, indicative of the $a_0(980)$ being a tetraquark state [358].

The $f_0(980)$ and $a_0(980)$ could also be $K\bar{K}$ molecular states [359–361], being close to the $K\bar{K}$ threshold and decaying strongly into $K\bar{K}$. For $q\bar{q}$ states, the expected $\gamma\gamma$ widths [362, 363] are not significantly larger than for molecular states [362, 364] and both predictions are consistent with data. Radiative decay of the $\phi(1020)$ into $a_0(980)$ and $f_0(980)$ were proposed to disentangle compact (tetraquark) structures from hadronic molecules. Following Refs. [365, 366] the data from KLOE [367, 368], CMD-2 [369] and SND [370] seem to favor these mesons to be tetraquark states. This is also supported by a BESIII analysis of $J/\psi(1S) \rightarrow \gamma\pi^0\pi^0$ data [371] and by a measurement of $a_0(980) - f_0(980)$ mixing at BESIII [372]. In Ref. [43] these states are made of four-quark cores and virtual $K\bar{K}$ clouds at the periphery, a view that is challenged in Ref. [373] showing that radiative ϕ decay data are consistent with molecular structures of light scalars.

As mentioned already, the $f_0(1500)$ [45] and the $f_1(1285)$ [353] have been proposed as tetraquarks, the latter also as $K^*\bar{K}$ molecule [288], together with the $f_1(1420)$ [296].

Another potential candidate for a tetraquark is the $\phi(2170)$. As an excited $q\bar{q}$ state of the $\phi(1020)$, this meson should decay strongly into K^+K^- and $K_S^0 K_L^0$, and also $K^*\bar{K}^*$. However, these decays are not observed. Hence, based on its observed decay into $f_0(980)\phi(1020)$ this meson could be $ss\bar{s}\bar{s}$ [374], where relative decay rates into various channels are predicted for both $q\bar{q}$ and tetraquark structures of the $f_0(980)$. However Refs. [375, 376] claim that the $\phi(2170)$ may not be a good candidate for the $ss\bar{s}\bar{s}$ state, but could qualify as an $su\bar{s}\bar{u}$ tetraquark [376].

More information on the $a_0(980)$, $f_0(980)$, $f_0(500)$ and $K_0^*(700)$ is provided by ‘Scalar Mesons below 1 GeV’ in the *Review*.

63.9 Baryonia

Nucleon-antinucleon ($N\bar{N}$) bound states and resonances (baryonium) were predicted a long time ago [377, 378], based on the strongly attractive $N\bar{N}$ meson exchange potential, which is obtained from the NN one by multiplying with the G -parity of the exchanged meson. Several candidates had been reported in the seventies by experiments at CERN, BNL and KEK, some of them being indisputably statistically significant (for details on the model and on experiments, see [379, 380] and references therein). Most potential models predict a sequence of deeply bound isoscalar baryonia with quantum numbers $J^{PC} = 2^{++}$, 1^{--} and 0^{++} , the latter being the mostly bound [381, 382]. The $f_2(1565)$ which is observed in $\bar{p}p$ annihilation only [383, 384], is a good candidate for the 2^{++} $\bar{p}p$ bound state.

Enhancements close to the $\bar{p}p$ threshold have also been reported in B decays [385–387]. The strong signal in $J/\psi(1S) \rightarrow \gamma\bar{p}p$

[388–390] could be due to a 0^{-+} baryonium [391], but could also be generated by the $N\bar{N}$ final state interaction [392–395]. The strong energy dependence of the cross section in $e^+e^- \rightarrow \bar{p}p$ [396, 397] and $\bar{p}p \rightarrow e^+e^-$ [398] is attributed to the $N\bar{N}$ final state interaction [399] (see also our comments on the $\rho(1900)$ at the end of section 63.5.2). Alternative explanations to baryonia have been proposed for the signals in $B \rightarrow \bar{p}pK$, such as the dynamics of the fragmentation mechanism [386].

63.10 Conclusions

The ground state nonets 1^1S_0 , 1^3S_1 , 1^1P_1 , 1^3P_2 , 1^1D_2 and 1^3D_3 (see fig. 63.1) are established (although more data are desirable for the $h_1(1415)$ in the 1^1P_1 nonet). There are uncertainties and ambiguities in all other nonets. In the pseudoscalar sector the $\eta(1440)$ consists of two states, one at 1405 MeV, the other at 1475 MeV, which could also be the manifestation of a single resonance decaying into two different final states. In this case the 1475 one could be the radial excitation of the η' and the 1405 the pseudoscalar ground state glueball predicted a long time ago by the bag model, although the lattice puts it above 2 GeV. In the 1^{++} nonet two isoscalars – the $f_1(1420)$ and $f_1(1510)$ – compete for the $s\bar{s}$ slot. The first radial excitation 2^3S_1 is complete, but questions have been raised as to the nature of the $\rho(1450)$ and its relation to the $\rho(1700)$. The classification of scalar mesons is not settled, with the ones below 1 GeV being tetraquark states or building the ground state nonet. The nature of the scalars in the 1.5 – 1.8 GeV region is unclear, obscured by the interference with the ground state scalar glueball predicted in this mass region. For example, the $f_0(1500)$ and the $f_0(1710)$ could be $q\bar{q}$ states ($n\bar{n}$ and $s\bar{s}$, respectively) or made of gluons mixed with $q\bar{q}$. The $f_0(1500)$, or alternatively the $f_0(1710)$, have been proposed as mostly gluonic. Scalar mesons above the $f_0(1710)$ need experimental confirmation. Another pair of scalars, $a_0(1710)$ and $f_0(1770)$, has been reported. An isovector meson with exotic (1^{-+}) quantum numbers, $\pi_1(1600)$, is observed around 1.6 GeV with mass not far below theoretical predictions, although a further 1^{-+} state, decaying into $\eta\pi$, cannot be entirely excluded around 1.4 GeV. An isoscalar partner, the $\eta_1(1855)$, has been reported. Above 1.8 GeV mesons are broad and overlap, which complicates the data analyses. This makes the classification difficult, in particular the identification of the 2^{++} glueball, expected in 2200 – 2300 MeV mass range.

References

- [1] C. Amsler and N. A. Tornqvist, Phys. Rept. **389**, 61 (2004).
- [2] D. V. Bugg, Phys. Rept. **397**, 257 (2004), [hep-ex/0412045].
- [3] E. Klempt and A. Zaitsev, Phys. Rept. **454**, 1 (2007), [arXiv:0708.4016].
- [4] C. A. Meyer and E. S. Swanson, Prog. Part. Nucl. Phys. **82**, 21 (2015), [arXiv:1502.07276].
- [5] R. De Vita, EPJ Web Conf. **66**, 01004 (2014).
- [6] A. Esposito, A. Pilloni and A. D. Polosa, Phys. Rept. **668**, 1 (2017), [arXiv:1611.07920].
- [7] F.-K. Guo *et al.*, Rev. Mod. Phys. **90**, 015004 (2018), [arXiv:1705.00141].
- [8] C. Amsler, *The Quark Structure of Hadrons: An Introduction to the Phenomenology and Spectroscopy*, volume 949 of *Lecture Notes in Physics*, Springer (2018).
- [9] C. Amsler *et al.* (Crystal Barrel), Phys. Lett. **B333**, 277 (1994).
- [10] A. Abele *et al.*, Phys. Rev. **D57**, 3860 (1998).
- [11] C. Amsler, Rev. Mod. Phys. **70**, 1293 (1998), [hep-ex/9708025].
- [12] S. Uehara *et al.* (Belle), Phys. Rev. **D80**, 032001 (2009), [arXiv:0906.1464].
- [13] C. Amsler, Phys. Lett. **B541**, 22 (2002), [hep-ph/0206104].
- [14] P. Rubin *et al.* (CLEO), Phys. Rev. **D78**, 072003 (2008), [arXiv:0807.4545].
- [15] R. Aaij *et al.* (LHCb), Phys. Rev. **D93**, 052018 (2016), [arXiv:1509.06628].

- [16] M. Albrecht *et al.* (Crystal Barrel), *Eur. Phys. J.* **C80**, 453 (2020), [arXiv:1909.07091].
- [17] C. Amsler *et al.* (Crystal Barrel), *Eur. Phys. J.* **C23**, 29 (2002).
- [18] C. Amsler *et al.* (Crystal Barrel), *Phys. Lett.* **B322**, 431 (1994).
- [19] C. Amsler *et al.* (Crystal Barrel), *Phys. Lett.* **B342**, 433 (1995).
- [20] A. Abele *et al.* (Crystal Barrel), *Phys. Lett.* **B380**, 453 (1996).
- [21] D. Barberis *et al.* (WA102), *Phys. Lett.* **B462**, 462 (1999), [hep-ex/9907055].
- [22] D. Barberis *et al.* (WA102), *Phys. Lett.* **B471**, 440 (2000), [hep-ex/9912005].
- [23] C. Amsler *et al.* (Crystal Barrel), *Phys. Lett.* **B353**, 571 (1995).
- [24] C. Amsler *et al.* (Crystal Barrel), *Phys. Lett.* **B355**, 425 (1995).
- [25] D. Barberis *et al.* (WA102), *Phys. Lett.* **B479**, 59 (2000), [hep-ex/0003033].
- [26] D. Barberis *et al.*, *Physics Letters B* **471**, 429 (2000), [hep-ex/9911041].
- [27] C. Adolph *et al.* (COMPASS), *Phys. Rev.* **D95**, 032004 (2017), [arXiv:1509.00992].
- [28] R. Aaij *et al.* (LHCb), *Phys. Rev.* **D89**, 092006 (2014), [arXiv:1402.6248].
- [29] R. Aaij *et al.* (LHCb), *Phys. Rev.* **D90**, 012003 (2014), [arXiv:1404.5673].
- [30] F. E. Close and A. Kirk, *Phys. Rev.* **D91**, 114015 (2015), [arXiv:1503.06942].
- [31] W. Ochs, *J. Phys.* **G40**, 043001 (2013), [arXiv:1301.5183].
- [32] D. V. Bugg, B. S. Zou and A. V. Sarantsev, *Nucl. Phys.* **B471**, 59 (1996).
- [33] P. d'Argent *et al.*, *JHEP* **05**, 143 (2017), [arXiv:1703.08505].
- [34] B. Aubert *et al.* (BaBar), *Phys. Rev.* **D79**, 072006 (2009), [arXiv:0902.2051].
- [35] J. R. Pelaez, A. Rodas and J. R. de Elvira, *Phys. Rev. Lett.* **130**, 051902 (2023), [arXiv:2206.14822].
- [36] R. Molina, D. Nicmorus and E. Oset, *Phys. Rev.* **D78**, 114018 (2008), [arXiv:0809.2233].
- [37] C. García-Recio *et al.*, *Phys. Rev.* **D87**, 096006 (2013), [arXiv:1304.1021].
- [38] D. Gülmez, U. G. Meißner and J. A. Oller, *Eur. Phys. J.* **C77**, 460 (2017), [arXiv:1611.00168].
- [39] M. Carver *et al.* (CLAS), *Phys. Rev. Lett.* **126**, 082002 (2021), [arXiv:2010.16006].
- [40] J.-J. Xie and E. Oset, *Eur. Phys. J. A* **51**, 111 (2015), [arXiv:1412.3234].
- [41] A. Abele *et al.* (Crystal Barrel), *Phys. Lett.* **B385**, 425 (1996).
- [42] C. Amsler *et al.* (Crystal Barrel), *Phys. Lett.* **B639**, 165 (2006).
- [43] F. E. Close and N. A. Tornqvist, *J. Phys.* **G28**, R249 (2002), [hep-ph/0204205].
- [44] J. R. Pelaez, *Phys. Rept.* **658**, 1 (2016), [arXiv:1510.00653].
- [45] L. Zou *et al.*, *Phys. Rev. D* **99**, 114024 (2019), [arXiv:1901.11205].
- [46] E. Klempt, *Physics Letters B* **820**, 136512 (2021), [arXiv:2104.09922].
- [47] H. Kim and K. S. Kim, *The European Physical Journal C* **82**, 1113 (2022), [arXiv:2209.02958].
- [48] N. A. Tornqvist, *Z. Phys.* **C68**, 647 (1995), [hep-ph/9504372].
- [49] E. van Beveren and G. Rupp, *Eur. Phys. J.* **C22**, 493 (2001), [hep-ex/0106077].
- [50] M. Boglione and M. R. Pennington, *Phys. Rev.* **D65**, 114010 (2002), [hep-ph/0203149].
- [51] L. S. Celenza *et al.*, *Phys. Rev. C* **61**, 035201 (2000).
- [52] M. Ablikim *et al.* (BES), *Phys. Lett. B* **607**, 243 (2005), [hep-ex/0411001].
- [53] M. Ablikim *et al.* (BES), *Phys. Rev. D* **72**, 092002 (2005), [hep-ex/0508050].
- [54] M. Ablikim *et al.* (BESIII), *Phys. Rev. D* **87**, 032008 (2013), [arXiv:1211.5668].
- [55] M. S. Kholodenko (VES), *Phys. Atom. Nucl.* **83**, 11, 1602 (2020).
- [56] F. E. Close and Q. Zhao, *Phys. Rev. D* **71**, 094022 (2005), [hep-ph/0504043].
- [57] A. Sarantsev *et al.*, *Physics Letters B* **816**, 136227 (2021), [arXiv:2103.09680].
- [58] E. Klempt and A. Sarantsev, *Physics Letters B* **826**, 136906 (2022), [arXiv:2112.04348].
- [59] M. Ablikim *et al.* (BESIII), *Phys. Rev. D* **104**, 012016 (2021), [arXiv:2011.08041].
- [60] M. Ablikim *et al.* (BESIII), *Phys. Rev. D* **105**, L051103 (2022), [arXiv:2110.07650].
- [61] M. Ablikim *et al.* (BESIII), *Phys. Rev. Lett.* **129**, 182001 (2022), [arXiv:2204.09614].
- [62] J. P. Lees *et al.* (BaBar), *Phys. Rev. D* **104**, 072002 (2021), [arXiv:2106.05157].
- [63] L. S. Geng and E. Oset, *Phys. Rev. D* **79**, 074009 (2009), [arXiv:0812.1199].
- [64] X. Zhu *et al.*, *Phys. Rev. D* **105**, 116010 (2022), [arXiv:2204.09384].
- [65] X. Zhu *et al.*, *Phys. Rev. D* **107**, 034001 (2023), [arXiv:2210.12992].
- [66] Z.-L. Wang and B.-S. Zou, *Phys. Rev. D* **104**, 114001 (2021), [arXiv:2107.14470].
- [67] Z.-Y. Wang *et al.*, *Phys. Rev. D* **107**, 116018 (2023), [arXiv:2306.06395].
- [68] S. Schacht and A. Soni, *Physics Letters B* **825**, 136855 (2022), [arXiv:arXiv:2110.07619].
- [69] W.-J. Lee and D. Weingarten, *Phys. Rev.* **D61**, 014015 (2000), [hep-lat/9910008].
- [70] G. S. Bali *et al.* (UKQCD), *Phys. Lett.* **B309**, 378 (1993), [hep-lat/9304012].
- [71] C. J. Morningstar and M. J. Peardon, *Phys. Rev.* **D56**, 4043 (1997), [hep-lat/9704011].
- [72] Y. Chen *et al.*, *Phys. Rev.* **D73**, 014516 (2006), [hep-lat/0510074].
- [73] J. Leutgeb and A. Rebhan, *Phys. Rev.* **D101**, 014006 (2020), [arXiv:1909.12352].
- [74] F. Brünner, J. Leutgeb and A. Rebhan, *Physics Letters B* **788**, 431 (2019), [arXiv:1807.10164].
- [75] M. Q. Huber, C. S. Fischer and H. Sanchis-Alepuz, *The European Physical Journal C* **80**, 1077 (2020), [arXiv:2004.00415].
- [76] S. R. Cotanch and R. A. Williams, *Phys. Lett. B* **621**, 269 (2005), [arXiv:nucl-th/0505074].
- [77] F. Hechenberger, J. Leutgeb and A. Rebhan, *Phys. Rev. D* **107**, 114020 (2023), [arXiv:2302.13379].
- [78] C. Amsler and F. E. Close, *Phys. Rev.* **D53**, 295 (1996), [hep-ph/9507326].
- [79] N. A. Tornqvist and M. Roos, *Phys. Rev. Lett.* **76**, 1575 (1996), [hep-ph/9511210].
- [80] A. V. Anisovich, V. V. Anisovich and A. V. Sarantsev, *Phys. Lett.* **B395**, 123 (1997), [hep-ph/9611333].

- [81] M. Boglione and M. R. Pennington, Phys. Rev. Lett. **79**, 1998 (1997), [hep-ph/9703257].
- [82] P. Minkowski and W. Ochs, Eur. Phys. J. **C9**, 283 (1999), [hep-ph/9811518].
- [83] F. E. Close and A. Kirk, Eur. Phys. J. **C21**, 531 (2001), [hep-ph/0103173].
- [84] H.-Y. Cheng, C.-K. Chua and K.-F. Liu, Phys. Rev. **D74**, 094005 (2006), [hep-ph/0607206].
- [85] T. Barnes *et al.*, Phys. Rev. **D55**, 4157 (1997), [hep-ph/9609339].
- [86] S. Janowski, F. Giacosa and D. H. Rischke, Phys. Rev. **D90**, 114005 (2014), [arXiv:1408.4921].
- [87] F. Br unner and A. Rebhan, Phys. Rev. Lett. **115**, 131601 (2015), [arXiv:1504.05815].
- [88] J. Ellis and J. L nik, Physics Letters B **150**, 289 (1985).
- [89] C.-D. Lu *et al.*, Eur. Phys. J. **A49**, 58 (2013), [arXiv:1301.0225].
- [90] J.-L. Ren *et al.* [arXiv:2311.16824].
- [91] F. E. Close and A. Kirk, Phys. Lett. **B397**, 333 (1997), [hep-ph/9701222].
- [92] F. E. Close, Phys. Lett. **B419**, 387 (1998), [hep-ph/9710450].
- [93] A. Kirk, Phys. Lett. **B489**, 29 (2000), [hep-ph/0008053].
- [94] M. Ablikim *et al.* (BES), Phys. Lett. **B603**, 138 (2004), [hep-ex/0409007].
- [95] M. Ablikim *et al.* (BES), Phys. Lett. **B607**, 243 (2005), [hep-ex/0411001].
- [96] S. Narison, Nuclear Physics B **509**, 312 (1998).
- [97] M. Chanowitz, Phys. Rev. Lett. **95**, 172001 (2005), [hep-ph/0506125].
- [98] M. Albaladejo and J. A. Oller, Phys. Rev. Lett. **101**, 252002 (2008), [arXiv:0801.4929].
- [99] F. Br unner and A. Rebhan, Phys. Rev. D **92**, 121902 (2015), [arXiv:1510.07605].
- [100] M. Acciarri *et al.* (L3), Phys. Lett. **B501**, 173 (2001), [hep-ex/0011037].
- [101] K. Abe *et al.* (Belle), Eur. Phys. J. **C32**, 323 (2003), [hep-ex/0309077].
- [102] R. Barate *et al.* (ALEPH), Phys. Lett. **B472**, 189 (2000), [hep-ex/9911022].
- [103] S. Uehara *et al.* (Belle), Phys. Rev. **D78**, 052004 (2008), [arXiv:0805.3387].
- [104] S. Uehara *et al.* (Belle), PTEP **2013**, 123C01 (2013), [arXiv:1307.7457].
- [105] A. H. Fariborz *et al.*, Phys. Rev. **D90**, 033009 (2014), [arXiv:1407.3870].
- [106] P. Minkowski and W. Ochs, Eur. Phys. J. **C39**, 71 (2005), [hep-ph/0404194].
- [107] A. Garmash *et al.* (Belle), Phys. Rev. **D71**, 092003 (2005), [hep-ex/0412066].
- [108] B. Aubert *et al.* (BaBar), Phys. Rev. **D74**, 032003 (2006), [hep-ex/0605003].
- [109] B. Aubert *et al.* (BaBar), Phys. Rev. Lett. **99**, 161802 (2007), [arXiv:0706.3885].
- [110] M. Ablikim *et al.*, Phys. Lett. **B642**, 441 (2006), [hep-ex/0603048].
- [111] M. Ablikim *et al.* (BESIII), Phys. Rev. **D87**, 092009 (2013), [Erratum: Phys. Rev. D87, 119901(2013)], [arXiv:1301.0053].
- [112] A. Rodas *et al.*, Eur. Phys. J. **C82**, 80 (2022), [arXiv:2110.00027].
- [113] A. Vereijken *et al.*, Phys. Rev. D **108**, 014023 (2023), [arXiv:2304.05225].
- [114] A. A. Godizov, Eur. Phys. J. C **76**, 361 (2016), [arXiv:1604.01689].
- [115] S. Donnachie *et al.*, *Pomeron Physics and QCD*, Cambridge Monographs on Particle Physics, Nuclear Physics and Cosmology, Cambridge University Press, p. 85 (2002).
- [116] C. Evangelista *et al.* (JETSET), Phys. Rev. D **57**, 5370 (1998), [hep-ex/9802016].
- [117] P. S. L. Booth *et al.*, Nucl. Phys. B **273**, 689 (1986).
- [118] A. Etkin *et al.*, Phys. Lett. B **201**, 568 (1988).
- [119] D. Barberis *et al.* (WA102), Phys. Lett. B **432**, 436 (1998), [hep-ex/9805018].
- [120] M. Ablikim *et al.* (BESIII), Phys. Rev. D **93**, 112011 (2016), [arXiv:1602.01523].
- [121] Y.-B. Yang *et al.* (CLQCD Collaboration), Phys. Rev. Lett. **111**, 091601 (2013), [arXiv:1304.3807].
- [122] E. Klempt *et al.*, Phys. Lett. B **830**, 137171 (2022), [arXiv:2205.07239].
- [123] I. Iatrakis, A. Ramamurti and E. Shuryak, Phys. Rev. D **94**, 045005 (2016), [arXiv:1602.05014].
- [124] F. Br unner, D. Parganlija and A. Rebhan, Phys. Rev. D **91**, 106002 (2015), [Erratum: Phys. Rev. D93, 109903 (2016)], [arXiv:1501.07906].
- [125] J. Z. Bai *et al.* (BES), Phys. Rev. Lett. **76**, 3502 (1996).
- [126] C. Amsler *et al.* (Crystal Barrel), Phys. Lett. B **520**, 175 (2001).
- [127] R. Aaij *et al.* (LHCb), Eur. Phys. J. C **78**, 443 (2018), [arXiv:1712.08609].
- [128] P. H. Baillon *et al.*, Nuovo Cim. **A50**, 393 (1967).
- [129] D. L. Scharre *et al.*, Phys. Lett. **97B**, 329 (1980).
- [130] C. Edwards *et al.*, Phys. Rev. Lett. **49**, 259 (1982), [Erratum: Phys. Rev. Lett.50,219(1983)].
- [131] J. E. Augustin *et al.* (DM2), Phys. Rev. **D42**, 10 (1990).
- [132] J. Z. Bai *et al.* (BES), Phys. Lett. **B594**, 47 (2004), [hep-ex/0403008].
- [133] G. S. Adams *et al.* (E852), Phys. Lett. **B516**, 264 (2001), [hep-ex/0107042].
- [134] S. Fukui *et al.*, Phys. Lett. **B267**, 293 (1991).
- [135] D. Alde *et al.* (GAMS), Phys. Atom. Nucl. **60**, 386 (1997), [Yad. Fiz.60,458(1997)].
- [136] J. J. Manak *et al.* (E852), Phys. Rev. **D62**, 012003 (2000), [hep-ex/0001051].
- [137] A. V. Anisovich *et al.*, Nucl. Phys. **A690**, 567 (2001).
- [138] C. Amsler *et al.*, Eur. Phys. J. **C33**, 23 (2004).
- [139] J. E. Augustin *et al.* (DM2), Phys. Rev. **D46**, 1951 (1992).
- [140] B. Aubert *et al.* (BaBar), Phys. Rev. Lett. **101**, 091801 (2008), [arXiv:0804.0411].
- [141] M. G. Rath *et al.*, Phys. Rev. **D40**, 693 (1989).
- [142] Z. Bai *et al.* (MARK-III), Phys. Rev. Lett. **65**, 2507 (1990).
- [143] A. Bertin *et al.* (OBELIX), Phys. Lett. **B361**, 187 (1995).
- [144] A. Bertin *et al.* (OBELIX), Phys. Lett. **B400**, 226 (1997).
- [145] C. Cicalo *et al.* (OBELIX), Phys. Lett. **B462**, 453 (1999).
- [146] F. Nichtiu *et al.* (OBELIX), Phys. Lett. **B545**, 261 (2002).
- [147] T. Bolton *et al.*, Phys. Rev. Lett. **69**, 1328 (1992).
- [148] M. Ablikim *et al.* (BES), Phys. Rev. **D77**, 032005 (2008), [arXiv:0712.1411].
- [149] M. Ablikim *et al.* (BESIII), Phys. Rev. **D87**, 092006 (2013), [arXiv:1303.6360].
- [150] M. Acciarri *et al.* (L3), Phys. Lett. **B501**, 1 (2001), [hep-ex/0011035].
- [151] F. E. Close, G. R. Farrar and Z.-p. Li, Phys. Rev. **D55**, 5749 (1997), [hep-ph/9610280].

- [152] D. M. Li, H. Yu and S. S. Fang, *Eur. Phys. J.* **C28**, 335 (2003).
- [153] R. Ahohe *et al.* (CLEO), *Phys. Rev.* **D71**, 072001 (2005), [hep-ex/0501026].
- [154] P. Achard *et al.* (L3), *JHEP* **03**, 018 (2007).
- [155] T. Gutsche, V. E. Lyubovitskij and M. C. Tichy, *Phys. Rev.* **D79**, 014036 (2009), [arXiv:0811.0668].
- [156] L. Faddeev, A. J. Niemi and U. Wiedner, *Phys. Rev.* **D70**, 114033 (2004), [hep-ph/0308240].
- [157] C. J. Morningstar and M. J. Peardon, *Phys. Rev.* **D60**, 034509 (1999), [hep-lat/9901004].
- [158] H.-Y. Cheng, H.-n. Li and K.-F. Liu, *Phys. Rev.* **D79**, 014024 (2009), [arXiv:0811.2577].
- [159] G. Li, Q. Zhao and C.-H. Chang, *J. Phys.* **G35**, 055002 (2008), [hep-ph/0701020].
- [160] T. Gutsche, V. E. Lyubovitskij and M. C. Tichy, *Phys. Rev.* **D80**, 014014 (2009), [arXiv:0904.3414].
- [161] B. A. Li, *Phys. Rev.* **D81**, 114002 (2010), [arXiv:0912.2323].
- [162] A. Masoni, C. Cicalo and G. L. Usai, *J. Phys.* **G32**, R293 (2006).
- [163] E. Klempt, *Int. J. Mod. Phys.* **A21**, 739 (2006).
- [164] J.-J. Wu *et al.*, *Phys. Rev. Lett.* **108**, 081803 (2012), [arXiv:1108.3772].
- [165] X.-G. Wu *et al.*, *Phys. Rev.* **D87**, 014023 (2013), [arXiv:1211.2148].
- [166] M.-C. Du and Q. Zhao, *Phys. Rev. D* **100**, 036005 (2019), [arXiv:1905.04207].
- [167] Y. Cheng, L. Qiu and Q. Zhao [arXiv:2302.01210].
- [168] F. Aceti *et al.*, *Phys. Rev.* **D86**, 114007 (2012), [arXiv:1209.6507].
- [169] M. Ablikim *et al.* (BESIII), *JHEP* **03**, 121 (2023), [arXiv:2209.11175].
- [170] S. X. Nakamura *et al.*, *Phys. Rev. D* **107**, L091505 (2023), [arXiv:2212.07904].
- [171] J. Pisut and M. Roos, *Nucl. Phys.* **B6**, 325 (1968).
- [172] G. D. Lafferty, *Z. Phys.* **C60**, 659 (1993).
- [173] A. Abele *et al.* (Crystal Barrel), *Phys. Lett.* **B402**, 195 (1997).
- [174] M. Benayoun *et al.*, *Eur. Phys. J.* **C31**, 525 (2003), [arXiv:nucl-th/0306078].
- [175] R. Barate *et al.* (ALEPH), *Z. Phys.* **C76**, 15 (1997).
- [176] L. M. Barkov *et al.*, *Nucl. Phys.* **B256**, 365 (1985).
- [177] S. Anderson *et al.* (CLEO), *Phys. Rev.* **D61**, 112002 (2000), [hep-ex/9910046].
- [178] M. Fujikawa *et al.* (Belle), *Phys. Rev.* **D78**, 072006 (2008), [arXiv:0805.3773].
- [179] K. Ackerstaff *et al.* (OPAL), *Eur. Phys. J.* **C7**, 571 (1999), [hep-ex/9808019].
- [180] M. Davier and C.-Z. Yuan, *Nucl. Phys. B - Proc. Suppl.* **123**, 47 (2003), [hep-ex/0211057].
- [181] S. Schael *et al.* (ALEPH), *Phys. Rept.* **421**, 191 (2005), [hep-ex/0506072].
- [182] R. R. Akhmetshin *et al.* (CMD-2), *Phys. Lett.* **B527**, 161 (2002), [hep-ex/0112031].
- [183] R. R. Akhmetshin *et al.* (CMD-2), *Phys. Lett.* **B578**, 285 (2004), [hep-ex/0308008].
- [184] M. Davier *et al.*, *Eur. Phys. J.* **C27**, 497 (2003), [hep-ph/0208177].
- [185] M. Davier *et al.*, *Eur. Phys. J.* **C31**, 503 (2003), [hep-ph/0308213].
- [186] A. Aloisio *et al.* (KLOE), *Phys. Lett.* **B606**, 12 (2005), [hep-ex/0407048].
- [187] F. Ambrosino *et al.* (KLOE), *Phys. Lett.* **B670**, 285 (2009), [arXiv:0809.3950].
- [188] F. Ambrosino *et al.* (KLOE), *Phys. Lett.* **B700**, 102 (2011), [arXiv:1006.5313].
- [189] D. Babusci *et al.* (KLOE), *Phys. Lett. B* **720**, 336 (2013), [arXiv:1212.4524].
- [190] M. N. Achasov *et al.*, *J. Exp. Theor. Phys.* **101**, 1053 (2005), [hep-ex/0506076].
- [191] M. N. Achasov *et al.*, *J. Exp. Theor. Phys.* **103**, 380 (2006), [hep-ex/0605013].
- [192] B. Aubert *et al.* (BaBar), *Phys. Rev. Lett.* **103**, 231801 (2009), [arXiv:0908.3589].
- [193] M. Ablikim *et al.* (BESIII), *Phys. Lett. B* **753**, 629 (2016), [Erratum: *Phys. Lett. B* 812, 135982 (2021)], [arXiv:1507.08188].
- [194] R. Alemany, M. Davier and A. Hocker, *Eur. Phys. J.* **C2**, 123 (1998), [hep-ph/9703220].
- [195] H. Czyz and J. H. Kuhn, *Eur. Phys. J.* **C18**, 497 (2001), [hep-ph/0008262].
- [196] V. Cirigliano, G. Ecker and H. Neufeld, *Phys. Lett.* **B513**, 361 (2001), [hep-ph/0104267].
- [197] V. Cirigliano *et al.*, *Eur. Phys. J.* **C23**, 121 (2002), [hep-ph/0110153].
- [198] K. Maltman and C. E. Wolfe, *Phys. Rev.* **D73**, 013004 (2006), [hep-ph/0509224].
- [199] C. E. Wolfe and K. Maltman, *Phys. Rev.* **D80**, 114024 (2009), [arXiv:0908.2391].
- [200] M. N. Achasov *et al.*, *Journal of High Energy Physics* **2021**, 113 (2021), [arXiv:2004.00263].
- [201] F. V. Ignatov *et al.* (CMD-3) (2023), [arXiv:2302.08834].
- [202] F. V. Ignatov *et al.* (CMD-3) (2023), [arXiv:2309.12910].
- [203] F. Jegerlehner and R. Szafron, *Eur. Phys. J.* **C71**, 1632 (2011), [arXiv:1101.2872].
- [204] M. Benayoun *et al.*, *Eur. Phys. J.* **C72**, 1848 (2012), [arXiv:1106.1315].
- [205] M. Benayoun *et al.*, *Eur. Phys. J. C* **73**, 2453 (2013), [arXiv:1210.7184].
- [206] M. Davier *et al.*, *Eur. Phys. J. C* **77**, 827 (2017), [arXiv:1706.09436].
- [207] C. Erkal and M. G. Olsson, *Z. Phys.* **C31**, 615 (1986).
- [208] A. Donnachie and H. Mirzaie, *Z. Phys.* **C33**, 407 (1987).
- [209] A. Donnachie and A. B. Clegg, *Z. Phys.* **C34**, 257 (1987).
- [210] A. Donnachie and A. B. Clegg, *Z. Phys.* **C51**, 689 (1991).
- [211] A. B. Clegg and A. Donnachie, *Z. Phys.* **C40**, 313 (1988).
- [212] A. B. Clegg and A. Donnachie, *Z. Phys.* **C62**, 455 (1994).
- [213] T. J. Killian *et al.*, *Phys. Rev.* **D21**, 3005 (1980).
- [214] S. Fukui *et al.*, *Phys. Lett.* **B202**, 441 (1988).
- [215] D. Bisello *et al.* (DM2), *Phys. Lett.* **B220**, 321 (1989).
- [216] A. Antonelli *et al.* (DM2), *Phys. Lett.* **B212**, 133 (1988).
- [217] A. Abele *et al.* (Crystal Barrel), *Phys. Lett.* **B391**, 191 (1997).
- [218] A. Bertin *et al.* (OBELIX), *Phys. Lett.* **B434**, 180 (1998).
- [219] A. Abele *et al.* (Crystal Barrel), *Phys. Lett.* **B468**, 178 (1999).
- [220] W.-F. Wang, *Phys. Rev. D* **103**, 056021 (2021), [arXiv:2012.15039].
- [221] K. W. Edwards *et al.* (CLEO), *Phys. Rev.* **D61**, 072003 (2000), [hep-ex/9908024].
- [222] J. P. Lees *et al.* (BaBar), *Phys. Rev.* **D86**, 032013 (2012), [arXiv:1205.2228].
- [223] F. E. Close and P. R. Page, *Phys. Rev.* **D56**, 1584 (1997), [hep-ph/9701425].

- [224] A. Donnachie and Yu. S. Kalashnikova, Phys. Rev. **D60**, 114011 (1999), [hep-ph/9901334].
- [225] R. R. Akhmetshin *et al.* (CMD-2), Phys. Lett. **B466**, 392 (1999), [hep-ex/9904024].
- [226] J. P. Alexander *et al.* (CLEO), Phys. Rev. **D64**, 092001 (2001), [hep-ex/0103021].
- [227] D. Matvienko *et al.* (Belle), Phys. Rev. **D92**, 012013 (2015), [arXiv:1505.03362].
- [228] R. R. Akhmetshin *et al.* (CMD-2), Phys. Lett. **B562**, 173 (2003), [hep-ex/0304009].
- [229] M. N. Achasov *et al.*, Phys. Rev. D **94**, 112001 (2016), [arXiv:1610.00235].
- [230] A. Abele *et al.* (CRYSTAL BARREL), Eur. Phys. J. **C21**, 261 (2001).
- [231] M. Bargiotti *et al.* (Obelix), Phys. Lett. **B561**, 233 (2003).
- [232] S. I. Bitukov *et al.*, Phys. Lett. **B188**, 383 (1987).
- [233] M. N. Achasov *et al.*, Eur. Phys. J. C **80**, 1139 (2020), [arXiv:2007.04527].
- [234] B. Aubert *et al.* (BaBar), Phys. Rev. **D77**, 092002 (2008), [arXiv:0710.4451].
- [235] N. N. Achasov and G. N. Shestakov, Phys. Atom. Nucl. **59**, 1262 (1996), [Yad. Fiz.59N7,1319(1996)].
- [236] L. G. Landsberg, Sov. J. Nucl. Phys. **55**, 1051 (1992), [Yad. Fiz.55,1896(1992)].
- [237] A. Abele *et al.* (Crystal Barrel), Phys. Lett. **B415**, 280 (1997).
- [238] V. M. Aulchenko *et al.*, JETP Lett. **45**, 145 (1987), [Pisma Zh. Eksp. Teor. Fiz.45,118(1987)].
- [239] D. Bisello *et al.*, Z. Phys. **C52**, 227 (1991).
- [240] P. Frenkiel *et al.*, Nucl. Phys. **B47**, 61 (1972).
- [241] G. Cosme *et al.*, Phys. Lett. **63B**, 352 (1976).
- [242] D. P. Barber *et al.* (LAMP2 Group), Z. Phys. **C4**, 169 (1980).
- [243] D. Aston *et al.*, Phys. Lett. **92B**, 211 (1980), [Erratum: Phys. Lett.95B,461(1980)].
- [244] M. Atkinson *et al.* (Omega Photon), Nucl. Phys. **B243**, 1 (1984).
- [245] J. E. Brau *et al.* (SLAC Hybrid Facility Photon), Phys. Rev. **D37**, 2379 (1988).
- [246] C. Amsler *et al.* (Crystal Barrel), Phys. Lett. **B311**, 362 (1993).
- [247] J. Layssac and F. M. Renard, Nuovo Cim. **A6**, 134 (1971).
- [248] D. Aston *et al.*, Nucl. Phys. Proc. Suppl. **21**, 105 (1991).
- [249] N. Hammoud *et al.*, Phys. Rev. D **102**, 054029 (2020), [arXiv:2009.06317].
- [250] M. Ablikim *et al.* (BES), Phys. Rev. Lett. **97**, 142002 (2006), [hep-ex/0606047].
- [251] G.-J. Ding and M.-L. Yan, Phys. Lett. **B643**, 33 (2006), [hep-ph/0607253].
- [252] F.-K. Guo *et al.*, Nucl. Phys. **A773**, 78 (2006), [hep-ph/0509050].
- [253] A. Zhang, T. Huang and T. G. Steele, Phys. Rev. **D76**, 036004 (2007), [hep-ph/0612146].
- [254] B. A. Li, Phys. Rev. **D76**, 094016 (2007), [hep-ph/0701159].
- [255] X. Liu *et al.*, Phys. Rev. **D75**, 074017 (2007), [hep-ph/0701022].
- [256] J. P. Lees *et al.* (BaBar), Phys. Rev. D **88**, 032013 (2013), [arXiv:1306.3600].
- [257] M. N. Achasov *et al.*, Phys. Rev. D **94**, 112006 (2016), [arXiv:1608.08757].
- [258] M. Ablikim *et al.*, Journal of High Energy Physics **2022**, 45 (2022), and references therein, [arXiv:2202.06447].
- [259] A. B. Clegg and A. Donnachie, Z. Phys. **C45**, 677 (1990).
- [260] D. Bisello *et al.*, Phys. Lett. **107B**, 145 (1981).
- [261] A. Castro *et al.*, LAL-88-58(1988), URL <https://doi.org/10.17182/hepdata.38181>.
- [262] M. Atkinson *et al.* (Omega Photon), Z. Phys. **C29**, 333 (1985).
- [263] B. Aubert *et al.* (BaBar), Phys. Rev. **D76**, 092005 (2007), [Erratum: Phys. Rev.D77,119902(2008)], [arXiv:0708.2461].
- [264] J. P. Lees *et al.* (BABAR Collaboration), Phys. Rev. D **86**, 032013 (2012), [arXiv:1205.2228].
- [265] M. Ablikim *et al.* (BESIII Collaboration), Phys. Rev. D **99**, 032001 (2019), [arXiv:1811.08742].
- [266] J. P. Lees *et al.* (BaBar Collaboration), Phys. Rev. D **101**, 012011 (2020), [arXiv:1912.04512].
- [267] S. Godfrey and N. Isgur, Phys. Rev. **D32**, 189 (1985).
- [268] P. L. Frabetti *et al.* (E687), Phys. Lett. **B514**, 240 (2001), [hep-ex/0106029].
- [269] P. L. Frabetti *et al.*, Phys. Lett. **B578**, 290 (2004), [hep-ex/0310041].
- [270] A. Antonelli *et al.* (FENICE), Phys. Lett. **B365**, 427 (1996).
- [271] B. Aubert *et al.* (BaBar), Phys. Rev. **D73**, 052003 (2006), [hep-ex/0602006].
- [272] R. R. Akhmetshin *et al.* (CMD-3), Phys. Lett. **B723**, 82 (2013), [arXiv:1302.0053].
- [273] R. R. Akhmetshin *et al.* (CMD-3), Phys. Lett. B **794**, 64 (2019), [arXiv:1808.00145].
- [274] A. E. Obrazovsky and S. I. Serednyakov, JETP Lett. **99**, 315 (2014), [arXiv:1402.5225].
- [275] J. Haidenbauer *et al.*, Phys. Rev. **D92**, 054032 (2015), [arXiv:1506.08120].
- [276] A. I. Milstein and S. G. Salnikov, Nucl. Phys. A **977**, 60 (2018), [arXiv:1804.01283].
- [277] M. Ablikim *et al.* (BESIII Collaboration), Phys. Rev. D **97**, 032013 (2018), [arXiv:1709.10236].
- [278] M. Ablikim *et al.* (BESIII), Phys. Rev. D **107**, 072005 (2023), [arXiv:2303.07629].
- [279] A. I. Milstein and S. G. Salnikov, JETP Lett. **117**, 905 (2023), [arXiv:2303.13551].
- [280] H.-Y. Cheng, Phys. Lett. **B707**, 116 (2012), [arXiv:1110.2249].
- [281] L. S. Geng *et al.*, Phys. Rev. D **75**, 014017 (2007), [hep-ph/0610217].
- [282] S. U. Chung *et al.*, Phys. Rev. Lett. **55**, 779 (1985), [Erratum: Phys. Rev. Lett.55,2093(1985)].
- [283] D. F. Reeves *et al.*, Phys. Rev. **D34**, 1960 (1986).
- [284] A. Birman *et al.*, Phys. Rev. Lett. **61**, 1557 (1988), [Erratum: Phys. Rev. Lett.62,1577(1989)].
- [285] C. Dionisi *et al.* (CERN-College de France-Madrid-Stockholm), Nucl. Phys. **B169**, 1 (1980).
- [286] H. J. Behrend *et al.* (CELLO), Z. Phys. **C42**, 367 (1989).
- [287] T. A. Armstrong *et al.* (WA76), Z. Phys. **C52**, 389 (1991).
- [288] F. Aceti, J.-J. Xie and E. Oset, Phys. Lett. **B750**, 609 (2015), [arXiv:1505.06134].
- [289] R. Aaij *et al.* (LHCb), Phys. Rev. Lett. **112**, 091802 (2014), [arXiv:1310.2145].
- [290] G. Gidal *et al.*, Phys. Rev. Lett. **59**, 2012 (1987).
- [291] C. Adolph *et al.* (COMPASS), Phys. Rev. Lett. **115**, 082001 (2015), [arXiv:1501.05732].
- [292] M. Aghasyan *et al.* (COMPASS), Phys. Rev. **D98**, 092003 (2018), [arXiv:1802.05913].
- [293] G. D. Alexeev *et al.*, Phys. Rev. Lett. **127**, 082501 (2021), [arXiv:2006.05342].
- [294] V. R. Debastiani *et al.*, Phys. Rev. **D95**, 034015 (2017), [arXiv:1611.05383].

- [295] S. Ishida *et al.*, Prog. Theor. Phys. **82**, 119 (1989).
- [296] R. S. Longacre, Phys. Rev. **D42**, 874 (1990).
- [297] D. Aston *et al.*, Phys. Lett. **B201**, 573 (1988).
- [298] P. F. Ermolov *et al.*, Sov. J. Nucl. Phys. **39**, 738 (1984), [Yad. Fiz.39,1170(1984)].
- [299] F. E. Close and A. Kirk, Z. Phys. **C76**, 469 (1997), [hep-ph/9706543].
- [300] P. Gavillet *et al.*, Z. Phys. **C16**, 119 (1982).
- [301] R. R. Akhmetshin *et al.*, Physics Letters B **836**, 137606 (2023), [arXiv:2207.04615].
- [302] J. Z. Bai *et al.* (BES), Phys. Lett. **B446**, 356 (1999).
- [303] M. Ablikim *et al.* (BESIII), Phys. Rev. Lett. **106**, 072002 (2011), [arXiv:1012.3510].
- [304] E. King *et al.*, Nucl. Phys. Proc. Suppl. **21**, 11 (1991).
- [305] D. Barberis *et al.* (WA102), Phys. Lett. **B413**, 225 (1997), [hep-ex/9707022].
- [306] H. Aihara *et al.* (TPC/Two Gamma), Phys. Rev. **D38**, 1 (1988).
- [307] D. A. Bauer *et al.* (TPC/Two Gamma), Phys. Rev. **D48**, 3976 (1993).
- [308] N. Isgur, R. Kokoski and J. Paton, Phys. Rev. Lett. **54**, 869 (1985).
- [309] F. E. Close and P. R. Page, Nucl. Phys. **B443**, 233 (1995), [hep-ph/9411301].
- [310] P. Lacock *et al.* (UKQCD), Phys. Lett. **B401**, 308 (1997), [hep-lat/9611011].
- [311] C. W. Bernard *et al.* (MILC), Phys. Rev. **D56**, 7039 (1997), [hep-lat/9707008].
- [312] P. R. Page, E. S. Swanson and A. P. Szczepaniak, Phys. Rev. **D59**, 034016 (1999), [hep-ph/9808346].
- [313] J. J. Dudek *et al.*, Phys. Rev. **D83**, 111502 (2011), [arXiv:1102.4299].
- [314] J. J. Dudek *et al.*, Phys. Rev. **D88**, 094505 (2013), [arXiv:1309.2608].
- [315] A. J. Woss *et al.*, Phys. Rev. D **103**, 054502 (2021), [arXiv:2009.10034].
- [316] C. A. Meyer and Y. Van Haarlem, Phys. Rev. C **82**, 025208 (2010), [arXiv:1004.5516].
- [317] D. R. Thompson *et al.* (E852), Phys. Rev. Lett. **79**, 1630 (1997), [hep-ex/9705011].
- [318] S. U. Chung *et al.* (E852), Phys. Rev. **D60**, 092001 (1999), [hep-ex/9902003].
- [319] G. S. Adams *et al.* (E862), Phys. Lett. **B657**, 27 (2007), [hep-ex/0612062].
- [320] D. Alde *et al.*, Phys. Lett. **B205**, 397 (1988).
- [321] Yu. D. Prokoshkin and S. A. Sadovsky, Phys. Atom. Nucl. **58**, 606 (1995), [Yad. Fiz.58N4,662(1995)].
- [322] Yu. D. Prokoshkin and S. A. Sadovsky, Phys. Atom. Nucl. **58**, 853 (1995), [Yad. Fiz.58,921(1995)].
- [323] A. Abele *et al.* (Crystal Barrel), Phys. Lett. **B423**, 175 (1998).
- [324] A. Abele *et al.* (Crystal Barrel), Phys. Lett. **B446**, 349 (1999).
- [325] A. Donnachie and P. R. Page, Phys. Rev. **D58**, 114012 (1998), [hep-ph/9808225].
- [326] M. Aghasyan *et al.* (COMPASS), Phys. Rev. D **98**, 092003 (2018), [arXiv:1802.05913].
- [327] G. D. Alexeev *et al.*, Phys. Rev. D **105**, 012005 (2022), [arXiv:arXiv:2108.01744].
- [328] E. I. Ivanov *et al.* (E852), Phys. Rev. Lett. **86**, 3977 (2001), [hep-ex/0101058].
- [329] J. Kuhn *et al.* (E852), Phys. Lett. **B595**, 109 (2004), [hep-ex/0401004].
- [330] M. Lu *et al.* (E852), Phys. Rev. Lett. **94**, 032002 (2005), [hep-ex/0405044].
- [331] Yu.P. Gouz *et al.*, Proc. XXVI Int. Conf. on HEP, Dallas (1992).
- [332] G. M. Beladidze *et al.* (VES), Phys. Lett. **B313**, 276 (1993).
- [333] C. Adolph *et al.* (COMPASS), Phys. Lett. B **740**, 303 (2015), [Erratum: Phys.Lett.B 811, 135913 (2020)], [arXiv:1408.4286].
- [334] A. Rodas *et al.* (JPAC), Phys. Rev. Lett. **122**, 042002 (2019), [arXiv:1810.04171].
- [335] B. Kopf *et al.*, Eur. Phys. J. C **81**, 12, 1056 (2021), [arXiv:2008.11566].
- [336] M. Ablikim *et al.* (BESIII), Phys. Rev. Lett. **129**, 192002 (2022), [Erratum: Phys.Rev.Lett. 130, 159901 (2023)], [arXiv:2202.00621].
- [337] M. Ablikim *et al.* (BESIII), Phys. Rev. D **106**, 072012 (2022), [Erratum: Phys.Rev.D 107, 079901 (2023)], [arXiv:2202.00623].
- [338] V. Shastry, C. S. Fischer and F. Giacosa, Phys. Lett. B **834**, 137478 (2022), [arXiv:2203.04327].
- [339] L. Qiu and Q. Zhao, Chin. Phys. C **46**, 5, 051001 (2022), [arXiv:2202.00904].
- [340] E. S. Swanson, Phys. Rev. D **107**, 074028 (2023), [arXiv:2302.01372].
- [341] X.-K. Dong, Y.-H. Lin and B.-S. Zou, Sci. ChinaPhys. Mech. Astron. **65**, 261011 (2022), [arXiv:2202.00863].
- [342] M. Alekseev *et al.* (COMPASS), Phys. Rev. Lett. **104**, 241803 (2010), [arXiv:0910.5842].
- [343] D. V. Amelin *et al.* (VES), Phys. Lett. **B356**, 595 (1995).
- [344] J. Adomeit *et al.* (Crystal Barrel), Z. Phys. **C71**, 227 (1996).
- [345] S. U. Chung, E. Klempt and J. G. Korner, Eur. Phys. J. **A15**, 539 (2002), [hep-ph/0211100].
- [346] F. E. Close and H. J. Lipkin, Phys. Lett. **B196**, 245 (1987).
- [347] F. Iddir and A. S. Safir, Phys. Lett. **B507**, 183 (2001), [hep-ph/0010121].
- [348] G. C. Rossi and G. Veneziano, Nucl. Phys. **B123**, 507 (1977).
- [349] J. L. Rosner, Phys. Rev. Lett. **21**, 950 (1968).
- [350] R. L. Jaffe, Phys. Rev. **D15**, 281 (1977).
- [351] M. G. Alford and R. L. Jaffe, Nucl. Phys. **B578**, 367 (2000), [hep-lat/0001023].
- [352] G. 't Hooft *et al.*, Phys. Lett. **B662**, 424 (2008), [arXiv:0801.2288].
- [353] S. Stone and L. Zhang, Phys. Rev. Lett. **111**, 062001 (2013), [arXiv:1305.6554].
- [354] E. M. Aitala *et al.* (E791), Phys. Rev. Lett. **86**, 765 (2001), [hep-ex/0007027].
- [355] H.-Y. Cheng, Phys. Rev. **D67**, 054021 (2003), [hep-ph/0212361].
- [356] R. Fleischer, R. Knegjens and G. Ricciardi, Eur. Phys. J. **C71**, 1832 (2011), [arXiv:1109.1112].
- [357] J. T. Daub, C. Hanhart and B. Kubis, JHEP **02**, 009 (2016), [arXiv:1508.06841].
- [358] S. Acharya *et al.* (ALICE), Physics Letters B **833**, 137335 (2022), [arXiv:2111.06611].
- [359] J. D. Weinstein and N. Isgur, Phys. Rev. **D41**, 2236 (1990).
- [360] G. Janssen *et al.*, Phys. Rev. **D52**, 2690 (1995), [arXiv:nucl-th/9411021].
- [361] M. P. Locher, V. E. Markushin and H. Q. Zheng, Eur. Phys. J. **C4**, 317 (1998), [hep-ph/9705230].
- [362] J. A. Oller and E. Oset, AIP Conf. Proc. **432**, 413 (1998), [hep-ph/9710557].
- [363] R. Delbourgo, D.-s. Liu and M. D. Scadron, Phys. Lett. **B446**, 332 (1999), [hep-ph/9811474].

- [364] C. Hanhart *et al.*, Phys. Rev. **D75**, 074015 (2007), [hep-ph/0701214].
- [365] F. E. Close, N. Isgur and S. Kumano, Nucl. Phys. **B389**, 513 (1993), [hep-ph/9301253].
- [366] N. N. Achasov, V. V. Gubin and V. I. Shevchenko, Phys. Rev. **D56**, 203 (1997), [hep-ph/9605245].
- [367] F. Ambrosino *et al.*, Physics Letters B **681**, 5 (2009), [arXiv:0904.2539].
- [368] F. Ambrosino *et al.*, Eur. Phys. J. C **49**, 473 (2007), [hep-ex/0609009].
- [369] R. R. Akhmetshin *et al.* (CMD-2), Phys. Lett. **B462**, 371 (1999), [hep-ex/9907005].
- [370] M. N. Achasov *et al.*, Phys. Lett. **B479**, 53 (2000), [hep-ex/0003031].
- [371] N. N. Achasov *et al.*, Phys. Rev. D **103**, 014010 (2021), [arXiv:2009.04191].
- [372] M. Ablikim *et al.* (BESIII Collaboration), Phys. Rev. Lett. **121**, 022001 (2018), [arXiv:1802.00583].
- [373] Yu. S. Kalashnikova *et al.*, Eur. Phys. J. **A24**, 437 (2005), [hep-ph/0412340].
- [374] H.-W. Ke and X.-Q. Li, Phys. Rev. D **99**, 036014 (2019), [arXiv:1810.07912].
- [375] F.-X. Liu *et al.*, Phys. Rev. D **103**, 016016 (2021), [arXiv:2008.01372].
- [376] S. S. Agaev, K. Azizi and H. Sundu, Phys. Rev. D **101**, 074012 (2020).
- [377] O. D. Dalkarov, V. B. Mandelzweig and I. S. Shapiro, Nucl. Phys. B **21**, 88 (1970).
- [378] G. Rossi and G. Veneziano, Physics Reports **63**, 153 (1980).
- [379] C. Amsler, Adv. Nucl. Phys. **18**, 183 (1987).
- [380] L. Montanet, Phys. Rept. **63**, 201 (1980).
- [381] C. B. Dover and J. M. Richard, Annals Phys. **121**, 70 (1979).
- [382] W. W. Buck, C. B. Dover and J. M. Richard, Annals Phys. **121**, 47 (1979).
- [383] B. May *et al.* (ASTERIX), Z. Phys. **C46**, 203 (1990).
- [384] A. Bertin *et al.* (OBELIX), Phys. Rev. **D57**, 55 (1998).
- [385] K. Abe *et al.* (Belle), Phys. Rev. Lett. **88**, 181803 (2002), [hep-ex/0202017].
- [386] M. Z. Wang *et al.* (Belle), Phys. Lett. **B617**, 141 (2005), [hep-ex/0503047].
- [387] K. Abe *et al.* (Belle), Phys. Rev. Lett. **89**, 151802 (2002), [hep-ex/0205083].
- [388] J. Z. Bai *et al.* (BES), Phys. Rev. Lett. **91**, 022001 (2003), [hep-ex/0303006].
- [389] J. P. Alexander *et al.* (CLEO), Phys. Rev. **D82**, 092002 (2010), [arXiv:1007.2886].
- [390] M. Ablikim *et al.* (BESIII), Phys. Rev. Lett. **108**, 112003 (2012), [arXiv:1112.0942].
- [391] G.-J. Ding and M.-L. Yan, Phys. Rev. **C72**, 015208 (2005), [hep-ph/0502127].
- [392] B. Loiseau and S. Wycech, Phys. Rev. **C72**, 011001 (2005), [hep-ph/0501112].
- [393] A. Sibirtsev *et al.*, Phys. Rev. **D71**, 054010 (2005), [hep-ph/0411386].
- [394] X.-W. Kang, J. Haidenbauer and U.-G. Meissner, JHEP **02**, 113 (2014), [arXiv:1311.1658].
- [395] X.-W. Kang, J. Haidenbauer and U.-G. Meissner, Phys. Rev. **D91**, 074003 (2015), [arXiv:1502.00880].
- [396] J. P. Lees *et al.* (BaBar), Phys. Rev. **D87**, 092005 (2013), [arXiv:1302.0055].
- [397] E. P. Solodov *et al.*, EPJ Web Conf. **212**, 07002 (2019).
- [398] G. Bardin *et al.*, Nucl. Phys. **B411**, 3 (1994).
- [399] J. Haidenbauer, X. W. Kang and U. G. Meissner, Nucl. Phys. **A929**, 102 (2014), [arXiv:1405.1628].

64. Scalar Mesons below 1 GeV

Revised August 2023 by T. Gutsche (Tübingen U.), C. Hanhart (FZ Jülich), R.E. Mitchell (Indiana U.) and S. Spanier (Tennessee U.).

64.1 Introduction

The identification of the light scalar mesons is a long-standing puzzle. Scalar resonances are difficult to resolve experimentally as they can have large decay widths, which cause a strong overlap between neighboring resonances and with background. In addition, in some cases, several decay channels open up within a short mass interval (*e.g.* at the $K\bar{K}$ and $\eta\eta$ thresholds), producing cusps in the line shapes of the nearby resonances. Furthermore, one expects non- $q\bar{q}$ scalar objects, such as hadronic molecules and multiquark states, in the mass range of interest (for reviews see, *e.g.*, Refs. [1–6]).

Light scalars are produced, for example, in πN scattering on polarized/unpolarized targets, $p\bar{p}$ annihilation, central hadronic production, $J/\psi(1S)$, B^- , D^- and K^- -meson decays, $\gamma\gamma$ formation, and ϕ radiative decays. Especially for the lightest scalar mesons simple parameterizations like Breit-Wigner functions and variants thereof fail — this is demonstrated explicitly on the example of the $f_0(500)$ or σ , *e.g.*, in Ref. [7]. Accordingly, more advanced theory tools are necessary to extract the resonance parameters from data. In the analyses available in the literature, fundamental properties of the amplitudes such as unitarity, analyticity, Lorentz invariance, and chiral and flavor symmetry are implemented at different levels of rigor. Especially, chiral symmetry implies the appearance of zeros, the so-called Adler zeros, close to the threshold in elastic S -wave scattering amplitudes involving soft (pseudo) Goldstone bosons [8, 9], which may be shifted or removed in associated production processes [10]. Moreover, especially for the lightest non-strange and strange scalar resonance precision extractions of pole parameters get complicated by the presence of both left-hand cuts as well as circular cuts (for a recent review on the subject see Ref. [5]). The methods employed are the K -matrix formalism, the N/D -method, the Dalitz-Tuan ansatz, the inverse amplitude method, unitarized quark models with coupled channels, effective chiral field theories and the linear sigma model, *etc.* Dynamics near the lowest two-body thresholds in some analyses are described by crossed channel (t , u) meson exchange or with an effective range parameterization instead of, or in addition to, resonant features in the s -channel. Dispersion theoretical approaches are applied to pin down the location of resonance poles for the low mass states [11–16] unambiguously — in particular the existence of a nonet of light scalar is not questioned anymore.

In parallel to the developments sketched above also lattice QCD entered the field of precision spectroscopy, since it was acknowledged that a study of resonances calls for a proper treatment of the scattering process employing *e.g.* the Lüscher method [17], later extended to coupled channels in Refs. [18–23]. This allowed for determinations of the poles of the $I = 1/2$ [24], the $I = 1$ [25] as well as the $I = 0$ [26, 27] light scalar mesons. Besides and additional firm confirmation of the existence of a nonet of light scalar mesons, via the quark mass dependence of the pole locations (here the most sophisticated analysis is reported in Ref. [28]) these studies allow for an alternative look on their nature [29–31].

The mass and width of a resonance are found from the position of the nearest pole in the process amplitude (S - or T -matrix) at an unphysical sheet of the complex energy plane, traditionally labeled as

$$\sqrt{s_{\text{Pole}}} = M - i\Gamma/2. \quad (64.1)$$

It is important to note that in general the pole of a Breit-Wigner parameterization does not agree with the S - or T -matrix pole. For a detailed discussion of this issue we refer to the review on *Resonances* in this Review of Particle Physics (RPP).

In this review we present proposed values for the mass parameters of the scalar resonances below 1 GeV. Note that those are labeled as ‘our estimate’ — it is not an average over the quoted analyses, but is chosen to include the bulk of the analyses. An averaging procedure is not justified, since the analyses use over-

lapping or sometimes even identical data sets so that they are not statistically independent.

In this note, we discuss the light scalars below 1 GeV organized in the *Listings* under the entries $K_0^*(700)$ (or κ) with isospin $I = 1/2$, $a_0(980)$ with $I = 1$, as well as $f_0(500)$ (or σ) and $f_0(980)$ both with $I = 0$. The $I = 2$ $\pi\pi$ and $I = 3/2$ $K\pi$ partial waves do not exhibit resonant behaviour.

64.2 The $K_0^*(700)$, also known as κ ($I = 1/2$)

The $K_0^*(700)$ shows up as a pole in the low energy πK scattering, although its presence and properties are difficult to establish, since it appears to have a very large width ($\Gamma \approx 500$ MeV) and resides close to the $K\pi$ threshold. Hadronic D^- and B^- -meson decays provide additional data points in the vicinity of the $K\pi$ threshold and are discussed in detail in the *Review on Multibody Charm Analyses* in this RPP. With a few exceptions discussed there, the three- or more-hadron final states are usually treated as non-interacting two-body systems. Precise information from semileptonic D decays, where the strongly interacting two-particle final states could be treated without approximation, is not available. BES II [32] (re-analyzed in [33]) finds a $K_0^*(700)$ -like structure in $J/\psi(1S)$ decays to $\bar{K}^{*0}(892)K^+\pi^-$ where $K_0^*(700)$ recoils against the $K^*(892)$. The decay $\tau^- \rightarrow K_S^0\pi^-\nu_\tau$ and is studied by Belle [34], with $K_0^*(700)$ parameters fixed to those of Ref. [32].

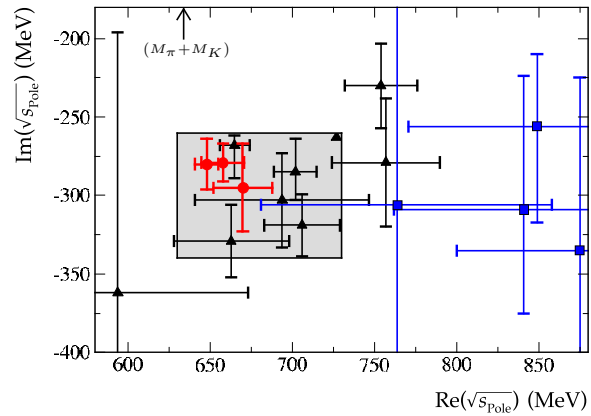


Figure 64.1: Location of the $K_0^*(700)$ (or κ) poles in the complex energy plane. Red circles denote the results of the most sophisticated analyses based on dispersion relations (see text for details), poles extracted from Breit-Wigner fits are shown as blue squares, while all other analyses quoted in the *Listings* are denoted by black triangles. The corresponding references are given in the listing. The arrow shows the location of the πK thresholds. The grey box indicates the range of pole locations classified as ‘our estimate’.

Some authors find a $K_0^*(700)$ pole in their phenomenological analysis (see, *e.g.*, [35–44]), while others do not need to include it in their fits (see, *e.g.*, [45–48]; note that in Ref. [49] only a K_0^* meson above 825 MeV was discarded using scattering data fits and analyticity, which is not in conflict with the properties quoted below). All works including constraints from chiral symmetry at low energies naturally find a light $K_0^*(700)$ below 800 MeV, see, *e.g.*, [50–56]. The analyses of Ref. [15, 16] are based on the Roy-Steiner equations, which include analyticity and crossing symmetry constraints. Ref. [57] uses the Padé method to extract pole parameters after refitting scattering data constrained to satisfy forward dispersion relations. All three arrive at compatible pole positions for the $K_0^*(700)$ that are also consistent with the pole parameters deduced from other theoretical methods. Due to their large uncertainties, the pole locations deduced from the Breit-Wigner fits appear to be just about consistent with the other determinations, but the real parts of all those analyses lie systematically higher. Moreover, phase shifts extracted from the Breit-Wigner functions for the $K_0^*(700)$ are very different from the known scalar πK phase shifts. The various poles are shown

in in Fig. 64.1. The compilation in this figure motivates the pole parameters of the $K_0^*(700)$, which we quote as ‘our estimate’, namely,

$$\sqrt{s_{\text{Pole}}^{\kappa}} = (630 - 730) - i(260 - 340) \text{ MeV} . \quad (64.2)$$

For an extensive discussion about the πK system in general and the κ meson in particular, see Ref. [58].

64.3 The $a_0(980)$ ($I = 1$)

The $a_0(980)$ couples strongly to the channels $\pi\eta$ and $K\bar{K}$. Independent of any model, the $K\bar{K}$ component must be large in the $a_0(980)$ wave function, since the mass of the $a_0(980)$ lies very close to the opening of the $K\bar{K}$ channel, to which it strongly couples [59,60]. This generates a pronounced cusp-like behavior in the resonant amplitude and to reveal its true coupling constants the presence of the $K\bar{K}$ channel cannot be ignored. All listed $a_0(980)$ measurements agree on a mass position value near 980 MeV, but the width deduced from the imaginary part of the pole location has values between 50 and 100 MeV, mostly due to the different models. For example, the analysis of the $p\bar{p}$ annihilation data [59] using a unitary K -matrix description finds a width determined from the T -matrix pole of 92 ± 8 MeV. Note that the width of the $a_0(980)$ line shape is typically smaller than what could be expected from the pole location.

The relative coupling $K\bar{K}/\pi\eta$ is determined indirectly from $f_1(1285)$ [61–63] or $\eta(1410)$ decays [64–66], from the line shape observed in the $\pi\eta$ decay mode [67–70], or from the coupled-channel analysis of the $\pi\eta$ and $K\bar{K}\pi$ final states of $p\bar{p}$ annihilation at rest [59].

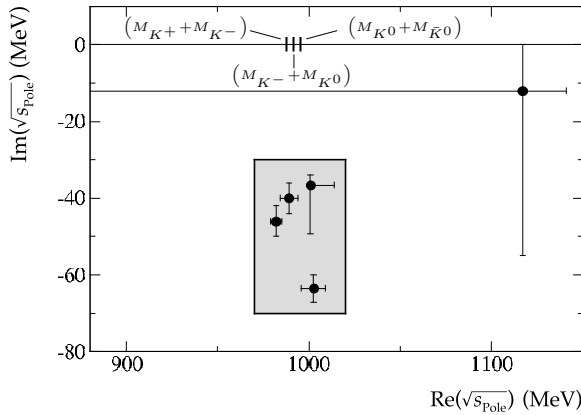


Figure 64.2: Location of the $a_0(980)$ poles from different extractions in the complex energy plane. The corresponding references are given in the Listings. Also shown are the thresholds for the K^+K^- and $K^0\bar{K}^0$ channels, relevant for $a_0(980)^0$, and for the K^-K^0 channel, relevant for the $a_0(980)^-$. The grey box indicates the range of pole locations classified as ‘our estimate’. Note that by default we take the pole located closest to the physical axis; thus the poles shown are not all on the same sheet.

For the extraction of the $a_0(980)$ pole locations, Refs. [52, 53, 55, 71] use unitarized chiral perturbation theory. Ref. [72] uses a similar formalism to extract the pole of the $a_0(980)$, employing the amplitude fixed in Ref. [73]. A dispersion theoretical approach to the isovector scalar $\pi\eta - K\bar{K}$ system is presented in Ref. [74] that may be refined further from studies of heavy meson decays [75]. Those efforts lead to a rather precise determination of the $a_0(980)$ pole location [76]. A value consistent for the mass parameter, but with a larger width, is found in the analysis of $p\bar{p}$ annihilation in flight data employing a K -matrix [77]. The poles presented in Refs. [55, 59, 70, 76, 77] are shown in Fig. 64.2 together with the range of pole parameters estimated by us from this compilation, namely,

$$\sqrt{s_{\text{Pole}}^{a_0(980)}} = (970 - 1020) - i(30 - 70) \text{ MeV} \quad (64.3)$$

indicated by the box.

64.4 The $f_0(500)$, also known as σ -meson ($I = 0$)

For discussions of the $\pi\pi$ S wave below the $K\bar{K}$ threshold and on the long history of the $f_0(500)$, which was suggested in linear sigma models more than 50 years ago, see the review [5]. Information on the $\pi\pi$ S -wave phase shift $\delta_f^J = \delta_0^0$ was already extracted many years ago from πN scattering [78–80], and near the $\pi\pi$ threshold from K_{e4} decays [81]. The kaon decays were later revisited leading to consistent data with very much improved statistics [82,83]. The reported $\pi\pi \rightarrow K\bar{K}$ cross sections [84–87] have large uncertainties. The πN data have been analyzed in combination with high-statistics data (see entries labeled as RVUE for re-analyses of the data). The $2\pi^0$ invariant mass spectra, extracted from $p\bar{p}$ annihilation at rest into $3\pi^0$ [88,89] and into $5\pi^0$ [90] and from central $p\bar{p}$ collision [91] do not show a distinct resonance structure below 900 MeV, but these data sets are consistently described with the standard solution for the $\pi\pi$ scalar isoscalar S -wave extracted from high energy $\pi N \rightarrow \pi\pi N$ data [79,92], which allows for the existence of the broad $f_0(500)$. An enhancement is observed in the $\pi^+\pi^-$ invariant mass near threshold in the decays $D^+ \rightarrow \pi^+\pi^-\pi^+$ [93–95] and $J/\psi(1S) \rightarrow \omega\pi^+\pi^-$ [96,97], and in $\psi(2S) \rightarrow J/\psi(1S)\pi^+\pi^-$ with very limited phase space [98,99].

The precise $f_0(500)$ (or σ) pole is difficult to establish because of its large width. The $\pi\pi$ scattering amplitude shows an unusual energy dependence due to the presence of the Adler zero in the unphysical regime close to the threshold [8,9], required by chiral symmetry. However, most of the analyses listed under $f_0(500)$ agree on a pole position near $(500 - i250)$ MeV. In particular, analyses of $\pi\pi$ data that include unitarity, are consistent with the near threshold $\pi\pi$ data from K_{e4} decays, and the chiral symmetry constraints from Adler zeroes and/or scattering lengths find a light $f_0(500)$, see, *e.g.*, [100,101].

Precise pole positions with an uncertainty of less than 20 MeV (see our table for the T -matrix pole in the Listings) are extracted using the Roy equations, which are twice subtracted dispersion relations derived from crossing symmetry and analyticity. In Ref. [12] the subtraction constants are fixed to the S -wave scattering lengths a_0^0 and a_0^2 derived from matching the Roy equations and two-loop chiral perturbation theory [11]. The only additional relevant input to fix the $f_0(500)$ pole is the $\pi\pi$ -wave phase shift at some higher energy point, chosen as 800 MeV. The analysis is improved further in Ref. [14]. Alternatively, in Ref. [13] Roy equations are used as constraints for a fit to data. In that reference also once-subtracted Roy-like equations, called GKP equations, are used, since the extrapolation into the complex plane based on the twice-subtracted equations leads to larger uncertainties, mainly due to the limited experimental information on the isospin $2\pi\pi$ scattering length. Ref. [102] uses Padé approximants for the analytic continuation. All these extractions find consistent results. Using only analyticity and unitarity to describe data from $K_{2\pi}$ and K_{e4} decays, Ref. [103] finds consistent values for the pole position and the scattering length a_0^0 . The importance of the $\pi\pi$ scattering data for fixing the $f_0(500)$ pole is nicely illustrated by comparing analyses of $p\bar{p} \rightarrow 3\pi^0$ omitting [88,104] or including [89,105] information on $\pi\pi$ scattering: while the former analyses find an extremely broad structure above 1 GeV, the latter find $f_0(500)$ masses of the order of 400 MeV.

From Fig. 64.3 we estimate the range of pole positions for the $f_0(500)$, namely,

$$\sqrt{s_{\text{Pole}}^{\sigma}} = (400 - 550) - i(200 - 350) \text{ MeV} . \quad (64.4)$$

The plot contains the poles from Refs. [40, 51, 53, 55, 56, 69, 71, 78, 89, 95, 98–101, 103, 105–124] as well as the advanced dispersion analyses [11–14, 102]. The extracted $f_0(500)$ pole position is very sensitive to the high accuracy low energy $\pi\pi$ scattering data [82, 83]. In fact, all analyses consistent with this data find poles within the accepted range indicated in the figure. As in case of the $K_0^*(700)$, poles extracted from Breit-Wigner analyses are shown as blue squares. Again we see that those poles have the tendency to appear at higher masses, although here the effect is not as pronounced as in case of the $K_0^*(700)$. One should not take this as an indication that using Breit-Wigners is justified in case of the $f_0(500)$, since $\pi\pi$ phase shifts extracted from Breit-Wigners

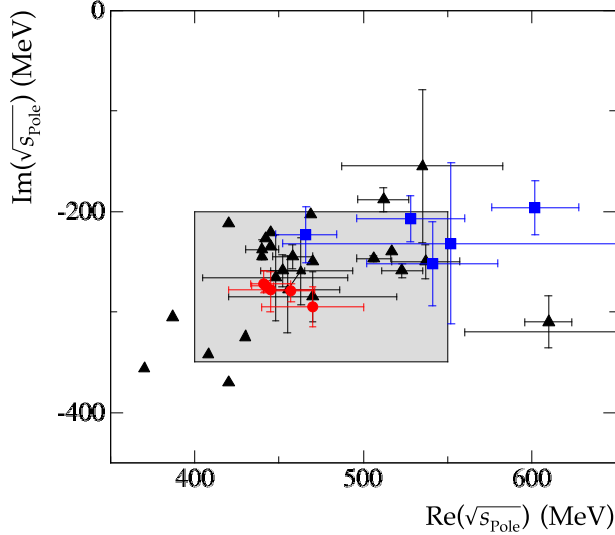


Figure 64.3: Location of the $f_0(500)$ (σ) poles in the complex energy plane. Circles denote the recent analyses based on Roy(-like) dispersion relations, poles extracted from Breit-Wigner fits are shown as blue squares, while all other analyses are denoted by triangles. The corresponding references are given in the *Listings*. The grey box indicates the range of pole locations classified as ‘our estimate’.

are in strong discrepancy with the scattering phase shifts.

If one uses just the most advanced dispersive analyses of Refs. [11–14], shown as solid dots in Fig. 64.3 to determine the pole location of the $f_0(500)$, the range narrows down to [5]

$$\sqrt{s_{\text{Pole}}^{\sigma}} = (449_{-16}^{+22}) - i(275 \pm 12) \text{ MeV}, \quad (64.5)$$

which is labeled as ‘conservative dispersive estimate’ in this reference.

Besides $\pi\pi$, the only other decay channel of the $f_0(500)$ is two photons. Due to the large full width of the $f_0(500)$ an extraction of its two-photon width directly from data is not possible. Thus, the values for $\Gamma(\gamma\gamma)$ quoted in the literature as well as the in *Listings* are based on the expression in the narrow width approximation [125] $\Gamma(\gamma\gamma) \simeq \alpha^2 |g_\gamma|^2 / (4 \text{Re}(\sqrt{s_{\text{Pole}}^{\sigma}}))$, where g_γ is derived from the residue at the $f_0(500)$ pole to two photons and α denotes the electromagnetic fine-structure constant (see also the review on *Resonances* in this issue of the RPP). The explicit form of the expression may vary between different authors due to different definitions of the coupling constant, however, the expression given for $\Gamma(\gamma\gamma)$ is free of ambiguities. According to Refs. [126–129], $\pi\pi$ and $\gamma\gamma$ scattering data sets are consistently described including $f_0(500)$ via the two step process of $\gamma\gamma \rightarrow \pi^+\pi^-$ with pion exchange in the t - and u -channel, followed by a final state interaction $\pi^+\pi^- \rightarrow \pi^0\pi^0$. The same conclusion is drawn in Ref. [130], where the $f_0(500) \rightarrow \gamma\gamma$ decay width is dominated by re-scattering. Therefore, it might be difficult to learn anything new about the nature of the $f_0(500)$ from its $\gamma\gamma$ coupling. For the most recent work on $\gamma\gamma \rightarrow \pi\pi$, see Refs. [56, 71, 103–105, 112–125, 128–133]. There are strong indications (*e.g.*, [134–164]) that the $f_0(500)$ pole cannot be classified as a $q\bar{q}$ state.

64.5 The $f_0(980)$ ($I = 0$)

The $f_0(980)$ couples predominantly to the $\pi\pi$ and $K\bar{K}$ channels and its signal overlaps strongly with the background represented mainly by the $f_0(500)$ and the $f_0(1370)$. This can lead to a dip in the $\pi\pi$ spectrum at the $K\bar{K}$ threshold. It changes from a dip into a peak structure in the $\pi^0\pi^0$ invariant mass spectrum of the reaction $\pi^-p \rightarrow \pi^0\pi^0n$ [138], with increasing four momentum transfer to the $\pi^0\pi^0$ system, which means increasing the $a_1(1260)$ exchange contribution in the amplitude, while the π exchange decreases. Also when a $(u\bar{u} + d\bar{d})$ source is switched to a $s\bar{s}$ source, as it appears when moving from $B_d \rightarrow J/\psi(1S)\pi\pi$ to $B_s \rightarrow J/\psi(1S)\pi\pi$,

the f_0 signal switches from a dip to a peak [152]. The $f_0(500)$ and the $f_0(980)$ are also observed in the data for radiative ϕ decays ($\phi \rightarrow f_0\gamma$) from SND [139,140], CMD2 [141], and KLOE [142,143].

Unitarized chiral perturbation theory is employed to extract the pole of the $f_0(980)$ in Refs. [52,53,55,71,72]. Two different dispersive analyses are used in Ref. [13] to simultaneously pin down the pole parameters of both the $f_0(500)$ and the $f_0(980)$. The poles extracted in Refs. [13,14,55,56,77,108,165,166] are shown in Fig. 64.4, together with the range of pole parameters estimated by us from this compilation, namely,

$$\sqrt{s_{\text{Pole}}^{f_0(980)}} = (980 - 1010) - i(20 - 35) \text{ MeV} \quad (64.6)$$

indicated by the box. A disclaimer is important here: Both the poles of $a_0(980)$ and of $f_0(980)$ are located very close to the kaon thresholds, with the charged and neutral thresholds being 8 MeV apart — to illustrate this point the pertinent thresholds are shown explicitly in Figs. 64.2 and 64.4. This observation leads to the prediction of an enhanced a_0 - f_0 mixing [167–170]. On the other hand, all analyses employed in the pole determinations quoted above are done assuming isospin symmetry. Future studies need to show the impact of isospin violation on the extraction of the $a_0(980)/f_0(980)$ pole parameters.

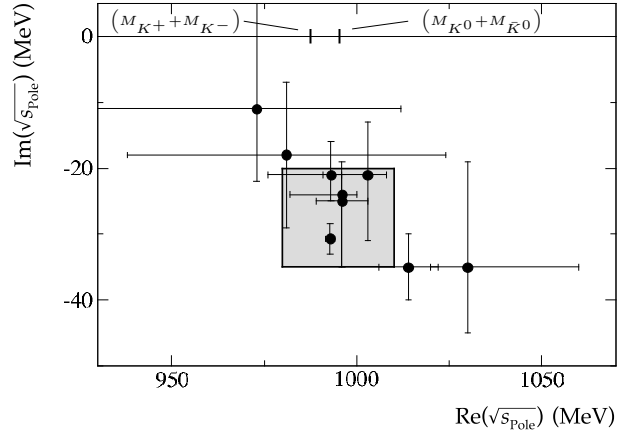


Figure 64.4: Location of the $f_0(980)$ poles from different extractions in the complex energy plane. The corresponding references are given in the *Listings*. Also shown are the thresholds for the K^+K^- and $K^0\bar{K}^0$ channels. The grey box indicates the range of pole locations classified as ‘our estimate’.

Analyses of $\gamma\gamma \rightarrow \pi\pi$ data [144–146] underline the importance of the $K\bar{K}$ coupling of the $f_0(980)$, while the resulting two-photon width of the $f_0(980)$ cannot be determined precisely [147]. The prominent appearance of the $f_0(980)$ in the semileptonic D_s decays and decays of B and B_s mesons implies a dominant ($s\bar{s}$) component: those decays occur via weak transitions that alternatively result in $\phi(1020)$ production. Ratios of decay rates of B and/or B_s mesons into $J/\psi(1S)$ plus $f_0(980)$ or $f_0(500)$ are proposed to extract the flavor mixing angle and to probe the tetraquark nature of those mesons within a certain model [148,149]. The resulting phenomenological fits of the LHCb collaboration [150,151] lead the authors to conclude that their data are incompatible with a model where $f_0(500)$ and $f_0(980)$ are formed from two quarks and two antiquarks (tetraquarks). However, a dispersive analysis of the same data that allows for a model independent inclusion of the hadronic final state interactions in Ref. [152] puts into question the conclusions of Ref. [150]. Moreover, the assumption underlying Ref. [150] that the production dynamics of $f_0(500)$ and $f_0(980)$ are equal such that they cancel in ratios appears to be not justified [5].

64.6 Interpretation of the scalars below 1 GeV

In the literature, many structures are discussed for the light scalar mesons, such as conventional $q\bar{q}$ mesons, compact $(qq)(\bar{q}\bar{q})$ structures (tetraquarks), or meson-meson bound states (hadronic

molecules). In reality, there can be superpositions of these components, and one often depends on models to determine the dominant one. Although we have seen progress in recent years, this question remains open. Here, we mention some of the present conclusions.

The $f_0(980)$ and $a_0(980)$ are often interpreted as compact tetraquark states [161–164, 171] or $K\bar{K}$ bound states [172]. The insight into their internal structure using two-photon widths [140, 173–179] is not conclusive. The $f_0(980)$ appears as a peak structure in D_s decays without $f_0(500)$ background. Based on that observation it is suggested that $f_0(980)$ has a large $s\bar{s}$ component, which according to Ref. [180] is surrounded by a virtual $K\bar{K}$ cloud (see also Ref. [181]). The inclusive production property of the $f_0(980)$ in Z^0 decays is consistent with mesons of other nonets [182]. However, as stated by the authors, the results should be taken as model-dependent measurements while presently no reliable predictions for production rates of non- $q\bar{q}$ states in Z^0 decay are available. Data sets on radiative decays ($\phi \rightarrow f_0\gamma$ and $\phi \rightarrow a_0\gamma$) from SND, CMD2, and KLOE (see above) are consistent with a prominent role of kaon loops. This observation is interpreted as evidence for a compact four-quark structure of the light scalars in Ref. [183], while it is claimed to point at a molecular nature in Ref. [184, 185]. Details of this controversy are given in the comments [186, 187]; see also Ref. [188]. There is now a rather broad consensus that the states $f_0(980)$ and $a_0(980)$, together with the $f_0(500)$ and the $K_0^*(700)$, form a nonet of predominantly four-quark states, where at larger distances the quarks recombine into a pair of pseudoscalar mesons creating a meson cloud (see, *e.g.*, Ref. [189]). Different QCD sum rule studies [190–195] do not agree on a tetraquark configuration for the same particle group.

Models that start directly from chiral Lagrangians, either in non-linear [52, 55, 100, 184] or in linear [196–202] realization, predict the existence of the $f_0(500)$ meson near 500 MeV. Here the $f_0(500)$, $a_0(980)$, $f_0(980)$, and $K_0^*(700)$ (in some models the $K_0^*(1430)$) would form a nonet (not necessarily $q\bar{q}$). In the linear sigma models the lightest pseudoscalars appear as their chiral partners.

In the non-linear approaches of Refs. [52] and [100] the above resonances together with the low mass vector states are generated starting from chiral perturbation theory predictions near the first open channel, and then by shifting the states to the resonance locations, using unitarity and analyticity.

Ref. [196] uses a framework with explicit resonances that are unitarized and coupled to the light pseudoscalars in a chirally invariant way. Evidence for a dominant non- $q\bar{q}$ nature of the lightest scalar resonances is derived from their mixing scheme. In Ref. [197] the scheme is extended and applied to the decay $\eta' \rightarrow \eta\pi\pi$, which leads to the same conclusions. In Ref. [203] the large N_c behavior of the poles is studied to identify the nature of the resonances generated from scattering equations. This leads to the observation that, while the light vector states behave consistent with what is predicted for $q\bar{q}$ states, the light scalars behave very differently. This finding provides strong support for a dominant non- $q\bar{q}$ nature of the light scalar resonances. Note, the more refined study of Ref. [134] which finds, in the case of the $f_0(500)$, indications for a subdominant $q\bar{q}$ component located around 1 GeV in addition to a dominant non- $q\bar{q}$ nature. Additional support for the dominant non- $q\bar{q}$ nature of the $f_0(500)$ is given in Ref. [204], where the connection between the pole of resonances and their Regge trajectories is analyzed. All works including constraints from chiral symmetry at low energies naturally find a light $K_0^*(700)$ below 800 MeV and a $f_0(500)$ below 600 MeV, see, *e.g.*, [50–55]. In these works the $K_0^*(700)$, $f_0(500)$, $f_0(980)$, and $a_0(980)$ appear to form a nonet [51, 54]. Additional evidence for this assignment is presented in Ref. [14], where the couplings of the nine states to $q\bar{q}$ sources are compared. Similar conclusions are reached in Ref. [205] where in the analyzed data the $f_0(980)$ for example appears as a peak structure in $J/\psi(1S) \rightarrow \phi\pi^+\pi^-$ while in $J/\psi(1S) \rightarrow \omega\pi^+\pi^-$ the signal is suppressed. The same low mass scalar nonet is also found earlier in the unitarized quark model of Ref. [111]. A recent phenomenological study based on a $q\bar{q}$ flavor scheme for the light scalars concludes that their glueball

content is ruled out because of low production rates in radiative $J/\psi(1S)$ decays [206].

There are, however, alternative interpretations of the light scalars. For example Ref. [207] (for a more recent, condensed discussion of the idea see Ref. [208]), also builds on chiral symmetry, but expands around an infrared fixed point such that the $f_0(500)$ appears as a QCD dilaton with a mass driven by the QCD scale anomaly. The phenomenology studied in that work appears consistent with this proposal. In Ref. [108, 130, 209, 210] data sets on $\pi\pi - \bar{K}K$ scattering, as well as $\gamma\gamma \rightarrow \pi\pi$, are analysed and the authors conclude that especially the $f_0(500)$ should have a significant gluon content. An extensive analysis on mass, width and decay couplings of the light scalars in a QCD spectral sum rule study [211] leads to ambiguous results for their internal structure. The $f_0(500)$ can equally well have tetraquark, molecular or gluonic content, while the states $f_0(980)$ and $a_0(980)$ can be of molecular or tetraquark nature. A scenario where the $f_0(500)$ and $f_0(980)$ result from quarkonia-gluon mixing is also possible. Note, however, that the large similarities of the features of the κ and the σ meson put into question both a dilaton and a glueball contribution to the latter, since neither of them can be present in the former.

A model independent method to identify hadronic molecules goes back to a proposal by Weinberg [212] (an extension of the formalism to virtual states is provided in Ref. [31]), which is shown to be equivalent to the pole counting arguments of [167–170, 213–218] in Ref. [216]. The formalism allows one to extract the amount of molecular component in the wave function from the effective coupling constant of a physical state to a nearby continuum channel. It can be applied to near threshold states only and provides strong evidence that the $f_0(980)$ is predominantly a $\bar{K}K$ molecule, while the situation turns out to be less clear for the $a_0(980)$ (see also Refs. [177, 179]). This is in line with the findings of Ref. [72], which reports an important role of the $\pi\eta$ channel to the formation of the $a_0(980)$ in addition to the $\bar{K}K$ channel, while the $f_0(980)$ also in this work appears to be predominantly a $\bar{K}K$ molecule. The relevance of both the $\bar{K}K$ and the $\pi\eta$ channels in a dynamically generated $a_0(980)$ is also pointed out in the description of the $\chi_{c1} \rightarrow \eta\pi^+\pi^-$ and $D_s^+ \rightarrow \pi^+\pi^0\eta$ reactions [219, 220]. A recent analysis on the compositeness of the $\pi\pi - K\bar{K}$ and $\pi\eta - K\bar{K}$ channels for the $f_0(980)$ and $a_0(980)$ resonances based on pole values and decay branchings is performed in Ref. [221]. While the $\bar{K}K$ configuration dominates in the $f_0(980)$, the meson-meson components are subdominant in $a_0(980)$. Further insights into $a_0(980)$ and $f_0(980)$ are expected from their mixing [167–170]. A corresponding signal predicted in Refs. [168, 169] is reported by BES III [222]. The importance of the molecular structure of $a_0(980)$, $f_0(980)$ and of their mixing in the reactions $\bar{B}_s^0 \rightarrow J/\psi(1S)\pi^+\pi^-$ and $\bar{B}_s^0 \rightarrow J/\psi(1S)\pi^0\eta$ is pointed out in Ref. [223].

In the unitarized quark model with coupled $q\bar{q}$ and meson-meson channels, the light scalars are interpreted as additional manifestations of bare $q\bar{q}$ confinement states, strongly mass shifted from the 1.3 - 1.5 GeV region and very distorted due to the strong 3P_0 coupling to S -wave two-meson decay channels [218, 224]. Thus, in these models the light scalar nonet comprising the $f_0(500)$, $f_0(980)$, $K_0^*(700)$, and $a_0(980)$, as well as the nonet consisting of the $f_0(1370)$, $f_0(1500)$ (or $f_0(1710)$), $K_0^*(1430)$, and $a_0(1450)$, respectively, are seen as two manifestations of the same bare input states (see also Ref. [225]). It should not remain unmentioned, however, that the heavier nonet lies rather close to the input nonet and that the light scalar one emerges only once the coupling to the two-meson channels is switched on, again highlighting that the meson-meson interaction is indispensable for the light scalars.

Acknowledgement

The authors would like to thank Eberhard Klempt, and Jose Ramon Pelaez for helpful input and discussions in the preparation of the review.

References

- [1] F. E. Close and N. A. Tornqvist, J. Phys. **G28**, R249 (2002), [hep-ph/0204205].
- [2] C. Amsler and N. A. Tornqvist, Phys. Rept. **389**, 61 (2004).

- [3] D. V. Bugg, Phys. Rept. **397**, 257 (2004), [hep-ex/0412045].
- [4] E. Klempt and A. Zaitsev, Phys. Rept. **454**, 1 (2007), [arXiv:0708.4016].
- [5] J. R. Peláez, Phys. Rept. **658**, 1 (2016), [arXiv:1510.00653].
- [6] J. R. Peláez, A. Rodas and J. R. de Elvira, Eur. Phys. J. ST **230**, 6, 1539 (2021), [arXiv:2101.06506].
- [7] S. Gardner and U.-G. Meissner, Phys. Rev. D **65**, 094004 (2002), [hep-ph/0112281].
- [8] S. L. Adler, Phys. Rev. **137**, B1022 (1965), [,140(1964)].
- [9] S. L. Adler, Phys. Rev. **139**, B1638 (1965), [,152(1965)].
- [10] J. A. Oller, Phys. Rev. **D71**, 054030 (2005), [hep-ph/0411105].
- [11] G. Colangelo, J. Gasser and H. Leutwyler, Nucl. Phys. **B603**, 125 (2001), [hep-ph/0103088].
- [12] I. Caprini, G. Colangelo, and H. Leutwyler, Phys. Rev. Lett. **96**, 132001 (2006).
- [13] R. Garcia-Martin *et al.*, Phys. Rev. Lett. **107**, 072001 (2011), [arXiv:1107.1635].
- [14] B. Moussallam, Eur. Phys. J. **C71**, 1814 (2011), [arXiv:1110.6074].
- [15] S. Descotes-Genon and B. Moussallam, Eur. Phys. J. **C 48**, 553 (2006), [hep-ph/0607133].
- [16] J. R. Peláez and A. Rodas, Phys. Rev. Lett. **124**, 17, 172001 (2020), [arXiv:2001.08153].
- [17] M. Luscher, Nucl. Phys. B **354**, 531 (1991).
- [18] S. He, X. Feng and C. Liu, JHEP **07**, 011 (2005), [hep-lat/0504019].
- [19] M. Doring *et al.*, Eur. Phys. J. A **47**, 139 (2011), [arXiv:1107.3988].
- [20] M. Doring *et al.*, Eur. Phys. J. A **47**, 163 (2011), [arXiv:1108.0676].
- [21] M. T. Hansen and S. R. Sharpe, Phys. Rev. D **86**, 016007 (2012), [arXiv:1204.0826].
- [22] P. Guo *et al.*, Phys. Rev. D **88**, 1, 014501 (2013), [arXiv:1211.0929].
- [23] R. A. Briceno and Z. Davoudi, Phys. Rev. D **88**, 9, 094507 (2013), [arXiv:1204.1110].
- [24] J. J. Dudek *et al.* (Hadron Spectrum), Phys. Rev. Lett. **113**, 18, 182001 (2014), [arXiv:1406.4158].
- [25] J. J. Dudek, R. G. Edwards and D. J. Wilson (Hadron Spectrum), Phys. Rev. D **93**, 9, 094506 (2016), [arXiv:1602.05122].
- [26] R. A. Briceno *et al.*, Phys. Rev. Lett. **118**, 2, 022002 (2017), [arXiv:1607.05900].
- [27] R. A. Briceno *et al.*, Phys. Rev. D **97**, 5, 054513 (2018), [arXiv:1708.06667].
- [28] A. Rodas, J. J. Dudek and R. G. Edwards (2023), [arXiv:2304.03762].
- [29] C. Hanhart, J. R. Peláez and G. Rios, Phys. Rev. Lett. **100**, 152001 (2008), [arXiv:0801.2871].
- [30] C. Hanhart, J. R. Peláez and G. Rios, Phys. Lett. B **739**, 375 (2014), [arXiv:1407.7452].
- [31] I. Matuschek *et al.*, Eur. Phys. J. A **57**, 3, 101 (2021), [arXiv:2007.05329].
- [32] M. Ablikim *et al.* (BES), Phys. Lett. **B633**, 681 (2006), [hep-ex/0506055].
- [33] F.-K. Guo *et al.*, Nucl. Phys. **A773**, 78 (2006), [hep-ph/0509050].
- [34] D. Epifanov *et al.* (Belle), Phys. Lett. **B654**, 65 (2007), [arXiv:0706.2231].
- [35] C. Cawfield *et al.* (CLEO), Phys. Rev. **D74**, 031108 (2006), [hep-ex/0606045].
- [36] A. V. Anisovich and A. V. Sarantsev, Phys. Lett. **B413**, 137 (1997), [hep-ph/9705401].
- [37] R. Delbourgo and M. D. Scadron, Int. J. Mod. Phys. **A13**, 657 (1998), [hep-ph/9807504].
- [38] C. M. Shakin and H. Wang, Phys. Rev. **D63**, 014019 (2001).
- [39] M. D. Scadron *et al.*, Nucl. Phys. **A724**, 391 (2003), [hep-ph/0211275].
- [40] D. V. Bugg, Phys. Lett. **B572**, 1 (2003), [Erratum: Phys. Lett. B595,556(2004)].
- [41] M. Ishida, Prog. Theor. Phys. Suppl. **149**, 190 (2003), [hep-ph/0212383].
- [42] H. Q. Zheng *et al.*, Nucl. Phys. **A733**, 235 (2004), [hep-ph/0310293].
- [43] Z. Y. Zhou and H. Q. Zheng, Nucl. Phys. **A775**, 212 (2006), [hep-ph/0603062].
- [44] J. M. Link *et al.* (FOCUS), Phys. Lett. **B653**, 1 (2007), [arXiv:0705.2248].
- [45] B. Aubert *et al.* (BaBar), Phys. Rev. **D76**, 011102 (2007), [arXiv:0704.3593].
- [46] S. Kopp *et al.* (CLEO), Phys. Rev. **D63**, 092001 (2001), [hep-ex/0011065].
- [47] J. M. Link *et al.* (FOCUS), Phys. Lett. **B535**, 43 (2002), [hep-ex/0203031].
- [48] J. M. Link *et al.* (FOCUS), Phys. Lett. **B621**, 72 (2005), [hep-ex/0503043].
- [49] S. N. Cherry and M. R. Pennington, Nucl. Phys. **A688**, 823 (2001), [hep-ph/0005208].
- [50] M. Jamin, J. A. Oller and A. Pich, Nucl. Phys. **B587**, 331 (2000), [hep-ph/0006045].
- [51] D. Black *et al.*, Phys. Rev. **D64**, 014031 (2001), [hep-ph/0012278].
- [52] J. A. Oller, E. Oset and J. R. Peláez, Phys. Rev. **D59**, 074001 (1999), [Erratum: Phys. Rev. D75,099903(2007)], [hep-ph/9804209].
- [53] J. A. Oller and E. Oset, Phys. Rev. **D60**, 074023 (1999), [hep-ph/9809337].
- [54] J. A. Oller, Nucl. Phys. **A727**, 353 (2003), [hep-ph/0306031].
- [55] J. R. Peláez, Mod. Phys. Lett. **A19**, 2879 (2004), [hep-ph/0411107].
- [56] I. Danilkin, O. Deineka and M. Vanderhaeghen, Phys. Rev. D **103**, 11, 114023 (2021), [arXiv:2012.11636].
- [57] J. R. Peláez, A. Rodas and J. Ruiz de Elvira, Eur. Phys. J. **C77**, 2, 91 (2017), [arXiv:1612.07966].
- [58] J. R. Peláez and A. Rodas, Phys. Rept. **969**, 1 (2022), [arXiv:2010.11222].
- [59] A. Abele *et al.*, Phys. Rev. **D57**, 3860 (1998).
- [60] M. Bargiotti *et al.* (OBELIX), Eur. Phys. J. **C26**, 371 (2003).
- [61] D. Barberis *et al.* (WA102), Phys. Lett. **B440**, 225 (1998), [hep-ex/9810003].
- [62] M. J. Corden *et al.*, Nucl. Phys. **B144**, 253 (1978).
- [63] C. Defoix *et al.*, Nucl. Phys. **B44**, 125 (1972).
- [64] Z. Bai *et al.* (MARK-III), Phys. Rev. Lett. **65**, 2507 (1990).
- [65] T. Bolton *et al.*, Phys. Rev. Lett. **69**, 1328 (1992).
- [66] C. Amsler *et al.* (Crystal Barrel), Phys. Lett. **B353**, 571 (1995).
- [67] S. M. Flatte, Phys. Lett. **63B**, 224 (1976).
- [68] C. Amsler *et al.* (Crystal Barrel), Phys. Lett. **B333**, 277 (1994).
- [69] G. Janssen *et al.*, Phys. Rev. **D52**, 2690 (1995), [arXiv:nucl-th/9411021].
- [70] D. V. Bugg, Phys. Rev. **D78**, 074023 (2008), [arXiv:0808.2706].

- [71] J. A. Oller and E. Oset, Nucl. Phys. **A620**, 438 (1997), [Erratum: Nucl. Phys. A652,407(1999)], [hep-ph/9702314].
- [72] H. A. Ahmed and C. W. Xiao, Phys. Rev. D **101**, 9, 094034 (2020), [arXiv:2001.08141].
- [73] C. W. Xiao, U. G. Meißner and J. A. Oller, Eur. Phys. J. A **56**, 1, 23 (2020), [arXiv:1907.09072].
- [74] M. Albaladejo and B. Moussallam, Eur. Phys. J. C **75**, 10, 488 (2015), [arXiv:1507.04526].
- [75] M. Albaladejo *et al.*, JHEP **04**, 010 (2017), [arXiv:1611.03502].
- [76] J. Lu and B. Moussallam, Eur. Phys. J. C **80**, 5, 436 (2020), [arXiv:2002.04441].
- [77] M. Albrecht *et al.* (Crystal Barrel), Eur. Phys. J. C **80**, 5, 453 (2020), [arXiv:1909.07091].
- [78] S. D. Protopopescu *et al.*, Phys. Rev. **D7**, 1279 (1973).
- [79] G. Grayer *et al.*, Nucl. Phys. **B75**, 189 (1974).
- [80] H. Becker *et al.* (CERN-Cracow-Munich), Nucl. Phys. **B151**, 46 (1979).
- [81] L. Rosselet *et al.*, Phys. Rev. **D15**, 574 (1977).
- [82] S. Pislak *et al.* (BNL-E865), Phys. Rev. Lett. **87**, 221801 (2001), [Erratum: Phys. Rev. Lett. 105,019901(2010)], [hep-ex/0106071].
- [83] J. R. Batley *et al.* (NA48-2), Eur. Phys. J. **C70**, 635 (2010).
- [84] W. Wetzel *et al.*, Nucl. Phys. **B115**, 208 (1976).
- [85] V. A. Polychronakos *et al.*, Phys. Rev. **D19**, 1317 (1979).
- [86] D. H. Cohen *et al.*, Phys. Rev. **D22**, 2595 (1980).
- [87] A. Etkin *et al.*, Phys. Rev. **D25**, 1786 (1982).
- [88] C. Amsler *et al.*, Phys. Lett. **B342**, 433 (1995).
- [89] C. Amsler *et al.* (Crystal Barrel), Phys. Lett. **B355**, 425 (1995).
- [90] A. Abele *et al.* (Crystal Barrel), Phys. Lett. **B380**, 453 (1996).
- [91] D.M. Alde *et al.*, Phys. Lett. **B397**, 350 (1997).
- [92] R. Kaminski, L. Lesniak and K. Rybicki, Z. Phys. **C74**, 79 (1997), [hep-ph/9606362].
- [93] E. M. Aitala *et al.* (E791), Phys. Rev. Lett. **86**, 770 (2001), [hep-ex/0007028].
- [94] J. M. Link *et al.* (FOCUS), Phys. Lett. **B585**, 200 (2004), [hep-ex/0312040].
- [95] G. Bonvicini *et al.* (CLEO), Phys. Rev. **D76**, 012001 (2007), [arXiv:0704.3954].
- [96] J. E. Augustin *et al.* (DM2), Nucl. Phys. **B320**, 1 (1989).
- [97] M. Ablikim *et al.* (BES), Phys. Lett. **B598**, 149 (2004), [hep-ex/0406038].
- [98] A. Gallegos, J. L. Lucio M. and J. Pestieau, Phys. Rev. **D69**, 074033 (2004), [hep-ph/0311133].
- [99] M. Ablikim *et al.* (BES), Phys. Lett. **B645**, 19 (2007), [hep-ex/0610023].
- [100] A. Dobado and J. R. Pelaez, Phys. Rev. **D56**, 3057 (1997), [hep-ph/9604416].
- [101] I. Caprini, Phys. Rev. **D77**, 114019 (2008), [arXiv:0804.3504].
- [102] P. Masjuan, J. Ruiz de Elvira, J.J. Sanz-Cillero, Phys. Rev. **D90**, 097901 (2014).
- [103] R. Garcia-Martin, J. R. Pelaez and F. J. Yndurain, Phys. Rev. **D76**, 074034 (2007), [hep-ph/0701025].
- [104] V.V. Anisovich *et al.*, Sov. Phys. Usp. **41**, 419 (1998).
- [105] V. V. Anisovich, Int. J. Mod. Phys. **A21**, 3615 (2006), [hep-ph/0510409].
- [106] M. Ablikim *et al.* (BESIII), Phys. Rev. Lett. **118**, 1, 012001 (2017), [arXiv:1606.03847].
- [107] M. Albaladejo and J. A. Oller, Phys. Rev. D **86**, 034003 (2012), [arXiv:1205.6606].
- [108] G. Mennessier, S. Narison and X. G. Wang, Phys. Lett. B **688**, 59 (2010), [arXiv:1002.1402].
- [109] M. Ablikim *et al.* (BES), Phys. Lett. B **598**, 149 (2004), [hep-ex/0406038].
- [110] P. Estabrooks, Phys. Rev. D **19**, 2678 (1979).
- [111] E. van Beveren *et al.*, Z. Phys. **C30**, 615 (1986), [arXiv:0710.4067].
- [112] B. S. Zou and D. V. Bugg, Phys. Rev. **D48**, R3948 (1993).
- [113] N. A. Tornqvist and M. Roos, Phys. Rev. Lett. **76**, 1575 (1996), [hep-ph/9511210].
- [114] R. Kaminski, L. Lesniak and J. P. Maillet, Phys. Rev. **D50**, 3145 (1994), [hep-ph/9403264].
- [115] N. N. Achasov and G. N. Shestakov, Phys. Rev. **D49**, 5779 (1994).
- [116] M. P. Locher, V. E. Markushin and H. Q. Zheng, Eur. Phys. J. **C4**, 317 (1998), [hep-ph/9705230].
- [117] T. Hannah, Phys. Rev. **D60**, 017502 (1999), [hep-ph/9905236].
- [118] R. Kaminski, L. Lesniak and B. Loiseau, Phys. Lett. **B413**, 130 (1997), [hep-ph/9707377].
- [119] R. Kaminski, L. Lesniak and B. Loiseau, Eur. Phys. J. **C9**, 141 (1999), [hep-ph/9810386].
- [120] M. Ishida *et al.*, Prog. Theor. Phys. **104**, 203 (2000), [hep-ph/0005251].
- [121] Y.S. Surovtsev *et al.*, Phys. Rev. **D61**, 054024 (2001).
- [122] M. Ishida *et al.*, Phys. Lett. **B518**, 47 (2001).
- [123] Z. Y. Zhou *et al.*, JHEP **02**, 043 (2005), [hep-ph/0406271].
- [124] D. V. Bugg, J. Phys. **G34**, 151 (2007), [hep-ph/0608081].
- [125] D. Morgan and M. R. Pennington, Z. Phys. **C48**, 623 (1990).
- [126] J. F. Donoghue, B. R. Holstein and Y. C. Lin, Phys. Rev. D **37**, 2423 (1988).
- [127] A. Dobado and J. R. Pelaez, Z. Phys. C **57**, 501 (1993).
- [128] M. R. Pennington, Phys. Rev. Lett. **97**, 011601 (2006).
- [129] M. R. Pennington, Mod. Phys. Lett. **A22**, 1439 (2007), [arXiv:0705.3314].
- [130] G. Mennessier, S. Narison and W. Ochs, Phys. Lett. **B665**, 205 (2008), [arXiv:0804.4452].
- [131] R. Garcia-Martin and B. Moussallam, Eur. Phys. J. **C70**, 155 (2010), [arXiv:1006.5373].
- [132] M. Hoferichter, D. R. Phillips and C. Schat, Eur. Phys. J. **C71**, 1743 (2011), [arXiv:1106.4147].
- [133] L.-Y. Dai and M. R. Pennington, Phys. Rev. **D90**, 3, 036004 (2014), [arXiv:1404.7524].
- [134] J. R. Pelaez and G. Rios, Phys. Rev. Lett. **97**, 242002 (2006), [hep-ph/0610397].
- [135] H.-X. Chen, A. Hosaka and S.-L. Zhu, Phys. Lett. **B650**, 369 (2007), [hep-ph/0609163].
- [136] F. Giacosa, Phys. Rev. **D75**, 054007 (2007), [hep-ph/0611388].
- [137] L. Maiani *et al.*, Eur. Phys. J. **C50**, 609 (2007), [hep-ph/0604018].
- [138] N. N. Achasov and G. N. Shestakov, Phys. Rev. **D58**, 054011 (1998), [hep-ph/9802286].
- [139] M. N. Achasov *et al.*, Phys. Lett. **B479**, 53 (2000), [hep-ex/0003031].
- [140] M. N. Achasov *et al.*, Phys. Lett. **B485**, 349 (2000), [hep-ex/0005017].
- [141] R. R. Akhmetshin *et al.* (CMD-2), Phys. Lett. **B462**, 371 (1999), [hep-ex/9907005].
- [142] A. Aloisio *et al.* (KLOE), Phys. Lett. **B536**, 209 (2002), [hep-ex/0204012].

- [143] F. Ambrosino *et al.* (KLOE), *Eur. Phys. J.* **C49**, 473 (2007), [hep-ex/0609009].
- [144] M. Boglione and M. R. Pennington, *Eur. Phys. J.* **C9**, 11 (1999), [hep-ph/9812258].
- [145] T. Mori *et al.* (Belle), *Phys. Rev.* **D75**, 051101 (2007), [hep-ex/0610038].
- [146] N. N. Achasov and G. N. Shestakov, *Phys. Rev.* **D77**, 074020 (2008), [arXiv:0712.0885].
- [147] M. R. Pennington *et al.*, *Eur. Phys. J.* **C56**, 1 (2008), [arXiv:0803.3389].
- [148] R. Fleischer, R. Knegjens and G. Ricciardi, *Eur. Phys. J.* **C71**, 1832 (2011), [arXiv:1109.1112].
- [149] S. Stone and L. Zhang, *Phys. Rev. Lett.* **111**, 6, 062001 (2013), [arXiv:1305.6554].
- [150] R. Aaij *et al.* (LHCb), *Phys. Rev.* **D90**, 1, 012003 (2014), [arXiv:1404.5673].
- [151] R. Aaij *et al.* (LHCb), *Phys. Rev.* **D89**, 9, 092006 (2014), [arXiv:1402.6248].
- [152] J. T. Daub, C. Hanhart and B. Kubis, *JHEP* **02**, 009 (2016), [arXiv:1508.06841].
- [153] D. Barberis *et al.* (WA102), *Phys. Lett.* **B462**, 462 (1999), [hep-ex/9907055].
- [154] D. Barberis *et al.* (WA102), *Phys. Lett.* **B479**, 59 (2000), [hep-ex/0003033].
- [155] M. Gaspero, *Nucl. Phys.* **A562**, 407 (1993).
- [156] A. Adamo *et al.*, *Nucl. Phys.* **A558**, 13C (1993).
- [157] C. Amsler *et al.* (Crystal Barrel), *Phys. Lett.* **B322**, 431 (1994).
- [158] A. Abele *et al.* (Crystal Barrel), *Eur. Phys. J.* **C19**, 667 (2001).
- [159] A. Abele *et al.* (CRYSTAL BARREL), *Eur. Phys. J.* **C21**, 261 (2001).
- [160] D. Barberis *et al.* (WA102), *Phys. Lett.* **B471**, 440 (2000), [hep-ex/9912005].
- [161] R. L. Jaffe, *Phys. Rev.* **D15**, 267 (1977).
- [162] M. G. Alford and R. L. Jaffe, *Nucl. Phys.* **B578**, 367 (2000), [hep-lat/0001023].
- [163] L. Maiani *et al.*, *Phys. Rev. Lett.* **93**, 212002 (2004), [hep-ph/0407017].
- [164] L. Maiani, A. D. Polosa and V. Riquer, *Phys. Lett.* **B651**, 129 (2007), [hep-ph/0703272].
- [165] V. V. Anisovich and A. V. Sarantsev, *Int. J. Mod. Phys. A* **24**, 2481 (2009).
- [166] A. V. Sarantsev *et al.*, *Phys. Lett. B* **816**, 136227 (2021), [arXiv:2103.09680].
- [167] N. N. Achasov, S. A. Devyanin and G. N. Shestakov, *Phys. Lett.* **88B**, 367 (1979).
- [168] J.-J. Wu, Q. Zhao and B. S. Zou, *Phys. Rev.* **D75**, 114012 (2007), [arXiv:0704.3652].
- [169] C. Hanhart, B. Kubis and J. R. Pelaez, *Phys. Rev.* **D76**, 074028 (2007), [arXiv:0707.0262].
- [170] L. Roca, *Phys. Rev.* **D88**, 014045 (2013), [arXiv:1210.4742].
- [171] G. 't Hooft *et al.*, *Phys. Lett.* **B662**, 424 (2008), [arXiv:0801.2288].
- [172] J. D. Weinstein and N. Isgur, *Phys. Rev.* **D41**, 2236 (1990).
- [173] T. Barnes, *Phys. Lett.* **165B**, 434 (1985).
- [174] Z. P. Li, F. E. Close and T. Barnes, *Phys. Rev.* **D43**, 2161 (1991).
- [175] R. Delbourgo, D.-s. Liu and M. D. Scadron, *Phys. Lett.* **B446**, 332 (1999), [hep-ph/9811474].
- [176] J. L. Lucio Martinez and M. Napsuciale, *Phys. Lett.* **B454**, 365 (1999), [hep-ph/9903234].
- [177] C. Hanhart *et al.*, *Phys. Rev.* **D75**, 074015 (2007), [hep-ph/0701214].
- [178] R. H. Lemmer, *Phys. Lett.* **B650**, 152 (2007), [hep-ph/0701027].
- [179] T. Branz, T. Gutsche and V. E. Lyubovitskij, *Eur. Phys. J.* **A37**, 303 (2008), [arXiv:0712.0354].
- [180] A. Deandrea *et al.*, *Phys. Lett.* **B502**, 79 (2001), [hep-ph/0012120].
- [181] K. M. Ecklund *et al.* (CLEO), *Phys. Rev.* **D80**, 052009 (2009), [arXiv:0907.3201].
- [182] K. Ackerstaff *et al.* (OPAL), *Eur. Phys. J. C* **4**, 19 (1998), [hep-ex/9802013].
- [183] N. N. Achasov and V. N. Ivanchenko, *Nucl. Phys.* **B315**, 465 (1989).
- [184] J. A. Oller, *Nucl. Phys.* **A714**, 161 (2003), [hep-ph/0205121].
- [185] Yu. S. Kalashnikova *et al.*, *Eur. Phys. J.* **A24**, 437 (2005), [hep-ph/0412340].
- [186] Yu. S. Kalashnikova *et al.*, *Phys. Rev.* **D78**, 058501 (2008), [arXiv:0711.2902].
- [187] N. N. Achasov and A. V. Kiselev, *Phys. Rev.* **D78**, 058502 (2008), [arXiv:0806.2993].
- [188] M. Boglione and M. R. Pennington, *Eur. Phys. J.* **C30**, 503 (2003), [hep-ph/0303200].
- [189] F. Giacosa and G. Pagliara, *Phys. Rev.* **C76**, 065204 (2007), [arXiv:0707.3594].
- [190] S. Narison, *Nucl. Phys. B Proc. Suppl.* **96**, 244 (2001).
- [191] H.-J. Lee, *Eur. Phys. J.* **A30**, 423 (2006), [hep-ph/0512212].
- [192] H.-X. Chen, A. Hosaka and S.-L. Zhu, *Phys. Rev.* **D76**, 094025 (2007), [arXiv:0707.4586].
- [193] J. Sugiyama *et al.*, *Phys. Rev.* **D76**, 114010 (2007), [arXiv:0707.2533].
- [194] T. Kojo and D. Jido, *Phys. Rev.* **D78**, 114005 (2008), [arXiv:0802.2372].
- [195] H.-J. Lee, K. S. Kim and H. Kim, *Phys. Rev. D* **100**, 3, 034021 (2019), [arXiv:1904.12311].
- [196] D. Black *et al.*, *Phys. Rev.* **D59**, 074026 (1999), [hep-ph/9808415].
- [197] A. H. Fariborz *et al.*, *Phys. Rev.* **D90**, 3, 033009 (2014), [arXiv:1407.3870].
- [198] M. D. Scadron, *Eur. Phys. J.* **C6**, 141 (1999), [hep-ph/9710317].
- [199] M. Ishida, *Prog. Theor. Phys.* **101**, 661 (1999), [hep-ph/9902260].
- [200] N. A. Tornqvist, *Eur. Phys. J.* **C11**, 359 (1999), [hep-ph/9905282].
- [201] M. Napsuciale and S. Rodriguez, *Phys. Lett.* **B603**, 195 (2004), [hep-ph/0403072].
- [202] M. Napsuciale and S. Rodriguez, *Phys. Rev.* **D70**, 094043 (2004), [hep-ph/0407037].
- [203] J. R. Pelaez, *Phys. Rev. Lett.* **92**, 102001 (2004), [hep-ph/0309292].
- [204] J. T. Londergan *et al.*, *Phys. Lett.* **B729**, 9 (2014), [arXiv:1311.7552].
- [205] L. Roca *et al.*, *Nucl. Phys. A* **744**, 127 (2004), [hep-ph/0405228].
- [206] E. Klempt, *Phys. Lett. B* **820**, 136512 (2021), [arXiv:2104.09922].
- [207] R. J. Crewther and L. C. Tunstall, *Phys. Rev. D* **91**, 3, 034016 (2015), [arXiv:1312.3319].
- [208] R. J. Crewther, *Universe* **6**, 7, 96 (2020), [arXiv:2003.11259].
- [209] R. Kaminski, G. Mennessier and S. Narison, *Phys. Lett. B* **680**, 148 (2009), [arXiv:0904.2555].

- [210] G. Mennessier, S. Narison and X. G. Wang, Phys. Lett. B **696**, 40 (2011), [arXiv:1009.2773].
- [211] R. Albuquerque, S. Narison and D. Rabietarivony, Nucl. Phys. A **1039**, 122743 (2023), [arXiv:2305.02421].
- [212] S. Weinberg, Phys. Rev. **130**, 776 (1963).
- [213] D. Morgan and M. R. Pennington, Phys. Lett. **B258**, 444 (1991), [Erratum: Phys. Lett.B269,477(1991)].
- [214] D. Morgan, Nucl. Phys. **A543**, 632 (1992).
- [215] N. A. Tornqvist, Phys. Rev. **D51**, 5312 (1995), [hep-ph/9403234].
- [216] V. Baru *et al.*, Phys. Lett. **B586**, 53 (2004), [hep-ph/0308129].
- [217] M. Ablikim *et al.* (BESIII), Phys. Rev. **D83**, 032003 (2011), [arXiv:1012.5131].
- [218] N. A. Tornqvist, Z. Phys. **C68**, 647 (1995), [hep-ph/9504372].
- [219] W.-H. Liang, J.-J. Xie and E. Oset, Eur. Phys. J. C **76**, 12, 700 (2016), [arXiv:1609.03864].
- [220] R. Molina *et al.*, Phys. Lett. B **803**, 135279 (2020), [arXiv:1908.11557].
- [221] Z.-Q. Wang *et al.*, Phys. Rev. D **105**, 7, 074016 (2022), [arXiv:2201.00492].
- [222] M. Ablikim *et al.* (BESIII), Phys. Rev. Lett. **121**, 2, 022001 (2018), [arXiv:1802.00583].
- [223] J.-T. Li *et al.*, Chin. Phys. C **46**, 8, 083108 (2022), [arXiv:2203.13786].
- [224] E. van Beveren and G. Rupp, Eur. Phys. J. **C22**, 493 (2001), [hep-ex/0106077].
- [225] M. Boglione and M. R. Pennington, Phys. Rev. **D65**, 114010 (2002), [hep-ph/0203149].

65. Rare Kaon Decays

Revised August 2023 by L. Littenberg (BNL) and G. Valencia (Monash U.).

65.1 Introduction

There are several useful reviews on rare kaon decays and related topics [1–13]. Activity in rare kaon decays can be divided roughly into four categories:

1. Searches for explicit violations of the Standard Model (SM)
2. The golden modes: $K \rightarrow \pi\nu\bar{\nu}$
3. Other constraints on SM parameters
4. Studies of strong interactions at low energy.

The paradigm of Category 1 is the lepton flavor violating decay $K_L \rightarrow \mu e$. Category 2 includes the two modes that can be calculated with negligible theoretical uncertainty, $K^+ \rightarrow \pi^+\nu\bar{\nu}$ and $K_L \rightarrow \pi^0\nu\bar{\nu}$. These modes can lead to precision determinations of CKM parameters or, in combination with other measurements of these parameters, they can constrain new interactions. They constitute the main focus of the current experimental kaon program. The search for new light particles through the reaction $K \rightarrow \pi X^0$ is a byproduct of these measurements. Category 3 is focused on decays with charged leptons, such as $K_L \rightarrow \pi^0\ell^+\ell^-$ or $K_L \rightarrow \ell^+\ell^-$ where $\ell \equiv e, \mu$. These modes are sensitive to CKM parameters, but they suffer from multiple hadronic uncertainties that can be addressed, at least in part, through a systematic study of the peripheral modes indicated in Fig. 65.1.

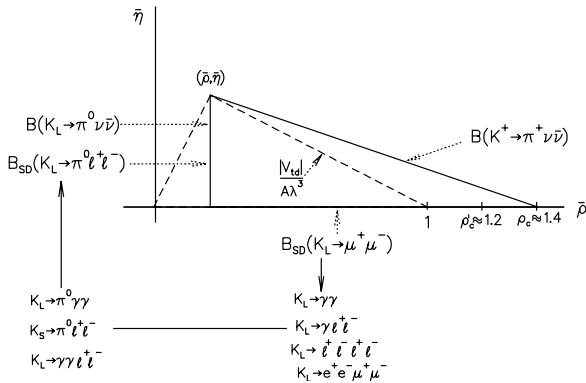


Figure 65.1: Role of rare kaon decays in determining the unitarity triangle. The solid arrows point to auxiliary modes needed to interpret the main results, or potential backgrounds to them.

The interplay between Categories 3-4 and their complementarity to Category 2 is illustrated in the figure. Category 4 includes reactions like $K^+ \rightarrow \pi^+\ell^+\ell^-$ where long distance contributions are dominant and which constitute a testing ground for the ideas of chiral perturbation theory. Other decays in this category are

$$B(K^+ \rightarrow \pi^+\nu\bar{\nu}(\gamma)) = \kappa_+(1 + \Delta_{EM}) \left[\left(\frac{\text{Im}(V_{ts}^* V_{td})}{\lambda^5} X_t \right)^2 + \left(\frac{\text{Re}(V_{cs}^* V_{cd})}{\lambda} P_c + \frac{\text{Re}(V_{ts}^* V_{td})}{\lambda^5} X_t \right)^2 \right]. \quad (65.1)$$

The parameters in Eq. 65.1 incorporate the *a priori* unknown hadronic matrix element in terms of the very well-measured K_{e3} rate [24] in κ_+ ; long distance QED corrections in Δ_{EM} [30]; the Inami-Lim function for the short distance top-quark contribution [31] including NLO QCD corrections [32,33] and the two-loop electroweak correction [29], all in X_t ; and the charm-quark contributions due to short distance effects including NNLO QCD corrections [34,35] and NLO electroweak corrections via P_c [36], which also includes certain long distance terms dubbed $\delta P_{c,u}$ [26,37].

$K_L \rightarrow \pi^0\gamma\gamma$ and $K_L \rightarrow \ell^+\ell^-\gamma$. The former is important in understanding a CP -conserving contribution to $K_L \rightarrow \pi^0\ell^+\ell^-$, whereas the latter could shed light on long distance contributions to $K_L \rightarrow \mu^+\mu^-$.

65.2 Explicit violations of the Standard Model

Much activity has focussed on searches for lepton flavor violation (LFV). This is motivated by the fact that many extensions of the minimal Standard Model violate lepton flavor and by the potential to access very high energy scales. For example, the tree-level exchange of a LFV vector boson of mass M_X that couples to left-handed fermions with electroweak strength and without mixing angles yields $B(K_L \rightarrow \mu e) = 4.7 \times 10^{-12} (148 \text{ TeV}/M_X)^4$ [2]. This simple dimensional analysis may be used to read from Table 65.1 that the reaction $K_L \rightarrow \mu e$ is already probing scales of over 100 TeV. Table 65.1 summarizes the present experimental situation vis-à-vis LFV. The decays $K_L \rightarrow \mu^\pm e^\mp$ and $K^+ \rightarrow \pi^+ e^\mp \mu^\pm$ (or $K_L \rightarrow \pi^0 e^\mp \mu^\pm$) provide complementary information on potential family number violating interactions, since the former is sensitive to parity-odd couplings and the latter is sensitive to parity-even couplings.

Limits on certain lepton-number violating (LNV) kaon decays also have been obtained, with special interest arising from their role in constraining possible extensions of the neutrino sector [14, 15], and we list those in the table as well. Related searches in μ and τ processes are discussed in our section “Tests of Conservation Laws.”

Table 65.1: Searches for lepton flavor and lepton number violation in K decay

LFV mode	90% CL upper limit	Experiment	Yr./Ref.	Type
$K^+ \rightarrow \pi^+ e^- \mu^+$	1.3×10^{-11}	BNL-865	2005/ [16]	LFV
$K^+ \rightarrow \pi^+ e^+ \mu^-$	6.6×10^{-11}	NA62	2021/ [17]	LFV
$K_L \rightarrow \mu e$	4.7×10^{-12}	BNL-871	1998/ [18]	LFV
$K_L \rightarrow \pi^0 e \mu$	7.6×10^{-11}	KTeV	2008/ [19]	LFV
$K_L \rightarrow \pi^0 \pi^0 e \mu$	1.7×10^{-10}	KTeV	2008/ [19]	LFV
$K^+ \rightarrow \pi^- e^+ e^+$	5.3×10^{-11}	NA62	2022/ [20]	LNV
$K^+ \rightarrow \pi^- \pi^0 e^+ e^+$	8.5×10^{-10}	NA62	2022/ [20]	LNV
$K^+ \rightarrow \pi^- \mu^+ \mu^+$	4.2×10^{-11}	NA62	2019/ [21]	LNV
$K_L \rightarrow e^\pm e^\pm \mu^\mp \mu^\mp$	4.12×10^{-11}	KTeV	2003/ [22]	LNV
$K^+ \rightarrow \pi^- \mu^+ e^+$	4.2×10^{-11}	NA62	2021/ [17]	LNV
$K^+ \rightarrow \mu^- \nu e^+ e^+$	8.1×10^{-11}	NA62	2023/ [23]	LNV/LFV

65.3 The golden modes: $K \rightarrow \pi\nu\bar{\nu}$

In the SM, the decay $K^+ \rightarrow \pi^+\nu\bar{\nu}$ is dominated by one-loop diagrams with top-quark intermediate states while long-distance contributions are known to be quite small [24–26]. This permits a precise calculation of this rate in terms of SM parameters. Studies of this process are thus motivated by the possibility of detecting non-SM physics when comparing with the results of global fits [27,28].

The branching ratio can be written in a compact form that exhibits the different ingredients that go into the calculation [29],

An interesting approximate way to cast this result in terms of the CKM parameters λ , V_{cb} , $\bar{\rho}$ and $\bar{\eta}$ (see our Section on “The Cabibbo-Kobayashi-Maskawa mixing matrix”) [9] is:

$$B(K^+ \rightarrow \pi^+\nu\bar{\nu}) \approx 1.6 \times 10^{-5} |V_{cb}|^4 [(\sigma\bar{\eta})^2 + (\rho_c - \bar{\rho})^2] \quad (65.2)$$

where $\rho_c \approx 1.45$ and $\sigma \equiv \frac{1}{(1 - \frac{1}{2}\lambda^2)^2}$. Thus, $B(K^+ \rightarrow \pi^+\nu\bar{\nu})$ determines an ellipse in the $\bar{\rho}$, $\bar{\eta}$ plane with center $(\rho_c, 0)$ and semiaxes $\approx \frac{1}{|V_{cb}|^2} \sqrt{\frac{B(K^+ \rightarrow \pi^+\nu\bar{\nu})}{1.6 \times 10^{-5}}}$ and $\frac{1}{\sigma|V_{cb}|^2} \sqrt{\frac{B(K^+ \rightarrow \pi^+\nu\bar{\nu})}{1.6 \times 10^{-5}}}$.

BNL-787 observed two candidate events [38, 39] in the clean high π^+ momentum and one event [40] in the low-momentum region. The successor experiment BNL-949 observed one more in the high-momentum region [41] and three more in the low-momentum region [42], yielding a branching ratio of $(1.73_{-1.05}^{+1.15}) \times 10^{-10}$ [43].

NA62 was commissioned in 2015 and took data in 2016, 2017 and 2018 and published results from those runs [44]. Twenty candidate events were observed, including an estimated background of 7.03, yielding $B(K^+ \rightarrow \pi^+ \nu \bar{\nu}) = (10.6_{-3.4}^{+4.0})_{\text{stat}} \pm 0.9_{\text{sys}} \times 10^{-11}$. They resumed data taking in 2023 after some upgrades to the detector with the goal of achieving a 20% measurement of the branching ratio by the next long shutdown of the accelerator.

Using the latest CKMfitter input (Jan. 2022) [27], we estimate $B(K^+ \rightarrow \pi^+ \nu \bar{\nu})_{SM} = (8.1 \pm 0.4) \times 10^{-11}$, near the lower end of the measurements of BNL-787/949 and NA62. Current parametric uncertainty in the CKM angles can result in numbers with central values differing from this one by up to 10% [45].

The second golden mode is the neutral counterpart to our preceding discussion: $K_L \rightarrow \pi^0 \nu \bar{\nu}$. It is dominantly CP -violating and free of hadronic uncertainties [24, 46, 47]. In the Standard Model, this mode is dominated by an intermediate top-quark state and does not suffer from the small uncertainty associated with the charm-quark intermediate state that affects $K^+ \rightarrow \pi^+ \nu \bar{\nu}$. The branching ratio is given by [9]:

$$B(K_L \rightarrow \pi^0 \nu \bar{\nu}) = \kappa_L \left(\frac{\text{Im}(V_{ts}^* V_{td})}{\lambda^5} X_t \right)^2 \approx 7.6 \times 10^{-5} |V_{cb}|^4 \eta^2. \quad (65.3)$$

As with the charged mode, the hadronic matrix element can be related to that measured in $K_{\ell 3}$ decay and is parameterized in κ_L .

Our estimate for the branching ratio within the SM, using the latest CKMfitter input (Jan. 2022) [27], is $(2.8 \pm 0.2) \times 10^{-11}$. Similarly to the charged kaon case, parametric uncertainty in the CKM angles can result in a central value that differs from this one by up to almost 20% [45].

Grossman and Nir (GN) [48] pointed out that, in a nearly model-independent manner, the two golden modes satisfy the relation $B(K_L \rightarrow \pi^0 \nu \bar{\nu}) \lesssim 4.3 B(K^+ \rightarrow \pi^+ \nu \bar{\nu})$. Using the BNL 787/949 90% CL bound on $K^+ \rightarrow \pi^+ \nu \bar{\nu}$, GN then predict $B(K_L \rightarrow \pi^0 \nu \bar{\nu}) < 1.46 \times 10^{-9}$. Using instead the latest NA62 result, the GN upper bound becomes $B(K_L \rightarrow \pi^0 \nu \bar{\nu}) < 8.14 \times 10^{-10}$ [13].

The KOTO experiment at J-PARC, whose goal is to make an initial observation of this decay, has been in operation since 2013. It has made a series of data collection runs and has reported on three data sets thus far. In 2018 it published a 90% CL upper limit of 3.0×10^{-9} [49], based on 2015 data. They have run almost every year since, making incremental improvements to the experimental configuration between runs. In 2021 they published a result on the data taken between 2016 and 2018 in which three events were observed in the signal region [50], whereas the expected background was 1.22 events, mainly from charged kaons produced by K_L interactions in the downstream collimator. Conservatively assuming the three events were due to background, they extracted a 90% CL upper limit of 4.9×10^{-9} . Subsequent hardware and analysis improvements reduced the expected background to 0.26 in a sample of similar sensitivity taken in 2021. No events were observed in the signal region and a 90% CL upper limit of 2.0×10^{-9} was established [51]. An increase of 3-5 in sensitivity is anticipated from runs planned in the next three years.

The current theoretical and experimental situation for the golden modes is summarized in Fig. 65.2. The red area corresponds to the 1σ SM prediction with the latest input available from CKMfitter (January 2022) [27]. The yellow region shows the result established by the combined BNL-787 and BNL-949 results, whereas the green region marks the new NA62 result for $K^+ \rightarrow \pi^+ \nu \bar{\nu}$. The black shaded region marks the GN exclusion, which lies significantly above the SM expectation leaving a large window for discovery of new physics contributions by experiments seeking to measure $B(K_L \rightarrow \pi^0 \nu \bar{\nu})$. The 90% CL upper

bound on this mode from the KOTO result published in 2018 [49] is shown as a dashed orange line, and is seen to still lie in the GN excluded zone.

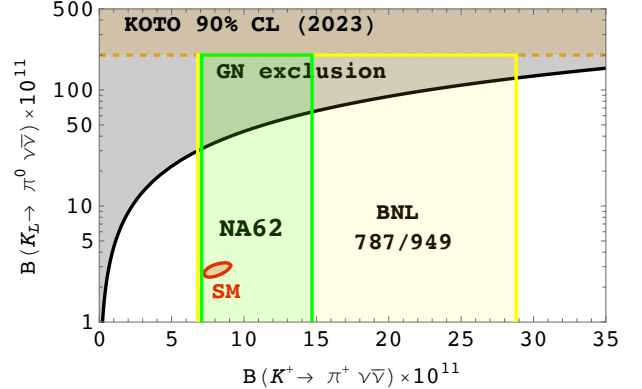


Figure 65.2: Summary of current situation for the golden modes $K \rightarrow \pi \nu \bar{\nu}$. The red ellipse shows the 1σ SM prediction with input from CKMfitter; the green (yellow) region corresponds to the NA62 (BNL787/949) 1σ measurement; and the dashed orange line marks the 90% CL KOTO upper bound. The black shaded region shows the GN exclusion.

Much theoretical work has explored beyond the SM scenarios that can populate this window as well as their correlations with other rare processes outside kaon physics. Although it would be relatively straightforward to establish the existence of new physics by observing deviations from their SM values in the $K \rightarrow \pi \nu \bar{\nu}$ modes, it would take much more extensive global fits to pinpoint the origin of any such deviation. Partial summaries with references focusing on quark flavor physics can be found in Refs. [9, 52–56]. Different possibilities emphasizing an interpretation of these modes as $K \rightarrow \pi + E_{\text{miss}}$ can be found in Refs. [57–59].

There is a subtlety in converting the GN bound extracted from measurements of $K^+ \rightarrow \pi^+ \nu \bar{\nu}$ into an upper bound for $K_L \rightarrow \pi^0 \nu \bar{\nu}$ as applied to KOTO [60]. This is due to a lack of sensitivity of the charged kaon experiments to a kinematic window near the pion mass. New physics appearing through a two body mode $K^+ \rightarrow \pi^+ X^0$, for an invisible X^0 with mass near the pion mass, has a much weaker constraint. The situation is illustrated in Fig. 65.3 which shows the BNL787/949 [43] and NA62 [61] 90% c.l. limits on $K^+ \rightarrow \pi^+ X^0$ as a function of m_{X^0} assuming X^0 is stable. The implied GN bound for $K_L \rightarrow \pi^0 X^0$, $B(K_L \rightarrow \pi^0 X^0) \lesssim 4.3 B(K^+ \rightarrow \pi^+ X^0)$ is shown as a blue line and can be compared with the actual KOTO [49] constraint on $K_L \rightarrow \pi^0 X^0$ in red. Notice that the upper bound derived from NA62 is lower than that derived from BNL787/949 except for a small mass window. For $120 \lesssim m_{X^0} \lesssim 150$ MeV, KOTO already has better sensitivity than that implied by the GN bound in this case. The possibility of new physics in this scenario has generated much theoretical speculation [62–72].

The search for a new light particle X^0 in $K^+ \rightarrow \pi^+ X^0$ has a long tradition covering both long-lived particles (*e.g.*, hyperphoton, axion, familon, *etc.*), and short-lived ones that decay to muon, electron, photon or neutrino pairs. The longstanding 90% CL upper limit on $K^+ \rightarrow \pi^+ X^0$ from BNL787/949 7.3×10^{-11} [41] for the case of massless X^0 has been slightly improved by NA62 to 5×10^{-11} as can be read from Fig. 65.3. These limits can also be reinterpreted in connection with a dark photon [73] or dark Z [74], and in this context NA48/2 also constrained the mode $B(K^\pm \rightarrow \pi^\pm A' \rightarrow \pi^\pm e^+ e^-)$ [75]. Complementary searches for new light particles in kaon experiments use modes with two pions and include the KTeV bound $B(K_L \rightarrow \pi^0 \pi^0 X^0 \rightarrow \pi^0 \pi^0 \mu^+ \mu^-) < 1 \times 10^{-10}$ [76] and the E391a bound $B(K_L \rightarrow \pi^0 \pi^0 X^0 \rightarrow \pi^0 \pi^0 \gamma \gamma) < 2.4 \times 10^{-7}$ [77].

Neutrino pair modes with one extra pion, $K \rightarrow \pi \pi \nu \bar{\nu}$, are similarly dominated by short distance contributions in the SM [78–80]. Even though they are theoretically clean, they occur with very

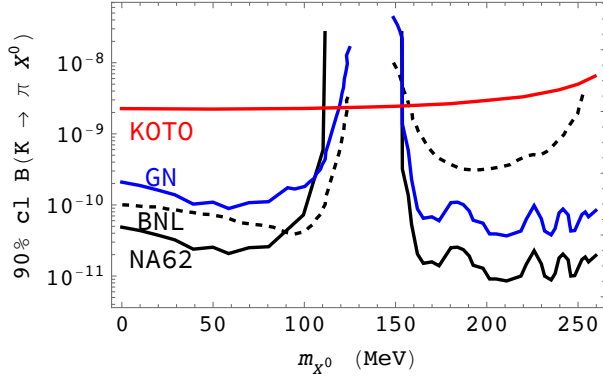


Figure 65.3: Summary of current situation for $K \rightarrow \pi X^0$. The solid (dashed) black line shows the exclusion limit for $K^+ \rightarrow \pi^+ X^0$ from NA62 (BNL787/949) assuming X^0 is stable. The blue line marks the constraint implied for $K_L \rightarrow \pi^0 X^0$ by the Grossman-Nir relation and the red line marks the current KOTO limit on $K^+ \rightarrow \pi^+ X^0$.

low rates with branching ratios of order 10^{-13} . The current best bound comes from KEK-391a, $B(K_L \rightarrow \pi^0 \pi^0 \nu \bar{\nu}) < 8.1 \times 10^{-7}$ at 90% CL [81]. There is also a bound for the charged kaon mode $B(K^+ \rightarrow \pi^+ \pi^0 \nu \bar{\nu}) < 4.3 \times 10^{-5}$ at 90% CL [82] from BNL-787. New physics contributions to these modes are discussed in [83].

65.4 Other constraints on Standard Model parameters

The decay $K_L \rightarrow \mu^+ \mu^-$ has a short distance contribution sensitive to the CKM parameter $\bar{\rho}$, given by [5]:

$$B_{SD}(K_L \rightarrow \mu^+ \mu^-) \approx 2.7 \times 10^{-4} |V_{cb}|^4 (\rho'_c - \bar{\rho})^2 \quad (65.4)$$

$$B_{CPV} \approx \left[15.7 |a_S|^2 \pm 1.4 \left(\frac{|V_{cb}|^2 \bar{\eta}}{10^{-4}} \right) |a_S| + 0.12 \left(\frac{|V_{cb}|^2 \bar{\eta}}{10^{-4}} \right)^2 \right] \times 10^{-12} \quad (65.5)$$

where the three terms correspond to the indirect CP violation, the interference, and the direct CP violation, respectively. The parameter a_S has been extracted by NA48/1 from a measurement of $K_S \rightarrow \pi^0 e^+ e^-$ with the result $|a_S| = 1.06^{+0.26}_{-0.21} \pm 0.07$ [99], as well as from a measurement of $K_S \rightarrow \pi^0 \mu^+ \mu^-$ with the result $|a_S| = 1.54^{+0.40}_{-0.32} \pm 0.06$ [100]. With current constraints on the CKM parameters, and assuming a positive sign for the interference term [98, 101], this implies that $B_{CPV}(K_L \rightarrow \pi^0 e^+ e^-) \approx (3.1 \pm 0.9) \times 10^{-11}$, where the three contributions to the central value from indirect, interference and direct CP violation are $(1.76, 0.9, 0.45) \times 10^{-11}$ respectively. It should be noted that more recent studies suggest a much larger uncertainty in the value of a_S [102].

$K_L \rightarrow \pi^0 e^+ e^-$ also has a CP -conserving component dominated by a two-photon intermediate state. This component can be decomposed into an absorptive and a dispersive part. The absorptive part can be extracted from the measurement of the low $m_{\gamma\gamma}$ region of the $K_L \rightarrow \pi^0 \gamma\gamma$ spectrum. The rate and the shape of the distribution $d\Gamma/dm_{\gamma\gamma}$ in $K_L \rightarrow \pi^0 \gamma\gamma$ are well described in chiral perturbation theory in terms of three (*a priori*) unknown parameters [103–106].

Both KTeV and NA48 have studied the mode $K_L \rightarrow \pi^0 \gamma\gamma$, reporting similar results. KTeV finds $B(K_L \rightarrow \pi^0 \gamma\gamma) = (1.29 \pm 0.03_{\text{stat}} \pm 0.05_{\text{sys}}) \times 10^{-6}$ [107], while NA48 finds $B(K_L \rightarrow \pi^0 \gamma\gamma) = (1.36 \pm 0.03_{\text{stat}} \pm 0.03_{\text{sys}} \pm 0.03_{\text{norm}}) \times 10^{-6}$ [108]. Both experiments are consistent with a negligible rate in the low $m_{\gamma\gamma}$ region, suggesting a very small CP -conserving component $B_{CP}(K_L \rightarrow \pi^0 e^+ e^-) \sim \mathcal{O}(10^{-13})$ [98, 106, 108]. There remains some model dependence in the estimate of the dispersive part of the CP -conserving $K_L \rightarrow \pi^0 e^+ e^-$ [98].

where ρ'_c depends on the charm quark mass and is approximately 1.2. This decay, however, is dominated by a long-distance contribution from a two-photon intermediate state. The absorptive (imaginary) part of the long-distance component is determined by the measured rate for $K_L \rightarrow \gamma\gamma$ to be $B_{\text{abs}}(K_L \rightarrow \mu^+ \mu^-) = (6.64 \pm 0.07) \times 10^{-9}$; and it almost completely saturates the observed rate $B(K_L \rightarrow \mu^+ \mu^-) = (6.84 \pm 0.11) \times 10^{-9}$ [84]. The difference between the observed rate and the absorptive component can be attributed to the (coherent) sum of the short-distance amplitude and the real part of the long-distance amplitude. The latter cannot be derived directly from experiment [85], but can be estimated with certain assumptions [86, 87].

By contrast, the decay $K_L \rightarrow e^+ e^-$ is completely dominated by long distance physics and is easier to estimate. The result, $B(K_L \rightarrow e^+ e^-) \sim 9 \times 10^{-12}$ [85, 88], is in good agreement with the BNL-871 measurement, $(8.7^{+5.7}_{-4.1}) \times 10^{-12}$ [89].

The mode $K_S \rightarrow \mu^+ \mu^-$ has a short distance contribution proportional to the square of the CKM parameter $\bar{\eta}$ entering at the 10^{-13} level [10]. It also has long distance contributions arising from the two photon intermediate state which result in a rate $B(K_S \rightarrow \mu^+ \mu^-)_{LD} = 5.1 \times 10^{-12}$ [10]. There is a 90% CL limit $B(K_S \rightarrow \mu^+ \mu^-) < 2.1 \times 10^{-10}$ from LHCb [90, 91]. The interplay between $K_L \rightarrow \mu^+ \mu^-$ and $K_S \rightarrow \mu^+ \mu^-$ has been the subject of [92, 93], and it has been pointed out that a measurement of time-dependent interference effects could be used to extract information on CKM angles from $K \rightarrow \mu^+ \mu^-$ measurements [94, 95].

The decay $K_L \rightarrow \pi^0 e^+ e^-$ is sensitive to the CKM parameter η through its CP -violating component. There are both direct and indirect CP -violating amplitudes that can interfere. The direct CP -violating amplitude is short distance dominated and has been calculated in detail within the SM [5]. The indirect CP -violating amplitude can be inferred from a measurement of $K_S \rightarrow \pi^0 e^+ e^-$. The complete CP -violating contribution to the rate can be written as [96–98]:

The related process, $K_L \rightarrow \pi^0 \gamma e^+ e^-$, is potentially an additional background to $K_L \rightarrow \pi^0 e^+ e^-$ in some region of phase space [109]. This process has been observed with a branching ratio of $(1.62 \pm 0.14_{\text{stat}} \pm 0.09_{\text{sys}}) \times 10^{-8}$ [110].

The decay $K_L \rightarrow \gamma\gamma e^+ e^-$ constitutes the dominant background to $K_L \rightarrow \pi^0 e^+ e^-$. It was first observed by BNL-845 [111], and subsequently confirmed with a much larger sample by KTeV [112]. It has been estimated that this background will enter at about the 10^{-10} level [113, 114], comparable to or larger than the signal level. Because of this, the observation of $K_L \rightarrow \pi^0 e^+ e^-$ at the SM level will depend on background subtraction with good statistics. Possible alternative strategies are discussed in [98] and references cited therein.

The 90% CL upper bound for the process $K_L \rightarrow \pi^0 e^+ e^-$ is 2.8×10^{-10} [114]. For the closely related muonic process, the published upper bound is $B(K_L \rightarrow \pi^0 \mu^+ \mu^-) < 3.8 \times 10^{-10}$ [115], compared with the SM prediction of $(1.9 \pm 0.5) \times 10^{-11}$. The latter assumes positive interference between the direct- and indirect- CP violating components and includes a CP -conserving component which contributes about 30% of the total [10, 116].

A study of $K_L \rightarrow \pi^0 \mu^+ \mu^-$ has indicated that it might be possible to extract the direct CP -violating contribution by a joint study of the Dalitz plot variables and the components of the μ^+ polarization [117]. The latter tends to be quite substantial so that large statistics may not be necessary.

Combined information from $K_L \rightarrow \pi^0 \ell^+ \ell^-$ as well as $K_L \rightarrow \mu^+ \mu^-$ complements the $K \rightarrow \pi \nu \bar{\nu}$ measurements in constraining physics beyond the SM [118].

65.5 Other long distance dominated modes

The rates and spectra for the decays $K^+ \rightarrow \pi^+ \ell^+ \ell^-$ ($\ell = e$ or μ) have been measured [119–124] and are successfully described with a parameterization inspired by chiral perturbation theory but with large corrections beyond leading order [96, 97] (see [102, 125] for a review). The most recent NA62 result shows good agreement between the electron and muon mode form factors [126]. NA62 has also obtained a first measurement of the forward-backward asymmetry in the muon mode [126].

The mode $K^+ \rightarrow \pi^+ \pi^0 e^+ e^-$, analyzed by NA48/2 [127], is also dominated by long distance physics but it has been argued that measuring asymmetries can provide information on the short distance components [128]. The current status of these modes is discussed in [129]. Contributions to $K^+ \rightarrow \pi^+ e^+ e^- e^+ e^-$ beyond the double Dalitz decay in $K^+ \rightarrow \pi^+ \pi^0$ are considered in [130], and have been measured by NA62 [131].

The decay $K^+ \rightarrow \pi^+ \gamma \gamma$ can be predicted in terms of one unknown parameter to leading order in χ PT, dubbed \hat{c} , resulting in a correlation between the rate and the diphoton mass spectrum [132]. Certain important corrections at the next order are also known [133]. The rate and spectrum were first measured by E787 [134], followed by NA48/2 [135] and NA62 [136]. The most recent measurement from NA62 [137], based on a sample of over 4000 events, finds $B(K^+ \rightarrow \pi^+ \gamma \gamma) = (9.73 \pm 0.17 \pm 0.08) \times 10^{-7}$ and a precise value for \hat{c} .

Much information has been recorded by KTeV and NA48 on the rates and spectrum for the Dalitz pair conversion modes $K_L \rightarrow \ell^+ \ell^- \gamma$ [138, 139], and $K_L \rightarrow \ell^+ \ell^- \ell'^+ \ell'^-$ for $\ell, \ell' = e$ or μ [22, 140]. LHCb has recently placed limits on $K_{L,S} \rightarrow \mu^+ \mu^- \mu^+ \mu^-$ [141]. All these results are used to test hadronic models and should eventually help unravel the underlying physics in $K_L \rightarrow \mu^+ \mu^-$ [87, 92, 142].

References

- [1] L. Littenberg and G. Valencia, *Ann. Rev. Nucl. Part. Sci.* **43**, 729 (1993), [hep-ph/9303225].
- [2] J. L. Ritchie and S. G. Wojcicki, *Rev. Mod. Phys.* **65**, 1149 (1993).
- [3] B. Winstein and L. Wolfenstein, *Rev. Mod. Phys.* **65**, 1113 (1993).
- [4] A. Pich, *Rept. Prog. Phys.* **58**, 563 (1995), [hep-ph/9502366].
- [5] G. Buchalla, A. J. Buras and M. E. Lautenbacher, *Rev. Mod. Phys.* **68**, 1125 (1996), [hep-ph/9512380].
- [6] G. D'Ambrosio and G. Isidori, *Int. J. Mod. Phys. A* **13**, 1 (1998), [hep-ph/9611284].
- [7] P. Buchholz and B. Renk, *Prog. Part. Nucl. Phys.* **39**, 253 (1997).
- [8] A. R. Barker and S. H. Kettell, *Ann. Rev. Nucl. Part. Sci.* **50**, 249 (2000), [hep-ex/0009024].
- [9] A. J. Buras, F. Schwab and S. Uhlig, *Rev. Mod. Phys.* **80**, 965 (2008), [hep-ph/0405132].
- [10] V. Cirigliano *et al.*, *Rev. Mod. Phys.* **84**, 399 (2012), [arXiv:1107.6001].
- [11] D. Bryman *et al.*, *Ann. Rev. Nucl. Part. Sci.* **61**, 331 (2011).
- [12] T. K. Komatsubara, *Prog. Part. Nucl. Phys.* **67**, 995 (2012), [arXiv:1203.6437].
- [13] A. Ceccucci, *Annual Review of Nuclear and Particle Science* **71**, 1 (2021), URL <https://doi.org/10.1146/annurev-nucl-102419-054905>.
- [14] A. Atre *et al.*, *JHEP* **05**, 030 (2009), [arXiv:0901.3589].
- [15] L. S. Littenberg and R. Shrock, *Phys. Lett.* **B491**, 285 (2000), [hep-ph/0005285].
- [16] A. Sher *et al.*, *Phys. Rev.* **D72**, 012005 (2005), [hep-ex/0502020].
- [17] E. Cortina Gil *et al.* (NA62), *Phys. Rev. Lett.* **127**, 13, 131802 (2021), [arXiv:2105.06759].
- [18] D. Ambrose *et al.* (BNL), *Phys. Rev. Lett.* **81**, 5734 (1998), [hep-ex/9811038].
- [19] E. Abouzaid *et al.* (KTeV), *Phys. Rev. Lett.* **100**, 131803 (2008), [arXiv:0711.3472].
- [20] E. Cortina Gil *et al.* (NA62), *Phys. Lett. B* **830**, 137172 (2022), [arXiv:2202.00331].
- [21] E. Cortina Gil *et al.* (NA62), *Phys. Lett.* **B797**, 134794 (2019), [arXiv:1905.07770].
- [22] A. Alavi-Harati *et al.* (KTeV), *Phys. Rev. Lett.* **90**, 141801 (2003), [hep-ex/0212002].
- [23] E. Cortina Gil *et al.* (NA62), *Phys. Lett. B* **838**, 137679 (2023), [arXiv:2211.04818].
- [24] J. S. Hagelin and L. S. Littenberg, *Prog. Part. Nucl. Phys.* **23**, 1 (1989).
- [25] M. Lu and M. B. Wise, *Phys. Lett.* **B324**, 461 (1994), [hep-ph/9401204].
- [26] A. F. Falk, A. Lewandowski and A. A. Petrov, *Phys. Lett.* **B505**, 107 (2001), [hep-ph/0012099].
- [27] J. Charles *et al.*, *Phys. Rev.* **D84**, 033005 (2011), [arXiv:1106.4041].
- [28] M. Bona *et al.* (UTfit), *JHEP* **03**, 049 (2008), [arXiv:0707.0636].
- [29] J. Brod, M. Gorbahn and E. Stamou, *Phys. Rev.* **D83**, 034030 (2011), [arXiv:1009.0947].
- [30] F. Mescia and C. Smith, *Phys. Rev.* **D76**, 034017 (2007), [arXiv:0705.2025].
- [31] T. Inami and C. S. Lim, *Prog. Theor. Phys.* **65**, 297 (1981), [Erratum: *Prog. Theor. Phys.* **65**, 1772 (1981)].
- [32] G. Buchalla and A. J. Buras, *Nucl. Phys.* **B548**, 309 (1999), [hep-ph/9901288].
- [33] M. Misiak and J. Urban, *Phys. Lett.* **B451**, 161 (1999), [hep-ph/9901278].
- [34] A. J. Buras *et al.*, *Phys. Rev. Lett.* **95**, 261805 (2005), [hep-ph/0508165].
- [35] A. J. Buras *et al.*, *JHEP* **11**, 002 (2006), [Erratum: *JHEP* **11**, 167 (2012)], [hep-ph/0603079].
- [36] J. Brod and M. Gorbahn, *Phys. Rev.* **D78**, 034006 (2008), [arXiv:0805.4119].
- [37] G. Isidori, F. Mescia and C. Smith, *Nucl. Phys.* **B718**, 319 (2005), [hep-ph/0503107].
- [38] S. Adler *et al.* (E787), *Phys. Rev. Lett.* **88**, 041803 (2002), [hep-ex/0111091].
- [39] S. Adler *et al.* (E787), *Phys. Rev. Lett.* **84**, 3768 (2000), [hep-ex/0002015].
- [40] S. S. Adler *et al.* (E787), *Phys. Lett.* **B537**, 211 (2002), [hep-ex/0201037].
- [41] V. V. Anisimovskiy *et al.* (E949), *Phys. Rev. Lett.* **93**, 031801 (2004), [hep-ex/0403036].
- [42] A. V. Artamonov *et al.* (E949), *Phys. Rev. Lett.* **101**, 191802 (2008), [arXiv:0808.2459].
- [43] A. V. Artamonov *et al.* (BNL-E949), *Phys. Rev.* **D79**, 092004 (2009), [arXiv:0903.0030].
- [44] E. Cortina Gil *et al.* (NA62), *JHEP* **06**, 093 (2021), [arXiv:2103.15389].
- [45] A. J. Buras *et al.*, *JHEP* **11**, 033 (2015), [arXiv:1503.02693].
- [46] L. S. Littenberg, *Phys. Rev.* **D39**, 3322 (1989).
- [47] G. Buchalla and G. Isidori, *Phys. Lett.* **B440**, 170 (1998), [hep-ph/9806501].
- [48] Y. Grossman and Y. Nir, *Phys. Lett.* **B398**, 163 (1997), [hep-ph/9701313].
- [49] J. K. Ahn *et al.* (KOTO), *Phys. Rev. Lett.* **122**, 021802 (2019), [arXiv:1810.09655].
- [50] J. K. Ahn *et al.* (KOTO), *Phys. Rev. Lett.* **126**, 121801 (2021), [arXiv:2012.07571].

- [51] K. Shiomi, “Latest results on the $K_L \rightarrow \pi^0 \nu \bar{\nu}$ search at the J-PARC KOTO experiment,” (2023), KOTO seminar at KEK Sept. 6, 2023.
- [52] G. D’Ambrosio and G. Isidori, Phys. Lett. **B530**, 108 (2002), [hep-ph/0112135].
- [53] D. Bryman *et al.*, Int. J. Mod. Phys. **A21**, 487 (2006), [hep-ph/0505171].
- [54] A. J. Buras, D. Buttazzo and R. Knegjens, JHEP **11**, 166 (2015), [arXiv:1507.08672].
- [55] X.-G. He, G. Valencia and K. Wong, Eur. Phys. J. **C78**, 472 (2018), [arXiv:1804.07449].
- [56] J. Aebischer, A. J. Buras and J. Kumar, JHEP **12**, 097 (2020), [arXiv:2006.01138].
- [57] M. Bordone *et al.*, Eur. Phys. J. **C77**, 618 (2017), [arXiv:1705.10729].
- [58] X.-G. He, J. Tandean and G. Valencia, Phys. Lett. **B797**, 134842 (2019), [arXiv:1904.04043].
- [59] F. F. Deppisch, K. Fridell and J. Harz, JHEP **12**, 186 (2020), [arXiv:2009.04494].
- [60] K. Fuyuto, W.-S. Hou and M. Kohda, Phys. Rev. Lett. **114**, 171802 (2015), [arXiv:1412.4397].
- [61] E. Cortina Gil *et al.* (NA62), JHEP **03**, 058 (2021), [arXiv:2011.11329].
- [62] T. Kitahara *et al.*, Phys. Rev. Lett. **124**, 071801 (2020), [arXiv:1909.11111].
- [63] D. Egana-Ugrinovic, S. Homiller and P. Meade, Phys. Rev. Lett. **124**, 191801 (2020), [arXiv:1911.10203].
- [64] P. S. B. Dev, R. N. Mohapatra and Y. Zhang, Phys. Rev. D **101**, 075014 (2020), [arXiv:1911.12334].
- [65] M. Fabbrichesi and E. Gabrielli, Eur. Phys. J. C **80**, 532 (2020), [arXiv:1911.03755].
- [66] Y. Liao *et al.*, Phys. Rev. D **102**, 055005 (2020), [arXiv:2005.00753].
- [67] R. Ziegler, J. Zupan and R. Zwicky, JHEP **07**, 229 (2020), [arXiv:2005.00451].
- [68] T. Li, X.-D. Ma and M. A. Schmidt, Phys. Rev. D **101**, 055019 (2020), [arXiv:1912.10433].
- [69] X.-G. He *et al.*, JHEP **08**, 034 (2020), [arXiv:2005.02942].
- [70] M. Hostert, K. Kaneta and M. Pospelov, Phys. Rev. D **102**, 055016 (2020), [arXiv:2005.07102].
- [71] S. Gori, G. Perez and K. Tobioka, JHEP **08**, 110 (2020), [arXiv:2005.05170].
- [72] T. B. de Melo *et al.*, Phys. Rev. D **103**, 115001 (2021), [arXiv:2102.06262].
- [73] M. Pospelov, Phys. Rev. **D80**, 095002 (2009), [arXiv:0811.1030].
- [74] H. Davoudiasl, H.-S. Lee and W. J. Marciano, Phys. Rev. **D89**, 095006 (2014), [arXiv:1402.3620].
- [75] J. R. Batley *et al.* (NA48/2), Phys. Lett. **B746**, 178 (2015), [arXiv:1504.00607].
- [76] E. Abouzaid *et al.* (KTeV), Phys. Rev. Lett. **107**, 201803 (2011), [arXiv:1105.4800].
- [77] Y. C. Tung *et al.* (E391a), Phys. Rev. Lett. **102**, 051802 (2009), [arXiv:0810.4222].
- [78] L. S. Littenberg and G. Valencia, Phys. Lett. **B385**, 379 (1996), [hep-ph/9512413].
- [79] C.-W. Chiang and F. J. Gilman, Phys. Rev. **D62**, 094026 (2000), [hep-ph/0007063].
- [80] C. Q. Geng, I. J. Hsu and Y. C. Lin, Phys. Rev. **D50**, 5744 (1994), [hep-ph/9406313].
- [81] R. Ogata *et al.* (E391a), Phys. Rev. **D84**, 052009 (2011), [arXiv:1106.3404].
- [82] S. Adler *et al.* (E787), Phys. Rev. **D63**, 032004 (2001), [hep-ex/0009055].
- [83] C.-Q. Geng and J. Tandean, Phys. Rev. D **102**, 115021 (2020), [arXiv:2009.00608].
- [84] D. Ambrose *et al.* (E871), Phys. Rev. Lett. **84**, 1389 (2000).
- [85] G. Valencia, Nucl. Phys. **B517**, 339 (1998), [hep-ph/9711377].
- [86] G. D’Ambrosio, G. Isidori and J. Portoles, Phys. Lett. **B423**, 385 (1998), [hep-ph/9708326].
- [87] G. Isidori and R. Unterdorfer, JHEP **01**, 009 (2004), [hep-ph/0311084].
- [88] D. Gomez Dumm and A. Pich, Phys. Rev. Lett. **80**, 4633 (1998), [hep-ph/9801298].
- [89] D. Ambrose *et al.* (BNL E871), Phys. Rev. Lett. **81**, 4309 (1998), [hep-ex/9810007].
- [90] R. Aaij *et al.* (LHCb), Eur. Phys. J. **C77**, 678 (2017), [arXiv:1706.00758].
- [91] R. Aaij *et al.* (LHCb), Phys. Rev. Lett. **125**, 231801 (2020), [arXiv:2001.10354].
- [92] G. D’Ambrosio and T. Kitahara, Phys. Rev. Lett. **119**, 201802 (2017), [arXiv:1707.06999].
- [93] V. Chobanova *et al.*, JHEP **05**, 024 (2018), [arXiv:1711.11030].
- [94] A. Dery *et al.*, JHEP **07**, 103 (2021), [arXiv:2104.06427].
- [95] A. Dery *et al.*, JHEP **03**, 014 (2023), [arXiv:2211.03804].
- [96] G. D’Ambrosio *et al.*, JHEP **08**, 004 (1998), [hep-ph/9808289].
- [97] C. Dib, I. Dunietz and F. J. Gilman, Phys. Rev. **D39**, 2639 (1989).
- [98] G. Buchalla, G. D’Ambrosio and G. Isidori, Nucl. Phys. **B672**, 387 (2003), [hep-ph/0308008].
- [99] J. R. Batley *et al.* (NA48/1), Phys. Lett. **B576**, 43 (2003), [hep-ex/0309075].
- [100] J. R. Batley *et al.* (NA48/1), Phys. Lett. **B599**, 197 (2004), [hep-ex/0409011].
- [101] S. Friot, D. Greynat and E. De Rafael, Phys. Lett. **B595**, 301 (2004), [hep-ph/0404136].
- [102] G. D’Ambrosio, D. Greynat and M. Knecht, JHEP **02**, 049 (2019), [arXiv:1812.00735].
- [103] G. Ecker, A. Pich and E. de Rafael, Phys. Lett. **B237**, 481 (1990).
- [104] L. Cappiello, G. D’Ambrosio and M. Miragliuolo, Phys. Lett. **B298**, 423 (1993).
- [105] A. G. Cohen, G. Ecker and A. Pich, Phys. Lett. **B304**, 347 (1993).
- [106] F. Gabbiani and G. Valencia, Phys. Rev. **D66**, 074006 (2002), [hep-ph/0207189].
- [107] E. Abouzaid *et al.* (KTeV), Phys. Rev. **D77**, 112004 (2008), [arXiv:0805.0031].
- [108] A. Lai *et al.* (NA48), Phys. Lett. **B536**, 229 (2002), [hep-ex/0205010].
- [109] J. F. Donoghue and F. Gabbiani, Phys. Rev. **D56**, 1605 (1997), [hep-ph/9702278].
- [110] E. Abouzaid *et al.* (KTeV), Phys. Rev. **D76**, 052001 (2007), [arXiv:0706.4074].
- [111] W. M. Morse *et al.*, Phys. Rev. **D45**, 36 (1992).
- [112] A. Alavi-Harati *et al.* (KTeV), Phys. Rev. **D64**, 012003 (2001), [hep-ex/0010059].
- [113] H. B. Greenlee, Phys. Rev. **D42**, 3724 (1990).
- [114] A. Alavi-Harati *et al.* (KTeV), Phys. Rev. Lett. **93**, 021805 (2004), [hep-ex/0309072].
- [115] A. Alavi-Harati *et al.* (KTeV), Phys. Rev. Lett. **84**, 5279 (2000), [hep-ex/0001006].
- [116] G. Isidori, C. Smith and R. Unterdorfer, Eur. Phys. J. **C36**, 57 (2004), [hep-ph/0404127].

- [117] M. V. Diwan, H. Ma and T. L. Trueman, Phys. Rev. **D65**, 054020 (2002), [hep-ph/0112350].
- [118] F. Mescia, C. Smith and S. Trine, JHEP **08**, 088 (2006), [hep-ph/0606081].
- [119] R. Appel *et al.* (E865), Phys. Rev. Lett. **83**, 4482 (1999), [hep-ex/9907045].
- [120] J. R. Batley *et al.* (NA48/2), Phys. Lett. **B677**, 246 (2009), [arXiv:0903.3130].
- [121] S. Adler *et al.* (E787), Phys. Rev. Lett. **79**, 4756 (1997), [hep-ex/9708012].
- [122] H. Ma *et al.* (e865), Phys. Rev. Lett. **84**, 2580 (2000), [hep-ex/9910047].
- [123] H. K. Park *et al.* (HyperCP), Phys. Rev. Lett. **88**, 111801 (2002), [hep-ex/01110033].
- [124] J. R. Batley *et al.* (NA48/2), Phys. Lett. **B697**, 107 (2011), [arXiv:1011.4817].
- [125] G. D'Ambrosio, D. Greynat and M. Knecht, Phys. Lett. B **797**, 134891 (2019), [arXiv:1906.03046].
- [126] E. Cortina Gil *et al.* (NA62), JHEP **11**, 011 (2022), [Addendum: JHEP 06, 040 (2023)], [arXiv:2209.05076].
- [127] J. R. Batley *et al.* (NA48/2), Phys. Lett. **B788**, 552 (2019), [arXiv:1809.02873].
- [128] L. Cappiello *et al.*, Eur. Phys. J. **C72**, 1872 (2012), [Erratum: Eur. Phys. J. **C72**, 2208 (2012)], [arXiv:1112.5184].
- [129] L. Cappiello, O. Catà and G. D'Ambrosio, Eur. Phys. J. **C78**, 265 (2018), [arXiv:1712.10270].
- [130] T. Husek, Phys. Rev. D **106**, 7, L071301 (2022), [arXiv:2207.02234].
- [131] E. Cortina Gil *et al.* (NA62) (2023), [arXiv:2307.04579].
- [132] G. Ecker, A. Pich and E. de Rafael, Nucl. Phys. **B303**, 665 (1988).
- [133] G. D'Ambrosio and J. Portoles, Phys. Lett. **B386**, 403 (1996), [Erratum: Phys. Lett. **B395**, 389 (1997)], [hep-ph/9606213].
- [134] P. Kitching *et al.* (E787), Phys. Rev. Lett. **79**, 4079 (1997), [hep-ex/9708011].
- [135] J. R. Batley *et al.* (NA48/2), Phys. Lett. **B730**, 141 (2014), [arXiv:1310.5499].
- [136] C. Lazzeroni *et al.* (NA62), Phys. Lett. **B732**, 65 (2014), [arXiv:1402.4334].
- [137] A. S. for NA62, "Study of the rare decay $K^+ \rightarrow \pi^+ \gamma \gamma$ at the NA62 experiment," (2022), international Conference on kaon physics KAON2022, URL <https://conference-indico.kek.jp/event/169/contributions/3462/>.
- [138] A. Alavi-Harati *et al.* (KTeV), Phys. Rev. Lett. **87**, 071801 (2001).
- [139] E. Abouzaid *et al.* (KTeV), Phys. Rev. Lett. **99**, 051804 (2007), [hep-ex/0702039].
- [140] V. Fanti *et al.* (NA48), Phys. Lett. **B458**, 553 (1999).
- [141] D. M. et. al. (LHCb) (2022), [arXiv:2212.04977].
- [142] G. D'Ambrosio, D. Greynat and G. Vulvert, Eur. Phys. J. **C73**, 2678 (2013), [arXiv:1309.5736].

66. CPT Invariance Tests in Neutral Kaon Decay

Revised August 2023 by M. Antonelli (INFN, Frascati), G. D'Ambrosio (INFN, Napoli) and M.S. Sozzi (Pisa U.).

CPT theorem is based on three assumptions: quantum field theory, locality, and Lorentz invariance, and thus it is a fundamental probe of our basic understanding of particle physics. Strangeness oscillation in $K^0 - \bar{K}^0$ system, described by the equation

$$i \frac{d}{dt} \begin{bmatrix} K^0 \\ \bar{K}^0 \end{bmatrix} = [M - i\Gamma/2] \begin{bmatrix} K^0 \\ \bar{K}^0 \end{bmatrix},$$

where M and Γ are hermitian matrices (see PDG review [1], references [2,3], and KLOE paper [4] for notations and previous literature), allows a very accurate test of *CPT* symmetry; indeed since *CPT* requires $M_{11} = M_{22}$ and $\Gamma_{11} = \Gamma_{22}$, the mass and width eigenstates, $K_{S,L}$, have a *CPT*-violating piece, δ , in addition to the usual *CPT*-conserving parameter ϵ :

$$K_{S,L} = \frac{1}{\sqrt{2(1+|\epsilon_{S,L}|^2)}} \left[(1 + \epsilon_{S,L}) K^0 \pm (1 - \epsilon_{S,L}) \bar{K}^0 \right]$$

$$\epsilon_{S,L} = \frac{-i\Im(M_{12}) - \frac{1}{2}\Im(\Gamma_{12}) \mp \frac{1}{2} [M_{11} - M_{22} - \frac{i}{2}(\Gamma_{11} - \Gamma_{22})]}{m_L - m_S + i(\Gamma_S - \Gamma_L)/2}$$

$$\equiv \epsilon \pm \delta. \quad (66.1)$$

Using the phase convention $\Im(\Gamma_{12}) = 0$, we determine the phase of ϵ to be $\varphi_{SW} \equiv \arctan \frac{2(m_L - m_S)}{\Gamma_S - \Gamma_L}$. Imposing unitarity to an arbitrary combination of K^0 and \bar{K}^0 wave functions, we obtain the Bell-Steinberger relation [5] connecting *CP* and *CPT* violation in the mass matrix to *CP* and *CPT* violation in the decay; in fact, neglecting $\mathcal{O}(\epsilon)$ corrections to the coefficient of the *CPT*-violating parameter, δ , we can write [4]

$$\left[\frac{\Gamma_S + \Gamma_L}{\Gamma_S - \Gamma_L} + i \tan \varphi_{SW} \right] \left[\frac{\Re(\epsilon)}{1 + |\epsilon|^2} - i\Im(\delta) \right] = \frac{1}{\Gamma_S - \Gamma_L} \sum_f A_L(f) A_S^*(f), \quad (66.2)$$

where $A_{L,S}(f) \equiv A(K_{L,S} \rightarrow f)$. We stress that this relation is phase-convention-independent. The advantage of the neutral kaon system is that only a few decay modes give significant contributions to the r.h.s. in Eq. (66.2); in fact, defining for the hadronic modes

$$\alpha_i \equiv \frac{1}{\Gamma_S} \langle A_L(i) A_S^*(i) \rangle = \eta_i \mathcal{B}(K_S \rightarrow i),$$

$$i = \pi^0 \pi^0, \pi^+ \pi^- (\gamma), 3\pi^0, \pi^0 \pi^+ \pi^- (\gamma), \quad (66.3)$$

the recent data from CPLEAR, KLOE, KTeV, and NA48 have led to the following determinations (the analysis described in Ref. [4] has been updated by using the recent measurements of K_L branching ratios from KTeV [6, 7], NA48 [8, 9], the results described in the *CP* violation in K_L decays minireview, and the KLOE result [10])

$$\alpha_{\pi^+ \pi^-} = ((1.121 \pm 0.010) + i(1.061 \pm 0.010)) \times 10^{-3},$$

$$\alpha_{\pi^0 \pi^0} = ((0.493 \pm 0.005) + i(0.471 \pm 0.005)) \times 10^{-3},$$

$$\alpha_{\pi^+ \pi^- \pi^0} = ((0 \pm 2) + i(0 \pm 2)) \times 10^{-6},$$

$$|\alpha_{\pi^0 \pi^0 \pi^0}| < 1.5 \times 10^{-6} \text{ at } 95\% \text{ CL.} \quad (66.4)$$

The semileptonic contribution to the right-handed side of Eq. (66.2) requires the determination of several observables: we

define [2,3]

$$\begin{aligned} \mathcal{A}(K^0 \rightarrow \pi^- l^+ \nu) &= \mathcal{A}_0(1 - y), \\ \mathcal{A}(K^0 \rightarrow \pi^+ l^- \nu) &= \mathcal{A}_0^*(1 + y^*)(x_+ - x_-)^*, \\ \mathcal{A}(\bar{K}^0 \rightarrow \pi^+ l^- \nu) &= \mathcal{A}_0^*(1 + y^*), \\ \mathcal{A}(\bar{K}^0 \rightarrow \pi^- l^+ \nu) &= \mathcal{A}_0(1 - y)(x_+ + x_-), \end{aligned} \quad (66.5)$$

where x_+ (x_-) describes the violation of the $\Delta S = \Delta Q$ rule in *CPT*-conserving (violating) decay amplitudes, and y parameterizes *CPT* violation for $\Delta S = \Delta Q$ transitions. Taking advantage of their tagged $K^0(\bar{K}^0)$ beams, CPLEAR has measured $\Im(x_+)$, $\Re(x_-)$, $\Im(\delta)$, and $\Re(\delta)$ [11]. These determinations have been improved in Ref. [4] by including the information $A_S - A_L = 4[\Re(\delta) + \Re(x_-)]$ (valid at first order in the small parameters), where $A_{L,S}$ are the K_L and K_S semileptonic charge asymmetries, respectively, from the PDG [12] and the new KLOE semileptonic measurement [13]. Here we are also including the *T*-violating asymmetry measurement from CPLEAR [14] with a finer binning than appearing in the published article.

Table 66.1: Values, errors, and correlation coefficients for $\Re(\delta)$, $\Im(\delta)$, $\Re(x_-)$, $\Im(x_+)$, and $A_S + A_L$ obtained from a combined fit, including KLOE [4,13] and CPLEAR [14].

	value	Correlations coefficients			
$\Re(\delta)$	$(4.3 \pm 2.7) \times 10^{-4}$	1			
$\Im(\delta)$	$(-0.9 \pm 0.6) \times 10^{-2}$	-0.40	1		
$\Re(x_-)$	$(-0.22 \pm 0.10) \times 10^{-2}$	-0.14	-0.30	1	
$\Im(x_+)$	$(0.06 \pm 0.19) \times 10^{-2}$	-0.12	-0.02	0.34	1
$A_S + A_L$	$(-0.23 \pm 0.38) \times 10^{-2}$	-0.12	-0.29	0.94	0.18 1

The value $A_S + A_L$ in Table 66.1 can be directly included in the semileptonic contributions to the Bell Steinberger relations in Eq. (66.2)

$$\begin{aligned} & \sum_{\pi l \nu} \langle A_L(\pi l \nu) A_S^*(\pi l \nu) \rangle \\ &= 2\Gamma(K_L \rightarrow \pi l \nu) (\Re(\epsilon) - \Re(y) - i(\Im(x_+) + \Im(\delta))) \\ &= 2\Gamma(K_L \rightarrow \pi l \nu) ((A_S + A_L)/4 - i(\Im(x_+) + \Im(\delta))). \end{aligned} \quad (66.6)$$

Defining

$$\alpha_{\pi l \nu} \equiv \frac{1}{\Gamma_S} \sum_{\pi l \nu} \langle A_L(\pi l \nu) A_S^*(\pi l \nu) \rangle + 2i \frac{\tau_{K_S}}{\tau_{K_L}} \mathcal{B}(K_L \rightarrow \pi l \nu) \Im(\delta), \quad (66.7)$$

we find:

$$\alpha_{\pi l \nu} = ((-0.1 \pm 0.2) + i(-0.1 \pm 0.5)) \times 10^{-5}. \quad (66.8)$$

Table 66.2: Summary of results: values, errors, and correlation coefficients for $\Re(\epsilon)$, $\Im(\delta)$, $\Re(\delta)$, and $\Re(x_-)$.

	value	Correlations coefficients			
$\Re(\epsilon)$	$(161.2 \pm 0.5) \times 10^{-5}$	+1			
$\Im(\delta)$	$(-0.3 \pm 1.4) \times 10^{-5}$	+0.08	1		
$\Re(\delta)$	$(2.6 \pm 2.5) \times 10^{-4}$	+0.00	-0.05	1	
$\Re(x_-)$	$(-2.7 \pm 1.0) \times 10^{-3}$	+0.05	0.13	-0.30	1

The analysis of semileptonic decay asymmetries implicitly assumes Lepton Flavour Universality (LFU) of any effect violating *CPT* or $\Delta S = \Delta Q$, through the use of a single set of x, y parameters, consistently with the availability of experimental information on A_S for the electron mode only. The explicit LFU assumption in the input BR measurements has been lifted exploiting the measurement of $BR(K_S \rightarrow \pi \mu \nu)$ Ref. [15], with no effect on the numerical results.

Inserting the values of the α parameters into Eq. (66.2), we find

$$\begin{aligned}\Re(\epsilon) &= (161.2 \pm 0.5) \times 10^{-5}, \\ \Im(\delta) &= (-0.3 \pm 1.4) \times 10^{-5}.\end{aligned}\quad (66.9)$$

The complete information on Eq. (66.9) is given in Table 66.2.

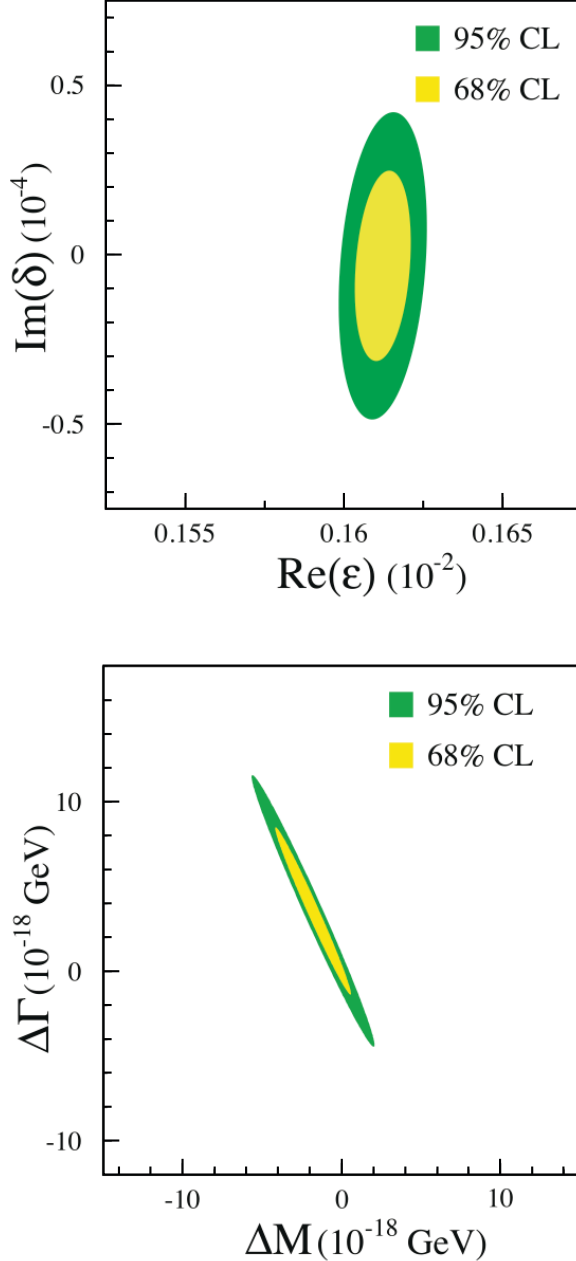


Figure 66.1: Top: allowed region at 68% and 95% C.L. in the $\Re(\epsilon)$, $\Im(\delta)$ plane. Bottom: allowed region at 68% and 95% C.L. in the ΔM , $\Delta \Gamma$ plane.

Now the agreement with *CPT* conservation, $\Im(\delta) = \Re(\delta) = \Re(x_-) = 0$, is at 18% C.L.

The allowed region in the $\Re(\epsilon) - \Im(\delta)$ plane at 68% CL and 95% C.L. is shown in the top panel of Fig. 66.1.

The process giving the largest contribution to the size of the allowed region is $K_L \rightarrow \pi^+ \pi^-$, through the uncertainty on ϕ_{+-} .

The limits on $\Im(\delta)$ and $\Re(\delta)$ can be used to constrain the $K^0 - \bar{K}^0$ mass and width difference

$$\delta = \frac{i(m_{K^0} - m_{\bar{K}^0}) + \frac{1}{2}(\Gamma_{K^0} - \Gamma_{\bar{K}^0})}{\Gamma_S - \Gamma_L} \cos \phi_{SW} e^{i\phi_{SW}} [1 + \mathcal{O}(\epsilon)].$$

The allowed region in the $\Delta M = (m_{K^0} - m_{\bar{K}^0})$, $\Delta \Gamma = (\Gamma_{K^0} - \Gamma_{\bar{K}^0})$ plane is shown in the bottom panel of Fig. 66.1. As a result, we improve on the previous limits (see for instance, P. Bloch in Ref. [12]) and in the limit $\Gamma_{K^0} - \Gamma_{\bar{K}^0} = 0$ we obtain

$$-4.0 \times 10^{-19} \text{ GeV} < m_{K^0} - m_{\bar{K}^0} < 4.0 \times 10^{-19} \text{ GeV} \quad \text{at 95 \% C.L.}$$

References

- [1] See the “*CP* Violation in Meson Decays,” in this *Review*.
- [2] L. Maiani, “*CP* And *CPT* Violation in Neutral Kaon Decays,” L. Maiani, G. Pancheri, and N. Paver, *The Second DAΦNE Physics Handbook*, Vol. 1,2.
- [3] G. D’Ambrosio, G. Isidori and A. Pugliese, in “2nd DAΦNE Physics Handbook:63-96,” 63–96 (1994), [hep-ph/9411389], URL <http://preprints.cern.ch/cgi-bin/setlink?base=preprint&categ=cern&id=th-7504-94>.
- [4] G. D’Ambrosio and G. Isidori (KLOE), *JHEP* **12**, 011 (2006), [hep-ex/0610034].
- [5] J. S. Bell and J. Steinberger, in “Wolfenstein, L. (ed.): *CP* violation, 42-57. (In Oxford International Symposium Conference on Elementary Particles),” 195–208, 221–222 (1966), (See Book Index).
- [6] T. Alexopoulos *et al.* (KTeV), *Phys. Rev.* **D70**, 092006 (2004), [hep-ex/0406002].
- [7] E. Abouzaid *et al.* (KTeV), *Phys. Rev.* **D83**, 092001 (2011), [arXiv:1011.0127].
- [8] A. Lai *et al.* (NA48), *Phys. Lett.* **B645**, 26 (2007), [hep-ex/0611052]; A. Lai *et al.* (NA48), *Phys. Lett.* **B602**, 41 (2004), [hep-ex/0410059].
- [9] We thank G. Isidori and M. Palutan for their contribution to the original analysis [4] performed with KLOE data.
- [10] D. Babusci *et al.* (KLOE), *Phys. Lett.* **B723**, 54 (2013), [arXiv:1301.7623].
- [11] A. Angelopoulos *et al.* (CPLEAR), *Phys. Lett.* **B444**, 52 (1998).
- [12] W. M. Yao *et al.* (Particle Data Group), *J. Phys.* **G33**, 1 (2006).
- [13] A. Anastasi *et al.* (KLOE-2), *JHEP* **09**, 021 (2018), [arXiv:1806.08654].
- [14] P. Bloch, M. Fidecaro, private communication of the data in a finer binning format; A. Angelopoulos *et al.* (CPLEAR), *Phys. Lett.* **B444**, 43 (1998).
- [15] D. Babusci *et al.* (KLOE-2), *Phys. Lett. B* **804**, 135378 (2020), [arXiv:1912.05990].

67. V_{ud} , V_{us} the Cabibbo Angle, and CKM Unitarity

Revised March 2024 by E. Blucher (Chicago U.), G. D'Ambrosio (INFN, Napoli) and W.J. Marciano (BNL).

The Cabibbo-Kobayashi-Maskawa (CKM) [1, 2] three-generation quark mixing matrix written in terms of the Wolfenstein parameters (λ, A, ρ, η) [3] nicely illustrates the orthonormality constraint of unitarity, as well as the central role played by λ .

$$V_{\text{CKM}} = \begin{pmatrix} V_{ud} & V_{us} & V_{ub} \\ V_{cd} & V_{cs} & V_{cb} \\ V_{td} & V_{ts} & V_{tb} \end{pmatrix} = \begin{pmatrix} 1 - \lambda^2/2 & \lambda & A\lambda^3(\rho - i\eta) \\ -\lambda & 1 - \lambda^2/2 & A\lambda^2 \\ A\lambda^3(1 - \rho - i\eta) & -A\lambda^2 & 1 \end{pmatrix} + \mathcal{O}(\lambda^4). \quad (67.1)$$

That cornerstone parameter is a carryover from the two-generation Cabibbo angle, $\lambda = \sin(\theta_{\text{Cabibbo}}) = V_{us}$. Its value is an important component in tests of CKM unitarity.

Up until 2003, the precise value of λ was controversial, with kaon decays (specifically $K \rightarrow \pi e \nu$) branching fractions suggesting [4] $\lambda \simeq 0.220$, while indirect determinations via V_{ud} obtained from nuclear β -decays combined with unitarity preferred a somewhat larger $\lambda \simeq 0.225 - 0.230$. This difference implied a 2 - 2.5 sigma deviation from the first row unitarity requirement

$$|V_{ud}|^2 + |V_{us}|^2 + |V_{ub}|^2 = 1, \quad (67.2)$$

a possible hint [5, 6] of new physics effects. Below, we describe the current status of V_{ud} and V_{us} , and their implication for the unitarity test in Eq. (67.2). (Since $|V_{ub}|^2 \simeq 1.7 \times 10^{-5}$ is negligibly small, it is ignored in this discussion.) Eq. (67.2) is currently the most stringent test of unitarity in the CKM matrix. As we shall see, it is again showing signs of a possible 2 to 3 sigma inconsistency.

67.1 V_{ud}

Precise values of V_{ud} have been obtained from superallowed nuclear, neutron, and pion beta decays. Currently, the best determination of V_{ud} comes from analysis of a set of 15 precisely measured superallowed nuclear beta-decays [5, 6] ($0^+ \rightarrow 0^+$ transitions). Measuring their half-lives, t , and Q values gives the decay rate factors, f , which lead to a precise determination of V_{ud} via [7–12]. Based on several decades of dedicated studies, Hardy and Towner recently updated the average of the half-life, $\overline{\mathcal{F}t}$, [6]

$$|V_{ud}|^2 = \frac{K}{2G_F^2(1 + \Delta_R^V)\overline{\mathcal{F}t}} = \frac{2912.95 \pm 0.54}{\overline{\mathcal{F}t}} = 0.94815 \pm 0.00060 \quad \text{for } \Delta_R^V = 2.454(19)\%, \quad (67.3)$$

where $K/(\hbar c)^6 = 2\pi^3 \hbar \ln 2 / (m_e c^2)^5 = 8120.27648(26) \times 10^{-10} \text{GeV}^{-4} \text{s}$, Δ_R^V denotes the so-called inner or universal electroweak radiative corrections (RC) to superallowed nuclear beta decays. A dispersion relation (DR) calculational approach [13] to quantum loop corrections, specifically the gamma-W box diagram, gives $\Delta_R^V = 0.02467(22)$. Actually the authors of Ref. [14] have combined the different theoretical calculations leading to $\Delta_R^V = 0.02467(27)$ and

$$V_{ud} = 0.97367(11)_{\text{exp}}(13)_{\Delta_R^V}(27)_{\text{NS}}(32)_{\text{total}} \text{ (superallowed)}. \quad (67.4)$$

As a result of its small uncertainty and more rigorous theoretical footing, we use this value below. A somewhat different approach [15] found $\Delta_R^V = 0.02426(32)$. These recent values are roughly consistent. Both are larger than the 2018 PDG value of 0.02361(38). Implications and possible nuclear physics modifications of those studies are still under scrutiny [16, 17]. Note that an additional uncertainty $(54)_{\text{NS}}$ from nuclear structure (NS) [17] has been recently included [6] in that master formula. This recent determination of V_{ud} has shifted significantly down compared to the 2018 PDG value of 0.97420(21). In addition, NS uncertainties are now the dominant contribution to the overall uncertainty.

Taken at face value, along with current V_{us} determinations (see subsection 67.2), the reduced V_{ud} would seem to violate the first row unitarity requirement, and thus suggest the presence of deviations from unitarity or unaccounted uncertainties.

Measurements of the neutron lifetime, τ_n , and the ratio of axial-vector/vector couplings, $g_A \equiv G_A/G_V$, via neutron decay asymmetries combined with the inner radiative corrections can also be used to determine V_{ud} via the precise formula [14, 18]

$$|V_{ud}|^2 = \frac{5024.7 \text{ s}}{\tau_n(1 + 3g_A)(1 + \Delta_R)}, \quad (67.5)$$

where $\Delta_R = 0.03983(27)$ represents radiative corrections [14]. We present the V_{ud} results using either the the current published world averages [19] or the best measured values for λ [20] and for τ_n [21]. The average leads to

$$\begin{aligned} \tau_n^{\text{ave}} &= 879.4(6) \text{ s} \quad (1.6 \text{ PDG scale factor}) \\ g_A^{\text{ave}} &= 1.2756(13), \quad (2.6 \text{ PDG scale factor}), \end{aligned} \quad (67.6)$$

$$|V_{ud}^{n,PDG}| = 0.97441(28)_{\tau_n}(82)_{\lambda}(13)_{\Delta_R}(88)_{\text{TOT}}, \quad (67.7)$$

while the best values lead to

$$|V_{ud}^{n,best}| = 0.97413(20)_{\tau_n}(35)_{\lambda}(13)_{\Delta_R}(42)_{\text{TOT}}. \quad (67.8)$$

Both central values are similar to the superallowed nuclear beta decay result reported above. Reconciliation with CKM unitarity suggests a shorter neutron lifetime near 878.5 s or a smaller g_A . We note that the most precise recent neutron lifetime update reported [21], $\tau_n = 877.75(34)$ s, has an uncertainty about half as big as the average given in Eq. 67.6. It corresponds to $|V_{ud}| = 0.9746(8)$, a value more in keeping with unitarity expectations; but too large an uncertainty from g_A to be meaningful. Future neutron studies [22] are expected to resolve any current inconsistencies and further reduce the uncertainties in g_A and τ_n making them a potentially better way to determine V_{ud} without the nuclear physics uncertainties.

The PIBETA experiment at PSI measured the very small ($\mathcal{O}(10^{-8})$) branching ratio for $\pi^+ \rightarrow \pi^0 e^+ \nu_e$ with about $\pm 0.6\%$ precision. Its result gives [23]

$$|V_{ud}| = 0.9739(27) \left[\frac{BR(\pi^+ \rightarrow e^+ \nu_e(\gamma))}{1.2325 \times 10^{-4}} \right]^{\frac{1}{2}}, \quad (67.9)$$

which is normalized using the very precisely measured $BR(\pi^+ \rightarrow e^+ \nu_e(\gamma)) = 1.2325(23) \times 10^{-4}$ [7], rather than the theoretical branching ratio of $1.2350(2) \times 10^{-4}$, which if used, would increase $|V_{ud}|$ to 0.9749(27). Theoretical uncertainties in pion beta decay are very small [24], leaving open more than an order of magnitude improvement of its experimental branching ratio before theory uncertainties become a problem. Although challenging, improved measurements of pion beta decay currently under discussion would allow this decay mode to compete with superallowed beta decays and future neutron decay efforts for the most precise direct $|V_{ud}|$ determination.

67.2 V_{us}

$|V_{us}|$ may be directly obtained from kaon decays, hyperon decays, and tau decays. Early determinations most often used $K\ell 3$ decays:

$$\Gamma_{K\ell 3} = \frac{G_F^2 M_K^5}{192\pi^3} S_{EW} (1 + \delta_K^\ell + \delta_{SU2}) C^2 |V_{us}|^2 f_+(0) I_K^\ell. \quad (67.10)$$

Here, ℓ refers to either e or μ , G_F is the Fermi constant, M_K is the kaon mass, S_{EW} is the short-distance radiative correction, δ_K^ℓ is the mode-dependent long-distance radiative correction, $f_+(0)$ is the calculated form factor at zero momentum transfer for the $\ell\nu$ system, and I_K^ℓ is the phase-space integral, which depends on measured semileptonic form factors. For charged kaon decays, δ_{SU2} is the deviation from one of the ratio of $f_+(0)$ for the charged to neutral kaon decay; it is zero for the neutral kaon. C^2 is 1 (1/2) for neutral (charged) kaon decays. Most early determinations of

$|V_{us}|$ were based solely on $K \rightarrow \pi e \nu$ decays; $K \rightarrow \pi \mu \nu$ decays were not used because of large uncertainties in I_K^μ . The experimental measurements are the semileptonic decay widths (based on the semileptonic branching fractions and lifetime) and form factors (allowing calculation of the phase space integrals). Theory is needed for S_{EW} , δ_K^e , δ_{SU2} , and $f_+(0)$.

Many measurements during the last 20 years have resulted in a shift in $|V_{us}|$. Most importantly, the $K \rightarrow \pi e \nu$ branching fractions are significantly different than much earlier PDG averages, probably as a result of inadequate treatment of radiation in older experiments. This effect was first observed by BNL E865 [25] in the charged kaon system and then by KTeV [26,27] in the neutral kaon system; subsequent measurements were made by KLOE [28–31], NA48 [32–34], and ISTRA+ [35]. Current averages (*e.g.*, by the PDG [36] or Flavianet [37]) of the semileptonic branching fractions are based only on recent, high-statistics experiments where the treatment of radiation is clear. In addition to measurements of branching fractions, new measurements of lifetimes [38] and form factors [39–43], have resulted in improved precision for all of the experimental inputs to $|V_{us}|$. Precise measurements of form factors for $K_{\mu 3}$ decay make it possible to use both semileptonic decay modes to extract V_{us} .

Following the analysis of Moulson [18,44] and the Flavianet group [37,45,46], along with recent improvements in the QED radiative corrections [47], one finds [48], after including the isospin violating effect, δ_{SU2} , the values of $|V_{us}|f_+(0)$ in Table 67.1. The average of these measurements, including correlation effects [18,48–50] gives [14]

$$f_+(0)|V_{us}| = 0.21656(35) \quad \text{FLAVIANET} \quad (67.11)$$

where the errors correspond to kaon experimental parameters and radiative corrections, respectively, leading, as we shall see, to $|V_{us}| = 0.22330(35)_{\text{exp}}(39)_{\text{LAT}}(8)_{\text{RC+IB}}(53)_{\text{TOT}}$.

Lattice QCD calculations of $f_+(0)$ have been carried out for 2, 2+1, and 2+1+1 quark flavors and range from about 0.96 to 0.97. Here, we illustrate recent FLAG (2020) updated averages [51] for 2+1 and 2+1+1 flavors:

$$\begin{aligned} f_+(0) &= 0.9677(27) \quad N_f = 2 + 1 \\ f_+(0) &= 0.9698(17) \quad N_f = 2 + 1 + 1 \end{aligned} \quad (67.12)$$

Updating the result for $N_f = 2 + 1 + 1$ we obtain for V_{us} from Eq. (67.11) and Eq. (67.12),

$$\begin{aligned} |V_{us}| &= 0.2238(4)_{\text{exp+RC}}(6)_{\text{lattice}} \quad (N_f = 2 + 1, K_{\ell 3} \text{ decays}) \\ &= 0.22330(4)_{\text{exp+RC}}(4)_{\text{lattice}} \quad (N_f = 2 + 1 + 1, K_{\ell 3} \text{ decays}) \end{aligned} \quad (67.13)$$

based on ref. [18] and ref. [48]

Table 67.1: $|V_{us}|f_+(0)$ from $K\ell 3$, based on ref. [18,48]

Decay Mode	$ V_{us} f_+(0)$
$K^\pm e 3$	0.2169(6)
$K^\pm \mu 3$	0.2168(10)
$K_L e 3$	0.2162(5)
$K_L \mu 3$	0.2165(6)
$K_S e 3$	0.2169(8)
$K_S \mu 3$	0.2125(47)
Average (including correlation effects [18,48])	0.21656(35)

A value of V_{us} can also be obtained from a comparison of the radiative inclusive decay rates for $K \rightarrow \mu \nu(\gamma)$ and $\pi \rightarrow \mu \nu(\gamma)$ combined with a lattice gauge theory calculation of f_{K^+}/f_{π^+} via

$$\frac{|V_{us}|f_{K^+}}{|V_{ud}|f_{\pi^+}} = 0.23871(20) \left[\frac{\Gamma(K \rightarrow \mu \nu(\gamma))}{\Gamma(\pi \rightarrow \mu \nu(\gamma))} \right]^{\frac{1}{2}} \quad (67.14)$$

with the small error coming from electroweak radiative corrections [52–54]; these corrections were confirmed by direct lattice calculation of the kaon and pion leptonic decay rates [53,54].

A recent fit [14,18] gives

$$\frac{|V_{us}|f_{K^+}}{|V_{ud}|f_{\pi^+}} = 0.27679(28)_{\text{BR}}(20)_{\text{corr}}. \quad (67.15)$$

Employing the FLAG [51] lattice QCD averages for the isospin broken decay constants

$$\frac{f_{K^+}}{f_{\pi^+}} = 1.1978(22) \quad N_f = 2 + 1 + 1 \quad (67.16)$$

leading to

$$\frac{|V_{us}|}{|V_{ud}|} = 0.23108(51) \quad (N_f = 2 + 1 + 1, K_{\mu 2} \text{ decays}). \quad (67.17)$$

Actually we can average the Cabibbo angle determinations from kaons: from $K_{\ell 3}$ decays in eqs. 67.11, 67.12 and from $K_{\mu 2}$ in eqs. 67.15, 67.16 with $N_f = 2 + 1 + 1$. Assuming 20% correlation between $(|V_{us}/V_{ud}|f_K/f_\pi)$ and (f_K/f_π) we obtain

$$V_{us} = 0.22431(85) \quad S = 2.5. \quad (67.18)$$

The result shown in Eq. 67.18 is what we use when we consider the first row test of CKM unitarity. The quoted uncertainty includes a scale factor of 2.5 to account for the discrepancies between the values of V_{us} obtained from $K\ell 3$ and $K\mu 2$ decays.

This is the current status of the Cabibbo Angle determination from the kaon sector, and theoretical and experimental progress is expected to clarify the situation soon.

It should be mentioned that hyperon decay fits suggest [55]

$$|V_{us}| = 0.2250(27) \quad (\text{Hyperon Decays}) \quad (67.19)$$

modulo SU(3) breaking effects that could shift that value up or down. We note that a representative effort [56] that incorporates SU(3) breaking found $V_{us} = 0.226(5)$. Strangeness changing tau decays, averaging both inclusive and exclusive measurements, give [57,58]

$$|V_{us}| = 0.2207(14) \quad (\text{Tau Decays}), \quad (67.20)$$

which differs by about 2 sigma from the kaon determination discussed above, and would, if combined with V_{ud} from super-allowed beta decays, lead to a 4 sigma deviation from unitarity. This discrepancy results mainly from the inclusive tau decay results that rely on Finite Energy Sum Rule techniques and assumptions, as well as experimental uncertainties. Recent investigation of that approach suggests a larger value for V_{us} , which is more in accord with other determinations [59].

Employing the values of V_{ud} and V_{us} with an error scale factor of 2 from Eq. (67.4) and the average obtained after rescaling the errors from mEq. 67.18 leads to the unitarity consistency check

$$|V_{ud}|^2 + |V_{us}|^2 + |V_{ub}|^2 = 0.9983(6)(4), \quad (67.21)$$

where the first error is the uncertainty from $|V_{ud}|^2$ and the second error is the uncertainty from the average $|V_{us}|^2$ in Eq. 67.18. One finds about an overall 2 sigma deviation from unitarity. (The deviation increases to 3 sigma if nuclear structure uncertainties are ignored.) That deviation could be due a problem with $|V_{ud}|$ theory (RC or NS), the lattice determination of $f_+(0)$ or new physics.

67.3 CKM Unitarity Constraints

The current 2 sigma experimental disagreement with unitarity, $|V_{ud}|^2 + |V_{us}|^2 + |V_{ub}|^2 = 0.9983(7)$, still provides strong confirmation of Standard Model radiative corrections (which range between 3-4% depending on the nucleus used) at a high significance level [60]. In addition, it implies constraints on “New Physics” effects at both the tree and quantum loop levels. Those effects could be in the form of contributions to nuclear beta decays, K decays and/or muon decays, with the last of these providing normalization via the muon lifetime [61], which is used to obtain the Fermi constant, $G_\mu = 1.1663787(6) \times 10^{-5} \text{GeV}^{-2}$.

In the following examples, we illustrate the implications of CKM unitarity for (1) exotic muon decays [62] (beyond ordinary

muon decay $\mu^+ \rightarrow e^+ \nu_e \bar{\nu}_\mu$) and (2) new heavy quark mixing V_{uD} [63]. Other examples in the literature [64, 65] include Z_χ boson quantum loop effects, supersymmetry, leptoquarks, compositeness etc.

References

- [1] N. Cabibbo, Phys. Rev. Lett. **10**, 531 (1963).
- [2] M. Kobayashi and T. Maskawa, Prog. Theor. Phys. **49**, 652 (1973).
- [3] L. Wolfenstein, Phys. Rev. Lett. **51**, 1945 (1983).
- [4] S. Eidelman *et al.* (Particle Data Group), Phys. Lett. B **592**, 1-4, 1 (2004).
- [5] I. Towner and J. Hardy, Rept. Prog. Phys. **73**, 046301 (2010).
- [6] J. C. Hardy and I. S. Towner, Phys. Rev. C **102**, 4, 045501 (2020).
- [7] W. J. Marciano and A. Sirlin, Phys. Rev. Lett. **71**, 3629 (1993).
- [8] A. Czarnecki, W. J. Marciano and A. Sirlin, Phys. Rev. D **70**, 093006 (2004), [hep-ph/0406324].
- [9] W. J. Marciano and A. Sirlin, Phys. Rev. Lett. **96**, 032002 (2006), [hep-ph/0510099].
- [10] I. Towner and J. Hardy, Phys. Rev. C **77**, 025501 (2008), [arXiv:0710.3181].
- [11] J. Hardy and I. Towner, Phys. Rev. C **79**, 055502 (2009), [arXiv:0812.1202].
- [12] J. Hardy and I. Towner, Phys. Rev. C **91**, 2, 025501 (2015), [arXiv:1411.5987].
- [13] C.-Y. Seng *et al.*, Phys. Rev. Lett. **121**, 24, 241804 (2018), [arXiv:1807.10197].
- [14] V. Cirigliano *et al.*, Phys. Lett. B **838**, 137748 (2023), [arXiv:2208.11707].
- [15] A. Czarnecki, W. J. Marciano and A. Sirlin, Phys. Rev. D **100**, 7, 073008 (2019), [arXiv:1907.06737].
- [16] C. Y. Seng, M. Gorchtein and M. J. Ramsey-Musolf, Phys. Rev. D **100**, 1, 013001 (2019), [arXiv:1812.03352].
- [17] M. Gorchtein, Phys. Rev. Lett. **123**, 4, 042503 (2019), [arXiv:1812.04229].
- [18] M. Moulson, talk at CKM2023, <https://indico.cern.ch/event/1184945/contributions/5540813/attachments/2717802/4721036/CKM202023.pdf>.
- [19] R. L. Workman *et al.* (Particle Data Group), PTEP **2022**, 083C01 (2022).
- [20] B. Märkisch *et al.*, Phys. Rev. Lett. **122**, 24, 242501 (2019), [arXiv:1812.04666].
- [21] F. M. Gonzalez *et al.* (UCN τ) (2021), [arXiv:2106.10375].
- [22] H. Abele, Prog. Part. Nucl. Phys. **60**, 1 (2008).
- [23] D. Pocanic *et al.*, Phys. Rev. Lett. **93**, 181803 (2004), [hep-ex/0312030]; A. Czarnecki, W. J. Marciano and A. Sirlin, Phys. Rev. D **101**, 9, 091301 (2020), [arXiv:1911.04685].
- [24] X. Feng *et al.*, Phys. Rev. Lett. **124**, 19, 192002 (2020), [arXiv:2003.09798].
- [25] A. Sher *et al.*, Phys. Rev. Lett. **91**, 261802 (2003), [hep-ex/0305042].
- [26] T. Alexopoulos *et al.* (KTeV), Phys. Rev. Lett. **93**, 181802 (2004), [hep-ex/0406001].
- [27] T. Alexopoulos *et al.* (KTeV), Phys. Rev. D **70**, 092006 (2004), [hep-ex/0406002].
- [28] F. Ambrosino *et al.* (KLOE), Phys. Lett. B **632**, 43 (2006), [hep-ex/0508027].
- [29] F. Ambrosino *et al.* (KLOE), Phys. Lett. B **638**, 140 (2006), [hep-ex/0603041].
- [30] F. Ambrosino *et al.* (KLOE), Phys. Lett. B **636**, 173 (2006), [hep-ex/0601026].
- [31] B. Sciascia (KLOE), PoS **HEP2005**, 287 (2006), [hep-ex/0510028].
- [32] A. Lai *et al.* (NA48), Phys. Lett. B **602**, 41 (2004), [hep-ex/0410059].
- [33] A. Lai *et al.* (NA48), Phys. Lett. B **645**, 26 (2007), [hep-ex/0611052].
- [34] J. Batley *et al.* (NA48/2), Eur. Phys. J. C **50**, 329 (2007), [Erratum: Eur.Phys.J.C 52, 1021–1023 (2007)], [hep-ex/0702015].
- [35] V. Romanovsky *et al.* (2007), [arXiv:0704.2052].
- [36] K. Olive *et al.* (Particle Data Group), Chin. Phys. C **38**, 090001 (2014).
- [37] M. Antonelli *et al.* (FlaviaNet Working Group on Kaon Decays), Eur. Phys. J. C **69**, 399 (2010), [arXiv:1005.2323]; For a detailed review, see; M. Antonelli *et al.*, Phys. Rept. **494**, 197 (2010), [arXiv:0907.5386].
- [38] F. Ambrosino *et al.* (KLOE), Phys. Lett. B **626**, 15 (2005), [hep-ex/0507088].
- [39] T. Alexopoulos *et al.* (KTeV), Phys. Rev. D **70**, 092007 (2004), [hep-ex/0406003].
- [40] E. Abouzaid *et al.* (KTeV), Phys. Rev. D **74**, 097101 (2006), [hep-ex/0608058].
- [41] F. Ambrosino *et al.* (KLOE), Phys. Lett. B **636**, 166 (2006), [hep-ex/0601038].
- [42] A. Lai *et al.* (NA48), Phys. Lett. B **604**, 1 (2004), [hep-ex/0410065].
- [43] O. Yushchenko *et al.*, Phys. Lett. B **589**, 111 (2004), [hep-ex/0404030].
- [44] M. Moulson, PoS **CKM2016**, 033 (2017), [arXiv:1704.04104].
- [45] E. Passemar, talk at CKM2018, <https://zenodo.org/record/2565480>.
- [46] Y. Aoki *et al.* (Flavour Lattice Averaging Group (FLAG)), Eur. Phys. J. C **82**, 10, 869 (2022), [arXiv:2111.09849].
- [47] C.-Y. Seng *et al.* (2021), [arXiv:2103.04843].
- [48] C.-Y. Seng *et al.* (2021), [arXiv:2107.14708].
- [49] C.-Y. Seng *et al.*, JHEP **07**, 071 (2022), [arXiv:2203.05217].
- [50] V. Cirigliano, talk at Cabibbo 60 - Convegno, Accademia Nazionale dei Lincei, <https://www.lincci.it/it/manifestazioni/cabibbo-60-convegno>.
- [51] S. Aoki *et al.* (Flavour Lattice Averaging Group), Eur. Phys. J. C **80**, 2, 113 (2020), [arXiv:1902.08191]; A. Bazavov *et al.*, Phys. Rev. Lett. **112**, 11, 112001 (2014), [arXiv:1312.1228]; N. Carrasco *et al.*, Phys. Rev. D **93**, 11, 114512 (2016), [arXiv:1602.04113]; A. Bazavov *et al.*, Phys. Rev. D **87**, 073012 (2013), [arXiv:1212.4993]; P. A. Boyle *et al.* (RBC/UKQCD), JHEP **06**, 164 (2015), [arXiv:1504.01692]; A. Bazavov *et al.*, Phys. Rev. D **98**, 7, 074512 (2018), [arXiv:1712.09262]; T. Blum *et al.* (RBC, UKQCD), Phys. Rev. D **93**, 7, 074505 (2016), [arXiv:1411.7017]; R. Dowdall *et al.*, Phys. Rev. D **88**, 074504 (2013), [arXiv:1303.1670]; N. Carrasco *et al.*, Phys. Rev. D **91**, 5, 054507 (2015), [arXiv:1411.7908]; E. Follana *et al.* (HPQCD, UKQCD), Phys. Rev. Lett. **100**, 062002 (2008), [arXiv:0706.1726]; A. Bazavov *et al.* (MILC), PoS **LATTICE2010**, 074 (2010), [arXiv:1012.0868]; S. Durr *et al.*, Phys. Rev. D **81**, 054507 (2010), [arXiv:1001.4692]; S. Durr *et al.*, Phys. Rev. D **95**, 5, 054513 (2017), [arXiv:1601.05998]; V. Bornyakov *et al.* (QCDSF), Phys. Lett. B **767**, 366 (2017), [arXiv:1612.04798].
- [52] V. Cirigliano and H. Neufeld, Phys. Lett. B **700**, 7 (2011), [arXiv:1102.0563]; W. J. Marciano, Phys. Rev. Lett. **93**, 231803 (2004), [hep-ph/0402299].
- [53] D. Giusti *et al.*, Phys. Rev. Lett. **120**, 7, 072001 (2018), [arXiv:1711.06537].
- [54] M. Di Carlo *et al.*, Phys. Rev. D **100**, 3, 034514 (2019), [arXiv:1904.08731].
- [55] N. Cabibbo, E. C. Swallow and R. Winston, Phys. Rev. Lett. **92**, 251803 (2004), [hep-ph/0307214].

- [56] V. Mateu and A. Pich, JHEP **10**, 041 (2005), [hep-ph/0509045].
- [57] Y. S. Amhis *et al.* (HFLAV) (2019), [arXiv:1909.12524].
- [58] Y. S. Amhis *et al.* (HFLAV), Phys. Rev. D **107**, 5, 052008 (2023), [arXiv:2206.07501].
- [59] R. J. Hudspith *et al.*, Phys. Lett. B **781**, 206 (2018), [arXiv:1702.01767]; P. Boyle *et al.* (RBC, UKQCD), Phys. Rev. Lett. **121**, 20, 202003 (2018), [arXiv:1803.07228].
- [60] A. Sirlin, Rev. Mod. Phys. **50**, 573 (1978), [Erratum: Rev.Mod.Phys. 50, 905 (1978)].
- [61] D. Webber *et al.* (MuLan), Phys. Rev. Lett. **106**, 041803 (2011), [arXiv:1010.0991].
- [62] K. Babu and S. Pakvasa (2002), [hep-ph/0204236].
- [63] W. Marciano and A. Sirlin, Phys. Rev. Lett. **56**, 22 (1986); P. Langacker and D. London, Phys. Rev. D **38**, 886 (1988).
- [64] W. Marciano and A. Sirlin, Phys. Rev. D **35**, 1672 (1987).
- [65] R. Barbieri *et al.*, Phys. Lett. B **156**, 348 (1985); K. Hagiwara, S. Matsumoto and Y. Yamada, Phys. Rev. Lett. **75**, 3605 (1995), [hep-ph/9507419]; A. Kurylov and M. Ramsey-Musolf, Phys. Rev. Lett. **88**, 071804 (2002), [hep-ph/0109222]; S. Bauman, J. Erler and M. Ramsey-Musolf, Phys. Rev. D **87**, 3, 035012 (2013), [arXiv:1204.0035].

68. CP Violation in K_L^0 Decays

Revised August 2023 by C.-J. Lin (LBNL).

The symmetries C (particle-antiparticle interchange) and P (space inversion) hold for strong and electromagnetic interactions. After the discovery of large C and P violation in the weak interactions, it appeared that the product CP was a good symmetry. In 1964 CP violation was observed in K^0 decays at a level given by the parameter $\epsilon \approx 2.3 \times 10^{-3}$.

A unified treatment of CP violation in K , D , B , and B_s mesons is given in “ CP Violation in Meson Decays” by D. Kirkby and Y. Nir in this *Review*. A more detailed review including a thorough discussion of the experimental techniques used to determine CP violation parameters is given in a book by K. Kleinknecht [1]. Here we give a concise summary of the formalism needed to define the parameters of CP violation in K_L decays, and a description of our fits for the best values of these parameters.

68.1 Formalism for CP violation in Kaon decay

CP violation has been observed in the semi-leptonic decays $K_L^0 \rightarrow \pi^\mp \ell^\pm \nu$, and in the nonleptonic decay $K_L^0 \rightarrow 2\pi$. The experimental numbers that have been measured are

$$A_L = \frac{\Gamma(K_L^0 \rightarrow \pi^- \ell^+ \nu) - \Gamma(K_L^0 \rightarrow \pi^+ \ell^- \nu)}{\Gamma(K_L^0 \rightarrow \pi^- \ell^+ \nu) + \Gamma(K_L^0 \rightarrow \pi^+ \ell^- \nu)} \quad (68.1a)$$

$$\eta_{+-} = A(K_L^0 \rightarrow \pi^+ \pi^-) / A(K_S^0 \rightarrow \pi^+ \pi^-) \\ = |\eta_{+-}| e^{i\phi_{+-}} \quad (68.1b)$$

$$\eta_{00} = A(K_L^0 \rightarrow \pi^0 \pi^0) / A(K_S^0 \rightarrow \pi^0 \pi^0) \\ = |\eta_{00}| e^{i\phi_{00}} \quad (68.1c)$$

CP violation can occur either in the $K^0 - \bar{K}^0$ mixing or in the decay amplitudes. Assuming CPT invariance, the mass eigenstates of the $K^0 - \bar{K}^0$ system can be written

$$|K_S\rangle = p|K^0\rangle + q|\bar{K}^0\rangle, \quad |K_L\rangle = p|K^0\rangle - q|\bar{K}^0\rangle. \quad (68.2)$$

If CP invariance held, we would have $q = p$ so that K_S would be CP -even and K_L CP -odd. (We define $|\bar{K}^0\rangle$ as $CP|K^0\rangle$.) CP violation in $K^0 - \bar{K}^0$ mixing is then given by the parameter ϵ where

$$\frac{p}{q} = \frac{(1 + \tilde{\epsilon})}{(1 - \tilde{\epsilon})}. \quad (68.3)$$

CP violation can also occur in the decay amplitudes

$$A(K^0 \rightarrow \pi\pi(I)) = A_I e^{i\delta_I}, \quad A(\bar{K}^0 \rightarrow \pi\pi(I)) = A_I^* e^{i\delta_I}, \quad (68.4)$$

where I is the isospin of $\pi\pi$, δ_I is the final-state phase shift, and A_I would be real if CP invariance held. The CP -violating observables are usually expressed in terms of ϵ and ϵ' defined by

$$\eta_{+-} = \epsilon + \epsilon', \quad \eta_{00} = \epsilon - 2\epsilon'. \quad (68.5a)$$

One can then show [2]

$$\epsilon = \tilde{\epsilon} + i \left(\text{Im } A_0 / \text{Re } A_0 \right), \quad (68.5b)$$

$$\sqrt{2}\epsilon' = i e^{i(\delta_2 - \delta_0)} (\text{Re } A_2 / \text{Re } A_0) \left(\text{Im } A_2 / \text{Re } A_2 - \text{Im } A_0 / \text{Re } A_0 \right), \quad (68.5c)$$

$$A_L = 2\text{Re } \epsilon / (1 + |\epsilon|^2) \approx 2\text{Re } \epsilon. \quad (68.5d)$$

In Eq. (68.5a), small corrections [3] of order $\epsilon' \times \text{Re}(A_2/A_0)$ are neglected, and Eq. (68.5d) assumes the $\Delta S = \Delta Q$ rule.

The quantities $\text{Im } A_0$, $\text{Im } A_2$, and $\text{Im } \tilde{\epsilon}$ depend on the choice of phase convention, since one can change the phases of K^0 and \bar{K}^0 by a transformation of the strange quark state $|s\rangle \rightarrow |s\rangle e^{i\alpha}$; of course, observables are unchanged. It is possible by a choice of phase convention to set $\text{Im } A_0$ or $\text{Im } A_2$ or $\text{Im } \tilde{\epsilon}$ to zero, but none of these is zero with the usual phase conventions in the Standard Model. The choice $\text{Im } A_0 = 0$ is called the Wu-Yang phase convention [4], in which case $\epsilon = \tilde{\epsilon}$. The value of ϵ' is independent of phase convention, and a nonzero value demonstrates CP violation

in the decay amplitudes, referred to as direct CP violation. The possibility that direct CP violation is essentially zero, and that CP violation occurs only in the mixing matrix, was referred to as the superweak theory [5].

By applying CPT invariance and unitarity the phase of ϵ is given approximately by

$$\phi_\epsilon \approx \tan^{-1} \frac{2(m_{K_L} - m_{K_S})}{\Gamma_{K_S} - \Gamma_{K_L}} \approx 43.52 \pm 0.05^\circ, \quad (68.6a)$$

while Eq. (68.5c) gives the phase of ϵ' to be

$$\phi_{\epsilon'} = \delta_2 - \delta_0 + \frac{\pi}{2} \approx 42.3 \pm 1.5^\circ, \quad (68.6b)$$

where the numerical value is based on an analysis of $\pi - \pi$ scattering using chiral perturbation theory [6]. The approximation in Eq. (68.6a) depends on the assumption that direct CP violation is very small in all K^0 decays. This is expected to be good to a few tenths of a degree, as indicated by the small value of ϵ' and of η_{+-} and η_{00} , the CP -violation parameters in the decays $K_S \rightarrow \pi^+ \pi^- \pi^0$ [7], and $K_S \rightarrow \pi^0 \pi^0 \pi^0$ [8]. The relation in Eq. (68.6a) is exact in the superweak theory, so this is sometimes called the superweak-phase ϕ_{SW} . An important point for the analysis is that $\cos(\phi_{\epsilon'} - \phi_\epsilon) \approx 1$. The consequence is that only two real quantities need be measured, the magnitude of ϵ and the value of (ϵ'/ϵ) , including its sign. The measured quantity $|\eta_{00}/\eta_{+-}|^2$ is very close to unity so that we can write

$$|\eta_{00}/\eta_{+-}|^2 \approx 1 - 6\text{Re}(\epsilon'/\epsilon) \approx 1 - 6\epsilon'/\epsilon, \quad (68.7a)$$

$$\text{Re}(\epsilon'/\epsilon) \approx \frac{1}{3}(1 - |\eta_{00}/\eta_{+-}|). \quad (68.7b)$$

From the experimental measurements in this edition of the *Review*, and the fits discussed in the next section, one finds

$$|\epsilon| = (2.228 \pm 0.011) \times 10^{-3}, \quad (68.8a)$$

$$\phi_\epsilon = (43.5 \pm 0.5)^\circ, \quad (68.8b)$$

$$\text{Re}(\epsilon'/\epsilon) \approx \epsilon'/\epsilon = (1.66 \pm 0.23) \times 10^{-3}, \quad (68.8c)$$

$$\phi_{+-} = (43.4 \pm 0.5)^\circ, \quad (68.8d)$$

$$\phi_{00} - \phi_{+-} = (0.34 \pm 0.32)^\circ, \quad (68.8e)$$

$$A_L = (3.32 \pm 0.06) \times 10^{-3}. \quad (68.8f)$$

Direct CP violation, as indicated by ϵ'/ϵ , is expected in the Standard Model. However, the numerical value cannot be reliably predicted because of theoretical uncertainties [9]. The value of A_L agrees with Eq. (68.5d). The values of ϕ_{+-} and $\phi_{00} - \phi_{+-}$ are used to set limits on CP violation [see “Tests of Conservation Laws”].

68.2 Fits for K_L^0 CP -violation parameters

In recent years, K_L^0 CP -violation experiments have improved our knowledge of CP -violation parameters,

and their consistency with the expectations of CPT invariance and unitarity. To determine the best values of the CP -violation parameters in $K_L^0 \rightarrow \pi^+ \pi^-$ and $\pi^0 \pi^0$ decay, we make two types of fits, one for the phases ϕ_{+-} and ϕ_{00} jointly with Δm and τ_S , and the other for the amplitudes $|\eta_{+-}|$ and $|\eta_{00}|$ jointly with the $K_L^0 \rightarrow \pi\pi$ branching fractions.

68.2.1 Fits to ϕ_{+-} , ϕ_{00} , $\Delta\phi$, Δm , and τ_S data

These are joint fits to the data on ϕ_{+-} , ϕ_{00} , the phase difference $\Delta\phi = \phi_{00} - \phi_{+-}$, the $K_L^0 - K_S^0$ mass difference Δm , and the K_S^0 mean life τ_S , including the effects of correlations.

Measurements of ϕ_{+-} and ϕ_{00} are highly correlated with Δm and τ_S . Some measurements of τ_S are correlated with Δm . The correlations are given in the footnotes of the ϕ_{+-} and ϕ_{00} sections of the K_L^0 Listings, and the τ_S section of the K_S^0 Listings.

In most cases, the correlations are quoted as 100%, with the value and error of ϕ_{+-} or ϕ_{00} given at a fixed value of Δm and τ_S , with additional terms specifying the dependence of the value on Δm and τ_S . These cases lead to diagonal bands in Figs. 68.1

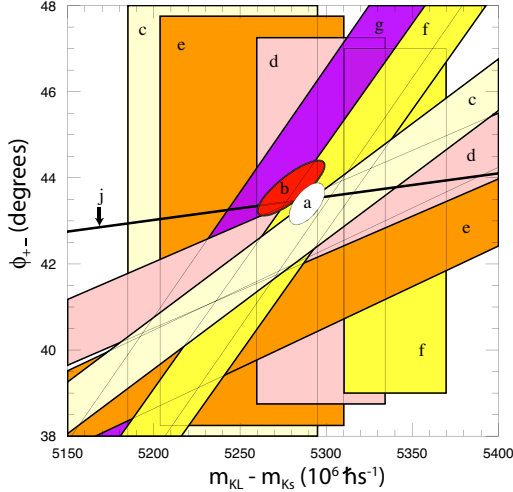


Figure 68.1: ϕ_{+-} vs Δm for experiments which do not assume CPT invariance. Δm measurements appear as vertical bands spanning $\Delta m \pm 1\sigma$, cut near the top and bottom to aid the eye. Most ϕ_{+-} measurements appear as diagonal bands spanning $\phi_{+-} \pm \sigma_\phi$. Data are labeled by letters: “b”–FNAL KTeV, “c”–CERN CPLEAR, “d”–FNAL E773, “e”–FNAL E731, “f”–CERN, “g”–CERN NA31, and are cited in Table 68.1. The narrow band “j” shows ϕ_{SW} . The ellipse “a” shows the $\chi^2 = 1$ contour of the fit result.

and 68.2. The KTeV experiment [10] quotes its results as values of Δm , τ_S , ϕ_ϵ , $\text{Re}(\epsilon'/\epsilon)$, and $\text{Im}(\epsilon'/\epsilon)$ with correlations, leading to the ellipses labeled “b.” The correlations for the KTeV measurements are given in the $\text{Im}(\epsilon'/\epsilon)$ section of the K_L^0 Listings. For small $|\epsilon'/\epsilon|$, $\phi_{+-} \approx \phi_\epsilon + \text{Im}(\epsilon'/\epsilon)$.

Table 68.1: References, Document ID’s, and sources corresponding to the letter labels in the figures. The data are given in the ϕ_{+-} and Δm sections of the K_L Listings, and the τ_S section of the K_S Listings.

Label	Source	PDG Document ID	Ref.
a	This Review	OUR FIT	
b	FNAL KTeV	ABOUZAID 11	[10]
c	CERN CPLEAR	APOSTOLAKIS 99C	[11]
d	FNAL E773	SCHWINGENHEUER 95	[12]
e	FNAL E731	GIBBONS 93,93C	[13], [14]
f	CERN	GEWENIGER 74B,74C	[15], [16]
g	CERN NA31	CAROSI 90	[17]
h	CERN NA48	LAI 02C	[18]
i	CERN NA31	BERTANZA 97	[19]
j	This Review	SUPERWEAK 16	

The data on τ_S , Δm , and ϕ_{+-} shown in Figs. 68.1 and 68.2 are combined with data on ϕ_{00} and $\phi_{00} - \phi_{+-}$ in two fits, one without assuming CPT , and the other with this assumption. The results without assuming CPT are shown as ellipses labeled “a.” These ellipses are seen to be in good agreement with the superweak phase

$$\phi_{SW} = \tan^{-1} \left(\frac{2\Delta m}{\Delta\Gamma} \right) = \tan^{-1} \left(\frac{2\Delta m \tau_S \tau_L}{\hbar(\tau_L - \tau_S)} \right). \quad (68.9)$$

In Figs. 68.1 and 68.2, ϕ_{SW} is shown as narrow bands labeled “j.”

Table 68.2 column 2, “Fit w/o CPT ,” gives the resulting fitted parameters, while Table 68.3 gives the correlation matrix for this fit. The white ellipses labeled “a” in Figure 68.1 and 68.2 are the $\chi^2 = 1$ contours for this fit.

For experiments which have dependencies on unseen fit parameters, that is, parameters other than those shown on the x or y

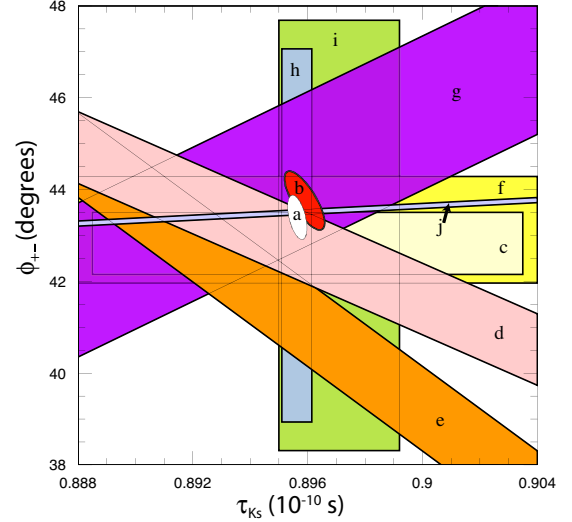


Figure 68.2: ϕ_{+-} vs τ_S . τ_S measurements appear as vertical bands spanning $\tau_S \pm 1\sigma$, some of which are cut near the top and bottom to aid the eye. Most ϕ_{+-} measurements appear as diagonal or horizontal bands spanning $\phi_{+-} \pm \sigma_\phi$. Data are labeled by letters: “b”–FNAL KTeV, “c”–CERN CPLEAR, “d”–FNAL E773, “e”–FNAL E731, “f”–CERN, “g”–CERN NA31, “h”–CERN NA48, “i”–CERN NA31, and are cited in Table 68.1. The narrow band “j” shows ϕ_{SW} . The ellipse “a” shows the fit result’s $\chi^2 = 1$ contour.

axis of the figure, their band positions are evaluated using the fit results and their band widths include the fitted uncertainty in the unseen parameters. This is also true for the ϕ_{SW} bands.

If CPT invariance and unitarity are assumed, then by Eq. (68.6a), the phase of ϵ is constrained to be approximately equal to

$$\phi_{SW} = (43.50258 \pm 0.00021)^\circ + 54.1(\Delta m - 0.5289)^\circ + 32.0(\tau_S - 0.89564) \quad (68.10)$$

where we have linearized the Δm and τ_S dependence of Eq. (68.9). The error ± 0.00021 is due to the uncertainty in τ_L . Here Δm has units 10^{10} h s^{-1} and τ_S has units 10^{-10} s .

If in addition we use the observation that $\text{Re}(\epsilon'/\epsilon) \ll 1$ and $\cos(\phi_{\epsilon'} - \phi_\epsilon) \simeq 1$, as well as the numerical value of $\phi_{\epsilon'}$ given in Eq. (68.6b), then Eqs. 68.5a, which are sketched in Fig 68.3, lead to the constraint

$$\begin{aligned} \phi_{00} - \phi_{+-} &\approx -3 \text{Im} \left(\frac{\epsilon'}{\epsilon} \right) \\ &\approx -3 \text{Re} \left(\frac{\epsilon'}{\epsilon} \right) \tan(\phi_{\epsilon'} - \phi_\epsilon) \\ &\approx 0.006^\circ \pm 0.008^\circ, \end{aligned} \quad (68.11)$$

so that $\phi_{+-} \approx \phi_{00} \approx \phi_\epsilon \approx \phi_{SW}$.

Table 68.2: Fit results for ϕ_{+-} , Δm , τ_S , ϕ_{00} , $\Delta\phi = \phi_{00} - \phi_{+-}$, and ϕ_ϵ without and with the CPT assumption

Quantity(units)	Fit w/o CPT	Fit w/ CPT
$\phi_{+-} (^\circ)$	43.4 ± 0.5 (S=1.2)	43.51 ± 0.05 (S=1.2)
$\Delta m (10^{10} \text{ h s}^{-1})$	0.5289 ± 0.0010	0.5293 ± 0.0009 (S=1.3)
$\tau_S (10^{-10} \text{ s})$	0.89564 ± 0.00033	0.8954 ± 0.0004 (S=1.1)
$\phi_{00} (^\circ)$	43.7 ± 0.6 (S=1.2)	43.52 ± 0.05 (S=1.3)
$\Delta\phi (^\circ)$	0.34 ± 0.32	0.006 ± 0.014 (S=1.7)
$\phi_\epsilon (^\circ)$	43.5 ± 0.5 (S=1.3)	43.52 ± 0.05 (S=1.2)
χ^2	16.4	20.0
# Deg. Free.	14	16

In the fit assuming CPT , we constrain $\phi_\epsilon = \phi_{SW}$ using the linear expression in Eq. (68.10), and constrain $\phi_{00} - \phi_{+-}$ using Eq. (68.11). These constraints are inserted into the Listings with the Document ID of SUPERWEAK 16. Some additional data for which the authors assumed CPT are added to this fit or substitute for other less precise data for which the authors did not make this assumption. See the Listings for details.

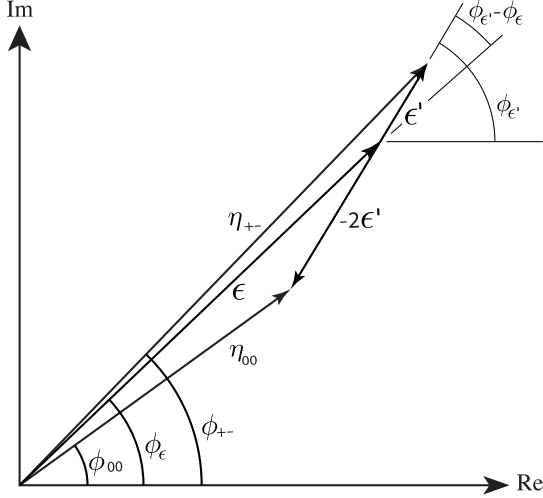


Figure 68.3: Sketch of Eqs. 68.5a. Not to scale

The results of this fit are shown in Table 68.2, column 3, “Fit w/ CPT ,” and the correlation matrix is shown in Table 68.4. The Δm precision is improved by the CPT assumption.

Table 68.3: Correlation matrix for the results of the fit without the CPT assumption

	ϕ_{+-}	Δm	τ_S	ϕ_{00}	$\Delta\phi$	ϕ_ϵ
ϕ_{+-}	1.000	0.596	-0.488	0.827	-0.040	0.976
Δm	0.596	1.000	-0.572	0.487	-0.035	0.580
τ_S	-0.488	-0.572	1.000	-0.423	-0.014	-0.484
ϕ_{00}	0.827	0.487	-0.423	1.000	0.529	0.929
$\Delta\phi$	-0.040	-0.035	-0.014	0.529	1.000	0.178
ϕ_ϵ	0.976	0.580	-0.484	0.929	0.178	1.000

Table 68.4: Correlation matrix for the results of the fit with the CPT assumption

	ϕ_{+-}	Δm	τ_S	ϕ_{00}	$\Delta\phi$	ϕ_ϵ
ϕ_{+-}	1.000	0.972	-0.311	0.957	-0.105	0.995
Δm	0.972	1.000	-0.509	0.958	-0.007	0.977
τ_S	-0.311	-0.509	1.000	-0.306	0.004	-0.312
ϕ_{00}	0.957	0.958	-0.306	1.000	0.189	0.981
$\Delta\phi$	-0.105	-0.007	0.004	0.189	1.000	-0.006
ϕ_ϵ	0.995	0.977	-0.312	0.981	-0.006	1.000

68.2.2 Fits for ϵ'/ϵ , $|\eta_{+-}|$, $|\eta_{00}|$, and $B(K_L \rightarrow \pi\pi)$

We list measurements of $|\eta_{+-}|$, $|\eta_{00}|$, $|\eta_{00}/\eta_{+-}|$, and ϵ'/ϵ . Independent information on $|\eta_{+-}|$ and $|\eta_{00}|$ can be obtained from measurements of the K_L^0 and K_S^0 lifetimes (τ_L , τ_S), and branching ratios (B) to $\pi\pi$, using the relations

$$|\eta_{+-}| = \left[\frac{B(K_L^0 \rightarrow \pi^+\pi^-)}{\tau_L} \frac{\tau_S}{B(K_S^0 \rightarrow \pi^+\pi^-)} \right]^{1/2}, \quad (68.12a)$$

$$|\eta_{00}| = \left[\frac{B(K_L^0 \rightarrow \pi^0\pi^0)}{\tau_L} \frac{\tau_S}{B(K_S^0 \rightarrow \pi^0\pi^0)} \right]^{1/2}. \quad (68.12b)$$

For historical reasons, the branching ratio fits and the CP -violation fits are done separately, but we want to include the

influence of $|\eta_{+-}|$, $|\eta_{00}|$, $|\eta_{00}/\eta_{+-}|$, and ϵ'/ϵ measurements on $B(K_L^0 \rightarrow \pi^+\pi^-)$ and $B(K_L^0 \rightarrow \pi^0\pi^0)$ and vice versa. We approximate a global fit to all of these measurements by first performing two independent fits: 1) BRFIT, a fit to the K_L^0 branching ratios, rates, and mean life, and 2) ETAFIT, a fit to the $|\eta_{+-}|$, $|\eta_{00}|$, $|\eta_{+-}/\eta_{00}|$, and ϵ'/ϵ measurements. The results from fit 1, along with the K_S^0 values from this edition, are used to compute values of $|\eta_{+-}|$ and $|\eta_{00}|$, which are included as measurements in the $|\eta_{00}|$ and $|\eta_{+-}|$ sections with a document ID of BRFIT 16. Thus, the fit values of $|\eta_{+-}|$ and $|\eta_{00}|$ given in this edition include both the direct measurements and the results from the branching ratio fit.

The process is reversed in order to include the direct $|\eta|$ measurements in the branching ratio fit. The results from fit 2 above (before including BRFIT 16 values) are used along with the K_L^0 and K_S^0 mean lives and the $K_S^0 \rightarrow \pi\pi$ branching fractions to compute the K_L^0 branching ratio $\Gamma(K_L^0 \rightarrow \pi^0\pi^0)/\Gamma(K_L^0 \rightarrow \pi^+\pi^-)$. This branching ratio value is included as a measurement in the branching ratio section with a document ID of ETAFIT 16. Thus, the K_L^0 branching ratio fit values in this edition include the results of the direct measurement of $|\eta_{00}/\eta_{+-}|$ and ϵ'/ϵ . Most individual measurements of $|\eta_{+-}|$ and $|\eta_{00}|$ enter our fits directly via the corresponding measurements of $\Gamma(K_L^0 \rightarrow \pi^+\pi^-)/\Gamma(\text{total})$ and $\Gamma(K_L^0 \rightarrow \pi^0\pi^0)/\Gamma(\text{total})$, and those that do not have too large errors to have any influence on the fitted values of these branching ratios. A more detailed discussion of these fits is given in the 1990 edition of this *Review* [20].

References

- [1] K. Kleinknecht, *Uncovering CP violation: Experimental clarification in the neutral K meson and B meson*, volume 195, Springer Verlag (2003).
- [2] B. Winstein and L. Wolfenstein, *Rev. Mod. Phys.* **65**, 1113 (1993).
- [3] M. S. Sozzi, *Eur. Phys. J.* **C36**, 37 (2004), [hep-ph/0401176].
- [4] T. T. Wu and C.-N. Yang, *Phys. Rev. Lett.* **13**, 380 (1964).
- [5] L. Wolfenstein, *Phys. Rev. Lett.* **13**, 562 (1964); L. Wolfenstein, *Comments Nucl. Part. Phys.* **21**, 5, 275 (1994).
- [6] G. Colangelo, J. Gasser and H. Leutwyler, *Nucl. Phys.* **B603**, 125 (2001), [hep-ph/0103088].
- [7] R. Adler *et al.* (CPLEAR), *Phys. Lett.* **B407**, 193 (1997); P. Bloch, *Proceedings of Workshop on K Physics* (Orsay 1996), ed. L. Iconomidou-Fayard, Edition Frontieres, Gif-sur-Yvette, France (1997) p. 307.
- [8] A. Lai *et al.* (NA48), *Phys. Lett.* **B610**, 165 (2005), [hep-ex/0408053].
- [9] G. Buchalla, A. J. Buras and M. E. Lautenbacher, *Rev. Mod. Phys.* **68**, 1125 (1996), [hep-ph/9512380]; S. Bosch *et al.*, *Nucl. Phys.* **B565**, 3 (2000), [hep-ph/9904408]; S. Bertolini, M. Fabbrichesi and J. O. Eeg, *Rev. Mod. Phys.* **72**, 65 (2000), [hep-ph/9802405].
- [10] E. Abouzaid *et al.* (KTeV), *Phys. Rev.* **D83**, 092001 (2011), [arXiv:1011.0127].
- [11] A. Apostolakis *et al.* (CPLEAR), *Phys. Lett.* **B458**, 545 (1999).
- [12] B. Schwingerheuer *et al.*, *Phys. Rev. Lett.* **74**, 4376 (1995).
- [13] L. K. Gibbons *et al.*, *Phys. Rev. Lett.* **70**, 1199 (1993).
- [14] L.K. Gibbons, Thesis, RX-1487, Univ. of Chicago, 1993.
- [15] C. Geweniger *et al.*, *Phys. Lett.* **48B**, 487 (1974).
- [16] C. Geweniger *et al.*, *Phys. Lett.* **52B**, 108 (1974).
- [17] R. Carosi *et al.* (NA31), *Phys. Lett.* **B237**, 303 (1990).
- [18] A. Lai *et al.* (NA48), *Phys. Lett.* **B537**, 28 (2002), [hep-ex/0205008].
- [19] L. Bertanza *et al.*, *Z. Phys.* **C73**, 629 (1997).
- [20] J. J. Hernandez *et al.* (Particle Data Group), *Phys. Lett.* **B239**, 1 (1990), [Erratum: *Phys. Lett.* **B253**, 524(1991)].

69. Review of Multibody Charm Analyses

Revised August 2023 by J. Rademacker (Bristol U.); written with D.M. Asner (BNL)

69.1 Overview

The study of multibody charm decays is a vibrant field, with vast and fast-increasing datasets, new developments in theory and experimental technique, and implications reaching beyond charm. This review is structured as follows: Sec. 69.2 summarizes key aspects of amplitude models that describe multibody charm decays, their application to data, and theory progress; Sec. 69.3 reviews the special role of charm threshold data in model-independent approaches; and Sec. 69.4 describes applications of multi-body charm analyses, focusing on Charge-Parity (CP) violation, charm mixing and the role of threshold data in this context. In Sec. 69.5, we conclude.

69.2 Kinematics & Models

The differential decay rate to a point $\mathbf{s} = (s_1, \dots, s_n)$ in n dimensional phase space can be expressed as

$$d\Gamma = |\mathcal{M}(\mathbf{s})|^2 \left| \frac{\partial^n \phi}{\partial(s_1 \dots s_n)} \right| d^n s \quad (69.1)$$

where $|\partial^n \phi / \partial(s_1 \dots s_n)|$ represents the density of states at \mathbf{s} , and \mathcal{M} the matrix element for the decay at that point in phase space, which is 2, 5, 8, ... dimensional for D decays to 3, 4, 5, ... spinless particles. Additional parameters are required to fully describe decays involving particles with non-zero spin in the initial or final state.

For the important case of D decays to three pseudoscalars, the decay kinematics can be represented in a two-dimensional Dalitz plot [1]. This is usually parameterized in terms of $s_{12} \equiv (p_1 + p_2)^2$ and $s_{23} \equiv (p_2 + p_3)^2$, where p_1 , p_2 , and p_3 are the four-momenta of the final-state particles. In terms of these variables, phase-space density is constant across the kinematically allowed region, so that any structure seen in the Dalitz plot is a direct consequence of the dynamics encoded in $|\mathcal{M}|^2$. Note that decays to four or more particles cannot be unambiguously described in terms of analogously-defined variables s_{ij} and s_{ijk} , which are all parity-even. Parity-odd kinematics are absent in three-body decays because the final-state momenta are confined to a plane; the use of parity-odd observables in four body decays is discussed in Sec. 69.4.4.

In the widely-used isobar approach, the matrix element \mathcal{M} is modeled as a sum of interfering decay amplitudes, each proceeding through resonant two-body decays [2–6]. See [2, 7, 8] for a review of resonance phenomenology. In most analyses, each resonance is described by a relativistic Breit-Wigner [9] or Flatté [10] lineshape, and the model includes a non-resonant term with a constant phase and magnitude. This approach has well-known theoretical limitations, such as the violation of unitarity and analyticity, which can break the relationship between magnitude and phase across phase space. This motivates the use of more sophisticated descriptions, especially for broad, overlapping resonances (frequently found in S-wave components) where these limitations are particularly problematic. In charm analyses, these approaches have included the K-matrix [11] which respects two-body unitarity; the use of LASS scattering data [12]; dispersive methods [13–16]; multi-meson models using chiral Lagrangians [17–20]; and methods based on chiral unitarity [21–24]; QCD factorization [25–28]; and quasi model-independent parameterizations that use generic lineshapes, with minimal theory input and many free parameters, for a subset of resonances [29–37].

An important example for a multibody charm decay is $D^0 \rightarrow K_S^0 \pi^+ \pi^-$, which is a key channel in CP violation and charm-mixing analyses. The latest analysis, published jointly by BaBar and Belle [38], describes the Dalitz plot with 1.1M $D^0 \rightarrow K_S^0 \pi^+ \pi^-$ events with 18 resonant components, including four doubly Cabibbo suppressed ones. The model uses a K-matrix description for the $\pi\pi$ S-wave based on [39] and input from LASS scattering data [12, 40] for the $K\pi$ S-wave, with no need to add a non-resonant component to describe the data. These data were re-analyzed by [25] in a QCD factorization framework, using lineshape parameterizations for the S [41, 42] and P wave [14] con-

tributions that preserve two-body unitarity and analyticity. The analyses give compatible results for the components they share.

The field of charm amplitude analyses remains very active. Publications since the last update of this review two years ago include Dalitz plot analyses of $D^0 \rightarrow K_L^0 \pi^+ \pi^-$, $D^0 \rightarrow K_S^0 \pi^+ \pi^-$, $D_s^+ \rightarrow K_S^0 K^+ \pi^0$, $D_s^+ \rightarrow K_S^0 K_S^0 \pi^+$, $D_s^+ \rightarrow K^+ \pi^- \pi^+$, $D_s^+ \rightarrow \pi^+ \pi^0 \eta'$, and $D_s^+ \rightarrow \pi^+ \pi^0 \pi^0$ by BESIII [43–48]; $D_s^+ \rightarrow \pi^+ \pi^- \pi^+$ by LHCb [36] and BESIII [35]; and $D^+ \rightarrow \pi^+ \pi^- \pi^+$ by LHCb [37]. LHCb studied the amplitude structure of $\Lambda_c \rightarrow p K^- \pi^+$ [49] and BESIII that of $\Lambda_c \rightarrow \Lambda \pi^+ \pi^0$ [50]. BESIII continued its series of four-body amplitude analyses with $D^+ \rightarrow K_S^0 \pi^+ \pi^0 \pi^0$ and $D_s^+ \rightarrow K^+ \pi^- \pi^+ \pi^0$ [51, 52], and performed a five-body amplitude analysis of $D_s^+ \rightarrow K^+ K^- \pi^+ \pi^+ \pi^-$ [53]. These analyses provide valuable insight into hadronic dynamics and have wider impact beyond that. The amplitude structure of $\Lambda_c \rightarrow p K^- \pi^+$ for example is found to have a high sensitivity to the Λ_c polarization, which can prove valuable in polarization measurements of Λ_b baryons decaying to Λ_c [49, 54]. The importance of charm amplitude analyses for CP violation and charm mixing is further discussed below. Comparing the $D^0 \rightarrow K_L^0 \pi^+ \pi^-$ amplitude structure with that of $D^0 \rightarrow K_S^0 \pi^+ \pi^-$ reveals U-spin breaking effects [43]. The D_s^+ and $D^+ \rightarrow \pi^+ \pi^- \pi^+$ analyses mentioned above, as well an earlier one by BaBar [31], analyse the $\pi^+ \pi^-$ S-wave using a quasi-model-independent approach. They observe substantial differences between the $\pi^+ \pi^+$ S-wave components observed in the two decays, and between the associated phase shift seen in either compared to that observed in scattering data [55–57]. These observations suggest that broad scalar meson resonances in these decays might be generated from meson-meson rescattering [37]; more broadly, they emphasize the importance of final state interactions in multibody decays.

Noteworthy is the increasing sophistication of recent amplitude analyses, most of which go substantially beyond the isobar model with Breit Wigner and Flatté lineshapes. However, with the notable exceptions of [15, 16, 23, 24, 58, 59], they remain within the isobar framework which describes the decay as a series of two-body processes, ignores long-range hadronic effects such as rescattering, and does not respect three (or four)-body unitarity and analyticity.

Several groups work on improved models. Dispersive techniques, which respect three-body unitarity and analyticity, have been applied to regions of the $D^+ \rightarrow K^- \pi^+ \pi^+$ and $D^+ \rightarrow K_S^0 \pi^0 \pi^+$ Dalitz plots below the η'/K threshold [15, 16], where they provide a good description of the data with fewer fit parameters than the isobar approach. Reference [58] uses a unitary coupled channel approach to describe $D^+ \rightarrow K^- \pi^+ \pi^+$, which has no restrictions on the kinematic range, but requires additional parameters to describe the Dalitz plot above the η'/K threshold. Using an effective chiral Lagrangian, the authors of reference [19] provide a description of the annihilation contribution to the decay amplitude which respects three-body unitarity. The approach provides a good description of LHCb's $D^+ \rightarrow K^+ K^- K^+$ data, with fewer parameters than an equivalent isobar model [59]. The same channel has more recently been re-analyzed by the authors of [23], who argue that the internal emission diagram should dominate and use a chiral unitarity-based approach to achieve a reasonable description of the data with two free parameters.

Limitations in the theoretical description of interfering resonances are the leading source of systematic uncertainty in many analyses. In some cases, the model uncertainty can be removed through model-independent methods, often relying on input from the charm threshold, as discussed in Sec. 69.3. The authors of [60] expand the scope and applicability of the quasi model-independent approach in amplitude fits. At the same time, increasingly sophisticated models are being developed, and applied to data. The authors of [20] and [61] provide valuable practical frameworks for sophisticated amplitude analyses.

69.3 Model Independent Methods and the Charm Threshold

Precision measurements of the CP -violation phase γ/ϕ_3 using $B^- \rightarrow DK^-$, $D \rightarrow K_S^0 \pi^+ \pi^-$ and related decay modes, as well as precision measurements of charm-mixing parameters in decay modes such as $D^0 \rightarrow K_S^0 \pi^+ \pi^-$, require input on the relative decay amplitudes of D^0 and \bar{D}^0 . In the above examples, $K_S^0 \pi^+ \pi^-$ can be replaced with other final state accessible to both D^0 and \bar{D}^0 [62–70]. While the magnitudes of the decay amplitudes can be measured precisely using the vast charm samples at the B factories and LHCb, obtaining the relative phases requires either amplitude models with reliable phase motion, or model-independent approaches. More details on the measurements of γ/ϕ_3 and charm mixing can be found in sections 69.4.1 and 69.4.2.

Model-independent measurements of relative phases between D^0 and \bar{D}^0 decay amplitudes rely on interference effects in the decays of well-defined coherent superpositions of D^0 and \bar{D}^0 . These are accessible at the charm threshold [65, 68, 70–75], where CLEO-c and BESIII operate. There, quantum-correlated D -meson pairs are produced, which have opposite CP and flavour content. For example if one (the tag) is identified as a CP eigenstate through its decay (e.g. to $K^+ K^-$ or $K_S \pi^0$) the other D meson is an eigenstate state with the opposite CP eigenvalue. The decay rate of a CP eigenstate $\frac{1}{\sqrt{2}}(D^0 \pm \bar{D}^0)$ is proportional to $|A_D|^2 + |\bar{A}_D|^2 \pm 2|A_D||\bar{A}_D| \cos(\delta_D)$, where A_D and \bar{A}_D are the D^0 and \bar{D}^0 decay amplitudes, and δ_D is their sought-after phase difference. Other quantum correlations give access to $\sin(\delta_D)$. For multibody decays, A_D , \bar{A}_D and δ_D vary across phase space. Model-independent phase information is measured either integrated over the entire phase space of the decay, or in sub-regions/bins. The results can be expressed in terms of one complex parameter $\mathcal{Z} = Re^{-i\delta} = c + is$ per pair of CP -conjugate bins; c and s are the average of $\cos(\delta_D)$ and $\sin(\delta_D)$ over that region of phase space. Amplitude models can be used to optimize the binning for sensitivity to γ/ϕ_3 , without introducing a model-dependent bias in the result [76]; novel unbinned approaches have the potential to further increase the precision on γ/ϕ_3 in future analyses [77–79].

CLEO-c data have been analyzed to provide binned \mathcal{Z} for the self-conjugate decays $D^0 \rightarrow K_{S,L}^0 \pi^+ \pi^-$, $K_{S,L}^0 K^+ K^-$, $\pi^+ \pi^- \pi^+ \pi^-$, and $K_S^0 \pi^- \pi^+ \pi^0$ and phase space-integrated values for $D^0, \bar{D}^0 \rightarrow K_S^0 K^+ \pi^-$, $K^+ \pi^- \pi^0$ and $K^+ \pi^- \pi^+ \pi^+$ [80–85]. BESIII significantly improved the precision for the $K_S^0 \pi^+ \pi^-$, $K_S^0 K^+ K^-$, $K^+ \pi^- \pi^0$ and $K^+ \pi^- \pi^+ \pi^-$ final states [86–89]. CLEO-c and BESIII $K^+ \pi^- \pi^+ \pi^-$ data were also analysed in four bins of five-dimensional phase space [89, 90] with a binning based on [33].

For self-conjugate decays such as $D^0 \rightarrow \pi^+ \pi^- \pi^0$, one can define the CP -even fraction F_+ which is +1 for a CP -even eigenstate and 0 for a CP -odd one [73]. F_+ is related to $Re(\mathcal{Z}) = c$, defined for a single CP -conjugate bin pair. For the purpose of γ/ϕ_3 measurements, this information allows the decay to be treated equivalently to a two-body decay, where γ/ϕ_3 is determined from relative decay rates in multiple decay modes, without the need to resolve the phase-space distribution. In the mathematical expressions for the decay rates, a factor $(2F_+ - 1)$ multiplies the γ/ϕ_3 -sensitive term, leading to best sensitivity for $F_+ = 1$ or $F_+ = 0$. $D^0 \rightarrow \pi^+ \pi^- \pi^0$ is found to be, with $F_+ = (97.3 \pm 1.7)\%$, compatible with being completely CP -even (CLEO-c data); a recent BESIII analysis of $D^0 \rightarrow K_{L,S} \pi^+ \pi^-$ finds $F_+ = (35.3 \pm 0.6 \pm 1.4)\%$ and $(55.6 \pm 0.6 \pm 1.2)\%$, respectively; $D^0 \rightarrow \pi^+ \pi^- \pi^+ \pi^-$ (BESIII, CLEO-c data), $D^0 \rightarrow K^+ K^- \pi^+ \pi^-$ (BESIII), $D^0 \rightarrow K^+ K^- \pi^0$ (CLEO-c data), are all predominantly CP even with F_+ ranging from 73% to 77%; $D^0 \rightarrow K_S^0 \pi^+ \pi^- \pi^0$ (BESIII, CLEO-c data), is predominantly CP odd with $F_+ = (23.5 \pm 10)\%$ [43, 74, 82, 83, 91–93]. In cases where results from both BESIII and CLEO-c data exist, BESIII's more precise results are quoted.

Comparing measured parameters like F_+ and \mathcal{Z} with those predicted from amplitude models provides a test of the models' phase motion. Model-predicted values for F_+ in $D^0 \rightarrow K_{L,S} \pi^+ \pi^-$ agree, with $(35.3 \pm 0.6 \pm 1.4)\%$ and $(55.6 \pm 0.6 \pm 1.2)\%$ [38, 43] well

with the measured values given above; as does the measured F_+ for $D^0 \rightarrow \pi^+ \pi^- \pi^+ \pi^-$, $F_+ = 0.769 \pm 0.023$ [92], with 0.729 ± 0.020 calculated from [32]; and the coherence factor $|\mathcal{Z}| = R$ measured in $D^0 \rightarrow K^\pm \pi^\mp \pi^\pm \pi^\mp$, $0.44_{-0.09}^{+0.10}$ [85, 94], with 0.459 ± 0.025 predicted by [33]. The latest bin-wise comparisons between model and data for $D^0 \rightarrow K_{L,S} \pi^+ \pi^-$, $K^\pm \pi^\mp \pi^\pm \pi^\mp$, $K^\pm \pi^\mp \pi^0$, $K_S^0 K^+ K^-$, and $\pi^+ \pi^- \pi^+ \pi^-$ can be found in [43, 82, 86–89, 89] and generally show good agreement. These results are a welcome surprise given the preceding discussion on the theoretical shortcomings of amplitude models.

69.4 Applications of multibody charm analyses for CP violation and mixing

Amplitude analyses provide sensitivity to both relative magnitudes and phases of the interfering decay amplitudes. It is especially the sensitivity to phases that makes amplitude analyses such a uniquely powerful tool for studying a wide range of phenomena. Here we concentrate on their critical role in CP violation and mixing measurements. Properties of light-meson resonances determined in D amplitude analyses are reported in the light-unflavored-meson section of this *Review*.

The closely related topics of multibody charm decays in measurements of CP violation in beauty decays to charm and charm mixing will be discussed in turn, followed by a review of searches for time-integrated CP violation in multibody charm decays.

69.4.1 CP violation in decays of Beauty to Charm

Neutral D mesons originating from $B^- \rightarrow DK^-$ (here denoted as D_{B^-}) are a superposition of D^0 and \bar{D}^0 with a relative phase that depends on the CKM unitarity triangle parameter γ/ϕ_3 ,

$$D_{B^-} \propto D^0 + r_B e^{i(\delta_B - \gamma)} \bar{D}^0,$$

where δ_B is a CP conserving strong phase, and $r_B \sim 0.1$ is the magnitude of the ratio of the $B^- \rightarrow \bar{D}^0 K^-$ and $B^- \rightarrow D^0 K^-$ decay amplitudes. In the corresponding CP -conjugate expression, γ/ϕ_3 changes sign. The amplitude analysis of the subsequent D_{B^\pm} decay to a state accessible to both D^0 and \bar{D}^0 allows the measurement of γ/ϕ_3 [62–69]. The method generalizes to similar B hadron decays, such as $B^0 \rightarrow DK^{*0}$, and, albeit with reduced sensitivity, to decays where the kaon is replaced by a pion.

Measurements based on this technique have been reported by BaBar [95, 96], Belle [97–99], Belle II [100], and LHCb [101–114]. Since it relies on $D^0 - \bar{D}^0$ interference, the phase differences between the relevant D^0 and \bar{D}^0 decay amplitudes are required in order to extract γ/ϕ_3 . Because the theoretical shortcomings of amplitude models discussed above make their phases unreliable, most recent γ/ϕ_3 measurements use amplitude model-independent approaches to obtain this information [98–105, 107–114]. These depend critically on information from the charm threshold described in Sec. 69.3. Charm mixing also results in a (time-dependent) $D^0 - \bar{D}^0$ superposition, that can be used to measure the relevant phase information as input to γ/ϕ_3 measurements. This method is particularly powerful in doubly Cabibbo-suppressed decays such as $D^0 \rightarrow K^+ \pi^- \pi^+ \pi^-$, and when used in combination with threshold data [115, 116]. Under some circumstances, with large data sets, the relevant strong phases and γ/ϕ_3 can be extracted simultaneously without external input, for example in simultaneous analysis of the $B^0 \rightarrow DK^+ \pi^-$ Dalitz plot and that of the subsequent $D \rightarrow K_S^0 \pi^+ \pi^-$ decay [117]. However, the global effort to measure γ/ϕ_3 to sub-degree precision will continue to rely critically on input from the charm threshold and BESIII's increasing datasets [118].

The most precise individual γ/ϕ_3 measurement with an uncertainty of $\sim 5^\circ$ results from LHCb's amplitude model-independent study of $D_{B^-} \rightarrow K_S^0 \pi^+ \pi^-$ and $D_{B^-} \rightarrow K_S^0 K^+ K^-$ [119], using input from the charm threshold [80, 87]. LHCb's analysis of $D_{B^-} \rightarrow K^+ \pi^- \pi^+ \pi^-$ decays leads to the second most precise individual γ/ϕ_3 measurement with $\gamma/\phi_3 = 55.8_{-5.8}^{+6.0} \pm 0.6_{-4.3}^{+6.7} \circ$ [113]. Here, the first uncertainty is due to $B^\pm \rightarrow DK^\pm$ statistics, the second systematic, and the third due to the uncertainty on charm-threshold input. This illustrates the importance of charm-threshold data, and the need for the analysis of larger threshold datasets to keep pace with the sharp increase in $B^\pm \rightarrow DK^\pm$ data

expected at the upgraded LHCb detector and Belle II. Further improvements in this mode are expected from including information on relative phases between D^0 and \bar{D}^0 amplitudes obtained from charm mixing [85, 94, 116].

The current world average on γ/ϕ_3 is dominated by LHCb who finds, combining its results with input from CLEO-c and BESIII in an amplitude-model independent approach, $\gamma = 63.8^{+3.5^\circ}_{-3.7^\circ}$ [111, 120]. Belle II, which is expected to reach excellent precision in γ/ϕ_3 , recently released its first γ/ϕ_3 result, based on Belle, Belle II and charm threshold data [100].

The interference between mixing and decay in $B^0 \rightarrow D^0 h^0$ with $h^0 = \pi^0, \eta, \omega$ provides sensitivity to β , which can be extracted from the Dalitz plot of the subsequent $D^0 \rightarrow K_S^0 \pi^+ \pi^-$ decay [38, 121–124]. The combined BaBar/Belle analysis based on this technique resolved the ambiguity in β present in other measurements [38].

Further details on CP violation in beauty and charm can be found in [125, 126].

69.4.2 Charm Mixing and CP violation

Time-dependent amplitude analyses in decays to final states that are accessible to both D^0 and \bar{D}^0 have unique sensitivity to mixing parameters. A Dalitz plot analysis of a self-conjugate final state, such as $K_S^0 \pi^+ \pi^-$ and $K_S^0 K^+ K^-$, allows a direct measurement of x and y , the normalized mass and width difference of the $D^0 - \bar{D}^0$ system's mass eigenstates [127]. This is in contrast to decays like $D^0 \rightarrow K^+ \pi^-$ which only provide access to decay-specific parameters x'^2, y' .

The phase differences between D^0 and \bar{D}^0 amplitudes across the Dalitz plot affect these measurements in the same way as those of γ/ϕ_3 in $B^+ \rightarrow DK^+$, and can be taken into account in an amplitude model-independent way using the same charm threshold results [65, 70–75, 125]. This approach recently resulted in the first observation of a non-zero mass difference between the neutral charm mass eigenstates by LHCb [128], using a model-independent analysis of $D^0 \rightarrow K_S^0 \pi^+ \pi^-$. The “bin flip” technique applied in this measurements exploits that CP -conjugate regions of the $D^0 \rightarrow K_S^0 \pi^+ \pi^-$ Dalitz plot have near-identical experimental efficiencies [129]. This measurement is also sensitive to CP violation in mixing and in the interference between mixing and decay, which is discussed further in [125, 126].

69.4.3 Everything, Everywhere, All at Once

The discussion above shows how closely related the measurements of γ/ϕ_3 , charm mixing, and the analysis of charm threshold data are, due to the shared charm parameters. While above, the emphasis was on the importance of charm as input to γ/ϕ_3 , and threshold data as input to charm mixing and γ/ϕ_3 , these relationships are in fact omnidirectional. This is demonstrated by LHCb's combined γ/ϕ_3 fit to γ/ϕ_3 -sensitive beauty decays to charm such as $B^- \rightarrow DK^-$, charm mixing, and charm threshold data. This combined analysis has a notable effect on charm parameters due to the input from beauty decays to charm [111].

69.4.4 Searches for time-integrated CPV in charm

The recent observation of direct CP violation in LHCb's analysis of $D^0 \rightarrow \pi^+ \pi^-$ and $D^0 \rightarrow K^+ K^-$ decays [130, 131], and the open question as to its Standard Model or beyond the Standard Model nature, add renewed interest in the search for CP violation in other decays.

Multibody decays, with their rich structure and varying strong phase across phase space, could potentially have particularly high sensitivity to CP violation. Comparing the results of amplitude fits for CP -conjugate decay modes provides a measure of CP violation, as for example done for $D^0 \rightarrow K_S^0 K^\pm \pi^\mp$, $D^0 \rightarrow K^+ K^- \pi^+ \pi^-$, and $D^0 \rightarrow \pi^+ \pi^- \pi^+ \pi^-$ using LHCb and CLEO-c data [32, 132–134]. A widely-used amplitude model-independent technique to search for local CP violation in multibody phase space is based on performing a χ^2 comparison of CP -conjugate phase-space distributions. This method was pioneered by BaBar [135] and developed further in [136–138] with results reported by BaBar [135, 139] and LHCb in $D^\pm \rightarrow K^+ K^- \pi^\pm$ [140, 141], CDF in $D^0 \rightarrow K_S^0 \pi^+ \pi^-$ [142], and LHCb in $D_{(s)}^+ \rightarrow K^+ K^- K^+$, $D^+ \rightarrow \pi^- \pi^+ \pi^+$, $D^0 \rightarrow K^+ K^- \pi^+ \pi^-$,

$D^0 \rightarrow \pi^+ \pi^- \pi^+ \pi^-$, and $\Xi_c^+ \rightarrow p K^- \pi^+$ [138, 143–145]. Unbinned methods can increase sensitivity [146, 147] and have been applied by LHCb to $D^+ \rightarrow \pi^- \pi^+ \pi^+$, $D^0 \rightarrow \pi^+ \pi^- \pi^0$, $D^0 \rightarrow \pi^+ \pi^- \pi^+ \pi^-$, and $\Xi_c^+ \rightarrow p K^- \pi^+$ [144, 145, 148–150].

An alternative model-independent approach is based on observables in four body decays that are odd under motion reversal (“naïve T ”) [151–159], which is equivalent to P for scalar particles [159]. One such observable is $C_T = \vec{p}_2 \cdot (\vec{p}_3 \times \vec{p}_4)$ where \vec{p}_i are the decay products' three momenta in the decay's center of mass frame. Comparing the P violating asymmetry $A_T \equiv \frac{\Gamma(C_T > 0) - \Gamma(C_T < 0)}{\Gamma(C_T > 0) + \Gamma(C_T < 0)}$ with its C -conjugate provides sensitivity to CP violation. Additional variables are proposed in [159], which also provides an excellent review of this topic. Searches for CP violation using P -odd variables have been carried out by BaBar, Belle, FOCUS, and LHCb in $D^0 \rightarrow K^+ K^- \pi^+ \pi^-$ [160–163], $D^+ \rightarrow K^+ K_S^0 \pi^+ \pi^-$, $D_s^+ \rightarrow K^+ K_S^0 \pi^+ \pi^-$ [164], $D^0 \rightarrow K_S^0 \pi^+ \pi^- \pi^0$ [165], and $D^0 \rightarrow \pi^+ \pi^- \pi^+ \pi^-$ [149].

Recently, LHCb performed the first full angular analysis of the rare decays $D^0 \rightarrow \pi^+ \pi^- \mu^+ \mu^-$ and $D^0 \rightarrow K^+ K^- \mu^+ \mu^-$. From this, several observables with sensitivity to physics beyond the Standard Model are constructed, including CP -violating ones. The results are in agreement with Standard-Model predictions [166, 167].

All results of analyses mentioned in this section are compatible with CP conservation. The observation of CP violation in two body charm decays [130, 131], and the vast data samples about to be collected, provide grounds for optimism that this may change in the foreseeable future.

69.5 Summary

Multibody charm decays offer a rich phenomenology, including unique sensitivity to CP violation and charm mixing. This is a highly dynamic field with many new results (some of which we presented here) and rapidly increasing, high quality datasets. These datasets constitute a huge opportunity, but also a challenge to improve the theoretical descriptions of soft hadronic effects in multibody decays. For some measurements, model-independent methods, many relying on input from the charm threshold, provide a way of removing model-induced uncertainties. At the same time, substantial progress in the theoretical description of multibody decays is being made.

References

- [1] R. Dalitz, Phil. Mag. Ser. 7 **44**, 1068 (1953).
- [2] M. Bauer, B. Stech and M. Wirbel, Z. Phys. C **34**, 103 (1987).
- [3] L.-L. Chau and H.-Y. Cheng, Phys. Rev. D **36**, 137 (1987), [Addendum: Phys.Rev.D 39, 2788–2791 (1989)].
- [4] P. F. Bedaque, A. K. Das and V. Mathur, Phys. Rev. D **49**, 269 (1994), [hep-ph/9307296].
- [5] K. Terasaki, Int. J. Mod. Phys. A **10**, 3207 (1995).
- [6] F. Buccella, M. Lusignoli and A. Pugliese, Phys. Lett. B **379**, 249 (1996), [hep-ph/9601343].
- [7] J. D. Jackson, Nuovo Cim. **34**, 1644 (1964).
- [8] See the note on Resonances in this Review.
- [9] E. P. Wigner, Phys. Rev. **70**, 15 (1946).
- [10] S. M. Flatte, Phys. Lett. B **63**, 224 (1976).
- [11] I. Aitchison, Nucl. Phys. A **189**, 417 (1972).
- [12] D. Aston *et al.*, Nucl. Phys. B **296**, 493 (1988).
- [13] R. Omnes, Nuovo Cim. **8**, 316 (1958).
- [14] C. Hanhart, Phys. Lett. B **715**, 170 (2012), [arXiv:1203.6839].
- [15] F. Nieknig and B. Kubis, JHEP **10**, 142 (2015), [arXiv:1509.03188].
- [16] F. Nieknig and B. Kubis, Phys. Lett. B **780**, 471 (2018), [arXiv:1708.00446].
- [17] P. Magalhães and M. Robilotta, Phys. Rev. D **92**, 9, 094005 (2015), [arXiv:1504.06346].

- [18] P. Magalhaes *et al.*, Phys. Rev. D **84**, 094001 (2011), [arXiv:1105.5120].
- [19] R. Aoude *et al.*, Phys. Rev. D **98**, 5, 056021 (2018), [arXiv:1805.11764].
- [20] P. C. Magalhães, A. C. dos Reis and M. R. Robilotta, Phys. Rev. D **102**, 7, 076012 (2020), [arXiv:2007.12304].
- [21] J. A. Oller, Phys. Rev. D **71**, 054030 (2005), [hep-ph/0411105].
- [22] G. Toledo, N. Ikeno and E. Oset, Eur. Phys. J. C **81**, 3, 268 (2021), [arXiv:2008.11312].
- [23] L. Roca and E. Oset, Phys. Rev. D **103**, 3, 034020 (2021), [arXiv:2011.05185].
- [24] J. Song, A. Feijoo and E. Oset, Phys. Rev. D **106**, 7, 074027 (2022), [arXiv:2205.04781].
- [25] J.-P. Dedonder *et al.*, Phys. Rev. D **89**, 9, 094018 (2014), [arXiv:1403.2971].
- [26] D. Boito *et al.*, Phys. Rev. D **96**, 11, 113003 (2017), [arXiv:1709.09739].
- [27] R. Klein *et al.*, JHEP **10**, 117 (2017), [arXiv:1708.02047].
- [28] J. P. Dedonder *et al.*, Phys. Rev. D **103**, 11, 114028 (2021), [arXiv:2105.03355].
- [29] E. Aitala *et al.* (E791), Phys. Rev. D **73**, 032004 (2006), [Erratum: Phys. Rev. D **74**, 059901 (2006)], [hep-ex/0507099].
- [30] G. Bonvicini *et al.* (CLEO), Phys. Rev. D **78**, 052001 (2008), [arXiv:0802.4214].
- [31] B. Aubert *et al.* (BaBar), Phys. Rev. D **79**, 032003 (2009), [arXiv:0808.0971].
- [32] P. d'Argent *et al.*, JHEP **05**, 143 (2017), [arXiv:1703.08505].
- [33] R. Aaij *et al.* (LHCb), Eur. Phys. J. C **78**, 6, 443 (2018), [arXiv:1712.08609].
- [34] M. Ablikim *et al.* (BESIII), Phys. Rev. D **104**, 1, 012016 (2021), [arXiv:2011.08041].
- [35] M. Ablikim *et al.* (BESIII), Phys. Rev. D **106**, 11, 112006 (2022), [arXiv:2108.10050].
- [36] R. Aaij *et al.* (LHCb), JHEP **07**, 204 (2023), [arXiv:2209.09840].
- [37] R. Aaij *et al.* (LHCb), JHEP **06**, 044 (2023), [arXiv:2208.03300].
- [38] I. Adachi *et al.* (BaBar, Belle), Phys. Rev. Lett. **121**, 26, 261801 (2018), [arXiv:1804.06152]; I. Adachi *et al.* (BaBar, Belle), Phys. Rev. D **98**, 11, 112012 (2018), [arXiv:1804.06153].
- [39] V. Anisovich and A. Sarantsev, Eur. Phys. J. A **16**, 229 (2003), [hep-ph/0204328].
- [40] Z. Y. Zhou and H. Q. Zheng, Nucl. Phys. A **775**, 212 (2006), [hep-ph/0603062].
- [41] B. El-Bennich *et al.*, Phys. Rev. D **79**, 094005 (2009), [Erratum: Phys. Rev. D **83**, 039903 (2011)], [arXiv:0902.3645].
- [42] J.-P. Dedonder *et al.*, Acta Phys. Polon. B **42**, 2013 (2011), [arXiv:1011.0960].
- [43] M. Ablikim *et al.* (BESIII) (2022), [arXiv:2212.09048].
- [44] M. Ablikim *et al.* (BESIII), JHEP **08**, 196 (2022), [arXiv:2205.08844].
- [45] M. Ablikim *et al.* (BESIII), Phys. Rev. Lett. **129**, 18, 182001 (2022), [arXiv:2204.09614].
- [46] M. Ablikim *et al.* (BESIII), Phys. Rev. D **105**, 5, L051103 (2022), [arXiv:2110.07650].
- [47] M. Ablikim *et al.* (BESIII), JHEP **04**, 058 (2022), [arXiv:2202.04232].
- [48] M. Ablikim *et al.* (BESIII), JHEP **01**, 052 (2022), [arXiv:2109.12660].
- [49] R. Aaij *et al.* (LHCb), Phys. Rev. D **108**, 1, 012023 (2023), [arXiv:2208.03262].
- [50] M. Ablikim *et al.* (BESIII), JHEP **12**, 033 (2022), [arXiv:2209.08464].
- [51] M. Ablikim *et al.* (BESIII) (2023), [arXiv:2305.15879].
- [52] M. Ablikim *et al.* (BESIII), JHEP **09**, 242 (2022), [arXiv:2205.13759].
- [53] M. Ablikim *et al.* (BESIII), JHEP **07**, 051 (2022), [arXiv:2203.06688].
- [54] R. Aaij *et al.* (LHCb), JHEP **07**, 228 (2023), [arXiv:2301.07010].
- [55] K. M. Watson, Phys. Rev. **88**, 1163 (1952).
- [56] B. Hyams *et al.*, Nuclear Physics B **64**, 134 (1973), ISSN 0550-3213, URL <https://www.sciencedirect.com/science/article/pii/0550321373906184>.
- [57] J. R. Batley *et al.* (NA48/2), Eur. Phys. J. C **70**, 635 (2010).
- [58] S. X. Nakamura, Phys. Rev. D **93**, 1, 014005 (2016), [arXiv:1504.02557].
- [59] R. Aaij *et al.* (LHCb), JHEP **04**, 063 (2019), [arXiv:1902.05884].
- [60] F. Krinner *et al.*, Phys. Rev. D **97**, 11, 114008 (2018), [arXiv:1710.09849].
- [61] M. Mikhasenko *et al.* (JPAC), Phys. Rev. D **101**, 3, 034033 (2020), [arXiv:1910.04566].
- [62] M. Gronau and D. Wyler, Phys. Lett. B **265**, 172 (1991).
- [63] M. Gronau and D. London, Phys. Lett. B **253**, 483 (1991).
- [64] A. Bondar, Proceedings of BINP special analysis meeting on Dalitz analysis, 24–26 Sep. 2002, unpublished.
- [65] A. Giri *et al.*, Phys. Rev. D **68**, 054018 (2003), [hep-ph/0303187].
- [66] A. Poluektov *et al.* (Belle), Phys. Rev. D **70**, 072003 (2004), [hep-ex/0406067].
- [67] D. Atwood, I. Dunietz and A. Soni, Phys. Rev. D **63**, 036005 (2001), [hep-ph/0008090].
- [68] D. Atwood and A. Soni, Phys. Rev. D **68**, 033003 (2003), [hep-ph/0304085].
- [69] J. Rademacker and G. Wilkinson, Phys. Lett. B **647**, 400 (2007), [hep-ph/0611272].
- [70] A. Bondar, A. Poluektov and V. Vorobiev, Phys. Rev. D **82**, 034033 (2010), [arXiv:1004.2350].
- [71] S. Malde and G. Wilkinson, Phys. Lett. B **701**, 353 (2011), [arXiv:1104.2731].
- [72] C. Thomas and G. Wilkinson, JHEP **10**, 185 (2012), [arXiv:1209.0172].
- [73] M. Nayak *et al.*, Phys. Lett. B **740**, 1 (2015), [arXiv:1410.3964].
- [74] S. Malde *et al.*, Phys. Lett. B **747**, 9 (2015), [arXiv:1504.05878].
- [75] S. Malde, C. Thomas and G. Wilkinson, Phys. Rev. D **91**, 9, 094032 (2015), [arXiv:1502.04560].
- [76] A. Bondar and A. Poluektov, Eur. Phys. J. C **55**, 51 (2008), [arXiv:0801.0840].
- [77] A. Poluektov, Eur. Phys. J. C **78**, 2, 121 (2018), [arXiv:1712.08326].
- [78] J. V. Backus *et al.* (2022), [arXiv:2211.05133].
- [79] J. Lane, E. Gersabeck and J. Rademacker (2023), [arXiv:2305.10787].
- [80] J. Libby *et al.* (CLEO), Phys. Rev. D **82**, 112006 (2010), [arXiv:1010.2817].
- [81] R. A. Briere *et al.* (CLEO), Phys. Rev. D **80**, 032002 (2009), [arXiv:0903.1681].
- [82] S. Harnew *et al.*, JHEP **01**, 144 (2018), [arXiv:1709.03467].
- [83] P. Resmi *et al.*, JHEP **01**, 082 (2018), [arXiv:1710.10086].
- [84] J. Insler *et al.* (CLEO), Phys. Rev. D **85**, 092016 (2012), [Erratum: Phys. Rev. D **94**, 099905 (2016)], [arXiv:1203.3804].

- [85] T. Evans *et al.*, Phys. Lett. B **757**, 520 (2016), [Erratum: Phys. Lett. B 765, 402–403 (2017)], [arXiv:1602.07430].
- [86] M. Ablikim *et al.* (BESIII), Phys. Rev. Lett. **124**, 24, 241802 (2020), [arXiv:2002.12791].
- [87] M. Ablikim *et al.* (BESIII), Phys. Rev. D **101**, 11, 112002 (2020), [arXiv:2003.00091].
- [88] M. Ablikim *et al.* (BESIII), Phys. Rev. D **102**, 5, 052008 (2020), [arXiv:2007.07959].
- [89] M. Ablikim *et al.* (BESIII), JHEP **05**, 164 (2021), [arXiv:2103.05988].
- [90] T. Evans *et al.*, Phys. Lett. B **802**, 135188 (2020), [arXiv:1909.10196].
- [91] M. Ablikim *et al.* (BESIII), Phys. Rev. D **107**, 3, 032009 (2023), [arXiv:2212.06489].
- [92] M. Ablikim *et al.* (BESIII, (The BESIII Collaboration)*), Phys. Rev. D **106**, 9, 092004 (2022), [arXiv:2208.10098].
- [93] C. Rosner *et al.* (BESIII), Phys. Rev. D **108**, 3, 032003 (2023), [arXiv:2305.03975].
- [94] R. Aaij *et al.* (LHCb), Phys. Rev. Lett. **116**, 24, 241801 (2016), [arXiv:1602.07224].
- [95] P. del Amo Sanchez *et al.* (BaBar), Phys. Rev. Lett. **105**, 121801 (2010), [arXiv:1005.1096].
- [96] J. Lees *et al.* (BaBar), Phys. Rev. D **84**, 012002 (2011), [arXiv:1104.4472].
- [97] A. Poluektov *et al.* (Belle), Phys. Rev. D **81**, 112002 (2010), [arXiv:1003.3360].
- [98] H. Aihara *et al.* (Belle), Phys. Rev. D **85**, 112014 (2012), [arXiv:1204.6561].
- [99] P. K. Resmi *et al.* (Belle), JHEP **10**, 178 (2019), [arXiv:1908.09499].
- [100] F. Abudinén *et al.* (Belle, Belle-II), JHEP **02**, 063 (2022), [Erratum: JHEP 12, 034 (2022)], [arXiv:2110.12125].
- [101] R. Aaij *et al.* (LHCb), Phys. Lett. B **726**, 151 (2013), [arXiv:1305.2050].
- [102] R. Aaij *et al.* (LHCb), Phys. Lett. B **723**, 44 (2013), [arXiv:1303.4646].
- [103] R. Aaij *et al.* (LHCb), Phys. Lett. B **718**, 43 (2012), [arXiv:1209.5869].
- [104] R. Aaij *et al.* (LHCb), JHEP **10**, 097 (2014), [arXiv:1408.2748].
- [105] R. Aaij *et al.* (LHCb), Phys. Lett. B **733**, 36 (2014), [arXiv:1402.2982].
- [106] R. Aaij *et al.* (LHCb), Nucl. Phys. B **888**, 169 (2014), [arXiv:1407.6211].
- [107] R. Aaij *et al.* (LHCb), Phys. Rev. D **91**, 11, 112014 (2015), [arXiv:1504.05442].
- [108] R. Aaij *et al.* (LHCb), JHEP **06**, 131 (2016), [arXiv:1604.01525].
- [109] R. Aaij *et al.* (LHCb), JHEP **12**, 087 (2016), [arXiv:1611.03076].
- [110] R. Aaij *et al.* (LHCb), JHEP **08**, 176 (2018), [Erratum: JHEP 10, 107 (2018)], [arXiv:1806.01202].
- [111] R. Aaij *et al.* (LHCb), JHEP **12**, 141 (2021), [arXiv:2110.02350]; LHCb-CONF-2022-003 (2022), URL <https://cds.cern.ch/record/2838029>.
- [112] R. Aaij *et al.* (LHCb), JHEP **07**, 099 (2022), [arXiv:2112.10617].
- [113] R. Aaij *et al.* (LHCb), JHEP **07**, 138 (2023), [arXiv:2209.03692].
- [114] R. Aaij *et al.* (LHCb), Eur. Phys. J. C **83**, 6, 547 (2023), [arXiv:2301.10328].
- [115] S. Harnew and J. Rademacker, Phys. Lett. B **728**, 296 (2014), [arXiv:1309.0134].
- [116] S. Harnew and J. Rademacker, JHEP **03**, 169 (2015), [arXiv:1412.7254].
- [117] D. Craik, T. Gershon and A. Poluektov, Phys. Rev. D **97**, 5, 056002 (2018), [arXiv:1712.07853].
- [118] M. Ablikim *et al.* (BESIII), Chin. Phys. C **44**, 4, 040001 (2020), [arXiv:1912.05983].
- [119] R. Aaij *et al.* (LHCb), JHEP **02**, 169 (2021), [arXiv:2010.08483].
- [120] Y. S. Amhis *et al.* (HFLAV), Eur. Phys. J. C **81**, 226 (2021), updated results and plots available at <https://hflav.web.cern.ch/>, [arXiv:1909.12524].
- [121] A. Bondar, T. Gershon and P. Krokovny, Phys. Lett. B **624**, 1 (2005), [hep-ph/0503174].
- [122] P. Krokovny *et al.* (Belle), Phys. Rev. Lett. **97**, 081801 (2006), [hep-ex/0605023].
- [123] B. Aubert *et al.* (BaBar), Phys. Rev. Lett. **99**, 231802 (2007), [arXiv:0708.1544].
- [124] V. Vorobyev *et al.* (Belle), Phys. Rev. D **94**, 5, 052004 (2016), [arXiv:1607.05813].
- [125] See the note on $D^0-\bar{D}^0$ Mixing in this *Review*.
- [126] See the note CP violation in the quark sector in this *Review*.
- [127] D. Asner *et al.* (CLEO), Phys. Rev. D **72**, 012001 (2005), [hep-ex/0503045].
- [128] R. Aaij *et al.* (LHCb), Phys. Rev. Lett. **127**, 11, 111801 (2021), [arXiv:2106.03744].
- [129] A. Di Canto *et al.*, Phys. Rev. D **99**, 1, 012007 (2019), [arXiv:1811.01032].
- [130] R. Aaij *et al.* (LHCb), Phys. Rev. Lett. **122**, 21, 211803 (2019), [arXiv:1903.08726].
- [131] (2022), [arXiv:2209.03179].
- [132] R. Aaij *et al.* (LHCb), Phys. Rev. D **93**, 5, 052018 (2016), [arXiv:1509.06628].
- [133] R. Aaij *et al.* (LHCb), JHEP **02**, 126 (2019), [arXiv:1811.08304].
- [134] M. Artuso *et al.* (CLEO), Phys. Rev. D **85**, 122002 (2012), [arXiv:1201.5716].
- [135] B. Aubert *et al.* (BaBar), Phys. Rev. D **78**, 051102 (2008), [arXiv:0802.4035].
- [136] I. Bediaga *et al.*, Phys. Rev. D **80**, 096006 (2009), [arXiv:0905.4233].
- [137] I. Bediaga *et al.*, Phys. Rev. D **86**, 036005 (2012), [arXiv:1205.3036].
- [138] R. Aaij *et al.* (LHCb), Phys. Lett. B **726**, 623 (2013), [arXiv:1308.3189].
- [139] J. Lees *et al.* (BaBar), Phys. Rev. D **87**, 5, 052010 (2013), [arXiv:1212.1856].
- [140] R. Aaij *et al.* (LHCb), Phys. Rev. D **84**, 112008 (2011), [arXiv:1110.3970].
- [141] R. Aaij *et al.* (LHCb), JHEP **06**, 112 (2013), [arXiv:1303.4906].
- [142] T. Aaltonen *et al.* (CDF), Phys. Rev. D **86**, 032007 (2012), [arXiv:1207.0825].
- [143] R. Aaij *et al.* (LHCb), JHEP **07**, 067 (2023), [arXiv:2303.04062].
- [144] R. Aaij *et al.* (LHCb), Phys. Lett. B **728**, 585 (2014), [arXiv:1310.7953].
- [145] R. Aaij *et al.* (LHCb), Eur. Phys. J. C **80**, 10, 986 (2020), [arXiv:2006.03145].
- [146] M. Williams, Phys. Rev. D **84**, 054015 (2011), [arXiv:1105.5338].
- [147] A. Davis *et al.*, JHEP **06**, 098 (2023), [arXiv:2301.13211].
- [148] R. Aaij *et al.* (LHCb), Phys. Lett. B **740**, 158 (2015), [arXiv:1410.4170].

- [149] R. Aaij *et al.* (LHCb), Phys. Lett. B **769**, 345 (2017), [arXiv:1612.03207].
- [150] R. Aaij *et al.* (LHCb) (2023), [arXiv:2306.12746].
- [151] E. Golowich and G. Valencia, Phys. Rev. D **40**, 112 (1989).
- [152] G. Valencia, Phys. Rev. D **39**, 3339 (1989).
- [153] W. Bensalem and D. London, Phys. Rev. D **64**, 116003 (2001), [hep-ph/0005018].
- [154] I. I. Bigi, in “KAON2001: International Conference on CP Violation,” (2001), [hep-ph/0107102].
- [155] W. Bensalem, A. Datta and D. London, Phys. Rev. D **66**, 094004 (2002), [hep-ph/0208054].
- [156] W. Bensalem, A. Datta and D. London, Phys. Lett. B **538**, 309 (2002), [hep-ph/0205009].
- [157] A. Datta and D. London, Int. J. Mod. Phys. A **19**, 2505 (2004), [hep-ph/0303159].
- [158] M. Gronau and J. L. Rosner, Phys. Rev. D **84**, 096013 (2011), [arXiv:1107.1232].
- [159] G. Durieux and Y. Grossman, Phys. Rev. D **92**, 7, 076013 (2015), [arXiv:1508.03054].
- [160] J. Link *et al.* (FOCUS), Phys. Lett. B **622**, 239 (2005), [hep-ex/0506012].
- [161] P. del Amo Sanchez *et al.* (BaBar), Phys. Rev. D **81**, 111103 (2010), [arXiv:1003.3397].
- [162] R. Aaij *et al.* (LHCb), JHEP **10**, 005 (2014), [arXiv:1408.1299].
- [163] J. Kim *et al.* (Belle), Phys. Rev. D **99**, 1, 011104 (2019), [arXiv:1810.06457].
- [164] J. Lees *et al.* (BaBar), Phys. Rev. D **84**, 031103 (2011), [arXiv:1105.4410].
- [165] K. Prasanth *et al.* (Belle), Phys. Rev. D **95**, 9, 091101 (2017), [arXiv:1703.05721].
- [166] R. Aaij *et al.* (LHCb), Phys. Rev. Lett. **128**, 22, 221801 (2022), [arXiv:2111.03327].
- [167] R. Aaij *et al.* (LHCb), Phys. Rev. Lett. **121**, 9, 091801 (2018), [arXiv:1806.10793].

70. D^0 - \bar{D}^0 Mixing

Revised September 2023 by D.M. Asner (BNL) and A.J. Schwartz (U. of Cincinnati).

The formalism for D^0 - \bar{D}^0 mixing is closely related to that for CP violation; for further details on the latter, see the note “ CP Violation in the Quark Sector” in this *Review*. The time evolution of the D^0 - \bar{D}^0 system is described by the Schrödinger equation

$$i \frac{\partial}{\partial t} \begin{pmatrix} D^0(t) \\ \bar{D}^0(t) \end{pmatrix} = \left(\mathbf{M} - \frac{i}{2} \mathbf{\Gamma} \right) \begin{pmatrix} D^0(t) \\ \bar{D}^0(t) \end{pmatrix}, \quad (70.1)$$

where the \mathbf{M} and $\mathbf{\Gamma}$ matrices are Hermitian, and CPT invariance requires that $M_{11} = M_{22} \equiv M$ and $\Gamma_{11} = \Gamma_{22} \equiv \Gamma$. The off-diagonal elements of \mathbf{M} and $\mathbf{\Gamma}$ are referred to as the dispersive and absorptive parts, respectively, of the mixing. The mass eigenstates D_1 and D_2 of the Hamiltonian $\mathbf{M} - i\mathbf{\Gamma}/2$ are defined as

$$|D_{1,2}\rangle \equiv p|D^0\rangle \pm q|\bar{D}^0\rangle, \quad (70.2)$$

where normalization imposes $|p|^2 + |q|^2 = 1$. If $p = \pm q$, then the mass eigenstates are CP eigenstates and CP is conserved in mixing. Our phase convention is $CP|D^0\rangle = -|\bar{D}^0\rangle$ and $\text{Arg}(q/p) \in [-\pi/2, \pi/2]$, which imply that, in the absence of CP violation in mixing, D_2 is CP -even and D_1 is CP -odd.

The eigenvalues of $\mathbf{M} - i\mathbf{\Gamma}/2$ are

$$\omega_{1,2} = \left(M - \frac{i}{2} \Gamma \right) \pm \frac{q}{p} \left(M_{12} - \frac{i}{2} \Gamma_{12} \right) \equiv m_{1,2} - \frac{i}{2} \Gamma_{1,2}, \quad (70.3)$$

where $m_{1,2}$ and $\Gamma_{1,2}$ are real and correspond to the masses and decay widths, respectively, of the $D_{1,2}$ mass eigenstates. As the trace $\Gamma_{11} + \Gamma_{22} = 2\Gamma$ is unchanged by diagonalizing $\mathbf{\Gamma}$, Γ must equal $(\Gamma_1 + \Gamma_2)/2$, the mean decay width. Solving for the eigenstates of the eigenvalues yields

$$\left(\frac{q}{p} \right)^2 = \frac{M_{12}^* - \frac{i}{2} \Gamma_{12}^*}{M_{12} - \frac{i}{2} \Gamma_{12}}. \quad (70.4)$$

If CP is conserved in mixing, then $(q/p)^2 = 1$ and M_{12} and Γ_{12} must be real. In this case, the difference in eigenvalues is $\Delta m \equiv m_2 - m_1 = 2M_{12}$ and $\Delta\Gamma \equiv \Gamma_2 - \Gamma_1 = 2\Gamma_{12}$. The signs of Δm and $\Delta\Gamma$ are difficult to predict from theory and thus must be determined experimentally.

We define dimensionless mixing parameters x and y as

$$x \equiv \frac{\Delta m}{\Gamma} \quad (70.5)$$

$$y \equiv \frac{\Delta\Gamma}{2\Gamma}. \quad (70.6)$$

These parameters are measured in several ways. The most precise values are obtained by measuring the time dependence of D^0 decays. For all methods, the initial flavor of the D^0 or \bar{D}^0 when produced must be determined. The most common method used for this is to reconstruct $D^{*+} \rightarrow D^0\pi^+$ or $D^{*-} \rightarrow \bar{D}^0\pi^-$ decays; the charge of the accompanying pion (which has low momentum in the lab frame and is often referred to as the “soft” pion) determines the flavor of the neutral D . BABAR and LHCb have also identified the flavor of the neutral D by reconstructing the semileptonic decays $B^+ \rightarrow \bar{D}^0\ell^+\nu$, $B^0 \rightarrow D^{*+}\ell^+\nu$, $B^- \rightarrow D^0\ell^-\nu$, and $\bar{B}^0 \rightarrow D^{*+}\ell^-\nu$; in this case the charge of the accompanying lepton determines the D flavor. Both experiments have used both tags together to select “double-tagged” $B \rightarrow D^{*\pm}\ell^\mp\nu$, $D^{*\pm} \rightarrow (D^0, \bar{D}^0)\pi^\pm$ decays, which have especially high purity. At e^+e^- collider experiments such as Belle, BABAR, and BESIII, the D flavor can also be determined by fully reconstructing a flavor-specific D decay on the “opposite side” of an event, i.e., recoiling against the signal-side D decay.

At BESIII, where $D\bar{D}$ pairs are produced near their threshold via $e^+e^- \rightarrow \psi(3770) \rightarrow D^0\bar{D}^0$, there is relatively little background and the purity of opposite-side tagging is equivalent to that achieved using $D^{*\pm}$ decays. However, BESIII operates at a symmetric e^+e^- collider, and the $D\bar{D}$ pairs are produced almost at rest in the lab frame. As a consequence, the D 's do

not travel any appreciable distance before decaying, and time-dependent analyses are not possible. To overcome this, measurements of mixing at BESIII utilize the quantum coherence of the initial $\psi(3770) \rightarrow D^0\bar{D}^0$ state and time-integrated measurements [1–5].

70.1 Time-Dependent Analyses

Our notation is as follows: Cabibbo-favored (CF) decay amplitudes are denoted $\bar{A}_f \equiv \langle f|H|\bar{D}^0\rangle$ and $A_f \equiv \langle f|H|D^0\rangle$; i.e, the final state is $f = K^+\ell^-\nu$, $K^+\pi^-$, $K^+\pi^-\pi^0$, etc. Doubly-Cabibbo-suppressed (DCS) decay amplitudes are denoted $\bar{A}_{\bar{f}} \equiv \langle \bar{f}|H|\bar{D}^0\rangle$ and $\bar{A}_{\bar{f}} \equiv \langle \bar{f}|H|D^0\rangle$. When discussing decay rates, we neglect constant phase-space factors, which divide out in ratios of rates to common final states.

Starting from a pure $|D^0\rangle$ or $|\bar{D}^0\rangle$ state at $t = 0$, the time-dependent decay rates to “wrong-sign” final states can be written

$$r(t) \equiv \left| \langle f|H|D^0(t)\rangle \right|^2 = |\bar{A}_f|^2 \left| \frac{q}{p} \right|^2 \left| g_+(t) \lambda_f^{-1} + g_-(t) \right|^2 \quad (70.7)$$

$$\bar{r}(t) \equiv \left| \langle \bar{f}|H|\bar{D}^0(t)\rangle \right|^2 = |A_{\bar{f}}|^2 \left| \frac{p}{q} \right|^2 \left| g_+(t) \lambda_{\bar{f}} + g_-(t) \right|^2, \quad (70.8)$$

where

$$\lambda_f \equiv \frac{q \bar{A}_f}{p A_f}, \quad \lambda_{\bar{f}} \equiv \frac{q \bar{A}_{\bar{f}}}{p A_{\bar{f}}}, \quad (70.9)$$

and

$$g_{\pm}(t) = \frac{1}{2} \left(e^{-i\omega_1 t} \pm e^{-i\omega_2 t} \right). \quad (70.10)$$

A change in convention for the relative phase of D^0 and \bar{D}^0 would cancel between q/p and \bar{A}_f/A_f or $\bar{A}_{\bar{f}}/A_{\bar{f}}$, leaving λ_f and $\lambda_{\bar{f}}$ unchanged. For multibody final states, these equations apply separately to each point in phase-space. Integrating over regions of phase-space can lead to enhanced sensitivity to CP violation; see the discussion below on multibody decays and the note “Review of Multibody Charm Analyses” in this *Review*. As the mixing parameters x and y are very small, $r(t)$ and $\bar{r}(t)$ are usually expanded to second order in x and y .

70.2 Semileptonic decays

Consider the final state $f = K^+\ell^-\bar{\nu}_\ell$, where $A_f = \bar{A}_{\bar{f}} = 0$ is an excellent approximation in the Standard Model. The final state f is accessible from a D^0 only via mixing,¹ and the decay rate is

$$r(t) = |\bar{A}_f|^2 \left| \frac{q}{p} \right|^2 |g_-(t)|^2 \approx |\bar{A}_f|^2 \left| \frac{q}{p} \right|^2 \left(\frac{x^2 + y^2}{4} \right) (\Gamma t)^2 e^{-\Gamma t}. \quad (70.11)$$

For $\bar{r}(t)$, q/p is replaced by p/q . In the Standard Model, CP violation in charm mixing is small and $|q/p| \approx 1$. In the limit of CP conservation, $r(t) = \bar{r}(t)$, and the time-integrated mixed decay rate relative to the time-integrated unmixed decay rate for semileptonic decays is

$$\frac{\int_0^\infty r(t) dt}{\int_0^\infty |\bar{A}_f|^2 e^{-\Gamma t} dt} = \frac{x^2 + y^2}{2} \equiv R_M. \quad (70.12)$$

Table 70.1 summarizes results for R_M from semileptonic decays. The world average from the Heavy Flavor Averaging Group (HFLAV) [6] is $R_M = (1.30 \pm 2.69) \times 10^{-4}$.

¹There exists a doubly Cabibbo-suppressed amplitude in which the c and \bar{u} quarks exchange a W , and then the resulting d quark (from c) decays semileptonically. We neglect this second-order process.

Table 70.1: Results for $R_M = (x^2 + y^2)/2$ in D^0 semileptonic decays. The HFLAV average assumes statistical and systematic uncertainties are uncorrelated. When a single uncertainty is listed, that corresponds to statistical and systematic uncertainties combined. The measurements with an asterisk (*) have been superseded and thus are not included in the HFLAV average.

Year	Experiment	Final state(s)	$R_M (\times 10^{-3})$	90% C.L. ($\times 10^{-3}$)
2008	Belle (492 fb $^{-1}$) [7]	$K^{(*)+}e^{-}\bar{\nu}_e$	$0.13 \pm 0.22 \pm 0.20$	< 0.61
2007	BABAR (344 fb $^{-1}$) [8]	$K^{(*)+}e^{-}\bar{\nu}_e$	$0.04^{+0.70}_{-0.60}$	(-1.3, 1.2)
2005	CLEO (9.0 fb $^{-1}$) [9]	$K^{(*)+}e^{-}\bar{\nu}_e$	$1.6 \pm 2.9 \pm 2.9$	< 7.8
1996	E791 (2×10^{10} evts) [10]	$K^+\ell^{-}\bar{\nu}_\ell$	$1.1^{+3.0+0.0}_{-2.7-0.1}$	< 5.0
HFLAV Average [6]			0.130 ± 0.269	
2005*	Belle (253 fb $^{-1}$) [11]	$K^{(*)+}e^{-}\bar{\nu}_e$	$0.02 \pm 0.47 \pm 0.14$	< 1.0
2004*	BABAR (87 fb $^{-1}$) [12]	$K^{(*)+}e^{-}\bar{\nu}_e$	$2.3 \pm 1.2 \pm 0.4$	< 4.2

70.3 Wrong-sign decays to hadronic non- CP eigenstates

Consider the final state $f = K^+\pi^-$, i.e., A_f and \bar{A}_f are CF, A_f and \bar{A}_f are DCS. Because CF and DCS decays proceed via tree-level amplitudes, and such amplitudes involve only the first two quark generations, direct CP violation is negligible². The ratios of decay amplitudes can be written

$$\frac{A_f}{\bar{A}_f} = -\sqrt{R_D^+} e^{-i\delta_f} \quad \frac{\bar{A}_f}{A_f} = -\sqrt{R_D^-} e^{-i\delta_f}, \quad (70.13)$$

where δ_f is the strong phase difference between the DCS and CF amplitudes. The minus sign originates from the weak phase difference between the amplitudes, specifically, the relative minus sign between V_{us} and V_{cd} (which produces a relative minus sign between $V_{cs}^*V_{ud}$ and $V_{us}^*V_{cd}$). The parameters R_D^+ and R_D^- are the ratios of the DCS decay rate to the CF decay rate. From the relevant CKM matrix elements, one estimates $R_D^+, R_D^- \sim \tan^4 \theta_c$, where θ_c is the Cabibbo angle.

With the parameterization of Eq. (70.13), Eq. (70.9) becomes

$$\lambda_f^{-1} = \frac{p}{q} \frac{A_f}{\bar{A}_f} = -\sqrt{R_D^+} \left| \frac{p}{q} \right| e^{-i(\delta_f + \phi)} \quad (70.14)$$

$$\lambda_{\bar{f}} = \frac{q}{p} \frac{\bar{A}_f}{A_f} = -\sqrt{R_D^-} \left| \frac{q}{p} \right| e^{-i(\delta_f - \phi)}, \quad (70.15)$$

where $\phi = \text{Arg}(q/p)$. The weak phase ϕ is independent of the final state f and is often referred to as “universal.” For convenience, we define the mean decay rate $R_D \equiv (R_D^+ + R_D^-)/2$, and the decay rate asymmetry $A_D \equiv (R_D^+ - R_D^-)/(R_D^+ + R_D^-)$.

With these definitions, we expand the decay rates in Eqs. (70.7) and (70.8) to second order in the small mixing parameters x and y to obtain [13,14]:

$$r(t) = \left| \bar{A}_f \right|^2 e^{-\Gamma t} \left[R_D (1 + A_D) + \sqrt{R_D (1 + A_D)} \left| \frac{q}{p} \right| y'_+(\Gamma t) + \left| \frac{q}{p} \right|^2 \frac{(x'_+{}^2 + y'_+{}^2)}{4} (\Gamma t)^2 \right] \quad (70.16)$$

and

$$\bar{r}(t) = \left| A_{\bar{f}} \right|^2 e^{-\Gamma t} \left[R_D (1 - A_D) + \sqrt{R_D (1 - A_D)} \left| \frac{p}{q} \right| y'_-(\Gamma t) + \left| \frac{p}{q} \right|^2 \frac{(x'_-{}^2 + y'_-{}^2)}{4} (\Gamma t)^2 \right], \quad (70.17)$$

where

$$x'_\pm = x \cos(\delta_f \pm \phi) + y \sin(\delta_f \pm \phi) \quad (70.18)$$

$$y'_\pm = y \cos(\delta_f \pm \phi) - x \sin(\delta_f \pm \phi). \quad (70.19)$$

²For two quark generations, the weak phases can be defined to eliminate all weak-phase differences.

Defining the “strong-phase-rotated” mixing parameters

$$x' \equiv x \cos \delta_f + y \sin \delta_f \quad (70.20)$$

$$y' \equiv y \cos \delta_f - x \sin \delta_f \quad (70.21)$$

gives

$$x'_\pm = x' \cos \phi \pm y' \sin \phi \quad (70.22)$$

$$y'_\pm = y' \cos \phi \mp x' \sin \phi, \quad (70.23)$$

i.e., x'_\pm and y'_\pm are obtained from x', y' via an additional “weak-phase rotation.” To summarize, parameters (x', y') are the mixing parameters (x, y) rotated by the strong phase δ_f , and parameters (x'_\pm, y'_\pm) are the parameters (x', y') rotated by the weak phase $+\phi$ for D^0 decays and $-\phi$ for \bar{D}^0 decays. Note that $x'^2 + y'^2 = x'^2 + y'^2 = x^2 + y^2 = x^2 + y^2$. In Eqs. (70.16) and (70.17), a fourth term $R_D (1 \pm A_D) (x'_\pm - y'_\pm)^2 (\Gamma t)^2 / 4$ has been dropped, as it is negligible relative to the other terms for the range of decay times measured by experiments.

Comparing Eqs. (70.16) and (70.17), one sees that $r(t) \neq \bar{r}(t)$ and CP is violated if either $A_D \neq 0$, $|q/p| \neq 1$, or $\phi \neq 0$. These three inequalities correspond, respectively, to the three types of CP violation: in the decay amplitudes ($R_D^+ \neq R_D^-$); in the mixing; and due to interference between a mixed decay amplitude (i.e., mixing is followed by decay) and an unmixed decay amplitude. Whereas CP violation in the decay amplitudes is parameterized by A_D , CP violation in mixing is parameterized by $A_M \equiv (|q/p| - |p/q|) / (|q/p| + |p/q|)$.

In the limit of CP conservation, $A_D = 0$, $|q/p| = 1$, and $\phi = 0$. In this case

$$r(t) = \bar{r}(t) = \left| A_{\bar{f}} \right|^2 e^{-\Gamma t} \left[R_D + \sqrt{R_D} y' (\Gamma t) + \frac{x'^2 + y'^2}{4} (\Gamma t)^2 \right], \quad (70.24)$$

and the total number of $D^0 \rightarrow f$ decays divided by the total number of $D^0 \rightarrow \bar{f}$ decays is

$$R = \frac{\int_0^\infty r(t) dt}{\int_0^\infty \left| A_{\bar{f}} \right|^2 e^{-\Gamma t} dt} = R_D + \sqrt{R_D} y' + \frac{x'^2 + y'^2}{2}. \quad (70.25)$$

The ratio R is more straightforward to measure than $r(t)$ or $\bar{r}(t)$, as there is no decay-time dependence. In Table 70.2 we report measurements of R , R_D , and A_D in $D^0 \rightarrow K^+\pi^-$ decays normalized to $D^0 \rightarrow K^-\pi^+$ decays, and results from HFLAV [15] obtained from a global fit to all relevant data that allows for both mixing and CP violation (see Section 70.7). The experiments typically perform a single fit for parameters R_D , x'^2 , and y' ; results for x'^2 and y' are listed in Table 70.3. Allowing for CP violation, the experiments measure parameters (R_D^+, x'^2, y'_+) and (R_D^-, x'^2, y'_-) [or equivalently (R_D, A_D) instead of (R_D^+, R_D^-)] by

Table 70.2: Results for R , R_D , and A_D as measured using $D^0 \rightarrow K^\pm \pi^\mp$ decays. When a single uncertainty is listed, that corresponds to statistical and systematic uncertainties combined. The measurements with an asterisk (*) have been superseded and thus are not included in the HFLAV global fit (Section 70.7). The measurements with a dagger (†) are not included in the HFLAV global fit due to much poorer precision.

Year	Experiment	$R (\times 10^{-3})$	$R_D (\times 10^{-3})$	$A_D (\%)$
2018	LHCb (5.0 fb ⁻¹ D^* tag) [16]	—	3.454 ± 0.031	-0.01 ± 0.91
2017	LHCb (3.0 fb ⁻¹ $B+D^*$ double tag) [17]	—	3.48 ± 0.10	-3.15 ± 3.31
2014	Belle (976 fb ⁻¹) [18]	3.86 ± 0.06	3.53 ± 0.13	—
2013	CDF (9.6 fb ⁻¹) [19]	4.30 ± 0.05	3.51 ± 0.35	—
2007	BABAR (384 fb ⁻¹) [20]	3.53 ± 0.08 ± 0.04	3.03 ± 0.16 ± 0.10	-2.1 ± 5.2 ± 1.5
HFLAV Fit Result [15]			3.434 ± 0.019	-0.70 ± 0.36
2013b*	LHCb (3.0 fb ⁻¹ D^* tag) [21]	—	3.568 ± 0.066	-0.7 ± 1.9
2013a*	LHCb (1.0 fb ⁻¹) [22]	4.25 ± 0.04	3.52 ± 0.15	—
2008*	CDF (1.5 fb ⁻¹) [23]	4.15 ± 0.10	3.04 ± 0.55	—
2006*	Belle (400 fb ⁻¹) [24]	3.77 ± 0.08 ± 0.05	3.64 ± 0.18	2.3 ± 4.7
2005†	FOCUS (234 evts) [25]	4.29 ^{+0.63} ± 0.27	5.17 ^{+1.47} ± 0.76	13 ⁺³³ ± 10
2000†	CLEO (9.0 fb ⁻¹) [26]	3.32 ^{+0.83} ± 0.40	4.8 ± 1.2 ± 0.4	-1 ⁺¹⁶ ± 1
1998†	E791 (5643 evts) [27]	6.8 ^{+3.4} ± 0.7	—	—

separately fitting the $D^0 \rightarrow K^+ \pi^-$ and $\bar{D}^0 \rightarrow K^- \pi^+$ event samples.

Extraction of the mixing parameters x and y from measurements of x' and y' requires knowledge of the strong phase difference $\delta_{K\pi}$. This can be determined from the decay rates of $D_\pm \rightarrow K^+ \pi^-$, where D_+ (D_-) denotes the CP -even (CP -odd) eigenstate. Since $|D_\pm\rangle = (|D^0\rangle \mp |\bar{D}^0\rangle)/\sqrt{2}$,

$$\sqrt{2} A(D_\pm \rightarrow K^+ \pi^-) = A(D^0 \rightarrow K^+ \pi^-) \mp A(\bar{D}^0 \rightarrow K^+ \pi^-). \quad (70.26)$$

Squaring this amplitude and using Eq. (70.13) yields the relation

$$\cos \delta_{K\pi} = \frac{|A(D_+ \rightarrow K^+ \pi^-)|^2 - |A(D_- \rightarrow K^+ \pi^-)|^2}{2|A(D^0 \rightarrow K^+ \pi^-)||A(\bar{D}^0 \rightarrow K^+ \pi^-)|}. \quad (70.27)$$

Measuring the right-hand side is possible if one can identify pure D_+ , D_- , D^0 , and \bar{D}^0 initial states. This is accomplished at CLEOC and BESIII utilizing the processes $e^+ e^- \rightarrow \psi(3770) \rightarrow \bar{D}^0 D^0 \rightarrow (f_{CP})(K^+ \pi^-)$, or $\psi(3770) \rightarrow \bar{D}^0 D^0 \rightarrow (f_{\bar{D}^0})(K^+ \pi^-)$, where f_{CP} denotes a CP -specific final state, and $f_{\bar{D}^0}$ denotes a \bar{D}^0 -flavor-specific final state. In the first case, quantum coherence and CP symmetry ensures that the $K^+ \pi^-$ state originates from a neutral D with CP opposite that of f_{CP} . In the second case, at the time when the \bar{D}^0 decays, the opposite side is D^0 . However, it can potentially mix to \bar{D}^0 before decaying to $K^+ \pi^-$, and this introduces some dependence on the mixing parameters x and y . This dependence is seen explicitly in the observable

$$A_{K\pi}^{CP} \equiv \frac{|A(D_- \rightarrow K^- \pi^+)|^2 - |A(D_+ \rightarrow K^- \pi^+)|^2}{|A(D_- \rightarrow K^- \pi^+)|^2 + |A(D_+ \rightarrow K^- \pi^+)|^2}. \quad (70.28)$$

To lowest order in the mixing parameters [28],

$$A_{K\pi}^{CP} = \frac{2\sqrt{R_D} \cos \delta_{K\pi} + y}{1 + R}, \quad (70.29)$$

where R is defined in Eq. (70.25). Such measurements are discussed in Section 70.5.

70.3.1 Wrong-sign decays to multibody final states

For multibody final states, Eqs. (70.13)-(70.25) apply to each point in phase-space.³ Although x and y do not vary across phase-space, knowledge of the resonant substructure is needed to determine the strong phase difference δ from point to point to extract x

and y . Alternatively, experimental knowledge of the strong phase difference between D^0 and \bar{D}^0 decay amplitudes across phase space [29] allow one to determine x and y independent of a decay model of resonant substructure. This phase information can be measured at the charm threshold, where CLEO-c and BESIII took data.

A time-dependent analysis at BABAR [30, 31] of $D^0 \rightarrow K^+ \pi^- \pi^0$ decays, relative to CF $\bar{D}^0 \rightarrow K^+ \pi^- \pi^0$ decays, determined the strong phase variation across the Dalitz plot and reported $x' = (2.61_{-0.68}^{+0.57} \pm 0.39)\%$ and $y' = (-0.06_{-0.64}^{+0.55} \pm 0.34)\%$. These mixing parameters are defined as

$$x'' = x \cos \delta_{K\pi\pi^0} + y \sin \delta_{K\pi\pi^0} \quad (70.30)$$

$$y'' = y \cos \delta_{K\pi\pi^0} - x \sin \delta_{K\pi\pi^0}, \quad (70.31)$$

in analogy with x' , y' , and $\delta_{K\pi}$ of Eqs. (70.20) and (70.21). Here, $\delta_{K\pi\pi^0}$ is the strong phase difference between the amplitudes $A(D^0 \rightarrow K^+ \rho^-)$ and $A(\bar{D}^0 \rightarrow K^+ \rho^-)$. The phase difference $\delta_{K\pi\pi^0}$ can be determined in a manner similar to that for $\delta_{K\pi}$: by using Eq. (70.27) and quantum-correlated measurements of the branching fractions $B(D_+ \rightarrow K^+ \rho^-)$, $B(D_- \rightarrow K^+ \rho^-)$, $B(D^0 \rightarrow K^+ \rho^-)$, and $B(\bar{D}^0 \rightarrow K^+ \rho^-)$ in $e^+ e^- \rightarrow \psi(3770)$ events.

For the decay modes D^0 and $\bar{D}^0 \rightarrow K^+ \pi^- \pi^+ \pi^-$, Belle measured $R = (0.324 \pm 0.008 \pm 0.007)\%$ [32]. Subsequently, a phase-space-integrated analysis from LHCb [33] measured the product of a “coherence factor” $R_D^{K3\pi}$ and the strong-phase-rotated mixing parameter $y''_{K3\pi}$. This measurement resulted in an observation of charm mixing with 8.2σ significance.

Both the sign and magnitude of x and y without strong phases entering or sign ambiguity can be determined by measuring the time-dependent resonant substructure of multibody D^0 decays to self-conjugate final states [34, 35]. For such decays, e.g., $D^0 \rightarrow K_S^0 \pi^+ \pi^-$, the DCS and CF decay amplitudes populate the same Dalitz plot, which allows for direct measurement of the strong phase difference. Belle [35, 36], BABAR [37], and CLEO [38] have measured the overall phase difference between $D^0 \rightarrow K^*(892)^- \pi^+$ and $D^0 \rightarrow K^*(892)^+ \pi^-$ to be $[173.9 \pm 0.7 \text{ (stat. only)}]^\circ$, $[177.6 \pm 1.1 \text{ (stat. only)}]^\circ$, and $[189 \pm 10 \pm 3_{-5}^{+15}]^\circ$, respectively. These results are close to the 180° expected from Cabibbo factors, i.e., the relative minus sign between $V_{cs}^* V_{ud}$ and $V_{us}^* V_{cd}$; thus they indicate a small strong phase. Four LHCb measurements [39–42] of x , y using $D^0 \rightarrow K_S^0 \pi^+ \pi^-$ decays are decay-model independent, as the model of resonances in the intermediate state is replaced by strong-phase measurements from CLEO-c [43] and BESIII [44]. Table 70.4 summarizes results from time-dependent analyses of self-conjugate multibody final states. World average values for the measurements listed are given later, as a result of the HFLAV global fit.

With regard to resonant substructure in $D^0 \rightarrow K_S^0 \pi^+ \pi^-$ decays, Belle [35, 36] measured the relative strong phase (statistical errors only) and the ratio R (central values only) of the DCS fit

³However, if the decay amplitudes involve the third generation, then A_f/\bar{A}_f and \bar{A}_f/A_f in Eq. (70.13) also have weak phase differences. However, this phase difference is estimated to be negligible for the sensitivity of current and foreseeable future experimental measurements.

Table 70.3: Results for x'^2 and y' , as measured using $D^0 \rightarrow K^\pm \pi^\mp$ decays. When a single uncertainty is listed, that corresponds to statistical and systematic uncertainties combined. The measurements with an asterisk (*) have been superseded and thus are not included in the HFLAV global fit. The measurements with a dagger (\dagger) are not included in the HFLAV global fit due to much poorer precision. All confidence limits and intervals correspond to 95% C.L. The Belle 2006 results restrict x'^2 to the physical region. The BABAR confidence intervals are obtained from the fit, whereas Belle uses a Feldman-Cousins method, and CDF uses a Bayesian method.

Year	Experiment	No CP violation		Allowing for CP violation	
		$x'^2 (\times 10^{-3})$	$y' (\%)$	$x'^2 (\times 10^{-3})$	$y' (\%)$
2018	LHCb (5.0 fb^{-1}) [D^* tag] [16]	0.039 ± 0.027	0.528 ± 0.052	$\begin{cases} D^0: 0.061 \pm 0.037 \\ \bar{D}^0: 0.016 \pm 0.039 \end{cases}$	$\begin{cases} 0.501 \pm 0.074 \\ 0.554 \pm 0.074 \end{cases}$
2017	LHCb (3.0 fb^{-1}) [$B+D^*$ double tag] [17]	0.028 ± 0.310	0.46 ± 0.37	$\begin{cases} D^0: -0.019 \pm 0.447 \\ \bar{D}^0: 0.079 \pm 0.433 \end{cases}$	$\begin{cases} 0.581 \pm 0.526 \\ 0.332 \pm 0.523 \end{cases}$
2014	Belle (976 fb^{-1}) [18]	0.09 ± 0.22	0.46 ± 0.34	—	—
2013	CDF (9.6 fb^{-1}) [19]	0.08 ± 0.18	0.43 ± 0.43	—	—
2007	BABAR (384 fb^{-1}) [20]	-0.22 ± 0.37	0.97 ± 0.54	$\begin{cases} D^0: -0.24 \pm 0.52 \\ \bar{D}^0: -0.20 \pm 0.50 \end{cases}$	$\begin{cases} 0.98 \pm 0.78 \\ 0.96 \pm 0.75 \end{cases}$
2006	Belle (400 fb^{-1}) [24]	$(0.18^{+0.21}_{-0.23})^*$	$(0.06^{+0.40}_{-0.39})^*$	< 0.72	$-2.8 < y' < 2.1$
2013b*	LHCb (3.0 fb^{-1}) [D^* tag] [21]	0.055 ± 0.049	0.48 ± 0.10	$\begin{cases} D^0: 0.049 \pm 0.070 \\ \bar{D}^0: 0.060 \pm 0.068 \end{cases}$	$\begin{cases} 0.51 \pm 0.14 \\ 0.45 \pm 0.14 \end{cases}$
2013a*	LHCb (1.0 fb^{-1}) [22]	-0.09 ± 0.13	0.72 ± 0.24	—	—
2008*	CDF (1.5 fb^{-1}) [23]	-0.12 ± 0.35	0.85 ± 0.76	—	—
2005 \dagger	FOCUS (234 evts) [25]	< 8.3	$-7.2 < y' < 4.1$	< 8.0	$-11.2 < y' < 6.7$
2000 \dagger	CLEO (9.0 fb^{-1}) [26]	0.00 ± 0.23	$-2.3^{+1.3}_{-1.4}$	0.00 ± 0.23	$-2.5^{+1.4}_{-1.6}$
1998 \dagger	E791 (5643 evts) [27]	< 17	< 13	—	—

Table 70.4: Results from time-dependent multibody analyses. The errors are statistical, systematic, and, when a third error is listed, due to the decay-model, respectively. The measurement with an asterisk (*) has been superseded and thus is not included in the HFLAV global fit. The measurement with a dagger (\dagger) is not included in the HFLAV global fit due to poorer precision. The 2019 LHCb result utilizes strong-phase measurements from CLEO-c [43] and thus is decay-model independent. The 2019–2023 LHCb fits determine CP -violating parameters Δx and Δy ; the translation of these parameters to $|q/p|$ and ϕ is given in Ref. [45].

No CP Violation				
Year	Experiment	Final state(s)	$x (\times 10^{-3})$	$y (\times 10^{-3})$
2023	LHCb (5.4 fb^{-1} B tag) [42]	$K_S^0 \pi^+ \pi^-$	$4.29 \pm 1.48 \pm 0.26$	$12.61 \pm 3.12 \pm 0.83$
2021	LHCb (5.4 fb^{-1} D^* tag) [41]	$K_S^0 \pi^+ \pi^-$	$3.97 \pm 0.46 \pm 0.29$	$4.59 \pm 1.20 \pm 0.85$
2019	LHCb (3.0 fb^{-1} B, D^* tags) [40]	$K_S^0 \pi^+ \pi^-$	$2.7 \pm 1.6 \pm 0.4$	$7.4 \pm 3.6 \pm 1.1$
2016	LHCb (1.0 fb^{-1} D^* tag) [39]	$K_S^0 \pi^+ \pi^-$	$-8.6 \pm 5.3 \pm 1.7$	$0.3 \pm 4.6 \pm 1.3$
2016	BABAR (468 fb^{-1}) [46]	$\pi^+ \pi^- \pi^0$	$15 \pm 12 \pm 6$	$2 \pm 9 \pm 5$
2014	Belle (921 fb^{-1}) [36]	$K_S^0 \pi^+ \pi^-$	$5.6 \pm 1.9^{+0.3+0.6}_{-0.9-0.9}$	$3.0 \pm 1.5^{+0.4+0.3}_{-0.5-0.6}$
2010	BABAR (469 fb^{-1}) [37]	$\begin{cases} K_S^0 \pi^+ \pi^- \\ K_S^0 K^+ K^- \end{cases}$	$1.6 \pm 2.3 \pm 1.2 \pm 0.8$	$5.7 \pm 2.0 \pm 1.3 \pm 0.7$
2007*	Belle (540 fb^{-1}) [35]	$K_S^0 \pi^+ \pi^-$	$8.0 \pm 2.9^{+0.9+1.0}_{-0.7-1.4}$	$3.3 \pm 2.4^{+0.8+0.6}_{-1.2-0.8}$
2005 \dagger	CLEO (9.0 fb^{-1}) [34]	$K_S^0 \pi^+ \pi^-$	$19^{+32}_{-33} \pm 4 \pm 4$	$-14 \pm 24 \pm 8 \pm 4$

With CP Violation				
Year	Experiment	Final state(s)	$ q/p $	ϕ
2023	LHCb (5.4 fb^{-1}) [42]	$K_S^0 \pi^+ \pi^-$	$\begin{cases} \Delta x \times 10^3 = \\ -0.77 \pm 0.93 \pm 0.28 \end{cases}$	$\begin{cases} \Delta y \times 10^3 = \\ 3.01 \pm 1.92 \pm 0.26 \end{cases}$
2021	LHCb (5.4 fb^{-1}) [41]	$K_S^0 \pi^+ \pi^-$	$\begin{cases} 0.996 \pm 0.052 \\ \Delta x \times 10^3 = \\ -0.27 \pm 0.18 \pm 0.01 \end{cases}$	$\begin{cases} (3.2^{+2.7}_{-2.9})^\circ \\ \Delta y \times 10^3 = \\ 0.20 \pm 0.36 \pm 0.13 \end{cases}$
2019	LHCb (3.0 fb^{-1}) [40]	$K_S^0 \pi^+ \pi^-$	$\begin{cases} 1.05^{+0.22}_{-0.17} \\ \Delta x \times 10^3 = \\ -0.53 \pm 0.70 \pm 0.22 \end{cases}$	$\begin{cases} (-5.2^{+6.3}_{-9.2})^\circ \\ \Delta y \times 10^3 = \\ 0.6 \pm 1.6 \pm 0.3 \end{cases}$
2014	Belle (921 fb^{-1}) [36]	$K_S^0 \pi^+ \pi^-$	$0.90^{+0.16+0.05+0.06}_{-0.15-0.04-0.05}$	$(-6 \pm 11 \pm 3^{+3}_{-4})^\circ$
2007* \ddagger	Belle (540 fb^{-1}) [35]	$K_S^0 \pi^+ \pi^-$	$0.86^{+0.30+0.06}_{-0.29-0.03} \pm 0.08$	$(-14^{+16+5+2}_{-18-3-4})^\circ$

\ddagger This result allows for all types of CP violation and is superseded by Ref. [36], which assumes no direct CP violation in CF or DCS decays.

fraction relative to the CF fit fraction for five excited K states: $K^*(892)^+ \pi^-$, $K_0^*(1430)^+ \pi^-$, $K_2^*(1430)^+ \pi^-$, $K^*(1410)^+ \pi^-$, and $K^*(1680)^+ \pi^-$. Similarly, BABAR [37, 47, 48] reported central values of R for $K^*(892)^+ \pi^-$, $K_0^*(1430)^+ \pi^-$, and $K_2^*(1430)^+ \pi^-$. The systematic uncertainties on R are not evaluated. Large differences in R are observed among these final states, which indicates significant hadronic effects.

70.4 Decays to CP Eigenstates

When the final state f is a CP eigenstate, there is no distinction between f and \bar{f} . Thus $A_f = A_{\bar{f}}$ and $\bar{A}_{\bar{f}} = \bar{A}_f$. We denote final states with CP eigenvalues ± 1 by f_\pm . Decays to CP eigenstates proceed mainly via singly Cabibbo-suppressed amplitudes. Such amplitudes can contain internal loops and thus involve the third quark generation; in this manner a weak phase would appear in

Table 70.5: Results for y_{CP} and A_Γ from D^0 decays to CP eigenstates. When a single uncertainty is listed, that corresponds to statistical and systematic uncertainties combined. The measurements with an asterisk (*) have been superseded.

Year	Experiment	Final state(s)	y_{CP} (%)	A_Γ ($\times 10^{-3}$)
2022 [‡]	LHCb (6 fb ⁻¹ D^* tag) [49]	$K^+K^- + \pi^+\pi^-$	$0.696 \pm 0.026 \pm 0.013$	—
2021	LHCb (8.4 fb ⁻¹ B, D^* tags) [50]	$K^+K^- + \pi^+\pi^-$	—	$0.10 \pm 0.11 \pm 0.03$
2021	LHCb (6 fb ⁻¹ D^* tag) [50]	$K^+K^- + \pi^+\pi^-$	—	$0.27 \pm 0.13 \pm 0.03$
2021	LHCb (6 fb ⁻¹ D^* tag) [50]	K^+K^-	—	$0.23 \pm 0.15 \pm 0.03$
2021	LHCb (6 fb ⁻¹ D^* tag) [50]	$\pi^+\pi^-$	—	$0.40 \pm 0.28 \pm 0.04$
2020	Belle (976 fb ⁻¹) [51]	$K_S^0 \omega$	$0.96 \pm 0.91^{+0.64}_{-0.62}$	—
2019	LHCb (3 fb ⁻¹ B tag) [52]	$K^+K^- + \pi^+\pi^-$	$0.57 \pm 0.13 \pm 0.09$	—
2017	LHCb (3 fb ⁻¹ D^* tag) [53]	$K^+K^- + \pi^+\pi^-$	—	$-0.13 \pm 0.28 \pm 0.10$
2017	LHCb (3 fb ⁻¹ D^* tag) [53]	K^+K^-	—	$-0.30 \pm 0.32 \pm 0.10$
2017	LHCb (3 fb ⁻¹ D^* tag) [53]	$\pi^+\pi^-$	—	$0.46 \pm 0.58 \pm 0.12$
2016	Belle (976 fb ⁻¹) [54]	$K^+K^- + \pi^+\pi^-$	$1.11 \pm 0.22 \pm 0.09$	$-0.3 \pm 2.0 \pm 0.7$
2015	LHCb (3 fb ⁻¹ B tag) [55]	$K^+K^- + \pi^+\pi^-$	—	-1.25 ± 0.73
2015	LHCb (3 fb ⁻¹ B tag) [55]	K^+K^-	—	$-1.34 \pm 0.77^{+0.26}_{-0.34}$
2015	LHCb (3 fb ⁻¹ B tag) [55]	$\pi^+\pi^-$	—	$-0.92 \pm 1.45^{+0.25}_{-0.33}$
2015	BES III (2.9 fb ⁻¹) [56]	$\left\{ \begin{array}{l} K^+K^-, \pi^+\pi^- \\ K_S^0 \pi^0, K_S^0 \pi^0 \pi^0 \\ K_S^0 \eta, K_S^0 \omega \end{array} \right.$	$-2.0 \pm 1.3 \pm 0.7$	—
2014	CDF (9.7 fb ⁻¹) [57]	$K^+K^- + \pi^+\pi^-$	—	-1.2 ± 1.2
2014	CDF (9.7 fb ⁻¹) [57]	K^+K^-	—	$-1.9 \pm 1.5 \pm 0.4$
2014	CDF (9.7 fb ⁻¹) [57]	$\pi^+\pi^-$	—	$-0.1 \pm 1.8 \pm 0.3$
2012	BABAR (468 fb ⁻¹) [58]	$K^+K^- + \pi^+\pi^-$	$0.72 \pm 0.18 \pm 0.12$	$0.9 \pm 2.6 \pm 0.6$
2009	Belle (673 fb ⁻¹) [59]	$K_S^0 K^+K^-$	$0.11 \pm 0.61 \pm 0.52$	—
2002	CLEO (9.0 fb ⁻¹) [60]	$K^+K^- + \pi^+\pi^-$	$-1.2 \pm 2.5 \pm 1.4$	—
2000	FOCUS (1×10^6 evts) [61]	K^+K^-	$3.42 \pm 1.39 \pm 0.74$	—
1999	E791 (2×10^{10} evts) [62]	K^+K^-	$0.73 \pm 2.89 \pm 1.03$	—
HFLAV Average [63]			0.719 \pm 0.113	0.089 \pm 0.113
2020*	LHCb (5.4 fb ⁻¹ B tag) [64]	K^+K^-	—	$-0.43 \pm 0.36 \pm 0.05$
2020*	LHCb (5.4 fb ⁻¹ B tag) [64]	$\pi^+\pi^-$	—	$0.22 \pm 0.70 \pm 0.08$
2013*	LHCb (1.0 fb ⁻¹ D^* tag) [65]	K^+K^-	—	$-0.35 \pm 0.62 \pm 0.12$
2013*	LHCb (1.0 fb ⁻¹ D^* tag) [65]	$\pi^+\pi^-$	—	$0.33 \pm 1.06 \pm 0.14$
2011* [§]	LHCb (29 pb ⁻¹ D^* tag) [66]	K^+K^-	$0.55 \pm 0.63 \pm 0.41$	$-5.9 \pm 5.9 \pm 2.1$
2009*	BABAR (384 fb ⁻¹) [67]	K^+K^-	$1.16 \pm 0.22 \pm 0.18$	—
2008*	BABAR (384 fb ⁻¹) [68]	$K^+K^- + \pi^+\pi^-$	$1.03 \pm 0.33 \pm 0.19$	$2.6 \pm 3.6 \pm 0.8$
2007*	Belle (540 fb ⁻¹) [69]	$K^+K^- + \pi^+\pi^-$	$1.31 \pm 0.32 \pm 0.25$	$0.1 \pm 3.0 \pm 1.5$
2003*	BABAR (91 fb ⁻¹) [70]	$K^+K^- + \pi^+\pi^-$	$0.8 \pm 0.4^{+0.5}_{-0.4}$	—
2001*	Belle (23.4 fb ⁻¹) [71]	K^+K^-	$-0.5 \pm 1.0^{+0.7}_{-0.8}$	—

[‡]This measurement has sufficient precision that y_{CP} for the normalization channel $D^0 \rightarrow K^- \pi^+$ must be accounted for. Thus, the measurement is $y_{CP}(h^+ h^-) - y_{CP}(K^- \pi^+)$. HFLAV accounts for this small correction in their global fit.

[§]This result for y_{CP} is not superseded, but it is not included in the HFLAV average due to having some correlations with the result of Ref. [52] but much worse precision.

the decay amplitude, leading to direct CP violation. However, such internal loop amplitudes are suppressed, and the presence of a weak phase is often neglected.

The mixing parameter y may be measured by comparing the rate for D^0 decays to CP eigenstates such as K^+K^- with the rate to flavor eigenstates such as $K^- \pi^+$ [14]. If decays to K^+K^- have a shorter effective lifetime than those to $K^- \pi^+$, then $\Gamma_+ > \Gamma_-$, or, since CP violation is very small, $\Gamma_2 > \Gamma_1$ and y is positive. For small mixing ($x, y \ll 1$), the decay rates for $D^0 \rightarrow f_\pm$ and $\bar{D}^0 \rightarrow \bar{f}_\pm$ have an approximately exponential time dependence:

$$r_\pm(t) \propto \exp(-\Gamma_\pm t) \quad (70.32)$$

$$\bar{r}_\pm(t) \propto \exp(-\bar{\Gamma}_\pm t), \quad (70.33)$$

where the effective decay widths are given by

$$\Gamma_\pm = \Gamma \left(1 \pm \left| \frac{q}{p} \right| (y \cos \phi - x \sin \phi) \right) \quad (70.34)$$

$$\bar{\Gamma}_\pm = \Gamma \left(1 \pm \left| \frac{p}{q} \right| (y \cos \phi + x \sin \phi) \right). \quad (70.35)$$

Thus, the effective decay rate to a CP eigenstate combining equal numbers of D^0 and \bar{D}^0 decays (e.g., an untagged sample with no production asymmetry) is

$$r_\pm(t) + \bar{r}_\pm(t) \propto e^{-(1 \pm y_{CP})\Gamma t}, \quad (70.36)$$

where

$$y_{CP} = \frac{1}{2} \left(\left| \frac{q}{p} \right| + \left| \frac{p}{q} \right| \right) y \cos \phi - \frac{1}{2} \left(\left| \frac{q}{p} \right| - \left| \frac{p}{q} \right| \right) x \sin \phi \quad (70.37)$$

$$\approx y \cos \phi - A_M x \sin \phi. \quad (70.38)$$

If CP is conserved, $y_{CP} = y$. Most measurements of y_{CP} have used $D^0 \rightarrow K^+K^-$ and $D^0 \rightarrow \pi^+\pi^-$ decays, which are CP -even, measured relative to $D^0 \rightarrow K^- \pi^+$. Belle measured y_{CP} also using $D^0 \rightarrow K_S^0 \omega$ decays [51], which are CP -odd, and $D^0 \rightarrow K_S^0 K^+K^-$ decays [59], which are dominated by the CP -odd final state $K_S^0 \phi$. Table 70.5 summarizes the current status of measurements.

In addition to y_{CP} , Belle [54], BABAR [58], CDF [57], and LHCb [50, 66] have reported measurements of the decay-rate asymmetry for CP -even final states:

$$A_\Gamma \equiv \frac{\Gamma_+ - \bar{\Gamma}_+}{\Gamma_+ + \bar{\Gamma}_+} = \frac{(1/\tau_+) - (1/\bar{\tau}_+)}{(1/\tau_+) + (1/\bar{\tau}_+)} = \frac{\bar{\tau}_+ - \tau_+}{\bar{\tau}_+ + \tau_+} \quad (70.39)$$

$$\approx \frac{1}{2} \left(\left| \frac{q}{p} \right| - \left| \frac{p}{q} \right| \right) y \cos \phi - \frac{1}{2} \left(\left| \frac{q}{p} \right| + \left| \frac{p}{q} \right| \right) x \sin \phi \quad (70.40)$$

$$\approx A_M y \cos \phi - x \sin \phi. \quad (70.41)$$

If CP is conserved, $A_\Gamma = 0$.

There is a contribution to Eq. (70.41) from direct CP violation, i.e., $|\bar{A}_f/A_f| \neq 1$ [72, 73]. For $f = K^+K^-$ and $\pi^+\pi^-$, this contribution can be estimated from measurements of $A_{CP}(K^+K^-)$ and $A_{CP}(\pi^+\pi^-)$ (see below) and is much smaller than the current uncertainty on A_M ; thus we neglect it here. We note that, when averaging A_Γ measurements over K^+K^- and $\pi^+\pi^-$ final states, the contribution from direct CP violation cancels, as it has the same magnitude but opposite signs for K^+K^- and $\pi^+\pi^-$ due to U -spin symmetry [73].

The asymmetry A_Γ is an asymmetry in the full decay widths. An asymmetry in partial widths is referred to as A_{CP} and is final-state dependent:

$$A_{CP} \equiv \frac{\Gamma(D^0 \rightarrow f) - \Gamma(\bar{D}^0 \rightarrow \bar{f})}{\Gamma(D^0 \rightarrow f) + \Gamma(\bar{D}^0 \rightarrow \bar{f})}. \quad (70.42)$$

Unlike A_Γ , which is measured by fitting decay time distributions, A_{CP} is measured by fitting for signal yields and (aside from acceptance effects) does not require measuring decay times. For neutral D decays, A_{CP} receives contributions from both direct (in the decay amplitudes) and indirect (due to mixing) processes: $A_{CP}(D^0 \rightarrow f) = A_{CP}^{\text{direct}} + A_{CP}^{\text{indirect}}$. The latter indirect contribution depends on the mixing parameters x and y :

$$\begin{aligned} A_{CP}^{\text{indirect}} &= \frac{1}{2} \left(\left| \frac{q}{p} \right| + \left| \frac{p}{q} \right| \right) x \sin \phi - \frac{1}{2} \left(\left| \frac{q}{p} \right| - \left| \frac{p}{q} \right| \right) y \cos \phi \\ &= -A_\Gamma. \end{aligned} \quad (70.43)$$

Numerous measurements of A_{CP} for decays to CP eigenstates are listed in this Review [74]. Table 70.6 summarizes the current status of measurements of the difference in A_{CP} for $D^0 \rightarrow K^+K^-$ and $D^0 \rightarrow \pi^+\pi^-$ decays: $\Delta A_{CP} \equiv A_{CP}(K^+K^-) - A_{CP}(\pi^+\pi^-)$. Within the Standard Model, $A_{CP}^{KK} \approx -A_{CP}^{\pi\pi}$ [75], and ΔA_{CP} essentially doubles any direct CP violation present. The difference is also advantageous experimentally, as several systematic uncertainties cancel. As A_{CP}^{direct} is independent of final state, it subtracts out of ΔA_{CP} . However, at hadron experiments such as LHCb, there is a difference in efficiencies between K^+K^- and $\pi^+\pi^-$ such that $\langle t \rangle_{KK} \neq \langle t \rangle_{\pi\pi}$, i.e., the mean decay times slightly differ. This difference leads to a small contribution to ΔA_{CP} from A_{CP}^{direct} [72]. The most recent ΔA_{CP} result from LHCb [76], based on 8.9 fb^{-1} of data, differs from zero with a statistical significance of 5.3σ . Thus, this measurement constitutes the first observation of CP violation in charm decays. These CP asymmetries are included in HFLAV's global fit for charm mixing parameters discussed below.

Table 70.6: Results for the difference in time-integrated CP asymmetries ΔA_{CP} between $D^0 \rightarrow K^+K^-$ and $D^0 \rightarrow \pi^+\pi^-$ decays. When a single uncertainty is listed, that corresponds to statistical and systematic uncertainties combined. The measurements with an asterisk (*) have been either superseded or combined with subsequent results and thus are not included in the HFLAV global fit.

Year	Experiment	$\Delta A_{CP} (\times 10^{-3})$
2019	LHCb (8.9 fb^{-1} B, D^* tags) [76]	-1.54 ± 0.29
2013	CDF (9.7 fb^{-1} D^* tag) [77]	$-6.2 \pm 2.1 \pm 1.0$
2008	BABAR (386 fb^{-1}) [78]	$2.4 \pm 6.2 \pm 2.6$
2008	Belle (540 fb^{-1}) [79]	$-8.6 \pm 6.0 \pm 0.7$
2016*	LHCb (3.0 fb^{-1} D^* tag) [80]	$-1.0 \pm 0.8 \pm 0.3$
2014*	LHCb (3.0 fb^{-1} B tag) [81]	$1.4 \pm 1.6 \pm 0.8$
2013*	LHCb (1.0 fb^{-1} B tag) [82]	$4.9 \pm 3.0 \pm 1.4$
2012*	LHCb (0.62 fb^{-1} D^* tag) [83]	$-8.2 \pm 2.1 \pm 1.1$
2012 [‡]	Belle (976 fb^{-1}) [84]	$-8.7 \pm 4.1 \pm 0.6$

[‡]This preliminary result was not published and thus is not included in the HFLAV global fit.

70.5 Quantum-correlated $D^0\bar{D}^0$ Analyses

Measurements of R_D , $\cos \delta_{K\pi}$, $\sin \delta_{K\pi}$, x , and y can be obtained from a combined fit to time-integrated yields of single-tagged (ST) and double-tagged (DT) $D^0\bar{D}^0$ events produced at the $\psi(3770)$ resonance. Single-tagged events are those in which either the D^0 or \bar{D}^0 decay is reconstructed (identified), and the other neutral D decays generically. Double-tagged events are those in which both the D^0 and \bar{D}^0 decays are identified. Due to quantum correlations, the decay of a D^0 , \bar{D}^0 , D_+ , or D_- projects the other neutral D into a state \bar{D}^0 , D^0 , D_- , or D_+ , respectively. The CP -specific D_- and D_+ decays (or, neglecting CP violation, D_1 and D_2 decays) include interference between D^0 and \bar{D}^0 amplitudes, and this provides sensitivity to R_D and $\cos \delta_{K\pi}$. The flavor-specific D^0 and \bar{D}^0 decays include interference between D_1 and D_2 amplitudes, and this provides sensitivity to x and y . For details of this method, see Refs. [1–5].

BESIII has reported results using 2.9 fb^{-1} of $e^+e^- \rightarrow \psi(3770)$ data, where the quantum-correlated $D^0\bar{D}^0$ pairs are produced in a $C = -1$ state. They measure $y_{CP} = (-2.0 \pm 1.3 \pm 0.7)\%$ [56] from DT yields using a CP -eigenstate tag for one D and a flavor-specific semileptonic tag for the other; and they measure $A_{K\pi}^{CP} = (13.2 \pm 1.1 \pm 0.7)\%$ [85] from DT yields using a CP tag for one D and a $K^\pm\pi^\mp$ tag for the other. For y_{CP} , the CP eigenstates used are K^-K^+ (f_+), $\pi^+\pi^-$ (f_+), $K_S^0\pi^0\pi^0$ (f_+), $K_S^0\pi^0$ (f_-), $K_S^0\eta$ (f_-), and $K_S^0\omega$ (f_-). For $A_{K\pi}^{CP}$, seven additional CP eigenstates are included: $\pi^0\pi^0$ (f_+), $K_S^0\eta'$ (f_-), $K_S^0\phi$ (f_-), $K_L^0\pi^0$ (f_+), $K_L^0\omega$ (f_+), $K_L^0\pi^0\pi^0$ (f_-), and $\pi^+\pi^-\pi^0$ (mixed CP). Using Eq. (70.29) and external inputs for the CP -even fraction of $D^0 \rightarrow \pi^+\pi^-\pi^0$ (from Ref. [86]) and values of R_D and y (from HFLAV [87]), BESIII obtains $\delta_{K\pi} = (7.6^{+10.4}_{-11.6})^\circ$ [85].

CLEO-c has reported results using 0.82 fb^{-1} of $e^+e^- \rightarrow \psi(3770)$ data [88–90]. The values for y , R_M , $\cos \delta_{K\pi}$, and $\sin \delta_{K\pi}$ are obtained from a combined fit to the ST (hadronic only) and DT yields. The DT yields include events in which one D is reconstructed in a hadronic mode and the other D is partially reconstructed in flavor-specific $D \rightarrow K^\mp e^\pm \nu$ and $D \rightarrow K^\mp \mu^\pm \nu$ modes. The CLEO-c analysis obtains $\cos \delta_{K\pi} = 0.81^{+0.22+0.07}_{-0.18-0.05}$ and $\sin \delta_{K\pi} = -0.01 \pm 0.41 \pm 0.04$. These fits allow $\cos \delta_{K\pi}$ and $\sin \delta_{K\pi}$ (and also x^2) to be unphysical. Constraining $\cos \delta_{K\pi}$ and $\sin \delta_{K\pi}$ to the physical range $[-1, +1]$ (i.e., interpreting $\delta_{K\pi}$ as an angle) and also using external inputs for x , y , and y_{CP} from HFLAV 2012 [91], CLEO-c obtains $\delta_{K\pi} = (18^{+11}_{-17})^\circ$ [90].

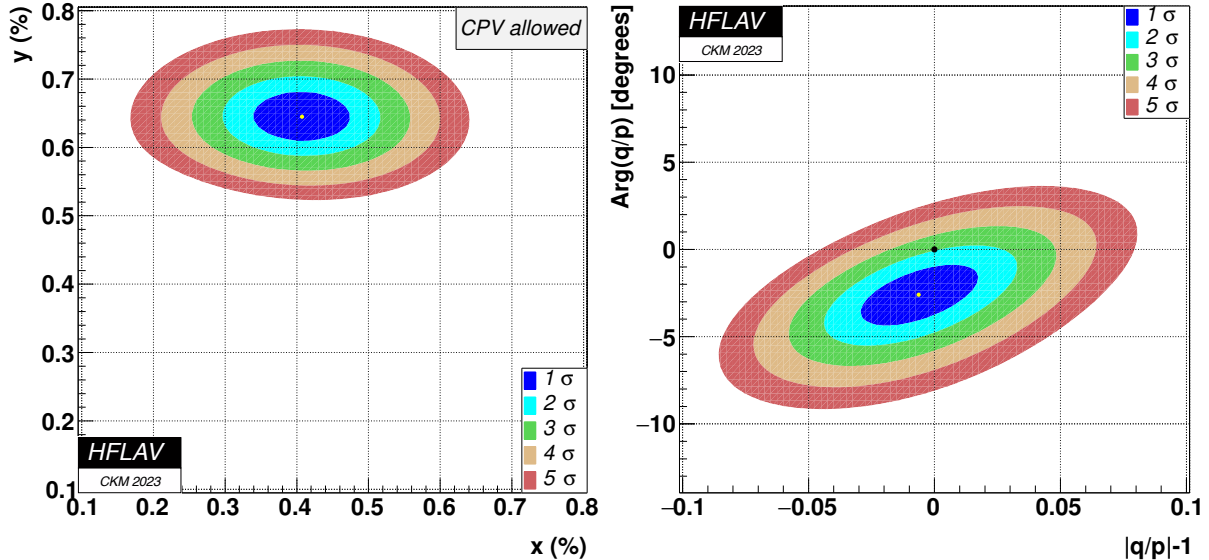
70.6 Summary of Experimental Results

The first evidence for D^0 - \bar{D}^0 mixing was obtained in 2007 by Belle [69] and BABAR [20]. These results were confirmed by CDF [92] and, much later, by LHCb [22]. There are now numerous measurements of D^0 - \bar{D}^0 mixing with various levels of sensitivity. For $D^0 \rightarrow K^+\pi^-$ decays, LHCb [21, 22], CDF [19], and Belle [18] each exclude the no-mixing hypothesis by more than five standard deviations. LHCb [33] reported the observation of charm mixing in $D^0 \rightarrow K^+\pi^-\pi^+\pi^-$ decays with 8.2σ significance. However, the strong phase difference for this decay is not known, and thus the mixing parameters x and y cannot be extracted. The most precise measurements of x and y are obtained from a time-dependent Dalitz plot analysis of $D^0 \rightarrow K_S^0\pi^+\pi^-$ decays. This method was developed at CLEO [93] and subsequently used at Belle [35, 36] and BABAR [37] with much higher statistics. BABAR has applied this method also to $D^0 \rightarrow K_S^0K^+K^-$ decays [37]. It has recently been used by LHCb with very high statistics [41, 42] to obtain the most precise values of x and y to date. This measurement resulted in the first observation ($> 5\sigma$ significance) of dispersive mixing ($x \neq 0$).

The experimental measurements establish that D^0 and \bar{D}^0 mesons mix. This mixing is presumably dominated by long-distance amplitudes, which are difficult to calculate. Under the assumption that the observed mixing is due entirely to non-Standard Model processes, significant constraints on new physics models can be obtained [94]. A significant limitation to interpreting charm mixing in terms of new physics is the theoretical uncertainty on Standard Model predictions [95, 96]. We note that the HFLAV global fit results for x and y (see below) indicate that

Table 70.7: HFLAV global fit results (see text) [15].

Parameter	No CP violation	No subleading amplitudes for indirect CPV	No subleading amplitudes in CF+DCS decays	All CP violation allowed	95% C.L. Interval (CPV allowed)
	Fit (a)	Fit (b)	Fit (c)	Fit (d)	
x (%)	$0.434^{+0.126}_{-0.139}$	0.407 ± 0.044	—	0.407 ± 0.044	[0.320, 0.493]
y (%)	0.646 ± 0.024	$0.643^{+0.024}_{-0.023}$	—	$0.645^{+0.024}_{-0.023}$	[0.600, 0.692]
$\delta_{K\pi}$ (°)	$11.5^{+3.6}_{-3.7}$	$11.3^{+3.6}_{-3.8}$	$10.9^{+3.6}_{-3.8}$	$11.4^{+3.5}_{-3.8}$	[3.7, 18.2]
R_D (%)	0.344 ± 0.002	0.344 ± 0.002	0.344 ± 0.002	0.344 ± 0.002	[0.340, 0.347]
A_D (%)	—	—	—	-0.77 ± 0.35	[-1.46, -0.08]
$ q/p $	—	1.005 ± 0.007	—	$0.994^{+0.016}_{-0.015}$	[0.96, 1.02]
ϕ (°)	—	-0.19 ± 0.26	—	$-2.6^{+1.1}_{-1.2}$	[-4.88, -0.37]
$\delta_{K\pi\pi}$ (°)	$23.1^{+22.8}_{-23.2}$	$24.5^{+21.4}_{-22.5}$	$24.4^{+21.5}_{-22.5}$	$24.6^{+21.4}_{-22.5}$	[-20.1, 65.7]
A_π (%)	—	0.202 ± 0.059	0.200 ± 0.059	0.218 ± 0.060	[0.10, 0.34]
A_K (%)	—	0.045 ± 0.053	0.043 ± 0.053	0.062 ± 0.054	[-0.04, 0.17]
x_{12} (%)	—	0.407 ± 0.044	0.407 ± 0.044	—	[0.321, 0.494]
y_{12} (%)	—	$0.643^{+0.024}_{-0.023}$	$0.641^{+0.024}_{-0.023}$	—	[0.595, 0.687]
ϕ_{12} (°)	—	$0.65^{+0.92}_{-0.90}$	—	—	[-1.13, 2.49]
ϕ_2^M (°)	—	—	0.48 ± 0.92	—	[-1.35, 2.32]
ϕ_2^T (°)	—	—	$2.40^{+1.55}_{-1.54}$	—	[-0.61, 5.45]
$\chi^2/\text{d.o.f.}$	100.6/(63-5) = 1.74	68.9/(63-8) = 1.25	66.5/(63-9) = 1.23	65.4/(63-10) = 1.23	

**Figure 70.1:** Two-dimensional 1σ - 5σ contours for (x, y) (left) and for $(|q/p|, \text{Arg}(q/p))$ (right) as obtained by HFLAV [15]. In the right plot, the black dot denotes the no- CP -violation point $(0, 0)$.

charm mixing is at the upper end of the range of these predictions. The current situation would benefit from knowledge of the strong phase difference $\delta_{K\pi\pi}$ between $\bar{D}^0 \rightarrow K^+\pi^-\pi^0$ and $D^0 \rightarrow K^+\pi^-\pi^0$ decays, and similarly the strong phase difference $\delta_{K\pi\pi\pi}$ between $\bar{D}^0 \rightarrow K^+\pi^-\pi^+\pi^-$ and $D^0 \rightarrow K^+\pi^-\pi^+\pi^-$ decays. Such knowledge would allow one to extract x and y from measurements of (x''^2, y'') and $(x''_{K3\pi}, y''_{K3\pi})$ for these three- and four-body decays.

With regard to CP violation, by combining four separate measurements from two data sets totalling 8.9 fb^{-1} of data, LHCb observed CP violation in D decays for the first time [76]. The observable measured is the difference $\Delta A_{CP} = A_{CP}(K^+K^-) - A_{CP}(\pi^+\pi^-)$, which is dominated by direct CP violation, i.e., the potential contributions from indirect CP violation mostly cancel. The amount of direct CP violation observed is small: $\Delta A_{CP} = (-0.154 \pm 0.029)\%$. A theory calculation indicates this value is consistent with Standard Model expectations [97]; however, new physics contributions cannot be excluded. A subsequent LHCb measurement of $A_{CP}(K^+K^-) = (0.068 \pm 0.056)\%$ differs from zero by only 1.2σ [98]; thus, the ΔA_{CP} result is interpreted

as indicating direct CP violation in $D^0 \rightarrow \pi^+\pi^-$ decays.

70.7 HFLAV Global Fit for Charm Mixing Parameters

The Heavy Flavor Averaging Group (HFLAV) performs global fits to all relevant mixing measurements to obtain world average values for the following parameters: mixing parameters x and y ; strong phase differences $\delta_{K\pi}$ and $\delta_{K\pi\pi^0}$; the ratio R_D of $D^0 \rightarrow K^+\pi^-$ and $\bar{D}^0 \rightarrow K^+\pi^-$ partial widths; direct CP -violating parameters $A_D(K^+\pi^-)$, $A_{CP}^{KK} \equiv A_K$, and $A_{CP}^{\pi\pi} \equiv A_\pi$; and indirect CP -violating parameters $|q/p|$, $\text{Arg}(q/p) \equiv \phi$, ϕ_{12} , ϕ_2^M , and ϕ_2^T . Four separate fits are performed: (a) assuming no CP violation; (b) assuming no subleading amplitudes for indirect CP violation; (c) assuming no subleading amplitudes in Cabibbo-favored and doubly Cabibbo-suppressed decays; and (d) allowing for all CP violation. Fits (b) and (c) correspond to theory expectations [73,99,100], with the latter being less restrictive. For fit (b), four fitted parameters are reduced to three using the relationship $\tan \phi = (x/y) \cdot (1 - |q/p|^2)/(1 + |q/p|^2)$ [99–101]; alternatively, one can fit for the three parameters $x_{12} \equiv 2|M_{12}|/\Gamma$,

$y_{12} \equiv |\Gamma_{12}|/\Gamma$, and $\phi_{12} \equiv \text{Arg}(M_{12}/\Gamma_{12})$, from which x , y , $|q/p|$, and ϕ can be derived. Details of these fits are given in Ref. [87].

The fits use Belle, BABAR, CDF, and LHCb measurements of $D^0 \rightarrow K^{(*)+}\ell^-\bar{\nu}$, K^+K^- , $\pi^+\pi^-$, $K^+\pi^-$, $K^+\pi^-\pi^0$, $K^+\pi^-\pi^+\pi^-$, $K_S^0\pi^+\pi^-$, $K_S^0K^+K^-$, and $\pi^+\pi^-\pi^0$ decays, as well as CLEO-c and BESIII measurements of $\cos\delta$, $\sin\delta$, and $A_{CP}(K^+\pi^-)$ obtained from quantum-correlated branching fractions measured in $e^+e^- \rightarrow \psi(3770) \rightarrow D^0\bar{D}^0$ reactions. Correlations among observables are taken into account by using the error matrices provided by the experiments. Three observables input to the fit are themselves world average values calculated by HFLAV: $R_M = (x^2 + y^2)/2$ from $D^0 \rightarrow K^{(*)+}\ell^-\bar{\nu}$ decays (Table 70.1), and y_{CP} and A_{CP} from $D^0 \rightarrow f_{CP}$ decays (Table 70.5). A measurement by LHCb of R_M using $D^0 \rightarrow K^+\pi^-\pi^+\pi^-$ decays is input separately.

The results of the fit as of September, 2023 are listed in Table 70.7. Confidence contours in the two dimensions (x, y) and ($|q/p|, \phi$) resulting from the fit are plotted in Fig. 70.1. These contours are obtained by allowing, for any point in the two-dimensional plane, all other fitted parameters to take their preferred values. The 1σ - 5σ boundaries drawn are the loci of points in which the χ^2 has risen above the minimum by 2.30, 6.18, 11.83, 19.33, and 28.67 units. The fit excludes the no-mixing point $x = y = 0$ at more than 11.5σ . The fit is consistent with CP conservation ($|q/p| = 1$, $\phi = 0$) at the 2σ level. The χ^2 of the all- CP -violation-allowed fit is 65.4 for $63-10 = 53$ degrees of freedom, which is satisfactory. One-dimensional likelihood functions for parameters are obtained by allowing, for any value of the parameter, all other fitted parameters to take their preferred values. The resulting likelihood functions give central values, 68.3% C.L. intervals, and 95% C.L. intervals as listed in Table 70.7.

From the results of the HFLAV global fit, we conclude the following: (1) Since CP violation is small and y_{CP} is positive, the CP -even state is shorter-lived, as in the $K^0\bar{K}^0$ system. (2) Since x is positive, the CP -even state is heavier, unlike in the $K^0\bar{K}^0$ system. (3) The strong phase difference $\delta_{K\pi}$ is small but probably nonzero: the 95% C.L. interval is $3.7^\circ < \delta_{K\pi} < 18.2^\circ$. (4) While direct CP violation has been observed in D decays, there is still no evidence for indirect CP violation, i.e., $|q/p| \neq 1$ or $\phi \neq 0$. Observing such CP violation at the current level of sensitivity would indicate new physics.

70.8 Future Data

Current results are based primarily upon CLEO-c (0.82 fb^{-1} of $e^+e^- \rightarrow \psi(3770)$ data), Belle and BABAR ($\sim 1.4 \text{ ab}^{-1}$ of $e^+e^- \rightarrow \Upsilon(4S)$ data), CDF (9.6 fb^{-1} of $p\bar{p}$ collision data at $\sqrt{s} = 1.96 \text{ TeV}$), and LHCb Runs 1 and 2 ($3.0 \text{ fb}^{-1} + 5.9 \text{ fb}^{-1}$ of pp collision data at $\sqrt{s} = 7, 8, 13 \text{ TeV}$).

BESIII has accumulated 8 fb^{-1} of $e^+e^- \rightarrow \psi(3770)$ data and plans to collect a total of 20 fb^{-1} by 2025. These data should provide strong phase measurements that would enable improved model-independent determinations of mixing parameters from Belle II and LHCb. In 2019, Belle II began accumulating 50 ab^{-1} of $e^+e^- \rightarrow \Upsilon(4S)$ data [102], which is expected to take approximately ten years to collect. At LHCb, Run 2 was completed in 2018, Run 3 is now in progress, and Run 4 is planned for 2027-30 [103]. The goal for Runs 3+4 is to accumulate an additional 50 fb^{-1} of pp data at $\sqrt{s} \approx 14 \text{ TeV}$ [104]. These data, along with the large e^+e^- dataset from Belle II, should provide more precise measurements of D^0 - \bar{D}^0 mixing and direct CP violation, and might possibly uncover indirect CP violation in the neutral D system.

References

[1] D. M. Asner and W. M. Sun, Phys. Rev. **D73**, 034024 (2006), [Erratum: Phys. Rev. **D77**, 019901 (2008)], [hep-ph/0507238].
 [2] D. Atwood and A. A. Petrov, Phys. Rev. **D71**, 054032 (2005), [hep-ph/0207165].
 [3] M. Gronau, Y. Grossman and J. L. Rosner, Phys. Lett. **B508**, 37 (2001), [hep-ph/0103110].
 [4] Z.-z. Xing, Phys. Rev. **D55**, 196 (1997), [hep-ph/9606422].

[5] M. Goldhaber and J. L. Rosner, Phys. Rev. **D15**, 1254 (1977).
 [6] Y. S. Amhis *et al.* (HFLAV), Eur. Phys. J. C **81**, 3, 226 (2021), [arXiv:1909.12524].
 [7] U. Bitenc *et al.* (Belle), Phys. Rev. **D77**, 112003 (2008), [arXiv:0802.2952].
 [8] B. Aubert *et al.* (BaBar), Phys. Rev. **D76**, 014018 (2007), [arXiv:0705.0704].
 [9] C. Cawfield *et al.* (CLEO), Phys. Rev. **D71**, 077101 (2005), [hep-ex/0502012].
 [10] E. M. Aitala *et al.* (E791), Phys. Rev. Lett. **77**, 2384 (1996), [hep-ex/9606016].
 [11] U. Bitenc *et al.* (Belle), Phys. Rev. **D72**, 071101 (2005), [hep-ex/0507020].
 [12] B. Aubert *et al.* (BaBar), Phys. Rev. **D70**, 091102 (2004), [hep-ex/0408066].
 [13] Y. Nir, Lectures given at 27th SLAC Summer Institute on Particle Physics: “ CP Violation in and Beyond the Standard Model (SSI 99),” Stanford, California, 7-16 July 1999. Published in Trieste 1999, *Particle Physics*, pp. 165-243.
 [14] S. Bergmann *et al.*, Phys. Lett. **B486**, 418 (2000), [hep-ph/0005181].
 [15] Heavy Flavor Averaging Group, https://hflav-eos.web.cern.ch/hflav-eos/charm/CKM23/results_mix_cpv.html.
 [16] R. Aaij *et al.* (LHCb), Phys. Rev. **D97**, 3, 031101 (2018), [arXiv:1712.03220].
 [17] R. Aaij *et al.* (LHCb), Phys. Rev. **D95**, 5, 052004 (2017), [Erratum: Phys. Rev. **D96**, 099907 (2017)], [arXiv:1611.06143].
 [18] B. R. Ko *et al.* (Belle), Phys. Rev. Lett. **112**, 11, 111801 (2014), [Addendum: Phys. Rev. Lett. **112**, 139903 (2014)], [arXiv:1401.3402].
 [19] T. A. Aaltonen *et al.* (CDF), Phys. Rev. Lett. **111**, 23, 231802 (2013), [arXiv:1309.4078].
 [20] B. Aubert *et al.* (BaBar), Phys. Rev. Lett. **98**, 211802 (2007), [hep-ex/0703020].
 [21] R. Aaij *et al.* (LHCb), Phys. Rev. Lett. **111**, 25, 251801 (2013), [arXiv:1309.6534].
 [22] R. Aaij *et al.* (LHCb), Phys. Rev. Lett. **110**, 10, 101802 (2013), [arXiv:1211.1230].
 [23] T. Aaltonen *et al.* (CDF), Phys. Rev. Lett. **100**, 121802 (2008), [arXiv:0712.1567].
 [24] L. M. Zhang *et al.* (Belle), Phys. Rev. Lett. **96**, 151801 (2006), [hep-ex/0601029].
 [25] J. M. Link *et al.* (FOCUS), Phys. Lett. **B618**, 23 (2005), [hep-ex/0412034].
 [26] R. Godang *et al.* (CLEO), Phys. Rev. Lett. **84**, 5038 (2000), [hep-ex/0001060].
 [27] E. M. Aitala *et al.* (E791), Phys. Rev. **D57**, 13 (1998), [hep-ex/9608018].
 [28] M. Ablikim *et al.* (BESIII), Phys. Lett. **B734**, 227 (2014), [arXiv:1404.4691].
 [29] See “Review of Multibody Charm Analyses” in this *Review*.
 [30] B. Aubert *et al.* (BaBar), Phys. Rev. Lett. **97**, 221803 (2006), [hep-ex/0608006].
 [31] B. Aubert *et al.* (BaBar), Phys. Rev. Lett. **103**, 211801 (2009), [arXiv:0807.4544].
 [32] E. White *et al.* (Belle), Phys. Rev. **D88**, 5, 051101 (2013), [arXiv:1307.5935].
 [33] R. Aaij *et al.* (LHCb), Phys. Rev. Lett. **116**, 24, 241801 (2016), [arXiv:1602.07224].
 [34] D. M. Asner *et al.* (CLEO), Phys. Rev. **D72**, 012001 (2005), [hep-ex/0503045].
 [35] K. Abe *et al.* (Belle), Phys. Rev. Lett. **99**, 131803 (2007), [arXiv:0704.1000].

- [36] T. Peng *et al.* (Belle), Phys. Rev. **D89**, 9, 091103 (2014), [arXiv:1404.2412].
- [37] P. del Amo Sanchez *et al.* (BaBar), Phys. Rev. Lett. **105**, 081803 (2010), [arXiv:1004.5053].
- [38] H. Muramatsu *et al.* (CLEO), Phys. Rev. Lett. **89**, 251802 (2002), [Erratum: Phys. Rev. Lett. **90**, 059901 (2003)], [hep-ex/0207067].
- [39] R. Aaij *et al.* (LHCb), JHEP **04**, 033 (2016), [arXiv:1510.01664].
- [40] R. Aaij *et al.* (LHCb), Phys. Rev. Lett. **122**, 23, 231802 (2019), [arXiv:1903.03074].
- [41] R. Aaij *et al.* (LHCb), Phys. Rev. Lett. **127**, 11, 111801 (2021), [arXiv:2106.03744].
- [42] R. Aaij *et al.* (LHCb), Phys. Rev. D **108**, 052005 (2023), [arXiv:2208.06512].
- [43] J. Libby *et al.* (CLEO), Phys. Rev. **D82**, 112006 (2010), [arXiv:1010.2817].
- [44] M. Ablikim *et al.* (BESIII), Phys. Rev. D **101**, 11, 112002 (2020), [arXiv:2003.00091].
- [45] A. Di Canto *et al.*, Phys. Rev. **D99**, 1, 012007 (2019), [arXiv:1811.01032].
- [46] J. P. Lees *et al.* (BaBar), Phys. Rev. **D93**, 11, 112014 (2016), [arXiv:1604.00857].
- [47] B. Aubert *et al.* (BaBar), Phys. Rev. Lett. **95**, 121802 (2005), [hep-ex/0504039].
- [48] B. Aubert *et al.* (BaBar), Phys. Rev. **D78**, 034023 (2008), [arXiv:0804.2089].
- [49] R. Aaij *et al.* (LHCb), Phys. Rev. D **105**, 9, 092013 (2022), [arXiv:2202.09106].
- [50] R. Aaij *et al.* (LHCb), Phys. Rev. D **104**, 7, 072010 (2021), [arXiv:2105.09889].
- [51] M. Nayak *et al.* (Belle), Phys. Rev. D **102**, 7, 071102 (2020), [arXiv:1912.10912].
- [52] R. Aaij *et al.* (LHCb), Phys. Rev. Lett. **122**, 1, 011802 (2019), [arXiv:1810.06874].
- [53] R. Aaij *et al.* (LHCb), Phys. Rev. Lett. **118**, 26, 261803 (2017), [arXiv:1702.06490].
- [54] M. Starič *et al.* (Belle), Phys. Lett. **B753**, 412 (2016), [arXiv:1509.08266].
- [55] R. Aaij *et al.* (LHCb), JHEP **04**, 043 (2015), [arXiv:1501.06777].
- [56] M. Ablikim *et al.* (BESIII), Phys. Lett. **B744**, 339 (2015), [arXiv:1501.01378].
- [57] T. A. Aaltonen *et al.* (CDF), Phys. Rev. **D90**, 11, 111103 (2014), [arXiv:1410.5435].
- [58] J. P. Lees *et al.* (BaBar), Phys. Rev. **D87**, 1, 012004 (2013), [arXiv:1209.3896].
- [59] A. Zupanc *et al.* (Belle), Phys. Rev. **D80**, 052006 (2009), [arXiv:0905.4185].
- [60] S. E. Csorna *et al.* (CLEO), Phys. Rev. **D65**, 092001 (2002), [hep-ex/0111024].
- [61] J. M. Link *et al.* (FOCUS), Phys. Lett. **B485**, 62 (2000), [hep-ex/0004034].
- [62] E. M. Aitala *et al.* (E791), Phys. Rev. Lett. **83**, 32 (1999), [hep-ex/9903012].
- [63] Heavy Flavor Averaging Group, https://hflav-eos.web.cern.ch/hflav-eos/charm/CKM23/results_mixing.html.
- [64] R. Aaij *et al.* (LHCb), Phys. Rev. **D101**, 1, 012005 (2020), [arXiv:1911.01114].
- [65] R. Aaij *et al.* (LHCb), Phys. Rev. Lett. **112**, 4, 041801 (2014), [arXiv:1310.7201].
- [66] R. Aaij *et al.* (LHCb), JHEP **04**, 129 (2012), [arXiv:1112.4698].
- [67] B. Aubert *et al.* (BaBar), Phys. Rev. **D80**, 071103 (2009), [arXiv:0908.0761].
- [68] B. Aubert *et al.* (BaBar), Phys. Rev. **D78**, 011105 (2008), [arXiv:0712.2249].
- [69] M. Staric *et al.* (BELLE), Phys. Rev. Lett. **98**, 211803 (2007), [65(2007)], [hep-ex/0703036].
- [70] B. Aubert *et al.* (BaBar), Phys. Rev. Lett. **91**, 121801 (2003), [hep-ex/0306003].
- [71] K. Abe *et al.* (Belle), Phys. Rev. Lett. **88**, 162001 (2002), [hep-ex/0111026].
- [72] M. Gersabeck *et al.*, J. Phys. G **39**, 045005 (2012), [arXiv:1111.6515].
- [73] A. L. Kagan and L. Silvestrini, Phys. Rev. D **103**, 5, 053008 (2021), [arXiv:2001.07207].
- [74] See the tabulation of A_{CP} results in the D^0 and D^+ Listings in this Review.
- [75] Y. Grossman, A. L. Kagan and Y. Nir, Phys. Rev. D **75**, 036008 (2007), [hep-ph/0609178].
- [76] R. Aaij *et al.* (LHCb), Phys. Rev. Lett. **122**, 21, 211803 (2019), [arXiv:1903.08726].
- [77] T. Aaltonen *et al.* (CDF), Phys. Rev. Lett. **109**, 111801 (2012), [arXiv:1207.2158].
- [78] B. Aubert *et al.* (BaBar), Phys. Rev. Lett. **100**, 061803 (2008), [arXiv:0709.2715].
- [79] M. Staric *et al.* (Belle), Phys. Lett. **B670**, 190 (2008), [arXiv:0807.0148].
- [80] R. Aaij *et al.* (LHCb), Phys. Rev. Lett. **116**, 19, 191601 (2016), [arXiv:1602.03160].
- [81] R. Aaij *et al.* (LHCb), JHEP **07**, 041 (2014), [arXiv:1405.2797].
- [82] R. Aaij *et al.* (LHCb), Phys. Lett. **B723**, 33 (2013), [arXiv:1303.2614].
- [83] R. Aaij *et al.* (LHCb), Phys. Rev. Lett. **108**, 111602 (2012), [arXiv:1112.0938].
- [84] B. R. Ko (Belle), in “7th International Workshop on the CKM Unitarity Triangle (CKM 2012) Cincinnati, Ohio, USA, September 28-October 2, 2012,” (2012), [arXiv:1212.5320].
- [85] M. Ablikim *et al.* (BESIII), Eur. Phys. J. C **82**, 11, 1009 (2022), [arXiv:2208.09402].
- [86] S. Malde *et al.*, Phys. Lett. B **747**, 9 (2015), [arXiv:1504.05878].
- [87] Y. S. Amhis *et al.* (Heavy Flavor Averaging Group, HFLAV), Phys. Rev. D **107**, 5, 052008 (2023), [arXiv:2206.07501].
- [88] J. L. Rosner *et al.* (CLEO), Phys. Rev. Lett. **100**, 221801 (2008), [arXiv:0802.2264].
- [89] D. M. Asner *et al.* (CLEO), Phys. Rev. **D78**, 012001 (2008), [arXiv:0802.2268].
- [90] D. M. Asner *et al.* (CLEO), Phys. Rev. **D86**, 112001 (2012), [arXiv:1210.0939].
- [91] Heavy Flavor Averaging Group, https://hflav-eos.web.cern.ch/hflav-eos/charm/March12/results_mix_cp.html.
- [92] T. Aaltonen *et al.* (CDF), Phys. Rev. Lett. **100**, 121802 (2008), [arXiv:0712.1567].
- [93] D. M. Asner *et al.* (CLEO), Phys. Rev. D **72**, 012001 (2005), [hep-ex/0503045].
- [94] E. Golowich *et al.*, Phys. Rev. **D76**, 095009 (2007), [arXiv:0705.3650].
- [95] G. Isidori *et al.*, Phys. Lett. **B711**, 46 (2012), [arXiv:1111.4987].
- [96] E. Franco, S. Mishima and L. Silvestrini, JHEP **05**, 140 (2012), [arXiv:1203.3131].

- [97] J. Brod, A. L. Kagan and J. Zupan, Phys. Rev. D **86**, 014023 (2012), [arXiv:1111.5000].
- [98] R. Aaij *et al.* (LHCb), Phys. Rev. Lett. **131**, 9, 091802 (2023), [arXiv:2209.03179].
- [99] Y. Grossman, Y. Nir and G. Perez, Phys. Rev. Lett. **103**, 071602 (2009), [arXiv:0904.0305].
- [100] A. L. Kagan and M. D. Sokoloff, Phys. Rev. **D80**, 076008 (2009), [arXiv:0907.3917].
- [101] M. Ciuchini *et al.*, Phys. Lett. **B655**, 162 (2007), [hep-ph/0703204].
- [102] W. Altmannshofer *et al.* (Belle-II), PTEP **2019**, 12, 123C01 (2019), [Erratum: PTEP 2020, 029201 (2020)], [arXiv:1808.10567].
- [103] CERN LHC Schedule, <https://lhc-commissioning.web.cern.ch/schedule/LHC-long-term.htm>.
- [104] R. Aaij *et al.* (LHCb) (2018), [arXiv:1808.08865].

71. D_s^+ Branching Fractions

Revised September 2021 by J.L. Rosner (Chicago U.) and C.G. Wohl (LBNL).

Figure 71.1 shows a partial breakdown of the D_s^+ branching fractions. The rest of this note is about how the figure was constructed. The values shown make heavy use of CLEO measurements of inclusive branching fractions [1]. For references to other data cited in the following, see the Listings. An addendum updates branching fractions to two-body final states reported by the BESIII Collaboration in 2020 [2], and the conclusion stresses modes still to be identified.

71.1 Modes with leptons

The bottom $(18.0 \pm 1.0)\%$ of Fig. 71.1 shows the fractions for the modes that include leptons. The measured $K^0 e^+ \nu_e$ and $K^{*0} e^+ \nu_e$ fractions have been doubled to take account of the corresponding $\mu^+ \nu_\mu$ fractions. The sum of the exclusive $X e^+ \nu_e$ fractions is $(6.0 \pm 0.3)\%$, consistent with an inclusive semileptonic measurement of $(6.5 \pm 0.4)\%$. There seems to be little missing here.

71.2 Inclusive hadronic $K\bar{K}$ fractions

The Cabibbo-favored $c \rightarrow s$ decay in D_s^+ decay produces a final state with both an s and an \bar{s} ; and thus modes with a $K\bar{K}$ pair or with an η , ω , η' , or ϕ predominate (as may already be seen in Fig. 71.1 in the semileptonic fractions). We consider the $K\bar{K}$ modes first. A complete picture of the exclusive $K\bar{K}$ charge modes is not yet possible, because branching fractions for many of those modes have not yet been measured. However, CLEO has measured the inclusive K^+ , K^- , K_S^0 , $K^+ K^-$, $K^+ K_S^0$, $K^- K_S^0$, and $2K_S^0$ fractions (these include modes with leptons) [1]. And each of these inclusive fractions with a K_S^0 is equal to the corresponding fraction with a K_L^0 : $f(K^+ K_L^0) = f(K^+ K_S^0)$, $f(2K_L^0) = f(2K_S^0)$, etc. Therefore, of all-inclusive fractions pairing a K^+ , K_S^0 , or K_L^0 with a K^- , K_S^0 , or K_L^0 , we know all but $f(K_S^0 K_L^0)$.

We can get that fraction. The total K_S^0 fraction is

$$f(K_S^0) = f(K^+ K_S^0) + f(K^- K_S^0) + 2f(2K_S^0) + f(K_S^0 K_L^0) + f(\text{single } K_S^0),$$

where $f(\text{single } K_S^0)$ is the sum of the branching fractions for modes such as $K_S^0 \pi^+ 2\pi^0$ with a K_S^0 and no second K . The $K_S^0 \pi^+ 2\pi^0$ mode is in fact the only unmeasured single- K_S^0 mode (throughout, we shall assume that fractions for modes with a K or $K\bar{K}$ and more than three pions are negligible), and we shall take its fraction to be the same as for the $K_S^0 2\pi^+ \pi^-$ mode, $(0.30 \pm 0.11)\%$. Any reasonable deviation from this value would be too small to matter much in the following. Adding the several small single- K_S^0 branching fractions, including those from semileptonic modes, we get $f(\text{single } K_S^0) = (1.7 \pm 0.2)\%$. Using this, we have:

$$\begin{aligned} f(K_S^0 K_L^0) &= f(K_S^0) - f(K^+ K_S^0) - f(K^- K_S^0) \\ &\quad - 2f(2K_S^0) - f(\text{single } K_S^0) \\ &= (19.0 \pm 1.1) - (5.8 \pm 0.5) - (1.9 \pm 0.4) \\ &\quad - 2 \times (1.7 \pm 0.3) - (1.7 \pm 0.2) \\ &= (6.2 \pm 1.4)\%. \end{aligned}$$

Here and below we treat the errors as uncorrelated, although often they are not. However, our main aim is to get numbers for Fig. 71.1; errors are secondary.

There is a check on our result: The ϕ inclusive branching fraction is $(15.7 \pm 1.0)\%$, of which 34%, or $(5.34 \pm 0.34)\%$ of D_s^+ decays, produces a $K_S^0 K_L^0$. Our $f(K_S^0 K_L^0) = (6.2 \pm 1.4)\%$ has to be at least this large—and it is, within the sizable error.

We now have all the inclusive $K\bar{K}$ fractions. We use $f(K^+ \bar{K}^0) = 2f(K^+ K_S^0)$, and likewise for $f(K^- K^0)$. For $K^+ K^-$ and $K_S^0 K_L^0$, we subtract off the contributions from $\phi \ell^+ \nu$ decay to

get the purely hadronic $K\bar{K}$ inclusive fractions:

$$\begin{aligned} f(K^+ K^-, \text{hadronic}) &= (15.8 \pm 0.7) - (2.1 \pm 0.3) \\ &= (13.7 \pm 0.8)\% \\ f(K^+ \bar{K}^0, \text{hadronic}) &= (11.6 \pm 1.0)\% \\ f(K^- K^0, \text{hadronic}) &= (3.8 \pm 0.8)\% \\ f(2K_S^0 + 2K_L^0, \text{hadronic}) &= (3.4 \pm 0.6)\% \\ f(K_S^0 K_L^0, \text{hadronic}) &= (6.2 \pm 1.4) - (1.5 \pm 0.2) \\ &= (4.7 \pm 1.4)\%. \end{aligned}$$

The fractions are shown in Fig. 71.1. They total $(37.2 \pm 2.2)\%$ of D_s^+ decays.

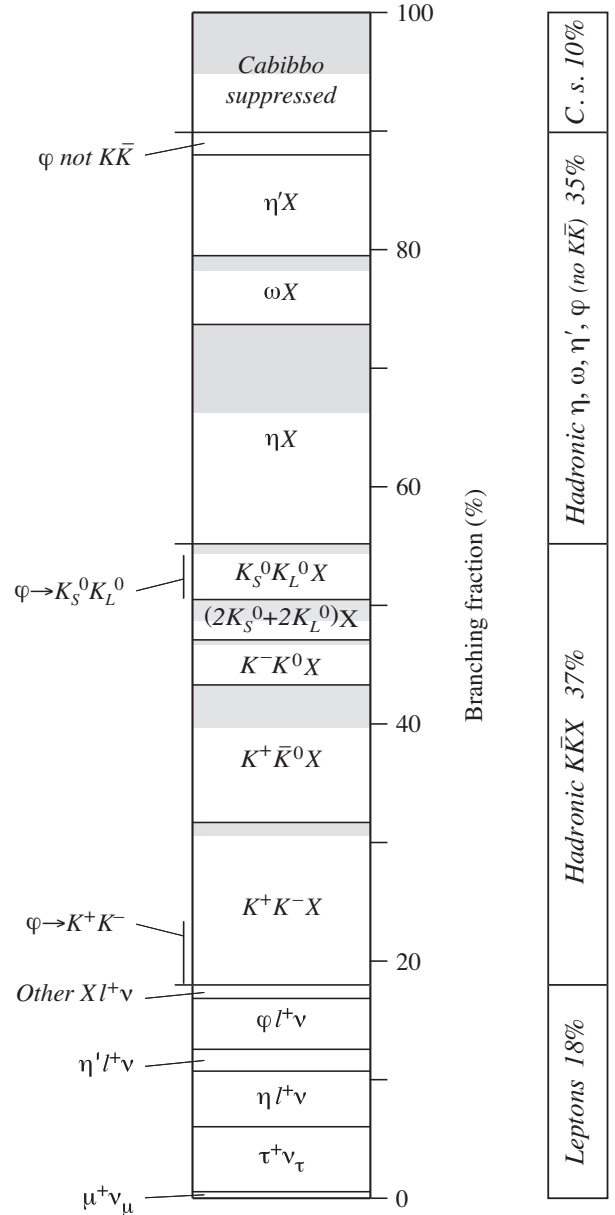


Figure 71.1: A partial breakdown of D_s^+ branching fractions. The hadronic bins in the left column show inclusive fractions. Shading within a bin shows how much of the inclusive fraction is not yet accounted for by adding up all the relevant exclusive fractions. The inclusive hadronic ϕ fraction is spread over three bins, in proportion to its decay fractions into $K^+ K^-$, $K_S^0 K_L^0$, and no- $K\bar{K}$ modes.

We can add more information to the figure by summing up measured branching fractions for exclusive modes within each bin:

K^+K^- modes—The sum of measured $K^+K^-\pi^+$, $K^+K^-\pi^+\pi^0$, and $K^+K^-\pi^+\pi^0$ branching fractions is $(12.6 \pm 0.6)\%$. That leaves $(1.1 \pm 1.0)\%$ for the $K^+K^-\pi^+2\pi^0$ mode, which is the only other K^+K^- mode with three or fewer pions. In Fig. 71.1, this unmeasured part of the K^+K^- bin is shaded.

$K^+\bar{K}^0$ modes—Two times the sum of the measured $K^+K_S^0$, $K^+K_S^0\pi^0$, and $K^+K_S^0\pi^+\pi^-$ branching fractions is $(8.0 \pm 0.5)\%$. This leaves $(3.6 \pm 1.1)\%$ for the unmeasured $K^+\bar{K}^0$ modes (there are three such modes with three or fewer pions). This is shaded in the figure.

K^-K^0 modes—Twice the $K^-K_S^02\pi^+$ fraction is $(3.4 \pm 0.2)\%$, which leaves about $(0.4 \pm 0.8)\%$ for $K^-K^02\pi^+\pi^0$, the only other K^-K^0 mode with three or fewer pions.

$2K_S^0+2K_L^0$ modes—The $2K_S^0\pi^+$ and $2K_S^02\pi^+\pi^-$ fractions sum to $(0.86 \pm 0.07)\%$; this times two (for the corresponding $2K_L^0$ modes) is $(1.72 \pm 0.14)\%$. This leaves about $(1.7 \pm 0.7)\%$ for other $2K_S^0+2K_L^0$ modes.

$K_S^0K_L^0$ modes—Most of the $K_S^0K_L^0$ fraction is accounted for by ϕ decays (see below).

71.3 Inclusive hadronic η , ω , η' , and ϕ fractions

These are easier. We start with the inclusive branching fractions, and then, to avoid double counting, subtract: (1) fractions for modes with leptons; (2) η mesons that are included in the inclusive η' fraction; and (3) K^+K^- and $K_S^0K_L^0$ from ϕ decays:

$$f(\eta \text{ hadronic}) = f(\eta \text{ inclusive}) - 0.65 f(\eta' \text{ inclusive}) \\ - f(\eta\ell^+\nu) = (18.5 \pm 3.0)\%$$

$$f(\omega \text{ hadronic}) = f(\omega \text{ inclusive}) - 0.026 f(\eta' \text{ inclusive}) \\ = (5.8 \pm 1.4)\%$$

$$f(\eta' \text{ hadronic}) = f(\eta' \text{ inclusive}) - f(\eta'\ell^+\nu) \\ = (8.5 \pm 1.5)\%$$

$$f(\phi \text{ hadronic, } \not\rightarrow K\bar{K}) = 0.17 [f(\phi \text{ inclusive}) - f(\phi\ell^+\nu)] \\ = (1.9 \pm 0.2)\% .$$

The factors 0.65, 0.026, and 0.17 are the $\eta' \rightarrow \eta$, $\eta' \rightarrow \omega$, and $\phi \not\rightarrow K\bar{K}$ branching fractions. Figure 71.1 shows the results; the sum is $(34.7 \pm 3.6)\%$, which is about equal to the hadronic $K\bar{K}$ total.

Note that the bin marked ϕ near the top of Fig. 71.1 includes neither the $\phi\ell^+\nu$ decays nor the 83% of other ϕ decays that produce a $K\bar{K}$ pair. There is twice as much ϕ in the $K_S^0K_L^0$ bin, and nearly three times as much in the K^+K^- bin. These contributions are indicated in those bins.

Again, we can show how much of each bin is accounted for by measured exclusive branching fractions: η modes—The sum of $\eta\pi^+$, $\eta\pi^+\pi^0$ (nearly all $\eta\rho^+$), and ηK^+ branching fractions is $(11.1 \pm 1.2)\%$, which leaves a good part of the inclusive hadronic η fraction, $(18.5 \pm 3.0)\%$, to be accounted for. This is shaded in the figure. ω modes—The sum of $\omega\pi^+$, $\omega\pi^+\pi^0$, and $\omega2\pi^+\pi^-$ fractions is $(4.6 \pm 0.9)\%$, which is nearly as large as the inclusive hadronic ω fraction, $(5.8 \pm 1.4)\%$. η' modes—The sum of $\eta'\pi^+$, $\eta'\rho^+$, and $\eta'K^+$ fractions is $(9.9 \pm 1.5)\%$, which is larger than but not in serious disagreement with the inclusive hadronic η' fraction, $(8.5 \pm 1.5)\%$.

71.4 Cabibbo-suppressed modes

The sum of the fractions for modes with a $K\bar{K}$, η , ω , η' , or leptons is $(89.9 \pm 4.4)\%$. The remaining $(10.1 \pm 4.4)\%$ is to

Cabibbo-suppressed modes, mainly single- K + pions and multiple-pion modes (see below). However, it should be noted that some small parts of the modes already discussed are Cabibbo-suppressed. For example, the $(1.1 \pm 0.2)\%$ of D_s^+ decays to $K^0\ell\nu$ or $K^{*0}\ell\nu$ is already in the $X\ell\nu$ bin in Fig. 71.1. And the inclusive measurements of η , ω , and η' fractions do not distinguish between (and therefore include both) Cabibbo-allowed and -suppressed modes. We shall not try to make a separation here.

K^0 + pions—Above, we found that $f(\text{single } K_S^0) = (1.7 \pm 0.2)\%$. Subtracting semileptonic fractions with a K_S^0 leaves $(1.3 \pm 0.2)\%$. The hadronic single- K^0 fraction is twice this, about $(2.6 \pm 0.4)\%$. The sum of measured $K^0\pi^+$, $K^0\pi^+\pi^0$, and $K^02\pi^+\pi^-$ fractions is $(1.8 \pm 0.3)\%$, about two-thirds as much.

K^+ + pions—The $K^+\pi^0$ and $K^+\pi^+\pi^-$ fractions sum to $(0.72 \pm 0.05)\%$. The total K^+ fraction wanted here is probably in the 1-to-2% range.

Multi-pions—The $2\pi^+\pi^-$, $\pi^+2\pi^0$, and $3\pi^+2\pi^-$ fractions total $(2.5 \pm 0.2)\%$. Modes not measured might double this.

The sum of the actually measured fractions is, including the semileptonics, $(4.9 \pm 0.3)\%$. The error on our Cabibbo-suppressed total, $(10.1 \pm 4.4)\%$ is too large to know how much we might be missing.

71.5 Addendum: Improved precision in some measurements

The Table compares measurements of branching fractions to pairs of two pseudoscalar mesons used in our 2019 update of the 2018 PDG review with values available in 2021 [2]. They have not changed much but are much better known.

Final state	2019 PDG avg or fit (%)	New BESIII entry in 2021 PDG (%)	2021 PDG avg or fit (%)
$K^+\eta'$	0.18 ± 0.06	0.268 ± 0.025	0.265 ± 0.025
$K^+\eta$	0.177 ± 0.035	0.162 ± 0.012	0.160 ± 0.011
$\eta\pi^+$	1.70 ± 0.09	1.741 ± 0.063	1.68 ± 0.10
$K^+K_S^0$	1.50 ± 0.05	1.502 ± 0.055	1.46 ± 0.04
$K_S^0\pi^+$	0.122 ± 0.006	0.1109 ± 0.005	0.110 ± 0.005
$K^+\pi^0$	0.063 ± 0.021	0.0748 ± 0.0057	0.074 ± 0.0057

Other recent BESIII additions include the measurements $\mathcal{B}(D_s \rightarrow \omega\pi^+, \omega K^+) = (1.77 \pm 0.32 \pm 0.13, 0.87 \pm 0.24 \pm 0.08) \times 10^{-3}$ [3] and $\mathcal{B}(D_s \rightarrow K_{S,L}K^+) = (1.425 \pm 0.038 \pm 0.031, 1.485 \pm 0.039 \pm 0.046)\%$ [4].

71.6 Concluding remarks

The shaded bands in the figure imply that about eight percent of the total D_s decay rate is into ηX , with X still to be accounted for. Unidentified Cabibbo-suppressed modes and the modes $K^+\bar{K}^0 X$ and $(2K_S^0+2K_L^0)X$ respectively correspond to $\sim (5, 3, 2)\%$ of the total. However, one can consider the vast majority of D_s decays to be represented by exclusive final states.

References

- [1] S. Dobbs *et al.* (CLEO), Phys. Rev. D **79**, 112008 (2009), [arXiv:0904.2417].
- [2] M. Ablikim *et al.* (BESIII), JHEP **08**, 146 (2020), [arXiv:2005.05072].
- [3] M. Ablikim *et al.* (BESIII), Phys. Rev. D **99**, 9, 091101 (2019), [arXiv:1811.00392].
- [4] M. Ablikim *et al.* (BESIII), Phys. Rev. D **99**, 11, 112005 (2019), [arXiv:1903.04164].

72. Leptonic Decays of Charged Pseudoscalar Mesons

Updated Aug. 2023 by R. A. Briere (Carnegie Mellon U.); written with J. L. Rosner (Chicago U.), S. L. Stone (Syracuse U.) and R. Van de Water (FNAL)

72.1 Introduction

This review updates one in Ref. [1]. Extensive use is made of results of the Flavor Lattice Averaging group (FLAG 21 and the 2023 online update), Ref. [2, 3].

Charged mesons formed from a quark and antiquark can decay to a lepton-neutrino pair when these objects annihilate via a virtual W boson. Figure 72.1 illustrates this process for the purely leptonic decay of a D^+ meson.

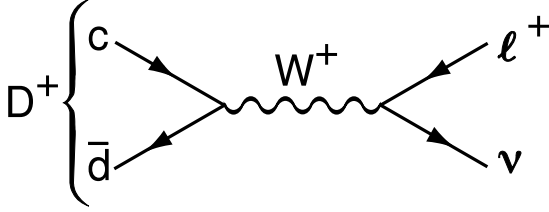


Figure 72.1: The annihilation process for pure D^+ leptonic decays in the standard model.

Similar quark-antiquark annihilations via a virtual W^+ to the $\ell^+\nu$ final states occur for the π^+ , K^+ , D_s^+ , and B^+ mesons. (Whenever pseudoscalar-meson charges are specified in this article, use of the charge-conjugate particles and corresponding decays are also implied.) Let P be any of these pseudoscalar mesons. To lowest order, the decay width is

$$\Gamma^{(0)}(P \rightarrow \ell\nu) = \frac{G_F^2}{8\pi} f_P^2 m_\ell^2 M_P \left(1 - \frac{m_\ell^2}{M_P^2}\right)^2 |V_{q_1 q_2}|^2. \quad (72.1)$$

Here M_P is the P mass, m_ℓ is the ℓ mass, $V_{q_1 q_2}$ is the Cabibbo-Kobayashi-Maskawa (CKM) matrix element between the quarks $q_1 \bar{q}_2$ in P , and G_F is the Fermi coupling constant. The decay constant f_P is proportional to the matrix element of the axial current between the one- P -meson state and the vacuum:

$$\langle 0 | \bar{q}_1 \gamma_\mu \gamma_5 q_2 | P(p) \rangle = i p_\mu f_P, \quad (72.2)$$

and can be thought of as proportional to the “wave function overlap” of the quark and antiquark. In this article, we use the convention in which $f_\pi \approx 130$ MeV. For brevity, we will often denote the purely leptonic decay width in Eq. (72.1) by $\Gamma^{(0)}$.

The decay of P^\pm starts with a spin-0 meson, and ends up with a left-handed neutrino or right-handed antineutrino. By angular momentum conservation, the ℓ^\pm must then also be left-handed or right-handed, respectively. In the $m_\ell = 0$ limit, the decay is forbidden, and can only occur as a result of the finite ℓ mass. This helicity suppression is the origin of the m_ℓ^2 factor in the decay width.

Experimentally, it is difficult to isolate events in which there are *only* a lepton and neutrino in the final state from those with a lepton, neutrino, and soft photon. Thus, radiative contributions must be removed from the experimental measurements *a posteriori* to obtain $\Gamma^{(0)}$. The radiative contributions can be broken into three pieces: the short-distance contribution to leptonic and semileptonic decays mediated by a W^\pm boson that accounts for electroweak corrections not included in the definition of G_F , the long-distance internal bremsstrahlung (IB) contribution, and the contribution from photon emission that depends upon the hadron’s structure. The universal electroweak correction was calculated at $\mathcal{O}(\alpha)$ by Sirlin [4], and increases the purely leptonic decay rate by ~ 1.8 – 2.2% depending on the decaying meson. The $\mathcal{O}(\alpha)$ IB contribution was calculated by Kinoshita [5], and again is universal for all leptonic decays at this order. Numerically, this universal long-distance contribution lowers the purely leptonic decay rate by ~ 0.4 – 2.4% , where the correction is smallest for pions and largest for $D_{(s)}$ mesons. The structure-dependent

contributions have been estimated within various effective theories to increase the purely leptonic rate by one to a few percent [6–11].

In this review, we treat the radiative corrections differently for the light, charm, and bottom meson systems for several reasons. First, the experimental uncertainties on the decay widths vary substantially. Thus, while the inclusion of radiative corrections is essential for the pion, kaon, and $D_{(s)}$ -meson decay widths, which have been measured to (sub)-percent precision, radiative corrections can be neglected (for now) for $B \rightarrow \tau\nu$ decay. Second, the photons are treated differently on the experimental side for the different decay processes. For pions and kaons, the experimental measurements of $\Gamma_{P\ell 2[\gamma]}$ are fully inclusive, while for $D_{(s)}$ mesons, the experiments impose cuts on the energy of any neutral cluster deposited in the calorimeter, which reduce the soft-photon background substantially. Some experiments also remove the QED bremsstrahlung in the leading-logarithmic approximation using the PHOTOS Monte-Carlo generator [12]. Third, the theoretical knowledge of the structure-dependent corrections varies for each meson system.

Once radiative corrections have been accounted for, measurements of purely leptonic decay branching fractions and lifetimes allow an experimental determination of the product $|V_{q_1 q_2}| f_P$. If the decay constant f_P is known to sufficient precision from theory, one can obtain the corresponding CKM element within the standard model. If, on the other hand, one takes the value of $|V_{q_1 q_2}|$ assuming CKM unitarity, one can infer an “experimental measurement” of the decay constant that can then be compared with theory.

The importance of measuring $\Gamma(P \rightarrow \ell\nu)$ depends on the particle being considered. Leptonic decays of charged pseudoscalar mesons occur at tree level within the standard model. Thus one does not expect large new-physics contributions to measurements of $\Gamma(P \rightarrow \ell\nu)$ for the lighter mesons $P = \pi^+, K^+$, and these processes, in principle, provide clean standard-model determinations of $|V_{ud}|$ and $|V_{us}|$. The situation is different for leptonic decays of charm and bottom mesons. The presence of new heavy particles such as charged Higgs bosons or leptoquarks could lead to observable effects in $\Gamma(P \rightarrow \ell\nu)$ for $P = D_{(s)}^+, B^+$ [13–17]. Thus, the determination of $|V_{ub}|$ from $B^+ \rightarrow \tau\nu$ decay, in particular, should be considered a probe of new physics. More generally, the ratio of leptonic decays to $\tau\nu$ over $\mu\nu$ final states probes lepton universality [13, 18].

The determinations of CKM elements from leptonic decays of charged pseudoscalar mesons provide complementary information to those from other decay processes. The decay $P \rightarrow \ell\nu$ proceeds in the standard model via the axial-vector current $\bar{q}_1 \gamma_\mu \gamma_5 q_2$, whereas semileptonic pseudoscalar meson decays $P_1 \rightarrow P_2 \ell\nu$ proceed via the vector current $\bar{q}_1 \gamma_\mu q_2$. Thus the comparison of determinations of $|V_{q_1 q_2}|$ from leptonic and semileptonic decays tests the $V - A$ structure of the standard-model electroweak charged-current interaction. More generally, a small right-handed admixture to the standard-model weak current would lead to discrepancies between $|V_{q_1 q_2}|$ obtained from leptonic pseudoscalar-meson decays, exclusive semileptonic pseudoscalar-meson decays, exclusive semileptonic baryon decays, and inclusive semileptonic decays [19, 20].

Both measurements of the decay rates $\Gamma(P \rightarrow \ell\nu)$ and theoretical calculations of the decay constants f_P for $P = \pi^+, K^+, D_{(s)}^+$ from numerical lattice-QCD calculations are now quite precise. As a result, the elements of the first row of the CKM matrix $|V_{ud}|$ and $|V_{us}|$ can be obtained to sub-percent precision from $\pi^+ \rightarrow \ell\nu$ and $K^+ \rightarrow \ell\nu$, where the limiting error is from continuum theory radiative corrections. The elements of the second row of the CKM matrix $|V_{cd(s)}|$ can be obtained from leptonic decays of charmed pseudoscalar mesons to few-percent precision, where here the limiting error is from experiment. These enable stringent tests of the unitarity of the first and second rows of the CKM matrix.

This review is organized as follows. Because the experimental and theoretical issues associated with measurements of pions and kaons, charmed mesons, and bottom mesons differ, we discuss each one separately. We begin with the pion and kaon sys-

tem in Sec. 72.2. First, in Sec. 72.2.1, we review current measurements of the experimental decay rates. We provide tables of branching-ratio measurements and determinations of the product $|V_{ud(s)}|f_{\pi^+(K^+)}$, as well as average values for these quantities including correlations and other effects needed to combine results. Then, in Sec. 72.2.2, we summarize the status of theoretical calculations of the decay constants. We provide tables of recent lattice-QCD results for f_{π^+} , f_{K^+} , and their ratio from calculations including dynamical u , d , s , and (in some cases c) quarks, along with averages including correlations and strong SU(2)-isospin breaking corrections as needed. We next discuss the charmed meson system in Sec. 72.3, again reviewing current experimental rate measurements in Sec. 72.3.1 and theoretical decay-constant calculations in Sec. 72.3.2. Last, we discuss the bottom meson system in Sec. 72.4, following the same organization as the two previous sections. For almost all of the decay constants presented in Secs. 72.2.2, 72.3.2, and 72.4.2, we take as our preferred values the four-flavor averages from the FLAG 21 review [2] as updated online in 2023 [3]. This 2023 web update contains only one relevant new result since the 2021 version, on f_{K^+}/f_{π^+} from ETM 21 [21].

After having established the status of both experimental measurements and theoretical calculations of leptonic charged pseudoscalar-meson decays, we discuss some implications for phenomenology in Sec. 72.5. For each process discussed in Secs. 72.2–72.4, we combine the average $\mathcal{B}(P \rightarrow \ell\nu)$ with the decay constant f_P to infer the associated CKM matrix element. We then compare these results with determinations of the same CKM elements from other processes. We also use the CKM elements obtained from leptonic decays to test the unitarity of the first and second rows of the CKM matrix. Further, as in previous reviews, we combine the experimental $\mathcal{B}(P \rightarrow \ell\nu)$ s with the associated CKM elements obtained from CKM unitarity to infer “experimental” values for the decay constants. The comparison of these values with theory provides a test of lattice and other QCD approaches, assuming that new-physics contributions to these processes are not significant.

72.2 Pions and kaons

72.2.1 Experimental rate measurements

Experimental rate measurements of pion and kaon leptonic decays are fully radiation inclusive. Following Refs. [22, 23], and references therein, we combine the $\mathcal{O}(\alpha)$ radiative corrections to the purely leptonic rate as follows:

$$\Gamma(P \rightarrow \ell\nu[\gamma]) = \Gamma^{(0)}(P \rightarrow \ell\nu) \left[1 + \frac{\alpha}{\pi} C_P \right], \quad (72.3)$$

where $P = \pi, K$. The full expressions for C_π and C_K are given in Eq. (114) of Ref. [8]. In addition to the universal short- [4] and long-distance [5] corrections, C_π and C_K include hadronic-structure dependent contributions [6] through $\mathcal{O}(\alpha p^4)$ in chiral perturbation theory (χ PT), where p is the pion or kaon momentum. The inclusion of radiative corrections to the purely leptonic rates is numerically important given the level of precision achieved on the experimental measurements of the $\pi^\pm \rightarrow \mu^\pm\nu$ and $K^\pm \rightarrow \mu^\pm\nu$ decay widths.

We evaluate $\delta_P \equiv (\alpha/\pi)C_P$ using experimentally-measured meson and lepton masses and coupling constants from the Particle Data Group [24], and taking the low-energy constants (LECs) that parametrize the hadronic contributions from Refs. [8, 25, 26]. Because the finite non-logarithmic parts of the LECs were estimated within the large- N_C approximation assuming that contributions from the lowest-lying resonances dominate, we conservatively assign a 100% uncertainty to the LECs, which leads to a ± 0.9 error in $C_{\pi,K}$.¹ We obtain the following correction factors to the indi-

vidual charged pion and kaon decay widths:

$$\delta_\pi = 0.0176(21) \quad \text{and} \quad \delta_K = 0.0107(21). \quad (72.4)$$

The error on the ratio of kaon-to-pion leptonic decay widths is under better theoretical control because the hadronic contributions from low-energy constants estimated within the large- N_C framework cancel at lowest order in the chiral expansion. For the ratio, we use the correction factor

$$\delta_{K/\pi} = -0.0069(17), \quad (72.5)$$

where we take the estimated error due to higher-order corrections in the chiral expansion from Ref. [28].

There have been no new measurements of the pion leptonic decay rate since the review of Ref. [29]. The sum of branching fractions for $\pi^- \rightarrow \mu^- \bar{\nu}$ and $\pi^- \rightarrow \mu^- \bar{\nu} \gamma$ is 99.98770(4)% [1]. Together with the lifetime 26.033(5) ns [1] this implies $\Gamma(\pi^- \rightarrow \mu^- \bar{\nu}[\gamma]) = 3.8408(7) \times 10^7 \text{ s}^{-1}$. We then subtract the estimated radiative correction factor δ_π in Eq. (72.4) to obtain the purely leptonic rate $\Gamma^{(0)}(\pi^- \rightarrow \mu^- \bar{\nu})$. Using this rate and the masses from the 2022' PDG review [1] in Eq. (72.1) gives

$$f_{\pi^+}|V_{ud}| = (127.13 \pm 0.01 \pm 0.13) \text{ MeV}, \quad (72.6)$$

where the errors are from the experimental rate measurement and the radiative correction factor, respectively.

The uncertainty on $f_{\pi^-}|V_{ud}|$ is dominated by that from theoretical estimate of the hadronic structure-dependent radiative corrections. The first direct lattice-QCD calculation of the radiative corrections to the pion and kaon leptonic decay rates was performed by the RM123-Soton Collaboration [11]. The results for both $\delta_\pi = 0.0153(19)$ and $\delta_K = 0.0088(9)$, which are given in the Gasser-Rusetsky-Scimemi scheme for separating strong and electromagnetic effects [30], are compatible with our chiral-perturbation-theory estimates above and have smaller quoted uncertainties, especially for δ_K . While independent confirmation of these results is needed, they demonstrate a promising approach for reducing the theoretical uncertainties on the pion and kaon leptonic decay rates in the future.

The world average for the $K \rightarrow \mu\nu$ decay rate was previously obtained from a global fit of several kaon-decay branching ratios and lifetime measurements by the FlaviaNet Working Group on Kaon Decays in 2014 [41]; we have now updated to the PDG [1]. The radiation-inclusive branching ratio $\mathcal{B}(K^+ \rightarrow \mu^+ \nu[\gamma]) = 63.56(11)\%$ and lifetime $\tau_{K^\pm} = 12.380(20)$ ns are now used; this is a very small change. These measurements imply $\Gamma(K^+ \rightarrow \mu^+ \nu[\gamma]) = 5.134(12) \times 10^7 \text{ s}^{-1}$. As before, we subtract δ_K in Eq. (72.4) from the radiation-inclusive decay width to obtain $\Gamma^{(0)}(K^+ \rightarrow \mu^+ \nu)$. We then use Eq. (72.1) to obtain

$$f_{K^+}|V_{us}| = (35.083 \pm 0.042 \pm 0.037) \text{ MeV}, \quad (72.7)$$

where the errors are from the experimental rate measurement and the radiative correction factor, respectively.

Short-distance radiative corrections cancel in the ratio of pion-to-kaon decay rates [42]:

$$\frac{\Gamma_{K\ell 2[\gamma]}}{\Gamma_{\pi\ell 2[\gamma]}} = \frac{|V_{us}^2|f_{K^-}^2}{|V_{ud}|^2 f_{\pi^-}^2} \frac{m_K(1 - m_\ell^2/m_K^2)^2}{m_\pi(1 - m_\ell^2/m_\pi^2)^2} (1 + \delta_{K/\pi}), \quad (72.8)$$

where $\delta_{K/\pi}$ is given in Eq. (72.5). The left-hand side of Eq. (72.8) is 1.3367(32), which implies

$$\frac{|V_{us}|f_{K^+}}{|V_{ud}|f_{\pi^+}} = 0.27599 \pm 0.00033 \pm 0.00024, \quad (72.9)$$

where the first uncertainty is from the branching fractions and the second is from $\delta_{K/\pi}$. Here, the estimated error on the hadronic structure-dependent radiative corrections is commensurate with the experimental error.

¹This uncertainty on $C_{\pi,K}$ is smaller than the error estimated by Marciano and Sirlin in Ref. [27], which predates the calculations of the hadronic-structure contributions in Refs. [6, 8, 25, 26]. The hadronic LECs incorporate the large short-distance electroweak logarithm discussed in Ref. [27], and their dependence on the chiral renormalization scale cancels the scale-dependence induced by chiral loops, thereby removing the dominant scale uncertainty of the Marciano–Sirlin analysis [27].

Table 72.1: Recent published lattice-QCD results for f_{π^+} , f_{K^+} , and their ratio. The upper and lower panels show $(2+1+1)$ -flavor and $(2+1)$ -flavor determinations, respectively. When two errors are shown, they are statistical and systematic, respectively. Results for f_{π} and f_K in the isospin symmetric limit $m_u = m_d$ are noted with a ‡; they are corrected for isospin breaking via Eq. (72.13) before computing the averages. The 2+1+1 FLAG 23 averages are dominated by the Fermilab/MILC values.

Reference	N_f	f_{π^+} (MeV)	f_{K^+} (MeV)	f_{K^+}/f_{π^+}
ETM 21 [21]	2+1+1	–	–	1.1957(44)(7)
CalLat 20 [31]	2+1+1	–	–	1.1942(32)(31)
Fermilab/MILC 17 [32] *	2+1+1	–	–	1.1950(15)($^{+6}_{-18}$)
ETM 14 [33] *	2+1+1	–	154.4(1.5)(1.3)	1.184(12)(11)
Fermilab/MILC 14 [10] * †	2+1+1	–	155.92(13)($^{+42}_{-34}$)	1.1956(10)($^{+26}_{-18}$) † ‡
HPQCD 13 [34] *	2+1+1	–	155.37(20)(27)	1.1916(15)(16)
FLAG 23 average [3]	2+1+1	–	155.7(3)	1.1934(19)
QCDSF/UKQCD 16 [35]	2+1	–	–	1.190(10)(13)
BMW 16 [36]	2+1	–	–	1.178(10)(26)
RBC/UKQCD 14 [37] ‡	2+1	130.19(89)	155.51(83)	1.1945(45)
MILC 10 [38]	2+1	129.2(0.4)(1.4)	156.1(4)($^{+6}_{-9}$)	1.197(2)($^{+3}_{-7}$)
BMW 10 [39] ‡	2+1	–	–	1.192(7)(6)
HPQCD/UKQCD 07 [40] ‡	2+1	132(2)	157(2)	1.189(2)(7)
FLAG 23 average [3]	2+1	130.2(8)	155.7(7)	1.1917(37)

*PDG 2014 value of $f_{\pi^+} = 130.41(21)$ MeV used to set absolute lattice scale.

†Superseded by f_{K^+}/f_{π^+} from Fermilab/MILC 17.

In summary, the main experimental results pertaining to charged pion and kaon leptonic decays are

$$|V_{ud}|f_{\pi^+} = (127.13 \pm 0.01 \pm 0.13) \text{ MeV}, \quad (72.10)$$

$$|V_{us}|f_{K^+} = (35.083 \pm 0.042 \pm 0.037) \text{ MeV}, \quad (72.11)$$

$$\frac{|V_{us}|f_{K^+}}{|V_{ud}|f_{\pi^+}} = 0.27599 \pm 0.00033 \pm 0.00024, \quad (72.12)$$

where the errors are from the experimental uncertainties in the branching fractions and the theoretical uncertainties in the radiative correction factors δ_P , respectively. These values contain small changes from earlier reviews [29, 43, 44].

72.2.2 Theoretical decay-constant calculations

Table 72.1 presents recent published results for the charged pion and kaon decay constants and their ratio from numerical lattice-QCD calculations with three ($N_f = 2+1$) or four flavors ($N_f = 2+1+1$) of dynamical quarks. The uncertainties on both the individual decay constants and their ratio are at the sub-percent level. The $SU(3)$ -breaking ratio f_{K^+}/f_{π^+} can be obtained with especially small errors because statistical errors associated with the Monte Carlo calculations are correlated between the numerator and denominator, as are some systematics. The results in Table 72.1 were obtained using several independent sets of gauge-field configurations, and a variety of lattice fermion actions that are sensitive to different systematic uncertainties.² Thus, the good agreement between them indicates that the lattice-QCD uncertainties are controlled and the associated error estimates are reliable.³

Table 72.1 also shows the three- and four-flavor averages for the pion and kaon decay constants and their ratio from the FLAG 23 review [2, 3] in the lines labeled “FLAG 23 average.” There is no four-flavor average for the pion decay constant in Table 72.1 because all of the four-flavor calculations use the quantity $f_{\pi^+} = 130.41(20)$ MeV [24] as an input to fix the absolute lattice scale needed to convert from lattice-spacing units to GeV [10, 33, 34].

All of the results in Table 72.1 were obtained using isospin-symmetric gauge-field configurations, *i.e.*, the dynamical up and

down quarks have the same mass. Fortunately, however, the dominant effect of strong-isospin breaking is easily included in lattice-QCD calculations as follows. Because the up-down mass difference $\Delta m_{ud} \equiv (m_u - m_d) \sim -2.5$ MeV [50, 52] is much less than typical hadronic scales, the strong-isospin breaking corrections to physical observables can be systematically expanded in the small parameter $\delta m_{ud} \equiv \Delta m_{ud}/\Lambda_{\text{QCD}}$. The leading strong-isospin-breaking corrections to pseudoscalar-meson decay constants arise from the light valence quarks in the initial- and final-state hadrons. (See, *e.g.*, the discussion in Ref. [53], for a detailed discussion of isospin-breaking effects in pion and kaon observables.) Thus, to include the effect of non-degenerate up- and down-quark masses, most recent lattice-QCD calculations of f_{π^+} and f_{K^+} evaluate the masses of the valence quarks in the pion at the physical m_u and m_d , and the mass of the valence light quark in the kaon at the physical m_u . This procedure yields a correction to the kaon decay constant below 0.5%. Consequently, strong-isospin breaking corrections from the light sea-quark masses — which are suppressed by an additional power of δm_{ud} — can be neglected given present uncertainties.

Some earlier lattice-QCD calculations, however, only provide the decay constants and their ratio in the $SU(2)$ isospin-symmetric limit [37, 39, 40]. The Flavour Lattice Averaging Group corrects these results for strong-isospin breaking using chiral perturbation theory before including them in the averages. The leading strong-isospin-breaking corrections to the pion and kaon decay constants in χ PT can be parametrized as [28, 60]

$$f_{\pi^+} = f_{\pi}, \quad f_{K^+} = f_K \sqrt{1 + \delta_{\text{SU}(2)}}, \quad (72.13)$$

where f_{π} and f_K denote the values of the decay constants in the isospin-symmetric limit. The pion decay constant does not receive corrections linear in $m_u - m_d$ because of the G -parity symmetry⁴ of the pion triplet, so at first order the δm_{ud} expansion, strong-isospin breaking corrections are characterized by a single parameter, $\delta_{\text{SU}(2)}$. Next-to-leading order χ PT yields numerical values for $\delta_{\text{SU}(2)}$ of approximately -0.004 . Recent direct lattice-QCD calculations of $\delta_{\text{SU}(2)}$ give larger values of around -0.005 to -0.008 [11, 32–34, 53, 61], but further studies are needed. Thus, to be conservative, FLAG includes an uncertainty of 100% on the χ PT estimate for $\delta_{\text{SU}(2)}$ when correcting those decay-constant values that are quoted in the isospin-symmetric limit.

²See the PDG mini-review on “Lattice Quantum Chromodynamics” [45–47] for a general review of numerical lattice-QCD calculations. Details on the different methods used in modern lattice-QCD calculations are provided in Appendix A of the FLAG “Review[s] of lattice results concerning low energy particle physics” [2, 48–50].

³See the review by Kronfeld [51] for a summary of the large body of evidence validating the methods employed in modern lattice-QCD calculations.

⁴This is a combination of charge conjugation, C , and an $e^{i\pi I_2}$ rotation in isospin space that maps the triplet onto itself.

Table 72.2: Experimental results for $\mathcal{B}(D^+ \rightarrow \mu^+\nu[\gamma])$, $\mathcal{B}(D^+ \rightarrow \tau^+\nu[\gamma])$, and $|V_{cd}|f_{D^+}$. The systematic errors on the inferred values of $|V_{cd}|f_{D^+}$ include those from the D^+ lifetime and mass. The error from radiative corrections is only included in the entries labeled “our average.” In the second CLEO line the τ^+ decays to $\mu^+\nu_\mu\bar{\nu}_\tau$.

Experiment	Mode	\mathcal{B}	$ V_{cd} f_{D^+}$ (MeV)
CLEO-c [54, 55]	$\mu^+\nu$	$(3.93 \pm 0.35 \pm 0.09) \times 10^{-4}$	$46.80 \pm 2.08 \pm 0.55$
CLEO-c [54, 55]	$\mu^+\nu + \tau^+\nu$	$(3.82 \pm 0.32 \pm 0.09) \times 10^{-4}$	$46.14 \pm 1.93 \pm 0.56$
BESIII [56]	$\mu^+\nu$	$(3.71 \pm 0.19 \pm 0.06) \times 10^{-4}$	$45.47 \pm 1.16 \pm 0.38$
Our average	Lines 2+3	$(3.74 \pm 0.17) \times 10^{-4}$	45.65 ± 1.19
CLEO-c [57, 58]	$\tau^+\nu$ ($\pi^+\bar{\nu}$)	$< 1.2 \times 10^{-3}$	
BESIII [59]	$\tau^+\nu$ ($\pi^+\bar{\nu}$)	$(1.20 \pm 0.24 \pm 0.12) \times 10^{-3}$	50.08 ± 5.62
Our average	$\mu^+\nu + \tau^+\nu$		45.82 ± 1.10

The errors on the decay-constant results in Table 72.1 obtained from $(2+1)$ -flavor lattice-QCD calculations do not include an estimate of the systematic uncertainty from the omission of charm sea quarks in the calculation. Consequently, when the uncertainty on the $(2+1+1)$ -flavor FLAG average is comparable to or better than that on the $(2+1)$ -flavor FLAG average, we simply use the four-flavor average as our preferred value. This is not possible, however, for the pion decay constant. To account for this, we first estimate the systematic uncertainty on pseudoscalar-meson decay constants associated with the omission of charm sea quarks. We then add this estimate in quadrature to the quoted error on the $(2+1)$ -flavor FLAG average for f_{π^+} to obtain our preferred value.

The error introduced by omitting charm sea quarks can be roughly estimated by expanding the charm-quark determinant in powers of $1/m_c$ [62]; the resulting leading contribution is of order $\alpha_s (A_{\text{QCD}}/2m_c)^2$ [63]. Taking the $\overline{\text{MS}}$ values $\bar{m}_c(\bar{m}_c) = 1.275$ GeV, $\bar{A}_{\text{QCD}} \sim 340$ MeV from FLAG [48], and $\bar{\alpha}_s(\bar{m}_c) \sim 0.4$, leads to an estimate of about 0.7% for the contribution to the decay constants from charm sea quarks. We can compare this power-counting estimate of charm sea-quark contributions with the observed differences between the $(2+1)$ - and $(2+1+1)$ -flavor lattice-QCD averages for kaon, $D_{(s)}$ -meson, and $B_{(s)}$ -decay constants in Tables 72.1, 72.4, and 72.6. Looking at Table 72.1, the three- and four-flavor averages for f_{K^+} agree to much better than our simple power-counting estimate. Inspection of Tables 72.4 and 72.6 shows, however, that charm sea-quark effects of this size are still allowed for both $D_{(s)}$ -meson and $B_{(s)}$ -meson decay constants.

Our final preferred theoretical values for the charged pion and kaon decay constants are

$$f_{\pi^+} = 130.2(1.2) \text{ MeV}, \quad f_{K^+} = 155.7(3) \text{ MeV}, \quad \frac{f_{K^+}}{f_{\pi^+}} = 1.193(2), \quad (72.14)$$

where f_{K^+} and f_{K^+}/f_{π^+} are simply the four-flavor FLAG 2023 averages [2, 3], and f_{π^+} is the three-flavor FLAG 2023 average with the error increased by the estimated 0.7% charm sea-quark contribution.

72.3 Charmed mesons

72.3.1 Experimental rate measurements

Measurements have been made of the branching fractions for D^+ and D_s^+ mesons decaying to both $\mu^+\nu$ and $\tau^+\nu$ final states. The CLEO-c and BESIII experiments have made measurements of D^+ decays using e^+e^- collisions at the $\psi(3770)$ resonant energy where D^-D^+ pairs are copiously produced. They fully reconstruct one of the D mesons; for concreteness, we will take this to be the D^- . Counting the number of these events provides the normalization for the branching fraction measurement. The experimental analyses then proceed by identifying a candidate μ^+ and forming the missing-mass squared, $MM^2 = (E_{\text{CM}} - E_{D^-})^2 - (\vec{p}_{\text{CM}} - \vec{p}_{D^-} - \vec{p}_{\mu^+})^2$, where E_{CM} and p_{CM} are the center-of-mass energy (which is known) and momentum (which equals zero in e^+e^- collisions). A peak at zero MM^2 implies the existence of a missing neutrino, and hence the $\mu^+\nu$ decay of the D^+ . CLEO-c does not explicitly identify the muon, so their data consists of a

combination of $\mu^+\nu$ and $\tau^+\nu$, $\tau^+ \rightarrow \pi^+\nu$ events. This permits them to do two fits: in one they fit for the individual components, and in the other they fix the ratio of $\tau^+\nu/\mu^+\nu$ events to be that given by the standard-model expectation. Thus, the former measurement should be used for new-physics searches, and the latter for standard-model predictions. Our average uses the fixed-ratio value; this ratio is implied by Eq. 72.1 which is necessary to extract $|V_{cd}|f_{D^+}$.

Table 72.2 shows the available measurements of $D^+ \rightarrow \mu^+\nu$, an upper limit on $D^+ \rightarrow \tau^+\nu$ from CLEO-c, and the first measurement of this decay from BESIII. To extract the values of $|V_{cd}|f_{D^+}$ via Eq. (72.1), we use [1] the mass $m_{D^+} = 1.86966(5)$ GeV and the lifetime $\tau_{D^+} = 1.033(5)$ ps, and apply radiative corrections as described below. For calculating the average $\mu^+\nu$ number, we use the CLEO-c result from $\mu^+\nu + \tau^+\nu$. Since the last review the D^+ lifetime is updated and the propagated uncertainties on $|V_{cd}|f_{D^+}$ from the last measurement [59] are corrected.

To obtain the purely leptonic rates $\Gamma^{(0)}(D^+ \rightarrow \mu^+(\tau^+)\nu)$, we subtract the radiative contributions as in Sec. 72.2.1, but use numerical values for the corrections appropriate for D mesons. First, we reduce both the $\mu^+\nu$ and $\tau^+\nu$ branching fractions in Table 72.2 by 1.8%, which is the universal short-distance electroweak contribution of Sirlin [4] evaluated using the D -meson mass for the factorization scale. We do not adjust the experimental rates by the universal long-distance correction [5]. This is because QED bremsstrahlung contributions have already been subtracted at leading-log order from the measurements in Table 72.2 using Monte-Carlo estimates computed with PHOTOS [12]. The $\mu^+\nu$ rates should also be reduced by the 1% estimate of the structure-dependent contributions from Dobrescu and Kronfeld [17]. This correction accounts for tree-level radiative processes in which the D meson decays into a real photon and an off-shell vector meson, which subsequently decays weakly to a charged lepton and neutrino. It is estimated using Eq. (12) of Burdman *et al.* [7] with the CLEO-c cut on the photon energy from Ref. [74], which is typical of all the measurements. We do not need to apply the structure-dependent correction to the $\mu^+\nu$ branching fractions in Table 72.2, however, because the experiments have already included it in their quoted results. Therefore, in summary, we reduce both the $D^+ \rightarrow \mu^+\nu$ and the $D^+ \rightarrow \tau^+\nu$ rates by 1.8% to account for radiative corrections. It is worth noting, however, that the universal long-distance electromagnetic contribution estimated for point-like charged mesons by Kinoshita [5], which we are not including because IB contributions are already subtracted from the measurements via PHOTOS, would *increase* both rates by about 2.5%.

We now discuss the D_s^+ decay process; there is no change since our previous review [1]. Measurements of D_s^+ leptonic decay branching fractions by several groups are listed in Table 72.3. We exclude older values obtained by normalizing to D_s^+ decay modes that are not well-defined. Many measurements, for example, used the $\phi\pi^+$ mode. This decay is a subset of the $D_s^+ \rightarrow K^+K^-\pi^+$ channel which has interferences from other modes populating the K^+K^- mass region near the ϕ , the most prominent of which is the $f_0(980)$. Thus, the extraction of the effective $\phi\pi^+$ rate is sensitive to the mass resolution of the experiment and the cuts used

Table 72.3: Experimental results for $\mathcal{B}(D_s^+ \rightarrow \mu^+\nu[\gamma])$, $\mathcal{B}(D_s^+ \rightarrow \tau^+\nu[\gamma])$, and $|V_{cs}|f_{D_s^+}$. The systematic errors on the inferred values of $|V_{cs}|f_{D_s^+}$ include those from the D_s^+ lifetime and mass. The entries labeled “our average” take into account correlations between systematic errors common to the experiments, and also include errors from radiative corrections.

Experiment	Mode	$\mathcal{B}(\%)$	$ V_{cs} f_{D_s^+}$ (MeV)
CLEO-c [57, 58]	$\mu^+\nu$	$0.565 \pm 0.045 \pm 0.017$	$247.6 \pm 9.9 \pm 4.1$
BaBar* [65]	$\mu^+\nu$	$0.602 \pm 0.038 \pm 0.034$	$254.3 \pm 8.0 \pm 7.4$
Belle [66]	$\mu^+\nu$	$0.531 \pm 0.028 \pm 0.020$	$238.8 \pm 6.3 \pm 4.8$
BESIII [67]	$\mu^+\nu$	$0.517 \pm 0.075 \pm 0.021$	$238.9 \pm 17.3 \pm 4.9$
BESIII [68]	$\mu^+\nu$	$0.535 \pm 0.013 \pm 0.016$	$240.9 \pm 2.9 \pm 4.0$
Our average	$\mu^+\nu$	0.543 ± 0.017	242.6 ± 4.0
CLEO-c [57, 58]	$\tau^+\nu (\pi^+\bar{\nu})$	$6.42 \pm 0.81 \pm 0.18$	$267.3 \pm 16.9 \pm 4.2$
CLEO-c [69]	$\tau^+\nu (\rho^+\bar{\nu})$	$5.52 \pm 0.57 \pm 0.21$	$247.9 \pm 12.8 \pm 5.0$
CLEO-c [70, 71]	$\tau^+\nu (e^+\nu\bar{\nu})$	$5.30 \pm 0.47 \pm 0.22$	$242.9 \pm 10.8 \pm 5.3$
BaBar [65]	$\tau^+\nu (e^+(\mu^+)\nu\bar{\nu})$	$5.00 \pm 0.35 \pm 0.49$	$236.9 \pm 8.3 \pm 11.7$
Belle [66]	$\tau^+\nu (\pi^+\bar{\nu})$	$6.04 \pm 0.43^{+0.46}_{-0.40}$	$260.3 \pm 9.3^{+10.1}_{-8.8}$
Belle [66]	$\tau^+\nu (e^+\nu\bar{\nu})$	$5.37 \pm 0.33^{+0.35}_{-0.31}$	$244.5 \pm 7.5^{+8.2}_{-7.4}$
Belle [66]	$\tau^+\nu (\mu^+\nu\bar{\nu})$	$5.86 \pm 0.37^{+0.34}_{-0.59}$	$255.4 \pm 8.0^{+7.6}_{-13.1}$
BESIII [67]	$\tau^+\nu (\pi^+\bar{\nu})$	$3.28 \pm 1.83 \pm 0.37$	$193 \pm 54 \pm 11$
BESIII [68]	$\tau^+\nu (\pi^+\bar{\nu})$	$5.21 \pm 0.25 \pm 0.17$	$240.8 \pm 5.8 \pm 4.3$
BESIII [72]	$\tau^+\nu (e^+\nu_e\bar{\nu})$	$5.27 \pm 0.10 \pm 0.12$	$242.2 \pm 2.3 \pm 3.2$
BESIII [73]	$\tau^+\nu (\pi^+\pi^0\bar{\nu})$	$5.29 \pm 0.25 \pm 0.20$	$242.7 \pm 5.7 \pm 4.0$
Our average	$\tau^+\nu$	5.33 ± 0.13	244.0 ± 3.1
Our average	$\mu^+\nu + \tau^+\nu$		243.5 ± 2.7

*We do not use a previous unpublished BaBar result from a subsample of data that uses a different technique for obtaining the branching fraction normalization [64].

to define the ϕ mass region [75].⁵

To find D_s decays in the $\mu^+\nu$ signal channels, the experiments rely on fully reconstructing all of the final state particles except for the neutrino and use a missing-mass technique to infer the existence of the neutrino. CLEO and BESIII use $e^+e^- \rightarrow D_s D_s^*$ collisions at 4170 MeV, while BaBar and Belle use $e^+e^- \rightarrow DK n \pi D_s^*$ collisions at energies near the $\Upsilon(4S)$. CLEO and BESIII do a similar analysis as was done for the D^+ above. BaBar and Belle do a similar MM^2 calculation by using the reconstructed hadrons, the photon from the D_s^{*+} decay and a detected μ^+ . To get the normalization they do a MM^2 fit without the μ^+ and use the signal at the D_s^+ mass squared to determine the total D_s^+ yield.

When selecting the $\tau^+ \rightarrow \pi^+\bar{\nu}$ and $\tau^+ \rightarrow \rho^+\bar{\nu}$ decay modes, CLEO uses both the calculation of the missing-mass and the fact that there should be no extra energy in the event beyond that deposited by the measured tagged D_s^- and the τ^+ decay products. The $\tau^+ \rightarrow e^+\nu\bar{\nu}$ mode, however, uses only extra energy. BaBar and Belle also use the extra energy to discriminate signal from background in their $\tau^+\nu$ measurements. BESIII uses $\tau^+ \rightarrow \pi^+\bar{\nu}$ decays, where they calculate the MM^2 and discriminate against μ^+ from $D_s^+ \rightarrow \mu^+\nu$ decays, and more recently $\tau^+ \rightarrow e^+\nu\bar{\nu}$ and $\tau^+ \rightarrow \pi^+\pi^0\bar{\nu}$ decays.

When extracting $|V_{cs}|f_{D_s^+}$ via Eq. (72.1), we first apply the -1.8% universal electroweak correction [4] to all of the $\mu^+\nu$ and $\tau^+\nu$ branching fractions in Table 72.3; this is the same as for D^+ mesons. We also decrease the BaBar and Belle $\mu^+\nu$ branching fractions by the 1% structure-dependent correction [17]. This correction was already included in CLEO and BESIII results for the $\mu^+\nu$ branching fractions in Table 72.3. We use the masses and lifetimes $m_{D_s^+} = 1.96834(7)$ GeV, $m_{\tau^+} = 1.77686(12)$ GeV, and $\tau_{D_s^+} = 0.504(4)$ ps [43]. The inferred values for $f_{D_s^+}|V_{cs}|$ are in good agreement for the $\mu^+\nu$ and $\tau^+\nu$ decay modes.

It is clear from the discussion of radiative corrections in this section that they are less well understood theoretically for D^+ and

D_s^+ meson decays than for pions and kaons. We therefore assign a 1.4% systematic uncertainty to the purely leptonic decay rates, which is half the size of the applied radiative corrections. This translates to a 0.7% error on the products of the decay constant times CKM matrix element. Putting everything together, the main experimental results pertaining to charmed meson leptonic decays are (see the bottom lines of Tables 72.2 and 72.3):

$$|V_{cd}|f_{D^+} = 45.82 \pm 1.05 \pm 0.32 = 45.82 \pm 1.10 \text{ MeV} \quad (72.15)$$

$$|V_{cs}|f_{D_s^+} = 243.5 \pm 2.1 \pm 1.7 = 243.5 \pm 2.7 \text{ MeV}, \quad (72.16)$$

where the errors are from the measured branching fractions and the applied radiative corrections, respectively.

72.3.2 Theoretical decay-constant calculations

Table 72.4 presents recent theoretical calculations of charmed heavy-light meson decay constants and their ratio in the isospin-symmetric limit $m_u = m_d$. (As in Sec. 72.2.2, we denote the physical D^+ -meson decay constant by f_{D^+} , and use f_D for the isospin-symmetric value.) The upper two panels show results from lattice-QCD calculations with three ($N_f = 2 + 1$) or four flavors ($N_f = 2 + 1 + 1$) of dynamical quarks. Although there are fewer available results than for the pion and kaon sector, both f_D and f_{D_s} have been obtained using multiple sets of gauge-field configurations with different lattice fermion actions, providing independent confirmation. For comparison, the bottom panel of Table 72.4 shows QCD-model calculations of the D - and D_s -meson decay constants for which uncertainty estimates are provided. The lattice and non-lattice results agree, but numerical lattice-QCD calculations have now reached significantly greater precision than other approaches.

The lattice-QCD decay-constant results in Table 72.4 were all obtained using isospin-symmetric gauge-field configurations. As discussed in Sec. 72.2.2, however, the leading strong-isospin breaking corrections to heavy-light pseudoscalar-meson decay constants can be accounted for by using the physical down (or up) quark in the D (or B) meson. Strong-isospin breaking corrections to heavy-strange meson decay constants are roughly an order-of-magnitude smaller because there are no light valence quarks involved. Re-

⁵We have not included the BaBar result for $\mathcal{B}(D_s^+ \rightarrow \mu^+\nu)$ reported in Ref. [76] because this measurement determined the ratio of the leptonic decay rate to the hadronic decay rate $\Gamma(D_s^+ \rightarrow \ell^+\nu)/\Gamma(D_s^+ \rightarrow \phi\pi^+)$.

Table 72.4: Recent theoretical determinations of f_D , f_{D_s} , and their ratio in the isospin-symmetric limit. The upper panels show results from lattice-QCD calculations with $(2+1+1)$ and $(2+1)$ dynamical quark flavors, respectively. Statistical and systematic errors are quoted separately. The bottom panel shows estimates from QCD sum rules (QCD SR). These are not used to obtain our preferred decay-constant values. The $2+1+1$ averages are dominated by the Fermilab/MILC values.

Reference	Method	N_f	f_D (MeV)	f_{D_s} (MeV)	f_{D_s}/f_D
Fermilab/MILC 17 [32]	LQCD	2+1+1	212.1(0.3)(0.5)	249.9(0.3)(0.3)	1.1782(06)(15)*
ETM 14 [33]	LQCD	2+1+1	207.4(3.7)(0.9)	247.2(3.9)(1.4)	1.192(19)(11)
FLAG 23 average [3]	LQCD	2+1+1	212.0(0.7)	249.9(0.5)	1.1783(16)
χ QCD 20A [77]	LQCD	2+1	213(5)	249(7)	1.16(3)
RBC/UKQCD 18A [78]†	LQCD	2+1	–	–	1.1740(51)(68)
RBC/UKQCD 17 [79]	LQCD	2+1	208.7(2.8)($^{+2.1}_{-1.8}$)	246.4(1.3)($^{+1.3}_{-1.9}$)	1.1667(77)($^{+5.7}_{-4.3}$)
χ QCD 14 [80]	LQCD	2+1	–	254(2)(4)	–
HPQCD 12 [81]	LQCD	2+1	208.3(1.0)(3.3)	–	1.187(4)(12)
Fermilab/MILC 11 [82]	LQCD	2+1	218.9(9.2)(6.6)	260.1(8.9)(6.1)	1.188(14)(21)
HPQCD 10 [83]	LQCD	2+1	–	248.0(1.4)(2.1)	–
FLAG 23 average [3]	LQCD	2+1	209.0(2.4)	248.0(1.6)	1.174(7)
Pullin 21 [84]	QCD SR		190(15)	226(17)	1.19(7)
Wang 15 [85]‡	QCD SR		208(10)	240(10)	1.15(6)
Gelhausen 13 [86]	QCD SR		201($^{+12}_{-13}$)	238($^{+13}_{-23}$)	1.15($^{+0.04}_{-0.05}$)
Narison 12 [87]	QCD SR		204(6)	246(6)	1.21(4)
Lucha 11 [88]	QCD SR		206.2(8.9)	245.3(16.3)	1.193(26)

*Ref. [32] provides values for f_D and f_{D_s} in the isospin-symmetric limit, but not for their ratio. Here we infer the central value from those of the individual decay constants, and take the statistical and systematic errors to be the same as for the physical ratio f_{D_s}/f_{D^+} .

†Slight difference from preliminary value quoted in 2019 FLAG review.

‡Obtained using $m_c^{\overline{\text{MS}}}$; results using m_c^{pole} are also given in the paper.

cently, the Fermilab Lattice and MILC Collaborations used this approach to calculate directly the dominant strong-isospin breaking corrections to both f_D and f_B , finding [32]

$$\begin{aligned} f_{D^+} - f_D &= +0.58(1)_{\text{stat}}(7)_{\text{syst}}(1)_{\text{EM scheme}} \text{ MeV}, \\ f_{B^+} - f_B &= -0.53(5)_{\text{stat}}(7)_{\text{syst}}(0)_{\text{EM scheme}} \text{ MeV}. \end{aligned} \quad (72.17)$$

These results agree with independent estimates of the strong-isospin-breaking corrections to heavy-light meson decay constants from QCD sum rules [89]. Combined with the determinations of f_D and f_B from the same work, Eq. (72.17) implies that the corrections to the SU(3)-flavor breaking ratios are

$$\frac{f_{D_s}}{f_{D^+}} = \frac{f_{D_s}}{f_D} (1 - 0.0027(3)), \quad \frac{f_{B_s}}{f_{B^+}} = \frac{f_{B_s}}{f_B} (1 + 0.0028(5)). \quad (72.18)$$

These estimated strong-isospin-breaking corrections to f_D and f_{D_s}/f_D above are commensurate with the uncertainties on the $(2+1+1)$ -flavor FLAG averages in Table 72.4. Consequently, it is important to account for isospin-breaking effects before combining the theoretical decay constants with the corresponding experimental decay rates.

To obtain the charged D^+ -meson decay constant, we apply the correction in Eq. (72.17) to the $(2+1+1)$ -flavor 2021 FLAG average for the D -meson decay constant in the isospin-symmetric limit. Similarly we use Eq. (72.18) to correct the $(2+1+1)$ -flavor 2021 FLAG average for f_{D_s}/f_D . We take the four-flavor FLAG 2021 average for f_{D_s} directly. Our final preferred theoretical values for the charmed pseudoscalar-meson decay constants are

$$\begin{aligned} f_{D^+} &= 212.0(7) \text{ MeV}, \\ f_{D_s} &= 249.9(5) \text{ MeV}, \\ \frac{f_{D_s}}{f_{D^+}} &= 1.1783(16). \end{aligned} \quad (72.19)$$

72.4 Bottom mesons

72.4.1 Experimental rate measurements

The Belle and BaBar collaborations have found evidence for $B^- \rightarrow \tau^- \bar{\nu}$ decay in $e^+e^- \rightarrow B^- B^+$ collisions at the $\Upsilon(4S)$ energy. The analysis relies on reconstructing a hadronic or semileptonic B decay tag, finding a τ candidate in the remaining track and photon candidates, and examining the extra energy in the event which should be close to zero for a real τ^- decay to $e^- \nu \bar{\nu}$ or $\mu^- \nu \bar{\nu}$ opposite a B^+ tag. The results are listed in Table 72.5. These are unchanged since the previous review [1].

Table 72.5: Experimental results for $\mathcal{B}(B^- \rightarrow \tau^- \bar{\nu})$ and $|V_{ub}|f_{B^+}$. To extract the values of $|V_{ub}|f_{B^+}$ via Eq. (72.1), we use the PDG values of the B^+ lifetime of 1.638 ± 0.004 ps, and the τ^+ and B^+ masses of 1.77686 and 5.27934 GeV, respectively.

Experiment	Tag	\mathcal{B} (units of 10^{-4})	$ V_{ub} f_{B^+}$ (MeV)
Belle [90]	Hadronic	$0.72^{+0.27}_{-0.25} \pm 0.11$	
Belle [91]	Semileptonic	$1.25 \pm 0.28 \pm 0.27$	
Belle [91]	Average	0.91 ± 0.22	0.72 ± 0.09
BaBar [92]	Hadronic	$1.83^{+0.53}_{-0.49} \pm 0.24$	
BaBar [93]	Semileptonic	$1.7 \pm 0.8 \pm 0.2$	
BaBar [92]	Average	1.79 ± 0.48	1.01 ± 0.14
Our average		1.06 ± 0.20	0.77 ± 0.07

Because there are large backgrounds under the signals for these measurements, as well as substantial systematic errors, the significances of the individual results are still below the 5σ discovery threshold. Belle quotes 4.6σ for their combined hadronic and semileptonic tags, while BaBar quotes 3.3σ and 2.3σ , for hadronic and semileptonic tags. Greater precision is necessary to determine if any effects beyond the standard model are present.

We do not correct the measured branching ratios in Table 72.5 for radiative corrections because the experimental uncertainties are so large. The relative radiative corrections are expected to be larger, however, for $B \rightarrow \mu\nu$ leptonic decays because the corrections are no longer helicity suppressed [9], and may be a significant fraction of the purely leptonic rate. More theoretical work is needed to understand radiative corrections to leptonic B decays in anticipation of future measurements with greater precision, and of new decay channels.

72.4.2 Theoretical decay-constant calculations

Table 72.6 presents recent theoretical calculations of bottom heavy-light meson decay constants and their ratio in the isospin-symmetric limit $m_u = m_d$. The upper two panels show results from lattice-QCD calculations with three ($N_f = 2+1$) or four flavors ($N_f = 2+1+1$) of dynamical quarks. For all decay constants, calculations using different gauge-field configurations, light-quark actions, and b -quark actions provide independent confirmation. For comparison, the bottom panel of Table 72.6 shows QCD-model calculations of the B^- and B_s^- -meson decay constants

Table 72.6: Recent theoretical determinations of f_B , f_{B_s} , and their ratio in the isospin-symmetric limit. The upper panels show results from lattice-QCD calculations with $(2+1+1)$ and $(2+1)$ dynamical quark flavors, respectively. When available, statistical and systematic errors are quoted separately. The bottom panel shows estimates from the relativistic potential model (RPM) and QCD sum rules (QCD SR), which are not used to obtain our preferred decay-constant values. The 2+1+1 FLAG 23 averages are dominated by the Fermilab/MILC values.

Reference	Method	N_f	f_B (MeV)	f_{B_s} (MeV)	f_{B_s}/f_B
Fermilab/MILC 17 [32]	LQCD	2+1+1	189.9(1.4)	230.7(1.2)	1.2146(49)
HPQCD 17 [94]*	LQCD	2+1+1	190(4)	229(5)	1.206(5)
ETM 16 [95]	LQCD	2+1+1	193(6)	229(5)	1.184(25)
HPQCD 13 [96]	LQCD	2+1+1	186(4)	224(5)	1.205(7)
FLAG 23 average [3]	LQCD	2+1+1	190.0(1.3)	230.3(1.3)	1.209(5)
Aoki 14 [97] [†]	LQCD	2+1	218.8(6.5)(30.8)	263.5(4.8)(36.7)	1.193(20)(44)
RBC/UKQCD 14 [98] [‡]	LQCD	2+1	195.6(6.4)(13.3)	235.4(5.2)(11.1)	1.223(14)(70)
HPQCD 12 [99]	LQCD	2+1	191(1)(8)	228(3)(10)	1.188(12)(13)
HPQCD 12 [99]	LQCD	2+1	189(3)(3)*	–	–
HPQCD 11 [100]	LQCD	2+1	–	225(3)(3)	–
Fermilab/MILC 11 [82]	LQCD	2+1	196.9(5.5)(7.0)	242.0(5.1)(8.0)	1.229(13)(23)
FLAG 23 average [3]	LQCD	2+1	192.0(4.3)	228.4(3.7)	1.201(16)
Pullin 21 [84]	QCD SR		192^{+20}_{-19}	225^{+21}_{-20}	1.17(7)
Sun 16 [101] [§]	RPM		219(15)	266(19)	1.21(9)
Wang 15 [85] [§]	QCD SR		194(15)	231(16)	1.19(10)
Baker 13 [102]	QCD SR		186(14)	222(12)	1.19(4)
Lucha 13 [103]	QCD SR		192.0(14.6)	228.0(19.8)	1.184(24)
Gelhausen 13 [86]	QCD SR		$207^{(+17)}_{(-9)}$	$242^{(+17)}_{(-12)}$	$1.17^{(+3)}_{(-4)}$
Narison 12 [87]	QCD SR		206(7)	234(5)	1.14(3)

* Average of new HPQCD 17 and previous HPQCD 13 results allowing for correlations between the two sets of results.

[†] Obtained with static b quarks (*i.e.*, $m_b \rightarrow \infty$).

[‡] Ref. [98] does not provide results in the isospin-symmetric limit, so we show f_{B^+} and f_{B_s}/f_{B^+} for this work.

[§] Obtained using $m_b^{\overline{\text{MS}}}$; results using m_b^{pole} are also given in the paper.

for which uncertainty estimates are provided. These are consistent with the lattice values, but with much larger uncertainties.

The lattice-QCD decay-constant results in Table 72.6 were all obtained using isospin-symmetric gauge-field configurations. Some calculations, however, account for the dominant effect of strong-isospin-breaking by using the correct value for the valence light-quark mass in the B meson (m_u for f_{B^+} and m_d for f_{B^0}). Early estimates of the strong-isospin-breaking correction obtained $f_{B^+} - f_B \sim -2$ MeV [96, 98], which would be significant given the present lattice-QCD uncertainties. It turns out, however, that these calculations inadvertently introduced a spurious sea-quark contribution, and therefore overestimated the size of the effect. A more recent calculation by the Fermilab/MILC Collaboration finds very little evidence for isospin violation ($f_{B^+} - f_B \sim -0.5$ MeV) [32], which is more than two times smaller than the total uncertainties on present lattice-QCD calculations. For this reason, we quote isospin averages in the current review. Our preferred theoretical values for the bottom pseudoscalar-meson decay constants are

$$\begin{aligned} f_B &= 190.0(1.3) \text{ MeV}, \\ f_{B_s} &= 230.3(1.3) \text{ MeV}, \\ \frac{f_{B_s}}{f_B} &= 1.209(5), \end{aligned} \quad (72.20)$$

which are simply the $N_f = 2+1+1$ FLAG 2023 averages [3]. Because the uncertainties on the three-flavor results in Table 72.6 are substantially larger than those on the four-flavor results, including them in the average leaves the central values unchanged, and decreases the errors only slightly.

72.5 Phenomenological implications

72.5.1 $|V_{ud}|$, $|V_{us}|$, and status of first-row unitarity

Using the average values for $f_{\pi^+}|V_{ud}|$, $f_{K^+}|V_{us}|$, and their ratio from Eqs. (72.10)–(72.12) and for f_{π^+} , f_{K^+} , and their ratio from Eq. (72.14), we obtain the following determinations of the CKM matrix elements $|V_{ud}|$, $|V_{us}|$, and their ratio from leptonic decays

within the standard model:

$$\begin{aligned} |V_{ud}| &= 0.9763(1)(90)(10), \quad |V_{us}| = 0.2253(3)(4)(2), \\ \frac{|V_{us}|}{|V_{ud}|} &= 0.2313(3)(4)(2), \end{aligned} \quad (72.21)$$

where the errors are from the experimental branching fraction(s), the pseudoscalar decay constant(s), and radiative corrections, respectively. These results enable a test of the unitarity of the first row of the CKM matrix from leptonic decays alone (the contribution from $|V_{ub}|$ is negligible). Using the values of $|V_{ud}|$ and $|V_{us}|$ from Eq. (72.21), we find

$$|V_{ud}|^2 + |V_{us}|^2 + |V_{ub}|^2 - 1 = 0.004(18), \quad (72.22)$$

which is consistent with three-generation unitarity at the few-percent level.

The determinations of $|V_{ud}|$ and $|V_{us}|$ from leptonic decays in Eq. (72.21) can be compared to those obtained from other processes. The result above for $|V_{ud}|$ agrees with the determination from super-allowed β -decay (a previous value of $|V_{ud}| = 0.97420(21)$ [104] has been updated to $|V_{ud}| = 0.97373(31)$ [105]) but has a considerably larger error, primarily due to the uncertainty in the theoretical determination of f_{π^+} .

The CKM element $|V_{us}|$ can be determined from semileptonic $K^+ \rightarrow \pi^0 \ell^+ \nu$ decay. Here experimental measurements provide a value for the product $f_+^{K\pi}(0)|V_{us}|$, where $f_+^{K\pi}(0)$ is the form factor at zero four-momentum transfer between the initial state kaon and the final state pion. We quote a recent analysis by Seng *et al.* [106] which finds $|V_{us}|f_+^{K\pi}(0) = 0.21635(38)(3)$, with the first error denoting experiment and the second reflecting uncertainty in higher order corrections. Choosing the 2021 2+1+1-flavor FLAG average for $f_+(0)^{K\pi} = 0.9698(17)$ [2] based on the calculations of ETM [107] and Fermilab/MILC [108] gives $|V_{us}| = 0.22309(39)_{\text{exp}}(39)_{\text{LQCD}}(3)_{\text{HO}}$ from semileptonic decay. The determinations of $|V_{us}|$ from leptonic and semileptonic kaon decays are both quite precise, with comparable errors, but the central values differ by 2.8 σ .

Finally, the combination of the ratio $|V_{us}|/|V_{ud}|$ from leptonic decays [Eq. (72.21)] with $|V_{ud}|$ from β decay implies an alternative determination of $|V_{us}| = 0.2252(5)$ which agrees with the value from leptonic kaon decay, but again disagrees with the semileptonic-decay result at the 2.8σ level.

Given the roughly 3σ tension between $|V_{us}|$ from leptonic and semileptonic kaon decays, it is important to scrutinize the uncertainties on the theoretical and experimental inputs to $|V_{us}|$ and other elements of the first row of the CKM matrix. Seng *et al.* have introduced a new approach for calculating radiative corrections to neutron and nuclear beta decays using dispersion relations [109–112]. These calculations imply a value of $|V_{ud}| = 0.97395(23)$, consistent with the updated analysis of Ref. [105]. An independent calculation of the radiative corrections by Czarnecki and Marciano using QCD sum rules yields similar results [113]. Using this value of $|V_{ud}|$ with the determination of $|V_{us}|$ from leptonic kaon decays in Eq. (72.21), we obtain $|V_{ud}|^2 + |V_{us}|^2 + |V_{ub}|^2 - 1 = -0.0007(5)$, again consistent with first-row unitarity.

Last, we combine the experimental measurement of $f_{\pi^+}|V_{ud}|$ in Eq. (72.10) with $|V_{ud}|$ from super-allowed β -decay [105] to infer an “experimental” value for the pion decay constant:

$$f_{\pi^-}^{\text{“exp”}} = 130.56(2)(4)(13) \text{ MeV}, \quad (72.23)$$

where the uncertainties are from the errors on Γ , $|V_{ud}|$, and higher-order corrections, respectively. Many recent (2+1+1)-flavor lattice-QCD calculations use this quantity to set the overall physical scale in their simulations, *e.g.*, Refs. [10, 32–34]. Conversely, comparing $f_{\pi^-}^{\text{“exp”}}$ with the 2021 FLAG (2+1)-flavor average $f_{\pi^+} = 130.2(8)$ MeV, which only includes lattice-QCD results that employ other observables to set the scale [35–40], provides a test of lattice-QCD methods. The values are in good agreement within present uncertainties. We do not quote an “experimental” value for the kaon decay constant because the value of $|V_{us}|$ is less clear given the approximately 3σ tension between the values of $|V_{us}|$ obtained from leptonic and semileptonic kaon decays.

72.5.2 $|V_{cd}|$, $|V_{cs}|$, and status of second-row unitarity

Using the average values for $|V_{cd}|f_{D^+}$ and $|V_{cs}|f_{D_s^+}$ from Eqs. (72.15) and (72.16), and for f_{D^+} and $f_{D_s^+}$ from Eq. (72.19), we obtain the following determinations of the CKM matrix elements $|V_{cd}|$ and $|V_{cs}|$ from leptonic decays within the standard model:

$$|V_{cd}| = 0.2161(50)(15)(7) \quad \text{and} \quad |V_{cs}| = 0.9744(84)(16)(20), \quad (72.24)$$

where the errors are from the measured branching fractions, radiative corrections, and decay constants, respectively. These results enable a test of the unitarity of the second row of the CKM matrix. Taking $|V_{cb}| = 40.8(1.4) \times 10^{-3}$ [1], we obtain

$$|V_{cd}|^2 + |V_{cs}|^2 + |V_{cb}|^2 - 1 = -0.002(22), \quad (72.25)$$

in agreement with three-generation unitarity.

The uncertainty on $|V_{cd}|$ in Eq. (72.24) is limited by the measurement error on the $D^+ \rightarrow \mu^+\nu$ decay rate. For $|V_{cs}|$, however, the experimental and radiative-correction errors are commensurate. The value of $|V_{cs}|$ from leptonic D_s decays decreased substantially from the value of 1.007(17) in an earlier version of this review [29, 114], and is now below unity as expected in the three-generation CKM framework. This change is due to our more consistent treatment of the radiative corrections, which lower the purely leptonic decay rates for $D_s^+ \rightarrow \mu^+\nu$ and $D_s^+ \rightarrow \tau^+\nu$. We emphasize, however, that we have taken a generous uncertainty on these estimates, and that more theoretical work is needed to really pin down the sizes of the radiative corrections to $D_{(s)}$ -meson leptonic decays.

The CKM matrix elements $|V_{cd}|$ and $|V_{cs}|$ can also be obtained from semileptonic $D^+ \rightarrow \pi^0\ell^+\nu$ and $D_s^+ \rightarrow K^0\ell^+\nu$ decays, respectively. Here experimental measurements determine the product of the form factor times the CKM element, and theory provides the value for the form factor at zero four-momentum transfer between the initial $D_{(s)}$ meson and the final pion or kaon.

The latest experimental averages (2023, with data as of 2021) from the Heavy Flavor Averaging Group (HFLAV) are $f_+^{D\pi}(0)|V_{cd}| = 0.1426(18)$ and $f_+^{DK}(0)|V_{cs}| = 0.7180(33)$ [115]. There were not enough published lattice-QCD calculations of the zero-momentum D -meson semileptonic form factors with $N_f \geq 3$ to permit an average by the FLAG Collaboration; instead, we summarize the 2+1+1 flavor results here. The newest calculation, from the Fermilab Lattice and MILC Collaborations [116] appeared after the FLAG 2023 online update [3]. They report $f_+^{D\pi}(0) = 0.6300(51)$ and $f_+^{DK}(0) = 0.7452(31)$; these results are the most precise and include both decay modes. For the decay $D \rightarrow K\ell\nu$, the HPQCD Collaboration [117] calculates $f_+^{DK}(0) = 0.7380(44)$, about 1.3σ lower. An update from HPQCD [118] gives $f_+^{DK}(0) = 0.7441(40)$, in agreement with Fermilab-MILC. Note that the two HPQCD results and Fermilab-MILC all share MILC gauge configurations and are hence not independent. The ETM Collaboration [119], has results for both decays, obtaining $f_+^{D\pi}(0) = 0.612(35)$ and $f_+^{DK}(0) = 0.765(31)$, which are consistent but less precise. A naive combination of the HFLAV $f(0)|V|$ products and the new Fermilab-MILC results gives results for $|V_{cd}|$ and $|V_{cs}|$ consistent with the leptonic decays in Eq. (72.24). However, as with the leptonic case, one must exercise some care with corrections; this is beyond the scope of the present review. We note that Ref. [116] presents a detailed discussion of CKM element extractions using their LQCD results, including consideration of QED, electroweak and isospin corrections; a comparison of leptonic and semileptonic results and unitarity tests are also included.

We can combine the experimental measurements of $f_{D^+}|V_{cd}|$ and $f_{D_s^+}|V_{cs}|$ from Tables 72.2 and 72.3 with $|V_{cd}| = 0.22486(67)$ and $|V_{cs}| = 0.97349(16)$ from the PDG 2022 global unitarity-triangle analysis [1] to infer “experimental” values for the decay constants within the standard model. We take the CKM elements from the global fit because they are based on many input quantities, thereby reducing the sensitivity to any one outlying measurement or calculation. We obtain for the decay constants

$$\begin{aligned} f_{D^+}^{\text{“exp”}} &= 203.8(4.7)(0.6)(1.4) \text{ MeV}, \\ f_{D_s^+}^{\text{“exp”}} &= 250.1(2.2)(0.04)(1.8) \text{ MeV}, \\ (f_{D_s^+}/f_{D^+})^{\text{“exp”}} &= 1.228(30)(4)(9). \end{aligned} \quad (72.26)$$

where the uncertainties are from the errors on $\Gamma^{(0)}$, CKM matrix elements, and radiative corrections, respectively. Here, the third uncertainty on the ratio is taken as 0.7%, the same as on the first two results, due to presumed partial cancellation. Possible further cancellation is not very relevant given the current statistical uncertainty. The “experimental” values f_{D^+} ($f_{D_s^+}/f_{D^+}$) are consistent within 1σ with the (2+1+1)-flavor lattice-QCD averages in Eq. (72.19). The CKM matrix element $|V_{cd}|$ is approximately equal to $|V_{us}|$, as first shown by Wolfenstein [120, 121]. Thus, resolving the inconsistencies between determinations of $|V_{us}|$ from leptonic and semileptonic decays discussed in Sec. 72.5.1 may benefit from the constraints observed here.

Last, we can test lepton-flavor universality in charm meson decays by checking the following relationship derived from Eq. (72.1):

$$\frac{\Gamma(D_s^+ \rightarrow \tau^+\nu)}{\Gamma(D_s^+ \rightarrow \mu^+\nu)} = \frac{m_\tau^2 (1 - m_\tau^2/M_{D_s}^2)^2}{m_\mu^2 (1 - m_\mu^2/M_{D_s}^2)^2} = 9.75, \quad (72.27)$$

where the uncertainties from the masses are negligible to the number of digits quoted. The measured ratio of $\tau^+\nu$ to $\mu^+\nu$ rates is 9.82 ± 0.40 , consistent with this standard-model expectation.

72.5.3 $|V_{ub}|$ and other applications

Using the average value for $|V_{ub}|f_{B^+}$ from Table 72.5, and for f_{B^+} from Eq. (72.20), we obtain the following determination of the CKM matrix element $|V_{ub}|$ from leptonic decays within the standard model:

$$|V_{ub}| = 4.05(37)(3) \times 10^{-3}, \quad (72.28)$$

where the errors are from experiment and theory, respectively. One should bear in mind when interpreting Eq. (72.28) that none of the experimental measurements of the branching fractions that enter the average for $|V_{ub}|f_{B^+}$ have individually reached the 5σ discovery level (see Sec. 72.4.1). Further, decays involving the third generation of quarks and leptons may be particularly sensitive to new physics associated with electroweak symmetry breaking due to their larger masses [13, 15], so Eq. (72.28) is more likely to be influenced by new physics than the determinations of the elements of the first and second rows of the CKM matrix in the previous sections.

The CKM element $|V_{ub}|$ can also be obtained from semileptonic B -meson decays. A long-standing $2\text{-}3\sigma$ tension between the determinations of $|V_{ub}|$ from exclusive $B \rightarrow \pi\ell\nu$ decay and from inclusive $B \rightarrow X_u\ell\nu$ decay has diminished somewhat; here, X_u denotes all hadronic states populated by the $b \rightarrow u$ weak transition [24, 122–126]. The currently most precise determination of $|V_{ub}|^{\text{excl}} = 3.73(14) \times 10^{-3}$ is obtained from a joint z -fit by FLAG [2] of the vector and scalar form factors $f_+^{B\pi}(q^2)$ and $f_0^{B\pi}(q^2)$ calculated in (2+1)-flavor lattice QCD [127–129] and experimental measurements of the differential decay rate from BaBar [130, 131] and Belle [132, 133]. This is consistent with the value of $|V_{ub}|^{\text{excl}} = 3.70(16) \times 10^{-3}$ obtained in the 2022 PDG review on semileptonic determinations of V_{cb}, V_{ub} [134]. On the other hand, the inclusive determination in that same review, obtained using the theoretical frameworks in Refs. [135–137], is $|V_{ub}|^{\text{incl}} = 4.13(26) \times 10^{-3}$ [1, 134]. This value is significantly lower than the $4.49(28) \times 10^{-3}$ value from the corresponding PDG 2018 review [134], reducing the exclusive-inclusive tension to less than 2σ . The value of $|V_{ub}|$ from leptonic $B \rightarrow \tau\nu$ decay in Eq. (72.28) lies between these inclusive and exclusive determinations, and is compatible (within large uncertainties) with both.

Given the large uncertainties on the experimental measurements of $\mathcal{B}(B^- \rightarrow \tau^-\bar{\nu})$, and the lingering tension between $|V_{ub}|$ obtained from inclusive and exclusive semileptonic B decays, we do not present an “experimental” value of the decay constant f_{B^+} .

72.6 Concluding remarks

The increasing precision of measurements of leptonic decays of charged pseudoscalar mesons has begun to require control over radiative corrections at a level superior to that presented here. Improvements will be called for both in theory and in experiment (for example, by BESIII and Belle II).

Unitarity of the CKM matrix is in reasonable shape. However, there is a lingering almost 3σ tension between the values of V_{us} determined by semileptonic and leptonic kaon decays. It will be interesting to follow experimental and theoretical developments on this quantity.

Acknowledgements

I thank J. L. Rosner for useful discussions on this review. Previous assistance from C. Davies, S. Gottlieb, S. Hashimoto, A. Kronfeld, H.-L. Ma, W. Marciano, and S. Stone is also acknowledged.

References

- [1] R. L. Workman *et al.* (Particle Data Group), PTEP **2022**, 083C01 (2022).
- [2] Y. Aoki *et al.* (Flavour Lattice Averaging Group (FLAG)), Eur. Phys. J. C **82**, 10, 869 (2022), [arXiv:2111.09849].
- [3] Y. Aoki *et al.* (Flavour Lattice Averaging Group (FLAG)) 2023 online web update.
- [4] A. Sirlin, Nucl. Phys. **B196**, 83 (1982).
- [5] T. Kinoshita, Phys. Rev. Lett. **2**, 477 (1959).
- [6] M. Knecht *et al.*, Eur. Phys. J. **C12**, 469 (2000), [hep-ph/9909284].
- [7] G. Burdman, J. T. Goldman and D. Wyler, Phys. Rev. **D51**, 111 (1995), [hep-ph/9405425].
- [8] V. Cirigliano and I. Rosell, JHEP **10**, 005 (2007), [arXiv:0707.4464].
- [9] D. Becirevic, B. Haas and E. Kou, Phys. Lett. **B681**, 257 (2009), [arXiv:0907.1845].
- [10] A. Bazavov *et al.* (Fermilab Lattice and MILC), Phys. Rev. **D90**, 074509 (2014), [arXiv:1407.3772].
- [11] M. Di Carlo *et al.*, Phys. Rev. **D100**, 034514 (2019), [arXiv:1904.08731].
- [12] E. Barberio and Z. Was, Comput. Phys. Commun. **79**, 291 (1994).
- [13] W.-S. Hou, Phys. Rev. **D48**, 2342 (1993).
- [14] A. G. Akeroyd and S. Recksiegel, Phys. Lett. **B554**, 38 (2003), [hep-ph/0210376].
- [15] A. G. Akeroyd and S. Recksiegel, J. Phys. **G29**, 2311 (2003), [hep-ph/0306037].
- [16] A. G. Akeroyd, Prog. Theor. Phys. **111**, 295 (2004), [hep-ph/0308260].
- [17] B. A. Dobrescu and A. S. Kronfeld, Phys. Rev. Lett. **100**, 241802 (2008), [arXiv:0803.0512].
- [18] J. L. Hewett, in “Heavy flavor physics. Proceedings, LISHEP 95, LAFEX International School on High-Energy Physics, session C, cbt Workshop, Rio de Janeiro, Brazil, February 21–23, 1995,” 171–187 (1995), [hep-ph/9505246], URL <http://www-public.slac.stanford.edu/sciDoc/docMeta.aspx?slacPubNumber=SLAC-PUB-6821>.
- [19] A. Crivellin, Phys. Rev. **D81**, 031301 (2010), [arXiv:0907.2461].
- [20] F. U. Bernlochner, Z. Ligeti and S. Turczyk, Phys. Rev. **D90**, 094003 (2014), [arXiv:1408.2516].
- [21] C. Alexandrou *et al.* (Extended Twisted Mass), Phys. Rev. D **104**, 7, 074520 (2021), [arXiv:2104.06747].
- [22] W. J. Marciano, Phys. Rev. Lett. **93**, 231803 (2004), [hep-ph/0402299].
- [23] V. Cirigliano *et al.*, Rev. Mod. Phys. **84**, 399 (2012), [arXiv:1107.6001].
- [24] K. A. Olive *et al.* (Particle Data Group), Chin. Phys. **C38**, 090001 (2014).
- [25] B. Ananthanarayan and B. Moussallam, JHEP **06**, 047 (2004), [hep-ph/0405206].
- [26] S. Descotes-Genon and B. Moussallam, Eur. Phys. J. **C42**, 403 (2005), [hep-ph/0505077].
- [27] W. J. Marciano and A. Sirlin, Phys. Rev. Lett. **71**, 3629 (1993).
- [28] V. Cirigliano and H. Neufeld, Phys. Lett. **B700**, 7 (2011), [arXiv:1102.0563].
- [29] J. L. Rosner, S. Stone and R. S. Van de Water (2015), review prepared for PDG 2015 edition, [arXiv:1509.02220].
- [30] J. Gasser, A. Rusetsky and I. Scimemi, Eur. Phys. J. **C32**, 97 (2003), [hep-ph/0305260].
- [31] N. Miller *et al.*, Phys. Rev. **D102**, 3, 034507 (2020), [arXiv:2005.04795].
- [32] A. Bazavov *et al.*, Phys. Rev. **D98**, 7, 074512 (2018), [arXiv:1712.09262].
- [33] N. Carrasco *et al.* (ETM), Phys. Rev. **D91**, 054507 (2015), [arXiv:1411.7908].
- [34] R. Dowdall *et al.* (HPQCD), Phys. Rev. **D88**, 074504 (2013), [arXiv:1303.1670].
- [35] V. G. Bornyakov *et al.* (QCDSF-UKQCD), Phys. Lett. **B767**, 366 (2017), [arXiv:1612.04798].
- [36] S. Durr *et al.*, Phys. Rev. **D95**, 5, 054513 (2017), [arXiv:1601.05998].
- [37] T. Blum *et al.* (RBC, UKQCD), Phys. Rev. **D93**, 074505 (2016), [arXiv:1411.7017].
- [38] A. Bazavov *et al.* (MILC), PoS **LATTICE2010**, 074 (2010), [arXiv:1012.0868].
- [39] S. Durr *et al.* (BMW), Phys. Rev. **D81**, 054507 (2010), [arXiv:1001.4692].

- [40] E. Follana *et al.* (HPQCD, UKQCD), Phys. Rev. Lett. **100**, 062002 (2008), [arXiv:0706.1726].
- [41] M. Moulson, in “8th International Workshop on the CKM Unitarity Triangle (CKM2014) Vienna, Austria, September 8-12, 2014,” (2014), [arXiv:1411.5252].
- [42] M. Antonelli *et al.* (FlaviaNet Working Group on Kaon Decays), Eur. Phys. J. **C69**, 399 (2010), [arXiv:1005.2323].
- [43] M. Tanabashi *et al.* (Particle Data Group), Phys. Rev. **D98**, 3, 030001 (2018).
- [44] P. A. Zyla *et al.* (Particle Data Group), PTEP **2020**, 8, 083C01 (2020).
- [45] S. Hashimoto, J. Laiho and S. R. Sharpe, Lattice Quantum Chromodynamics <http://pdg.lbl.gov/2019/reviews/rpp2018-rev-lattice-qcd.pdf> (2017), review prepared for PDG 2018 edition.
- [46] S. Hashimoto, J. Laiho and S. R. Sharpe, Lattice Quantum Chromodynamics pdg.lbl.gov/2020/reviews/rpp2020-rev-lattice-qcd.pdf (2020), review prepared for PDG 2020 edition.
- [47] S. Hashimoto, J. Laiho and S. R. Sharpe, Lattice Quantum Chromodynamics pdg.lbl.gov/2022/reviews/rpp2022-rev-lattice-qcd.pdf (2021), review prepared for PDG 2022 edition.
- [48] S. Aoki *et al.* (Flavour Lattice Averaging Group), Eur. Phys. J. **C74**, 2890 (2014), [arXiv:1310.8555].
- [49] S. Aoki *et al.*, Eur. Phys. J. **C77**, 2, 112 (2017), [arXiv:1607.00299].
- [50] S. Aoki *et al.* (Flavour Lattice Averaging Group), Eur. Phys. J. **C80**, 2, 113 (2020), [arXiv:1902.08191].
- [51] A. S. Kronfeld, Ann. Rev. Nucl. Part. Sci. **62**, 265 (2012), [arXiv:1203.1204].
- [52] A. V. Manohar, C. T. Sachrajda and R. M. Barnett, Quark Masses <http://pdg.lbl.gov/2019/reviews/rpp2018-rev-quark-masses.pdf> (2018), review prepared for PDG 2018 update.
- [53] G. M. de Divitiis *et al.*, JHEP **04**, 124 (2012), [arXiv:1110.6294].
- [54] M. Artuso *et al.* (CLEO), Phys. Rev. Lett. **95**, 251801 (2005), [hep-ex/0508057].
- [55] B. I. Eisenstein *et al.* (CLEO), Phys. Rev. **D78**, 052003 (2008), [arXiv:0806.2112].
- [56] M. Ablikim *et al.* (BESIII), Phys. Rev. **D89**, 051104 (2014), [arXiv:1312.0374].
- [57] M. Artuso *et al.* (CLEO), Phys. Rev. Lett. **99**, 071802 (2007), [arXiv:0704.0629].
- [58] J. P. Alexander *et al.* (CLEO), Phys. Rev. **D79**, 052001 (2009), [arXiv:0901.1216].
- [59] M. Ablikim *et al.* (BESIII), Phys. Rev. Lett. **123**, 21, 211802 (2019), [arXiv:1908.08877].
- [60] J. Gasser and H. Leutwyler, Nucl. Phys. **B250**, 465 (1985).
- [61] G. M. de Divitiis *et al.* (RM123), Phys. Rev. **D87**, 11, 114505 (2013), [arXiv:1303.4896].
- [62] M. Nobes (2005), [hep-lat/0501009].
- [63] A. Bazavov *et al.* (Fermilab Lattice, MILC), Phys. Rev. **D93**, 11, 113016 (2016), [arXiv:1602.03560].
- [64] J. P. Lees *et al.* (BaBar) (2010), [arXiv:1003.3063].
- [65] P. del Amo Sanchez *et al.* (BaBar), Phys. Rev. **D82**, 091103 (2010), [Erratum: Phys. Rev. **D91**, 019901 (2015)], [arXiv:1008.4080].
- [66] A. Zupanc *et al.* (Belle), JHEP **1309**, 139 (2013), [arXiv:1307.6240].
- [67] M. Ablikim *et al.* (BESIII), Phys. Rev. **D94**, 7, 072004 (2016), [arXiv:1608.06732].
- [68] M. Ablikim *et al.* (BESIII), Phys. Rev. **D104**, 5, 052009 (2021), [arXiv:2102.11734].
- [69] P. Naik *et al.* (CLEO), Phys. Rev. **D80**, 112004 (2009), [arXiv:0910.3602].
- [70] K. M. Ecklund *et al.* (CLEO), Phys. Rev. Lett. **100**, 161801 (2008), [arXiv:0712.1175].
- [71] P. U. E. Onyisi *et al.* (CLEO), Phys. Rev. **D79**, 052002 (2009), [arXiv:0901.1147].
- [72] M. Ablikim *et al.* (BESIII), Phys. Rev. Lett. **127**, 17, 171801 (2021), [arXiv:2106.02218].
- [73] M. Ablikim *et al.* (BESIII), Phys. Rev. **D104**, 3, 032001 (2021), [arXiv:2105.07178].
- [74] T. K. Pedlar *et al.* (CLEO), Phys. Rev. **D76**, 072002 (2007), [arXiv:0704.0437].
- [75] J. P. Alexander *et al.* (CLEO), Phys. Rev. Lett. **100**, 161804 (2008), [arXiv:0801.0680].
- [76] B. Aubert *et al.* (BaBar), Phys. Rev. Lett. **98**, 141801 (2007), [hep-ex/0607094].
- [77] Y. Chen *et al.* (χ QCD), Chin. Phys. C **45**, 2, 023109 (2021), [arXiv:2008.05208].
- [78] P. A. Boyle *et al.* (RBC/UKQCD) (2018), [arXiv:1812.08791].
- [79] P. A. Boyle *et al.*, JHEP **12**, 008 (2017), [arXiv:1701.02644].
- [80] Y.-B. Yang *et al.* (χ QCD), Phys. Rev. **D92**, 034517 (2015), [arXiv:1410.3343].
- [81] H. Na *et al.* (HPQCD), Phys. Rev. **D86**, 054510 (2012), [arXiv:1206.4936].
- [82] A. Bazavov *et al.* (Fermilab Lattice and MILC), Phys. Rev. **D85**, 114506 (2012), [arXiv:1112.3051].
- [83] C. T. H. Davies *et al.* (HPQCD), Phys. Rev. **D82**, 114504 (2010), [arXiv:1008.4018].
- [84] B. Pullin and R. Zwicky (2021), [arXiv:2106.13617].
- [85] Z.-G. Wang, Eur. Phys. J. **C75**, 427 (2015), [arXiv:1506.01993].
- [86] P. Gelhausen *et al.*, Phys. Rev. **D88**, 014015 (2013), [arXiv:1305.5432].
- [87] S. Narison, Phys. Lett. **B718**, 1321 (2013), [arXiv:1209.2023].
- [88] W. Lucha, D. Melikhov and S. Simula, Phys. Lett. **B701**, 82 (2011), [arXiv:1101.5986].
- [89] W. Lucha, D. Melikhov and S. Simula, Eur. Phys. J. **C78**, 2, 168 (2018), [Erratum: Eur. Phys. J. **C78**, 936 (2018)], [arXiv:1702.07537].
- [90] I. Adachi *et al.* (Belle), Phys. Rev. Lett. **110**, 131801 (2013), [arXiv:1208.4678].
- [91] B. Kronenbitter *et al.* (Belle), Phys. Rev. **D92**, 051102 (2015), [arXiv:1503.05613].
- [92] J. P. Lees *et al.* (BaBar), Phys. Rev. **D88**, 031102 (2013), [arXiv:1207.0698].
- [93] B. Aubert *et al.* (BaBar), Phys. Rev. **D81**, 051101 (2010), [arXiv:0912.2453].
- [94] C. Hughes, C. T. H. Davies and C. J. Monahan, Phys. Rev. **D97**, 5, 054509 (2018), [arXiv:1711.09981].
- [95] A. Bussone *et al.* (ETM), Phys. Rev. **D93**, 11, 114505 (2016), [arXiv:1603.04306].
- [96] R. Dowdall *et al.* (HPQCD), Phys. Rev. Lett. **110**, 222003 (2013), [arXiv:1302.2644].
- [97] Y. Aoki *et al.*, Phys. Rev. **D91**, 114505 (2015), [arXiv:1406.6192].
- [98] N. H. Christ *et al.* (RBC/UKQCD), Phys. Rev. **D91**, 054502 (2015), [arXiv:1404.4670].
- [99] H. Na *et al.* (HPQCD), Phys. Rev. **D86**, 034506 (2012), [arXiv:1202.4914].
- [100] C. McNeile *et al.* (HPQCD), Phys. Rev. **D85**, 031503 (2012), [arXiv:1110.4510].

- [101] H.-K. Sun and M.-Z. Yang, Phys. Rev. **D95**, 11, 113001 (2017), [arXiv:1609.08958].
- [102] M. J. Baker *et al.*, JHEP **07**, 032 (2014), [arXiv:1310.0941].
- [103] W. Lucha, D. Melikhov and S. Simula, Phys.Rev. **D88**, 056011 (2013), [arXiv:1305.7099].
- [104] J. Hardy and I. S. Towner, PoS **CKM2016**, 028 (2016).
- [105] J. C. Hardy and I. S. Towner, Phys. Rev. **C102**, 4, 045501 (2020).
- [106] C.-Y. Seng *et al.*, Phys. Rev. **D105**, 1, 013005 (2022), [arXiv:2107.14708].
- [107] N. Carrasco *et al.*, Phys. Rev. **D93**, 11, 114512 (2016), [arXiv:1602.04113].
- [108] A. Bazavov *et al.* (Fermilab Lattice and MILC), Phys. Rev. Lett. **112**, 112001 (2014), [arXiv:1312.1228].
- [109] C.-Y. Seng *et al.*, Phys. Rev. Lett. **121**, 241804 (2018), [arXiv:1807.10197].
- [110] C. Y. Seng, M. Gorchtein and M. J. Ramsey-Musolf, Phys. Rev. **D100**, 013001 (2019), [arXiv:1812.03352].
- [111] M. Gorchtein, Phys. Rev. Lett. **123**, 042503 (2019), [arXiv:1812.04229].
- [112] C.-Y. Seng and U.-G. Meissner, Phys. Rev. Lett. **122**, 211802 (2019), [arXiv:1903.07969].
- [113] A. Czarnecki, W. J. Marciano and A. Sirlin, Phys. Rev. D **100**, 7, 073008 (2019), [arXiv:1907.06737].
- [114] C. Patrignani *et al.* (Particle Data Group), Chin. Phys. **C40**, 10, 100001 (2016).
- [115] Y. S. Amhis *et al.* (Heavy Flavor Averaging Group, HFLAV), Phys. Rev. D **107**, 5, 052008 (2023), [arXiv:2206.07501].
- [116] A. Bazavov *et al.* (Fermilab Lattice, MILC), Phys. Rev. D **107**, 9, 094516 (2023), [arXiv:2212.12648].
- [117] B. Chakraborty *et al.* ((HPQCD Collaboration)), Phys. Rev. **D104**, 3, 034505 (2021), [arXiv:2104.09883].
- [118] W. G. Parrott, C. Boucharad and C. T. H. Davies ((HPQCD collaboration)§, HPQCD), Phys. Rev. D **107**, 1, 014510 (2023), [arXiv:2207.12468].
- [119] V. Lubicz *et al.* (ETM), Phys. Rev. **D96**, 5, 054514 (2017), [Errata: Phys. Rev. **D99**, 099902 (2019), Phys. Rev. **D100**, 079901 (2019)], [arXiv:1706.03017].
- [120] L. Wolfenstein, Phys. Rev. Lett. **51**, 1945 (1983).
- [121] J. Charles *et al.* (CKMfitter Group), Eur. Phys. J. **C41**, 1 (2005), updated results and plots available at: <http://ckmfitter.in2p3.fr>, [hep-ph/0406184].
- [122] M. Antonelli *et al.*, Phys. Rept. **494**, 197 (2010), [arXiv:0907.5386].
- [123] J. N. Butler *et al.* (Quark Flavor Physics Working Group), in “Community Summer Study 2013: Snowmass on the Mississippi (CSS2013) Minneapolis, MN, USA, July 29-August 6, 2013,” (2013), [arXiv:1311.1076], URL <http://www.slac.stanford.edu/econf/C1307292/docs/IntensityFrontier/QuarkF1-15.pdf>.
- [124] Y. Amhis *et al.* (Heavy Flavor Averaging Group) (2014), [arXiv:1412.7515].
- [125] A. J. Bevan *et al.* (Belle, BaBar), Eur. Phys. J. **C74**, 3026 (2014), [arXiv:1406.6311].
- [126] Y. Amhis *et al.* (HFLAV), Eur. Phys. J. **C77**, 12, 895 (2017), [arXiv:1612.07233].
- [127] E. Dalgic *et al.*, Phys. Rev. **D73**, 074502 (2006), [Erratum: Phys. Rev. **D75**, 119906 (2007)], [hep-lat/0601021].
- [128] J. M. Flynn *et al.* (RBC/UKQCD), Phys. Rev. **D91**, 074510 (2015), [arXiv:1501.05373].
- [129] J. A. Bailey *et al.* (Fermilab Lattice, MILC), Phys. Rev. **D92**, 014024 (2015), [arXiv:1503.07839].
- [130] P. del Amo Sanchez *et al.* (BaBar), Phys. Rev. **D83**, 032007 (2011), [arXiv:1005.3288].
- [131] J. P. Lees *et al.* (BaBar), Phys. Rev. **D86**, 092004 (2012), [arXiv:1208.1253].
- [132] H. Ha *et al.* (Belle), Phys. Rev. **D83**, 071101 (2011), [arXiv:1012.0090].
- [133] A. Sibidanov *et al.* (Belle), Phys.Rev. **D88**, 032005 (2013), [arXiv:1306.2781].
- [134] A. X. El-Khadra and P. Urquijo, Semileptonic b -Hadron Decays, Determination of V_{cb} , V_{ub} <http://pdg.lbl.gov/2022/reviews/rpp2022-rev-vcb-vub.pdf> (2021), review prepared for PDG 2022 update.
- [135] B. O. Lange, M. Neubert and G. Paz, Phys. Rev. D **72**, 073006 (2005), [hep-ph/0504071].
- [136] J. R. Andersen and E. Gardi, JHEP **01**, 097 (2006), [hep-ph/0509360].
- [137] P. Gambino *et al.*, JHEP **10**, 058 (2007), [arXiv:0707.2493].

73. Production and Decay of *b*-flavored Hadrons

Revised March 2024 by P. Eerola (Research Council of Finland), M. Kreps (Warwick U.) and Y. Kwon (Yonsei U., Seoul).

The *b* quark belongs to the third generation of quarks and is the weak-doublet partner of the *t* quark. The existence of the third-generation quark doublet was proposed in 1973 by Kobayashi and Maskawa [1] in their model of the quark mixing matrix (“CKM” matrix), and confirmed four years later by the first observation of a $b\bar{b}$ meson [2]. In the KM model, *CP* violation is explained within the Standard Model (SM) by an irreducible phase of the 3×3 unitary matrix. The regular pattern of the three lepton and quark families is one of the most intriguing puzzles in particle physics. The existence of families gives rise to many of the free parameters in the SM, including the fermion masses, and the elements of the CKM matrix.

Since the *b* quark is the lighter element of the third-generation quark doublet, the decays of *b*-flavored hadrons occur via generation-changing processes through CKM matrix. Because of this, and the fact that the CKM matrix is close to a 3×3 unitary matrix, many interesting features such as loop and box diagrams, flavor oscillations, as well as large *CP* asymmetries, can be observed in the weak decays of *b*-flavored hadrons.

The CKM matrix is parameterized by three real parameters and one complex phase. This complex phase is the source of *CP* violation in *B* meson decays in the Standard Model. A crucial milestone was the first observation of *CP* violation in the *B* meson system in 2001, by the BaBar [3] and Belle [4] collaborations. They measured a large value for the parameter $\sin 2\beta$ ($= \sin 2\phi_1$) [5], almost four decades after the discovery of a small *CP* asymmetry in neutral kaons. A more detailed discussion of the CKM matrix and *CP* violation can be found elsewhere in this Review [6,7].

The structure of this mini-review is organized as follows. After a discussion of *b*-quark production and current results on spectroscopy, we discuss lifetimes of *b*-flavored hadrons. We then discuss some basic properties of *B*-meson decays, followed by summaries of dominant hadronic, rare hadronic, and electroweak penguin decays of *B*-mesons. There are separate mini-reviews for $B^0 - \bar{B}^0$ mixing [8] and the extraction of the CKM matrix elements V_{cb} and V_{ub} from *B*-meson decays [9] in this Review.

73.1 Production and spectroscopy

The bound states of a \bar{b} antiquark and a *u*, *d*, *s*, or *c* quark are referred to as the B_u (B^+), B_d (B^0), B_s (B_s^0), and B_c (B_c^+) mesons, respectively. The B_c^+ is the heaviest of the ground-state *b*-flavored mesons, and the most difficult to produce: it was observed for the first time in the semileptonic mode by CDF in 1998 [10], but its mass was accurately determined only in 2006, from the fully reconstructed mode $B_c^+ \rightarrow J/\psi\pi^+$ [11]. Many exclusive decay channels can now be used for the accurate mass measurements, given the large statistics available at the LHC. Currently the most precise measurement is made by LHCb and yields $m(B_c^+) = 6274.47 \pm 0.27 \pm 0.17 \text{ MeV}/c^2$ [12], combining $B_c^+ \rightarrow J/\psi\pi^+$, $B_c^+ \rightarrow J/\psi\pi^+\pi^-\pi^+$, $B_c^+ \rightarrow J/\psi p\bar{p}\pi^+$, $B_c^+ \rightarrow J/\psi D_s^+$, $B_c^+ \rightarrow J/\psi D^0 K^+$ and $B_c^+ \rightarrow B_s^0\pi^+$ decay modes.

The first excited meson is called the B^* meson, while B^{**} is the generic name for the four orbitally excited ($L = 1$) *B*-meson states that correspond to the *P*-wave mesons in the charm system, D^{**} . Excited states of the B_s^0 meson are similarly named B_s^* and B_s^{**} .

Of the possible bound $\bar{b}b$ states, the $\Upsilon(nS)$ and $\chi_{bJ}(nP)$ states are well studied. The pseudoscalar ground state η_b has been observed for the first time by BaBar [13] indirectly through the decay $\Upsilon(3S) \rightarrow \gamma\eta_b$, and then confirmed by Babar in $\Upsilon(2S)$ decays [14] and CLEO in $\Upsilon(3S)$ decays [15]. The most accurate mass and width measurements come now from Belle, using decays $\Upsilon(5S) \rightarrow h_b(1P)\pi^+\pi^-$, $h_b(1P) \rightarrow \gamma\eta_b(1S)$ [16], $\Upsilon(4S) \rightarrow \eta h_b(1P)$, $h_b(1P) \rightarrow \gamma\eta_b(1S)$ [17], and $\Upsilon(2S) \rightarrow \gamma\eta_b(1S)$ [18]. Belle has also reported first evidence for the $\eta_b(2S)$ in the $h_b(2P) \rightarrow \eta_b(2S)\gamma$ transition [16]. In addition, Belle has observed $T_{b\bar{b}1}(10610)$ (was $Z_b(10610)$) and $T_{b\bar{b}1}(10650)$ (was $Z_b(10650)$) states in the processes $\Upsilon(5S) \rightarrow \Upsilon(nS)\pi^+\pi^-$ ($n = 1, 2, 3$) and $\Upsilon(5S) \rightarrow h_b(mP)\pi^+\pi^-$ ($m = 1, 2$) [19]. These $T_{b\bar{b}1}$ states are

observed to decay to $\Upsilon(nS)\pi^\pm$ and $h_b(mP)\pi^\pm$, hence electrically charged and do not belong to ordinary $q\bar{q}$ mesons. For classification and naming of these and other states, see Ref. [20].

Experimental studies of *b* decays have been performed in e^+e^- collisions at the $\Upsilon(4S)$ (ARGUS, CLEO, Belle, BaBar) and $\Upsilon(5S)$ (CLEO, Belle) resonances. The $e^+e^- \rightarrow b\bar{b}$ production cross-section at the $\Upsilon(4S)$ ($\Upsilon(5S)$) resonance is about 1.1 nb (0.3 nb). The full data samples of BaBar and Belle are 560 fb^{-1} and 1020 fb^{-1} , respectively, of which 433 fb^{-1} and 710 fb^{-1} are at the $\Upsilon(4S)$ resonance. Since the $\Upsilon(4S)$ decays dominantly to a pair of *B* mesons (either B^+B^- or $B^0\bar{B}^0$), a precise knowledge of the energy-momentum of one *B* meson (the ‘tagging *B*’) enables deducing the properties of the other *B* (the ‘signal *B*’). This property has been exploited by both BaBar and Belle, in particular, to measure inclusive decay modes as well as final states with missing neutrinos. The Belle II experiment at SuperKEKB has started recording data in 2019, and the experiment has so far collected about 428 fb^{-1} of data by summer 2022, when their long shutdown 1 started. Of collected data, 363 fb^{-1} is at the $\Upsilon(4S)$ resonance. At the *Z* resonance (SLC, LEP) all species of *b*-flavored hadrons could be studied for the first time. The $e^+e^- \rightarrow b\bar{b}$ production cross-section at the *Z* resonance is about 6.6 nb .

High-energy $p\bar{p}$ (Tevatron) and pp collisions (LHC) produce *b*-flavored hadrons of all species with large cross-sections. At the Tevatron ($\sqrt{s} = 1.96 \text{ TeV}$) the visible cross section $\sigma(p\bar{p} \rightarrow bX, |\eta| < 1)$ is about $30 \mu\text{b}$. CDF and D0 experiments at the Tevatron have accumulated by the end of their running about 10 fb^{-1} each.

At the LHC pp collider at $\sqrt{s} = 7 - 13 \text{ TeV}$, the visible *b*-hadron cross section at the LHCb experiment with pseudorapidity acceptance $2 < \eta < 5$ has been measured to be $\sim 72 \mu\text{b}$ at 7 TeV and $\sim 144 \mu\text{b}$ at 13 TeV [21] (cross section at 13 TeV corrected in Erratum). LHCb has collected about 1 fb^{-1} at 7 TeV, 2 fb^{-1} at 8 TeV, and close to 5.9 fb^{-1} at 13 TeV during LHC Runs 1 and 2. CMS and ATLAS have collected each about 5 fb^{-1} of data at $\sqrt{s} = 7, 20 \text{ fb}^{-1}$ at 8 TeV and about 150 fb^{-1} at 13 TeV during LHC Runs 1 and 2. The latest LHC Run 3 at 13.6 TeV started in summer 2022, with upgraded detectors. By the time of the writing (March 2024), LHC has delivered about 70 fb^{-1} to ATLAS and CMS experiments, and about 300 pb^{-1} to the LHCb experiment with major detector upgrades.

In hadron collisions, production happens as $b\bar{b}$ pairs via leading order flavor creation or higher order processes such as gluon-splitting. Single *b*-quarks can be produced by flavor excitation. The total *b*-production cross section is an interesting test of our understanding of leading and higher order QCD processes. With a wealth of measurements at LHC and at Tevatron (see Ref. [21] and references therein), and improved calculations [22], there is a reasonable agreement between measurements and predictions.

Each quark of a $b\bar{b}$ pair produced in hadron collisions hadronizes separately and incoherently from the other, but it is still possible to obtain a statistical indication of the charge of a produced b/\bar{b} quark (“flavor tag” or “charge tag”) from the accompanying particles produced in the hadronization process, or from the decay products of the other quark. The momentum spectrum of produced *b*-quarks typically peaks near the *b*-quark mass, and extends to much higher momenta, dropping by about a decade for every ten GeV. Typical decay lengths are of the order of a centimeter at 13 TeV pp collisions; the resolution for the decay vertex must be more precise than this to resolve the fast oscillations of B_s^0 mesons.

In e^+e^- colliders, since the *B* mesons are very slow in the $\Upsilon(4S)$ rest frame, asymmetric beam energies are used to boost the decay products to allow time-dependent measurements that are crucial for the study of *CP* violation. At KEKB, the boost was $\beta\gamma = 0.43$, while PEP-II used a slightly larger boost, $\beta\gamma = 0.55$. The typical *B*-meson decay length is dilated from $\approx 20 \mu\text{m}$ to $\approx 200 \mu\text{m}$. At SuperKEKB the boost is lower, $\beta\gamma = 0.28$, which puts more demanding requirements on the track reconstruction precision at Belle II to reach a resolution in decay time measurements similar to Belle. The two *B* mesons produced in $\Upsilon(4S)$ decay are in

a coherent quantum state, which makes it easier than in hadron collisions to infer the charge state of one B meson from observation of the other; however, the coherence also requires determination of the decay time of both mesons, rather than just one, in order to perform time-dependent CP -violation measurements. For B_s^0 , which can be produced at $\Upsilon(5S)$ the situation is less favourable, as boost is not high enough to provide sufficient time resolution to resolve the fast B_s^0 oscillations.

For the measurement of branching fractions, the initial composition of the data sample must be known. The $\Upsilon(4S)$ resonance decays predominantly to $B^0\bar{B}^0$ and B^+B^- ; the current experimental upper limit for non- $B\bar{B}$ decays of the $\Upsilon(4S)$ is less than 4% at the 95% confidence level (CL) [23]. The observed modes of this category are decays to lower Υ states and a pion pair, η , or η' , measured branching fractions being of order $10^{-4} - 10^{-5}$ [24], and decays to $h_b(1P)\eta$ with branching fraction of order 10^{-3} [17].

The ratio f_+/f_0 of the fractions of charged to neutral B productions from $\Upsilon(4S)$ decays has been measured by CLEO, BaBar, and Belle in various ways. They typically use pairs of isospin-related decays of B^+ and B^0 , such that it can be assumed that $\Gamma(B^+ \rightarrow x^+) = \Gamma(B^0 \rightarrow x^0)$. In this way, the ratio of the number of events observed in these modes is proportional to $(f_+\tau_+)/ (f_0\tau_0)$ [25]. BaBar has also performed an independent measurement of f_0 with a different method that does not require isospin symmetry or the value of the lifetime ratio, based on the number of events with one or two reconstructed $B^0 \rightarrow D^{*+}\ell^+\nu$ decays [26]. The combined result, from the current average of τ_+/τ_0 , is $f_+/f_0 = 1.058 \pm 0.024$ [27]. The result is consistent within 2.4σ with equal production of B^+B^- and $B^0\bar{B}^0$ pairs, and we assume $f_+/f_0 = 1$ in this mini-review except where explicitly stated otherwise. This assumption is also supported by the near equality of the B^+ and B^0 masses: our fit yields $m(B^0) = 5279.72 \pm 0.08$ MeV/ c^2 , $m(B^+) = 5279.41 \pm 0.07$ MeV/ c^2 , and $m(B^0) - m(B^+) = 0.31 \pm 0.05$ MeV/ c^2 .

Data collected at the $\Upsilon(5S)$ resonance gave CLEO, Belle and BaBar access to B_s^0 decays. In $\Upsilon(5S)$ decays there are seven possible final states including a pair of non-strange B mesons and 0, 1 or 2 pions, and three final states with a pair of strange B mesons ($B_s^0\bar{B}_s^0$, $B_s^+\bar{B}_s^0$, and $B_s^0\bar{B}_s^+$). The fraction of events with a pair of B_s^0 mesons over the total number of events with a pair of b -flavored hadrons has been measured to be $f_s[\Upsilon(5S)] = 0.199_{-0.029}^{+0.030}$ [28], of which 88% is $B_s^0\bar{B}_s^0$ events. However, the small boost of B_s^0 mesons produced in this way prevents resolution of their fast oscillations for time-dependent measurements; these are only accessible in hadron collisions (or at the Z peak).

In high-energy collisions, the produced b or \bar{b} quarks can hadronize with different probabilities into the full spectrum of b -hadrons, either in their ground or excited states. The hadronization does not have to be identical in $p\bar{p}$ or pp collisions and in Z decay, because of the different momentum distributions of the b -quark in these processes; the sample used in the $p\bar{p}$ measurements has momenta close to the b mass, rather than $m_Z/2$ in Z decay. The available data from Tevatron and LHC show that the production fractions f_d , f_u , f_s , and f_{baryon} of B^0 , B^+ , B_s^+ , and b baryons, respectively, of weakly decaying b hadrons depend on the kinematics of the produced b hadron. Recently LHCb experiment found evidence for dependence of b -quark hadronization on multiplicity in pp collisions [29]. The production fractions of b hadrons are discussed in more detail in the $B^0 - \bar{B}^0$ mixing section in this Review [8].

Excited B -meson states have been thoroughly studied by CLEO, LEP, CUSB, D0 and CDF (an admixture of B mesons) and LHCb (B^{*+} -meson). The current world average of the $B^* - B$ mass difference is 45.21 ± 0.21 MeV/ c^2 . Excited B_s^* -meson states have observed in $\Upsilon(5S)$ decays by CUSB, CLEO and Belle.

For orbitally excited $B_{(s)}$ meson states, with relative angular momentum $L=1$ of the two quarks, there exist four states $(J, j_q) = (0, 1/2), (1, 1/2), (1, 3/2), (2, 3/2)$, where j_q is the total angular momentum of the light u , d or s quark and J is the total angular momentum of the B meson. These states are collectively called as $B_{(s)}^{**}$ mesons. The $j_q = 1/2$ states are named $B_{(s)0}^*$ ($J = 0$) and $B_{(s)1}$ ($J = 1$) mesons, while the states with

$j_q = 3/2$ are named $B_{(s)1}$ ($J = 1$) and $B_{(s)2}^*$ ($J = 2$) mesons. The states with $j_q = 1/2$ can decay through an S -wave transition and are expected to have a large width, but the $j_q = 3/2$ states are narrow D -wave decays. Evidence for B^{**} production has been initially obtained at LEP as a broad $B\pi$ resonance [30] or a B^+K^- enhancement [31]. Detailed results have been obtained for the narrow states $B_1(5721)^{0,+}$ and $B_2(5747)^{0,+}$ at the Tevatron and by LHCb, and clear enhancements compatible with the higher mass states $B_J(5840)^{0,+}$ and $B_J(5970)^{0,+}$ have been observed [32]. Also the narrow B_s^{**} states $B_{s1}(5830)^0$ and $B_{s2}(5840)^0$ have been measured at the CDF [32], LHCb [33], and CMS [34].

Excited states of B_c^+ mesons will provide important information about the strong potential. A $B_c^+ \pi^+ \pi^-$ resonance has been observed for the first time by ATLAS [35]. The mass of the resonance has been measured precisely by CMS and LHCb as 6871.2 ± 1.0 MeV/ c^2 [36]. The resonance may be interpreted as the second S -wave state of the B_c^+ meson, $B_c^+(2S)$, but the quantum numbers are to be confirmed.

Baryon states containing a b quark are labeled according to the same scheme used for non- b baryons, with the addition of a b subscript [20]. The first observed b baryon was the Λ_b^0 (quark composition udb). Thanks to the large samples accumulated at the Tevatron and specially at the LHC many new b baryons have been found. The masses of all these new baryons have been measured to a precision of a few MeV/ c^2 , and found to be in agreement with predictions from Heavy Quark Effective Theory (HQET).

Clear signals of four strongly-decaying baryon states, Σ_b^+ , Σ_b^{*+} (uub), Σ_b^- , Σ_b^{*-} (ddb) have been obtained by CDF [37] and LHCb [38]. LHCb has also observed two new mass peaks in the $\Lambda_b^0 \pi^\pm$ systems, consistent with single resonances and named as $\Sigma_b^\pm(6097)$ [38]. The nature of these resonances is, however, not yet clear. The isodoublet of strange b baryons $\Xi_b^0(usb)$ and $\Xi_b^\pm(ds b)$ has been observed by CDF and D0 [39]. Masses, lifetimes, and branching ratios have been accurately measured by LHCb [40–42] and CDF [43]. LHCb has also measured several parameters sensitive to P and CP violation [42, 44]. Other observed Ξ_b baryons are spin-3/2 states $\Xi_b(5945)^0$ (Ξ_b^{*0}) [45, 46], $\Xi_b^{*-}(5955)^-$ [46, 47] and $\Xi_b(6100)^-$ [46, 48], a spin-1/2 state $\Xi_b'(5935)^-$ [46, 47], and resonance states $\Xi_b^-(6227)$ [41, 49], $\Xi_b^0(6327)$ [50] and $\Xi_b^0(6333)$ [50]. The doubly-strange bottom baryon Ω_b^- has been observed first by D0 and CDF [51]. Mass and mean life have been measured precisely by LHCb [52] and CDF [43]. LHCb has also observed four excited Ω_b^- states $\Omega_b^-(6316)$, $\Omega_b^-(6330)$, $\Omega_b^-(6340)$ and $\Omega_b^-(6350)$ [53].

The so-called exotic states have raised a lot of interest recently. While many exotic states were seen in the charm sector, in bottom sector there are fewer seen. The D0 Collaboration claimed a narrow state $X(5568)$ decaying into a $B_s^0 \pi^\pm$ final state [54]. While this would be an interesting addition to the observed states as the first exotic state with constituent quarks with four different flavours (b, s, u, d), analysis by LHCb yields negative result [55]. Also CMS finds no such a state [56].

73.2 Lifetimes

Precise lifetimes are key in extracting the weak parameters that are important for understanding the role of the CKM matrix in CP violation, such as the determination of V_{cb} and $B_s^0 - \bar{B}_s^0$ mixing parameters. In the naive spectator model, the heavy-flavored hadrons can decay only via the external spectator mechanism, and thus, the lifetimes of all mesons and baryons containing b quarks would be equal. Non-spectator effects, such as the interference between contributing amplitudes, modify this simple picture and give rise to a lifetime hierarchy for b -flavored hadrons similar to the one in the charm sector. However, since the lifetime differences are expected to scale as $1/m_Q^2$, where m_Q is the mass of the heavy quark, the variations in the b system are expected to be only 10% or less [57, 58]. We expect:

$$\tau(B^+) \geq \tau(B^0) \approx \tau(B_s^0) > \tau(\Lambda_b^0) \gg \tau(B_c^+) . \quad (73.1)$$

For the B_c^+ , both quarks decay weakly, so the lifetime is much shorter.

Measurements of the lifetimes of the different b -flavored hadrons thus provide a means to determine the importance of non-spectator mechanisms in the b sector. Availability of large samples of fully-reconstructed decays of different b -hadron species has resulted in precise measurements with small statistical and systematic uncertainties ($\sim 1\%$). The world averages given in Table 73.1 have been determined by the Heavy Flavor Averaging Group (HFLAV) [59].

Table 73.1: Summary of the world-average b -hadron lifetime measurements. For the B_s^0 lifetimes, see text below.

Particle	Lifetime [ps]
B^+	1.638 ± 0.004
B^0	1.517 ± 0.004
B_s^0	1.520 ± 0.005
$B_s^0 \text{ (L)}$	1.429 ± 0.006
$B_s^0 \text{ (H)}$	1.623 ± 0.008
B_c^+	0.510 ± 0.009
A_b^0	1.471 ± 0.009
Ξ_b^-	1.572 ± 0.040
Ξ_b^0	1.480 ± 0.030
Ω_b^-	$1.64^{+0.18}_{-0.17}$

The B_s^0 lifetime in Table 73.1 is defined as $1/\Gamma_s$, where Γ_s is the average width of the light (L) and heavy (H) mass eigenstates, $(\Gamma_L + \Gamma_H)/2$. In the absence of CP violation, the light (heavy) B_s^0 mass eigenstate is the CP -even (CP -odd) eigenstate. Thus, the lifetime of the light (heavy) mass eigenstate can be measured from CP -even (odd) final states. The lifetimes can also be obtained from time-dependent angular analysis of $B_s^0 \rightarrow J/\psi\phi$ decays.

The short B_c^+ lifetime is in good agreement with predictions [60]. With large samples of B_c^+ mesons at the LHC precision on the lifetimes can still improve. The measurement using semileptonic decays gives $\tau_{B_c^+} = 0.509 \pm 0.008 \pm 0.012$ ps [61] while using decays $B_c^+ \rightarrow J/\psi\pi^+$ yields $\tau_{B_c^+} = 0.5134 \pm 0.0110 \pm 0.0057$ ps [62]. Each of these is more precise than the combination of all previous experiments.

The recent A_b^0 lifetime measurements from LHC experiments and CDF are precise and favour lifetime close to the lifetime of B^0 meson, in agreement with theory.

For precision comparisons with theory, lifetime ratios are more sensitive. Experimentally it is found [59]:

$$\frac{\tau_{B^+}}{\tau_{B^0}} = 1.076 \pm 0.004, \quad \frac{\tau_{B_s^0}}{\tau_{B^0}} = 1.002 \pm 0.004,$$

$$\frac{\tau_{A_b^0}}{\tau_{B^0}} = 0.969 \pm 0.006,$$

while recent Heavy Quark Expansion (HQE) predictions give [58]:

$$\frac{\tau_{B^+}}{\tau_{B^0}} = 1.04^{+0.05}_{-0.01} \pm 0.02 \pm 0.01, \quad \frac{\tau_{B_s^0}}{\tau_{B^0}} = 1.001 \pm 0.002,$$

$$\frac{\tau_{A_b^0}}{\tau_{B^0}} = 0.935 \pm 0.054.$$

The ratio of B^+ to B^0 lifetimes has a precision of better than 1%, and is significantly different from 1.0, in agreement with predictions [57]. The ratio of B_s^0 to B^0 lifetimes is expected to be very close to 1.0.

For a detailed discussion on neutral B^0 and B_s^0 oscillation and relevant CP violation measurements see Ref. [8].

73.3 Features of decays

The ground states of b -flavored hadrons decay via weak interactions. In most decays of the b -flavored hadrons, where the b -quark is accompanied by lighter partner quarks (d , u , s , or c), the decay modes are well described by the decay of the b quark (spectator

model) [63]. The dominant decay mode of a b quark is $b \rightarrow cW^{*-}$ (referred to as a “tree” or “spectator” decay), where the virtual W materializes either into a pair of leptons $\ell\bar{\nu}$ (“semileptonic decay”), or into a pair of quarks which then hadronizes. The transition $b \rightarrow u$ is suppressed by $|V_{ub}/V_{cb}|^2 \sim (0.1)^2$ relative to $b \rightarrow c$ transitions. The decays in which the spectator quark combines with one of the quarks from W^* to form one of the final state hadrons are suppressed by a factor $\sim (1/3)^2$, because the colors of the two quarks from different sources must match (“color-suppression”).

Semileptonic B decays $B \rightarrow X_c\ell\nu$ and $B \rightarrow X_u\ell\nu$ provide an excellent way to measure the magnitude of the CKM elements $|V_{cb}|$ and $|V_{ub}|$ respectively, because the strong interaction effects are much simplified due to the two leptons in the final state. Both exclusive and inclusive decays can be used with dominant uncertainties being complementary. For exclusive decay analysis, knowledge of the form factors for the exclusive hadronic system $X_{c(u)}$ is required. For inclusive analysis, it is usually necessary to restrict the available phase-space of the decay products to suppress backgrounds; subsequently uncertainties are introduced in the extrapolation to the full phase-space. Moreover, restriction to a small corner of the phase-space may result in breakdown of the operator-product expansion scheme, thus making theoretical calculations unreliable. A more detailed discussion of B semileptonic decays and the extraction of $|V_{cb}|$ and $|V_{ub}|$ is given elsewhere in this Review [9]. While traditionally B^0 and B^+ decays were used, over time also other B hadron studies became available. Most notably, determination of $|V_{ub}|$ using $A_b^0 \rightarrow p\mu^-\bar{\nu}_\mu$ decays by LHCb [64] was more precise than expected. Besides, there have been measurements of inclusive semileptonic decay rates of B_s^0 [65] and B_c^+ [66] mesons. One of the latest additions in this area is the observation of the $B_s^0 \rightarrow K^-\mu^+\nu_\mu$ decays by LHCb using only a fraction of their available data [67].

On the other hand, hadronic B decays are complicated because of strong interaction effects caused by the surrounding cloud of light quarks and gluons. While this complicates the extraction of CKM matrix elements, it also provides a great opportunity to study perturbative and non-perturbative QCD, hadronization, and Final State Interaction (FSI) effects.

Many aspects of B decays can be understood through the Heavy Quark Effective Theory (HQET) [68]. This has been particularly successful for semileptonic decays. For further discussion of HQET, see for instance Ref. [69]. For hadronic decays, one typically uses effective Hamiltonian calculations that rely on a perturbative expansion with Wilson coefficients. In addition, some form of the factorization hypothesis is commonly used, where, in analogy with semileptonic decays, two-body hadronic decays of B mesons are expressed as the product of two independent hadronic currents, one describing the formation of a charm meson (in case of the dominant $b \rightarrow cW^{*-}$ decays), and the other describing the hadronization of the remaining $\bar{u}d$ (or $\bar{c}s$) system from the virtual W^- . Qualitatively, for B decays with a large energy release, e.g. $b \rightarrow uW^{*-}$ transitions, the $\bar{u}d$ pair (produced as a color singlet) travels fast enough to leave the interaction region without influencing the meson containing the spectator quark. This is known to work well for the dominant spectator decays [70]. There are several common implementations of these ideas for hadronic B decays, the most common of which are QCD factorization (QCDF) [71], perturbative QCD (pQCD) [72], and soft collinear effective theory (SCET) [73].

The transitions $b \rightarrow s$ and $b \rightarrow d$ are flavor-changing neutral-current (FCNC) processes. Although they are not allowed in the SM as a tree-process, they can occur via loop diagrams (denoted “penguin” decays). The rates for $b \rightarrow s$ penguin decays are comparable to the CKM-suppressed $b \rightarrow u$ tree processes. Pure-penguin decays were first established by the observation of $B \rightarrow K^*(892)\gamma$ [74]. Penguin processes involving $b \rightarrow d$ transitions are further suppressed by CKM, and have been observed for $B \rightarrow (\rho/\omega)\gamma$ decays [75, 76]. LHCb has observed a $b \rightarrow d$ penguin transition in the $B^+ \rightarrow \pi^+\mu^+\mu^-$ mode and measured its branching fraction to be $(1.83 \pm 0.24 \pm 0.05) \times 10^{-8}$ [77].

Other decay processes discussed in this Review include W -exchange (a W is exchanged between initial-state quarks), penguin annihilation (the gluon from a penguin loop attaches to

the spectator quark, similar to an exchange diagram), and pure-annihilation (the initial quarks annihilate to a virtual W , which then decays). Some observed decay modes such as $B^0 \rightarrow D_s^- K^+$, may be interpreted as evidence of a W -exchange process [78]. The evidence for the purely leptonic decay $B^+ \rightarrow \tau^+ \nu$ from Belle [79] and BaBar [80] is the first sign of a pure annihilation decay. The average branching fraction is $(1.09 \pm 0.24) \times 10^{-4}$, which is somewhat larger than, though consistent with, the value expected in the SM. A substantial region of parameter space of charged Higgs mass vs. $\tan\beta$ is excluded by the measurements of this mode. A dedicated discussion of purely leptonic decays of charged pseudoscalar mesons is given elsewhere in this *Review* [81].

73.4 Dominant hadronic decays

Most of the hadronic B decays involve $b \rightarrow c$ transition at the quark level, resulting in a charmed hadron or charmonium in the final state. Other types of hadronic decays are very rare and will be discussed separately in the next section. The experimental results on hadronic B decays have steadily improved over the years, and the measurements have reached sufficient precision to challenge our understanding of the dynamics of these decays. With good particle detection and hadron identification capabilities of B -factory detectors, a substantial fraction (roughly on the order of a few per mill) of hadronic B decay events can be fully reconstructed. In particular, good performances for detecting π^0 and other neutral particles helped Belle and BaBar to make comprehensive measurements of the decays $\bar{B}^0 \rightarrow D^{(*)0} h^0$ [82], where h^0 stands for light neutral mesons such as $\pi^0, \eta^{(\prime)}, \rho^0, \omega$. The measurements are being complemented by LHCb, in decays like $\bar{B}^0 \rightarrow D^0 \pi^+ \pi^-$ [83], where no neutral particles reconstruction is needed. These decays proceed through color-suppressed diagrams, hence they provide useful tests on the factorization models.

Because of the kinematic constraint of $\Upsilon(4S) \rightarrow B\bar{B}$, the energy sum of the final-state particles of a B meson decay is always equal to one half of the total energy in the center of mass frame. As a result, the two variables, ΔE (energy difference) and M_B (B candidate mass with a beam-energy constraint) are very effective for reducing combinatorial background both from $\Upsilon(4S)$ and $e^+e^- \rightarrow q\bar{q}$ continuum events. In particular, the energy-constraint in M_B improves the signal resolution by almost an order of magnitude.

The kinematically clean environment of B meson decays provides an excellent opportunity to search for new states. For instance, quark-level $b \rightarrow c\bar{c}s$ decays have been used to search for new charmonium and charm-strange mesons and study their properties in detail. While narrow charm-strange states $D_{s0}^*(2317)$ [84] and $D_{s1}(2460)$ [85] were discovered by BaBar and CLEO, respectively, the properties of these new states were revealed by studying the B meson decays, $B \rightarrow DD_{s0}^*(2317)$ and $B \rightarrow DD_{s1}(2460)$ by Belle [86] and BaBar [87]. Another example is Dalitz plot analysis of decay $B_s^0 \rightarrow \bar{D}^0 K^- \pi^+$ in which the decay to spin-3 resonance was observed for the first time [88]. One of the most significant improvements in the past decade is establishment of decays $B^+ \rightarrow D^0 K^+$ and $B^+ \rightarrow D^0 K^*(892)^+$ with D^0 decaying to final state common to D^0 and \bar{D}^0 [89]. This allows direct determination of CKM angle $\gamma(= \phi_3)$ to be $65.9_{-3.5}^{+3.3}$.

Information on B_s^0, B_c^+ and Λ_b^0 decays have been remarkably improved with recent studies of large samples from LHCb. Noticeable additions in B_s include decay modes to $D_s^{(*)+} D_s^{(*)-}, \bar{D}^0 \bar{K}^0$, and $J/\psi \bar{K}^*(892)^0$. The $B_s^0 \rightarrow D_s^{(*)+} D_s^{(*)-}$ decays were first observed by CDF [90], followed by Belle [91]. LHCb has improved the precision with $\mathcal{B}(B_s^0 \rightarrow D_s^{(*)+} D_s^{(*)-}) = (3.07 \pm 0.22 \pm 0.33)\%$ [92], which suggests that $B_s^0 \rightarrow D_s^{(*)+} D_s^{(*)-}$ decays do not saturate the CP -even modes of the B_s decays. The $B_s^0 \rightarrow \bar{D}^0 \bar{K}^0$ decay occurs mostly via a color-suppressed tree diagram, and has a small theoretical uncertainty in the SM, thus this mode can significantly improve the determination of the CP -violation angle ϕ_s . LHCb has observed this decay and the branching fraction is $(4.3 \pm 0.5 \pm 0.7) \times 10^{-4}$ [93]. The $B_s^0 \rightarrow J/\psi \bar{K}^*(892)^0$ decay can be used to constrain the penguin pollution in determining ϕ_s . LHCb has updated the branching fraction and measured the CP asymmetries of this decay, thereby constraining the penguin pol-

lution in ϕ_s [94], although a much more stringent constraint on penguin pollution can come from $B^0 \rightarrow J/\psi \rho^0$ which has been observed by BaBar [95] and LHCb [96]. The $B_c^+ \rightarrow B_s^0 \pi^+$ decay is unique as the only observed mode of b -flavored hadron decays where the partner quark decays (c in this case) while the b quark remains a spectator. LHCb has observed this mode [97] and measured $\mathcal{B}(B_c^+ \rightarrow B_s^0 \pi^+)/\mathcal{B}(B_c^+ \rightarrow J/\psi \pi^+) = (91 \pm 10 \pm 8 \pm 3)$ [98]. In addition, LHCb [99] and ATLAS [100] have measured $B_c^+ \rightarrow J/\psi D_s^{(*)+}$, which, by comparing with $B_c^+ \rightarrow B_s^0 \pi^+$, provides a ratio of exclusive $b \rightarrow c$ and $c \rightarrow s$ decays of B_c^+ . For $\Lambda_b^0 \rightarrow \Lambda_c^+ \pi^+ \pi^- \pi^-$ [101], not only the total rate is measured, but also structure involving decays through excited Λ_c and Σ_c baryons.

In addition, a variety of exotic particles that do not fit the conventional meson spectroscopy have been discovered in B decays. Belle found the $X(3872)$ state by studying $B^+ \rightarrow J/\psi \pi^+ \pi^- K^+$ [102], which was confirmed by CDF [103], D0 [104] and BaBar [105]. Production of $X(3872)$ has been studied by the LHC experiments, LHCb [106], CMS [107] and ATLAS [108].

A charged charmonium-like state $X(4430)^\pm$ that decays to $\psi(2S)\pi^\pm$ was observed by Belle in $B \rightarrow \psi(2S)K\pi^\pm$ [109]. Since it is charged, it could not be an ordinary charmonium state. A high-statistics study by LHCb confirmed the existence of the $X(4430)^\pm$ in decays $B \rightarrow \psi(2S)K\pi^\pm$ [110], demonstrated its resonance character by studying the phase motion, unambiguously determined its spin-parity, and saw evidence for another state. In a Dalitz plot analysis of $\bar{B}^0 \rightarrow J/\psi K^- \pi^+$ [111], Belle has found another state, labeled as $X(4200)^+$ in this *Review*, adding to the list of exotic charged charmonium-like states. In an amplitude analysis of the decay $\Lambda_b^0 \rightarrow J/\psi p K^-$, LHCb observed exotic structures, labeled as $P_c(4380)^+$ and $P_c(4450)^+$ in this *Review*, in the $J/\psi p$ channel [112]. The subsequent analysis with significantly increased statistics observed additional state and resolved the peak at 4450 MeV/ c^2 as being due to the two states close in the mass [113]. The structure in the $J/\psi p$ channel was also seen in the $B_s^0 \rightarrow J/\psi p \bar{p}$ decays [114] and in the $J/\psi \Lambda$ channel in $B^+ \rightarrow J/\psi \Lambda p$ and $\Xi_b^- \rightarrow J/\psi \Lambda K^-$ decays [115]. They are referred to as charmonium-pentaquark states. More detailed discussions of exotic meson-like states and pentaquarks are given elsewhere in this *Review* [116].

73.5 Rare hadronic decays

All B -meson decays that do not occur through the $b \rightarrow c$ transition are usually called rare B decays. These include both semileptonic and hadronic $b \rightarrow u$ decays that are suppressed at leading order by the small CKM matrix element V_{ub} , as well as higher-order $b \rightarrow s(d)$ processes such as electroweak and gluonic penguin decays. In this section, we review hadronic rare B decays, while electroweak penguin decays and others are discussed in the next.

Charmless B meson decays into two-body hadronic final states such as $B \rightarrow \pi\pi$ and $K\pi$ are experimentally clean, and provide good opportunities to probe new physics and search for indirect and direct CP violations. Since the final state particles in these decays tend to have larger momenta than average B decay products, the event environment is cleaner than for $b \rightarrow c$ decays. Branching fractions are typically around 10^{-5} . Over the past decade, many such modes have been observed not only by e^+e^- collider experiments such as BaBar and Belle, but also by hadron collider experiments such as CDF ($p\bar{p}$) and LHCb (pp). In the latter cases, huge data samples of the modes with all charged final-state particles have been reconstructed by triggering on the impact parameter of the charged tracks. This has also allowed observation of charmless decays of the B_s , in final states such as $\phi\phi$ [117], K^+K^- [118, 119], and $K^-\pi^+$ [119, 120], and of charmless decays of the Λ_b^0 baryon [120]. The large samples available at LHCb experiment allow to perform also time-dependent CP violation measurements [121]. Charmless B_s modes are related to corresponding B^0 modes by U-spin symmetry, and are determined by similar amplitudes. Combining the observables from B_s^0 and B^0 modes is a further way of eliminating hadronic uncertainties and extracting relevant CKM information [122].

Because of relatively high-momenta for final state particles, the dominant source of background in e^+e^- collisions is $q\bar{q}$ contin-

uum events; sophisticated background suppression techniques exploiting event shape variables are essential for these analyses. In hadron collisions, the dominant background comes from QCD or partially reconstructed heavy flavors, and is similarly suppressed by a combination of kinematic and isolation requirements. The results are in general consistent among the experiments.

Most rare decay modes including $B^0 \rightarrow K^+\pi^-$ have contributions from both $b \rightarrow u$ tree and $b \rightarrow sg$ penguin processes. If the size of the two contributions are comparable, the interference between them may result in direct CP violation, seen experimentally as a charge asymmetry in the decay rate measurement. BaBar [123], Belle [124], CDF [118], and LHCb [121, 125] have measured the direct CP violating asymmetry in $B^0 \rightarrow K^+\pi^-$ decays. Direct CP violation has been observed in this decay with a significance of more than 5σ . The world average value of the asymmetry is now rather precise, $A_{CP}(K^+\pi^-) = -0.0834 \pm 0.0032$. The CP asymmetry in $B^+ \rightarrow K^+\pi^0$ mode has been measured by BaBar [126], *Belle [124] and LHCb [127] with the average value $A_{CP}(K^+\pi^0) = 0.030 \pm 0.013$. These two asymmetries differ significantly, in contrast to a naive expectation based on simplified picture in the SM. For more detailed tests, there are sum rules [128] that relate the decay rates and decay-rate asymmetries between the four $K\pi$ charge states. A crucial ingredient of the sum rule test is $A_{CP}(K^0\pi^0)$. Currently, measured values are reported by both BaBar [129] and Belle [130]. Using the $A_{CP}(K^0\pi^0)$ value of Ref. [130], Belle reports the sum rule test result that is consistent with zero within 1.9σ [124]. With the future improvements via Belle II and upgraded LHCb, the measurements are expected to become precise enough to shape a definite conclusion. The CP asymmetry in the π^+K^- mode has also been measured in B_s^0 decays, by CDF [118] and LHCb [121, 125]. The combined value is $A_{CP}(B_s^0 \rightarrow \pi^+K^-) = 0.224 \pm 0.012$.

In addition to $B_{(s)} \rightarrow K\pi$ modes, significant ($> 3\sigma$) non-zero CP asymmetries have been measured in several other rare decay modes: $A_{CP}(B^+ \rightarrow \rho^0 K^+) = 0.37 \pm 0.10$ [131], $A_{CP}(B^+ \rightarrow \eta K^+) = -0.37 \pm 0.08$ [132], $A_{CP}(B^0 \rightarrow \eta K^0) = 0.19 \pm 0.05$ [133], and $A_{CP}(B^+ \rightarrow f_2(1270)K^+) = -0.68^{+0.19}_{-0.17}$ [131]. In at least the first two cases, a large direct CP violation might be expected since the penguin amplitude is suppressed so the tree and penguin amplitudes may have comparable magnitudes. There are also measurements by LHCb of CP asymmetries in several 3-body modes: $A_{CP}(B^+ \rightarrow \pi^+\pi^-\pi^+) = 0.057 \pm 0.013$, $A_{CP}(B^+ \rightarrow K^+\pi^-\pi^+) = 0.027 \pm 0.008$, $A_{CP}(B^+ \rightarrow K^+K^-\pi^+) = -0.122 \pm 0.0021$, and $A_{CP}(B^+ \rightarrow K^+K^-K^+) = -0.033 \pm 0.008$ [134]. Many of these analyses now include Dalitz plot treatments with many intermediate resonances.

BaBar [135] and Belle [124, 136] have observed the decays $B^+ \rightarrow \bar{K}^0 K^+$ and $B^0 \rightarrow K^0 \bar{K}^0$. The world-average branching fractions are $\mathcal{B}(B^0 \rightarrow K^0 \bar{K}^0) = (1.21 \pm 0.16) \times 10^{-6}$ and $\mathcal{B}(B^+ \rightarrow \bar{K}^0 K^+) = (1.31 \pm 0.17) \times 10^{-6}$. These are the first observations of hadronic $b \rightarrow d$ transitions, with significance bigger than 5σ for all four measurements. CP asymmetries have been measured for these modes, but with large errors. LHCb has observed $B^0 \rightarrow K^+ K^-$ mode which occurs via a weak-annihilation process and is the rarest hadronic B -meson decay thus far observed, with $\mathcal{B}(B^0 \rightarrow K^+ K^-) = (7.80 \pm 1.52) \times 10^{-8}$ [137]. $B_s^0 \rightarrow K^+ K^-$ decay mode, which occurs mostly via $b \rightarrow s$ penguin process, has been observed by Belle [138], CDF [139] and LHCb [119]. The average branching fraction is $\mathcal{B}(B_s^0 \rightarrow K^+ K^-) = (26.6 \pm 2.2) \times 10^{-6}$. Belle has also observed $B_s^0 \rightarrow K^0 \bar{K}^0$ [140] which also occurs via $b \rightarrow s$ penguin transition in the SM. This was recently confirmed by LHCb [141]. The average branching fraction is $(1.76 \pm 0.31) \times 10^{-5}$.

The decay $B^0 \rightarrow \pi^+\pi^-$ can be used to extract the CKM angle α (for details see elsewhere in this Review [142]). This is complicated by the presence of significant contributions from penguin diagrams. An isospin analysis [143] can be used to untangle the penguin complications. The decay $B^0 \rightarrow \pi^0\pi^0$ is crucial in this analysis. Both BaBar and Belle have observed $B^0 \rightarrow \pi^0\pi^0$, with a mild tension in the measured branching fractions: $(1.83 \pm 0.25) \times 10^{-6}$ for BaBar [123] and $(1.31 \pm 0.26) \times 10^{-6}$ for Belle [144]. It turns out that the amount of penguin pollution in the $B \rightarrow \pi\pi$ system is

rather large. In the past few years, measurements in the $B^0 \rightarrow \rho\rho$ system have produced more precise values of α , since penguin amplitudes are generally smaller for decays with vector mesons. An important ingredient in the analysis is the $B^0 \rightarrow \rho^0\rho^0$ branching fraction. The average of measurements from BaBar [145] and Belle [146] yields a branching fraction of $(0.96 \pm 0.15) \times 10^{-6}$. This is only 3% of the $\rho^+\rho^-$ branching fraction, much smaller than the corresponding ratio ($\gtrsim 20\%$) in the $\pi\pi$ system.

Since $B \rightarrow \rho\rho$ has two vector mesons in the final state, the CP eigenvalue of the final state depends on the longitudinal polarization fraction f_L for the decay. Therefore, a measurement of f_L is needed to extract the CKM angle α . Both BaBar and Belle have measured f_L for the decays $\rho^+\rho^-$ [147] and $\rho^+\rho^0$ [148] and in both cases the measurements show $f_L > 0.9$, making a complete angular analysis unnecessary. In $B^0 \rightarrow \rho^0\rho^0$, f_L is measured by BaBar [145], Belle [146] and LHCb [149], with the average value being $0.71^{+0.08}_{-0.09}$.

By analyzing the angular distributions of the B decays to two vector mesons, we can learn a lot about both weak- and strong-interaction dynamics in B decays. Decays that are penguin-dominated surprisingly have values of f_L near 0.5. The list of such decays has now grown to include $B \rightarrow \phi K^*(892)$, $B \rightarrow \rho K^*(892)$, and $B \rightarrow \omega K^*(892)$. The reasons for this "polarization puzzle" are not fully understood. A detailed description of the angular analysis of B decays to two vector mesons can be found in a separate mini-review [150] in this Review.

73.6 Electroweak penguin decays

Electroweak penguin decays are one-loop FCNC decays proceeding through penguin or box Feynman diagrams with final state including real photon or pair of leptons. Such decays were first observed by CLEO experiment when it observed decay $B \rightarrow K^*(892)\gamma$ [74]. Since then significant amount of experimental information was obtained. Branching fractions for these decays are 10^{-5} or less, which makes them excellent candidates for searches for new physics beyond SM. Often several observables are available, which allows for stringent tests of the SM.

Starting with radiative decays, experimentally easiest to study are exclusive decays with a fully reconstructed final state. The best studied decay in this class is $B \rightarrow K^*(892)\gamma$ seen by CLEO, Belle, BaBar experiments [151, 152] with world average branching fraction $\mathcal{B}(B^0 \rightarrow K^*(892)^0\gamma) = (41.8 \pm 2.5) \times 10^{-6}$. Decays through several other kaon resonances such as $B \rightarrow K_1(1270)\gamma$, $K_2^*(1430)\gamma$, etc. were studied at B-factories [153, 154]. It is worth to mention decay $B^+ \rightarrow K^+\pi^+\pi^-\gamma$ for which besides measurements of the branching fraction [154, 155] one can also use the angular distribution to access photon polarization. Such a measurement was done by the LHCb experiment, which was able to clearly demonstrate that the photon in $B^+ \rightarrow K^+\pi^+\pi^-\gamma$ decay is polarized [156]. Unfortunately given non-trivial hadronic structure, more work is needed before turning this into test of the SM. The exclusive radiative decays $B_s^0 \rightarrow \phi\gamma$ was seen by the Belle and LHCb experiments [157] with an average branching fraction of $(3.4 \pm 0.4) \times 10^{-5}$ and more recently also decay $A_b \rightarrow A\gamma$ was observed by LHCb [158].

Compared to $b \rightarrow s\gamma$, the $b \rightarrow d\gamma$ transitions such as $B \rightarrow \rho\gamma$, are suppressed by the CKM elements ratio $|V_{td}/V_{ts}|^2$. Both Belle and BaBar have observed these decays [75, 76]. The world average $\mathcal{B}(B \rightarrow (\rho, \omega)\gamma) = (1.30 \pm 0.23) \times 10^{-6}$. This can be used to calculate $|V_{td}/V_{ts}|$ [159]; the measured values are $0.195^{+0.025}_{-0.024}$ from Belle [75] and $0.233^{+0.033}_{-0.032}$ from BaBar [76].

The observed radiative penguin branching fractions can constrain a large class of SM extensions [160]. However, due to the uncertainties in the hadronization, only the inclusive $b \rightarrow s\gamma$ rate can be reliably compared with theoretical calculations. This rate can be measured from the endpoint of the inclusive photon spectrum in B decay. By combining the measurements of $B \rightarrow X_s\gamma$ from the CLEO, BaBar, and Belle experiments [161, 162], HFLAV obtains the average: $\mathcal{B}(B \rightarrow X_s\gamma) = (3.49 \pm 0.19) \times 10^{-4}$ [59] for $E_\gamma \geq 1.6$ GeV, averaging over B^+ and B^0 . Consistent but less precise results have been reported by ALEPH for inclusive b -hadrons produced at the Z , which includes also contribution from B_s^0 and A_b^0 hadrons. Using the sum of seven exclusive final

states, the BaBar experiment measured the branching fraction of inclusive $b \rightarrow d\gamma$ decays to be $(9.2 \pm 2.0 \pm 2.3) \times 10^{-6}$ [163]. The measured branching fraction can be compared to theoretical calculations. Recent calculations of $\mathcal{B}(b \rightarrow s\gamma)$ at NNLO level predict for the $E_\gamma \geq 1.6$ GeV values of $(3.36 \pm 0.23) \times 10^{-4}$ for $b \rightarrow s\gamma$ and $(1.68 \pm 0.17) \times 10^{-5}$ for $b \rightarrow d\gamma$ decays [164].

The CP asymmetry in $b \rightarrow s\gamma$ is extensively studied theoretically both in the SM and beyond [165]. According to the SM, the CP asymmetry in $b \rightarrow s\gamma$ is smaller than 1%, but some non-SM models allow significantly larger CP asymmetry ($\sim 10\%$) without altering the branching fraction. The current world average is $A_{CP} = 0.015 \pm 0.011$, again dominated by BaBar and Belle [166, 167]. In addition to the CP asymmetry, BaBar and Belle also measured the isospin asymmetry $\Delta_{0-} = -0.005 \pm 0.020$ in $b \rightarrow s\gamma$ measured using sum of exclusive decays [166, 168]. An alternative measurement using full reconstruction of the companion B in the hadronic decay modes yields a consistent, but less precise result [169]. Both Belle and BaBar experiments measured the isospin asymmetry in exclusive $B \rightarrow K^*(892)\gamma$ decay with average of $6.3 \pm 1.7\%$ [152] and therefore providing evidence for the non-zero isospin asymmetry.

In addition, experiments have measured the inclusive photon energy spectrum for $b \rightarrow s\gamma$, and by analyzing the shape of the spectrum they obtain the first and second moments for photon energies. Belle has measured these moments covering the widest range in the photon energy ($1.7 < E_\gamma < 2.8$ GeV) [162]. The measurement by BaBar has slightly smaller range with lower limit at 1.8 GeV [170]. These results can be used to extract non-perturbative HQET parameters that are needed for precise determination of the CKM matrix element V_{ub} (see further discussion elsewhere in this *Review* [171]).

Additional information on FCNC processes can be obtained from $b \rightarrow s\ell^+\ell^-$ decays. These processes are studied as a function of dilepton invariant mass squared, q^2 . Different q^2 regions are sensitive to different physics. Starting at the very low q^2 decays exhibit sensitivity to the same physics as the radiative decays. Then for the q^2 in region 1.1 to 6.0 GeV²/c⁴ the SM and new physics have best chance to compete. At the high q^2 above the $\psi(2S)$ mass, the interference of SM and new physics is to some extent complementary to that in lower q^2 . Regions around J/ψ and $\psi(2S)$ is normally excluded from measurements as these are dominated by the $b \rightarrow c$ transitions to charmonia. For exclusive decays, theory predictions require calculations of hadronic form factors. With current theory predictions, the most useful are measurements within the q^2 regions 1.1 to 6.0 GeV²/c⁴ and from 16.0 GeV²/c⁴ up to the kinematic limit. From this reason in the listing we provide results mainly in those two regions.

Similar as for radiative decays, also for the $b \rightarrow s\ell^+\ell^-$ decays the inclusive measurements provide some benefits. Both Belle and BaBar performed such measurement without reconstructing hadronic part exclusively and measure a branching fraction of $(5.8 \pm 1.3) \times 10^{-6}$ [172]. Unfortunately this measurement is not trivially possible at hadron colliders and also does not easily allow the angular distributions of the decay products to be exploited. One alternative is to extract information on the inclusive decay as sum of exclusive decays. Such a measurement was performed by Belle [173], but in this case the difficulty lies in extrapolation for the missing hadronic states.

Turning to the exclusive decays, the initial measurements performed by B-factories typically averaged between charged and neutral B mesons as well as between e^+e^- and $\mu^+\mu^-$ final states. The experiments CDF, LHCb, ATLAS and CMS are much better suited for the $\mu^+\mu^-$ final states compared to the e^+e^- final states. As such most measurements at hadron colliders are done only with $\mu^+\mu^-$ pairs and by separating charged and neutral B mesons. Recently, however, with much increased statistics, LHCb measured several final states with e^+e^- , to make a series of tests of e/μ universality in $B \rightarrow K^{(*)}\ell^+\ell^-$ decays. At hadron colliders other b hadrons are produced and as such CDF and LHCb experiments did observe also $B_s^0 \rightarrow \phi\mu^+\mu^-$ [174, 175], $\Lambda_b^0 \rightarrow \Lambda\mu^+\mu^-$ [174, 176] and $\Lambda_b^0 \rightarrow pK^-\mu^+\mu^-$ decays [177]. The averages of the total branching fractions integrated over whole q^2 regions are $(5.6 \pm 0.6) \times 10^{-7}$ for $B^+ \rightarrow K^+e^+e^-$, $(4.53 \pm 0.35) \times 10^{-7}$ for

$B^+ \rightarrow K^+\mu^+\mu^-$, $(1.03_{-0.17}^{+0.19}) \times 10^{-6}$ for $B^0 \rightarrow K^*(892)^0e^+e^-$ and $(0.94 \pm 0.05) \times 10^{-6}$ for $B^0 \rightarrow K^*(892)^0\mu^+\mu^-$ decays [178–182]. The total branching fractions for $B_s^0 \rightarrow \phi\mu^+\mu^-$ and $\Lambda_b^0 \rightarrow \Lambda\mu^+\mu^-$ decays are $(8.4 \pm 0.4) \times 10^{-7}$ [174, 175, 183] and $(1.08 \pm 0.28) \times 10^{-6}$ [174, 176] respectively. With increased precision of $B^0 \rightarrow K^*(892)^0\ell^+\ell^-$ decay, there is a question on what fraction of the seen branching fraction is due to the $K^*(892)^0$ resonance and what fraction is due to the $K\pi$ in s -wave. This has been studied by LHCb which found that the $K\pi$ in s -wave fraction varies between 1% and about 10% depending on the q^2 region [182]. It should be noted, that for all relevant B meson decays the branching fractions so far studied are consistently below the SM expectation.

In the $b \rightarrow s\ell^+\ell^-$ decays angular distributions offer rich source of information. The full angular analysis was performed for decays $B^+ \rightarrow K^+\ell^+\ell^-$, $B^0 \rightarrow K^0\ell^+\ell^-$, $B^+ \rightarrow K^*(892)^+\ell^+\ell^-$, $B^0 \rightarrow K^*(892)^0\ell^+\ell^-$, $B_s^0 \rightarrow \phi\mu^+\mu^-$ and $\Lambda_b^0 \rightarrow \Lambda\mu^+\mu^-$ decays [184–192]. An attempt to increase sensitivity to the NP was made by constructing observables, which have reduced theory uncertainties and measurements of these are done. Most notably the observable called P'_5 [193] shows a discrepancy with the SM in the q^2 region which is highly sensitive to new physics [186–188]. Measurements of the CP asymmetries [177, 178, 181, 194, 195] and the isospin asymmetry [179–181, 194] were also performed. All these measurements are well consistent with the small A_{CP} and small isospin asymmetry expected in the SM [196]. With statistics available at the LHC, the measurement of phase difference between long- and short-distance contribution in $B^+ \rightarrow K^+\mu^+\mu^-$ decays became possible [197].

With the data samples available at LHC, the lepton universality in $b \rightarrow s\ell^+\ell^-$ can be tested. While in the SM decays to electron-positron and muon pairs are expected to be same up to small corrections due to the different masses of leptons, in extensions of the SM this does not have to hold. The angular analysis of $B^0 \rightarrow K^*(892)^0e^+e^-$ decays was performed by LHCb at low dilepton invariant masses [198] and Belle in several regions over whole q^2 range [188]. The LHCb measurement yields the most stringent constraint on the photon polarization. The result on lepton universality test which over past few years attracted most attention is the ratio of branching fractions between $B^+ \rightarrow K^+\mu^+\mu^-$ and $B^+ \rightarrow K^+e^+e^-$ and between $B^0 \rightarrow K^*(892)^0\mu^+\mu^-$ and $B^0 \rightarrow K^*(892)^0e^+e^-$ decays [179, 199]. The measurements by LHCb showed mild discrepancy from the SM, with significance of 3.1σ for $B^+ \rightarrow K^+\ell^+\ell^-$ and about 2.4σ for $B^0 \rightarrow K^*(892)^0\ell^+\ell^-$. The latest analysis in Ref. [200] identified previously missed hadronic misidentification background. With better handling of such background the results are now consistent with the SM. LHCb experiment performed similar test with $\Lambda_b^0 \rightarrow pK^-\ell^+\ell^-$ decays [201], $B^0 \rightarrow K_S^0\ell^+\ell^-$ and $B^+ \rightarrow K^*(892)^+\ell^+\ell^-$ [202].

While $b \rightarrow d\ell^+\ell^-$ decays are further suppressed, they recently became accessible. Signals were observed for $B^+ \rightarrow \pi^+\mu^+\mu^-$ [77], $B^0 \rightarrow \pi^+\pi^-\mu^+\mu^-$ [203] and $\Lambda_b^0 \rightarrow p\pi^-\mu^+\mu^-$ [204] decays. Search for the $B_s^0 \rightarrow \bar{K}^*(892)^0\mu^+\mu^-$ at LHCb is complicated by large background from $B^0 \rightarrow K^*(892)^0\mu^+\mu^-$ and current significance for the decay is 3.4σ [205]. The total branching fractions are only quantities measured and these are about 2×10^{-8} for the meson decays and about 7×10^{-8} for the Λ_b^0 decay.

A closely related process is $B \rightarrow X_s\nu\bar{\nu}$. Since the neutrinos are not detected, the final state is a strange hadron system X_s plus missing energy-momentum. Depending on X_s , the SM branching fraction is $\mathcal{O}(10^{-6})$. New physics effects beyond SM, e.g. those from dark sector models can greatly enhance the yield of X_s plus missing energy. BaBar [206], Belle [207], and Belle II [208] have searched for these decays and determined the upper limits in the range $\mathcal{O}(10^{-5})$.

Finally the decays $B_{(s)}^0 \rightarrow e^+e^-$ and $\mu^+\mu^-$ are interesting since they only proceed at second order in weak interactions in the SM, but may have large contributions from supersymmetric loops, proportional to $(\tan\beta)^6$. First limits were published more than 30 years ago and since then experiments at Tevatron, B-factories and LHC gradually improved those and effectively ex-

cluded whole models of new physics and significantly constrained allowed parameter space of others. For the decays to $\mu^+\mu^-$, Tevatron experiments pushed the limits down to roughly factor of 5-10 above the SM expectation [209]. The long journey in the search for these decays culminated in 2012, when first evidence for $B_s^0 \rightarrow \mu^+\mu^-$ decay was seen [210]. Subsequently, LHC experiments ATLAS [211], CMS [212] and LHCb [213] observed statistically significant signal for $B_s^0 \rightarrow \mu^+\mu^-$ decay. The average branching fraction is found to be $(3.01 \pm 0.435) \times 10^{-9}$. In experiments at hadron colliders searches for $B^0 \rightarrow \mu^+\mu^-$ decays are performed at the same time. The $B(B^0 \rightarrow \mu^+\mu^-)$ is extracted in simultaneously with $B(B_s^0 \rightarrow \mu^+\mu^-)$ and is found to be $(0.07^{+0.13}_{-0.11}) \times 10^{-9}$. The limits for the e^+e^- modes are: $< 9.4 \times 10^{-9}$ and $< 2.5 \times 10^{-9}$, respectively, for B_s^0 and B^0 [214]. The searches for decays to $\tau^+\tau^-$ are more challenging with current best limits of $B(B^0 \rightarrow \tau^+\tau^-) < 2.1 \times 10^{-3}$ and $B(B_s^0 \rightarrow \tau^+\tau^-) < 6.8 \times 10^{-3}$ at 95% C.L. [215]. All existing measurements of B^0 and B_s^0 decays to same flavour dilepton pair is consistent with SM expectation [216]. With $B_s^0 \rightarrow \mu^+\mu^-$ decay observed, it was suggested that the effective lifetime is useful further test of the decay [217]. Attempt was made by LHCb and CMS experiments, but its precision is not yet sufficient to provide test of the SM [212, 213]. It will take couple of years until interesting precision is reached. The searches were also performed for lepton flavour violating decays to two leptons with best limits in $e^\pm\mu^\mp$ channel, where limits are $< 1.3 \times 10^{-9}$ for B^0 and $< 6.3 \times 10^{-9}$ for B_s^0 , at 95% confidence level [218].

Several theory groups performed global analysis of electroweak decays concluding that significant tension between data and SM is present [219]. The tension can be relieved by new physics beyond SM. For more detailed reviews see e.g. Ref. [220].

73.7 Summary and Outlook

The study of B mesons continues to be one of the most productive fields in particle physics. With the two asymmetric B -factory experiments Belle and BaBar, we now have a combined data sample of well over 1 ab^{-1} . CP violation has been firmly established in many decays of B mesons. Evidence for direct CP violation has been observed. Many rare decays resulting from hadronic $b \rightarrow u$ transitions and $b \rightarrow s(d)$ penguin decays have been observed, and the emerging pattern is still full of surprises. Despite the remarkable successes of the B -factory experiments, many fundamental questions in the flavor sector remain unanswered.

At Fermilab, CDF and D0 each has accumulated about 10 fb^{-1} , which is the equivalent of about 10^{12} b -hadrons produced. In spite of the low trigger efficiency of hadronic experiments, a selection of modes have been reconstructed in large quantities, giving a start to a program of studies on B_s and b -flavored baryons, in which a first major step has been the determination of the B_s oscillation frequency.

As Tevatron and B -factories finished their data taking few year ago, the experiments at the LHC have become very active. LHCb has collected about 1 fb^{-1} at 7 TeV, 2 fb^{-1} at 8 TeV, and close to 5.9 fb^{-1} at 13 TeV during LHC Runs 1 and 2. CMS and ATLAS have collected each about 5 fb^{-1} of data at $\sqrt{s} = 7 \text{ TeV}$, 20 fb^{-1} at 8 TeV and about 150 fb^{-1} at 13 TeV during LHC Runs 1 and 2. The latest LHC Run 3 at 13.6 TeV started in summer 2022, with upgraded detectors. By the time of the writing (summer 2023), LHC has delivered about 70 fb^{-1} to ATLAS and CMS experiments. LHCb, which is dedicated to the studies of b - and c -hadrons, has a data sample that is for many decays larger than the sum of all previous experiments. With it, we are entering to regime of precision physics even for many rare decays, which allows much more detailed measurements.

The Belle II experiment at the SuperKEKB has started recording data in 2019 and has by summer 2022 collected about 428 fb^{-1} of data, when their long shutdown 1 started. The aim to increase sample to $\sim 50 \text{ ab}^{-1}$ will make it possible to explore the indirect evidence of new physics beyond the SM in the heavy-flavor particles (b , c , and τ), in a way that is complementary to the LHC. The LHCb Collaboration is commissioning upgrade of its detector and is planning on nominal running from 2024. The aim of the upgrade was to increase flexibility of the trigger, which will

allow about a factor of five increase in instantaneous luminosity and of about a factor of two in efficiencies on triggering on purely hadronic decays. The plan is to integrate about 50 fb^{-1} of data during LHC runs 3 and 4.

These experiments promise a rich spectrum of rare and precise measurements that have the potential to fundamentally affecting our understanding of the SM and CP -violating phenomena.

References

- [1] M. Kobayashi and T. Maskawa, *Prog. Theor. Phys.* **49**, 652 (1973).
- [2] S. W. Herb *et al.*, *Phys. Rev. Lett.* **39**, 252 (1977).
- [3] B. Aubert *et al.* (BaBar), *Phys. Rev. Lett.* **87**, 091801 (2001), [hep-ex/0107013].
- [4] K. Abe *et al.* (Belle), *Phys. Rev. Lett.* **87**, 091802 (2001), [hep-ex/0107061].
- [5] Currently two different notations (ϕ_1, ϕ_2, ϕ_3) and (α, β, γ) are used in the literature for CKM unitarity angles. In this mini-review, we use the latter notation following the other mini-reviews in this *Review*. The two notations are related by $\phi_1 = \beta$, $\phi_2 = \alpha$ and $\phi_3 = \gamma$.
- [6] See the “ CP Violation in Meson Decays” by D. Kirkby and Y. Nir in this *Review*.
- [7] See the “CKM Quark Mixing Matrix,” by A. Cecucci, Z. Ligeti, and Y. Sakai, in this *Review*.
- [8] See the note on “ $B^0 - \bar{B}^0$ mixing,” by O. Schneider in this *Review*.
- [9] See the “Determination of $|V_{cb}|$ and $|V_{ub}|$,” by R. Kowalewski and T. Mannel in this *Review*.
- [10] F. Abe *et al.* (CDF), *Phys. Rev. Lett.* **81**, 2432 (1998), [hep-ex/9805034]; F. Abe *et al.* (CDF), *Phys. Rev.* **D58**, 112004 (1998), [hep-ex/9804014].
- [11] A. Abulencia *et al.* (CDF), *Phys. Rev. Lett.* **96**, 082002 (2006), [hep-ex/0505076].
- [12] R. Aaij *et al.* (LHCb), *JHEP* **07**, 123 (2020), [arXiv:2004.08163].
- [13] B. Aubert *et al.* (BaBar), *Phys. Rev. Lett.* **101**, 071801 (2008), [Erratum: *Phys. Rev. Lett.* **102**, 029901 (2009)], [arXiv:0807.1086].
- [14] B. Aubert *et al.* (BaBar), *Phys. Rev. Lett.* **103**, 161801 (2009), [arXiv:0903.1124].
- [15] G. Bonvicini *et al.* (CLEO), *Phys. Rev.* **D81**, 031104 (2010), [arXiv:0909.5474].
- [16] R. Mizuk *et al.* (Belle), *Phys. Rev. Lett.* **109**, 232002 (2012), [arXiv:1205.6351].
- [17] U. Tamponi *et al.* (Belle), *Phys. Rev. Lett.* **115**, 14, 142001 (2015), [arXiv:1506.08914].
- [18] B. Fulsom *et al.* (Belle), *Phys. Rev. Lett.* **121**, 232001 (2018), [arXiv:1807.01201].
- [19] A. Bondar *et al.* (Belle), *Phys. Rev. Lett.* **108**, 122001 (2012), [arXiv:1110.2251].
- [20] See the note on “Naming scheme for hadrons,” by M. Roos and C.G. Wohl in this *Review*.
- [21] R. Aaij *et al.* (LHCb), *Phys. Rev. Lett.* **118**, 5, 052002 (2017), [Erratum: *Phys. Rev. Lett.* **119**, 169901 (2017)], [arXiv:1612.05140].
- [22] M. Cacciari *et al.*, *JHEP* **10**, 137 (2012), [arXiv:1205.6344]; B. A. Kniehl *et al.*, *Phys. Rev.* **D84**, 094026 (2011), [arXiv:1109.2472]; M. Cacciari, M. L. Mangano and P. Nason, *Eur. Phys. J.* **C75**, 12, 610 (2015), [arXiv:1507.06197].
- [23] B. Barish *et al.* (CLEO), *Phys. Rev. Lett.* **76**, 1570 (1996).
- [24] E. Guido *et al.* (Belle), *Phys. Rev. Lett.* **121**, 062001 (2018), [arXiv:1803.10303]; E. Guido *et al.* (Belle), *Phys. Rev.* **D96**, 052005 (2017), [arXiv:1707.04973]; A. Sokolov *et al.* (Belle), *Phys. Rev.* **D79**, 051103 (2009), [arXiv:0901.1431]; B. Aubert *et al.* (BaBar), *Phys. Rev.* **D78**, 112002 (2008), [arXiv:0807.2014].

- [25] J. P. Alexander *et al.* (CLEO), Phys. Rev. Lett. **86**, 2737 (2001), [hep-ex/0006002]; S. B. Athar *et al.* (CLEO), Phys. Rev. **D66**, 052003 (2002), [hep-ex/0202033]; N. C. Hastings *et al.* (Belle), Phys. Rev. **D67**, 052004 (2003), [hep-ex/0212033].
- [26] B. Aubert *et al.* (BaBar), Phys. Rev. Lett. **95**, 042001 (2005), [hep-ex/0504001].
- [27] Y. Amhis *et al.* (HFLAV), Eur. Phys. J. **C77**, 12, 895 (2017), [arXiv:1612.07233].
- [28] Y. S. Amhis *et al.* (HFLAV), Eur. Phys. J. **C 81**, 3, 226 (2021), [arXiv:1909.12524].
- [29] R. Aaij *et al.* (LHCb) (2022), [arXiv:2204.13042].
- [30] P. Abreu *et al.* (DELPHI), Phys. Lett. **B345**, 598 (1995).
- [31] R. Akers *et al.* (OPAL), Z. Phys. **C66**, 19 (1995).
- [32] T. A. Aaltonen *et al.* (CDF), Phys. Rev. **D90**, 1, 012013 (2014), [arXiv:1309.5961]; R. Aaij *et al.* (LHCb), JHEP **04**, 024 (2015), [arXiv:1502.02638].
- [33] R. Aaij *et al.* (LHCb), Phys. Rev. Lett. **110**, 15, 151803 (2013), [arXiv:1211.5994].
- [34] A. M. Sirunyan *et al.* (CMS), Eur. Phys. J. **C78**, 939 (2018), [arXiv:1809.03578].
- [35] G. Aad *et al.* (ATLAS), Phys. Rev. Lett. **113**, 21, 212004 (2014), [arXiv:1407.1032].
- [36] A. Sirunyan *et al.* (CMS), Phys. Rev. Lett. **122**, 132001 (2019), [arXiv:1902.00571]; R. Aaij *et al.* (LHCb), Phys. Rev. Lett. **122**, 232001 (2019), [arXiv:1904.00081].
- [37] T. Aaltonen *et al.* (CDF), Phys. Rev. Lett. **99**, 202001 (2007), [arXiv:0706.3868]; T. Aaltonen *et al.* (CDF), Phys. Rev. **D85**, 092011 (2012), [arXiv:1112.2808].
- [38] R. Aaij *et al.* (LHCb), Phys. Rev. Lett. **122**, 012001 (2019), [arXiv:1809.07752].
- [39] V. M. Abazov *et al.* (D0), Phys. Rev. Lett. **99**, 052001 (2007), [arXiv:0706.1690]; T. Aaltonen *et al.* (CDF), Phys. Rev. Lett. **99**, 052002 (2007), [arXiv:0707.0589].
- [40] R. Aaij *et al.* (LHCb), Phys. Rev. Lett. **113**, 032001 (2014), [arXiv:1405.7223]; R. Aaij *et al.* (LHCb), Phys. Lett. **B736**, 154 (2014), [arXiv:1405.1543]; R. Aaij *et al.* (LHCb), Phys. Rev. **D89**, 3, 032001 (2014), [arXiv:1311.4823]; R. Aaij *et al.* (LHCb), Phys. Rev. Lett. **113**, 24, 242002 (2014), [arXiv:1409.8568]; R. Aaij *et al.* (LHCb), Phys. Rev. Lett. **115**, 24, 241801 (2015), [arXiv:1510.03829]; R. Aaij *et al.* (LHCb), Phys. Rev. Lett. **118**, 7, 071801 (2017), [arXiv:1612.02244]; R. Aaij *et al.* (LHCb), Phys. Lett. **B722**, 265 (2017), [arXiv:1701.05274]; R. Aaij *et al.* (LHCb), JHEP **02**, 98 (2018), [arXiv:1711.05490]; R. Aaij *et al.* (LHCb), Phys. Rev. **D99**, 052006 (2019), [arXiv:1901.07075]; R. Aaij *et al.* (LHCb), Phys. Rev. Lett. **124**, 11, 111802 (2020), [arXiv:1912.02110].
- [41] R. Aaij *et al.* (LHCb Collaboration), Phys. Rev. **D 103**, 012004 (2021), [arXiv:2010.14485], URL <https://link.aps.org/doi/10.1103/PhysRevD.103.012004>.
- [42] R. Aaij *et al.* (LHCb), Phys. Rev. **D104**, 052010 (2021), [arXiv:2104.15074].
- [43] T. A. Aaltonen *et al.* (CDF), Phys. Rev. **D89**, 7, 072014 (2014), [arXiv:1403.8126].
- [44] R. Aaij *et al.* (LHCb), JHEP **08**, 039 (2018), [arXiv:1805.03941]; R. Aaij *et al.* (LHCb), Eur. Phys. J. **C 79**, 9, 745 (2019), [arXiv:1903.06792]; R. Aaij *et al.* (LHCb), Eur. Phys. J. **C79**, 9, 745 (2019), [arXiv:1903.06792].
- [45] S. Chatrchyan *et al.* (CMS), Phys. Rev. Lett. **108**, 252002 (2012), [arXiv:1204.5955]; R. Aaij *et al.* (LHCb), JHEP **1605**, 161 (2016), [arXiv:1604.03896].
- [46] R. Aaij *et al.* (LHCb Collaboration), Phys. Rev. Lett. **131**, 171901 (2023), [arXiv:2307.13399], URL <https://link.aps.org/doi/10.1103/PhysRevLett.131.171901>.
- [47] R. Aaij *et al.* (LHCb), Phys. Rev. Lett. **114**, 062004 (2015), [arXiv:1411.4849].
- [48] A. M. Sirunyan *et al.* (CMS Collaboration), Phys. Rev. Lett. **126**, 252003 (2021), [arXiv:2102.04524], URL <https://link.aps.org/doi/10.1103/PhysRevLett.126.252003>.
- [49] R. Aaij *et al.* (LHCb), Phys. Rev. Lett. **121**, 072002 (2018), [arXiv:1805.09418].
- [50] R. Aaij *et al.* (LHCb Collaboration), Phys. Rev. Lett. **128**, 162001 (2022), [arXiv:2110.04497], URL <https://link.aps.org/doi/10.1103/PhysRevLett.128.162001>.
- [51] V. M. Abazov *et al.* (D0), Phys. Rev. Lett. **101**, 232002 (2008), [arXiv:0808.4142]; T. Aaltonen *et al.* (CDF), Phys. Rev. **D80**, 072003 (2009), [arXiv:0905.3123].
- [52] R. Aaij *et al.* (LHCb), Phys. Rev. Lett. **110**, 18, 182001 (2013), [arXiv:1302.1072]; R. Aaij *et al.* (LHCb), Phys. Lett. **B736**, 154 (2014), [arXiv:1405.1543]; R. Aaij *et al.* (LHCb), Phys. Rev. **D93**, 9, 092007 (2016), [arXiv:1604.01412]; R. Aaij *et al.* (LHCb), Phys. Rev. **D104**, L091102 (2021), [arXiv:2107.03419].
- [53] R. Aaij *et al.* (LHCb Collaboration), Phys. Rev. Lett. **124**, 082002 (2020), [arXiv:2001.00851], URL <https://link.aps.org/doi/10.1103/PhysRevLett.124.082002>.
- [54] V. M. Abazov *et al.* (D0), Phys. Rev. Lett. **117**, 2, 022003 (2016), [arXiv:1602.07588]; V. M. Abazov *et al.* (D0), Phys. Rev. **D97**, 092004 (2018), [arXiv:1712.10176].
- [55] R. Aaij *et al.* (LHCb), Phys. Rev. Lett. **117**, 15, 152003 (2016), [Addendum: Phys. Rev. Lett.118,no.10,109904(2017)], [arXiv:1608.00435].
- [56] A. Sirunyan *et al.* (CMS), Phys. Rev. Lett. **120**, 202005 (2018), [arXiv:1712.06144].
- [57] C. Tarantino, Eur. Phys. J. **C33**, S895 (2004), [hep-ph/0310241]; F. Gabbiani, A. I. Onishchenko and A. A. Petrov, Phys. Rev. **D70**, 094031 (2004), [hep-ph/0407004]; F. Gabbiani, A. I. Onishchenko and A. A. Petrov, Phys. Rev. **D68**, 114006 (2003), [hep-ph/0303235].
- [58] A. Lenz, Int. J. Mod. Phys. **A30**, 10, 1543005 (2015), [arXiv:1405.3601].
- [59] Y. S. Amhis *et al.* (Heavy Flavor Averaging Group, HFLAV), Phys. Rev. **D 107**, 5, 052008 (2023), [arXiv:2206.07501].
- [60] C.-H. Chang *et al.*, Phys. Rev. **D64**, 014003 (2001), [hep-ph/0007162]; V. V. Kiselev, A. E. Kovalsky and A. K. Likhoded, Nucl. Phys. **B585**, 353 (2000), [hep-ph/0002127]; A. Yu. Anisimov *et al.*, Phys. Lett. **B452**, 129 (1999), [hep-ph/9812514]; M. Beneke and G. Buchalla, Phys. Rev. **D53**, 4991 (1996), [hep-ph/9601249].
- [61] R. Aaij *et al.* (LHCb), Eur. Phys. J. **C74**, 5, 2839 (2014), [arXiv:1401.6932].
- [62] R. Aaij *et al.* (LHCb), Phys. Lett. **B742**, 29 (2015), [arXiv:1411.6899].
- [63] The B_c is a special case, where a weak decay of the c quark is also possible, but the spectator model still applies.
- [64] R. Aaij *et al.* (LHCb), Nature Phys. **11**, 743 (2015), [arXiv:1504.01568].
- [65] J. P. Lees *et al.* (BaBar), Phys. Rev. **D85**, 011101 (2012), [arXiv:1110.5600]; C. Oswald *et al.* (Belle), Phys. Rev. **D87**, 7, 072008 (2013), [Erratum: Phys. Rev. **D90**, 119901 (2014)], [arXiv:1212.6400]; C. Oswald *et al.* (Belle), Phys. Rev. **D92**, 7, 072013 (2015), [arXiv:1504.02004].
- [66] T. A. Aaltonen *et al.* (CDF), Phys. Rev. **D93**, 5, 052001 (2016), [arXiv:1601.03819].
- [67] R. Aaij *et al.* (LHCb), Phys. Rev. Lett. **126**, 8, 081804 (2021), [arXiv:2012.05143].
- [68] B. Grinstein, Nucl. Phys. **B339**, 253 (1990); H. Georgi, Phys. Lett. **B240**, 447 (1990); A. F. Falk *et al.*, Nucl. Phys. **B343**, 1 (1990); E. Eichten and B. R. Hill, Phys. Lett. **B234**, 511 (1990).
- [69] "Heavy-Quark and Soft-Collinear Effective Theory" by C.W. Bauer and M. Neubert in this *Review*.

- [70] M. Neubert, “Aspects of QCD Factorization,” hep-ph/0110093, *Proceedings of HF9*, Pasadena (2001) and references therein; Z. Ligeti, M. E. Luke and M. B. Wise, *Phys. Lett.* **B507**, 142 (2001), [hep-ph/0103020].
- [71] M. Beneke *et al.*, *Phys. Rev. Lett.* **83**, 1914 (1999), [hep-ph/9905312]; M. Beneke *et al.*, *Nucl. Phys.* **B591**, 313 (2000), [hep-ph/0006124]; M. Beneke *et al.*, *Nucl. Phys.* **B606**, 245 (2001), [hep-ph/0104110]; M. Beneke and M. Neubert, *Nucl. Phys.* **B675**, 333 (2003), [hep-ph/0308039].
- [72] Y.-Y. Keum, H.-n. Li and A. I. Sanda, *Phys. Lett.* **B504**, 6 (2001), [hep-ph/0004004]; Y. Y. Keum, H.-N. Li and A. I. Sanda, *Phys. Rev.* **D63**, 054008 (2001), [hep-ph/0004173]; Y.-Y. Keum and H.-n. Li, *Phys. Rev.* **D63**, 074006 (2001), [hep-ph/0006001]; C.-D. Lu, K. Ukai and M.-Z. Yang, *Phys. Rev.* **D63**, 074009 (2001), [hep-ph/0004213]; C.-D. Lu and M.-Z. Yang, *Eur. Phys. J.* **C23**, 275 (2002), [hep-ph/0011238].
- [73] C. W. Bauer, S. Fleming and M. E. Luke, *Phys. Rev.* **D63**, 014006 (2000), [hep-ph/0005275]; C. W. Bauer *et al.*, *Phys. Rev.* **D63**, 114020 (2001), [hep-ph/0011336]; C. W. Bauer and I. W. Stewart, *Phys. Lett.* **B516**, 134 (2001), [hep-ph/0107001].
- [74] R. Ammar *et al.* (CLEO), *Phys. Rev. Lett.* **71**, 674 (1993).
- [75] N. Taniguchi *et al.* (Belle), *Phys. Rev. Lett.* **101**, 111801 (2008), [Erratum: *Phys. Rev. Lett.* **101**, 129904 (2008)], [arXiv:0804.4770].
- [76] B. Aubert *et al.* (BaBar), *Phys. Rev.* **D78**, 112001 (2008), [arXiv:0808.1379].
- [77] R. Aaij *et al.* (LHCb), *JHEP* **10**, 034 (2015), [arXiv:1509.00414].
- [78] P. Krokovny *et al.* (Belle), *Phys. Rev. Lett.* **89**, 231804 (2002), [hep-ex/0207077]; B. Aubert *et al.* (BaBar), *Phys. Rev. Lett.* **98**, 081801 (2007), [hep-ex/0604012].
- [79] B. Kronenbitter *et al.* (Belle), *Phys. Rev.* **D92**, 5, 051102 (2015), [arXiv:1503.05613]; I. Adachi *et al.* (Belle), *Phys. Rev. Lett.* **110**, 13, 131801 (2013), [arXiv:1208.4678].
- [80] J. P. Lees *et al.* (BaBar), *Phys. Rev.* **D88**, 3, 031102 (2013), [arXiv:1207.0698]; B. Aubert *et al.* (BaBar), *Phys. Rev.* **D81**, 051101 (2010), [arXiv:0912.2453].
- [81] See the “Leptonic decays of charged pseudoscalar mesons,” by R. Briere, J. Rosner, S. Stone, and R. Van de Water, in this *Review*.
- [82] J. P. Lees *et al.* (BaBar), *Phys. Rev.* **D84**, 112007 (2011), [Erratum: *Phys. Rev.* **D87**, 039901 (2013)], [arXiv:1107.5751]; S. Blyth *et al.* (Belle), *Phys. Rev.* **D74**, 092002 (2006), [hep-ex/0607029].
- [83] R. Aaij *et al.* (LHCb), *Phys. Rev. D* **92**, 3, 032002 (2015), [arXiv:1505.01710].
- [84] B. Aubert *et al.* (BaBar), *Phys. Rev. Lett.* **90**, 242001 (2003), [hep-ex/0304021].
- [85] D. Besson *et al.* (CLEO), *Phys. Rev.* **D68**, 032002 (2003), [Erratum: *Phys. Rev.* **D75**, 119908(2007)], [hep-ex/0305100].
- [86] P. Krokovny *et al.* (Belle), *Phys. Rev. Lett.* **91**, 262002 (2003), [hep-ex/0308019]; Y. Mikami *et al.* (Belle), *Phys. Rev. Lett.* **92**, 012002 (2004), [hep-ex/0307052].
- [87] B. Aubert *et al.* (BaBar), *Phys. Rev. Lett.* **93**, 181801 (2004), [hep-ex/0408041].
- [88] R. Aaij *et al.* (LHCb), *Phys. Rev. Lett.* **113**, 162001 (2014), [arXiv:1407.7574].
- [89] R. Aaij *et al.* (LHCb), *JHEP* **12**, 141 (2021), [arXiv:2110.02350]; F. Abudinén *et al.* (Belle, Belle-II), *JHEP* **02**, 063 (2022), [Erratum: *JHEP* **12**, 034 (2022)], [arXiv:2110.12125].
- [90] T. Aaltonen *et al.* (CDF), *Phys. Rev. Lett.* **108**, 201801 (2012), [arXiv:1204.0536].
- [91] S. Esen *et al.* (Belle), *Phys. Rev.* **D87**, 3, 031101 (2013), [arXiv:1208.0323].
- [92] R. Aaij *et al.* (LHCb), *Phys. Rev.* **D93**, 9, 092008 (2016), [arXiv:1602.07543].
- [93] R. Aaij *et al.* (LHCb), *Phys. Rev. Lett.* **116**, 16, 161802 (2016), [arXiv:1603.02408].
- [94] R. Aaij *et al.* (LHCb), *JHEP* **11**, 082 (2015), [arXiv:1509.00400].
- [95] B. Aubert *et al.* (BaBar), *Phys. Rev.* **D76**, 031101 (2007), [arXiv:0704.1266].
- [96] R. Aaij *et al.* (LHCb), *Phys. Rev.* **D90**, 1, 012003 (2014), [arXiv:1404.5673].
- [97] R. Aaij *et al.* (LHCb), *Phys. Rev. Lett.* **111**, 18, 181801 (2013), [arXiv:1308.4544].
- [98] R. Aaij *et al.* (LHCb), *JHEP* **07**, 066 (2023), [arXiv:2210.12000].
- [99] R. Aaij *et al.* (LHCb), *Phys. Rev.* **D87**, 11, 112012 (2013), [Addendum: *Phys. Rev.* **D89**, 019901 (2014)], [arXiv:1304.4530].
- [100] G. Aad *et al.* (ATLAS), *Eur. Phys. J.* **C76**, 1, 4 (2016), [arXiv:1507.07099]; G. Aad *et al.* (ATLAS), *JHEP* **08**, 087 (2022), [arXiv:2203.01808].
- [101] R. Aaij *et al.* (LHCb), *Phys. Rev.* **D84**, 092001 (2011), [Erratum: *Phys. Rev.* **D85**, 039904(2012)], [arXiv:1109.6831]; T. Aaltonen *et al.* (CDF), *Phys. Rev.* **D85**, 032003 (2012), [arXiv:1112.3334].
- [102] S. K. Choi *et al.* (Belle), *Phys. Rev. Lett.* **91**, 262001 (2003), [hep-ex/0309032].
- [103] D. Acosta *et al.* (CDF), *Phys. Rev. Lett.* **93**, 072001 (2004), [hep-ex/0312021].
- [104] V. M. Abazov *et al.* (D0), *Phys. Rev. Lett.* **93**, 162002 (2004), [hep-ex/0405004].
- [105] B. Aubert *et al.* (BaBar), *Phys. Rev.* **D71**, 071103 (2005), [hep-ex/0406022].
- [106] R. Aaij *et al.* (LHCb), *Eur. Phys. J.* **C72**, 1972 (2012), [arXiv:1112.5310].
- [107] S. Chatrchyan *et al.* (CMS), *JHEP* **04**, 154 (2013), [arXiv:1302.3968].
- [108] M. Aaboud *et al.* (ATLAS), *JHEP* **01**, 117 (2017), [arXiv:1610.09303].
- [109] S. K. Choi *et al.* (Belle), *Phys. Rev. Lett.* **100**, 142001 (2008), [arXiv:0708.1790]; R. Mizuk *et al.* (Belle), *Phys. Rev.* **D80**, 031104 (2009), [arXiv:0905.2869].
- [110] R. Aaij *et al.* (LHCb), *Phys. Rev. Lett.* **112**, 22, 222002 (2014), [arXiv:1404.1903]; R. Aaij *et al.* (LHCb), *Phys. Rev.* **D92**, 11, 112009 (2015), [arXiv:1510.01951].
- [111] K. Chilikin *et al.* (Belle), *Phys. Rev.* **D90**, 11, 112009 (2014), [arXiv:1408.6457].
- [112] R. Aaij *et al.* (LHCb), *Phys. Rev. Lett.* **115**, 072001 (2015), [arXiv:1507.03414].
- [113] R. Aaij *et al.* (LHCb), *Phys. Rev. Lett.* **122**, 22, 222001 (2019), [arXiv:1904.03947].
- [114] R. Aaij *et al.* (LHCb), *Phys. Rev. Lett.* **128**, 6, 062001 (2022), [arXiv:2108.04720].
- [115] R. Aaij *et al.* (LHCb), *Phys. Rev. Lett.* **131**, 3, 031901 (2023), [arXiv:2210.10346]; R. Aaij *et al.* (LHCb), *Sci. Bull.* **66**, 1278 (2021), [arXiv:2012.10380].
- [116] See the “Non- $q\bar{q}$ mesons,” by C. Amsler and C. Hanhart, and “Pentaquarks,” by M. Karliner and T. Skwarnicki, in this *Review*.
- [117] T. Aaltonen *et al.* (CDF), *Phys. Rev. Lett.* **107**, 261802 (2011), [arXiv:1107.4999]; R. Aaij *et al.* (LHCb), *JHEP* **10**, 053 (2015), [arXiv:1508.00788].
- [118] T. A. Aaltonen *et al.* (CDF), *Phys. Rev. Lett.* **113**, 24, 242001 (2014), [arXiv:1403.5586].

- [119] R. Aaij *et al.* (LHCb), JHEP **10**, 037 (2012), [arXiv:1206.2794].
- [120] T. Aaltonen *et al.* (CDF), Phys. Rev. Lett. **103**, 031801 (2009), [arXiv:0812.4271].
- [121] R. Aaij *et al.* (LHCb), Phys. Rev. D **98**, 3, 032004 (2018), [arXiv:1805.06759]; R. Aaij *et al.* (LHCb), JHEP **12**, 155 (2019), [arXiv:1907.10003]; R. Aaij *et al.* (LHCb) (2023), [arXiv:2304.06198].
- [122] R. Fleischer, Phys. Lett. **B459**, 306 (1999), [hep-ph/9903456]; D. London and J. Matias, Phys. Rev. **D70**, 031502 (2004), [hep-ph/0404009].
- [123] J. P. Lees *et al.* (BaBar), Phys. Rev. **D87**, 5, 052009 (2013), [arXiv:1206.3525].
- [124] Y. T. Duh *et al.* (Belle), Phys. Rev. **D87**, 3, 031103 (2013), [arXiv:1210.1348].
- [125] R. Aaij *et al.* (LHCb), JHEP **03**, 075 (2021), [arXiv:2012.05319].
- [126] B. Aubert *et al.* (BaBar), Phys. Rev. **D76**, 091102 (2007), [arXiv:0707.2798].
- [127] R. Aaij *et al.* (LHCb), Phys. Lett. B **726**, 646 (2013), [arXiv:1308.1277]; R. Aaij *et al.* (LHCb), Phys. Rev. Lett. **126**, 9, 091802 (2021), [arXiv:2012.12789].
- [128] M. Gronau and J. L. Rosner, Phys. Rev. **D71**, 074019 (2005), [hep-ph/0503131]; M. Gronau, Phys. Lett. **B627**, 82 (2005), [hep-ph/0508047].
- [129] B. Aubert *et al.* (BaBar), Phys. Rev. D **79**, 052003 (2009), [arXiv:0809.1174].
- [130] M. Fujikawa *et al.* (Belle), Phys. Rev. D **81**, 011101 (2010), [arXiv:0809.4366].
- [131] B. Aubert *et al.* (BaBar), Phys. Rev. **D78**, 012004 (2008), [arXiv:0803.4451]; A. Garmash *et al.* (Belle), Phys. Rev. Lett. **96**, 251803 (2006), [hep-ex/0512066].
- [132] C. T. Hoi *et al.* (Belle), Phys. Rev. Lett. **108**, 031801 (2012), [arXiv:1110.2000]; B. Aubert *et al.* (BaBar), Phys. Rev. **D80**, 112002 (2009), [arXiv:0907.1743].
- [133] B. Aubert *et al.* (BaBar), Phys. Rev. Lett. **97**, 201802 (2006), [hep-ex/0608005]; C. H. Wang *et al.* (Belle), Phys. Rev. **D75**, 092005 (2007), [hep-ex/0701057].
- [134] R. Aaij *et al.* (LHCb), Phys. Rev. **D90**, 11, 112004 (2014), [arXiv:1408.5373]; C.-L. Hsu *et al.* (Belle), Phys. Rev. D **96**, 3, 031101 (2017), [arXiv:1705.02640].
- [135] B. Aubert *et al.* (BaBar), Phys. Rev. Lett. **97**, 171805 (2006), [hep-ex/0608036].
- [136] K. Abe *et al.* (Belle), Phys. Rev. Lett. **98**, 181804 (2007), [hep-ex/0608049].
- [137] R. Aaij *et al.* (LHCb), Phys. Rev. Lett. **118**, 8, 081801 (2017), [arXiv:1610.08288].
- [138] C. C. Peng *et al.* (Belle), Phys. Rev. **D82**, 072007 (2010), [arXiv:1006.5115].
- [139] T. Aaltonen *et al.* (CDF), Phys. Rev. Lett. **106**, 181802 (2011), [arXiv:1103.5762].
- [140] B. Pal *et al.* (Belle), Phys. Rev. Lett. **116**, 16, 161801 (2016), [arXiv:1512.02145].
- [141] R. Aaij *et al.* (LHCb), Phys. Rev. D **102**, 1, 012011 (2020), [arXiv:2002.08229].
- [142] See the “Determination of CKM angles from B hadrons,” by T. Gershon, M. Kenzie, and K. Trabelsi, in this *Review*.
- [143] M. Gronau and D. London, Phys. Rev. Lett. **65**, 3381 (1990).
- [144] T. Julius *et al.* (Belle), Phys. Rev. **D96**, 3, 032007 (2017), [arXiv:1705.02083].
- [145] B. Aubert *et al.* (BaBar), Phys. Rev. **D78**, 071104 (2008), [arXiv:0807.4977].
- [146] P. Vanhovefer *et al.* (Belle), Phys. Rev. **D89**, 072008 (2014), [Addendum: Phys. Rev. D89 119903 (2014)], [arXiv:1212.4015].
- [147] B. Aubert *et al.* (BaBar), Phys. Rev. **D76**, 052007 (2007), [arXiv:0705.2157]; P. Vanhoefer *et al.* (Belle), Phys. Rev. D **93**, 3, 032010 (2016), [Addendum: Phys.Rev.D 94, 099903 (2016)], [arXiv:1510.01245].
- [148] B. Aubert *et al.* (BaBar), Phys. Rev. Lett. **102**, 141802 (2009), [arXiv:0901.3522]; J. Zhang *et al.* (Belle), Phys. Rev. Lett. **91**, 221801 (2003), [hep-ex/0306007].
- [149] R. Aaij *et al.* (LHCb), Phys. Lett. **B747**, 468 (2015), [arXiv:1503.07770].
- [150] See the “Polarization in B Decays,” by A. Gritsan in this *Review*.
- [151] T. E. Coan *et al.* (CLEO), Phys. Rev. Lett. **84**, 5283 (2000), [hep-ex/9912057].
- [152] B. Aubert *et al.* (BaBar), Phys. Rev. Lett. **103**, 211802 (2009), [arXiv:0906.2177]; T. Horiguchi *et al.* (Belle), Phys. Rev. Lett. **119**, 19, 191802 (2017), [arXiv:1707.00394].
- [153] B. Aubert *et al.* (BaBar), Phys. Rev. **D70**, 091105 (2004), [hep-ex/0409035]; S. Nishida *et al.* (Belle), Phys. Lett. **B610**, 23 (2005), [hep-ex/0411065]; B. Aubert *et al.* (BaBar), Phys. Rev. **D74**, 031102 (2006), [hep-ex/0603054].
- [154] H. Yang *et al.* (Belle), Phys. Rev. Lett. **94**, 111802 (2005), [hep-ex/0412039].
- [155] B. Aubert *et al.* (BaBar), Phys. Rev. Lett. **98**, 211804 (2007), [Erratum: Phys. Rev. Lett.100,199905(2008)], [hep-ex/0507031]; P. del Amo Sanchez *et al.* (BaBar), Phys. Rev. **D93**, 5, 052013 (2016), [arXiv:1512.03579].
- [156] R. Aaij *et al.* (LHCb), Phys. Rev. Lett. **112**, 16, 161801 (2014), [arXiv:1402.6852].
- [157] J. Wicht *et al.* (Belle), Phys. Rev. Lett. **100**, 121801 (2008), [arXiv:0712.2659]; D. Dutta *et al.* (Belle), Phys. Rev. **D91**, 1, 011101 (2015), [arXiv:1411.7771]; R. Aaij *et al.* (LHCb), Nucl. Phys. **B867**, 1 (2013), [arXiv:1209.0313].
- [158] R. Aaij *et al.* (LHCb), Phys. Rev. Lett. **123**, 3, 031801 (2019), [arXiv:1904.06697].
- [159] A. Ali, E. Lunghi and A. Ya. Parkhomenko, Phys. Lett. **B595**, 323 (2004), [hep-ph/0405075]; P. Ball, G. W. Jones and R. Zwicky, Phys. Rev. **D75**, 054004 (2007), [hep-ph/0612081].
- [160] J. L. Hewett, Phys. Rev. Lett. **70**, 1045 (1993), [hep-ph/9211256].
- [161] S. Chen *et al.* (CLEO), Phys. Rev. Lett. **87**, 251807 (2001), [hep-ex/0108032]; J. P. Lees *et al.* (BaBar), Phys. Rev. **D86**, 112008 (2012), [arXiv:1207.5772].
- [162] A. Limosani *et al.* (Belle), Phys. Rev. Lett. **103**, 241801 (2009), [arXiv:0907.1384]; T. Saito *et al.* (Belle), Phys. Rev. **D91**, 5, 052004 (2015), [arXiv:1411.7198].
- [163] P. del Amo Sanchez *et al.* (BaBar), Phys. Rev. **D82**, 051101 (2010), [arXiv:1005.4087].
- [164] M. Misiak *et al.*, Phys. Rev. Lett. **114**, 22, 221801 (2015), [arXiv:1503.01789]; M. Czakon *et al.*, JHEP **04**, 168 (2015), [arXiv:1503.01791]; R. Bause *et al.*, Eur. Phys. J. C **83**, 5, 419 (2023), [arXiv:2209.04457].
- [165] L. Wolfenstein and Y. L. Wu, Phys. Rev. Lett. **73**, 2809 (1994), [hep-ph/9410253]; G. M. Asatrian and A. Ioannian, Phys. Rev. **D54**, 5642 (1996), [hep-ph/9603318]; M. Ciuchini, E. Gabrielli and G. F. Giudice, Phys. Lett. **B388**, 353 (1996), [Erratum: Phys. Lett.B393,489(1997)], [hep-ph/9604438]; S. Baek and P. Ko, Phys. Rev. Lett. **83**, 488 (1999), [hep-ph/9812229]; A. L. Kagan and M. Neubert, Phys. Rev. **D58**, 094012 (1998), [hep-ph/9803368]; K. Kiers, A. Soni and G.-H. Wu, Phys. Rev. **D62**, 116004 (2000), [hep-ph/0006280].
- [166] S. Watanuki *et al.* (Belle), Phys. Rev. D **99**, 3, 032012 (2019), [arXiv:1807.04236].
- [167] J. P. Lees *et al.* (BaBar), Phys. Rev. **D90**, 9, 092001 (2014), [arXiv:1406.0534].

- [168] B. Aubert *et al.* (BaBar), Phys. Rev. **D72**, 052004 (2005), [hep-ex/0508004].
- [169] B. Aubert *et al.* (BaBar), Phys. Rev. **D77**, 051103 (2008), [arXiv:0711.4889].
- [170] J. P. Lees *et al.* (BaBar), Phys. Rev. Lett. **109**, 191801 (2012), [arXiv:1207.2690].
- [171] See the “Semileptonic *b*-Hadron Decays, Determination of V_{cb} , V_{ub} ,” by T. Mannel and P. Urquijo in this *Review*.
- [172] M. Iwasaki *et al.* (Belle), Phys. Rev. **D72**, 092005 (2005), [hep-ex/0503044]; J. P. Lees *et al.* (BaBar), Phys. Rev. Lett. **112**, 211802 (2014), [arXiv:1312.5364].
- [173] Y. Sato *et al.* (Belle), Phys. Rev. **D93**, 3, 032008 (2016), [Addendum: Phys. Rev. D93, no.5, 059901 (2016)], [arXiv:1402.7134].
- [174] T. Aaltonen *et al.* (CDF), Phys. Rev. Lett. **107**, 201802 (2011), [arXiv:1107.3753].
- [175] R. Aaij *et al.* (LHCb), JHEP **07**, 084 (2013), [arXiv:1305.2168]; R. Aaij *et al.* (LHCb), JHEP **09**, 179 (2015), [arXiv:1506.08777].
- [176] R. Aaij *et al.* (LHCb), Phys. Lett. **B725**, 25 (2013), [arXiv:1306.2577].
- [177] R. Aaij *et al.* (LHCb), JHEP **06**, 108 (2017), [arXiv:1703.00256].
- [178] B. Aubert *et al.* (BaBar), Phys. Rev. Lett. **102**, 091803 (2009), [arXiv:0807.4119].
- [179] S. Choudhury *et al.* (BELLE), JHEP **03**, 105 (2021), [arXiv:1908.01848].
- [180] R. Aaij *et al.* (LHCb), JHEP **06**, 133 (2014), [arXiv:1403.8044].
- [181] J. T. Wei *et al.* (Belle), Phys. Rev. Lett. **103**, 171801 (2009), [arXiv:0904.0770].
- [182] R. Aaij *et al.* (LHCb), JHEP **11**, 047 (2016), [Erratum: JHEP **04**, 142 (2017)], [arXiv:1606.04731].
- [183] R. Aaij *et al.* (LHCb), Phys. Rev. Lett. **127**, 15, 151801 (2021), [arXiv:2105.14007].
- [184] T. Aaltonen *et al.* (CDF), Phys. Rev. Lett. **108**, 081807 (2012), [arXiv:1108.0695].
- [185] R. Aaij *et al.* (LHCb), JHEP **05**, 082 (2014), [arXiv:1403.8045].
- [186] A. M. Sirunyan *et al.* (CMS), Phys. Lett. B **781**, 517 (2018), [arXiv:1710.02846].
- [187] R. Aaij *et al.* (LHCb), Phys. Rev. Lett. **125**, 1, 011802 (2020), [arXiv:2003.04831].
- [188] S. Wehle *et al.* (Belle), Phys. Rev. Lett. **118**, 11, 111801 (2017), [arXiv:1612.05014].
- [189] M. Aaboud *et al.* (ATLAS), JHEP **10**, 047 (2018), [arXiv:1805.04000].
- [190] R. Aaij *et al.* (LHCb), Phys. Rev. Lett. **126**, 16, 161802 (2021), [arXiv:2012.13241].
- [191] R. Aaij *et al.* (LHCb), JHEP **11**, 043 (2021), [arXiv:2107.13428].
- [192] R. Aaij *et al.* (LHCb), JHEP **09**, 146 (2018), [arXiv:1808.00264].
- [193] S. Descotes-Genon *et al.*, JHEP **01**, 048 (2013), [arXiv:1207.2753].
- [194] J. P. Lees *et al.* (BaBar), Phys. Rev. **D86**, 032012 (2012), [arXiv:1204.3933].
- [195] R. Aaij *et al.* (LHCb), JHEP **09**, 177 (2014), [arXiv:1408.0978].
- [196] J. Lyon and R. Zwicky, Phys. Rev. **D88**, 9, 094004 (2013), [arXiv:1305.4797].
- [197] R. Aaij *et al.* (LHCb), Eur. Phys. J. **C77**, 3, 161 (2017), [arXiv:1612.06764].
- [198] R. Aaij *et al.* (LHCb), JHEP **12**, 081 (2020), [arXiv:2010.06011].
- [199] R. Aaij *et al.* (LHCb), Phys. Rev. Lett. **122**, 19, 191801 (2019), [arXiv:1903.09252]; R. Aaij *et al.* (LHCb), JHEP **08**, 055 (2017), [arXiv:1705.05802]; R. Aaij *et al.* (LHCb), Nature Phys. **18**, 3, 277 (2022), [arXiv:2103.11769]; A. Abdesselam *et al.* (Belle), Phys. Rev. Lett. **126**, 16, 161801 (2021), [arXiv:1904.02440].
- [200] R. Aaij *et al.* (LHCb), Phys. Rev. Lett. **131**, 5, 051803 (2023), [arXiv:2212.09152].
- [201] R. Aaij *et al.* (LHCb), JHEP **05**, 040 (2020), [arXiv:1912.08139].
- [202] R. Aaij *et al.* (LHCb), Phys. Rev. Lett. **128**, 19, 191802 (2022), [arXiv:2110.09501].
- [203] R. Aaij *et al.* (LHCb), Phys. Lett. **B743**, 46 (2015), [arXiv:1412.6433].
- [204] R. Aaij *et al.* (LHCb), JHEP **04**, 029 (2017), [arXiv:1701.08705].
- [205] R. Aaij *et al.* (LHCb), JHEP **07**, 020 (2018), [arXiv:1804.07167].
- [206] J. P. Lees *et al.* (BaBar), Phys. Rev. D **87**, 11, 112005 (2013), [arXiv:1303.7465].
- [207] J. Grygier *et al.* (Belle), Phys. Rev. D **96**, 9, 091101 (2017), [Addendum: Phys. Rev. D97, 099902 (2018)], [arXiv:1702.03224].
- [208] F. Abudinén *et al.* (Belle-II), Phys. Rev. Lett. **127**, 18, 181802 (2021), [arXiv:2104.12624].
- [209] T. Aaltonen *et al.* (CDF), Phys. Rev. Lett. **107**, 191801 (2011), [Addendum: Phys. Rev. Lett. **107**, 239903 (2011)], [arXiv:1107.2304]; V. M. Abazov *et al.* (D0), Phys. Rev. **D87**, 7, 072006 (2013), [arXiv:1301.4507].
- [210] R. Aaij *et al.* (LHCb), Phys. Rev. Lett. **110**, 2, 021801 (2013), [arXiv:1211.2674].
- [211] M. Aaboud *et al.* (ATLAS), JHEP **04**, 098 (2019), [arXiv:1812.03017].
- [212] A. M. Sirunyan *et al.* (CMS), JHEP **04**, 188 (2020), [arXiv:1910.12127].
- [213] R. Aaij *et al.* (LHCb), Phys. Rev. Lett. **118**, 19, 191801 (2017), [arXiv:1703.05747]; R. Aaij *et al.* (LHCb), Phys. Rev. Lett. **128**, 4, 041801 (2022), [arXiv:2108.09284].
- [214] R. Aaij *et al.* (LHCb), Phys. Rev. Lett. **124**, 21, 211802 (2020), [arXiv:2003.03999].
- [215] R. Aaij *et al.* (LHCb), Phys. Rev. Lett. **118**, 25, 251802 (2017), [arXiv:1703.02508].
- [216] C. Bobeth *et al.*, Phys. Rev. Lett. **112**, 101801 (2014), [arXiv:1311.0903].
- [217] K. De Bruyn *et al.*, Phys. Rev. Lett. **109**, 041801 (2012), [arXiv:1204.1737]; A. J. Buras *et al.*, JHEP **07**, 77 (2013), [arXiv:1303.3820].
- [218] R. Aaij *et al.* (LHCb), JHEP **03**, 078 (2018), [arXiv:1710.04111].
- [219] J. Aebischer *et al.*, Eur. Phys. J. C **80**, 3, 252 (2020), [arXiv:1903.10434]; F. Beaujean, C. Bobeth and D. van Dyk, Eur. Phys. J. **C74**, 2897 (2014), [Erratum: Eur. Phys. J. **C74**, 3179 (2014)], [arXiv:1310.2478]; M. Algueró *et al.*, JHEP **07**, 096 (2019), [arXiv:1902.04900]; M. Algueró *et al.*, Eur. Phys. J. C **79**, 8, 714 (2019), [Addendum: Eur. Phys. J. C **80**, 511 (2020)], [arXiv:1903.09578]; M. Algueró *et al.*, Eur. Phys. J. C **82**, 4, 326 (2022), [arXiv:2104.08921]; A. Arbey *et al.*, Phys. Rev. D **100**, 1, 015045 (2019), [arXiv:1904.08399]; W. Altmannshofer and P. Stangl, Eur. Phys. J. C **81**, 10, 952 (2021), [arXiv:2103.13370]; T. Hurth *et al.*, Phys. Lett. B **824**, 136838 (2022), [arXiv:2104.10058].
- [220] T. Blake, G. Lanfranchi and D. M. Straub, Prog. Part. Nucl. Phys. **92**, 50 (2017), [arXiv:1606.00916]; J. Albrecht, S. Reichert and D. van Dyk, Int. J. Mod. Phys. A **33**, 1830016 (2018), [arXiv:1806.05010]; J. Albrecht, D. van Dyk and C. Langenbruch, Prog. Part. Nucl. Phys. **120**, 103885 (2021), [arXiv:2107.04822].

74. Polarization in B Decays

Revised July 2023 by A.V. Gritsan (Johns Hopkins U.).

We review the notation used in polarization measurements in particle production and decay, with a particular emphasis on the B decays and the CP -violating observables in polarization measurements. We look at several examples of vector-vector and vector-tensor B meson decays, while more details about the theory and experimental results in B decays can be found in a separate mini-review [1] in this *Review*.

Figure 74.1 illustrates angular observables in an example of the sequential process $ab \rightarrow X \rightarrow P_1 P_2 \rightarrow (p_{11} p_{12})(p_{21} p_{22})$ [2]. The angular distributions are of particular interest because they are sensitive to spin correlations and reveal properties of particles and their interactions, such as quantum numbers and couplings. In the case of a spin-zero particle X , such as B meson or a Higgs boson, there are no spin correlations in the production mechanism and the decay chain is to be analyzed. The angular distribution of decay products can be expressed as a function of three helicity angles which describe the alignment of the particles in the decay chain. The analyzer of the B -daughter polarization is normally chosen for two-body decays, as the direction of the daughters in the center-of-mass of the parent (*e.g.*, $\rho \rightarrow 2\pi$) [3], and for three-body decays as the normal to the decay plane (*e.g.*, $\omega \rightarrow 3\pi$) [4]. An equivalent set of transversity angles is sometimes used in polarization analyses [5]. The differential decay width depends on complex amplitudes $A_{\lambda_1 \lambda_2}$, corresponding to the X -daughter helicity states λ_i .

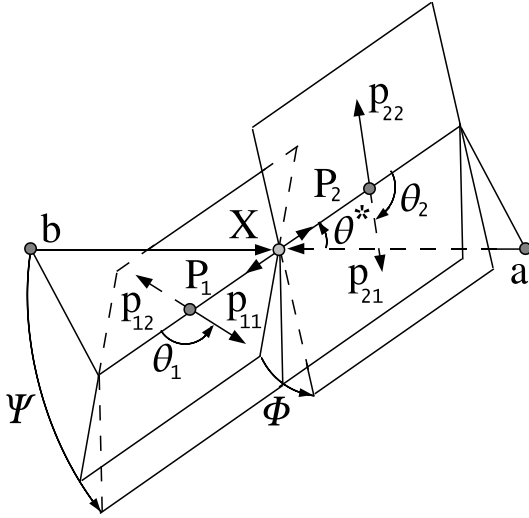


Figure 74.1: Definition of the production and helicity angles in the sequential process $ab \rightarrow X \rightarrow P_1 P_2 \rightarrow (p_{11} p_{12})(p_{21} p_{22})$. The three helicity angles include θ_1 and θ_2 , defined in the rest frame of the two daughters P_1 and P_2 , and Φ , defined in the X frame as the angle between the two decay planes. The two production angles θ^* and Ψ are defined in the X frame, where Ψ is the angle between the production plane and the average of the two decay planes.

In the case of a spin-zero B -meson decay, its daughter helicities are constrained to $\lambda_1 = \lambda_2 = \lambda$. Therefore we simplify amplitude notation as A_λ . Moreover, most B -decay polarization analyses are limited to the case when the spin of one of the B -meson daughters is 1. In that case, there are only three independent amplitudes corresponding to $\lambda = 0$ or ± 1 [6], where the last two can be expressed in terms of parity-even and parity-odd amplitudes $A_{\parallel, \perp} = (A_{+1} \pm A_{-1})/\sqrt{2}$. The overall decay amplitude involves three complex terms proportional to the above amplitudes and the Wigner d functions of helicity angles. The exact angular dependence would depend on the quantum numbers of the B -meson daughters and of their decay products, and can be found in the literature [6, 7]. When both B -meson daughters are tensor mesons and the smaller of the two daughter spins is $J_1 > 1$, this formalism

can be easily extended by introducing the parity-even and parity-odd amplitudes of higher order $A_{\parallel, \perp n} = (A_{+n} \pm A_{-n})/\sqrt{2}$, with $1 < n \leq J_1$, while the general angular parameterization may be found in Ref. [7]. However, we limit the following discussion to $J_1 = 1$. The differential decay rate would involve six real quantities α_i , including interference terms,

$$\frac{d\Gamma}{\Gamma d \cos \theta_1 d \cos \theta_2 d\Phi} = \sum_i \alpha_i f_i(\cos \theta_1, \cos \theta_2, \Phi), \quad (74.1)$$

where each $f_i(\cos \theta_1, \cos \theta_2, \Phi)$ has unique angular dependence specific to particle quantum numbers, and the α_i parameters are defined as:

$$\alpha_1 = \frac{|A_0|^2}{\sum |A_\lambda|^2} = f_L, \quad (74.2)$$

$$\alpha_2 = \frac{|A_\parallel|^2 + |A_\perp|^2}{\sum |A_\lambda|^2} = (1 - f_L), \quad (74.3)$$

$$\alpha_3 = \frac{|A_\parallel|^2 - |A_\perp|^2}{\sum |A_\lambda|^2} = (1 - f_L - 2f_\perp), \quad (74.4)$$

$$\alpha_4 = \frac{\Im m(A_\perp A_\parallel^*)}{\sum |A_\lambda|^2} = \sqrt{f_\perp(1 - f_L - f_\perp)} \sin(\phi_\perp - \phi_\parallel), \quad (74.5)$$

$$\alpha_5 = \frac{\Re e(A_\parallel A_0^*)}{\sum |A_\lambda|^2} = \sqrt{f_L(1 - f_L - f_\perp)} \cos(\phi_\parallel), \quad (74.6)$$

$$\alpha_6 = \frac{\Im m(A_\perp A_0^*)}{\sum |A_\lambda|^2} = \sqrt{f_\perp f_L} \sin(\phi_\perp), \quad (74.7)$$

where the amplitudes have been expressed with the help of polarization parameters f_L , f_\perp , ϕ_\parallel , and ϕ_\perp defined in Table 74.1. Note that the terms proportional to $\Re e(A_\perp A_\parallel^*)$, $\Im m(A_\parallel A_0^*)$, and $\Re e(A_\perp A_0^*)$ are absent in Eqs. (2-7). However, these terms may appear for some three-body decays of a B -meson daughter, see Ref. [7].

Table 74.1: Rate, polarization, and CP -asymmetry parameters defined for the B -meson decays to mesons with non-zero spin. Numerical examples are shown for the average of the $B^0 \rightarrow \varphi K^*(892)^0$ decay measurements obtained from BABAR [8], Belle [9], and LHCb [10]. The first six parameters are defined under the assumption of no CP violation in decay, while they are averaged between the \bar{B} and B parameters in general. The last six parameters involve differences between the \bar{B} and B meson decay parameters. The phase convention δ_0 is chosen with respect to a single A_{00} amplitude from a reference B decay mode, which is $B^0 \rightarrow \varphi K^*(1430)^0$ for numerical results.

parameter	definition	average
\mathcal{B}	$\Gamma/\Gamma_{\text{total}}$	$(10.1^{+0.6}_{-0.5}) \times 10^{-6}$
f_L	$ A_0 ^2/\sum A_\lambda ^2$	0.497 ± 0.017
f_\perp	$ A_\perp ^2/\sum A_\lambda ^2$	0.225 ± 0.015
$\phi_\parallel - \pi$	$\arg(A_\parallel/A_0) - \pi$	-0.712 ± 0.058
$\phi_\perp - \pi$	$\arg(A_\perp/A_0) - \pi$	-0.615 ± 0.056
$\delta_0 - \pi$	$\arg(A_{00}/A_0) - \pi$	-0.26 ± 0.10
A_{CP}	$(\bar{\Gamma} - \Gamma)/(\bar{\Gamma} + \Gamma)$	-0.003 ± 0.038
A_{CP}^0	$(\bar{f}_L - f_L)/(\bar{f}_L + f_L)$	-0.007 ± 0.030
A_{CP}^\perp	$(\bar{f}_\perp - f_\perp)/(\bar{f}_\perp + f_\perp)$	-0.014 ± 0.057
$\Delta\phi_\parallel$	$(\bar{\phi}_\parallel - \phi_\parallel)/2$	$+0.051 \pm 0.053$
$\Delta\phi_\perp$	$(\bar{\phi}_\perp - \phi_\perp - \pi)/2$	$+0.075 \pm 0.050$
$\Delta\delta_0$	$(\bar{\delta}_0 - \delta_0)/2$	$+0.13 \pm 0.08$

Overall, six real parameters describe three complex amplitudes A_0 , A_\parallel , and A_\perp . These could be chosen to be the four polarization

parameters f_L , f_\perp , ϕ_\parallel , and ϕ_\perp , one overall size normalization, such as decay rate Γ , or branching fraction \mathcal{B} , and one overall phase δ_0 . The phase convention is arbitrary for an isolated B decay mode. However, for several B decays, the relative phase could produce meaningful and observable effects through interference with other B decays with the same final states, such as for $B \rightarrow VK_J^*$ with $J = 0, 1, 2, 3, 4, \dots$. The phase could be referenced to the single $B \rightarrow VK_0^*$ amplitude A_{00} in such a case, as shown in Table 74.1. Here V stands for any spin-one vector meson.

Moreover, CP violation can be tested in the angular distribution of the decay as the difference between the B and \bar{B} . Each of the six real parameters describing the three complex amplitudes would have a counterpart CP -asymmetry term, corresponding to three direct- CP asymmetries in three amplitudes, and three CP -violating phase differences, equivalent to the phase measurements from the mixing-induced CP asymmetries in the time evolution of B -decays [1]. In Table 74.1 and Ref. [11], these are chosen to be the direct- CP asymmetries in the overall decay rate \mathcal{A}_{CP} , in the f_L fraction \mathcal{A}_{CP}^0 , and in the f_\perp fraction \mathcal{A}_{CP}^\perp , and three weak phase differences:

$$\Delta\phi_\parallel = \frac{1}{2}\arg(\bar{A}_\parallel A_0/A_\parallel \bar{A}_0), \quad (74.8)$$

$$\Delta\phi_\perp = \frac{1}{2}\arg(\bar{A}_\perp A_0/A_\perp \bar{A}_0) - \frac{\pi}{2}, \quad (74.9)$$

$$\Delta\delta_0 = \frac{1}{2}\arg(\bar{A}_{00} A_0/A_{00} \bar{A}_0). \quad (74.10)$$

The $\frac{\pi}{2}$ term in Eq. (74.8) reflects the fact that A_\perp and \bar{A}_\perp differ in phase by π if CP is conserved. The two parameters $\Delta\phi_\parallel$ and $\Delta\phi_\perp$ are equivalent to triple-product asymmetries constructed from the vectors describing the decay angular distribution [12]. The CP -violating phase difference in the reference decay mode [11] is, in the Wolfenstein CKM quark-mixing phase convention,

$$\Delta\phi_{00} = \frac{1}{2}\arg(A_{00}/\bar{A}_{00}). \quad (74.11)$$

This can be measured only together with the mixing-induced phase difference for some of the neutral B -meson decays similar to other mixing-induced CP asymmetry measurements [1].

It may not always be possible to have a phase-reference decay mode which would define δ_0 and $\Delta\delta_0$ parameters. In that case, it may be possible to define the phase difference directly similarly to Eq. (74.11):

$$\Delta\phi_0 = \frac{1}{2}\arg(A_0/\bar{A}_0). \quad (74.12)$$

One can measure the angles of the CKM unitarity triangle, assuming Standard Model contributions to the $\Delta\phi_0$ and B -mixing phases. Examples include measurements of $\beta = \phi_1$ with $B \rightarrow J/\psi K^*$ and $\alpha = \phi_2$ with $B \rightarrow \rho\rho$.

Most of the B decays that arise from tree-level $b \rightarrow c$ transitions have the amplitude hierarchy $|A_0| > |A_+| > |A_-|$ which is expected from analyses based on quark-helicity conservation [13]. The larger the mass of the vector-meson daughters, the weaker the inequality. The B meson decays to heavy vector particles with charm, such as $B \rightarrow J/\psi K^*$, $\psi(2S)K^*$, $\chi_{c1}K^*$, $D^*\rho$, D^*K^* , D^*D^* , and $D^*D_s^*$, show a substantial fraction of the amplitudes corresponding to transverse polarization of the vector mesons ($A_{\pm 1}$), in agreement with the factorization prediction. The detailed amplitude analysis of the $B \rightarrow J/\psi K^*$ decays has been performed by the BABAR [14], Belle [15], CDF [16], CLEO [17], D0 [18], and LHCb [19] collaborations. Most analyses are performed under the assumption of the absence of direct CP violation. The parameter values are given in the particle listing of this Review. The difference between the strong phases ϕ_\parallel and ϕ_\perp deviates significantly from zero. The measurements [14, 15] of CP -violating terms similar to those in $B \rightarrow \varphi K^*$ [8] shown in Table 74.1 are consistent with zero.

In addition, the mixing-induced CP -violating asymmetry is measured in the $B^0 \rightarrow J/\psi K^{*0}$ decay [1, 14, 15] where angular analysis allows one to separate CP -eigenstate amplitudes. This allows one to resolve the sign ambiguity of the $\cos 2\beta$ ($\cos 2\phi_1$) term that appears in the time-dependent angular distribution due

to interference of parity-even and parity-odd terms. This analysis relies on the knowledge of discrete ambiguities in the strong phases ϕ_\parallel and ϕ_\perp , as discussed below. The BABAR experiment used a method based on the dependence on the $K\pi$ invariant mass of the interference between the S - and P -waves to resolve the discrete ambiguity in the determination of the strong phases ($\phi_\parallel, \phi_\perp$) in $B \rightarrow J/\psi K^*$ decays [14]. The result is in agreement with the amplitude hierarchy expectation [13]. The CDF [20], D0 [21], LHCb [22], and ATLAS [23] experiments have studied the $B_s^0 \rightarrow J/\psi(K^+K^-)$, $J/\psi(\pi^+\pi^-)$, $\psi(K^+\pi^-)$ decays and provided the lifetime, polarization, and phase measurements.

The amplitude hierarchy $|A_0| \gg |A_+| \gg |A_-|$ was expected in B decays to light vector particles in both penguin transitions [24, 25] and tree-level transitions [13]. There is confirmation by the BABAR and Belle experiments of predominantly longitudinal polarization in the tree-level $b \rightarrow u$ transition, such as $B^0 \rightarrow \rho^+\rho^-$ [26], $B^+ \rightarrow \rho^0\rho^+$ [27], and $B^+ \rightarrow \omega\rho^+$ [28]; this is consistent with the analysis of the quark helicity conservation [13]. Because the longitudinal amplitude dominates the decay, a detailed amplitude analysis is not possible with current B samples, and limits on the transverse amplitude fraction are obtained. The small branching fractions of $B^0 \rightarrow \rho^0\rho^0, \omega\rho^0, \omega\omega$ [28–31] indicate that $b \rightarrow d$ penguin pollution is small in the charmless, strangeless vector-vector B decays. There is a measurement of large longitudinal polarization in $B^0 \rightarrow \rho^0\rho^0$ [29–31] decays. The fraction of transverse polarization is large in decays to heavier mesons such as $B^0 \rightarrow a_1(1260)^+a_1(1260)^-$ [32].

The interest in the polarization and CP -asymmetry measurements in penguin transition, such as $b \rightarrow s$ decays $B \rightarrow \varphi K^*$, ρK^* , ωK^* , or $B_s^0 \rightarrow \varphi\varphi, K^*K^*$, and $b \rightarrow d$ decay $B \rightarrow K^*\bar{K}^*$, is motivated by their potential sensitivity to physics beyond the Standard Model. The decay amplitudes for $B \rightarrow \varphi K^*$ have been measured by the BABAR, Belle, and LHCb experiments [9–11, 33, 34]. The fractions of longitudinal polarization are $f_L = 0.50 \pm 0.05$ for the $B^+ \rightarrow \varphi K^{*+}$ decay and $f_L = 0.497 \pm 0.017$ for the $B^0 \rightarrow \varphi K^{*0}$ decay. These indicate significant departure from the naive expectation of predominant longitudinal polarization, suggesting other contributions to the decay amplitude, previously neglected, either within the Standard Model, such as penguin annihilation [35] or QCD rescattering [36], or from physics beyond the Standard Model [37]. The complete set of twelve amplitude parameters measured in the $B^0 \rightarrow \varphi K^{*0}$ decay is given in Table 74.1. Several other parameters could be constructed from the above twelve parameters, as suggested in Ref. [38].

The discrete ambiguity in the phase ($\phi_\parallel, \phi_\perp, \Delta\phi_\parallel, \Delta\phi_\perp$) measurements has been resolved by BABAR in favor of $|A_+| \gg |A_-|$ through interference between the S - and P -waves of $K\pi$. The search for vector-tensor and vector-axialvector $B \rightarrow \varphi K_J^{(*)}$ decays with $J = 1, 2, 3, 4$ revealed a large fraction of longitudinal polarization in the decay $B \rightarrow \varphi K_2^*(1430)$ with $f_L = 0.90_{-0.07}^{+0.06}$ [11, 39], but large contribution of transverse amplitude in $B \rightarrow \varphi K_1(1270)$ with $f_L = 0.46_{-0.15}^{+0.13}$ [40].

Like $B \rightarrow \varphi K^*$, the decays $B \rightarrow \rho K^*$ and $B \rightarrow \omega K^*$ may be sensitive to New Physics. Measurements of the longitudinal polarization fraction in $B \rightarrow \rho K^*$ [41] and in both vector-vector and vector-tensor final states of $B \rightarrow \omega K_J^*$ [28] by BABAR and Belle reveal a large fraction of transverse polarization, indicating an anomaly similar to $B \rightarrow \varphi K^*$ except for a different pattern in vector-tensor final states. An angular analysis of the $B^0 \rightarrow \rho^0 K^{*0}$ decay mode by LHCb [42] provides much higher precision and indicates remarkably small longitudinal polarization fraction and a significant direct CP asymmetry observed in angular distributions of $B \rightarrow VV$ decays for the first time. A large transverse polarization is also observed in the $B_s^0 \rightarrow \varphi\varphi$ decay by CDF [43] and LHCb [44], $B_s^0 \rightarrow K^{*0}\bar{K}^{*0}$ decays by LHCb [45], and $B_s^0 \rightarrow \varphi K^{*0}$ decays by LHCb [46]. At the same time, measurement of the polarization in the $b \rightarrow d$ penguin decays $B \rightarrow K^*\bar{K}^*$ indicates a large fraction of longitudinal polarization [45, 47]. The LHCb experiment has also provided the very first polarization results on the tensor-tensor, as well as vector-tensor, decays of the B_s^0 meson in the $(K\pi)(K\pi)$ final state [45]. The polarization pattern in penguin-dominated B -meson decays is not fully understood [35–37].

The three-body semileptonic B -meson decays, such as $B \rightarrow V\ell_1\ell_2$, share many features with the two-body $B \rightarrow VV$ decays. Their differential decay width can be parameterized with the two helicity angles defined in the V and $(\ell_1\ell_2)$ frames and with the azimuthal angle, as defined in Fig. 74.1. However, since the $(\ell_1\ell_2)$ pair does not come from an on-shell particle, the angular distribution is unique to each point in the dilepton mass $m_{\ell\ell}$ spectrum. The polarization measurements as a function of $m_{\ell\ell}$ provide complementary information on physics beyond the Standard Model, as discussed for $B \rightarrow K^*\ell^+\ell^-$ and $B_s \rightarrow \phi\ell^+\ell^-$ decays in Ref. [48]. The data in these modes have been analyzed by the BABAR, Belle, CDF, CMS, ATLAS, and LHCb experiments [49–54].

The examples of the angular distributions and observables in $B \rightarrow K^*\ell^+\ell^-$ are discussed in Ref. [48]. Two angular observables have been measured in this decay in certain ranges of the dilepton mass $m_{\ell\ell}$. One parameter is the fraction of longitudinal polarization F_L , which is determined by the K^* angular distribution and is similar to f_L defined for exclusive two-body decays. The other parameter is the forward-backward asymmetry of the lepton pair A_{FB} , which is the asymmetry of the decay rate with positive and negative values of $\cos\theta_1$. A complete set of observables and angular terms has been adopted by the LHCb collaboration [54] following Ref. [48] with the F_L , A_{FB} , and $S_3 - S_9$ coefficients in the angular distributions. Additional set of optimized observables $P_i^{(\prime)}$ is derived from those, for example $P_2 = 2A_{FB}/(3 - 3F_L)$ and $P_5' = S_5/\sqrt{F_L(1 - F_L)}$. These observables have the advantage that the leading form-factor uncertainties cancel. There have been hints of deviations from SM in the measurement of P_5' and lepton flavor universality [49–54].

In summary, there has been considerable interest in the polarization measurements of B -meson decays because they reveal both weak- and strong-interaction dynamics [35–37, 55]. New measurements will further elucidate the pattern of spin alignment measurements in rare B decays, and further test the Standard Model and strong interaction dynamics, including the non-factorizable contributions to the B -decay amplitudes.

References

- [1] P. Eerola, M. Kreps, and Y. Kwon, “Production and Decay of b -Flavored Hadrons,” mini-review in this *Review*.
- [2] Y. Gao *et al.*, Phys. Rev. D **81**, 075022 (2010), [arXiv:1001.3396].
- [3] M. Jacob and G. Wick, Annals Phys. **7**, 404 (1959).
- [4] S. Berman and M. Jacob, Phys. Rev. **139**, B1023 (1965).
- [5] I. Dunietz *et al.*, Phys. Rev. D **43**, 2193 (1991).
- [6] G. Kramer and W. Palmer, Phys. Rev. D **45**, 193 (1992).
- [7] A. Datta *et al.*, Phys. Rev. D **77**, 114025 (2008), [arXiv:0711.2107].
- [8] B. Aubert *et al.* (BaBar), Phys. Rev. D **78**, 092008 (2008), [arXiv:0808.3586].
- [9] M. Prim *et al.* (Belle), Phys. Rev. D **88**, 7, 072004 (2013), [arXiv:1308.1830].
- [10] R. Aaij *et al.* (LHCb), JHEP **05**, 069 (2014), [arXiv:1403.2888].
- [11] B. Aubert *et al.* (BaBar), Phys. Rev. Lett. **93**, 231804 (2004), [hep-ex/0408017]; B. Aubert *et al.* (BaBar), Phys. Rev. Lett. **98**, 051801 (2007), [hep-ex/0610073]; B. Aubert *et al.* (BaBar), Phys. Rev. D **78**, 092008 (2008), [arXiv:0808.3586].
- [12] G. Valencia, Phys. Rev. D **39**, 3339 (1989); A. Datta and D. London, Int. J. Mod. Phys. A **19**, 2505 (2004), [hep-ph/0303159].
- [13] A. Ali *et al.*, Z. Phys. C **1**, 269 (1979); M. Suzuki, Phys. Rev. D **64**, 117503 (2001), [hep-ph/0106354].
- [14] B. Aubert *et al.* (BaBar), Phys. Rev. D **71**, 032005 (2005), [hep-ex/0411016]; B. Aubert *et al.* (BaBar), Phys. Rev. D **76**, 031102 (2007), [arXiv:0704.0522].
- [15] R. Itoh *et al.* (Belle), Phys. Rev. Lett. **95**, 091601 (2005), [hep-ex/0504030]; M. Prim *et al.* (Belle), Phys. Rev. D **88**, 7, 072004 (2013), [arXiv:1308.1830].
- [16] T. Affolder *et al.* (CDF), Phys. Rev. Lett. **85**, 4668 (2000), [hep-ex/0007034]; D. Acosta *et al.* (CDF), Phys. Rev. Lett. **94**, 101803 (2005), [hep-ex/0412057].
- [17] C. Jessop *et al.* (CLEO), Phys. Rev. Lett. **79**, 4533 (1997), [hep-ex/9702013].
- [18] V. Abazov *et al.* (D0), Phys. Rev. Lett. **102**, 032001 (2009), [arXiv:0810.0037].
- [19] R. Aaij *et al.* (LHCb), Phys. Rev. D **88**, 052002 (2013), [arXiv:1307.2782].
- [20] T. Aaltonen *et al.* (CDF), Phys. Rev. Lett. **100**, 121803 (2008), [arXiv:0712.2348]; T. Aaltonen *et al.* (CDF), Phys. Rev. D **85**, 072002 (2012), [arXiv:1112.1726].
- [21] V. Abazov *et al.* (D0), Phys. Rev. Lett. **98**, 121801 (2007), [hep-ex/0701012]; V. M. Abazov *et al.* (D0), Phys. Rev. D **85**, 032006 (2012), [arXiv:1109.3166].
- [22] R. Aaij *et al.* (LHCb), Phys. Rev. Lett. **108**, 101803 (2012), [arXiv:1112.3183]; R. Aaij *et al.* (LHCb), Phys. Rev. Lett. **114**, 4, 041801 (2015), [arXiv:1411.3104]; R. Aaij *et al.* (LHCb), Phys. Lett. B **747**, 484 (2015), [arXiv:1503.07112]; R. Aaij *et al.* (LHCb), JHEP **11**, 082 (2015), [arXiv:1509.00400]; R. Aaij *et al.* (LHCb), JHEP **08**, 037 (2017), [arXiv:1704.08217].
- [23] G. Aad *et al.* (ATLAS), Eur. Phys. J. C **81**, 4, 342 (2021), [arXiv:2001.07115].
- [24] H.-Y. Cheng and K.-C. Yang, Phys. Lett. B **511**, 40 (2001), [hep-ph/0104090]; C.-H. Chen, Y.-Y. Keum and H.-n. Li, Phys. Rev. D **66**, 054013 (2002), [hep-ph/0204166].
- [25] A. L. Kagan, Phys. Lett. B **601**, 151 (2004), [hep-ph/0405134]; Y. Grossman, Int. J. Mod. Phys. A **19**, 907 (2004), [hep-ph/0310229].
- [26] B. Aubert *et al.* (BaBar), Phys. Rev. D **76**, 052007 (2007), [arXiv:0705.2157]; P. Vanhoefer *et al.* (Belle), Phys. Rev. D **93**, 3, 032010 (2016), [Erratum: Phys. Rev. D **94**, 099903 (2016)], [arXiv:1510.01245].
- [27] J. Zhang *et al.* (Belle), Phys. Rev. Lett. **91**, 221801 (2003), [hep-ex/0306007]; B. Aubert *et al.* (BaBar), Phys. Rev. Lett. **102**, 141802 (2009), [arXiv:0901.3522].
- [28] B. Aubert *et al.* (BaBar), Phys. Rev. D **74**, 051102 (2006), [hep-ex/0605017]; B. Aubert *et al.* (BaBar), Phys. Rev. D **79**, 052005 (2009), [arXiv:0901.3703].
- [29] B. Aubert *et al.* (BaBar), Phys. Rev. D **78**, 071104 (2008), [arXiv:0807.4977].
- [30] I. Adachi *et al.* (Belle), Phys. Rev. D **89**, 7, 072008 (2014), [Erratum: Phys. Rev. D **89**, 119903 (2014)], [arXiv:1212.4015].
- [31] R. Aaij *et al.* (LHCb), Phys. Lett. B **747**, 468 (2015), [arXiv:1503.07770].
- [32] B. Aubert *et al.* (BaBar), Phys. Rev. D **80**, 092007 (2009), [arXiv:0907.1776].
- [33] K.-F. Chen *et al.* (Belle), Phys. Rev. Lett. **94**, 221804 (2005), [hep-ex/0503013].
- [34] B. Aubert *et al.* (BaBar), Phys. Rev. Lett. **99**, 201802 (2007), [arXiv:0705.1798].
- [35] A. L. Kagan, Phys. Lett. B **601**, 151 (2004), [hep-ph/0405134]; H.-n. Li and S. Mishima, Phys. Rev. D **71**, 054025 (2005), [hep-ph/0411146]; C.-H. Chen *et al.*, Phys. Rev. D **72**, 054011 (2005), [hep-ph/0507012]; M. Beneke, J. Rohrer and D. Yang, Phys. Rev. Lett. **96**, 141801 (2006), [hep-ph/0512258]; C.-H. Chen and C.-Q. Geng, Phys. Rev. D **75**, 054010 (2007), [hep-ph/0701023]; A. Datta *et al.*, Phys. Rev. D **76**, 034015 (2007), [arXiv:0705.3915]; M. Beneke, J. Rohrer and D. Yang, Nucl. Phys. B **774**, 64 (2007), [hep-ph/0612290]; H.-Y. Cheng and K.-C. Yang, Phys. Rev. D **78**, 094001 (2008), [Erratum: Phys. Rev. D **79**, 039903 (2009)], [arXiv:0805.0329].

- [36] C. W. Bauer *et al.*, Phys. Rev. D **70**, 054015 (2004), [hep-ph/0401188]; P. Colangelo, F. De Fazio and T. Pham, Phys. Lett. B **597**, 291 (2004), [hep-ph/0406162]; M. Ladisa *et al.*, Phys. Rev. D **70**, 114025 (2004), [hep-ph/0409286]; H.-Y. Cheng, C.-K. Chua and A. Soni, Phys. Rev. D **71**, 014030 (2005), [hep-ph/0409317]; H.-Y. Cheng and K.-C. Yang, Phys. Rev. D **83**, 034001 (2011), [arXiv:1010.3309].
- [37] Y. Grossman, Int. J. Mod. Phys. A **19**, 907 (2004), [hep-ph/0310229]; E. Alvarez *et al.*, Phys. Rev. D **70**, 115014 (2004), [hep-ph/0410096]; P. K. Das and K.-C. Yang, Phys. Rev. D **71**, 094002 (2005), [hep-ph/0412313]; C.-H. Chen and C.-Q. Geng, Phys. Rev. D **71**, 115004 (2005), [hep-ph/0504145]; Y.-D. Yang, R.-M. Wang and G.-R. Lu, Phys. Rev. D **72**, 015009 (2005), [hep-ph/0411211]; K.-C. Yang, Phys. Rev. D **72**, 034009 (2005), [Erratum: Phys. Rev. D **72**, 059901 (2005)], [hep-ph/0506040]; S. Baek *et al.*, Phys. Rev. D **72**, 094008 (2005), [hep-ph/0508149]; C.-S. Huang *et al.*, Phys. Rev. D **73**, 034026 (2006), [hep-ph/0511129]; C.-H. Chen and H. Hatanaka, Phys. Rev. D **73**, 075003 (2006), [hep-ph/0602140]; A. Faessler *et al.*, Phys. Rev. D **75**, 074029 (2007), [hep-ph/0702020].
- [38] D. London, N. Sinha and R. Sinha, Phys. Rev. D **69**, 114013 (2004), [hep-ph/0402214].
- [39] B. Aubert *et al.* (BaBar), Phys. Rev. D **76**, 051103 (2007), [arXiv:0705.0398].
- [40] B. Aubert *et al.* (BaBar), Phys. Rev. Lett. **101**, 161801 (2008), [arXiv:0806.4419].
- [41] J. Zhang *et al.* (Belle), Phys. Rev. Lett. **95**, 141801 (2005), [hep-ex/0408102]; B. Aubert *et al.* (BaBar), Phys. Rev. Lett. **97**, 201801 (2006), [hep-ex/0607057]; P. del Amo Sanchez *et al.* (BaBar), Phys. Rev. D **83**, 051101 (2011), [arXiv:1012.4044]; J. Lees *et al.* (BaBar), Phys. Rev. D **85**, 072005 (2012), [arXiv:1112.3896].
- [42] R. Aaij *et al.* (LHCb), JHEP **05**, 026 (2019), [arXiv:1812.07008].
- [43] T. Aaltonen *et al.* (CDF), Phys. Rev. Lett. **107**, 261802 (2011), [arXiv:1107.4999].
- [44] R. Aaij *et al.* (LHCb), Phys. Lett. B **713**, 369 (2012), [arXiv:1204.2813]; R. Aaij *et al.* (LHCb), Phys. Rev. D **90**, 05, 052011 (2014), [arXiv:1407.2222]; R. Aaij *et al.* (LHCb), JHEP **12**, 155 (2019), [arXiv:1907.10003]; R. Aaij *et al.* (LHCb) (2023), [arXiv:2304.06198].
- [45] R. Aaij *et al.* (LHCb), Phys. Lett. B **709**, 50 (2012), [arXiv:1111.4183]; R. Aaij *et al.* (LHCb), JHEP **07**, 166 (2015), [arXiv:1503.05362]; R. Aaij *et al.* (LHCb), JHEP **07**, 032 (2019), [arXiv:1905.06662].
- [46] R. Aaij *et al.* (LHCb), JHEP **11**, 092 (2013), [arXiv:1306.2239].
- [47] B. Aubert *et al.* (BaBar), Phys. Rev. Lett. **100**, 081801 (2008), [arXiv:0708.2248]; B. Aubert *et al.* (BaBar), Phys. Rev. D **79**, 051102 (2009), [arXiv:0901.1223].
- [48] G. Burdman, Phys. Rev. D **52**, 6400 (1995), [hep-ph/9505352]; F. Kruger and J. Matias, Phys. Rev. D **71**, 094009 (2005), [hep-ph/0502060]; E. Lunghi and J. Matias, JHEP **04**, 058 (2007), [hep-ph/0612166]; W. Altmannshofer *et al.*, JHEP **01**, 019 (2009), [arXiv:0811.1214]; J. Matias *et al.*, JHEP **04**, 104 (2012), [arXiv:1202.4266]; S. Descotes-Genon *et al.*, JHEP **01**, 048 (2013), [arXiv:1207.2753].
- [49] B. Aubert *et al.* (BaBar), Phys. Rev. D **79**, 031102 (2009), [arXiv:0804.4412]; J. Lees *et al.* (BaBar), Phys. Rev. D **93**, 5, 052015 (2016), [arXiv:1508.07960].
- [50] J.-T. Wei *et al.* (Belle), Phys. Rev. Lett. **103**, 171801 (2009), [arXiv:0904.0770]; S. Wehle *et al.* (Belle), Phys. Rev. Lett. **118**, 11, 111801 (2017), [arXiv:1612.05014]; A. Abdesselam *et al.* (Belle), Phys. Rev. Lett. **126**, 16, 161801 (2021), [arXiv:1904.02440].
- [51] T. Aaltonen *et al.* (CDF), Phys. Rev. Lett. **108**, 081807 (2012), [arXiv:1108.0695].
- [52] S. Chatrchyan *et al.* (CMS), Phys. Lett. B **727**, 77 (2013), [arXiv:1308.3409]; V. Khachatryan *et al.* (CMS), Phys. Lett. B **753**, 424 (2016), [arXiv:1507.08126]; A. M. Sirunyan *et al.* (CMS), Phys. Lett. B **781**, 517 (2018), [arXiv:1710.02846]; A. M. Sirunyan *et al.* (CMS), JHEP **04**, 124 (2021), [arXiv:2010.13968].
- [53] M. Aaboud *et al.* (ATLAS), JHEP **10**, 047 (2018), [arXiv:1805.04000].
- [54] R. Aaij *et al.* (LHCb), JHEP **08**, 131 (2013), [arXiv:1304.6325]; R. Aaij *et al.* (LHCb), JHEP **04**, 064 (2015), [arXiv:1501.03038]; R. Aaij *et al.* (LHCb), JHEP **02**, 104 (2016), [arXiv:1512.04442]; R. Aaij *et al.* (LHCb), JHEP **11**, 047 (2016), [Erratum: JHEP **04**, 142 (2017)], [arXiv:1606.04731]; R. Aaij *et al.* (LHCb), JHEP **12**, 065 (2016), [arXiv:1609.04736]; R. Aaij *et al.* (LHCb), JHEP **08**, 055 (2017), [arXiv:1705.05802]; R. Aaij *et al.* (LHCb), Phys. Rev. Lett. **125**, 1, 011802 (2020), [arXiv:2003.04831]; R. Aaij *et al.* (LHCb), Phys. Rev. Lett. **126**, 16, 161802 (2021), [arXiv:2012.13241]; R. Aaij *et al.* (LHCb), JHEP **09**, 179 (2015), [arXiv:1506.08777]; R. Aaij *et al.* (LHCb), JHEP **11**, 043 (2021), [arXiv:2107.13428]; R. Aaij *et al.* (LHCb), Phys. Rev. Lett. **128**, 19, 191802 (2022), [arXiv:2110.09501]; R. Aaij *et al.* (LHCb), Phys. Rev. D **108**, 3, 032002 (2023), [arXiv:2212.09153].
- [55] C.-H. Chen and H.-N. Li, Phys. Rev. D **71**, 114008 (2005), [hep-ph/0504020].

75. $B^0-\bar{B}^0$ Mixing

Revised March 2024 by O. Schneider (EPFL).

There are two neutral $B^0-\bar{B}^0$ meson systems, $B_d^0-\bar{B}_d^0$ and $B_s^0-\bar{B}_s^0$ (generically denoted $B_q^0-\bar{B}_q^0$, $q = s, d$), which exhibit particle-antiparticle mixing [1]. This mixing phenomenon is described in Ref. [2]. In the following, we adopt the notation introduced in Ref. [2], and assume CPT conservation throughout. In each system, the light (L) and heavy (H) mass eigenstates,

$$|B_{L,H}\rangle = p|B_q^0\rangle \pm q|\bar{B}_q^0\rangle, \quad (75.1)$$

have a mass difference $\Delta m_q = m_H - m_L > 0$, a total decay width difference $\Delta\Gamma_q = \Gamma_L - \Gamma_H$ and an average decay width $\Gamma_q = (\Gamma_L + \Gamma_H)/2$. In the absence of CP violation in the mixing, $|q/p| = 1$, the differences are given by $\Delta m_q = 2|M_{12}|$ and $|\Delta\Gamma_q| = 2|\Gamma_{12}|$, where M_{12} and Γ_{12} are the off-diagonal elements of the mass and decay matrices [2]. The evolution of a pure $|B_q^0\rangle$ or $|\bar{B}_q^0\rangle$ state at $t = 0$ is given by

$$|B_q^0(t)\rangle = g_+(t)|B_q^0\rangle + \frac{q}{p}g_-(t)|\bar{B}_q^0\rangle, \quad (75.2)$$

$$|\bar{B}_q^0(t)\rangle = g_+(t)|\bar{B}_q^0\rangle + \frac{p}{q}g_-(t)|B_q^0\rangle, \quad (75.3)$$

which means that the flavor states remain unchanged (+) or oscillate into each other (-) with time-dependent probabilities proportional to

$$|g_{\pm}(t)|^2 = \frac{e^{-\Gamma_q t}}{2} \left[\cosh\left(\frac{\Delta\Gamma_q}{2}t\right) \pm \cos(\Delta m_q t) \right]. \quad (75.4)$$

In the absence of CP violation, the time-integrated mixing probability $\int |g_-(t)|^2 dt / (\int |g_-(t)|^2 dt + \int |g_+(t)|^2 dt)$ is given by

$$\chi_q = \frac{x_q^2 + y_q^2}{2(x_q^2 + 1)}, \quad \text{where } x_q = \frac{\Delta m_q}{\Gamma_q}, \quad y_q = \frac{\Delta\Gamma_q}{2\Gamma_q}. \quad (75.5)$$

75.1 Standard Model predictions and phenomenology

In the Standard Model, the transitions $B_q^0 \rightarrow \bar{B}_q^0$ and $\bar{B}_q^0 \rightarrow B_q^0$ are due to the weak interaction. They are described, at the lowest order, by box diagrams involving two W bosons and two up-type quarks (see Fig. 75.1), as is the case for $K^0 - \bar{K}^0$ mixing. However, the long range interactions arising from intermediate virtual states are negligible for the neutral B meson systems, because the large B mass is off the region of hadronic resonances. The calculation of the dispersive and absorptive parts of the box diagrams yields the following predictions for the off-diagonal element of the mass and decay matrices [3],

$$M_{12} = -\frac{G_F^2 m_W^2 \eta_B m_{B_q} B_{B_q} f_{B_q}^2}{12\pi^2} S_0(m_t^2/m_W^2) (V_{tq}^* V_{tb})^2, \quad (75.6)$$

$$\Gamma_{12} = \frac{G_F^2 m_b^2 \eta_B' m_{B_q} B_{B_q} f_{B_q}^2}{8\pi} \times \left[(V_{tq}^* V_{tb})^2 + V_{tq}^* V_{tb} V_{cq}^* V_{cb} \mathcal{O}\left(\frac{m_c^2}{m_b^2}\right) + (V_{cq}^* V_{cb})^2 \mathcal{O}\left(\frac{m_c^4}{m_b^4}\right) \right], \quad (75.7)$$

where G_F is the Fermi constant, m_W the W boson mass, and m_i the mass of quark i ; m_{B_q} , f_{B_q} and B_{B_q} are the B_q^0 mass, weak decay constant and bag parameter, respectively. The known function $S_0(x)$ can be approximated very well by $0.784 x_i^{0.76}$ [4], and V_{ij} are the elements of the CKM matrix [5]. The QCD corrections η_B and η_B' are of order unity. The only non-negligible contributions to M_{12} are from box diagrams involving two top quarks. The phases of M_{12} and Γ_{12} satisfy

$$\phi_M - \phi_\Gamma = \pi + \mathcal{O}\left(\frac{m_c^2}{m_b^2}\right), \quad (75.8)$$

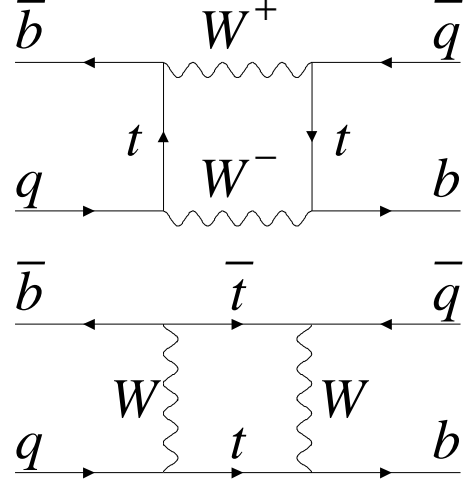


Figure 75.1: Dominant box diagrams for the $B_q^0 \rightarrow \bar{B}_q^0$ transitions ($q = d$ or s). Similar diagrams exist where one or both t quarks are replaced with c or u quarks.

implying that the mass eigenstates have mass and width differences of opposite signs. This means that, like in the $K^0-\bar{K}^0$ system, the heavy state is expected to have a smaller decay width than that of the light state: $\Gamma_H < \Gamma_L$. Hence, $\Delta\Gamma_q = \Gamma_L - \Gamma_H$ is expected to be positive in the Standard Model.

Furthermore, the quantity

$$\left| \frac{\Gamma_{12}}{M_{12}} \right| \simeq \frac{3\pi}{2} \frac{m_b^2}{m_W^2} \frac{1}{S_0(m_t^2/m_W^2)} \sim \mathcal{O}\left(\frac{m_b^2}{m_t^2}\right) \quad (75.9)$$

is small, and a power expansion of $|q/p|^2$ yields

$$\left| \frac{q}{p} \right|^2 = 1 + \left| \frac{\Gamma_{12}}{M_{12}} \right| \sin(\phi_M - \phi_\Gamma) + \mathcal{O}\left(\left| \frac{\Gamma_{12}}{M_{12}} \right|^2\right). \quad (75.10)$$

Therefore, considering both Eqs. (75.8) and (75.9), the CP -violating parameter

$$1 - \left| \frac{q}{p} \right|^2 \simeq \text{Im}\left(\frac{\Gamma_{12}}{M_{12}}\right) \quad (75.11)$$

is expected to be very small: $\sim \mathcal{O}(10^{-3})$ for the $B_d^0-\bar{B}_d^0$ system and $\lesssim \mathcal{O}(10^{-4})$ for the $B_s^0-\bar{B}_s^0$ system [6].

In the approximation of negligible CP violation in mixing, the ratio $\Delta\Gamma_q/\Delta m_q$ is equal to the small quantity $|\Gamma_{12}/M_{12}|$ of Eq. (75.9); it is hence independent of CKM matrix elements, *i.e.*, the same for the $B_d^0-\bar{B}_d^0$ and $B_s^0-\bar{B}_s^0$ systems. Calculations [7] yield $\sim 5 \times 10^{-3}$ with a $\sim 15\%$ uncertainty. Given the published experimental knowledge [8] on the mixing parameter x_q

$$\begin{cases} x_d = 0.7697 \pm 0.0035 & (B_d^0-\bar{B}_d^0 \text{ system}) \\ x_s = 26.99 \pm 0.09 & (B_s^0-\bar{B}_s^0 \text{ system}) \end{cases}, \quad (75.12)$$

the Standard Model thus predicts that $\Delta\Gamma_d/\Gamma_d$ is very small (below 1%), but $\Delta\Gamma_s/\Gamma_s$ considerably larger ($\sim 10\%$). These width differences are caused by the existence of final states to which both the B_q^0 and \bar{B}_q^0 mesons can decay. Such decays involve $b \rightarrow c\bar{c}q$ quark-level transitions, which are Cabibbo-suppressed if $q = d$ and Cabibbo-allowed if $q = s$.

A complete set of Standard Model predictions for all mixing parameters in both the $B_d^0-\bar{B}_d^0$ and $B_s^0-\bar{B}_s^0$ systems can be found in Ref. [7].

75.2 Experimental issues and methods for oscillation analyses

Time-integrated measurements of $B^0-\bar{B}^0$ mixing were published for the first time in 1987 by UA1 [9] and ARGUS [10], and since then by many other experiments. These measurements are typically based on counting same-sign and opposite-sign lepton pairs from the semileptonic decay of the produced $b\bar{b}$ pairs. Such analyses cannot easily separate the contributions from the different b -hadron species, therefore, the clean environment of $\Upsilon(4S)$ machines (where only B_d^0 and charged B_u mesons are produced) is in principle best suited to measure χ_d .

However, better sensitivity is obtained from time-dependent analyses aiming at the direct measurement of the oscillation frequencies Δm_d and Δm_s , from the proper time distributions of B_d^0 or B_s^0 candidates identified through their decay in (mostly) flavor-specific modes, and suitably tagged as mixed or unmixed. This is particularly true for the $B_s^0-\bar{B}_s^0$ system, where the large value of x_s implies maximal mixing, *i.e.*, $\chi_s \simeq 1/2$. In such analyses, the B_d^0 or B_s^0 mesons are either fully reconstructed, partially reconstructed from a charm meson, selected from a lepton with the characteristics of a $b \rightarrow \ell^-$ decay, or selected from a reconstructed displaced vertex. At high-energy colliders (LEP, SLC, Tevatron, LHC), the proper time $t = \frac{m_B}{p}L$ is measured from the distance L between the production vertex and the B decay vertex, and from an estimate of the B momentum p . At asymmetric B factories (SuperKEKB, KEKB, PEP-II), producing $e^+e^- \rightarrow \Upsilon(4S) \rightarrow B_d^0 \bar{B}_d^0$ events with a boost $\beta\gamma$ ($= 0.28, 0.425, 0.55$), the proper time difference between the two B candidates is estimated as $\Delta t \simeq \frac{\Delta z}{\beta\gamma c}$, where Δz is the spatial separation between the two B decay vertices along the boost direction. In all cases, the good resolution needed on the vertex positions is obtained with silicon detectors.

The average statistical significance \mathcal{S} of a B_q^0 oscillation signal can be approximated as [11]

$$\mathcal{S} \approx \sqrt{N/2} f_{\text{sig}} (1 - 2\eta) e^{-(\Delta m_q \sigma_t)^2/2}, \quad (75.13)$$

where N is the number of selected and tagged candidates, f_{sig} is the fraction of signal in that sample, η is the total mistag probability, and σ_t is the resolution on proper time (or proper time difference). The quantity \mathcal{S} decreases very quickly as Δm_q increases; this dependence is controlled by σ_t , which is therefore a critical parameter for Δm_s analyses. At high-energy colliders, the proper time resolution $\sigma_t \sim \frac{m_B}{\langle p \rangle} \sigma_L \oplus t \frac{\sigma_p}{p}$ includes a constant contribution due to the decay length resolution σ_L (typically 0.04–0.3 ps), and a term due to the relative momentum resolution σ_p/p (typically 10–20% for partially reconstructed decays), which increases with proper time. At B factories, the boost of the B mesons is estimated from the known beam energies, and the term due to the spatial resolution dominates (typically 0.7–1.5 ps because of the much smaller B boost).

In order to tag a B_q^0 candidate as mixed or unmixed, it is necessary to determine its flavor both in the initial state and in the final state. The initial and final state mistag probabilities, η_i and η_f , degrade \mathcal{S} by a total factor $(1 - 2\eta) = (1 - 2\eta_i)(1 - 2\eta_f)$. In lepton-based analyses, the final state is tagged by the charge of the lepton from $b \rightarrow \ell^-$ decays; the largest contribution to η_f is then due to $\bar{b} \rightarrow \bar{c} \rightarrow \ell^-$ decays. Alternatively, the charge of a reconstructed charm meson (D^{*-} from B_d^0 or D_s^- from B_s^0), or that of a kaon hypothesized to come from a $b \rightarrow c \rightarrow s$ decay [12], can be used. For fully-inclusive analyses based on topological vertexing, final-state tagging techniques include jet-charge [13] and charge-dipole [14, 15] methods. At high-energy colliders, the methods to tag the initial state (*i.e.*, the state at production), can be divided into two groups: the ones that tag the initial charge of the \bar{b} quark contained in the B_q^0 candidate itself (same-side tag), and the ones that tag the initial charge of the other b quark produced in the event (opposite-side tag). On the same side, the sign of a charged pion, kaon or proton from the primary vertex is correlated with the production state of the B_q^0 meson if that particle is a decay product of a B^{**} state or the first in the fragmentation chain [16, 17]. Jet- and vertex-charge

techniques work on both sides and on the opposite side, respectively. Finally, the charge of a lepton from $b \rightarrow \ell^-$, of a kaon from $b \rightarrow c \rightarrow s$ or of a charm hadron from $b \rightarrow c$ [18] can be used as an opposite-side tag, keeping in mind that its performance is degraded due to integrated mixing. At SLC, the beam polarization produced a sizeable forward-backward asymmetry in the $Z \rightarrow b\bar{b}$ decays, and provided another very interesting and effective initial state tag based on the polar angle of the B_q^0 candidate [14]. Initial state tags have also been combined to reach $\eta_i \sim 26\%$ at LEP [17, 19] or 22% at SLD [14] with full efficiency. In the case $\eta_f = 0$, this corresponds to an effective tagging efficiency $Q = \epsilon D^2 = \epsilon(1 - 2\eta)^2$, where ϵ is the tagging efficiency, in the range 23–31%. The equivalent figure achieved by CDF during Tevatron Run I was $\sim 3.5\%$ (see tagging summary on page 160 of Ref. [20]), reflecting the fact that tagging is more difficult at hadron colliders. The CDF and DØ analyses of Tevatron Run II data reached $\epsilon D^2 = (1.8 \pm 0.1)\%$ [21] and $(2.5 \pm 0.2)\%$ [22] for opposite-side tagging, while same-side kaon tagging (for B_s^0 analyses) contributed an additional 3.7–4.8% at CDF [21], and pushed the combined performance to $(4.7 \pm 0.5)\%$ at DØ [23]. LHCb, operating in the forward region at the LHC where the environment is different in terms of track multiplicity and b -hadron production kinematics, has reported $\epsilon D^2 = (2.10 \pm 0.25)\%$ [24] for opposite-side tagging, $(1.80 \pm 0.26)\%$ [25] for same-side kaon tagging, and $(2.11 \pm 0.11)\%$ [26] for same-side pion and proton tagging: the combined figure ranges typically between $(3.73 \pm 0.15)\%$ [27] and $(6.3 \pm 0.5)\%$ [28] depending on the mode in which the tagged B_s^0 meson is reconstructed, and reaches up to $(8.1 \pm 0.6)\%$ [29] for hadronic B_d^0 modes. ATLAS [30] and CMS [31] have reported $\epsilon D^2 \sim 1.75\%$ and $\epsilon D^2 \sim 10\%$ using opposite-side tagging of $B_s^0 \rightarrow J/\psi\phi$ decays.

At B factories, the flavor of a B_d^0 meson at production cannot be determined, since the two neutral B mesons produced in a $\Upsilon(4S)$ decay evolve in a coherent P -wave state where they keep opposite flavors at any time. However, as soon as one of them decays, the other follows a time-evolution given by Eqs. (75.2) or (75.3), where t is replaced with Δt (which will take negative values half of the time). Hence, the “initial state” tag of a B can be taken as the final-state tag of the other B . Effective tagging efficiencies of 30% are achieved by BaBar and Belle [32], using different techniques including $b \rightarrow \ell^-$ and $b \rightarrow c \rightarrow s$ tags. It is worth noting that, in this case, mixing of the other B (*i.e.*, the coherent mixing occurring before the first B decay) does not contribute to the mistag probability.

Before the experimental observation of a decay-width difference, oscillation analyses typically neglected $\Delta\Gamma_q$ in Eq. (75.4), and described the time dependence with the functions $\Gamma_q e^{-\Gamma_q t} (1 \pm \cos(\Delta m_q t))/2$ (high-energy colliders) or $\Gamma_d e^{-\Gamma_d |\Delta t|} (1 \pm \cos(\Delta m_d \Delta t))/4$ (asymmetric $\Upsilon(4S)$ machines). As can be seen from Eq. (75.4), a non-zero value of $\Delta\Gamma_q$ would effectively reduce the oscillation amplitude with a small time-dependent factor that would be very difficult to distinguish from time resolution effects. Measurements of Δm_q are usually extracted from the data using a maximum likelihood fit.

75.3 Δm_d and $\Delta\Gamma_d$ measurements

Many $B_d^0-\bar{B}_d^0$ oscillations analyses have been published [33] by the ALEPH [34], DELPHI [15, 35], L3 [36], OPAL [37, 38], CDF [16], DØ [22], BaBar [39], Belle [40], Belle II [41], and LHCb [42–45] collaborations. Although a variety of different techniques have been used, the individual Δm_d results obtained at LEP and Tevatron have remarkably similar precision. Their average is compatible with the more precise measurements at the asymmetric B factories and the LHC. The systematic uncertainties are not negligible; they are often dominated by sample composition, mistag probability, or b -hadron lifetime contributions. Before being combined, the measurements are adjusted on the basis of a common set of input values, including the b -hadron lifetimes and fractions published in this *Review*. Some measurements are statistically correlated. Systematic correlations arise both from common physics sources (fragmentation fractions, lifetimes, branching ratios of b hadrons), and from purely experimental or algorithmic effects (efficiency, resolu-

tion, tagging, background description). Combining all measurements [15, 16, 22, 34–45] and accounting for all identified correlations yields $\Delta m_d = 0.5069 \pm 0.0016(\text{stat}) \pm 0.0011(\text{syst}) \text{ ps}^{-1}$ [8], a result dominated by the latest LHCb measurement with $B^0 \rightarrow D^{(*)-} \mu^+ \nu_\mu X$ decays [45].

On the other hand, ARGUS and CLEO have published time-integrated measurements [46–48], which average to $\chi_d = 0.182 \pm 0.015$. Following Ref. [48], the width difference $\Delta\Gamma_d$ could in principle be extracted from the measured value of $1/\Gamma_d$ and the above averages for Δm_d and χ_d (see Eq. (75.5)), provided that $\Delta\Gamma_d$ has a negligible impact on the Δm_d and $1/\Gamma_d$ analyses that have assumed $\Delta\Gamma_d = 0$. However, $\Delta\Gamma_d/\Gamma_d$ is too small and the knowledge of χ_d too imprecise to provide useful sensitivity on $\Delta\Gamma_d/\Gamma_d$. Direct time-dependent studies published by DELPHI [15], BaBar [49], Belle [50], LHCb [51], ATLAS [52] and CMS [53] provide stronger constraints, which can be combined to yield [8]

$$\Delta\Gamma_d/\Gamma_d = +0.001 \pm 0.010. \quad (75.14)$$

This determination is compatible both with zero and with the Standard Model prediction of $(4.0 \pm 0.9) \times 10^{-3}$ [54].

Assuming $\Delta\Gamma_d = 0$ and no CP violation in mixing, and using the B_d^0 lifetime average of $1.517 \pm 0.004 \text{ ps}$ [8], the Δm_d and χ_d results are combined to yield the world average

$$\Delta m_d = 0.5069 \pm 0.0019 \text{ ps}^{-1} \quad (75.15)$$

or, equivalently,

$$\chi_d = 0.1860 \pm 0.0011. \quad (75.16)$$

This Δm_d value provides an estimate of $2|M_{12}|$, and can be used with Eq. (75.6) to extract $|V_{td}|$ within the Standard Model [55]. The main experimental uncertainties on the result come from m_t and Δm_d , but are still completely negligible with respect to the uncertainty due to the hadronic matrix element $f_{B_d} \sqrt{B_{B_d}} = 225 \pm 9 \text{ MeV}$ [56] obtained from three-flavor lattice QCD calculations.

75.4 Δm_s and $\Delta\Gamma_s$ measurements

After many years of intense search at LEP and SLC, B_s^0 - \bar{B}_s^0 oscillations were first observed in 2006 by CDF using 1 fb^{-1} of Tevatron Run II data [21]. LHCb then observed B_s^0 - \bar{B}_s^0 oscillations independently with $B_s^0 \rightarrow D_s^- \pi^+$ [42, 57], $B_s^0 \rightarrow D_s^- \mu^+ \nu X$ [44] and $B_s^0 \rightarrow J/\psi K^+ K^-$ [27] decays using up to 3 fb^{-1} of LHC Run 1 data. More recently measurements based on additional LHC Run 2 data have been published by CMS with $B_s^0 \rightarrow J/\psi \phi$ decays [31], and by LHCb with $B_s^0 \rightarrow D_s^- \pi^+ \pi^- \pi^+$ [58], $B_s^0 \rightarrow D_s^- \pi^+$ [59] and $B_s^0 \rightarrow J/\psi K^+ K^-$ [60] decays. Taking systematic correlations into account, the average [8] of all published measurements of Δm_s [21, 27, 31, 42, 44, 57–60] is

$$\Delta m_s = 17.765 \pm 0.004(\text{stat}) \pm 0.004(\text{syst}) \text{ ps}^{-1}, \quad (75.17)$$

with an impressive precision dominated by the most recent $B_s^0 \rightarrow D_s^- \pi^+$ result [59] (see Fig. 75.2).

The information on $|V_{ts}|$ obtained in the framework of the Standard Model is hampered by the hadronic uncertainty, as in the B_d^0 case. However, several uncertainties cancel in the frequency ratio

$$\frac{\Delta m_s}{\Delta m_d} = \frac{m_{B_s}}{m_{B_d}} \xi^2 \left| \frac{V_{ts}}{V_{td}} \right|^2, \quad (75.18)$$

where the SU(3) flavor-symmetry breaking factor $\xi = (f_{B_s} \sqrt{B_{B_s}})/(f_{B_d} \sqrt{B_{B_d}})$ is obtained as 1.206 ± 0.017 from a combination of three-flavor lattice QCD calculations [56] dominated by the results of Ref. [61], or as $1.2014^{+0.0065}_{-0.0072}$ from QCD sum rules [62]. Using the measurements of Eqs. (75.15) and (75.17), one can extract

$$\left| \frac{V_{td}}{V_{ts}} \right| = \begin{cases} 0.2054 \pm 0.0004 \pm 0.0029 \text{ (lattice QCD)} \\ 0.2045 \pm 0.0004^{+0.0011}_{-0.0012} \text{ (QCD sum rules)} \end{cases}, \quad (75.19)$$

in good agreement with (but much more precise than) the value obtained from the ratio of the $b \rightarrow d\gamma$ and $b \rightarrow s\gamma$ transition rates observed at the B factories [55].

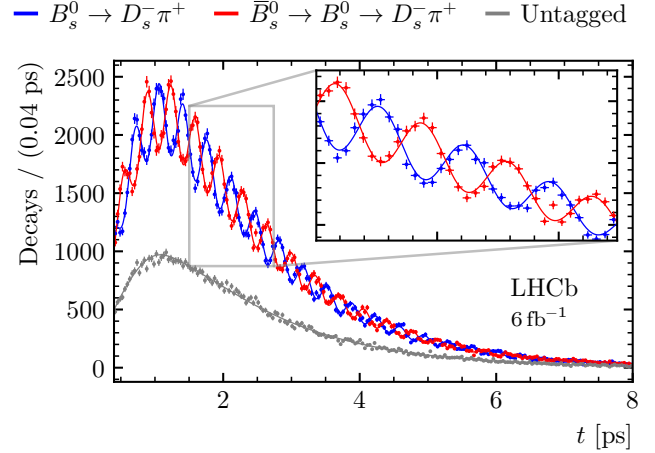


Figure 75.2: Proper decay-time distributions of background-subtracted $B_s^0 \rightarrow D_s^- \pi^+$ decays tagged as unmixed (blue), tagged as mixed (red) or untagged (grey) in the Run 2 data of the LHCb experiment, displaying B_s^0 - \bar{B}_s^0 oscillations [59].

The CKM matrix can be constrained using experimental results on observables such as Δm_d , Δm_s , $|V_{ub}/V_{cb}|$, ϵ_K , and $\sin(2\beta)$ together with theoretical inputs and unitarity conditions [55, 63, 64]. The constraint from our knowledge on the ratio $\Delta m_s/\Delta m_d$ is more effective in limiting the position of the apex of the CKM unitarity triangle than the one obtained from the Δm_d measurements alone, due to the reduced hadronic uncertainty in Eq. (75.18). We also note that the experimental value of Δm_s from Eq. (75.17) is consistent with the Standard Model predictions obtained from CKM fits where no experimental information on Δm_s is used, e.g., $17.89 \pm 0.65 \text{ ps}^{-1}$ [63] or $17.26^{+0.63}_{-0.41} \text{ ps}^{-1}$ [64]. It is also consistent with the prediction $18.23 \pm 0.62 \text{ ps}^{-1}$ from Ref. [7].

Information on $\Delta\Gamma_s$ can be obtained from the study of the proper time distribution of untagged B_s^0 samples [65]. In the case of an inclusive B_s^0 selection [66], or a flavor-specific (semileptonic or hadronic) B_s^0 decay selection [19, 67–69], both the short- and long-lived components are present, and the proper decay-time distribution is a superposition of two exponentials with decay constants $\Gamma_{L,H} = \Gamma_s \pm \Delta\Gamma_s/2$. In principle, this provides sensitivity to both Γ_s and $(\Delta\Gamma_s/\Gamma_s)^2$. Ignoring $\Delta\Gamma_s$ and fitting for a single exponential leads to an estimate of $1/\Gamma_s$ (called effective lifetime) with a relative bias proportional to $(\Delta\Gamma_s/\Gamma_s)^2$. An alternative approach, sensitive to first order in $\Delta\Gamma_s/\Gamma_s$, is to determine the effective lifetime of untagged B_s^0 decays to pure CP eigenstates; measurements exist for $B_s^0 \rightarrow D_s^+ D_s^-$ [68], $B_s^0 \rightarrow K^+ K^-$ [69, 70], $B_s^0 \rightarrow J/\psi \eta$ [71, 72], $B_s^0 \rightarrow J/\psi f_0(980)$ [73], $B_s^0 \rightarrow J/\psi \pi^+ \pi^-$ [53, 74, 75], $B_s^0 \rightarrow J/\psi K_S^0$ [76], and $B_s^0 \rightarrow \mu^+ \mu^-$ [77]. The extraction of $1/\Gamma_s$ and $\Delta\Gamma_s$ from such measurements, discussed in detail in Ref. [78], requires additional information in the form of theoretical assumptions or external inputs on weak phases and hadronic parameters. In what follows, we only use the effective lifetimes of decays to CP -even ($D_s^+ D_s^-$, $J/\psi \eta$) and CP -odd ($J/\psi f_0(980)$, $J/\psi \pi^+ \pi^-$) final states where CP conservation can be assumed. In addition $\Delta\Gamma_s$ can be extracted from the decay-time distributions of B_s^0 decays to CP -even and CP -odd final states, as has been done by LHCb with $B_s^0 \rightarrow J/\psi \eta'$ and $B_s^0 \rightarrow J/\psi \pi^+ \pi^-$, respectively [79].

The best sensitivity to $1/\Gamma_s$ and $\Delta\Gamma_s$ is achieved by the time-dependent measurements of the $B_s^0 \rightarrow J/\psi K^+ K^-$ (including $B_s^0 \rightarrow J/\psi \phi$) and $B_s^0 \rightarrow \psi(2S) \phi$ decay rates performed at CDF [80], DØ [81], ATLAS [30, 82], CMS [31, 83] and LHCb [27, 60, 84–86], where the CP -even and CP -odd amplitudes are separated statistically through a full angular analysis (see Fig. 75.3). The LHCb collaboration analyzes the $B_s^0 \rightarrow J/\psi K^+ K^-$ decay considering that the $K^+ K^-$ system can be in a P-wave or S-wave state, and measures the dependence of the strong phase difference between the P-wave and S-wave amplitudes as a function of the $K^+ K^-$ invariant mass [27, 60, 87];

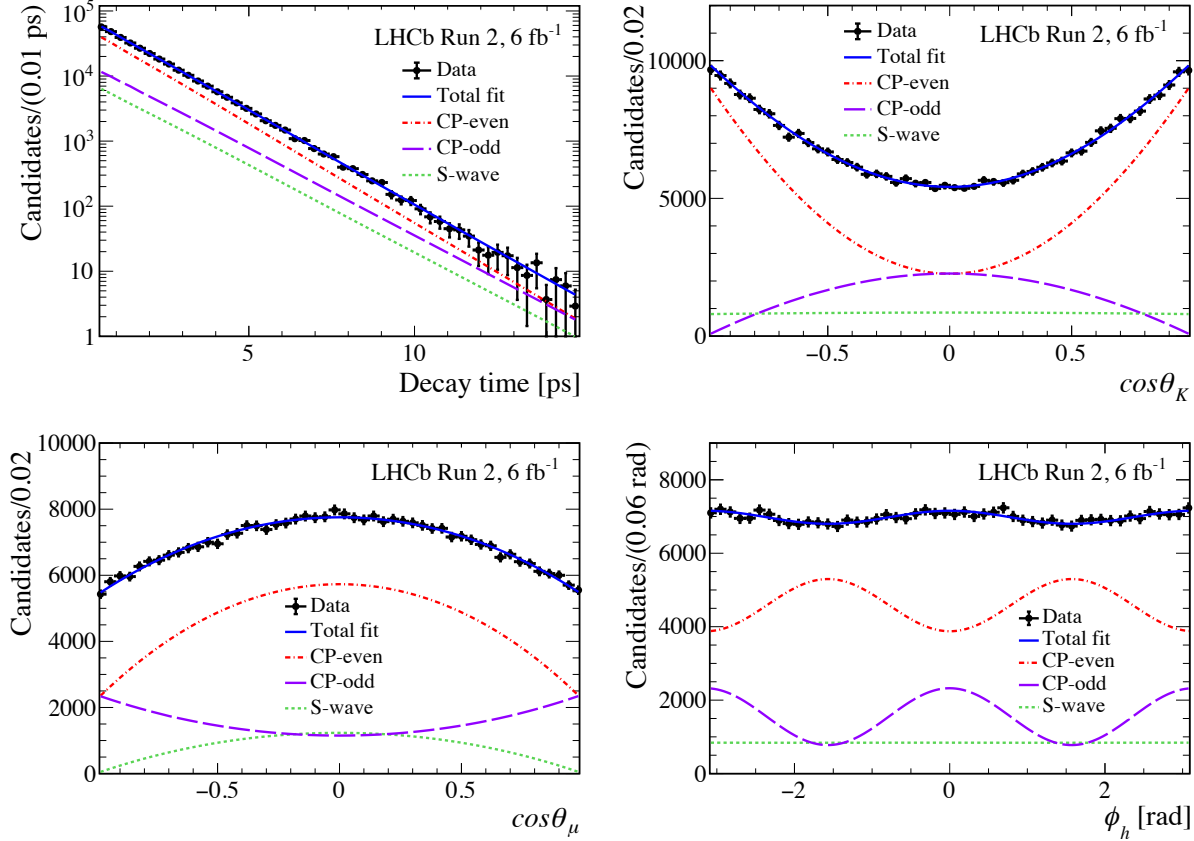


Figure 75.3: Distributions of the proper decay-time and of the three decay angles of background-subtracted $B_s^0 \rightarrow J/\psi K^+ K^-$ decays reconstructed by LHCb in the vicinity of the ϕ resonance [60]. The kaon pair is predominantly in a P-wave state (from the ϕ decay) which can be CP-even or CP-odd, while a small S-wave state is CP-odd. The curves show the projections of a four-dimensional fit allowing the various components to be disentangled. The different lifetimes of the CP-even and CP-odd components is evident from the decay-time distribution.

this allows the unambiguous determination of the sign of $\Delta\Gamma_s$, which is found to be positive. All these studies use both untagged and tagged B_s^0 candidates and are optimized for the measurement of the phase $\phi_s^{c\bar{c}s}$ that describes CP violation in the interference between $B_s^0-\bar{B}_s^0$ mixing and decay in $b \rightarrow c\bar{c}s$ transitions. The published $B_s^0 \rightarrow J/\psi K^+ K^-$, $J/\psi\phi$ and $\psi(2S)\phi$ analyses [27, 30, 31, 60, 80–86] are combined in a multi-dimensional fit including all measured parameters and their correlations. To account for a tension in the time and angular parameters, scale factors are applied on the combined uncertainty of each parameter where a discrepancy arise. For example, the scale factors on the uncertainties of $\Delta\Gamma_s$, Γ_s and $\phi_s^{c\bar{c}s}$ are 1.84, 2.45 and 1.00, respectively. The averages are then further refined by applying constraints from the published lifetime measurements with flavor-specific [19, 67–69] and pure CP [53, 68, 71–75] final states, to yield [8, 88]

$$\Delta\Gamma_s = +0.083 \pm 0.005 \text{ ps}^{-1} \text{ and } 1/\Gamma_s = 1.520 \pm 0.005 \text{ ps}, \quad (75.20)$$

or, equivalently,

$$1/\Gamma_L = 1.429 \pm 0.006 \text{ ps} \text{ and } 1/\Gamma_H = 1.622 \pm 0.008 \text{ ps}, \quad (75.21)$$

in good agreement with the Standard Model predictions $\Delta\Gamma_s^{\text{SM}} = +0.091 \pm 0.015 \text{ ps}^{-1}$ [7] and $\Delta\Gamma_s^{\text{SM}} = +0.076 \pm 0.017 \text{ ps}^{-1}$ [89]. Estimates of $\Delta\Gamma_s/\Gamma_s$ obtained from measurements of the $B_s^0 \rightarrow D_s^{(*)+} D_s^{(*)-}$ branching fractions are not included in the average, since they are based on the questionable [90] assumption that these decays account for all CP -even final states.

From Eqs. (75.5), (75.17) and (75.20), one gets

$$\chi_s = 0.499318 \pm 0.000005. \quad (75.22)$$

75.5 CP -violation studies

Evidence for CP violation in $B_q^0-\bar{B}_q^0$ mixing has been searched for, both with flavor-specific and inclusive B_q^0 decays, in samples where the initial flavor state is tagged, usually with a lepton from the other b -hadron in the event. In the case of semileptonic (or other flavor-specific) decays, where the final-state tag is also available, the following asymmetry [2]

$$\mathcal{A}_{\text{SL}}^q = \frac{N(\bar{B}_q^0(t) \rightarrow \ell^+ \nu_\ell X) - N(B_q^0(t) \rightarrow \ell^- \bar{\nu}_\ell X)}{N(\bar{B}_q^0(t) \rightarrow \ell^+ \nu_\ell X) + N(B_q^0(t) \rightarrow \ell^- \bar{\nu}_\ell X)} \simeq 1 - |q/p|_q^2 \quad (75.23)$$

has been measured either in time-integrated analyses at CLEO [48, 91], BaBar [92], CDF [93], DØ [94–96] and LHCb [97], or in time-dependent analyses at LEP [38, 98], BaBar [49, 99] and Belle [100]. In the inclusive case, also investigated at LEP [98, 101], no final-state tag is used, and the asymmetry [102]

$$\begin{aligned} & \frac{N(\bar{B}_q^0(t) \rightarrow \text{all}) - N(B_q^0(t) \rightarrow \text{all})}{N(\bar{B}_q^0(t) \rightarrow \text{all}) + N(B_q^0(t) \rightarrow \text{all})} \\ & \simeq \mathcal{A}_{\text{SL}}^q \left[\sin^2 \left(\frac{\Delta m_q t}{2} \right) - \frac{x_q}{2} \sin(\Delta m_q t) \right] \end{aligned} \quad (75.24)$$

must be measured as a function of the proper time to extract information on CP violation. In addition LHCb has studied the time dependence of the charge asymmetry of $B^0 \rightarrow D^{(*)-} \mu^+ \nu_\mu X$ decays without tagging the initial state [103], which would be equal to

$$\frac{N(D^{(*)-} \mu^+ \nu_\mu X) - N(D^{(*)+} \mu^- \bar{\nu}_\mu X)}{N(D^{(*)-} \mu^+ \nu_\mu X) + N(D^{(*)+} \mu^- \bar{\nu}_\mu X)} = \mathcal{A}_{\text{SL}}^d \frac{1 - \cos(\Delta m_d t)}{2} \quad (75.25)$$

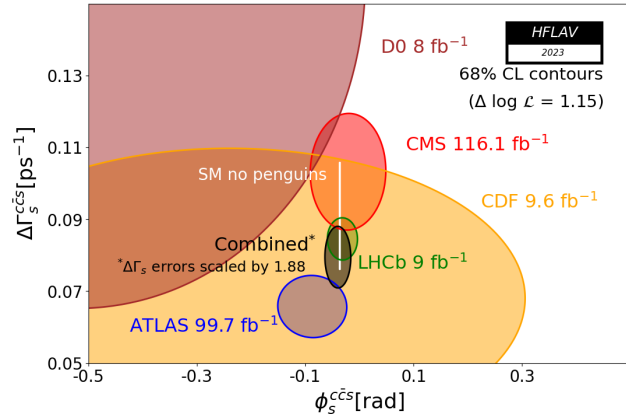


Figure 75.4: 68% CL contours in the $(\phi_s^{ccs}, \Delta\Gamma_s)$ plane, showing all measurements from CDF [80], DØ [81], ATLAS [30, 82], CMS [31, 83] and LHCb [27, 60, 75, 84–86, 104, 105] using B_s^0 decays governed by the $b \rightarrow c\bar{c}s$ transition. Their average [8] is represented as the black ellipse, where the combined uncertainty on $\Delta\Gamma_s$ has been multiplied by 1.88. The very thin white rectangle represents the Standard Model predictions of $-2\beta_s$ [63, 64] and $\Delta\Gamma_s$ [7].

in absence of detection and production asymmetries.

The DØ collaboration measured a like-sign dimuon charge asymmetry in semileptonic b decays that deviates by 2.8σ from the tiny Standard Model prediction and concluded, from a more refined analysis in bins of muon impact parameters, that the overall discrepancy is at the level of 3.6σ [94]. In all other cases, asymmetries compatible with zero (and the Standard Model [7]) have been found, with a precision limited by the available statistics. Several of the analyses at high energy don’t disentangle the B_d^0 and B_s^0 contributions, and either quote a mean asymmetry or a measurement of $\mathcal{A}_{\text{SL}}^d$ assuming $\mathcal{A}_{\text{SL}}^s = 0$: we no longer include these in the average. An exception is the dimuon DØ analysis [94], which separates the two contributions by exploiting their dependence on the muon impact parameter cut. The resulting measurements of $\mathcal{A}_{\text{SL}}^d$ and $\mathcal{A}_{\text{SL}}^s$ are then both compatible with the Standard Model. They are also correlated. We therefore perform a two-dimensional average of the measurements of Refs. [48, 49, 91, 92, 94–97, 99, 100, 103] and obtain [8]

$$\mathcal{A}_{\text{SL}}^d = -0.0021 \pm 0.0017 \Leftrightarrow |q/p|_d = 1.0010 \pm 0.0008, \quad (75.26)$$

$$\mathcal{A}_{\text{SL}}^s = -0.0006 \pm 0.0028 \Leftrightarrow |q/p|_s = 1.0003 \pm 0.0014, \quad (75.27)$$

with a correlation coefficient of -0.054 between $\mathcal{A}_{\text{SL}}^d$ and $\mathcal{A}_{\text{SL}}^s$. These results show no evidence of CP violation and are compatible with the very small Standard Model predictions, $\mathcal{A}_{\text{SL}}^{d,\text{SM}} = -(5.1 \pm 0.5) \times 10^{-4}$ and $\mathcal{A}_{\text{SL}}^{s,\text{SM}} = +(2.2 \pm 0.2) \times 10^{-5}$ [7], but have insufficient precision yet to constrain the Standard Model.

CP violation induced by $B_s^0-\bar{B}_s^0$ mixing in $b \rightarrow c\bar{c}s$ decays is controlled by the small weak phase ϕ_s^{ccs} . Measuring ϕ_s^{ccs} requires tagging the initial flavour of the decaying B_s^0 meson. In addition to the previously mentioned $B_s^0 \rightarrow J/\psi K^+ K^-$ (including $B_s^0 \rightarrow J/\psi\phi$) and $B_s^0 \rightarrow \psi(2S)\phi$ studies, the decay modes $B_s^0 \rightarrow J/\psi\pi^+\pi^-$ (including $B_s^0 \rightarrow J/\psi f_0(980)$) [75, 105] and $B_s^0 \rightarrow D_s^+ D_s^-$ [104] have also been analyzed by LHCb to measure ϕ_s^{ccs} , without the need for an angular analysis. The $J/\psi\pi^+\pi^-$ final state has been shown indeed to be (very close to) a pure CP -odd state [106]. In the $B_s^0 \rightarrow J/\psi\phi$ and $B_s^0 \rightarrow J/\psi K^+ K^-$ analyses, ϕ_s^{ccs} is obtained together with several other observables, including $\Delta\Gamma_s$, Γ_s , the longitudinal and perpendicular ϕ polarisation amplitudes, the S-wave amplitude, and strong phases. In order to account for all correlations, the full sets of measurements provided by the different analyses are combined in a multi-dimensional fit [8] of which ϕ_s^{ccs} is just one of the free parameters. As already mentioned the $B_s^0 \rightarrow J/\psi\phi$ analyses of ATLAS, CMS and LHCb show a poor overall compatibility, mostly in the lifetime and angular parameters, corresponding approximately to

3 standard deviations. Therefore, scale factors are applied on the combined uncertainty of each parameter where a discrepancy arises. For the parameters already in agreement, such as ϕ_s^{ccs} , no scale factor is applied. The combined result based on all published analyses [27, 30, 31, 60, 75, 80–86, 104, 105] is

$$\phi_s^{ccs} = -0.040 \pm 0.016. \quad (75.28)$$

A two-dimensional projection of the overall situation in the $(\phi_s^{ccs}, \Delta\Gamma_s)$ plane is shown in Fig. 75.4. The experimental determination of ϕ_s^{ccs} is still statistically limited. It is consistent with the Standard Model prediction, which is equal to $-2\beta_s = -2\arg(-V_{ts}V_{tb}^*)/(V_{cs}V_{cb}^*) = -0.0367 \pm 0.0010$ [63] or $-0.0376^{+0.0006}_{-0.0005}$ [64] assuming negligible Penguin pollution.

CP violation induced by $B_s^0-\bar{B}_s^0$ mixing in $b \rightarrow s\bar{s}s$ decays is controlled by the weak phase ϕ_s^{sss} , which is an observable different from ϕ_s^{ccs} . In the Standard Model, such pure gluonic Penguin decays have an amplitude with a CKM phase that cancels that of the mixing amplitude, and hence ϕ_s^{sss} is expected to be essentially zero. LHCb has performed a flavour-tagged time-dependent angular analysis of $B_s^0 \rightarrow \phi\phi$ decays [28, 107], similar to that of $B_s^0 \rightarrow J/\psi\phi$ decays, and measured

$$\phi_s^{sss} = -0.074 \pm 0.069, \quad (75.29)$$

in agreement with the Standard Model prediction.

75.6 Summary

$B^0-\bar{B}^0$ mixing has been and still is a field of intense study. The mass differences in the $B_d^0-\bar{B}_d^0$ and $B_s^0-\bar{B}_s^0$ systems are known to relative precisions of 0.38% and 0.03%, respectively. The non-zero decay width difference in the $B_s^0-\bar{B}_s^0$ system is well established, with a relative difference of $\Delta\Gamma_s/\Gamma_s = (12.7 \pm 0.7)\%$, meaning that the heavy state of the $B_s^0-\bar{B}_s^0$ system lives $\sim 14\%$ longer than the light state. In contrast, the relative decay width difference in the $B_d^0-\bar{B}_d^0$ system, $\Delta\Gamma_d/\Gamma_d = (0.1 \pm 1.0)\%$, is still consistent with zero. CP violation in $B_d^0-\bar{B}_d^0$ or $B_s^0-\bar{B}_s^0$ mixing has not been observed yet, with precisions on the semileptonic asymmetries below 0.3%. CP violation induced by $B_s^0-\bar{B}_s^0$ mixing in B_s^0 decays has not yet been observed either, with uncertainties on the ϕ_s^{ccs} and ϕ_s^{sss} phases of 16 mrad and 69 mrad, respectively. All observations so far remain consistent with the Standard Model expectations.

However, the measurements where New Physics might show up are still statistically limited. More results are awaited from the LHC experiments and Belle II, with promising prospects for the investigation of the CP -violating phase $\arg(-M_{12}/\Gamma_{12})$ and improved determination of the ϕ_s^{ccs} and ϕ_s^{sss} phases.

Mixing studies have clearly reached the stage of precision measurements, where much effort is needed, both on the experimental and theoretical sides, in particular to further reduce the hadronic uncertainties of lattice QCD calculations. In the long term, a stringent check of the consistency of the B_d^0 and B_s^0 mixing amplitudes (magnitudes and phases) with all other measured flavor-physics observables will be possible within the Standard Model, leading to very tight limits on (or otherwise a long-awaited surprise about) New Physics.

References

- [1] T. D. Lee and C. S. Wu, *Ann. Rev. Nucl. Part. Sci.* **16**, 511 (1966); I. I. Bigi and A. I. Sanda, *Camb. Monogr. Part. Phys. Nucl. Phys. Cosmol.* **9**, 1 (2009), second edition, first published in 2000; G. C. Branco, L. Lavoura and J. P. Silva, *Int. Ser. Monogr. Phys.* **103**, 1 (1999).
- [2] See the review on CP violation in the quark sector by T. Gershon and Y. Nir in this publication.
- [3] A. J. Buras, W. Slominski and H. Steger, *Nucl. Phys.* **B245**, 369 (1984).
- [4] T. Inami and C. S. Lim, *Prog. Theor. Phys.* **65**, 297 (1981), erratum *ibid.* **65**, 1772 (1981); for the power-like approximation, see A. J. Buras and R. Fleischer, page 91 in “Heavy

- Flavours II,” eds. A. J. Buras and M. Lindner, Singapore World Scientific (1998).
- [5] M. Kobayashi and T. Maskawa, *Prog. Theor. Phys.* **49**, 652 (1973).
- [6] I. I. Bigi *et al.*, in “*CP violation*,” ed. C. Jarlskog, Singapore World Scientific (1989).
- [7] J. Albrecht, F. Bernlochner, A. Lenz and A. Rusov (2024), [arXiv:2402.04224].
- [8] Y. S. Amhis *et al.* (HFLAV), *Phys. Rev. D* **107**, 052008 (2023), [arXiv:2206.07501]; the combined results on b -hadron lifetimes and mixing parameters published in this *Review* have been obtained by the corresponding subgroup of the Heavy Flavor Averaging (HFLAV) group in March 2024 as updates of the averages published in Chapter 5 of the above paper; for more information, see <https://hflav.web.cern.ch/>.
- [9] C. Albajar *et al.* (UA1), *Phys. Lett.* **B186**, 247 (1987), erratum *ibid.* **B197**, 565 (1987).
- [10] H. Albrecht *et al.* (ARGUS), *Phys. Lett.* **B192**, 245 (1987).
- [11] H. G. Moser and A. Roussarie, *Nucl. Instrum. Meth.* **A384**, 491 (1997).
- [12] SLD collab., SLAC-PUB-7228, SLAC-PUB-7229, and SLAC-PUB-7230, *28th Int. Conf. on High Energy Physics*, Warsaw (1996); J. L. Wittlin, *A measurement of the time dependence of $B_d^0-\bar{B}_d^0$ mixing with kaon tagging*, Ph.D. thesis, Massachusetts U., Amherst (2001), URL <http://wwwlib.umi.com/dissertations/fullcit?p3027272>.
- [13] ALEPH collab., contrib. 596 to *Int. Europhysics Conf. on High Energy Physics*, Jerusalem (1997).
- [14] K. Abe *et al.* (SLD), *Phys. Rev.* **D67**, 012006 (2003), [hep-ex/0209002].
- [15] J. Abdallah *et al.* (DELPHI), *Eur. Phys. J.* **C28**, 155 (2003), [hep-ex/0303032].
- [16] F. Abe *et al.* (CDF), *Phys. Rev. Lett.* **80**, 2057 (1998), [hep-ex/9712004]; F. Abe *et al.* (CDF), *Phys. Rev.* **D59**, 032001 (1999), [hep-ex/9806026]; F. Abe *et al.* (CDF), *Phys. Rev.* **D60**, 051101 (1999); F. Abe *et al.* (CDF), *Phys. Rev.* **D60**, 072003 (1999), [hep-ex/9903011]; T. Affolder *et al.* (CDF), *Phys. Rev.* **D60**, 112004 (1999), [hep-ex/9907053].
- [17] R. Barate *et al.* (ALEPH), *Eur. Phys. J.* **C4**, 367 (1998); R. Barate *et al.* (ALEPH), *Eur. Phys. J.* **C7**, 553 (1999), [hep-ex/9811018].
- [18] R. Aaij *et al.* (LHCb), *JINST* **10**, P10005 (2015), [arXiv:1507.07892].
- [19] P. Abreu *et al.* (DELPHI), *Eur. Phys. J.* **C16**, 555 (2000), [hep-ex/0107077].
- [20] K. Anikeev *et al.* (2002), [hep-ph/0201071].
- [21] A. Abulencia *et al.* (CDF), *Phys. Rev. Lett.* **97**, 242003 (2006), [hep-ex/0609040].
- [22] V. M. Abazov *et al.* (DØ), *Phys. Rev.* **D74**, 112002 (2006), [hep-ex/0609034].
- [23] V. M. Abazov *et al.* (DØ), *Phys. Rev. Lett.* **101**, 241801 (2008), [arXiv:0802.2255].
- [24] R. Aaij *et al.* (LHCb), *Eur. Phys. J.* **C72**, 2022 (2012), [arXiv:1202.4979].
- [25] R. Aaij *et al.* (LHCb), *JINST* **11**, P05010 (2016), [arXiv:1602.07252].
- [26] R. Aaij *et al.* (LHCb), *Eur. Phys. J.* **C77**, 238 (2017), [arXiv:1610.06019].
- [27] R. Aaij *et al.* (LHCb), *Phys. Rev. Lett.* **114**, 041801 (2015), [arXiv:1411.3104].
- [28] R. Aaij *et al.* (LHCb), *Phys. Rev. Lett.* **131**, 17, 171802 (2023), [arXiv:2304.06198].
- [29] R. Aaij *et al.* (LHCb), *Phys. Rev. Lett.* **117**, 261801 (2016), [arXiv:1608.06620].
- [30] G. Aad *et al.* (ATLAS), *Eur. Phys. J.* **C81**, 342 (2021), [arXiv:2001.07115].
- [31] A. M. Sirunyan *et al.* (CMS), *Phys. Lett.* **B816**, 136188 (2021), [arXiv:2007.02434].
- [32] B. Aubert *et al.* (BaBar), *Phys. Rev. Lett.* **94**, 161803 (2005), [hep-ex/0408127]; K. F. Chen *et al.* (Belle), *Phys. Rev.* **D72**, 012004 (2005), [hep-ex/0504023].
- [33] Throughout this document we omit references of results that have been replaced by new published measurements.
- [34] D. Buskulic *et al.* (ALEPH), *Z. Phys.* **C75**, 397 (1997).
- [35] P. Abreu *et al.* (DELPHI), *Z. Phys.* **C76**, 579 (1997).
- [36] M. Acciarri *et al.* (L3), *Eur. Phys. J.* **C5**, 195 (1998).
- [37] G. Alexander *et al.* (OPAL), *Z. Phys.* **C72**, 377 (1996); K. Ackerstaff *et al.* (OPAL), *Z. Phys.* **C76**, 417 (1997), [hep-ex/9707010]; G. Abbiendi *et al.* (OPAL), *Phys. Lett.* **B493**, 266 (2000), [hep-ex/0010013].
- [38] K. Ackerstaff *et al.* (OPAL), *Z. Phys.* **C76**, 401 (1997), [hep-ex/9707009].
- [39] B. Aubert *et al.* (BaBar), *Phys. Rev. Lett.* **88**, 221802 (2002), [hep-ex/0112044]; B. Aubert *et al.* (BaBar), *Phys. Rev.* **D66**, 032003 (2002), [hep-ex/0201020]; B. Aubert *et al.* (BaBar), *Phys. Rev. Lett.* **88**, 221803 (2002), [hep-ex/0112045]; B. Aubert *et al.* (BaBar), *Phys. Rev.* **D67**, 072002 (2003), [hep-ex/0212017]; B. Aubert *et al.* (BaBar), *Phys. Rev.* **D73**, 012004 (2006), [hep-ex/0507054].
- [40] N. C. Hastings *et al.* (Belle), *Phys. Rev.* **D67**, 052004 (2003), [hep-ex/0212033]; Y. Zheng *et al.* (Belle), *Phys. Rev.* **D67**, 092004 (2003), [hep-ex/0211065]; K. Abe *et al.* (Belle), *Phys. Rev.* **D71**, 072003 (2005), erratum *ibid.* **D71**, 079903 (2005), [hep-ex/0408111].
- [41] F. Abudinén *et al.* (Belle II), *Phys. Rev.* **D107**, L091102 (2023), [arXiv:2302.12791].
- [42] R. Aaij *et al.* (LHCb), *Phys. Lett.* **B709**, 177 (2012), [arXiv:1112.4311].
- [43] R. Aaij *et al.* (LHCb), *Phys. Lett.* **B719**, 318 (2013), [arXiv:1210.6750].
- [44] R. Aaij *et al.* (LHCb), *Eur. Phys. J.* **C73**, 2655 (2013), [arXiv:1308.1302].
- [45] R. Aaij *et al.* (LHCb), *Eur. Phys. J.* **C76**, 412 (2016), [arXiv:1604.03475].
- [46] H. Albrecht *et al.* (ARGUS), *Z. Phys.* **C55**, 357 (1992); H. Albrecht *et al.* (ARGUS), *Phys. Lett.* **B324**, 249 (1994).
- [47] J. E. Bartelt *et al.* (CLEO), *Phys. Rev. Lett.* **71**, 1680 (1993).
- [48] B. H. Behrens *et al.* (CLEO), *Phys. Lett.* **B490**, 36 (2000), [hep-ex/0005013].
- [49] B. Aubert *et al.* (BaBar), *Phys. Rev. Lett.* **92**, 181801 (2004), [hep-ex/0311037]; B. Aubert *et al.* (BaBar), *Phys. Rev.* **D70**, 012007 (2004), [hep-ex/0403002].
- [50] T. Higuchi *et al.*, *Phys. Rev.* **D85**, 071105 (2012), [arXiv:1203.0930].
- [51] R. Aaij *et al.* (LHCb), *JHEP* **04**, 114 (2014), [arXiv:1402.2554].
- [52] M. Aaboud *et al.* (ATLAS), *JHEP* **06**, 081 (2016), [arXiv:1605.07485].
- [53] A. M. Sirunyan *et al.* (CMS), *Eur. Phys. J.* **C78**, 457 (2018), erratum *ibid.* **C78**, 561 (2018), [arXiv:1710.08949].
- [54] M. Artuso, G. Borissov and A. Lenz, *Rev. Mod. Phys.* **88**, 045002 (2016), [arXiv:1511.09466].
- [55] See the review on the CKM quark-mixing matrix by A. Cecucci, Z. Ligeti, and Y. Sakai in this publication.
- [56] S. Aoki *et al.* (Flavour Lattice Averaging Group) (2019), [arXiv:1902.08191].
- [57] R. Aaij *et al.* (LHCb), *New J. Phys.* **15**, 053021 (2013), [arXiv:1304.4741].

- [58] R. Aaij *et al.* (LHCb), JHEP **03**, 137 (2021), [arXiv:2011.12041].
- [59] R. Aaij *et al.* (LHCb), Nature Phys. **18**, 1 (2022), [arXiv:2104.04421].
- [60] R. Aaij *et al.* (LHCb), Phys. Rev. Lett. **132**, 051802 (2024), [arXiv:2308.01468].
- [61] A. Bazavov *et al.* (Fermilab Lattice and MILC), Phys. Rev. **D93**, 113016 (2016), [arXiv:1602.03560].
- [62] D. King, A. Lenz and T. Rauh, JHEP **05**, 034 (2019), [arXiv:1904.00940].
- [63] M. Bona *et al.* (UTfit), Rend. Lincei Sci. Fis. Nat. **34**, 37 (2023), [arXiv:2212.03894]; updated results at <http://www.utfit.org/>.
- [64] J. Charles *et al.* (CKMfitter), Phys. Rev. **D91**, 073007 (2015), [arXiv:1501.05013]; updated results at <http://ckmfitter.in2p3.fr/>.
- [65] K. Hartkorn and H. G. Moser, Eur. Phys. J. **C8**, 381 (1999).
- [66] M. Acciarri *et al.* (L3), Phys. Lett. **B438**, 417 (1998).
- [67] D. Buskulic *et al.* (ALEPH), Phys. Lett. **B377**, 205 (1996); K. Ackerstaff *et al.* (OPAL), Phys. Lett. **B426**, 161 (1998), [hep-ex/9802002]; F. Abe *et al.* (CDF), Phys. Rev. **D59**, 032004 (1999), [hep-ex/9808003]; V. M. Abazov *et al.* (DØ), Phys. Rev. Lett. **114**, 062001 (2015), [arXiv:1410.1568]; T. Aaltonen *et al.* (CDF), Phys. Rev. Lett. **107**, 272001 (2011), [arXiv:1103.1864]; R. Aaij *et al.* (LHCb), Phys. Rev. Lett. **113**, 172001 (2014), [arXiv:1407.5873]; R. Aaij *et al.* (LHCb), Phys. Rev. Lett. **119**, 101801 (2017), [arXiv:1705.03475].
- [68] R. Aaij *et al.* (LHCb), Phys. Rev. Lett. **112**, 111802 (2014), [arXiv:1312.1217].
- [69] R. Aaij *et al.* (LHCb), Phys. Lett. **B736**, 446 (2014), [arXiv:1406.7204].
- [70] R. Aaij *et al.* (LHCb), Phys. Lett. **B707**, 349 (2012), [arXiv:1111.0521].
- [71] R. Aaij *et al.* (LHCb), Phys. Lett. **B762**, 484 (2016), [arXiv:1607.06314].
- [72] R. Aaij *et al.* (LHCb), Eur. Phys. J. **C83**, 7, 629 (2023), [arXiv:2206.03088].
- [73] T. Aaltonen *et al.* (CDF), Phys. Rev. **D84**, 052012 (2011), [arXiv:1106.3682]; V. M. Abazov *et al.* (DØ), Phys. Rev. **D94**, 012001 (2016), [arXiv:1603.01302].
- [74] R. Aaij *et al.* (LHCb), Phys. Rev. **D87**, 112010 (2013), [arXiv:1304.2600].
- [75] R. Aaij *et al.* (LHCb), Phys. Lett. **B797**, 134789 (2019), [arXiv:1903.05530].
- [76] R. Aaij *et al.* (LHCb), Nucl. Phys. **B873**, 275 (2013), [arXiv:1304.4500].
- [77] R. Aaij *et al.* (LHCb), Phys. Rev. Lett. **128**, 041801 (2022), [arXiv:2108.09284]; R. Aaij *et al.* (LHCb), Phys. Rev. **D105**, 012010 (2022), [arXiv:2108.09283]; A. Tumasyan *et al.* (CMS), Phys. Lett. **B842**, 137955 (2023), [arXiv:2212.10311]; G. Aad *et al.* (ATLAS), JHEP **09**, 199 (2023), [arXiv:2308.01171].
- [78] R. Fleischer and R. Kneijens, Eur. Phys. J. **C71**, 1789 (2011), [arXiv:1109.5115].
- [79] R. Aaij *et al.* (LHCb), submitted to JHEP, [arXiv:2310.12649].
- [80] T. Aaltonen *et al.* (CDF), Phys. Rev. Lett. **109**, 171802 (2012), [arXiv:1208.2967].
- [81] V. M. Abazov *et al.* (DØ), Phys. Rev. **D85**, 032006 (2012), [arXiv:1109.3166].
- [82] G. Aad *et al.* (ATLAS), Phys. Rev. **D90**, 052007 (2014), [arXiv:1407.1796]; G. Aad *et al.* (ATLAS), JHEP **08**, 147 (2016), [arXiv:1601.03297].
- [83] V. Khachatryan *et al.* (CMS), Phys. Lett. **B757**, 97 (2016), [arXiv:1507.07527].
- [84] R. Aaij *et al.* (LHCb), Eur. Phys. J. **C81**, 1026 (2021), [arXiv:2105.14738].
- [85] R. Aaij *et al.* (LHCb), JHEP **08**, 037 (2017), [arXiv:1704.08217].
- [86] R. Aaij *et al.* (LHCb), Phys. Lett. **B762**, 253 (2016), [arXiv:1608.04855].
- [87] R. Aaij *et al.* (LHCb), Phys. Rev. Lett. **108**, 241801 (2012), [arXiv:1202.4717].
- [88] Including the result of Ref. [79], which has not been accepted by a journal at the time of writing this review, changes $\Delta\Gamma_s$ to $+0.084 \pm 0.004 \text{ ps}^{-1}$ and $1/\Gamma_H$ to $1.623 \pm 0.008 \text{ ps}$.
- [89] M. Gerlach, U. Nierste, P. Reeck, V. Shtabovenko and M. Steinhauser (2024), [arXiv:2403.08316].
- [90] A. Lenz and U. Nierste, JHEP **06**, 072 (2007), [hep-ph/0612167].
- [91] D. E. Jaffe *et al.* (CLEO), Phys. Rev. Lett. **86**, 5000 (2001), [hep-ex/0101006].
- [92] J. P. Lees *et al.* (BaBar), Phys. Rev. Lett. **114**, 081801 (2015), [arXiv:1411.1842].
- [93] F. Abe *et al.* (CDF), Phys. Rev. **D55**, 2546 (1997).
- [94] V. M. Abazov *et al.* (DØ), Phys. Rev. **D89**, 012002 (2014), [arXiv:1310.0447].
- [95] V. M. Abazov *et al.* (DØ), Phys. Rev. **D86**, 072009 (2012), [arXiv:1208.5813].
- [96] V. M. Abazov *et al.* (DØ), Phys. Rev. Lett. **110**, 011801 (2013), [arXiv:1207.1769].
- [97] R. Aaij *et al.* (LHCb), Phys. Rev. Lett. **117**, 061803 (2016), erratum *ibid.* **118**, 129903 (2017), [arXiv:1605.09768].
- [98] R. Barate *et al.* (ALEPH), Eur. Phys. J. **C20**, 431 (2001).
- [99] J. P. Lees *et al.* (BaBar), Phys. Rev. Lett. **111**, 101802 (2013), erratum *ibid.* **111**, 159901 (2013), [arXiv:1305.1575].
- [100] E. Nakano *et al.* (Belle), Phys. Rev. **D73**, 112002 (2006), [hep-ex/0505017].
- [101] G. Abbiendi *et al.* (OPAL), Eur. Phys. J. **C12**, 609 (2000), [hep-ex/9901017].
- [102] M. Beneke, G. Buchalla and I. Dunietz, Phys. Lett. **B393**, 132 (1997), [hep-ph/9609357]; I. Dunietz, Eur. Phys. J. **C7**, 197 (1999), [hep-ph/9806521].
- [103] R. Aaij *et al.* (LHCb), Phys. Rev. Lett. **114**, 041601 (2015), [arXiv:1409.8586].
- [104] R. Aaij *et al.* (LHCb), Phys. Rev. Lett. **113**, 211801 (2014), [arXiv:1409.4619].
- [105] R. Aaij *et al.* (LHCb), Phys. Lett. **B736**, 186 (2014), [arXiv:1405.4140].
- [106] R. Aaij *et al.* (LHCb), Phys. Rev. **D86**, 052006 (2012), [arXiv:1204.5643].
- [107] R. Aaij *et al.* (LHCb), Phys. Rev. **D90**, 052011 (2014), [arXiv:1407.2222].

76. Semileptonic b -Hadron Decays, Determination of V_{cb} , V_{ub}

Revised August 2023 by A.X. El-Khadra (Physics, Illinois U.) and P. Urquijo (School of Phys. U. of Melbourne).

76.1 Introduction

Precision determinations of $|V_{ub}|$ and $|V_{cb}|$ are central to testing the CKM sector of the Standard Model, and complement the measurements of CP asymmetries in B decays. The length of the side of the unitarity triangle opposite the well-measured angle β is proportional to the ratio $|V_{ub}|/|V_{cb}|$; its precise determination is a high priority of the heavy-flavor physics program.

The transitions $b \rightarrow c\ell\bar{\nu}_\ell$ and $b \rightarrow u\ell\bar{\nu}_\ell$ ($\ell = e, \mu$) each provide two avenues for determining these CKM matrix elements, namely through measurements of inclusive decay rates, $\bar{B} \rightarrow X\ell\bar{\nu}_\ell$ with a sum over all possible hadronic states X or of exclusive rates, where the final state hadron is a specific meson ($X = D, D^*, \pi, \rho$ etc.).

Purely leptonic decays, such as $B_c^- \rightarrow \tau\bar{\nu}$, $B^- \rightarrow \tau\bar{\nu}$, and $B^- \rightarrow \mu\bar{\nu}$, provide a third avenue that is theoretically very simple (see the RPP mini-review [1]). However, we do not use this information at present since none of the measurements have reached a competitive level of precision. Hence the results presented here are solely obtained from exclusive and inclusive semileptonic b -hadron decays. This article and the values quoted here update the previous review [2].

The theoretical methods underlying the different determinations of $|V_{qb}|$ are quite mature. The theoretical approach for inclusive determinations uses the fact that the mass m_b of the b quark is large compared to the scale Λ_{QCD} that determines low-energy hadronic physics. Thus the basis for precise calculations is a systematic expansion in powers of Λ/m_b , where $\Lambda \sim 500 - 700$ MeV is a hadronic scale of the order of Λ_{QCD} . Such an expansion can be formulated in the framework of an effective field theory which is described in a separate RPP mini-review [3]. Exclusive determinations rely on non-perturbatively calculated form factors, that encode the low-energy dynamics of the hadronic transition. Here, lattice QCD provides an, in principle, ab-initio method to calculate the non-perturbative QCD contributions to the exclusive decay amplitudes. Thanks to a combination of improved theoretical methods, better algorithms, and large increases in computational power, precise lattice QCD results are now available for the processes that are used in exclusive $|V_{ub}|$ and $|V_{cb}|$ determinations. State-of-the-art lattice QCD calculations are based on gauge-field ensembles that include realistic sea quark effects for degenerate up/down and strange quarks (aka $2 + 1$ -flavor ensembles), and increasingly, also for charm (aka $2 + 1 + 1$ -flavor ensembles). They employ ensembles generated at three (or more) lattice spacings, different spatial volumes, among other parameter variations to allow for quantification of the underlying systematic errors, and include detailed systematic error analyses. This is described in a separate RPP mini-review [4]. The lattice-QCD results discussed in this review are all state-of-the-art with fully quantified uncertainties, and therefore play a central role in exclusive $|V_{qb}|$ determinations. In the case of exclusive $\bar{B} \rightarrow D^{(*)}\ell\bar{\nu}_\ell$ decays, heavy quark symmetry (HQS) and heavy quark effective theory (HQET) yield constraints on the form factors that can be used to improve exclusive $|V_{cb}|$ determinations, especially when lattice QCD form factor results are incomplete, as was the case until very recently for $\bar{B} \rightarrow D^*\ell\bar{\nu}_\ell$. Light-cone sum rules (LCSR) provide another nonperturbative approach to compute form factors. However, while the lattice-QCD results employed in this review have well-quantified uncertainties, LCSR results suffer, in general, from hard-to-quantify systematic errors. The two methods typically provide results in opposite regions of phase space. Lattice-QCD calculations work best at low hadronic recoil or high momentum transfer (q^2) to the leptons, while LCSR calculations provide estimates at high recoil, near $q^2 = 0$. In general, we don't use form factor inputs obtained from LCSR in this review.

The measurements discussed in this review are of branching fractions, ratios of branching fractions, and decay kinematic distributions. The determinations of $|V_{cb}|$ and $|V_{ub}|$ also require a measurement of the total decay widths of the corresponding b hadrons, determined from lifetimes, which is the subject of a

separate RPP mini-review [5]. The measurements of inclusive semileptonic decays relevant to this review come primarily from $e^+e^- B$ factories operating at the $\Upsilon(4S)$ resonance, while the measurements of exclusive semileptonic decays come from both the $e^+e^- B$ factories and from the LHCb experiment at CERN.

Semileptonic B -meson decay amplitudes to electrons and muons are well measured and consistent with Standard Model W -boson exchange. As they are expected to be insensitive to the effects of non-Standard-Model physics, they are used to extract $|V_{qb}|$. However, semileptonic decays to tau-lepton final states, such as $\bar{B} \rightarrow D^{(*)}\tau\bar{\nu}_\tau$, may be sensitive to effects from beyond the Standard Model particles due to the large mass of the τ lepton. The currently observed tensions between Standard Model theory and experiment for these decays indicate that semitauonic decays must be studied further. For rare decays, tests of lepton-flavor universality violations (LFUV) in ratios involving μ/e final states provide CKM-free tests of the SM. These and other flavor dependent angular analyses are also included in this review.

Many of the numerical results quoted in this review have been provided by the Heavy Flavor Averaging Group (HFLAV) [6].

76.2 Determination of $|V_{cb}|$

Summary: The determination of $|V_{cb}|$ from inclusive decays has a relative uncertainty of about 1.5%; the limitations arise mainly from our ignorance of higher-order perturbative and non-perturbative corrections. Exclusive $\bar{B} \rightarrow D^*\ell\bar{\nu}_\ell$ decays provide a determination of $|V_{cb}|$ with a relative precision of about 2%, with comparable contributions from theory and experiment to the total uncertainty; the value determined from $\bar{B} \rightarrow D\ell\bar{\nu}_\ell$ decays is consistent and has an uncertainty of 2.5%. The values obtained from the inclusive and exclusive B decay determinations discussed below are:

$$|V_{cb}| = (42.2 \pm 0.5) \times 10^{-3} \quad (\text{inclusive}) \quad (76.1)$$

$$|V_{cb}| = (39.8 \pm 0.6) \times 10^{-3} \quad (\text{exclusive}). \quad (76.2)$$

An average of these determinations has $p(\chi^2) = 1\%$, so we scale the error by $\sqrt{\chi^2/1} = 3.0$ to find

$$|V_{cb}| = (41.1 \pm 1.2) \times 10^{-3} \quad (\text{average}). \quad (76.3)$$

Given the only marginal consistency, of approximately 3.0σ , this average should be treated with caution.

76.2.1 $|V_{cb}|$ from exclusive decays

Exclusive determinations of $|V_{cb}|$ make use of semileptonic B decays into the ground state charmed mesons D and D^* . The corresponding hadronic matrix elements can be parameterized in terms of six independent form factors, which depend on the variable $w \equiv v \cdot v'$, where v and v' are the four velocities of the initial and final-state hadrons. In the rest frame of the decay this variable corresponds to the Lorentz factor of the final state $D^{(*)}$ meson. Determinations of $|V_{cb}|$ from experimental measurements of $\bar{B} \rightarrow D^{(*)}\ell\bar{\nu}_\ell$ decay rates require precise knowledge of these form factors. Fortunately, lattice QCD results for all relevant form factors, including their recoil dependence, are now available [7–12]. Heavy Quark Symmetry (HQS) [13, 14] predicts that in the infinite mass limit the six form factors collapse into a single one, which is normalized at the “zero recoil point” $w = 1$, the point of maximum momentum transfer to the leptons. Heavy Quark Effective Theory (HQET) provides a framework for obtaining the corrections to the HQS prediction in a systematic expansion in powers of Λ_{QCD}/m_c which is discussed in a separate RPP mini-review [3].

76.2.2 $\bar{B} \rightarrow D^*\ell\bar{\nu}_\ell$

The decay rate for $\bar{B} \rightarrow D^*\ell\bar{\nu}_\ell$, assuming massless leptons, is given by

$$\frac{d\Gamma}{dw}(\bar{B} \rightarrow D^*\ell\bar{\nu}_\ell) = \frac{G_F^2 m_B^5}{48\pi^3} |V_{cb}|^2 |\eta_{\text{EW}}|^2 (w^2 - 1)^{1/2} P(w) |\mathcal{F}(w)|^2, \quad (76.4)$$

where $P(w)$ is a phase space factor,

$$P(w) = r^3(1-r)^2(w+1)^2 \left(1 + \frac{4w}{w+1} \frac{1-2rw+r^2}{(1-r)^2} \right), \quad (76.5)$$

with $r = m_{D^*}/m_B$. The decay amplitude $\mathcal{F}(w)$ can be expressed in terms of the form factors which parametrize the vector and axial vector current matrix elements

$$\frac{\langle D^*(v', \epsilon) | \bar{c} \gamma^\mu b | B(v) \rangle}{\sqrt{m_B m_{D^*}}} = h_V(w) \varepsilon^{\mu\nu\rho\sigma} v_{B,\nu} v_{D^*,\rho} \epsilon_\sigma^*, \quad (76.6)$$

$$\begin{aligned} \frac{\langle D^*(v', \epsilon) | \bar{c} \gamma^\mu \gamma^5 b | B(v) \rangle}{\sqrt{m_B m_{D^*}}} &= i h_{A_1}(w) (1+w) \epsilon^{*\mu} \\ &\quad - i [h_{A_2}(w) v_B^\mu + h_{A_3}(w) v_{D^*}^\mu] \epsilon^* \cdot v_B, \end{aligned} \quad (76.7)$$

and the ratios

$$R_1(w) = \frac{h_V(w)}{h_{A_1}(w)}, \quad R_2(w) = \frac{h_{A_3}(w) + r h_{A_2}(w)}{h_{A_1}(w)}, \quad (76.8)$$

as

$$\begin{aligned} P(w) |\mathcal{F}(w)|^2 &= |h_{A_1}(w)|^2 \times \left\{ 2 \frac{r^2 - 2rw + 1}{(1-r)^2} \left[1 + \frac{w-1}{w+1} R_1^2(w) \right] \right. \\ &\quad \left. + \left[1 + \frac{w-1}{1-r} (1 - R_2(w)) \right]^2 \right\}. \end{aligned} \quad (76.9)$$

Note that \mathcal{F} at $w = 1$ is unity by HQS in the infinite-mass limit [15–18]. The effect of assuming massless leptons is typically very small, but for the muon case can be non-negligible in fits to data at high hadronic recoil.

The factor $\eta_{EW} = 1.0066 \pm 0.0050$ accounts for the leading electroweak corrections to the four-fermion operator mediating the semileptonic decay [19], and includes an estimated uncertainty for missing long-distance and structure-dependent QED corrections [20]. While some QED radiative corrections are included in the experimental analysis, the Coulomb correction, which arises when the final-state hadron is charged, is not taken into account.

The determination of $|V_{cb}|$ requires knowledge of the normalization, where one commonly uses a theoretical calculation of the zero recoil input, $\mathcal{F}(1)$. Theoretical knowledge of the shapes of the form factors provides crucial compatibility checks between theory and experiment, and improves the precision of the determinations.

Model-independent shape parametrizations of the form factors make use of analyticity and unitarity constraints and are expressed in terms of the variable

$$z = \frac{\sqrt{w+1} - \sqrt{2N}}{\sqrt{w+1} + \sqrt{2N}}, \quad (76.10)$$

originating from a conformal transformation, where $N = (t_+ - t_0)/(t_+ - t_-)$, $t_\pm = (m_B \pm m_{D^*})^2$, and the choice of t_0 determines the kinematic point at which $z = 0$. The form factors (generically denoted as F) may then be written as [21–25]

$$F(z) = \frac{1}{P_F(z) \phi_F(z)} \sum_{n=0}^{\infty} a_n z^n \quad (76.11)$$

where the sum is bounded, $\sum |a_n| < 1$. Furthermore, the function $P_F(z)$ takes into account the resonances in the $(\bar{c}b)$ system below the $\bar{D}B$ threshold, and the weighting functions $\phi_F(z)$ are derived from the unitarity constraint on the corresponding form factor. With the conventional choice $N = 1$, $z = 0$ when $w = 1$ and kinematic range of the decay corresponds to $0 \leq z \leq 0.06$. As a result, only very few terms are needed in the series in z . We refer to Eq. (76.11) as the ‘‘BGL’’ expansion.

The Caprini-Lellouch-Neubert (CLN) parametrization [26] yields a simple form

$$h_{A_1}(w) = h_{A_1}(1) \left[1 - 8\rho^2 z + (53\rho^2 - 15)z^2 - (231\rho^2 - 91)z^3 \right] \quad (76.12)$$

with the slope ρ and normalization $h_{A_1}(1)$ as the only parameters, albeit at the cost of introducing model dependence. Furthermore, the ratios $R_1(w)$ and $R_2(w)$ are expanded in $w - 1$. However, this simple CLN parametrization does not account for higher-order corrections in the $1/m_{c,b}$ expansion, which are now relevant [25, 27–33]. In addition, the numerical values of the coefficients use outdated knowledge and should include uncertainties. Thus, this report focuses on recent analyses that employ different combinations of HQET expansions through $\mathcal{O}(\alpha_s/m_{b,c}, 1/m_{b,c}^2)$, lattice form factors at non-zero recoil, as well as the model-independent BGL expansion. Typical fits include up to three parameters a_n in Eq. (76.11) for the different form factors.

There now exist three independent lattice QCD calculations by Fermilab/MILC [9], HPQCD [10], and JLQCD [11] of the $B \rightarrow D^* \ell \bar{\nu}_\ell$ form factors at non-zero recoil. The three groups each employ statistically independent gauge-field ensembles and use different lattice actions for the heavy and light quarks. To obtain results in the continuum and at the physical point, all three analyses first perform chiral-continuum fits and systematic error studies on the corresponding lattice form factor data. The resulting continuum form factors are smooth functions (bands) obtained over recoil ranges which depend on the respective simulation details. In a second step, BGL-expansion fits are used to obtain the form factors over the entire recoil range. We note that the interplay between choices for the ChPT-based continuum extrapolations and BGL coefficients needs further investigation [34]. A comparison of the resulting $|\mathcal{F}(w)|^2$ amplitudes is shown in Fig. 76.1. While the lattice results are reasonably consistent in the low-recoil region, there is some variation in the slopes, as is evident from the spread between the bands at large recoil.

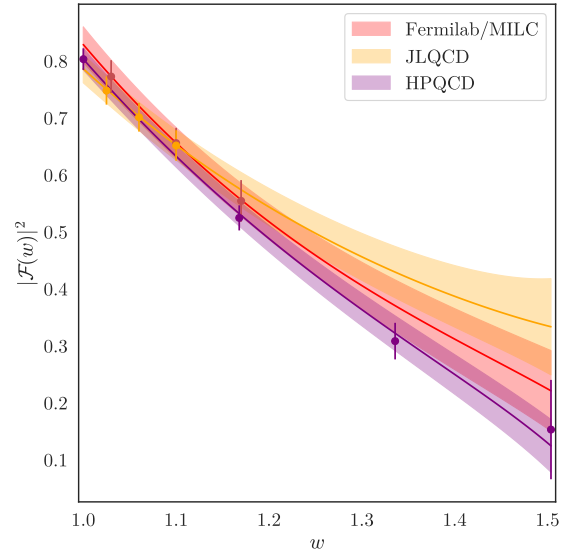


Figure 76.1: Comparison of lattice QCD results for $|\mathcal{F}(w)|^2$ obtained by the Fermilab Lattice and MILC collaborations (red), HPQCD (purple), and JLQCD (yellow). Plot courtesy of A. Vaquero.

Prior lattice calculations obtained results for only the form factor at the zero-recoil point, $\mathcal{F}(1)$, [20, 35] with a total uncertainty at the (1-2)% level. A weighted average of the $\mathcal{F}(1)$ results from Refs. [10, 11, 20] yields

$$\mathcal{F}(1) = 0.903 \pm 0.012. \quad (76.13)$$

The lattice QCD results in Refs. [9–11] appeared (or were published) after the most recent FLAG review [36], and will therefore be included in the next FLAG review. Non-lattice estimates based on zero-recoil sum rules for the form factor tend to yield lower central values for $\mathcal{F}(1)$ [37–39]. The sum rules indicate that $\mathcal{F}(1) < 0.92$ [37, 38, 40, 41], while an explicit estimate that includes excited state contributions yields $\mathcal{F}(1) \approx 0.86$ [39, 42].

Lattice-QCD form factors at non-zero recoil provide valuable shape constraints, and hence enable more refined $|V_{cb}|$ determinations. However, since they were not available until recently, some $|V_{cb}|$ determinations in the literature use the value for $\mathcal{F}(1)$ from Eq. (76.13) as the only quantitative lattice input. We discuss these first, before turning to results for $|V_{cb}|$ which employ the lattice-QCD form factors at non-zero recoil from Refs. [9–11].

While Light Cone Sum Rules (LCSR) can provide constraints on the form factors at maximum recoil, the underlying systematic errors are not fully quantified. A modern LCSR calculation [43] quotes uncertainties in the $\lesssim 20\%$ range for the $\bar{B} \rightarrow D^{(*)}\ell\bar{\nu}_\ell$ form factors at $q^2 = 0$.

Dispersive methods [44] can also be used to provide additional constraints on form factors calculated in lattice QCD. Recent work [45, 46] introduces the dispersive matrix method, which includes a strategy for computing the susceptibilities that are also needed inputs in z -expansion fits. They are calculable in lattice QCD from two-point correlation functions, which must be analyzed with the same care as the form factors themselves. The susceptibilities have also been computed in perturbative QCD in Ref. [47]. The two sets of results in Refs. [46, 47] differ in some cases outside of the quoted error bars, with a significance of up to 2.5σ . A test of the dispersive matrix approach for the $D \rightarrow K\ell\nu$ form factors, which can be computed in lattice-QCD over the entire kinematic range, is presented in Ref. [45]. The implementation of the dispersive matrix in Ref. [48] imposes unitarity constraints on the input data via a so-called unitarity filter. The filter has the effect of altering the shapes of the form factor bands while reducing the uncertainties from extrapolating the form factors over the entire kinematic range. Subsequently, the authors of Ref. [48] determine $|V_{cb}|$ from a bin-by-bin analysis of the experimental data, which avoids the common shape constraints in joint z -expansion fits. In follow-up work, this method has also been applied to other semileptonic decay channels [49–51]. A more recent proposal [52] employs Bayesian inference to implement unitarity constraints, which allows for a straightforward combination of inputs from multiple lattice calculations while including experimental data in joint z -expansion fits.

Many experiments [53–65] have measured the differential decay rate as a function of w , employing a variety of methods: using either B^+ or B^0 decays, with or without B -tagging, and with or without explicit reconstruction of the transition pion from $D^* \rightarrow D$ decays. In Ref. [6] a subset of the available experimental measurements were input to a four-dimensional fit for $\eta_{EW}\mathcal{F}(1)|V_{cb}|$, $\rho_{A_1}^2$ and the form-factor ratios $R_1 \propto A_2/A_1$ and $R_2 \propto V/A_1$. The fit has a p -value of 0.9%, so we scale the uncertainty by a factor $\sqrt{\chi^2/23}$ to give $\eta_{EW}\mathcal{F}(1)|V_{cb}| = (35.00 \pm 0.49) \times 10^{-3}$ (CLN).

The leading sources of uncertainty on $\eta_{EW}\mathcal{F}(1)|V_{cb}|$ are due to detection efficiencies and $D^{(*)}$ decay branching fractions. Note that the $\bar{B} \rightarrow D^*\ell\bar{\nu}_\ell$ form factor in the fit is parameterized using the CLN form, which has the drawbacks discussed previously.

Using the value from Eq. (76.13) for $\mathcal{F}(1)$ and accounting for the electroweak correction gives

$$|V_{cb}| = (38.5 \pm 0.5 \pm 0.6) \times 10^{-3} \quad (\bar{B} \rightarrow D^*\ell\bar{\nu}_\ell, \text{ LQCD, CLN}). \quad (76.14)$$

A safer approach is to use the more general BGL form-factor parameterization [22–25, 29]. The BABAR and Belle experiments have published analyses with BGL based parameterizations at a given order in the expansion [62–64]. A preliminary measurement from Belle II [65] has also been performed with a BGL based parameterization. The main results from these measurements are summarised in Table 76.1 after multiplying through the value of $\mathcal{F}(1)$ quoted in the nominal result of each respective study. These results have not yet been combined by the Heavy Flavor Averaging Group.

The Belle analysis [62] and the Belle II analysis [65] are both based on untagged approaches in the mode $\bar{B}^0 \rightarrow D^{*+}\ell\bar{\nu}_\ell$ and measure 1- d projections in bins of the hadronic recoil w , and angular variables $\cos\theta_\ell$, $\cos\theta_V$, and χ . The BABAR analysis [63] and the recent Belle analysis [64] are based on hadronic tagged samples using both charged and neutral B decays. BABAR performs a full 4- d unbinned analysis of neutral and charged B de-

cay modes, while Belle uses unfolded 1- d projections of w , $\cos\theta_\ell$, $\cos\theta_V$, and χ . Only the BGL form factors are directly determined in these tagged analysis, not the normalization, which is taken from the world average $\bar{B} \rightarrow D^*\ell\bar{\nu}_\ell$ branching fractions.

The studies in Refs. [62, 64, 65] publish the fully-differential decay rate data and associated covariance matrices. The BGL fit results in the Belle, Belle II and BABAR measurements are all consistent with corresponding results from fits with the CLN parameterization, Eq. (76.14). Each study reports fit results at low order in the three BGL expansion terms when non-zero lattice data is not used as an additional constraint, ranging from zero-order to second-order. Studies of the impact of higher order expansions based on the Belle published decay rate data have been reported in Refs. [30, 31], as well as in the recent Belle and Belle II studies [64, 65], where it is shown that the fit uncertainty on $|V_{cb}|$ increases substantially with respect to the results reported at lower order, while the parameter correlations approach 1. This is due to larger number of degrees of freedom allowed in the higher order expansions, which are not sufficiently constrained without lattice-QCD inputs at nonzero recoil.

In Ref. [9], BGL expansion fits to the FNAL/MILC lattice QCD form factors show that they are insensitive to truncation effects beyond quadratic order. These form factors were subsequently used in Ref. [9] to extract $|V_{cb}|$ from combined BGL fits to the Belle [62] and synthetic BABAR [63] $\bar{B} \rightarrow D^*\ell\bar{\nu}_\ell$ data, yielding $|V_{cb}| = (38.74 \pm 0.78) \times 10^{-3}$. The p -values for the combined (experiment+lattice QCD) BGL fits reported in Ref. [9] are small, reflecting tensions between the data sets. For a fit combining only the Belle data with the lattice-QCD form factors, Ref. [9] quotes $|V_{cb}| = 38.60(86) \times 10^{-3}$, while a fit combining the experimental data with only the lattice QCD $\mathcal{F}(1)$ yields $|V_{cb}| = 39.75(92) \times 10^{-3}$. Similarly, Refs. [10, 11] present analyses based on the BGL expansion, combining the respective lattice form factor results with the new Belle data [64]. The HPQCD collaboration [10] reports $|V_{cb}| = 39.31(74) \times 10^{-3}$, while the JLQCD collaboration [11] reports $|V_{cb}| = 39.19(90) \times 10^{-3}$. All these determinations are consistent with the result presented in Eq. (76.15) as well as with other exclusive determinations, where the HPQCD value needs to be shifted due to their inclusion of the Coulomb factor in η_{EW} . As noted in Refs. [9–11, 64, 65], the form factor shapes and $R_2(w)$ ratio predicted from FNAL/MILC [9] and HPQCD [10] are in tension with experimental data yielding small p -values, while those from JLQCD [11] are not. Furthermore, the $R_2(w)$ ratio results from Refs. [9, 10] are also in tension with HQET expectations (see, for example, Refs. [30, 32, 33, 67]). These tensions must be understood better in order to improve the precision of $|V_{cb}|$ extractions. Indeed, ongoing experimental analyses as well as theoretical work may resolve them in the near future.

For this review, we take a naive combination of the results in Table 76.1, assuming minimal correlations between measurements, and correct for the value of $\mathcal{F}(1)\eta_{EW}$. In the future we expect HFLAV to perform a combined global fit analysis. The combination has a p -value of 8%. The nominal result for $|V_{cb}|$ is therefore

$$|V_{cb}| = (39.7 \pm 0.7) \times 10^{-3} \quad (\bar{B} \rightarrow D^*\ell\bar{\nu}_\ell, \text{ LQCD, BGL}), \quad (76.15)$$

where the uncertainty contains contributions from experimental, lattice QCD, and η_{EW} sources. We note that despite the improvements in the experimental data, theoretical inputs, and $|V_{cb}|$ extraction methods, this new exclusive determination of $|V_{cb}|$, while higher in central value compared to earlier ones, is still in tension with the inclusive determinations discussed in Section 76.2.5 and summarized in Eq. (76.32).

76.2.3 $\bar{B} \rightarrow D\ell\bar{\nu}_\ell$

The differential rate for $\bar{B} \rightarrow D\ell\bar{\nu}_\ell$ is given by

$$\begin{aligned} \frac{d\Gamma}{dw}(\bar{B} \rightarrow D\ell\bar{\nu}_\ell) = & \\ & \frac{G_F^2}{48\pi^3} |V_{cb}|^2 (m_B + m_D)^2 m_D^3 (w^2 - 1)^{3/2} (\eta_{EW}\mathcal{G}(w))^2. \end{aligned} \quad (76.16)$$

Table 76.1: $\mathcal{F}(1)\eta_{EW}|V_{cb}|$ results from $B \rightarrow D^*\ell\nu$ with BGL expansion fits. Note that the tagged analyses combined results from B^- and \bar{B}^0 decays, while the untagged analyses study only \bar{B}^0 decays. The final column listed the non-zero recoil lattice QCD data used in each study.

Measurement	Tag	$\mathcal{F}(1)\eta_{EW} V_{cb} \times 10^3$	Fit inputs
Belle [66]	Untagged	35.22 ± 0.95	FNAL/MILC [20]
Babar [63]	Tagged	34.98 ± 0.65	FNAL/MILC [9], HPQCD [10], JLQCD [11]
Belle [64]	Tagged	37.00 ± 0.56	
Belle II [65]	Untagged	36.94 ± 0.91	FNAL/MILC [9]

The form factor is defined in terms of

$$\frac{\langle D(v') | \bar{c}\gamma^\mu b | B(v) \rangle}{\sqrt{m_B m_D}} = h_+(w) (v_B + v_D)^\mu + h_-(w) (v_B - v_D)^\mu \quad (76.17)$$

and reads

$$\mathcal{G}(w) = h_+(w) - \frac{m_B - m_D}{m_B + m_D} h_-(w), \quad (76.18)$$

where $h_+(1)$ is normalized to unity due to HQS and $h_-(1)$ vanishes in the infinite-mass limit. Thus

$$\mathcal{G}(1) = 1 + \mathcal{O}\left(\left(\frac{m_B - m_D}{m_B + m_D}\right)^2 \frac{\Lambda_{\text{QCD}}}{m_c}\right) \quad (76.19)$$

and the corrections to the HQS prediction are of order Λ_{QCD}/m_c in contrast to the case of $\mathcal{F}(1)$. The lattice-QCD result for the normalization, $\mathcal{G}(1)$, obtained in Ref. [7] is

$$\mathcal{G}(1) = 1.054 \pm 0.004 \pm 0.008. \quad (76.20)$$

We first turn to $|V_{cb}|$ extractions that rely on only the normalization $\mathcal{G}(1)$ from Eq. (76.20). The most precise measurements of $\bar{B} \rightarrow D\ell\bar{\nu}_\ell$ [60, 68, 69] dominate the CLN average [6] value, $\eta_{EW}\mathcal{G}(1)|V_{cb}| = (41.53 \pm 0.98) \times 10^{-3}$. Note that this average corresponds to measurements that are fit to the CLN form factor parameterization; the same concerns expressed above for $\bar{B} \rightarrow D^*\ell\bar{\nu}_\ell$ apply here. Using the value from Eq. (76.20) for $\mathcal{G}(1)$ and accounting for the electroweak correction as above gives

$$|V_{cb}| = (39.1 \pm 0.9 \pm 0.4) \times 10^{-3} \quad (\bar{B} \rightarrow D\ell\bar{\nu}_\ell, \text{LQCD, CLN}), \quad (76.21)$$

where the first uncertainty is from experiment, and the second combines the lattice QCD uncertainty in Eq. (76.20) with the electroweak correction.

For the $\bar{B} \rightarrow D\ell\bar{\nu}_\ell$ modes, theoretical input on the shape of the form factor, especially near $w \sim 1$, is especially beneficial to $|V_{cb}|$ determinations, since experimental measurements of the differential decays rate near zero recoil are affected by the more severe phase space suppression, compared to the D^* case. Hence the best $|V_{cb}|$ determinations from exclusive $\bar{B} \rightarrow D\ell\bar{\nu}_\ell$ decays employ lattice-QCD form factors obtained over a range of $w \geq 1$ [7, 8], where Ref. [70] provides a lattice average of the two results. Using the BCL parameterization (z -expansion from Ref. [71]) for the form factors, they can be combined with binned measurements from Belle [69] and BABAR [68]. Only Ref. [69] published the full measurement covariance matrix, while Ref. [68] provides the statistical uncertainty covariance. Nevertheless, Ref. [69] is more precise and dominates the average [70], giving

$$|V_{cb}| = (40.1 \pm 1.0) \times 10^{-3} \quad (\bar{B} \rightarrow D\ell\bar{\nu}_\ell, \text{LQCD, BCL}). \quad (76.22)$$

This result is consistent with the value reported in Ref. [47], which is based on the same experimental and lattice inputs.

The $|V_{cb}|$ averages from $\bar{B} \rightarrow D^*\ell\bar{\nu}_\ell$ and $\bar{B} \rightarrow D\ell\bar{\nu}_\ell$ decays using the BGL (Eq. (76.15)) and BCL (Eq. (76.22)) forms, respectively, are reasonably consistent. The correlations between the lattice uncertainties for $\bar{B} \rightarrow D^*\ell\bar{\nu}_\ell$ and $\bar{B} \rightarrow D\ell\bar{\nu}_\ell$ are discussed in Ref. [36], and considered to be 100% for the statistical uncertainty component. We assume an experimental uncertainty correlation of order 20% and combine the results of Eq. (76.15) and Eq. (76.22), giving

$$|V_{cb}| = (39.8 \pm 0.6) \times 10^{-3} \quad (\text{exclusive}). \quad (76.23)$$

76.2.4 $B_s \rightarrow D_s^{(*)-} \mu^+ \nu_\mu$

Semileptonic decays of B_s mesons are being studied extensively by the LHCb experiment. On the theory side, lattice QCD calculations of the corresponding form factors can proceed using the same methods and gauge-field ensembles as for B -meson decays. In fact, the presence of a strange spectator quark in the B_s -meson decay amplitudes tends to yield smaller statistical and systematic errors in the lattice computation. Nevertheless, to-date there are still fewer lattice-QCD results for B_s -meson form factors available than for the B -meson case, but this situation is expected to change. For the case of the $B_s \rightarrow D_s$ transition, two lattice QCD calculations of the form factors over a range of recoil momenta have been performed by the HPQCD collaboration, the first on 2 + 1-flavor gauge field ensembles (generated by the MILC collaboration) using NRQCD b -quarks [72]. The second calculation uses the 2 + 1 + 1-flavor gauge-field ensembles (also generated by MILC), employing the HISQ action for all valence quarks [73]. The all-HISQ approach avoids the need to compute renormalization factors separately, at the cost of requiring an extrapolation to the physical b -quark mass at the lattice spacings used in Ref. [73]. For the $B_s \rightarrow D_s^{*-}$ transition, Refs. [35, 74] provide lattice QCD results for the form factor at zero recoil, where Ref. [74] uses a similar set-up as Ref. [73] and reads

$$\mathcal{F}^{B_s \rightarrow D_s^*}(1) = 0.9020(96)_{\text{stat}}(90)_{\text{sys}}. \quad (76.24)$$

A lattice QCD calculation of the $B_s \rightarrow D_s^{*-}$ form factors at non-zero recoil, employing 2+1+1-flavor gauge-field ensembles (generated by MILC) in an all-HISQ approach was presented in Ref. [12] and updated in Ref. [10].

LHCb has extracted $|V_{cb}|$ from semileptonic B_s^0 decays [75]. The measurement uses both $B_s^0 \rightarrow D_s^- \mu^+ \nu_\mu$ and $B_s^0 \rightarrow D_s^{*-} \mu^+ \nu_\mu$ decays. The value of $|V_{cb}|$ is determined from the observed yields of B_s^0 decays normalized to those of B^0 decays after correcting for the relative reconstruction and selection efficiencies. The normalization channels are $B^0 \rightarrow D^- \mu^+ \nu_\mu$ and $B^0 \rightarrow D^{*-} \mu^+ \nu_\mu$ decays, where the D^- is reconstructed with the same decay mode of the D_s ($D_s^- \rightarrow [K^+ K^-]_\phi \pi^-$). The shape of the form factors are extracted using $p_\perp(D_s)$, which is the component of the D_s^- momentum perpendicular to the B_s^0 flight direction. This variable is correlated with q^2 and the helicity angles in the $B_s^0 \rightarrow D_s^{*-} \mu^+ \nu_\mu$ decay. For the $B_s \rightarrow D_s^- \mu^+ \nu_\mu$ decay, for example, $|V_{cb}|$ is related to the measured ratio of signal yields, N_{sig} , and the normalization channel yields, N_{ref} , through the relation

$$\begin{aligned} \frac{N_{\text{sig}}}{N_{\text{ref}}} &= \xi \frac{f_s \mathcal{B}(D_s^- \rightarrow K^+ K^- \pi^-)}{f_d \mathcal{B}(D^- \rightarrow K^+ K^- \pi^-)} \frac{1}{\mathcal{B}(B^0 \rightarrow D^- \mu \nu_\mu)} \tau_s \\ &\quad \times \int \frac{d\Gamma(B_s \rightarrow D_s \mu \nu_\mu)}{dw}, \end{aligned}$$

where τ_s is the B_s lifetime, and ξ is the efficiency ratio between the signal and the normalization. The analysis uses the lattice-QCD form factors obtained for $B_s \rightarrow D_s^-$ over the full kinematic range in Ref. [73] and the zero-recoil result for the $B_s \rightarrow D_s^{*-}$ form factor from Ref. [74]. Fits to both the CLN parameterization and a 5-parameter version of BGL were performed. The result for $|V_{cb}|$, updated with the most recent determination of f_s/f_d and $\mathcal{B}(D_s^- \rightarrow K^- K^+ \pi^-)$ from Ref. [76], are $|V_{cb}|_{\text{CLN}} = (40.8 \pm 0.6 \pm 0.9 \pm 1.1) \times 10^{-3}$, and $|V_{cb}|_{\text{BGL}} = (41.7 \pm 0.8 \pm 0.9 \pm 1.1) \times 10^{-3}$, where the first uncertainty is statistical, the second systematic and the third due to the limited knowledge of the external inputs,

in particular the constant $f_s/f_d \times \mathcal{B}(D_s^- \rightarrow K^+ K^- \pi^-)$. The determination of $|V_{cb}|$ in Ref. [12], using the lattice form factors obtained therein combined with LHCb data yields a consistent result, $|V_{cb}| = 42.7(1.5)_{\text{lat}}(1.7)_{\text{exp}}(0.4)_{\text{EM}} \times 10^{-3}$. The results obtained are consistent with the exclusive determinations of $|V_{cb}|$ using the B^0 and B^+ decays but are not used in the overall average in this review at this stage. These channels are important in the measurement of the ratio $|V_{ub}|/|V_{cb}|$, which cancels out the B_s normalisation uncertainties, discussed in Section 76.5. LHCb also perform measurements of the $B_s^0 \rightarrow D_s^{*-} \mu^+ \nu_\mu$ differential decay rate [77]. Fits are performed to extract the form factors in CLN and BGL parametrizations.

76.2.5 $|V_{cb}|$ from inclusive decays

Measurements of the total semileptonic branching decay rate, along with moments of the lepton energy and hadronic invariant mass spectra in inclusive semileptonic $b \rightarrow c$ transitions, can be used for a precision determination of $|V_{cb}|$. The total semileptonic decay rate can be calculated quite reliably in terms of non-perturbative parameters that can be extracted from the information contained in the moments.

76.2.6 Inclusive semileptonic rate

The theoretical foundation for the calculation of the total semileptonic rate is the Operator Product Expansion (OPE) which yields the Heavy Quark Expansion (HQE) [78, 79]. Details can be found in the RPP mini-review on Effective Theories [3].

The OPE result for the total rate can be written schematically (details can be found, *e.g.*, in Ref. [80]) as

$$\begin{aligned} \Gamma = & |V_{cb}|^2 \frac{G_F^2 m_b^5(\mu)}{192\pi^3} |\eta_{\text{EW}}|^2 \times \\ & \left[z_0^{(0)}(r) + \frac{\alpha_s(\mu)}{\pi} z_0^{(1)}(r) + \left(\frac{\alpha_s(\mu)}{\pi} \right)^2 z_0^{(2)}(r) + \dots \right. \\ & + \frac{\mu_\pi^2}{m_b^2} \left(z_2^{(0)}(r) + \frac{\alpha_s(\mu)}{\pi} z_2^{(1)}(r) + \dots \right) \\ & + \frac{\mu_G^2}{m_b^2} \left(y_2^{(0)}(r) + \frac{\alpha_s(\mu)}{\pi} y_2^{(1)}(r) + \dots \right) \\ & + \frac{\rho_D^3}{m_b^3} \left(z_3^{(0)}(r) + \frac{\alpha_s(\mu)}{\pi} z_3^{(1)}(r) + \dots \right) \\ & \left. + \frac{\rho_{LS}^3}{m_b^3} \left(y_3^{(0)}(r) + \frac{\alpha_s(\mu)}{\pi} y_3^{(1)}(r) + \dots \right) + \dots \right] \quad (76.25) \end{aligned}$$

where r is the ratio m_c/m_b and the y_i and z_i are perturbatively calculable Wilson coefficients functions that appear at different orders of the heavy mass expansion.

The parameters μ_π^2 , μ_G^2 , ρ_D^3 and ρ_{LS}^3 constitute the non-perturbative input into the heavy quark expansion; they correspond to certain matrix elements to be discussed below. In the same way the HQE can be set up for the moments of distributions of charged-lepton energy, hadronic invariant mass and hadronic energy, *e.g.*

$$\langle E_e^n \rangle_{E_e > E_{\text{cut}}} = \int_{E_{\text{cut}}}^{E_{\text{max}}} \frac{d\Gamma}{dE_e} E_e^n dE_e \Big/ \int_{E_{\text{cut}}}^{E_{\text{max}}} \frac{d\Gamma}{dE_e} dE_e. \quad (76.26)$$

The coefficients of the HQE are known up to order $1/m_b^5$ at tree level [81–84]. The leading term $z_0^{(i)}$ is the parton model, and is known completely through order α_s^2 [85–87] and now also at α_s^3 [88]. The terms of order $\alpha_s^{n+1} \beta_0^n$ (where $\beta_0 = (33 - 2n_f)/3$) have been included following the BLM procedure [80, 89–92]. Corrections of order $\alpha_s \mu_\pi^2/m_b^2$ have been computed in Ref. [93] and Ref. [94], while the $\alpha_s \mu_G^2/m_b^2$ terms have been calculated in Ref. [95] and Ref. [96], and the $\alpha_s \rho_D^3/m_b^3$ corrections in Refs. [97, 98].

Starting at order $1/m_b^3$ contributions with an infrared sensitivity to the charm mass, m_c , appear [81, 83, 99, 100]. At order $1/m_b^3$ this “intrinsic charm” contribution manifests as a $\log(m_c)$ in the coefficient of the Darwin term ρ_D^3 . At higher orders, terms such

as $1/m_b^3 \times 1/m_c^2$ and $\alpha_s(m_c)1/m_b^3 \times 1/m_c$ appear; numerically these terms may be comparable in size to the contributions of order $1/m_b^4$.

The HQE parameters are given in terms of forward matrix elements of local operators; the parameters entering the expansion for orders up to $1/m_b^3$ are $(D_\perp^\mu = (g_{\mu\nu} - v_\mu v_\nu) D^\nu)$, where $v = p_B/M_B$ is the four-velocity of the B meson)

$$\begin{aligned} \bar{\Lambda} &= M_B - m_b, \\ \mu_\pi^2 &= -\langle B | \bar{b} (iD_\perp)^2 b | B \rangle, \\ \mu_G^2 &= \langle B | \bar{b} (iD_\perp^\mu) (iD_\perp^\nu) \sigma_{\mu\nu} b | B \rangle, \\ \rho_D^3 &= \langle B | \bar{b} (iD_{\perp\mu}) (ivD) (iD_\perp^\mu) b | B \rangle, \\ \rho_{LS}^3 &= \langle B | \bar{b} (iD_\perp^\mu) (ivD) (iD_\perp^\nu) \sigma_{\mu\nu} b | B \rangle. \end{aligned} \quad (76.27)$$

These parameters still depend on the heavy quark mass. Sometimes the infinite mass limits of these parameters $\bar{\Lambda} \rightarrow \bar{\Lambda}_{\text{HQET}}$, $\mu_\pi^2 \rightarrow -\lambda_1$, $\mu_G^2 \rightarrow 3\lambda_2$, $\rho_D^3 \rightarrow \rho_1$ and $\rho_{LS}^3 \rightarrow 3\rho_2$, are used instead. Beyond $1/m^3$ the number of independent HQE parameters starts to proliferate [84, 101]. In general, there are 13 parameters (at tree level) up to order $1/m^4$ and 31 (at tree level) up to order $1/m^5$, not including $\bar{\Lambda}$. A framework to compute observables at higher order in $1/m$ [84, 102] has been used to estimate the HQE parameters of the orders $1/m^4$ and $1/m^5$. Their impact on the $|V_{cb}|$ determination has been studied in Ref. [103]. However, as pointed out in Ref. [104] one may reduce the number of independent parameters in the HQE by exploiting reparametrization invariance, which is a symmetry of the HQE stemming from Lorentz invariance of QCD. For a subset of observables this allows us to reduce the number of parameters to three up to order $1/m^3$ (ρ_{LS}^3 can be absorbed into μ_G^2 by a re-definition) and to 8 up to order $1/m^4$ [105].

The perturbative QCD expansion for the decay rate does not converge, in general. In addition, the expansion coefficients in the rates and spectra depend strongly on the scheme used for m_b (or equivalently on $\bar{\Lambda}$). It is well known (see *e.g.* [106]) that using the pole mass definition for heavy quark masses leads to particularly badly behaved expansions. This motivates the use of “short-distance” mass definitions, such as the kinetic scheme [37] or the $1S$ scheme [107–109]. Both schemes are well suited for the HQE, since they allow the choice of the renormalization scale $\mu \leq m_b$. Furthermore, in both schemes, the masses can be extracted from other observables with sufficient precision, enabling a precise determination of $|V_{cb}|$, despite of the strong quark-mass dependence of the total rate.

The $1S$ scheme eliminates the b quark pole mass by relating it to the perturbative expression for the mass of the $1S$ state of the Υ system. The b quark mass in the $1S$ scheme is half of the perturbatively calculated mass of the $1S$ state of the Υ system. The best determination of the b quark mass in the $1S$ scheme is obtained from sum rules for $e^+e^- \rightarrow b\bar{b}$ [110]. A second alternative is the so-called “kinetic mass” $m_b^{\text{kin}}(\mu)$, which enters the non-relativistic expression for the kinetic energy of a heavy quark, and is defined using heavy-quark sum rules [37]. The relation between m_b^{kin} and $m_b^{\overline{MS}}$ is known through three-loop order [111].

Finally, we note that the theoretical description of inclusive decays employed here, is based on the assumption of quark-hadron duality. While there is no evidence of violations of quark-hadron duality, the theoretical uncertainties due to such violations are not well quantified [3].

76.2.7 Determination of HQE Parameters and $|V_{cb}|$

Several experiments have measured moments in $B \rightarrow X_c \ell \bar{\nu}_\ell$ decays [112–120] as a function of the minimum lepton momentum. Recently, moments measurements have been performed as a function of lepton invariant mass squared, q^2 [121, 122]. The measurements of the moments of the electron energy spectrum ($0^{\text{th}}\text{--}3^{\text{rd}}$) and of the squared hadronic mass spectrum ($0^{\text{th}}\text{--}2^{\text{nd}}$) have statistical uncertainties that are roughly equal to their systematic uncertainties. The 3^{rd} order hadronic mass spectrum moments have also been measured by some experiments, with relatively large statistical uncertainty. The sets of moments mea-

sured within each experiment have strong correlations; their use in a global fit requires fully specified statistical and systematic covariance matrices. Measurements of photon energy moments (0th-2nd) in $B \rightarrow X_s \gamma$ decays [123–127] as a function of the minimum accepted photon energy are also used in some fits; the dominant uncertainties on these measurements are statistical.

Global fits [120, 124, 128–134] to the moments of the electron energy spectrum and the squared hadronic mass spectrum have been performed in the $1S$ and kinetic schemes. The semileptonic moments alone determine a linear combination of m_b and m_c very accurately but leave the orthogonal combination poorly determined (See e.g. [135]); additional input is required to allow a precise determination of m_b . This additional information can come from the radiative $B \rightarrow X_s \gamma$ moments (with the caveat that the OPE for $b \rightarrow s \gamma$ breaks down beyond leading order in Λ_{QCD}/m_b), which provide complementary information on m_b and μ_π^2 , or from precise determinations of the charm and beauty quark masses [36, 70, 136]. The values obtained in the kinetic scheme fits [6, 132, 133] with these two constraints are consistent. Based on the charm and beauty quark mass constraints [36, 134] $m_c^{\overline{\text{MS}}}(3 \text{ GeV}) = 0.988 \pm 0.007 \text{ GeV}$, and $m_b^{\overline{\text{MS}}} = 4.198 \pm 0.012 \text{ GeV}$ a fit in the kinetic scheme [134] obtains

$$|V_{cb}| = (42.16 \pm 0.51) \times 10^{-3} \quad (76.28)$$

where the error include experimental and theoretical uncertainties. This analysis [134] includes calculations of the third-order corrections to the semi-leptonic $b \rightarrow c \ell \nu$ decay width [88] and mass relations [111, 137]. Theoretical uncertainties from higher orders in $1/m$ as well as in α_s are estimated and included in performing the fits. Similar values for the parameters are obtained with a variety of assumptions about the theoretical uncertainties and their correlations. The χ^2/dof is well below unity, which could suggest that the theoretical uncertainties may be overestimated. However, while one could obtain a satisfactory fit with smaller uncertainties, this would result in unrealistically small uncertainties on the extracted HQE parameters, which are used as input to other calculations (e.g. the determination of $|V_{ub}|$).

A fit to the measured moments in the $1S$ scheme [6, 124, 131] gives

$$|V_{cb}| = (41.98 \pm 0.45) \times 10^{-3}, \quad (76.29)$$

$$m_b^{1S} = (4.691 \pm 0.037) \text{ GeV}. \quad (76.30)$$

This fit uses moments measurements from semileptonic and radiative decays and constrains the chromomagnetic operator using the B^*-B and D^*-D mass differences, but does not include the constraint on m_c nor all known higher order corrections.

Measurements of higher order moments and moments of additional variables, such as q^2 , can further improve the sensitivity of the fits to higher-order terms in the HQE [105]. The q^2 moments depend on a reduced set of operators, thereby possibly making it easier to extract higher-order terms from data. A fit to the q^2 moments measured by the Belle [121] and Belle II [122] experiments combined with the world average inclusive branching fractions, finds [138]:

$$|V_{cb}| = (41.69 \pm 0.63) \times 10^{-3}, \quad (76.31)$$

which is compatible with the fit to the other moments. Note there is a strong correlation with the other determinations due to the use of common inputs for the branching fractions.

These fits give consistent results for $|V_{cb}|$ and, after translation to a common renormalization scheme, for m_b . We take the fit in the kinetic scheme [134], which includes higher-order perturbative corrections, as the inclusive determination of $|V_{cb}|$:

$$|V_{cb}| = (42.2 \pm 0.5) \times 10^{-3} \text{ (inclusive)}. \quad (76.32)$$

76.3 Determination of $|V_{ub}|$

Summary: Currently the best determinations of $|V_{ub}|$ are from $\bar{B} \rightarrow \pi \ell \bar{\nu}_\ell$ decays, where combined fits to theory and experimental data as a function of q^2 provide a precision of about 4%; the uncertainties from experiment and theory are comparable in size. Determinations based on inclusive semileptonic B decays are based

on different observables and use different strategies to suppress the $b \rightarrow c$ background. Most of the determinations are consistent and provide a precision of about 7%, with comparable contributions to the uncertainty from experiment and theory.

The values obtained from inclusive and exclusive B decay determinations are

$$|V_{ub}| = (4.13 \pm 0.12 \pm_{0.14}^{0.13} \pm 0.18) \times 10^{-3} \text{ (inclusive)}, \quad (76.33)$$

$$|V_{ub}| = (3.70 \pm 0.10 \pm 0.12) \times 10^{-3} \text{ (exclusive)}, \quad (76.34)$$

where the last uncertainty on the inclusive result was added by the authors of this review and is discussed below. The exclusive and inclusive determinations are independent, and the dominant uncertainties are on multiplicative factors. The results from the two determinations are compatible to within two standard deviations.

This can be compared to the values derived from $|V_{ub}|/|V_{cb}|$ ratio measurements, described in the next section. Taking the value for this ratio from Eq. (76.54), and $|V_{cb}|$ from Eq. (76.3) we obtain.

$$|V_{ub}| = (3.43 \pm 0.32) \times 10^{-3} \text{ (B}_s, \Lambda_b), \quad (76.35)$$

We choose to combine only the direct determinations of $|V_{ub}|$, based on the inclusive and exclusive B measurements. In the combination they are weighted by their relative errors, where the uncertainties are treated as normally distributed. The resulting average has $p(\chi^2) = 15\%$, so we scale the error by $\sqrt{\chi^2/1} = 1.4$ to find

$$|V_{ub}| = (3.82 \pm 0.20) \times 10^{-3} \text{ (average)}. \quad (76.36)$$

In a future update we may consider the constraints in the $|V_{ub}|$ - $|V_{cb}|$ plane from the direct determinations together with the LHCb $|V_{ub}|/|V_{cb}|$ results, although the agreement among all inputs is somewhat marginal.

76.3.1 $|V_{ub}|$ from inclusive decays

The theoretical description of inclusive $\bar{B} \rightarrow X_u \ell \bar{\nu}_\ell$ decays is based on the Heavy Quark Expansion and leads to a predicted total decay rate with uncertainties below 5% [108, 139]. However, the total decay rate is hard to measure due to the large background from CKM-favored $\bar{B} \rightarrow X_c \ell \bar{\nu}_\ell$ transitions, and hence the theoretical methods differ from the $\bar{B} \rightarrow X_c \ell \bar{\nu}_\ell$ case. For a calculation of the partial decay rate in regions of phase space where $\bar{B} \rightarrow X_c \ell \bar{\nu}_\ell$ decays are suppressed one cannot use the HQE as for $b \rightarrow c$, rather one needs to introduce non-perturbative distribution functions, the “shape functions” (SF) [140, 141]. Their exact form is not known, but its moments can be related to the HQE parameters known e.g from the $b \rightarrow c$ case.

The shape functions become important when the light-cone momentum component $P_+ \equiv E_X - |P_X|$ is not large compared to Λ_{QCD} , as is the case near the endpoint of the $\bar{B} \rightarrow X_u \ell \bar{\nu}_\ell$ lepton spectrum. Partial rates for $\bar{B} \rightarrow X_u \ell \bar{\nu}_\ell$ are predicted and measured in a variety of kinematic regions that differ in their sensitivity to shape-function effects.

At leading order in $1/m_b$ only a single shape function (SF) appears, which is universal for all heavy-to-light transitions [140, 141] and can be extracted in $\bar{B} \rightarrow X_s \gamma$ decays. At subleading order in $1/m_b$, several shape functions appear [142], along with small “resolved photon contributions” specific for $\bar{B} \rightarrow X_s \gamma$ [143–145], and thus the prescriptions that relate directly the partial rates for $\bar{B} \rightarrow X_s \gamma$ and $\bar{B} \rightarrow X_u \ell \bar{\nu}_\ell$ decays [146–154] are limited to leading order in $1/m_b$.

Existing approaches use parametrizations of the leading SF that respect constraints on the normalization and on the first and second moments, which are given in terms of the HQE parameters $\bar{\Lambda} = M_B - m_b$ and μ_π^2 , respectively. The relations between SF moments and the HQE parameters are known to second order in α_s [155]; as a result, measurements of HQE parameters from global fits to $\bar{B} \rightarrow X_c \ell \bar{\nu}_\ell$ and $\bar{B} \rightarrow X_s \gamma$ moments can be used to constrain the SF moments, as well as to provide accurate values of m_b and other parameters for use in determining $|V_{ub}|$. Flexible parametrizations of the SF using orthogonal basis functions [156] or artificial neural networks [157] allow global fits to inclusive B

meson decay data [145] that incorporate the known short-distance contributions and renormalization properties of the SF.

HFLAV performs fits on the basis of several approaches, with varying degrees of model dependence. We will consider here the approaches documented in Ref. [158] (BLNP), Ref. [159] (GGOU) and Ref. [160] (DGE).

The triple differential rate in the variables

$$P_\ell = M_B - 2E_\ell, \quad P_- = E_X + |\vec{P}_X|, \quad P_+ = E_X - |\vec{P}_X| \quad (76.37)$$

is

$$\frac{d^3\Gamma}{dP_+ dP_- dP_\ell} = \frac{G_F^2 |V_{ub}|^2}{16\pi^2} (M_B - P_+) \quad (76.38)$$

$$\left\{ (P_- - P_\ell)(M_B - P_- + P_\ell - P_+) \mathcal{F}_1 \right.$$

$$\left. + (M_B - P_-)(P_- - P_+) \mathcal{F}_2 + (P_- - P_\ell)(P_\ell - P_+) \mathcal{F}_3 \right\}.$$

The “structure functions”, \mathcal{F}_i , can be calculated using factorization theorems that have been proven to subleading order in the $1/m_b$ expansion [161].

The BLNP [158] calculation uses these factorization theorems to write the \mathcal{F}_i terms as functions of perturbatively calculable hard coefficients and jet functions, which are convolved with the (soft) light-cone distribution functions. The calculation of $\mathcal{O}(\alpha_s^2)$ contributions [162,163] is not yet complete and is not included in the $|V_{ub}|$ determination given below.

The leading order term in the $1/m_b$ expansion of the \mathcal{F}_i terms contains a single non-perturbative function and is calculated to subleading order in α_s , while at subleading order in the $1/m_b$ expansion there are several independent non-perturbative functions that have been calculated only at tree level in the α_s expansion.

A distinct approach (GGOU) [159] uses a hard, Wilsonian cut-off that matches the definition of the kinetic mass. The non-perturbative input is similar to what is used in BLNP, but the shape functions are defined differently. In particular, they are defined at finite m_b and depend on the light-cone component k_+ of the b quark momentum and on the momentum transfer q^2 to the leptons. These functions include subleading effects to all orders; as a result they are non-universal, with one shape function corresponding to each structure function in Eq. (76.38). Their k_+ moments can be computed in the OPE.

Going to subleading order in α_s requires the definition of a renormalization scheme for the HQE parameters and for the SF. The relation between the moments of the SF and the forward matrix elements of local operators appearing the HQE is plagued by ultraviolet problems and requires additional renormalization. A scheme for improving this behavior was suggested in Refs. [158,164], which introduce a definition of the quark mass (the so-called shape-function scheme) based on the first moment of the measured $\bar{B} \rightarrow X_s \gamma$ photon energy spectrum. Likewise, the HQE parameters can be defined from measured moments of spectra, corresponding to moments of the SF.

There are various ideas to model the SF, but this requires additional assumptions. One approach (DGE) is the so-called “dressed gluon exponentiation” [160], where the perturbative result is continued into the infrared regime using the renormalon structure obtained in the large β_0 limit, where β_0 has been defined following Eq. (76.25). Other approaches make even stronger assumptions, such as in Ref. [165], which assumes an analytic behavior for the strong coupling in the infrared to perform an extrapolation of perturbation theory.

In order to reduce sensitivity to SF uncertainties, measurements that use a combination of cuts on the leptonic momentum transfer q^2 and the hadronic invariant mass m_X , as suggested in Ref. [166,167], have been made. In general, experimental measurements of $\bar{B} \rightarrow X_u \ell \bar{\nu}_\ell$ into charm-dominated regions (in order to reduce SF uncertainties) are sensitive to the modeling of $\bar{B} \rightarrow X_u \ell \bar{\nu}_\ell$ and $\bar{B} \rightarrow X_c \ell \bar{\nu}_\ell$ decays. The measurements quoted below have used a variety of functional forms to parametrize the leading SF; a specific error budget for one determination is quoted in the next section. In no case is the parametrization uncertainty estimated to be more than a 2% on $|V_{ub}|$.

Weak Annihilation [159,168,169] (WA) can in principle contribute significantly in the high- q^2 region of $\bar{B} \rightarrow X_u \ell \bar{\nu}_\ell$ decays. Estimates based on semileptonic D_s decays [100,166,167,169] lead to a $\sim 2\%$ uncertainty on the total $\bar{B} \rightarrow X_u \ell \bar{\nu}_\ell$ rate from the $\Upsilon(4S)$. The q^2 spectrum of the WA contribution is not well known, but from the OPE it is expected to contribute predominantly at high q^2 . Other theoretical investigations [100,170,171], a direct search [172], and $\mathcal{B}(B^0 \rightarrow X_u \ell \bar{\nu})/\mathcal{B}(B^+ \rightarrow X_u \ell \bar{\nu})$ ratio measurements [173–176] indicate that WA is a small effect, but may become a significant source of uncertainty for $|V_{ub}|$ measurements that accept only a small fraction of the full $\bar{B} \rightarrow X_u \ell \bar{\nu}_\ell$ phase space.

76.3.2 Measurements

We summarize the measurements used in the determination of $|V_{ub}|$ below. Given the improved precision and more rigorous theoretical interpretation of more recent measurements, determinations [177–180] done with LEP data are not considered in this review.

Inclusive electron momentum measurements [181,182] reconstruct a single charged electron to determine a partial decay rate for $\bar{B} \rightarrow X_u \ell \bar{\nu}_\ell$ near the kinematic endpoint. This results in a selection efficiency of order 50% and only modest sensitivity to the modeling of detector response. The inclusive electron momentum spectrum from $B\bar{B}$ events, after subtraction of the $e^+e^- \rightarrow q\bar{q}$ continuum background, is fitted to a model $\bar{B} \rightarrow X_u \ell \bar{\nu}_\ell$ spectrum and several components ($D\ell\bar{\nu}_\ell$, $D^*\ell\bar{\nu}_\ell$, ...) of the $\bar{B} \rightarrow X_c \ell \bar{\nu}_\ell$ background; the dominant uncertainties are related to this subtraction and modelling. The decay rate can be cleanly extracted for $E_e > 2.3$ GeV, but this is deep in the SF region, where theoretical uncertainties are large. More recent measurements have increased the accessed phase space. The resulting $|V_{ub}|$ values for various E_e cuts are given in Table 76.2.

The most recent BABAR measurement [183] is based on the inclusive electron spectrum and determines the partial branching fraction and $|V_{ub}|$ for $E_e > 0.8$ GeV. The analysis shows that the partial branching fraction measurements can have signal model dependence when the kinematic acceptance includes regions dominated by $\bar{B} \rightarrow X_c \ell \bar{\nu}_\ell$ background. The model dependence enters primarily through the partial branching fractions, and arises because the signal yield fit has sensitivity to $\bar{B} \rightarrow X_u \ell \bar{\nu}_\ell$ decays only in regions with good signal to noise.

An untagged “neutrino reconstruction” measurement [184] from BABAR uses a combination [185] of a high-energy electron with a measurement of the missing momentum vector. This allows $S/B \sim 0.7$ for $E_e > 2.0$ GeV and a $\approx 5\%$ selection efficiency, but at the cost of a smaller accepted phase space for $\bar{B} \rightarrow X_u \ell \bar{\nu}_\ell$ decays and uncertainties associated with the determination of the missing momentum.

The large samples accumulated at the B factories allow studies in which one B meson is fully reconstructed and the recoiling B decays semileptonically [186–189]. The experiments can fully reconstruct a “tag” B candidate in about 0.5% (0.3%) of B^+B^- ($B^0\bar{B}^0$) events. An electron or muon with center-of-mass momentum above 1.0 GeV is required amongst the charged tracks not assigned to the tag B and the remaining particles are assigned to the X_u system. The full set of kinematic properties (E_ℓ , m_X , q^2 , etc.) are available for studying the semileptonically decaying B , making possible selections that accept up to 90% of the full $\bar{B} \rightarrow X_u \ell \bar{\nu}_\ell$ rate; however, the sensitivity to $\bar{B} \rightarrow X_u \ell \bar{\nu}_\ell$ decays is still driven by the regions where $\bar{B} \rightarrow X_c \ell \bar{\nu}_\ell$ decays are suppressed. Despite requirements (e.g. on the square of the missing mass) aimed at rejecting events with additional missing particles, undetected or mis-measured particles from $\bar{B} \rightarrow X_c \ell \bar{\nu}_\ell$ decay (e.g., K_L^0 and additional neutrinos) remain an important source of uncertainty.

A recent recoil method measurement of partial branching fractions in three phase-space regions, covering about 31% to 86% of the accessible phase space, was performed by Belle [173], where machine learning techniques were used to reduce background levels. The measurement contains substantial decay model updates and supersedes previous measurements from Belle [187,188]. The measurement of the partial branching fraction obtained in the $E_\ell^B > 1$ GeV region, the most precise one, is used to obtain

$|V_{ub}|$ [173]. Belle also reports measurements of the background subtracted, and unfolded differential decay spectra in bins of m_X , m_X and q^2 , P_+ and E_ℓ [190] for use in global fit analyses.

Earlier measurements by BABAR [186] were also performed with cuts on m_X , m_X and q^2 , P_+ and E_ℓ using the recoil method. In each case the experimental systematic uncertainties have significant contributions from the modeling of $\bar{B} \rightarrow X_u \ell \bar{\nu}_\ell$ and $\bar{B} \rightarrow X_c \ell \bar{\nu}_\ell$ decays and from the detector response to charged particles, photons and neutral hadrons.

To reduce modelling uncertainties associated to $\bar{B} \rightarrow X_c \ell \bar{\nu}_\ell$ decays a recent Belle tagged measurement [176] uses a novel data driven approach to correct the kinematics and normalisation of this background component, while using less restrictive event selection with higher efficiency than the other recent Belle result. In the analysis the ratio $|V_{ub}|/|V_{cb}|$ is directly extracted from inclusive decays for the first time. While a value for $|V_{ub}|$ is provided here, it is not yet included in the combination.

The corresponding $|V_{ub}|$ values are given in Table 76.2.

76.3.3 $|V_{ub}|$ from inclusive partial rates

The measured partial rates and theoretical calculations from BLNP, GGOU and DGE described previously are used to determine $|V_{ub}|$ from all measured partial $\bar{B} \rightarrow X_u \ell \bar{\nu}_\ell$ rates [6]; selected values are given in Table 76.2. The correlations amongst the multiple BABAR recoil-based measurements [186] are fully accounted for in the average. The statistical correlations amongst the other measurements used in the average are small (due to small overlaps among signal events and large differences in S/B ratios) and have been ignored. Correlated systematic and theoretical errors are taken into account, both within an experiment and between experiments. As an illustration of the relative sizes of the uncertainties entering $|V_{ub}|$ we give the error breakdown for the GGOU average: statistical—1.3%; experimental—1.6%; $\bar{B} \rightarrow X_c \ell \bar{\nu}_\ell$ modeling—0.9%; $\bar{B} \rightarrow X_u \ell \bar{\nu}_\ell$ modeling—1.7%; HQE parameters (m_b)—1.8%; higher-order corrections—1.5%; q^2 modeling—1.3%; Weak Annihilation— $^{+0.0}_{-1.1}\%$; SF parametrization—0.1%.

The averages quoted here are based on the following m_b values: $m_b^{SF} = 4.582 \pm 0.023 \pm 0.018$ GeV for BLNP, $m_b^{\text{kin}} = 4.554 \pm 0.018$ GeV for GGOU, and $m_b^{MS} = 4.188 \pm 0.043$ GeV for DGE. The m_b^{kin} value is determined in a global fit to moments in the kinetic scheme [6]; this value is translated into m_b^{SF} and m_b^{MS} at fixed order in α_s . The second uncertainty quoted on m_b arises from the scheme translation.

Hadronization uncertainties also impact the $|V_{ub}|$ determination. The theoretical expressions are valid at the parton level and do not incorporate any resonant structure (e.g. $\bar{B} \rightarrow \pi \ell \bar{\nu}_\ell$); this must be added to the simulated $\bar{B} \rightarrow X_u \ell \bar{\nu}_\ell$ event samples, since the detailed final state multiplicity and structure impacts the estimates of experimental acceptance and efficiency. The experiments have adopted procedures to input resonant structure while preserving the appropriate behavior in the kinematic variables (q^2 , E_ℓ , m_X) averaged over the sample, but these prescriptions are *ad hoc* and ultimately require *in situ* calibration. The resulting uncertainties have been estimated to be ~ 1 -2% on $|V_{ub}|$. A recent inclusive $|V_{ub}|$ Belle measurement is the first to perform a fit to final state pion multiplicity for *in situ* calibration of the hadronization models used. The measurement simultaneously extracts inclusive and exclusive $|V_{ub}|$, with compatible results [191].

All calculations yield compatible $|V_{ub}|$ values and similar error estimates. The arithmetic mean of the values and errors of the HFLAV combinations listed in Table 76.2 is $|V_{ub}| = (4.13 \pm 0.12_{\text{exp}} \pm 0.13_{\text{theo}}) \times 10^{-3}$, although there is a spread of approximately 10% in the evaluations with the three theoretical models. For reasons discussed below, we assign an additional uncertainty due to model dependence that is not reflected in the HFLAV averages. As highlighted in the BABAR analysis [173,183], model dependence entering measurement procedures can be sizeable, and is not consistently treated across analyses. Many of the analyses shown in Table 76.2 were based on partial branching fraction measurements determined in a single model (i.e. the one used by that analysis when simulating $\bar{B} \rightarrow X_u \ell \bar{\nu}_\ell$ decays), although in some cases simulated events were weighted to match the expected spectra in other models and the differences

introduced as systematic uncertainties, e.g. Ref. [188]. The $|V_{ub}|$ value quoted by HFLAV for each model are, typically, derived from this unique partial branching fraction combined with another model-specific partial rate calculation. The model dependence in the partial branching fraction is sensitive to how the model predictions compare in the restricted region with good signal-to-noise, not by how they compare when integrated over the full kinematic range used in the fit. Ideally this effect needs to be accounted for by the experiments; the published information is insufficient to determine it. To account for the range in results using the different theoretical models, we take half of the spread of the averages as an additional systematic uncertainty, denoted Δ_{model} . With this addition, the inclusive $|V_{ub}|$ average is

$$|V_{ub}| = (4.13 \pm 0.12_{\text{exp}} \pm 0.13_{\text{theo}} \pm 0.18_{\Delta_{\text{model}}}) \times 10^{-3} \quad (\text{inclusive}). \quad (76.39)$$

76.3.4 $|V_{ub}|$ from exclusive decays

Exclusive charmless semileptonic decays offer a complementary means of determining $|V_{ub}|$. For the experiments, the specification of the final state provides better background rejection, but the branching fraction to a specific final state is typically only a few percent of that for inclusive decays. For theory, the calculation of the form factors for decays of B -mesons into exclusive final states is challenging, but brings in a different set of uncertainties from those encountered in inclusive decays. In this review we focus on $\bar{B} \rightarrow \pi \ell \bar{\nu}_\ell$, as it is the most promising decay mode for both experiment and theory. However, we also discuss $\bar{B}_s \rightarrow K \ell \bar{\nu}_\ell$ decays, for which there are recent interesting results. Measurements of other exclusive $\bar{B} \rightarrow X_u \ell \bar{\nu}_\ell$ decays can be found in Refs. [192–205].

76.3.5 $\bar{B} \rightarrow \pi \ell \bar{\nu}_\ell$ form factor calculations

The relevant form factors for the decay $\bar{B} \rightarrow \pi \ell \bar{\nu}_\ell$ are usually defined as

$$\langle \pi(p_\pi) | V^\mu | B(p_B) \rangle = f_+(q^2) \left[p_B^\mu + p_\pi^\mu - \frac{m_B^2 - m_\pi^2}{q^2} q^\mu \right] + f_0(q^2) \frac{m_B^2 - m_\pi^2}{q^2} q^\mu \quad (76.40)$$

in terms of which the rate becomes (in the limit $m_\ell \rightarrow 0$)

$$\frac{d\Gamma}{dq^2} = \frac{G_F^2 |V_{ub}|^2}{24\pi^3} |p_\pi|^3 |f_+(q^2)|^2, \quad (76.41)$$

where p_π is the pion momentum in the B meson rest frame.

Lattice-QCD calculations of the form factors for the $B \rightarrow \pi \ell \bar{\nu}$ and $B_s \rightarrow K \ell \bar{\nu}$ transitions are available from the Fermilab/MILC [206,207], HPQCD [208], RBC/UKQCD [209,210], and JLQCD [211] collaborations. The lattice form factors are obtained in the large q^2 region, $q_{\text{max}}^2 > q^2 \gtrsim 15 \text{ GeV}^2$ and the calculations differ in actions employed for the b quark. While HPQCD [208] is using lattice-nonrelativistic QCD, the results from Fermilab/MILC [206,207] and RBC/UKQCD [209] are obtained with relativistic b quark actions based on the Fermilab approach [212], albeit using independently generated gauge-field configurations. The JLQCD collaboration is using all-domain-wall-fermion set-up, The results agree within the quoted errors. For the $B \rightarrow \pi$ form factor $f_+(q^2 = 20 \text{ GeV}^2)$, Ref. [206] quotes uncertainty of 3.4%, where the leading contribution is due to the chiral-continuum extrapolation fit, which includes statistical and heavy-quark discretization errors.

The extrapolation to small values of q^2 can be performed using guidance from analyticity and unitarity together with a conformal mapping of the kinematical variables onto the complex unit disc, which yields series in the variable

$$z = \frac{\sqrt{t_+ - q^2} - \sqrt{t_+ - t_0}}{\sqrt{t_+ - q^2} + \sqrt{t_+ - t_0}}, \quad (76.42)$$

where $t_\pm = (M_B \pm m_\pi)^2$ and the choice of t_0 determines the range of z that corresponds to the kinematic range of the decay. Setting $t_0 = t_-$ results in $z = 0$ when $q^2 = q_{\text{max}}^2$. The choice $t_0 = (m_B + m_\pi)/(\sqrt{m_B} - \sqrt{m_\pi})^2$ centers the kinematic range around $z = 0$, so that $|z| < 0.3$.

Table 76.2: $|V_{ub}|$ (in units of 10^{-5}) from inclusive $\bar{B} \rightarrow X_u \ell \bar{\nu}_\ell$ measurements. The first uncertainty on $|V_{ub}|$ is experimental, while the second includes both theoretical and HQE parameter uncertainties. The values are generally listed in order of increasing kinematic acceptance, f_u (0.19 to 0.90), except for the BABAR $E_e > 0.8$ GeV measurement; those below the horizontal bar are based on recoil methods. The Belle 2023 measurement is not yet included in the combination.

Ref.	cut (GeV)	BLNP	GGOU	DGE
CLEO [181]	$E_e > 2.1$	$422 \pm 49^{+29}_{-34}$	$423 \pm 49^{+22}_{-31}$	$386 \pm 45^{+25}_{-27}$
BABAR [184]	$E_e - q^2$	$471 \pm 32^{+33}_{-38}$	not available	$435 \pm 29^{+28}_{-30}$
Belle [182]	$E_e > 1.9$	$493 \pm 46^{+26}_{-29}$	$495 \pm 46^{+16}_{-21}$	$482 \pm 45^{+23}_{-23}$
BABAR [183]	$E_e > 0.8$	$441 \pm 12^{+27}_{-27}$	$396 \pm 10^{+17}_{-17}$	$385 \pm 11^{+8}_{-7}$
<hr/>				
BABAR [186]	$q^2 > 8$ $m_X < 1.7$	$432 \pm 23^{+26}_{-28}$	$433 \pm 23^{+24}_{-27}$	$424 \pm 22^{+18}_{-21}$
BABAR [186]	$P_+ < 0.66$	$409 \pm 25^{+25}_{-25}$	$425 \pm 26^{+26}_{-27}$	$417 \pm 25^{+28}_{-37}$
BABAR [186]	$m_X < 1.7$	$403 \pm 22^{+22}_{-22}$	$410 \pm 23^{+17}_{-17}$	$422 \pm 23^{+21}_{-21}$
BABAR [186]	$E_\ell > 1.3$	$433 \pm 24^{+19}_{-21}$	$444 \pm 24^{+9}_{-10}$	$445 \pm 24^{+12}_{-13}$
Belle [173]	$E_\ell > 1$	$405 \pm 23^{+18}_{-20}$	$415 \pm 24^{+8}_{-9}$	$416 \pm 24^{+11}_{-12}$
Belle [176]	$E_\ell > 1$	$415 \pm 24^{+18}_{-20}$	$425 \pm 25^{+8}_{-9}$	$426 \pm 25^{+11}_{-12}$
<hr/>				
HFLAV [6]	Combination	$428 \pm 13^{+20}_{-21}$	$419 \pm 12^{+11}_{-12}$	$392 \pm 10^{+9}_{-10}$

We note that the $\bar{B}_s \rightarrow K \ell \bar{\nu}_\ell$ decay is an example where the implementation of unitarity bounds is complicated by the fact that the location of the cut in the q^2 plane is different from the $B_s K$ threshold, because the cut starts at $B\pi$ production threshold. Modifications of the unitarity constraints in this and similar examples are discussed in Refs. [210, 213–216].

The "BCL" parameterization of Ref. [71] is commonly used for these decays, as it is consistent with the asymptotic scaling ($q^2 \rightarrow \infty$) as well as near threshold, $q^2 = t_+$. As pointed out in Ref. [217] the unitarity sum of the z -expansion coefficients for f_+ is expected to be of order $(\Lambda/m)^3$, hence yielding a rapidly converging series. We note that relatively small differences in different lattice QCD form factor results can be amplified by a long extrapolation to the low- q^2 region. However, such extrapolations are not needed, when lattice form factors are combined with experimental measurements of the differential decay rate. The joint fits provide constraints on the shape of the form factor over the entire kinematic range, in addition to enabling precise determinations of $|V_{ub}|$ [218].

LCSR calculations provide estimates for the product $f_B f_+(q^2)$, valid in the region $0 < q^2 \lesssim 12$ GeV. The determination of $f_+(q^2)$ itself requires knowledge of the decay constant f_B , which is usually obtained by replacing f_B by its two-point QCD (SVZ) sum rule [219] in terms of perturbative and condensate contributions. The advantage of this procedure is the approximate cancellation of various theoretical uncertainties in the ratio $(f_B f_+)/f_B$. The LCSR for $f_B f_+$ is based on the light-cone OPE of the relevant vacuum-to-pion correlation function, calculated in full QCD at finite b -quark mass. The resulting expressions comprise a triple expansion: in the twist, t , of the operators near the light-cone, in α_s , and in the deviation of the pion distribution amplitudes from their asymptotic form, which is fixed from conformal symmetry. The state-of-the-art calculations include the leading twists two, three and four with full one-loop α_s corrections [220, 221] and partial two-loop corrections [222]. Higher-twist contributions have been investigated in Ref. [223] and two-particle higher twist contributions are studied in Ref. [43]. Nevertheless, estimates based on LCSR generally suffer from difficult to quantify systematic uncertainties.

A detailed statistical analysis including the various correlations has been performed in Ref. [224], also including unitarity bounds on the form factor. The results obtained are numerically compatible with the lattice QCD calculations of the form factor. A more recent analysis [225] employs a modified BCL expansion to extrapolate the LCSR form factors obtained at low q^2 to the high q^2 region, where good agreement with lattice QCD form factor predictions is found. The LCSR form factors can be combined with experimental data in joint z -expansion fits to determine $|V_{ub}|$.

76.3.6 $\bar{B} \rightarrow \pi \ell \bar{\nu}_\ell$ measurements

The $\bar{B} \rightarrow \pi \ell \bar{\nu}_\ell$ measurements fall into two broad classes: untagged, in which case the reconstruction of the missing momentum of the event serves as an estimator for the unseen neutrino, and tagged, in which the second B meson in the event is fully reconstructed in either a hadronic or semileptonic decay mode. The tagged measurements have better q^2 resolution, high and uniform acceptance and S/B as high as 10, but lower statistical power. The untagged measurements have higher background (S/B < 1) and make slightly more restrictive kinematic cuts, but still provide statistical power precision on the q^2 dependence of the form factor.

CLEO has analyzed $\bar{B} \rightarrow \pi \ell \bar{\nu}_\ell$ and $\bar{B} \rightarrow \rho \ell \bar{\nu}_\ell$ using an untagged analysis [199–201]. Similar analyses have been done at BABAR [202–205] and Belle [226]. The leading systematic uncertainties in the untagged $\bar{B} \rightarrow \pi \ell \bar{\nu}_\ell$ analyses are associated with modeling the missing momentum reconstruction, with background from $\bar{B} \rightarrow X_u \ell \bar{\nu}_\ell$ decays and $e^+ e^- \rightarrow q \bar{q}$ continuum events, and with varying the form factor used to model $\bar{B} \rightarrow \rho \ell \bar{\nu}_\ell$ decays.

Analyses [194, 227] based on reconstructing a B in the $\bar{D}^{(*)} \ell^+ \nu_\ell$ decay mode and looking for a $\bar{B} \rightarrow \pi \ell \bar{\nu}_\ell$ or $\bar{B} \rightarrow \rho \ell \bar{\nu}_\ell$ decay amongst the remaining particles in the event make use of the fact that the B and \bar{B} are back-to-back in the $\Upsilon(4S)$ frame to construct a discriminant variable that provides a signal-to-noise ratio above unity for all q^2 bins. A related technique was discussed in Ref. [228]. BABAR [227] and Belle [192] have used their samples of B mesons reconstructed in hadronic decay modes to measure exclusive charmless semileptonic decays, resulting in very clean but smaller samples. The dominant systematic uncertainties in the tagged analyses arise from tag calibration.

$|V_{ub}|$ can be obtained from the average $\bar{B} \rightarrow \pi \ell \bar{\nu}_\ell$ branching fraction and the measured q^2 spectrum. Fits to the q^2 spectrum using a theoretically motivated parametrization (e.g. "BCL" from Ref. [71]) remove most of the model dependence from theoretical uncertainties in the shape of the spectrum. The most sensitive method for determining $|V_{ub}|$ from $\bar{B} \rightarrow \pi \ell \bar{\nu}_\ell$ decays employs a simultaneous fit [6, 206, 217, 218, 229, 230] to measured experimental partial rates and lattice points versus q^2 (or z) to determine $|V_{ub}|$ and the first few coefficients of the expansion of the form factor in z . We quote the result from Ref. [6], which uses as experimental input an average of the measurements in Refs. [192, 202, 205, 226] and an average [231] of the LQCD input from Refs. [206] and [209]. The p -value of the q^2 measurement average is 6%. The average for the total $B^0 \rightarrow \pi^- \ell^+ \nu_\ell$ branching fraction is obtained by summing up the partial branching fractions:

$$\mathcal{B}(B^0 \rightarrow \pi^- \ell^+ \nu_\ell) = (1.50 \pm 0.02_{\text{stat}} \pm 0.06_{\text{syst}}) \times 10^{-4} \quad (76.43)$$

The corresponding value of $|V_{ub}|$ with this approach is found to

be

$$|V_{ub}| = (3.70 \pm 0.10 \pm 0.12) \times 10^{-3} \quad (\text{exclusive}), \quad (76.44)$$

where the first uncertainty is experimental and the second is from theory. A consistent result for $|V_{ub}|$ was reported in Ref. [36], which uses the same experimental and lattice-QCD inputs. Adding additional constraints using input from LCSR [222] gives [6] $|V_{ub}| = (3.67 \pm 0.09 \pm 0.12) \times 10^{-3}$ (exclusive, LQCD+LCSR). Other recent LCSR estimates [225, 232] have been used to obtain consistent results for $|V_{ub}|$, albeit with slightly higher central values. Ref. [232] also presents results for $|V_{ub}|$ from joint fits that exclude some of the experimental data in order to bring the exclusive values into agreement with the inclusive ones.

76.3.7 $\bar{B}_s \rightarrow K\ell\bar{\nu}_\ell$

The LHCb experiment have conducted the first observation of the decay $B_s^0 \rightarrow K^- \mu^+ \nu_\mu$ and the measurements of its branching fraction normalised to the $B_s^0 \rightarrow D_s^- \mu^+ \nu_\mu$ decays [233]. The measurement has been performed in two bins of q^2 , derived using the B_s^0 flight direction and the known B_s^0 mass. The analysis uses a BDT classifier to suppress semileptonic b -hadron background. The results of the partial branching fractions have been translated into measurements of $|V_{ub}|/|V_{cb}|$ using form factor calculations from LCSR for $q^2 < 7 \text{ GeV}^2$ [234], and a recent LQCD calculation for $q^2 > 7 \text{ GeV}^2$ [207]. The results are

$$|V_{ub}|/|V_{cb}| = 0.0607 \pm 0.0021 \pm 0.0030, \quad q^2 < 7 \text{ GeV}^2 (76.45)$$

$$|V_{ub}|/|V_{cb}| = 0.0946 \pm 0.0041 \pm 0.0068, \quad q^2 > 7 \text{ GeV}^2 (76.46)$$

where the first uncertainties include also experimental and external input sources, and the latter are due to the form factor calculations. The sizeable discrepancy between the values of $|V_{ub}|/|V_{cb}|$ for the low and high q^2 , requires further theoretical and experimental investigation. On the theory side, FLAG [36] perform a joint z -fit to the lattice QCD results in Refs. [207–209], with error inflation to account for the tensions between lattice results for f_0 . They then use the form factors for $\bar{B}_s \rightarrow K\ell\bar{\nu}_\ell$ and $\bar{B}_s \rightarrow D_s^* \ell\bar{\nu}_\ell$ to determine the ratio $|V_{ub}|/|V_{cb}|$ in combination with the LHCb measurements in the high- and low- q^2 regions, finding good agreement between the two:

$$|V_{ub}|/|V_{cb}| = 0.0819 \pm 0.0029 \pm 0.0072, \quad q^2 < 7 \text{ GeV}^2 (76.47)$$

$$|V_{ub}|/|V_{cb}| = 0.0860 \pm 0.0038 \pm 0.0037, \quad q^2 > 7 \text{ GeV}^2 (76.48)$$

While the experimental measurement has higher purity in the low q^2 region, the lattice QCD form factors are constrained more reliably in high- q^2 region. RBC/UKQCD recently presented in Ref. [210] an update of their previous calculation. They studied the effect of different strategies for obtaining the form factors $f_{+,0}$ in the continuum limit, finding sizeable differences for f_0 , but not f_+ . This issue needs to be studied further. In particular, such differences were not seen in a similar study, albeit for D -meson decay form factors [235]. However, the resulting effect on $|V_{ub}|/|V_{cb}|$ is relatively small, as the f_0 form factor enters the determination only via the kinematic constraint at $q^2 = 0$. A very recent analysis in Ref. [236] combines the lattice QCD form factors from Refs. [208, 210] with the LHCb data in $|V_{ub}|/|V_{cb}|$ determinations that are compatible with Eq. (76.48). When they combine their updated LCSR results with the low- q^2 LHCb data, they find $|V_{ub}|/|V_{cb}| = 0.057 \pm 0.005$, compatible with Eq. (76.45), and hence also in tension with Eq. (76.48). Experimental measurements of the differential rates in smaller bins would provide valuable shape constraints and additional compatibility tests, improving the reliability of the $|V_{ub}|/|V_{cb}|$ determinations by reducing the need for extrapolations of form factors.

76.4 Semileptonic b -baryon decays

Summary: A significant sample of Λ_b^0 baryons is available at the LHCb experiment, and methods have been developed to study their semileptonic decays. Both $\Lambda_b^0 \rightarrow p\mu\bar{\nu}$ and $\Lambda_b^0 \rightarrow \Lambda_c^+ \mu\bar{\nu}$ decays have been measured at LHCb, and the ratio of branching fractions to these two decay modes is used to determine the ratio $|V_{ub}|/|V_{cb}|$.

76.4.1 $\Lambda_b^0 \rightarrow \Lambda_c^+ \mu\bar{\nu}$ and $\Lambda_b^0 \rightarrow p\mu\bar{\nu}$

The $\Lambda_b^0 \rightarrow \Lambda_c^+$ and $\Lambda_b^0 \rightarrow p$ semileptonic transitions are described in terms of six form factors each. The three form factors corresponding to the vector current can be defined as [237]

$$\begin{aligned} \langle F(p', s') | \bar{q} \gamma_\mu b | \Lambda_b^0(p, s) \rangle = & \bar{u}_F(p', s') \left\{ f_0(q^2) (M_{\Lambda_b^0} - m_F) \frac{q_\mu}{q^2} \right. \\ & + f_+(q^2) \frac{M_{\Lambda_b^0} + m_F}{s_+} \left(p_\mu + p'_\mu - \frac{q_\mu}{q^2} (M_{\Lambda_b^0}^2 - m_F^2) \right) \\ & \left. + f_\perp(q^2) \left(\gamma_\mu - \frac{2m_F}{s_+} p_\mu - \frac{2M_{\Lambda_b^0}}{s_+} p'_\mu \right) \right\} u_{\Lambda_b^0}(p, s), \end{aligned} \quad (76.49)$$

where $F = p$ or Λ_c^+ and where we define $s_\pm = (M_{\Lambda_b^0} \pm m_F)^2 - q^2$. At vanishing momentum transfer, $q^2 \rightarrow 0$, the kinematic constraint $f_0(0) = f_+(0)$ holds. The form factors are defined in such a way that they correspond to time-like (scalar), longitudinal and transverse polarization with respect to the momentum-transfer q^μ for f_0 , f_+ and f_\perp , respectively. Likewise, the expression for the axial-vector current is

$$\begin{aligned} \langle F(p', s') | \bar{q} \gamma_\mu \gamma_5 b | \Lambda_b^0(p, s) \rangle = & -\bar{u}_F(p', s') \gamma_5 \left\{ g_0(q^2) (M_{\Lambda_b^0} + m_F) \frac{q_\mu}{q^2} \right. \\ & + g_+(q^2) \frac{M_{\Lambda_b^0} - m_F}{s_-} \left(p_\mu + p'_\mu - \frac{q_\mu}{q^2} (M_{\Lambda_b^0}^2 - m_F^2) \right) \\ & \left. + g_\perp(q^2) \left(\gamma_\mu + \frac{2m_F}{s_-} p_\mu - \frac{2M_{\Lambda_b^0}}{s_-} p'_\mu \right) \right\} u_{\Lambda_b^0}(p, s), \end{aligned} \quad (76.50)$$

with the kinematic constraint $g_0(0) = g_+(0)$ at $q^2 \rightarrow 0$.

In the heavy-quark limit, where both the b and c quarks are treated as heavy, all the form factors reduce to the Isgur Wise function ξ_B for baryons [237]:

$$f_0 = f_+ = f_\perp = g_0 = g_+ = g_\perp = \xi_B \quad (76.51)$$

With a light baryon in the final state, the form factors are related through the heavy quark symmetries of the Λ_b^0 , reducing the number of independent form factors to two. It should be noted that the differential $\Lambda_b^0 \rightarrow (p/\Lambda_c^+) \mu\bar{\nu}$ decay rates peak at high q^2 , so that the kinematic regions where both lattice QCD calculations and experimental measurements are precise are well matched.

The form factors for Λ_b^0 decays have been studied with lattice QCD [238]. Based on these results the differential rates for both $\Lambda_b^0 \rightarrow \Lambda_c^+ \mu\bar{\nu}$ as well as for $\Lambda_b^0 \rightarrow p\mu\bar{\nu}$ can be predicted in the full phase space. In particular, for the experimentally interesting region they find the ratio of decay rates to be [238]

$$\frac{\mathcal{B}(\Lambda_b^0 \rightarrow p\mu\bar{\nu})_{q^2 > 15 \text{ GeV}^2}}{\mathcal{B}(\Lambda_b^0 \rightarrow \Lambda_c^+ \mu\bar{\nu})_{q^2 > 7 \text{ GeV}^2}} = (1.471 \pm 0.095 \pm 0.109) \left| \frac{V_{ub}}{V_{cb}} \right|^2 \quad (76.52)$$

where the first uncertainty is statistical and the second, systematic.

76.4.2 Measurements at LHCb

The LHCb experiment has measured the branching fractions of the semileptonic decays $\Lambda_b^0 \rightarrow \Lambda_c^+ \mu\bar{\nu}$ and $\Lambda_b^0 \rightarrow p\mu\bar{\nu}$, from which they determine $|V_{ub}|/|V_{cb}|$. This is the first such determination at a hadron collider, the first to use a b baryon decay, and the first observation of $\Lambda_b^0 \rightarrow p\mu\bar{\nu}$. Excellent vertex resolution allows the $p\mu$ and production vertices to be separated, which permits the calculation of the transverse momentum p_\perp of the $p\mu$ pair relative to the Λ_b^0 flight direction. The corrected mass, $m_{\text{corr}} = \sqrt{p_\perp^2 + m_{p\mu}^2} + p_\perp$, peaks at the Λ_b^0 mass for signal decays and provides good discrimination against background combinations. The topologically similar decay $\Lambda_b^0 \rightarrow \Lambda_c^+ \mu\bar{\nu}$ is also measured, which eliminates the need to know the production cross-section or absolute efficiencies. Using vertex and Λ_b^0 mass constraints,

q^2 can be determined up to a two-fold ambiguity. The LHCb analysis requires both solutions to be in the high q^2 region to minimise contamination from the low q^2 region. Their result [239], rescaled [6] to take into account the recent branching fraction measurement [240] $\mathcal{B}(\Lambda_c^+ \rightarrow pK^-\pi^+) = (6.28 \pm 0.32)\%$, is

$$\frac{\mathcal{B}(A_b^0 \rightarrow p\mu\bar{\nu})_{q^2 > 15\text{GeV}^2}}{\mathcal{B}(A_b^0 \rightarrow \Lambda_c^+\mu\bar{\nu})_{q^2 > 7\text{GeV}^2}} = (0.92 \pm 0.04 \pm 0.07) \times 10^{-2} \quad (76.53)$$

The largest systematic uncertainty is from the measured $\mathcal{B}(\Lambda_c^+ \rightarrow pK^-\pi^+)$; uncertainties due to trigger, tracking and the Λ_c^+ selection efficiency are each about 3%.

A LHCb analysis [241] measures the normalized q^2 spectrum and finds good agreement with the shape calculated with lattice QCD [238].

The decay rate for $A_b^0 \rightarrow p\mu\bar{\nu}$ peaks at high q^2 where the calculation of the associated form factors using lattice QCD is under good control. Using the measured ratio from Eq. (76.53) along with the calculated ratio from Ref. [238] (see Eq. (76.52)) results in [6]

$$|V_{ub}|/|V_{cb}| = 0.079 \pm 0.004 \pm 0.004(A_b). \quad (76.54)$$

where the first uncertainty is experimental and the second is from the LQCD calculation.

76.5 The ratio $|V_{ub}|/|V_{cb}|$

The ratio of matrix elements, $|V_{ub}|/|V_{cb}|$, is often required when testing the compatibility of a set of measurements with theoretical predictions. It can be determined from the ratio of branching fractions and has been directly measured by the LHCb (quoted in the previous sections) and Belle experiments. It can also be calculated based on the $|V_{ub}|$ and $|V_{cb}|$ values quoted earlier in this review.

The average of the LHCb results extracted at high q^2 from B_s and A_b decays, taken to be uncorrelated, is

$$|V_{ub}|/|V_{cb}| = 0.083 \pm 0.004 \quad (A_b, B_s). \quad (76.55)$$

The first direct extraction of this ratio from inclusive B decays was recently performed by Belle [176]. Belle measures the ratio of $\bar{B} \rightarrow X_u\ell\bar{\nu}_\ell$ and $\bar{B} \rightarrow X_c\ell\bar{\nu}_\ell$ branching fractions with a lepton energy threshold of 1.0 GeV. The partial decay widths, omitting the CKM factors, are taken from BLNP and GGOU for $|V_{ub}|$ and the kinetic scheme for $|V_{cb}|$ to extract the ratio of CKM factors. The results are found to be

$$|V_{ub}|/|V_{cb}| = 0.097 \pm 0.008 \quad (\text{BLNP}), \quad (76.56)$$

$$|V_{ub}|/|V_{cb}| = 0.100 \pm 0.006 \quad (\text{GGOU}). \quad (76.57)$$

These values are in excellent agreement with $|V_{ub}|/|V_{cb}|$ from independent inclusive determinations, given below, but involve non-zero correlations in both the theoretical and experimental uncertainties. We will therefore leave it out of the combination for this edition.

Given the similarities in the theoretical frameworks used for charmed and charmless decays, we choose to also quote separate ratios of $|V_{ub}|/|V_{cb}|$ for inclusive and exclusive B decays, as discussed earlier:

$$|V_{ub}|/|V_{cb}| = 0.098 \pm 0.006 \quad (\text{inclusive}), \quad (76.58)$$

$$|V_{ub}|/|V_{cb}| = 0.093 \pm 0.004 \quad (\text{exclusive}). \quad (76.59)$$

The respective determinations of $|V_{ub}|$ and $|V_{cb}|$ are taken to be uncorrelated in the ratio, although there could be some small cancellations of the uncertainties in both the experimental and the theoretical input. We average the B decay values, along with the B_s and baryonic result in Eq. (76.55), weighting by relative errors to find

$$|V_{ub}|/|V_{cb}| = 0.089 \pm 0.005 \quad (\text{average}). \quad (76.60)$$

where the uncertainty has been scaled by a factor $\sqrt{\chi^2/2} = 1.6$.

76.6 Lepton flavour universality violation

76.6.1 Semitauonic decays

Summary: Semileptonic decays to third-generation leptons provide sensitivity to non-Standard Model amplitudes, such as from a charged Higgs boson [242–245] and from leptoquarks [246–252]. The ratios of branching fractions of semileptonic decays involving tau leptons to those involving $\ell = e/\mu$, $R(D^{(*)}) \equiv \mathcal{B}(\bar{B} \rightarrow D^{(*)}\tau\bar{\nu}_\tau)/\mathcal{B}(\bar{B} \rightarrow D^{(*)}\ell\bar{\nu}_\ell)$, are predicted with good precision and consistency in the Standard Model [7–11, 27, 28, 30, 47, 48], using a variety of different strategies. Because this ratio is independent of $|V_{cb}|$, it can, in principle, be computed entirely from within the Standard Model, without using experimental decay rate data. For example, in Refs. [7, 9] the lattice-QCD only ratios are obtained as:

$$\begin{aligned} R(D)^{\text{LQCD, FNAL-MILC}} &= 0.284 \pm 0.014, \\ R(D^*)^{\text{LQCD, FNAL-MILC}} &= 0.265 \pm 0.013. \end{aligned} \quad (76.61)$$

Without constraints from experimental data at large recoil, such SM-theory only evaluations tend to be less precise than those obtained from joint fits that employ experimental data as well as Standard-Model theory inputs (lattice-QCD form factors, HQET constraints, etc.). Other recent lattice-QCD only results are found in Refs. [10, 11]. Here we use an average of Refs. [27, 28, 47, 48, 253] for $R(D)$ and Refs. [27, 28, 30, 63, 253] for $R(D^*)$.

$$\begin{aligned} R(D)^{\text{SM+Exp}} &= 0.298 \pm 0.004, \\ R(D^*)^{\text{LQCD+Exp}} &= 0.254 \pm 0.005. \end{aligned} \quad (76.62)$$

These use various combinations of experimental data, lattice-QCD form factor inputs, HQET constraints, and LCSR estimates and are consistent with the values quoted above.

Measurements [254–261], of these ratios yield higher values; averaging B -tagged measurements of $R(D)$ and $R(D^*)$ at the $\Upsilon(4S)$ and at LHCb yields [6]

$$\begin{aligned} R(D)^{\text{meas}} &= 0.357 \pm 0.029, \\ R(D^*)^{\text{meas}} &= 0.284 \pm 0.012, \end{aligned} \quad (76.63)$$

with a linear correlation of -0.37 . These values exceed the Standard Model predictions of Eq. (76.62) by 2.0σ and 2.2σ , respectively. A variety of new physics models have been proposed to explain this excess, see eg. Refs. [242–249] as well as reviews in Refs. [262–264].

76.6.2 Sensitivity of $\bar{B} \rightarrow D^{(*)}\tau\bar{\nu}_\tau$ to additional amplitudes

In addition to the helicity amplitudes present for decays to $e\bar{\nu}_e$ and $\mu\bar{\nu}_\mu$, decays proceeding through $\tau\bar{\nu}_\tau$ include a scalar amplitude H_s . The differential decay rate is given by [266]

$$\begin{aligned} \frac{d\Gamma}{dq^2} &= \frac{G_F^2 |V_{cb}|^2 |\mathbf{p}_{D^{(*)}}^*|^2}{96\pi^3 m_B^2} \left(1 - \frac{m_\tau^2}{q^2} \right)^2 \\ &\left[(|H_+|^2 + |H_-|^2 + |H_0|^2) \left(1 + \frac{m_\tau^2}{2q^2} \right) + \frac{3m_\tau^2}{2q^2} |H_s|^2 \right], \end{aligned} \quad (76.64)$$

where $|\mathbf{p}_{D^{(*)}}^*|$ is the 3-momentum of the $D^{(*)}$ in the \bar{B} rest frame and the helicity amplitudes H depend on the four-momentum transfer q^2 . All four helicity amplitudes contribute to $\bar{B} \rightarrow D^*\tau\bar{\nu}_\tau$, while only H_0 and H_s contribute to $\bar{B} \rightarrow D\tau\bar{\nu}_\tau$; as a result, new physics contributions can produce larger effects in the latter mode. Semi-leptonic B decays into a τ lepton provide a stringent test of the two-Higgs doublet model of type II (2HDM-II), i.e. where the two Higgs doublets couple separately to up- and down-type quarks. The distinct feature of the 2HDM-II is that the contributions of the charged scalars scale as $m_\tau^2/m_{H^\pm}^2$, since the couplings to the charged Higgs particles are proportional to the mass of the lepton. As a consequence, one may expect visible effects in decays into a τ , but only small effects for decays into e and μ . The present data disfavors the 2HDM-II, see below.

Table 76.3: Measurements of $R(D)$ and $R(D^*)$, their correlations, ρ , and the combined averages [6].

		$R(D) \times 10^2$	$R(D^*) \times 10^2$	ρ
BABAR [254, 255]	B^0, B^+	$44.0 \pm 5.8 \pm 4.2$	$33.2 \pm 2.4 \pm 1.8$	-0.27
Belle [256]	B^0, B^+	$37.5 \pm 6.4 \pm 2.6$	$29.3 \pm 3.8 \pm 1.5$	-0.49
Belle [257, 265]	B^0, B^+		$27.0 \pm 3.5 \pm_{-2.5}^{+2.8}$	
Belle [258]	B^0, B^+	$30.7 \pm 3.7 \pm 1.6$	$28.3 \pm 1.8 \pm 1.4$	-0.51
LHCb [261]	$B^+ (R(D)), B^0$	$44.1 \pm 6.0 \pm 6.6$	$28.1 \pm 1.8 \pm 2.4$	-0.43
LHCb [260]	B^0		$25.7 \pm 1.2 \pm 1.8$	
Belle II [259]	B^0, B^+		$26.2 \pm_{-3.9-3.2}^{+4.1+3.5}$	
Average	B^0, B^+	35.7 ± 2.9	28.4 ± 1.2	-0.40

76.6.3 Measurement of $R(D^{(*)})$

$\bar{B} \rightarrow D^{(*)}\tau\bar{\nu}_\tau$ decays have been studied at the $\Upsilon(4S)$ resonance and in pp collisions. At the $\Upsilon(4S)$, the majority of experimental measurements are based on signatures that consist of a D or D^* meson, an electron or muon (denoted here by ℓ) from the decay $\tau \rightarrow \ell\nu_\tau\bar{\nu}_\ell$, a fully-reconstructed decay of the second B meson in the event, and multiple missing neutrinos. One analysis reconstructs the τ in a hadronic mode. The analyses that use hadronic B tags separate signal decays from $\bar{B} \rightarrow D^{(*)}\ell\bar{\nu}_\ell$ decays using the lepton momentum and the measured missing mass squared; decays with only a single missing neutrino peak sharply at zero in this variable, while the signal is spread out to positive values. When a semileptonic B tag is used, the discrimination between signal and $\bar{B} \rightarrow D^{(*)}\ell\bar{\nu}_\ell$ decays comes from the calorimeter energy that is not associated with any particle used in the reconstruction of the B meson candidates, the measured missing mass squared and the cosine of the angle between the $D^*\ell$ system and its parent B meson, which is calculated under the assumption that only one particle (a neutrino) is missing. In both these approaches, background from $\bar{B} \rightarrow D^{(*)}\ell\bar{\nu}_\ell$ decays with one or more unreconstructed particles is challenging to separate from signal, as is background from $\bar{B} \rightarrow D^{(*)}H_c X$ (where H_c is a hadron containing a \bar{c} quark) decays. The leading sources of systematic uncertainty are due to the limited size of simulation samples used in constructing the PDFs, the composition of the D^{**} states, efficiency corrections, and cross-feed (swapping soft particles between the signal and tag B).

The most precise measurement from Belle [258] uses semileptonic B tags and leptonic τ decays to simultaneously measure $R(D^*)$ and $R(D)$. The measurement combines results from charged and neutral B decays for both $R(D^*)$ and $R(D)$, and is compatible with the Standard Model expectation to approximately 1σ . The first result from Belle II [259] uses a hadronic tag to measure $R(D^*)$ in $\bar{B} \rightarrow D^*\tau^-\bar{\nu}_\tau$ decays with a 189 fb $^{-1}$ dataset. The statistical power of the Belle II dataset has been found to outperform that of Belle in this channel.

In addition to the ratio measurements, the Belle experiment has performed polarization measurements of the τ [257] and D^* [267] respectively. The τ polarization measurement uses hadronic B tags and τ^- decays to $\pi^-\nu_\tau$ or $\rho^-\nu_\tau$. The main discriminant variables are the measured missing mass squared and the unassociated calorimeter energy. This measurement provides the first determination of the τ polarization in the $\bar{B} \rightarrow D^*\tau\bar{\nu}_\tau$ decay, $\mathcal{P}_\tau(D^*) = -0.38 \pm 0.51 \pm_{-0.16}^{+0.21}$, compatible with the Standard Model expectation [30], $\mathcal{P}_\tau(D^*) = -0.476 \pm_{-0.034}^{+0.037}$.

The main uncertainties on the $R(D^*)$ measurement come from the composition of the hadronic B background and from modeling of semileptonic B decays and mis-reconstructed D^* mesons. The D^* polarization measurement uses an inclusive tag approach based on Refs. [268, 269], and reconstructs the τ decays in $\ell\nu_\tau\bar{\nu}_\ell$ and $\pi^+\bar{\nu}_\tau$ channels. The main discriminant variables are X_{miss} , a quantity that approximates missing mass but does not depend on tag B reconstruction, the visible energy of the event, and the beam-energy constrained mass, M_{bc} , of the inclusively reconstructed tag side B . This measurement provides the first determination of the D^* longitudinal polarization fraction in the $\bar{B} \rightarrow D^*\tau\bar{\nu}_\tau$ decay, $\mathcal{F}_L(D^*) = -0.38 \pm 0.60 \pm_{-0.04}^{+0.08}$, compatible with the Standard Model expectation [270] within 1.7σ .

The LHCb experiment has performed a simultaneous analysis of $R(D^*)$ and $R(D)$ where $\tau \rightarrow \mu\nu_\tau\bar{\nu}_\mu$. The reconstructed decay modes are $\bar{B}^0 \rightarrow D^{*+}\tau^-\bar{\nu}_\tau$ with $D^{*+} \rightarrow D^0\pi^+$, $B^- \rightarrow D^{*0}\tau^-\bar{\nu}_\tau$ with $D^{*0} \rightarrow D^0\pi^0$ and $D^{*0} \rightarrow D^0\pi^0$, and $B^- \rightarrow D^0\tau^-\bar{\nu}_\tau$. Their analysis [261] takes advantage of the measurable flight lengths of b and c hadrons and τ leptons. A multivariate discriminant is used to select decays where no additional charged particles are consistent with coming from the signal decay vertices. The separation between the primary and B decay vertices is used to calculate the momentum of the B decay products transverse to the B flight direction. The longitudinal component of the B momentum can be estimated based on the visible decay products; this allows a determination of the B rest frame, with modest resolution, and enables the calculation of similar discrimination variables to those available at the $e^+e^- B$ factories. The (rest frame) muon energy, missing mass-squared and q^2 are used in a 3- d fit.

A complementary LHCb result [260] on $R(D^*)$ uses three-prong τ decays that take advantage of their excellent vertex resolution to isolate the τ decay from hadronic background. A 3- d fit is performed to determine the signal yield, based on the $\tau\nu_\tau$ pair q^2 , the τ lifetime, as well as a boosted decision tree classifier based on isolation, invariant mass and flight distance information. The leading sources of systematic uncertainty are due to the size of the simulation sample used in constructing the fit templates, uncertainties in modelling the background from hadronic $\bar{B} \rightarrow D^{(*)}H_c X$ decays, as well as reconstruction and trigger effects. The result is normalized to $B^0 \rightarrow D^{*-}\pi^+\pi^-\pi^+$ and found to be 1σ from the Standard Model expectation (using the expectation value quoted here). An analogous measurement of $B_c \rightarrow J/\psi\tau\bar{\nu}_\tau$ was performed by the LHCb measurement [271], in leptonic τ decays. The result, $R(J/\psi) = 0.71 \pm 0.17 \pm 0.18$, while relatively high is compatible to within 2σ of a recent Standard Model evaluation [272] based on a lattice-QCD calculation [273] of the form factors. Systematic uncertainties are dominated by form factors, as B_c decays are relatively unexplored.

Measurements from BABAR [254, 255], Belle [256–258], Belle II [259] and LHCb [260, 261] result in values for $R(D)$ and $R(D^*)$ that exceed Standard Model predictions. Table 76.3 lists these values and their average. The simultaneous measurements of $R(D)$ and $R(D^*)$ have linear correlation coefficients of -0.27 (BABAR [254, 255]), -0.49 (Belle hadronic tag [256]), -0.51 (Belle semileptonic tag [258]), and 0.43 (LHCb $\tau^- \rightarrow \mu^-\nu_\tau\bar{\nu}_\mu$); the $R(D)$ and $R(D^*)$ averages have a correlation of -0.40 . Two early untagged Belle measurements [268, 269] are subject to larger systematic uncertainties, with a breakdown of the respective contributions that is inconsistent with the more recent determinations, hence they cannot be reliably combined in the average. All three experiments assume the Standard Model kinematic distributions for $\bar{B} \rightarrow D^{(*)}\tau\bar{\nu}_\tau$ in their determinations of the branching fraction ratios.

The measurement combination in the $R(D) - R(D^*)$ plane is shown in Fig. 76.2, compared with the predictions in Eq. (76.61) (LQCD) and Eq. (76.62) (Experiment+LQCD+HQET). The measurement combination is based on Ref. [6] and online updates with the inclusion of recent results from LHCb and Belle II. The tension between the Standard Model prediction in Eq. (76.62) and the measurements is at the level of 2.0σ ($R(D)$) and 2.2σ ($R(D^*)$); if one considers these deviations together the significance is 3.3σ . This motivates speculation on possible new physics contributions.

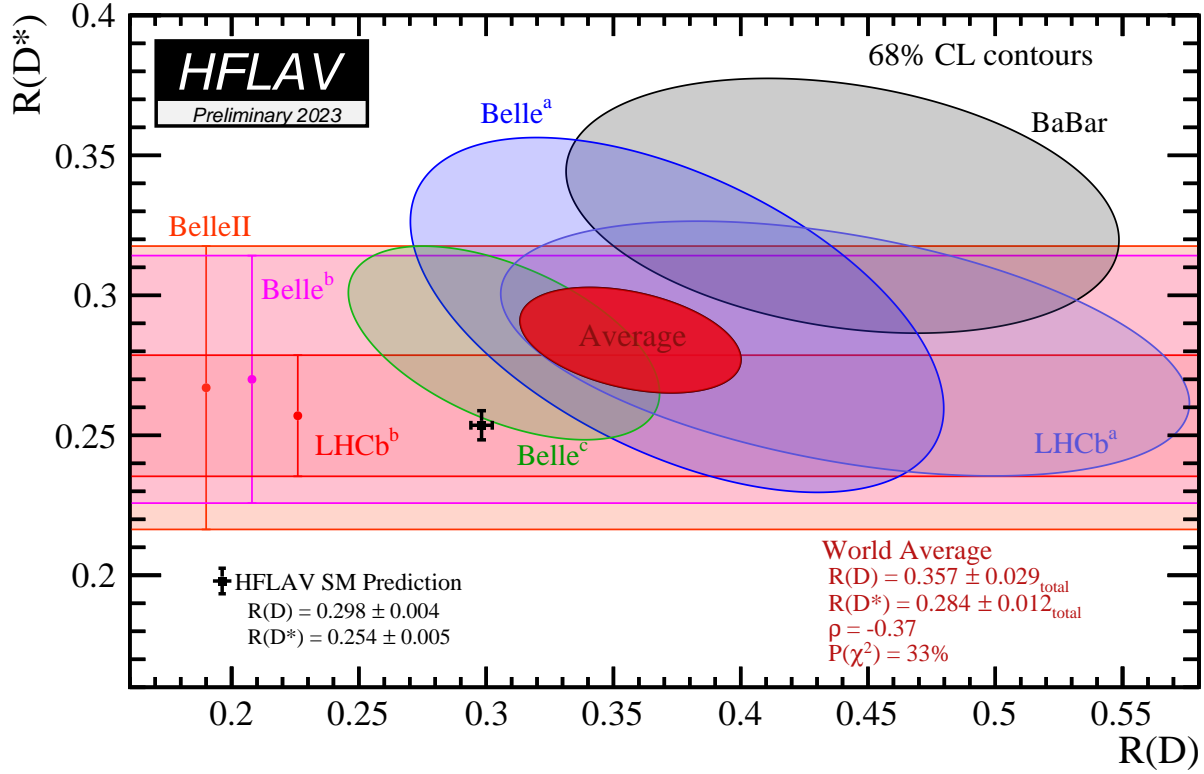


Figure 76.2: Measurements of $R(D)$ and $R(D^*)$ and their two-dimensional average compared with the average predictions for $R(D)$ and $R(D^*)$ given in Eq. 76.62. Contours correspond to 68% CL. The experiment-lattice QCD-HQET predictions and the experimental average deviate from each other by 3.3σ .

The measurements reported in Refs. [259, 260, 265] are all in reasonable agreement with the Standard-Model predictions. There is some tension in the combination coming from the BABAR measurement and the most recent LHCb measurement [261]. The BABAR measurement is the only one to claim a deviation from the Standard Model of more than 3σ , although the p -value of the full combination is an acceptable 33%.

The current discussion of $R(D)$ and $R(D^*)$ may be embedded in the theoretical analysis of the other anomalies that have been observed in semileptonic FCNC ($b \rightarrow s\ell\ell$) transitions. More sophisticated approaches fit the data to a general effective Hamiltonian. Matching this effective Hamiltonian to simplified models, the current situation of the anomalies seems to be compatible with scenarios with an additional Z' or a leptoquark scenario, see eg. [246–252].

76.6.4 Measurements of $R(X)$

We note that in addition to exclusive modes, inclusive modes also offer an opportunity to test the presence of non-Standard Model contributions, although typically with lower precision. The first measurement of $R(X)$ from a B -factory was recently performed by Belle II [274], $R(X) = 0.228 \pm 0.039$, and found to be compatible with an average of Standard Model predictions $R(X) = 0.223 \pm 0.005$ [275–277]. Prior measurements of the branching fractions of $b \rightarrow X\tau\nu$ were performed by LEP experiments and also found to be compatible with Standard Model predictions.

76.6.5 Ratios of semileptonic decay rates with e to μ final states

Several tests of lepton flavor universality in semileptonic B decays have recently been undertaken at Belle and Belle II. This includes ratios of rates to electron and muon modes (i.e. $R(e/\mu)$) performed as part of CKM matrix element extraction analyses (Table 76.4), as well as dedicated flavour dependent angular anal-

yses [278]. Refs. [62, 64, 65] provide measurements of LFUV in $\bar{B} \rightarrow D^*\ell\bar{\nu}$ decays at Belle (untagged, and hadron tagged) and Belle II (hadron tagged). The corresponding theoretical prediction is $\mathcal{B}(B \rightarrow D^*e\nu)/\mathcal{B}(B \rightarrow D^*\mu\nu) = 1.0041 \pm 0.0001$ [33]. Refs. [176, 279] provide measurements of LFUV in $B \rightarrow X_c\ell\bar{\nu}$ in hadron tagged events at Belle and Belle II, where the theoretical expectation is $\mathcal{B}(B \rightarrow X_c e\nu)/\mathcal{B}(B \rightarrow X_c \mu\nu) = 1.006 \pm 0.001$ [276]. Finally, Ref. [173] provides a result for LFUV in $B \rightarrow X_u\ell\nu$ decays where the ratio is expected to be close to 1, as in the $B \rightarrow X_c\ell\nu$ case. With the exception of the charmless decay measurement, the experimental uncertainties are dominated by lepton identification uncertainties that do not cancel in the ratios. All results are found to be highly compatible with SM expectations.

Table 76.4: Measurements of $R(e/\mu) = \mathcal{B}(B \rightarrow X_e\nu)/\mathcal{B}(B \rightarrow X_\mu\nu)$ where the specific decay process is listed.

Ref.	Decay	$R(e/\mu) \times 100$
Belle [64]	$B \rightarrow D^*\ell\bar{\nu}$	$99.2 \pm 2.3 \pm 2.3$
Belle [62]	$B^0 \rightarrow D^{*+}\ell\nu$	$101 \pm 1 \pm 3$
Belle II [65]	$B^0 \rightarrow D^{*+}\ell\nu$	$99.8 \pm 0.9 \pm 2.0$
Belle II [279]	$B \rightarrow X_c\ell\nu$	$100.7 \pm 0.9 \pm 1.9$
Belle [176]	$B \rightarrow X_c\ell\nu$	$100.3 \pm 0.5 \pm 2.4$
Belle [173]	$B \rightarrow X_u\ell\nu$	$97 \pm 9 \pm 4$

76.7 Conclusion

The study of semileptonic B meson decays continues to be an active area for both theory and experiment. The application of HQE calculations to inclusive decays is well established, and fits to moments of $\bar{B} \rightarrow X_c\ell\bar{\nu}_\ell$ decays provide precise values for $|V_{cb}|$ and, in conjunction with input on m_c or from $B \rightarrow X_s\gamma$ decays, provide precise and consistent values for m_b . Recent developments

will make use of more types of moments and better theoretical inputs to constrain higher order effects. Further into the future, new nonperturbative methods to compute inclusive decay rates, for example, in lattice QCD [280–282], may provide interesting new insights.

The determination of $|V_{ub}|$ from inclusive $\bar{B} \rightarrow X_u \ell \bar{\nu}_\ell$ decays is based on multiple calculational approaches and independent measurements over a variety of kinematic regions, all of which provide consistent results. Further progress in this area is possible, but will require better theoretical control over higher-order terms, improved experimental knowledge of the $\bar{B} \rightarrow X_c \ell \bar{\nu}_\ell$ background and improvements to the modeling of the $\bar{B} \rightarrow X_u \ell \bar{\nu}_\ell$ signal distributions.

In both $b \rightarrow u$ and $b \rightarrow c$ exclusive channels there has been significant recent progress in lattice-QCD calculations, resulting in improved precision on both $|V_{ub}|$ and $|V_{cb}|$. These calculations now provide information on the form factors well away from the high q^2 region, allowing better use of experimental data. For $|V_{cb}|$ recent measurements have provided binned data enabling model-independent fits.

The values from the inclusive and exclusive determinations of $|V_{cb}|$ and $|V_{ub}|$ are only marginally consistent. This is a long-standing puzzle that the recent improvements have, unfortunately, not yet resolved.

Both $|V_{cb}|$ and $|V_{ub}|$ are indispensable inputs into unitarity triangle fits. In particular, knowing $|V_{ub}|$ with good precision allows a test of CKM unitarity in a most direct way, by comparing the length of the $|V_{ub}|$ side of the unitarity triangle with the measurement of $\sin(2\beta)$. This comparison of a “tree” process ($b \rightarrow u$) with a “loop-induced” process ($B^0 - \bar{B}^0$ mixing) provides sensitivity to possible contributions from new physics.

The observation of semileptonic decays into τ leptons has opened a new window to the physics of the third generation. The measurements indicate a tension between the data and Standard-Model predictions, which could be a hint for new physics, manifesting itself as a violation of lepton universality beyond the Standard-Model couplings to the Higgs. It should be noted that none of the most recent measurements alone claim discovery of a deviation from the Standard Model. Combining the data of the semitaonic decays with the anomalies observed in the FCNC $b \rightarrow s \ell \ell$ transitions allows an interpretation in terms of additional Z' or in terms of additional leptiquarks, but the current data does not allow us to draw a definite conclusion.

Acknowledgements

We thank J. Flynn, E. Kou, C. Schwanda, and K. Vos for useful discussions and comments on this review, and A. Vaquero for creating Fig. 76.1. Previous assistance from D. Ferlewicz, P. Gambino, S. Hashimoto, Z. Ligeti, and M. Rotondo is also acknowledged.

References

- [1] See “Leptonic Decays of Charged Pseudoscalar Mesons” by J.L. Rosner, S.L. Stone, and R. Van de Water in this *Review*.
- [2] R. L. Workman and Others (Particle Data Group), *PTEP* **2022**, 083C01 (2022).
- [3] See “Heavy-Quark and Soft-Collinear Effective Theory” by C.W. Bauer and M. Neubert in this *Review*.
- [4] See “Lattice Quantum Chromodynamics” by S. Hashimoto, J. Laiho, and S.R. Sharpe in this *Review*.
- [5] See “Production and Decay of b -Flavored Hadrons” by P. Eerola, M. Kreps and Y. Kwon in this *Review*.
- [6] Y. S. Amhis *et al.* (Heavy Flavor Averaging Group, HFLAV), *Phys. Rev. D* **107**, 5, 052008 (2023), [arXiv:2206.07501].
- [7] J. A. Bailey *et al.* (Fermilab Lattice and MILC), *Phys. Rev. D* **92**, 3, 034506 (2015), [arXiv:1503.07237].
- [8] H. Na *et al.* (HPQCD), *Phys. Rev. D* **92**, 5, 054510 (2015), [Erratum: *Phys. Rev. D* 93, no.11, 119906 (2016)], [arXiv:1505.03925].
- [9] A. Bazavov *et al.* (Fermilab Lattice, MILC), *Eur. Phys. J. C* **82**, 12, 1141 (2022), [Erratum: *Eur. Phys. J. C* 83, 21 (2023)], [arXiv:2105.14019].
- [10] J. Harrison and C. T. H. Davies (2023), [arXiv:2304.03137].
- [11] Y. Aoki *et al.* (JLQCD) (2023), [arXiv:2306.05657].
- [12] J. Harrison and C. T. H. Davies (HPQCD), *Phys. Rev. D* **105**, 9, 094506 (2022), [arXiv:2105.11433].
- [13] N. Isgur and M. B. Wise, *Phys. Lett.* **B232**, 113 (1989); N. Isgur and M. B. Wise, *Phys. Lett.* **B237**, 527 (1990).
- [14] M. A. Shifman and M. B. Voloshin, *Sov. J. Nucl. Phys.* **47**, 511 (1988), [*Yad. Fiz.* 47, 801 (1988)].
- [15] A. V. Manohar and M. B. Wise, *Camb. Monogr. Part. Phys. Nucl. Phys. Cosmol.* **10**, 1 (2000).
- [16] H. Georgi, *Phys. Lett.* **B240**, 447 (1990).
- [17] A. F. Falk *et al.*, *Nucl. Phys.* **B343**, 1 (1990).
- [18] E. Eichten and B. R. Hill, *Phys. Lett.* **B234**, 511 (1990).
- [19] A. Sirlin, *Nucl. Phys.* **B196**, 83 (1982).
- [20] J. A. Bailey *et al.* (Fermilab Lattice, MILC), *Phys. Rev. D* **89**, 11, 114504 (2014), [arXiv:1403.0635].
- [21] C. G. Boyd, B. Grinstein and R. F. Lebed, *Phys. Rev. Lett.* **74**, 4603 (1995), [hep-ph/9412324].
- [22] C. G. Boyd, B. Grinstein and R. F. Lebed, *Phys. Lett. B* **353**, 306 (1995), [hep-ph/9504235].
- [23] C. G. Boyd, B. Grinstein and R. F. Lebed, *Nucl. Phys. B* **461**, 493 (1996), [hep-ph/9508211].
- [24] C. G. Boyd, B. Grinstein and R. F. Lebed, *Phys. Rev. D* **56**, 6895 (1997), [hep-ph/9705252].
- [25] B. Grinstein and A. Kobach, *Phys. Lett.* **B771**, 359 (2017), [arXiv:1703.08170].
- [26] I. Caprini, L. Lellouch and M. Neubert, *Nucl. Phys.* **B530**, 153 (1998), [hep-ph/9712417].
- [27] M. Bordone, M. Jung and D. van Dyk (2019), [arXiv:1908.09398].
- [28] F. U. Bernlochner *et al.*, *Phys. Rev. D* **95**, 11, 115008 (2017), [erratum: *Phys. Rev. D* 97, no.5, 059902 (2018)], [arXiv:1703.05330].
- [29] D. Bigi, P. Gambino and S. Schacht, *Phys. Lett.* **B769**, 441 (2017), [arXiv:1703.06124].
- [30] P. Gambino, M. Jung and S. Schacht, *Phys. Lett.* **B795**, 386 (2019), [arXiv:1905.08209].
- [31] F. U. Bernlochner, Z. Ligeti and D. J. Robinson, *Phys. Rev. D* **100**, 1, 013005 (2019), [arXiv:1902.09553].
- [32] F. U. Bernlochner *et al.*, *Phys. Rev. D* **96**, 9, 091503 (2017), [arXiv:1708.07134].
- [33] F. U. Bernlochner *et al.*, *Phys. Rev. D* **106**, 9, 096015 (2022), [arXiv:2206.11281].
- [34] M. Jung, private communication.
- [35] J. Harrison, C. Davies and M. Wingate (HPQCD), *Phys. Rev. D* **97**, 5, 054502 (2018), [arXiv:1711.11013].
- [36] Y. Aoki *et al.* (Flavour Lattice Averaging Group (FLAG)), *Eur. Phys. J. C* **82**, 10, 869 (2022), [arXiv:2111.09849].
- [37] I. I. Y. Bigi *et al.*, *Phys. Rev. D* **52**, 196 (1995), [hep-ph/9405410].
- [38] A. Kapustin *et al.*, *Phys. Lett.* **B375**, 327 (1996), [hep-ph/9602262].
- [39] P. Gambino, T. Mannel and N. Uraltsev, *Phys. Rev. D* **81**, 113002 (2010), [arXiv:1004.2859].
- [40] M. A. Shifman, N. G. Uraltsev and A. I. Vainshtein, *Phys. Rev. D* **51**, 2217 (1995), [Erratum: *Phys. Rev. D* 52, 3149 (1995)], [hep-ph/9405207].
- [41] A. Czarnecki, K. Melnikov and N. Uraltsev, *Phys. Rev. D* **57**, 1769 (1998), [hep-ph/9706311].
- [42] P. Gambino, T. Mannel and N. Uraltsev, *JHEP* **10**, 169 (2012), [arXiv:1206.2296].

- [43] N. Gubernari, A. Kokulu and D. van Dyk, JHEP **01**, 150 (2019), [arXiv:1811.00983].
- [44] L. Lellouch, Nucl. Phys. B **479**, 353 (1996), [hep-ph/9509358].
- [45] M. Di Carlo *et al.*, Phys. Rev. D **104**, 5, 054502 (2021), [arXiv:2105.02497].
- [46] G. Martinelli, S. Simula and L. Vittorio (2021), [arXiv:2105.07851].
- [47] D. Bigi and P. Gambino, Phys. Rev. **D94**, 9, 094008 (2016), [arXiv:1606.08030].
- [48] G. Martinelli, S. Simula and L. Vittorio, Phys. Rev. D **105**, 3, 034503 (2022), [arXiv:2105.08674].
- [49] G. Martinelli, S. Simula and L. Vittorio, Eur. Phys. J. C **82**, 12, 1083 (2022), [arXiv:2109.15248].
- [50] G. Martinelli, S. Simula and L. Vittorio, JHEP **08**, 022 (2022), [arXiv:2202.10285].
- [51] G. Martinelli *et al.*, Phys. Rev. D **106**, 9, 093002 (2022), [arXiv:2204.05925].
- [52] J. M. Flynn, A. Jüttner and J. T. Tsang (2023), [arXiv:2303.11285].
- [53] D. Buskulic *et al.* (ALEPH), Phys. Lett. **B395**, 373 (1997).
- [54] G. Abbiendi *et al.* (OPAL), Phys. Lett. **B482**, 15 (2000), [hep-ex/0003013].
- [55] P. Abreu *et al.* (DELPHI), Phys. Lett. **B510**, 55 (2001), [hep-ex/0104026].
- [56] J. Abdallah *et al.* (DELPHI), Eur. Phys. J. **C33**, 213 (2004), [hep-ex/0401023].
- [57] N. E. Adam *et al.* (CLEO), Phys. Rev. **D67**, 032001 (2003), [hep-ex/0210040].
- [58] B. Aubert *et al.* (BaBar), Phys. Rev. **D77**, 032002 (2008), [arXiv:0705.4008].
- [59] B. Aubert *et al.* (BaBar), Phys. Rev. Lett. **100**, 231803 (2008), [arXiv:0712.3493].
- [60] B. Aubert *et al.* (BaBar), Phys. Rev. **D79**, 012002 (2009), [arXiv:0809.0828].
- [61] W. Dungen *et al.* (Belle), Phys. Rev. **D82**, 112007 (2010), [arXiv:1010.5620].
- [62] E. Waheed *et al.* (Belle), Phys. Rev. D **100**, 5, 052007 (2019), [Erratum: Phys.Rev.D 103, 079901 (2021)], [arXiv:1809.03290].
- [63] J. P. Lees *et al.* (BaBar), Phys. Rev. Lett. **123**, 9, 091801 (2019), [arXiv:1903.10002].
- [64] M. T. Prim *et al.* (Belle), Phys. Rev. D **108**, 1, 012002 (2023), [arXiv:2301.07529].
- [65] I. Adachi *et al.* (Belle-II), Phys. Rev. D **108**, 9, 092013 (2023), [arXiv:2310.01170].
- [66] D. Ferlewicz, P. Urquijo and E. Waheed, Phys. Rev. D **103**, 7, 073005 (2021), [arXiv:2008.09341].
- [67] D. Bigi, P. Gambino and S. Schacht, JHEP **11**, 061 (2017), [arXiv:1707.09509].
- [68] B. Aubert *et al.* (BaBar), Phys. Rev. Lett. **104**, 011802 (2010), [arXiv:0904.4063].
- [69] R. Glattauer *et al.* (Belle), Phys. Rev. **D93**, 3, 032006 (2016), [arXiv:1510.03657].
- [70] S. Aoki *et al.* (Flavour Lattice Averaging Group) (2019), [arXiv:1902.08191].
- [71] C. Bourrely, I. Caprini and L. Lellouch, Phys. Rev. **D79**, 013008 (2009), [Erratum: Phys.Rev.D82,099902(2010)], [arXiv:0807.2722].
- [72] C. J. Monahan *et al.*, Phys. Rev. D **95**, 11, 114506 (2017), [arXiv:1703.09728].
- [73] E. McLean *et al.*, Phys. Rev. D **101**, 7, 074513 (2020), [arXiv:1906.00701].
- [74] E. McLean *et al.*, Phys. Rev. D **99**, 11, 114512 (2019), [arXiv:1904.02046].
- [75] R. Aaij *et al.* (LHCb), Phys. Rev. D **101**, 7, 072004 (2020), [arXiv:2001.03225].
- [76] R. Aaij *et al.* (LHCb), Phys. Rev. D **104**, 3, 032005 (2021), [arXiv:2103.06810].
- [77] R. Aaij *et al.* (LHCb), JHEP **12**, 144 (2020), [arXiv:2003.08453].
- [78] A. V. Manohar and M. B. Wise, Phys. Rev. **D49**, 1310 (1994), [hep-ph/9308246].
- [79] I. I. Y. Bigi *et al.*, Phys. Rev. Lett. **71**, 496 (1993), [201(1993)], [hep-ph/9304225]; I. I. Y. Bigi *et al.*, Phys. Lett. **B323**, 408 (1994), [hep-ph/9311339].
- [80] D. Benson *et al.*, Nucl. Phys. **B665**, 367 (2003), [hep-ph/0302262].
- [81] M. Gremm and A. Kapustin, Phys. Rev. **D55**, 6924 (1997), [hep-ph/9603448].
- [82] B. M. Dassing, T. Mannel and S. Turczyk, JHEP **03**, 087 (2007), [hep-ph/0611168].
- [83] I. I. Bigi, N. Uraltsev and R. Zwicky, Eur. Phys. J. **C50**, 539 (2007), [hep-ph/0511158].
- [84] T. Mannel, S. Turczyk and N. Uraltsev, JHEP **11**, 109 (2010), [arXiv:1009.4622].
- [85] A. Pak and A. Czarnecki, Phys. Rev. **D78**, 114015 (2008), [arXiv:0808.3509].
- [86] S. Biswas and K. Melnikov, JHEP **02**, 089 (2010), [arXiv:0911.4142].
- [87] P. Gambino, JHEP **09**, 055 (2011), [arXiv:1107.3100].
- [88] M. Fael, K. Schönwald and M. Steinhauser, Phys. Rev. D **104**, 1, 016003 (2021), [arXiv:2011.13654].
- [89] P. Gambino and N. Uraltsev, Eur. Phys. J. **C34**, 181 (2004), [hep-ph/0401063].
- [90] V. Aquila *et al.*, Nucl. Phys. **B719**, 77 (2005), [hep-ph/0503083].
- [91] M. E. Luke, M. J. Savage and M. B. Wise, Phys. Lett. B **343**, 329 (1995), [hep-ph/9409287].
- [92] M. E. Luke, M. J. Savage and M. B. Wise, Phys. Lett. B **345**, 301 (1995), [hep-ph/9410387].
- [93] T. Becher, H. Boos and E. Lunghi, JHEP **12**, 062 (2007), [arXiv:0708.0855].
- [94] A. Alberti *et al.*, Nucl. Phys. **B870**, 16 (2013), [arXiv:1212.5082].
- [95] A. Alberti, P. Gambino and S. Nandi, JHEP **01**, 147 (2014), [arXiv:1311.7381].
- [96] T. Mannel, A. A. Pivovarov and D. Rosenthal, Phys. Rev. **D92**, 5, 054025 (2015), [arXiv:1506.08167].
- [97] T. Mannel and A. A. Pivovarov, Phys. Rev. D **100**, 9, 093001 (2019), [arXiv:1907.09187].
- [98] T. Mannel, D. Moreno and A. A. Pivovarov, Phys. Rev. D **105**, 5, 054033 (2022), [arXiv:2112.03875].
- [99] C. Breidenbach *et al.*, Phys. Rev. **D78**, 014022 (2008), [arXiv:0805.0971].
- [100] I. Bigi *et al.*, JHEP **04**, 073 (2010), [arXiv:0911.3322].
- [101] A. Kobach and S. Pal, Phys. Lett. **B772**, 225 (2017), [arXiv:1704.00008].
- [102] J. Heinonen and T. Mannel, Nucl. Phys. **B889**, 46 (2014), [arXiv:1407.4384].
- [103] P. Gambino, K. J. Healey and S. Turczyk, Phys. Lett. **B763**, 60 (2016), [arXiv:1606.06174].
- [104] T. Mannel and K. K. Vos, JHEP **06**, 115 (2018), [arXiv:1802.09409].
- [105] M. Fael, T. Mannel and K. Keri Vos, JHEP **02**, 177 (2019), [arXiv:1812.07472].

- [106] I. I. Y. Bigi *et al.*, Phys. Rev. **D50**, 2234 (1994), [hep-ph/9402360].
- [107] A. H. Hoang, Z. Ligeti and A. V. Manohar, Phys. Rev. Lett. **82**, 277 (1999), [hep-ph/9809423].
- [108] A. H. Hoang, Z. Ligeti and A. V. Manohar, Phys. Rev. **D59**, 074017 (1999), [hep-ph/9811239].
- [109] A. H. Hoang and T. Teubner, Phys. Rev. **D60**, 114027 (1999), [hep-ph/9904468].
- [110] A. Hoang, P. Ruiz-Femenia and M. Stahlhofen, JHEP **10**, 188 (2012), [arXiv:1209.0450].
- [111] M. Fael, K. Schönwald and M. Steinhauser, Phys. Rev. Lett. **125**, 5, 052003 (2020), [arXiv:2005.06487].
- [112] S. E. Csorna *et al.* (CLEO), Phys. Rev. **D70**, 032002 (2004), [hep-ex/0403052].
- [113] A. H. Mahmood *et al.* (CLEO), Phys. Rev. **D70**, 032003 (2004), [hep-ex/0403053].
- [114] B. Aubert *et al.* (BaBar), Phys. Rev. **D69**, 111103 (2004), [hep-ex/0403031].
- [115] B. Aubert *et al.* (BaBar), Phys. Rev. **D69**, 111104 (2004), [hep-ex/0403030].
- [116] C. Schwanda *et al.* (Belle), Phys. Rev. **D75**, 032005 (2007), [hep-ex/0611044].
- [117] P. Urquijo *et al.* (Belle), Phys. Rev. **D75**, 032001 (2007), [hep-ex/0610012].
- [118] J. Abdallah *et al.* (DELPHI), Eur. Phys. J. **C45**, 35 (2006), [hep-ex/0510024].
- [119] D. Acosta *et al.* (CDF), Phys. Rev. **D71**, 051103 (2005), [hep-ex/0502003].
- [120] B. Aubert *et al.* (BaBar), Phys. Rev. **D81**, 032003 (2010), [arXiv:0908.0415].
- [121] R. van Tonder *et al.* (Belle), Phys. Rev. D **104**, 11, 112011 (2021), [arXiv:2109.01685].
- [122] F. Abudinén *et al.* (Belle-II), Phys. Rev. D **107**, 7, 072002 (2023), [arXiv:2205.06372].
- [123] A. Limosani *et al.* (Belle), Phys. Rev. Lett. **103**, 241801 (2009), [arXiv:0907.1384].
- [124] C. Schwanda *et al.* (Belle), Phys. Rev. **D78**, 032016 (2008), [arXiv:0803.2158].
- [125] B. Aubert *et al.* (BaBar), Phys. Rev. **D72**, 052004 (2005), [hep-ex/0508004].
- [126] B. Aubert *et al.* (BaBar), Phys. Rev. Lett. **97**, 171803 (2006), [hep-ex/0607071].
- [127] S. Chen *et al.* (CLEO), Phys. Rev. Lett. **87**, 251807 (2001), [hep-ex/0108032].
- [128] M. Battaglia *et al.*, eConf **C0304052**, WG102 (2003), [Phys. Lett. B556,41(2003)], [hep-ph/0210319].
- [129] B. Aubert *et al.* (BaBar), Phys. Rev. Lett. **93**, 011803 (2004), [hep-ex/0404017].
- [130] O. Buchmüller and H. Flächer, hep-ph/0507253 updated in Ref. [283].
- [131] C. W. Bauer *et al.*, Phys. Rev. **D70**, 094017 (2004), updated in Ref. [283], [hep-ph/0408002].
- [132] P. Gambino and C. Schwanda, Phys. Rev. **D89**, 1, 014022 (2014), [arXiv:1307.4551].
- [133] A. Alberti *et al.*, Phys. Rev. Lett. **114**, 6, 061802 (2015), [arXiv:1411.6560].
- [134] M. Bordone, B. Capdevila and P. Gambino, Phys. Lett. B **822**, 136679 (2021), [arXiv:2107.00604].
- [135] M. Antonelli *et al.*, Phys. Rept. **494**, 197 (2010), see section 5.4.2, [arXiv:0907.5386].
- [136] See “Quark Masses” by A.V. Manohar, L.P. Lellouch, and R.M. Barnett in this *Review*.
- [137] M. Fael, K. Schönwald and M. Steinhauser, Phys. Rev. D **103**, 1, 014005 (2021), [arXiv:2011.11655].
- [138] F. Bernlochner *et al.*, JHEP **10**, 068 (2022), [arXiv:2205.10274].
- [139] N. Uraltsev, Int. J. Mod. Phys. **A14**, 4641 (1999), [hep-ph/9905520].
- [140] M. Neubert, Phys. Rev. **D49**, 4623 (1994), [hep-ph/9312311]; M. Neubert, Phys. Rev. **D49**, 3392 (1994), [hep-ph/9311325].
- [141] I. I. Y. Bigi *et al.*, Int. J. Mod. Phys. **A9**, 2467 (1994), [hep-ph/9312359].
- [142] C. W. Bauer, M. E. Luke and T. Mannel, Phys. Rev. **D68**, 094001 (2003), [hep-ph/0102089].
- [143] M. Benzke *et al.*, Phys. Rev. Lett. **106**, 141801 (2011), [arXiv:1012.3167].
- [144] A. Gunawardana and G. Paz, JHEP **11**, 141 (2019), [arXiv:1908.02812].
- [145] F. U. Bernlochner *et al.* (SIMBA), Phys. Rev. Lett. **127**, 10, 102001 (2021), [arXiv:2007.04320].
- [146] M. Neubert, Phys. Lett. **B513**, 88 (2001), [hep-ph/0104280].
- [147] M. Neubert, Phys. Lett. **B543**, 269 (2002), [hep-ph/0207002].
- [148] A. K. Leibovich, I. Low and I. Z. Rothstein, Phys. Rev. **D61**, 053006 (2000), [hep-ph/9909404].
- [149] A. K. Leibovich, I. Low and I. Z. Rothstein, Phys. Rev. **D62**, 014010 (2000), [hep-ph/0001028].
- [150] A. K. Leibovich, I. Low and I. Z. Rothstein, Phys. Lett. **B486**, 86 (2000), [hep-ph/0005124].
- [151] A. K. Leibovich, I. Low and I. Z. Rothstein, Phys. Lett. **B513**, 83 (2001), [hep-ph/0105066].
- [152] A. H. Hoang, Z. Ligeti and M. Luke, Phys. Rev. **D71**, 093007 (2005), [hep-ph/0502134].
- [153] B. O. Lange, M. Neubert and G. Paz, JHEP **10**, 084 (2005), [hep-ph/0508178].
- [154] B. O. Lange, JHEP **01**, 104 (2006), [hep-ph/0511098].
- [155] M. Neubert, Phys. Lett. **B612**, 13 (2005), [hep-ph/0412241].
- [156] Z. Ligeti, I. W. Stewart and F. J. Tackmann, Phys. Rev. **D78**, 114014 (2008), [arXiv:0807.1926].
- [157] P. Gambino, K. J. Healey and C. Mondino, Phys. Rev. **D94**, 1, 014031 (2016), [arXiv:1604.07598].
- [158] B. O. Lange, M. Neubert and G. Paz, Phys. Rev. **D72**, 073006 (2005), [hep-ph/0504071].
- [159] P. Gambino *et al.*, JHEP **10**, 058 (2007), [arXiv:0707.2493].
- [160] J. R. Andersen and E. Gardi, JHEP **01**, 097 (2006), [hep-ph/0509360].
- [161] M. Beneke *et al.*, JHEP **06**, 071 (2005), [hep-ph/0411395].
- [162] C. Greub, M. Neubert and B. D. Pecjak, Eur. Phys. J. **C65**, 501 (2010), [arXiv:0909.1609].
- [163] M. Brucherseifer, F. Caola and K. Melnikov, Phys. Lett. **B721**, 107 (2013), [arXiv:1302.0444].
- [164] T. Mannel and S. Recksiegel, Phys. Rev. **D60**, 114040 (1999), [hep-ph/9904475].
- [165] U. Aglietti *et al.*, Eur. Phys. J. **C59**, 831 (2009), [arXiv:0711.0860].
- [166] C. W. Bauer, Z. Ligeti and M. E. Luke, Phys. Rev. **D64**, 113004 (2001), [hep-ph/0107074].
- [167] C. W. Bauer, Z. Ligeti and M. E. Luke, Phys. Lett. **B479**, 395 (2000), [hep-ph/0002161].
- [168] I. I. Y. Bigi and N. G. Uraltsev, Nucl. Phys. **B423**, 33 (1994), [hep-ph/9310285].
- [169] M. B. Voloshin, Phys. Lett. **B515**, 74 (2001), [hep-ph/0106040].
- [170] Z. Ligeti, M. Luke and A. V. Manohar, Phys. Rev. **D82**, 033003 (2010), [arXiv:1003.1351].

- [171] P. Gambino and J. F. Kamenik, Nucl. Phys. **B840**, 424 (2010), [arXiv:1004.0114].
- [172] J. L. Rosner *et al.* (CLEO), Phys. Rev. Lett. **96**, 121801 (2006), [hep-ex/0601027].
- [173] L. Cao *et al.* (Belle), Phys. Rev. D **104**, 1, 012008 (2021), [arXiv:2102.00020].
- [174] B. Aubert *et al.* (BaBar), in “23rd International Symposium on Lepton-Photon Interactions at High Energy (LP07),” (2007), [arXiv:0708.1753].
- [175] J. P. Lees *et al.* (BaBar), Phys. Rev. D **86**, 032004 (2012), [arXiv:1112.0702].
- [176] M. Hohmann *et al.* (Belle) (2023), [arXiv:2311.00458].
- [177] R. Barate *et al.* (ALEPH), Eur. Phys. J. **C6**, 555 (1999).
- [178] M. Acciarri *et al.* (L3), Phys. Lett. **B436**, 174 (1998).
- [179] G. Abbiendi *et al.* (OPAL), Eur. Phys. J. **C21**, 399 (2001), [hep-ex/0107016].
- [180] P. Abreu *et al.* (DELPHI), Phys. Lett. **B478**, 14 (2000), [hep-ex/0105054].
- [181] A. Bornheim *et al.* (CLEO), Phys. Rev. Lett. **88**, 231803 (2002), [hep-ex/0202019].
- [182] A. Limosani *et al.* (Belle), Phys. Lett. **B621**, 28 (2005), [hep-ex/0504046].
- [183] J. P. Lees *et al.* (BaBar), Phys. Rev. **D95**, 7, 072001 (2017), [arXiv:1611.05624].
- [184] B. Aubert *et al.* (BaBar), Phys. Rev. Lett. **95**, 111801 (2005), [Erratum: Phys. Rev. Lett.97,019903(2006)], [hep-ex/0506036].
- [185] R. V. Kowalewski and S. Menke, Phys. Lett. **B541**, 29 (2002), [hep-ex/0205038].
- [186] J. P. Lees *et al.* (BaBar), Phys. Rev. **D86**, 032004 (2012), [arXiv:1112.0702].
- [187] I. Bizjak *et al.* (Belle), Phys. Rev. Lett. **95**, 241801 (2005), [hep-ex/0505088].
- [188] P. Urquijo *et al.* (Belle), Phys. Rev. Lett. **104**, 021801 (2010), [arXiv:0907.0379].
- [189] B. Aubert *et al.* (BaBar), Phys. Rev. Lett. **96**, 221801 (2006), [hep-ex/0601046].
- [190] L. Cao *et al.* (Belle), Phys. Rev. Lett. **127**, 26, 261801 (2021), [arXiv:2107.13855].
- [191] L. Cao *et al.* (Belle) (2023), [arXiv:2303.17309].
- [192] A. Sibidanov *et al.* (Belle), Phys. Rev. **D88**, 3, 032005 (2013), [arXiv:1306.2781].
- [193] B. Aubert *et al.* (BaBar), Phys. Rev. Lett. **90**, 181801 (2003), [eConfC0304052,WG117(2003)], [hep-ex/0301001].
- [194] T. Hokuue *et al.* (Belle), Phys. Lett. **B648**, 139 (2007), [hep-ex/0604024].
- [195] B. Aubert *et al.* (BaBar), Phys. Rev. **D79**, 052011 (2009), [arXiv:0808.3524].
- [196] J. P. Lees *et al.* (BaBar), Phys. Rev. **D88**, 7, 072006 (2013), [arXiv:1308.2589].
- [197] J. P. Lees *et al.* (BaBar), Phys. Rev. **D87**, 3, 032004 (2013), [Erratum: Phys. Rev.D87,no.9,099904(2013)], [arXiv:1205.6245].
- [198] C. Schwanda *et al.* (Belle), Phys. Rev. Lett. **93**, 131803 (2004), [hep-ex/0402023].
- [199] N. E. Adam *et al.* (CLEO), Phys. Rev. Lett. **99**, 041802 (2007), [hep-ex/0703041].
- [200] S. B. Athar *et al.* (CLEO), Phys. Rev. **D68**, 072003 (2003), superceded by Ref. [201], [hep-ex/0304019].
- [201] R. Gray *et al.* (CLEO), Phys. Rev. **D76**, 012007 (2007), [Addendum: Phys. Rev.D76,no.3,039901(2007)], [hep-ex/0703042].
- [202] P. del Amo Sanchez *et al.* (BaBar), Phys. Rev. **D83**, 032007 (2011), supercedes Ref. [203], [arXiv:1005.3288].
- [203] B. Aubert *et al.* (BaBar), Phys. Rev. **D72**, 051102 (2005), [hep-ex/0507003].
- [204] P. del Amo Sanchez *et al.* (BaBar), Phys. Rev. **D83**, 052011 (2011), updated in Ref. [205], [arXiv:1010.0987].
- [205] J. P. Lees *et al.* (BaBar), Phys. Rev. **D86**, 092004 (2012), [arXiv:1208.1253].
- [206] J. A. Bailey *et al.* (Fermilab Lattice, MILC), Phys. Rev. **D92**, 1, 014024 (2015), [arXiv:1503.07839].
- [207] A. Bazavov *et al.* (Fermilab Lattice, MILC), Phys. Rev. **D100**, 3, 034501 (2019), [arXiv:1901.02561].
- [208] C. M. Bouchard *et al.*, Phys. Rev. **D90**, 054506 (2014), [arXiv:1406.2279].
- [209] J. M. Flynn *et al.*, Phys. Rev. **D91**, 7, 074510 (2015), [arXiv:1501.05373].
- [210] J. M. Flynn *et al.* (RBC/UKQCD), Phys. Rev. D **107**, 11, 114512 (2023), [arXiv:2303.11280].
- [211] B. Colquhoun *et al.* (JLQCD), Phys. Rev. D **106**, 5, 054502 (2022), [arXiv:2203.04938].
- [212] A. X. El-Khadra, A. S. Kronfeld and P. B. Mackenzie, Phys. Rev. D **55**, 3933 (1997), [hep-lat/9604004].
- [213] A. Berns and H. Lamm, JHEP **12**, 114 (2018), [arXiv:1808.07360].
- [214] N. Gubernari, D. van Dyk and J. Virto, JHEP **02**, 088 (2021), [arXiv:2011.09813].
- [215] T. Blake *et al.*, Phys. Rev. D **108**, 9, 094509 (2023), [arXiv:2205.06041].
- [216] N. Gubernari *et al.*, JHEP **09**, 133 (2022), [arXiv:2206.03797].
- [217] T. Becher and R. J. Hill, Phys. Lett. **B633**, 61 (2006), [hep-ph/0509090].
- [218] M. C. Arnesen *et al.*, Phys. Rev. Lett. **95**, 071802 (2005), [hep-ph/0504209].
- [219] M. A. Shifman, A. I. Vainshtein and V. I. Zakharov, Nucl. Phys. **B147**, 385 (1979); M. A. Shifman, A. I. Vainshtein and V. I. Zakharov, Nucl. Phys. **B147**, 448 (1979).
- [220] P. Ball and R. Zwicky, Phys. Rev. **D71**, 014015 (2005), [hep-ph/0406232].
- [221] G. Duplancic *et al.*, JHEP **04**, 014 (2008), [arXiv:0801.1796].
- [222] A. Bharucha, JHEP **05**, 092 (2012), [arXiv:1203.1359].
- [223] A. V. Rusov, Eur. Phys. J. **C77**, 7, 442 (2017), [arXiv:1705.01929].
- [224] I. Sentitemsu Imsong *et al.*, JHEP **02**, 126 (2015), [arXiv:1409.7816].
- [225] D. Lejjak, B. Melić and D. van Dyk, JHEP **07**, 036 (2021), [arXiv:2102.07233].
- [226] H. Ha *et al.* (Belle), Phys. Rev. **D83**, 071101 (2011), [arXiv:1012.0090].
- [227] B. Aubert *et al.* (BaBar), Phys. Rev. Lett. **101**, 081801 (2008), [arXiv:0805.2408].
- [228] W. S. Brower and H. P. Paar, Nucl. Instrum. Meth. **A421**, 411 (1999), [hep-ex/9710029].
- [229] P. Ball, eConf **C070512**, 016 (2007), [arXiv:0705.2290].
- [230] J. M. Flynn and J. Nieves, Phys. Lett. **B649**, 269 (2007), [hep-ph/0703284].
- [231] S. Aoki *et al.*, Eur. Phys. J. **C77**, 2, 112 (2017), [arXiv:1607.00299].
- [232] A. Biswas *et al.*, JHEP **07**, 082 (2021), [arXiv:2103.01809].
- [233] R. Aaij *et al.* (LHCb), Phys. Rev. Lett. **126**, 8, 081804 (2021), [arXiv:2012.05143].
- [234] A. Khodjamirian and A. V. Rusov, JHEP **08**, 112 (2017), [arXiv:1703.04765].
- [235] A. Bazavov *et al.* (Fermilab Lattice, MILC), Phys. Rev. D **107**, 9, 094516 (2023), [arXiv:2212.12648].

- [236] C. Bolognani, D. van Dyk and K. K. Vos (2023), [arXiv:2308.04347].
- [237] T. Feldmann and M. W. Y. Yip, Phys. Rev. **D85**, 014035 (2012), [Erratum: Phys. Rev. D86,079901(2012)], [arXiv:1111.1844].
- [238] W. Detmold, C. Lehner and S. Meinel, Phys. Rev. **D92**, 3, 034503 (2015), [arXiv:1503.01421].
- [239] R. Aaij *et al.* (LHCb), Nature Phys. **11**, 743 (2015), [arXiv:1504.01568].
- [240] M. Ablikim *et al.* (BESIII), Phys. Rev. Lett. **116**, 5, 052001 (2016), [arXiv:1511.08380].
- [241] R. Aaij *et al.* (LHCb), Phys. Rev. **D96**, 11, 112005 (2017), [arXiv:1709.01920].
- [242] M. Tanaka, Z. Phys. **C67**, 321 (1995), [hep-ph/9411405].
- [243] H. Itoh, S. Komine and Y. Okada, Prog. Theor. Phys. **114**, 179 (2005), [hep-ph/0409228].
- [244] U. Nierste, S. Trine and S. Westhoff, Phys. Rev. **D78**, 015006 (2008), [arXiv:0801.4938].
- [245] M. Tanaka and R. Watanabe, Phys. Rev. **D82**, 034027 (2010), [arXiv:1005.4306].
- [246] A. Datta, M. Duraisamy and D. Ghosh, Phys. Rev. **D86**, 034027 (2012), [arXiv:1206.3760].
- [247] D. Becirevic, N. Kosnik and A. Tayduganov, Phys. Lett. **B716**, 208 (2012), [arXiv:1206.4977].
- [248] S. Fajfer *et al.*, Phys. Rev. Lett. **109**, 161801 (2012), [arXiv:1206.1872].
- [249] A. Crivellin, C. Greub and A. Kokulu, Phys. Rev. **D86**, 054014 (2012), [arXiv:1206.2634].
- [250] M. Bauer and M. Neubert, Phys. Rev. Lett. **116**, 14, 141802 (2016), [arXiv:1511.01900].
- [251] I. Doršner *et al.*, Phys. Rept. **641**, 1 (2016), [arXiv:1603.04993].
- [252] A. Celis *et al.*, Phys. Lett. **B771**, 168 (2017), [arXiv:1612.07757].
- [253] S. Jaiswal, S. Nandi and S. K. Patra, JHEP **12**, 060 (2017), [arXiv:1707.09977].
- [254] J. P. Lees *et al.* (BaBar), Phys. Rev. Lett. **109**, 101802 (2012), [arXiv:1205.5442].
- [255] J. P. Lees *et al.* (BaBar), Phys. Rev. **D88**, 7, 072012 (2013), [arXiv:1303.0571].
- [256] M. Huschle *et al.* (Belle), Phys. Rev. **D92**, 7, 072014 (2015), [arXiv:1507.03233].
- [257] S. Hirose *et al.* (Belle), Phys. Rev. Lett. **118**, 21, 211801 (2017), [arXiv:1612.00529].
- [258] G. Caria *et al.* (Belle), Phys. Rev. Lett. **124**, 16, 161803 (2020), [arXiv:1910.05864].
- [259] I. Adachi *et al.* (Belle-II) (2024), [arXiv:2401.02840].
- [260] R. Aaij *et al.* (LHCb), Phys. Rev. D **108**, 1, 012018 (2023), [arXiv:2305.01463].
- [261] R. Aaij *et al.* (LHCb), Phys. Rev. Lett. **131**, 111802 (2023), [arXiv:2302.02886].
- [262] M. Blanke, PoS **LeptonPhoton2019**, 015 (2019), [arXiv:1908.09713].
- [263] S. Descotes-Genon, PoS **ALPS2019**, 016 (2020).
- [264] D. London and J. Matias, Ann. Rev. Nucl. Part. Sci. **72**, 37 (2022), [arXiv:2110.13270].
- [265] S. Hirose *et al.* (Belle), Phys. Rev. **D97**, 1, 012004 (2018), [arXiv:1709.00129].
- [266] J. G. Korner and G. A. Schuler, Z. Phys. **C46**, 93 (1990).
- [267] A. Abdesselam *et al.* (Belle), in “10th International Workshop on the CKM Unitarity Triangle (CKM 2018) Heidelberg, Germany, September 17-21, 2018,” (2019), [arXiv:1903.03102].
- [268] A. Matyja *et al.* (Belle), Phys. Rev. Lett. **99**, 191807 (2007), [arXiv:0706.4429].
- [269] A. Bozek *et al.* (Belle), Phys. Rev. **D82**, 072005 (2010), [arXiv:1005.2302].
- [270] M. Tanaka and R. Watanabe, Phys. Rev. **D87**, 3, 034028 (2013), [arXiv:1212.1878].
- [271] R. Aaij *et al.* (LHCb), Phys. Rev. Lett. **120**, 12, 121801 (2018), [arXiv:1711.05623].
- [272] J. Harrison, C. T. H. Davies and A. Lytle (LATTICE-HPQCD), Phys. Rev. Lett. **125**, 22, 222003 (2020), [arXiv:2007.06956].
- [273] J. Harrison, C. T. H. Davies and A. Lytle (HPQCD), Phys. Rev. D **102**, 9, 094518 (2020), [arXiv:2007.06957].
- [274] I. Adachi *et al.* (Belle-II) (2023), [arXiv:2311.07248].
- [275] M. Freytsis, Z. Ligeti and J. T. Ruderman, Phys. Rev. D **92**, 5, 054018 (2015), [arXiv:1506.08896].
- [276] M. Rahimi and K. K. Vos, JHEP **11**, 007 (2022), [arXiv:2207.03432].
- [277] Z. Ligeti, M. Luke and F. J. Tackmann, Phys. Rev. D **105**, 7, 073009 (2022), [arXiv:2112.07685].
- [278] I. Adachi *et al.* (Belle-II), Phys. Rev. Lett. **131**, 18, 181801 (2023), [arXiv:2308.02023].
- [279] L. Aggarwal *et al.* (Belle-II), Phys. Rev. Lett. **131**, 5, 051804 (2023), [arXiv:2301.08266].
- [280] P. Gambino and S. Hashimoto, Phys. Rev. Lett. **125**, 3, 032001 (2020), [arXiv:2005.13730].
- [281] P. Gambino *et al.*, JHEP **07**, 083 (2022), [arXiv:2203.11762].
- [282] A. Barone *et al.*, JHEP **07**, 145 (2023), [arXiv:2305.14092].
- [283] Y. Amhis *et al.* (HFLAV), Eur. Phys. J. **C77**, 12, 895 (2017), [arXiv:1612.07233].

77. Determination of CKM angles from B hadrons

Revised February 2024 by T. Gershon (Warwick U.), M. Kenzie (Cambridge U.) and K. Trabelsi (U. Paris-Saclay, IJCLab).

77.1 Introduction

The Cabibbo–Kobayashi–Maskawa (CKM) description of quark mixing [1, 2] leads to a number of triangle relations between pairs of CKM matrix elements. One of these,

$$V_{ud}V_{ub}^* + V_{cd}V_{cb}^* + V_{td}V_{tb}^* = 0, \quad (77.1)$$

is of particular interest since (i) all its terms are of comparable magnitude, and (ii) its properties can be measured through studies of oscillations and decays of B mesons. As the area of this unitary triangle is a measure of the amount of CP violation in the Standard Model [3], it is of particular interest to determine the values of its angles and to test the consistency of the CKM paradigm with the experimental measurements. The angles are defined as

$$\alpha = \arg \left[-\frac{V_{td}V_{tb}^*}{V_{ud}V_{ub}^*} \right], \quad \beta = \arg \left[-\frac{V_{cd}V_{cb}^*}{V_{td}V_{tb}^*} \right], \quad (77.2)$$

$$\gamma = \arg \left[-\frac{V_{ud}V_{ub}^*}{V_{cd}V_{cb}^*} \right],$$

with an alternative notation $(\phi_2, \phi_1, \phi_3) \equiv (\alpha, \beta, \gamma)$ also widely used in the literature.

In this mini-review, the most precise methods to determine the CKM angles are described, with a particular focus on nontrivial aspects of the combination of results. More detailed discussions of these points can be found in Ref. [4]. A similar mini-review on the side of the unitarity triangle adjacent to the angle γ can be found in Ref. [5]. A detailed overview of the CKM quark-mixing matrix is given in Ref. [6] while CP violation in the quark sector is discussed in Ref. [7].

77.2 β

The relative weak (*i.e.* CP -violating) phase between the amplitude for any CKM-favoured B^0 meson decay to a CP eigenstate and that for the decay following B^0 – \bar{B}^0 oscillation is twice the angle β . The decay-time-dependent CP asymmetry can be expressed as

$$A_{f_{CP}}(t) \equiv \frac{d\Gamma/dt[\bar{B}_{\text{phys}}^0(t) \rightarrow f_{CP}] - d\Gamma/dt[B_{\text{phys}}^0(t) \rightarrow f_{CP}]}{d\Gamma/dt[\bar{B}_{\text{phys}}^0(t) \rightarrow f_{CP}] + d\Gamma/dt[B_{\text{phys}}^0(t) \rightarrow f_{CP}]}, \quad (77.3a)$$

$$= S_f \sin(\Delta m t) - C_f \cos(\Delta m t), \quad (77.3b)$$

where the notation $B_{\text{phys}}^0(t)$ ($\bar{B}_{\text{phys}}^0(t)$) denotes a neutral B meson that decays at time t into the final state f_{CP} , and is known (“tagged”) at time $t = 0$ to have flavour content corresponding to B^0 (\bar{B}^0). In Eq. (77.3b), Δm denotes the mass difference between the two physical eigenstates of the B^0 – \bar{B}^0 system, while the corresponding decay-width difference is assumed to be negligible [8]; moreover CPT symmetry and the absence of CP violation in B^0 – \bar{B}^0 mixing is assumed throughout this mini-review.

In the general case, one can write

$$S_f \equiv \frac{2\text{Im}(\lambda_f)}{1 + |\lambda_f|^2} \quad \text{and} \quad C_f \equiv \frac{1 - |\lambda_f|^2}{1 + |\lambda_f|^2}, \quad (77.4)$$

where the parameter $\lambda_f = \frac{q}{p} \frac{\bar{A}_f}{A_f}$ is defined in terms of p and q , which define the flavour content of the mass eigenstates of the B^0 – \bar{B}^0 system [8], and the amplitudes \bar{A}_f (A_f) for a \bar{B}^0 (B^0) decay to the final state f_{CP} . In the limit that the decay amplitude is dominated by a CKM-favoured transition, as is the case for $B^0 \rightarrow J/\psi K_S^0$ decays, one obtains simple relations: $S_f = -\eta_{CP} \sin(2\beta)$ and $C_f = 0$, where η_{CP} is the CP eigenvalue of the final state [9, 10]. This method has been pursued intensively by experiments. The current world averages, combining results for

several charmonium-kaon final states but dominated by results on $B^0 \rightarrow J/\psi K_S^0$ (CP odd) and $B^0 \rightarrow J/\psi K_L^0$ (CP even), are [4]

$$-\eta_{CP} S_f = 0.709 \pm 0.011, \quad C_f = +0.004 \pm 0.010. \quad (77.5)$$

Despite the large number of signal events in the data, the dominant uncertainties are still statistical. One important source of potential systematic correlation between results from different experiments is that due to “tag-side interference” [11],² which is common to measurements exploiting production through the $e^+e^- \rightarrow \Upsilon(4S) \rightarrow B^0\bar{B}^0$ process, including the latest results from BaBar [12] and Belle [13]. It does not, however, affect the results from LHCb [14] that now have better statistical sensitivity. Another common source of systematic uncertainty is due to knowledge of the value of Δm , but since this quantity has been measured precisely [8] the effect remains small.

The interpretation of the value of $-\eta_{CP} S_f$ from Eq. (77.5) as $\sin(2\beta)$ assumes negligible contributions from subleading amplitudes with a different weak phase to that of the tree diagram (*i.e.* to that of the CKM matrix elements $V_{cb}V_{cs}^*$). This potential additional contribution is often referred to as “penguin pollution”. All existing data, including the value of C_f in Eq. (77.5), as well as several explicit calculations [15–18], are consistent with penguin pollution in B^0 meson decays to charmonium-kaon decays being negligible at the current level of precision. Therefore, the value of $-\eta_{CP} S_f$ is generally converted to $\sin(2\beta)$ without any correction or additional uncertainty being assigned due to this assumption. This gives [4]

$$\beta = (22.6_{-0.4}^{+0.5})^\circ, \quad (77.6)$$

where only the solution consistent with the Standard Model is reported (methods to resolve the trigonometric ambiguity in the result are discussed below). It is also possible to use data-driven methods, typically based on flavour symmetries plus some additional assumptions, to constrain the effects of penguin pollution [19–21]. In this case it is necessary to consider each charmonium-kaon final state separately, since the penguin pollution to each may differ. The most common approach [19], which relies on experimental information on $B^0 \rightarrow J/\psi\pi^0$ decays, currently gives an additional uncertainty on $\sin(2\beta)$ from $B^0 \rightarrow J/\psi K_S^0$ of around 0.01.

It is possible to avoid the issue of penguin pollution in the measurement of β by using B^0 meson decays to a charm- and light-meson final state, such as $D_{CP}\pi^0$ (where D_{CP} represents a D^0 meson decaying into a CP eigenstate), instead of the charmonium-kaon final states. These decays do have a CKM-suppressed contribution ($V_{ub}V_{cd}^*$ instead of $V_{cb}V_{cs}^*$), which can in principle bias the determination of $\sin(2\beta)$ from S_f , but this can be calculated and is known to be negligible at current precision. The requirement that the neutral D meson decays to a final state that is common to both D^0 and \bar{D}^0 , such as the CP -even eigenstate K^+K^- , reduces the sample size that is available for analysis. Consequently, the world average [4], $\sin(2\beta) = 0.71 \pm 0.09$, with these channels is not as precise as that from the charmonium-kaon states.

Converting experimental results on $\sin(2\beta)$ into constraints on β leads to a trigonometric ambiguity in the range $[0^\circ, 180^\circ]$. This can be resolved with experimental measurements of $\cos(2\beta)$, which can be obtained from decay-time-dependent analyses of B^0 meson decays to multibody (non- CP -eigenstate) final states. Among the charmonium-kaon decays, study of $B^0 \rightarrow J/\psi K^*(892)^0$ with $K^*(892)^0 \rightarrow K_S^0\pi^0$ is the most promising approach, but due to the limited sample size that has been analysed to date the precision is not sufficient to resolve the ambiguity conclusively. The charm- and light-meson channels such as $B^0 \rightarrow D\pi^0$ with $D \rightarrow K_S^0\pi^+\pi^-$ have been shown to provide good statistical power for this purpose, with a joint analysis of BaBar and Belle data giving $\cos(2\beta) = 0.91 \pm 0.25$ [22, 23], sufficient to rule out the alternative solution for β .

77.3 α

In the limit that only tree amplitudes contribute to B^0 meson decays to light mesons, such as $B^0 \rightarrow \pi^+\pi^-$, then the observables of the decay-time-dependent CP asymmetry of Eq. (77.3) would allow a straight-forward determination of 2α : $S_f = +\eta_{CP} \sin(2\alpha)$

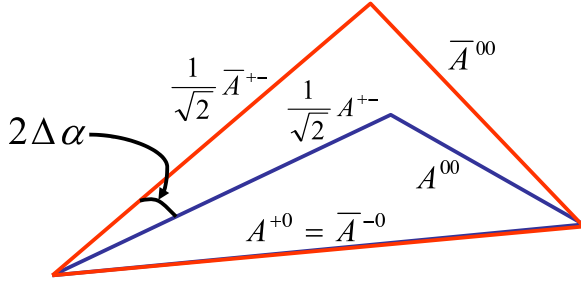


Figure 77.1: Isospin triangles for $B \rightarrow \pi\pi$ decays, reproduced from Ref. [24]. Here, the relative phase between A^{+0} and \bar{A}^{-0} has been rotated away to simplify the picture. The total relative phase probed by $S_{\pi^+\pi^-}$ is arg $\left(\frac{q}{p} \frac{\bar{A}^{+-}}{A^{+-}}\right) = 2\alpha - 2\Delta\alpha$, including contributions from $B^0\text{-}\bar{B}^0$ mixing, the tree-level amplitudes and the correction $\Delta\alpha$, and exploiting the unitarity requirement $\alpha + \beta + \gamma = 180^\circ$.

and $C_f = 0$. In general, however, the determination of α is complicated by the presence of contributions from $b \rightarrow d(u\bar{u})$ neutral-current penguin transitions, which have a similar level of CKM-suppression as the $b \rightarrow u(\bar{u})$ charged-current tree amplitudes but have a different weak phase. Consequently, one obtains instead for $B^0 \rightarrow \pi^+\pi^-$

$$S_{\pi^+\pi^-} = \sqrt{1 - C_{\pi^+\pi^-}^2} \sin(2\alpha - 2\Delta\alpha), \quad (77.7)$$

where $\Delta\alpha$ is the *a priori* unknown penguin contribution.

This contribution from the penguin amplitude can be accounted for in an analysis relating the amplitudes for isospin partner decays, *e.g.* A^{+-} for $B^0 \rightarrow \pi^+\pi^-$, A^{+0} for $B^+ \rightarrow \pi^+\pi^0$, A^{00} for $B^0 \rightarrow \pi^0\pi^0$ decays and $(\bar{A}^{+-}, \bar{A}^{-0}, \bar{A}^{00})$ for their charge conjugates. The isospin analysis relies on the fact that there is no penguin contribution to A^{+0} and \bar{A}^{-0} , because $\pi^\pm\pi^0$ is a pure isospin-2 state, and the ($\Delta I = \frac{1}{2}$) QCD-penguin amplitudes only contribute to the isospin-0 final state. One therefore obtains the following isospin triangle relations [25]

$$A^{+0} = \frac{1}{\sqrt{2}} A^{+-} + A^{00} \quad \text{and} \quad \bar{A}^{-0} = \frac{1}{\sqrt{2}} \bar{A}^{+-} + \bar{A}^{00}, \quad (77.8)$$

from which it is possible to determine $\Delta\alpha$, as shown in Fig. 77.1.

Since the determination of $\Delta\alpha$ and thus also α requires construction of amplitude-level relations, it is not appropriate to simply average results of α from different experiments. Instead, measurements of each of the observable quantities needed to determine α are input into a combination. For the $B \rightarrow \pi\pi$ system, the inputs are the branching fractions of $B^0 \rightarrow \pi^+\pi^-$, $B^+ \rightarrow \pi^+\pi^0$ and $B^0 \rightarrow \pi^0\pi^0$ decays, the lifetimes of the B^+ and B^0 mesons (which relate the branching fractions to amplitude-level quantities), and the $S_{\pi^+\pi^-}$, $C_{\pi^+\pi^-}$ and $C_{\pi^0\pi^0}$ observables. Potential sources of correlation must be taken into account, but these are predominantly systematic in origin and thus have a small effect on the combination, since the measurements are statistically limited. An exception is that the LHCb measurements of $(S_{\pi^+\pi^-}, C_{\pi^+\pi^-})$ [26, 27] have a significant statistical correlation due to the fact that the time variable of Eq. (77.3) is the difference between production and decay, and hence is in the range $[0, \infty]$. This correlation is largely absent for measurements from BaBar [28] and Belle [29], where the difference between the signal and tagging B meson decay times is measured, and hence $t \in [-\infty, \infty]$. The combination itself can be performed with different statistical approaches; the procedure described in detail in Ref. [30], based on a frequentist treatment, is used here. The knowledge of $C_{\pi^0\pi^0}$ [28, 31] is currently the limiting factor in the precision on α from the $B \rightarrow \pi\pi$ system, and is likely to remain so for some time due to the difficulty to reconstruct this final state.

In general, the isospin triangle construction gives a four-fold ambiguity on $2\Delta\alpha$ (each triangle can face either up or down), leading to an eight-fold ambiguity on α in the range $[0^\circ, 180^\circ]$.

This is reduced if either or both of the triangles are flat, or if the two triangles have sides of identical length. The ambiguities can also be reduced if measurement of the $S_{\pi^0\pi^0}$ (or equivalent) observable is available, since this can be combined with the corresponding $\Delta\alpha$ parameter from the right-hand corner of the triangle in Fig. 77.1 to provide an additional constraint. None of these possibilities are realised in the $B \rightarrow \pi\pi$ system; in particular a decay-time-dependent analysis of $B^0 \rightarrow \pi^0\pi^0$ is extremely challenging experimentally due to the absence of any charged particle originating from the B decay position. Nonetheless, solutions consistent with $\alpha = 0$ can be rejected on physical grounds [24].

The isospin analysis can also be performed with the $B \rightarrow \rho\rho$ system, which contains two vector particles in the final state and so does not have a fixed CP eigenvalue. In principle the analysis can be performed separately for each $\rho\rho$ polarization state, but in practise it is found that the longitudinal polarization fraction, f_L , is close to unity, and hence the final state is approximately CP -even. Compared to $B^0 \rightarrow \pi\pi$, the $\rho\rho$ modes benefit experimentally from a higher branching fraction and smaller penguin contributions, so that the isospin triangles are flatter, reducing the ambiguities. (The value of $\Delta\alpha$ in the $B \rightarrow \rho\rho$ system, obtained from the isospin analysis, has a single solution in $[0, \pi]$ at $(3 \pm 5)^\circ$, while for $B \rightarrow \pi\pi$ there are two solutions at 13° and 27° with $\Delta\alpha \in [7, 33]^\circ$ at 68.3% confidence level (CL). The isospin analysis with either final state has an ambiguity under $\Delta\alpha \leftrightarrow -\Delta\alpha$.) For the BaBar [32] and Belle [33] experiments, the high branching fraction and smaller penguin contribution compensate for the increased difficulty to reconstruct the $\rho\rho$ final state relative to $\pi\pi$. Moreover, in contrast to $S_{\pi^0\pi^0}$, measurement of $S_{\rho^0\rho^0}$ is possible due to the four charged pion final state, following $\rho^0 \rightarrow \pi^+\pi^-$ decay, as has been demonstrated by BaBar [34].

In the $B \rightarrow \rho\pi$ system there are more amplitudes to consider, so that the isospin relation corresponds to a pentagon rather than a triangle and Eq. (77.8) is modified to become

$$\begin{aligned} \sqrt{2}(A^{+0} + A^{0+}) &= A^{+-} + A^{-+} + 2A^{00} \quad \text{and} \\ \sqrt{2}(\bar{A}^{-0} + \bar{A}^{0-}) &= \bar{A}^{+-} + \bar{A}^{-+} + 2\bar{A}^{00}. \end{aligned} \quad (77.9)$$

As in Eq. (77.8), the left-hand sides of these expressions correspond to a pure isospin-2 final state, and therefore the ratio of the right-hand sides gives a pure phase term that, accounting for the $B^0\text{-}\bar{B}^0$ mixing phase that also contributes to the measured quantities, is 2α . The relative amplitudes for B^0 and \bar{B}^0 decays to $\rho^+\pi^-$, $\rho^-\pi^+$ and $\rho^0\pi^0$ can all be determined from a decay-time-dependent analysis of the $\pi^+\pi^-\pi^0$ Dalitz plot, so that study of this channel alone allows determination of α [35]. This analysis in principle leads to a single solution for α in $[0^\circ, 180^\circ]$, but the precision of current measurements [36–38] is limited.

The isospin analysis used to determine α is believed to be valid to high precision, and theoretical uncertainties in the procedure are usually neglected. Nonetheless, it should be noted that the analysis assumes the absence of electroweak penguin amplitudes, which can contribute to $\Delta I = \frac{3}{2}$ transitions with a different weak phase to that of the tree amplitudes [39, 40]. Moreover, isospin-breaking effects such as (π^0, η, η') mixing would impact on the relations of Eq. (77.8). A further complication in the $B \rightarrow \rho\rho$ system is the effect of the non-zero ρ meson width [41]. Estimates of the size of these effects on the determined value of α are typically at the 1° level or less [30]. By contrast, methods to determine α using SU(3) or other flavour symmetries are generally considered to have larger theoretical uncertainties and are not included here.

The world average obtained for the angle α from isospin analysis of $B \rightarrow \pi\pi$, $\rho\pi$ and $\rho\rho$ decays is [4]

$$\alpha = (84.1_{-3.8}^{+4.5})^\circ, \quad (77.10)$$

where the quoted uncertainty is at the 68.3% CL and does not include effects due to isospin-breaking. This world average, together with results split by decay mode, is shown in Fig. 77.2. The combination has a total of 57 experimental inputs from which 24 parameters are determined, and an overall χ^2 of 22.4, which corresponds to a p-value of 91%. Thus, there is excellent overall consistency between the inputs, despite the tension apparent in

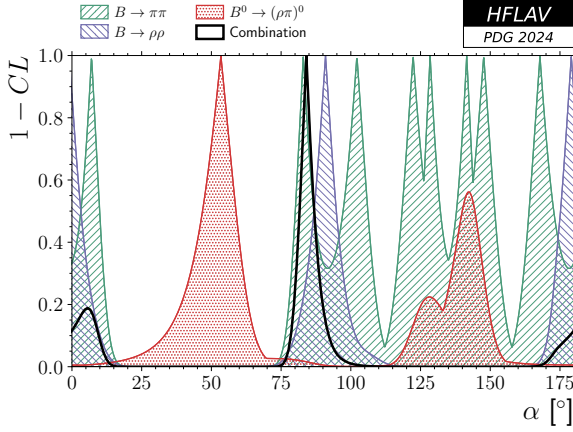


Figure 77.2: World average of α , as well as contributions from individual modes, in terms of $1-CL$.

Fig. 77.2 between the results from $B^0 \rightarrow (\rho\pi)^0$ and the others. The combination gives a single best-fit for α in $[0^\circ, 180^\circ]$, but an ambiguous solution exists at $\alpha \leftrightarrow \alpha + 180^\circ$. A secondary minimum close to zero is disfavoured [30].

77.4 γ

The angle γ is the weak phase between Cabibbo-favoured $b \rightarrow c$ and suppressed $b \rightarrow u$ quark transitions and can be determined by exploiting interference between them. Explicitly, the ratio of suppressed to favoured amplitudes is parameterized by

$$r_B e^{i(\delta_B \pm \gamma)} = \frac{A_{\text{sup}}}{A_{\text{fav}}}, \quad (77.11)$$

where r_B is the ratio of amplitude magnitudes, δ_B the strong phase difference and the $+$ or $-$ sign depends on whether the transition involves a \bar{b} or b quark, respectively. Measurement of γ in this way has negligible theoretical uncertainty in the Standard Model [42], and therefore this approach provides a benchmark against which determinations from other methods, typically involving loop diagrams, can be compared.

Interference between these amplitudes is realised in $B^+ \rightarrow DK^+$ decays, where D represents an admixture of D^0 and \bar{D}^0 mesons. The simplest case is that of D decays to CP -eigenstates (GLW method [43, 44]), either CP -even such as K^+K^- ($CP+$) or CP -odd such as $K_S^0\pi^0$ ($CP-$). The normalized decay rate and CP asymmetry are given by

$$R_{CP\pm} = \frac{\Gamma(B^- \rightarrow D_{CP\pm}K^-) + \Gamma(B^+ \rightarrow D_{CP\pm}K^+)}{\Gamma(B^- \rightarrow D^0K^-) + \Gamma(B^+ \rightarrow \bar{D}^0K^+)} \\ = 1 + r_B^2 \pm 2r_B \cos(\delta_B) \cos(\gamma), \quad (77.12a)$$

$$A_{CP\pm} = \frac{\Gamma(B^- \rightarrow D_{CP\pm}K^-) - \Gamma(B^+ \rightarrow D_{CP\pm}K^+)}{\Gamma(B^- \rightarrow D_{CP\pm}K^-) + \Gamma(B^+ \rightarrow D_{CP\pm}K^+)} \\ = \frac{\pm 2r_B \sin(\delta_B) \sin(\gamma)}{1 + r_B^2 \pm 2r_B \cos(\delta_B) \cos(\gamma)}. \quad (77.12b)$$

These relations assume the absence of direct CP violation in the charm system; experimentally allowed deviations from this assumption are too small to cause a significant bias on γ [7, 45]. It is convenient to determine the $R_{CP\pm}$ quantities through a double ratio, normalizing to $B^+ \rightarrow D\pi^+$ decays involving the same final states, since this cancels potential sources of systematic uncertainty due to the branching fractions of the D decays that are used; small possible effects of CP violation in $B^+ \rightarrow D\pi^+$ decays are a source of systematic uncertainty in this procedure. The GLW method can be extended to include final states that are almost CP -eigenstates [46], as is the case in $D \rightarrow \pi^+\pi^-\pi^0$ and $D \rightarrow K^+K^-\pi^0$ decays, via inclusion of a factor encoding the fraction of CP -even (or CP -odd) content, F_{\pm} , which dilutes the sensitivity to γ by reducing the size of the interference terms (the terms linear with r_B) in Eq. (77.12).

For other D decays, the ratio of amplitudes for the D^0 and \bar{D}^0 decays to the final state of interest has to be accounted for in the formalism. The ADS method [47, 48] uses D decays to final states such as $K^\mp\pi^\pm$, which involve interference between Cabibbo-favoured (CF) and doubly-Cabibbo-suppressed (DCS) transitions. The observables in this case are

$$A_{\text{ADS}} = \frac{\Gamma(B^- \rightarrow [K^+\pi^-]_D K^-) - \Gamma(B^+ \rightarrow [K^-\pi^+]_D K^+)}{\Gamma(B^- \rightarrow [K^+\pi^-]_D K^-) + \Gamma(B^+ \rightarrow [K^-\pi^+]_D K^+)} \\ = \frac{2r_B r_D \sin(\delta_B + \delta_D) \sin(\gamma)}{r_B^2 + r_D^2 + 2r_B r_D \cos(\delta_B + \delta_D) \cos(\gamma)}, \quad (77.13a)$$

$$R_{\text{ADS}} = \frac{\Gamma(B^- \rightarrow [K^+\pi^-]_D K^-) + \Gamma(B^+ \rightarrow [K^-\pi^+]_D K^+)}{\Gamma(B^- \rightarrow [K^-\pi^+]_D K^-) + \Gamma(B^+ \rightarrow [K^+\pi^-]_D K^+)} \\ = r_B^2 + r_D^2 + 2r_B r_D \cos(\delta_B + \delta_D) \cos(\gamma), \quad (77.13b)$$

where r_D and δ_D are the amplitude magnitude ratio and strong phase difference between the CF and DCS D decay. An alternative pair of observables, (R_-, R_+) , is also sometimes used, where R_- (R_+) is the ratio of decay rates between the suppressed and favoured transitions for B^- (B^+) decays. The R_- and R_+ observables are statistically independent, while A_{ADS} and R_{ADS} are not (in particular, the uncertainty on A_{ADS} depends on the central value of R_{ADS}). However, the pair (R_-, R_+) has more correlated sources of systematic uncertainty compared to $(A_{\text{ADS}}, R_{\text{ADS}})$. The observables of Eq. (77.13) are therefore usually preferred once a significant signal is established. The ADS method can also be extended to include decays to multibody final states, such as $D \rightarrow K^\pm\pi^\mp\pi^0$ and $D \rightarrow K^\pm\pi^\mp\pi^+\pi^-$, by addition of a coherence factor [49] which appears in the interference terms of Eq. (77.13) and accounts for dilution of the sensitivity due to variation of the decay amplitude across the phase space of the final state. A similar method can be used for singly Cabibbo-suppressed D decays to non- CP eigenstates such as K^*K [50].

For D decays to multibody self-conjugate final states (BPGGSZ method [51, 52]), such as $D \rightarrow K_S^0\pi^+\pi^-$, one can write the partial decay rate as a function of the position in the phase space in terms of the ‘‘Cartesian parameters’’ $x_{\pm} + iy_{\pm} = r_B e^{i(\delta_B \pm \gamma)}$:

$$d\Gamma(B^\pm \rightarrow [K_S^0\pi^+\pi^-]_D K^\pm) = A_{(\mp, \pm)}^2 + r_B^2 A_{(\pm, \mp)}^2 \\ + 2A_{(\pm, \mp)} A_{(\mp, \pm)} [x_{\pm} c_{D(\pm, \mp)} + y_{\pm} s_{D(\pm, \mp)}], \quad (77.14)$$

where the notation $(+, -)$ is shorthand for the dependence on the Dalitz-plot position — the squared invariant masses of $K_S^0\pi^+$ and $K_S^0\pi^-$ combinations, respectively. The quantities $A_{(+, -)}$ and $A_{(-, +)}$ represent the magnitudes of the D^0 and \bar{D}^0 decay amplitudes at the position $(+, -)$ and are interchangeable with their CP conjugate amplitudes because CP conservation is assumed in the D decay (i.e. $A_{(-, +)} = \bar{A}_{(+, -)}$). The quantities $c_{D(\pm, \mp)}$ and $s_{D(\pm, \mp)}$ are the cosine and sine of the strong phase difference, $\delta_{D(+, -)} = \arg(\bar{A}_{(+, -)}) - \arg(A_{(+, -)})$, between the \bar{D}^0 and D^0 amplitudes. These quantities can be determined from an amplitude model, although this leads to a hard-to-quantify systematic uncertainty associated to the composition of the model. An alternative, ‘‘model-independent’’, approach involves dividing the phase space into appropriate bins. In this case, the analysis benefits from external input on the values of c_D and s_D integrated over each bin. Measurements of these external parameters have been performed for the $D \rightarrow K_S^0\pi^+\pi^-$ decay by the CLEO-c and BES-III collaborations [53–56]. The use of common input values for these parameters in model-independent determinations of γ with the BPGGSZ method by different experiments is a source of correlation between experiments that is currently negligible but will become more significant as the available B meson data samples increase in size.

The discussion above refers to $B^+ \rightarrow DK^+$ decays, but analogous measurements can be made also for additional channels such as $B^+ \rightarrow D^*K^+$ (with $D^* \rightarrow D\pi^0, D\gamma$) and $B^+ \rightarrow DK^{*+}$ (with $K^{*+} \rightarrow K_S^0\pi^+, K^+\pi^0$). In the limit that these can be treated purely as two-body decays, the expressions for $B^+ \rightarrow DK^+$ are modified only by ensuring the r_B and δ_B parameters are specific to each B decay. Moreover, for $B^+ \rightarrow D^*K^+$ decays an effective

shift of the strong phase by π between $D^* \rightarrow D\pi^0$ and $D\gamma$ decays [57] has to be taken into account. In case the finite width of the decaying resonance is non-negligible, as is the case for the $K^*(892)$ state, additional amplitudes can contribute leading to a dilution of the sensitivity, which can be accounted for in the formalism through the introduction of a relevant coherence factor. For the $B^0 \rightarrow DK^{*0}$ decay, full amplitude analysis of the $B^0 \rightarrow DK^+\pi^-$ Dalitz plot provides additional sensitivity compared to the quasi-two-body approach [58, 59].

It is also possible to measure γ using decay-time-dependent analysis of the B_s^0 meson [60]. The weak phase arising in the interference between direct decay of $B_s^0 \rightarrow D_s^\mp K^\pm$ and decay via mixing is $(\gamma - 2\beta_s)$, where β_s is the angle associated with $B_s^0 \rightarrow J/\psi\phi$ decays in a similar way to the relation between β and $B^0 \rightarrow J/\psi K_S^0$ decays described in Sec. 77.2. Sufficient information can be obtained from the tagged, decay-time-dependent rates of $B_s^0 \rightarrow D_s^\mp K^\pm$ decays that this weak phase can be determined, up to an ambiguity, together with the strong phase difference between, and the ratio of the magnitudes of, the suppressed and favoured amplitudes. Since β_s is known to good precision [8], measurements of the decay-time-dependent CP -asymmetry observables in $B_s^0 \rightarrow D_s^\mp K^\pm$ decays can be used to infer constraints on γ . Alternatively, if effects of penguin pollution in $B_s^0 \rightarrow J/\psi\phi$ decays [17, 18] are a concern, as they will become in the future, results from the $B_s^0 \rightarrow D_s^\mp K^\pm$ mode can be combined with an independent precise measurement of γ to provide a penguin-free determination of β_s .

The average for γ requires a non-trivial combination due the complicated relations between the observables and the physics parameters of interest, such as in Eqs. (77.12), (77.13) and (77.14). Moreover, hadronic parameters such as r_B and δ_B defined in Eq. (77.11) are common to all different D decay modes (but differ for each B decay mode). Thus, it is not correct to simply average results for γ obtained by different experiments or in different channels. Instead, measurements of rate asymmetries, rate ratios and the Cartesian parameters are taken as inputs to the combination, from which results are obtained not only for γ but also for the hadronic parameters. Independent measurements of auxiliary parameters such as r_D and δ_D are also treated as inputs to the combination. In some cases the B decay data can help to reduce uncertainties on these auxiliary parameters and therefore a simultaneous fit of charm and beauty data can provide stronger constraints [61]; this approach however is not currently used for the world average.

The precision to which γ can be measured with a particular B decay is approximately inversely proportional to the value of r_B . Thus, results from channels with smaller yields but larger values of r_B , such as $B^0 \rightarrow DK^{*0}$ and $B_s^0 \rightarrow D_s^\mp K^\pm$ ($r_B \approx 0.3$ – 0.4), can have a significant impact on the world average and are included in the combination. By contrast the $B^+ \rightarrow D\pi^+$ mode, for which large samples are available but $r_B \approx 0.005$, has little impact and is also more sensitive to potential systematic biases; hence it is not included. The sensitivity of the world average at present is dominated by results from $B^+ \rightarrow DK^+$, where $r_B \approx 0.1$, in particular results with the GLW [62], ADS [62] and BPGGSZ [63] methods.

The world average obtained for the angle γ , obtained by combining results from $B^+ \rightarrow DK^+$, D^*K^+ , DK^{*+} , $DK^+\pi^+\pi^-$, $B^0 \rightarrow DK^+\pi^-$, $B_s^0 \rightarrow D_s^\mp K^\pm$ and $B_s^0 \rightarrow D_s^\mp K^\pm\pi^+\pi^-$ decays, is [4]

$$\gamma = (65.7 \pm 3.0)^\circ, \quad (77.15)$$

where the quoted uncertainty is at the 68.3% CL.

Effects related to charm and kaon mixing and CP violation are generally negligible at the current level of precision, in particular for modes with $r_B \gtrsim 0.1$. An exception is that a dependence of the selection efficiency on the charm decay time can induce a dependence of the observables on charm mixing parameters [64]. Such effects can be important at hadron collider experiments such as LHCb, but can be and are corrected for. Interactions of neutral kaons with detector material can also cause a bias in determination of γ from modes with low values of r_B [65], such as the BPGGSZ method applied to $B^+ \rightarrow D\pi^+$, but are negligible in modes with larger r_B values. A further subtlety is that the

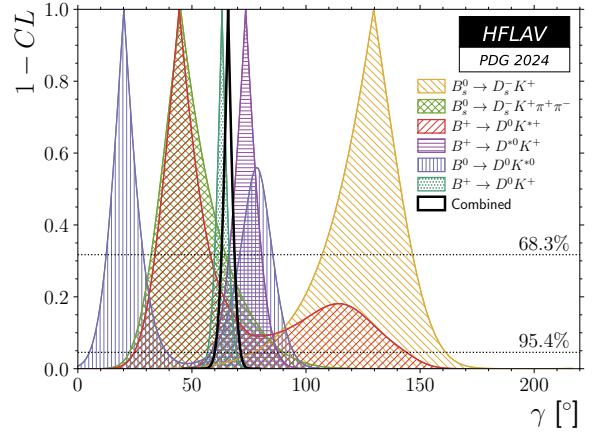


Figure 77.3: World average of $\gamma \equiv \phi_3$, as well as contributions from individual modes, in terms of $1-\text{CL}$.

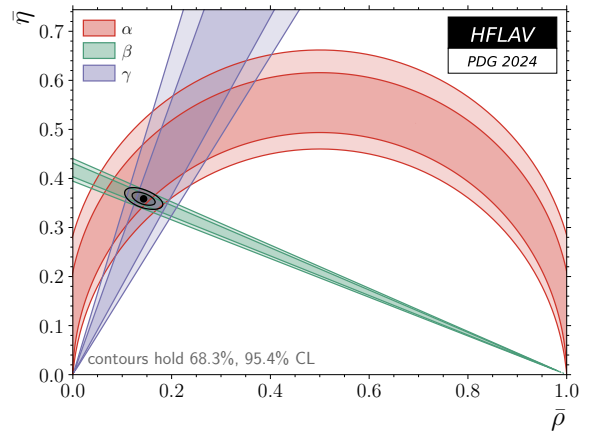


Figure 77.4: Constraints from the measurements of the angles of the CKM unitarity triangle in the $(\bar{\rho}, \bar{\eta})$ plane.

identification of the weak phase between suppressed and favoured amplitudes in $B \rightarrow DK$ decays with γ , as defined in Eq. (77.2), assumes that the 2×2 submatrix of the CKM matrix is real, *i.e.* that $\arg[V_{ud}V_{us}^*/(V_{cd}V_{cs}^*)] = 0$. This is true to an excellent approximation in the Standard Model, and is known experimentally from independent studies of the charm system [45] to contribute negligible bias to current measurements. Nonetheless, in future it will be possible to test directly this assumption by comparing the value of γ obtained from the $B \rightarrow DK$ and $B \rightarrow D\pi$ systems.

Effects from correlated uncertainties between amplitude models and strong phase differences in charm decays are negligible and are not explicitly accounted for in the combination, nor are effects related to charm and kaon mixing and CP violation. This world average, together with results split by decay mode, is shown in Fig. 77.3. The combination has a total of 173 experimental inputs from which 36 parameters are determined, and an overall χ^2 of 159.5, which corresponds to a p-value of 9% indicating reasonable agreement between the inputs. The combination gives a single solution for γ in $[0^\circ, 180^\circ]$, but an ambiguous solution exists at $\gamma \Leftrightarrow \gamma + 180^\circ$.

77.5 Summary

Experimental progress has resulted in all three angles of the CKM unitarity triangle being measured with good accuracy, with β known to subdegree precision and both α and γ known to better than 5° . The constraints from these three measurements in the $(\bar{\rho}, \bar{\eta})$ plane are shown in Fig. 77.4; further discussion and comparison with constraints from independent measurements can be found in Ref. [6]. The determinations of all three angles remain statistically limited, but it will be a challenge for experiments to

ensure that this remains the case as the precision improves. Consequently, the correct treatment of sources of correlation between the measurements that go into the world average combinations is becoming increasingly important.

References

- [1] N. Cabibbo, Phys. Rev. Lett. **10**, 531 (1963).
- [2] M. Kobayashi and T. Maskawa, Prog. Theor. Phys. **49**, 652 (1973).
- [3] C. Jarlskog, Phys. Rev. Lett. **55**, 1039 (1985).
- [4] Y. S. Amhis *et al.* (HFLAV), Phys. Rev. D **107**, 5, 052008 (2023), updated averages are available online at hflav.web.cern.ch, [arXiv:2206.07501].
- [5] See the review on “Semileptonic b -Hadron Decays, Determination of V_{cb} , V_{ub} ” in this *Review*.
- [6] See the review on “Cabibbo-Kobayashi-Maskawa Mixing Matrix,” in this *Review*.
- [7] See the review on “ CP Violation in the Quark Sector,” in this *Review*.
- [8] See the review on “ $B^0-\bar{B}^0$ Mixing” in this *Review*.
- [9] A. Carter and A. Sanda, Phys. Rev. **D23**, 1567 (1981).
- [10] I. Bigi and A. Sanda, Nucl. Phys. **B193**, 85 (1981).
- [11] O. Long *et al.*, Phys. Rev. **D68**, 034010 (2003), [hep-ex/0303030].
- [12] B. Aubert *et al.* (BaBar), Phys. Rev. **D79**, 072009 (2009), [arXiv:0902.1708].
- [13] I. Adachi *et al.*, Phys. Rev. Lett. **108**, 171802 (2012), [arXiv:1201.4643].
- [14] R. Aaij *et al.* (LHCb), Phys. Rev. Lett. **132**, 021801 (2024), [arXiv:2309.09728].
- [15] H.-n. Li and S. Mishima, JHEP **03**, 009 (2007), [hep-ph/0610120].
- [16] M. Jung, Phys. Rev. **D86**, 053008 (2012), [arXiv:1206.2050].
- [17] K. De Bruyn and R. Fleischer, JHEP **1503**, 145 (2015), [arXiv:1412.6834].
- [18] P. Frings, U. Nierste and M. Wiebusch, Phys. Rev. Lett. **115**, 061802 (2015), [arXiv:1503.00859].
- [19] M. Ciuchini, M. Pierini and L. Silvestrini, Phys. Rev. Lett. **95**, 221804 (2005), [hep-ph/0507290].
- [20] S. Faller *et al.*, Phys. Rev. **D79**, 014030 (2009), [arXiv:0809.0842].
- [21] Z. Ligeti and D. Robinson, Phys. Rev. Lett. **115**, 251801 (2015), [arXiv:1507.06671].
- [22] I. Adachi *et al.* (BaBar, Belle), Phys. Rev. Lett. **121**, 261801 (2018), [arXiv:1804.06152].
- [23] I. Adachi *et al.* (BaBar, Belle), Phys. Rev. **D98**, 112012 (2018), [arXiv:1804.06153].
- [24] M. Antonelli *et al.*, Phys. Rept. **494**, 197 (2010), [arXiv:0907.5386].
- [25] M. Gronau and D. London, Phys. Rev. Lett. **65**, 3381 (1990).
- [26] R. Aaij *et al.* (LHCb), Phys. Rev. **D98**, 032004 (2018), [arXiv:1805.06759].
- [27] R. Aaij *et al.* (LHCb), JHEP **03**, 075 (2021), [arXiv:2012.05319].
- [28] J. P. Lees *et al.* (BaBar), Phys. Rev. **D87**, 052009 (2013), [arXiv:1206.3525].
- [29] I. Adachi *et al.* (Belle), Phys. Rev. **D88**, 092003 (2013), [arXiv:1302.0551].
- [30] J. Charles *et al.*, Eur. Phys. J. **C77**, 574 (2017), [arXiv:1705.02981].
- [31] T. Julius *et al.* (Belle), Phys. Rev. **D96**, 032007 (2017), [arXiv:1705.02083].
- [32] B. Aubert *et al.* (BaBar), Phys. Rev. **D76**, 052007 (2007), [arXiv:0705.2157].
- [33] P. Vanhoefer *et al.* (Belle), Phys. Rev. **D93**, 032010 (2016), [Addendum *ibid.*: **D94** 099903 (2016)], [arXiv:1510.01245].
- [34] B. Aubert *et al.* (BaBar), Phys. Rev. **D78**, 071104 (2008), [arXiv:0807.4977].
- [35] A. E. Snyder and H. R. Quinn, Phys. Rev. **D48**, 2139 (1993).
- [36] J. P. Lees *et al.* (BaBar), Phys. Rev. **D88**, 012003 (2013), [arXiv:1304.3503].
- [37] A. Kusaka *et al.* (Belle), Phys. Rev. Lett. **98**, 221602 (2007), [hep-ex/0701015].
- [38] A. Kusaka *et al.* (Belle), Phys. Rev. **D77**, 072001 (2008), [arXiv:0710.4974].
- [39] M. Gronau and J. Zupan, Phys. Rev. **D71**, 074017 (2005), [hep-ph/0502139].
- [40] S. Gardner, Phys. Rev. **D72**, 034015 (2005), [hep-ph/0505071].
- [41] A. Falk *et al.*, Phys. Rev. **D69**, 011502 (2004), [hep-ph/0310242].
- [42] J. Brod and J. Zupan, JHEP **01**, 051 (2014), [arXiv:1308.5663].
- [43] M. Gronau and D. London, Phys. Lett. **B253**, 483 (1991).
- [44] M. Gronau and D. Wyler, Phys. Lett. **B265**, 172 (1991).
- [45] See the review on “ $D^0-\bar{D}^0$ Mixing” in this *Review*.
- [46] M. Nayak *et al.*, Phys. Lett. **B740**, 1 (2015), [arXiv:1410.3964].
- [47] D. Atwood, I. Dunietz and A. Soni, Phys. Rev. Lett. **78**, 3257 (1997), [hep-ph/9612433].
- [48] D. Atwood, I. Dunietz and A. Soni, Phys. Rev. **D63**, 036005 (2001), [hep-ph/0008090].
- [49] D. Atwood and A. Soni, Phys. Rev. **D68**, 033003 (2003), [hep-ph/0304085].
- [50] Y. Grossman, Z. Ligeti and A. Soffer, Phys. Rev. **D67**, 071301 (2003), [hep-ph/0210433].
- [51] A. Giri *et al.*, Phys. Rev. **D68**, 054018 (2003), [hep-ph/0303187].
- [52] A. Bondar, *Proceedings of BINP special analysis meeting on Dalitz analysis*, 24-26 Sep. 2002, unpublished.
- [53] R. Briere *et al.* (CLEO), Phys. Rev. **D80**, 032002 (2009), [arXiv:0903.1681].
- [54] J. Libby *et al.* (CLEO), Phys. Rev. **D82**, 112006 (2010), [arXiv:1010.2817].
- [55] M. Ablikim *et al.* (BESIII), Phys. Rev. Lett. **124**, 241802 (2020), [arXiv:2002.12791].
- [56] M. Ablikim *et al.* (BESIII), Phys. Rev. **D101**, 112002 (2020), [arXiv:2003.00091].
- [57] A. Bondar and T. Gershon, Phys. Rev. **D70**, 091503 (2004), [hep-ph/0409281].
- [58] T. Gershon, Phys. Rev. **D79**, 051301 (2009), [arXiv:0810.2706].
- [59] T. Gershon and M. Williams, Phys. Rev. **D80**, 092002 (2009), [arXiv:0909.1495].
- [60] R. Aleksan, I. Dunietz and B. Kayser, Z. Phys. **C54**, 653 (1992).
- [61] R. Aaij *et al.* (LHCb), JHEP **12**, 141 (2021), [arXiv:2110.02350].
- [62] R. Aaij *et al.* (LHCb), JHEP **04**, 081 (2021), [arXiv:2012.09903].
- [63] R. Aaij *et al.* (LHCb), JHEP **02**, 169 (2021), [arXiv:2010.08483].
- [64] M. Rama, Phys. Rev. **D89**, 014021 (2014), [arXiv:1307.4384].
- [65] M. Bjørn and S. Malde, JHEP **07**, 106 (2019), [arXiv:1904.01129].

78. Spectroscopy of Mesons Containing Two Heavy Quarks

Revised March 2024 by J. J. Hernández-Rey (IFIC, Valencia), C. Lourenço (CERN), R.E. Mitchell (Indiana U.), S. Navas (Granada U.) and C. Patrignani (Bologna U.).

A golden age for heavy quarkonium physics dawned at the turn of this century, initiated by the confluence of exciting advances in quantum chromodynamics (QCD) and an explosion of related experimental activity. The subsequent broad spectrum of breakthroughs, surprises, and continuing puzzles had not been anticipated. Indeed, CLEO-c, BESIII, and the B-factories, later joined by ATLAS, CMS and LHCb, have made a series of groundbreaking observations. For an extensive presentation of the status of heavy quarkonium physics, the reader is referred to several reviews [1–9]. This note focuses on experimental developments in heavy quarkonium spectroscopy with very few theoretical comments. Possible theoretical interpretations of the states not predicted by the quark model are presented in the review “Heavy non- $q\bar{q}$ mesons”. Note that in this review we follow the new naming scheme for hadrons (see the review “Naming scheme for hadrons” in the current edition of the RPP).

This review covers states discovered since 2003, the year that marked the unexpected discovery of the $X(3872)$ [10]. The $X(3872)$, now called $\chi_{c1}(3872)$, was the first of the mesons containing two heavy quarks that could not be easily accommodated by the $q\bar{q}$ quark model. Its discovery was a watershed event in meson spectroscopy. In earlier versions of this write-up the particles were sorted according to an assumed *conventional* or *unconventional* nature with respect to the quark model. However, since this classification is not always unambiguous, we here follow Ref. [11] and sort the states into three groups, namely states below (*cf.* Table 78.1), above (*cf.* Table 78.2), and near (*cf.* Table 78.3) the lowest open-flavor thresholds. Due to the presence of many open-flavor thresholds, we note that the division of states between “above” and “near” open-flavor thresholds is not absolute.

78.1 States Below Open-Flavor Threshold

Table 78.1 lists properties of recently observed heavy quarkonium states located below the lowest open-flavor thresholds. Those are expected to be (at least prominently) conventional quarkonia. The majority of charmonium ($c\bar{c}$) and bottomonium ($b\bar{b}$) states were established prior to 2003.

78.1.1 Charmonium

The $h_c(1P)$ is the 1^1P_1 charmonium state, the singlet partner of the long-known χ_{cJ} triplet 1^3P_J . After being firmly established in 2005 through the process $\psi(2S) \rightarrow \pi^0 h_c(1P)$ [12], it has since been studied extensively by BESIII using large samples of $\psi(2S)$ decays. Exclusive hadronic decays of the $h_c(1P)$, strongly suppressed relative to the dominant radiative transition $h_c(1P) \rightarrow \gamma \eta_c(1S)$, were first observed in 2019 [13] and additional decays were found in 2020 [14] and 2022 [15].

Belle reported an observation of the $\psi_2(1D)$ decaying to $\gamma \chi_{c1}(1P)$ with J^{PC} presumed to be 2^{--} [16]. This state is listed in Table 78.1 as $\psi_2(3823)$. Its existence was confirmed with high significance by BESIII [17, 18]. While the negative C-parity is indeed established by its observed decay channel, the assignment of $J = 2$ was made by matching to the closest quark model state (1^3D_2) and requires experimental confirmation.

The 1^1D_2 state, or the $\eta_{c2}(1D)$, with a mass expected near 3820 MeV, has not yet been observed. Recently Belle performed a search in $B \rightarrow \eta_{c2}(1D)K(\pi)$ decays in the mass range 3795–3845 MeV and found no signal [19]. Thus, the $\eta_{c2}(1D)$ remains the only unobserved conventional charmonium state that does not have open-charm decays.

78.1.2 Bottomonium

The ground state of bottomonium, $\eta_b(1S)$, is well established. After the initial reports from BaBar in radiative decays of the $\Upsilon(3S)$ (observation) [20] and $\Upsilon(2S)$ (evidence) [21], Belle confirmed the existence of the $\eta_b(1S)$ with more than 5σ significance in radiative decays of the newly discovered $h_b(1P)$ [22, 23] and $h_b(2P)$ [22] (see next paragraph), as well as in $\Upsilon(2S)$ radiative decays [24]. Belle has also reported strong evidence for

the $\eta_b(2S)$ [22], but it still needs confirmation at the 5σ level. Note that there are hints of tension in the $\eta_b(1S)$ mass as measured in radiative M1 and E1 transitions. In the M1 transition $\Upsilon(2S) \rightarrow \gamma \eta_b(1S)$ Belle measures a mass of $9394.8_{-3.1}^{+2.7+4.5}$ MeV [24], while in the E1 transitions $h_b(1P, 2P) \rightarrow \gamma \eta_b(1S)$ Belle measures $9402.4 \pm 1.5 \pm 1.8$ MeV [22]. This tension may point to an incomplete understanding of the $\eta_b(1S)$ lineshape in different production mechanisms.

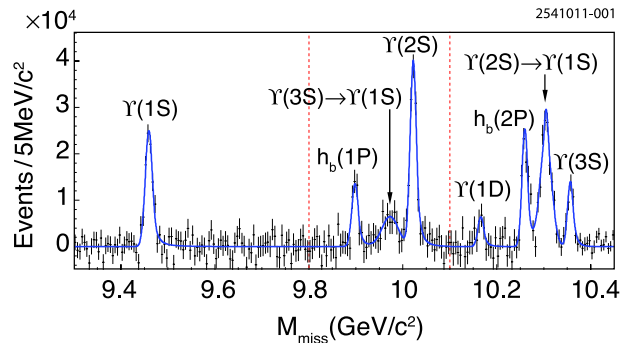


Figure 78.1: From Belle [25], the mass recoiling against $\pi^+\pi^-$ pairs, M_{miss} , in e^+e^- collision data taken near the peak of the $\Upsilon(10860)$. The smooth combinatorial and $K_S^0 \rightarrow \pi^+\pi^-$ background contributions have been subtracted. The fit to the various labeled signal contributions is overlaid (*curve*). The fit is performed separately in three regions with boundaries indicated by the vertical dashed lines.

The $h_b(1P)$, the bottomonium counterpart of the $h_c(1P)$, and the next excited state, the $h_b(2P)$, were simultaneously discovered by Belle using dipion transitions from the $\Upsilon(10860)$ [25] (Fig. 78.1). The same analysis also showed the $\Upsilon_J(1D)$, the lowest-lying D -wave triplet of the $b\bar{b}$ system, but did not resolve the $J = 1, 2, 3$ components. The search for the $h_b(1P)$ was directly inspired by a CLEO result [26], which found a surprisingly copious production of $e^+e^- \rightarrow \pi^+\pi^-h_c(1P)$ as well as an indication that $\psi(4230) \rightarrow \pi^+\pi^-h_c(1P)$ occurs at a comparable rate with the signature mode $\psi(4230) \rightarrow \pi^+\pi^-J/\psi(1S)$. The presence of $\Upsilon(nS)$ peaks in Fig. 78.1 at rates two orders of magnitude larger than expected, along with separate studies with exclusive decays $\Upsilon(nS) \rightarrow \mu^+\mu^-$, allow precise calibration of the $\pi^+\pi^-$ recoil mass spectrum and very accurate measurements of the $h_b(1P)$ and $h_b(2P)$ masses. Both corresponding hyperfine splittings are consistent with zero within an uncertainty of about 1.5 MeV (lowered to 1.1 MeV for the $h_b(1P)$ in Ref. [27]). Belle later observed the transition $\Upsilon(4S) \rightarrow h_b(1P)\eta$ [23] and the corresponding 1P hyperfine splitting was also found to be compatible with zero at a similar precision level.

Just before Christmas 2011, ATLAS offered the world a beautiful gift, in the form of the discovery of the $\chi_b(3P)$ quarkonium state [28], observed by combining dimuons from $\Upsilon(1S)$ or $\Upsilon(2S)$ decays with photons emitted in the radiative $\chi_b(3P)$ decays (Fig. 78.2, bottom left panel). The new resonance, with a mass of $10530 \pm 5(\text{stat}) \pm 9(\text{syst})$ MeV, was soon confirmed by D0 [29]. Also LHCb observed the $\chi_b(3P)$ peak, using the full Run 1 event sample, corresponding to an integrated luminosity of 3 fb^{-1} [30] (Fig. 78.2, middle left panel). Finally, CMS used 80 fb^{-1} of 13 TeV pp collisions, collected in 2016 and 2017, to show two well-resolved $\chi_{b1}(3P)$ and $\chi_{b2}(3P)$ peaks [31], separated by a mass difference of $10.60 \pm 0.64(\text{stat}) \pm 0.17(\text{syst})$ MeV (Fig. 78.2, top left panel). The remarkable precision of the individual mass measurements, with relative uncertainties as small as 50 ppm, shows that the LHC experiments can provide important results in the field of hadron spectroscopy, especially in the case of heavy particles, which require very high collision energies and large event samples.

78.1.3 B_c System

The B_c^\pm family is quite special because these (charged) quarkonium states consist of two heavy quarks of different flavor. Among

Table 78.1: New states below the open-flavor thresholds in the $c\bar{c}$, $b\bar{c}$, and $b\bar{b}$ regions, ordered by mass. Masses m and widths Γ represent the PDG23 weighted averages with statistical and systematic uncertainties added in quadrature. In the Production column, the state is always denoted by X . Ellipses (...) indicate inclusively selected event topologies, *i.e.*, additional particles not directly detected by experiment. A question mark (?) indicates an unmeasured value. The Discovery Year column gives the date of the first measurement cited. The Summary Table column indicates whether or not the state appears in the summary tables, usually requiring at least two independent experiments with significance of $>5\sigma$. Refer to the particle listings for references and further information.

PDG Name	Former Name	m (MeV)	Γ (MeV)	$I^G(J^{PC})$	Production	Decay	Discovery Year	Summary Table
$h_c(1P)$		3525.37 ± 0.14	$0.78^{+0.30}_{-0.27}$	$0^-(1^{+-})$	$\psi(2S) \rightarrow \pi^0 X$ $p\bar{p} \rightarrow X$ $e^+e^- \rightarrow \pi\pi X$	$\gamma\eta_c(1S)$ hadrons (see listings)	2004	YES
$\psi_2(3823)$	$X(3823)$	3823.51 ± 0.34	< 2.9	$0^-(2^{--})$	$B \rightarrow KX$ $e^+e^- \rightarrow \pi^+\pi^-X$	$\gamma\chi_{c1}(1P)$ $\pi^+\pi^-J/\psi(1S)$	2013	YES
B_c^+		6274.47 ± 0.32	stable	$0(0^-)$	$p\bar{p} \rightarrow X\dots$ $pp \rightarrow X\dots$	$\pi^+J/\psi(1S)$ (see listings)	2007	YES
$B_c^+(2S)$		6871.2 ± 1.0	?	$0(0^-)$	$pp \rightarrow X\dots$	$B_c^+\pi^+\pi^-$	2014	YES
$\eta_b(1S)$		9398.7 ± 2.0	10^{+5}_{-4}	$0^+(0^{++})$	$\Upsilon(2S, 3S) \rightarrow \gamma X$ $h_b(1P, 2P) \rightarrow \gamma X$	hadrons (see listings)	2008	YES
$h_b(1P)$		9899.3 ± 0.8	?	$0^-(1^{+-})$	$\Upsilon(10860) \rightarrow \pi^+\pi^-X$ $\Upsilon(3S) \rightarrow \pi^0 X$ $\Upsilon(4S) \rightarrow \eta X$	$\gamma\eta_b(1S)$	2011	YES
$\eta_b(2S)$		$9999.0^{+4.5}_{-4.0}$	< 24	$0^+(0^{++})$	$T_{bb}^+(10610) \rightarrow \pi^+ X$ $T_{bb}^+(10650) \rightarrow \pi^+ X$ $h_b(2P) \rightarrow \gamma X$	hadrons	2012	NO
$\Upsilon_2(1D)$		10163.7 ± 1.4	?	$0^-(2^{--})$	$\Upsilon(3S) \rightarrow \gamma\gamma X$ $\Upsilon(10860) \rightarrow \pi^+\pi^-X$	$\gamma\gamma\Upsilon(1S)$ $\pi^+\pi^-\Upsilon(1S)$	2004	YES
$h_b(2P)$		10259.8 ± 1.2	?	$0^-(1^{+-})$	$\Upsilon(10860) \rightarrow \pi^+\pi^-X$ $\Upsilon(10860) \rightarrow \pi^+\pi^-X$ $T_{bb}^+(10610) \rightarrow \pi^+ X$ $T_{bb}^+(10650) \rightarrow \pi^+ X$	$\gamma\eta_b(1S, 2S)$	2011	YES
$\chi_{b1}(3P)$		10513.42 ± 0.67	?	$0^+(1^{++})$	$pp \rightarrow X\dots$	$\gamma\Upsilon(1S, 2S, 3S)$	2011	YES
$\chi_{b2}(3P)$		10524.02 ± 0.78	?	$0^+(2^{++})$	$pp \rightarrow X\dots$	$\gamma\Upsilon(3S)$	2011	YES

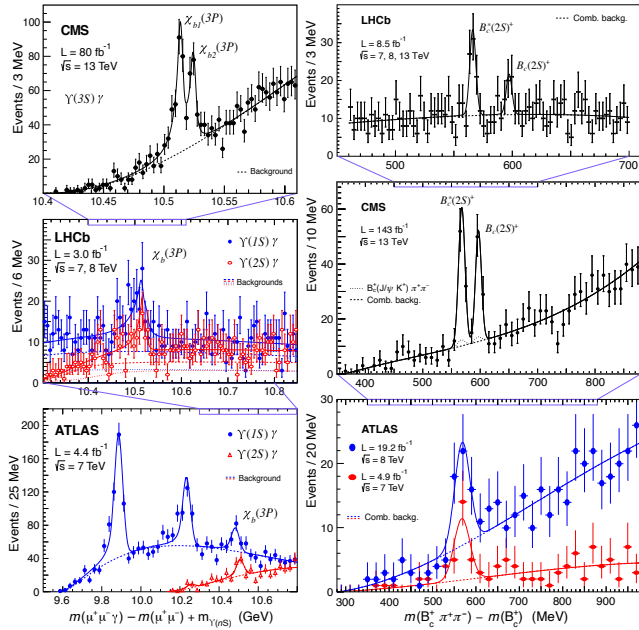


Figure 78.2: (Left Column) Invariant mass distributions measured by the ATLAS [28] (bottom), LHCb [30] (middle) and CMS [31] (top) experiments in their searches for the $\chi_b(3P)$ states through their radiative decays to one of the S-wave bottomonia. (Right Column) Invariant mass distributions measured by the ATLAS [32] (bottom), CMS [33] (middle) and LHCb [34] (top) experiments in their searches for B_c^\pm excited states decaying to the B_c^\pm ground state with the emission of two charged pions.

other interesting properties, this means that they cannot annihili-

late into gluons, the excited states only decaying to the pseudoscalar ground state, B_c^\pm , via electromagnetic and pionic transitions.

On the basis of an event sample collected in the Run 1 of the LHC, corresponding to an integrated luminosity of 24 fb^{-1} , adding the 7 and 8 TeV data, the ATLAS Collaboration observed a resonance in the $B_c^+\pi^+\pi^-$ invariant mass spectrum [32] (Fig. 78.2, bottom right panel). This peak, observed with a significance of 5.2 standard deviations and a mass of $6842 \pm 4(\text{stat}) \pm 5(\text{syst}) \text{ MeV}$, was immediately recognized as the $B_c(2S)^\pm$ state, the first radial excitation in the B_c^\pm family. Profiting from the much larger Run 2 event sample, collected in the 2015, 2016, 2017 and 2018 running periods and corresponding to 143 fb^{-1} of 13 TeV pp collisions, as well as from a measurement resolution of around 6 MeV, the CMS Collaboration could observe *two* well-resolved peaks, separated by $29.1 \pm 1.5(\text{stat}) \pm 0.7(\text{syst}) \text{ MeV}$ [33] (Fig. 78.2, middle right panel). The existence of two peaks, rather than a single one, is established with a significance of 6.5 standard deviations. The “right peak” has a mass of $6871.0 \pm 1.2(\text{stat}) \pm 0.8(\text{syst}) \pm 0.8(B_c^+)$ MeV, where the last term is the uncertainty in the B_c^+ mass, and is identified as the $B_c(2S)^\pm$ state, which decays directly to the B_c^\pm , emitting two (easy to detect) pions. The CMS observation, reported a couple of months after the end of the LHC Run 2, was soon followed by the corresponding LHCb result [34] (Fig. 78.2, top right panel), which confirmed the existence of the two states and reported a second measurement of the $B_c(2S)^\pm$ mass, $6872.1 \pm 1.3(\text{stat}) \pm 0.1(\text{syst}) \pm 0.8(B_c^+)$ MeV.

The “left peak” is interpreted as being the $B_c^*(2S)^\pm$ signal. It is observed at a mass lower than the real value because the experiments are unable to detect the low-energy photon emitted in the decay chain, $B_c^*(2S)^\pm \rightarrow B_c^\pm \pi^+\pi^-$ followed by $B_c^\pm \rightarrow B_c^\pm \gamma$ (Fig. 78.3). Its energy, expected to be in the range 40–80 MeV, leads to a very small probability that the photon converts into an e^+e^- pair and the two electrons are reconstructed. The relative ordering of the two peaks is based on a generally-agreed assumption: the $M(B_c^{*\pm}) - M(B_c^\pm)$ mass difference is larger than the $M(B_c^*(2S)^\pm) - M(B_c(2S)^\pm)$ differ-

ence. Naturally, these observations provide evidence for the existence of the $B_c^*(1S)^\pm$ state. They also provide measurements of two interesting mass differences, between the masses of the pseudoscalar mesons, $M(B_c(2S)^\pm) - M(B_c(1S)^\pm) = 596.1$ MeV, and of the vector mesons, $M(B_c^*(2S)^\pm) - M(B_c^*(1S)^\pm) = 567.0$ MeV (Fig. 78.3).

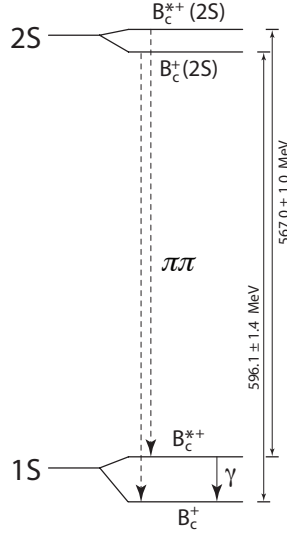


Figure 78.3: Diagram showing the decays mentioned in the text.

78.2 States Above Open-Flavor Threshold

Many states have been discovered both above and near the lowest open-flavor thresholds. They are displayed in Tables 78.2 and 78.3, respectively. With the exception of the $\psi_3(3842)$ and the tensor state located at 3930 MeV (now called $\chi_{c2}(3930)$), which have properties consistent with those expected for the $\psi_3(1^3D_3)$ and $\chi_{c2}(2^3P_2)$, respectively, none of these states can easily be assigned a place in the quark model spectrum of the charmonium or bottomonium families. The theoretical interpretation of these states remains under discussion.

78.2.1 Charmonium

Using proton-proton collisions, LHCb observed a narrow state, the $\psi_3(3842)$ resonance, in the decay modes $\psi_3(3842) \rightarrow D^0\bar{D}^0$ and D^+D^- [35]. The mass and width of this state are measured to be $3842.71 \pm 0.16 \pm 0.12$ MeV and $2.79 \pm 0.51 \pm 0.35$ MeV, respectively. The observed mass and narrow width are consistent with expectations for the spin-3 $\psi_3(1^3D_3)$ charmonium. Accordingly, the state is given the name $\psi_3(3842)$ in the listings, with the remark that the quantum numbers are fixed from the quark model and need to be confirmed.

The $\chi_{c2}(3930)$, which is a natural candidate for the $\chi_{c2}(2^3P_2)$ quark model state, was originally seen by Belle [36] and later confirmed by BaBar [37] in the $\gamma\gamma$ process $e^+e^- \rightarrow e^+e^-D\bar{D}$. This interpretation was strengthened by the more recent LHCb observation of the $\chi_{c2}(3930)$ alongside the $\psi_3(3842)$ in proton-proton collisions [35].

Unlike the $\chi_{c2}(2^3P_2)$, the identification of the $\chi_{c0}(2^3P_0)$ quark model state remains controversial. The original candidate was the $\chi_{c0}(3915)$, discovered by Belle in the $\gamma\gamma$ process $e^+e^- \rightarrow e^+e^- \omega J/\psi(1S)$ [38]. In a subsequent measurement by BaBar, its quantum numbers were determined to be $J^{PC} = 0^{++}$ [39]. However, its identification as the $\chi_{c0}(2^3P_0)$ quark model state was soon challenged [40, 41]. In addition, it was pointed out in Ref. [42] that if the assumption of helicity-2 dominance is abandoned and, instead, one allows for a sizeable helicity-0 component, a $J^{PC} = 2^{++}$ assignment is possible. This could imply that it is the same as the $\chi_{c2}(3930)$, but to explain the large helicity-0 component a sizeable portion of non- $q\bar{q}$ is necessary [42]. A more recent LHCb amplitude analysis of the process $B^+ \rightarrow D^+D^-K^+$ finds distinct 0^{++} and 2^{++} components decaying to D^+D^- [43],

which are currently identified in the listings as the $\chi_{c0}(3915)$ and $\chi_{c2}(3930)$, respectively.

An alternative candidate for the $\chi_{c0}(2^3P_0)$ (here referred to as the $\chi_{c0}(3860)$) was reported in Ref. [44] with properties more consistent with expectation: its mass is close to the potential model expectations, it decays to $D\bar{D}$, and the preferred quantum numbers are $J^{PC} = 0^{++}$ (this hypothesis is favored over the 2^{++} one with a 2.5σ significance).

In the excited vector charmonium spectrum, the $\psi(4040)$, $\psi(4160)$, and $\psi(4415)$ are prominent in the inclusive e^+e^- hadronic cross section and are naturally identified as the 3^3S_1 , 2^3D_1 , and 4^3S_1 $c\bar{c}$ quark model states, respectively. In addition to these long-established states, however, another set of peaks has been found in exclusive e^+e^- cross sections. Unlike conventional vector charmonia, they do not appear in the inclusive hadronic cross section and they apparently do not decay to $D\bar{D}$. The PDG summary table currently lists the $\psi(4230)$, $\psi(4360)$, and $\psi(4660)$ within this category. The first of these to be discovered was originally known as the $Y(4260)$ (now the $\psi(4230)$), seen by BaBar [45] and Belle [46, 47] in $e^+e^- \rightarrow \pi^+\pi^-J/\psi(1S)$ using initial state radiation. In a more recent high-statistics scan of $e^+e^- \rightarrow \pi^+\pi^-J/\psi(1S)$, BESIII demonstrated that the lineshape in this mass range is highly non-trivial [48]. The latter observation was interpreted by the authors as the presence of two states. However, this lineshape is also consistent with other possible interpretations, such as one assuming a molecular structure for the $\psi(4230)$ [49]. The data of Ref. [48] also called for a significant downward shift of the mass of what was originally called the $Y(4260)$ (or, more formally, the $\psi(4260)$) with the $\psi(4230)$ in the listings.

BESIII observed the $\chi_{c1}(3872)$, also known as $X(3872)$, in $e^+e^- \rightarrow \gamma\chi_{c1}(3872)$ in the $\psi(4230)$ mass range [51], which could allow for additional insight into the structure of both states (see the review on heavy non- $q\bar{q}$ mesons). BESIII also performed a recent study of the process $e^+e^- \rightarrow \pi^+\pi^-\psi(2S)$ and found evidence for a lower mass state, possibly the $\psi(4230)$, in addition to the more dominant $\psi(4360)$ [52].

Another interesting question is whether a heavier $\pi^+\pi^-\psi(2S)$ state, the $\psi(4660)$, discovered by Belle [53, 54] and confirmed by BaBar [55], is identical to the $A_c^+\bar{A}_c^-$ resonance observed by Belle with a nearby mass and width [56]. Most probably it is, the $A_c^+\bar{A}_c^-$ being one more decay mode of the $\psi(4660)$ (see the review on heavy non- $q\bar{q}$ mesons for more details). Note that this is the interpretation adopted in the particle listings. In addition, Belle reported the first observation of a vector charmonium-like state decaying to $D_s^+D_{s1}(2536)$ with a significance of 5.9σ [57]. Its measured mass and width are $4625.9_{-11.5}^{+13.9} \pm 0.4$ MeV and $49.8_{-6.0}^{+6.2} \pm 0.4$ MeV, respectively, consistent with those of the $\psi(4660)$. Therefore, $D_s^+D_{s1}(2536)$ appears as an additional decay mode of the $\psi(4660)$ in the listings.

A series of isovector states¹ containing $c\bar{c}$ have been found in B decays to $K\pi(c\bar{c})$, where the isovector state decays to $\pi(c\bar{c})$ and $(c\bar{c})$ stands for $J/\psi(1S)$, $\psi(2S)$, or $\chi_{c1}(1P)$. They are manifestly non- $q\bar{q}$. The $T_{c\bar{c}1}(4430)$ (originally called the $Z_c(4430)$), decaying to $\pi\psi(2S)$, is the most well established. Based on a full amplitude analysis of $B^0 \rightarrow K^+\pi^-\psi(2S)$ decays, Belle determined the spin-parity of the $T_{c\bar{c}1}(4430)$ to be $J^P = 1^+$ [58]. From their study of $B^0 \rightarrow K^+\pi^-J/\psi(1S)$ decays, Belle also found evidence for the decay mode $T_{c\bar{c}1}(4430) \rightarrow \pi J/\psi(1S)$ [59], which has an order of magnitude lower branching fraction than the discovery mode $T_{c\bar{c}1}(4430) \rightarrow \pi\psi(2S)$. In the same analysis, Belle reported evidence for one more charged state, dubbed $T_{c\bar{c}1}(4200)$, decaying to $\pi J/\psi(1S)$. The observation of the $T_{c\bar{c}1}(4430)$ in $\pi\psi(2S)$, as well as its quantum number assignments, were confirmed by LHCb [60] with a much larger data sample, leading to improved mass and width values, consistent with earlier measurements; the experiment even reports a resonant behavior of the $T_{c\bar{c}1}(4430)$ amplitude. The $T_{c\bar{c}1}(4430)$ was not confirmed (or excluded) by BaBar [61].

Table 78.2: As in Table 78.1, but for states above the first open-flavor thresholds in the $c\bar{c}$ and $b\bar{b}$ regions, ordered by mass.

PDG Name	Former Name(s)	m (MeV)	Γ (MeV)	$I^G(J^{PC})$	Production	Decay	Discovery Year	Summary Table
$\psi_3(3842)$		3842.71 ± 0.20	2.79 ± 0.62	$0^-(3^{--})^*$	$pp \rightarrow X\dots$	$D\bar{D}$	2019	YES
$\chi_{c0}(3860)$		3862^{+48}_{-35}	201^{+177}_{-106}	$0^+(0^{++})$	$e^+e^- \rightarrow J/\psi(1S)X$	$D\bar{D}$	2017	NO
$\chi_{c0}(3915)$	$X(3915)$, $Y(3940)$	3922.1 ± 1.8	20 ± 4	$0^+(0/2^{++})$	$B \rightarrow KX$	$\omega J/\psi(1S)$	2004	YES
$\chi_{c2}(3930)$	$\chi_{c2}(2P)$, $Z(3930)$	3922.5 ± 1.0	35.2 ± 2.2	$0^+(2^{++})$	$e^+e^- \rightarrow e^+e^-X$	$D\bar{D}$ $D\bar{D}$	2005	YES
$X(3940)$		3942^{+9}_{-8}	37^{+27}_{-17}	$?^?(?^{??})$	$e^+e^- \rightarrow J/\psi(1S)X$	$D\bar{D}^*$	2007	NO
$T_{c\bar{c}}(4050)$	$Z_1(4050)$ $X(4050)$	4051^{+24}_{-43}	82^{+51}_{-28}	$1^-(?^{?+})$	$\bar{B}^0 \rightarrow K^-X$	$\pi^+\chi_{c1}(1P)$	2008	NO
$T_{c\bar{c}}(4055)$	$Z_c(4055)$ $X(4055)$	4054 ± 3	45 ± 13	$1^+(?^{?-})$	$e^+e^- \rightarrow \pi^-X$	$\pi^+\psi(2S)$	2015	NO
$T_{c\bar{c}}(4100)$	$X(4100)$	4096^{+27}_{-30}	152^{+83}_{-68}	$1^-(?^{??})$	$\bar{B}^0 \rightarrow K^-X$	$\pi^+\eta_c(1S)$	2018	NO
$\chi_{c1}(4140)$	$Y(4140)$	4146.5 ± 3.0	19^{+7}_{-5}	$0^+(1^{++})$	$B^+ \rightarrow K^+X$	$\phi J/\psi(1S)$	2009	YES
$X(4160)$		4153^{+23}_{-21}	136^{+60}_{-35}	$?^?(?^{??})$	$e^+e^- \rightarrow J/\psi(1S)X$	$D^*\bar{D}^*$	2007	NO
$T_{c\bar{c}1}(4200)$	$Z_c(4200)$	4196^{+35}_{-32}	370^{+99}_{-149}	$1^+(1^{+-})$	$B^+ \rightarrow K^+X$	$\phi J/\psi(1S)$	2014	NO
$\psi(4230)$	$Y(4230)$ $Y(4260)$	4222.1 ± 2.3	49 ± 7	$0^-(1^{--})$	$\bar{B}^0 \rightarrow K^-X$	$J/\psi(1S)\pi^+$ $\pi^+\pi^-J/\psi(1S)$ $\omega\chi_{c0}(1P)$ $\pi^+\pi^-h_c(1P)$ (see listings)	2015	YES
$T_{c\bar{c}0}(4240)$	$Z_c(4240)$ $R_{c0}(4240)$	4239^{+48}_{-21}	220^{+118}_{-88}	$1^+(0^{--})$	$\bar{B}^0 \rightarrow K^-X$	$\pi^+\psi(2S)$	2014	NO
$T_{c\bar{c}}(4250)$	$Z_2(4250)$ $X(4250)$	4248^{+185}_{-45}	177^{+321}_{-72}	$1^-(?^{?+})$	$\bar{B}^0 \rightarrow K^-X$	$\pi^+\chi_{c1}(1P)$	2008	NO
$\chi_{c1}(4274)$	$Y(4274)$	4286^{+8}_{-9}	51 ± 7	$0^+(1^{++})$	$B^+ \rightarrow K^+X$	$\phi J/\psi(1S)$	2011	YES
$X(4350)$		$4350.6^{+4.7}_{-5.1}$	13^{+18}_{-10}	$0^+(?^{?+})$	$e^+e^- \rightarrow e^+e^-X$	$\phi J/\psi(1S)$	2009	NO
$\psi(4360)$	$Y(4360)$	4374 ± 7	118 ± 12	$0^-(1^{--})$	$e^+e^- \rightarrow X$	$\pi^+\pi^-\psi(2S)$ $\pi^+\pi^-J/\psi(1S)$	2007	YES
$T_{c\bar{c}1}(4430)$	$Z_c(4430)$	4478^{+15}_{-18}	181 ± 31	$1^+(1^{+-})$	$\bar{B}^0 \rightarrow K^-X$	$\pi^+\psi(2S)$ $\pi^+J/\psi(1S)$	2007	YES
$\chi_{c0}(4500)$	$X(4500)$	4474 ± 4	77^{+12}_{-10}	$0^+(0^{++})$	$B^+ \rightarrow K^+X$	$\phi J/\psi(1S)$	2017	NO
$X(4630)$		4626^{+24}_{-111}	174^{+137}_{-78}	$0^+(?^{?+})$	$B^+ \rightarrow K^+X$	$\phi J/\psi(1S)$	2021	NO
$\psi(4660)$	$Y(4660)$, $X(4660)$	4641 ± 10	72^{+13}_{-11}	$0^-(1^{--})$	$e^+e^- \rightarrow X$	$\pi^+\pi^-\psi(2S)$ $\Lambda_c^+\bar{\Lambda}_c^-$ $D_s^+D_{s1}(2536)$ $\phi J/\psi(1S)$	2007	YES
$\chi_{c1}(4685)$		4684^{+15}_{-17}	126^{+40}_{-44}	$0^+(1^{++})$	$B^+ \rightarrow K^+X$	$\phi J/\psi(1S)$	2021	NO
$\chi_{c0}(4700)$	$X(4700)$	4694^{+16}_{-5}	87^{+18}_{-10}	$0^+(0^{++})$	$B^+ \rightarrow K^+X$	$\phi J/\psi(1S)$	2017	NO
$T_{c\bar{c}\bar{c}}(6900)$	$X(6900)$	6899 ± 12	153 ± 29	$0^+(?^{?+})$	$pp \rightarrow X\dots$	$J/\psi(1S)J/\psi(1S)$	2020	NO
$\Upsilon(10753)$		$10752.7^{+5.9}_{-6.0}$	36^{+18}_{-12}	$?^?(1^{--})$	$e^+e^- \rightarrow X$	$\pi\pi\Upsilon(1S, 2S, 3S)$	2019	NO
$\Upsilon(10860)$	$\Upsilon(5S)$	$10885.2^{+2.6}_{-1.6}$	37 ± 4	$0^-(1^{--})$	$e^+e^- \rightarrow X$	$B_{(s)}^{(*)}\bar{B}_{(s)}^{(*)}(\pi)$ $\pi\pi\Upsilon(1S, 2S, 3S)$ $\pi^+\pi^-h_b(1P, 2P)$ $\eta\Upsilon(1S, 2S)$ $\pi^+\pi^-\Upsilon(1D)$ (see listings)	1985	YES
$\Upsilon(11020)$	$\Upsilon(6S)$	11000 ± 4	24^{+8}_{-6}	$0^-(1^{--})$	$e^+e^- \rightarrow X$	$B_{(s)}^{(*)}\bar{B}_{(s)}^{(*)}(\pi)$ $\pi\pi\Upsilon(1S, 2S, 3S)$ $\pi^+\pi^-h_b(1P, 2P)$ (see listings)	1985	YES

*Quantum numbers fixed from the quark model and need confirmation.

Belle also reported an observation of two charged states decaying to $\pi\chi_{c1}(1P)$ in an analysis of $B^0 \rightarrow K^+\pi^-\chi_{c1}(1P)$ decays [62]. These were originally called $Z_1(4050)^\pm$ and $Z_2(4250)^\pm$, but are referred to in Table 78.2 as $T_{c\bar{c}}(4050)$ and $T_{c\bar{c}}(4250)$. These states were not confirmed by BaBar [63]. Belle observes signals with 5.0σ significance for both the $T_{c\bar{c}}(4050)$ and $T_{c\bar{c}}(4250)$,

¹These isovector states were originally called Z_c . They are now referred to as $T_{c\bar{c}}$. See the naming scheme review.

whereas BaBar reports 1.1σ and 2.0σ effects, respectively, setting upper limits that are not inconsistent with Belle's measured rates. The situation remains unresolved.

The decay $B^+ \rightarrow K^+\phi J/\psi(1S)$ appears to be especially rich in resonant substructure. The $Y(4140)$ (now the $\chi_{c1}(4140)$), decaying to $\phi J/\psi(1S)$, was first observed in 2008 by CDF [64, 65], and confirmed by D0 and CMS [66, 67]. However, a second structure, the $Y(4274)$ (now the $\chi_{c1}(4274)$), could not be established

unambiguously. Neither of the two states was seen in B decays at Belle [68], LHCb [69] and BaBar [70], or in $\gamma\gamma$ collisions at Belle [71]. The real breakthrough happened when LHCb performed a full amplitude analysis of $B^+ \rightarrow K^+\phi/J/\psi(1S)$ with $J/\psi(1S) \rightarrow \mu^+\mu^-$, $\phi \rightarrow K^+K^-$ decays and showed that the data cannot be described in a model that contains only excited kaon states decaying into $K^+\phi$ [72, 73]. They observe two 1^{++} states with masses close to those originally reported by CDF (the $\chi_{c1}(4140)$ and $\chi_{c1}(4274)$), but the width of the one at 4140 MeV is much larger. In addition, they find two significant 0^{++} structures at 4500 and 4700 MeV (the $\chi_{c0}(4500)$ and $\chi_{c0}(4700)$). The LHCb analysis was extended even further in Ref. [74] with a factor of six increase in statistics: the $\chi_{c1}(4140)$, $\chi_{c1}(4274)$, $\chi_{c0}(4500)$, and $\chi_{c0}(4700)$ were confirmed, and two new states, the $X(4630)$ and $\chi_{c1}(4685)$ were reported, also decaying to $\phi J/\psi(1S)$.

78.2.2 Resonances in the $J/\psi(1S)$ -pair mass spectrum

Based on proton-proton event samples collected at $\sqrt{s} = 7, 8$ and 13 TeV, corresponding to an integrated luminosity of 9 fb^{-1} , the LHCb Collaboration reported the observation of a narrow structure in the invariant mass distribution of $J/\psi(1S)$ pairs [75]. The new resonance, denoted as $T_{cc\bar{c}\bar{c}}(6900)$ (also $X(6900)$), is clearly seen at a mass of 6.9 GeV in the bottom panel of Fig. 78.4, as indicated by the red curve. The ATLAS Collaboration has also

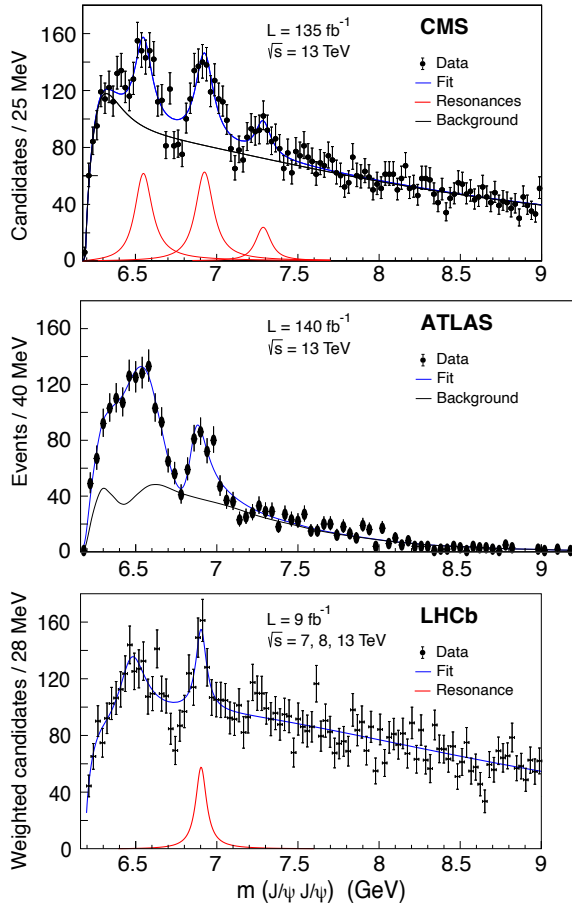


Figure 78.4: $J/\psi(1S)$ -pair invariant mass distributions measured by the LHCb [75] (bottom), ATLAS [76] (middle), and CMS [77] (top) experiments.

observed the $T_{cc\bar{c}\bar{c}}(6900)$ resonance in the di- $J/\psi(1S)$ mass spectrum, using 140 fb^{-1} of pp collisions at $\sqrt{s} = 13 \text{ TeV}$ [76], as can be seen in the middle panel of Fig. 78.4. More recently, also the CMS Collaboration reported the observation of the $T_{cc\bar{c}\bar{c}}(6900)$ in the $J/\psi(1S)$ -pair mass distribution, using 135 fb^{-1} of 13 TeV pp collisions [77]. Thanks to its good mass resolution and relatively large event yields, CMS determined the mass and width of the $T_{cc\bar{c}\bar{c}}(6900)$ with the best precision among the three measure-

ments. Furthermore, another resonance is seen with a significance exceeding 5 standard deviations, at a mass of 6.55 GeV, as shown in the top panel of Fig. 78.4. The measured values of the masses and widths of the new states depend on whether the model used to fit the distributions includes interference effects between the resonances and the underlying continuum (and also among the resonances). The larger event samples presently being collected by the LHC experiments will surely lead to significantly improved measurements, as well as to complementary results (including determinations of spin-parity quantum numbers), so that one can expect near-future progress in our understanding of the nature of these “narrow structures”.

78.2.3 Bottomonium

Belle reported a new measurement of the $e^+e^- \rightarrow \Upsilon(nS)\pi^+\pi^-$ ($n = 1, 2, 3$) cross sections at energies from 10.52 to 11.02 GeV [78]. They observed, with a 5.2σ significance, a new structure in the energy dependence of the cross sections. If described by a Breit–Wigner function, its mass and width are $10752.7 \pm 5.9_{-1.1}^{+0.7} \text{ MeV}$ and $35.5_{-11.3}^{+17.6+3.9}_{-3.3} \text{ MeV}$, respectively. The new structure could have a resonant origin and correspond to the not yet observed $\Upsilon(3D)$ state, provided $S-D$ mixing is enhanced, or an exotic state, e.g., a compact tetraquark or hadrobottomonium. It could also be a non-resonant effect due to rescattering. The $\Upsilon(10750)$ was confirmed in a global K -matrix fit to exclusive and inclusive $e^+e^- \rightarrow b\bar{b}$ cross sections in Ref. [79].

We no longer mention a hypothetical $Y_b(10888)$ state since a new analysis of the $\Upsilon(10860)$ energy range does not show evidence for an additional state with a mass different from that of the $\Upsilon(10860)$ [80]. After the mass of the $\eta_b(1S)$ was shifted upwards by about 10 MeV based on the Belle measurements [22, 23], all of the bottomonium states mentioned above fit into their respective spectroscopies, roughly where expected. An independent experimental confirmation of the shifted masses came from the Belle observation of $\Upsilon(4S) \rightarrow \eta_b(1P)$ decays [23]. This process turns out to be the strongest observed transition of the $\Upsilon(4S)$ to lower bottomonium states.

78.3 States Near Open-Flavor Threshold

A number of states, listed in Table 78.3, appear near open-flavor thresholds, which is likely an important factor in their theoretical interpretation [81].

78.3.1 Charmonium

The $\chi_{c1}(3872)$, also known as $X(3872)$, is widely studied and seen in many transitions — see Table 78.3. Yet its interpretation remains unsettled (see the heavy non- $q\bar{q}$ review). Its unique experimental features include: it has $J^{PC} = 1^{++}$ [82, 83], yet it is too light to be the $\chi_{c1}(2^3P_1)$ quark model state; its mass is within 200 keV of the $D^0\bar{D}^{*0}$ threshold; it shows substantial isospin-breaking in its decays to $\rho J/\psi(1S)$ and $\pi^0\chi_{c1}(1P)$; and it is extremely narrow. Using a large sample of inclusively produced $\chi_{c1}(3872)$ decaying to $\pi^+\pi^-J/\psi(1S)$, LHCb recently determined the decay width of the $\chi_{c1}(3872)$ under two different assumptions [84]. Assuming a Flatté-inspired line shape and exploiting the strong coupling of the $\chi_{c1}(3872)$ to $D^0\bar{D}^{*0}$, LHCb performed the first exploration of the pole structure of the $\chi_{c1}(3872)$, finding a FWHM width of $0.22_{-0.08}^{+0.06+0.25}_{-0.17} \text{ MeV}$. On the other hand, assuming a Breit–Wigner line shape, its width was found to be $1.39 \pm 0.24 \pm 0.10 \text{ MeV}$. While the former analysis has a more firm theoretical foundation, the LHCb detector resolution did not allow for a distinction between the different line shapes.

In addition to the $T_{c\bar{c}}$ (also known as Z_c) states found in B decays, discussed above, several isovector states with masses near DD^* and $D^*\bar{D}^*$ thresholds appear to be unique to e^+e^- annihilation. In 2013, a state named $T_{c\bar{c}1}(3900)$ (originally $Z_c(3900)$) was unearthed in the charmonium region at BESIII [86] and Belle [47] in the process $e^+e^- \rightarrow \pi^\mp T_{c\bar{c}1}(3900)^\pm$ with $T_{c\bar{c}1}(3900)^\pm \rightarrow \pi^\pm J/\psi(1S)$. The corresponding spectrum from BESIII is shown in Fig. 78.5. An analysis of CLEO data [87] confirmed this finding and also provided evidence for a neutral partner. A nearby signal was also seen in the DD^* channel [88] whose quantum numbers were fixed to 1^{+-} . BESIII reported its neutral partner in both $J/\psi(1S)\pi^0$ [89] and DD^* [90] decay modes. The masses extracted

Table 78.3: As in Table 78.1, but for states near the first open-flavor thresholds in the $c\bar{c}$ and $b\bar{b}$ regions, ordered by mass. Updated from Ref. [85] with kind permission, copyright (2011), Springer, and from Ref. [11] with kind permission from the authors.

PDG Name	Former Name	m (MeV)	Γ (MeV)	$J^G(J^{PC})$	Production	Decay	Discovery Year	Summary Table
$\chi_{c1}(3872)$	$X(3872)$	3871.64 ± 0.06	1.19 ± 0.21	$0^+(1^{++})$	$B \rightarrow KX$ $p\bar{p} \rightarrow X\dots$ $pp \rightarrow X\dots$ $e^+e^- \rightarrow \gamma X$	$\pi^+\pi^- J/\psi(1S)$ $3\pi J/\psi(1S)$ $D^{*0}\bar{D}^0$ $\gamma J/\psi(1S)$ $\gamma\psi(2S)$ $\pi^0\chi_{c1}(1P)$	2003	YES
$T_{cc}(3875)$		3874.83 ± 0.11	$0.410^{+0.172}_{-0.175}$	$?(?)$	$pp \rightarrow X\dots$	$D^0D^0\pi$	2022	NO
$T_{c\bar{c}1}(3900)$	$Z_c(3900)$	3887.1 ± 2.6	28.4 ± 2.6	$1^+(1^{+-})$	$\psi(4230) \rightarrow \pi^- X$ $\psi(4230) \rightarrow \pi^0 X$	$\pi^+ J/\psi(1S)$ $\pi^0 J/\psi(1S)$ $(D\bar{D}^*)^+$ $(D\bar{D}^*)^0$	2013	YES
$T_{c\bar{c}\bar{s}1}(4000)$	$Z_{cs}(4000)$	$3980 - 4010$	$5 - 150$	$\frac{1}{2}(1^+)$	$e^+e^- \rightarrow KX$ $B^+ \rightarrow \phi X$	$D_s D^* + D_s^* D$ $K^+ J/\psi(1S)$	2021	NO
$T_{c\bar{c}}(4020)$	$Z_c(4020)$ $X(4020)$	4024.1 ± 1.9	13 ± 5	$1^+(?^-)$	$\psi(4230, 4360) \rightarrow \pi^- X$ $\psi(4230, 4360) \rightarrow \pi^0 X$	$\pi^+ h_c(1P)$ $\pi^0 h_c(1P)$ $(D^* \bar{D}^*)^+$ $(D^* \bar{D}^*)^0$	2013	YES
$T_{c\bar{c}\bar{s}1}(4220)$	$Z_{cs}(4220)$	4216^{+49}_{-38}	233^{+110}_{-90}	$\frac{1}{2}(1^+)$	$B^+ \rightarrow \phi X$	$K^+ J/\psi(1S)$	2021	NO
$T_{b\bar{b}1}(10610)$	$Z_b(10610)$	10607.2 ± 2.0	18.4 ± 2.4	$1^+(1^{+-})$	$\Upsilon(10860) \rightarrow \pi^- X$ $\Upsilon(10860) \rightarrow \pi^0 X$	$\pi^+ \Upsilon(1S, 2S, 3S)$ $\pi^0 \Upsilon(1S, 2S, 3S)$ $\pi^+ h_b(1P, 2P)$ $(B\bar{B}^*)^+$	2011	YES
$T_{b\bar{b}1}(10650)$	$Z_b(10650)$	10652.2 ± 1.5	11.5 ± 2.2	$1^+(1^{+-})$	$\Upsilon(10860) \rightarrow \pi^- X$	$\pi^+ \Upsilon(1S, 2S, 3S)$ $\pi^+ h_b(1P, 2P)$ $(B^* \bar{B}^*)^+$	2011	YES

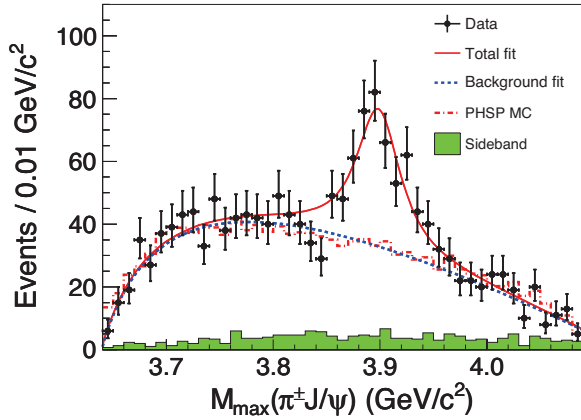


Figure 78.5: The $\pi^\pm J/\psi(1S)$ invariant mass distribution from BESIII [86] e^+e^- collision data taken at a center-of-mass energy near 4260 MeV.

from these experiments in different decay modes agree within 2σ . However, since the extraction of the mass and width parameters did not allow for an interference with the background and Breit–Wigner line shapes are used, which is not justified near thresholds, there might be some additional systematic uncertainty in the mass values. Therefore, in the RPP listings as well as in Table 78.3 both structures appear under the name $T_{c\bar{c}1}(3900)$. BESIII also reported the observation of another charged state, the $T_{c\bar{c}}(4020)^\pm$ (originally called $Z_c(4020)^\pm$), in two decay modes: $h_c(1P)\pi^\pm$ [91] and $(D^* \bar{D}^*)^\pm$ [92]. The neutral partners have also been observed by BESIII in the $h_c(1P)\pi^0$ [93] and $(D^* \bar{D}^*)^0$ [94] final states. The $T_{c\bar{c}}$ states show some remarkable similarities to the $T_{b\bar{b}}$ states (discussed below), e.g. they decay dominantly to $D^{(*)} \bar{D}^*$ channels. However, current analyses suggest that the mass of the $T_{c\bar{c}1}(3900)$ might be somewhat above the $D\bar{D}^*$ threshold. If confirmed, this feature would challenge a possible $D\bar{D}^*$ -molecular interpretation with S -wave interactions only — prominent D -waves can shift molecular poles above threshold (see the discussion in Sec. 78.3.3).

Finally, 3.5σ evidence for one more charged charmonium-like state at 4055 MeV decaying into $\psi(2S)\pi^\pm$ was reported by Belle in their analysis of the process $e^+e^- \rightarrow \psi(2S)\pi^+\pi^-$ [54]. The same process was studied by BESIII, where there appears to be complications in the Dalitz plot requiring further investigation [52].

An isospin-1/2 state with open strangeness, the $T_{c\bar{c}\bar{s}1}(4000)$, has been reported near $D_s D^*$ threshold by both BESIII [95, 96] and LHCb [74]. BESIII observes the charged $T_{c\bar{c}\bar{s}1}(4000)$ in the process $e^+e^- \rightarrow K^+(D_s^- D^{*0} + D_s^{*-} D^0)$ [95] and the neutral $T_{c\bar{c}\bar{s}1}(4000)$ in the process $e^+e^- \rightarrow K_S(D_s^- D^{*+} + D_s^{*-} D^+)$ [96]. LHCb observes the charged version in $B^+ \rightarrow \phi(K^+ J/\psi(1S))$ [74], although with a much larger decay width. The same LHCb analysis also finds a higher mass $T_{c\bar{c}\bar{s}}$ candidate, the $T_{c\bar{c}\bar{s}1}(4220)$. A search by BESIII for a heavier partner $T'_{c\bar{c}\bar{s}}$ near $D_s^* D^*$ threshold was negative [97].

78.3.2 Double Charm

The most striking recent result, however, is due to the observation by LHCb [98, 99] of a doubly charmed state, the $T_{cc}(3875)^+$, in the inclusive cross section of $D^{*+} D^0 \rightarrow D^0 D^0 \pi^+$ (see Fig. 78.6). The statistical significance is overwhelming, the minimal quark content is $cc\bar{u}\bar{d}$, and the width is approximately what would be expected for an isoscalar ground state having $J^P = 1^+$. The integrated luminosity used in this study was 9 fb^{-1} . The larger integrated luminosity of the event sample to be collected by the end of the LHC Run 3, together with improved analysis techniques, might bring the T_{bc} states within reach.

78.3.3 Bottomonium

New results on the η_b , h_b , and $T_{b\bar{b}}$ mostly come from Belle [22, 23, 25, 27, 80, 100–106], all from analyses of 121.4 fb^{-1} of e^+e^- collision data collected near the peak of the $\Upsilon(10860)$ resonance, as well as from an additional 25 fb^{-1} of data collected during the scans of the c.m. energy range 10.63–11.05 GeV. The η_b , h_b , and $T_{b\bar{b}}$ appear in the decay chains $\Upsilon(10860) \rightarrow \pi^- T_{b\bar{b}}^+$, $T_{b\bar{b}}^+ \rightarrow \pi^+(b\bar{b})$, and, when the $b\bar{b}$ forms an $h_b(1P)$, frequently decaying as $h_b(1P) \rightarrow \gamma\eta_b$.

Belle soon noticed that, for events in the peaks of Fig. 78.1 corresponding to the processes $e^+e^- \rightarrow \pi^+\pi^-\Upsilon(1S, 2S, 3S)$ and $\pi^+\pi^-h_b(1P, 2P)$, there seemed to be two intermediate charged

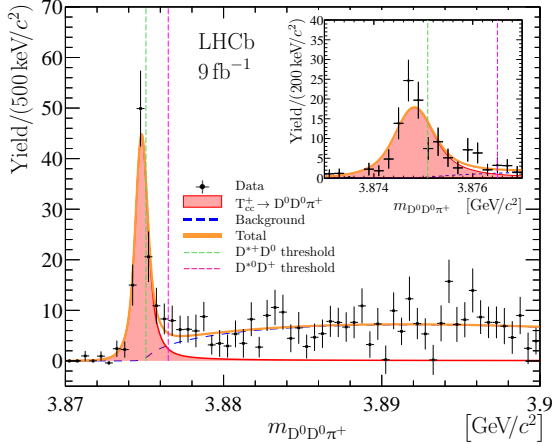


Figure 78.6: The $D^0 D^0 \pi^+$ invariant mass distribution from LHCb [98,99]

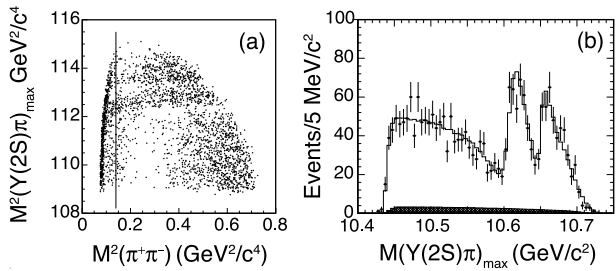


Figure 78.7: From Belle [100] e^+e^- collision data taken near the peak of the $\Upsilon(10860)$ for events with a $\pi^+\pi^-$ -missing mass consistent with an $\Upsilon(2S) \rightarrow \mu^+\mu^-$, (a) the maximum of the two possible single π^\pm -missing-mass-squared combinations vs. the $\pi^+\pi^-$ -mass-squared; and (b) projection of the maximum of the two possible single π^\pm -missing-mass combinations overlaid with a fit (curve). Events to the left of the vertical line in (a) are excluded from the amplitude analysis. The hatched histogram in (b) corresponds to the combinatorial background. The two horizontal stripes in (a) and two peaks in (b) correspond to the two $T_{b\bar{b}}$ states.

states in the $\pi^\pm\Upsilon$ and $\pi^\pm h_b$ channels, called the $T_{b\bar{b}}^-(10610)$ and the $T_{b\bar{b}}^-(10650)$. For example, Fig. 78.7 shows a Dalitz plot for events restricted to the $\Upsilon(2S)$ region of $\pi^+\pi^-$ recoil mass, with $\Upsilon(2S) \rightarrow \mu^+\mu^-$ [100]. The two bands observed in the maximum of the two $M[\pi^\pm\Upsilon(2S)]^2$ values also appear in the $\Upsilon(1S)$, $\Upsilon(3S)$, $h_b(1P)$, and $h_b(2P)$ samples. Belle fits all subsamples to resonant plus non-resonant amplitudes, allowing for interference (notably, between $\pi^-T_{b\bar{b}}^+$ and $\pi^+T_{b\bar{b}}^-$), and finds consistent pairs of $T_{b\bar{b}}^-$ masses for all bottomonium transitions, and comparable strengths of the two states. A recent angular analysis assigned $J^P = 1^+$ for both $T_{b\bar{b}}$ states [101], which must also have negative G -parity. Transitions through $T_{b\bar{b}}$ to the $h_b(nP)$ saturate the observed $\pi^+\pi^- h_b(nP)$ cross sections. While the two masses of the $T_{b\bar{b}}$ states as extracted from Breit–Wigner fits for the various channels are just a few MeV above the $B^*\bar{B}$ and B^*B^* thresholds, more refined analyses using only S -waves find pole locations right below the corresponding thresholds either on the physical [107] or the unphysical [108] sheet. Once D -waves are included, the pole of the $T_{b\bar{b}}^-(10650)$ moves above the $B^*\bar{B}^*$ threshold [109]. Regardless of their proximity to the corresponding thresholds, both states predominantly decay into these open-flavor channels [103, 110] with branching fractions that exceed 80% and 70%, respectively, at 90% CL. This feature provides strong evidence for their molecular nature.

78.4 Concluding Remarks

The discovery of the $\chi_{c1}(3872)$ (also known as the $X(3872)$) in 2003 ushered in an era of tremendous progress in experimental heavy quark meson spectroscopy, even though many issues remain unsettled. As shown in Tables 78.1 to 78.3, more than 40 new states have been reported during this period, many of which were unanticipated. While the states below open-flavor thresholds (Table 78.1) appear to be well-explained by the conventional $q\bar{q}$ quark model, a thorough understanding of the suite of states above (Table 78.2) and near (Table 78.3) open-flavor thresholds remains elusive. After nearly two decades, experimental progress remains rapid with the continuation of BESIII, the commencement of the Belle II program, and the imminent accumulation of additional data at the LHC.

References

- [1] N. Brambilla *et al.*, Phys. Rept. **873**, 1 (2020), [arXiv:1907.07583].
- [2] Y.-R. Liu *et al.*, Prog. Part. Nucl. Phys. **107**, 237 (2019), [arXiv:1903.11976].
- [3] S. L. Olsen, T. Skwarnicki and D. Zieminska, Rev. Mod. Phys. **90**, 1, 015003 (2018), [arXiv:1708.04012].
- [4] A. Ali, J. S. Lange and S. Stone, Prog. Part. Nucl. Phys. **97**, 123 (2017), [arXiv:1706.00610].
- [5] F.-K. Guo *et al.*, Rev. Mod. Phys. **90**, 1, 015004 (2018), [arXiv:1705.00141].
- [6] R. F. Lebed, R. E. Mitchell and E. S. Swanson, Prog. Part. Nucl. Phys. **93**, 143 (2017), [arXiv:1610.04528].
- [7] A. E. Bondar, R. V. Mizuk and M. B. Voloshin, Mod. Phys. Lett. A **32**, 04, 1750025 (2017), [arXiv:1610.01102].
- [8] H.-X. Chen *et al.*, Rept. Prog. Phys. **86**, 2, 026201 (2023), [arXiv:2204.02649].
- [9] M. Mai, U.-G. Meißner and C. Urbach, Phys. Rept. **1001**, 1 (2023), [arXiv:2206.01477].
- [10] S. K. Choi *et al.* (Belle), Phys. Rev. Lett. **91**, 262001 (2003), [hep-ex/0309032].
- [11] N. Brambilla *et al.*, Eur. Phys. J. **C74**, 10, 2981 (2014), [arXiv:1404.3723].
- [12] J. L. Rosner *et al.* (CLEO), Phys. Rev. Lett. **95**, 102003 (2005), [hep-ex/0505073].
- [13] M. Ablikim *et al.* (BESIII), Phys. Rev. D **99**, 7, 072008 (2019), [arXiv:1810.12023].
- [14] M. Ablikim *et al.* (BESIII), Phys. Rev. D **102**, 112007 (2020), [arXiv:2010.12092].
- [15] M. Ablikim *et al.* (BESIII), JHEP **05**, 108 (2022), [Erratum: JHEP 03, 022 (2023)], [arXiv:2203.10439].
- [16] V. Bhardwaj *et al.* (Belle), Phys. Rev. Lett. **111**, 3, 032001 (2013), [arXiv:1304.3975].
- [17] M. Ablikim *et al.* (BESIII), Phys. Rev. Lett. **115**, 1, 011803 (2015), [arXiv:1503.08203].
- [18] M. Ablikim *et al.* (BESIII), Phys. Rev. Lett. **129**, 10, 102003 (2022), [arXiv:2203.05815].
- [19] K. Chilikin *et al.* (Belle) (2020), [arXiv:2003.08335].
- [20] B. Aubert *et al.* (BaBar), Phys. Rev. Lett. **101**, 071801 (2008), [Erratum: Phys.Rev.Lett. 102, 029901 (2009)], [arXiv:0807.1086].
- [21] B. Aubert *et al.* (BaBar), Phys. Rev. Lett. **103**, 161801 (2009), [arXiv:0903.1124].
- [22] R. Mizuk *et al.* (Belle), Phys. Rev. Lett. **109**, 232002 (2012), [arXiv:1205.6351].
- [23] U. Tamponi *et al.* (Belle), Phys. Rev. Lett. **115**, 14, 142001 (2015), [arXiv:1506.08914].
- [24] B. G. Fulsom *et al.* (Belle), Phys. Rev. Lett. **121**, 23, 232001 (2018), [arXiv:1807.01201].
- [25] I. Adachi *et al.* (Belle), Phys. Rev. Lett. **108**, 032001 (2012), [arXiv:1103.3419].

- [26] T. K. Pedlar *et al.* (CLEO), Phys. Rev. Lett. **107**, 041803 (2011), [arXiv:1104.2025].
- [27] I. Adachi (Belle), in “8th International Workshop On Heavy Quarkonium (QWG2011) Darmstadt, Germany, October 3-7, 2011,” (2011), [arXiv:1110.3934].
- [28] G. Aad *et al.* (ATLAS), Phys. Rev. Lett. **108**, 152001 (2012), [arXiv:1112.5154].
- [29] V. M. Abazov *et al.* (D0), Phys. Rev. D **86**, 031103 (2012), [arXiv:1203.6034].
- [30] R. Aaij *et al.* (LHCb), JHEP **10**, 088 (2014), [arXiv:1409.1408].
- [31] A. M. Sirunyan *et al.* (CMS), Phys. Rev. Lett. **121**, 092002 (2018), [arXiv:1805.11192].
- [32] G. Aad *et al.* (ATLAS), Phys. Rev. Lett. **113**, 212004 (2014), [arXiv:1407.1032].
- [33] A. M. Sirunyan *et al.* (CMS), Phys. Rev. Lett. **122**, 132001 (2019), [arXiv:1902.00571].
- [34] R. Aaij *et al.* (LHCb), Phys. Rev. Lett. **122**, 232001 (2019), [arXiv:1904.00081].
- [35] R. Aaij *et al.* (LHCb), JHEP **07**, 035 (2019), [arXiv:1903.12240].
- [36] S. Uehara *et al.* (Belle), Phys. Rev. Lett. **96**, 082003 (2006), [hep-ex/0512035].
- [37] B. Aubert *et al.* (BaBar), Phys. Rev. D **81**, 092003 (2010), [arXiv:1002.0281].
- [38] K. Abe *et al.* (Belle), Phys. Rev. Lett. **94**, 182002 (2005), [hep-ex/0408126].
- [39] J. P. Lees *et al.* (BaBar), Phys. Rev. **D86**, 072002 (2012), [arXiv:1207.2651].
- [40] F.-K. Guo and U.-G. Meissner, Phys. Rev. **D86**, 091501 (2012), [arXiv:1208.1134].
- [41] S. L. Olsen, Phys. Rev. **D91**, 5, 057501 (2015), [arXiv:1410.6534].
- [42] Z.-Y. Zhou, Z. Xiao and H.-Q. Zhou, Phys. Rev. Lett. **115**, 2, 022001 (2015), [arXiv:1501.00879].
- [43] R. Aaij *et al.* (LHCb), Phys. Rev. D **102**, 112003 (2020), [arXiv:2009.00026].
- [44] K. Chilikin *et al.* (Belle), Phys. Rev. **D95**, 112003 (2017), [arXiv:1704.01872].
- [45] B. Aubert *et al.* (BaBar), Phys. Rev. Lett. **95**, 142001 (2005), [hep-ex/0506081].
- [46] C. Z. Yuan *et al.* (Belle), Phys. Rev. Lett. **99**, 182004 (2007), [arXiv:0707.2541].
- [47] Z. Q. Liu *et al.* (Belle), Phys. Rev. Lett. **110**, 252002 (2013), [arXiv:1304.0121].
- [48] M. Ablikim *et al.* (BESIII), Phys. Rev. Lett. **118**, 9, 092001 (2017), [arXiv:1611.01317].
- [49] M. Cleven *et al.*, Phys. Rev. **D90**, 7, 074039 (2014), [arXiv:1310.2190].
- [50] M. Ablikim *et al.* (BESIII), Phys. Rev. Lett. **118**, 9, 092002 (2017), [arXiv:1610.07044].
- [51] M. Ablikim *et al.* (BESIII), Phys. Rev. Lett. **112**, 9, 092001 (2014), [arXiv:1310.4101].
- [52] M. Ablikim *et al.* (BESIII), Phys. Rev. **D96**, 3, 032004 (2017), [erratum: Phys. Rev. D99, no.1, 019903(2019)], [arXiv:1703.08787].
- [53] X. L. Wang *et al.* (Belle), Phys. Rev. Lett. **99**, 142002 (2007), [arXiv:0707.3699].
- [54] X. L. Wang *et al.* (Belle), Phys. Rev. **D91**, 112007 (2015), [arXiv:1410.7641].
- [55] J. P. Lees *et al.* (BaBar), Phys. Rev. **D89**, 11, 111103 (2014), [arXiv:1211.6271].
- [56] G. Pakhlova *et al.* (Belle), Phys. Rev. Lett. **101**, 172001 (2008), [arXiv:0807.4458].
- [57] S. Jia *et al.* (Belle), Phys. Rev. **D100**, 11, 111103 (2019), [arXiv:1911.00671].
- [58] K. Chilikin *et al.* (Belle), Phys. Rev. **D88**, 7, 074026 (2013), [arXiv:1306.4894].
- [59] K. Chilikin *et al.* (Belle), Phys. Rev. **D90**, 11, 112009 (2014), [arXiv:1408.6457].
- [60] R. Aaij *et al.* (LHCb), Phys. Rev. Lett. **112**, 22, 222002 (2014), [arXiv:1404.1903].
- [61] B. Aubert *et al.* (BaBar), Phys. Rev. **D79**, 112001 (2009), [arXiv:0811.0564].
- [62] R. Mizuk *et al.* (Belle), Phys. Rev. **D78**, 072004 (2008), [arXiv:0806.4098].
- [63] J. P. Lees *et al.* (BaBar), Phys. Rev. **D85**, 052003 (2012), [arXiv:1111.5919].
- [64] T. Aaltonen *et al.* (CDF), Phys. Rev. Lett. **102**, 242002 (2009), [arXiv:0903.2229].
- [65] T. Aaltonen *et al.* (CDF), Mod. Phys. Lett. **A32**, 26, 1750139 (2017), [arXiv:1101.6058].
- [66] V. M. Abazov *et al.* (D0), Phys. Rev. **D89**, 1, 012004 (2014), [arXiv:1309.6580].
- [67] S. Chatrchyan *et al.* (CMS), Phys. Lett. **B734**, 261 (2014), [arXiv:1309.6920].
- [68] J. Brodzicka, Conf. Proc. **C0908171**, 299 (2009), [299(2009)].
- [69] R. Aaij *et al.* (LHCb), Phys. Rev. **D85**, 091103 (2012), [arXiv:1202.5087].
- [70] J. P. Lees *et al.* (BaBar), Phys. Rev. **D91**, 1, 012003 (2015), [arXiv:1407.7244].
- [71] C. P. Shen *et al.* (Belle), Phys. Rev. Lett. **104**, 112004 (2010), [arXiv:0912.2383].
- [72] R. Aaij *et al.* (LHCb), Phys. Rev. **D95**, 1, 012002 (2017), [arXiv:1606.07898].
- [73] R. Aaij *et al.* (LHCb), Phys. Rev. Lett. **118**, 2, 022003 (2017), [arXiv:1606.07895].
- [74] R. Aaij *et al.* (LHCb), Phys. Rev. Lett. **127**, 8, 082001 (2021), [arXiv:2103.01803].
- [75] R. Aaij *et al.* (LHCb), Sci. Bull. **65**, 1983 (2020), [arXiv:2006.16957].
- [76] G. Aad *et al.* (ATLAS) (2023), [arXiv:2304.08962].
- [77] A. Hayrapetyan *et al.* (CMS) (2023), [arXiv:2306.07164].
- [78] R. Mizuk *et al.* (Belle), JHEP **10**, 220 (2019), [arXiv:1905.05521].
- [79] N. Hüsken, R. E. Mitchell and E. S. Swanson, Phys. Rev. D **106**, 9, 094013 (2022), [arXiv:2204.11915].
- [80] D. Santel *et al.* (Belle), Phys. Rev. **D93**, 1, 011101 (2016), [arXiv:1501.01137].
- [81] F.-K. Guo, X.-H. Liu and S. Sakai, Prog. Part. Nucl. Phys. **112**, 103757 (2020), [arXiv:1912.07030].
- [82] R. Aaij *et al.* (LHCb), Phys. Rev. Lett. **110**, 222001 (2013), [arXiv:1302.6269].
- [83] R. Aaij *et al.* (LHCb), Phys. Rev. **D92**, 1, 011102 (2015), [arXiv:1504.06339].
- [84] R. Aaij *et al.* (LHCb), Phys. Rev. D **102**, 9, 092005 (2020), [arXiv:2005.13419].
- [85] N. Brambilla *et al.*, Eur. Phys. J. **C71**, 1534 (2011), [arXiv:1010.5827].
- [86] M. Ablikim *et al.* (BESIII), Phys. Rev. Lett. **110**, 252001 (2013), [arXiv:1303.5949].
- [87] T. Xiao *et al.*, Phys. Lett. **B727**, 366 (2013), [arXiv:1304.3036].
- [88] M. Ablikim *et al.* (BESIII), Phys. Rev. Lett. **112**, 2, 022001 (2014), [arXiv:1310.1163].
- [89] M. Ablikim *et al.* (BESIII), Phys. Rev. Lett. **115**, 11, 112003 (2015), [arXiv:1506.06018].

- [90] M. Ablikim *et al.* (BESIII), Phys. Rev. Lett. **115**, 22, 222002 (2015), [arXiv:1509.05620].
- [91] M. Ablikim *et al.* (BESIII), Phys. Rev. Lett. **111**, 24, 242001 (2013), [arXiv:1309.1896].
- [92] M. Ablikim *et al.* (BESIII), Phys. Rev. Lett. **112**, 13, 132001 (2014), [arXiv:1308.2760].
- [93] M. Ablikim *et al.* (BESIII), Phys. Rev. Lett. **113**, 21, 212002 (2014), [arXiv:1409.6577].
- [94] M. Ablikim *et al.* (BESIII), Phys. Rev. Lett. **115**, 18, 182002 (2015), [arXiv:1507.02404].
- [95] M. Ablikim *et al.* (BESIII), Phys. Rev. Lett. **126**, 10, 102001 (2021), [arXiv:2011.07855].
- [96] M. Ablikim *et al.* (BESIII), Phys. Rev. Lett. **129**, 11, 112003 (2022), [arXiv:2204.13703].
- [97] M. Ablikim *et al.* ((BESIII), BESIII), Chin. Phys. C **47**, 3, 033001 (2023), [arXiv:2211.12060].
- [98] R. Aaij *et al.* (LHCb), Nature Phys. **18**, 7, 751 (2022), [arXiv:2109.01038].
- [99] R. Aaij *et al.* (LHCb), Nature Commun. **13**, 1, 3351 (2022), [arXiv:2109.01056].
- [100] A. Bondar *et al.* (Belle), Phys. Rev. Lett. **108**, 122001 (2012), [arXiv:1110.2251].
- [101] A. Garmash *et al.* (Belle), Phys. Rev. **D91**, 7, 072003 (2015), [arXiv:1403.0992].
- [102] P. Krokovny *et al.* (Belle), Phys. Rev. **D88**, 5, 052016 (2013), [arXiv:1308.2646].
- [103] I. Adachi *et al.* (Belle) (2012), [arXiv:1209.6450].
- [104] K. F. Chen *et al.* (Belle), Phys. Rev. Lett. **100**, 112001 (2008), [arXiv:0710.2577].
- [105] P. Krokovny (Belle Collab.), talk given at Les Rencontres de Physique de la Vallee d'Aoste, La Thuile, Aosta Valley, Italy, 2012.
- [106] A. Abdesselam *et al.* (Belle), Phys. Rev. Lett. **117**, 14, 142001 (2016), [arXiv:1508.06562].
- [107] M. Cleven *et al.*, Eur. Phys. J. **A47**, 120 (2011), [arXiv:1107.0254].
- [108] F. K. Guo *et al.*, Phys. Rev. **D93**, 7, 074031 (2016), [arXiv:1602.00940].
- [109] Q. Wang *et al.*, Phys. Rev. D **98**, 7, 074023 (2018), [arXiv:1805.07453].
- [110] A. Garmash *et al.* (Belle), Phys. Rev. Lett. **116**, 21, 212001 (2016), [arXiv:1512.07419].

79. Heavy Non- $q\bar{q}$ Mesons

Revised March 2024 by T. Gutsche (Tübingen U.), C. Hanhart (FZ Jülich) and R.E. Mitchell (Indiana U.).

The constituent quark model describes the observed meson spectrum as bound $q\bar{q}$ states grouped into SU(N) flavor multiplets (see the ‘Quark Model’ in this issue of the *Review of Particle Physics*). However, the self coupling of gluons in QCD suggests that additional mesons made of bound gluons (glueballs), or $q\bar{q}$ -pairs with an excited gluon (hybrids), may exist. Furthermore, multi-quark color singlet states such as $qq\bar{q}\bar{q}$ (tetraquarks as compact diquark-antidiquark systems and ‘molecular’ bound states of two mesons) or $qqq\bar{q}\bar{q}$ (six-quark, ‘baryonium’ or quasinuclear baryon-antibaryon bound states) have also been predicted. The focus of this review is on the current understanding of exotic states that apparently do not fit into the constituent quark model and contain at least one heavy quark (charm or bottom — the lifetime of the top quark is too short to allow it to hadronise). Light non- $q\bar{q}$ candidates (made of u , d and s quarks) are discussed in ‘Scalar Mesons below 1 GeV’ and ‘Spectroscopy of Light Meson Resonances’ in this *Review*.

There are candidates for exotic states with both quantum numbers not allowed and quantum number allowed for $q\bar{q}$ states. For the latter class it is up to now unclear to what extent a mixing of conventional and unconventional states occurs. While Refs. [1–4] report a significant mixing, Refs. [5, 6] describe a scenario where the mixing especially between molecular structures and $q\bar{q}$ states is suppressed.

The review is split into 3 parts, discussing separately heavy–light systems, heavy–heavy systems, as well as systems with more than two heavy quarks. For a more detailed discussion of the experimental and/or theoretical status on exotic meson candidates in the doubly heavy meson sector we refer to Refs. [7–13]. Reviews with main focus on tetraquarks and molecular states are presented in Ref. [14] and in Ref. [15], respectively.

The naming scheme for hadrons has been updated by the Particle Data Group in 2023, and now covers the heavy “exotic” tetraquark ($qq\bar{q}\bar{q}$) and pentaquark ($qqqq\bar{q}$) candidates recently discovered. We use the new naming scheme in the following. See “Naming Scheme for Hadrons” in this *Review* for details and a table mapping old and new particle names.

79.1 Heavy-light systems

79.1.1 Positive parity open charm ground states

Two very narrow states, $D_{s0}^*(2317)^\pm$ and $D_{s1}(2460)^\pm$, were observed at B factories [16, 17]. They lie far below the predicted masses for the two expected broad P -wave $c\bar{s}$ mesons. However, strong cusp effects, due to the nearby DK (DK^*) thresholds, could shift their masses downwards and quench the observed widths, still allowing for a conventional explanation of these states [18]. Such an effect was also claimed for the $a_0(980)$ and $f_0(980)$ mesons, which lie just below the $K\bar{K}$ threshold. In contrast to this picture, many authors favour exotic explanations for these lightest positive parity charmed states, such as four-quark states [19–22] or DK (DK^*) molecules [23–28]. Both states are isoscalars and thus strong isospin-violating decays are possible only to the isovector channels $D_s^{(*)\pm}\pi^0$, leading to very small widths. For compact structures the hadronic decay is driven by $\eta - \pi^0$ mixing and one finds widths below 10 keV [18, 29]. In contrast to this a hadronic width typically larger than 100 keV would be the unequivocal signature for a prominent molecular nature of $D_{s0}^*(2317)^\pm$ [25, 27, 28, 30, 31], since then meson loops generating enhanced isospin violation due to the energy difference between the $D^{*0}K^+$ and the $D^{*+}K^0$ thresholds would contribute significantly. The most refined analysis in the molecular scenario [30], where the parameters of the formalism are constrained by a large bulk of lattice QCD data on singly charmed systems, reports a prediction for the width in the range (104–116) keV. The currently measured upper bound for the width is 3.8 MeV.

It should be stressed that – akin to $q\bar{q}$ mesons – multi-quark states also appear in multiplets. An important probe for the structure of hadrons is therefore the spectra, and in particular the SU(3) flavor multiplets within the different scenarios. For example the tetraquark model advocated in Refs. [22, 32] finds

that the $D_{s0}^*(2317)^\pm$ should be degenerate with its non-strange partner state $D_0^*(2300)$ in line with the currently available experimental analyses. However, Ref. [33] showed that the recent LHCb data for $B \rightarrow D\pi\pi$ [34, 35] call for a significantly lighter lightest non-strange scalar charmed meson as soon as constraints from the chiral symmetry of QCD are employed in the analysis. This claim is in line with the recent lattice QCD study of Ref. [36]. In fact, experimental as well as lattice data turn out to be consistent with the predictions from unitarised chiral perturbation theory pioneered for these systems in Ref. [24]. For more recent calculations see Refs. [30, 37, 38]. Moreover, all these latter calculations predict that there should be in addition an about 300 MeV heavier flavor exotic state, formally a member of a flavor sextet and absent for $c\bar{q}$ states, that indeed shows up in the above mentioned LHCb data [38] — why this state was not reported in the lattice study of Ref. [39] is explained in Ref. [40] by its being located on a hidden Riemann-sheet. Thus, in this picture the structure that appears as $D_0^*(2300)$ in the *Listings* originates from the interplay of two poles, similar to the $\Lambda(1405)$ in the baryon sector, see ‘Pole structure of the $\Lambda(1405)$ region’ in this *Review*. Two poles in the non-strange scalar sector are also generated in the tetraquark picture of Ref. [22], but in this work the real parts of the poles are located at 2308 MeV and 2666 MeV, in conflict with the data mentioned above. In the refined analysis of Ref. [32] it is shown, however, that the exact pole locations and even the ordering of the higher multiplets depend on the details of the model.

Lattice QCD allows for predictions of the flavor partner states in the B -sector. The most recent analysis can be found in Ref. [41]. In this work also a comparison with theoretical predictions can be found. Unfortunately an experimental confirmation for those states is difficult with existing facilities. Radiative decays are predicted to be the most prominent decay channels [31], since the above mentioned isospin violation from meson loops is suppressed in the B sector as a consequence of the tiny $B^\pm - B^0$ mass difference.

79.1.2 The $T_{cs0}^*(2870)$ and $T_{cs1}^*(2900)$

Manifestly exotic candidates around 2.9 GeV were reported in Refs. [42, 43] by LHCb in the $\bar{D}K$ system. Since the strong interaction preserves the quark flavor and the final state contains an \bar{s} as well as a \bar{c} , color neutrality calls for a minimum quark content of $ud\bar{c}\bar{s}$. The explanation for those states include compact tetraquarks [44–46], hadronic molecules with a prominent D^*K^* component [47–51], or kinematic effects such as cusps or triangle singularities without nearby poles [52, 53]. The different pictures are contrasted and observable differences between them are discussed in Ref. [54].

79.1.3 The $T_{cs0}^*(2900)^0$ and $T_{cs0}^*(2900)^{++}$

There is a very recent report by LHCb [55] on the observation of a doubly charged open-charm tetraquark candidate together with a neutral partner in the $D_s\pi$ channel, with masses near 2.9 GeV. The results imply two states with $c\bar{s}u\bar{d}$ or $c\bar{s}u\bar{d}$ flavor structures. Although masses and widths are consistent with the T_{cs} states of Refs. [42, 43], the strangeness quantum numbers do not match. The first explanation for those states in coupled-channel studies is based on a kinematic effect such as a cusp [56], while a molecular structure with a dominant D^*K^* component is claimed to be excluded [57].

79.2 Heavy-heavy systems

With the discovery of the $\chi_{c1}(3872)^1$ in $B^\pm \rightarrow K^\pm X$ ($X \rightarrow J/\psi(1S)\pi^+\pi^-$) by Belle [58] in 2003, soon confirmed by BaBar [59], many searches for states beyond the standard $q\bar{q}$ quark model were initiated in the charm and bottom sectors. For an updated collection of the currently available experimental information on multi-quark states we refer to ‘Spectroscopy of mesons containing two heavy quarks’ in this *Review*, and in particular to Table 78.2. Moreover, in the decay $A_b^0 \rightarrow J/\psi(1S)K^-p$ the LHCb collaboration has recently reported the observation of new baryons decaying into $J/\psi(1S)p$, which are candidates for heavy pentaquark

¹ The $\chi_{c1}(3872)$ is also known as the $X(3872)$. According to the PDG naming scheme, the primary name for a meson expresses its quantum numbers.

states [60,61]. They are discussed in some depth in ‘Pentaquarks’ in this *Review*.

When restricting ourselves to confirmed states we are faced with several states that do not seem to fit into the mass and quantum number schemes of $q\bar{q}$ quark models. This is clear for the five established charged states ($T_{c\bar{c}1}(3900)^\pm$, $T_{c\bar{c}}(4020)^\pm$ and $T_{c\bar{c}1}(4430)^\pm$ in the charmonium sector, and $T_{b\bar{b}1}(10610)^\pm$ and $T_{b\bar{b}1}(10650)^\pm$ in the bottomonium sector). The neutral states ($\chi_{c1}(3872)$, $\psi(4230)$, $\psi(4360)$, and $\psi(4660)$)² also challenge the quark model since their masses and decay properties are in conflict with expectations. Although so far seen just by a single experiment in a single channel [62,63], the $T_{cc}(3875)$ should not remain unmentioned.

79.2.1 The $\chi_{c1}(3872)$

The quantum numbers of the $\chi_{c1}(3872)$ have been determined by LHCb to be $J^{PC} = 1^{++}$, first by assuming zero angular momentum between the $J/\psi(1S)$ and the dipion [64] and then by relaxing this constraint [65]. The $\chi_{c1}(3872)$ cannot be identified with the $\chi_{c1}(2^3P_1)$ since the latter is predicted to lie about 100 MeV higher in mass [66]. Instead, the $X(3940)$ reported by Belle in $e^+e^- \rightarrow J/\psi(1S)X$, decaying into $D^*\bar{D}$ but not into $D\bar{D}$ [67] could be the $\chi_{c1}(2^3P_1)$. The $\chi_{c2}(3930)$ 2^3P_2 tensor partner was reported by Belle at 3931 MeV in $\gamma\gamma$ interactions [68].

The $\chi_{c1}(3872)$ lies within 200 keV of the $D^0\bar{D}^{*0}$ threshold and its width is very small — recent Breit-Wigner analyses by LHCb [69,70] result in an average value of $\Gamma = (1.19 \pm 0.21)$ MeV as indicated in the *Listings*; employing the Flatté formalism of Ref. [71] under the constraint that the $D^*\bar{D}$ decay channel dominates, results in $\Gamma = 0.22_{-0.19}^{+0.18}$ MeV, where the standard convention is applied to use twice the imaginary part of the pole location as width. In the future those values can be refined more by either a direct measurement of the width that should be possible at the planned PANDA experiment [72,73] or by exploiting the interplay of a triangle singularity and the $\chi_{c1}(3872)$ pole [74–76]. Therefore the most natural explanation for this state is a $1^{++} D\bar{D}^*$ molecule [77], for which strong isospin breaking is predicted [77,78], since the distance of the pole of the $\chi_{c1}(3872)$ to the $D^0\bar{D}^{*0}$ threshold is significantly smaller than to the D^+D^{*-} threshold. Indeed, the comparable rates for $\omega J/\psi(1S)$ and $\rho^0 J/\psi(1S)$ are consistent with an interpretation of $\chi_{c1}(3872)$ as an isoscalar $D\bar{D}^*$ molecule, when the different widths of the ρ and ω are taken into account [79]. Similarly, a dominant molecular $D^0\bar{D}^{*0}$ structure in the $\chi_{c1}(3872)$ with further subleading hadronic components is used to explain strong and radiative decays involving $J/\psi(1S)$ and $\psi(2S)$ in the final states [80,81]. From an effective field theory point of view these radiative transitions are not well suited to identify the molecular admixture in the $\chi_{c1}(3872)$, since there appears a counter term at leading order, diminishing the sensitivity to the long ranged molecular component [82].

A four-quark state $c\bar{q}c\bar{q}'$ is another possible interpretation of the $\chi_{c1}(3872)$ [21] but a charged partner of the $\chi_{c1}(3872)$ has not been observed (e.g. not in $B^- \rightarrow \bar{K}^0 X^-$ nor in $B^0 \rightarrow K^+ X^-$, where $X^- \rightarrow J/\psi(1S)\pi^-\pi^0$ [83]) — see [84] for a possible explanation of this non-observation within the tetraquark approach assuming specific diquark correlations and the more recent discussion in Ref. [85]. The claim that $\chi_{c1}(3872)$ must be a compact (tetraquark) state, since it is also produced at very high p_T in $p\bar{p}$ collisions [86] and in high multiplicity final states [87], was challenged in [88] and [89], respectively, which in particular stress the importance of rescattering, see also Refs. [90,91].

The high statistics measurement of the $\chi_{c1}(3872)$ lineshape of Ref. [69] also allowed for an extraction of the effective range for the $D^0\bar{D}^{*0}$ interaction. At face value, the values provided in this publication indicate a large and negative effective range [92], which could be interpreted as a signature of a prominent compact component in the $\chi_{c1}(3872)$ wave function — this follows from the famous Weinberg compositeness criterion [93]. The effect of the one-pion exchange on the effective range turns out to

be small [94–97] and should therefore not invalidate the Weinberg-type analysis. However, it was argued in Ref. [98] that once the effect of the large isospin violation as well as the strong correlations between the effective parameters appearing in Ref. [71] are subtracted, the effective range is consistent with a purely molecular $\chi_{c1}(3872)$. There is no consensus yet how to interpret the line shapes of $\chi_{c1}(3872)$.

79.2.2 The $\psi(4230)$ and $\psi(4360)$

A broad structure, originally called $Y(4260)$, decaying into $J/\psi(1S)\pi^+\pi^-$ was reported by BaBar in initial state radiation $e^+e^- \rightarrow (\gamma_{\text{ISR}})Y(4260)$ [99]. A subsequent measurement with significantly improved precision was reported by BESIII [100], and revealed that the original $Y(4260)$ cannot be described with a simple resonant lineshape. Fitting the BESIII data with two Breit-Wigner distributions leads to a narrower and lighter structure (referred to in the *Listings* as the $\psi(4230)$), but also requires a second state at 4320 MeV. However, note that the $D_1(2420)\bar{D}$ molecular model for the $\psi(4230)$ can describe the same data with just one single pole [101]. How many vector states are in the mass range between 4220 MeV and 4400 MeV is not yet settled, but knowing this is crucial to allow for further progress.

There are no charmonium states expected in this mass region with quantum numbers 1^{--} from quark models using the Cornell type of interaction, although this might not be true for some screened versions thereof — for a recent discussion we refer to Ref. [102]. In addition, a charmonium state at this mass is expected to have significant couplings to one or more of the $\bar{D}^{(*)}D^{(*)}$ channels [103,104], a feature that is not observed for the $\psi(4230)$. This state could be a hybrid charmonium with a spin-1 [105,106] or a spin-0 [107,108] $\bar{c}c$ core. However, provided that the observation of $\psi(4230)$ decay into $h_c(1P)\pi\pi$ by BESIII [109] is confirmed, the hybrid hypothesis would be under pressure, since the spin of the heavy quarks (coupled to zero in the $h_c(1P)$) should be conserved in leading order in the expansion in $(\Lambda_{\text{QCD}}/m_c)$. (The individual conservation of the heavy quark spin and the total angular momentum of the light quark cloud is a consequence of the heavy-quark spin symmetry, see ‘Heavy-Quark and Soft-Collinear Effective Theory’ in this issue of the *Review*.) The same criticism applies to the hadrocharmonium interpretation of the $\psi(4230)$, which describes this state as spin-1 quarkonium surrounded by a light quark cloud [110]. To circumvent the spin-symmetry argument, Ref. [111] argues that $\psi(4230)$ and $\psi(4360)$ could be mixtures of two hadrocharmonia with spin-triplet and spin-singlet heavy quark pairs. The same kind of mixing could also be at work for hybrid structures. Hybrids can also be treated employing the Born-Oppenheimer EFT originally suggested in Ref. [112,113]. Those studies revealed that while the $\psi(4230)$ is in principle a good candidate for a hybrid state [114], its decays are incompatible with this assignment [115].

A dominant $D_1(2420)\bar{D}$ component in the $\psi(4230)$ [116] explains naturally why the $T_{c\bar{c}1}(3900)^\pm$ (interpreted by the authors as a $D\bar{D}^*$ bound state) is seen in $\psi(4230) \rightarrow \pi^\mp T_{c\bar{c}1}(3900)^\pm$. A similar mechanism is also found in Ref. [117] linking in addition the $J/\psi(1S)\pi^+\pi^-$ and $\psi(2S)\pi^+\pi^-$ decays of the $\psi(4230)$. Furthermore, a copious production of $\chi_{c1}(3872)$ in $\psi(4230)$ radiative decays was predicted from the prominent $D_1\bar{D}$ component of the $\psi(4230)$ [118], which was confirmed by BESIII [119]. Possible charmonia components both in $\psi(4230)$ and $\chi_{c1}(3872)$ can influence the radiative transition but they are shown to be of subleading order [120]. It was proposed that $\psi(4360)$ as a $D_1\bar{D}^*$ bound state could be the spin partner of the $\psi(4230)$ [121,122]. In Ref. [123] a dynamical model is presented that identifies the vector states $\psi(4230)$, $\psi(4360)$ and $\psi(4415)$ as $D\bar{D}_1$, $D^*\bar{D}_1$ and $D^*\bar{D}_2$ molecular states, respectively. Moreover, an exotic 0^{--} state is predicted as $D^*\bar{D}_1$ molecule with a mass of 4366 ± 18 MeV and a width of less than 10 MeV.

The tetraquark picture calls for four ground state vector states — once the parameters of the model are fixed from some candidate states in the negative and positive parity sector, states with other quantum numbers can be predicted. Possible scenarios are for instance discussed in Ref. [124] which builds on a tailor-made spin-spin interaction [125] to describe the $\chi_{c1}(3872)$, both $T_{c\bar{c}1}(3900)^\pm$ and $T_{c\bar{c}}(4020)^\pm$ and even the $T_{c\bar{c}1}(4430)^\pm$

² The $\psi(4230)$, $\psi(4360)$, and $\psi(4660)$ are also known as the $Y(4230)$, $Y(4360)$, and $Y(4660)$, respectively. Before improved mass measurements, the $\psi(4230)$ was originally called the $\psi(4260)$ or $Y(4260)$.

confirmed by Belle [126] and LHCb [127]. This model also explains the copious production of $\chi_{c1}(3872)$ in $\psi(4230)$ radiative decays mentioned above [125, 128]. However, tetraquark models (in most cases based on diquark-antidiquark configurations) tend to predict many additional charged and neutral states which have not yet been discovered. In particular, as for the conventional $\bar{q}q$ structures one should expect nearly degenerate isoscalar and isovector states in analogy to the near degeneracy of $\rho(770)$ and $\omega(782)$. The problem and possible explanations are discussed in some detail in Refs. [84, 85].

Ref. [129] found a sizeable SU(3) flavor octet contribution when analysing the $\pi\pi$ final state from $\psi(4230) \rightarrow J/\psi(1S)\pi^+\pi^-$, which is consistent with both a molecular and a tetraquark interpretation of $\psi(4230)$, but at odds with a hybrid or a $\bar{c}c$ interpretation.

79.2.3 The $\psi(4660)$

In the mass range above 4600 MeV, the number of poles is also not yet settled. Experimental signals are seen in the $\psi(2S)\pi\pi$, $A_c^+ \bar{A}_c^-$, $D_s \bar{D}_{s1}$, and $D_s \bar{D}_{s2}^*$ final states. In the Listings these structures go into one node, $\psi(4660)$, due to their proximity in parameter values. Moreover, various theoretical works describe these states in a combined analysis [130–132]. The signal in the hidden strangeness mode around 4630 MeV still calls for confirmation and might be yet another realisation of the same state, but there are already speculations about its nature. While Ref. [133] argues in favor of a $D_s^{(*)} \bar{D}_{s1}(2536)$ or $D_s^{(*)} \bar{D}_{s2}(2573)$ [134] molecular nature, Ref. [135] does not confirm these claims. Ref. [136] identifies the structure as P -wave $[cs][\bar{c}\bar{s}]$ tetraquark state. Other explanations of the $\psi(4660)$ include a $\psi(2S)f_0(980)$ molecule [137] and a $\Lambda_c^+ \bar{\Lambda}_c^-$ baryonium [130]. Also in this mass range studies of the partner states, driven either by spin or flavor symmetry will be very valuable — see e.g. the predictions in Ref. [138].

79.2.4 The $T_{c\bar{c}1}(3900)$, $T_{c\bar{c}}(4020)$, $T_{b\bar{b}1}(10610)$, and $T_{b\bar{b}}(10650)$

The isovector states $T_{c\bar{c}1}(3900)$ and $T_{c\bar{c}}(4020)$, first observed by BESIII [139, 140], decay predominantly into $\bar{D}D^*$ and \bar{D}^*D^* , respectively, while the $T_{b\bar{b}1}(10610)$ and $T_{b\bar{b}}(10650)$, first observed by Belle [141, 142], decay predominantly into $\bar{B}B^*$ and \bar{B}^*B^* [143], respectively, although all four were discovered in the decay mode heavy quarkonium plus pion. This suggests that these states are close relatives and their interactions are connected via heavy quark flavor symmetry. A molecular interpretation for the bottomonium states was proposed shortly after the discovery of the two $T_{b\bar{b}}$ states [144] and also shortly after that of the $T_{c\bar{c}1}(3900)$ [116]. This picture is confirmed within the meson exchange model of Ref. [145]. Decay patterns of $T_{c\bar{c}1}(3900)$ and the two $T_{b\bar{b}}$ were also shown to be consistent with a molecular interpretation [146–148]. However, some of their properties also appear to be consistent with tetraquark structures [149]. If the molecular picture were correct for the $T_{b\bar{b}}$ states, spin symmetry would lead to the existence of spin partner states [150–152], which are still to be found. In Ref. [153] it was shown that the actual pole locations of these partner states would be good probes of one-pion exchange in the molecular potential, which makes the experimental search for those states even more interesting.

79.2.5 The $T_{c\bar{c}1}(4200)$ and $T_{c\bar{c}1}(4430)$

The heaviest confirmed charged state in the charmonium sector is the $T_{c\bar{c}1}(4430)^\pm$ observed by Belle [126]. It is interpreted as hadrocharmonium [110], $\bar{D}_1 D^*$ molecule [154], as well as tetraquark [125]. Alternatively, in [155, 156] the $T_{c\bar{c}1}(4430)^\pm$ is explained as a cross-channel effect enhanced by a triangle singularity from open charm states. These works were criticised in Ref. [157] where an alternative triangle consisting of a K^* , a π , and the $\psi(4230)$, is proposed to generate the $T_{c\bar{c}1}(4430)$. The Argand diagram shows an anticlockwise circle, in line with the experimental analysis [127], while the one of Ref. [156] shows a clockwise motion. By replacing the $\psi(4230)$ with the $\psi(3770)$, and changing the K^* , one can also interpret the $T_{c\bar{c}1}(4200)$ as a kinematic effect [157]. A possible interpretation of $T_{c\bar{c}1}(3900)$ and $T_{c\bar{c}}(4020)$ as crossed channel effects is put forward in Ref. [158]. It remains to be seen, however, if this kind of explanation is also

capable of explaining the observations of these lowest $T_{c\bar{c}}$ states, also at other total energies.

79.2.6 The $T_{c\bar{c}\bar{s}1}(4000)$

There is recent evidence for a charged charmonium-like state with strangeness, $T_{c\bar{c}\bar{s}1}(4000)$, from BESIII [159] and LHCb [160]. The possible existence of a strange partner to the $T_{c\bar{c}}$ near the $D_s \bar{D}^*$ thresholds has been predicted in molecular models [161, 162], for tetraquarks [163, 164], for hadrocharmonium structures [164, 165], and as a coupled-channel effect [166]. Later on this state is interpreted in Refs. [167, 168] as a member of the same multiquark octet and in Refs. [169–171] as a member of the same molecular one as the $T_{c\bar{c}1}(3900)$. Ref. [168] is also able to describe the recent LHCb data in the $J/\psi(1S)K^-$ system [160], although the extracted total width for their lowest $T_{c\bar{c}\bar{s}}$ state is an order of magnitude larger than that found by BESIII. Refs. [172, 173] claim that both the molecular components and the compact tetraquark core are relevant to describe the $T_{c\bar{c}1}(3900)$ and $T_{c\bar{c}\bar{s}1}(4000)$ resonances. Again, in [174] the $T_{c\bar{c}\bar{s}1}(4000)$ can be explained as a coupled-channel effect producing the enhancement close to threshold.

Ref. [169] comes to the conclusion that an understanding of the experimental data for the $T_{c\bar{c}\bar{s}1}(4000)$ calls for the inclusion of both triangle diagrams as well as a pole term. The authors conclude from their calculations that $T_{c\bar{c}\bar{s}1}(4000)$ and $T_{c\bar{c}1}(3900)$ are members of the same SU(3) multiplet. This conclusion was confirmed in Ref. [175] and the study extended to higher energies. The fit of the experimental data allowed for two solutions, one where the $T_{c\bar{c}}(4020)$ is a spin partner of the mentioned isovector states and one where it is not. Data e.g. for $e^+e^- \rightarrow K^+D^{*-}D^{*0}$ is claimed to be decisive which scenario is indeed realised.

It should be stressed that the various scenarios, while describing much of the available data, also make decisive predictions, e.g. yet unobserved quantum numbers [124, 176]. The forthcoming data on heavy meson spectroscopy from various facilities should provide a much deeper understanding of how QCD forms matter out of quarks and gluons.

79.2.7 The $T_{cc}(3875)$

There is a recent report and follow-up by LHCb [62, 63] on the observation of a narrow peak in the $D^0 D^0 \pi^+$ mass spectrum just below the $D^{*+} D^0$ threshold. The observed state is a candidate for an isoscalar double-charm T_{cc}^+ tetraquark configuration with a quark content of $cc\bar{u}\bar{d}$. Unsuccessful searches in $D^+ D^0 \pi^+$ and $D^+ D^+$ mass spectra disfavour the isovector assignment. The $D^0 \pi^+$ mass distribution indicates that the T_{cc}^+ proceeds through the formation of a D^* in the intermediate state. The additional proximity to the $D^* D^0$ mass threshold favors the $J^P = 1^+$ assignment. The T_{cc}^+ has a remarkable narrow width and lies very close to the $D^{*+} D^0$ threshold [63], comparable to the properties of the $\chi_{c1}(3872)$ [177].

A first evaluation in the context of QCD sum rules [178] results in mass and width values consistent with the assumption of a compact diquark-antidiquark structure of the T_{cc}^+ . A pole analysis performed with $D^0 D^0 \pi^+ - D^{*+} D^0$ coupled-channels [179] suggests that the T_{cc}^+ has its origin in a $D^{*+} D^0$ virtual state resulting from the attraction in this channel and the coupling to $D^0 D^0 \pi^+$. The interpretation of the observed T_{cc}^+ as a $D^* D$ molecular structure was pursued in quark models [180–183] and the Bethe-Salpeter framework [184]. Predictions depend on fine model details and are usually accompanied by additional partner states, like an isovector molecule or higher radial excitations. In analogy to the case of the $\chi_{c1}(3872)$ in Ref. [177] the production of T_{cc}^+ in high-energy proton-proton collisions at the LHC is studied. Effects of a charm-meson triangle singularity on the inclusive production of T_{cc}^+ from the rescattering of DD leads to a narrow peak in the $T_{cc}^+ \pi^+$ invariant mass distribution. A spin 2 partner of the T_{cc}^+ is predicted in Refs. [182, 183], who's hadronic decays are studied in Ref. [185].

As for the $\chi_{c1}(3872)$ one can employ the effective range deduced from experiment for the effective range in the DD^* -channel as a measure of the nature of the $T_{cc}(3875)$. Also here isospin violations are significant. It turns out that in a calculation where the one-pion exchange is kept fully non-perturbative, its effect on the

effective range is small and positive [183], while it is small and negative when being treated perturbatively [97, 186].

First lattice studies are also available for the $T_{cc}(3875)$ [187–189], all performed at pion masses slightly larger than physical such that the D^* and with this also the $T_{cc}(3875)$ are stable. They all find that at these pion masses the T_{cc} is a virtual state. In Ref. [190] it was stressed, however, that all those analyses should be redone, since the proximity of a left-hand cut invalidates the method used.

79.3 Systems containing four heavy quarks

79.3.1 The $T_{cc\bar{c}\bar{c}}(6900)$

LHCb reported the observation of pronounced structures in a double- $J/\psi(1S)$ invariant mass distribution [191] thus pointing at states with $cc\bar{c}\bar{c}$ quarks contents. First results on di- $J/\psi(1S)$ and $J/\psi(1S)\psi(2S)$ invariant mass distributions in proton-proton collision data by the CMS [192] and ATLAS [193] Collaborations confirm and extend the resonance structures seen by LHCb. Belle reported on a first search for a double-charmonium state with $e^+e^- \rightarrow \eta_c J/\psi(1S)$ near threshold via the ISR process. No significant signal of the double charmonium state is found in several bins of the invariant mass of $\eta_c J/\psi(1S)$ [194]. Recently the COMPASS [195] Collaboration also studied double $J/\psi(1S)$ production in pion scattering off nuclear targets. No significant signatures that could be associated with tetraquarks are found in the double $J/\psi(1S)$ mass spectrum, although the COMPASS data sample is limited.

From quark models the possible existence of bound states like this was discussed already long ago [196, 197]. There are now also many model calculations available in the literature. For discussions of those data from the compact tetraquark perspective see Refs. [198–204]. Most of these quark model calculations assign the reported structure to a $cc\bar{c}\bar{c}$ state in the $2S$ multiplet with near-degenerate $J^P = 0^+, 1^+$ and 2^+ configurations. The dominance of a compact tetraquark component in the apparently exotic structure is also supported by the coupled multichannel study of Ref. [205]. The full coupled-channel study of Ref. [206] leads to a rich spectrum of $c\bar{c}-c\bar{c}$ states where parts are candidates for the observed double $J/\psi(1S)$ structures. For direct analyses of the data within the tetraquark approach, see, e.g., Ref. [207]. Also QCD sum rule studies of the system were published, but do not give consistent results: For example Ref. [208] interprets the structure at 6900 MeV as a hybrid state, Ref. [209] as a tetraquark, and Ref. [210] states that both molecular and tetraquark interpretations are possible. An alternative view on the LHCb double- $J/\psi(1S)$ data is provided in Refs. [211–213] where the analyses are performed using coupled channel T -matrices. In these works the structures in the data emerge from the interplay of thresholds and resonances with the non-trivial prediction that there should exist, if this dynamical picture were correct, a state located very near the double- $J/\psi(1S)$ threshold which can be searched for experimentally. In Ref. [214] it was shown that a $J/\psi(1S)J/\psi(1S)$ scattering potential sufficiently strong to bind is in fact consistent with our current understanding of $\pi J/\psi(1S)$ scattering as well as the strength of the $\pi\pi$ interactions.

In contrast, Ref. [215, 216] explains the double- $J/\psi(1S)$ data as cusps without nearby poles. This claim can be tested experimentally: if this explanation were correct, there should not be any narrow near threshold structure in the channel that generates the cusp, for that would call for a non-perturbative interaction in that channel, as pointed out in Ref. [217].

References

- [1] Y. S. Kalashnikova and A. V. Nefediev, Phys. Rev. D **80**, 074004 (2009), [arXiv:0907.4901].
- [2] M. Takizawa and S. Takeuchi, PTEP **2013**, 093D01 (2013), [arXiv:1206.4877].
- [3] P. G. Ortega, D. R. Entem and F. Fernandez, J. Phys. G **40**, 065107 (2013), [arXiv:1205.1699].
- [4] S. Coito, G. Rupp and E. van Beveren, Eur. Phys. J. C **73**, 3, 2351 (2013), [arXiv:1212.0648].
- [5] I. K. Hammer, C. Hanhart and A. V. Nefediev, Eur. Phys. J. A **52**, 11, 330 (2016), [arXiv:1607.06971].
- [6] C. Hanhart and A. Nefediev, Phys. Rev. D **106**, 11, 114003 (2022), [arXiv:2209.10165].
- [7] N. Brambilla *et al.*, Eur. Phys. J. **C71**, 1534 (2011), [arXiv:1010.5827].
- [8] H.-X. Chen *et al.*, Phys. Rept. **639**, 1 (2016), [arXiv:1601.02092].
- [9] A. Ali, J. S. Lange and S. Stone, Prog. Part. Nucl. Phys. **97**, 123 (2017), [arXiv:1706.00610].
- [10] R. F. Lebed, R. E. Mitchell and E. S. Swanson, Prog. Part. Nucl. Phys. **93**, 143 (2017), [arXiv:1610.04528].
- [11] S. L. Olsen, T. Skwarnicki and D. Zieminska, Rev. Mod. Phys. **90**, 1, 015003 (2018), [arXiv:1708.04012].
- [12] Y.-R. Liu *et al.*, Prog. Part. Nucl. Phys. **107**, 237 (2019), [arXiv:1903.11976].
- [13] N. Brambilla *et al.*, Phys. Rept. **873**, 1 (2020), [arXiv:1907.07583].
- [14] A. Esposito, A. Pilloni and A. D. Polosa, Phys. Rept. **668**, 1 (2017), [arXiv:1611.07920].
- [15] F.-K. Guo *et al.*, Rev. Mod. Phys. **90**, 1, 015004 (2018), [arXiv:1705.00141].
- [16] B. Aubert *et al.* (BaBar), Phys. Rev. Lett. **90**, 242001 (2003), [hep-ex/0304021].
- [17] D. Besson *et al.* (CLEO), Phys. Rev. **D68**, 032002 (2003), [Erratum: Phys. Rev. D **75**, 119908 (2007)], [hep-ex/0305100].
- [18] S. Godfrey, Phys. Lett. **B568**, 254 (2003), [hep-ph/0305122].
- [19] H.-Y. Cheng and W.-S. Hou, Phys. Lett. **B566**, 193 (2003), [hep-ph/0305038].
- [20] K. Terasaki, Phys. Rev. **D68**, 011501 (2003), [hep-ph/0305213].
- [21] L. Maiani *et al.*, Phys. Rev. **D71**, 014028 (2005), [hep-ph/0412098].
- [22] V. Dmitrasinovic, Phys. Rev. Lett. **94**, 162002 (2005).
- [23] T. Barnes, F. E. Close and H. J. Lipkin, Phys. Rev. **D68**, 054006 (2003), [hep-ph/0305025].
- [24] E. E. Kolomeitsev and M. F. M. Lutz, Phys. Lett. **B582**, 39 (2004), [hep-ph/0307133].
- [25] A. Faessler *et al.*, Phys. Rev. **D76**, 014005 (2007), [arXiv:0705.0254].
- [26] A. Faessler *et al.*, Phys. Rev. D **76**, 114008 (2007), [arXiv:0709.3946].
- [27] M. F. M. Lutz and M. Soyeur, Nucl. Phys. **A813**, 14 (2008), [arXiv:0710.1545].
- [28] L. Liu *et al.*, Phys. Rev. **D87**, 1, 014508 (2013), [arXiv:1208.4535].
- [29] P. Colangelo and F. De Fazio, Phys. Lett. **B570**, 180 (2003), [hep-ph/0305140].
- [30] X.-Y. Guo, Y. Heo and M. F. M. Lutz, Phys. Rev. **D98**, 1, 014510 (2018), [arXiv:1801.10122].
- [31] H.-L. Fu *et al.*, Eur. Phys. J. A **58**, 4, 70 (2022), [arXiv:2111.09481].
- [32] V. Dmitrasinovic, Phys. Rev. D **86**, 016006 (2012).
- [33] M.-L. Du *et al.*, Phys. Rev. Lett. **126**, 19, 192001 (2021), [arXiv:2012.04599].
- [34] R. Aaij *et al.* (LHCb), Phys. Rev. **D94**, 7, 072001 (2016), [arXiv:1608.01289].
- [35] R. Aaij *et al.* (LHCb), Phys. Rev. D **94**, 7, 072001 (2016), [arXiv:1608.01289].
- [36] L. Gayer *et al.* (Hadron Spectrum), JHEP **07**, 123 (2021), [arXiv:2102.04973].
- [37] M. Albaladejo *et al.*, Phys. Lett. **B767**, 465 (2017), [arXiv:1610.06727].
- [38] M.-L. Du *et al.*, Phys. Rev. **D98**, 9, 094018 (2018), [arXiv:1712.07957].

- [39] G. Moir *et al.*, JHEP **10**, 011 (2016), [arXiv:1607.07093].
- [40] A. Asokan *et al.*, Eur. Phys. J. C **83**, 9, 850 (2023), [arXiv:2212.07856].
- [41] R. J. Hudspith and D. Mohler, Phys. Rev. D **107**, 11, 114510 (2023), [arXiv:2303.17295].
- [42] R. Aaij *et al.* (LHCb), Phys. Rev. D **102**, 112003 (2020), [arXiv:2009.00026].
- [43] R. Aaij *et al.* (LHCb), Phys. Rev. Lett. **125**, 242001 (2020), [arXiv:2009.00025].
- [44] M. Karliner and J. L. Rosner, Phys. Rev. D **102**, 9, 094016 (2020), [arXiv:2008.05993].
- [45] X.-G. He, W. Wang and R. Zhu, Eur. Phys. J. C **80**, 11, 1026 (2020), [arXiv:2008.07145].
- [46] Z.-G. Wang, Int. J. Mod. Phys. A **35**, 30, 2050187 (2020), [arXiv:2008.07833].
- [47] R. Molina and E. Oset, Phys. Lett. B **811**, 135870 (2020), [arXiv:2008.11171].
- [48] Y. Huang *et al.*, Eur. Phys. J. C **80**, 10, 973 (2020), [arXiv:2008.07959].
- [49] M.-Z. Liu, J.-J. Xie and L.-S. Geng, Phys. Rev. D **102**, 9, 091502 (2020), [arXiv:2008.07389].
- [50] B. Wang and S.-L. Zhu, Eur. Phys. J. C **82**, 5, 419 (2022), [arXiv:2107.09275].
- [51] Z.-L. Yue, C.-J. Xiao and D.-Y. Chen, Phys. Rev. D **107**, 3, 034018 (2023), [arXiv:2212.03018].
- [52] T. J. Burns and E. S. Swanson, Phys. Lett. B **813**, 136057 (2021), [arXiv:2008.12838].
- [53] X.-H. Liu *et al.*, Eur. Phys. J. C **80**, 12, 1178 (2020), [arXiv:2008.07190].
- [54] T. J. Burns and E. S. Swanson, Phys. Rev. D **103**, 1, 014004 (2021), [arXiv:2009.05352].
- [55] R. Aaij *et al.* (LHCb), Phys. Rev. D **108**, 1, 012017 (2023), [arXiv:2212.02717].
- [56] R. Molina and E. Oset, Phys. Rev. D **107**, 5, 056015 (2023), [arXiv:2211.01302].
- [57] H.-W. Ke *et al.*, Phys. Rev. D **106**, 11, 114032 (2022), [arXiv:2210.06215].
- [58] S. K. Choi *et al.* (Belle), Phys. Rev. Lett. **91**, 262001 (2003), [hep-ex/0309032].
- [59] B. Aubert *et al.* (BaBar), Phys. Rev. D **71**, 071103 (2005), [hep-ex/0406022].
- [60] R. Aaij *et al.* (LHCb), Phys. Rev. Lett. **115**, 072001 (2015), [arXiv:1507.03414].
- [61] R. Aaij *et al.* (LHCb), Phys. Rev. Lett. **122**, 22, 222001 (2019), [arXiv:1904.03947].
- [62] R. Aaij *et al.* (LHCb), Nature Phys. **18**, 7, 751 (2022), [arXiv:2109.01038].
- [63] R. Aaij *et al.* (LHCb), Nature Commun. **13**, 1, 3351 (2022), [arXiv:2109.01056].
- [64] R. Aaij *et al.* (LHCb), Phys. Rev. Lett. **110**, 222001 (2013), [arXiv:1302.6269].
- [65] R. Aaij *et al.* (LHCb), Phys. Rev. D **92**, 1, 011102 (2015), [arXiv:1504.06339].
- [66] T. Barnes and S. Godfrey, Phys. Rev. D **69**, 054008 (2004), [hep-ph/0311162].
- [67] K. Abe *et al.* (Belle), Phys. Rev. Lett. **98**, 082001 (2007), [hep-ex/0507019].
- [68] S. Uehara *et al.* (Belle), Phys. Rev. Lett. **96**, 082003 (2006), [hep-ex/0512035].
- [69] R. Aaij *et al.* (LHCb), Phys. Rev. D **102**, 9, 092005 (2020), [arXiv:2005.13419].
- [70] R. Aaij *et al.* (LHCb), JHEP **08**, 123 (2020), [arXiv:2005.13422].
- [71] C. Hanhart *et al.*, Phys. Rev. D **76**, 034007 (2007), [arXiv:0704.0605].
- [72] G. Barucca *et al.* (PANDA), Eur. Phys. J. A **55**, 3, 42 (2019), [arXiv:1812.05132].
- [73] G. Barucca *et al.* (PANDA), Eur. Phys. J. A **57**, 6, 184 (2021), [arXiv:2101.11877].
- [74] F.-K. Guo, Phys. Rev. Lett. **122**, 20, 202002 (2019), [arXiv:1902.11221].
- [75] E. Braaten, L.-P. He and K. Ingles, Phys. Rev. D **100**, 3, 031501 (2019), [arXiv:1904.12915].
- [76] S. Sakai, H.-J. Jing and F.-K. Guo, Phys. Rev. D **102**, 11, 114041 (2020), [arXiv:2008.10829].
- [77] N. A. Tornqvist, Phys. Lett. **B590**, 209 (2004), [hep-ph/0402237].
- [78] E. S. Swanson, Phys. Lett. **B588**, 189 (2004), [hep-ph/0311229].
- [79] D. Gamermann and E. Oset, Phys. Rev. D **80**, 014003 (2009), [arXiv:0905.0402].
- [80] Y.-b. Dong *et al.*, Phys. Rev. D **77**, 094013 (2008), [arXiv:0802.3610].
- [81] Y. Dong *et al.*, Phys. Rev. D **79**, 094013 (2009), [arXiv:0903.5416].
- [82] F.-K. Guo *et al.*, Phys. Lett. B **742**, 394 (2015), [arXiv:1410.6712].
- [83] B. Aubert *et al.* (BaBar), Phys. Rev. D **71**, 031501 (2005), [hep-ex/0412051].
- [84] L. Maiani, A. D. Polosa and V. Riquer, Phys. Lett. **B778**, 247 (2018), [arXiv:1712.05296].
- [85] L. Maiani, A. D. Polosa and V. Riquer, Phys. Rev. D **102**, 3, 034017 (2020), [arXiv:2005.08764].
- [86] C. Bignamini *et al.*, Phys. Rev. Lett. **103**, 162001 (2009), [arXiv:0906.0882].
- [87] A. Esposito *et al.*, Eur. Phys. J. C **81**, 669 (2021), [arXiv:2006.15044].
- [88] P. Artoisenet and E. Braaten, Phys. Rev. D **81**, 114018 (2010), [arXiv:0911.2016].
- [89] E. Braaten *et al.*, Phys. Rev. D **103**, 7, L071901 (2021), [arXiv:2012.13499].
- [90] F.-K. Guo *et al.*, JHEP **05**, 138 (2014), [arXiv:1403.4032].
- [91] M. Albaladejo *et al.*, Chin. Phys. C **41**, 12, 121001 (2017), [arXiv:1709.09101].
- [92] A. Esposito *et al.*, Phys. Rev. D **105**, 3, L031503 (2022), [arXiv:2108.11413].
- [93] S. Weinberg, Phys. Rev. **137**, B672 (1965).
- [94] V. Baru *et al.*, Phys. Rev. D **84**, 074029 (2011), [arXiv:1108.5644].
- [95] M. Jansen, H. W. Hammer and Y. Jia, Phys. Rev. D **89**, 1, 014033 (2014), [arXiv:1310.6937].
- [96] E. Braaten, Phys. Rev. D **91**, 11, 114007 (2015), [arXiv:1503.04791].
- [97] A. Esposito *et al.*, Phys. Lett. B **847**, 138285 (2023), [arXiv:2307.11400].
- [98] V. Baru *et al.*, Phys. Lett. B **833**, 137290 (2022), [arXiv:2110.07484].
- [99] B. Aubert *et al.* (BaBar), Phys. Rev. Lett. **95**, 142001 (2005), [hep-ex/0506081].
- [100] M. Ablikim *et al.* (BESIII), Phys. Rev. Lett. **118**, 9, 092001 (2017), [arXiv:1611.01317].
- [101] M. Cleven *et al.*, Phys. Rev. D **90**, 7, 074039 (2014), [arXiv:1310.2190].
- [102] C. Hanhart and E. Klempt, Int. J. Mod. Phys. A **35**, 05, 2050019 (2020), [arXiv:1906.11971].
- [103] T. Barnes, S. Godfrey and E. S. Swanson, Phys. Rev. D **72**, 054026 (2005), [hep-ph/0505002].

- [104] L.-C. Gui *et al.*, Phys. Rev. D **98**, 1, 016010 (2018), [arXiv:1801.08791].
- [105] F. E. Close and P. R. Page, Phys. Lett. **B628**, 215 (2005), [hep-ph/0507199].
- [106] M. Berwein *et al.*, Phys. Rev. **D92**, 11, 114019 (2015), [arXiv:1510.04299].
- [107] E. Kou and O. Pene, Phys. Lett. **B631**, 164 (2005), [hep-ph/0507119].
- [108] Yu. S. Kalashnikova and A. V. Nefediev, Phys. Rev. **D77**, 054025 (2008), [arXiv:0801.2036].
- [109] M. Ablikim *et al.* (BESIII), Phys. Rev. Lett. **111**, 24, 242001 (2013), [arXiv:1309.1896].
- [110] M. B. Voloshin, Prog. Part. Nucl. Phys. **61**, 455 (2008), [arXiv:0711.4556].
- [111] X. Li and M. B. Voloshin, Mod. Phys. Lett. **A29**, 12, 1450060 (2014), [arXiv:1309.1681].
- [112] E. Braaten, C. Langmack and D. H. Smith, Phys. Rev. D **90**, 1, 014044 (2014), [arXiv:1402.0438].
- [113] N. Brambilla *et al.*, Phys. Rev. D **97**, 1, 016016 (2018), [arXiv:1707.09647].
- [114] N. Brambilla *et al.*, Phys. Rev. D **101**, 5, 054040 (2020), [arXiv:1908.11699].
- [115] N. Brambilla *et al.*, Phys. Rev. D **107**, 5, 054034 (2023), [arXiv:2212.09187].
- [116] Q. Wang, C. Hanhart and Q. Zhao, Phys. Rev. Lett. **111**, 13, 132003 (2013), [arXiv:1303.6355].
- [117] Y. Dong *et al.*, Phys. Rev. D **89**, 3, 034018 (2014), [arXiv:1310.4373].
- [118] F.-K. Guo *et al.*, Phys. Lett. **B725**, 127 (2013), [arXiv:1306.3096].
- [119] M. Ablikim *et al.* (BESIII), Phys. Rev. Lett. **112**, 9, 092001 (2014), [arXiv:1310.4101].
- [120] Y. Dong *et al.*, Phys. Rev. D **90**, 7, 074032 (2014), [arXiv:1404.6161].
- [121] Q. Wang *et al.*, Phys. Rev. **D89**, 3, 034001 (2014), [arXiv:1309.4303].
- [122] V. Baru *et al.*, Phys. Rev. **D91**, 3, 034002 (2015), [arXiv:1501.02924].
- [123] T. Ji *et al.*, Phys. Rev. Lett. **129**, 10, 102002 (2022), [arXiv:2205.10994].
- [124] A. Ali *et al.*, Eur. Phys. J. **C78**, 1, 29 (2018), [arXiv:1708.04650].
- [125] L. Maiani *et al.*, Phys. Rev. **D89**, 114010 (2014), [arXiv:1405.1551].
- [126] K. Chilikin *et al.* (Belle), Phys. Rev. **D88**, 7, 074026 (2013), [arXiv:1306.4894].
- [127] R. Aaij *et al.* (LHCb), Phys. Rev. Lett. **112**, 22, 222002 (2014), [arXiv:1404.1903].
- [128] L. Maiani, A. D. Polosa and V. Riquer, Symmetry **13**, 5, 751 (2021), [arXiv:2103.14356].
- [129] Y.-H. Chen *et al.*, Phys. Rev. **D99**, 7, 074016 (2019), [arXiv:1902.10957].
- [130] G. Cotugno *et al.*, Phys. Rev. Lett. **104**, 132005 (2010), [arXiv:0911.2178].
- [131] F.-K. Guo *et al.*, Phys. Rev. **D82**, 094008 (2010), [arXiv:1005.2055].
- [132] L.-Y. Dai, J. Haidenbauer and U. G. Meissner, Phys. Rev. **D96**, 11, 116001 (2017), [arXiv:1710.03142].
- [133] J. He *et al.*, Eur. Phys. J. C **80**, 3, 246 (2020), [arXiv:1912.08420].
- [134] F.-L. Wang and X. Liu, Phys. Rev. D **102**, 9, 094006 (2020), [arXiv:2008.13484].
- [135] H.-W. Ke, X.-H. Liu and X.-Q. Li, Chin. Phys. C **44**, 9, 093104 (2020), [arXiv:2004.03167].
- [136] J.-R. Zhang, Phys. Rev. D **102**, 5, 054006 (2020), [arXiv:2004.10985].
- [137] F.-K. Guo, C. Hanhart and U.-G. Meissner, Phys. Lett. B **665**, 26 (2008), [arXiv:0803.1392].
- [138] F.-K. Guo, C. Hanhart and U.-G. Meissner, Phys. Rev. Lett. **102**, 242004 (2009), [arXiv:0904.3338].
- [139] M. Ablikim *et al.* (BESIII), Phys. Rev. Lett. **110**, 252001 (2013), [arXiv:1303.5949].
- [140] M. Ablikim *et al.* (BESIII), Phys. Rev. Lett. **112**, 2, 022001 (2014), [arXiv:1310.1163].
- [141] P. Krokovny *et al.* (Belle), Phys. Rev. **D88**, 5, 052016 (2013), [arXiv:1308.2646].
- [142] A. Bondar *et al.* (Belle), Phys. Rev. Lett. **108**, 122001 (2012), [arXiv:1110.2251].
- [143] A. Garmash *et al.* (Belle), Phys. Rev. Lett. **116**, 21, 212001 (2016), [arXiv:1512.07419].
- [144] A. E. Bondar *et al.*, Phys. Rev. **D84**, 054010 (2011), [arXiv:1105.4473].
- [145] Z.-M. Ding, H.-Y. Jiang and J. He, Eur. Phys. J. C **80**, 12, 1179 (2020), [arXiv:2011.04980].
- [146] Y. Dong *et al.*, Phys. Rev. D **88**, 1, 014030 (2013), [arXiv:1306.0824].
- [147] F. Goerke *et al.*, Phys. Rev. D **94**, 9, 094017 (2016), [arXiv:1608.04656].
- [148] F. Goerke *et al.*, Phys. Rev. D **96**, 5, 054028 (2017), [arXiv:1707.00539].
- [149] A. Ali *et al.*, Phys. Rev. **D91**, 1, 017502 (2015), [arXiv:1412.2049].
- [150] M. B. Voloshin, Phys. Rev. **D84**, 031502 (2011), [arXiv:1105.5829].
- [151] T. Mehen and J. W. Powell, Phys. Rev. **D84**, 114013 (2011), [arXiv:1109.3479].
- [152] V. Baru *et al.*, JHEP **06**, 158 (2017), [arXiv:1704.07332].
- [153] V. Baru *et al.*, Phys. Rev. **D99**, 9, 094013 (2019), [arXiv:1901.10319].
- [154] T. Branz, T. Gutsche and V. E. Lyubovitskij, Phys. Rev. **D82**, 054025 (2010), [arXiv:1005.3168].
- [155] P. Pakhlov, Phys. Lett. **B702**, 139 (2011), [arXiv:1105.2945].
- [156] P. Pakhlov and T. Uglov, Phys. Lett. **B748**, 183 (2015), [arXiv:1408.5295].
- [157] S. X. Nakamura and K. Tsushima, Phys. Rev. **D100**, 5, 051502 (2019), [arXiv:1901.07385].
- [158] J.-Z. Wang *et al.*, Eur. Phys. J. C **80**, 11, 1040 (2020), [arXiv:2007.02263].
- [159] M. Ablikim *et al.* (BESIII), Phys. Rev. Lett. **126**, 10, 102001 (2021), [arXiv:2011.07855].
- [160] R. Aaij *et al.* (LHCb), Phys. Rev. Lett. **127**, 8, 082001 (2021), [arXiv:2103.01803].
- [161] S. H. Lee, M. Nielsen and U. Wiedner, J. Korean Phys. Soc. **55**, 424 (2009), [arXiv:0803.1168].
- [162] J. M. Dias, X. Liu and M. Nielsen, Phys. Rev. D **88**, 9, 096014 (2013), [arXiv:1307.7100].
- [163] D. Ebert, R. N. Faustov and V. O. Galkin, Eur. Phys. J. C **58**, 399 (2008), [arXiv:0808.3912].
- [164] J. Ferretti and E. Santopinto, JHEP **04**, 119 (2020), [arXiv:2001.01067].
- [165] M. B. Voloshin, Phys. Lett. B **798**, 135022 (2019), [arXiv:1901.01936].
- [166] D.-Y. Chen, X. Liu and T. Matsuki, Phys. Rev. Lett. **110**, 23, 232001 (2013), [arXiv:1303.6842].
- [167] L. Meng, B. Wang and S.-L. Zhu, Phys. Rev. D **102**, 11, 111502 (2020), [arXiv:2011.08656].

- [168] P. G. Ortega, D. R. Entem and F. Fernandez, Phys. Lett. B **818**, 136382 (2021), [arXiv:2103.07871].
- [169] Z. Yang *et al.*, Phys. Rev. D **103**, 7, 074029 (2021), [arXiv:2011.08725].
- [170] B. Wang, L. Meng and S.-L. Zhu, Phys. Rev. D **103**, 2, L021501 (2021), [arXiv:2011.10922].
- [171] M.-L. Du *et al.*, Phys. Rev. D **105**, 7, 074018 (2022), [arXiv:2201.08253].
- [172] R. M. Albuquerque, S. Narison and D. Rabietarivony, Phys. Rev. D **103**, 7, 074015 (2021), [arXiv:2101.07281].
- [173] Z.-H. Guo and J. A. Oller, Phys. Rev. D **103**, 5, 054021 (2021), [arXiv:2012.11904].
- [174] N. Ikeno, R. Molina and E. Oset, Phys. Lett. B **814**, 136120 (2021), [arXiv:2011.13425].
- [175] V. Baru *et al.*, Phys. Rev. D **105**, 3, 034014 (2022), [arXiv:2110.00398].
- [176] M. Cleven *et al.*, Phys. Rev. D **92**, 1, 014005 (2015), [arXiv:1505.01771].
- [177] E. Braaten *et al.*, Phys. Rev. D **106**, 3, 034033 (2022), [arXiv:2202.03900].
- [178] S. S. Agaev, K. Azizi and H. Sundu, Nucl. Phys. B **975**, 115650 (2022), [arXiv:2108.00188].
- [179] L.-Y. Dai *et al.*, Phys. Rev. D **105**, 5, L051507 (2022), [arXiv:2108.06002].
- [180] C. Deng and S.-L. Zhu, Phys. Rev. D **105**, 5, 054015 (2022), [arXiv:2112.12472].
- [181] P. G. Ortega *et al.*, Phys. Lett. B **841**, 137918 (2023), [arXiv:2211.06118].
- [182] M. Albaladejo, Phys. Lett. B **829**, 137052 (2022), [arXiv:2110.02944].
- [183] M.-L. Du *et al.*, Phys. Rev. D **105**, 1, 014024 (2022), [arXiv:2110.13765].
- [184] H.-W. Ke, X.-H. Liu and X.-Q. Li, Eur. Phys. J. C **82**, 2, 144 (2022), [arXiv:2112.14142].
- [185] Z.-S. Jia *et al.*, Phys. Rev. D **107**, 7, 074029 (2023), [arXiv:2211.02479].
- [186] M. Mikhasenko (2022), [arXiv:2203.04622].
- [187] M. Padmanath and S. Prelovsek, Phys. Rev. Lett. **129**, 3, 032002 (2022), [arXiv:2202.10110].
- [188] S. Chen *et al.*, Phys. Lett. B **833**, 137391 (2022), [arXiv:2206.06185].
- [189] Y. Lyu *et al.*, Phys. Rev. Lett. **131**, 16, 161901 (2023), [arXiv:2302.04505].
- [190] M.-L. Du *et al.*, Phys. Rev. Lett. **131**, 13, 131903 (2023), [arXiv:2303.09441].
- [191] R. Aaij *et al.* (LHCb), Sci. Bull. **65**, 23, 1983 (2020), [arXiv:2006.16957].
- [192] A. Hayrapetyan *et al.* (CMS) (2023), [arXiv:2306.07164].
- [193] Y. Xu (ATLAS), Acta Phys. Polon. Supp. **16**, 3, 21 (2023), [arXiv:2209.12173].
- [194] J. H. Yin *et al.* (Belle) (2023), [arXiv:2305.17947].
- [195] G. D. Alexeev *et al.* (COMPASS), Phys. Lett. B **838**, 137702 (2023), [arXiv:2204.01817].
- [196] J. P. Ader, J. M. Richard and P. Taxil, Phys. Rev. D **25**, 2370 (1982).
- [197] Y. Iwasaki, Prog. Theor. Phys. **54**, 492 (1975).
- [198] L. Maiani, Sci. Bull. **65**, 1949 (2020), [arXiv:2008.01637].
- [199] K.-T. Chao and S.-L. Zhu, Sci. Bull. **65**, 23, 1952 (2020), [arXiv:2008.07670].
- [200] J.-M. Richard, Sci. Bull. **65**, 1954 (2020), [arXiv:2008.01962].
- [201] R. N. Faustov, V. O. Galkin and E. M. Savchenko, Phys. Rev. D **102**, 11, 114030 (2020), [arXiv:2009.13237].
- [202] J. F. Giron and R. F. Lebed, Phys. Rev. D **102**, 7, 074003 (2020), [arXiv:2008.01631].
- [203] X. Jin *et al.*, Eur. Phys. J. C **80**, 11, 1083 (2020), [arXiv:2006.13745].
- [204] Q.-F. Lü, D.-Y. Chen and Y.-B. Dong, Eur. Phys. J. C **80**, 9, 871 (2020), [arXiv:2006.14445].
- [205] Z.-H. Guo and J. A. Oller, Phys. Rev. D **103**, 3, 034024 (2021), [arXiv:2011.00978].
- [206] P. G. Ortega, D. R. Entem and F. Fernández, Phys. Rev. D **108**, 9, 094023 (2023), [arXiv:2307.00532].
- [207] M. Karliner and J. L. Rosner, Phys. Rev. D **102**, 11, 114039 (2020), [arXiv:2009.04429].
- [208] B.-D. Wan and C.-F. Qiao, Phys. Lett. B **817**, 136339 (2021), [arXiv:2012.00454].
- [209] B.-C. Yang, L. Tang and C.-F. Qiao, Eur. Phys. J. C **81**, 4, 324 (2021), [arXiv:2012.04463].
- [210] R. M. Albuquerque *et al.*, Phys. Rev. D **102**, 9, 094001 (2020), [arXiv:2008.01569].
- [211] X.-K. Dong *et al.*, Phys. Rev. Lett. **126**, 13, 132001 (2021), [arXiv:2009.07795].
- [212] C. Gong *et al.*, Phys. Lett. B **824**, 136794 (2022), [arXiv:2011.11374].
- [213] Z.-R. Liang, X.-Y. Wu and D.-L. Yao, Phys. Rev. D **104**, 3, 034034 (2021), [arXiv:2104.08589].
- [214] X.-K. Dong *et al.*, Sci. Bull. **66**, 24, 2462 (2021), [arXiv:2107.03946].
- [215] J.-Z. Wang *et al.*, Phys. Rev. D **103**, 7, 071503 (2021), [arXiv:2008.07430].
- [216] J.-Z. Wang, X. Liu and T. Matsuki, Phys. Lett. B **816**, 136209 (2021), [arXiv:2012.03281].
- [217] F.-K. Guo *et al.*, Phys. Rev. D **91**, 5, 051504 (2015), [arXiv:1411.5584].

80. Baryon Decay Parameters

Revised August 2019 by E.D. Commins (UC Berkeley).

80.1 Baryon semileptonic decays

The typical spin-1/2 baryon semileptonic decay is described by a matrix element, the hadronic part of which may be written as:

$$\bar{B}_f \left[f_1(q^2)\gamma_\lambda + i f_2(q^2)\sigma_{\lambda\mu}q^\mu + g_1(q^2)\gamma_\lambda\gamma_5 + g_3(q^2)\gamma_5q_\lambda \right] B_i . \quad (80.1)$$

Here B_i and \bar{B}_f are spinors describing the initial and final baryons, and $q = p_i - p_f$, while the terms in f_1 , f_2 , g_1 , and g_3 account for vector, induced tensor (“weak magnetism”), axial vector, and induced pseudoscalar contributions [1]. Second-class current contributions are ignored here. In the limit of zero momentum transfer, f_1 reduces to the vector coupling constant g_V , and g_1 reduces to the axial-vector coupling constant g_A . The latter coefficients are related by Cabibbo’s theory [2], generalized to six quarks (and three mixing angles) by Kobayashi and Maskawa [3]. The g_3 term is negligible for transitions in which an e^\pm is emitted, and gives a very small correction, which can be estimated by PCAC [4], for μ^\pm modes. Recoil effects include weak magnetism, and are taken into account adequately by considering terms of first order in

$$\delta = \frac{m_i - m_f}{m_i + m_f} , \quad (80.2)$$

where m_i and m_f are the masses of the initial and final baryons.

The experimental quantities of interest are the total decay rate, the lepton-neutrino angular correlation, the asymmetry coefficients in the decay of a polarized initial baryon, and the polarization of the decay baryon in its own rest frame for an unpolarized initial baryon. Formulae for these quantities are derived by standard means [5] and are analogous to formulae for nuclear beta decay [6]. We use the notation of Ref. [6] in the Listings for neutron beta decay. For comparison with experiments at higher q^2 , it is necessary to modify the form factors at $q^2 = 0$ by a “dipole” q^2 dependence, and for high-precision comparisons to apply appropriate radiative corrections [7].

The ratio g_A/g_V may be written as

$$g_A/g_V = |g_A/g_V| e^{i\phi_{AV}} . \quad (80.3)$$

The presence of a “triple correlation” term in the transition probability, proportional to $\text{Im}(g_A/g_V)$ and of the form

$$\sigma_i \cdot (p_\ell \times p_\nu) \quad (80.4)$$

for initial baryon polarization or

$$\sigma_f \cdot (p_\ell \times p_\nu) \quad (80.5)$$

for final baryon polarization, would indicate failure of time-reversal invariance. The phase angle ϕ has been measured precisely only in neutron decay (and in ^{19}Ne nuclear beta decay), and the results are consistent with T invariance.

80.2 Hyperon nonleptonic decays

The amplitude for a spin-1/2 hyperon decaying into a spin-1/2 baryon and a spin-0 meson may be written in the form

$$M = G_F m_\pi^2 \cdot \bar{B}_f (A - B\gamma_5) B_i , \quad (80.6)$$

where A and B are constants [1]. The transition rate is proportional to

$$R = 1 + \gamma \hat{\omega}_f \cdot \hat{\omega}_i + (1 - \gamma)(\hat{\omega}_f \cdot \hat{\mathbf{n}})(\hat{\omega}_i \cdot \hat{\mathbf{n}}) + \alpha(\hat{\omega}_f \cdot \hat{\mathbf{n}} + \hat{\omega}_i \cdot \hat{\mathbf{n}}) + \beta \hat{\mathbf{n}} \cdot (\hat{\omega}_f \times \hat{\omega}_i) , \quad (80.7)$$

where $\hat{\mathbf{n}}$ is a unit vector in the direction of the final baryon momentum, and $\hat{\omega}_i$ and $\hat{\omega}_f$ are unit vectors in the directions of the

initial and final baryon spins. (The sign of the last term in the above equation was incorrect in our 1988 and 1990 editions.) The parameters α , β , and γ are defined as

$$\begin{aligned} \alpha &= 2 \text{Re}(s^*p)/(|s|^2 + |p|^2) , \\ \beta &= 2 \text{Im}(s^*p)/(|s|^2 + |p|^2) , \\ \gamma &= (|s|^2 - |p|^2)/(|s|^2 + |p|^2) , \end{aligned} \quad (80.8)$$

where $s = A$ and $p = |\mathbf{p}_f| B/(E_f + m_f)$; here E_f and \mathbf{p}_f are the energy and momentum of the final baryon. The parameters α , β , and γ satisfy

$$\alpha^2 + \beta^2 + \gamma^2 = 1 \quad (80.9)$$

If the hyperon polarization is \mathbf{P}_Y , the polarization \mathbf{P}_B of the decay baryons is

$$\mathbf{P}_B = \frac{(\alpha + \mathbf{P}_Y \cdot \hat{\mathbf{n}})\hat{\mathbf{n}} + \beta(\mathbf{P}_Y \times \hat{\mathbf{n}}) + \gamma\hat{\mathbf{n}} \times (\mathbf{P}_Y \times \hat{\mathbf{n}})}{1 + \alpha\mathbf{P}_Y \cdot \hat{\mathbf{n}}} . \quad (80.10)$$

Here \mathbf{P}_B is defined in the rest system of the baryon, obtained by a Lorentz transformation along $\hat{\mathbf{n}}$ from the hyperon rest frame, in which $\hat{\mathbf{n}}$ and \mathbf{P}_Y are defined.

An additional useful parameter ϕ is defined by

$$\beta = (1 - \alpha^2)^{1/2} \sin\phi . \quad (80.11)$$

In the Listings, we compile α and ϕ for each decay, since these quantities are most closely related to experiment and are essentially uncorrelated. When necessary, we have changed the signs of reported values to agree with our sign conventions. In the Baryon Summary Table, we give α , ϕ , and Δ (defined below) with errors, and also give the value of γ without error.

Time-reversal invariance requires, in the absence of final-state interactions, that s and p be relatively real, and therefore that $\beta = 0$. However, for the decays discussed here, the final-state interaction is strong. Thus

$$s = |s| e^{i\delta_s} \quad \text{and} \quad p = |p| e^{i\delta_p} , \quad (80.12)$$

where δ_s and δ_p are the pion-baryon s - and p -wave strong interaction phase shifts. We then have

$$\beta = \frac{-2|s||p|}{|s|^2 + |p|^2} \sin(\delta_s - \delta_p) . \quad (80.13)$$

One also defines $\Delta = -\tan^{-1}(\beta/\alpha)$. If T invariance holds, $\Delta = \delta_s - \delta_p$. For $\Lambda \rightarrow p\pi^-$ decay, the value of Δ may be compared with the s - and p -wave phase shifts in low-energy π^-p scattering, and the results are consistent with T invariance.

See also the note on “Radiative Hyperon Decays” in this *Review*.

References

- [1] E. Commins and P. Bucksbaum, *Weak Interactions of Leptons and Quarks* (1983), ISBN 978-0-521-27370-1, (Cambridge, USA: University Press, 473p.).
- [2] N. Cabibbo, Phys. Rev. Lett. **10**, 531 (1963).
- [3] M. Kobayashi and T. Maskawa, Prog. Theor. Phys. **49**, 652 (1973).
- [4] M. Goldberger and S. Treiman, Phys. Rev. **111**, 354 (1958).
- [5] P. Frampton and W.-K. Tung, Phys. Rev. D **3**, 1114 (1971).
- [6] J. Jackson, S. Treiman and H. Wyld, Nucl. Phys. **4**, 206 (1957).
- [7] Y. Yokoo, S. Suzuki and M. Morita, Prog. Theor. Phys. **50**, 1894 (1973).

81. N and Δ Resonances

Revised August 2019 by V.D. Burkert (Jefferson Lab), V. Crede (Florida State U.), U. Thoma (Bonn U.), L. Tiator (KPH, JGU Mainz) and R.L. Workman (George Washington U.).

81.1 Introduction

The excited states of the nucleon have been studied in a large number of formation and production experiments. Until recently, the Breit-Wigner masses and widths, the pole positions, and the elasticities of the N and Δ resonances in the Baryon Summary Table came largely from partial-wave analyses of πN total, elastic, and charge-exchange scattering data. The most comprehensive analyses were carried out by the Karlsruhe-Helsinki (KH80) [1], Carnegie Mellon-Berkeley (CMB80) [2], and George Washington U (GWU) [3] groups. Partial-wave analyses have also been performed on much smaller πN reaction data sets to get ηN , KA , and $K\Sigma$ branching fractions (see the Listings for references). Other branching fractions come from analyses of $\pi N \rightarrow \pi\pi N$ data.

In recent years, a large amount of data on photoproduction of many final states has been accumulated, and these data are beginning to tell us much about the properties of baryon resonances. A survey of data on photoproduction can be found in the proceedings of recent conferences [4] and workshops [5], and in recent reviews [6, 7].

81.2 Naming scheme for baryon resonances

In the past, when nearly all resonance information came from elastic πN scattering, it was common to label resonances with the incoming partial wave $L_{2I,2J}$, as in $\Delta(1232)P_{33}$ and $N(1680)F_{15}$. However, most recent information has come from γN experiments. Therefore, we have replaced $L_{2I,2J}$ with the spin-parity J^P of the state, as in $\Delta(1232)3/2^+$ and $N(1680)5/2^+$; this name gives intrinsic properties of the resonance that are independent of the specific particles and reactions used to study them. This applies equally to all baryons, including Ξ resonances and charm baryons that are not produced in formation experiments. We do not, however, attach the mass or spin-parity to the names of the ground-state (“stable”) baryons $N, \Lambda, \Sigma, \Xi, \Omega, A_c, \dots$.

81.3 Using the N and Δ listings

Tables 81.1 and 81.2 list all the N and Δ entries in the Baryon Listings and give our evaluation of the overall status and the status channel by channel. Only the established resonances (overall status 3 or 4 stars) are promoted to the Baryon Summary Table. We long ago omitted from the Listings information from old analyses, prior to KH80 and CMB80, which can be found in earlier editions. A rather complete survey of older results was given in our 1982 edition [8].

As a rule, we award an overall status **** or *** only to those resonances which are derived from analyses of data sets that include precision differential cross sections and polarization observables, and are confirmed by independent analyses. All other signals are given ** or * status. New results that are not accompanied by proper error evaluation are less valuable for evaluating star ratings. The following criteria are guidelines for future error analysis.

1. Uncertainties in resonance parameters: The publication should have a detailed discussion on how the uncertainties of parameters were estimated. This requires that the error estimates go beyond the simple fit error as e.g. given by MINUIT, and the robustness of the results should be demonstrated.

2. Fit quality: Concrete measures for the fit quality should be provided. The reduced global χ^2 value of the fit, while useful, is insufficient. Other possibilities include quoting variations of local χ^2 values in kinematic regions where evidence for new resonances, or significantly improved information on resonance parameters, is claimed.

3. Weight factors in observables: Analyses sometimes use weight factors for certain data sets to either increase or reduce their impact on the results. This has been particularly important when polarization observables are involved, which often are sensitive to resonance amplitudes through interferences, but usually have much poorer statistics than differential cross section data. To evaluate sensitivities, the resulting resonance parameters should

be checked against variations of the specific weight factors.

Table 81.1: The status of the N resonances and their decays. Sub-threshold decay modes are omitted. Only resonances with an overall status of *** or **** are included in the main Baryon Summary Table.

Particle	J^P	Status as seen in																			
		overall	$N\gamma$	$N\pi$	$\Delta\pi$	$N\sigma$	$N\eta$	AK	ΣK	$N\rho$	$N\omega$	$N\eta'$									
N	$1/2^+$	****																			
$N(1440)$	$1/2^+$	****	****	****	****	****	****	****	****	****	****	****	****	****	****	****	****	****	****	****	****
$N(1520)$	$3/2^-$	****	****	****	****	****	****	****	****	****	****	****	****	****	****	****	****	****	****	****	****
$N(1535)$	$1/2^-$	****	****	****	****	****	****	****	****	****	****	****	****	****	****	****	****	****	****	****	****
$N(1650)$	$1/2^-$	****	****	****	****	****	****	****	****	****	****	****	****	****	****	****	****	****	****	****	****
$N(1675)$	$5/2^-$	****	****	****	****	****	****	****	****	****	****	****	****	****	****	****	****	****	****	****	****
$N(1680)$	$5/2^+$	****	****	****	****	****	****	****	****	****	****	****	****	****	****	****	****	****	****	****	****
$N(1700)$	$3/2^-$	****	****	****	****	****	****	****	****	****	****	****	****	****	****	****	****	****	****	****	****
$N(1710)$	$1/2^+$	****	****	****	****	****	****	****	****	****	****	****	****	****	****	****	****	****	****	****	****
$N(1720)$	$3/2^+$	****	****	****	****	****	****	****	****	****	****	****	****	****	****	****	****	****	****	****	****
$N(1860)$	$5/2^+$	****	****	****	****	****	****	****	****	****	****	****	****	****	****	****	****	****	****	****	****
$N(1875)$	$3/2^-$	****	****	****	****	****	****	****	****	****	****	****	****	****	****	****	****	****	****	****	****
$N(1880)$	$1/2^+$	****	****	****	****	****	****	****	****	****	****	****	****	****	****	****	****	****	****	****	****
$N(1895)$	$1/2^-$	****	****	****	****	****	****	****	****	****	****	****	****	****	****	****	****	****	****	****	****
$N(1900)$	$3/2^+$	****	****	****	****	****	****	****	****	****	****	****	****	****	****	****	****	****	****	****	****
$N(1990)$	$7/2^+$	****	****	****	****	****	****	****	****	****	****	****	****	****	****	****	****	****	****	****	****
$N(2000)$	$5/2^+$	****	****	****	****	****	****	****	****	****	****	****	****	****	****	****	****	****	****	****	****
$N(2040)$	$3/2^+$	****	****	****	****	****	****	****	****	****	****	****	****	****	****	****	****	****	****	****	****
$N(2060)$	$5/2^-$	****	****	****	****	****	****	****	****	****	****	****	****	****	****	****	****	****	****	****	****
$N(2100)$	$1/2^+$	****	****	****	****	****	****	****	****	****	****	****	****	****	****	****	****	****	****	****	****
$N(2120)$	$3/2^-$	****	****	****	****	****	****	****	****	****	****	****	****	****	****	****	****	****	****	****	****
$N(2190)$	$7/2^-$	****	****	****	****	****	****	****	****	****	****	****	****	****	****	****	****	****	****	****	****
$N(2220)$	$9/2^+$	****	****	****	****	****	****	****	****	****	****	****	****	****	****	****	****	****	****	****	****
$N(2250)$	$9/2^-$	****	****	****	****	****	****	****	****	****	****	****	****	****	****	****	****	****	****	****	****
$N(2300)$	$1/2^+$	****	****	****	****	****	****	****	****	****	****	****	****	****	****	****	****	****	****	****	****
$N(2570)$	$5/2^-$	****	****	****	****	****	****	****	****	****	****	****	****	****	****	****	****	****	****	****	****
$N(2600)$	$11/2^-$	****	****	****	****	****	****	****	****	****	****	****	****	****	****	****	****	****	****	****	****
$N(2700)$	$13/2^+$	****	****	****	****	****	****	****	****	****	****	****	****	****	****	****	****	****	****	****	****

**																					
*																					

Table 81.2: The status of the Δ resonances and their decays. Sub-threshold decay modes are omitted. Only resonances with an overall status of *** or **** are included in the main Baryon Summary Table.

Particle	J^P	Status as seen in						
		overall	$N\gamma$	$N\pi$	$\Delta\pi$	ΣK	$N\rho$	$\Delta\eta$
$\Delta(1232)$	$3/2^+$	****	****	****	****	****	****	****
$\Delta(1600)$	$3/2^+$	****	****	****	****	****	****	****
$\Delta(1620)$	$1/2^-$	****	****	****	****	****	****	****
$\Delta(1700)$	$3/2^-$	****	****	****	****	****	****	****
$\Delta(1750)$	$1/2^+$	****	****	****	****	****	****	****
$\Delta(1900)$	$1/2^-$	****	****	****	****	****	****	****
$\Delta(1905)$	$5/2^+$	****	****	****	****	****	****	****
$\Delta(1910)$	$1/2^+$	****	****	****	****	****	****	****
$\Delta(1920)$	$3/2^+$	****	****	****	****	****	****	****
$\Delta(1930)$	$5/2^-$	****	****	****	****	****	****	****
$\Delta(1940)$	$3/2^-$	****	****	****	****	****	****	****
$\Delta(1950)$	$7/2^+$	****	****	****	****	****	****	****
$\Delta(2000)$	$5/2^+$	****	****	****	****	****	****	****
$\Delta(2150)$	$1/2^-$	****	****	****	****	****	****	****
$\Delta(2200)$	$7/2^-$	****	****	****	****	****	****	****
$\Delta(2300)$	$9/2^+$	****	****	****	****	****	****	****
$\Delta(2350)$	$5/2^-$	****	****	****	****	****	****	****
$\Delta(2390)$	$7/2^+$	****	****	****	****	****	****	****
$\Delta(2400)$	$9/2^-$	****	****	****	****	****	****	****
$\Delta(2420)$	$11/2^+$	****	****	****	****	****	****	****
$\Delta(2750)$	$13/2^-$	****	****	****	****	****	****	****
$\Delta(2950)$	$15/2^+$	****	****	****	****	****	****	****

**								
*								

Claims of evidence for new baryon states must be based on a sufficiently complete set of partial waves in the fit. The robustness of signals must be demonstrated, e.g. by examining the effect of higher partial waves in the fit.

81.4 Properties of resonances

Resonances are defined by poles of the S -matrix, whether in scattering, production or decay matrix elements. These are poles

in the complex plane in s , as discussed in the new review on *Resonances*. As is traditional, we quote here the pole positions in the complex energy $w = \sqrt{s}$ plane. Crucially, the position of the pole of the S -matrix is independent of the process, and the production and decay properties factorize. This is the rationale for listing the pole position first for each resonance. These key properties of the S -matrix pole are in contrast to other quantities related to resonance phenomena, such as Breit-Wigner parameters or any K -matrix pole. Breit-Wigner parameters depend on the formalism used, such as angular-momentum barrier factors, or cut-off parameters, and the assumed or modeled background. However, the accurate determination of pole parameters from the analysis of data on the real energy axis is not necessarily simple, or even straightforward. It requires the implementation of the correct analytic structure of the relevant (often coupled) channels.

In principle, there are two ways to extract pole parameters from experimental data: (i) analytic continuation of theoretical single- or multi-channel models into the complex energy plane or (ii) local expansions of the partial-wave T -matrix amplitudes in the complex energy plane in the vicinity of a pole.

At present, poles are usually extracted using the first method [9–14], but considerable effort has been put into the development of alternate approaches, such as the speed plot [15], time delay [16], N/D method [17], regularization procedure [18], or Padé approximation [19].

Methods of the second type are based on the idea to use first or higher-order derivatives in energy to reduce the importance of, or totally eliminate, the background contribution. One either has to model the background contribution and introduce model dependence, or one is faced with numerical derivatives of single-energy data. In both cases, one reaches almost unsurmountable difficulties.

An alternate way to extract pole parameters from partial waves has been proposed by introducing a Laurent+Pietarinen (L+P) expansion [20–22]

$$T(W) = \sum_{i=1}^N \frac{Res_i}{W - W_i} + \sum_{j=1}^M \sum_{n=0}^{n_{max}} c_n^j \left(\frac{\alpha_j - \sqrt{x_j - W}}{\alpha_j + \sqrt{x_j - W}} \right)^n, \quad (81.1)$$

where $T(W)$ is a given partial wave amplitude, W_i and Res_i are the N complex pole positions and residues. The background is parameterized with M Pietarinen functions, where α_j are positive range parameters and x_j are real or complex branch points; c_n^j are real expansion coefficients.

The main idea of this procedure is to find the simplest analytic function, with well-defined poles and cuts, regardless of whether they are generated by a theoretical model or some energy-independent procedure. Instead of searching for the function which reproduces the input amplitudes over the complete complex energy plane, on all Riemann sheets, a representation is searched only in a limited complex energy range, near the real axis, which is defined by the radius of convergence of the Laurent decomposition, and which contains the input amplitudes. All details are found in Ref. [21]. Applications of the method can be found in [20–27].

81.5 Photoproduction

A new approach to the nucleon excitation spectrum is provided by dedicated facilities at the Universities of Bonn, Grenoble, and Mainz, and at the national laboratories Jefferson Lab in the US and SPring-8 in Japan. High-precision cross sections and polarization observables for the photoproduction of pseudoscalar mesons provide a data set that is approaching a “complete experiment,” one that fully constrains the four complex amplitudes describing the spin-structure of the reaction [28]. A large number of photoproduction reactions has been studied.

In pseudoscalar meson photoproduction, the four independent helicity amplitudes can be expressed in terms of the four CGLN [29] amplitudes allowed by Lorentz and gauge invariance. These amplitudes can be expanded in a series of electric and magnetic multipoles. Except for $J = 1/2$, one electric and one magnetic multipole contributes to each J^P combination.

For a given state, these two amplitudes determine the resonance photo-decay helicity amplitudes $A_{1/2}$ and $A_{3/2}$. As described below, this resonance extraction has been carried out either assuming a Breit-Wigner resonance or at the pole.

If a Breit-Wigner parametrization is used, the $N\gamma$ partial width, Γ_γ , is given in terms of the helicity amplitudes $A_{1/2}$ and $A_{3/2}$ by

$$\Gamma_\gamma = \frac{k_{\text{BW}}^2}{\pi} \frac{2m_N}{(2J+1)m_{\text{BW}}} \left(|A_{1/2}|^2 + |A_{3/2}|^2 \right). \quad (81.2)$$

Here m_N and m_{BW} are the nucleon and resonance masses, J is the resonance spin, and k_{BW} is the photon c.m. decay momentum. Most earlier analyses have provided these real quantities $A_{1/2}$ and $A_{3/2}$.

More recent studies have quoted related complex quantities, evaluated at the T -matrix pole. These complex helicity amplitudes, $\tilde{A}_{1/2}$ and $\tilde{A}_{3/2}$, can be cast onto the form

$$\tilde{A}_h = \sqrt{\frac{\pi(2J+1)w_{\text{pole}}}{m_N k_{\text{pole}}^2}} \frac{Res(T_h(\gamma N \rightarrow N b))}{\sqrt{Res(T(N b \rightarrow N b))}} \quad (81.3)$$

where the residues (Res) are evaluated at the pole position, w_{pole} , and $k_{\text{pole}}^2 = (w_{\text{pole}}^2 - m_N^2)^2 / 4w_{\text{pole}}^2$ [30]. For Breit-Wigner amplitudes, $w_{\text{pole}} = m_{\text{BW}}$ and $\tilde{A}_h = A_h$. Similar relations for the photo and electro couplings at the pole position can be found in [31, 32].

The determination of eight real numbers from four complex amplitudes (with one overall phase undetermined) requires at least seven independent measurements. At least one further measurement is required to resolve discrete ambiguities that result from the fact that data are proportional to squared amplitudes. Photon beams and nucleon targets can be polarized (with linear or circular polarization P_\perp , P_\odot and \vec{T} , respectively); the recoil polarization of the outgoing baryon \vec{R} can be measured. The experiments can be divided into three classes: (1) the beam and target are polarized (BT); (2) the beam is polarized and the recoil baryon polarization is measured (BR); (3) the target is polarized and the recoil polarization is measured (TR). Different sign conventions are used in the literature, as summarized in [33].

One of the best studied reactions is $\gamma p \rightarrow AK^+$. Published data include differential cross sections, the beam asymmetry Σ , the target asymmetry T , the recoil polarization P , and the BR double-polarization variables $C_{x'}$, $C_{z'}$, $O_{x'}$, and $O_{z'}$. For the photoproduction of pions and etas, off proton and neutron targets, differential cross sections, single- and double-polarization asymmetries have been measured, mainly for pions.

81.6 Electroproduction

Electroproduction of mesons provides information on the internal structure of resonances. The helicity amplitudes are functions of the (squared) momentum transfer $Q^2 = -(e-e')^2$, where e and e' are the 4-momenta of the incident and scattered electron, and a third amplitude, $S_{1/2}$, measures the resonance response to the longitudinal component of the virtual photon. Most data stem from the reactions $e^- p \rightarrow e^- n\pi^+$ and $e^- p \rightarrow e^- p\pi^0$ but also the reactions $e^- p \rightarrow e^- p\eta$, $e^- p \rightarrow e^- p\pi^+\pi^-$, and $e^- p \rightarrow e^- \Lambda(\Sigma^0)K^+$ have been studied. The data and their interpretation are reviewed in Refs. [34, 35].

The transition to the $\Delta(1232)3/2^+$ is often quantified in terms of the magnetic dipole transition moment M_{1+} (or the magnetic transition form factor $G_{M,As}^*(Q^2)$) [36], and the electric and scalar quadrupole transition moments E_{1+} and S_{1+} . Figure 81.1 shows the strength of the $p \rightarrow \Delta^+$ transition plotted versus the photon virtuality Q^2 . At $Q^2 = 0$, M_{1+} dominates the resonance transition strength. The two amplitudes E_{1+} and S_{1+} imply a quadrupole deformation of the transition to the lowest excited state. The magnitude of $R_{EM} = E_{1+}/M_{1+}$ remains nearly constant, while the magnitude of $R_{SM} = S_{1+}/M_{1+}$ increases rapidly up to 25% at the highest Q^2 value.

Figure 81.2 shows the transverse and scalar helicity amplitudes for the $N(1440)1/2^+$, $N(1520)3/2^-$, and $N(1535)1/2^-$ resonances from JLab [34]. Similar results have been achieved at

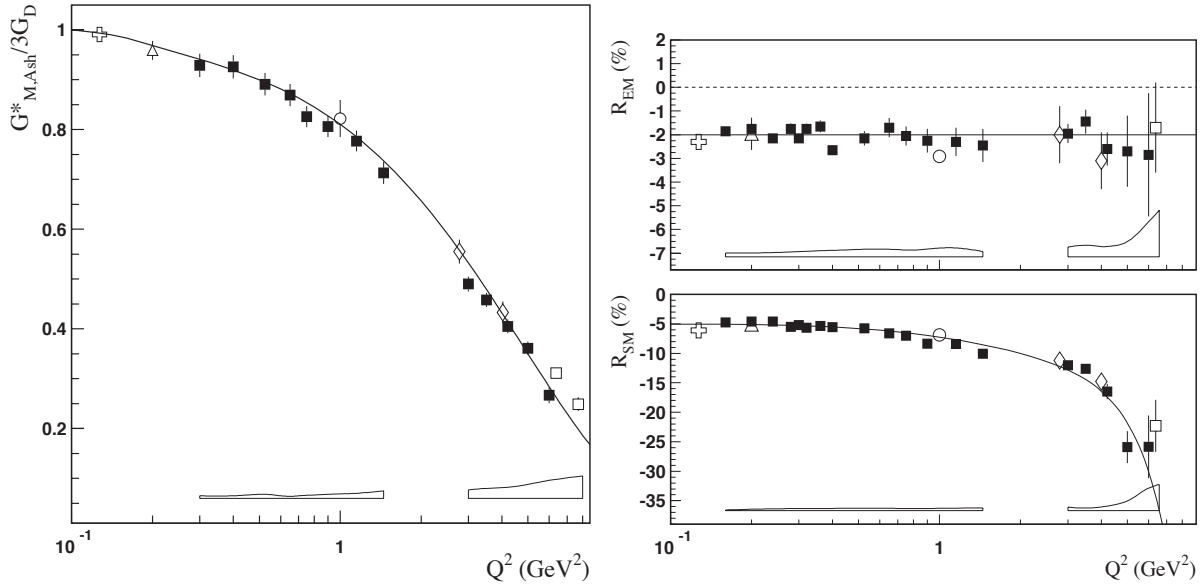


Figure 81.1: Left: The magnetic transition form factor for the $\gamma^* p \rightarrow \Delta^+(1232)$ transition versus the photon virtuality Q^2 . Right: The electric and scalar quadrupole ratios R_{EM} and R_{SM} . The different symbols are results from different experiments at JLab (squares, diamonds) and MAMI (triangle, cross). The boxes near the horizontal axis indicate model uncertainties of the squares. Curves to guide the eyes.

Mainz [35]. For the states $N(1440)1/2^+$ and $N(1520)3/2^-$, helicity amplitudes and $\pi\Delta$ and ρp decays were determined at JLab in an analysis of $\pi^+\pi^-p$ electroproduction [37]. The data show distinctly different Q^2 dependencies that indicate different internal structures.

The $N(1520)3/2^-$ helicity amplitudes reveal the dominance of its three-quark nature: the $A_{3/2}$ amplitude is large at the photon point and decreases rapidly $\sim Q^{-5}$ with increasing Q^2 ; $A_{1/2}$ is small at the photon point, increases rapidly with Q^2 and then falls off with $\sim Q^{-3}$. Quantitative agreement with the data is, however, achieved only when meson cloud effects are included.

At high Q^2 , both amplitudes for $N(1440)1/2^+$ are qualitatively described by light front quark models [38]: at short distances the resonance behaves as expected from a radial excitation of the nucleon. On the other hand, $A_{1/2}$ changes sign at about 0.6 GeV^2 . This remarkable behavior has not been observed before for any nucleon form factor or transition amplitude. Obviously, an important change in the structure occurs when the resonance is probed as a function of Q^2 .

The Q^2 dependence of $A_{1/2}$ of the $N(1535)1/2^-$ resonance exhibits the expected Q^{-3} dependence, except for small Q^2 values where meson cloud effects set in.

Figure 81.3 shows the transverse and scalar amplitudes for three states in the 3rd nucleon resonance region, the $\Delta(1620)1/2^-$, the $N(1675)5/2^-$ and $N(1680)5/2^+$. The latter two states have nearly degenerate masses and are parity partners. In the quark model picture, the transverse amplitudes for $N(1675)5/2^-$ on the proton are suppressed due to the Moorhouse selection rule, allowing for a quantitative evaluation of the meson-baryon contributions. The data show significant meson-baryon strength in the $A_{1/2}$ amplitude even at quite high Q^2 , while $A_{3/2}$ drops much faster with Q^2 . $N(1680)5/2^+$ shows qualitatively the features predicted in constituent quark models, a dominant $A_{3/2}$ at the real photon point that drops rapidly with increasing Q^2 , while $A_{1/2}$ becomes the dominant contribution at high Q^2 , indicating a switch of the helicity structure in the resonance transition at short distances.

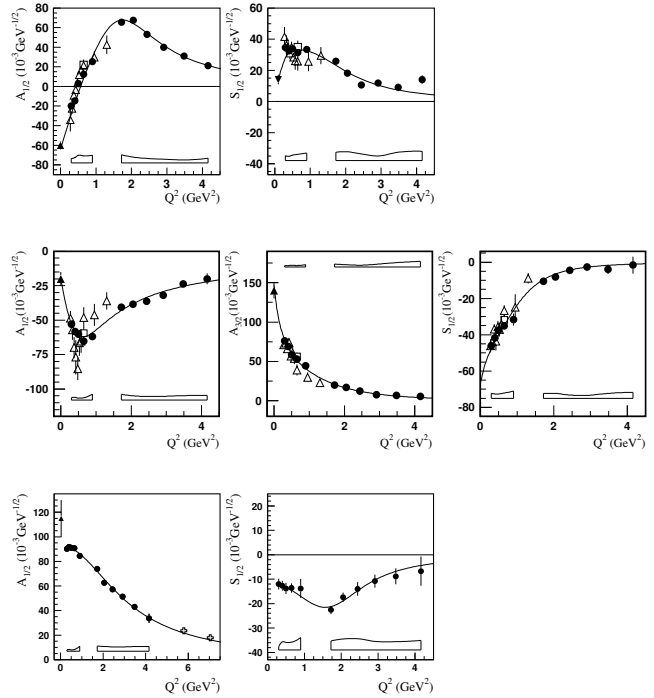


Figure 81.2: Transverse and scalar (longitudinal) helicity amplitudes for $\gamma p \rightarrow N(1440)1/2^+$ (top), $\gamma p \rightarrow N(1520)3/2^-$ (center), and $\gamma p \rightarrow N(1535)1/2^-$ (bottom) as extracted from the JLab/CLAS data in $n\pi^+$ production (full circles), MAMI/A1 data in $p\pi^0$ production (full down triangle), in $p\pi^+\pi^-$ (open triangles), and combined single and double pion production (open squares). The solid triangle is the PDG 2014 value at $Q^2 = 0$. The open boxes are the model uncertainties of the full circles.

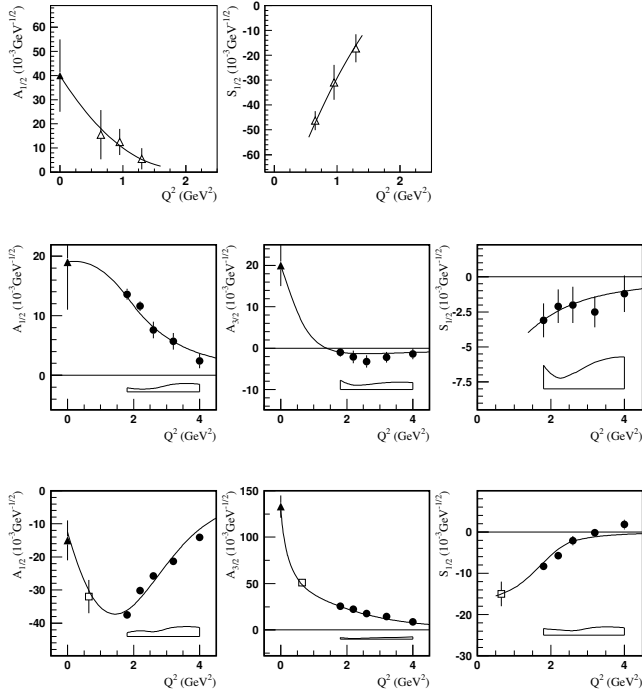


Figure 81.3: Transverse and scalar helicity amplitudes for $\gamma p \rightarrow \Delta(1620)1/2^-$ (top), $\gamma p \rightarrow N(1675)5/2^-$ (center), and $\gamma p \rightarrow N(1680)5/2^+$ (bottom) as extracted from the JLab/CLAS data in $n\pi^+$ production (full circles), $p\pi^+\pi^-$ (open triangles), combined single and double pion production (open square). The solid triangle is the 2014 PDG value at $Q^2 = 0$. The open boxes are the model uncertainties of the full circles. The curves are to guide the eye.

81.7 Partial wave analyses

Several PWA groups are now actively involved in the analysis of the new data. The GWU group maintains a nearly complete database covering reactions from πN and KN elastic scattering to $\gamma N \rightarrow N\pi$, $N\eta$, and $N\eta'$. It is presently the only group determining πN elastic amplitudes from scattering data in sliced energy bins. Given the high-precision of photoproduction data already or soon to be collected, the spectrum of N and Δ resonances will in the near future be better known.

Fits to the data are performed by various groups with the aim to understand the reaction dynamics and to identify N and Δ resonances. For practical reasons, approximations have to be made. We mention several analyses here: (1) The Mainz unitary isobar model [39] focuses on the correct treatment of the low-energy domain. Resonances are added to the unitary amplitude as a sum of Breit-Wigner amplitudes. This model also obtains resonance transition form factors and helicity amplitudes from electroproduction [35]. (2) For $N\pi$ electroproduction, the Yerevan/JLab group uses both the unitary isobar model and the dispersion relation approach developed in [38]. A phenomenological model was developed to extract resonance couplings and partial decay widths from exclusive $\pi^+\pi^-p$ electroproduction [37]. (3) Multichannel analyses using K-matrix parameterizations derive background terms from a chiral Lagrangian - providing a microscopical description of the background - (Giessen [40,41]) or from phenomenology (KSU [42,43], Bonn-Gatchina [44]). (4) Several groups (EBAC-Jlab [45,46], ANL-Osaka [47], Dubna-Mainz-Taipch [48], Bonn-Jülich [49–51], Valencia [52]) use dynamical reaction models, driven by chiral Lagrangians, which take dispersive parts of intermediate states into account. Several other groups have made important contributions. The Giessen group pioneered multichannel analyses of large data sets on pion- and photo-induced reactions [40,41]. The Bonn-Gatchina group included recent high-statistics data and reported systematic searches for new baryon resonances in all relevant partial waves. A summary of their re-

sults can be found in [44].

References

- [1] G. Höhler, Pion-Nucleon Scattering, Landolt-Börnstein Vol. I/9b2 (1983), ed. H. Schopper, Springer Verlag.
- [2] R. E. Cutkosky *et al.*, in “VI International Conference on Baryon Resonances,” 19 (1980), Toronto, ed. N. Isgur.
- [3] R. Arndt *et al.*, Phys. Rev. C **74**, 045205 (2006), [arXiv:nucl-th/0605082].
- [4] “Hadron 2011: 14th International Conference on Hadron Spectroscopy”, München, Germany, June, 13 - 17, 2011, published in eConf.
- [5] “NSTAR 2013: 9th International Workshop on the Physics of Excited Nucleons”, 27-30 May 2013, Peñíscola, Spain.
- [6] E. Klempt and J.-M. Richard, Rev. Mod. Phys. **82**, 1095 (2010), [arXiv:0901.2055].
- [7] V. Crede and W. Roberts, Rept. Prog. Phys. **76**, 076301 (2013), [arXiv:1302.7299].
- [8] M. Roos *et al.* (Particle Data Group), Phys. Lett. B **111**, 1 (1982).
- [9] M. Doring *et al.*, Nucl. Phys. A **829**, 170 (2009), [arXiv:0903.4337].
- [10] N. Suzuki *et al.*, Phys. Rev. Lett. **104**, 042302 (2010), [arXiv:0909.1356].
- [11] R. Cutkosky *et al.*, Phys. Rev. D **20**, 2839 (1979).
- [12] R. Arndt *et al.*, Phys. Rev. C **69**, 035213 (2004), [arXiv:nucl-th/0311089].
- [13] M. Batinić *et al.*, Phys. Rev. C **51**, 2310 (1995), [Erratum: Phys.Rev.C 57, 1004–1005 (1998)], [arXiv:nucl-th/9501011]; M. Batinić *et al.*, Phys. Scr. **58**, 15 (1998).
- [14] A. Anisovich *et al.*, Eur. Phys. J. A **48**, 15 (2012), and references therein., [arXiv:1112.4937].
- [15] G. Höhler, PiN Newslett. **1993**, 9, 1 (1993).
- [16] N. Kelkar and M. Nowakowski, Phys. Rev. A **78**, 012709 (2008), and references therein., [arXiv:0805.0608].
- [17] G. F. Chew and S. Mandelstam, Phys. Rev. **119**, 467 (1960).
- [18] S. Ceci *et al.*, Phys. Rev. D **77**, 116007 (2008), [hep-ph/0609236].
- [19] P. Masjuan and J. J. Sanz-Cillero, Eur. Phys. J. C **73**, 2594 (2013), [arXiv:1306.6308].
- [20] A. Švarc *et al.*, Phys. Rev. C **88**, 3, 035206 (2013), [arXiv:1307.4613].
- [21] A. Švarc *et al.*, Phys. Rev. C **89**, 4, 045205 (2014), [arXiv:1401.1947].
- [22] A. Švarc *et al.*, Phys. Lett. B **755**, 452 (2016), [arXiv:1512.07403].
- [23] A. Švarc *et al.*, Phys. Rev. C **89**, 6, 065208 (2014), [arXiv:1404.1544].
- [24] A. Švarc *et al.*, Phys. Rev. C **91**, 1, 015207 (2015), [arXiv:1405.6474].
- [25] L. Tiator *et al.*, Phys. Rev. C **94**, 6, 065204 (2016), [arXiv:1606.00371].
- [26] A. Anisovich *et al.*, Eur. Phys. J. A **53**, 12, 242 (2017), [arXiv:1712.07537].
- [27] A. Anisovich *et al.*, Phys. Rev. Lett. **119**, 6, 062004 (2017), [arXiv:1712.07549].
- [28] C. Fasano, F. Tabakin and B. Saghai, Phys. Rev. C **46**, 2430 (1992).
- [29] G. Chew *et al.*, Phys. Rev. **106**, 1345 (1957).
- [30] R. Workman, L. Tiator and A. Sarantsev, Phys. Rev. C **87**, 6, 068201 (2013), [arXiv:1304.4029].
- [31] N. Suzuki, T. Sato and T.-S. Lee, Phys. Rev. C **82**, 045206 (2010), [arXiv:1006.2196].
- [32] H. Kamano, Phys. Rev. C **88**, 045203 (2013), [arXiv:1305.6678].

- [33] A. Sandorfi *et al.*, AIP Conf. Proc. **1432**, 1, 219 (2012), [arXiv:1108.5411].
- [34] I. Aznauryan and V. Burkert, Prog. Part. Nucl. Phys. **67**, 1 (2012), [arXiv:1109.1720].
- [35] L. Tiator *et al.*, Eur. Phys. J. ST **198**, 141 (2011), [arXiv:1109.6745]; S. Štajner *et al.*, Phys. Rev. Lett. **119**, 2, 022001 (2017).
- [36] W. Ash *et al.*, Phys. Lett. B **24**, 165 (1967).
- [37] V. Mokeev *et al.* (CLAS), Phys. Rev. C **86**, 035203 (2012), [arXiv:1205.3948].
- [38] I. Aznauryan, Phys. Rev. C **67**, 015209 (2003), [arXiv:nucl-th/0206033].
- [39] D. Drechsel, S. Kamalov and L. Tiator, Eur. Phys. J. A **34**, 69 (2007), [arXiv:0710.0306].
- [40] G. Penner and U. Mosel, Phys. Rev. C **66**, 055211 (2002), [arXiv:nucl-th/0207066].
- [41] G. Penner and U. Mosel, Phys. Rev. C **66**, 055212 (2002), [arXiv:nucl-th/0207069].
- [42] D. Manley and E. Saleski, Phys. Rev. D **45**, 4002 (1992).
- [43] M. Shrestha and D. Manley, Phys. Rev. C **86**, 055203 (2012), [arXiv:1208.2710].
- [44] A. Anisovich *et al.*, Eur. Phys. J. A **48**, 15 (2012), [arXiv:1112.4937].
- [45] A. Matsuyama, T. Sato and T.-S. Lee, Phys. Rept. **439**, 193 (2007), [arXiv:nucl-th/0608051].
- [46] T. Sato and T.-S. Lee, J. Phys. G **36**, 073001 (2009), [arXiv:0902.3653].
- [47] H. Kamano *et al.*, Phys. Rev. C **88**, 3, 035209 (2013), [arXiv:1305.4351].
- [48] G. Y. Chen *et al.*, Phys. Rev. C **76**, 035206 (2007), [arXiv:nucl-th/0703096].
- [49] M. Doring *et al.*, Phys. Lett. B **681**, 26 (2009), [arXiv:0903.1781].
- [50] M. Doring *et al.*, Nucl. Phys. A **829**, 170 (2009), [arXiv:0903.4337].
- [51] D. Ronchen *et al.*, Eur. Phys. J. A **49**, 44 (2013), [arXiv:1211.6998].
- [52] S. Sarkar, E. Oset and M. Vicente Vacas, Nucl. Phys. A **750**, 294 (2005), [Erratum: Nucl.Phys.A 780, 90–90 (2006)], [arXiv:nucl-th/0407025].

82. Λ and Σ Resonances

Revised August 2021 by V.D. Burkert (Jefferson Lab), V. Crede (Florida State U.), E. Klempt (Bonn U.), U. Thoma (Bonn U.), L. Tiator (KPH, JGU Mainz) and R.L. Workman (George Washington U.).

82.1 Introduction

For several decades, there has been very little new experimental data bearing on the properties of Λ and Σ resonances. An exception was the study at JLab of the reactions $\gamma p \rightarrow K^+ \Sigma^\pm \pi^\mp$ and $\gamma p \rightarrow K^+ \Sigma^0 \pi^0$ [1], which established the spin and parity of the $\Lambda(1405)$ [2]. There was also from BNL new data on the very low energy region of $K^- p$ scattering [3–7]. Otherwise, the field is starved for data. Recent analyses (see below) have improved what we know about the *properties* of the known Λ and Σ resonances, but the *established* resonances are the same ones that were listed in our 1984 edition [8] except for the $\Sigma(2250)$ which we consider 2-star only due to its unknown spin-parity. The 1990 Review [9] gave a full report of the status of Lambda and Sigma hyperons, and included Argand plots from the partial-wave analyses. The 2018 Review [10] has a short survey of the $\Sigma(1670)$ -region.

In the last few years, four groups have re-analyzed $K^- p$ reactions using more extensive collections of the old data. These analyses justify an update of the status of the Λ and Σ resonances. Although they have not established any new resonances, they have provided at least some evidence for new states and have given a better understanding of the old ones.

Tables 82.1 and 82.2 give our evaluation of the status, both overall and channel by channel, of each Λ and Σ resonance in the Particle Listings. In making these evaluations, we considered, in addition to the four analyses [11–14], the ratings that predated them. The ratings use a 1- to 4-star system. For more details on the evaluation of the overall star ratings, see [15]. The main Summary Table includes only established states with an overall status of 3 or 4 stars; as has already been noted, these are the same fourteen Λ resonances (including $\Lambda(1116)$) and nine Σ resonances instead of the former ten (including $\Sigma(1193)3/2^+$, and $\Sigma(1385)3/2^+$) that had long been in the Table. In addition, there are seven 1-star and two 2-star Λ 's, and fourteen 1-star and three 2-star Σ 's in the Particle Listings.

82.2 New analyses

The new analysis progress was pioneered by the Kent group which collected a large fraction of the available data and performed a comprehensive partial wave analysis [11, 16]. $K^- p$ scattering into a pseudoscalar meson and an octet baryon is governed by two complex amplitudes; hence four quantities need to be measured to fully construct the amplitudes (up to an arbitrary phase per energy and angular bin). Discussions of complete experiments also generally assume perfect data (no experimental uncertainties); realistic uncertainties further complicate the task of amplitude extraction. Here, the available data are limited to the differential cross section and the target or hyperon recoil polarization P ; data on the polarization transfer do not exist. The authors of Ref. [16] overcame this difficulty by using start values for the partial wave amplitudes determined in [17] and/or from an energy-dependent fit and by freezing or releasing sets of amplitudes. The resulting amplitudes were fitted with a unitary multichannel parameterization [11].

The JPAC group presented a coupled-channel fit to the $\bar{K}N$ partial waves derived by the Kent group [13]. The JPAC approach was based on the K -matrix formalism. Special attention was paid to the analytical properties of the amplitudes determined by the square-root unitary branch points and the continuation to the complex angular momentum plane. The fit described the Kent partial waves reasonably well. However, when observables were calculated from their partial-wave amplitudes, significant discrepancies became apparent. The results were therefore not included in the RPP.

The ANL-Osaka group derived the energy-dependent amplitudes in fits to a large subset of the data collected in Ref. [16] and further data sets described in Ref. [18]. Their fits were based on

a phenomenological SU(3) Lagrangian [18]. The two ANL-Osaka models agree on the leading contributions but differ significantly in cases with weaker candidates [12].

Table 82.1: The status of the Λ resonances. Only those with an overall status of *** or **** are included in the main Baryon Summary Table. Decay channels other than $N\bar{K}$ and $\Sigma\pi$ are only given for *** and **** resonances.

Particle	J^P	Overall status	Status as seen in —		
			$N\bar{K}$	$\Sigma\pi$	Other channels
$\Lambda(1116)$	$1/2^+$	****			$N\pi$ (weak decay)
$\Lambda(1380)$	$1/2^-$	**	**	**	
$\Lambda(1405)$	$1/2^-$	****	****	****	
$\Lambda(1520)$	$3/2^-$	****	****	****	$\Lambda\pi\pi, \Lambda\gamma, \Sigma\pi\pi$
$\Lambda(1600)$	$1/2^+$	****	***	****	$\Lambda\pi\pi, \Sigma(1385)\pi$
$\Lambda(1670)$	$1/2^-$	****	****	****	$\Lambda\eta$
$\Lambda(1690)$	$3/2^-$	****	****	**	$\Lambda\pi\pi, \Sigma(1385)\pi$
$\Lambda(1710)$	$1/2^+$	*	*	*	
$\Lambda(1800)$	$1/2^-$	***	***	**	$\Lambda\pi\pi, N\bar{K}^*$
$\Lambda(1810)$	$1/2^+$	***	**	**	$N\bar{K}^*$
$\Lambda(1820)$	$5/2^+$	****	****	****	$\Sigma(1385)\pi$
$\Lambda(1830)$	$5/2^-$	****	****	****	$\Sigma(1385)\pi$
$\Lambda(1890)$	$3/2^+$	****	****	**	$\Sigma(1385)\pi, N\bar{K}^*$
$\Lambda(2000)$	$1/2^-$	*	*	*	
$\Lambda(2050)$	$3/2^-$	*	*	*	
$\Lambda(2070)$	$3/2^+$	*	*	*	
$\Lambda(2080)$	$5/2^-$	*	*	*	
$\Lambda(2085)$	$7/2^+$	**	**	*	
$\Lambda(2100)$	$7/2^-$	****	****	**	$N\bar{K}^*$
$\Lambda(2110)$	$5/2^+$	***	**	**	$N\bar{K}^*$
$\Lambda(2325)$	$3/2^-$	*	*		
$\Lambda(2350)$	$9/2^+$	***	***	*	
$\Lambda(2585)$		*	*		

The Bonn-Gatchina (BnGa) group added further (old) data to those analyzed in Ref. [16]. The data set was fitted in a modified K -matrix approach and the resulting amplitudes were compared with those from Refs. [16, 18]. New resonances were found, other states, mostly one and two-star states could not be confirmed; all resonances were tested for their statistical significance. Additional states with any set of quantum numbers were tested and were found to produce only small improvements in the fit [14]. In Ref. [19], properties of the full set of contributing hyperons were reported.

The star ratings of Λ and Σ resonances given in our earlier editions, and the new results from the Kent, ANL-Osaka and BnGa groups were used to update the star rating of the hyperon resonances. In [19], the overall star rating is directly estimated, for [11] we estimate the star rating from the branching-ratio uncertainties. In [12], two solutions are given but no uncertainties for branching ratios. The overall star ratings are based on the evidence for the resonances in the new analyses as well as their consistency including also the results of earlier analyses given in [20]. For further details see also [15].

We decided to remove the three so-called *bumps* $\Sigma(1480)$, $\Sigma(1560)$, $\Sigma(1670)$, and $\Sigma(1690)$ as well as $\Sigma(1620)$ from production experiments. The entries from $\Sigma(1770)1/2^+$ are now listed under $\Sigma(1660)1/2^+$ and $\Sigma(1880)1/2^+$, the entries from $\Sigma(1730)3/2^+$ and $\Sigma(1840)3/2^+$ are now combined to one $\Sigma(1780)3/2^+$. The one-star $\Sigma(2000)1/2^-$ is combined with a new one-star $\Sigma(2160)1/2^-$ to a single one-star $\Sigma(2110)1/2^-$. Apart from $\Lambda(1380)1/2^-$, four further new resonances were included in the Listings: $\Lambda(2070)3/2^+$, $\Lambda(2080)5/2^-$, $\Sigma(2010)3/2^-$, and $\Sigma(2230)3/2^+$, all with one star.

Table 82.2: The status of the Σ resonances. Only those with an overall status of *** or **** are included in the main Baryon Summary Table. Decay channels other than $N\bar{K}$, $\Lambda\pi$ and $\Sigma\pi$ are only given for *** and **** resonances.

Particle	J^P	Overall status	Status as seen in —			Other channels
			$N\bar{K}$	$\Lambda\pi$	$\Sigma\pi$	
$\Sigma(1193)$	$1/2^+$	****				$N\pi$ (weak decay)
$\Sigma(1385)$	$3/2^+$	****				$\Lambda\gamma$
$\Sigma(1580)$	$3/2^-$	*	*	*	*	
$\Sigma(1620)$	$1/2^-$	*	*	*	*	
$\Sigma(1660)$	$1/2^+$	***	***	***	***	
$\Sigma(1670)$	$3/2^-$	****	****	****	****	
$\Sigma(1750)$	$1/2^-$	***	***	**	***	$\Sigma\eta$
$\Sigma(1775)$	$5/2^-$	****	****	****	**	
$\Sigma(1780)$	$3/2^+$	*	*	*	*	
$\Sigma(1880)$	$1/2^+$	**	**	*		
$\Sigma(1900)$	$1/2^-$	**	**	*	**	
$\Sigma(1910)$	$3/2^-$	***	*	*	**	
$\Sigma(1915)$	$5/2^+$	****	***	***	***	
$\Sigma(1940)$	$3/2^+$	*	*		*	
$\Sigma(2010)$	$3/2^-$	*	*	*		
$\Sigma(2030)$	$7/2^+$	****	****	****	**	$\Delta(1232)\bar{K}, N\bar{K}^*, \Sigma(1385)\pi$
$\Sigma(2070)$	$5/2^+$	*	*		*	
$\Sigma(2080)$	$3/2^+$	*		*		
$\Sigma(2100)$	$7/2^-$	*	*	*	*	
$\Sigma(2110)$	$1/2^-$	*	*	*	*	
$\Sigma(2230)$	$3/2^+$	*	*	*	*	
$\Sigma(2250)$		**	**	*	*	
$\Sigma(2455)$		*	*			
$\Sigma(2620)$		*	*			
$\Sigma(3000)$		*	*	*		
$\Sigma(3170)$		*				

82.3 Sign conventions for resonance couplings

In terms of the isospin-0 and isospin-1 elastic scattering amplitudes A_0 and A_1 , the amplitude for $K^-p \rightarrow \bar{K}^0 n$ scattering is $\pm(A_1 - A_0)/2$, where the sign depends on conventions used in conjunction with the Clebsch-Gordan coefficients (such as, is the baryon or the meson the “first” particle). If this reaction is partial-wave analyzed and if the overall phase is chosen so that, say, the $\Sigma(1775)5/2^- (D_{15})$ amplitude at resonance points along the positive imaginary axis (points “up”), then any Σ at resonance will point “up” and any Λ at resonance will point “down” (along the negative imaginary axis). Thus the phase at resonance determines the isospin. The above ignores background amplitudes in the resonating partial waves.

That is the basic idea. In a similar but somewhat more complicated way, the phases of the $\bar{K}N \rightarrow \Lambda\pi$ and $\bar{K}N \rightarrow \Sigma\pi$ amplitudes for a resonating wave help determine the SU(3) multiplet to which the resonance belongs. Again, a convention has to be adopted for some overall arbitrary phases: which way is “up”? Our convention is that of Levi-Setti [21] and is shown in Fig. 82.1, which also compares experimental results with theoretical predictions for the signs of several resonances. In the Listings, a + or – sign in front of a measurement of an inelastic resonance coupling indicates the sign (the *absence* of a sign means that the sign is not determined, *not* that it is positive). Also other decay modes can be used to assign a hyperon to a SU(3) multiplet [22, 23]. Modern analyses determine properties of resonances at the pole position. In these analyses, the + or – sign is replaced by a phase. Background amplitudes can lead to significant phase shifts, and an additional phase shift due to rescattering is admitted in some analyses. In comparison to quark model predictions [19, 24], three Λ spin doublets can be identified as being mainly SU(3) singlets: the well-known ($\Lambda(1405)1/2^-$, $\Lambda(1520)3/2^-$), the ($\Lambda(2080)5/2^-$, $\Lambda(2100)7/2^-$), and ($\Lambda(2070)3/2^+$, $\Lambda(2110)5/2^+$).

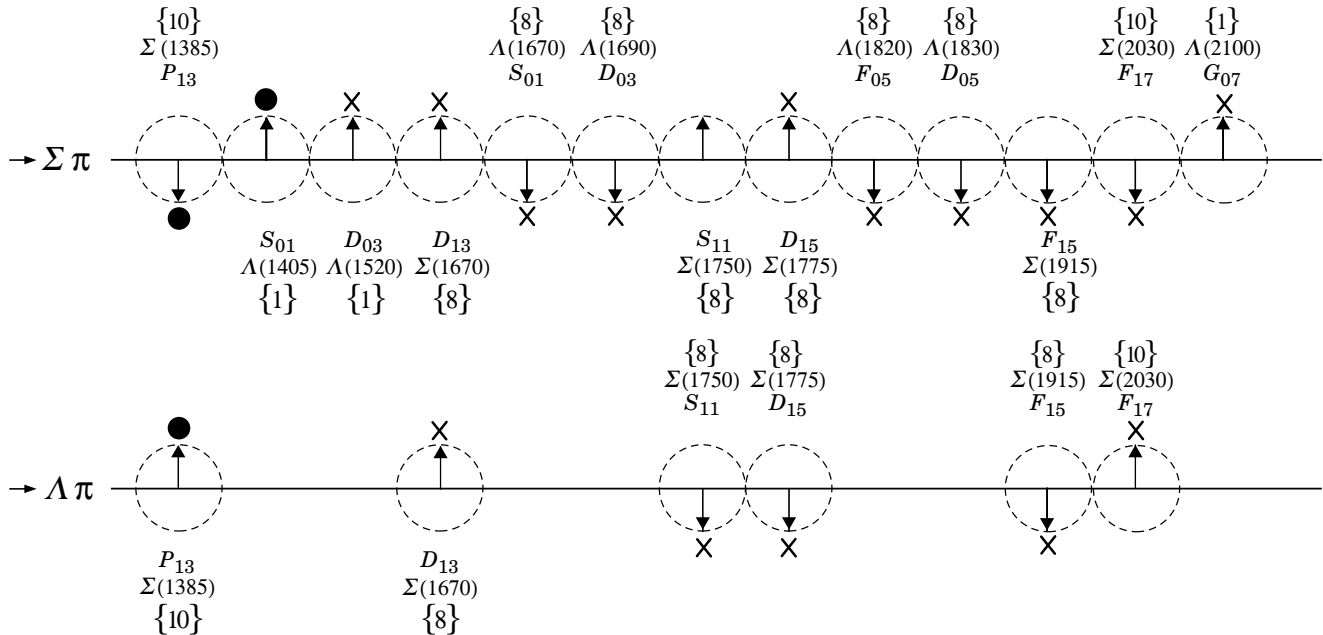


Figure 82.1: The signs of the imaginary parts of resonating amplitudes in the $\bar{K}N \rightarrow \Lambda\pi$ and $\Sigma\pi$ channels. The signs of the $\Sigma(1385)$ and $\Lambda(1405)$, marked with a •, are set by convention, and then the others are determined relative to them. The signs required by the SU(3) assignments of the resonances are shown with an arrow, and the experimentally determined signs are shown with an X.

82.4 The $\Lambda(1405)$

In coupled-channels calculations based on the chiral SU(3) effective field theory, the strongly attractive forces between $N\bar{K}$

and $\Sigma\pi$ generate five poles, one SU(3) singlet pole, two Λ octet poles and two (or one) octet Σ poles (see Section 83). In quark models, these five states are $\Lambda(1405)$, $\Lambda(1670)$, $\Lambda(1800)$, $\Sigma(1620)$,

and $\Sigma(1750)$. The octet states are found 100 to 150 MeV above the corresponding nucleon resonances. In chiral SU(3) effective field theories, at least three of these states are seen in the 1300 to 1600 MeV mass range. The appearance of two Λ poles in this mass range, a narrow SU(3) octet at ~ 1420 MeV and a wider SU(3) singlet at ~ 1380 MeV, was unexpected. This approach has been pursued by a number of groups; for a summary of the results see our Review 83, “Pole Structure of the $\Lambda(1405)$ Region”. In the Listings, we have introduced the $\Lambda(1380)$ as a new candidate resonance (with two stars), named in accordance with its approximate pole position. The second SU(3) octet Λ state is the well-known $\Lambda(1670)$. The masses of the two associated Σ states are uncertain so far, and no new entries are introduced in the Listings.

In traditional approaches only one resonance was seen in this mass region, the narrow state at 1405 MeV. It was reported to be the SU(3) singlet state a long time ago in Ref. [25], in agreement with the quark-model expectations but in contrast to the findings based on coupled-channels calculations within chiral SU(3) effective field theories. In the Listings, the $\Lambda(1405)$ has been retained with its traditional name. In quark models, this state is identified with the SU(3) singlet state, the two Λ octet states with $\Lambda(1670)$ and $\Lambda(1800)$, and the two Σ states with $\Sigma(1620)$ and $\Sigma(1750)$.

82.5 Uncertainties on masses and widths

The uncertainties quoted on resonance parameters from partial-wave analyses are often only statistical, and the parameters can change beyond these uncertainties when a different parametrization of the waves is used. Furthermore, the different analyses use more or less the same data, so it is not really appropriate to treat the different determinations of the resonance parameters as independent or to average them. In any case, the spread of the masses, widths, and branching fractions from the different analyses is certainly a better indication of the uncertainties than are the quoted uncertainties. In the Listings, we usually give a range reflecting the spread of the values rather than a particular value with error.

82.6 Production experiments

Partial-wave analyses of course separate partial waves, whereas a peak in a cross section or an invariant mass distribution usually cannot be disentangled from background and analyzed for its quantum numbers; and more than one resonance may be contributing to the peak. The $\Sigma(1385)$ and $\Lambda(1405)$ lie below the $\bar{K}N$ threshold and nearly everything about $\Sigma(1385)$ is learned from production experiments. Our knowledge on $\Lambda(1405)$ benefits greatly from photoproduction of the three $\Sigma\pi$ charge states [1, 2] and from the precise measurement of the energy shift and width of the kaonic hydrogen atom [26].

Production and formation experiments agree quite well in the case of $\Lambda(1520)$ and results have been combined. Above this mass, no new results on peak hunting have been reported for about 40 years. For these early results, we refer the reader to our earlier editions. In photoproduction with energetic photons [27, 28] or at LHCb [29], hyperons are produced abundantly. So far, no attempt has been made to extract hyperon properties from these data. New data on hyperon spectroscopy can be expected from J-PARC [30], JLAB [31], and the forthcoming PANDA experiment [32].

References

- [1] K. Moriya *et al.* (CLAS), Phys. Rev. **C87**, 3, 035206 (2013), [arXiv:1301.5000].
- [2] K. Moriya *et al.* (CLAS), Phys. Rev. Lett. **112**, 8, 082004 (2014), [arXiv:1402.2296].
- [3] A. Starostin *et al.* (Crystal Ball), Phys. Rev. **C64**, 055205 (2001).
- [4] S. Prakhov *et al.*, Phys. Rev. **C69**, 042202 (2004).
- [5] S. Prakhov *et al.* (Crystal Ball), Phys. Rev. **C70**, 034605 (2004).
- [6] R. Manweiler *et al.*, Phys. Rev. **C77**, 015205 (2008).
- [7] S. Prakhov *et al.*, Phys. Rev. **C80**, 025204 (2009), [arXiv:0812.1888].
- [8] C. G. Wohl *et al.* (Particle Data Group), Rev. Mod. Phys. **56**, S1 (1984).
- [9] J. J. Hernandez *et al.* (Particle Data Group), Phys. Lett. **B239**, 1 (1990), [Erratum: Phys. Lett. B253,524(1991)].
- [10] M. Tanabashi *et al.* (Particle Data Group), Phys. Rev. **D98**, 3, 030001 (2018).
- [11] H. Zhang *et al.*, Phys. Rev. **C88**, 3, 035205 (2013), [arXiv:1305.4575].
- [12] H. Kamano *et al.*, Phys. Rev. **C92**, 2, 025205 (2015), [Erratum: Phys. Rev. C95, no.4, 049903(2017)], [arXiv:1506.01768].
- [13] C. Fernandez-Ramirez *et al.*, Phys. Rev. **D93**, 3, 034029 (2016), [arXiv:1510.07065].
- [14] M. Matveev *et al.*, Eur. Phys. J. **A55**, 10, 179 (2019), [arXiv:1907.03645].
- [15] E. Klempt *et al.* (Baryon@PDG Group), Eur. Phys. J. A **56**, 10, 261 (2020), [arXiv:2007.04232].
- [16] H. Zhang *et al.*, Phys. Rev. **C88**, 3, 035204 (2013), [arXiv:1305.3598].
- [17] J. Tulpan, PhD Dissertation, Kent State University (2007).
- [18] H. Kamano *et al.*, Phys. Rev. **C90**, 6, 065204 (2014), [arXiv:1407.6839].
- [19] A. V. Sarantsev *et al.*, Eur. Phys. J. **A55**, 10, 180 (2019), [arXiv:1907.13387].
- [20] J. Beringer *et al.* (Particle Data Group), Phys. Rev. **D86**, 010001 (2012).
- [21] R. Levi Setti, Conf. Proc. **C690625**, 339 (1969).
- [22] V. Guzey and M. V. Polyakov, Annalen Phys. **13**, 673 (2004).
- [23] V. Guzey and M. V. Polyakov (2005), [hep-ph/0512355].
- [24] U. Loring, B. C. Metsch and H. R. Petry, Eur. Phys. J. **A10**, 447 (2001), [hep-ph/0103290].
- [25] R. D. Tripp *et al.*, Phys. Rev. Lett. **21**, 1721 (1968).
- [26] M. Bazzi *et al.* (SIDDHARTA), Phys. Lett. **B704**, 113 (2011), [arXiv:1105.3090].
- [27] K. Moriya *et al.* (CLAS), Phys. Rev. **C88**, 045201 (2013), [Addendum: Phys. Rev. C88, no.4, 049902(2013)], [arXiv:1305.6776].
- [28] B. Dey *et al.* (CLAS), Phys. Rev. **C89**, 5, 055208 (2014), [Addendum: Phys. Rev. C90, no.1, 019901(2014)], [arXiv:1403.2110].
- [29] R. Aaij *et al.* (LHCb), Phys. Rev. Lett. **115**, 072001 (2015), [arXiv:1507.03414].
- [30] K. Hicks and H. Sako, Proposal for J-PARC E45.
- [31] M. Amarian *et al.* (KLF) (2020), [arXiv:2008.08215].
- [32] F. Iazzi (PANDA), AIP Conf. Proc. **1743**, 1, 050006 (2016).

83. Pole Structure of the $\Lambda(1405)$ Region

Revised June 2021 by T. Hyodo (Tokyo Metropolitan U.) and U.-G. Meißner (Bonn U.; FZ Jülich).

The $\Lambda(1405)$ resonance emerges in the meson-baryon scattering amplitude with the strangeness $S = -1$ and isospin $I = 0$. It is the archetype of what is called a dynamically generated resonance, as pioneered by Dalitz and Tuan [1]. The most powerful and systematic approach for the low-energy regime of the strong interactions is chiral perturbation theory (ChPT), see e.g. Ref. [2]. A perturbative calculation is, however, not applicable to this sector because of the existence of the $\Lambda(1405)$ just below the $\bar{K}N$ threshold. In this case, ChPT has to be combined with a non-perturbative resummation technique, just as in the case of the nuclear forces. By solving the Lippmann-Schwinger equation with the interaction kernel determined by ChPT and using a particular regularization, in Ref. [3] a successful description of the low-energy K^-p scattering data as well as the mass distribution of the $\Lambda(1405)$ was achieved (for further developments, see Ref. [4–7] and references therein).

The study of the pole structure was initiated by Ref. [8], which finds two poles of the scattering amplitude in the complex energy plane between the $\bar{K}N$ and $\pi\Sigma$ thresholds. The spectrum in experiments exhibits one effective resonance shape, while the existence of two poles results in the reaction-dependent lineshape [9]. The origin of this two-pole structure is attributed to the two attractive channels of the leading order interaction in the SU(3) basis (singlet and octet) [9] and in the isospin basis ($\bar{K}N$ and $\pi\Sigma$) [10]. It is remarkable that the sign and the strength of the leading order interaction is determined by a low-energy theorem of chiral symmetry, i.e. the so-called Weinberg-Tomozawa term. The two-pole nature of the $\Lambda(1405)$ is qualitatively different from the case of the N(1440) resonance. Two poles of the N(1440) appear on different Riemann sheets of the complex energy plane separated by the $\pi\Delta$ branch point. These poles reflect a single state, with a nearby pole and a more distant shadow pole. In contrast, the two poles in the $\Lambda(1405)$ region on the same Riemann sheet (where $\pi\Sigma$ channels are unphysical and all other channels physical, correspondingly to the one, connected to the real axis between the $\pi\Sigma$ and $\bar{K}N$ thresholds) are generated from two attractive forces mentioned above [9, 10].

Recently, various new experimental results on the $\Lambda(1405)$ have become available [4]. Among these, the most striking measurement is the precise determination of the energy shift and width of kaonic hydrogen by the SIDDHARTA collaboration [11, 12], which provides a quantitative and stringent constraint on the K^-p amplitude at threshold through the improved Deser formula [13]. Systematic studies with error analyses based on the next-to-leading order ChPT interaction including the SIDDHARTA constraint have been performed by various groups [14–18]. All these studies confirm that the new kaonic hydrogen data are compatible with the scattering data above threshold.

The results of the pole positions of $\Lambda(1405)$ in the various approaches are summarized in Table 83.1. We may regard the difference among the calculations as a systematic error, which stems from the various approximations of the Bethe-Salpeter equation, the fitting procedure, and also the inclusion of SU(3) breaking effects such as the choice of the various meson decay constants, and so on. A detailed comparison of the various approaches that enter the table is given in Ref. [19]. A recent analysis including also the $J^P = 1/2^+$ P-wave contribution (and also an explicit $\Sigma(1385)$ $3/2^+$ state) gives results consistent with the findings reported above, with the pole positions at $(1364 - i43)$ MeV and $(1430 - i15)$ MeV, respectively [20].

The main component for the $\Lambda(1405)$ is the pole 1, whose position converges within a relatively small region near the $\bar{K}N$ threshold. On the other hand, the position of the pole 2 shows a sizeable scatter. Detailed studies of the $\pi\Sigma$ spectrum in various reaction processes, together with the precise experimental lineshape (see e.g. the recent precise photoproduction data from the LEPS collaboration [21] and from the CLAS collaboration [22, 23], electroproduction data from the CLAS collaboration [24], and proton-proton collision data from COSY [25] and the HADES collaboration [26]), will shed light on the position of the second pole.

The $\pi\Sigma$ spectra from the CLAS data are analyzed in Ref. [27] and Ref. [18]. It was shown in Ref. [18] that several solutions, which agree with the scattering data, are ruled out if confronted with the recent CLAS data. The remaining solutions are collected as solution #2 and solution #4 in Table 83.1. The HADES data are analyzed in Ref. [28] and Ref. [29]. Although the result of the pole found in Ref. [28] is not compatible with other results, the authors of Ref. [29] invoke the anomalous triangle singularity mechanism to argue that the invariant mass distribution of the $\pi\Sigma$ system is found at lower masses than in other reactions. It is thus desirable to perform more comprehensive analyses of $\pi\Sigma$ spectra together with the systematic error analysis of the scattering data.

Table 83.1: Comparison of the pole positions of $\Lambda(1405)$ in the complex energy plane from next-to-leading order chiral unitary coupled-channel approaches including the SIDDHARTA constraint. The lower two results also include the CLAS photoproduction data.

approach	pole 1 [MeV]	pole 2 [MeV]
Refs. [14, 15], NLO	$1424_{-23}^{+7} - i 26_{-14}^{+3}$	$1381_{-6}^{+18} - i 81_{-8}^{+19}$
Ref. [17], Fit II	$1421_{-2}^{+3} - i 19_{-5}^{+8}$	$1388_{-9}^{+9} - i 114_{-25}^{+24}$
Ref. [18], solution #2	$1434_{-2}^{+2} - i 10_{-1}^{+2}$	$1330_{-5}^{+4} - i 56_{-11}^{+17}$
Ref. [18], solution #4	$1429_{-7}^{+8} - i 12_{-3}^{+2}$	$1325_{-15}^{+15} - i 90_{-18}^{+12}$

References

- [1] R. Dalitz and S. Tuan, Phys. Rev. Lett. **2**, 425 (1959).
- [2] V. Bernard, N. Kaiser and U.-G. Meißner, Int. J. Mod. Phys. E **4**, 193 (1995), [hep-ph/9501384].
- [3] N. Kaiser, P. Siegel and W. Weise, Nucl. Phys. A **594**, 325 (1995), [arXiv:nucl-th/9505043].
- [4] T. Hyodo and D. Jido, Prog. Part. Nucl. Phys. **67**, 55 (2012), [arXiv:1104.4474].
- [5] U.-G. Meißner, Symmetry **12**, 6, 981 (2020), [arXiv:2005.06909].
- [6] M. Mai, Eur. Phys. J. ST **230**, 6, 1593 (2021), [arXiv:2010.00056].
- [7] T. Hyodo and M. Niiyama, Prog. Part. Nucl. Phys. **120**, 103868 (2021), [arXiv:2010.07592].
- [8] J. Oller and U.-G. Meißner, Phys. Lett. B **500**, 263 (2001), [hep-ph/0011146].
- [9] D. Jido *et al.*, Nucl. Phys. A **725**, 181 (2003), [arXiv:nucl-th/0303062].
- [10] T. Hyodo and W. Weise, Phys. Rev. C **77**, 035204 (2008), [arXiv:0712.1613].
- [11] M. Bazzi *et al.* (SIDDHARTA), Phys. Lett. B **704**, 113 (2011), [arXiv:1105.3090].
- [12] M. Bazzi *et al.* (SIDDHARTA), Nucl. Phys. A **881**, 88 (2012), [arXiv:1201.4635].
- [13] U.-G. Meißner, U. Raha and A. Rusetsky, Eur. Phys. J. C **35**, 349 (2004), [hep-ph/0402261].
- [14] Y. Ikeda, T. Hyodo and W. Weise, Phys. Lett. B **706**, 63 (2011), [arXiv:1109.3005].
- [15] Y. Ikeda, T. Hyodo and W. Weise, Nucl. Phys. A **881**, 98 (2012), [arXiv:1201.6549].
- [16] M. Mai and U.-G. Meißner, Nucl. Phys. A **900**, 51 (2013), [arXiv:1202.2030].
- [17] Z.-H. Guo and J. Oller, Phys. Rev. C **87**, 3, 035202 (2013), [arXiv:1210.3485].
- [18] M. Mai and U.-G. Meißner, Eur. Phys. J. A **51**, 3, 30 (2015), [arXiv:1411.7884].
- [19] A. Cieplý *et al.*, Nucl. Phys. A **954**, 17 (2016), [arXiv:1603.02531].
- [20] D. Sadasivan, M. Mai and M. Döring, Phys. Lett. B **789**, 329 (2019), [arXiv:1805.04534].

-
- [21] M. Niyama *et al.*, Phys. Rev. C **78**, 035202 (2008), [arXiv:0805.4051].
- [22] K. Moriya *et al.* (CLAS), Phys. Rev. C **87**, 3, 035206 (2013), [arXiv:1301.5000].
- [23] K. Moriya *et al.* (CLAS), Phys. Rev. Lett. **112**, 8, 082004 (2014), [arXiv:1402.2296].
- [24] H. Lu *et al.* (CLAS), Phys. Rev. C **88**, 045202 (2013), [arXiv:1307.4411].
- [25] I. Zychor *et al.*, Phys. Lett. B **660**, 167 (2008), [arXiv:0705.1039].
- [26] G. Agakishiev *et al.* (HADES), Phys. Rev. C **87**, 025201 (2013), [arXiv:1208.0205].
- [27] L. Roca and E. Oset, Phys. Rev. C **87**, 5, 055201 (2013), [arXiv:1301.5741].
- [28] M. Hassanvand *et al.*, Phys. Rev. C **87**, 5, 055202 (2013), [Addendum: Phys.Rev.C 88, 019905 (2013)], [arXiv:1210.7725].
- [29] M. Bayar *et al.*, Phys. Rev. C **97**, 3, 035203 (2018), [arXiv:1710.03964].

84. Pentaquarks

Revised March 2024 by M. Karliner (Tel Aviv U.) and T. Skwarnicki (Syracuse U.).

Experimental searches for pentaquark hadrons comprised of light flavors have a long and vivid history. No undisputed candidates had been found in 50 years. The first wave of claimed observations of pentaquark candidates containing a strange antiquark occurred in the early seventies, see e.g. a review in the 1976 edition of Particle Data Group listings for $Z_0(1780)$, $Z_0(1865)$ and $Z_1(1900)$ [1]. The last mention of these candidates can be found in the 1992 edition [2] with the perhaps prophetic comment “the results permit no definite conclusion - the same story for 20 years. [...] The skepticism about baryons not made of three quarks, and lack of any experimental activity in this area, make it likely that another 20 years will pass before the issue is decided.” A decade later, a second wave of observations occurred, possibly motivated by specific theoretical predictions for their existence [3–5]. The evidence for pentaquarks was based on observations of peaks in the invariant mass distributions of their decay products. More data and subsequent more sensitive experiments did not confirm these claims [6]. In the last mention of the best known candidate from that period, $\Theta(1540)^+$, the 2006 Particle Data Group listing [7] included a statement: “The conclusion that pentaquarks in general, and that Θ^+ , in particular, do not exist, appears compelling,” which well reflected the prevailing mood in the particle physics community until a study of $\Lambda_b^0 \rightarrow J/\psi p K^-$ ($J/\psi \rightarrow \mu^+ \mu^-$) decays by LHCb [8] (charge conjugate modes are implied). From an analysis of 3 fb⁻¹ Run 1 data at 7 and 8 TeV at the LHC, the LHCb collaboration reported a significant $J/\psi p$ structure in $\Lambda_b^0 \rightarrow J/\psi p K^-$ decays [8]. The exotic character of this structure, with the minimal quark content of $uudc\bar{c}$, was demonstrated in a nearly model-independent way in Ref. [9], where it was shown that the $J/\psi p$ mass ($m_{J/\psi p}$) peak near 4450 MeV was too narrow to be accounted for by $\Lambda^* \rightarrow p K^-$ reflections (Λ^* denotes a generic Λ excitation), reinforcing the results from the earlier model-dependent six-dimensional amplitude analysis of invariant masses and decay angles describing the Λ_b^0 decay in the same data [8]. The LHCb 6 fb⁻¹ Run 2 LHC data at 13 TeV, together with the improvements in the data selection for both runs, resulted in a nine-fold increase in the number of reconstructed $\Lambda_b^0 \rightarrow J/\psi p K^-$ decays (246,000 events) [10] and observation of new narrow $J/\psi p$ structures which were too faint to had been significant in the Run 1 data analysis. A second horizontal band is observed in the Dalitz plot (Fig. 84.1) near 4312 MeV in the $J/\psi p$ mass.

The 4450 MeV structure also appears to consist of two narrower peaks at 4440 and 4457 MeV. Performing a rigorous six-

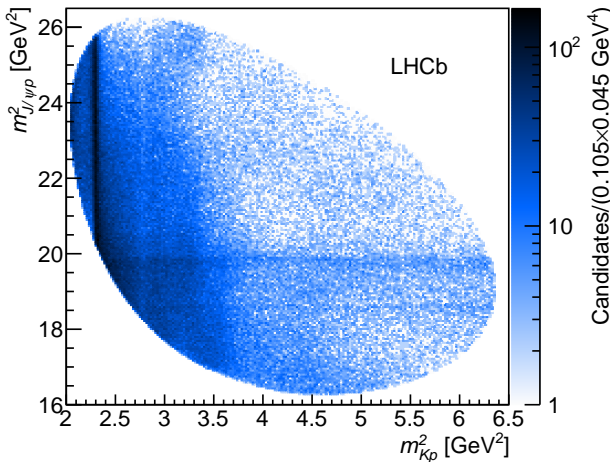


Figure 84.1: Dalitz plot distributions for $\Lambda_b^0 \rightarrow J/\psi p K^-$ decays as observed by LHCb.

dimensional amplitude analysis of these faint $J/\psi p$ structures is challenging and has not been accomplished yet. Fortunately, the newly observed peaks are so narrow that it is not necessary to construct an amplitude model to prove that these states are not arti-

facts of interfering Λ^* resonances, as was previously demonstrated in Ref. [9]. Their masses and widths have been characterized by the LHCb (see Table 84.1) from one-dimensional fits to $J/\psi p$ mass distributions, with different levels of suppression of the Λ^* contributions, which peak at the lower $p K^-$ masses (Fig. 84.1). Such analysis is not sensitive to any broad $J/\psi p$ contributions. The histograms analyzed by the LHCb are available in tabular form at <https://www.hepdata.net/record/89271>.

The fit chosen by the LHCb for the central mass and width values is displayed in Fig. 84.2. The $P_{c\bar{c}}(4312)^+$ state (formerly known as $P_c(4312)^+$) peaks right below the $\Sigma_c^+ \bar{D}^0$ threshold and has statistical significance over 7.6σ . The $P_{c\bar{c}}(4457)^+$ state peaks right below the $\Sigma_c^+ \bar{D}^{*0}$ threshold, while the $P_{c\bar{c}}(4440)^+$ state peaks about 20 MeV below it. The significance of the two-peak versus one-peak hypothesis for the 4450 MeV structure is over 5.4σ , rendering the single peak interpretation of this region obsolete. The six-dimensional amplitude analysis reported in Ref. [8], which in addition to the structure near 4450 MeV, provided also evidence for the broad $P_{c\bar{c}}(4380)^+$ state, is obsolete since it used the single $P_{c\bar{c}}(4450)^+$ state and it lacked the $P_{c\bar{c}}(4312)^+$ state. Furthermore, it used the helicity formalism in which the half-integer spin of the proton was not aligned properly between the different Λ_b^0 decay chains [11, 12]. The newer one-dimensional analysis by LHCb [10] was not sensitive to wide $P_{c\bar{c}}^+$ states. The LHCb result from the six-dimensional amplitude analysis of the Cabibbo suppressed channel $\Lambda_b^0 \rightarrow J/\psi p \pi^-$ [13], which contains a statistically marginal evidence for the sum of the $P_{c\bar{c}}^+$ and the $T_{c\bar{c}}^-$ (formerly known as $Z_c(4200)^-$) contributions, took extensive input from Ref. [8] and, like the $P_{c\bar{c}}(4380)^+$ state, should be treated with caution until the both amplitude analyses are completed on the enlarged data sets with the modified helicity formalism.

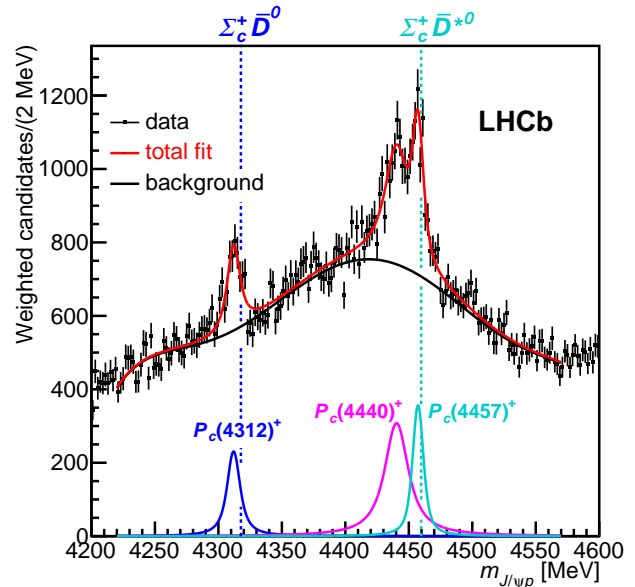


Figure 84.2: Fit to the $J/\psi p$ mass distribution, in which events were weighted to suppress $\Lambda^* \rightarrow p K^-$ backgrounds, of three Breit-Wigner functions and a sixth-order polynomial background. This fit was used to determine the central values of the masses and widths of the $P_{c\bar{c}}^+$ states (formerly known as P_c^+) reported by LHCb. The mass thresholds for the $\Sigma_c^+ \bar{D}^0$ and $\Sigma_c^+ \bar{D}^{*0}$ final states are superimposed.

While $\Sigma_c \bar{D}^{(*)}$ states had been predicted [14–17] before the first LHCb results [8], after these results became known, many theoretical groups interpreted the $P_{c\bar{c}}(4450)^+$ and $P_{c\bar{c}}(4380)^+$ states in terms of diquarks and triquarks as building blocks of a compact pentaquark [18–24]. In a different strategy, a tentative attempt has been made to treat the full 5-body dynamics, leading to states below the lowest threshold for spontaneous dissociation [25]. In the first implementation of the former approach [18], the pen-

Table 84.1: Summary of the narrow $P_{c\bar{c}}^+$ (formerly known as P_c^+) properties, interpreted as Breit-Wigner resonances. The central values are based on the fit displayed in Fig. 84.2.

State	M [MeV]	Γ [MeV] (95% CL)	\mathcal{R} [%]
$P_{c\bar{c}}(4312)^+$	$4311.9 \pm 0.7^{+6.8}_{-0.6}$	$9.8 \pm 2.7^{+3.7}_{-4.5}$ (< 27)	$0.30 \pm 0.07^{+0.34}_{-0.09}$
$P_{c\bar{c}}(4440)^+$	$4440.3 \pm 1.3^{+4.1}_{-4.7}$	$20.6 \pm 4.9^{+8.7}_{-10.1}$ (< 49)	$1.11 \pm 0.33^{+0.22}_{-0.10}$
$P_{c\bar{c}}(4457)^+$	$4457.3 \pm 0.6^{+4.1}_{-1.7}$	$6.4 \pm 2.0^{+5.7}_{-1.9}$ (< 20)	$0.53 \pm 0.16^{+0.15}_{-0.13}$

taquark mass splitting was generated mostly by the change of angular momentum between the sub-components (L) from zero to one, which would also make the heavier state narrower and of opposite parity. Explicit modeling of multi-quark systems [26] questions if centrifugal barrier factor provides enough width suppression via spatial separation of c and \bar{c} quarks at these masses, as the phase space for $J/\psi p$ decay is very large (more than 400 MeV). Also, the observed mass splitting was too small to be only due to the mechanism proposed in Ref. [18] and required fine-tuning of such models. A variation of this model, in which the heavy (cu) diquark couples with heavy \bar{c} to form colored triquark attracting the light diquark (ud), has been re-implemented for the narrow $P_{c\bar{c}}^+$ states [27]. In this model, the $P_{c\bar{c}}(4440)^+$ and $P_{c\bar{c}}(4457)^+$ states are accommodated via spin-orbit interactions for the $L = 1$ states, while the $P_{c\bar{c}}(4312)^+$ is one of the $L = 0$ states. However, the mass prediction for the latter is off by (-72 ± 29) MeV [27]. This work was later extended to $SU(3)_F$ [28]. The width dilemma becomes more severe in view of the narrow widths of the newly observed states (Table 84.1), especially for the $L = 0$ $P_{c\bar{c}}(4312)^+$ state, and requires a different origin of potential barrier between c and \bar{c} than angular momentum [27, 29], which remains a subject of theoretical controversy. Measurement of spin-parity of $P_{c\bar{c}}(4312)^+$, $P_{c\bar{c}}(4440)^+$ and $P_{c\bar{c}}(4457)^+$ will be crucial for testing these and alternative theoretical ideas discussed in the following.

More effective width suppression mechanism is offered by a loosely bound charmed baryon-anticharmed meson molecular model, in which c and \bar{c} can be separated by much larger distances, resulting in a smaller probability of them getting close enough to each other in order to make a J/ψ . Since molecular binding energy cannot be large, such molecules are in S -wave, so it has been realized early on that their masses must be near the sum of the baryon and meson masses and their spin and parity are inherited from their constituent hadrons, see e.g. discussion in [17]. The mass coincidence of the $P_{c\bar{c}}(4312)^+$ and of $P_{c\bar{c}}(4457)^+$ states, with the two related thresholds, $\Sigma_c^+ \bar{D}^0$ and $\Sigma_c^+ \bar{D}^{*0}$, provides very strong experimental evidence in favor of this interpretation. Given how close $P_{c\bar{c}}(4312)^+$ is to the $\Sigma_c^+ \bar{D}^0$ threshold, it might be a virtual rather than a bound state [30]. Since the spins of Σ_c^+ and of \bar{D}^{*0} can be combined in two different ways, the narrow $P_{c\bar{c}}(4440)^+$ peak also finds natural explanation in this physical picture. It cannot be a virtual state since it is sufficiently below the $\Sigma_c^+ \bar{D}^{*0}$ threshold.

It is worth stressing that other baryon-meson combinations, $\Lambda_c^{(*)+} \bar{D}^{(*)0}$ and $\chi_{c,J} p$ are not expected to bind [14, 31]. Before the first pentaquark observation [8] heavy quark symmetry was used to show that, in addition to the three $\Sigma_c \bar{D}^{(*)0}$ states, one expects four $\Sigma_c^* \bar{D}^{(*)0}$ states, for a total of seven [32]. Indeed, additional states at, or below, the $\Sigma_c^+ \bar{D}$ and $\Sigma_c^+ \bar{D}^*$ thresholds, are expected [33–36]. Since Σ_c^+ width is likely around 15 MeV [37], more than the width of either $P_{c\bar{c}}(4312)^+$ or $P_{c\bar{c}}(4457)^+$, it is important to keep in mind that a molecule is typically as broad as the constituents¹ [38–40]. There is no significant evidence for $\Sigma_c \bar{D}^{(*)}$ states in the present LHCb data set [10, 41]. Larger data sets are expected from the Upgraded LHCb experiment. For a review on hadronic molecules, and a recent survey in a particular approach, see respectively Refs. [42, 43].

It is useful to consider the $P_{c\bar{c}}(4312)^+$, $P_{c\bar{c}}(4440)^+$ and $P_{c\bar{c}}(4457)^+$ narrow pentaquarks together with several analogous exotic states with hidden charm and bottom in the meson sector. This provides additional significant motivation for the molecular model. At least five exotic mesons are close to thresholds of

two heavy-light mesons: $\chi_{c1}(3872)$ (formerly known as $X(3872)$) [44–47], $T_{bb1}(10610)$ and $T_{bb1}(10650)$ (formerly $Z_b(10610)$ and $Z_b(10650)$) in the bottomonium sector [48–52] and $T_{cc1}(3900)$ (formerly $Z_c(3900)$) [53–57] and $T_{cc1}(4020)$ (formerly $Z_c(4020)$) [58–60] in the charmonium sector (see Table II in Ref. [61]; for reviews of experimental information see Ref. [62, 63], as well as *Spectroscopy of Mesons Containing Two Heavy Quarks* and *Heavy Non- $q\bar{q}$ Mesons* in the current Review of Particle Properties). These states share several important features: a) their masses are near thresholds and their spin and parity correspond to S -wave combination of the two mesons; b) they are very narrow, despite very large phase space for decay into quarkonium + pion(s); c) the branching fractions for “fall apart” mode into two mesons are much larger than branching fractions for decay into quarkonium and pion(s). So far, there is no experimental evidence for states at two pseudoscalar thresholds ($D\bar{D}$ and $B\bar{B}$), suggesting that pseudoscalar exchange is essential for binding in meson-meson systems.

The above provide a strong hint that these states are deuteron-like loosely bound states of two heavy mesons [64–72]. It is then natural to conjecture that similar bound states might exist of two heavy baryons [73, 74], or a meson and a baryon or a baryon and an antibaryon, leading to a rather accurate prediction of the $P_{c\bar{c}}(4457)^+$ mass as $3/2^- \Sigma_c \bar{D}^*$ molecule (the mass threshold is 4460 MeV for $\Sigma_c^+ \bar{D}^{*0}$ and 4464 MeV for $\Sigma_c^+ \bar{D}^{*-}$) [17, 61], following similar predictions obtained in a wider framework of doubly heavy baryon-meson hadronic molecules, which might include mixtures of various two-hadron states [14–16, 31]. However, single pion exchange is not possible in $\Sigma_c^+ \bar{D}^0$ system. Thus the existence of $P_{c\bar{c}}(4312)^+$ suggests a more general binding mechanism in baryon-meson molecules, e.g. vector or two-pion exchanges, and/or coupled-channel interactions. Two-pion exchange in $D\bar{D}$ system is highly suppressed, because the intermediate state is $D^* \bar{D}^*$, which is 282 MeV heavier than $D\bar{D}$. On the other hand, in the $\Sigma_c \bar{D}$ system the intermediate $\Lambda_c^+ \bar{D}^*$ state is only 25 MeV lighter than $\Sigma_c \bar{D}$, and therefore does not have to suffer significant suppression, providing a possible binding mechanism [75]. In a generic hadronic molecule it is essential that the two hadrons are heavy, in order to minimize the repulsive kinetic energy [73, 74, 76].

Following the initial LHCb discovery [8], several groups carried out a detailed analysis of the $P_{c\bar{c}}^+$ states as hadronic molecules [77–86] followed by further analyses [35, 87–111] after the updated LHCb results [10]. Partial widths of all the allowed decay channels for the $P_{c\bar{c}}$ states have been estimated within a specific model in the molecular picture [112]. The most striking suggestion is that $P_{c\bar{c}}(4312)^+$ decays are totally dominated by the $\Lambda_c^+ \bar{D}^{*0}$ channel. This channel is also suggested to be very prominent in decays of $P_{c\bar{c}}(4440)^+$ and $P_{c\bar{c}}(4457)^+$. But other scenarios are possible, as shown by a recent theoretical analysis, allowing for the most general scattering potential of the baryon-meson system consistent with QCD symmetries at leading order in a momentum counting [113]. They found that both large and vanishing transitions to $\Lambda_c^+ \bar{D}^{(*)0}$ channels are allowed. Clearly, experimental determination of the branching fraction of these channels is of high priority.

The $P_{c\bar{c}}$ states have also been interpreted as so called hadro-charmonium [114], a bound state of relatively compact charmonium states with light hadronic matter. It was proposed that $P_{c\bar{c}}(4440)^+$ and $P_{c\bar{c}}(4457)^+$ are spin-split $\psi(2S)p$ bound states with $J^P = \frac{1}{2}^-$ and $\frac{3}{2}^-$, while $P_{c\bar{c}}(4312)^+$ is a $\chi_{c0} p$ bound state with $J^P = \frac{1}{2}^+$ [115]. While very interesting from the theoretical point of view, it is not at all clear why the binding energies

¹This feature gets changed if systems are more deeply bound.

between charmonia and the nucleon should conspire to produce states so close to the $\Sigma_c \bar{D}$ and $\Sigma_c \bar{D}^*$ thresholds. Moreover, the predicted widths of $P_{c\bar{c}}(4440)^+$ and $P_{c\bar{c}}(4457)^+$ are too big by a factor ~ 2 -3. One should also keep in mind that the molecular and hadro-charmonium pictures provide opposite predictions for the parity of $P_{c\bar{c}}(4312)^+$. In principle LHCb can check the spin and parity through partial wave analysis, but at present it is not known if systematic uncertainties can be sufficiently reduced to make such an analysis conclusive.

Shortly after the initial experimental discovery it was conjectured that the $P_{c\bar{c}}(4450)^+$ reflects the presence of a triangle singularity near the $\chi_{c1} p$ threshold [116–119]. These explanations are no longer viable, since the $P_{c\bar{c}}(4440)^+$ mass is not at any threshold and the $P_{c\bar{c}}(4312)^+$ and $P_{c\bar{c}}(4457)^+$ peak slightly below the $\Sigma_c^+ \bar{D}^0$ and $\Sigma_c^+ \bar{D}^{*0}$ thresholds. The $P_{c\bar{c}}(4457)^+$ mass is exactly at $\Lambda_c^+ \bar{D}^0$ threshold, but LHCb has demonstrated that the observed peaking is narrower in the data than expected from the triangle diagram when a realistic width of the excited D_s^- state exchanged in the triangle is used (Supplemental Material in Ref. [10]).

More extensive pre-2019 reviews of some of the theoretical issues can be found in Refs. [120,121]. Two recent relevant reviews are Refs. [122,123].

So far the $P_{c\bar{c}}^+$ states have been observed by only one experiment in only one channel. It is essential to explore other possible experimental channels, such as $P_{c\bar{c}}^+ \rightarrow \Lambda_c^+ \bar{D}^{(*)0}$, $\eta c p$ [113]. These channels are however much more experimentally challenging than $P_{c\bar{c}}^+ \rightarrow J/\psi p$. Proposals have also been made to search for heavy pentaquarks in photo-production [124–131]. Ref. [132] discusses photoproduction within the string-junction physical picture of the pentaquarks. Photoproduction is also related to recent work on $J/\psi(\eta_c)N$ scattering on the lattice [133] and on computation of $J/\psi(\eta_c)N$ and $\Upsilon(\eta_b)N$ cross sections [134]. In addition, pentaquark production has been discussed in the context of antiproton-deuteron collisions [135], of heavy ion collisions at LHC [136], in pA collisions [137] and in pion-induced processes [138–140]. The GlueX Collaboration reported negative search results for the $P_{c\bar{c}}^+$ states in photo-production at JLAB [141,142], $\gamma p \rightarrow (J/\psi \rightarrow e^+ e^-) p$. Within the large experimental errors and considerable theoretical model dependence these results do not contradict the molecular interpretations of the narrow $P_{c\bar{c}}^+$ states. In particular, vector-meson dominance often assumed in theoretical modelling may not hold for near-threshold J/ψ production, and $\Lambda_c \bar{D}^{(*)0}$ intermediate states may significantly contribute to the $J/\psi p$ production complicating probing for the $P_{c\bar{c}}^+$ states [143,144].

As noted in e.g. [17], bottom analogues of the $P_{c\bar{c}}^+$ might well exist, but experimental search for such states involves very significant challenges. It is therefore hardly surprising that they have not been observed so far. A detailed discussion is beyond the scope of the current review.

The LHCb collaboration obtained a 3.1σ evidence for a $P_{c\bar{c}}^+ \rightarrow J/\psi p$ state in the four-dimensional amplitude analysis of about $800 B_s^0 \rightarrow J/\psi p \bar{p}$ ($J/\psi \rightarrow \mu^+ \mu^-$) decays [145]. The mass of the state, $4337_{-4}^{+7} \pm 2$ MeV, is not compatible with the $P_{c\bar{c}}(4312)^+$ state at 3.1 standard deviations. The width is relatively small, $29_{-12}^{+26} \pm 14$ MeV. The present data do not provide sufficient discrimination between various J^P assignments. Its mass is about 19 MeV higher than the $\Sigma_c^+ \bar{D}^0$ threshold and about 16 MeV lower than the $\chi_{c0} p$ threshold. At present, no specific explanation for this structure has been proposed, but some intriguing ideas have been raised in Ref. [146]. Since the statistical significance of this evidence is marginal, more data are required before this state is considered experimentally established.

Similarly inconclusive 3.1σ evidence for a $P_{c\bar{c}s}^0 \rightarrow J/\psi \Lambda$ structure was observed by the LHCb collaboration in the six-dimensional amplitude analysis of about 1750 $\Xi_b^- \rightarrow J/\psi \Lambda K^-$ ($J/\psi \rightarrow \mu^+ \mu^-$, $\Lambda \rightarrow p \pi^-$) decays [12]. The strange counterparts of $P_{c\bar{c}}^+$ states have been predicted in both molecular and compact pentaquark models [15,99,101,147–149]. When interpreted as a single peak, its mass, $4458.8 \pm 2.9_{-1.1}^{+4.7}$ MeV, is 15 MeV above the $\Xi_c^0 \bar{D}^0$ threshold and 18 MeV below the $\Xi_c^0 \bar{D}^{*0}$ threshold. Its width, $17.3 \pm 6.5_{-5.7}^{+8.0}$ MeV, is relatively narrow, thus plausibly

could be interpreted as a loosely bound $\Xi_c^0 \bar{D}^{*0}$ state. However, in the latter model two states are expected with J^P equal to $1/2^-$ and $3/2^-$. In fact, the LHCb data are consistent with such hypothesis, under which 4454.9 ± 2.7 MeV ($\Gamma = 7.5 \pm 9.7$ MeV) and 4467.8 ± 3.7 MeV ($\Gamma = 5.2 \pm 5.3$ MeV) mass (width) estimates are obtained (statistical errors only). It is worth noting, that the $SU(3)$ flavor structure of $\Xi_c^0 \bar{D}^{*0}$ states is different from that of $\Sigma_c^+ \bar{D}^{*0}$ states, since Ξ_c^0 belongs to the charmed baryon triplet, together with Ξ_c^+ and Λ_c^+ , where the two light quarks form a spin-zero diquark, unlike Σ_c^+ , which together with Ξ_c^0 and Ω_c^0 belongs to the charmed baryon sextet, where the two light quarks form a spin-1 diquark. More data are required to experimentally establish this structure, clarify its composition, and determine the related quantum numbers.

If the two states at 4455 MeV and 4468 MeV indeed correspond to a $\Xi_c^0 \bar{D}^{*0}$ molecule, there perhaps exist two other states, corresponding to $\Xi_c' \bar{D}^*$ [15,99,101,147–149], with a mass shifted upwards by approximately $\Xi_c' - \Xi_c$ mass difference [150,151], i.e. about 108 MeV [37].

More recently, the LHCb experiment observed highly significant ($> 14\sigma$) pentaquark state $P_{c\bar{c}s}(4338)^0 \rightarrow J/\psi \Lambda$ (formerly known as $P_{c\bar{c}s}(4338)$) in the six-dimensional amplitude analysis of $4620 \pm 70 B^- \rightarrow J/\psi \Lambda \bar{p}$ decays [152]. Its mass $4338.2 \pm 0.7 \pm 0.4$ MeV is right at the $\Xi_c \bar{D}$ threshold (Fig. 84.3), its width is narrow $7.0 \pm 1.2 \pm 1.3$ MeV, and its spin is $1/2$, with a preference for negative parity, which all fits the molecular model very well. This makes the $P_{c\bar{c}s}(4338)^0$ state a likely $\Xi_c^0 \bar{D}^0$ analog of the $P_{c\bar{c}}(4312)^+$ state in $\Sigma_c^0 \bar{D}^0$ system. In addition, as in the $P_{c\bar{c}s}(4459)^0$ case, a $\Xi_c' \bar{D}$ state is expected, for a total of three additional strange pentaquarks [151]. Experimental determination whether yet additional $\Xi_c^{(*)'} \bar{D}^{(*)0}$ states actually exist will provide a useful testing ground for the various theoretical approaches which have been used to predict them.

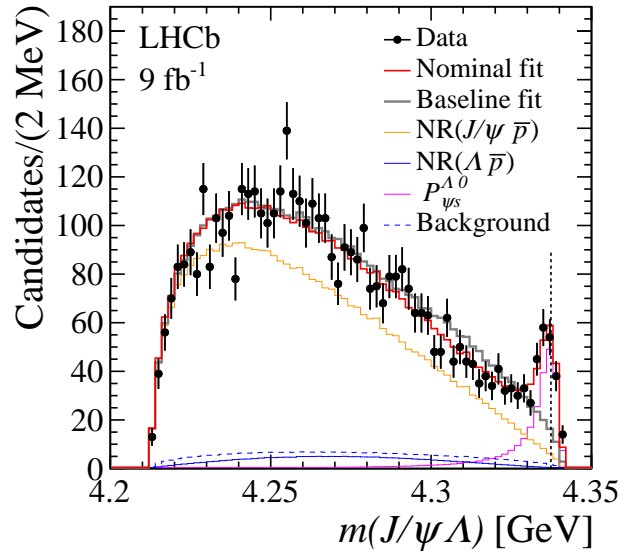


Figure 84.3: Distribution of invariant $J/\psi \Lambda$ mass, with the projection of the amplitude fit model superimposed. The model without the $P_{c\bar{c}s}(4338)^0$ state (labeled as $P_{\psi s}^{\Lambda 0}$) is also shown in grey. The $\Xi_c^+ D^-$ baryon-meson threshold is indicated with a vertical dashed line.

In hidden-charm exotics discussed above, the charmed and the anticharmed quarks can form a charmonium and thereby decouple from the light quarks. The molecular model provides an efficient mechanism to suppress such decays, thus making these states narrow. Compact direct color couplings between quarks are missing an obvious width suppression mechanism, thus could lead to broader states. In fact, there is plenty of evidence for them in form of broader tetraquark mass structures in $J/\psi \phi$ [153–159], $J/\psi J/\psi$ [160–162], $T_{c\bar{c}1}(4430)^+ \rightarrow \psi(2S)\pi^+$ (formerly

$Z_c(4430)^+$ [163–165] and others, although alternative explanations of these structures have been also proposed. Analogous configurations may also exist for pentaquarks, but there is no firm evidence for them yet.

The hidden-charm exotic states, should not be confused with exotic hadrons containing two heavy quarks, rather than a heavy quark and a heavy antiquark. Decoupling from the light quarks is impossible in exotics which contain two heavy quarks. This has far-reaching consequences. The first tetraquark of the latter type, i.e. containing two heavy quarks, has been reported by LHCb [166, 167]. A comprehensive discussion of tetraquark candidates can be found in the “Heavy non- QQ Mesons” review.

References

- [1] T. G. Trippe *et al.* (Particle Data Group), *Rev. Mod. Phys.* **48**, S1 (1976), [Erratum: *Rev. Mod. Phys.* 48,497(1976)].
- [2] K. Hikasa *et al.* (Particle Data Group), *Phys. Rev.* **D45**, S1 (1992), [Erratum: *Phys. Rev.* D46,5210(1992)].
- [3] M. Praszalowicz, *Skyrmions and Anomalies, p.112, M. Jezabek Ed.*, World Scientific Publishing (1987), ISBN 9971503506.
- [4] D. Diakonov, V. Petrov and M. V. Polyakov, *Z. Phys.* **A359**, 305 (1997), [hep-ph/9703373].
- [5] H. Weigel, *Eur. Phys. J.* **A2**, 391 (1998), [hep-ph/9804260].
- [6] K. H. Hicks, *Eur.Phys.J.* **H37**, 1 (2012).
- [7] W. M. Yao *et al.* (Particle Data Group), *J. Phys.* **G33**, 1 (2006).
- [8] R. Aaij *et al.* (LHCb), *Phys. Rev. Lett.* **115**, 072001 (2015), [arXiv:1507.03414].
- [9] R. Aaij *et al.* (LHCb), *Phys. Rev. Lett.* **117**, 8, 082002 (2016), [arXiv:1604.05708].
- [10] R. Aaij *et al.* (LHCb), *Phys. Rev. Lett.* **122**, 22, 222001 (2019), [arXiv:1904.03947].
- [11] M. Wang *et al.*, *Chin. Phys. C* **45**, 6, 063103 (2021), [arXiv:2012.03699].
- [12] R. Aaij *et al.* (LHCb), *Sci. Bull.* **66**, 1391 (2021), [arXiv:2012.10380].
- [13] R. Aaij *et al.* (LHCb), *Phys. Rev. Lett.* **117**, 8, 082003 (2016), [Addendum: *Phys. Rev. Lett.* 118,119901(2017)], [arXiv:1606.06999].
- [14] Z.-C. Yang *et al.*, *Chin. Phys.* **C36**, 6 (2012), [arXiv:1105.2901].
- [15] J.-J. Wu *et al.*, *Phys. Rev. Lett.* **105**, 232001 (2010), [arXiv:1007.0573].
- [16] J.-J. Wu, T. S. H. Lee and B. S. Zou, *Phys. Rev.* **C85**, 044002 (2012), [arXiv:1202.1036].
- [17] M. Karliner and J. L. Rosner, *Phys. Rev. Lett.* **115**, 12, 122001 (2015), [arXiv:1506.06386].
- [18] L. Maiani, A. D. Polosa and V. Riquer, *Phys. Lett.* **B749**, 289 (2015), [arXiv:1507.04980].
- [19] R. F. Lebed, *Phys. Lett.* **B749**, 454 (2015), [arXiv:1507.05867].
- [20] V. V. Anisovich *et al.* (2015), [arXiv:1507.07652].
- [21] G.-N. Li, X.-G. He and M. He, *JHEP* **12**, 128 (2015), [arXiv:1507.08252].
- [22] R. Ghosh, A. Bhattacharya and B. Chakrabarti, *Phys. Part. Nucl. Lett.* **14**, 4, 550 (2017), [arXiv:1508.00356].
- [23] Z.-G. Wang, *Eur. Phys. J.* **C76**, 2, 70 (2016), [arXiv:1508.01468].
- [24] R. Zhu and C.-F. Qiao, *Phys. Lett.* **B756**, 259 (2016), [arXiv:1510.08693].
- [25] J. M. Richard, A. Valcarce and J. Vijande, *Phys. Lett.* **B774**, 710 (2017), [arXiv:1710.08239].
- [26] E. Hiyama *et al.*, *Phys. Rev.* **C98**, 4, 045208 (2018), [arXiv:1803.11369].
- [27] A. Ali and A. Y. Parkhomenko, *Phys. Lett.* **B793**, 365 (2019), [arXiv:1904.00446].
- [28] A. Ali *et al.*, *JHEP* **10**, 256 (2019), [arXiv:1907.06507].
- [29] L. Maiani, A. D. Polosa and V. Riquer, *Phys. Lett.* **B778**, 247 (2018), [arXiv:1712.05296].
- [30] C. Fernandez-Ramirez *et al.* (JPAC), *Phys. Rev. Lett.* **123**, 9, 092001 (2019), [arXiv:1904.10021].
- [31] W. L. Wang *et al.*, *Phys. Rev.* **C84**, 015203 (2011), [arXiv:1101.0453].
- [32] J.-J. Wu *et al.*, *Phys. Rev. C* **84**, 015202 (2011), [arXiv:1011.2399].
- [33] C. W. Xiao, J. Nieves and E. Oset, *Phys. Rev.* **D88**, 056012 (2013), [arXiv:1304.5368].
- [34] C. W. Xiao, J. Nieves and E. Oset, *Phys. Rev.* **D100**, 1, 014021 (2019), [arXiv:1904.01296].
- [35] M.-Z. Liu *et al.*, *Phys. Rev. Lett.* **122**, 24, 242001 (2019), [arXiv:1903.11560].
- [36] G.-J. Wang *et al.*, *Phys. Rev. D* **102**, 3, 036012 (2020), [arXiv:1911.09613].
- [37] P. A. Zyla *et al.* (Particle Data Group), *PTEP* **2020**, 8, 083C01 (2020).
- [38] C. Hanhart, Yu. S. Kalashnikova and A. V. Nefediev, *Phys. Rev.* **D81**, 094028 (2010), [arXiv:1002.4097].
- [39] A. A. Filin *et al.*, *Phys. Rev. Lett.* **105**, 019101 (2010), [arXiv:1004.4789].
- [40] F.-K. Guo and U.-G. Meissner, *Phys. Rev.* **D84**, 014013 (2011), [arXiv:1102.3536].
- [41] M.-L. Du *et al.*, *Phys. Rev. Lett.* **124**, 7, 072001 (2020), [arXiv:1910.11846].
- [42] F.-K. Guo *et al.*, *Rev. Mod. Phys.* **90**, 1, 015004 (2018), [arXiv:1705.00141].
- [43] X.-K. Dong, F.-K. Guo and B.-S. Zou (2021), [arXiv:2108.02673].
- [44] S. K. Choi *et al.* (Belle), *Phys. Rev. Lett.* **91**, 262001 (2003), [hep-ex/0309032].
- [45] D. Acosta *et al.* (CDF), *Phys. Rev. Lett.* **93**, 072001 (2004), [hep-ex/0312021].
- [46] B. Aubert *et al.* (BaBar), *Phys. Rev.* **D71**, 071103 (2005), [hep-ex/0406022].
- [47] V. M. Abazov *et al.* (D0), *Phys. Rev. Lett.* **93**, 162002 (2004), [hep-ex/0405004].
- [48] M. Karliner and H. J. Lipkin (2008), [arXiv:0802.0649].
- [49] K. F. Chen *et al.* (Belle), *Phys. Rev. Lett.* **100**, 112001 (2008), [arXiv:0710.2577].
- [50] A. Bondar *et al.* (Belle), *Phys. Rev. Lett.* **108**, 122001 (2012), [arXiv:1110.2251].
- [51] P. Krokovny *et al.* (Belle), *Phys. Rev.* **D88**, 5, 052016 (2013), [arXiv:1308.2646].
- [52] A. Garmash *et al.* (Belle), *Phys. Rev.* **D91**, 7, 072003 (2015), [arXiv:1403.0992].
- [53] M. Ablikim *et al.* (BESIII), *Phys. Rev. Lett.* **110**, 252001 (2013), [arXiv:1303.5949].
- [54] Z. Q. Liu *et al.* (Belle), *Phys. Rev. Lett.* **110**, 252002 (2013), [arXiv:1304.0121].
- [55] T. Xiao *et al.*, *Phys. Lett.* **B727**, 366 (2013), [arXiv:1304.3036].
- [56] M. Ablikim *et al.* (BESIII), *Phys. Rev. Lett.* **112**, 2, 022001 (2014), [arXiv:1310.1163].
- [57] M. Ablikim *et al.* (BESIII), *Phys. Rev. Lett.* **115**, 11, 112003 (2015), [arXiv:1506.06018].
- [58] M. Ablikim *et al.* (BESIII), *Phys. Rev. Lett.* **111**, 24, 242001 (2013), [arXiv:1309.1896].
- [59] M. Ablikim *et al.* (BESIII), *Phys. Rev. Lett.* **113**, 21, 212002 (2014), [arXiv:1409.6577].

- [60] M. Ablikim *et al.* (BESIII), Phys. Rev. Lett. **112**, 13, 132001 (2014), [arXiv:1308.2760].
- [61] M. Karliner, Acta Phys. Polon. **B47**, 117 (2016).
- [62] M. Karliner, J. L. Rosner and T. Skwarnicki, Ann. Rev. Nucl. Part. Sci. **68**, 17 (2018), [arXiv:1711.10626].
- [63] S. L. Olsen, T. Skwarnicki and D. Zieminska, Rev. Mod. Phys. **90**, 1, 015003 (2018), [arXiv:1708.04012].
- [64] M. B. Voloshin and L. B. Okun, JETP Lett. **23**, 333 (1976), [Pisma Zh. Eksp. Teor. Fiz.23,369(1976)].
- [65] A. De Rujula, H. Georgi and S. Glashow, Phys. Rev. Lett. **38**, 317 (1977).
- [66] N. A. Tornqvist, Phys. Rev. Lett. **67**, 556 (1991).
- [67] N. A. Tornqvist, Z. Phys. **C61**, 525 (1994), [hep-ph/9310247].
- [68] N. A. Tornqvist, Phys. Lett. **B590**, 209 (2004), [hep-ph/0402237].
- [69] C. E. Thomas and F. E. Close, Phys. Rev. **D78**, 034007 (2008), [arXiv:0805.3653].
- [70] M. Suzuki, Phys. Rev. **D72**, 114013 (2005), [hep-ph/0508258].
- [71] S. Fleming *et al.*, Phys. Rev. **D76**, 034006 (2007), [hep-ph/0703168].
- [72] T. E. O. Ericson and G. Karl, Phys. Lett. **B309**, 426 (1993).
- [73] M. Karliner, H. J. Lipkin and N. A. Tornqvist, in “Proceedings, 14th International Conference on Hadron spectroscopy (Hadron 2011),” (2011), [arXiv:1109.3472], URL <http://inspirehep.net/record/927616/files/arXiv:1109.3472.pdf>.
- [74] M. Karliner, H. J. Lipkin and N. A. Tornqvist, Nucl. Phys. Proc. Suppl. **225-227**, 102 (2012).
- [75] M. Karliner, Hidden Charm Molecular Pentaquarks: Some Open Questions in Proc. Bled Mini-Workshop, Slovenia, July 15-19, 2019, B. Golli *et al.*, Eds., p. 25, <http://www-f1.ijs.si/BledPub/bled2019.pdf>.
- [76] X.-Q. Li and X. Liu, Eur. Phys. J. **C74**, 12, 3198 (2014), [arXiv:1409.3332].
- [77] R. Chen *et al.*, Phys. Rev. Lett. **115**, 13, 132002 (2015), [arXiv:1507.03704].
- [78] H.-X. Chen *et al.*, Phys. Rev. Lett. **115**, 17, 172001 (2015), [arXiv:1507.03717].
- [79] L. Roca, J. Nieves and E. Oset, Phys. Rev. **D92**, 9, 094003 (2015), [arXiv:1507.04249].
- [80] J. He, Phys. Lett. **B753**, 547 (2016), [arXiv:1507.05200].
- [81] H. Huang *et al.*, Eur. Phys. J. **C76**, 11, 624 (2016), [arXiv:1510.04648].
- [82] L. Roca and E. Oset, Eur. Phys. J. **C76**, 11, 591 (2016), [arXiv:1602.06791].
- [83] Q.-F. Lü and Y.-B. Dong, Phys. Rev. **D93**, 7, 074020 (2016), [arXiv:1603.00559].
- [84] Y. Shimizu, D. Suenaga and M. Harada, Phys. Rev. **D93**, 11, 114003 (2016), [arXiv:1603.02376].
- [85] C.-W. Shen *et al.*, Nucl. Phys. **A954**, 393 (2016), [arXiv:1603.04672].
- [86] Y. Yamaguchi *et al.*, Phys. Rev. **D96**, 11, 114031 (2017), [arXiv:1709.00819].
- [87] J. F. Giron, R. F. Lebed and C. T. Peterson, JHEP **05**, 061 (2019), [arXiv:1903.04551].
- [88] R. Chen *et al.*, Phys. Rev. **D100**, 1, 011502 (2019), [arXiv:1903.11013].
- [89] F.-K. Guo *et al.*, Phys. Rev. **D99**, 9, 091501 (2019), [arXiv:1903.11503].
- [90] J. He, Eur. Phys. J. **C79**, 5, 393 (2019), [arXiv:1903.11872].
- [91] H. Huang, J. He and J. Ping (2019), [arXiv:1904.00221].
- [92] Y. Shimizu, Y. Yamaguchi and M. Harada (2019), [arXiv:1904.00587].
- [93] Z.-H. Guo and J. A. Oller, Phys. Lett. **B793**, 144 (2019), [arXiv:1904.00851].
- [94] C.-J. Xiao *et al.*, Phys. Rev. **D100**, 1, 014022 (2019), [arXiv:1904.00872].
- [95] Z.-G. Wang, Int. J. Mod. Phys. A **35**, 01, 2050003 (2020), [arXiv:1905.02892].
- [96] L. Meng *et al.*, Phys. Rev. **D100**, 1, 014031 (2019), [arXiv:1905.04113].
- [97] F. Giannuzzi, Phys. Rev. **D99**, 9, 094006 (2019), [arXiv:1903.04430].
- [98] Q. Wu and D.-Y. Chen, Phys. Rev. D **100**, 11, 114002 (2019), [arXiv:1906.02480].
- [99] C.-W. Shen, J.-J. Wu and B.-S. Zou, Phys. Rev. **D100**, 5, 056006 (2019), [arXiv:1906.03896].
- [100] F. Stancu, Eur. Phys. J. C **79**, 11, 957 (2019), [arXiv:1902.07101].
- [101] C. W. Xiao, J. Nieves and E. Oset, Phys. Lett. B **799**, 135051 (2019), [arXiv:1906.09010].
- [102] M. B. Voloshin, Phys. Rev. **D100**, 3, 034020 (2019), [arXiv:1907.01476].
- [103] S. Sakai, H.-J. Jing and F.-K. Guo, Phys. Rev. D **100**, 7, 074007 (2019), [arXiv:1907.03414].
- [104] Z.-G. Wang and X. Wang, Chin. Phys. C **44**, 103102 (2020), [arXiv:1907.04582].
- [105] Y. Yamaguchi *et al.*, Phys. Rev. D **101**, 9, 091502 (2020), [arXiv:1907.04684].
- [106] Y.-J. Xu *et al.*, Phys. Rev. D **102**, 3, 034028 (2020), [arXiv:1907.05097].
- [107] M. Pavon Valderrama, Phys. Rev. D **100**, 9, 094028 (2019), [arXiv:1907.05294].
- [108] F.-Z. Peng *et al.*, Nucl. Phys. B **983**, 115936 (2022), [arXiv:1907.05322].
- [109] M.-Z. Liu *et al.*, Phys. Rev. D **103**, 5, 054004 (2021), [arXiv:1907.06093].
- [110] Y.-W. Pan *et al.*, Phys. Rev. D **102**, 1, 011504 (2020), [arXiv:1907.11220].
- [111] T. J. Burns and E. S. Swanson, Phys. Rev. D **100**, 11, 114033 (2019), [arXiv:1908.03528].
- [112] Y.-H. Lin and B.-S. Zou, Phys. Rev. **D100**, 5, 056005 (2019), [arXiv:1908.05309].
- [113] M.-L. Du *et al.*, JHEP **08**, 157 (2021), [arXiv:2102.07159].
- [114] S. Dubynskiy and M. B. Voloshin, Phys. Lett. **B666**, 344 (2008), [arXiv:0803.2224].
- [115] M. I. Eides, V. Y. Petrov and M. V. Polyakov, Mod. Phys. Lett. A **35**, 18, 2050151 (2020), [arXiv:1904.11616].
- [116] F.-K. Guo *et al.*, Phys. Rev. **D92**, 7, 071502 (2015), [arXiv:1507.04950].
- [117] U.-G. Meissner and J. A. Oller, Phys. Lett. **B751**, 59 (2015), [arXiv:1507.07478].
- [118] X.-H. Liu, Q. Wang and Q. Zhao, Phys. Lett. **B757**, 231 (2016), [arXiv:1507.05359].
- [119] M. Mikhasenko (2015), [arXiv:1507.06552].
- [120] T. J. Burns, Eur. Phys. J. **A51**, 11, 152 (2015), [arXiv:1509.02460].
- [121] H.-X. Chen *et al.*, Phys. Rept. **639**, 1 (2016), [arXiv:1601.02092].
- [122] Y.-R. Liu *et al.*, Prog. Part. Nucl. Phys. **107**, 237 (2019), [arXiv:1903.11976].
- [123] N. Brambilla *et al.*, Phys. Rept. **873**, 1 (2020), [arXiv:1907.07583].
- [124] Y. Huang *et al.*, J. Phys. **G41**, 11, 115004 (2014), [arXiv:1305.4434].

- [125] Q. Wang, X.-H. Liu and Q. Zhao, Phys. Rev. **D92**, 034022 (2015), [arXiv:1508.00339].
- [126] V. Kubarovsky and M. B. Voloshin, Phys. Rev. **D92**, 3, 031502 (2015), [arXiv:1508.00888].
- [127] M. Karliner and J. L. Rosner, Phys. Lett. **B752**, 329 (2016), [arXiv:1508.01496].
- [128] A. N. Hiller Blin *et al.*, Phys. Rev. **D94**, 3, 034002 (2016), [arXiv:1606.08912].
- [129] X. Cao and J.-p. Dai, Phys. Rev. **D100**, 5, 054033 (2019), [arXiv:1904.06015].
- [130] X.-Y. Wang, X.-R. Chen and J. He, Phys. Rev. **D99**, 11, 114007 (2019), [arXiv:1904.11706].
- [131] J.-J. Wu, T. S. H. Lee and B.-S. Zou, Phys. Rev. **C100**, 3, 035206 (2019), [arXiv:1906.05375].
- [132] G. C. Rossi and G. Veneziano (2019), [arXiv:1909.01753].
- [133] U. Skerbis and S. Prelovsek, Phys. Rev. **D99**, 9, 094505 (2019), [arXiv:1811.02285].
- [134] C. W. Xiao and U. G. Meissner, Phys. Rev. **D92**, 11, 114002 (2015), [arXiv:1508.00924].
- [135] M. B. Voloshin, Phys. Rev. **D99**, 9, 093003 (2019), [arXiv:1903.04422].
- [136] R.-Q. Wang *et al.*, Phys. Rev. **C94**, 4, 044913 (2016), [arXiv:1601.02835].
- [137] I. Schmidt and M. Siddikov, Phys. Rev. **D93**, 9, 094005 (2016), [arXiv:1601.05621].
- [138] Q.-F. L^u *et al.*, Phys. Rev. **D93**, 3, 034009 (2016), [arXiv:1510.06271].
- [139] X.-H. Liu and M. Oka, Nucl. Phys. **A954**, 352 (2016), [arXiv:1602.07069].
- [140] X.-Y. Wang *et al.*, Phys. Lett. **B797**, 134862 (2019), [arXiv:1906.04044].
- [141] A. Ali *et al.* (GlueX), Phys. Rev. Lett. **123**, 7, 072001 (2019), [arXiv:1905.10811].
- [142] S. Adhikari *et al.* (GlueX), Phys. Rev. C **108**, 2, 025201 (2023), [arXiv:2304.03845].
- [143] M.-L. Du *et al.*, Eur. Phys. J. C **80**, 11, 1053 (2020), [arXiv:2009.08345].
- [144] D. Winney *et al.* (Joint Physics Analysis Center), Phys. Rev. D **108**, 5, 054018 (2023), [arXiv:2305.01449].
- [145] R. Aaij *et al.* (LHCb), Phys. Rev. Lett. **128**, 062001 (2021), [arXiv:2108.04720].
- [146] B. Wang, L. Meng and S.-L. Zhu, JHEP **11**, 108 (2019), [arXiv:1909.13054].
- [147] R. Chen, J. He and X. Liu, Chin. Phys. C **41**, 10, 103105 (2017), [arXiv:1609.03235].
- [148] E. Santopinto and A. Giachino, Phys. Rev. D **96**, 1, 014014 (2017), [arXiv:1604.03769].
- [149] B. Wang, L. Meng and S.-L. Zhu, Phys. Rev. D **101**, 3, 034018 (2020), [arXiv:1912.12592].
- [150] M. Karliner and J. L. Rosner, Sci. Bull. **66**, 13, 1256 (2021), [arXiv:2104.15077].
- [151] M. Karliner and J. L. Rosner, Phys. Rev. D **106**, 3, 036024 (2022), [arXiv:2207.07581].
- [152] R. Aaij *et al.* (LHCb), Phys. Rev. Lett. **131**, 3, 031901 (2023), [arXiv:2210.10346].
- [153] T. Aaltonen *et al.* (CDF), Phys. Rev. Lett. **102**, 242002 (2009), [arXiv:0903.2229].
- [154] T. Aaltonen *et al.* (CDF), Mod. Phys. Lett. A **32**, 26, 1750139 (2017), [arXiv:1101.6058].
- [155] S. Chatrchyan *et al.* (CMS), Phys. Lett. B **734**, 261 (2014), [arXiv:1309.6920].
- [156] R. Aaij *et al.* (LHCb), Phys. Rev. Lett. **118**, 2, 022003 (2017), [arXiv:1606.07895].
- [157] R. Aaij *et al.* (LHCb), Phys. Rev. D **95**, 1, 012002 (2017), [arXiv:1606.07898].
- [158] R. Aaij *et al.* (LHCb), Phys. Rev. Lett. **127**, 8, 082001 (2021), [arXiv:2103.01803].
- [159] LHCb (LHCb) (2023), [arXiv:2301.04899].
- [160] R. Aaij *et al.* (LHCb), Sci. Bull. **65**, 23, 1983 (2020), [arXiv:2006.16957].
- [161] A. Hayrapetyan *et al.* (CMS) (2023), [arXiv:2306.07164].
- [162] G. Aad *et al.* (ATLAS) (2023), [arXiv:2304.08962].
- [163] S. K. Choi *et al.* (Belle), Phys. Rev. Lett. **100**, 142001 (2008), [arXiv:0708.1790].
- [164] K. Chilikin *et al.* (Belle), Phys. Rev. D **88**, 7, 074026 (2013), [arXiv:1306.4894].
- [165] R. Aaij *et al.* (LHCb), Phys. Rev. Lett. **112**, 22, 222002 (2014), [arXiv:1404.1903].
- [166] R. Aaij *et al.* (LHCb), Nature Phys. **18**, 7, 751 (2022), [arXiv:2109.01038].
- [167] R. Aaij *et al.* (LHCb), Nature Commun. **13**, 1, 3351 (2022), [arXiv:2109.01056].



Hypothetical Particles and Concepts

85. Extra dimensions (rev.)	1021
86. W' -boson searches (rev.)	1029
87. Z' -boson searches (rev.)	1033
88. Supersymmetry: theory (rev.)	1038
89. Supersymmetry: experiment (rev.)	1058
90. Axions and other similar particles (rev.)	1079
91. Quark and lepton compositeness, searches for (rev.)	1098
92. Dynamical electroweak symmetry breaking:	1104
implications of the H^0 (rev.)	
93. Grand unified theories (rev.)	1119
94. Leptoquarks (rev.)	1134
95. Magnetic monopoles (rev.)	1138



85. Extra Dimensions

Revised August 2023 by Z. Demiragli (Boston U.) and A. Pomarol (U. Autònoma de Barcelona; IFAE).

85.1 Introduction

Proposals for a spacetime with more than three spatial dimensions date back to the 1920s, mainly through the work of Kaluza and Klein, in an attempt to unify the forces of nature [1]. Although their initial idea failed, the formalism that they and others developed is still useful nowadays. Around 1980, string theory proposed again to enlarge the number of space dimensions, this time as a requirement for describing a consistent theory of quantum gravity. The extra dimensions were supposed to be compactified at a scale close to the Planck scale, and thus not testable experimentally in the near future.

A different approach was given by Arkani-Hamed, Dimopoulos, and Dvali (ADD) in their seminal paper in 1998 [2], where they showed that the weakness of gravity could be explained by postulating two or more flat extra dimensions in which only gravity could propagate. The size of these extra dimensions should range between roughly a millimeter and $\sim 1/\text{TeV}$, leading to possible observable consequences in current and future experiments. A year later, Randall and Sundrum (RS) [3] found a new possibility using a warped geometry, postulating a five-dimensional Anti-de Sitter (AdS) spacetime with a compactification scale of order $1/\text{TeV}$. The origin of the smallness of the electroweak scale versus the Planck scale was explained by the gravitational redshift factor present in the warped AdS metric. As in the ADD model, originally only gravity was assumed to propagate in the extra dimensions, although it was soon clear that this was not necessary in warped extra dimensions and also the SM gauge fields [4, 5] and SM fermions [6, 7] could propagate in the five-dimensional spacetime.

The physics of warped extra-dimensional models has an alternative interpretation by means of the AdS/CFT correspondence [8–10]. Models with warped extra dimensions are related to four-dimensional strongly-interacting theories, allowing an understanding of the properties of five-dimensional fields as those of four-dimensional composite states [11]. This approach has opened new directions for tackling outstanding questions in particle physics, such as the flavor problem, grand unification, and the origin of electroweak symmetry breaking or supersymmetry breaking.

85.1.1 Experimental Constraints

Constraints on extra-dimensional models arise from astrophysical and cosmological considerations, tabletop experiments exploring gravity at sub-mm distances, and collider experiments. Collider limits on extra-dimensional models are dominated by LHC results, which can be found on the public WWW pages of ATLAS [12] and CMS [13]. This review includes the most recent limits, most of which are published results based on 140 fb^{-1} LHC data collected in 2015–18 at a center-of-mass energy of 13 TeV and legacy results from 20 fb^{-1} of 8 TeV data collected in Run 1. For most of the models, Run 2 results surpass the sensitivity of Run 1.

85.1.2 Kaluza-Klein Theories

Field theories with compact extra dimensions can be written as theories in ordinary four dimensions (4D) by performing a Kaluza-Klein (KK) reduction. As an illustration, consider a simple example, namely a field theory of a complex scalar in flat five-dimensional (5D) spacetime. The action will be given by ¹

$$S_5 = - \int d^4x dy M_5 \left[|\partial_\mu \phi|^2 + |\partial_y \phi|^2 + \lambda_5 |\phi|^4 \right], \quad (85.1)$$

where y refers to the extra (fifth) dimension. A universal scale M_5 has been extracted in front of the action in order to keep the 5D field with the same mass-dimension as in 4D. This theory is perturbative for energies $E \lesssim \ell_5 M_5 / \lambda_5$ where $\ell_5 = 24\pi^3$ [14].

Let us now consider that the fifth dimension is compact with the topology of a circle S^1 of radius R , which corresponds to the identification of y with $y + 2\pi R$. In such a case, the 5D complex scalar field can be expanded in a Fourier series:

$$\phi(x, y) = \frac{1}{\sqrt{2\pi R M_5}} \sum_{n=-\infty}^{\infty} e^{iny/R} \phi^{(n)}(x), \quad (85.2)$$

that, inserted in Eq. (85.1) and integrating over y , gives

$$S_5 = S_4^{(0)} + S_4^{(n)}, \quad (85.3)$$

where

$$S_4^{(0)} = - \int d^4x \left[|\partial_\mu \phi^{(0)}|^2 + \lambda_4 |\phi^{(0)}|^4 \right], \quad (85.4)$$

and,

$$S_4^{(n)} = - \int d^4x \sum_{n \neq 0} \left[|\partial_\mu \phi^{(n)}|^2 + \left(\frac{n}{R} \right)^2 |\phi^{(n)}|^2 \right] + \text{quartic interactions}. \quad (85.5)$$

The $n = 0$ mode self-coupling is given by

$$\lambda_4 = \frac{\lambda_5}{2\pi R M_5}. \quad (85.6)$$

The above action corresponds to a 4D theory with a massless scalar $\phi^{(0)}$, referred to as the zero mode, and an infinite tower of massive modes $\phi^{(n)}$ with $n > 0$, known as KK modes. The KK reduction thus allows a treatment of 5D theories as 4D field theories with an infinite number of fields. At energies smaller than $1/R$, the KK modes can be neglected, leaving the zero-mode action of Eq. (85.4). The strength of the interaction of the zero-mode, given by Eq. (85.6), decreases as R increases. Thus, for a large extra dimension $R \gg 1/M_5$, the massless scalar is very weakly coupled.

85.2 Large Extra Dimensions for Gravity

85.2.1 The ADD Scenario

The ADD scenario [2, 15] (for a review see, for example, [16]) assumes a $D = 4 + \delta$ dimensional spacetime, with δ compactified spatial dimensions. The apparent weakness of gravity arises since it propagates in the higher-dimensional space. The SM is assumed to be localized in a 4D subspace, a 3-brane, as can be found in certain string theory constructions [17, 18]. Gravity is described by the Einstein-Hilbert action in $D = 4 + \delta$ spacetime dimensions

$$S_D = - \frac{\bar{M}_D^{2+\delta}}{2} \int d^4x d^\delta y \sqrt{-g} \mathcal{R} + \int d^4x \sqrt{-g_{\text{ind}}} \mathcal{L}_{\text{SM}}, \quad (85.7)$$

where x labels the ordinary four coordinates, y the δ extra coordinates, g refers to the determinant of the D -dimensional metric whose Ricci scalar is defined by \mathcal{R} , and \bar{M}_D is called the reduced Planck scale of the D -dimensional theory. In the second term of Eq. (85.7), which gives the gravitational interactions of SM fields, the D -dimensional metric reduces to the induced metric on the 3-brane where the SM fields propagate. The extra dimensions are assumed to be flat and compactified in a volume V_δ . As an example, consider a toroidal compactification of equal radii R and volume $V_\delta = (2\pi R)^\delta$. After a KK reduction, one finds that the fields that couple to the SM are the spin-2 gravitational field $G_{\mu\nu}(x, y)$ and a tower of spin-0 KK graviscalars [19]. The graviscalars, however, only couple to SM fields through the trace of the energy-momentum tensor, resulting in weaker couplings to the SM fields. The Fourier expansion of the spin-2 field is given by

$$G_{\mu\nu}(x, y) = G_{\mu\nu}^{(0)}(x) + \frac{1}{\sqrt{V_\delta}} \sum_{\vec{n} \neq 0} e^{i\vec{n} \cdot \vec{y}/R} G_{\mu\nu}^{(\vec{n})}(x), \quad (85.8)$$

where $\vec{y} = (y_1, y_2, \dots, y_\delta)$ are the extra-dimensional coordinates and $\vec{n} = (n_1, n_2, \dots, n_\delta)$. Eq. (85.8) contains a massless state,

¹Our convention for the metric is $\eta_{MN} = \text{Diag}(-1, 1, 1, 1, 1)$.

the 4D graviton $G_{\mu\nu}^{(0)}$, and its KK tower $G_{\mu\nu}^{(\vec{n})}$ with masses $m_{\vec{n}}^2 = |\vec{n}|^2/R^2$. At energies below $1/R$ the action is that of the zero mode

$$S_4^{(0)} = -\frac{\bar{M}_D^{2+\delta}}{2} \int d^4x V_\delta \sqrt{-g^{(0)}} \mathcal{R}^{(0)} + \int d^4x \sqrt{-g_{\text{ind}}^{(0)}} \mathcal{L}_{\text{SM}}, \quad (85.9)$$

where we can identify the 4D reduced Planck mass, $M_P \equiv 1/\sqrt{8\pi G_N} \simeq 2.4 \times 10^{18}$ GeV, as a function of the D -dimensional parameters:

$$M_P^2 = V^\delta \bar{M}_D^{2+\delta} \equiv R^\delta M_D^{2+\delta}. \quad (85.10)$$

Fixing M_D at around the electroweak scale $M_D \sim \text{TeV}$ to avoid introducing a new mass scale in the model, Eq. (85.10) gives a prediction for R :

$$\delta = 1, 2, \dots, 6 \rightarrow R \sim 10^9 \text{ km}, 0.5 \text{ mm}, \dots, 0.1 \text{ MeV}^{-1}. \quad (85.11)$$

The option $\delta = 1$ is clearly ruled out, as it leads to modifications of Newton's law at solar system distances. However this is not the case for $\delta \geq 2$, and possible observable consequences can be sought in present and future experiments.

Consistency of the model requires a stabilization mechanism for the radii of the extra dimensions, to the values shown in Eq. (85.11). The fact that we need $R \gg 1/M_D$ leads to a new hierarchy problem, the solution of which might require imposing supersymmetry in the extra-dimensional bulk (for the case of two extra dimensions see for example [20]).

85.2.2 Tests of the Gravitational Force Law at Sub-mm Distances

The KK modes of the graviton give rise to deviations from Newton's law of gravitation for distances $\lesssim R$. Such deviations are usually parameterized by a modified Newtonian potential of the form

$$V(r) = -G_N \frac{m_1 m_2}{r} \left[1 + \alpha e^{-r/\lambda} \right]. \quad (85.12)$$

For a 2-torus compactification, $\alpha = 16/3$ and $\lambda = R$. Searches for deviations from Newton's law of gravitation have been performed in several experiments [21–24]. From Ref. [23] we have the constraint $R < 30 \mu\text{m}$ at 95% CL for $\delta = 2$, corresponding to $M_D > 4.0$ TeV. We see then that bounds from Newton's law deviations are already pushing the scale M_D beyond the TeV for two extra dimensions.

85.2.3 Astrophysical and Cosmological Constraints

The light KK gravitons could be copiously produced in stars, carrying away energy. Ensuring that the graviton luminosity is low enough to preserve the agreement of stellar models with observations provides powerful bounds on the scale M_D . The most stringent bound arises from supernova SN1987A, giving $M_D > 27$ (2.4) TeV for $\delta = 2$ (3) [25]. After a supernova explosion, most of the KK gravitons stay gravitationally trapped in the remnant neutron star. The requirement that neutron stars are not excessively heated by KK decays into photons leads to $M_D > 1700$ (76) TeV for $\delta = 2$ (3) [26].

Cosmological constraints are also quite stringent [27]. To avoid overclosure of the Universe by relic gravitons one needs $M_D > 7$ TeV for $\delta = 2$. Relic KK gravitons decaying into photons contribute to the cosmic diffuse gamma radiation, from which one can derive the bound $M_D > 100$ TeV for $\delta = 2$.

We must mention however that bounds coming from the decays of KK gravitons into photons can be reduced if we assume that KK gravitons decay mainly into other non-SM states. This could happen, for example, if there were other 3-branes with hidden sectors residing on them [15].

85.2.4 Collider Signals

85.2.4.1 Graviton and Other Particle Production

Although each KK graviton has a purely gravitational coupling, suppressed by $1/M_P$, inclusive processes in which one sums over the almost continuous spectrum of available gravitons have cross sections suppressed only by powers of M_D . Processes involving gravitons are therefore detectable in collider experiments if $M_D \sim \text{TeV}$. A number of experimental searches for evidence of

large extra dimensions have been performed at colliders, and interpreted in the context of the ADD model.

One signature arises from direct graviton emission. By making a derivative expansion of Einstein gravity, one can construct an effective theory, valid for energies much lower than M_D , and use it to make predictions for graviton-emission processes at colliders [19, 28, 29]. Gravitons produced in the final state would escape detection, giving rise to missing transverse momentum ($p_{\text{T}}^{\text{miss}}$). The results quoted below are 95% CL lower limits on M_D for a range of values of δ between 2 and 6, with more stringent limits corresponding to lower δ values.

At hadron colliders, experimentally sensitive channels include the jet (j) + $p_{\text{T}}^{\text{miss}}$ and γ + $p_{\text{T}}^{\text{miss}}$ final states. ATLAS (CMS) j + $p_{\text{T}}^{\text{miss}}$ results with 139 (137) fb^{-1} of 13 TeV data provide limits of $M_D > 5.9 - 11.2$ TeV [30] ($M_D > 5.5 - 10.7$ TeV [31]). For these analyses, both experiments are assuming leading order (LO) cross sections. Since the effective theory is only valid for energies much less than M_D , the results are quoted for the full space, and include the information that suppressing the graviton cross section by a factor M_D^4/s^2 for $\sqrt{s} > M_D$, where \sqrt{s} is the parton-level center-of-mass energy of the hard collision, weakens the limits on M_D by a negligible amount for $\delta = 2$ ($\sim 3\%$ for $\delta = 6$). Less stringent limits are obtained by CMS [32] from analysis of 36 fb^{-1} of 13 TeV data in the γ + $p_{\text{T}}^{\text{miss}}$ final state ($M_D > 2.85 - 2.90$ TeV for $\delta = 3 - 6$). The analogous ATLAS search [33] uses full Run 2 statistics but does not quote ADD interpretation of the results.

In models in which the ADD scenario is embedded in a string theory at the TeV scale [18], we expect the string scale M_s to be smaller than M_D , and therefore expect production of string resonances at the LHC [34]. A result from CMS analyzing the dijet invariant mass distribution for 137 fb^{-1} of 13 TeV data excludes string resonances that decay predominantly to $q + g$ with masses below 7.9 TeV [35]. ATLAS dijet analysis [36] provides their results in the context of model-independent limits on the cross section times acceptance for generic resonances of a variety of possible widths, from which one can deduce similar lower mass limits ~ 8 TeV for string resonances decaying to $q + g$.

85.2.4.2 Virtual graviton effects

One can also search for virtual graviton effects, the calculation of which however depends on the ultraviolet cut-off of the theory and is therefore very model dependent. In the literature, several different formulations exist [19, 29, 37] for the dimension-eight operator for gravity exchange at tree level:

$$\mathcal{L}_8 = \pm \frac{4}{M_{TT}^4} \left(T_{\mu\nu} T^{\mu\nu} - \frac{1}{\delta + 2} T_\mu^\mu T_\nu^\nu \right), \quad (85.13)$$

where $T_{\mu\nu}$ is the energy-momentum tensor and M_{TT} is related to M_D by some model-dependent coefficient [38]. The relations with the parametrization of Refs. [37] and [19] are, respectively, $M_{TT} = M_S$ and $M_{TT} = (2/\pi)^{1/4} \Lambda_T$. The experimental results below are given as 95% CL lower limits on M_{TT} , including in some cases the possibility of both constructive or destructive interference, depending on the sign chosen in Eq. (9).

The most stringent limits arise from LHC analyses of the dijet angular distribution. Using 35.9 fb^{-1} of 13 TeV data, CMS [39] obtains results that correspond to an approximate limit of $M_{TT} \gtrsim 9$ TeV.

The next most restrictive results come from the analyses of diphoton ($M_{TT} > 6.1$ TeV from ATLAS [40] and $M_{TT} > 7.0$ TeV from CMS [41]) and dilepton mass spectra ($M_{TT} > 6.5$ TeV from CMS [42]). The complete Run 2 (139 fb^{-1}) analysis of ATLAS di-lepton data [43] does not quote the limits on ADD.

At the one-loop level, gravitons can also generate dimension-six operators with coefficients that are also model dependent. Experimental bounds on these operators can also give stringent constraints on M_D [38].

85.2.4.3 Black Hole Production

The physics at energies $\sqrt{s} \sim M_D$ is sensitive to the details of the unknown quantum theory of gravity. Nevertheless, in the transplanckian regime, $\sqrt{s} \gg M_D$, one can rely on a semiclassical description of gravity to obtain predictions. An interesting feature

of transplanckian physics is the creation of black holes [44,45] (for a review see, for example, [46]). A black hole is expected to be formed in a collision in which the impact parameter is smaller than the Schwarzschild radius [47]:

$$R_S = \frac{1}{M_D} \left[\frac{2^\delta \pi^{\delta-3/2}}{\delta+2} \Gamma\left(\frac{\delta+3}{2}\right) \frac{M_{BH}}{M_D} \right]^{1/(\delta+1)}, \quad (85.14)$$

where M_{BH} is the mass of the black hole, which would roughly correspond to the total energy in the collision. The cross section for black hole production can be estimated to be of the same order as the geometric area $\sigma \sim \pi R_S^2$. For $M_D \sim \text{TeV}$, this gives a production of $\sim 10^7$ black holes at the $\sqrt{s} = 14$ TeV LHC with an integrated luminosity of 30 fb^{-1} [44,45]. A black hole would provide a striking experimental signature since it is expected to thermally radiate with a Hawking temperature $T_H = (\delta+1)/(4\pi R_S)$, and therefore would evaporate democratically into all SM states. Nevertheless, given the present constraints on M_D , the LHC will not be able to reach energies much above M_D . This implies that predictions based on the semiclassical approximation could receive sizable modifications from model-dependent quantum-gravity effects.

The most stringent limits on microscopic black holes arise from LHC searches which observed no excesses above the SM background in high-multiplicity final states. The results are usually quoted as model-independent limits on the cross section for new physics in the final state and kinematic region analyzed. These results can then be used to provide constraints of models of low-scale gravity and weakly-coupled string theory. In addition, limits are sometimes quoted on particular implementations of models, which are used as benchmarks to illustrate the sensitivity.

A CMS analysis [48] of multi-object final states using 36 fb^{-1} of 13 TeV data, excludes semiclassical black holes below masses of up to 10.1 TeV for $M_D = 2$ TeV and $\delta = 6$. Analogous Run 2 ATLAS analysis [49], using 3.0 fb^{-1} of 13 TeV data, excludes black hole masses up to 9.0–9.7 TeV, depending on M_D , for $\delta = 6$. Another ATLAS search [50] for an excess of events with multiple high transverse momentum objects, including charged leptons and jets, using 3.2 fb^{-1} of 13 TeV data, excludes semiclassical black holes below masses of ~ 8.7 TeV for $M_D = 2$ TeV and $\delta = 6$.

A complementary approach is to look for jet extinction at high transverse momenta, as we expect hard short distance scattering processes to be highly suppressed at energies above M_D [51]. The CMS analysis [52] of inclusive jet p_T spectrum in 10.7 fb^{-1} of 8 TeV data set a lower limit of 3.3 TeV on the extinction mass scale.

For black hole masses near M_D , the semi-classical approximation is not valid, and one could instead expect quantum black holes (QBH) that decay primarily into two-body final states [53]. In the context of both ADD model with $\delta = 6$ the QBHs have been searched in few final state analysis (based on 2.3 fb^{-1} [54]), dijet [36,39,55], (same and different flavor) dilepton [56–60], photon+jet [61,62] and lepton+jet [63] channels by both ATLAS and CMS experiments. The Run 2 results at 13 TeV provide lower limits on QBH masses of up-to 9.4 TeV in an ADD model with $\delta = 6$. The strongest constraints are from dijet searches.

In weakly-coupled string models the semiclassical description of gravity fails in the energy range between M_s and M_s/g_s^2 where stringy effects are important. In this regime one expects, instead of black holes, the formation of string balls, made of highly excited long strings, that could be copiously produced at the LHC for $M_s \sim \text{TeV}$ [64], and would evaporate thermally at the Hagedorn temperature giving rise to high-multiplicity events. The same analyses used to search for black holes can be interpreted in the context of string balls. For example, for the case of $\delta = 6$ with $M_s = M_D/1.26 = 3$ TeV, the ATLAS multiple high transverse momentum object analysis [49] excludes string balls with masses below 6.5 to 9.0 TeV for values of $0.2 < g_s < 0.8$. The CMS multi-object analysis [48] studies string ball production in two scenarios, both assuming $\delta = 6$. For the constant $g_s = 0.2$ and $1 < M_s < 3.5$ TeV the string ball masses below 7.2 to 9.4 TeV are excluded, while at constant $M_s = 3.6$ TeV and $0.2 < g_s < 0.4$ masses below 7.2 to 8.1 TeV are excluded.

85.3 TeV-Scale Extra Dimensions

85.3.1 Warped Extra Dimensions

The RS model [3] is the most attractive setup of warped extra dimensions at the TeV scale, since it provides an alternative solution to the hierarchy problem. The RS model is based on a 5D theory with the extra dimension compactified in an orbifold, S^1/Z_2 , a circle S^1 with the extra identification of y with $-y$. This corresponds to the segment $y \in [0, \pi R]$, a manifold with boundaries at $y = 0$ and $y = \pi R$. Let us now assume that this 5D theory has a cosmological constant in the bulk Λ , and on the two boundaries Λ_0 and $\Lambda_{\pi R}$. The action is given by

$$S_5 = - \int d^4x dy \left\{ \sqrt{-g} \left[\frac{1}{2} M_5^3 \mathcal{R} + \Lambda \right] + \sqrt{-g_0} \delta(y) \Lambda_0 + \sqrt{-g_{\pi R}} \delta(y - \pi R) \Lambda_{\pi R} \right\}, \quad (85.15)$$

where g_0 and $g_{\pi R}$ are the values of the determinant of the induced metric on the two respective boundaries. Einstein's equations can be solved, giving in this case the metric

$$ds^2 = a(y)^2 dx^\mu dx^\nu \eta_{\mu\nu} + dy^2, \quad a(y) = e^{-ky}, \quad (85.16)$$

where $k = \sqrt{-\Lambda/6M_5^3}$. Consistency of the solution requires $\Lambda_0 = -\Lambda_{\pi R} = -\Lambda/k$. The metric in Eq. (85.16) corresponds to a 5D AdS space. The factor $a(y)$ is called the “warp” factor and determines how 4D scales change as a function of the position in the extra dimension. In particular, this implies that energy scales for 4D fields localized at the boundary at $y = \pi R$ are redshifted by a factor $e^{-k\pi R}$ with respect to those localized at $y = 0$. For this reason, the boundaries at $y = 0$ and $y = \pi R$ are usually referred to as the ultraviolet (UV) and infrared (IR) boundaries, respectively.

As in the ADD case, we can perform a KK reduction and obtain the low-energy effective theory of the 4D massless graviton. In this case we obtain

$$M_P^2 = \int_0^{\pi R} dy e^{-2ky} M_5^3 = \frac{M_5^3}{2k} (1 - e^{-2k\pi R}). \quad (85.17)$$

Taking $M_5 \sim k \sim M_P$, we can generate an IR-boundary scale of order $ke^{-k\pi R} \sim \text{TeV}$ for an extra dimension of radius $R \simeq 11/k$. Mechanisms to stabilize R to this value have been proposed [65,66] that, contrary to the ADD case, do not require introducing any new small or large parameter. Therefore a natural solution to the hierarchy problem can be achieved in this framework if the Higgs field, whose vacuum expectation value (VEV) is responsible for electroweak symmetry breaking, is localized at the IR-boundary where the effective mass scales are of order TeV. The radion field is generically heavy in models with a stabilized R . Nevertheless, it has been recently discussed that under some conditions a naturally light radion can arise [67–70]. In these cases the radion is identified with the dilaton, the Nambu-Goldstone boson associated to the spontaneous breaking of scale invariance, and its mass can be naturally below $ke^{-k\pi R} \sim \text{TeV}$.

In the RS model [3], all the SM fields were assumed to be localized on the IR-boundary. Nevertheless, for the hierarchy problem, only the Higgs field has to be localized there. SM gauge bosons and fermions can propagate in the 5D bulk [4–7] (for a review see, for example, [71,72]). By performing a KK reduction from the 5D action of a gauge boson, we find [4,5]

$$\frac{1}{g_4^2} = \int_0^{\pi R} dy \frac{1}{g_5^2} = \frac{\pi R}{g_5^2}, \quad (85.18)$$

where g_D ($D = 4, 5$) is the gauge coupling in D -dimensions. Therefore the 4D gauge couplings can be of order one, as is the case of the SM, if one demands $g_5^2 \sim \pi R$. Using $kR \sim 10$ and $g_4 \sim 0.5$, one obtains the 5D gauge coupling

$$g_5 \sim 4/\sqrt{k}. \quad (85.19)$$

Boundary kinetic terms for the gauge bosons can modify this relation, allowing for larger values of $g_5\sqrt{k}$.

Fermions propagating in a warped extra dimension have 4D massless zero-modes with wavefunctions which vary as $f_0 \sim \exp[(1/2 - c_f k)y]$, where $c_f k$ is their 5D mass [7,73]. Depending on the free parameter $c_f k$, fermions can be localized either towards the UV-boundary ($c_f > 1/2$) or IR-boundary ($c_f < 1/2$). Since the Higgs boson is localized on the IR-boundary, one can generate exponentially suppressed Yukawa couplings by having the fermion zero-modes localized towards the UV-boundary, generating naturally the light SM fermion spectrum [7]. A large overlap with the wavefunction of the Higgs is needed for the top quark, in order to generate its large mass, thus requiring it to be localized towards the IR-boundary. In conclusion, the large mass hierarchies present in the SM fermion spectrum can be easily obtained in warped models via suitable choices of the order-one parameters c_f [74]. In these scenarios, deviations in flavor physics from the SM predictions are expected to arise from flavor-changing KK gluon couplings [75], putting certain constraints on the parameters of the models and predicting new physics effects to be observed in B -physics processes (see, for example, [76,77]).

The masses of the KK states can also be calculated. One finds [7]

$$m_n \simeq \left(n + \frac{\alpha}{2} - \frac{1}{4} \right) \pi k e^{-\pi k R}, \quad (85.20)$$

where $n = 1, 2, \dots$ and $\alpha = \{c_f - 1/2, 0, 1\}$ for KK fermions, KK gauge bosons and KK gravitons, respectively. Their masses are of order $k e^{-\pi k R} \sim \text{TeV}$ (for this reason we refer to these scenarios as TeV-scale extra dimensions). The first KK state of the gauge bosons would be the lightest, while gravitons are expected to be the heaviest.

85.3.1.1 Models of Electroweak Symmetry Breaking

Theories in warped extra dimensions can be used to implement symmetry breaking at low energies by boundary conditions (for a review see, for example, [78]). For example, for a $U(1)$ gauge symmetry in the 5D bulk, this can be easily achieved by imposing a Dirichlet boundary condition on the IR-boundary for the gauge-boson field, $A_\mu|_{y=\pi R} = 0$. This makes the zero-mode gauge boson get a mass, given by $m_A = g_4 \sqrt{2k/g_5^2} e^{-\pi k R}$. A very different situation occurs if the Dirichlet boundary condition is imposed on the UV-boundary, $A_\mu|_{y=0} = 0$. In this case the zero-mode gauge boson disappears from the spectrum. Finally, if a Dirichlet boundary condition is imposed on the two boundaries, one obtains a massless 4D scalar corresponding to the fifth component of the 5D gauge boson, A_5 . Thus, different scenarios can be implemented by appropriately choosing the 5D bulk gauge symmetry, \mathcal{G}_5 , and the symmetries to which it reduces on the UV and IR-boundary, \mathcal{H}_{UV} and \mathcal{H}_{IR} , respectively. In all cases the KK spectrum comes in representations of the group \mathcal{G}_5 .

Among the most interesting scenarios are those called gauge-Higgs unified models, where the Higgs boson appears as the fifth component of a 5D gauge boson, A_5 . The Higgs mass is protected by the 5D gauge invariance and can only get a nonzero value from non-local one-loop effects [79]. To guarantee the relation $M_W^2 \simeq M_Z^2 \cos^2 \theta_W$, a custodial $SU(2)_V$ symmetry is needed in the bulk and IR-boundary [80]. The simplest realization [81,82] has

$$\begin{aligned} \mathcal{G}_5 &= SU(3)_c \times SO(5) \times U(1)_X, \\ \mathcal{H}_{IR} &= SU(3)_c \times SO(4) \times U(1)_X, \\ \mathcal{H}_{UV} &= G_{SM}. \end{aligned}$$

The Higgs boson gets a potential at the one-loop level that triggers a VEV, breaking the electroweak symmetry. In these models there is a light Higgs boson whose mass can be around 125 GeV, as required by the discovered Higgs boson [83]. This state, as will be explained in Sec. 85.3.2, behaves as a composite pseudo-Nambu-Goldstone boson with couplings that deviate from the SM Higgs [84]. The present experimental determination of the Higgs couplings at the LHC, that agrees with the SM predictions, put important constraints on these scenarios [83]. The lightest KK modes of the model are color fermions with charges $Q = -1/3, 2/3$ and $5/3$ [85].

85.3.1.2 Constraints from Electroweak Precision Tests

Models in which the SM gauge bosons propagate in 1/TeV-sized extra dimensions give generically large corrections to electroweak observables. When the SM fermions are confined on a boundary these corrections are universal and can be parameterized by four quantities: \widehat{S} , \widehat{T} , W and Y , as defined in Ref. [86]. For warped models, where the 5D gauge coupling of Eq. (85.19) is large, the most relevant parameter is \widehat{T} , which gives the bound $m_{KK} \gtrsim 10 \text{ TeV}$ [71]. When a custodial symmetry is imposed [80], the main constraint comes from the \widehat{S} parameter, requiring $m_{KK} \gtrsim 3 \text{ TeV}$, independent of the value of g_5 . Corrections to the $Z b_L \bar{b}_L$ coupling can also be important [71], especially in warped models for electroweak symmetry breaking as the ones described above.

85.3.1.3 Kaluza-Klein Searches

The main prediction of 1/TeV-sized extra dimensions is the presence of a discretized KK spectrum, with masses around the TeV scale, associated with the SM fields that propagate in the extra dimension.

In the RS model [3], only gravity propagates in the 5D bulk. Experimental searches have been performed for the lightest KK graviton through its decay to a variety of SM particle-antiparticle pairs. The results are usually interpreted in the plane of the dimensionless coupling k/M_P versus m_1 , where M_P is the reduced Planck mass defined previously and m_1 is the mass of the lightest KK excitation of the graviton. Since the AdS curvature $\sim k$ cannot exceed the cut-off scale of the model, which is estimated to be $\ell_5^{1/3} M_5$ [38], one must demand $k \ll \sqrt{2\ell_5} M_P \simeq 40 M_P$. The most stringent limits currently arise from LHC searches for resonances in the dilepton and diphoton final states, using 13 TeV collisions. Searches with the $\gamma\gamma$ final state are an especially powerful approach, given that these final states have a branching fraction twice that of any individual lepton flavor. The CMS analysis [41] of 36 fb⁻¹ of 13 TeV data excludes KK gravitons below 2.3 to 4.6 TeV, depending on the value of the coupling k/M_P , which is varied between 0.01 and 0.2, while ATLAS [87] uses the full 139 fb⁻¹ and provides a lower limit on the KK graviton mass of 4.5 TeV for the coupling parameter 0.1. The CMS [42] dilepton analyses, combining results from the ee and $\mu\mu$ channels, exclude KK gravitons with masses 2.47–4.78 TeV for k/M_P values of 0.01–0.1. The ATLAS [88] analysis of 139 fb⁻¹ of Run 2 data does not include a RS KK graviton interpretation of the results. Less stringent limits on the KK graviton mass can be derived from analyses of the dijet [35,36,89,90], HH [91–99], and VV [100–104] final states, where V can represent either a W or Z boson.

In addition, both ATLAS and CMS experiments directly search for heavy radions, with masses above 1 TeV where the dominant decay mode is to pairs of bosons. The main production mechanism is gluon fusion. ATLAS [102] (CMS [105]) excludes radion masses below 3.2 TeV (3.1 TeV) for a radion decaying into WW, ZZ . Radions are also searched in final states with pairs of Higgs bosons HH [91,94,96,97,99,106], and dijet final states [107] with additional gluons. Bounds for a light radion (1 keV–10 GeV mass range) can be found in [108].

In warped extra-dimensional models in which the SM fields propagate in the 5D bulk, the couplings of the KK graviton to $ee/\mu\mu/\gamma\gamma$ are suppressed [109], and the above bounds do not apply. Furthermore, the KK graviton is the heaviest KK state (see Eq. (85.20)), and therefore experimental searches for KK gauge bosons and fermions are more appropriate discovery channels in these scenarios. For the scenarios discussed above in which only the Higgs boson and the top quark are localized close to the IR-boundary, the KK gauge bosons mainly decay into top quarks, longitudinal W/Z bosons, and Higgs bosons. Couplings to light SM fermions are suppressed by a factor $g/\sqrt{g_5^2 k} \sim 0.2$ [7] for the value of Eq. (85.19) that is considered from now on. Searches have been made for evidence of the lightest KK excitation of the gluon, through its decay to $t\bar{t}$ pairs. The searches take into account the natural KK gluon width, which is typically $\sim 15\%$ of its mass. The decay of a heavy particle to $t\bar{t}$ would tend to produce highly boosted top (anti-)quarks in the final state. Products of the subsequent top decays would therefore tend to be close to each other in the detector. In the case of $t \rightarrow Wb \rightarrow jjb$ decays, the three

jets could overlap with one another and not be individually reconstructed with the standard jet algorithms, while $t \rightarrow Wb \rightarrow \ell\nu b$ decays could result in the lepton failing standard isolation requirements due to its proximity to the b -jet; in both cases, the efficiency for properly reconstructing the final state would fall as the mass of the original particle increases. To avoid the loss in sensitivity which would result, a number of techniques, known generally as top quark tagging [110, 111], have been developed to reconstruct and identify highly boosted top quarks, for example by using a single wide jet to contain all the decay products of a hadronic top decay. The large backgrounds from QCD jets can then be reduced by requiring the jet mass be consistent with that of a top quark, and also by examining the substructure of the wide jet for indication that it resulted from the hadronic decay of a top quark. These techniques are key to extending to very high masses the range of accessible resonances decaying to $t\bar{t}$ pairs. While the ATLAS search in 139 fb⁻¹ of Run 2 data [112] does not provide a KK interpretation, dedicated analysis from CMS [113] of 36 fb⁻¹ of 13 TeV data combines di-lepton, lepton-plus-jet, and all-hadronic $t\bar{t}$ decays and excludes KK gluons with masses below 4.55 TeV. ATLAS uses all-hadronic [114] and lepton-plus-jet [115] final states to exclude KK gluons up to 3.4 and 3.8 TeV respectively with 36fb⁻¹ of 13 TeV data. The results are not directly comparable between the two LHC experiments, since they employ in their respective analyses different implementations of the theoretical model. For masses between 3 and 5 TeV, the cross-section limits are around 20 fb for CMS analysis of 36 fb⁻¹ and 30 fb (4 fb) for ATLAS analyses of 36 (139) fb⁻¹.

A gauge boson KK excitation could be also sought through its decay to longitudinal W/Z bosons. Recent analyses from ATLAS [116] (and CMS [117]) with 139 (137) fb⁻¹ of 13 TeV data searching for heavy vector resonances decaying to a W or Z boson and a Higgs in the $q\bar{q}b\bar{b}$ final state have set a lower limit on the mass of these KK of 3.2 (3.7) TeV (warped models are equivalent to the Model B considered in the analyses with $g_V \sim g_5\sqrt{k}$). The decay to a pair of intermediate vector bosons has also been exploited to search for KK gravitons in models in which the SM fields propagate in the 5D bulk. The analyses typically reconstruct hadronic W/Z decays using variants of the boosted techniques mentioned previously. An ATLAS analysis [118] combines leptonic and hadronic final states from the KK graviton decay $G^* \rightarrow VV$, where V can represent either a W or Z boson, exclude KK gravitons with masses below 2.3 TeV, for a value of $k/M_P = 1$. CMS VV analyses [105, 119, 120] using 137 fb⁻¹ of 13 TeV data also exclude KK gravitons with masses below 1.8 TeV in the context of bulk gravitons for a maximum value of $k/M_P = 0.5$.

The lightest KK states are, in certain models, the partners of the top quark. For example, in 5D composite Higgs models these are colored states with charges $Q = -1/3, 2/3$ and $5/3$ (arising from $SU(2)_L$ doublets with $Y = 7/6, 1/6$), and masses expected to be below the TeV [85]. They can be either singly or pair-produced, and mainly decay into a combination of W/Z with top/bottom quarks [121–124]. An exhaustive review of these searches can be found in Ref. [125]. Of particular note, the $Q = 5/3$ state decays mainly into $W^+t \rightarrow W^+W^+b$, giving a very clean signature of a pair of same-sign leptons in the final state. An analysis by ATLAS [126] searching in the lepton-plus-jets final state for evidence of pair production of the $Q = 5/3$ state provides a lower mass limit of 1.25 TeV. A CMS analysis [127] searching for pair production of the $Q = 5/3$ state using both lepton-plus-jets and same sign lepton final states excludes masses below 1.3 TeV. Similarly, searches for single production of the $Q = 5/3$ state [128], also excludes masses up to 0.9 to 1.5 TeV depending on the model parameters. Both LHC experiments have searched for pair production of vector-like quarks T and B of charges $Q = 2/3$ and $-1/3$ respectively, assuming the allowable decays are $T \rightarrow Wb/Zt/Ht$ and $B \rightarrow Wt/Zb/Hb$. In each case, it is assumed the branching fractions of the three decay modes sum to unity, but the individual branching fractions, which are model-dependent, are allowed to vary within this constraint. Both ATLAS [129–131] and CMS [132, 133] obtain lower limits on the mass of the T and B vector-like quarks up to 1.5 TeV and 1.6 TeV respectively.

Analyses from ATLAS [134–138] and CMS [128, 139–142] also

search for a single top partner and single bottom partner production, the cross section for which is model-dependent [143] but does not carry the kinematic penalty for producing two heavy objects.

85.3.2 Connection with Strongly Coupled Models via the AdS/CFT Correspondence

The AdS/CFT correspondence [8] provides a connection between warped extra-dimensional models and strongly-coupled theories in ordinary 4D. Although the exact connection is only known for certain cases, the AdS/CFT techniques have been very useful to obtain, at the qualitative level, a 4D holographic description of the various phenomena in warped extra-dimensional models [11, 72].

The connection goes as follows. The physics of the bulk AdS₅ models can be interpreted as that of a 4D conformal field theory (CFT) which is strongly coupled. The extra-dimensional coordinate y plays the role of the renormalization scale μ of the CFT by means of the identification $\mu \equiv ke^{-ky}$. Therefore the UV-boundary corresponds in the CFT to a UV cut-off scale at $\Lambda_{UV} = k \sim M_P$, breaking explicitly conformal invariance, while the IR-boundary can be interpreted as a spontaneous breaking of the conformal symmetry at energies $ke^{-k\pi R} \sim \text{TeV}$. Fields localized on the UV-boundary are elementary fields external to the CFT, while fields localized on the IR-boundary and KK states correspond to composite resonances of the CFT. Furthermore, local gauge symmetries in the 5D models, \mathcal{G}_5 , correspond to global symmetries of the CFT, while the UV-boundary symmetry can be interpreted as a gauging of the subgroup \mathcal{H}_{UV} of \mathcal{G}_5 in the CFT. Breaking gauge symmetries by IR-boundary conditions corresponds to the spontaneous breaking $\mathcal{G}_5 \rightarrow \mathcal{H}_{IR}$ in the CFT at energies $\sim ke^{-k\pi R}$. Using this correspondence one can easily derive the 4D massless spectrum of the compactified AdS₅ models. One also has the identification $k^3/M_5^3 \approx 16\pi^2/N^2$ and $g_5^2 k \approx 16\pi^2/N^r$ ($r = 1$ or 2 for CFT fields in the fundamental or adjoint representation of the gauge group), where N plays the role of the number of colors of the CFT. Therefore the weak-coupling limit in AdS₅ corresponds to a large- N expansion in the CFT.

Following the above AdS/CFT dictionary one can understand the RS solution to the hierarchy problem from a 4D viewpoint. The equivalent 4D model is a CFT with a TeV mass gap and a Higgs boson emerging as a composite state. In the particular case where the Higgs is the fifth-component of the gauge-boson, A_5 [144], this corresponds to models, similar to those proposed in Ref. [145–148], where the Higgs is a composite pseudo-Nambu-Goldstone boson arising from the spontaneous breaking $\mathcal{G}_5 \rightarrow \mathcal{H}_{IR}$ in the CFT. The AdS/CFT dictionary tells us that KK states must behave as composite resonances. For example, if the SM gauge bosons propagate in the 5D bulk, the lowest KK $SU(2)_L$ -gauge boson must have properties similar to those of the Techni-rho ρ_T [125] with a coupling to longitudinal W/Z bosons given by $g_5\sqrt{k} \approx g_{\rho_T}$, while the coupling to elementary fermions is $g^2/\sqrt{g_5^2 k} \approx g^2 F_{\rho_T}/M_{\rho_T}$.

Fermions in compactified AdS₅ also have a simple 4D holographic interpretation. The 4D massless mode described in Sec. 85.3.1 corresponds to an external fermion ψ_i linearly coupled to a fermionic CFT operator \mathcal{O}_i : $\mathcal{L}_{\text{int}} = \lambda_i \bar{\psi}_i \mathcal{O}_i + h.c.$. The dimension of the operator \mathcal{O}_i is related to the 5D fermion mass according to $\text{Dim}[\mathcal{O}_i] = |c_f + 1/2| - 1$. Therefore, by varying c_f one varies $\text{Dim}[\mathcal{O}_i]$, making the coupling λ_i irrelevant ($c_f > 1/2$), marginal ($c_f = 1/2$) or relevant ($c_f < 1/2$). When irrelevant, the coupling is exponentially suppressed at low energies, and then the coupling of ψ_i to the CFT (and eventually to the composite Higgs) is very small. When relevant, the coupling grows in the IR and becomes as large as g_5 (in units of k), meaning that the fermion is as strongly coupled as the CFT states [81]. In this latter case ψ_i behaves as a composite fermion.

85.3.3 Linear dilaton geometry

The warp factor $a(y)$ in Eq. (85.16) can be different from the exponential considered above, giving rise to a different KK mass spectrum. A particularly interesting case is the linear dilaton geometry [149] where the KK states become very narrowly-spaced. These scenarios can also be understood in 4D via the clockwork mechanism [150], and for this reason are usually referred to as

Clockwork/Linear Dilaton (CW/LD) models. The collider phenomenology becomes different in these models since the decay of the narrowly-spaced KK spectrum appears as a periodic signal in the invariant mass of the decaying products. An excellent detector resolution is needed in order to resolve these KK modes which can be done by looking at 2 electrons or 2 photons in the final state. A search for this type of KK gravitons decaying into ee [151] and $\gamma\gamma$ [151, 152] put bounds for M_5 in the range of 10 TeV to 1 TeV for values of the lightest KK graviton mass (referred as k in [151, 152]) in the range of few TeVs.

85.3.4 Flat Extra Dimensions

Models with quantum gravity at the TeV scale, as in the ADD scenario, can have extra (flat) dimensions of $1/\text{TeV}$ size, as happens in string scenarios (see, for example, [153]). All SM fields may propagate in these extra dimensions, leading to the possibility of observing their corresponding KK states.

A simple example is to assume that the SM gauge bosons propagate in a flat five-dimensional orbifold S^1/Z_2 of radius R , with the fermions localized on a 4D boundary. The KK gauge bosons behave as sequential SM gauge bosons with a coupling to fermions enhanced by a factor $\sqrt{2}$ [153]. The experimental limits on such sequential gauge bosons could therefore be recast as limits on KK gauge bosons. Such an interpretation of the ATLAS 7 TeV dilepton analysis [154] yielded the bound $1/R > 4.16$ TeV, while a CMS 8 TeV search with a lepton and missing transverse energy in the final state [155] give $1/R > 3.4$ TeV. Indirect bounds from LEP2 require however $1/R \gtrsim 6$ TeV [86, 156], a bound that can considerably improve in the future by high-energy measurements of the dilepton invariant mass spectrum from Drell-Yan processes at the LHC [157]. More recent LHC limits on leptonically decaying gauge bosons [88, 158–162] are not interpreted as bounds on $1/R$ by the collaborations, but the published results allow for independent derivation of such bounds.

An alternative scenario, known as Universal Extra Dimensions (UED) [163] (for a review see, for example, [164]), assumes that all SM fields propagate universally in a flat orbifold S^1/Z_2 with an extra Z_2 parity, called KK-parity, that interchanges the two boundaries. In this case, the lowest KK state is stable and is a Dark Matter candidate. At colliders, the KK particles would have to be created in pairs, and would then cascade decay to the lightest KK particle, which would be stable and escape detection. The UED mass-spectrum depends not only on the extra-dimensional radius R , but also on the cut-off of the 5D theory Λ , since quantum corrections sensitive to ΛR induce mass-splittings between the KK states. Experimental signatures, such as jets or leptons and p_T^{miss} , would be similar to those of typical R -parity conserving SUSY searches. An interpretation of the recent LHC experimental SUSY searches for UED models has been presented in Refs. [165, 166]. A lower bound $1/R > 1.4 - 1.5$ TeV was derived for ΛR in the range $5 - 35$ [165]. A recent analysis is given in Ref. [167] where it is shown that the minimal UED model is ruled out when LHC data is combined with Dark Matter relic density data. Extensions to the minimal UED model where boundary terms are included can however be compatible with experiments [167].

Finally, realistic models of electroweak symmetry breaking can also be constructed with flat extra spatial dimensions, similarly to those in the warped case, requiring, however, the presence of sizeable boundary kinetic terms [168]. There is also the possibility of breaking supersymmetry by boundary conditions [169]. Models of this type could explain naturally the presence of a Higgs boson lighter than $M_D \sim \text{TeV}$ (see, for example, [170–172]).

References

- [1] For a comprehensive collection of the original papers see, “Modern Kaluza-Klein Theories”, edited by T. Appelquist *et al.*, Addison-Wesley (1987).
- [2] N. Arkani-Hamed, S. Dimopoulos and G. Dvali, Phys. Lett. **B429**, 263 (1998), [hep-ph/9803315].
- [3] L. Randall and R. Sundrum, Phys. Rev. Lett. **83**, 3370 (1999), [hep-ph/9905221].
- [4] H. Davoudiasl, J. L. Hewett and T. G. Rizzo, Phys. Lett. **B473**, 43 (2000), [hep-ph/9911262].
- [5] A. Pomarol, Phys. Lett. **B486**, 153 (2000), [hep-ph/9911294].
- [6] S. Chang *et al.*, Phys. Rev. **D62**, 084025 (2000), [hep-ph/9912498].
- [7] T. Gherghetta and A. Pomarol, Nucl. Phys. **B586**, 141 (2000), [hep-ph/0003129].
- [8] J. M. Maldacena, Int. J. Theor. Phys. **38**, 1113 (1999), [Adv. Theor. Math. Phys.2,231(1998)], [hep-th/9711200].
- [9] E. Witten, Adv. Theor. Math. Phys. **2**, 253 (1998), [hep-th/9802150].
- [10] S. S. Gubser, I. R. Klebanov and A. M. Polyakov, Phys. Lett. **B428**, 105 (1998), [hep-th/9802109].
- [11] N. Arkani-Hamed, M. Porrati and L. Randall, JHEP **08**, 017 (2001), [hep-th/0012148].
- [12] ATLAS public results are available on WWW at <https://twiki.cern.ch/twiki/bin/view/AtlasPublic>.
- [13] CMS public results are available on WWW at <https://cms-results.web.cern.ch/cms-results/public-results/publications>.
- [14] Z. Chacko, M. A. Luty and E. Ponton, JHEP **07**, 036 (2000), [hep-ph/9909248].
- [15] N. Arkani-Hamed, S. Dimopoulos and G. R. Dvali, Phys. Rev. **D59**, 086004 (1999), [hep-ph/9807344].
- [16] R. Rattazzi, hep-ph/0607055 (2006); I. Antoniadis, Yellow report CERN-2002-002 (2002).
- [17] J. D. Lykken, Phys. Rev. **D54**, R3693 (1996), [hep-th/9603133].
- [18] I. Antoniadis *et al.*, Phys. Lett. **B436**, 257 (1998), [hep-ph/9804398].
- [19] G. F. Giudice, R. Rattazzi and J. D. Wells, Nucl. Phys. **B544**, 3 (1999), [hep-ph/9811291].
- [20] N. Arkani-Hamed *et al.*, Phys. Rev. **D62**, 105002 (2000), [hep-ph/9912453].
- [21] E. G. Adelberger *et al.*, Prog. Part. Nucl. Phys. **62**, 102 (2009).
- [22] J. Murata and S. Tanaka, Class. Quant. Grav. **32**, 3, 033001 (2015), [arXiv:1408.3588].
- [23] W.-H. Tan *et al.*, Phys. Rev. Lett. **116**, 13, 131101 (2016).
- [24] J. G. Lee *et al.*, Phys. Rev. Lett. **124**, 101101 (2020), [arXiv:2002.11761].
- [25] C. Hanhart *et al.*, Phys. Lett. **B509**, 1 (2001), [arXiv:astro-ph/0102063].
- [26] S. Hannestad and G. G. Raffelt, Phys. Rev. **D67**, 125008 (2003), [Erratum: Phys. Rev.D69,029901(2004)], [hep-ph/0304029].
- [27] L. J. Hall and D. Tucker-Smith, Phys. Rev. **D60**, 085008 (1999), [hep-ph/9904267].
- [28] E. A. Mirabelli, M. Perelstein and M. E. Peskin, Phys. Rev. Lett. **82**, 2236 (1999), [hep-ph/9811337].
- [29] T. Han, J. D. Lykken and R.-J. Zhang, Phys. Rev. **D59**, 105006 (1999), [hep-ph/9811350].
- [30] G. Aad *et al.* (ATLAS), Phys. Rev. D **103**, 112006 (2021), [arXiv:2102.10874].
- [31] A. Tumasyan *et al.* (CMS), JHEP **11**, 153 (2021), [arXiv:2107.13021].
- [32] A. M. Sirunyan *et al.* (CMS), JHEP **02**, 074 (2019), [arXiv:1810.00196].
- [33] G. Aad *et al.* (ATLAS), JHEP **02**, 226 (2021), [arXiv:2011.05259].
- [34] S. Cullen, M. Perelstein and M. E. Peskin, Phys. Rev. **D62**, 055012 (2000), [hep-ph/0001166].
- [35] A. M. Sirunyan *et al.* (CMS), JHEP **05**, 033 (2020), [arXiv:1911.03947].

- [36] G. Aad *et al.* (ATLAS), JHEP **03**, 145 (2020), [arXiv:1910.08447].
- [37] J. L. Hewett, Phys. Rev. Lett. **82**, 4765 (1999), [hep-ph/9811356].
- [38] G. F. Giudice and A. Strumia, Nucl. Phys. **B663**, 377 (2003), [hep-ph/0301232].
- [39] A. M. Sirunyan *et al.* (CMS), Eur. Phys. J. **C78**, 9, 789 (2018), [arXiv:1803.08030].
- [40] M. Aaboud *et al.* (ATLAS), Phys. Lett. **B775**, 105 (2017), [arXiv:1707.04147].
- [41] A. M. Sirunyan *et al.* (CMS), Phys. Rev. **D98**, 9, 092001 (2018), [arXiv:1809.00327].
- [42] A. M. Sirunyan *et al.*, JHEP **07**, 7 (2021), [arXiv:2103.02708].
- [43] G. Aad *et al.*, JHEP **11**, 005 (2020), [arXiv:2006.12946].
- [44] S. B. Giddings and S. D. Thomas, Phys. Rev. **D65**, 056010 (2002), [hep-ph/0106219].
- [45] S. Dimopoulos and G. L. Landsberg, Phys. Rev. Lett. **87**, 161602 (2001), [hep-ph/0106295].
- [46] P. Kanti, Int. J. Mod. Phys. **A19**, 4899 (2004), [hep-ph/0402168].
- [47] R. C. Myers and M. J. Perry, Annals Phys. **172**, 304 (1986).
- [48] A. M. Sirunyan *et al.* (CMS), JHEP **11**, 042 (2018), [arXiv:1805.06013].
- [49] G. Aad *et al.* (ATLAS), JHEP **03**, 026 (2016), [arXiv:1512.02586].
- [50] M. Aaboud *et al.* (ATLAS), Phys. Lett. **B760**, 520 (2016), [arXiv:1606.02265].
- [51] C. Kilic *et al.*, Phys. Rev. **D89**, 1, 016003 (2014), [arXiv:1207.3525].
- [52] V. Khachatryan *et al.* (CMS), Phys. Rev. **D90**, 3, 032005 (2014), [arXiv:1405.7653].
- [53] P. Meade and L. Randall, JHEP **05**, 003 (2008), [arXiv:0708.3017].
- [54] A. M. Sirunyan *et al.* (CMS), Phys. Lett. **B774**, 279 (2017), [arXiv:1705.01403].
- [55] G. Aad *et al.* (ATLAS), Phys. Lett. B **754**, 302 (2016), [arXiv:1512.01530].
- [56] G. Aad *et al.* (ATLAS) (2023), [arXiv:2307.08567].
- [57] M. Aaboud *et al.* (ATLAS), Eur. Phys. J. C **76**, 10, 541 (2016), [arXiv:1607.08079].
- [58] M. Aaboud *et al.* (ATLAS), Phys. Rev. **D98**, 9, 092008 (2018), [arXiv:1807.06573].
- [59] A. Tumasyan *et al.* (CMS), JHEP **05**, 227 (2023), [arXiv:2205.06709].
- [60] A. M. Sirunyan *et al.* (CMS), JHEP **04**, 073 (2018), [arXiv:1802.01122].
- [61] A. Tumasyan *et al.* (CMS) (2023), [arXiv:2305.07998].
- [62] M. Aaboud *et al.* (ATLAS), Eur. Phys. J. C **78**, 2, 102 (2018), [arXiv:1709.10440].
- [63] G. Aad *et al.* (ATLAS) (2023), [arXiv:2307.14967].
- [64] S. Dimopoulos and R. Emparan, Phys. Lett. **B526**, 393 (2002), [hep-ph/0108060].
- [65] W. D. Goldberger and M. B. Wise, Phys. Rev. Lett. **83**, 4922 (1999), [hep-ph/9907447].
- [66] J. Garriga and A. Pomarol, Phys. Lett. **B560**, 91 (2003), [hep-th/0212227].
- [67] See talk by R. Rattazzi at Planck 2010, CERN, <https://indico.cern.ch/getFile.py/access?contribId=163&resId=0&materialId=slides&confId=75810>.
- [68] B. Bellazzini *et al.*, Eur. Phys. J. **C74**, 2790 (2014), [arXiv:1305.3919].
- [69] F. Coradeschi *et al.*, JHEP **11**, 057 (2013), [arXiv:1306.4601].
- [70] E. Megias and O. Pujolas, JHEP **08**, 081 (2014), [arXiv:1401.4998].
- [71] E. P. H. Davoudiasl, S. Gopalakrishna and J. Santiago, New J. Phys. **12**, 075011 (2010), [arXiv:0908.1968].
- [72] T. Gherghetta, in “Physics of the large and the small, TASI 09, proceedings of the Theoretical Advanced Study Institute in Elementary Particle Physics, Boulder, Colorado, USA, 1-26 June 2009,” 165–232 (2011), [arXiv:1008.2570].
- [73] Y. Grossman and M. Neubert, Phys. Lett. **B474**, 361 (2000), [hep-ph/9912408].
- [74] S. J. Huber and Q. Shafi, Phys. Lett. **B498**, 256 (2001), [hep-ph/0010195].
- [75] A. Delgado, A. Pomarol and M. Quiros, JHEP **01**, 030 (2000), [hep-ph/9911252].
- [76] K. Agashe, G. Perez and A. Soni, Phys. Rev. **D71**, 016002 (2005), [hep-ph/0408134].
- [77] M. Bauer *et al.*, JHEP **09**, 017 (2010), [arXiv:0912.1625].
- [78] A. Pomarol, Int. J. Mod. Phys. **A24**, 61 (2009), [In Kane, Gordon (ed.) *et al.: Perspectives on LHC physics*, 259(2008)].
- [79] Y. Hosotani, Phys. Lett. **126B**, 309 (1983).
- [80] K. Agashe *et al.*, JHEP **08**, 050 (2003), [hep-ph/0308036].
- [81] K. Agashe, R. Contino and A. Pomarol, Nucl. Phys. **B719**, 165 (2005), [hep-ph/0412089].
- [82] For a review see, for example, R. Contino, arXiv:1005.4269.
- [83] See, for example, PDG review of Higgs boson in this *Review*.
- [84] G. F. Giudice *et al.*, JHEP **06**, 045 (2007), [hep-ph/0703164].
- [85] R. Contino, L. Da Rold and A. Pomarol, Phys. Rev. **D75**, 055014 (2007), [hep-ph/0612048].
- [86] R. Barbieri *et al.*, Nucl. Phys. **B703**, 127 (2004), [hep-ph/0405040].
- [87] G. Aad *et al.* (ATLAS) (2021), [arXiv:2102.13405].
- [88] G. Aad *et al.* (ATLAS), Phys. Lett. **B796**, 68 (2019), [arXiv:1903.06248].
- [89] A. M. Sirunyan *et al.* (CMS), JHEP **08**, 130 (2018), [arXiv:1806.00843].
- [90] G. Aad *et al.* (ATLAS), Phys. Rev. Lett. **125**, 13, 131801 (2020), [arXiv:2005.02983].
- [91] A. M. Sirunyan *et al.* (CMS), Phys. Rev. Lett. **122**, 12, 121803 (2019), [arXiv:1811.09689].
- [92] M. Aaboud *et al.* (ATLAS), JHEP **01**, 030 (2019), [arXiv:1804.06174].
- [93] G. Aad *et al.* (ATLAS), Phys. Lett. B **800**, 135103 (2020), [arXiv:1906.02025].
- [94] G. Aad *et al.* (ATLAS), Phys. Rev. D **106**, 5, 052001 (2022), [arXiv:2112.11876].
- [95] G. Aad *et al.* (ATLAS), JHEP **11**, 163 (2020), [arXiv:2007.14811].
- [96] A. M. Sirunyan *et al.* (CMS), Phys. Rev. D **102**, 3, 032003 (2020), [arXiv:2006.06391].
- [97] A. Tumasyan *et al.* (CMS), JHEP **05**, 005 (2022), [arXiv:2112.03161].
- [98] A. Tumasyan *et al.* (CMS) (2021), [arXiv:2106.10361].
- [99] A. Tumasyan *et al.* (CMS), JHEP **07**, 095 (2023), [arXiv:2206.10268].
- [100] G. Aad *et al.* (ATLAS), JHEP **09**, 091 (2019), [Erratum: JHEP 06, 042 (2020)], [arXiv:1906.08589].
- [101] A. M. Sirunyan *et al.* (CMS) (2019), [arXiv:1906.05977].
- [102] G. Aad *et al.* (ATLAS), Eur. Phys. J. C **80**, 12, 1165 (2020), [arXiv:2004.14636].
- [103] G. Aad *et al.* (ATLAS), Eur. Phys. J. C **81**, 4, 332 (2021), [arXiv:2009.14791].

- [104] A. Tumasyan *et al.* (CMS), Phys. Lett. B **844**, 137813 (2023), [arXiv:2210.00043].
- [105] A. Tumasyan *et al.* (CMS), Phys. Rev. D **105**, 3, 032008 (2022), [arXiv:2109.06055].
- [106] A. M. Sirunyan *et al.* (CMS), JHEP **01**, 051 (2019), [arXiv:1808.01365].
- [107] A. Tumasyan *et al.* (CMS), Phys. Lett. B **832**, 137263 (2022), [arXiv:2201.02140].
- [108] F. Abu-Ajamieh, J. S. Lee and J. Terning, JHEP **10**, 050 (2018), [arXiv:1711.02697].
- [109] K. Agashe *et al.*, Phys. Rev. **D76**, 036006 (2007), [hep-ph/0701186].
- [110] M. Aaboud *et al.* (ATLAS), Eur. Phys. J. C **79**, 5, 375 (2019), [arXiv:1808.07858].
- [111] A. M. Sirunyan *et al.* (CMS), JINST **15**, 06, P06005 (2020), [arXiv:2004.08262].
- [112] G. Aad *et al.* (ATLAS), JHEP **10**, 061 (2020), [arXiv:2005.05138].
- [113] A. M. Sirunyan *et al.* (CMS), JHEP **04**, 031 (2019), [arXiv:1810.05905].
- [114] M. Aaboud *et al.* (ATLAS), Phys. Rev. **D99**, 9, 092004 (2019), [arXiv:1902.10077].
- [115] M. Aaboud *et al.* (ATLAS), Eur. Phys. J. C **78**, 7, 565 (2018), [arXiv:1804.10823].
- [116] G. Aad *et al.* (ATLAS), Phys. Rev. D **102**, 11, 112008 (2020), [arXiv:2007.05293].
- [117] A. M. Sirunyan *et al.* (CMS), Eur. Phys. J. C **81**, 8, 688 (2021), [arXiv:2102.08198].
- [118] M. Aaboud *et al.* (ATLAS), Phys. Rev. **D98**, 5, 052008 (2018), [arXiv:1808.02380].
- [119] A. Tumasyan *et al.* (CMS), Phys. Rev. D **106**, 1, 012004 (2022), [arXiv:2109.08268].
- [120] A. Tumasyan *et al.* (CMS), JHEP **04**, 087 (2022), [arXiv:2111.13669].
- [121] R. Contino and G. Servant, JHEP **06**, 026 (2008), [arXiv:0801.1679].
- [122] J. A. Aguilar-Saavedra, JHEP **11**, 030 (2009), [arXiv:0907.3155].
- [123] J. Mrazek and A. Wulzer, Phys. Rev. **D81**, 075006 (2010), [arXiv:0909.3977].
- [124] G. Dissertori *et al.*, JHEP **09**, 019 (2010), [arXiv:1005.4414].
- [125] See, for example, PDG review of Technicolor searches in this volume.
- [126] M. Aaboud *et al.* (ATLAS), JHEP **10**, 141 (2017), [arXiv:1707.03347].
- [127] A. M. Sirunyan *et al.* (CMS), JHEP **03**, 082 (2019), [arXiv:1810.03188].
- [128] A. M. Sirunyan *et al.* (CMS), Eur. Phys. J. C **79**, 90 (2019), [arXiv:1809.08597].
- [129] G. Aad *et al.* (ATLAS), Eur. Phys. J. C **83**, 8, 719 (2023), [arXiv:2212.05263].
- [130] G. Aad *et al.* (ATLAS), Phys. Lett. B **843**, 138019 (2023), [arXiv:2210.15413].
- [131] M. Aaboud *et al.* (ATLAS), Phys. Rev. Lett. **121**, 21, 211801 (2018), [arXiv:1808.02343].
- [132] A. Tumasyan *et al.* (CMS), JHEP **07**, 020 (2023), [arXiv:2209.07327].
- [133] A. M. Sirunyan *et al.* (CMS), Phys. Rev. D **102**, 112004 (2020), [arXiv:2008.09835].
- [134] G. Aad *et al.* (ATLAS) (2023), [arXiv:2308.02595].
- [135] G. Aad *et al.* (ATLAS) (2023), [arXiv:2307.07584].
- [136] G. Aad *et al.* (ATLAS) (2023), [arXiv:2305.03401].
- [137] G. Aad *et al.* (ATLAS), Phys. Rev. D **105**, 9, 092012 (2022), [arXiv:2201.07045].
- [138] M. Aaboud *et al.* (ATLAS), JHEP **05**, 164 (2019), [arXiv:1812.07343].
- [139] (2023), [arXiv:2302.12802].
- [140] A. Tumasyan *et al.* (CMS), JHEP **05**, 093 (2022), [arXiv:2201.02227].
- [141] A. M. Sirunyan *et al.* (CMS), JHEP **01**, 036 (2020), [arXiv:1909.04721].
- [142] A. M. Sirunyan *et al.* (CMS), JHEP **06**, 031 (2018), [arXiv:1802.01486].
- [143] A. De Simone *et al.*, JHEP **04**, 004 (2013), [arXiv:1211.5663].
- [144] R. Contino, Y. Nomura and A. Pomarol, Nucl. Phys. **B671**, 148 (2003), [hep-ph/0306259].
- [145] D. B. Kaplan and H. Georgi, Phys. Lett. **136B**, 183 (1984).
- [146] D. B. Kaplan, H. Georgi and S. Dimopoulos, Phys. Lett. B **136**, 187 (1984).
- [147] T. Banks, Nucl. Phys. B **243**, 125 (1984).
- [148] H. Georgi, D. B. Kaplan and P. Galison, Phys. Lett. **143B**, 152 (1984).
- [149] I. Antoniadis *et al.*, Phys. Rev. Lett. **108**, 081602 (2012), [arXiv:1102.4043].
- [150] G. F. Giudice and M. McCullough, JHEP **02**, 036 (2017), [arXiv:1610.07962].
- [151] G. Aad *et al.* (ATLAS) (2023), [arXiv:2305.10894].
- [152] A. M. Sirunyan *et al.* (CMS), Phys. Rev. D **98**, 9, 092001 (2018), [arXiv:1809.00327].
- [153] I. Antoniadis and K. Benakli, Int. J. Mod. Phys. **A15**, 4237 (2000), [hep-ph/0007226].
- [154] G. Aad *et al.* (ATLAS), JHEP **11**, 138 (2012), [arXiv:1209.2535].
- [155] V. Khachatryan *et al.* (CMS), Phys. Rev. **D91**, 9, 092005 (2015), [arXiv:1408.2745].
- [156] K. Cheung and G. L. Landsberg, Phys. Rev. **D65**, 076003 (2002), [hep-ph/0110346].
- [157] M. Farina *et al.*, Phys. Lett. **B772**, 210 (2017), [arXiv:1609.08157].
- [158] M. Aaboud *et al.* (ATLAS), Eur. Phys. J. C **78**, 5, 401 (2018), [arXiv:1706.04786].
- [159] G. Aad *et al.* (ATLAS) (2019), [arXiv:1906.05609].
- [160] A. M. Sirunyan *et al.* (CMS), JHEP **06**, 128 (2018), [arXiv:1803.11133].
- [161] A. M. Sirunyan *et al.* (CMS), JHEP **06**, 120 (2018), [arXiv:1803.06292].
- [162] A. Tumasyan *et al.* (CMS), JHEP **09**, 051 (2023), [arXiv:2212.12604].
- [163] T. Appelquist, H.-C. Cheng and B. A. Dobrescu, Phys. Rev. **D64**, 035002 (2001), [hep-ph/0012100].
- [164] A. Datta, K. Kong and K. T. Matchev, New J. Phys. **12**, 075017 (2010), [arXiv:1002.4624].
- [165] N. Deutschmann, T. Flacke and J. S. Kim, Phys. Lett. **B771**, 515 (2017), [arXiv:1702.00410].
- [166] J. Beuria *et al.*, Comput. Phys. Commun. **226**, 187 (2018), [arXiv:1702.00413].
- [167] Avnish *et al.*, Phys. Rev. D **103**, 115011 (2021), [arXiv:2012.15137].
- [168] G. Panico, M. Safari and M. Serone, JHEP **02**, 103 (2011), [arXiv:1012.2875].
- [169] J. Scherk and J. H. Schwarz, Phys. Lett. **82B**, 60 (1979).
- [170] A. Pomarol and M. Quiros, Phys. Lett. **B438**, 255 (1998), [hep-ph/9806263].
- [171] I. Antoniadis *et al.*, Nucl. Phys. **B544**, 503 (1999), [hep-ph/9810410].
- [172] R. Barbieri, L. J. Hall and Y. Nomura, Phys. Rev. **D63**, 105007 (2001), [hep-ph/0011311].

86. W' -Boson Searches

Revised September 10, 2023 by B.A. Dobrescu (FNAL) and S. Willocq (U. Massachusetts).

The W' boson is a massive hypothetical particle of spin 1 and electric charge ± 1 , which is a color singlet and is predicted in various extensions of the Standard Model (SM).

86.1 W' couplings to quarks and leptons

The Lagrangian terms describing the couplings of a W'^{\pm} boson to fermions are given by

$$\frac{W'^{\pm}}{\sqrt{2}} \left[\bar{u}_i (C_{qij}^R P_R + C_{qij}^L P_L) \gamma^\mu d_j + \bar{\nu}_i (C_{\ell ij}^R P_R + C_{\ell ij}^L P_L) \gamma^\mu e_j \right]. \quad (86.1)$$

Here, u, d, ν , and e are the SM fermions in the mass eigenstate basis, $i, j = 1, 2, 3$ label the fermion generation, and $P_{R,L} = (1 \pm \gamma_5)/2$. The coefficients C_{qij}^L , C_{qij}^R , $C_{\ell ij}^L$, and $C_{\ell ij}^R$ are complex dimensionless parameters. If $C_{\ell ij}^R \neq 0$, then the i th generation includes a right-handed neutrino. Using this notation, the SM W couplings are $C_q^L = g V_{\text{CKM}}$, $C_\ell^L = g \approx 0.63$ and $C_q^R = C_\ell^R = 0$.

Unitarity considerations imply that the W' boson is associated with a spontaneously-broken gauge symmetry. This is true even when it is a composite particle (*e.g.* ρ^\pm -like bound states [1]) if its mass is much smaller than the compositeness scale, or a Kaluza-Klein mode in theories where the W boson propagates in extra dimensions [2]. The simplest extension of the electroweak gauge group that includes a W' boson is $SU(2)_1 \times SU(2)_2 \times U(1)$, but larger groups are encountered in some theories. A generic property of these gauge theories is that they also include a Z' boson [3]; the W' -to- Z' mass ratio is often a free parameter.

A tree-level mass mixing may be induced between the electrically-charged gauge bosons. Upon diagonalization of their mass matrix, the W -to- Z mass ratio and the couplings of the observed W boson are shifted from the SM values. Their measurements imply that the mixing angle, θ_+ , between the gauge eigenstates must be smaller than about 10^{-2} [4]. In certain theories the mixing is negligible (*e.g.*, due to a new parity [5]), even when the W' mass is near the electroweak scale. Note that $SU(2)$ gauge invariance suppresses the kinetic mixing between the W and W' bosons (in contrast to the case of a Z' boson [3]).

The W' coupling to WZ is fixed by Lorentz and gauge invariances, and to leading order in θ_+ is given by [6]

$$\frac{g \theta_+ i}{\cos \theta_W} \left[W_\mu'^+ (W_\nu^- Z^{\nu\mu} + Z_\nu W^{-\mu\nu}) + Z^\nu W^{-\mu} W_{\nu\mu}'^+ \right] + \text{H.c.}, \quad (86.2)$$

where $W^{\mu\nu} \equiv \partial^\mu W^\nu - \partial^\nu W^\mu$, etc. The θ_W dependence shown here corrects the one given in Ref. [7], which has been referred to as the Extended Gauge Model by the experimental collaborations. The W' coupling to Wh^0 , where h^0 is the SM Higgs boson, is

$$-\xi_h g_{W'} M_W W_\mu'^+ W^{\mu-} h^0 + \text{H.c.}, \quad (86.3)$$

where $g_{W'}$ is the gauge coupling of the W' boson, and the coefficient ξ_h satisfies $\xi_h \leq 1$ in simple Higgs sectors [6].

In models based on the “left-right symmetric” gauge group [8], $SU(2)_L \times SU(2)_R \times U(1)_{B-L}$, the SM fermions that couple to the W boson transform as doublets under $SU(2)_L$ while the other fermions transform as doublets under $SU(2)_R$. Consequently, the W' boson couples primarily to right-handed fermions; its coupling to left-handed fermions arises due to the θ_+ mixing, so that C_q^L is proportional to the CKM matrix and its elements are much smaller than the diagonal elements of C_q^R . Generically, C_q^R does not need to be proportional to V_{CKM} .

There are many other models based on the $SU(2)_1 \times SU(2)_2 \times U(1)$ gauge symmetry. In the “alternate left-right” model [9], all the couplings shown in Eq. (86.1) vanish, but there are some new fermions such that the W' boson couples to pairs involving a SM fermion and a new fermion. In the “unified SM” [10], the left-handed quarks are doublets under one $SU(2)$, and the left-handed leptons are doublets under a different $SU(2)$, leading to a mostly leptophobic W' boson: $C_{\ell ij}^L \ll C_{qij}^L$ and $C_{\ell ij}^R = C_{qij}^R = 0$. Fermions of different generations may also transform

as doublets under different $SU(2)$ gauge groups [11]. In particular, the couplings to third generation quarks may be enhanced [12].

It is also possible that the W' couplings to SM fermions are highly suppressed. For example, if the quarks and leptons are singlets under one $SU(2)$ [13], then the couplings are proportional to the tiny mixing angle θ_+ . Similar suppressions may arise if some vectorlike fermions mix with the SM fermions [14].

Gauge groups that embed the electroweak symmetry, such as $SU(3)_W \times U(1)$ or $SU(4)_W \times U(1)$, also include one or more W' bosons [15].

86.2 Collider searches

At hadron colliders, W' bosons can be detected through resonant pair production of fermions (f and f') or electroweak bosons with a net electric charge equal to ± 1 . When W' has a width much smaller than its mass ($\Gamma_{W'}/M_{W'} \lesssim 7\%$), the contribution of the s -channel W' exchange to the total rate for $pp \rightarrow f\bar{f}'X$, where X is any final state, may be approximated by the branching fraction $B(W' \rightarrow f\bar{f}')$ times the production cross section [16], which may be written as

$$\sigma(pp \rightarrow W'X) \simeq \frac{\pi}{6s} \sum_{i,j} [(C_{qij}^L)^2 + (C_{qij}^R)^2] w_{ij} (M_{W'}^2/s, M_{W'}). \quad (86.4)$$

The functions w_{ij} include the information about proton structure, and are given to leading order in α_s by

$$w_{ij}(z, \mu) = \int_z^1 \frac{dx}{x} \left[u_i(x, \mu) \bar{d}_j\left(\frac{z}{x}, \mu\right) + \bar{u}_i(x, \mu) d_j\left(\frac{z}{x}, \mu\right) \right], \quad (86.5)$$

where $u_i(x, \mu)$ and $d_i(x, \mu)$ are the parton distributions inside the proton at the factorization scale μ and parton momentum fraction x for the up- and down-type quarks of the i th generation, respectively. QCD corrections to W' production are sizable (they also include quark-gluon initial states), but preserve the above factorization of couplings at next-to-leading order [17].

The most commonly studied W' signal consists of a high-momentum electron or muon and large missing transverse momentum. The signal transverse mass distribution forms a Jacobian peak with its endpoint at $M_{W'}$ (see Fig. 1 (top) of Ref. [18]). Given that the branching fractions for $W' \rightarrow e\nu$ and $W' \rightarrow \mu\nu$ could be very different, the results in these channels should be presented separately. Searches in these channels often implicitly assume that the left-handed couplings vanish (no interference between W and W'), and that the right-handed neutrino is light compared to the W' boson and escapes the detector. An example of parameter values that satisfy these assumptions is $C_q^R = g V_{\text{CKM}}$, $C_\ell^R = g$, $C_q^L = C_\ell^L = 0$, which define a model that preserves lepton universality and predicts the same total cross section as the Sequential SM used in many W' searches. However, if a W' boson were discovered and the final state fermions have left-handed helicity, then the effects of $W - W'$ interference could be observed [22], providing information about the W' couplings. The effects of the W' width on interference are discussed in Ref. [23].

In the $e\nu$ channel, the ATLAS and CMS collaborations set limits on the W' production cross section times branching fraction $\sigma \times B$ (and thus indirectly on the W' couplings). These limits are set for $M_{W'}$ in the 0.15–7 TeV range and are based on approximately 140 fb^{-1} at $\sqrt{s} = 13 \text{ TeV}$ [18, 19], with the most stringent limits reproduced in Fig. 86.1. ATLAS sets the strongest mass limit $M_{W'} > 6.0 \text{ TeV}$ in the Sequential SM (all limits in this mini-review are at the 95% CL). The coupling limits are much weaker for $M_{W'} < 150 \text{ GeV}$, a range last explored with the Tevatron at $\sqrt{s} = 1.8 \text{ TeV}$ [24].

In the $\mu\nu$ channel, ATLAS and CMS set rate limits for $M_{W'}$ in the 0.15–7 TeV range [18, 19], with the strongest mass lower limit of 5.6 TeV in the Sequential SM set by CMS [19] using 138 fb^{-1} of $\sqrt{s} = 13 \text{ TeV}$ data, as shown in Fig. 86.1. When combined with the $e\nu$ channel assuming lepton universality, the upper limit on the $\sqrt{s} = 13 \text{ TeV}$ cross section times branching fraction to $\ell\nu$ varies between 0.05 and 2.1 fb for $M_{W'}$ values between 1 and 6 TeV [18]. Only weak limits on $W' \rightarrow \mu\nu$ exist for $M_{W'} < 150 \text{ GeV}$ [25]. Note that masses of the order of the electroweak

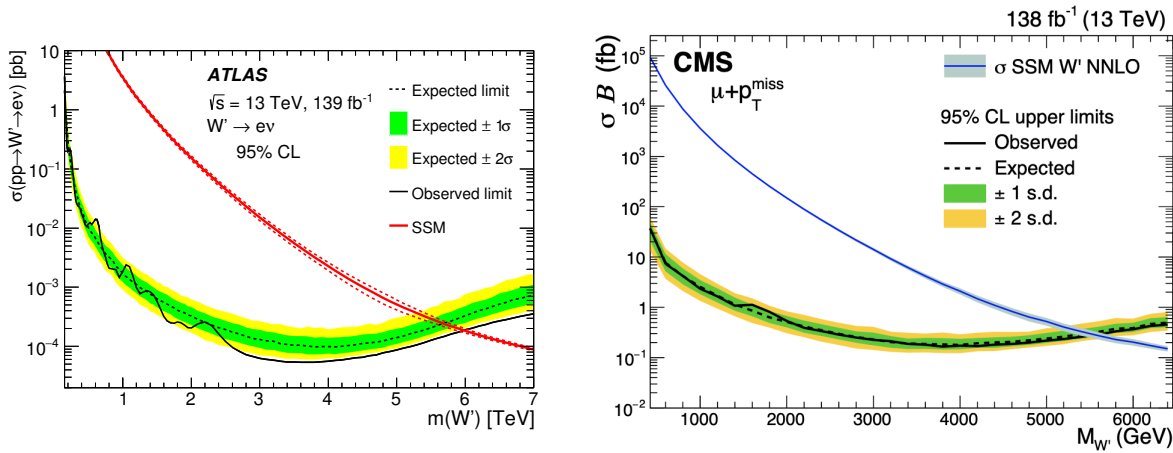


Figure 86.1: Upper limit on $\sigma(pp \rightarrow W' X) \times B(W' \rightarrow \ell\nu)$ in the $e\nu$ channel from ATLAS [18] (left) and the $\mu\nu$ channel from CMS [19] (right). The red (black) line shows the theoretical prediction in the Sequential SM in the $e\nu$ ($\mu\nu$) channel.

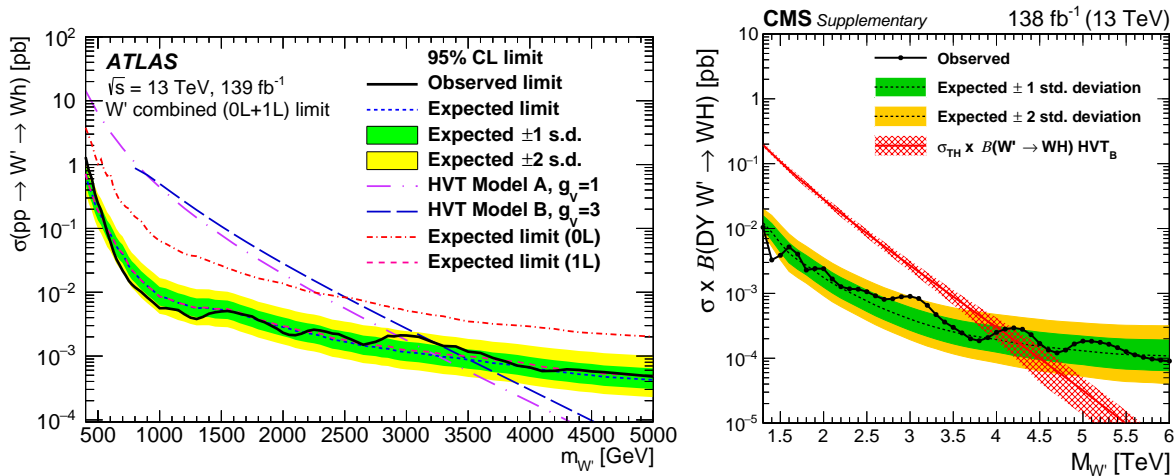


Figure 86.2: Upper limits on W' production cross section times branching fraction into a W and a SM Higgs boson decaying into heavy-flavor quarks, from ATLAS [20] (left) and CMS [21] (right).

scale are interesting from a theoretical point of view, while lepton universality does not necessarily apply to a W' boson.

Searches for $W' \rightarrow \tau\nu$ have been performed at 13 TeV by CMS with 138 fb $^{-1}$ [26], and by ATLAS with 139 fb $^{-1}$ [27]. Limits are set on $\sigma \times B$ for $M_{W'}$ between 0.5 and 6 TeV. A mass lower limit of 5.0 TeV is set in the Sequential SM, and the upper limit on the cross section times branching fraction to $\tau\nu$ at 13 TeV varies between 0.4 and 9 fb for $M_{W'}$ values between 1 and 5 TeV [27].

The W' decay into a charged lepton and a right-handed neutrino, ν_R , may also be followed by the ν_R decay through a virtual W' boson into a charged lepton and two quark jets. The CMS [28] and ATLAS [29] searches in the $eejj$ and $\mu\mu jj$ channels have set limits at $\sqrt{s} = 13$ TeV on the cross section times branching fractions as a function of the ν_R mass and of $M_{W'}$. No requirement is placed on the charge of the lepton pair. A related W' search in the $\tau\tau jj$ channel with hadronic τ decays was also performed by CMS [30].

The $t\bar{b}$ channel is particularly important because a W' boson that couples only to right-handed fermions cannot decay to leptons when the right-handed neutrinos are heavier than $M_{W'}$. Additional motivations are provided by a W' boson with enhanced couplings to the third generation [12], and by a leptophobic W' boson. The usual signature for $W' \rightarrow t\bar{b}$ consists of a leptonically-decaying W boson and two b -jets. Recent studies have also incorporated the fully hadronic decay channel for $M_{W'} \gg m_t$ with the use of jet substructure techniques to tag highly boosted top-jets.

For a detailed discussion of this channel, see Ref. [31].

Searches for dijet resonances may be used to set limits on $W' \rightarrow q\bar{q}'$. ATLAS [32] and CMS [33] provide similar coverage in the ~ 1.5 –8 TeV mass range with 139 and 137 fb $^{-1}$ of data, respectively, collected at $\sqrt{s} = 13$ TeV. Interpretation in terms of W' decays with 139 fb $^{-1}$ of 13 TeV data yields a W' mass lower limit of 4.0 TeV in the Sequential SM [32]. For masses in the range ~ 0.5 –1.5 TeV, analyses based on jets reconstructed online provide the best sensitivity because they circumvent trigger bandwidth limitations [34, 35]. For W' masses below ~ 0.5 TeV, the best limits are set in novel analyses exploiting boosted technologies and initial state radiation [36–39]. Cross-section limits for W' masses below ~ 1.5 TeV can be derived from the dijet limits on Z' bosons summarized in Ref. [3].

In some theories [5] the W' couplings to SM fermions are suppressed by discrete symmetries. W' production then occurs in pairs, through a photon or Z boson. The decay modes are model-dependent and often involve other new particles. The ensuing collider signals arise from cascade decays and often include missing transverse momentum or boosted multi-jet topologies. Even when single production of W' is large enough, it is possible that its main decay mode is into a new particle and a SM one. An example is a search performed by CMS [40] for W' decays into a vector-like quark and a top or a bottom quark. The final state studied in this analysis involves a boosted SM Higgs or Z boson, as well as a $t\bar{t}$ or $b\bar{b}$ pair, with all heavy particles decaying into

jets. Another example is a search performed by ATLAS [41] for W' decays into a W boson and a Z' boson, the latter decaying into a jet pair.

Searches for WZ resonances at the LHC have focused on the process $pp \rightarrow W' \rightarrow WZ$ with the production mainly from $u\bar{d} \rightarrow W'$, assuming SM-like couplings to quarks. ATLAS and CMS have set upper limits on the $W'WZ$ coupling for $M_{W'}$ in the 0.2–5.0 TeV range with a combination of fully leptonic, semi-leptonic and fully hadronic channels with $\sim 36 - 139 \text{ fb}^{-1}$ at 13 TeV [42–44] (see also Ref. [31]). Recent constraints with 138–139 fb^{-1} at 13 TeV were also set in individual channels by ATLAS [45–47] and CMS [21, 48–50]. The strongest lower limit on the W' mass is set by ATLAS [46] in the semi-leptonic channel with a lower limit on $M_{W'}$ of 3.9 TeV [46] in the context of the Heavy Vector Triplet (HVT) weakly-coupled scenario A [51]. A similar result is obtained by CMS in the fully-hadronic channel [21]. A fermiophobic W' boson that couples to WZ may be produced at hadron colliders in association with a Z boson, or via WZ fusion. This would give rise to $(WZ)Z$ and $(WZ)jj$ final states [52]. Results of the search for the latter are reported in Refs. [21, 42, 46, 48, 50].

W' bosons have also been searched for in final states with a W boson and a SM Higgs boson in the channels $W \rightarrow \ell\nu$ or $W \rightarrow q\bar{q}'$ and $h^0 \rightarrow b\bar{b}$ by ATLAS [20, 53] and CMS [21, 50] with 138–139 fb^{-1} at $\sqrt{s} = 13 \text{ TeV}$. CMS also searched for W' bosons in the $q\bar{q}'\tau\tau$ final state [54]. Cross-section limits are set for W' masses between 0.4 and 6.0 TeV. The most stringent upper limit on the cross section is set by the ATLAS analysis with $W \rightarrow \ell\nu$ at low $M_{W'}$ and the CMS analysis with $W \rightarrow q\bar{q}'$ at high $M_{W'}$, as shown in Fig. 86.2.

At lepton colliders, W' bosons may be produced in pairs via their photon coupling, which is model independent. At LEP-II, although dedicated searches for W' bosons have not been performed, the large cross section for $e^+e^- \rightarrow \gamma^* \rightarrow W'^+W'^-$ and small backgrounds suggest that any W' is ruled out up to the kinematic limit, $M_{W'} < \sqrt{s}/2 \approx 105 \text{ GeV}$, for most decay modes. Sensitivity to $M_{W'}$ above \sqrt{s} could be achieved [55] using the $e^+e^- \rightarrow \gamma\nu\bar{\nu}$ process via a t -channel W' exchange, if the W' coupling to $e\nu$ is large enough.

86.3 Low-energy constraints

The properties of W' bosons are also constrained by measurements of processes at energies much below $M_{W'}$. The bounds on $W - W'$ mixing [4] are mostly due to the change in W properties compared to the SM. Limits on deviations in the ZWW couplings provide a leading constraint for fermiophobic W' bosons [14].

Constraints arising from low-energy effects of W' exchange are strongly model-dependent. If the W' couplings to quarks are not suppressed, then box diagrams involving a W and a W' boson contribute to neutral meson-mixing. In the case of W' couplings to right-handed quarks as in the left-right symmetric model, the limit from $K_L - K_S$ mixing is severe: $M_{W'} > 2.9 \text{ TeV}$ for $C_q^R = gV_{CKM}$ [56]. However, if no correlation between the W' and W couplings is assumed, then the limit on $M_{W'}$ may be significantly relaxed [57].

W' exchange also contributes at tree level to various low-energy processes. In particular, it would impact the measurement of the Fermi constant G_F in muon decay, which in turn would change the predictions of many other electroweak processes. A recent test of parity violation in polarized muon decay [58] has set limits of about 600 GeV on $M_{W'}$, assuming W' couplings to right-handed leptons as in left-right symmetric models and a light ν_R . There are also W' contributions to the neutron electric dipole moment, β decays, and other processes [4].

If right-handed neutrinos have Majorana masses, then there are tree-level contributions to neutrinoless double-beta decay, and a limit on $M_{W'}$ versus the ν_R mass may be derived [59]. For ν_R masses below a few GeV, the W' boson contributes to leptonic and semileptonic B meson decays, so that limits may be placed on various combinations of W' parameters [57]. For ν_R masses below $\sim 30 \text{ MeV}$, the most stringent constraints on $M_{W'}$ are due to the limits on ν_R emission from supernovae [60].

References

- [1] M. Bando, T. Kugo and K. Yamawaki, Phys. Rept. **164**, 217 (1988).
- [2] H.-C. Cheng *et al.*, Phys. Rev. D **64**, 065007 (2001), [hep-th/0104179].
- [3] See the Section on “ Z' -boson searches” in this *Review*.
- [4] See the particle listings for W' in this *Review*.
- [5] H.-C. Cheng and I. Low, JHEP **09**, 051 (2003), [hep-ph/0308199].
- [6] B. A. Dobrescu and Z. Liu, JHEP **10**, 118 (2015), [arXiv:1507.01923].
- [7] G. Altarelli, B. Mele and M. Ruiz-Altaba, Z. Phys. C **45**, 109 (1989), [Erratum: Z. Phys. C **47**, 676 (1990)].
- [8] R. N. Mohapatra and J. C. Pati, Phys. Rev. D **11**, 566 (1975).
- [9] K. S. Babu, X.-G. He and E. Ma, Phys. Rev. D **36**, 878 (1987).
- [10] H. Georgi, E. E. Jenkins and E. H. Simmons, Nucl. Phys. B **331**, 541 (1990).
- [11] X.-y. Li and E. Ma, J. Phys. G **19**, 1265 (1993), [hep-ph/9208210].
- [12] D. J. Muller and S. Nandi, Phys. Lett. B **383**, 345 (1996), [hep-ph/9602390].
- [13] A. Donini *et al.*, Nucl. Phys. B **507**, 51 (1997), [hep-ph/9705450].
- [14] R. S. Chivukula *et al.*, Phys. Rev. D **74**, 075011 (2006), [hep-ph/0607124].
- [15] F. Pisano and V. Pleitez, Phys. Rev. D **46**, 410 (1992), [hep-ph/9206242].
- [16] V. D. Barger and R. J. N. Phillips, *Collider Physics* (1996), ISBN 978-0201149456.
- [17] Z. Sullivan, Phys. Rev. D **66**, 075011 (2002), [hep-ph/0207290].
- [18] G. Aad *et al.* (ATLAS), Phys. Rev. D **100**, 052013 (2019), [arXiv:1906.05609].
- [19] A. Tumasyan *et al.* (CMS), JHEP **07**, 067 (2022), [arXiv:2202.06075].
- [20] G. Aad *et al.* (ATLAS), JHEP **06**, 016 (2023), [arXiv:2207.00230].
- [21] A. Tumasyan *et al.* (CMS), Phys. Lett. B **844**, 137813 (2023), [arXiv:2210.00043].
- [22] T. G. Rizzo, JHEP **05**, 037 (2007), [arXiv:0704.0235].
- [23] E. Accomando *et al.*, Phys. Rev. D **85**, 115017 (2012), [arXiv:1110.0713].
- [24] F. Abe *et al.* (CDF), Phys. Rev. Lett. **74**, 2900 (1995).
- [25] F. Abe *et al.* (CDF), Phys. Rev. Lett. **67**, 2609 (1991).
- [26] A. Tumasyan *et al.* (CMS), JHEP **09**, 051 (2023), [arXiv:2212.12604].
- [27] G. Aad *et al.* (ATLAS) (2024), [arXiv:2402.16576].
- [28] A. Tumasyan *et al.* (CMS), JHEP **04**, 047 (2022), [arXiv:2112.03949].
- [29] G. Aad *et al.* (ATLAS), Eur. Phys. J. C **83**, 12, 1164 (2023), [arXiv:2304.09553].
- [30] A. M. Sirunyan *et al.* (CMS), JHEP **03**, 170 (2019), [arXiv:1811.00806].
- [31] K.M. Black *et al.*, “Dynamical electroweak symmetry breaking” in this *Review*.
- [32] G. Aad *et al.* (ATLAS), JHEP **03**, 145 (2020), [arXiv:1910.08447].
- [33] A. M. Sirunyan *et al.* (CMS), JHEP **05**, 033 (2020), [arXiv:1911.03947].
- [34] M. Aaboud *et al.* (ATLAS), Phys. Rev. Lett. **121**, 081801 (2018), [arXiv:1804.03496].

- [35] A. M. Sirunyan *et al.* (CMS), JHEP **08**, 130 (2018), [arXiv:1806.00843].
- [36] M. Aaboud *et al.* (ATLAS), Phys. Lett. B **788**, 316 (2019), [arXiv:1801.08769].
- [37] M. Aaboud *et al.* (ATLAS), Phys. Lett. B **795**, 56 (2019), [arXiv:1901.10917].
- [38] A. M. Sirunyan *et al.* (CMS), Phys. Rev. D **100**, 112007 (2019), [arXiv:1909.04114].
- [39] A. M. Sirunyan *et al.* (CMS), Phys. Rev. Lett. **123**, 231803 (2019), [arXiv:1905.10331].
- [40] A. Tumasyan *et al.* (CMS), JHEP **09**, 088 (2022), [arXiv:2202.12988].
- [41] G. Aad *et al.* (ATLAS), JHEP **07**, 202 (2023), [arXiv:2211.08945].
- [42] M. Aaboud *et al.* (ATLAS), Phys. Rev. D **98**, 052008 (2018), [arXiv:1808.02380].
- [43] ATLAS Collab., ATLAS-CONF-2022-028, May 2022.
- [44] A. M. Sirunyan *et al.* (CMS), Phys. Lett. B **798**, 134952 (2019), [arXiv:1906.00057].
- [45] G. Aad *et al.* (ATLAS), JHEP **09**, 091 (2019), [Erratum: JHEP **06** (2020) 042], [arXiv:1906.08589].
- [46] G. Aad *et al.* (ATLAS), Eur. Phys. J. C **80**, 1165 (2020), [arXiv:2004.14636].
- [47] G. Aad *et al.* (ATLAS), Eur. Phys. J. C **83**, 633 (2023), [arXiv:2207.03925].
- [48] A. Tumasyan *et al.* (CMS), Phys. Rev. D **106**, 012004 (2022), [arXiv:2109.08268].
- [49] A. Tumasyan *et al.* (CMS), JHEP **04**, 087 (2022), [arXiv:2111.13669].
- [50] A. Tumasyan *et al.* (CMS), Phys. Rev. D **105**, 032008 (2022), [arXiv:2109.06055].
- [51] D. Pappadopulo *et al.*, JHEP **09**, 060 (2014), [arXiv:1402.4431].
- [52] H.-J. He *et al.*, Phys. Rev. D **78**, 031701 (2008), [arXiv:0708.2588].
- [53] G. Aad *et al.* (ATLAS), Phys. Rev. D **102**, 112008 (2020), [arXiv:2007.05293].
- [54] A. M. Sirunyan *et al.* (CMS), JHEP **01**, 051 (2019), [arXiv:1808.01365].
- [55] S. Godfrey *et al.*, Phys. Rev. D **61**, 113009 (2000), [hep-ph/0001074].
- [56] Y. Zhang *et al.*, Phys. Rev. D **76**, 091301 (2007), [arXiv:0704.1662].
- [57] P. Langacker and S. U. Sankar, Phys. Rev. D **40**, 1569 (1989).
- [58] J. F. Bueno *et al.* (TWIST), Phys. Rev. D **84**, 032005 (2011), [arXiv:1104.3632].
- [59] G. Prezeau, M. Ramsey-Musolf and P. Vogel, Phys. Rev. D **68**, 034016 (2003), [hep-ph/0303205].
- [60] G. G. Raffelt, Ann. Rev. Nucl. Part. Sci. **49**, 163 (1999), [hep-ph/9903472].

87. Z' -Boson Searches

Revised September 2023 by B.A. Dobrescu (FNAL) and S. Willocq (U. Massachusetts).

The Z' boson is a massive, electrically-neutral and color-singlet hypothetical particle of spin 1. This particle is predicted in many extensions of the Standard Model (SM) and has been the object of extensive phenomenological studies [1].

87.1 Z' boson couplings

The couplings of a Z' boson to the first-generation fermions are given by

$$\begin{aligned} Z'_\mu \left(g_u^L \bar{u}_L \gamma^\mu u_L + g_d^L \bar{d}_L \gamma^\mu d_L + g_u^R \bar{u}_R \gamma^\mu u_R + g_d^R \bar{d}_R \gamma^\mu d_R \right. \\ \left. + g_\nu^L \bar{\nu}_L \gamma^\mu \nu_L + g_e^L \bar{e}_L \gamma^\mu e_L + g_e^R \bar{e}_R \gamma^\mu e_R \right), \end{aligned} \quad (87.1)$$

where u, d, ν, e are the quark and lepton fields in the mass eigenstate basis, and the coefficients $g_u^L, g_d^L, g_u^R, g_d^R, g_\nu^L, g_e^L, g_e^R$ are real dimensionless parameters. If the Z' couplings to quarks and leptons are generation-independent, then these seven parameters describe the couplings of the Z' boson to all SM fermions. More generally, however, the Z' couplings to fermions are generation-dependent, in which case Eq. (87.1) may be written with generation indices $i, j = 1, 2, 3$ labeling the quark and lepton fields, and with the seven coefficients promoted to 3×3 Hermitian matrices (e.g., $g_{e,ij}^L \bar{e}_L^i \gamma^\mu e_L^j$, where e_L^2 is the left-handed muon, etc.).

The parameters describing the Z' boson interactions with quarks and leptons are subject to some theoretical constraints. Quantum field theories that include a heavy spin-1 particle are well behaved at high energies only if that particle is a gauge boson associated with a spontaneously broken gauge symmetry. Quantum effects preserve the gauge symmetry only if the couplings of the gauge boson to fermions satisfy the anomaly equations [2]. Furthermore, the fermion charges under the new gauge symmetry are constrained by the requirement that the quarks and leptons get masses from gauge-invariant interactions with the Higgs fields.

The relation between the couplings displayed in Eq. (87.1) and the gauge charges z_f^L and z_f^R of the fermions $f = u, d, \nu, e$ involves the unitary 3×3 matrices V_f^L and V_f^R that transform the gauge eigenstate fermions f_L^i and f_R^i , respectively, into the mass eigenstates. The Z' couplings also depend on the mixings of the new gauge boson in the gauge eigenstate basis (\tilde{Z}'_μ). The main mixings are a kinetic mixing $(-\chi/2)B^{\mu\nu}\tilde{Z}'_{\mu\nu}$ with the hypercharge gauge boson B^μ (χ is a dimensionless parameter), and a mass mixing $\delta M^2 \tilde{Z}'^\mu \tilde{Z}'_\mu$ with the linear combination (\tilde{Z}'_μ) of neutral bosons that couples as the SM Z boson [3]. Since both the kinetic and mass mixings shift the mass and couplings of the Z boson, electroweak measurements impose upper limits on χ and $\delta M^2/(M_{Z'}^2 - M_Z^2)$ of the order of 10^{-3} [4]. Keeping only linear terms in these two small quantities, the couplings of the mass-eigenstate Z' boson are given by

$$\begin{aligned} g_{f,ij}^L = g_z V_{fii'}^L z_{f'i'}^L (V_f^L)_{i'j}^\dagger \\ + \frac{e}{c_W} \left(\frac{s_W \chi M_{Z'}^2 + \delta M^2}{2s_W (M_{Z'}^2 - M_Z^2)} \sigma_f^3 - \epsilon Q_f \right), \end{aligned} \quad (87.2)$$

$$g_{f,ij}^R = g_z V_{fii'}^R z_{f'i'}^R (V_f^R)_{i'j}^\dagger - \frac{e}{c_W} \epsilon Q_f, \quad (87.3)$$

where g_z is the new gauge coupling, Q_f is the electric charge of f , e is the electromagnetic gauge coupling, s_W and c_W are the sine and cosine of the weak mixing angle, $\sigma_f^3 = +1$ for $f = u, \nu$ and $\sigma_f^3 = -1$ for $f = d, e$, and

$$\epsilon = \frac{\chi (M_{Z'}^2 - c_W^2 M_Z^2) + s_W \delta M^2}{M_{Z'}^2 - M_Z^2}. \quad (87.4)$$

The interaction of the Z' boson with a pair of W bosons has

the form

$$\begin{aligned} \left[i (W_\mu^- Z'_\nu - W_\nu^- Z'_\mu) \partial^\mu W^{+\nu} + \text{H.c.} \right] \\ + i (W_\mu^+ W_\nu^- - W_\nu^+ W_\mu^-) \partial^\mu Z'^{\nu} \end{aligned} \quad (87.5)$$

with a coefficient of order $M_W^2/M_{Z'}^2$ [5]. The Z' also couples to one SM Higgs boson and one Z boson, $Z'_\mu Z^\mu h^0$, with a coefficient of order M_Z .

87.2 Z' models

A simple origin of a Z' boson is a new $U(1)'$ gauge symmetry. In that case, the matricial equalities $z_u^L = z_d^L$ and $z_\nu^L = z_e^L$ are required by the SM $SU(2)_W$ gauge symmetry. Given that the $U(1)'$ interaction is not asymptotically free, the theory may be well-behaved at high energies (e.g., by embedding $U(1)'$ in a non-Abelian gauge group) only if the charges are commensurate numbers, i.e. any ratio of charges is a rational number. Satisfying the anomaly equations [6] with rational numbers is highly nontrivial, and typically new fermions charged under $U(1)'$ are necessary.

If the couplings are generation-independent ($V_f^{L,R}$ are then unit matrices in Eq. (87.2)) and the mixings of \tilde{Z}' are negligible, then there are five commensurate couplings: $g_u^R, g_d^R, g_e^R, g_q^L$ ($q = u$ or d), g_l^L ($l = \nu$ or e). Four sets of charges are displayed in Table 87.1, each of them spanned by a free parameter x [6]. The first set, labeled $B - xL$, has charges proportional to the baryon number minus x times the lepton number. These charges allow all SM Yukawa couplings to the Higgs doublet which is neutral under $U(1)_{B-xL}$, so that there is no tree-level $\tilde{Z} - \tilde{Z}'$ mixing. For $x = 1$ one recovers the $U(1)_{B-L}$ group, which is non-anomalous in the presence of one “right-handed neutrino” (a chiral fermion that is a singlet under the SM gauge group) per generation. For $x \neq 1$, it is necessary to include some fermions that are vectorlike (i.e. their mass terms are gauge invariant) with respect to the electroweak gauge group and chiral with respect to $U(1)_{B-xL}$. In the particular cases $x = 0$ or $x \gg 1$, the Z' is leptophobic or quark-phobic, respectively.

The second set, $U(1)_{10+x5}$, has charges that commute with the representations of the $SU(5)$ grand unified group. Here x is related to the mixing angle between the two $U(1)$ bosons encountered in the $E_6 \rightarrow SU(5) \times U(1) \times U(1)$ symmetry breaking patterns of grand unified theories [1,7]. With these charges, two Higgs doublets are typically required to generate masses for both up- and down- type fermions. This set leads to $\tilde{Z} - \tilde{Z}'$ mass mixing at tree level, such that for a Z' mass close to the electroweak scale, the measurements at the Z -pole require some fine tuning between the charges and VEVs of the two Higgs doublets. Vectorlike quarks charged under the electroweak gauge group are required (except for $x = -3$) to make this set anomaly free. The particular cases $x = -3, 1, -1/2$ are usually labeled $U(1)_\chi$, $U(1)_\psi$, and $U(1)_\eta$, respectively. Under the third set, $U(1)_{d-xu}$, the weak-doublet quarks are neutral, and the ratio of u_R and d_R charges is $-x$. For $x = 1$, this is the “right-handed” group $U(1)_R$. For $x = 0$, the charges are those of the E_6 -inspired $U(1)_I$ group, which requires new quarks and leptons. Other generation-independent sets of $U(1)'$ charges are given in Ref. [8].

In the absence of new fermions charged under the SM group, the most general generation-independent charge assignment is $U(1)_{q+xu}$, which is a linear combination of hypercharge and $B-L$. Many other anomaly-free solutions exist if generation-dependent charges are allowed. An example is $B - xL_e - yL_\mu + (y-3)L_\tau$, with x, y free parameters. This allows all fermion masses to be generated by Yukawa couplings to a single Higgs doublet, without inducing tree-level flavor-changing neutral current (FCNC) processes. There are also lepton-flavor dependent charges that allow neutrino masses to arise only from operators of high dimensionality [9].

If the $SU(2)_W$ -doublet quarks have generation-dependent $U(1)'$ charges, then the mass eigenstate quarks have flavor off-diagonal couplings to the Z' boson (see Eq. (87.1), and note that $V_u^L (V_d^L)^\dagger$

Table 87.1: Examples of generation-independent $U(1)'$ charges for quarks and leptons. The parameter x is an arbitrary rational number. Gauge anomaly cancellation requires certain new fermions [6].

fermion	$U(1)_{B-xL}$	$U(1)_{10+x5}$	$U(1)_{d-xu}$	$U(1)_{q+xu}$
(u_L, d_L)	1/3	1/3	0	1/3
u_R	1/3	-1/3	$-x/3$	$x/3$
d_R	1/3	$-x/3$	1/3	$(2-x)/3$
(ν_L, e_L)	$-x$	$x/3$	$(-1+x)/3$	-1
e_R	$-x$	-1/3	$x/3$	$-(2+x)/3$

is the CKM matrix). These are severely constrained by measurements of FCNC processes, which in this case are mediated at tree-level by Z' boson exchange [10]. The constraints are relaxed if the first and second generation charges are the same, although they are increasingly tightened by the measurements of B meson properties [11]. If only the $SU(2)_W$ -singlet quarks have generation-dependent $U(1)'$ charges, there is more freedom in adjusting the flavor off-diagonal couplings because the $V_{u,d}^R$ matrices are not observable in the SM.

The anomaly equations for $U(1)'$ could be circumvented only if there is an axion with certain dimension-5 couplings to the gauge bosons. However, such a scenario violates unitarity unless the quantum field theory description breaks down at a scale near $M_{Z'}$ [12]. It is possible, though, that the SM fermions are not charged under the $U(1)'$, but have mass mixing with some vectorlike fermions which are charged under $U(1)'$, implying that the physical fermions have couplings to the Z' [13]. For example, if the only SM quarks that have large mixings with some vectorlike quarks are the b quarks, then the only currently known particles that couple to the Z' would be the physical b quarks.

Z' bosons may also arise from larger gauge groups. These may extend the electroweak group, as in $SU(2) \times SU(2) \times U(1)$, or may embed the electroweak group, as in $SU(3)_W \times U(1)$ [14]. If the larger group is spontaneously broken down to $SU(2)_W \times U(1)_Y \times U(1)'$ at a scale $v_* \gg M_{Z'}/g_z$, then the above discussion applies up to corrections of order $M_{Z'}^2/(g_z v_*)^2$. For $v_* \sim M_{Z'}/g_z$, additional gauge bosons have masses comparable to $M_{Z'}$, including at least a W' boson [14]. If the larger gauge group breaks together with the electroweak symmetry directly to the electromagnetic $U(1)_{em}$, then the left-handed fermion charges are no longer correlated ($z_u^L \neq z_d^L$, $z_\nu^L \neq z_e^L$) and a $Z'W^+W^-$ coupling is induced.

If the electroweak gauge bosons propagate in extra dimensions, then their Kaluza-Klein (KK) excitations include a series of Z' boson pairs. Each of these pairs can be associated with a different $SU(2) \times U(1)$ gauge group in four dimensions. The properties of the KK particles depend strongly on the extra dimensional theory [15]. For example, in universal extra dimensions there is a parity that forces all couplings of Eq. (87.1) to vanish in the case of the lightest KK bosons, while allowing couplings to pairs of fermions involving a SM and a heavy vectorlike fermion. There are also 4-dimensional gauge theories (*e.g.* little Higgs with T parity) with Z' bosons exhibiting similar properties. By contrast, in a warped extra dimension, the couplings of Eq. (87.1) may be sizable even when SM fields propagate along the extra dimension.

Z' bosons may also be composite particles. For example, in confining gauge theories [16], the ρ -like bound state is a spin-1 boson that may be interpreted as arising from a spontaneously broken gauge symmetry [17].

87.3 Non-resonant Z' signatures at colliders

In the presence of the couplings shown in Eq. (87.1), the Z' boson may be produced in the s -channel at colliders, and would decay to pairs of fermions. The decay width into a pair of electrons is given by

$$\Gamma(Z' \rightarrow e^+e^-) \simeq \left[(g_e^L)^2 + (g_e^R)^2 \right] \frac{M_{Z'}}{24\pi}, \quad (87.6)$$

where small corrections from electroweak loops are not included. The decay width into $q\bar{q}$ is similar, except for an additional color factor of 3, QCD radiative corrections, and fermion mass corrections. Thus, one may compute the Z' branching fractions in terms of the couplings of Eq. (87.1). However, other decay channels, such as WW or a pair of new particles, could have large widths and need to be added to the total decay width.

As mentioned above, there are theories in which the Z' couplings are controlled by a discrete symmetry that forbids decays into a pair of SM particles. Typically, such theories involve several new particles, which may be produced only in pairs and undergo cascade decays through Z' bosons, leading to signals involving missing transverse momentum. Given that the cascade decays depend on the properties of new particles other than the Z' boson (see, *e.g.* Ref. [18]), this case is not discussed further here.

The Z' contribution to the cross sections for $e^+e^- \rightarrow f\bar{f}$ proceeds through an s -channel Z' exchange (when $f = e$, there are also t - and u -channel exchanges). For $M_{Z'} < \sqrt{s}$, the Z' appears as an $f\bar{f}$ resonance in the radiative return process where photon emission tunes the effective center-of-mass energy to $M_{Z'}$. The agreement between the LEP-II measurements and the SM predictions implies that either the Z' couplings are smaller than or of order 10^{-2} , or else $M_{Z'}$ is above 209 GeV, the maximum energy of LEP-II. In the latter case, the Z' exchange may be approximated up to corrections of order $s/M_{Z'}^2$, by the contact interactions

$$\frac{g_z^2}{M_{Z'}^2 - s} \left[\bar{e}\gamma_\mu (z_e^L P_L + z_e^R P_R) e \right] \left[\bar{f}\gamma^\mu (z_f^L P_L + z_f^R P_R) f \right], \quad (87.7)$$

where $P_{L,R}$ are chirality projection operators, and the relation between Z' couplings and charges (see Eq. (87.2) in the limit where the mass and kinetic mixings are neglected) is used, assuming generation-independent charges. The four LEP collaborations have set limits on the coefficients of such operators for all possible chiral structures and for various combinations of fermions [19]. Thus, one may derive bounds on $(M_{Z'}/g_z) |z_e^L z_f^L|^{-1/2}$ and the analogous combinations of LR , RL and RR charges, which are typically on the order of a few TeV. LEP-II limits were derived [6] on the four sets of charges shown in Table 87.1.

Somewhat stronger bounds can be set on $M_{Z'}/g_z$ for specific sets of Z' couplings if the effects of several operators (87.7) are combined. Dedicated analyses by the LEP collaborations have set limits on Z' bosons for particular values of the gauge coupling (see section 3.5 of Ref. [19]). For example, $M_{Z_{SSM}} > 1.76$ TeV for a “sequential” Z' of same couplings as the SM Z boson, while $M_{Z_\chi} > 0.785$ TeV for the Z' associated with $U(1)_\chi$ assuming a unification condition for the gauge coupling.

87.4 Searches at hadron colliders

Z' bosons with couplings to quarks (see Eq. (87.1)) may be produced at hadron colliders in the s -channel and would show up as resonances in the invariant mass distribution of the decay products. The cross section for producing a Z' boson at the LHC, which then decays to some $f\bar{f}$ final state, takes the form [22]

$$\sigma(pp \rightarrow Z'X \rightarrow f\bar{f}X) \simeq \frac{\pi}{6s} \sum_q c_q^f w_q(s, M_{Z'}^2) \quad (87.8)$$

for flavor-diagonal couplings to quarks. Here, we have neglected the interference with the SM contribution to $f\bar{f}$ production, which is a good approximation for a narrow Z' resonance (deviations from the narrow width approximation are discussed in Ref. [23]). The coefficients

$$c_q^f = \left[(g_q^L)^2 + (g_q^R)^2 \right] B(Z' \rightarrow f\bar{f}) \quad (87.9)$$

contain all the dependence on the Z' couplings, while the functions w_q include all the information about parton distributions and QCD corrections [6, 8]. This factorization holds exactly to NLO and the deviations from it induced at NNLO are very small. Note that the w_u and w_d functions are substantially larger than the w_q functions for the other quarks. Eq. (87.8) also applies to

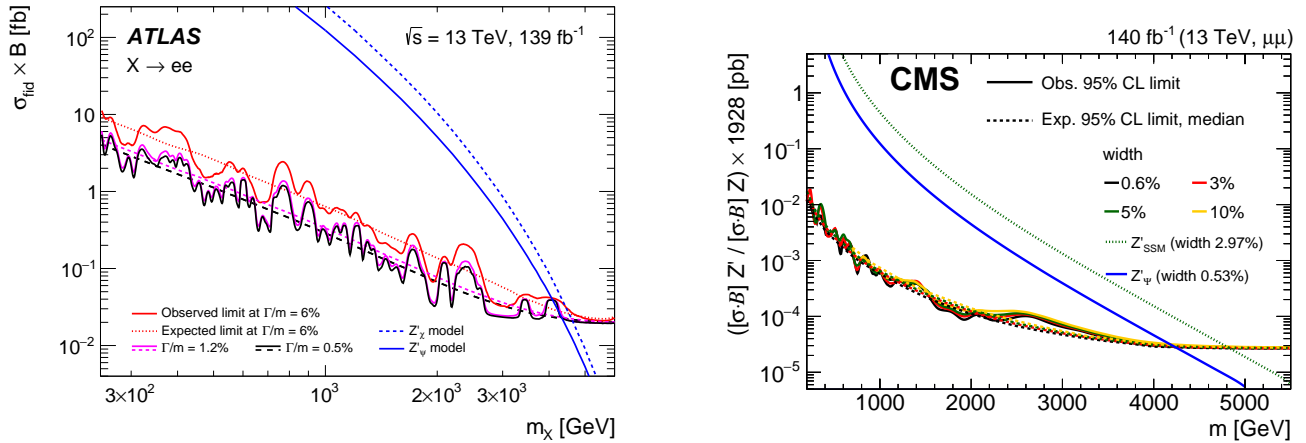


Figure 87.1: Upper limits on the cross section for Z' production times the branching fraction for $Z' \rightarrow e^+e^-$ (left panel, set by ATLAS [20]) or $Z' \rightarrow \mu^+\mu^-$ (right panel, set by CMS [21]) as a function of $M_{Z'}$. The lines labeled by Z'_ψ and Z'_χ are theoretical predictions for the $U(1)_{10+x5}$ models in Table 87.1 with $x = -3$ and $x = +1$, respectively, for g_z fixed by an E_6 unification condition. The Z'_{SSM} line corresponds to Z' couplings equal to those of the Z boson.

the Tevatron, except for changing the pp initial state to $p\bar{p}$, which implies that the $w_q(s, M_{Z'}^2)$ functions are replaced by some other functions $\bar{w}_q((1.96 \text{ TeV})^2, M_{Z'}^2)$.

It is common to present results of Z' searches as limits on the cross section versus $M_{Z'}$ (see for example Fig. 87.1). An alternative is to plot exclusion curves for fixed $M_{Z'}$ values in the $c_u^f - c_d^f$ planes, allowing a simple derivation of the mass limit within any Z' model. CMS upper limits in the $c_\ell^u - c_\ell^d$ plane ($\ell = e$ or μ) for different $M_{Z'}$ are shown in Ref. [21] (for Tevatron limits, see Refs. [8, 24]).

The discovery of a dilepton resonance at the LHC would determine the Z' mass and width. A measurement of the total cross section would define a band in the $c_u^e - c_d^e$ plane. Angular distributions can be used to measure several combinations of Z' parameters (angular distributions were used in Ref. [25] to improve the Tevatron sensitivity). Even though the original quark direction in a pp collider is unknown, the leptonic forward-backward asymmetry A_{FB}^ℓ can be extracted from the kinematics of the dilepton system, and is sensitive to parity-violating couplings. A fit to the Z' rapidity distribution can distinguish between the couplings to up and down quarks. These measurements, combined with off-peak observables, have the potential to differentiate among various Z' models [26]. In some cases, A_{FB}^ℓ may provide discovery sensitivity that is competitive with the mass distribution [27]. The spin of the Z' boson may be determined from angular distributions [28].

Searches for Z' decays into e^+e^- and $\mu^+\mu^-$ by the ATLAS and CMS collaborations [20, 21] have set 95% C.L. upper cross-section limits as low as 0.02 fb (see Fig. 87.1), with the mass lower limits in specific models as high as 4.9 TeV in a single channel. Cross section limits in the dimuon channel for low mass regions, below 200 GeV but not near the Z mass, have been set at the LHC by CMS [29, 30] and LHCb [31].

The $Z' \rightarrow \tau^+\tau^-$ decay has been searched for by ATLAS with 36 fb^{-1} of 13 TeV data [32], and a limit $M_{Z'} > 2.4 \text{ TeV}$ has been set in the case of a sequential Z' . Limits on heavy scalars in the $\tau^+\tau^-$ final state, set by ATLAS [33] and CMS [34] with the full Run 2 datasets, can be recast into limits on Z' . Limits in the flavor-violating leptonic final states have also been reported by ATLAS [35] and CMS [36] at 13 TeV, for resonances in the $e^\pm\mu^\mp$, $e^\pm\tau^\mp$ and $\mu^\pm\tau^\mp$ channels.

Final states with higher background, jj , $b\bar{b}$ and $t\bar{t}$, are also important as they probe various combinations of Z' couplings to quarks. Besides the improved sensitivity at masses of several TeV, the LHC searches in the dijet channel have been also extended to masses as low as 10 GeV, through the use of new techniques involving boosted topologies and initial state radiation [37]. Limits from such Z' searches in hadronic final states are summarized in Fig. 87.2.

Searches for the $Z' \rightarrow b\bar{b}$ decay have been performed for two production mechanisms. ATLAS [39] and CMS [40] searched for $b\bar{b}$ resonances using the full Run 2 datasets, setting limits under the assumption that the Z' boson couples to light quarks and thus is produced in the s -channel. The CMS upper limit on the cross-section times the $Z' \rightarrow b\bar{b}$ branching fraction decreases from 40 fb at $M_{Z'} = 1.8 \text{ TeV}$ to 0.4 fb at $M_{Z'} = 8 \text{ TeV}$. The ATLAS search covered the 1.3 TeV – 5 TeV mass range, setting a lower mass limit of 2.7 TeV for the Z'_{SSM} . Independent of any other couplings, if the Z' couples to the b quark, then it can be produced in association with a $b\bar{b}$ pair, and it decays to a second $b\bar{b}$ pair, which forms a resonance. The cross-section limit for that process, set by ATLAS [41] with 103 fb^{-1} of 13 TeV data, is between 0.1 and 0.2 pb for $M_{Z'}$ in the 1.3 – 3 TeV range. For a vector coupling g_b of Z' to b quarks, *i.e.*, $g_b^T = g_b^R = g_b$ using the notation of Eq. (87.1), the limit is $M_{Z'} > 1.45 \text{ TeV}$ when $g_b = 1$.

Another search that depends on the Z' couplings to the b quark for production (more precisely, for a $b\bar{b}$, $s\bar{b}$ or $b\bar{s}$ initial state) was performed by CMS [42], under the assumption that the Z' boson decays into a muon pair. Searches for the $Z' \rightarrow t\bar{t}$ decay are discussed in Ref. [16].

Heavy resonances decaying into Zh^0 with $Z \rightarrow \ell^+\ell^-$, $\nu\bar{\nu}$ or $q\bar{q}$ and $h^0 \rightarrow b\bar{b}$ have been studied by ATLAS [43, 44] and CMS [45, 46] using the full 13 TeV dataset. CMS also searched for Z' bosons in the $q\bar{q}\tau\tau$ final state [47]. The most stringent constraint on Z' production in the context of the Heavy Vector Triplet (HVT) model weakly-coupled scenario A [48] is set in the semi-leptonic channel, with a mass lower limit of 3.5 TeV [45].

Searches for a Z' boson lighter than the SM Z and which couples to leptons have been performed in the 4-lepton final state. ATLAS [49] and CMS [50] focused on the Z decays into a muon pair followed by the radiation of a narrow Z' boson which decays itself into a muon pair. A related CMS search [51] for Z decays into four leptons, but without requiring that a pair of leptons form a narrow resonance, was used to set limits on Z' couplings to electrons or muons as a function of mass, which are relevant for large widths. ATLAS [52] considered the $h^0 \rightarrow ZZ'$ and $h^0 \rightarrow Z'Z'$ processes followed by the leptonic decays of both spin-1 bosons.

The $pp \rightarrow Z'X \rightarrow W^+W^-X$ process has also been searched for at the LHC. The channel where the Z' boson is produced through its couplings to quarks, and the W bosons decay hadronically, has been explored using boosted techniques to analyze the 13 TeV data [46, 53–55] with a mass lower limit of 3.5 TeV in the HVT model A [54]. A search in the $e\nu\mu\nu$ final state sets cross-section limits at lower Z' mass [56]. The Z' boson may also be produced through its couplings to W bosons [57], which has been explored with the use of forward jets consistent with a vector boson fusion event topology [46, 54, 55]. The latter process provides a test of

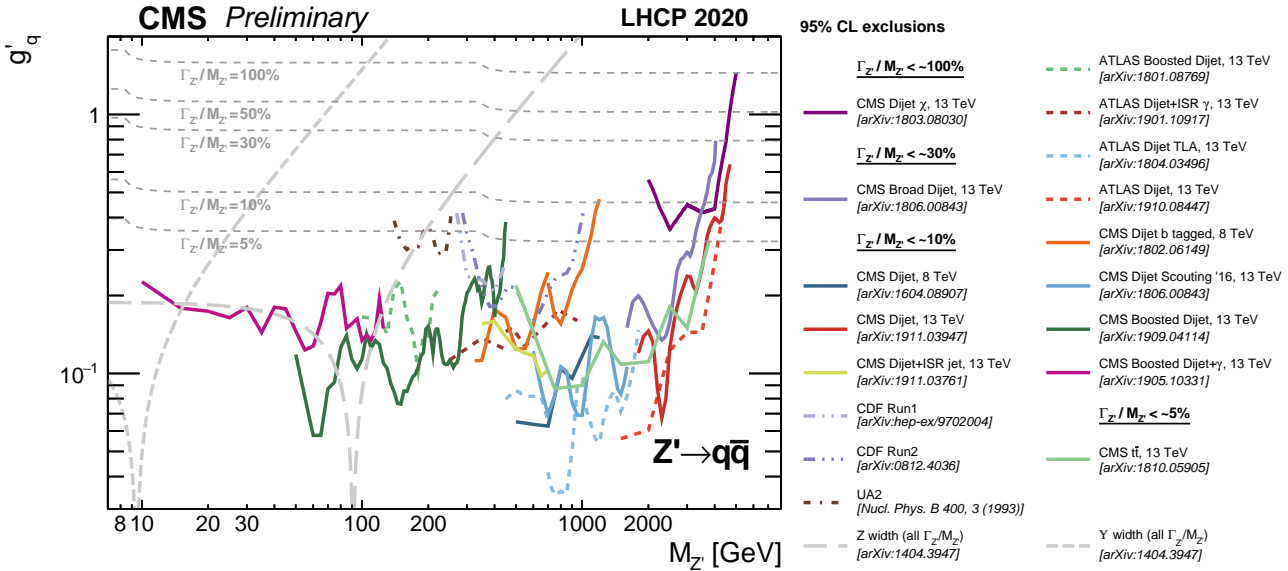


Figure 87.2: Upper limits on the Z' coupling to quarks as a function of $M_{Z'}$ based on various searches performed by the ATLAS, CMS, CDF, and UA2 experiments [38].

fermiophobic Z' models.

At the Tevatron, the CDF and $D\bar{O}$ collaborations have searched for Z' bosons in the e^+e^- [58], $\mu^+\mu^-$ [59], $e^\pm\mu^\mp$ [60], $\tau^+\tau^-$ [61], $t\bar{t}$ [62], jj [63] and W^+W^- [64] final states. These limits have been mostly superseded by the LHC results.

87.5 Low-energy constraints

Z' boson properties are also constrained by a variety of low-energy experiments [65]. Polarized electron-nucleon scattering and atomic parity violation are sensitive to electron-quark contact interactions, which get contributions from Z' exchange that can be expressed in terms of the couplings introduced in Eq. (87.1) and $M_{Z'}$. Further corrections to the electron-quark contact interactions are induced in the presence of $\tilde{Z}-\tilde{Z}'$ mixing because of the shifts in the Z couplings to quarks and leptons [3]. Deep-inelastic neutrino-nucleon scattering is similarly affected by Z' bosons. Other low-energy observables are discussed in [4]. Viable models with Z' bosons much lighter than the Z boson have been constructed, despite many additional experimental constraints [66]. Limits on the Z' coupling to leptons in the mass range 0.02–10.2 GeV have been set in e^+e^- collisions by BaBar [67], assuming a dark photon, *i.e.*, a Z' boson whose couplings arise only from the kinetic mixing with the hypercharge gauge boson.

In some models, the lower limits on $M_{Z'}$ set by low-energy data are above 1 TeV. For example, $M_{Z'_\chi} > 1.1$ TeV and $M_{Z'_\eta} > 0.43$ TeV assuming that the Higgs sectors consist of electroweak doublets and singlets only [4], while the gauge coupling is fixed by an $SO(10)$ unification condition for $U(1)_\chi$ and $U(1)_\eta$. For more general models, see Refs. [1, 6, 68]. The mass bounds from direct searches at the LHC [20, 21] exceed the electroweak constraints by a factor of three or more for the models mentioned here. This conclusion could change if the collider bounds are weakened by exotic decay channels [69].

Although the LHC data are most constraining for many Z' models, one should be careful in assessing the relative reach of various experiments given the freedom in Z' couplings. For example, a Z' coupled to $B-yL_\mu+(y-3)L_\tau$ has implications for the muon $g-2$, neutrino oscillations or τ decays, and would be hard to see in processes involving first-generation fermions. Moreover, the combination of LHC searches and low-energy measurements could allow a precise determination of the Z' parameters [70].

References

[1] A. Leike, Phys. Rept. **317**, 143 (1999), [hep-ph/9805494].

- [2] T. P. Cheng and L. F. Li, *Gauge Theory of Elementary Particle Physics* (1984), ISBN 9780198519614.
- [3] K. S. Babu, C. F. Kolda and J. March-Russell, Phys. Rev. D **57**, 6788 (1998), [hep-ph/9710441].
- [4] J. Erler *et al.*, JHEP **08**, 017 (2009), [arXiv:0906.2435].
- [5] B. A. Dobrescu and P. J. Fox, JHEP **05**, 047 (2016), [arXiv:1511.02148].
- [6] M. Carena *et al.*, Phys. Rev. D **70**, 093009 (2004), [hep-ph/0408098].
- [7] F. Del Aguila, M. Cvetič and P. Langacker, Phys. Rev. D **52**, 37 (1995), [hep-ph/9501390].
- [8] E. Accomando *et al.*, Phys. Rev. D **83**, 075012 (2011), [arXiv:1010.6058].
- [9] M.-C. Chen, A. de Gouvea and B. A. Dobrescu, Phys. Rev. D **75**, 055009 (2007), [hep-ph/0612017].
- [10] P. Langacker and M. Plumacher, Phys. Rev. D **62**, 013006 (2000), [hep-ph/0001204].
- [11] A. J. Buras, F. De Fazio and J. Girrbach, JHEP **02**, 116 (2013), [arXiv:1211.1896].
- [12] L. E. Ibanez and G. G. Ross, Phys. Lett. B **332**, 100 (1994), [hep-ph/9403338].
- [13] P. J. Fox *et al.*, Phys. Rev. D **84**, 115006 (2011), [arXiv:1104.4127].
- [14] See the Section on “ W' searches” in this Review.
- [15] J. Parsons and A. Pomarol, “Extra dimensions” in this Review.
- [16] K.M. Black *et al.*, “Dynamical electroweak symmetry breaking” in this Review.
- [17] M. Bando, T. Kugo and K. Yamawaki, Phys. Rept. **164**, 217 (1988).
- [18] J. Y. Araz *et al.*, JHEP **02**, 092 (2018), [arXiv:1711.06302].
- [19] S. Schael *et al.* (ALEPH, DELPHI, L3, OPAL, LEP Electroweak), Phys. Rept. **532**, 119 (2013), [arXiv:1302.3415].
- [20] G. Aad *et al.* (ATLAS), Phys. Lett. B **796**, 68 (2019), [arXiv:1903.06248].
- [21] A. M. Sirunyan *et al.* (CMS), JHEP **07**, 208 (2021), [arXiv:2103.02708].
- [22] G. Paz and J. Roy, Phys. Rev. D **97**, 075025 (2018), [arXiv:1711.02655].

- [23] E. Accomando *et al.*, JHEP **10**, 153 (2013), [arXiv:1304.6700].
- [24] A. Abulencia *et al.* (CDF), Phys. Rev. Lett. **95**, 252001 (2005), [hep-ex/0507104].
- [25] A. Abulencia *et al.* (CDF), Phys. Rev. Lett. **96**, 211801 (2006), [hep-ex/0602045].
- [26] F. Petriello and S. Quackenbush, Phys. Rev. D **77**, 115004 (2008), [arXiv:0801.4389].
- [27] E. Accomando *et al.*, JHEP **01**, 127 (2016), [arXiv:1503.02672].
- [28] P. Osland *et al.*, Phys. Rev. D **79**, 115021 (2009), [arXiv:0904.4857].
- [29] A. M. Sirunyan *et al.* (CMS), Phys. Rev. Lett. **124**, 13, 131802 (2020), [arXiv:1912.04776].
- [30] A. Hayrapetyan *et al.* (CMS), JHEP **12**, 070 (2023), [arXiv:2309.16003].
- [31] R. Aaij *et al.* (LHCb), JHEP **10**, 156 (2020), [arXiv:2007.03923].
- [32] M. Aaboud *et al.* (ATLAS), JHEP **01**, 055 (2018), [arXiv:1709.07242].
- [33] G. Aad *et al.* (ATLAS), Phys. Rev. Lett. **125**, 051801 (2020), [arXiv:2002.12223].
- [34] A. Tumasyan *et al.* (CMS), JHEP **07**, 073 (2023), [arXiv:2208.02717].
- [35] G. Aad *et al.* (ATLAS), JHEP **23**, 082 (2020), [arXiv:2307.08567].
- [36] A. Tumasyan *et al.* (CMS), JHEP **05**, 227 (2023), [arXiv:2205.06709].
- [37] A. M. Sirunyan *et al.* (CMS), Phys. Rev. Lett. **123**, 231803 (2019), [arXiv:1905.10331].
- [38] CMS Collab., <https://twiki.cern.ch/twiki/bin/view/CMSPublic/SummaryPlotsEX013TeV>.
- [39] G. Aad *et al.* (ATLAS), JHEP **03**, 145 (2020), [arXiv:1910.08447].
- [40] A. Tumasyan *et al.* (CMS), Phys. Rev. D **108**, 012009 (2023), [arXiv:2205.01835].
- [41] G. Aad *et al.* (ATLAS), Phys. Rev. D **105**, 012001 (2022), [arXiv:2108.09059].
- [42] A. Hayrapetyan *et al.* (CMS), JHEP **10**, 043 (2023), [arXiv:2307.08708].
- [43] G. Aad *et al.* (ATLAS), JHEP **06**, 016 (2023), [arXiv:2207.00230].
- [44] G. Aad *et al.* (ATLAS), Phys. Rev. D **102**, 112008 (2020), [arXiv:2007.05293].
- [45] A. M. Sirunyan *et al.* (CMS), Eur. Phys. J. C **81**, 688 (2021), [arXiv:2102.08198].
- [46] A. Tumasyan *et al.* (CMS), Phys. Lett. B **844**, 137813 (2023), [arXiv:2210.00043].
- [47] A. M. Sirunyan *et al.* (CMS), JHEP **01**, 051 (2019), [arXiv:1808.01365].
- [48] D. Pappadopulo *et al.*, JHEP **09**, 060 (2014), [arXiv:1402.4431].
- [49] G. Aad *et al.* (ATLAS), JHEP **07**, 090 (2023), [arXiv:2301.09342].
- [50] A. M. Sirunyan *et al.* (CMS), Phys. Lett. B **792**, 345 (2019), [arXiv:1808.03684].
- [51] CMS Collab., CMS PAS SMP-19-007, Aug. 2023.
- [52] G. Aad *et al.* (ATLAS), JHEP **03**, 041 (2022), [arXiv:2110.13673].
- [53] G. Aad *et al.* (ATLAS), JHEP **09**, 091 (2019), [arXiv:1906.08589].
- [54] G. Aad *et al.* (ATLAS), Eur. Phys. J. C **80**, 1165 (2020), [arXiv:2004.14636].
- [55] A. Tumasyan *et al.* (CMS), Phys. Rev. D **105**, 032008 (2022), [arXiv:2109.06055].
- [56] ATLAS Collab., ATLAS-CONF-2022-066, Nov. 2022.
- [57] H.-J. He *et al.*, Phys. Rev. D **78**, 031701 (2008), [arXiv:0708.2588].
- [58] V. M. Abazov *et al.* (D0), Phys. Lett. B **695**, 88 (2011), [arXiv:1008.2023].
- [59] T. Aaltonen *et al.* (CDF), Phys. Rev. Lett. **106**, 121801 (2011), [arXiv:1101.4578].
- [60] A. Abulencia *et al.* (CDF), Phys. Rev. Lett. **96**, 211802 (2006), [hep-ex/0603006].
- [61] D. Acosta *et al.* (CDF), Phys. Rev. Lett. **95**, 131801 (2005), [hep-ex/0506034].
- [62] T. Aaltonen *et al.* (CDF), Phys. Rev. D **84**, 072004 (2011), [arXiv:1107.5063].
- [63] T. Aaltonen *et al.* (CDF), Phys. Rev. D **79**, 112002 (2009), [arXiv:0812.4036].
- [64] T. Aaltonen *et al.* (CDF), Phys. Rev. Lett. **104**, 241801 (2010), [arXiv:1004.4946].
- [65] V. D. Barger *et al.*, Phys. Rev. D **57**, 391 (1998), [hep-ph/9707412].
- [66] R. Harnik, J. Kopp and P. A. N. Machado, JCAP **1207**, 026 (2012), [arXiv:1202.6073].
- [67] J. P. Lees *et al.* (BaBar), Phys. Rev. Lett. **113**, 201801 (2014), [arXiv:1406.2980].
- [68] E. Rojas and J. Erler, JHEP **10**, 063 (2015), [arXiv:1505.03208].
- [69] J. Kang and P. Langacker, Phys. Rev. D **71**, 035014 (2005), [hep-ph/0412190].
- [70] Y. Li, F. Petriello and S. Quackenbush, Phys. Rev. D **80**, 055018 (2009), [arXiv:0906.4132].

88. Supersymmetry, Part I (Theory)

Revised August 2023 by B.C. Allanach (DAMTP, Cambridge U.) and H.E. Haber (UC Santa Cruz).

88.1	Introduction	1038
88.2	Structure of the MSSM	1038
88.2.1	R-parity and the lightest supersymmetric particle	1039
88.2.2	The goldstino and gravitino	1039
88.2.3	Hidden sectors and the structure of SUSY breaking	1040
88.2.4	SUSY and extra dimensions	1040
88.2.5	Split-SUSY	1040
88.3	Parameters of the MSSM	1041
88.3.1	The SUSY-conserving parameters	1041
88.3.2	The SUSY-breaking parameters	1041
88.3.3	MSSM-124	1041
88.4	The supersymmetric-particle spectrum	1042
88.4.1	The charginos and neutralinos	1042
88.4.2	The squarks and sleptons	1043
88.5	The supersymmetric Higgs sector	1043
88.5.1	The tree-level Higgs sector	1043
88.5.2	The radiatively-corrected Higgs sector	1044
88.6	Restricting the MSSM parameter freedom	1044
88.6.1	Gaugino mass relations	1045
88.6.2	Constrained versions of the MSSM: mSUGRA, CMSSM, etc.	1046
88.6.3	Gauge-mediated SUSY breaking	1046
88.6.4	The phenomenological MSSM	1047
88.6.5	Simplified models	1047
88.7	Experimental data confronts the MSSM	1047
88.7.1	Naturalness constraints and the little hierarchy	1048
88.7.2	Indirect constraints on supersymmetric models	1049
88.8	Massive neutrinos in weak-scale SUSY	1050
88.8.1	The supersymmetric seesaw	1050
88.8.2	R-parity-violating SUSY	1050
88.9	Extensions beyond the MSSM	1051

88.1 Introduction

Supersymmetry (SUSY) is a generalization of the space-time symmetries of quantum field theory that transforms fermions into bosons and vice versa [1]. The existence of such a non-trivial extension of the Poincaré symmetry of ordinary quantum field theory was initially surprising, and its form is highly constrained by theoretical principles [2]. SUSY also provides a framework for the unification of particle physics and gravity [3–5] at the Planck energy scale, $M_P \sim 10^{19}$ GeV, where the gravitational interactions become comparable in strength to the gauge interactions. Moreover, supersymmetry can stabilize the hierarchy between the energy scale that characterizes electroweak symmetry breaking, $M_{EW} \sim 100$ GeV, and the Planck scale [6–9] against large radiative corrections. The stability of this large gauge hierarchy with respect to radiative quantum corrections is not possible to maintain in the Standard Model (SM) without an unnatural fine-tuning of the parameters of the fundamental theory at the Planck scale. In contrast, in a supersymmetric extension of the SM, it is possible to maintain the gauge hierarchy while providing a natural framework for elementary scalar fields.

If supersymmetry were an exact symmetry of nature, then particles and their superpartners, which differ in spin by half a unit, would be degenerate in mass. Since superpartners have not (yet) been observed, supersymmetry must be a broken symmetry. Nevertheless, the stability of the gauge hierarchy can still be maintained if the SUSY breaking is soft [10, 11], and the corresponding SUSY-breaking mass parameters are no larger than a few TeV. Whether this is still plausible in light of recent SUSY searches at the LHC (see Sec. 89) will be discussed in Sec. 88.7.

In particular, soft-SUSY-breaking terms of the Lagrangian involve combinations of fields with total mass dimension of three or

less, with some restrictions on the dimension-three terms as elucidated in Ref. [10]. The impact of the soft terms becomes negligible at energy scales much larger than the size of the SUSY-breaking masses. Thus, a theory of weak-scale supersymmetry, where the effective scale of supersymmetry breaking is tied to the scale of electroweak symmetry breaking, provides a natural framework for the origin and the stability of the gauge hierarchy [6–9].

At present, there is no unambiguous experimental evidence for the breakdown of the SM at or below the TeV scale. The expectations for new TeV-scale physics beyond the SM are based primarily on three theoretical arguments. First, in a theory with an elementary scalar field of mass m and interaction strength λ (e.g., a quartic scalar self-coupling, the square of a gauge coupling or the square of a Yukawa coupling), the stability with respect to quantum corrections requires the existence of an energy cutoff roughly of order $(16\pi^2/\lambda)^{1/2}m$, beyond which new physics must enter [12]. A significantly larger energy cutoff would require an unnatural fine-tuning of parameters that govern the effective low-energy theory. Applying this argument to the SM leads to an expectation of new physics at the TeV scale [9].

Second, the unification of the three SM gauge couplings at a very high energy close to the Planck scale is possible if new physics beyond the SM (which modifies the running of the gauge couplings above the electroweak scale) is present. The minimal supersymmetric extension of the SM, where superpartner masses lie below a few TeV, provides an example of successful gauge coupling unification [13].

Third, the existence of dark matter that makes up approximately one quarter of the energy density of the universe, cannot be explained within the SM of particle physics [14]. Remarkably, a stable weakly-interacting massive particle (WIMP) whose mass and interaction rate are governed by new physics associated with the TeV-scale can be consistent with the observed density of dark matter (this is the so-called WIMP miracle, which is reviewed in Ref. [15]). The lightest supersymmetric particle (LSP), if stable, is a promising (although not the unique) candidate for the dark matter [16–20]. Further aspects of dark matter can be found in Sec. 27.

88.2 Structure of the MSSM

The minimal supersymmetric extension of the SM (MSSM) consists of the fields of the two-Higgs-doublet extension of the SM and the corresponding superpartner fields [21–25]. A particle and its superpartner together form a supermultiplet. The corresponding field content of the supermultiplets of the MSSM and their gauge quantum numbers are shown in Table 88.1. The electric charge $Q = T_3 + \frac{1}{2}Y$ is determined in terms of the third component of the weak isospin (T_3) and the U(1) weak hypercharge (Y).

The gauge supermultiplets consist of the gluons and their gluino fermionic superpartners and the SU(2) × U(1) gauge bosons and their gaugino fermionic superpartners. The matter supermultiplets consist of three generations of left-handed quarks and leptons and their scalar superpartners (squarks and sleptons, collectively referred to as sfermions), and the corresponding antiparticles. The Higgs supermultiplets consist of two complex Higgs doublets, their higgsino fermionic superpartners, and the corresponding antiparticles. The enlarged Higgs sector of the MSSM constitutes the minimal structure needed to guarantee the cancellation of gauge anomalies [27] generated by the higgsino superpartners that can appear as internal lines in triangle diagrams with three external electroweak gauge bosons. Moreover, without a second Higgs doublet, one cannot generate mass for both “up”-type and “down”-type quarks (and charged leptons) in a way consistent with the underlying SUSY [28–30].

In the most elegant treatment of SUSY, spacetime is extended to superspace which consists of the spacetime coordinates and new anticommuting fermionic coordinates θ and θ^\dagger [25, 31, 32]. Each supermultiplet is represented by a superfield that is a function of the superspace coordinates. The fields of a given supermultiplet (which are functions of the spacetime coordinates) are coefficients of the θ and θ^\dagger expansion of the corresponding superfield.

Vector superfields contain the gauge-boson fields and their gaugino partners. Chiral superfields contain the spin-0 and spin-

Table 88.1: The fields of the MSSM and their representations under the $SU(3) \times SU(2) \times U(1)$ gauge group are listed. For simplicity, only one generation of quarks and leptons is exhibited. For each lepton, quark, and Higgs supermultiplet (each denoted by a hatted upper-case letter), there is a corresponding antiparticle multiplet of charge-conjugated fermions and their associated scalar partners [26].

Field Content of the MSSM						
Super-multiplets	Super-field	Bosonic fields	Fermionic partners	SU(3)	SU(2)	U(1)
gluon/gluino	\hat{V}_8	g	\tilde{g}	8	1	0
gauge boson/ gaugino	\hat{V} \hat{V}'	W^\pm, W^0 B	$\tilde{W}^\pm, \tilde{W}^0$ \tilde{B}	1 1	3 1	0 0
slepton/ lepton	\hat{L} \hat{E}^c	$(\tilde{\nu}_L, \tilde{e}_L^-)$ \tilde{e}_R^+	$(\nu, e^-)_L$ e_L^c	1 1	2 1	-1 2
squark/ quark	\hat{Q} \hat{U}^c \hat{D}^c	(\tilde{u}_L, d_L) \tilde{u}_R^* d_R^*	$(u, d)_L$ u_L^c d_L^c	3 $\bar{3}$ $\bar{3}$	2 1 1	1/3 -4/3 2/3
Higgs boson/ higgsino	\hat{H}_d \hat{H}_u	(H_d^0, H_d^-) (H_u^+, H_u^0)	$(\tilde{H}_d^0, \tilde{H}_d^-)$ $(\tilde{H}_u^+, \tilde{H}_u^0)$	1 1	2 2	-1 1

1/2 fields of the matter or Higgs supermultiplets. A general supersymmetric Lagrangian is determined by three functions of the chiral superfields [4]: the superpotential, the Kähler potential, and the gauge kinetic function (which can be appropriately generalized to accommodate higher derivative terms [33]). Minimal forms for the Kähler potential and gauge kinetic function, which generate canonical kinetic energy terms for all the fields, are required for renormalizable globally supersymmetric theories. A renormalizable superpotential, which is at most cubic in the chiral superfields, yields supersymmetric Yukawa couplings and mass terms. A combination of gauge invariance and SUSY produces couplings of gaugino fields to matter (or Higgs) fields and their corresponding superpartners. The (renormalizable) MSSM Lagrangian is then constructed by including all possible supersymmetric interaction terms (of dimension four or less) that satisfy $SU(3) \times SU(2) \times U(1)$ gauge invariance and $B-L$ conservation (where B = baryon number and L = lepton number). Finally, the most general soft-supersymmetry-breaking terms consistent with these symmetries are added [10, 11, 34].

Although the MSSM is the focus of much of this review, there is some motivation for considering non-minimal supersymmetric extensions of the SM [35]. For example, extra structure is needed to generate non-zero neutrino masses as discussed in Sec. 88.8. In addition, in order to address some theoretical issues and tensions associated with the MSSM, it has been fruitful to introduce one additional singlet Higgs superfield. The resulting next-to-minimal supersymmetric extension of the Standard Model (NMSSM) [36] is briefly considered in Sec. 88.4–88.7 and 88.9. Finally, one is always free to add additional fields to the SM along with the corresponding superpartners. However, only certain choices for the new fields (*e.g.*, the addition of complete $SU(5)$ multiplets) will preserve the successful gauge coupling unification of the MSSM. Some examples will be briefly mentioned in Sec. 88.9.

88.2.1 R -parity and the lightest supersymmetric particle

The (renormalizable) SM Lagrangian possesses an accidental global $B-L$ symmetry due to the fact that B and L -violating operators composed of SM fields must have dimension $d = 5$ or larger [37]. Consequently, B and L -violating effects are suppressed by $(M_{\text{EW}}/M)^{d-4}$, where M is the characteristic mass scale of the physics that generates the corresponding higher dimensional operators. Indeed, values of M of order the grand unification scale or larger may be responsible for the observed (approximate) stability of the proton and suppression of neutrino masses. Unfortunately, these results are not guaranteed in a generic supersymmetric extension of the SM. For example, it is possible to construct gauge invariant supersymmetric dimension-four B and L -violating operators made up of fields of SM particles and their superpartners. Such operators, if simultaneously present in the theory, would typically yield a proton decay rate many orders of magnitude larger

than the current experimental bound. It is for this reason that $B-L$ conservation is *imposed* on the supersymmetric Lagrangian when defining the MSSM, which is sufficient for eliminating all B and L -violating operators of dimension $d \leq 4$.

As a consequence of the $B-L$ symmetry, the MSSM possesses a multiplicative R -parity invariance, where $R = (-1)^{3(B-L)+2S}$ for a particle of spin S [38]. This implies that all the particles of the SM have even R -parity, whereas the corresponding superpartners have odd R -parity. The conservation of R -parity in scattering and decay processes has a critical impact on supersymmetric phenomenology. For example, any initial state in a scattering experiment will involve ordinary (R -even) particles. Consequently, it follows that supersymmetric particles must be produced in pairs. In general, these particles are highly unstable and decay into lighter states. Moreover, R -parity invariance also implies that the LSP is absolutely stable, and must eventually be produced at the end of a decay chain initiated by the decay of a heavy unstable supersymmetric particle. In order to be consistent with cosmological constraints, a stable LSP is almost certainly electrically and color neutral [18]. Consequently, the LSP in an R -parity-conserving theory is weakly interacting with ordinary matter, *i.e.*, it behaves like a stable heavy neutrino and will escape collider detectors without being directly observed. Thus, the canonical signature for conventional R -parity-conserving supersymmetric theories is missing (transverse) momentum, due to the escape of the LSP. Moreover, as noted in Sec. 88.1 and reviewed in Refs. [19] and [20], the stability of the LSP in R -parity-conserving SUSY makes it a promising candidate for dark matter.

The possibility of relaxing the R -parity invariance of the MSSM (which would generate new B and/or L -violating interactions) will be addressed in Sec. 88.8.2. However, note that in R -parity violating (RPV) models, the LSP is no longer stable and thus would not be a viable candidate for the dark matter (unless its lifetime was significantly longer than the age of the universe). In such scenarios, one has to look elsewhere to explain the origin of dark matter.

88.2.2 The goldstino and gravitino

In the MSSM, SUSY breaking is accomplished by including the most general renormalizable soft-SUSY-breaking terms consistent with the $SU(3) \times SU(2) \times U(1)$ gauge symmetry and R -parity invariance. These terms parameterize our ignorance of the fundamental mechanism of supersymmetry breaking. If supersymmetry breaking occurs spontaneously, then a massless Goldstone fermion called the goldstino ($\tilde{G}_{1/2}$) must exist. The goldstino would then be the LSP, and could play an important role in supersymmetric phenomenology [39].

However, the goldstino degrees of freedom are physical only in models of spontaneously-broken global SUSY. If SUSY is a local symmetry, then the theory must incorporate gravity; the resulting

theory is called supergravity [5, 40]. In models of spontaneously-broken supergravity, the goldstino is “absorbed” by the gravitino (\tilde{G}), the spin-3/2 superpartner of the graviton, via the super-Higgs mechanism [41]. Consequently, the goldstino is removed from the physical spectrum and the gravitino acquires a mass (denoted by $m_{3/2}$). If $m_{3/2}$ is smaller than the mass of the lightest superpartner of the SM particles, then the gravitino is the LSP.

In processes with center-of-mass energy $E \gg m_{3/2}$, one can employ the goldstino–gravitino equivalence theorem [42], which implies that the interactions of the helicity $\pm\frac{1}{2}$ gravitino (whose properties approximate those of the goldstino) dominate those of the helicity $\pm\frac{3}{2}$ gravitino. The interactions of gravitinos with other light fields can be described by a low-energy effective Lagrangian that is determined by fundamental principles [43].

88.2.3 Hidden sectors and the structure of SUSY breaking

It is very difficult (perhaps impossible) to construct a realistic model of spontaneously-broken weak-scale supersymmetry where the supersymmetry breaking arises solely as a consequence of the interactions of the particles of the MSSM. A more successful scheme posits a theory with at least two distinct sectors: a visible sector consisting of the particles of the MSSM [34] and a sector where SUSY breaking is generated. It is often (but not always) assumed that particles of the hidden sector are neutral with respect to the SM gauge group. The effects of the hidden sector supersymmetry breaking are then transmitted to the MSSM by some mechanism (often involving the mediation by particles that comprise an additional messenger sector). Two theoretical scenarios that exhibit this structure are gravity-mediated and gauge-mediated SUSY breaking.

Supergravity models provide a natural mechanism for transmitting the SUSY breaking of the hidden sector to the particle spectrum of the MSSM. In models of gravity-mediated SUSY breaking, gravity is the messenger of supersymmetry breaking [44–48]. More precisely, supersymmetry breaking is mediated by effects of gravitational strength (*i.e.* suppressed by inverse powers of the Planck mass). The soft-SUSY-breaking parameters with dimensions of mass arise as model-dependent multiples of the gravitino mass $m_{3/2}$. In this scenario, $m_{3/2}$ is of order the electroweak-symmetry-breaking scale, while the gravitino couplings are roughly gravitational in strength [3, 49].¹

Under certain theoretical assumptions that govern the structure of the Kähler potential (the so-called sequestered form introduced in Ref. [51]), SUSY breaking is due entirely to the super-conformal (super-Weyl) anomaly, which is common to all supergravity models [51]. In particular, gaugino masses are radiatively generated at one-loop, and squark and slepton squared-mass matrices are flavor-diagonal. In sequestered scenarios, sfermion squared-masses arise at two-loops, which implies that gluino and sfermion masses are of the same order of magnitude. This approach is called anomaly-mediated SUSY breaking (AMSB). Indeed, anomaly mediation is more generic than originally conceived, and provides a ubiquitous source of SUSY breaking [52]. However in the simple formulation of AMSB as applied to the MSSM, the squared-masses of the sleptons are negative (known as the tachyonic slepton problem). It may be possible to cure this otherwise fatal flaw in non-minimal extensions of the MSSM [53]. Alternatively, one can assert that anomaly mediation is not the sole source of SUSY breaking in the sfermion sector. In non-sequestered scenarios, sfermion squared-masses can arise at tree-level, in which case squark masses would be parametrically larger than the loop-suppressed gaugino masses [54].

In gauge-mediated supersymmetry breaking (GMSB), gauge forces transmit the supersymmetry breaking to the MSSM. A typical structure of such models involves a hidden sector where SUSY is broken, a messenger sector consisting of particles (messengers) with nontrivial $SU(3) \times SU(2) \times U(1)$ quantum numbers, and the visible sector consisting of the fields of the MSSM [55–58]. The direct coupling of the messengers to the hidden sector generates a supersymmetry-breaking spectrum in the messenger sector.

Supersymmetry breaking is then transmitted to the MSSM via the virtual exchange of the messenger fields. In models of direct gauge mediation, there is no separate hidden sector. In particular, the sector in which the SUSY breaking originates includes fields that carry nontrivial SM quantum numbers, which allows for the direct transmission of SUSY breaking to the MSSM [59].

In models of gauge-mediated SUSY breaking with a minimal Kähler potential, the gravitino is the LSP [16], as its mass can range from a few eV (in the case of low SUSY breaking scales) up to a few GeV (in the case of high SUSY breaking scales). In particular, the gravitino is a potential dark matter candidate (for a review and guide to the literature, see Ref. [20]). The couplings of the helicity $\pm\frac{1}{2}$ components of \tilde{G} to the particles of the MSSM (which approximate those of the goldstino as previously noted in Sec. 88.2.2) are significantly stronger than gravitational strength and amenable to experimental collider analyses.

The mass ranges of the gravitino in either gravity-mediated or gauge-mediated SUSY breaking are further constrained by cosmological considerations [60, 61]. In particular, there is a danger of over-abundance of gravitinos if it is the dark matter or, if it decays before nucleosynthesis, modifications to the successful predictions of light element abundances. Avoiding these cosmological gravitino problems imposes strong constraints on gravity-mediated and gauge-mediated SUSY breaking models.

The concept of a hidden sector is more general than SUSY. Hidden valley models [62] posit the existence of a hidden sector of new particles and interactions that are very weakly coupled to particles of the SM. The impact of a hidden valley on supersymmetric phenomenology at colliders can be significant if the LSP lies in the hidden sector [63].

88.2.4 SUSY and extra dimensions

Approaches to SUSY breaking have also been developed in the context of theories in which the number of spatial dimensions is greater than three. In particular, a number of SUSY-breaking mechanisms have been proposed that are inherently extra-dimensional [64]. The size of the extra dimensions can be significantly larger than M_{P}^{-1} ; in some cases of order $(\text{TeV})^{-1}$ or even larger (see, *e.g.*, Sec. 85 and Ref. [65]).

For example, in one approach the fields of the MSSM live on some brane (a lower-dimensional manifold embedded in a higher-dimensional spacetime), while the sector of the theory that breaks SUSY lives on a second spatially-separated brane. Two examples of this approach are AMSB [51] and gaugino-mediated SUSY breaking [66]. In both cases, SUSY breaking is transmitted through fields that live in the bulk (the higher-dimensional space between the two branes). This setup has some features in common with both gravity-mediated and gauge-mediated SUSY breaking (*e.g.*, hidden and visible sectors and messengers).

Since a higher dimensional theory must be compactified to four spacetime dimensions, one can also generate a source of SUSY breaking by employing boundary conditions on the compactified space that distinguish between fermions and bosons. This is the so-called Scherk-Schwarz mechanism [67]. The phenomenology of such models can be strikingly different from that of the usual MSSM [68].

88.2.5 Split-SUSY

If SUSY is not connected with the origin of the electroweak scale, it may still be possible that some remnant of the superparticle spectrum survives down to the TeV-scale or below. This is the idea of split-SUSY [69, 70], in which scalar superpartners of the quarks and leptons are significantly heavier than 1 TeV, whereas the fermionic superpartners of the gauge and Higgs bosons have masses on the order of 1 TeV or below. With the exception of a single light neutral scalar whose properties are practically indistinguishable from those of the SM Higgs boson, all other Higgs bosons are also assumed to be very heavy. Among the supersymmetric particles, only the fermionic superpartners may be kinematically accessible at the LHC.

In models of split SUSY, the top squark masses cannot be arbitrarily large, as these parameters enter in the radiative corrections to the mass of the observed Higgs boson [71–73]. In the MSSM, a Higgs boson mass of 125 GeV (see Sec. 11) implies an upper bound

¹However, such a gravitino typically plays no direct role in supersymmetric phenomenology at colliders (except perhaps indirectly in the case where the gravitino is the LSP [50]).

on the top squark mass scale in the range of 10 to 10^8 TeV [74–76], depending on the value of the ratio of the two neutral Higgs field vacuum expectation values, although this mass range can be somewhat extended by varying other relevant MSSM parameters. In some approaches, gaugino masses are one-loop suppressed relative to the sfermion masses, corresponding to the so-called mini-split SUSY spectrum [72, 77]. The higgsino mass scale may or may not be likewise suppressed depending on the details of the model [78].

The SUSY breaking required to produce such a split-SUSY spectrum would destabilize the gauge hierarchy, and thus would not provide an explanation for the scale of electroweak symmetry breaking. Nevertheless, models of split-SUSY can account for the dark matter (which is assumed to be the LSP gaugino or higgsino) and gauge coupling unification, thereby preserving two of the desirable features of weak-scale SUSY. Finally, as a consequence of the very large squark and slepton masses, neutral flavor changing and CP-violating effects, which can be problematic in models with TeV-scale SUSY-breaking masses, are sufficiently reduced to avoid conflict with experimental observations.

88.3 Parameters of the MSSM

The parameters of the MSSM are conveniently described by considering separately the supersymmetry-conserving and the supersymmetry-breaking sectors. A careful discussion of the conventions used here in defining the tree-level MSSM parameters can be found in Refs. [25, 79, 80]. For simplicity, consider first the case of one generation of quarks, leptons, and their scalar superpartners.

88.3.1 The SUSY-conserving parameters

The parameters of the supersymmetry-conserving sector consist of: (i) gauge couplings, g_s , g , and g' , corresponding to the SM gauge group $SU(3) \times SU(2) \times U(1)$ respectively; (ii) a supersymmetry-conserving higgsino mass parameter μ ; and (iii) Higgs-fermion Yukawa couplings, λ_u , λ_d , and λ_e , of one generation of left- and right-handed quarks and leptons, and their superpartners to the Higgs bosons and higgsinos. Because there is no right-handed neutrino/sneutrino in the MSSM as defined here, a Yukawa coupling λ_ν is not included. The complex μ parameter and Yukawa couplings enter via the most general renormalizable R-parity-conserving superpotential,

$$W_{\text{MSSM}} = \lambda_d \hat{H}_d \hat{Q} \hat{D}^c - \lambda_u \hat{H}_u \hat{Q} \hat{U}^c + \lambda_e \hat{H}_d \hat{L} \hat{E}^c + \mu \hat{H}_u \hat{H}_d, \quad (88.1)$$

where the superfields are defined in Table 1 and the gauge group indices are suppressed. More explicitly, the so-called “ μ -term” can be written out as $\mu \epsilon^{ab} (\hat{H}_u)_a (\hat{H}_d)_b$ with an implicit sum over repeated indices, where ϵ^{ab} is used to tie together the $SU(2)$ weak isospin indices $a, b \in \{1, 2\}$ in a gauge-invariant way (where $\epsilon^{12} = -\epsilon^{21} = 1$ and $\epsilon^{11} = \epsilon^{22} = 0$). Likewise, the term $\hat{H}_u \hat{Q} \hat{U}^c$ can be written out as $\epsilon^{ab} (\hat{H}_u)_a \hat{Q}_{ib} (\hat{U}^c)^i$, where $i \in \{1, 2, 3\}$ is the $SU(3)$ color index. Finally, $\hat{H}_d \hat{Q} \hat{D}^c$ can be written out as $\epsilon^{ab} (\hat{H}_d)_a \hat{Q}_{ib} (\hat{D}^c)^i$, with an analogous expression for $\hat{H}_d \hat{L} \hat{E}^c$.

88.3.2 The SUSY-breaking parameters

The supersymmetry-breaking sector contains the following sets of parameters: (i) three complex gaugino Majorana mass parameters, M_3 , M_2 , and M_1 , associated with the $SU(3)$, $SU(2)$, and $U(1)$ subgroups of the SM; (ii) five sfermion squared-mass parameters, M_Q^2 , M_U^2 , M_D^2 , M_L^2 , and M_E^2 , corresponding to the five electroweak gauge multiplets, *i.e.*, superpartners of the left-handed fields $(u, d)_L$, u_L^c , d_L^c , $(\nu, e^-)_L$, and e_L^c , where the superscript c indicates a charge-conjugated fermion field [26]; and (iii) three Higgs-squark-squark and Higgs-slepton-slepton trilinear interaction terms, with complex coefficients $T_U \equiv \lambda_u A_U$, $T_D \equiv \lambda_d A_D$, and $T_E \equiv \lambda_e A_E$ (which define the “ A -parameters”), following the notation employed in Ref. [80]. It is conventional to separate out the factors of the Yukawa couplings in defining the A -parameters [3, 25] (originally motivated by a simple class of gravity-mediated SUSY-breaking models). If the A -parameters are parametrically of the same order (or smaller) relative to other SUSY-breaking mass parameters, then in most cases only the third generation A -parameters will be phenomenologically relevant.

Finally, we have (iv) two real squared-mass parameters, $m_{H_d}^2$ and $m_{H_u}^2$ (also called m_1^2 and m_2^2 , respectively, in the literature), and one complex squared-mass parameter, $m_{12}^2 \equiv \mu B$ (the latter defines the “ B -parameter”), which appear in the MSSM tree-level scalar Higgs potential [30],

$$V = (m_{H_d}^2 + |\mu|^2) H_d^\dagger H_d + (m_{H_u}^2 + |\mu|^2) H_u^\dagger H_u + (m_{12}^2 H_u H_d + \text{h.c.}) + \frac{1}{8} (g^2 + g'^2) (H_d^\dagger H_d - H_u^\dagger H_u)^2 + \frac{1}{2} g^2 |H_d^\dagger H_u|^2, \quad (88.2)$$

where the $SU(2)$ -invariant combination of the complex doublet scalar fields H_u and H_d that appears in Eq. (88.2) is given by $H_u H_d \equiv \epsilon^{ab} (H_u)_a (H_d)_b = H_u^+ H_d^- - H_u^0 H_d^0$. Note that the quartic Higgs couplings are related to the gauge couplings g and g' as a consequence of SUSY. The breaking of the $SU(2) \times U(1)$ electroweak symmetry group to $U(1)_{\text{EM}}$ is only possible after incorporating the SUSY-breaking Higgs squared-mass parameters $m_{H_d}^2$, $m_{H_u}^2$ (which can be negative) and m_{12}^2 . After minimizing the Higgs scalar potential, these three squared-mass parameters can be re-expressed in terms of the two Higgs vacuum expectation values, $\langle H_d^0 \rangle \equiv v_d/\sqrt{2}$ and $\langle H_u^0 \rangle \equiv v_u/\sqrt{2}$, and the CP-odd Higgs mass m_A [cf. Eqs. (88.4) and (88.5) below]. One is always free to rephrase the Higgs doublet fields such that v_d and v_u (also called v_1 and v_2 , respectively, in the literature) are both real and positive.

The quantity, $v_d^2 + v_u^2 = 4m_W^2/g^2 = (2G_F^2)^{-1/2} \simeq (246 \text{ GeV})^2$, is fixed by the Fermi constant, G_F , whereas the ratio

$$\tan \beta = v_u/v_d \quad (88.3)$$

is a free parameter such that $0 < \beta < \pi/2$. By employing the tree-level conditions resulting from the minimization of the scalar potential, one can eliminate the diagonal and off-diagonal Higgs squared-masses in favor of $m_Z^2 = \frac{1}{4}(g^2 + g'^2)(v_d^2 + v_u^2)$, the CP-odd Higgs mass m_A and the parameter $\tan \beta$,

$$\sin 2\beta = \frac{2m_{12}^2}{m_{H_d}^2 + m_{H_u}^2 + 2|\mu|^2} = \frac{2m_{12}^2}{m_A^2}, \quad (88.4)$$

$$\frac{1}{2} m_Z^2 = -|\mu|^2 + \frac{m_{H_d}^2 - m_{H_u}^2 \tan^2 \beta}{\tan^2 \beta - 1}. \quad (88.5)$$

One must also guard against the existence of charge and/or color breaking global minima due to non-zero vacuum expectation values for the squark and charged slepton fields. This possibility can be avoided if the A -parameters are not unduly large [45, 81, 82]. Additional constraints must also be respected to avoid the possibility of directions in scalar field space in which the full tree-level scalar potential can become unbounded from below [82]. A computer program has been developed to calculate vacuum stability bounds in general models at the one-loop level [83], and has been applied to the MSSM in Ref. [84].

Note that SUSY-breaking mass terms for the fermionic superpartners of the scalar fields and non-holomorphic trilinear scalar interactions (*i.e.*, interactions that mix scalar fields and their complex conjugates) have not been included above in the soft-SUSY-breaking sector. These terms can potentially destabilize the gauge hierarchy [10] in models with a gauge-singlet superfield. The latter is not present in the MSSM; hence as noted in Ref. [11], these so-called non-standard soft-SUSY-breaking terms are benign. The phenomenological impact of non-holomorphic soft SUSY-breaking terms has been reconsidered in Refs. [85–87]. However, in the most common approaches to constructing a fundamental theory of SUSY-breaking, the coefficients of these terms (which have dimensions of mass) are significantly suppressed compared to the TeV-scale [88]. Consequently, we follow the usual approach and omit these terms from further consideration.

88.3.3 MSSM-124

The total number of independent physical parameters that define the MSSM (in its most general form) is quite large, primarily due to the soft-supersymmetry-breaking sector. In particular, in the case of three generations of quarks, leptons, and their superpartners, M_Q^2 , M_U^2 , M_D^2 , M_L^2 , and M_E^2 are hermitian 3×3

matrices, and A_U , A_D , and A_E are complex 3×3 matrices. In addition, M_1 , M_2 , M_3 , B , and μ are in general complex parameters. Finally, as in the SM, the Higgs-fermion Yukawa couplings, λ_f ($f = u, d$, and e), are complex 3×3 matrices that are related to the quark and lepton mass matrices via: $M_f = \lambda_f v_f / \sqrt{2}$, where $v_e = v_d$ [with v_u and v_d as defined above Eq. (88.3)].

However, not all these parameters are physical. Some of the MSSM parameters can be eliminated by expressing interaction eigenstates in terms of the mass eigenstates, with an appropriate redefinition of the MSSM fields to remove unphysical degrees of freedom. The analysis of Ref. [89] shows that the MSSM possesses 124 independent real degrees of freedom. Of these, 18 correspond to SM parameters (including the QCD vacuum angle θ_{QCD}), one corresponds to a Higgs sector parameter (the analogue of the SM Higgs mass), and 105 are genuinely new parameters of the model. The latter include: five real parameters and three CP-violating phases in the gaugino/higgsino sector, 21 squark and slepton (sfermion) masses, 36 real mixing angles to define the sfermion mass eigenstates, and 40 CP-violating phases that can appear in sfermion interactions. The most general parameterization of the R-parity-conserving MSSM (without additional theoretical assumptions) will be denoted henceforth as MSSM-124 [90].

88.4 The supersymmetric-particle spectrum

The supersymmetric particles (sparticles) differ in spin by half a unit from their SM partners. The superpartners of the gauge and Higgs bosons are fermions, whose names are obtained by appending “ino” to the end of the corresponding SM particle name. The gluino is the color-octet Majorana fermion partner of the gluon with mass $M_{\tilde{g}} = |M_3|$. The superpartners of the electroweak gauge and Higgs bosons (the gauginos and higgsinos) can mix due to $SU(2) \times U(1)$ breaking effects. As a result, the physical states of definite mass are parameter dependent linear combinations of the charged or neutral gauginos and higgsinos, called charginos and neutralinos, respectively (sometimes collectively called electroweakinos). The neutralinos are Majorana fermions, which can lead to some distinctive phenomenological signatures [91,92]. The superpartners of the quarks and leptons are spin-zero bosons: the squarks, charged sleptons, and sneutrinos, respectively. A complete set of Feynman rules for the sparticles of the MSSM can be found in Refs. [93,94]. The MSSM Feynman rules also are implicitly contained in a number of amplitude generation and Feynman diagram software packages (see *e.g.*, Refs. [95–97]).

It should be noted that all mass formulae quoted below in this Section are tree-level results. Radiative loop corrections will modify these results and must be included in any precision study of supersymmetric phenomenology [98]. Beyond tree level, the definition of the supersymmetric parameters becomes convention-dependent. For example, one can define physical couplings or running couplings, which differ beyond the tree level. This provides a challenge to any effort that attempts to extract supersymmetric parameters from data. The SUSY Les Houches Accord (SLHA) [80,99] has been adopted, which establishes a set of conventions for specifying generic file structures for supersymmetric model specifications and input parameters, supersymmetric mass and coupling spectra, and decay tables. These provide a universal interface between spectrum calculation programs, decay packages, and high energy physics event generators.

88.4.1 The charginos and neutralinos

The mixing of the charged gauginos (\tilde{W}^\pm) and charged higgsinos (\tilde{H}_u^\pm and \tilde{H}_d^\pm) is described (at tree-level) by a 2×2 complex mass matrix [100,101],

$$M_C \equiv \begin{pmatrix} M_2 & \frac{1}{\sqrt{2}} g v_u \\ \frac{1}{\sqrt{2}} g v_d & \mu \end{pmatrix}. \quad (88.6)$$

To determine the physical chargino states and their masses, one must perform a singular value decomposition [102] of the complex matrix M_C [25,103]:

$$U^* M_C V^{-1} = \text{diag}(M_{\tilde{\chi}_1^\pm}, M_{\tilde{\chi}_2^\pm}), \quad (88.7)$$

where U and V are unitary matrices, and the right-hand side of Eq. (88.7) is the diagonal matrix of (real non-negative) chargino masses. Explicit formulae for the singular value decomposition of M_C can be found in Ref. [104]. The physical chargino states are denoted by $\tilde{\chi}_1^\pm$ and $\tilde{\chi}_2^\pm$. These are linear combinations of the charged gaugino and higgsino states determined by the matrix elements of U and V [100,101]. The chargino masses correspond to the singular values [102] of M_C , *i.e.*, the positive square roots of the eigenvalues of $M_C^\dagger M_C$:

$$M_{\tilde{\chi}_1^\pm, \tilde{\chi}_2^\pm}^2 = \frac{1}{2} \left\{ |\mu|^2 + |M_2|^2 + 2m_W^2 \mp \sqrt{(|\mu|^2 + |M_2|^2 + 2m_W^2)^2 - 4|\mu M_2 - m_W^2 \sin 2\beta|^2} \right\}, \quad (88.8)$$

in a convention where v_u and v_d are real and positive, and where the states are ordered such that $M_{\tilde{\chi}_1^\pm} \leq M_{\tilde{\chi}_2^\pm}$. The relative phase of μ^* and M_2 is physical and potentially observable [105].

The mixing of the neutral gauginos (\tilde{B} and \tilde{W}^0) and neutral higgsinos (\tilde{H}_d^0 and \tilde{H}_u^0) is described (at tree-level) by a 4×4 complex symmetric mass matrix [100,101],

$$M_N \equiv \begin{pmatrix} M_1 & 0 & -\frac{1}{2} g' v_d & \frac{1}{2} g' v_u \\ 0 & M_2 & \frac{1}{2} g v_d & -\frac{1}{2} g v_u \\ -\frac{1}{2} g' v_d & \frac{1}{2} g v_d & 0 & -\mu \\ \frac{1}{2} g' v_u & -\frac{1}{2} g v_u & -\mu & 0 \end{pmatrix}. \quad (88.9)$$

To determine the physical neutralino states and their masses, one must perform an Autonne-Takagi factorization [102,106] (also called Takagi diagonalization in Refs. [25,103,107]) of the complex symmetric matrix M_N :

$$W^T M_N W = \text{diag}(M_{\tilde{\chi}_1^0}, M_{\tilde{\chi}_2^0}, M_{\tilde{\chi}_3^0}, M_{\tilde{\chi}_4^0}), \quad (88.10)$$

where W is a unitary matrix (which is called N^{-1} in Refs. [21,30]) and the right-hand side of Eq. (88.10) is the diagonal matrix of (real non-negative) neutralino masses. The physical neutralino states are denoted by $\tilde{\chi}_i^0$ (for $i = 1, \dots, 4$), where the states are ordered such that $M_{\tilde{\chi}_1^0} \leq M_{\tilde{\chi}_2^0} \leq M_{\tilde{\chi}_3^0} \leq M_{\tilde{\chi}_4^0}$. The $\tilde{\chi}_i^0$ are the linear combinations of the neutral gaugino and higgsino states determined by the matrix elements of W . The neutralino masses correspond to the singular values of M_N , *i.e.*, the positive square roots of the eigenvalues of $M_N^\dagger M_N$. Exact formulae for these masses can be found in Refs. [108,109]. A numerical algorithm for determining the mixing matrix W has been given in Ref. [110].

If a chargino or neutralino state approximates a particular gaugino or higgsino state, it is convenient to employ the corresponding nomenclature. Specifically, if $|M_1|$ and $|M_2|$ are small compared to m_Z and $|\mu|$, then the lightest neutralino $\tilde{\chi}_1^0$ would be nearly a pure photino, $\tilde{\gamma}$, the superpartner of the photon. If $|M_1|$ and m_Z are small compared to $|M_2|$ and $|\mu|$, then the lightest neutralino would be nearly a pure bino, \tilde{B} , the superpartner of the weak hypercharge gauge boson. If $|M_2|$ and m_Z are small compared to $|M_1|$ and $|\mu|$, then the lightest chargino pair and neutralino would constitute a triplet of roughly mass-degenerate pure winos, \tilde{W}^\pm , and \tilde{W}_3^0 , the superpartners of the weak $SU(2)$ gauge bosons. Finally, if $|\mu|$ and m_Z are small compared to $|M_1|$ and $|M_2|$, then the lightest chargino pair and neutralino would be nearly pure higgsino states, the superpartners of the Higgs bosons. Each of the above cases leads to a strikingly different phenomenology.

In the NMSSM, an additional Higgs singlet superfield is added to the MSSM. This superfield comprises two real Higgs scalar degrees of freedom and an associated neutral higgsino degree of freedom. Consequently, there are five neutralino mass eigenstates that are obtained by a Takagi-diagonalization of the 5×5 neutralino mass matrix. In many cases, the fifth neutralino state is dominated by its $SU(2) \times U(1)$ singlet component, and thus is very weakly coupled to the SM particles and their superpartners.

88.4.2 The squarks and sleptons

For a given Dirac fermion f , there are two superpartners, \tilde{f}_L and \tilde{f}_R , where the L and R subscripts simply identify the scalar partners that are related by SUSY to the left-handed and right-handed fermions, $f_{L,R} \equiv \frac{1}{2}(1 \mp \gamma_5)f$, respectively. (There is no $\tilde{\nu}_R$ in the MSSM.) However, \tilde{f}_L - \tilde{f}_R mixing is possible, in which case \tilde{f}_L and \tilde{f}_R are not mass eigenstates. For three generations of squarks, one must diagonalize 6×6 matrices corresponding to the basis $(\tilde{q}_{iL}, \tilde{q}_{iR})$, where $i = 1, 2, 3$ are the generation labels. For simplicity, only the one-generation case is illustrated in detail below.

Using the notation of the third family, the one-generation tree-level squark squared-mass matrix is given by [25, 111],

$$\mathcal{M}^2 = \begin{pmatrix} M_Q^2 + m_q^2 + L_q & m_q X_q^* \\ m_q X_q & M_R^2 + m_q^2 + R_q \end{pmatrix}, \quad (88.11)$$

where

$$X_q \equiv A_q - \mu^* (\cot \beta)^{2T_{3q}}, \quad (88.12)$$

and $T_{3q} = \frac{1}{2} [-\frac{1}{2}]$ for $q = t [b]$. The diagonal squared-masses are governed by soft-SUSY-breaking squared-masses M_Q^2 and $M_R^2 \equiv M_U^2 [M_D^2]$ for $q = t [b]$, the corresponding quark masses $m_t [m_b]$ and the electroweak correction terms:

$$\begin{aligned} L_q &\equiv (T_{3q} - e_q \sin^2 \theta_W) m_Z^2 \cos 2\beta, \\ R_q &\equiv e_q \sin^2 \theta_W m_Z^2 \cos 2\beta, \end{aligned} \quad (88.13)$$

where $e_q = \frac{2}{3} [-\frac{1}{3}]$ for $q = t [b]$. The off-diagonal squark squared-masses are proportional to the corresponding quark masses and depend on $\tan \beta$, the soft-SUSY-breaking A -parameters and the higgsino mass parameter μ . Assuming that the A -parameters are parametrically of the same order (or smaller) relative to other SUSY-breaking mass parameters, it then follows that the first and second generation \tilde{q}_L - \tilde{q}_R mixing is smaller than that of the third generation where mixing can be enhanced by factors of m_t and $m_b \tan \beta$.

In the case of third generation \tilde{q}_L - \tilde{q}_R mixing, the squark mass eigenstates (usually denoted by \tilde{q}_1 and \tilde{q}_2 , with $m_{\tilde{q}_1} < m_{\tilde{q}_2}$) are determined by diagonalizing the 2×2 matrix \mathcal{M}^2 given by Eq. (88.11). The corresponding squared-masses and mixing angle are given by [111]:

$$\begin{aligned} m_{\tilde{q}_{1,2}}^2 &= \frac{1}{2} \left[\text{Tr} \mathcal{M}^2 \mp \sqrt{(\text{Tr} \mathcal{M}^2)^2 - 4 \det \mathcal{M}^2} \right], \\ \sin 2\theta_{\tilde{q}} &= \frac{2m_q |X_q|}{m_{\tilde{q}_2}^2 - m_{\tilde{q}_1}^2}. \end{aligned} \quad (88.14)$$

The one-generation results above also apply to the charged sleptons, with the obvious substitutions: $q \rightarrow \ell$ with $T_{3\ell} = -\frac{1}{2}$ and $e_\ell = -1$, and the replacement of the SUSY-breaking parameters: $M_Q^2 \rightarrow M_L^2$, $M_R^2 \rightarrow M_E^2$, and $A_q \rightarrow A_\tau$. For the neutral sleptons, $\tilde{\nu}_R$ does not exist in the MSSM, so $\tilde{\nu}_L$ is a mass eigenstate.

In the case of three generations, the SUSY-breaking scalar-squared masses $[M_Q^2, M_U^2, M_D^2, M_L^2, \text{ and } M_E^2]$ and the A -parameters $[A_U, A_D, \text{ and } A_E]$ are now 3×3 matrices as noted in Sec. 88.3.3. The diagonalization of the 6×6 squark mass matrices yields \tilde{f}_{iL} - \tilde{f}_{jR} mixing. In practice, since the \tilde{f}_L - \tilde{f}_R mixing is appreciable only for the third generation, this additional complication can often be neglected (although see Ref. [112] for examples in which the mixing between the second and third generation squarks is relevant).

88.5 The supersymmetric Higgs sector

Consider first the MSSM Higgs sector [29, 30, 113]. Despite the large number of potential CP-violating phases among the MSSM-124 parameters, the tree-level MSSM Higgs potential given by Eq. (88.2) is automatically CP-conserving. This follows from the fact that the only potentially complex parameter (m_{12}^2) of the

MSSM Higgs potential can be chosen real and positive by rephasing the Higgs fields, in which case $\tan \beta$ is a real positive parameter. Consequently, the physical neutral Higgs scalars are CP-eigenstates (at tree-level). The MSSM Higgs sector contains five physical spin-zero particles: a charged Higgs boson pair (H^\pm), two CP-even neutral Higgs bosons (denoted by h^0 and H^0 where $m_h < m_H$), and one CP-odd neutral Higgs boson (A^0). The discovery of a SM-like Higgs boson at the LHC with a mass of 125 GeV (see Sec. 11) strongly suggests that this state should be identified with h^0 , although the possibility that the 125 GeV state should be identified with H^0 cannot yet be completely ruled out [114].

In the NMSSM [36], the scalar component of the singlet Higgs superfield adds two additional neutral states to the Higgs sector. In this model, the tree-level Higgs sector can exhibit explicit CP-violation. If CP is conserved, then the two extra neutral scalar states are CP-even and CP-odd, respectively. These states can potentially mix with the neutral Higgs states of the MSSM. If scalar states exist that are dominantly singlet, then they are weakly coupled to SM gauge bosons and fermions through their small mixing with the MSSM Higgs scalars. Consequently, it is possible that one (or both) of the singlet-dominated states is considerably lighter than the Higgs boson that was observed at the LHC.

88.5.1 The tree-level Higgs sector

The tree-level properties of the Higgs sector are determined by the Higgs potential given by Eq. (88.2). The quartic interaction terms are manifestly supersymmetric (although these are modified by SUSY-breaking effects at the loop level). In general, the quartic couplings arise from two sources: (i) the supersymmetric generalization of the scalar potential (the so-called “ F -terms”), and (ii) interaction terms related by SUSY to the coupling of the scalar fields and the gauge fields, whose coefficients are proportional to the corresponding gauge couplings (the so-called “ D -terms”).

In the MSSM, F -term contributions to the quartic Higgs self-couplings are absent. As a result, the strengths of the MSSM quartic Higgs interactions are fixed in terms of the gauge couplings, as noted below Eq. (88.2). Consequently, all the tree-level MSSM Higgs-sector parameters depend only on two quantities: $\tan \beta$ [defined in Eq. (88.3)] and one Higgs mass usually taken to be m_A . For example, the tree-level squared mass of the charged Higgs boson is given by

$$m_{H^\pm}^2 = m_A^2 + m_W^2, \quad (88.15)$$

where $m_A^2 = m_{H_d}^2 + m_{H_u}^2 + 2|\mu|^2$ [cf. Eq. (88.5)] and

$$H^\pm = H_d^\pm \sin \beta + H_u^\pm \cos \beta, \quad A = \sqrt{2} (\text{Im} H_d^0 \sin \beta + \text{Im} H_u^0 \cos \beta). \quad (88.16)$$

The CP-even scalar mass eigenstate fields h and H are identified by diagonalizing the 2×2 squared-mass matrix

$$\mathcal{M}^2 = \begin{pmatrix} m_A^2 \sin^2 \beta + m_Z^2 \cos^2 \beta & -(m_A^2 + m_Z^2) \sin \beta \cos \beta \\ -(m_A^2 + m_Z^2) \sin \beta \cos \beta & m_A^2 \cos^2 \beta + m_Z^2 \sin^2 \beta \end{pmatrix}. \quad (88.17)$$

In particular,

$$h = -(\sqrt{2} \text{Re} H_d^0 - v_d) \sin \alpha + (\sqrt{2} \text{Re} H_u^0 - v_u) \cos \alpha, \quad (88.18)$$

$$H = (\sqrt{2} \text{Re} H_d^0 - v_d) \cos \alpha + (\sqrt{2} \text{Re} H_u^0 - v_u) \sin \alpha, \quad (88.19)$$

with corresponding tree-level squared masses,

$$m_{H,h}^2 = \frac{1}{2} \left(m_A^2 + m_Z^2 \pm \sqrt{(m_A^2 + m_Z^2)^2 - 4m_Z^2 m_A^2 \cos^2 2\beta} \right), \quad (88.20)$$

and mixing angle α given by

$$\cos \alpha = \sqrt{\frac{m_A^2 \sin^2 \beta + m_Z^2 \cos^2 \beta - m_h^2}{m_H^2 - m_h^2}}, \quad (88.21)$$

in a convention where $|\alpha| \leq \pi/2$. However, because the off-diagonal elements of \mathcal{M}^2 are negative, it follows that $-\pi/2 \leq$

$\alpha \leq 0$ [104]. In light of Eq. (88.20), the tree-level mass of the lighter CP-even Higgs boson is bounded [29,30],

$$m_h \leq m_Z |\cos 2\beta| \leq m_Z. \quad (88.22)$$

This bound can be substantially modified when radiative corrections are included, as discussed in Sec. 88.5.2.

In the NMSSM, we set $\mu = 0$ in Eq. 88.1 and then add two additional terms to the superpotential,

$$W_{\text{NMSSM}} \supset \lambda \hat{H}_u \hat{H}_d \hat{S} + \frac{1}{3} \kappa \hat{S}^3, \quad (88.23)$$

where \hat{S} is a singlet Higgs superfield. In the NMSSM as defined here, all terms in W_{NMSSM} are cubic in the superfields due to the presence of a discrete \mathbb{Z}_3 symmetry. An effective μ -term is generated, $\mu_{\text{eff}} = \lambda \langle S \rangle$, where $\langle S \rangle$ is the vacuum expectation value of the scalar field component of \hat{S} . Moreover, due to the term proportional to λ in Eq. 88.23, there is now an F -term contribution to the quartic Higgs self-couplings. Consequently, the tree-level bound for the mass of the lightest CP-even MSSM Higgs boson is modified [115],

$$m_h^2 \leq m_Z^2 \cos^2 2\beta + \frac{1}{2} \lambda^2 v^2 \sin^2 2\beta, \quad (88.24)$$

where $v \equiv (v_u^2 + v_d^2)^{1/2} = 246$ GeV. By requiring that λ remain finite after renormalization-group evolution up to the Planck scale, one finds that λ is constrained to lie below about 0.7–0.8 at the electroweak scale [36] (although larger values of λ have also been considered in Ref. [116]).

The tree-level Higgs couplings to gauge bosons and the Higgs boson self-couplings are governed by the electroweak gauge couplings and the parameter $\cos(\beta - \alpha)$. Explicitly,

$$\cos(\beta - \alpha) = \frac{m_Z^2 \sin 2\beta \cos 2\beta}{\sqrt{(m_H^2 - m_h^2)(m_H^2 - m_Z^2 \cos^2 2\beta)}}. \quad (88.25)$$

Note that $\cos(\beta - \alpha) \rightarrow 0$ in the limit of $m_H \gg m_h, m_Z$. In this *decoupling limit* [117], the properties of h coincide with those of the SM Higgs boson. In light of the LHC Higgs data [118,119], which are compatible with the SM predictions (see Sec. 11), one can conclude that if h is identified with the observed Higgs boson then H, A and H^\pm must be substantially heavier (most likely of order 500 GeV or larger [120]).

The tree-level Higgs-quark and Higgs-lepton interactions of the MSSM are derived from the superpotential given in Eq. (88.1). The corresponding Higgs-fermion Yukawa couplings can be expressed in terms of the fermion masses and the separate parameters $\cos(\beta - \alpha)$ and $\tan \beta$. In particular, the Higgs sector of the MSSM is a Type-II two-Higgs doublet model [121], in which one Higgs doublet (H_d) couples exclusively to the right-handed down-type quark (or lepton) fields and the second Higgs doublet (H_u) couples exclusively to the right-handed up-type quark fields. Consequently, the diagonalization of the fermion mass matrices simultaneously diagonalizes the matrix of Yukawa couplings, resulting in flavor-diagonal tree-level couplings of the neutral Higgs bosons h^0, H^0 and A^0 to quark and lepton pairs. One can again check that in the decoupling limit where $\cos(\beta - \alpha) \rightarrow 0$, the couplings of h reduce to those of the SM.

88.5.2 The radiatively-corrected Higgs sector

When radiative corrections are incorporated, additional parameters of the supersymmetric model enter via virtual supersymmetric particles that appear in loops. The impact of these corrections can be significant [122]. The qualitative behavior of these radiative corrections can be most easily seen in the large top-squark mass limit, where in addition, both the splitting of the two diagonal entries and the off-diagonal entries of the top-squark squared-mass matrix [Eq. (88.11)] are small in comparison to the geometric mean of the two top-squark squared-masses, $M_S^2 \equiv M_{t_1} M_{t_2}$. In this case (assuming $m_A > m_Z$), the predicted upper bound for

m_h is approximately given by [123]

$$m_h^2 \lesssim m_Z^2 \cos^2 2\beta + \frac{3g^2 m_t^4}{8\pi^2 m_W^2} \left[\ln \left(\frac{M_S^2}{m_t^2} \right) + \frac{X_t^2}{M_S^2} \left(1 - \frac{X_t^2}{12M_S^2} \right) \right], \quad (88.26)$$

where $X_t \equiv A_t - \mu \cot \beta$ [cf. Eq. (88.12)] is proportional to the off-diagonal entry of the top-squark squared-mass matrix (where for simplicity, A_t and μ are taken to be real). The Higgs mass upper limit specified by Eq. (88.26) is saturated when $\tan \beta$ is large (*i.e.*, $\cos^2 2\beta \sim 1$) and $X_t = \sqrt{6} M_S$, which defines the so-called maximal mixing scenario.

In applying the radiatively corrected MSSM Higgs sector to the analysis of LHC Higgs data, the authors of Refs. [124,125] suggested that a reasonable approximation would consist of retaining the leading corrections employed in deriving Eq. (88.26), while discarding all other subleading terms. This procedure was implemented by simply replacing $\mathcal{M}_{22}^2 \rightarrow \mathcal{M}_{22}^2 + \Delta \mathcal{M}_{22}^2$ in the 22 element of the CP-even Higgs squared-mass matrix given in Eq. (88.17), since $\Delta \mathcal{M}_{22}^2$ contains the leading contributions that govern the Higgs mass radiative corrections. One can now re-diagonalize the CP-even Higgs squared-mass matrix and determine $\Delta \mathcal{M}_{22}^2$ in terms of the parameters $m_A, \tan \beta$ and the measured Higgs mass (*e.g.*, $m_h \simeq 125$ GeV, if h is identified with the observed Higgs boson). This framework was dubbed the hMSSM in Ref. [124].

Although the hMSSM can be readily applied to LHC data to derive interesting constraints on the MSSM Higgs sector, it can lead to results that are not robust in a more general MSSM parameter scan. Indeed, a more complete treatment of the radiative corrections can yield results that cannot be accounted for by the hMSSM framework. Examples of benchmark points of the MSSM parameter space that cannot be reproduced by the hMSSM analysis are discussed in 11.6.1.1.

The set of approximations employed in obtaining Eq. (88.26) somewhat overestimates the value of m_h . The most complete treatment of the MSSM Higgs mass radiative corrections, which incorporate renormalization group improvement, the two loop, and the leading three-loop contributions [73,126], yields a predicted value of m_h shown in Fig. 88.1, as a function of X_t (assumed for simplicity to be real).

In the NMSSM with $m_h \simeq 125$ GeV, the dominant radiative correction to Eq. (88.24) is the same as the one given in Eq. (88.26). However, in contrast to the MSSM, one does not need as large a boost from radiative corrections to achieve a Higgs mass of 125 GeV in certain regimes of the NMSSM parameter space (*e.g.*, $\tan \beta \sim 2$ and $\lambda \sim 0.7$ [127]).

88.6 Restricting the MSSM parameter freedom

In Sections 88.4 and 88.5, we surveyed the parameters that comprise the MSSM-124. However, the MSSM-124 is not a phenomenologically viable theory over much of its parameter space. In particular, a generic point of the MSSM-124 parameter space exhibits: (i) no conservation of the separate lepton numbers $L_e, L_\mu,$ and L_τ ; (ii) unsuppressed flavor-changing neutral currents (FCNCs); and (iii) new sources of CP violation that are inconsistent with the experimental bounds.

In addition, one-loop radiative corrections can introduce CP-violating effects in the Higgs sector that depend on some of the CP-violating phases among the MSSM-124 parameters [128]. This phenomenon is most easily understood in a scenario where $m_A \ll M_S$ (*i.e.*, all five physical Higgs states are significantly lighter than the SUSY breaking scale). In this case, one can integrate out the heavy superpartners to obtain a low-energy effective theory with two Higgs doublets. The resulting effective two-Higgs doublet model will now contain all possible Higgs self-interaction terms (both CP-conserving and CP-violating) and Higgs-fermion interactions (beyond those of Type-II) that are consistent with electroweak gauge invariance [129].

For example, the MSSM contains new sources of CP violation [130]. Indeed, for TeV-scale sfermion and gaugino masses, some combinations of the complex phases of the gaugino-mass parameters, the A -parameters, and μ must be less than about 10^{-2} – 10^{-3} to avoid generating electric dipole moments for the

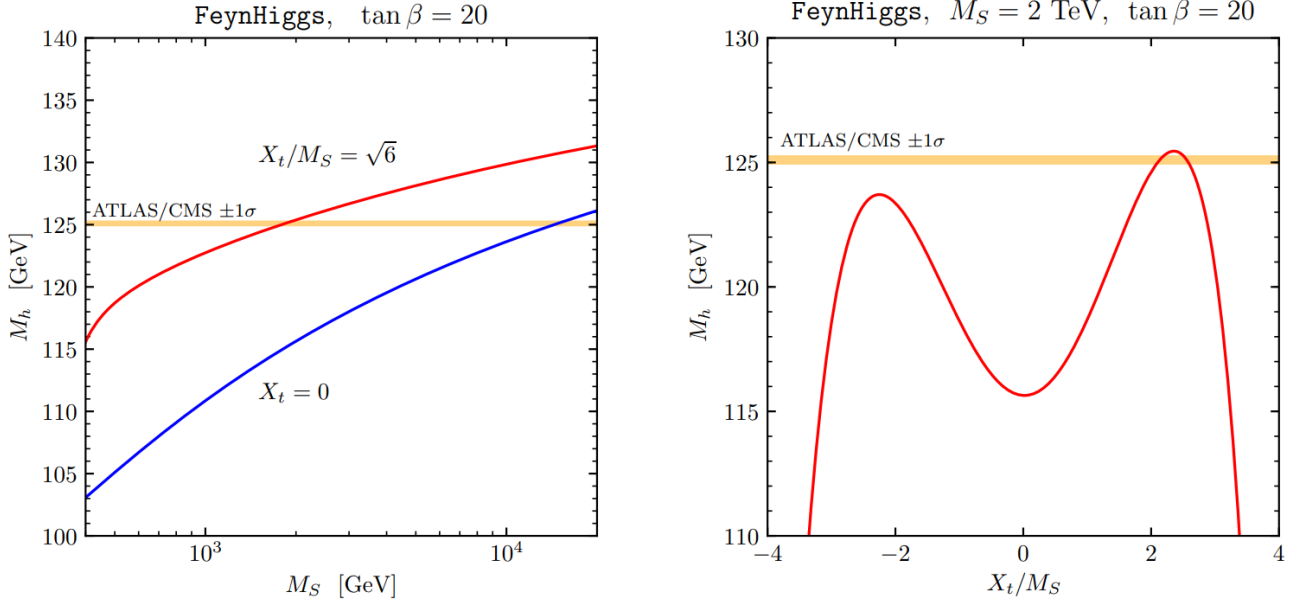


Figure 88.1: The lighter CP-even Higgs mass in the MSSM as a function of a common SUSY mass parameter M_S and of the stop mixing parameter X_t (normalized to M_S). Figure taken from Ref. [73].

neutron, electron, and atoms [131–133] in conflict with observed data [134, 135]. The rarity of FCNCs [136–138] places additional constraints on the off-diagonal matrix elements of the squark and slepton soft-SUSY-breaking squared-masses and A -parameters (see Sec. 88.3.3).

The MSSM-124 is also theoretically incomplete as it provides no explanation for the fundamental origin of the supersymmetry-breaking parameters. The successful unification of the MSSM gauge couplings at a grand unified mass scale M_{GUT} , close to the Planck scale [7, 70, 139–141],

$$g_s(M_{\text{GUT}}) = g(M_{\text{GUT}}) = \sqrt{\frac{5}{3}} g'(M_{\text{GUT}}), \quad (88.27)$$

suggests that the high-energy structure of the theory may be considerably simpler than its low-energy realization.² In a top-down approach, the dynamics that governs the theory at high energies is used to derive the effective broken-supersymmetric theory at the TeV scale.

In this Section, we examine a number of theoretical frameworks that potentially yield phenomenologically viable regions of the MSSM-124 parameter space. The resulting supersymmetric particle spectrum is then a function of a relatively small number of input parameters. This is accomplished by imposing a simple structure on the soft SUSY-breaking parameters at a common high-energy scale M_X (typically chosen to be the Planck scale, M_P , the grand unified theory scale, M_{GUT} , or the messenger scale, M_{mess}). These serve as initial conditions for the MSSM renormalization group equations (RGEs), which are given in the two-loop approximation in Ref. [142]. An automated program to compute RGEs for the MSSM and other supersymmetric models of new physics has been developed in Ref. [143]. Solving these equations numerically, one can then derive the low-energy MSSM parameters relevant for phenomenology. A number of software packages exist that numerically calculate the spectrum of supersymmetric particles, consistent with theoretical conditions on SUSY breaking at high energies and some experimental data at low energies [73, 144].

²Generically, the normalization of the U(1) hypercharges exhibited in Table 88.1 is a matter of convention. In particular, the U(1) hypercharges can be rescaled by absorbing the scaling factor into a redefinition of the hypercharge gauge coupling g' . However, the embedding of the hypercharge U(1) generator into the Lie algebra of a grand unified simple gauge group fixes the normalization of the U(1) hypercharges and results in the rescaled hypercharge gauge coupling shown in Eq. (88.27).

Examples of viable frameworks are provided by models of gravity-mediated, anomaly-mediated, and gauge-mediated SUSY breaking. In some of these approaches, one of the diagonal Higgs squared-mass parameters is driven negative by renormalization group evolution [145]. In such models, electroweak symmetry breaking is generated radiatively, and the resulting electroweak symmetry-breaking scale is intimately tied to the scale of low-energy SUSY breaking.

88.6.1 Gaugino mass relations

One prediction of many supersymmetric grand unified models is the unification of the (tree-level) gaugino mass parameters³ at some high-energy scale, M_X ,

$$M_1(M_X) = M_2(M_X) = M_3(M_X) = m_{1/2}. \quad (88.28)$$

Due to renormalization group running, in the one-loop approximation the effective low-energy gaugino mass parameters (at the electroweak scale) are related,

$$M_3 = (g_s^2/g^2)M_2 \simeq 3.5M_2, \quad M_1 = (5g'^2/3g^2)M_2 \simeq 0.5M_2. \quad (88.29)$$

Eq. (88.29) can arise more generally in gauge-mediated SUSY-breaking models where the gaugino masses are generated at the messenger scale M_{mess} (which typically lies significantly below the unification scale where the gauge couplings unify). In this case, the gaugino mass parameters are proportional to the corresponding squared gauge couplings at the messenger scale.

When Eq. (88.29) is satisfied, the chargino and neutralino masses and mixing angles depend only on three unknown parameters: the gluino mass, μ , and $\tan\beta$. It then follows that the lightest neutralino must be heavier than 46 GeV due to the non-observation of charginos at LEP [147]. If in addition $|\mu| \gg |M_1| \gtrsim m_Z$, then the lightest neutralino is nearly a pure bino, an assumption often made in supersymmetric particle searches at colliders. Although Eq. (88.29) is often assumed in many phenomenological studies, a truly model-independent approach would take the gaugino mass parameters M_1 , M_2 , and M_3 to be independent parameters to be determined by experiment. Indeed, an approximately massless neutralino *cannot* be ruled out at present by a model-independent analysis [148].

It is possible that the tree-level masses of the gauginos are zero. In this case, the gaugino mass parameters arise at one-loop and

³Non-universal gaugino mass parameters can also be a viable option in grand unified models with non-minimal gauge kinetic functions [146].

do not satisfy Eq. (88.29). For example, the gaugino masses in AMSB models arise entirely from a model-independent contribution derived from the super-conformal anomaly [51, 149]. In this case, Eq. (88.29) is replaced (in the one-loop approximation) by:

$$M_i \simeq \frac{b_i g_i^2}{16\pi^2} m_{3/2}, \quad (88.30)$$

where $m_{3/2}$ is the gravitino mass and the b_i are the coefficients of the MSSM gauge beta-functions corresponding to the corresponding U(1), SU(2), and SU(3) gauge groups, $(b_1, b_2, b_3) = (\frac{33}{5}, 1, -3)$. Eq. (88.30) yields $M_1 \simeq 2.8M_2$ and $M_3 \simeq -8.3M_2$, which implies that the lightest chargino pair and neutralino comprise a nearly mass-degenerate triplet of winos, $\tilde{W}^\pm, \tilde{W}^0$ (cf. Table 1), over most of the MSSM parameter space. For example, if $|\mu| \gg m_Z, |M_2|$, then Eq. (88.30) implies that $M_{\tilde{\chi}^\pm} \simeq M_{\tilde{\chi}^0} \simeq M_2$ [150]. Alternatively, one can construct an AMSB model where $|\mu|, m_Z \ll M_2$, which yields an LSP that is an approximate higgsino state [151]. In both cases, the corresponding supersymmetric phenomenology differs significantly from the standard phenomenology based on Eq. (88.29) [152, 153].

Finally, it should be noted that the unification of gaugino masses (and scalar masses) can be accidental. In particular, the energy scale where unification takes place may not be directly related to any physical scale. One version of this phenomenon has been called mirage unification and can occur in certain theories of fundamental SUSY breaking [154].

88.6.2 Constrained versions of the MSSM: mSUGRA, CMSSM, etc.

In the minimal supergravity (mSUGRA) framework [3–5, 25, 44–46], the minimal form of the Kähler potential is employed, which yields standard kinetic energy terms for the MSSM fields [48]. As a result, the soft supersymmetry-breaking parameters at the high-energy scale M_X take a particularly simple form in which the scalar squared-masses and the A -parameters are flavor-diagonal and universal [46]:

$$\begin{aligned} M_Q^2(M_X) &= M_U^2(M_X) = M_D^2(M_X) = m_0^2 \mathbf{1}, \\ M_L^2(M_X) &= M_E^2(M_X) = m_0^2 \mathbf{1}, \\ m_1^2(M_X) &= m_2^2(M_X) = m_0^2, \\ A_U(M_X) &= A_D(M_X) = A_E(M_X) = A_0 \mathbf{1}, \end{aligned} \quad (88.31)$$

where $\mathbf{1}$ is a 3×3 identity matrix in generation space. As in the SM, this approach exhibits minimal flavor violation (see *e.g.* Refs. [155, 156]), whose unique source is the nontrivial flavor structure of the Higgs-fermion Yukawa couplings. The gaugino masses are also unified according to Eq. (88.28).

Renormalization group evolution is then used to derive the values of the supersymmetric parameters at the low-energy (electroweak) scale. For example, to compute squark masses, one should use the low-energy values for M_Q^2 , M_U^2 , and M_D^2 in Eq. (88.11). Through the renormalization group running with boundary conditions specified in Eq. (88.29) and Eq. (88.31), one can show that the low-energy values of M_Q^2 , M_U^2 , and M_D^2 depend primarily on m_0^2 and $m_{1/2}^2$. A number of useful approximate analytic expressions for superpartner masses in terms of the mSUGRA parameters can be found in Ref. [157].

One can count the number of independent parameters in the mSUGRA framework. In addition to 18 SM parameters (excluding the Higgs mass), one must specify $m_0, m_{1/2}, A_0$, the Planck-scale values for μ and B -parameters (denoted by μ_0 and B_0), and the gravitino mass $m_{3/2}$. Without additional model assumptions, $m_{3/2}$ is independent of the parameters that govern the mass spectrum of the superpartners of the SM [46]. In principle, A_0, B_0, μ_0 , and $m_{3/2}$ can be complex, although in the mSUGRA approach, these parameters are taken to be real for simplicity.

As previously noted, renormalization group evolution is used to compute the low-energy values of the mSUGRA parameters, which then fixes all the parameters of the low-energy MSSM. In

particular, the two Higgs vacuum expectation values (or equivalently, m_Z and $\tan\beta$) can be expressed as a function of the Planck-scale supergravity parameters. In light of Eq. (88.4) and Eq. (88.5), a common procedure is to determine μ_0 and B_0 in terms of m_Z and $\tan\beta$ [the sign of μ_0 , denoted $\text{sgn}(\mu_0)$ below, is not fixed in this process]. In this case, the MSSM spectrum and its interaction strengths are fixed by five parameters:

$$m_0, A_0, m_{1/2}, \tan\beta, \text{ and } \text{sgn}(\mu_0), \quad (88.32)$$

and an independent gravitino mass $m_{3/2}$ (in addition to the 18 parameters of the SM). In Ref. [158], this framework was dubbed the constrained minimal supersymmetric extension of the SM (CMSSM). Additional relations such as $B_0 = A_0 - m_0$ and $m_{3/2} = m_0$ comprise the original mSUGRA proposal [44, 48, 159].

One can also relax the universality of scalar masses by decoupling the squared-masses of the Higgs bosons and the squarks/sleptons. This leads to the non-universal Higgs mass models (NUHMs), thereby adding one or two new parameters to the CMSSM depending on whether the diagonal Higgs scalar squared-mass parameters ($m_{H_d}^2$ and $m_{H_u}^2$) are set equal (NUHM1 [160]) or taken to be independent (NUHM2 [161]) at the high energy scale M_X . Clearly, this modification preserves the minimal flavor violation of the mSUGRA approach. Nevertheless, the mSUGRA approach and its NUHM generalizations are probably too simplistic. Theoretical considerations suggest that the universality of Planck-scale soft SUSY-breaking parameters is not generic [162]. In particular, effective operators at the Planck scale exist that do not respect flavor universality, and it is difficult to find a theoretical principle that would forbid them.

In the framework of supergravity, if anomaly mediation is the sole source of SUSY breaking, then the gaugino mass parameters, diagonal scalar squared-mass parameters, and the SUSY-breaking trilinear scalar interaction terms (proportional to $\lambda_f A_F$) are determined in terms of the beta functions of the gauge and Yukawa couplings and the anomalous dimensions of the squark and slepton fields [51, 149, 153]. As noted in Sec. 88.2.3, this approach yields tachyonic sleptons in the MSSM unless additional sources of SUSY breaking are present. In the minimal AMSB (mAMSB) scenario, a universal squared-mass parameter, m_0^2 , is added to the AMSB expressions for the diagonal scalar squared-masses [153]. Thus, the mAMSB spectrum and its interaction strengths are determined by four parameters, $m_0^2, m_{3/2}, \tan\beta$ and $\text{sgn}(\mu_0)$.

The mAMSB scenario appears to be ruled out based on the observed value of the Higgs boson mass, assuming an upper limit on M_S of a few TeV, since the mAMSB constraint on A_F implies that the maximal mixing scenario cannot be achieved [cf. Eq. (88.26)]. Indeed, under the stated assumptions, the mAMSB Higgs mass upper bound lies below the observed Higgs mass value [163]. Thus within the AMSB scenario, either an additional SUSY-breaking contribution to $\lambda_f A_F$ and/or new ingredients beyond the MSSM are required.

88.6.3 Gauge-mediated SUSY breaking

In contrast to models of gravity-mediated SUSY breaking, the flavor universality of the fundamental soft SUSY-breaking squark and slepton squared-mass parameters is guaranteed in gauge-mediated SUSY breaking (GMSB) because the supersymmetry breaking is communicated to the sector of MSSM fields via gauge interactions [56, 58]. In GMSB models, the mass scale of the messenger sector (or its equivalent) is sufficiently below the Planck scale such that the additional SUSY-breaking effects mediated by supergravity can be neglected.

In the minimal GMSB approach, there is one effective mass scale, A , that determines all low-energy scalar and gaugino mass parameters through loop effects, while the resulting A -parameters are suppressed. In addition, the minimal form of the Kähler potential is employed. In order that the resulting superpartner masses be of order 1 TeV, one must have $A \sim \mathcal{O}(100 \text{ TeV})$. The origin of the μ and B -parameters is model-dependent, and lies somewhat outside the purview of gauge-mediated SUSY breaking [164].

The simplest GMSB models appear to be ruled out based on the observed value of the Higgs boson mass. Due to suppressed A pa-

rameters, it is difficult to boost the contributions of the radiative corrections in Eq. (88.26) to obtain a Higgs mass as large as 125 GeV. However, this conflict can be alleviated in more complicated GMSB models [165]. To analyze these generalized GMSB models, it has been especially fruitful to develop model-independent techniques that encompass all known GMSB models [166]. These techniques are well-suited for a comprehensive analysis [167] of the phenomenological profile of gauge-mediated SUSY breaking.

The gravitino is the LSP in minimal GMSB models, as noted in Sec. 88.2.3. As a result, the next-to-lightest supersymmetric particle (NLSP) now plays a crucial role in the phenomenology of supersymmetric particle production and decays. Note that unlike the LSP, the NLSP can be charged. In GMSB models, the most likely candidates for the NLSP are $\tilde{\chi}_1^0$ and $\tilde{\tau}_R^\pm$. The NLSP will decay into its superpartner plus a gravitino (*e.g.*, $\tilde{\chi}_1^0 \rightarrow \gamma\tilde{G}$, $\tilde{\chi}_1^0 \rightarrow Z\tilde{G}$, $\tilde{\chi}_1^0 \rightarrow h^0\tilde{G}$ or $\tilde{\tau}_1^\pm \rightarrow \tau^\pm\tilde{G}$), with lifetimes and branching ratios that depend on the model parameters. There are also GMSB scenarios in which there are several nearly degenerate co-NLSPs, any one of which can be produced at the penultimate step of a supersymmetric decay chain [168]. For example, in the slepton co-NLSP case, all three right-handed sleptons are close enough in mass and thus can each play the role of the NLSP.

Different choices for the identity of the NLSP and its decay rate lead to a variety of distinctive supersymmetric phenomenologies [58, 169]. For example, a long-lived $\tilde{\chi}_1^0$ -NLSP that decays outside collider detectors leads to supersymmetric decay chains with missing energy in association with leptons and/or hadronic jets (this case is indistinguishable from the standard phenomenology of the $\tilde{\chi}_1^0$ -LSP). On the other hand, if $\tilde{\chi}_1^0 \rightarrow \gamma\tilde{G}$ is the dominant decay mode, and the decay occurs inside the detector, then nearly all supersymmetric particle decay chains would produce a photon. In contrast, in the case of a $\tilde{\tau}_1^\pm$ -NLSP, the $\tilde{\tau}_1^\pm$ would either be long-lived or would decay inside the detector into a τ -lepton plus missing energy.

A number of attempts have been made to address the origins of the μ and B -parameters in GMSB models based on the field content of the MSSM (see, *e.g.*, Refs. [164, 170]). An alternative approach is to consider GMSB models based on the NMSSM [171]. The vacuum expectation value of the additional singlet Higgs superfield can be used to generate effective μ and B -parameters [172]. Such models provide an alternative GMSB framework for achieving a Higgs mass of 125 GeV, while still being consistent with LHC bounds on supersymmetric particle masses.

88.6.4 The phenomenological MSSM

Any of the theoretical assumptions described in the previous three subsections must be tested experimentally and could turn out to be wrong. To facilitate the exploration of MSSM phenomena in a more model-independent way while respecting the constraints noted at the beginning of this Section, the phenomenological MSSM (pMSSM) has been introduced [173].

The pMSSM is governed by 19 independent real supersymmetric parameters: the three gaugino mass parameters M_1 , M_2 and M_3 , the Higgs sector parameters m_A and $\tan\beta$, the Higgsino mass parameter μ , five sfermion squared-mass parameters for the degenerate first and second generations (M_Q^2 , M_U^2 , M_D^2 , M_L^2 and M_E^2), the five corresponding sfermion squared-mass parameters for the third generation, and three third-generation A -parameters (A_t , A_b and A_τ). The first and second generation A -parameters are typically neglected in pMSSM studies, as their phenomenological consequences are negligible in most applications. One counterexample arises when considering the A_μ dependence of the anomalous magnetic moment of the muon, which can be as significant as other contributions due to superpartner mediated radiative corrections [174]. Since its initial proposal, the pMSSM approach has been extended to include a 20th parameter, A_μ [175]. It also has been further extended to include CP-violating SUSY-breaking parameters in Ref. [176].

The 19-parameter pMSSM is often further constrained to expedite scans over the parameter space. For example, in Ref. [177], the number of pMSSM parameters is reduced to ten by assuming one common squark squared-mass parameter for the first two

generations, a second common squark squared-mass parameter for the third generation, a common (charged) slepton squared-mass parameter and a common third generation A parameter. In Ref. [178] an eleven parameter pMSSM is defined by allowing for a different stau squared-mass parameter from that of the first two generation charged sleptons. Other applications of the pMSSM approach (with a reduced pMSSM parameter space) to supersymmetric particle searches, and a discussion of the implications for past and future LHC and dark matter studies can be found in Refs. [177, 179, 180].

88.6.5 Simplified models

As Sec. 89 demonstrates, experiments present their searches for supersymmetric particles primarily in terms of simplified models. Simplified models for supersymmetric searches [181] are defined mostly by the empirical objects and kinematic variables involved in the search. Their interpretation by an experimental collaboration usually involves only a small number of supersymmetric particles (often two or three). Other supersymmetric particles are assumed to play no role (this may happen by virtue of them being too heavy to be produced). Experimental bounds from non-observation of a signal are usually presented in terms of the physical masses of the supersymmetric particles involved. Bounds may be presented on the relevant supersymmetric particle masses assuming certain values for the branching ratio of certain supersymmetric particle decays, or as an upper bound on the signal production cross-section as a function of the relevant supersymmetric particle masses.

For example, consider a search for hadronic jets plus missing transverse momentum. One can match such a search to the simplified model of squark pair production followed by the subsequent decay of each squark into a quark (which appears as a jet) and a neutralino LSP that produces the missing transverse momentum, *i.e.* $\tilde{q}\tilde{q} \rightarrow (q\tilde{\chi}_1^0)(q\tilde{\chi}_1^0)$. Excluded cross-sections resulting from the non-observation of a signal (which in this case could consist of some specified minimum value of missing transverse momentum and at least two hard jets) may be exhibited in the squark mass versus LSP mass plane.

Simplified models have the apparent advantage that they have fewer free parameters than more complete supersymmetric models, whose greater number of free parameters makes it difficult to present excluded regions in any generality. If limits are quoted on supersymmetric particle masses without reference to the signal production cross-section from a simplified model analysis, then there is a potential pitfall—namely, mass limits can differ from those obtained in full models because there may be contributions to the signal coming from processes involving supersymmetric particles other than those assumed. For example, in the $\tilde{q}\tilde{q} \rightarrow q\tilde{\chi}_1^0 q\tilde{\chi}_1^0$ process mentioned above, the simplified model analysis does not account for the interference with tree-level t -channel gluino contributions. Nevertheless, simplified model bounds quoted purely in terms of supersymmetric particle masses may still approximately hold over sizable regions of parameter space of more complete models, within which the simplified model is embedded. When simplified model limits are phrased as bounds on signal cross-sections, the aforementioned pitfall is sidestepped. Simplified models thus remain an efficient tool for organizing and presenting the results of supersymmetric particle searches. A comparison between supersymmetric particle search constraints in the context of simplified models and the corresponding constraints obtained in the more complete pMSSM can be found in Ref. [182].

88.7 Experimental data confronts the MSSM

At present, there is no significant evidence for weak-scale SUSY from the data analyzed by the LHC experiments. Recent LHC data have been employed in ruling out the existence of colored supersymmetric particles (primarily the gluino and the first generation of squarks) with masses below about 2 TeV (see Fig. 89.14). Moreover, given that the mass of the observed Higgs boson is 125 GeV, the results exhibited in Fig. 88.1 tend to favor a mass scale of the top squarks somewhat above 2 TeV. However, the precise mass limits are very model dependent. For example, as Fig. 89.13 demonstrates, regions of the pMSSM parameter space can be identified in which lighter squarks and gluinos below 1 TeV cannot be

definitely ruled out. Under the assumption of gaugino mass unification [cf. Eq. (88.29)], LHC searches result in a lower bound on neutralino and chargino masses of roughly 200 GeV. It is difficult to place general bounds on neutralino and chargino masses, since the limit in terms of masses from direct searches tends to be particularly model dependent. Nevertheless, one must confront the tension that exists between the theoretical expectations for the magnitude of the SUSY-breaking parameters and the non-observation of supersymmetric phenomena at colliders.

88.7.1 Naturalness constraints and the little hierarchy

In Sec. 88.1, weak-scale SUSY was motivated as a natural solution to the hierarchy problem, which could provide an understanding of the origin of the electroweak symmetry-breaking scale without a significant fine-tuning of the fundamental parameters that govern the MSSM. In this context, the weak scale soft supersymmetry-breaking masses must be generally of the order of 1 TeV or below [183]. This requirement is most easily seen in the determination of m_Z by the scalar potential minimum condition. In light of Eq. (88.5), to avoid the fine-tuning of MSSM parameters, the soft SUSY-breaking squared-masses $m_{H_d}^2$ and $m_{H_u}^2$ and the higgsino squared-mass $|\mu|^2$ should all be roughly of $\mathcal{O}(m_Z^2)$. Many authors have proposed quantitative measures of fine-tuning [183–188]. One of the simplest measures is the one advocated by Barbieri and Giudice [183] (which was also introduced previously in Ref. [184]),

$$\Delta_i \equiv \left| \frac{\partial \ln m_Z^2}{\partial \ln p_i} \right|, \quad \Delta \equiv \max \Delta_i, \quad (88.33)$$

where the p_i are the MSSM parameters at the high-energy scale M_X , which are set by the fundamental SUSY-breaking dynamics. The theory is more fine-tuned as Δ becomes larger. However, different measures of fine-tuning yield quantitatively different results; in particular, calculating minimal fine-tuning based on the high-scale parameters [as defined in Eq. (88.33)] yields a difference by a factor ~ 10 to fine-tuning based on TeV-scale parameters [189, 190].

One can apply the fine-tuning measure to any explicit model of SUSY breaking. For example, in the approaches discussed in Sec. 88.6, the p_i are parameters of the model at the energy scale M_X where the soft SUSY-breaking operators are generated by the dynamics of SUSY breaking. Renormalization group evolution then determines the values of the parameters appearing in Eq. (88.5) at the electroweak scale. In this way, Δ is sensitive to all the SUSY-breaking parameters of the model (see *e.g.* Ref. [191]). The computation of Δ is often based on Eq. (88.5), which is a tree-level condition. However, the fine-tuning measure obtained at tree level can be somewhat reduced in value when loop corrections are included while remaining consistent with all experimental constraints [87, 192].

One way of taking fine-tuning into account in fits to data using Bayesian statistics is to have a prior probability distribution proportional to $1/\Delta$ [193] so that fine-tuning is balanced against the fit to empirical data. In such a Bayesian approach, it is important to choose the prior probability distribution carefully, since prior probability densities that are flat in one set of variables may not be flat in another, more fundamental set. One can in fact derive a different measure of fine-tuning resulting from a Jacobian factor when transforming to other variables.⁴ By comparing the results of several Bayesian fits with different (but reasonable) prior probability distributions, one can assess the robustness of the fit with respect to their variation, mitigating for subjectivity in the interpretation of the fine-tuning measure.

As anticipated, there is a tension between the present experimental lower limits on the masses of colored supersymmetric particles [195, 196] and the expectation that supersymmetry-breaking is associated with the electroweak symmetry-breaking scale. Moreover, this tension is exacerbated [197] by the observed value of the

Higgs mass ($m_h \simeq 125$ GeV), which is not far from the MSSM upper bound ($m_h \lesssim 135$ GeV) [which depends on the top-squark mass and mixing as noted in Sec. 88.5.2]. If M_{SUSY} characterizes the scale of supersymmetric particle masses, then one would crudely expect $\Delta \sim M_{\text{SUSY}}^2/m_Z^2$. For example, if $M_{\text{SUSY}} \sim 1$ TeV then one expects a $\Delta^{-1} \sim 1\%$ fine-tuning of the MSSM parameters to achieve the observed value of m_Z . This separation of the electroweak symmetry-breaking and SUSY-breaking scales is an example of the little hierarchy problem [198, 199].

The fine-tuning parameter Δ can depend quite sensitively on the structure of the SUSY-breaking dynamics, such as the value of M_X and relations among SUSY-breaking parameters in the fundamental high energy theory [200]. For example, in so-called focus point SUSY models [187, 201], all squark masses can be as heavy as 5 TeV *without* significant fine-tuning. This can be attributed to a focusing behavior of the renormalization group evolution when certain relations hold among the high-energy values of the scalar squared-mass SUSY-breaking parameters. Although the focus point region of the CMSSM still yields an uncomfortably high value of Δ due to the observed Higgs mass of 125 GeV, one can achieve moderate values of Δ in models with NUHM2 boundary conditions for the scalar masses [197].

Among the colored superpartners, the third generation squarks typically have the most significant impact on the naturalness constraints [202], while their masses are the least constrained by the LHC data. Hence, in the absence of any relation between third generation squarks and those of the first two generations, the naturalness constraints due to present LHC data can be considerably weaker than those obtained in the CMSSM. Indeed, models with first and second generation squark masses in the multi-TeV range do not necessarily require significant fine tuning. Such models have the added benefit that undesirable FCNCs mediated by squark exchange are naturally suppressed [203]. Other MSSM mass spectra that are compatible with moderate fine tuning have been considered in Refs. [200] and [204].

The lower bounds on squark and gluino masses may not be as large as suggested by the experimental analyses based on the CMSSM or simplified models. For example, mass bounds for the gluino and the first and second generation squarks based on the CMSSM can often be evaded in alternative or extended MSSM models, *e.g.*, compressed SUSY [205] and stealth SUSY [206]. Moreover, the experimental upper limits for the third generation squark masses (which have a more direct impact on the fine-tuning measure) are weaker than the corresponding mass limits for other colored supersymmetric states.

Among the uncolored superpartners, the higgsinos are typically the most impacted by the naturalness constraints. Eq. (88.5) suggests that the masses of the two neutral higgsinos and charged higgsino pair (which are governed by $|\mu|$) should not be significantly larger than m_Z to avoid an unnatural fine-tuning of the supersymmetric parameters, which would imply the existence of light higgsinos (whose masses are not well constrained, as they are difficult to detect directly at the LHC due to their soft decay products). However, it may be possible to avoid the conclusion that $\mu \sim \mathcal{O}(m_Z)$ if additional correlations among the SUSY breaking mass parameters and μ are present. Such a scenario can be realized in models in which the boundary conditions for SUSY breaking are generated by approximately conformal strong dynamics. For example, in the so-called scalar-sequestering model of Ref. [207], values of $|\mu| > 1$ TeV can be achieved while naturally maintaining the observed value of m_Z .

Finally, one can also consider extensions of the MSSM in which the degree of fine-tuning is relaxed. For example, it has already been noted in Sec. 88.5 that it is possible to accommodate the observed Higgs mass more easily in the NMSSM due to contributions to m_h^2 proportional to the parameter λ^2 . This means that one does not have to rely on a large contribution from radiative corrections to boost the Higgs mass sufficiently above its tree-level bound. This allows for smaller top squark masses, which are more consistent with the demands of naturalness. The reduction of the fine-tuning in various NMSSM models was initially advocated in Ref. [208], and subsequently treated in more detail in Refs. [116, 209]. Naturalness can also be relaxed in extended su-

⁴For example, one may consider the parameters μ and m_{12}^2 to be more fundamental than $\tan \beta$ and M_Z . In this case, one would choose a flat prior probability distribution in μ and m_{12}^2 rather than in $\tan \beta$ and M_Z [186, 194]. The Jacobian factor is then obtained from Eq. (88.4) and Eq. (88.5).

persymmetric models with vector-like quarks [210] and in gauge extensions of the MSSM [211].

The experimental absence of any new physics beyond the SM at the LHC suggests that the principle of naturalness is presently under significant stress [212]. Nevertheless, one must be very cautious when drawing conclusions about the viability of weak-scale SUSY to explain the origin of electroweak symmetry breaking, since different measures of fine-tuning noted above can lead to different assessments [189, 190]. Moreover, the maximal value of Δ that determines whether weak-scale SUSY is a fine-tuned model (should it be $\Delta \sim 10?$ $100?$ $1000?$) is ultimately subjective. Thus, it is premature to conclude that weak-scale SUSY is on the verge of exclusion. It might be possible to sharpen the upper bounds on superpartner masses based on naturalness arguments, which ultimately will either confirm or refute the weak scale SUSY hypothesis [213]. Of course, if evidence for supersymmetric phenomena in the multi-TeV regime were to be established at a future collider facility (with an energy reach beyond the LHC [214]), it would be viewed as a spectacularly successful explanation of the large gauge hierarchy between the (multi-)TeV scale and Planck scale. In this case, the remaining little hierarchy, characterized by the somewhat large value of the fine-tuning parameter Δ discussed above, would be regarded as a less pressing issue.

88.7.2 Indirect constraints on supersymmetric models

While direct empirical searches for supersymmetric particles provide various limits on their properties, indirect constraints can depend more sensitively on details of the whole model. The cold dark matter relic density inferred from cosmological fits to observational data is one such example of an indirect constraint. In supersymmetric models where the LSP is stable (and thus is a dark matter candidate), its thermally-produced relic density depends upon the scattering of various supersymmetric particles into dark matter particles and SM particles. The resulting relic density can depend sensitively on the masses of the non-LSP supersymmetric particles as well as on the mass of the LSP. In a typical model, an appreciable region of the parameter space is ruled out because it yields an overabundance of dark matter (see for example Ref. [215] for a fit to a seven parameter version of the pMSSM). However, subsequent tweaks to the supersymmetric model that yield an unstable LSP, such as the introduction of R-parity violating effects, can mean that the relic density no longer constrains the parameter space.

There are a number of indirect constraints based on low-energy measurements that are sensitive to the effects of new physics via supersymmetric loop effects. For example, the virtual exchange of supersymmetric particles can contribute to the muon anomalous magnetic moment, $a_\mu \equiv \frac{1}{2}(g-2)_\mu$, as reviewed in Ref. [216]. The SM prediction for a_μ , which employs dispersion relations and low energy e^+e^- scattering data to determine the hadronic corrections [217], exhibits a deviation of 5σ from the experimentally observed value [218]. The deviation of Ref. [217] from the measured value of a_μ [218] is difficult to accommodate in the constrained models of Sec. 88.6.2 and 88.6.3 given the present sparticle mass bounds [196]. Nevertheless, such a deviation can be consistent in the context of a more general version of the MSSM [219].

However, the Budapest-Marseille-Wupertal (BMW) lattice determination of the leading hadronic contribution to the muon magnetic moment obtained in Ref. [220] yields a significantly smaller deviation from the SM prediction [221]. Indeed, there is a tension of almost 4σ between the BMW lattice calculation and the corresponding dispersive estimate based on the same e^+e^- data, as stated in Ref. [222] where the relevant references are cited. Moreover, Ref. [222] notes that crucial parts of the BMW calculation have recently been cross checked by other lattice groups. In addition, various tensions exist among the relevant sets of e^+e^- scattering data that are used in the dispersive estimate, some of which have appeared after the publication of Ref. [217]. Thus, the deviation of the measured value of a_μ from the corresponding SM prediction still needs to be clarified.

The precision of the measured value of a_μ is not sensitive to the experimental error associated with the measured value of the fine structure constant, α . In contrast, the comparison of the SM prediction with the experimental measurement of the anomalous

magnetic moment of the electron, a_e , depends critically on the value of α . Using the experimentally determined value of α given in Ref. [223] yields a SM prediction for a_e that is 2.4σ above its measured value [224]. However, this previous determination of α is in tension at the 5σ level with a more recent measurement of the fine structure constant [225]. The latter yields a SM prediction for a_e that is 1.6σ below its measured value [225].

Measurements of the fine structure constant, a_e and a_μ jointly constrain the pMSSM parameter space [226] due to shifts originating from supersymmetric loop effects. In particular, if the supersymmetric interpretation of the deviation in the measured value of a_μ from its SM prediction is combined with the experimental limits on the electron electric dipole moment [135], then the resulting upper bounds on MSSM CP-violating phases are even more constraining [227] than previously noted at the beginning of Sec. 88.6.

Flavor transitions in radiative, leptonic and semi-leptonic b quark decays [228] provide a fertile ground for physics beyond the SM. For example, the rare inclusive decay $b \rightarrow s\gamma$ is a sensitive probe of the virtual effects of new physics beyond the SM. The experimental measurements of $B \rightarrow X_s + \gamma$ [229] are in agreement with the theoretical SM predictions of Ref. [230]. Since supersymmetric loop corrections can contribute an observable shift from the SM predictions, the absence of any significant deviation places useful constraints on the MSSM parameter space [231].

The rare decays $B_s \rightarrow \mu^+\mu^-$ and $B_d \rightarrow \mu^+\mu^-$ are especially sensitive to supersymmetric loop effects, with some loop contributions scaling as $\tan^6\beta$ when $\tan\beta \gg 1$ [232]. At present, a combination [233] of the measurements of these rare decay modes [234] is in slight tension at the 1.6σ level with the predicted SM rates [235]. Such a tension can be resolved by the aforementioned supersymmetric loop effects [232].

Several tensions exist between SM predictions and measurements of some other experimental observables that probe $b \rightarrow s\mu^+\mu^-$ transitions, although the level of tension depends upon the theoretical treatment of the SM analysis. In a certain angular distribution parameter (denoted by P'_5) extracted from $B^0 \rightarrow K^{*0}\mu^+\mu^-$ decays, the tension is around the 4σ level [236]. An even larger discrepancy is observed in a combination of angular distributions and rates derived from $B^\pm \rightarrow K^\pm\mu^+\mu^-$ and $B^0 \rightarrow K^0\mu^+\mu^-$ [237]. Finally, there is a 3.6σ deviation in the branching ratio of $B_s \rightarrow \phi\mu^+\mu^-$ for di-muon invariant mass squared values between 1.1 GeV^2 and 6.0 GeV^2 [238]. Finally, a recent measurement of $B^+ \rightarrow K^+\nu\bar{\nu}$ by the Belle II Collaboration [239] obtained a branching fraction that is roughly four times larger than the SM prediction [240], corresponding to 2.7σ above the SM expectation. However, it is unlikely that this result can be attributed to new contributions from the MSSM [241], as the latter are expected to be negligible in comparison with the SM.

The decays $B^\pm \rightarrow \tau^\pm\nu_\tau$ and $\bar{B} \rightarrow D^{(*)}\tau^-\bar{\nu}_\tau$ are noteworthy, since in models with extended Higgs sectors such as the MSSM, these processes possess tree-level charged Higgs exchange contributions that can compete with the dominant W -exchange. As Sec. 72 shows, experimental measurements of $B^\pm \rightarrow \tau^\pm\nu_\tau$ are currently consistent with SM expectations [242]. The BaBar Collaboration measured values of the rates for $\bar{B} \rightarrow D\tau^-\bar{\nu}_\tau$ and $\bar{B} \rightarrow D^*\tau^-\bar{\nu}_\tau$ [243] which exhibited a combined 3.4σ discrepancy from the SM predictions, which was also not compatible with the Type-II Higgs Yukawa couplings employed by the MSSM. Subsequent measurements by the LHCb and Belle Collaborations were compatible with the BaBar measurements although they displayed less deviation from the SM expectations; the combined difference between the measured values of the $\bar{B} \rightarrow D\tau^-\bar{\nu}_\tau$ and $\bar{B} \rightarrow D^*\tau^-\bar{\nu}_\tau$ decay rates relative to the corresponding SM values has a significance of 3.3 standard deviations [244].

In summary, although there are a few hints of possible deviations from the SM in B decays, none of the discrepancies by themselves are significant enough to conclusively imply the existence of new physics beyond the SM. Moreover, the absence of evidence for sizable deviations in other B -physics observables from their SM predictions can place useful constraints on the MSSM parameter space [138, 195, 245, 246].

The CDF Collaboration has reported a measurement of the W

boson mass [247] that is 7σ above the SM prediction. Supersymmetric models have been shown to be able to accommodate the measured value by the CDF Collaboration at the 2σ level [248]. However, other measurements, including a more recent determination by ATLAS Collaboration [249], are consistent with SM predictions for m_W (see Sec. 10 for further details).

88.8 Massive neutrinos in weak-scale SUSY

In the minimal version of the SM and its supersymmetric extension, there are no right-handed neutrinos, and Majorana mass terms for the left-handed neutrinos are absent. However, given the overwhelming evidence for neutrino masses and mixing (see Sec. 14 and [250]), any viable model of the fundamental particles must provide a mechanism for generating neutrino masses [251]. In extended supersymmetric models, various mechanisms exist for producing massive neutrinos [252]. Although one can devise models for generating massive Dirac neutrinos [253], the most common approaches for incorporating neutrino masses are based on L -violating supersymmetric extensions of the MSSM, which generate massive Majorana neutrinos. Two classes of L -violating supersymmetric models will now be considered.

88.8.1 The supersymmetric seesaw

Neutrino masses can be incorporated into the SM by introducing $SU(3)\times SU(2)\times U(1)$ singlet right-handed neutrinos (ν_R) whose mass parameters are very large, typically near the grand unification scale. In addition, one must also include a standard Yukawa couplings between the lepton doublets, the Higgs doublet, and ν_R . The Higgs vacuum expectation value then induces an off-diagonal ν_L - ν_R mass on the order of the electroweak scale. Diagonalizing the neutrino mass matrix (in the three-generation model) yields three superheavy neutrino states, and three very light neutrino states that are identified with the light neutrinos observed in nature. This is the seesaw mechanism [254].

It is straightforward to construct a supersymmetric generalization of the seesaw model of neutrino masses [255, 256] by promoting the right-handed neutrino field to a superfield $\widehat{N}^c = (\widetilde{\nu}_R; \nu_R)$. Integrating out the heavy right-handed neutrino supermultiplet yields a new term in the superpotential [cf. Eq. (88.1)] of the form

$$W_{\text{seesaw}} = \frac{f}{M_R} (\widehat{H}_U \widehat{L}) (\widehat{H}_U \widehat{L}), \quad (88.34)$$

where M_R is the mass scale of the right-handed neutrino sector and f is a dimensionless constant. Note that lepton number is broken by two units by Eq. (88.34), which implies that R-parity invariance is preserved. The supersymmetric analogue of the Majorana neutrino mass term in the sneutrino sector leads to sneutrino-antisneutrino mixing phenomena [256, 257]. In addition, new Higgs-slepton interaction terms can probe the structure of the supersymmetric seesaw model [258]. The right-handed sneutrino that resides in \widehat{L} also provides an intriguing dark matter candidate [259].

The SUSY Les Houches Accord [80, 99], mentioned at the end of the introduction to Sec. 88.4, has been extended to the supersymmetric seesaw (and other extensions of the MSSM) in Ref. [260].

88.8.2 R-parity-violating SUSY

It is possible to incorporate massive neutrinos in renormalizable supersymmetric models while retaining the minimal particle content of the MSSM by relaxing the assumption of R-parity invariance. The most general R-parity-violating model involving the MSSM spectrum introduces many new parameters to both the SUSY-conserving and the SUSY-breaking sectors [80, 261]. Each new interaction term violates either B or L conservation. For example, starting from the MSSM superpotential given in Eq. (88.1) [suitably generalized to three generations of quarks, leptons and their superpartners], consider the effect of adding the following new terms:

$$W_{\text{RPV}} = (\lambda_L)_{pmn} \widehat{L}_p \widehat{L}_m \widehat{E}_n^c + (\lambda'_L)_{pmn} \widehat{L}_p \widehat{Q}_m \widehat{D}_n^c + (\lambda_B)_{pmn} \widehat{U}_p^c \widehat{D}_m^c \widehat{D}_n^c + (\mu_L)_p \widehat{H}_u \widehat{L}_p, \quad (88.35)$$

where p , m , and n are generation indices, and gauge group indices are suppressed. Eq. (88.35) yields new scalar-fermion Yukawa

couplings consisting of all possible combinations involving two SM fermions and one scalar superpartner.

Note that the term in Eq. (88.35) proportional to λ_B violates B , while the other three terms violate L . The L -violating term in Eq. (88.35) proportional to μ_L is the RPV analog of the $\mu \widehat{H}_u \widehat{H}_d$ term of the MSSM superpotential, in which the $Y = -1$ Higgs/higgsino supermultiplet \widehat{H}_d is replaced by the slepton/lepton supermultiplet \widehat{L}_p .

Phenomenological constraints derived from data on various low-energy B - and L -violating processes can be used to establish limits on each of the coefficients $(\lambda_L)_{pmn}$, $(\lambda'_L)_{pmn}$, and $(\lambda_B)_{pmn}$ taken one at a time [261, 262]. If more than one coefficient is simultaneously non-zero, then the limits are in general more complicated [263]. All possible RPV terms cannot be simultaneously present and unsuppressed; otherwise the proton decay rate would be many orders of magnitude larger than the present experimental bound. One way to avoid proton decay is to impose B or L invariance (either one alone would suffice). Otherwise, one must accept the requirement that certain RPV coefficients must be extremely suppressed.

One particularly interesting class of RPV models is one in which B is conserved, but L is violated. It is possible to enforce baryon number conservation (and the stability of the proton), while allowing for lepton-number-violating interactions by imposing a discrete \mathbb{Z}_3 baryon triality symmetry on the low-energy theory [264], in place of the standard \mathbb{Z}_2 R-parity. Since the distinction between the Higgs and matter supermultiplets is lost in RPV models where L is violated, the mixing of sleptons and Higgs bosons, the mixing of neutrinos and neutralinos, and the mixing of charged leptons and charginos are now possible, leading to more complicated mass matrices and mass eigenstates than in the MSSM. The treatment of neutrino masses and mixing in this framework can be found, *e.g.*, in Ref. [265].

Alternatively, one can consider imposing a lepton parity such that all lepton superfields are odd [264, 266]. In this case, only the B -violating term in Eq. (88.35) survives, and L is conserved. Models of this type have been considered in Ref. [267]. Since L is conserved in these models, the mixing of the lepton and Higgs superfields is forbidden. Moreover, neutrino masses (and mixing) are not generated if lepton parity is an exact symmetry. However, one expects that lepton parity cannot be exact due to quantum gravity effects. Remarkably, the standard \mathbb{Z}_2 R-parity and the \mathbb{Z}_3 baryon triality are stable with respect to quantum gravity effects, as they can be identified as residual discrete symmetries that arise from spontaneously broken non-anomalous gauge symmetries [264].

The symmetries employed above to either remove or suppress R-parity violating operators were flavor independent. In contrast, there exist a number of motivated scenarios based on flavor symmetries that can also yield the suppression as required by the experimental data (*e.g.*, see Ref. [268]).

The supersymmetric phenomenology of the RPV models exhibits features that are distinct from that of the MSSM [261]. The LSP is no longer stable, which implies that not all supersymmetric decay chains must yield missing-energy events at colliders. A comprehensive examination of the phenomenology of the MSSM extended by a single R-parity violating coupling at the unification scale and its implications for LHC searches has been given in Ref. [269]. As an example, the sparticle mass bounds obtained in searches for R-parity-conserving SUSY can be considerably relaxed in certain RPV models due to the absence of large missing transverse momentum signatures [270]. This can alleviate some of the tension with naturalness (introduced in Sec. 88.7.1).

Nevertheless, the loss of the missing-energy signature is often compensated by other striking signals (which depend on which R-parity-violating parameters are dominant). For example, supersymmetric particles in RPV models can be singly produced (in contrast to R-parity-conserving models where supersymmetric particles must be produced in pairs). The phenomenology of pair-produced supersymmetric particles is also modified in RPV models due to new decay chains not present in R-parity-conserving SUSY models [261].

In RPV models with lepton number violation (these include

weak-scale SUSY models with baryon triality mentioned above), both $\Delta L = 1$ and $\Delta L = 2$ phenomena are allowed, leading to neutrino masses and mixing [271], neutrinoless double-beta decay [272], sneutrino-antisneutrino mixing [273], and resonant s -channel production of sneutrinos in e^+e^- collisions [274] and in charged sleptons in $p\bar{p}$ and pp collisions [275], respectively.

88.9 Extensions beyond the MSSM

Extensions of the MSSM have been proposed to solve a variety of theoretical problems [35]. One such problem involves the μ parameter of the MSSM. Although μ is a SUSY-preserving parameter, it must be of order the effective SUSY-breaking scale of the MSSM to yield a consistent supersymmetric phenomenology [276]. Any natural solution to the so-called μ -problem must incorporate a symmetry that enforces $\mu = 0$ and a small symmetry-breaking parameter that generates a value of μ that is not parametrically larger than the effective SUSY-breaking scale [277]. A number of proposed mechanisms in the literature (*e.g.*, see Ref. [276–278]) provide concrete examples of a natural solution to the μ -problem of the MSSM.

In extensions of the MSSM, other compelling solutions to the μ -problem are possible. For example, one can replace μ by the vacuum expectation value of a new $SU(3)\times SU(2)\times U(1)$ singlet scalar field, as noted below Eq. 88.23. This is the NMSSM, which yields phenomena that were briefly discussed in Sections 88.4–88.7. The NMSSM superpotential consists only of trilinear terms whose coefficients are dimensionless. There are some advantages to extending the NMSSM further to the ‘USSM’ [107] by adding a new broken $U(1)$ gauge symmetry [279], under which the singlet field is charged.

Alternatively, one can consider a generalized version of the NMSSM (called the GNMSSM in Ref. [209]), where all possible renormalizable terms in the superpotential are allowed, which yield new supersymmetric mass terms (analogous to the μ term of the MSSM). A discussion of the parameters of the GNMSSM can be found in Ref. [80]. Although the GNMSSM does not solve the μ -problem, it does exhibit regions of parameter space in which the degree of fine-tuning is relaxed, as discussed in Sec. 88.7.1.

The generation of the μ -term may be connected with the solution to the strong CP problem [280]. Models of this type, which include new gauge singlet fields that are charged under the Peccei-Quinn (PQ) symmetry [281], were first proposed in Ref. [276]. The breaking of the PQ symmetry is thus intimately tied to SUSY breaking, while naturally yielding a value of μ that is of order the electroweak symmetry breaking scale [282].

All supersymmetric models discussed so far in this review possess self-conjugate fermions—the Majorana gluinos and neutralinos. However, it is possible to add additional chiral superfields in the adjoint representation. The spin-1/2 components of these new superfields can pair up with the gauginos to form Dirac gauginos [283, 284]. Such states appear in models of so-called supersoft SUSY breaking [285], in some generalized GMSB models [286], and in R-symmetric SUSY models [287, 288]. Such approaches often lead to improved naturalness and/or significantly relaxed flavor constraints. The implications of models of Dirac gauginos on the observed Higgs boson mass and its properties are addressed in Ref. [289].

For completeness, we briefly note other MSSM extensions considered in the literature. These include an enlarged electroweak gauge group beyond $SU(2)\times U(1)$ [290]; the addition of new Higgs supermultiplets beyond the doublets and singlets of the MSSM/NMSSM [291]; and/or the addition of new (possibly exotic) matter supermultiplets [210, 292, 293] such as vector-like fermions and their superpartners.

References

[1] *The Supersymmetric World—The Beginnings of the Theory*, World Scientific, Singapore (2000), edited by G. Kane and M. Shifman, contains an early history of supersymmetry and a guide to the original literature.
 [2] R. Haag, J. T. Lopuszanski and M. Sohnius, Nucl. Phys. **B88**, 257 (1975); S. R. Coleman and J. Mandula, Phys. Rev. **159**, 1251 (1967).
 [3] H. P. Nilles, Phys. Rept. **110**, 1 (1984).

[4] S. Weinberg, *The Quantum Theory of Fields, Volume III: Supersymmetry* (Cambridge University Press, Cambridge, UK, 2000).
 [5] P. Nath, *Supersymmetry, Supergravity, and Unification* (Cambridge University Press, Cambridge, UK, 2017).
 [6] E. Witten, Nucl. Phys. **B188**, 513 (1981).
 [7] S. Dimopoulos and H. Georgi, Nucl. Phys. **B193**, 150 (1981).
 [8] N. Sakai, Z. Phys. **C11**, 153 (1981).
 [9] L. Susskind, Phys. Rept. **104**, 181 (1984).
 [10] L. Girardello and M. T. Grisaru, Nucl. Phys. **B194**, 65 (1982).
 [11] L. J. Hall and L. Randall, Phys. Rev. Lett. **65**, 2939 (1990); I. Jack and D. R. T. Jones, Phys. Lett. **B457**, 101 (1999), [hep-ph/9903365].
 [12] V. F. Weisskopf, Phys. Rev. **56**, 72 (1939).
 [13] See *e.g.*, N. Polonsky, *Supersymmetry: Structure and phenomena. Extensions of the standard model*, Lect. Notes Phys. Monogr. **68**, 1 (2001).
 [14] G. Bertone, D. Hooper and J. Silk, Phys. Rept. **405**, 279 (2005), [hep-ph/0404175].
 [15] D. Hooper, “TASI 2008 Lectures on Dark Matter,” in *The Dawn of the LHC Era, Proceedings of the 2008 Theoretical and Advanced Study Institute in Elementary Particle Physics*, Boulder, Colorado, 2–27 June 2008, edited by Tao Han (World Scientific, Singapore, 2009).
 [16] H. Pagels and J. R. Primack, Phys. Rev. Lett. **48**, 223 (1982).
 [17] H. Goldberg, Phys. Rev. Lett. **50**, 1419 (1983).
 [18] J. R. Ellis *et al.*, Nucl. Phys. **B238**, 453 (1984).
 [19] G. Jungman, M. Kamionkowski, and K. Griest, Phys. Reports **267**, 195 (1996).
 [20] F. D. Steffen, Eur. Phys. J. **C59**, 557 (2009), [arXiv:0811.3347].
 [21] H. E. Haber and G. L. Kane, Phys. Rept. **117**, 75 (1985).
 [22] S. P. Martin, *A Supersymmetry Primer*, [hep-ph/9709356].
 [23] M. Drees, R. Godbole, and P. Roy, *Theory and Phenomenology of Sparticles* (World Scientific, Singapore, 2005).
 [24] H. Baer and X. Tata, *Weak Scale Supersymmetry: from Superfields to Scattering Events* (Cambridge University Press, Cambridge, UK, 2006).
 [25] H.K. Dreiner, H.E. Haber, and S.P. Martin, *From Spinors to Supersymmetry* (Cambridge University Press, Cambridge, UK, 2023).
 [26] Our notation for the charge-conjugated fields follows the notation of P. Langacker, *The Standard Model and Beyond*, 2nd edition (CRC Press, Boca Raton, FL, 2017).
 [27] H. Georgi and S. L. Glashow, Phys. Rev. **D6**, 429 (1972).
 [28] P. Fayet, Nucl. Phys. **B90**, 104 (1975).
 [29] K. Inoue *et al.*, Prog. Theor. Phys. **67**, 1889 (1982).
 [30] J. F. Gunion and H. E. Haber, Nucl. Phys. **B272**, 1 (1986), [Erratum: **B402**, 567 (1993)].
 [31] A. Salam and J. A. Strathdee, Nucl. Phys. **B76**, 477 (1974).
 [32] J. Wess and J. Bagger, *Supersymmetry and Supergravity* (Princeton University Press, Princeton, NJ, 1992).
 [33] I. L. Buchbinder, S. Kuzenko and Z. Yarevskaya, Nucl. Phys. **B411**, 665 (1994); I. Antoniadis, E. Dudas and D. M. Ghilencea, JHEP **03**, 045 (2008), [arXiv:0708.0383]; E. Dudas and D. M. Ghilencea, JHEP **06**, 124 (2015), [arXiv:1503.08319].
 [34] D. J. H. Chung *et al.*, Phys. Rept. **407**, 1 (2005), [hep-ph/0312378].

- [35] S. Khalil and S. Moretti, *Supersymmetry Beyond Minimality: From Theory to Experiment* (CRC Press, Boca Raton, FL, 2018).
- [36] J. R. Ellis *et al.*, Phys. Rev. **D39**, 844 (1989); U. Ellwanger and C. Hugonie, Eur. Phys. J. **C25**, 297 (2002), [hep-ph/9909260]; U. Ellwanger, C. Hugonie and A. M. Teixeira, Phys. Rept. **496**, 1 (2010), [arXiv:0910.1785]; M. Maniatis, Int. J. Mod. Phys. **A25**, 3505 (2010), [arXiv:0906.0777].
- [37] S. Weinberg, Phys. Rev. Lett. **43**, 1566 (1979); S. Weinberg, Phys. Rev. **D22**, 1694 (1980); F. Wilczek and A. Zee, Phys. Rev. Lett. **43**, 1571 (1979); H. A. Weldon and A. Zee, Nucl. Phys. **B173**, 269 (1980).
- [38] P. Fayet, Phys. Lett. **69B**, 489 (1977); G. R. Farrar and P. Fayet, Phys. Lett. **76B**, 575 (1978).
- [39] P. Fayet, Phys. Lett. **84B**, 421 (1979); P. Fayet, Phys. Lett. **86B**, 272 (1979).
- [40] D.Z. Freedman and A. Van Proeyen, *Supergravity* (Cambridge University Press, Cambridge, UK, 2012); M. Rausch de Traubenberg and M. Valenzuela, *A Supergravity Primer* (World Scientific, Singapore, 2020).
- [41] S. Deser and B. Zumino, Phys. Rev. Lett. **38**, 1433 (1977); E. Cremmer *et al.*, Phys. Lett. **79B**, 231 (1978).
- [42] R. Casalbuoni *et al.*, Phys. Lett. **B215**, 313 (1988); R. Casalbuoni *et al.*, Phys. Rev. **D39**, 2281 (1989); A. L. Maroto and J. R. Pelaez, Phys. Rev. **D62**, 023518 (2000), [hep-ph/9912212].
- [43] Z. Komargodski and N. Seiberg, JHEP **09**, 066 (2009), [arXiv:0907.2441]; I. Antoniadis *et al.*, Nucl. Phys. B **841**, 157 (2010), [arXiv:1006.1662]; D. M. Ghilencea, Mod. Phys. Lett. A **31**, 12, 1630011 (2016), [arXiv:1512.07484].
- [44] A.H. Chamseddine, R. Arnowitt, and P. Nath, Phys. Rev. Lett. **49**, 970 (1982); R. Barbieri, S. Ferrara and C. A. Savoy, Phys. Lett. **119B**, 343 (1982); L. E. Ibanez, Nucl. Phys. **B218**, 514 (1983); H. P. Nilles, M. Srednicki and D. Wyler, Phys. Lett. **120B**, 346 (1983); H. P. Nilles, M. Srednicki and D. Wyler, Phys. Lett. **124B**, 337 (1983); E. Cremmer, P. Fayet and L. Girardello, Phys. Lett. **122B**, 41 (1983); N. Ohta, Prog. Theor. Phys. **70**, 542 (1983).
- [45] L. Alvarez-Gaume, J. Polchinski and M. B. Wise, Nucl. Phys. B **221**, 495 (1983).
- [46] L. J. Hall, J. D. Lykken and S. Weinberg, Phys. Rev. **D27**, 2359 (1983).
- [47] S. K. Soni and H. A. Weldon, Phys. Lett. **126B**, 215 (1983); Y. Kawamura, H. Murayama and M. Yamaguchi, Phys. Rev. **D51**, 1337 (1995), [hep-ph/9406245].
- [48] See, *e.g.*, A. Brignole, L.E. Ibáñez, and C. Muñoz, in *Perspectives on Supersymmetry II*, edited by G.L. Kane (World Scientific, Singapore, 2010) pp. 244–268.
- [49] A. B. Lahanas and D. V. Nanopoulos, Phys. Rept. **145**, 1 (1987).
- [50] J. L. Feng, A. Rajaraman and F. Takayama, Phys. Rev. Lett. **91**, 011302 (2003), [hep-ph/0302215]; J. L. Feng, A. Rajaraman and F. Takayama, Phys. Rev. **D68**, 063504 (2003), [hep-ph/0306024]; J. L. Feng, A. Rajaraman and F. Takayama, Int. J. Mod. Phys. **D13**, 2355 (2004), [hep-th/0405248].
- [51] L. Randall and R. Sundrum, Nucl. Phys. **B557**, 79 (1999), [hep-th/9810155].
- [52] F. D’Eramo, J. Thaler and Z. Thomas, JHEP **06**, 151 (2012), [arXiv:1202.1280]; F. D’Eramo, J. Thaler and Z. Thomas, JHEP **09**, 125 (2013), [arXiv:1307.3251]; S. P. de Alwis, Phys. Rev. **D77**, 105020 (2008), [arXiv:0801.0578]; S. P. de Alwis, JHEP **01**, 006 (2013), [arXiv:1206.6775]; K. Harigaya and M. Ibe, Phys. Rev. **D90**, 085028 (2014), [arXiv:1409.5029].
- [53] I. Jack, D. R. T. Jones and R. Wild, Phys. Lett. **B535**, 193 (2002), [hep-ph/0202101]; B. Murakami and J. D. Wells, Phys. Rev. **D68**, 035006 (2003), [hep-ph/0302209]; R. Kitano, G. D. Kribs and H. Murayama, Phys. Rev. **D70**, 035001 (2004), [hep-ph/0402215]; R. Hodgson *et al.*, Nucl. Phys. **B728**, 192 (2005), [hep-ph/0507193]; D. R. T. Jones and G. G. Ross, Phys. Lett. **B642**, 540 (2006), [hep-ph/0609210].
- [54] S. Asai *et al.*, Phys. Lett. **B653**, 81 (2007), [arXiv:0705.3086].
- [55] M. Dine, W. Fischler and M. Srednicki, Nucl. Phys. **B189**, 575 (1981); S. Dimopoulos and S. Raby, Nucl. Phys. **B192**, 353 (1981); S. Dimopoulos and S. Raby, Nucl. Phys. **B219**, 479 (1983); M. Dine and W. Fischler, Phys. Lett. **110B**, 227 (1982); C. R. Nappi and B. A. Ovrut, Phys. Lett. **113B**, 175 (1982); L. Alvarez-Gaume, M. Claudson and M. B. Wise, Nucl. Phys. **B207**, 96 (1982).
- [56] M. Dine and A. E. Nelson, Phys. Rev. **D48**, 1277 (1993), [hep-ph/9303230]; M. Dine, A. E. Nelson and Y. Shirman, Phys. Rev. **D51**, 1362 (1995), [hep-ph/9408384].
- [57] M. Dine *et al.*, Phys. Rev. **D53**, 2658 (1996), [hep-ph/9507378].
- [58] G. F. Giudice and R. Rattazzi, Phys. Rept. **322**, 419 (1999), [hep-ph/9801271].
- [59] E. Poppitz and S. P. Trivedi, Phys. Rev. **D55**, 5508 (1997), [hep-ph/9609529]; H. Murayama, Phys. Rev. Lett. **79**, 18 (1997), [hep-ph/9705271]; M. A. Luty and J. Terning, Phys. Rev. **D57**, 6799 (1998), [hep-ph/9709306]; K. Agashe, Phys. Lett. **B435**, 83 (1998), [hep-ph/9804450]; N. Arkani-Hamed, J. March-Russell and H. Murayama, Nucl. Phys. **B509**, 3 (1998), [hep-ph/9701286]; C. Csaki, Y. Shirman and J. Terning, JHEP **05**, 099 (2007), [hep-ph/0612241]; M. Ibe and R. Kitano, Phys. Rev. **D77**, 075003 (2008), [arXiv:0711.0416].
- [60] S. Weinberg, Phys. Rev. Lett. **48**, 1303 (1982); M. Kawasaki, F. Takahashi and T. T. Yanagida, Phys. Rev. D **74**, 043519 (2006), [hep-ph/0605297].
- [61] M. Kawasaki *et al.*, Phys. Rev. **D78**, 065011 (2008), [arXiv:0804.3745].
- [62] M. J. Strassler and K. M. Zurek, Phys. Lett. **B651**, 374 (2007), [hep-ph/0604261]; T. Han *et al.*, JHEP **07**, 008 (2008), [arXiv:0712.2041].
- [63] M. J. Strassler [hep-ph/0607160]; K. M. Zurek, Phys. Rev. **D79**, 115002 (2009), [arXiv:0811.4429].
- [64] See *e.g.*, M. Quiros, in *Particle Physics and Cosmology: The Quest for Physics Beyond the Standard Model(s), Proceedings of the 2002 Theoretical Advanced Study Institute in Elementary Particle Physics (TASI 2002)*, edited by H.E. Haber and A.E. Nelson (World Scientific, Singapore, 2004) pp. 549–601; C. Csaki, in *ibid.*, pp. 605–698.
- [65] V.A. Rubakov, Sov. Phys. Usp. **44**, 871 (2001); J. L. Hewett and M. Spiropulu, Ann. Rev. Nucl. Part. Sci. **52**, 397 (2002), [hep-ph/0205106].
- [66] Z. Chacko, M. A. Luty and E. Ponton, JHEP **07**, 036 (2000), [hep-ph/9909248]; D. E. Kaplan, G. D. Kribs and M. Schmaltz, Phys. Rev. **D62**, 035010 (2000), [hep-ph/9911293]; Z. Chacko *et al.*, JHEP **01**, 003 (2000), [hep-ph/9911323].
- [67] J. Scherk and J. H. Schwarz, Phys. Lett. **82B**, 60 (1979); J. Scherk and J. H. Schwarz, Nucl. Phys. **B153**, 61 (1979).
- [68] R. Barbieri, L. J. Hall and Y. Nomura, Phys. Rev. **D66**, 045025 (2002), [hep-ph/0106190]; R. Barbieri, L. J. Hall and Y. Nomura, Nucl. Phys. **B624**, 63 (2002), [hep-th/0107004]; I. Garcia Garcia, K. Howe and J. March-Russell, JHEP **12**, 005 (2015), [arXiv:1510.07045].
- [69] J. D. Wells, Phys. Rev. **D71**, 015013 (2005), [hep-ph/0411041].
- [70] N. Arkani-Hamed and S. Dimopoulos, JHEP **06**, 073 (2005), [hep-th/0405159]; G. F. Giudice and A. Romanino, Nucl. Phys. **B699**, 65 (2004), [Erratum: **B706**, 487 (2005)], [hep-ph/0406088].

- [71] G. F. Giudice and A. Strumia, Nucl. Phys. **B858**, 63 (2012), [arXiv:1108.6077].
- [72] A. Arvanitaki *et al.*, JHEP **02**, 126 (2013), [arXiv:1210.0555]; N. Arkani-Hamed *et al.* (2012), [arXiv:1212.6971].
- [73] P. Slavich *et al.*, Eur. Phys. J. C **81**, 450 (2021), [arXiv:2012.15629].
- [74] E. Bagnaschi *et al.*, JHEP **09**, 092 (2014), [arXiv:1407.4081].
- [75] J. Pardo Vega and G. Villadoro, JHEP **07**, 159 (2015), [arXiv:1504.05200].
- [76] B. C. Allanach and A. Voigt, Eur. Phys. J. **C78**, 573 (2018), [arXiv:1804.09410].
- [77] Y. Kahn, M. McCullough and J. Thaler, JHEP **11**, 161 (2013), [arXiv:1308.3490].
- [78] L. J. Hall and Y. Nomura, JHEP **01**, 082 (2012), [arXiv:1111.4519]; M. Ibe and T. T. Yanagida, Phys. Lett. **B709**, 374 (2012), [arXiv:1112.2462].
- [79] H. E. Haber and L. Stephenson Haskins (2018), *Supersymmetric Theory and Models*, in *Anticipating the Next Discoveries in Particle Physics*, Proceedings of the 2016 Theoretical Advanced Study Institute in Elementary Particle Physics, edited by Rouven Essig and Ian Low (World Scientific, Singapore, 2018) pp. 355-499, [arXiv:1712.05926].
- [80] B. C. Allanach *et al.*, Comput. Phys. Commun. **180**, 8 (2009), [arXiv:0801.0045].
- [81] J. M. Frere, D. R. T. Jones and S. Raby, Nucl. Phys. **B222**, 11 (1983); J. P. Derendinger and C. A. Savoy, Nucl. Phys. **B237**, 307 (1984); J. F. Gunion, H. E. Haber and M. Sher, Nucl. Phys. **B306**, 1 (1988); D. Chowdhury *et al.*, JHEP **02**, 110 (2014), [Erratum: **03**, 149 (2018)], [arXiv:1310.1932]; W. G. Hollik, JHEP **08**, 126 (2016), [arXiv:1606.08356].
- [82] J. A. Casas, A. Lleyda and C. Munoz, Nucl. Phys. **B471**, 3 (1996), [hep-ph/9507294].
- [83] J. E. Camargo-Molina *et al.*, Eur. Phys. J. C **73**, 2588 (2013), [arXiv:1307.1477].
- [84] N. Blinov and D. E. Morrissey, JHEP **03**, 106 (2014), [arXiv:1310.4174].
- [85] C. S. Ün *et al.*, Phys. Rev. **D91**, 105033 (2015), [arXiv:1412.1440].
- [86] G. G. Ross, K. Schmidt-Hoberg and F. Staub, Phys. Lett. **B759**, 110 (2016), [arXiv:1603.09347].
- [87] G. G. Ross, K. Schmidt-Hoberg and F. Staub, JHEP **03**, 021 (2017), [arXiv:1701.03480].
- [88] S. P. Martin, Phys. Rev. **D61**, 035004 (2000), [hep-ph/9907550].
- [89] S. Dimopoulos and D. W. Sutter, Nucl. Phys. **B452**, 496 (1995), [hep-ph/9504415]; D. W. Sutter, Stanford Ph.D. thesis (1995), [hep-ph/9704390].
- [90] H. E. Haber, Nucl. Phys. B Proc. Suppl. **62**, 469 (1998), [hep-ph/9709450].
- [91] R. M. Barnett, J. F. Gunion and H. E. Haber, Phys. Lett. **B315**, 349 (1993), [hep-ph/9306204]; H. Baer, X. Tata and J. Woodside, Phys. Rev. **D41**, 906 (1990).
- [92] S. M. Bilenky, N. P. Nedelcheva and E. K. Khristova, Phys. Lett. **161B**, 397 (1985); S. M. Bilenky, E. K. Khristova and N. P. Nedelcheva, Bulg. J. Phys. **13**, 283 (1986); G. A. Moortgat-Pick and H. Fraas, Eur. Phys. J. **C25**, 189 (2002), [hep-ph/0204333].
- [93] J. Rosiek, Phys. Rev. **D41**, 3464 (1990), [Erratum: hep-ph/9511250].
- [94] M. Kuroda (1999), [hep-ph/9902340].
- [95] J. Alwall *et al.*, JHEP **09**, 028 (2007), [arXiv:0706.2334].
- [96] T. Hahn, Comput. Phys. Commun. **140**, 418 (2001), [hep-ph/0012260].
- [97] A. Pukhov *et al.*, INP-MSU-98-41/542 (1998), [hep-ph/9908288]; E. Boos *et al.* (CompHEP Collaboration), Nucl. Instrum. Meth. A **534**, 250 (2004), [hep-ph/0403113], URL <https://theory.sinp.msu.ru/doku.php/compheap/start>.
- [98] D. M. Pierce *et al.*, Nucl. Phys. **B491**, 3 (1997), [hep-ph/9606211].
- [99] P. Z. Skands *et al.*, JHEP **07**, 036 (2004), [hep-ph/0311123].
- [100] For further details, see *e.g.*, Appendix C of Ref. [21] and Appendix A of Ref. [30].
- [101] J. L. Kneur and G. Moutaka, Phys. Rev. **D59**, 015005 (1999), [hep-ph/9807336].
- [102] R.A. Horn and C.R. Johnson, *Matrix Analysis*, 2nd Edition (Cambridge University Press, Cambridge, UK, 2003).
- [103] H. K. Dreiner, H. E. Haber and S. P. Martin, Phys. Rept. **494**, 1 (2010), [arXiv:0812.1594].
- [104] H. E. Haber, Int. J. Mod. Phys. A **36**, 2130003 (2021), [arXiv:2009.03990].
- [105] S. Pokorski, J. Rosiek and C. A. Savoy, Nucl. Phys. B **570**, 81 (2000), [hep-ph/9906206].
- [106] L. Autonne, Annals de l'Université de Lyon, Nouvelle Série I, Fasc. **38**, 1 (1915); T. Takagi, Japan J. Math. **1**, 83 (1925).
- [107] S. Y. Choi *et al.*, Nucl. Phys. **B778**, 85 (2007), [hep-ph/0612218].
- [108] S. Y. Choi *et al.*, Eur. Phys. J. **C22**, 563 (2001), [Addendum: Eur. Phys. J. **C23**, 769 (2002)], [hep-ph/0108117].
- [109] M. M. El Kheishen, A. A. Aboshousha and A. A. Shafik, Phys. Rev. **D45**, 4345 (1992).
- [110] T. Hahn (2006), [arXiv:physics/0607103].
- [111] J. R. Ellis and S. Rudaz, Phys. Lett. **128B**, 248 (1983); F. Browning, D. Chang and W.-Y. Keung, Phys. Rev. **D64**, 015010 (2001), [hep-ph/0012258]; A. Bartl *et al.*, Phys. Lett. **B573**, 153 (2003), [hep-ph/0307317]; A. Bartl *et al.*, Phys. Rev. **D70**, 035003 (2004), [hep-ph/0311338].
- [112] K.-i. Hikasa and M. Kobayashi, Phys. Rev. **D36**, 724 (1987); F. Gabbiani and A. Masiero, Nucl. Phys. **B322**, 235 (1989); P. Brax and C. A. Savoy, Nucl. Phys. **B447**, 227 (1995), [hep-ph/9503306].
- [113] J.F. Gunion *et al.*, *The Higgs Hunter's Guide* (Westview Press, Boulder, CO, 2000); M. Carena and H. E. Haber, Prog. Part. Nucl. Phys. **50**, 63 (2003), [hep-ph/0208209]; A. Djouadi, Phys. Rept. **459**, 1 (2008), [hep-ph/0503173].
- [114] E. Bagnaschi *et al.*, Eur. Phys. J. **C79**, 617 (2019), [arXiv:1808.07542].
- [115] H. E. Haber and M. Sher, Phys. Rev. **D35**, 2206 (1987).
- [116] L. J. Hall, D. Pinner and J. T. Ruderman, JHEP **04**, 131 (2012), [arXiv:1112.2703].
- [117] J. F. Gunion and H. E. Haber, Phys. Rev. D **67**, 075019 (2003), [hep-ph/0207010].
- [118] ATLAS Collaboration, Nature **607**, 52 (2022), [Erratum: Nature **612**, E24 (2022)], [arXiv:2207.00092].
- [119] A. Tumasyan *et al.* (CMS Collaboration), Nature **607**, 60 (2022), [arXiv:2207.00043].
- [120] G. Aad *et al.* (ATLAS Collaboration), Phys. Rev. D **101**, 012002 (2020), [arXiv:1909.02845].
- [121] L. J. Hall and M. B. Wise, Nucl. Phys. **B187**, 397 (1981).
- [122] H. E. Haber and R. Hempfling, Phys. Rev. Lett. **66**, 1815 (1991); Y. Okada, M. Yamaguchi and T. Yanagida, Prog. Theor. Phys. **85**, 1 (1991); J. R. Ellis, G. Ridolfi and F. Zwirner, Phys. Lett. **B257**, 83 (1991).
- [123] H. E. Haber, R. Hempfling and A. H. Hoang, Z. Phys. C **75**, 539 (1997), [hep-ph/9609331].
- [124] A. Djouadi *et al.*, Eur. Phys. J. C **73**, 2650 (2013), [arXiv:1307.5205].
- [125] A. Djouadi *et al.*, JHEP **06**, 168 (2015), [arXiv:1502.05653].

- [126] P. Draper and H. Rzehak, Phys. Rept. **619**, 1 (2016), [arXiv:1601.01890].
- [127] M. Carena *et al.*, Phys. Rev. **D93**, 035013 (2016), [arXiv:1510.09137].
- [128] A. Pilaftsis and C. E. M. Wagner, Nucl. Phys. **B553**, 3 (1999), [hep-ph/9902371]; D. A. Demir, Phys. Rev. **D60**, 055006 (1999), [hep-ph/9901389]; S. Y. Choi, M. Drees and J. S. Lee, Phys. Lett. **B481**, 57 (2000), [hep-ph/0002287]; M. Carena *et al.*, Nucl. Phys. **B586**, 92 (2000), [hep-ph/0003180]; M. Carena *et al.*, Phys. Lett. **B495**, 155 (2000), [hep-ph/0009212]; M. Carena *et al.*, Nucl. Phys. **B625**, 345 (2002), [hep-ph/0111245]; M. Frank *et al.*, JHEP **02**, 047 (2007), [hep-ph/0611326]; S. Heinemeyer *et al.*, Phys. Lett. **B652**, 300 (2007), [arXiv:0705.0746].
- [129] H. E. Haber and J. D. Mason, Phys. Rev. **D77**, 115011 (2008), [arXiv:0711.2890].
- [130] S. Khalil, Int. J. Mod. Phys. **A18**, 1697 (2003), [hep-ph/0212050].
- [131] W. Fischler, S. Paban and S. D. Thomas, Phys. Lett. **B289**, 373 (1992), [hep-ph/9205233].
- [132] A. Masiero and L. Silvestrini, in *Perspectives on Supersymmetry*, edited by G.L. Kane (World Scientific, Singapore, 1998) pp. 423–441.
- [133] M. Pospelov and A. Ritz, Annals Phys. **318**, 119 (2005), [hep-ph/0504231].
- [134] C. Abel *et al.*, Phys. Rev. Lett. **124**, 081803 (2020), [arXiv:2001.11966].
- [135] T. S. Roussy *et al.*, Science **381**, 46 (2023), [arXiv:2212.11841].
- [136] F. Gabbiani *et al.*, Nucl. Phys. **B477**, 321 (1996), [hep-ph/9604387].
- [137] M. J. Ramsey-Musolf and S. Su, Phys. Rept. **456**, 1 (2008), [hep-ph/0612057].
- [138] M. Carena, A. Menon and C. E. M. Wagner, Phys. Rev. **D79**, 075025 (2009), [arXiv:0812.3594].
- [139] M. B. Einhorn and D. R. T. Jones, Nucl. Phys. **B196**, 475 (1982).
- [140] W. J. Marciano and G. Senjanovic, Phys. Rev. **D25**, 3092 (1982).
- [141] R.N. Mohapatra, *Unification and Supersymmetry*, Third Edition (Springer Science, New York, 2003).
- [142] S. P. Martin and M. T. Vaughn, Phys. Rev. **D50**, 2282 (1994), [Erratum: **D78**, 039903 (2008)], [hep-ph/9311340]; R. M. Fonseca *et al.*, Nucl. Phys. **B854**, 28 (2012), [arXiv:1107.2670]; F. Staub, Comput. Phys. Commun. **182**, 808 (2011), [arXiv:1002.0840].
- [143] F. Staub, Comput. Phys. Commun. **185**, 1773 (2014), [arXiv:1309.7223]; F. Staub, Adv. High Energy Phys. **2015**, 840780 (2015), [arXiv:1503.04200]; The SARAH homepage is <https://sarah.hepforge.org/>; R. M. Fonseca, Comput. Phys. Commun. **183**, 2298 (2012), [arXiv:1106.5016]; The Susyno homepage is <https://renatofonseca.net/susyno>.
- [144] B. C. Allanach, Comput. Phys. Commun. **143**, 305 (2002), [hep-ph/0104145]; The SOFTSUSY homepage is <https://ballanach.github.io/softsusy/>; A. Djouadi, J.-L. Kneur and G. Moultaka, Comput. Phys. Commun. **176**, 426 (2007), [hep-ph/0211331]; The Suspect homepage is <http://suspect.in2p3.fr/>; F. E. Paige *et al.* (2003), [hep-ph/0312045]; Isajet may be obtained from <http://www.nhn.ou.edu/~isajet/>; W. Porod, Comput. Phys. Commun. **153**, 275 (2003), [hep-ph/0301101]; Spheno may be obtained from <https://spheno.hepforge.org/>; P. Athron *et al.*, Comput. Phys. Commun. **190**, 139 (2015), [arXiv:1406.2319]; The FlexibleSUSY homepage is <https://flexiblesusy.hepforge.org/>.
- [145] L. E. Ibanez and G. G. Ross, Phys. Lett. **110B**, 215 (1982).
- [146] M. Drees, Phys. Lett. B **158**, 409 (1985); J. R. Ellis *et al.*, Phys. Lett. B **155**, 381 (1985); S. P. Martin, Phys. Rev. D **79**, 095019 (2009), [arXiv:0903.3568].
- [147] J. Abdallah *et al.* (DELPHI Collaboration), Eur. Phys. J. **C31**, 421 (2003), [hep-ex/0311019].
- [148] H. K. Dreiner *et al.*, Eur. Phys. J. **C62**, 547 (2009), [arXiv:0901.3485].
- [149] G. F. Giudice *et al.*, JHEP **12**, 027 (1998), [hep-ph/9810442]; A. Pomarol and R. Rattazzi, JHEP **05**, 013 (1999), [hep-ph/9903448]; D.-W. Jung and J. Y. Lee, JHEP **03**, 123 (2009), [arXiv:0902.0464].
- [150] J. F. Gunion and H. E. Haber, Phys. Rev. **D37**, 2515 (1988); S. Y. Choi, M. Drees and B. Gaissmaier, Phys. Rev. **D70**, 014010 (2004), [hep-ph/0403054].
- [151] H. Baer, V. Barger and D. Sengupta, Phys. Rev. **D98**, 015039 (2018), [arXiv:1801.09730].
- [152] J. L. Feng *et al.*, Phys. Rev. Lett. **83**, 1731 (1999), [hep-ph/9904250]; J. F. Gunion and S. Mrenna, Phys. Rev. **D62**, 015002 (2000), [hep-ph/9906270].
- [153] T. Gherghetta, G. F. Giudice and J. D. Wells, Nucl. Phys. **B559**, 27 (1999), [hep-ph/9904378].
- [154] M. Endo, M. Yamaguchi and K. Yoshioka, Phys. Rev. **D72**, 015004 (2005), [hep-ph/0504036]; K. Choi, K. S. Jeong and K.-i. Okumura, JHEP **09**, 039 (2005), [hep-ph/0504037]; O. Loaiza-Brito *et al.*, AIP Conf. Proc. **805**, 198 (2005), [hep-th/0509158].
- [155] G. D'Ambrosio *et al.*, Nucl. Phys. B **645**, 155 (2002), [hep-ph/0207036].
- [156] C. Smith, Acta Phys. Polon. Supp. **3**, 53 (2010), [arXiv:0909.4444].
- [157] M. Drees and S.P. Martin, in *Electroweak Symmetry Breaking and New Physics at the TeV Scale*, edited by T. Barklow *et al.* (World Scientific, Singapore, 1996) pp. 146–215.
- [158] G. L. Kane *et al.*, Phys. Rev. **D49**, 6173 (1994), [hep-ph/9312272].
- [159] J. R. Ellis *et al.*, Phys. Lett. **B573**, 162 (2003), [hep-ph/0305212]; J. R. Ellis *et al.*, Phys. Rev. **D70**, 055005 (2004), [hep-ph/0405110].
- [160] H. Baer *et al.*, Phys. Rev. **D71**, 095008 (2005), [hep-ph/0412059].
- [161] V. Berezhinsky *et al.*, Astropart. Phys. **5**, 1 (1996), [hep-ph/9508249]; J. R. Ellis *et al.*, Nucl. Phys. **B652**, 259 (2003), [hep-ph/0210205].
- [162] L. E. Ibanez and D. Lust, Nucl. Phys. **B382**, 305 (1992), [hep-th/9202046]; B. de Carlos, J. A. Casas and C. Munoz, Phys. Lett. **B299**, 234 (1993), [hep-ph/9211266]; V. S. Kaplunovsky and J. Louis, Phys. Lett. **B306**, 269 (1993), [hep-th/9303040]; A. Brignole, L. E. Ibanez and C. Munoz, Nucl. Phys. **B422**, 125 (1994), [Erratum: **B436**, 747 (1995)], [hep-ph/9308271].
- [163] A. Arbey *et al.*, Phys. Rev. **D87**, 115020 (2013), [arXiv:1304.0381].
- [164] G. R. Dvali, G. F. Giudice and A. Pomarol, Nucl. Phys. **B478**, 31 (1996), [hep-ph/9603238].
- [165] P. Draper *et al.*, Phys. Rev. **D85**, 095007 (2012), [arXiv:1112.3068].
- [166] P. Meade, N. Seiberg and D. Shih, Prog. Theor. Phys. Suppl. **177**, 143 (2009), [arXiv:0801.3278]; M. Buican *et al.*, JHEP **03**, 016 (2009), [arXiv:0812.3668].
- [167] A. Rajaraman *et al.*, Phys. Lett. **B678**, 367 (2009), [arXiv:0903.0668]; L. M. Carpenter *et al.*, Phys. Rev. **D79**, 035002 (2009), [arXiv:0805.2944].
- [168] S. Ambrosanio, G. D. Kribs and S. P. Martin, Nucl. Phys. **B516**, 55 (1998), [hep-ph/9710217].
- [169] For a review and guide to the literature, see J.F. Gunion and H.E. Haber, in *Perspectives on Supersymmetry II*, edited by G.L. Kane (World Scientific, Singapore, 2010) pp. 420–445.

- [170] T. S. Roy and M. Schmaltz, Phys. Rev. **D77**, 095008 (2008), [arXiv:0708.3593].
- [171] A. de Gouvea, A. Friedland and H. Murayama, Phys. Rev. **D57**, 5676 (1998), [hep-ph/9711264].
- [172] T. Han, D. Marfatia and R.-J. Zhang, Phys. Rev. **D61**, 013007 (2000), [hep-ph/9906508]; Z. Chacko and E. Ponton, Phys. Rev. **D66**, 095004 (2002), [hep-ph/0112190]; A. Delgado, G. F. Giudice and P. Slavich, Phys. Lett. **B653**, 424 (2007), [arXiv:0706.3873]; T. Liu and C. E. M. Wagner, JHEP **06**, 073 (2008), [arXiv:0803.2895].
- [173] A. Djouadi, J.L. Kneur, and G. Moultaka, Comp. Phys. Comm. **176**, 426 (2007); C. F. Berger *et al.*, JHEP **02**, 023 (2009), [arXiv:0812.0980]; B. Allanach *et al.*, Phys. Rev. **D92**, 015006 (2015), [arXiv:1502.05836].
- [174] S. P. Martin and J. D. Wells, Phys. Rev. **D64**, 035003 (2001), [hep-ph/0103067].
- [175] S. S. AbdusSalam *et al.*, Phys. Rev. D **81**, 095012 (2010), [arXiv:0904.2548].
- [176] J. Berger *et al.*, Phys. Rev. **D93**, 035017 (2016), [arXiv:1510.08840].
- [177] K. J. de Vries *et al.*, Eur. Phys. J. **C75**, 422 (2015), [arXiv:1504.03260].
- [178] E. Bagnaschi *et al.*, Eur. Phys. J. **C78**, 256 (2018), [arXiv:1710.11091].
- [179] M. Cahill-Rowley *et al.*, Phys. Rev. **D90**, 095017 (2014), [arXiv:1407.7021]; M. Cahill-Rowley *et al.*, Phys. Rev. **D91**, 055011 (2015), [arXiv:1405.6716].
- [180] G. Bertone *et al.*, JCAP **1604**, 037 (2016), [arXiv:1507.07008].
- [181] N. Arkani-Hamed *et al.* (2007), [hep-ph/0703088]; J. Alwall *et al.*, Phys. Rev. **D79**, 015005 (2009), [arXiv:0809.3264]; J. Alwall, P. Schuster and N. Toro, Phys. Rev. **D79**, 075020 (2009), [arXiv:0810.3921]; D. S. M. Alves, E. Izaguirre and J. G. Wacker, Phys. Lett. **B702**, 64 (2011), [arXiv:1008.0407]; D. S. M. Alves, E. Izaguirre and J. G. Wacker, JHEP **10**, 012 (2011), [arXiv:1102.5338]; D. Alves (LHC New Physics Working Group), J. Phys. **G39**, 105005 (2012), [arXiv:1105.2838].
- [182] F. Ambrogio *et al.*, Eur. Phys. J. **C78**, 215 (2018), [arXiv:1707.09036].
- [183] R. Barbieri and G. F. Giudice, Nucl. Phys. B **306**, 63 (1988).
- [184] J. R. Ellis *et al.*, Mod. Phys. Lett. **A1**, 57 (1986).
- [185] G. W. Anderson and D. J. Castano, Phys. Lett. **B347**, 300 (1995), [hep-ph/9409419]; G. W. Anderson and D. J. Castano, Phys. Rev. **D52**, 1693 (1995), [hep-ph/9412322]; G. W. Anderson and D. J. Castano, Phys. Rev. **D53**, 2403 (1996), [hep-ph/9509212]; P. Athron and D. J. Miller, Phys. Rev. **D76**, 075010 (2007), [arXiv:0705.2241].
- [186] M. E. Cabrera, J. A. Casas and R. Ruiz de Austri, JHEP **03**, 075 (2009), [arXiv:0812.0536]; H. Baer *et al.*, Phys. Rev. Lett. **109**, 161802 (2012), [arXiv:1207.3343].
- [187] J. L. Feng, K. T. Matchev and T. Moroi, Phys. Rev. **D61**, 075005 (2000), [hep-ph/9909334].
- [188] D. M. Ghilencea and G. G. Ross, Nucl. Phys. **B868**, 65 (2013), [arXiv:1208.0837].
- [189] H. Baer, V. Barger and D. Mickelson, Phys. Rev. **D88**, 095013 (2013), [arXiv:1309.2984].
- [190] M. van Beekveld, S. Caron and R. Ruiz de Austri, JHEP **01**, 147 (2020), [arXiv:1906.10706].
- [191] G. L. Kane and S. F. King, Phys. Lett. **B451**, 113 (1999), [hep-ph/9810374]; M. Bastero-Gil, G. L. Kane and S. F. King, Phys. Lett. **B474**, 103 (2000), [hep-ph/9910506]; J. A. Casas, J. R. Espinosa and I. Hidalgo, JHEP **01**, 008 (2004), [hep-ph/0310137]; H. Abe, T. Kobayashi and Y. Omura, Phys. Rev. **D76**, 015002 (2007), [hep-ph/0703044]; R. Essig and J.-F. Fortin, JHEP **04**, 073 (2008), [arXiv:0709.0980].
- [192] B. de Carlos and J. A. Casas, Phys. Lett. **B309**, 320 (1993), [hep-ph/9303291]; S. Cassel, D. M. Ghilencea and G. G. Ross, Nucl. Phys. **B825**, 203 (2010), [arXiv:0903.1115]; S. Cassel, D. M. Ghilencea and G. G. Ross, Nucl. Phys. **B835**, 110 (2010), [arXiv:1001.3884]; D. M. Ghilencea, H. M. Lee and M. Park, JHEP **07**, 046 (2012), [arXiv:1203.0569].
- [193] B. C. Allanach, Phys. Lett. B **635**, 123 (2006), [hep-ph/0601089].
- [194] B. C. Allanach *et al.*, JHEP **08**, 023 (2007), [arXiv:0705.0487].
- [195] O. Buchmueller *et al.*, Eur. Phys. J. **C74**, 2922 (2014), [arXiv:1312.5250].
- [196] P. Bechtle *et al.*, Eur. Phys. J. **C76**, 96 (2016), [arXiv:1508.05951]; C. Han *et al.*, Phys. Lett. B **769**, 470 (2017), [arXiv:1612.02296]; P. Athron *et al.* (GAMBIT Collaboration), Eur. Phys. J. C **77**, 824 (2017), [arXiv:1705.07935].
- [197] H. Baer *et al.*, Phys. Rev. **D89**, 115019 (2014), [arXiv:1404.2277].
- [198] R. Barbieri and A. Strumia, in “4th Rencontres du Vietnam: Physics at Extreme Energies (Particle Physics and Astrophysics) Hanoi, Vietnam, July 19-25, 2000,” (2000), [hep-ph/0007265].
- [199] L. Giusti, A. Romanino and A. Strumia, Nucl. Phys. **B550**, 3 (1999), [hep-ph/9811386]; H.-C. Cheng and I. Low, JHEP **09**, 051 (2003), [hep-ph/0308199]; H.-C. Cheng and I. Low, JHEP **08**, 061 (2004), [hep-ph/0405243]; R. Harnik *et al.*, Phys. Rev. **D70**, 015002 (2004), [hep-ph/0311349].
- [200] H. Baer *et al.*, Phys. Rev. **D87**, 035017 (2013), [arXiv:1210.3019]; H. Baer *et al.*, Phys. Rev. **D87**, 115028 (2013), [arXiv:1212.2655]; J. L. Feng, Ann. Rev. Nucl. Part. Sci. **63**, 351 (2013), [arXiv:1302.6587].
- [201] J. L. Feng, K. T. Matchev and T. Moroi, Phys. Rev. Lett. **84**, 2322 (2000), [hep-ph/9908309]; J. L. Feng and F. Wilczek, Phys. Lett. **B631**, 170 (2005), [hep-ph/0507032]; D. Horton and G. G. Ross, Nucl. Phys. **B830**, 221 (2010), [arXiv:0908.0857].
- [202] M. Drees, Phys. Rev. **D33**, 1468 (1986); S. Dimopoulos and G. F. Giudice, Phys. Lett. **B357**, 573 (1995), [hep-ph/9507282]; A. Pomarol and D. Tommasini, Nucl. Phys. **B466**, 3 (1996), [hep-ph/9507462].
- [203] M. Dine, A. Kagan and S. Samuel, Phys. Lett. **B243**, 250 (1990); A. G. Cohen, D. B. Kaplan and A. E. Nelson, Phys. Lett. **B388**, 588 (1996), [hep-ph/9607394].
- [204] C. Brust *et al.*, JHEP **03**, 103 (2012), [arXiv:1110.6670].
- [205] S. P. Martin, Phys. Rev. **D75**, 115005 (2007), [hep-ph/0703097]; S. P. Martin, Phys. Rev. **D78**, 055019 (2008), [arXiv:0807.2820].
- [206] J. Fan, M. Reece and J. T. Ruderman, JHEP **11**, 012 (2011), [arXiv:1105.5135]; J. Fan, M. Reece and J. T. Ruderman, JHEP **07**, 196 (2012), [arXiv:1201.4875].
- [207] H. Murayama, Y. Nomura and D. Poland, Phys. Rev. **D77**, 015005 (2008), [arXiv:0709.0775]; G. Perez, T. S. Roy and M. Schmaltz, Phys. Rev. **D79**, 095016 (2009), [arXiv:0811.3206].
- [208] R. Dermisek and J. F. Gunion, Phys. Rev. Lett. **95**, 041801 (2005), [hep-ph/0502105]; Phys. Rev. **D75**, 095019 (2007); R. Dermisek and J. F. Gunion, Phys. Rev. **D76**, 095006 (2007), [arXiv:0705.4387].
- [209] G. G. Ross and K. Schmidt-Hoberg, Nucl. Phys. **B862**, 710 (2012), [arXiv:1108.1284]; G. G. Ross, K. Schmidt-Hoberg and F. Staub, JHEP **08**, 074 (2012), [arXiv:1205.1509]; A. Kaminska, G. G. Ross and K. Schmidt-Hoberg, JHEP **11**, 209 (2013), [arXiv:1308.4168].
- [210] S. P. Martin and J. D. Wells, Phys. Rev. **D86**, 035017 (2012), [arXiv:1206.2956].

- [211] B. Bellazzini *et al.*, Phys. Rev. **D79**, 095003 (2009), [arXiv:0902.0015].
- [212] M. Dine, Ann. Rev. Nucl. Part. Sci. **65**, 43 (2015), [arXiv:1501.01035].
- [213] H. Baer, V. Barger and M. Savoy, Phys. Rev. **D93**, 035016 (2016), [arXiv:1509.02929].
- [214] M.L. Mangano, editor, *Physics at the FCC-hh, a 100 TeV pp collider*, CERN Yellow Report, CERN-2017-003-M (2017).
- [215] P. Athron *et al.* (GAMBIT), Eur. Phys. J. C **77**, 879 (2017), [arXiv:1705.07917].
- [216] D. Stockinger, J. Phys. **G34**, R45 (2007), [hep-ph/0609168]; P. Athron *et al.*, Eur. Phys. J. **C76**, 62 (2016), [arXiv:1510.08071].
- [217] T. Aoyama *et al.*, Phys. Rept. **887**, 1 (2020), [arXiv:2006.04822].
- [218] D. P. Aguillard *et al.* (Muon $g - 2$ Collaboration), Phys. Rev. Lett. **131**, 16, 161802 (2023), [arXiv:2308.06230].
- [219] M. Endo *et al.*, JHEP **07**, 075 (2021), [arXiv:2104.03217]; M. Van Beekveld *et al.*, SciPost Phys. **11**, 049 (2021), [arXiv:2104.03245]; M. Chakraborti, S. Heinemeyer and I. Saha, Eur. Phys. J. C **81**, 1114 (2021), [arXiv:2104.03287]; S. Baum *et al.*, JHEP **01**, 025 (2022), [arXiv:2104.03302]; P. Athron *et al.*, JHEP **09**, 080 (2021), [arXiv:2104.03691].
- [220] S. Borsanyi *et al.*, Nature **593**, 51 (2021), [arXiv:2002.12347].
- [221] C. Lehner, Nature Rev. Phys. **4**, 14 (2022).
- [222] H. Wittig, in “Proceedings of the 57th Rencontres de Moriond on Electroweak Interactions and Unified Theories,” (2023), [arXiv:2306.04165]; S. Kuberski *et al.*, JHEP **03**, 172 (2024), [arXiv:2401.11895].
- [223] D. Hanneke, S. Fogwell and G. Gabrielse, Phys. Rev. Lett. **100**, 120801 (2008), [arXiv:0801.1134].
- [224] R. H. Parker *et al.*, Science **360**, 191 (2018), [arXiv:1812.04130].
- [225] L. Morel *et al.*, Nature **588**, 61 (2020).
- [226] B. Dutta and Y. Mimura, Phys. Lett. **B790**, 563 (2019), [arXiv:1811.10209]; M. Endo and W. Yin, JHEP **08**, 122 (2019), [arXiv:1906.08768]; M. Badziak and K. Sakurai, JHEP **10**, 024 (2019), [arXiv:1908.03607]; S. Li, Y. Xiao and J. M. Yang, Eur. Phys. J. C **82**, 276 (2022), [arXiv:2107.04962].
- [227] T. Ibrahim and P. Nath, Phys. Rev. D **62**, 015004 (2000), [hep-ph/9908443]; R. L. Arnowitt, B. Dutta and Y. Santoso, Phys. Rev. D **64**, 113010 (2001), [hep-ph/0106089]; C. Han (2021), [arXiv:2104.03292].
- [228] J. Albrecht, D. van Dyk and C. Langenbruch, Prog. Part. Nucl. Phys. **120**, 103885 (2021), [arXiv:2107.04822].
- [229] J. P. Lees *et al.* (BaBar Collaboration), Phys. Rev. Lett. **109**, 191801 (2012), [arXiv:1207.2690]; J. P. Lees *et al.* (BaBar Collaboration), Phys. Rev. **D86**, 112008 (2012), [arXiv:1207.5772]; T. Saito *et al.* (Belle Collaboration), Phys. Rev. D **91**, 5, 052004 (2015), [arXiv:1411.7198].
- [230] M. Misiak *et al.*, Phys. Rev. Lett. **114**, 221801 (2015), [arXiv:1503.01789]; M. Czakon *et al.*, JHEP **04**, 168 (2015), [arXiv:1503.01791]; M. Misiak, A. Rehman and M. Steinhauser, JHEP **06**, 175 (2020), [arXiv:2002.01548].
- [231] H. Baer and M. Brhlik, Phys. Rev. **D55**, 3201 (1997), [hep-ph/9610224]; M. Ciuchini *et al.*, Phys. Rev. **D67**, 075016 (2003), [Erratum: **D68**, 079901 (2003)], [hep-ph/0212397]; T. Hurth, Rev. Mod. Phys. **75**, 1159 (2003), [hep-ph/0212304]; F. Mahmoudi, JHEP **12**, 026 (2007), [arXiv:0710.3791]; K. A. Olive and L. Velasco-Sevilla, JHEP **05**, 052 (2008), [arXiv:0801.0428].
- [232] S. R. Choudhury and N. Gaur, Phys. Lett. **B451**, 86 (1999), [hep-ph/9810307]; K. S. Babu and C. F. Kolda, Phys. Rev. Lett. **84**, 228 (2000), [hep-ph/9909476]; G. Isidori and A. Retico, JHEP **11**, 001 (2001), [hep-ph/0110121]; G. Isidori and A. Retico, JHEP **09**, 063 (2002), [hep-ph/0208159].
- [233] B. Allanach and J. Davighi, JHEP **04**, 033 (2023), [arXiv:2211.11766].
- [234] A. Tumasyan *et al.* (CMS Collaboration), Phys. Lett. B **842**, 137955 (2023), [arXiv:2212.10311]; M. Aaboud *et al.* (ATLAS Collaboration), JHEP **04**, 098 (2019), [arXiv:1812.03017]; R. Aaij *et al.* (LHCb Collaboration), Phys. Rev. Lett. **118**, 191801 (2017), [arXiv:1703.05747].
- [235] C. Bobeth *et al.*, Phys. Rev. Lett. **112**, 101801 (2014), [arXiv:1311.0903].
- [236] R. Aaij *et al.* (LHCb Collaboration), Phys. Rev. Lett. **125**, 011802 (2020), [arXiv:2003.04831].
- [237] N. Gubernari *et al.*, JHEP **09**, 133 (2022), [arXiv:2206.03797].
- [238] R. Aaij *et al.* (LHCb Collaboration), Phys. Rev. Lett. **127**, 151801 (2021), [arXiv:2105.14007].
- [239] I. Adachi *et al.* (Belle-II Collaboration) (2023), [arXiv:2311.14647].
- [240] W. G. Parrott, C. Bouchard and C. T. H. Davies (HPQCD Collaboration), Phys. Rev. D **107**, 1, 014511 (2023), [Erratum: **D107**, 119903 (2023)], [arXiv:2207.13371].
- [241] S. Bertolini *et al.*, Nucl. Phys. B **353**, 591 (1991); T. M. Aliev, G. Turan and O. Yilmaz, Nuovo Cim. A **106**, 1059 (1993).
- [242] M. Bona *et al.* (UTfit Collaboration), Phys. Lett. **B687**, 61 (2010), [arXiv:0908.3470].
- [243] J. P. Lees *et al.* (BaBar Collaboration), Phys. Rev. Lett. **109**, 101802 (2012), [arXiv:1205.5442]; J. P. Lees *et al.* (BaBar Collaboration), Phys. Rev. **D88**, 072012 (2013), [arXiv:1303.0571].
- [244] Y. S. Amhis *et al.* (Heavy Flavor Averaging Group, HFLAV), Phys. Rev. D **107**, 052008 (2023), [arXiv:2206.07501].
- [245] F. Mahmoudi, S. Neshatpour and J. Orloff, JHEP **08**, 092 (2012), [arXiv:1205.1845]; A. Arbey *et al.*, JHEP **11**, 132 (2017), [arXiv:1707.00426].
- [246] H. Eberl *et al.*, Phys. Rev. D **104**, 075025 (2021), [arXiv:2106.15228].
- [247] T. Aaltonen *et al.* (CDF Collaboration), Science **376**, 170 (2022).
- [248] J. M. Yang and Y. Zhang, Sci. Bull. **67**, 1430 (2022), [arXiv:2204.04202]; P. Athron *et al.*, Phys. Rev. D **106**, 095023 (2022), [arXiv:2204.05285]; J. Gu *et al.*, Chin. Phys. C **46**, 123107 (2022), [arXiv:2204.05296].
- [249] ATLAS Collaboration, (2023), ATLAS-CONF-2023-004.
- [250] P. F. de Salas *et al.*, JHEP **02**, 071 (2021), [arXiv:2006.11237]; I. Esteban *et al.*, JHEP **09**, 178 (2020), [arXiv:2007.14792].
- [251] K. Zuber, Phys. Rept. **305**, 295 (1998), [hep-ph/9811267]; S. F. King, J. Phys. **G42**, 123001 (2015), [arXiv:1510.02091]; S. F. King, Prog. Part. Nucl. Phys. **94**, 217 (2017), [arXiv:1701.04413].
- [252] For a review of neutrino masses in supersymmetry, see *e.g.*, B. Mukhopadhyaya, Proc. Indian National Science Academy **A70**, 239 (2004); M. Hirsch and J. W. F. Valle, New J. Phys. **6**, 76 (2004), [hep-ph/0405015].
- [253] F. Borzumati and Y. Nomura, Phys. Rev. **D64**, 053005 (2001), [hep-ph/0007018].
- [254] P. Minkowski, Phys. Lett. **67B**, 421 (1977); M. Gell-Mann, P. Ramond, and R. Slansky, in *Supergravity*, edited by D. Freedman and P. van Nieuwenhuizen (North Holland, Amsterdam, 1979) p. 315; T. Yanagida, Prog. Theor. Phys. **64**, 1103 (1980); R. N. Mohapatra and G. Senjanovic, Phys. Rev. Lett. **44**, 912 (1980); R. N. Mohapatra and G. Senjanovic, Phys. Rev. **D23**, 165 (1981).

- [255] J. Hisano *et al.*, Phys. Lett. **B357**, 579 (1995), [hep-ph/9501407]; J. Hisano *et al.*, Phys. Rev. **D53**, 2442 (1996), [hep-ph/9510309]; J. A. Casas and A. Ibarra, Nucl. Phys. **B618**, 171 (2001), [hep-ph/0103065]; J. R. Ellis *et al.*, Phys. Rev. **D66**, 115013 (2002), [hep-ph/0206110]; A. Masiero, S. K. Vempati and O. Vives, New J. Phys. **6**, 202 (2004), [hep-ph/0407325]; E. Arganda *et al.*, Phys. Rev. **D71**, 035011 (2005), [hep-ph/0407302]; F. R. Joaquim and A. Rossi, Phys. Rev. Lett. **97**, 181801 (2006), [hep-ph/0604083]; J. R. Ellis and O. Lebedev, Phys. Lett. **B653**, 411 (2007), [arXiv:0707.3419].
- [256] Y. Grossman and H. E. Haber, Phys. Rev. Lett. **78**, 3438 (1997), [hep-ph/9702421]; A. Dedes, H. E. Haber and J. Rosiek, JHEP **11**, 059 (2007), [arXiv:0707.3718].
- [257] M. Hirsch, H. V. Klapdor-Kleingrothaus and S. G. Kovalenko, Phys. Lett. **B398**, 311 (1997), [hep-ph/9701253]; L. J. Hall, T. Moroi and H. Murayama, Phys. Lett. **B424**, 305 (1998), [hep-ph/9712515]; K. Choi, K. Hwang and W. Y. Song, Phys. Rev. Lett. **88**, 141801 (2002), [hep-ph/0108028]; T. Honkavaara, K. Huitu and S. Roy, Phys. Rev. **D73**, 055011 (2006), [hep-ph/0512277].
- [258] Y. Liu, S. Moretti and H. Waltari (2023), [arXiv:2307.05550].
- [259] T. Faber *et al.*, Phys. Rev. D **101**, 055029 (2020), [arXiv:1909.11686].
- [260] L. Basso *et al.*, Comput. Phys. Commun. **184**, 698 (2013), [arXiv:1206.4563].
- [261] M. Chemtob, Prog. Part. Nucl. Phys. **54**, 71 (2005), [hep-ph/0406029]; R. Barbier *et al.*, Phys. Rept. **420**, 1 (2005), [hep-ph/0406039].
- [262] H. Dreiner, in *Perspectives on Supersymmetry II*, edited by G.L. Kane (World Scientific, Singapore, 2010) pp. 565–583.
- [263] B. C. Allanach, A. Dedes and H. K. Dreiner, Phys. Rev. **D60**, 075014 (1999), [hep-ph/9906209].
- [264] L. E. Ibanez and G. G. Ross, Nucl. Phys. **B368**, 3 (1992); L. E. Ibanez, Nucl. Phys. **B398**, 301 (1993), [hep-ph/9210211].
- [265] A. Dedes, S. Rimmer and J. Rosiek, JHEP **08**, 005 (2006), [hep-ph/0603225]; B. C. Allanach and C. H. Kom, JHEP **04**, 081 (2008), [arXiv:0712.0852]; H. K. Dreiner *et al.*, Phys. Rev. **D84**, 113005 (2011), [arXiv:1106.4338].
- [266] H. K. Dreiner, C. Luhn and M. Thormeier, Phys. Rev. **D73**, 075007 (2006), [hep-ph/0512163].
- [267] K. Tamvakis, Phys. Lett. **B382**, 251 (1996), [hep-ph/9604343]; G. Eyal and Y. Nir, JHEP **06**, 024 (1999), [hep-ph/9904473]; A. Florez *et al.*, Phys. Rev. **D87**, 095010 (2013), [arXiv:1303.0278].
- [268] C. Csaki, Y. Grossman and B. Heidenreich, Phys. Rev. **D85**, 095009 (2012), [arXiv:1111.1239].
- [269] D. Dercks *et al.*, Eur. Phys. J. **C77**, 856 (2017), [arXiv:1706.09418].
- [270] B. C. Allanach and B. Gripaios, JHEP **05**, 062 (2012), [arXiv:1202.6616]; M. Asano, K. Rolbiecki and K. Sakurai, JHEP **01**, 128 (2013), [arXiv:1209.5778]; N. Chamoun *et al.*, JHEP **08**, 142 (2014), [arXiv:1407.2248].
- [271] J. C. Romao, Nucl. Phys. Proc. Suppl. **81**, 231 (2000), [hep-ph/9907466]; Y. Grossman and S. Rakshit, Phys. Rev. **D69**, 093002 (2004), [hep-ph/0311310].
- [272] R. N. Mohapatra, Phys. Rev. **D34**, 3457 (1986); K. S. Babu and R. N. Mohapatra, Phys. Rev. Lett. **75**, 2276 (1995), [hep-ph/9506354]; M. Hirsch, H. V. Klapdor-Kleingrothaus and S. G. Kovalenko, Phys. Rev. Lett. **75**, 17 (1995); M. Hirsch, H. V. Klapdor-Kleingrothaus and S. G. Kovalenko, Phys. Rev. **D53**, 1329 (1996), [hep-ph/9502385].
- [273] Y. Grossman and H. E. Haber, Phys. Rev. **D59**, 093008 (1999), [hep-ph/9810536].
- [274] S. Dimopoulos and L. J. Hall, Phys. Lett. **B207**, 210 (1988); J. Kalinowski *et al.*, Phys. Lett. **B406**, 314 (1997), [hep-ph/9703436]; J. Erler, J. L. Feng and N. Polonsky, Phys. Rev. Lett. **78**, 3063 (1997), [hep-ph/9612397].
- [275] H. K. Dreiner, P. Richardson and M. H. Seymour, Phys. Rev. **D63**, 055008 (2001), [hep-ph/0007228].
- [276] J. E. Kim and H. P. Nilles, Phys. Lett. **138B**, 150 (1984).
- [277] J. E. Kim and H. P. Nilles, Mod. Phys. Lett. **A9**, 3575 (1994), [hep-ph/9406296].
- [278] G. F. Giudice and A. Masiero, Phys. Lett. **B206**, 480 (1988); J. A. Casas and C. Munoz, Phys. Lett. **B306**, 288 (1993), [hep-ph/9302227]; K. J. Bae *et al.*, Phys. Rev. **D99**, 115027 (2019), [arXiv:1902.10748].
- [279] M. Cvetič *et al.*, Phys. Rev. **D56**, 2861 (1997), [Erratum: **D58**, 119905 (1998)], [hep-ph/9703317].
- [280] R. D. Peccei, Lect. Notes Phys. **741**, 3 (2008), [hep-ph/0607268].
- [281] R. D. Peccei and H. R. Quinn, Phys. Rev. Lett. **38**, 1440 (1977); R. D. Peccei and H. R. Quinn, Phys. Rev. **D16**, 1791 (1977).
- [282] H. Murayama, H. Suzuki and T. Yanagida, Phys. Lett. **B291**, 418 (1992); T. Gherghetta and G. L. Kane, Phys. Lett. **B354**, 300 (1995), [hep-ph/9504420]; K. J. Bae, H. Baer and H. Serce, Phys. Rev. **D91**, 015003 (2015), [arXiv:1410.7500]; H. Baer, V. Barger and D. Sengupta, Phys. Lett. **B790**, 58 (2019), [arXiv:1810.03713].
- [283] P. Fayet, Phys. Lett. **78B**, 417 (1978).
- [284] K. Benakli, Fortsch. Phys. **59**, 1079 (2011), [arXiv:1106.1649].
- [285] P. J. Fox, A. E. Nelson and N. Weiner, JHEP **08**, 035 (2002), [hep-ph/0206096].
- [286] K. Benakli and M. D. Goodsell, Nucl. Phys. **B816**, 185 (2009), [arXiv:0811.4409]; K. Benakli and M. D. Goodsell, Nucl. Phys. **B840**, 1 (2010), [arXiv:1003.4957].
- [287] U. Sarkar and R. Adhikari, Phys. Rev. **D55**, 3836 (1997), [hep-ph/9608209]; R. Fok *et al.*, Phys. Rev. **D87**, 055018 (2013), [arXiv:1208.2784].
- [288] G. D. Kribs, E. Poppitz and N. Weiner, Phys. Rev. **D78**, 055010 (2008), [arXiv:0712.2039].
- [289] K. Benakli, M. D. Goodsell and F. Staub, JHEP **06**, 073 (2013), [arXiv:1211.0552].
- [290] J. L. Hewett and T. G. Rizzo, Phys. Rept. **183**, 193 (1989).
- [291] A. Delgado, G. Nardini and M. Quiros, Phys. Rev. **D86**, 115010 (2012), [arXiv:1207.6596].
- [292] S. F. King, S. Moretti and R. Nevzorov, Phys. Lett. **B634**, 278 (2006), [hep-ph/0511256]; S. F. King, S. Moretti and R. Nevzorov, Phys. Rev. **D73**, 035009 (2006), [hep-ph/0510419].
- [293] H. Kawase, JHEP **12**, 094 (2011), [arXiv:1110.3861]; N. Escudero, C. Munoz and A. M. Teixeira, Phys. Rev. D **73**, 055015 (2006), [hep-ph/0512046]; B. Dutta and Y. Mimura, Phys. Lett. B **790**, 589 (2019), [arXiv:1810.08413]; W. Altmannshofer *et al.*, JHEP **07**, 118 (2021), [arXiv:2104.08293].

89. Supersymmetry, Part II (Experiment)

Revised August 2023 by M. D’Onofrio (Liverpool U.) and F. Moortgat (CERN; Ghent U.).

89.1 Introduction

Supersymmetry (SUSY), a transformation relating fermions to bosons and vice versa [1–9] is one of the most compelling possible extensions of the Standard Model of particle physics (SM).

On theoretical grounds SUSY is motivated as a generalization of space-time symmetries. A low-energy realization of SUSY, *i.e.*, SUSY at the TeV scale, is, however, not a necessary consequence. Instead, low-energy SUSY is motivated by the possible cancellation of quadratic divergences in radiative corrections to the Higgs boson mass [10–15]. Furthermore, it is intriguing that a weakly interacting, (meta)stable supersymmetric particle might make up some or all of the dark matter in the Universe [16–18]. In addition, SUSY predicts that gauge couplings, as measured experimentally at the electroweak scale, unify at an energy scale $\mathcal{O}(10^{16})$ GeV (“GUT scale”) near the Planck scale [19–25].

In the minimal supersymmetric extension to the Standard Model, the so called MSSM [11, 26, 27], a supersymmetry transformation relates every chiral fermion and gauge boson in the SM to a supersymmetric partner with half a unit of spin difference, but otherwise with the same properties (such as mass) and quantum numbers. The MSSM Higgs sector contains two doublets, which give mass to the up-type and down-type quarks, respectively. After electroweak symmetry breaking, five Higgs bosons arise, of which two are charged. The supersymmetric partners of chiral fermions are squarks (\tilde{q}) and sleptons ($\tilde{\ell}$, $\tilde{\nu}$), and the “gauginos” for gauge bosons. The supersymmetric partners of the Higgs doublets are known as “higgsinos.” The weak gauginos and higgsinos mix, giving rise to charged mass eigenstates called “charginos” ($\tilde{\chi}^{\pm}$), and neutral mass eigenstates called “neutralinos” ($\tilde{\chi}^0$). These are often collectively referred to as electroweakinos (EWkinos). The SUSY partners of the gluons are known as “gluinos” (\tilde{g}). The fact that such particles are not yet observed leads to the conclusion that, if supersymmetry is realized, it is a broken symmetry. A description of SUSY in the form of an effective Lagrangian with only “soft” SUSY breaking terms and SUSY particle masses of the order of TeV maintains the cancellation of quadratic divergences of soft SUSY breaking scalar mass squared parameters.

The phenomenology of SUSY is to a large extent defined by the SUSY breaking mechanism and the SUSY breaking scale. These determine the SUSY particle masses, the mass hierarchy, the field contents of physical particles, and their decay modes. In addition, phenomenology crucially depends on whether the multiplicative quantum number of R -parity [27], $R = (-1)^{3(B-L)+2S}$, where B and L are baryon and lepton numbers and S is the spin, is conserved or violated. If R -parity is conserved, SUSY particles (sparticles), which have odd R -parity, are produced in pairs and the decays of each SUSY particle must involve an odd number of lighter SUSY particles. The lightest SUSY particle (LSP) is then stable and often assumed to be a weakly interacting massive particle (WIMP). If R -parity is violated, new terms λ_{ijk} , λ'_{ijk} and λ''_{ijk} appear in the superpotential, where ijk are generation indices; λ -type couplings appear between lepton superfields only, λ'' -type are between quark superfields only, and λ' -type couplings connect the two. R -parity violation implies lepton and/or baryon number violation. More details of the theoretical framework of SUSY are discussed elsewhere in this volume [28].

The discovery of a Higgs boson with a mass around 125 GeV imposes constraints on SUSY models, which are discussed elsewhere [28, 29]. Low-energy data from flavor physics experiments, high-precision electroweak observables as well as astrophysical data also impose strong constraints on the allowed SUSY parameter space. Recent examples of such data include measurements of the rare B-meson decay $B_s \rightarrow \mu^+ \mu^-$ [30–32], measurements of the anomalous magnetic moment of the muon [33, 34], and accurate determinations of the cosmological dark matter relic density constraint [35, 36].

Indirect constraints can be more sensitive to higher SUSY mass scales than experiments searching for direct sparticle production

at colliders, but the interpretation of these results is often strongly model dependent. In contrast, direct searches for sparticle production at collider experiments, which are the main topic of this review, are less subject to interpretation ambiguities and therefore they play a crucial role in the search for SUSY. Further discussion on indirect constraints can be found in 88.7.2.

89.2 Overview of the experimental search programme

The electron-positron collider LEP was operational at CERN between 1989 and 2000. In the initial phase, center-of-mass energies around the Z -peak were probed, but after 1995 the LEP experiments collected a significant amount of luminosity at higher center-of-mass energies, some 235 pb^{-1} per experiment at $\sqrt{s} \geq 204 \text{ GeV}$, with a maximum \sqrt{s} of 209 GeV. Searches for new physics at e^+e^- colliders benefit from the clean experimental environment and the fact that momentum balance can be measured not only in the plane transverse to the beam, but also in the direction along the beam (up to the beam pipe holes), defined as the longitudinal direction. Searches at LEP are dominated by the data samples taken at the highest center-of-mass energies.

The CDF and D0 experiments at the Tevatron, a proton-antiproton collider at a center-of-mass energy of up to 1.96 TeV, had an extensive search program for supersymmetric particles. CDF and D0 collected integrated luminosities between 10 and 11 fb^{-1} each up to the end of collider operations in 2011.

The electron-proton collider HERA provided collisions to the H1 and ZEUS experiments between 1992 and 2007, at a center-of-mass energy up to 318 GeV. A total integrated luminosity of approximately 0.5 fb^{-1} was collected by each experiment. Since at HERA baryons collide with leptons, SUSY searches typically look for R -parity violating production of single SUSY particles.

The Large Hadron Collider (LHC) at CERN started proton-proton operation at a center-of-mass energy of 7 TeV in 2010. By the end of 2011 the ATLAS and CMS experiments had collected about 5 fb^{-1} of integrated luminosity each, and the LHCb experiment had collected approximately 1 fb^{-1} . In 2012, the LHC operated at a center-of-mass energy of 8 TeV, and ATLAS and CMS collected approximately 20 fb^{-1} each, whereas LHCb collected 2 fb^{-1} . In 2015, the LHC started Run 2, with a center-of-mass energy of 13 TeV. At the end of Run 2 in November 2018, ATLAS and CMS had both collected approximately 140 fb^{-1} , and LHCb had collected almost 6 fb^{-1} . The Run 3 of the LHC started in July 2022 with a center-of-mass energy of 13.6 TeV. Almost 70 fb^{-1} of data have been collected by ATLAS and CMS at the time of writing (August 2023), and LHCb collected around 1.3 fb^{-1} .

At the LHC, cross sections of QCD-mediated processes are the largest achievable at colliders, which is reflected in the higher sensitivity for SUSY particles carrying color charge, squarks and gluinos, with respect to LEP, Tevatron and HERA. In particular, proton-proton collisions at the LHC differ from proton-antiproton collisions at the Tevatron in the sense that there are no valence anti-quarks in the proton, and that gluon-initiated processes play a more dominant role. The increased center-of-mass energy of the LHC compared to the Tevatron significantly extends the kinematic reach for SUSY searches. This is reflected foremost in the sensitivity for squarks and gluinos, but also for SUSY particles produced via electroweak processes.

In this review we report results of direct searches for SUSY particles at colliders up to August 2023, mostly covering data analyses at the ATLAS and CMS experiments with reference to results from LEP, HERA and the Tevatron. For more details on LEP and Tevatron constraints, see earlier PDG reviews [37]. Analyses on the Run 3 datasets are still in progress hence the results reported for ATLAS and CMS are based on Run 1 and Run 2 data. Results are categorized depending on the targeted SUSY particles, the nature of their production and decays, and the assumption on R -parity. Brief summaries of search techniques and approaches adopted for interpretation of the results are given in Section 89.3 and 89.4, respectively. Sections 89.5–89.8 focus on results for promptly-decaying gluinos and first and second generation squarks, top and bottom squarks, electroweakinos (charginos,

neutralinos) and sleptons. Limits obtained for sparticle masses assuming R -parity violating models are also reported. Results of dedicated searches for long-lived (LL) SUSY particles are reported in Section 89.9. Finally, Section 89.10 provides examples of global reinterpretations of SUSY searches.

89.3 Experimental search techniques

Large background contributions from Standard Model processes pose challenges to the trigger and analysis. Such backgrounds are dominated by multijet production processes, including, particularly at the LHC, those of top quark production, as well as jet production in association with vector bosons. The proton's momentum is shared between its parton constituents, and in each collision only a fraction of the total center-of-mass energy is available in the hard parton-parton scattering. Since the parton momenta in the longitudinal direction are not known on an event-by-event basis, use of momentum conservation constraints in an analysis is restricted to the transverse plane, leading to the definition of transverse variables, such as the missing transverse momentum, and the transverse mass.

Under the assumption of R -parity conservation (RPC), the typical SUSY search signature for squarks and gluinos at hadron colliders contains high- p_T jets, which are produced in the decay chains of heavy squarks and gluinos, and significant missing transverse momentum originating from the two LSPs produced at the end of the decay chains, which escape experimental detection. Electroweakino decays are often characterised by the presence of leptons, for instance from W and Z bosons in the decay chain, plus missing transverse momentum. Standard Model backgrounds with missing transverse momentum include leptonic W/Z -boson decays, associated production of jets and a Z -boson decaying into neutrinos, semi-leptonic heavy-flavor decays to neutrinos, top-quark pair production with one or both W bosons decaying leptonically, and multijet events that may be affected by instrumental effects such as jet mis-measurement.

Selection variables designed to separate the SUSY signal from the Standard Model backgrounds include transverse variables such as H_T , E_T^{miss} , and m_{eff} . The quantities H_T and E_T^{miss} refer to the measured transverse energy and the missing transverse momentum in the event, respectively. They are usually defined as the scalar sum of the transverse jet momenta or of the transverse energies of calorimeter clusters measured in the event (H_T), or the magnitude (E_T^{miss}) of the negative vector sum of transverse momenta of reconstructed objects like jets and leptons in the event (E_T^{miss}). The quantity m_{eff} is referred to as the effective mass of the event and is defined as $m_{\text{eff}} = H_T + E_T^{\text{miss}}$. The peak of the m_{eff} distribution for SUSY signal events correlates with the SUSY mass scale, in particular with the mass difference between the primary produced SUSY particle and the LSP [38], whereas the Standard Model backgrounds dominate at low m_{eff} . An additional reduction of multijet backgrounds can be achieved by demanding isolated leptons or photons in the final states; in such events the lepton or photon transverse momentum may be added to H_T or m_{eff} for further signal-background separation. Other kinematic variables and approaches developed to increase the sensitivity to pair production of heavy sparticles with TeV-scale masses focusing on the kinematics of their decays are the α_T [39–43], *razor* [44], *stransverse mass* (m_{T2}) [45], and *contransverse mass* (m_{CT}) [46] variables. The *super-razor* [47] and *recursive jigsaw reconstruction* [48] techniques are topological event reconstruction methods also used in searches for sparticles with masses in the TeV-range. In case massive, unstable SM particles such as top quarks, vector bosons or the Higgs boson arise in the decay chain, dedicated procedures are employed for their reconstruction and identification. If these are produced with a significant boost, their decay products will typically overlap and become collimated (boosted) in the direction of the parent particle. Their hadronic decay products can be reconstructed as a single large-radius jet (see studies from ATLAS [49]), and *jet-substructure* [50] techniques can be adopted. Machine-learning (ML) approaches are also used to identify and classify hadronic decays of highly Lorentz-boosted bosons and top quarks, see as example recent studies from CMS [51].

Most analyses still use simple combinations of selections on

kinematic variables (often referred to as *cut-and-count* analyses) and exploit multiple signal regions defined by categorizing events on the basis of several variables and their correlations. An example is provided in Fig. 89.1 from Ref. [52]: 39 signal regions are set to search for top squarks in events with one lepton, jets and missing transverse momentum. Regions depend on jet multiplicities, reconstructed top-quark candidates and thresholds applied to the most discriminant variables used for optimisation.

In recent years, shape analyses or analyses using more sophisticated techniques, e.g. machine learning, have been also developed. ML techniques often allow analyses to better capture the complexity of the events and achieve improved sensitivity with respect to counting experiments. For example, Boosted Decision Trees (BDTs) allow analyses to exploit simultaneously the discriminating power of multiple variables and that of correlations among objects in the events. Deep Neural Networks (NN) are also employed for objects reconstruction and to use directly detector-recorded energies and momenta of produced particles instead of first deriving a restricted set of physical variables. Among others, currently in use are Convolutional NN for image classification techniques, Recurrent NN, parametric NN and Generative Adversarial Networks.

Variables and approaches reported above are also used in searches for R -parity violating (RPV) SUSY models where signal events are often characterised by the presence of multiple leptons and/or jets, and little or no missing transverse momentum. However, if R -parity violating couplings are small, sparticles might be long-lived and may travel macroscopic distances before decaying. Similarly, long lifetimes may be due to small mass splittings, as in the case of pure higgsino/wino scenarios, or to heavy mediators, as in Split SUSY models [53, 54]. The identification of long-lived particles requires dedicated tools and their signatures can be very diverse. At the LHC, customized techniques (also based on NN) have been developed, for example, to reconstruct significantly displaced decay vertices or short track segments, and to identify tracks with atypical properties or unusual ionization, small and localized deposits of energy inside of the calorimeters without associated tracks, or stopped particles that decay out of time with collisions. For an overview, see Ref. [55].

89.4 Interpretation of search results

Since the mechanism by which SUSY is broken is unknown, a general approach to SUSY via the most general soft SUSY breaking Lagrangian adds a significant number of new free parameters. For the minimal supersymmetric standard model, MSSM, *i.e.*, the model with the minimal particle content, these comprise 105 new real degrees of freedom. A phenomenological analysis of SUSY searches leaving all these parameters free is not feasible. For the practical interpretation of SUSY searches at colliders several approaches are taken to reduce the number of free parameters.

One approach is to assume a SUSY breaking mechanism and lower the number of free parameters through the assumption of additional constraints. Before the start of the LHC, interpretations of experimental results were often performed in constrained models of gravity mediated [56, 57], gauge-mediated [58–60], and anomaly mediated [61, 62] SUSY breaking. The most popular model was the constrained MSSM (CMSSM) [56, 63, 64], which in the literature is also referred to as minimal supergravity, or MSUGRA. These constrained SUSY models are theoretically well motivated and provide a rich spectrum of experimental signatures. However, with universality relations imposed on the soft SUSY breaking parameters, they do not cover all possible kinematic signatures and mass relations of SUSY. Furthermore, the Higgs mass measurement from LHC Run 1, together with other collider and non-collider measurements, limits substantially the allowed SUSY parameter space for these models. This indicates that very constrained models like the CMSSM are no longer good benchmark scenarios to solely characterize the results of SUSY searches at the LHC and efforts have been made to complement them with more flexible approaches.

A broader and more comprehensive subset of the MSSM can be studied via the so-called phenomenological-MSSM, or pMSSM [65–68]. It is derived from the MSSM, using experimental data to eliminate parameters that are free in principle but have

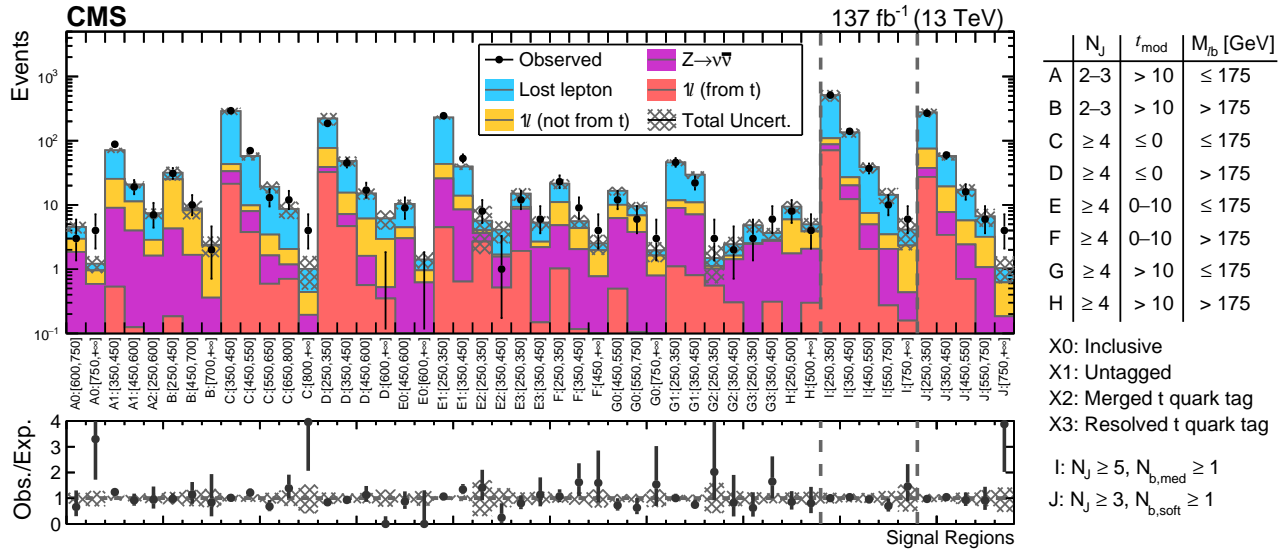


Figure 89.1: Example of multiple signal regions set for a typical SUSY search at the LHC. For definition of regions and acronyms specific for this search, see corresponding paper.

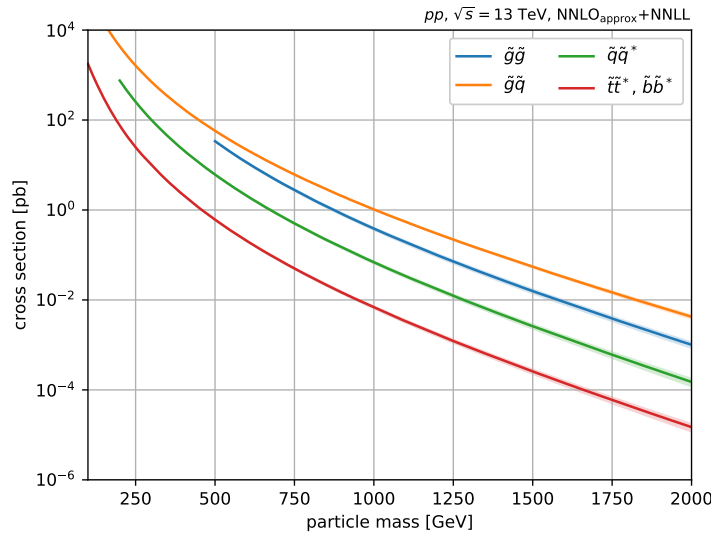


Figure 89.2: Cross sections for pair production of gluinos and squarks as a function of their mass at the LHC for a center-of-mass energy of 13 TeV. They are calculated at approximately next-to-next-to-leading-order (NNLO) including the resummation of soft gluon emission at the next-to-next-to-leading logarithmic accuracy.

already been highly constrained by measurements of *e.g.*, flavor mixing and *CP*-violation. This effective approach reduces the number of free parameters in the MSSM to typically 19 or even less, making it a practical compromise between the full MSSM and highly constrained models such as the CMSSM.

Even less dependent on fundamental assumptions are interpretations in terms of so-called simplified models [69–72]. Such models assume a limited set of SUSY particle production and decay modes and leave open the possibility to vary masses and other parameters freely. Therefore, simplified models enable comprehensive studies of individual SUSY topologies, and are useful for optimization of the experimental searches over a wide parameter space without limitations on fundamental kinematic properties such as masses, production cross sections, and decay modes.

As a consequence, ATLAS and CMS have adopted simplified models as the primary framework to provide interpretations of their searches. In addition to using simplified models that describe prompt decays of SUSY particles, the experiments are now also

focusing more on the use of simplified models that allow for decays of long-lived SUSY particles as they can arise in different SUSY scenarios (see Section 89.9 for further discussion). Today, almost every individual search provides interpretations of their results in one or several simplified models that are characteristic of SUSY topologies probed by the analysis.

While simplified models are very convenient for the interpretation of individual SUSY production and decay topologies, care must be taken when applying these limits to more complex SUSY spectra. In particular, the branching ratio of SUSY particles into a specific final state is often assumed to be 100% and in many of the quoted limits the LSP is assumed to be massless. Therefore, simplified model limits should be seen as an approximation of the constraints that can be placed on sparticle masses in more complex SUSY spectra. Only on a case-by-case basis can it be determined whether the limit of a given simplified model represents a good approximation of the true underlying constraint that can be applied on a sparticle mass in a complex SUSY spectrum.

In the following, we will point out explicitly the assumptions that have entered the limits when quoting interpretations from simplified models.

Since none of the searches performed so far have shown significant excess above the SM background prediction, the interpretation of the presented results are exclusion limits on SUSY parameter space. Unless stated differently, all quoted exclusion limits are at the 95% confidence level. Finally, we note that many of the recent publications by ATLAS and CMS also present results in terms of model-independent limits such that their discovery potential is statistically quantified independently on a particular model.

89.5 Exclusion limits on gluino, first and second generation squark masses in RPC scenarios

Colored SUSY particles such as squarks and gluinos are produced via the strong interaction and have the highest cross sections at hadron colliders. Limits on squark masses of the order 100 GeV have been set by the LEP experiments [73], in the decay to quark plus neutralino, and for a mass difference between squark and quark plus neutralino of typically at least a few GeV. However, hadron collider experiments are able to set much more stringent mass limits.

The main production mechanisms at hadron colliders are squark-squark, squark-gluino and gluino-gluino production; when “squark” is used “antisquark” is also implied. Pair production usually involves both the s -channel and t -channel parton-parton interactions. However, since there is a negligible amount of bottom and top quark content in the proton, top and bottom squark production proceeds through s -channel diagrams only. Experimental analyses of squark and/or gluino production typically assume the first and second generation squarks to be approximately degenerate in mass. Cross section calculations at the center-of-mass energy of 13 TeV shown in Fig. 89.2 (from Ref. [74]) assume mass degeneracy of left- and right-handed u, d, s, c squarks. Other sparticle masses are considered decoupled, *i.e.* their masses are assumed to have a very high value (above 10 TeV). The LHC experiments also provide simplified model limits on individual first or second generation squarks. Top and bottom squarks have the same production cross section, identical to that of a single light squark.

In this section, we focus on results assuming R -parity conservation. Limits set by the Tevatron experiments on the gluino mass assume the framework of the CMSSM, with $\tan\beta = 5$ (CDF) or $\tan\beta = 3$ (D0). Furthermore, the common trilinear term A_0 is set to 0 and the higgsino mass term μ is assumed to be less than 0. The resulting lower mass limits are about 310 GeV for all squark masses, or 390 GeV for the case $m_{\tilde{q}} = m_{\tilde{g}}$ [75,76].

ATLAS and CMS limits on the gluino mass have been established in the framework of simplified models. Assuming only gluino pair production, three main primary decay chains of the gluino have been considered by the LHC experiments for interpretations of their search results. The first decay chain, $\tilde{g} \rightarrow q\bar{q}\tilde{\chi}_1^0$, assumes gluino mediated production of first and second generation squarks (on-shell or off-shell) which leads to four light flavor quarks in the final state. Therefore, inclusive all-hadronic analyses searching for multijet plus E_T^{miss} final states are utilized to put limits on this simplified model. These limits are derived as a function of the gluino and neutralino (LSP) mass. As shown in Fig. 89.3 (left) the CMS collaboration [77] excludes in this simplified model gluino masses below approximately 2.1 TeV for a light neutralino mass below about 600 GeV. In scenarios where neutralinos are not very light, the efficiency of the analyses is reduced by the fact that jets are less energetic, and there is less missing transverse momentum in the event. This leads to weaker limits when the mass difference $\Delta m = m_{\tilde{g}} - m_{\tilde{\chi}_1^0}$ is reduced. For example, for neutralino masses above about 1.2 TeV no limit on the gluino mass can be set for this decay chain. Therefore, limits on gluino masses are strongly affected by the assumption of the neutralino mass. Similar results for this simplified model have been obtained by ATLAS [78]. A second simplified model postulates a decay chain where $\tilde{g} \rightarrow q\bar{q}W\tilde{\chi}_1^0$, assuming that the intermediate (on-shell or off-shell) squark is left-handed and de-

cays to a chargino and a quark, with the chargino decaying to a W boson and the LSP. This leads to two W bosons and four light flavor quarks plus E_T^{miss} in the final state. Both leptonic and hadronic decays of the W can be considered. In this scenario, the ATLAS collaboration [79,80] excludes gluino masses below approximately 2.2 TeV for a sufficiently light neutralino and assuming the chargino mass is halfway between the gluino and neutralino mass, see Fig. 89.3 (right). Again, for neutralino masses above about 1.2 TeV, there exists no limit on the gluino mass for this decay chain. A similar reach has been obtained by the CMS collaboration [81,81,82], where the most recent results are obtained using novel algorithms based on deep neural networks that identify hadronically decaying W bosons.

Gluino decays are not limited to first and second generation squarks: another important decay chain of the gluino considered for interpretation in simplified models is $\tilde{g} \rightarrow b\bar{b}\tilde{\chi}_1^0$. In this case the decay is mediated via bottom squarks and thus leads to four jets originating from b -quarks and E_T^{miss} in the final state. For this topology as well, inclusive all-hadronic searches provide the highest sensitivity. In this case, the use of secondary vertex reconstruction for the identification of jets originating from the b -quarks in the event provides a powerful handle to reject SM background contributions. Therefore, in addition to a multijet plus E_T^{miss} signature these searches also require between 1 and 4 jets to be tagged as b -jets. As shown in Fig. 89.4 (left), for this simplified model CMS [77] excludes gluino masses below ≈ 2.3 TeV for a sufficiently light neutralino, while for neutralino masses above ≈ 1.5 TeV no limit on the gluino mass can be set. Comparable limits for this simplified model are provided by searches from ATLAS [83,84], with the most recent results pushing the boundary of gluino masses to 2.44 TeV in the case of a massless neutralino.

If kinematically allowed, decays of gluinos to top squarks via $\tilde{g} \rightarrow \tilde{t}t$ are also possible. This defines the next important simplified model characterizing gluino pair production, $\tilde{g} \rightarrow t\bar{t}\tilde{\chi}_1^0$, which leads to a “four tops” final state, $ttt\bar{t}\tilde{\chi}_1^0\tilde{\chi}_1^0$. The topology of this decay is very rich in different experimental signatures: as many as four isolated leptons, four b -jets, several light flavor quark jets, and significant missing transverse momentum from the neutrinos in the W decay and from the two neutralinos. As shown in Fig. 89.4 (right), the ATLAS search [83] rules out gluinos with masses below ≈ 2.4 TeV for light neutralinos in this model. For neutralino masses above ≈ 1.4 TeV, no limit can be placed on the gluino mass. The CMS multiple b -jet search [85] and the search in full-hadronic events using identification techniques for boosted top-quarks in the final state [86] result in gluino mass limits of ≈ 2.3 TeV.

Assuming gluinos to be heavier than squarks, squarks will predominantly decay to a quark and a neutralino or chargino, if kinematically allowed. The decay may involve the lightest neutralino (typically the LSP) or chargino, but, depending on the masses and couplings of the gauginos and on the handedness of the squarks, may involve heavier neutralinos or charginos. For pair production of first and second generation squarks, the simplest decay modes involve two jets and missing transverse momentum, with potential extra jets stemming from initial state or final state radiation (ISR/FSR) or from decay modes with longer decay chains (cascades). In cascades, isolated photons or leptons may appear from the decays of sparticles such as neutralinos or charginos.

Limits on first and second generation squark masses set by the Tevatron experiments assume the CMSSM, and amount to lower limits of about 380 GeV for all gluino masses, or 390 GeV for the case $m_{\tilde{q}} = m_{\tilde{g}}$ [75,76]. At the LHC, limits on squark masses have been set using up to approximately 140 fb^{-1} of data at 13 TeV. Interpretations in simplified models typically characterize squark pair production considering only one decay chain at the time for the squark, for instance $\tilde{q} \rightarrow q\tilde{\chi}_1^0$. It is usually assumed that the left and right-handed $\tilde{u}, \tilde{d}, \tilde{s}$ and \tilde{c} squarks are degenerate in mass. Furthermore, it is assumed that the mass of the gluino is very high (above 10 TeV) and thus contributions of the corresponding t -channel diagrams to squark pair production are negligible. Therefore, the total production cross section

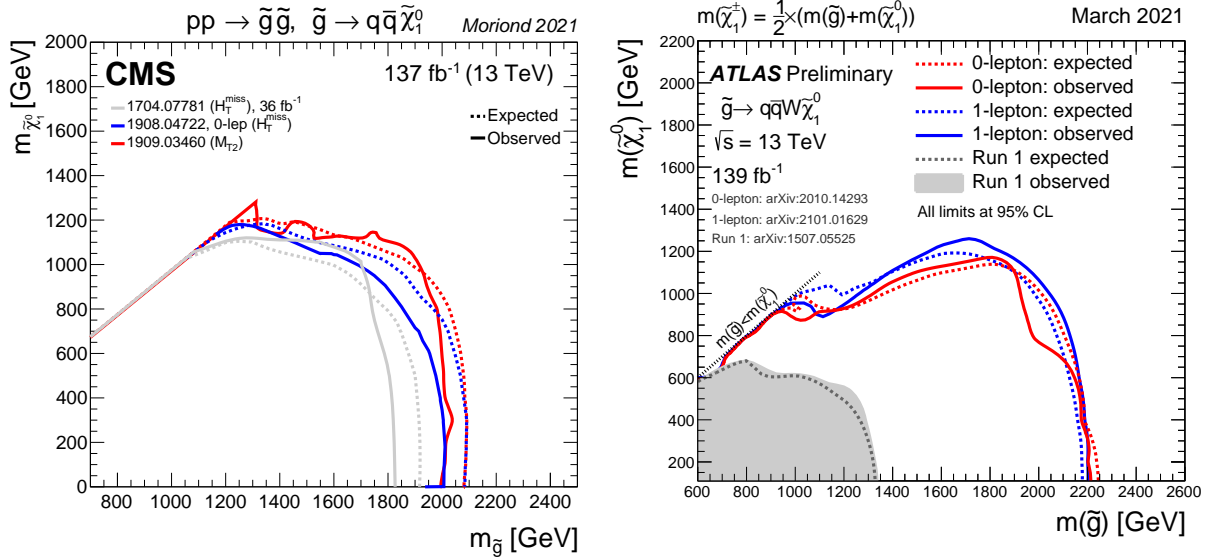


Figure 89.3: Lower mass limits, at 95% C.L., on gluino pair production for various decay chains in the framework of simplified models. Left: $\tilde{g} \rightarrow q\bar{q}\tilde{\chi}_1^0$, result of the CMS collaboration. Right: $\tilde{g} \rightarrow q\bar{q}W\tilde{\chi}_1^0$, result of the ATLAS collaboration.

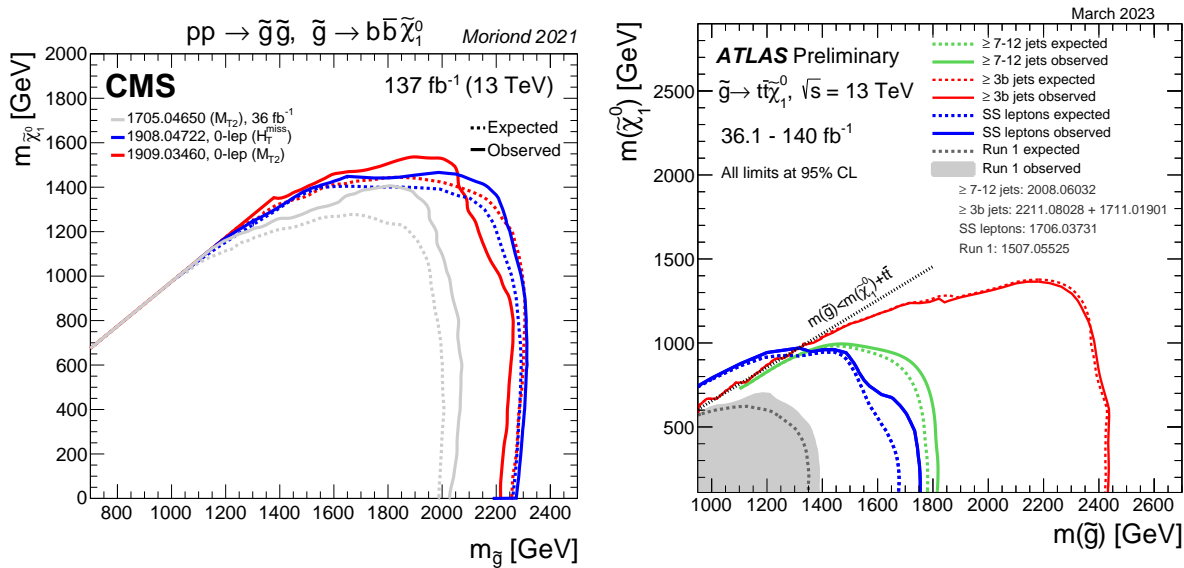


Figure 89.4: Lower mass limits, at 95% C.L., on gluino pair production for various decay chains in the framework of simplified models. Left: $\tilde{g} \rightarrow b\bar{b}\tilde{\chi}_1^0$. Right: $\tilde{g} \rightarrow t\bar{t}\tilde{\chi}_1^0$. Results from the CMS and ATLAS collaborations.

for this simplified model is eight times the production cross section of an individual squark (e.g. \tilde{u}_L). Under these assumptions, CMS obtains a lower squark mass limit of ≈ 1.75 TeV for light neutralinos [85], as shown in Fig. 89.5 (left). Only for neutralino masses below ≈ 800 GeV can any squark masses be excluded. Searches for new physics in monojet channels are sensitive to very compressed scenarios, and masses up to 900 GeV are excluded for $\Delta m = m_{\tilde{q}}, m_{\tilde{\chi}_1^0} \approx 5$ GeV [87].

If the assumption of mass degenerate first and second generation squarks is dropped and only the production of a single light squark is assumed, the limits weaken significantly. For example, the CMS limit on degenerate squarks of 1750 GeV for light neutralinos drops to ≈ 1300 GeV for pair production of a single light squark, and for neutralinos heavier than ≈ 600 GeV no squark mass limit can be placed. It should be noted that this limit is not a result of a simple scaling of the above mentioned mass limits assuming eight-fold mass degeneracy but it also takes into account that for an eight times lower production cross section the analyses must probe kinematic regions of phase space that are closer to the

ones of SM background production.

A summary of results of the ATLAS searches also targeting more complicated decay chains, where e.g. intermediate bosons are produced as well, can be seen in Fig. 89.5 (right). Depending on the topology, the exclusion limit can reach up to ≈ 2 TeV (this value is only reached in gaugino-mediated simplified models [88]). Recent results include a search in two-opposite-sign, same-flavor dilepton final state events [89] targeting squarks decaying through the next-to-lightest neutralino via a slepton or a Z boson and exclude mass up to ≈ 1550 GeV for a massless neutralino. Squarks decaying via charginos and next-to-lightest neutralinos in long decay chains including W and Z bosons are constrained with searches for same-sign dilepton or three-lepton final state events [90]: in this case, masses up to ≈ 1.7 TeV are excluded.

For single light squarks ATLAS also reports results of a dedicated search for pair production of scalar partners of charm quarks [91]. Assuming that the scalar-charm state exclusively decays into a charm quark and a neutralino, scalar-charm masses

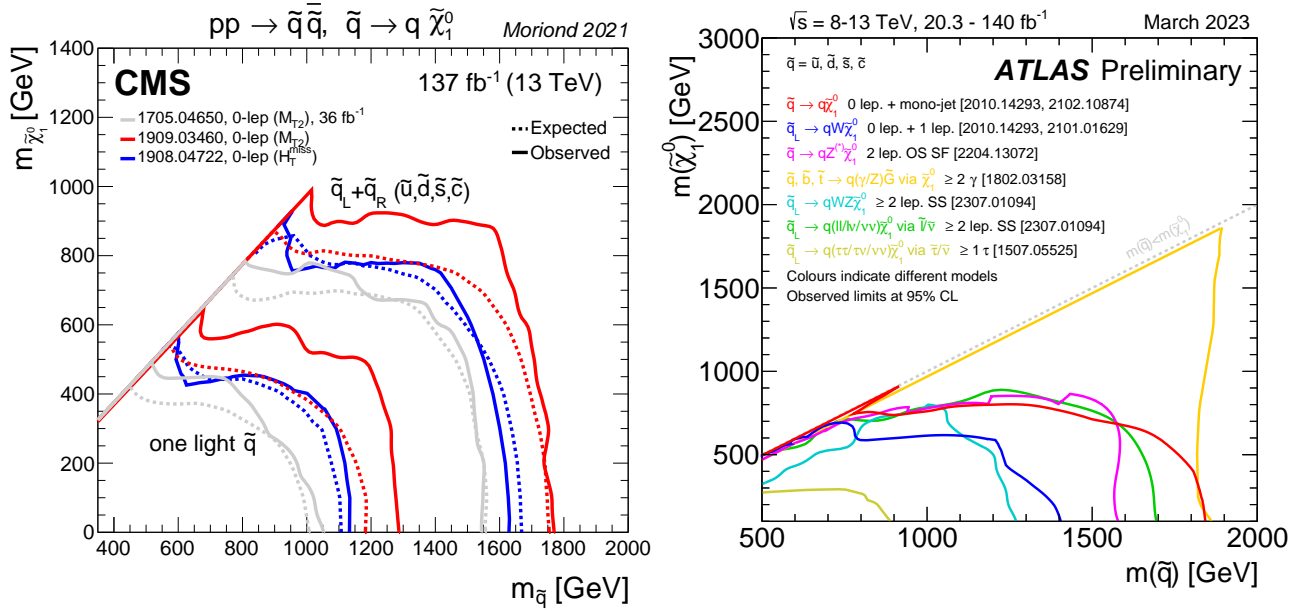


Figure 89.5: Left: 95% C.L. exclusion contours in the framework of simplified models assuming a single decay chain of $\tilde{q} \rightarrow q\tilde{\chi}_1^0$, obtained by the CMS collaboration. Right: Assuming more complicated decay chains including W or Z bosons, obtained by the ATLAS collaboration.

up to 800 GeV are excluded for neutralino masses below 260 GeV.

Table 89.1: Summary of squark mass and gluino mass limits using different interpretation approaches assuming R -parity conservation. Masses in this table are provided in GeV. Further details about the assumptions and analyses from which these limits are obtained are discussed in the corresponding sections of the text.

Model	Assumption	$m_{\tilde{q}}$	$m_{\tilde{g}}$
Simplified models $\tilde{g}\tilde{g}$			
$\tilde{g} \rightarrow q\tilde{q}\tilde{\chi}_1^0$	$m_{\tilde{\chi}_1^0} = 0$	-	≈ 2300
	$m_{\tilde{\chi}_1^0} > \approx 1200$	-	no limit
$\tilde{g} \rightarrow b\tilde{b}\tilde{\chi}_1^0$	$m_{\tilde{\chi}_1^0} = 0$	-	≈ 2440
	$m_{\tilde{\chi}_1^0} > \approx 1600$	-	no limit
$\tilde{g} \rightarrow t\tilde{t}\tilde{\chi}_1^0$	$m_{\tilde{\chi}_1^0} = 0$	-	≈ 2400
	$m_{\tilde{\chi}_1^0} > \approx 1400$	-	no limit
Simplified models $\tilde{q}\tilde{q}$			
$\tilde{q} \rightarrow q\tilde{\chi}_1^0$	$m_{\tilde{\chi}_1^0} = 0$	≈ 1900	-
	$m_{\tilde{\chi}_1^0} > \approx 800$	no limit	-
$\tilde{u}_L \rightarrow q\tilde{\chi}_1^0$	$m_{\tilde{\chi}_1^0} = 0$	≈ 1300	-
	$m_{\tilde{\chi}_1^0} > \approx 600$	no limit	-

A summary of the most important squark and gluino mass limits for different interpretation approaches assuming R -parity conservation is shown in Table 89.1. For gluino masses rather similar limits of about 2.3 – 2.4 TeV are obtained from different model assumptions, indicating that the LHC is indeed probing direct gluino production at the TeV scale and beyond. However, for neutralino masses above approximately 1.2 to 1.6 TeV, even in the best case scenarios, ATLAS and CMS searches do not place any limits on the gluino mass. Limits on direct squark production, on the other hand, depend strongly on the chosen model. For neutralino masses above ≈ 600 GeV no limits on any direct squark pair production scenario are placed by the LHC.

89.6 Exclusion limits on bottom and top squarks masses in RPC scenarios

Besides placing stringent limits on first and second generation squark masses, the LHC experiments also search for the production of third generation squarks. SUSY at the TeV-scale is often motivated by naturalness arguments, most notably as a solution to cancel quadratic divergences in radiative corrections to the Higgs boson mass. In this context, the most relevant terms for SUSY phenomenology arise from the interplay between the masses of the third generation squarks and the Yukawa coupling of the top quark to the Higgs boson. This motivates a potential constraint on the masses of the top squarks and the left-handed bottom squark. Due to the large top quark mass, significant mixing between \tilde{t}_L and \tilde{t}_R is expected, leading to a lighter mass state \tilde{t}_1 and a heavier mass state \tilde{t}_2 . In the MSSM, the lightest top squark (\tilde{t}_1) can be the lightest squark.

Bottom squarks are expected to decay predominantly to $b\tilde{\chi}_1^0$ giving rise to the characteristic multi b -jet and E_T^{miss} signature. Direct production of bottom squark pairs has been searched for at the Tevatron and at the LHC. Limits from the Tevatron are $m_{\tilde{b}} > 247$ GeV for a massless neutralino [92, 93]. ATLAS has set a lower limit of $m_{\tilde{b}} > 1250$ GeV for massless neutralinos in this model [94] exploiting the two b -jets and missing transverse momentum analysis. For $m_{\tilde{\chi}_1^0} \approx 800$ GeV or higher no limit can be placed on direct bottom squark pair production in this simplified model. Limits from CMS are comparable [85]. Reinterpretations of the monojet analysis results can be used to constrain very compressed scenarios, with exclusion of masses up to 550 GeV in case of $\Delta m = m_{\tilde{b}} - m_{\tilde{\chi}_1^0} \approx 5$ GeV [87]. Further bottom squark decay modes have also been searched for by ATLAS [95–97] and CMS [77, 98, 99], for instance targeting more complex decay chains that include Higgs bosons in the cascade.

The top squark decay modes depend on the SUSY mass spectrum, and on the \tilde{t}_L - \tilde{t}_R mixture of the top squark mass eigenstate. If kinematically allowed, the two-body decays $\tilde{t} \rightarrow t\tilde{\chi}_1^0$ (which requires $m_{\tilde{t}} - m_{\tilde{\chi}_1^0} > m_t$) and $\tilde{t} \rightarrow b\tilde{\chi}_1^\pm$ (which requires $m_{\tilde{t}} - m_{\tilde{\chi}_1^\pm} > m_b$) are expected to dominate. If not, the top squark decay may proceed either via the two-body decay $\tilde{t} \rightarrow c\tilde{\chi}_1^0$ or through $\tilde{t} \rightarrow b\tilde{f}'\tilde{\chi}_1^0$ (where f and f' denote a fermion-antifermion pair with appropriate quantum numbers). For $m_{\tilde{t}} - m_{\tilde{\chi}_1^0} > m_b$ the latter decay chain represents a four-body decay with a W boson,

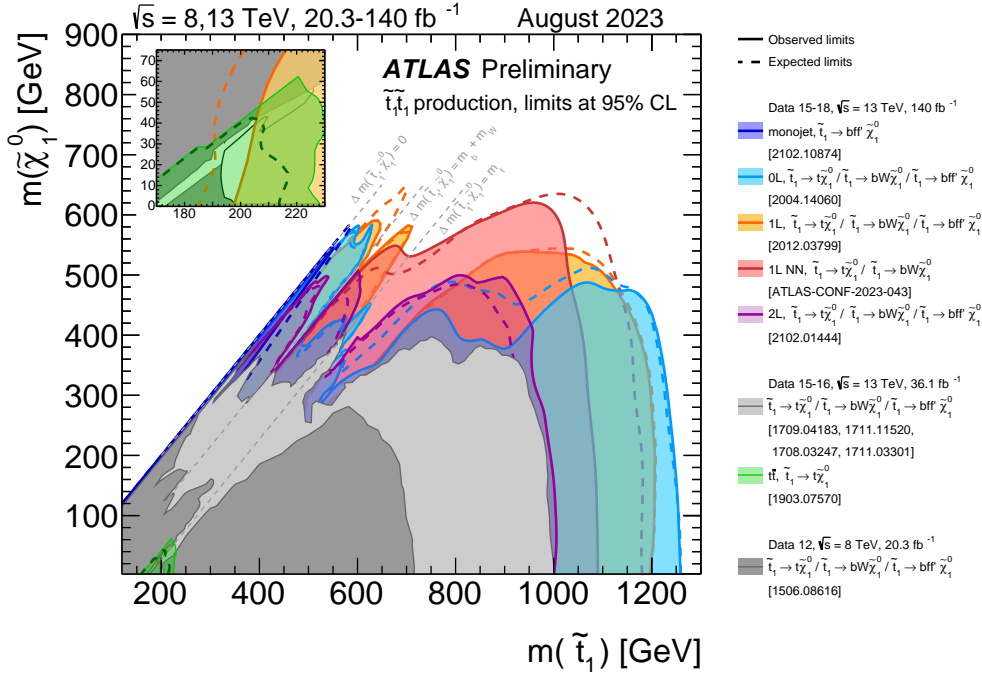


Figure 89.6: A summary of the 95% C.L. exclusion contours in the stop-neutralino mass plane for various possible decay chains, including two-, three- and four-body decays, as obtained in dedicated analyses by ATLAS.

charged Higgs H^\pm , slepton $\tilde{\ell}$, or light flavor squark \tilde{q} , exchange. If the exchanged W boson and/or sleptons are kinematically allowed to be on-shell, the three-body decays $\tilde{t} \rightarrow Wb\tilde{\chi}_1^0$ and/or $\tilde{t} \rightarrow b\nu\tilde{\ell}$ ($\tilde{\nu}\ell$) will become dominant. For further discussion on top squark decays see for example Ref. [100].

Limits from LEP on the \tilde{t}_1 mass are $m_{\tilde{t}} > 96$ GeV in the charm plus neutralino final state, and > 93 GeV in the lepton, b -quark and sneutrino final state [73].

The Tevatron experiments have performed a number of searches for top squarks, often assuming direct pair production. In the $b\tilde{\nu}$ decay channel, and assuming a 100% branching fraction, limits are set as $m_{\tilde{t}} > 210$ GeV for $m_{\tilde{\nu}} < 110$ GeV and $m_{\tilde{t}} - m_{\tilde{\nu}} > 30$ GeV, or $m_{\tilde{t}} > 235$ GeV for $m_{\tilde{\nu}} < 50$ GeV [101, 102]. In the $\tilde{t} \rightarrow c\tilde{\chi}_1^0$ decay mode, a top squark with a mass below 180 GeV is excluded for a neutralino lighter than 95 GeV [103, 104]. In both analyses, no limits on the top squark can be set for heavy sneutrinos or neutralinos. In the $\tilde{t} \rightarrow b\tilde{\chi}_1^\pm$ decay channel, searches for a relatively light top squark have been performed in the dilepton final state [105, 106]. The CDF experiment sets limits in the $\tilde{t} - \tilde{\chi}_1^0$ mass plane for various branching fractions of the chargino decay to leptons and for two values of $m_{\tilde{\chi}_1^\pm}$. For $m_{\tilde{\chi}_1^\pm} = 105.8$ GeV and $m_{\tilde{\chi}_1^0} = 47.6$ GeV, top squarks between 128 and 135 GeV are excluded for W -like leptonic branching fractions of the chargino.

The LHC experiments have improved these limits substantially and developed dedicated searches for all potential top-squark decay mode. This is well depicted in Fig. 89.6, where a summary of the limits on the top squark mass are reported for the single decay chain of $\tilde{t} \rightarrow t\tilde{\chi}_1^0$ as well as for the three-body and four-body decay modes. Interpretations are carried out in simplified models hence care must be taken when interpreting these limits in the context of more complete SUSY models.

The most important searches for the top squark decay topology are dedicated searches requiring zero or one isolated lepton, modest E_T^{miss} , and four or more jets out of which at least one jet must be reconstructed as a b -jet [52, 77, 85, 86, 107–109]. For example, using an all-hadronic analysis, CMS excludes top squarks with masses below about 1300 GeV in this model for light neutralinos, while for $m_{\tilde{\chi}_1^0} > 700$ GeV no limits can be provided [86]. Equivalent constraints are set by the ATLAS all-hadronic search [107].

Analyses targeting final state events characterised by the presence of one lepton (electron or muon) have similar albeit lower sensitivity in the $\tilde{t} \rightarrow t\tilde{\chi}_1^0$ decay mode, see for instance the recent ATLAS result [109] using NN methods.

Single and di-lepton analyses are most sensitive to models where the top squark decay exclusively proceeds via the chargino mediated decay chain $\tilde{t} \rightarrow b\tilde{\chi}_1^\pm, \tilde{\chi}_1^\pm \rightarrow W^{(*)}\tilde{\chi}_1^0$. In this case, top squark mass exclusion limits vary strongly with the assumptions made on the $\tilde{t} - \tilde{\chi}_1^\pm - \tilde{\chi}_1^0$ mass hierarchy. For example, for $m_{\tilde{\chi}_1^\pm} = (m_{\tilde{t}} + m_{\tilde{\chi}_1^0})/2$, a stop mass below ≈ 1150 GeV for a light $\tilde{\chi}_1^0$ is excluded by CMS, while no limit can be placed for $m_{\tilde{\chi}_1^0} > 550$ GeV [52]. These limits, however, can weaken significantly when other assumptions about the mass hierarchy or the decay of the charginos are imposed [52, 110–112].

Other analyses with zero, one or two leptons target this kinematic region [113–119], also providing sensitivity in the case of alternative decay modes of the top squark, *i.e.* including tau sleptons [112, 120–122] or Higgs and Z bosons in the decay chain [123].

If the decays $\tilde{t} \rightarrow t\tilde{\chi}_1^0$ and $\tilde{t} \rightarrow b\tilde{\chi}_1^\pm, \tilde{\chi}_1^\pm \rightarrow W^{(*)}\tilde{\chi}_1^0$ are kinematically forbidden, the decay chains $\tilde{t} \rightarrow Wb\tilde{\chi}_1^0$ and $\tilde{t} \rightarrow c\tilde{\chi}_1^0$ can become important. The one-lepton ATLAS search [108] provides for the kinematic region $m_{\tilde{t}} - m_{\tilde{\chi}_1^\pm} > m_b + m_W$ lower limits on the top squark mass of ≈ 700 GeV for a neutralino lighter than ≈ 570 GeV, as also shown in Fig. 89.6. For the kinematic region in which even the production of real W bosons is not allowed, ATLAS and CMS improve the Tevatron limit on $\tilde{t} \rightarrow c\tilde{\chi}_1^0$ substantially. Based on a monojet analysis [87] ATLAS excludes top squark masses below $m_{\tilde{\chi}_1^0} \approx 550$ GeV along the kinematic boundary for the $\tilde{t} \rightarrow c\tilde{\chi}_1^0$ decay. The ATLAS monojet analysis also places similar boundaries for the other decay chain relevant in this phase region, $\tilde{t} \rightarrow bf\tilde{\chi}_1^0$. Other analyses, such as the search in events with one leptons and jets, are also sensitive to this decay mode: the ATLAS one-lepton analysis excludes up to ≈ 650 GeV for $\Delta m = m_{\tilde{t}} - m_{\tilde{\chi}_1^0} \approx 50$ GeV [108]. The CMS collaboration uses the hadronic searches [86, 114, 116] to place constraints on stop decay into charm-quark and excludes $m_{\tilde{t}} \approx 630$ GeV for $\Delta m = m_{\tilde{t}} - m_{\tilde{\chi}_1^0} \approx 50$ GeV [86]. Constraints are also set in case of

$\tilde{t} \rightarrow b\bar{f}'\tilde{\chi}_1^0$, with CMS excluding masses up to 480 and 700 GeV for $\Delta m = m_{\tilde{t}}, m_{\tilde{\chi}_1^0} \approx 10$ and 80 GeV, respectively [124].

Table 89.2: Summary of bottom and top squark mass limits using different interpretation approaches assuming R -parity conservation. Masses in this table are provided in GeV. Further details about the assumptions and analyses from which these limits are obtained are discussed in the corresponding sections of the text.

Model	Assumption	$m_{\tilde{q}}$
$\tilde{b} \rightarrow b\tilde{\chi}_1^0$	$m_{\tilde{\chi}_1^0} = 0$ $m_{\tilde{\chi}_1^0} > \approx 700$	≈ 1250 no limit
$\tilde{t} \rightarrow t\tilde{\chi}_1^0$	$m_{\tilde{\chi}_1^0} = 0$ $m_{\tilde{\chi}_1^0} > \approx 600$	≈ 1300 no limit
$\tilde{t} \rightarrow b\tilde{\chi}_1^\pm$	$m_{\tilde{\chi}_1^0} = 0$	≈ 1150
$(m_{\tilde{\chi}_1^\pm} = (m_{\tilde{t}} - m_{\tilde{\chi}_1^0})/2)$	$m_{\tilde{\chi}_1^0} > \approx 550$	no limit
$\tilde{t} \rightarrow Wb\tilde{\chi}_1^0$	$m_{\tilde{\chi}_1^0} < \approx 570$	≈ 700
$(m_W < m_{\tilde{t}} - m_{\tilde{\chi}_1^0} < m_t)$		
$\tilde{t} \rightarrow c\tilde{\chi}_1^0$	$m_{\tilde{t}} - m_{\tilde{\chi}_1^0} \approx 50$	≈ 630
	$m_{\tilde{t}} \approx m_{\tilde{\chi}_1^0}$	≈ 550
$\tilde{t} \rightarrow b\bar{f}'\tilde{\chi}_1^0$	$m_{\tilde{t}} - m_{\tilde{\chi}_1^0} \approx 50$	≈ 650
$(m_{\tilde{t}} - m_{\tilde{\chi}_1^0} < m_W)$	$m_{\tilde{t}} \approx m_{\tilde{\chi}_1^0}$	≈ 550

In general, the variety of top squark decay chains in the phase space region where $\tilde{t} \rightarrow t\tilde{\chi}_1^0$ is kinematically forbidden represents a challenge for the experimental search program but more data and refined analyses in Run 2 have further improved the sensitivity in this difficult but important region of SUSY parameter space, and more is expected for future Runs of the LHC. Precision SM measurements can also provide important insights to such challenging regions. For instance, analyses of $t\bar{t}$ spin correlations can be used to set constraints on top squark masses close to the top-quark mass. ATLAS [125] excludes the mass region between 150 and 230 GeV for kinematically allowed values of the neutralino mass. CMS [126] results cover a similar mass range.

89.7 Exclusion limits on the masses of charginos, neutralinos and sleptons in RPC scenarios

Charginos, neutralinos and sleptons are produced through electroweak interactions and their cross sections depend on the assumptions made for mass and mixing parameters.

Charginos and neutralinos carry no color charge and the mixing of the charged wino and higgsino states (for charginos), and the neutral bino, wino and higgsino states (for neutralinos), is determined by a limited number of parameters. For charginos these are the wino mass parameter M_2 , the higgsino mass parameter μ , and $\tan\beta$, and for neutralinos these are the same parameters plus the bino mass parameter M_1 . If one of the parameters M_1 , M_2 or μ is substantially smaller than the others, the chargino/neutralino composition would be dominated by specific states, which are referred to as bino-like ($M_1 \ll M_2, \mu$), wino-like ($M_2 \ll M_1, \mu$), or higgsino-like ($\mu \ll M_1, M_2$). If gaugino mass unification at the GUT scale is assumed, a relation between M_1 and M_2 at the electroweak scale follows: $M_1 = 5/3 \tan^2\theta_W M_2 \approx 0.5M_2$, with θ_W the weak mixing angle. The largest production rates at hadron machines are obtained when the LSP is bino-like and the lightest chargino and next-to-lightest neutralino are wino-like, forming an approximately mass degenerate $SU(2)$ triplet. If the higgsino mass is much smaller than the gaugino masses, the two lightest neutralinos and the lightest chargino form an approximately mass degenerate Dirac $SU(2)$ doublet, production rates are lower and the mass spectrum is compressed.

In models with slepton and gaugino mass unification at the GUT scale, the superpartner of the right-handed lepton, $\tilde{\ell}_R$, is expected to be lighter than the left-handed one, $\tilde{\ell}_L$. Cross sections depend on the L-R mixing which in turn depends on the mass of the fermion and other parameters. For tau sleptons there may

be considerable mixing between the L and R states, leading to a significant mass difference between the lighter $\tilde{\tau}_1$ and the heavier $\tilde{\tau}_2$.

Fig. 89.7 [127, 128] (see also Ref. [74] for further details) shows typical production cross sections at hadron colliders for electroweakinos under various assumptions and considering a center-of-mass energy of 13 TeV. For masses of several hundreds of GeV, they are at least two orders of magnitude smaller than for colored SUSY particles. Thanks to the large data samples collected at the LHC, the sensitivity of LEP and Tevatron searches for direct chargino/neutralino or slepton production has been surpassed in several regions of SUSY parameter space.

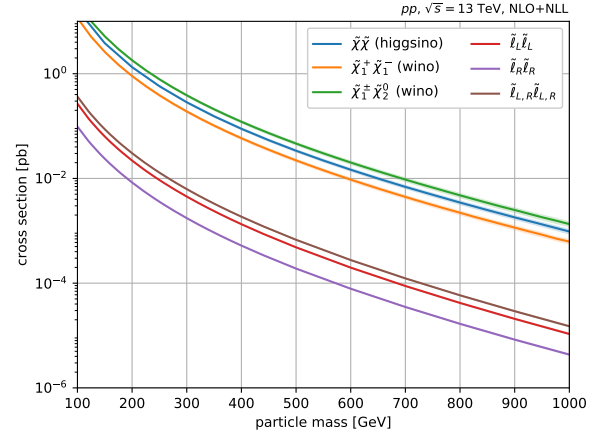


Figure 89.7: Cross sections for pair production of charginos, neutralinos and sleptons calculated for 13 TeV centre-of-mass energy at NLO plus next-to-leading-log (NLL) precision. Wino-like $\tilde{\chi}_1^\pm \tilde{\chi}_2^0$ and $\tilde{\chi}_1^+ \tilde{\chi}_1^-$ productions are calculated in a limit of mass-degenerate $\tilde{\chi}_1^\pm$ and $\tilde{\chi}_2^0$, light bino $\tilde{\chi}_1^0$, and with all the other particles assumed to be heavy and decoupled. Higgsino-like cross sections assume mass-degenerate $\tilde{\chi}_1^\pm$, $\tilde{\chi}_2^0$ and $\tilde{\chi}_1^0$. For slepton pair cross sections, left(right)-handed only or 50% mixed states are considered.

89.7.1 Exclusion limits on chargino masses

The lightest chargino $\tilde{\chi}_1^\pm$ is searched for either considering pair production, or through associated production of $\tilde{\chi}_1^\pm$ and the next-to-lightest neutralino, $\tilde{\chi}_2^0$, if they are assumed to be degenerate in mass. If kinematically allowed, two body decay modes such as $\tilde{\chi}^\pm \rightarrow \bar{f}f'$ (including $\tilde{\nu}\nu$ and $\tilde{\ell}\nu$) are dominant. If not, three-body decays $\tilde{\chi}^\pm \rightarrow f\bar{f}'\tilde{\chi}_1^0$, mediated through virtual W bosons or sfermions, become dominant. If sfermions are heavy, the W mediation dominates, and $f\bar{f}'$ are distributed with branching fractions similar to W decay products (barring phase space effects for small mass gaps between $\tilde{\chi}^\pm$ and $\tilde{\chi}_1^0$). If, on the other hand, sleptons are light enough to play a significant role in the decay, leptonic final states will be enhanced.

At LEP, $\tilde{\chi}_1^+ \tilde{\chi}_1^-$ is the dominant production process. Charginos have been searched for in fully-hadronic, semi-leptonic and fully leptonic decay modes [129, 130]. A general lower limit on the lightest chargino mass of 103.5 GeV is derived, except in corners of phase space with low electron sneutrino mass, where destructive interference in chargino production, or two-body decay modes, play a role. The limit is also affected if the mass difference between $\tilde{\chi}_1^\pm$ and $\tilde{\chi}_1^0$ is small; dedicated searches for such scenarios set a lower limit of 92 GeV.

At the Tevatron, charginos have been searched for via associated production of $\tilde{\chi}_1^\pm \tilde{\chi}_2^0$ [131, 132]. Decay modes involving multilepton final states provide the best discrimination against the large multijet background. Analyses have looked for at least three charged isolated leptons, for two leptons with missing transverse momentum, or for two leptons with the same charge. Depending

on the $(\tilde{\chi}_1^\pm - \tilde{\chi}_1^0)$ and/or $(\tilde{\chi}_2^0 - \tilde{\chi}_1^0)$ mass differences, leptons may have soft transverse momentum.

At the LHC, the search strategy is similar to that at the Tevatron but it also exploits the large datasets collected to target missing momentum and fully-hadronic final states and consider $\tilde{\chi}_1^+ \tilde{\chi}_1^-$ production only i.e. releasing the assumption of $\tilde{\chi}_1^\pm, \tilde{\chi}_2^0$ mass degeneracy. Furthermore, compressed SUSY spectra are searched for considering low-momentum leptons recoiling against an ISR jet.

Chargino pair production is searched for in the dilepton plus missing momentum final state. In a simplified model interpretation of the results where only the $\tilde{\chi}_1^+ \tilde{\chi}_1^-$ process is considered and assuming mediation of the chargino decay by light sleptons (\tilde{e} and $\tilde{\mu}$), ATLAS [133] and CMS [134] set limits on the chargino mass up to 1 TeV for massless LSPs, but no limits on the chargino mass can be set for $\tilde{\chi}_1^0$ heavier than 480 GeV. Limits are fairly robust against variation of the slepton mass, unless the mass gap between sparticles becomes small enough that the charged lepton has a too low-momentum to be reconstructed. For decays mediated through $\tilde{\tau}$ or $\tilde{\nu}_\tau$, limits of 630 GeV are set by ATLAS [135] for LSPs not heavier than 200 GeV. The CMS experiment provides similar limits [136].

In case slepton masses are higher than the mass of the chargino, searches are performed for charginos decaying via a W boson. ATLAS sets limits on this kind of simplified models [133] for pure-wino charginos: masses below 420 GeV are excluded for massless LSPs, but no limits are set for LSPs heavier than 120 GeV. In the challenging case where the difference between chargino and LSP masses is close to that of the W boson, dedicated searches have been carried out by ATLAS [137], excluding chargino masses up to 140 GeV. Searches have also been carried out in the single lepton final state. ATLAS excludes chargino masses between 260 and 520 GeV for a massless LSP [138].

Further extension of the sensitivity in the high-mass region is achieved by ATLAS [139] and CMS [140] exploiting the large branching ratio of fully-hadronic final states and the identification of boosted W bosons through large-radius jets and jet substructure information. Considering only wino-like chargino pair production in case of a massless LSP, ATLAS excludes a region between 630 GeV and 760 GeV, while CMS excludes between 290 GeV and 670 GeV. No limits are set for LSP masses above 200 GeV.

Several final states characterised by the presence of missing transverse momentum are studied to set limits on the chargino mass through $\tilde{\chi}_1^\pm \tilde{\chi}_2^0$ associated production. Usually, wino-like $\tilde{\chi}_1^\pm$ and $\tilde{\chi}_2^0$ and bino-like $\tilde{\chi}_1^0$ are assumed with $m_{\tilde{\chi}_1^\pm} = m_{\tilde{\chi}_2^0}$, leaving $m_{\tilde{\chi}_1^\pm}$ and $m_{\tilde{\chi}_1^0}$ free. Again, the branching fraction of leptonic final states is determined by the slepton masses. If the decay is predominantly mediated by a light $\tilde{\ell}_L$, i.e. $\tilde{\ell}_R$ is assumed to be heavy, the three charged-lepton flavors will be produced in equal amounts, and a multi-lepton signature is favored. It is assumed that $\tilde{\ell}_L$ and sneutrino masses are equal, and diagrams with sneutrinos are included. In this scenario, ATLAS [141] and CMS [142] exclude chargino masses below 1450 GeV for massless LSPs; no limits are set for LSP masses above 1 TeV. If the decay is dominated by a light $\tilde{\ell}_R$, the chargino cannot be a pure wino but needs to have a large higgsino component, preferring the decays to tau leptons. Limits are set in various scenarios. If, like for $\tilde{\ell}_L$, a flavor-democratic scenario is assumed (τ -enriched scenario), CMS sets limits of 1150 GeV on the chargino mass for massless LSPs, but under the assumption that both $\tilde{\chi}_1^\pm$ and $\tilde{\chi}_2^0$ decay leads to tau leptons in the final state (τ -dominated scenario), the chargino mass limit deteriorates to 970 GeV for massless LSPs [142]. ATLAS assumes a simplified model in which staus are significantly lighter than the other sleptons and search for a similar multi-tau final state, setting a lower limit on the chargino mass of 760 GeV in this model [135].

If sleptons are heavy, the chargino is assumed to decay to a W boson plus LSP, and the $\tilde{\chi}_2^0$ into Z plus LSP (WZ searches) or H plus LSP (WH searches). Searches for the WZ channel exploit events with either two same-sign leptons or three leptons, a single

lepton, or with no leptons (all-hadronic). If $\tilde{\chi}_2^0$ decays through a Higgs boson with $m_H = 125$ GeV, search strategies depend on the SM-like Higgs decay modes and branching fractions. Higgs bosons in the final state are identified by either two jets originating from bottom quarks ($h \rightarrow b\bar{b}$), two photons ($h \rightarrow \gamma\gamma$), or leptons from the WW , ZZ or $\tau\tau$ decay modes. Interpretations are also provided in scenarios where the $\tilde{\chi}_2^0$ does not decay exclusively into a Z or H boson and the LSP.

ATLAS has searched for $\tilde{\chi}_1^\pm \tilde{\chi}_2^0$ production in events with three leptons and missing momentum and wino-like chargino masses below 640 GeV are excluded for massless LSPs [143]. Results have also been reported for searches including same-sign lepton signal regions [144] and single lepton searches [138]. Limits are reduced in case of higgsino-like scenarios, with exclusion down to 210 GeV. CMS [142] excludes chargino masses below 650 GeV for massless LSPs using events with two leptons of the same sign, or with three or more leptons targeting final states with W and Z bosons. No constraints are set for $\tilde{\chi}_1^0$ masses above 300 GeV.

Additional constraints on the chargino mass are placed exploiting all-hadronic analyses. A wino-like (higgsino-like) chargino with mass up to 1060 (900) GeV is excluded by ATLAS [139] when the LSP mass is below 400 (240) GeV and the mass splitting is larger than 400 (450) GeV. CMS [140] excludes wino-like charginos with mass up to 970 GeV for massless LSP.

Searches exploiting the presence of b -jets are most sensitive in the high-mass chargino region if $\tilde{\chi}_2^0$ decays through a Higgs boson, while analyses targeting photon pair or leptonic decays provide the best sensitivity in the region of low masses. CMS [145] sets lower limits on the chargino mass up to 820 GeV for massless LSPs, but vanish for LSP masses above 350 GeV using events with at least one lepton and missing transverse momentum in the final state. Similar sensitivity is achieved by the ATLAS analyses [146–148].

In both the wino region (a characteristic of anomaly-mediated SUSY breaking models) and the higgsino region of the MSSM, the mass splitting between $\tilde{\chi}_1^\pm$ and $\tilde{\chi}_1^0$ is small. The chargino decay products are very soft and may escape detection. These compressed spectra are hard to detect, and have triggered dedicated search strategies. ATLAS [149] and CMS [150] have performed searches for charginos and neutralinos in a compressed mass spectrum using initial state radiation and two or three low-momentum (soft) leptons. For wino-like charginos, assuming degenerate $\tilde{\chi}_1^\pm$ and $\tilde{\chi}_2^0$, exclusion contours in the chargino-mass versus $\Delta m(\tilde{\chi}_1^\pm - \tilde{\chi}_1^0)$ plane are derived. As an example, such charginos are excluded by CMS (ATLAS) below 280 (240) GeV for $\Delta m(\tilde{\chi}_1^\pm - \tilde{\chi}_1^0) = 10$ GeV. Considering the higgsino model, the masses probed by CMS reach up to 215 GeV for a mass difference of 7.5 GeV and 150 GeV in the highly compressed region with a mass difference of 3 GeV. CMS has also searched for chargino-pair production through vector-boson-fusion [151], also targeting compressed mass spectra. Assuming degenerate $\tilde{\chi}_1^\pm$ and $\tilde{\chi}_2^0$, charginos with a mass below 112 GeV are excluded for $\Delta m(\tilde{\chi}_1^\pm - \tilde{\chi}_1^0) = 1$ GeV. CMS has published further searches for such compressed spectra with a soft tau lepton [152].

89.7.2 Exclusion limits on neutralino masses

In a considerable part of the MSSM parameter space, and in particular when demanding that the LSP carries no electric or color charge, the lightest neutralino $\tilde{\chi}_1^0$ is the LSP. If R -parity is conserved, such a $\tilde{\chi}_1^0$ is stable. Since it is weakly interacting, it will typically escape detectors unseen. Limits on the invisible width of the Z boson apply to neutralinos with a mass below 45.5 GeV, but depend on the Z -neutralino coupling. Such a coupling could be small or even absent; in such a scenario there is no general lower limit on the mass of the lightest neutralino [153]. In models with gaugino mass unification and sfermion mass unification at the GUT scale, a lower limit on the neutralino mass is derived from limits from direct searches, notably for charginos and sleptons, and amounts to 47 GeV [154]. Assuming a constrained model like the CMSSM, this limit increases to 50 GeV at LEP; however the strong constraints now set by the LHC increase such CMSSM-derived $\tilde{\chi}_1^0$ mass limits to well above a few hundred GeV (the latest reinterpretation only uses Run 1 data and indicates 200 GeV [155–

157]).

In gauge-mediated SUSY breaking models (GMSB), the LSP is typically a gravitino, and the phenomenology is determined by the nature of the next-to-lightest supersymmetric particle (NLSP). A NLSP neutralino will decay to a gravitino and a SM particle whose nature is determined by the neutralino composition. Final states with two high p_T photons and missing momentum are searched for, and interpreted in gauge mediation models with bino-like neutralinos [158–164].

Assuming the production of at least two neutralinos per event, neutralinos with large non-bino components can also be searched for by their decay in final states with missing momentum plus any two bosons out of the collection γ, Z, H . A number of searches at the LHC have tried to cover the rich phenomenology predicted by the general gauge mediation model (GGM) where $\tilde{\chi}_1^0$ might decay with various BR in the Z and H decay modes [98, 147, 161, 165–175]. As an example, strong constraints for decay modes involving Z and H bosons arise from full-hadronic searches on higgsino-like scenarios: ATLAS [139] excludes higgsino production with decays into a massless gravitino LSP in a mass range between 450 (500) GeV and 940 (850) GeV assuming BR = 1 (0.5) for the Z plus gravitino decay mode. Assuming only H plus gravitino decays, CMS [176] excludes a higgsino mass range between 175 GeV and 1025 GeV. Assuming a mix of γ, Z, H decays, a CMS search [164] in the photonic final state excludes higgsinos up to 1.05 TeV.

Heavier neutralinos, in particular $\tilde{\chi}_2^0$, have been searched for in their decays to the lightest neutralino plus a γ , a Z boson or a Higgs boson. Limits on electroweak production of $\tilde{\chi}_2^0$ plus $\tilde{\chi}_1^\pm$ from all-hadronic, same-sign dilepton and trilepton analyses have been discussed in the section on charginos; the assumption of equal mass of $\tilde{\chi}_2^0$ and $\tilde{\chi}_1^\pm$ make the limits on chargino masses apply to $\tilde{\chi}_2^0$ as well. Multilepton analyses have also been used to set limits on $\tilde{\chi}_2^0 \tilde{\chi}_3^0$ production; assuming equal mass and decay through light sleptons, limits are set up to 680 GeV for massless LSPs [177]. Again, compressed spectra with small mass differences between the heavier neutralinos and the LSP form the most challenging region.

In $\tilde{\chi}_2^0$ decays to $\tilde{\chi}_1^0$ and a lepton pair, the lepton pair invariant mass distribution may show a structure that can be used to measure the $\tilde{\chi}_2^0 - \tilde{\chi}_1^0$ mass difference in case of a signal [38]. This structure, however, can also be used in the search strategy itself, as demonstrated by ATLAS [178, 179] and CMS [98, 180].

Fig. 89.8 summarizes some of the most recent results from ATLAS and CMS for chargino pair or chargino and next-to-lightest neutralino pair productions comparing results obtained with various assumptions. The limits on weak gauginos in simplified models are also summarized in Table 89.3. Only results for promptly decaying charginos and neutralinos are included: limits from searches focusing on long-lived particle scenarios are reported in Section 89.9. A combination of several searches for the electroweak production of winos, binos, higgsinos, and sleptons has also been recently presented by CMS [181].

Interpretations of the search results outside simplified models, such as in the phenomenological MSSM [182–187], show that the simplified model limits can translate into accurate constraints but must also be interpreted with care. Electroweak gauginos in models that are compatible with the relic density of dark matter in the Universe, for example, have particularly tuned mixing parameters and mass spectra, which are not always captured by the simplified models used.

89.7.3 Exclusion limits on slepton masses

The most model-independent searches for selectrons, smuons and staus originate from the LEP experiments [188]. Smuon production only takes place via s -channel γ^*/Z exchange. Search results are often quoted for $\tilde{\mu}_R$, since it is typically lighter than $\tilde{\mu}_L$ and has a weaker coupling to the Z boson; limits are therefore conservative. Decays are expected to be dominated by $\tilde{\mu}_R \rightarrow \mu \tilde{\chi}_1^0$, leading to two non-back-to-back muons and missing momentum. Slepton mass limits are calculated in the MSSM under the assumption of gaugino mass unification at the GUT scale, and depend on the mass difference between the smuon and $\tilde{\chi}_1^0$. A $\tilde{\mu}_R$

Table 89.3: Summary of weak gaugino mass limits in simplified models, assuming R -parity conservation. Masses in the table are provided in GeV. Further details about assumptions and corresponding analyses are discussed in the text. Details on constraints for compressed scenarios from soft-lepton searches are not represented in the table.

Assumption	m_χ
$\tilde{\chi}_1^\pm$, all $\Delta m(\tilde{\chi}_1^\pm, \tilde{\chi}_1^0)$	> 92
$\tilde{\chi}_1^\pm$ $\Delta m > 5$, $m_{\tilde{\nu}} > 300$	> 103.5
$\tilde{\chi}_1^\pm$, $m_{(\tilde{\ell}, \nu)} = (m_{\tilde{\chi}_1^\pm} + m_{\tilde{\chi}_1^0})/2$	
$m_{\tilde{\chi}_1^0} \approx 0$	> 1000
$\tilde{\chi}_1^\pm$, $m_{\tilde{\chi}_1^0} > 480$	no LHC limit
$\tilde{\chi}_1^\pm$, $m_{\tilde{\ell}} > m_{\tilde{\chi}_1^\pm}$	
$m_{\tilde{\chi}_1^0} \approx 0$	> 420 and 290 – 760
$\tilde{\chi}_1^\pm$, $m_{\tilde{\chi}_1^0} > 120$	no LHC limit
$m_{\tilde{\chi}_1^\pm} = m_{\tilde{\chi}_2^0}$, $m_{\tilde{\ell}_L} = (m_{\tilde{\chi}_1^\pm} + m_{\tilde{\chi}_1^0})/2$	
$m_{\tilde{\chi}_1^0} \approx 0$	> 1450
$m_{\tilde{\chi}_1^0} > 1000$	no LHC limit
$m_{\tilde{\chi}_1^\pm} = m_{\tilde{\chi}_2^0}$, $m_{\tilde{\ell}_R} = (m_{\tilde{\chi}_1^\pm} + m_{\tilde{\chi}_1^0})/2$	flavor-democratic
$m_{\tilde{\chi}_1^0} \approx 0$	> 1150
$m_{\tilde{\chi}_1^0} > 700$	no LHC limit
$m_{\tilde{\chi}_1^\pm} = m_{\tilde{\chi}_2^0}$, $m_{\tilde{\tau}} = (m_{\tilde{\chi}_1^\pm} + m_{\tilde{\chi}_1^0})/2$	$\tilde{\tau}$ -dominated
$m_{\tilde{\chi}_1^0} \approx 0$	> 970
$m_{\tilde{\chi}_1^0} > 450$	no LHC limit
$m_{\tilde{\chi}_1^\pm} = m_{\tilde{\chi}_2^0}$, $m_{\tilde{\ell}} > m_{\tilde{\chi}_1^\pm}$, $\text{BF}(WZ) = 1$	
$m_{\tilde{\chi}_1^0} \approx 0$	> 960
$m_{\tilde{\chi}_1^0} > 300$	no LHC limit
$m_{\tilde{\chi}_1^\pm} = m_{\tilde{\chi}_2^0}$, $m_{\tilde{\ell}} > m_{\tilde{\chi}_1^\pm}$, $\text{BF}(WH) = 1$	
$m_{\tilde{\chi}_1^0} \approx 0$, wino-like $\tilde{\chi}_1^\pm$	> 1060
$m_{\tilde{\chi}_1^0} \approx 0$, higgsino-like $\tilde{\chi}_1^\pm$	> 900
$m_{\tilde{\chi}_1^0} > 400(240)$	no LHC limit wino(higgsino)-like

with a mass below 94 GeV is excluded for $m_{\tilde{\mu}_R} - m_{\tilde{\chi}_1^0} > 10$ GeV. The selectron case is similar to the smuon case, except that an additional production mechanism is provided by t -channel neutralino exchange. The \tilde{e}_R lower mass limit is 100 GeV for $m_{\tilde{\chi}_1^0} < 85$ GeV. Due to the t -channel neutralino exchange, $\tilde{e}_R \tilde{e}_L$ pair production was possible at LEP, and a lower limit of 73 GeV was set on the selectron mass regardless of the neutralino mass by scanning over MSSM parameter space [189]. The potentially large mixing between $\tilde{\tau}_L$ and $\tilde{\tau}_R$ not only makes the $\tilde{\tau}_1$ light, but can also make its coupling to the Z boson small. LEP lower limits on the $\tilde{\tau}$ mass range between 87 and 93 GeV depending on the $\tilde{\chi}_1^0$ mass, for $m_{\tilde{\tau}} - m_{\tilde{\chi}_1^0} > 7$ GeV [188].

At the LHC, pair production of sleptons is not only heavily suppressed with respect to pair production of colored SUSY particles but the cross section is also almost two orders of magnitude smaller than the one of pair production of charginos and neutralinos. With the full data sets of Run 1 and Run 2, however, ATLAS and CMS have surpassed the sensitivity of the LEP analyses under certain assumptions.

ATLAS and CMS have searched for direct production of selectron pairs and smuon pairs at the LHC, with each slepton decaying to its corresponding SM partner lepton and the $\tilde{\chi}_1^0$ LSP. In simplified models, ATLAS [133] and CMS [180] set lower mass limits on sleptons of 700 GeV for degenerate $\tilde{\ell}_L$ and $\tilde{\ell}_R$, for a massless $\tilde{\chi}_1^0$ and assuming equal selectron and smuon masses, as shown in Fig. 89.9. The limits deteriorate with increasing $\tilde{\chi}_1^0$ mass due to decreasing missing momentum and lepton momentum. As a consequence, no limits are set for $\tilde{\chi}_1^0$ masses above 400 GeV. Limits are also derived without the assumption of slepton mass degeneracy [133, 190]. A dedicated search for sleptons with small mass difference between $\tilde{\ell}$ and $\tilde{\chi}_1^0$ is performed by ATLAS [149] demanding

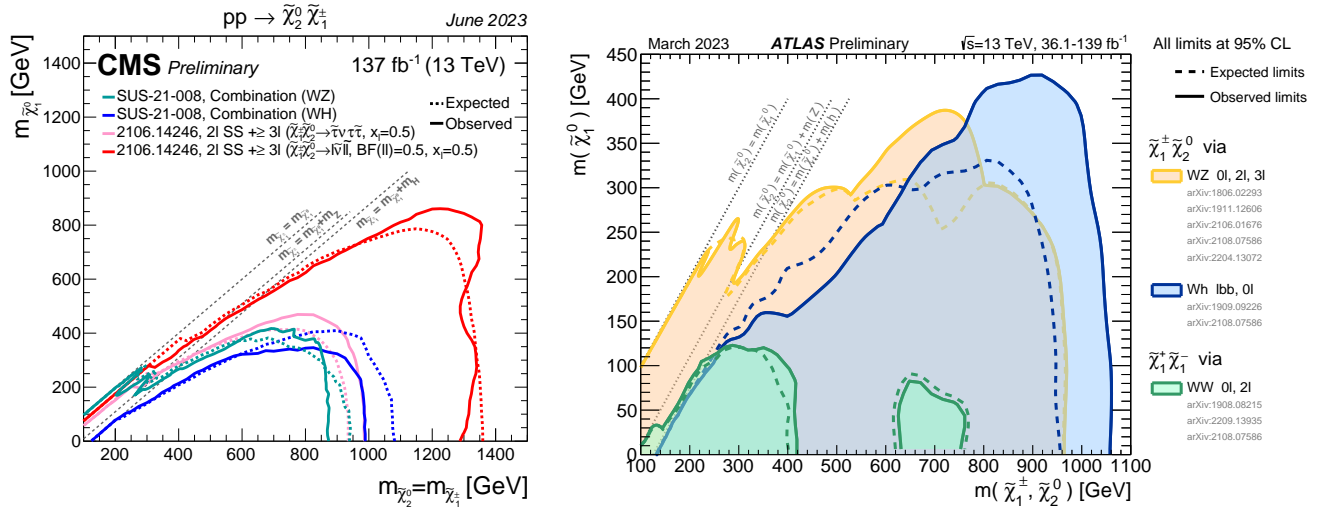


Figure 89.8: LHC exclusion limits on chargino and neutralino masses in a number of simplified models. Left: CMS limits on chargino and neutralino masses for pair production of charginos, pair production of heavier neutralinos, or pair production of chargino and neutralino, under a variety of assumptions including light sleptons mediating the decays. Right: ATLAS limits on chargino and neutralino masses for pair production of chargino and neutralino, under the assumption of decoupled sleptons, and chargino/neutralino decay through on- or off-shell W and Z or H .

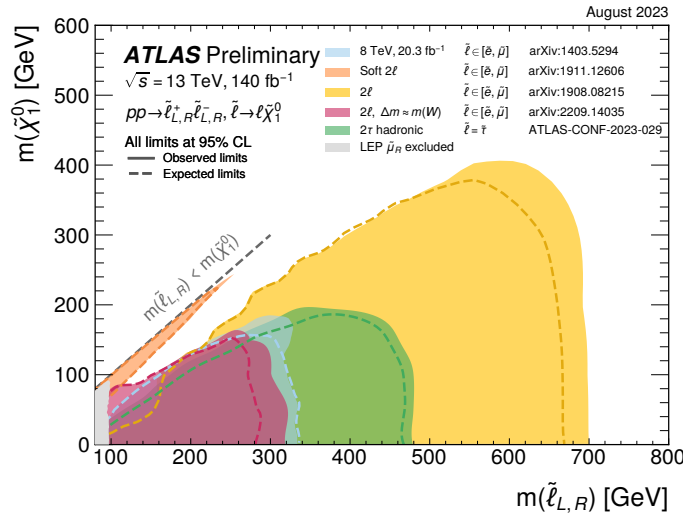


Figure 89.9: LHC exclusion limits on slepton (selectron, smuon and stau) masses, assuming equal masses of selectrons and smuons, degeneracy of $\tilde{\ell}_L$ and $\tilde{\ell}_R$, and a 100% branching fraction for $\tilde{\ell} \rightarrow \ell \tilde{\chi}_1^0$.

the presence of ISR jets. Although no sensitivity is achieved for intermediate mass differences between the slepton and the LSP, slepton masses up to 260 GeV are excluded for slepton-LSP mass differences of 10-20 GeV. ATLAS [137] followed up with a dedicated search in the challenging regime where the mass difference between the slepton and the LSP is close to the W mass. Sleptons with masses up to 150 GeV are excluded for a mass-splitting between the sleptons and the LSP of 50 GeV.

ATLAS and CMS have also searched for $\tilde{\tau}$ -pair production. In simplified models, ATLAS excludes $\tilde{\tau}$ masses between 120 and 390 GeV assuming light $\tilde{\chi}_1^0$, combining the production of degenerate left- and right-handed $\tilde{\tau}$ s [191]. The CMS analysis [192] covers lower masses and closes the mass gap with LEP. In a search for hadronic final states, CMS [193] excludes purely left-handed $\tilde{\tau}$ s with masses between 115 and 340 GeV for massless LSP. A recent ATLAS search [194] for stau pair production in the fully hadronic final state excludes, for a massless LSP, degenerate left- and right-handed $\tilde{\tau}$ s with masses up to 480 GeV, purely left-handed $\tilde{\tau}$ s with masses up to 410 GeV and purely right-handed $\tilde{\tau}$ s with masses up

to 330 GeV.

In gauge-mediated SUSY breaking models, sleptons can be (co-)NLSPs, *i.e.*, the next-to-lightest SUSY particles and almost degenerate in mass, decaying to a lepton and a gravitino. This decay can either be prompt, or the slepton can have a non-zero lifetime. Combining several analyses, lower mass limits on $\tilde{\mu}_R$ of 96.3 GeV and on $\tilde{\tau}_R$ of 66 GeV are set for all slepton lifetimes at LEP [195]. In a considerable part of parameter space in these models, the $\tilde{\tau}$ is the NLSP. The LEP experiments have set lower limits on the mass of such a $\tilde{\tau}$ between 87 and 97 GeV, depending on the $\tilde{\tau}$ lifetime. ATLAS and CMS have searched for final states with τ s, jets and missing transverse momentum, and have interpreted the results in GMSB models setting limits on the model parameters [196, 197]. CMS has interpreted a multilepton analysis in terms of limits on gauge mediation models with slepton NLSP [198]. CDF has put limits on gauge mediation models at high $\tan\beta$ and slepton NLSP using an analysis searching for like-charge light leptons and taus [199].

The invisible width of the Z boson puts a lower limit on the

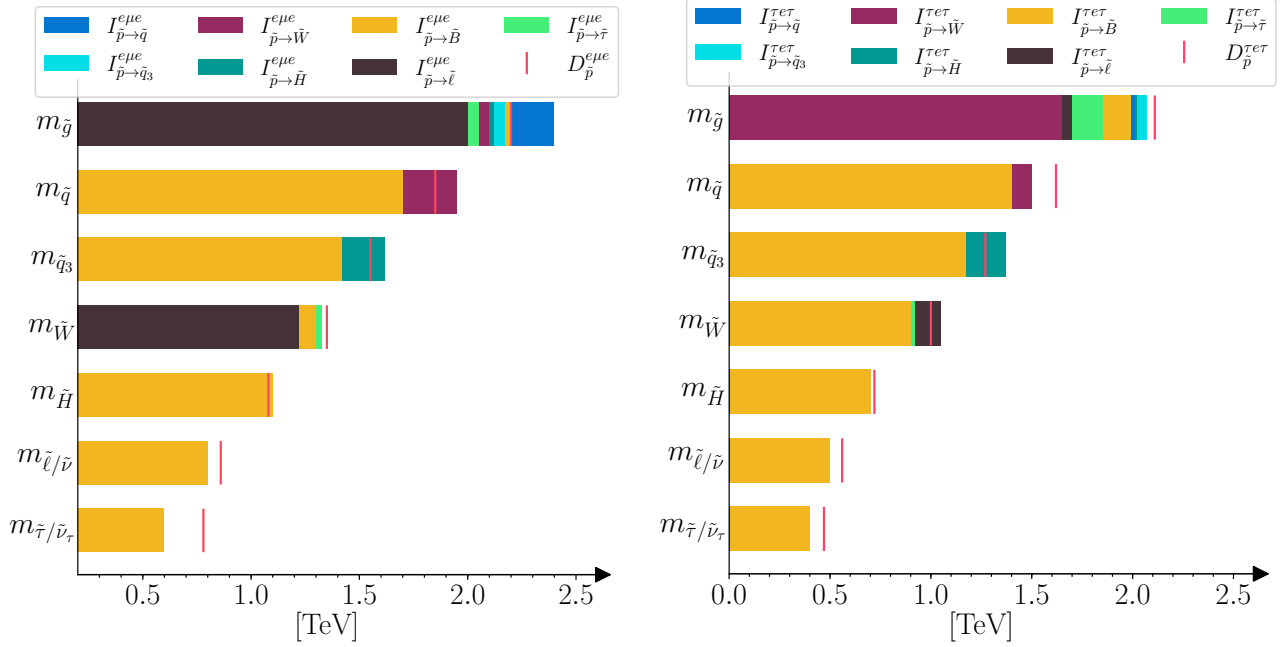


Figure 89.10: Summary of 95% C.L. limits on sparticle masses in RPV models, for λ_{121} (left), and for λ_{313} (right). The vertical red line represents the direct production mass bound when the sparticle under consideration is the LSP.

sneutrino mass of about 45 GeV. Tighter limits are derived from other searches, notably for gauginos and sleptons, under the assumption of gaugino and sfermion mass universality at the GUT scale, and amount to approximately 94 GeV in the MSSM [200].

The limits on sleptons in simplified models are summarized in Table 89.4.

Table 89.4: Summary of slepton mass limits from LEP and LHC, assuming R -parity conservation and 100% branching fraction for $\tilde{\ell} \rightarrow \ell \tilde{\chi}_1^0$. Masses in this table are provided in GeV.

Assumption	$m_{\tilde{\ell}}$
$\tilde{\mu}_R, \Delta m(\tilde{\mu}_R, \tilde{\chi}_1^0) > 10$	> 94
$\tilde{e}_R, \Delta m(\tilde{e}_R, \tilde{\chi}_1^0) > 10$	> 94
$\tilde{e}_R, \text{any } \Delta m$	> 73
$\tilde{\tau}_R, \Delta m(\tilde{\tau}_R, \tilde{\chi}_1^0) > 7$	> 87
$\tilde{\nu}_e, \Delta m(\tilde{e}_R, \tilde{\chi}_1^0) > 10$	> 94
$m_{\tilde{e}_{L,R}} = m_{\tilde{\mu}_{L,R}}, m_{\tilde{\chi}_1^0} \approx 0$	> 700
$m_{\tilde{\chi}_1^0} \gtrsim 400$	no LHC limit
$m_{\tilde{\tau}_L} = m_{\tilde{\tau}_R}, m_{\tilde{\chi}_1^0} \approx 0$	> 480
$m_{\tilde{\chi}_1^0} \gtrsim 200$	no LHC limit
$m_{\tilde{\tau}_L}, m_{\tilde{\chi}_1^0} \approx 0$	> 410
$m_{\tilde{\chi}_1^0} \gtrsim 150$	no LHC limit
$m_{\tilde{\tau}_R}, m_{\tilde{\chi}_1^0} \approx 0$	> 330
$m_{\tilde{\chi}_1^0} \gtrsim 100$	no LHC limit

89.8 Exclusion limits on promptly decaying sparticle masses in RPV scenarios

The large variety of possible configurations for non-zero λ , λ' and λ'' couplings in RPV SUSY scenarios leads to a huge number of potential signatures to be investigated in the strong and electroweak sectors. The lightest supersymmetric particle can be any particle, although most of the models considered at the LHC assume that to be the lightest neutralino, and can decay promptly or displaced. Cascade decays of sparticles down to the LSP can also be prompt or displaced depending on the strength of the couplings involved, although typically such cascades are dominated by gauge couplings which are prompt. In this section,

we review dedicated searches for scenarios with small non-zero RPV couplings but still large enough to allow prompt decays of the sparticles involved (see Section 89.9 for examples of dedicated signatures searches for non-prompt decays).

Prompt RPV gluino and squark decays are searched for in final states generally characterised by the presence of multiple leptons or jets and moderate or no missing transverse momentum.

Searches in multilepton final states [90, 166, 201–205] set lower gluino mass limits between 1 and 2.5 TeV for decays mediated by λ and λ' couplings, with strong dependence on the couplings involved, the neutralino mass and the lepton flavor. Multijet final states have been used to search for fully hadronic gluino decays involving λ'' couplings, by CDF [206], ATLAS [96, 207–210] and CMS [211–213]. Lower gluino mass limits range between 600 and 2000 GeV depending on neutralino mass and flavor content of the final state. ATLAS [214] also searched in events characterised by high jet multiplicity, at least one isolated light lepton and either zero or at least three b -tagged jets, reaching as high as 2.4 TeV in gluino mass. If gluinos decay via top squark into tbd final states through a non-zero λ''_{313} coupling, a search for same-sign/three-lepton events can be effective. ATLAS [90] sets a lower limit of 1.65 TeV for a top squark with a mass below 1.45 TeV.

RPV production of single squarks via a λ' -type coupling has been studied at HERA. In such models, a lower limit on the squark mass of the order of 275 GeV has been set for electromagnetic-strength-like couplings $\lambda' = 0.3$ [215]. At the LHC, prompt [202, 205, 216] R -parity violating squark decays have been searched for, with mass limits very model-dependent.

Dedicated searches for RPV top squarks (at production and/or in decays) have been carried out in the past decades. Production of single top squarks has been searched for at LEP, HERA, and the Tevatron. For example, an analysis from the ZEUS collaboration [217] makes an interpretation of its search result assuming top squarks to be produced via a λ' coupling and decay either to $b\tilde{\chi}_1^\pm$ or R -parity-violating to a lepton and a jet. Limits are set on λ'_{131} as a function of the top squark mass in a MSSM framework with gaugino mass unification at the GUT scale. CMS and ATLAS have performed several searches for top squarks using a variety of multilepton and/or multijet final states and Run 2 data. The λ' -mediated top squark decay $\tilde{t} \rightarrow b\ell$ has been studied by ATLAS for prompt decays [218], and by ATLAS and CMS for non-prompt decays [219–221], setting limits up to 1.4–1.6 TeV in simplified models for this mode. CMS also searched for the λ' -mediated

decay $\tilde{t} \rightarrow blqq$, setting lower stop mass limits of 890 GeV (e) or 1000 GeV (μ) [222]. The fully hadronic R -parity violating top squark decays $\tilde{t} \rightarrow bs$, $\tilde{t} \rightarrow ds$, and $\tilde{t} \rightarrow bd$, involving λ'' , have been searched for by ATLAS [202, 208, 223–225], and CMS [226, 227]. Other recent searches target top squarks decaying through cascades into several b - and light-quarks, for example as in [228]. The most recent results set lower top squark mass limits up to 1.35 TeV in top-squark mass [214] if decays include top- and b -quarks [214] lower top squark mass limits are up to 1.35 TeV in top-squark mass. Constraints on masses up to 670 GeV are found if the top squarks decays include top- and light-quarks [229].

Various searches for multi-lepton and lepton plus jets events are interpreted in a model with RPV decays of charginos and neutralinos (including the LSP) involving a non-zero λ [166, 201, 205] or λ' [202, 210, 230, 231] coupling. Neutralino decays involving non-zero λ'' lead to fully hadronic final states, and searches for multi-jet events and jet-pair resonances are used to set limits, typically on the production of colored particles like top squarks or gluinos, which are assumed to be the primary produced sparticles in these interpretations, as discussed earlier. For instance, the ATLAS search [214] in events with one lepton and high jet multiplicity excludes up to 320 (365) GeV in higgsino (wino) masses. If top quarks arise in the decay of the neutralino, lepton-enriched final state events are also relevant, see for example preliminary results in [144]. The multilepton search in [232] set limits on the production of charginos and neutralinos for a minimal SUSY model with an approximate $B - L$ symmetry. In this case, charginos and neutralinos with masses between 100 GeV and 1.1 TeV are excluded depending on the assumed decay BR into a lepton plus a W, Z or H boson. Finally, recent results from ATLAS [144] set the first experimental constraints on bilinear RPV models (bRPV) with degenerate higgsino masses exploiting same-sign/three-lepton signatures, excluding masses smaller than 440 GeV.

Limits also exist on sleptons in RPV models, both from LEP and the Tevatron experiments. From LEP, lower limits on $\tilde{\mu}_R$ and \tilde{e}_R masses in such models are 97 GeV, and the limits on the stau mass are very close: 96 GeV [233]. CMS has searched for resonant smuon production in a modified CMSSM scenario [234], putting limits on λ'_{211} as a function of $m_0, m_{1/2}$. Production of pairs of sneutrinos in R -parity violating models has been searched for at LEP [233]. Assuming fully leptonic decays via λ -type couplings, lower mass limits between 85 and 100 GeV are set. At the Tevatron [235, 236] and at the LHC [234, 237–239], searches have focused on scenarios with resonant production of a sneutrino decaying to $e\mu, \mu\tau$ and $e\tau$ final states. Limits have been set on sneutrino masses as a function of the value of relevant RPV couplings. As an example, the LHC experiments exclude a resonant tau sneutrino with a mass below 3.9 TeV for $\lambda_{312} = \lambda_{321} > 0.07$ and $\lambda'_{311} > 0.11$ [240].

Formulating a general assessment of the existing bounds on RPV SUSY models is becoming increasingly important in order to evaluate loopholes and potential new search directions. A classification of all potential RPV signatures at the LHC for small couplings has been recently published [241] to evaluate the coverage of the most general RPV-MSSM setup, without making any assumptions about the sparticle spectrum details. Small RPV couplings imply that sparticles are pair-produced at the LHC as in the RPC-MSSM case. Figure 89.10 shows a summary of the 95% C.L. limits on sparticle masses in RPV models for two types of λ couplings, compared to the direct production mass bound when the sparticle under consideration is the LSP. This is done to quantify the impact of possible assumptions made on the nature, mass and coupling choices for the LSP which in turn might lead to different leptons, jets and top-quark multiplicities. As underlined in [241], changes in exclusion limits on sparticle masses are at most around 20%.

Finally, RPV signatures are often similar to signatures of Stealth SUSY [242–244]. In these scenarios, squarks can decay to a quark and a chargino (neutralino), which can subsequently decay to a singlino \tilde{S} and a W^\pm (photon), with the \tilde{S} decaying to two gluons and a soft gravitino \tilde{G} . Dedicated CMS searches [245, 246] exclude squark masses up to 1.85 TeV in the photon channel and up to 550 GeV in the charged lepton channel. Gluino masses up

to 2.1 TeV are excluded in the di-photon channel [246]. Limits have also been placed on top squarks in stealth SUSY scenarios, where the top squark decays to a top quark, a gluon and a \tilde{S} , and the \tilde{S} subsequently decays to a \tilde{G} and two gluons. In such a scenario, top squark masses up to 870 GeV have been excluded by CMS [229].

89.9 Exclusion limits on long-lived particles

Long-lived sparticles arise in many different SUSY models. In particular in co-annihilation scenarios, where the NLSP and LSP are nearly mass-degenerate, this is rather common in order to obtain the correct Dark Matter relic density. Prominent examples are scenarios featuring stau co-annihilation, or models of SUSY breaking, e.g. minimal anomaly-mediated SUSY breaking (AMSB), in which the appropriate Dark Matter density is obtained by co-annihilation of the LSP with an almost degenerate long-lived wino. R -parity violating SUSY models might also lead to non-prompt decays. Searches for events with a displaced hadronic vertex, with or without a matched lepton, are for instance interpreted in a model with RPV neutralino decays involving a non-zero λ' coupling [231]. However, in general, other sparticles can also be long-lived and it is desirable to establish a comprehensive search program for these special long-lived cases, which lead to distinct experimental search signatures. Past experiments have performed dedicated searches for long-lived SUSY signatures, but given the absence of any experimental evidence for SUSY so far, more effort and focus has gone into such searches at the LHC recently. Signatures interpreted in terms of SUSY models include disappearing tracks, identification of tracks with atypical properties or unusual ionization, small and localized deposits of energy inside of the calorimeters without associated tracks, or stopped particles that decay out of time with collisions. Some examples are reported below with interpretations provided for gluinos, squarks and electroweak SUSY particles in a variety of SUSY models.

If the decay of gluinos is suppressed, for example if squark masses are high, gluinos may live longer than typical hadronization times. It is expected that such gluinos will hadronize to long-living strongly interacting particles known as R-hadrons. In particular, if the suppression of the gluino decay is strong, as in the case that the squark masses are much higher than the TeV scale, these R-hadrons can be (semi-)stable in collider timescales. Searches for such R-hadrons exploit the typical signature of stable charged massive particles in the detector. R-hadrons decaying in the detector are searched for using dE/dx measurements and searches for displaced vertices. As shown in the left plot of Fig. 89.11, the ATLAS experiment excludes semi-stable gluino R-hadrons with masses below 1.9 – 2.3 TeV for all lifetimes in a simplified model where such gluinos always form R-hadrons, and decay into jets and a light neutralino, by combining a number of analyses [208, 247–250]. A combination of CMS searches for long-lived particles, as shown in Fig. 89.12, reaches similar limits [251–255].

Alternatively, since such R-hadrons are strongly interacting, they may be stopped in the calorimeter or in other material, and decay later into energetic jets. These decays are searched for by identifying the jets [256–258] or muons [258] outside the time window associated with bunch-bunch collisions. As shown in Fig. 89.12, the CMS collaboration sets limits on such stopped R-hadrons over 13 orders of magnitude in gluino lifetime, up to masses of 1390 GeV [258]. Recent results from ATLAS [259] sets constraint on the mass of gluino R-hadrons using large out-of-time energy deposits in the calorimeters. Also in this case, masses of up to 1.4 TeV are excluded for gluino lifetimes of $10^{-5} - 10^3$ s.

Top squarks can also be long-lived and hadronize to a R-hadron, for example in the scenario where the top squark is the next-to-lightest SUSY particle, with a small mass difference to the LSP. Searches for massive stable charged particles are sensitive to such top squarks. Tevatron limits are approximately $m_{\tilde{t}} > 300$ GeV [260, 261]. ATLAS sets a limit of 1340 GeV on such top squarks [249], the CMS limits are comparable [253]. Intermediate lifetimes of top squarks decaying through RPV coupling into a quark and a lepton are also targeted by ATLAS and CMS. Limits on top squarks decaying into a quark and a muon

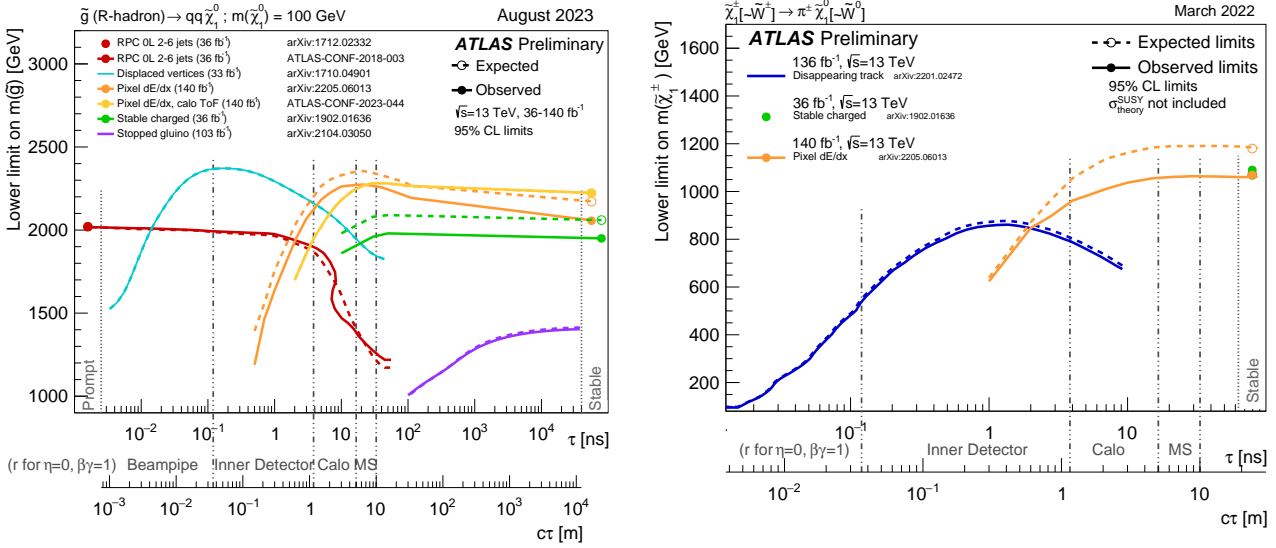
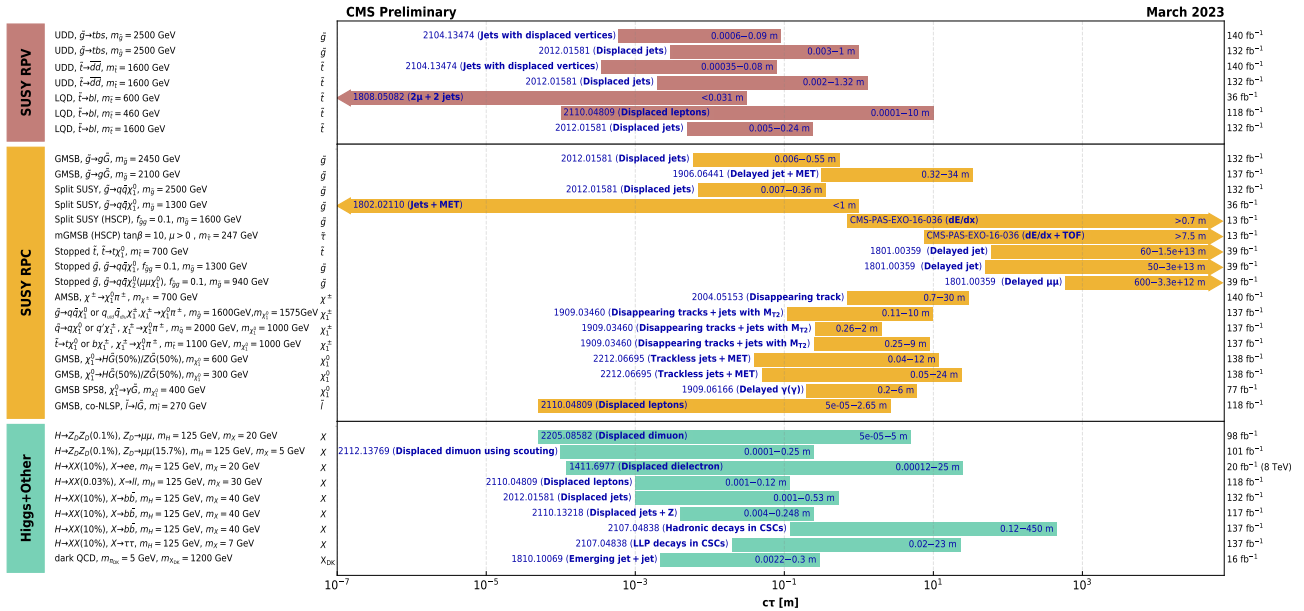


Figure 89.11: Limits at 95% C.L. on the gluino mass in R-hadron models (left), and on the chargino mass in a model where the wino-like chargino is almost degenerate with the LSP (right), as a function of gluino or chargino lifetime, as obtained by ATLAS.

Overview of CMS long-lived particle searches



Selection of observed exclusion limits at 95% C.L. (theory uncertainties are not included). The y-axis tick labels indicate the studied long-lived particle.

Figure 89.12: Excluded regions, at 95% C.L., in the lifetimes of long-lived particles in several models, as obtained by CMS.

are set by ATLAS [262] using events that pass a muon or missing-transverse-momentum trigger and contain a displaced muon track and a displaced vertex. Masses up to 1.7 TeV are excluded for a lifetime of 0.1 ns, and masses below 1.3 TeV are excluded for lifetimes between 0.01 ns and 30 ns. CMS [263] utilizes events with two leptons with transverse impact parameter values between 0.01 and 10 cm not required to form a common vertex to exclude top squarks with masses between 100 and at least 460 GeV for $0.01 < c\tau_0 < 1000$ cm, where $c\tau_0$ is the proper decay length.

In addition to colored sparticles, sparticles like charginos may also be long-lived, especially in scenarios with compressed mass spectra. Charginos decaying in the detectors away from the primary vertex could lead to signatures such as kinked-tracks, or apparently disappearing tracks, since, for example, the pion in $\tilde{\chi}_1^\pm \rightarrow \pi^\pm \tilde{\chi}_1^0$ might be too soft to be reconstructed. At the LHC, searches have been performed for such disappearing tracks,

and interpreted within anomaly-mediated SUSY breaking models [264–267]. The right plot of Fig. 89.11 shows constraints for different ATLAS searches on the chargino mass-vs-lifetime plane for an AMSB model ($\tan\beta = 5$, $\mu > 0$) in which a wino-like $\tilde{\chi}_1^\pm$ decays to a soft pion and an almost mass-degenerated wino-like $\tilde{\chi}_1^0$ [249, 250, 265–268]. The disappearing track search [267] provides constraints also for higgsino-like models. Results from [268] exploiting anomalously large specific ionisation losses dE/dx are extrapolated to the stable regime. For a similar AMSB-like model, CMS excludes $c\tau$ values between 0.15 and 18 m for a chargino mass of 505 GeV [264], see Fig. 89.12. Their most recent results [269] expand and improve the constraints on masses of charginos as well as of colored sparticles by making use of electron and muon plus disappearing track signatures, measurements of the dE/dx ionization energy loss of candidate tracks, and by re-analyzing the fully hadronic signatures using ML techniques.

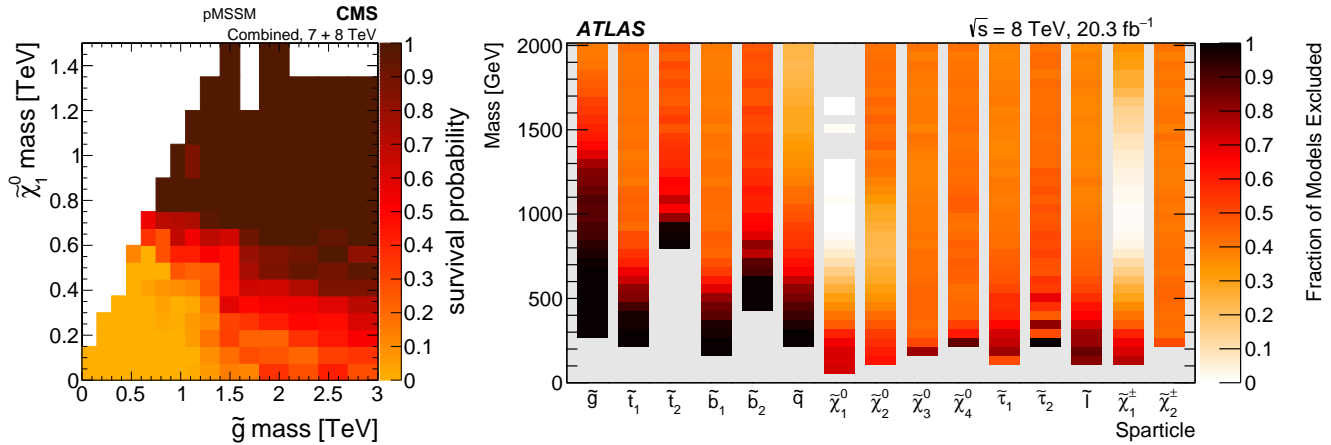


Figure 89.13: The plot on the left shows the survival probability of a pMSSM parameter space model in the gluino-neutralino mass plane after the application of the relevant CMS search results. The plot on the right shows a graphical representation of the ATLAS exclusion power in a pMSSM model. Each vertical bar is a one-dimensional projection of the fraction of models points excluded for each sparticle by ATLAS analyses. The experimental results are obtained from data taken at $\sqrt{s} = 7$ and 8 TeV.

Charginos with a lifetime longer than the time needed to pass through the detector appear as charged stable massive particles. Limits have been derived by the LEP experiments [270], by D0 at the Tevatron [261], and by the LHC experiments [249, 271], and such charginos with mass below 1090 GeV are excluded.

In gauge mediation models, NLSP neutralino decays need not be prompt, and experiments have searched for late decays with photons in the final state. CDF has searched for delayed $\tilde{\chi}_1^0 \rightarrow \gamma \tilde{G}$ decays using the timing of photon signals in the calorimeter [272]. CMS has used the same technique at the LHC [273]. Results are given as exclusion contours in the neutralino mass versus lifetime plane, and for example in a GMSB model with a neutralino mass of 300 GeV, $c\tau$ values between 10 and 2000 cm are excluded [273]. D0 has looked at the direction of showers in the electromagnetic calorimeter with a similar goal [274], and ATLAS has searched for photon candidates that do not point back to the primary vertex, as well as for delayed photons [275].

Charged slepton decays may be kinematically suppressed, for example in the scenario of a NLSP slepton with a very small mass difference to the LSP. Such a slepton may appear to be a stable charged massive particle. Interpretation of searches at LEP for such signatures within GMSB models with a stau NLSP or slepton co-NLSP exclude masses up to 99 GeV [270]. Searches for stable charged particles at the Tevatron [260, 261] and at the LHC [249, 253] are also interpreted in terms of limits on stable charged sleptons. The limits obtained at the LHC exclude stable staus with masses below 430 GeV when produced directly in pairs, and below 660 GeV when staus are produced both directly and indirectly in the decay of other particles in a GMSB model. Recent results from ATLAS and CMS set constraints on long-lived charged slepton with intermediate lifetimes. ATLAS searches for charged sleptons with large impact parameters and exclude selectron, smuon and stau masses up to 720 GeV, 680 GeV, and 340 GeV, respectively, in case of lifetimes of 0.1 ns. They also exclude smuons with lifetimes down to 1 ps for a smuon mass of 100 GeV, and smuon masses up to 520 GeV are excluded for a proper lifetime of 10 ps [276]. CMS [193] targets long-lived stau with $c\tau$ of about 0.1 mm excluding masses between 115 and 220 GeV for the case that the LSP is nearly massless.

89.10 Global interpretations

Apart from the interpretation of direct searches for sparticle production at colliders in terms of limits on masses of individual SUSY particles, model-dependent interpretations of allowed SUSY parameter space are derived from global SUSY fits. Typically these fits combine the results from collider experiments with indirect constraints on SUSY as obtained from low-energy experiments, flavor physics, high-precision electroweak results, and astrophysical data.

In the pre-LHC era these fits were mainly dominated by indirect constraints. Even for very constrained models like the CMSSM, the allowed parameter space, in terms of squark and gluino masses, ranged from several hundreds of GeV to a few TeV. Furthermore, these global fits indicated that squarks and gluino masses in the range of 500 to 1000 GeV were the preferred region of parameter space, although values as high as a few TeV were allowed with lower probabilities [277–284].

With ATLAS and CMS now probing mass scales around 1 TeV and beyond, the importance of the direct searches for global analyses of allowed SUSY parameter space has increased. For example, imposing the new experimental limits on constrained supergravity models pushes the most likely values of first generation squark and gluino masses significantly beyond 2 TeV, typically resulting in overall values of fit quality much worse than those in the pre-LHC era [155–157, 185, 285–292]. The measured value of m_h pushes the sparticle masses upwards. Although these constrained models are not yet ruled out, the extended experimental limits impose very tight constraints on the allowed parameter space.

For this reason, the emphasis of global SUSY fits has shifted towards less-constrained SUSY models. Interpretations in the pMSSM [183–187, 271, 285, 293] as well as in simplified models, have been useful to generalize SUSY searches, for example to redesign experimental analyses in order to increase their sensitivity for compressed spectra, where the mass of the LSP is much closer to squark and gluino masses than predicted by the CMSSM. As shown in Table 89.1, for neutralino masses above 0.5–1 TeV the current set of ATLAS and CMS searches, interpreted in simplified models, cannot exclude the existence of squarks or gluinos with masses only marginally above the neutralino mass. However, as these exclusion limits are defined in the context of simplified models, they are only valid for the assumptions in which these models are defined.

Fig. 89.13 shows graphically the LHC exclusion power in the pMSSM based on searches performed at $\sqrt{s} = 7$ and 8 TeV as reported by ATLAS [183] and CMS [184]. The plot on the left shows the survival probability in the gluino-neutralino mass plane, which is a measure of the parameter space that remains after inclusion of the relevant CMS search results. As can be seen, gluino masses below about 1.2 TeV are almost fully excluded. This result agrees well with the typical exclusion obtained at 8 TeV in simplified models for gluino production. However, as shown in the right plot of Fig. 89.13, when a similar analysis for other sparticles is performed it becomes apparent that exclusions on the pMSSM parameter space can be significantly less stringent than simplified model limits might suggest. This is especially apparent for the electroweak sector, where even at rather low masses several of the pMSSM test points still survive the constraint of ATLAS searches at $\sqrt{s} = 7$ and 8 TeV. This again indicates that care

ATLAS SUSY Searches* - 95% CL Lower Limits
August 2023

ATLAS Preliminary
 $\sqrt{s} = 13$ TeV

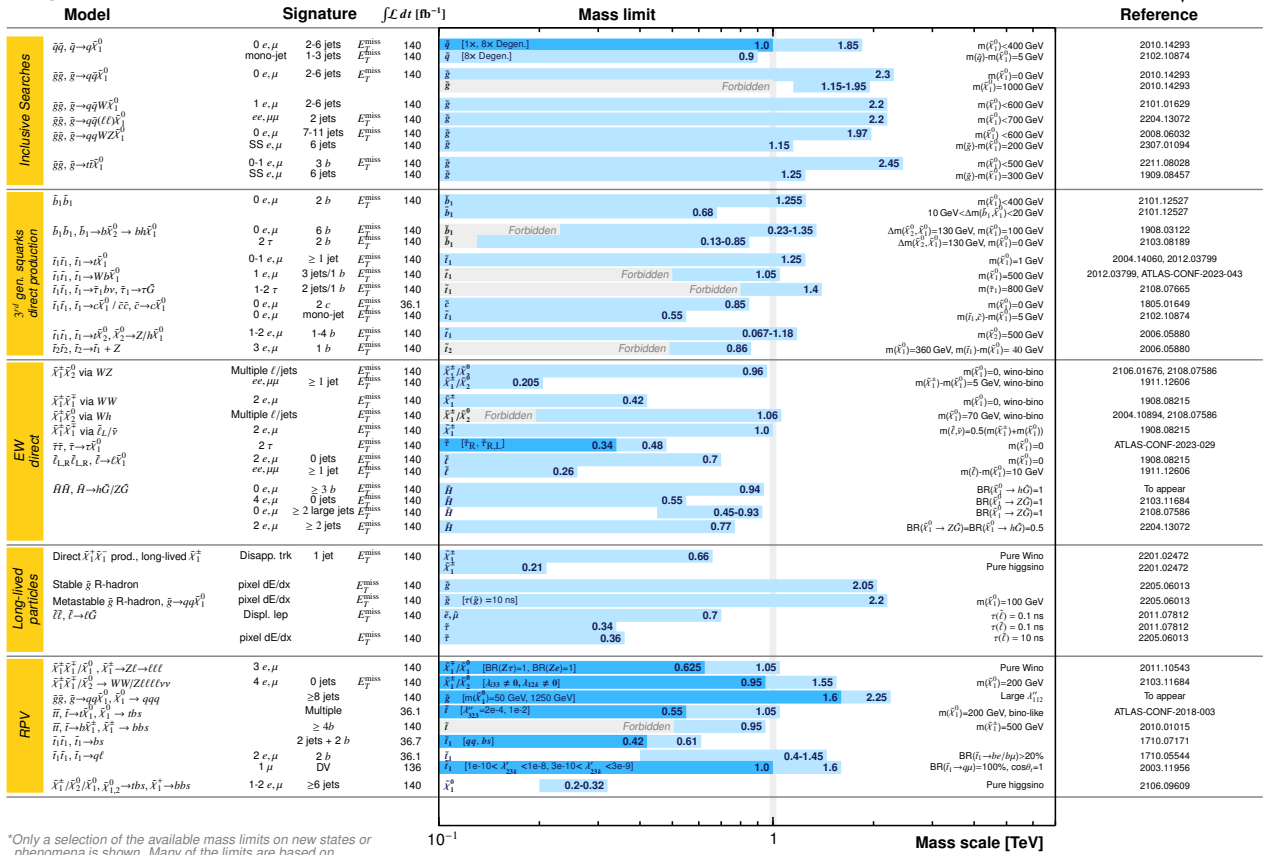


Figure 89.14: Overview of the current landscape of SUSY searches at the LHC (updated on August 2023). The plot shows exclusion mass limits of ATLAS for different searches and interpretation assumptions. The corresponding results of the CMS experiment are similar.

must be taken when interpreting results from the LHC searches and there are still several scenarios where sparticles below the 1 TeV scale are not excluded, even when considering the most recent results at $\sqrt{s} = 13$ TeV. Interpretations in the pMSSM of searches performed on the full Run 2 dataset are in preparation and will offer further insights on the validity of constraints obtained with simplified models and, thus, guidance towards the future LHC runs and beyond.

Furthermore, the discovery of a Higgs boson with a mass around 125 GeV has triggered many studies regarding the compatibility of SUSY parameter space with this new particle (see for example [294, 295]). Much of it is still work in progress and it will be interesting to see how the interplay between the results from direct SUSY searches and more precise measurements of the properties of the Higgs boson will unfold in the future.

89.11 Summary and Outlook

The absence of any observation of new phenomena at the first run of the LHC at $\sqrt{s} = 7/8$ TeV, and after the second run at $\sqrt{s} = 13$ TeV, places significant constraints on SUSY parameter space. An overview of the current landscape of SUSY searches and limits at the LHC is shown in Figure 89.14, where a summary of results from the ATLAS experiment [296] (CMS results are similar [297]), is reported for illustration purposes. Inclusive searches probe production of gluinos at about 2.45 TeV, first and second generation squarks in the range of about 1 to 1.9 TeV, third generation squarks at scales around 600 GeV to 1.2 TeV, electroweak gauginos at scales around 400 – 1100 GeV, and sleptons around 700 GeV. However, depending on the assumptions made on the underlying SUSY spectrum these limits can also weaken considerably.

With the LHC having reached almost its maximum energy of about $\sqrt{s} = 14$ TeV and analyses explored the full Run 2 dataset, future sensitivity improvements will have to originate from more data, the improvement of experimental analysis techniques and the focus on special signatures like the ones arising in long-lived sparticle decays. Therefore, it is expected that the current landscape of SUSY searches and corresponding exclusion limits at the LHC, especially for strongly produced sparticles in RPC scenarios, will not change as rapidly anymore as it did in the past, when the LHC underwent several successive increases of collision energy.

The interpretation of results at the LHC has moved away from constrained models like the CMSSM towards a large set of simplified models, or the pMSSM. Quoted limits in simplified models are only valid under the explicit assumptions made in these models. The addition of more comprehensive interpretations in the pMSSM complement those and therefore enable an even more refined understanding of the probed SUSY parameter space.

In this context, the limit range of 1.5 – 2.45 TeV on generic colored SUSY particles only holds for light neutralinos, in the R -parity conserving MSSM. Limits on third generation squarks and electroweak gauginos also only hold for light neutralinos, and under specific assumptions for decay modes and slepton masses. Constraints in R -parity violating SUSY models strongly depend also on the assumed non-zero couplings.

The next LHC runs, with \sqrt{s} between 13 and 14 TeV and significantly larger integrated luminosities (notably the High-Luminosity LHC), will provide a large data sample for future SUSY searches. As mentioned above, the improvement in sensitivity will largely have to come from a larger data set, and evolution of trigger and analysis techniques, since there will be no significant energy increase at the LHC anymore. Although the sensi-

tivity for colored sparticles will increase somewhat as well, the expanded data set will be particularly beneficial for electroweak gaugino searches, and for the more difficult final states presented by compressed particle spectra, stealth SUSY, long-lived sparticles, or R -parity violating scenarios.

References

- [1] H. Miyazawa, Prog. Theor. Phys. **36**, 6, 1266 (1966).
- [2] Y. A. Golfand and E. P. Likhthman, JETP Lett. **13**, 323 (1971).
- [3] J.-L. Gervais and B. Sakita, Nucl. Phys. **B34**, 632 (1971).
- [4] D. V. Volkov and V. P. Akulov, Phys. Lett. **46B**, 109 (1973).
- [5] J. Wess and B. Zumino, Phys. Lett. **49B**, 52 (1974).
- [6] J. Wess and B. Zumino, Nucl. Phys. **B70**, 39 (1974).
- [7] A. Salam and J. A. Strathdee, Nucl. Phys. **B76**, 477 (1974).
- [8] H. P. Nilles, Phys. Rept. **110**, 1 (1984).
- [9] H. E. Haber and G. L. Kane, Phys. Rept. **117**, 75 (1985).
- [10] E. Witten, Nucl. Phys. **B188**, 513 (1981).
- [11] S. Dimopoulos and H. Georgi, Nucl. Phys. **B193**, 150 (1981).
- [12] M. Dine, W. Fischler and M. Srednicki, Nucl. Phys. **B189**, 575 (1981).
- [13] S. Dimopoulos and S. Raby, Nucl. Phys. **B192**, 353 (1981).
- [14] N. Sakai, Z. Phys. **C11**, 153 (1981).
- [15] R. K. Kaul and P. Majumdar, Nucl. Phys. **B199**, 36 (1982).
- [16] H. Goldberg, Phys. Rev. Lett. **50**, 1419 (1983).
- [17] J. R. Ellis *et al.*, Nucl. Phys. **B238**, 453 (1984).
- [18] G. Jungman, M. Kamionkowski and K. Griest, Phys. Rept. **267**, 195 (1996), [hep-ph/9506380].
- [19] S. Dimopoulos, S. Raby and F. Wilczek, Phys. Rev. **D24**, 1681 (1981).
- [20] W. J. Marciano and G. Senjanovic, Phys. Rev. **D25**, 3092 (1982).
- [21] M. B. Einhorn and D. R. T. Jones, Nucl. Phys. **B196**, 475 (1982).
- [22] L. E. Ibanez and G. G. Ross, Phys. Lett. **105B**, 439 (1981).
- [23] U. Amaldi, W. de Boer and H. Furstenuau, Phys. Lett. **B260**, 447 (1991).
- [24] P. Langacker and N. Polonsky, Phys. Rev. **D52**, 3081 (1995), [hep-ph/9503214].
- [25] J. R. Ellis, S. Kelley and D. V. Nanopoulos, Phys. Lett. B **260**, 131 (1991).
- [26] P. Fayet, Phys. Lett. **64B**, 159 (1976).
- [27] G. R. Farrar and P. Fayet, Phys. Lett. **76B**, 575 (1978).
- [28] B.C. Allanach and H.E. Haber, *Supersymmetry, Part I (Theory)*, in this Review.
- [29] M. Carena *et al.*, *Status of Higgs Boson Physics*, in this Review.
- [30] A. M. Sirunyan *et al.* (CMS), JHEP **04**, 188 (2020), [arXiv:1910.12127].
- [31] M. Aaboud *et al.* (ATLAS), JHEP **04**, 098 (2019), [arXiv:1812.03017].
- [32] R. Aaij *et al.* (LHCb), Phys. Rev. Lett. **118**, 19, 191801 (2017), [arXiv:1703.05747].
- [33] A. Höcker and W.J. Marciano, *Muon Anomalous Magnetic Moment*, in this Review.
- [34] B. Abi *et al.* (Muon g-2), Phys. Rev. Lett. **126**, 14, 141801 (2021), [arXiv:2104.03281].
- [35] G. Hinshaw *et al.* (WMAP), Astrophys. J. Suppl. **208**, 19 (2013), [arXiv:1212.5226].
- [36] N. Aghanim *et al.* (Planck Collaboration), A&A **641**, A1 (2020).
- [37] K. Nakamura *et al.* (Particle Data Group), J. Phys. **G37**, 075021 (2010).
- [38] I. Hinchliffe *et al.*, Phys. Rev. **D55**, 5520 (1997), [hep-ph/9610544].
- [39] L. Randall and D. Tucker-Smith, Phys. Rev. Lett. **101**, 221803 (2008), [arXiv:0806.1049].
- [40] V. Khachatryan *et al.* (CMS), Phys. Lett. **B698**, 196 (2011), [arXiv:1101.1628].
- [41] S. Chatrchyan *et al.* (CMS), Phys. Rev. Lett. **107**, 221804 (2011), [arXiv:1109.2352].
- [42] S. Chatrchyan *et al.* (CMS), JHEP **01**, 077 (2013), [arXiv:1210.8115].
- [43] S. Chatrchyan *et al.* (CMS), Eur. Phys. J. **C73**, 9, 2568 (2013), [arXiv:1303.2985].
- [44] S. Chatrchyan *et al.* (CMS), Phys. Rev. **D85**, 012004 (2012), [arXiv:1107.1279].
- [45] C. G. Lester and D. J. Summers, Phys. Lett. **B463**, 99 (1999), [hep-ph/9906349].
- [46] D. R. Tovey, JHEP **04**, 034 (2008), [arXiv:0802.2879].
- [47] M. R. Buckley *et al.*, Phys. Rev. **D89**, 5, 055020 (2014), [arXiv:1310.4827].
- [48] P. Jackson, C. Rogan and M. Santoni, Phys. Rev. **D95**, 3, 035031 (2017), [arXiv:1607.08307].
- [49] G. Aad *et al.* (ATLAS), Eur. Phys. J. C **81**, 4, 334 (2021), [arXiv:2009.04986].
- [50] J. M. Butterworth *et al.*, Phys. Rev. Lett. **100**, 242001 (2008), [arXiv:0802.2470].
- [51] A. M. Sirunyan *et al.* (CMS), JINST **15**, 06, P06005 (2020), [arXiv:2004.08262].
- [52] A. M. Sirunyan *et al.* (CMS), JHEP **05**, 032 (2020), [arXiv:1912.08887].
- [53] N. Arkani-Hamed and S. Dimopoulos, JHEP **06**, 073 (2005), [hep-th/0405159].
- [54] G. F. Giudice and A. Romanino, Nucl. Phys. B **699**, 65 (2004), [Erratum: Nucl.Phys.B 706, 487–487 (2005)], [hep-ph/0406088].
- [55] J. Alimena *et al.*, J. Phys. G **47**, 9, 090501 (2020), [arXiv:1903.04497].
- [56] A.H. Chamseddine, R. Arnowitt, and P. Nath, Phys. Rev. Lett. **49**, 970 (1982).
- [57] E. Cremmer *et al.*, Nucl. Phys. **B212**, 413 (1983).
- [58] P. Fayet, Phys. Lett. **70B**, 461 (1977).
- [59] M. Dine, A. E. Nelson and Y. Shirman, Phys. Rev. **D51**, 1362 (1995), [hep-ph/9408384].
- [60] P. Meade, N. Seiberg and D. Shih, Prog. Theor. Phys. Suppl. **177**, 143 (2009), [arXiv:0801.3278].
- [61] G. F. Giudice *et al.*, JHEP **12**, 027 (1998), [hep-ph/9810442].
- [62] L. Randall and R. Sundrum, Nucl. Phys. **B557**, 79 (1999), [hep-th/9810155].
- [63] R. L. Arnowitt and P. Nath, Phys. Rev. Lett. **69**, 725 (1992).
- [64] G. L. Kane *et al.*, Phys. Rev. **D49**, 6173 (1994), [hep-ph/9312272].
- [65] A. Djouadi *et al.* (MSSM Working Group), in “GDR (Groupement De Recherche) - Supersymetrie,” (1998), [hep-ph/9901246].
- [66] A. Djouadi, J.-L. Kneur and G. Moultaka, Comput. Phys. Commun. **176**, 426 (2007), [hep-ph/0211331].
- [67] C. F. Berger *et al.*, JHEP **02**, 023 (2009), [arXiv:0812.0980].
- [68] H. Baer *et al.*, in “Workshop on Physics at Current Accelerators and the Supercollider Argonne, Illinois, June 2-5, 1993,” 0703-720 (1993), [hep-ph/9305342], URL http://lss.fnal.gov/cgi-bin/find_paper.pl?other/ssc/sscl-preprint-441.

- [69] R. M. Barnett, H. E. Haber and G. L. Kane, Nucl. Phys. **B267**, 625 (1986).
- [70] H. Baer, D. Karatas and X. Tata, Phys. Lett. **B183**, 220 (1987).
- [71] J. Alwall, P. Schuster and N. Toro, Phys. Rev. **D79**, 075020 (2009), [arXiv:0810.3921].
- [72] J. Alwall *et al.*, Phys. Rev. **D79**, 015005 (2009), [arXiv:0809.3264].
- [73] LEP2 SUSY Working Group, ALEPH, DELPHI, L3 and OPAL experiments, note LEPSUSYWG/04-02.1, <http://lepsusy.web.cern.ch/lepsusy>.
- [74] LHC SUSY cross sections working group, <https://twiki.cern.ch/twiki/bin/view/LHCPhysics/SUSYCrossSections>.
- [75] T. Aaltonen *et al.* (CDF), Phys. Rev. Lett. **102**, 121801 (2009), [arXiv:0811.2512].
- [76] V. M. Abazov *et al.* (D0), Phys. Lett. **B660**, 449 (2008), [arXiv:0712.3805].
- [77] A. M. Sirunyan *et al.* (CMS) (2019), [arXiv:1908.04722].
- [78] ATLAS Collab., ATLAS-CONF-2019-040 (2019).
- [79] G. Aad *et al.* (ATLAS), Eur. Phys. J. C **81**, 7, 600 (2021), [arXiv:2101.01629].
- [80] G. Aad *et al.* (ATLAS), JHEP **02**, 143 (2021), [arXiv:2010.14293].
- [81] A. Tumasyan *et al.* (CMS), JHEP **09**, 149 (2023), [arXiv:2211.08476].
- [82] A. M. Sirunyan *et al.* (CMS), JHEP **10**, 244 (2019), [arXiv:1908.04722].
- [83] G. Aad *et al.* (ATLAS), Eur. Phys. J. C **83**, 7, 561 (2023), [arXiv:2211.08028].
- [84] ATLAS Collab., ATLAS-CONF-2018-041 (2018).
- [85] A. M. Sirunyan *et al.* (CMS) (2019), [arXiv:1909.03460].
- [86] A. M. Sirunyan *et al.* (CMS), Phys. Rev. D **104**, 5, 052001 (2021), [arXiv:2103.01290].
- [87] G. Aad *et al.* (ATLAS Collaboration), Phys. Rev. D **103**, 112006 (2021), URL <https://link.aps.org/doi/10.1103/PhysRevD.103.112006>.
- [88] M. Aaboud *et al.* (ATLAS), Phys. Rev. D **97**, 9, 092006 (2018), [arXiv:1802.03158].
- [89] G. Aad *et al.* (ATLAS), Eur. Phys. J. C **83**, 6, 515 (2023), [arXiv:2204.13072].
- [90] G. Aad *et al.* (ATLAS) (2023), [arXiv:2307.01094].
- [91] M. Aaboud *et al.* (ATLAS), JHEP **09**, 050 (2018), [arXiv:1805.01649].
- [92] T. Aaltonen *et al.* (CDF), Phys. Rev. Lett. **105**, 081802 (2010), [arXiv:1005.3600].
- [93] V. M. Abazov *et al.* (D0), Phys. Lett. **B693**, 95 (2010), [arXiv:1005.2222].
- [94] G. Aad *et al.* (ATLAS), JHEP **05**, 093 (2021), [arXiv:2101.12527].
- [95] G. Aad *et al.* (ATLAS), JHEP **12**, 060 (2019), [arXiv:1908.03122].
- [96] G. Aad *et al.* (ATLAS), JHEP **06**, 046 (2020), [arXiv:1909.08457].
- [97] G. Aad *et al.* (ATLAS), Phys. Rev. D **104**, 3, 032014 (2021), [arXiv:2103.08189].
- [98] A. M. Sirunyan *et al.* (CMS), JHEP **03**, 076 (2018), [arXiv:1709.08908].
- [99] A. M. Sirunyan *et al.* (CMS), Eur. Phys. J. C **80**, 8, 752 (2020), [arXiv:2001.10086].
- [100] C. Boehm, A. Djouadi and Y. Mambrini, Phys. Rev. **D61**, 095006 (2000), [hep-ph/9907428].
- [101] T. Aaltonen *et al.* (CDF), Phys. Rev. **D82**, 092001 (2010), [arXiv:1009.0266].
- [102] V. M. Abazov *et al.* (D0), Phys. Lett. **B696**, 321 (2011), [arXiv:1009.5950].
- [103] T. Aaltonen *et al.* (CDF), JHEP **10**, 158 (2012), [arXiv:1203.4171].
- [104] V. M. Abazov *et al.* (D0), Phys. Lett. **B665**, 1 (2008), [arXiv:0803.2263].
- [105] T. Aaltonen *et al.* (CDF), Phys. Rev. Lett. **104**, 251801 (2010), [arXiv:0912.1308].
- [106] V. M. Abazov *et al.* (D0), Phys. Lett. **B674**, 4 (2009), [arXiv:0901.1063].
- [107] G. Aad *et al.* (ATLAS), Eur. Phys. J. C **80**, 8, 737 (2020), [arXiv:2004.14060].
- [108] G. Aad *et al.* (ATLAS), JHEP **04**, 174 (2021), [arXiv:2012.03799].
- [109] Technical report, CERN, Geneva (2023), all figures including auxiliary figures are available at <https://atlas.web.cern.ch/Atlas/GROUPS/PHYSICS/CONFNOTES/ATLAS-CONF-2023-043>, URL <https://cds.cern.ch/record/2869241>.
- [110] M. Aaboud *et al.* (ATLAS), JHEP **06**, 108 (2018), [arXiv:1711.11520].
- [111] M. Aaboud *et al.* (ATLAS), Phys. Rev. **D98**, 3, 032008 (2018), [arXiv:1803.10178].
- [112] A. M. Sirunyan *et al.* (CMS), JHEP **02**, 015 (2020), [arXiv:1910.12932].
- [113] G. Aad *et al.* (ATLAS), JHEP **04**, 165 (2021), [arXiv:2102.01444].
- [114] A. M. Sirunyan *et al.* (CMS), Eur. Phys. J. C **77**, 10, 710 (2017), [arXiv:1705.04650].
- [115] A. M. Sirunyan *et al.* (CMS), Phys. Rev. **D96**, 3, 032003 (2017), [arXiv:1704.07781].
- [116] A. M. Sirunyan *et al.* (CMS), JHEP **10**, 005 (2017), [arXiv:1707.03316].
- [117] A. M. Sirunyan *et al.* (CMS), JHEP **10**, 019 (2017), [arXiv:1706.04402].
- [118] A. M. Sirunyan *et al.* (CMS), Eur. Phys. J. C **81**, 1, 3 (2021), [arXiv:2008.05936].
- [119] A. M. Sirunyan *et al.* (CMS), JHEP **03**, 101 (2019), [arXiv:1901.01288].
- [120] A. Tumasyan *et al.* (CMS), JHEP **07**, 110 (2023), [arXiv:2304.07174].
- [121] M. Aaboud *et al.* (ATLAS), Phys. Rev. D **98**, 3, 032008 (2018), [arXiv:1803.10178].
- [122] G. Aad *et al.* (ATLAS) (2021), [arXiv:2108.07665].
- [123] G. Aad *et al.* (ATLAS), Eur. Phys. J. C **80**, 11, 1080 (2020), [arXiv:2006.05880].
- [124] A. Tumasyan *et al.* (CMS), JHEP **06**, 060 (2023), [arXiv:2301.08096].
- [125] M. Aaboud *et al.* (ATLAS), Eur. Phys. J. C **80**, 8, 754 (2020), [arXiv:1903.07570].
- [126] CMS Collab. CMS-PAS-SUS-18-003 (2018).
- [127] B. Fuks *et al.*, JHEP **10**, 081 (2012), [arXiv:1207.2159].
- [128] B. Fuks *et al.*, Eur. Phys. J. C **73**, 2480 (2013), [arXiv:1304.0790].
- [129] LEP2 SUSY Working Group, ALEPH, DELPHI, L3 and OPAL experiments, note LEPSUSYWG/01-03.1, <http://lepsusy.web.cern.ch/lepsusy>.
- [130] LEP2 SUSY Working Group, ALEPH, DELPHI, L3 and OPAL experiments, note LEPSUSYWG/02-04.1, <http://lepsusy.web.cern.ch/lepsusy>.
- [131] CDF Collab., CDF Note 10636 (2011).
- [132] V. M. Abazov *et al.* (D0), Phys. Lett. **B680**, 34 (2009), [arXiv:0901.0646].

- [133] G. Aad *et al.* (ATLAS), *Eur. Phys. J. C* **80**, 2, 123 (2020), [arXiv:1908.08215].
- [134] A. M. Sirunyan *et al.* (CMS), *JHEP* **11**, 079 (2018), [arXiv:1807.07799].
- [135] M. Aaboud *et al.* (ATLAS), *Eur. Phys. J.* **C78**, 2, 154 (2018), [arXiv:1708.07875].
- [136] A. M. Sirunyan *et al.* (CMS), *JHEP* **11**, 151 (2018), [arXiv:1807.02048].
- [137] G. Aad *et al.* (ATLAS), *JHEP* **06**, 031 (2023), [arXiv:2209.13935].
- [138] G. Aad *et al.* (ATLAS), *JHEP* **12**, 167 (2023), [arXiv:2310.08171].
- [139] G. Aad *et al.* (ATLAS), *Phys. Rev. D* **104**, 11, 112010 (2021), [arXiv:2108.07586].
- [140] A. Tumasyan *et al.* (CMS), *Phys. Lett. B* **842**, 137460 (2023), [arXiv:2205.09597].
- [141] M. Aaboud *et al.* (ATLAS), *Eur. Phys. J.* **C78**, 12, 995 (2018), [arXiv:1803.02762].
- [142] A. Tumasyan *et al.* (CMS), *JHEP* **04**, 147 (2022), [arXiv:2106.14246].
- [143] G. Aad *et al.* (ATLAS), *Eur. Phys. J. C* **81**, 12, 1118 (2021), [arXiv:2106.01676].
- [144] G. Aad *et al.* (ATLAS), *JHEP* **11**, 150 (2023), [arXiv:2305.09322].
- [145] A. Tumasyan *et al.* (CMS), *JHEP* **10**, 045 (2021), [arXiv:2107.12553].
- [146] M. Aaboud *et al.* (ATLAS), *Phys. Rev.* **D100**, 1, 012006 (2019), [arXiv:1812.09432].
- [147] G. Aad *et al.* (ATLAS), *JHEP* **10**, 005 (2020), [arXiv:2004.10894].
- [148] G. Aad *et al.* (ATLAS), *Eur. Phys. J. C* **80**, 8, 691 (2020), [arXiv:1909.09226].
- [149] G. Aad *et al.* (ATLAS), *Phys. Rev. D* **101**, 5, 052005 (2020), [arXiv:1911.12606].
- [150] A. Tumasyan *et al.* (CMS), *JHEP* **04**, 091 (2022), [arXiv:2111.06296].
- [151] A. M. Sirunyan *et al.* (CMS), *JHEP* **08**, 150 (2019), [arXiv:1905.13059].
- [152] A. M. Sirunyan *et al.* (CMS), *Phys. Rev. Lett.* **124**, 4, 041803 (2020), [arXiv:1910.01185].
- [153] H. K. Dreiner *et al.*, *Eur. Phys. J.* **C62**, 547 (2009), [arXiv:0901.3485].
- [154] LEP2 SUSY Working Group, ALEPH, DELPHI, L3 and OPAL experiments, note LEPSUSYWG/04-07.1, <http://lepsusy.web.cern.ch/lepsusy>.
- [155] O. Buchmueller *et al.*, *Eur. Phys. J.* **C74**, 6, 2922 (2014), [arXiv:1312.5250].
- [156] C. Strege *et al.*, *JCAP* **1304**, 013 (2013), [arXiv:1212.2636].
- [157] A. Fowlie *et al.*, *Phys. Rev.* **D86**, 075010 (2012), [arXiv:1206.0264].
- [158] LEP2 SUSY Working Group, ALEPH, DELPHI, L3 and OPAL experiments, note LEPSUSYWG/04-09.1, <http://lepsusy.web.cern.ch/lepsusy>.
- [159] T. Aaltonen *et al.* (CDF), *Phys. Rev. Lett.* **104**, 011801 (2010), [arXiv:0910.3606].
- [160] V. M. Abazov *et al.* (D0), *Phys. Rev. Lett.* **105**, 221802 (2010), [arXiv:1008.2133].
- [161] M. Aaboud *et al.* (ATLAS), *Phys. Rev.* **D97**, 9, 092006 (2018), [arXiv:1802.03158].
- [162] A. M. Sirunyan *et al.* (CMS), *JHEP* **06**, 143 (2019), [arXiv:1903.07070].
- [163] A. M. Sirunyan *et al.* (CMS), *Phys. Lett. B* **801**, 135183 (2020), [arXiv:1907.00857].
- [164] A. Hayrapetyan *et al.* (CMS), *JHEP* **10**, 046 (2023), [arXiv:2307.16216].
- [165] M. Aaboud *et al.* (ATLAS), *Phys. Rev.* **D98**, 9, 092002 (2018), [arXiv:1806.04030].
- [166] M. Aaboud *et al.* (ATLAS), *Phys. Rev.* **D98**, 3, 032009 (2018), [arXiv:1804.03602].
- [167] M. Aaboud *et al.* (ATLAS), *Phys. Rev.* **D99**, 1, 012001 (2019), [arXiv:1808.03057].
- [168] G. Aad *et al.* (ATLAS), *Phys. Rev. D* **104**, 11, 112010 (2021), [arXiv:2108.07586].
- [169] A. M. Sirunyan *et al.* (CMS), *JHEP* **03**, 166 (2018), [arXiv:1709.05406].
- [170] A. M. Sirunyan *et al.* (CMS), *JHEP* **03**, 160 (2018), [arXiv:1801.03957].
- [171] A. M. Sirunyan *et al.* (CMS), *Eur. Phys. J.* **C79**, 5, 444 (2019), [arXiv:1901.06726].
- [172] A. M. Sirunyan *et al.* (CMS), *JHEP* **01**, 154 (2019), [arXiv:1812.04066].
- [173] A. M. Sirunyan *et al.* (CMS), *Phys. Lett.* **B780**, 118 (2018), [arXiv:1711.08008].
- [174] A. M. Sirunyan *et al.* (CMS), *Phys. Rev.* **D97**, 3, 032007 (2018), [arXiv:1709.04896].
- [175] A. M. Sirunyan *et al.* (CMS), *Phys. Lett.* **B779**, 166 (2018), [arXiv:1709.00384].
- [176] A. Tumasyan *et al.* (CMS), *JHEP* **05**, 014 (2022), [arXiv:2201.04206].
- [177] G. Aad *et al.* (ATLAS), *Phys. Rev.* **D93**, 5, 052002 (2016), [arXiv:1509.07152].
- [178] M. Aaboud *et al.* (ATLAS), *Eur. Phys. J.* **C78**, 8, 625 (2018), [arXiv:1805.11381].
- [179] M. Aaboud *et al.* (ATLAS), *Eur. Phys. J.* **C77**, 3, 144 (2017), [arXiv:1611.05791].
- [180] A. M. Sirunyan *et al.* (CMS), *JHEP* **04**, 123 (2021), [arXiv:2012.08600].
- [181] A. Tumasyan *et al.* (CMS) (2023).
- [182] A. Arbey, M. Battaglia and F. Mahmoudi, *Eur. Phys. J. C* **72**, 1847 (2012), [arXiv:1110.3726].
- [183] G. Aad *et al.* (ATLAS), *JHEP* **10**, 134 (2015), [arXiv:1508.06608].
- [184] V. Khachatryan *et al.* (CMS), *JHEP* **10**, 129 (2016), [arXiv:1606.03577].
- [185] P. Athron *et al.* (GAMBIT), *Eur. Phys. J.* **C77**, 12, 879 (2017), [arXiv:1705.07917].
- [186] K. J. de Vries *et al.*, *Eur. Phys. J.* **C75**, 9, 422 (2015), [arXiv:1504.03260].
- [187] C. Strege *et al.*, *JHEP* **09**, 081 (2014), [arXiv:1405.0622].
- [188] LEP2 SUSY Working Group, ALEPH, DELPHI, L3 and OPAL experiments, note LEPSUSYWG/04-01.1, <http://lepsusy.web.cern.ch/lepsusy>.
- [189] A. Heister *et al.* (ALEPH), *Phys. Lett.* **B544**, 73 (2002), [hep-ex/0207056].
- [190] A. M. Sirunyan *et al.* (CMS), *Phys. Lett.* **B790**, 140 (2019), [arXiv:1806.05264].
- [191] G. Aad *et al.* (ATLAS), *Phys. Rev. D* **101**, 3, 032009 (2020), [arXiv:1911.06660].
- [192] A. M. Sirunyan *et al.* (CMS) (2019), [arXiv:1907.13179].
- [193] A. Tumasyan *et al.* (CMS), *Phys. Rev. D* **108**, 1, 012011 (2023), [arXiv:2207.02254].
- [194] G. Aad *et al.* (ATLAS) (2023).
- [195] LEP2 SUSY Working Group, ALEPH, DELPHI, L3 and OPAL experiments, note LEPSUSYWG/02-09.2, <http://lepsusy.web.cern.ch/lepsusy>.
- [196] M. Aaboud *et al.* (ATLAS), *Phys. Rev.* **D99**, 1, 012009 (2019), [arXiv:1808.06358].

- [197] S. Chatrchyan *et al.* (CMS), Eur. Phys. J. **C73**, 2493 (2013), [arXiv:1301.3792].
- [198] S. Chatrchyan *et al.* (CMS), Phys. Rev. **D90**, 032006 (2014), [arXiv:1404.5801].
- [199] T. Aaltonen *et al.* (CDF), Phys. Rev. Lett. **110**, 20, 201802 (2013), [arXiv:1302.4491].
- [200] DELPHI Collab., Eur. Phys. J. **C31**, 412 (2003).
- [201] G. Aad *et al.* (ATLAS), JHEP **07**, 167 (2021), [arXiv:2103.11684].
- [202] M. Aaboud *et al.* (ATLAS), JHEP **09**, 084 (2017), [arXiv:1706.03731].
- [203] CMS Collab., CMS-PAS-SUS-19-008 (2019).
- [204] V. Khachatryan *et al.* (CMS), Phys. Rev. **D94**, 11, 112009 (2016), [arXiv:1606.08076].
- [205] CMS Collab., CMS-PAS-SUS-13-010 (2013).
- [206] T. Aaltonen *et al.* (CDF), Phys. Rev. Lett. **107**, 042001 (2011), [arXiv:1105.2815].
- [207] M. Aaboud *et al.* (ATLAS), Phys. Lett. **B785**, 136 (2018), [arXiv:1804.03568].
- [208] ATLAS Collab., ATLAS-CONF-2018-003 (2018).
- [209] ATLAS Collab., ATLAS-CONF-2016-057 (2016).
- [210] M. Aaboud *et al.* (ATLAS), JHEP **09**, 088 (2017), [arXiv:1704.08493].
- [211] A. M. Sirunyan *et al.* (CMS), Phys. Lett. **B783**, 114 (2018), [arXiv:1712.08920].
- [212] S. Chatrchyan *et al.* (CMS), Phys. Lett. **B730**, 193 (2014), [arXiv:1311.1799].
- [213] V. Khachatryan *et al.* (CMS), Phys. Lett. **B770**, 257 (2017), [arXiv:1608.01224].
- [214] G. Aad *et al.* (ATLAS) (2021), [arXiv:2106.09609].
- [215] F. D. Aaron *et al.* (H1), Eur. Phys. J. **C71**, 1572 (2011), [arXiv:1011.6359].
- [216] ATLAS Collab., ATLAS-CONF-2015-018 (2015).
- [217] S. Chekanov *et al.* (ZEUS), Eur. Phys. J. **C50**, 269 (2007), [hep-ex/0611018].
- [218] M. Aaboud *et al.* (ATLAS), Phys. Rev. **D97**, 3, 032003 (2018), [arXiv:1710.05544].
- [219] ATLAS Collab., ATLAS-CONF-2019-006 (2019).
- [220] A. M. Sirunyan *et al.* (CMS), Phys. Rev. **D99**, 3, 032014 (2019), [arXiv:1808.05082].
- [221] CMS Collab., CMS-PAS-EXO-16-022 (2016).
- [222] V. Khachatryan *et al.* (CMS), Phys. Lett. **B760**, 178 (2016), [arXiv:1602.04334].
- [223] M. Aaboud *et al.* (ATLAS), Eur. Phys. J. **C 78**, 3, 250 (2018), [arXiv:1710.07171].
- [224] G. Aad *et al.* (ATLAS) (2019), [arXiv:1909.08457].
- [225] M. Aaboud *et al.* (ATLAS), Eur. Phys. J. **C78**, 3, 250 (2018), [arXiv:1710.07171].
- [226] V. Khachatryan *et al.* (CMS), Phys. Rev. **D95**, 1, 012009 (2017), [arXiv:1610.05133].
- [227] V. Khachatryan *et al.* (CMS), Phys. Lett. **B747**, 98 (2015), [arXiv:1412.7706].
- [228] G. Aad *et al.* (ATLAS), Eur. Phys. J. **C 81**, 1, 11 (2021), [Erratum: Eur.Phys.J.C 81, 249 (2021)], [arXiv:2010.01015].
- [229] A. M. Sirunyan *et al.* (CMS), Phys. Rev. **D 104**, 3, 032006 (2021), [arXiv:2102.06976].
- [230] G. Aad *et al.* (ATLAS), Phys. Rev. **D92**, 7, 072004 (2015), [arXiv:1504.05162].
- [231] V. Khachatryan *et al.* (CMS), Phys. Rev. **D91**, 1, 012007 (2015), [arXiv:1411.6530].
- [232] G. Aad *et al.* (ATLAS), Phys. Rev. **D 103**, 112003 (2021), [arXiv:2011.10543].
- [233] LEP2 SUSY Working Group, ALEPH, DELPHI, L3 and OPAL experiments, note LEPSUSYWG/02-10.1, <http://lepsusy.web.cern.ch/lepsusy>.
- [234] A. M. Sirunyan *et al.* (CMS), Eur. Phys. J. **C79**, 4, 305 (2019), [arXiv:1811.09760].
- [235] T. Aaltonen *et al.* (CDF), Phys. Rev. Lett. **105**, 191801 (2010), [arXiv:1004.3042].
- [236] V. M. Abazov *et al.* (D0), Phys. Rev. Lett. **105**, 191802 (2010), [arXiv:1007.4835].
- [237] G. Aad *et al.* (ATLAS), Phys. Rev. Lett. **115**, 3, 031801 (2015), [arXiv:1503.04430].
- [238] M. Aaboud *et al.* (ATLAS), Eur. Phys. J. **C76**, 10, 541 (2016), [arXiv:1607.08079].
- [239] V. Khachatryan *et al.* (CMS), Eur. Phys. J. **C76**, 6, 317 (2016), [arXiv:1604.05239].
- [240] G. Aad *et al.* (ATLAS), JHEP **23**, 082 (2020), [arXiv:2307.08567].
- [241] H. K. Dreiner *et al.*, JHEP **07**, 215 (2023), [arXiv:2306.07317].
- [242] J. Fan, M. Reece and J. T. Ruderman, JHEP **11**, 012 (2011), [arXiv:1105.5135].
- [243] J. Fan, M. Reece and J. T. Ruderman, JHEP **07**, 196 (2012), [arXiv:1201.4875].
- [244] J. Fan *et al.*, JHEP **07**, 016 (2016), [arXiv:1512.05781].
- [245] V. Khachatryan *et al.* (CMS), Phys. Lett. **B 743**, 503 (2015), [arXiv:1411.7255].
- [246] (2023).
- [247] Technical report, CERN, Geneva (2023), all figures including auxiliary figures are available at <https://atlas.web.cern.ch/Atlas/GROUPS/PHYSICS/CONFNOTES/ATLAS-CONF-2023-044>, URL <https://cds.cern.ch/record/2870112>.
- [248] M. Aaboud *et al.* (ATLAS), Phys. Rev. **D97**, 5, 052012 (2018), [arXiv:1710.04901].
- [249] M. Aaboud *et al.* (ATLAS), Phys. Rev. **D99**, 9, 092007 (2019), [arXiv:1902.01636].
- [250] G. Aad *et al.* (ATLAS), Eur. Phys. J. **C75**, 9, 407 (2015), [arXiv:1506.05332].
- [251] A. M. Sirunyan *et al.* (CMS), Phys. Lett. **B797**, 134876 (2019), [arXiv:1906.06441].
- [252] A. M. Sirunyan *et al.* (CMS), JHEP **05**, 025 (2018), [arXiv:1802.02110].
- [253] CMS Collab., CMS-PAS-EXO-16-036 (2016).
- [254] A. M. Sirunyan *et al.* (CMS), Phys. Lett. **B 806**, 135502 (2020), [arXiv:2004.05153].
- [255] A. M. Sirunyan *et al.* (CMS), Phys. Rev. **D 104**, 1, 012015 (2021), [arXiv:2012.01581].
- [256] V. M. Abazov *et al.* (D0), Phys. Rev. Lett. **99**, 131801 (2007), [arXiv:0705.0306].
- [257] G. Aad *et al.* (ATLAS), Phys. Rev. **D88**, 11, 112003 (2013), [arXiv:1310.6584].
- [258] A. M. Sirunyan *et al.* (CMS), JHEP **05**, 127 (2018), [arXiv:1801.00359].
- [259] G. Aad *et al.* (ATLAS), JHEP **07**, 173 (2021), [arXiv:2104.03050].
- [260] T. Aaltonen *et al.* (CDF), Phys. Rev. Lett. **103**, 021802 (2009), [arXiv:0902.1266].
- [261] V. M. Abazov *et al.* (D0), Phys. Rev. **D87**, 5, 052011 (2013), [arXiv:1211.2466].
- [262] G. Aad *et al.* (ATLAS), Phys. Rev. **D 102**, 3, 032006 (2020), [arXiv:2003.11956].
- [263] A. Tumasyan *et al.* (CMS), Eur. Phys. J. **C 82**, 2, 153 (2022), [arXiv:2110.04809].

- [264] A. M. Sirunyan *et al.* (CMS), JHEP **08**, 016 (2018), [arXiv:1804.07321].
- [265] M. Aaboud *et al.* (ATLAS), JHEP **06**, 022 (2018), [arXiv:1712.02118].
- [266] G. Aad *et al.* (ATLAS), Phys. Rev. **D88**, 11, 112006 (2013), [arXiv:1310.3675].
- [267] G. Aad *et al.* (ATLAS), Eur. Phys. J. C **82**, 7, 606 (2022), [arXiv:2201.02472].
- [268] G. Aad *et al.* (ATLAS), JHEP **2306**, 158 (2023), [arXiv:2205.06013].
- [269] Technical report, CERN, Geneva (2023), URL <https://cds.cern.ch/record/2859611>.
- [270] LEP2 SUSY Working Group, ALEPH, DELPHI, L3 and OPAL experiments, note LEPSUSYWG/02-05.1, <http://lepsusy.web.cern.ch/lepsusy>.
- [271] V. Khachatryan *et al.* (CMS), Eur. Phys. J. **C75**, 7, 325 (2015), [arXiv:1502.02522].
- [272] T. Aaltonen *et al.* (CDF), Phys. Rev. **D88**, 3, 031103 (2013), [arXiv:1307.0474].
- [273] A. M. Sirunyan *et al.* (CMS) (2019), [arXiv:1909.06166].
- [274] V. M. Abazov *et al.* (D0), Phys. Rev. Lett. **101**, 111802 (2008), [arXiv:0806.2223].
- [275] G. Aad *et al.* (ATLAS), Phys. Rev. **D90**, 11, 112005 (2014), [arXiv:1409.5542].
- [276] G. Aad *et al.* (ATLAS), JHEP **12**, 081 (2023), [arXiv:2307.14759].
- [277] O. Buchmueller *et al.*, Eur. Phys. J. **C71**, 1722 (2011), [arXiv:1106.2529].
- [278] E. A. Baltz and P. Gondolo, JHEP **10**, 052 (2004), [hep-ph/0407039].
- [279] B. C. Allanach and C. G. Lester, Phys. Rev. **D73**, 015013 (2006), [hep-ph/0507283].
- [280] R. Ruiz de Austri, R. Trotta and L. Roszkowski, JHEP **05**, 002 (2006), [hep-ph/0602028].
- [281] R. Lafaye *et al.*, Eur. Phys. J. **C54**, 617 (2008), [arXiv:0709.3985].
- [282] M. Shaposhnikov, JHEP **08**, 008 (2008), [arXiv:0804.4542].
- [283] R. Trotta *et al.*, JHEP **12**, 024 (2008), [arXiv:0809.3792].
- [284] P. Bechtle *et al.*, Eur. Phys. J. **C66**, 215 (2010), [arXiv:0907.2589].
- [285] E. Bagnaschi *et al.*, Eur. Phys. J. C **78**, 256, 1 (2018).
- [286] J. Costa *et al.*, Eur. Phys. J. C **78**, 158, 1 (2018).
- [287] E. Bagnaschi *et al.*, Eur. Phys. J. **C77**, 4, 268 (2017), [arXiv:1612.05210].
- [288] E. Bagnaschi *et al.*, Eur. Phys. J. **C77**, 2, 104 (2017), [arXiv:1610.10084].
- [289] L. A. Harland-Lang, V. A. Khoze and M. G. Ryskin, Eur. Phys. J. **C76**, 1, 9 (2016), [arXiv:1508.02718].
- [290] E. A. Bagnaschi *et al.*, Eur. Phys. J. **C75**, 500 (2015), [arXiv:1508.01173].
- [291] O. Buchmueller *et al.*, Eur. Phys. J. **C74**, 12, 3212 (2014), [arXiv:1408.4060].
- [292] M. Citron *et al.*, Phys. Rev. **D87**, 3, 036012 (2013), [arXiv:1212.2886].
- [293] F. Ambrogio *et al.*, Eur. Phys. J. C **78**, 3, 215 (2018), [arXiv:1707.09036].
- [294] E. Bagnaschi *et al.*, Eur. Phys. J. C **79**, 2, 149 (2019), [arXiv:1810.10905].
- [295] A. Arbey *et al.*, Phys. Rev. D **106**, 5, 055002 (2022), [arXiv:2201.00070].
- [296] Supersymmetry Physics Results, ATLAS experiment, <http://twiki.cern.ch/twiki/bin/view/AtlasPublic/SupersymmetryPublicResults/>.
- [297] Supersymmetry Physics Results, CMS experiment, <http://cms-results.web.cern.ch/cms-results/public-results/publications/SUS/index.html>.

90. Axions and Other Similar Particles

Revised August 2023 by L. J. Rosenberg (U. Washington), G. Rybka (U. Washington) and B. Safdi (UC Berkeley).

90.1 Introduction

In this section, we list coupling-strength and mass limits for light neutral scalar or pseudoscalar bosons that couple weakly to normal matter and radiation. Such bosons may arise from the spontaneous breaking of a global U(1) symmetry, resulting in a massless Nambu-Goldstone (NG) boson. If there is a small explicit symmetry breaking, either already in the Lagrangian or due to quantum effects such as anomalies, the boson acquires a mass and is called a pseudo-NG boson. Typical examples are axions (a) [1–4] and majorons [5, 6], associated, respectively, with a spontaneously broken Peccei-Quinn PQ and lepton-number symmetry. Axions may also arise in extra dimension constructions as the zero-modes of higher-dimensional gauge fields compactified on internal manifolds; in this case, the absence of a local contribution to the axion mass is due to the higher-dimensional gauge symmetry [7, 8].

A common feature of these light bosons ϕ is that their coupling to Standard-Model particles is suppressed by the energy scale that characterizes the symmetry breaking, *i.e.*, the decay constant f . For example, in models where the axion arises as a Goldstone boson, the interaction Lagrangian at energy scales below f is

$$\mathcal{L} = f^{-1} J^\mu \partial_\mu \phi, \quad (90.1)$$

where J^μ is the Noether current of the spontaneously broken global symmetry. If f is very large, these new particles interact very weakly. Detecting them would provide a window to physics far beyond what can be probed at accelerators.

Axions are of particular interest because the PQ mechanism is a compelling scheme to preserve CP -symmetry in QCD. Moreover, the cold dark matter (CDM) of the Universe may well consist of axions and they are searched for in dedicated experiments with a realistic chance of discovery.

Originally it was assumed that the PQ scale f_a was related to the electroweak symmetry-breaking scale $v_{EW} = (\sqrt{2}G_F)^{-1/2} = 246.22$ GeV. However, the associated “standard” and “variant” axions were quickly excluded—we refer to the Listings for detailed limits. Here we focus on “invisible axions” with $f_a \gg v_{EW}$ as the main possibility.

Axions have a characteristic two-photon vertex, inherited from their mixing with π^0 and η . This coupling allows for the main search strategy based on axion-photon conversion in external magnetic fields [9], an effect that also can be of astrophysical interest. While for axions the product “ $a\gamma\gamma$ interaction strength \times mass” is essentially fixed by the corresponding π^0 properties, one may consider a more general class of axion-like particles (ALPs) where the two parameters (coupling and mass) are independent. A number of experiments explore this more general ALP parameter space. ALPs populating the latter are predicted to arise generically, in addition to the axion, in low-energy effective field theories emerging from string theory [7, 8, 10–16]. The latter may contain also very light Abelian vector bosons under which the Standard-Model particles are not charged: so-called hidden-sector photons, dark photons or paraphotons. They share a number of phenomenological features with the axion and ALPs, notably the possibility of hidden photon-to-photon conversion and of hidden photon dark matter [17–19]. Their physics cases and the current constraints are compiled in Refs. [20–23].

90.2 Theory

90.2.1 Peccei-Quinn mechanism and axions

The QCD Lagrangian includes a CP -violating term $\mathcal{L}_\Theta = -\bar{\Theta}(\alpha_s/8\pi)G^{\mu\nu a}\tilde{G}_{\mu\nu}^a$, where $-\pi \leq \bar{\Theta} \leq +\pi$ is the effective Θ parameter after diagonalizing quark masses, $G_{\mu\nu}^a$ is the color field strength tensor, and $\tilde{G}^{a,\mu\nu} \equiv \epsilon^{\mu\nu\lambda\rho}G_{\lambda\rho}^a/2$, with $\epsilon^{0123} = 1$, its dual. This term induces an electric dipole moment (EDM) of the neutron of strength $d_n = C_{EDM}e\bar{\Theta}$. The coefficient C_{EDM} is calculated using QCD sum rules as $C_{EDM} = 2.4(1.0) \times 10^{-16}$ cm [24], while lattice QCD computations find $C_{EDM} = 1.48(14)(31) \times 10^{-16}$ cm [25] including statistical and

systematic uncertainties. Experimental upper bounds on the latter, $|d_n| < 1.8 \times 10^{-26}$ e cm [26, 27], imply $|\bar{\Theta}| \lesssim 10^{-10}$ even though $\bar{\Theta} = \mathcal{O}(1)$ is otherwise completely satisfactory. Note that the proton has a similar EDM as the neutron, but it is less strongly constrained at present; this could change in the future [28]. The proton EDM may be written as $d_p = C_{EDM}^p e\bar{\Theta}$, with $C_{EDM}^p = -3.8(11)(8)$ [25]. The opposite signs of the neutron and proton EDMs may be understood from the opposite signs of their magnetic moments. The spontaneously broken global PQ symmetry U(1)_{PQ} was introduced to solve the “strong CP problem” [1, 2] of small $\bar{\Theta}$, the axion being the pseudo-NG boson of U(1)_{PQ} [3, 4]. This symmetry is broken due to the axion’s anomalous triangle coupling to gluons,

$$\mathcal{L} = \left(\frac{a}{f_a} - \bar{\Theta} \right) \frac{\alpha_s}{8\pi} G^{\mu\nu a} \tilde{G}_{\mu\nu}^a, \quad (90.2)$$

where a is the axion field and f_a the axion decay constant. Color anomaly factors have been absorbed in the normalization of f_a which is defined by this Lagrangian. Thus normalized, f_a is the quantity that enters all low-energy phenomena [29]. Non-perturbative topological fluctuations of the gluon fields in QCD induce a potential for a whose minimum is at $a = \bar{\Theta} f_a$, thereby canceling the $\bar{\Theta}$ term in the QCD Lagrangian and thus restoring CP symmetry.

The resulting axion mass, in units of the PQ scale f_a , is identical to the square root of the topological susceptibility in QCD, $m_a f_a = \sqrt{\chi}$. The latter can be evaluated further [30, 31], exploiting the chiral limit (masses of up and down quarks much smaller than the scale of QCD), yielding $m_a f_a = \sqrt{\chi} \approx f_\pi m_\pi$, where $m_\pi \approx 135$ MeV and $f_\pi \approx 92$ MeV. In more detail one finds, by including $\mathcal{O}(\alpha)$ QED corrections and next-to-next-to-leading order (NNLO) corrections in chiral perturbation theory [32],

$$m_a = 5.691(51) \left(\frac{10^9 \text{ GeV}}{f_a} \right) \text{meV}. \quad (90.3)$$

A direct calculation of the topological susceptibility via QCD lattice simulations finds almost the same central value, albeit with an about five times larger error bar [33].

The QCD axion acquires a variety of couplings to low-energy Standard Model observables, as we discuss in detail in this review. The most model-independent couplings are those of the axion to the neutron and proton EDM operators. While the axion removes the static neutron and proton EDMs, displacements of the axion field a from its vacuum expectation value induce field-dependent EDMs, which are characterized through the operator

$$\mathcal{L}_{aN\gamma} = -\frac{i}{2} g_{aN\gamma} a \bar{\Psi}_N \sigma_{\mu\nu} \gamma_5 \Psi_N F^{\mu\nu}, \quad (90.4)$$

with $N = n, p$ for neutrons or protons, respectively. The coupling $g_{aN\gamma}$ is related to C_{EDM} by $g_{aN\gamma} = eC_{EDM}/f_a$ and similarly for $g_{ap\gamma}$. Direct probes of the axion-EDM operators are difficult, though by studying the thermal production of axions in the early universe one can broadly constrain, using Planck and Baryon Acoustic Oscillation (BAO) data, $m_a \lesssim 0.3$ eV [34]. In the presence of an oscillatory relic axion DM field, this operator induces an oscillating neutron EDM; this effect forms the basis of the CASPEr experiment [35, 36] that is discussed more later in this review. Non-linearly realized discrete-symmetries may be used to suppress the QCD axion mass below the prediction in Eq. (90.3), in which case a variety of cosmological and terrestrial constraints on the operator in Eq. (90.4) are also relevant [37–44]

Axions with $f_a \gg v_{EW}$ evade almost all current experimental limits. One generic class of models invokes “hadronic axions” where new heavy quarks carry U(1)_{PQ} charges, leaving ordinary quarks and leptons without tree-level axion couplings. The archetype is the KSVZ model [45, 46], where in addition the heavy new quarks are electrically neutral. Another generic class of axion models requires at least two Higgs doublets and ordinary quarks and leptons carry PQ charges, the archetype being the DFSZ model [47, 48]; in this case the quarks and leptons may

where $C_{a\pi} = 2(C_p - C_n)/(3g_A)$ and g_A is the nucleon axial charge $g_A = 1.2723(23)$. Additionally, there are axion-pion-nucleon interactions of the form

$$\mathcal{L}_{a\pi N} = \frac{C_{a\pi N}}{2f_\pi f_a} \partial_\mu a \left(i\pi^+ \bar{p}\gamma^\mu n - i\pi^- \bar{n}\gamma^\mu p \right), \quad (90.14)$$

where $C_{a\pi N} = (C_{ap} - C_{an})/(\sqrt{2}g_A)$.

90.3 Laboratory Searches

90.3.1 Light shining through walls

Searching for “invisible axions” is extremely challenging due to their extraordinarily feeble coupling to normal matter and radiation. Currently, the most promising approaches rely on the axion-two-photon interaction, allowing for axion-photon conversion in external electric or magnetic fields [9]. For the Coulomb field of a charged particle, the conversion can be viewed as a scattering process, $\gamma + Ze \leftrightarrow Ze + a$, called Primakoff effect [178]. In the other extreme of a macroscopic field, usually a large-scale B -field, the momentum transfer is small, the interaction is coherent over a large distance, and the conversion can be viewed as an axion-photon oscillation phenomenon in analogy to neutrino flavor oscillations [179].

Photons propagating through a transverse magnetic field, with incident \mathbf{E}_γ and magnetic field \mathbf{B} parallel, may convert into axions. For $m_a^2 L/2\omega \ll 2\pi$, where L is the length of the B field region and ω the photon energy, the resultant axion beam is coherent with the incident photon beam and the conversion probability is $\Pi \sim (1/4)(g_{a\gamma\gamma}BL)^2$. One such realization uses a laser beam propagating down the bore of a superconducting dipole magnet (like, say, the bending magnets in high-energy accelerators). If another magnet is in line with the first, but shielded by an optical barrier, then photons may be regenerated from the pure axion beam [180, 181]. The overall probability is $P(\gamma \rightarrow A \rightarrow \gamma) = \Pi^2$.

The first such Light-Shining-through-Walls (LSW) experiment was performed by the BFRT (Brookhaven-Fermilab-Rochester-Trieste) collaboration. It utilized two magnets of length $L = 4.4$ m and $B = 3.7$ T and found $|g_{a\gamma\gamma}| < 6.7 \times 10^{-7}$ GeV $^{-1}$ at 95% CL for $m_a < 1$ meV [182, 183]. More recently, several such experiments were performed (see Listings) [98, 101, 184–188]. The current best limit, $|g_{a\gamma\gamma}| < 3.5 \times 10^{-8}$ GeV $^{-1}$ at 95% CL for $m_a \lesssim 0.3$ meV (see Fig. 90.1), has been achieved by the OSQAR (Optical Search for QED Vacuum Birefringence, Axions, and Photon Regeneration) experiment, which exploited two 9 T LHC dipole magnets and an 18.5 W continuous wave laser emitting at the wavelength of 532 nm [101]. The ALPS I (Any Light Particle Search I) experiment achieved a similar sensitivity [98], see Fig. 90.1. Some of these experiments have also reported limits for scalar bosons where the photon \mathbf{E}_γ must be chosen perpendicular to the magnetic field \mathbf{B} .

The concept of resonantly enhanced photon regeneration may open unexplored regions of coupling strength [189–191]. In this scheme, both the production and detection magnets are within Fabry-Perot optical cavities and actively locked in frequency. The $\gamma \rightarrow a \rightarrow \gamma$ rate is enhanced by a factor $\mathcal{F}\mathcal{F}'/\pi^2$ relative to a single-pass experiment, where \mathcal{F} and \mathcal{F}' are the finesses of the two cavities. The resonant enhancement could be of order $10^{(10-12)}$, improving the $g_{a\gamma\gamma}$ sensitivity by $10^{(2.5-3)}$. The experiment ALPS II (Any Light Particle Search II) is based on this concept and aims at an improvement of the current laboratory bound on $g_{a\gamma\gamma}$ by a factor $\sim 10^3$ [192]. ALPS II began operations in 2023.

Resonantly enhanced photon regeneration has already been exploited in experiments searching for “radiowaves shining through a shielding” [193–196]. For $m_a \lesssim 10^{-5}$ eV, the upper bound on $g_{a\gamma\gamma}$ established by the CROWS (CERN Resonant Weakly Interacting sub-eV Particle Search) experiment [100] is slightly less stringent than the one set by OSQAR, see Fig. 90.1.

90.3.2 Photon polarization

An alternative to regenerating the lost photons is to use the beam itself to detect conversion: the polarization of light propagating through a transverse B field undergoes dichroism and birefringence [197]. Dichroism: The E_\parallel component, but not E_\perp , is

depleted by axion production, causing a small rotation of linearly polarized light. For $m_a^2 L/2\omega \ll 2\pi$, the effect is independent of m_a . For heavier axions, it oscillates and diminishes as m_a increases, and it vanishes for $m_a > \omega$. Birefringence: This effect occurs because there is mixing of virtual axions in the E_\parallel state, but not for E_\perp . Hence, linearly polarized light will develop elliptical polarization. Higher-order QED also induces vacuum magnetic birefringence (VMB). A search for these effects was performed in the same dipole magnets of the BFRT experiment mentioned before [198]. The dichroic rotation gave a stronger limit than the ellipticity rotation: $|g_{a\gamma\gamma}| < 3.6 \times 10^{-7}$ GeV $^{-1}$ at 95% CL, for $m_a < 5 \times 10^{-4}$ eV. The ellipticity limits are better at higher masses, as they fall off smoothly and do not terminate at m_a .

90.3.3 Long-range forces

New bosons would mediate new long-range forces, which are severely constrained by “fifth force” experiments [199]. Those looking for new mass-spin couplings provide significant constraints on pseudoscalar bosons [200–205], see for example in Fig. 90.3 the limit on the axion-neutron coupling [206] from torsion balance tests of the gravitational inverse square law [207]. Presently, the most restrictive limits are obtained from combining long-range force measurements with stellar cooling arguments [208, 209]. For the moment, any of these limits are far from realistic values expected for the QCD axion. Still, these efforts provide constraints on more general low-mass bosons.

In Ref. [210], a method was proposed that can extend the search for axion-mediated spin-dependent forces by several orders of magnitude. By combining techniques used in nuclear magnetic resonance and short-distance tests of gravity, this method appears to be sensitive to the QCD axion in the $\mu\text{eV} - \text{meV}$ mass range, independent of the cosmic axion abundance, if axions have a CP -violating interaction with nuclei as large as the current experimental bound on the electric dipole moment of the neutron allows. (Note that the CP -violation already present in the Standard Model is sufficient for generating an axion-mediated force, though in this case the signal appears too small to be detectable for the QCD axion in the foreseeable future [210].) The ARIADNE (Axion Resonant InterAction Detection Experiment) is under development and employs this approach to search for axion-mediated spin-dependent short-range interactions between a hyper-polarized 3-He sample and an unpolarized tungsten source mass [211]. The method relies on superconducting magnetic shielding to screen the sample from ordinary magnetic field noise. Experimental tests to demonstrate the requirements of ARIADNE, including characterization of the magnetic field backgrounds, are under way [212, 213].

90.4 Axions from Astrophysical Sources

90.4.1 Stellar energy-loss limits

Axions are produced in hot astrophysical plasmas, and can thus transport energy out of stars. The coupling strength of these particles with normal matter and radiation is bounded by the constraint that stellar lifetimes or energy-loss rates are not in conflict with observation [214, 215].

We begin this discussion with our Sun and concentrate first on the axion-photon coupling. In the Sun axions are produced by the Primakoff process $\gamma + Ze \rightarrow Ze + a$. Integrating this process over a standard solar model yields the axion luminosity [216]

$$L_a = g_{10}^2 \times 1.85 \times 10^{-3} L_\odot, \quad (90.15)$$

where $g_{10} = |g_{a\gamma\gamma}| \times 10^{10}$ GeV. The maximum of the spectrum is at 3.0 keV, the average at 4.2 keV, and the number flux at Earth is $g_{10}^2 \times 3.75 \times 10^{11}$ cm $^{-2}$ s $^{-1}$. The solar photon luminosity is fixed, so energy losses due to the Primakoff process require enhanced nuclear energy production and thus enhanced neutrino fluxes. The all-flavor measurements by SNO (Sudbury Neutrino Observatory), together with a standard solar model, imply $L_a \lesssim 0.10 L_\odot$, corresponding to $g_{10} \lesssim 7$ [217], mildly superseding a similar limit from helioseismology (sound speed, surface helium and convective radius) [218]. In Ref. [147], this limit was improved to $g_{10} < 4.1$ (at 3σ), see Fig. 90.1, exploiting a new statistical analysis that combined helioseismology and solar neutrino observations, including

theoretical and observational errors, and accounting for tensions between input parameters of solar models, in particular the solar element abundances. Going beyond the axion-photon coupling, Ref. [217] considered also a non-zero axion-electron coupling and obtained the bound on the latter displayed in Fig. 90.2.

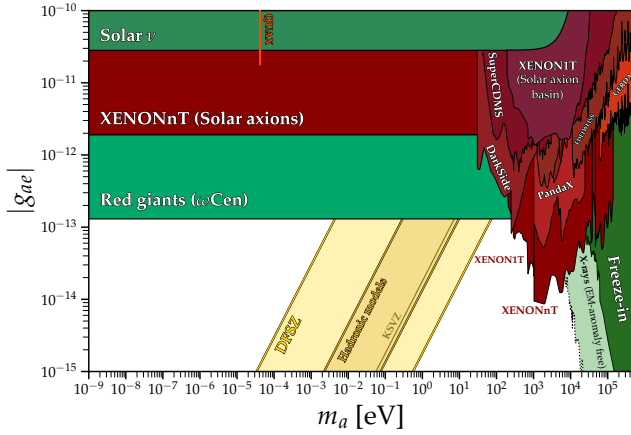


Figure 90.2: Exclusion plot for ALP-electron coupling as described in the text. Figure courtesy of Ciaran O’Hare [61], contains data from refs. [168, 217, 219–228]. The hadronic QCD axion-electron coupling arises at one loop and is given in Eq. (90.9); varying E/N between $5/3$ and $44/3$ gives the indicated hadronic axion band. The KSVZ axion has $E/N = 0$, while the DFSZ axion-electron coupling has the tree-level coupling given in Eq. (90.10) that depends on the unknown but bounded value of $\tan\beta$ (see text for details).

A more restrictive limit derives from globular-cluster (GC) stars that allow for detailed tests of stellar-evolution theory. The stars on the horizontal branch (HB) in the color-magnitude diagram have reached helium burning with a core-averaged energy release of about $80 \text{ erg g}^{-1} \text{ s}^{-1}$, compared to Primakoff axion losses of $g_{10}^2 30 \text{ erg g}^{-1} \text{ s}^{-1}$. The accelerated consumption of helium reduces the HB lifetime by about $80/(80 + 30 g_{10}^2)$. In contrast, the red giant (RG) branch stars are not strongly affected by Primakoff losses, since unlike for the HB stars the plasma frequency in the RG stellar cores is below the temperature. Thus, Primakoff production reduces the R -parameter, which is the number of observed HB branch stars to RG branch stars in a GC. Measurements of the R -parameter in a large sample of 39 Galactic GCs

give a weak indication of non-standard losses which may be accounted by Primakoff-like axion emission, if the photon coupling is in the range $|g_{a\gamma\gamma}| = (2.9 \pm 1.8) \times 10^{-11} \text{ GeV}^{-1}$ [122, 229]. Still, the upper bound found in this analysis,

$$|g_{a\gamma\gamma}| < 6.6 \times 10^{-11} \text{ GeV}^{-1} \text{ (95\% CL)}, \quad (90.16)$$

represents one of the strongest limits on $g_{a\gamma\gamma}$ for a wide mass range. More recently, the R_2 -parameter has emerged as a potentially more sensitive probe of axions; the R_2 -parameter is defined as the ratio of the asymptotic giant branch (AGB) stars to the HB stars in a GC. AGB stars have more efficient Primakoff production than HB stars, meaning that R_2 is expected to decrease for increasing $|g_{a\gamma\gamma}|$. Ref. [123] used an R_2 measurement based off of 48 GCs as observed by the Hubble Space Telescope [230] to constrain

$$|g_{a\gamma\gamma}| < 4.7 \times 10^{-11} \text{ GeV}^{-1} \text{ (95\% CL)}. \quad (90.17)$$

The constraint above on $g_{a\gamma\gamma}$ may be translated to $f_a > 4.8 \times 10^7 \text{ GeV}$ ($m_a < 0.12 \text{ eV}$), using $E/N = 0$ as in the KSVZ model, or to $f_a > 1.8 \times 10^7 \text{ GeV}$ ($m_a < 0.32 \text{ eV}$), for the DFSZ axion model, with $E/N = 8/3$, see Fig. 90.1.

If axions couple directly to electrons, the dominant emission processes are atomic axio-recombination and axio-deexcitation, axio-bremsstrahlung in electron-ion or electron-electron collisions, and Compton scattering [231]. Stars in the RG branch of the

color-magnitude diagram of GCs are particularly sensitive to these processes: they would lead to an extension of the latter to larger brightness. In fact, the tip of the RG branch (TRGB) – the brightest point of the RG branch – provides the currently most sensitive method to test the axion coupling to electrons. The strongest bounds on it are derived from analyses of the TRGB in several GCs [232] and in the Galactic GC ω Centauri [226]. The two analyses lead to very similar results,

$$|g_{aee}| < 1.48 \times 10^{-13} \text{ (95\% CL)} \text{ and } |g_{aee}| < 1.3 \times 10^{-13} \text{ (95\% CL)}, \quad (90.18)$$

respectively, see Fig. 90.2. Reference [232] finds also a small hint for extra cooling, corresponding to $|g_{aee}| = 0.60^{+0.32}_{-0.58} \times 10^{-13}$, while Ref. [226] does not find any evidence for exotic cooling.

Bremsstrahlung is also efficient in white dwarfs (WDs), where the Primakoff and Compton processes are suppressed by the large plasma frequency. A comparison of the predicted and observed luminosity function of WDs can be used to put limits on $|g_{aee}|$ [233, 234]. An analysis based on detailed WD cooling treatment and data on the WD luminosity function (WDLF) of the Galactic disk found that electron couplings above $|g_{aee}| \gtrsim 3 \times 10^{-13}$ are disfavoured [235]. Lower couplings cannot be discarded from the current knowledge of the WDLF of the Galactic disk [235–237]. These probes may be improved by the Rubin Observatory Large Synoptic Survey Telescope (LSST), which is expected to increase the sample of WDs in the Galactic halo to hundreds of thousands [238]. For pulsationally unstable WDs (ZZ Ceti stars), the period decrease \dot{P}/P is a measure of the cooling speed. The corresponding observations of a handful pulsating WDs imply additional cooling that can be interpreted in terms of axion energy losses [239–243], though with axion-electron coupling values likely incompatible with other constraints [244].

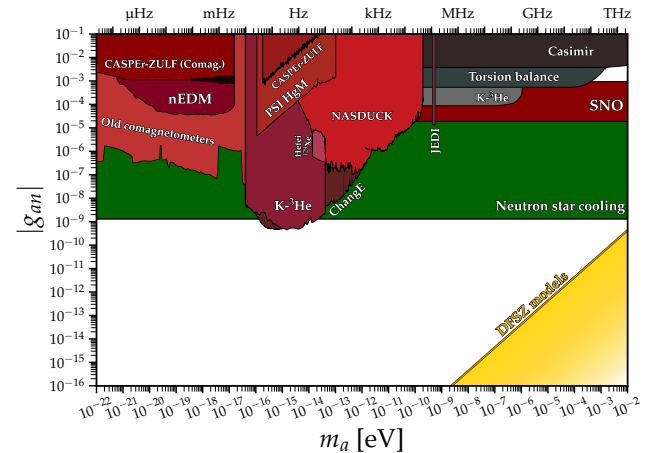


Figure 90.3: Exclusion plot for ALP-neutron coupling as described in the text. Figure courtesy of Ciaran O’Hare [61], includes data from refs. [40, 42, 206, 245–255]. The hadronic axion model prediction is given in Eq. (90.11) with vanishing quark couplings, while the DFSZ model prediction depends on $\tan\beta$ as is found in Eq. (90.12), giving the shaded yellow region above. Note that for a fine-tuned value of $\tan\beta$ g_{an} can be taken to zero. On the other hand, the neutron star cooling constraints [254] also probe the axion-proton coupling g_{ap} at a comparable level (not shown), and both g_{an} and g_{ap} cannot simultaneously be taken to zero in the DFSZ model.

Analogous constraints derive from neutron stars (NS) cooling. Broadly speaking, there are two classes of NS cooling searches for axions. One approach uses the proto-NS formed after SN 1987A to constrain the axion luminosity produced during the first seconds of the proto-NS when the neutrino luminosity is measured with terrestrial experiments. The second class of NS cooling constraints consider older NSs, typically much older than $\sim 100 \text{ yr}$, and constrains the axion luminosity using the surface temperature as measured with photons versus the age of NS as measured

through *e.g.* kinematic considerations. We begin with a discussion of the limits from SN 1987A.

Numerical simulations reveal that the energy-loss rate due to axions in a nuclear medium at the density $3 \times 10^{14} \text{ g cm}^{-3}$ and temperature 30 MeV should not exceed about $1 \times 10^{19} \text{ erg g}^{-1} \text{ s}^{-1}$ to be consistent with the neutrino signal observed from SN 1987A [256]. The energy-loss rate from nucleon bremsstrahlung, $N + N \rightarrow N + N + a$, is $(C_N/2f_a)^2(T^4/\pi^2 m_N)F$. Here F is a numerical factor that represents an integral over the dynamical spin-density structure function because axions couple to the nucleon spin. For realistic conditions, even after considerable effort, one is limited to a heuristic estimate leading to $F \approx 1$ [215]. The SN 1987A limits are of particular interest for hadronic axions where the bounds on $|g_{aee}|$ are moot. Using a proton fraction of 0.3, $g_{ann} = 0$, $F = 1$, and $T = 30 \text{ MeV}$, one finds $f_a > 4 \times 10^8 \text{ GeV}$ and $m_a < 16 \text{ meV}$ [215]. A more detailed numerical calculation [257] with state of the art SN models, again assuming $g_{ann} = 0$, found that a coupling larger than $|g_{app}| \gtrsim 6 \times 10^{-10}$, would shorten significantly the timescale of the neutrino emission. This result is, not surprisingly, rather close to the estimate in Ref. [215]. Improving the calculation of axion emission via nucleon-nucleon bremsstrahlung beyond the basic one-pion exchange approximation appears to loosen the bound [258, 259]. The latter analysis finds a reduction of the axion emissivity by an order of magnitude if one takes into account the non-vanishing mass of the exchanged pion, the contribution from two-pion exchange, effective in-medium nucleon masses and multiple nucleon scattering, leading to the result [259]

$$g_{ann}^2 + 0.61 g_{app}^2 + 0.53 g_{ann} g_{app} < 8.26 \times 10^{-19}, \quad (90.19)$$

which is consistent with the original estimate in [215]. This analysis, however, still neglects another very efficient mechanism for axion production in a SN: the pion production process, $\pi^- + p \rightarrow a + n$, also induced by the axion coupling to nucleons. Pion production was recognized long ago as being competitive with nucleon bremsstrahlung [260–262]. However, only recently it was shown that the pion abundance in the early stages of a SN is much larger than previously expected [263]. It was shown in Ref. [264] that pion induced processes dominate over bremsstrahlung and so strengthen the bound on the axion-nucleon coupling. On the other hand, given the modeling uncertainties and the sparse data from SN 1987A, the constraint on the axion-nucleon couplings from SN 1987A should be considered more as indicative than as a sharp bound [257]. Furthermore, note that if axions interact sufficiently strongly they are trapped. Only about three orders of magnitude in g_{aNN} , where $N = n, p$, or m_a are excluded. For even larger couplings, the axion flux would have been negligible, yet it would have triggered additional events in the detectors, excluding a further range [265].

Further bounds on the axion-nucleon coupling can be derived from observations of the cooling of older NSs. Recently, strong constraints were obtained by modeling the cooling of the “Magnificent Seven” (M7) NSs in the presence of axions [254]. Axion emission would accelerate NS cooling. Thus, if the age and temperature of a NS are independently known, then by modeling axion-induced cooling in conjunction with the standard NS cooling mechanisms, in particular cooling via neutrino emission from the bulk of the NS and thermal emission from the NS surface, one is able to constrain the axion’s coupling strength. Ref. [254] used a sample of four of the M7 along with PSR J0659 to constrain $m_a < 16 \text{ meV}$ for the KSVZ QCD axion at 95% CL and $m_a \lesssim 5 \text{ meV}$ ($m_a \lesssim 30 \text{ meV}$) in the DFSZ scenario for asymptotically large (small) $\tan \beta$. For axions that couple exclusively to neutrons (protons) Ref. [254] constrains $|g_{ann}| < 1.3 \times 10^{-9}$ ($|g_{app}| < 1.5 \times 10^{-9}$), as illustrated in Fig. 90.3. The five NSs used in that work are unique in that their ages, all in the range 0.1–1 Myr, are known by kinematic measurements (*e.g.*, tracing back to the SN remnant), while their surface temperatures are measured in the X-ray band. Beyond statistical uncertainties on these measurements, there are a number of confounding systematic uncertainties that must be accounted for in NS cooling analyses, including uncertainties related to the core-surface temperature relation, which involves the chemical composition of the

NS envelope. The NS equation of state and the superfluid critical temperatures of the dense nuclear matter are also sources of uncertainty. Note that axions are predominantly produced by nuclear bremsstrahlung [266, 267] except for temperatures near the superfluid critical temperature, when Cooper pair breaking and formation (PBF) processes may efficiently produce axions [268, 269]. Given the large densities it is crucial to account for medium dependent couplings when computing the axion luminosities [270].

The young NS in the supernova remnant Cassiopeia A (Cas A) was previously thought to strongly constrain axions, at a level similar to the NS cooling bound described above, due to PBF axion production [271]. This is because it was observed that Cas A was cooling rapidly, which may be explained by neutrino cooling with neutron superfluidity and proton superconductivity [272, 273]. However, it is possible that the excessive cooling of Cas A is at least in part instrumental in origin [274]. Fully accounting for uncertainties on both the NS properties and the data, constraints from young NSs such as Cas A and the NS in the supernova remnant HESS J1731-347 [275] appear to be subdominant compared to the limits from SN 1987A and the M7 [254].

Finally, let us note that if $m_a \sim \text{meV}$, SNe would lose a large fraction of their energy as axions. This would lead to a diffuse SN axion background in the Universe with an energy density comparable to the extra-galactic background light [276]. However, there is no apparent way of detecting it or the axion burst from the next nearby SN. On the other hand, neutrino detectors such as IceCube, Super-Kamiokande or a future mega-ton water Cherenkov detector will probe exactly the mass region of interest by measuring the neutrino pulse duration of the next Galactic SN [257].

90.4.2 Searches for solar axions and ALPs

Instead of using stellar energy losses to derive axion limits, one can also search directly for these fluxes, notably from the Sun. The main focus has been on ALPs with a two-photon vertex. They are produced by the Primakoff process with a flux given by Eq. (90.15) and an average energy of 4.2 keV, and can be detected at Earth with the reverse process in a macroscopic B -field (“axion helioscope”) [9]. In order to extend the sensitivity in mass towards larger values, one can endow the photon with an effective mass in a gas, ω_{plas} , and tune the mass to match the axion’s dispersion relation ($\omega_{\text{plas}} = m_a$) [277].

An early implementation of these ideas used a conventional dipole magnet, with a conversion volume of variable-pressure gas with a xenon proportional chamber as x-ray detector [278]. The conversion magnet was fixed in orientation and collected data for about 1000 s/day. Axions were excluded for $|g_{a\gamma\gamma}| < 3.6 \times 10^{-9} \text{ GeV}^{-1}$ for $m_a < 0.03 \text{ eV}$, and $|g_{a\gamma\gamma}| < 7.7 \times 10^{-9} \text{ GeV}^{-1}$ for $0.03 < m_a < 0.11 \text{ eV}$ at 95% CL.

Later, the Tokyo axion helioscope used a superconducting magnet on a tracking mount, viewing the Sun continuously. They reported $|g_{a\gamma\gamma}| < 6 \times 10^{-10} \text{ GeV}^{-1}$ for $m_a < 0.3 \text{ eV}$ [279, 280]. This experiment was recommissioned and a similar limit for masses around 1 eV was reported [281].

The most recent helioscope CAST (CERN Axion Solar Telescope) uses a decommissioned LHC dipole magnet on a tracking mount. The hardware includes grazing-incidence x-ray optics with solid-state x-ray detectors, as well as x-ray Micromegas position-sensitive gaseous detectors. Exploiting an IAXO (see below) pathfinder system, CAST has established the limit

$$|g_{a\gamma\gamma}| < 6.6 \times 10^{-11} \text{ GeV}^{-1} \quad (95\% \text{ CL}), \quad (90.20)$$

for $m_a < 0.02 \text{ eV}$ [99]. To cover larger masses, the magnet bores are filled with a gas at varying pressure. The runs with ^4He cover masses up to about 0.4 eV [282], providing the high-mass component of the CAST limits shown in Fig. 90.1. To cover yet larger masses, ^3He was used to achieve a larger pressure at cryogenic temperatures. Limits up to 1.17 eV allowed CAST to “cross the axion line” for the KSVZ model [283–285], see Fig. 90.1.

Sensitivity to significantly smaller values of $g_{a\gamma\gamma}$ can be achieved with a next-generation axion helioscope with a much larger magnetic-field cross section. Realistic design options for this “International Axion Observatory” (IAXO) have been studied in some detail [286] and its physics potential has been reviewed

recently [287]. Such a next-generation axion helioscope may also push the sensitivity in the product of couplings to photons and to electrons, $g_{a\gamma}g_{aee}$, into a range beyond stellar energy-loss limits and test the hypothesis that WD, RG, and HB cooling is dominated by axion emission [288,289]. As a first step towards IAXO, an intermediate experimental stage called BabyIAXO is currently under preparation at DESY [290].

Direct detection experiments searching for dark matter (DM) consisting of weakly interacting massive particles have also the capability to search for solar axions and ALPs. For low masses, $m_a \lesssim 100$ eV, the XENONnT experiment [291] has provided the most stringent bound among those experiments on the axion-electron coupling constant,

$$|g_{aee}| < 1.9 \times 10^{-12} \quad (90\% \text{ CL}), \quad (90.21)$$

see Fig. 90.2, by exploiting the axio-electric effect in liquid xenon. Slightly less stringent limits were set by PandaX-II [292] and by LUX [293]. However, this technique has not reached the sensitivity of energy-loss considerations in stars.

90.4.3 Conversion of astrophysical axion fluxes

Large-scale B fields exist in astrophysics that can induce axion-photon oscillations. In practical cases, the strength of B is much smaller than in the laboratory, whereas the conversion region L is much larger. Therefore, while the product BL can be large, realistic sensitivities are usually restricted to very low-mass particles, far away from the “QCD axion band” in a plot like Fig. 90.1.

One example of this is SN 1987A, which would have emitted a burst of ALPs due to the Primakoff production in its core. They would have partially converted into γ -rays in the Galactic B -field. The lack of a gamma-ray signal in the GRS instrument of the SMM satellite in coincidence with the observation of the neutrinos emitted from SN 1987A therefore provides a strong bound on their coupling to photons [294,295]. This bound has been revisited and the underlying physics has been brought to the current state-of-the-art, as far as modeling of the supernova and the Milky-Way magnetic field are concerned, resulting in the limit [151, 152] $|g_{a\gamma\gamma}| < 5.2 \times 10^{-12} \text{ GeV}^{-1}$ for $m_a \lesssim 5 \times 10^{-10} \text{ eV}$.

Reference [119] reports no evidence of a γ -ray burst in observations of extragalactic SNe with the Fermi Large Area Telescope (LAT). Under the assumption that at least one SN was contained within the LAT field of view, the authors derive an upper bound on the axion photon coupling which is about a factor of 5 weaker than the one from SN 1987A, see Fig. 90.1.

The cumulative emission of ALPs from all past core-collapse SNe would lead to a diffuse gamma-ray flux peaked at energies $\sim 50 - 100$ MeV which can convert in the Galactic magnetic field into photons. Using Fermi-LAT measurements of the diffuse γ -ray flux, Ref. [296] obtains a conservative bound on the photon coupling, $|g_{a\gamma\gamma}| < 5 \times 10^{-10} \text{ GeV}^{-1}$, for $m_a \lesssim 10^{-11} \text{ eV}$, see Fig. 90.1, which can be decreased by nearly three orders of magnitude, if an ALP-nucleon coupling of maximal phenomenologically allowed strength, $|g_{aNN}| \sim 10^{-9}$, is allowed.

Hot, young stars, such as Wolf-Rayet stars, efficiently produce ALPs with energies $\sim 10 - 100$ keV via the Primakoff effect. Large numbers of those stars are hosted by the Galactic Quintuplet and Westerlund 1 super star clusters (SSCs). The non-observation of hard X-rays originating from axion-photon conversion in the Galactic magnetic field in archival NuSTAR (Nuclear Spectroscopic Telescope Array) data from these SSCs leads to a bound on the axion-photon coupling [159], $|g_{a\gamma\gamma}| < 3.6 \times 10^{-12} \text{ GeV}^{-1}$, for $m_a \lesssim 5 \times 10^{-11} \text{ eV}$, see Fig. 90.1. A somewhat weaker bound in the same mass range was established exploiting NuSTAR data on Betelgeuse [105].

A hard X-ray excess in data from the nearby M7 isolated NSs [297] may be explained by ALPs produced in the cores of those stars and converted in the surrounding magnetic fields, with $|g_{aNN}g_{a\gamma\gamma}| \in (2 \times 10^{-21}, 10^{-18}) \text{ GeV}^{-1}$, for $m_a \lesssim 10^{-5} \text{ eV}$ [298]. The non-observation of an X-ray excess from the magnetic WD RE J0317-853 [299] by Chandra yields the constraint $|g_{aee}g_{a\gamma\gamma}| \lesssim 1.3 \times 10^{-25} \text{ GeV}^{-1}$, for $m_a \ll 10^{-5} \text{ eV}$ [128], which provides a non-trivial constraint on the ratio g_{aee}/g_{aNN} for axion models explaining the M7 X-ray excess.

In addition to being produced in NS cores, axions may also be produced in NS magnetospheres. In particular, it has recently been shown that axions could be copiously produced in the polar-cap regions of NS magnetospheres due to time-varying, un-screened electric fields [145]. Those axions could then convert to photons in the outer regions of the NS magnetosphere, leading to observable, broadband radio flux. The absence of such radio flux sets competitive constraints on ALPs, as indicated by the “pulsars” constraint in Fig. 90.1.

90.4.4 Conversion of astrophysical photon fluxes

Magnetically induced oscillations between photons and ALPs can modify the photon fluxes from distant sources in various ways, featuring (i) frequency-dependent dimming, (ii) modified polarization, and (iii) avoiding absorption by propagation in the form of axions. For example, dimming of SNe Ia could influence the interpretation in terms of cosmic acceleration [300], although it has become clear that photon-ALP conversion could only be a subdominant effect [301].

Polarization measurements are particularly powerful probes of photon-to-axion conversion since only photons polarized parallel to astrophysical magnetic fields may convert into axions, meaning that in the presence of large-scale ordered magnetic fields axions tend to leave distinct polarization signatures in passing radiation. Searches for linear polarization from radio galaxies (see, *e.g.*, Ref. [302]) and quasars [303] may approach in sensitivity $|g_{a\gamma\gamma}| \sim \text{few} \times 10^{-13} \text{ GeV}^{-1}$, albeit with uncertainties related to the underlying modeling assumptions. Recently, robust limits at the level $|g_{a\gamma\gamma}| \leq 5.4 \times 10^{-12} \text{ GeV}^{-1}$ at 95% CL have been derived from optical polarization measurements of nearby magnetic WDs [129] (see also [304]), see Fig. 90.1. The magnetic fields of magnetic WDs may be well-measured through the Zeeman splitting of bound-bound transitions in the WD atmospheres.

Remarkably, it appears that the Universe could be too transparent to TeV γ -rays that should be absorbed by pair production on the extra-galactic background light [109,305–308]. The situation is not conclusive at present [309–312], but the possible role of photon-ALP oscillations in TeV γ -ray astronomy is tantalizing [313–315]. On the other hand, much of this parameter space is excluded by the previously-discussed WD polarization probes. Fortunately, the region in ALP parameter space, $g_{a\gamma\gamma} \sim 10^{-12} - 10^{-10} \text{ GeV}^{-1}$ for $m_a \lesssim 10^{-7} \text{ eV}$ [316], required to explain the anomalous TeV transparency of the Universe, could be conceivably probed by the next generation of laboratory experiments (ALPS II) and helioscopes (IAXO) mentioned above.

This parameter region can also be probed by searching for an irregular behavior of the gamma ray spectrum of distant active galactic nuclei (AGN), expected to arise from photon-ALP mixing in a limited energy range. In this type of studies, the uncertainty in the magnetic field around the source needs to be taken into account. This typically leads to a range of limits on the ALP-photon coupling that depend on the modeling assumptions. The H.E.S.S. collaboration has set a limit of $|g_{a\gamma\gamma}| \lesssim 2.1 \times 10^{-11} \text{ GeV}^{-1}$, for $1.5 \times 10^{-8} \text{ eV} \lesssim m_a \lesssim 6.0 \times 10^{-8} \text{ eV}$, from the non-observation of an irregular behavior of the spectrum of the AGN PKS 2155-304 [317]. The Fermi-LAT collaboration has put an even more stringent limit on the ALP-photon coupling [118] from observations of the gamma ray spectrum of NGC 1275, the central galaxy of the Perseus cluster, see Fig. 90.1. A similar analysis has been carried out in Ref. [318], using Fermi-LAT data of PKS 2155-304, and in Ref. [131], using ARGO-YBJ and Fermi-LAT data of Mrk 421, see Fig. 90.1. However, these constraints were obtained under certain theoretical assumptions about magnetic fields surrounding the sources, not confirmed yet by direct astronomical observations in these particular directions; this introduces large systematic uncertainties in the reported constraints [319].

Evidence for spectral irregularities has been reported in Galactic sources, such as pulsars and supernova remnants, and has been interpreted as hints for ALPs [334,335] (see also discussion in Ref. [336] and references therein). However, the inferred ALP parameters, $|g_{a\gamma\gamma}| \sim 10^{-10} \text{ GeV}^{-1}$, $m_a \sim \text{neV}$, are in tension with the CAST helioscope bounds. Reference [336] updated the analysis of the pulsar signal region including astrophysical nuisance parameters and correctly deriving confidence intervals on ALP

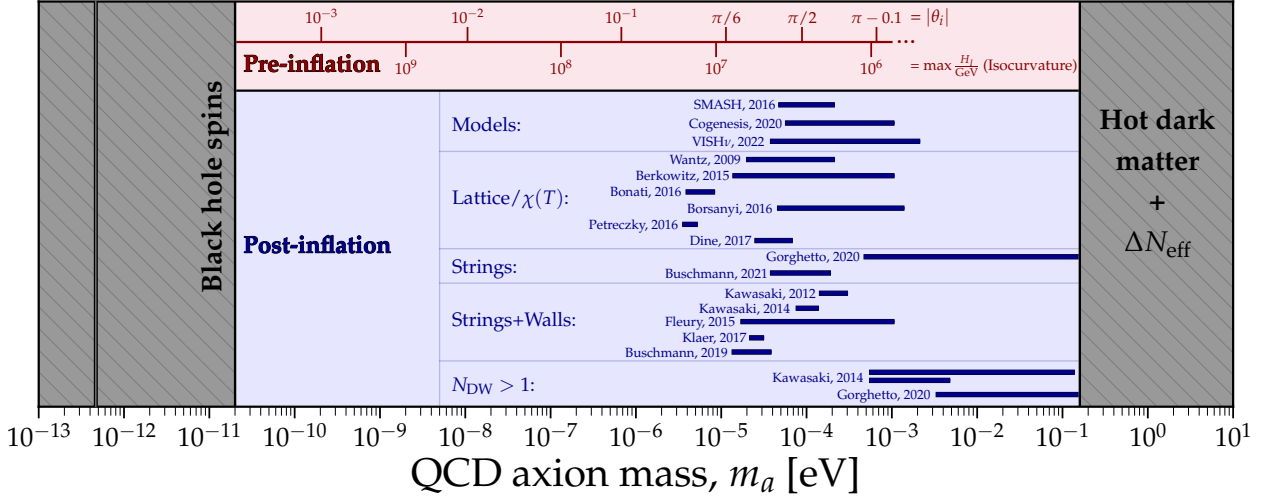


Figure 90.4: QCD axion mass predictions for obtaining the correct DM abundance assuming the PQ symmetry is and is not restored after inflation and, in the case the PQ symmetry is restored after inflation, depending on the domain wall number N . Figure courtesy of Ciaran O’Hare [61], includes data from refs. [18, 33, 320–333]. The lower-end of the possible mass range is bounded by BH superradiance constraints and the theoretical requirement that f_a be below the Planck scale, while the upper end is bounded by the somewhat model-dependent NS cooling constraints (not shown), which exclude QCD axion masses above roughly ~ 15 – 30 meV, depending on the UV completion. At even higher masses there are strong constraints from the production of DM in the early universe, which behaves as hot DM and contributes to ΔN_{eff} .

parameters by means of Monte Carlo simulations. The tension with the CAST bounds can be evaded if environmental effects in matter, which would suppress the ALP production in dense astrophysical plasmas like the solar interior, are invoked. If this explanation is correct, the claimed ALP signal would be in reach of the next-generation LSW experiment ALPS II. Other ways to make the CAST bound compatible with photon-ALP conversions in the low-density Galactic medium are invoking photon-ALP-dark photon oscillations [337] or the existence of a number of ‘hidden’ ALPs [338].

At smaller masses, $m_a \lesssim 10^{-12}$ eV, galaxy clusters become highly efficient at interconverting ALPs and photons at X-ray energies. Constraints on spectral irregularities in the spectra of luminous X-ray sources (Hydra A, M87, NGC 1275, NGC 3862, Seyfert galaxy 2E3140; taken by Chandra and XMM-Newton) located in or behind galaxy clusters then lead to stringent upper limits on the ALP-photon coupling [110–112, 339–341], (for the limits exploiting spectra from Hydra and M87 from Refs. [110] and [111], respectively, see Fig. 90.1). Reference [112] recently performed the most sensitive x-ray searches for ALPs to date by employing Chandra’s High-Energy Transmission Gratings that allow for an unsurpassed spectral resolution. New observations of the AGN NGC 1275 then led to the bound $|g_{a\gamma\gamma}| < 8 \times 10^{-13}$ GeV $^{-1}$ at 99.7% C.L. for ultra-light ALPs, as illustrated in Fig. 90.1. On the other hand, magnetic field modeling uncertainties in the clusters may not be fully accounted for in these analyses [319].

90.4.5 Finite density effects for the QCD axion

If the QCD axion sector has a discrete, \mathbb{Z}_N , shift symmetry, its potential is much shallower, and its mass, in units of its decay constant, $m_a f_a \simeq (3\pi)^{-1/4} N^{3/4} 2^{-N/2} m_\pi f_\pi$, is smaller than the one of the canonical QCD axion by an exponential factor $\propto 2^{-N/2}$ [57, 58]. This opens up the parameter space over which one should search for a QCD axion towards the left of the yellow canonical QCD axion band in Fig. 90.1, Fig. 90.2, and Fig. 90.3. Novel bounds apply to this exceptionally light QCD axion due to finite density effects [342–344]. In fact, in dense stellar media, the minimum of the axion potential may be shifted to π . This has a number of phenomenological consequences that span from the modification of nuclear processes in stars due to $\theta = \mathcal{O}(\pi)$ to modifications in the orbital decay of binary systems (and subsequently in the emitted gravitational waves). Recently strong constraints have been set using the modification of the WD mass-radius relation due to such axions [345].

In fact, $\theta \sim 1$ in the solar core would lead to an increased proton-neutron mass difference, which would prohibit the neutrino line corresponding to the ${}^7\text{Be}$ - ${}^7\text{Li}$ mass difference observed by Borexino [346].

Moreover, the fact that the position of the minimum of the axion potential depends on the nuclear density of the medium may also source a long-range force between dense stars [342]. This new long-range force sourced by the axion can be constrained by the measurement of the orbital decay of double pulsar or NS-pulsar binaries [342]. The gravitational wave signal of NS-NS mergers or black hole (BH) - NS mergers would also be modified by these axionic long-range forces [342, 343]. There is also a corresponding bound [344] exploiting the gravitational waves observation from the binary NS inspiral GW170817 detected by LIGO (Laser Interferometer Gravitational-Wave Observatory) and Virgo [347].

90.4.6 Superradiance of black holes

Light bosonic fields such as axions or ALPs can affect the dynamics and gravitational wave emission of rapidly rotating astrophysical BHs through the superradiance mechanism. When the boson’s Compton wavelength is of order of the size of the BH’s ergoregion, they form gravitational bound states around the BH. Their occupation number grows exponentially by extracting energy and angular momentum from the black hole, forming a coherent axion or ALP bound state emitting gravitational waves. When accretion cannot replenish the spin of the BH, superradiance dominates the BH spin evolution; this is true for both supermassive and stellar mass BHs. The existence of destabilizing light bosonic fields thus leads to exclusion regions in the mass versus spin plot of rotating BHs. Stellar BH spin measurements exploiting well-studied binaries and two independent techniques exclude a mass range – up to self-interaction caveats discussed below – 6×10^{-13} eV $< m_a < 2 \times 10^{-11}$ eV at 2σ , which for the axion excludes 3×10^{17} GeV $< f_a < 1 \times 10^{19}$ GeV [12, 348, 349], see Fig. 90.4. These bounds apply when gravitational interactions dominate over the axion self-interaction, which is largely true for the QCD axion in this mass range. On the other hand, Mehta *et al.* [350, 351] considered superradiance bounds for string theory ALPs with a quartic self-coupling (of either sign) given by $\lambda = m_a^2/f_a^2$, using the bosonova model of Ref. [349], and found that for $m_a \sim 10^{-12}$ eV the superradiant cloud, and thus the constraints, are destroyed for $f_a \lesssim 10^{11} - 10^{12}$ GeV, depending precisely on the mass and the source.

Baryakhtar *et al.* [352] used a more advanced model for the ef-

fect of self-interactions on superradiant evolution, and a different (frequentist) statistical methodology, leading to more conservative bounds from stellar mass BHs (region near 10^{-12} eV). In particular, Baryakhtar *et al.* [352] found that QCD axions are only excluded for $m_a \lesssim 6 \times 10^{-12} M_\odot$ instead of the $2 \times 10^{-11} M_\odot$, as claimed in [350,351]. Baryakhtar *et al.* [352] also vetoed supermassive BHs (SMBHs) with spins measured at low significance, and thus found no ALP bounds in the SMBH region (near 10^{-18} eV); Mehta *et al.* [350, 351, 353], in contrast, included SMBHs in a (quasi-)Bayesian analysis with a flat prior on the spin and found non-trivial constraints. In summary, it appears likely that the lower end of the QCD axion mass range is excluded by superradiance, with the requirement $m_a \gtrsim 10^{-11}$ eV, but the exact location of this limit is still debated. It is also too early to claim that ultra-light ALP parameter space is excluded by SMBHs, though this may change with future work.

Long lasting, monochromatic gravitational wave signals, which can be distinguished from ordinary astrophysical sources by their clustering in a narrow frequency range, are expected to be produced by axions or ALPs annihilating to gravitons. Gravitational waves could also be sourced by axions/ALPs transitioning between energy levels of the effective gravitational atom. Accordingly, the gravitational wave detector Advanced LIGO should be sensitive to the axion in the $m_a \lesssim 10^{-10}$ eV region. LIGO measurements of BH spins in binary merger events could also provide statistical evidence for the presence of an axion [354, 355]. Similar signatures could arise for supermassive and intermediate mass BHs for particles with masses $\lesssim 10^{-15}$ eV. Gravitational waves from such sources could be detected at lower-frequency observatories such as LISA (Laser Interferometer Space Antenna). First attempts to use LIGO/Virgo data to search for monochromatic signatures of axion superradiance were recently made in [356, 357].

90.5 Cosmic Axions

90.5.1 Cosmic axion populations

There are two distinct populations of cosmic relic axion populations: a non-thermal one behaving as CDM, and a thermal one comprising a HDM component, in analogy to massive neutrinos. For $m_a \lesssim 0.01$ eV, thermal axions are dominantly produced by processes involving quarks and gluons [358, 359], while, for larger masses, the dominant thermalization process is $\pi + \pi \leftrightarrow \pi + a$ [173, 360, 361]. A number of evaluations exploiting cosmological precision data have found restrictive constraints on a possible HDM fraction that translate into an upper bound on the axion mass, $m_a \lesssim 1$ eV, if a LO axion-pion chiral effective field theory (EFT) analysis of the axion-pion thermalization rate is used [362–365]. Recently, it was found that the NLO contribution exceeds the LO contributions for masses below $m_a \lesssim 1.2 (0.12/C_{a\pi})$ eV [366]. Therefore, in order to assess the reach in sensitivity of future cosmological data sets, one has to improve the EFT description or to compute axion-pion scattering via lattice QCD techniques. Alternatively, recently Ref. [367] used pion-pion scattering data to overcome the EFT description issues and found the constraint $m_a \lesssim 0.24$ eV, see Fig. 90.4.

For $m_a \gtrsim 10$ eV, axions may decay faster than the age of the Universe (see Eq. (90.7)), depending on the decay constant, which would remove the cosmic axion population while injecting photons. If the axions were in thermal equilibrium in the early Universe, which depends on the inflationary reheat temperature and assumptions about the pre-BBN cosmology [368, 369], this excess radiation provides additional limits on the axion- or ALP-photon coupling up to very large masses [368, 369]. Such photons could contribute to the extragalactic background light (EBL), could ionize primordial hydrogen and thus contribute to the optical depth after recombination, or could spoil the agreement of big bang nucleosynthesis (BBN) with observations. The corresponding up-to-date bounds from Refs. [166, 167] are displayed in Fig. 90.1. It has recently been shown that there is an *irreducible axion background* [168] that arises from axion freeze-in before BBN; decays of that axion population provide strong constraints on axions with masses above roughly 100 eV (see Fig. 90.1). For high enough decay constants, high-mass axions ($m_a \gtrsim 10$ eV) can account for the

DM abundance through the misalignment mechanism, described in more detail below, though additional entropy dilution or fine-tuning is needed to avoid overproducing the DM abundance [370] (see also [371] for heavy axion production through lepton-flavor-violating decays). The decay of such high-mass axions to photon pairs could leave narrow spectral features in *e.g.* optical or X-ray backgrounds [126, 138–140, 161, 163, 372, 373] (see Fig. 90.1).

The main cosmological interest in axions at present derives from their possible role as CDM. In addition to thermal processes, axions are abundantly produced by the misalignment (MIS) mechanism [374–376]. The axion DM abundance crucially depends on the cosmological history. Let us first consider the so called *pre-inflationary PQ symmetry breaking scenario*, in which the PQ symmetry is broken before and during inflation and not restored afterwards. After the breakdown of the PQ symmetry, the axion field relaxes somewhere in the bottom of the “wine-bottle-bottom” potential. Near the QCD epoch, topological fluctuations of the gluon fields such as instantons explicitly break the PQ symmetry. This tilting of the “wine-bottle-bottom” drives the axion field toward the CP -conserving minimum, thereby exciting coherent oscillations of the axion field that ultimately represent a condensate of CDM. The fractional cosmic mass density in this homogeneous field mode, created by the MIS mechanism, is [33, 377–379],

$$\begin{aligned} \Omega_a^{\text{MIS}} h^2 &\approx 0.12 \left(\frac{f_a}{9 \times 10^{11} \text{ GeV}} \right)^{1.165} F \Theta_i^2 \\ &\approx 0.12 \left(\frac{6 \mu\text{eV}}{m_a} \right)^{1.165} F \Theta_i^2, \end{aligned} \quad (90.22)$$

where h is the present-day Hubble expansion parameter in units of $100 \text{ km s}^{-1} \text{ Mpc}^{-1}$, and $-\pi \leq \Theta_i \leq \pi$ is the initial “misalignment angle” relative to the CP -conserving position attained in the causally connected region which evolved into today’s observable Universe. $F = F(\Theta_i, f_a)$ is a factor accounting for anharmonicities in the axion potential. For $F \Theta_i^2 = \mathcal{O}(1)$, m_a should be above $\sim 6 \mu\text{eV}$ in order that the cosmic axion density does not exceed the observed CDM density, $\Omega_{\text{CDM}} h^2 = 0.12$. However, much smaller axion masses (much higher PQ scales) are still possible if entropy is diluted for example by the late decay of a scalar condensate (see for example [380] and references therein) or the initial value Θ_i just happens to be small enough in today’s observable Universe (“anthropic axion window” [381]). In the latter cosmological scenario, however, quantum fluctuations of the axion field during inflation are expected to lead to isocurvature density fluctuations which get imprinted to the temperature fluctuations of the CMB [382, 383]. Their non-observation puts severe constraints on the Hubble expansion rate H_I during inflation [384–389], which read, in the simplest cosmological inflationary scenario,

$$H_I \lesssim 5.7 \times 10^8 \text{ GeV} \left(\frac{5 \text{ neV}}{m_a} \right)^{0.4175}, \quad (90.23)$$

if axions represent all of DM. In Ref. [390] an alternative to the MIS mechanism was proposed: the so-called kinetic MIS mechanism. In this case, the axion field is assumed to have an initial velocity which may be generated, *e.g.*, by a hypothesized explicit breaking of the axion shift symmetry in the early universe. The amount of QCD axion dark matter generated by the kinetic MIS mechanism can fit the observed dark matter abundance for any $f_a \lesssim 1.5 \times 10^{11}$ GeV, down to the minimum value allowed by the SN 1987A constraint.

In the above prediction of the fractional cosmic mass density in axions, the exponent, 1.165, arises from the non-trivial temperature dependence of the topological susceptibility $\chi(T) = m_A^2(T) f_A^2$ at temperatures slightly above the QCD quark-hadron phase transition. Lattice QCD calculations of this exponent [33, 323, 325, 391–393], but also Ref. [324], found it to be remarkably close to the prediction of the dilute instanton gas approximation [394] which was previously exploited. Therefore, the state-of-the-art prediction of the axion mass relevant for DM for a fixed initial misalignment angle Θ_i differs from the previous prediction by just a factor of order one.

In the *post-inflationary PQ symmetry breaking scenario*, on the other hand, Θ_i will take on different values in different patches of

the present Universe. The average contribution is [33, 377–379]

$$\Omega_a^{\text{MIS}} h^2 \approx 0.12 \left(\frac{30 \mu\text{eV}}{m_a} \right)^{1.165}. \quad (90.24)$$

The decay of cosmic strings and domain walls gives rise to a further population of CDM axions, whose abundance suffers from significant uncertainties [321, 327–329, 378, 379, 395–403] which arise from the difficulty in understanding the energy loss process of topological defects and the generated axion spectrum in a quantitative way. In fact, in the present state-of-the-art it is still possible that the CDM contribution from the decay of topological defects is subdominant [327] or overwhelmingly large [328] in comparison to the one from the MIS mechanism. Correspondingly, the plausible range of axion masses providing all of CDM in scenarios with postinflationary PQ symmetry breaking is still rather large, namely [327, 328]

$$m_a \approx 26 \mu\text{eV} - 0.5 \text{ meV}, \quad (90.25)$$

for models with short-lived (requiring unit color anomaly $N = 1$) domain walls, such as the KSVZ model. On the other hand, the most recent adaptive mesh refinement axion string simulations, which are able to evolve over larger dynamic ranges than static lattice simulations, suggest the mass range $m_a \approx 40 - 180 \mu\text{eV}$ [321]. For models with long-lived ($N > 1$) domain walls, such as an accidental DFSZ model [404], where the PQ symmetry is broken by higher dimensional Planck suppressed operators, the mass is predicted to be significantly higher [287, 329, 404–406],

$$m_a \approx (0.58 - 130) \text{ meV}. \quad (90.26)$$

However, the upper part of the predicted range is in conflict with stellar energy-loss limits on the axion. The pre- and post-inflationary mass predictions are summarized in Fig. 90.4.

In this post-inflationary PQ symmetry breakdown scenario, the spatial axion density variations are large at the QCD transition, and they are not erased by free streaming. Gravitationally bound “axion miniclusters” form before and around matter-radiation equality [407–409]. A significant fraction of CDM axions can reside in these bound objects [400, 410]. Remarkably, the minicluster fraction can be bounded by gravitational lensing [411–413], although more simulations are required to understand whether miniclusters are dense enough and survive in sufficient quantities for lensing bounds to apply.

The non-thermal production mechanisms attributed to axions are generic to light bosonic weakly interacting particles such as ALPs [18]. The relic abundance is set by the epoch when the axion mass becomes significant, $3H(t) \approx m_a(t)$, and ALP field oscillations begin. For ALPs to contribute to the DM density this epoch must precede that of matter radiation equality. For a temperature independent ALP mass this leads to the bound:

$$m_a \gtrsim 7 \times 10^{-28} \text{ eV} \left(\frac{\Omega_m h^2}{0.15} \right)^{1/2} \left(\frac{1 + z_{\text{eq}}}{3.4 \times 10^3} \right)^{3/2}. \quad (90.27)$$

ALPs lighter than this bound are allowed if their cosmic energy density is small, but they are quite distinct from other forms of DM [414]. Ignoring anharmonicities in the ALP potential, and taking the ALP mass to be temperature independent, the relic density in DM ALPs due to the MIS mechanism is given by

$$\Omega_{\text{ALP}}^{\text{MIS}} h^2 = 0.12 \left(\frac{m_a}{4.7 \times 10^{-19} \text{ eV}} \right)^{1/2} \left(\frac{f_a}{10^{16} \text{ GeV}} \right)^2 \times \left(\frac{\Omega_m h^2}{0.15} \right)^{3/4} \left(\frac{1 + z_{\text{eq}}}{3.4 \times 10^3} \right)^{-3/4} \Theta_i^2. \quad (90.28)$$

An ALP decay constant near the GUT scale gives the correct relic abundance for *ultralight ALPs* (ULAs) with $m_{\text{ULA}} \approx 10^{-19} \text{ eV}$ [415, 416]. ULAs encompass the entire Earth in a single Compton wavelength, and for large occupation numbers are modelled as a coherent classical field. The coherence time is determined by the mass and virial velocity in the Milky Way,

$\tau_{\text{coh}} \sim 1/m_{\text{ULA}} v_{\text{vir}}^2$, with the detailed properties described by a stochastic model with an approximately Rayleigh Jeans distribution [417]. Natural models for ULAs can be found in string and M-theory compactifications [7, 8, 10–15], in field theory with accidental symmetries [418, 419], or new hidden strongly coupled sectors [420, 421].

In addition to the gravitational potential energy, the ULA field also carries gradient energy. On scales where the gradient energy is non-negligible, ULAs acquire an effective pressure and do not behave as CDM. The gradient energy opposes gravitational collapse, leading to a Jeans scale below which perturbations are stable [422]. The Jeans scale suppresses linear cosmological structure formation relative to CDM [423–425]. The Jeans scale at matter-radiation equality in the case that ULAs make up all of CDM is:

$$k_{\text{J,eq}} = 8.7 \text{ Mpc}^{-1} \left(\frac{1 + z_{\text{eq}}}{3.4 \times 10^3} \right)^{-1/4} \left(\frac{h^2 \Omega_{\text{ALP}}^{\text{MIS}}}{0.12} \right)^{1/4} \times \left(\frac{m_{\text{ULA}}}{10^{-22} \text{ eV}} \right)^{1/2}. \quad (90.29)$$

On non-linear scales the gradient energy leads to the existence of a class of pseudo-solitons known as oscillatons, or axion stars [426]. Axion stars are expected to form in all cosmological scenarios, and for all types of ALPs, including the QCD axion [427–429]. Some axion stars may explode into radio photons, heating the interstellar medium [104].

Cosmological and astrophysical observations are consistent with the CDM model, and departures from it are only allowed on the scales of the smallest observed DM structures with $M \sim 10^{6-8} M_{\odot}$. The CMB power spectrum and galaxy auto-correlation power spectrum limit the ULA mass to $m_{\text{ULA}} \gtrsim \mathcal{O}(\text{few}) \times 10^{-24} \text{ eV}$ from linear theory of structure formation [414, 430]. Analytic models [431] and N -body simulations [432] for non-linear structures show that halo formation is suppressed in ULA models relative to CDM. This leads to constraints on the ULA mass of $m_{\text{ULA}} > 10^{-22} \text{ eV}$ from observations of high- z galaxies [432–434], and $m_{\text{ULA}} > 2 \times 10^{-20} \text{ eV}$ from the Lyman-alpha forest flux power spectrum [435]. Including the effects of anharmonicities on structure formation with ALPs can weaken these bounds if the misalignment angle $\Theta_i \approx \pi$ [436]. A comprehensive study of Milky Way satellites by the DES collaboration resulted in the bound $m_{\text{ULA}} > 2.9 \times 10^{-21} \text{ eV}$ [437].

Cosmological simulations that treat gradient energy in the ULA field beyond the N -body approximation have just recently become available [427, 438–440], and show, among other things, evidence for the formation of axion stars in the centres of ULA halos (various consequences of axion stars are considered in Refs. [441]). These central axion stars have been conjectured to play a role in the apparently cored density profiles of dwarf spheroidal galaxies, and other central galactic regions [127, 427, 442–446]. However, the relationship between the halo mass and the axion star mass [447] leads to problems with this scenario in some galaxies [448–450]. It should be emphasised that many of the conclusions about the role of ULA axion stars in galactic dynamics are based on use of simulation results that do not contain baryons and feedback could be important [451–453].

Inside DM halos the axion gradient energy causes coherence on the de Broglie wavelength and fluctuations on the coherence time [427, 454]. These fluctuations can be thought of as short-lived quasiparticles and lead to relaxation processes that can be described statistically [416, 455] (this relaxation processes also leads to the gravitational condensation of axion stars [428]). The typical relaxation time is:

$$t \sim 10^{10} \text{ years} \left(\frac{m_{\text{ULA}}}{10^{-22} \text{ eV}} \right)^3 \left(\frac{v}{100 \text{ km s}^{-1}} \right)^2 \left(\frac{r}{5 \text{ kpc}} \right)^4, \quad (90.30)$$

where v and r are the velocity and radius of the orbit in the host DM halo.

Relaxation processes such as these are not observed in galaxies, though there are some circumstances where they may be desirable [416]. An absence of observed relaxation can be used to set

limits on the ULA mass. An absence of Milky Way disk thickening excludes $m_{\text{ULA}} > 0.6 \times 10^{-22}$ eV [456], while stellar streams give the stronger bound $m_{\text{ULA}} > 1.5 \times 10^{-22}$ eV [457]. The survival of the old star cluster in Eridanus II [458] excludes the range of masses 10^{-21} eV $\lesssim m_{\text{ULA}} \lesssim 10^{-19}$ eV [459]. Recently Ref. [460] finds that ULA DM is excluded for $m_{\text{ULA}} \lesssim 3 \times 10^{-19}$ eV at 99% CL because such DM would kinematically heat the stars in the Segue I and Segue II ultra-faint dwarf galaxies to a level inconsistent with their observed dynamics.

Finally, one should note that the beyond-CDM physics of ULAs (Jeans scale, relaxation, axion star formation) of course also applies to the QCD axion on smaller length scales. This is of particular interest inside axion miniclusters [407, 408, 428, 429].

90.5.2 Electron recoil searches

In a DM direct detection experiment, a DM ALP featuring a coupling to the electron can be absorbed by the target material, leading to a mono-energetic electronic recoil signal peaked at m_a . This mechanism allowed the EDELWEISS [461], PandaX [221], SuperCDMS [222] and XENON1T [462] collaborations to put the bounds on the axion-electron coupling displayed in Fig. 90.2 in the keV mass range. As discussed in the last sub-section, additionally dynamics beyond the standard misalignment mechanism are needed to explain the axion DM abundance for keV-scale axion masses (e.g., [370, 371]). Moreover, such models are subject to stringent constraints from axion decays to photons [370].

90.5.3 Telescope searches

The two-photon decay is extremely slow for axions with masses in the CDM regime, but could be detectable for eV masses. The signature would be a quasi-monochromatic emission line from galaxies and galaxy clusters. The expected optical line intensity for DFSZ axions is similar to the continuum night emission. A search for optical line emission in two Abell clusters using spectra from the VIMOS (Visible Multi-Object Spectrograph) integral field unit at the Very Large Telescope (VLT) excludes axions and ALPs with a two photon coupling bigger than $\sim 5 \times 10^{-12}$ GeV $^{-1}$ in the mass range between 4.5 and 5.5 eV [163], see Fig. 90.1. Spectral data on the dwarf spheroidal galaxy Leo T from the Multi Unit Spectroscopic Explorer (MUSE) at the VLT improve these constraints by more than an order of magnitude for ALP masses between 2.7 and 5.3 eV [162], see Fig. 90.1.

Very low-mass axions in halos produce a weak quasi-monochromatic radio line. Virial velocities in undisrupted dwarf galaxies are very low, and the axion decay line would therefore be extremely narrow. A search with the Haystack radio telescope on three nearby dwarf galaxies gave a limit $|g_{a\gamma\gamma}| < 1.0 \times 10^{-9}$ GeV $^{-1}$ at 96% CL for $298 < m_a < 363$ μeV [161]. However, this combination of m_a and $g_{a\gamma\gamma}$ does not exclude plausible axion models.

A monochromatic signal is also produced in the conversion of DM axions in the background of slowly varying galactic B-fields [463]. The signal is, however, sensitive to magnetic field power on the scale of the axion mass [464]. Present and future radio telescopes appear to be able to probe ALP DM in the mass range 0.1 – 100 μeV for couplings $g_{a\gamma\gamma} \gtrsim 10^{-13}$ GeV $^{-1}$ [464] – unfortunately not reaching down to the benchmark QCD axion sensitivity.

Resonant conversion of QCD axion or ALP DM in NS magnetospheres may give a detectable signal from individual NSs and populations of NSs for axion masses in the μeV range [465, 466]. Recent analyses of radio data in the frequency range 1-40 GHz from several NSs have found no evidence for a narrow peak predicted from this mechanism and therefore put bounds on the axion-photon coupling around 10^{-11} GeV $^{-2}$ for $m_a \sim 10$ μeV [133–136], see Fig. 90.1. However, these limits may still suffer from uncertainties because the line intensity is difficult to predict in detail in the complicated environments of NSs [135, 467–470]. Still, next-generation radio telescopes such as the Square Kilometer Array (SKA) may reach sensitivity to QCD axion-strength couplings [136]. Stimulated ALP decays in high radiation environments may be detectable, by e.g. the future SKA, down to $g_{a\gamma\gamma} \gtrsim 10^{-11}$ GeV $^{-1}$, for masses between μeV and 0.1 meV [471]. Furthermore, in condensed ALP dark matter structures such as

ALP stars, a parametric instability may lead to an exponential enhancement of the photon flux from ALP-photon conversion by a factor $\sim \exp\left[|g_{a\gamma\gamma}| \int ds \rho_a^{1/2}(s)\right]$, where the integral is along any photon trajectory through the ALP overdensity [472, 473].

Photon propagation on an ULA DM background can induce birefringence that can be compared with upper limits from the CMB [106, 141, 474] and may also be probed with other sources such as pulsars [475].

90.5.4 Microwave cavity experiments

Over a large part of the plausible m_a range for CDM, Galactic halo axions may be detected by their resonant conversion into a quasi-monochromatic microwave signal in a high-Q electromagnetic cavity permeated by a strong, static B field [9, 476, 477]. The cavity frequency is tunable, and the signal is maximized when the cavity resonant frequency is the total axion energy, rest mass plus kinetic energy, of $\nu = (m_a/2\pi)[1 + \mathcal{O}(10^{-6})]$, the width above the rest mass representing the axions' virial distribution in the galaxy near Earth. The frequency spectrum may also contain finer structure from axions more recently fallen into the galactic potential and not yet completely virialized [478, 479] or otherwise incompletely thermalized.

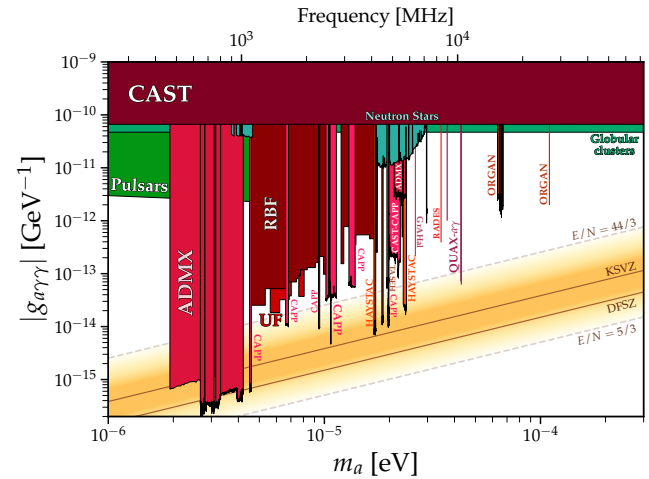


Figure 90.5: Exclusion plot for ALP-photon coupling with closeup on the parameter space of RF cavity experiments as described in the text. This is a zoom-in of Fig. 90.1 that highlights regions probed by axion DM direct detection experiments. In particular, note that all of the terrestrial experiments shaded in red, except that of CAST, assume that the axion is 100% of the local DM. Figure courtesy of Ciaran O’Hare [61], including data from Refs. [43, 64–68, 76, 78, 81–84, 86, 87, 91, 93, 99, 122, 123, 145, 216, 480–484]

The feasibility of this technique was established in early experiments (RBF (Rochester-Brookhaven-Florida) and UF (University of Florida)) of relatively small sensitive volume, $\mathcal{O}(1)$ liter), with HFET-based microwave amplifiers, setting limits in the range $4.5 < m_a < 16.3$ μeV [91, 95, 482], but lacking by 2–3 orders of magnitude the sensitivity required to detect realistic axions, see Fig. 90.5.

Later, the first generation of ADMX ($B \sim 8$ T, $V \sim 200$ liters) achieved sensitivity to KSVZ axions, assuming they saturate the local DM density and are well virialized, over the mass range 1.9–3.3 μeV [485]. Should halo axions have a significant narrow component not yet virialized, ADMX was sensitive to DFSZ axions over the entire mass range [486]. The corresponding 90% CL exclusion regions shown in Fig. 90.5 assume a local CDM density of 7.5×10^{-25} g cm $^{-3}$ (450 MeV cm $^{-3}$).

Somewhat later, the ADMX experiment commissioned an upgrade [64] that replaced the microwave HFET amplifiers by near-quantum-limited low-noise dc SQUID microwave amplifiers [487] and, more recently, with Josephson parametric amplifiers (related

to the earlier dc SQUID amplifiers), also with noise near-quantum-limited [481]. With its large volume and low noise, ADMX has achieved an unprecedented axion DM sensitivity in the mass range between 2.7 and 4.2 μeV [66–68, 480], down to the DFSZ benchmark axion-photon coupling over much of the range, see Fig. 90.5. This apparatus is also sensitive to certain other hypothetical light bosons, such as hidden photons or chameleons, over a limited parameter space [18, 488, 489].

ADMX continues to scan at DFSZ sensitivity, and has since been joined by an array of haloscopes. One of the CAPP experiments has also achieved DFSZ sensitivity over a small range of frequencies near 4.55 μeV [76]. A number of other experiments from the CAPP group have operated at higher frequencies, many with KSVZ or near KSVZ sensitivity. [72–74, 74, 75] The HAYSTAC experiment also operates at or near KSVZ sensitivity and was the first to demonstrate near-quantum limited noise using a Josephson parametric amplifier [82, 490], and demonstrated ‘state-squeezing’ to increase scan speed by nearly a factor of 2. [83, 84] Other haloscopes operating at or near KSVZ over narrow bands include TASEH [93] and QUAX-a γ [90]. The ORGAN experiment is the highest frequency haloscope, operating with a small cavity and sensitive to axion-like-particle masses up to 67.1 μeV , though not yet with sensitivity to the KSVZ model. [86, 87] There are also a number of other haloscopes sensitive to axion-like-particles with couplings above those predicted by KSVZ. [65, 81, 88, 89, 483] Fig. 90.5 shows the exclusions on axion-photon coupling from these haloscopes to date.

90.5.5 New concepts for axion DM direct detection

Other new concepts for searching for axion DM are also being investigated. ‘Plasma haloscopes’ are under development by the ALPHA consortium [491]. This concept uses a metamaterial consisting of a parallel-wire array, thereby inducing an effective photon mass which is tunable by adjusting wire separation, and sensitive to axion masses 35–400 μeV . Another detector concept exploits the fact that a magnetized mirror would radiate photons in the background of axion DM, which could be collected like in a dish antenna [492]. The proposed MADMAX experiment will place a stack of dielectric layers in a magnetic field in order to resonantly enhance the photon signal, aiming a sensitivity to probe the mass range 40 $\mu\text{eV} \lesssim m_a \lesssim 200 \mu\text{eV}$ [493, 494]. Optical dielectric haloscopes with single photon signal detection have been proposed to search for axions in the 50 meV – 10 eV mass range [495]. Other semi-resonant or nonresonant axion haloscope ideas to read high mass axions that are based around similar principles but novel configurations include BREAD [496] and CADEX [497].

Absorption of axions on molecular transitions can be sensitive to the axion pseudoscalar coupling $g_{aN\gamma}$ to nucleons or the pseudoscalar coupling g_{aee} to electrons in the 0.5 – 20 eV range [498]. It has also been pointed out that the coupling induced by an axion field between photonic modes [96, 499] or atomic states [500] separated by an energy equal to the axion mass may be leveraged for axion detection, though the implementation may be challenging. Certain magnetic topological insulators are conjectured to contain axion-polaritons, quasiparticles composed of magnons and the electric field, with magnetically tunable mass in the meV to eV range [501–503]. Axion dark matter leads to resonant photon emission from such materials, which can be detected [504, 505].

In the intermediate mass region, $\text{neV} \lesssim m_a \lesssim 0.1 \mu\text{eV}$, one may exploit a cooled LC circuit and precision magnetometry to search for the oscillating electric current induced by DM axions in a strong magnetic field [506, 507]. A number of small-scale pathfinder experiments have implemented this approach: ABRACADABRA [62, 63] used a nonresonant configuration in a toroidal magnet for a broadband search, ADMX-SLIC [70] used a resonant configuration in a solenoid magnet for a narrowband search, SHAFT [92] used a nonresonant configuration in a toroidal magnet enhanced with a ferromagnetic core, BASE [80] used antiprotons in a Penning trap as the LC circuit, and DANCE [508] used a laser interferometer. The exclusion limits from these experiments are shown in Fig. 90.1; none are yet sensitive to the QCD axion. Future work in this direction is expected to have much more competitive limits [509, 510].

The oscillating Galactic DM axion field induces oscillating nu-

clear electric dipole moments (EDMs) [35],

$$d_N(t) = g_{aN\gamma} \sqrt{2\rho_{\text{ADM}}} \cos(m_a t) / m_a, \quad (90.31)$$

where $g_{aN\gamma}$ is the coupling of the axion to the nucleon EDM operator, defined in Eq. (90.4). An analysis of the ratio of spin-precession frequencies of stored ultracold neutrons and ^{199}Hg atoms measured by neutron EDM experiments for an axion-induced oscillating neutron EDM revealed no signal consistent with axion DM, excluding a sizeable region of parameter space in the mass region $10^{-24} \text{eV} \leq m_a \leq 10^{-17} \text{eV}$ [40], which surpass the limits on anomalous energy loss of SN 1987A by more than seven orders of magnitude and are competitive with the ones from the requirement of successful BBN established in [38].¹ In fact, the oscillating dark matter axion field could increase the neutron-proton mass difference at neutron freeze-out and thus result in the underproduction of ^4He during BBN. The oscillating EDMs cause also the precession of nuclear spins in a nucleon spin polarized sample in the presence of an electric field. The resulting transverse magnetization can be searched for by exploiting magnetic-resonance (MR) techniques, which are most sensitive in the range of low oscillation frequencies corresponding to sub-neV axion masses. The aim of the corresponding Cosmic Axion Spin Precession Experiment (CASPER) [36] is to probe axion DM in the anthropic window, $f_a \gtrsim 10^{15} \text{GeV}$ ($m_a \lesssim \text{neV}$), motivated from Grand Unification [511–514]. There are two interactions probed through MR: the electric dipole coupling as searched for by CASPER-electric (with first result presented in [39]) and an interaction between the axion field gradient and the nuclear spin, which is aimed for by CASPER-Gradient. In the meantime, the latter has been explored through comagnetometry between a variety of nuclei: H- ^{12}C in CASPER-ZULF [246, 247], Xe-Rb in NAS-DUCK [515], and K- ^3He [251, 252]. The exclusions from these searches are shown in Fig. 90.3. Sub- μeV ALP masses can also be probed by using the storage ring EDM method proposed in Ref. [516] which exploits a combination of B and E-fields to produce a resonance between the $g - 2$ spin precession frequency and the DM ALP field oscillation frequency. This method, however, does not reach the sensitivity to probe the QCD axion prediction for $g_{aN\gamma}$. An eventually non-zero axion electron coupling g_{aee} will lead to an electron spin precession about the axion DM wind [517, 518]. The QUAX a-e experiment exploits MR inside a magnetized material [519]. Because of the higher Larmor frequency of the electron, it is sensitive in the classic window. Its first run established the bound in the mass range 42.4 to 43.2 μeV [227], slightly better than the solar ν bound, shown in Fig. 90.2.

90.6 Conclusions

There is a strengthening physics case for very weakly coupled light particles beyond the Standard Model. The elegant solution of the strong CP problem proposed by Peccei and Quinn yields a particularly strong motivation for the axion. In many theoretically appealing ultraviolet completions of the Standard Model axions and ALPs occur automatically. Moreover, they are natural CDM candidates. Perhaps the first hints of their existence have already been seen in the anomalous excessive cooling of stars and the anomalous transparency of the Universe for very high energy gamma rays. Interestingly, a significant portion of previously unexplored, but phenomenologically very interesting and theoretically very well motivated axion and ALP parameter space can be explored in the foreseeable future by a number of terrestrial experiments searching for axion/ALP DM, for solar axions/ALPs, and for light apparently shining through a wall.

90.7 Acknowledgements

It is a pleasure to thank Masha Baryakhtar, Francesca Calore, Luca Di Luzio, Andrew Geraci, Maurizio Giannotti, Igor Irastorza, David J.E. Marsh, Alessandro Mirizzi, Ciaran O’Hare, Georg Raffelt, Ken’ichi Saikawa, Yannis Semertzidis, Guenter

¹These limits are still to the left of the canonical QCD axion line. However, as already mention in non-minimal models where the QCD axion is a mediator between strongly interacting hidden sectors enjoying a discrete, \mathbb{Z}_N , shift symmetry, the QCD axion line can be shifted to the left in discrete steps, without any fine tuning [57, 58, 421].

Sigl, Sergey Troitsky, and Lindley Winslow for discussions, suggestions, and comments on this review. Particular thanks to Ciaran O’Hare for maintaining a publicly accessible collection of axion plots and providing updates to accommodate this review [61].

References

- [1] R. D. Peccei and H. R. Quinn, *Phys. Rev. Lett.* **38**, 1440 (1977).
- [2] R. D. Peccei and H. R. Quinn, *Phys. Rev.* **D16**, 1791 (1977).
- [3] S. Weinberg, *Phys. Rev. Lett.* **40**, 223 (1978).
- [4] F. Wilczek, *Phys. Rev. Lett.* **40**, 279 (1978).
- [5] Y. Chikashige, R.N. Mohapatra, and R.D. Peccei, *Phys. Lett.* **B98**, 265 (1981).
- [6] G. B. Gelmini and M. Roncadelli, *Phys. Lett.* **99B**, 411 (1981).
- [7] E. Witten, *Phys. Lett. B* **149**, 351 (1984).
- [8] P. Svrcek and E. Witten, *JHEP* **06**, 051 (2006), [hep-th/0605206].
- [9] P. Sikivie, *Phys. Rev. Lett.* **51**, 1415 (1983) and Erratum *ibid.*, **52**, 695 (1984).
- [10] J. P. Conlon, *JHEP* **05**, 078 (2006), [hep-th/0602233].
- [11] K.-S. Choi *et al.*, *Phys. Lett.* **B675**, 381 (2009), [arXiv:0902.3070].
- [12] A. Arvanitaki *et al.*, *Phys. Rev.* **D81**, 123530 (2010), [arXiv:0905.4720].
- [13] B. S. Acharya, K. Bobkov and P. Kumar, *JHEP* **11**, 105 (2010), [arXiv:1004.5138].
- [14] M. Cicoli, M. Goodsell and A. Ringwald, *JHEP* **10**, 146 (2012), [arXiv:1206.0819].
- [15] J. Halverson, C. Long and P. Nath, *Phys. Rev.* **D96**, 5, 056025 (2017), [arXiv:1703.07779].
- [16] M. Demirtas *et al.*, *JHEP* **04**, 138 (2020), [arXiv:1808.01282].
- [17] A. E. Nelson and J. Scholtz, *Phys. Rev. D* **84**, 103501 (2011), [arXiv:1105.2812].
- [18] P. Arias *et al.*, *JCAP* **1206**, 013 (2012), [arXiv:1201.5902].
- [19] P. W. Graham, J. Mardon and S. Rajendran, *Phys. Rev. D* **93**, 10, 103520 (2016), [arXiv:1504.02102].
- [20] J. Jaeckel and A. Ringwald, *Ann. Rev. Nucl. Part. Sci.* **60**, 405 (2010), [arXiv:1002.0329].
- [21] A. Ringwald, *Phys. Dark Univ.* **1**, 116 (2012), [arXiv:1210.5081].
- [22] J. Jaeckel, *Frascati Phys. Ser.* **56**, 172 (2012), [arXiv:1303.1821].
- [23] A. Caputo *et al.*, *Phys. Rev. D* **104**, 9, 095029 (2021), [arXiv:2105.04565].
- [24] M. Pospelov and A. Ritz, *Nucl. Phys.* **B573**, 177 (2000), [hep-ph/9908508].
- [25] J. Liang *et al.* (2023), [arXiv:2301.04331].
- [26] C. A. Baker *et al.*, *Phys. Rev. Lett.* **97**, 131801 (2006), [hep-ex/0602020].
- [27] C. Abel *et al.* (nEDM), *Phys. Rev. Lett.* **124**, 8, 081803 (2020), [arXiv:2001.11966].
- [28] J. Alexander *et al.* (2022), [arXiv:2205.00830].
- [29] H. Georgi, D. B. Kaplan and L. Randall, *Phys. Lett.* **169B**, 73 (1986).
- [30] R. J. Crewther, *Phys. Lett.* **70B**, 349 (1977).
- [31] P. Di Vecchia and G. Veneziano, *Nucl. Phys.* **B171**, 253 (1980).
- [32] M. Gorghetto and G. Villadoro, *JHEP* **03**, 033 (2019), [arXiv:1812.01008].
- [33] S. Borsanyi *et al.*, *Nature* **539**, 7627, 69 (2016), [arXiv:1606.07494].
- [34] L. Caloni *et al.*, *JCAP* **09**, 021 (2022), [arXiv:2205.01637].
- [35] P. W. Graham and S. Rajendran, *Phys. Rev.* **D88**, 035023 (2013), [arXiv:1306.6088].
- [36] D. Budker *et al.*, *Phys. Rev.* **X4**, 2, 021030 (2014), [arXiv:1306.6089].
- [37] I. Schulthess *et al.*, *Phys. Rev. Lett.* **129**, 19, 191801 (2022), [arXiv:2204.01454].
- [38] K. Blum *et al.*, *Phys. Lett. B* **737**, 30 (2014), [arXiv:1401.6460].
- [39] D. Aybas *et al.*, *Phys. Rev. Lett.* **126**, 14, 141802 (2021), [arXiv:2101.01241].
- [40] C. Abel *et al.*, *Phys. Rev.* **X7**, 4, 041034 (2017), [arXiv:1708.06367].
- [41] T. S. Roussy *et al.*, *Phys. Rev. Lett.* **126**, 17, 171301 (2021), [arXiv:2006.15787].
- [42] S. Karanth *et al.* (JEDI Collaboration), *Phys. Rev. X* **13**, 031004 (2023), URL <https://link.aps.org/doi/10.1103/PhysRevX.13.031004>.
- [43] X. Zhang *et al.*, *Phys. Rev. Lett.* **130**, 251002 (2023), URL <https://link.aps.org/doi/10.1103/PhysRevLett.130.251002>.
- [44] G. Lucente *et al.*, *Phys. Rev. D* **105**, 12, 123020 (2022), [arXiv:2203.15812].
- [45] J. E. Kim, *Phys. Rev. Lett.* **43**, 103 (1979).
- [46] M. A. Shifman, A. I. Vainshtein and V. I. Zakharov, *Nucl. Phys.* **B166**, 493 (1980).
- [47] M. Dine, W. Fischler and M. Srednicki, *Phys. Lett.* **104B**, 199 (1981).
- [48] A. R. Zhitnitsky, *Sov. J. Nucl. Phys.* **31**, 260 (1980), [*Yad. Fiz.*31,497(1980)].
- [49] L. Di Luzio *et al.*, *Phys. Rept.* **870**, 1 (2020), [arXiv:2003.01100].
- [50] J. E. Kim and G. Carosi, *Rev. Mod. Phys.* **82**, 557 (2010), [arXiv:0807.3125].
- [51] G. Grilli di Cortona *et al.*, *JHEP* **01**, 034 (2016), [arXiv:1511.02867].
- [52] J. E. Kim, *Phys. Rev.* **D58**, 055006 (1998), [hep-ph/9802220].
- [53] L. Di Luzio, F. Mescia and E. Nardi, *Phys. Rev. Lett.* **118**, 3, 031801 (2017), [arXiv:1610.07593].
- [54] L. Di Luzio, F. Mescia and E. Nardi, *Phys. Rev. D* **96**, 7, 075003 (2017), [arXiv:1705.05370].
- [55] M. Farina *et al.*, *JHEP* **01**, 095 (2017), [arXiv:1611.09855].
- [56] P. Agrawal *et al.*, *JHEP* **02**, 006 (2018), [arXiv:1709.06085].
- [57] A. Hook, *Phys. Rev. Lett.* **120**, 26, 261802 (2018), [arXiv:1802.10093].
- [58] L. Di Luzio *et al.*, *JHEP* **05**, 184 (2021), [arXiv:2102.00012].
- [59] A. V. Sokolov and A. Ringwald, *JHEP* **06**, 123 (2021), [arXiv:2104.02574].
- [60] J. Diehl and E. Koutsangelas, *Phys. Rev. D* **107**, 9, 095020 (2023), [arXiv:2302.04667].
- [61] C. O’Hare, *cajohare/AxionLimits: AxionLimits* (2023), URL <https://doi.org/10.5281/zenodo.3932430>.
- [62] J. L. Ouellet *et al.* (ABRACADABRA), *Phys. Rev. Lett.* **122**, 12, 121802 (2019), [arXiv:1810.12257].
- [63] C. P. Salemi *et al.*, *Phys. Rev. Lett.* **127**, 8, 081801 (2021), [arXiv:2102.06722].
- [64] S. J. Asztalos *et al.* (ADMX), *Phys. Rev. Lett.* **104**, 041301 (2010), [arXiv:0910.5914].
- [65] C. Boutan *et al.* (ADMX), *Phys. Rev. Lett.* **121**, 26, 261302 (2018), [arXiv:1901.00920].
- [66] N. Du *et al.* (ADMX), *Phys. Rev. Lett.* **120**, 15, 151301 (2018), [arXiv:1804.05750].
- [67] T. Braine *et al.* (ADMX), *Phys. Rev. Lett.* **124**, 10, 101303 (2020), [arXiv:1910.08638].

- [68] C. Bartram *et al.* (ADMX Collaboration), Phys. Rev. Lett. **127**, 261803 (2021), URL <https://link.aps.org/doi/10.1103/PhysRevLett.127.261803>.
- [69] C. Bartram *et al.*, Review of Scientific Instruments **94**, 4, 044703 (2023), ISSN 0034-6748, URL <https://doi.org/10.1063/5.0122907>.
- [70] N. Crisosto *et al.*, Phys. Rev. Lett. **124**, 24, 241101 (2020), [arXiv:1911.05772].
- [71] S. Lee *et al.*, Phys. Rev. Lett. **124**, 10, 101802 (2020), [arXiv:2001.05102].
- [72] J. Jeong *et al.*, Phys. Rev. Lett. **125**, 22, 221302 (2020), [arXiv:2008.10141].
- [73] O. Kwon *et al.* (CAPP), Phys. Rev. Lett. **126**, 19, 191802 (2021), [arXiv:2012.10764].
- [74] Y. Lee *et al.*, Phys. Rev. Lett. **128**, 24, 241805 (2022), [arXiv:2206.08845].
- [75] J. Kim *et al.*, Phys. Rev. Lett. **130**, 091602 (2023), URL <https://link.aps.org/doi/10.1103/PhysRevLett.130.091602>.
- [76] A. K. Yi *et al.*, Phys. Rev. Lett. **130**, 071002 (2023), URL <https://link.aps.org/doi/10.1103/PhysRevLett.130.071002>.
- [77] B. Yang *et al.* (2023), [arXiv:2308.09077].
- [78] C. M. Adair *et al.*, Nature Commun. **13**, 1, 6180 (2022), [arXiv:2211.02902].
- [79] Y. Oshima *et al.* (2023), [arXiv:2303.03594].
- [80] J. A. Devlin *et al.*, Phys. Rev. Lett. **126**, 4, 041301 (2021), [arXiv:2101.11290].
- [81] T. Grenet *et al.* (2021), [arXiv:2110.14406].
- [82] L. Zhong *et al.* (HAYSTAC), Phys. Rev. D **97**, 9, 092001 (2018), [arXiv:1803.03690].
- [83] K. M. Backes *et al.* (HAYSTAC), Nature **590**, 7845, 238 (2021), [arXiv:2008.01853].
- [84] M. J. Jewell *et al.* (HAYSTAC) (2023), [arXiv:2301.09721].
- [85] J. Heinze *et al.* (2023), [arXiv:2307.01365].
- [86] B. T. McAllister *et al.*, Phys. Dark Univ. **18**, 67 (2017), [arXiv:1706.00209].
- [87] A. P. Quiskamp *et al.*, Sci. Adv. **8**, 27, abq3765 (2022), [arXiv:2203.12152].
- [88] D. Alesini *et al.*, Phys. Rev. D **99**, 10, 101101 (2019), [arXiv:1903.06547].
- [89] D. Alesini *et al.*, Phys. Rev. D **103**, 10, 102004 (2021), [arXiv:2012.09498].
- [90] D. Alesini *et al.*, Phys. Rev. D **106**, 5, 052007 (2022), [arXiv:2208.12670].
- [91] S. De Panfilis *et al.*, Phys. Rev. Lett. **59**, 839 (1987).
- [92] A. V. Gramolin *et al.*, Nature Phys. **17**, 1, 79 (2021), [arXiv:2003.03348].
- [93] H. Chang *et al.* (TASEH), Phys. Rev. Lett. **129**, 11, 111802 (2022), [arXiv:2205.05574].
- [94] A. Arza *et al.*, Phys. Rev. D **105**, 9, 095007 (2022), [arXiv:2112.09620].
- [95] C. Hagmann *et al.*, Phys. Rev. **D42**, 1297 (1990).
- [96] C. A. Thomson *et al.*, Phys. Rev. Lett. **126**, 8, 081803 (2021), [Erratum: Phys.Rev.Lett. 127, 019901 (2021)], [arXiv:1912.07751].
- [97] C. A. Thomson *et al.*, Phys. Rev. D **107**, 112003 (2023), URL <https://link.aps.org/doi/10.1103/PhysRevD.107.112003>.
- [98] K. Ehret *et al.* (ALPS), Phys. Lett. **B689**, 149 (2010), [arXiv:1004.1313].
- [99] V. Anastassopoulos *et al.* (CAST), Nature Phys. **13**, 584 (2017), [arXiv:1705.02290].
- [100] M. Betz *et al.*, Phys. Rev. **D88**, 7, 075014 (2013), [arXiv:1310.8098].
- [101] R. Ballou *et al.* (OSQAR), Phys. Rev. **D92**, 9, 092002 (2015), [arXiv:1506.08082].
- [102] F. Della Valle *et al.*, Eur. Phys. J. **C76**, 1, 24 (2016), [arXiv:1510.08052].
- [103] Y. Kirita *et al.* (SAPPHIRES), JHEP **10**, 176 (2022), [arXiv:2208.09880].
- [104] M. Escudero *et al.* (2023), [arXiv:2302.10206].
- [105] M. Xiao *et al.*, Phys. Rev. Lett. **126**, 3, 031101 (2021), [arXiv:2009.09059].
- [106] P. A. R. Ade *et al.* (BICEP/Keck Collaboration), Phys. Rev. D **105**, 022006 (2022), URL <https://link.aps.org/doi/10.1103/PhysRevD.105.022006>.
- [107] A. Keller *et al.*, Astrophys. J. **927**, 1, 71 (2022), [arXiv:2112.03439].
- [108] M. H. Chan, Sci. Rep. **11**, 20087 (2021), [arXiv:2109.11734].
- [109] K. Kohri and H. Kodama, Phys. Rev. **D96**, 5, 051701 (2017), [arXiv:1704.05189].
- [110] D. Wouters and P. Brun, Astrophys. J. **772**, 44 (2013), [arXiv:1304.0989].
- [111] M. C. D. Marsh *et al.*, JCAP **1712**, 12, 036 (2017), [arXiv:1703.07354].
- [112] C. S. Reynolds *et al.*, Astrophys. J. **890**, 1, 59 (2020), [arXiv:1907.05475].
- [113] J. S. Reynés *et al.*, Mon. Not. Roy. Astron. Soc. **510**, 1, 1264 (2021), [arXiv:2109.03261].
- [114] F. Capozzi *et al.* (2023), [arXiv:2303.07426].
- [115] H. Liu *et al.* (2023), [arXiv:2303.07370].
- [116] B. Bolliet, J. Chluba and R. Battye, Mon. Not. Roy. Astron. Soc. **507**, 3, 3148 (2021), [arXiv:2012.07292].
- [117] M. A. Buen-Abad, J. Fan and C. Sun (2020), [arXiv:2011.05993].
- [118] M. Ajello *et al.* (Fermi-LAT), Phys. Rev. Lett. **116**, 16, 161101 (2016), [arXiv:1603.06978].
- [119] M. Meyer and T. Petrushevskaya, Phys. Rev. Lett. **124**, 23, 231101 (2020), [Erratum: Phys.Rev.Lett. 125, 119901 (2020)], [arXiv:2006.06722].
- [120] J. Davies, M. Meyer and G. Cotter (2022), [arXiv:2211.03414].
- [121] J. L. Bernal *et al.* (2022), [arXiv:2208.13794].
- [122] A. Ayala *et al.*, Phys. Rev. Lett. **113**, 19, 191302 (2014), [arXiv:1406.6053].
- [123] M. J. Dolan, F. J. Hiskens and R. R. Volkas, JCAP **10**, 096 (2022), [arXiv:2207.03102].
- [124] S. Jacobsen, T. Linden and K. Freese (2022), [arXiv:2203.04332].
- [125] A. Abramowski *et al.* (H.E.S.S.), Phys. Rev. D **88**, 10, 102003 (2013), [arXiv:1311.3148].
- [126] F. Calore *et al.*, Mon. Not. Roy. Astron. Soc. **520**, 3, 4167 (2023), [arXiv:2209.06299].
- [127] D. Wadekar and G. R. Farrar, Phys. Rev. D **103**, 123028 (2021), URL <https://link.aps.org/doi/10.1103/PhysRevD.103.123028>.
- [128] C. Dessert, A. J. Long and B. R. Safdi, Phys. Rev. Lett. **128**, 071102 (2022), URL <https://link.aps.org/doi/10.1103/PhysRevLett.128.071102>.
- [129] C. Dessert, D. Dunsby and B. R. Safdi, Phys. Rev. D **105**, 10, 103034 (2022), [arXiv:2203.04319].
- [130] M. M. Ivanov *et al.*, JCAP **02**, 059 (2019), [arXiv:1811.10997].
- [131] H.-J. Li *et al.*, Phys. Rev. D **103**, 8, 083003 (2021), [arXiv:2008.09464].

- [132] H.-J. Li, X.-J. Bi and P.-F. Yin, *Chin. Phys. C* **46**, 8, 085105 (2022), [arXiv:2110.13636].
- [133] J. W. Foster *et al.*, *Phys. Rev. Lett.* **125**, 17, 171301 (2020), [arXiv:2004.00011].
- [134] J. Darling, *Astrophys. J. Lett.* **900**, 2, L28 (2020), [arXiv:2008.11188].
- [135] R. A. Battye *et al.*, *Phys. Rev. D* **105**, L021305 (2022), URL <https://link.aps.org/doi/10.1103/PhysRevD.105.L021305>.
- [136] J. W. Foster *et al.*, *Phys. Rev. Lett.* **129**, 25, 251102 (2022), [arXiv:2202.08274].
- [137] R. A. Battye *et al.* (2023), [arXiv:2303.11792].
- [138] K. Perez *et al.*, *Phys. Rev. D* **95**, 12, 123002 (2017), [arXiv:1609.00667].
- [139] K. C. Y. Ng *et al.*, *Phys. Rev. D* **99**, 083005 (2019), [arXiv:1901.01262].
- [140] B. M. Roach *et al.*, *Phys. Rev. D* **107**, 2, 023009 (2023), [arXiv:2207.04572].
- [141] M. A. Fedderke, P. W. Graham and S. Rajendran, *Phys. Rev. D* **100**, 1, 015040 (2019), [arXiv:1903.02666].
- [142] S. Adachi *et al.* (POLARBEAR Collaboration), *Phys. Rev. D* **108**, 043017 (2023), URL <https://link.aps.org/doi/10.1103/PhysRevD.108.043017>.
- [143] A. Castillo *et al.*, *JCAP* **06**, 06, 014 (2022), [arXiv:2201.03422].
- [144] T. Liu, X. Lou and J. Ren, *Phys. Rev. Lett.* **130**, 121401 (2023), URL <https://link.aps.org/doi/10.1103/PhysRevLett.130.121401>.
- [145] D. Noordhuis *et al.* (2022), [arXiv:2209.09917].
- [146] C. Severino and I. Lopes, *The Astrophysical Journal* **943**, 2, 95 (2023), URL <https://dx.doi.org/10.3847/1538-4357/aca897>.
- [147] N. Vinyoles *et al.*, *JCAP* **1510**, 10, 015 (2015), [arXiv:1501.01639].
- [148] N. H. Nguyen, E. H. Tanin and M. Kamionkowski (2023), [arXiv:2307.11216].
- [149] J. Jaeckel, P. C. Malta and J. Redondo, *Phys. Rev. D* **98**, 5, 055032 (2018), [arXiv:1702.02964].
- [150] E. Müller *et al.* (2023), [arXiv:2304.01060].
- [151] A. Payez *et al.*, *JCAP* **1502**, 02, 006 (2015), [arXiv:1410.3747].
- [152] S. Hoof and L. Schulz, *JCAP* **03**, 054 (2023), [arXiv:2212.09764].
- [153] G. Lucente *et al.*, *JCAP* **12**, 008 (2020), [arXiv:2008.04918].
- [154] A. Caputo, G. Raffelt and E. Vitagliano, *Phys. Rev. D* **105**, 3, 035022 (2022), [arXiv:2109.03244].
- [155] A. Caputo *et al.*, *Phys. Rev. Lett.* **128**, 22, 221103 (2022), [arXiv:2201.09890].
- [156] M. Diamond *et al.*, *Phys. Rev. D* **107**, 10, 103029 (2023), [arXiv:2303.11395].
- [157] W. DeRocco *et al.*, *Phys. Rev. Lett.* **129**, 10, 101101 (2022), [arXiv:2205.05700].
- [158] C. Beaufort *et al.* (2023), [arXiv:2303.06968].
- [159] C. Dessert, J. W. Foster and B. R. Safdi, *Phys. Rev. Lett.* **125**, 26, 261102 (2020), [arXiv:2008.03305].
- [160] K. R. Ferguson *et al.* (SPT-3G), *Phys. Rev. D* **106**, 4, 042011 (2022), [arXiv:2203.16567].
- [161] B. D. Blout *et al.*, *Astrophys. J.* **546**, 825 (2001), [arXiv:astro-ph/0006310].
- [162] M. Regis *et al.*, *Phys. Lett. B* **814**, 136075 (2021), [arXiv:2009.01310].
- [163] D. Grin *et al.*, *Phys. Rev. D* **75**, 105018 (2007), [arXiv:astro-ph/0611502].
- [164] K. Nakayama and W. Yin, *Phys. Rev. D* **106**, 10, 103505 (2022), [arXiv:2205.01079].
- [165] P. Carena, G. Lucente and E. Vitagliano (2023), [arXiv:2301.06560].
- [166] D. Cadamuro and J. Redondo, *JCAP* **1202**, 032 (2012), [arXiv:1110.2895].
- [167] P. F. Depta, M. Hufnagel and K. Schmidt-Hoberg, *JCAP* **05**, 009 (2020), [arXiv:2002.08370].
- [168] K. Langhoff, N. J. Outmezguine and N. L. Rodd, *Phys. Rev. Lett.* **129**, 24, 241101 (2022), [arXiv:2209.06216].
- [169] G. Raffelt and D. Seckel, *Phys. Rev. Lett.* **60**, 1793 (1988).
- [170] M. Carena and R. D. Peccei, *Phys. Rev.* **D40**, 652 (1989).
- [171] K. Choi, K. Kang and J. E. Kim, *Phys. Rev. Lett.* **62**, 849 (1989).
- [172] M. Srednicki, *Nucl. Phys.* **B260**, 689 (1985).
- [173] S. Chang and K. Choi, *Phys. Lett.* **B316**, 51 (1993), [hep-ph/9306216].
- [174] G. C. Branco *et al.*, *Phys. Rept.* **516**, 1 (2012), [arXiv:1106.0034].
- [175] C.-Y. Chen and S. Dawson, *Phys. Rev.* **D87**, 055016 (2013), [arXiv:1301.0309].
- [176] R. Balkin *et al.*, *JHEP* **07**, 221 (2020), [arXiv:2003.04903].
- [177] K. Choi *et al.*, *JHEP* **02**, 143 (2022), [arXiv:2110.01972].
- [178] D. A. Dicus *et al.*, *Phys. Rev.* **D18**, 1829 (1978).
- [179] G. Raffelt and L. Stodolsky, *Phys. Rev.* **D37**, 1237 (1988).
- [180] A. A. Anselm, *Yad. Fiz.* **42**, 1480 (1985).
- [181] K. van Bibber *et al.*, *Phys. Rev. Lett.* **59**, 759 (1987).
- [182] G. Ruoso *et al.*, *Z. Phys.* **C56**, 505 (1992).
- [183] R. Cameron *et al.*, *Phys. Rev.* **D47**, 3707 (1993).
- [184] M. Fouche *et al.*, *Phys. Rev.* **D78**, 032013 (2008), [arXiv:0808.2800].
- [185] P. Pugno *et al.* (OSQAR), *Phys. Rev.* **D78**, 092003 (2008), [arXiv:0712.3362].
- [186] A. S. Chou *et al.* (GammeV (T-969)), *Phys. Rev. Lett.* **100**, 080402 (2008), [arXiv:0710.3783].
- [187] A. Afanasev *et al.*, *Phys. Rev. Lett.* **101**, 120401 (2008), [arXiv:0806.2631].
- [188] P. Pugno *et al.* (OSQAR), *Eur. Phys. J.* **C74**, 8, 3027 (2014), [arXiv:1306.0443].
- [189] F. Hoogeveen and T. Ziegenhagen, *Nucl. Phys.* **B358**, 3 (1991).
- [190] P. Sikivie, D. B. Tanner and K. van Bibber, *Phys. Rev. Lett.* **98**, 172002 (2007), [hep-ph/0701198].
- [191] G. Mueller *et al.*, *Phys. Rev.* **D80**, 072004 (2009), [arXiv:0907.5387].
- [192] M. Diaz Ortiz *et al.*, *Physics of the Dark Universe* **35**, 100968 (2022), ISSN 2212-6864, URL <https://www.sciencedirect.com/science/article/pii/S2212686422000115>.
- [193] F. Hoogeveen, *Phys. Lett.* **B288**, 195 (1992).
- [194] J. Jaeckel and A. Ringwald, *Phys. Lett.* **B659**, 509 (2008), [arXiv:0707.2063].
- [195] F. Caspers, J. Jaeckel and A. Ringwald, *JINST* **4**, P11013 (2009), [arXiv:0908.0759].
- [196] R. Povey, J. Hartnett and M. Tobar, *Phys. Rev.* **D82**, 052003 (2010), [arXiv:1003.0964].
- [197] L. Maiani, R. Petronzio and E. Zavattini, *Phys. Lett.* **B175**, 359 (1986).
- [198] Y. Semertzidis *et al.*, *Phys. Rev. Lett.* **64**, 2988 (1990).
- [199] E. Fischbach and C. Talmadge, *Nature* **356**, 207 (1992).
- [200] J. E. Moody and F. Wilczek, *Phys. Rev.* **D30**, 130 (1984).
- [201] A. N. Youdin *et al.*, *Phys. Rev. Lett.* **77**, 2170 (1996).

- [202] W.-T. Ni *et al.*, Phys. Rev. Lett. **82**, 2439 (1999).
- [203] D. F. Phillips *et al.*, Phys. Rev. **D63**, 111101 (2001), [arXiv:physics/0008230].
- [204] B. R. Heckel *et al.*, Phys. Rev. Lett. **97**, 021603 (2006), [hep-ph/0606218].
- [205] S. A. Hoedl *et al.*, Phys. Rev. Lett. **106**, 041801 (2011).
- [206] E. G. Adelberger *et al.*, Phys. Rev. Lett. **98**, 131104 (2007), [hep-ph/0611223].
- [207] D. J. Kapner *et al.*, Phys. Rev. Lett. **98**, 021101 (2007), [hep-ph/0611184].
- [208] G. Raffelt, Phys. Rev. **D86**, 015001 (2012), [arXiv:1205.1776].
- [209] C. A. J. O'Hare and E. Vitagliano, Phys. Rev. D **102**, 11, 115026 (2020), [arXiv:2010.03889].
- [210] A. Arvanitaki and A. A. Geraci, Phys. Rev. Lett. **113**, 16, 161801 (2014), [arXiv:1403.1290].
- [211] A. A. Geraci *et al.* (ARIADNE), Springer Proc. Phys. **211**, 151 (2018), [arXiv:1710.05413].
- [212] H. Fosbinder-Elkins *et al.* (2017), [arXiv:1710.08102].
- [213] N. Aggarwal *et al.* (ARIADNE Collaboration), Phys. Rev. Res. **4**, 013090 (2022), URL <https://link.aps.org/doi/10.1103/PhysRevResearch.4.013090>.
- [214] M. S. Turner, Phys. Rept. **197**, 67 (1990).
- [215] G. G. Raffelt, Lect. Notes Phys. **741**, 51 (2008), [51(2006)], [hep-ph/0611350].
- [216] S. Andriamonje *et al.* (CAST), JCAP **0704**, 010 (2007), [hep-ex/0702006].
- [217] P. Gondolo and G. G. Raffelt, Phys. Rev. **D79**, 107301 (2009), [arXiv:0807.2926].
- [218] H. Schlattl, A. Weiss and G. Raffelt, Astropart. Phys. **10**, 353 (1999), [hep-ph/9807476].
- [219] P. Agnes *et al.* (DarkSide), Phys. Rev. Lett. **130**, 10, 101002 (2023), [arXiv:2207.11968].
- [220] M. Agostini *et al.* (GERDA), Phys. Rev. Lett. **125**, 1, 011801 (2020), [arXiv:2005.14184].
- [221] C. Fu *et al.* (PandaX), Phys. Rev. Lett. **119**, 18, 181806 (2017), [arXiv:1707.07921].
- [222] T. Aralis *et al.* (SuperCDMS), Phys. Rev. D **101**, 5, 052008 (2020), [Erratum: Phys.Rev.D 103, 039901 (2021)], [arXiv:1911.11905].
- [223] E. Aprile *et al.* (XENON), Phys. Rev. D **102**, 7, 072004 (2020), [arXiv:2006.09721].
- [224] E. Aprile *et al.* (XENON Collaboration), Phys. Rev. Lett. **129**, 161805 (2022), URL <https://link.aps.org/doi/10.1103/PhysRevLett.129.161805>.
- [225] K. Van Tilburg, Phys. Rev. D **104**, 2, 023019 (2021), [arXiv:2006.12431].
- [226] F. Capozzi and G. Raffelt, Phys. Rev. D **102**, 8, 083007 (2020), [arXiv:2007.03694].
- [227] N. Crescini *et al.* (QUAX), Phys. Rev. Lett. **124**, 17, 171801 (2020), [arXiv:2001.08940].
- [228] R. Z. Ferreira, M. C. D. Marsh and E. Müller, Phys. Rev. Lett. **128**, 22, 221302 (2022), [arXiv:2202.08858].
- [229] O. Straniero *et al.*, in "Proceedings, 11th Patras Workshop on Axions, WIMPs and WISPs (Axion-WIMP 2015): Zaragoza, Spain, June 22-26, 2015," 77-81 (2015).
- [230] T. Constantino *et al.*
- [231] J. Redondo, Journal of Cosmology and Astroparticle Physics **2013**, 12, 008 (2013).
- [232] O. Straniero *et al.*, Astron. Astrophys. **644**, A166 (2020), [arXiv:2010.03833].
- [233] G. G. Raffelt, Phys. Lett. **166B**, 402 (1986).
- [234] S. I. Blinnikov and N. V. Dunina-Barkovskaya, Mon. Not. Roy. Astron. Soc. **266**, 289 (1994).
- [235] M. M. Miller Bertolami *et al.*, JCAP **1410**, 10, 069 (2014), [arXiv:1406.7712].
- [236] J. Isern *et al.*, Astrophys. J. **682**, L109 (2008), [arXiv:0806.2807].
- [237] J. Isern *et al.*, J. Phys. Conf. Ser. **172**, 012005 (2009), [arXiv:0812.3043].
- [238] A. Drlica-Wagner *et al.* (LSST Dark Matter Group) (2019), [arXiv:1902.01055].
- [239] J. Isern *et al.*, Astron. & Astrophys. **512**, A86 (2010).
- [240] A. H. Corsico *et al.*, Mon. Not. Roy. Astron. Soc. **424**, 2792 (2012), [arXiv:1205.6180].
- [241] A. H. Corsico *et al.*, JCAP **1212**, 010 (2012), [arXiv:1211.3389].
- [242] A. H. Corsico *et al.*, The Astronomy and Astrophysics Review **27**, 1, 7 (2019), URL <https://doi.org/10.1007/s00159-019-0118-4>.
- [243] M. J. Dolan, F. J. Hiskens and R. R. Volkas, Journal of Cosmology and Astroparticle Physics **2021**, 09, 010 (2021), URL <https://doi.org/10.1088/1475-7516/2021/09/010>.
- [244] J. Isern, S. Torres and A. Rebassa-Mansergas, Front. Astron. Space Sci. **9**, 815517 (2022), [arXiv:2202.02052].
- [245] V. M. Mostepanenko and G. L. Klimchitskaya, Universe **6**, 9, 147 (2020), [arXiv:2009.04517].
- [246] T. Wu *et al.*, Phys. Rev. Lett. **122**, 19, 191302 (2019), [arXiv:1901.10843].
- [247] A. Garcon *et al.*, Sci. Adv. **5**, 10, eaax4539 (2019), [arXiv:1902.04644].
- [248] K. Wei *et al.* (2023), [arXiv:2306.08039].
- [249] M. Jiang *et al.*, Nature Phys. **17**, 12, 1402 (2021), [arXiv:2102.01448].
- [250] I. M. Bloch *et al.* (NASDUCK) (2022), [arXiv:2209.13588].
- [251] I. M. Bloch *et al.*, JHEP **01**, 167 (2020), [arXiv:1907.03767].
- [252] G. Vasilakis *et al.*, Physical Review Letters **103**, 26 (2009), ISSN 1079-7114, URL <http://dx.doi.org/10.1103/PhysRevLett.103.261801>.
- [253] J. Lee *et al.*, Phys. Rev. X **13**, 011050 (2023), URL <https://link.aps.org/doi/10.1103/PhysRevX.13.011050>.
- [254] M. Buschmann *et al.*, Phys. Rev. Lett. **128**, 9, 091102 (2022), [arXiv:2111.09892].
- [255] A. Bhusal, N. Houston and T. Li, Phys. Rev. Lett. **126**, 9, 091601 (2021), [arXiv:2004.02733].
- [256] G.G. Raffelt, *Stars as Laboratories for Fundamental Physics*, (Univ. of Chicago Press, Chicago, 1996).
- [257] T. Fischer *et al.*, Phys. Rev. **D94**, 8, 085012 (2016), [arXiv:1605.08780].
- [258] J. H. Chang, R. Essig and S. D. McDermott, JHEP **09**, 051 (2018), [arXiv:1803.00993].
- [259] P. Carezza *et al.*, JCAP **10**, 10, 016 (2019), [Erratum: JCAP 05, E01 (2020)], [arXiv:1906.11844].
- [260] M. S. Turner, Phys. Rev. D **45**, 1066 (1992).
- [261] G. Raffelt and D. Seckel, Phys. Rev. D **52**, 1780 (1995), [arXiv:astro-ph/9312019].
- [262] W. Keil *et al.*, Phys. Rev. D **56**, 2419 (1997), [arXiv:astro-ph/9612222].
- [263] B. Fore and S. Reddy, Phys. Rev. C **101**, 3, 035809 (2020), [arXiv:1911.02632].
- [264] P. Carezza *et al.*, Phys. Rev. Lett. **126**, 7, 071102 (2021), [arXiv:2010.02943].
- [265] J. Engel, D. Seckel and A. C. Hayes, Phys. Rev. Lett. **65**, 960 (1990).
- [266] N. Iwamoto, Phys. Rev. Lett. **53**, 1198 (1984).
- [267] N. Iwamoto, Phys. Rev. D **64**, 043002 (2001).
- [268] A. Sedrakian, Phys. Rev. **D93**, 6, 065044 (2016), [arXiv:1512.07828].

- [269] J. Keller and A. Sedrakian, Nucl. Phys. **A897**, 62 (2013), [arXiv:1205.6940].
- [270] T. Fischer, Astron. Astrophys. **593**, A103 (2016), [arXiv:1608.05004].
- [271] K. Hamaguchi *et al.*, Phys. Rev. **D98**, 10, 103015 (2018), [arXiv:1806.07151].
- [272] D. Page *et al.*, Phys. Rev. Lett. **106**, 081101 (2011), [arXiv:1011.6142].
- [273] P. S. Shternin *et al.*, Mon. Not. Roy. Astron. Soc. **412**, L108 (2011), [arXiv:1012.0045].
- [274] B. Posselt and G. G. Pavlov, Astrophys. J. **864**, 2, 135 (2018), [arXiv:1808.00531].
- [275] M. V. Beznogov *et al.*, Phys. Rev. **C98**, 3, 035802 (2018), [arXiv:1806.07991].
- [276] G. G. Raffelt, J. Redondo and N. Viaux Maira, Phys. Rev. **D84**, 103008 (2011), [arXiv:1110.6397].
- [277] K. van Bibber *et al.*, Phys. Rev. **D39**, 2089 (1989).
- [278] D. M. Lazarus *et al.*, Phys. Rev. Lett. **69**, 2333 (1992).
- [279] S. Moriyama *et al.*, Phys. Lett. **B434**, 147 (1998), [hep-ex/9805026].
- [280] Y. Inoue *et al.*, Phys. Lett. **B536**, 18 (2002), [arXiv:astro-ph/0204388].
- [281] Y. Inoue *et al.*, Phys. Lett. **B668**, 93 (2008), [arXiv:0806.2230].
- [282] E. Arik *et al.* (CAST), JCAP **0902**, 008 (2009), [arXiv:0810.4482].
- [283] S. Aune *et al.* (CAST), Phys. Rev. Lett. **107**, 261302 (2011), [arXiv:1106.3919].
- [284] M. Arik *et al.* (CAST), Phys. Rev. Lett. **112**, 9, 091302 (2014), [arXiv:1307.1985].
- [285] M. Arik *et al.* (CAST), Phys. Rev. **D92**, 2, 021101 (2015), [arXiv:1503.00610].
- [286] E. Armengaud *et al.*, JINST **9**, T05002 (2014), [arXiv:1401.3233].
- [287] E. Armengaud *et al.* (IAXO), JCAP **1906**, 06, 047 (2019), [arXiv:1904.09155].
- [288] M. Giannotti *et al.*, JCAP **1710**, 10, 010 (2017), [arXiv:1708.02111].
- [289] K. Barth *et al.*, JCAP **1305**, 010 (2013), [arXiv:1302.6283].
- [290] A. Abeln *et al.* (BabyIAXO), JCAP **2105**, 05, 137 (2021), [arXiv:2010.12076].
- [291] E. Aprile *et al.* (XENON), Phys. Rev. Lett. **129**, 16, 161805 (2022), [arXiv:2207.11330].
- [292] X. Zhou *et al.*, Chinese Physics Letters **38**, 10, 109902 (2021), URL <https://dx.doi.org/10.1088/0256-307X/38/10/109902>.
- [293] D. S. Akerib *et al.* (LUX), Phys. Rev. Lett. **118**, 26, 261301 (2017), [arXiv:1704.02297].
- [294] J. W. Brockway, E. D. Carlson and G. G. Raffelt, Phys. Lett. **B383**, 439 (1996), [arXiv:astro-ph/9605197].
- [295] J. A. Grifols, E. Masso and R. Toldra, Phys. Rev. Lett. **77**, 2372 (1996), [arXiv:astro-ph/9606028].
- [296] F. Calore *et al.*, Phys. Rev. D **102**, 12, 123005 (2020), [arXiv:2008.11741].
- [297] C. Dessert, J. W. Foster and B. R. Safdi, Astrophys. J. **904**, 1, 42 (2020), [arXiv:1910.02956].
- [298] M. Buschmann *et al.*, Phys. Rev. Lett. **126**, 2, 021102 (2021), [arXiv:1910.04164].
- [299] C. Dessert, A. J. Long and B. R. Safdi, Phys. Rev. Lett. **123**, 6, 061104 (2019), [arXiv:1903.05088].
- [300] C. Csaki, N. Kaloper and J. Terning, Phys. Rev. Lett. **88**, 161302 (2002), [hep-ph/0111311].
- [301] A. Mirizzi, G.G. Raffelt, and P.D. Serpico, Lect. Notes Phys. **741**, 115 (2008).
- [302] D. Horns *et al.*, Phys. Rev. **D85**, 085021 (2012), [arXiv:1203.2184].
- [303] A. Payez, J. R. Cudell and D. Hutsemekers, JCAP **1207**, 041 (2012), [arXiv:1204.6187].
- [304] R. Gill and J. S. Heyl, Phys. Rev. **D84**, 085001 (2011), [arXiv:1105.2083].
- [305] A. Dominguez, M. A. Sanchez-Conde and F. Prada, JCAP **1111**, 020 (2011), [arXiv:1106.1860].
- [306] W. Essey and A. Kusenko, Astrophys. J. **751**, L11 (2012), [arXiv:1111.0815].
- [307] D. Horns and M. Meyer, JCAP **1202**, 033 (2012), [arXiv:1201.4711].
- [308] G. I. Rubtsov and S. V. Troitsky, JETP Lett. **100**, 6, 355 (2014), [Pisma Zh. Eksp. Teor. Fiz.100,no.6,397(2014)], [arXiv:1406.0239].
- [309] D. A. Sanchez, S. Fegan and B. Giebels, Astron. Astrophys. **554**, A75 (2013), [arXiv:1303.5923].
- [310] J. Biteau and D. A. Williams, Astrophys. J. **812**, 1, 60 (2015), [arXiv:1502.04166].
- [311] A. Dominguez and M. Ajello, Astrophys. J. **813**, 2, L34 (2015), [arXiv:1510.07913].
- [312] A. Korochkin, G. Rubtsov and S. Troitsky, JCAP **12**, 002 (2019), [arXiv:1810.03443].
- [313] A. De Angelis, G. Galanti and M. Roncadelli, Phys. Rev. **D84**, 105030 (2011), [Erratum: Phys. Rev.D87,no.10,109903(2013)], [arXiv:1106.1132].
- [314] M. Simet, D. Hooper and P. D. Serpico, Phys. Rev. **D77**, 063001 (2008), [arXiv:0712.2825].
- [315] M. A. Sanchez-Conde *et al.*, Phys. Rev. **D79**, 123511 (2009), [arXiv:0905.3270].
- [316] M. Meyer, D. Horns and M. Raue, Phys. Rev. **D87**, 3, 035027 (2013), [arXiv:1302.1208].
- [317] A. Abramowski *et al.* (H.E.S.S.), Phys. Rev. **D88**, 10, 102003 (2013), [arXiv:1311.3148].
- [318] C. Zhang *et al.*, Phys. Rev. **D97**, 6, 063009 (2018), [arXiv:1802.08420].
- [319] M. Libanov and S. Troitsky, Phys. Lett. B **802**, 135252 (2020), [arXiv:1908.03084].
- [320] G. Ballesteros *et al.*, Phys. Rev. Lett. **118**, 071802 (2017), URL <https://link.aps.org/doi/10.1103/PhysRevLett.118.071802>.
- [321] M. Buschmann *et al.*, Nature Commun. **13**, 1, 1049 (2022), [arXiv:2108.05368].
- [322] C. Bonati *et al.*, JHEP **03**, 155 (2016), [arXiv:1512.06746].
- [323] E. Berkowitz, M. I. Buchoff and E. Rinaldi, Phys. Rev. **D92**, 3, 034507 (2015), [arXiv:1505.07455].
- [324] M. Dine *et al.*, Phys. Rev. **D96**, 9, 095001 (2017), [arXiv:1705.00676].
- [325] P. Petreczky, H.-P. Schadler and S. Sharma, Phys. Lett. **B762**, 498 (2016), [arXiv:1606.03145].
- [326] L. Fleury and G. D. Moore, Journal of Cosmology and Astroparticle Physics **2016**, 01, 004 (2016), URL <https://dx.doi.org/10.1088/1475-7516/2016/01/004>.
- [327] V. B. Klaer and G. D. Moore, JCAP **1711**, 11, 049 (2017), [arXiv:1708.07521].
- [328] M. Gorghetto, E. Hardy and G. Villadoro, SciPost Phys. **10**, 050 (2021), [arXiv:2007.04990].
- [329] M. Kawasaki, K. Saikawa and T. Sekiguchi, Phys. Rev. **D91**, 6, 065014 (2015), [arXiv:1412.0789].
- [330] R. T. Co, L. J. Hall and K. Harigaya, Journal of High Energy Physics **2021**, 1, 172 (2021), ISSN 1029-8479, URL [https://doi.org/10.1007/JHEP01\(2021\)172](https://doi.org/10.1007/JHEP01(2021)172).
- [331] N. Blinov *et al.*, Phys. Rev. D **100**, 015049 (2019), URL <https://link.aps.org/doi/10.1103/PhysRevD.100.015049>.

- [332] C. A. J. O'Hare *et al.*, Phys. Rev. D **105**, 055025 (2022), URL <https://link.aps.org/doi/10.1103/PhysRevD.105.055025>.
- [333] L. D. Luzio *et al.*, Journal of Cosmology and Astroparticle Physics **2021**, 10, 001 (2021), URL <https://dx.doi.org/10.1088/1475-7516/2021/10/001>.
- [334] Z.-Q. Xia *et al.*, Phys. Rev. **D97**, 6, 063003 (2018), [arXiv:1801.01646].
- [335] J. Majumdar, F. Calore and D. Horns, JCAP **1804**, 04, 048 (2018), [arXiv:1801.08813].
- [336] G. A. Pallathadka *et al.* (2020), [arXiv:2008.08100].
- [337] K. Choi *et al.*, Phys. Rev. D **101**, 4, 043007 (2020), [arXiv:1806.09508].
- [338] F. Chadha-Day (2021), [arXiv:2107.12813].
- [339] M. Berg *et al.*, Astrophys. J. **847**, 2, 101 (2017), [arXiv:1605.01043].
- [340] J. P. Conlon *et al.*, JCAP **1707**, 07, 005 (2017), [arXiv:1704.05256].
- [341] L. Chen and J. P. Conlon, Mon. Not. Roy. Astron. Soc. **479**, 2, 2243 (2018), [arXiv:1712.08313].
- [342] A. Hook and J. Huang, JHEP **06**, 036 (2018), [arXiv:1708.08464].
- [343] J. Huang *et al.*, Phys. Rev. D **99**, 6, 063013 (2019), [arXiv:1807.02133].
- [344] J. Zhang *et al.* (2021), [arXiv:2105.13963].
- [345] R. Balkin *et al.* (2022), [arXiv:2211.02661].
- [346] G. Bellini *et al.* (Borexino), Phys. Rev. D **89**, 11, 112007 (2014), [arXiv:1308.0443].
- [347] B. P. Abbott *et al.* (LIGO Scientific, Virgo), Phys. Rev. Lett. **119**, 16, 161101 (2017), [arXiv:1710.05832].
- [348] A. Arvanitaki and S. Dubovsky, Phys. Rev. **D83**, 044026 (2011), [arXiv:1004.3558].
- [349] A. Arvanitaki, M. Baryakhtar and X. Huang, Phys. Rev. **D91**, 8, 084011 (2015), [arXiv:1411.2263].
- [350] V. M. Mehta *et al.* (2020), [arXiv:2011.08693].
- [351] V. M. Mehta *et al.*, JCAP **07**, 033 (2021), [arXiv:2103.06812].
- [352] M. Baryakhtar *et al.*, Phys. Rev. D **103**, 9, 095019 (2021), [arXiv:2011.11646].
- [353] M. J. Stott (2020), [arXiv:2009.07206].
- [354] A. Arvanitaki *et al.*, Phys. Rev. **D95**, 4, 043001 (2017), [arXiv:1604.03958].
- [355] K. K. Y. Ng *et al.*, Phys. Rev. D **103**, 6, 063010 (2021), [arXiv:1908.02312].
- [356] C. Palomba *et al.*, Phys. Rev. Lett. **123**, 171101 (2019), [arXiv:1909.08854].
- [357] L. Sun, R. Brito and M. Isi, Phys. Rev. D **101**, 6, 063020 (2020), [Erratum: Phys.Rev.D 102, 089902 (2020)], [arXiv:1909.11267].
- [358] E. Masso, F. Rota and G. Zsembinszki, Phys. Rev. D **66**, 023004 (2002), [hep-ph/0203221].
- [359] P. Graf and F. D. Steffen, Phys. Rev. D **83**, 075011 (2011), [arXiv:1008.4528].
- [360] Z. G. Berezhiani, A. S. Sakharov and M. Y. Khlopov, Sov. J. Nucl. Phys. **55**, 1063 (1992).
- [361] S. Hannestad, A. Mirizzi and G. Raffelt, JCAP **07**, 002 (2005), [hep-ph/0504059].
- [362] S. Hannestad *et al.*, JCAP **08**, 001 (2010), [arXiv:1004.0695].
- [363] M. Archidiacono *et al.*, JCAP **10**, 020 (2013), [arXiv:1307.0615].
- [364] E. Di Valentino *et al.*, Phys. Lett. B **752**, 182 (2016), [arXiv:1507.08665].
- [365] W. Giarè *et al.*, Mon. Not. Roy. Astron. Soc. **505**, 2, 2703 (2021), [arXiv:2011.14704].
- [366] L. Di Luzio, G. Martinelli and G. Piazza, Phys. Rev. Lett. **126**, 24, 241801 (2021), [arXiv:2101.10330].
- [367] A. Notari, F. Rompineve and G. Villadoro, Phys. Rev. Lett. **131**, 1, 011004 (2023), [arXiv:2211.03799].
- [368] E. Masso and R. Toldra, Phys. Rev. D **52**, 1755 (1995), [hep-ph/9503293].
- [369] E. Masso and R. Toldra, Phys. Rev. **D55**, 7967 (1997), [hep-ph/9702275].
- [370] J. W. Foster *et al.*, JHEP **12**, 119 (2022), [arXiv:2208.10504].
- [371] P. Panci *et al.*, Phys. Lett. B **841**, 137919 (2023), [arXiv:2209.03371].
- [372] E. Todarello *et al.* (2023), [arXiv:2307.07403].
- [373] J. W. Foster *et al.*, Phys. Rev. Lett. **127**, 5, 051101 (2021), [arXiv:2102.02207].
- [374] J. Preskill, M. B. Wise and F. Wilczek, Phys. Lett. **B120**, 127 (1983).
- [375] L. F. Abbott and P. Sikivie, Phys. Lett. **B120**, 133 (1983).
- [376] M. Dine and W. Fischler, Phys. Lett. **B120**, 137 (1983).
- [377] K. J. Bae, J.-H. Huh and J. E. Kim, JCAP **0809**, 005 (2008), [arXiv:0806.0497].
- [378] O. Wantz and E. P. S. Shellard, Phys. Rev. **D82**, 123508 (2010), [arXiv:0910.1066].
- [379] G. Ballesteros *et al.*, JCAP **1708**, 08, 001 (2017), [arXiv:1610.01639].
- [380] R. T. Co, F. D'ErAMO and L. J. Hall, Phys. Rev. D **94**, 7, 075001 (2016), [arXiv:1603.04439].
- [381] M. Tegmark *et al.*, Phys. Rev. **D73**, 023505 (2006), [arXiv:astro-ph/0511774].
- [382] A. D. Linde, Phys. Lett. **158B**, 375 (1985).
- [383] D. Seckel and M. S. Turner, Phys. Rev. **D32**, 3178 (1985).
- [384] M. Beltran, J. Garcia-Bellido and J. Lesgourgues, Phys. Rev. **D75**, 103507 (2007), [hep-ph/0606107].
- [385] M. P. Hertzberg, M. Tegmark and F. Wilczek, Phys. Rev. **D78**, 083507 (2008), [arXiv:0807.1726].
- [386] J. Hamann *et al.*, JCAP **0906**, 022 (2009), [arXiv:0904.0647].
- [387] P. A. R. Ade *et al.* (Planck), Astron. Astrophys. **571**, A22 (2014), [arXiv:1303.5082].
- [388] P. A. R. Ade *et al.* (Planck), Astron. Astrophys. **594**, A20 (2016), [arXiv:1502.02114].
- [389] B. Bolliet, J. Chluba and R. Battye, Monthly Notices of the Royal Astronomical Society **507**, 3, 3148 (2021), ISSN 0035-8711, URL <https://doi.org/10.1093/mnras/stab1997>.
- [390] R. T. Co, L. J. Hall and K. Harigaya, Phys. Rev. Lett. **124**, 25, 251802 (2020), [arXiv:1910.14152].
- [391] S. Borsanyi *et al.*, Phys. Lett. **B752**, 175 (2016), [arXiv:1508.06917].
- [392] R. Kitano and N. Yamada, JHEP **10**, 136 (2015), [arXiv:1506.00370].
- [393] Y. Taniguchi *et al.*, Phys. Rev. **D95**, 5, 054502 (2017), [arXiv:1611.02411].
- [394] R. D. Pisarski and L. G. Yaffe, Phys. Lett. **97B**, 110 (1980).
- [395] S. Chang, C. Hagmann and P. Sikivie, Phys. Rev. **D59**, 023505 (1999), [hep-ph/9807374].
- [396] C. Hagmann, S. Chang and P. Sikivie, Phys. Rev. **D63**, 125018 (2001), [hep-ph/0012361].
- [397] T. Hiramatsu *et al.*, Phys. Rev. **D83**, 123531 (2011), [arXiv:1012.5502].
- [398] T. Hiramatsu *et al.*, Phys. Rev. **D85**, 105020 (2012), [Erratum: Phys. Rev.D86,089902(2012)], [arXiv:1202.5851].

- [399] M. Gorghetto, E. Hardy and G. Villadoro, *JHEP* **07**, 151 (2018), [arXiv:1806.04677].
- [400] M. Buschmann, J. W. Foster and B. R. Safdi, *Phys. Rev. Lett.* **124**, 16, 161103 (2020), [arXiv:1906.00967].
- [401] M. Hindmarsh *et al.*, *Phys. Rev. Lett.* **124**, 2, 021301 (2020), [arXiv:1908.03522].
- [402] M. Dine *et al.*, *Journal of Cosmology and Astroparticle Physics* **2021**, 11, 041 (2021), URL <https://dx.doi.org/10.1088/1475-7516/2021/11/041>.
- [403] M. Hindmarsh *et al.*, *Phys. Rev. D* **103**, 10, 103534 (2021), [arXiv:2102.07723].
- [404] A. Ringwald and K. Saikawa, *Phys. Rev.* **D93**, 8, 085031 (2016), [Addendum: *Phys. Rev. D* **94**, no.4, 049908(2016)], [arXiv:1512.06436].
- [405] T. Hiramatsu *et al.*, *JCAP* **1301**, 001 (2013), [arXiv:1207.3166].
- [406] K. A. Beyer and S. Sarkar, *SciPost Phys.* **15**, 003 (2023), [arXiv:2211.14635].
- [407] C. J. Hogan and M. J. Rees, *Phys. Lett.* **B205**, 228 (1988).
- [408] E. W. Kolb and I. I. Tkachev, *Phys. Rev. Lett.* **71**, 3051 (1993), [hep-ph/9303313].
- [409] B. Eggemeier *et al.*, *Phys. Rev. Lett.* **125**, 4, 041301 (2020), [arXiv:1911.09417].
- [410] A. Vaquero, J. Redondo and J. Stadler, *Journal of Cosmology and Astroparticle Physics* **2019**, 04, 012 (2019), URL <https://dx.doi.org/10.1088/1475-7516/2019/04/012>.
- [411] E. W. Kolb and I. I. Tkachev, *Astrophys. J.* **460**, L25 (1996), [arXiv:astro-ph/9510043].
- [412] M. Fairbairn, D. J. E. Marsh and J. Quevillon, *Phys. Rev. Lett.* **119**, 2, 021101 (2017), [arXiv:1701.04787].
- [413] A. Katz *et al.*, *JCAP* **1812**, 005 (2018), [arXiv:1807.11495].
- [414] R. Hlozek *et al.*, *Phys. Rev.* **D91**, 10, 103512 (2015), [arXiv:1410.2896].
- [415] D. J. E. Marsh, *Phys. Rept.* **643**, 1 (2016), [arXiv:1510.07633].
- [416] L. Hui *et al.*, *Phys. Rev.* **D95**, 4, 043541 (2017), [arXiv:1610.08297].
- [417] G. P. Centers *et al.*, *Nature Communications* **12**, 1, 7321 (2021), ISSN 2041-1723, URL <https://doi.org/10.1038/s41467-021-27632-7>.
- [418] A. G. Dias *et al.*, *JHEP* **06**, 037 (2014), [arXiv:1403.5760].
- [419] J. E. Kim and D. J. E. Marsh, *Phys. Rev.* **D93**, 2, 025027 (2016), [arXiv:1510.01701].
- [420] H. Davoudiasl and C. W. Murphy, *Phys. Rev. Lett.* **118**, 14, 141801 (2017), [arXiv:1701.01136].
- [421] L. Di Luzio *et al.*, *JCAP* **10**, 001 (2021), [arXiv:2102.01082].
- [422] M. Khlopov, B. A. Malomed and I. B. Zeldovich, *Mon. Not. Roy. Astron. Soc.* **215**, 575 (1985).
- [423] W. Hu, R. Barkana and A. Gruzinov, *Phys. Rev. Lett.* **85**, 1158 (2000), [arXiv:astro-ph/0003365].
- [424] L. Amendola and R. Barbieri, *Phys. Lett.* **B642**, 192 (2006), [hep-ph/0509257].
- [425] D. J. E. Marsh and P. G. Ferreira, *Phys. Rev.* **D82**, 103528 (2010), [arXiv:1009.3501].
- [426] E. Seidel and W. M. Suen, *Phys. Rev. Lett.* **66**, 1659 (1991).
- [427] H.-Y. Schive, T. Chiueh and T. Broadhurst, *Nature Phys.* **10**, 496 (2014), [arXiv:1406.6586].
- [428] D. G. Levkov, A. G. Panin and I. I. Tkachev, *Phys. Rev. Lett.* **121**, 15, 151301 (2018), [arXiv:1804.05857].
- [429] B. Eggemeier and J. C. Niemeyer, *Phys. Rev. D* **100**, 6, 063528 (2019), [arXiv:1906.01348].
- [430] R. Hlozek, D. J. E. Marsh and D. Grin, *Mon. Not. Roy. Astron. Soc.* **476**, 3, 3063 (2018), [arXiv:1708.05681].
- [431] D. J. E. Marsh and J. Silk, *Mon. Not. Roy. Astron. Soc.* **437**, 3, 2652 (2014), [arXiv:1307.1705].
- [432] H.-Y. Schive *et al.*, *Astrophys. J.* **818**, 1, 89 (2016), [arXiv:1508.04621].
- [433] B. Bozek *et al.*, *Mon. Not. Roy. Astron. Soc.* **450**, 1, 209 (2015), [arXiv:1409.3544].
- [434] P. S. Corasaniti *et al.*, *Phys. Rev.* **D95**, 8, 083512 (2017), [arXiv:1611.05892].
- [435] K. K. Rogers and H. V. Peiris, *Phys. Rev. Lett.* **126**, 7, 071302 (2021), [arXiv:2007.12705].
- [436] H.-Y. Schive and T. Chiueh, *Mon. Not. Roy. Astron. Soc.* **473**, 1, L36 (2018), [arXiv:1706.03723].
- [437] E. O. Nadler *et al.* (DES), *Phys. Rev. Lett.* **126**, 091101 (2021), [arXiv:2008.00022].
- [438] B. Schwabe, J. C. Niemeyer and J. F. Engels, *Phys. Rev.* **D94**, 4, 043513 (2016), [arXiv:1606.05151].
- [439] J. Veltmaat and J. C. Niemeyer, *Phys. Rev.* **D94**, 12, 123523 (2016), [arXiv:1608.00802].
- [440] P. Mocz *et al.*, *Mon. Not. Roy. Astron. Soc.* **471**, 4, 4559 (2017), [arXiv:1705.05845].
- [441] D. G. Levkov, A. G. Panin and I. I. Tkachev, *Phys. Rev. Lett.* **118**, 011301 (2017); T. Helfer *et al.*, *JCAP* **1703**, 03, 055 (2017), [arXiv:1609.04724]; J. Eby *et al.*, *Journal of High Energy Physics* **2018**, 1, 66 (2018), ISSN 1029-8479, URL [https://doi.org/10.1007/JHEP01\(2018\)066](https://doi.org/10.1007/JHEP01(2018)066).
- [442] D. J. E. Marsh and A.-R. Pop, *Mon. Not. Roy. Astron. Soc.* **451**, 3, 2479 (2015), [arXiv:1502.03456].
- [443] S.-R. Chen, H.-Y. Schive and T. Chiueh, *Mon. Not. Roy. Astron. Soc.* **468**, 2, 1338 (2017), [arXiv:1606.09030].
- [444] A. X. González-Morales *et al.*, *Mon. Not. Roy. Astron. Soc.* **472**, 2, 1346 (2017), [arXiv:1609.05856].
- [445] I. De Martino *et al.*, *Phys. Dark Univ.* **28**, 100503 (2020), [arXiv:1807.08153].
- [446] T. Broadhurst *et al.*, *Phys. Rev. D* **101**, 8, 083012 (2020), [arXiv:1902.10488].
- [447] H.-Y. Schive *et al.*, *Phys. Rev. Lett.* **113**, 26, 261302 (2014), [arXiv:1407.7762].
- [448] V. H. Robles, J. S. Bullock and M. Boylan-Kolchin, *Mon. Not. Roy. Astron. Soc.* **483**, 1, 289 (2019), [arXiv:1807.06018].
- [449] V. Desjacques and A. Nusser, *Monthly Notices of the Royal Astronomical Society* **488**, 4, 4497 (2019), ISSN 0035-8711, URL <https://doi.org/10.1093/mnras/stz1978>.
- [450] M. Safarzadeh and D. N. Spergel, *The Astrophysical Journal* **893**, 1, 21 (2020), URL <https://dx.doi.org/10.3847/1538-4357/ab7db2>.
- [451] A. Pontzen and F. Governato, *Nature* **506**, 171 (2014), [arXiv:1402.1764].
- [452] P. Mocz *et al.*, *Phys. Rev. Lett.* **123**, 14, 141301 (2019), [arXiv:1910.01653].
- [453] J. Veltmaat, B. Schwabe and J. C. Niemeyer, *Phys. Rev. D* **101**, 8, 083518 (2020), [arXiv:1911.09614].
- [454] J. Veltmaat, J. C. Niemeyer and B. Schwabe, *Phys. Rev.* **D98**, 4, 043509 (2018), [arXiv:1804.09647].
- [455] B. Bar-Or, J.-B. Fouvry and S. Tremaine, *Astrophys. J.* **871**, 1, 28 (2019), [arXiv:1809.07673].
- [456] B. V. Church, P. Mocz and J. P. Ostriker, *MNRAS* **485**, 2861 (2019), [arXiv:1809.04744].
- [457] N. C. Amorisco and A. Loeb (2018), [arXiv:1808.00464].
- [458] T. S. Li *et al.* (DES), *Astrophys. J.* **838**, 1, 8 (2017), [arXiv:1611.05052].
- [459] D. J. E. Marsh and J. C. Niemeyer, *Phys. Rev. Lett.* **123**, 5, 051103 (2019), [arXiv:1810.08543].
- [460] N. Dalal and A. Kravtsov, *Phys. Rev. D* **106**, 6, 063517 (2022), [arXiv:2203.05750].

- [461] E. Armengaud *et al.* (EDELWEISS), Phys. Rev. D **98**, 8, 082004 (2018), [arXiv:1808.02340].
- [462] E. Aprile *et al.* (XENON), Phys. Rev. Lett. **123**, 25, 251801 (2019), [arXiv:1907.11485].
- [463] K. Kelley and P. J. Quinn, Astrophys. J. **845**, 1, L4 (2017), [arXiv:1708.01399].
- [464] G. Sigl, Phys. Rev. **D96**, 10, 103014 (2017), [arXiv:1708.08908].
- [465] A. Hook *et al.*, Phys. Rev. Lett. **121**, 24, 241102 (2018), [arXiv:1804.03145].
- [466] B. R. Safdi, Z. Sun and A. Y. Chen, Phys. Rev. D **99**, 12, 123021 (2019), [arXiv:1811.01020].
- [467] S. J. Witte *et al.* (2021), [arXiv:2104.07670].
- [468] R. A. Battye *et al.*, Journal of High Energy Physics **2021**, 9, 105 (2021), ISSN 1029-8479, URL [https://doi.org/10.1007/JHEP09\(2021\)105](https://doi.org/10.1007/JHEP09(2021)105).
- [469] A. J. Millar *et al.* (2021), [arXiv:2107.07399].
- [470] J. I. McDonald, B. Garbrecht and P. Millington (2023), [arXiv:2307.11812].
- [471] A. Caputo *et al.*, JCAP **1903**, 03, 027 (2019), [arXiv:1811.08436].
- [472] P. Carena, A. Mirizzi and G. Sigl, Phys. Rev. D **101**, 10, 103016 (2020), [arXiv:1911.07838].
- [473] D. G. Levkov, A. G. Panin and I. I. Tkachev, Phys. Rev. D **102**, 2, 023501 (2020), [arXiv:2004.05179].
- [474] T. Fujita *et al.*, Phys. Rev. D **103**, 4, 043509 (2021), [arXiv:2011.11894].
- [475] T. Liu, G. Smoot and Y. Zhao (2019), [arXiv:1901.10981].
- [476] P. Sikivie, Phys. Rev. **D32**, 2988 (1985), [Erratum: Phys. Rev. D **36**, 974 (1987)].
- [477] R. Bradley *et al.*, Rev. Mod. Phys. **75**, 777 (2003).
- [478] P. Sikivie and J. R. Ipser, Phys. Lett. **B291**, 288 (1992).
- [479] P. Sikivie, I. I. Tkachev and Y. Wang, Phys. Rev. Lett. **75**, 2911 (1995), [arXiv:astro-ph/9504052].
- [480] C. Bartram *et al.* (ADMX), Phys. Rev. D **103**, 3, 032002 (2021), [arXiv:2010.06183].
- [481] R. Khatriwada *et al.*, Review of Scientific Instruments **92**, 12, 124502 (2021), ISSN 0034-6748, URL <https://doi.org/10.1063/5.0037857>.
- [482] W. Wuensch *et al.*, Phys. Rev. **D40**, 3153 (1989).
- [483] A. A. Melcón *et al.* (CAST), JHEP **21**, 075 (2020), [arXiv:2104.13798].
- [484] B. T. McAllister *et al.*, Annalen der Physik **n/a**, n/a, 2200622 (2022), URL <https://onlinelibrary.wiley.com/doi/abs/10.1002/andp.202200622>.
- [485] S. J. Asztalos *et al.* (ADMX), Phys. Rev. **D69**, 011101 (2004), [arXiv:astro-ph/0310042].
- [486] L. Duffy *et al.*, Phys. Rev. Lett. **95**, 091304 (2005), [arXiv:astro-ph/0505237]; J. Hoskins *et al.*, Phys. Rev. **D84**, 121302 (2011), [arXiv:1109.4128].
- [487] S. J. Asztalos *et al.* (ADMX), Nucl. Instrum. Meth. **A656**, 39 (2011), [arXiv:1105.4203].
- [488] G. Rybka *et al.* (ADMX), Phys. Rev. Lett. **105**, 051801 (2010), [arXiv:1004.5160].
- [489] A. Wagner *et al.* (ADMX), Phys. Rev. Lett. **105**, 171801 (2010), [arXiv:1007.3766].
- [490] B. M. Brubaker *et al.*, Phys. Rev. Lett. **118**, 6, 061302 (2017), [arXiv:1610.02580].
- [491] A. J. Millar *et al.* (Endorsers), Phys. Rev. D **107**, 055013 (2023), URL <https://link.aps.org/doi/10.1103/PhysRevD.107.055013>.
- [492] D. Horns *et al.*, JCAP **1304**, 016 (2013), [arXiv:1212.2970].
- [493] A. Caldwell *et al.* (MADMAX Working Group), Phys. Rev. Lett. **118**, 9, 091801 (2017), [arXiv:1611.05865].
- [494] P. Brun *et al.* (MADMAX), Eur. Phys. J. **C79**, 3, 186 (2019), [arXiv:1901.07401].
- [495] M. Baryakhtar, J. Huang and R. Lasenby, Phys. Rev. **D98**, 3, 035006 (2018), [arXiv:1803.11455].
- [496] J. Liu *et al.* (BREAD Collaboration), Phys. Rev. Lett. **128**, 131801 (2022), URL <https://link.aps.org/doi/10.1103/PhysRevLett.128.131801>.
- [497] B. Aja *et al.*, Journal of Cosmology and Astroparticle Physics **2022**, 11, 044 (2022), URL <https://dx.doi.org/10.1088/1475-7516/2022/11/044>.
- [498] A. Arvanitaki, S. Dimopoulos and K. Van Tilburg, Phys. Rev. **X8**, 4, 041001 (2018), [arXiv:1709.05354].
- [499] A. Berlin *et al.*, JHEP **07**, 07, 088 (2020), [arXiv:1912.11048].
- [500] P. Sikivie, Phys. Rev. Lett. **113**, 20, 201301 (2014), [Erratum: Phys. Rev. Lett. **125**, 029901 (2020)], [arXiv:1409.2806].
- [501] R. Li *et al.*, Nature Phys. **6**, 284 (2010), [arXiv:0908.1537].
- [502] K. Ishiwata, Phys. Rev. D **104**, 1, 016004 (2021), [arXiv:2103.02848].
- [503] L. Cao *et al.*, Phys. Rev. B **104**, 054421 (2021), URL <https://link.aps.org/doi/10.1103/PhysRevB.104.054421>.
- [504] D. J. E. Marsh *et al.*, Phys. Rev. Lett. **123**, 12, 121601 (2019), [arXiv:1807.08810].
- [505] J. Schütte-Engel *et al.*, JCAP **08**, 066 (2021), [arXiv:2102.05366].
- [506] P. Sikivie, N. Sullivan, and D. B. Tanner, Phys. Rev. Lett. **112**, 131301 (2014).
- [507] Y. Kahn, B. R. Safdi and J. Thaler, Phys. Rev. Lett. **117**, 14, 141801 (2016), [arXiv:1602.01086].
- [508] Y. Oshima *et al.*, Phys. Rev. D **108**, 072005 (2023), URL <https://link.aps.org/doi/10.1103/PhysRevD.108.072005>.
- [509] L. Brouwer *et al.* (DMRadio), Phys. Rev. D **106**, 10, 103008 (2022), [arXiv:2204.13781].
- [510] L. Brouwer *et al.* (DMRadio), Phys. Rev. D **106**, 11, 112003 (2022), [arXiv:2203.11246].
- [511] M. B. Wise, H. Georgi and S. L. Glashow, Phys. Rev. Lett. **47**, 402 (1981).
- [512] A. Ernst, A. Ringwald and C. Tamarit, JHEP **02**, 103 (2018), [arXiv:1801.04906].
- [513] L. Di Luzio, A. Ringwald and C. Tamarit, Phys. Rev. **D98**, 9, 095011 (2018), [arXiv:1807.09769].
- [514] P. F. Pérez, C. Murgui and A. D. Plascencia, Journal of High Energy Physics **2019**, 11, 93 (2019), ISSN 1029-8479, URL [https://doi.org/10.1007/JHEP11\(2019\)093](https://doi.org/10.1007/JHEP11(2019)093).
- [515] I. M. Bloch *et al.* (NASDUCK) (2021), [arXiv:2105.04603].
- [516] S. P. Chang *et al.*, Phys. Rev. **D99**, 8, 083002 (2019), [arXiv:1710.05271].
- [517] L. Krauss *et al.*, Phys. Rev. Lett. **55**, 1797 (1985).
- [518] R. Barbieri *et al.*, Phys. Lett. B **226**, 357 (1989).
- [519] R. Barbieri *et al.*, Phys. Dark Univ. **15**, 135 (2017), [arXiv:1606.02201].

91. Searches for Quark and Lepton Compositeness

Revised October 2023 by K. Hikasa (Tohoku U.), M. Tanabashi (Nagoya U.; KMI, Nagoya U.), K. Terashi (ICEPP, Tokyo U.) and N. Varelas (U. of Illinois at Chicago).

91.1 Limits on contact interactions

If quarks and leptons are made of constituents, then at the scale of constituent binding energies (compositeness scale) there should appear new interactions among them. At energies much below the compositeness scale (Λ), these interactions are suppressed by inverse powers of Λ . The dominant effect of the compositeness of fermion ψ should come from the lowest dimensional interactions with four fermions (contact terms), whose most general flavor-diagonal color-singlet chirally invariant form reads [1, 2]

$$\mathcal{L} = \mathcal{L}_{LL} + \mathcal{L}_{RR} + \mathcal{L}_{LR} + \mathcal{L}_{RL},$$

with

$$\begin{aligned} \mathcal{L}_{LL} &= \frac{g_{\text{contact}}^2}{2\Lambda^2} \sum_{i,j} \eta_{LL}^{ij} (\bar{\psi}_L^i \gamma_\mu \psi_L^i) (\bar{\psi}_L^j \gamma^\mu \psi_L^j), \\ \mathcal{L}_{RR} &= \frac{g_{\text{contact}}^2}{2\Lambda^2} \sum_{i,j} \eta_{RR}^{ij} (\bar{\psi}_R^i \gamma_\mu \psi_R^i) (\bar{\psi}_R^j \gamma^\mu \psi_R^j), \\ \mathcal{L}_{LR} &= \frac{g_{\text{contact}}^2}{2\Lambda^2} \sum_{i,j} \eta_{LR}^{ij} (\bar{\psi}_L^i \gamma_\mu \psi_L^i) (\bar{\psi}_R^j \gamma^\mu \psi_R^j), \\ \mathcal{L}_{RL} &= \frac{g_{\text{contact}}^2}{2\Lambda^2} \sum_{i,j} \eta_{RL}^{ij} (\bar{\psi}_R^i \gamma_\mu \psi_R^i) (\bar{\psi}_L^j \gamma^\mu \psi_L^j), \end{aligned} \quad (91.1)$$

where i, j are the indices of fermion species. Color and other indices are suppressed in Eq. (91.1). Chiral invariance provides a natural explanation why quark and lepton masses are much smaller than their inverse size (inverse radius) Λ . Note $\eta_{\alpha\beta}^{ij} = \eta_{\beta\alpha}^{ji}$, thus \mathcal{L}_{LR} and \mathcal{L}_{RL} are identical. Therefore, in order to specify the contact interaction among the same fermion species $i = j$, it is enough to use η_{LL} , η_{RR} and η_{LR} . We will suppress the indices of fermion species hereafter. We may determine the scale Λ unambiguously by using the above form of the effective interactions; the conventional method [1] is to fix its scale by setting $g_{\text{contact}}^2/4\pi = g_{\text{contact}}^2(\Lambda)/4\pi = 1$ for the new strong interaction coupling and by setting the largest magnitude of the coefficients $\eta_{\alpha\beta}$ to be unity. In the following, we denote

$$\Lambda = \Lambda_{LL}^\pm, \Lambda_{RR}^\pm, \Lambda_{VV}^\pm, \Lambda_{AA}^\pm, \Lambda_{V-A}^\pm, \quad (91.2)$$

for $(\eta_{LL}, \eta_{RR}, \eta_{LR}) = (\pm 1, 0, 0)$, $(0, \pm 1, 0)$, $(\pm 1, \pm 1, \pm 1)$, $(\pm 1, \pm 1, \mp 1)$, $(0, 0, \pm 1)$. Such interactions can arise by interchanging constituents (when the fermions have common constituents), and/or by exchanging the binding quanta (whenever binding quanta couple to constituents of both particles).

Fermion scattering amplitude induced from the contact interaction in Eq. (91.1) interferes with the Standard Model (SM) amplitude destructively or constructively [2]. The sign of interference depends on the sign of $\eta_{\alpha\beta}$ ($\alpha, \beta = L, R$). For instance, in the parton level $qq \rightarrow qq$ scattering cross section in the Λ_{LL}^\pm model, the contact interaction amplitude and the SM gluon exchange amplitude interfere destructively for $\eta_{LL} = +1$, while they interfere constructively for $\eta_{LL} = -1$. In models of quark compositeness, the quark scattering cross sections induced from the contact interactions receive sizable QCD radiative corrections. The exact next-to-leading order (NLO) QCD corrections to the quark scatterings cross sections induced by the contact interactions are given in [3].

Over the last three decades experiments at the CERN Sp \bar{p} S [4, 5], the Fermilab Tevatron [6, 7], and the CERN LHC [8–12] have searched for quark contact interactions, characterized by the four-fermion effective Lagrangian in Eq. (91.1), using jet final states. These searches have been performed primarily by studying the angular distribution of the two highest transverse momentum, p_T , jets (dijets), and the inclusive jet p_T spectrum. The variable $\chi = \exp(|y_1 - y_2|)$ is used to measure the dijet angular distribution, where y_1 and y_2 are the rapidities of the two jets with

the highest transverse momenta. For collinear massless parton scattering, χ is related to the polar scattering angle θ^* in the partonic center-of-mass frame by $\chi = (1 + |\cos \theta^*|)/(1 - |\cos \theta^*|)$. The choice of χ is motivated by the fact that the angular distribution for Rutherford scattering, which is proportional to $1/(1 - \cos \theta^*)^2$, is independent of χ . In perturbative QCD the χ distributions are relatively uniform and only mildly modified by higher-order QCD or electroweak corrections. Signatures of quark contact interactions exhibit more isotropic angular distribution than QCD and can be identified as an excess at low values of χ . In the inclusive jet cross section measurement, quark contact interaction effects are searched for as deviations from the predictions of perturbative QCD in the tails of the high- p_T jet spectrum [11].

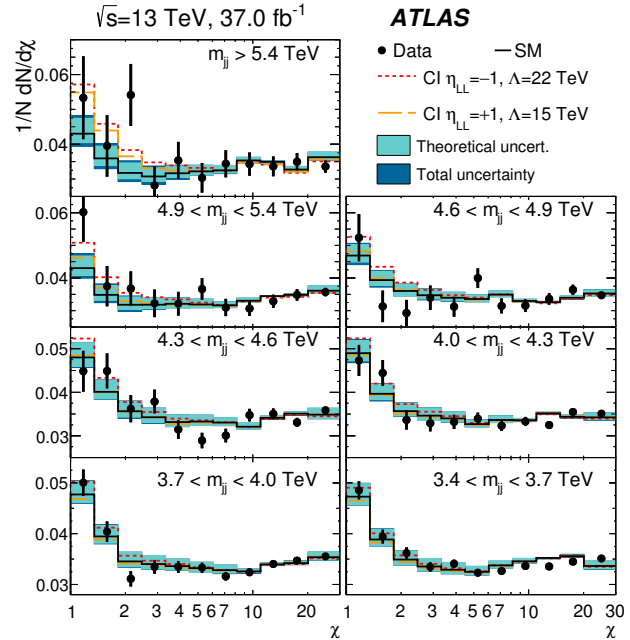


Figure 91.1: Normalized dijet angular distributions in several dijet mass (m_{jj}) ranges. The data distributions are compared to PYTHIA8 predictions with NLO and electroweak corrections applied (solid line) and with the predictions including a contact interaction (CI) term in which only left-handed quarks participate of compositeness scale $\Lambda_{LL}^+ = 15$ TeV (dashed line) and $\Lambda_{LL}^- = 22$ TeV (dotted line). The theoretical uncertainties and the total theoretical and experimental uncertainties in the predictions are displayed as shaded bands around the SM prediction. Figure adopted from [9].

Recent results from the LHC, using data collected at proton-proton center-of-mass energy of $\sqrt{s} = 13$ TeV, extend previous limits on quark contact interactions. Figure 91.1 shows the normalized dijet angular distributions for several dijet mass ranges measured in ATLAS [9] at $\sqrt{s} = 13$ TeV. The data distributions are compared with SM predictions, estimated using PYTHIA8 [13] with GEANT4-based [14] ATLAS detector simulation and corrected to NLO QCD calculation provided by NLO Jet++ [15] including electroweak corrections [16]. Predictions including a contact interaction term in which only left-handed quarks participate at compositeness scale $\Lambda_{LL}^+ = 15$ TeV ($\Lambda_{LL}^- = 22$ TeV) with destructive (constructive) interference are also shown. Over a wide range of χ and dijet mass the data are well described by the SM predictions. Using the dijet angular distributions measured at high dijet masses and $\sqrt{s} = 13$ TeV, the ATLAS [9] and CMS [12] Collaborations have set 95% confidence level (C.L.) lower limits on the contact interaction scale Λ , ranging from 9.2 to 29.5 TeV for different quark contact interaction models that correspond to various combinations of $(\eta_{LL}, \eta_{RR}, \eta_{LR})$, as summarized in Figure 91.2. The contact interaction scale limits extracted using the dijet angular distributions include the exact NLO QCD corrections to dijet production induced by contact interactions [3]. In proton-

proton collisions, the Λ_{LL}^\pm and Λ_{RR}^\pm contact interaction models result in identical tree-level cross sections and NLO QCD corrections and yield the same exclusion limits. For Λ_{VV}^\pm and Λ_{AA}^\pm , the contact interaction predictions are identical at tree level, but exhibit different NLO QCD corrections and yield different exclusion limits.

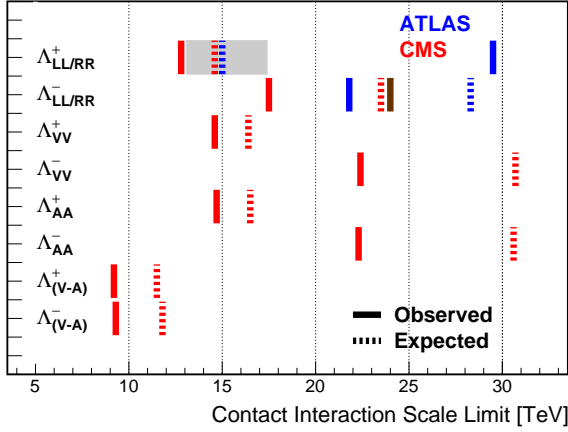


Figure 91.2: Observed (solid lines) and expected (dashed lines) 95% C.L. lower limits on the contact interaction scale Λ for different contact interaction models from ATLAS [9] and CMS [12] using the dijet angular distributions. The contact interaction models used for the dijet angular distributions include the exact NLO QCD corrections to dijet production. The shaded band for the $\Lambda_{LL/RR}^+$ model indicates the range of contact interaction scale that was not excluded in ATLAS [9], due to an observed excess in the data that produced a weaker limit. The observed 95% C.L. lower limit on the Λ_{LL}^- from CMS [17] is shown as the second solid line in brown.

If leptons (l) and quarks (q) are composite with common constituents, the interaction of these constituents will manifest itself in the form of a $llqq$ -type four-fermion contact interaction Lagrangian at energies below the compositeness scale Λ . The $llqq$ terms in the contact interaction Lagrangian can be expressed as

$$\begin{aligned}\mathcal{L}_{LL} &= \frac{g_{\text{contact}}^2}{\Lambda^2} \sum_{i,j} \eta_{LL}^{ij} (\bar{q}_L^i \gamma_\mu q_L^i) (\bar{l}_L^j \gamma^\mu l_L^j), \\ \mathcal{L}_{RR} &= \frac{g_{\text{contact}}^2}{\Lambda^2} \sum_{i,j} \eta_{RR}^{ij} (\bar{q}_R^i \gamma_\mu q_R^i) (\bar{l}_R^j \gamma^\mu l_R^j), \\ \mathcal{L}_{LR} &= \frac{g_{\text{contact}}^2}{\Lambda^2} \sum_{i,j} \eta_{LR}^{ij} (\bar{q}_L^i \gamma_\mu q_L^i) (\bar{l}_R^j \gamma^\mu l_R^j), \\ \mathcal{L}_{RL} &= \frac{g_{\text{contact}}^2}{\Lambda^2} \sum_{i,j} \eta_{RL}^{ij} (\bar{q}_R^i \gamma_\mu q_R^i) (\bar{l}_L^j \gamma^\mu l_L^j).\end{aligned}\quad (91.3)$$

Searches on quark-lepton compositeness have been reported from experiments at LEP [18–21], HERA [22, 23], the Tevatron [24, 25], and recently from the ATLAS [26, 27] and CMS [28, 29] experiments at the LHC. The most stringent searches for $llqq$ contact interactions are performed by the LHC experiments using high-mass oppositely-charged lepton pairs produced through the $q\bar{q} \rightarrow l^+l^-$ Drell-Yan process. The contact interaction amplitude of the $u\bar{u} \rightarrow l^+l^-$ process ($l = e$ or μ) interferes with the corresponding SM amplitude constructively (destructively) for $\eta_{\alpha\beta}^{ul} = -1$ ($\eta_{\alpha\beta}^{ul} = +1$). The ATLAS Collaboration, using a 139 fb^{-1} dataset at $\sqrt{s} = 13 \text{ TeV}$, has extracted limits on the $llqq$ contact interaction for the right-right ($\eta_{RR} = \pm 1$, $\eta_{LL} = \eta_{LR} = \eta_{RL} = 0$), left-left ($\eta_{LL} = \pm 1$, $\eta_{RR} = \eta_{LR} = \eta_{RL} = 0$), and left-right ($\eta_{LR} = \eta_{RL} = \pm 1$, $\eta_{RR} = \eta_{LL} = 0$) models. In

Ref. [27], ATLAS used a background estimate directly obtained from data. Combining the dielectron and dimuon channels, the 95% C.L. lower limits on the $llqq$ contact interaction scale Λ are 36 TeV (27 TeV) for the right-right model, 36 TeV (26 TeV) for the left-left model, and 33 TeV (29 TeV) for the left-right model, each with constructive (destructive) interference [27]. The CMS Collaboration, using a 140 fb^{-1} dataset at 13 TeV, has set 95% C.L. exclusion limits on the $llqq$ contact interaction scale that range from $\Lambda_{LL} > 23.9 \text{ TeV}$ for the destructive interference to $\Lambda_{RR} > 36.4 \text{ TeV}$ for the constructive interference, for the left-left and the right-right models, respectively [29].

Note that the contact interactions arising from the compositeness of quarks and leptons in Eq. (91.1) can also be regarded as a part of more general dimension-six operators in the context of low-energy standard-model effective field theory (SMEFT). For a complete list of SM gauge-invariant dimension-six operators, see [30, 31]. A computation of the one-loop anomalous dimension matrix for SMEFT operators are found in Refs. [32–34]. See also Refs. [35–37] for recent reviews. Ref. [17] sets limits on the Wilson coefficients of the contact interaction operators in the SMEFT framework, using the CMS data of the inclusive jet production cross sections together with the deep inelastic scattering data from HERA and the CMS $t\bar{t}$ cross section data. The results are translated into a 95% C.L. exclusion limit on the quark compositeness $\Lambda_{LL}^- > 24 \text{ TeV}$, which is shown as the second solid line in brown in Figure 91.2. In models where the SM fermions get their masses through the mixing with the composite states, the top-quark is expected to show compositeness properties [38] resulting in the $t\bar{t}t\bar{t}$ contact interaction operators in the SMEFT context. An enhancement of the four-top-quark production cross section is expected at hadron colliders in these models [39]. The ATLAS Collaboration has extracted 95% C.L. observed (expected) limits on the $t\bar{t}t\bar{t}$ contact interaction operator $|C_{4t}|/\Lambda^2 < 1.9 \text{ TeV}^{-2}$ (1.6 TeV^{-2}) using their 36.1 fb^{-1} data at $\sqrt{s} = 13 \text{ TeV}$ [40]. Consistent SMEFT reinterpretations of top-quark data, and high energy non-resonant dijet and dilepton data are provided, e.g., in Refs. [41, 42].

Interactions of hypothetical dark matter candidate particles with SM particles through mediators can also be described as contact interactions at low energy. See “Searches for WIMPs and Other Particles” in this volume for limits on the interactions involving dark matter candidate particles.

91.2 Limits on excited fermions

Another typical consequence of compositeness is the appearance of excited leptons and quarks (l^* and q^*). Phenomenologically, an excited lepton is defined to be a heavy lepton which shares a leptonic quantum number with one of the existing leptons (an excited quark is defined similarly). For example, an excited electron e^* is characterized by a nonzero transition-magnetic coupling with electrons. The smallness of the lepton mass and the success of QED prediction for $g-2$ suggest chirality conservation, i.e., an excited lepton should not couple to both left- and right-handed components of the corresponding lepton [43–45].

Excited leptons may be classified by $SU(2) \times U(1)$ quantum numbers. Typical examples are:

1. Sequential type

$$\begin{pmatrix} \nu^* \\ l^* \end{pmatrix}_L, \quad [\nu_R^*], \quad l_R^*.$$

ν_R^* is necessary if we assume ν^* has a Dirac mass.

2. Mirror type

$$[\nu_L^*], \quad l_L^*, \quad \begin{pmatrix} \nu^* \\ l^* \end{pmatrix}_R.$$

3. Homodoublet type

$$\begin{pmatrix} \nu^* \\ l^* \end{pmatrix}_L, \quad \begin{pmatrix} \nu^* \\ l^* \end{pmatrix}_R.$$

Similar classification can be made for excited quarks.

Excited fermions can be pair produced via their minimal gauge couplings. The couplings of excited leptons with Z are given by

$$\frac{e}{2 \sin \theta_W \cos \theta_W} \left[(-1 + 2 \sin^2 \theta_W) \bar{l}^* \gamma^\mu l^* Z_\mu + \bar{\nu}^* \gamma^\mu \nu^* Z_\mu \right]$$

in the homodoublet model. The corresponding couplings of excited quarks can be easily obtained. Although form factor effects can be present for the gauge couplings at $q^2 \neq 0$, they are usually neglected.

Excited fermions may also be produced via the contact interactions with ordinary quarks and leptons [46]

$$\mathcal{L} = \frac{g_{\text{contact}}^2}{\Lambda^2} \left[\eta'_{LL} (\bar{\psi}_L \gamma_\mu \psi_L) (\bar{\psi}_L^* \gamma^\mu \psi_L^*) + (\eta''_{LL} (\bar{\psi}_L \gamma_\mu \psi_L) (\bar{\psi}_L^* \gamma^\mu \psi_L) + \text{h.c.}) + \dots \right]. \quad (91.4)$$

Again, the coefficient is conventionally taken $g_{\text{contact}}^2 = 4\pi$. It is widely assumed $\eta'_{LL} = \eta''_{LL} = 1$, $\eta'_{LR} = \eta''_{LR} = \eta'_{RL} = \eta''_{RL} = \eta'_{RR} = \eta''_{RR} = 0$ in experimental analyses for simplicity.

In addition, transition-magnetic type couplings with a gauge boson are expected. These couplings can be generally parameterized as follows:

$$\begin{aligned} \mathcal{L} = & \frac{\lambda_\gamma^{(\psi^*)} e}{2m_{\psi^*}} \bar{\psi}^* \sigma^{\mu\nu} (\eta_L \frac{1-\gamma_5}{2} + \eta_R \frac{1+\gamma_5}{2}) \psi F_{\mu\nu} \\ & + \frac{\lambda_Z^{(\psi^*)} e}{2m_{\psi^*}} \bar{\psi}^* \sigma^{\mu\nu} (\eta_L \frac{1-\gamma_5}{2} + \eta_R \frac{1+\gamma_5}{2}) \psi Z_{\mu\nu} \\ & + \frac{\lambda_W^{(l^*)} g}{2m_{l^*}} \bar{l}^* \sigma^{\mu\nu} \frac{1-\gamma_5}{2} \nu W_{\mu\nu} \\ & + \frac{\lambda_W^{(\nu^*)} g}{2m_{\nu^*}} \bar{\nu}^* \sigma^{\mu\nu} (\eta_L \frac{1-\gamma_5}{2} + \eta_R \frac{1+\gamma_5}{2}) l W_{\mu\nu}^\dagger \\ & + \text{h.c.}, \end{aligned} \quad (91.5)$$

where $g = e/\sin \theta_W$, $\psi = \nu$ or l , $F_{\mu\nu} = \partial_\mu A_\nu - \partial_\nu A_\mu$ is the photon field strength, $Z_{\mu\nu} = \partial_\mu Z_\nu - \partial_\nu Z_\mu$, etc.. The normalization of the coupling is chosen such that

$$\max(|\eta_L|, |\eta_R|) = 1.$$

Chirality conservation requires

$$\eta_L \eta_R = 0. \quad (91.6)$$

These couplings in Eq. (91.5) can arise from $SU(2) \times U(1)$ -invariant higher-dimensional interactions. A well-studied model is the interaction of homodoublet type l^* with the Lagrangian (see [47, 48])

$$\mathcal{L} = \frac{1}{2\Lambda} \bar{L}^* \sigma^{\mu\nu} (gf \frac{\tau^a}{2} W_{\mu\nu}^a + g' f' Y B_{\mu\nu}) \frac{1-\gamma_5}{2} L + \text{h.c.}, \quad (91.7)$$

where L denotes the lepton doublet (ν, l), Λ is the compositeness scale, g, g' are $SU(2)$ and $U(1)_Y$ gauge couplings, and $W_{\mu\nu}^a$ and $B_{\mu\nu}$ are the field strengths for $SU(2)$ and $U(1)_Y$ gauge fields. These couplings satisfy the relation

$$\lambda_W = -\sqrt{2} \sin^2 \theta_W (\lambda_Z \cot \theta_W + \lambda_\gamma), \quad (91.8)$$

with $\lambda_{W,Z,\gamma}$ being defined in Eq. (91.5) with $\lambda_{W,Z,\gamma} = \lambda_{W,Z,\gamma}^{(l^*)}$ or $\lambda_{W,Z,\gamma} = \lambda_{W,Z,\gamma}^{(\nu^*)}$. Here $(\eta_L, \eta_R) = (1, 0)$ is assumed. It should be noted that the electromagnetic radiative decay of l^* (ν^*) is forbidden if $f = -f'$ ($f = f'$).

Additional coupling with gluons is possible for excited quarks:

$$\begin{aligned} \mathcal{L} = & \frac{1}{2\Lambda} \bar{Q}^* \sigma^{\mu\nu} \left(g_s f_s \frac{\lambda^a}{2} G_{\mu\nu}^a + gf \frac{\tau^a}{2} W_{\mu\nu}^a + g' f' Y B_{\mu\nu} \right) \\ & \times \frac{1-\gamma_5}{2} Q + \text{h.c.}, \end{aligned} \quad (91.9)$$

where Q denotes a quark doublet, g_s is the QCD gauge coupling, and $G_{\mu\nu}^a$ the gluon field strength.

If leptons are made of color triplet and antitriplet constituents, we may expect their color-octet partners. Transitions between the octet leptons (l_8) and the ordinary lepton (l) may take place via the dimension-five interactions

$$\mathcal{L} = \frac{1}{2\Lambda} \sum_l \left\{ \bar{l}_8^\alpha g_S F_{\mu\nu}^\alpha \sigma^{\mu\nu} (\eta_L l_L + \eta_R l_R) + \text{h.c.} \right\} \quad (91.10)$$

where the summation is over charged leptons and neutrinos. The leptonic chiral invariance implies $\eta_L \eta_R = 0$ as before.

Searches for the excited quarks and leptons have been performed over the last decades in experiments at the LEP [49–52], HERA [53, 54], Tevatron [55, 56], and LHC [57–89]. Most stringent constraints, which are described below at 95% confidence level, come from the LHC experiments.

The signature of excited quarks q^* at hadron colliders is characterized by a narrow resonant peak in the reconstructed invariant mass distribution of the q^* decay products. The decays via the transition-magnetic type operator in Eq. (91.9) are considered for excited quarks in LHC searches, and the final states to search for are dijet (qg) [57, 58, 70–73] or a jet in association with a photon ($q\gamma$) [59, 60, 74, 75, 89] or a weak gauge boson (qW, qZ) [76, 77]. All analyses consider only spin-1/2 excited states of first generation quarks (u^*, d^*) with degenerate masses, expected to be predominantly produced in proton-proton collisions except for the excited b quark searches described below. Only the minimal gauge interactions and the transition-magnetic couplings with the form given in Eq. (91.9) are considered in the production process, and hence the contact interactions in Eq. (91.4) are not considered. The compositeness scale Λ is taken to be the same as the excited quark mass m_{q^*} . The transition-magnetic coupling coefficients f_s, f and f' are assumed to be equal to 1 (denoted by f).

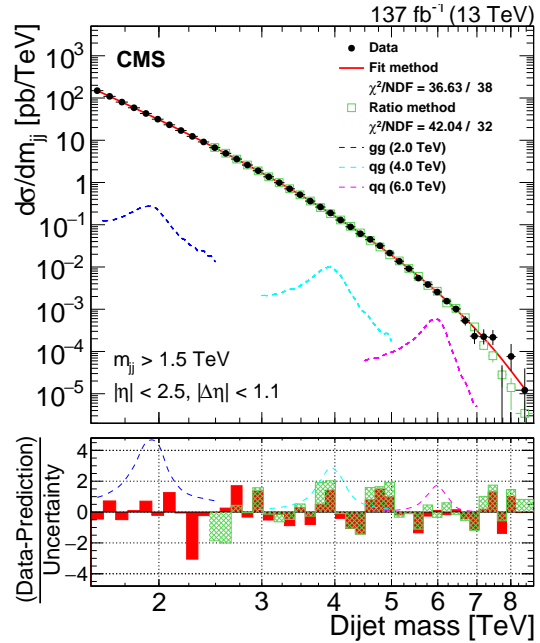


Figure 91.3: Dijet mass distribution measured by CMS using wide jets reconstructed from two highest transverse momentum jets by adding nearby jets within $\Delta R = \sqrt{\Delta\eta^2 + \Delta\phi^2} < 1.1$. The data distribution is compared to a fit representing a smooth background spectrum (solid curve) and the background prediction obtained from the $\Delta\eta_{jj}$ control regions (open squares), denoted as Ratio method, at $m_{jj} > 2.4$ TeV. The excited quark signal with mass of 4.0 TeV (labeled as qg) is shown together with other benchmark signals. Shown at the bottom panel is the difference between the data and the fitted parametrization from the fit method or the data and the background prediction from the Ratio method, divided by the statistical uncertainty of the data. Figure adopted from [73].

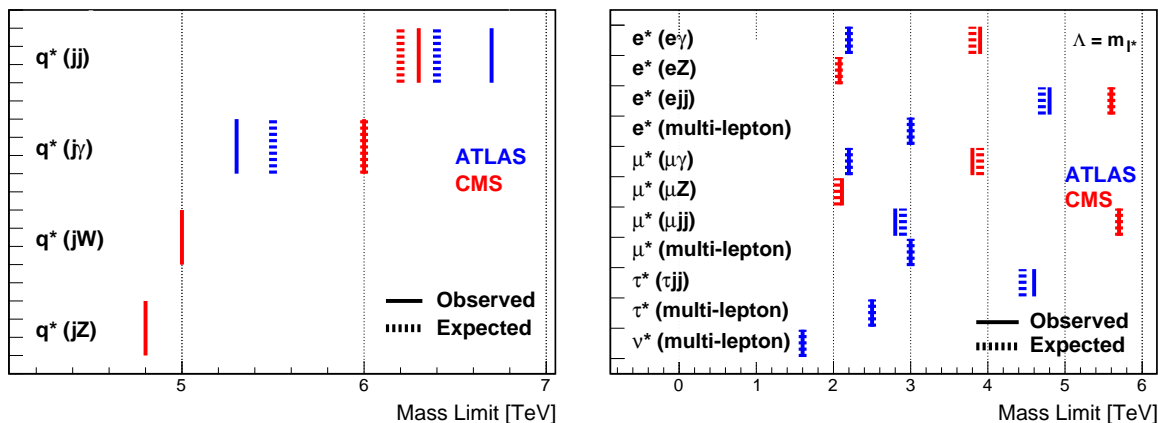


Figure 91.4: 95% C.L. lower mass limits for the excited quarks (left) and excited leptons (right) at ATLAS [58, 60, 66–68, 88] and CMS [73, 75, 77, 80–82, 89] experiments. Shown are the most stringent limits for each final state (denoted in parentheses) of the excited fermions from both experiments. Only first generation quarks (u, d) with transition-magnetic type interactions with $f_s = f = f' = 1$ are considered for the excited quarks. The excited lepton limits are given for the production via contact interactions with $\Lambda = m_{l^*}$.

With proton-proton collision data recorded at $\sqrt{s} = 13$ TeV at the LHC, the excited quark masses are excluded in dijet resonance searches up to 6.7 TeV in ATLAS using 139 fb^{-1} [58] and 6.3 TeV in CMS using 137 fb^{-1} [73]. Figure 91.3 shows the dijet mass (m_{jj}) distribution measured in CMS [73] by using the two highest p_T jets reconstructed with the anti- k_T algorithm [90] of a distance parameter of 0.4, and by combining nearby jets within $\Delta R = \sqrt{\Delta\eta^2 + \Delta\phi^2} < 1.1$ around the leading two jets. The measured dijet mass spectrum is compared to a fit with smoothly falling background shape (solid curve) at $m_{jj} > 1.5$ TeV and the background prediction obtained from $\Delta\eta_{jj}$ control regions (open squares), denoted as Ratio method, at $m_{jj} > 2.4$ TeV to look for a narrow resonance. Here $\Delta\eta_{jj}$ is the pseudorapidity separation between the two jets. An excited quark signal with mass of 4.0 TeV is shown in the figure (denoted by qg) as one of the benchmark signals considered in the analysis.

The photon + jet resonance searches, targeting excited quarks decaying into a quark and a photon ($q^* \rightarrow q + \gamma$), have excluded q^* masses up to 5.3 TeV in ATLAS [60] and 6.0 TeV in CMS [89] using collision data at $\sqrt{s} = 13$ TeV. The W/Z boson + jet final states are examined to look for the $q^* \rightarrow q + W$ and $q + Z$ signal in CMS [77], exploiting jet substructure technique designed to provide sensitivity for highly-boosted hadronically decaying W and Z bosons. The lower mass limit of 5.0 (4.8) TeV is obtained from the $W + \text{jet}$ ($Z + \text{jet}$) search using dataset recorded at $\sqrt{s} = 13$ TeV.

The excited b quarks (b^*) are also considered in the present searches at the LHC. Assuming the similar production processes to the first-generation excited quarks, the b^* has been searched for in final states containing at least one jet identified as originating from a b quark (b -tagging). The searches using two jets including at least one b -tagged jet have been performed at 8 and 13 TeV [58, 61, 62, 71, 85], resulting in b^* lower mass limits of 3.2 TeV in ATLAS using 139 fb^{-1} at $\sqrt{s} = 13$ TeV [58] and 4.0 TeV in CMS using 138 fb^{-1} at $\sqrt{s} = 13$ TeV [85]. The CMS Collaboration also performed a search for $b^* \rightarrow b + \gamma$ in events with a b -tagged jet in association with a photon using data at $\sqrt{s} = 13$ TeV [89], and excluded b^* masses up to 2.2 TeV. For the same coupling strength, the observed lower mass bounds on the excited bottom quarks extends to 3.8 TeV, when the production mode from contact interactions Eq. (91.4) is also considered. Excited b quarks with charged-current decay into a W -boson and a top quark ($b^* \rightarrow t + W$) were looked for in both ATLAS and CMS using the full 8 TeV data [63, 78] and in CMS using the full 13 TeV data [86, 87]. For the left(right)-handed couplings, CMS excluded the masses below 2.6(2.8) TeV in the fully hadronic final states [86] and 3.0(3.2) TeV in the lepton+jets final states [87].

The excited top quarks (t^*) have also been searched for at

the LHC. The CMS Collaboration performed the search for pair-produced t^* quarks with the assumption of the t^* quark decay into a top quark and a gluon, in events with a charged lepton, missing transverse momentum and multiple jets including b -tagged jets at $\sqrt{s} = 8$ TeV [84] and 13 TeV [83]. With 35.9 fb^{-1} data at 13 TeV, CMS excluded the t^* masses below 1.2 TeV for spin 3/2 t^* quarks [83].

Searches for excited leptons l^* are also performed at the LHC using proton-proton collision data recorded at $\sqrt{s} = 7$ and 8 TeV [65–69, 79, 80] as well as at 13 TeV [81]. Considering single l^* production in contact interactions (Eq. (91.4)) and electromagnetic radiative decay to a SM lepton and a photon ($l^* \rightarrow l + \gamma$ where $l = e, \mu$), the excited electron and muon masses are excluded for $\Lambda = m_{l^*}$ up to 3.9 and 3.8 TeV, respectively, using 35.9 fb^{-1} at $\sqrt{s} = 13$ TeV in CMS [81] and 2.2 TeV using 13 fb^{-1} at $\sqrt{s} = 8$ TeV in ATLAS [66].

With the full 20.3 fb^{-1} data at $\sqrt{s} = 8$ TeV, the inclusive search on multi-lepton signatures with 3 or more charged leptons in ATLAS [67] further constrains the excited charged leptons and neutrinos. Considering both the transition-magnetic (Eq. (91.7)) and contact interaction (Eq. (91.4)) processes, the lower mass limits for the e^*, μ^*, τ^* and ν^* (for every excited neutrino flavor) are obtained to be 3.0, 3.0, 2.5 and 1.6 TeV, respectively, for $\Lambda = m_{e^*}, m_{\mu^*}, m_{\tau^*}$ and m_{ν^*} . The rate of pair-produced excited leptons is independent of Λ for the minimal gauge interaction processes, and it allows to improve search sensitivity with multi-lepton signatures at high Λ , especially for excited neutrinos because the predominant $\nu_l^* \rightarrow l + W$ decays result in a higher acceptance for ≥ 3 charged lepton final states.

Both ATLAS and CMS Collaborations performed searches for singly produced excited leptons. The single excited leptons, both produced and decaying in contact interaction processes (Eq. (91.4)), were searched for in CMS with 77.4 fb^{-1} at 13 TeV [82] and in ATLAS with 20.3 fb^{-1} at 8 TeV [68] and 139 fb^{-1} at 13 TeV [88] using the final states with two leptons and two jets ($q\bar{q} \rightarrow ll^* \rightarrow llq\bar{q}$). The CMS search [82] considered both excited electrons and excited muons, using the invariant mass of the combination of the two leptons and two jets as a discriminating variable to separate signal from background. The ATLAS search considered excited muons [68] and excited τ leptons [88]. The single excited electrons, produced in contact interactions and decayed either in contact interaction or charged-current processes, were considered in ATLAS using 36.1 fb^{-1} at 13 TeV [69] in the final states with two electrons and two jets ($q\bar{q} \rightarrow ee^* \rightarrow eeq\bar{q}$) or an electron, missing transverse momentum and a hadronically decaying W -boson candidate ($q\bar{q} \rightarrow ee^* \rightarrow e\nu W$). The excited electron (muon) mass was excluded up to 5.6 (5.7) TeV in CMS [82] at $\Lambda = m_{e^*}$ ($\Lambda = m_{\mu^*}$), which is the best limit to date on the ex-

cited electrons (muons). The excited τ lepton mass was excluded up to 4.6 TeV in ATLAS [88] at $\Lambda = m_{\tau^*}$.

The CMS Collaboration also performed an excited lepton search in the final states containing a Z boson [80], probing the excited leptons produced in contact interactions and decayed in neutral-current processes ($l^* \rightarrow l + Z$) with $f = f' = 1$ or $f = -f' = 1$. The leptonic and hadronic decays of Z bosons have been considered in the search, and the most stringent limits are obtained from the hadronic Z decay to be 2.08 (2.34) TeV and 2.11 (2.37) TeV for the e^* and μ^* , respectively, with $f = f' = 1$ ($f = -f' = 1$) at $\Lambda = m_{l^*}$.

Figure 91.4 summarizes the most stringent 95% C.L. lower mass limits for excited quarks and leptons obtained from the LHC experiments.

References

- [1] E. Eichten, K. D. Lane and M. E. Peskin, Phys. Rev. Lett. **50**, 811 (1983).
- [2] E. Eichten *et al.*, Rev. Mod. Phys. **56**, 579 (1984), [Addendum: Rev.Mod.Phys. 58, 1065–1073 (1986)].
- [3] J. Gao *et al.*, Phys. Rev. Lett. **106**, 142001 (2011), [arXiv:1101.4611].
- [4] G. Arnison *et al.* (UA1), Phys. Lett. B **177**, 244 (1986).
- [5] J. Appel *et al.* (UA2), Phys. Lett. B **160**, 349 (1985).
- [6] F. Abe *et al.* (CDF), Phys. Rev. Lett. **62**, 613 (1989); F. Abe *et al.* (CDF), Phys. Rev. Lett. **69**, 2896 (1992); F. Abe *et al.* (CDF), Phys. Rev. Lett. **77**, 5336 (1996), [Erratum: Phys.Rev.Lett. 78, 4307 (1997)], [hep-ex/9609011].
- [7] B. Abbott *et al.* (D0), Phys. Rev. Lett. **80**, 666 (1998), [hep-ex/9707016]; B. Abbott *et al.* (D0), Phys. Rev. Lett. **82**, 2457 (1999), [hep-ex/9807014]; B. Abbott *et al.* (D0), Phys. Rev. D **62**, 031101 (2000), [hep-ex/9912023]; B. Abbott *et al.* (D0), Phys. Rev. D **64**, 032003 (2001), [hep-ex/0012046]; V. Abazov *et al.* (D0), Phys. Rev. Lett. **103**, 191803 (2009), [arXiv:0906.4819].
- [8] G. Aad *et al.* (ATLAS), Phys. Lett. B **694**, 327 (2011), [arXiv:1009.5069]; G. Aad *et al.* (ATLAS), New J. Phys. **13**, 053044 (2011), [arXiv:1103.3864]; G. Aad *et al.* (ATLAS), JHEP **01**, 029 (2013), [arXiv:1210.1718]; G. Aad *et al.* (ATLAS), Phys. Rev. Lett. **114**, 22, 221802 (2015), [arXiv:1504.00357]; G. Aad *et al.* (ATLAS), Phys. Lett. B **754**, 302 (2016), [arXiv:1512.01530].
- [9] M. Aaboud *et al.* (ATLAS), Phys. Rev. D **96**, 5, 052004 (2017), [arXiv:1703.09127].
- [10] V. Khachatryan *et al.* (CMS), Phys. Rev. Lett. **105**, 262001 (2010), [arXiv:1010.4439]; V. Khachatryan *et al.* (CMS), Phys. Rev. Lett. **106**, 201804 (2011), [arXiv:1102.2020]; S. Chatrchyan *et al.* (CMS), JHEP **05**, 055 (2012), [arXiv:1202.5535]; V. Khachatryan *et al.* (CMS), Phys. Lett. B **746**, 79 (2015), [arXiv:1411.2646]; A. M. Sirunyan *et al.* (CMS), JHEP **07**, 013 (2017), [arXiv:1703.09986].
- [11] S. Chatrchyan *et al.* (CMS), Phys. Rev. D **87**, 5, 052017 (2013), [arXiv:1301.5023].
- [12] A. M. Sirunyan *et al.* (CMS), Eur. Phys. J. C **78**, 9, 789 (2018), [arXiv:1803.08030].
- [13] T. Sjostrand, S. Mrenna and P. Z. Skands, Comput. Phys. Commun. **178**, 852 (2008), [arXiv:0710.3820].
- [14] S. Agostinelli *et al.* (GEANT4), Nucl. Instrum. Meth. A **506**, 250 (2003), :GEANT4: a simulation toolkit.
- [15] Z. Nagy, Phys. Rev. Lett. **88**, 122003 (2002), [hep-ph/0110315]; Z. Nagy, Phys. Rev. D **68**, 094002 (2003), [hep-ph/0307268].
- [16] S. Dittmaier, A. Huss and C. Speckner, JHEP **11**, 095 (2012), [arXiv:1210.0438].
- [17] A. Tumasyan *et al.* (CMS), JHEP **02**, 142 (2022), [Addendum: JHEP 12, 035 (2022)], [arXiv:2111.10431].
- [18] S. Schael *et al.* (ALEPH), Eur. Phys. J. C **49**, 411 (2007), [hep-ex/0609051].
- [19] J. Abdallah *et al.* (DELPHI), Eur. Phys. J. C **45**, 589 (2006), [hep-ex/0512012].
- [20] M. Acciarri *et al.* (L3), Phys. Lett. B **489**, 81 (2000), [hep-ex/0005028].
- [21] K. Ackerstaff *et al.* (OPAL), Phys. Lett. B **391**, 221 (1997); G. Abbiendi *et al.* (OPAL), Eur. Phys. J. C **33**, 173 (2004), [hep-ex/0309053].
- [22] F. Aaron *et al.* (H1), Phys. Lett. B **705**, 52 (2011), [arXiv:1107.2478].
- [23] S. Chekanov *et al.* (ZEUS), Phys. Lett. B **591**, 23 (2004), [hep-ex/0401009].
- [24] F. Abe *et al.* (CDF), Phys. Rev. Lett. **68**, 1463 (1992); F. Abe *et al.* (CDF), Phys. Rev. Lett. **79**, 2198 (1997); T. Affolder *et al.* (CDF), Phys. Rev. Lett. **87**, 231803 (2001), [hep-ex/0107008]; A. Abulencia *et al.* (CDF), Phys. Rev. Lett. **96**, 211801 (2006), [hep-ex/0602045].
- [25] B. Abbott *et al.* (D0), Phys. Rev. Lett. **82**, 4769 (1999), [hep-ex/9812010].
- [26] G. Aad *et al.* (ATLAS), Phys. Rev. D **84**, 011101 (2011), [arXiv:1104.4398]; G. Aad *et al.* (ATLAS), Phys. Lett. B **712**, 40 (2012), [arXiv:1112.4462]; G. Aad *et al.* (ATLAS), Phys. Rev. D **87**, 1, 015010 (2013), [arXiv:1211.1150]; G. Aad *et al.* (ATLAS), Eur. Phys. J. C **74**, 12, 3134 (2014), [arXiv:1407.2410]; M. Aaboud *et al.* (ATLAS), Phys. Lett. B **761**, 372 (2016), [arXiv:1607.03669]; M. Aaboud *et al.* (ATLAS), JHEP **10**, 182 (2017), [arXiv:1707.02424].
- [27] G. Aad *et al.* (ATLAS), JHEP **11**, 005 (2020), [Erratum: JHEP 04, 142 (2021)], [arXiv:2006.12946].
- [28] S. Chatrchyan *et al.* (CMS), Phys. Rev. D **87**, 3, 032001 (2013), [arXiv:1212.4563]; V. Khachatryan *et al.* (CMS), JHEP **04**, 025 (2015), [arXiv:1412.6302]; A. M. Sirunyan *et al.* (CMS), JHEP **04**, 114 (2019), [arXiv:1812.10443].
- [29] A. M. Sirunyan *et al.* (CMS), JHEP **07**, 208 (2021), [arXiv:2103.02708].
- [30] W. Buchmuller and D. Wyler, Nucl. Phys. B **268**, 621 (1986).
- [31] B. Grzadkowski *et al.*, JHEP **10**, 085 (2010), [arXiv:1008.4884].
- [32] E. E. Jenkins, A. V. Manohar and M. Trott, JHEP **10**, 087 (2013), [arXiv:1308.2627].
- [33] E. E. Jenkins, A. V. Manohar and M. Trott, JHEP **01**, 035 (2014), [arXiv:1310.4838].
- [34] R. Alonso *et al.*, JHEP **04**, 159 (2014), [arXiv:1312.2014].
- [35] I. Brivio and M. Trott, Phys. Rept. **793**, 1 (2019), [arXiv:1706.08945].
- [36] A. V. Manohar (2018), [arXiv:1804.05863].
- [37] A. Falkowski, Eur. Phys. J. C **83**, 7, 656 (2023).
- [38] A. Pomarol and J. Serra, Phys. Rev. D **78**, 074026 (2008), [arXiv:0806.3247].
- [39] C. Degrande *et al.*, JHEP **03**, 125 (2011), [arXiv:1010.6304].
- [40] M. Aaboud *et al.* (ATLAS), Phys. Rev. D **99**, 5, 052009 (2019), [arXiv:1811.02305].
- [41] D. Barducci *et al.* (2018), [arXiv:1802.07237]; S. Alte, M. König and W. Shepherd, JHEP **01**, 094 (2018), [arXiv:1711.07484]; S. Alte, M. König and W. Shepherd, JHEP **07**, 144 (2019), [arXiv:1812.07575]; J. Ellis *et al.*, JHEP **04**, 279 (2021), [arXiv:2012.02779].
- [42] The ATLAS and CMS Collaborations (2022), updated results and plots available at <https://twiki.cern.ch/twiki/bin/view/LHCPhysics/LHCTopWGSummaryPlots>, URL <https://cds.cern.ch/record/2840588/files/ATL-PHYS-PUB-2022-048.pdf>.
- [43] F. Renard, Phys. Lett. B **116**, 264 (1982).
- [44] F. del Aguila, A. Mendez and R. Pascual, Phys. Lett. B **140**, 431 (1984).
- [45] M. Suzuki, Phys. Lett. B **143**, 237 (1984).

- [46] U. Baur, M. Spira and P. Zerwas, *Phys. Rev. D* **42**, 815 (1990).
- [47] K. Hagiwara, D. Zeppenfeld and S. Komamiya, *Z. Phys. C* **29**, 115 (1985).
- [48] N. Cabibbo, L. Maiani and Y. Srivastava, *Phys. Lett. B* **139**, 459 (1984).
- [49] D. Decamp *et al.* (ALEPH), *Phys. Rept.* **216**, 253 (1992); R. Barate *et al.* (ALEPH), *Eur. Phys. J. C* **4**, 571 (1998).
- [50] P. Abreu *et al.* (DELPHI), *Nucl. Phys. B* **367**, 511 (1991); J. Abdallah *et al.* (DELPHI), *Eur. Phys. J. C* **37**, 405 (2004), [hep-ex/0409058].
- [51] O. Adriani *et al.* (L3), *Phys. Rept.* **236**, 1 (1993); P. Achard *et al.* (L3), *Phys. Lett. B* **531**, 28 (2002), [hep-ex/0202025]; P. Achard *et al.* (L3), *Phys. Lett. B* **568**, 23 (2003), [hep-ex/0306016].
- [52] G. Abbiendi *et al.* (OPAL), *Phys. Lett. B* **544**, 57 (2002), [hep-ex/0206061]; G. Abbiendi *et al.* (OPAL), *Phys. Lett. B* **602**, 167 (2004), [hep-ex/0412011].
- [53] C. Adloff *et al.* (H1), *Phys. Lett. B* **525**, 9 (2002), [hep-ex/0110037]; F. Aaron *et al.* (H1), *Phys. Lett. B* **663**, 382 (2008), [arXiv:0802.1858]; F. Aaron *et al.* (H1), *Phys. Lett. B* **666**, 131 (2008), [arXiv:0805.4530].
- [54] S. Chekanov *et al.* (ZEUS), *Phys. Lett. B* **549**, 32 (2002), [hep-ex/0109018].
- [55] D. Acosta *et al.* (CDF), *Phys. Rev. Lett.* **94**, 101802 (2005), [hep-ex/0410013]; A. Abulencia *et al.* (CDF), *Phys. Rev. Lett.* **97**, 191802 (2006), [hep-ex/0606043]; T. Aaltonen *et al.* (CDF), *Phys. Rev. D* **79**, 112002 (2009), [arXiv:0812.4036].
- [56] V. Abazov *et al.* (D0), *Phys. Rev. D* **73**, 111102 (2006), [hep-ex/0604040]; V. Abazov *et al.* (D0), *Phys. Rev. D* **77**, 091102 (2008), [arXiv:0801.0877]; V. Abazov *et al.* (D0), *Phys. Rev. Lett.* **103**, 191803 (2009), [arXiv:0906.4819].
- [57] G. Aad *et al.* (ATLAS), *Phys. Lett. B* **708**, 37 (2012), [arXiv:1108.6311]; G. Aad *et al.* (ATLAS), *JHEP* **01**, 029 (2013), [arXiv:1210.1718]; G. Aad *et al.* (ATLAS), *Phys. Rev. D* **91**, 5, 052007 (2015), [arXiv:1407.1376]; G. Aad *et al.* (ATLAS), *Phys. Lett. B* **754**, 302 (2016), [arXiv:1512.01530]; M. Aaboud *et al.* (ATLAS), *Phys. Rev. D* **96**, 5, 052004 (2017), [arXiv:1703.09127].
- [58] G. Aad *et al.* (ATLAS), *JHEP* **03**, 145 (2020), [arXiv:1910.08447].
- [59] G. Aad *et al.* (ATLAS), *Phys. Rev. Lett.* **108**, 211802 (2012), [arXiv:1112.3580]; G. Aad *et al.* (ATLAS), *Phys. Lett. B* **728**, 562 (2014), [arXiv:1309.3230]; G. Aad *et al.* (ATLAS), *JHEP* **03**, 041 (2016), [arXiv:1512.05910].
- [60] M. Aaboud *et al.* (ATLAS), *Eur. Phys. J. C* **78**, 2, 102 (2018), [arXiv:1709.10440].
- [61] M. Aaboud *et al.* (ATLAS), *Phys. Rev. D* **98**, 032016 (2018), [arXiv:1805.09299].
- [62] M. Aaboud *et al.* (ATLAS), *Phys. Lett. B* **759**, 229 (2016), [arXiv:1603.08791].
- [63] G. Aad *et al.* (ATLAS), *JHEP* **02**, 110 (2016), [arXiv:1510.02664].
- [64] G. Aad *et al.* (ATLAS), *Phys. Lett. B* **721**, 171 (2013), [arXiv:1301.1583].
- [65] G. Aad *et al.* (ATLAS), *Phys. Rev. D* **85**, 072003 (2012), [arXiv:1201.3293].
- [66] G. Aad *et al.* (ATLAS), *New J. Phys.* **15**, 093011 (2013), [arXiv:1308.1364].
- [67] G. Aad *et al.* (ATLAS), *JHEP* **08**, 138 (2015), [arXiv:1411.2921].
- [68] G. Aad *et al.* (ATLAS), *New J. Phys.* **18**, 7, 073021 (2016), [Erratum: *New J. Phys.* **21**, 109501 (2019)], [arXiv:1601.05627].
- [69] M. Aaboud *et al.* (ATLAS), *Eur. Phys. J. C* **79**, 9, 803 (2019), [arXiv:1906.03204].
- [70] S. Chatrchyan *et al.* (CMS), *Phys. Lett. B* **704**, 123 (2011), [arXiv:1107.4771]; S. Chatrchyan *et al.* (CMS), *JHEP* **01**, 013 (2013), [arXiv:1210.2387]; S. Chatrchyan *et al.* (CMS), *Phys. Rev. D* **87**, 11, 114015 (2013), [arXiv:1302.4794].
- [71] V. Khachatryan *et al.* (CMS), *Phys. Rev. D* **91**, 5, 052009 (2015), [arXiv:1501.04198].
- [72] V. Khachatryan *et al.* (CMS), *Phys. Rev. Lett.* **116**, 7, 071801 (2016), [arXiv:1512.01224]; V. Khachatryan *et al.* (CMS), *Phys. Rev. Lett.* **117**, 3, 031802 (2016), [arXiv:1604.08907]; A. M. Sirunyan *et al.* (CMS), *Phys. Lett. B* **769**, 520 (2017), [Erratum: *Phys. Lett. B* **772**, 882–883 (2017)], [arXiv:1611.03568]; A. M. Sirunyan *et al.* (CMS), *JHEP* **08**, 130 (2018), [arXiv:1806.00843].
- [73] A. M. Sirunyan *et al.* (CMS), *JHEP* **05**, 033 (2020), [arXiv:1911.03947].
- [74] V. Khachatryan *et al.* (CMS), *Phys. Lett. B* **738**, 274 (2014), [arXiv:1406.5171].
- [75] A. M. Sirunyan *et al.* (CMS), *Phys. Lett. B* **781**, 390 (2018), [arXiv:1711.04652].
- [76] S. Chatrchyan *et al.* (CMS), *Phys. Lett. B* **722**, 28 (2013), [arXiv:1210.0867]; S. Chatrchyan *et al.* (CMS), *Phys. Lett. B* **723**, 280 (2013), [arXiv:1212.1910]; V. Khachatryan *et al.* (CMS), *JHEP* **08**, 173 (2014), [arXiv:1405.1994].
- [77] A. M. Sirunyan *et al.* (CMS), *Phys. Rev. D* **97**, 7, 072006 (2018), [arXiv:1708.05379].
- [78] V. Khachatryan *et al.* (CMS), *JHEP* **01**, 166 (2016), [arXiv:1509.08141].
- [79] S. Chatrchyan *et al.* (CMS), *Phys. Lett. B* **704**, 143 (2011), [arXiv:1107.1773]; S. Chatrchyan *et al.* (CMS), *Phys. Lett. B* **720**, 309 (2013), [arXiv:1210.2422].
- [80] V. Khachatryan *et al.* (CMS), *JHEP* **03**, 125 (2016), [arXiv:1511.01407].
- [81] A. M. Sirunyan *et al.* (CMS), *JHEP* **04**, 015 (2019), [arXiv:1811.03052].
- [82] A. M. Sirunyan *et al.* (CMS), *JHEP* **05**, 052 (2020), [arXiv:2001.04521].
- [83] A. M. Sirunyan *et al.* (CMS), *Phys. Lett. B* **778**, 349 (2018), [arXiv:1711.10949].
- [84] S. Chatrchyan *et al.* (CMS), *JHEP* **06**, 125 (2014), [arXiv:1311.5357].
- [85] A. Tumasyan *et al.* (CMS), *Phys. Rev. D* **108**, 1, 012009 (2023), [arXiv:2205.01835].
- [86] A. M. Sirunyan *et al.* (CMS), *JHEP* **12**, 106 (2021), [arXiv:2104.12853].
- [87] A. Tumasyan *et al.* (CMS), *JHEP* **04**, 048 (2022), [arXiv:2111.10216].
- [88] G. Aad *et al.* (ATLAS), *JHEP* **06**, 199 (2023), [arXiv:2303.09444].
- [89] A. Tumasyan *et al.* (CMS), *JHEP* **12**, 189 (2023), [arXiv:2305.07998].
- [90] M. Cacciari, G. P. Salam and G. Soyez, *JHEP* **04**, 063 (2008), [arXiv:0802.1189].

92. Dynamical Electroweak Symmetry Breaking: Implications of the H^0

Revised August 2023 by K.M. Black (Wisconsin U.), R. Sekhar Chivukula (UC San Diego) and A. Lister (U. of British Columbia).

92.1 Introduction and Phenomenology

In theories of dynamical electroweak symmetry breaking, the electroweak interactions are broken to electromagnetism by the vacuum expectation value of a composite operator, typically a fermion bilinear. In these theories, the longitudinal components of the massive weak bosons are identified with composite Nambu-Goldstone bosons arising from dynamical symmetry breaking in a strongly-coupled extension of the standard model. Viable theories of dynamical electroweak symmetry breaking must also explain (or at least accommodate) the presence of an additional composite scalar state to be identified with the H^0 scalar boson [1,2] – a state unlike any other observed previously.

Theories of dynamical electroweak symmetry breaking can be classified by the nature of the composite singlet state to be associated with the H^0 and the corresponding dimensional scales f , the analog of the pion decay-constant in QCD, and Λ , the scale of the underlying strong dynamics.¹ Of particular importance is the ratio v/f , where $v^2 = 1/(\sqrt{2}G_F) \approx (246 \text{ GeV})^2$, since this ratio measures the expected size of the deviations of the couplings of a composite Higgs boson from those expected in the standard model. The basic possibilities, and the additional states that they predict, are described below.

92.1.1 Technicolor, $v/f \simeq 1$, $\Lambda \simeq 1 \text{ TeV}$

Technicolor models [7–9] provided the first examples of theories of dynamical electroweak symmetry breaking. These theories incorporate a new asymptotically free gauge theory (“technicolor”) and additional massless fermions (“technifermions” transforming under a vectorial representation of the gauge group). The global chiral symmetry of the fermions is spontaneously broken by the formation of a technifermion condensate, just as the approximate chiral symmetry in QCD is broken down to isospin by the formation of a quark condensate. The $SU(2)_W \times U(1)_Y$ interactions are embedded in the global technifermion chiral symmetries in such a way that the only unbroken gauge symmetry after chiral symmetry breaking is $U(1)_{em}$.² The theories naturally provide the Nambu-Goldstone bosons “eaten” by the W and Z bosons. There would also typically be additional heavy states (e.g. vector mesons, analogous to the ρ and ω mesons in QCD) with TeV masses [13,14], and the WW and ZZ scattering amplitudes would be expected to be strong at energies of order 1 TeV.

There are various possibilities for the scalar H^0 in technicolor models. First, the H^0 could be identified as a singlet scalar resonance, analogous to the σ particle expected in pion-scattering in QCD [15,16]. Alternatively, the H^0 could be identified as a dilaton, a (pseudo-)Goldstone boson of scale invariance in theories of “walking technicolor” [17–21].³ Finally, the H^0 could be identified as an additional isosinglet state if the chiral symmetry breaking pattern of the technicolor theory provides for such a state.⁴ In all of these cases, however, one expects large deviations in the couplings of this particle from those of the standard model Higgs boson. Since the couplings observed for the H^0 approximate those of the Higgs boson to the 10% level, models of this kind are very highly constrained.

¹In a strongly interacting theory “Naive Dimensional Analysis” [3,4] implies that, in the absence of fine-tuning, $\Lambda \simeq g^* f$ where $g^* \simeq 4\pi$ is the typical size of a strong coupling in the low-energy theory [5,6]. This estimate is modified in the presence of multiple flavors or colors [7].

²For a review of technicolor models, see [10–12].

³If both the electroweak symmetry and the approximate scale symmetry are broken only by electroweak doublet condensate(s), then the decay-constants for scale and electroweak symmetry breaking may be approximately equal – differing only by terms formally proportional to the amount of explicit scale-symmetry breaking.

⁴In this case, however, the coupling strength of the singlet state to WW and ZZ pairs would be comparable to the couplings to gluon and photon pairs, and these would all arise from loop-level couplings in the underlying technicolor theory [22].

92.1.2 The Higgs doublet as a pseudo-Nambu-Goldstone Boson, $v/f < 1$, $\Lambda > 1 \text{ TeV}$

In technicolor models, the symmetry-breaking properties of the underlying strong dynamics necessarily breaks the electroweak gauge symmetries. An alternative possibility is that the underlying strong dynamics itself does not break the electroweak interactions, and that the entire quartet of bosons in the Higgs doublet (including the state associated with the H^0) are composite (pseudo-) Nambu-Goldstone particles [23–25]. In this case, the underlying dynamics can occur at energies exceeding 1 TeV and additional interactions with the top-quark mass generating sector (and possibly with additional weakly-coupled gauge bosons) cause the vacuum energy to be minimized when the composite Higgs doublet gains a vacuum expectation value [26,27]. In these theories, the couplings of the remaining singlet scalar state would naturally be equal to that of the standard model Higgs boson up to corrections of order $(v/f)^2$ and, therefore, constraints on the size of deviations of the H^0 couplings from that of the standard model Higgs [28] give rise to lower bounds on the scales f and Λ .⁵

The electroweak gauge interactions, as well as the interactions responsible for the top-quark mass, explicitly break the chiral symmetries of the composite Higgs model and lead generically to sizable corrections to the mass-squared of the Higgs-doublet – the so-called “Little Hierarchy Problem” [29]. “Little Higgs” theories [30–33] are examples of composite Higgs models in which the (collective) symmetry-breaking structure is selected so as to suppress these contributions to the Higgs mass-squared.

Composite Higgs models typically require a larger global symmetry of the underlying theory, and hence additional relatively light (compared to Λ) scalar particles, extra electroweak vector bosons (e.g. an additional $SU(2) \times U(1)$ gauge group), and vector-like partners of the top-quark of charge $+2/3$ and possibly also $+5/3$ [34]. In addition to these states, one would expect the underlying dynamics to yield additional scalar and vector resonances with masses of order Λ . If the theory respects a custodial symmetry [35], the couplings of these additional states to the electroweak and Higgs boson will be related – and, for example, one might expect a charged vector resonance to have similar branching ratios to WZ and WH . Different composite Higgs models utilize different mechanisms for arranging for the hierarchy of scales $v < f$ and arranging for a scalar Higgs self-coupling small enough to produce an H^0 of mass of order 125 GeV, for a review see [36]. If the additional states in these models carry color, they can provide additional contributions to Higgs production via gluon fusion [37]. The extent to which Higgs production at the LHC conforms with standard model predictions provides additional constraints (typically lower bounds on the masses of the additional colored states of order 0.7 TeV) on these models.

In addition, if the larger symmetry of the underlying composite Higgs theory does not commute with the standard model gauge group, then the additional states found in those models – especially those related to the top-quark, which tend to have the largest couplings to the electroweak sector – may be *colorless*. For example, in twin Higgs models [38], the top-partners carry no standard model charges. The phenomenology of the additional states in twin Higgs theories is rather different, since lacking color the production of these particles at the LHC will be suppressed – and, their decays may occur only via the electroweak symmetry breaking sector, leading to their being long-lived.

92.1.3 Top-Condensate, Top-Color, Top-Seesaw and related theories, $v/f < 1$, $\Lambda > 1 \text{ TeV}$

A final alternative is to consider a strongly interacting theory with a high (compared to a TeV) underlying dynamical scale that would naturally break the electroweak interactions, but whose

⁵In these models v/f is an adjustable parameter, and in the limit $v/f \rightarrow 1$ they reduce, essentially, to the technicolor models discussed in the previous subsection. Our discussion here is consistent with that given there, since we expect corrections to the SM Higgs couplings to be large for $v/f \simeq 1$. Current measurements constrain the couplings of the H^0 to equal those predicted for the Higgs in the standard model to about the 10% level [28], suggesting that f must have values of order a TeV or higher and, therefore, a dynamical scale Λ of at least several TeV.

strength is adjusted (“fine-tuned”) to produce electroweak symmetry breaking at 1 TeV. This alternative is possible if the electroweak (quantum) phase transition is continuous (second order) in the strength of the strong dynamics [39]. If the fine-tuning can be achieved, the underlying strong interactions will produce a light composite Higgs bound state with couplings equal to that of the standard model Higgs boson up to corrections of order $(1 \text{ TeV}/\Lambda)^2$. As in theories in which electroweak symmetry breaking occurs through vacuum alignment, therefore, constraints on the size of deviations of the H^0 couplings from that of the standard model Higgs give rise to lower bounds on the scale Λ . Formally, in the limit $\Lambda \rightarrow \infty$ (a limit which requires arbitrarily fine adjustment of the strength of the high-energy interactions), these theories are equivalent to a theory with a fundamental Higgs boson – and the fine adjustment of the coupling strength is a manifestation of the hierarchy problem of theories with a fundamental scalar particle.

In many of these theories the top-quark itself interacts strongly (at high energies), potentially through an extended color gauge sector [40, 40–44]. In these theories, top-quark condensation (or the condensation of an admixture of the top with additional vector-like quarks) is responsible for electroweak symmetry breaking, and the H^0 is identified with a bound state involving the third generation of quarks. These theories typically include an extra set of massive color-octet vector bosons (top-gluons), and an extra $U(1)$ interaction (giving rise to a top-color Z') which couple preferentially to the third generation and whose masses define the scale Λ of the underlying physics.

92.1.4 Flavor

In addition to the electroweak symmetry breaking dynamics described above, which gives rise to the masses of the W and Z particles, additional interactions must be introduced to produce the masses of the standard model fermions. Two general avenues have been suggested for these new interactions. In “extended technicolor” (ETC) theories [45, 46], the gauge interactions in the underlying strongly interacting theory are extended to incorporate flavor. This extended gauge symmetry is broken down (possibly sequentially, at several different mass scales) to the residual strong interaction responsible for electroweak symmetry breaking. The massive gauge-bosons corresponding to the broken symmetries then mediate interactions between mass operators for the quarks/leptons and the corresponding bilinears of the strongly-interacting fermions, giving rise to the masses of the ordinary fermions after electroweak symmetry breaking.

In the case of “partial compositeness” [47], the additional flavor-dependent interactions arise from mixing between the ordinary quarks and leptons and massive composite fermions in the strongly-interacting underlying theory. Theories incorporating partial compositeness include additional vector-like partners of the ordinary quarks and leptons, typically with masses of order a TeV or less.

In both cases, the effects of flavor interactions on the electroweak properties of the ordinary quarks and leptons are likely to be most pronounced in the third generation of fermions.⁶ The additional particles present in these theories, especially the additional scalars, often couple more strongly to heavier fermions.

Moreover, since the flavor interactions must give rise to quark mixing, we expect that a generic theory of this kind could give rise to large flavor-changing neutral-currents [46]. In ETC theories, these constraints are typically somewhat relaxed if the theory incorporates approximate generational flavor symmetries [48], the theory has a slowly running coupling constant or “walks” [17–21], or if $\Lambda > 1 \text{ TeV}$ [49]. In theories of partial compositeness, the masses of the ordinary fermions depend on the scaling-dimension of the operators corresponding to the composite fermions with which they mix. This leads to a new mechanism for generating the mass-hierarchy of the observed quarks and leptons that, potentially, ameliorates flavor-changing neutral current problems and can provide new contributions to the composite Higgs poten-

tial which allow for $v/f < 1$ [50–54].

Alternatively, one can assume that the underlying flavor dynamics respect flavor symmetries (“minimal” [55, 56] or “next-to-minimal” [57] flavor violation) that suppress flavor-changing neutral currents in the two light generations. Additional considerations apply when extending these arguments to potential explanation of neutrino masses (see, for example, [58, 59]).

92.1.5 Theoretical Considerations

Since the underlying high-energy dynamics in these theories are strongly coupled, there are no reliable calculation techniques that can be applied to analyze their properties. Instead, most phenomenological studies depend on the construction of a “low-energy” effective theory describing additional scalar, fermion, or vector boson degrees of freedom, which incorporates the relevant symmetries and, when available, dynamical principles. In some cases, motivated by the AdS/CFT correspondence [60], the strongly-interacting theories described above have been investigated by analyzing a dual compactified five-dimensional gauge theory. In these cases, the AdS/CFT “dictionary” is used to map the features of the underlying strongly coupled high-energy dynamics onto the low-energy weakly coupled dual theory [61].

More recently, progress has been made in investigating strongly-coupled models using lattice gauge theory [62–65]. These calculations offer the prospect of establishing which strongly coupled theories of electroweak symmetry breaking have a particle with properties consistent with those observed for the H^0 – and for establishing concrete predictions for these theories at the LHC [66].

92.1.6 Summary

The theoretical ideas and models reviewed here motivate searches for a wide variety of new states. Heavy vector bound states decaying to dibosons and additional scalar states appear naturally in both technicolor (92.1.1) and composite Higgs models (92.1.2). Composite Higgs models based on collective symmetry breaking naturally include W' , Z' , and vector-like quark states (especially for the third-generation, and potentially including charge $+5/3$ custodial top-partner quarks). Vector-like states are also natural for any theory including partial compositeness in order to address the flavor problem (92.1.4). Top-condensate and related models (92.1.3) predict the existence of colorons which preferentially couple to third-generation quarks. Finally, the new states discussed here also occur in extra-dimensional models [61], which is understandable given that many strongly-coupled theories can be viewed as compactified five-dimensional gauge theories via duality (92.1.5). We turn now to a review the status of experimental searches related to dynamical electroweak symmetry breaking.

92.2 Experimental Searches

As discussed above, the extent to which the couplings of the H^0 conform to the expectations for a standard model Higgs boson constrains the viability of each of these models. Measurements of the H^0 couplings, and their interpretation in terms of effective field theory, are summarized in the H^0 review in this volume. In what follows, we will focus on searches for the additional particles that might be expected to accompany the singlet scalar: extra scalars, fermions, and vector bosons. In some cases, detailed model-specific searches have been made for the particles described above (though generally not yet taking account of the demonstrated existence of the H^0 boson).

In most cases, however, generic searches (e.g. for extra W' or Z' particles, extra scalars in the context of multi-Higgs models, or for fourth-generation quarks) are quoted that can be used – when appropriately translated – to derive bounds on a specific model of interest.

The mass scale of the new particles implied by the interpretations of the low mass of H^0 discussed above, and existing studies from the Tevatron and lower-energy colliders, suggests that only the Large Hadron Collider has any real sensitivity. A number of analyses already carried out by ATLAS and CMS use relevant final states and might have been expected to observe a deviation from standard model expectations – in no case so far has any such deviation been reported. The detailed implications of these

⁶Indeed, from this point of view, the vector-like partners of the top-quark in top-seesaw and little Higgs models can be viewed as incorporating partial compositeness to explain the origin of the top quark’s large mass.

searches in various model frameworks are described below.

Except where otherwise noted, all limits in this section are quoted at a confidence level of 95%. The searches at $\sqrt{s} = 8$ TeV (Run 1) are based on 20.3 fb $^{-1}$ of data recorded by ATLAS, and an integrated luminosity of 19.7 fb $^{-1}$ analyzed by CMS. The datasets collected at $\sqrt{s} = 13$ TeV during Run 2 of the LHC since 2015 are based on analyses with varied integrated luminosities ranging from ~ 2 -140 fb $^{-1}$.

92.2.1 Searches for Z' or W' Bosons

Massive vector bosons or particles with similar decay channels would be expected to arise in Little Higgs theories, in theories of Technicolor, or models involving a dilaton, adjusted to produce a light Higgs boson, consistent with the observed H^0 . These particles would be expected to decay to pairs of vector bosons, or to third generation quarks, or to leptons. The generic searches for W' and Z' vector bosons listed below can, therefore, be used to constrain models incorporating a composite Higgs-like boson.

A general review of searches for Z' and W' bosons is also included in this volume [67, 68]. In the context of the dynamical electroweak symmetry breaking models, we emphasize their decays to third generation fermions by including a detailed overview, while also briefly summarizing the other searches.

$Z' \rightarrow \ell\ell$:

ATLAS [69] and CMS [70] have both searched for Z' production with $Z' \rightarrow e\bar{e}$ or $\mu\bar{\mu}$. No deviation from the standard model prediction was seen in the dielectron and dimuon invariant mass spectra, by either the ATLAS or the CMS analysis, and lower limits on possible Z' boson masses were set. A Z'_{SSM} with couplings equal to the standard model Z' (a “sequential standard model” Z') and a mass below 5.1 TeV was excluded by ATLAS, while CMS set a lower mass limit of 5.15 TeV. The experiments also place limits on the parameters of extra dimension models and in the case of ATLAS on the parameters of a minimal walking technicolor model [17–21], consistent with a 125 GeV Higgs boson [71]. For a general review of searches in these channels see the PDG review of Z' prime in this volume [67].

In addition, both experiments have also searched for Z' decaying to a ditau final state [72, 73]. An excess in $\tau^+\tau^-$ could have interesting implications for models in which lepton universality is not a requirement and enhanced couplings to the third generation are allowed. This analysis led to lower limits on the mass of a Z'_{SSM} of 2.4 and 2.1 TeV from ATLAS and CMS respectively.

$Z' \rightarrow q\bar{q}$:

The ability to relatively cleanly select $t\bar{t}$ pairs at the LHC together with the existence of enhanced couplings to the third generation in many models makes it worthwhile to search for new particles decaying in this channel. Both ATLAS [74] and CMS [75] have carried out searches for new particles decaying into $t\bar{t}$.

Both ATLAS and CMS searched for $t\bar{t}$ in the all hadronic mode [76] [77] in both the resolved and boosted regions. No evidence of resonance production were seen and limits were produced for various models including the Z' boson in topcolor-assisted technicolor which excludes masses less than 3.1 to 3.6 TeV (ATLAS) depending on the details of the model and 3.3, 5.25, and 6.65 TeV for widths of 1, 10 and 30 percent relative to the mass of the resonance.

ATLAS also presented results on the lepton plus jets final state, where the top quark pair decays as $t\bar{t} \rightarrow WbWb$ with one W boson decaying leptonically and the other hadronically; CMS used final states where both, one or neither W decays leptonically and then combined the results. The $t\bar{t}$ invariant mass spectrum was analyzed for any excess, and no evidence for any resonance was seen. ATLAS excluded a narrow ($\Gamma/m = 1.2\%$) leptophobic topcolor Z' boson with masses between 0.7 and 2.1 TeV and with $\Gamma/m = 3\%$ between 0.7 and 3.2 TeV. CMS set limits on leptophobic Z' bosons for three different assumed widths $\Gamma/m = 1.0\%$, $\Gamma/m = 10.0\%$, and $\Gamma/m = 30.0\%$ of 3.9 TeV to 4.0 TeV and exclude RS KK gluons up to 3.3 TeV.

Both ATLAS [78] and CMS [79] have also searched for resonances decaying into $q\bar{q}$, qg or gg using the dijet invariant mass spectrum. Excited quarks are excluded up to masses of 6.7 TeV and model-independent upper limits on cross sections with a

Gaussian signal shape were set. CMS excluded string resonances with masses below 7.9 TeV, scalar diquarks below 7.5 TeV, axigluons and colorons below 6.6 TeV, excited quarks below 6.3 TeV, color-octet scalars below 3.7 TeV, W' bosons below 3.6 TeV, Z' bosons with SM-like couplings below 2.9 TeV and between 3.1 TeV and 3.3 TeV, Randall–Sundrum Gravitons below 2.6 TeV.

$W' \rightarrow \ell\nu$:

Both LHC experiments have also searched for massive charged vector bosons. In this section we include a summary of the results, with emphasis on final states with third generation fermions, while the details on other decays are discussed in the mini-review of W' [68]. ATLAS searched for a heavy W' decaying to $e\nu$ or $\mu\nu$ and found no excess over the standard model expectation. A sequential standard model (SSM) W' boson (assuming zero branching ratio to WZ) with mass less than 7 TeV was excluded [80] using the 139 fb $^{-1}$ dataset at $\sqrt{s} = 13$ TeV. Model independent cross-section limits as a function of mass were also set. Based on a similar dataset, the CMS experiment excluded a SSM W' boson with mass up to 5.7 TeV [81] and presented upper limits on the production of generic W' bosons decaying into this final state using a model-independent approach.

CMS [82] has carried out a complementary search in the $\tau\nu$ final state. As noted above, such searches place limits on models with enhanced couplings to the third generation. No excess was observed and limits between 2.0 and 2.7 TeV were set on the mass of a W' decaying preferentially to the third generation; a W' with universal fermion couplings was also excluded for masses less than 2.7 TeV.

$W' \rightarrow t\bar{b}$:

Heavy new gauge bosons can couple to left-handed fermions like the SM W boson or to right-handed fermions. W' bosons that couple only to right-handed fermions (W'_R) may not have leptonic decay modes, depending on the mass of the right-handed neutrino. For these W' bosons, the $t\bar{b}$ ($t\bar{b} + \bar{t}b$) decay mode is especially important because in many models the W' boson is expected to have enhanced couplings to the third generation of quarks relative to those in the first and second generations. It is also the hadronic decay mode with the best signal-to-background. ATLAS and CMS have performed searches for W' bosons via the $W' \rightarrow t\bar{b}$ decay channel in the lepton+jets and all-hadronic final state.

The CMS lepton+jets search [83–86], $W' \rightarrow t\bar{b} \rightarrow Wbb \rightarrow \ell\nu bb$, proceeded via selecting events with an isolated lepton (electron or muon), and at least two jets, one of which is identified to originate from a b -quark. The mass of the W' boson ($M_{t\bar{b}}$) was reconstructed using the four-momentum vectors of the final state objects ($b\bar{b}\ell\nu$). The distribution of $M_{t\bar{b}}$ is used as the search discriminant. A search [86] using 35.9 fb $^{-1}$ of data, collected at $\sqrt{s} = 13$ TeV, led to an exclusion of W'_R bosons with masses below 3.4 TeV (3.6 TeV) if $M_{W'_R} \gg M_{\nu_R}$ ($M_{W'_R} < M_{\nu_R}$), where M_{ν_R} is the mass of the right-handed neutrino.

The CMS search for $W' \rightarrow t\bar{b}$ decays using the all-hadronic final state focused on W' masses above 1 TeV [85, 87]. In this region, the top quark gets a large Lorentz boost and hence the three hadronic products from its decay merge into a single large-radius jet. Deep neural network(DNN) algorithms are used to identify the jet initiated by the bottom quark. Techniques including DNN, which rely on substructure information of the jets [88] are employed to identify boosted all hadronic W boson and top quark [87] decays. The W' candidate mass was computed from back-to-back boosted top-tagged jet and a low mass b -tagged jet. From this all-hadronic search, W' bosons were excluded for masses up to 3.4 TeV [87].

ATLAS has searched for W'_R bosons in the $t\bar{b}$ final state both for lepton+jets [89] and all-hadronic [90] decays of the top. No significant deviations from the standard model were seen in either analysis and limits were set on the $W' \rightarrow t\bar{b}$ cross section times branching ratio and W' bosons with both purely right and purely left-handed coupling and limits are set between 0.5 and 6 TeV for different values of the coupling strength.

In addition, the above studies also provided upper limits on the W' effective couplings to right- and left-handed fermions.

In Fig. 92.1 (bottom) the upper limits on W' couplings normalized to the SM W boson couplings derived by ATLAS [90] are shown. The top panel of Fig. 92.1 shows the upper limits for arbitrary combinations of left- and right-handed couplings of the W' boson to fermions set using a model independent approach by CMS [86].

92.2.2 Searches for Resonances decaying to Vector Bosons and/or Higgs Bosons

Both ATLAS and CMS have used the data collected at $\sqrt{s} = 13$ TeV to search for resonances decaying to pairs of bosons. Overall no significant excesses were seen in the full datasets that were analyzed and the results are interpreted in models with heavy vector triplets (HVT) [92], models with strong gravity and extra spatial dimensions, and model independent limits as a function of mass are set. For a full review of models including extra spatial dimensions and the interpretation of many of these results in that context please see the review of extra dimensions in this volume [61].

Utilizing data collected at $\sqrt{s} = 13$ TeV, ATLAS [93] and CMS [94], have both looked for a resonant state decaying into VV (with $V = W$ or Z), VH (with H representing the SM Higgs boson), and HH . ATLAS has searched in the $qqqq$, $\nu\nu qq$, $lvqq$, $llqq$, $lv\nu\nu$, $ll\nu\nu$, $lvll$, $llll$, $qqbb$, $\nu\nu bb$, $lvbb$, and $llbb$ final states and combined the results. While CMS analyzed the $qqqq$, $\nu\nu qq$, $lvqq$, $llqq$, $ll\nu\nu$, $\nu\nu bb$, $lvbb$, $llbb$, $bbbb$, $\tau\tau bb$, and $qq\tau\tau$ final states.

The combined limits are expressed both as limits on the cross-section as a function resonance mass as well as constraints on the coupling of the heavy boson triplet to quarks, leptons, and the Higgs boson.

$X \rightarrow WZ$:

ATLAS searched for new heavy resonances decaying into WZ in the channels $WZ \rightarrow qqqq$ [95], $lvqq$ [96], and $lvll$ [97]. In the fully leptonic channel, the invariant mass of the WZ pair is obtained by considering all possible four lepton permutations in each event. The dominant background is Standard Model continuum WZ production, ZZ production where one lepton is not identified or falls outside the detector acceptance, and top quark plus vector boson production. No resonant production is seen in data and lower limits on the mass of a HVT decaying into WZ are set at 2260 (2460) GeV assuming a coupling constant of $g_V = 1$ ($g_V = 3$). In the $WZ \rightarrow lvqq$ mode, ATLAS searches in both the cases that the quarks are observed as individual jets (resolved) and where they merge into one jet in the detector (boosted) which probe the low and high p_T regime of the Z boson. No significant excess is seen in either channel and combined lower mass limits are placed at 2900 (3000) GeV for $g_V = 1$ ($g_V = 3$) in the HVT model. In the all hadronic decay mode, ATLAS searched for two high p_T hadronically decaying vector bosons looking for a resonant structure. No excess is seen and limits are placed exclude 1200-3000 (1200-3300) GeV for $g_V = 1$ ($g_V = 3$) in the HVT model.

CMS searched for new heavy resonances in the ZV final state using the semi-leptonic decay channels excluding W masses up to 1800 GeV in HVT two models with $g_V = 1$ and 3 and in the ZZ channel excludes gravitons up to 1200 GeV. The CMS collaboration searched for $VV \rightarrow qqqq$ [98] in the large R dijet search. The W and Z boson are identified through the mass of the large R jet and substructure variables. No excess is seen and limits are set for charged HVT bosons with masses lower than 3200 (3800) GeV for $g_V = 1$ ($g_V = 3$). Cross-section limits as function of mass are reported for the charged spin-1 resonance interpretation and are placed at 44.4 fb at 1.4 TeV to 0.7 pb at 4 TeV. In the $\nu\nu qq$ final state [99], the CMS collaboration searched for a charged spin 1 resonance decaying into a VZ final state with a Z boson decaying into a pair of neutrinos and the other boson decaying into two collimated quarks reconstructed as a large R -jet. The transverse mass of the VZ candidate is reconstructed and utilized to search for evidence of resonant VZ production. No excess is seen and lower mass limits are placed on the charged resonance at 3100 (3400) GeV for $g_V = 1$ ($g_V = 3$). In the $2l2q$ final state, the CMS collaboration searched for a heavy resonance decaying into ZV [100] looking for events with one large R -jet consistent with the hadronic decay of a vector boson and a Z boson reconstructed in the charged lepton decay channel (e or μ).

Limits are set for a HVT W' with a lower mass of 2270 (2330) for $g_V = 1$ ($g_V = 3$).

$X \rightarrow WW$:

ATLAS searched for a new heavy resonance decaying into WW in the channels $WW \rightarrow qqqq$ [95], $lvqq$ [96], and $lv\nu$ [101]. In the case where both W s decay leptonically, ATLAS utilized the transverse mass of the two lepton and two neutrino final state and searched for an excess in this distribution between 200 GeV and 5 TeV. No excess is seen and a HVT is excluded for masses below 1300 GeV. Vector boson fusion is also considered and cross-section limits as a function of mass are placed ranging from 1.3 pb to 0.006 pb at 200 GeV to 3 TeV, respectively. In the $lvqq$ mode, ATLAS completed a companion analysis to the $WZ \rightarrow$ analysis discussed above and places lower mass limits of 2850 (3150) GeV for $g_V = 1$ ($g_V = 3$) in the HVT model. ATLAS also interprets the all hadronic mode analysis in the hypothesis that $WW \rightarrow qqqq$ and places limits on a HVT boson decaying into WW in the all hadronic mode between 1200 and 2200 (1200 and 2800) GeV for $g_V = 1$ ($g_V = 3$).

The CMS collaboration searched for $VV \rightarrow qqqq$ [98] in the large R dijet search. The W and Z boson are identified through the mass of the large R jet and substructure variables. No excess is seen and limits are set for charged HVT bosons with masses lower than 2700 (2800) GeV for $g_V = 1$ ($g_V = 3$). Cross-section limits as function of mass are reported for the uncharged spin-1 resonance interpretation and are placed at 41.6 fb at 1.4 TeV to 0.6 pb at 4 TeV.

$X \rightarrow VH$:

ATLAS searched for a new heavy resonance decaying into WH and ZH in the $qqbb$ (WH and ZH) [102], $lvbb$ (WH), $\nu\nu bb$ (ZH), $llbb$ (ZH) [103] modes. In the all hadronic mode, ATLAS searched for boosted VH production looking for two large R jets where the larger invariant mass large R jet is interpreted as the Higgs boson decay products while the lesser invariant mass jet is taken to be the hadronically decaying vector boson requiring b -tagging on the Higgs boson subjects. The invariant mass is reconstructed and a search is performed for resonant production of ZH . None is found and limits from 1100 to 2500 (1300 to 3800) GeV are placed for $g_V = 1$ ($g_V = 3$). ATLAS also searched for XH where the W or Z boson decays into $\nu\nu$, lv , and ll . The analysis searched for both resolved and merged (boosted) b -jets from the decay of the Higgs boson and defines the signal regions based on the number of reconstructed charged leptons (0,1,or 2). In the dilepton channel the invariant mass is explicitly reconstructed of the entire diboson system, the single lepton channel reconstructs the diboson final state constraining the lepton and missing transverse momentum utilizing the known W boson mass, while the 0 charged lepton channel reconstructs the transverse mass of the diboson system. No excess is seen in any channel and limits on the production of a HVT are placed at 2800 GeV (2930) GeV for $g_V = 1$ ($g_V = 3$).

The CMS Collaboration searched for a heavy resonance decaying into VH [104] searching for a resonances decaying into a Higgs boson and a hadronically decaying W or Z boson. The search identifies events with two large- R jets using substructure variables and requires one large- R jets is tagged with a pair of b -hadrons clustered in a single jet. The invariant mass of the VH bosons is reconstructed and evidence for resonance production is sought. No excess is seen and limits are placed. With $g_V = 1$ (3) a narrow W' resonance with $m_{W'} < 2470(3150)$ GeV and $m_{Z'} < 1150(1190)$.

The CMS collaboration searched for a heavy resonance decaying into a pair of boosted Higgs boson with $HH \rightarrow bbWW^*$ in the single and dilepton channel [105]. Events are categorized according to lepton flavor and multiplicity, along with discriminators that characterize the compatibility with having jets arising from the decay of boosted Higgs and W bosons. The reconstructed Higgs and diHiggs mass distributions are fit and used as the final discriminators. No significant deviations in the 12 sub-categories are seen and 95% confidence limits on spin-0 bosons are set from 24.5 fb at 0.8 TeV to 0.78 fb at 4.5 TeV and spin-2 bosons from 16.7 fb at 0.8 TeV to 0.67 fb at 4.5 TeV. A similar search in the

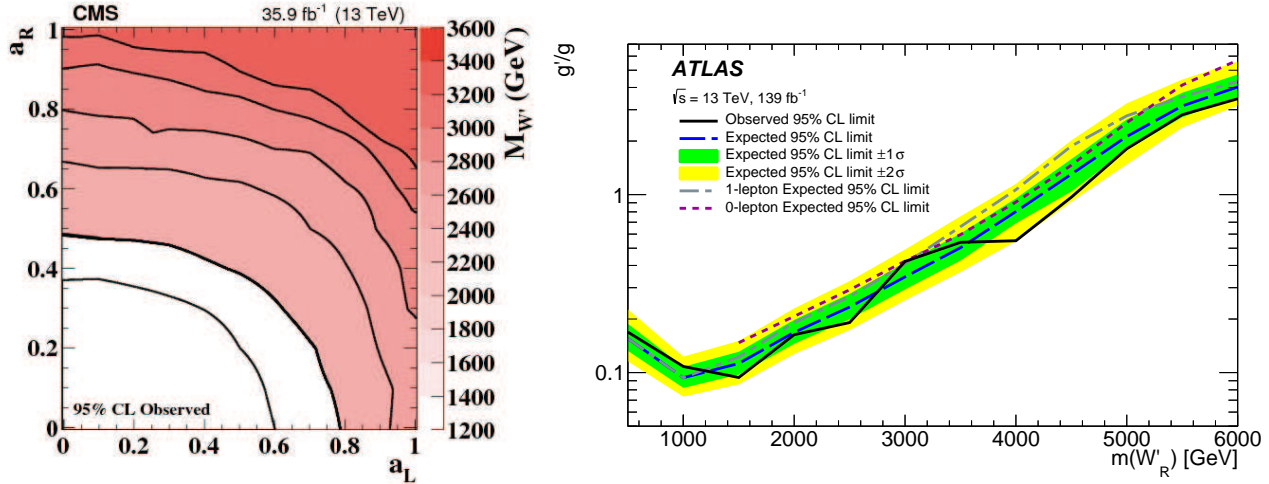


Figure 92.1: Left panel: Observed limits on the W' boson mass as function of the left-handed (a_L) and right-handed (a_R) couplings. Black lines represent contours of equal W' boson mass [86]. Right panel: Observed and expected regions, on the g'/g vs mass of the W' boson plane, that are excluded at 95% CL, for right-handed W' bosons [91] showing the exclusion of the values of a hypothetical right-handed coupling of a heavy W particle.

four b -quark final state is used to set limits range 9.74 to 0.29 fb and 4.94 to 0.19 fb in the spin-0 bosons and spin-2 gravitons (respectively) interpretation with masses of 1-3 TeV [106].

$X \rightarrow H\gamma$ or $V\gamma$:

Both CMS and ATLAS search for heavy resonances decaying into either a vector boson and a photon or a Higgs boson or a photon. These searches are motivated generically by the fact that new heavy gauge bosons are generically predicted to decay to either a Higgs boson or a vector boson and a photon by one loop decays [107]. ATLAS searched for a heavy resonances decaying into a Higgs boson and a photon and sets limits from 0.7 to 4 TeV from 11.6 fb to 0.11 fb [108]. ATLAS searched for a heavy resonance decaying into XH where $XH \rightarrow qqbb$ [109] and sets limits from 1 to 4 TeV. CMS searched for a heavy resonance decaying into a W boson and a photon [110] setting limits for narrow resonances range between 0.17 fb at 6.0 TeV and 55 fb at 0.7 TeV.

Summary of Searches with Diboson Final States:

Both ATLAS [93] and CMS [94] provide plots summarizing the various searched results and limits combining. The results are shown in the context of HVT models and models of strong gravity with extra spatial dimensions. No excess is seen in any search and limits on the 4.3 (4.5) TeV (ATLAS) and (CMS). Inclusion of decays directly to fermions increase these limits to 5.3 (5.5) TeV and 5.0 (5.2) TeV from the ATLAS and CMS combinations, respectively. Both collaborations also place varying limits on the coupling strength as a function of HVT boson mass as well.

Searches for Triboson Resonances:

The CMS collaboration presents the first search for massive triboson resonances in both the semi-leptonic [111] and fully hadronic final state [112]. Three boson final states can be produced via the decay of Kaluza-Klein (KK) states decaying via $W_{KK} \rightarrow WR$ with $R \rightarrow WW$ where R is a scalar radion. The search utilizes novel deep neural networks to perform optimal separation between signal and background and searched for evidence of resonance structure in the triboson invariant mass-spectrum. No excesses above SM backgrounds are seen and $M_{W_{KK}}$ and radion masses are excluded up to $M_{W_{KK}} = 3.4$ TeV and $M_R = 1$ TeV and up to $M_{W_{KK}} = 3.6$ TeV and $M_R = 0.35$ TeV. $M_{W_{KK}}$ below 3 TeV are excluded for $0.6 < \frac{M_R}{M_{W_{KK}}} < 0.7$ in the semi-leptonic final state and up to $M_{W_{KK}} = 3.0$ TeV and $M_R = 200$ GeV and up to $M_{W_{KK}} = 1.5$ TeV and $M_R = 1.5$ TeV in the fully hadronic final state.

92.2.3 Vector-like third generation quarks

Vector-like quarks (VLQ) have non-chiral couplings to W bosons, i.e. their left- and right-handed components couple in

the same way. They therefore have vectorial couplings to W bosons. Vector-like quarks arise in Little Higgs theories, top-coloron-models, and theories of a composite Higgs boson with partial compositeness. In the following, the notation T quark refers to a vector-like quark with charge $2/3$ and the notation B quark refers to a vector-like quark with charge $-1/3$, the same charges as the SM top and b quarks respectively. The exotic vector-like quarks $X_{5/3}$ and $Y_{-4/3}$ have charges $5/3$, and $-4/3$ respectively. Vector-like quarks couple with SM quarks with Yukawa interactions and may exist as $SU(2)$ singlets (T , and B), doublets $[(X_{5/3}, T), (T, B), (B, Y_{-4/3})]$, or triplets $[(X_{5/3}, T, B), (T, B, Y_{-4/3})]$. At the LHC, VLQs can be pair produced via the dominant gluon-gluon fusion process. VLQs can also be produced singly by their electroweak effective couplings to a weak boson and a standard model quark. The single production rate is expected to dominate over the rate of pair production at large VLQ masses. T quarks can decay to bW , tZ , or tH^0 . Weak isospin singlets are expected to decay to all three final states with (asymptotic) branching fractions of 50%, 25%, 25%, respectively. Weak isospin doublets are expected to decay exclusively to tZ and to tH^0 [113] with equal branching ratios. Analogously, B quarks can decay to tW , bZ , or bH^0 . The $Y_{-4/3}$ and $X_{5/3}$ quarks decay exclusively to bW and to tW . While these are taken as the benchmark scenarios, other representations and decays to exotic new particles are possible [114–116], and hence the final results are interpreted for many allowed branching fraction combinations.

Given the multiple decay modes of the VLQs, the final state signatures of both pair produced and the singly produced VLQs are fairly rich with leptons, jets, b -jets, and missing energy. Depending on the mass of the VLQ, the top quarks and $W/Z/H^0$ bosons may be Lorentz boosted and identified using jet substructure techniques. Thus the searches are performed using lepton+jets signatures, multi-lepton and all-hadronic decays. In addition, T or B quarks with their antiparticles can result in events with same-sign leptons, for example if the decay $T \rightarrow tH \rightarrow bWW^+W^-$ is present, followed by leptonic decays of two same-sign W bosons. In the following subsections, while we describe the searches for each of the decay modes of the VLQs, the same analysis can be re-interpreted to obtain the sensitivity to a combination with varied branching fractions to the different decay modes.

In the following sections, the results obtained for T (B) quarks assuming 100% branching ratio to Wb (Wt) are also applicable to heavy vector-like $Y_{-4/3}$ ($X_{5/3}$) with charge $4/3$ ($5/3$).

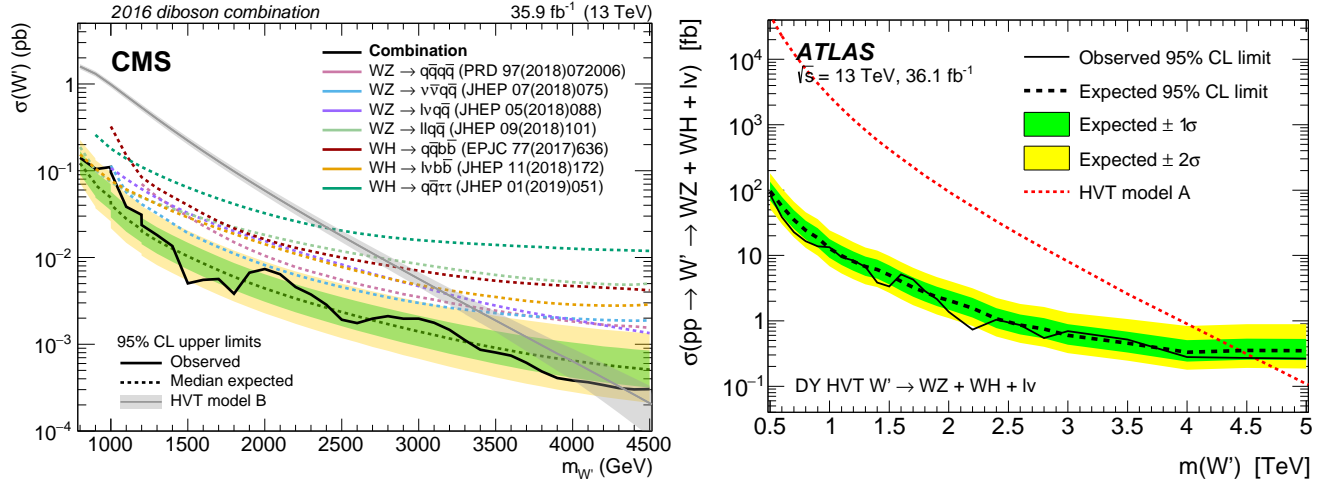


Figure 92.2: Left panel: Observed limits from W' to diboson from CMS [94]. Right panel: Observed limits from W' to diboson decays from ATLAS [93].

92.2.3.1 Searches for T quarks that decay to W , Z and H^0 bosons

$T/Y \rightarrow bW$:

CMS has searched for pair production of heavy T quarks that decay exclusively to bW [117–119]. The analysis selected events with exactly one charged lepton, assuming that the W boson from the second T quark decays hadronically. Under this hypothesis, a 2-constraint kinematic fit can be performed to reconstruct the mass of the T quark as a narrow mass peak with a mass resolution of around 7%. In Refs. [118] and [119], the two-dimensional distribution of reconstructed mass vs S_T was used to test for the signal, where S_T is the scalar sum of the missing p_T and the transverse momenta of the lepton and the leading four jets. This analysis, when combined with the search in the fully hadronic final state [120] excluded new quarks that decay 100% to bW for masses below 0.89 TeV [119]. At times the hadronically-decaying W boson is produced with a large Lorentz boost, leading to the W decay products merged into a large-radius jet. Algorithms such as jet pruning [121] were used to remove contributions from soft, wide angle radiation, from large-radius jets, leading to better discrimination between jets from multijet events and those arising from decays of the heavy particles. If the mass of the boosted jet was compatible with the W boson mass, then the W boson candidate jet and its subjets were used in the kinematic reconstruction of the T quark. No excess over standard model backgrounds was observed. Upper limits on the production cross section as a function of the mass of T quarks were measured. By comparing them with the predicted cross section for vector like quark pair production, the strong pair production of T quarks was excluded for masses below 1.30 TeV (1.28 TeV expected) [117].

Another “cut-based” search for pair produced T quarks in the all-hadronic final state targeting the Wb decay mode [122], relies on mass reconstruction of two highest p_T Wb combinations using boosted W boson candidates with $p_T > 200$ GeV and b -tagged jets. H_T is used as the signal discriminator, with selected events divided into nine categories based on the multiplicity of W and b -jets in the event. From this search T quarks with pure Wb decays are excluded for masses below 1.04 TeV (1.07 TeV expected).

An analogous search has been carried out by ATLAS [123, 124] for the pair production of heavy T quarks. It used the lepton+jets final state with an isolated electron or muon and at least four jets, including a b -jet, and required reconstruction of the T quark mass. Given that the mass range for the T quark being explored was from a 0.4 TeV to a couple of TeV, the W boson from the T quark may fall in two categories: those with a high boost leading to merged decay products, and others where the two jets from the W boson were resolved. In addition, the selection was optimized to require large angular separation between the high p_T W bosons and the b -jets.

The $T \rightarrow Wb$ candidates were constructed from both the leptonically and hadronically decaying W bosons by pairing them with the two highest p_T b -tagged jets in the event. The pairing of b -jets with W bosons which minimizes the difference between the masses of leptonically decaying T ($m_{lep}(T)$) and the hadronic T ($m_{had}(T)$) was chosen. Finally, $m_{lep}(T)$ was used as the discriminating variable in a signal region defined by high S'_T (here S'_T is defined as the scalar sum of the missing p_T , the p_T of the lepton and jets), and the opening angle between the lepton and the neutrino ($\Delta R(e, \nu)$). With the 36.1 fb^{-1} data collected during Run 2 at $\sqrt{s} = 13$ TeV, assuming 100% branching ratio to the Wb decay, the observed lower limit on the T mass was 1.35 TeV, and in the $SU(2)$ singlet scenario, the lower mass limit was obtained to be 1.17 TeV [123].

A targeted search for a T quark, produced singly in association with a light flavor quark and a b quark and decaying into bW , was carried out by CMS at $\sqrt{s}=13$ TeV and a dataset corresponding to 2.3 fb^{-1} [125]. The analysis used lepton+jets events, with at least one b -tagged jet with large transverse momentum, and a jet in the forward η region. Selected events were required to have $S'_T > 500$ GeV, where S'_T is defined as the scalar sum of the transverse momenta of the lepton, the leading central jet, and the missing transverse momentum. The invariant mass of the T candidate was used as the discriminating variable and was reconstructed using the four-vectors of the leptonically decaying W boson and the leading central jet. No excess over the standard model prediction was observed. As the VLQ width is proportional to the square of the coupling, upper limits were set on the production cross section assuming a narrow width VLQ with coupling greater than 0.5. For Y/T quarks with a coupling of 0.5 and a 100% branching fraction for the decay to bW the excluded masses were in the range from 0.85 to 1.40 TeV [125]. A similar search [126, 127] was performed by ATLAS for a singly produced T or $Y_{-4/3}$ quark decaying to Wb using a dataset corresponding to 36.1 fb^{-1} . The search was performed using lepton+jets events with a high p_T b -tagged jet, and at least one forward jet. The reconstructed mass of the $T/Y_{-4/3}$ quark, was used as the discriminating variable and showed no excess above the expectation from SM. Interference effects with the SM background are included in the study. This search led to 95% CL upper limits on the mixing angle $|\sin(\theta_L)|$ (C_L^{Wb}) in the range of 0.18–0.35 (0.25–0.49) for singlet T quark mass between 0.8–1.2 TeV. This search also provided limits as a function of the $Y_{-4/3}$ quark mass, on the coupling of the $Y_{-4/3}$ quark to bW , and the mixing parameter $|\sin\theta_R|$ (C_R^{Wb}) for a $(B, Y_{-4/3})$ doublet model [126]. For VLQ masses between 0.08–1.8 TeV, the limits on $|\sin(\theta_R)|$ (C_R^{Wb}) are in the range 0.17–0.55 (0.24–0.77), and for $Y_{-4/3}$ quark mass between 0.9–1.25 TeV, the limits on $|\sin\theta_R|$ are around 0.18–0.19 and below the constraints from electroweak precision observables.

For $Y_{-4/3}$ quark in the triplets $(T, B, Y_{-4/3})$, limits on $|\sin(\theta_L)|$ (C_L^{Wb}) are between 0.16–0.39 (0.31–0.78) for masses between 0.8 GeV–1.6 TeV [126].

$T \rightarrow tH^0$:

ATLAS has performed a search for $T\bar{T}$ production with $T \rightarrow tH^0$ [124, 128]. Given the dominant decay mode $H^0 \rightarrow b\bar{b}$, these events are characterized by a large number of jets, many of which are b -jets. Thus the event selection required one isolated electron or muon and high jet multiplicity (including b -tagged jets). The sample is categorized by the jet multiplicity (5 and ≥ 6 jets in the 1-lepton channel; 6 and ≥ 7 jets in the 0-lepton channel), b tag multiplicity (2, 3 and ≥ 4) and mass-tagged jet multiplicity (0, 1 and ≥ 2). The distributions of m_{eff} , defined as the scalar sum of the lepton and jet p_T and the missing p_T , for each category were used as the discriminant for the final signal and background separation. No excess of events was found. Weak isospin doublet T quarks were excluded below 1.16 TeV.

A search by ATLAS for pair produced VLQs with an all-hadronic final state signature yields an exclusion of pure decays $T \rightarrow tH^0$ upto a T quark mass of 2.3 TeV [129].

The CMS search for $T\bar{T}$ production, with $T \rightarrow tH^0$ decays has been performed in lepton+jets, multilepton and all-hadronic final states. The lepton+jets analysis [130] emphasizes the presence of a large number of b -tagged jets, and combines it with other kinematic variables in a Boosted Decision Tree (BDT) to enhance signal to background discrimination. The multilepton analysis [130] was optimized for the presence of b -jets and the large hadronic activity. For $\mathcal{B}(T \rightarrow tH^0) = 1$, the combined lepton+jets and multilepton analyses led to a lower limit on T quark masses of 0.71 TeV. A search for $T \rightarrow tH^0$ in all-hadronic decays [131], optimized for a high mass T quark, and based on identifying boosted top quark jets has been carried out by CMS. This search aimed to resolve subjects within the jets arising from boosted top quark decays, including b tagging of the subjects. A likelihood discriminator was defined based on the distributions of H_T and the invariant mass of the two b -jets in the events for signal and background. No excess above background expectations was observed. Assuming 100% branching ratio for $T \rightarrow tH^0$, this analysis led to a lower limit of 0.75 TeV on the mass of the T quark.

Searches for T quarks at $\sqrt{s}=13$ TeV, based on a 2.6 fb^{-1} dataset [132] have been performed by CMS using the lepton+jets final state. This search has been optimized for high mass T quarks by exploiting techniques to identify W or Higgs bosons decaying hadronically with large transverse momenta. The boosted W channel excluded T quarks decaying only to bW with masses below 0.91 TeV, and the boosted tH channel excluded T quarks decaying only to tH for masses below 0.89 TeV.

A CMS search for $T \rightarrow tH^0$ with $H^0 \rightarrow \gamma\gamma$ decays has been performed [133] in pair production of T quarks. To identify the Higgs boson produced in the decay of the heavy T quark, and the subsequent $H^0 \rightarrow \gamma\gamma$ decay, the analysis focused on identification of two photons in events with one or more high p_T lepton+jets or events with no leptons and large hadronic activity. A search for a resonance in the invariant mass distribution of the two photons in events with large hadronic activity defined by the H_T variable showed no excess above the prediction from standard model processes. The analysis resulted in exclusion of T quark masses below 0.54 TeV.

A search for electroweak single production of T quarks decaying to tH^0 using boosted topologies in fully hadronic [134] and lepton+jets [135] in the final states has been performed by CMS. The electroweak couplings of the T quarks to the SM third generation quarks are highly model dependent, and hence these couplings determine the rates of the single T quark production. In both analyses, T quark invariant mass was reconstructed using the boosted Higgs boson jet and the top quark. Higgs boson jets were identified using jet substructure techniques and subject b tagging. For the lepton+jets analysis, the top quark was reconstructed from the leptonically decaying W and the b jet, while in the all-hadronic analysis the top quark jet was tagged using substructure analysis. There was no excess of events observed above background. Exclusion limits on the product of the production cross

section and the branching fraction $(\sigma(pp \rightarrow Tqt/b) \times \mathcal{B}(T \rightarrow tH^0))$ were derived for the T quark masses in the range 0.70–1.8 TeV. From the lepton+jets analysis, for a mass of 1.0 TeV, values of $(\sigma(pp \rightarrow Tqt/b) \times \mathcal{B}(T \rightarrow tH^0))$ greater than 0.8 and 0.7 pb were excluded assuming left- and right-handed coupling of the T quark to standard model fermions, respectively [135]. For the all-hadronic analysis, upper limits between 0.31 and 0.93 pb were obtained on $(\sigma(pp \rightarrow Tqt/b) \times \mathcal{B}(T \rightarrow tH^0))$ for T quark masses in the range 1.0–1.8 TeV [134]. ATLAS performs a similar search [136] for single production of vector-like T quarks decaying into a Higgs Boson and a top quark and places limits between 1 and 1.7 TeV depending on the coupling

$T \rightarrow tZ$:

Both ATLAS and CMS search for T quarks that decay exclusively into tZ in pp collisions at $\sqrt{s} = 13$ TeV. No excesses were found in either search.

ATLAS performs a search [137] optimized for pair production of vector-like top quarks decaying into tZ where the Z boson subsequently decays into neutrino pairs, utilizing 139 fb^{-1} of data. The search selected events with one lepton, multiple jets, and significant missing transverse momentum. No significant excesses were found and lower limits on the mass of a vector like top quark were placed, excluding masses below 1.59 TeV (weak-isospin doublet) and 1.47 TeV (pure tZ mode).

Another search by ATLAS for pair produced T decaying to tZ has been carried out by reconstructing the high transverse momentum Z boson from a pair of opposite-sign same-flavor leptons, using events with two or three charged leptons [138]. The final analysis is based on three final state signatures. In the trilepton events, at least one b -tagged jet is required and H_T , formed from all hadronic jets and charged leptons, is used as the discriminating variable. In events with two leptons, at least 2 b -jets are requested and events with zero or one high p_T top-tagged jet, use H_T as the discriminator. The second dilepton analysis with two top-tagged high p_T jets focuses on hadronically decaying heavy resonances and the invariant mass of the Z boson and the highest p_T b -tagged jet is found to be a good discriminating variable. No excess was observed over the background expectations. Limits were placed at a heavy vector like top of 1.6 TeV.

ATLAS has subsequently carried out a search [139] for singly produced T quarks decaying to tZ where the Z boson decays into neutrino pairs. The search is carried out using 36.1 fb^{-1} of data in events with two different final state signatures: one with jets and significant missing p_T (0L) and the other with a single lepton, jets and missing p_T (1L). Events are divided into signal and dedicated W +jets and $t\bar{t}$ background control regions. The sensitivity to the T quark signal is extracted using distributions of missing p_T for the 1L and the distribution of T quark transverse mass constructed from missing p_T and the high p_T large-radius top-tagged jet, for 0L analysis. There is no excess found over the expected background and lower limits on the production of T singlets are obtained as a function of the left- and right-handed couplings $c_{L,W}$ and $c_{R,W}$ to top quarks and W bosons, where c_W above 0.7 is excluded for T quark mass of 1.4 TeV. The limits on c_W are also recasted into expected and observed 95% CL upper limits for the mixing angle (θ_L) of a singlet T with the top quark.

CMS searched [140] for single production of T quarks decaying into tZ with the Z boson decaying to pairs of charged leptons (electrons and muons) and the top quark decaying hadronically using 35.9 fb^{-1} of data. Limits were placed on T quarks with masses between 0.7 and 1.7 TeV excluding the product of cross section and branching fraction above values of 0.27 to 0.04 pb. Additionally, limits on the product of cross section and branching fractions for a Z' boson decaying into tZ were set between 0.13 and 0.06 pb for Z' boson masses in the range from 1.5 to 2.5 TeV.

Similar searches by ATLAS for singly produced T decaying to Zt have been performed in final state signatures with two or three charged leptons [141]. The analysis relies on tagging b -jets and high p_T large-radius jets originating from top-quarks. Additional selections are devised to reduce the contributions from pair production of T quarks. For events with dilepton analysis, the discriminating variable is the mass of the T quark formed using the invariant mass of the Z boson candidate and the highest p_T top-

tagged jet, while for the trilepton analysis, the variable S_T is used to search for an excess of data over the expected SM background. No excess above the SM expectations is observed. The two final states (dilepton and trileptons) are combined to obtain the final results. For the coupling parameter κ_T between 0.1–1.6, the 95% CL upper limits on the production cross section times branching fraction into Zt is between 0.16–0.18 (0.03–0.05) pb at T quark mass of 0.7 (2) TeV.

The search by the ATLAS experiment for VLQ pair production optimized to search for $T \rightarrow tZ$ decays [142] in a dataset with 139 fb^{-1} of luminosity has been performed in final states with either two leptons or three or more leptons. A multi-class boosted object tagger based on DNN techniques for large-radius jets is used to categorize events according to the number of high p_T boosted H^0 , Z/W , and top quark jets. The discriminant in the signal to evaluate the sensitivity depends on the number of leptons in the event. For the two lepton analysis, the discriminant is the mass of the T quark which is constructed from b and Z candidates, while for the three or more lepton analysis, H_T computed using the p_T of the jets and leptons is used as the discriminant. This analysis excludes T quark masses up to 1.27 GeV (1.46 GeV), for the singlet (doublet) configuration [142].

Combination of $T \rightarrow tZ/tH^0$:

The search performed by the ATLAS experiment for electroweak single production of T quark decaying to tH^0 and tZ uses a dataset corresponding to 139 fb^{-1} of integrated luminosity, and events with a single lepton with multiple jets and b -jets in the final state [143]. The single production channel for VLQs probes κ , the universal coupling constant, which also controls the production cross section and the resonance width of the VLQ. The analysis uses techniques to tag boosted jets, and categorizes events by numbers of jets and b -jets. The event discriminant is the “effective mass” (m_{eff}) observable, defined as the scalar sum of the p_T of all central jets, p_T of leptons and the missing p_T in the event. No significant excess is observed. Limits on the mass of T quark and universal coupling strength (κ) are obtained. For singlet T quarks, values of κ above 0.5 are excluded for all masses below 1.8 TeV. For T quark mass of 1.6 TeV, κ above 0.41 is excluded [143].

A CMS search published in 2020 concentrates on the electroweak production of the T quark with $T \rightarrow tH^0$, and $T \rightarrow tZ$ decays, where subsequently both H^0 and Z Bosons decay hadronically, leading to fully hadronic final states [144]. The search focuses on evidence of T quarks produced in association with a b quark ($qg \rightarrow T\bar{b}q'$) or a top quark ($qg \rightarrow T\bar{t}q$). The production cross sections are model dependent, as the electroweak production depends on the strength of the T quark coupling, TbW (TtZ), for the charged-current (neutral-current) process, at the production vertex. The searches are split into two domains depending on the mass of the T quark and consider a wide range of widths of the T quark from a few percent to about 30% of the T quark mass. The event selection relies primarily on the large number of jets and on efficient identification of jets from b -quarks, in addition to double- b jet decays of the H^0 and Z bosons. The final sensitivity is derived by the search for a resonant peak in the tH^0/Z invariant mass spectrum. For low mass T quark searches, three independent regions based on the b -tagged jet requirements are examined. For T quark masses above 1 TeV, which result in highly Lorentz-boosted top quarks and H^0 or Z boson, large-area jets are used to form the T quark. This search reports upper limits at 95% confidence level on $\sigma B(T \rightarrow tH)$ and $\sigma B(T \rightarrow tZ)$ between 2 pb and 20 fb for T masses between 0.6 to 2.6 TeV in the Tbq and Ttq production channels. The analysis also reports combined results for $T \rightarrow tH$ and $T \rightarrow tZ$ associated production with a bottom quark and provides constraints on T quarks in the T singlet model for masses below 1.00 TeV. For an expected fractional width of 30%, the expected sensitivity extends to 1.28 TeV, comparable to the most stringent results.

Combination of $T \rightarrow bW/tZ/tH^0$:

Most of the analyses described above target an individual decay mode of the T quark, with 100% branching ratio to either bW , tZ or tH^0 and are optimized accordingly. However, they have

varied sensitivity to all three decay modes and the results can be interpreted as a function of branching ratios to each of the three decay modes, assuming the total adds up to unity ($B(tH) + B(tZ) + B(Wb) = 1$).

Combinations of analyses have been performed by both ATLAS and CMS. The limits set by ATLAS searches in $W(\ell\nu)b + X$, $H(bb)b + X$, $Z(\nu\bar{\nu})$, $Z(\ell\ell)t/b + X$, dileptons with same-sign charge, trileptons, all-hadronic final states have been combined and the results obtained for various sets of branching fractions for T quark decays to bW , tH^0 and tZ are shown in Fig. 92.3 (left). In the combined analysis, ATLAS sets lower T quarks mass limit of 1.31 TeV for all possible values of the branching fractions to the three decay modes [123, 145, 146]. In Fig. 92.3, exclusion is shown in the plane of $B(T \rightarrow Ht)$ versus $B(T \rightarrow Wb)$, for different values of the T quark mass. The default branching ratio values for the weak-isospin singlet and doublet cases are also shown in Fig. 92.3 as yellow circle and star symbols respectively. Assuming a weak isospin (T, B) doublet and $|V_{Tb}| \ll |V_{tB}|$, T quark mass below 1.37 TeV is excluded.

A CMS analysis for pair production of T combines three channels with lepton final states: single lepton, two leptons with the same sign of the electric charge (SS), or at least three leptons (trilepton) [147]. For various combinations of branching fractions for T quark decays to bW , tH^0 and tZ , the combined results exclude T quarks with masses below 1.14–1.3 TeV and are shown in Figure 92.3 (right). Single lepton events are classified into 16 signal categories and 6 background control regions based on multiplicity of b -tagged, high p_T H^0 and W -tagged jets. The discriminating variables are H_T for H^0 -tagged events and the minimum invariant mass constructed from the lepton and the b jet, $\min[M_{lb}]$, for zero H^0 -tagged events. For the same-sign dilepton and trilepton analyses, the non-prompt backgrounds due to misidentified jets and leptons are derived from data control regions. In the trilepton analysis the S_T variable is used as the signal discriminator binned in four categories based on the lepton flavor combinations (eee , $ee\mu$, $e\mu\mu$, $\mu\mu\mu$). The single lepton analysis is most sensitive for $tHbW$ and $WbWb$ decay modes, within the SS dilepton analysis $tHtH$ and $tHtZ$ have the best efficiency and for trileptons the $tZtZ$ and $tHtZ$ decays modes have the highest efficiency. CMS excludes singlet (doublet) T quark masses below 1.2 (1.28) TeV. Masses below 800 GeV were excluded in previous searches. For T quark masses in the range 0.8–1.8 TeV, cross sections smaller than 30.4–9.4 fb (21.2–6.1 fb) are excluded for the singlet (doublet) scenario.

Another inclusive search for pair produced T in the all-hadronic final state [122] has been performed by CMS using the boosted event shape tagger (BEST NN) neural network technique to classify jets in six categories W , Z , H^0 , t , b , and light. This search does not focus on a given VLQ mode, but on various combinations of the boson and quark jets in the final state. Anti- k_T jets with a distance parameter of 0.8 are used. The BEST NN algorithm simultaneously classifies jets according to heavy object type. For each of the six particle hypotheses, it boosts each jet constituent into corresponding frame along the jet momentum direction, and calculates event shape and angular variables in the boosted frame, with the expectation that when boosting to the correct rest frame, jet constituents will be isotropic and show the expected N-prong structure of the decaying object in its rest frame. A neural network is trained using the event shape and angular variables in the boosted frame to classify jets according to one of those six possibilities (W , Z , H , t , b , or light). The analysis bins the events into 126 categories depending on the number of W , Z , H , t , b , or light jets in the final state with a maximum of four such objects. For each category H_T^{AK8} , the scalar sum of p_T of all AK8 jets, is used as the signal discriminator. A scan over a combination of various branching fractions is also performed. This search excludes T quark masses in the range 0.74–1.37 TeV for the tH decay mode in the NN analysis.

An inclusive search for VLQs has been carried out by CMS targeted at heavy T quarks decaying to any combination of bW , tZ , or tH^0 as described in [130]. Selected events have at least one isolated charged lepton. Events were categorized according to number and flavor of the leptons, the number of jets, and the

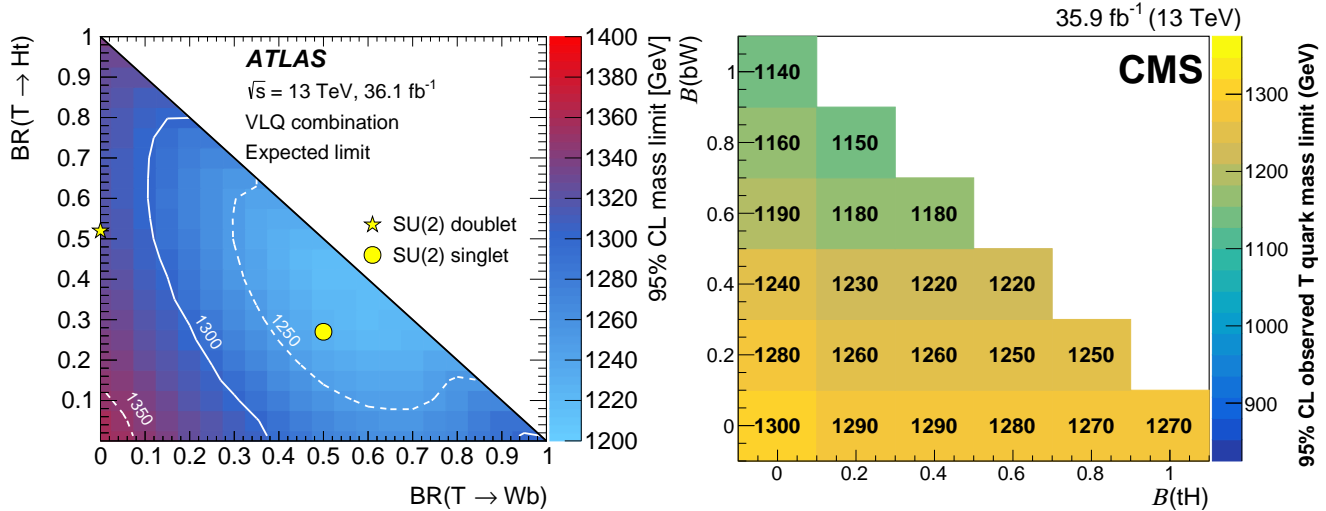


Figure 92.3: Left panel: observed limits on the mass of the T quark in the plane of $\mathcal{B}(T \rightarrow tH^0)$ versus $\mathcal{B}(T \rightarrow bW)$ from a combination [145] of all ATLAS searches for TT production. The markers indicate the default branching ratios for the SU(2) singlet and doublet scenarios. Right panel: the observed lower limits on the T quark mass (in GeV), from CMS searches after combining all lepton channels [147], for various branching fraction scenarios. $\mathcal{B}(T \rightarrow Wb) + \mathcal{B}(T \rightarrow tZ) + \mathcal{B}(T \rightarrow tH^0) = 1$ is assumed.

presence of hadronic vector boson and top quark decays that are merged into a single jet. The use of jet substructure to identify hadronic decays significantly increases the acceptance for high T quark masses. No excess above standard model backgrounds was observed. Limits on the pair production cross section of the new quarks are set, combining all event categories, for all combinations of branching fractions into the three final states. For T quarks that exclusively decay to $bW/tZ/tH^0$, masses below 0.70/0.78/0.71 TeV are excluded.

92.2.3.2 Searches for B quarks that decay to W , Z and H^0 bosons

ATLAS and CMS have performed searches for pair production of heavy B quarks which subsequently decay to Wt , bZ or bH^0 . The searches have been carried out in final states with single leptons, dileptons (with same charge or opposite charge), multileptons, as well as in fully hadronic final states.

$B \rightarrow bH^0$:

A search for B pair-produced events has been performed by the CMS experiment [123] using 137 fb^{-1} of data where the B decays into a b/\bar{b} quark and either a H^0 or a Z boson. This search concentrates on final states with fully hadronic signatures, and utilizes different jet multiplicity categories to account for two resolved jets or merged single jets from H^0 or Z boson to $b\bar{b}$ decays, depending on the p_T of the H^0 or Z bosons. Nine final state categories are used, depending on the number of observed jets and the reconstructed event mode. No significant excess over expected background is observed. For the case $\mathcal{B}(B \rightarrow bH) = 100\%$ (50%), VLQs with masses below 1.57 (1.45) TeV are ruled out.

Using 36.1 fb^{-1} of data, ATLAS has performed a search for pair produced VLQs with all-hadronic final state signature [148]. While this analysis provides exclusion limits for all third generation VLQs, it provides the strongest results for the $B \rightarrow bH^0$ decay mode and excludes decays with $\mathcal{B}(B \rightarrow [H']) = \infty$ scenario for B masses upto 1.01 TeV. The limits are also cast in a two-dimensional plane of branching ratio values of $B \rightarrow bH^0$ vs. $B \rightarrow Wb$. This analysis required the presence of high p_T jets and multiple b tags. It used a multi-class DNN to classify jets arising from W , Z , H^0 bosons and top-quarks. In addition, the matrix element method was used to compute the likelihood for the event to arise from a particular VLQ final state and to construct the final discriminator. To increase the sensitivity of the analysis, processes with the same number of top quarks, W/Z bosons, and H^0 Higgs bosons are combined into a single hypothesis.

ATLAS has performed a search for single production of a vector-like B quark decaying to a b -quark and a H^0 boson, with $H^0 \rightarrow b\bar{b}$

decay, using a dataset corresponding to an integrated luminosity of 139 fb^{-1} [149]. The all hadronic final state signature relies on identification of at least 3 b -jets, with an additional soft forward jet from the spectator quark. Large area jets are used to identify boosted H^0 decays. This analysis results in excluding the single production of a VLQ (B , Y) doublet with relative width larger than 5% between masses of 1.0 TeV and 2.0 TeV [150]. The CMS experiment has searched for a single vector-like quark decaying into tH or tZ in the all hadronic final state with 138 fb^{-1} of data in the all hadronic channel constraining both the boson invariant mass and the tH or tZ invariant mass and searching for a resonance. No significant excess is found and cross-section limits are placed between 600 GeV and 1200 GeV between 600 and 68 fb [151].

$B \rightarrow Wt$:

A search for $B \rightarrow tW$ in B pair produced events has been performed by ATLAS [123] using lepton+jets events with one hadronically decaying W and one leptonically decaying W utilizing 36.1 fb^{-1} of data at $\sqrt{s} = 13 \text{ TeV}$. The search was optimized for T production decaying into Wb . Since the analysis was optimized for $T \rightarrow Wb$ rather than Wt decays the analysis does not reconstruct the full B mass. As discussed earlier, the hadronically and leptonically decaying heavy quarks were required to have similar reconstructed masses (within 300 GeV). The interpretation of the $T \rightarrow Wb$ in the context of $B \rightarrow tW$ production led to the exclusion of heavy B like VLQs for masses less than 1.25 TeV and 1.08 TeV, assuming a 100% branching fraction to tW or SU(2) singlet B scenario, respectively.

A similar search by CMS [152], using 19.8 fb^{-1} of $\sqrt{s} = 8 \text{ TeV}$ data, selected events with one lepton and four or more jets, with at least one b -tagged jet, significant missing p_T , and further categorized them based on the number of jets tagged as arising from the decay of boosted W , Z or H^0 bosons. The S_T distributions of the events in different categories showed no excess of events above the expected background and yielded a lower limit on the B quark mass of 0.73 TeV for $BR(B \rightarrow Wt) = 1$.

CMS [132] also searched for pair production of both TT and BB with collisions from 2.5 fb^{-1} of $\sqrt{s} = 13 \text{ TeV}$ data. The analysis searched for events with one high p_T lepton, multiple jets, and highly boosted W or Higgs bosons decaying hadronically. The analysis focused on pair production and selects events with either a boosted W or Higgs candidate and then proceeds to search for anomalous production in excess of standard model production. Seeing no significant excesses CMS then proceeded to set limits in many different interpretations. The strongest was from the $B \rightarrow Wt$ interpretation leading to excluding heavy vector-like B quarks with mass less than 0.73 TeV.

The all-hadronic inclusive analysis [122] performed by CMS using the BEST NN technique to classify $W/Z/H^0/t/b$ /light jets also gives exclusion limits on B quark production for various combinations of branching fractions for decays to tW , bZ , bH^0 . By considering categories based on various combinations of the boson and quark jets in the final state it excludes B quarks with masses up to 1230 GeV, for B decays to tW with a 100% branching fraction.

Electroweak production of single heavy $B+b$ production has been studied by CMS in the decay to tW with the lepton+jets final state [153]. Single lepton events with hadronic jets, including a forward jet, and missing p_T are selected and divided into 10 different categories based on lepton flavor (e/μ), top-tagged, W -tagged, and 0/1/2 b -tagged jets. The B quark mass m_{reco} is fully reconstructed from lepton, jets, and missing p_T , where the neutrino four-momentum is computed using the missing p_T and the W mass constraint. For events within the top-tagged category, the high p_T top-tagged hadronic jet and the leptonically decaying W boson are used to compute m_{reco} . The m_{reco} distribution are used as the signal discriminator. In the absence of an excess over the expected SM background, the exclusion limits on the production cross section for B quark masses between 0.7-2 TeV varies between 0.3 to 0.03 pb. In addition, B quarks with left-handed couplings and a relative width of 10, 20, and 30% are excluded for masses below 1.49, 1.59, and 1.66 TeV respectively.

$B \rightarrow bZ$:

As mentioned above, a search for B pair produced events, with final states with fully hadronic signature, using 137 fb^{-1} of data, has been performed by the CMS experiment [123]. In this search, the B decays into a b/\bar{b} quark and either a H^0 or a Z boson. For the case $\mathcal{B}(B \rightarrow bZ) = 100\%(50\%)$, VLQs with masses below 1.39 (1.45) TeV are ruled out by this analysis.

A search by CMS [154] for the pair-production of a heavy B quark and its antiparticle has been performed, where one of the heavy B quark decays to bZ . Events with a Z boson decaying to e^+e^- or $\mu^+\mu^-$ and at least one b jet are selected. The signal from $B \rightarrow bZ$ decays is expected to appear as a local enhancement in the bZ mass distribution. No such enhancement was found and B quarks that decay 100% into bZ are excluded below 0.70 TeV. This analysis also set upper limits on the branching fraction for $B \rightarrow bZ$ decays of 30-100% in the B quark mass range 0.45-0.70 TeV. A complementary search has been carried out by ATLAS for new heavy quarks decaying into a Z boson and a b -quark [155]. Selected dilepton events contain a high transverse momentum Z boson that decays leptonically, together with two b -jets. If the dilepton events have an extra lepton in addition to those from the Z boson, then only one b -jet is required. No significant excess of events above the standard model expectation was observed, and mass limits were set depending on the assumed branching ratios, as shown in Fig. 92.4. In a weak-isospin singlet scenario, a B quark with mass lower than 0.65 TeV was excluded, while for a particular weak-isospin doublet scenario, a B quark with mass lower than 0.73 TeV was ruled out.

The search by ATLAS for $B \rightarrow bZ$ decays [142] in final states with either two leptons or three or more leptons using a multi-class boosted object tagger to categorize events according to the number of high p_T boosted H^0 , Z/W , and top quark jets excludes B quark masses up to 1.20 GeV (1.32 GeV), for the singlet (doublet) configuration [142].

In addition to pair production, ATLAS has also searched for the electroweak production of single B quarks, which is accompanied by a b -jet and a light jet [155]. The dilepton selection for double B production was modified for the single B production study by requiring the presence of an additional energetic jet in the forward region. An upper limit of 200 fb was obtained for the process $\sigma(pp \rightarrow B\bar{b}q) \times \mathcal{B}(B \rightarrow Zb)$ with a heavy B quark mass at 0.70 TeV. This search indicated that the electroweak mixing parameter X_{Bb} below 0.5 is neither expected nor observed to be excluded for any values of B quark mass.

Combination of $B \rightarrow tW/bZ/bH^0$:

ATLAS has combined the various analyses targeted for specific decay modes to obtain the most sensitive limit on the

pair production of B quarks [123, 124, 145]. Various searches ($W(\ell\nu)t + X, Z(\ell\ell)t/b + X$, same sign charge dilepton events, trilepton events, and all-hadronic) are combined to obtain lower limit on the mass of the B quark [in the plane of $BR(B \rightarrow Wt)$ vs $BR(B \rightarrow bH^0)$]. The searches were optimized for 100% branching fractions and hence are most sensitive at large $BR(B \rightarrow Wt)$, and also at large $BR(B \rightarrow bH^0)$. For all possible values of branching ratios in the three decay modes tW , bZ , or bH^0 , the lower limits on the B quark mass was found to be 1.03 TeV and shown in Fig. 92.4 (left) as a function of the B quark branching ratios.

CMS combined three channels with lepton final states: single lepton, two leptons with the same sign of the electric charge (SS), or at least three leptons (trilepton) [147]. For various combinations of branching fractions for B quark decays to tW , bH^0 and bZ , the combined results exclude b quarks with masses below 0.91–1.24 TeV and are shown in Figure 92.4 (right); the details are provided earlier in subsection 92.2.3.1. The single lepton analysis is most sensitive for $tHbW$ and $WbWb$ decay modes, within the SS dilepton analysis $tHtH$ and $tHtZ$ have the best efficiency and for trileptons the $tZtZ$ and $tHtZ$ decays modes have the highest efficiency. CMS excludes singlet (doublet) B quark masses below 1.17 (0.94) TeV. Masses below 800 GeV were excluded in previous searches. For B quark masses in the range 0.8–1.8 TeV, cross sections smaller than 40.6–9.4 fb (101–49.0 fb) are excluded for the singlet (doublet) scenario.

92.2.3.3 Searches for top-partner quark $X_{5/3}$

Searches for a heavy top vector-like quark $X_{5/3}$, with exotic charge $\pm 5/3$, such as that proposed in Refs. [156, 157], have been performed by both ATLAS and CMS [123, 158].

The analyses assumed pair-production or single production of $X_{5/3}$ with $X_{5/3}$ decaying with 100% branching fraction to tW . Searches for $X_{5/3}$ have been performed using two final state signatures: same-sign leptons and lepton+jets.

The analysis based on searching for same-sign leptons, from the two W bosons from one of the $X_{5/3}$, has smaller backgrounds compared to the lepton+jets signature. Requiring same-sign leptons eliminates most of the standard model background processes, leaving those with smaller cross sections: $t\bar{t}W$, $t\bar{t}Z$, WWW , and same-sign WW . In addition, backgrounds from instrumental effects due to charge misidentification were considered. Assuming pair production of $X_{5/3}$, the analysis by CMS using H_T as the discriminating variable restrict the $X_{5/3}$ mass to be higher than 1.16 (1.10) TeV for a right (left) handed chirality particle [158–160]. The limits obtained by ATLAS, by classifying the signal region by number of b -jets, H_T , and missing p_T in the event, led to a lower mass limit on $X_{5/3}$ of 1.19 TeV [161, 162].

Searches for $X_{5/3}$ using leptons+jets final state signatures are based on either full or partial reconstruction of the T mass from the lepton, jets (including b -jets) and missing p_T . The CMS search [158, 163] also utilized jet substructure techniques to identify boosted $X_{5/3}$ topologies. The discriminating variable used was the mass constructed from the lepton and b -tagged jet, $M_{(\ell,b)}$, which corresponds to the visible mass of the leptonically decaying top quark. To optimize the search sensitivity, the events were further separated into categories based on lepton flavor (e, μ), the number of b -tagged jets, the number of W -tagged jets, and the number of t -tagged jets. In the absence of a signal, the CMS analysis excluded $X_{5/3}$ quark masses with right-handed (left-handed) couplings below 1.32 (1.30) TeV [163]. Combining the lepton+jets with the same-sign leptons analyses leads to a slight improvement and excludes $X_{5/3}$ quark masses with right-handed (left-handed) couplings below 1.33 (1.30) TeV.

The ATLAS lepton+jets search for $X_{5/3}$ utilized events with high p_T W bosons and b -jets. The search described earlier for T pair production, with $T \rightarrow Wb$ decays, can be reinterpreted as a search for $X \rightarrow tW$. This analysis excluded $X_{5/3}$ with masses below 1.25 TeV [123].

The single $X_{5/3}$ production cross section depends on the coupling constant λ of the tWX vertex. ATLAS has performed an analysis of same-sign dileptons which includes both the single and pair production. This analysis led to a lower limit on the mass of the $X_{5/3}$ of 0.75 TeV for both values of $\lambda = 0.5$ and 1.0 [164].

Single heavy $X_{5/3}+t$ production has been studied by CMS in

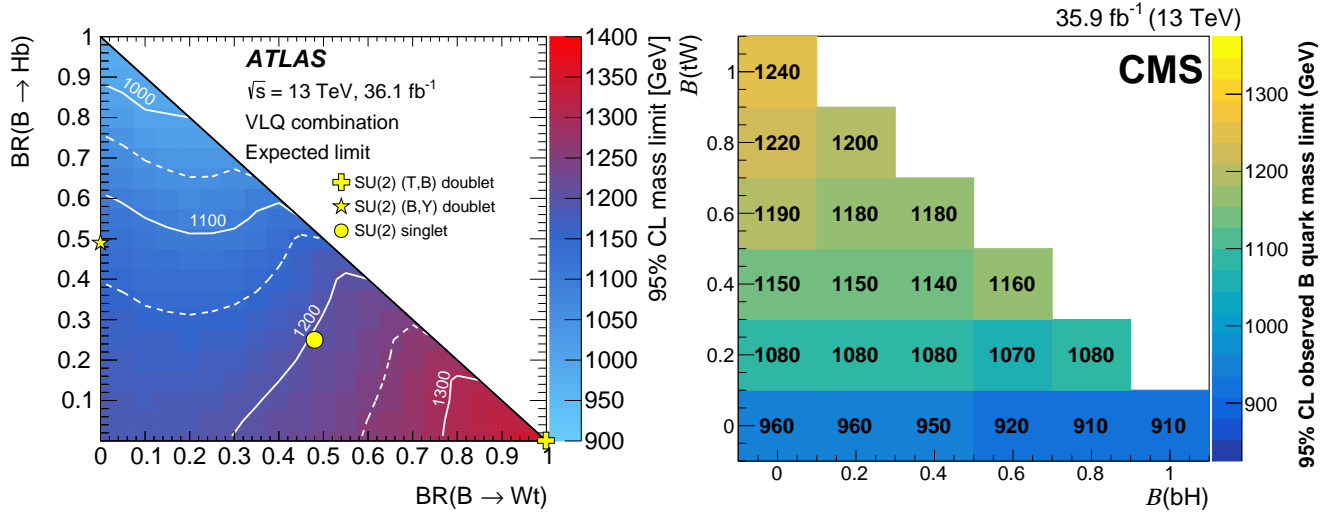


Figure 92.4: Observed limits on the mass of the B quark in the plane of $BR(B \rightarrow bH^0)$ versus $BR(B \rightarrow tW)$ from ATLAS searches [145] on the left panel, and CMS searches [147] on the right panel, for BB production. $B(B \rightarrow \mathcal{H}) + B(B \rightarrow \mathcal{Z}) + B(B \rightarrow \mathcal{W}) = 1$ is assumed. The yellow markers indicate the branching ratios for the SU(2) singlet and doublet scenarios.

the decay to tW with the lepton+jets final state [153]. The description of the analysis is provided earlier in the discussion of $B \rightarrow WtX$ decays, where the reconstructed mass of $X_{5/3}$, m_{reco} distribution is used as the signal discriminator. In the absence of an excess over the expected SM background, the exclusion limits on the production cross section for $X_{5/3}$ quark masses between 0.7–2 TeV varies between 0.3 to 0.03 pb, depending on the width of $X_{5/3}$ between 1–10%. In addition, $X_{5/3}$ quarks with left-handed couplings and a relative width of 10, 20, and 30% are excluded for masses below 0.92, 1.3, and 1.45 TeV respectively.

92.2.4 Heavy resonances decaying to VLQ

CMS has performed search for VLQ production in the decay of massive resonances such as Z' and W' bosons.

$Z' \rightarrow tT$: Specifically searches are presented by CMS in Refs. [165] and [166] for massive spin-1 Z' resonances decaying to a top quark and a heavy VLQ top quark partner T . The results of this search for a heavy spin-1 resonance are interpreted in the context of two different models. In the G^* model which predicts ten VLQs ($T, B, \bar{T}, \bar{B}, T_{5/3}, T_{2/3}, T', B', B_{-1/3}, B_{-4/3}$) with the mass relationship $M(T_{5/3}) = M(T_{2/3}) = M(T)\cos(\phi_L)$. For the benchmark scenario [167], $\cos(\phi_L) = 0.84$ and the branching fractions $T \rightarrow tH^0, tZ, Wb$ are 0.25, 0.25 and 0.5 respectively. The ρ^0 model predicts a multiplet of four new VLQs $T, B, X_{2/3}, X_{5/3}$, and in the benchmark scenario [168], the branching fractions $T \rightarrow tH^0, tZ, Wb$ are 0.5, 0.5 and 0 respectively.

Two of the three decays of the $Z' \rightarrow tT$ with $T \rightarrow tH^0, tZ, Wb$ are characterized by the presence of two top quark decays and a boson (H^0/Z). A search [166] by CMS, optimized for $T \rightarrow tH/Zt$ decays was carried out in the lepton+jets final state using a dataset corresponding to an integrated luminosity of 35.9 fb^{-1} . Jet substructure techniques are used to identify (or tag) the high p_T large-radius jets originating from H^0, Z bosons and merged top quarks. The mass of the Z' boson is used as the signal discriminator and constructed using H^0 or Z -tagged dijet, the hadronic and leptonic top quark four vectors. For the leptonic top quark reconstruction ($t \rightarrow b\nu_e$), the neutrino four vector is obtained from the event missing p_T using the W boson mass constraint. While the high p_T hadronic top quark jets from decays of massive Z' bosons are mostly merged and identified by top tagging techniques, those from T decays maybe resolved. The reconstructed Z' candidate events are classified into six different categories requiring the presence of either a H^0 -tagged jet with 2 b -tagged subjets or one b -tagged subjet or a Z -tagged boson, each with either zero or one top-tagged jet. This search does not observe any significant deviation in data over the expectation from standard model backgrounds. Within the context of the G^* model, for a T mass of 1.2 (1.5) TeV, this search excludes G^* [167] resonances

with masses between 1.5–2.3 (2.0–2.4) TeV.

The search in the all-hadronic final state is based on a 2.6 fb^{-1} dataset [165], and optimized for $T \rightarrow Wb$ decays. Jet substructure techniques are deployed for tagging jets from high p_T W boson and top quarks. Events are categorized into two groups based on the presence of b -tagged subjets in the top-tagged jet. The multi-tjet background estimation is challenging and determined using side-bands defined by inverting the b -tagging requirement. Upper limits on the cross section for $Z' \rightarrow tT$ are obtained in the range of 0.13–10 pb.

$W' \rightarrow Tb/Bt$: W' bosons are predicted to decay to VLQ third generation partners T, B quarks within composite Higgs and warped extra dimensional models [169]. In the benchmark scenarios of this framework, W' decays to Tb or Bt are equally distributed and the subsequent VLQ decays $T \rightarrow tH$ and $B \rightarrow bH^0$ each are assumed to have a branching fraction of 0.5. The search for $W' \rightarrow Tb/bH^0 \rightarrow tbH^0$ is performed using a sample of 35.9 fb^{-1} by CMS [170] in the final state with all-hadronic decays of both the Higgs boson ($H^0 \rightarrow b\bar{b}$) and the top quark. Both the H^0 boson and the top quark are expected to be boosted in the decay of a heavy W' , and hence jet substructure techniques, including subjet b -tagging and double b -tagging are deployed to identify the H^0 -tagged and the top-tagged jets. The three particle mass m_{tbH^0} , is used as the signal discriminant to observe the W' resonance. There is no excess observed in data above the expected SM background. This search excludes W' production cross section above 0.01–0.43 pb for masses between 1.5–4.0 TeV.

92.2.5 Colorons and Colored Scalars

These particles are associated with top-condensate and top-seesaw models, which involve an enlarged color gauge group. The new particles decay to dijets, $t\bar{t}$, and $b\bar{b}$.

Direct searches for colorons, color-octet scalars and other heavy objects decaying to $q\bar{q}, qg, q\bar{q}$, or gg have been performed using LHC data from pp collisions at $\sqrt{s} = 7, 8$ and 13 TeV. Based on the analysis of dijet events from a data sample corresponding to a luminosity of 19.6 fb^{-1} , at $\sqrt{s} = 8$ TeV, the CMS experiment excluded pair production of colorons with mass between 1.20–3.60 and 3.90–4.08 TeV [171]. Analyses of inclusive 8- and 10-jet final states with low missing transverse momentum by CMS [172], set limits in several benchmark models. Colorons (axigluons) with masses between 0.6 and 0.75 (up to 1.15) TeV were excluded, and gluinos in R -parity violating supersymmetric scenarios were ruled out from 0.6 up to 1.1 TeV.

A search for pair-produced colorons based on an integrated luminosity of 5.0 fb^{-1} at $\sqrt{s} = 7$ TeV by CMS excluded colorons with masses between 0.25 TeV and 0.74 TeV, assuming colorons decay 100% into $q\bar{q}$ [174]. This analysis was based on events with

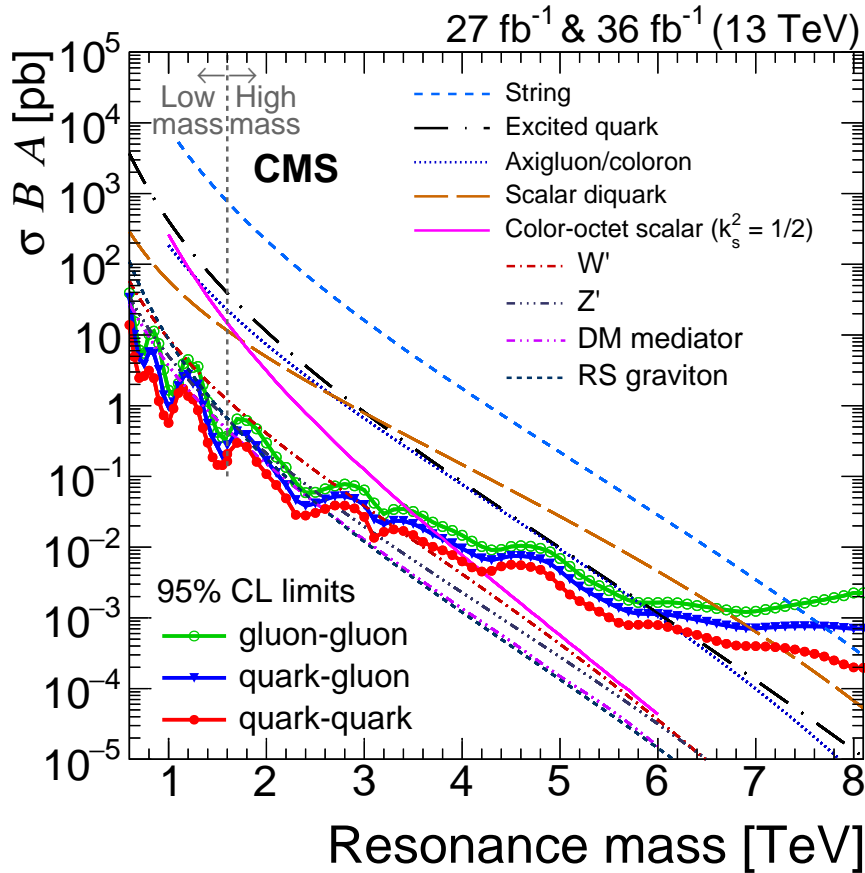


Figure 92.5: Observed 95% C.L. limits on $\sigma \times B \times A$ for string resonances, excited quarks, axigluons, colorons, E6 diquarks, s8 resonances, W' and Z' bosons, and Randall–Sundrum Gravitons g_{KK} from [173].

at least four jets and two dijet combinations with similar dijet mass. Color-octet scalars (s8) with masses between 1.20–2.79 TeV were excluded by CMS [171], and below 2.7 TeV by ATLAS [175].

These studies have now been extended to take advantage of the increased center-of-mass energy during Run 2 of the LHC. Using 35.9 fb^{-1} of data collected at $\sqrt{s} = 13 \text{ TeV}$, searches for narrow resonances have been performed by CMS. An analysis of the dijet invariant mass spectrum formed using wide jets [173, 176, 177], separated by $\Delta\eta_{jj} \leq 1.3$, led to limits on new particles decaying to parton pairs (qq , qg , gg). Specific exclusions on the masses of colorons and color-octet scalars were obtained and are shown in Fig. 92.5. Exclusions have been obtained for axigluons and colorons below 6.1 TeV, and color-octet scalars below 3.4 TeV.

Additional searches for dijet resonances have been performed by both ATLAS [178–180] and CMS [181, 182], though they have not been interpreted in the context of coloron production.

92.3 Conclusions

As the above analyses have demonstrated, there is already substantial sensitivity to possible new particles predicted to accompany the H^0 in dynamical frameworks of electroweak symmetry breaking. No significant hints of any deviations from the standard model have been observed, and limits typically at the scale of a few hundred GeV to a few TeV are set.

Given the need to better understand the H^0 and to determine in detail how it behaves, such analyses continue to be a major theme of Run 3 of the LHC, and we look forward to increased sensitivity as a result of the higher luminosity at the increased center of mass energy of collisions.

References

- [1] G. Aad *et al.* (ATLAS), Phys. Lett. **B716**, 1 (2012), [arXiv:1207.7214].
- [2] S. Chatrchyan *et al.* (CMS), Phys. Lett. **B716**, 30 (2012), [arXiv:1207.7235].

- [3] S. Weinberg, Physica **A96**, 1-2, 327 (1979).
- [4] A. Manohar and H. Georgi, Nucl. Phys. **B234**, 189 (1984).
- [5] H. Georgi, Nucl. Phys. **B266**, 274 (1986).
- [6] R. S. Chivukula, in “Flavor physics for the millennium. Proceedings, Theoretical Advanced Study Institute in elementary particle physics, TASI 2000, Boulder, USA, June 4-30, 2000,” 731–772 (2000), [hep-ph/0011264].
- [7] R. S. Chivukula, M. J. Dugan and M. Golden, Phys. Rev. **D47**, 2930 (1993), [hep-ph/9206222].
- [8] S. Weinberg, Phys. Rev. **D13**, 974 (1976), [Addendum: Phys. Rev.D19,1277(1979)].
- [9] L. Susskind, Phys. Rev. **D20**, 2619 (1979).
- [10] K. Lane (2002), [hep-ph/0202255].
- [11] C. T. Hill and E. H. Simmons, Phys. Rept. **381**, 235 (2003), [Erratum: Phys. Rept.390,553(2004)], [hep-ph/0203079].
- [12] R. Shrock, in “The origin of mass and strong coupling gauge theories. Proceedings, 5th International Workshop, SCGT’06, Nagoya, Japan November 21-24, 2006,” 227–241 (2007), [hep-ph/0703050].
- [13] E. Eichten *et al.*, Rev. Mod. Phys. **56**, 579 (1984), [Addendum: Rev. Mod. Phys.58,1065(1986)].
- [14] E. Eichten *et al.*, Phys. Rev. **D34**, 1547 (1986).
- [15] R. S. Chivukula and V. Koulovassilopoulos, Phys. Lett. **B309**, 371 (1993), [hep-ph/9304293].
- [16] R. Foadi, M. T. Frandsen and F. Sannino, Phys. Rev. **D87**, 9, 095001 (2013), [arXiv:1211.1083].
- [17] B. Holdom, Phys. Lett. **150B**, 301 (1985).
- [18] K. Yamawaki, M. Bando, and K.-i. Matumoto, Phys. Rev. Lett. **56**, 1335 (1986).

- [19] T. W. Appelquist, D. Karabali and L. C. R. Wijewardhana, Phys. Rev. Lett. **57**, 957 (1986).
- [20] T. Appelquist and L. C. R. Wijewardhana, Phys. Rev. **D35**, 774 (1987).
- [21] T. Appelquist and L. C. R. Wijewardhana, Phys. Rev. **D36**, 568 (1987).
- [22] E. Eichten, K. Lane and A. Martin (2012), [arXiv:1210.5462].
- [23] D. B. Kaplan and H. Georgi, Phys. Lett. **136B**, 183 (1984).
- [24] D. B. Kaplan, H. Georgi and S. Dimopoulos, Phys. Lett. **136B**, 187 (1984).
- [25] G. Ferretti and D. Karateev, JHEP **03**, 077 (2014), [arXiv:1312.5330].
- [26] M. E. Peskin, Nucl. Phys. **B175**, 197 (1980).
- [27] J. Preskill, Nucl. Phys. **B177**, 21 (1981).
- [28] See “Status of Higgs Boson Physics” review in this volume.
- [29] R. Barbieri and A. Strumia, in “4th Rencontres du Vietnam: Physics at Extreme Energies (Particle Physics and Astrophysics) Hanoi, Vietnam, July 19-25, 2000,” (2000), [hep-ph/0007265].
- [30] N. Arkani-Hamed, A. G. Cohen and H. Georgi, Phys. Lett. **B513**, 232 (2001), [hep-ph/0105239].
- [31] N. Arkani-Hamed *et al.*, JHEP **08**, 020 (2002), [hep-ph/0202089].
- [32] N. Arkani-Hamed *et al.*, JHEP **07**, 034 (2002), [hep-ph/0206021].
- [33] M. Schmaltz and D. Tucker-Smith, Ann. Rev. Nucl. Part. Sci. **55**, 229 (2005), [hep-ph/0502182].
- [34] K. Agashe *et al.*, Phys. Lett. **B641**, 62 (2006), [hep-ph/0605341].
- [35] P. Sikivie *et al.*, Nucl. Phys. **B173**, 189 (1980).
- [36] B. Bellazzini, C. Csáki and J. Serra, Eur. Phys. J. **C74**, 5, 2766 (2014), [arXiv:1401.2457].
- [37] R. Essig *et al.*, JHEP **09**, 085 (2017), [arXiv:1707.03399].
- [38] Z. Chacko, H.-S. Goh and R. Harnik, Phys. Rev. Lett. **96**, 231802 (2006), [hep-ph/0506256].
- [39] R. S. Chivukula, A. G. Cohen and K. D. Lane, Nucl. Phys. **B343**, 554 (1990).
- [40] V. A. Miransky, M. Tanabashi and K. Yamawaki, Mod. Phys. Lett. **A4**, 1043 (1989).
- [41] W. A. Bardeen, C. T. Hill and M. Lindner, Phys. Rev. **D41**, 1647 (1990).
- [42] C. T. Hill, Phys. Lett. **B266**, 419 (1991).
- [43] B. A. Dobrescu and C. T. Hill, Phys. Rev. Lett. **81**, 2634 (1998), [hep-ph/9712319].
- [44] R. S. Chivukula *et al.*, Phys. Rev. **D59**, 075003 (1999), [hep-ph/9809470].
- [45] S. Dimopoulos and L. Susskind, Nucl. Phys. **B155**, 237 (1979), [2,930(1979)].
- [46] E. Eichten and K. D. Lane, Phys. Lett. **90B**, 125 (1980).
- [47] D. B. Kaplan, Nucl. Phys. **B365**, 259 (1991).
- [48] T. Appelquist, M. Piai and R. Shrock, Phys. Rev. **D69**, 015002 (2004), [hep-ph/0308061].
- [49] R.S. Chivukula, B.A. Dobrescu, and E.H. Simmons, Phys. Lett. **B401**, 74 (1997).
- [50] Y. Grossman and M. Neubert, Phys. Lett. **B474**, 361 (2000), [hep-ph/9912408].
- [51] S. J. Huber and Q. Shafi, Phys. Lett. **B498**, 256 (2001), [hep-ph/0010195].
- [52] T. Gherghetta and A. Pomarol, Nucl. Phys. **B586**, 141 (2000), [hep-ph/0003129].
- [53] K. Agashe, R. Contino and A. Pomarol, Nucl. Phys. **B719**, 165 (2005), [hep-ph/0412089].
- [54] G. F. Giudice *et al.*, JHEP **06**, 045 (2007), [hep-ph/0703164].
- [55] R. S. Chivukula and H. Georgi, Phys. Lett. **B188**, 99 (1987).
- [56] G. D’Ambrosio *et al.*, Nucl. Phys. **B645**, 155 (2002), [hep-ph/0207036].
- [57] K. Agashe *et al.* (2005), [hep-ph/0509117].
- [58] T. Appelquist and R. Shrock, Phys. Lett. **B548**, 204 (2002), [hep-ph/0204141].
- [59] K. Sakai, Nucl. Phys. **B867**, 429 (2013), [arXiv:1207.4057].
- [60] J. M. Maldacena, Int. J. Theor. Phys. **38**, 1113 (1999), [Adv. Theor. Math. Phys.2,231(1998)], [hep-th/9711200].
- [61] For a review, see C. Csaki, J. Hubisz, and P. Meade, hep-ph/0510275 (2005), and “Extra Dimensions” review in this volume.
- [62] C. Pica, PoS **LATTICE2016**, 015 (2016), [arXiv:1701.07782].
- [63] B. Svetitsky, EPJ Web Conf. **175**, 01017 (2018), [arXiv:1708.04840].
- [64] O. Witzel, PoS **LATTICE2018**, 006 (2019), [arXiv:1901.08216].
- [65] V. Drach, PoS **LATTICE2019**, 242 (2020), [arXiv:2005.01002].
- [66] T. Appelquist *et al.*, Phys. Rev. **D93**, 11, 114514 (2016), [arXiv:1601.04027].
- [67] PDG review on “ Z' -Boson Searches” in this volume.
- [68] PDG review on “ W' -Boson Searches” in this volume.
- [69] M. Aaboud *et al.* (ATLAS), Phys. Lett. **B**, 68 (2019), [arXiv:1903.06248].
- [70] CMS Collaboration, Technical Report CMS-PAS-EXO-19-019, CERN, Geneva (2019), URL <http://cds.cern.ch/record/2684757>.
- [71] G. Aad *et al.* (ATLAS), Phys. Rev. **D90**, 5, 052005 (2014), [arXiv:1405.4123].
- [72] M. Aaboud *et al.* (ATLAS), JHEP **01**, 055 (2018), [arXiv:1709.07242].
- [73] CMS Collaboration, JHEP **0217**, 48 (2017).
- [74] ATLAS Collaboration, ATLAS-CONF-2016-014 (2016).
- [75] CMS Collaboration, JHEP **0717**, 001 (2016).
- [76] M. Aaboud *et al.* (ATLAS), Phys. Rev. D. **99**, 092004 (2019), [arXiv:1902.10077].
- [77] A. M. Sirunyan *et al.* (CMS), JHEP **04**, 031 (2019), [arXiv:1810.05905].
- [78] ATLAS Collaboration, ATLAS-CONF-2019-007 (2019).
- [79] CMS Collaboration, CMS-PAS-EXO-19-012 (2019).
- [80] M. Aaboud *et al.* (ATLAS), Accepted by Phys. Rev. [arXiv:1906.05609].
- [81] A. Tumasyan *et al.* (CMS), JHEP **07**, 067 (2022), [arXiv:2202.06075].
- [82] V. Khachatryan *et al.* (CMS), Phys. Lett. **B755**, 196 (2016), [arXiv:1508.04308].
- [83] S. Chatrchyan *et al.* (CMS), JHEP **05**, 108 (2014), [arXiv:1402.2176].
- [84] V. Khachatryan *et al.* (CMS), JHEP **02**, 122 (2016), [arXiv:1509.06051].
- [85] A. M. Sirunyan *et al.* (CMS), JHEP **08**, 029 (2017), [arXiv:1706.04260].
- [86] A. M. Sirunyan *et al.* (CMS), Phys. Lett. **B777**, 39 (2018), [arXiv:1708.08539].
- [87] A. M. Sirunyan *et al.* (CMS), Phys. Lett. B **820**, 136535 (2021), [arXiv:2104.04831].

- [88] CMS Collaboration, Technical Report CMS-PAS-JME-15-002, CERN, Geneva (2016), URL <http://cds.cern.ch/record/2126325>.
- [89] G. Aad *et al.* (ATLAS), Phys. Lett. **B788**, 347 (2019), [arXiv:1807.10473].
- [90] G. Aad *et al.* (ATLAS) (2023), [arXiv:2308.08521].
- [91] G. Aad *et al.* (ATLAS), Phys. Lett. **B743**, 235 (2015), [arXiv:1410.4103].
- [92] D. Pappadopulo *et al.*, JHEP **09**, 060 (2014), [arXiv:1402.4431].
- [93] M. Aaboud *et al.* (ATLAS), Phys. Rev. **D98**, 5, 052008 (2018), [arXiv:1601.04027].
- [94] A. M. Sirunyan *et al.* (CMS), Phys. Lett. **B798**, 134952 (2019), [arXiv:1906.00057].
- [95] M. Aaboud *et al.* (ATLAS), Phys. Lett. **B**, 91 (2017), [arXiv:1708.04445].
- [96] M. Aaboud *et al.* (ATLAS), JHEP **03**, 042 (2018), [arXiv:1710.07235].
- [97] M. Aaboud *et al.* (ATLAS), Phys. Lett. **B**, 68 (2018), [arXiv:1806.10532].
- [98] A. M. Sirunyan *et al.* (CMS), Phys. Rev. **D97**, 072006, [arXiv:1708.05379].
- [99] A. M. Sirunyan *et al.* (CMS), JHEP **07**, 075, [arXiv:1802.09407].
- [100] A. M. Sirunyan *et al.* (CMS), JHEP **09**, 101, [arXiv:1803.10093].
- [101] M. Aaboud *et al.* (ATLAS), Eur. Phys. J. **C**, 78 (2017), [arXiv:1710.01123].
- [102] M. Aaboud *et al.* (ATLAS), Phys. Lett. **B**, 774 (2017), [arXiv:1707.06858].
- [103] M. Aaboud *et al.* (ATLAS), JHEP **B**, 174 (2018), [arXiv:1712.06518].
- [104] A. M. Sirunyan *et al.* (CMS), Eur. Phys. J. **C**, 636, [arXiv:1707.01303].
- [105] CMS Collaboration (CMS), Technical Report CMS-PAS-B2G-20-007 (2021).
- [106] CMS Collaboration (CMS), Technical Report CMS-PAS-B2G-20-004 (2021).
- [107] Eur. Phys. J. **C** **74**, 704 (2017).
- [108] A. Collaboration, PRL **125**, 251802 (2020).
- [109] A. Collaboration, Physics Letters B **779**, 24 (2018).
- [110] A. Tumasyan *et al.* (CMS), Phys. Lett. **B** **826**, 136888 (2022), [arXiv:2106.10509].
- [111] CMS Collaboration (CMS), Technical Report CMS-PAS-B2G-20-001 (2021).
- [112] CMS Collaboration (CMS), Technical Report CMS-PAS-B2G-20-002 (2021).
- [113] F. del Aguila *et al.*, Nucl. Phys. **B334**, 1 (1990).
- [114] J. Serra, Journal of High Energy Physics **2015**, 9 (2015), ISSN 1029-8479, URL [http://dx.doi.org/10.1007/JHEP09\(2015\)176](http://dx.doi.org/10.1007/JHEP09(2015)176).
- [115] A. Anandkrishnan *et al.*, Physical Review D **93**, 7 (2016), ISSN 2470-0029, URL <http://dx.doi.org/10.1103/PhysRevD.93.075009>.
- [116] M. Chala, Physical Review D **96**, 1 (2017), ISSN 2470-0029, URL <http://dx.doi.org/10.1103/PhysRevD.96.015028>.
- [117] A. M. Sirunyan *et al.* (CMS), Phys. Lett. **B779**, 82 (2018), [arXiv:1710.01539].
- [118] CMS Collaboration, Technical Report CMS-PAS-B2G-12-017 (2014).
- [119] V. Khachatryan *et al.* (CMS), Phys. Rev. **D93**, 1, 012003 (2016), [arXiv:1509.04177].
- [120] CMS Collaboration, Technical Report CMS-PAS-B2G-12-013 (2012).
- [121] S. D. Ellis, C. K. Vermilion and J. R. Walsh, Phys. Rev. **D80**, 051501 (2009), [arXiv:0903.5081].
- [122] A. M. Sirunyan *et al.* (CMS), Phys. Rev. **D** **100**, 7, 072001 (2019), [arXiv:1906.11903].
- [123] M. Aaboud *et al.* (ATLAS), JHEP **10**, 141 (2017), [arXiv:1707.03347].
- [124] G. Aad *et al.* (ATLAS), JHEP **08**, 105 (2015), [arXiv:1505.04306].
- [125] A. M. Sirunyan *et al.* (CMS), Phys. Lett. **B772**, 634 (2017), [arXiv:1701.08328].
- [126] M. Aaboud *et al.* (ATLAS), JHEP **05**, 164 (2019), [arXiv:1812.07343].
- [127] G. Aad *et al.* (ATLAS), Eur. Phys. J. **C76**, 8, 442 (2016), [arXiv:1602.05606].
- [128] ATLAS Collaboration (ATLAS), Technical Report ATLAS-CONF-2016-104 (2016).
- [129] J. H. Foo (ATLAS), PoS **LHCP2022**, 321 (2023).
- [130] S. Chatrchyan *et al.* (CMS), Phys. Lett. **B729**, 149 (2014), [arXiv:1311.7667].
- [131] V. Khachatryan *et al.* (CMS), JHEP **06**, 080 (2015), [arXiv:1503.01952].
- [132] A. M. Sirunyan *et al.* (CMS), JHEP **11**, 085 (2017), [arXiv:1706.03408].
- [133] CMS Collaboration, cds.cern.ch/record/1709129 (2014).
- [134] A. M. Sirunyan *et al.* (CMS), JHEP **04**, 136 (2017), [arXiv:1612.05336].
- [135] V. Khachatryan *et al.* (CMS), Phys. Lett. **B771**, 80 (2017), [arXiv:1612.00999].
- [136] G. Aad *et al.* (ATLAS), JHEP **08**, 153 (2023), [arXiv:2305.03401].
- [137] G. Aad *et al.* (ATLAS), Eur. Phys. J. **C** **83**, 8, 719 (2023), [arXiv:2212.05263].
- [138] G. Aad *et al.* (ATLAS), Phys. Lett. **B** **843**, 138019 (2023), [arXiv:2210.15413].
- [139] M. Aaboud *et al.* (ATLAS), JHEP **05**, 041 (2019), [arXiv:1812.09743].
- [140] A. M. Sirunyan *et al.* (CMS), Phys. Lett. **B781**, 574 (2018), [arXiv:1708.01062].
- [141] M. Aaboud *et al.* (ATLAS), Phys. Rev. **D98**, 11, 112010 (2018), [arXiv:1806.10555].
- [142] ATLAS Collaboration (ATLAS), Technical report, CERN, Geneva (2021), URL <https://cds.cern.ch/record/2773300>.
- [143] ATLAS Collaboration (ATLAS), Technical report, CERN, Geneva (2021), URL <https://cds.cern.ch/record/2779174>.
- [144] A. M. Sirunyan *et al.* (CMS), JHEP **01**, 036 (2020), [arXiv:1909.04721].
- [145] M. Aaboud *et al.* (ATLAS), Phys. Rev. Lett. **121**, 21, 211801 (2018), [arXiv:1808.02343].
- [146] M. Aaboud *et al.* (ATLAS), JHEP **08**, 052 (2017), [arXiv:1705.10751].
- [147] A. M. Sirunyan *et al.* (CMS), JHEP **08**, 177 (2018), [arXiv:1805.04758].
- [148] M. Aaboud *et al.* (ATLAS), Phys. Rev. **D98**, 9, 092005 (2018), [arXiv:1808.01771].
- [149] ATLAS Collaboration (ATLAS), Technical report, CERN, Geneva (2021), URL <https://cds.cern.ch/record/2760012>.
- [150] G. Aad *et al.* (ATLAS) (2023), [arXiv:2308.02595].
- [151] (2023).
- [152] CMS Collaboration, Technical Report CMS-PAS-B2G-12-019 (2012).

- [153] A. M. Sirunyan *et al.* (CMS), Eur. Phys. J. **C79**, 90 (2019), [arXiv:1809.08597].
- [154] V. Khachatryan *et al.* (CMS), Phys. Rev. **D93**, 11, 112009 (2016), [arXiv:1507.07129].
- [155] G. Aad *et al.* (ATLAS), JHEP **11**, 104 (2014), [arXiv:1409.5500].
- [156] R. Contino and G. Servant, JHEP **06**, 026 (2008), [arXiv:0801.1679].
- [157] J. Mrazek and A. Wulzer, Phys. Rev. **D81**, 075006 (2010), [arXiv:0909.3977].
- [158] A. M. Sirunyan *et al.* (CMS), JHEP **08**, 073 (2017), [arXiv:1705.10967].
- [159] CMS Collaboration, Technical Report CMS-PAS-B2G-16-019 (2017).
- [160] S. Chatrchyan *et al.* (CMS), Phys. Rev. Lett. **112**, 17, 171801 (2014), [arXiv:1312.2391].
- [161] M. Aaboud *et al.* (ATLAS), JHEP **12**, 039 (2018), [arXiv:1807.11883].
- [162] G. Aad *et al.* (ATLAS), Phys. Rev. **D91**, 11, 112011 (2015), [arXiv:1503.05425].
- [163] A. M. Sirunyan *et al.* (CMS), JHEP **03**, 082 (2019), [arXiv:1810.03188].
- [164] G. Aad *et al.* (ATLAS), JHEP **10**, 150 (2015), [arXiv:1504.04605].
- [165] A. M. Sirunyan *et al.* (CMS), JHEP **09**, 053 (2017), [arXiv:1703.06352].
- [166] A. M. Sirunyan *et al.* (CMS), Eur. Phys. J. **C79**, 3, 208 (2019), [arXiv:1812.06489].
- [167] C. Bini, R. Contino and N. Vignaroli, JHEP **01**, 157 (2012), [arXiv:1110.6058].
- [168] D. Greco and D. Liu, JHEP **12**, 126 (2014), [arXiv:1410.2883].
- [169] N. Vignaroli, Phys. Rev. **D89**, 9, 095027 (2014), [arXiv:1404.5558].
- [170] A. M. Sirunyan *et al.* (CMS), JHEP **03**, 127 (2019), [arXiv:1811.07010].
- [171] V. Khachatryan *et al.* (CMS), Phys. Rev. **D91**, 5, 052009 (2015), [arXiv:1501.04198].
- [172] V. Khachatryan *et al.* (CMS), Phys. Lett. **B770**, 257 (2017), [arXiv:1608.01224].
- [173] A. M. Sirunyan *et al.* (CMS), JHEP **08**, 130 (2018), [arXiv:1806.00843].
- [174] S. Chatrchyan *et al.* (CMS), Phys. Rev. Lett. **110**, 14, 141802 (2013), [arXiv:1302.0531].
- [175] G. Aad *et al.* (ATLAS), Phys. Rev. **D91**, 5, 052007 (2015), [arXiv:1407.1376].
- [176] A. M. Sirunyan *et al.* (CMS), Phys. Lett. **B769**, 520 (2017), [Erratum: Phys. Lett. **B772**, 882(2017)], [arXiv:1611.03568].
- [177] CMS Collaboration, Technical Report CMS-PAS-EXO-15-001 (2015).
- [178] G. Aad *et al.* (ATLAS), JHEP **06**, 151 (2020), [arXiv:2002.11325].
- [179] G. Aad *et al.* (ATLAS), Phys. Rev. Lett. **125**, 13, 131801 (2020), [arXiv:2005.02983].
- [180] M. Aaboud *et al.* (ATLAS), Phys. Rev. D **96**, 5, 052004 (2017), [arXiv:1703.09127].
- [181] A. M. Sirunyan *et al.* (CMS), Phys. Lett. B **805**, 135448 (2020), [arXiv:1911.03761].
- [182] A. M. Sirunyan *et al.* (CMS), JHEP **05**, 033 (2020), [arXiv:1911.03947].

93. Grand Unified Theories

Revised August 2023 by A. Hebecker (Heidelberg U.), J. Hisano (Nagoya U.; KMI, Nagoya U.) and N. Nagata (UTokyo).

93.1 The standard model

The Standard Model (SM) may be defined as the renormalizable field theory with gauge group $G_{SM} = SU(3)_C \times SU(2)_L \times U(1)_Y$, with 3 generations of fermions in the representation

$$(\mathbf{3}, \mathbf{2})_{1/3} + (\bar{\mathbf{3}}, \mathbf{1})_{-4/3} + (\bar{\mathbf{3}}, \mathbf{1})_{2/3} + (\mathbf{1}, \mathbf{2})_{-1} + (\mathbf{1}, \mathbf{1})_2, \quad (93.1)$$

and a scalar Higgs doublet H transforming as $(\mathbf{1}, \mathbf{2})_1$. Here and below we use boldface numbers to specify the dimension of representations of non-Abelian groups (in this case fundamental and antifundamental) and lower indices for $U(1)$ charges. The fields of Eq. (93.1) should also be familiar as $[Q, u^c, d^c, L, e^c]$, with $Q = (u, d)$ and $L = (\nu, e)$ being the quark and lepton $SU(2)$ -doublets and u^c, d^c, e^c charge conjugate $SU(2)$ -singlets.¹ Especially after the discovery of the Higgs, this model is remarkably complete and consistent with almost all experimental data.

A notable exception are neutrino masses, which are known to be non-zero but are absent in the SM even after the Higgs acquires its vacuum expectation value (VEV). The minimalist attitude is to allow for the dimension-five operator $(HL)^2$ [1], which induces (Majorana) neutrino masses. In the seesaw mechanism [2–4] this operator is generated by integrating out heavy singlet fermions (right-handed (r.h.) neutrinos). Alternatively, neutrinos can have Dirac masses if light singlet neutrinos are added to the SM spectrum.

Conceptual problems of the SM include the absence of a Dark Matter candidate, of a mechanism for generating the baryon asymmetry of the Universe, and of any reason for the observed smallness of the θ parameter of QCD (θ_{QCD}). In addition, the apparently rather complex group-theoretic data of Eq. (93.1) remains unexplained. Together with the abundance of seemingly arbitrary coupling constants, this disfavors the SM as a candidate fundamental theory, even before quantum gravity problems arise at energies near the Planck mass M_P .

To be precise, there are 19 SM parameters which have to be fitted to data: Three gauge couplings² g_3, g_2 and g_1 , 13 parameters associated with the Yukawa couplings (9 charged fermion masses, three mixing angles and one CP phase in the CKM matrix.), the Higgs mass and quartic coupling, and θ_{QCD} . In addition, Majorana neutrinos introduce 3 more masses and 6 mixing angles and phases. As we will see, the paradigm of grand unification addresses mainly the group theoretic data of Eq. (93.1) and the values of the three gauge couplings. In many concrete realizations, it then impacts also the other mentioned issues of the SM, such as the family structure and fermion mass hierarchy.

More specifically, after precision measurements of the Weinberg angle θ_W in the LEP experiments, supersymmetric GUTs (SUSY GUTs) have become the leading candidates in the search for ‘Physics beyond the SM’. Supersymmetry (SUSY) is a symmetry between bosons and fermions which requires the addition of superpartners to the SM spectrum. If SUSY is motivated as a solution to the gauge hierarchy problem (i.e. to the naturalness or fine-tuning problem of the electroweak scale) [5], superpartners have to be present near the weak scale. Assuming a minimal Higgs sector, SUSY GUTs [6] then lead to the prediction of θ_W , in good agreement with subsequent observations [7]. However, the non-discovery of new particles at the LHC puts into question the presence of new physics at the TeV scale in general and in particular of low-scale supersymmetry. Still, SUSY may be present just outside the presently explored energy domain.

The measured Higgs mass (125 GeV) is in principle consistent with this picture, assuming superpartners in the region of roughly 10 TeV. Such heavy superpartners then induce radiative corrections raising the Higgs mass above the Z boson mass m_Z [8, 9]. However, from the vantage point of the hierarchy problem, heavy

superpartners are problematic: They also contribute to SUSY-breaking Higgs mass parameters and thereby to the Higgs potential, tending to raise the Z mass. As a result, the incarnation of SUSY in terms of the minimal supersymmetric SM (MSSM) is becoming questionable. Turning the logic around, one may say that compared to expectations based on the MSSM with superpartner masses below about 1 TeV, the measured Higgs mass value of 125 GeV is somewhat too high [10]. Independently, the LHC has disfavored light colored superpartners (which does not imply that *all* superpartners are heavy). These facts represent new hints for future work on SUSY GUTs or on GUTs without TeV-scale supersymmetry.

93.2 Basic group theory and charge quantization

93.2.1 $SU(4)_C \times SU(2)_L \times SU(2)_R$

Historically, the first attempt at unification was the Pati-Salam model with gauge group $G_{PS} = SU(4)_C \times SU(2)_L \times SU(2)_R$ [11]. It unifies SM fermions in the sense that one generation (plus an extra SM singlet) now comes from the $(\mathbf{4}, \mathbf{2}, \mathbf{1}) + (\bar{\mathbf{4}}, \mathbf{1}, \mathbf{2})$ of G_{PS} . This is easy to verify from the breaking pattern $SU(4)_C \rightarrow SU(3)_C \times U(1)_{B-L}$ together with the identification of SM hypercharge as a linear combination between $B-L$ (baryon minus lepton number) and the T_3 generator of $SU(2)_R$. This model explains charge quantization, that is, why all electric charges are integer multiples of some smallest charge in the SM. Concretely, the $\mathbf{4}$ and $\bar{\mathbf{4}}$ of $SU(4)_C$ identify lepton number as the 4th colour and the tracelessness of the diagonal generator implies that quark charges are expressed in terms of $1/N_c$ fractions of lepton charges. However, G_{PS} is not simple (containing three simple factors), and thus it does not predict gauge coupling unification.

93.2.2 $SU(5)$

Since G_{SM} has rank four (two for $SU(3)_C$ and one for $SU(2)_L$ and $U(1)_Y$, respectively), the rank-four group $SU(5)$ is the minimal choice for unification in a simple group [12]. The three SM gauge coupling constants derive from a universal coupling α_G at the GUT scale M_G . Explicitly embedding G_{SM} in $SU(5)$ is straightforward, with $SU(3)_C$ and $SU(2)_L$ corresponding e.g. to the upper-left 3×3 and lower-right 2×2 blocks, respectively, in traceless 5×5 matrices for $SU(5)$ generators of the fundamental representation. The $U(1)_Y$ corresponds to matrices generated by $\text{diag}(-2/3, -2/3, -2/3, 1, 1)$ and hence commutes with $SU(3)_C \times SU(2)_L \subset SU(5)$. It is then easy to derive how one SM generation precisely comes from the $\mathbf{10} + \bar{\mathbf{5}}$ of $SU(5)$ (where $\mathbf{10}$ is the antisymmetric rank-2 tensor):

$$\mathbf{10} : \begin{pmatrix} 0 & u_b^c & -u_g^c & u_r & d_r \\ -u_b^c & 0 & u_r^c & u_g & d_g \\ u_g^c & -u_r^c & 0 & u_b & d_b \\ -u_r & -u_g & -u_b & 0 & e^c \\ -d_r & -d_g & -d_b & -e^c & 0 \end{pmatrix} \quad \text{and} \quad \bar{\mathbf{5}} : \begin{pmatrix} d_r^c \\ d_g^c \\ d_b^c \\ e \\ -\nu_e \end{pmatrix}. \quad (93.2)$$

In addition to charge quantization this structure explains why the l.h. quark and lepton states fall in $SU(2)_L$ doublets while the r.h. states are singlets.

Since $SU(5)$ has 24 generators, $SU(5)$ GUTs have 12 new gauge bosons known as X bosons (or X/Y bosons) in addition to the SM. X bosons form an $SU(3)_C$ -triplet and $SU(2)_L$ -doublet. Their interaction connects quarks and leptons such that baryon and lepton numbers are not conserved and nucleon decay is predicted. Furthermore, $U(1)_Y$ hypercharge is automatically quantized since it is embedded in $SU(5)$.

In order to break the electroweak symmetry at the weak scale and give mass to quarks and leptons, Higgs doublets are needed. In the minimal $SU(5)$ model, they can sit in either a $\mathbf{5}_H$ or $\bar{\mathbf{5}}_H$. The three additional states are referred to as color-triplet Higgs scalars. Their couplings also violate baryon and lepton numbers, inducing nucleon decay. In order not to violently disagree with the non-observation of nucleon decay, the triplet mass must be greater than $\sim 10^{11}$ GeV [13]. Moreover, in SUSY GUTs [6], in order to cancel anomalies as well as give mass to both up and down quarks, both Higgs multiplets $\mathbf{5}_H$ and $\bar{\mathbf{5}}_H$ are required. As we shall discuss later, nucleon decay now constrains the Higgs triplets to have

¹ In our convention the electric charge is $Q = T_3 + Y/2$ and all our spinor fields are left-handed (l.h.).

² Equivalently, the $SU(2)_L$ and $U(1)_Y$ couplings are denoted as $g = g_2$ and $g' = \sqrt{3/5} g_1$. One also uses $\alpha_s = \alpha_3 = (g_3^2/4\pi)$, $\alpha_{EM} = (e^2/4\pi)$ with $e = g \sin \theta_W$ and $\sin^2 \theta_W = (g')^2/(g^2 + (g')^2)$.

mass significantly greater than M_G in the minimal SUSY $SU(5)$ GUT since integrating out the Higgs triplets generates dimension-five baryon-number-violating operators [14]. The mass splitting between doublet and triplet in the $\mathbf{5}_H$ (and $\bar{\mathbf{5}}_H$) comes from their interaction with the $SU(5)$ breaking sector.

93.2.3 $SO(10)$

While $SU(5)$ allows for the minimal GUT models, unification is not complete: Two independent representations, $\mathbf{10}$ and $\bar{\mathbf{5}}$, are required for one SM generation. A further representation, an $SU(5)$ singlet, has to be added to serve as r.h. neutrino in the seesaw mechanism. In this case, the r.h. neutrino masses are not necessarily related to the GUT scale. By contrast, a single $\mathbf{16}$ -dimensional spinor representation of $SO(10)$ accommodates a full SM generation together with an extra singlet, potentially providing a r.h. neutrino [15]. This is most easily understood from the breaking pattern $SO(10) \rightarrow SU(5) \times U(1)_X$ and the associated branching rule³ $\mathbf{16} = \mathbf{10}_{-1} + \bar{\mathbf{5}}_3 + \mathbf{1}_{-4}$. Here the indices refer to charges under the $U(1)_X$ subgroup, which is orthogonal to $SU(5)$ and reflects the fact that $SO(10)$ has rank five. From the above, it is easy to see that $U(1)_X$ charges can be given as $2Y - 5(B - L)$. Intriguingly, all representations of $SO(10)$ are anomaly free in four dimensions (4d). Thus, the absence of anomalies in an $SU(5)$ -GUT or a SM generation can be viewed as deriving from this feature.

We now describe in more detail how one family of quarks and leptons appears in the $\mathbf{16}$. To understand this, recall that the Γ -matrices of the 10d Clifford algebra give rise to five independent, anticommuting ‘creation-annihilation’ operators $\Gamma^{a\pm} = (\Gamma^{2a-1} \pm i\Gamma^{2a})/2$ with $a = 1, \dots, 5$. These correspond to five fermionic harmonic oscillators or ‘spin’ $1/2$ systems. The 32-dimensional tensor product of those is reducible since the 10d rotation generators $M_{mn} = -i[\Gamma^m, \Gamma^n]/4$ ($m, n = 1, \dots, 10$) always flip an even number of ‘spins’. This gives rise to the $\mathbf{16}$ as displayed in Table 93.1. Next, one also recalls that the natural embedding of $SU(5)$ in $SO(10)$ relies on ‘pairing up’ the 10 real dimensions to produce 5 complex dimensions, $\mathbb{R}^{10} \equiv \mathbb{C}^5$, similarly to the pairing up of Γ^m s used above. This makes it clear how to associate one $|\pm\rangle$ system to each complex dimension of $SU(5)$, which explains the labeling of the ‘spin’ columns in Table 93.1: The first three and last two ‘spins’ correspond to $SU(3)_C$ and $SU(2)_L$, respectively. In fact, an $SU(3)_C$ rotation just raises one color index and lowers another, changing colors $\{r, g, b\}$, or changes relative phases between the three spin states. Similarly, an $SU(2)_L$ rotation raises one weak index and lowers another, thereby flipping the weak isospin from up to down or vice versa, or changes the relative phase between the two spin states. In this representation $U(1)_Y$ hypercharge is simply given by $Y = -2/3(\sum \text{color spins}) + (\sum \text{weak spins})$. $SU(5)$ rotations corresponding to X bosons then raise (or lower) a color index, while at the same time lowering (or raising) a weak index. It is easy to see that such rotations can mix the states $\{Q, u^c, e^c\}$ and $\{d^c, L\}$ among themselves and ν^c is a singlet. Since $SO(10)$ has 45 generators, additional 21 gauge bosons are introduced including the $U(1)_X$ above. The 20 new $SO(10)$ rotations not in $SU(5)$ are then given by either raising any two spins or lowering them. With these rotations, $\mathbf{1}$ and $\bar{\mathbf{5}}$ are connected with $\mathbf{10}$. The last $SO(10)$ rotation changes phases of states with weight $2(\sum \text{color spins}) + 2(\sum \text{weak spins})$, which corresponds to $U(1)_X$.

$SO(10)$ has two inequivalent maximal subgroups and hence breaking patterns, $SO(10) \rightarrow SU(5) \times U(1)_X$ and $SO(10) \rightarrow SU(4)_C \times SU(2)_L \times SU(2)_R$. In the first case, one can carry on breaking to $G_{SM} \subset SU(5)$ precisely as in the minimal $SU(5)$ case above. Alternatively, one can identify $U(1)_Y$ as an appropriate linear combination of $U(1)_X$ and the $U(1)$ factor from $SU(5)$, leading to the so-called flipped $SU(5)$ [17] as an intermediate step in breaking $SO(10)$ to G_{SM} . In the second case, we have an intermediate Pati-Salam model thanks to the branching rule $\mathbf{16} = (\mathbf{4}, \mathbf{2}, \mathbf{1}) + (\bar{\mathbf{4}}, \mathbf{1}, \mathbf{2})$. Finally, $SO(10)$ can break directly to the SM at M_G . Gauge coupling unification remains intact in

Table 93.1: Quantum numbers of $\mathbf{16}$ -dimensional representation of $SO(10)$.

state	Y	Color	Weak	$SU(5)$	$SO(10)$
ν^c	0	---	--	1	16
e^c	2	---	++	10	
u_r	1/3	+--	-+		
d_r	1/3	+--	+-		
u_g	1/3	-+-	-+		
d_g	1/3	-+-	+-		
u_b	1/3	--+	-+		
d_b	1/3	--+	+-		
u_r^c	-4/3	-++	--		
u_g^c	-4/3	+-+	--		
u_b^c	-4/3	++-	--		
d_r^c	2/3	-++	++	$\bar{\mathbf{5}}$	
d_g^c	2/3	+-+	++		
d_b^c	2/3	++-	++		
ν	-1	+++	-+		
e	-1	+++	+-		

the case of this ‘direct’ breaking and for the breaking pattern $SO(10) \rightarrow SU(5) \rightarrow G_{SM}$ (with $SU(5)$ broken at M_G). In the case of intermediate-scale Pati-Salam or flipped $SU(5)$ models, gauge coupling predictions are modified. The Higgs multiplets in the minimal $SO(10)$ come from the fundamental representation, $\mathbf{10}_H = \mathbf{5}_H + \bar{\mathbf{5}}_H$. Note, only in $SO(10)$ does the representation type distinguish SM matter from Higgs fields.

93.2.4 Beyond $SO(10)$

Finally, larger symmetry groups can be considered. For example, the exceptional group E_6 has maximal subgroup $SO(10) \times U(1)$ [18]. Its fundamental representation branches as $\mathbf{27} = \mathbf{16}_1 + \mathbf{10}_{-2} + \mathbf{1}_4$. Another maximal subgroup is $SU(3)_C \times SU(3)_L \times SU(3)_R \subset E_6$ with branching rule $\mathbf{27} = (\mathbf{3}, \mathbf{3}, \mathbf{1}) + (\bar{\mathbf{3}}, \mathbf{1}, \bar{\mathbf{3}}) + (\mathbf{1}, \bar{\mathbf{3}}, \bar{\mathbf{3}})$. Independently of any underlying E_6 , the group $[SU(3)]^3$ with additional permutation symmetry Z_3 interchanging the three factors can be considered. This is known as ‘trinification’ [19]. The $E_6 \rightarrow [SU(3)]^3$ breaking pattern has been used in phenomenological analyses of the heterotic string [20]. However, in larger symmetry groups, such as E_6 , $SU(6)$, etc., there are now many more states which have not been observed and must be removed from the effective low-energy theory.

Intriguingly, the logic by which G_{SM} is a maximal subgroup of $SU(5)$, which together with $U(1)_X$ is a maximal subgroup of $SO(10)$, continues in a very elegant and systematic way up to the largest exceptional group. The resulting famous breaking chain $E_8 \rightarrow E_7 \rightarrow E_6 \rightarrow SO(10) \rightarrow SU(5) \rightarrow G_{SM}$ together with the special role played by E_8 in group and in string theory is a tantalizing hint at deeper structures. However, since all representations of E_8 and E_7 are real and can not lead to 4d chiral fermions, this is necessarily outside the 4d GUT framework.

93.3 GUT breaking and doublet-triplet splitting

In the standard, 4d field-theoretic approach to GUTs, the unified gauge group is broken spontaneously by an appropriate GUT Higgs sector. Scalar potentials (or superpotentials in SUSY GUTs) exist whose vacua spontaneously break $SU(5)$ or $SO(10)$. While these potentials are ad hoc (just like the Higgs potential in the SM), the most naive expectation is that all their dimensional parameters are $O(M_G)$. In the simplest case of $SU(5)$, the $\mathbf{24}$ (adjoint) GUT Higgs develops a VEV along the G_{SM} -singlet direction as $\langle \Phi \rangle \propto \text{diag}(-2/3, -2/3, -2/3, 1, 1)$. In order for $SO(10)$ to break to $SU(5)$, the $\mathbf{16}$ or $\mathbf{126}$, which have a G_{SM} -singlet with non-zero $U(1)_X$ charge, get a VEV.

The masses of doublet and triplet in the $\mathbf{5}_H$ (and $\bar{\mathbf{5}}_H$) generically split due to their coupling to the GUT Higgs. In addition, both the doublet and the triplet masses also get an equal contribution from an $SU(5)$ -invariant GUT-scale mass term. Without any further structure, an extreme fine-tuning between two large effects is then necessary to keep the doublet mass at the electroweak scale. Supersymmetry plays an important role in for-

³ Useful references on group theory in the present context include [16] and refs. therein.

bidding large radiative correction to the doublet mass due to the non-renormalization theorem [5]. However, even in this case we have to fine tune parameters at tree level. This is the doublet-triplet splitting problem which, in the SUSY context, is clearly related to the μ -term problem of the MSSM (the smallness of the coefficient of $\mu H_u H_d$).

Several mechanisms for natural doublet-triplet splitting have been suggested under the assumption of supersymmetry, such as the sliding singlet [21], missing partner [22], missing VEV [23], and pseudo-Nambu-Goldstone boson mechanisms [24]. Particular examples of the missing partner mechanism for $SU(5)$ [25], the missing VEV mechanism for $SO(10)$ [26, 27] and the pseudo-Nambu-Goldstone boson mechanism for $SU(6)$ [28] have been shown to be consistent with gauge coupling unification and nucleon decay. From the GUT-scale perspective, one is satisfied if the triplets are naturally heavy and the doublets are massless. In other words, one wants to ensure that the fundamental superpotential term $\mu H_u H_d$ is absent ($\mu \simeq 0$) while the corresponding term for the Higgs triplets is large. We note however that implementing this by a global symmetry is problematic, see e.g. [29–31].

Once a model with vanishing fundamental μ term has been realized, an *effective* μ term of order the SUSY breaking scale can then be induced by, for example, higher-mass-dimension terms in the Kahler potential [32]. For a review of the μ problem and some suggested solutions in SUSY GUTs and string theory, see [30, 33–35] and references therein.

In general, GUT-breaking sectors successfully resolving the doublet-triplet splitting problem, dynamically stabilizing all GUT-scale VEVs and allowing for realistic neutrino masses and Yukawa couplings (including the GUT-symmetry violation in the latter) require a number of ingredients. However, for validity of the effective theory, introduction of higher or many representations is limited, otherwise a Landau pole may appear below the Planck scale. In addition, GUTs are only effective theories below the Planck scale in the 4d field-theoretic approach. Since M_G is close to this scale, the effects of higher-dimension operators are not obviously negligible. In particular, operators including the GUT-breaking Higgs may affect low-energy predictions, such as quark and lepton masses.

Thus, especially in the context of GUT breaking and doublet-triplet splitting, models beyond 4d field theory appear attractive. While this is mainly the subject of the next section, some advantages can already be noted: In models with extra dimensions, in particular string constructions, GUT breaking may occur due to boundary conditions in the compactified dimensions [36–39]. No complicated GUT breaking sector is then required. Moreover, boundary conditions can give mass only to the triplet, leaving the doublet massless. This is similar to the ‘missing partner mechanism’ since the effective mass term does not ‘pair up’ the triplets from $\mathbf{5}_H$ and $\bar{\mathbf{5}}_H$ but rather each of them with further fields which are automatically present in the higher-dimensional theory. This can eliminate dimension-five nucleon decay (cf. Sec. 93.6).

93.4 String-theoretic and higher-dimensional unified models

As noted earlier, the GUT scale is dangerously close to the scale of quantum gravity. It may hence be necessary to discuss unified models of particle physics in the latter, more ambitious context. Among the models of quantum gravity, superstring or M-theory stands out as the best-studied and technically most developed proposal, possessing in particular a high level of internal, mathematical consistency. For our purposes, it is sufficient to know that five 10d and one 11d low-energy effective supergravity theories arise in this setting (cf. [40] and refs. therein).

Grand unification is realized most naturally in the context of the two ‘heterotic’ theories with gauge groups $E_8 \times E_8$ and $SO(32)$, respectively [38, 41] (see [42] for some of the more recent results). Justified in part by the intriguing breaking path $E_8 \rightarrow \dots \rightarrow G_{SM}$ mentioned above, the focus has historically largely been on $E_8 \times E_8$. To describe particle physics, solutions of the 10d theory with geometry $\mathbb{R}^{1,3} \times M_6$ are considered, where M_6 is a Calabi-Yau (CY) 3-fold (with 6 real dimensions) [38]. The background solution involves expectation values of higher-

dimensional components of the $E_8 \times E_8$ gauge fields. This includes both Wilson lines [36] and non-vanishing field-strength and leads, in general, to a reduced gauge symmetry and to chirality in the resulting 4d effective theory. The 4d fermions arise from 10d gauginos.

Given an appropriate embedding⁴ of G_{SM} in $E_8 \times E_8$, gauge coupling unification is automatic at leading order. Corrections arise mainly through (string)-loop effects and are similar to the familiar field-theory thresholds of 4d GUTs⁵ [43]. Thus, one may say that coupling unification is a generic prediction in spite of the complete absence⁶ of a 4d GUT at any energy scale. This absence is both an advantage and a weakness. On the up side, GUT breaking and doublet-triplet splitting [45] are more naturally realized and dimension-five nucleon decay is relatively easy to avoid. On the down side, there is no reason to expect full GUT representations in the matter sector and flavor model building is much less tied to the GUT structure than in 4d.

Let us pause to explain the beautiful idea behind the advertised solution of the doublet-triplet splitting problem: One starts with a simply connected CY X and mods out the action of a discrete group G (say \mathbb{Z}_2). In the absence of fixed points, X/G is smooth and has a non-contractible 1-cycle. Furthermore, let G also act on the gauge bundle, according to an embedding $G \rightarrow E_8$. Now the parallel transport around the 1-cycle is tied to a gauge rotation (one says a non-trivial Wilson-line is present). Moreover, this Wilson line can not be continuously turned off since, e.g. in the case of \mathbb{Z}_2 , its square is the unit element of the group. The induced ‘Wilson-line breaking’, which comes on top of the breaking by non-zero field strengths, may remove certain sub-representations (e.g. the triplet of $SU(5) \rightarrow G_{SM}$) while keeping others exactly massless. A simpler and, due to fixed points, singular version of this will appear below in the context of orbifold GUTs.

One technical problem of heterotic constructions is the dependence on the numerous size and shape parameters of M_6 (the so-called moduli), the stabilization of which is poorly understood (see [46] for recent developments). Another is the sheer mathematical complexity of the analysis, involving in particular the study of (non-Abelian) gauge-bundles on CY spaces [47] (see however [48]).

An interesting aspect of heterotic string constructions is represented by orbifold models [37]. Here the internal space is given by a six-torus, modded out by a discrete symmetry group (e.g. T^6/\mathbb{Z}_n). More recent progress is reported in [49, 50], including in particular the systematic exploration of the phenomenological advantages of so-called ‘non-prime’ (referring to n) orbifolds. The symmetry breaking to G_{SM} as well as the survival of Higgs doublets without triplet partners is ensured by the appropriate embedding of the discrete orbifold group in $E_8 \times E_8$. String theory on such spaces, which are locally flat but include singularities, is much more calculable than in the CY case. The orbifold geometries can be viewed as singular limits of CYs.

An even simpler approach to unified models, which includes many of the advantages of full-fledged string constructions, is provided by Orbifold GUTs [39]. These are (mostly) 5d or 6d SUSY field theories with unified gauge group (e.g. $SU(5)$ or $SO(10)$), broken in the process of compactifying to 4d. To give a particularly simple example, consider $SU(5)$ on $\mathbb{R}^{1,3} \times S^1/(\mathbb{Z}_2 \times \mathbb{Z}'_2)$. Here the compact space is an interval of length $\pi R/2$ and the embedding of \mathbb{Z}'_2 in the hypercharge direction of $SU(5)$ realizes the breaking to G_{SM} . Concretely, 5d X bosons are given Dirichlet BCs at one endpoint of the interval and thus have no Kaluza-Klein (KK) zero mode. Their lightest modes have mass $\sim 1/R$, making the KK-scale the effective GUT scale. As an implication, the boundary theory has no $SU(5)$ invariance. Nevertheless, since the $SU(5)$ -symmetric 5d bulk dominates 4d gauge couplings, unifica-

⁴ All embeddings of G_{SM} in one E_8 factor which are consistent with a breaking-pattern $E_8 \rightarrow SU(5) \rightarrow G_{SM}$ are suitable (cf. for example the natural breaking chain from E_8 to G_{SM} through maximal subgroups mentioned at the end of Sect. 93.3). Other embeddings can change the ratios between the three resulting G_{SM} couplings at the GUT scale by group-theoretic factors. Crucially, due to the single 10d gauge coupling, no continuous tuning is possible.

⁵Field-theory thresholds of 4d GUTs are discussed in 93.5.

⁶ See however [44].

tion remains a prediction. Many other features but also problems of 4d GUTs can be circumvented, especially doublet-triplet splitting is easily realized.

With the advent of the string-theory ‘flux landscape’ [51], which is best understood in 10d type-IIB supergravity, the focus in string model building has shifted to this framework. While type II string theories have no gauge group in 10d, brane-stacks support gauge dynamics. A particularly appealing setting (see e.g. [52]) is provided by type IIB models with D7 branes (defining 8d submanifolds). However, in the $SO(10)$ context the **16** is not available and, for $SU(5)$, the top-Yukawa coupling vanishes at leading order [53]. As a crucial insight, this can be overcome on the non-perturbative branch of type IIB, also known as F-theory [54, 55]. This setting allows for more general branes, thus avoiding constraints of the Dp -brane framework. GUT breaking can be realized using hypercharge flux (the VEV of the $U(1)_Y$ field strength), an option not available in heterotic models. The whole framework combines the advantages of the heterotic or higher-dimensional unification approach with the more recent progress in understanding moduli stabilization. It thus represents at this moment the most active and promising branch of theory-driven GUT model building (see e.g. [56] and refs. therein).

As a result of the flux-breaking, a characteristic ‘type IIB’ or ‘F-theoretic’ tree-level correction to gauge unification arises [57]. The fact that this correction can be rather significant numerically is occasionally held against the framework of F-theory GUTs. However, at a parametric level, this correction nevertheless behaves like a 4d threshold, i.e., it provides $\mathcal{O}(1)$ additive contributions to the inverse 4d gauge couplings $\alpha_i^{-1}(M_G)$.

A final important issue in string GUTs is the so-called string-scale/GUT-scale problem [58]. It arises since, in heterotic compactifications, the Planck scale and the high-scale value of the gauge coupling unambiguously fix the string-scale to about 10^{18} GeV. As the compactification radius R is raised above the string length, the GUT scale (identified with $1/R$) goes down and the string coupling goes up. Within the domain of perturbative string theory, a gap of about a factor ~ 20 remains between the lowest GUT scale achievable in this way and the phenomenological goal of 2×10^{16} GeV. The situation can be improved by venturing into the non-perturbative regime [58], by considering ‘anisotropic’ geometries with hierarchically different radii R [58, 59] or by including GUT scale threshold corrections [60, 61].

In F-theory GUTs, the situation is dramatically improved since the gauge theory lives only in four out of the six compact dimensions. This allows for models with a ‘decoupling limit’, where the GUT scale is parametrically below the Planck scale [55]. However, moduli stabilization may not be without problems in such constructions, in part due to a tension between the required large volume and the desirable low SUSY breaking scale.

93.5 Gauge coupling unification

The quantitative unification of the three SM gauge couplings at the energy scale M_G is one of the cornerstones of the GUT paradigm. It is obviously of direct phenomenological relevance. Gauge coupling unification is well understood in the framework of effective field theory (EFT) [62]. In the simplest case, the relevant EFT at energies $\mu \gg M_G$ has a unified gauge symmetry (say $SU(5)$ for definiteness) and a single running gauge coupling $\alpha_G(\mu)$. At energies $\mu \ll M_G$, states with mass $\sim M_G$ (such as X bosons, GUT Higgs, color-triplet Higgs) have to be integrated out. The EFT now has three independent couplings and SM (or SUSY SM) matter content. One-loop renormalization group equations readily allow for an extrapolation to the weak scale,

$$\alpha_i^{-1}(m_Z) = \alpha_G^{-1}(M_G) + \frac{b_i}{2\pi} \log\left(\frac{M_G}{m_Z}\right) + \delta_i, \quad (93.4)$$

($i = 1, 2, 3$). Here we defined δ_i to absorb all sub-leading effects, such as threshold corrections at or near the weak scale (e.g. from superpartners and the additional Higgs bosons in the case of the MSSM) and at the GUT scale, and also higher-order corrections. We will discuss them momentarily.

It is apparent from Eq. (93.3) that the three low-scale couplings can be very different. This is due to the large energy range

$m_Z \ll \mu \ll M_G$ and the non-universal β -function coefficients ($b_i^{\text{SM}} = \{41/10, -19/6, -7\}$ or $b_i^{\text{MSSM}} = \{33/5, 1, -3\}$). Incomplete GUT multiplets, such as gauge and Higgs bosons in the SM and also their superpartners and the additional Higgs bosons in the MSSM, contribute to the differences between the β functions. Inverting the argument, one expects that extrapolating the measured couplings to the high scale, we find quantitative unification at $\mu \sim M_G$. While this fails in the SM, it works intriguingly well in the MSSM (cf. Fig. 93.1).

The three equations contained in Eq. (93.3) can be used to determine the three ‘unknowns’ $\alpha_3(m_Z)$, $\alpha_G(M_G)$ and M_G , assuming that all other parameters entering the equations are given. Focusing on the SUSY case and using the $\overline{\text{MS}}$ coupling constants $\alpha_{\text{EM}}^{-1}(m_Z)$ and $\sin^2 \theta_W(m_Z)$ from [64],

$$\alpha_{\text{EM}}^{-1}(m_Z) = 127.951 \pm 0.009, \quad (93.4)$$

$$\sin^2 \theta_W(m_Z) = 0.23122 \pm 0.00004, \quad (93.5)$$

as input, one determines $\alpha_{1,2}^{-1}(m_Z)$, which then gives

$$\alpha_G^{-1}(M_G) \simeq 24.3 \quad \text{and} \quad M_G \simeq 2 \times 10^{16} \text{ GeV}. \quad (93.6)$$

Here we have set $\delta_i = 0$ for simplicity. Crucially, one in addition obtains a prediction for the low-energy observable α_3 ,

$$\alpha_3^{-1}(m_Z) = -\frac{5}{7}\alpha_1^{-1}(m_Z) + \frac{12}{7}\alpha_2^{-1}(m_Z) + \Delta_3, \quad (93.7)$$

where

$$\Delta_3 = \frac{5}{7}\delta_1 - \frac{12}{7}\delta_2 + \delta_3. \quad (93.8)$$

Here we followed the elegant formulation in Ref. [65] of the classical analyses of [7]. Of course, it is a matter of convention which of the three low-energy gauge coupling parameters one ‘predicts’ and indeed, early works on the subject discussed the prediction of $\sin^2 \theta_W$ in terms of α_{EM} and α_3 [66, 67].

Remarkably, the leading order result (i.e. Eq. (93.7) with $\delta_i = 0$) is in excellent agreement with experiments [64]:

$$\alpha_3^{\text{LO}}(m_Z) = 0.117 \quad \text{vs.} \quad \alpha_3^{\text{EXP}}(m_Z) = 0.1179 \pm 0.0009. \quad (93.9)$$

However, this near perfection is to some extent accidental. To see this, we now discuss the various contributions to the δ_i (and hence to Δ_3).

The two-loop running correction from the gauge sector $\Delta_3^{(2)}$ and the low-scale threshold correction $\Delta_3^{(l)}$ from superpartners can be summarized as [65]

$$\Delta_3^{(2)} \simeq -0.82 \quad \text{and} \quad \Delta_3^{(l)} \simeq \frac{19}{28\pi} \log\left(\frac{m_{\text{SUSY}}}{m_Z}\right). \quad (93.10)$$

The relevant scale m_{SUSY} can be estimated as [68]

$$m_{\text{SUSY}} \rightarrow m_H^{3/19} m_{\tilde{H}}^{12/19} m_{\tilde{W}}^{4/19} \times \left(\frac{m_{\tilde{W}}}{m_g}\right)^{28/19} \left(\frac{m_{\tilde{t}}}{m_{\tilde{q}}}\right)^{3/19}, \quad (93.11)$$

where m_H stands for the masses of non-SM Higgs states and superpartner masses are given in self-evident notation. Detailed analyses including the above effects are best done using appropriate software packages, such as SOFTSUSY [63] (or alternatively SuSpect [69] or SPheno [70]). See also [63] for references to the underlying theoretical two-loop analyses.

To get a very rough feeling for these effects, let us assume that all superpartners are degenerate at $m_{\text{SUSY}} = 1$ TeV, except for heavier gluinos: $m_{\tilde{W}}/m_{\tilde{g}} \simeq 1/3$. This gives $\Delta_3^{(2)} \simeq -0.35 + 0.22 \ln(m_{\text{SUSY}}/m_Z) \simeq 0.18$. The resulting prediction of $\alpha_3(m_Z) \simeq 0.126$ significantly upsets the perfect one-loop agreement found earlier. Before discussing this issue further, it is useful to introduce yet another important type of correction, the high or GUT scale thresholds.

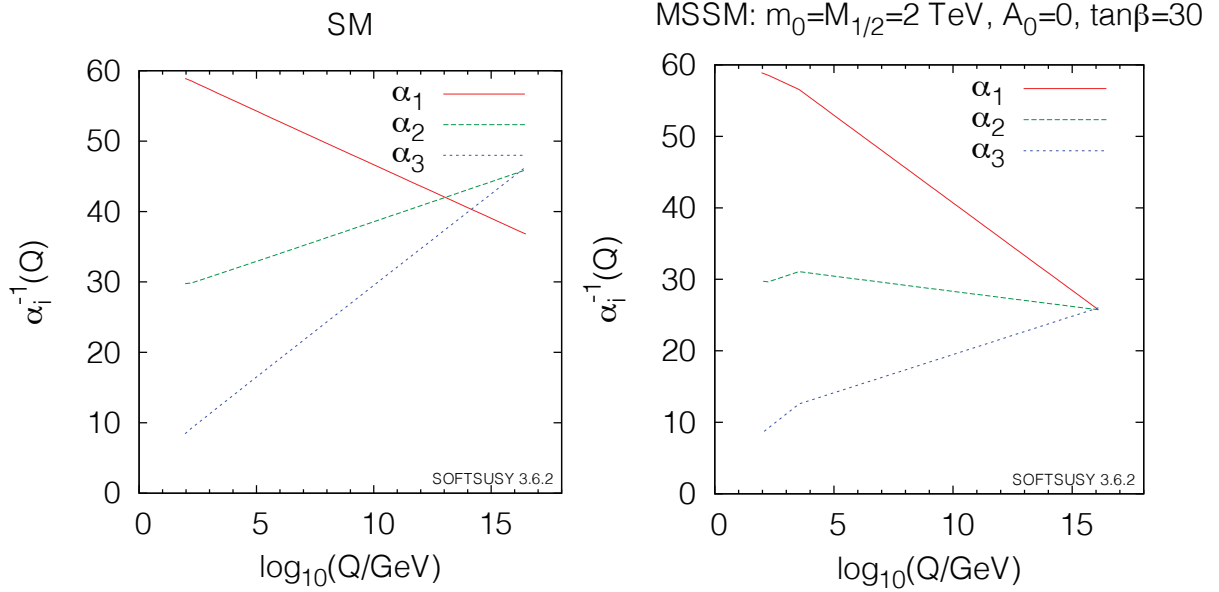


Figure 93.1: Running couplings in SM and MSSM using two-loop RG evolution. The SUSY threshold at 2 TeV is clearly visible on the MSSM side. (We thank Ben Allanach for providing the plots created using SOFTSUSY [63].)

To discuss high scale thresholds, let us set all other corrections to zero for the moment and write down a version of Eq. (93.3) that captures the running near and above the GUT scale more correctly. The threshold correction at one-loop level can be evaluated accurately by the simple step-function approximation for the β functions in the $\overline{\text{DR}}$ scheme⁷ [74],

$$\alpha_i^{-1}(m_Z) = \alpha_G^{-1}(\mu) + \frac{1}{2\pi} \left[b_i \ln \frac{\mu}{m_Z} + b_i^C \ln \frac{\mu}{M_C} + b_i^X \ln \frac{\mu}{M_X} + b_i^\Phi \ln \frac{\mu}{M_\Phi} \right]. \quad (93.12)$$

Here we started the running at some scale $\mu \gg M_G$, including the contribution of the minimal set of states relevant for the transition from the high-scale $SU(5)$ model to the MSSM. These are the color-triplet Higgs multiplets with mass M_C , massive vector multiplets of X -bosons with mass M_X (including GUT Higgs degrees of freedom), and the remaining GUT-Higgs fields and superpartners with mass M_Φ . The coefficients $b_i^{C,X,\Phi}$ can be found in Ref. [75]. Crucially, the b_i in Eq. (93.12) conspire to make the running GUT-universal at high scales, such that the resulting prediction for α_3 does not depend on the value of μ .

To relate this to our previous discussion, we can, for example, define $M_G \equiv M_X$ and then choose $\mu = M_G$ in Eq. (93.12). This gives the high-scale threshold corrections

$$\delta_i^{(h)} = \frac{1}{2\pi} \left[b_i^C \ln \frac{M_G}{M_C} + b_i^\Phi \ln \frac{M_G}{M_\Phi} \right], \quad (93.13)$$

and a corresponding correction $\Delta_3^{(h)}$. To get some intuition for the magnitude, one can furthermore assume $M_\Phi = M_G$, finding (with $b_i^C = \{2/5, 0, 1\}$)

$$\Delta_3^{(h)} = \frac{9}{14\pi} \ln \left(\frac{M_G}{M_C} \right). \quad (93.14)$$

To obtain the desired effect of $-\Delta_3^{(2)} - \Delta_3^{(l)} \simeq +0.64$, the triplet Higgs would have to be by about a factor 20 lighter than the GUT scale. While this is ruled out by nucleon decay in the minimal model [76] as will be discussed Sec. 93.6, it is also clear that

threshold corrections of this order of magnitude can, in general, be realized with a certain amount of GUT-scale model building, e.g. in specific $SU(5)$ [25] or $SO(10)$ [26,27] constructions. Corrections can also be much larger or of different sign if, as is required in many fully realistic 4d GUT models, many additional (and in particular higher) representations are introduced. Thus, there is considerable model building freedom. Nevertheless, a significant constraint from getting the right GUT threshold corrections while keeping the triplet Higgs heavy remains.

The above analysis implicitly assumes universal soft SUSY breaking masses at the GUT scale, which directly affect the spectrum of SUSY particles at the weak scale. In the simplest case we have a universal gaugino mass $M_{1/2}$, a universal mass for squarks and sleptons m_{16} and a universal Higgs mass m_{10} , as motivated by $SO(10)$. In some cases, threshold corrections to gauge coupling unification can be exchanged for threshold corrections to soft SUSY parameters (see [77] and refs. therein). For example, if gaugino masses were not unified at M_G and, in particular, gluinos were lighter than winos at the weak scale (cf. Eq. (93.11)), then it is possible that, due to weak scale threshold corrections, a much smaller or even slightly negative threshold correction at the GUT scale would be consistent with gauge coupling unification [78].

It is also noteworthy that perfect unification can be realized without significant GUT-scale corrections, simply by slightly raising the (universal) SUSY breaking scale. In this case the dark matter abundance produced by thermal processes in the early Universe (if the lightest neutralino is the dark matter particle) is too high. However, even if the gaugino mass in the MSSM is about 1 TeV to explain the dark matter abundance, if the Higgsino and the non-SM Higgs boson masses are about 10-100 TeV, the effective SUSY scale can be raised [79]. This setup is realized in split SUSY [80] or the pure gravity mediation model [81] based on anomaly mediation [82]. Since the squarks and sleptons are much heavier than the gaugino masses in those setups, a gauge hierarchy problem is reintroduced. The facts that no superpartners have so far been seen at the LHC and that the observed Higgs mass favors heavier stop masses than about 1 TeV force one to accept a certain amount of fine-tuning anyway.

For non-SUSY GUTs or GUTs with a very high SUSY breaking scale to fit the data, new light states in incomplete GUT multiplets or multiple GUT breaking scales are required. For example, non-SUSY models $SO(10) \rightarrow SU(4)_C \times SU(2)_L \times SU(2)_R \rightarrow \text{SM}$, with the second breaking scale of order an intermediate scale, determined by light neutrino masses using the see-saw mechanism, can fit the low-energy data for gauge couplings [83] and at the

⁷The $\overline{\text{DR}}$ scheme is frequently used in a supersymmetric regularization [71]. The renormalization transformation of the gauge coupling constants from $\overline{\text{MS}}$ to $\overline{\text{DR}}$ scheme is given in Ref. [72]. For an alternative treatment using holomorphic gauge couplings and NSVZ β -functions see e.g. [73].

same time survive nucleon decay bounds [84]. Alternatively, one can appeal to string-theoretic corrections discussed in Sec. 93.4 to compensate for a high SUSY breaking scale. This has, for example, been concretely analyzed in the context of F-theory GUTs in [85]. Similarly, one may even wonder whether particularly large GUT threshold corrections could be sufficient to ensure non-SUSY precision unification. Notice here that the gauge coupling unification predicts just one parameter. When introducing new states, typically one can fit the data by choice of their masses. This is not the case in SUSY GUTs with low-scale SUSY breaking scale where the masses are constrained by fine-tuning.

In 5d or 6d orbifold GUTs, certain ‘‘GUT scale’’ threshold corrections come from the Kaluza-Klein modes between the compactification scale, $M_c \sim 1/R$, and the effective cutoff scale M_* . In string theory, this cutoff scale is the string scale. Gauge coupling unification at two loops then constrains the values of M_c and M_* .⁸ Often, one finds M_c to be lower than the 4d GUT scale. Since the X -bosons, responsible for nucleon decay, get mass at the compactification scale, this has significant consequences for nucleon decay.

Finally, it has been shown that non-supersymmetric GUTs in warped 5d orbifolds can be consistent with gauge coupling unification. This assumes (in 4d language) that the r.h. top quark and the Higgs doublets are composite-like objects with a compositeness scale in the TeV range [87].

93.6 Nucleon decay

Quarks and leptons are indistinguishable in any 4d GUT, and both the baryon (B) and lepton number (L) are not conserved. This leads to baryon-number-violating nucleon decay. In addition to baryon-number violation, lepton-number violation is also required for nucleon decay since, in the SM, leptons are the only free fermions which are lighter than nucleons. The lowest-dimension operators relevant for nucleon decay are $(B+L)$ violating dimension-six four-fermion-terms in the SM, and all baryon-violating operators with dimension less than seven preserve $(B-L)$ [1, 88].

In $SU(5)$ GUTs, the dimension-six operators are induced by X boson exchange. These operators are suppressed by $(1/M_X^2)$ (M_X is the X boson mass), and the nucleon lifetime is given by $\tau_N \propto M_X^4/(\alpha_G^2 m_p^5)$ (m_p is proton mass). The dominant decay mode of the proton (and the baryon-violating decay mode of the neutron), via X boson exchange, is $p \rightarrow e^+ \pi^0$ ($n \rightarrow e^+ \pi^-$). In any simple gauge symmetry, with one universal GUT coupling α_G and scale M_X , the nucleon lifetime from gauge boson exchange is calculable. Hence, the GUT scale may be directly observed via the extremely rare decay of the nucleon. The present experimental bounds on the modes come from Super-Kamiokande. With 450 kton-years of data they find $\tau_p/\text{Br}(p \rightarrow e^+ \pi^0) > 2.4 \times 10^{34}$ years at 90% CL [89]. In addition, Hyper-Kamiokande [90] is planned to reach to $\tau_p/\text{Br}(p \rightarrow e^+ \pi^0) \sim 10^{35}$ years. The reader may consult [91] for other planned experiments and some historical context. The hadronic matrix elements for baryon-number-violating operators are evaluated with lattice QCD simulations [92]. In SUSY $SU(5)$ GUTs, the lower bound on the X boson mass from null results in nucleon decay searches is approaching 10^{16} GeV [93], which is close to the GUT scale suggested by gauge coupling unification. On the other hand, the prediction for nucleon decay in non-SUSY GUTs is hard to quantify. The reason is that gauge couplings do not unify with just the SM particle content. Once extra states or large thresholds are included to ensure precision unification, a certain range of unification scales is allowed.

In SUSY GUTs there are additional sources for baryon and/or lepton-number violation – dimension-four and five operators [14]. These arise since, in the SUSY SM, quarks and leptons have scalar partners (squarks and sleptons). Although our notation does not change, when discussing SUSY models our fields are chiral superfields and both fermionic and bosonic matter is implicitly represented by those. In this language, baryon- and/or lepton-number-violating dimension-four and five operators are given as

⁸ It is interesting to note that a ratio $M_*/M_c \sim 100$, needed for gauge coupling unification to work in orbifold GUTs, is typically the maximum value for this ratio consistent with perturbativity [86].

so-called F terms of products of chiral superfields, which contain two fermionic components and the rest scalars or products of scalars. Within the context of $SU(5)$ the dimension-four and five operators have the form

$$(10 \bar{5} \bar{5}) \supset (u^c d^c d^c) + (Q L d^c) + (e^c L L),$$

$$(10 10 10 \bar{5}) \supset (Q Q Q L) + (u^c u^c d^c e^c) \\ + B\text{- and }L\text{-conserving terms,}$$

respectively.

The dimension-four operators in $(10 \bar{5} \bar{5})$ violate either baryon number or lepton number. The nucleon lifetime is extremely short if both types of dimension-four operators are present in the SUSY SM since squark or slepton exchange induces the dangerous dimension-six SM operators. Even in the case that they violate baryon number or lepton number only but not both, they are constrained by various phenomena [94]. For example, the primordial baryon number in the Universe is washed out unless the dimensionless coupling constants are less than 10^{-7} . Both types of operators can be eliminated by requiring R parity, which distinguishes Higgs from ordinary matter multiplets. R parity [95] or its cousin, matter parity [6, 96], act as $F \rightarrow -F$, $H \rightarrow H$ with $F = \{10, \bar{5}\}$, $H = \{\bar{5}_H, 5_H\}$ in $SU(5)$.⁹ In $SU(5)$, the Higgs multiplet $\bar{5}_H$ and the matter multiplets $\bar{5}$ have identical gauge quantum numbers. In E_6 , Higgs and matter multiplets could be unified within the fundamental 27 representation. Only in $SO(10)$ are Higgs and matter multiplets distinguished by their gauge quantum numbers. The Z_4 center of $SO(10)$ distinguishes 10_s from 16_s and can be associated with R parity [97].

The baryon-number violating dimension-five operators have a dimensionful coupling. They are generated by integrating out the color-triplet Higgs with GUT-scale mass in SUSY GUTs such that the coefficient is suppressed by $1/M_G$. Note that both triplet Higgsinos (due to their fermionic nature) and Higgs scalars (due to their mass-enhanced trilinear coupling with matter) contribute to the operators. The dimension-five operators include squarks and/or sleptons. To allow for nucleon decay, these must be converted to light quarks or leptons by exchange of a gaugino or Higgsino in the SUSY SM. The nucleon lifetime is proportional to $M_G^2 m_{\text{SUSY}}^2/m_p^5$, where m_{SUSY} is the SUSY breaking scale. Thus, dimension-five operators may predict a shorter nucleon lifetime than dimension-six operators. Unless accidental cancellations are present, the dominant decay modes from dimension-five operators include a K meson, such as $p \rightarrow K^+ \bar{\nu}$ ($n \rightarrow K^0 \bar{\nu}$). This is due to a simple symmetry argument: The operators are given as $(Q_i Q_j Q_k L_l)$ and $(u_i^c u_j^c d_k^c e_l^c)$, where $i, j, k, l (= 1, 2, 3)$ are family indices and color and weak indices are implicit. They must be invariant under $SU(3)_C$ and $SU(2)_L$ so that their color and weak doublet indices must be anti-symmetrized. Since these operators are given by bosonic superfields, they must be totally symmetric under interchange of all indices. Thus, the first operator vanishes for $i = j = k$ and the second vanishes for $i = j$. Hence a second or third generation member exists in the dominant modes of nucleon decay unless these modes are accidentally suppressed [96].

The Super-Kamiokande bounds on the proton lifetime severely constrain the dimension-five operators. With 306 kton-years of data they find $\tau_p/\text{Br}(p \rightarrow K^+ \bar{\nu}) > 6.61 \times 10^{33}$ years at 90% CL [98]. In the minimal SUSY $SU(5)$, $\tau_p/\text{Br}(p \rightarrow K^+ \bar{\nu})$ is smaller than about 10^{31} years if the triplet Higgs mass is 10^{16} GeV and $m_{\text{SUSY}} = 1$ TeV [99]. The triplet Higgs mass bound from nucleon decay is then in conflict with gauge coupling unification so that this model is considered to be ruled out [76].

Since nucleon decay induced by the triplet Higgs is a severe problem in SUSY GUTs, various proposals for its suppression have been made. First, some accidental symmetry or accidental structure in non-minimal Higgs sectors in $SU(5)$ or $SO(10)$ theories may suppress the dimension-five operators [22, 26, 27, 100].

⁹ This forbids the dimension-four operator $(10 \bar{5} \bar{5})$, but allows the Yukawa couplings for quark and lepton masses of the form $(10 \bar{5} \bar{5}_H)$ and $(10 10 5_H)$. It also forbids the dimension-three, lepton-number-violating operator $(\bar{5} 5_H) \supset (L H_u)$ as well as the dimension-five, baryon-number-violating operator $(10 10 10 \bar{5}_H) \supset (Q Q Q H_d) + \dots$

Symmetries to suppress the dimension-five operators are typically broken by the VEVs responsible for the color-triplet Higgs masses. Consequently, the dimension-five operators are generically generated via the triplet Higgs exchange in SUSY $SU(5)$ GUTs, as mentioned above. In other words, the nucleon decay is suppressed if the Higgs triplets in $\bar{\mathbf{5}}_H$ and $\mathbf{5}_H$ do not have a common mass term but, instead, their mass terms involve partners from other $SU(5)$ multiplets. Second, the SUSY breaking scale may be around $\mathcal{O}(10\text{--}100)$ TeV in order to explain the observed Higgs boson mass at the LHC. In this case, nucleon decay is automatically suppressed [80,101,102]. Third, accidental cancellations among diagrams due to a fine-tuned structure of squark and slepton flavor mixing might suppress nucleon decay [103]. Last, we have also implicitly assumed a hierarchical structure for Yukawa matrices in the analysis. It is however possible to fine-tune a hierarchical structure for quarks and leptons which baffles the family structure so that the nucleon decay is suppressed [104]. The upper bound on the proton lifetime from some of these theories is approximately a factor of 10 above the experimental bounds. Future experiments with larger neutrino detectors, such as JUNO [105], Hyper-Kamiokande [90], DUNE [106] and Theia [107], are planned and will have higher sensitivities to nucleon decay.

Are there ways to avoid the stringent predictions for proton decay discussed above? Orbifold GUTs and string theories, see Sec. 93.4, contain grand unified symmetries realized in higher dimensions. In the process of compactification and GUT symmetry breaking, the triplet Higgs states may be removed (projected out of the massless sector of the theory). In such models, the nucleon decay due to dimension-five operators can be severely suppressed or eliminated completely. However, nucleon decay due to dimension-six operators may be enhanced, since the gauge-bosons mediating proton decay obtain mass at the compactification scale, M_c , which is typically less than the 4d GUT scale (cf. Sec. 93.5). Alternatively, the same projections which eliminate the triplet Higgs may rearrange the quark and lepton states such that the massless states of one family come from different higher-dimensional GUT multiplets. This can suppress or completely eliminate even dimension-six proton decay. Thus, enhancement or suppression of dimension-six proton decay is model-dependent. In some complete 5d orbifold GUT models [65, 108] the lifetime for the decay $\tau_p/\text{Br}(p \rightarrow e^+\pi^0)$ can be near the bound of 1×10^{34} years with, however, large model-dependence and/or theoretical uncertainties. In other cases, the modes $p \rightarrow K^+\bar{\nu}$ and $p \rightarrow K^0\mu^+$ may be dominant [65]. Thus, interestingly, the observation of nucleon decay may distinguish string or higher-dimensional GUTs from 4d ones.

In orbifold GUTs or string theory, new discrete symmetries consistent with SUSY GUTs can forbid all dimension-three and four baryon- and lepton-number-violating operators. Even the μ term and dimension-five baryon- and lepton-number-violating operators can be forbidden to all orders in perturbation theory [35]. The μ term and dimension-five baryon- and lepton-number-violating operators may then be generated, albeit sufficiently suppressed, via non-perturbative effects. The simplest example of this is a Z_4^R symmetry which is the unique discrete R symmetry consistent with $SO(10)$ [35]. Even though it forbids the dimension-five proton decay operator to the desired level, it allows the required dimension-five neutrino mass term. In this case, proton decay is dominated by dimension-six operators, leading to decays such as $p \rightarrow e^+\pi^0$.

93.7 Yukawa coupling unification

In the SM, masses and mixings for quarks and leptons come from the Yukawa couplings with the Higgs doublet, but the values of these couplings remain a mystery. GUTs provide at least a partial understanding since each generation is embedded in unified multiplet(s). Specifically, since quarks and leptons are two sides of the same coin, the GUT symmetry relates the Yukawa couplings (and hence the masses) of quarks and leptons.

In $SU(5)$, there are two types of independent renormalizable Yukawa interactions given by $\lambda_{ij}(\mathbf{10}_i \mathbf{10}_j \mathbf{5}_H) + \lambda'_{ij}(\mathbf{10}_i \bar{\mathbf{5}}_j \bar{\mathbf{5}}_H)$. These contain the SM interactions $\lambda_{ij}(Q_i u_j^c H_u) + \lambda'_{ij}(Q_i d_j^c H_d + e_i^c L_j H_d)$. Here $i, j (= 1, 2, 3)$

are, as before, family indices. Hence, at the GUT scale we have tree-level relations between Yukawa coupling constants for charged lepton and down quark masses, such as $\lambda_b = \lambda_\tau$ in which $\lambda_{b/\tau}$ are the bottom quark / τ lepton Yukawa coupling constants [109,110]. In $SO(10)$, there is only one type of independent renormalizable Yukawa interaction given by $\lambda_{ij}(\mathbf{16}_i \mathbf{16}_j \mathbf{10}_H)$, leading to relations among all Yukawa coupling constants and quark and lepton masses within one generation [111,112] (such as $\lambda_t = \lambda_b = \lambda_\tau$, with λ_t the top quark Yukawa coupling constant).

In addition to gauge coupling unification, the ratio of bottom quark and τ lepton mass has been a central target in the study of GUTs since it was found that this ratio was almost consistent with observations after including the QCD correction [109]. Today the quark masses and the gauge coupling constants are known precisely such that, as discussed below, the ratio of bottom quark and τ lepton mass has become a target of precision analyses in the GUT context.

93.7.1 The third generation, $b\text{--}\tau$ or $t\text{--}b\text{--}\tau$ unification

Third generation Yukawa couplings are larger than those of the first two generations. Hence, the fermion mass relations predicted from renormalizable GUT interactions which we introduced above are expected to be more reliable. In order to compare them with data, we have to include the radiative correction to these relations from the RG evolution between GUT and fermion mass scale, from integrating out heavy particles at the GUT scale, and from weak scale thresholds.

Since testing Yukawa coupling unification is only possible in models with successful gauge coupling unification, we here focus on SUSY GUTs. In the MSSM, top and bottom quark and τ lepton masses are related to the Yukawa coupling constants at the scale m_Z as

$$\begin{aligned} m_t(m_Z) &= \lambda_t(m_Z) v_u (1 + \delta m_t/m_t), \\ m_{b/\tau}(m_Z) &= \lambda_{b/\tau}(m_Z) v_d (1 + \delta m_{b/\tau}/m_{b/\tau}), \end{aligned}$$

where $\langle H_u^0 \rangle \equiv v_u = \sin \beta v/\sqrt{2}$, $\langle H_d^0 \rangle \equiv v_d = \cos \beta v/\sqrt{2}$, $v_u/v_d \equiv \tan \beta$ and $v \sim 246$ GeV is fixed by the Fermi constant, G_μ . Here, $\delta m_f/m_f$ ($f = t, b, \tau$) represents the threshold correction due to integrating out SUSY partners. For the bottom quark mass, it is found [113] that the dominant corrections come from the gluino-sbottom and from the Higgsino-stop loops,

$$\begin{aligned} \left(\frac{\delta m_b}{m_b}\right)_{g_3} &\sim \frac{g_3^2}{6\pi^2} \frac{m_{\tilde{g}} \mu}{m_{\text{SUSY}}^2} \tan \beta \quad \text{and} \\ \left(\frac{\delta m_b}{m_b}\right)_{\lambda_t} &\sim \frac{\lambda_t^2}{16\pi^2} \frac{A_t \mu}{m_{\text{SUSY}}^2} \tan \beta, \end{aligned} \quad (93.16)$$

where $m_{\tilde{g}}$, μ , and A_t stand for gluino and Higgsino masses and trilinear stop coupling, respectively. Note that Eq. (93.16) only illustrates the structure of the corrections – non-trivial functional dependences on several soft parameters $\sim m_{\text{SUSY}}$ have been suppressed. For the full one-loop correction to the bottom quark mass see, for example, Ref. [114].

Note also that the corrections do not go to zero as SUSY particles become much heavier than m_Z . They may change the bottom quark mass at the $\mathcal{O}(10)\%$ level for $\tan \beta = \mathcal{O}(10)$. The total effect is sensitive to the relative phase between gluino and Higgsino masses since $A_t \sim -m_{\tilde{g}}$ due to the infrared fixed point nature of the RG equation for A_t [115] in settings where SUSY breaking terms come from Planck scale dynamics, such as gravity mediation. The τ lepton mass also receives a similar correction, though only at the few % level. The top quark mass correction, not being proportional to $\tan \beta$, is at most 10% [116].

Including one loop threshold corrections at m_Z and additional RG running, one finds the top, bottom and τ pole masses. In SUSY GUTs, $b\text{--}\tau$ unification has two possible solutions with $\tan \beta \sim 1$ or $\mathcal{O}(10)$. The small $\tan \beta$ solution may be realized in the MSSM if superpartner masses are $\mathcal{O}(10)$ TeV, as suggested by the observed Higgs mass [101]. The large $\tan \beta$ limit such as $\tan \beta \sim 40\text{--}50$ overlaps the $SO(10)$ symmetry relation [116,117]. When $\tan \beta$ is large, there are significant threshold corrections to

down quark masses as mentioned above, and Yukawa unification is only consistent with low-energy data in a restricted region of SUSY parameter space, with important consequences for SUSY searches [116, 118]. More recent analyses of Yukawa unification after LHC Run-I are found in Ref. [119].

Gauge coupling unification is also successful in the scenario of split supersymmetry [80], in which squarks and sleptons have mass at a scale $\tilde{m} \gg m_Z$, while gauginos and/or Higgsinos have masses of order the weak scale. Unification of b - τ Yukawa couplings requires $\tan\beta$ to be fine-tuned close to 1 [101]. If by contrast, $\tan\beta \gtrsim 1.5$, b - τ Yukawa unification only works for $\tilde{m} \lesssim 10^4$ GeV. This is because the effective theory between the gaugino mass scale and \tilde{m} includes only one Higgs doublet, as in the standard model. As a result, the large top quark Yukawa coupling tends to increase the ratio λ_b/λ_τ due to the vertex correction, which is absent in supersymmetric theories, as one runs down in energy below \tilde{m} . This is opposite to what happens in the MSSM where the large top quark Yukawa coupling lowers the ratio λ_b/λ_τ [110].

93.7.2 Beyond leading order: three-family models

Simple Yukawa unification is not possible for the first two generations. Indeed, the simplest implementation of $SU(5)$ implies $\lambda_s = \lambda_\mu$, $\lambda_d = \lambda_e$ and hence $\lambda_s/\lambda_d = \lambda_\mu/\lambda_e$. This is an RG-invariant relation which extrapolates to $m_s/m_d = m_\mu/m_e$ at the weak scale, in serious disagreement with data ($m_s/m_d \sim 20$ and $m_\mu/m_e \sim 200$). An elegant solution to this problem was given by Georgi and Jarlskog [120] (for a recent analysis in the SUSY context see [121]).

More generally, we have to recall that in all of the previous discussion of Yukawa couplings, we assumed renormalizable interactions as well as the minimal matter and Higgs content. Since the GUT scale is close to the Planck scale, higher-dimension operators involving the GUT-breaking Higgs may modify the predictions, especially for lower generations. An example is provided by the operators $\mathbf{10} \bar{\mathbf{5}} \bar{\mathbf{5}}_H \mathbf{24}_H$ with $\mathbf{24}_H$ the GUT-breaking Higgs of $SU(5)$. We can fit parameters to the observed fermion masses with these operators, though some fine-tuning is introduced in doing so. The SM Higgs doublet may come in part from higher representations of the GUT group. For example, the $\mathbf{45}$ of $SU(5)$ includes an $SU(2)_L$ doublet with appropriate $U(1)_Y$ charge [120]. This $\mathbf{45}$ can, in turn, come from the $\mathbf{120}$ or $\mathbf{126}$ of $SO(10)$ after its breaking to $SU(5)$ [122, 123]. These fields may also have renormalizable couplings with quarks and leptons. The relations among the Yukawa coupling constants in the SM are modified if the SM Higgs doublet is a linear combination of several such doublets from different $SU(5)$ multiplets. Finally, the SM fermions may not be embedded in GUT multiplets in the minimal way. Indeed, if all quarks and leptons are embedded in $\mathbf{16}$ s of $SO(10)$, the renormalizable interactions with $\mathbf{10}_H$ cannot explain the observed CKM mixing angles. This situation improves when extra matter multiplets, such as $\mathbf{10}$, are introduced: After $U(1)_X$, which distinguishes the $\bar{\mathbf{5}}$ s coming from the $\mathbf{16}$ and the $\mathbf{10}$ of $SO(10)$, is broken (e.g. by a VEV of $\mathbf{16}_H$ or $\mathbf{126}_H$), the r.h. down quarks and l.h. leptons in the SM can be linear combinations of components in $\mathbf{16}$ s and $\mathbf{10}$ s. As a result, $\lambda \neq \lambda'$ in $SU(5)$ [124].

To construct realistic three-family models, some or all of the above effects can be used. Even so, to achieve significant predictions for fermion masses and mixing angles grand unification alone is not sufficient. Other ingredients, for example additional global family symmetries are needed (in particular, non-Abelian symmetries can strongly reduce the number of free parameters). These family symmetries constrain the set of effective higher-dimensional fermion mass operators discussed above. In addition, sequential breaking of the family symmetry can be correlated with the hierarchy of fermion masses [125]. One simple, widely known idea in this context is to ensure that each $\mathbf{10}_i$ enters Yukawa interactions together with a suppression factor e^{3-i} (ϵ being a small parameter). This way one automatically generates a stronger hierarchy in up-type quark Yukawas as compared to down-type quark and lepton Yukawas and no hierarchy for neutrinos, which agrees with observations at the $\mathcal{O}(1)$ -level. Three-family models exist which fit all the data, including neutrino masses and mixing [27, 126].

Finally, a particularly ambitious variant of unification is to re-

quire that the fermions of all three generations come from a single representation of a large gauge group. A somewhat weaker assumption is that the flavor group (e.g. $SU(3)$) unifies with the SM gauge group in a simple gauge group at some energy scale $M \geq M_G$. Early work on such ‘flavor-unified GUTs’, see e.g. [124, 127], has been reviewed in [128, 129]. For a selection of more recent papers see [130]. In such settings, Yukawa couplings are generally determined by gauge couplings together with symmetry breaking VEVs. This is reminiscent of heterotic string GUTs, where all couplings come from the 10d gauge coupling. However, while the $E_8 \rightarrow SU(3) \times E_6$ branching rule $\mathbf{248} = (\mathbf{8}, \mathbf{1}) + (\mathbf{1}, \mathbf{78}) + (\mathbf{3}, \mathbf{27}) + (\bar{\mathbf{3}}, \mathbf{27})$ looks very suggestive in this context, the way in which most modern heterotic models arrive at three generations is actually more complicated.

93.8 Neutrino masses

We see from atmospheric and solar neutrino oscillation observations, along with long baseline accelerator and reactor experiments, that neutrinos have finite masses. By adding three ‘sterile’ neutrinos ν_i^c with Yukawa couplings $\lambda_{\nu,ij}$ ($\nu_i^c L_j H_u$) ($i, j = 1, 2, 3$), one easily obtains three massive Dirac neutrinos with mass $m_\nu = \lambda_\nu v_u$, analogously to quark and charged lepton masses. However, in order to obtain a τ neutrino with mass of order 0.1 eV, one requires the exceedingly small coupling ratio $\lambda_{\nu\tau}/\lambda_\tau \lesssim 10^{-10}$. By contrast, in GUTs the seesaw mechanism *naturally* explains such tiny neutrino masses as follows [2–4]: The sterile neutrinos have no SM gauge quantum numbers so that there is no symmetry other than global lepton number which forbids the Majorana mass term $\frac{1}{2} M_{ij} \nu_i^c \nu_j^c$. Note also that sterile neutrinos can be identified with the r.h. neutrinos necessarily contained in complete families of $SO(10)$ or Pati-Salam models. Since the Majorana mass term violates $U(1)_X$ in $SO(10)$, one might expect $M_{ij} \sim M_G$. The heavy sterile neutrinos can be integrated out, defining an effective low-energy theory with only three light active Majorana neutrinos with the effective dimension-five operator

$$-\mathcal{L}_{eff} = \frac{1}{2} c_{ij} (L_i H_u) (L_j H_u), \quad (93.17)$$

where $c = \lambda_\nu^T M^{-1} \lambda_\nu$. This then leads to a 3×3 Majorana neutrino mass matrix $m = m_\nu^T M^{-1} m_\nu$.

The seesaw mechanism implemented by r.h. neutrinos is sometimes called the type-I seesaw model. There are variant models in which the dimension-five operator for neutrino masses is induced in different ways: In the type-II model, an $SU(2)_L$ triplet Higgs boson Σ is introduced to have couplings ΣL^2 and also ΣH_u^2 [122, 131]. In the type-III model, an $SU(2)_L$ triplet of fermions $\tilde{\Sigma}$ with a Yukawa coupling $\tilde{\Sigma} L H_u$ is introduced [132]. In these models, the dimension-five operator is induced by integrating out the triplet Higgs boson or fermions. Such models can also be implemented in GUTs by introducing Higgs bosons in the $\mathbf{15}$ or fermions in the $\mathbf{24}$ in $SU(5)$ GUTs or the $\mathbf{126}$ in $SO(10)$ GUTs. Notice that the gauge non-singlet fields in the type-II and III models have masses at the intermediate scale. Thus, gauge coupling unification is not automatic if these variant mechanisms are implemented in SUSY GUTs.

Atmospheric neutrino oscillations discovered by Super-Kamiokande [133] require neutrino masses with $\Delta m_\nu^2 \sim 2.5 \times 10^{-3}$ eV² with maximal mixing [64], in the simplest scenario of two neutrino dominance. With hierarchical neutrino masses this implies $m_{\nu\tau} = \sqrt{\Delta m_\nu^2} \sim 0.05$ eV. Next, we can try to relate the neutrino Yukawa coupling to the top quark Yukawa coupling, $\lambda_{\nu\tau} = \lambda_t$ at the GUT scale, as in $SO(10)$ or $SU(4) \times SU(2)_L \times SU(2)_R$ models. This gives $M \sim 10^{14}$ GeV, which is remarkably close to the GUT scale.

Neutrinos pose a special problem for GUTs. The question is why the quark mixing angles in the CKM matrix are small while there are two large lepton mixing angles in the PMNS matrix. Global fits of neutrino masses and mixing angles can, for example, be found in Refs. [134] and [135]. For SUSY GUT models which fit quark and lepton masses, see Ref. [136, 137] for reviews. Finally, for a compilation of the range of SUSY GUT predictions for neutrino mixing, see [138].

We should also note that, both within and independently of the GUT framework, much work has been devoted to neutrino-mass and more generally flavor model building on the basis of discrete symmetries (see e.g. [137, 139]). A more recent interesting twist in this context is the use of the (non-linearly realized) modular group $SL(2, \mathbb{Z})$ as a discrete flavor symmetry [140]. This group plays a key role in string theory as the group of large diffeomorphisms of the 2-torus, the latter appearing as the string worldsheet and, more relevant in the present context, as part of the compactification space of torus orbifold models (cf. also Sect. 93.4). For a selection from the recent significant activity in these directions see e.g. [141].

93.9 Selected topics

93.9.1 Global symmetries

As we discussed, global symmetries are frequently introduced to control higher-dimension operators in GUT models. This is particularly important in the context of nucleon decay but also plays a role in GUT-based flavor model building and cosmological applications, such as baryogenesis and inflation. However, we should note that appealing to global symmetries to suppress specific interactions may not be as straightforward as it naively seems. Indeed, there are two possibilities: On the one hand, the relevant symmetry might be gauged at a higher scale. Effects of the VEVs responsible for the spontaneous breaking are then in principle dangerous and need to be quantified. On the other hand, the symmetry might be truly only global. This must e.g. be the case for anomalous symmetries, which are then also violated by field-theoretic non-perturbative effects. The latter can in principle be exponentially small. It is, however, widely believed that global symmetries are always broken in quantum gravity (see e.g. [142]). One then needs to understand which power or functional form the Planck scale suppression of the relevant interaction has. For example, dimension-five baryon number violating operators suppressed by just one unit of the Planck or string scale are completely excluded in the supersymmetric models.

In view of the above, it is also useful to recall that in string models 4d global symmetries generally originate in higher-dimensional gauge symmetries [40, 143]. Here ‘global’ implies that the gauge boson has acquired a Stückelberg-mass. This is a necessity in the anomalous case (Green-Schwarz mechanism [144]) but can also happen to non-anomalous symmetries. One expects no symmetry violation beyond the well-understood non-perturbative effects. Discrete symmetries arise as subgroups of continuous gauge symmetries, such as $\mathbb{Z}_N \subset U(1)$. In particular, non-anomalous subgroups of Stückelberg-massive $U(1)$ s represent unbroken discrete gauge symmetries and as such are non-perturbatively exact (see e.g. [145]). Of course, such discrete gauge symmetries may also arise as remnants of continuous gauge symmetries after conventional 4d spontaneous breaking.

93.9.2 Anomaly constraints vs. GUT paradigm

As emphasized at the very beginning, the fact that the SM fermions of one generation fill out the $\mathbf{10} + \mathbf{\bar{5}}$ of $SU(5)$ appears to provide overwhelming evidence for some form of GUT embedding. However, one should be aware that a counterargument can be made which is related to the issue of ‘charge quantization by anomaly cancellation’ (see [146, 147] for some early papers and [148] for a more detailed reference list): Imagine we only knew that the low-energy gauge group were G_{SM} and the matter content included the $(\mathbf{3}, \mathbf{2})_Y$, i.e. a ‘quark doublet’ with $U(1)$ -charge Y . One can then ask which possibilities exist of adding further matter to ensure the cancellation of all triangle anomalies. It turns out that this problem has only three different, minimal¹⁰ solutions [147]. One of those is precisely a single SM generation, with the apparent ‘ $SU(5)$ -ness’ emerging accidentally. Thus, if one randomly picks models from the set of consistent gauge theories, preconditioning on G_{SM} and $(\mathbf{3}, \mathbf{2})_Y$, one may easily end up with ‘ $\mathbf{10} + \mathbf{\bar{5}}$ ’ of an $SU(5)$ that is in no way dynamically present. This is precisely what happens in the context of non-GUT string model building [149].

¹⁰ Adding extra vector-like sets of fields, e.g. two fermions which only transform under $U(1)$ and have charges Y and $-Y$, is considered to violate minimality.

93.9.3 Topological defects and phase transitions

Of the various topological defects which may exist in the broken phase of GUT models, the most famous ones are magnetic monopoles. These are typically localized classical solutions carrying magnetic charge under an unbroken $U(1)$ symmetry [150]. These magnetic monopoles with mass of order M_G/α_G can be produced during a possible GUT phase transition in the early Universe. The flux of magnetic monopoles is experimentally found to be less than $\sim 10^{-16} \text{ cm}^{-2} \text{ s}^{-1} \text{ sr}^{-1}$ [151]. Many more are however predicted, hence the GUT monopole problem. In fact, one of the original motivations for inflation was to solve the monopole problem by exponential expansion after the GUT phase transition [152] and hence dilution of the monopole density. Other possible solutions to the monopole problem include: sweeping them away by domain walls [153], $U(1)$ electromagnetic symmetry breaking at high temperature [154] or GUT symmetry non-restoration [155]. Parenthetically, it was also shown that GUT monopoles can catalyze nucleon decay [156]. A significantly stronger bound on the monopole flux can then be obtained by considering X-ray emission from radio pulsars due to monopole capture and the subsequent nucleon decay catalysis [157].

Note that the present upper bound on the inflationary vacuum energy density is very close to the GUT scale, $V_{inf}^{1/4} = (1.88 \times 10^{16} \text{ GeV}) \times (r/0.10)^{1/4}$, with the scalar-to-tensor ratio constrained to $r < 0.036$ [158]. This guarantees that reheating does not lead to temperatures above M_G and hence the monopole problem is solved by inflation (unless M_G is unexpectedly low).

As already noted, topological defects other than monopoles are also common, see e.g. [159]. They can be cosmologically relevant in GUT models based on a gauge group larger than $SU(5)$, say, $SO(10)$, where an intermediate gauge theory may appear. The breaking of this intermediate gauge symmetry can a priori occur anywhere between the GUT and the electroweak scale. Right-handed neutrino masses favor a value near $\mathcal{O}(10^{14})$ GeV and non-SUSY coupling unification may profit from such a two-step GUT breaking scheme (cf. Sect. 93.5). Crucially for the present context, the last breaking step may occur after inflation, generating topological defects (like cosmic strings) which are not diluted. Their signature can be probed through gravitational waves [160], with the metastable string case being of particular phenomenological interest [161, 162]. Metastability arises because the nucleation of a monopole-anti-monopole pair, each of which serves as an endpoint for the string, allow the cosmic string to break. The lifetime becomes long and hence the string stable as the ratio between monopole mass and the square root of the string tension grows. This is related to the ratio of scales of the two symmetry breaking steps. It is of phenomenological interest that metastability allows the string network to evade the recent bound of $G\mu \lesssim 10^{-10}$ (or $\sqrt{\mu} \lesssim 10^{14} \text{ GeV}$) [162]. Moreover the spectrum is blue-tilted compared to the stable string case. Finally, we note that if the intermediate gauge symmetry breaking proceeds with a (strong) first order phase transition, this could also generate gravitational waves [162, 163]. However, due to the relatively high energy scales involved the peak frequency tends to be high, with signals hopefully to be explored in future gravitational wave experiments.

93.9.4 Flavor violation

Yukawa interactions of GUT-scale particles with quarks and leptons may leave imprints on the flavor violation induced by SUSY breaking parameters [164]. To understand this, focus first on the MSSM with universal Planck-scale boundary conditions (as e.g. in gravity mediation). Working in a basis where up-quark and lepton Yukawas are diagonal, one finds that the large top-quark Yukawa coupling reduces the l.h. squark mass squareds in the third generation radiatively. It turns out that only the l.h. down-type squark mass matrix has sizable off-diagonal terms in the flavor basis after CKM-rotation. However, in GUTs the color-triplet Higgs has flavor violating interactions from the Yukawa coupling $\lambda_{ij} (\mathbf{10}_i \mathbf{10}_j \mathbf{5}_H)$, such that flavor-violating r.h. slepton mass terms are radiatively generated in addition [165]. In $SU(5)$ extension of the type-I seesaw model, where r.h. neutrinos are introduced as $SU(5)$ singlets with interactions $\lambda_{ij}^u (\mathbf{1}_i \mathbf{\bar{5}}_j \mathbf{5}_H)$, the doublet and color-triplet Higgses acquire another type of Yukawa

coupling, respectively. They then radiatively generate flavor-violating l.h. slepton [166] and r.h. down squark masses [167]. These flavor-violating SUSY breaking terms induce new contributions to FCNC processes in quark and lepton sectors, such as $\mu \rightarrow e\gamma$ and $K^0\text{--}\bar{K}^0$ and $B^0\text{--}\bar{B}^0$ mixing. Note that even if the flavor-universal SUSY breaking terms are generated at M_G , the r.h. neutrino Yukawa coupling may induce sizable flavor violation in l.h. slepton masses due to the running between M_G and the right-handed-neutrino mass scale.

EDMs are also induced when both l.h. and r.h. squarks/sleptons have flavor-violating mass terms with relative phases, as discussed for $SV(10)$ in [168] or for $SU(5)$ with r.h. neutrinos in [169]. Thus, such low-energy observables constrain GUT-scale interactions.

93.9.5 From GUT baryogenesis to leptogenesis and B/L -violating transitions

During inflation, any conserved quantum number is extremely diluted. Thus, one expects the observed baryon asymmetry of the Universe to originate at reheating or in the subsequent cosmological evolution. In detail, the situation is slightly more involved: Both baryon number B and lepton number L are global symmetries of the SM. However, $(B+L)$ is anomalous and violated by thermal fluctuations in the early Universe, via so-called sphaleron processes. Moreover, it is violated in GUT models, as is most apparent in proton decay. By contrast, $(B-L)$ is anomaly free and preserved by both the SM as well as $SU(5)$ or $SO(10)$ gauge interactions.

Now, the old idea of GUT baryogenesis [170,171] is to generate a $(B+L)$ and hence a baryon asymmetry by the out-of-equilibrium decay of the color-triplet Higgs. However such an asymmetry, generated at GUT temperatures, is washed out by sphalerons¹¹. This can be overcome [173] using lepton-number violating interaction of neutrinos to create a $(B-L)$ from the $(B+L)$ asymmetry, before sphaleron processes become sufficiently fast at $T < 10^{12}$ GeV. This $(B-L)$ asymmetry can then survive the subsequent sphaleron dominated phase. Note that this does not work in the minimal SUSY GUT setting, with the triplet Higgs above the GUT scale. The reason is that a correspondingly high reheating temperature would be required which, as explained above, is ruled out by Planck data.

However, the most widely accepted simple way out of the dilemma is to directly generate a net $(B-L)$ asymmetry dynamically in the early Universe, also using r.h. neutrinos. Indeed, we have seen that neutrino oscillations suggest a new scale of physics of order 10^{14} GeV. This scale is associated with heavy Majorana neutrinos in the seesaw mechanism. If in the early Universe, the decay of the heavy neutrinos is out of equilibrium and violates both lepton number and CP , then a net lepton number may be generated. This lepton number will then be partially converted into baryon number via electroweak processes [174]. This mechanism is called leptogenesis.

If the three heavy Majorana neutrino masses are hierarchical, the net lepton number is produced by decay of the lightest one, and it is proportional to the CP asymmetry in the decay. The CP asymmetry is bounded from above, and the lightest neutrino mass is required to be larger than 10^9 GeV in order to explain the observed baryon asymmetry [175]. This implies that the reheating temperature after inflation should be larger than 10^9 GeV so that the heavy neutrinos are thermally produced¹². In supersymmetric models, there is a tension between leptogenesis and Big Bang Nucleosynthesis (BBN) if gravitinos decay in the BBN era. The gravitino problem gives a constraint on the reheating temperature $\lesssim 10^{6-10}$ GeV though the precise value depends on the SUSY breaking parameters [177]. Recent reviews of leptogenesis can be found in Ref. [178].

One of the important tests of leptogenesis are searches for neutrinoless double- β ($0\nu\beta\beta$) decays¹³. In a $0\nu\beta\beta$ decay, only two

¹¹ To be precise, if lepton flavor numbers L_i ($i = 1-3$) are nonzero and $(L_i - L_j) \neq 0$ ($i \neq j$), one may obtain nonzero values for B and L even if $(B-L) = 0$ [172].

¹² This constraint may be avoided in resonant leptogenesis [176], in which the right-handed neutrinos are required to be almost degenerate in mass.

¹³ Another important test of leptogenesis would be the observation of CP violation in neutrino oscillations. Strictly speaking, the CP phase in the

electrons but no (anti-)neutrinos are emitted by the decaying nucleus. This is in contrast to ordinary double- β decay. Thus, $0\nu\beta\beta$ decays are lepton-number-violating with $\Delta L = 2$. At the nucleon level, this is described by dimension-nine effective operators for $nn \rightarrow ppee$. These operators may in turn come from SM operators of with dimension less than nine, in combination with SM weak interactions. The lowest one is the dimension-five operator generating the Majorana neutrino mass terms (Eq. (93.17)). Thus, if the lepton-number violating effective interactions come from physics at energies much above the weak scale, the $0\nu\beta\beta$ decay rates are proportional to the Majorana neutrino masses. The latest experimental results are reviewed in [64]. For recent studies of the $0\nu\beta\beta$ decay including SM operators up to mass dimension nine, see [179] and refs. therein.

In addition to L -violation, one can consider $(B-L)$ and B -violating phenomena. They are interesting in their own right and may also be relevant to baryogenesis. The relevant operators have higher mass dimension than the familiar dimension-six $(B+L)$ -violating operators (cf. Sec. 93.6). They may be predicted in $SO(10)$ GUTs with an intermediate scale, at which baryogenesis is realized, such as in [180]. First, one may have nucleon decays with $\Delta(B-L) = 2$, such as $n \rightarrow e^-\pi^+$. This is induced by dimension-seven effective operators in the SM, which are suppressed by the SM Higgs VEV or derivatives. Second, there are neutron-antineutron ($n\text{--}\bar{n}$) oscillations, which are induced by $\Delta B = 2$ dimension-nine effective operators in the SM. The upper bound on the mean time for $n\text{--}\bar{n}$ transitions is directly derived using free neutrons [181]. It is also constrained from the lower limit on the lifetime for neutrons bound in ^{16}O , derived by Super-Kamiokande [182]. Their results are very similar. Super-Kamiokande also searches for dinucleon decays with $\Delta B = 2$, such as $pp \rightarrow \pi^+\pi^+$ and $nn \rightarrow \pi^\pm\pi^\mp$ [183].

93.9.6 The QCD Axion

The axion is a hypothetical pseudoscalar particle which is capable of resolving the strong CP problem [184] and may potentially be related to GUT physics. In particular, the strength of the direct coupling of the QCD axion to photons, relative to its coupling to gluons, may be seen as a phenomenological signature of grand unification. It is quantified by the predicted anomaly ratio $E/N = 8/3$ (see [185–187]). This ratio follows from the GUT normalization of the relevant generators together with the completeness of GUT multiplets contributing to the anomaly.¹⁴ It hence arises in axion models of both DFSZ [188] and KSVZ [189] type as long as the Peccei-Quinn symmetry commutes with the GUT group (see e.g. [190]). Specifically in the case of a DFSZ axion, extra $SU(2)$ multiplets contribute to the running of gauge couplings between Peccei-Quinn and GUT scale, potentially affecting unification. By contrast, the KSVZ axion can be implemented without such effects.

We also note that, in bottom-up approaches and in the presence of split GUT multiplets, other anomaly ratios can appear (cf. e.g. [191]). Their embedding in a UV GUT structure, possibly with explicit GUT symmetry breaking, requires case-by-case study. The ratio $E/N = 8/3$ also arises in string-theoretic GUTs [186,192]. In this case, the axion does not come from the phase of a complex scalar but is a fundamental shift-symmetric real field, coupling through a higher-dimension operator directly to the product of the GUT field-strength and its dual.

93.10 Conclusion

Most conservatively, grand unification means that (some of) the SM gauge interactions of $U(1)_Y$, $SU(2)_L$ and $SU(3)_C$ become part of a larger, unifying gauge symmetry at a high energy scale. In most models, especially in the simplest and most appealing variants of $SU(5)$ and $SO(10)$ unification, the statement is much stronger: One expects the three gauge couplings to unify (up to small threshold corrections) at a unique scale, M_G , and the proton to be unstable due to exchange of gauge bosons of the larger

PMNS matrix does not contribute to ϵ_1 in the seesaw model. Nevertheless, the observation of CP violation in neutrino oscillations would suggest that the seesaw mechanism is associated with a large CP violation, similarly to the quark sector.

¹⁴See e.g. eq. (312) of [187]

symmetry group. Supersymmetric grand unified theories provide, by far, the most predictive and economical framework allowing for perturbative unification. Many more details than could be discussed in the present article can be found in some of the classic reviews [128, 193] and the four books [194] (see also [195] for two recent overviews).

Thus, the three classical pillars of GUTs are gauge coupling unification at $M_G \sim 2 \times 10^{16}$ GeV, low-energy supersymmetry (with a large SUSY desert), and nucleon decay. The first of these may be viewed as predicting the value of the strong coupling – a prediction which has already been verified (see Fig. 93.1). Numerically, this prediction remains intact even if SUSY partner masses are somewhat above the weak scale. However, at the conceptual level a continuously increasing lower bound on the SUSY scale is nevertheless problematic for the GUT paradigm: Indeed, if the independent, gauge-hierarchy-based motivation for SUSY is completely abandoned, the SUSY scale and hence α_3 become simply free parameters and the first two pillars crumble. Thus, it is important to keep pushing bounds on proton decay which, although again not completely universal in all GUT constructions, is arguably a more generic part of the GUT paradigm than low-energy SUSY.

Whether or not Yukawa couplings unify is more model dependent. However, irrespective of possible (partial) Yukawa unification, there certainly exists a very interesting and potentially fruitful interplay between flavor model building and grand unification. Especially in the neutrino sector this is strongly influenced by the developing experimental situation.

It is probably fair to say that, due to limitations of the 4d approach, including especially remaining ambiguities (free parameters or ad hoc assumptions) in models of flavor and GUT breaking, the string theoretic approach has become more important in GUT model building. In this framework, challenges include learning how to deal with the many vacua of the ‘landscape’ as well as, for each vacuum, developing the tools for reliably calculating detailed, phenomenological observables. Finally, due to limitations of space, the present article has barely touched on the interesting cosmological implications of GUTs. They may become more important in the future, especially in the case that a high inflationary energy scale is established observationally.

References

- [1] S. Weinberg, Phys. Rev. Lett. **43**, 1566 (1979).
- [2] P. Minkowski, Phys. Lett. **67B**, 421 (1977).
- [3] T. Yanagida, in *Proceedings of the Workshop on the Unified Theory and the Baryon Number of the Universe*, eds. O. Sawada and A. Sugamoto, KEK report No. 79-18, Tsukuba, Japan, 1979; S. Glashow, Quarks and leptons, published in *Proceedings of the Cargèse Lectures*, M. Levy (ed.), Plenum Press, New York, (1980); M. Gell-Mann, P. Ramond and R. Slansky, in *Supergravity*, ed. P. van Nieuwenhuizen *et al.*, North-Holland, Amsterdam, (1979), p. 315 [arXiv:1306.4669].
- [4] F. Wilczek, eConf **C790823**, 437 (1979); E. Witten, Phys. Lett. **91B**, 81 (1980); R. N. Mohapatra and G. Senjanovic, Phys. Rev. Lett. **44**, 912 (1980), [231(1979)].
- [5] G. 't Hooft, NATO Sci. Ser. B **59**, 135 (1980); M. J. G. Veltman, Acta Phys. Polon. **B12**, 437 (1981); L. Maiani, Gif-sur-Yvette Summer School on Particle Physics, 11th, Gif-sur-Yvette, France, 1979 (Inst. Nat. Phys. Nucl. Phys. Particules, Paris, 1979); E. Witten, Nucl. Phys. **B188**, 513 (1981).
- [6] S. Dimopoulos, S. Raby and F. Wilczek, Phys. Rev. **D24**, 1681 (1981); S. Dimopoulos and H. Georgi, Nucl. Phys. **B193**, 150 (1981); L. E. Ibanez and G. G. Ross, Phys. Lett. **105B**, 439 (1981); N. Sakai, Z. Phys. **C11**, 153 (1981); M. B. Einhorn and D. R. T. Jones, Nucl. Phys. **B196**, 475 (1982); W. J. Marciano and G. Senjanovic, Phys. Rev. **D25**, 3092 (1982).
- [7] U. Amaldi, W. de Boer and H. Furstenau, Phys. Lett. **B260**, 447 (1991); J. R. Ellis, S. Kelley and D. V. Nanopoulos, Phys. Lett. **B260**, 131 (1991); P. Langacker and M.-x. Luo, Phys. Rev. **D44**, 817 (1991); C. Giunti, C.W. Kim and U.W. Lee, Mod. Phys. Lett. **A6**, 1745 (1991); P. Langacker and N. Polonsky, Phys. Rev. **D47**, 4028 (1993), [hep-ph/9210235]; M. Carena, S. Pokorski and C. E. M. Wagner, Nucl. Phys. **B406**, 59 (1993), [hep-ph/9303202]; See also the review by S. Dimopoulos, S.A. Raby and F. Wilczek, Physics Today, p. 25 October (1991).
- [8] Y. Okada, M. Yamaguchi and T. Yanagida, Prog. Theor. Phys. **85**, 1 (1991); J. R. Ellis, G. Ridolfi and F. Zwirner, Phys. Lett. **B257**, 83 (1991); H. E. Haber and R. Hempfling, Phys. Rev. Lett. **66**, 1815 (1991).
- [9] M. Carena *et al.*, Phys. Lett. **B355**, 209 (1995), [hep-ph/9504316]; G. Degrassi *et al.*, Eur. Phys. J. **C28**, 133 (2003), [hep-ph/0212020]; P. Kant *et al.*, JHEP **08**, 104 (2010), [arXiv:1005.5709].
- [10] J. L. Feng *et al.*, Phys. Rev. Lett. **111**, 131802 (2013), [arXiv:1306.2318]; S. Heinemeyer (2014), [arXiv:1405.3781]; P. Draper and H. Rzehak, Phys. Rept. **619**, 1 (2016), [arXiv:1601.01890].
- [11] J. C. Pati and A. Salam, Phys. Rev. **D8**, 1240 (1973); For more discussion on the standard charge assignments in this formalism, see A. Davidson, Phys. Rev. **D20**, 776 (1979) and R.N. Mohapatra and R.E. Marshak, Phys. Lett. **B91**, 222 (1980); see also J. C. Pati, Int. J. Mod. Phys. A **32**, 1741013 (2017), arXiv:1706.09531 for a recent account.
- [12] H. Georgi and S. L. Glashow, Phys. Rev. Lett. **32**, 438 (1974).
- [13] J. R. Ellis, M. K. Gaillard and D. V. Nanopoulos, Phys. Lett. **80B**, 360 (1979), [Erratum: Phys. Lett.82B,464(1979)]; E. Golowich, Phys. Rev. **D24**, 2899 (1981).
- [14] S. Weinberg, Phys. Rev. **D26**, 287 (1982); N. Sakai and T. Yanagida, Nucl. Phys. **B197**, 533 (1982).
- [15] H. Georgi, Particles and Fields, *Proceedings of the APS Div. of Particles and Fields*, ed. C. Carlson, p. 575 (1975); H. Fritzsch and P. Minkowski, Annals Phys. **93**, 193 (1975).
- [16] R. Slansky, Phys. Rept. **79**, 1 (1981); H. Georgi, Front. Phys. **54**, 1 (1982); R. Feger and T. W. Kephart, Comput. Phys. Commun. **192**, 166 (2015), [arXiv:1206.6379]; N. Yamatsu, PTEP **2016**, 4, 043B02 (2016), [arXiv:1512.05559].
- [17] S. M. Barr, Phys. Lett. **112B**, 219 (1982); J. P. Derendinger, J. E. Kim and D. V. Nanopoulos, Phys. Lett. **139B**, 170 (1984); I. Antoniadis *et al.*, Phys. Lett. **B194**, 231 (1987); I. Antoniadis *et al.*, Phys. Lett. **B231**, 65 (1989).
- [18] F. Gursev, P. Ramond and P. Sikivie, Phys. Lett. **60B**, 177 (1976).
- [19] A. de Rujula, H. Georgi and S. L. Glashow, *5th Workshop on Grand Unification*, ed. K. Kang, H. Fried and P. Frampton, World Scientific, Singapore (1984), p. 88; See also earlier paper by Y. Achiman and B. Stech, p. 303, “New Phenomena in Lepton-Hadron Physics,” ed. D.E.C. Fries and J. Wess, Plenum, NY (1979).
- [20] B. R. Greene *et al.*, Nucl. Phys. **B278**, 667 (1986); B. R. Greene *et al.*, Nucl. Phys. **B292**, 606 (1987); B. R. Greene, C. A. Lutken and G. G. Ross, Nucl. Phys. **B325**, 101 (1989); J. E. Kim, Phys. Lett. **B591**, 119 (2004), [hep-ph/0403196].
- [21] E. Witten, Phys. Lett. **105B**, 267 (1981).
- [22] A. Masiero *et al.*, Phys. Lett. **115B**, 380 (1982); B. Grinstein, Nucl. Phys. **B206**, 387 (1982).
- [23] S. Dimopoulos and F. Wilczek, *Proceedings Erice Summer School*, ed. A. Zichichi (1981); M. Srednicki, Nucl. Phys. **B202**, 327 (1982).
- [24] K. Inoue, A. Kakuto and H. Takano, Prog. Theor. Phys. **75**, 664 (1986).
- [25] Y. Yamada, Z. Phys. **C60**, 83 (1993); J. Hisano *et al.*, Phys. Lett. **B342**, 138 (1995), [hep-ph/9406417]; G. Altarelli, F. Feruglio and I. Masina, JHEP **11**, 040 (2000), [hep-ph/0007254].

- [26] K. S. Babu and S. M. Barr, *Phys. Rev.* **D48**, 5354 (1993), [hep-ph/9306242]; K. S. Babu and S. M. Barr, *Phys. Rev.* **D50**, 3529 (1994), [hep-ph/9402291]; K. S. Babu, J. C. Pati and Z. Tavartkiladze, *JHEP* **06**, 084 (2010), [arXiv:1003.2625].
- [27] K. S. Babu and R. N. Mohapatra, *Phys. Rev. Lett.* **74**, 2418 (1995), [hep-ph/9410326]; V. Lucas and S. Raby, *Phys. Rev.* **D54**, 2261 (1996), [hep-ph/9601303]; T. Blazek *et al.*, *Phys. Rev.* **D56**, 6919 (1997), [hep-ph/9611217]; S. M. Barr and S. Raby, *Phys. Rev. Lett.* **79**, 4748 (1997), [hep-ph/9705366]; K. S. Babu, J. C. Pati and F. Wilczek, *Nucl. Phys.* **B566**, 33 (2000), [hep-ph/9812538]; R. Dermisek, A. Mafi and S. Raby, *Phys. Rev.* **D63**, 035001 (2001), [hep-ph/0007213].
- [28] R. Barbieri, G. R. Dvali and A. Strumia, *Nucl. Phys.* **B391**, 487 (1993); Z. Berezhiani, C. Csaki and L. Randall, *Nucl. Phys.* **B444**, 61 (1995), [hep-ph/9501336]; Q. Shafi and Z. Tavartkiladze, *Phys. Lett.* **B522**, 102 (2001), [hep-ph/0105140].
- [29] M. W. Goodman and E. Witten, *Nucl. Phys. B* **271**, 21 (1986).
- [30] E. Witten, in “Supersymmetry and unification of fundamental interactions. Proceedings, 10th International Conference, SUSY’02, Hamburg, Germany, June 17-23, 2002,” 472–491 (2001), [hep-ph/0201018], URL http://www-library.desy.de/preparch/desy/proc/proc02-02/Proceedings/susy02/special/hertz_pr.ps.
- [31] K. Harigaya, M. Ibe and M. Suzuki, *JHEP* **09**, 155 (2015), [arXiv:1505.05024].
- [32] G. F. Giudice and A. Masiero, *Phys. Lett.* **B206**, 480 (1988); J. E. Kim and H. P. Nilles, *Mod. Phys. Lett.* **A9**, 3575 (1994), [hep-ph/9406296].
- [33] L. Randall and C. Csaki, in “Supersymmetry and unification of fundamental interactions. Proceedings, International Workshop, SUSY 95, Palaiseau, France, May 15-19, 1995,” 99–109 (1995), [235(1995)], [hep-ph/9508208]; M. Dine, Y. Nir and Y. Shadmi, *Phys. Rev.* **D66**, 115001 (2002), [hep-ph/0206268].
- [34] A. Hebecker, J. March-Russell and R. Ziegler, *JHEP* **08**, 064 (2009), [arXiv:0801.4101]; F. Brummer *et al.*, *JHEP* **08**, 011 (2009), [arXiv:0906.2957]; F. Brummer *et al.*, *JHEP* **04**, 006 (2010), [arXiv:1003.0084].
- [35] H. M. Lee *et al.*, *Phys. Lett.* **B694**, 491 (2011), [arXiv:1009.0905]; R. Kappl *et al.*, *Nucl. Phys.* **B847**, 325 (2011), [arXiv:1012.4574]; H. M. Lee *et al.*, *Nucl. Phys.* **B850**, 1 (2011), [arXiv:1102.3595].
- [36] Y. Hosotani, *Phys. Lett.* **126B**, 309 (1983).
- [37] L. J. Dixon *et al.*, *Nucl. Phys.* **B261**, 678 (1985), [678(1985)]; L. J. Dixon *et al.*, *Nucl. Phys.* **B274**, 285 (1986); L. E. Ibanez, H. P. Nilles and F. Quevedo, *Phys. Lett.* **B187**, 25 (1987); L. E. Ibanez *et al.*, *Phys. Lett.* **B191**, 282 (1987).
- [38] P. Candelas *et al.*, *Nucl. Phys.* **B258**, 46 (1985).
- [39] Y. Kawamura, *Prog. Theor. Phys.* **103**, 613 (2000), [hep-ph/9902423]; Y. Kawamura, *Prog. Theor. Phys.* **105**, 999 (2001), [hep-ph/0012125]; G. Altarelli and F. Feruglio, *Phys. Lett.* **B511**, 257 (2001), [hep-ph/0102301]; L. J. Hall and Y. Nomura, *Phys. Rev.* **D64**, 055003 (2001), [hep-ph/0103125]; A. Hebecker and J. March-Russell, *Nucl. Phys.* **B613**, 3 (2001), [hep-ph/0106166]; T. Asaka, W. Buchmuller and L. Covi, *Phys. Lett.* **B523**, 199 (2001), [hep-ph/0108021]; L. J. Hall *et al.*, *Phys. Rev.* **D65**, 035008 (2002), [hep-ph/0108071]; R. Dermisek and A. Mafi, *Phys. Rev.* **D65**, 055002 (2002), [hep-ph/0108139]; H. D. Kim and S. Raby, *JHEP* **01**, 056 (2003), [hep-ph/0212348].
- [40] L.E. Ibanez and A.M. Uranga, “String theory and particle physics: An introduction to string phenomenology,” Cambridge University Press 2012; K.-S. Choi and J. E. Kim, *Lect. Notes Phys.* **696**, 1 (2006); R. Blumenhagen *et al.*, *Phys. Rept.* **445**, 1 (2007), [hep-th/0610327].
- [41] D. J. Gross *et al.*, *Phys. Rev. Lett.* **54**, 502 (1985).
- [42] V. Braun *et al.*, *JHEP* **05**, 043 (2006), [hep-th/0512177]; V. Bouchard and R. Donagi, *Phys. Lett.* **B633**, 783 (2006), [hep-th/0512149]; L. B. Anderson *et al.*, *Phys. Rev.* **D84**, 106005 (2011), [arXiv:1106.4804].
- [43] L. J. Dixon, V. Kaplunovsky and J. Louis, *Nucl. Phys.* **B355**, 649 (1991).
- [44] G. Aldazabal *et al.*, *Nucl. Phys.* **B452**, 3 (1995), [hep-th/9410206]; Z. Kakushadze *et al.*, *Int. J. Mod. Phys.* **A13**, 2551 (1998), [hep-th/9710149].
- [45] E. Witten, *Nucl. Phys.* **B258**, 75 (1985).
- [46] S. Gukov *et al.*, *Phys. Rev.* **D69**, 086008 (2004), [hep-th/0310159]; G. Curio, A. Krause and D. Lust, *Fortsch. Phys.* **54**, 225 (2006), [hep-th/0502168]; L. B. Anderson *et al.*, *Phys. Rev.* **D83**, 106011 (2011), [arXiv:1102.0011].
- [47] R. Friedman, J. Morgan and E. Witten, *Commun. Math. Phys.* **187**, 679 (1997), [hep-th/9701162].
- [48] R. Blumenhagen, G. Honecker and T. Weigand, *JHEP* **08**, 009 (2005), [hep-th/0507041]; L. B. Anderson *et al.*, *JHEP* **01**, 047 (2014), [arXiv:1307.4787].
- [49] T. Kobayashi, S. Raby and R.-J. Zhang, *Phys. Lett.* **B593**, 262 (2004), [hep-ph/0403065].
- [50] S. Forste *et al.*, *Phys. Rev.* **D70**, 106008 (2004), [hep-th/0406208]; T. Kobayashi, S. Raby and R.-J. Zhang, *Nucl. Phys.* **B704**, 3 (2005), [hep-ph/0409098]; W. Buchmuller *et al.*, *Nucl. Phys.* **B712**, 139 (2005), [hep-ph/0412318]; W. Buchmuller *et al.*, *Phys. Rev. Lett.* **96**, 121602 (2006), [hep-ph/0511035]; W. Buchmuller *et al.*, *Nucl. Phys.* **B785**, 149 (2007), [hep-th/0606187]; O. Lebedev *et al.*, *Phys. Lett.* **B645**, 88 (2007), [hep-th/0611095]; J. E. Kim, J.-H. Kim and B. Kyae, *JHEP* **06**, 034 (2007), [hep-ph/0702278]; O. Lebedev *et al.*, *Phys. Rev.* **D77**, 046013 (2008), [arXiv:0708.2691].
- [51] S. B. Giddings, S. Kachru and J. Polchinski, *Phys. Rev.* **D66**, 106006 (2002), [hep-th/0105097]; S. Kachru *et al.*, *Phys. Rev.* **D68**, 046005 (2003), [hep-th/0301240].
- [52] R. Blumenhagen *et al.*, *Nucl. Phys.* **B815**, 1 (2009), [arXiv:0811.2936].
- [53] R. Blumenhagen *et al.*, *Nucl. Phys.* **B616**, 3 (2001), [hep-th/0107138].
- [54] R. Donagi and M. Wijnholt, *Adv. Theor. Math. Phys.* **15**, 5, 1237 (2011), [arXiv:0802.2969].
- [55] C. Beasley, J. J. Heckman and C. Vafa, *JHEP* **01**, 058 (2009), [arXiv:0802.3391]; C. Beasley, J. J. Heckman and C. Vafa, *JHEP* **01**, 059 (2009), [arXiv:0806.0102].
- [56] T. Weigand, *Class. Quant. Grav.* **27**, 214004 (2010), [arXiv:1009.3497]; J. J. Heckman, *Ann. Rev. Nucl. Part. Sci.* **60**, 237 (2010), [arXiv:1001.0577]; M. Cvetic, I. Garcia-Etxebarria and J. Halverson, *JHEP* **01**, 073 (2011), [arXiv:1003.5337]; A. Maharana and E. Palti, *Int. J. Mod. Phys.* **A28**, 1330005 (2013), [arXiv:1212.0555]; S. Krippendorff, S. Schafer-Nameki and J.-M. Wong, *JHEP* **11**, 008 (2015), [arXiv:1507.05961].
- [57] R. Donagi and M. Wijnholt, *Adv. Theor. Math. Phys.* **15**, 6, 1523 (2011), [arXiv:0808.2223]; R. Blumenhagen, *Phys. Rev. Lett.* **102**, 071601 (2009), [arXiv:0812.0248]; K.-S. Choi and J. E. Kim, *Phys. Rev.* **D83**, 065016 (2011), [arXiv:1012.0847]; C. Mayrhofer, E. Palti and T. Weigand, *JHEP* **09**, 082 (2013), [arXiv:1303.3589]; G. K. Leon-taris and Q. Shafi, *Phys. Rev.* **D96**, 6, 066023 (2017), [arXiv:1706.08372].
- [58] E. Witten, *Nucl. Phys.* **B471**, 135 (1996), [hep-th/9602070].
- [59] A. Hebecker and M. Trapletti, *Nucl. Phys.* **B713**, 173 (2005), [hep-th/0411131].
- [60] B. Dundee and S. Raby (2008), [arXiv:0808.0992].

- [61] G. G. Ross (2004), [hep-ph/0411057].
- [62] H. Georgi, H. R. Quinn and S. Weinberg, Phys. Rev. Lett. **33**, 451 (1974); S. Weinberg, Phys. Lett. **91B**, 51 (1980); L. J. Hall, Nucl. Phys. **B178**, 75 (1981).
- [63] B. C. Allanach, Comput. Phys. Commun. **143**, 305 (2002), [hep-ph/0104145].
- [64] R. L. Workman *et al.* (Particle Data Group), PTEP **2022**, 083C01 (2022).
- [65] M. L. Alciati *et al.*, JHEP **03**, 054 (2005), [hep-ph/0501086].
- [66] See talks on proposed and running nucleon decay experiments, and theoretical talks by P. Langacker, p. 131, and W.J. Marciano and A. Sirlin, p. 151, in *The Second Workshop on Grand Unification*, eds. J.P. Leveille *et al.*, Birkhäuser, Boston (1981).
- [67] W.J. Marciano, p. 190, *Eighth Workshop on Grand Unification*, ed. K. Wali, World Scientific Publishing Co., Singapore (1987).
- [68] M.S. Carena *et al.*, in Ref. [7].
- [69] A. Djouadi, J.-L. Kneur and G. Moultaka, Comput. Phys. Commun. **176**, 426 (2007), [hep-ph/0211331].
- [70] W. Porod and F. Staub, Comput. Phys. Commun. **183**, 2458 (2012), [arXiv:1104.1573].
- [71] W. Siegel, Phys. Lett. **94B**, 37 (1980).
- [72] I. Antoniadis, C. Kounnas, and R. Lacaze, Nucl. Phys. **B221**, 377 (1983).
- [73] M. A. Shifman, Int. J. Mod. Phys. **A11**, 5761 (1996), [hep-ph/9606281]; N. Arkani-Hamed and H. Murayama, JHEP **06**, 030 (2000), [hep-th/9707133]; I. Jack, D. R. T. Jones and A. Pickering, Phys. Lett. **B435**, 61 (1998), [hep-ph/9805482].
- [74] M.B. Einhorn and D.R.T. Jones in Ref. [6]; I. Antoniadis, C. Kounnas and K. Tamvakis, Phys. Lett. **119B**, 377 (1982).
- [75] J. Hisano, H. Murayama and T. Yanagida, Phys. Rev. Lett. **69**, 1014 (1992); J. Hisano, H. Murayama and T. Yanagida, Nucl. Phys. B **402**, 46 (1993), [hep-ph/9207279].
- [76] H. Murayama and A. Pierce, Phys. Rev. **D65**, 055009 (2002), [hep-ph/0108104].
- [77] G. Anderson *et al.*, eConf **C960625**, SUP107 (1996) [hep-ph/9609457].
- [78] L. Roszkowski and M. A. Shifman, Phys. Rev. **D53**, 404 (1996), [hep-ph/9503358]; S. Raby, M. Ratz and K. Schmidt-Hoberg, Phys. Lett. **B687**, 342 (2010), [arXiv:0911.4249].
- [79] J. Hisano, T. Kuwahara and N. Nagata, Phys. Lett. **B723**, 324 (2013), [arXiv:1304.0343].
- [80] N. Arkani-Hamed, A. Delgado and G. F. Giudice, Nucl. Phys. **B741**, 108 (2006), [hep-ph/0601041].
- [81] M. Ibe, T. Moroi and T. T. Yanagida, Phys. Lett. **B644**, 355 (2007), [hep-ph/0610277].
- [82] G. F. Giudice *et al.*, JHEP **12**, 027 (1998), [hep-ph/9810442]; L. Randall and R. Sundrum, Nucl. Phys. **B557**, 79 (1999), [hep-th/9810155].
- [83] R. N. Mohapatra and M. K. Parida, Phys. Rev. **D47**, 264 (1993), [hep-ph/9204234].
- [84] D.-G. Lee *et al.*, Phys. Rev. **D51**, 229 (1995), [hep-ph/9404238].
- [85] L. E. Ibanez *et al.*, JHEP **07**, 195 (2012), [arXiv:1206.2655].
- [86] K. R. Dienes, E. Dudas and T. Gherghetta, Phys. Rev. Lett. **91**, 061601 (2003), [hep-th/0210294].
- [87] K. Agashe, R. Contino and R. Sundrum, Phys. Rev. Lett. **95**, 171804 (2005), [hep-ph/0502222].
- [88] F. Wilczek and A. Zee, Phys. Rev. Lett. **43**, 1571 (1979).
- [89] A. Takenaka *et al.* (Super-Kamiokande), Phys. Rev. D **102**, 11, 112011 (2020), [arXiv:2010.16098].
- [90] K. Abe *et al.* (Hyper-Kamiokande) (2018), [arXiv:1805.04163].
- [91] P. S. B. Dev *et al.* (2022), [arXiv:2203.08771].
- [92] J.-S. Yoo *et al.*, Phys. Rev. D **105**, 7, 074501 (2022), [arXiv:2111.01608].
- [93] J. Hisano, T. Kuwahara and Y. Omura, Nucl. Phys. **B898**, 1 (2015), [Erratum: Nucl. Phys.B907,476(2016)], [arXiv:1503.08561].
- [94] R. Barbier *et al.*, Phys. Rept. **420**, 1 (2005), [hep-ph/0406039]; F. Domingo *et al.*, JHEP **02**, 066 (2019), [arXiv:1810.08228].
- [95] G. R. Farrar and P. Fayet, Phys. Lett. **76B**, 575 (1978).
- [96] S. Dimopoulos, S. Raby and F. Wilczek, Phys. Lett. **112B**, 133 (1982); J. R. Ellis, D. V. Nanopoulos and S. Rudaz, Nucl. Phys. **B202**, 43 (1982).
- [97] C. S. Aulakh *et al.*, Nucl. Phys. **B597**, 89 (2001), [hep-ph/0004031].
- [98] S. Mine (Super Kamiokande), J. Phys. Conf. Ser. **718**, 6, 062044 (2016).
- [99] T. Goto and T. Nihei, Phys. Rev. **D59**, 115009 (1999), [hep-ph/9808255].
- [100] G. D. Coughlan *et al.*, Phys. Lett. **160B**, 249 (1985); J. L. Chkareuli and I. G. Gogoladze, Phys. Rev. **D58**, 055011 (1998), [hep-ph/9803335].
- [101] G. F. Giudice and A. Romanino, Nucl. Phys. **B699**, 65 (2004), [Erratum: Nucl. Phys.B706,487(2005)], [hep-ph/0406088].
- [102] J. Hisano *et al.*, JHEP **07**, 038 (2013), [arXiv:1304.3651].
- [103] B. Bajc, P. Fileviez Perez and G. Senjanovic, Phys. Rev. **D66**, 075005 (2002), [hep-ph/0204311].
- [104] K.-S. Choi, Phys. Lett. **B668**, 392 (2008), [arXiv:0807.2766].
- [105] A. Abusleme *et al.* (JUNO), Prog. Part. Nucl. Phys. **123**, 103927 (2022), [arXiv:2104.02565]; A. Abusleme *et al.* (JUNO) (2022), [arXiv:2212.08502].
- [106] B. Abi *et al.* (DUNE), Eur. Phys. J. C **81**, 4, 322 (2021), [arXiv:2008.12769].
- [107] M. Askins *et al.* (Theia), Eur. Phys. J. C **80**, 5, 416 (2020), [arXiv:1911.03501]; M. Askins *et al.* (Theia), in “Snowmass 2021,” (2022), [arXiv:2202.12839].
- [108] L. J. Hall and Y. Nomura, Phys. Rev. **D66**, 075004 (2002), [hep-ph/0205067]; H. D. Kim, S. Raby and L. Schradin, JHEP **05**, 036 (2005), [hep-ph/0411328].
- [109] M.S. Chanowitz, J.R. Ellis and M.K. Gaillard, Nucl. Phys. **B128**, 506 (1977); A. J. Buras *et al.*, Nucl. Phys. **B135**, 66 (1978).
- [110] K. Inoue *et al.*, Prog. Theor. Phys. **67**, 1889 (1982); L. E. Ibanez and C. Lopez, Nucl. Phys. **B233**, 511 (1984).
- [111] H. Georgi and D. V. Nanopoulos, Nucl. Phys. **B159**, 16 (1979); J. A. Harvey, P. Ramond and D. B. Reiss, Phys. Lett. **92B**, 309 (1980); J. A. Harvey, D. B. Reiss and P. Ramond, Nucl. Phys. **B199**, 223 (1982).
- [112] T. Banks, Nucl. Phys. **B303**, 172 (1988); M. Olechowski and S. Pokorski, Phys. Lett. **B214**, 393 (1988); S. Pokorski, Nucl. Phys. Proc. Suppl. **13**, 606 (1990); B. Ananthanarayan, G. Lazarides and Q. Shafi, Phys. Rev. **D44**, 1613 (1991); Q. Shafi and B. Ananthanarayan, ICTP Summer School lectures (1991); S. Dimopoulos, L. J. Hall and S. Raby, Phys. Rev. Lett. **68**, 1984 (1992); S. Dimopoulos, L. J. Hall and S. Raby, Phys. Rev. **D45**, 4192 (1992); G. W. Anderson *et al.*, Phys. Rev. **D47**, R3702 (1993), [hep-ph/9209250]; B. Ananthanarayan, G. Lazarides and Q. Shafi, Phys. Lett. **B300**, 245 (1993); G. Anderson *et al.*, Phys. Rev. **D49**, 3660 (1994), [hep-ph/9308333]; B. Ananthanarayan, Q. Shafi and X. M. Wang, Phys. Rev. **D50**, 5980 (1994), [hep-ph/9311225].

- [113] L. J. Hall, R. Rattazzi and U. Sarid, *Phys. Rev.* **D50**, 7048 (1994), [hep-ph/9306309]; M. Carena *et al.*, *Nucl. Phys.* **B426**, 269 (1994), [hep-ph/9402253].
- [114] A. Anandakrishnan, B. C. Bryant and S. Raby, *JHEP* **05**, 088 (2015), [arXiv:1411.7035].
- [115] M. Lanzagorta and G. G. Ross, *Phys. Lett.* **B364**, 163 (1995), [hep-ph/9507366].
- [116] K. Tobe and J. D. Wells, *Nucl. Phys.* **B663**, 123 (2003), [hep-ph/0301015].
- [117] G. Ross and M. Serna, *Phys. Lett.* **B664**, 97 (2008), [arXiv:0704.1248].
- [118] T. Blazek, R. Dermisek and S. Raby, *Phys. Rev. Lett.* **88**, 111804 (2002), [hep-ph/0107097]; T. Blazek, R. Dermisek and S. Raby, *Phys. Rev.* **D65**, 115004 (2002), [hep-ph/0201081]; D. Auto *et al.*, *JHEP* **06**, 023 (2003), [hep-ph/0302155]; R. Dermisek *et al.*, *JHEP* **04**, 037 (2003), [hep-ph/0304101]; R. Dermisek *et al.*, *JHEP* **09**, 029 (2005), [hep-ph/0507233].
- [119] A. Anandakrishnan, S. Raby and A. Wingerter, *Phys. Rev.* **D87**, 5, 055005 (2013), [arXiv:1212.0542]; M. Adeel Ajaib *et al.*, *JHEP* **07**, 139 (2013), [arXiv:1303.6964]; Z. Poh and S. Raby, *Phys. Rev.* **D92**, 1, 015017 (2015), [arXiv:1505.00264]; M. Badziak, M. Olechowski and S. Pokorski, *JHEP* **10**, 088 (2013), [arXiv:1307.7999].
- [120] H. Georgi and C. Jarlskog, *Phys. Lett.* **86B**, 297 (1979).
- [121] S. Antusch and M. Spinrath, *Phys. Rev.* **D79**, 095004 (2009), [arXiv:0902.4644].
- [122] G. Lazarides, Q. Shafi and C. Wetterich, *Nucl. Phys.* **B181**, 287 (1981).
- [123] T. E. Clark, T.-K. Kuo and N. Nakagawa, *Phys. Lett.* **115B**, 26 (1982); K. S. Babu and R. N. Mohapatra, *Phys. Rev. Lett.* **70**, 2845 (1993), [hep-ph/9209215].
- [124] R. Barbieri and D. V. Nanopoulos, *Phys. Lett.* **91B**, 369 (1980).
- [125] C. D. Froggatt and H. B. Nielsen, *Nucl. Phys.* **B147**, 277 (1979).
- [126] R. Barbieri *et al.*, *Nucl. Phys.* **B493**, 3 (1997), [hep-ph/9610449]; T. Blazek, S. Raby and K. Tobe, *Phys. Rev.* **D60**, 113001 (1999), [hep-ph/9903340]; T. Blazek, S. Raby and K. Tobe, *Phys. Rev.* **D62**, 055001 (2000), [hep-ph/9912482]; Q. Shafi and Z. Tavartkiladze, *Phys. Lett.* **B487**, 145 (2000), [hep-ph/9910314]; C. H. Albright and S. M. Barr, *Phys. Rev. Lett.* **85**, 244 (2000), [hep-ph/0002155]; Z. Berezhiani and A. Rossi, *Nucl. Phys.* **B594**, 113 (2001), [hep-ph/0003084]; C. H. Albright and S. M. Barr, *Phys. Rev.* **D64**, 073010 (2001), [hep-ph/0104294]; M.-C. Chen and K. T. Mahanthappa, *Int. J. Mod. Phys.* **A18**, 5819 (2003), [hep-ph/0305088]; R. Dermisek and S. Raby, *Phys. Lett.* **B622**, 327 (2005), [hep-ph/0507045].
- [127] H. Georgi, *Nucl. Phys.* **B156**, 126 (1979); P. H. Frampton, *Phys. Lett.* **88B**, 299 (1979); P. Frampton and S. Nandi, *Phys. Rev. Lett.* **43**, 1460 (1979); J.E. Kim, *Phys. Rev. Lett.* **45**, 1916 (1980), *Phys. Rev.* **D23**, 2706 (1981) and *Phys. Rev.* **D26**, 674 (1982); Y. Fujimoto, *Phys. Rev.* **D26**, 3183 (1982).
- [128] P. Langacker, *Phys. Rept.* **72**, 185 (1981).
- [129] H. Georgi, *Conf. Proc. C* **820726**, 705 (1982).
- [130] S. M. Barr, *Phys. Rev.* **D78**, 055008 (2008), [arXiv:0805.4808]; Y. Goto, Y. Kawamura and T. Miura, *Phys. Rev.* **D88**, 5, 055016 (2013), [arXiv:1307.2631]; J. E. Kim, *JHEP* **06**, 114 (2015), [arXiv:1503.03104]; C.H. Albright, R.P. Feger and T.W. Kephart, arXiv:1601.07523; M. Reig, J. W. F. Valle, C. A. Vaquera-Araujo and F. Wilczek, arXiv:1706.03116.
- [131] M. Magg and C. Wetterich, *Phys. Lett.* **94B**, 61 (1980); J. Schechter and J. W. F. Valle, *Phys. Rev.* **D22**, 2227 (1980); R. N. Mohapatra and G. Senjanovic, *Phys. Rev.* **D23**, 165 (1981); G. B. Gelmini and M. Roncadelli, *Phys. Lett.* **99B**, 411 (1981).
- [132] R. Foot *et al.*, *Z. Phys.* **C44**, 441 (1989).
- [133] Y. Fukuda *et al.* (Super-Kamiokande), *Phys. Rev. Lett.* **81**, 1562 (1998), [hep-ex/9807003].
- [134] M.C. Gonzalez-Garcia and M. Yokoyama, Review of 'Neutrino Masses, Mixing, and Oscillations' in Ref. [64].
- [135] I. Esteban *et al.*, *JHEP* **09**, 178 (2020), [arXiv:2007.14792].
- [136] G. Altarelli, *Soryushiron Kenkyu Electron.* **116**, A29 (2008), [arXiv:0711.0161].
- [137] S. F. King and C. Luhn, *Rept. Prog. Phys.* **76**, 056201 (2013), [arXiv:1301.1340].
- [138] C. H. Albright and M.-C. Chen, *Phys. Rev.* **D74**, 113006 (2006), [hep-ph/0608137].
- [139] G. Altarelli and F. Feruglio, *Rev. Mod. Phys.* **82**, 2701 (2010), [arXiv:1002.0211]; H. Ishimori *et al.*, *Prog. Theor. Phys. Suppl.* **183**, 1 (2010), [arXiv:1003.3552].
- [140] F. Feruglio, *Are neutrino masses modular forms?*, 227–266 (2019), [arXiv:1706.08749].
- [141] T. Kobayashi, K. Tanaka and T. H. Tatsuishi, *Phys. Rev. D* **98**, 1, 016004 (2018), [arXiv:1803.10391]; J. T. Penedo and S. T. Petcov, *Nucl. Phys. B* **939**, 292 (2019), [arXiv:1806.11040]; Y. Almumin *et al.*, *JHEP* **05**, 078 (2021), [arXiv:2102.11286]; H. P. Nilles, S. Ramos-Sánchez and P. K. S. Vaudrevange, *JHEP* **02**, 045 (2020), [arXiv:2001.01736].
- [142] R. Kallosh *et al.*, *Phys. Rev.* **D52**, 912 (1995), [hep-th/9502069].
- [143] H. Ruegg and M. Ruiz-Altaba, *Int. J. Mod. Phys.* **A19**, 3265 (2004), [hep-th/0304245].
- [144] M. B. Green and J. H. Schwarz, *Phys. Lett.* **149B**, 117 (1984).
- [145] L. E. Ibanez and G. G. Ross, *Nucl. Phys.* **B368**, 3 (1992); M. Berasaluze-Gonzalez *et al.*, *JHEP* **12**, 113 (2011), [arXiv:1106.4169].
- [146] N.G. Deshpande, OITS-107; C. Q. Geng and R. E. Marshak, *Phys. Rev.* **D39**, 693 (1989); A. Font, L. E. Ibanez and F. Quevedo, *Phys. Lett.* **B228**, 79 (1989); K. S. Babu and R. N. Mohapatra, *Phys. Rev. Lett.* **63**, 938 (1989).
- [147] R. Foot *et al.*, *Phys. Rev.* **D39**, 3411 (1989).
- [148] M. Nowakowski and A. Pilaftsis, *Phys. Rev.* **D48**, 259 (1993), [hep-ph/9304312].
- [149] T. P. T. Dijkstra, L. R. Huiszoon and A. N. Schellekens, *Phys. Lett.* **B609**, 408 (2005), [hep-th/0403196]; F. Gmeiner *et al.*, *JHEP* **01**, 004 (2006), [hep-th/0510170]; B. Gato-Rivera and A. N. Schellekens, *Nucl. Phys.* **B883**, 529 (2014), [arXiv:1401.1782].
- [150] G. 't Hooft, *Nucl. Phys.* **B79**, 276 (1974) A.M. Polyakov, *Pis'ma Zh. Eksp. Teor. Fiz.* **20**, 430 (1974) [Sov. Phys. JETP Lett. **20**, 194 (1974)]; For a pedagogical introduction, see S. Coleman, in *Aspects of Symmetry*, Selected Erice Lectures, Cambridge University Press, Cambridge, (1985), and P. Goddard and D. Olive, *Rept. on Prog. in Phys.* **41**, 1357 (1978).
- [151] M. Ambrosio *et al.* (MACRO), *Eur. Phys. J.* **C25**, 511 (2002), [hep-ex/0207020]; S. Balestra *et al.* (2011), [arXiv:1105.5587]; L. Patrizzii and M. Spurio, *Ann. Rev. Nucl. Part. Sci.* **65**, 279 (2015), [arXiv:1510.07125].
- [152] For a review, see A.D. Linde, *Particle Physics and Inflationary Cosmology*, Harwood Academic, Switzerland (1990).
- [153] G. R. Dvali, H. Liu and T. Vachaspati, *Phys. Rev. Lett.* **80**, 2281 (1998), [hep-ph/9710301].
- [154] P. Langacker and S.-Y. Pi, *Phys. Rev. Lett.* **45**, 1 (1980).
- [155] G. R. Dvali, A. Melfo and G. Senjanovic, *Phys. Rev. Lett.* **75**, 4559 (1995), [hep-ph/9507230].
- [156] V. Rubakov, *Nucl. Phys.* **B203**, 311 (1982) and Institute of Nuclear Research Report No. P-0211, Moscow (1981), unpublished; C. G. Callan, Jr., *Phys. Rev.* **D26**, 2058 (1982); F. Wilczek, *Phys. Rev. Lett.* **48**, 1146 (1982); S. Dawson and A. N. Schellekens, *Phys. Rev.* **D27**, 2119 (1983).

- [157] K. Freese, M. S. Turner and D. N. Schramm, *Phys. Rev. Lett.* **51**, 1625 (1983).
- [158] P. A. R. Ade *et al.* (BICEP, Keck), *Phys. Rev. Lett.* **127**, 15, 151301 (2021), [arXiv:2110.00483].
- [159] A. Vilenkin, *Phys. Rept.* **121**, 263 (1985); M. B. Hindmarsh and T. W. B. Kibble, *Rept. Prog. Phys.* **58**, 477 (1995), [hep-ph/9411342]; R. Jeannerot, J. Rocher and M. Sakellariadou, *Phys. Rev. D* **68**, 103514 (2003), [hep-ph/0308134].
- [160] B. P. Abbott *et al.* (LIGO Scientific, Virgo), *Phys. Rev. D* **97**, 10, 102002 (2018), [arXiv:1712.01168]; S. F. King *et al.*, *Phys. Rev. Lett.* **126**, 2, 021802 (2021), [arXiv:2005.13549]; S. Chigusa, Y. Nakai and J. Zheng, *Phys. Rev. D* **104**, 3, 035031 (2021), [arXiv:2011.04090]; E. J. Chun and L. Velasco-Sevilla, *Phys. Rev. D* **106**, 3, 035008 (2022), [arXiv:2112.14483].
- [161] A. Vilenkin, *Nucl. Phys. B* **196**, 240 (1982); A. Monin and M. B. Voloshin, *Phys. Rev. D* **78**, 065048 (2008), [arXiv:0808.1693]; W. Buchmuller *et al.*, *Phys. Lett. B* **809**, 135764 (2020), [arXiv:1912.03695]; J. A. Dror *et al.*, *Phys. Rev. Lett.* **124**, 4, 041804 (2020), [arXiv:1908.03227]; W. Buchmuller, V. Domcke and K. Schmitz, *Phys. Lett. B* **811**, 135914 (2020), [arXiv:2009.10649].
- [162] A. Afzal *et al.* (NANOGrav), *Astrophys. J. Lett.* **951**, 1, L11 (2023), [arXiv:2306.16219].
- [163] C. Caprini *et al.*, *JCAP* **04**, 001 (2016), [arXiv:1512.06239]; C. Caprini *et al.*, *JCAP* **03**, 024 (2020), [arXiv:1910.13125]; M. B. Hindmarsh *et al.*, *SciPost Phys. Lect. Notes* **24**, 1 (2021), [arXiv:2008.09136]; A. Mazumdar and G. White, *Rept. Prog. Phys.* **82**, 7, 076901 (2019), [arXiv:1811.01948].
- [164] L. J. Hall, V. A. Kostelecky and S. Raby, *Nucl. Phys.* **B267**, 415 (1986).
- [165] R. Barbieri and L. J. Hall, *Phys. Lett.* **B338**, 212 (1994), [hep-ph/9408406]; R. Barbieri, L. J. Hall and A. Strumia, *Nucl. Phys.* **B445**, 219 (1995), [hep-ph/9501334].
- [166] F. Borzumati and A. Masiero, *Phys. Rev. Lett.* **57**, 961 (1986); J. Hisano *et al.*, *Phys. Lett.* **B357**, 579 (1995), [hep-ph/9501407]; J. Hisano *et al.*, *Phys. Rev.* **D53**, 2442 (1996), [hep-ph/9510309]; J. Hisano and D. Nomura, *Phys. Rev.* **D59**, 116005 (1999), [hep-ph/9810479].
- [167] T. Moroi, *JHEP* **03**, 019 (2000), [hep-ph/0002208]; D. Chang, A. Masiero and H. Murayama, *Phys. Rev.* **D67**, 075013 (2003), [hep-ph/0205111].
- [168] S. Dimopoulos and L. J. Hall, *Phys. Lett.* **B344**, 185 (1995), [hep-ph/9411273].
- [169] J. Hisano *et al.*, *Phys. Lett.* **B604**, 216 (2004), [hep-ph/0407169].
- [170] A. Yu. Ignatiev *et al.*, *Phys. Lett.* **76B**, 436 (1978); M. Yoshimura, *Phys. Rev. Lett.* **41**, 281 (1978), [Erratum: *Phys. Rev. Lett.* **42**, 746 (1979)].
- [171] D. Toussaint *et al.*, *Phys. Rev.* **D19**, 1036 (1979); S. Weinberg, *Phys. Rev. Lett.* **42**, 850 (1979); M. Yoshimura, *Phys. Lett.* **88B**, 294 (1979); S. M. Barr, G. Segre and H. A. Weldon, *Phys. Rev.* **D20**, 2494 (1979); D. V. Nanopoulos and S. Weinberg, *Phys. Rev.* **D20**, 2484 (1979); A. Yildiz and P. H. Cox, *Phys. Rev.* **D21**, 906 (1980).
- [172] H. K. Dreiner and G. G. Ross, *Nucl. Phys.* **B410**, 188 (1993), [hep-ph/9207221].
- [173] M. Fukugita and T. Yanagida, *Phys. Rev. Lett.* **89**, 131602 (2002), [hep-ph/0203194].
- [174] M. Fukugita and T. Yanagida, *Phys. Lett.* **B174**, 45 (1986).
- [175] S. Davidson and A. Ibarra, *Phys. Lett.* **B535**, 25 (2002), [hep-ph/0202239]; K. Hamaguchi, H. Murayama and T. Yanagida, *Phys. Rev.* **D65**, 043512 (2002), [hep-ph/0109030].
- [176] A. Pilaftsis and T. E. J. Underwood, *Phys. Rev.* **D72**, 113001 (2005), [hep-ph/0506107].
- [177] M. Kawasaki *et al.*, *Phys. Rev.* **D78**, 065011 (2008), [arXiv:0804.3745].
- [178] W. Buchmuller, R. D. Peccei and T. Yanagida, *Ann. Rev. Nucl. Part. Sci.* **55**, 311 (2005), [hep-ph/0502169]; C. S. Fong, E. Nardi and A. Riotto, *Adv. High Energy Phys.* **2012**, 158303 (2012), [arXiv:1301.3062].
- [179] V. Cirigliano *et al.*, *JHEP* **12**, 097 (2018), [arXiv:1806.02780].
- [180] K. S. Babu and R. N. Mohapatra, *Phys. Rev.* **D86**, 035018 (2012), [arXiv:1203.5544]; K. S. Babu and R. N. Mohapatra, *Phys. Lett.* **B715**, 328 (2012), [arXiv:1206.5701]; K. S. Babu and R. N. Mohapatra, *Phys. Rev. Lett.* **109**, 091803 (2012), [arXiv:1207.5771].
- [181] M. Baldo-Ceolin *et al.*, *Z. Phys.* **C63**, 409 (1994).
- [182] K. Abe *et al.* (Super-Kamiokande), *Phys. Rev. D* **103**, 1, 012008 (2021), [arXiv:2012.02607].
- [183] J. Gustafson *et al.* (Super-Kamiokande), *Phys. Rev.* **D91**, 7, 072009 (2015), [arXiv:1504.01041].
- [184] R. D. Peccei and H. R. Quinn, *Phys. Rev. Lett.* **38**, 1440 (1977); F. Wilczek, *Phys. Rev. Lett.* **40**, 279 (1978); S. Weinberg, *Phys. Rev. Lett.* **40**, 223 (1978); G. Grilli di Cortona *et al.*, *JHEP* **01**, 034 (2016), [arXiv:1511.02867].
- [185] A. Ringwald, L.J. Rosenberg and G. Rybka, Review of 'Axions and other Similar Particles' in Ref. [64].
- [186] P. Svrcek and E. Witten, *JHEP* **06**, 051 (2006), [hep-th/0605206].
- [187] L. Di Luzio *et al.*, *Phys. Rept.* **870**, 1 (2020), [arXiv:2003.01100].
- [188] M. Dine, W. Fischler and M. Srednicki, *Phys. Lett.* **104B**, 199 (1981); A. R. Zhitnitsky, *Sov. J. Nucl. Phys.* **31**, 260 (1980), [*Yad. Fiz.* **31**, 497 (1980)].
- [189] J. E. Kim, *Phys. Rev. Lett.* **43**, 103 (1979); M. A. Shifman, A. I. Vainshtein and V. I. Zakharov, *Nucl. Phys. B* **166**, 493 (1980).
- [190] J. Hisano, H. Murayama and T. Yanagida, *Phys. Lett. B* **291**, 263 (1992); R. T. Co, F. D'ErAMO and L. J. Hall, *Phys. Rev. D* **94**, 7, 075001 (2016), [arXiv:1603.04439].
- [191] G. F. Giudice, R. Rattazzi and A. Strumia, *Phys. Lett. B* **715**, 142 (2012), [arXiv:1204.5465]; K. J. Bae, H. Baer and H. Serce, *JCAP* **06**, 024 (2017), [arXiv:1705.01134].
- [192] J. P. Conlon, *JHEP* **05**, 078 (2006), [hep-th/0602233].
- [193] K. R. Dienes, *Phys. Rept.* **287**, 447 (1997), [hep-th/9602045]; P. Nath and P. Fileviez Perez, *Phys. Rept.* **441**, 191 (2007), [hep-ph/0601023].
- [194] G.G. Ross, "Grand Unified Theories", Benjamin/Cummings, 1984.; R. N. Mohapatra, *Unification and Supersymmetry. The Frontiers of Quark-Lepton Physics*, Springer, Berlin (1986), ISBN 978-1-4757-1930-7, 978-1-4757-1928-4; P. Nath, *Supersymmetry, Supergravity, and Unification*, Cambridge Monographs on Mathematical Physics, Cambridge University Press (2016), ISBN 978-0-521-19702-1, 978-1-316-98396-6; S. Raby, *Lect. Notes Phys.* **939**, 1 (2017).
- [195] P. Nath, *Int. J. Mod. Phys.* **A33**, 20, 1830017 (2018), [arXiv:1807.05302]; D. Croon *et al.*, *Front.in Phys.* **7**, 76 (2019), [arXiv:1903.04977].

94. Leptoquarks

Revised October 2023 by S. Rolli (DOE) and M. Tanabashi (Nagoya U.; KMI, Nagoya U.).

Leptoquarks are hypothetical particles carrying both baryon number (B) and lepton number (L). The possible quantum numbers of leptoquark states can be restricted by assuming that their direct interactions with the ordinary Standard Model (SM) fermions are dimensionless and invariant under the SM gauge group. Table 94.1 shows the list of all possible quantum numbers with this assumption [1]. The columns of $SU(3)_C$, $SU(2)_W$, and $U(1)_Y$ in Table 94.1 indicate the QCD representation, the weak isospin representation, and the weak hypercharge, respectively. The spin of a leptoquark state is taken to be 1 (vector leptoquark) or 0 (scalar leptoquark).

If we do not require leptoquark states to couple directly with SM fermions, different assignments of quantum numbers become possible [2, 3].

Leptoquark states are expected to exist in various extensions of the SM. The Pati-Salam model [4] is an example predicting the existence of a leptoquark state. Leptoquark states also exist in grand unification theories based on $SU(5)$ [5], $SO(10)$ [6] which includes Pati-Salam color $SU(4)$, and larger gauge groups. The existence of leptoquarks at TeV-scale also affect the renormalization group of the standard model gauge coupling strengths and may allow for the gauge coupling unification required by the grand unification theories [7]. Scalar quarks in supersymmetric models with R -parity violation may also have leptoquark-type Yukawa

couplings. The bounds on the leptoquark states can therefore be applied to constrain R -parity-violating supersymmetric models [8, 9]. Scalar leptoquarks are expected to exist at the TeV scale in extended technicolor models [10, 11] where leptoquark states appear as the bound states of techni-fermions. Compositeness of quarks and leptons also provides examples of models which may have light leptoquark states [12].

Bounds on leptoquark states are obtained both directly and indirectly. Direct limits are from their production cross sections at colliders, while indirect limits are calculated from bounds on leptoquark-induced two-quark two-lepton interactions, which are obtained from low-energy experiments, or from collider experiments below threshold. The quantum number assignment of Table 94.1 allows several leptoquark states to couple to both left- and right-handed quarks simultaneously. Such leptoquark states are called non-chiral and may cause low-energy interactions

$$(\bar{u}_R q_{Li})(\bar{e}_R \ell_{Lj}) \epsilon^{ij} \quad (\bar{d}_R q_{Li})(\bar{\ell}_L^j e_R). \quad (94.1)$$

Here i, j are indices for the weak isospin. These two-quark two-lepton interactions affect the $(\pi \rightarrow e\nu)/(\pi \rightarrow \mu\nu)$ ratio [13]. Non-chiral scalar leptoquarks also contribute to the anomalous magnetic moments of charged leptons [14, 15]. On the other hand, the exchanges of the chiral leptoquarks produce effective two-quark two-lepton interactions

$$\begin{aligned} (\bar{q}_L^i \gamma^\mu q_{Li})(\bar{\ell}_L^j \gamma_\mu \ell_{Lj}), & \quad (\bar{q}_L^i \gamma^\mu q_{Li})(\bar{e}_R \gamma_\mu e_R), & \quad (\bar{q}_L^i \gamma^\mu (\vec{\sigma})^i q_{Lj}) \cdot (\bar{\ell}_L^k \gamma_\mu (\vec{\sigma})^k \ell_{Ll}), \\ (\bar{u}_R \gamma^\mu u_R)(\bar{\ell}_L^j \gamma_\mu \ell_{Lj}), & \quad (\bar{u}_R \gamma^\mu u_R)(\bar{e}_R \gamma_\mu e_R), & \\ (\bar{d}_R \gamma^\mu d_R)(\bar{\ell}_L^j \gamma_\mu \ell_{Lj}), & \quad (\bar{d}_R \gamma^\mu d_R)(\bar{e}_R \gamma_\mu e_R) \end{aligned} \quad (94.2)$$

below the leptoquark mass scale. Note that labels for the generations of quarks and leptons are suppressed in (94.1) and (94.2). If a leptoquark couples to quarks (leptons) belonging to more than a single generation in the mass eigenbasis, it can induce two-quark two-lepton interactions causing flavor-changing neutral currents (lepton-family-number violations). Since indirect limits provide more stringent constraints on non-chiral or flavor-violating leptoquarks, in the searches of leptoquark states at collider experiments, it is often assumed that a leptoquark state couples only to a single generation of quarks and a single generation of leptons in a chiral interaction, for which indirect limits become much weaker. Additionally, this assumption gives strong constraints on models of leptoquarks.

Refs. [16–18] give extensive lists of the bounds on the leptoquark-induced two-quark two-lepton interactions. For the isoscalar scalar and vector leptoquarks S_0 and V_0 , for example, which couple with the first- (second-) generation left-handed quark, and the first-generation left-handed lepton, the bounds $\lambda^2 < 0.07 \times (M_{LQ}/1 \text{ TeV})^2$ for S_0 , and $\lambda^2 < 0.4 \times (M_{LQ}/1 \text{ TeV})^2$ for V_0 ($\lambda^2 < 0.7 \times (M_{LQ}/1 \text{ TeV})^2$ for S_0 , and $\lambda^2 < 0.5 \times (M_{LQ}/1 \text{ TeV})^2$ for V_0) with λ being the leptoquark coupling strength, can be derived from the limits listed in Ref. [18]. See also Refs. [19, 20] for earlier studies. The e^+e^- collider experiments are sensitive to the indirect effects coming from t - and u -channel exchanges of leptoquarks in the $e^+e^- \rightarrow q\bar{q}$ process. The HERA experiments give bounds on the leptoquark-induced two-quark two-lepton interaction. It should also be stressed that the measurements of the high-mass Drell-Yan cross sections, $pp \rightarrow \ell\nu$ and $pp \rightarrow \ell^+\ell^-$, are also sensitive to these leptoquark-induced interactions. For detailed bounds obtained in this way, see e.g., Ref. [17], and the Heavy Boson Particle Listings for “Indirect Limits for Leptoquarks” and their references.

Note that the two-quark two-lepton interactions arising from the leptoquark exchanges in Eq.(94.1) and Eq.(94.2) can also be regarded as a part of more general dimension-six operators in the context of low-energy standard-model effective field theory (SMEFT). For a complete list of SM gauge-invariant dimension-

six operators, see [21, 22]. A computation of the one-loop anomalous dimension matrix for SMEFT operators are found in Refs. [23–25]. The leptoquark induced two-quark two-lepton interactions often cause lepton-flavor non-universalities in heavy quark decays. The $R(D)$, $R(D^*)$ anomaly observed in the semi-leptonic B decays [26] may be explained in models with TeV scale leptoquarks.

Collider experiments provide direct limits on the leptoquark states through limits on the pair- and single-production cross sections. The leading-order cross sections of the parton processes

$$\begin{aligned} q + \bar{q} &\rightarrow \text{LQ} + \overline{\text{LQ}} \\ g + g &\rightarrow \text{LQ} + \overline{\text{LQ}} \\ e + q &\rightarrow \text{LQ} \end{aligned} \quad (94.3)$$

may be written as [27]

$$\begin{aligned} \hat{\sigma}_{\text{LO}} [q\bar{q} \rightarrow \text{LQ} + \overline{\text{LQ}}] &= \frac{2\alpha_s^2 \pi}{27\hat{s}} \beta^3, \\ \hat{\sigma}_{\text{LO}} [gg \rightarrow \text{LQ} + \overline{\text{LQ}}] &= \frac{\alpha_s^2 \pi}{96\hat{s}} \\ &\times \left[\beta(41 - 31\beta^2) + (18\beta^2 - \beta^4 - 17) \log \frac{1+\beta}{1-\beta} \right], \\ \hat{\sigma}_{\text{LO}} [eq \rightarrow \text{LQ}] &= \frac{\pi\lambda^2}{4} \delta(\hat{s} - M_{\text{LQ}}^2) \end{aligned} \quad (94.4)$$

for a scalar leptoquark. Here $\sqrt{\hat{s}}$ is the invariant energy of the parton subprocess, and $\beta \equiv \sqrt{1 - 4M_{\text{LQ}}^2/\hat{s}}$. The leptoquark Yukawa coupling is given by λ . The cross sections of the pair productions of scalar leptoquarks in pp collisions at the LHC energies have been computed in Refs. [28, 29] at the next-to-leading order in QCD. Leptoquarks are also produced singly at hadron colliders through $g + q \rightarrow \text{LQ} + \ell$ [30], which allows extending to higher

Table 94.1: Possible leptoquarks and their quantum numbers.

Spin	$3B+L$	$SU(3)_c$	$SU(2)_W$	$U(1)_Y$	Allowed coupling
0	-2	3	1	1/3	$\bar{q}_L^c \ell_L$ or $\bar{u}_R^c e_R$
0	-2	$\bar{3}$	1	4/3	$\bar{d}_R^c e_R$
0	-2	$\bar{3}$	3	1/3	$\bar{q}_L^c \ell_L$
1	-2	$\bar{3}$	2	5/6	$\bar{q}_L^c \gamma^\mu e_R$ or $\bar{d}_R^c \gamma^\mu \ell_L$
1	-2	$\bar{3}$	2	-1/6	$\bar{u}_R^c \gamma^\mu \ell_L$
0	0	3	2	7/6	$\bar{q}_L e_R$ or $\bar{u}_R \ell_L$
0	0	3	2	1/6	$\bar{d}_R \ell_L$
1	0	3	1	2/3	$\bar{q}_L \gamma^\mu \ell_L$ or $\bar{d}_R \gamma^\mu e_R$
1	0	3	1	5/3	$\bar{u}_R \gamma^\mu e_R$
1	0	3	3	2/3	$\bar{q}_L \gamma^\mu \ell_L$

masses the collider reach in the leptoquark search [31], depending on the leptoquark Yukawa coupling. The next-to-leading order computations for the single production of the leptoquark states at the LHC energies have been performed in Refs. [32–35]. Since protons contain leptons inside, it is possible to target lepton-induced processes at high energy pp colliders. The single leptoquark production cross sections induced from the lepton-quark collisions at the LHC have been computed in Refs. [36,37]. Ref. [38] performed searches for the leptoquark states produced in lepton-quark collisions at the LHC.

See Ref. [17] for a comprehensive review on the leptoquark phenomenology in precision experiments and particle colliders.

Leptoquark states which couple only to left- or right-handed quarks are called chiral leptoquarks. Leptoquark states which couple only to the first (second, third) generation are referred as the first- (second-, third-) generation leptoquarks.

The LHC, Tevatron and LEP experiments have been searching for pair production of the leptoquark states, which arises from the leptoquark gauge interaction. Due to the typical decay of the leptoquark into charged and neutral leptons and quarks, the searches are carried on in signatures including high p_T charged leptons, high E_T jets and large missing transverse energy. Additionally, searches for pair produced LQs are often organized by the decay mode of the pair of LQs, via the decay parameter β , which represents the branching fraction into a charge lepton vs a neutrino: $\beta = 1$ for LQs decaying into a charged lepton with 100% branching fraction, $\beta = 0.5$ for LQs decaying into a charged lepton with 50% branching fraction. The gauge couplings of a scalar leptoquark are determined uniquely according to its quantum numbers in Table 94.1. Since all of the leptoquark states belong to color-triplet representation, the scalar leptoquark QCD-induced pair-production cross section at the Tevatron and LHC can be determined solely as a function of the leptoquark mass without making further assumptions. This is in contrast to the indirect or single-production limits, which give constraints in the leptoquark mass-coupling plane.

Older results from the Tevatron run can be found here: [39–42].

Since the previous version of this review, both ATLAS and CMS continue to update their results concerning searches for first, second, and third generation LQs and leptoquark states which couple only with the i -th generation quarks and the j -th generation leptons ($i \neq j$) without causing conflicts with severe indirect constraints. The datasets were almost all collected at center of mass energy of 13 TeV and corresponding to the latest integrated luminosity collected before the shutdown of the LHC occurring in 2019 and 2020.

It is worthy to note that organizing LQs by flavor quantum number first before organizing them by gauge quantum number is becoming more common and advantageous because it relates more closely to some of the experimental searches being performed. The traditional nomenclature for 1st, 2nd, and 3rd generation LQ encourages only looking for the diagonal elements in a flavor matrix of possibilities, which has been the traditional experimental search strategy.

Current results extend previous mass limits for scalar leptoquarks to > 1435 GeV (first generation, CMS, $\beta = 1$, $\sqrt{s} = 13$ TeV) and > 1270 GeV (first generation, CMS, $\beta = 0.5$, $\sqrt{s} = 13$ TeV) [43]; > 1800 GeV (first generation, ATLAS, $\beta = 1$, $\sqrt{s} =$

13 TeV) [44] and > 1290 GeV (first generation, ATLAS, $\beta = 0.5$, $\sqrt{s} = 13$ TeV) [45]; > 1530 GeV (second generation, CMS, $\beta = 1$, $\sqrt{s} = 13$ TeV) and > 1285 GeV (second generation, CMS, $\beta = 0.5$, $\sqrt{s} = 13$ TeV) [46]; and > 1700 GeV (second generation, ATLAS, $\beta = 1$, $\sqrt{s} = 13$ TeV) [44] and > 1230 GeV (second generation, ATLAS, $\beta = 0.5$, $\sqrt{s} = 13$ TeV) [45]. All limits are presented at 95% C.L.

As for third generation leptoquarks, CMS results are the following: 1) assuming that all leptoquarks decay to a top quark and a τ lepton, the existence of pair produced, third-generation leptoquark up to a mass of 1120 GeV ($\beta = 1$, 13 TeV) is excluded at 95% confidence level [47]; 2) assuming that all leptoquarks decay to a bottom quark and a τ lepton, the existence of pair produced, third-generation leptoquark up to a mass of 1020 GeV ($\beta = 1$, 13 TeV) is excluded at 95% confidence level [48]; 3) assuming that all leptoquarks decay to a bottom quark and a τ neutrino, the existence of pair produced, third-generation leptoquark up to a mass of 1185 GeV ($\beta = 0$, 13 TeV) is excluded at 95% confidence level [49]. In a recent paper [50] signatures of top quark τ lepton ν bottom and top $\tau \nu$ - not previously explored in dedicated searches, were analyzed in the context of searches for scalar leptoquark of charge $-1/3e$ coupling to a top quark plus a τ lepton ($t\tau$) or a bottom quark plus a neutrino ($b\nu$), or a vector particle of charge $+2/3e$, coupling to $t\nu$ or $b\tau$. These choices are motivated by models that can explain a series of anomalies observed in the measurement of B meson decays. The data are found to be in agreement with the standard model prediction. Lower limits at 95% confidence level are set on the LQ mass in the range 0.98–1.73 TeV, depending on the LQ spin and its coupling λ to a lepton and a quark, and assuming equal couplings for the two LQ decay modes considered. These are the most stringent constraints to date on the existence of leptoquarks in this scenario.

In [51] ATLAS present the result of searches for pair production of third-generation scalar leptoquarks decaying into a top quark and a τ -lepton, using 139 fb^{-1} of data collected at 13 TeV. Scalar leptoquarks decaying exclusively into $t\tau$ are excluded up to masses of 1.43 TeV while, for a branching fraction of 50% into $t\tau$, the lower mass limit is 1.22 TeV. In two recent papers [52] and [53] ATLAS searched for pair-produced scalar or vector leptoquarks decaying into a b -quark and a τ -lepton and single production of vector leptoquarks with electric charge of $2/3e$ and scalar leptoquarks with an electric charge of $4/3e$. For pair production of scalar leptoquarks, masses below 1490 GeV are excluded assuming a 100% branching ratio, while for vector leptoquarks the corresponding limit is 1690 GeV (1960 GeV) in the minimal-coupling (Yang–Mills) scenario. For single vector leptoquark production two models are considered: the Yang–Mills and Minimal coupling models. In the Yang–Mills (Minimal coupling) scenario, vector leptoquarks with a mass below 1.58 (1.35) TeV are excluded for a gauge coupling of 1.0 and below 2.05 (1.99) TeV for a gauge coupling of 2.5. In the case of single scalar leptoquark production, masses below 1.28 TeV (1.53 TeV) are excluded for a Yukawa coupling of 1.0 (2.5). Additionally, a search for pair production of leptoquarks with decays into third-generation leptons and quarks. in final states with hadronically decaying τ leptons, b -jets, and missing transverse momentum was performed in [54]: depending on the branching fraction into charged leptons, leptoquarks with masses up to around 1.25 TeV can be excluded at

the 95% confidence level for the case of scalar leptoquarks and up to 1.8 TeV (1.5 TeV) for vector leptoquarks in a Yang–Mills (minimal-coupling) scenario.

It is also possible to consider leptoquark states which couple only with the i -th generation quarks and the j -th generation leptons ($i \neq j$) without causing conflicts with severe indirect constraints. Such couplings have received renewed attention because they may provide an explanation to anomalies in rare B –meson decays and the anomalous magnetic moment of the muon. See Ref. [55, 56] and [57] and references therein for collider search strategies and limits on the pair production cross sections of this class of leptoquark states. In this framework, in [58] and [47] CMS presents a non-traditional search for pair production of LQs coupled to a top quark and a leptons. As no deviation from the Standard Model prediction was observed, scalar LQs decaying exclusively into top quark and lepton are excluded below 1.12–1.42 TeV depending on the lepton flavor. In [59] ATLAS conducted a search for pair production of scalar and vector leptoquarks, each decaying into first and second generation leptons and a third generation quarks. This is part of leptoquark search using ATLAS data to investigate cross-generational couplings that could provide explanations for recently observed anomalies in B meson decays. All possible decays of the pair-produced leptoquarks into quarks of the third generation and charged or neutral leptons of the first or second generation with exactly one electron or muon in the final state are investigated. No significant deviations from the Standard Model expectation are observed. Upper limits on the production cross-section are provided for different models as a function of the leptoquark mass and the branching ratio of the leptoquark into the charged or neutral lepton. Some of these models have the goal of providing an explanation for the recent B-anomalies. In such models, a vector leptoquark decays into charged and neutral leptons of the second generation with a similar branching fraction. Lower limits of 1.9 TeV and 1.7 TeV are set on the leptoquark mass for these two models.

The magnetic-dipole-type and the electric-quadrupole-type interactions of a vector leptoquark are not determined even if we fix its gauge quantum numbers as listed in the Table 94.1 [60]. The production of vector leptoquarks depends in general on additional assumptions, where the leptoquark couplings and their pair production cross sections are enhanced relative to the scalar leptoquark contributions. The most stringent limits on vector LQ production are now from CMS [61] where previous searches for squarks and gluinos have been reinterpreted to constrain models of leptoquark production. LQ masses below 1530 GeV are excluded assuming the Yang–Mills case with coupling $\kappa = 1$, or 1115 GeV in the minimal coupling case where $\kappa = 0$, placing the most stringent constraint to date from pair production of vector LQs. These results and the ones in [62] were updated in [49] where searches for phenomena beyond the standard model (BSM) were performed using events with hadronic jets and significant transverse momentum imbalance to constrain a range of BSM models including the pair production of scalar and vector leptoquarks each decaying to a neutrino and a top, bottom, or light-flavor quark.

The leptoquark pair-production cross sections in e^+e^- collisions depend on the leptoquark $SU(2) \times U(1)$ quantum numbers and Yukawa coupling with electron [63].

Searches for first generation leptoquark singly produced were performed by the HERA experiments. Since the leptoquark single-production cross section depends on its Yukawa coupling, the leptoquark mass limits from HERA are usually displayed in the mass-coupling plane. For leptoquark Yukawa coupling $\lambda = 0.1$, early ZEUS Collaboration bounds on the first-generation leptoquarks range from 248 to 290 GeV, depending on the leptoquark species [64]. The ZEUS Collaboration has recently released a new paper [65] where data corresponding to a luminosity of around 1 fb^{-1} have been used in the framework of $eeqq$ contact interactions (CI) to set limits on possible high-energy contributions beyond the Standard Model to electron-quark scattering. The analysis of the ep data has been based on simultaneous fits of parton distribution functions including contributions of Contact Interaction (CI) couplings to ep scattering. Several general

CI models and scenarios with heavy leptoquarks were considered. As unambiguous deviations from the SM cannot be established, limits for CI compositeness scales and LQ mass scales were set that are in the TeV range. The H1 Collaboration has a comprehensive summary of searches for first generation leptoquarks using the full data sample collected in ep collisions at HERA (446 pb^{-1}). No evidence of production of leptoquarks was observed in final states with a large transverse momentum electron or large missing transverse momentum. For a coupling strength $\lambda = 0.3$, first generation leptoquarks with masses up to 800 GeV are excluded at 95% C.L. [66].

At the LHC, the CMS collaboration performed searches for single production of first and second generation leptoquarks [67], which is complementary to the HERA searches in the high λ region (for coupling strength $\lambda = 1.0$, first generation leptoquarks are excluded for masses up to 1.73 TeV and second generation leptoquark are excluded up to masses of 530 GeV). CMS also recently searched for third generation LQ decaying into τ and bottom in [68]. Assuming unit Yukawa coupling (λ), a third generation scalar leptoquark is excluded for masses below 740 GeV. Limits are also set on λ of the hypothesized leptoquark as a function of its mass. Above $\lambda = 1.4$, the results provide the best upper limit on the mass of a third-generation scalar leptoquark decaying to a τ lepton and a bottom quark.

Searches for LQ will continue with more LHC data, particularly in light of the renewed interest in this type of particle to explain violation of lepton flavor universality and other anomalies, which point to explanations laying outside the Standard Model.

References

- [1] W. Buchmuller, R. Ruckl and D. Wyler, Phys. Lett. B **191**, 442 (1987), [Erratum: Phys.Lett.B 448, 320–320 (1999)].
- [2] K. Babu, C. F. Kolda and J. March-Russell, Phys. Lett. B **408**, 261 (1997), [hep-ph/9705414].
- [3] J. L. Hewett and T. G. Rizzo, Phys. Rev. D **58**, 055005 (1998), [hep-ph/9708419].
- [4] J. C. Pati and A. Salam, Phys. Rev. D **10**, 275 (1974), [Erratum: Phys.Rev.D 11, 703–703 (1975)].
- [5] H. Georgi and S. Glashow, Phys. Rev. Lett. **32**, 438 (1974).
- [6] H. Georgi, AIP Conf. Proc. **23**, 575 (1975); H. Fritzsch and P. Minkowski, Annals Phys. **93**, 193 (1975).
- [7] H. Murayama and T. Yanagida, Mod. Phys. Lett. A **7**, 147 (1992).
- [8] G. R. Farrar and P. Fayet, Phys. Lett. B **76**, 575 (1978).
- [9] R. Barbier *et al.*, Phys. Rept. **420**, 1 (2005), [hep-ph/0406039].
- [10] For a review, see, E. Farhi and L. Susskind, Phys. Rept. **74**, 277 (1981).
- [11] K. D. Lane and M. Ramana, Phys. Rev. D **44**, 2678 (1991).
- [12] See, for example, B. Schrempp and F. Schrempp, Phys. Lett. **153B**, 101 (1985).
- [13] O. U. Shanker, Nucl. Phys. B **204**, 375 (1982).
- [14] U. Mahanta, Eur. Phys. J. C **21**, 171 (2001), [hep-ph/0102176].
- [15] K.-M. Cheung, Phys. Rev. D **64**, 033001 (2001), [hep-ph/0102238].
- [16] M. Carpentier and S. Davidson, Eur. Phys. J. C **70**, 1071 (2010), [arXiv:1008.0280].
- [17] I. Doršner *et al.*, Phys. Rept. **641**, 1 (2016), [arXiv:1603.04993].
- [18] S. Davidson and A. Saporta, Phys. Rev. D **99**, 1, 015032 (2019), [arXiv:1807.10288].
- [19] S. Davidson, D. C. Bailey and B. A. Campbell, Z. Phys. C **61**, 613 (1994), [hep-ph/9309310].
- [20] M. Leurer, Phys. Rev. D **49**, 333 (1994), [hep-ph/9309266]; M. Leurer, Phys. Rev. D **50**, 536 (1994), [hep-ph/9312341].
- [21] W. Buchmuller and D. Wyler, Nucl. Phys. B **268**, 621 (1986).

- [22] B. Grzadkowski *et al.*, JHEP **10**, 085 (2010), [arXiv:1008.4884].
- [23] E. E. Jenkins, A. V. Manohar and M. Trott, JHEP **10**, 087 (2013), [arXiv:1308.2627].
- [24] E. E. Jenkins, A. V. Manohar and M. Trott, JHEP **01**, 035 (2014), [arXiv:1310.4838].
- [25] R. Alonso *et al.*, JHEP **04**, 159 (2014), [arXiv:1312.2014].
- [26] Y. S. Amhis *et al.* (Heavy Flavor Averaging Group, HFLAV), Phys. Rev. D **107**, 5, 052008 (2023), updated results and plots available at <https://hf1av.web.cern.ch/>, [arXiv:2206.07501].
- [27] T. Plehn *et al.*, Z. Phys. C **74**, 611 (1997), [hep-ph/9703433]; M. Kramer *et al.*, Phys. Rev. Lett. **79**, 341 (1997), [hep-ph/9704322].
- [28] M. Kramer *et al.*, Phys. Rev. D **71**, 057503 (2005), [hep-ph/0411038].
- [29] T. Mandal, S. Mitra and S. Seth, Phys. Rev. D **93**, 3, 035018 (2016), [arXiv:1506.07369].
- [30] J. Hewett and S. Pakvasa, Phys. Rev. D **37**, 3165 (1988); O. J. Eboli and A. V. Olinto, Phys. Rev. D **38**, 3461 (1988); A. Dobado, M. J. Herrero and C. Munoz, Phys. Lett. B **207**, 97 (1988); V. D. Barger *et al.*, Phys. Lett. B **220**, 464 (1989); M. De Montigny and L. Marleau, Phys. Rev. D **40**, 2869 (1989), [Erratum: Phys.Rev.D 56, 3156 (1997)].
- [31] A. Belyaev *et al.*, JHEP **09**, 005 (2005), [hep-ph/0502067].
- [32] A. Alves, O. Eboli and T. Plehn, Phys. Lett. B **558**, 165 (2003), [hep-ph/0211441].
- [33] T. Mandal, S. Mitra and S. Seth, JHEP **07**, 028 (2015), [arXiv:1503.04689].
- [34] J. B. Hammett and D. A. Ross, JHEP **07**, 148 (2015), [arXiv:1501.06719].
- [35] I. Doršner and A. Greljo, JHEP **05**, 126 (2018), [arXiv:1801.07641].
- [36] L. Buonocore *et al.*, Phys. Rev. Lett. **125**, 23, 231804 (2020), [arXiv:2005.06475].
- [37] A. Greljo and N. Selimovic, JHEP **03**, 279 (2021), [arXiv:2012.02092].
- [38] A. Hayrapetyan *et al.* (CMS) (2023), [arXiv:2308.06143].
- [39] V. Abazov *et al.* (D0), Phys. Lett. B **681**, 224 (2009), [arXiv:0907.1048].
- [40] A. Abulencia *et al.* (CDF), Phys. Rev. D **73**, 051102 (2006), [hep-ex/0512055].
- [41] V. Abazov *et al.* (D0), Phys. Lett. B **671**, 224 (2009), [arXiv:0808.4023].
- [42] V. M. Abazov *et al.* (D0), Phys. Lett. B **693**, 95 (2010), [arXiv:1005.2222].
- [43] A. M. Sirunyan *et al.* (CMS), Phys. Rev. D **99**, 5, 052002 (2019), [arXiv:1811.01197].
- [44] G. Aad *et al.* (ATLAS), JHEP **10**, 112 (2020), [arXiv:2006.05872].
- [45] M. Aaboud *et al.* (ATLAS), Eur. Phys. J. C **79**, 9, 733 (2019), [arXiv:1902.00377].
- [46] A. M. Sirunyan *et al.* (CMS), Phys. Rev. D **99**, 3, 032014 (2019), [arXiv:1808.05082].
- [47] A. Tumasyan *et al.* (CMS), Phys. Rev. D **105**, 11, 112007 (2022), [arXiv:2202.08676].
- [48] A. M. Sirunyan *et al.* (CMS), JHEP **03**, 170 (2019), [arXiv:1811.00806].
- [49] A. M. Sirunyan *et al.* (CMS), Eur. Phys. J. C **80**, 1, 3 (2020), [arXiv:1909.03460].
- [50] A. M. Sirunyan *et al.* (CMS), Phys. Lett. B **819**, 136446 (2021), [arXiv:2012.04178].
- [51] G. Aad *et al.* (ATLAS), JHEP **06**, 179 (2021), [arXiv:2101.11582].
- [52] G. Aad *et al.* (ATLAS), Search for leptoquark pair production decaying into $te^- \bar{t}e^+$ or $t\mu^- \bar{t}\mu^+$ in multi-lepton final states in pp collisions at 13 TeV with the ATLAS detector (2023), [arXiv:2306.17642].
- [53] G. Aad *et al.* (ATLAS), JHEP **10**, 001 (2023), [arXiv:2305.15962].
- [54] G. Aad *et al.* (ATLAS), Phys. Rev. D **104**, 11, 112005 (2021), [arXiv:2108.07665].
- [55] B. Diaz, M. Schmaltz and Y.-M. Zhong, JHEP **10**, 097 (2017), [arXiv:1706.05033].
- [56] M. Schmaltz and Y.-M. Zhong, JHEP **01**, 132 (2019), [arXiv:1810.10017].
- [57] D. Müller, EPJ Web Conf. **179**, 01015 (2018), [arXiv:1801.03380].
- [58] A. M. Sirunyan *et al.* (CMS), Phys. Rev. Lett. **121**, 24, 241802 (2018), [arXiv:1809.05558].
- [59] G. Aad *et al.* (ATLAS), JHEP **2306**, 188 (2023), [arXiv:2210.04517].
- [60] J. Blumlein, E. Boos and A. Kryukov, Z. Phys. C **76**, 137 (1997), [hep-ph/9610408].
- [61] A. M. Sirunyan *et al.* (CMS), Phys. Rev. D **98**, 3, 032005 (2018), [arXiv:1805.10228].
- [62] S. Chatrchyan *et al.* (CMS), JHEP **12**, 055 (2012), [arXiv:1210.5627].
- [63] J. Blumlein and R. Ruckl, Phys. Lett. B **304**, 337 (1993).
- [64] S. Chekanov *et al.* (ZEUS), Phys. Rev. D **68**, 052004 (2003), [hep-ex/0304008].
- [65] H. Abramowicz *et al.* (ZEUS), Phys. Rev. D **99**, 9, 092006 (2019), [arXiv:1902.03048].
- [66] F. Aaron *et al.* (H1), Phys. Lett. B **704**, 388 (2011), [arXiv:1107.3716].
- [67] V. Khachatryan *et al.* (CMS), Phys. Rev. D **93**, 3, 032005 (2016), [Erratum: Phys.Rev.D 95, 039906 (2017)], [arXiv:1509.03750].
- [68] A. Sirunyan *et al.* (CMS), JHEP **07**, 115 (2018), [arXiv:1806.03472].

95. Magnetic Monopoles

Revised March 2024 by D. Milstead (Stockholm U.) and E.J. Weinberg (Columbia U.).

95.1 Theory of magnetic monopoles

The symmetry between electric and magnetic fields in the source-free Maxwell's equations naturally suggests that electric charges might have magnetic counterparts, known as magnetic monopoles. Although the greatest interest has been in the supermassive monopoles that are a firm prediction of all grand unified theories, one cannot exclude the possibility of lighter monopoles.

In either case, the magnetic charge is constrained by a quantization condition first found by Dirac [1]. Consider a monopole with magnetic charge Q_M and a Coulomb magnetic field

$$\mathbf{B} = \frac{Q_M}{4\pi} \frac{\hat{\mathbf{r}}}{r^2}. \quad (95.1)$$

Any vector potential \mathbf{A} whose curl is equal to \mathbf{B} must be singular along some line running from the origin to spatial infinity. This Dirac string singularity could potentially be detected through the extra phase that the wavefunction of a particle with electric charge Q_E would acquire if it moved along a loop encircling the string. For the string to be unobservable, this phase must be a multiple of 2π . Requiring that this be the case for any pair of electric and magnetic charges gives the condition that all charges be integer multiples of minimum charges Q_E^{\min} and Q_M^{\min} obeying

$$Q_E^{\min} Q_M^{\min} = 2\pi. \quad (95.2)$$

(For monopoles which also carry an electric charge, called dyons [2], the quantization conditions on their electric charges can be modified. However, the constraints on magnetic charges, as well as those on all purely electric particles, will be unchanged.)

Another way to understand this result is to note that the conserved orbital angular momentum of a point electric charge moving in the field of a magnetic monopole has an additional component, with

$$\mathbf{L} = m\mathbf{r} \times \mathbf{v} - 4\pi Q_E Q_M \hat{\mathbf{r}} \quad (95.3)$$

Requiring the radial component of \mathbf{L} to be quantized in half-integer units yields Eq. 95.2.

If there are unbroken gauge symmetries in addition to the U(1) of electromagnetism, the above analysis must be modified [3, 4]. For example, a monopole could have both a U(1) magnetic charge and a color magnetic charge. The latter could combine with the color charge of a quark to give an additional contribution to the phase factor associated with a loop around the Dirac string, so that the U(1) charge could be the Dirac charge $Q_M^D \equiv 2\pi/e$, the result that would be obtained by substituting the electron charge into Eq. (95.2). On the other hand, for monopoles without color-magnetic charge, one would simply insert the quark electric charges into Eq. 95.2 and conclude that Q_M must be a multiple of $6\pi/e$.

The prediction of GUT monopoles arises from the work of 't Hooft [5] and Polyakov [6], who showed that certain spontaneously broken gauge theories have nonsingular classical solutions that lead to magnetic monopoles in the quantum theory. The simplest example occurs in a theory where the vacuum expectation value of a triplet Higgs field ϕ breaks an SU(2) gauge symmetry down to the U(1) of electromagnetism and gives a mass M_V to two of the gauge bosons. In order to have finite energy, ϕ must approach a vacuum value at infinity. However, there is a continuous family of possible vacua, since the scalar field potential determines only the magnitude v of $\langle \phi \rangle$, but not its orientation in the internal SU(2) space. In the monopole solution, the direction of ϕ in internal space is correlated with the position in physical space; *i.e.*, $\phi^a \sim v\hat{r}^a$. The stability of the solution follows from the fact that this twisting Higgs field cannot be smoothly deformed to a spatially uniform vacuum configuration. Reducing the energetic cost of the spatial variation of ϕ requires a nonzero gauge potential, which turns out to yield the magnetic field corresponding to a charge $Q_M = 4\pi/e$. Numerical solution of the classical field equations shows that the mass of this monopole is

$$M_{\text{mon}} \sim \frac{4\pi M_V}{e^2}. \quad (95.4)$$

The essential ingredient here was the fact that the Higgs fields at spatial infinity could be arranged in a topologically nontrivial configuration. A discussion of the general conditions under which this is possible is beyond the scope of this review, so we restrict ourselves to the two phenomenologically most important cases.

The first is the standard electroweak theory, with SU(2) \times U(1) broken to U(1). There are no topologically nontrivial configurations of the Higgs field, and hence no topologically stable monopole solutions. Although electroweak scale monopoles are thus not required, there have been claims that they might not be ruled out. For example, there have been a variety of proposals in this direction involving modifications of the Lagrangian.

The second case is when any simple Lie group is broken to a subgroup with a U(1) factor, a case that includes all grand unified theories. Here the spectrum of states must include a topologically stable monopole whose mass is determined by the mass scale of the symmetry breaking that allows nontrivial topology. For example, an SU(5) model with

$$\text{SU}(5) \xrightarrow{M_X} \text{SU}(3) \times \text{SU}(2) \times \text{U}(1) \xrightarrow{M_W} \text{SU}(3) \times \text{U}(1) \quad (95.5)$$

has a monopole [7] with $Q_M = 2\pi/e$ and mass

$$M_{\text{mon}} \sim \frac{4\pi M_X}{g^2}, \quad (95.6)$$

where g is the SU(5) gauge coupling. For a unification scale of 10^{16} GeV, these monopoles would have a mass $M_{\text{mon}} \sim 10^{17} - 10^{18}$ GeV.

In theories with several stages of symmetry breaking, monopoles of different mass scales can arise. In an SO(10) theory with

$$\text{SO}(10) \xrightarrow{M_1} \text{SU}(4) \times \text{SU}(2) \times \text{SU}(2) \xrightarrow{M_2} \text{SU}(3) \times \text{SU}(2) \times \text{U}(1) \quad (95.7)$$

there is a monopole with $Q_M = 2\pi/e$ and mass $\sim 4\pi M_1/g^2$ and a much lighter monopole with $Q_M = 4\pi/e$ and mass $\sim 4\pi M_2/g^2$ [8].

The central core of a GUT monopole contains the fields of the superheavy gauge bosons that mediate baryon number violation, so one might expect that baryon number conservation could be violated in baryon-monopole scattering. The surprising feature, pointed out by Callan [9] and Rubakov [10], is that these processes are not suppressed by powers of the gauge boson mass. Instead, the cross-sections for catalysis processes such as $p + \text{monopole} \rightarrow e^+ + \pi^0 + \text{monopole}$ are essentially geometric; *i.e.*, $\sigma_{\Delta B} \sim 10^{-27} \text{ cm}^2$, where $\beta = v/c$. Note, however, that this catalysis is model-dependent and is not even a universal property of all GUT monopoles.

95.2 Production and Annihilation

GUT monopoles are far too massive to be produced in any foreseeable accelerator. However, they could have been produced in the early Universe as topological defects arising via the Kibble mechanism [11] in a symmetry-breaking phase transition. Estimates of the initial monopole abundance, and of the degree to which it can be reduced by monopole-antimonopole annihilation, predict a present-day monopole abundance that exceeds by many orders of magnitude the astrophysical and experimental bounds described below [12]. Cosmological inflation and other proposed solutions to this primordial monopole problem generically lead to present-day abundances exponentially smaller than could be plausibly detected, although potentially observable abundances can be obtained in scenarios with carefully tuned parameters.

If monopoles light enough to be produced at colliders exist, one would expect that these could be produced by analogs of the electromagnetic processes that produce pairs of electrically charged particles. Because of the large size of the magnetic charge, this is a strong coupling problem for which perturbation theory cannot be trusted. Indeed, the problem of obtaining reliable quantitative estimates of the production cross-sections remains an open one, on which there is no clear consensus.

95.3 Astrophysical and Cosmological Bounds

If there were no galactic magnetic field, one would expect monopoles in the galaxy to have typical velocities of the order of $10^{-3}c$, comparable to the virial velocity in the galaxy (relevant if the monopoles cluster with the galaxy) and the peculiar velocity of the galaxy with respect to the CMB rest frame (relevant if the monopoles are not bound to the galaxy). This situation is modified by the existence of a galactic magnetic field $B \sim 3\mu\text{G}$. A monopole with the Dirac charge and mass M would be accelerated by this field to a velocity

$$v_{\text{mag}} \sim \begin{cases} c, & M \lesssim 10^{11} \text{ GeV}, \\ 10^{-3}c \left(\frac{10^{17} \text{ GeV}}{M} \right)^{1/2}, & M \gtrsim 10^{11} \text{ GeV}. \end{cases} \quad (95.8)$$

Accelerating these monopoles drains energy from the magnetic field. Parker [13] obtained an upper bound on the flux of monopoles in the galaxy by requiring that the rate of this energy loss be small compared to the time scale on which the galactic field can be regenerated. With reasonable choices for the astrophysical parameters (see Ref. [14] for details), this Parker bound is

$$F < \begin{cases} 10^{-15} \text{ cm}^{-2} \text{ sr}^{-1} \text{ sec}^{-1}, & M \lesssim 10^{17} \text{ GeV}, \\ 10^{-15} \left(\frac{M}{10^{17} \text{ GeV}} \right) \text{ cm}^{-2} \text{ sr}^{-1} \text{ sec}^{-1}, & M \gtrsim 10^{17} \text{ GeV}. \end{cases} \quad (95.9)$$

Applying similar arguments to an earlier seed field that was the progenitor of the current galactic field leads to a tighter bound [15],

$$F < \left[\frac{M}{10^{17} \text{ GeV}} + (3 \times 10^{-6}) \right] 10^{-16} \text{ cm}^{-2} \text{ sr}^{-1} \text{ sec}^{-1}. \quad (95.10)$$

Considering magnetic fields in galactic clusters gives a bound [16] which, although less secure, is about three orders of magnitude lower than the Parker bound.

A flux bound can also be inferred from the total mass of monopoles in the Universe. If the monopole mass density is a fraction Ω_M of the critical density, and the monopoles were uniformly distributed throughout the Universe, there would be a monopole flux

$$F_{\text{uniform}} = 1.3 \times 10^{-16} \Omega_M \left(\frac{10^{17} \text{ GeV}}{M} \right) \left(\frac{v}{10^{-3}c} \right) \text{ cm}^{-2} \text{ sr}^{-1} \text{ sec}^{-1}. \quad (95.11)$$

If we assume that $\Omega_M \sim 0.1$, this gives a stronger constraint than the Parker bound for $M \sim 10^{15}$ GeV. However, monopoles with masses $\sim 10^{17}$ GeV are not ejected by the galactic field and can be gravitationally bound to the galaxy. In this case their flux within the galaxy is increased by about five orders of magnitude for a given value of Ω_M , and the mass density bound only becomes stronger than the Parker bound for $M \sim 10^{18}$ GeV.

A much more stringent flux bound applies to GUT monopoles that catalyze baryon number violation. The essential idea is that compact astrophysical objects would capture monopoles at a rate proportional to the galactic flux. These monopoles would then catalyze proton decay, with the energy released in the decay leading to an observable increase in the luminosity of the object. A variety of bounds, based on neutron stars [17–21], white dwarfs [22], and Jovian planets [23] have been obtained. These depend in the obvious manner on the catalysis cross section, but also on the details of the astrophysical scenarios; *e.g.*, on how much the accumulated density is reduced by monopole-antimonopole annihilation, and on whether monopoles accumulated in the progenitor star survive its collapse to a white dwarf or neutron star. The bounds obtained in this manner lie in the range

$$F \left(\frac{\sigma_{\Delta B \beta}}{10^{-27} \text{ cm}^2} \right) \sim (10^{-18} - 10^{-29}) \text{ cm}^{-2} \text{ sr}^{-1} \text{ sec}^{-1}. \quad (95.12)$$

It is important to remember that not all GUT monopoles catalyze baryon number nonconservation. In particular, the intermediate mass monopoles that arise in some GUTs at later stages

of symmetry-breaking are examples of theoretically motivated monopoles that are exempt from the bound of the above equation.

95.4 Searches for Magnetic Monopoles

To date there have been no confirmed observations of exotic particles possessing magnetic charge. Precision measurements of the properties of known particles have led to tight limits on the values of magnetic charge they may possess. Using the induction method (see below), the electron's magnetic charge has been found to be $Q_e^m < 10^{-24} Q_M^D$ [24]. Furthermore, measurements of the anomalous magnetic moment of the muon have been used to place a model dependent lower limit of 120 GeV on the monopole mass¹ [25]. Nevertheless, guided mainly by Dirac's argument and the predicted existence of monopoles from spontaneous symmetry breaking mechanisms, searches have been routinely made for monopoles produced at accelerators, in cosmic rays, and bound in matter [26]. Although the resultant limits from such searches are usually made under the assumption of a particle possessing only magnetic charge, most of the searches are also sensitive to dyons.

95.5 Search Techniques

Search strategies are determined by the expected interactions of monopoles as they pass through matter. These would give rise to a number of striking characteristic signatures. Since a complete description of monopole search techniques falls outside of the scope of this minireview, only the most common methods are described below. More comprehensive descriptions of search techniques can be found in Refs. [27, 28].

The induction method exploits the long-range electromagnetic interaction of the monopole with the quantum state of a superconducting ring which would lead to a monopole which passes through such a ring inducing a permanent current. The induction technique typically uses Superconducting Quantum Interference Devices (SQUID) technology for detection and is employed for searches for monopoles in cosmic rays and matter. Another approach is to exploit the electromagnetic energy loss of monopoles. Monopoles with Dirac charge would typically lose energy at a rate which is several thousand times larger than that expected from particles possessing the elementary electric charge. Consequently, scintillators, gas chambers and nuclear track detectors (NTDs) have been used in cosmic ray and collider experiments. A further approach, which has been used at colliders, is to search for particles describing a non-helical path in a uniform magnetic field.

95.5.1 Searches for Monopoles Bound in Matter

Monopoles have been sought in a range of bulk materials which it is assumed would have absorbed incident cosmic ray monopoles over a long exposure time of order million years. Materials which have been studied include moon rock, meteorites, manganese modules, and sea water [29, 30]. A stringent upper limit on the monopoles per nucleon ratio of $\sim 10^{-29}$ has been obtained [30].

95.5.2 Searches in Cosmic Rays

Direct searches for monopoles in cosmic rays refer to those experiments in which the passage of the monopole is measured by an active detector. Searches made assuming a catalysis processes in which GUT monopoles could induce nucleon decay are discussed in the next section. To interpret the results of the non-catalysis searches, the cross section for the catalysis process is typically either set to zero [31] or assigned a modest value (1mb) [32].

Although early cosmic ray searches using the induction technique [33] and NTDs [34] observed monopole candidates, none of these apparent observations have been confirmed. Recent experiments have typically employed large scale detectors. The MACRO experiment at the Gran Sasso underground laboratory comprised three different types of detector: liquid scintillator, limited stream tubes, and NTDs, which provided a total acceptance of $\sim 10000 \text{ m}^2$ for an isotropic flux. As shown in Fig. 95.1, this experiment has so far provided the most extensive β -dependent flux limits for GUT monopoles with Dirac charge [32]. Also shown

¹Where no ambiguity is likely to arise, a reference to a monopole implies a particle possessing Dirac charge.

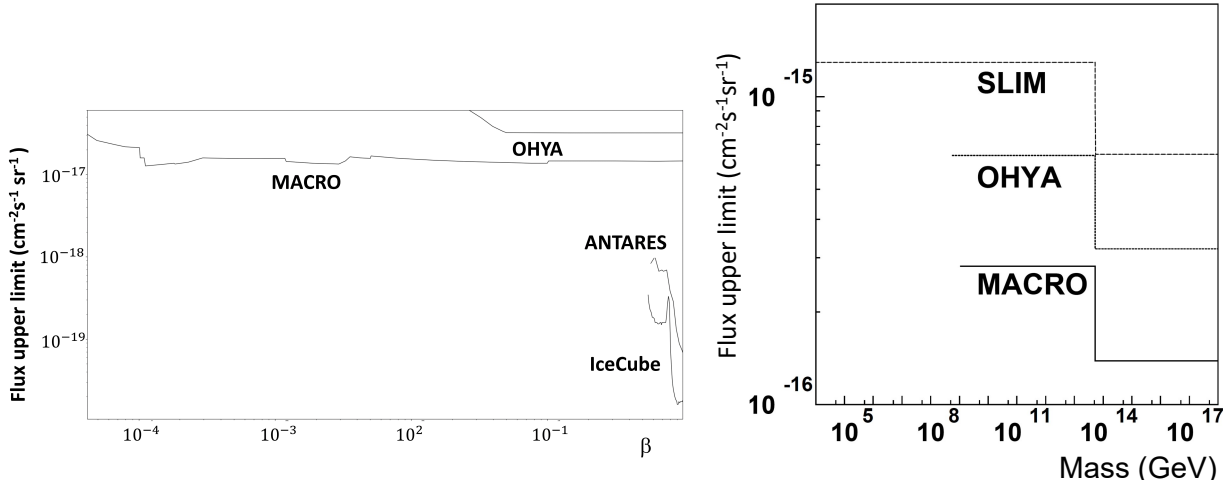


Figure 95.1: Left: upper flux limits for GUT monopoles as a function of β . Right: upper flux limits for monopoles as a function of monopole mass for $\beta > 0.05$.

are limits from an experiment at the OHYA mine in Japan [31], which used a 2000m^2 array of NTDs, and from the IceCube [35,36] and Antares [37] experiments which each employ the Cerenkov method.

In Fig. 95.1, upper flux limits are also shown as a function of monopole mass for monopole speed $\beta > 0.05$. In addition to MACRO and OHYA flux limits, results from the SLIM [38] high-altitude experiment are shown. The SLIM experiment provided a good sensitivity to intermediate mass monopoles ($10^5 \lesssim M \lesssim 10^{12}$ GeV).

In addition to the results shown in Fig. 95.1, the NoVA experiment [39] has recently set an upper limit on monopole flux of $2 \times 10^{-14} \text{ cm}^{-2}\text{s}^{-1}\text{sr}^{-1}$ for speeds $6 \times 10^{-4} < \beta < 10^{-3}$ for masses greater than 5×10^8 GeV. Stringent constraints on the flux of ultra-relativistic monopoles have been obtained at the Pierre Auger Observatory [40] which was sensitive to monopoles with γ values ranging from 10^9 to 10^{12} , leading to flux limits in the range $10^{-15} - 2.5 \times 10^{-21} \text{ cm}^{-2}\text{s}^{-1}\text{sr}^{-1}$. The RICE [41] and ANITA-II experiments [42] at the South Pole have also sought ultra-relativistic monopoles with γ values of $10^7 \lesssim \gamma \lesssim 10^{12}$ and $10^9 \lesssim \gamma \lesssim 10^{13}$, respectively, and which produced flux limits as low as $2.5 \times 10^{-21} \text{ cm}^{-2}\text{s}^{-1}\text{sr}^{-1}$.

95.5.3 Searches via the Catalysis of Nucleon-Decay

Searches have been performed for evidence of the catalysed decay of a nucleon by a monopole, as predicted by the Callan-Rubakov mechanism. The searches are thus sensitive to the assumed value of the catalysis decay cross section. Searches have been made with the Soudan [43] and Macro [44] experiments, using tracking detectors. Searches at IMB [45], the underwater Lake Baikal experiment [46,47] and the IceCube experiment [48] which exploit the Cerenkov effect have also been made. The resulting β -dependent flux limits from these experiments typically vary between $\sim 10^{-18}$ and $\sim 10^{-14} \text{ cm}^{-2}\text{s}^{-1}\text{sr}^{-1}$. A search for low energy neutrinos (assumed to be produced from induced proton decay in the sun) was made at Super-Kamiokande [49]. A model- and β -dependent limit of $6.3 \times 10^{-24} (\frac{\beta}{10^{-3}})^2 \text{ cm}^{-2}\text{s}^{-1}\text{sr}^{-1}$ was obtained.

95.5.4 Searches at Colliders

Searches have been performed at hadron-hadron, electron-positron and lepton-hadron experiments. Collider searches can be broadly classed as being direct or indirect. In a direct search, evidence of the passage of a monopole through material, such as a charged particle track, is sought. In indirect searches, virtual monopole processes are assumed to influence the production rates of certain final states.

95.5.4.1 Direct Searches at Colliders

Collider experiments typically express their results in terms of upper limits on a production cross section and/or monopole mass. To calculate these limits, ansatzes are used to model the kinematics of monopole-antimonopole pair production processes since perturbative field theory cannot be used to calculate the rate and kinematic properties of produced monopoles. Limits therefore suffer from a degree of model-dependence, implying that a comparison between the results of different experiments can be problematic, in particular when this concerns excluded mass regions. A conservative approach with as little model-dependence as possible is thus to present representative values of the upper cross-section limits as a function of the centre-of-mass energy of the collisions, as shown in Fig. 95.2 for recent results from high energy colliders.

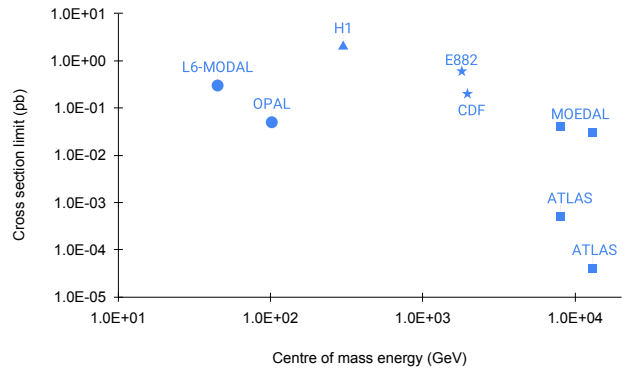


Figure 95.2: Upper limits on the production cross sections of monopoles from various collider-based experiments. Results from lepton-hadron (triangle), electron-positron (filled circle), proton-antiproton (star) and proton-proton (filled square) experiments are shown.

Searches for monopoles produced at the highest available energies in hadron-hadron collisions were made in pp collisions at the LHC by the ATLAS [50–53] and MoEDAL [54–57] experiments. ATLAS looked for highly ionising particles leaving a characteristic energy deposition profile in the tracker and calorimeter. MoEDAL used a NTD to tag highly ionising particles and the induction method to search for stopped monopoles. The charge-dependent mass limits extend up to around 4 TeV. The ATLAS experiment has considered hypotheses of monopoles with charges between $0.5Q_M^D$ and $2Q_M^D$ while MoEDAL has quoted limits for monopoles in the charge range Q_M^D to $5Q_M^D$. Models considered include monopole-pair production via photon fusion along with,

as is commonly used in hadron-hadron collisions, Drell-Yan processes [58]. MoEDAL has also looked for monopole produced via the Schwinger mechanism in the intense magnetic field created in PbPb collisions [57]. Tevatron searches have also been carried out by the CDF [59] and E882 [60] experiments. The CDF experiment used a dedicated time-of-flight system whereas the E882 experiment employed the induction technique to search for stopped monopoles in discarded detector material which had been part of the CDF and D0 detectors using periods of luminosity. Earlier searches at the Tevatron, such as [61], used NTDs and were based on comparatively modest amounts of integrated luminosity. Lower energy hadron-hadron experiments have employed a variety of search techniques including plastic track detectors [62] and searches for trapped monopoles [63].

The only LEP-2 search was made by OPAL [64] which quoted cross section limits for the production of monopoles possessing masses up to around 103 GeV. At LEP-1, searches were made with NTDs deployed around an interaction region. This allowed a range of charges to be sought for masses up to ~ 45 GeV. The L6-MODAL experiment [65] gave limits for monopoles with charges in the range $0.9Q_M^D$ and $3.6Q_M^D$, whilst an earlier search by the MODAL experiment was sensitive to monopoles with charges as low as $0.1Q_M^D$ [66]. The deployment of NTDs around the beam interaction point was also used at earlier e^+e^- colliders such as KEK [67] and PETRA [68]. Searches at e^+e^- facilities have also been made for particles following non-helical trajectories [69, 70].

There has so far been one search for monopole production in lepton-hadron scattering. Using the induction method, monopoles were sought which could have stopped in the aluminium beampipe which had been used by the H1 experiment at HERA [71]. Cross section limits were set for monopoles with charges in the range $Q_M^D - 6Q_M^D$ for masses up to around 140 GeV.

95.5.4.2 Indirect Searches at Colliders

It has been proposed that virtual monopoles can mediate processes which give rise to multi-photon final-states [72,73]. Photon-based searches were made by the D0 [74] and L3 [75] experiments. The D0 work led to spin-dependent lower mass limits of between 610 and 1580 GeV, while L3 reported a lower mass limit of 510 GeV. However, it should be stressed that uncertainties on the theoretical calculations which were used to derive these limits are difficult to estimate.

References

- [1] P. A. M. Dirac, Proc. Roy. Soc. Lond. **A133**, 821, 60 (1931).
- [2] J. S. Schwinger, Science **165**, 757 (1969).
- [3] F. Englert and P. Windey, Phys. Rev. **D14**, 2728 (1976).
- [4] P. Goddard, J. Nuyts and D. I. Olive, Nucl. Phys. **B125**, 1 (1977).
- [5] G. 't Hooft, Nucl. Phys. **B79**, 276 (1974).
- [6] A. M. Polyakov, JETP Lett. **20**, 194 (1974).
- [7] C. P. Dokos and T. N. Tomaras, Phys. Rev. **D21**, 2940 (1980).
- [8] G. Lazarides and Q. Shafi, Phys. Lett. **94B**, 149 (1980).
- [9] C. G. Callan, Jr., Phys. Rev. **D26**, 2058 (1982).
- [10] V. A. Rubakov, Nucl. Phys. **B203**, 311 (1982).
- [11] T. W. B. Kibble, J. Phys. **A9**, 1387 (1976).
- [12] J. Preskill, Phys. Rev. Lett. **43**, 1365 (1979).
- [13] E. N. Parker, Astrophys. J. **160**, 383 (1970).
- [14] M. S. Turner, E. N. Parker and T. J. Bogdan, Phys. Rev. **D26**, 1296 (1982).
- [15] F. C. Adams *et al.*, Phys. Rev. Lett. **70**, 2511 (1993).
- [16] Y. Rephaeli and M. S. Turner, Phys. Lett. **121B**, 115 (1983).
- [17] E. W. Kolb, S. A. Colgate and J. A. Harvey, Phys. Rev. Lett. **49**, 1373 (1982).
- [18] S. Dimopoulos, J. Preskill and F. Wilczek, Phys. Lett. **119B**, 320 (1982).
- [19] K. Freese, M. S. Turner and D. N. Schramm, Phys. Rev. Lett. **51**, 1625 (1983).
- [20] E. W. Kolb and M. S. Turner, Astrophys. J. **286**, 702 (1984).
- [21] J. A. Harvey, Nucl. Phys. **B236**, 255 (1984).
- [22] K. Freese and E. Krasteva, Phys. Rev. **D59**, 063007 (1999), [arXiv:astro-ph/9804148].
- [23] J. Arafune, M. Fukugita and S. Yanagita, Phys. Rev. **D32**, 2586 (1985).
- [24] L. L. Vant-Hull, Phys. Rev. **173**, 1412 (1968).
- [25] S. Graf, A. Schaefer and W. Greiner, Phys. Lett. **B262**, 463 (1991).
- [26] Review of Particle Physics 2024 (*this paper*), listing on *Searches for Magnetic Monopoles*.
- [27] L. Patrizii and M. Spurio, Ann. Rev. Nucl. Part. Sci. **65**, 279 (2015), [arXiv:1510.07125].
- [28] M. Fairbairn *et al.*, Phys. Rept. **438**, 1 (2007), [hep-ph/0611040].
- [29] J. M. Kovalik and J. L. Kirschvink, Phys. Rev. **A33**, 1183 (1986).
- [30] H. Jeon and M. J. Longo, Phys. Rev. Lett. **75**, 1443 (1995), [Erratum: Phys. Rev. Lett.76,159(1996)], [hep-ex/9508003].
- [31] S. Orito *et al.*, Phys. Rev. Lett. **66**, 1951 (1991).
- [32] M. Ambrosio *et al.* (MACRO), Eur. Phys. J. **C25**, 511 (2002), [hep-ex/0207020].
- [33] B. Cabrera, Phys. Rev. Lett. **48**, 1378 (1982).
- [34] P. B. Price *et al.*, Phys. Rev. Lett. **35**, 487 (1975).
- [35] M. G. Aartsen *et al.* (IceCube), Eur. Phys. J. **C76**, 3, 133 (2016), [arXiv:1511.01350].
- [36] R. Abbasi *et al.* (IceCube), Phys. Rev. Lett. **128**, 5, 051101 (2022), [arXiv:2109.13719].
- [37] A. Albert *et al.* (ANTARES), JHEAp **34**, 1 (2022), [arXiv:2202.13786].
- [38] S. Balestra *et al.*, Eur. Phys. J. **C55**, 57 (2008), [arXiv:0801.4913].
- [39] M. A. Acero *et al.* (NOvA), Phys. Rev. D **103**, 1, 012007 (2021), [arXiv:2009.04867].
- [40] A. Aab *et al.* (Pierre Auger), Phys. Rev. **D94**, 8, 082002 (2016), [arXiv:1609.04451].
- [41] D. P. Hogan *et al.*, Phys. Rev. **D78**, 075031 (2008), [arXiv:0806.2129].
- [42] M. Detrixhe *et al.* (ANITA-II), Phys. Rev. **D83**, 023513 (2011), [arXiv:1008.1282].
- [43] J. E. Bartelt *et al.*, Phys. Rev. D **36**, 1990 (1987), [Erratum: Phys.Rev.D 40, 1701 (1989)].
- [44] M. Ambrosio *et al.* (MACRO), Eur. Phys. J. **C26**, 163 (2002), [hep-ex/0207024].
- [45] R. Becker-Szendy *et al.*, Phys. Rev. **D49**, 2169 (1994).
- [46] V. A. Balkanov *et al.* (Baikal), Prog. Part. Nucl. Phys. **40**, 391 (1998), [arXiv:astro-ph/9801044].
- [47] O. N. Gaponenko, Phys. At. Nucl. **84**, 3, 287 (2021).
- [48] M. G. Aartsen *et al.* (IceCube), Eur. Phys. J. **C74**, 7, 2938 (2014), [Erratum: Eur. Phys. J.C79,no.2,124(2019)], [arXiv:1402.3460].
- [49] K. Ueno *et al.* (Super-Kamiokande), Astropart. Phys. **36**, 131 (2012), [arXiv:1203.0940].
- [50] G. Aad *et al.* (ATLAS), Phys. Rev. **D93**, 5, 052009 (2016), [arXiv:1509.08059].
- [51] G. Aad *et al.* (ATLAS), Phys. Rev. Lett. **124**, 3, 031802 (2020), [arXiv:1905.10130].
- [52] G. Aad *et al.* (ATLAS), Phys. Rev. Lett. **124**, 3, 031802 (2020), [arXiv:1905.10130].
- [53] G. Aad *et al.* (ATLAS), JHEP **11**, 112 (2023), [arXiv:2308.04835].
- [54] B. Acharya *et al.* (MoEDAL), Phys. Rev. Lett. **118**, 6, 061801 (2017), [arXiv:1611.06817].

- [55] B. Acharya *et al.* (MoEDAL), Phys. Rev. Lett. **123**, 2, 021802 (2019), [arXiv:1903.08491].
- [56] B. Acharya *et al.* (MoEDAL), Eur. Phys. J. C **82**, 8, 694 (2022), [arXiv:2112.05806].
- [57] B. Acharya *et al.* (MoEDAL), Nature **602**, 7895, 63 (2022), [arXiv:2106.11933].
- [58] S. Baines *et al.*, Eur. Phys. J. **C78**, 11, 966 (2018), [Erratum: Eur. Phys. J. C79, no.2, 166 (2019)], [arXiv:1808.08942].
- [59] A. Abulencia *et al.* (CDF), Phys. Rev. Lett. **96**, 201801 (2006), [hep-ex/0509015].
- [60] G. R. Kalbfleisch *et al.*, Phys. Rev. **D69**, 052002 (2004), [hep-ex/0306045].
- [61] P. B. Price, G.-X. Ren and K. Kinoshita, Phys. Rev. Lett. **59**, 2523 (1987).
- [62] B. Aubert *et al.*, Phys. Lett. **120B**, 465 (1983).
- [63] R. A. Carrigan, F. A. Nezrick and B. P. Strauss, Phys. Rev. **D8**, 3717 (1973).
- [64] G. Abbiendi *et al.* (OPAL), Phys. Lett. **B663**, 37 (2008), [arXiv:0707.0404].
- [65] J. L. Pinfold *et al.*, Phys. Lett. **B316**, 407 (1993).
- [66] K. Kinoshita *et al.*, Phys. Rev. **D46**, R881 (1992).
- [67] K. Kinoshita *et al.*, Phys. Lett. **B228**, 543 (1989).
- [68] P. Musset, M. Price and E. Lohrmann, Phys. Lett. **128B**, 333 (1983).
- [69] T. Gentile *et al.* (CLEO), Phys. Rev. **D35**, 1081 (1987).
- [70] W. Braunschweig *et al.* (TASSO), Z. Phys. **C38**, 543 (1988).
- [71] A. Aktas *et al.* (H1), Eur. Phys. J. **C41**, 133 (2005), [hep-ex/0501039].
- [72] A. De Rujula, Nucl. Phys. **B435**, 257 (1995), [hep-th/9405191].
- [73] I. F. Ginzburg and A. Schiller, Phys. Rev. **D60**, 075016 (1999), [hep-ph/9903314].
- [74] B. Abbott *et al.* (D0), Phys. Rev. Lett. **81**, 524 (1998), [hep-ex/9803023].
- [75] M. Acciarri *et al.* (L3), Phys. Lett. **B345**, 609 (1995).

INDEX

Index

- a* meson resonances
- $a_0(980)$ 34, 1444
 - $a_0(1710)$ 1509
 - $a_0(1450)$ 36, 1478
 - $a_0(1950)$ 1520
 - $a_1(1260)$ 35, 1455
 - $a_1(1640)$ 37, 1494
 - $a_2(1320)$ 35, 1465
 - $a_2(1700)$ 38, 1508
 - $a_4(1970)$ [*was* $a_4(2040)$] 39, 1521
- A-parameter 1041
- ABC, approximate Bayesian computation 719
- Absolute monochromatic magnitude 138
- Accelerating Universe evidence 486
- Accelerator parameters 569
- Accelerator parameters for neutrino beam lines 574
- Accelerator-based ν detectors 635
- Accelerator-induced radioactivity 681
- Acceptance-rejection method (Von Neumann) 748
- Acoustic oscillations, baryon 493
- Activation function 724
- Active learning 718, 719
- Activity, unit of 679
- AD, automatic differentiation 735
- AdaBoost, adaptive boost 724
- ADAM, Adaptive Momentum Estimation 735
- AdS, anti-de Sitter spacetime 1021
- AdS/CFT
- correspondence 1021, 1105
 - dictionary 1025, 1105
- Advanced acceleration schemes 567
- Age of the Universe 139, 446
- Air shower extensive, EAS 649
- Aleatoric uncertainty 739
- Algorithms for Monte Carlo 749
- α_s , QCD coupling constant 137
- Amplitudes, Lorentz invariant 777
- AMS, approximate median significance 739
- AMSB, anomaly-mediated SUSY breaking 1040
- Angular-diameter distance, d_A 446
- Anisotropy of CMB 486, 524
- Annihilating dark matter 532
- Anomalous dimension quark mass (\overline{MS}) 834
- Anomaly detection 718, 741
- Anomaly-mediated SUSY breaking, AMSB 1040
- Anthropic approach 449
- Anthropic axion window 1086
- Antineutrino flux from reactor 308
- Antineutrinos, right-handed 929
- Astronomical unit 138
- Astrophysics 499
- Asymptotic freedom 153
- Asymptotics, total hadronic cross sections behaviour 423
- ATLAS – Toroidal LHC Apparatus, LHC 218
- Atmospheric
- Cherenkov detectors 651
 - fluorescence detector 649
 - Fly’s Eye 649
 - HiRes (high resolution) Fly’s Eye 649
 - Pierre Auger observatory 649
 - Telescope Array 649
 - neutrino flux 303
- Atmospheric pressure 137
- Atomic
- and nuclear properties of materials, table 144
 - mass unit 137
- Atomic weights of elements 131
- Attention 725, 729
- Attenuation length for photons 583
- Auger observatory 649, 1140
- Authors and consultants 12
- Auto-encoder 716, 718
- Averaging of data 15
- Averaging, unconstrained 16
- Avogadro constant 137
- Axial vector mesons $\ell = 1; 1^{++}$ or 1^{+-} 323
- Axial-vector mesons
- $K_{1A}-K_{1B}$ mixing 874, 879
 - $f_1(1285), f_1(1420), f_1(1510)$ 879, 880
- Axion as dark matter 502, 1079
- Axion searches 1079
- Axion stars 1087
- Axion-like particles (ALP) 1079
- Axion-photon mixing 532
- Axions (A^0) and other very light bosons searches 27, 1271
- $B\bar{B}$ mixing 955
- $b\bar{b}$ mesons 83, 2023
- B decay, CP violation in 287, 952
- B decays polarization, note 951
- B mesons
- $B_{sJ}(6063)^0$ 1892
 - $B_{sJ}(6114)^0$ 1892
 - B^* 69, 1860
 - B^0 61, 1751
 - B^\pm 54, 1682
 - B^\pm/B^0 admixture 67, 1828
 - $B^\pm/B^0/B_s^0/B$ -baryon admixture 68, 1851
 - $B_1(5721)$ 69, 1861
 - $B_2^*(5747)$ 69, 1862
 - $B_J^*(5732)$ [*was* B^{**}] 1861
 - $B_J(5840)$ 1862
 - $B_J(5970)$ 69, 1863
 - B_c^+ 72, 1893
 - $B_c(2S)^\pm$ 72, 1897
 - $B_{s1}(5830)^0$ 71, 1890
 - $B_{s2}^*(5840)^0$ 71, 1891
 - $B_{sJ}^*(5850)$ 1891
 - $B_{sJ}(6063)^0$ 1892
 - $B_{sJ}(6114)^0$ 1892
 - B_s^* 71, 1890
 - B_s^0 70, 1865
- b' quark (4^{th} generation), searches for 32, 859, 1398
- b -baryon admixture 111, 2283
- b -flavored Hadrons, production and decay 940
- b -quark fragmentation 397, 858
- $b_1(1235)$ meson 35, 1454
- Background
- cosmic microwave, CMB 524
 - cosmic ray radiation 680
 - relic cosmic neutrino 491
 - relic light gravitons 1022
- Background cosmology parameters 526
- Backpropagation 719, 735
- Bagging, bootstrap aggregating 723
- Balitsky-Fadin-Kuraev-Lipatov (BFKL) limit 156
- Barkas correction 578
- Baryogenesis 450
- Baryon
- acoustic oscillations 461, 486, 493
 - decay parameters, note on 1001
 - density of the Universe 138
 - Hyperon nonleptonic decays 1001
 - magnetic moments 332, 337
 - number conservation 120
 - oscillation spectroscopic survey 486
 - resonances, naming scheme 1002
 - resonances, SU(3) classification of 327
 - semileptonic decays 1001
- Baryon quick reference table 89
- Baryon-to-photon ratio 138, 476
- Baryonia 874, 881
- $\rho(1900)$ 879
 - $f_2(1565)$ 881
- Baryons in quark model 327

- Batch 735, 737
- Bayes' theorem 466, 689
- Bayesian
- approach 698
 - intervals 704
 - method 694
 - statistics 704
- Bayesian machine learning 740
- Bayesian optimization 717, 722
- BBN, Big-Bang nucleosynthesis 474
- Beam collimation 561, 566
- Beam cooling 561
- Beam dynamics 559
- Beam momentum, c.m. energy and momentum vs 777
- Beam-beam interaction 562
- Beamstrahlung 562, 564
- Becquerel, unit of radioactivity 679
- BEPC 569
- BEPC-II 569
- β function of QCD 153
- Beta distribution 692, 750
- Beta function 560
- β -rays, from radioactive sources 685
- Betatron tune 560
- Bethe equation 576
- Beyond the general relativity physics 532
- Beyond the SM physics, BSM 270, 478, 502, 755
- Bhabha cross section 581
- Bi-directional RNN 729
- Bias of an estimator 694
- Big-Bang cosmology 444, 457
- Big-Bang nucleosynthesis (BBN) 474
- Binary classification 714, 715, 721
- Binary pulsars, strong-self-gravity 438
- Bino 1042
- Binomial distribution 692, 749
- Biological damage from radiation 679
- Birks' law 595
- Black holes
- binary 438
 - coalescing 435
 - horizon 433
 - microscopic, searches 1023
 - production 1022
 - strong gravitational fields 432
 - supermassive 438
- Bloch correction 578
- BMA, Bayesian model averaging 740
- BN, batch normalization 726, 736
- Bohr magneton 137
- Bohr radius 137
- Boiling points of cryogenic gases, table 144
- Boltzmann constant k 137, 138
- Booklet, Particle Physics, how to get 11
- Boosting 723
- Bose-Einstein correlations 418, 760, 815
- Bosons, Nambu-Goldstone composite 1104
- BOSS, baryon oscillation spectroscopic survey 486
- Bottleneck 716, 732
- Bottom baryons 108, 2263
- Bottom mesons
- experimental rate measurements 934
 - production and decay 940
 - theoretical decay-constant calculations 934
- Bottom mesons (B, B^*) 54, 1682
- Bottom, Charmed mesons ($B_c, B_c(2S)$) 72, 1893
- Bottom, Strange mesons (B_s, B_s^*, X) 70, 1865
- Bottom-changing neutral currents, tests for 121
- Bottomonium 83, 2023
- Bragg additivity 580
- Brane 478, 1022, 1040, 1122
- Breit-Wigner distribution 750
- Bremstrahlung
- at very high energies 584
 - by e^\pm 582
 - by muons 586
- B_s^0 decay, CP violation in 287
- BSM, beyond Standard Model 502
- Bubble chambers 635
- Bubble Universes 449
- $c\bar{c}$ mesons (including possibly non- $q\bar{q}$ states) 72, 1898
- C (charge conjugation), tests of conservation 114
- c -quark fragmentation 397
- Cabibbo angle 904
- Calorimeter
- electromagnetic (ECAL) 627
 - hadronic (HCAL) 627
 - homogeneous 627
 - sampling 627
- CBR – Cosmic background radiation (see CMB) 524
- CDM, cold dark matter 499
- Central limit theorem 691
- CEPC 564
- Cepheid variable stars 485
- CESR (Cornell) 570
- CESR-C (Cornell) 570
- CFT, 4d conformal field theory 1025
- Chandrasekhar mass 138
- Change of random variables 690
- Channels 720, 725, 737
- Characteristic functions 690
- Charge conjugation (C) conservation 114
- Charge conjugation of $q\bar{q}$ states 323
- Charge conservation 117
- Charged Higgs bosons (H^\pm and $H^{\pm\pm}$) searches 27, 1248
- Chargino mass limits 1065
- Charginos 1042
- Charm decays, CP violation in 285
- Charm mixing and CP violation 913
- Charm-changing neutral currents, tests for 121
- Charmed baryons ($\Lambda_c^+, \Sigma_c, \Xi_c, \Omega_c^+$) 103, 2234
- Charmed baryons, note on 103, 2234
- Charmed mesons
- experimental rate measurements 932
 - theoretical decay-constant calculations 933
- Charmed mesons (D, D^*, D_J) 43, 1592
- Charmed, Strange mesons (D_s, D_s^*, D_{sJ}, X) 50, 1657
- Chemical potential 360, 447
- Chemical potential, neutrino 532
- Cherenkov detectors 599
- at accelerators
 - differential 599
 - ring imaging 599
 - threshold 599
 - tracking 598 - electromagnetic calorimeters 598
 - fast particle counter 598
 - nonaccelerator
 - atmospheric 651
 - deep underground 652
 - particle identification PID 598
- Cherenkov radiation 587
- χ^2 distribution 691, 749
- χ_b and χ_c mesons
- $\chi_{b0}(1P)$ 85, 2031
 - $\chi_{b0}(2P)$ 86, 2043
 - $\chi_{b1}(1P)$ 85, 2033
 - $\chi_{b1}(2P)$ 86, 2045
 - $\chi_{b1}(3P)$ 87, 2053
 - $\chi_{b2}(1P)$ 85, 2035
 - $\chi_{b2}(2P)$ 87, 2047
 - $\chi_{b2}(3P)$ 87, 2053
 - $\chi_{c0}(1P)$ 75, 1935
 - $\chi_{c0}(3860)$ 1996
 - $\chi_{c0}(3915)$ [*was* $X(3915)$] 81, 2000

- $\chi_{c0}(4500)$ [*was* $X(4500)$] 2019
 $\chi_{c0}(4700)$ [*was* $X(4700)$] 2022
 $\chi_{c1}(1P)$ 76, 1945
 $\chi_{c1}(3872)$ [*aka* $X(3872)$] 81, 1996
 $\chi_{c1}(4140)$ [*was* $X(4140)$] 82, 2005
 $\chi_{c1}(4274)$ [*was* $X(4274)$] 83, 2014
 $\chi_{c1}(4685)$ 2022
 $\chi_{c2}(1P)$ 77, 1956
 $\chi_{c2}(3930)$ 81, 2001
Chiral perturbation theory 354, 837, 889, 896
Chiral superfields 1038
Chromaticity 561
Chromomagnetic dipole moment 850
Circular Colliders 559
Circular Higgs factories 564
CKM (Cabibbo-Kobayashi-Maskawa) quark mixing matrix 980
CKM angles
 α 980
 β 980
 γ 982
from B hadrons determination, note 980
CKM matrix elements 980
CKM quark-mixing matrix, note on 270
CKM unitarity constraints 905
Classical electron radius 137
Classification 711, 714, 718, 721, 722, 726, 732, 740
Clebsch-Gordan coefficients 772, 773
CLIC (CERN) future collider 570
Clustering 716, 732
CMB
Planck satellite 461, 519, 527
anisotropy 453, 486
anisotropy power spectrum 524
COBE satellite 483, 524
Compton distortion 530
concordance with baryon density 477
cosmic microwave background 524
cosmic variance 525
detectors 666
dipole 524
future Simons observatory 488
lensing 494
LiteBIRD satellite 529
Lorentz-boosted temperature pattern 524
mean temperature, monopole 524
monopole 524
multipoles 524
non-Gaussianity 451, 467, 525
polarization 528
primordial perturbation 526
radiation density of Universe 138
scalar perturbations 526
sky map 524
Solar System motion 524
spectrum 524
tensor perturbations 526
Wilkinson Microwave Anisotropy Probe, *WMAP* ... 524
WMAP satellite 519
CMB–Cosmic microwave background 450, 486
CMS – Compact Muon Solenoid, LHC 218
CMSSM, Constrained MSSM 1046, 1059
CNN, convolutional neural network 714, 720, 725, 737
CNO cycle, solar neutrino 302
COBE – COsmic Background Explorer 524
Coherent radio Cherenkov radiation detectors 657
Cold dark matter (CDM) 452
Cold dark matter density 138
Collaboration databases 22
Collaborations
Planck 485
ALEPH 815, 956
ALICE 412
ALPHA 359
ANITA 659
ARIANNA 660
ATLAS 412, 503, 815, 985, 1029
B-factories 985
BaBar 830, 934, 940, 956, 985, 1049
Belle 830, 934, 940, 956, 985, 1049
BelleII 956
BERT 1081
BESIII 985
CALICE 631
CCFR 638
CDF 815, 940, 956
CJ 380
CLEO 940
CLEO-c 985
CMS 503, 815, 985, 1029, 1035, 1070, 1136
COMPASS 872
COMPETE 413, 423
CTA 651
D0 421, 815, 941, 956, 1036
DAMIC-M 507
DELPHI 815, 956
DREAM/RD52 633
DSSV 372
eBOSS 518
ETM 936
Event Horizon Telescope 439
Fermi-LAT 1084
Fermilab-MILC 936
FLAG 936
GlueX 1014
GRAND 661
H.E.S.S. 651, 1084
H1 398, 1136
HERA 398, 1069
HFLAV 936
HPQCD 359, 936
HWPf 637
L3 815, 956
Lattice QCD 838
LEP 815, 817, 1034, 1069
LHC 815, 1035
LHCb 815, 940, 952, 956, 985, 994, 1035, 1049
LIGO-Virgo 435
LVC 435
LVK 435
MAGIC 651
MAMI 872
MILC 934
MOSCAB 507
NEWS-G 507
NEWSdm 508
NINJA 638
NuTeV 638
OPAL 815, 956
PDG, Particle Data Group 2
PIBETA 871
RBC/UKQCD 969
RD51 607
RM123-Soton 930
RNO-G 660
SLD 819
Sp \bar{p} 1098
Tevatron 815, 1036, 1069
TOTEM 410
Tunka-Rex 660
UA4 421
VERITAS 651
WMAP 487
ZEUS 398, 1069, 1136
Collider parameters 569
Colliders 559
future 564

- present 563
 recent 562
 Colliders based on Energy Recovery Linacs 566
 Collinear and infrared safety 158, 161
 Collinear factorization 156
 Color confinement 1086
 Color factor 153, 163
 Color reconnection 815
 Color reconnection phenomenon 418, 761
 Colorons (axigluons) search 1114
 Comments, e-mail address to contact 11
 Compact Linear Collider (CLIC) 566
 Compactification 1087
 Compensation
 intrinsic 632
 software 632
 Composite Higgs boson 243
 Compton wavelength, electron 137
 Concordance cosmology 483
 Conditional probability density function 690
 Confidence intervals 703
 frequentist 704
 Gaussian 15
 Poisson 706
 Confinement 360
 -deconfinement quarks-hadrons transition 448
 color 1086
 harmonic 328
 linear 328, 757
 Conformal field theory, CFT 1025
 Conservation laws 114
 Consistency of an estimator 694
 Constancy of constants tests 437
 Constrained fit 829
 Constrained fits, procedures for 16
 Constrained MSSM, CMSSM 1046, 1059
 Constraints, parameter estimation with 697
 Consultants 12
 Contour-improved perturbation theory (CIPT) 168
 Conversion constant 137
 Conversion probability for photons to e^+e^- 583
 Convolution kernel 725
 Convolution, 1×1 725
 Convolution, kernel size 725
 Convolution, padding 725
 Convolution, stride 725
 Convolution-transpose 726
 Copernican Principle 444
 Correlation coefficient, definition 690
 Correlation matrices 829
 Cosmic acceleration, dark energy 515
 Cosmic background radiation temperature 524
 Cosmic microwave background, CMB 450, 486, 524
 Cosmic neutrino background, $C\nu B$ 491
 Cosmic ray(s)
 background in counters 680
 fluorescence detectors FDs 649
 radio detection of air showers 660
 ultra-high energy, UHE 658
 Cosmic topology 485
 Cosmological
 constant Λ 138, 444, 457, 515, 526
 density parameter, Ω 445
 equation of state 445
 mass density parameter 444
 parameters, note on 482
 standard model 532
 Cosmological probes
 CMB 530
 galaxy peculiar velocities 487
 integrated Sachs-Wolfe effect 487
 redshift 444
 supernovae 485
 Cosmology 482, 499
 Λ CDM 499
 Big-Bang 444, 457, 499
 modern 499
 outlook for the future 488
 Robertson-Walker metric 457
 scalar field 458
 standard 502
 standard early Universe 457
 standard neutrino 491
 Coupling between matter and gravity 437
 Coupling constant in QCD 137, 153
 Coupling unification 1122
 Covariance matrix 696
 Covariance, definition 690
 Coverage 704
 CP , tests of conservation 114
 CP violation
 and $D^0 - \bar{D}^0$ mixing 917
 charm mixing 913
 classification of effects 282
 in $B\bar{B}$ mixing 958
 in B and B_s^0 mixing and decay 287
 in B decay 940
 in K_L^0 decay 284
 in K_L^0 decay, note on 908
 in charm 285
 in decays of Beauty to Charm 912
 in the quark sector, note 280
 interference between tree and penguin amplitudes .. 287
 overview 114, 280
 the CKM matrix 283
 the Kobayashi-Maskawa mechanism 283
 CPT invariance tests in neutral kaon decay 902
 CPT tests of conservation 117
 Critical density in cosmology 444
 Critical density of the Universe 138
 Critical energy
 for electrons 583
 for muons 586
 Cross sections and related quantities, plots of 807
 e^+e^- annihilation cross section near M_Z 810
 Pseudorapidity distribution in pp and $\bar{p}p$ interactions 807
 Average hadron multiplicities in e^+e^- annihilation events 808
 nucleon structure functions 367
 Cross sections, relations for 779, 792
 Cross-entropy loss 715
 Cross-validation 713
 Cryogenic beam vacuum system 566
 Cryogenic gases, boiling points, table 144
 Crystal accelerator 567
 Cumulative distribution function, definition 689
 Curie, unit of radioactivity 679
 Curvature 139

 d functions 772
 D mesons
 D^0, \bar{D}^0 46, 1610
 D^\pm 43, 1592
 $D(3000)^0$ 1655
 $D^*(2007)^0$ 50, 1646
 $D^*(2010)^\pm$ 50, 1647
 $D^*(2640)^\pm$ 1654
 $D_0^*(2300)$ [*was* $D_0^*(2400)$] 50, 1648
 $D_0(2550)^0$ 1653
 $D_1^*(2600)^0$ [*was* $D_J^*(2600)$] 1653
 $D_1^*(2760)^0$ 1655
 $D_1(2420)$ 50, 1649
 $D_1(2430)^0$ 50, 1650
 $D_2^*(2460)$ 50, 1651
 $D_2(2740)^0$ [*was* $D(2740)^0$] 1654
 $D_3^*(2750)$ 50, 1654

- $D_{s0}^*(2317)^\pm$ 53, 1674
 $D_{s0}^*(2590)^\pm$ 1678
 $D_{s1}^*(2700)^\pm$ 53, 1678
 $D_{s1}^*(2860)^\pm$ 1679
 $D_{s1}(2460)^\pm$ 53, 1675
 $D_{s1}(2536)^\pm$ 53, 1676
 $D_{s2}^*(2573)$ 53, 1677
 $D_{s3}^*(2860)^\pm$ 53, 1679
 $D_{sJ}(3040)^\pm$ 1680
 $D_s^{*\pm}$ 53, 1673
 D_s^\pm 50, 1657
 D^0 - \bar{D}^0 mixing, note on 917
DAΦNE 569
 d_A , angular-diameter distance 486, 531
Dalitz plot, relations for 778
Damage, biological, from radiation 679
Dark energy 445, 484, 515
 cosmic acceleration 515
 density parameter 138
 equation of state parameter 139
 equation of state parameter w 486, 515
 Euclid satellite 470
 experiments 518
 observational probes
 baryon acoustic oscillations, BAO 517
 CMB anisotropies 517
 Type Ia supernovae 517
 weak gravitational lensing 517
 parameter, Ω_N 445
 quintessence 454
 repulsive gravity 516
Dark energy spectroscopic instrument (DESI) 487, 518
Dark matter 452, 484
 annihilating 532
 CDM cosmology 499
 cusp-core problem 501
 density distribution 500
 detectors 666
 Gaia satellite 501
 Galactic halo shape 500
 genesis, cannibalization 500
 genesis, DM anti-DM asymmetry 500
 genesis, freeze-in 500
 genesis, freeze-out 499
 genesis, non-thermal production 500
 genesis, primordial black holes 500
 laboratory detection 503
 missing satellites problem 501
 non-baryonic 499
 Too-big-to-fail problem 501
 velocity distribution 501
Dark matter astrophysical detection
 cosmic-ray antimatter 510
 cosmology 510
 gamma rays 508
 multi-wavelength 510
 neutrinos 509
 PBH detection 510
 staller physics 510
Dark matter candidates
 axions 502
 dark photon 502
 gaugino 1041
 gravitino 1040
 higgsino 1041
 sterile neutrinos 502
 WIMPs 502
Dark matter properties
 darkness 499
 mass lower and upper limits 499
 self-interactions 499
 stability 499
Data 22
 Data augmentation 721, 738, 739
 Data manifold 721
 Data, averaging and fitting procedures 15
 Data, selecting and treatment 15
Databases
 availability online 20
 conferences 21
 experiments 21
 high-energy physics 20
 Insitutions 21
 INSPIRE 20
 Authors 21
 Conferences 21
 Experiments 21
 Insitutions 21
 Jobs 22
 Journals 21
 Literature 20
 Seminars 21
 institutions 21
 journals 21
 literature 20
 ADS 20
 arXiv.org 20
 INSPIRE 20
 MathSciNet 21
 OSTI 21
 ORCID 21
 particle physics 20
 PDG API 20
 PDGLive, PDG web browser 20
 Review of Particle Physics (RPP) 20
 ROR 21
 RPP computer-readable files 20
Day, sidereal 138
 dE/dx 575
Decay parameters, Michel 832
Decays, kinematics and phase space for 777
Deceleration parameter, q_0 445
Decision trees 712
Decoder 716, 726, 731, 733
Deep inelastic scattering, DIS 155, 367, 412, 635
Deep learning 725
Deep Sets 720, 731
Degree of freedom, number of 696
 $\Delta B = 1$, weak-neutral currents, tests for 114
 $\Delta B = 2$, tests for 114
 $\Delta C = 1$, weak-neutral currents, tests for 114
 $\Delta C = 2$, tests for 114
 Δ resonances
 $\Delta(1232)$ 97, 2137
 $\Delta(1600)$ 97, 2139
 $\Delta(1620)$ 97, 2141
 $\Delta(1700)$ 97, 2142
 $\Delta(1750)$ 2144
 $\Delta(1900)$ 97, 2145
 $\Delta(1905)$ 98, 2146
 $\Delta(1910)$ 98, 2148
 $\Delta(1920)$ 98, 2149
 $\Delta(1930)$ 98, 2151
 $\Delta(1940)$ 2152
 $\Delta(1950)$ 98, 2153
 $\Delta(2000)$ 2155
 $\Delta(2150)$ 2156
 $\Delta(2200)$ 98, 2156
 $\Delta(2300)$ 2157
 $\Delta(2350)$ 2157
 $\Delta(2390)$ 2158
 $\Delta(2400)$ 2158
 $\Delta(2420)$ 98, 2159
 $\Delta(2750)$ 2159
 $\Delta(2950)$ 2160

- $\Delta S = 1$, weak-neutral currents, tests for 114
 $\Delta S = \Delta Q$ tests of 114
 $\Delta T = 1$, weak-neutral currents, tests for 114
 $\Delta(\sim 3000 \text{ Region})$ Partial-Wave Analyses 2160
 δ -rays 579
DenseNet 727
Density
 of CMB photons 138
 of materials, table 144
 of Universe, critical 138
 parameter of the Universe Ω_0 138
Density effect in energy loss rate 576
Density estimation 715, 719, 732, 739, 740
DESI – dark energy spectroscopic instrument .. 470, 487, 518
Detectors
 bubble chambers 635
 calorimeters
 electromagnetic 629
 Cherenkov 598, 651
 CMB detectors 666
 coherent radio Cherenkov radiation 657
 Dark matter 666
 fluorescence, atmospheric 649
 for rare events 661
 gas-filled 601
 drift chamber 603, 634
 high rate effects 604
 micro-pattern 605
 micro-strip chamber 607
 multi-wire proportional chambers, MWPC 603
 resistive plate chambers, RPC 611
 time-projection chambers, TPC 607
 transition radiation, TRD 609
 gravitation wave observatory, Virgo 435
 hadronic shower 591
 ice-based 659
 inorganic scintillator 596
 Kinetic Inductance Detectors (KIDs) 666
 LAr Time projection chambers 613
 laser interferometer gravitation observatory, LIGO .. 435
 liquid ionization chamber 634
 liquid scintillator 652
 Low Temperature Detectors (LTDs) 665
 low-noise readout 623
 low-radioactivity background techniques 670
 Magnetic Metallic Calorimeters (MMCs) 668
 Neutrino cryogenic detectors 666
 neutrino telescopes 654
 neutrino, calibration of 685
 neutrinos
 accelerator-based 635
 bubble chambers 635
 Cherenkov 637
 emulsion 638
 iron tracking calorimeters 636
 liquid argon TPC 637
 plastic scintillators 637
 noble liquid 654
 organic scintillator 594
 proton decay 652
 radio-detection of cosmic ray air showers 660
 rare event search
 $0\nu\beta$ decay 664
 WIMPs 663
 semiconductor 617
 (D)MAPS 619
 3D-Si 619
 DEPFET 619
 hybrid pixels 619
 LGAD 620
 microstrip 619
 monolithic pixels 619
 radiation damage 621
 silicon driftchamber 619
 Semiconductor Thermistors 667
 showers 629
 superconducting solenoid magnets for 639
 superconducting toroidal magnets for 640
 Superconducting Tunnel Junctions (STJs) 666
 Transition Edge Sensors (TESs) 667
 water Cherenkov 653
 wire chambers 613
Deuterium abundance 474
Deuteron mass 137
Deuteron structure function 379
DIEHARD 748
Dielectric constant of gaseous elements, table 145
Dielectric laser accelerator 567
Dielectric suppression of bremsstrahlung 582
Dielectric wakefield accelerators 567
Differentiable simulator 719
Differential Cherenkov detectors 599
Diffraction and high energy soft QCD 406
Diffractive parton distribution 412
Diffractive processes 406
Dirac gauginos 1051
Dirac neutrinos 296
Direct CP asymmetry in B decays 952
Directories, online, people, and organizations 20
DIS, deep inelastic scattering 367, 412
Discriminative model 711, 713, 732
Disk density 138
Dispersion relation 422, 888, 904
Distance ladders 485
Distance-redshift relation 444, 446, 482, 485, 516
Distribution shift 712
Dokshitzer-Gribov-Lipatov-Altarelli-Parisi
 (DGLAP) equations 156
Domain adaptation 738
Domain shift 712, 738
Donnachie-Landshoff pp -scattering amplitude 407
Dose rate from γ ray sources 681
Dose, radioactivity, unit of absorbed 680
Double PDFs 372
Double- β decay 1343
Doubly charmed baryons 2262
Drell-Yan process 220, 346, 375, 1026
Drift chambers 603
Drift velocities of electrons 634
Dropout 714, 725
 D_s^+ branching fractions, note on 927
Dual problem 721
Dual readout 632
Dynamic Graph CNN 731
Dynamical electroweak symmetry breaking 1104

 e (electron) 28, 1297
 e (natural log base) 137
 e^- Compton wavelength 137
Early stopping 712, 714, 724, 735, 736
Early Universe 457, 474
Earth
 equatorial radius 138
 mass 138
Eddington luminosity 138
Edge 731
Education databases 22
Effective
 number of neutrinos 139
Effective dose of radioactivity 679
Effective field theories (EFTs) 341
Effective skin depth δ 146
Efficiency of an estimator 694
EFT – effective field theories 341
Elastic cross sections 412
Elastic scattering 406

- ELBO, Evidence Lower Bound Objective 715, 732, 733
- Electric charge (Q) conservation 117
- Electric dipole moment, EDM 115
- Electrical resistivity of elements, table 145
- Electromagnetic
- calorimeters 629
 - cascades 585
 - effects 337
 - field equations 146
 - relations 146
 - showers, lateral distribution 586
 - showers, longitudinal distribution 585
- Electron
- charge magnitude e 137
 - configuration of element, table 142
 - critical energy 583
 - cyclotron frequency/field e/m_e 137
 - drift velocities 634
 - mass 137
 - radius, classical 137
 - volt eV 137
- Electron and photon interactions in matter 581
- Electron-Ion Collider (EIC) 564
- Electron-positron collider rings 563
- Electron-positron colliders – future 565
- Electronic energy loss by heavy particles 575
- Electronic structure of the elements 142
- Electroweak
- dynamical symmetry breaking 1104
 - penguin decay 944, 952
- Electroweak Symmetry Breaking (EWSB) 211
- Electroweak corrections 158, 166
- Elements
- electronic structure of 142
 - ionization energies of 142
- Elements, periodic table of 131
- Embedding 720
- Emission probability 685
- Emittance 560
- Empirical risk 712
- Encoder 716, 726, 731, 733
- Encoder-decoder 727, 729
- Energy and momentum (c.m.) vs beam momentum 777
- Energy density
- of CBR 138
 - of dark energy 138
 - of relativistic particles 138
- Energy loss
- (fractional) for e^\pm in lead 582
 - at low energies 577
 - by electrons 582
 - by photons 583
 - density effect 576
 - higher order corrections 577
 - rate for heavy charged particles 576
 - rate for muons at high energies 586
 - rate in compounds and mixtures 580
 - rate, form factor corrections 576
 - rate, most probable 579
 - rate, restricted 576, 579
 - scaling with mass 576
- Energy Recovery Linac 566
- Energy resolution (calorimeter) 627
- constant term 627
 - stochastic term 627
- Energy-energy correlation 163
- Ensemble methods 723
- Entropy density 138, 448, 449
- e^+e^- annihilation
- cross-section formulae 792
 - two-photon process 793
- Epistemic uncertainty 739
- ϵ_0 (permittivity of free space) 137, 146
- Equivalence principle, experimental tests of 437
- Equivalence principle, GR 431
- Equivalent noise charge 624
- Error function 691
- Error propagation 738
- Errors, treatment of 15
- Established nonets for the meson 324
- Estimator 694
- η mesons
- η 33, 1416
 - $\eta_1(1855)$ 1517
 - $\eta(1295)$ 35, 1464
 - $\eta(1405)$ 36, 1472
 - $\eta(1475)$ 36, 1483
 - $\eta(1760)$ 1512
 - $\eta(2225)$ 1533
 - $\eta'(958)$ 34, 1435
 - $\eta_2(1645)$ 37, 1495
 - $\eta_2(1870)$ 38, 1518
 - $\eta_c(1S)$ 72, 1898
 - $\eta_c(2S)$ 78, 1967
 - $\eta_b(1S)$ 83, 2023
 - $\eta_b(2S)$ 2037
- Event pile up 566
- Event shape 163
- EWSB, Electroweak Symmetry Breaking 211
- Excitation energy 576
- Excited fermions searches 1099
- Excited leptons searches 1099
- Exotic quantum numbers 874
- Expansion of the Universe 445
- Expectation value, definition 689
- Experiment databases 21
- Experimental design optimization 717, 718
- Experimental rate measurements
- bottom mesons 934
 - charmed mesons 932
 - pions and kaons 930
- Experimental sensitivity 708
- Experimental tests of gravitational theory 431
- Exploding gradient 724, 729, 736
- Extensions to the cosmological standard model 483
- Extensive air shower, EAS 649
- Extra Dimensions 113, 1040, 2352
- Extra Dimensions, note on 1021
- f, F mesons
- $f_0(980)$ 34, 1442
 - $f_0(1370)$ 36, 1469
 - $f_0(1500)$ 36, 1484
 - $f_0(1710)$ 38, 1510
 - $f_0(2020)$ 39, 1523
 - $f_0(2100)$ 1526
 - $f_0(2200)$ 1531
 - $f_0(2330)$ 1535
 - $f_1(1285)$ 35, 1461
 - $f_1(1420)$ 36, 1475
 - $f_1(1510)$ 1486
 - $f_2'(1525)$ 37, 1487
 - $f_2(1270)$ 35, 1457
 - $f_2(1430)$ 1478
 - $f_2(1565)$ 37, 1491
 - $f_2(1640)$ 1495
 - $f_2(1810)$ 1515
 - $f_2(1910)$ 1519
 - $f_2(1950)$ 39, 1520
 - $f_2(2010)$ 39, 1523
 - $f_2(2150)$ 1526
 - $f_2(2300)$ 39, 1534
 - $f_2(2340)$ 39, 1535
 - $f_4(2050)$ 39, 1524
 - $f_4(2300)$ 1534
 - $f_6(2510)$ 1537

- $f_J(2220)$ 1531
 $f_0(600)$ [was $f_0(500)$ was σ] 33, 1422
 $f_0(1770)$ 1513
 $f_0(2470)$ 1537
 F_2 structure function, plots 379
Factorization scale 155, 156
FCC-ee (Future Circular Collider) 564
FCC-hh (Future Circular Collider) 566
Feature engineering 716
Feature map 725
Feature vector 712, 724
Fermi constant 1041
Fermi coupling constant $G_F/(hc)^3$ 137
Fermi plateau 577
Fermions
 left-handed 1106
 right-handed 1106
Feynman's x variable 780
Field equations, electromagnetic 146
Filter 724
Fine tuning 1048
Fine-structure constant, α 137
Fine-structure constant, time variation 532
Fine-tuning 737
Fit to Z electroweak measurements 817
Fit, technical implementation 830
Fits to data 15
Fixed-order perturbation theory (FOPT) 168
Flat extra dimension 1026
Flatness of Universe 488
Flavor number scheme (FNS) 156
Flavor anomalies 1049
Flavor symmetric couplings 876
Flavor transitions (oscillations) neutrino 301
Flavor-changing neutral currents, tests for 121
Flavour Lattice Averaging Group (FLAG) 168
Fluctuation amplitude σ_8 138
Fluctuation amplitude at $8 h^{-1}$ Mpc scale 139
Fluctuations in energy loss 579
Fluorescence detector, atmospheric 649
Flux conversion 138
Fly's Eye fluorescence detector 649
FODO cell 560
Forbidden states in quark model 148
Force, Lorentz 146
Form factors for radiative pion and kaon decays, note on 871
Four-quark states 327, 891
Fourth generation b' quark searches 859
Fragmentation
 functions, scaling violations in 390
 heavy-quark 397
 in e^+e^- annihilation 389
 longitudinal 392
 models 393
Fragmentation function 160
Fragmentation functions in
 e^+e^- , ep , and pp collisions, note on 389
Free quark searches 32, 1403
Frequentist
 approach 694
 confidence intervals 704
 statistics 704
Friedman equation 446
Friedmann constraint equation 457
Friedmann-Lemaître equations 444
Further states mesons 2072

 g (gluon) 25, 1186
g-2 muon anomalous magnetic moment 824
Galaxy clustering 470, 486
Galaxy power spectrum 486
 γ (photon) 25, 1185
 γ (Euler constant) 137
Gamma collider 566
Gamma distribution 692, 749
Gamma factory 567
 γ -rays, from radioactive sources 685
 $\gamma\gamma$ collisions 876
GAN, Generative Adversarial Network 732, 733, 738
Gas electron multiplier (GEM) 605
Gas-filled detectors
 electron drift velocity 601, 634
 gas properties 601
 high rate effects 604
 mobility of ions 602
 Townsend coefficient 602
Gauge and Higgs bosons
 H^0 Higgs 26, 1220
 W 25, 1187
 Z 25, 1200
 γ (photon) 25, 1185
 g (gluon) 25, 1186
 Searches
 graviton 25, 1186
Gauge and Higgs bosons searches
 W' , Z' 27, 1253
 axion 27, 1271
 charged Higgs $H^\pm, H^{\pm\pm}$ 27, 1248
Gauge coupling unification 1122
Gauge hierarchy 1038
Gauge kinetic function 1039
Gauge supermultiplet 1038
Gauge symmetry principle 295
Gauge-mediated supersymmetry breaking, GMSB 1046
Gaugino 1039, 1042
Gaugino mass unification 1045
Gaussian
 n -dimensional ellipsoid 691
 (Normal) distribution 692
 confidence intervals 705
 distribution, MC algorithm 749
 distribution, Multivariate 691
General relativity predictions 431
 equivalence principle 431
 gravitational waves 432
 isotropy of space 437
 quasi-stationary, weak-field 432
 radiative gravity tests 439
 strong fields, neutron stars, black holes 432
 universality of free fall tests 437
General relativity, GR 431
General-purpose Monte Carlo generators, (GPMC) 752
Generalization 712, 713
Generalized NMSSM, GNMSSM 1051
Generative model 712, 713, 732, 740
Generator of SU(3) transformation 773
Geometric deep learning 731
GIM – Glashow-Iliopoulos-Maiani mechanism 227
Glashow-Iliopoulos-Maiani (GIM) mechanism 117, 227
Global fit in SM 275
Glueballs 326, 874, 875
 $\eta(1405)$ 878
 $f_2(1950)$ 877
 $f_0(1500)$, $f_0(1710)$ 876
 lattice calculations 875
 scalar 876
 tensor 877
Gluino 1039
Gluino mass limits 1061
Gluino searches 243
Gluon field, SU(3) valued 834
Gluon induced jets 163
GMSB, gauge-mediated supersymmetry breaking 1046
GNMSSM, generalized NMSSM 1051
GNN, graph neural network 720, 731
Goldstino 1039

- GP, Gaussian Process 713, 718, 722
- GPMC generators
 General-purpose Monte Carlo generators 752
 HERWIG 752
 PHOTOS 755
 PYTHIA 752
 SHERPA 752
 uncertainties and tuning 761
- GR, general relativity 431
- Gradient boosting 724
- Gradient clipping 736
- Gradient descent 712, 714, 719, 724, 735
- Grand unified theories, GUTs 1119
- Graviscalar searches 1021
- Gravitational
 constant G_N 137
 acceleration g_N 137
 lensing 451
 radiation 434
 theory, experimental tests of 431
 wave speed 435
 waves in GR 432
- Gravitational lensing 487, 527, 529
- Gravitational-wave first observed, GW170817 485
- Gravitino 1040
- Graviton
 disperse 440
 mass 440
 Randall-Sundrum 1106
 searches 1022
- Graviton searches 25, 1186
- Gravity
 in extra dimensions 1021
 tests 435
- Gray, unit of absorbed dose of radiation 679
- Group normalization 737
- GRU, Gated Recurrent Unit 729
- GUTs
 baryon-number-violating nucleon decay 1124
 basic group theory, charge quantization 1119
 breaking 1120
 doublet-triplet splitting 1120
 monopoles prediction 1138
 neutrino masses 1126
 Pati-Salam model 1119
 Yukawa coupling unification 1125
- GUTs, grand unified theories 1119
- h* mesons
 $h_1(1170)$ 35, 1454
 $h_1(1415)$ [*was* $h_1(1380)$] 36, 1475
 $h_1(1595)$ 1492
 $h_b(1P)$ 85, 2035
 $h_b(2P)$ 86, 2047
 $h_c(1P)$ 77, 1954
- H^0 (Higgs boson) 26, 1220
- Hadron colliders 562
- Hadron colliders – future 565
- Hadron level 160
- Hadronic
 calorimeters 591
 shower detectors 591
- Hadronic Molecules 891
- Hadronization model 160
- Hadronization corrections 161
- Hagedorn temperature 1023
- Half-lives of radioactive nuclides 685
- Harrison–Zeldovich spectrum 482
- Hawking temperature 1023
- h/e ratio 631
- He initialization 736
- Heavy baryons 330
- Heavy charged lepton searches 30, 1331
- Heavy neutral leptons searches 1367
- Heavy Quark Expansion (HQE) 966
- Heavy quarks masses 839
- Heavy vector-like quark B 1113
- Heavy vector-like quark T 1109
- Heavy-quark
 effective theory (HQET) 341
 expansion for inclusive decays 342
 fragmentation 397
 spin-flavor symmetry 341
- Heavy-quark and soft-collinear effective theory, note on 341
- Heavy-quarkonium spectroscopy 985
- Helium-3 abundance 475
- Helium-4 abundance 475
- HERA 562
- HERA (DESY) collider parameters 572
- Hessian 735
- HFLAV charm mixing global fit 923
- Hidden sector 1040
- Hidden state 727
- Hidden valley models 1040
- Hierarchy problem 1022
- Higgs and electroweak factories 564
- Higgs boson
 ATLAS and CMS total inefficiency 218
 double charged search 253
 in MSSM 243
 LHC runs at $\sqrt{s} = 7, 8, 13$ & 13.6 TeV 218
 mass 212
 new physics models 242
 quantum numbers 212
 self coupling 229
 trilinear self coupling 217
 vector boson fusion (VBF) 218
 width 235
 Yukawa coupling to fermions 220
- Higgs boson physics 211
- Higgs boson quantum numbers 231
- Higgs production in e^+e^- annihilation 794
- Higgsino 1039
- High energy diffraction experiments 412
- High energy diffraction, theoretical description 407
- High energy soft QCD and diffraction, note on 406
- High intensity beams 561
- High-field accelerator magnets 566
- High-frequency surface impedance 146
- Highlights of this edition of the RPP 6
- History of measurements, discussion 17
- History plots 19
- HL-LHC 563
- HMSSM 1044
- Holographic model 875–877
- Horizon scale 526
- Hot Big-Bang cosmology 474
- HQE parameters and V_{cb} 966
- HQET – Heavy-quark effective theory 341
- HST, Hubble space telescope 485
- Hubble
 constant H_0 482, 526, 531
 cosmic topology 485
 expansion 445
 expansion rate 138, 499
 flow 518
 length c/H_0 138, 446
 parameter $H(t)$ 444
 radius 526
 relativistic species 484
 scaling factor for expansion rate 138
 space telescope HST 485
 varying constants 484
- Hubble’s law 444
- Huber loss 713
- Hybrid inflation model 459

- Hybrid mesons 880
 $\eta_1(1855)$ 880
 $\pi(1800)$, $\pi_1(2015)$ 880
 $\pi_1(1600)$ 880
 $\rho(1450)$ 879
Hybrid states 327
Hyperbolic tangent activation 724, 729
Hypercharge 322, 1033, 1119
- Ice-based detectors 659
ID particle codes for MC 768
Ideal mixing 874
Ideal mixing in quark model 325
Ideograms, criteria for presentation 16
ILC, future International Linear Collider (Japan) 570
Image data 720, 725
Imaging Cherenkov detectors 599
Impedance of free space 146
Impedance, relations for 146
Importance sampling 750
Importance sampling in Monte Carlo calculations 748
Inception 725
Inclusive hadronic reactions 794
Inclusive reactions, kinematics for 779, 794
Inconsistent data, treatment of 16
Independence of random variables 690
Inductive bias 714, 720, 732
Inelastic cross sections 412
Inference 714, 719, 738, 741
Inflation
 CMB photons 457
 de Sitter limit $\epsilon \rightarrow 0$ 460
 effective field theory of 467
 Friedman equation 457
 future probes of 470
 motivation 457
 multi-field 469
 of early Universe 449, 457, 482
 quantum fluctuations 459
 reheating 458
 slow-roll 458, 525
Inflation models
 R^2 inflation 463
 axion monodromy 463
 chaotic with power-law potentials 463
 D-brane 463
 Higgs 464
 Hilltop 463
 natural 463
 pioneering 462
 supergravity 465
 supersymmetric 464
Inflation primordial perturbations 459
 density from single-field 460
 gravitational waves 459
 metric 459
 observational bounds 461
Inflaton
 field fluctuations 460
 Higgs scalar field as candidate 465
Inflaton scalar field 433, 449, 459
Information horizon 447
Infrared and collinear safety 158, 161
Initialization 724, 735, 736
Inorganic scintillators 596
Input normalization 736
Instance normalization 737
Integer encoding 720
Integrated Sachs-Wolfe effect 454, 486, 515, 526
Inter-galactic medium clustering 487
Interaction length 627
International Linear Collider (ILC) 564
International System (SI) units 140
- Interpretability 712, 726, 730
Introduction 11
Inverse problem 719
Inverse transform method in Monte Carlo 748
Invisible energy (calorimetry) 631
Ion colliders 564
Ionization
 energies of the elements 142
 energy loss at minimum, table 144
 history of the Universe 484
Ionization history 484
Ionization yields for charged particles 580
IoU, Intersection over Union 726
Isotropy of space tests 437
- $J/\psi(1S)$ 73, 1907
Jansky 138
Jet algorithm
 cone 162
 sequential recombination 162
Jet definition 162
Jet shape 163
Jet substructure 163
 J/ψ radiative decay 876, 877
JS, Jensen-Shannon divergence 734
- K factor 161
 K stable mesons
 K^0 40, 1553
 K^\pm 39, 1538
 K_L^0 41, 1558
 K_L^0 decay, CP violation in 908
 K_S^0 40, 1554
 K , K^* meson resonances
 $K(1460)$ 42, 1583
 $K(1630)$ 1584
 $K(1830)$ 1587
 $K(3100)$ 1591
 $K_1(1270)$ 42, 1577
 $K_1(1400)$ 42, 1578
 $K_1(1650)$ 42, 1584
 $K^*(892)$ 42, 1574
 $K^*(1410)$ 42, 1579
 $K^*(1680)$ 43, 1584
 $K_0^*(1430)$ [*was* $\kappa(1350)$] 42, 1580
 $K_0^*(1950)$ 43, 1588
 $K_2^*(1430)$ 42, 1581
 $K_2^*(1980)$ 43, 1588
 $K_2(1580)$ 1584
 $K_2(1770)$ 43, 1585
 $K_2(1820)$ 43, 1587
 $K_2(2250)$ 1590
 $K_3^*(1780)$ 43, 1586
 $K_3^*(2320)$ 1590
 $K_4^*(2045)$ 43, 1589
 $K_4(2500)$ 1590
 $K_5^*(2380)$ 1590
k-means clustering 716
 K_L^0 decay, CP violation in 284
Kähler potential 1039
Kaluza-Klein
 excitations 769, 1034
 modes 1021, 1029, 1124
 reduction 1021
 searches 1024
 theories 435, 1021
Kaon decay, CPT invariance tests in neutral 902
KEKB (KEK) collider parameters 570
Kernel machines 712
Kernel trick 721
Kinematic limits
 sequential two-body decay 778
 three-body decays 778

- Kinematics, decays, and scattering 777
 Kinetic Inductance Detectors (KIDs) 666
 Kinetic Sunyaev-Zeldovich effect 454
 KL, Kullback-Leibler divergence 715, 732–734
 Knock-on electrons, energetic 579
 Kobayashi-Maskawa (Cabibbo-) mixing matrix 270
 KRR, kernel ridge regression 722

 l.h., left-handed 1119
 L1 loss 713
 L2 loss 713
 L2 regularization 714
 Label 712, 718
 LAGEOS – laser geodynamics satellite 438
 Lagged-Fibonacci-based random number generator 748
 Lagrangian, QCD 153, 834
 Λ QCD parameter 154
 Λ and Σ resonances 1007, 1009
 Λ baryons 98, 2161
 $\Lambda_c(2910)^+$ 2246
 Λ 98, 2161
 $\Lambda(1405)$ 99, 2164
 $\Lambda(1520)$ 99, 2165
 $\Lambda(1600)$ 99, 2167
 $\Lambda(1670)$ 99, 2168
 $\Lambda(1690)$ 99, 2170
 $\Lambda(1710)$ 2171
 $\Lambda(1800)$ 99, 2172
 $\Lambda(1810)$ 99, 2173
 $\Lambda(1820)$ 99, 2174
 $\Lambda(1830)$ 99, 2176
 $\Lambda(1890)$ 99, 2177
 $\Lambda(2000)$ 2179
 $\Lambda(2050)$ 2179
 $\Lambda(2070)$ 2180
 $\Lambda(2085)$ 2181
 $\Lambda(2100)$ 100, 2182
 $\Lambda(2110)$ 100, 2184
 $\Lambda(2325)$ 2185
 $\Lambda(2350)$ 100, 2185
 $\Lambda(2585)$ 2186
 Λ_b^0 108, 2263
 $\Lambda_b(5912)^0$ 108, 2271
 $\Lambda_b(5920)^0$ 109, 2272
 $\Lambda_b(6070)^0$ 109, 2272
 $\Lambda_b(6146)^0$ 109, 2272
 $\Lambda_b(6152)^0$ 109, 2273
 Λ_c^+ 103, 2234
 $\Lambda_c(2595)^+$ 104, 2243
 $\Lambda_c(2625)^+$ 104, 2244
 $\Lambda_c(2765)^+$ or $\Sigma_c(2765)$ 2245
 $\Lambda_c(2860)^+$ 104, 2245
 $\Lambda_c(2880)^+$ 104, 2245
 $\Lambda_c(2940)^+$ 105, 2246
 $\Lambda(1405)$ region, pole structure, note on 1010
 Λ , cosmological constant 444
 Λ CDM, minimal cosmological model 491
 Landau distribution 579
 Landau–Yang theorem 231
 Landau–Pomeranchuk-Migdal (LPM) effect 582
 LAr Time projection chambers, detector 613
 LARES – laser relativity satellite 438
 Large extra dimensions 799, 1021
 Large rapidity gap 406
 Large-scale structure of the Universe 452
 Last scattering surface, LSS 526
 Lattice calculations of spectroscopy 334
 Lattice QCD 350, 834, 957, 1086
 Layer normalization 737
 LBL, long baseline 299
 Leaky ReLU 724
 Learning rate 712, 735
 Least squares 696

 Left-handed
 fermions 1106
 leptons 1119
 neutrinos 929
 quarks 1119
 sleptons 1128
 Left-handed (l.h.) 1119
 Left-handedness of neutrinos 295
 LEP 563
 LEP (CERN) 570
 Lepton
 conservation, tests of 120
 family number conservation 117
 left-handed 1119
 mixing 297
 Lepton flavour universality violation 972
 Lepton PDF 156
 Lepton-flavor violation, LFV 117
 Leptonic decays of charged pseudoscalar mesons,
 note on 929
 phenomenological implications 935
 Leptons
 (see individual entries for e , μ , τ and ν) 28, 1297
 Leptoproduction kinematics 792
 Leptoquark review 1134
 Leptoquark searches 1134
 Lethal dose from penetrating ionizing radiation 680
 LFV – lepton-flavor violation 117
 LHC 563
 LHC (CERN) collider parameters 572
 LHC (CERN) heavy ion collider parameters 573
 LHeC 566
 Light
 speed in vacuum of 137
 year (deprecated unit) 138
 Light meson spectrum 874
 Light Quarks — u , d , s 1371
 Light quarks masses 836
 Light unflavored mesons 33, 1411
 Lightest supersymmetric particle, LSP 1038
 LIGO, Laser interferometer gravitational observatory 435
 Likelihood-ratio trick 714, 719, 740
 Limits 703
 Linear colliders 562, 564
 Linear confinement 328, 757
 Linear Higgs factories 564
 Linear regression 713
 Linear-theory mass dispersion σ_8 483
 Liquid ionization chambers 634
 Lithium-7 abundance 477
 Little hierarchy 1048
 Local dark matter density 138
 Local disk density 138
 Local Group velocity with respect to CMB 138
 Log-normal distribution 692
 Logistic activation 724
 Logistic regression 713
 Logits 725, 730
 Lomonosov satellite. γ -ray burst,
 high-energy cosmic rays 649
 Long baseline neutrino sources (LBL) 299, 1126
 Long-lived sparticles masses limits 1070
 Longitudinal fragmentation 392
 Longitudinal structure function, plots of 379
 Lorentz force 146
 Lorentz invariant amplitudes 777
 Lorentz transformations of four-vectors 777
 Loss 712, 713
 Low Temperature Detectors (LTDs) 665
 Low-radioactivity background techniques 670
 LQCD
 heavy quark masses 354
 heavy quarks 352

- light quarks masses 353
Monte Carlo method 355
QED 353
scattering amplitudes and resonances 357
status of simulations 357
Wilson fermion action 351
Wilson gauge action 350
LQCD, lattice quantum chromodynamics calculations 350
LSP, lightest supersymmetric particle 1038
LSTM, Long Short-Term Memory 729
Luminosity 559, 561
 muon collider 566
 circular collider 562
 linear collider 564
Luminosity conversion 138
Luminosity distance d_L 446
Lund string model 757
Ly α forest 451
M-theory 1087
Machine learning 163, 711
MAE, mean-absolute error 713
MAF, Masked Autoregressive Flow 734
Magnetic fields, primordial 532
Magnetic Metallic Calorimeters (MMCs) 668
Magnetic monopoles 1127
 GUTs prediction 1138
 note on 1138
Magnetic monopoles searches 112, 2289
Majorana neutrinos 296
mAMSB, minimal AMSB 1046
Mandelstam variables 779
MAP, maximum a posteriori 714, 719, 740
Marginal probability density function 690
Markov chain 750
Mass attenuation coefficient for photons 583
Mass matrix
 light quark 837
 neutrino 296
Masses
 heavy quarks 839
 light quarks 836
Matter supermultiplet 1038
Matter, passage of particles through 575
Maximal mixing scenario 1044
Maximum energy transfer to e^- in single collision 576
Maximum likelihood 695
Maximum-margin classifier 721
Maxwell equations 146
MC – Monte Carlo 768
MDP, Markov decision process 717
Mean energy loss rate in H₂ liquid, He gas, C, Al, Fe, Sn 576
Mean excitation energy 575, 576
Mean range in H₂ liquid, He gas, C, Fe, Pb 576
Mean sidereal day 138
Median, definition 689
Meson cloud 891, 1004
Meson electromagnetic radius 872
Meson multiplets in quark model 323
Meson nonets (established) 324
Meson quick reference table 88
Meson-meson bound states 891
Mesons
 Further states 2072
 axial vector $\ell = 1; 1^{++}$ or 1^{+-} 323
 bottomonium 985
 charmonium 985
 conventional 985
 pseudoscalar $\ell = 0, 0^{-+}$ 323
 scalar $\ell = 1, 0^{++}$ 323, 888
 tensor $\ell = 1, 2^{++}$ 323
 thresholds 985
 unconventional 985
 vector $\ell = 0, 1^{--}$ 323
 XYZ 985
Messenger scale 1045
Metric prefixes, commonly used 140
Michel parameters 832
Micro-mesh gaseous structure (MicroMegas) 605
Micro-pattern gas detectors, MPGD 605
MicroMegas, micro-mesh gaseous structure 605
Microwave background 450
Mihheev-Smirnov-Wolfenstein effect for solar neutrinos 301
Minimal
 7-parameter model, Λ CDM + $\sum m_\nu$ 495
 cosmological model Λ CDM 491
Minimal AMSB, mAMSB 1046
Minimal supergravity, mSUGRA 1046, 1059
Minimal supersymmetric SM, MSSM 1038
Minimum ionization 576
MIP (minimum ionizing particle) 576, 601
Mixing angle, weak ($\sin^2 \hat{\theta}(M_Z)$) 137
Mixing, D^0 - \bar{D}^0 , note on 917
Mixing matrix 298
Mixing, singlet-octet in quark model 334
MLP, multi-layer perceptron 720, 724, 731
Modified gravity 484
Modified minimal subtraction scheme ($\overline{\text{MS}}$) 153
Molar volume 137
Molecular states 874, 881
Molière radius 586
Momenta, measurement of, in a magnetic field 640
Monopoles
 catalysis of nucleon decay 1140
 Kibble mechanism 1138
 Parker bound 1139
Monte Carlo
 acceptance-rejection method 748
 calculations, importance sampling in 748
 codes for radiation protection studies 683
 DIEHARD 748
 inverse transform method 748
 Lagged-Fibonacci-based generator 748
 LQCD 355
 neutrino event generators 764
 particle numbering scheme 768
 random number generators 748
 RANLUX generator 748
 techniques 748
Monte Carlo algorithm for
 χ^2 distribution 749
 beta distribution 750
 binomial distribution 749
 Breit-Wigner distribution 750
 exponential decay 749
 Gamma distribution 749
 Gaussian distribution 749
 Poisson distribution 749
 sine and cosine of random angle 749
 Student's t distribution 749
Monte Carlo dropout 740
Monte Carlo event generators 752
MPGD, micro-pattern gas detectors 607
MPNN, Message Passing Neural Network 732
 $\overline{\text{MS}}$ factorization scheme 156
 $\overline{\text{MS}}$ mass 154
MSE, mean-squared error 713, 740
MSSM current experimental status 1047
MSSM Higgs boson phenomenology 245
MSSM parameters 1041
MSSM, minimal supersymmetric SM 1038
MSSM-124 1041
mSUGRA, minimal supergravity 1046, 1059
 μ -term 1041, 1044, 1051
 μ (muon) 28, 1298
 μ_0 (permeability of free space) 137, 146

- Multi-arm bandits 717
- Multi-class classification 715, 725, 730
- Multi-head attention 731
- Multi-wire proportional chamber, MWPC 603
- Multibody charm analyses, review of 911
- Multibody decay kinematics 779
- Multinomial distributions 691
- Multiple parton-parton interactions, MPI 160
- Multiple Coulomb scattering 580
- Multiple parton-parton interactions, MPI 411, 759
- Multiplets, meson in quark model 323
- Multiplets, $SU(n)$ 774
- Multiplexing 668
- Multivariate Gaussian distribution 691
- Multiverse 449, 470
- Muon
- anomalous magnetic moment 824
 - critical energy 586
 - energy loss rate at high energies 586
- Muon Anomalous Magnetic Moment 822
- Muon collider 566
- Muon collider, neutrino radiation hazard 566
- Muon decay parameters 826
- MWPC, Multi-wire proportional chamber
- maximum wire tension 603
 - wire stability 603
- Møller cross section 581
- n (neutron) 93, 2091
- N and Δ Resonances 94, 2096
- N and Δ Resonances, note on 1002
- N baryons
- $N(1440)$ 94, 2096
 - $N(1520)$ 94, 2098
 - $N(1535)$ 94, 2100
 - $N(1650)$ 94, 2102
 - $N(1675)$ 94, 2104
 - $N(1680)$ 94, 2107
 - $N(1700)$ 95, 2109
 - $N(1710)$ 95, 2111
 - $N(1720)$ 95, 2113
 - $N(1860)$ 2115
 - $N(1875)$ 95, 2116
 - $N(1880)$ 95, 2118
 - $N(1895)$ 96, 2120
 - $N(1900)$ 96, 2122
 - $N(1990)$ 2124
 - $N(2000)$ 2125
 - $N(2040)$ 2126
 - $N(2060)$ 96, 2126
 - $N(2100)$ 96, 2128
 - $N(2120)$ 96, 2130
 - $N(2190)$ 96, 2131
 - $N(2220)$ 97, 2133
 - $N(2250)$ 97, 2134
 - $N(2300)$ 2135
 - $N(2570)$ 2135
 - $N(2600)$ 97, 2135
 - $N(2700)$ 2136
- N 's and Δ 's note 94, 2096
- N (~ 3000 Region) Partial-Wave Analyses 2136
- n -body differential cross sections 777
- n -body phase space 777
- Nambu-Goldstone bosons 1023, 1079
- Nambu-Goldstone composite bosons 1104
- Names, hadrons 15, 148
- Naming scheme for baryon resonances 1002
- Naturalness 1048
- Network-in-network 725
- Neural network 712, 714, 724, 732, 735, 736, 740
- Neuron 724
- Neutral Higgs bosons searches 27, 1237
- Neutralinos 1042
- Neutralino mass limits 1066
- Neutrino detectors (deep, large, enclosed volume) 652
- heavy water 654
 - liquid scintillator 652
 - noble
 - time-projection chamber 654
 - table of detectors 652
 - water-filled 653
- Neutrino detectors, cryogenic detectors 666
- Neutrino telescopes
- AMANDA, South Pole 655
 - ANTARES, Med. Sea 655
 - backgrounds 654
 - DUMAND, Pacific Ocean 655
 - effective area 655
 - GVD, Lake Baikal 655
 - IceCube, South Pole 655
 - KM3NeT, Med. Sea 655
 - NEMO, Med. Sea 655
 - NESTOR, Med. Sea 655
 - NT-200, Lake Baikal 655
 - P-ONE, Pacific Ocean 655
 - technical realisation 655
- Neutrino(s)
- astrophysical 654
 - atmospheric
 - detectors 652
 - atmospheric flux 303
 - beam lines at high-energy proton synchrotrons 574
 - chemical potential 532
 - cosmological constraints 491
 - current temperature 491
 - Dirac 296
 - left-handed 295, 929
 - Majorana 296
 - mass density parameter, Ω_ν 482
 - mass hierarchy 654
 - mass matrix 296
 - mass, cosmological limit 487
 - masses 495
 - masses, mixing, and oscillations, note on 295
 - mixing 30, 1348
 - Monte Carlo event generators 764
 - neutrinoless double- β decay 316
 - non-standard 494
 - oscillation search 301
 - properties 30, 1332
 - reactor
 - detectors 652
 - relic background 491
 - right-handed 295, 1119
 - see-saw mechanism 296
 - solar flux 302
 - solar, pp chain 302
 - solar, CNO cycle 302
 - sterile 295, 297, 314
 - supernova burst
 - detectors 652
 - Neutrinoless double- β decay searches 316
 - Neutrinos
 - density of the Universe 139
 - Neutrinos in cosmology, note on 491
 - Neutron 93, 2091
 - Neutron mass 137
 - Neutrons at accelerators 680
 - Neutrons, from radioactive sources 685
 - New heavy bosons
 - (W' , Z' , leptoquarks, etc.) searches 27, 1253
 - New Physics (NP) beyond SM 297, 952
 - NEWS-G collaboration 507
 - NEWSdm collaboration 508
 - Newtonian gravitation constant G_N 138
 - Next-to-lightest supersymmetric particle, NLSP 1047

- Next-to-minimal supersymmetric SM, NMSSM 1039
- NF, Normalizing Flow 718, 719, 732, 734
- NICA 564
- NLSP, next-to-lightest supersymmetric particle 1047
- NMS, Non-Maximum Suppression 726
- NMSSM, next-to-minimal supersymmetric SM 1039
- Node 731
- Noise
- equivalent noise analysis 623
 - equivalent noise charge (ENC) 624
 - in analog signal processing 623
 - in digital signal processing 626
 - in timing measurements 626
 - noise origins 623
- Nomenclature for hadrons 148
- Non-Gaussianity CMB 451, 467, 525
- Non-perturbative corrections 161
- Non-standard neutrinos
- interactions beyond weak force 494
 - sterile neutrinos 494
 - unstable neutrinos 494
- Non $q\bar{q}$ candidates
- $ccc\bar{c}$ state 997
 - Double- $J/\psi(1S)$ invariant mass 997
 - four heavy quarks 997
 - heavy-heavy systems 994
 - heavy-light systems 994
- Normal (Gaussian) distribution 692
- Normal distribution 691
- NP, new physics beyond SM 297
- Neutrino properties 30, 1332
- Nuclear
- and atomic properties of materials, table 144
 - interaction length, table 144
 - magneton 137
- Nuclear PDFs 372
- Nucleon decay 1124
- Nucleosynthesis 450
- Nuclides, radioactive, commonly used 685
- Number density of baryons 138
- Number density of CMB photons 138
- Number of degree of freedom 696
- Number of neutrino types
- and sum of neutrino masses 30, 1341
- Numbering scheme for particles 768
- Object detection 726
- Observations, the light element abundance 474
- Occupational radiation dose, U.S. maximum permissible 680
- Octet-singlet mixing in quark model 324
- Odderon in soft QCD 421
- Ω baryons
- $\Omega_c(3185)^0$ 107, 2261
 - $\Omega_c(3327)^0$ 107, 2261
 - Ω^- 102, 2231
 - $\Omega(2012)^-$ 103, 2232
 - $\Omega(2250)^-$ 103, 2233
 - $\Omega(2380)^-$ 2233
 - $\Omega(2470)^-$ 2233
 - Ω_b^- 110, 2283
 - $\Omega_b(6316)^-$ 110, 2282
 - $\Omega_b(6330)^-$ 110, 2282
 - $\Omega_b(6340)^-$ 110, 2282
 - $\Omega_b(6350)^-$ 110, 2283
 - Ω_c^0 107, 2258
 - $\Omega_c(2770)^0$ 107, 2259
 - $\Omega_c(3000)^0$ 107, 2259
 - $\Omega_c(3050)^0$ 107, 2260
 - $\Omega_c(3065)^0$ 107, 2260
 - $\Omega_c(3090)^0$ 107, 2260
 - $\Omega_c(3120)^0$ 107, 2261
- Ω_{dm} , dark matter density 484
- ω mesons
- $\omega(2220)$ 1532
 - $\omega(782)$ 34, 1430
 - $\omega(1420)$ 36, 1477
 - $\omega(1650)$ 37, 1495
 - $\omega_3(1670)$ 37, 1497
- Ω , cosmological density parameter 445
- Ω_m , mass density parameter 445
- Ω_Λ , scaled cosmological constant 445
- Ω_ν , neutrino mass density parameter 482
- Ω_{tot} , total energy density of Universe 488
- Ω_v , vacuum energy parameter 445
- One-hot encoding 720
- One-shot learning 737
- OOD, out-of-distribution 718
- Optimal control 717
- Optimization 712
- Organic scintillator 594
- Other light mesons 2072
- Other particle searches 2374
- Overfitting 712–714, 716, 735, 736
- p (proton) 93, 2081
- P (parity), tests of conservation 114
- PAE, Probabilistic Auto-Encoder 733
- Parameter estimation 694
- Parameter estimation with constraints 697
- Parameterizing the Universe 482
- Paraphotons, searches 1079
- Pardethadcal 630
- Parity of $q\bar{q}$ states 323
- Parsec 138
- Partial Conserved Axial Current, PCAC 765, 872
- Partial wave analyses, PWA 1005
- Particle
- ID numbers for MC 768
 - identification detectors, PID 598
 - nomenclature 148
 - symbol style conventions 148
- Particle flow 628
- Particle flow confusion 628
- Particle level 160
- Particle nomenclature 15
- Particle Physics Booklet, how to get 11
- Parton
- density functions 752
 - distribution function, PDF 412
 - distributions 371
- Parton distribution function (PDF) 155
- Parton level 161
- Parton shower 160
- Parton-shower formalism 754
- Passage of particles through matter 575
- Pati-Salam model 1119, 1134
- $\bar{p}p$ annihilation 875
- PBN, primordial black holes 510
- P_c , exotic baryons
- $P_{c\bar{c}s}(4338)^0$ 111, 2285
 - $P_{c\bar{c}s}(4459)^0$ 2286
 - $P_c(4312)^+$ 2285
 - $P_c(4380)^+$ 2285
 - $P_c(4440)$ 2285
 - $P_c(4457)^+$ 2286
- PCA, principle component analysis 716, 733
- PCAC, Partial Conserved Axial Current 765, 872
- PDF, parton distribution function 412
- PdgLive, interactive access to RPP 11
- PDGLive, PDG web presentation 20
- Peccei-Quinn mechanism and axion 1079
- Penguin decays, electroweak 944, 952
- Penguin-dominated modes 274
- Pentaquarks
- $P_{c\bar{c}}(4312)^+$ 1012
 - $P_{c\bar{c}}(4440)^+$ 1012

- $P_{c\bar{c}}(4457)^+$ 1012
 search 1012
 PEP-II (SLAC) collider parameters 570
 Periodic table of the elements 131
 Permeability μ_0 of free space 137, 146
 Permittivity ϵ_0 of free space 137, 146
 Permutation invariant 720, 731
 Perturbation of early Universe 482
 Perturbation theory, chiral 889, 896
 Phase space, Lorentz invariant 777
 Phase space, relations for 777
 Phenomenological MSSM, pMSSM 1047, 1059
 ϕ mesons
 $\phi(1020)$ 34, 1446
 $\phi(1680)$ 37, 1499
 $\phi(2170)$ 39, 1529
 $\phi_3(1850)$ 38, 1517
 Photon
 attenuation length 583
 cross section in carbon and lead, contributions to ... 583
 pair production cross section 583
 structure functions F_2^{γ} 396
 to e^+e^- conversion probability 583
 total cross sections (C and Pb) 583
 ultra-high energy 585
 Photon and electron interactions with matter 581
 Photon collider 566
 Photon detectors 591
 Photon PDF 156
 Photon-dark photon-paraphoton conversion 1079
 Photoproduction 157
 Physical constants 137
 Physics beyond general relativity 532
 π mesons
 π^0 33, 1414
 π^\pm 33, 1411
 $\pi(1300)$ 35, 1464
 $\pi_1(1400)$ 1471
 $\pi_1(1600)$ 37, 1493
 $\pi_2(1670)$ 37, 1497
 $\pi_2(1880)$ 38, 1518
 $\pi_2(2005)$ 1523
 $\pi_2(2100)$ 1525
 $\pi(1800)$ 38, 1514
 π value 137
 PID, particle identification detectors 598
 Pions and kaons
 experimental rate measurements 930
 theoretical decay-constant calculations 931
 Pixel detectors
 DEPFET pixels 620
 DMAPS 620
 hybrid pixels 620
 monolithic pixels 620
 PixelCNN 734
Planck
 constant h 137
 constant, reduced 137
 length 138
 mass 138
 Plasma acceleration 567
 Plasma energy 575
 pMSSM, phenomenological MSSM 1047
 POEMMA – probe of extreme multi-mes. astrophys. 649
 Point Net 731
 Poisson distribution 692, 749
 Polarization in B decays, note on 951
 Polarization in penguin-dominated B decays 952
 Pole mass 154
 Pole structure of the $\Lambda(1405)$ region, note on 1010
 Pomeron effective trajectory 416
 Pomeron in soft QCD 415
 mixing matrix (PMNS) 298
 Pooling 725
 Pooling, average 726
 Pooling, max 726
 Potentials, electromagnetic 146
 Power correction 154
 pp -scattering amplitude by Donnachie-Landshoff 407
 Preconfinement 757
 Prefixes, metric, commonly used 140
 PReLU, Parametric ReLU 724
 Present-day CMB
 dipole amplitude 138
 temperature 138
 Pressureless matter parameter 138
 Primordial
 helium fraction 138
 Primordial element abundance 474
 Primordial magnetic fields 532
 Princeton Tritium Observatory for Light, Early universe,
 Massive-neutrino Yield (PTOLEMY) 496
 Probability 689
 Probability density function, definition 689
 Probability, Kolmogorovs definition 689
 Production and Decay of b -flavored Hadrons 940
 Propagation of errors 690
 Proton
 cyclotron frequency/field e/m_p 137
 decay 1124
 mass 137
 structure function 367
 structure function, plots 379
 Proton (see p) 93, 2081
 Proton decay detectors 652
 Proton structure functions 155
 Pseudorapidity 406, 780
 Pseudoscalar mesons 877
 $\eta(1405)$, $\eta(1475)$ 877
 $\eta(1295)$ 877, 878
 Pseudoscalar mesons $\ell = 0$, 0^{-+} 323
 ψ mesons
 $\psi_2(3823)$ [*was* $\psi(3823)$; *was* $X(3823)$] 81, 1995
 $\psi_2(3842)$ 81, 1996
 $\psi(2S)$ 78, 1970
 $\psi(3770)$ 80, 1988
 $\psi(4040)$ 81, 2002
 $\psi(4160)$ 82, 2005
 $\psi(4230)$ [*aka* $Y(4230)$; *was* $\psi(4260)$] 82, 2009
 $\psi(4360)$ [*aka* $Y(4360)$; *was* $X(4360)$] 83, 2015
 $\psi(4415)$ 83, 2017
 $\psi(4660)$ [*aka* $Y(4660)$; *was* $X(4660)$] 83, 2020
 PTOLEMY, neutrino background direct detection 496
 Pulsars, binary 438
 QCD
 Λ parameter 761
 $\overline{\text{MS}}$ renormalization scheme 153
 β function 153
 color factor 153, 163
 coupling constant 153
 jets 162
 Lagrangian 153
 lagrangian 834
 Λ parameter 154
 Lattice 350
 lattice 834, 1086
 photon structure functions 396
 renormalization group equation (RGE) 153
 running coupling 153, 172
 structure functions 369
 Quality factor for biological damage due to radiation 679
 Quantum
 fluctuations, inflation 459
 gravity theory 1021

- numbers in quark model 322
- Quark
 - masses review 32, 1371
 - masses, note on 834
- Quark induced jets 163
- Quark model
 - baryon resonances in 327
 - ideal mixing in 325
 - meson multiplets in 323
 - mixing, singlet-octet in 334
 - quantum numbers in 322
- Quark-antiquark annihilations $c\bar{d} \rightarrow W^+ \rightarrow \ell^+\nu$ 929
- Quark-mixing CKM matrix 270
- Quark-parton model 155
- Quarks 32, 1371
 - and lepton compositeness searches 113, 1098, 2348
 - b 32, 1377
 - c 32, 1375
 - d 32, 1371
 - fragmentation in e^+e^- annihilation, heavy 397
 - left-handed 1119
 - model 322
 - model assignments 328
 - model, dynamical ingredients 333
 - properties of 322
 - s 32, 1371
 - t 32, 1379
 - u 32, 1371
- Quasi-stationary general relativity 432
- R-CNN, region convolutional neural network 726
- R-parity 1039, 1058, 1134
- R-parity conserving 1039
- R-parity violation, RPV 1050
- r.h., right-handed 1119
- Rad, unit of absorbed dose of radiation 679
- Radiation
 - dominated epoch 448
 - Cherenkov 587
 - coherent radio Cherenkov radiation 588
 - gravitational 434
 - length 582
 - length of materials, table 144
 - length, approximate algorithm 582
 - protection 679
 - protection instrumentation 682
 - transition 588
 - weighting factor 679
- Radiation damage
 - in silicon detectors 621
- Radiation length 627
- Radiative
 - gravity test, GR prediction 439
- Radiative loss by muons 586
- Radio-detection of cosmic ray air shower 660
- Radioactive nuclides, half-lives of 685
- Radioactive sources, commonly used 685
- Radioactivity
 - accelerator-induced 681
 - accelerators prompt neutrons 680
 - ambient dose equivalent 679
 - and radiation protection 679
 - Becquerel, unit of 679
 - biological damage from chronic exposure 679
 - Cancer induction 680
 - cosmic ray background radiation 680
 - dose rate from γ ray sources 681
 - effective dose 679
 - effective dose limits 680
 - fluence, Φ 679
 - kerma, K 679
 - lethal dose from 680
 - long-term risk 679
 - natural annual background 680
 - personal dosimeters 683
 - rem, roentgen equivalent for man 682
 - unit of absorbed dose, gray 679
 - unit of activity 679
 - weighting factor 679
- Radion searches 1023
- Randall-Sundrum
 - model 799, 1024
 - warped geometry 1021
- Randall-Sundrum graviton 1106
- Random angle, MC algorithm for sine and cosine of 749
- Random Forests 723
- Random number generators 748
- RANLUX Monte Carlo generator 748
- Rapidity 779
- Rare event search
 - $0\nu\beta$ decay 664
 - WIMPs 663
- Rare kaon decay, constraints on CKM parameters 898
- Reactor
 - antineutrino flux 308
 - antineutrino oscillation 308
- Readout
 - detector 623
 - low-noise 623
- Receptive field 725
- Recombination scheme 162
- Redshift 444
 - $z \simeq 1100$, reionization 525
 - age at half reionization 139
 - age when acceleration was zero 139
 - age when optical depth equals unity 139
 - at half reionization 139
 - at which optical depth equals unity 139
 - comoving size of sound horizon at z_* 139
 - matter-radiation equality 139
 - when acceleration was zero 139
- Redshift distortion 486
- Refractive index of materials, table 144
- Regge pole approach 406
- Regge poles multiple exchange 407
- Reggeon field theory 407
- Regression 711, 713, 721, 722, 726, 732, 740
- Regularization 712, 714, 736, 740
- Reionization of the Universe 484, 486
- Reionization optical depth 138
- Relativistic kinematics 777
- Relativistic rise 576
- Relativistic transformation of electromagnetic fields 146
- ReLU, Rectified Linear Unit 724, 736
- Rem, roentgen equivalent for man 679
- Renormalization group
 - quark mass 834
- Renormalization group equation (RGE) 153, 1045
- Renormalon 155, 839
- Representation learning 716
- Representations, $SU(n)$ 774
- Repulsive gravity, dark energy 516
- Resistive plate chambers 611
- Resistivity of metals 146
- ResNet, Residual Network 727, 729
- Resonances
 - bound state 782
 - branch points 781
 - Breit-Wigner parameterization 786
 - Chew-Mandelstam function 787
 - effective-range expansion 788
 - Flatte parameterization 786
 - \mathcal{K} -matrix parameterization 787
 - left-hand cut 782
 - Mandelstam variables 781
 - partial-wave decomposition 784

- physical sheet 782
 pole couplings 785
 pole residues 785
 properties of resonances 785
 resonance pole mass 785
 resonance pole position 785
 resonance pole width 785
 Riemann sheets 781
 right-hand cut 782
 \mathcal{S} -matrix properties 781
 scattering-length approximation 788
 triangle singularity 782
 unphysical sheet 782
 virtual state 782
 Watson theorem 785
 Restricted energy loss rate 576, 579
 Resummation 159
 Review of multibody charm analyses 911
 Review of Particle Physics overview 11
 RG - renormalization group 345, 351
 RGE, renormalization group equation 1045
 RHIC 563
 RHIC (Brookhaven) collider parameters 572
 RHIC (Brookhaven) heavy ion collider parameters 573
 ρ mesons
 $\rho(770)$ 33, 1424
 $\rho(1450)$ 36, 1479
 $\rho(1570)$ 1492
 $\rho(1700)$ 38, 1504
 $\rho(1900)$ 1519
 $\rho(2150)$ 1528
 $\rho_3(1690)$ 38, 1501
 $\rho_3(1990)$ 1522
 $\rho_3(2250)$ 1533
 $\rho_5(2350)$ 1536
 Right-handed
 antineutrinos 929
 fermions 1106
 neutrinos 295, 1119
 sleptons 1127
 top quark 1124
 Right-handed (r.h.) 1119
 Risk 712, 739
 Risk minimization 712, 713
 RL, reinforcement learning 711, 717
 RMSprop 735
 RNN, recurrent neural network 720, 727
 RNNSearch 730
 Robertson-Walker metric 444, 457, 482
 Robustness of an estimator 694
 ROC, receiver operating characteristic curve 712, 714
 ROI, region of interest 726
 Rotational invariance 721
 Rounding errors, treatment of 17
 Rounding, PDG rules 17
 RPC, resistive plate chambers 611
 RPN, Region Proposal Network 726
 RPP authors and affiliations 2
 RPP criteria for measured data 15
 RPV, R-parity violation 1050
 Running coupling in QCD 153, 172
 Running spectral index, $k_0 = 0.05 \text{ Mpc}^{-1}$ 139
 Rydberg energy 137

 \mathcal{S} -matrix
 approach to Z 817
 for two-body scattering 777
 Sachs-Wolfe effect 453, 526
 Sachs-Wolfe effect, integrated 454, 486, 515, 526
 Sampling 719
 Satellite
 Planck, CMB 461, 519, 524, 527
 COBE, monopole 524

 Euclid, dark energy 470
 Gaia, density distribution 501
 LAGEOS, test of gravity 438
 LARES, test of gravity 438
 LiteBIRD, inflation, CMB 529
 Lomonosov, γ -ray bursts 649
 POEMMA, cosmic rays 649
 SMM, sun radiation 1084
 SPHEREx, inflation 470
 WMAP, CMB 519
 Scalar field cosmology 458
 Scalar mesons 874
 $a_0(1450)$ 875
 $a_0(980)$, $f_0(980)$, $f_0(500)$, $K_0^*(700)$ 880
 $f_0(1370)$, $f_0(1500)$, $f_0(1710)$ 875
 $f_0(1770)$, $a_0(1710)$ 875
 nonets 880
 SU(3) couplings 876
 Scalar mesons $\ell = 1, 0^{++}$ 323, 888
 Scalar mesons below 1 GeV, note on 888
 Scalar spectral index 138
 Scale dependence 154
 Scale factor, definition of 16
 Scaled cosmological constant, Ω_Λ 445
 Scaled dot-product attention 730
 Scaled Hubble constant 445
 Scaling factor for Hubble expansion rate 138
 Scaling for cosmological constant 138
 Scaling violations in fragmentation functions 390
 Scattering, relations for 792
 SCET – soft-collinear effective theory 343
 Scherk-Schwarz mechanism 1040
 Schwarzschild
 radius of a black hole 1023
 radius of the Earth 138
 radius of the Sun 138
 Scintillation neutrino detectors 637
 Scintillator parameters 594
 Searches
 W' bosons 1029, 1106
 Z' bosons 1033, 1106
 b' quark fourth generation 859
 new light particles in rare K decay 897
 axiguons 1106, 1114
 axion like particles (ALP) 1083
 axions (A^0) 502, 1079
 charginos 245
 colorons 1114
 dark matter 113, 2359
 dark photon 228
 doubly charged Higgs boson 253
 dyons 1139
 excited fermions 1099
 excited leptons 1099
 extra dimensions 502, 1021
 gluinos 243
 graviscalar 1021
 graviton 1022
 heavy charged lepton 30, 1331
 heavy neutral leptons 1367
 heavy non- $q\bar{q}$ mesons 994
 leptoquark 1134
 light Higgsinos 243
 magnetic monopoles 112, 1127, 1138, 2289
 neutralino 245
 neutrino oscillation or flavor transition 301
 neutrinoless double- β decay 316
 paraphotons 1079
 pentaquarks 1012
 quark and lepton compositeness 113, 1098, 2348
 radion 1023
 rare events 661
 sleptons 245

- SM explicit violations 896, 897
solar axions 1083
squarks 243, 245
supersymmetric particle 112, 2292
technicolor 251, 502, 1104, 1134
technifermions
 spontaneously broken chiral symmetry 1104
WIMP 113, 2359
Selection and treatment of data 15
Self-attention 731
Self-supervised learning 715
Semantic segmentation 726
Semiconductor
 detectors 617
 materials 617, 623
 radiation damage 621
 type inversion 622
Semiconductor Thermistors 667
Semileptonic b -hadron decays,
 determination of V_{cb} , V_{ub} 962
Semitauonic decays 972
Sequential data 720, 727
Sequential two-body decay, kinematic limits 778
sfermion 1038
SGD, Stochastic Gradient Descent 735
Shape functions, SF 272, 343
Shared weights 725, 729
Shell correction 577
Shower detectors 629
Showers, electromagnetic
 lateral distribution of 586
 longitudinal distribution of 585
SI units, complete set 140
Sidereal day 138
Sievert, unit of radiation dose equivalent 679
 σ 33, 1422
 Σ baryons
 Σ^+ 100, 2187
 Σ^- 100, 2190
 Σ^0 100, 2189
 Σ_b^* 109, 2273
 $\Sigma_b(6097)^+$ 109, 2274
 $\Sigma_b(6097)^-$ 109, 2274
 Σ_b 109, 2273
 $\Sigma(1385)$ 101, 2192
 $\Sigma(1580)$ 2195
 $\Sigma(1620)$ 2196
 $\Sigma(1660)$ 101, 2197
 $\Sigma(1670)$ 101, 2198
 $\Sigma(1750)$ 101, 2200
 $\Sigma(1775)$ 101, 2202
 $\Sigma(1780)$ 2204
 $\Sigma(1880)$ 2205
 $\Sigma(1900)$ 2205
 $\Sigma(1910)$ 101, 2206
 $\Sigma(1915)$ 101, 2207
 $\Sigma(2010)$ 2209
 $\Sigma(2030)$ 101, 2210
 $\Sigma(2070)$ 2213
 $\Sigma(2080)$ 2213
 $\Sigma(2100)$ 2213
 $\Sigma(2110)$ 2214
 $\Sigma(2250)$ 2216
 $\Sigma(2455)$ 2217
 $\Sigma(2620)$ 2217
 $\Sigma(3000)$ 2217
 $\Sigma(3170)$ 2217
 $\Sigma_c(2455)$ 105, 2246
 $\Sigma_c(2520)$ 105, 2247
 $\Sigma_c(2800)$ 105, 2248
 Σ baryons ($S = -1$, $I = 1$) 100, 2187
 σ_8 fluctuation amplitude at $8 h^{-1}$ Mpc scale 138
Sign conventions for resonance couplings 1008
Silicon detector 617
 radiation damage 621
 timing measurement 620
Silk damping 527
Simplified models 1047
Simulation-based inference 714, 719, 732, 735, 740
Singlet-octet mixing in quark model 324
Skip connection 727, 729, 731, 736
Slack variable 721
SLC (SLAC) 563, 570
sleptons 1043
sleptons masses limits 1067
SLHA, SUSY Les Houches accord 1042
Sloan Digital Sky Survey (SDSS) 487
Slow-roll inflation 525
SMM – solar maximum mission satellite 1084
SN1987A
 light gravitons luminosity 1022
Sneutrino masses limits 1067
sneutrinos 1043
SNO - sudbury neutrino observatory 1081
Soft supersymmetry breaking 1038
Soft-collinear effective theory (SCET) 343
Softmax 715, 725, 729
Software 22
Solar
 ν experiment 302
 ν fluxes 302
 ν problem 302
 constant, nominal 138
 distance from Galactic center 138
 equatorial radius, nominal 138
 escape velocity from the Galaxy 138
 luminosity, nominal 138
 mass 138
 photosphere temperature, nominal 138
 Schwarzschild radius of 138
 standard model 302
 velocity with respect to CMB 138
Solid angle 138
Sparticle 1042
Specific heats of elements, table 145
Spectroscopy of mesons
 containing two heavy quarks, note on 985
Speed of light in vacuum c 137
Sphaleron 1128
SPHEREx – spectro-photometer for history
 of epoch reionization, satellite 470
Spherical harmonics 772
Spin polarisation 561
Spin-dependent structure functions 372
Spin-flavor symmetry 341
Split supersymmetry 1040
Splitting functions 156
SPPC 566
Squark mass limits 1061
squarks 1043
String theory 478
SSM, standard solar model 302
Standard
 gravitational acceleration 137
 neutrino cosmology 491
 particle numbering for MC 768
 Solar Model (SSM) 302
Standard cosmological model 483
Standard model of particle physics
 as EFT of more fundamental theory 341
Standard model, cosmological 532
Starobinsky model of gravity 454
Statistical procedures 15
Statistics, note on 694
Status of LQCD simulations 357
Stefan-Boltzmann constant 137

- Sterile neutrinos 295, 314
 Stopping power for heavy charged projectiles 575
 Strangeness-changing neutral currents, tests for 114
 String theory 1079
 Strong coupling constant 137, 163, 167
 Strong fields, neutron stars, black holes in GR 432
 Structure functions 367
 Student's t distribution 692, 749
 $SU(n)$ multiplets 774
 $SU(3)$
 classification of baryon resonances 327
 isoscalar factors, note on 773
 multiplets 327
 representation matrices, note on 773
 transformation, generators of 773
 $SU(5)$ 331
 $SU(6)$ multiplets 327
 Sudbury
 neutrino observatory, SNO 1081
 Sum of neutrino masses 139
 Sum rules 838
 Summary tables, organization of 11
 Sunyaev-Zeldovich effect 454, 486, 517, 530
 Sunyaev-Zeldovich effect, kinetic 454
 Super tau-charm factories 566
 Super-conformal anomaly 1040
 Super-Higgs mechanism 1040
 Superconducting Tunnel Junctions (STJs) 666
 Supergravity 1040
 SuperKEKB (KEK) collider parameters 570
 Supermassive GUT monopoles 1138
 Supermultiplet 1038
 Supernovae
 as cosmological probes 485
 Type Ia 485, 495
 Type II 485
 Superpartners 1038
 Superpotential 1039
 Superspace 1038
 Supersymmetric particle searches 112, 2292
 Supersymmetric particle spectrum 1042
 Supersymmetry breaking 1040
 Supersymmetry, SUSY 1038
 Supervised learning 711–713, 718, 721, 732
 Survival probability, relations for 777
 SUSY Les Houches accord, SLHA 1042
 SUSY, supersymmetry 1038
 SVM, support vector machine 720, 721
 SVR, support vector regression 721, 722
 Symmetry breaking 1125
 Synchrotron oscillations 561
 Synchrotron radiation 147, 561
 Synchrotron tune 561
 Systematic errors, treatment of 15
 SZ, Sunyaev-Zeldovich effect 530

 t (quark) 844
 T (time reversal), tests of conservation 114
 t' (4^{th} Generation) Quark, Searches for 32, 1401
 Tabular data 720
 τ lepton 28, 1303
 τ branching fractions, note on 829
 τ decay parameters, note on 832
 Technicolor 112, 2347
 electroweak symmetry breaking 1104
 Technifermion condensat formation 1104
 Telescope Array (TA) 649
 Tensor mesons 876, 877
 Tensor mesons $\ell = 1, 2^{++}$ 323
 Tensor-to-scalar field perturbations ratio, 139
 Testing dataset 712, 714, 716
 Tests of conservation laws 89
 Tetraquark candidates
 K_0^* (700) 891
 $T_{c\bar{c}1}$ (4430) 996
 X (3872) 995
 ψ (4230) 996
 a_0 (980) 891
 f_0 (500) 890
 f_0 (980) 890
 Tetraquark states 880
 ϕ (2170) 881
 a_0 (980), f_0 (980) 880
 Tetraquarks 326, 874
 $T_{c\bar{s}0}^*$ (2900) 2062
 $T_{c\bar{s}0}^*$ (2870)⁰ 2062
 $T_{c\bar{s}1}^*$ (2900)⁰ 2062
 $T_{c\bar{c}}$ (3875)⁺ 2062
 $T_{b\bar{b}1}$ (10610) 88, 2069
 $T_{b\bar{b}1}^-$ (10650)⁺ 88, 2071
 $T_{b\bar{s}}$ (5568)⁺ 2069
 $T_{c\bar{c}s1}$ (4000) 2064
 $T_{c\bar{c}s1}$ (4220)⁺ 2067
 $T_{c\bar{c}0}$ (4240)⁺ 2067
 $T_{c\bar{c}1}$ (3900) 88, 2063
 $T_{c\bar{c}1}$ (4200)⁺ 2067
 $T_{c\bar{c}1}$ (4430)⁺ 88, 2068
 $T_{c\bar{c}}$ (4020) 88, 2065
 $T_{c\bar{c}}$ (4050)⁺ 2066
 $T_{c\bar{c}}$ (4055)⁺ 2066
 $T_{c\bar{c}}$ (4100)⁺ 2067
 $T_{c\bar{c}}$ (4250)⁺ 2068
 $T_{c\bar{c}c}$ (6900)⁰ 2069
 Tevatron 562
 Tevatron collider parameters 572
 Theoretical decay-constant calculations
 Bottom mesons 934
 charmed mesons 933
 pions and kaons 931
 Thermal
 conductivity of elements, table 145
 expansion coefficients of elements, table 145
 history of the Universe 447
 θ_W , Weinberg angle 295
 Third generation vector-like quarks 1108
 Thomson cross section σ_T 137
 Three-body
 decay kinematics 778
 decays, kinematic limits 778
 phase space 778
 Threshold Cherenkov detectors 599
 Thrust 163
 Time variation of the fine-structure constant 532
 Time-projection chambers, TPC 607, 661
 Timing measurement
 noise 626
 silicon detectors 620
 Top quark t 844
 Top quark mass 857
 Top quark, note on 844
 Top-changing neutral currents, tests for 121
 Total cross sections 412
 Total energy density of Universe, Ω_{tot} 488
 Total lepton number conservation 120
 TPC, Time-projection chambers 661
 Training 712, 714, 718, 724, 741
 Training dataset 712–716
 Transfer learning 737
 Transformation of electromagnetic fields, relativistic 146
 Transformer 720, 730, 737
 Transition Edge Sensors (TESs) 667
 Transition radiation 588
 Transition radiation detectors, TRD 609
 Translational invariance 720, 725
 Transverse variables 780
 Trees 720, 722

- Triangle singularity 326, 878, 879
Triangles, unitarity, note on 270
Trilepton events 1110
Trilinear coupling 217
Tropical year 138
Two-body
 decay 777
 differential cross sections 779
 partial decay rate 777
 reactions 779
 scattering kinematics 777
Two-Higgs-doublet models 248
Two-photon processes in e^+e^- annihilation 794
Type Ia supernovae 485, 495
Type II supernovae 485
- U-Net 726
ULA, ultralight axion-like particles 1087
Ultralight axion-like particles (ULAs) 1087
Uncertainty quantification 738, 740
Unconstrained averaging 16
Underfitting 712
Underlying event (UE) 160
Unified atomic mass unit 137
Unified theories, grand 1119
Uniform distribution 692
Units and conversion factors 359
Units, electromagnetic 146
Units, SI, complete set 140
Universal approximation 712, 714, 725
Universal Extra Dimension, UED 798, 1026
Universality of free fall tests GR 437
Universe
 accelerating evidence 486
 age of 446, 488
 as a particle detector 496
 baryon density of 138, 475
 bubble 449
 composition 444, 446
 cosmological structure 448
 critical density of 138
 curvature of 445
 density fluctuations 451
 density parameter of 138
 entropy density 449
 flatness 488
 global description of 482
 Hubble expansion of 444, 482
 inflation 482
 large-scale structure of 446, 452
 matter-dominated 450
 parametrizing 482
 perturbation 482
 phase transitions 449
 radiation content at early times 448
 thermal history of 447, 457
 thermodynamic equilibrium 448
Unsupervised learning 711, 712, 715, 718
 Υ (bb) mesons
 $\Upsilon(1S)$ 84, 2024
 $\Upsilon(2S)$ 85, 2037
 $\Upsilon_2(1D)$ [*was* $\Upsilon(1D)$] 86, 2043
 $\Upsilon(3S)$ 87, 2049
 $\Upsilon(4S)$ [*was* $\Upsilon(10580)$] 87, 2054
 $\Upsilon(10753)$ 2056
 $\Upsilon(10860)$ 87, 2056
 $\Upsilon(11020)$ 88, 2060
- Vacuum energy parameter Ω_ν 445
Vacuum expectation value (VEV) 1023
VAE, Variational Auto-Encoder 732, 733
Validation dataset 713
Values of particle properties, historical perspective of 19
- Vanishing gradient 724, 727, 729, 736
Variance, definition 689
Variational inference 715, 719, 732, 733, 740
Varying constants
 gravitational G_N , fine structure α 484
VBF – vector boson fusion 218
 V_{cb} and V_{ub} CKM Matrix Elements 1859
 V_{cb} and V_{ub} determination of, note on 962
 V_{cb} determination 962
Vector mesons 878
 ρ excitations 878
 $\rho(1570) - C(1480)$ 879
 $\rho(1900)$ 879
 $\rho(770)$ 878
Vector mesons $\ell = 0, 1^{--}$ 323
Vector superfields 1038
Vector-like quarks, VLQ 1108
VEPP-2000 569
VEPP-4M 569
Virgo, gravitational observatory 435
Virtual graviton process 799
VLQ, vector like quarks 1108
Von Neuman’s acceptance-rejection method in MC 748
 V_{ub} determination 967
 V_{ub}/V_{cb} determination 971
 V_{ud} determination 904
 $V_{ud}, V_{us}, V_{ub}, V_{cd}, V_{cs}, V_{cb}, V_{td}, V_{ts}, V_{tb}$ 270
 V_{us} determination 904
- W and Z resonant production 793
 W boson 25, 1187
 mass 815
 width 815
 w , dark energy equation of state parameter 445
 W - W' mixing 1031
Warped extra dimensions 1021
Wasserstein distance 718, 732, 734
Wasserstein GAN 734
Wavelength of 1 eV/ c particle 137
WaveNet 734
Weak decay form factors 342
Weak gauge bosons pairs production 793
Weak neutral currents
 tests ($\Delta B = \Delta C = \Delta S = \Delta T = 1$) 114
Weak-field general relativity 432
Weak-mixing angle ($\sin^2 \hat{\theta}(M_Z)$) 137
Weakly supervised learning 714
Weakly-interacting massive particle, WIMP 1038
Weight matrix 724
Weinberg angle θ_W 295
White-dwarf, weak-self-gravity 438
Wien displacement law constant $b = \lambda_m axT$ 137
WIMP 502
 miracle 500, 1038
WIMP dark matter searches 113, 2359
WIMP, weakly-interacting massive particle 1038
Wino 1042
WMAP, Wilkinson Microwave Anisotropy Probe 486
Wolfenstein parameters 270, 904, 936
World average of $\alpha_s(m_Z^2)$ 168, 172
 W' -boson searches 1029, 1114
Wrapped extra dimension 799
- X mesons
 $X_0(2900)$ 2062
 $X_1(2900)$ 2062
 $X(1835)$ 1516
 $X(2370)$ 1536
 $X(3872)$ [*aka* $\chi_{c1}(3872)$] 81, 1996
 $X(3940)$ 2002
 $X(4020)^\pm$ 88, 2065
 $X(4050)^\pm$ 2066
 $X(4055)^\pm$ 2066

$X(4100)^\pm$	2067	Ξ_c^+	105, 2249
$X(4160)$	2008	Ξ_c^0	105, 2250
$X(4250)^\pm$	2068	$\Xi_c(2645)$	106, 2253
$X(4350)$	2015	$\Xi_c(2790)$	106, 2253
$X(4630)$	2019	$\Xi_c(2815)$	106, 2254
$X(5568)^\pm$	2069	$\Xi_c(2923)$	2255
x variable (of Feynman's)	780	$\Xi_c(2930)$	2255
Xavier initialization	736	$\Xi_c(2970)$	106, 2256
xF_3 structure function, plots of	379	$\Xi_c'^+$	106, 2252
Ξ baryons		$\Xi_c(3055)$	106, 2257
$\Xi_b(6087)^0$	110, 2279	$\Xi_c(3080)$	106, 2257
$\Xi_b(6095)^0$	110, 2279	$\Xi_c(3123)$	2257
$\Xi_b(6227)^-$	110, 2280	$\Xi_c'^0$	106, 2253
$\Xi_b(6327)^0$	110, 2280		
$\Xi_b(6333)^0$	110, 2281		
$\Xi_c(2882)$	2255		
Ξ^-	102, 2221		
Ξ^0	101, 2218		
Ξ_{bc}^0	2281		
$\Xi(1530)$	102, 2224		
$\Xi(1620)$	2225		
$\Xi(1690)$	102, 2225		
$\Xi(1820)$	102, 2226		
$\Xi(1950)$	102, 2227		
$\Xi(2030)$	102, 2228		
$\Xi(2120)$	2229		
$\Xi(2250)$	2229		
$\Xi(2370)$	2230		
$\Xi(2500)$	2230		
Ξ_{cc}^{++}	107, 2262		
Ξ_{cc}^+	2262		
Ξ_b^-	109, 2275		
Ξ_b^0	109, 2277		
$\Xi_b(6100)^-$	110, 2279		
$\Xi_b(6227)^-$	110, 2280		
$\Xi_b(6227)^0$	110, 2280		
$\Xi_b'(5935)^-$	109, 2278		
$\Xi_b(5945)^0$	110, 2278		
$\Xi_b(5955)^-$	110, 2279		
		Year, sidereal	138
		Year, tropical	138
		Young diagrams (tableaux)	774
		Young's modulus of solid elements, table	145
		Yukawa coupling	
		Higgs to fermions direct observation	220
		leptoquark-type	1134
		unification	1125
		Z boson	25, 1200
		branching ratios	818
		mass	817
		note on	817
		width	810, 817
		Z' -boson searches, note on	1033
		Z' or W' bosons, searches for	1106
		$Z_c(4200)$ [<i>was</i> $X(4200)^\pm$]	2067
		$Z_b(10610)$ [<i>was</i> $X(10610)$]	88, 2069
		$Z_b(10650)$ [<i>was</i> $X(10650)^\pm$]	88, 2071
		$Z_c(3900)$ [<i>was</i> $X(3900)$]	88, 2063
		$Z_c(4430)$ [<i>was</i> $X(4430)^\pm$]	88, 2068
		Zero-shot learning	737
		Z' -boson searches	1114

VOLUME II: TABLE OF CONTENTS

PARTICLE LISTINGS*

Illustrative key and abbreviations	1171
Gauge and Higgs bosons	
(γ , gluon, graviton, W , Z , Higgs, Axions)	1185
Leptons	
(e , μ , τ , Heavy-charged lepton searches, Neutrino properties, Number of neutrino types Double- β decay, Neutrino mixing, Heavy-neutral lepton searches)	1297
Quarks	
(u , d , s , c , b , t , b' , t' (4^{th} gen.), Free quarks)	1371
Mesons	
Light unflavored (π , ρ , a , b) (η , ω , f , ϕ , h)	1411
Strange (K , K^*)	1538
Charmed (D , D^*)	1592
Charmed, strange (D_s , D_s^* , D_{sJ})	1657
Bottom (B , V_{cb}/V_{ub} , B^* , B_J^*)	1681
Bottom, strange (B_s , B_s^* , B_{sJ}^*)	1865
Bottom, charmed (B_c)	1893
$c\bar{c}$ (η_c , $J/\psi(1S)$, χ_c , h_c , ψ)	1898
$b\bar{b}$ (η_b , Υ , χ_b , h_b)	2023
Other mesons (T_c , T_b tetraquarks)	2062
Baryons	
N	2081
Δ	2137
Λ	2161
Σ	2187
Ξ	2218
Ω	2231
Charmed (Λ_c , Σ_c , Ξ_c , Ω_c)	2234
Doubly charmed (Ξ_{cc})	2262
Bottom (Λ_b , Σ_b , Ξ_b , Ω_b , b -baryon admixture)	2263
Exotic baryons (P_c pentaquarks)	2285
Searches not in Other Sections	
Magnetic monopole searches	2289
Supersymmetric particle searches	2292
Technicolor	2347
Searches for quark and lepton compositeness	2348
Extra dimensions	2352
WIMP and dark matter searches	2359
Other particle searches	2374

*The divider sheets give more detailed indices for each main section of the Particle Listings.

INTRODUCTION TO THE PARTICLE LISTINGS

Illustrative key	1171
Abbreviations	1172





Illustrative Key to the Particle Listings

Name of particle. "Old" name used before 1986 renaming scheme also given if different. See the section "Naming Scheme for Hadrons" for details.

$a_0(1200)$

$$I^G(J^{PC}) = 1^-(0^{++})$$

Particle quantum numbers (where known).

OMITTED FROM SUMMARY TABLE
Evidence not compelling, may be a kinematic effect.

Indicates particle omitted from Particle Physics Summary Table, implying particle's existence is not confirmed.

Quantity tabulated below.

$a_0(1200)$ MASS

General comments on particle.

Top line gives our best value (and error) of quantity tabulated here, based on weighted average of measurements used. Could also be from fit, best limit, estimate, or other evaluation. See next page for details.

VALUE (MeV)	EVTS	DOCUMENT ID	TECN	CHG	COMMENT
1206 ± 7 OUR AVERAGE					
1210 ± 8 ± 9	3000	FENNER 87	MMS	-	3.5 $\pi^- p$
1198 ± 10		PIERCE 83	ASPK	+	2.1 $K^- p$
1216 ± 11 ± 9	1500	MERRILL 81	HBC	0	3.2 $K^- p$
• • • We do not use the following data for averages, fits, limits, etc. • • •					
1192 ± 16	200	LYNCH 81	HBC	±	2.7 $\pi^- p$
Systematic error was added quadratically by us in our 1986 edition.					

"Document id" for this result; full reference given below.

Measurement technique. (See abbreviations on next page.)

Footnote number linking measurement to text of footnote.

$a_0(1200)$ WIDTH

Scale factor > 1 indicates possibly inconsistent data.

Number of events above background.

Measured value used in averages, fits, limits, etc.

VALUE (MeV)	EVTS	DOCUMENT ID	TECN	CHG	COMMENT
41 ± 11 OUR AVERAGE					Error includes scale factor of 1.8. See the ideogram below.
50 ± 8		PIERCE 83	ASPK	+	2.1 $K^- p$
70 +30 -20	200	LYNCH 81	HBC	±	2.7 $\pi^- p$
25 ± 5 ± 7		MERRILL 81	HBC	0	3.2 $K^- p$
• • • We do not use the following data for averages, fits, limits, etc. • • •					
<60		FENNER 87	MMS	-	3.5 $\pi^- p$

Reaction producing particle, or general comments.

"Change bar" indicates result added or changed since previous edition.

Charge(s) of particle(s) detected.

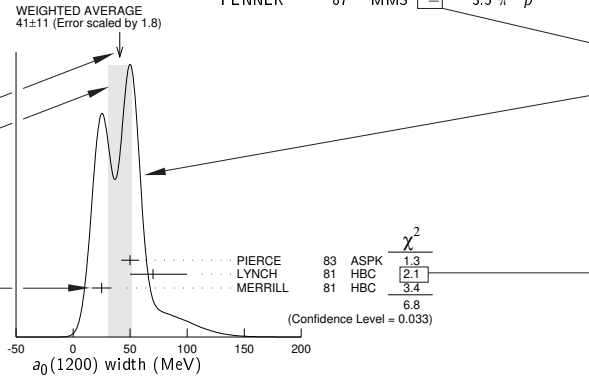
Error in measured value (often statistical only; followed by systematic if separately known; the two are combined in quadrature for averaging and fitting.)

Measured value *not used* in averages, fits, limits, etc. See the Introductory Text for explanations.

Arrow points to weighted average.

Shaded pattern extends ±1σ (scaled by "scale factor" S) from weighted average.

Value and error for each experiment.



Ideogram to display possibly inconsistent data. Curve is sum of Gaussians, one for each experiment (area of Gaussian = 1/error; width of Gaussian = ±error). See Introductory Text for discussion.

Contribution of experiment to χ^2 (if no entry present, experiment not used in calculating χ^2 or scale factor because of very large error).

$a_0(1200)$ DECAY MODES

Partial decay mode (labeled by Γ_i).

Mode	Fraction (Γ_i/Γ)	Scale factor/ Confidence level
Γ_1 3π	(65.2 ± 1.3) %	S=1.7
Γ_2 $K\bar{K}$	(34.8 ± 1.3) %	S=1.7
Γ_3 $\eta\pi^\pm$	< 5 × 10 ⁻⁴	CL=95%

Our best value for branching fraction as determined from data averaging, fitting, evaluating, limit selection, etc. This list is basically a compact summary of results in the Branching Ratio section below.

$a_0(1200)$ BRANCHING RATIOS

Branching ratio.

Our best value (and error) of quantity tabulated, as determined from constrained fit (using *all significant* measured branching ratios for this particle).

Weighted average of measurements of this ratio only.

Footnote (referring to LYNCH 81).

$\Gamma(3\pi)/\Gamma_{total}$	Γ_1/Γ
0.652 ± 0.013 OUR FIT	
0.643 ± 0.010 OUR AVERAGE	
0.64 ± 0.01	PIERCE 83 ASPK + 2.1 $K^- p$
0.74 ± 0.06	MERRILL 81 HBC 0 3.2 $K^- p$
• • • We do not use the following data for averages, fits, limits, etc. • • •	
0.48 ± 0.15	² LYNCH 81 HBC ± 2.7 $\pi^- p$
² Data has questionable background subtraction.	
$\Gamma(K\bar{K})/\Gamma_{total}$	Γ_2/Γ
0.348 ± 0.013 OUR FIT	
0.35 ± 0.05	PIERCE 83 ASPK + 2.1 $K^- p$
$\Gamma(K\bar{K})/\Gamma(3\pi)$	Γ_2/Γ_1
0.535 ± 0.030 OUR FIT	
0.50 ± 0.03	MERRILL 81 HBC 0 3.2 $K^- p$
$\Gamma(\eta(\text{neutral decay})\pi^\pm)/\Gamma_{total}$	0.71 Γ_3/Γ
<3.5	
95	PIERCE 83 ASPK + 2.1 $K^- p$

Branching ratio in terms of partial decay mode(s) Γ_i above.

Confidence level for measured upper limit.

References, ordered inversely by year, then author.

"Document id" used on data entries above.

Journal, report, preprint, etc. (See abbreviations on next page.)

$a_0(1200)$ REFERENCES

FENNER 87	PRL 55 14	H. Fenner et al.	(SLAC)
PIERCE 83	PL 123B 230	J.H. Pierce	(FNAL) JP
LYNCH 81	PR D24 610	G.R. Lynch et al.	(CLEO Collab.)
MERRILL 81	PRL 47 143	D.W. Merrill et al.	(SACL, CERN)

Partial list of author(s) in addition to first author.

Quantum number determinations in this reference.

Institution(s) of author(s). (See abbreviations on next page.)

Abbreviations Used in the Particle Listings

Indicator of Procedure Used to Obtain Our Result

OUR AVERAGE	From a weighted average of selected data.
OUR FIT	From a constrained or overdetermined multiparameter fit of selected data.
OUR EVALUATION	Not from a direct measurement, but evaluated from measurements of other quantities.
OUR ESTIMATE	Based on the observed range of the data. Not from a formal statistical procedure.
OUR LIMIT	For special cases where the limit is evaluated by us from measured ratios or other data. Not from a direct measurement.

Measurement Techniques

(i.e., Detectors and Methods of Analysis)

A1	A1 Collaboration at MAMI
A2MM	A2 spectrometer at the Mainz Microtron, MAMI
ABRA	ABRACADABRA QCD axion dark matter search
ACCM	ACCMOR Collaboration
ADMX	Axion Dark Matter Experiment
AEMS	Argonne effective mass spectrometer
ALCE	ALICE detector at CERN LHC
ALEP	ALEPH – CERN LEP detector
ALPS	Photon regeneration experiment
AMND	AMANDA South Pole neutrino detector
AMY	AMY detector at KEK-TRISTAN
ANAI	Direct DM detection exp. with NaI at Canfranc Underground Lab, Spain
ANIC	ANTARES and IceCube combined analysis
ANIT	Antarctic Impulsive Transient Antenna balloon mission
ANTR	ANTARES underwater neutrino telescope in the Western Mediterranean Sea
APEX	FNAL APEX Collab.
ARG	ARGUS detector at DORIS
ARGD	Fit to semicircular amplitude path on Argand diagram
ASP	Anomalous single-photon detector
ASPK	Automatic spark chambers
ASTE	ASTERIX detector at LEAR
ASTR	Astronomy
ATLS	ATLAS detector at CERN LHC
AUGE	Pierre Auger Observatory
AURG	Resonant-mass gravitational wave AURIGA detector
B787	BNL experiment 787 detector
B791	BNL experiment 791 detector
B845	BNL experiment 845 detector
B852	BNL E-852
B865	BNL E865 detector
B871	BNL experiment 871 detector
B949	BNL E949 detector at AGS
BABR	BaBar Collab.
BAIK	Lake Baikal neutrino telescope
BAKS	Baksan underground scintillation telescope
BC	Bubble chamber
BDMP	Beam dump
BEAT	CERN BEATRICE Collab.
BEBC	Big European bubble chamber at CERN
BEL2	Belle II Collab.
BELL	Belle Collab.
BES	BES Beijing Spectrometer at Beijing Electron-Positron Collider
BES2	BES Beijing Spectrometer at Beijing Electron-Positron Collider
BES3	BES Beijing Spectrometer at Beijing Electron-Positron Collider
BEST	Baksan Experiment on Sterile Transitions
BIS2	BIS-2 spectrometer at Serpukhov
BKEI	BENKEI spectrometer system at KEK Proton Synchrotron
BOLO	Bolometer, a cryogenic thermal detector
BONA	Bonanza nonmagnetic detector at DORIS
BORX	BOREXINO
BPWA	Barrelet-zero partial-wave analysis
BRAS	BRASS: Broadband Radiometric Axion/ALPs Search Setup
C100	COSINE-100 experiment in South Korea
CALO	Calorimeter
CAPP	CAPP18T haloscope detector
CASK	CULTASK: CAPPs Ultra Low Temperature Axion Search in Korea
CASP	Cosmic Axion Spin Precession Experiments
CAST	CAST experiment at CERN
CBAL	Crystal Ball detector at SLAC-SPEAR or DORIS
CBAR	Crystal Barrel detector at CERN-LEAR
CBOX	Crystal Box at LAMPF

CBTP	CBELSA/TAPS Collaboration
CC	Cloud chamber
CCFR	Columbia-Chicago-Fermilab-Rochester detector
CCM	Coherent CAPTAIN-Mills 10-ton liquid Ar detector at Los Alamos
CDEX	China Dark Matter Experiment
CDF	Collider detector at Fermilab
CDF2	CDF-II Collab.
CDHS	CDHS neutrino detector at CERN
CDM2	CDMS II, Cryogenic Dark Matter Search at Soudan Underground Lab.
CDMS	CDMS Collaboration
CELL	CELLO detector at DESY
CGNT	CoGeNT dark matter search experiment
CHER	Cherenkov detector
CHM2	CHARM-II neutrino detector (glass) at CERN
CHOZ	Nuclear Power Station near Chooz, France
CHRM	CHARM neutrino detector (marble) at CERN
CHRS	CHORUS Collaboration – CERN SPS
CIB	Cosmic Infrared Background
CIBS	CERN-IHEP boson spectrometer
CLAS	Jefferson CLAS Collab.
CLE2	CLEO II detector at CESR
CLE3	CLEO III detector at CESR
CLEC	CLEO-c detector at CESR
CLEO	Cornell magnetic detector at CESR
CMB	Cosmic Microwave Background
CMD	Cryogenic magnetic detector at VEPP-2M, Novosibirsk
CMD2	Cryogenic magnetic detector 2 at VEPP-2M, Novosibirsk
CMD3	Cryogenic magnetic detector 3 at VEPP-2000, Novosibirsk
CMS	CMS detector at CERN LHC
CNTR	Counters
COHR	COHERENT experiment at the SNS, Oak Ridge
COMB	Combined analysis of data from independent experiments.
COMP	COMPASS experiment at the CERN SPS
CONN	CONNIE: Coherent Neutrino-Nucleus Interaction Experiment
COSM	Cosmology and astrophysics
COSY	COSY-TOF Collaboration
COUP	COUPP (the Chicagoland Observatory for Underground Particle Physics) Collab.
CPLR	CPLEAR Collaboration
CRBT	Crystal Ball and TAPS detector at MAMI
CRES	CRESST cryogenic detector
CRYB	Crystal Ball at BNL
CRYM	Crystal Ball detector at Mainz Microtron MAMI
CSB2	Columbia U. - Stony Brook BGO calorimeter inserted in NaI array
CSME	COSME Collaboration
CUOR	CUORICINO experiment at Gran Sasso Laboratory.
CUSB	Columbia U. - Stony Brook segmented NaI detector at CESR
D0	D0 detector at Fermilab Tevatron Collider
DAMA	DAMA, dark matter detector at Gran Sasso National Lab.
DAMP	The DArk Matter Particle Explorer, DAMPE, detector
DANC	DANCE axion search experiment
DASP	DESY double-arm spectrometer
DAYA	Daya Bay Collaboration
DBC	Deuterium bubble chamber
DCHZ	Double Chooz Collaboration
DEAP	DEAP-3600 DM search with argon at SNOLAB
DISP	Graviton mass measurement based on dispersion measure
DLCO	DELCO detector at SLAC-SPEAR or SLAC-PEP
DLPH	DELPHI detector at LEP
DM1	Magnetic detector no. 1 at Orsay DCI collider
DM2	Magnetic detector no. 2 at Orsay DCI collider
DMIC	DAMIC Dark Matter in CCD experiment at Fermilab
DMTP	Dark Matter Time Projection Chamber (DMTPC) directional detection experiment
DONU	DONUT Collab.
DORR	DOSUE-RR Collab., dark photon dark matter search
DPWA	Energy-dependent partial-wave analysis
DRFT	Directional dark matter detector at Boulby Underground Science Facility
DS50	DarkSide-50 Liquid Argon TPC at Gran Sasso National Laboratory
E137	SLAC E137 beam-dump experiment
E621	Fermilab E621 detector
E653	Fermilab E653 detector
E665	Fermilab E665 detector
E687	Fermilab E687 detector

Abbreviations Used in the Particle Listings

E691	Fermilab E691 detector	IACT	Imaging Air Cherenkov Telescope
E705	Fermilab E705 Spectrometer-Calorimeter	ICAR	ICARUS experiment at Gran Sasso Laboratory.
E731	Fermilab E731 Spectrometer-Calorimeter	ICCB	IceCube neutrino detector at South Pole
E756	Fermilab E756 detector	IGEX	IGEX Collab.
E760	Fermilab E760 detector	IMB	Irvine-Michigan-Brookhaven underground Cherenkov detector
E761	Fermilab E761 detector	IMB3	Irvine-Michigan-Brookhaven underground Cherenkov detector
E771	Fermilab E771 detector	INDU	Magnetic induction
E773	Fermilab E773 Spectrometer-Calorimeter	IPWA	Energy-independent partial-wave analysis
E789	Fermilab E789 detector	ISTR	IHEP ISTRA+ spectrometer-calorimeter
E791	Fermilab E791 detector	JADE	JADE detector at DESY
E799	Fermilab E799 Spectrometer-Calorimeter	JPAC	Joint Physics Analysis Center (JPAC) Collaboration
E835	Fermilab E835 detector	K246	KEK E246 detector with polarimeter
EDE2	EDELWEISS II dark matter search Collaboration	K2K	KEK to Super-Kamiokande
EDE3	EDELWEISS III dark matter search Collaboration	K391	KEK E391a detector
EDEL	EDELWEISS dark matter search Collaboration	K470	KEK-E470 Stopping K detector
EDGS	EDGES: Global EoR (Epoch of Reionization) Signature experiment	KAM2	KAMIOKANDE-II underground Cherenkov detector
EHS	Four-pi detector at CERN	KAMI	KAMIOKANDE underground Cherenkov detector
ELEC	Electronic combination	KAR2	KARMEN2 calorimeter at the ISIS neutron spallation source at Rutherford
EMC	European muon collaboration detector at CERN	KARM	KARMEN calorimeter at the ISIS neutron spallation source at Rutherford
EMUL	Emulsions	KEDR	detector operating at VEPP-4M collider (Novosibirsk)
EPTA	The European Pulsar Timing Array	KIMS	Korea Invisible Mass Search experiment at YangYang, Korea
ESR	Electron spin resonance spectroscopy	KLND	KamLand Collab. (Japan)
EXO2	Enriched Xenon Observatory 200-kg liquid Xe TPC	KLOE	KLOE detector at DAFNE (the Frascati e+e- collider Italy)
FASR	FASER light dark matter search at LHC	KOLR	Kolar Gold Field underground detector
FAST	Fiber Active Scintillator Target detector at PSI	KOTO	KOTO experiment with K_L^0 beam at J-PARC
FBC	Freon bubble chamber	KTEV	KTeV Collaboration
FENI	FENICE (at the ADONE collider of Frascati)	L3	L3 detector at LEP
FIT	Fit to previously existing data	LASR	Laser
FLAT	Large Area Telescope onboard the Fermi Gamma-Ray Space Telescope (Fermi-LAT)	LASS	Large-angle superconducting solenoid spectrometer at SLAC
FMPS	Fermilab Multiparticle Spectrometer	LATT	Lattice calculations
FOCS	FNAL E831 FOCUS Collab.	LEBC	Little European bubble chamber at CERN
FRAB	ADONE $B\bar{B}$ group detector	LEGS	BNL LEGS Collab.
FRAG	ADONE $\gamma\gamma$ group detector	LENA	Nonmagnetic lead-glass NaI detector at DORIS
FRAM	ADONE MEA group detector	LEP	From combination of all 4 LEP experiments: ALEPH, DELPHI, L3, OPAL
FREJ	FREJUS Collaboration – modular flash chamber detector (calorimeter)	LEPS	Low-Energy Pion Spectrometer at the Paul Scherrer Institute
FUNK	Finding U(1)'s of a Novel Kind experiment	LGW	Lead Glass Wall collaboration at SPEAR/SLAC
GA24	Hodoscope Cherenkov γ calorimeter (IHEP GAMS-2000) (CERN GAMS-4000)	LHC	Combined analysis of LHC experiments
GALX	GALLEX solar neutrino detector in the Gran Sasso Underground Lab.	LHCB	LHCb detector at CERN LHC
GAM2	IHEP hodoscope Cherenkov γ calorimeter GAMS-2000	L+P	Multichannel L + P model fit
GAM4	CERN hodoscope Cherenkov γ calorimeter GAMS-4000	LSD	Mont Blanc liquid scintillator detector
GAMS	IHEP hodoscope Cherenkov γ calorimeter GAMS-4 π	LSND	Liquid Scintillator Neutrino Detector
GLUX	GlueX exotic hybrid mesons search at JLAB	LSW	Light Shining through a Wall
GNME	Global Network of Optical Magnetometers for Exotic searches (GNOME)	LUX	Large Underground Xenon experiment at SURF
GNO	Gallium Neutrino Observatory in the Gran Sasso Underground Lab.	LZ	LUX-ZEPLIN dark matter Xe CPT detector at SURF
GOLI	CERN Goliath spectrometer	MAC	MAC detector at PEP/SLAC
GRAL	GRAAL Collaboration	MAJD	Majorana Demonstrator experiment at SURF
H1	H1 detector at DESY/HERA	MBNE	Fermilab MiniBooNE neutrino experiment
HAWC	High Altitude Water Cherenkov Observatory experiment at Sierra Negra, Mexico	MBR	Molecular beam resonance technique
HBC	Hydrogen bubble chamber	MCBN	Fermilab MicroBooNE neutrino experiment
HDBC	Hydrogen and deuterium bubble chambers	MCRO	MACRO detector in Gran Sasso
HDES	HADES Collaboration at GSI in Darmstadt	MD1	Magnetic detector at VEPP-4, Novosibirsk
HDMO	Heidelberg-Moscow Experiment	MDHI	Multilayer Dielectric Haloscope Investigation
HDMS	Heidelberg Dark Matter Search Experiment	MDRP	Millikan drop measurement
HEBC	Helium bubble chamber	MEG	Muon to electron conversion detector at PSI
HEPT	Helium proportional tubes	MGFL	MAGIC and Fermi-LAT Collaborations
HERA	H1 and ZEUS Collaborations at DESY/HERA	MGIC	MAGIC Telescopes gamma-ray observatory
HERB	HERA-B detector at DESY/HERA	MICA	Underground mica deposits
HERM	HERMES detector at DESY/HERA	MICR	MICROSCOPE satellite test of weak equivalence principle
HESS	High Energy Stereoscopic System gamma-ray instrument	MINS	Fermilab MINOS experiment
HFR	HighFlow Reactor at the Institut Laue-Langevin	MIRA	MIRABELLE Liquid-hydrogen bubble chamber
HFS	Hyperfine structure	MLEV	Magnetic levitation
HLBC	Heavy-liquid bubble chamber	MLS	Modified Laurent Series
HOME	Homestake underground scintillation detector	MMS	Missing mass spectrometer
HPGE	High-purity Germanium detector	MOEDAL	MoEDAL magnetic monopoles search experiment at LHC
HPS	Heavy Photon Search experiment at JLAB	MPS	Multiparticle spectrometer at BNL
HPW	Harvard-Pennsylvania-Wisconsin detector	MPS2	Multiparticle spectrometer upgrade at BNL
HRS	SLAC high-resolution spectrometer	MPSF	Multiparticle spectrometer at Fermilab
HYBR	Hybrid: bubble chamber + electronics	MPWA	Model-dependent partial-wave analysis
HYCP	HyperCP Collab. (FNAL E-871)	MRK1	SLAC Mark-I detector
HYST	HAYSTAC axion search experiment	MRK2	SLAC Mark-II detector
		MRK3	SLAC Mark-III detector
		MRKJ	Mark-J detector at DESY
		MRS	Magnetic resonance spectrometer
		MUG2	Muon (g-2)
		MWPC	Multi-Wire Proportional Chamber

Abbreviations Used in the Particle Listings

NA14	CERN NA14	SNSP	SNSPD, Superconducting Nanowire Single-Photon Detectors
NA31	CERN NA31 Spectrometer-Calorimeter	SOU2	Soudan 2 underground detector
NA32	CERN NA32 Spectrometer	SOUND	Soudan underground detector
NA48	CERN NA48 Collaboration	SPEC	Spectrometer
NA49	CERN NA49 Collaboration	SPED	From maximum of speed plot or resonant amplitude
NA60	CERN NA60 Collaboration	SPHR	Bonn SAPHIR Collab.
NA62	CERN NA62 Experiment	SPNX	SPHINX spectrometer at IHEP accelerator
NA64	CERN SPS NA64 Experiment	SPRK	Spark chamber
NAGE	NEWAGE, New generation WIMP-search experiment with advanced gaseous tracking	SQID	SQUID device
NAIA	NAIAD (NaI Advanced Detector) dark matter search experiment	STRC	Streamer chamber
ND	NaI detector at VEPP-2M, Novosibirsk	SVD2	SVD-2 experiment at IHEP, Protvino
NEOS	NEOS Collaboration	T2K	T2K Collaboration
NEWS	NEWS-G direct dark matter search at LSM	TASE	Taiwan Axion Search Experiment with a Haloscope, TASEH, experiment
NICE	Serpukhov nonmagnetic precision spectrometer	TASS	DESY TASSO detector
NMR	Nuclear magnetic resonance	TEVA	Combined analysis of CDF and DØ experiments
NOMD	NOMAD Collaboration, CERN SPS	TEXO	TEXONO Collab., ultra low energy Ge detector at Kuo-Sheng Laboratory
NOVA	NOvA experiment with Fermilab's NuMI neutrino beam	THEO	Theoretical or heavily model-dependent result
NTEV	NuTeV Collab. at Fermilab	TNF	TNF-IHEP facility at 70 GeV IHEP accelerator
nTRV	neutron Time-Reversal Violation	TOF	Time-of-flight
NUSX	Mont Blanc NUSEX underground detector	TOPZ	TOPAZ detector at KEK-TRISTAN
OBLX	OBELIX detector at LEAR	TPC	TPC detector at PEP/SLAC
OKA	OKA collaboration at U70 accelerator in Protvino, Russia	TPS	Tagged photon spectrometer at Fermilab
OLYA	Detector at VEPP-2M and VEPP-4, Novosibirsk	TRAP	Penning trap
OMEG	CERN OMEGA spectrometer	TWST	TWIST spectrometer at TRIUMF
OPAL	OPAL detector at LEP	UA1	UA1 detector at CERN
OPER	OPERA experiment with emulsion tracking at Gran Sasso	UA2	UA2 detector at CERN
ORGN	ORGAN (Oscillating Resonant Group AxioN) experiment	UA5	UA5 detector at CERN
ORPH	ADMX-Orpheus Dark Matter Experiment	UCNA	UCNA collaboration using polarized ultracold neutrons at LANSCE
OSPK	Optical spark chamber	UKDM	UK Dark Matter Collab.
PIBE	The PIBETA detector at the Paul Scherrer Institute (PSI), Switzerland.	UPLD	UPLOAD, upconversion low-noise oscillator axion detection experiment
PICA	PICASSO dark matter search experiment	VES	Vertex Spectrometer Facility at 70 GeV IHEP accelerator
PICO	PICO bubble chamber experiment in SNOLAB underground laboratory	VLBI	Very Long Baseline Interferometer
PIE3	π E3 beam-line of Paul Scherrer Institute	VNS	VENUS detector at KEK-TRISTAN
PLAS	Plastic detector	VRTS	Very Energetic Radiation Imaging Telescope Array System (VERITAS)
PLUT	DESY PLUTO detector	WA75	CERN WA75 experiment
PMLA	PAMELA space spectrometer on Resurs-DK1 satellite	WA82	CERN WA82 experiment
PNDX	PandaX dual-phase liquid xenon dark matter experiment at Jin-Ping	WA89	CERN WA89 experiment
PPTA	Parkes Pulsar Timing Array	WARP	Liquid argon detector for CDM searches at Gran Sasso
PRMX	The PRIMEX detector in Hall B at TJNAF	WASA	WASA detector at CELSIUS, Uppsala and at COSY, Juelich
PWA	Partial-wave analysis	WDMX	WISP Dark Matter eXperiment (WISPDIMX) for direct hidden photon search
QUAX	QUAX axion search experiment	WIRE	Wire chamber
QULP	QUALIPHIDE, quantum limited photons in the dark exp.	X100	XENON100 dark matter search experiment at Gran Sasso National Laboratory
RADE	CAST-RADES haloscope search for axions.	XE10	XENON10 experiment at Gran Sasso National Laboratory
RDK2	NIST rare radioactive decay experiment	XE1T	XENON1T dark matter search experiment at Gran Sasso National Laboratory
REDE	Resonance depolarization	XEBC	Xenon bubble chamber
RENO	RENO Collaboration	XENT	XENONnT dark matter search experiment at Gran Sasso National Laboratory
RICE	Radio Ice Cherenkov Experiment	XMAS	XMASS, liquid xenon scintillation detector at Kamioka Observatory
RVUE	Review of previous data	YUKA	Graviton mass measurement based on Yukawa potential
SAGE	US - Russian Gallium Experiment	ZEP2	ZEPLIN-II dark matter detector
SAPH	SAPPHIRES collaboration search for sub-eV Axion LPs	ZEP3	ZEPLIN-III dark matter detector at Palmer Underground Lab.
SCDM	SuperCDMS experiment at Soudan Underground Lab.	ZEPL	ZEPLIN-I galactic dark matter detector
SELX	FNAL SELEX Collab.	ZEUS	ZEUS detector at DESY/HERA
SENS	Sub-Electron-Noise Skipper CCD Experimental Instrument (SENSEI)		
SFM	CERN split-field magnet		
SHF	SLAC Hybrid Facility Photon Collaboration		
SHFT	Search for Halo Axions with Ferromagnetic Toroids		
SHUK	SHUKET: search for U(1) dark matter with an electromagnetic telescope		
SIGM	Serpukhov CERN-IHEP magnetic spectrometer (SIGMA)		
SILI	Silicon detector		
SIMP	SIMPLE, dark matter detector at Laboratori Nazionali del Sud		
SKAM	Super-Kamiokande Collab.		
SLAX	Solar Axion Experiment in Canfranc Underground Laboratory		
SLD	SLC Large Detector for e^+e^- colliding beams at SLAC		
SLIC	ADMX SLIC (Superconducting LC Circuit Investigating Cold Axions)		
SMPL	SIMPLE, Superheated Instrument for Massive Particle Experiments		
SND	Novosibirsk Spherical neutral detector at VEPP-2M		
SNDR	SINDRUM spectrometer at PSI		
SNO	SNO Collaboration (Sudbury Neutrino Observatory)		
SNO+	SNO+ Collaboration (Sudbury Neutrino Observatory)		

Conferences

Conferences are generally referred to by the location at which they were held (e.g., HAMBURG, TORONTO, CORNELL, BRIGHTON, etc.).

Journals

AA	Astronomy and Astrophysics
ADVP	Advances in Physics
AFIS	Anales de Fisica
AJP	American Journal of Physics
AL	Astronomy Letters
ANP	Annals of Physics
ANPL	Annals of Physics (Leipzig)
ANYAS	Annals of the New York Academy of Sciences
AP	Atomic Physics

Abbreviations Used in the Particle Listings

ANSM	St. Anselm Coll.	Manchester, NH, USA	BRUX	Univ. Libre de Bruxelles ; Physique des Particules Elémentaires	Bruxelles, Belgium
AQUI	Univ. di LAquila	Aquila , Italy	BRUXT	Univ. Libre de Bruxelles ; Physique Théorique	Bruxelles, Belgium
ARCBO	Arecibo Observatory	Arecibo, PR, USA	BUCH	Univ. of Bucharest	Bucharest-Magurele, Romania
ARIZ	Univ. of Arizona	Tucson, AZ, USA	BUDA	Wigner Research Centre for Physics	Budapest , Hungary
ARZS	Arizona State Univ.	Tempe, AZ, USA	BUFF	SUNY at Buffalo	Buffalo, NY, USA
ASCI	Russian Academy of Sciences	Moscow , Russian Federation	BURE	Inst. des Hautes Etudes Scien- tifiques	Bures-sur-Yvette , France
AST	Academia Sinica	Nankang, Taipei, Taiwan	CAEN	Lab. de Physique Corpuscu- laire, ENSICAEN	Caen , France
ASTAR	Institute of Materials	Singapore, Singapore	CAGL	Univ. degli Studi di Cagliari	Monserrato (CA), Italy
ATEN	NCSR " Demokritos "	Aghia Paraskevi, Greece	CAGLI	INFN , Sezione di Cagliari	Monserrato (CA), Italy
ATHU	Univ. of Athens	Athens, Greece	CAIR	Cairo University	Orman, Giza, Cairo, Egypt
AUCK	Univ. of Auckland	Auckland, New Zealand	CAIW	Carnegie Inst. of Washing- ton	Washington, DC, USA
BAKU	Natl. Azerbaijan Academy of Sciences , Inst. of Physics	Baku , Azerbaijan	CALB	Univ. della Calabria	Cosenza, Italy
BANG	Indian Inst. of Science	Bangalore , India	CALC	Univ. of Calcutta	Calcutta, India
BANGB	Bangabasi College	Calcutta, India	CAMB	DAMTP	Cambridge, United Kingdom
BARC	Univ. Autónoma de Barcelona ; Dept. de Física	Bellaterra (Barcelona), Spain	CAMP	Univ. Estadual de Campinas (UNICAMP)	Campinas , SP, Brazil
BARCE	Univ. Autónoma de Barcelona ; Inst. de Física de Altas Energías	Bellaterra (Barcelona), Spain	CANB	Australian National Univ.	Canberra, ACT, Australia
BARI	Univ. e del Politecnico di Bari	Bari, Italy	CANTB	Inst. de Física de Cantabria (CSIC-Univ. Cantabria)	Santander, Spain
BART	Univ. of Delaware ; Bartol Research Inst.	Newark, DE, USA	CAPE	University of Cape Town	Rondebosch, Cape Town, South Africa
BASL	Inst. für Physik der Univ. Basel	Basel, Switzerland	CARA	Univ. Central de Venezuela	Caracas, Venezuela
BAYR	Univ. Bayreuth	Bayreuth, Germany	CARL	Carleton Univ.	Ottawa, ON, Canada
BCEN	Centre d'Etudes Nucleaires de Bordeaux-Gradignan	Gradignan, France	CARLC	Carleton College	Northfield, MN, USA
BCIP	Natl. Inst. for Physics & Nu- clear Eng. "Horia Hulubei" (IFIN-HH)	Bucharest -Magurele, Romania	CASE	Case Western Reserve Univ.	Cleveland, OH, USA
BELJ	Beijing Univ.	Beijing, China	CAST	China Center of Advanced Science and Technology	Beijing, China
BELJT	Inst. of Theoretical Physics	Beijing , China	CATA	Univ. di Catania	Catania, Italy
BELG	Inter-University Inst. for High Energies (ULB-VUB)	Brussel , Belgium	CATH	Catholic Univ. of America	Washington, DC, USA
BELL	AT & T Bell Labs	Murray Hill, NJ, USA	CAVE	Cavendish Lab.	Cambridge, United Kingdom
BERG	Univ. of Bergen	Bergen, Norway	CBNM	CBNM	Geel , Belgium
BERL	DESY , Deutsches Elektronen-Synchrotron	Zeuthen , Germany	CBPF	Centro Brasileiro de Pesquisas Físicas - BIB/CDI/CBPF	Rio de Janeiro , RJ, Brazil
BERN	Univ. of Berne	Berne, Switzerland	CCAC	Allegheny College	Meadville, PA, USA
BGNA	Univ. di Bologna , & INFN , Sezione di Bologna; Via Irne- rio, 46, I-40126 Bologna; Viale C. Berti Pichat, n. 6/2	Bologna, Italy	CDEF	Univ. Paris VII, Denis Diderot	Paris, France
BHAB	Bhabha Atomic Research Center	Trombay, Bombay, India	CEA	Cambridge Electron Acceler- ator (Historical in <i>Review</i>)	Cambridge , MA, USA
BHEP	Inst. of High Energy Physics	Beijing , China	CEADE	Center for Apl. Studies for Nuclear Physics	Havana, Cuba
BIEL	Univ. Bielefeld	Bielefeld, Germany	CEBAF	Jefferson Lab—Thomas Jefferson National Accel- erator Facility	Newport News , VA, USA
BING	SUNY at Binghamton	Binghamton, NY, USA	CENG	Centre d'Etudes Nucleaires	Grenoble , France
BIRK	Birkbeck College, Univ. of London	London, United Kingdom	CERN	CERN , European Organiza- tion for Nuclear Research	Genève, Switzerland
BIRM	Univ. of Birmingham	Edgbaston, Birmingham, United Kingdom	CFPA	Univ. of California, (Berke- ley)	Berkeley, CA, USA
BLSU	Bloomsburg Univ.	Bloomsburg, PA, USA	CHIC	Univ. of Chicago	Chicago, IL, USA
BNL	Brookhaven National Lab.	Upton, NY, USA	CIAE	State Nuclear Power Re- search Inst.	Beijing , China
BNORM	Beijing Normal Univ.	Beijing, China	CINC	Univ. of Cincinnati	Cincinnati, OH, USA
BOCH	Ruhr Univ. Bochum	Bochum, Germany	CINV	CINVESTAV-IPN Centro de Investigacion y de Estudios Avanzados del IPN	México , DF, Mexico
BOHR	Niels Bohr Inst.	Copenhagen Ø, Denmark	CIT	California Inst. of Tech.	Pasadena, CA, USA
BOIS	Boise State Univ.	Boise, ID, USA	CLER	Univ. de Clermont-Ferrand	Aubière, France
BOMB	Univ. of Bombay	Bombay, India	CLEV	Cleveland State Univ.	Cleveland, OH, USA
BONN	Univ. of Bonn	Bonn, Germany	CMNS	Comenius Univ. (FMFI UK)	Bratislava , Slovakia
BORD	Centre d'Etudes Nucléaires de Bordeaux Gradignan (CENBG)	Gradignan, France	CMU	Carnegie Mellon Univ.	Pittsburgh, PA, USA
BOSE	S.N. Bose National Centre for Basis Sciences	Calcutta, India	CNEA	Comisión Nacional de En- ergía Atómica	Buenos Aires, Argentina
BOSK	" Rudjer Bošković " Inst.	Zagreb, Croatia	CNRC	Centre for Research in Parti- cle Physics	Ottawa, ON, Canada
BOST	Boston Univ.	Boston, MA, USA	CNRS	National Center for Scientific Research	Paris, France
BRAN	Brandeis Univ.	Waltham, MA, USA	CNYIT	C. N. Yang Institute	New York, USA
BRCO	Univ. of British Columbia	Vancouver, BC, Canada	COIM	Univ. de Coimbra	Coimbra , Portugal
BRIS	Univ. of Bristol	Bristol, United Kingdom	COLO	Univ. of Colorado	Boulder, CO, USA
BROW	Brown Univ.	Providence, RI, USA	COLU	Columbia Univ.	New York, NY, USA
BRUN	Brunel Univ.	Uxbridge, Middlesex, United Kingdom	CONC	Concordia University	Montreal, PQ, Canada
			CORN	Cornell Univ.	Ithaca, NY, USA

Abbreviations Used in the Particle Listings

COSU	Colorado State Univ.	Fort Collins, CO, USA	GIFU	Gifu Univ.	Gifu, Japan
CPPM	Centre National de la Recherche Scientifique, Luminy	Marseille , France	GLAS	Univ. of Glasgow	Glasgow, United Kingdom
CRAC	Henryk Niewodniczański Inst. of Nuclear Physics	Kraków , Poland	GMAS	George Mason Univ.	Fairfax, VA, USA
CRNL	Chalk River Labs.	Chalk River, ON, Canada	GOET	Univ. Göttingen	Göttingen, Germany
CSEB	California State University	Hayward, USA	GOML	Gomel State Univ.	Gomel, Belarus
CSOK	Oklahoma Central State Univ.	Edmond, OK, USA	GRAN	Univ. de Granada	Granada, Spain
CST	Univ. of Science and Technology of China	Hefei , Anhui 230026, China	GRAZ	Univ. Graz	Graz, Austria
CSULB	California State Univ.	Long Beach, CA, USA	GRON	Univ. of Groningen	Groningen, The Netherlands
CSUS	California State Univ.	Sacramento, CA, USA	GSCO	Geological Survey of Canada	Ottawa, ON, Canada
CTUP	Czech Technical University	Prague, Czech Republic	GSI	GSI Helmholtzzentrum für Schwerionenforschung GmbH	Darmstadt , Germany
CUNY	City College of New York	New York, NY, USA	GUAN	Univ. de Guanajuato	León, Gto., Mexico
CURCP	Univ. Pierre et Marie Curie (Paris VI), LCP	Paris, France	GUEL	Univ. of Guelph	Guelph, ON, Canada
CURIN	Univ. Pierre et Marie Curie (Paris VI), LPNHE	Paris, France	GWU	George Washington Univ.	Washington, DC, USA
CURIT	Univ. Pierre et Marie Curie (Paris VI), LPTHE	Paris, France	HAHN	Hahn-Meitner Inst. Berlin GmbH	Berlin, Germany
DALH	Dalhousie Univ.	Halifax, NS, Canada	HAIF	Technion – Israel Inst. of Tech.	Technion, Haifa, Israel
DALI	Dalian Univ. of Tech.	Dalian, China	HAMB	Univ. Hamburg	Hamburg, Germany
DARE	Daresbury Lab	Cheshire, United Kingdom	HANN	Univ. Hannover	Hannover, Germany
DARM	Tech. Hochschule Darmstadt	Darmstadt, Germany	HARC	Houston Advanced Research Ctr.	The Woodlands, TX, USA
DELA	Univ. of Delaware ; Dept. of Physics & Astronomy	Newark, DE, USA	HARV	Harvard Univ.	Cambridge, MA, USA
DELH	Univ. of Delhi	Delhi, India	HARV	Harvard Univ. (LPPC)	Cambridge, MA, USA
DESY	DESY , Deutsches Elektronen-Synchrotron	Hamburg , Germany	HAWA	Univ. of Hawai'i	Honolulu, HI, USA
DFAB	Escuela de Ingenieros	Bilbao , Spain	HEBR	Hebrew Univ.	Jerusalem, Israel
DOE	Department of Energy	Washington, DC, USA	HEID	Univ. Heidelberg ; (unspecified division) (Historical in <i>Review</i>)	Heidelberg, Germany
DORT	Technische Univ. Dortmund	Dortmund, Germany	HEIDH	Ruprecht-Karls Univ. Heidelberg	Heidelberg, Germany
DUKE	Duke Univ.	Durham, NC, USA	HEIDP	Univ. Heidelberg ; Physics Inst.	Heidelberg, Germany
DURH	Univ. of Durham	Durham, United Kingdom	HEIDT	Ruprecht-Karls-Univ. Heidelberg	Heidelberg, Germany
DUUC	University College Dublin	Dublin, Ireland	HELS	Univ. of Helsinki	University of Helsinki, Finland
ECT	Europ. Cent. for Theor. Studies in Nucl. Phys.	Trento, Italy	HIAS	Hangzhou Inst. for Advanced Studies	Hangzhou, China
EDIN	Univ. of Edinburgh	Edinburgh, United Kingdom	HINR	Inst. of Nuclear Research (ATOMKI)	Debrecen , Hungary
EFI	Univ. of Chicago, The Enrico Fermi Inst.	Chicago , IL, USA	HIRO	Hiroshima Univ.	Higashi-Hiroshima, Japan
ELMT	Elmhurst College	Elmhurst, IL, USA	HOUS	Univ. of Houston	Houston, TX, USA
ENSP	l'École Normale Supérieure	Paris , France	HPC	Hewlett-Packard Corp.	Cupertino, CA, USA
EOTV	Eötvös University	Budapest, Hungary	HSCA	Harvard-Smithsonian Center for Astrophysics	Cambridge, MA, USA
EPOL	École Polytechnique	Palaiseau , France	HYDER	Indian Inst. of Technology	Hyderabad, India
ERLA	Univ. Erlangen-Nurnberg	Erlangen, Germany	HZDR	Helmholtz-Zentrum Dresden-Rossendorf	Dresden, Germany
ESAP	ESAP Territorial Meta	Villavicencio, Colombia	IAC	Instituto de Astrofísica de Canarias	Tenerife, Spain
ETH	Eidg. Technische Hochschule	Zürich, Switzerland	IAS	Inst. for Advanced Study	Princeton, NJ, USA
FERR	Univ. di Ferrara	Ferrara, Italy	IASD	Dublin Inst. for Advanced Studies	Dublin, Ireland
FIRZ	Univ. degli Studi di Firenze	Sesto Fiorentino, Italy	IBAR	Ibaraki Univ.	Ibaraki, Japan
FISK	Fisk Univ.	Nashville, TN, USA	IBM	IBM Corp.	Palo Alto, CA, USA
FLOR	Univ. of Florida	Gainesville, FL, USA	IBMY	IBM	Yorktown Heights, NY, USA
FNAL	Fermilab	Batavia, IL, USA	IBS	Inst. for Boson Studies	Pasadena, CA, USA
FOM	FOM , Stichting voor Fundamenteel Onderzoek der Materie	JP Utrecht , The Netherlands	ICC	Universitat de Barcelona	Barcelona, Spain
FRAN	Frankfurt Inst. for Advanced Studies (FIAS)	Frankfurt am Main, Germany	ICCUB	Institut Ciències del Cosmos, Universitat Barcelona	Barcelona, Spain
FRAS	Lab. Nazionali di Frascati dell' INFN	Frascati (Roma), Italy	ICEPP	The Univ. of Tokyo	Tokyo, Japan
FREIB	Albert-Ludwigs Univ.	Freiburg , Germany	ICREA	Instituci Catalana de Recerca i Estudis Avanats	Barcelona, Spain
FREIE	Freie Univ. Berlin	Berlin, Germany	ICRR	Univ. of Tokyo	Chiba, Japan
FRIB	Univ. de Fribourg	Fribourg, Switzerland	ICTP	Abdus Salam International Centre for Theoretical Physics	Trieste , Italy
FSU	Florida State Univ.; High Energy Physics	Tallahassee, FL, USA	IFIC	IFIC (Instituto de Física Corpuscular)	Paterna (Valencia) , Spain
FSUSC	Florida State Univ.; SCS (School of Computational Science)	Tallahassee, FL, USA	IFRJ	Univ. Federal do Rio de Janeiro	Rio de Janeiro, RJ, Brazil
FUKI	Fukui Univ.	Fukui, Japan	IFT	Instituto de Física Teórica	Madrid, Spain
FUKU	Fukushima Univ.	Fukushima, Japan	IIT	Illinois Inst. of Tech.	Chicago, IL, USA
GENO	Univ. di Genova	Genova, Italy	IITB	Indian Inst. of Tech. IIT Bombay	Powai, Mumbai, India
GEOR	E. Andronikashvili Inst. of Physics	Tbilisi, Republic of Georgia	IITI	Indian Inst. of Tech. \ef IIT Indore	Simrol, Indore, India
GESC	General Electric Co.	Schenectady, NY, USA	IITJ	Indian Inst. of Tech. Jodhpur	Jodhpur, India
GEVA	Univ. de Genève	Genève, Switzerland	ILL	Univ. of Illinois at Urbana-Champaign	Urbana, IL, USA
GIES	Univ. Giessen	Giessen, Germany			

Abbreviations Used in the Particle Listings

ILLC	Univ. of Illinois at Chicago	Chicago, IL, USA	KOSI	Inst. of Experimental Physics SAS	Košice , Slovakia
ILLG	Inst. Laue-Langevin	Grenoble, France	KYOT	Kyoto Univ.; Dept. of Physics, Graduate School of Science	Kyoto, Japan
IND	Indiana Univ.	Bloomington, IN, USA	KYOTU	Kyoto Univ.; Yukawa Inst. for Theor. Physics	Kyoto, Japan
INEL	E G and G Idaho , Inc.	Idaho Falls, ID, USA	KYUN	Kyungpook National Univ.	Daegu, Republic of Korea
INFN	Ist. Nazionale di Fisica Nucleare (Generic INFN, unknown location)	Various places, Italy	KYUSH	Kyushu Univ.; Elementary Particle Theory Group; Exp. Particle Physics Group; Research Center for Advanced Particle Physics	Fukuoka, Japan
INFNL	INFN , Sezione di Lecce	Lecce, Italy	LALO	LAL , Laboratoire de l'Accélérateur Linéaire	Orsay , France
INNS	Univ. of Innsbruck	Innsbruck , Austria	LANC	Lancaster Univ.	Lancaster, United Kingdom
INPK	Henryk Niewodniczański Inst. of Nuclear Physics	Kraków , Poland	LANL	Los Alamos National Lab. (LANL)	Los Alamos, NM, USA
INRM	INR , Inst. for Nucl. Research	Moscow , Russian Federation	LAPL	Univ. Nacional de La Plata	La Plata, Argentina
INUS	KEK , High Energy Accelerator Research Organization	Tokyo, Japan	LAPP	LAPP , Lab. d'Annecy-le-Vieux de Phys. des Particules	Annecy-le-Vieux , France
IOAN	Univ. of Ioannina	Ioannina, Greece	LAPTh	LAPTh Lab. d'Annecy-le-Vieux de Phys. Théorique	Annecy-le-Vieux CEDEX, France
IOFF	A.F. Ioffe Phys. Tech. Inst.	St. Petersburg , Russian Federation	LASL	U.C. Los Alamos Scientific Lab. (Old name for LANL)	Los Alamos, NM, USA
IOWA	Univ. of Iowa	Iowa City, IA, USA	LATV	Latvian State Univ.	Riga, Latvia
IPN	IPN , Inst. de Phys. Nucl.	Orsay , France	LAUS	EPFL Lausanne	Lausanne, Switzerland
IPNP	Univ. Pierre et Marie Curie (Paris VI)	Paris, France	LAVL	Univ. Laval	Quebec, QC, Canada
IRAD	Inst. du Radium (Historical)	Paris , France	LBL	Lawrence Berkeley National Lab.	Berkeley, CA, USA
ISNG	Lab. de Physique Subatomique et de Cosmologie (LPSC)	Grenoble , France	LCGT	Univ. di Torino	Turin, Italy
ISU	Iowa State Univ.	Ames, IA, USA	LEBD	Lebedev Physical Inst.	Moscow , Russian Federation
ISUT	Isfahan University of Technology	Isfahan, Iran	LECE	Univ. di Lecce	Lecce, Italy
ITEP	ITEP , Inst. of Theor. and Exp. Physics	Moscow , Russian Federation	LEED	Univ. of Leeds	Leeds, United Kingdom
ITHA	Ithaca College	Ithaca, NY, USA	LEGN	Lab. Naz. di Legnaro	Legnaro , Italy
IUPU	Indiana Univ., Purdue Univ. Indianapolis	Indianapolis, IN, USA	LEHI	Lehigh Univ.	Bethlehem, PA, USA
JADA	Jadavpur Univ.	Calcutta, India	LEHM	Lehman College of CUNY	Bronx, NY, USA
JAGL	Jagiellonian Univ.	Kraków , Poland	LEID	Univ. Leiden	Leiden, The Netherlands
JHU	Johns Hopkins Univ.	Baltimore, MD, USA	LEMO	Le Moyne Coll.	Syracuse, NY, USA
JINR	JINR , Joint Inst. for Nucl. Research	Dubna , Russian Federation	LENSU	Saint-Petersburg State Univ.	St. Petersburg , Russian Federation
JPL	Jet Propulsion Laboratory	Pasadena, USA	LEUV	Katholieke Univ. Leuven	Leuven, Belgium
JULI	Forschungszentrum Jülich	Jülich, Germany	LIEG	Univ. de Liège	Liège, Belgium
JYV	Univ. of Jyväskylä	Jyväskylä, Finland	LINZ	Univ. Linz	Linz, Austria
KAGO	Univ. of Kagoshima	Kagoshima-shi, Japan	LISB	Inst. Nacional de Investigacion Cientifica	Lisboa CODEX, Portugal
KAIST	Korea Advanced Inst. of Science and Technology	Yusung ku, Daejeon, Republic of Korea	LISBT	Centro de Física Teórica de Partículas (CFTP)	Lisboa , Portugal
KANP	Indian Inst. of Tech.	Kanpur , UT, India	LIVP	Univ. of Liverpool	Liverpool, United Kingdom
KANS	Univ. of Kansas	Lawrence, KS, USA	LJUB	Univerza v Ljubljani	Ljubljana, Slovenia
KARL	Univ. Karlsruhe (Historical in <i>Review</i>)	Karlsruhe, Germany	LLL	Lawrence Livermore Lab. (Old name for LLNL)	Livermore, CA, USA
KARLE	Karlsruhe Inst. of Technology (KIT); Inst. for Experimental Nuclear Physics	Karlsruhe, Germany	LLNL	Lawrence Livermore National Lab.	Livermore, CA, USA
KARLK	Karlsruhe Inst. of Technology (KIT)	Eggenstein-Leopoldshafen, Germany	LNUDA	Liaoning Normal Univ.	Dalian, China
KARLT	Karlsruhe Inst. of Technology (KIT); Inst. for Theoretical Physics	Karlsruhe, Germany	LOCK	Lockheed Palo Alto Res. Lab	Palo Alto, CA, USA
KAZA	Kazakh Inst. of High Energy Physics	Alma Ata, Kazakhstan	LOIC	Imperial College of Science Tech. & Medicine	London, United Kingdom
KEK	KEK , High Energy Accelerator Research Organization	Ibaraki-ken, Japan	LOKC	Univ. of London , King's College	London, United Kingdom
KENT	Univ. of Kent	Canterbury, United Kingdom	LOQM	Queen Mary, Univ. of London	London, United Kingdom
KEYN	Open Univ.	Milton Keynes, United Kingdom	LOUC	University College London	London, United Kingdom
KFTI	Kharkov Inst. of Physics and Tech. (NSC KIPT)	Kharkov, Ukraine	LOUV	Univ. Catholique de Louvain	Louvain-la-Neuve, Belgium
KIAE	Kurchatov Inst.	Moscow , Russian Federation	LOWC	Westfield College (Historical, see LOQM (Queen Mary and Westfield joined))	London, United Kingdom
KIAM	Keldysh Inst. of Applied Math., Acad. Sci., Russia	Moscow , Russian Federation	LRL	U.C. Lawrence Radiation Lab. (Old name for LBL)	Berkeley , CA, USA
KIDR	Vinča Inst. of Nuclear Sciences	Belgrade, Serbia	LSU	Louisiana State Univ.	Baton Rouge, LA, USA
KIEV	Institute for Nuclear Research	Kyiv , Ukraine	LUND	Fysiska Institutionen	Lund , Sweden
KINK	Kinki Univ.	Osaka, Japan	LUND	Lund Univ.	Lund, Sweden
KIT	Karlsruhe Institute for Technology	Karlsruhe, Germany	LYON	Institute de Physique Nucléaire de Lyon (IPN)	Villeurbanne, France
KNTY	Univ. of Kentucky	Lexington, KY, USA	MADE	UAM/CSIC , Inst. de Física Teórica	Madrid , Cantoblanco, Spain
KOBE	Kobe Univ.	Kobe, Japan	MADR	C.I.E.M.A.T	Madrid , Spain
KOMAB	Univ. of Tokyo , Komaba	Tokyo, Japan	MADU	Univ. Autónoma de Madrid	Cantoblanco, Madrid, Spain
KONAN	Konan Univ.	Kobe, Japan			

Abbreviations Used in the Particle Listings

MAINZ	Johannes-Gutenberg- Univ. ; Inst. für Kernphysik, J.-J.-Becher-Weg 45; Inst. für Physik, Staudingerweg 7	Mainz, Germany	NBS	U.S National Bureau of Standards (Old name for NIST)	Gaithersburg, MD, USA
MANI	Univ. of Manitoba	Winnipeg, MB, Canada	NBSB	National Inst. Standards Tech.	Boulder, CO, USA
MARB	Univ. Marburg	Marburg, Germany	NCAR	National Center for Atmo- spheric Research	Boulder, CO, USA
MARS	Centre de Physique des Par- ticules de Marseille	Marseille, France	NCSU	North Carolina State Univ.	Raleigh, NC, USA
MASA	Univ. of Massachusetts Amherst	Amherst, MA, USA	NDAM	Univ. of Notre Dame	Notre Dame, IN, USA
MASB	Univ. of Massachusetts Boston	Boston, MA, USA	NEAS	Northeastern Univ.	Boston, MA, USA
MASD	Univ. of Massachusetts Dartmouth	North Dartmouth, MA, USA	NEBR	Univ. of Nebraska	Lincoln, NE, USA
MCGI	McGill Univ.	Montreal, QC, Canada	NEUC	Univ. de Neuchâtel	Neuchâtel, Switzerland
MCHS	Univ. of Manchester	Manchester, United Kingdom	NICEA	Univ. de Nice	Nice, France
MCMS	McMaster Univ.	Hamilton, ON, Canada	NICEO	Observatoire de Nice	Nice, France
MDRA	Univ. of Madras	Madras, India	NIHO	Nihon Univ.	Tokyo, Japan
MEHTA	Harish-Chandra Research Inst.	Allahabad, India	NIIG	Niigata Univ.	Niigata, Japan
MEIS	Meisei Univ.	Tokyo, Japan	NIJM	Radboud Univ. Nijmegen	AJ Nijmegen , The Nether- lands
MELB	Univ. of Melbourne	Victoria, Australia	NIRS	Nat. Inst. Radiological Sci- ences	Chiba , Japan
MEUD	Observatoire de Meudon	Meudon, France	NIST	National Institute of Stan- dards & Technology	Gaithersburg, MD, USA
MICH	Univ. of Michigan	Ann Arbor, MI, USA	NIU	Northern Illinois Univ.	De Kalb, IL, USA
MILA	Univ. di Milano	Milano, Italy	NJU	Nanjing University	Nanjing, China
MILAI	INFN , Sez. di Milano	Milano, Italy	NMSU	New Mexico State Univ.; Dept. of Physics, MSC 3D; Part. & Nucl. Phys. Group, Box 30001/Dept.	Las Cruces, NM, USA
MINN	Univ. of Minnesota	Minneapolis, MN, USA	NORD	Nordita	Stockholm, Sweden
MIPT	Moscow Institute of Physics and Technology	Moscow, Russian Federation	NOTT	Univ. of Nottingham	Nottingham, United Kingdom
MISS	Univ. of Mississippi	University, MS, USA	NOVM	Inst. of Mathematics	Novosibirsk , Russian Federa- tion
MISSR	Univ. of Missouri	Rolla, MO, USA	NOVO	BINP, Budker Inst. of Nu- clear Physics	Novosibirsk , Russian Federa- tion
MIT	MIT Massachusetts Inst. of Technology	Cambridge, MA, USA	NOVOU	Novosibirsk State University	Novosibirsk, Russian Federation
MIU	Maharishi International Univ.	Fairfield, IA, USA	NPLT	National Physical Laboratory	Teddington, United Kingdom
MIYA	Miyazaki Univ.	Miyazaki-shi, Japan	NPOL	Polytechnic of North Lon- don	London, United Kingdom
MONP	Univ. de Montpellier II	Montpellier, France	NRL	Naval Research Lab	Washington, DC, USA
MONS	Univ. of Mons	Mons , Belgium	NSF	National Science Founda- tion	Arlington, VA, USA
MONT	Univ. de Montréal ; Pavillon René-J.-A.-Lévesque	Montréal, PQ, Canada	NTHU	National Tsing Hua Univ.	Hsinchu, Taiwan
MONTC	Univ. de Montréal ; Centre de recherches mathématiques	Montréal, PQ, Canada	NTUA	National Tech. Univ. of Athens	Athens, Greece
MOSU	Skobeltsyn Inst. of Nuclear Physics, Lomonosov Moscow State Univ.; Experimental HEP Division; Theoretical HEP Division	Moscow , Russian Federation	NWES	Northwestern Univ.	Evanston, IL, USA
MPCM	Max Planck Inst. für Chemie	Mainz , Germany	NYU	New York Univ.	New York, NY, USA
MPEI	Moscow Physical Engi- neering Inst.	Moscow, Russian Federation	OBER	Oberlin College	Oberlin, OH, USA
MPIG	Max-Planck -Institute für Astrophysik	Garching, Germany	OCH	Ochanomizu Univ.	Tokyo, Japan
MPIK	Max-Planck-Inst. für Kern- physik	Heidelberg , Germany	OHIO	Ohio Univ.	Athens, OH, USA
MPIM	Max-Planck-Inst. für Physik	München , Germany	OKAY	Okayama Univ.	Okayama, Japan
MPP	Max Planck Institute for Physics	Munich, Germany	OKLA	Univ. of Oklahoma	Norman, OK, USA
MRION	Mirion Technologies Canberra	Meriden, CT, USA	OKSU	Oklahoma State Univ.	Stillwater, OK, USA
MSST	Mississippi State University	Mississippi State, MS, USA	OPAV	Silesian University	Opava, Czech Republic
MSU	Michigan State Univ.	East Lansing, MI, USA	OREG	Univ. of Oregon ; Inst. of Theoretical Science; U.O. Center for High Energy Physics	Eugene, OR, USA
MTHO	Mount Holyoke College	South Hadley, MA, USA	ORNL	Oak Ridge National Labora- tory	Oak Ridge, TN, USA
MULH	Centre Univ. du Haut-Rhin	Mulhouse, France	ORSAY	Univ. de Paris Sud 11	Orsay CEDEX, France
MUNI	Ludwig-Maximilians-Univ. München	Garching, Germany	ORST	Oregon State Univ.	Corvallis, OR, USA
MURA	Midwestern Univ. Research Assoc. (Historical in <i>Review</i>)	Stroughton, WI, USA	OSAK	Osaka Univ.	Osaka, Japan
MURC	Univ. of Murcia	Murcia, Spain	OSKC	Osaka City Univ.	Osaka, Japan
NAAS	North Americal Aviation Sci- ence Center (Historical in <i>Review</i>)	Thousand Oaks, CA, USA	OSLO	Univ. of Oslo	Oslo, Norway
NAGO	Nagoya Univ.	Nagoya, Japan	OSU	Ohio State Univ.	Columbus, OH, USA
NANJ	Nanjing Univ.	Nanjing, China	OTTA	Univ. of Ottawa	Ottawa, ON, Canada
NANKA	NanKai University	Tianjin, China	OXF	University of Oxford	Oxford, United Kingdom
NAPL	Univ. di Napoli "Federico II"	Napoli, Italy	OXFTP	Univ. of Oxford	Oxford, United Kingdom
NAPLI	INFN, Sezione di Napoli	NAPOLI, Italy	PADO	Univ. degli Studi di Padova	Padova, Italy
NASA	NASA	Greenbelt, MD, USA	PARIN	LPNHE, IN²P³/CNRS	Paris, France
NBI	Niels Bohr Institut	Copenhagen, Denmark	PARIS	Univ. de Paris (Historical)	Paris , France
			PARIT	Univ. Paris VII, LPTHE	Paris, France
			PARM	INFN , Gruppo Collegato di Parma	Parma, Italy
			PAST	Institut Pasteur	Paris , France
			PATR	Univ. of Patras	Patras, Greece
			PAVI	Univ. di Pavia	Pavia, Italy
			PAVII	INFN, Sez. di Pavia	Pavia , Italy

Abbreviations Used in the Particle Listings

PENN	Univ. of Pennsylvania	Philadelphia, PA, USA	SCIT	Science Univ. of Tokyo	Tokyo, Japan
PERIM	Perimeter Institute for Theoretical Physics	Ontario, Canada	SCOT	Scottish Univ. Research and Reactor Ctr.	Glasgow, United Kingdom
PGIA	INFN, Sezione di Perugia	Perugia, Italy	SCUC	Univ. of South Carolina	Columbia, SC, USA
PISA	Univ. di Pisa	Pisa, Italy	SEAT	Seattle Pacific Coll.	Seattle, WA, USA
PISAI	INFN, Sez. di Pisa	Pisa, Italy	SEIB	Austrian Research Center, Seibersdorf LTD.	Seibersdorf, Austria
PITT	Univ. of Pittsburgh	Pittsburgh, PA, USA	SEO	Korea Univ. ; Dept. of Physics; HEP Group	Seoul, Republic of Korea
PLAT	SUNY at Plattsburgh	Plattsburgh, NY, USA	SEOUL	Seoul National Univ. ; Center for Theoretical Physics; Dept. of Physics & Astronomy, Coll. of Natural Sciences	Seoul, Republic of Korea
PLRM	Univ. di Palermo	Palermo, Italy	SERP	IHEP, Inst. for High Energy Physics	Protvino, Russian Federation
PNL	Battelle Memorial Inst.	Richland, WA, USA	SETO	Seton Hall Univ.	South Orange, NJ, USA
PNPI	Petersburg Nuclear Physics Inst. of Russian Academy of Sciences	Gatchina, Russian Federation	SFLA	Univ. of South Florida	Tampa, FL, USA
PPA	Princeton-Penn. Proton Accelerator (Historical in <i>Review</i>)	Princeton, NJ, USA	SFRA	Simon Fraser University	Burnaby, BC, Canada
PRAG	Inst. of Physics, ASCR	Prague , Czech Republic	SFSU	California State Univ.	San Francisco , CA, USA
PRIN	Princeton Univ.	Princeton, NJ, USA	SHAMS	Ain Shams University	Abbassia, Cairo, Egypt
PSI	Paul Scherrer Institute	Villigen , Switzerland	SHDN	Shandong Univ.	Jinan, Shandong, China
PSLL	Physical Science Lab	Las Cruces, NM, USA	SHDNQ	Shandong Univ.	Qingdao, Shandong, China
PSU	Penn State Univ.	University Park, PA, USA	SHEF	Univ. of Sheffield	Sheffield, United Kingdom
PUCB	Pontificia Univ. Católica do Rio de Janeiro	Rio de Janeiro, RJ, Brazil	SHMP	Univ. of Southampton	Southampton, United Kingdom
PUEB	Univ. Autonoma de Puebla	Puebla , Pue, Mexico	SHRZ	Shiraz Univ.	Shiraz, Iran
PURD	Purdue Univ.	West Lafayette, IN, USA	SIEG	Univ. Siegen	Siegen, Germany
QUKI	Queen's Univ.	Kingston, ON, Canada	SILES	Univ. of Silesia	Katowice, Poland
RAL	STFC Rutherford Appleton Lab.	Chilton, Didcot, Oxfordshire, United Kingdom	SIN	Swiss Inst. of Nuclear Research (Old name for VILL)	Villigen , Switzerland
REGE	Univ. Regensburg	Regensburg, Germany	SING	National Univ. of Singapore	Kent Ridge, Singapore
REHO	Weizmann Inst. of Science	Rehovot, Israel	SISSA	Scuola Internazionale Superiore di Studi Avanzati	Trieste , Italy
REZ	Nuclear Physics Inst. AVČR	Řež , Czech Republic	SLAC	SLAC National Accelerator Laboratory	Menlo Park, CA, USA
RGSUL	Univ. Federal do Rio Grande do Sul (UFRGS)	Porto Alegre, RS, Brazil	SLOV	Inst. of Physics, Slovak Acad. of Sciences	Bratislava 45 , Slovakia
RHBL	Royal Holloway, Univ. of London	Egham, Surrey, United Kingdom	SMU	Southern Methodist Univ.	Dallas, TX, USA
RHEL	Rutherford High Energy Lab (Old name for RAL)	Chilton, Didcot, Oxon., United Kingdom	SNSP	Scuola Normale Superiore	Pisa , Italy
RICE	Rice Univ.	Houston, TX, USA	SOFI	Inst. for Nuclear Research and Nuclear Energy	Sofia , Bulgaria
RIKEN	Riken Nishina Center for Accelerator-Based Science	Saitama, Japan	SOFU	Univ. of Sofia "St. Kliment Ohridski"	Sofia, Bulgaria
RIKK	Rikkyo Univ.	Tokyo, Japan	SORB	Sorbonne Université	Paris, France
RIS	Rowland Inst. for Science	Cambridge, MA, USA	SPAUL	Univ. de São Paulo	São Paulo, SP, Brazil
RISC	Rockwell International	Thousand Oaks, CA, USA	SPIFT	Inst. de Física Teórica (IFT)	São Paulo , SP, Brazil
RISL	Universities Research Reactor	Risley , Warrington, United Kingdom	SSL	Univ. of California (Berkeley)	Berkeley, CA, USA
RISO	Riso National Laboratory	Roskilde, Denmark	STAN	Stanford Univ.	Stanford, CA, USA
RITS	Royal Inst. of Technology (KTH)	Stockholm , Sweden	STEV	Stevens Inst. of Tech.	Hoboken, NJ, USA
RL	Rutherford High Energy Lab (Old name for RAL)	Chilton, Didcot, Oxon., United Kingdom	STFN	Jozef Stefan Institute	Ljubljana , Slovenia
RMCS	Royal Military Coll. of Science	Swindon, Wilts., United Kingdom	STLO	St. Louis Univ.	St. Louis, MO, USA
ROCH	Univ. of Rochester	Rochester, NY, USA	STOH	Stockholm Univ.	Stockholm, Sweden
ROCK	Rockefeller Univ.	New York, NY, USA	STON	SUNY at Stony Brook	Stony Brook, NY, USA
ROMA	Univ. di Roma (Historical)	Roma , Italy	STRB	Inst. Pluridisciplinaire Hubert Curien (CNRS)	Strasbourg , France
ROMA2	Univ. di Roma , "Tor Vergata"	Roma, Italy	STUT	Univ. Stuttgart	Stuttgart, Germany
ROMA3	INFN, Sez. di Roma Tre	Roma , Italy	STUTM	Max-Planck-Inst.	Stuttgart , Germany
ROMAI	INFN, Sez. di Roma	Roma, Italy	SUGI	Sugiyama Jogakuen Univ.	Aichi, Japan
ROSE	Rose-Hulman Inst. of Technology	Terre Haute, IN, USA	SUNG	Sungkyunkwan Univ.	Suwon, Republic of Korea
RPI	Rensselaer Polytechnic Inst.	Troy, NY, USA	SURR	Univ. of Surrey	Guildford, Surrey, United Kingdom
RUTG	Rutgers , the State Univ. of New Jersey	Piscataway, NJ, USA	SUSS	Univ. of Sussex	Brighton, United Kingdom
S0GA	Sogang University	Seoul, Republic of Korea	SVR	Savannah River Labs.	Aiken, SC, USA
SACL	CEA Saclay , IRFU	Gif-sur-Yvette, France	SYDN	Univ. of Sydney	Sydney, NSW, Australia
SACL5	CEA Saclay - IPhT	Gif-sur-Yvette, France	SYRA	Syracuse Univ.	Syracuse, NY, USA
SACLD	CEA Saclay (Essonne)	Gif-sur-Yvette, France	TAJK	Acad. Sci., Tadjzhik SSR	Dushanbe , Tadjzhikstan
SAGA	Saga Univ.	Saga-shi, Japan	TAMU	Texas A&M Univ.	College Station, TX, USA
SAHA	Saha Inst. of Nuclear Physics	Bidhan Nagar, Calcutta, India	TATA	Tata Inst. of Fundamental Research	Bombay, India
SANG	Kyoto Sangyo Univ.	Kyoto-shi, Japan	TBIL	Tbilisi State University	Tbilisi, Republic of Georgia
SANI	Ist. Superiore di Sanità	Roma , Italy	TELA	Tel-Aviv Univ.	Tel Aviv, Israel
SASK	Univ. of Saskatchewan	Saskatoon, SK, Canada	TELE	Teledyne Brown Engineering	Huntsville, AL, USA
SASSO	Lab. Naz. Gran Sasso dell'INFN	Assergi (AQ), Italy	TEMP	Temple Univ.	Philadelphia, PA, USA
SAVO	Univ. de Savoie	Chambery, France	TENN	Univ. of Tennessee	Knoxville, TN, USA
SBER	California State Univ.	San Bernardino , CA, USA	TEXA	Univ. of Texas at Austin	Austin, TX, USA
SCHAF	W.J. Schafer Assoc.	Livermore, DA, USA	TGAK	Tokyo Gakuji Univ.	Tokyo, Japan
			TGU	Tohoku Gakuin Univ.	Miyagi, Japan

Abbreviations Used in the Particle Listings

THES	Aristotle Univ. of Thessaloniki (AUniv)	Thessaloniki, Greece	UPPS	Uppsala Univ.	Uppsala , Sweden
TINT	Tokyo Inst. of Technology	Tokyo, Japan	UPR	Univ. of Puerto Rico	San Juan , PR, USA
TISA	Sagamihara Inst. of Space & Astronautical Sci.	Kanagawa, Japan	URI	Univ. of Rhode Island	Kingston, RI, USA
TMSK	Tomsk Polytechnic Univ.	Tomsk , Russian Federation	USC	Univ. of Southern California	Los Angeles, CA, USA
TMTC	Tokyo Metropolitan Coll. Tech.	Tokyo, Japan	USDC	Univ. Santiago de Cali	Cali, Colombia
TMU	Tokyo Metropolitan Univ.	Tokyo, Japan	USF	Univ. of San Francisco	San Francisco, CA, USA
TNTO	Univ. of Toronto	Toronto, ON, Canada	USTA	Univ. Santo Toms	Bogota, Colombia
TOHO	Toho Univ.	Chiba, Japan	UTAH	Univ. of Utah	Salt Lake City, UT, USA
TOHOK	Tohoku Univ.	Sendai, Japan	UTOL	Univ. del Tolima	Ibague, Colombia
TOKA	Tokai Univ.	Shimizu, Japan	UTRE	Univ. of Utrecht	Utrecht, The Netherlands
TOKAH	Tokai Univ.	Hiratsuka, Japan	UTRO	Norwegian Univ. of Science & Technology	Trondheim, Norway
TOKMS	Univ. of Tokyo ; Meson Science Laboratory	Tokyo, Japan	UVA	Univ. of Virginia	Charlottesville, VA, USA
TOKU	Univ. of Tokushima	Tokushima-shi, Japan	UZINR	Acad. Sci., Ukrainian SSR	Uzhgorod , Ukraine
TOKY	Univ. of Tokyo ; High-Energy Physics Theory Group	Tokyo, Japan	VALE	Univ. de Valencia	Burjassot, Valencia , Spain
TOKYC	Univ. of Tokyo ; Dept. of Chemistry	Tokyo, Japan	VALP	Valparaiso Univ.	Valparaiso, IN, USA
TORI	Univ. degli Studi di Torino	Torino, Italy	VAND	Vanderbilt Univ.	Nashville, TN, USA
TPTI	Uzbek Academy of Sciences	Tashkent , Republic of Uzbekistan	VASS	Vassar College	Poughkeepsie, NY, USA
TRIN	Trinity College Dublin	Dublin, Ireland	VICT	Univ. of Victoria	Victoria, BC, Canada
TRIU	TRIUMF	Vancouver, BC, Canada	VIEN	Inst. für Hochenergiephysik (HEPHY)	Vienna , Austria
TRST	Univ. di Trieste	Trieste, Italy	VILL	Inst. for Part. Phys. and Astrophys. IPA at PSI	Villigen, Switzerland
TRSTI	INFN , Sez. di Trieste	Trieste, Italy	VPI	Virginia Tech.	Blacksburg, VA, USA
TRSTT	Univ. degli Studi di Trieste	Trieste , Italy	VRIJ	Vrije Univ.	HV Amsterdam , The Netherlands
TSIN	Tsinghua Univ.	Beijing, China	WABRN	Eidgenössisches Amt für Messwesen	Waber , Switzerland
TSUK	Univ. of Tsukuba	Ibaraki-ken, Japan	WARS	Univ. of Warsaw	Warsaw, Poland
TTAM	Tamagawa Univ.	Tokyo, Japan	WASCR	Waseda Univ.; Cosmic Ray Division	Tokyo, Japan
TUAT	Tokyo Univ. of Agriculture Tech.	Tokyo, Japan	WASH	Univ. of Washington ; Elem. Particle Experiment (EPE); Particle Astrophysics (PA)	Seattle, WA, USA
TUBIN	Univ. Tübingen	Tübingen, Germany	WASU	Waseda Univ.; Dept. of Physics, High Energy Physics Group	Tokyo, Japan
TUFTS	Tufts Univ.	Medford, MA, USA	WATER	Univ. of Waterloo	Waterloo, ON, Canada
TUM	Tech. Univ. München	Garching, Germany	WAUS	Univ. of Western Australia	Perth, WA, Australia
TUW	Technische Univ. Wien	Vienna, Austria	WAYN	Wayne State Univ.	Detroit, MI, USA
TUZL	Tuzla Univ.	Tuzla, Argentina	WESL	Wesleyan Univ.	Middletown, CT, USA
UBA	Univ. de Buenos Aires	Buenos Aires, Argentina	WIEN	Univ. Wien	Vienna, Austria
UCB	Univ. of California (Berkeley)	Berkeley, CA, USA	WILL	Coll. of William and Mary	Williamsburg, VA, USA
UCD	Univ. of California (Davis)	Davis, CA, USA	WINR	National Centre for Nuclear Research	Warsaw , Poland
UCI	Univ. of California (Irvine)	Irvine, CA, USA	WISC	Univ. of Wisconsin	Madison, WI, USA
UCLA	Univ. of California (Los Angeles)	Los Angeles, CA, USA	WITW	Univ. of the Witwatersrand	Wits, South Africa
UCND	Union Carbide Corp.	Oak Ridge, TN, USA	WMIU	Western Michigan Univ.	Kalamazoo, MI, USA
UCR	Univ. of California (Riverside)	Riverside, CA, USA	WONT	The Univ. of Western Ontario	London, ON, Canada
UCSB	Univ. of California (Santa Barbara) ; Physics Dept., High Energy Physics Experiment	Santa Barbara, CA, USA	WOOD	Woodstock College (No longer in existence)	Woodstock, MD, USA
UCSBT	Univ. of California (Santa Barbara) ; Kavli Inst. for Theoretical Physics	Santa Barbara, CA, USA	WROC	University of Wroclaw	Wroclaw, Poland
UCSC	Univ. of California (Santa Cruz)	Santa Cruz, CA, USA	WUPP	Bergische Univ. Wuppertal	Wuppertal , Germany
UCSD	Univ. of California (San Diego)	La Jolla, CA, USA	WURZ	Univ. Würzburg	Würzburg, Germany
UGAZ	Univ. of Gaziantep	Gaziantep, Turkey	WUSL	Washington Univ.	St. Louis, MO, USA
ULL	Universidad de La Laguna	La Laguna, Spain	WYOM	Univ. of Wyoming	Laramie, WY, USA
UMD	Univ. of Maryland	College Park, MD, USA	YALE	Yale Univ.	New Haven, CT, USA
UNAM	Univ. Nac. Autónoma de México (UNAM)	México , DF, Mexico	YARO	Yaroslavl State Univ.	Yaroslavl, Russian Federation
UNAM	Univ. Nacional Autónoma de México (UNAM)	México , DF, Mexico	YCC	Yokohama Coll. of Commerce	Yokohama, Japan
UNC	Univ. of North Carolina	Greensboro, NC, USA	YERE	Yerevan Physics Inst.	Yerevan, Armenia
UNCCH	Univ. of North Carolina at Chapel Hill	Chapel Hill, NC, USA	YOKO	Yokohama National Univ.	Yokohama-shi, Japan
UNCS	Union College	Schenectady, NY, USA	YORKC	York Univ.	Toronto, Canada
UNESP	UNESP	Botucatu, Brazil	ZAGR	Zagreb Univ.	Zagreb, Croatia
UNH	Univ. of New Hampshire	Durham, NH, USA	ZARA	Univ. de Zaragoza	Zaragoza, Spain
UNM	Univ. of New Mexico	Albuquerque, NM, USA	ZEEM	Univ. van Amsterdam	TV Amsterdam, The Netherlands
UOEH	Univ. of Occupational and Environmental Health	Kitakyushu , Japan	ZHON	Zhongshan (Sun Yat-Sen) Univ.	Guangzhou, China
UPCIT	Univ. Paris Cite	Paris, France	ZHZH	Zhengzhou Univ.	Zhengzhou, Henan, China
UPNJ	Uppsala College	East Orange, NJ, USA	ZURI	Univ. Zürich	Zürich, Switzerland

GAUGE AND HIGGS BOSONS

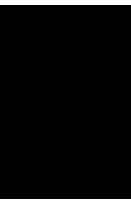
γ	1185
g (gluon)	1186
graviton	1186
W	1187
Z	1200
H	1220
Neutral Higgs Bosons, Searches for	1237
Charged Higgs Bosons (H^\pm and $H^{\pm\pm}$), Searches for	1248
New Heavy Bosons	1253
Axions (A^0) and Other Very Light Bosons	1271

Notes in the Listings

Triple gauge couplings (TGC's)	1190
Anomalous $ZZ\gamma$, $Z\gamma\gamma$, and ZZV couplings	1216
Anomalous W/Z quartic couplings (rev.)	1217

Related Reviews in Volume 1

54. Mass and width of the W boson (rev.)	815
55. Z boson	817





GAUGE AND HIGGS BOSONS

γ (photon)

$$I(J^{PC}) = 0,1(1^{--})$$

γ MASS

Results prior to 2008 are critiqued in GOLDHABER 10. All experimental results published prior to 2005 are summarized in detail by TU 05.

The following conversions are useful: 1 eV = 1.783 × 10⁻³³ g = 1.957 × 10⁻⁶ m_e; λ_C = (1.973 × 10⁻⁷ m) × (1 eV/m_e).

VALUE (eV)	CL%	DOCUMENT ID	COMMENT
<1 × 10⁻¹⁸		1 RYUTOV 07	MHD of solar wind
••• We do not use the following data for averages, fits, limits, etc. •••			
<2.1 × 10 ⁻¹⁵	68	2 WANG 23B	Fast Radio Bursts
<2 × 10 ⁻¹⁴		3 BONETTI 17	Fast Radio Bursts, FRB 121102
<1.8 × 10 ⁻¹⁴		4 BONETTI 16	Fast Radio Bursts, FRB 150418
<1.9 × 10 ⁻¹⁵		5 RETINO 16	Ampere's Law in solar wind
<2.3 × 10 ⁻⁹	95	6 EGOROV 14	Lensed quasar position
		7 ACCIOLY 10	Anomalous magn. mom.
<1 × 10 ⁻²⁶		8 ADELBERGER 07A	Proca galactic field
no limit feasible		8 ADELBERGER 07A	γ as Higgs particle
<1 × 10 ⁻¹⁹		9 TU 06	Torque on rotating magnetized toroid
<1.4 × 10 ⁻⁷		ACCIOLY 04	Dispersion of GHz radio waves by sun
<2 × 10 ⁻¹⁶		10 FULLEKRUG 04	Speed of 5-50 Hz radiation in atmosphere
<7 × 10 ⁻¹⁹		11 LUO 03	Torque on rotating magnetized toroid
<1 × 10 ⁻¹⁷		12 LAKES 98	Torque on toroid balance
<6 × 10 ⁻¹⁷		13 RYUTOV 97	MHD of solar wind
<8 × 10 ⁻¹⁶	90	14 FISCHBACH 94	Earth magnetic field
<5 × 10 ⁻¹³		15 CHERNIKOV 92	Ampere's Law null test
<1.5 × 10 ⁻⁹	90	16 RYAN 85	Coulomb's Law null test
<3 × 10 ⁻²⁷		17 CHIBISOV 76	Galactic magnetic field
<6 × 10 ⁻¹⁶	99.7	18 DAVIS 75	Jupiter's magnetic field
<7.3 × 10 ⁻¹⁶		HOLLWEG 74	Alfven waves
<6 × 10 ⁻¹⁷		19 FRANKEN 71	Low freq. res. circuit
<2.4 × 10 ⁻¹³		20 KROLL 71A	Dispersion in atmosphere
<1 × 10 ⁻¹⁴		21 WILLIAMS 71	Tests Coulomb's Law
<2.3 × 10 ⁻¹⁵		GOLDHABER 68	Satellite data

- RYUTOV 07 extends the method of RYUTOV 97 to the radius of Pluto's orbit.
- WANG 23B use fast radio burst photon mass dependent dispersion relation to determine an upper limit of the photon mass.
- BONETTI 17 uses frequency-dependent time delays of repeating FRB with well-determined redshift, assuming the DM is caused by expected dispersion in IGM. There are several uncertainties, leading to mass limit 2.2 × 10⁻¹⁴ eV.
- BONETTI 16 uses frequency-dependent time delays of FRB, assuming the DM is caused by expected dispersion in IGM. There are several uncertainties, leading to mass limit 1.8 × 10⁻¹⁴ eV, if indeed the FRB is at the initially reported redshift.
- RETINO 16 looks for deviations from Ampere's law in the solar wind, using Cluster four spacecraft data. Authors quote a range of limits from 1.9 × 10⁻¹⁵ eV to 7.9 × 10⁻¹⁴ eV depending on the assumptions of the vector potential from the interplanetary magnetic field.
- EGOROV 14 studies chromatic dispersion of lensed quasar positions ("gravitational rainbows") that could be produced by any of several mechanisms, among them via photon mass. Limit not competitive but obtained on cosmological distance scales.
- ACCIOLY 10 limits come from possible alterations of anomalous magnetic moment of electron and gravitational deflection of electromagnetic radiation. Reported limits are not "claimed" by the authors and in any case are not competitive.
- When trying to measure *m* one must distinguish between measurements performed on large and small scales. If the photon acquires mass by the Higgs mechanism, the large-scale behavior of the Proca regime for all scales, the very existence of the galactic field implies *m* < 10⁻²⁶ eV, as correctly calculated by YAMAGUCHI 59 and CHIBISOV 76.
- TU 06 continues the work of LUO 03, with extended LAKES 98 method, reporting the improved limit μ²A = (0.7 ± 1.7) × 10⁻¹³ T/m if A = 0.2 μG out to 4 × 10²² m. Reported result μ = (0.9 ± 1.5) × 10⁻⁵² g reduces to the frequentist mass limit 1.2 × 10⁻¹⁹ eV (FELDMAN 98).
- FULLEKRUG 04 adopted KROLL 71A method with newer and better Schumann resonance data. Result questionable because assumed frequency shift with photon mass is assumed to be linear. It is quadratic according to theorem by GOLDHABER 71B, KROLL 71, and PARK 71.
- LUO 03 extends LAKES 98 technique to set a limit on μ²A, where μ⁻¹ is the Compton wavelength λ_C of the massive photon and A is the ambient vector potential. The important departure is that the apparatus rotates, removing sensitivity to the direction of A. They take A = 10¹² Tm, due to "cluster level fields." But see comment of GOLDHABER 03 and reply by LUO 03b.
- LAKES 98 reports limits on torque on a toroid Cavendish balance, obtaining a limit on μ²A < 2 × 10⁻⁹ Tm/m² via the Maxwell-Proca equations, where μ⁻¹ is the characteristic length associated with the photon mass and A is the ambient vector potential in the Lorentz gauge. Assuming A ≈ 1 × 10¹² Tm due to cluster fields he obtains μ⁻¹ > 2 × 10¹⁰ m, corresponding to μ < 1 × 10⁻¹⁷ eV. A more conservative limit, using A ≈ (1 μG) × (600 pc) based on the galactic field, is μ⁻¹ > 1 × 10⁹ m or μ < 2 × 10⁻¹⁶ eV.

- RYUTOV 97 uses a magnetohydrodynamics argument concerning survival of the Sun's field to the radius of the Earth's orbit. "To reconcile observations to theory, one has to reduce [the photon mass] by approximately an order of magnitude compared with" per DAVIS 75. "Secure limit, best by this method" (per GOLDHABER 10).
- FISCHBACH 94 analysis is based on terrestrial magnetic fields; approach analogous to DAVIS 75. Similar result based on a much smaller planet probably follows from more precise B field mapping. "Secure limit, best by this method" (per GOLDHABER 10).
- CHERNIKOV 92, motivated by possibility that photon exhibits mass only below some unknown critical temperature, searches for departure from Ampere's Law at 1.24 K. See also RYAN 85.
- RYAN 85, motivated by possibility that photon exhibits mass only below some unknown critical temperature, sets mass limit at < (1.5 ± 1.4) × 10⁻⁴² g based on Coulomb's Law departure limit at 1.36 K. We report the result as frequentist 90% CL (FELDMAN 98).
- CHIBISOV 76 depends in critical way on assumptions such as applicability of virial theorem. Some of the arguments given only in unpublished references.
- DAVIS 75 analysis of Pioneer-10 data on Jupiter's magnetic field. "Secure limit, best by this method" (per GOLDHABER 10).
- FRANKEN 71 method is of dubious validity (KROLL 71A, JACKSON 99, GOLDHABER 10, and references therein).
- KROLL 71A used low frequency Schumann resonances in cavity between the conducting earth and resistive ionosphere, overcoming objections to resonant-cavity methods (JACKSON 99, GOLDHABER 10, and references therein). "Secure limit, best by this method" (per GOLDHABER 10).
- WILLIAMS 71 is landmark test of Coulomb's law. "Secure limit, best by this method" (per GOLDHABER 10).

γ CHARGE

OKUN 06 has argued that schemes in which all photons are charged are inconsistent. He says that if a neutral photon is also admitted to avoid this problem, then other problems emerge, such as those connected with the emission and absorption of charged photons by charged particles. He concludes that in the absence of a self-consistent phenomenological basis, interpretation of experimental data is at best difficult.

VALUE (e)	CHARGE	DOCUMENT ID	TECN	COMMENT
<1 × 10⁻⁴⁶	mixed	1 ALTSCHUL 07B	VLBI	Aharonov-Bohm effect
<1 × 10⁻³⁵	single	2 CAPRINI 05	CMB	Isotropy constraint
••• We do not use the following data for averages, fits, limits, etc. •••				
<1 × 10 ⁻³²	single	1 ALTSCHUL 07B	VLBI	Aharonov-Bohm effect
<3 × 10 ⁻³³	mixed	3 KOBYCHEV 05	VLBI	Smear as function of B·E _γ
<4 × 10 ⁻³¹	single	3 KOBYCHEV 05	VLBI	Deflection as function of B·E _γ
<8.5 × 10 ⁻¹⁷		4 SEMERTZIDIS 03		Laser light deflection in B-field
<3 × 10 ⁻²⁸	single	5 SIVARAM 95	CMB	For Ω _M = 0.3, h ² = 0.5
<5 × 10 ⁻³⁰		6 RAFFELT 94	TOF	Pulsar f ₁ - f ₂
<2 × 10 ⁻²⁸		7 COCCONI 92	VLBA	radio telescope resolution
<2 × 10 ⁻³²		COCCONI 88	TOF	Pulsar f ₁ - f ₂ TOF

- ALTSCHUL 07B looks for Aharonov-Bohm phase shift in addition to geometric phase shift in radio interference fringes (VSOP mission).
- CAPRINI 05 uses isotropy of the cosmic microwave background to place stringent limits on possible charge asymmetry of the Universe. Charge limits are set on the photon, neutrino, and dark matter particles. Valid if charge asymmetries produced by different particles are not anticorrelated.
- KOBYCHEV 05 considers a variety of observable effects of photon charge for extragalactic compact radio sources. Best limits if source observed through a foreground cluster of galaxies.
- SEMERTZIDIS 03 reports the first laboratory limit on the photon charge in the last 30 years. Straightforward improvements in the apparatus could attain a sensitivity of 10⁻²⁰ e.
- SIVARAM 95 requires that CMB photon charge density not overwhelm gravity. Result scales as Ω_M h².
- RAFFELT 94 notes that COCCONI 88 neglects the fact that the time delay due to dispersion by free electrons in the interstellar medium has the same photon energy dependence as that due to bending of a charged photon in the magnetic field. His limit is based on the assumption that the entire observed dispersion is due to photon charge. It is a factor of 200 less stringent than the COCCONI 88 limit.
- See COCCONI 92 for less stringent limits in other frequency ranges. Also see RAFFELT 94 note.

γ REFERENCES

WANG 23B	JCAP 2309 025	B. Wang et al.
BONETTI 17	PL B768 326	L. Bonetti et al.
BONETTI 16	PL B757 548	L. Bonetti et al.
RETINO 16	ASP 82 49	A. Retino, A.D.A.M. Spallicci, A. Vaivads (CURCP+)
EGOROV 14	MNRAS 437 L90	P. Egorov et al.
ACCIOLY 10	PR D82 065026	A. Accioly, J. Helayel-Nieto, E. Scatena (LABEX+)
GOLDHABER 10	RMP 82 939	A.S. Goldhaber, M.M. Nieto (STON, LANL)
ADELBERGER 07A	PRL 98 010402	E. Adelberger, G. Dvali, A. Gruzinov (WASH, NYU)
ALTSCHUL 07B	PRL 98 261801	B. Altschul (IND)
	ASP 29 290	B. Altschul (SUCU)
RYUTOV 07	PPCF 49 B429	D.D. Ryutov (LLNL)
OKUN 06	APP B37 555	L.B. Okun (ITEP)
TU 06	PL A352 267	L.-C. Tu et al.
CAPRINI 05	JCAP 0502 006	C. Caprini, P.G. Ferreira (GEVA, OXFPT)
KOBYCHEV 05	AL 31 147	V.V. Kobychiev, S.B. Popov (KIEV, PADO)
TU 05	RPP 68 77	L.-C. Tu, J. Luo, G.T. Gillies
ACCIOLY 04	PR D69 107501	A. Accioly, R. Paszko
FULLEKRUG 04	PRL 93 043901	M. Fullekrug
GOLDHABER 03	PRL 91 149101	A.S. Goldhaber, M.M. Nieto
LUO 03	PRL 90 081801	J. Luo et al.
LUO 03B	PRL 91 149102	J. Luo et al.
SEMERTZIDIS 03	PR D67 017701	Y.K. Semertzidis, G.T. Danby, D.M. Lazarus
JACKSON 99	Classical Electrodynamics	J.D. Jackson (3rd ed., J. Wiley and Sons (1999))

Gauge & Higgs Boson Particle Listings

$\gamma, g, \text{graviton}$

FELDMAN	98	PR D57 3873	G.J. Feldman, R.D. Cousins	
LAKES	98	PRL 80 1826	R. Lakes	(WIS C)
RYUTOV	97	PPCF 39 A73	D.D. Ryutov	(LLNL)
SIVARAM	95	AJP 63 473	C. Sivaram	(BANG)
FISCHBACH	94	PRL 73 514	E. Fischbach <i>et al.</i>	(PURD, JHU+)
RAFFELT	94	PR D90 7729	G. Raffelt	(MPIM)
CHERNIKOV	92	PRL 68 3383	M.A. Chernikov <i>et al.</i>	(ETH)
		Also PRL 69 2399 (errat.)	M.A. Chernikov <i>et al.</i>	(ETH)
COCCONI	92	AJP 60 750	G. Cocconi	(CERN)
COCCONI	88	PL B206 705	G. Cocconi	(CERN)
RYAN	85	PR D32 802	J.J. Ryan, F. Accetta, R.H. Austin	(PRIN)
CHIBISOV	76	SPU 19 624	G.V. Chibisov	(LEBD)
		Translated from UFN 119 551.		
DAVIS	75	PRL 35 1402	L. Davis, A.S. Goldhaber, M.M. Nieto	(CIT, STON+)
HOLLWEG	74	PRL 32 961	J.V. Hollweg	(NCAR)
FRANKEN	71	PRL 26 115	P.A. Franken, G.W. Ampulski	(MICH)
GOLDHABER	71B	RMP 43 277	A.S. Goldhaber, M.M. Nieto	(STON, BOHR, UCSB)
KROLL	71	PRL 26 1395	N.M. Kroll	(SLAC)
KROLL	71A	PRL 27 340	N.M. Kroll	(SLAC)
PARK	71	PRL 26 1393	D. Park, E.R. Williams	(WILC)
WILLIAMS	71	PRL 26 721	E.R. Williams, J.E. Fuller, H.A. Hill	(WESL)
GOLDHABER	68	PRL 21 567	A.S. Goldhaber, M.M. Nieto	(STON)
YAMAGUCHI	59	PTPS 11 37	Y. Yamaguchi	

$<1.2 \times 10^{-22}$	5	ABBOTT	16	DISP	Combined dispersion limit from two BH mergers
$<2.9 \times 10^{-21}$	13	ZAKHAROV	16	YUKA	S2 star orbit
$<5 \times 10^{-23}$	14	BRITO	13	MGRV	Spinning black holes bounds
$<6 \times 10^{-32}$	15	GRUZINOV	05	MGRV	Solar System observations
$<6 \times 10^{-32}$	16	CHOUDHURY	04	YUKA	Weak gravitational lensing
$<9.0 \times 10^{-34}$	17	GRSHTEIN	04	MGRV	From Ω_{tot} value assuming RTG
$<8 \times 10^{-20}$	18,19	FINN	02	DISP	Binary pulsar orbital period decrease
$<7 \times 10^{-23}$		TALMADGE	88	YUKA	Solar system planetary astrometric data
$<1.3 \times 10^{-29}$	20	GOLDHABER	74	YUKA	Rich clusters
$<7 \times 10^{-28}$		HARE	73	YUKA	Galaxy
$<8 \times 10^4$		HARE	73	YUKA	2 γ decay

g (gluon)

$$I(J^P) = 0(1^-)$$

SU(3) color octet

Mass $m = 0$. Theoretical value. A mass as large as a few MeV may not be precluded, see YNDURAIN 95.

gluon spin

VALUE	DOCUMENT ID	TECN	COMMENT
••• We do not use the following data for averages, fits, limits, etc. •••			
	ABREU 92E	DLPH	Spin 1, not 0
	ALEXANDER 91H	OPAL	Spin 1, not 0
	BEHREND 82D	CELL	Spin 1, not 0
	BERGER 80D	PLUT	Spin 1, not 0
	BRANDELIK 80C	TASS	Spin 1, not 0

gluon REFERENCES

YNDURAIN	95	PL B345 524	F.J. Yndurain	(MADU)
ABREU	92E	PL B274 498	P. Abreu <i>et al.</i>	(DELPHI Collab.)
ALEXANDER	91H	ZPHY C52 543	G. Alexander <i>et al.</i>	(OPAL Collab.)
BEHREND	82D	PL B110 329	H.J. Behrend <i>et al.</i>	(CELLO Collab.)
BERGER	80D	PL B97 459	C. Berger <i>et al.</i>	(PLUTO Collab.)
BRANDELIK	80C	PL B97 453	R. Brandelik <i>et al.</i>	(TASSO Collab.)

graviton

$$J = 2$$

graviton MASS

It is likely that the graviton is massless. More than fifty years ago Van Dam and Veltman (VANDAM 70), Iwasaki (IWASAKI 70), and Zakharov (ZAKHAROV 70) almost simultaneously showed that in the linear approximation a theory with a finite graviton mass does not approach GR as the mass approaches zero. Attempts have been made to evade this "vDVZ discontinuity" by invoking modified gravity or nonlinear theory by De Rahm (DE-RHAM 17) and others. More recently, the analysis of gravitational wave dispersion has led to bounds that are largely independent of the underlying model, even if not the strongest. We quote the best of these as our best limit.

Experimental limits have been set based on a Yukawa potential (YUKA), dispersion relation (DISP), or other modified gravity theories (MGRV).

The following conversions are useful: 1 eV = 1.783×10^{-33} g = $1.957 \times 10^{-6} m_e$; $\lambda_C = (1.973 \times 10^{-7} \text{ m}) \times (1 \text{ eV}/m_e)$.

VALUE (eV)	DOCUMENT ID	TECN	COMMENT
$<1.76 \times 10^{-23}$	1	ABBOTT	21 DISP LIGO Virgo catalog GWTC-2
••• We do not use the following data for averages, fits, limits, etc. •••			
$<8 \times 10^{-34}$	2	DEFELICE	21 MGRV Normal branch Minimal Theory of Massive Gravity
$<3.2 \times 10^{-23}$	3	BERNUS	20 YUKA Planetary ephemeris INPOP19a
$<2 \times 10^{-28}$	4	SHAO	20 DISP Binary pulsar Galileon radiation
$<4.7 \times 10^{-23}$	5	ABBOTT	19 DISP LIGO Virgo catalog GWTC-1
$<7 \times 10^{-23}$	6	BERNUS	19 YUKA Planetary ephemeris INPOP17b
$<3.1 \times 10^{-20}$	7	MIAO	19 DISP Binary pulsar orbital decay rate
$<1.4 \times 10^{-29}$	8	DESAI	18 YUKA Gal cluster Abell 1689
$<5 \times 10^{-30}$	9	GUPTA	18 YUKA Using SPT-SZ
$<3 \times 10^{-30}$	9	GUPTA	18 YUKA Using Planck all-sky SZ
$<1.3 \times 10^{-29}$	9	GUPTA	18 YUKA Using redMaPPer SDSS-DR8
$<6 \times 10^{-30}$	10	RANA	18 YUKA Weak lensing in massive clusters
$<8 \times 10^{-30}$	11	RANA	18 YUKA SZ effect in massive clusters
$<1.0 \times 10^{-23}$	12	WILL	18 YUKA Perihelion advances of planets
$<7 \times 10^{-23}$	5	ABBOTT	17 DISP Combined dispersion limit from three BH mergers

- ABBOTT 21 assumed modified gravitational-wave dispersion to establish a limit on graviton mass, using LIGO-Virgo O1-O3a binary black hole (BBH) events.
- DEFELICE 21 studies the normal branch of the Minimal Theory of Massive Gravity (MTMG) to find that after five parameters are adjusted to obtain agreement with all presently available data, today's squared mass $m_g^2 = (2.5^{+4.5}_{-4.8}) \times 10^{-67} \text{ eV}^2$ or $m_g < 8.4 \times 10^{-33} \text{ eV}$, both at the 95% CL.
- BERNUS 20 use the latest solution of the ephemeris INPOP (19a) in order to improve the constraint in BERNUS 19 on the existence of a Yukawa suppression to the Newtonian potential, generically associated to a gravitons mass.
- SHAO 20 sets limit, 95% CL, based on non-observation of excess gravitational radiation in 14 well-timed binary pulsars in the context of the cubic Galileon model.
- ABBOTT 19, ABBOTT 17, and ABBOTT 16 assumed modified gravitational waves dispersion to establish limits on graviton mass.
- BERNUS 19 use the planetary ephemeris INPOP 17b to constraint the existence of a Yukawa suppression to the Newtonian potential, generically associated to a gravitons mass.
- MIAO 19 90% CL limit is based on orbital period decay rates of 9 binary pulsars using a Bayesian prior uniform in graviton mass. Limit becomes $< 5.2 \times 10^{-21} \text{ eV}$ for a prior uniform in $\ln(m_g)$.
- DESAI 18 limit based on dynamical mass models of galaxy cluster Abell 1689.
- GUPTA 18 obtains graviton mass limits using stacked clusters from 3 disparate surveys.
- RANA 18 limit, 68% CL, obtained using weak lensing mass profiles out to the radius at which the cluster density falls to 200 times the critical density of the Universe. Limit is based on the fractional change between Newtonian and Yukawa accelerations for the 50 most massive galaxy clusters in the Local Cluster Substructure Survey. Limits for other CL's and other density cuts are also given.
- RANA 18 limit, 68% CL, obtained using mass measurements via the SZ effect out to the radius at which the cluster density falls to 500 times the critical density of the Universe for 182 optically confirmed galaxy clusters in an Atacama Cosmology Telescope survey. Limits for other CL's and other density cuts are also given.
- WILL 18 limit from perihelion advances of the planets, notably Earth, Mars, and Saturn. Alternate analysis yields $< 6 \times 10^{-24}$.
- ZAKHAROV 16 constrains range of Yukawa gravity interaction from S2 star orbit about black hole at Galactic center. The limit is $< 2.9 \times 10^{-21} \text{ eV}$ for $\delta = 100$.
- BRITO 13 explore massive graviton (spin-2) fluctuations around rotating black holes.
- GRUZINOV 05 uses the DGP model (DVALI 00) showing that non-perturbative effects restore continuity with Einstein's equations as the graviton mass approaches zero, then bases his limit on Solar System observations.
- CHOUDHURY 04 concludes from a study of weak-lensing data that masses heavier than about the inverse of 100 Mpc seem to be ruled out if the gravitation field has the Yukawa form.
- GRSHTEIN 04 use non-Einstein field relativistic theory of gravity (RTG), with a massive graviton, to obtain the 95% CL mass limit implied by the value of $\Omega_{tot} = 1.02 \pm 0.02$ current at the time of publication.
- FINN 02 analyze the orbital decay rates of PSR B1913+16 and PSR B1534+12 with a possible graviton mass as a parameter. The combined frequentist mass limit is at 90% CL.
- As of 2020, limits on dP/dt are now about 0.1% (see T. Damour, "Experimental tests of gravitational theory," in this Review).
- GOLDHABER 74 establish this limit considering the binding of galactic clusters, corrected to Planck $h_0 = 0.67$.

graviton REFERENCES

ABBOTT	21	PR D103 122002	R. Abbott <i>et al.</i>	(LIGO and Virgo Collabs.)
DEFELICE	21	JCAP 2112 011	A. De Felice, S. Mukohyama, M.C. Pookkillath	
BERNUS	20	PR D102 021501	L. Bernus <i>et al.</i>	
SHAO	20	PR D102 024069	L. Shao, N. Wex, S.-Y. Zhou	
ABBOTT	19	PR D100 104036	B.P. Abbott <i>et al.</i>	(LIGO and Virgo Collabs.)
BERNUS	19	PRL 123 161103	L. Bernus <i>et al.</i>	
MIAO	19	PR D99 123015	X. Miao, L. Shao, B.-Q. Ma	
DESAI	18	PL B778 325	S. Desai	(HYDER)
GUPTA	18	ANP 399 85	S. Gupta, S. Desai	
RANA	18	PL B781 220	A. Rana <i>et al.</i>	(DELHI)
WILL	18	CQG 35 17LT01	C.M. Will	
ABBOTT	17	PRL 118 221101	B.P. Abbott <i>et al.</i>	(LIGO and Virgo Collabs.)
DE-RHAM	17	RMP 89 025004	C. de Rahm <i>et al.</i>	
ABBOTT	16	PRL 116 061102	B.P. Abbott <i>et al.</i>	(LIGO and Virgo Collabs.)
ZAKHAROV	16	JCAP 1605 045	A.F. Zakharov <i>et al.</i>	
BRITO	13	PR D08 023514	R. Brito, V. Cardoso, P. Pani	(LISB, MISS, HSCA+)
GRUZINOV	05	MAST 10 311	A. Gruzinov	(NYU)
CHOUDHURY	04	ASP 21 559	S.R. Choudhury <i>et al.</i>	(DELPH, MELB)
GRSHTEIN	04	PAN 67 1596	S.S. Gershtein <i>et al.</i>	(SERP)
		Translated from YAF 67 1618.		
FINN	02	PR D65 044022	L.S. Finn, P.J. Sutton	
DVALI	00	PL B485 208	G.R. Dvali, G. Gabadadze, M. Porrati	(NYU)
TALMADGE	88	PRL 61 1159	C. Talmadge <i>et al.</i>	(JPL)
GOLDHABER	74	PR D9 1119	A.S. Goldhaber, M.M. Nieto	(LANL, STON)
HARE	73	CJP 51 431	M.G. Hare	(SASK)
IWASAKI	70	PR D2 2255	Y. Iwasaki	
VANDAM	70	NP B22 397	H. van Dam, M. Veltman	(UTRE)
ZAKHAROV	70	JETPL 12 312	V.I. Zakharov <i>et al.</i>	



J = 1

See the related review(s):
Mass and Width of the W Boson

W MASS

The W-mass listed here corresponds to the mass parameter in a Breit-Wigner distribution with mass-dependent width. To obtain the world averages of various measurements, common systematic uncertainties between experiments are evaluated and accounted for in combinations [SCHAEEL 13A, AMOROSO 24].

Until 2022, the measurements of the W-boson mass at lepton and hadron colliders, LEP-2 (ALEPH, DELPHI, L3, and OPAL), Tevatron (CDF and D0), and LHC (ALEPH and LHCb), were in good agreement with each other [PDG 22]. However, with the new CDF result [AALTONEN 22] based on their complete Run-II data set, this is no longer the case.

The LHC-TeV MW Working Group, including W-mass experts from CDF, D0, ATLAS, CMS and LHCb [AMOROSO 24], has examined this issue in depth. They report that a combination of all W-mass measurements corrected to a common theory description and PDF set, has a probability of compatibility of 0.5% only, and is therefore disfavoured. A 91% probability of compatibility is obtained when the CDF-II measurement is removed. The corresponding value of the W boson mass is 80369.2 ± 13.3 MeV, which we quote as the World Average.

More information is given in [M. Grunewald and A. Gurtu, Mass and Width of the W Boson review, PDG 24] and in [AMOROSO 24].

VALUE (GeV)	EVTs	DOCUMENT ID	TECN	COMMENT
80.3692 ± 0.0133 OUR EVALUATION		(AMOROSO 24)		
80.4335 ± 0.0094		(AALTONEN 22 CDF)		
80.354 ± 0.023 ± 0.022	2.4M	¹ AAIJ	22c LHCb	$E_{cm}^{pp} = 13$ TeV
80.4335 ± 0.0064 ± 0.0069	4.2M	² AALTONEN	22 CDF	$E_{cm}^{pp} = 1.96$ TeV
80.370 ± 0.007 ± 0.017	13.7M	³ AABOUD	18j ATLS	$E_{cm}^{pp} = 7$ TeV
80.375 ± 0.011 ± 0.020	2177k	⁴ ABAZOV	12f D0	$E_{cm}^{pp} = 1.96$ TeV
80.336 ± 0.055 ± 0.039	10.3k	⁵ ABDALLAH	08a DLPH	$E_{cm}^{ee} = 161$ -209 GeV
80.415 ± 0.042 ± 0.031	11830	⁶ ABBIENDI	06 OPAL	$E_{cm}^{ee} = 170$ -209 GeV
80.270 ± 0.046 ± 0.031	9909	⁷ ACHARD	06 L3	$E_{cm}^{ee} = 161$ -209 GeV
80.440 ± 0.043 ± 0.027	8692	⁸ SCHAEEL	06 ALEP	$E_{cm}^{ee} = 161$ -209 GeV
80.483 ± 0.084	49247	⁹ ABAZOV	02d D0	$E_{cm}^{pp} = 1.8$ TeV
• • • We do not use the following data for averages, fits, limits, etc. • • •				
80.520 ± 0.070 ± 0.092		¹⁰ ANDREEV	18a H1	$e^{\pm}p$
80.387 ± 0.012 ± 0.015	1095k	¹¹ AALTONEN	12e CDF	$E_{cm}^{pp} = 1.96$ TeV
80.367 ± 0.013 ± 0.022	1677k	¹² ABAZOV	12f D0	$E_{cm}^{pp} = 1.96$ TeV
80.401 ± 0.021 ± 0.038	500k	¹³ ABAZOV	09AB D0	$E_{cm}^{pp} = 1.96$ TeV
80.413 ± 0.034 ± 0.034	115k	¹⁴ AALTONEN	07f CDF	$E_{cm}^{pp} = 1.96$ TeV
82.87 ± 1.82 $^{+0.30}_{-0.16}$	1500	¹⁵ AKTAS	06 H1	$e^{\pm}p \rightarrow \bar{\nu}_e(\nu_e)X$, $\sqrt{s} \approx 300$ GeV
80.3 ± 2.1 ± 1.2 ± 1.0	645	¹⁶ CHEKANOV	02c ZEUS	$e^-p \rightarrow \nu_e X$, $\sqrt{s} = 318$ GeV
80.433 ± 0.079	53841	¹⁷ AFFOLDER	01e CDF	$E_{cm}^{pp} = 1.8$ TeV
81.4 $^{+2.7}_{-2.6}$ ± 2.0 $^{+3.3}_{-3.0}$	1086	¹⁸ BREITWEG	00d ZEUS	$e^+p \rightarrow \bar{\nu}_e X$, $\sqrt{s} \approx 300$ GeV
80.84 ± 0.22 ± 0.83	2065	¹⁹ ALITTI	92b UA2	See W/Z ratio below
80.79 ± 0.31 ± 0.84		²⁰ ALITTI	90b UA2	$E_{cm}^{pp} = 546,630$ GeV
80.0 ± 3.3 ± 2.4	22	²¹ ABE	89i CDF	$E_{cm}^{pp} = 1.8$ TeV
82.7 ± 1.0 ± 2.7	149	²² ALBAJAR	89 UA1	$E_{cm}^{pp} = 546,630$ GeV
81.8 $^{+6.0}_{-5.3}$ ± 2.6	46	²³ ALBAJAR	89 UA1	$E_{cm}^{pp} = 546,630$ GeV
89 ± 3 ± 6	32	²⁴ ALBAJAR	89 UA1	$E_{cm}^{pp} = 546,630$ GeV
81. ± 5.	6	ARNISON	83 UA1	$E_{cm}^{ee} = 546$ GeV
80. $^{+10.}_{-6.}$	4	BANNER	83b UA2	Repl. by ALITTI 90b

¹ AAIJ 22c analyse W production in the muon decay channel, with the transverse momentum of the muon required to be between 28 and 52 GeV. Analysing the distribution of the muon charge divided by the muon transverse momentum of approximately 2.4 million selected W candidates, a value of $M_W = 80354 \pm 23(\text{stat.}) \pm 10(\text{exp.}) \pm 17(\text{theo.}) \pm 9(\text{PDF})$ MeV is obtained; we combine the three systematic uncertainties in quadrature.

² AALTONEN 22 select a data sample of about 4 million W boson candidates in 8.8 fb⁻¹ of Run-II data. The mass is determined using the transverse mass, transverse lepton momentum and transverse missing momentum distributions of W decays into electrons or muons, accounting for correlations. This measurement supersedes AALTONEN 12e, but is not used in OUR EVALUATION.

³ AABOUD 18j select 4.61M $W^+ \rightarrow \mu^+ \nu_\mu$, 3.40M $W^+ \rightarrow e^+ \nu_e$, 3.23M $W^- \rightarrow \mu^- \bar{\nu}_\mu$ and 2.49M $W^- \rightarrow e^- \bar{\nu}_e$ events in 4.6 fb⁻¹ pp data at 7 TeV. The W mass is determined using the transverse mass and transverse lepton momentum distributions,

accounting for correlations. The systematic error includes 0.011 GeV experimental and 0.014 GeV modelling uncertainties.

⁴ Combination of results from ABAZOV 12f and ABAZOV 09AB as quoted in ABAZOV 12f.

⁵ ABDALLAH 08a use direct reconstruction of the kinematics of $W^+ W^- \rightarrow q\bar{q}\ell\nu$ and $W^+ W^- \rightarrow q\bar{q}q\bar{q}$ events for energies 172 GeV and above. The W mass was also extracted from the dependence of the WW cross section close to the production threshold and combined appropriately to obtain the final result. The systematic error includes ±0.025 GeV due to final state interactions and ±0.009 GeV due to LEP energy uncertainty.

⁶ ABBIENDI 06 use direct reconstruction of the kinematics of $W^+ W^- \rightarrow q\bar{q}\ell\nu_\ell$ and $W^+ W^- \rightarrow q\bar{q}q\bar{q}$ events. The result quoted here is obtained combining this mass value with the results using $W^+ W^- \rightarrow \ell\nu_\ell\ell'\nu_{\ell'}$ events in the energy range 183-207 GeV (ABBIENDI 03c) and the dependence of the WW production cross-section on m_W at threshold. The systematic error includes ±0.009 GeV due to the uncertainty on the LEP beam energy.

⁷ ACHARD 06 use direct reconstruction of the kinematics of $W^+ W^- \rightarrow q\bar{q}\ell\nu_\ell$ and $W^+ W^- \rightarrow q\bar{q}q\bar{q}$ events in the C.M. energy range 189-209 GeV. The result quoted here is obtained combining this mass value with those obtained from a direct W mass reconstruction at 172 and 183 GeV and with those from the dependence of the WW production cross-section on m_W at 161 and 172 GeV (ACCIARRI 99).

⁸ SCHAEEL 06 use direct reconstruction of the kinematics of $W^+ W^- \rightarrow q\bar{q}\ell\nu_\ell$ and $W^+ W^- \rightarrow q\bar{q}q\bar{q}$ events in the C.M. energy range 183-209 GeV. The result quoted here is obtained combining this mass value with those obtained from the dependence of the W pair production cross-section on m_W at 161 and 172 GeV (BARATE 97 and BARATE 97s respectively). The systematic error includes ±0.009 GeV due to possible effects of final state interactions in the $q\bar{q}q\bar{q}$ channel and ±0.009 GeV due to the uncertainty on the LEP beam energy.

⁹ ABAZOV 02d improve the measurement of the W-boson mass including $W \rightarrow e\nu_e$ events in which the electron is close to a boundary of a central electromagnetic calorimeter module. Properly combining the results obtained by fitting $m_T(W)$, $p_T(e)$, and $p_T(\nu)$, this sample provides a mass value of 80.574 ± 0.405 GeV. The value reported here is a combination of this measurement with all previous DØ W-boson mass measurements.

¹⁰ ANDREEV 18a obtain this result in a combined electroweak and QCD analysis using all deep-inelastic e^+p and e^-p neutral current and charged current scattering cross sections published by the H1 Collaboration, including data with longitudinally polarized lepton beams.

¹¹ AALTONEN 12e select 470k $W \rightarrow e\nu$ decays and 625k $W \rightarrow \mu\nu$ decays in 2.2 fb⁻¹ of Run-II data. The mass is determined using the transverse mass, transverse lepton momentum and transverse missing energy distributions, accounting for correlations. This result supersedes AALTONEN 07f. AALTONEN 14d gives more details on the procedures followed by the authors. This measurement is superseded by AALTONEN 22.

¹² ABAZOV 12f select 1677k $W \rightarrow e\nu$ decays in 4.3 fb⁻¹ of Run-II data. The mass is determined using the transverse mass and transverse lepton momentum distributions, accounting for correlations.

¹³ ABAZOV 09AB study the transverse mass, transverse electron momentum, and transverse missing energy in a sample of 0.5 million $W \rightarrow e\nu$ decays selected in Run-II data. The quoted result combines all three methods, accounting for correlations.

¹⁴ AALTONEN 07f obtain high purity $W \rightarrow e\nu_e$ and $W \rightarrow \mu\nu_\mu$ candidate samples totaling 63,964 and 51,128 events respectively. The W mass value quoted above is derived by simultaneously fitting the transverse mass and the lepton, and neutrino p_T distributions.

¹⁵ AKTAS 06 fit the Q^2 dependence ($300 < Q^2 < 30,000$ GeV²) of the charged-current differential cross section with a propagator mass. The first error is experimental and the second corresponds to uncertainties due to input parameters and model assumptions.

¹⁶ CHEKANOV 02c fit the Q^2 dependence ($200 < Q^2 < 60,000$ GeV²) of the charged-current differential cross sections with a propagator mass fit. The last error is due to the uncertainty on the probability density functions.

¹⁷ AFFOLDER 01e fit the transverse mass spectrum of 30115 $W \rightarrow e\nu_e$ events ($M_W = 80.473 \pm 0.065 \pm 0.092$ GeV) and of 14740 $W \rightarrow \mu\nu_\mu$ events ($M_W = 80.465 \pm 0.100 \pm 0.103$ GeV) obtained in the run IB (1994-95). Combining the electron and muon results, accounting for correlated uncertainties, yields $M_W = 80.470 \pm 0.089$ GeV. They combine this value with their measurement of ABE 95P reported in run IA (1992-93) to obtain the quoted value.

¹⁸ BREITWEG 00d fit the Q^2 dependence ($200 < Q^2 < 225,000$ GeV²) of the charged-current differential cross sections with a propagator mass fit. The last error is due to the uncertainty on the probability density functions.

¹⁹ ALITTI 92b result has two contributions to the systematic error (±0.83); one (±0.81) cancels in m_W/m_Z and one (±0.17) is noncancelling. These were added in quadrature. We choose the ALITTI 92b value without using the LEP m_Z value, because we perform our own combined fit.

²⁰ There are two contributions to the systematic error (±0.84): one (±0.81) which cancels in m_W/m_Z and one (±0.21) which is non-cancelling. These were added in quadrature.

²¹ ABE 89i systematic error dominated by the uncertainty in the absolute energy scale.

²² ALBAJAR 89 result is from a total sample of 299 $W \rightarrow e\nu$ events.

²³ ALBAJAR 89 result is from a total sample of 67 $W \rightarrow \mu\nu$ events.

²⁴ ALBAJAR 89 result is from $W \rightarrow \tau\nu$ events.

W/Z MASS RATIO

VALUE	EVTs	DOCUMENT ID	TECN	COMMENT
0.88136 ± 0.00015		¹ PDG	24	
• • • We do not use the following data for averages, fits, limits, etc. • • •				
0.8821 ± 0.0011 ± 0.0008	28323	² ABBOTT	98n D0	$E_{cm}^{pp} = 1.8$ TeV
0.88114 ± 0.00154 ± 0.00252	5982	³ ABBOTT	98p D0	$E_{cm}^{pp} = 1.8$ TeV
0.8813 ± 0.0036 ± 0.0019	156	⁴ ALITTI	92b UA2	$E_{cm}^{pp} = 630$ GeV

¹ This value was obtained using the world average values of m_Z and m_W as presented in these listings.

² ABBOTT 98n obtain this from a study of 28323 $W \rightarrow e\nu_e$ and 3294 $Z \rightarrow e^+e^-$ decays. Of this latter sample, 2179 events are used to calibrate the electron energy scale.

³ ABBOTT 98p obtain this from a study of 5982 $W \rightarrow e\nu_e$ events. The systematic error includes an uncertainty of ±0.00175 due to the electron energy scale.

Gauge & Higgs Boson Particle Listings

W

⁴ Scale error cancels in this ratio.

$m_Z - m_W$				
VALUE (GeV)	DOCUMENT ID	TECN	COMMENT	
10.818 ± 0.013	¹ PDG	24		
••• We do not use the following data for averages, fits, limits, etc. •••				
10.4 ± 1.4 ± 0.8	ALBAJAR	89 UA1	$E_{cm}^{pp} = 546,630$ GeV	
11.3 ± 1.3 ± 0.9	ANSARI	87 UA2	$E_{cm}^{pp} = 546,630$ GeV	

¹ This value was obtained using the world average values of m_Z and m_W as presented in these listings.

$m_{W^+} - m_{W^-}$				
Test of CPT invariance.				
VALUE (GeV)	EVTS	DOCUMENT ID	TECN	COMMENT
-0.029 ± 0.028 OUR AVERAGE				
-0.029 ± 0.013 ± 0.025	13.7M	¹ AABOUD	18J ATLS	$E_{cm}^{pp} = 7$ TeV
-0.19 ± 0.58	1722	ABE	90G CDF	$E_{cm}^{pp} = 1.8$ TeV

¹ AABOUD 18J select 4.61M $W^+ \rightarrow \mu^+ \nu_\mu$, 3.40M $W^+ \rightarrow e^+ \nu_e$, 3.23M $W^- \rightarrow \mu^- \bar{\nu}_\mu$ and 2.49M $W^- \rightarrow e^- \bar{\nu}_e$ events in 4.6 fb⁻¹ pp data at 7 TeV. The W mass is determined using the transverse mass and transverse lepton momentum distributions, accounting for correlations. The systematic error includes 0.007 GeV experimental and 0.024 GeV modelling uncertainties.

W WIDTH				
The W width listed here corresponds to the width parameter in a Breit-Wigner distribution with mass-dependent width. To obtain the world average, common systematic uncertainties between experiments are properly taken into account. The LEP-2 average W width based on published results is 2.195 ± 0.083 GeV [SCHAEL 13A]. The combined Tevatron data yields an average W width of 2.046 ± 0.049 GeV [FERMILAB-TM-2460-E].				
OUR FIT uses these average LEP and Tevatron width values and combines them assuming no correlations.				

VALUE (GeV)	EVTS	DOCUMENT ID	TECN	COMMENT
2.085 ± 0.042 OUR FIT				
2.028 ± 0.072	5272	¹ ABZOV	09AK D0	$E_{cm}^{pp} = 1.96$ GeV
2.032 ± 0.045 ± 0.057	6055	² AALTONEN	08B CDF	$E_{cm}^{pp} = 1.96$ TeV
2.404 ± 0.140 ± 0.101	10.3k	³ ABDALLAH	08A DLPH	$E_{cm}^{ee} = 183-209$ GeV
1.996 ± 0.096 ± 0.102	10729	⁴ ABBIENDI	06 OPAL	$E_{cm}^{ee} = 170-209$ GeV
2.18 ± 0.11 ± 0.09	9795	⁵ ACHARD	06 L3	$E_{cm}^{ee} = 172-209$ GeV
2.14 ± 0.09 ± 0.06	8717	⁶ SCHAEL	06 ALEP	$E_{cm}^{ee} = 183-209$ GeV
2.23 $\begin{smallmatrix} +0.15 \\ -0.14 \end{smallmatrix}$ ± 0.10	294	⁷ ABZOV	02E D0	$E_{cm}^{pp} = 1.8$ TeV
2.05 ± 0.10 ± 0.08	662	⁸ AFFOLDER	00M CDF	$E_{cm}^{pp} = 1.8$ TeV
••• We do not use the following data for averages, fits, limits, etc. •••				
2.152 ± 0.066	79176	⁹ ABBOTT	00B D0	Extracted value
2.064 ± 0.060 ± 0.059		¹⁰ ABE	95W CDF	Extracted value
2.10 $\begin{smallmatrix} +0.14 \\ -0.13 \end{smallmatrix}$ ± 0.09	3559	¹¹ ALITTI	92 UA2	Extracted value
2.18 $\begin{smallmatrix} +0.26 \\ -0.24 \end{smallmatrix}$ ± 0.04		¹² ALBAJAR	91 UA1	Extracted value

¹ ABZOV 09AK obtain this result fitting the high-end tail (100-200 GeV) of the transverse mass spectrum in $W \rightarrow e\nu$ decays.

² AALTONEN 08B obtain this result fitting the high-end tail (90-200 GeV) of the transverse mass spectrum in semileptonic $W \rightarrow e\nu_e$ and $W \rightarrow \mu\nu_\mu$ decays.

³ ABDALLAH 08A use direct reconstruction of the kinematics of $W^+ W^- \rightarrow q\bar{q}\ell\nu$ and $W^+ W^- \rightarrow q\bar{q}q\bar{q}$ events. The systematic error includes ±0.065 GeV due to final state interactions.

⁴ ABBIENDI 06 use direct reconstruction of the kinematics of $W^+ W^- \rightarrow q\bar{q}\ell\nu_\ell$ and $W^+ W^- \rightarrow q\bar{q}q\bar{q}$ events. The systematic error includes ±0.003 GeV due to the uncertainty on the LEP beam energy.

⁵ ACHARD 06 use direct reconstruction of the kinematics of $W^+ W^- \rightarrow q\bar{q}\ell\nu_\ell$ and $W^+ W^- \rightarrow q\bar{q}q\bar{q}$ events in the C.M. energy range 189-209 GeV. The result quoted here is obtained combining this value of the width with the result obtained from a direct W mass reconstruction at 172 and 183 GeV (ACCIARRI 99).

⁶ SCHAEL 06 use direct reconstruction of the kinematics of $W^+ W^- \rightarrow q\bar{q}\ell\nu_\ell$ and $W^+ W^- \rightarrow q\bar{q}q\bar{q}$ events. The systematic error includes ±0.05 GeV due to possible effects of final state interactions in the $q\bar{q}q\bar{q}$ channel and ±0.01 GeV due to the uncertainty on the LEP beam energy.

⁷ ABZOV 02E obtain this result fitting the high-end tail (90-200 GeV) of the transverse-mass spectrum in semileptonic $W \rightarrow e\nu_e$ decays.

⁸ AFFOLDER 00M fit the high transverse mass (100-200 GeV) $W \rightarrow e\nu_e$ and $W \rightarrow \mu\nu_\mu$ events to obtain $\Gamma(W) = 2.04 \pm 0.11(\text{stat}) \pm 0.09(\text{syst})$ GeV. This is combined with the earlier CDF measurement (ABE 95C) to obtain the quoted result.

⁹ ABBOTT 00B measure $R = 10.43 \pm 0.27$ for the $W \rightarrow e\nu_e$ decay channel. They use the SM theoretical predictions for $\sigma(W)/\sigma(Z)$ and $\Gamma(W \rightarrow e\nu_e)$ and the world average for $B(Z \rightarrow e\bar{e})$. The value quoted here is obtained combining this result (2.169 ± 0.070 GeV) with that of ABBOTT 99H.

¹⁰ ABE 95W measured $R = 10.90 \pm 0.32 \pm 0.29$. They use $m_W = 80.23 \pm 0.18$ GeV, $\sigma(W)/\sigma(Z) = 3.35 \pm 0.03$, $\Gamma(W \rightarrow e\nu) = 225.9 \pm 0.9$ MeV, $\Gamma(Z \rightarrow e^+e^-) = 83.98 \pm 0.18$ MeV, and $\Gamma(Z) = 2.4969 \pm 0.0038$ GeV.

¹¹ ALITTI 92 measured $R = 10.4 \pm 0.7 \pm 0.3$. The values of $\sigma(Z)$ and $\sigma(W)$ come from $O(\alpha_s^2)$ calculations using $m_W = 80.14 \pm 0.27$ GeV, and $m_Z = 91.175 \pm 0.021$ GeV along with the corresponding value of $\sin^2\theta_W = 0.2274$. They use $\sigma(W)/\sigma(Z) = 3.26 \pm 0.07 \pm 0.05$ and $\Gamma(Z) = 2.487 \pm 0.010$ GeV.

¹² ALBAJAR 91 measured $R = 9.5 \pm 1.1 \pm 1.0$ (stat. + syst.). $\sigma(W)/\sigma(Z)$ is calculated in QCD at the parton level using $m_W = 80.18 \pm 0.28$ GeV and $m_Z = 91.172 \pm 0.031$ GeV along with $\sin^2\theta_W = 0.2322 \pm 0.0014$. They use $\sigma(W)/\sigma(Z) = 3.23 \pm 0.05$ and $\Gamma(Z) = 2.498 \pm 0.020$ GeV. This measurement is obtained combining both the electron and muon channels.

W⁺ DECAY MODES

W^- modes are charge conjugates of the modes below.

Mode	Fraction (Γ_i/Γ)	Confidence level
Γ_1 $\ell^+ \nu$	[a] (10.86 ± 0.09) %	
Γ_2 $e^+ \nu$	(10.71 ± 0.16) %	
Γ_3 $\mu^+ \nu$	(10.63 ± 0.15) %	
Γ_4 $\tau^+ \nu$	(11.38 ± 0.21) %	
Γ_5 hadrons	(67.41 ± 0.27) %	
Γ_6 $\pi^+ \gamma$	< 7 × 10 ⁻⁶	95%
Γ_7 $D_s^+ \gamma$	< 6 × 10 ⁻⁴	95%
Γ_8 cX	(33.3 ± 2.6) %	
Γ_9 c \bar{X}	(31 $\begin{smallmatrix} +13 \\ -11 \end{smallmatrix}$) %	
Γ_{10} invisible	[b] (1.4 ± 2.9) %	
Γ_{11} $\pi^+ \pi^+ \pi^-$	< 1.01 × 10 ⁻⁶	95%

[a] ℓ indicates each type of lepton (e , μ , and τ), not sum over them.

[b] This represents the width for the decay of the W boson into a charged particle with momentum below detectability, $p < 200$ MeV.

W PARTIAL WIDTHS

 $\Gamma(\text{invisible})$ Γ_{10}

This represents the width for the decay of the W boson into a charged particle with momentum below detectability, $p < 200$ MeV.

VALUE (MeV)	DOCUMENT ID	TECN	COMMENT
30 $\begin{smallmatrix} +52 \\ -48 \end{smallmatrix}$ ± 33	¹ BARATE	99I ALEP	$E_{cm}^{ee} = 161+172+183$ GeV
••• We do not use the following data for averages, fits, limits, etc. •••			
	² BARATE	99L ALEP	$E_{cm}^{ee} = 161+172+183$ GeV

¹ BARATE 99I measure this quantity using the dependence of the total cross section σ_{WW} upon a change in the total width. The fit is performed to the WW measured cross sections at 161, 172, and 183 GeV. This partial width is < 139 MeV at 95%CL.

² BARATE 99L use W -pair production to search for effectively invisible W decays, tagging with the decay of the other W boson to Standard Model particles. The partial width for effectively invisible decay is < 27 MeV at 95%CL.

W BRANCHING RATIOS

Overall fits are performed to determine the branching ratios of the W boson. Averages on $W \rightarrow e\nu$, $W \rightarrow \mu\nu$, and $W \rightarrow \tau\nu$, and their correlations are obtained by combining results from the four LEP experiments properly taking into account the common systematic uncertainties and their correlations [SCHAEL 13A]. A first fit determines the three individual leptonic branching ratios $B(W \rightarrow e\nu)$, $B(W \rightarrow \mu\nu)$, and $B(W \rightarrow \tau\nu)$. This fit has a $\chi^2 = 6.3$ for 9 degrees of freedom. The correlation coefficients between the branching fractions are 0.14 ($e-\mu$), -0.20 ($e-\tau$), -0.12 ($\mu-\tau$). A second fit assumes lepton universality and determines the leptonic branching ratio $B(W \rightarrow \ell\nu)$ and the hadronic branching ratio is derived as $B(W \rightarrow \text{hadrons}) = 1 - 3 B(W \rightarrow \ell\nu)$. This fit has a $\chi^2 = 15.4$ for 11 degrees of freedom.

 $\Gamma(\ell^+ \nu)/\Gamma_{\text{total}}$ Γ_i/Γ

ℓ indicates average over e , μ , and τ modes, not sum over modes.

VALUE (units 10 ⁻²)	EVTS	DOCUMENT ID	TECN	COMMENT
10.86 ± 0.09 OUR FIT				
10.89 ± 0.01 ± 0.08		TUMASYAN	22f CMS	$E_{cm}^{pp} = 13$ TeV
10.86 ± 0.12 ± 0.08	16438	ABBIENDI	07A OPAL	$E_{cm}^{ee} = 161-209$ GeV
10.85 ± 0.14 ± 0.08	13600	ABDALLAH	04G DLPH	$E_{cm}^{ee} = 161-209$ GeV
10.83 ± 0.14 ± 0.10	11246	ACHARD	04J L3	$E_{cm}^{ee} = 161-209$ GeV
10.96 ± 0.12 ± 0.05	16116	SCHAEL	04A ALEP	$E_{cm}^{ee} = 183-209$ GeV
••• We do not use the following data for averages, fits, limits, etc. •••				
11.02 ± 0.52	11858	¹ ABBOTT	99H D0	$E_{cm}^{pp} = 1.8$ TeV
10.4 ± 0.8	3642	² ABE	92I CDF	$E_{cm}^{pp} = 1.8$ TeV

¹ ABBOTT 99H measure $R \equiv [\sigma_{WW} B(W \rightarrow \ell\nu_\ell)]/[\sigma_Z B(Z \rightarrow \ell\ell)] = 10.90 \pm 0.52$ combining electron and muon channels. They use $m_W = 80.39 \pm 0.06$ GeV and the SM theoretical predictions for $\sigma(W)/\sigma(Z)$ and $B(Z \rightarrow \ell\ell)$.

² 1216 ± 38 $\begin{smallmatrix} +27 \\ -31 \end{smallmatrix}$ $W \rightarrow \mu\nu$ events from ABE 92I and 2426 $W \rightarrow e\nu$ events of ABE 91C. ABE 92I give the inverse quantity as 9.6 ± 0.7 and we have inverted.

$\Gamma(e^+\nu)/\Gamma_{total}$ Γ_2/Γ

VALUE (units 10^{-2})	EVTs	DOCUMENT ID	TECN	COMMENT
10.71 ± 0.16 OUR FIT				
10.83 ± 0.01 ± 0.10		TUMASYAN	22F CMS	$E_{cm}^{pp} = 13$ TeV
10.71 ± 0.25 ± 0.11	2374	ABBIENDI	07A OPAL	$E_{cm}^{ee} = 161-209$ GeV
10.55 ± 0.31 ± 0.14	1804	ABDALLAH	04G DLPH	$E_{cm}^{ee} = 161-209$ GeV
10.78 ± 0.29 ± 0.13	1576	ACHARD	04J L3	$E_{cm}^{ee} = 161-209$ GeV
10.78 ± 0.27 ± 0.10	2142	SCHAEEL	04A ALEP	$E_{cm}^{ee} = 183-209$ GeV
10.61 ± 0.28		¹ ABAZOV	04D TEVA	$E_{cm}^{pp} = 1.8$ TeV

• • • We do not use the following data for averages, fits, limits, etc. • • •

¹ABAZOV 04D take into account all correlations to properly combine the CDF (ABE 95W) and DØ (ABBOTT 00b) measurements of the ratio R in the electron channel. The ratio R is defined as $[\sigma_W \cdot B(W \rightarrow e\nu_e)] / [\sigma_Z \cdot B(Z \rightarrow ee)]$. The combination gives $R^{Tevatron} = 10.59 \pm 0.23$. σ_W / σ_Z is calculated at next-to-next-to-leading order (3.360 ± 0.051). The branching fraction $B(Z \rightarrow ee)$ is taken from this Review as (3.363 ± 0.004)%.

$\Gamma(\mu^+\nu)/\Gamma_{total}$ Γ_3/Γ

VALUE (units 10^{-2})	EVTs	DOCUMENT ID	TECN	COMMENT
10.63 ± 0.15 OUR FIT				
10.94 ± 0.01 ± 0.08		TUMASYAN	22F CMS	$E_{cm}^{pp} = 13$ TeV
10.78 ± 0.24 ± 0.10	2397	ABBIENDI	07A OPAL	$E_{cm}^{ee} = 161-209$ GeV
10.65 ± 0.26 ± 0.08	1998	ABDALLAH	04G DLPH	$E_{cm}^{ee} = 161-209$ GeV
10.03 ± 0.29 ± 0.12	1423	ACHARD	04J L3	$E_{cm}^{ee} = 161-209$ GeV
10.87 ± 0.25 ± 0.08	2216	SCHAEEL	04A ALEP	$E_{cm}^{ee} = 183-209$ GeV

$\Gamma(\mu^+\nu)/\Gamma(e^+\nu)$ Γ_3/Γ_2

VALUE	EVTs	DOCUMENT ID	TECN	COMMENT
1.002 ± 0.006 OUR AVERAGE				
1.009 ± 0.009		TUMASYAN	22F CMS	$E_{cm}^{pp} = 13$ TeV
1.003 ± 0.010		¹ AABOUD	17Q ATLS	$E_{cm}^{pp} = 7$ TeV
0.980 ± 0.018		² AAIJ	16AJ LHCB	$E_{cm}^{pp} = 8$ TeV
0.993 ± 0.019		SCHAEEL	13A LEP	$E_{cm}^{ee} = 130-209$ GeV
0.89 ± 0.10	13k	³ ABACHI	95D D0	$E_{cm}^{pp} = 1.8$ TeV
1.02 ± 0.08	1216	⁴ ABE	92I CDF	$E_{cm}^{pp} = 1.8$ TeV
1.00 ± 0.14 ± 0.08	67	ALBAJAR	89 UA1	$E_{cm}^{pp} = 546,630$ GeV
1.24 $\begin{smallmatrix} +0.6 \\ -0.4 \end{smallmatrix}$	14	ARNISON	84D UA1	Repl. by ALBAJAR 89

• • • We do not use the following data for averages, fits, limits, etc. • • •

¹AABOUD 17Q make a precise determination of $W \rightarrow e\nu$ and $W \rightarrow \mu\nu$ production in the following fiducial phase space: lepton pseudo-rapidity range $|\eta| < 2.5$, lepton and neutrino transverse momenta larger than 25 GeV each, and W transverse mass larger than 25 GeV. They determine the ratio of the W branching fractions $B(W \rightarrow e\nu)/B(W \rightarrow \mu\nu) = 0.9967 \pm 0.0004 \pm 0.0101 = 0.997 \pm 0.010$.

²AAIJ 16AJ make precise measurements of forward $W \rightarrow e\nu$ and $W \rightarrow \mu\nu$ production in proton-proton collisions at 8 TeV and determine the ratio of the W branching fractions $B(W \rightarrow e\nu)/B(W \rightarrow \mu\nu) = 1.020 \pm 0.002 \pm 0.019$.

³ABACHI 95D obtain this result from the measured $\sigma_W B(W \rightarrow \mu\nu) = 2.09 \pm 0.23 \pm 0.11$ nb and $\sigma_W B(W \rightarrow e\nu) = 2.36 \pm 0.07 \pm 0.13$ nb in which the first error is the combined statistical and systematic uncertainty, the second reflects the uncertainty in the luminosity.

⁴ABE 92I obtain $\sigma_W B(W \rightarrow \mu\nu) = 2.21 \pm 0.07 \pm 0.21$ and combine with ABE 91C $\sigma_W B(W \rightarrow e\nu)$ to give a ratio of the couplings from which we derive this measurement.

$\Gamma(\tau^+\nu)/\Gamma_{total}$ Γ_4/Γ

VALUE (units 10^{-2})	EVTs	DOCUMENT ID	TECN	COMMENT
11.38 ± 0.21 OUR FIT				
10.77 ± 0.05 ± 0.21		TUMASYAN	22F CMS	$E_{cm}^{pp} = 13$ TeV
11.14 ± 0.31 ± 0.17	2177	ABBIENDI	07A OPAL	$E_{cm}^{ee} = 161-209$ GeV
11.46 ± 0.39 ± 0.19	2034	ABDALLAH	04G DLPH	$E_{cm}^{ee} = 161-209$ GeV
11.89 ± 0.40 ± 0.20	1375	ACHARD	04J L3	$E_{cm}^{ee} = 161-209$ GeV
11.25 ± 0.32 ± 0.20	2070	SCHAEEL	04A ALEP	$E_{cm}^{ee} = 183-209$ GeV

$\Gamma(\tau^+\nu)/\Gamma(e^+\nu)$ Γ_4/Γ_2

VALUE	EVTs	DOCUMENT ID	TECN	COMMENT
1.015 ± 0.020 OUR AVERAGE				Error includes scale factor of 1.3. See the ideogram below.
0.994 ± 0.021		TUMASYAN	22F CMS	$E_{cm}^{pp} = 13$ TeV
1.063 ± 0.027		SCHAEEL	13A LEP	$E_{cm}^{ee} = 130-209$ GeV
0.961 ± 0.061	980	¹ ABBOTT	00D D0	$E_{cm}^{pp} = 1.8$ TeV
0.94 ± 0.14	179	² ABE	92E CDF	$E_{cm}^{pp} = 1.8$ TeV
1.04 ± 0.08 ± 0.08	754	³ ALITTI	92F UA2	$E_{cm}^{pp} = 630$ GeV
1.02 ± 0.20 ± 0.12	32	ALBAJAR	89 UA1	$E_{cm}^{pp} = 546,630$ GeV
0.995 ± 0.112 ± 0.083	198	ALITTI	91c UA2	Repl. by ALITTI 92F
1.02 ± 0.20 ± 0.10	32	ALBAJAR	87 UA1	Repl. by ALBAJAR 89

• • • We do not use the following data for averages, fits, limits, etc. • • •

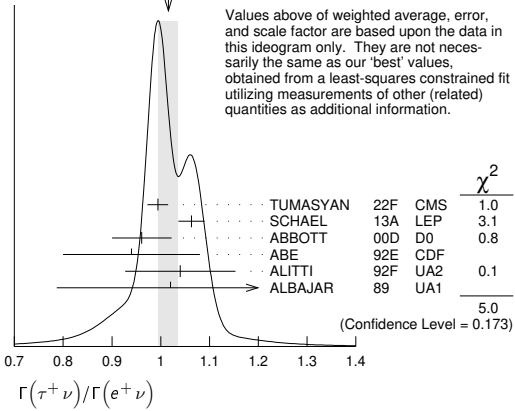
¹ABBOTT 00D measure $\sigma_W \times B(W \rightarrow \tau\nu_\tau) = 2.22 \pm 0.09 \pm 0.10 \pm 0.10$ nb. Using the ABBOTT 00b result $\sigma_W \times B(W \rightarrow e\nu_e) = 2.31 \pm 0.01 \pm 0.05 \pm 0.10$ nb, they quote the ratio of the couplings from which we derive this measurement.

²ABE 92E use two procedures for selecting $W \rightarrow \tau\nu_\tau$ events. The missing E_T trigger leads to $132 \pm 14 \pm 8$ events and the τ trigger to $47 \pm 9 \pm 4$ events. Proper statistical and

systematic correlations are taken into account to arrive at $\sigma_B(W \rightarrow \tau\nu) = 2.05 \pm 0.27$ nb. Combined with ABE 91C result on $\sigma_B(W \rightarrow e\nu)$, ABE 92E quote a ratio of the couplings from which we derive this measurement.

³This measurement is derived by us from the ratio of the couplings of ALITTI 92F.

WEIGHTED AVERAGE
1.015 ± 0.020 (Error scaled by 1.3)

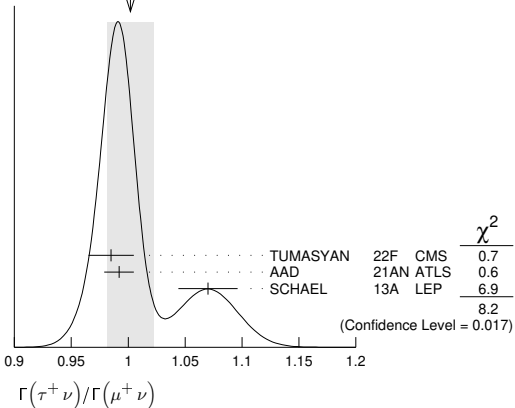


$\Gamma(\tau^+\nu)/\Gamma(\mu^+\nu)$ Γ_4/Γ_3

VALUE	DOCUMENT ID	TECN	COMMENT
1.002 ± 0.020 OUR AVERAGE			Error includes scale factor of 2.0. See the ideogram below.
0.985 ± 0.020	TUMASYAN 22F CMS	$E_{cm}^{pp} = 13$ TeV	
0.992 ± 0.007 ± 0.011	¹ AAD 21AN ATLS	$E_{cm}^{pp} = 13$ TeV	
1.070 ± 0.026	SCHAEEL 13A LEP	$E_{cm}^{ee} = 130-209$ GeV	

¹AAD 21AN study $t\bar{t}$ production, with the W bosons in top-quark decay decaying to electrons or taus, with the tau decaying further into a muon. Analyzing the muon impact parameter and its transverse momentum, the contributions from prompt muons (arising from W decay) and non-prompt muons (arising from tau decay) are separated, allowing a measurement of the ratio of the W branching fractions into taus and muons, $R(\tau/\mu) = 0.992 \pm 0.007 \pm 0.011$ where the first error is statistical and the second systematic.

WEIGHTED AVERAGE
1.002 ± 0.020 (Error scaled by 2.0)



$\Gamma(\text{hadrons})/\Gamma_{total}$ Γ_5/Γ

OUR FIT value is obtained by a fit to the lepton branching ratio data assuming lepton universality.

VALUE (units 10^{-2})	EVTs	DOCUMENT ID	TECN	COMMENT
67.41 ± 0.27 OUR FIT				
67.32 ± 0.02 ± 0.23		TUMASYAN	22F CMS	$E_{cm}^{pp} = 13$ TeV
67.41 ± 0.37 ± 0.23	16438	ABBIENDI	07A OPAL	$E_{cm}^{ee} = 161-209$ GeV
67.45 ± 0.41 ± 0.24	13600	ABDALLAH	04G DLPH	$E_{cm}^{ee} = 161-209$ GeV
67.50 ± 0.42 ± 0.30	11246	ACHARD	04J L3	$E_{cm}^{ee} = 161-209$ GeV
67.13 ± 0.37 ± 0.15	16116	SCHAEEL	04A ALEP	$E_{cm}^{ee} = 183-209$ GeV

$\Gamma(\pi^+\gamma)/\Gamma_{total}$ Γ_6/Γ

A stronger limit of $< 7 \times 10^{-6}$ is obtained from $\Gamma(W^+ \rightarrow \pi^+\gamma)/\Gamma(W^+ \rightarrow e^+\nu)$ measurements.

VALUE	CL%	DOCUMENT ID	COMMENT
< 1.50 × 10⁻⁵	95	¹ SIRUNYAN 21I	$E_{cm}^{pp} = 13$ TeV

• • • We do not use the following data for averages, fits, limits, etc. • • •

¹SIRUNYAN 21I search for the rare decay of a W boson into a charged pion accompanied by a photon. A signal is not observed, and an upper limit on the branching fraction $B(W \rightarrow \pi\gamma) < 1.50 \times 10^{-5}$ is obtained at 95% C.L.

Gauge & Higgs Boson Particle Listings

W

 $\Gamma(\pi^+\gamma)/\Gamma(e^+\nu)$ Γ_6/Γ_2

VALUE	CL%	DOCUMENT ID	TECN	COMMENT
$< 6.4 \times 10^{-5}$	95	AALTONEN	12W CDF	$E_{cm}^{pp} = 1.96$ TeV
••• We do not use the following data for averages, fits, limits, etc. •••				
$< 7 \times 10^{-4}$	95	ABE	98H CDF	$E_{cm}^{pp} = 1.8$ TeV
$< 4.9 \times 10^{-3}$	95	¹ ALITTI	92D UA2	$E_{cm}^{pp} = 630$ GeV
$< 58 \times 10^{-3}$	95	² ALBAJAR	90 UA1	$E_{cm}^{pp} = 546, 630$ GeV
¹ ALITTI 92D limit is 3.8×10^{-3} at 90%CL.				
² ALBAJAR 90 obtain < 0.048 at 90%CL.				

 $\Gamma(D_s^+\gamma)/\Gamma(e^+\nu)$ Γ_7/Γ_2

VALUE	CL%	DOCUMENT ID	TECN	COMMENT
$< 1.2 \times 10^{-2}$	95	ABE	98P CDF	$E_{cm}^{pp} = 1.8$ TeV

 $\Gamma(D_s^+\gamma)/\Gamma(\mu^+\nu)$ Γ_7/Γ_3

VALUE	CL%	DOCUMENT ID	TECN	COMMENT
$< 6.1 \times 10^{-3}$	95	¹ AAIJ	23AMLHCB	$E_{cm}^{pp} = 13$ TeV
¹ AAIJ 23AM also quotes the branching fraction limit $B(W^+ \rightarrow D_s^+\gamma) < 6.5 \times 10^{-4}$, using the known $W \rightarrow \mu\nu$ branching fraction.				

 $\Gamma(cX)/\Gamma(\text{hadrons})$ Γ_8/Γ_5

VALUE	EVTS	DOCUMENT ID	TECN	COMMENT
0.49 ± 0.04	OUR AVERAGE			
$0.481 \pm 0.042 \pm 0.032$	3005	¹ ABBIENDI	00V OPAL	$E_{cm}^{ee} = 183 + 189$ GeV
$0.51 \pm 0.05 \pm 0.03$	746	² BARATE	99M ALEP	$E_{cm}^{ee} = 172 + 183$ GeV
¹ ABBIENDI 00v tag $W \rightarrow cX$ decays using measured jet properties, lifetime information, and leptons produced in charm decays. From this result, and using the additional measurements of $\Gamma(W)$ and $B(W \rightarrow \text{hadrons})$, $ V_{cs} $ is determined to be $0.969 \pm 0.045 \pm 0.036$.				
² BARATE 99M tag c jets using a neural network algorithm. From this measurement $ V_{cs} $ is determined to be $1.00 \pm 0.11 \pm 0.07$.				

 $R_{c5} = \Gamma(c\bar{s})/\Gamma(\text{hadrons})$ Γ_9/Γ_5

VALUE	DOCUMENT ID	TECN	COMMENT
$0.46^{+0.19}_{-0.14} \pm 0.07$	¹ ABREU	98N DLPH	$E_{cm}^{ee} = 161+172$ GeV
¹ ABREU 98N tag c and s jets by identifying a charged kaon as the highest momentum particle in a hadronic jet. They also use a lifetime tag to independently identify a c jet, based on the impact parameter distribution of charged particles in a jet. From this measurement $ V_{cs} $ is determined to be $0.94^{+0.32}_{-0.26} \pm 0.13$.			

 $\Gamma(\pi^+\pi^+\pi^-)/\Gamma_{\text{total}}$ Γ_{11}/Γ

VALUE (units 10^{-6})	CL%	DOCUMENT ID	TECN	COMMENT
< 1.01	95	¹ SIRUNYAN	19BG CMS	$E_{cm}^{pp} = 13$ TeV
¹ SIRUNYAN 19BG search for the rare decay of a W boson into three charged pions. Three pion candidates are required in each event, with transverse momentum larger than 35 GeV, 35 GeV, 18 GeV, respectively, while the transverse momentum of the three-pion system is required to be larger than 40 GeV. Analyzing the three-pion invariant mass, no excess is observed in the W mass region, leading to the 95% C.L. upper limit on the branching fraction.				

AVERAGE PARTICLE MULTIPLICITIES IN HADRONIC W DECAY

Summed over particle and antiparticle, when appropriate.

 $\langle N_{\pi^\pm} \rangle$

VALUE	DOCUMENT ID	TECN	COMMENT
15.70 ± 0.35	¹ ABREU,P	00F DLPH	$E_{cm}^{ee} = 189$ GeV
¹ ABREU,P 00F measure $\langle N_{\pi^\pm} \rangle = 31.65 \pm 0.48 \pm 0.76$ and $15.51 \pm 0.38 \pm 0.40$ in the fully hadronic and semileptonic final states respectively. The value quoted is a weighted average without assuming any correlations.			

 $\langle N_{K^\pm} \rangle$

VALUE	DOCUMENT ID	TECN	COMMENT
2.20 ± 0.19	¹ ABREU,P	00F DLPH	$E_{cm}^{ee} = 189$ GeV
¹ ABREU,P 00F measure $\langle N_{K^\pm} \rangle = 4.38 \pm 0.42 \pm 0.12$ and $2.23 \pm 0.32 \pm 0.17$ in the fully hadronic and semileptonic final states respectively. The value quoted is a weighted average without assuming any correlations.			

 $\langle N_p \rangle$

VALUE	DOCUMENT ID	TECN	COMMENT
0.92 ± 0.14	¹ ABREU,P	00F DLPH	$E_{cm}^{ee} = 189$ GeV
¹ ABREU,P 00F measure $\langle N_p \rangle = 1.82 \pm 0.29 \pm 0.16$ and $0.94 \pm 0.23 \pm 0.06$ in the fully hadronic and semileptonic final states respectively. The value quoted is a weighted average without assuming any correlations.			

 $\langle N_{\text{charged}} \rangle$

VALUE	DOCUMENT ID	TECN	COMMENT
19.39 ± 0.08	OUR AVERAGE		
$19.38 \pm 0.05 \pm 0.08$	¹ ABBIENDI	06A OPAL	$E_{cm}^{ee} = 189-209$ GeV
19.44 ± 0.17	² ABREU,P	00F DLPH	$E_{cm}^{ee} = 183+189$ GeV

$19.3 \pm 0.3 \pm 0.3$	³ ABBIENDI	99N OPAL	$E_{cm}^{ee} = 183$ GeV
19.23 ± 0.74	⁴ ABREU	98C DLPH	$E_{cm}^{ee} = 172$ GeV

¹ABBIENDI 06A measure $\langle N_{\text{charged}} \rangle = 38.74 \pm 0.12 \pm 0.26$ when both W bosons decay hadronically and $\langle N_{\text{charged}} \rangle = 19.39 \pm 0.11 \pm 0.09$ when one W boson decays semileptonically. The value quoted here is obtained under the assumption that there is no color reconnection between W bosons; the value is a weighted average taking into account correlations in the systematic uncertainties.

²ABREU,P 00F measure $\langle N_{\text{charged}} \rangle = 39.12 \pm 0.33 \pm 0.36$ and $38.11 \pm 0.57 \pm 0.44$ in the fully hadronic final states at 189 and 183 GeV respectively, and $\langle N_{\text{charged}} \rangle = 19.49 \pm 0.31 \pm 0.27$ and $19.78 \pm 0.49 \pm 0.43$ in the semileptonic final states. The value quoted is a weighted average without assuming any correlations.

³ABBIENDI 99N use the final states $W^+W^- \rightarrow q\bar{q}\ell\bar{\nu}_\ell$ to derive this value.

⁴ABREU 98C combine results from both the fully hadronic as well semileptonic WW final states after demonstrating that the W decay charged multiplicity is independent of the topology within errors.

TRIPLE GAUGE COUPLINGS (TGC'S)

Revised April 2017 by M.W. Grunewald (U. College Dublin) and A. Gurtu (Formerly Tata Inst.).

Fourteen independent couplings, seven each for ZWW and γWW , completely describe the VWW vertices within the most general framework of the electroweak Standard Model (SM) consistent with Lorentz invariance and U(1) gauge invariance. Of each of the seven TGCs, three conserve C and P individually, three violate CP, and one violates C and P individually while conserving CP. Assumption of C and P conservation and electromagnetic gauge invariance reduces the number of independent VWW couplings to five: one common set [1,2] is $(\kappa_\gamma, \kappa_Z, \lambda_\gamma, \lambda_Z, g_1^Z)$, where $\kappa_\gamma = \kappa_Z = g_1^Z = 1$ and $\lambda_\gamma = \lambda_Z = 0$ in the Standard Model at tree level. The parameters κ_Z and λ_Z are related to the other three due to constraints of gauge invariance as follows: $\kappa_Z = g_1^Z - (\kappa_\gamma - 1) \tan^2 \theta_W$ and $\lambda_Z = \lambda_\gamma$, where θ_W is the weak mixing angle. The W magnetic dipole moment, μ_W , and the W electric quadrupole moment, q_W , are expressed as $\mu_W = e(1 + \kappa_\gamma + \lambda_\gamma)/2M_W$ and $q_W = -e(\kappa_\gamma - \lambda_\gamma)/M_W^2$.

Precision measurements of suitable observables at LEP1 has already led to an exploration of much of the TGC parameter space. At LEP2, the VWW coupling arises in W-pair production via s-channel exchange, or in single W production via the radiation of a virtual photon off the incident e^+ or e^- . At the Tevatron and the LHC, hard-photon bremsstrahlung off a produced W or Z signals the presence of a triple-gauge vertex. In order to extract the value of one TGC, the others are generally kept fixed to their SM values. While most analyses use the above gauge constraints in the extraction of TGCs, one analysis of W-pair events also determines the real and imaginary parts of all 14 couplings using unconstrained single-parameter fits [3]. The results are consistent. Some experiments have determined limits on the couplings under various non-LEP scenarios and assuming different values of the form factor Λ , where the coupling parameters are scaled by $1/(1 + s/\Lambda^2)^2$. For practical reasons it is not possible to quote all such determinations in the listings. For that the individual papers may be consulted. Recently, EFT-inspired sets of couplings [4,5], such as $c_{WWW}/\Lambda^2, c_W/\Lambda^2, c_B/\Lambda^2$ which are linearly related to the couplings discussed above, are also determined by the LHC experiments.

References

1. K. Hagiwara *et al.*, Nucl. Phys. **B282**, 253 (1987).

2. G. Gounaris *et al.*, CERN 96-01 p. 525.
3. S. Schael *et al.* (ALEPH Collab.), Phys. Lett. **B614**, 7 (2005).
4. K. Hagiwara *et al.*, Phys. Rev. **D48**, 2182 (1993).
5. C. Degrande *et al.*, Annals Phys. **335** (2013) 21-32.

 g_1^Z

OUR FIT below is taken from [SCHAE13A].

VALUE	EVTS	DOCUMENT ID	TECN	COMMENT
0.984^{+0.018}_{-0.020}				OUR FIT
0.975 ^{+0.033} _{-0.030}	7872	1 ABDALLAH	10 DLPH	$E_{cm}^{ee} = 189\text{--}209$ GeV
1.001 \pm 0.027 \pm 0.013	9310	2 SCHAE1	05A ALEP	$E_{cm}^{ee} = 183\text{--}209$ GeV
0.987 ^{+0.034} _{-0.033}	9800	3 ABBIENDI	04D OPAL	$E_{cm}^{ee} = 183\text{--}209$ GeV
0.966 ^{+0.034} _{-0.032} \pm 0.015	8325	4 ACHARD	04D L3	$E_{cm}^{ee} = 161\text{--}209$ GeV
• • •				We do not use the following data for averages, fits, limits, etc. • • •
		5 SIRUNYAN	20BA CMS	$E_{cm}^{pp} = 13$ TeV
		6 SIRUNYAN	19CL CMS	$E_{cm}^{pp} = 13$ TeV
		7 SIRUNYAN	18BZ CMS	$E_{cm}^{pp} = 13$ TeV
		8 AABOUD	17s ATLS	$E_{cm}^{pp} = 7+8$ TeV
		9 AABOUD	17u ATLS	$E_{cm}^{pp} = 8$ TeV
		10 KHACHATRYAN	17o CMS	$E_{cm}^{pp} = 8$ TeV
		11 SIRUNYAN	17X CMS	$E_{cm}^{pp} = 8$ TeV
		12 AAD	16AR ATLS	$E_{cm}^{pp} = 8$ TeV
		13 AAD	16P ATLS	$E_{cm}^{pp} = 8$ TeV
		14 AAD	14Y ATLS	$E_{cm}^{pp} = 8$ TeV
		15 AAD	13AL ATLS	$E_{cm}^{pp} = 7$ TeV
		16 CHATRCHYAN	13BF CMS	$E_{cm}^{pp} = 7$ TeV
		17 AAD	12CD ATLS	$E_{cm}^{pp} = 7$ TeV
		18 AALTONEN	12AC CDF	$E_{cm}^{pp} = 1.96$ TeV
		19 ABAZOV	12AG D0	$E_{cm}^{pp} = 1.96$ TeV
	34	20 ABAZOV	11 D0	$E_{cm}^{pp} = 1.96$ TeV
	334	21 AALTONEN	10K CDF	$E_{cm}^{pp} = 1.96$ TeV
1.04 \pm 0.09		22 ABAZOV	09AD D0	$E_{cm}^{pp} = 1.96$ TeV
		23 ABAZOV	09AJ D0	$E_{cm}^{pp} = 1.96$ TeV
1.07 ^{+0.08} _{-0.12}	1880	24 ABDALLAH	08C DLPH	Superseded by ABDALLAH 10
	13	25 ABAZOV	07Z D0	$E_{cm}^{pp} = 1.96$ TeV
	2.3	26 ABAZOV	05s D0	$E_{cm}^{pp} = 1.96$ TeV
0.98 \pm 0.07 \pm 0.01	2114	27 ABREU	01i DLPH	$E_{cm}^{ee} = 183+189$ GeV
	331	28 ABBOTT	99i D0	$E_{cm}^{pp} = 1.8$ TeV

¹ ABDALLAH 10 use data on the final states $e^+e^- \rightarrow jj\ell\nu, jijj, jX, \ell X$, at center-of-mass energies between 189–209 GeV at LEP2, where $j = \text{jet}$, $\ell = \text{lepton}$, and X represents missing momentum. The fit is carried out keeping all other parameters fixed at their SM values.

² SCHAE1 05A study single-photon, single- W , and WW -pair production from 183 to 209 GeV. The result quoted here is derived from the WW -pair production sample. Each parameter is determined from a single-parameter fit in which the other parameters assume their Standard Model values.

³ ABBIENDI 04D combine results from W^+W^- in all decay channels. Only CP -conserving couplings are considered and each parameter is determined from a single-parameter fit in which the other parameters assume their Standard Model values. The 95% confidence interval is $0.923 < g_1^Z < 1.054$.

⁴ ACHARD 04D study WW -pair production, single- W production and single-photon production with missing energy from 189 to 209 GeV. The result quoted here is obtained from the WW -pair production sample including data from 161 to 183 GeV, ACCIARRI 99Q. Each parameter is determined from a single-parameter fit in which the other parameters assume their Standard Model values.

⁵ SIRUNYAN 20BA study electroweak production of a W boson in association with two jets, using W decays in the electron or muon channel. The isolated muons (electrons) are required to have a transverse momentum larger than 25 (30) GeV, while the transverse momentum of the two jets has to be larger than 50 and 30 GeV. A total of 2.382 (1.051) million events are selected in the muon (electron) channel, with a Standard Model expectation of 2.39 ± 0.17 (1.054 ± 0.058) million events. Analyzing the transverse momentum distribution of the charged leptons from W decay, the following 95% C.L. limit is obtained: $0.971 < g_1^Z < 1.044$. Combining this result with that from the closely-related electroweak Z -jet-jet production SIRUNYAN 18BZ, the limit becomes: $0.979 < g_1^Z < 1.034$.

⁶ SIRUNYAN 19CL study WW and WZ production in lepton + jet events, with one W boson decaying leptonically (electron or muon), and another W or Z boson decaying hadronically, reconstructed as a single massive large-radius jet. In the electron channel 2,456 (2,235) events are selected in the $W(W/Z)$ category, while in the muon channel 3,996 (3,572) events are selected in the $W(W/Z)$ category. Analyzing the di-boson invariant mass distribution, the following 95% C.L. limit is obtained: $0.9939 < g_1^Z < 1.0074$.

⁷ SIRUNYAN 18BZ study $pp \rightarrow Z$ jet jet events at 13 TeV where $Z \rightarrow e^+e^-/\mu^+\mu^-$. Isolated electrons and muons are selected with p_T of the leading/sub-leading lepton $> 30/20$ GeV and $|\eta| < 2.4$, with the di-lepton invariant mass within 15 GeV of the Z mass. The two highest p_T jets are selected with p_T of the leading/sub-leading jet $> 50/30$ GeV respectively and dijet invariant mass > 200 GeV. Templates in the transverse momentum of the Z are utilized to set limits on the triple gauge couplings in the EFT and the LEP parametrizations. The following 95% C.L. limit is obtained: $0.965 < g_1^Z < 1.042$.

⁸ AABOUD 17s analyze electroweak production of a W boson in association with two jets at high dijet invariant mass, with the W boson decaying to electron or muon plus neutrino. In the signal region of dijet mass larger than 1 TeV and leading-jet transverse momentum larger than 600 GeV, 30 events are observed in the data with 39 ± 4 events expected in the Standard Model, yielding the following limit at 95% CL for the form factor cut-off scale $\Lambda_{FF} \rightarrow \infty$: $0.87 < g_1^Z < 1.12$.

⁹ AABOUD 17u analyze production of WW or WZ boson pairs with one W boson decaying to electron or muon plus neutrino, and the other W or Z boson decaying hadronically. The hadronic decay system is reconstructed as either a resolved two-jet system or as a single large jet. Analyzing the transverse momentum distribution of the hadronic system above 100 GeV yields the following limit at 95% CL for the form factor cut-off scale $\Lambda_{FF} \rightarrow \infty$: $0.979 < g_1^Z < 1.024$.

¹⁰ KHACHATRYAN 17o analyze WZ production where each boson decays into electrons or muons. Events are required to have a tri-lepton invariant mass larger than 100 GeV, with one of the lepton pairs having an invariant mass within 20 GeV of the Z boson mass. The Z transverse momentum spectrum is analyzed to set a 95% C.L. limit of: $0.982 < g_1^Z < 1.035$.

¹¹ SIRUNYAN 17X study $pp \rightarrow WW/WZ \rightarrow \ell\nu q\bar{q}$ production at 8 TeV where ℓ is an electron or muon with $p_T > 30$ or 25 GeV respectively. Suitable cuts are put on the p_T of the dijet system and the missing E_T of the event yielding a total of 285 and 204 WW events observed in the electron and muon channels. The following 95% C.L. limit is obtained: $0.9913 < g_1^Z < 1.024$.

¹² AAD 16AR study WW production in pp collisions and select 6636 WW candidates in decay modes with electrons or muons with an expected background of 1546 ± 157 events. Assuming the LEP formulation and setting the form-factor Λ to infinity, a fit to the transverse momentum distribution of the leading charged lepton, leads to a 95% C.L. range of $0.984 < g_1^Z < 1.027$.

¹³ AAD 16P study WZ production in pp collisions and select 2091 WZ candidates in 4 decay modes with electrons and muons, with an expected background of 1825 ± 7 events. Analyzing the WZ transverse momentum distribution, the resulting 95% C.L. limit is: $0.981 < g_1^Z < 1.029$.

¹⁴ AAD 14Y determine the electroweak Z -dijet cross section in 8 TeV pp collisions. $Z \rightarrow ee$ and $Z \rightarrow \mu\mu$ decays are selected with the di-lepton $p_T > 20$ GeV and mass in the 81–101 GeV range. Minimum two jets are required with $p_T > 55$ and 45 GeV and no additional jets with $p_T > 25$ GeV in the rapidity interval between them. The normalized p_T balance between the Z and the two jets is required to be < 0.15 . This leads to a selection of 900 events with dijet mass > 1 TeV. The number of signal and background events expected is 261 and 592 respectively. A Poisson likelihood method is used on an event by event basis to obtain the 95% CL limit $0.5 < g_1^Z < 1.26$ for a form factor value $\Lambda = \infty$.

¹⁵ AAD 13AL study WW production in pp collisions and select 1325 WW candidates in decay modes with electrons or muons with an expected background of 369 ± 61 events. Assuming the LEP formulation and setting the form-factor $\Lambda = \infty$, a fit to the transverse momentum distribution of the leading charged lepton, leads to a 95% C.L. range of $0.961 < g_1^Z < 1.052$. Supersedes AAD 12Ac.

¹⁶ CHATRCHYAN 13BF determine the W^+W^- production cross section using unlike sign di-lepton (e or μ) events with high p_T . The leptons have $p_T > 20$ GeV/c and are isolated. 1134 candidate events are observed with an expected SM background of 247 ± 34 . The p_T distribution of the leading lepton is fitted to obtain 95% C.L. limits of $0.905 \leq g_1^Z \leq 1.095$.

¹⁷ AAD 12CD study WZ production in pp collisions and select 317 WZ candidates in three $\ell\nu$ decay modes with an expected background of 68.0 ± 10.0 events. The resulting 95% C.L. range is: $0.943 < g_1^Z < 1.093$. Supersedes AAD 12v.

¹⁸ AALTONEN 12AC study WZ production in $p\bar{p}$ collisions and select 63 WZ candidates in three $\ell\nu$ decay modes with an expected background of 7.9 ± 1.0 events. Based on the cross section and shape of the Z transverse momentum spectrum, the following 95% C.L. range is reported: $0.92 < g_1^Z < 1.20$ for a form factor of $\Lambda = 2$ TeV.

¹⁹ ABAZOV 12AG combine new results with already published results on $W\gamma$, WW and WZ production in order to determine the couplings with increased precision, superseding ABAZOV 08R, ABAZOV 11AC, ABAZOV 09AJ, ABAZOV 09AD. The 68% C.L. result for a formfactor cutoff of $\Lambda = 2$ TeV is $g_1^Z = 1.022^{+0.032}_{-0.030}$.

²⁰ ABAZOV 11 study the $p\bar{p} \rightarrow 3\ell\nu$ process arising in WZ production. They observe 34 WZ candidates with an estimated background of 6 events. An analysis of the p_T spectrum of the Z boson leads to a 95% C.L. limit of $0.944 < g_1^Z < 1.154$, for a form factor $\Lambda = 2$ TeV.

²¹ AALTONEN 10K study $p\bar{p} \rightarrow W^+W^-$ with $W \rightarrow e/\mu\nu$. The p_T of the leading (second) lepton is required to be > 20 (10) GeV. The final number of events selected is 654 of which 320 ± 47 are estimated to be background. The 95% C.L. interval is $0.76 < g_1^Z < 1.34$ for $\Lambda = 1.5$ TeV and $0.78 < g_1^Z < 1.30$ for $\Lambda = 2$ TeV.

²² ABAZOV 09AD study the $p\bar{p} \rightarrow \ell\nu 2\text{jet}$ process arising in WW and WZ production. They select 12,473 (14,392) events in the electron (muon) channel with an expected di-boson signal of 436 (527) events. The results on the anomalous couplings are derived from an analysis of the p_T spectrum of the 2-jet system and quoted at 68% C.L. and for a form factor of 2 TeV. This measurement is not used for obtaining the mean as it is for a specific form factor. The 95% confidence interval is $0.88 < g_1^Z < 1.20$.

²³ ABAZOV 09AJ study the $p\bar{p} \rightarrow 2\ell 2\nu$ process arising in WW production. They select 100 events with an expected WW signal of 65 events. An analysis of the p_T spectrum of the two charged leptons leads to 95% C.L. limits of $0.86 < g_1^Z < 1.3$, for a form factor $\Lambda = 2$ TeV.

Gauge & Higgs Boson Particle Listings

W

- ²⁴ ABDALLAH 08c determine this triple gauge coupling from the measurement of the spin density matrix elements in $e^+e^- \rightarrow W^+W^- \rightarrow (qq)(\ell\nu)$, where $\ell = e$ or μ . Values of all other couplings are fixed to their standard model values.
- ²⁵ ABAZOV 07z set limits on anomalous TGCs using the measured cross section and $p_T(Z)$ distribution in WZ production with both the W and the Z decaying leptonically into electrons and muons. Setting the other couplings to their standard model values, the 95% C.L. limit for a form factor scale $\Lambda = 2$ TeV is $0.86 < g_1^Z < 1.35$.
- ²⁶ ABAZOV 05s study $\bar{p}p \rightarrow WZ$ production with a subsequent trilepton decay to $\ell\nu\ell'\bar{\ell}'$ (ℓ and $\ell' = e$ or μ). Three events (estimated background 0.71 ± 0.08 events) with WZ decay characteristics are observed from which they derive limits on the anomalous WWZ couplings. The 95% CL limit for a form factor scale $\Lambda = 1.5$ TeV is $0.51 < g_1^Z < 1.66$, fixing λ_Z and κ_Z to their Standard Model values.
- ²⁷ ABREU 01i combine results from e^+e^- interactions at 189 GeV leading to W^+W^- and $W\nu_e$ final states with results from ABREU 99L at 183 GeV. The 95% confidence interval is $0.84 < g_1^Z < 1.13$.
- ²⁸ ABBOTT 99i perform a simultaneous fit to the $W\gamma$, $WW \rightarrow$ dilepton, $WW/WZ \rightarrow e\nu jj$, $WW/WZ \rightarrow \mu\nu jj$, and $WZ \rightarrow$ trilepton data samples. For $\Lambda = 2.0$ TeV, the 95%CL limits are $0.63 < g_1^Z < 1.57$, fixing λ_Z and κ_Z to their Standard Model values, and assuming Standard Model values for the $WW\gamma$ couplings.

 κ_γ

OUR FIT below is taken from [SCHAEL 13A].

VALUE	EVTS	DOCUMENT ID	TECN	COMMENT
0.982 ± 0.042 OUR FIT				
1.024 ^{+0.077} _{-0.081}	7872	1 ABDALLAH	10 DLPH	$E_{cm}^{ee} = 189-209$ GeV
0.971 ± 0.055 ± 0.030	10689	2 SCHAEEL	05A ALEP	$E_{cm}^{ee} = 183-209$ GeV
0.88 ^{+0.09} _{-0.08}	9800	3 ABBIENDI	04D OPAL	$E_{cm}^{ee} = 183-209$ GeV
1.013 ^{+0.067} _{-0.064} ± 0.026	10575	4 ACHARD	04D L3	$E_{cm}^{ee} = 161-209$ GeV
• • • We do not use the following data for averages, fits, limits, etc. • • •				
		5 AABOUD	17U ATLS	$E_{cm}^{pp} = 8$ TeV
		6 SIRUNYAN	17X CMS	$E_{cm}^{pp} = 8$ TeV
		7 CHATRCHYAN 14AB	CMS	$E_{cm}^{pp} = 7$ TeV
		8 AAD	13AN ATLS	$E_{cm}^{pp} = 7$ TeV
		9 CHATRCHYAN 13BF	CMS	$E_{cm}^{pp} = 7$ TeV
		10 ABAZOV	12AG D0	$E_{cm}^{pp} = 1.96$ TeV
		11 ABAZOV	11AC D0	$E_{cm}^{pp} = 1.96$ TeV
		12 CHATRCHYAN 11M	CMS	$E_{cm}^{pp} = 7$ TeV
	334	13 AALTONEN	10K CDF	$E_{cm}^{pp} = 1.96$ TeV
	53	14 AARON	09B H1	$E_{cm}^{pp} = 0.3$ TeV
1.07 ^{+0.26} _{-0.29}		15 ABAZOV	09AD D0	$E_{cm}^{pp} = 1.96$ TeV
		16 ABAZOV	09AJ D0	$E_{cm}^{pp} = 1.96$ TeV
		17 ABAZOV	08R D0	$E_{cm}^{pp} = 1.96$ TeV
0.68 ^{+0.17} _{-0.15}	1880	18 ABDALLAH	08c DLPH	Superseded by ABDALLAH 10
	1617	19 AALTONEN	07L CDF	$E_{cm}^{pp} = 1.96$ GeV
	17	20 ABAZOV	06H D0	$E_{cm}^{pp} = 1.96$ TeV
	141	21 ABAZOV	05J D0	$E_{cm}^{pp} = 1.96$ TeV
1.25 ^{+0.21} _{-0.20} ± 0.06	2298	22 ABREU	01i DLPH	$E_{cm}^{ee} = 183+189$ GeV
		23 BREITWEG	00 ZEUS	$e^+p \rightarrow e^+W^+X$, $\sqrt{s} \approx 300$ GeV
0.92 ± 0.34	331	24 ABBOTT	99i D0	$E_{cm}^{pp} = 1.8$ TeV

- ¹ ABDALLAH 10 use data on the final states $e^+e^- \rightarrow jj\ell\nu, jjjj, jjX, \ell X$, at center-of-mass energies between 189–209 GeV at LEP2, where $j = \text{jet}$, $\ell = \text{lepton}$, and X represents missing momentum. The fit is carried out keeping all other parameters fixed at their SM values.
- ² SCHAEEL 05A study single-photon, single- W , and WW -pair production from 183 to 209 GeV. Each parameter is determined from a single-parameter fit in which the other parameters assume their Standard Model values.
- ³ ABBIENDI 04D combine results from W^+W^- in all decay channels. Only CP -conserving couplings are considered and each parameter is determined from a single-parameter fit in which the other parameters assume their Standard Model values. The 95% confidence interval is $0.73 < \kappa_\gamma < 1.07$.
- ⁴ ACHARD 04D study WW -pair production, single- W production and single-photon production with missing energy from 189 to 209 GeV. The result quoted here is obtained including data from 161 to 183 GeV, ACCIARRI 99Q. Each parameter is determined from a single-parameter fit in which the other parameters assume their Standard Model values.
- ⁵ AABOUD 17u analyze production of WW or WZ boson pairs with one W boson decaying to electron or muon plus neutrino, and the other W or Z boson decaying hadronically. The hadronic decay system is reconstructed as either a resolved two-jet system or as a single large jet. Analysing the transverse momentum distribution of the hadronic system above 100 GeV yields the following limit at 95% CL for the form factor cut-off scale $\Lambda_{FP} \rightarrow \infty$: $0.939 < \kappa_\gamma < 1.064$.
- ⁶ SIRUNYAN 17x study $pp \rightarrow WW/WZ \rightarrow \ell\nu q\bar{q}$ production at 8 TeV where ℓ is an electron or muon with $p_T > 30$ or 25 GeV respectively. Suitable cuts are put on the p_T of the dijet system and the missing E_T of the event yielding a total of 285 and 204 WW events observed in the electron and muon channels. The following 95% C.L. limit is obtained: $0.956 < \kappa_\gamma < 1.063$.

- ⁷ CHATRCHYAN 14AB measure $W\gamma$ production cross section for $p_T^\gamma > 15$ GeV and $R(\ell\gamma) > 0.7$, which is the separation between the γ and the final state charged lepton (e or μ) in the azimuthal angle-pseudorapidity ($\phi - \eta$) plane. After background subtraction the number of $e\nu\gamma$ and $\mu\nu\gamma$ events is determined to be 3200 ± 325 and 4970 ± 543 respectively, compatible with expectations from the SM. This leads to a 95% CL limit of $0.62 < \kappa_\gamma < 1.29$, assuming other parameters have SM values.
- ⁸ AAD 13AN study $W\gamma$ production in pp collisions. In events with no additional jet, 4449 (6578) W decays to electron (muon) are selected, with an expected background of 1662 ± 262 (2538 \pm 362) events. Analysing the photon p_T spectrum above 100 GeV yields a 95% C.L. limit of $0.59 < \kappa_\gamma < 1.46$. Supersedes AAD 12Bx.
- ⁹ CHATRCHYAN 13BF determine the W^+W^- production cross section using unlike sign di-lepton (e or μ) events with high p_T . The leptons have $p_T > 20$ GeV/c and are isolated. 1134 candidate events are observed with an expected SM background of 247 ± 34 . The p_T distribution of the leading lepton is fitted to obtain 95% C.L. limits of $0.79 \leq \kappa_\gamma \leq 1.22$.
- ¹⁰ ABAZOV 12AG combine new results with already published results on $W\gamma$, WW and WZ production in order to determine the couplings with increased precision, superseding ABAZOV 08R, ABAZOV 11AC, ABAZOV 09AJ, ABAZOV 09AD. The 68% C.L. result for a formfactor cutoff of $\Lambda = 2$ TeV is $1.048^{+0.106}_{-0.105}$.
- ¹¹ ABAZOV 11AC study $W\gamma$ production in $p\bar{p}$ collisions at 1.96 TeV, with the W decay products containing an electron or a muon. They select 196 (363) events in the electron (muon) mode, with a SM expectation of 190 (372) events. A likelihood fit to the photon E_T spectrum above 15 GeV yields at 95% C.L. the result: $0.6 < \kappa_\gamma < 1.4$ for a formfactor $\Lambda = 2$ TeV.
- ¹² CHATRCHYAN 11M study $W\gamma$ production in pp collisions at $\sqrt{s} = 7$ TeV using 36 pb^{-1} pp data with the W decaying to electron and muon. The total cross section is measured for photon transverse energy $E_T^\gamma > 10$ GeV and spatial separation from charged leptons in the plane of pseudo rapidity and azimuthal angle $\Delta R(\ell, \gamma) > 0.7$. The number of candidate (background) events is 452 (228 ± 21) for the electron channel and 520 (277 ± 25) for the muon channel. Setting other couplings to their standard model value, they derive a 95% CL limit of $-0.11 < \kappa_\gamma < 2.04$.
- ¹³ AALTONEN 10K study $p\bar{p} \rightarrow W^+W^-$ with $W \rightarrow e/\mu\nu$. The p_T of the leading (second) lepton is required to be > 20 (10) GeV. The final number of events selected is 654 of which 320 ± 47 are estimated to be background. The 95% C.L. interval is $0.37 < \kappa_\gamma < 1.72$ for $\Lambda = 1.5$ TeV and $0.43 < \kappa_\gamma < 1.65$ for $\Lambda = 2$ TeV.
- ¹⁴ AARON 09B study single- W production in ep collisions at 0.3 TeV C.M. energy. They select 53 $W \rightarrow e/\mu$ events with a standard model expectation of 54.1 ± 7.4 events. Fitting the transverse momentum spectrum of the hadronic recoil system they obtain a 95% C.L. limit of $-3.7 < \kappa_\gamma < -1.5$ or $0.3 < \kappa_\gamma < 1.5$, where the ambiguity is due to the quadratic dependence of the cross section to the coupling parameter.
- ¹⁵ ABAZOV 09AD study the $p\bar{p} \rightarrow \ell\nu 2\text{jet}$ process arising in WW and WZ production. They select 12,473 (14,392) events in the electron (muon) channel with an expected di-boson signal of 436 (527) events. The results on the anomalous couplings are derived from an analysis of the p_T spectrum of the 2-jet system and quoted at 68% C.L. and for a form factor of 2 TeV. This measurement is not used for obtaining the mean as it is for a specific form factor. The 95% confidence interval is $0.56 < \kappa_\gamma < 1.55$.
- ¹⁶ ABAZOV 09AJ study the $p\bar{p} \rightarrow 2\ell 2\nu$ process arising in WW production. They select 100 events with an expected WW signal of 65 events. An analysis of the p_T spectrum of the two charged leptons leads to 95% C.L. limits of $0.46 < \kappa_\gamma < 1.83$, for a form factor $\Lambda = 2$ TeV.
- ¹⁷ ABAZOV 08R use 0.7 fb^{-1} $p\bar{p}$ data at $\sqrt{s} = 1.96$ TeV to select 263 $W\gamma + X$ events, of which 187 constitute signal, with the W decaying into an electron or a muon, which is required to be well separated from a photon with $E_T > 9$ GeV. A likelihood fit to the photon E_T spectrum yields a 95% CL limit $0.49 < \kappa_\gamma < 1.51$ with other couplings fixed to their Standard Model values.
- ¹⁸ ABDALLAH 08c determine this triple gauge coupling from the measurement of the spin density matrix elements in $e^+e^- \rightarrow W^+W^- \rightarrow (qq)(\ell\nu)$, where $\ell = e$ or μ . Values of all other couplings are fixed to their standard model values.
- ¹⁹ AALTONEN 07L set limits on anomalous TGCs using the $p_T(W)$ distribution in WW and WZ production with the W decaying to an electron or muon and the Z to 2 jets. Setting other couplings to their standard model value, the 95% C.L. limits are $0.54 < \kappa_\gamma < 1.39$ for a form factor scale $\Lambda = 1.5$ TeV.
- ²⁰ ABAZOV 06H study $\bar{p}p \rightarrow WW$ production with a subsequent decay $WW \rightarrow e^+\nu_e e^-\bar{\nu}_e, WW \rightarrow e^\pm\nu_e\mu^\mp\nu_\mu$, or $WW \rightarrow \mu^+\nu_\mu\mu^-\bar{\nu}_\mu$. The 95% C.L. limit for a form factor scale $\Lambda = 1$ TeV is $-0.05 < \kappa_\gamma < 2.29$, fixing $\lambda_\gamma = 0$. With the assumption that the $WW\gamma$ and WWZ couplings are equal the 95% C.L. one-dimensional limit ($\Lambda = 2$ TeV) is $0.68 < \kappa < 1.45$.
- ²¹ ABAZOV 05i perform a likelihood fit to the photon E_T spectrum of $W\gamma + X$ events, where the W decays to an electron or muon which is required to be well separated from the photon. For $\Lambda = 2.0$ TeV the 95% CL limits are $0.12 < \kappa_\gamma < 1.96$. In the fit λ_γ is kept fixed to its Standard Model value.
- ²² ABREU 01i combine results from e^+e^- interactions at 189 GeV leading to W^+W^- , $W\nu_e$, and $\nu\bar{\nu}\gamma$ final states with results from ABREU 99L at 183 GeV. The 95% confidence interval is $0.87 < \kappa_\gamma < 1.68$.
- ²³ BREITWEG 00 search for W production in events with large hadronic p_T . For $p_T > 20$ GeV, the upper limit on the cross section gives the 95%CL limit $-3.7 < \kappa_\gamma < 2.5$ (for $\lambda_\gamma = 0$).
- ²⁴ ABBOTT 99i perform a simultaneous fit to the $W\gamma$, $WW \rightarrow$ dilepton, $WW/WZ \rightarrow e\nu jj$, $WW/WZ \rightarrow \mu\nu jj$, and $WZ \rightarrow$ trilepton data samples. For $\Lambda = 2.0$ TeV, the 95%CL limits are $0.75 < \kappa_\gamma < 1.39$.

 λ_γ

OUR FIT below is taken from [SCHAEL 13A].

VALUE	EVTS	DOCUMENT ID	TECN	COMMENT
-0.022 ± 0.019 OUR FIT				
0.002 ± 0.035	7872	1 ABDALLAH	10 DLPH	$E_{cm}^{ee} = 189-209$ GeV
-0.012 ± 0.027 ± 0.011	10689	2 SCHAEEL	05A ALEP	$E_{cm}^{ee} = 183-209$ GeV
-0.060 ^{+0.034} _{-0.033}	9800	3 ABBIENDI	04D OPAL	$E_{cm}^{ee} = 183-209$ GeV
-0.021 ^{+0.035} _{-0.034} ± 0.017	10575	4 ACHARD	04D L3	$E_{cm}^{ee} = 161-209$ GeV

• • • We do not use the following data for averages, fits, limits, etc. • • •

		5	CHATRCHYAN14AB	CMS	$E_{cm}^{pp} = 7$ TeV
		6	AAD	13AN ATLS	$E_{cm}^{pp} = 7$ TeV
		7	ABAZOV	12AG D0	$E_{cm}^{pp} = 1.96$ TeV
		8	ABAZOV	11AC D0	$E_{cm}^{pp} = 1.96$ TeV
		9	CHATRCHYAN11M	CMS	$E_{cm}^{pp} = 7$ TeV
	53	10	AARON	09B H1	$E_{cm}^{ep} = 0.3$ TeV
0.00 ± 0.06		11	ABAZOV	09AD D0	$E_{cm}^{pp} = 1.96$ TeV
		12	ABAZOV	09AJ D0	$E_{cm}^{pp} = 1.96$ TeV
		13	ABAZOV	08R D0	$E_{cm}^{pp} = 1.96$ TeV
0.16 \pm 0.12 -0.13	1880	14	ABDALLAH	08c DLPH LAH 10	Superseded by ABDAL-
	1617	15	AALTONEN	07L CDF	$E_{cm}^{pp} = 1.96$ GeV
		16	ABAZOV	06H D0	$E_{cm}^{pp} = 1.96$ TeV
	141	17	ABAZOV	05J D0	$E_{cm}^{pp} = 1.96$ TeV
0.05 ± 0.09 ± 0.01	2298	18	ABREU	01I DLPH	$E_{cm}^{ee} = 183+189$ GeV
		19	BREITWEG	00 ZEUS	$e^+p \rightarrow e^+W^{\pm}X$, $\sqrt{s} \approx 300$ GeV
0.00 \pm 0.10 -0.09	331	20	ABBOTT	99I D0	$E_{cm}^{pp} = 1.8$ TeV

- 1 ABDALLAH 10 use data on the final states $e^+e^- \rightarrow jj\ell\nu, jjjj, jjX, \ell X$, at center-of-mass energies between 189–209 GeV at LEP2, where $j = \text{jet}$, $\ell = \text{lepton}$, and X represents missing momentum. The fit is carried out keeping all other parameters fixed at their SM values.
- 2 SCHAE 05A study single-photon, single- W , and WW -pair production from 183 to 209 GeV. Each parameter is determined from a single-parameter fit in which the other parameters assume their Standard Model values.
- 3 ABBIENDI 04d combine results from W^+W^- in all decay channels. Only CP -conserving couplings are considered and each parameter is determined from a single-parameter fit in which the other parameters assume their Standard Model values. The 95% confidence interval is $-0.13 < \lambda_\gamma < 0.01$.
- 4 ACHARD 04d study WW -pair production, single- W production and single-photon production with missing energy from 189 to 209 GeV. The result quoted here is obtained including data from 161 to 183 GeV, ACCIARRI 99q. Each parameter is determined from a single-parameter fit in which the other parameters assume their Standard Model values.
- 5 CHATRCHYAN 14AB measure $W\gamma$ production cross section for $p_T^\gamma > 15$ GeV and $R(\ell\gamma) > 0.7$, which is the separation between the γ and the final state charged lepton (e or μ) in the azimuthal angle-pseudorapidity ($\phi - \eta$) plane. After background subtraction the number of $e\nu\gamma$ and $\mu\nu\gamma$ events is determined to be 3200 ± 325 and 4970 ± 543 respectively, compatible with expectations from the SM. This leads to a 95% CL limit of $-0.050 < \lambda_\gamma < 0.037$, assuming all other parameters have SM values.
- 6 AAD 13AN study $W\gamma$ production in pp collisions. In events with no additional jet, 4449 (6578) W decays to electron (muon) are selected, with an expected background of 1662 ± 262 (2538 ± 362) events. Analysing the photon p_T spectrum above 100 GeV yields a 95% C.L. limit of $-0.065 < \lambda_\gamma < 0.061$. Supersedes AAD 12Bx.
- 7 ABAZOV 12AG combine new results with already published results on $W\gamma$, WW and WZ production in order to determine the couplings with increased precision, superseding ABAZOV 08R, ABAZOV 11AC, ABAZOV 09AJ, ABAZOV 09AD. The 68% C.L. result for a formfactor cutoff of $\Lambda = 2$ TeV is $\lambda_\gamma = 0.007^{+0.021}_{-0.022}$.
- 8 ABAZOV 11AC study $W\gamma$ production in $p\bar{p}$ collisions at 1.96 TeV, with the W decay products containing an electron or a muon. They select 196 (363) events in the electron (muon) mode, with a SM expectation of 190 (372) events. A likelihood fit to the photon E_T spectrum above 15 GeV yields at 95% C.L. the result: $-0.08 < \lambda_\gamma < 0.07$ for a formfactor $\Lambda = 2$ TeV.
- 9 CHATRCHYAN 11M study $W\gamma$ production in pp collisions at $\sqrt{s} = 7$ TeV using 36 pb^{-1} pp data with the W decaying to electron and muon. The total cross section is measured for photon transverse energy $E_T^\gamma > 10$ GeV and spatial separation from charged leptons in the plane of pseudo rapidity and azimuthal angle $\Delta R(\ell, \gamma) > 0.7$. The number of candidate (background) events is 452 (228 ± 21) for the electron channel and 520 (277 ± 25) for the muon channel. Setting other couplings to their standard model value, they derive a 95% CL limit of $-0.18 < \lambda_\gamma < 0.17$.
- 10 AARON 09B study single- W production in ep collisions at 0.3 TeV C.M. energy. They select 53 $W \rightarrow e/\mu$ events with a standard model expectation of 54.1 ± 7.4 events. Fitting the transverse momentum spectrum of the hadronic recoil system they obtain a 95% C.L. limit of $-2.5 < \lambda_\gamma < 2.5$.
- 11 ABAZOV 09AD study the $p\bar{p} \rightarrow \ell\nu 2\text{jet}$ process arising in WW and WZ production. They select 12,473 (14,392) events in the electron (muon) channel with an expected di-boson signal of 436 (527) events. The results on the anomalous couplings are derived from an analysis of the p_T spectrum of the 2-jet system and quoted at 68% C.L. and for a form factor of 2 TeV. This measurement is not used for obtaining the mean as it is for a specific form factor. The 95% confidence interval is $-0.10 < \lambda_\gamma < 0.11$.
- 12 ABAZOV 09AJ study the $p\bar{p} \rightarrow 2\ell 2\nu$ process arising in WW production. They select 100 events with an expected WW signal of 65 events. An analysis of the p_T spectrum of the two charged leptons leads to 95% C.L. limits of $-0.14 < \lambda_\gamma < 0.18$, for a form factor $\Lambda = 2$ TeV.
- 13 ABAZOV 08R use 0.7 fb^{-1} $p\bar{p}$ data at $\sqrt{s} = 1.96$ TeV to select 263 $W\gamma + X$ events, of which 187 constitute signal, with the W decaying into an electron or a muon, which is required to be well separated from a photon with $E_T > 9$ GeV. A likelihood fit to the photon E_T spectrum yields a 95% C.L. limit $-0.12 < \lambda_\gamma < 0.13$ with other couplings fixed to their Standard Model values.
- 14 ABDALLAH 08c determine this triple gauge coupling from the measurement of the spin density matrix elements in $e^+e^- \rightarrow W^+W^- \rightarrow (qq)(\ell\nu)$, where $\ell = e$ or μ . Values of all other couplings are fixed to their standard model values.
- 15 AALTONEN 07L set limits on anomalous TGCs using the $p_T(W)$ distribution in WW and WZ production with the W decaying to an electron or muon and the Z to 2 jets. Setting other couplings to their standard model value, the 95% C.L. limits are $-0.18 < \lambda_\gamma < 0.17$ for a form factor scale $\Lambda = 1.5$ TeV.

- 16 ABAZOV 06H study $p\bar{p} \rightarrow WW$ production with a subsequent decay $WW \rightarrow e^+\nu_e e^-\bar{\nu}_e$, $WW \rightarrow e^+\nu_e \mu^+\bar{\nu}_\mu$ or $WW \rightarrow \mu^+\nu_\mu \mu^-\bar{\nu}_\mu$. The 95% C.L. limit for a form factor scale $\Lambda = 1$ TeV is $-0.97 < \lambda_\gamma < 1.04$, fixing $\kappa_\gamma = 1$. With the assumption that the $WW\gamma$ and WWZ couplings are equal the 95% C.L. one-dimensional limit ($\Lambda = 2$ TeV) is $-0.29 < \lambda < 0.30$.
- 17 ABAZOV 05J perform a likelihood fit to the photon E_T spectrum of $W\gamma + X$ events, where the W decays to an electron or muon which is required to be well separated from the photon. For $\Lambda = 2.0$ TeV the 95% CL limits are $-0.20 < \lambda_\gamma < 0.20$. In the fit κ_γ is kept fixed to its Standard Model value.
- 18 ABREU 01i combine results from e^+e^- interactions at 189 GeV leading to W^+W^- , $W\nu_e$, and $\nu\bar{\nu}$ final states with results from ABREU 99L at 183 GeV. The 95% confidence interval is $-0.11 < \lambda_\gamma < 0.23$.
- 19 BREITWEG 00 search for W production in events with large hadronic p_T . For $p_T > 20$ GeV, the upper limit on the cross section gives the 95%CL limit $-3.2 < \lambda_\gamma < 3.2$ for κ_γ fixed to its Standard Model value.
- 20 ABBOTT 99I perform a simultaneous fit to the $W\gamma$, $WW \rightarrow$ dilepton, $WW/WZ \rightarrow e\nu jj$, $WW/WZ \rightarrow \mu\nu jj$, and $WZ \rightarrow$ trilepton data samples. For $\Lambda = 2.0$ TeV, the 95%CL limits are $-0.18 < \lambda_\gamma < 0.19$.

κ_Z

This coupling is CP -conserving (C - and P -separately conserving).

VALUE	$E_{\nu\nu}$	EVTS	DOCUMENT ID	TECN	COMMENT
$0.924^{+0.059}_{-0.056} \pm 0.024$	7171	1	ACHARD	04D L3	$E_{cm}^{ee} = 189$ –209 GeV
• • • We do not use the following data for averages, fits, limits, etc. • • •					
		2	SIRUNYAN	20BA CMS	$E_{cm}^{pp} = 13$ TeV
		3	SIRUNYAN	19CL CMS	$E_{cm}^{pp} = 13$ TeV
		4	AABOUD	17s ATLS	$E_{cm}^{pp} = 7+8$ TeV
		5	KHACHATRY...	17o CMS	$E_{cm}^{pp} = 8$ TeV
		6	AAD	16AR ATLS	$E_{cm}^{pp} = 8$ TeV
		7	AAD	16P ATLS	$E_{cm}^{pp} = 8$ TeV
		8	AAD	13AL ATLS	$E_{cm}^{pp} = 7$ TeV
		9	AAD	12CD ATLS	$E_{cm}^{pp} = 7$ TeV
		10	AALTONEN	12AC CDF	$E_{cm}^{pp} = 1.96$ TeV
	34	11	ABAZOV	11 D0	$E_{cm}^{pp} = 1.96$ TeV
	17	12	ABAZOV	06H D0	$E_{cm}^{pp} = 1.96$ TeV
	2.3	13	ABAZOV	05s D0	$E_{cm}^{pp} = 1.96$ TeV

- 1 ACHARD 04d study WW -pair production, single- W production and single-photon production with missing energy from 189 to 209 GeV. The result quoted here is obtained using the WW -pair production sample. Each parameter is determined from a single-parameter fit in which the other parameters assume their Standard Model values.
- 2 SIRUNYAN 20BA study electroweak production of a W boson in association with two jets, using W decays in the electron or muon channel. The isolated muons (electrons) are required to have a transverse momentum larger than 25 (30) GeV, while the transverse momentum of the two jets has to be larger than 50 and 30 GeV. A total of 2,382 (1,051) million events are selected in the muon (electron) channel, with a Standard Model expectation of 2.39 ± 0.17 (1.054 ± 0.058) million events. Analysing the transverse momentum distribution of the charged leptons from W decay, the following 95% C.L. limit is obtained: $0.956 < \kappa_Z < 1.044$. Combining this result with that from the closely-related electroweak Z -jet-jet production SIRUNYAN 18Bz, the limit becomes: $0.957 < \kappa_Z < 1.042$.
- 3 SIRUNYAN 19CL study WW and WZ production in lepton + jet events, with one W boson decaying leptonically (electron or muon), and another W or Z boson decaying hadronically, reconstructed as a single massive large-radius jet. In the electron channel 2,456 (2,235) events are selected in the $WW(WZ)$ category, while in the muon channel 3,996 (3,572) events are selected in the $WW(WZ)$ category. Analysing the di-boson invariant mass distribution, the following 95% C.L. limit is obtained: $0.9921 < \kappa_Z < 1.0082$.
- 4 AABOUD 17s analyze electroweak production of a W boson in association with two jets at high dijet invariant mass, with the W boson decaying to electron or muon plus neutrino. In the signal region of dijet mass larger than 1 TeV and leading-jet transverse momentum larger than 600 GeV, 30 events are observed in the data with 39 ± 4 events expected in the Standard Model, yielding the following limit at 95% CL for the form factor cut-off scale $\Lambda_{FF} \rightarrow \infty$: $0.85 < \kappa_Z < 1.16$.
- 5 KHACHATRYAN 17o analyze WZ production where each boson decays into electrons or muons. Events are required to have a tri-lepton invariant mass larger than 100 GeV, with one of the lepton pairs having an invariant mass within 20 GeV of the Z boson mass. The Z transverse momentum spectrum is analyzed to set a 95% C.L. limit of: $0.79 < \kappa_Z < 1.25$.
- 6 AAD 16AR study WW production in pp collisions and select 6636 WW candidates in decay modes with electrons or muons with an expected background of 1546 ± 157 events. Assuming the LEP formulation and setting the form-factor Λ to infinity, a fit to the transverse momentum distribution of the leading charged lepton, leads to a 95% C.L. range of $0.975 < \kappa_Z < 1.020$.
- 7 AAD 16p study WZ production in pp collisions and select 2091 WZ candidates in 4 decay modes with electrons and muons, with an expected background of 1825 ± 7 events. Analysing the WZ transverse momentum distribution, the resulting 95% C.L. limit is: $0.81 < \kappa_Z < 1.30$.
- 8 AAD 13AL study WW production in pp collisions and select 1325 WW candidates in decay modes with electrons or muons with an expected background of 369 ± 61 events. Assuming the LEP formulation and setting the form-factor $\Lambda = \text{infinity}$, a fit to the transverse momentum distribution of the leading charged lepton, leads to a 95% C.L. range of $0.957 < \kappa_Z < 1.043$. Supersedes AAD 12AC.
- 9 AAD 12CD study WZ production in pp collisions and select 317 WZ candidates in three $\ell\nu$ decay modes with an expected background of 68.0 ± 10.0 events. The resulting 95% C.L. range is: $0.63 < \kappa_Z < 1.57$. Supersedes AAD 12v.
- 10 AALTONEN 12AC study WZ production in $p\bar{p}$ collisions and select 63 WZ candidates in three $\ell\nu$ decay modes with an expected background of 7.9 ± 1.0 events. Based on

Gauge & Higgs Boson Particle Listings

W

the cross section and shape of the Z transverse momentum spectrum, the following 95% C.L. range is reported: $0.61 < \kappa_Z < 1.90$ for a form factor of $\Lambda = 2$ TeV.

- 11 ABAZOV 11 study the $p\bar{p} \rightarrow 3\ell\nu$ process arising in WZ production. They observe 34 WZ candidates with an estimated background of 6 events. An analysis of the p_T spectrum of the Z boson leads to a 95% C.L. limit of $0.600 < \kappa_Z < 1.675$, for a form factor $\Lambda = 2$ TeV.
- 12 ABAZOV 06H study $p\bar{p} \rightarrow WW$ production with a subsequent decay $WW \rightarrow e^+\nu_e e^-\bar{\nu}_e$, $WW \rightarrow e^\pm\nu_e\mu^\mp\nu_\mu$ or $WW \rightarrow \mu^\pm\nu_\mu\mu^\mp\nu_\mu$. The 95% C.L. limit for a form factor scale $\Lambda = 2$ TeV is $0.55 < \kappa_Z < 1.55$, fixing $\lambda_Z=0$. With the assumption that the $WW\gamma$ and WWZ couplings are equal the 95% C.L. one-dimensional limit ($\Lambda = 2$ TeV) is $0.68 < \kappa < 1.45$.
- 13 ABAZOV 05s study $p\bar{p} \rightarrow WZ$ production with a subsequent trilepton decay to $\ell\nu\ell'\bar{\ell}'$ (ℓ and $\ell' = e$ or μ). Three events (estimated background 0.71 ± 0.08 events) with WZ decay characteristics are observed from which they derive limits on the anomalous WWZ couplings. The 95% CL limit for a form factor scale $\Lambda = 1$ TeV is $-1.0 < \kappa_Z < 3.4$, fixing λ_Z and g_1^Z to their Standard Model values.

 λ_Z

This coupling is CP -conserving (C - and P -separately conserving).

VALUE	EVTS	DOCUMENT ID	TECN	COMMENT
$-0.088^{+0.060}_{-0.057} \pm 0.023$	7171	1 ACHARD 04D L3	$E_{cm}^{ee} = 189-209$ GeV	
• • • We do not use the following data for averages, fits, limits, etc. • • •				
		2 SIRUNYAN 20BA CMS	$E_{cm}^{pp} = 13$ TeV	
		3 SIRUNYAN 19CL CMS	$E_{cm}^{pp} = 13$ TeV	
		4 SIRUNYAN 18BZ CMS	$E_{cm}^{pp} = 13$ TeV	
		5 AABOUD 17s ATLS	$E_{cm}^{pp} = 7+8$ TeV	
		6 AABOUD 17U ATLS	$E_{cm}^{pp} = 8$ TeV	
		7 KHACHATRYAN 17o CMS	$E_{cm}^{pp} = 8$ TeV	
		8 SIRUNYAN 17X CMS	$E_{cm}^{pp} = 8$ TeV	
		9 AAD 16AR ATLS	$E_{cm}^{pp} = 8$ TeV	
		10 AAD 16P ATLS	$E_{cm}^{pp} = 8$ TeV	
		11 AAD 14Y ATLS	$E_{cm}^{pp} = 8$ TeV	
		12 AAD 13AL ATLS	$E_{cm}^{pp} = 7$ TeV	
		13 CHATRCHYAN 13BF CMS	$E_{cm}^{pp} = 7$ TeV	
		14 AAD 12CD ATLS	$E_{cm}^{pp} = 7$ TeV	
		15 AALTONEN 12AC CDF	$E_{cm}^{pp} = 1.96$ TeV	
	34	16 ABAZOV 11 D0	$E_{cm}^{pp} = 1.96$ TeV	
	334	17 AALTONEN 10K CDF	$E_{cm}^{pp} = 1.96$ TeV	
	13	18 ABAZOV 07Z D0	$E_{cm}^{pp} = 1.96$ TeV	
	17	19 ABAZOV 06H D0	$E_{cm}^{pp} = 1.96$ TeV	
	2.3	20 ABAZOV 05s D0	$E_{cm}^{pp} = 1.96$ TeV	

- 1 ACHARD 04D study W^+W^- pair production, single- W production and single-photon production with missing energy from 189 to 209 GeV. The result quoted here is obtained using the W^+W^- pair production sample. Each parameter is determined from a single-parameter fit in which the other parameters assume their Standard Model values.
- 2 SIRUNYAN 20BA study electroweak production of a W boson in association with two jets, using W decays in the electron or muon channel. The isolated muons (electrons) are required to have a transverse momentum larger than 25 (30) GeV, while the transverse momentum of the two jets has to be larger than 50 and 30 GeV. A total of 2.382 (1.051) million events are selected in the muon (electron) channel, with a Standard Model expectation of 2.39 ± 0.17 (1.054 ± 0.058) million events. Analysing the transverse momentum distribution of the charged leptons from W decay, the following 95% C.L. limit is obtained: $-0.0088 < \lambda_Z < 0.0095$. Combining this result with that from the closely-related electroweak Z-jet-jet production SIRUNYAN 18BZ, the limit becomes: $-0.0071 < \lambda_Z < 0.0076$.
- 3 SIRUNYAN 19CL study WW and WZ production in lepton + jet events, with one W boson decaying leptonically (electron or muon), and another W or Z boson decaying hadronically, reconstructed as a single massive large-radius jet. In the electron channel 2,456 (2,235) events are selected in the $WW(WZ)$ category, while in the muon channel 3,996 (3572) events are selected in the $WW(WZ)$ category. Analysing the di-boson invariant mass distribution, the following 95% C.L. limit is obtained: $-0.0065 < \lambda_Z < 0.0066$.
- 4 SIRUNYAN 18BZ study $pp \rightarrow Z$ jet events at 13 TeV where $Z \rightarrow e^+e^-/\mu^+\mu^-$. Isolated electrons and muons are selected with p_T of the leading/sub-leading lepton $> 30/20$ GeV and $|\eta| < 2.4$, with the di-lepton invariant mass within 15 GeV of the Z mass. The two highest p_T jets are selected with p_T of the leading/sub-leading jet $> 50/30$ GeV respectively and dijet invariant mass > 200 GeV. Templates in the transverse momentum of the Z are utilized to set limits on the triple gauge couplings in the EFT and the LEP parametrizations. The following 95% C.L. limit is obtained: $-0.010 < \lambda_Z < 0.010$.
- 5 AABOUD 17s analyze electroweak production of a W boson in association with two jets at high dijet invariant mass, with the W boson decaying to electron or muon plus neutrino. In the signal region of dijet mass larger than 1 TeV and leading-jet transverse momentum larger than 600 GeV, 30 events are observed in the data with 39 ± 4 events expected in the Standard Model, yielding the following limit at 95% CL for the form factor cut-off scale $\Lambda_{FF} \rightarrow \infty$: $-0.053 < \lambda_Z < 0.042$.
- 6 AABOUD 17U analyze production of WW or WZ boson pairs with one W boson decaying to electron or muon plus neutrino, and the other W or Z boson decaying hadronically. The hadronic decay system is reconstructed as either a resolved two-jet system or as a single large jet. Analysing the transverse momentum distribution of the hadronic system above 100 GeV yields the following limit at 95% CL for the form factor cut-off scale $\Lambda_{FF} \rightarrow \infty$: $-0.013 < \lambda_Z < 0.013$.
- 7 KHACHATRYAN 17o analyse WZ production where each boson decays into electrons or muons. Events are required to have a tri-lepton invariant mass larger than 100 GeV, with one of the lepton pairs having an invariant mass within 20 GeV of the Z boson mass. The Z transverse momentum spectrum is analyzed to set a 95% C.L. limit of: $-0.018 < \lambda_Z < 0.016$.
- 8 SIRUNYAN 17X study $pp \rightarrow WW/WZ \rightarrow \ell\nu q\bar{q}$ production at 8 TeV where ℓ is an electron or muon with $p_T > 30$ or 25 GeV respectively. Suitable cuts are put on the p_T of the dijet system and the missing E_T of the event yielding a total of 285 and 204 WW events observed in the electron and muon channels. The following 95% C.L. limit is obtained: $-0.011 < \lambda_Z < 0.011$.
- 9 AAD 16AR study WW production in pp collisions and select 6636 WW candidates in decay modes with electrons or muons with an expected background of 1546 ± 157 events. Assuming the LEP formulation and setting the form-factor Λ to infinity, a fit to the transverse momentum distribution of the leading charged lepton, leads to a 95% C.L. range of $-0.019 < \lambda_Z < 0.019$.
- 10 AAD 16P study WZ production in pp collisions and select 2091 WZ candidates in 4 decay modes with electrons and muons, with an expected background of 1825 ± 7 events. Analysing the WZ transverse momentum distribution, the resulting 95% C.L. limit is: $-0.016 < \lambda_Z < 0.016$.
- 11 AAD 14Y determine the electroweak Z-dijet cross section in 8 TeV pp collisions. $Z \rightarrow ee$ and $Z \rightarrow \mu\mu$ decays are selected with the di-lepton $p_T > 20$ GeV and mass in the 81-101 GeV range. Minimum two jets are required with $p_T > 55$ and 45 GeV and no additional jets with $p_T > 25$ GeV in the rapidity interval between them. The normalized p_T balance between the Z and the two jets is required to be < 0.15 . This leads to a selection of 900 events with dijet mass > 1 TeV. The number of signal and background events expected is 261 and 592 respectively. A Poisson likelihood method is used on an event by event basis to obtain the 95% CL limit $-0.15 < \lambda_Z < 0.13$ for a form factor value $\Lambda = \infty$.
- 12 AAD 13AL study WW production in pp collisions and select 1325 WW candidates in decay modes with electrons or muons with an expected background of 369 ± 61 events. Assuming the LEP formulation and setting the form-factor $\Lambda = \infty$, a fit to the transverse momentum distribution of the leading charged lepton, leads to a 95% C.L. range of $-0.062 < \lambda_Z < 0.059$. Supersedes AAD 12AC.
- 13 CHATRCHYAN 13BF determine the W^+W^- production cross section using unlike sign di-lepton (e or μ) events with high p_T . The leptons have $p_T > 20$ GeV/c and are isolated. 1134 candidate events are observed with an expected SM background of 247 ± 34 . The p_T distribution of the leading lepton is fitted to obtain 95% C.L. limits of $-0.048 \leq \lambda_Z \leq 0.048$.
- 14 AAD 12CD study WZ production in pp collisions and select 317 WZ candidates in three $\ell\nu$ decay modes with an expected background of 68.0 ± 10.0 events. The resulting 95% C.L. range is: $-0.046 < \lambda_Z < 0.047$. Supersedes AAD 12v.
- 15 AALTONEN 12AC study WZ production in $p\bar{p}$ collisions and select 63 WZ candidates in three $\ell\nu$ decay modes with an expected background of 7.9 ± 1.0 events. Based on the cross section and shape of the Z transverse momentum spectrum, the following 95% C.L. range is reported: $-0.08 < \lambda_Z < 0.10$ for a form factor of $\Lambda = 2$ TeV.
- 16 ABAZOV 11 study the $p\bar{p} \rightarrow 3\ell\nu$ process arising in WZ production. They observe 34 WZ candidates with an estimated background of 6 events. An analysis of the p_T spectrum of the Z boson leads to a 95% C.L. limit of $-0.077 < \lambda_Z < 0.093$, for a form factor $\Lambda = 2$ TeV.
- 17 AALTONEN 10K study $p\bar{p} \rightarrow W^+W^-$ with $W \rightarrow e/\mu\nu$. The p_T of the leading (second) lepton is required to be > 20 (10) GeV. The final number of events selected is 654 of which 320 ± 47 are estimated to be background. The 95% C.L. interval is $-0.16 < \lambda_Z < 0.16$ for $\Lambda = 1.5$ TeV and $-0.14 < \lambda_Z < 0.15$ for $\Lambda = 2$ TeV.
- 18 ABAZOV 07Z set limits on anomalous TGCs using the measured cross section and $p_T(Z)$ distribution in WZ production with both the W and the Z decaying leptonically into electrons and muons. Setting the other couplings to their standard model values, the 95% C.L. limit for a form factor scale $\Lambda = 2$ TeV is $-0.17 < \lambda_Z < 0.21$.
- 19 ABAZOV 06H study $p\bar{p} \rightarrow WW$ production with a subsequent decay $WW \rightarrow e^+\nu_e e^-\bar{\nu}_e$, $WW \rightarrow e^\pm\nu_e\mu^\mp\nu_\mu$ or $WW \rightarrow \mu^\pm\nu_\mu\mu^\mp\nu_\mu$. The 95% C.L. limit for a form factor scale $\Lambda = 2$ TeV is $-0.39 < \lambda_Z < 0.39$, fixing $\kappa_Z=1$. With the assumption that the $WW\gamma$ and WWZ couplings are equal the 95% C.L. one-dimensional limit ($\Lambda = 2$ TeV) is $-0.29 < \lambda < 0.30$.
- 20 ABAZOV 05s study $p\bar{p} \rightarrow WZ$ production with a subsequent trilepton decay to $\ell\nu\ell'\bar{\ell}'$ (ℓ and $\ell' = e$ or μ). Three events (estimated background 0.71 ± 0.08 events) with WZ decay characteristics are observed from which they derive limits on the anomalous WWZ couplings. The 95% CL limit for a form factor scale $\Lambda = 1.5$ TeV is $-0.48 < \lambda_Z < 0.48$, fixing g_1^Z and κ_Z to their Standard Model values.

 g_1^Z

This coupling is CP -conserving but C - and P -violating.

VALUE	EVTS	DOCUMENT ID	TECN	COMMENT
-0.07 ± 0.09 OUR AVERAGE				Error includes scale factor of 1.1.
$-0.04^{+0.13}_{-0.12}$	9800	1 ABBIENDI 04D OPAL	$E_{cm}^{ee} = 183-209$ GeV	
$0.00 \pm 0.13 \pm 0.05$	7171	2 ACHARD 04D L3	$E_{cm}^{ee} = 189-209$ GeV	
$-0.44^{+0.23}_{-0.22} \pm 0.12$	1154	3 ACCIARRI 99Q L3	$E_{cm}^{ee} = 161+172+183$ GeV	

- • • We do not use the following data for averages, fits, limits, etc. • • •
- 0.31 \pm 0.23 4 EBOLI 00 THEO LEP1, SL+ Tevatron
- 1 ABBIENDI 04D combine results from W^+W^- in all decay channels. Only CP -conserving couplings are considered and each parameter is determined from a single-parameter fit in which the other parameters assume their Standard Model values. The 95% confidence interval is $-0.28 < g_1^Z < +0.21$.
- 2 ACHARD 04D study W^+W^- pair production, single- W production and single-photon production with missing energy from 189 to 209 GeV. The result quoted here is obtained using the W^+W^- pair production sample. Each parameter is determined from a single-parameter fit in which the other parameters assume their Standard Model values.
- 3 ACCIARRI 99Q study W -pair, single- W , and single photon events.
- 4 EBOLI 00 extract this indirect value of the coupling studying the non-universal one-loop contributions to the experimental value of the $Z \rightarrow b\bar{b}$ width ($\Lambda=1$ TeV is assumed).

$\tilde{\kappa}_Z^{\ell}$ This coupling is *CP*-violating (*C*-violating and *P*-conserving).

VALUE	EVTS	DOCUMENT ID	TECN	COMMENT
-0.30 ± 0.17 OUR AVERAGE				
-0.39 ^{+0.19} _{-0.20}	1880	1 ABDALLAH	08c DLPH	$E_{cm}^{ee} = 189\text{--}209$ GeV
-0.02 ^{+0.32} _{-0.33}	1065	2 ABBIENDI	01H OPAL	$E_{cm}^{ee} = 189$ GeV

1 ABDALLAH 08c determine this triple gauge coupling from the measurement of the spin density matrix elements in $e^+e^- \rightarrow W^+W^- \rightarrow (qq)(\ell\nu)$, where $\ell = e$ or μ . Values of all other couplings are fixed to their standard model values.

2 ABBIENDI 01H study W -pair events, with one leptonically and one hadronically decaying W . The coupling is extracted using information from the W production angle together with decay angles from the leptonically decaying W .

$\tilde{\kappa}_Z$ This coupling is *CP*-violating (*C*-conserving and *P*-violating).

VALUE	EVTS	DOCUMENT ID	TECN	COMMENT
-0.12^{+0.06}_{-0.04} OUR AVERAGE				
-0.09 ^{+0.08} _{-0.05}	1880	1 ABDALLAH	08c DLPH	$E_{cm}^{ee} = 189\text{--}209$ GeV
-0.20 ^{+0.10} _{-0.07}	1065	2 ABBIENDI	01H OPAL	$E_{cm}^{ee} = 189$ GeV

- • • We do not use the following data for averages, fits, limits, etc. • • •
 - 3 AABOUD 17s ATLS $E_{cm}^{pp} = 7+8$ TeV
 - 4 BLINOV 11 LEP $E_{cm}^{ee} = 183\text{--}207$ GeV
- 1 ABDALLAH 08c determine this triple gauge coupling from the measurement of the spin density matrix elements in $e^+e^- \rightarrow W^+W^- \rightarrow (qq)(\ell\nu)$, where $\ell = e$ or μ . Values of all other couplings are fixed to their standard model values.
- 2 ABBIENDI 01H study W -pair events, with one leptonically and one hadronically decaying W . The coupling is extracted using information from the W production angle together with decay angles from the leptonically decaying W .
- 3 AABOUD 17s analyze electroweak production of a W boson in association with two jets at high dijet invariant mass, with the W boson decaying to electron or muon plus neutrino. In the signal region of dijet mass larger than 1 TeV and leading-jet transverse momentum larger than 600 GeV, 30 events are observed in the data with 39 ± 4 events expected in the Standard Model, yielding the following limit at 95% CL for the form factor cut-off scale $\Lambda_{FF} \rightarrow \infty$: $-0.56 < \tilde{\kappa}_Z < 0.56$.
- 4 BLINOV 11 use the LEP-average $e^+e^- \rightarrow W^+W^-$ cross section data for $\sqrt{s} = 183\text{--}207$ GeV to determine an upper limit on the TGC $\tilde{\kappa}_Z$. The average values of the cross sections as well as their correlation matrix, and standard model expectations of the cross sections are taken from the LEPEWWG note hep-ex/0612034. At 95% confidence level $|\tilde{\kappa}_Z| < 0.13$.

$\tilde{\lambda}_Z$ This coupling is *CP*-violating (*C*-conserving and *P*-violating).

VALUE	EVTS	DOCUMENT ID	TECN	COMMENT
-0.09 ± 0.07 OUR AVERAGE				
-0.08 ± 0.07	1880	1 ABDALLAH	08c DLPH	$E_{cm}^{ee} = 189\text{--}209$ GeV
-0.18 ^{+0.24} _{-0.16}	1065	2 ABBIENDI	01H OPAL	$E_{cm}^{ee} = 189$ GeV

- • • We do not use the following data for averages, fits, limits, etc. • • •
 - 3 AABOUD 17s ATLS $E_{cm}^{pp} = 7+8$ TeV
 - 4 BLINOV 11 LEP $E_{cm}^{ee} = 183\text{--}207$ GeV
- 1 ABDALLAH 08c determine this triple gauge coupling from the measurement of the spin density matrix elements in $e^+e^- \rightarrow W^+W^- \rightarrow (qq)(\ell\nu)$, where $\ell = e$ or μ . Values of all other couplings are fixed to their standard model values.
- 2 ABBIENDI 01H study W -pair events, with one leptonically and one hadronically decaying W . The coupling is extracted using information from the W production angle together with decay angles from the leptonically decaying W .
- 3 AABOUD 17s analyze electroweak production of a W boson in association with two jets at high dijet invariant mass, with the W boson decaying to electron or muon plus neutrino. In the signal region of dijet mass larger than 1 TeV and leading-jet transverse momentum larger than 600 GeV, 30 events are observed in the data with 39 ± 4 events expected in the Standard Model, yielding the following limit at 95% CL for the form factor cut-off scale $\Lambda_{FF} \rightarrow \infty$: $-0.047 < \tilde{\lambda}_Z < 0.046$.
- 4 BLINOV 11 use the LEP-average $e^+e^- \rightarrow W^+W^-$ cross section data for $\sqrt{s} = 183\text{--}207$ GeV to determine an upper limit on the TGC $\tilde{\lambda}_Z$. The average values of the cross sections as well as their correlation matrix, and standard model expectations of the cross sections are taken from the LEPEWWG note hep-ex/0612034. At 95% confidence level $|\tilde{\lambda}_Z| < 0.31$.

W ANOMALOUS MAGNETIC MOMENT

The full magnetic moment is given by $\mu_W = e(1+\kappa+\lambda)/2m_W$. In the Standard Model, at tree level, $\kappa = 1$ and $\lambda = 0$. Some papers have defined $\Delta\kappa = 1-\kappa$ and assume that $\lambda = 0$. Note that the electric quadrupole moment is given by $-e(\kappa-\lambda)/m_W^2$. A description of the parameterization of these moments and additional references can be found in HAGIWARA 87 and BAUR 88. The parameter Λ appearing in the theoretical limits below is a regularization cutoff which roughly corresponds to the energy scale where the structure of the W boson becomes manifest.

VALUE ($e/2m_W$)	EVTS	DOCUMENT ID	TECN	COMMENT
2.22^{+0.20}_{-0.19}	2298	1 ABREU	01i DLPH	$E_{cm}^{ee} = 183+189$ GeV

• • • We do not use the following data for averages, fits, limits, etc. • • •

2 ABE	95G	CDF
3 ALITTI	92C	UA2
4 SAMUEL	92	THEO
5 SAMUEL	91	THEO
6 GRIFOLS	88	THEO
7 GROTC	87	THEO
8 VANDERBIJ	87	THEO
9 GRAU	85	THEO
10 SUZUKI	85	THEO
11 HERZOG	84	THEO

- 1 ABREU 01i combine results from e^+e^- interactions at 189 GeV leading to W^+W^- , $W\nu_e$, and $\nu\bar{\nu}\gamma$ final states with results from ABREU 99L at 183 GeV to determine Δg_Z^f , $\Delta\kappa_\gamma$, and λ_γ . $\Delta\kappa_\gamma$ and λ_γ are simultaneously floated in the fit to determine μ_W .
- 2 ABE 95G report $-1.3 < \kappa < 3.2$ for $\lambda=0$ and $-0.7 < \lambda < 0.7$ for $\kappa=1$ in $p\bar{p} \rightarrow e\nu_e\gamma X$ and $\mu\nu_\mu\gamma X$ at $\sqrt{s} = 1.8$ TeV.
- 3 ALITTI 92C measure $\kappa = 1 \pm 2.6$ and $\lambda = 0 \pm 1.7$ in $p\bar{p} \rightarrow e\nu_e\gamma + X$ at $\sqrt{s} = 630$ GeV. At 95%CL they report $-3.5 < \kappa < 5.9$ and $-3.6 < \lambda < 3.5$.
- 4 SAMUEL 92 use preliminary CDF and UA2 data and find $-2.4 < \kappa < 3.7$ at 96%CL and $-3.1 < \lambda < 4.2$ at 95%CL respectively. They use data for $W\gamma$ production and radiative W decay.
- 5 SAMUEL 91 use preliminary CDF data for $p\bar{p} \rightarrow W\gamma X$ to obtain $-11.3 \leq \Delta\kappa \leq 10.9$. Note that their $\kappa = 1 - \Delta\kappa$.
- 6 GRIFOLS 88 uses deviation from ρ parameter to set limit $\Delta\kappa \lesssim 65 (M_W^2/\Lambda^2)$.
- 7 GROTC 87 finds the limit $-37 < \Delta\kappa < 73.5$ (90% CL) from the experimental limits on $e^+e^- \rightarrow \nu\bar{\nu}\gamma$ assuming three neutrino generations and $-19.5 < \Delta\kappa < 56$ for four generations. Note their $\Delta\kappa$ has the opposite sign as our definition.
- 8 VANDERBIJ 87 uses existing limits to the photon structure to obtain $|\Delta\kappa| < 33 (m_W/\Lambda)$. In addition VANDERBIJ 87 discusses problems with using the ρ parameter of the Standard Model to determine $\Delta\kappa$.
- 9 GRAU 85 uses the muon anomaly to derive a coupled limit on the anomalous magnetic dipole and electric quadrupole (λ) moments $1.05 > \Delta\kappa \ln(\Lambda/m_W) + \lambda/2 > -2.77$. In the Standard Model $\lambda = 0$.
- 10 SUZUKI 85 uses partial-wave unitarity at high energies to obtain $|\Delta\kappa| \lesssim 190 (m_W/\Lambda)^2$. From the anomalous magnetic moment of the muon, SUZUKI 85 obtains $|\Delta\kappa| \lesssim 2.2/\ln(\Lambda/m_W)$. Finally SUZUKI 85 uses deviations from the ρ parameter and obtains a very qualitative, order-of-magnitude limit $|\Delta\kappa| \lesssim 150 (m_W/\Lambda)^4$ if $|\Delta\kappa| \ll 1$.
- 11 HERZOG 84 consider the contribution of W -boson to muon magnetic moment including anomalous coupling of $WW\gamma$. Obtain a limit $-1 < \Delta\kappa < 3$ for $\Lambda \gtrsim 1$ TeV.

$c_{WWW}/\Lambda^2, c_W/\Lambda^2, c_B/\Lambda^2$

These couplings are used in EFT-based approaches to anomalous couplings. They are linearly related to the couplings discussed above.

VALUE	DOCUMENT ID	TECN	COMMENT
• • • We do not use the following data for averages, fits, limits, etc. • • •			
1 TUMASYAN	22AB	CMS	$E_{cm}^{pp} = 13$ TeV
2 TUMASYAN	22E	CMS	$E_{cm}^{pp} = 13$ TeV
3 AAD	21AC	ATLS	$E_{cm}^{pp} = 13$ TeV
4 AAD	21W	ATLS	$E_{cm}^{pp} = 13$ TeV
5 SIRUNYAN	21G	CMS	$E_{cm}^{pp} = 13$ TeV
6 SIRUNYAN	20BA	CMS	$E_{cm}^{pp} = 13$ TeV
7 SIRUNYAN	20BF	CMS	$E_{cm}^{pp} = 13$ TeV
8 AABOUD	19BA	ATLS	$E_{cm}^{pp} = 13$ TeV
9 SIRUNYAN	19AD	CMS	$E_{cm}^{pp} = 13$ TeV
10 SIRUNYAN	19CL	CMS	$E_{cm}^{pp} = 13$ TeV
11 AABOUD	18Q	ATLS	$E_{cm}^{pp} = 13$ TeV
12 SIRUNYAN	18BZ	CMS	$E_{cm}^{pp} = 13$ TeV
13 AABOUD	17S	ATLS	$E_{cm}^{pp} = 7+8$ TeV
14 AABOUD	17U	ATLS	$E_{cm}^{pp} = 8$ TeV
15 KHACHATRY...	17O	CMS	$E_{cm}^{pp} = 8$ TeV
16 SIRUNYAN	17X	CMS	$E_{cm}^{pp} = 8$ TeV
17 AAD	16AR	ATLS	$E_{cm}^{pp} = 8$ TeV
18 AAD	16P	ATLS	$E_{cm}^{pp} = 8$ TeV
19 KHACHATRY...	16BI	CMS	$E_{cm}^{pp} = 8$ TeV

- 1 TUMASYAN 22AB study WZ production, measuring cross sections and various distributions. Analysing the WZ invariant mass distribution, the following 95% C.L. limits are derived in units of TeV^{-2} : $-2.5 < c_W/\Lambda^2 < 0.3$, $-1.0 < c_{WWW}/\Lambda^2 < 1.2$, $-43 < c_b/\Lambda^2 < 113$, $-0.62 < \tilde{c}_{WWW}/\Lambda^2 < 0.53$, $-32 < \tilde{c}_W/\Lambda^2 < 32$.
- 2 TUMASYAN 22E measure $W\gamma$ production where the W boson decays to electrons or muons. Analysing the photon transverse momentum distribution in bins of lepton azimuth, the following 95% C.L. limit is derived in units of TeV^{-2} : $-0.062 < c_3W/\Lambda^2 < 0.052$. This limit is derived including the non-SM, SM and their interference effects.
- 3 AAD 21AC study the differential cross-section for the electroweak production of dijets in association with a Z boson, where the Z boson decays to electrons or muons. The number of events selected in the data is 10,870 (12,125) in the electron (muon) channel. Analysing the distribution of the azimuthal separation of the two jets, the following 95% C.L. limits are derived in units of TeV^{-2} : $-2.7 < c_W W W/\Lambda^2 < 5.8$, $-1.6 < \tilde{c}_W W W/\Lambda^2 < 2.0$, $-0.19 < c_W/\Lambda^2 < 0.41$, $-0.11 < \tilde{c}_W/\Lambda^2 < 0.14$, $-6.31 < c_{HWB}/\Lambda^2 < 1.01$, $0.23 < \tilde{c}_{HWB}/\Lambda^2 < 2.35$.

Gauge & Higgs Boson Particle Listings

W

- ⁴ AAD 21w analyze W^+W^- production in association with at least one jet. Events with exactly one oppositely-charged electron-muon pair and at least one hadronic jet of transverse momentum larger than 30 GeV (120 GeV) are selected. In the data, 89,239 (5,825) events are found, with a total Standard-Model expectation of 91600 ± 2500 (5980 ± 150). Analyzing the electron-muon invariant mass distribution, the following limit at 95% C.L. is obtained: $-0.33 < c_W/\Lambda^2 < 0.33$ ($-0.60 < c_W/\Lambda^2 < 0.58$), for a fixed choice of $\Lambda = 1$ TeV.
- ⁵ SIRUNYAN 21G measure W production where the W decays into electrons or muons. In the data, 385,224 (395,818) events are selected in the electron (muon) channel, with a total Standard-Model expectation of 396913 ± 54686 (396257 ± 22837) events. Analysing the photon transverse momentum distribution, the following 95% C.L. limits are derived in units of TeV^{-2} : $-0.90 < c_{WW}/\Lambda^2 < 0.91$, $-40 < c_B/\Lambda^2 < 41$, $-0.45 < c_{\overline{W}W}/\Lambda^2 < 0.45$, $-20 < c_{\overline{W}}/\Lambda^2 < 20$.
- ⁶ SIRUNYAN 20BA study electroweak production of a W boson in association with two jets, using W decays in the electron or muon channel. The isolated muons (electrons) are required to have a transverse momentum larger than 25 (30) GeV, while the transverse momentum of the two jets has to be larger than 50 and 30 GeV. A total of 2.382 (1.051) million events are selected in the muon (electron) channel, with a Standard Model expectation of 2.39 ± 0.17 (1.054 ± 0.058) million events. Analysing the transverse momentum distribution of the charged leptons from W decay, the following 95% C.L. limits are obtained in units of TeV^{-2} : $-2.3 < c_{WW}/\Lambda^2 < 2.5$, $-8.8 < c_W/\Lambda^2 < 16$, $-45 < c_B/\Lambda^2 < 46$. Combining these results with those from the closely-related electroweak Z -jet-jet production SIRUNYAN 18BZ, the limits become: $-1.8 < c_{WW}/\Lambda^2 < 2.0$, $-5.8 < c_W/\Lambda^2 < 10$, $-43 < c_B/\Lambda^2 < 45$.
- ⁷ SIRUNYAN 20BF study W^+W^- production with the W bosons decaying to electrons or muons. The leading (subleading) lepton is required to have a transverse momentum larger than 25 (20) GeV. Events with a same-flavor di-lepton invariant mass within 15 GeV of the Z mass are rejected, as are event with a third lepton of transverse momentum larger than 10 GeV. In the same- (different-) flavor category a total of 9,604 (20,270) events are selected while the number of expected events is 9640 ± 490 (20280 ± 430). Analysing the different-flavor di-lepton invariant mass distribution, the following 95% C.L. limits are obtained in units of TeV^{-2} : $-1.8 < c_{WW}/\Lambda^2 < 1.8$, $-3.6 < c_W/\Lambda^2 < 2.8$, $-9.4 < c_B/\Lambda^2 < 8.5$.
- ⁸ AABOUD 19BA study WW production in decay modes with an electron and a muon. The charged leptons are each required to have a transverse momentum larger than 27 GeV and rapidity less than 2.5. The electron-muon system is required to have a mass larger than 55 GeV and a transverse momentum larger than 30 GeV. The missing transverse energy must be larger than 20 GeV. Events containing a jet with transverse momentum exceeding 35 GeV and rapidity smaller than 4.5 are rejected. A total of 12,659 events are selected in the data, with an expected background of 4240 ± 477 events. Analysing the transverse momentum spectrum of the leading charged lepton, the following 95% C.L. limits are derived in units of TeV^{-2} : $-3.4 < c_{WW}/\Lambda^2 < 3.3$, $-7.4 < c_W/\Lambda^2 < 4.1$, $-21 < c_B/\Lambda^2 < 18$, $-1.6 < c_{\overline{W}W}/\Lambda^2 < 1.6$, $-76 < c_{\overline{W}}/\Lambda^2 < 76$.
- ⁹ SIRUNYAN 19AD study inclusive WZ production, with W and Z decaying to electrons or muons. The leading (subleading) charged lepton candidate from the Z boson decay is required to have a transverse momentum larger than 25 GeV (10 GeV). The charged lepton candidate from the W boson decay is required to have a transverse momentum larger than 25 GeV. The invariant mass of the two leptons from Z decay is required to be within 15 GeV of the Z mass, while the invariant mass of the tri-lepton system is required to exceed 100 GeV. A total of 3,831 tri-lepton events are observed, with a fitted SM WZ signal of 3166 ± 62 events and a fitted background of 666 ± 45 events. The approximated WZ invariant mass distribution is analyzed to set 95% C.L. limits as follows: $-4.1 < c_W/\Lambda^2 < 1.1$, $-2.0 < c_{WW}/\Lambda^2 < 2.1$, $-100 < c_B/\Lambda^2 < 160$, in units of TeV^{-2} .
- ¹⁰ SIRUNYAN 19CL study WW and WZ production in lepton + jet events, with one W boson decaying leptonically (electron or muon), and another W or Z boson decaying hadronically, reconstructed as a single massive large-radius jet. In the electron channel 2,456 (2,235) events are selected in the $W(W)Z$ category, while in the muon channel 3,996 (3,572) events are selected in the $W(W)Z$ category. Analysing the di-boson invariant mass distribution, the following 95% C.L. limits are obtained in units of TeV^{-2} : $-1.58 < c_{WW}/\Lambda^2 < 1.59$, $-2.00 < c_W/\Lambda^2 < 2.65$, $-8.78 < c_B/\Lambda^2 < 8.54$.
- ¹¹ AABOUD 18Q study $pp \rightarrow ZZ$ events at $\sqrt{s} = 13$ TeV with $Z \rightarrow e^+e^-$ or $Z \rightarrow \mu^+\mu^-$. The number of events observed in the $4e$, $2e2\mu$, and 4μ channels is 249, 465, and 303 respectively. Analysing the p_T spectrum of the leading Z boson, the following the following 95% C.L. limits are derived in units of TeV^{-4} : $-5.9 < c_{\overline{B}W}/\Lambda^4 < 5.9$, $-3.0 < c_{WW}/\Lambda^4 < 3.0$, $-3.3 < c_{BW}/\Lambda^4 < 3.3$, $-2.7 < c_{BB}/\Lambda^4 < 2.8$.
- ¹² SIRUNYAN 18BZ study $pp \rightarrow Z$ jet jet events at 13 TeV where $Z \rightarrow e^+e^-/\mu^+\mu^-$. Isolated electrons and muons are selected with p_T of the leading/sub-leading lepton $> 30/20$ GeV and $|\eta| < 2.4$, with the di-lepton invariant mass within 15 GeV of the Z mass. The two highest p_T jets are selected with p_T of the leading/sub-leading jet $> 50/30$ GeV respectively and dijet invariant mass > 200 GeV. Templates in the transverse momentum of the Z are utilized to set limits on the triple gauge couplings in the EFT and the LEP parametrizations. The following 95% C.L. limits are obtained in units of TeV^{-2} : $-2.6 < c_{WW}/\Lambda^2 < 2.6$ and $-8.4 < c_W/\Lambda^2 < 10.1$.
- ¹³ AABOUD 17s analyze electroweak production of a W boson in association with two jets at high dijet invariant mass, with the W boson decaying to electron or muon plus neutrino. In the signal region of dijet mass larger than 1 TeV and leading-jet transverse momentum larger than 600 GeV, 30 events are observed in the data with 39 ± 4 events expected in the Standard Model, yielding the following limits at 95% CL for the form factor cut-off scale $\Lambda_{FF} \rightarrow \infty$: $-33 < c_W/\Lambda^2 < 30$, $-170 < c_B/\Lambda^2 < 160$, $-13 < c_{WW}/\Lambda^2 < 9$, $-580 < c_{\overline{W}}/\Lambda^2 < 580$, $-11 < c_{\overline{W}W}/\Lambda^2 < 11$, in units of TeV^{-2} .
- ¹⁴ AABOUD 17u analyze production of WW or WZ boson pairs with one W boson decaying to electron or muon plus neutrino, and the other W or Z boson decaying hadronically. The hadronic decay system is reconstructed as either a resolved two-jet system or as a single large jet. Analysing the transverse momentum distribution of the hadronic system above 100 GeV yields the following limits at 95% CL for the form factor cut-off scale $\Lambda_{FF} \rightarrow \infty$: $-3.1 < c_{WW}/\Lambda^2 < 3.1$, $-19 < c_B/\Lambda^2 < 20$, $-5.1 < c_W/\Lambda^2 < 5.8$, in units of TeV^{-2} .
- ¹⁵ KHACHATRYAN 17o analyse WZ production where each boson decays into electrons or muons. Events are required to have a tri-lepton invariant mass larger than 100 GeV,

with one of the lepton pairs having an invariant mass within 20 GeV of the Z boson mass. The Z transverse momentum spectrum is analyzed to set 95% C.L. limits of: $-260 < c_B/\Lambda^2 < 210$, $-4.2 < c_W/\Lambda^2 < 8.0$, $-4.6 < c_{WW}/\Lambda^2 < 4.2$, in units of TeV^{-2} .

- ¹⁶ SIRUNYAN 17X study $pp \rightarrow WW/WZ \rightarrow \ell\nu q\bar{q}$ production at 8 TeV where ℓ is an electron or muon with $p_T > 30$ or 25 GeV respectively. Suitable cuts are put on the p_T of the dijet system and the missing E_T of the event yielding a total of 285 and 204 WV events observed in the electron and muon channels. The following 95% C.L. limits in units of TeV^{-2} are obtained: $-2.7 < c_{WW}/\Lambda^2 < 2.7$, $-14 < c_B/\Lambda^2 < 17$, $-2.0 < c_W/\Lambda^2 < 5.7$.
- ¹⁷ AAD 16AR study WV production in pp collisions and select 6636 WW candidates in decay modes with electrons or muons with an expected background of 1546 ± 157 events. Assuming an EFT formulation, a fit to the transverse momentum distribution of the leading charged lepton, leads to 95% C.L. ranges of: $-4.61 < c_{WW}/\Lambda^2 < 4.60$, $-5.87 < c_W/\Lambda^2 < 10.54$ and $-20.9 < c_B/\Lambda^2 < 26.3$, in units of TeV^{-2} .
- ¹⁸ AAD 16P study WZ production in pp collisions and select 2091 WZ candidates in 4 decay modes with electrons and muons, with an expected background of 1825 ± 7 events. Analysing the WZ transverse momentum distribution, the resulting 95% C.L. limits are: $-3.9 < c_{WW}/\Lambda^2 < 4.0$, $-4.3 < c_W/\Lambda^2 < 6.8$, and $-320 < c_B/\Lambda^2 < 210$, in units of TeV^{-2} .
- ¹⁹ KHACHATRYAN 16Bl determine the W^+W^- production cross section using unlike sign di-lepton (e or μ) events with high p_T . The leptons have $p_T > 20$ GeV/ c and are isolated. Events are required to have no jets above p_T of 30 GeV/ c . 4847 (2233) events are selected with different (same) flavor leptons, with an expected total background of 1179 ± 123 (643 ± 73) events. Analysing the di-lepton invariant mass spectrum, the following values are obtained: $c_{WW}/\Lambda^2 = 0.1 \pm 3.2$, $c_W/\Lambda^2 = -3.6^{+5.0}_{-4.5}$ and $c_B/\Lambda^2 = -3.2^{+15.0}_{-14.5}$, in units of TeV^{-2} . The limits at 95% C.L. are: $-5.7 < c_{WW}/\Lambda^2 < 5.9$, $-11.4 < c_W/\Lambda^2 < 5.4$ and $-29.2 < c_B/\Lambda^2 < 23.9$, in units of TeV^{-2} .

ANOMALOUS W/Z QUARTIC COUPLINGS

Revised March 2024 by M.W. Grunewald (U. College Dublin) and A. Gurtu (CERN; TIFR Mumbai).

Quartic couplings, $WWZZ$, $WWZ\gamma$, $WW\gamma\gamma$, and $ZZ\gamma\gamma$, were studied at LEP and Tevatron at energies at which the Standard Model predicts negligible contributions to multiboson production. Thus, to parametrize limits on these couplings, an effective theory approach is adopted which supplements the Standard Model Lagrangian with higher dimensional operators which include quartic couplings. The LEP collaborations chose the lowest dimensional representation of operators (dimension 6) which presumes the $SU(2) \times U(1)$ gauge symmetry is broken by means other than the conventional Higgs scalar doublet [1–3]. In this representation possible quartic couplings, a_0, a_c, a_n , are expressed in terms of the following dimension-6 operators [1,2];

$$L_6^0 = -\frac{e^2}{16\Lambda^2} a_0 F^{\mu\nu} F_{\mu\nu} \vec{W}^\alpha \cdot \vec{W}_\alpha$$

$$L_6^c = -\frac{e^2}{16\Lambda^2} a_c F^{\mu\alpha} F_{\mu\beta} \vec{W}^\beta \cdot \vec{W}_\alpha$$

$$L_6^n = -i\frac{e^2}{16\Lambda^2} a_n \epsilon_{ijk} W_{\mu\alpha}^{(i)} W_\nu^{(j)} W^{(k)\alpha} F^{\mu\nu}$$

$$\tilde{L}_6^0 = -\frac{e^2}{16\Lambda^2} \tilde{a}_0 F^{\mu\nu} \tilde{F}_{\mu\nu} \vec{W}^\alpha \cdot \vec{W}_\alpha$$

$$\tilde{L}_6^n = -i\frac{e^2}{16\Lambda^2} \tilde{a}_n \epsilon_{ijk} W_{\mu\alpha}^{(i)} W_\nu^{(j)} W^{(k)\alpha} \tilde{F}^{\mu\nu}$$

where F, W are photon and W fields, L_6^0 and L_6^c conserve C, P separately (\tilde{L}_6^0 conserves only C) and generate anomalous $W^+W^-\gamma\gamma$ and $ZZ\gamma\gamma$ couplings, L_6^n violates CP (\tilde{L}_6^n violates both C and P) and generates an anomalous $W^+W^-Z\gamma$ coupling, and Λ is an energy scale for new physics. For the $ZZ\gamma\gamma$ coupling the CP -violating term represented by L_6^n does not contribute. These couplings are assumed to be real and to vanish at tree level in the Standard Model.

Within the same framework as above, a more recent description of the quartic couplings [3] treats the anomalous parts of the $WW\gamma\gamma$ and $ZZ\gamma\gamma$ couplings separately, leading to two sets parametrized as a_0^V/Λ^2 and a_c^V/Λ^2 , where $V = W$ or Z .

With the discovery of a Higgs at the LHC in 2012, it is then useful to go to the next higher dimensional representation (dimension 8 operators) in which the gauge symmetry is

broken by the conventional Higgs scalar doublet [3,4]. There are 14 operators which can contribute to the anomalous quartic coupling signal. Some of the operators have analogues in the dimension 6 scheme. The CMS collaboration, [5], have used this parametrization, in which the connections between the two schemes are also summarized:

$$\begin{aligned} \mathcal{L}_{AQGC} = & -\frac{e^2 a_0^W}{8 \Lambda^2} F_{\mu\nu} F^{\mu\nu} W^{+\alpha} W_a^- \\ & -\frac{e^2 a_c^W}{16 \Lambda^2} F_{\mu\nu} F^{\mu\alpha} (W^{+\nu} W_a^- + W^{-\nu} W_a^+) \\ & -e^2 g^2 \frac{\kappa_0^W}{\Lambda^2} F_{\mu\nu} Z^{\mu\nu} W^{+\alpha} W_a^- \\ & -\frac{e^2 g^2 \kappa_c^W}{2 \Lambda^2} F_{\mu\nu} Z^{\mu\alpha} (W^{+\nu} W_a^- + W^{-\nu} W_a^+) \\ & + \frac{f_{T,0}}{\Lambda^4} Tr[\widehat{W}_{\mu\nu} \widehat{W}^{\mu\nu}] \times Tr[\widehat{W}_{\alpha\beta} \widehat{W}^{\alpha\beta}] \end{aligned}$$

The energy scale of possible new physics is Λ , and $g = e/\sin(\theta_W)$, e being the unit electric charge and θ_W the Weinberg angle. The field tensors are described in [3,4].

The two dimension 6 operators a_0^W/Λ^2 and a_c^W/Λ^2 are associated with the $WW\gamma\gamma$ vertex. Among dimension 8 operators, κ_0^W/Λ^2 and κ_c^W/Λ^2 are associated with the $WWZ\gamma$ vertex, whereas the parameter $f_{T,0}/\Lambda^4$ contributes to both vertices. There is a relationship between these two dimension 6 parameters and the dimension 8 parameters $f_{M,i}/\Lambda^4$ as follows [3]:

$$\frac{a_0^W}{\Lambda^2} = -\frac{4M_W^2}{g^2} \frac{f_{M,0}}{\Lambda^4} - \frac{8M_W^2}{g'^2} \frac{f_{M,2}}{\Lambda^4}$$

$$\frac{a_c^W}{\Lambda^2} = -\frac{4M_W^2}{g^2} \frac{f_{M,1}}{\Lambda^4} - \frac{8M_W^2}{g'^2} \frac{f_{M,3}}{\Lambda^4}$$

where $g' = e/\cos(\theta_W)$ and M_W is the invariant mass of the W boson. This relation provides a translation between limits on dimension 6 operators $a_{0,c}^W$ and $f_{M,j}/\Lambda^4$. It is further required [4] that $f_{M,0} = 2f_{M,2}$ and $f_{M,1} = 2f_{M,3}$ which suppresses contributions to the $WWZ\gamma$ vertex. The complete set of Lagrangian contributions as presented in [4] corresponds to 19 anomalous couplings in total – $f_{S,i}$, $i = 1, 2$, $f_{M,i}$, $i = 0, \dots, 8$ and $f_{T,i}$, $i = 0, \dots, 9$ – each scaled by $1/\Lambda^4$.

Another approach to couplings is the so called K-matrix framework [7], in which the anomalous couplings can be expressed in terms of two parameters α_4 and α_5 , which account for all BSM effects.

The LHC collaborations have published couplings results based on various theoretical frameworks. It is hoped that the collaborations will agree to use at least one common set of parameters to express these limits to enable the reader to make a comparison, and to allow for a possible LHC combination.

References

1. G. Belanger and F. Boudjema, Phys. Lett. **B288**, 201 (1992).
2. J.W. Stirling and A. Werthenbach, Eur. Phys. J. **C14**, 103 (2000);
J.W. Stirling and A. Werthenbach, Phys. Lett. **B466**, 369

(1999);

A. Denner *et al.*, Eur. Phys. J. **C20**, 201 (2001);

G. Montagna *et al.*, Phys. Lett. **B515**, 197 (2001).

3. G. Belanger *et al.*, Eur. Phys. J. **C13**, 283 (2000).
4. O.J.P. Éboli, M.C. Gonzalez-Garcia, and S.M. Lietti, Phys. Rev. **D69**, 095005 (2004);
O.J.P. Éboli, M.C. Gonzalez-Garcia, and J.K. Mizukoshi, Phys. Rev. **D77**, 073005 (2006).
5. S. Chatrchyan *et al.*, Phys. Rev. **D90**, 032008 (2014);
S. Chatrchyan *et al.*, Phys. Rev. Lett. **114**, 051801 (2015).
6. G. Aad *et al.*, Phys. Rev. Lett. **113**, 141803 (2014).
7. A. Albateanu, W. Killian, and J. Reuter, JHEP **0811**, 010 (2008).

a_0/Λ^2 , a_c/Λ^2 , a_n/Λ^2 , κ_0^W/Λ^2 , κ_c^W/Λ^2 , $f_{T,0}/\Lambda^4$, $f_{M,i}/\Lambda^4$, α_4 , α_5 , $F_{S,i}/\Lambda^4$, $F_{M,i}/\Lambda^4$, $F_{T,i}/\Lambda^4$

Anomalous W quartic couplings are measured by the experiments at LEP, the Tevatron, and the LHC. Some of the recent results from the Tevatron and LHC experiments individually surpass the combined LEP-2 results in precision (see below). As discussed in the review on the ‘‘Anomalous W/Z quartic couplings (QGCS),’’ the measurements are typically done using different operator expansions which then do not allow the results to be compared and averaged. At least one common framework should be agreed upon for the use in the future publications by the experiments.

Some publications from LHC experiments derive limits for various assumed values of the form-factor cutoff Λ_{FF} . The values quoted below are for $\Lambda_{FF} \rightarrow \infty$.

VALUE	DOCUMENT ID	TECN	COMMENT
••• We do not use the following data for averages, fits, limits, etc. •••			
1	AAD	24c ATLS	$E_{cm}^{pp} = 13$ TeV
2	AAD	23BH ATLS	$E_{cm}^{pp} = 13$ TeV
3	AAD	23K ATLS	$E_{cm}^{pp} = 13$ TeV
4	TUMASYAN	23AK CMS	$E_{cm}^{pp} = 13$ TeV
5	TUMASYAN	23AM CMS	$E_{cm}^{pp} = 13$ TeV
6	SIRUNYAN	21 CMS	$E_{cm}^{pp} = 13$ TeV
7	TUMASYAN	21A CMS	$E_{cm}^{pp} = 13$ TeV
8	TUMASYAN	21B CMS	$E_{cm}^{pp} = 13$ TeV
9	SIRUNYAN	20 CMS	$E_{cm}^{pp} = 13$ TeV
10	SIRUNYAN	20AL CMS	$E_{cm}^{pp} = 13$ TeV
11	SIRUNYAN	20BD CMS	$E_{cm}^{pp} = 13$ TeV
12	SIRUNYAN	19BM CMS	$E_{cm}^{pp} = 13$ TeV
13	SIRUNYAN	19BP CMS	$E_{cm}^{pp} = 13$ TeV
14	SIRUNYAN	19CQ CMS	$E_{cm}^{pp} = 13$ TeV
15	SIRUNYAN	18CC CMS	$E_{cm}^{pp} = 13$ TeV
16	AABOUD	17AA ATLS	$E_{cm}^{pp} = 8$ TeV
17	AABOUD	17AG ATLS	$E_{cm}^{pp} = 8$ TeV
18	AABOUD	17D ATLS	$E_{cm}^{pp} = 8$ TeV
19	AABOUD	17J ATLS	$E_{cm}^{pp} = 8$ TeV
20	AABOUD	17M ATLS	$E_{cm}^{pp} = 8$ TeV
21	KHACHATRY..17AA	CMS	$E_{cm}^{pp} = 8$ TeV
22	KHACHATRY..17M	CMS	$E_{cm}^{pp} = 8$ TeV
23	SIRUNYAN	17AD CMS	$E_{cm}^{pp} = 13$ TeV
24	SIRUNYAN	17AR CMS	$E_{cm}^{pp} = 8$ TeV
25	AABOUD	16E ATLS	$E_{cm}^{pp} = 8$ TeV
26	AAD	16Q ATLS	$E_{cm}^{pp} = 8$ TeV
27	KHACHATRY...16AX	CMS	$E_{cm}^{pp} = 8$ TeV
28	AAD	15N ATLS	$E_{cm}^{pp} = 8$ TeV
29	KHACHATRY...15D	CMS	$E_{cm}^{pp} = 8$ TeV
30	AAD	14AM ATLS	
31	CHATRCHYAN14Q	CMS	
32	ABAZOV	13D D0	
33	CHATRCHYAN13AA	CMS	
34	ABBIENDI	04B OPAL	
35	ABBIENDI	04L OPAL	
36	HEISTER	04A ALEP	
37	ABDALLAH	03I DLPH	
38	ACHARD	02F L3	

¹ AAD 24c study the production of four charged leptons (electrons or muons) in association with two jets. Analysing the 4-lepton invariant mass distribution and the di-jet invariant mass distribution leads to the following 95% C.L. limits: $-0.98 < f_{T,0}/\Lambda^4 < 0.93$, $-1.2 < f_{T,1}/\Lambda^4 < 1.2$, $-2.5 < f_{T,2}/\Lambda^4 < 2.4$, $-2.5 < f_{T,5}/\Lambda^4 < 2.4$, $-3.9 < f_{T,6}/\Lambda^4 < 3.9$, $-8.5 < f_{T,7}/\Lambda^4 < 8.1$, $-2.1 < f_{T,8}/\Lambda^4 < 2.1$, $-4.5 < f_{T,9}/\Lambda^4 < 4.5$, in units of TeV^{-4} . The article also reports limits on these couplings by cutting the EFT expansion at various values of the cut-off scale.

- ²AAD 23BH study $pp \rightarrow Z\gamma\gamma$ events with the Z boson decaying to electron or muon pairs. The number of observed data events is 148 for the electron mode and 171 for the muon mode. The respective number of (data-background) events is $105.5 \pm 12.2(\text{stat}) \pm 8.1(\text{syst})$ and $120.4 \pm 13.1(\text{stat}) \pm 9.4(\text{syst})$. The corresponding number of predicted signal events is 91.5 ± 0.9 and 119.5 ± 1.0 using SHERPA (NLO), and 91.0 ± 1.0 and 118.1 ± 1.2 using MADGRAPH 5 AMC (NLO), where the error is statistical only. Analysing the transverse momentum distribution of the dilepton system, the following 95% C.L. limits are derived: $-9.87 < f_{T,0}/\Lambda^4 < 9.33$, $-9.88 < f_{T,1}/\Lambda^4 < 9.34$, $-20.31 < f_{T,2}/\Lambda^4 < 18.68$, $-4.64 < f_{T,5}/\Lambda^4 < 4.54$, $-7.04 < f_{T,6}/\Lambda^4 < 6.94$, $-15.55 < f_{T,7}/\Lambda^4 < 15.04$, $-1.64 < f_{T,8}/\Lambda^4 < 1.61$, $-3.26 < f_{T,9}/\Lambda^4 < 3.26$, in units of TeV^{-4} .
- ³AAD 23K measure Z production in association with a photon and two jets in proton-proton collisions at 13 TeV CM energy, where the Z boson decays into neutrinos. Within a sensitive fiducial phase-space region, 356 signal events are selected, with an expectation of 357 ± 30 . Analysing the photon transverse energy distribution, the following 95% C.L. limits are derived in units of TeV^{-4} : $-0.094 < f_{T,0}/\Lambda^4 < 0.084$, $-0.088 < f_{T,5}/\Lambda^4 < 0.099$, $-0.059 < f_{T,8}/\Lambda^4 < 0.059$, $-0.13 < f_{T,9}/\Lambda^4 < 0.13$, $-4.6 < f_{M,0}/\Lambda^4 < 4.6$, $-7.7 < f_{M,1}/\Lambda^4 < 7.7$, $-1.9 < f_{M,2}/\Lambda^4 < 1.9$.
- ⁴TUMASYAN 23AK study electroweak $W\gamma$ production in association with 2 jets. The events selected for the couplings analysis are required to have a dijet invariant mass in excess of 800 GeV, jet-jet separation of at least 2.5 in rapidity, invariant mass of the $W\gamma$ system larger than 150 GeV and transverse photon momentum larger than 100 GeV. Analysing the $W\gamma$ invariant mass distribution, varying one coupling at a time while fixing the others to their Standard Model value, leads to the following 95% C.L. limits: $-5.6 < f_{M,0}/\Lambda^4 < 5.5$, $-7.8 < f_{M,1}/\Lambda^4 < 8.1$, $-1.9 < f_{M,2}/\Lambda^4 < 1.9$, $-2.7 < f_{M,3}/\Lambda^4 < 2.7$, $-3.7 < f_{M,4}/\Lambda^4 < 3.6$, $-3.9 < f_{M,5}/\Lambda^4 < 3.9$, $-14 < f_{M,7}/\Lambda^4 < 14$, $-0.47 < f_{T,0}/\Lambda^4 < 0.51$, $-0.31 < f_{T,1}/\Lambda^4 < 0.34$, $-0.85 < f_{T,2}/\Lambda^4 < 1.0$, $-0.31 < f_{T,5}/\Lambda^4 < 0.33$, $-0.25 < f_{T,6}/\Lambda^4 < 0.27$, $-0.67 < f_{T,7}/\Lambda^4 < 0.73$, in units of TeV^{-4} .
- ⁵TUMASYAN 23AM use the combined CMS-TOTEM detector system to study exclusive $\gamma\gamma \rightarrow WW$ and $\gamma\gamma \rightarrow ZZ$ production in pp collisions at 13 TeV. The W and Z are identified through their hadronic decays with the added requirements of the invariant mass of the di-boson pair to be larger than 1 TeV, and the relative beam proton momentum loss between 0.04 and 0.20. The following limits are obtained at 95% C.L.: (i) on the dimension-6 (LEP like) couplings, in units of GeV^{-2} : $|a_0^W/\Lambda^2| < 4.3 \times 10^{-6}$, $|a_C^W/\Lambda^2| < 1.6 \times 10^{-5}$, $|a_0^Z/\Lambda^2| < 0.9 \times 10^{-5}$, $|a_C^Z/\Lambda^2| < 4.0 \times 10^{-5}$. (ii) on the dimension-8 operators, in units of TeV^{-4} : $|f_{M,0}/\Lambda^4| < 66.0$, $|f_{M,1}/\Lambda^4| < 245.5$, $|f_{M,2}/\Lambda^4| < 9.8$, $|f_{M,3}/\Lambda^4| < 73.0$, $|f_{M,4}/\Lambda^4| < 36.0$, $|f_{M,5}/\Lambda^4| < 67.0$, $|f_{M,7}/\Lambda^4| < 490.9$.
- ⁶SIRUNYAN 21 study electroweak Z-pair production in association with two jets, with the Z bosons decaying to oppositely-charged electron or muon pairs. Leptons with high transverse momentum are selected, with the di-lepton invariant mass of the two Z boson candidates between 60 GeV and 120 GeV, and the four-lepton invariant mass larger than 180 GeV. A total of 365 events are selected in the data, while the number of expected events is 370 ± 48 . Analysing the four-lepton invariant mass distribution, the following 95% C.L. limits are derived: $-0.24 < f_{T,0}/\Lambda^4 < 0.22$, $-0.31 < f_{T,1}/\Lambda^4 < 0.31$, $-0.63 < f_{T,2}/\Lambda^4 < 0.59$, $-0.43 < f_{T,8}/\Lambda^4 < 0.43$, $-0.92 < f_{T,9}/\Lambda^4 < 0.92$, in units of TeV^{-4} .
- ⁷TUMASYAN 21A study electroweak $Z\gamma$ production in association with two jets, where the Z boson decays to electron or muon pairs and the pair of two jets has high invariant mass, superseding SIRUNYAN 20AL. The number of observed (expected) electron events in the barrel and endcap regions are 375 (349 ± 9) and 174 (166 ± 6) events, respectively, while for muon events the respective numbers are 584 (612 ± 13) and 320 (303 ± 8). Analysing the $Z\gamma$ invariant mass distribution, the following 95% C.L. limits are derived: $-15.8 < f_{M,0}/\Lambda^4 < 16.0$, $-35.0 < f_{M,1}/\Lambda^4 < 34.7$, $-6.55 < f_{M,2}/\Lambda^4 < 6.49$, $-13.0 < f_{M,3}/\Lambda^4 < 13.0$, $-13.0 < f_{M,4}/\Lambda^4 < 12.7$, $-22.2 < f_{M,5}/\Lambda^4 < 21.3$, $-56.6 < f_{M,7}/\Lambda^4 < 55.9$, $-0.64 < f_{T,0}/\Lambda^4 < 0.57$, $-0.81 < f_{T,1}/\Lambda^4 < 0.90$, $-1.68 < f_{T,2}/\Lambda^4 < 1.54$, $-0.58 < f_{T,5}/\Lambda^4 < 0.64$, $-1.30 < f_{T,6}/\Lambda^4 < 1.33$, $-2.15 < f_{T,7}/\Lambda^4 < 2.43$, $-0.47 < f_{T,8}/\Lambda^4 < 0.47$, $-0.91 < f_{T,9}/\Lambda^4 < 0.91$, in units of TeV^{-4} .
- ⁸TUMASYAN 21B measure W or Z boson production in association with two photons, using the leptonic decays modes of W and Z with electrons or muons. The number of selected $W \rightarrow e(\mu)\nu$ events is 1987 (2384) and the number of selected $Z \rightarrow ee(\mu\mu)$ events is 110 (272) respectively. Analysing the transverse momentum of the di-photon system, the following 95% C.L. limits are derived in units of TeV^{-4} . In the W production channel, the observed limits are: $-39.9 < f_{M,2}/\Lambda^4 < 39.5$, $-63.8 < f_{M,3}/\Lambda^4 < 65.0$, $-1.30 < f_{T,0}/\Lambda^4 < 1.30$, $-1.70 < f_{T,1}/\Lambda^4 < 1.66$, $-3.64 < f_{T,2}/\Lambda^4 < 3.64$, $-0.52 < f_{T,5}/\Lambda^4 < 0.60$, $-0.60 < f_{T,6}/\Lambda^4 < 0.68$, $-1.16 < f_{T,7}/\Lambda^4 < 1.16$. In the Z production channel, the observed limits are: $-5.70 < f_{T,0}/\Lambda^4 < 5.46$, $-5.70 < f_{T,1}/\Lambda^4 < 5.46$, $-11.4 < f_{T,2}/\Lambda^4 < 10.9$, $-2.92 < f_{T,5}/\Lambda^4 < 2.92$, $-3.80 < f_{T,6}/\Lambda^4 < 3.88$, $-7.88 < f_{T,7}/\Lambda^4 < 7.72$, $-1.06 < f_{T,8}/\Lambda^4 < 1.10$, $-1.82 < f_{T,9}/\Lambda^4 < 1.82$, in units of TeV^{-4} .
- ⁹SIRUNYAN 20 study WZ and same-sign WW production in association with two jets, using the leptonic decays modes of the W and Z bosons with electrons or muons. Overall, 524 WZ events and 229 WW events are selected, with a Standard Model expectation of 535 ± 52 and 216 ± 21 events, respectively. Analysing the transverse mass spectrum of the di-boson system and the di-jet invariant mass, the following 95% C.L. limits are derived, not using any unitarization procedure: $-0.25 < f_{T,0}/\Lambda^4 < 0.28$, $-0.12 < f_{T,1}/\Lambda^4 < 0.14$, $-0.35 < f_{T,2}/\Lambda^4 < 0.48$, $-2.7 < f_{M,0}/\Lambda^4 < 2.9$, $-4.1 < f_{M,1}/\Lambda^4 < 4.2$, $-5.4 < f_{M,6}/\Lambda^4 < 5.8$, $-5.7 < f_{M,7}/\Lambda^4 < 6.0$, $-5.7 < f_{S,0}/\Lambda^4 < 6.1$, $-16 < f_{S,1}/\Lambda^4 < 17$, in units of TeV^{-4} . The article also reports limits on these couplings by cutting the EFT expansion at the unitarity limit.
- ¹⁰SIRUNYAN 20AL study electroweak production of a Z boson and a photon in association with two jets in the electron and muon decay modes of the Z. A signal with a significance of 3.9 standard deviations is observed, compared to a Standard Model expectation of 5.2 standard deviations. Combining with KHACHATRYAN 17AA data at 8 TeV the final observed and expected signal significance is 4.7 and 5.5 standard deviations. Analysing the Z-photon invariant mass distribution, the following 95% C.L. limits are derived: $-19.5 < f_{M,0}/\Lambda^4 < 20.3$, $-40.5 < f_{M,1}/\Lambda^4 < 39.5$, $-8.22 < f_{M,2}/\Lambda^4 < 8.10$, $-17.7 < f_{M,3}/\Lambda^4 < 17.9$, $-15.3 < f_{M,4}/\Lambda^4 < 15.8$, $-25.1 < f_{M,5}/\Lambda^4 < 24.5$, $-38.9 < f_{M,6}/\Lambda^4 < 40.6$, $-60.3 < f_{M,7}/\Lambda^4 < 62.5$, $-0.74 < f_{T,0}/\Lambda^4 < 0.69$, $-0.98 < f_{T,1}/\Lambda^4 < 0.96$, $-1.97 < f_{T,2}/\Lambda^4 < 1.86$, $-0.70 < f_{T,5}/\Lambda^4 < 0.75$, $-1.64 < f_{T,6}/\Lambda^4 < 1.68$, $-2.59 < f_{T,7}/\Lambda^4 < 2.82$, $-0.47 < f_{T,8}/\Lambda^4 < 0.47$, $-1.27 < f_{T,9}/\Lambda^4 < 1.27$, in units of TeV^{-4} .
- ¹¹SIRUNYAN 20BD study electroweak $W\gamma$ production in association with two jets, where the W boson decays to electron or muon and the two jets have high invariant mass. The number of observed (expected) electron events with the photon in the barrel and endcap regions are 393 (397.1 ± 18.5) and 159 (145.2 ± 10.0) respectively, while for muon events the respective numbers are 565 (537.9 ± 21.4) and 201 (188.2 ± 10.5). Analysing the $W\gamma$ invariant mass distribution, the following 95% C.L. limits are derived: $-8.1 < f_{M,0}/\Lambda^4 < 8.0$, $-12 < f_{M,1}/\Lambda^4 < 12$, $-2.8 < f_{M,2}/\Lambda^4 < 2.8$, $-4.4 < f_{M,3}/\Lambda^4 < 4.4$, $-5.0 < f_{M,4}/\Lambda^4 < 5.0$, $-8.3 < f_{M,5}/\Lambda^4 < 8.3$, $-16 < f_{M,6}/\Lambda^4 < 16$, $-21 < f_{M,7}/\Lambda^4 < 20$, $-0.6 < f_{T,0}/\Lambda^4 < 0.6$, $-0.4 < f_{T,1}/\Lambda^4 < 0.4$, -0.4 , $-1.0 < f_{T,2}/\Lambda^4 < 1.2$, $-0.5 < f_{T,5}/\Lambda^4 < 0.5$, $-0.4 < f_{T,6}/\Lambda^4 < 0.4$, $-0.9 < f_{T,7}/\Lambda^4 < 0.9$, in units of TeV^{-4} .
- ¹²SIRUNYAN 19BM search for the final state $W^+W^-W^\pm$ using W decays to electrons or muons. Two event samples are considered, events with three leptons, or events with two oppositely charged leptons accompanied by two jets. In a kinematic region selected to enhance the effect of anomalous couplings, no events are selected in the data, and 95% C.L. upper limits are obtained as follows: $-1.2 < f_{T,0}/\Lambda^4 < 1.2$, $-3.3 < f_{T,1}/\Lambda^4 < 3.3$, $-2.7 < f_{T,2}/\Lambda^4 < 2.6$, in units of TeV^{-4} and without application of a form factor.
- ¹³SIRUNYAN 19BP study WZ plus 2 jets production, using W and Z decay channels with electrons or muons. In the data, 75 events are selected, with a fitted SM signal of 15.1 ± 1.6 events and a fitted background of 62.4 ± 2.8 events. The transverse mass distribution of the WZ system is analyzed to set the following limits at 95% C.L., in units of TeV^{-4} : $-9.15 < f_{M,0}/\Lambda^4 < 9.15$, $-9.15 < f_{M,1}/\Lambda^4 < 9.45$, $-26.5 < f_{S,0}/\Lambda^4 < 27.5$, $-41.2 < f_{S,1}/\Lambda^4 < 42.8$, $-0.75 < f_{T,0}/\Lambda^4 < 0.81$, $-0.49 < f_{T,1}/\Lambda^4 < 0.55$, $-1.49 < f_{T,2}/\Lambda^4 < 1.85$.
- ¹⁴SIRUNYAN 19CQ search for anomalous electroweak production of vector boson pairs in association with two jets. Events are selected by requiring two jets with a large invariant mass and rapidity separation, one or two leptons (electrons or muons), and a W or Z boson decaying hadronically. In the WV (ZV) channel, 347 (47) events are selected in the data, with a total expected background of 352 ± 19 (50.3 ± 5.8) events. Analysing the mass distribution of the WV or ZV system, the following 95% C.L. limits are obtained: $-2.7 < f_{S,0}/\Lambda^4 < 2.7$, $-3.4 < f_{S,1}/\Lambda^4 < 3.4$, $-0.69 < f_{M,0}/\Lambda^4 < 0.70$, $-2.0 < f_{M,1}/\Lambda^4 < 2.1$, $-1.3 < f_{M,6}/\Lambda^4 < 1.3$, $-3.4 < f_{M,7}/\Lambda^4 < 3.4$, $-0.12 < f_{T,0}/\Lambda^4 < 0.11$, $-0.12 < f_{T,1}/\Lambda^4 < 0.13$, $-0.28 < f_{T,2}/\Lambda^4 < 0.28$, in units of TeV^{-4} .
- ¹⁵SIRUNYAN 18CC study pp collisions at $\sqrt{s} = 13$ TeV leading to a pair of same-sign W pairs decaying leptonically (e or μ) associated with a pair of jets. Isolated leptons with $p_T > 25$ (20) GeV for the leading (trailing) lepton, with $|\eta| < 2.5$ (2.4) for e (μ) and jets with $p_T > 30$ GeV, $|\eta| < 5.0$, $|\Delta\eta_{jj}| > 2.5$ and $m_{jj} > 500$ GeV is required. Further cuts are applied to minimize $Z \rightarrow ee$ events, non-promt leptons and hadronically decaying taus. The number of selected events is 201, with an expected SM signal of 66.9 ± 2.4 and background of 138 ± 13 events. Analysing the dilepton invariant mass spectrum the following 95% C.L. limits are derived: $-7.7 < f_{S,0}/\Lambda^4 < 7.7$, $-21.6 < f_{S,1}/\Lambda^4 < 21.8$, $-6.0 < f_{M,0}/\Lambda^4 < 5.9$, $-8.7 < f_{M,1}/\Lambda^4 < 9.1$, $-11.9 < f_{M,6}/\Lambda^4 < 11.8$, $-13.3 < f_{M,7}/\Lambda^4 < 12.9$, $-0.62 < f_{T,0}/\Lambda^4 < 0.65$, $-0.28 < f_{T,1}/\Lambda^4 < 0.31$, $-0.89 < f_{T,2}/\Lambda^4 < 1.02$.
- ¹⁶AABOUD 17AA analyze $W^\pm W^\pm$ production in association with two jets and W decay modes with electrons or muons. In the kinematic region of VBS the effect of anomalous QGCs is enhanced by requiring the transverse mass of the WW system to be larger than 400 GeV. In the data, 8 events are selected with a total background expected from SM processes of 3.8 ± 0.6 events. Assuming the other QGC coupling to have the SM value of zero, the observed event yield is used to determine 95% CL limits on the QGCs: $-0.14 < \alpha_4 < 0.15$ and $-0.22 < \alpha_5 < 0.22$. Supersedes AAD 14AM.
- ¹⁷AABOUD 17AG determine the $W\gamma\gamma$ and $WZ\gamma$ cross sections in 8 TeV pp interactions by studying the final states $e\nu\mu\nu\gamma$ and $e\nu j\gamma$ or $\mu\nu j\gamma$. Upper limits on the production cross sections are derived in a fiducial region optimized for BSM physics. These are used to derive the following 95% C.L. upper limits for quartic couplings assuming the form scale factor, $\Lambda_{FF} = \infty$ (all in units of 10^3TeV^{-4}): $-0.3 < f_{M,0}/\Lambda^4 < 0.3$, $-0.5 < f_{M,1}/\Lambda^4 < 0.5$, $-1.8 < f_{M,2}/\Lambda^4 < 1.8$, $-1.1 < f_{M,4}/\Lambda^4 < 1.1$, $-1.7 < f_{M,5}/\Lambda^4 < 1.7$, $-0.6 < f_{M,6}/\Lambda^4 < 0.6$, $-1.1 < f_{M,7}/\Lambda^4 < 1.1$, $-0.1 < f_{T,0}/\Lambda^4 < 0.1$, $-0.2 < f_{T,1}/\Lambda^4 < 0.2$, $-0.4 < f_{T,4}/\Lambda^4 < 0.4$, $-1.5 < f_{T,5}/\Lambda^4 < 1.6$, $-1.9 < f_{T,6}/\Lambda^4 < 1.9$, $-4.3 < f_{T,7}/\Lambda^4 < 4.3$.
- ¹⁸AABOUD 17D analyze electroweak diboson (WV , $V = W, Z$) production in association with a high-mass dijet system. In the data, 32 events are selected with an expected total background of 32 ± 12 events. Analysing the transverse mass distribution of the WV system, the following limits are set at 95% C.L.: $-0.024 < \alpha_4 < 0.030$ and $-0.028 < \alpha_5 < 0.033$.
- ¹⁹AABOUD 17J analyze the $Z\gamma$ production in association with a high-mass dijet system, with the Z boson decaying into a pair of electrons, muons, or neutrinos. In the charged lepton (neutrino) channel, events are selected with a dijet mass larger than 500 (600) GeV and a transverse photon energy larger than 250 (150) GeV, with 2 (4) events selected in the data and 0.30 ± 0.08 (1.6 ± 0.5) expected background events. The observed event yield is used to determine 95% CL limits as follows: $-4.1 \times 10^3 <$

- $f_{T,9}/\Lambda^4 < 4.2 \times 10^3$, $-1.9 \times 10^3 < f_{T,8}/\Lambda^4 < 2.1 \times 10^3$, $-1.9 \times 10^1 < f_{T,0}/\Lambda^4 < 1.6 \times 10^1$, $-1.6 \times 10^2 < f_{M,0}/\Lambda^4 < 1.8 \times 10^2$, $-3.5 \times 10^2 < f_{M,1}/\Lambda^4 < 3.4 \times 10^2$, $-8.9 \times 10^2 < f_{M,2}/\Lambda^4 < 8.9 \times 10^2$, $-1.7 \times 10^3 < f_{M,3}/\Lambda^4 < 1.7 \times 10^3$, in units of TeV^{-4} and without application of a form factor.
- 20** AABOUD 17M analyze tri-boson $W^\pm W^\pm W^\mp$ production in decay channels with three charged leptons or two like-sign charged leptons with two jets, where the lepton can be an electron or muon. In the data, 24 tri-lepton events and 21 di-lepton plus jets events are selected, compared to a total event yield expected in the SM of 30.8 ± 3.0 and 21.9 ± 2.0 , respectively. Analysing the tri-lepton transverse mass or the transverse momentum sum of the two leptons, two jets and the missing transverse energy, the following limits at 95% CL are derived for the form factor cut-off scale $\Lambda_{FF} \rightarrow \infty$: $-0.13 < f_{S,0}/\Lambda^4 < 0.18$, $-0.21 < f_{S,1}/\Lambda^4 < 0.27$, in units of 10^4 TeV^{-4} , which are converted into the following limits: $-0.49 < \alpha_4 < 0.75$ and $-0.48 < \alpha_5 < 0.62$.
- 21** KHACHATRYAN 17AA analyse electroweak production of $Z\gamma$ in association with two hadronic jets, with the Z boson decaying to electron or muon pairs. Events with photon transverse momentum larger than 60 GeV and di-jet invariant mass larger than 400 GeV are selected. The $Z\gamma$ invariant mass spectrum is analysed to set 95% C.L. limits as follows: $-71 < f_{M,0}/\Lambda^4 < 75$, $-190 < f_{M,1}/\Lambda^4 < 182$, $-32 < f_{M,2}/\Lambda^4 < 31$, $-58 < f_{M,3}/\Lambda^4 < 59$, $-3.8 < f_{T,0}/\Lambda^4 < 3.4$, $-4.4 < f_{T,1}/\Lambda^4 < 4.4$, $-9.9 < f_{T,2}/\Lambda^4 < 9.0$, $-1.8 < f_{T,8}/\Lambda^4 < 1.8$, $-4.0 < f_{T,9}/\Lambda^4 < 4.0$, in units of TeV^{-4} and without application of a form factor.
- 22** KHACHATRYAN 17M analyse electroweak production of $W\gamma$ in association with two hadronic jets, with the W boson decaying to electrons or muons. Events with photon transverse momentum larger than 200 GeV and di-jet invariant mass larger than 200 GeV are selected. The W transverse momentum spectrum is analysed to set 95% C.L. limits as follows: $-77 < f_{M,0}/\Lambda^4 < 74$, $-125 < f_{M,1}/\Lambda^4 < 129$, $-26 < f_{M,2}/\Lambda^4 < 26$, $-43 < f_{M,3}/\Lambda^4 < 44$, $-40 < f_{M,4}/\Lambda^4 < 40$, $-65 < f_{M,5}/\Lambda^4 < 65$, $-129 < f_{M,6}/\Lambda^4 < 129$, $-164 < f_{M,7}/\Lambda^4 < 162$, $-5.4 < f_{T,0}/\Lambda^4 < 5.6$, $-3.8 < f_{T,1}/\Lambda^4 < 4.0$, $-11 < f_{T,2}/\Lambda^4 < 12$, $-3.8 < f_{T,5}/\Lambda^4 < 3.8$, $-2.7 < f_{T,6}/\Lambda^4 < 3.0$, $-7.3 < f_{T,7}/\Lambda^4 < 7.7$, in units of TeV^{-4} and without application of a form factor.
- 23** SIRUNYAN 17AD study pp collisions at $\sqrt{s} = 13$ TeV to determine the cross section of $ZZjj$ with the Z decaying to ee or $\mu\mu$. The ZZ mass distribution is used to set upper limits on the anomalous quartic couplings. The 95% upper limits for the relevant quartic couplings in units of TeV^{-4} are: $-0.46 < f_{T,0}/\Lambda^4 < 0.44$, $-0.61 < f_{T,1}/\Lambda^4 < 0.61$, $-1.2 < f_{T,2}/\Lambda^4 < 1.2$, $-0.84 < f_{T,8}/\Lambda^4 < 0.84$, $-1.8 < f_{T,9}/\Lambda^4 < 1.8$.
- 24** SIRUNYAN 17AR study pp collisions at $\sqrt{s} = 8$ TeV to determine the cross section of $pp \rightarrow W\gamma\gamma$ and $pp \rightarrow Z\gamma\gamma$ where $W \rightarrow \ell\nu$ and $Z \rightarrow \ell^+\ell^-$, ℓ being an electron or a muon. The number of W events in the e and μ channels is 63 and 108 respectively, and the number of Z events in the e and μ channels is 117 and 141. To increase sensitivity, the transverse momentum of the leading photon is required to be larger than 70 GeV. The 95% C.L. upper limits in units of TeV^{-4} are $-701 < f_{M,2}/\Lambda^4 < 683$, $-1170 < f_{M,3}/\Lambda^4 < 1220$, $-33.5 < f_{T,0}/\Lambda^4 < 34.0$, $-44.3 < f_{T,1}/\Lambda^4 < 44.8$, $-93.8 < f_{T,2}/\Lambda^4 < 93.2$.
- 25** AABOUD 16E study WW production in two-photon mediated pp collisions at 8 TeV where the W boson decays into an electron or muon, probing the $\gamma\gamma WW$ vertex for anomalous quartic gauge couplings. The lepton p_T is required to be larger than 30 GeV. Limits on anomalous couplings are determined from events with p_T larger than 120 GeV where the aQGC effect is enhanced and the SM background reduced; in the data corresponding to an integrated luminosity of 20.2fb^{-1} , 1 event is selected with an expected SM background of 0.37 ± 0.13 events. The 95% C.L. limits without a form-factor cutoff ($\Lambda_{\text{cutoff}} \rightarrow \infty$) are as follows: $-1.7 < a_0^W/\Lambda^2 < 1.7$ and $-6.4 < a_C^W/\Lambda^2 < 6.3$ in units of 10^{-6} GeV^{-2} . In terms of another set of variables: $-6.6 < f_{M,0}/\Lambda^4 < 6.6$ and $-24 < f_{M,1}/\Lambda^4 < 25$ in units of $10^{-11} \text{ GeV}^{-4}$.
- 26** AAD 16Q study $Z\gamma\gamma$ production in pp collisions. In events with no additional jets, 29 (22) Z decays to electron (muon) pairs are selected, with an expected background of 3.3 ± 1.1 (6.5 ± 2.0) events, as well as 19 Z decays to neutrino pairs with an expected background of 8.3 ± 4.4 events. Analysing the photon transverse momentum distribution for $m_{\gamma\gamma}$ above 200 GeV (300 GeV) for lepton (neutrino) events, yields the 95% C.L. limits: $-1.6 \times 10^4 < f_{M,2}/\Lambda^4 < 1.6 \times 10^4$, $-2.9 \times 10^4 < f_{M,3}/\Lambda^4 < 2.7 \times 10^4$, $-0.86 \times 10^2 < f_{T,0}/\Lambda^4 < 1.03 \times 10^2$, $-0.69 \times 10^3 < f_{T,5}/\Lambda^4 < 0.68 \times 10^3$, $-0.74 \times 10^4 < f_{T,9}/\Lambda^4 < 0.74 \times 10^4$ in units of TeV^{-4} and without application of a form factor Λ_{FF} .
- 27** KHACHATRYAN 16AX searches for anomalous $WW\gamma\gamma$ quartic gauge couplings in the two-photon-mediated process $pp \rightarrow ppWW$, assuming the $WW\gamma\gamma$ triple gauge boson couplings to be at their Standard Model values. 13 events containing an $e^\pm\mu^\mp$ pair with $p_T(e, \mu) > 30$ GeV are selected in a total luminosity of 19.7 fb^{-1} , with an expected $\gamma\gamma \rightarrow WW$ signal of 5.3 ± 0.1 events and an expected background of 3.9 ± 0.5 events. When combining with the data collected at 7 TeV (KHACHATRYAN 13AA), and not assuming a form factor, the following 1-parameter limits at 95% C.L. are obtained from the $p_T(e, \mu)$ spectrum: $|a_0^W/\Lambda^2| < 1.1 \times 10^{-6} \text{ GeV}^{-2}$ ($a_C^W = 0$), and $|a_C^W/\Lambda^2| < 4.1 \times 10^{-6} \text{ GeV}^{-2}$ ($a_0^W = 0$). In terms of another set of variables: $|f_{M,0}/\Lambda^4| < 4.2 \times 10^{-12} \text{ GeV}^{-4}$, $|f_{M,1}/\Lambda^4| < 16 \times 10^{-12} \text{ GeV}^{-4}$, $|f_{M,2}/\Lambda^4| < 2.1 \times 10^{-12} \text{ GeV}^{-4}$, $|f_{M,3}/\Lambda^4| < 7.8 \times 10^{-12} \text{ GeV}^{-4}$.
- 28** AAD 15N study $W\gamma\gamma$ events in 8 TeV pp interactions, where the W decays into an electron or a muon. The events are characterized by an isolated lepton, a missing transverse energy due to the decay neutrino, and two isolated photons, with the p_T of the lepton and the photons being > 20 GeV. The number of candidate events observed in the electron channel for $N(\text{jet}) \geq 0$ and $N(\text{jet}) = 0$ is 47 and 15, the corresponding numbers for the muon channel being 110 and 53. The backgrounds expected are 30.2 ± 7.4 , 8.7 ± 3.0 , 52.1 ± 12.2 , and 24.4 ± 8.3 respectively. The 95% C.L. limits on the values of the parameters $f_{T,0}/\Lambda^4$, $f_{M,2}/\Lambda^4$ and $f_{M,3}/\Lambda^4$ are -0.9 – 0.9×10^2 , -0.8 – 0.8×10^4 , and -1.5 – 1.4×10^4 respectively, without application of a form factor Λ_{FF} .
- 29** KHACHATRYAN 15D study vector-boson-scattering tagged by two jets, requiring two same-sign charged leptons arising from $W^\pm W^\pm$ production and decay. The two jets must have a transverse momentum larger than 30 GeV, while the leptons, electrons or muons, must have a transverse momentum > 20 GeV. The dijet mass is required to be > 500 GeV, the dilepton mass > 50 GeV, with additional requirement of differing from the Z mass by > 15 GeV. In the two categories $W^+ W^+$ and $W^- W^-$, 10 and 2 data events are observed in a data sample corresponding to an integrated luminosity of 19.4 fb^{-1} , with an expected background of 3.1 ± 0.6 and 2.6 ± 0.5 events. Analysing the distribution of the dilepton invariant mass, the following limits at 95% C.L. are obtained, in units of TeV^{-4} : $-38 < f_{S,0}/\Lambda^4 < 40$, $-118 < f_{S,1}/\Lambda^4 < 120$, $-33 < f_{M,0}/\Lambda^4 < 32$, $-44 < f_{M,1}/\Lambda^4 < 47$, $-65 < f_{M,6}/\Lambda^4 < 63$, $-70 < f_{M,7}/\Lambda^4 < 66$, $-4.2 < f_{T,0}/\Lambda^4 < 4.6$, $-1.9 < f_{T,1}/\Lambda^4 < 2.2$, $-5.2 < f_{T,2}/\Lambda^4 < 6.4$.
- 30** AAD 14AM analyze electroweak production of WW jet jet same-charge diboson plus two jets production, with the W bosons decaying to electron or muon, to study the quartic $WWWW$ coupling. In a kinematic region enhancing the electroweak production over the strong production, 34 events are observed in the data while 29.8 ± 2.4 events are expected with a background of 15.9 ± 1.9 events. Assuming the other QGC coupling to have the SM value of zero, the observed event yield is used to determine 95% C.L. limits on the quartic gauge couplings: $-0.14 < \alpha_4 < 0.16$ and $-0.23 < \alpha_5 < 0.24$.
- 31** KHACHATRYAN 14Q study $WV\gamma$ production in 8 TeV pp collisions, in the single lepton final state, with $W \rightarrow \ell\nu$, $Z \rightarrow \text{dijet}$ or $W \rightarrow \ell\nu$, $W \rightarrow \text{dijet}$, the dijet mass resolution precluding differentiation between the W and Z. p_T and pseudo-rapidity cuts are put on the lepton, the photon and the two jets to minimize backgrounds. The dijet mass is required to be between 70–100 GeV and $|\Delta\eta_{jj}| < 1.4$. The selected number of muon (electron) events are 183 (139), with SM expectation being 194.2 ± 11.5 (147.9 ± 10.7) including signal and background. The photon E_T distribution is used to set limits on the anomalous quartic couplings. The following 95% C.L. limits are deduced (all in units of TeV^{-2} or TeV^{-4}): $-21 < a_0^W/\Lambda^2 < 20$, $-34 < a_C^W/\Lambda^2 < 32$, $-12 < \kappa_0^W/\Lambda^2 < 10$ and $-18 < \kappa_C^W/\Lambda^2 < 17$; and $-25 < f_{T,0}/\Lambda^4 < 24 \text{ TeV}^{-4}$.
- 32** ABAZOV 13D searches for anomalous $WW\gamma\gamma$ quartic gauge couplings in the two-photon-mediated process $pp \rightarrow ppWW$, assuming the $WW\gamma\gamma$ triple gauge boson couplings to be at their Standard Model values. 946 events containing an e^+e^- pair with missing energy are selected in a total luminosity of 9.7 fb^{-1} , with an expectation of 983 \pm 108 events from Standard-Model processes. The following 1-parameter limits at 95% CL are obtained: $|a_0^W/\Lambda^2| < 4.3 \times 10^{-4} \text{ GeV}^{-2}$ ($a_C^W = 0$), $|a_C^W/\Lambda^2| < 1.5 \times 10^{-3} \text{ GeV}^{-2}$ ($a_0^W = 0$).
- 33** KHACHATRYAN 13AA searches for anomalous $WW\gamma\gamma$ quartic gauge couplings in the two-photon-mediated process $pp \rightarrow ppWW$, assuming the $WW\gamma\gamma$ triple gauge boson couplings to be at their Standard Model values. 2 events containing an $e^\pm\mu^\mp$ pair with $p_T(e, \mu) > 30$ GeV are selected in a total luminosity of 5.05 fb^{-1} , with an expected $ppWW$ signal of 2.2 ± 0.4 events and an expected background of 0.84 ± 0.15 events. The following 1-parameter limits at 95% CL are obtained from the $p_T(e, \mu)$ spectrum: $|a_0^W/\Lambda^2| < 4.0 \times 10^{-6} \text{ GeV}^{-2}$ ($a_C^W = 0$), $|a_C^W/\Lambda^2| < 1.5 \times 10^{-5} \text{ GeV}^{-2}$ ($a_0^W = 0$).
- 34** ABBIENDI 04B select 187 $e^+e^- \rightarrow W^+W^-\gamma$ events in the C.M. energy range 180–209 GeV, where $E_\gamma > 2.5$ GeV, the photon has a polar angle $|\cos\theta_\gamma| < 0.975$ and is well isolated from the nearest jet and charged lepton, and the effective masses of both fermion-antifermion systems agree with the W mass within $3 \Gamma_W$. The measured differential cross section as a function of the photon energy and photon polar angle is used to extract the 95% CL limits: $-0.020 \text{ GeV}^{-2} < a_0/\Lambda^2 < 0.020 \text{ GeV}^{-2}$, $-0.053 \text{ GeV}^{-2} < a_C/\Lambda^2 < 0.037 \text{ GeV}^{-2}$ and $-0.16 \text{ GeV}^{-2} < a_n/\Lambda^2 < 0.15 \text{ GeV}^{-2}$.
- 35** ABBIENDI 04L select 20 $e^+e^- \rightarrow \nu\bar{\nu}\gamma\gamma$ acoplanar events in the energy range 180–209 GeV and 176 $e^+e^- \rightarrow q\bar{q}\gamma\gamma$ events in the energy range 130–209 GeV. These samples are used to constrain possible anomalous $W^+W^-\gamma\gamma$ and $ZZ\gamma\gamma$ quartic couplings. Further combining with the $W^+W^-\gamma$ sample of ABBIENDI 04B the following one-parameter 95% CL limits are obtained: $-0.007 < a_0^Z/\Lambda^2 < 0.023 \text{ GeV}^{-2}$, $-0.029 < a_C^Z/\Lambda^2 < 0.029 \text{ GeV}^{-2}$, $-0.020 < a_0^W/\Lambda^2 < 0.020 \text{ GeV}^{-2}$, $-0.052 < a_C^W/\Lambda^2 < 0.037 \text{ GeV}^{-2}$.
- 36** In the CM energy range 183 to 209 GeV HEISTER 04A select 30 $e^+e^- \rightarrow \nu\bar{\nu}\gamma\gamma$ events with two acoplanar, high energy and high transverse momentum photons. The photon-photon acoplanarity is required to be $> 5^\circ$, $E_\gamma/\sqrt{s} > 0.025$ (the more energetic photon having energy $> 0.2\sqrt{s}$), $p_{T,\gamma}/E_{\text{beam}} > 0.05$ and $|\cos\theta_\gamma| < 0.94$. A likelihood fit to the photon energy and recoil missing mass yields the following one-parameter 95% CL limits: $-0.012 < a_0^Z/\Lambda^2 < 0.019 \text{ GeV}^{-2}$, $-0.041 < a_C^Z/\Lambda^2 < 0.044 \text{ GeV}^{-2}$, $-0.060 < a_0^W/\Lambda^2 < 0.055 \text{ GeV}^{-2}$, $-0.099 < a_C^W/\Lambda^2 < 0.093 \text{ GeV}^{-2}$.
- 37** ABDALLAH 03i select 122 $e^+e^- \rightarrow W^+W^-\gamma$ events in the C.M. energy range 189–209 GeV, where $E_\gamma > 5$ GeV, the photon has a polar angle $|\cos\theta_\gamma| < 0.95$ and is well isolated from the nearest charged fermion. A fit to the photon energy spectra yields $a_C/\Lambda^2 = 0.000^{+0.019}_{-0.040} \text{ GeV}^{-2}$, $a_0/\Lambda^2 = -0.004^{+0.018}_{-0.010} \text{ GeV}^{-2}$, $\bar{a}_0/\Lambda^2 = -0.007^{+0.019}_{-0.008} \text{ GeV}^{-2}$, $a_n/\Lambda^2 = -0.09^{+0.16}_{-0.05} \text{ GeV}^{-2}$, and $\bar{a}_n/\Lambda^2 = +0.05^{+0.07}_{-0.15} \text{ GeV}^{-2}$, keeping the other parameters fixed to their Standard Model values (0). The 95% CL limits are: $-0.063 \text{ GeV}^{-2} < a_C/\Lambda^2 < +0.032 \text{ GeV}^{-2}$, $-0.020 \text{ GeV}^{-2} < a_0/\Lambda^2 < +0.020 \text{ GeV}^{-2}$, $-0.18 \text{ GeV}^{-2} < \bar{a}_n/\Lambda^2 < +0.14 \text{ GeV}^{-2}$, $-0.16 \text{ GeV}^{-2} < \bar{a}_n/\Lambda^2 < +0.17 \text{ GeV}^{-2}$.
- 38** ACHARD 02f select 86 $e^+e^- \rightarrow W^+W^-\gamma$ events at 192–207 GeV, where $E_\gamma > 5$ GeV and the photon is well isolated. They also select 43 acoplanar $e^+e^- \rightarrow \nu\bar{\nu}\gamma\gamma$ events in this energy range, where the photon energies are > 5 GeV and > 1 GeV and the photon polar angles are between 14° and 166° . All these 43 events are in the recoil mass region corresponding to the Z (75 – 110 GeV). Using the shape and normalization of the photon spectra in the $W^+W^-\gamma$ events, and combining with the 42 event sample from 189 GeV data (ACCIARRI 00T), they obtain: $a_0/\Lambda^2 = 0.000 \pm 0.010 \text{ GeV}^{-2}$, $a_C/\Lambda^2 = -0.013 \pm 0.023 \text{ GeV}^{-2}$, and $a_n/\Lambda^2 = -0.002 \pm 0.076 \text{ GeV}^{-2}$. Further combining the analyses of $W^+W^-\gamma$ events with the low recoil mass region of $\nu\bar{\nu}\gamma\gamma$ events (including samples collected at 183 + 189 GeV), they obtain the following one-parameter 95% CL

standard model. Keeping this term as free parameter leads to a somewhat larger error on the fitted Z mass. See ACCIARRI 00q and ABBIENDI 04g for a detailed investigation of both these issues.

VALUE (GeV)	EVTS	DOCUMENT ID	TECN	COMMENT
91.1880 ± 0.0020 OUR AVERAGE				
91.1923 ± 0.0071		1 AALTONEN 22	CDF	$E_{cm}^{p\bar{p}} = 1.8$ TeV
91.1876 ± 0.0021		2 LEP-SLC 06	LEP	$E_{cm}^{ee} = 88-94$ GeV
• • • We do not use the following data for averages, fits, limits, etc. • • •				
91.084 ± 0.107		3 ANDREEV 18A	H1	$e^\pm p$
91.1872 ± 0.0033		4 ABBIENDI 04G	OPAL	$E_{cm}^{ee} = LEP1 + 130-209$ GeV
91.272 ± 0.032 ± 0.033		5 ACHARD 04C	L3	$E_{cm}^{ee} = 183-209$ GeV
91.1852 ± 0.0030	4.57M	6 ABBIENDI 01A	OPAL	$E_{cm}^{ee} = 88-94$ GeV
91.1863 ± 0.0028	4.08M	7 ABREU 00F	DLPH	$E_{cm}^{ee} = 88-94$ GeV
91.1898 ± 0.0031	3.96M	8 ACCIARRI 00C	L3	$E_{cm}^{ee} = 88-94$ GeV
91.1875 ± 0.0039	3.97M	9 ACCIARRI 00Q	L3	$E_{cm}^{ee} = LEP1 + 130-189$ GeV
91.1885 ± 0.0031	4.57M	10 BARATE 00C	ALEP	$E_{cm}^{ee} = 88-94$ GeV
91.151 ± 0.008		11 MIYABAYASHI 95	TOPZ	$E_{cm}^{ee} = 57.8$ GeV
91.74 ± 0.28 ± 0.93	156	12 ALITTI 92B	UA2	$E_{cm}^{p\bar{p}} = 630$ GeV
90.9 ± 0.3 ± 0.2	188	13 ABE 89C	CDF	$E_{cm}^{p\bar{p}} = 1.8$ TeV
91.14 ± 0.12	480	14 ABRAMS 89B	MRK2	$E_{cm}^{ee} = 89-93$ GeV
93.1 ± 1.0 ± 3.0	24	15 ALBAJAR 89	UA1	$E_{cm}^{p\bar{p}} = 546,630$ GeV

- AALTONEN 22 analyse Z decays in the di-muon and di-electron channels using their full Run-II data set. They obtain Z mass values of 91192.0 ± 6.4 (stat.) ± 4.0 (syst.) MeV and 91194.3 ± 13.8 (stat.) ± 7.6 (syst.) MeV, respectively. Combining these results using the systematic uncertainty contributions and their correlations as given in AALTONEN 22, we obtain an average of 91192.3 ± 5.8 (stat.) ± 4.1 (syst.) MeV.
- This result combines ABBIENDI 01A, ABREU 00F, ACCIARRI 00C, BARATE 00C, taking correlated uncertainties into account.
- ANDREEV 18A obtain this result in a combined electroweak and QCD analysis using all deep-inelastic e^+p and e^-p neutral current and charged current scattering cross sections published by the H1 Collaboration, including data with longitudinally polarized lepton beams.
- ABBIENDI 04G obtain this result using the S-matrix formalism for a combined fit to their cross section and asymmetry data at the Z peak and their data at 130–209 GeV. The authors have corrected the measurement for the 34 MeV shift with respect to the Breit-Wigner fits.
- ACHARD 04C select $e^+e^- \rightarrow Z\gamma$ events with hard initial-state radiation. Z decays to $q\bar{q}$ and muon pairs are considered. The fit results obtained in the two samples are found consistent to each other and combined considering the uncertainty due to ISR modelling as fully correlated.
- ABBIENDI 01A error includes approximately 2.3 MeV due to statistics and 1.8 MeV due to LEP energy uncertainty. This result is included in the LEP average LEP-SLC 06.
- The error includes 1.6 MeV due to LEP energy uncertainty. This result is included in the LEP average LEP-SLC 06.
- The error includes 1.8 MeV due to LEP energy uncertainty. This result is included in the LEP average LEP-SLC 06.
- ACCIARRI 00Q interpret the s-dependence of the cross sections and lepton forward-backward asymmetries in the framework of the S-matrix formalism. They fit to their cross section and asymmetry data at high energies, using the results of S-matrix fits to Z-peak data (ACCIARRI 00C) as constraints. The 130–189 GeV data constrains the γ/Z interference term. The authors have corrected the measurement for the 34.1 MeV shift with respect to the Breit-Wigner fits. The error contains a contribution of ± 2.3 MeV due to the uncertainty on the γZ interference.
- BARATE 00C error includes approximately 2.4 MeV due to statistics, 0.2 MeV due to experimental systematics, and 1.7 MeV due to LEP energy uncertainty. This result is included in the LEP average LEP-SLC 06.
- MIYABAYASHI 95 combine their low energy total hadronic cross-section measurement with the ACTON 93D data and perform a fit using an S-matrix formalism. As expected, this result is below the mass values obtained with the standard Breit-Wigner parametrization.
- Enters fit through W/Z mass ratio given in the W Particle Listings. The ALITTI 92B systematic error (± 0.93) has two contributions: one (± 0.92) cancels in m_W/m_Z and one (± 0.12) is noncancelling. These were added in quadrature.
- First error of ABE 89 is combination of statistical and systematic contributions; second is mass scale uncertainty.
- ABRAMS 89B uncertainty includes 35 MeV due to the absolute energy measurement.
- ALBAJAR 89 result is from a total sample of 33 Z $\rightarrow e^+e^-$ events.

Z WIDTH

OUR EVALUATION is obtained using the fit procedure and correlations as determined by the LEP Electroweak Working Group (see the note “The Z boson” and ref. LEP-SLC 06). Corrections as discussed in VOUTSINAS 20 and JANOT 20 are also included.

VALUE (GeV)	EVTS	DOCUMENT ID	TECN	COMMENT
2.4955 ± 0.0023 OUR EVALUATION				
2.4955 ± 0.0023		1 JANOT 20		
• • • We do not use the following data for averages, fits, limits, etc. • • •				
2.4955 ± 0.0023		2 VOUTSINAS 20		
2.4952 ± 0.0023		LEP-SLC 06		$E_{cm}^{ee} = 88-94$ GeV
2.4943 ± 0.0041		3 ABBIENDI 04G	OPAL	$E_{cm}^{ee} = LEP1 + 130-209$ GeV
2.4948 ± 0.0041	4.57M	4 ABBIENDI 01A	OPAL	$E_{cm}^{ee} = 88-94$ GeV
2.4876 ± 0.0041	4.08M	5 ABREU 00F	DLPH	$E_{cm}^{ee} = 88-94$ GeV

2.5024 ± 0.0042	3.96M	6 ACCIARRI 00C	L3	$E_{cm}^{ee} = 88-94$ GeV
2.5025 ± 0.0041	3.97M	7 ACCIARRI 00Q	L3	$E_{cm}^{ee} = LEP1 + 130-189$ GeV
2.4951 ± 0.0043	4.57M	8 BARATE 00C	ALEP	$E_{cm}^{ee} = 88-94$ GeV
2.50 ± 0.21 ± 0.06		9 ABREU 96R	DLPH	$E_{cm}^{ee} = 91.2$ GeV
3.8 ± 0.8 ± 1.0	188	ABE 89C	CDF	$E_{cm}^{p\bar{p}} = 1.8$ TeV
2.42 +0.45 -0.35	480	10 ABRAMS 89B	MRK2	$E_{cm}^{ee} = 89-93$ GeV
2.7 +1.2 -1.0 ± 1.3	24	11 ALBAJAR 89	UA1	$E_{cm}^{p\bar{p}} = 546,630$ GeV
2.7 ± 2.0 ± 1.0	25	12 ANSARI 87	UA2	$E_{cm}^{p\bar{p}} = 546,630$ GeV

- JANOT 20 applies a correction to LEP-SLC 06 using an updated Bhabha cross section calculation. This result also includes a correction to account for correlated luminosity bias as presented in VOUTSINAS 20.
- VOUTSINAS 20 applies a correction to LEP-SLC 06 to account for correlated luminosity bias.
- ABBIENDI 04G obtain this result using the S-matrix formalism for a combined fit to their cross section and asymmetry data at the Z peak and their data at 130–209 GeV. The authors have corrected the measurement for the 1 MeV shift with respect to the Breit-Wigner fits.
- ABBIENDI 01A error includes approximately 3.6 MeV due to statistics, 1 MeV due to event selection systematics, and 1.3 MeV due to LEP energy uncertainty.
- The error includes 1.2 MeV due to LEP energy uncertainty.
- The error includes 1.3 MeV due to LEP energy uncertainty.
- ACCIARRI 00Q interpret the s-dependence of the cross sections and lepton forward-backward asymmetries in the framework of the S-matrix formalism. They fit to their cross section and asymmetry data at high energies, using the results of S-matrix fits to Z-peak data (ACCIARRI 00C) as constraints. The 130–189 GeV data constrains the γ/Z interference term. The authors have corrected the measurement for the 0.9 MeV shift with respect to the Breit-Wigner fits.
- BARATE 00C error includes approximately 3.8 MeV due to statistics, 0.9 MeV due to experimental systematics, and 1.3 MeV due to LEP energy uncertainty.
- ABREU 96R obtain this value from a study of the interference between initial and final state radiation in the process $e^+e^- \rightarrow Z \rightarrow \mu^+\mu^-$.
- ABRAMS 89B uncertainty includes 50 MeV due to the miniSAM background subtraction error.
- ALBAJAR 89 result is from a total sample of 33 Z $\rightarrow e^+e^-$ events.
- Quoted values of ANSARI 87 are from direct fit. Ratio of Z and W production gives either $\Gamma(Z) < (1.09 \pm 0.07) \times \Gamma(W)$, CL = 90% or $\Gamma(Z) = (0.82^{+0.19}_{-0.14} \pm 0.06) \times \Gamma(W)$. Assuming Standard-Model value $\Gamma(W) = 2.65$ GeV then gives $\Gamma(Z) < 2.89 \pm 0.19$ or $= 2.17^{+0.50}_{-0.37} \pm 0.16$.

Z DECAY MODES

Mode	Fraction (Γ_i/Γ)	Scale factor/ Confidence level
Γ_1 e^+e^-	(3.3632 ± 0.0042) %	
Γ_2 $\mu^+\mu^-$	(3.3662 ± 0.0066) %	
Γ_3 $\tau^+\tau^-$	(3.3696 ± 0.0083) %	
Γ_4 $\ell^+\ell^-$	[a] (3.3658 ± 0.0023) %	
Γ_5 $\mu^+\mu^-\mu^+\mu^-$		
Γ_6 $\ell^+\ell^-\ell^+\ell^-$	[b] (4.55 ± 0.17) × 10 ⁻⁶	
Γ_7 invisible	(20.000 ± 0.055) %	
Γ_8 hadrons	(69.911 ± 0.056) %	
Γ_9 $(u\bar{u} + c\bar{c})/2$	(11.6 ± 0.6) %	
Γ_{10} $(d\bar{d} + s\bar{s} + b\bar{b})/3$	(15.6 ± 0.4) %	
Γ_{11} $c\bar{c}$	(12.03 ± 0.21) %	
Γ_{12} $b\bar{b}$	(15.12 ± 0.05) %	
Γ_{13} $b\bar{b}b\bar{b}$	(3.6 ± 1.3) × 10 ⁻⁴	
Γ_{14} ggg	< 1.1	CL=95%
Γ_{15} $\pi^0\gamma$	< 2.01	× 10 ⁻⁵ CL=95%
Γ_{16} $\eta\gamma$	< 5.1	× 10 ⁻⁵ CL=95%
Γ_{17} $\rho^0\gamma$	< 4.0	× 10 ⁻⁶ CL=95%
Γ_{18} $\omega\gamma$	< 3.9	× 10 ⁻⁶ CL=95%
Γ_{19} $\eta'(958)\gamma$	< 4.2	× 10 ⁻⁵ CL=95%
Γ_{20} $\phi\gamma$	< 7	× 10 ⁻⁷ CL=95%
Γ_{21} $\gamma\gamma$	< 1.46	× 10 ⁻⁵ CL=95%
Γ_{22} $\pi^0\pi^0$	< 1.52	× 10 ⁻⁵ CL=95%
Γ_{23} $\gamma\gamma\gamma$	< 2.2	× 10 ⁻⁶ CL=95%
Γ_{24} $\pi^\pm W^\mp$	[c] < 7	× 10 ⁻⁵ CL=95%
Γ_{25} $\rho^\pm W^\mp$	[c] < 8.3	× 10 ⁻⁵ CL=95%
Γ_{26} $J/\psi(1S)X$	(3.51 +0.23 -0.25) × 10 ⁻³	S=1.1
Γ_{27} $J/\psi(1S)\gamma$	< 1.2	× 10 ⁻⁶ CL=95%
Γ_{28} $\psi(2S)X$	(1.60 ± 0.29) × 10 ⁻³	
Γ_{29} $\psi(2S)\gamma$	< 2.4	× 10 ⁻⁶ CL=95%
Γ_{30} $J/\psi(1S)\ell^+\ell^-$		
Γ_{31} $J/\psi(1S)J/\psi(1S)$	< 2.2	× 10 ⁻⁶ CL=95%
Γ_{32} $\chi_{c1}(1P)X$	(2.9 ± 0.7) × 10 ⁻³	
Γ_{33} $\chi_{c2}(1P)X$	< 3.2	× 10 ⁻³ CL=90%
Γ_{34} $\Upsilon(1S)X + \Upsilon(2S)X + \Upsilon(3S)X$	(1.0 ± 0.5) × 10 ⁻⁴	
Γ_{35} $\Upsilon(1S)X$	< 4.4	× 10 ⁻⁵ CL=95%

Gauge & Higgs Boson Particle Listings

Z

Γ_{36}	$\gamma(1S)\gamma$	< 1.1	$\times 10^{-6}$	CL=95%
Γ_{37}	$\gamma(2S)X$	< 1.39	$\times 10^{-4}$	CL=95%
Γ_{38}	$\gamma(2S)\gamma$	< 1.3	$\times 10^{-6}$	CL=95%
Γ_{39}	$\gamma(3S)X$	< 9.4	$\times 10^{-5}$	CL=95%
Γ_{40}	$\gamma(3S)\gamma$	< 2.4	$\times 10^{-6}$	CL=95%
Γ_{41}	$\gamma(1, 2, 3S)\gamma(1, 2, 3S)$	< 1.5	$\times 10^{-6}$	CL=95%
Γ_{42}	$D^0\gamma$	< 2.2	$\times 10^{-3}$	CL=95%
Γ_{43}	$(D^0/\bar{D}^0)X$	(20.7 \pm 2.0) %		
Γ_{44}	$D^\pm X$	(12.2 \pm 1.7) %		
Γ_{45}	$D^*(2010)^\pm X$	[c] (11.4 \pm 1.3) %		
Γ_{46}	$D_{s1}(2536)^\pm X$	(3.6 \pm 0.8) $\times 10^{-3}$		
Γ_{47}	$D_{sJ}(2573)^\pm X$	(5.8 \pm 2.2) $\times 10^{-3}$		
Γ_{48}	$D^*(2629)^\pm X$	searched for		
Γ_{49}	BX			
Γ_{50}	B^+X			
Γ_{51}	B^+X	[d] (6.08 \pm 0.13) %		
Γ_{52}	$B_s^0 X$	[d] (1.59 \pm 0.13) %		
Γ_{53}	$B_c^\pm X$	searched for		
Γ_{54}	$\Lambda_c^+ X$	(1.54 \pm 0.33) %		
Γ_{55}	$\Xi_c^0 X$	seen		
Γ_{56}	$\Xi_b X$	seen		
Γ_{57}	b -baryon X	[d] (1.38 \pm 0.22) %		
Γ_{58}	anomalous γ + hadrons	[e] < 3.2	$\times 10^{-3}$	CL=95%
Γ_{59}	$e^+ e^- \gamma$	[e] < 5.2	$\times 10^{-4}$	CL=95%
Γ_{60}	$\mu^+ \mu^- \gamma$	[e] < 5.6	$\times 10^{-4}$	CL=95%
Γ_{61}	$\tau^+ \tau^- \gamma$	[e] < 7.3	$\times 10^{-4}$	CL=95%
Γ_{62}	$\ell^+ \ell^- \gamma \gamma$	[f] < 6.8	$\times 10^{-6}$	CL=95%
Γ_{63}	$q\bar{q}\gamma\gamma$	[f] < 5.5	$\times 10^{-6}$	CL=95%
Γ_{64}	$\nu\bar{\nu}\gamma\gamma$	[f] < 3.1	$\times 10^{-6}$	CL=95%
Γ_{65}	$e^\pm \mu^\mp$	LF [c] < 2.62	$\times 10^{-7}$	CL=95%
Γ_{66}	$e^\pm \tau^\mp$	LF [c] < 5.0	$\times 10^{-6}$	CL=95%
Γ_{67}	$\mu^\pm \tau^\mp$	LF [c] < 6.5	$\times 10^{-6}$	CL=95%
Γ_{68}	$p e$	L,B < 1.8	$\times 10^{-6}$	CL=95%
Γ_{69}	$p \mu$	L,B < 1.8	$\times 10^{-6}$	CL=95%

[a] ℓ indicates each type of lepton (e , μ , and τ), not sum over them.

[b] Here ℓ indicates e or μ .

[c] The value is for the sum of the charge states or particle/antiparticle states indicated.

[d] This value is updated using the product of (i) the $Z \rightarrow b\bar{b}$ fraction from this listing and (ii) the b -hadron fraction in an unbiased sample of weakly decaying b -hadrons produced in Z -decays provided by the Heavy Flavor Averaging Group (HFLAV, http://www.slac.stanford.edu/xorg/hflav/osc/PDG_2009/#FRACZ).

[e] See the Particle Listings below for the γ energy range used in this measurement.

[f] For $m_{\gamma\gamma} = (60 \pm 5)$ GeV.

Z PARTIAL WIDTHS

$\Gamma(e^+ e^-)$ Γ_1
For the LEP experiments, this parameter is not directly used in the overall fit but is derived using the fit results; see the note "The Z boson" and ref. LEP-SLC 06.

VALUE (MeV)	EVTS	DOCUMENT ID	TECN	COMMENT
83.91 \pm 0.12 OUR FIT				
83.66 \pm 0.20	137.0k	ABBIENDI	01A OPAL	$E_{cm}^{ee} = 88-94$ GeV
83.54 \pm 0.27	117.8k	ABREU	00F DLPH	$E_{cm}^{ee} = 88-94$ GeV
84.16 \pm 0.22	124.4k	ACCIARRI	00c L3	$E_{cm}^{ee} = 88-94$ GeV
83.88 \pm 0.19		BARATE	00c ALEP	$E_{cm}^{ee} = 88-94$ GeV
82.89 \pm 1.20 \pm 0.89		¹ ABE	95J SLD	$E_{cm}^{ee} = 91.31$ GeV

¹ ABE 95J obtain this measurement from Bhabha events in a restricted fiducial region to improve systematics. They use the values 91.187 and 2.489 GeV for the Z mass and total decay width to extract this partial width.

$\Gamma(\mu^+ \mu^-)$ Γ_2
This parameter is not directly used in the overall fit but is derived using the fit results; see the note "The Z boson" and ref. LEP-SLC 06.

VALUE (MeV)	EVTS	DOCUMENT ID	TECN	COMMENT
83.99 \pm 0.18 OUR FIT				
84.03 \pm 0.30	182.8k	ABBIENDI	01A OPAL	$E_{cm}^{ee} = 88-94$ GeV
84.48 \pm 0.40	157.6k	ABREU	00F DLPH	$E_{cm}^{ee} = 88-94$ GeV
83.95 \pm 0.44	113.4k	ACCIARRI	00c L3	$E_{cm}^{ee} = 88-94$ GeV
84.02 \pm 0.28		BARATE	00c ALEP	$E_{cm}^{ee} = 88-94$ GeV

$\Gamma(\tau^+ \tau^-)$ Γ_3
This parameter is not directly used in the overall fit but is derived using the fit results; see the note "The Z boson" and ref. LEP-SLC 06.

VALUE (MeV)	EVTS	DOCUMENT ID	TECN	COMMENT
84.08 \pm 0.22 OUR FIT				
83.94 \pm 0.41	151.5k	ABBIENDI	01A OPAL	$E_{cm}^{ee} = 88-94$ GeV
83.71 \pm 0.58	104.0k	ABREU	00F DLPH	$E_{cm}^{ee} = 88-94$ GeV
84.23 \pm 0.58	103.0k	ACCIARRI	00c L3	$E_{cm}^{ee} = 88-94$ GeV
84.38 \pm 0.31		BARATE	00c ALEP	$E_{cm}^{ee} = 88-94$ GeV

$\Gamma(\ell^+ \ell^-)$ Γ_4
 ℓ indicates each type of lepton (e , μ , and τ), not sum over them.

In our fit $\Gamma(\ell^+ \ell^-)$ is defined as the partial Z width for the decay into a pair of massless charged leptons. This parameter is not directly used in the 5-parameter fit assuming lepton universality but is derived using the fit results. See the note "The Z boson" and ref. LEP-SLC 06.

VALUE (MeV)	EVTS	DOCUMENT ID	TECN	COMMENT
83.984 \pm 0.086 OUR FIT				
83.82 \pm 0.15	471.3k	ABBIENDI	01A OPAL	$E_{cm}^{ee} = 88-94$ GeV
83.85 \pm 0.17	379.4k	ABREU	00F DLPH	$E_{cm}^{ee} = 88-94$ GeV
84.14 \pm 0.17	340.8k	ACCIARRI	00c L3	$E_{cm}^{ee} = 88-94$ GeV
84.02 \pm 0.15	500k	BARATE	00c ALEP	$E_{cm}^{ee} = 88-94$ GeV

$\Gamma(\text{invisible})$ Γ_7

The Z boson also decays to final states invisible in any detector, for example, the decay to a neutrino pair as predicted in the Standard Model. Measurements of $\Gamma(\text{invisible})$ fall into two categories: direct or indirect. Direct measurements look for final states with missing energy, missing momentum, or missing mass, corresponding to the invisible decay of a produced Z boson, including single-photon final states which arise from initial-state radiation. The indirect determination is based on Z lineshape analyses performed at the LEP collider, where the invisible decay width is calculated by subtracting all visible partial decay widths from the total decay width of the Z boson. Within the framework of the Standard Model these two determinations should be identical, but not in non-SM scenarios.

VALUE (MeV)	EVTS	DOCUMENT ID	TECN	COMMENT
499.2 \pm 1.5 OUR AVERAGE				
523 \pm 3 \pm 16		1 TUMASYAN	23E CMS	$E_{cm}^{pp} = 13$ TeV
499.0 \pm 1.5		2 LEP-SLC	06 LEP	$E_{cm}^{ee} = 88-94$ GeV
498 \pm 12 \pm 12	1791	3 ACCIARRI	98G L3	$E_{cm}^{ee} = 88-94$ GeV
539 \pm 26 \pm 17	410	3 AKERS	95c OPAL	$E_{cm}^{ee} = 88-94$ GeV
450 \pm 34 \pm 34	258	3 BUSKULIC	93L ALEP	$E_{cm}^{ee} = 88-94$ GeV
540 \pm 80 \pm 40	52	3 ADEVA	92 L3	$E_{cm}^{ee} = 88-94$ GeV
498.1 \pm 2.6		4 ABBIENDI	01A OPAL	$E_{cm}^{ee} = 88-94$ GeV
498.1 \pm 3.2		4 ABREU	00F DLPH	$E_{cm}^{ee} = 88-94$ GeV
499.1 \pm 2.9		4 ACCIARRI	00c L3	$E_{cm}^{ee} = 88-94$ GeV
499.1 \pm 2.5		4 BARATE	00c ALEP	$E_{cm}^{ee} = 88-94$ GeV

• • • We do not use the following data for averages, fits, limits, etc. • • •

¹ TUMASYAN 23E analyses leptonic Z decay modes, with the invisible Z decay identified by missing momentum.
² The LEP Collaborations perform a combined fit to their line-shape results and determine this quantity as a difference between the total width and the sum of all the visible widths, assuming lepton universality. This result combines ABBIENDI 01A, ABREU 00F, ACCIARRI 00c, BARATE 00c, taking correlated uncertainties into account.
³ This analysis selects single-photon events arising from initial state radiation.
⁴ This is an indirect determination of $\Gamma(\text{invisible})$ from a fit to the visible Z decay modes. It is included in the determination of the LEP average LEP-SLC 06 reported above.

$\Gamma(\text{hadrons})$ Γ_8
This parameter is not directly used in the 5-parameter fit assuming lepton universality, but is derived using the fit results. See the note "The Z boson" and ref. LEP-SLC 06.

VALUE (MeV)	EVTS	DOCUMENT ID	TECN	COMMENT
1744.4 \pm 2.0 OUR FIT				
1745.4 \pm 3.5	4.10M	ABBIENDI	01A OPAL	$E_{cm}^{ee} = 88-94$ GeV
1738.1 \pm 4.0	3.70M	ABREU	00F DLPH	$E_{cm}^{ee} = 88-94$ GeV
1751.1 \pm 3.8	3.54M	ACCIARRI	00c L3	$E_{cm}^{ee} = 88-94$ GeV
1744.0 \pm 3.4	4.07M	BARATE	00c ALEP	$E_{cm}^{ee} = 88-94$ GeV

Z BRANCHING RATIOS

OUR FIT is obtained using the fit procedure and correlations as determined by the LEP Electroweak Working Group (see the note "The Z boson" and ref. LEP-SLC 06).

$\Gamma(\mu^+ \mu^-)/\Gamma(e^+ e^-)$ Γ_2/Γ_1

VALUE	DOCUMENT ID	TECN	COMMENT
1.0001 \pm 0.0024 OUR AVERAGE			
0.9974 \pm 0.0050	¹ AABOUD	17Q ATLS	$E_{cm}^{pp} = 7$ TeV
1.0009 \pm 0.0028	² LEP-SLC	06	$E_{cm}^{ee} = 88-94$ GeV

¹ AABOUD 17Q make a precise determination of $Z \rightarrow ee$ and $Z \rightarrow \mu\mu$ production in the lepton pseudo-rapidity range $|\eta| < 2.5$ and determine the ratio of the Z branching fractions $B(Z \rightarrow ee)/B(Z \rightarrow \mu\mu) = 1.0026 \pm 0.0013 \pm 0.0048 = 1.0026 \pm 0.0050$.

² This parameter is not directly used in the overall fit but is derived using the fit results; see the note "The Z boson" and ref. LEP-SLC 06.

$\Gamma(\tau^+\tau^-)/\Gamma(e^+e^-)$ Γ_3/Γ_1

VALUE	DOCUMENT ID	TECN	COMMENT
1.0020 ± 0.0032 OUR AVERAGE			
1.02 ± 0.06	¹ AAIJ	18AR LHCb	$E_{cm}^{pp} = 8$ TeV
1.0019 ± 0.0032	² LEP-SLC	06	$E_{cm}^{ee} = 88-94$ GeV

¹ AAIJ 18AR obtain the result from the ratio of the measured $pp \rightarrow Z + X$ cross sections in the corresponding Z decay channels.

² This parameter is not directly used in the overall fit but is derived using the fit results; see the note "The Z boson" and ref. LEP-SLC 06.

 $\Gamma(\tau^+\tau^-)/\Gamma(\mu^+\mu^-)$ Γ_3/Γ_2

VALUE	DOCUMENT ID	TECN	COMMENT
1.0010 ± 0.0026 OUR AVERAGE			
1.01 ± 0.05	¹ AAIJ	18AR LHCb	$E_{cm}^{pp} = 8$ TeV
1.0010 ± 0.0026	² LEP-SLC	06	$E_{cm}^{ee} = 88-94$ GeV

¹ AAIJ 18AR obtain the result from the ratio of the measured $pp \rightarrow Z + X$ cross sections in the corresponding Z decay channels.

² This parameter is not directly used in the overall fit but is derived using the fit results; see the note "The Z boson" and ref. LEP-SLC 06.

 $\Gamma(\ell^+\ell^-\ell^+\ell^-)/\Gamma_{total}$ Γ_6/Γ

Here ℓ indicates either e or μ . The branching fractions in this node are given within the phase-space defined by the requirements that (i) the 4-lepton invariant mass is between 80 GeV and 100 GeV, and (ii) any opposite-sign same-flavor lepton pair has a di-lepton invariant mass larger than 4 GeV.

VALUE (units 10^{-6})	EVTs	DOCUMENT ID	TECN	COMMENT
4.55 ± 0.17 OUR AVERAGE				
4.41 ± 0.13 ± 0.27		¹ AAD	21AQ ATLS	$E_{cm}^{pp} = 13$ TeV
4.70 ± 0.32 ± 0.25		² AABOUD	19N ATLS	$E_{cm}^{pp} = 13$ TeV
4.83 ^{+0.23+0.35} _{-0.22-0.32}	509	³ SIRUNYAN	18BT CMS	$E_{cm}^{pp} = 13$ TeV
4.9 ^{+0.8+0.4} _{-0.7-0.2}	39	⁴ KHACHATRYAN	16CC CMS	$E_{cm}^{pp} = 13$ TeV
4.31 ± 0.34 ± 0.17	172	⁵ AAD	14N ATLS	$E_{cm}^{pp} = 7, 8$ TeV
4.6 ^{+1.0} _{-0.9} ± 0.2	28	⁵ CHATRCHYAN	12BN CMS	$E_{cm}^{pp} = 7$ TeV

¹ AAD 21AQ analyze differential cross-sections in four-lepton events. Based on the measured cross section in the $Z \rightarrow 4\ell$ channel, a branching fraction of $B(Z \rightarrow 4\ell) = (4.41 \pm 0.13 \pm 0.23 \pm 0.09 \pm 0.12) \times 10^{-6}$ is obtained, where the uncertainties are statistical, systematic, theory and luminosity, respectively.

² AABOUD 19N reports $(4.70 \pm 0.32 \pm 0.21 \pm 0.14) \times 10^{-6}$, where the uncertainties are statistical, systematic, and luminosity. We have combined the latter two in quadrature.

³ SIRUNYAN 18BT report the $Z \rightarrow 4\ell$ branching fraction = $(4.83 \pm 0.23 \pm 0.29 \pm 0.08 \pm 0.12) \times 10^{-6}$, where the uncertainties are statistical, systematic, due to theory, and luminosity. The last three have been added in quadrature to obtain the total systematic error.

⁴ KHACHATRYAN 16CC reports $(4.9 \pm 0.8 \pm 0.3 \pm 0.2 \pm 0.1) \times 10^{-6}$ value, where the uncertainties are statistical, systematic, theory, and due to luminosity. We have combined uncertainties in quadrature.

⁵ CHATRCHYAN 12BN reports $(4.2 \pm 0.9 \pm 0.2) \times 10^{-6}$ value. Their result (both central value and uncertainties) is scaled up by 10% to account for the different phase-space definition used here (see RAINBOLT 19).

 $\Gamma(\text{hadrons})/\Gamma(e^+e^-)$ Γ_8/Γ_1

VALUE	EVTs	DOCUMENT ID	TECN	COMMENT
20.804 ± 0.050 OUR FIT				
20.902 ± 0.084	137.0k	¹ ABBIENDI	01A OPAL	$E_{cm}^{ee} = 88-94$ GeV
20.88 ± 0.12	117.8k	ABREU	00F DLPH	$E_{cm}^{ee} = 88-94$ GeV
20.816 ± 0.089	124.4k	ACCIARRI	00c L3	$E_{cm}^{ee} = 88-94$ GeV
20.677 ± 0.075		² BARATE	00c ALEP	$E_{cm}^{ee} = 88-94$ GeV
27.0 ^{+11.7} _{-8.8}	12	³ ABRAMS	89D MRK2	$E_{cm}^{ee} = 89-93$ GeV

¹ ABBIENDI 01A error includes approximately 0.067 due to statistics, 0.040 due to event selection systematics, 0.027 due to the theoretical uncertainty in t -channel prediction, and 0.014 due to LEP energy uncertainty.

² BARATE 00c error includes approximately 0.062 due to statistics, 0.033 due to experimental systematics, and 0.026 due to the theoretical uncertainty in t -channel prediction.

³ ABRAMS 89D have included both statistical and systematic uncertainties in their quoted errors.

 $\Gamma(\text{hadrons})/\Gamma(\mu^+\mu^-)$ Γ_8/Γ_2

OUR FIT is obtained using the fit procedure and correlations as determined by the LEP Electroweak Working Group (see the note "The Z boson" and ref. LEP-SLC 06).

VALUE	EVTs	DOCUMENT ID	TECN	COMMENT
20.785 ± 0.033 OUR FIT				
20.811 ± 0.058	182.8k	¹ ABBIENDI	01A OPAL	$E_{cm}^{ee} = 88-94$ GeV
20.65 ± 0.08	157.6k	ABREU	00F DLPH	$E_{cm}^{ee} = 88-94$ GeV
20.861 ± 0.097	113.4k	ACCIARRI	00c L3	$E_{cm}^{ee} = 88-94$ GeV
20.799 ± 0.056		² BARATE	00c ALEP	$E_{cm}^{ee} = 88-94$ GeV
18.9 ^{+7.1} _{-5.3}	13	³ ABRAMS	89D MRK2	$E_{cm}^{ee} = 89-93$ GeV

¹ ABBIENDI 01A error includes approximately 0.050 due to statistics and 0.027 due to event selection systematics.

² BARATE 00c error includes approximately 0.053 due to statistics and 0.021 due to experimental systematics.

³ ABRAMS 89D have included both statistical and systematic uncertainties in their quoted errors.

 $\Gamma(\text{hadrons})/\Gamma(\tau^+\tau^-)$ Γ_8/Γ_3

OUR FIT is obtained using the fit procedure and correlations as determined by the LEP Electroweak Working Group (see the note "The Z boson" and ref. LEP-SLC 06).

VALUE	EVTs	DOCUMENT ID	TECN	COMMENT
20.764 ± 0.045 OUR FIT				
20.832 ± 0.091	151.5k	¹ ABBIENDI	01A OPAL	$E_{cm}^{ee} = 88-94$ GeV
20.84 ± 0.13	104.0k	ABREU	00F DLPH	$E_{cm}^{ee} = 88-94$ GeV
20.792 ± 0.133	103.0k	ACCIARRI	00c L3	$E_{cm}^{ee} = 88-94$ GeV
20.707 ± 0.062		² BARATE	00c ALEP	$E_{cm}^{ee} = 88-94$ GeV
15.2 ^{+4.8} _{-3.9}	21	³ ABRAMS	89D MRK2	$E_{cm}^{ee} = 89-93$ GeV

¹ ABBIENDI 01A error includes approximately 0.055 due to statistics and 0.071 due to event selection systematics.

² BARATE 00c error includes approximately 0.054 due to statistics and 0.033 due to experimental systematics.

³ ABRAMS 89D have included both statistical and systematic uncertainties in their quoted errors.

 $\Gamma(\text{hadrons})/\Gamma(\ell^+\ell^-)$ Γ_8/Γ_4

ℓ indicates each type of lepton (e , μ , and τ), not sum over them.

Our fit result is obtained requiring lepton universality.

VALUE	EVTs	DOCUMENT ID	TECN	COMMENT
20.767 ± 0.025 OUR FIT				
20.823 ± 0.044	471.3k	¹ ABBIENDI	01A OPAL	$E_{cm}^{ee} = 88-94$ GeV
20.730 ± 0.060	379.4k	ABREU	00F DLPH	$E_{cm}^{ee} = 88-94$ GeV
20.810 ± 0.060	340.8k	ACCIARRI	00c L3	$E_{cm}^{ee} = 88-94$ GeV
20.725 ± 0.039	500k	² BARATE	00c ALEP	$E_{cm}^{ee} = 88-94$ GeV
18.9 ^{+3.6} _{-3.2}	46	ABRAMS	89B MRK2	$E_{cm}^{ee} = 89-93$ GeV

¹ ABBIENDI 01A error includes approximately 0.034 due to statistics and 0.027 due to event selection systematics.

² BARATE 00c error includes approximately 0.033 due to statistics, 0.020 due to experimental systematics, and 0.005 due to the theoretical uncertainty in t -channel prediction.

 $\Gamma((u\bar{u} + c\bar{c})/2)/\Gamma(\text{hadrons})$ Γ_9/Γ_8

This quantity is the branching ratio of $Z \rightarrow$ "up-type" quarks to $Z \rightarrow$ hadrons. Except ACKERSTAFF 97T the values of $Z \rightarrow$ "up-type" and $Z \rightarrow$ "down-type" branchings are extracted from measurements of $\Gamma(\text{hadrons})$, and $\Gamma(Z \rightarrow \gamma + \text{jets})$ where γ is a high-energy (>5 or 7 GeV) isolated photon. As the experiments use different procedures and slightly different values of M_Z , $\Gamma(\text{hadrons})$ and α_s in their extraction procedures, our average has to be taken with caution.

VALUE	DOCUMENT ID	TECN	COMMENT
1.166 ± 0.009 OUR AVERAGE			
0.172 ^{+0.011} _{-0.010}	¹ ABBIENDI	04E OPAL	$E_{cm}^{ee} = 91.2$ GeV
0.160 ± 0.019 ± 0.019	² ACKERSTAFF	97T OPAL	$E_{cm}^{ee} = 88-94$ GeV
0.137 ^{+0.038} _{-0.054}	³ ABREU	95x DLPH	$E_{cm}^{ee} = 88-94$ GeV
0.137 ± 0.033	⁴ ADRIANI	93 L3	$E_{cm}^{ee} = 91.2$ GeV

¹ ABBIENDI 04E select photons with energy > 7 GeV and use $\Gamma(\text{hadrons}) = 1744.4 \pm 2.0$ MeV and $\alpha_s = 0.1172 \pm 0.002$ to obtain $\Gamma_u = 300 \pm 19$ MeV.

² ACKERSTAFF 97T measure $\Gamma_{u\bar{u}}/(\Gamma_{d\bar{d}} + \Gamma_{u\bar{u}} + \Gamma_{s\bar{s}}) = 0.258 \pm 0.031 \pm 0.032$. To obtain this branching ratio authors use $R_c + R_b = 0.380 \pm 0.010$. This measurement is fully negatively correlated with the measurement of $\Gamma_{d\bar{d},s\bar{s}}/(\Gamma_{d\bar{d}} + \Gamma_{u\bar{u}} + \Gamma_{s\bar{s}})$ given in the next data block.

³ ABREU 95x use $M_Z = 91.187 \pm 0.009$ GeV, $\Gamma(\text{hadrons}) = 1725 \pm 12$ MeV and $\alpha_s = 0.123 \pm 0.005$. To obtain this branching ratio we divide their value of $C_{2/3} = 0.91 \pm 0.25 \pm 0.36$ by their value of $(3C_{1/3} + 2C_{2/3}) = 6.66 \pm 0.05$.

⁴ ADRIANI 93 use $M_Z = 91.181 \pm 0.022$ GeV, $\Gamma(\text{hadrons}) = 1742 \pm 19$ MeV and $\alpha_s = 0.125 \pm 0.009$. To obtain this branching ratio we divide their value of $C_{2/3} = 0.92 \pm 0.22$ by their value of $(3C_{1/3} + 2C_{2/3}) = 6.720 \pm 0.076$.

 $\Gamma((d\bar{d} + s\bar{s} + b\bar{b})/3)/\Gamma(\text{hadrons})$ Γ_{10}/Γ_8

This quantity is the branching ratio of $Z \rightarrow$ "down-type" quarks to $Z \rightarrow$ hadrons. Except ACKERSTAFF 97T the values of $Z \rightarrow$ "up-type" and $Z \rightarrow$ "down-type" branchings are extracted from measurements of $\Gamma(\text{hadrons})$, and $\Gamma(Z \rightarrow \gamma + \text{jets})$ where γ is a high-energy (>5 or 7 GeV) isolated photon. As the experiments use different procedures and slightly different values of M_Z , $\Gamma(\text{hadrons})$ and α_s in their extraction procedures, our average has to be taken with caution.

VALUE	DOCUMENT ID	TECN	COMMENT
0.223 ± 0.006 OUR AVERAGE			
0.218 ± 0.007	¹ ABBIENDI	04E OPAL	$E_{cm}^{ee} = 91.2$ GeV
0.230 ± 0.010 ± 0.010	² ACKERSTAFF	97T OPAL	$E_{cm}^{ee} = 88-94$ GeV
0.243 ^{+0.036} _{-0.026}	³ ABREU	95x DLPH	$E_{cm}^{ee} = 88-94$ GeV
0.243 ± 0.022	⁴ ADRIANI	93 L3	$E_{cm}^{ee} = 91.2$ GeV

¹ ABBIENDI 04E select photons with energy > 7 GeV and use $\Gamma(\text{hadrons}) = 1744.4 \pm 2.0$ MeV and $\alpha_s = 0.1172 \pm 0.002$ to obtain $\Gamma_d = 381 \pm 12$ MeV.

² ACKERSTAFF 97T measure $\Gamma_{d\bar{d},s\bar{s}}/(\Gamma_{d\bar{d}} + \Gamma_{u\bar{u}} + \Gamma_{s\bar{s}}) = 0.371 \pm 0.016 \pm 0.016$. To obtain this branching ratio authors use $R_c + R_b = 0.380 \pm 0.010$. This measurement is fully negatively correlated with the measurement of $\Gamma_{u\bar{u}}/(\Gamma_{d\bar{d}} + \Gamma_{u\bar{u}} + \Gamma_{s\bar{s}})$ presented in the previous data block.

Gauge & Higgs Boson Particle Listings

Z

³ ABREU 95x use $M_Z = 91.187 \pm 0.009$ GeV, $\Gamma(\text{hadrons}) = 1725 \pm 12$ MeV and $\alpha_s = 0.123 \pm 0.005$. To obtain this branching ratio we divide their value of $C_{1/3} = 1.62 \pm 0.24$ by their value of $(3C_{1/3} + 2C_{2/3}) = 6.66 \pm 0.05$.

⁴ ADRIANI 93 use $M_Z = 91.181 \pm 0.022$ GeV, $\Gamma(\text{hadrons}) = 1742 \pm 19$ MeV and $\alpha_s = 0.125 \pm 0.009$. To obtain this branching ratio we divide their value of $C_{1/3} = 1.63 \pm 0.15$ by their value of $(3C_{1/3} + 2C_{2/3}) = 6.720 \pm 0.076$.

$$R_c = \Gamma(c\bar{c})/\Gamma(\text{hadrons}) \quad \Gamma_{11}/\Gamma_8$$

OUR FIT is obtained by a simultaneous fit to several c - and b -quark measurements as explained in the note "The Z boson" and ref. LEP-SLC 06.

The Standard Model predicts $R_c = 0.1723$ for $m_t = 174.3$ GeV and $M_H = 150$ GeV.

VALUE	DOCUMENT ID	TECN	COMMENT
0.1721 ± 0.0030 OUR FIT			
0.1744 ± 0.0031 ± 0.0021	¹ ABE	05F SLD	$E_{cm}^{ee} = 91.28$ GeV
0.1665 ± 0.0051 ± 0.0081	² ABREU	00 DLPH	$E_{cm}^{ee} = 88-94$ GeV
0.1698 ± 0.0069	³ BARATE	00B ALEP	$E_{cm}^{ee} = 88-94$ GeV
0.180 ± 0.011 ± 0.013	⁴ ACKERSTAFF	98E OPAL	$E_{cm}^{ee} = 88-94$ GeV
0.167 ± 0.011 ± 0.012	⁵ ALEXANDER	96R OPAL	$E_{cm}^{ee} = 88-94$ GeV
0.1623 ± 0.0085 ± 0.0209	⁶ ABREU	95D DLPH	$E_{cm}^{ee} = 88-94$ GeV

• • • We do not use the following data for averages, fits, limits, etc. • • •

¹ ABE 05F use hadronic Z decays collected during 1996-98 to obtain an enriched sample of $c\bar{c}$ events using a double tag method. The single c -tag is obtained with a neural network trained to perform flavor discrimination using as input several signatures (corrected secondary vertex mass, vertex decay length, multiplicity and total momentum of the hemisphere). A multitag approach is used, defining 4 regions of the output value of the neural network and R_c is extracted from a simultaneous fit to the count rates of the 4 different tags. The quoted systematic error includes an uncertainty of ± 0.0006 due to the uncertainty on R_b .

² ABREU 00 obtain this result properly combining the measurement from the D^{*+} production rate ($R_c = 0.1610 \pm 0.0104 \pm 0.0077 \pm 0.0043$ (BR)) with that from the overall charm counting ($R_c = 0.1692 \pm 0.0047 \pm 0.0063 \pm 0.0074$ (BR)) in $c\bar{c}$ events. The systematic error includes an uncertainty of ± 0.0054 due to the uncertainty on the charmed hadron branching fractions.

³ BARATE 00B use exclusive decay modes to independently determine the quantities $R_c \times f(c \rightarrow X)$, $X = D^0, D^+, D_s^+$, and A_c . Estimating $R_c \times f(c \rightarrow \Xi_c / \Omega_c) = 0.0034$, they simply sum over all the charm decays to obtain $R_c = 0.1738 \pm 0.0047 \pm 0.0088 \pm 0.0075$ (BR). This is combined with all previous ALEPH measurements (BARATE 98T and BUSKULIC 94G, $R_c = 0.1681 \pm 0.0054 \pm 0.0062$) to obtain the quoted value.

⁴ ACKERSTAFF 98E use an inclusive/exclusive double tag. In one jet D^{*+} mesons are exclusively reconstructed in several decay channels and in the opposite jet a slow pion (opposite charge inclusive D^{*+}) tag is used. The b content of this sample is measured by the simultaneous detection of a lepton in one jet and an inclusively reconstructed D^{*+} meson in the opposite jet. The systematic error includes an uncertainty of ± 0.006 due to the external branching ratios.

⁵ ALEXANDER 96R obtain this value via direct charm counting, summing the partial contributions from D^0, D^+, D_s^+ , and A_c^+ , and assuming that strange-charmed baryons account for the 15% of the A_c^+ production. An uncertainty of ± 0.005 due to the uncertainties in the charm hadron branching ratios is included in the overall systematics.

⁶ ABREU 95D perform a maximum likelihood fit to the combined p and p_T distributions of single and dilepton samples. The second error includes an uncertainty of ± 0.0124 due to models and branching ratios.

$$R_b = \Gamma(b\bar{b})/\Gamma(\text{hadrons}) \quad \Gamma_{12}/\Gamma_8$$

OUR FIT is obtained by a simultaneous fit to several c - and b -quark measurements as explained in the note "The Z boson" and ref. LEP-SLC 06.

The Standard Model predicts $R_b = 0.21581$ for $m_t = 174.3$ GeV and $M_H = 150$ GeV.

VALUE	DOCUMENT ID	TECN	COMMENT
0.21629 ± 0.00066 OUR FIT			
0.21594 ± 0.00094 ± 0.00075	¹ ABE	05F SLD	$E_{cm}^{ee} = 91.28$ GeV
0.2174 ± 0.0015 ± 0.0028	² ACCIARRI	00 L3	$E_{cm}^{ee} = 89-93$ GeV
0.2178 ± 0.0011 ± 0.0013	³ ABBIENDI	99B OPAL	$E_{cm}^{ee} = 88-94$ GeV
0.21634 ± 0.00067 ± 0.00060	⁴ ABREU	99B DLPH	$E_{cm}^{ee} = 88-94$ GeV
0.2159 ± 0.0009 ± 0.0011	⁵ BARATE	97F ALEP	$E_{cm}^{ee} = 88-94$ GeV
0.2145 ± 0.0089 ± 0.0067	⁶ ABREU	95D DLPH	$E_{cm}^{ee} = 88-94$ GeV
0.219 ± 0.006 ± 0.005	⁷ BUSKULIC	94G ALEP	$E_{cm}^{ee} = 88-94$ GeV
0.251 ± 0.049 ± 0.030	⁸ JACOBSEN	91 MRK2	$E_{cm}^{ee} = 91$ GeV

¹ ABE 05F use hadronic Z decays collected during 1996-98 to obtain an enriched sample of $b\bar{b}$ events using a double tag method. The single b -tag is obtained with a neural network trained to perform flavor discrimination using as input several signatures (corrected secondary vertex mass, vertex decay length, multiplicity and total momentum of the hemisphere; the key tag is obtained requiring the secondary vertex corrected mass to be above the D -meson mass). ABE 05F obtain $R_b = 0.21604 \pm 0.00098 \pm 0.00074$ where the systematic error includes an uncertainty of ± 0.00012 due to the uncertainty on R_c . The value reported here is obtained properly combining with ABE 98D. The quoted systematic error includes an uncertainty of ± 0.00012 due to the uncertainty on R_c .

² ACCIARRI 00 obtain this result using a double-tagging technique, with a high p_T lepton tag and an impact parameter tag in opposite hemispheres.

³ ABBIENDI 99B tag $Z \rightarrow b\bar{b}$ decays using leptons and/or separated decay vertices. The b -tagging efficiency is measured directly from the data using a double-tagging technique.

⁴ ABREU 99B obtain this result combining in a multivariate analysis several tagging methods (impact parameter and secondary vertex reconstruction, complemented by event

shape variables). For R_c different from its Standard Model value of 0.172, R_b varies as $-0.024 \times (R_c - 0.172)$.

⁵ BARATE 97F combine the lifetime-mass hemisphere tag (BARATE 97E) with event shape information and lepton tag to identify $Z \rightarrow b\bar{b}$ candidates. They further use c - and ud -selection tags to identify the background. For R_c different from its Standard Model value of 0.172, R_b varies as $-0.019 \times (R_c - 0.172)$.

⁶ ABREU 95D perform a maximum likelihood fit to the combined p and p_T distributions of single and dilepton samples. The second error includes an uncertainty of ± 0.0023 due to models and branching ratios.

⁷ BUSKULIC 94G perform a simultaneous fit to the p and p_T spectra of both single and dilepton events.

⁸ JACOBSEN 91 tagged $b\bar{b}$ events by requiring coincidence of ≥ 3 tracks with significant impact parameters using vertex detector. Systematic error includes lifetime and decay uncertainties (± 0.014).

$$\Gamma(b\bar{b}b\bar{b})/\Gamma(\text{hadrons}) \quad \Gamma_{13}/\Gamma_8$$

VALUE (units 10^{-4})	DOCUMENT ID	TECN	COMMENT
5.2 ± 1.9 OUR AVERAGE			
3.6 ± 1.7 ± 2.7	¹ ABBIENDI	01G OPAL	$E_{cm}^{ee} = 88-94$ GeV
6.0 ± 1.9 ± 1.4	² ABREU	99U DLPH	$E_{cm}^{ee} = 88-94$ GeV

¹ ABBIENDI 01G use a sample of four-jet events from hadronic Z decays. To enhance the $b\bar{b}b\bar{b}$ signal, at least three of the four jets are required to have a significantly detached secondary vertex.

² ABREU 99U force hadronic Z decays into 3jets to use all the available phase space and require a b tag for every jet. This decay mode includes primary and secondary $4b$ production, e.g. from gluon splitting to $b\bar{b}$.

$$\Gamma(ggg)/\Gamma(\text{hadrons}) \quad \Gamma_{14}/\Gamma_8$$

VALUE	CL%	DOCUMENT ID	TECN	COMMENT
< 1.6 × 10⁻²	95	¹ ABREU	96S DLPH	$E_{cm}^{ee} = 88-94$ GeV

¹ This branching ratio is slightly dependent on the jet-finder algorithm. The value we quote is obtained using the JADE algorithm, while using the DURHAM algorithm ABREU 96S obtain an upper limit of 1.5×10^{-2} .

$$\Gamma(\pi^0\gamma)/\Gamma_{\text{total}} \quad \Gamma_{15}/\Gamma$$

VALUE	CL%	DOCUMENT ID	TECN	COMMENT
< 2.01 × 10⁻⁵	95	AALTONEN	14E CDF	$E_{cm}^{pp} = 1.96$ TeV
< 5.2 × 10 ⁻⁵	95	¹ ACCIARRI	95G L3	$E_{cm}^{ee} = 88-94$ GeV
< 5.5 × 10 ⁻⁵	95	ABREU	94B DLPH	$E_{cm}^{ee} = 88-94$ GeV
< 2.1 × 10 ⁻⁴	95	DECAMP	92 ALEP	$E_{cm}^{ee} = 88-94$ GeV
< 1.4 × 10 ⁻⁴	95	AKRAWY	91F OPAL	$E_{cm}^{ee} = 88-94$ GeV

¹ This limit is for both decay modes $Z \rightarrow \pi^0\gamma/\gamma\gamma$ which are indistinguishable in ACCIARRI 95G.

$$\Gamma(\eta\gamma)/\Gamma_{\text{total}} \quad \Gamma_{16}/\Gamma$$

VALUE	CL%	DOCUMENT ID	TECN	COMMENT
< 7.6 × 10 ⁻⁵	95	ACCIARRI	95G L3	$E_{cm}^{ee} = 88-94$ GeV
< 8.0 × 10 ⁻⁵	95	ABREU	94B DLPH	$E_{cm}^{ee} = 88-94$ GeV
< 5.1 × 10⁻⁵	95	DECAMP	92 ALEP	$E_{cm}^{ee} = 88-94$ GeV
< 2.0 × 10 ⁻⁴	95	AKRAWY	91F OPAL	$E_{cm}^{ee} = 88-94$ GeV

$$\Gamma(\rho^0\gamma)/\Gamma_{\text{total}} \quad \Gamma_{17}/\Gamma$$

VALUE	CL%	EVTS	DOCUMENT ID	TECN	COMMENT
< 4.0 × 10⁻⁶	95	12.5k	¹ AABOUD	18AU ATLS	$E_{cm}^{pp} = 13$ TeV

¹ AABOUD 18AU search for the $Z \rightarrow \rho\gamma$ decay mode where the ρ is identified through its decay $\rho \rightarrow \pi^+\pi^-$. In the data corresponding to 32.3 fb^{-1} , 12,583 events are selected for $635 < m(\pi^+\pi^-) < 915$ MeV. See erratum AABOUD 23A.

$$\Gamma(\omega\gamma)/\Gamma_{\text{total}} \quad \Gamma_{18}/\Gamma$$

VALUE	CL%	DOCUMENT ID	TECN	COMMENT
< 3.9 × 10⁻⁶	95	AAD	23Bs ATLS	$E_{cm}^{pp} = 13$ TeV
< 6.5 × 10 ⁻⁴	95	ABREU	94B DLPH	$E_{cm}^{ee} = 88-94$ GeV

• • • We do not use the following data for averages, fits, limits, etc. • • •

$$\Gamma(\eta'(958)\gamma)/\Gamma_{\text{total}} \quad \Gamma_{19}/\Gamma$$

VALUE	CL%	DOCUMENT ID	TECN	COMMENT
< 4.2 × 10⁻⁵	95	DECAMP	92 ALEP	$E_{cm}^{ee} = 88-94$ GeV

$$\Gamma(\phi\gamma)/\Gamma_{\text{total}} \quad \Gamma_{20}/\Gamma$$

VALUE	CL%	EVTS	DOCUMENT ID	TECN	COMMENT
< 7 × 10⁻⁷	95	3.3k	¹ AABOUD	18AU ATLS	$E_{cm}^{pp} = 13$ TeV
< 8.3 × 10 ⁻⁶	95	1.0k	² AABOUD	16k ATLS	$E_{cm}^{pp} = 13$ TeV

¹ AABOUD 18AU search for the $Z \rightarrow \phi\gamma$ decay mode where the ϕ is identified through its decay $\phi \rightarrow K^+K^-$. In the data corresponding to 32.3 fb^{-1} , 3,364 events are selected for $1012 < m(K^+K^-) < 1028$ MeV. See erratum AABOUD 23A.

² AABOUD 16k search for the $Z \rightarrow \phi\gamma$ decay mode where the ϕ is identified through its decay into K^+K^- . In the data corresponding to a total luminosity of 2.7 fb^{-1} , 1065 events are selected and their $K^+K^-\gamma$ invariant mass spectrum is analyzed.

$\Gamma(\gamma\gamma)/\Gamma_{\text{total}}$					Γ_{21}/Γ
This decay would violate the Landau-Yang theorem.					
VALUE	CL%	DOCUMENT ID	TECN	COMMENT	
$<1.46 \times 10^{-5}$	95	AALTONEN	14E CDF	$E_{\text{cm}}^{pp} = 1.96$ TeV	
$<5.2 \times 10^{-5}$	95	¹ ACCIARRI	95G L3	$E_{\text{cm}}^{ee} = 88-94$ GeV	
$<5.5 \times 10^{-5}$	95	ABREU	94B DLPH	$E_{\text{cm}}^{ee} = 88-94$ GeV	
$<1.4 \times 10^{-4}$	95	AKRAWY	91F OPAL	$E_{\text{cm}}^{ee} = 88-94$ GeV	

¹ This limit is for both decay modes $Z \rightarrow \pi^0 \gamma / \gamma \gamma$ which are indistinguishable in ACCIARRI 95G.

$\Gamma(\pi^0 \pi^0)/\Gamma_{\text{total}}$					Γ_{22}/Γ
VALUE	CL%	DOCUMENT ID	TECN	COMMENT	
$<1.52 \times 10^{-5}$	95	AALTONEN	14E CDF	$E_{\text{cm}}^{pp} = 1.96$ TeV	

$\Gamma(\gamma\gamma\gamma)/\Gamma_{\text{total}}$					Γ_{23}/Γ
VALUE	CL%	DOCUMENT ID	TECN	COMMENT	
$<2.2 \times 10^{-6}$	95	AAD	16L ATLS	$E_{\text{cm}}^{pp} = 8$ TeV	
••• We do not use the following data for averages, fits, limits, etc. •••					
$<1.0 \times 10^{-5}$	95	¹ ACCIARRI	95c L3	$E_{\text{cm}}^{ee} = 88-94$ GeV	
$<1.7 \times 10^{-5}$	95	¹ ABREU	94B DLPH	$E_{\text{cm}}^{ee} = 88-94$ GeV	
$<6.6 \times 10^{-5}$	95	AKRAWY	91F OPAL	$E_{\text{cm}}^{ee} = 88-94$ GeV	

¹ Limit derived in the context of composite Z model.

$\Gamma(\pi^\pm W^\mp)/\Gamma_{\text{total}}$					Γ_{24}/Γ
The value is for the sum of the charge states indicated.					
VALUE	CL%	DOCUMENT ID	TECN	COMMENT	
$<7 \times 10^{-5}$	95	DECAMP	92 ALEP	$E_{\text{cm}}^{ee} = 88-94$ GeV	

$\Gamma(\rho^\pm W^\mp)/\Gamma_{\text{total}}$					Γ_{25}/Γ
The value is for the sum of the charge states indicated.					
VALUE	CL%	DOCUMENT ID	TECN	COMMENT	
$<8.3 \times 10^{-5}$	95	DECAMP	92 ALEP	$E_{\text{cm}}^{ee} = 88-94$ GeV	

$\Gamma(J/\psi(1S)X)/\Gamma_{\text{total}}$					Γ_{26}/Γ
VALUE (units 10^{-3})	EVTS	DOCUMENT ID	TECN	COMMENT	
$3.51^{+0.23}_{-0.25}$ OUR AVERAGE				Error includes scale factor of 1.1.	
$3.21 \pm 0.21^{+0.19}_{-0.28}$	553	¹ ACCIARRI	99F L3	$E_{\text{cm}}^{ee} = 88-94$ GeV	
$3.9 \pm 0.2 \pm 0.3$	511	² ALEXANDER	96B OPAL	$E_{\text{cm}}^{ee} = 88-94$ GeV	
$3.73 \pm 0.39 \pm 0.36$	153	³ ABREU	94P DLPH	$E_{\text{cm}}^{ee} = 88-94$ GeV	

¹ ACCIARRI 99F combine $\mu^+ \mu^-$ and $e^+ e^- J/\psi(1S)$ decay channels. The branching ratio for prompt $J/\psi(1S)$ production is measured to be $(2.1 \pm 0.6 \pm 0.4^{+0.4}_{-0.2}(\text{theor.})) \times 10^{-4}$.

² ALEXANDER 96B identify $J/\psi(1S)$ from the decays into lepton pairs. $(4.8 \pm 2.4)\%$ of this branching ratio is due to prompt $J/\psi(1S)$ production (ALEXANDER 96N).

³ Combining $\mu^+ \mu^-$ and $e^+ e^-$ channels and taking into account the common systematic errors. $(7.7^{+6.3}_{-5.4})\%$ of this branching ratio is due to prompt $J/\psi(1S)$ production.

$\Gamma(J/\psi(1S)\gamma)/\Gamma_{\text{total}}$					Γ_{27}/Γ
VALUE	CL%	DOCUMENT ID	TECN	COMMENT	
$<1.2 \times 10^{-6}$	95	AAD	23CD ATLS	$E_{\text{cm}}^{pp} = 13$ TeV	
••• We do not use the following data for averages, fits, limits, etc. •••					
$<1.4 \times 10^{-6}$	95	¹ SIRUNYAN	19AJ CMS	$E_{\text{cm}}^{pp} = 13$ TeV	
$<2.3 \times 10^{-6}$	95	² AABOUD	18BL ATLS	$E_{\text{cm}}^{pp} = 13$ TeV	
$<2.6 \times 10^{-6}$	95	³ AAD	15I ATLS	$E_{\text{cm}}^{pp} = 8$ TeV	

¹ SIRUNYAN 19AJ study $Z \rightarrow J/\psi \gamma$ with $J/\psi \rightarrow \mu^+ \mu^-$. Candidate events are selected by requiring a pair of oppositely charged muons and a well isolated photon. The leading (subleading) muon is required to have a transverse momentum larger than 20 GeV (4 GeV), while the photon must have a transverse energy larger than 33 GeV. Requiring the invariant mass of the $\mu\mu$ ($\mu\mu\gamma$) system in the range 3.0 to 3.2 (81 to 101) GeV, selects 183 data events which is consistent with the expected background. The 95% C.L. limit on the Z branching fraction is obtained assuming the J/ψ to be unpolarized.

² AABOUD 18BL study $Z \rightarrow J/\psi \gamma$ in 13 TeV pp interactions. Two triggers were used: isolated photon of $p_T > 35(25)$ GeV and a muon with $p_T > 18(24)$ GeV. The J/ψ is detected via its dimuon decay and it is required that the azimuthal angle between the photon and the J/ψ in the plane transverse to the beam direction is $> \pi/2$. The number of observed/expected background events is 92/89 ± 6 in the dimuon mass range 2.9–3.3 GeV leading to the quoted 95% C.L. limit.

³ AAD 15I use events with the highest p_T muon in the pair required to have $p_T > 20$ GeV, the dimuon mass required to be within 0.2 GeV of the $J/\psi(1S)$ mass and it's transverse momentum required to be > 36 GeV. The photon is also required to have it's $p_T > 36$ GeV.

$\Gamma(\psi(2S)X)/\Gamma_{\text{total}}$					Γ_{28}/Γ
VALUE (units 10^{-3})	EVTS	DOCUMENT ID	TECN	COMMENT	
1.60 ± 0.29 OUR AVERAGE					
$1.6 \pm 0.5 \pm 0.3$	39	¹ ACCIARRI	97J L3	$E_{\text{cm}}^{ee} = 88-94$ GeV	
$1.6 \pm 0.3 \pm 0.2$	46.9	² ALEXANDER	96B OPAL	$E_{\text{cm}}^{ee} = 88-94$ GeV	
$1.60 \pm 0.73 \pm 0.33$	5.4	³ ABREU	94P DLPH	$E_{\text{cm}}^{ee} = 88-94$ GeV	

¹ ACCIARRI 97J measure this branching ratio via the decay channel $\psi(2S) \rightarrow \ell^+ \ell^-$ ($\ell = \mu, e$).

² ALEXANDER 96B measure this branching ratio via the decay channel $\psi(2S) \rightarrow J/\psi \pi^+ \pi^-$, with $J/\psi \rightarrow \ell^+ \ell^-$.

³ ABREU 94P measure this branching ratio via decay channel $\psi(2S) \rightarrow J/\psi \pi^+ \pi^-$, with $J/\psi \rightarrow \mu^+ \mu^-$.

$\Gamma(\psi(2S)\gamma)/\Gamma_{\text{total}}$					Γ_{29}/Γ
VALUE	CL%	DOCUMENT ID	TECN	COMMENT	
$<2.4 \times 10^{-6}$	95	AAD	23CD ATLS	$E_{\text{cm}}^{pp} = 13$ TeV	
••• We do not use the following data for averages, fits, limits, etc. •••					
$<4.5 \times 10^{-6}$	95	¹ AABOUD	18BL ATLS	$E_{\text{cm}}^{pp} = 13$ TeV	

¹ AABOUD 18BL study $Z \rightarrow \psi(2S)\gamma$ in 13 TeV pp interactions. Two triggers were used: isolated photon of $p_T > 35(25)$ GeV and a muon with $p_T > 18(24)$ GeV. The $\psi(2S)$ is detected via its dimuon decay and it is required that the azimuthal angle between the photon and the $\psi(2S)$ in the plane transverse to the beam direction is $> \pi/2$. The number of observed/expected background events is 43/42 ± 5 in the dimuon mass range 3.5–3.9 GeV leading to the quoted 95% C.L. limit.

$\Gamma(J/\psi(1S)\ell^+ \ell^-)/\Gamma(\mu^+ \mu^- \mu^+ \mu^-)$					Γ_{30}/Γ_5
VALUE	CL%	DOCUMENT ID	TECN	COMMENT	
$0.67 \pm 0.18 \pm 0.05$		¹ SIRUNYAN	18DZ CMS	pp at 13 TeV	

¹ SIRUNYAN 18DZ observe the decay $Z \rightarrow \Psi \ell^+ \ell^-$ in pp collisions at $\sqrt{s} = 13$ TeV, where Ψ includes J/ψ as well as $\psi(2S) \rightarrow J/\psi X$, and $\ell^+ \ell^-$ represents an electron or muon pair while the J/ψ is detected via its $\mu^+ \mu^-$ decay channel. To reduce systematic errors they determine the ratio of the branching fraction of this decay to that of $Z \rightarrow \mu^+ \mu^- \mu^+ \mu^-$ within phase-space cuts imposed on lepton transverse momentum and pseudo rapidity, dilepton invariant mass, and J/ψ transverse momentum. The number of selected $\Psi \mu^+ \mu^-$ ($\Psi e^+ e^-$) candidate events is 29 (18). Analyzing the $\mu^+ \mu^-$ and $\mu^+ \mu^- \ell^+ \ell^-$ invariant mass distributions, a yield of 13.0 ± 3.9 (11.2 ± 3.4) events for the $\Psi \mu^+ \mu^-$ ($\Psi e^+ e^-$) mode is obtained. The ratio of the branching fractions is determined as $0.67 \pm 0.18 \pm 0.05$ within the selected phase-space cuts. Assuming extrapolation to full phase space cancels in the ratio, and using their measured value of $B(Z \rightarrow \mu^+ \mu^- \mu^+ \mu^-) = (1.20 \pm 0.08) \times 10^{-6}$, they estimate $B(Z \rightarrow J/\psi \ell^+ \ell^-) = 8 \times 10^{-7}$.

$\Gamma(J/\psi(1S) J/\psi(1S))/\Gamma_{\text{total}}$					Γ_{31}/Γ
VALUE	CL%	EVTS	DOCUMENT ID	TECN	COMMENT
$<2.2 \times 10^{-6}$	95	189	¹ SIRUNYAN	19BR CMS	$E_{\text{cm}}^{pp} = 13$ TeV

¹ SIRUNYAN 19BR search for Z decays to a pair of J/ψ mesons in the channel $J/\psi \rightarrow \mu^+ \mu^-$. The invariant masses of the higher/lower- p_T J/ψ candidates have to be within 0.1/0.15 GeV of the nominal J/ψ mass. A total of 189 events are selected in the 40–140 GeV 4-muon invariant mass range. An un-binned extended maximum likelihood fit leads to the 95% C.L. upper limit, obtained assuming the J/ψ mesons to be unpolarised.

$\Gamma(\chi_{c1}(1P)X)/\Gamma_{\text{total}}$					Γ_{32}/Γ
VALUE (units 10^{-3})	EVTS	DOCUMENT ID	TECN	COMMENT	
2.9 ± 0.7 OUR AVERAGE					
$2.7 \pm 0.6 \pm 0.5$	33	¹ ACCIARRI	97J L3	$E_{\text{cm}}^{ee} = 88-94$ GeV	
$5.0 \pm 2.1^{+1.5}_{-0.9}$	6.4	² ABREU	94P DLPH	$E_{\text{cm}}^{ee} = 88-94$ GeV	

¹ ACCIARRI 97J measure this branching ratio via the decay channel $\chi_{c1} \rightarrow J/\psi + \gamma$, with $J/\psi \rightarrow \ell^+ \ell^-$ ($\ell = \mu, e$). The $M(\ell^+ \ell^- \gamma) - M(\ell^+ \ell^-)$ mass difference spectrum is fitted with two gaussian shapes for χ_{c1} and χ_{c2} .

² This branching ratio is measured via the decay channel $\chi_{c1} \rightarrow J/\psi + \gamma$, with $J/\psi \rightarrow \mu^+ \mu^-$.

$\Gamma(\chi_{c2}(1P)X)/\Gamma_{\text{total}}$					Γ_{33}/Γ
VALUE	CL%	DOCUMENT ID	TECN	COMMENT	
$<3.2 \times 10^{-3}$	90	¹ ACCIARRI	97J L3	$E_{\text{cm}}^{ee} = 88-94$ GeV	

¹ ACCIARRI 97J derive this limit via the decay channel $\chi_{c2} \rightarrow J/\psi + \gamma$, with $J/\psi \rightarrow \ell^+ \ell^-$ ($\ell = \mu, e$). The $M(\ell^+ \ell^- \gamma) - M(\ell^+ \ell^-)$ mass difference spectrum is fitted with two gaussian shapes for χ_{c1} and χ_{c2} .

$\Gamma(\Upsilon(1S)X + \Upsilon(2S)X + \Upsilon(3S)X)/\Gamma_{\text{total}}$					$\Gamma_{34}/\Gamma = (\Gamma_{35} + \Gamma_{37} + \Gamma_{39})/\Gamma$
VALUE (units 10^{-4})	EVTS	DOCUMENT ID	TECN	COMMENT	
$1.0 \pm 0.4 \pm 0.22$	6.4	¹ ALEXANDER	96F OPAL	$E_{\text{cm}}^{ee} = 88-94$ GeV	

¹ ALEXANDER 96F identify the Υ (which refers to any of the three lowest bound states) through its decay into $e^+ e^-$ and $\mu^+ \mu^-$. The systematic error includes an uncertainty of ± 0.2 due to the production mechanism.

$\Gamma(\Upsilon(1S)X)/\Gamma_{\text{total}}$					Γ_{35}/Γ
VALUE	CL%	DOCUMENT ID	TECN	COMMENT	
$<4.4 \times 10^{-5}$	95	¹ ACCIARRI	99F L3	$E_{\text{cm}}^{ee} = 88-94$ GeV	

¹ ACCIARRI 99F search for $\Upsilon(1S)$ through its decay into $\ell^+ \ell^-$ ($\ell = e$ or μ).

$\Gamma(\Upsilon(1S)\gamma)/\Gamma_{\text{total}}$					Γ_{36}/Γ
VALUE	CL%	DOCUMENT ID	TECN	COMMENT	
$<1.1 \times 10^{-6}$	95	AAD	23CD ATLS	$E_{\text{cm}}^{pp} = 13$ TeV	
••• We do not use the following data for averages, fits, limits, etc. •••					
$<2.8 \times 10^{-6}$	95	¹ AABOUD	18BL ATLS	$E_{\text{cm}}^{pp} = 13$ TeV	
$<3.4 \times 10^{-6}$	95	² AAD	15I ATLS	$E_{\text{cm}}^{pp} = 8$ TeV	

¹ AABOUD 18BL study $Z \rightarrow \Upsilon(1S)\gamma$ in 13 TeV pp interactions. Two triggers were used: isolated photon of $p_T > 35(25)$ GeV and a muon with $p_T > 18(24)$ GeV. The $\Upsilon(1S)$ is detected via its dimuon decay and it is required that the azimuthal angle between the photon and the $\Upsilon(1S)$ in the plane transverse to the beam direction is $> \pi/2$. The number of observed/expected background events is 115/126 ± 8 in the dimuon mass range 9.0–10.0 GeV leading to the quoted 95% C.L. limit.

² AAD 15I use events with the highest p_T muon in the pair required to have $p_T > 20$ GeV, the dimuon mass required to be in the range 8–12 GeV and it's transverse momentum required to be > 36 GeV. The photon is also required to have it's $p_T > 36$ GeV.

Gauge & Higgs Boson Particle Listings

Z

 $\Gamma(\mathcal{T}(2S)X)/\Gamma_{\text{total}}$ Γ_{37}/Γ

VALUE	CL%	DOCUMENT ID	TECN	COMMENT
$<13.9 \times 10^{-5}$	95	1 ACCIARRI	97R L3	$E_{\text{cm}}^{\text{pe}} = 88\text{--}94$ GeV

¹ ACCIARRI 97R search for $\mathcal{T}(2S)$ through its decay into $\ell^+ \ell^-$ ($\ell = e$ or μ).

 $\Gamma(\mathcal{T}(2S)\gamma)/\Gamma_{\text{total}}$ Γ_{38}/Γ

VALUE	CL%	DOCUMENT ID	TECN	COMMENT
$<1.3 \times 10^{-6}$	95	AAD	23CD ATLS	$E_{\text{cm}}^{\text{pp}} = 13$ TeV

• • • We do not use the following data for averages, fits, limits, etc. • • •

$<1.7 \times 10^{-6}$	95	1 AABOUD	18BL ATLS	$E_{\text{cm}}^{\text{pp}} = 13$ TeV
$<6.5 \times 10^{-6}$	95	2 AAD	15i ATLS	$E_{\text{cm}}^{\text{pp}} = 8$ TeV

¹ AABOUD 18BL study $Z \rightarrow \mathcal{T}(2S)\gamma$ in 13 TeV pp interactions. Two triggers were used: isolated photon of $p_{\mathcal{T}} > 35(25)$ GeV and a muon with $p_{\mathcal{T}} > 18(24)$ GeV. The $\mathcal{T}(2S)$ is detected via its dimuon decay and it is required that the azimuthal angle between the photon and the $\mathcal{T}(2S)$ in the plane transverse to the beam direction is $> \pi/2$. The number of observed/expected background events is 106/121 \pm 8 in the dimuon mass range 9.5–10.5 GeV leading to the quoted 95% C.L. limit.

² AAD 15i use events with the highest $p_{\mathcal{T}}$ muon in the pair required to have $p_{\mathcal{T}} > 20$ GeV, the dimuon mass required to be in the range 8–12 GeV and its transverse momentum required to be > 36 GeV. The photon is also required to have its $p_{\mathcal{T}} > 36$ GeV.

 $\Gamma(\mathcal{T}(3S)X)/\Gamma_{\text{total}}$ Γ_{39}/Γ

VALUE	CL%	DOCUMENT ID	TECN	COMMENT
$<9.4 \times 10^{-5}$	95	1 ACCIARRI	97R L3	$E_{\text{cm}}^{\text{pe}} = 88\text{--}94$ GeV

¹ ACCIARRI 97R search for $\mathcal{T}(3S)$ through its decay into $\ell^+ \ell^-$ ($\ell = e$ or μ).

 $\Gamma(\mathcal{T}(3S)\gamma)/\Gamma_{\text{total}}$ Γ_{40}/Γ

VALUE	CL%	DOCUMENT ID	TECN	COMMENT
$<2.4 \times 10^{-6}$	95	AAD	23CD ATLS	$E_{\text{cm}}^{\text{pp}} = 13$ TeV

• • • We do not use the following data for averages, fits, limits, etc. • • •

$<4.8 \times 10^{-6}$	95	1 AABOUD	18BL ATLS	$E_{\text{cm}}^{\text{pp}} = 13$ TeV
$<5.4 \times 10^{-6}$	95	2 AAD	15i ATLS	$E_{\text{cm}}^{\text{pp}} = 8$ TeV

¹ AABOUD 18BL study $Z \rightarrow \mathcal{T}(3S)\gamma$ in 13 TeV pp interactions. Two triggers were used: isolated photon of $p_{\mathcal{T}} > 35(25)$ GeV and a muon with $p_{\mathcal{T}} > 18(24)$ GeV. The $\mathcal{T}(3S)$ is detected via its dimuon decay and it is required that the azimuthal angle between the photon and the $\mathcal{T}(3S)$ in the plane transverse to the beam direction is $> \pi/2$. The number of observed/expected background events is 112/113 \pm 8 in the dimuon mass range 10.0–11.0 GeV leading to the quoted 95% C.L. limit.

² AAD 15i use events with the highest $p_{\mathcal{T}}$ muon in the pair required to have $p_{\mathcal{T}} > 20$ GeV, the dimuon mass required to be in the range 8–12 GeV and its transverse momentum required to be > 36 GeV. The photon is also required to have its $p_{\mathcal{T}} > 36$ GeV.

 $\Gamma(\mathcal{T}(1, 2, 3S) \mathcal{T}(1, 2, 3S))/\Gamma_{\text{total}}$ Γ_{41}/Γ

VALUE	CL%	EVTS	DOCUMENT ID	TECN	COMMENT
$<1.5 \times 10^{-6}$	95	106	1 SIRUNYAN	19BR CMS	$E_{\text{cm}}^{\text{pp}} = 13$ TeV

¹ SIRUNYAN 19BR search for Z decays to a pair of \mathcal{T} mesons in the channel $\mathcal{T} \rightarrow \mu^+ \mu^-$. The invariant mass of the \mathcal{T} candidates has to be in the range of 8.5 to 11 GeV. A total of 106 events are selected in the 20–140 GeV 4-muon invariant mass range. An un-binned extended maximum likelihood fit leads to the 95% C.L. upper limit, obtained assuming the \mathcal{T} mesons to be unpolarised.

 $\Gamma(D^0\gamma)/\Gamma(\mu^+ \mu^-)$ Γ_{42}/Γ_2

VALUE	CL%	DOCUMENT ID	TECN	COMMENT
$<6.4 \times 10^{-2}$	95	1 AAIJ	23AMLHCB	$E_{\text{cm}}^{\text{pp}} = 13$ TeV

¹ AAIJ 23AM also quotes the branching fraction limit $B(Z \rightarrow D^0\gamma) < 2.1 \times 10^{-3}$, using the known $Z \rightarrow \mu\mu$ branching fraction.

 $\Gamma((D^0/\bar{D}^0)X)/\Gamma(\text{hadrons})$ Γ_{43}/Γ_8

VALUE	EVTS	DOCUMENT ID	TECN	COMMENT
$0.296 \pm 0.019 \pm 0.021$	369	1 ABREU	93i DLPH	$E_{\text{cm}}^{\text{pe}} = 88\text{--}94$ GeV

¹ The (D^0/\bar{D}^0) states in ABREU 93i are detected by the $K\pi$ decay mode. This is a corrected result (see the erratum of ABREU 93i).

 $\Gamma(D^\pm X)/\Gamma(\text{hadrons})$ Γ_{44}/Γ_8

VALUE	EVTS	DOCUMENT ID	TECN	COMMENT
$0.174 \pm 0.016 \pm 0.018$	539	1 ABREU	93i DLPH	$E_{\text{cm}}^{\text{pe}} = 88\text{--}94$ GeV

¹ The D^\pm states in ABREU 93i are detected by the $K\pi\pi$ decay mode. This is a corrected result (see the erratum of ABREU 93i).

 $\Gamma(D^*(2010)^\pm X)/\Gamma(\text{hadrons})$ Γ_{45}/Γ_8

VALUE	EVTS	DOCUMENT ID	TECN	COMMENT
0.163 ± 0.019 OUR AVERAGE				Error includes scale factor of 1.3.
$0.155 \pm 0.010 \pm 0.013$	358	1 ABREU	93i DLPH	$E_{\text{cm}}^{\text{pe}} = 88\text{--}94$ GeV
0.21 ± 0.04	362	2 DECAMP	91J ALEP	$E_{\text{cm}}^{\text{pe}} = 88\text{--}94$ GeV

¹ $D^*(2010)^\pm$ in ABREU 93i are reconstructed from $D^0\pi^\pm$, with $D^0 \rightarrow K^-\pi^+$. The new CLEO II measurement of $B(D^{*\pm} \rightarrow D^0\pi^\pm) = (68.1 \pm 1.6)\%$ is used. This is a corrected result (see the erratum of ABREU 93i).

² DECAMP 91J report $B(D^{*+}(2010) \rightarrow D^0\pi^+) B(D^0 \rightarrow K^-\pi^+) \Gamma(D^*(2010)^\pm X) / \Gamma(\text{hadrons}) = (5.11 \pm 0.34) \times 10^{-3}$. They obtained the above number assuming $B(D^0 \rightarrow K^-\pi^+) = (3.62 \pm 0.34 \pm 0.44)\%$ and $B(D^*(2010)^\pm \rightarrow D^0\pi^\pm) = (55 \pm 4)\%$. We have rescaled their original result of 0.26 ± 0.05 taking into account the new CLEO II branching ratio $B(D^*(2010)^\pm \rightarrow D^0\pi^\pm) = (68.1 \pm 1.6)\%$.

 $\Gamma(D_{s1}(2536)^\pm X)/\Gamma(\text{hadrons})$ Γ_{46}/Γ_8

VALUE (%)	EVTS	DOCUMENT ID	TECN	COMMENT
$0.52 \pm 0.09 \pm 0.06$	92	1 HEISTER	02B ALEP	$E_{\text{cm}}^{\text{pe}} = 88\text{--}94$ GeV

¹ HEISTER 02B reconstruct this meson in the decay modes $D_{s1}(2536)^\pm \rightarrow D^{*\pm} K^0$ and $D_{s1}(2536)^\pm \rightarrow D^{*0} K^\pm$. The quoted branching ratio assumes that the decay width of the $D_{s1}(2536)$ is saturated by the two measured decay modes.

 $\Gamma(D_{sJ}(2573)^\pm X)/\Gamma(\text{hadrons})$ Γ_{47}/Γ_8

VALUE (%)	EVTS	DOCUMENT ID	TECN	COMMENT
$0.83 \pm 0.29 \pm 0.07$	64	1 HEISTER	02B ALEP	$E_{\text{cm}}^{\text{pe}} = 88\text{--}94$ GeV

¹ HEISTER 02B reconstruct this meson in the decay mode $D_{sJ}(2573)^\pm \rightarrow D^0 K^\pm$. The quoted branching ratio assumes that the detected decay mode represents 45% of the full decay width.

 $\Gamma(D^{*0}(2629)^\pm X)/\Gamma(\text{hadrons})$ Γ_{48}/Γ_8

VALUE (%)	DOCUMENT ID	TECN	COMMENT
searched for	1 ABBIENDI	01N OPAL	$E_{\text{cm}}^{\text{pe}} = 88\text{--}94$ GeV

¹ ABBIENDI 01N searched for the decay mode $D^{*0}(2629)^\pm \rightarrow D^{*\pm}\pi^+\pi^-$ with $D^{*+} \rightarrow D^0\pi^+$, and $D^0 \rightarrow K^-\pi^+$. They quote a 95% CL limit for $Z \rightarrow D^{*0}(2629)^\pm \times B(D^{*0}(2629)^\pm \rightarrow D^{*\pm}\pi^+\pi^-) < 3.1 \times 10^{-3}$.

 $\Gamma(B^* X) / [\Gamma(BX) + \Gamma(B^* X)]$ $\Gamma_{50}/(\Gamma_{49} + \Gamma_{50})$

As the experiments assume different values of the b -baryon contribution, our average should be taken with caution.

VALUE	EVTS	DOCUMENT ID	TECN	COMMENT
0.75 ± 0.04 OUR AVERAGE				
$0.760 \pm 0.036 \pm 0.083$		1 ACKERSTAFF	97M OPAL	$E_{\text{cm}}^{\text{pe}} = 88\text{--}94$ GeV
$0.771 \pm 0.026 \pm 0.070$		2 BUSKULIC	96D ALEP	$E_{\text{cm}}^{\text{pe}} = 88\text{--}94$ GeV
$0.72 \pm 0.03 \pm 0.06$		3 ABREU	95R DLPH	$E_{\text{cm}}^{\text{pe}} = 88\text{--}94$ GeV
$0.76 \pm 0.08 \pm 0.06$	1378	4 ACCIARRI	95B L3	$E_{\text{cm}}^{\text{pe}} = 88\text{--}94$ GeV

¹ ACKERSTAFF 97M use an inclusive B reconstruction method and assume a $(13.2 \pm 4.1)\%$ b -baryon contribution. The value refers to a b -flavored meson mixture of B_u, B_d , and B_s .

² BUSKULIC 96D use an inclusive reconstruction of B hadrons and assume a $(12.2 \pm 4.3)\%$ b -baryon contribution. The value refers to a b -flavored mixture of B_u, B_d , and B_s .

³ ABREU 95R use an inclusive B -reconstruction method and assume a $(10 \pm 4)\%$ b -baryon contribution. The value refers to a b -flavored meson mixture of B_u, B_d , and B_s .

⁴ ACCIARRI 95B assume a 9.4% b -baryon contribution. The value refers to a b -flavored mixture of B_u, B_d , and B_s .

 $\Gamma(B^+ X)/\Gamma(\text{hadrons})$ Γ_{51}/Γ_8

"OUR EVALUATION" is obtained using our current values for $f(\bar{b} \rightarrow B^+)$ and $R_b = \Gamma(b\bar{b})/\Gamma(\text{hadrons})$. We calculate $\Gamma(B^+ X)/\Gamma(\text{hadrons}) = R_b \times f(\bar{b} \rightarrow B^+)$.

VALUE	DOCUMENT ID	TECN	COMMENT
0.0869 ± 0.0019 OUR EVALUATION			(Produced by HFLAV)
0.0887 ± 0.0030	1 ABDALLAH	03K DLPH	$E_{\text{cm}}^{\text{pe}} = 88\text{--}94$ GeV

¹ ABDALLAH 03K measure the production fraction of B^+ mesons in hadronic Z decays $f(B^+) = (40.99 \pm 0.82 \pm 1.11)\%$. The value quoted here is obtained multiplying this production fraction by our value of $R_b = \Gamma(\bar{b}b)/\Gamma(\text{hadrons})$.

 $\Gamma(B_s^0 X)/\Gamma(\text{hadrons})$ Γ_{52}/Γ_8

"OUR EVALUATION" is obtained using our current values for $f(\bar{b} \rightarrow B_s^0)$ and $R_b = \Gamma(b\bar{b})/\Gamma(\text{hadrons})$. We calculate $\Gamma(B_s^0 X)/\Gamma(\text{hadrons}) = R_b \times f(\bar{b} \rightarrow B_s^0)$.

VALUE	DOCUMENT ID	TECN	COMMENT
0.0227 ± 0.0019 OUR EVALUATION			(Produced by HFLAV)
seen	1 ABREU	92M DLPH	$E_{\text{cm}}^{\text{pe}} = 88\text{--}94$ GeV
seen	2 ACTON	92N OPAL	$E_{\text{cm}}^{\text{pe}} = 88\text{--}94$ GeV
seen	3 BUSKULIC	92E ALEP	$E_{\text{cm}}^{\text{pe}} = 88\text{--}94$ GeV

¹ ABREU 92M reported value is $\Gamma(B_s^0 X) * B(B_s^0 \rightarrow D_s \mu \nu_\mu X) * B(D_s \rightarrow \phi\pi)/\Gamma(\text{hadrons}) = (18 \pm 8) \times 10^{-5}$.

² ACTON 92N find evidence for B_s^0 production using $D_s\text{-}\ell$ correlations, with $D_s^+ \rightarrow \phi\pi^+$ and $K^*(892) K^+$. Assuming R_b from the Standard Model and averaging over the e and μ channels, authors measure the product branching fraction to be $f(\bar{b} \rightarrow B_s^0) * B(B_s^0 \rightarrow D_s^- \ell^+ \nu_\ell X) * B(D_s^- \rightarrow \phi\pi^-) = (3.9 \pm 1.1 \pm 0.8) \times 10^{-4}$.

³ BUSKULIC 92E find evidence for B_s^0 production using $D_s\text{-}\ell$ correlations, with $D_s^+ \rightarrow \phi\pi^+$ and $K^*(892) K^+$. Using $B(D_s^+ \rightarrow \phi\pi^+) = (2.7 \pm 0.7)\%$ and summing up the e and μ channels, the weighted average product branching fraction is measured to be $B(\bar{b} \rightarrow B_s^0) * B(B_s^0 \rightarrow D_s^- \ell^+ \nu_\ell X) = 0.040 \pm 0.011 \pm 0.010$.

 $\Gamma(B_c^\pm X)/\Gamma(\text{hadrons})$ Γ_{53}/Γ_8

VALUE	DOCUMENT ID	TECN	COMMENT
searched for	1 ACKERSTAFF	98o OPAL	$E_{\text{cm}}^{\text{pe}} = 88\text{--}94$ GeV
searched for	2 ABREU	97E DLPH	$E_{\text{cm}}^{\text{pe}} = 88\text{--}94$ GeV
searched for	3 BARATE	97H ALEP	$E_{\text{cm}}^{\text{pe}} = 88\text{--}94$ GeV

¹ ACKERSTAFF 98o searched for the decay modes $B_c^- \rightarrow J/\psi\pi^+, J/\psi a_1^+$, and $J/\psi\ell^+ \nu_\ell$, with $J/\psi \rightarrow \ell^+ \ell^-$, $\ell = e, \mu$. The number of candidates (background) for

the three decay modes is $2(0.63 \pm 0.2)$, $0(1.10 \pm 0.22)$, and $1(0.82 \pm 0.19)$ respectively. Interpreting the $2B_c \rightarrow J/\psi\pi^+$ candidates as signal, they report $\Gamma(B_c^+ X) \times B(B_c \rightarrow J/\psi\pi^+)/\Gamma(\text{hadrons}) = (3.8_{-2.4}^{+5.0} \pm 0.5) \times 10^{-5}$. Interpreted as background, the 90% CL bounds are $\Gamma(B_c^+ X) \times B(B_c \rightarrow J/\psi\pi^+)/\Gamma(\text{hadrons}) < 1.06 \times 10^{-4}$, $\Gamma(B_c^+ X) \times B(B_c \rightarrow J/\psi a_1^+)/\Gamma(\text{hadrons}) < 5.29 \times 10^{-4}$, $\Gamma(B_c^+ X) \times B(B_c \rightarrow J/\psi\ell^+\nu_\ell)/\Gamma(\text{hadrons}) < 6.96 \times 10^{-5}$.

² ABREU 97E searched for the decay modes $B_c \rightarrow J/\psi\pi^+$, $J/\psi\ell^+\nu_\ell$, and $J/\psi(3\pi)^+$, with $J/\psi \rightarrow \ell^+\ell^-$, $\ell = e, \mu$. The number of candidates (background) for the three decay modes is 1 (1.7), 0 (0.3), and 1 (2.3) respectively. They report the following 90% CL limits: $\Gamma(B_c^+ X) \times B(B_c \rightarrow J/\psi\pi^+)/\Gamma(\text{hadrons}) < (1.05-0.84) \times 10^{-4}$, $\Gamma(B_c^+ X) \times B(B_c \rightarrow J/\psi\ell\nu_\ell)/\Gamma(\text{hadrons}) < (5.8-5.0) \times 10^{-5}$, $\Gamma(B_c^+ X) \times B(B_c \rightarrow J/\psi(3\pi)^+)/\Gamma(\text{hadrons}) < 1.75 \times 10^{-4}$, where the ranges are due to the predicted B_c lifetime (0.4-1.4) ps.

³ BARATE 97H searched for the decay modes $B_c \rightarrow J/\psi\pi^+$ and $J/\psi\ell^+\nu_\ell$ with $J/\psi \rightarrow \ell^+\ell^-$, $\ell = e, \mu$. The number of candidates (background) for the two decay modes is 0 (0.44) and 2 (0.81) respectively. They report the following 90% CL limits: $\Gamma(B_c^+ X) \times B(B_c \rightarrow J/\psi\pi^+)/\Gamma(\text{hadrons}) < 3.6 \times 10^{-5}$ and $\Gamma(B_c^+ X) \times B(B_c \rightarrow J/\psi\ell^+\nu_\ell)/\Gamma(\text{hadrons}) < 5.2 \times 10^{-5}$.

$\Gamma(\Lambda_c^+ X)/\Gamma(\text{hadrons})$ Γ_{54}/Γ_8

VALUE	DOCUMENT ID	TECN	COMMENT
0.022 ± 0.005 OUR AVERAGE			
0.024 ± 0.005 ± 0.006	¹ ALEXANDER 96R	OPAL	$E_{\text{cm}}^{\text{ee}} = 88-94$ GeV
0.021 ± 0.003 ± 0.005	² BUSKULIC 96V	ALEP	$E_{\text{cm}}^{\text{ee}} = 88-94$ GeV

¹ ALEXANDER 96R measure $R_b \times f(b \rightarrow \Lambda_c^+ X) \times B(\Lambda_c^+ \rightarrow pK^-\pi^+) = (0.122 \pm 0.023 \pm 0.010)\%$ in hadronic Z decays; the value quoted here is obtained using our best value $B(\Lambda_c^+ \rightarrow pK^-\pi^+) = (5.0 \pm 1.3)\%$. The first error is the total experiment's error and the second error is the systematic error due to the branching fraction uncertainty.

² BUSKULIC 96V obtain the production fraction of Λ_c^+ baryons in hadronic Z decays $f(b \rightarrow \Lambda_c^+ X) = 0.110 \pm 0.014 \pm 0.006$ using $B(\Lambda_c^+ \rightarrow pK^-\pi^+) = (4.4 \pm 0.6)\%$; we have rescaled using our best value $B(\Lambda_c^+ \rightarrow pK^-\pi^+) = (5.0 \pm 1.3)\%$ obtaining $f(b \rightarrow \Lambda_c^+ X) = 0.097 \pm 0.013 \pm 0.025$ where the first error is their total experiment's error and the second error is the systematic error due to the branching fraction uncertainty. The value quoted here is obtained multiplying this production fraction by our value of $R_b = \Gamma(b\bar{b})/\Gamma(\text{hadrons})$.

$\Gamma(\Xi_c^0 X)/\Gamma(\text{hadrons})$ Γ_{55}/Γ_8

VALUE	DOCUMENT ID	TECN	COMMENT
• • • We do not use the following data for averages, fits, limits, etc. • • •			
seen	¹ ABDALLAH 05c	DLPH	$E_{\text{cm}}^{\text{ee}} = 88-94$ GeV

¹ ABDALLAH 05c searched for the charmed strange baryon Ξ_c^0 in the decay channel $\Xi_c^0 \rightarrow \Xi^-\pi^+$ ($\Xi^- \rightarrow \Lambda\pi^-$). The production rate is measured to be $f_{\Xi_c^0} \times B(\Xi_c^0 \rightarrow \Xi^-\pi^+) = (4.7 \pm 1.4 \pm 1.1) \times 10^{-4}$ per hadronic Z decay.

$\Gamma(\Xi_b X)/\Gamma(\text{hadrons})$ Γ_{56}/Γ_8

Here Ξ_b is used as a notation for the strange b -baryon states Ξ_b^- and Ξ_b^0 .

VALUE	DOCUMENT ID	TECN	COMMENT
• • • We do not use the following data for averages, fits, limits, etc. • • •			
seen	¹ ABDALLAH 05c	DLPH	$E_{\text{cm}}^{\text{ee}} = 88-94$ GeV
seen	² BUSKULIC 96T	ALEP	$E_{\text{cm}}^{\text{ee}} = 88-94$ GeV
seen	³ ABREU 95v	DLPH	$E_{\text{cm}}^{\text{ee}} = 88-94$ GeV

¹ ABDALLAH 05c searched for the beauty strange baryon Ξ_b in the inclusive semileptonic decay channel $\Xi_b \rightarrow \Xi^-\ell^+\nu_\ell X$. Evidence for the Ξ_b production is seen from the observation of $\Xi\bar{\Xi}$ production accompanied by a lepton of the same sign. From the excess of "right-sign" pairs $\Xi\bar{\Xi}\ell^+\ell^-$ compared to "wrong-sign" pairs $\Xi\bar{\Xi}\ell^\pm\ell^\pm$ the production rate is measured to be $B(b \rightarrow \Xi_b) \times B(\Xi_b \rightarrow \Xi^-\ell^+ X) = (3.0 \pm 1.0 \pm 0.3) \times 10^{-4}$ per lepton species, averaged over electrons and muons.

² BUSKULIC 96T investigate Ξ -lepton correlations and find a significant excess of "right-sign" pairs $\Xi\bar{\Xi}\ell^+\ell^-$ compared to "wrong-sign" pairs $\Xi\bar{\Xi}\ell^\pm\ell^\pm$. This excess is interpreted as evidence for Ξ_b semileptonic decay. The measured product branching ratio is $B(b \rightarrow \Xi_b) \times B(\Xi_b \rightarrow X_c X \ell^+ \nu_\ell) \times B(X_c \rightarrow \Xi^- X') = (5.4 \pm 1.1 \pm 0.8) \times 10^{-4}$ per lepton species, averaged over electrons and muons, with X_c a charmed baryon.

³ ABREU 95v observe an excess of "right-sign" pairs $\Xi\bar{\Xi}\ell^+\ell^-$ compared to "wrong-sign" pairs $\Xi\bar{\Xi}\ell^\pm\ell^\pm$ in jets; this excess is interpreted as evidence for the beauty strange baryon Ξ_b production, with $\Xi_b \rightarrow \Xi^-\ell^+\nu_\ell X$. They find that the probability for this signal to come from non b -baryon decays is less than 5×10^{-4} and that Λ_b decays can account for less than 10% of these events. The Ξ_b production rate is then measured to be $B(b \rightarrow \Xi_b) \times B(\Xi_b \rightarrow \Xi^-\ell^+ X) = (5.9 \pm 2.1 \pm 1.0) \times 10^{-4}$ per lepton species, averaged over electrons and muons.

$\Gamma(b\text{-baryon } X)/\Gamma(\text{hadrons})$ Γ_{57}/Γ_8

"OUR EVALUATION" is obtained using our current values for $f(b \rightarrow b\text{-baryon})$ and $R_b = \Gamma(b\bar{b})/\Gamma(\text{hadrons})$. We calculate $\Gamma(b\text{-baryon } X)/\Gamma(\text{hadrons}) = R_b \times f(b \rightarrow b\text{-baryon})$.

VALUE	DOCUMENT ID	TECN	COMMENT
0.0197 ± 0.0032 OUR EVALUATION	(Produced by HFLAV)		
0.0221 ± 0.0015 ± 0.0058	¹ BARATE 98v	ALEP	$E_{\text{cm}}^{\text{ee}} = 88-94$ GeV

¹ BARATE 98v use the overall number of identified protons in b -hadron decays to measure $f(b \rightarrow b\text{-baryon}) = 0.102 \pm 0.007 \pm 0.027$. They assume $\text{BR}(b\text{-baryon} \rightarrow pX) = (58 \pm 6)\%$ and $\text{BR}(B_s^0 \rightarrow pX) = (8.0 \pm 4.0)\%$. The value quoted here is obtained multiplying this production fraction by our value of $R_b = \Gamma(b\bar{b})/\Gamma(\text{hadrons})$.

$\Gamma(\text{anomalous } \gamma + \text{hadrons})/\Gamma_{\text{total}}$ Γ_{58}/Γ

Limits on additional sources of prompt photons beyond expectations for final-state bremsstrahlung.

VALUE	CL%	DOCUMENT ID	TECN	COMMENT
< 3.2 × 10⁻³	95	¹ AKRAWY 90J	OPAL	$E_{\text{cm}}^{\text{ee}} = 88-94$ GeV
		¹ AKRAWY 90J report $\Gamma(\gamma X) < 8.2$ MeV at 95%CL. They assume a three-body $\gamma q\bar{q}$ distribution and use $E(\gamma) > 10$ GeV.		

$\Gamma(e^+ e^- \gamma)/\Gamma_{\text{total}}$ Γ_{59}/Γ

VALUE	CL%	DOCUMENT ID	TECN	COMMENT
< 5.2 × 10⁻⁴	95	¹ ACTON 91B	OPAL	$E_{\text{cm}}^{\text{ee}} = 91.2$ GeV
		¹ ACTON 91B looked for isolated photons with $E > 2\%$ of beam energy (> 0.9 GeV).		

$\Gamma(\mu^+ \mu^- \gamma)/\Gamma_{\text{total}}$ Γ_{60}/Γ

VALUE	CL%	DOCUMENT ID	TECN	COMMENT
< 5.6 × 10⁻⁴	95	¹ ACTON 91B	OPAL	$E_{\text{cm}}^{\text{ee}} = 91.2$ GeV
		¹ ACTON 91B looked for isolated photons with $E > 2\%$ of beam energy (> 0.9 GeV).		

$\Gamma(\tau^+ \tau^- \gamma)/\Gamma_{\text{total}}$ Γ_{61}/Γ

VALUE	CL%	DOCUMENT ID	TECN	COMMENT
< 7.3 × 10⁻⁴	95	¹ ACTON 91B	OPAL	$E_{\text{cm}}^{\text{ee}} = 91.2$ GeV
		¹ ACTON 91B looked for isolated photons with $E > 2\%$ of beam energy (> 0.9 GeV).		

$\Gamma(\ell^+ \ell^- \gamma)/\Gamma_{\text{total}}$ Γ_{62}/Γ

VALUE	CL%	DOCUMENT ID	TECN	COMMENT
< 6.8 × 10⁻⁶	95	¹ ACTON 93E	OPAL	$E_{\text{cm}}^{\text{ee}} = 88-94$ GeV
		¹ For $m_{\gamma\gamma} = 60 \pm 5$ GeV.		

$\Gamma(q\bar{q}\gamma\gamma)/\Gamma_{\text{total}}$ Γ_{63}/Γ

VALUE	CL%	DOCUMENT ID	TECN	COMMENT
< 5.5 × 10⁻⁶	95	¹ ACTON 93E	OPAL	$E_{\text{cm}}^{\text{ee}} = 88-94$ GeV
		¹ For $m_{\gamma\gamma} = 60 \pm 5$ GeV.		

$\Gamma(\nu\bar{\nu}\gamma\gamma)/\Gamma_{\text{total}}$ Γ_{64}/Γ

VALUE	CL%	DOCUMENT ID	TECN	COMMENT
< 3.1 × 10⁻⁶	95	¹ ACTON 93E	OPAL	$E_{\text{cm}}^{\text{ee}} = 88-94$ GeV
		¹ For $m_{\gamma\gamma} = 60 \pm 5$ GeV.		

$\Gamma(e^\pm \mu^\mp)/\Gamma_{\text{total}}$ Γ_{65}/Γ

Test of lepton family number conservation. The value is for the sum of the charge states indicated.

VALUE	CL%	DOCUMENT ID	TECN	COMMENT
< 2.62 × 10⁻⁷	95	AAD 23AQ	ATLS	$E_{\text{cm}}^{\text{pp}} = 13$ TeV
< 7.5 × 10 ⁻⁷	95	AAD 14AU	ATLS	$E_{\text{cm}}^{\text{pp}} = 8$ TeV
< 2.5 × 10 ⁻⁶	95	ABREU 97c	DLPH	$E_{\text{cm}}^{\text{ee}} = 88-94$ GeV
< 1.7 × 10 ⁻⁶	95	AKERS 95w	OPAL	$E_{\text{cm}}^{\text{ee}} = 88-94$ GeV
< 0.6 × 10 ⁻⁵	95	ADRIANI 93i	L3	$E_{\text{cm}}^{\text{ee}} = 88-94$ GeV
< 2.6 × 10 ⁻⁵	95	DECAMP 92	ALEP	$E_{\text{cm}}^{\text{ee}} = 88-94$ GeV

$\Gamma(e^\pm \mu^\mp)/\Gamma(e^+ e^-)$ Γ_{65}/Γ_1

Test of lepton family number conservation. The value is for the sum of the charge states indicated.

VALUE	CL%	DOCUMENT ID	TECN	COMMENT
< 0.07	90	ALBAJAR 89	UA1	$E_{\text{cm}}^{\text{pp}} = 546,630$ GeV

$\Gamma(e^\pm \tau^\mp)/\Gamma_{\text{total}}$ Γ_{66}/Γ

Test of lepton family number conservation. The value is for the sum of the charge states indicated.

VALUE	CL%	DOCUMENT ID	TECN	COMMENT
< 5.0 × 10⁻⁶	95	AAD 21AV	ATLS	$E_{\text{cm}}^{\text{pp}} = 13$ TeV
• • • We do not use the following data for averages, fits, limits, etc. • • •				
< 8.1 × 10 ⁻⁶	95	AAD 21AO	ATLS	$E_{\text{cm}}^{\text{pp}} = 13$ TeV
< 5.8 × 10 ⁻⁵	95	AABOUD 18CN	ATLS	$E_{\text{cm}}^{\text{pp}} = 13$ TeV
< 2.2 × 10 ⁻⁵	95	ABREU 97c	DLPH	$E_{\text{cm}}^{\text{ee}} = 88-94$ GeV
< 9.8 × 10 ⁻⁶	95	AKERS 95w	OPAL	$E_{\text{cm}}^{\text{ee}} = 88-94$ GeV
< 1.3 × 10 ⁻⁵	95	ADRIANI 93i	L3	$E_{\text{cm}}^{\text{ee}} = 88-94$ GeV
< 1.2 × 10 ⁻⁴	95	DECAMP 92	ALEP	$E_{\text{cm}}^{\text{ee}} = 88-94$ GeV

$\Gamma(\mu^\pm \tau^\mp)/\Gamma_{\text{total}}$ Γ_{67}/Γ

Test of lepton family number conservation. The value is for the sum of the charge states indicated.

VALUE	CL%	DOCUMENT ID	TECN	COMMENT
< 6.5 × 10⁻⁶	95	AAD 21AV	ATLS	$E_{\text{cm}}^{\text{pp}} = 13$ TeV
• • • We do not use the following data for averages, fits, limits, etc. • • •				
< 9.5 × 10 ⁻⁶	95	AAD 21AO	ATLS	$E_{\text{cm}}^{\text{pp}} = 13$ TeV
< 1.3 × 10 ⁻⁵	95	AABOUD 18CN	ATLS	$E_{\text{cm}}^{\text{pp}} = 8, 13$ TeV
< 1.2 × 10 ⁻⁵	95	ABREU 97c	DLPH	$E_{\text{cm}}^{\text{ee}} = 88-94$ GeV
< 1.7 × 10 ⁻⁵	95	AKERS 95w	OPAL	$E_{\text{cm}}^{\text{ee}} = 88-94$ GeV
< 1.9 × 10 ⁻⁵	95	ADRIANI 93i	L3	$E_{\text{cm}}^{\text{ee}} = 88-94$ GeV
< 1.0 × 10 ⁻⁴	95	DECAMP 92	ALEP	$E_{\text{cm}}^{\text{ee}} = 88-94$ GeV

Gauge & Higgs Boson Particle Listings

Z

$\Gamma(p\bar{e})/\Gamma_{\text{total}}$ Γ_{68}/Γ
 Test of baryon number and lepton number conservations. Charge conjugate states are implied.

VALUE	CL%	DOCUMENT ID	TECN	COMMENT
$<1.8 \times 10^{-6}$	95	¹ ABBIENDI	99I OPAL	$E_{\text{cm}}^{\text{ee}} = 88\text{--}94$ GeV

¹ ABBIENDI 99I give the 95%CL limit on the partial width $\Gamma(Z^0 \rightarrow p\bar{e}) < 4.6$ KeV and we have transformed it into a branching ratio.

$\Gamma(p\bar{\mu})/\Gamma_{\text{total}}$ Γ_{69}/Γ
 Test of baryon number and lepton number conservations. Charge conjugate states are implied.

VALUE	CL%	DOCUMENT ID	TECN	COMMENT
$<1.8 \times 10^{-6}$	95	¹ ABBIENDI	99I OPAL	$E_{\text{cm}}^{\text{ee}} = 88\text{--}94$ GeV

¹ ABBIENDI 99I give the 95%CL limit on the partial width $\Gamma(Z^0 \rightarrow p\bar{\mu}) < 4.4$ KeV and we have transformed it into a branching ratio.

AVERAGE PARTICLE MULTIPLICITIES IN HADRONIC Z DECAY

Summed over particle and antiparticle, when appropriate.

$\langle N_{\gamma} \rangle$

VALUE	DOCUMENT ID	TECN	COMMENT
$20.97 \pm 0.02 \pm 1.15$	ACKERSTAFF 98A	OPAL	$E_{\text{cm}}^{\text{ee}} = 91.2$ GeV

$\langle N_{\pi^{\pm}} \rangle$

VALUE	DOCUMENT ID	TECN	COMMENT
17.03 ± 0.16 OUR AVERAGE			
17.007 ± 0.209	ABE	04C SLD	$E_{\text{cm}}^{\text{ee}} = 91.2$ GeV
$17.26 \pm 0.10 \pm 0.88$	ABREU	98L DLPH	$E_{\text{cm}}^{\text{ee}} = 91.2$ GeV
17.04 ± 0.31	BARATE	98V ALEP	$E_{\text{cm}}^{\text{ee}} = 91.2$ GeV
17.05 ± 0.43	AKERS	94P OPAL	$E_{\text{cm}}^{\text{ee}} = 91.2$ GeV

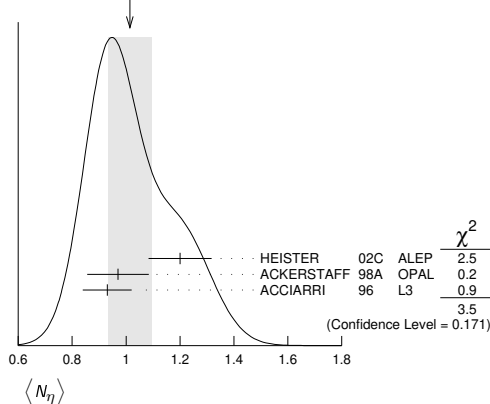
$\langle N_{\pi^0} \rangle$

VALUE	DOCUMENT ID	TECN	COMMENT
9.76 ± 0.26 OUR AVERAGE			
$9.55 \pm 0.06 \pm 0.75$	ACKERSTAFF 98A	OPAL	$E_{\text{cm}}^{\text{ee}} = 91.2$ GeV
$9.63 \pm 0.13 \pm 0.63$	BARATE	97J ALEP	$E_{\text{cm}}^{\text{ee}} = 91.2$ GeV
$9.90 \pm 0.02 \pm 0.33$	ACCIARRI	96 L3	$E_{\text{cm}}^{\text{ee}} = 91.2$ GeV
$9.2 \pm 0.2 \pm 1.0$	ADAM	96 DLPH	$E_{\text{cm}}^{\text{ee}} = 91.2$ GeV

$\langle N_{\eta} \rangle$

VALUE	DOCUMENT ID	TECN	COMMENT
1.01 ± 0.08 OUR AVERAGE			Error includes scale factor of 1.3. See the ideogram below.
$1.20 \pm 0.04 \pm 0.11$	HEISTER	02C ALEP	$E_{\text{cm}}^{\text{ee}} = 91.2$ GeV
$0.97 \pm 0.03 \pm 0.11$	ACKERSTAFF 98A	OPAL	$E_{\text{cm}}^{\text{ee}} = 91.2$ GeV
$0.93 \pm 0.01 \pm 0.09$	ACCIARRI	96 L3	$E_{\text{cm}}^{\text{ee}} = 91.2$ GeV

WEIGHTED AVERAGE
 1.01 ± 0.08 (Error scaled by 1.3)



$\langle N_{\rho^{\pm}} \rangle$

VALUE	DOCUMENT ID	TECN	COMMENT
2.57 ± 0.15 OUR AVERAGE			
$2.59 \pm 0.03 \pm 0.16$	¹ BEDDALL	09	ALEPH archive, $E_{\text{cm}}^{\text{ee}} = 91.2$ GeV
$2.40 \pm 0.06 \pm 0.43$	ACKERSTAFF 98A	OPAL	$E_{\text{cm}}^{\text{ee}} = 91.2$ GeV

¹ BEDDALL 09 analyse 3.2 million hadronic Z decays as archived by ALEPH collaboration and report a value of $2.59 \pm 0.03 \pm 0.15 \pm 0.04$. The first error is statistical, the second systematic, and the third arises from extrapolation to full phase space. We combine the systematic errors in quadrature.

$\langle N_{\rho^0} \rangle$

VALUE	DOCUMENT ID	TECN	COMMENT
1.24 ± 0.10 OUR AVERAGE			Error includes scale factor of 1.1.
1.19 ± 0.10	ABREU	99J DLPH	$E_{\text{cm}}^{\text{ee}} = 91.2$ GeV
$1.45 \pm 0.06 \pm 0.20$	BUSKULIC	96H ALEP	$E_{\text{cm}}^{\text{ee}} = 91.2$ GeV

$\langle N_{\omega} \rangle$

VALUE	DOCUMENT ID	TECN	COMMENT
1.02 ± 0.06 OUR AVERAGE			
$1.00 \pm 0.03 \pm 0.06$	HEISTER	02C ALEP	$E_{\text{cm}}^{\text{ee}} = 91.2$ GeV
$1.04 \pm 0.04 \pm 0.14$	ACKERSTAFF 98A	OPAL	$E_{\text{cm}}^{\text{ee}} = 91.2$ GeV
$1.17 \pm 0.09 \pm 0.15$	ACCIARRI	97D L3	$E_{\text{cm}}^{\text{ee}} = 91.2$ GeV

$\langle N_{\eta'} \rangle$

VALUE	DOCUMENT ID	TECN	COMMENT
0.17 ± 0.05 OUR AVERAGE			Error includes scale factor of 2.4.
$0.14 \pm 0.01 \pm 0.02$	ACKERSTAFF 98A	OPAL	$E_{\text{cm}}^{\text{ee}} = 91.2$ GeV
0.25 ± 0.04	¹ ACCIARRI	97D L3	$E_{\text{cm}}^{\text{ee}} = 91.2$ GeV
$0.068 \pm 0.018 \pm 0.016$	² BUSKULIC	92D ALEP	$E_{\text{cm}}^{\text{ee}} = 91.2$ GeV

¹ ACCIARRI 97D obtain this value averaging over the two decay channels $\eta' \rightarrow \pi^+ \pi^- \eta$ and $\eta' \rightarrow \rho^0 \gamma$.
² BUSKULIC 92D obtain this value for $x > 0.1$.

$\langle N_{\phi(980)} \rangle$

VALUE	DOCUMENT ID	TECN	COMMENT
0.147 ± 0.011 OUR AVERAGE			
0.164 ± 0.021	ABREU	99J DLPH	$E_{\text{cm}}^{\text{ee}} = 91.2$ GeV
$0.141 \pm 0.007 \pm 0.011$	ACKERSTAFF 98Q	OPAL	$E_{\text{cm}}^{\text{ee}} = 91.2$ GeV

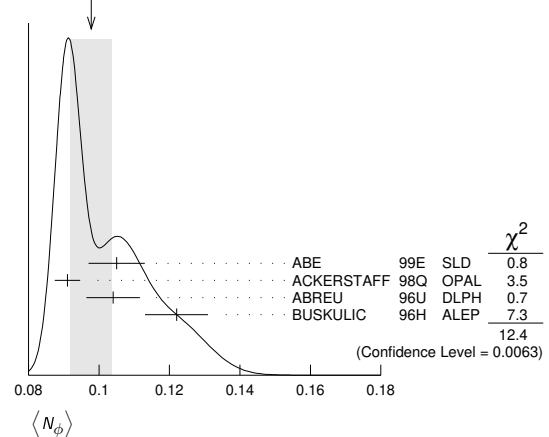
$\langle N_{\rho(980)^{\pm}} \rangle$

VALUE	DOCUMENT ID	TECN	COMMENT
$0.27 \pm 0.04 \pm 0.10$	ACKERSTAFF 98A	OPAL	$E_{\text{cm}}^{\text{ee}} = 91.2$ GeV

$\langle N_{\phi} \rangle$

VALUE	DOCUMENT ID	TECN	COMMENT
0.098 ± 0.006 OUR AVERAGE			Error includes scale factor of 2.0. See the ideogram below.
0.105 ± 0.008	ABE	99E SLD	$E_{\text{cm}}^{\text{ee}} = 91.2$ GeV
$0.091 \pm 0.002 \pm 0.003$	ACKERSTAFF 98Q	OPAL	$E_{\text{cm}}^{\text{ee}} = 91.2$ GeV
$0.104 \pm 0.003 \pm 0.007$	ABREU	96U DLPH	$E_{\text{cm}}^{\text{ee}} = 91.2$ GeV
$0.122 \pm 0.004 \pm 0.008$	BUSKULIC	96H ALEP	$E_{\text{cm}}^{\text{ee}} = 91.2$ GeV

WEIGHTED AVERAGE
 0.098 ± 0.006 (Error scaled by 2.0)



$\langle N_{\phi(1270)} \rangle$

VALUE	DOCUMENT ID	TECN	COMMENT
0.169 ± 0.025 OUR AVERAGE			Error includes scale factor of 1.4.
0.214 ± 0.038	ABREU	99J DLPH	$E_{\text{cm}}^{\text{ee}} = 91.2$ GeV
$0.155 \pm 0.011 \pm 0.018$	ACKERSTAFF 98Q	OPAL	$E_{\text{cm}}^{\text{ee}} = 91.2$ GeV

$\langle N_{\phi(1285)} \rangle$

VALUE	DOCUMENT ID	TECN	COMMENT
0.165 ± 0.051	¹ ABDALLAH	03H DLPH	$E_{\text{cm}}^{\text{ee}} = 91.2$ GeV

¹ ABDALLAH 03H assume a $K\bar{K}\pi$ branching ratio of $(9.0 \pm 0.4)\%$.

$\langle N_{\phi(1420)} \rangle$

VALUE	DOCUMENT ID	TECN	COMMENT
0.056 ± 0.012	¹ ABDALLAH	03H DLPH	$E_{\text{cm}}^{\text{ee}} = 91.2$ GeV

¹ ABDALLAH 03H assume a $K\bar{K}\pi$ branching ratio of 100%.

$\langle N_{\eta'(1525)} \rangle$

VALUE	DOCUMENT ID	TECN	COMMENT
0.012 ± 0.006	ABREU	99J DLPH	$E_{\text{cm}}^{\text{ee}} = 91.2$ GeV

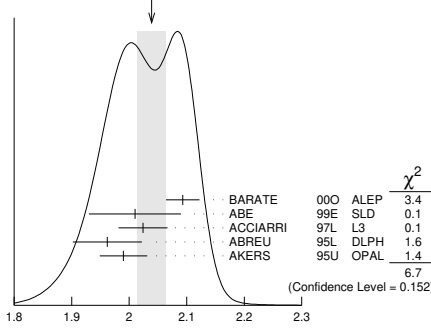
$\langle N_{K^\pm} \rangle$

VALUE	DOCUMENT ID	TECN	COMMENT
2.24 ± 0.04 OUR AVERAGE			
2.203 ± 0.071	ABE	04c	SLD $E_{cm}^{ee} = 91.2$ GeV
2.21 ± 0.05 ± 0.05	ABREU	98L	DLPH $E_{cm}^{ee} = 91.2$ GeV
2.26 ± 0.12	BARATE	98v	ALEP $E_{cm}^{ee} = 91.2$ GeV
2.42 ± 0.13	AKERS	94P	OPAL $E_{cm}^{ee} = 91.2$ GeV

$\langle N_{K^0} \rangle$

VALUE	DOCUMENT ID	TECN	COMMENT
2.039 ± 0.025 OUR AVERAGE	Error includes scale factor of 1.3.		See the ideogram below.
2.093 ± 0.004 ± 0.029	BARATE	00o	ALEP $E_{cm}^{ee} = 91.2$ GeV
2.01 ± 0.08	ABE	99E	SLD $E_{cm}^{ee} = 91.2$ GeV
2.024 ± 0.006 ± 0.042	ACCIARRI	97L	L3 $E_{cm}^{ee} = 91.2$ GeV
1.962 ± 0.022 ± 0.056	ABREU	95L	DLPH $E_{cm}^{ee} = 91.2$ GeV
1.99 ± 0.01 ± 0.04	AKERS	95U	OPAL $E_{cm}^{ee} = 91.2$ GeV

WEIGHTED AVERAGE
2.039±0.025 (Error scaled by 1.3)



$\langle N_{K^*(892)^\pm} \rangle$

VALUE	DOCUMENT ID	TECN	COMMENT
0.72 ± 0.05 OUR AVERAGE			
0.712 ± 0.031 ± 0.059	ABREU	95L	DLPH $E_{cm}^{ee} = 91.2$ GeV
0.72 ± 0.02 ± 0.08	ACTON	93	OPAL $E_{cm}^{ee} = 91.2$ GeV

$\langle N_{K^*(892)^0} \rangle$

VALUE	DOCUMENT ID	TECN	COMMENT
0.739 ± 0.022 OUR AVERAGE			
0.707 ± 0.041	ABE	99E	SLD $E_{cm}^{ee} = 91.2$ GeV
0.74 ± 0.02 ± 0.02	ACKERSTAFF	97S	OPAL $E_{cm}^{ee} = 91.2$ GeV
0.77 ± 0.02 ± 0.07	ABREU	96U	DLPH $E_{cm}^{ee} = 91.2$ GeV
0.83 ± 0.01 ± 0.09	BUSKULIC	96H	ALEP $E_{cm}^{ee} = 91.2$ GeV
0.97 ± 0.18 ± 0.31	ABREU	93	DLPH $E_{cm}^{ee} = 91.2$ GeV

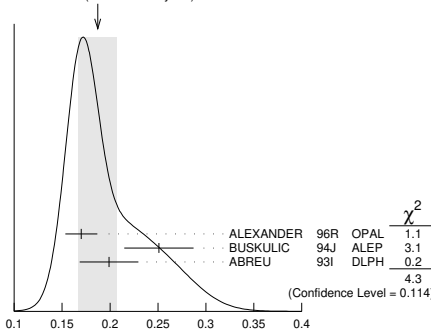
$\langle N_{K_2^*(1430)} \rangle$

VALUE	DOCUMENT ID	TECN	COMMENT
0.073 ± 0.023			
••• We do not use the following data for averages, fits, limits, etc. •••			
0.19 ± 0.04 ± 0.06	¹ AKERS	95X	OPAL $E_{cm}^{ee} = 91.2$ GeV
	¹ AKERS	95X	obtain this value for $x < 0.3$.

$\langle N_{D^\pm} \rangle$

VALUE	DOCUMENT ID	TECN	COMMENT
0.187 ± 0.020 OUR AVERAGE	Error includes scale factor of 1.5.		See the ideogram below.
0.170 ± 0.009 ± 0.014	ALEXANDER	96R	OPAL $E_{cm}^{ee} = 91.2$ GeV
0.251 ± 0.026 ± 0.025	BUSKULIC	94J	ALEP $E_{cm}^{ee} = 91.2$ GeV
0.199 ± 0.019 ± 0.024	¹ ABREU	93I	DLPH $E_{cm}^{ee} = 91.2$ GeV

WEIGHTED AVERAGE
0.187±0.020 (Error scaled by 1.5)



¹ See ABREU 95 (erratum).

$\langle N_{D^0} \rangle$

VALUE	DOCUMENT ID	TECN	COMMENT
0.462 ± 0.026 OUR AVERAGE			
0.465 ± 0.017 ± 0.027	ALEXANDER	96R	OPAL $E_{cm}^{ee} = 91.2$ GeV
0.518 ± 0.052 ± 0.035	BUSKULIC	94J	ALEP $E_{cm}^{ee} = 91.2$ GeV
0.403 ± 0.038 ± 0.044	¹ ABREU	93I	DLPH $E_{cm}^{ee} = 91.2$ GeV
	¹ See ABREU 95 (erratum).		

$\langle N_{D_s^\pm} \rangle$

VALUE	DOCUMENT ID	TECN	COMMENT
0.131 ± 0.010 ± 0.018	ALEXANDER	96R	OPAL $E_{cm}^{ee} = 91.2$ GeV

$\langle N_{D^*(2010)^\pm} \rangle$

VALUE	DOCUMENT ID	TECN	COMMENT
0.183 ± 0.008 OUR AVERAGE			
0.1854 ± 0.0041 ± 0.0091	¹ ACKERSTAFF	98E	OPAL $E_{cm}^{ee} = 91.2$ GeV
0.187 ± 0.015 ± 0.013	BUSKULIC	94J	ALEP $E_{cm}^{ee} = 91.2$ GeV
0.171 ± 0.012 ± 0.016	² ABREU	93I	DLPH $E_{cm}^{ee} = 91.2$ GeV

¹ ACKERSTAFF 98E systematic error includes an uncertainty of ± 0.0069 due to the branching ratios $B(D^{*+} \rightarrow D^0 \pi^+) = 0.683 \pm 0.014$ and $B(D^0 \rightarrow K^- \pi^+) = 0.0383 \pm 0.0012$.

² See ABREU 95 (erratum).

$\langle N_{D_{s1}^*(2536)^+} \rangle$

VALUE (units 10^{-3})	DOCUMENT ID	TECN	COMMENT
••• We do not use the following data for averages, fits, limits, etc. •••			
2.9 ± 0.7 -0.6 ± 0.2	¹ ACKERSTAFF	97W	OPAL $E_{cm}^{ee} = 91.2$ GeV

¹ ACKERSTAFF 97W obtain this value for $x > 0.6$ and with the assumption that its decay width is saturated by the D^*K final states.

$\langle N_{B^*} \rangle$

VALUE	DOCUMENT ID	TECN	COMMENT
0.28 ± 0.01 ± 0.03	¹ ABREU	95R	DLPH $E_{cm}^{ee} = 91.2$ GeV
	¹ ABREU 95R	quote this value for a flavor-averaged excited state.	

$\langle N_{J/\psi(1S)} \rangle$

VALUE	DOCUMENT ID	TECN	COMMENT
0.0056 ± 0.0003 ± 0.0004	¹ ALEXANDER	96B	OPAL $E_{cm}^{ee} = 91.2$ GeV
	¹ ALEXANDER 96B	identify $J/\psi(1S)$ from the decays into lepton pairs.	

$\langle N_{\psi(2S)} \rangle$

VALUE	DOCUMENT ID	TECN	COMMENT
0.0023 ± 0.0004 ± 0.0003	ALEXANDER	96B	OPAL $E_{cm}^{ee} = 91.2$ GeV

$\langle N_p \rangle$

VALUE	DOCUMENT ID	TECN	COMMENT
1.046 ± 0.026 OUR AVERAGE			
1.054 ± 0.035	ABE	04c	SLD $E_{cm}^{ee} = 91.2$ GeV
1.08 ± 0.04 ± 0.03	ABREU	98L	DLPH $E_{cm}^{ee} = 91.2$ GeV
1.00 ± 0.07	BARATE	98v	ALEP $E_{cm}^{ee} = 91.2$ GeV
0.92 ± 0.11	AKERS	94P	OPAL $E_{cm}^{ee} = 91.2$ GeV

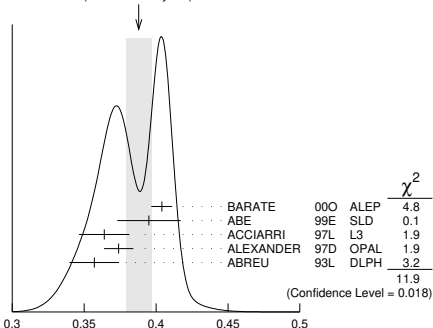
$\langle N_{\Delta(1232)^{++}} \rangle$

VALUE	DOCUMENT ID	TECN	COMMENT
0.087 ± 0.033 OUR AVERAGE	Error includes scale factor of 2.4.		
0.079 ± 0.009 ± 0.011	ABREU	95W	DLPH $E_{cm}^{ee} = 91.2$ GeV
0.22 ± 0.04 ± 0.04	ALEXANDER	95D	OPAL $E_{cm}^{ee} = 91.2$ GeV

$\langle N_\Lambda \rangle$

VALUE	DOCUMENT ID	TECN	COMMENT
0.388 ± 0.009 OUR AVERAGE	Error includes scale factor of 1.7.		See the ideogram below.
0.404 ± 0.002 ± 0.007	BARATE	00o	ALEP $E_{cm}^{ee} = 91.2$ GeV
0.395 ± 0.022	ABE	99E	SLD $E_{cm}^{ee} = 91.2$ GeV
0.364 ± 0.004 ± 0.017	ACCIARRI	97L	L3 $E_{cm}^{ee} = 91.2$ GeV
0.374 ± 0.002 ± 0.010	ALEXANDER	97D	OPAL $E_{cm}^{ee} = 91.2$ GeV
0.357 ± 0.003 ± 0.017	ABREU	93L	DLPH $E_{cm}^{ee} = 91.2$ GeV

WEIGHTED AVERAGE
0.388±0.009 (Error scaled by 1.7)



Gauge & Higgs Boson Particle Listings

Z

 $\langle N_{\Lambda(1520)} \rangle$

VALUE	DOCUMENT ID	TECN	COMMENT
0.0224 ± 0.0027 OUR AVERAGE			
0.029 ± 0.005 ± 0.005	ABREU 00P	DLPH	$E_{cm}^{ee} = 91.2$ GeV
0.0213 ± 0.0021 ± 0.0019	ALEXANDER 97D	OPAL	$E_{cm}^{ee} = 91.2$ GeV

 $\langle N_{\Sigma^+} \rangle$

VALUE	DOCUMENT ID	TECN	COMMENT
0.107 ± 0.010 OUR AVERAGE			
0.114 ± 0.011 ± 0.009	ACCIARRI 00J	L3	$E_{cm}^{ee} = 91.2$ GeV
0.099 ± 0.008 ± 0.013	ALEXANDER 97E	OPAL	$E_{cm}^{ee} = 91.2$ GeV

 $\langle N_{\Sigma^-} \rangle$

VALUE	DOCUMENT ID	TECN	COMMENT
0.082 ± 0.007 OUR AVERAGE			
0.081 ± 0.002 ± 0.010	ABREU 00P	DLPH	$E_{cm}^{ee} = 91.2$ GeV
0.083 ± 0.006 ± 0.009	ALEXANDER 97E	OPAL	$E_{cm}^{ee} = 91.2$ GeV

 $\langle N_{\Sigma^+ + \Sigma^-} \rangle$

VALUE	DOCUMENT ID	TECN	COMMENT
0.181 ± 0.018 OUR AVERAGE			
0.182 ± 0.010 ± 0.016	¹ ALEXANDER 97E	OPAL	$E_{cm}^{ee} = 91.2$ GeV
0.170 ± 0.014 ± 0.061	ABREU 95o	DLPH	$E_{cm}^{ee} = 91.2$ GeV

¹ We have combined the values of $\langle N_{\Sigma^+} \rangle$ and $\langle N_{\Sigma^-} \rangle$ from ALEXANDER 97E adding the statistical and systematic errors of the two final states separately in quadrature. If isospin symmetry is assumed this value becomes $0.174 \pm 0.010 \pm 0.015$.

 $\langle N_{\Sigma^0} \rangle$

VALUE	DOCUMENT ID	TECN	COMMENT
0.076 ± 0.010 OUR AVERAGE			
0.095 ± 0.015 ± 0.013	ACCIARRI 00J	L3	$E_{cm}^{ee} = 91.2$ GeV
0.071 ± 0.012 ± 0.013	ALEXANDER 97E	OPAL	$E_{cm}^{ee} = 91.2$ GeV
0.070 ± 0.010 ± 0.010	ADAM 96B	DLPH	$E_{cm}^{ee} = 91.2$ GeV

 $\langle N_{\Sigma^+ + \Sigma^- + \Sigma^0} \rangle / 3$

VALUE	DOCUMENT ID	TECN	COMMENT
0.084 ± 0.005 ± 0.008	ALEXANDER 97E	OPAL	$E_{cm}^{ee} = 91.2$ GeV

 $\langle N_{\Sigma(1385)^+} \rangle$

VALUE	DOCUMENT ID	TECN	COMMENT
0.0239 ± 0.0009 ± 0.0012	ALEXANDER 97D	OPAL	$E_{cm}^{ee} = 91.2$ GeV

 $\langle N_{\Sigma(1385)^-} \rangle$

VALUE	DOCUMENT ID	TECN	COMMENT
0.0240 ± 0.0010 ± 0.0014	ALEXANDER 97D	OPAL	$E_{cm}^{ee} = 91.2$ GeV

 $\langle N_{\Sigma(1385)^+ + \Sigma(1385)^-} \rangle$

VALUE	DOCUMENT ID	TECN	COMMENT
0.046 ± 0.004 OUR AVERAGE			
0.0479 ± 0.0013 ± 0.0026	ALEXANDER 97D	OPAL	$E_{cm}^{ee} = 91.2$ GeV
0.0382 ± 0.0028 ± 0.0045	ABREU 95o	DLPH	$E_{cm}^{ee} = 91.2$ GeV

 $\langle N_{\Xi^-} \rangle$

VALUE	DOCUMENT ID	TECN	COMMENT
0.0258 ± 0.0009 OUR AVERAGE			
0.0247 ± 0.0009 ± 0.0025	ABDALLAH 06E	DLPH	$E_{cm}^{ee} = 91.2$ GeV
0.0259 ± 0.0004 ± 0.0009	ALEXANDER 97D	OPAL	$E_{cm}^{ee} = 91.2$ GeV

 $\langle N_{\Xi(1530)^0} \rangle$

VALUE	DOCUMENT ID	TECN	COMMENT
0.0059 ± 0.0011 OUR AVERAGE			
0.0045 ± 0.0005 ± 0.0006	ABDALLAH 05C	DLPH	$E_{cm}^{ee} = 91.2$ GeV
0.0068 ± 0.0005 ± 0.0004	ALEXANDER 97D	OPAL	$E_{cm}^{ee} = 91.2$ GeV

 $\langle N_{\Xi^-} \rangle$

VALUE	DOCUMENT ID	TECN	COMMENT
0.00164 ± 0.00028 OUR AVERAGE			
0.0018 ± 0.0003 ± 0.0002	ALEXANDER 97D	OPAL	$E_{cm}^{ee} = 91.2$ GeV
0.0014 ± 0.0002 ± 0.0004	ADAM 96B	DLPH	$E_{cm}^{ee} = 91.2$ GeV

 $\langle N_{\Lambda_c^+} \rangle$

VALUE	DOCUMENT ID	TECN	COMMENT
0.078 ± 0.012 ± 0.012	ALEXANDER 96R	OPAL	$E_{cm}^{ee} = 91.2$ GeV

 $\langle N_D \rangle$

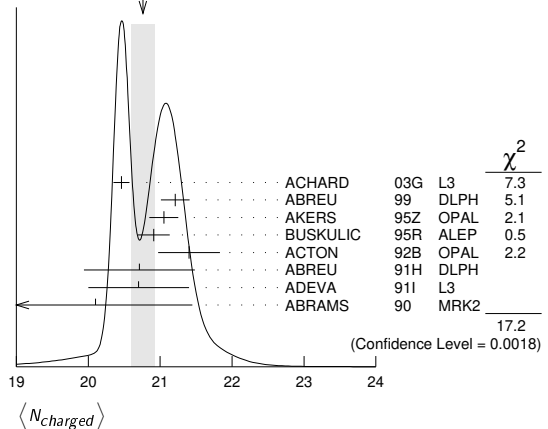
VALUE (units 10^{-6})	DOCUMENT ID	TECN	COMMENT
5.9 ± 1.8 ± 0.5	¹ SCHAEEL 06A	ALEP	$E_{cm}^{ee} = 91.2$ GeV

¹ SCHAEEL 06A obtain this anti-deuteron production rate per hadronic Z decay in the anti-deuteron momentum range from 0.62 to 1.03 GeV/c.

 $\langle N_{\text{charged}} \rangle$

VALUE	DOCUMENT ID	TECN	COMMENT
20.76 ± 0.16 OUR AVERAGE			Error includes scale factor of 2.1. See the ideogram below.
20.46 ± 0.01 ± 0.11	ACHARD 03G	L3	$E_{cm}^{ee} = 91.2$ GeV
21.21 ± 0.01 ± 0.20	ABREU 99	DLPH	$E_{cm}^{ee} = 91.2$ GeV
21.05 ± 0.20	AKERS 95Z	OPAL	$E_{cm}^{ee} = 91.2$ GeV
20.91 ± 0.03 ± 0.22	BUSKULIC 95R	ALEP	$E_{cm}^{ee} = 91.2$ GeV
21.40 ± 0.43	ACTON 92B	OPAL	$E_{cm}^{ee} = 91.2$ GeV
20.71 ± 0.04 ± 0.77	ABREU 91H	DLPH	$E_{cm}^{ee} = 91.2$ GeV
20.7 ± 0.7	ADEVA 91I	L3	$E_{cm}^{ee} = 91.2$ GeV
20.1 ± 1.0 ± 0.9	ABRAMS 90	MRK2	$E_{cm}^{ee} = 91.1$ GeV

WEIGHTED AVERAGE
20.76 ± 0.16 (Error scaled by 2.1)



Z HADRONIC POLE CROSS SECTION

OUR EVALUATION is obtained using the fit procedure and correlations as determined by the LEP Electroweak Working Group (see the note "The Z boson" and ref. LEP-SLC 06). Corrections as discussed in VOUTSINAS 20 and JANOT 20 are also included. This quantity is defined as

$$\sigma_h^0 = \frac{12\pi}{M_Z^2} \frac{\Gamma(e^+e^-)\Gamma(\text{hadrons})}{\Gamma_Z^2}$$

It is one of the parameters used in the Z lineshape fit.

VALUE (nb)	EVTS	DOCUMENT ID	TECN	COMMENT
41.4802 ± 0.0325 OUR EVALUATION				
41.4802 ± 0.0325		¹ JANOT 20	20	
• • • We do not use the following data for averages, fits, limits, etc. • • •				
41.500 ± 0.037		² VOUTSINAS 20	20	
41.541 ± 0.037		LEP-SLC 06		$E_{cm}^{ee} = 88-94$ GeV
41.501 ± 0.055	4.10M	³ ABBIENDI 01A	OPAL	$E_{cm}^{ee} = 88-94$ GeV
41.578 ± 0.069	3.70M	ABREU 00F	DLPH	$E_{cm}^{ee} = 88-94$ GeV
41.535 ± 0.055	3.54M	ACCIARRI 00C	L3	$E_{cm}^{ee} = 88-94$ GeV
41.559 ± 0.058	4.07M	⁴ BARATE 00C	ALEP	$E_{cm}^{ee} = 88-94$ GeV
42 ± 4	450	ABRAMS 89B	MRK2	$E_{cm}^{ee} = 89.2-93.0$ GeV

¹ JANOT 20 applies a correction to LEP-SLC 06 using an updated Bhabha cross section calculation. This result also includes a correction to account for correlated luminosity bias as presented in VOUTSINAS 20.

² VOUTSINAS 20 applies a correction to LEP-SLC 06 to account for correlated luminosity bias.

³ ABBIENDI 01A error includes approximately 0.031 due to statistics, 0.033 due to event selection systematics, 0.029 due to uncertainty in luminosity measurement, and 0.011 due to LEP energy uncertainty.

⁴ BARATE 00C error includes approximately 0.030 due to statistics, 0.026 due to experimental systematics, and 0.025 due to uncertainty in luminosity measurement.

Z VECTOR COUPLINGS

These quantities are the effective vector couplings of the Z to charged leptons and quarks. Their magnitude is derived from a measurement of the Z lineshape and the forward-backward lepton asymmetries as a function of energy around the Z mass. The relative sign among the vector to axial-vector couplings is obtained from a measurement of the Z asymmetry parameters, A_e , A_μ , and A_τ . By convention the sign of g_A^e is fixed to be negative (and opposite to that of g_V^e obtained using ν_e scattering measurements). For the light quarks, the sign of the couplings is assigned consistently with this assumption. The LEP/SLD-based fit values quoted below correspond to global nine- or five-parameter fits to lineshape, lepton forward-backward asymmetry, and A_e , A_μ , and A_τ measurements. See the note "The Z boson" and ref. LEP-SLC 06 for details. Where $p\bar{p}$ and $e\bar{p}$ data is quoted, OUR FIT value corresponds to a weighted average of this with the LEP/SLD fit result.

g_V^e

VALUE	EVTS	DOCUMENT ID	TECN	COMMENT
-0.03817 ± 0.00047 OUR FIT				
-0.058 ± 0.016 ± 0.007	5026	1 ACOSTA	05M CDF	$E_{cm}^{p\bar{p}} = 1.96$ TeV
-0.0346 ± 0.0023	137.0k	2 ABBIENDI	01o OPAL	$E_{cm}^{ee} = 88-94$ GeV
-0.0412 ± 0.0027	124.4k	3 ACCIARRI	00c L3	$E_{cm}^{ee} = 88-94$ GeV
-0.0400 ± 0.0037		BARATE	00c ALEP	$E_{cm}^{ee} = 88-94$ GeV
-0.0414 ± 0.0020		4 ABE	95j SLD	$E_{cm}^{ee} = 91.31$ GeV

¹ ACOSTA 05M determine the forward-backward asymmetry of e^+e^- pairs produced via $q\bar{q} \rightarrow Z/\gamma^* \rightarrow e^+e^-$ in 15 M(e^+e^-) effective mass bins ranging from 40 GeV to 600 GeV. These results are used to obtain the vector and axial-vector couplings of the Z to e^+e^- , assuming the quark couplings are as predicted by the standard model. Higher order radiative corrections have not been taken into account.

² ABBIENDI 01o use their measurement of the τ polarization in addition to the lineshape and forward-backward lepton asymmetries.

³ ACCIARRI 00c use their measurement of the τ polarization in addition to forward-backward lepton asymmetries.

⁴ ABE 95j obtain this result combining polarized Bhabha results with the A_{LR} measurement of ABE 94c. The Bhabha results alone give $-0.0507 \pm 0.0096 \pm 0.0020$.

 g_V^{μ}

VALUE	EVTS	DOCUMENT ID	TECN	COMMENT
-0.0367 ± 0.0023 OUR FIT				
-0.0388 ± 0.0060 -0.0064	182.8k	1 ABBIENDI	01o OPAL	$E_{cm}^{ee} = 88-94$ GeV
-0.0386 ± 0.0073	113.4k	2 ACCIARRI	00c L3	$E_{cm}^{ee} = 88-94$ GeV
-0.0362 ± 0.0061		BARATE	00c ALEP	$E_{cm}^{ee} = 88-94$ GeV
-0.0413 ± 0.0060	66143	3 ABBIENDI	01k OPAL	$E_{cm}^{ee} = 89-93$ GeV

• • • We do not use the following data for averages, fits, limits, etc. • • •

¹ ABBIENDI 01o use their measurement of the τ polarization in addition to the lineshape and forward-backward lepton asymmetries.

² ACCIARRI 00c use their measurement of the τ polarization in addition to forward-backward lepton asymmetries.

³ ABBIENDI 01k obtain this from an angular analysis of the muon pair asymmetry which takes into account effects of initial state radiation on an event by event basis and of initial-final state interference.

 g_V^{τ}

VALUE	EVTS	DOCUMENT ID	TECN	COMMENT
-0.0366 ± 0.0010 OUR FIT				
-0.0365 ± 0.0023	151.5k	1 ABBIENDI	01o OPAL	$E_{cm}^{ee} = 88-94$ GeV
-0.0384 ± 0.0026	103.0k	2 ACCIARRI	00c L3	$E_{cm}^{ee} = 88-94$ GeV
-0.0361 ± 0.0068		BARATE	00c ALEP	$E_{cm}^{ee} = 88-94$ GeV

¹ ABBIENDI 01o use their measurement of the τ polarization in addition to the lineshape and forward-backward lepton asymmetries.

² ACCIARRI 00c use their measurement of the τ polarization in addition to forward-backward lepton asymmetries.

 g_V^e

VALUE	EVTS	DOCUMENT ID	TECN	COMMENT
-0.03783 ± 0.00041 OUR FIT				
-0.0358 ± 0.0014	471.3k	1 ABBIENDI	01o OPAL	$E_{cm}^{ee} = 88-94$ GeV
-0.0397 ± 0.0020	379.4k	2 ABREU	00f DLPH	$E_{cm}^{ee} = 88-94$ GeV
-0.0397 ± 0.0017	340.8k	3 ACCIARRI	00c L3	$E_{cm}^{ee} = 88-94$ GeV
-0.0383 ± 0.0018	500k	BARATE	00c ALEP	$E_{cm}^{ee} = 88-94$ GeV

¹ ABBIENDI 01o use their measurement of the τ polarization in addition to the lineshape and forward-backward lepton asymmetries.

² Using forward-backward lepton asymmetries.

³ ACCIARRI 00c use their measurement of the τ polarization in addition to forward-backward lepton asymmetries.

 g_V^p

VALUE	EVTS	DOCUMENT ID	TECN	COMMENT
0.266 ± 0.034 OUR AVERAGE				
0.270 ± 0.037		1 ANDREEV	18A H1	$e^\pm p$
0.201 ± 0.112	156k	2 ABAZOV	11D D0	$E_{cm}^{p\bar{p}} = 1.97$ TeV
0.24 +0.28 -0.11		3 LEP-SLC	06	$E_{cm}^{ee} = 88-94$ GeV
0.399 +0.152 -0.188 ± 0.066	5026	4 ACOSTA	05M CDF	$E_{cm}^{p\bar{p}} = 1.96$ TeV
0.14 +0.09 -0.09		5 ABRAMOWICZ16A	ZEUS	
0.144 +0.066 -0.058		6 ABT	16	
0.27 ± 0.13	1500	7 AKTAS	06 H1	$e^\pm p \rightarrow \bar{\nu}_e(\nu_e)X$, $\sqrt{s} \approx 300$ GeV

• • • We do not use the following data for averages, fits, limits, etc. • • •

¹ ANDREEV 18A obtain this result in a combined electroweak and QCD analysis using all deep-inelastic e^+p and e^-p neutral current and charged current scattering cross sections published by the H1 Collaboration, including data with longitudinally polarized lepton beams.

² ABAZOV 11D study $p\bar{p} \rightarrow Z/\gamma^* e^+e^-$ events using 5 fb⁻¹ data at $\sqrt{s} = 1.96$ TeV. The candidate events are selected by requiring two isolated electromagnetic showers with $E_T > 25$ GeV, at least one electron in the central region and the di-electron mass in the range 50–1000 GeV. From the forward-backward asymmetry, determined as a function of

the di-electron mass, they derive the axial and vector couplings of the u - and d -quarks and the value of $\sin^2\theta_{eff}^l = 0.2309 \pm 0.0008(\text{stat}) \pm 0.0006(\text{syst})$.

³ LEP-SLC 06 is a combination of the results from LEP and SLC experiments using light quark tagging. s - and d -quark couplings are assumed to be identical.

⁴ ACOSTA 05M determine the forward-backward asymmetry of e^+e^- pairs produced via $q\bar{q} \rightarrow Z/\gamma^* \rightarrow e^+e^-$ in 15 M(e^+e^-) effective mass bins ranging from 40 GeV to 600 GeV. These results are used to obtain the vector and axial-vector couplings of the Z to the light quarks, assuming the electron couplings are as predicted by the Standard Model. Higher order radiative corrections have not been taken into account.

⁵ ABRAMOWICZ 16A determine the Z^0 couplings to u - and d -quarks using the ZEUS polarised data from Run II together with the unpolarised data from both ZEUS and H1 Collaborations for Run I and unpolarised H1 data from Run II.

⁶ ABT 16 determine the Z^0 couplings to u - and d -quarks using the same techniques and data as ABRAMOWICZ 16A but additionally use the published H1 polarised data.

⁷ AKTAS 06 fit the neutral current ($1.5 \leq Q^2 \leq 30,000$ GeV²) and charged current ($1.5 \leq Q^2 \leq 15,000$ GeV²) differential cross sections. In the determination of the u -quark couplings the electron and d -quark couplings are fixed to their standard model values.

 g_V^d

VALUE	EVTS	DOCUMENT ID	TECN	COMMENT
-0.38 ± 0.04 -0.05 OUR AVERAGE				
-0.488 ± 0.092		1 ANDREEV	18A H1	$e^\pm p$
-0.351 ± 0.251	156k	2 ABAZOV	11D D0	$E_{cm}^{p\bar{p}} = 1.97$ TeV
-0.33 +0.05 -0.07		3 LEP-SLC	06	$E_{cm}^{ee} = 88-94$ GeV
-0.226 +0.635 -0.290 ± 0.090	5026	4 ACOSTA	05M CDF	$E_{cm}^{p\bar{p}} = 1.96$ TeV
-0.41 +0.25 -0.20		5 ABRAMOWICZ16A	ZEUS	
-0.503 +0.171 -0.103		6 ABT	16	
-0.33 ± 0.33	1500	7 AKTAS	06 H1	$e^\pm p \rightarrow \bar{\nu}_e(\nu_e)X$, $\sqrt{s} \approx 300$ GeV

¹ ANDREEV 18A obtain this result in a combined electroweak and QCD analysis using all deep-inelastic e^+p and e^-p neutral current and charged current scattering cross sections published by the H1 Collaboration, including data with longitudinally polarized lepton beams.

² ABAZOV 11D study $p\bar{p} \rightarrow Z/\gamma^* e^+e^-$ events using 5 fb⁻¹ data at $\sqrt{s} = 1.96$ TeV. The candidate events are selected by requiring two isolated electromagnetic showers with $E_T > 25$ GeV, at least one electron in the central region and the di-electron mass in the range 50–1000 GeV. From the forward-backward asymmetry, determined as a function of the di-electron mass, they derive the axial and vector couplings of the u - and d -quarks and the value of $\sin^2\theta_{eff}^l = 0.2309 \pm 0.0008(\text{stat}) \pm 0.0006(\text{syst})$.

³ LEP-SLC 06 is a combination of the results from LEP and SLC experiments using light quark tagging. s - and d -quark couplings are assumed to be identical.

⁴ ACOSTA 05M determine the forward-backward asymmetry of e^+e^- pairs produced via $q\bar{q} \rightarrow Z/\gamma^* \rightarrow e^+e^-$ in 15 M(e^+e^-) effective mass bins ranging from 40 GeV to 600 GeV. These results are used to obtain the vector and axial-vector couplings of the Z to the light quarks, assuming the electron couplings are as predicted by the Standard Model. Higher order radiative corrections have not been taken into account.

⁵ ABRAMOWICZ 16A determine the Z^0 couplings to u - and d -quarks using the ZEUS polarised data from Run II together with the unpolarised data from both ZEUS and H1 Collaborations for Run I and unpolarised H1 data from Run II.

⁶ ABT 16 determine the Z^0 couplings to u - and d -quarks using the same techniques and data as ABRAMOWICZ 16A but additionally use the published H1 polarised data.

⁷ AKTAS 06 fit the neutral current ($1.5 \leq Q^2 \leq 30,000$ GeV²) and charged current ($1.5 \leq Q^2 \leq 15,000$ GeV²) differential cross sections. In the determination of the d -quark couplings the electron and u -quark couplings are fixed to their standard model values.

Z AXIAL-VECTOR COUPLINGS

These quantities are the effective axial-vector couplings of the Z to charged leptons and quarks. Their magnitude is derived from a measurement of the Z lineshape and the forward-backward lepton asymmetries as a function of energy around the Z mass. The relative sign among the vector to axial-vector couplings is obtained from a measurement of the Z asymmetry parameters, A_e , A_μ , and A_τ . By convention the sign of g_A^e is fixed to be negative (and opposite to that of g_V^e obtained using ν_e scattering measurements). For the light quarks, the sign of the couplings is assigned consistently with this assumption. The LEP/SLD-based fit values quoted below correspond to global nine- or five-parameter fits to lineshape, lepton forward-backward asymmetry, and A_e , A_μ , and A_τ measurements. See the note "The Z boson" and ref. LEP-SLC 06 for details. Where $p\bar{p}$ and $e p$ data is quoted, OUR FIT value corresponds to a weighted average of this with the LEP/SLD fit result.

 g_A^e

VALUE	EVTS	DOCUMENT ID	TECN	COMMENT
-0.50111 ± 0.00035 OUR FIT				
-0.528 ± 0.123 ± 0.059	5026	1 ACOSTA	05M CDF	$E_{cm}^{p\bar{p}} = 1.96$ TeV
-0.50062 ± 0.00062	137.0k	2 ABBIENDI	01o OPAL	$E_{cm}^{ee} = 88-94$ GeV
-0.5015 ± 0.0007	124.4k	3 ACCIARRI	00c L3	$E_{cm}^{ee} = 88-94$ GeV
-0.50166 ± 0.00057		BARATE	00c ALEP	$E_{cm}^{ee} = 88-94$ GeV
-0.4977 ± 0.0045		4 ABE	95j SLD	$E_{cm}^{ee} = 91.31$ GeV

¹ ACOSTA 05M determine the forward-backward asymmetry of e^+e^- pairs produced via $q\bar{q} \rightarrow Z/\gamma^* \rightarrow e^+e^-$ in 15 M(e^+e^-) effective mass bins ranging from 40 GeV to 600

Gauge & Higgs Boson Particle Listings

Z

GeV. These results are used to obtain the vector and axial-vector couplings of the Z to e^+e^- , assuming the quark couplings are as predicted by the standard model. Higher order radiative corrections have not been taken into account.

- ² ABBIENDI 01o use their measurement of the τ polarization in addition to the lineshape and forward-backward lepton asymmetries.
³ ACCIARRI 00c use their measurement of the τ polarization in addition to forward-backward lepton asymmetries.
⁴ ABE 95j obtain this result combining polarized Bhabha results with the A_{LR} measurement of ABE 94c. The Bhabha results alone give $-0.4968 \pm 0.0039 \pm 0.0027$.

g_A^u	VALUE	EVTS	DOCUMENT ID	TECN	COMMENT
	-0.50120 ± 0.00054				OUR FIT
	-0.50117 ± 0.00099	182.8k	¹ ABBIENDI 01o	OPAL	$E_{cm}^{ee} = 88-94$ GeV
	-0.5009 ± 0.0014	113.4k	² ACCIARRI 00c	L3	$E_{cm}^{ee} = 88-94$ GeV
	-0.50046 ± 0.00093		BARATE 00c	ALEP	$E_{cm}^{ee} = 88-94$ GeV
•••	We do not use the following data for averages, fits, limits, etc. •••				
	-0.520 ± 0.015	66143	³ ABBIENDI 01k	OPAL	$E_{cm}^{ee} = 89-93$ GeV

- ¹ ABBIENDI 01o use their measurement of the τ polarization in addition to the lineshape and forward-backward lepton asymmetries.
² ACCIARRI 00c use their measurement of the τ polarization in addition to forward-backward lepton asymmetries.
³ ABBIENDI 01k obtain this from an angular analysis of the muon pair asymmetry which takes into account effects of initial state radiation on an event by event basis and of initial-final state interference.

g_A^s	VALUE	EVTS	DOCUMENT ID	TECN	COMMENT
	-0.50204 ± 0.00064				OUR FIT
	-0.50165 ± 0.00124	151.5k	¹ ABBIENDI 01o	OPAL	$E_{cm}^{ee} = 88-94$ GeV
	-0.5023 ± 0.0017	103.0k	² ACCIARRI 00c	L3	$E_{cm}^{ee} = 88-94$ GeV
	-0.50216 ± 0.00100		BARATE 00c	ALEP	$E_{cm}^{ee} = 88-94$ GeV

- ¹ ABBIENDI 01o use their measurement of the τ polarization in addition to the lineshape and forward-backward lepton asymmetries.
² ACCIARRI 00c use their measurement of the τ polarization in addition to forward-backward lepton asymmetries.

g_A^c	VALUE	EVTS	DOCUMENT ID	TECN	COMMENT
	-0.50123 ± 0.00026				OUR FIT
	-0.50089 ± 0.00045	471.3k	¹ ABBIENDI 01o	OPAL	$E_{cm}^{ee} = 88-94$ GeV
	-0.5007 ± 0.0005	379.4k	ABREU 00f	DLPH	$E_{cm}^{ee} = 88-94$ GeV
	-0.50153 ± 0.00053	340.8k	² ACCIARRI 00c	L3	$E_{cm}^{ee} = 88-94$ GeV
	-0.50150 ± 0.00046	500k	BARATE 00c	ALEP	$E_{cm}^{ee} = 88-94$ GeV

- ¹ ABBIENDI 01o use their measurement of the τ polarization in addition to the lineshape and forward-backward lepton asymmetries.
² ACCIARRI 00c use their measurement of the τ polarization in addition to forward-backward lepton asymmetries.

g_A^d	VALUE	EVTS	DOCUMENT ID	TECN	COMMENT
	0.519 ± 0.028				OUR AVERAGE
	0.548 ± 0.036		¹ ANDREEV 18A	H1	$e^\pm p$
	0.501 ± 0.110	156k	² ABAZOV 11D	D0	$E_{cm}^{pp} = 1.97$ TeV
	0.47 ± 0.05		³ LEP-SLC 06		$E_{cm}^{ee} = 88-94$ GeV
	0.441 ± 0.207	± 0.067	⁴ ACOSTA 05M	CDF	$E_{cm}^{pp} = 1.96$ TeV
	-0.173	5026			
•••	We do not use the following data for averages, fits, limits, etc. •••				
	0.50 ± 0.12		⁵ ABRAMOWICZ16A	ZEUS	
	0.532 ± 0.107		⁶ ABT 16		
	0.57 ± 0.08	1500	⁷ AKTAS 06	H1	$e^\pm p \rightarrow \bar{\nu}_e(\nu_e)X$, $\sqrt{s} \approx 300$ GeV

- ¹ ANDREEV 18A obtain this result in a combined electroweak and QCD analysis using all deep-inelastic e^+p and e^-p neutral current and charged current scattering cross sections published by the H1 Collaboration, including data with longitudinally polarized lepton beams.
² ABAZOV 11D study $p\bar{p} \rightarrow Z/\gamma^* e^+e^-$ events using 5 fb⁻¹ data at $\sqrt{s} = 1.96$ TeV. The candidate events are selected by requiring two isolated electromagnetic showers with $E_T > 25$ GeV, at least one electron in the central region and the di-electron mass in the range 50–1000 GeV. From the forward-backward asymmetry, determined as a function of the di-electron mass, they derive the axial and vector couplings of the u - and d -quarks and the value of $\sin^2\theta_{eff}^l = 0.2309 \pm 0.0008(\text{stat}) \pm 0.0006(\text{syst})$.
³ LEP-SLC 06 is a combination of the results from LEP and SLC experiments using light quark tagging. s - and d -quark couplings are assumed to be identical.
⁴ ACOSTA 05M determine the forward-backward asymmetry of e^+e^- pairs produced via $q\bar{q} \rightarrow Z/\gamma^* \rightarrow e^+e^-$ in 15 M(e^+e^-) effective mass bins ranging from 40 GeV to 600 GeV. These results are used to obtain the vector and axial-vector couplings of the Z to the light quarks, assuming the electron couplings are as predicted by the Standard Model. Higher order radiative corrections have not been taken into account.
⁵ ABRAMOWICZ 16A determine the Z⁰ couplings to u - and d -quarks using the ZEUS polarised data from Run II together with the unpolarised data from both ZEUS and H1 Collaborations for Run I and unpolarised H1 data from Run II.
⁶ ABT 16 determine the Z⁰ couplings to u - and d -quarks using the same techniques and data as ABRAMOWICZ 16A but additionally use the published H1 polarised data.
⁷ AKTAS 06 fit the neutral current ($1.5 \leq Q^2 \leq 30,000$ GeV²) and charged current ($1.5 \leq Q^2 \leq 15,000$ GeV²) differential cross sections. In the determination of the u -quark couplings the electron and d -quark couplings are fixed to their standard model values.

g_A^d	VALUE	EVTS	DOCUMENT ID	TECN	COMMENT
	-0.527 ± 0.040				OUR AVERAGE
	-0.619 ± 0.108		¹ ANDREEV 18A	H1	$e^\pm p$
	-0.497 ± 0.165	156k	² ABAZOV 11D	D0	$E_{cm}^{pp} = 1.97$ TeV
	-0.52 ± 0.05		³ LEP-SLC 06		$E_{cm}^{ee} = 88-94$ GeV
	-0.016 ± 0.346	± 0.091	⁴ ACOSTA 05M	CDF	$E_{cm}^{pp} = 1.96$ TeV
	-0.536	5026			
•••	We do not use the following data for averages, fits, limits, etc. •••				
	-0.56 ± 0.41		⁵ ABRAMOWICZ16A	ZEUS	
	-0.15				
	-0.409 ± 0.373		⁶ ABT 16		
	-0.213				
	-0.80 ± 0.24	1500	⁷ AKTAS 06	H1	$e^\pm p \rightarrow \bar{\nu}_e(\nu_e)X$, $\sqrt{s} \approx 300$ GeV

- ¹ ANDREEV 18A obtain this result in a combined electroweak and QCD analysis using all deep-inelastic e^+p and e^-p neutral current and charged current scattering cross sections published by the H1 Collaboration, including data with longitudinally polarized lepton beams.
² ABAZOV 11D study $p\bar{p} \rightarrow Z/\gamma^* e^+e^-$ events using 5 fb⁻¹ data at $\sqrt{s} = 1.96$ TeV. The candidate events are selected by requiring two isolated electromagnetic showers with $E_T > 25$ GeV, at least one electron in the central region and the di-electron mass in the range 50–1000 GeV. From the forward-backward asymmetry, determined as a function of the di-electron mass, they derive the axial and vector couplings of the u - and d -quarks and the value of $\sin^2\theta_{eff}^l = 0.2309 \pm 0.0008(\text{stat}) \pm 0.0006(\text{syst})$.
³ LEP-SLC 06 is a combination of the results from LEP and SLC experiments using light quark tagging. s - and d -quark couplings are assumed to be identical.
⁴ ACOSTA 05M determine the forward-backward asymmetry of e^+e^- pairs produced via $q\bar{q} \rightarrow Z/\gamma^* \rightarrow e^+e^-$ in 15 M(e^+e^-) effective mass bins ranging from 40 GeV to 600 GeV. These results are used to obtain the vector and axial-vector couplings of the Z to the light quarks, assuming the electron couplings are as predicted by the Standard Model. Higher order radiative corrections have not been taken into account.
⁵ ABRAMOWICZ 16A determine the Z⁰ couplings to u - and d -quarks using the ZEUS polarised data from Run II together with the unpolarised data from both ZEUS and H1 Collaborations for Run I and unpolarised H1 data from Run II.
⁶ ABT 16 determine the Z⁰ couplings to u - and d -quarks using the same techniques and data as ABRAMOWICZ 16A but additionally use the published H1 polarised data.
⁷ AKTAS 06 fit the neutral current ($1.5 \leq Q^2 \leq 30,000$ GeV²) and charged current ($1.5 \leq Q^2 \leq 15,000$ GeV²) differential cross sections. In the determination of the d -quark couplings the electron and u -quark couplings are fixed to their standard model values.

Z COUPLINGS TO NEUTRAL LEPTONS

Averaging over neutrino species, the invisible Z decay width determines the effective neutrino coupling $g^{\nu e}$. For $g^{\nu e}$ and $g^{\nu\mu}$, $\nu_e e$ and $\nu_\mu e$ scattering results are combined with g_A^e and g_V^e measurements at the Z mass to obtain $g^{\nu e}$ and $g^{\nu\mu}$ following NOVIKOV 93c.

$g^{\nu e}$	VALUE	DOCUMENT ID	COMMENT
	0.50076 ± 0.00076	¹ LEP-SLC 06	$E_{cm}^{ee} = 88-94$ GeV

- ¹ From invisible Z-decay width.

$g^{\nu e}$	VALUE	DOCUMENT ID	TECN	COMMENT
	0.528 ± 0.085	¹ VILAIN 94	CHM2	From $\nu_\mu e$ and $\nu_e e$ scattering
	1.05 ± 0.15			
	-0.18			

- ¹ VILAIN 94 derive this value from their value of $g^{\nu\mu}$ and their ratio $g^{\nu e}/g^{\nu\mu} = 1.05 \pm 0.15 - 0.18$.

$g^{\nu\mu}$	VALUE	DOCUMENT ID	TECN	COMMENT
	0.502 ± 0.017	¹ VILAIN 94	CHM2	From $\nu_\mu e$ scattering

- ¹ VILAIN 94 derive this value from their measurement of the couplings $g_A^{e\nu\mu} = -0.503 \pm 0.017$ and $g_V^{e\nu\mu} = -0.035 \pm 0.017$ obtained from $\nu_\mu e$ scattering. We have re-evaluated this value using the current PDG values for g_A^e and g_V^e .

Z ASYMMETRY PARAMETERS

For each fermion-antifermion pair coupling to the Z these quantities are defined as

$$A_f = \frac{2g_V^f g_A^f}{(g_V^f)^2 + (g_A^f)^2}$$

where g_V^f and g_A^f are the effective vector and axial-vector couplings. For their relation to the various lepton asymmetries see the note "The Z boson" and ref. LEP-SLC 06.

A_e

Using polarized beams, this quantity can also be measured as $(\sigma_L - \sigma_R)/(\sigma_L + \sigma_R)$, where σ_L and σ_R are the e^+e^- production cross sections for Z bosons produced with left-handed and right-handed electrons respectively.

VALUE	EVTS	DOCUMENT ID	TECN	COMMENT
0.1515 ± 0.0019 OUR AVERAGE				
0.1454 ± 0.0108 ± 0.0036	144810	¹ ABBIENDI	01o OPAL	$E_{cm}^{ee} = 88-94$ GeV
0.1516 ± 0.0021	559000	² ABE	01B SLD	$E_{cm}^{ee} = 91.24$ GeV
0.1504 ± 0.0068 ± 0.0008		³ HEISTER	01 ALEP	$E_{cm}^{ee} = 88-94$ GeV
0.1382 ± 0.0116 ± 0.0005	105000	⁴ ABREU	00E DLPH	$E_{cm}^{ee} = 88-94$ GeV
0.1678 ± 0.0127 ± 0.0030	137092	⁵ ACCIARRI	98H L3	$E_{cm}^{ee} = 88-94$ GeV
0.162 ± 0.041 ± 0.014	89838	⁶ ABE	97 SLD	$E_{cm}^{ee} = 91.27$ GeV
0.202 ± 0.038 ± 0.008		⁷ ABE	95J SLD	$E_{cm}^{ee} = 91.31$ GeV

¹ ABBIENDI 01o fit for A_e and A_τ from measurements of the τ polarization at varying τ production angles. The correlation between A_e and A_τ is less than 0.03.

² ABE 01B use the left-right production and left-right forward-backward decay asymmetries in leptonic Z decays to obtain a value of 0.1544 ± 0.0060 . This is combined with left-right production asymmetry measurement using hadronic Z decays (ABE 00B) to obtain the quoted value.

³ HEISTER 01 obtain this result fitting the τ polarization as a function of the polar production angle of the τ .

⁴ ABREU 00E obtain this result fitting the τ polarization as a function of the polar τ production angle. This measurement is a combination of different analyses (exclusive τ decay modes, inclusive hadronic 1-prong reconstruction, and a neural network analysis).

⁵ Derived from the measurement of forward-backward τ polarization asymmetry.

⁶ ABE 97 obtain this result from a measurement of the observed left-right charge asymmetry, $A_Q^{obs} = 0.225 \pm 0.056 \pm 0.019$, in hadronic Z decays. If they combine this value of A_Q^{obs} with their earlier measurement of A_{LR}^{obs} they determine A_e to be $0.1574 \pm 0.0197 \pm 0.0067$ independent of the beam polarization.

⁷ ABE 95J obtain this result from polarized Bhabha scattering.

A_μ

This quantity is directly extracted from a measurement of the left-right forward-backward asymmetry in $\mu^+ \mu^-$ production at SLC using a polarized electron beam. This double asymmetry eliminates the dependence on the Z-e-e coupling parameter A_e .

VALUE	EVTS	DOCUMENT ID	TECN	COMMENT
0.142 ± 0.015				
0.142 ± 0.015	16844	¹ ABE	01B SLD	$E_{cm}^{ee} = 91.24$ GeV
0.153 ± 0.012	1.7M	² AAD	15BT ATLS	$E_{cm}^{pp} = 7$ TeV

• • • We do not use the following data for averages, fits, limits, etc. • • •

¹ ABE 01B obtain this direct measurement using the left-right production and left-right forward-backward polar angle asymmetries in $\mu^+ \mu^-$ decays of the Z boson obtained with a polarized electron beam.

² AAD 15BT study $pp \rightarrow Z \rightarrow \ell^+ \ell^-$ events where ℓ is an electron or a muon in the dilepton mass region 70–1000 GeV. The background in the Z peak region is estimated to be < 1% for the muon channel. The muon asymmetry parameter is derived from the measured forward-backward asymmetry assuming the value of the quark asymmetry parameter from the SM. For this reason it is not used in the average.

A_τ

The LEP Collaborations derive this quantity from the measurement of the τ polarization in $Z \rightarrow \tau^+ \tau^-$. The SLD Collaboration directly extracts this quantity from its measured left-right forward-backward asymmetry in $Z \rightarrow \tau^+ \tau^-$ produced using a polarized e^- beam. This double asymmetry eliminates the dependence on the Z-e-e coupling parameter A_e .

VALUE	EVTS	DOCUMENT ID	TECN	COMMENT
0.143 ± 0.004 OUR AVERAGE				
0.1456 ± 0.0076 ± 0.0057	144810	¹ ABBIENDI	01o OPAL	$E_{cm}^{ee} = 88-94$ GeV
0.136 ± 0.015	16083	² ABE	01B SLD	$E_{cm}^{ee} = 91.24$ GeV
0.1451 ± 0.0052 ± 0.0029		³ HEISTER	01 ALEP	$E_{cm}^{ee} = 88-94$ GeV
0.1359 ± 0.0079 ± 0.0055	105000	⁴ ABREU	00E DLPH	$E_{cm}^{ee} = 88-94$ GeV
0.1476 ± 0.0088 ± 0.0062	137092	ACCIARRI	98H L3	$E_{cm}^{ee} = 88-94$ GeV

¹ ABBIENDI 01o fit for A_e and A_τ from measurements of the τ polarization at varying τ production angles. The correlation between A_e and A_τ is less than 0.03.

² ABE 01B obtain this direct measurement using the left-right production and left-right forward-backward polar angle asymmetries in $\tau^+ \tau^-$ decays of the Z boson obtained with a polarized electron beam.

³ HEISTER 01 obtain this result fitting the τ polarization as a function of the polar production angle of the τ .

⁴ ABREU 00E obtain this result fitting the τ polarization as a function of the polar τ production angle. This measurement is a combination of different analyses (exclusive τ decay modes, inclusive hadronic 1-prong reconstruction, and a neural network analysis).

A_S

The SLD Collaboration directly extracts this quantity by a simultaneous fit to four measured s-quark polar angle distributions corresponding to two states of e^- polarization (positive and negative) and to the $K^+ K^-$ and $K_S^0 K_S^0$ strange particle tagging modes in the hadronic final states.

VALUE	EVTS	DOCUMENT ID	TECN	COMMENT
0.895 ± 0.066 ± 0.062				
0.895 ± 0.066 ± 0.062	2870	¹ ABE	00D SLD	$E_{cm}^{ee} = 91.2$ GeV

¹ ABE 00D tag $Z \rightarrow s\bar{s}$ events by an absence of B or D hadrons and the presence in each hemisphere of a high momentum K^\pm or K_S^0 .

A_C

This quantity is directly extracted from a measurement of the left-right forward-backward asymmetry in $c\bar{c}$ production at SLC using polarized electron beam. This double asymmetry eliminates the dependence on the Z-e-e coupling parameter A_e . OUR FIT is obtained by a simultaneous fit to several c- and b-quark measurements as explained in the note "The Z boson" and ref. LEP-SLC 06.

VALUE	EVTS	DOCUMENT ID	TECN	COMMENT
0.670 ± 0.027 OUR FIT				
0.6712 ± 0.0224 ± 0.0157		¹ ABE	05 SLD	$E_{cm}^{ee} = 91.24$ GeV
0.583 ± 0.055 ± 0.055		² ABE	02G SLD	$E_{cm}^{ee} = 91.24$ GeV
0.688 ± 0.041		³ ABE	01c SLD	$E_{cm}^{ee} = 91.25$ GeV

• • • We do not use the following data for averages, fits, limits, etc. • • •

¹ ABE 05 use hadronic Z decays collected during 1996–98 to obtain an enriched sample of $c\bar{c}$ events tagging on the invariant mass of reconstructed secondary decay vertices. The charge of the underlying c-quark is obtained with an algorithm that takes into account the net charge of the vertex as well as the charge of tracks emanating from the vertex and identified as kaons. This yields (9970 events) $A_C = 0.6747 \pm 0.0290 \pm 0.0233$. Taking into account all correlations with earlier results reported in ABE 02G and ABE 01c, they obtain the quoted overall SLD result.

² ABE 02G tag b and c quarks through their semileptonic decays into electrons and muons. A maximum likelihood fit is performed to extract simultaneously A_b and A_c .

³ ABE 01c tag $Z \rightarrow c\bar{c}$ events using two techniques: exclusive reconstruction of D^{*+}, D^+ and D^0 mesons and the soft pion tag for $D^{*+} \rightarrow D^0 \pi^+$. The large background from D mesons produced in $b\bar{b}$ events is separated efficiently from the signal using precision vertex information. When combining the A_C values from these two samples, care is taken to avoid double counting of events common to the two samples, and common systematic errors are properly taken into account.

A_b

This quantity is directly extracted from a measurement of the left-right forward-backward asymmetry in $b\bar{b}$ production at SLC using polarized electron beam. This double asymmetry eliminates the dependence on the Z-e-e coupling parameter A_e . OUR FIT is obtained by a simultaneous fit to several c- and b-quark measurements as explained in the note "The Z boson" and ref. LEP-SLC 06.

VALUE	EVTS	DOCUMENT ID	TECN	COMMENT
0.923 ± 0.020 OUR FIT				
0.9170 ± 0.0147 ± 0.0145		¹ ABE	05 SLD	$E_{cm}^{ee} = 91.24$ GeV
0.907 ± 0.020 ± 0.024	48028	² ABE	03F SLD	$E_{cm}^{ee} = 91.24$ GeV
0.919 ± 0.030 ± 0.024		³ ABE	02G SLD	$E_{cm}^{ee} = 91.24$ GeV
0.855 ± 0.088 ± 0.102	7473	⁴ ABE	99L SLD	$E_{cm}^{ee} = 91.27$ GeV

• • • We do not use the following data for averages, fits, limits, etc. • • •

¹ ABE 05 use hadronic Z decays collected during 1996–98 to obtain an enriched sample of $b\bar{b}$ events tagging on the invariant mass of reconstructed secondary decay vertices. The charge of the underlying b-quark is obtained with an algorithm that takes into account the net charge of the vertex as well as the charge of tracks emanating from the vertex and identified as kaons. This yields (25917 events) $A_b = 0.9173 \pm 0.0184 \pm 0.0173$. Taking into account all correlations with earlier results reported in ABE 03F, ABE 02G and ABE 99L, they obtain the quoted overall SLD result.

² ABE 03F obtain an enriched sample of $b\bar{b}$ events tagging on the invariant mass of a 3-dimensional topologically reconstructed secondary decay. The charge of the underlying b quark is obtained using a self-calibrating track-charge method. For the 1996–1998 data sample they measure $A_b = 0.906 \pm 0.022 \pm 0.023$. The value quoted here is obtained combining the above with the result of ABE 98I (1993–1995 data sample).

³ ABE 02G tag b and c quarks through their semileptonic decays into electrons and muons. A maximum likelihood fit is performed to extract simultaneously A_b and A_c .

⁴ ABE 99L obtain an enriched sample of $b\bar{b}$ events tagging with an inclusive vertex mass cut. For distinguishing b and \bar{b} quarks they use the charge of identified K^\pm .

TRANSVERSE SPIN CORRELATIONS IN $Z \rightarrow \tau^+ \tau^-$

The correlations between the transverse spin components of $\tau^+ \tau^-$ produced in Z decays may be expressed in terms of the vector and axial-vector couplings:

$$C_{TT} = \frac{|g_A^\tau|^2 - |g_V^\tau|^2}{|g_A^\tau|^2 + |g_V^\tau|^2}$$

$$C_{TN} = -2 \frac{|g_A^\tau| |g_V^\tau|}{|g_A^\tau|^2 + |g_V^\tau|^2} \sin(\phi_{g_V^\tau} - \phi_{g_A^\tau})$$

C_{TT} refers to the transverse-transverse (within the collision plane) spin correlation and C_{TN} refers to the transverse-normal (to the collision plane) spin correlation.

The longitudinal τ polarization $P_\tau (= -A_\tau)$ is given by:

$$P_\tau = -2 \frac{|g_A^\tau| |g_V^\tau|}{|g_A^\tau|^2 + |g_V^\tau|^2} \cos(\phi_{g_V^\tau} - \phi_{g_A^\tau})$$

Here ϕ is the phase and the phase difference $\phi_{g_V^\tau} - \phi_{g_A^\tau}$ can be obtained using both the measurements of C_{TN} and P_τ .

C_{TT}

VALUE	EVTS	DOCUMENT ID	TECN	COMMENT
1.01 ± 0.12 OUR AVERAGE				
0.87 ± 0.20 ^{+0.10} _{-0.12}	9.1k	ABREU	97G DLPH	$E_{cm}^{ee} = 91.2$ GeV
1.06 ± 0.13 ± 0.05	120k	BARATE	97D ALEP	$E_{cm}^{ee} = 91.2$ GeV

Gauge & Higgs Boson Particle Listings

Z

C_{TN}	VALUE	EVTS	DOCUMENT ID	TECN	COMMENT
$0.08 \pm 0.13 \pm 0.04$	120k	1	BARATE	97D ALEP	$E_{cm}^e = 91.2$ GeV

¹ BARATE 97D combine their value of C_{TN} with the world average $P_\tau = -0.140 \pm 0.007$ to obtain $\tan(\Phi_{g_V^\tau} - \Phi_{g_A^\tau}) = -0.57 \pm 0.97$.

FORWARD-BACKWARD $e^+e^- \rightarrow f\bar{f}$ CHARGE ASYMMETRIES

These asymmetries are experimentally determined by tagging the respective lepton or quark flavor in e^+e^- interactions. Details of heavy flavor (c - or b -quark) tagging at LEP are described in the note on "The Z boson" and ref. LEP-SLC 06. The Standard Model predictions for LEP data have been (re)computed using the ZFITTER package (version 6.36) with input parameters $M_Z = 91.187$ GeV, $M_{top} = 174.3$ GeV, $M_{Higgs} = 150$ GeV, $\alpha_s = 0.119$, $\alpha^{(5)}(M_Z) = 1/128.877$ and the Fermi constant $G_F = 1.16637 \times 10^{-5}$ GeV⁻² (see the note on "The Z boson" for references). For non-LEP data the Standard Model predictions are as given by the authors of the respective publications.

 $A_{FB}^{(0,e)}$ CHARGE ASYMMETRY IN $e^+e^- \rightarrow e^+e^-$

OUR FIT is obtained using the fit procedure and correlations as determined by the LEP Electroweak Working Group (see the note "The Z boson" and ref. LEP-SLC 06). For the Z peak, we report the pole asymmetry defined by $(3/4)A_e^2$ as determined by the nine-parameter fit to cross-section and lepton forward-backward asymmetry data.

ASYMMETRY (%)	STD. MODEL	\sqrt{s} (GeV)	DOCUMENT ID	TECN
1.45 ± 0.25 OUR FIT				
0.89 ± 0.44	1.57	91.2	¹ ABBIENDI 01A	OPAL
1.71 ± 0.49	1.57	91.2	ABREU 00F	DLPH
1.06 ± 0.58	1.57	91.2	ACCIARRI 00C	L3
1.88 ± 0.34	1.57	91.2	² BARATE 00C	ALEP

¹ ABBIENDI 01A error includes approximately 0.38 due to statistics, 0.16 due to event selection systematics, and 0.18 due to the theoretical uncertainty in t -channel prediction.
² BARATE 00C error includes approximately 0.31 due to statistics, 0.06 due to experimental systematics, and 0.13 due to the theoretical uncertainty in t -channel prediction.

 $A_{FB}^{(0,\mu)}$ CHARGE ASYMMETRY IN $e^+e^- \rightarrow \mu^+\mu^-$

OUR FIT is obtained using the fit procedure and correlations as determined by the LEP Electroweak Working Group (see the note "The Z boson" and ref. LEP-SLC 06). For the Z peak, we report the pole asymmetry defined by $(3/4)A_e A_\mu$ as determined by the nine-parameter fit to cross-section and lepton forward-backward asymmetry data.

ASYMMETRY (%)	STD. MODEL	\sqrt{s} (GeV)	DOCUMENT ID	TECN
1.69 ± 0.13 OUR FIT				
1.59 ± 0.23	1.57	91.2	¹ ABBIENDI 01A	OPAL
1.65 ± 0.25	1.57	91.2	ABREU 00F	DLPH
1.88 ± 0.33	1.57	91.2	ACCIARRI 00C	L3
1.71 ± 0.24	1.57	91.2	² BARATE 00C	ALEP

• • • We do not use the following data for averages, fits, limits, etc. • • •

9 ± 30	-1.3	20	³ ABREU 95M	DLPH
7 ± 26	-8.3	40	³ ABREU 95M	DLPH
-11 ± 33	-24.1	57	³ ABREU 95M	DLPH
-62 ± 17	-44.6	69	³ ABREU 95M	DLPH
-56 ± 10	-63.5	79	³ ABREU 95M	DLPH
-13 ± 5	-34.4	87.5	³ ABREU 95M	DLPH
$-29.0 \pm 5.0 \pm 0.5$	-32.1	56.9	⁴ ABE 90I	VNS
$-9.9 \pm 1.5 \pm 0.5$	-9.2	35	HEGNER 90	JADE
0.05 ± 0.22	0.026	91.14	⁵ ABRAMS 89D	MRK2
-43.4 ± 17.0	-24.9	52.0	⁶ BACALA 89	AMY
-11.0 ± 16.5	-29.4	55.0	⁶ BACALA 89	AMY
-30.0 ± 12.4	-31.2	56.0	⁶ BACALA 89	AMY
-46.2 ± 14.9	-33.0	57.0	⁶ BACALA 89	AMY
-29 ± 13	-25.9	53.3	ADACHI 88C	TOPZ
$+5.3 \pm 5.0 \pm 0.5$	-1.2	14.0	ADEVA 88	MRKJ
$-10.4 \pm 1.3 \pm 0.5$	-8.6	34.8	ADEVA 88	MRKJ
$-12.3 \pm 5.3 \pm 0.5$	-10.7	38.3	ADEVA 88	MRKJ
$-15.6 \pm 3.0 \pm 0.5$	-14.9	43.8	ADEVA 88	MRKJ
-1.0 ± 6.0	-1.2	13.9	BRAUNSCH... 88D	TASS
$-9.1 \pm 2.3 \pm 0.5$	-8.6	34.5	BRAUNSCH... 88D	TASS
$-10.6 \pm 2.2 \pm 0.5$	-8.9	35.0	BRAUNSCH... 88D	TASS
$-17.6 \pm 4.4 \pm 0.5$	-15.2	43.6	BRAUNSCH... 88D	TASS
$-4.8 \pm 6.5 \pm 1.0$	-11.5	39	BEHREND 87C	CELL
$-18.8 \pm 4.5 \pm 1.0$	-15.5	44	BEHREND 87C	CELL
$+2.7 \pm 4.9$	-1.2	13.9	BARTEL 86C	JADE
$-11.1 \pm 1.8 \pm 1.0$	-8.6	34.4	BARTEL 86C	JADE
$-17.3 \pm 4.8 \pm 1.0$	-13.7	41.5	BARTEL 86C	JADE

$-22.8 \pm 5.1 \pm 1.0$	-16.6	44.8	BARTEL 86C	JADE
$-6.3 \pm 0.8 \pm 0.2$	-6.3	29	ASH 85	MAC
$-4.9 \pm 1.5 \pm 0.5$	-5.9	29	DERRICK 85	HRS
-7.1 ± 1.7	-5.7	29	LEVI 83	MRK2
-16.1 ± 3.2	-9.2	34.2	BRANDELIK 82C	TASS

¹ ABBIENDI 01A error is almost entirely on account of statistics.

² BARATE 00C error is almost entirely on account of statistics.

³ ABREU 95M perform this measurement using radiative muon-pair events associated with high-energy isolated photons.

⁴ ABE 90I measurements in the range $50 \leq \sqrt{s} \leq 60.8$ GeV.

⁵ ABRAMS 89D asymmetry includes both $9 \mu^+ \mu^-$ and $15 \tau^+ \tau^-$ events.

⁶ BACALA 89 systematic error is about 5%.

 $A_{FB}^{(0,\tau)}$ CHARGE ASYMMETRY IN $e^+e^- \rightarrow \tau^+\tau^-$

OUR FIT is obtained using the fit procedure and correlations as determined by the LEP Electroweak Working Group (see the note "The Z boson" and ref. LEP-SLC 06). For the Z peak, we report the pole asymmetry defined by $(3/4)A_e A_\tau$ as determined by the nine-parameter fit to cross-section and lepton forward-backward asymmetry data.

ASYMMETRY (%)	STD. MODEL	\sqrt{s} (GeV)	DOCUMENT ID	TECN
1.88 ± 0.17 OUR FIT				
1.45 ± 0.30	1.57	91.2	¹ ABBIENDI 01A	OPAL
2.41 ± 0.37	1.57	91.2	ABREU 00F	DLPH
2.60 ± 0.47	1.57	91.2	ACCIARRI 00C	L3
1.70 ± 0.28	1.57	91.2	² BARATE 00C	ALEP

• • • We do not use the following data for averages, fits, limits, etc. • • •

$-32.8 \pm 6.4 \pm 1.5$	-32.1	56.9	³ ABE 90I	VNS
$-8.1 \pm 2.0 \pm 0.6$	-9.2	35	HEGNER 90	JADE
-18.4 ± 19.2	-24.9	52.0	⁴ BACALA 89	AMY
-17.7 ± 26.1	-29.4	55.0	⁴ BACALA 89	AMY
-45.9 ± 16.6	-31.2	56.0	⁴ BACALA 89	AMY
-49.5 ± 18.0	-33.0	57.0	⁴ BACALA 89	AMY
-20 ± 14	-25.9	53.3	ADACHI 88C	TOPZ
$-10.6 \pm 3.1 \pm 1.5$	-8.5	34.7	ADEVA 88	MRKJ
$-8.5 \pm 6.6 \pm 1.5$	-15.4	43.8	ADEVA 88	MRKJ
$-6.0 \pm 2.5 \pm 1.0$	8.8	34.6	BARTEL 85F	JADE
$-11.8 \pm 4.6 \pm 1.0$	14.8	43.0	BARTEL 85F	JADE
$-5.5 \pm 1.2 \pm 0.5$	-0.063	29.0	FERNANDEZ 85A	MAC
-4.2 ± 2.0	0.057	29	LEVI 83	MRK2
-10.3 ± 5.2	-9.2	34.2	BEHREND 82	CELL
-0.4 ± 6.6	-9.1	34.2	BRANDELIK 82C	TASS

¹ ABBIENDI 01A error includes approximately 0.26 due to statistics and 0.14 due to event selection systematics.

² BARATE 00C error includes approximately 0.26 due to statistics and 0.11 due to experimental systematics.

³ ABE 90I measurements in the range $50 \leq \sqrt{s} \leq 60.8$ GeV.

⁴ BACALA 89 systematic error is about 5%.

 $A_{FB}^{(0,\ell)}$ CHARGE ASYMMETRY IN $e^+e^- \rightarrow \ell^+\ell^-$

For the Z peak, we report the pole asymmetry defined by $(3/4)A_\ell^2$ as determined by the five-parameter fit to cross-section and lepton forward-backward asymmetry data assuming lepton universality. For details see the note "The Z boson" and ref. LEP-SLC 06.

ASYMMETRY (%)	STD. MODEL	\sqrt{s} (GeV)	DOCUMENT ID	TECN
1.71 ± 0.10 OUR FIT				
1.45 ± 0.17	1.57	91.2	¹ ABBIENDI 01A	OPAL
1.87 ± 0.19	1.57	91.2	ABREU 00F	DLPH
1.92 ± 0.24	1.57	91.2	ACCIARRI 00C	L3
1.73 ± 0.16	1.57	91.2	² BARATE 00C	ALEP

¹ ABBIENDI 01A error includes approximately 0.15 due to statistics, 0.06 due to event selection systematics, and 0.03 due to the theoretical uncertainty in t -channel prediction.

² BARATE 00C error includes approximately 0.15 due to statistics, 0.04 due to experimental systematics, and 0.02 due to the theoretical uncertainty in t -channel prediction.

 $A_{FB}^{(0,u)}$ CHARGE ASYMMETRY IN $e^+e^- \rightarrow u\bar{u}$

ASYMMETRY (%)	STD. MODEL	\sqrt{s} (GeV)	DOCUMENT ID	TECN
$4.0 \pm 6.7 \pm 2.8$	7.2	91.2	¹ ACKERSTAFF 97T	OPAL

¹ ACKERSTAFF 97T measure the forward-backward asymmetry of various fast hadrons made of light quarks. Then using SU(2) isospin symmetry and flavor independence for down and strange quarks authors solve for the different quark types.

 $A_{FB}^{(0,s)}$ CHARGE ASYMMETRY IN $e^+e^- \rightarrow s\bar{s}$

The s -quark asymmetry is derived from measurements of the forward-backward asymmetry of fast hadrons containing an s quark.

ASYMMETRY (%)	STD. MODEL	\sqrt{s} (GeV)	DOCUMENT ID	TECN
9.8 ± 1.1 OUR AVERAGE				
$10.08 \pm 1.13 \pm 0.40$	10.1	91.2	¹ ABREU 00B	DLPH

6.8 ± 3.5 ± 1.1 10.1 91.2 2 ACKERSTAFF 97T OPAL

¹ ABREU 00B tag the presence of an *s* quark requiring a high-momentum-identified charged kaon. The *s*-quark pole asymmetry is extracted from the charged-kaon asymmetry taking the expected *d*- and *u*-quark asymmetries from the Standard Model and using the measured values for the *c*- and *b*-quark asymmetries.

² ACKERSTAFF 97T measure the forward-backward asymmetry of various fast hadrons made of light quarks. Then using SU(2) isospin symmetry and flavor independence for down and strange quarks authors solve for the different quark types. The value reported here corresponds then to the forward-backward asymmetry for "down-type" quarks.

———— $A_{FB}^{(0,c)}$ CHARGE ASYMMETRY IN $e^+e^- \rightarrow c\bar{c}$ ————

OUR FIT, which is obtained by a simultaneous fit to several *c*- and *b*-quark measurements as explained in the note "The Z boson" and ref. LEP-SLC 06, refers to the **Z pole** asymmetry. The experimental values, on the other hand, correspond to the measurements carried out at the respective energies.

ASYMMETRY (%)	STD. MODEL	\sqrt{s} (GeV)	DOCUMENT ID	TECN
7.07 ± 0.35 OUR FIT				
6.31 ± 0.93 ± 0.65	6.35	91.26	¹ ABDALLAH 04F DLPH	
5.68 ± 0.54 ± 0.39	6.3	91.25	² ABBIENDI 03P OPAL	
6.45 ± 0.57 ± 0.37	6.10	91.21	³ HEISTER 02H ALEP	
6.59 ± 0.94 ± 0.35	6.2	91.235	⁴ ABREU 99Y DLPH	
6.3 ± 0.9 ± 0.3	6.1	91.22	⁵ BARATE 98O ALEP	
6.3 ± 1.2 ± 0.6	6.1	91.22	⁶ ALEXANDER 97C OPAL	
8.3 ± 3.8 ± 2.7	6.2	91.24	⁷ ADRIANI 92D L3	

• • • We do not use the following data for averages, fits, limits, etc. • • •

3.1 ± 3.5 ± 0.5	-3.5	89.43	¹ ABDALLAH 04F DLPH	
11.0 ± 2.8 ± 0.7	12.3	92.99	¹ ABDALLAH 04F DLPH	
-6.8 ± 2.5 ± 0.9	-3.0	89.51	² ABBIENDI 03P OPAL	
-14.6 ± 2.0 ± 0.8	12.2	92.95	² ABBIENDI 03P OPAL	
-12.4 ± 15.9 ± 2.0	-9.6	88.38	³ HEISTER 02H ALEP	
-2.3 ± 2.6 ± 0.2	-3.8	89.38	³ HEISTER 02H ALEP	
-0.3 ± 8.3 ± 0.6	0.9	90.21	³ HEISTER 02H ALEP	
10.6 ± 7.7 ± 0.7	9.6	92.05	³ HEISTER 02H ALEP	
11.9 ± 2.1 ± 0.6	12.2	92.94	³ HEISTER 02H ALEP	
12.1 ± 11.0 ± 1.0	14.2	93.90	³ HEISTER 02H ALEP	
-4.96 ± 3.68 ± 0.53	-3.5	89.434	⁴ ABREU 99Y DLPH	
11.80 ± 3.18 ± 0.62	12.3	92.990	⁴ ABREU 99Y DLPH	
-1.0 ± 4.3 ± 1.0	-3.9	89.37	⁵ BARATE 98O ALEP	
11.0 ± 3.3 ± 0.8	12.3	92.96	⁵ BARATE 98O ALEP	
3.9 ± 5.1 ± 0.9	-3.4	89.45	⁶ ALEXANDER 97C OPAL	
15.8 ± 4.1 ± 1.1	12.4	93.00	⁶ ALEXANDER 97C OPAL	
-12.9 ± 7.8 ± 5.5	-13.6	35	BEHREND 90D CELL	
7.7 ± 13.4 ± 5.0	-22.1	43	BEHREND 90D CELL	
-12.8 ± 4.4 ± 4.1	-13.6	35	ELSEN 90 JADE	
-10.9 ± 12.9 ± 4.6	-23.2	44	ELSEN 90 JADE	
-14.9 ± 6.7	-13.3	35	OULD-SAADAA 89 JADE	

¹ ABDALLAH 04F tag *b*- and *c*-quarks using semileptonic decays combined with charge flow information from the hemisphere opposite to the lepton. Enriched samples of $c\bar{c}$ and $b\bar{b}$ events are obtained using lifetime information.

² ABBIENDI 03P tag heavy flavors using events with one or two identified leptons. This allows the simultaneous fitting of the *b* and *c* quark forward-backward asymmetries as well as the average B^0 - \bar{B}^0 mixing.

³ HEISTER 02H measure simultaneously *b* and *c* quark forward-backward asymmetries using their semileptonic decays to tag the quark charge. The flavor separation is obtained with a discriminating multivariate analysis.

⁴ ABREU 99Y tag $Z \rightarrow b\bar{b}$ and $Z \rightarrow c\bar{c}$ events by an exclusive reconstruction of several *D* meson decay modes (D^{*+} , D^0 , and D^+ with their charge-conjugate states).

⁵ BARATE 98O tag $Z \rightarrow c\bar{c}$ events requiring the presence of high-momentum reconstructed D^{*+} , D^+ , or D^0 mesons.

⁶ ALEXANDER 97C identify the *b* and *c* events using a D/D^* tag.

⁷ ADRIANI 92D use both electron and muon semileptonic decays.

———— $A_{FB}^{(0,b)}$ CHARGE ASYMMETRY IN $e^+e^- \rightarrow b\bar{b}$ ————

OUR FIT, which is obtained by a simultaneous fit to several *c*- and *b*-quark measurements as explained in the note "The Z boson" and ref. LEP-SLC 06, refers to the **Z pole** asymmetry. The experimental values, on the other hand, correspond to the measurements carried out at the respective energies.

ASYMMETRY (%)	STD. MODEL	\sqrt{s} (GeV)	DOCUMENT ID	TECN
9.92 ± 0.16 OUR FIT				
9.58 ± 0.32 ± 0.14	9.68	91.231	¹ ABDALLAH 05 DLPH	
10.04 ± 0.56 ± 0.25	9.69	91.26	² ABDALLAH 04F DLPH	
9.72 ± 0.42 ± 0.15	9.67	91.25	³ ABBIENDI 03P OPAL	
9.77 ± 0.36 ± 0.18	9.69	91.26	⁴ ABBIENDI 02I OPAL	
9.52 ± 0.41 ± 0.17	9.59	91.21	⁵ HEISTER 02H ALEP	
10.00 ± 0.27 ± 0.11	9.63	91.232	⁶ HEISTER 01H ALEP	
7.62 ± 1.94 ± 0.85	9.64	91.235	⁷ ABREU 99Y DLPH	
9.60 ± 0.66 ± 0.33	9.69	91.26	⁸ ACCIARRI 99D L3	
9.31 ± 1.01 ± 0.55	9.65	91.24	⁹ ACCIARRI 98U L3	
9.4 ± 2.7 ± 2.2	9.61	91.22	¹⁰ ALEXANDER 97C OPAL	

• • • We do not use the following data for averages, fits, limits, etc. • • •

6.37 ± 1.43 ± 0.17	5.8	89.449	¹ ABDALLAH 05 DLPH	
10.41 ± 1.15 ± 0.24	12.1	92.990	¹ ABDALLAH 05 DLPH	
6.7 ± 2.2 ± 0.2	5.7	89.43	² ABDALLAH 04F DLPH	
11.2 ± 1.8 ± 0.2	12.1	92.99	² ABDALLAH 04F DLPH	
4.7 ± 1.8 ± 0.1	5.9	89.51	³ ABBIENDI 03P OPAL	
10.3 ± 1.5 ± 0.2	12.0	92.95	³ ABBIENDI 03P OPAL	
5.82 ± 1.53 ± 0.12	5.9	89.50	⁴ ABBIENDI 02I OPAL	
12.21 ± 1.23 ± 0.25	12.0	92.91	⁴ ABBIENDI 02I OPAL	
-13.1 ± 13.5 ± 1.0	3.2	88.38	⁵ HEISTER 02H ALEP	
5.5 ± 1.9 ± 0.1	5.6	89.38	⁵ HEISTER 02H ALEP	
-0.4 ± 6.7 ± 0.8	7.5	90.21	⁵ HEISTER 02H ALEP	
11.1 ± 6.4 ± 0.5	11.0	92.05	⁵ HEISTER 02H ALEP	
10.4 ± 1.5 ± 0.3	12.0	92.94	⁵ HEISTER 02H ALEP	
13.8 ± 9.3 ± 1.1	12.9	93.90	⁵ HEISTER 02H ALEP	
4.36 ± 1.19 ± 0.11	5.8	89.472	⁶ HEISTER 01D ALEP	
11.72 ± 0.97 ± 0.11	12.0	92.950	⁶ HEISTER 01D ALEP	
5.67 ± 7.56 ± 1.17	5.7	89.434	⁷ ABREU 99Y DLPH	
8.82 ± 6.33 ± 1.22	12.1	92.990	⁷ ABREU 99Y DLPH	
6.11 ± 2.93 ± 0.43	5.9	89.50	⁸ ACCIARRI 99D L3	
13.71 ± 2.40 ± 0.44	12.2	93.10	⁸ ACCIARRI 99D L3	
4.95 ± 5.23 ± 0.40	5.8	89.45	⁹ ACCIARRI 98U L3	
11.37 ± 3.99 ± 0.65	12.1	92.99	⁹ ACCIARRI 98U L3	
-8.6 ± 10.8 ± 2.9	5.8	89.45	¹⁰ ALEXANDER 97C OPAL	
-2.1 ± 9.0 ± 2.6	12.1	93.00	¹⁰ ALEXANDER 97C OPAL	
-71 ± 34 ± 7	-58	58.3	SHIMONAKA 91 TOPZ	
-22.2 ± 7.7 ± 3.5	-26.0	35	BEHREND 90D CELL	
-49.1 ± 16.0 ± 5.0	-39.7	43	BEHREND 90D CELL	
-28 ± 11	-23	35	BRAUNSCH... 90 TASS	
-16.6 ± 7.7 ± 4.8	-24.3	35	ELSEN 90 JADE	
-33.6 ± 22.2 ± 5.2	-39.9	44	ELSEN 90 JADE	
3.4 ± 7.0 ± 3.5	-16.0	29.0	BAND 89 MAC	
-72 ± 28 ± 13	-56	55.2	SAGAWA 89 AMY	

¹ ABDALLAH 05 obtain an enriched samples of $b\bar{b}$ events using lifetime information. The quark (or antiquark) charge is determined with a neural network using the secondary vertex charge, the jet charge and particle identification.

² ABDALLAH 04F tag *b*- and *c*-quarks using semileptonic decays combined with charge flow information from the hemisphere opposite to the lepton. Enriched samples of $c\bar{c}$ and $b\bar{b}$ events are obtained using lifetime information.

³ ABBIENDI 03P tag heavy flavors using events with one or two identified leptons. This allows the simultaneous fitting of the *b* and *c* quark forward-backward asymmetries as well as the average B^0 - \bar{B}^0 mixing.

⁴ ABBIENDI 02I tag $Z^0 \rightarrow b\bar{b}$ decays using a combination of secondary vertex and lepton tags. The sign of the *b*-quark charge is determined using an inclusive tag based on jet, vertex, and kaon charges.

⁵ HEISTER 02H measure simultaneously *b* and *c* quark forward-backward asymmetries using their semileptonic decays to tag the quark charge. The flavor separation is obtained with a discriminating multivariate analysis.

⁶ HEISTER 01D tag $Z \rightarrow b\bar{b}$ events using the impact parameters of charged tracks complemented with information from displaced vertices, event shape variables, and lepton identification. The *b*-quark direction and charge is determined using the hemisphere charge method along with information from fast kaon tagging and charge estimators of primary and secondary vertices. The change in the quoted value due to variation of A_{FB}^c and R_b is given as $+0.103(A_{FB}^c - 0.0651) - 0.440(R_b - 0.21585)$.

⁷ ABREU 99Y tag $Z \rightarrow b\bar{b}$ and $Z \rightarrow c\bar{c}$ events by an exclusive reconstruction of several *D* meson decay modes (D^{*+} , D^0 , and D^+ with their charge-conjugate states).

⁸ ACCIARRI 99D tag $Z \rightarrow b\bar{b}$ events using high *p* and *p* \bar{T} leptons. The analysis determines simultaneously a mixing parameter $\chi_b = 0.1192 \pm 0.0068 \pm 0.0051$ which is used to correct the observed asymmetry.

⁹ ACCIARRI 98U tag $Z \rightarrow b\bar{b}$ events using lifetime and measure the jet charge using the hemisphere charge.

¹⁰ ALEXANDER 97C identify the *b* and *c* events using a D/D^* tag.

CHARGE ASYMMETRY IN $e^+e^- \rightarrow q\bar{q}$

Summed over five lighter flavors.

Experimental and Standard Model values are somewhat event-selection dependent. Standard Model expectations contain some assumptions on B^0 - \bar{B}^0 mixing and on other electroweak parameters.

ASYMMETRY (%)	STD. MODEL	\sqrt{s} (GeV)	DOCUMENT ID	TECN
-0.76 ± 0.12 ± 0.15		91.2	¹ ABREU 92I DLPH	
4.0 ± 0.4 ± 0.63	4.0	91.3	² ACTON 92L OPAL	
9.1 ± 1.4 ± 1.6	9.0	57.9	ADACHI 91 TOPZ	
-0.84 ± 0.15 ± 0.04		91	DECAMP 91B ALEP	
8.3 ± 2.9 ± 1.9	8.7	56.6	STUART 90 AMY	
11.4 ± 2.2 ± 2.1	8.7	57.6	ABE 89L VNS	
6.0 ± 1.3	5.0	34.8	GREENSHAW 89 JADE	
8.2 ± 2.9	8.5	43.6	GREENSHAW 89 JADE	

¹ ABREU 92I has 0.14 systematic error due to uncertainty of quark fragmentation.

² ACTON 92L use the weight function method on 259k selected $Z \rightarrow$ hadrons events. The systematic error includes a contribution of 0.2 due to B^0 - \bar{B}^0 mixing effect, 0.4 due to Monte Carlo (MC) fragmentation uncertainties and 0.3 due to MC statistics. ACTON 92L derive a value of $\sin^2\theta_W^{\text{eff}}$ to be $0.2321 \pm 0.0017 \pm 0.0028$.

Gauge & Higgs Boson Particle Listings

Z

CHARGE ASYMMETRY IN $p\bar{p} \rightarrow Z \rightarrow e^+e^-$

ASYMMETRY (%)	STD MODEL	\sqrt{s} (GeV)	DOCUMENT ID	TECN
••• We do not use the following data for averages, fits, limits, etc. •••				
5.2 ± 5.9 ± 0.4		91	ABE	91E CDF

ANOMALOUS ZZ γ , Z $\gamma\gamma$, AND ZZV COUPLINGS

Revised September 2013 by M.W. Gr unewald (U. College Dublin and U. Ghent) and A. Gurtu (Formerly Tata Inst.).

In on-shell $Z\gamma$ production, deviations from the Standard Model for the $Z\gamma\gamma^*$ and $Z\gamma Z^*$ couplings may be described in terms of eight parameters, h_i^V ($i = 1, 4; V = \gamma, Z$) [1]. The parameters h_i^γ describe the $Z\gamma\gamma^*$ couplings and the parameters h_i^Z the $Z\gamma Z^*$ couplings. In this formalism h_1^V and h_2^V lead to CP -violating and h_3^V and h_4^V to CP -conserving effects. All these anomalous contributions to the cross section increase rapidly with center-of-mass energy. In order to ensure unitarity, these parameters are usually described by a form-factor representation, $h_i^V(s) = h_{i0}^V/(1 + s/\Lambda^2)^n$, where Λ is the energy scale for the manifestation of a new phenomenon and n is a sufficiently large power. By convention one uses $n = 3$ for $h_{1,3}^V$ and $n = 4$ for $h_{2,4}^V$. Usually limits on h_i^V 's are put assuming some value of Λ , sometimes ∞ .

In on-shell ZZ production, deviations from the Standard Model for the $ZZ\gamma^*$ and ZZZ^* couplings may be described by means of four anomalous couplings f_i^V ($i = 4, 5; V = \gamma, Z$) [2]. As above, the parameters f_i^γ describe the $ZZ\gamma^*$ couplings and the parameters f_i^Z the ZZZ^* couplings. The anomalous couplings f_5^V lead to violation of C and P symmetries while f_4^V introduces CP violation. Also here, formfactors depending on a scale Λ are used.

All these couplings h_i^V and f_i^V are zero at tree level in the Standard Model; they are measured in e^+e^- , $p\bar{p}$ and pp collisions at LEP, Tevatron and LHC.

References

- U. Baur and E.L. Berger, Phys. Rev. **D47**, 4889 (1993).
- K. Hagiwara *et al.*, Nucl. Phys. **B282**, 253 (1987).

h_γ^V

Combining the LEP-2 results taking into account the correlations, the following 95% CL limits are derived [SCHAEL 13a]:

$$\begin{aligned} -0.12 < h_1^Z < +0.11, & \quad -0.07 < h_2^Z < +0.07, \\ -0.19 < h_3^Z < +0.06, & \quad -0.04 < h_4^Z < +0.13, \\ -0.05 < h_1^\gamma < +0.05, & \quad -0.04 < h_2^\gamma < +0.02, \\ -0.05 < h_3^\gamma < +0.00, & \quad +0.01 < h_4^\gamma < +0.05. \end{aligned}$$

Some of the recent results from the Tevatron and LHC experiments individually surpass the combined LEP-2 results in precision (see below).

VALUE	DOCUMENT ID	TECN	COMMENT
••• We do not use the following data for averages, fits, limits, etc. •••			
1 AAD	16Q ATLS	$E_{cm}^{p\bar{p}} = 8$ TeV	
2 KHACHATRY...16AE	CMS	$E_{cm}^{p\bar{p}} = 8$ TeV	
3 KHACHATRY...15AC	CMS	$E_{cm}^{p\bar{p}} = 8$ TeV	
4 CHATRCHYAN14AB	CMS	$E_{cm}^{p\bar{p}} = 7$ TeV	
5 AAD	13AN ATLS	$E_{cm}^{p\bar{p}} = 7$ TeV	
6 CHATRCHYAN13BI	CMS	$E_{cm}^{p\bar{p}} = 7$ TeV	
7 ABAZOV	12S D0	$E_{cm}^{p\bar{p}} = 1.96$ TeV	
8 AALTONEN	11S CDF	$E_{cm}^{p\bar{p}} = 1.96$ TeV	
9 CHATRCHYAN11M	CMS	$E_{cm}^{p\bar{p}} = 7$ TeV	

10 ABAZOV	09L D0	$E_{cm}^{p\bar{p}} = 1.96$ TeV
11 ABAZOV	07M D0	$E_{cm}^{p\bar{p}} = 1.96$ TeV
12 ABDALLAH	07C DLPH	$E_{cm}^{e\bar{e}} = 183$ –208 GeV
13 ACHARD	04H L3	$E_{cm}^{e\bar{e}} = 183$ –208 GeV
14 ABBIENDI,G	00C OPAL	$E_{cm}^{e\bar{e}} = 189$ GeV
15 ABBOTT	98M D0	$E_{cm}^{p\bar{p}} = 1.8$ TeV
16 ABREU	98K DLPH	$E_{cm}^{e\bar{e}} = 161, 172$ GeV

- AAD 16Q study $Z\gamma$ production in pp collisions. In events with no additional jets, 10268 (12738) Z decays to electron (muon) pairs are selected, with an expected background of 1291 ± 340 (1537 ± 408) events, as well as 1039 Z decays to neutrino pairs with an expected background of 450 ± 96 events. Analyzing the photon transverse momentum distribution above 250 GeV (400 GeV) for lepton (neutrino) events, yields the 95% C.L. limits: $-7.8 \times 10^{-4} < h_3^Z < 8.6 \times 10^{-4}$, $-3.0 \times 10^{-6} < h_4^Z < 2.9 \times 10^{-6}$, $-9.5 \times 10^{-4} < h_3^\gamma < 9.9 \times 10^{-4}$, $-3.2 \times 10^{-6} < h_4^\gamma < 3.2 \times 10^{-6}$.
- KHACHATRYAN 16AE determine the $Z\gamma \rightarrow \nu\bar{\nu}\gamma$ cross section by selecting events with a photon of $E_T > 145$ GeV and $\cancel{E}_T > 140$ GeV. 630 candidate events are observed with an expected SM background of 269 ± 26 . The E_T spectrum of the photon is used to set 95% C.L. limits as follows: $-1.5 \times 10^{-3} < h_3^Z < 1.6 \times 10^{-3}$, $-3.9 \times 10^{-6} < h_4^Z < 4.5 \times 10^{-6}$, $-1.1 \times 10^{-3} < h_3^\gamma < 0.9 \times 10^{-3}$, $-3.8 \times 10^{-6} < h_4^\gamma < 4.3 \times 10^{-6}$.
- KHACHATRYAN 15AC study $Z\gamma$ events in 8 TeV pp interactions, where the Z decays into 2 same-flavor, opposite sign leptons (e or μ) and a photon with $p_T > 15$ GeV. The p_T of a lepton is required to be > 20 GeV/ c , their effective mass > 50 GeV, and the photon should have a separation $\Delta R > 0.7$ with each lepton. The observed p_T distribution of the photons is used to extract the 95% C.L. limits: $-3.8 \times 10^{-3} < h_3^Z < 3.7 \times 10^{-3}$, $-3.1 \times 10^{-5} < h_4^Z < 3.0 \times 10^{-5}$, $-4.6 \times 10^{-3} < h_3^\gamma < 4.6 \times 10^{-3}$, $-3.6 \times 10^{-5} < h_4^\gamma < 3.5 \times 10^{-5}$.
- CHATRCHYAN 14AB measure $Z\gamma$ production cross section for $p_T^\gamma > 15$ GeV and $R(\ell\gamma) > 0.7$, which is the separation between the γ and the final state charged lepton (e or μ) in the azimuthal angle-pseudorapidity ($\phi - \eta$) plane. The di-lepton mass is required to be > 50 GeV. After background subtraction the number of $e\bar{e}\gamma$ and $\mu\mu\gamma$ events is determined to be 3160 ± 120 and 5030 ± 233 respectively, compatible with expectations from the SM. This leads to a 95% CL limits of $-1 \times 10^{-2} < h_3^\gamma < 1 \times 10^{-2}$, $-9 \times 10^{-5} < h_4^\gamma < 9 \times 10^{-5}$, $-9 \times 10^{-3} < h_3^Z < 9 \times 10^{-3}$, $-8 \times 10^{-5} < h_4^Z < 8 \times 10^{-5}$, assuming h_1^V and h_2^V have SM values, $V = \gamma$ or Z .
- AAD 13AN study $Z\gamma$ production in pp collisions. In events with no additional jet, 1417 (2031) Z decays to electron (muon) pairs are selected, with an expected background of 156 ± 54 (244 ± 64) events, as well as 662 Z decays to neutrino pairs with an expected background of 302 ± 42 events. Analysing the photon p_T spectrum above 100 GeV yields the 95% C.L. limits: $-0.013 < h_3^Z < 0.014$, $-8.7 \times 10^{-5} < h_4^Z < 8.7 \times 10^{-5}$, $-0.015 < h_3^\gamma < 0.016$, $-9.4 \times 10^{-5} < h_4^\gamma < 9.2 \times 10^{-5}$. Supersedes AAD 12Bx.
- CHATRCHYAN 13BI determine the $Z\gamma \rightarrow \nu\bar{\nu}\gamma$ cross section by selecting events with a photon of $E_T > 145$ GeV and a $\cancel{E}_T > 130$ GeV. 73 candidate events are observed with an expected SM background of 30.2 ± 6.5 . The E_T spectrum of the photon is used to set 95% C.L. limits as follows: $|h_3^Z| < 2.7 \times 10^{-3}$, $|h_4^Z| < 1.3 \times 10^{-5}$, $|h_3^\gamma| < 2.9 \times 10^{-3}$, $|h_4^\gamma| < 1.5 \times 10^{-5}$.
- ABAZOV 12S study $Z\gamma$ production in $p\bar{p}$ collisions at $\sqrt{s} = 1.96$ TeV using 6.2 fb^{-1} of data where the Z decays to electron (muon) pairs and the photon has at least 10 GeV of transverse momentum. In data, 304 (308) di-electron (di-muon) events are observed with an expected background of 255 ± 16 (285 ± 24) events. Based on the photon p_T spectrum, and including also earlier data and the $Z \rightarrow \nu\bar{\nu}$ decay mode (from ABAZOV 09L), the following 95% C.L. limits are reported: $|h_{03}^Z| < 0.026$, $|h_{04}^Z| < 0.0013$, $|h_{03}^\gamma| < 0.027$, $|h_{04}^\gamma| < 0.0014$ for a form factor scale of $\Lambda = 1.5$ TeV.
- AALTONEN 11S study $Z\gamma$ events in $p\bar{p}$ interactions at $\sqrt{s} = 1.96$ TeV with integrated luminosity 5.1 fb^{-1} for $Z \rightarrow e^+e^-/\mu^+\mu^-$ and 4.9 fb^{-1} for $Z \rightarrow \nu\bar{\nu}$. For the charged lepton case, the two leptons must be of the same flavor with the transverse momentum/energy of one > 20 GeV and the other > 10 GeV. The isolated photon must have $E_T > 50$ GeV. They observe 91 events with 87.2 ± 7.8 events expected from standard model processes. For the $\nu\bar{\nu}$ case they require solitary photons with $E_T > 25$ GeV and missing $E_T > 25$ GeV and observe 85 events with standard model expectation of 85.9 ± 5.6 events. Taking the form factor $\Lambda = 1.5$ TeV they derive 95% C.L. limits as $|h_3^{Z,\gamma}| < 0.022$ and $|h_4^{Z,\gamma}| < 0.0009$.
- CHATRCHYAN 11M study $Z\gamma$ production in pp collisions at $\sqrt{s} = 7$ TeV using 36 pb^{-1} pp data, where the Z decays to e^+e^- or $\mu^+\mu^-$. The total cross sections are measured for photon transverse energy $E_T^\gamma > 10$ GeV and spatial separation from charged leptons in the plane of pseudo rapidity and azimuthal angle $\Delta R(\ell,\gamma) > 0.7$ with the dilepton invariant mass requirement of $M_{\ell\ell} > 50$ GeV. The number of $e^+e^-\gamma$ and $\mu^+\mu^-\gamma$ candidates is 81 and 90 with estimated backgrounds of 20.5 ± 2.5 and 27.3 ± 3.2 events respectively. The 95% CL limits for $ZZ\gamma$ couplings are $-0.05 < h_3^Z < 0.06$ and $-0.0005 < h_4^Z < 0.0005$, and for $Z\gamma\gamma$ couplings are $-0.07 < h_3^\gamma < 0.07$ and $-0.0005 < h_4^\gamma < 0.0006$.
- ABAZOV 09L study $Z\gamma, Z \rightarrow \nu\bar{\nu}$ production in $p\bar{p}$ collisions at 1.96 TeV C.M. energy. They select 51 events with a photon of transverse energy E_T^γ larger than 90 GeV, with an expected background of 17 events. Based on the photon E_T spectrum and including also Z decays to charged leptons (from ABAZOV 07M), the following 95% CL limits are reported: $|h_{30}^Z| < 0.033$, $|h_{40}^Z| < 0.0017$, $|h_{30}^\gamma| < 0.033$, $|h_{40}^\gamma| < 0.0017$.
- ABAZOV 07M use 968 $p\bar{p} \rightarrow e^+e^-/\mu^+\mu^-X$ candidates, at 1.96 TeV center of mass energy, to tag $p\bar{p} \rightarrow Z\gamma$ events by requiring $E_T(\gamma) > 7$ GeV, lepton-gamma separation $\Delta R_{\ell\gamma} > 0.7$, and di-lepton invariant mass > 30 GeV. The cross section is in agreement with the SM prediction. Using these $Z\gamma$ events they obtain 95% C.L. limits on each h_i^V , keeping all others fixed at their SM values. They report: $-0.083 < h_{30}^Z <$

- 0.082, $-0.0053 < h_{40}^Z < 0.0054$, $-0.085 < h_{30}^\gamma < 0.084$, $-0.0053 < h_{40}^\gamma < 0.0054$, for the form factor scale $\Lambda = 1.2$ TeV.
- 12 Using data collected at $\sqrt{s} = 183\text{--}208$, ABDALLAH 07c select 1,877 $e^+e^- \rightarrow Z\gamma$ events with $Z \rightarrow q\bar{q}$ or $\nu\bar{\nu}$, 171 $e^+e^- \rightarrow ZZ$ events with $Z \rightarrow q\bar{q}$ or lepton pair (except an explicit τ pair), and 74 $e^+e^- \rightarrow Z\gamma^*$ events with a $q\bar{q}\mu^+\mu^-$ or $q\bar{q}e^+e^-$ signature, to derive 95% CL limits on h_i^γ . Each limit is derived with other parameters set to zero. They report: $-0.23 < h_1^Z < 0.23$, $-0.30 < h_3^Z < 0.16$, $-0.14 < h_1^\gamma < 0.14$, $-0.049 < h_3^\gamma < 0.044$.
- 13 ACHARD 04H select 3515 $e^+e^- \rightarrow Z\gamma$ events with $Z \rightarrow q\bar{q}$ or $\nu\bar{\nu}$ at $\sqrt{s} = 189\text{--}209$ GeV to derive 95% CL limits on h_i^γ . For deriving each limit the other parameters are fixed at zero. They report: $-0.153 < h_1^Z < 0.141$, $-0.087 < h_2^Z < 0.079$, $-0.220 < h_3^Z < 0.112$, $-0.068 < h_4^Z < 0.148$, $-0.057 < h_1^\gamma < 0.057$, $-0.050 < h_2^\gamma < 0.023$, $-0.059 < h_3^\gamma < 0.004$, $-0.004 < h_4^\gamma < 0.042$.
- 14 ABBIENDI, G 00c study $e^+e^- \rightarrow Z\gamma$ events (with $Z \rightarrow q\bar{q}$ and $Z \rightarrow \nu\bar{\nu}$) at 189 GeV to obtain the central values (and 95% CL limits) of these couplings: $h_1^Z = 0.000 \pm 0.100$ ($-0.190, 0.190$), $h_2^Z = 0.000 \pm 0.068$ ($-0.128, 0.128$), $h_3^Z = -0.074_{-0.103}^{+0.102}$ ($-0.269, 0.119$), $h_4^Z = 0.046 \pm 0.068$ ($-0.084, 0.175$), $h_1^\gamma = 0.000 \pm 0.061$ ($-0.115, 0.115$), $h_2^\gamma = 0.000 \pm 0.041$ ($-0.077, 0.077$), $h_3^\gamma = -0.080_{-0.041}^{+0.039}$ ($-0.164, -0.006$), $h_4^\gamma = 0.064_{-0.030}^{+0.033}$ ($+0.007, +0.134$). The results are derived assuming that only one coupling at a time is different from zero.
- 15 ABBOTT 98M study $p\bar{p} \rightarrow Z\gamma + X$, with $Z \rightarrow e^+e^-, \mu^+\mu^-, \nu\bar{\nu}$ at 1.8 TeV, to obtain 95% CL limits at $\Lambda = 750$ GeV: $|h_{30}^Z| < 0.36$, $|h_{40}^Z| < 0.05$ (keeping $h_i^\gamma = 0$), and $|h_{30}^\gamma| < 0.37$, $|h_{40}^\gamma| < 0.05$ (keeping $h_i^Z = 0$). Limits on the CP-violating couplings are $|h_{10}^Z| < 0.36$, $|h_{20}^Z| < 0.05$ (keeping $h_i^\gamma = 0$), and $|h_{10}^\gamma| < 0.37$, $|h_{20}^\gamma| < 0.05$ (keeping $h_i^Z = 0$).
- 16 ABREU 98k determine a 95% CL upper limit on $\sigma(e^+e^- \rightarrow \gamma + \text{invisible particles}) < 2.5$ pb using 161 and 172 GeV data. This is used to set 95% CL limits on $|h_{30}^\gamma| < 0.8$ and $|h_{30}^Z| < 1.3$, derived at a scale $\Lambda = 1$ TeV and with $n = 3$ in the form factor representation.

 f_i^γ

Combining the LEP-2 results taking into account the correlations, the following 95% CL limits are derived [SCHAEEL 13A]:

$$\begin{aligned} -0.28 < f_4^Z < +0.32, & \quad -0.34 < f_5^Z < +0.35, \\ -0.17 < f_4^\gamma < +0.19, & \quad -0.35 < f_5^\gamma < +0.32. \end{aligned}$$

Some of the recent results from the Tevatron and LHC experiments individually surpass the combined LEP-2 results in precision (see below).

VALUE	DOCUMENT ID	TECN	COMMENT
• • • We do not use the following data for averages, fits, limits, etc. • • •			
1	AAD	23CH	$E_{cm}^{pp} = 13$ TeV
2	SIRUNYAN	21q CMS	$E_{cm}^{pp} = 13$ TeV
3	AABOUD	19AY ATLS	$E_{cm}^{pp} = 13$ TeV
4	AABOUD	18q ATLS	$E_{cm}^{pp} = 13$ TeV
5	SIRUNYAN	18BT CMS	$E_{cm}^{pp} = 13$ TeV
6	KHACHATRYAN...15B	CMS	$E_{cm}^{pp} = 8$ TeV
7	KHACHATRYAN...15BC	CMS	$E_{cm}^{pp} = 7, 8$ TeV
8	AAD	13z ATLS	$E_{cm}^{pp} = 7$ TeV
9	CHATRCHYAN13B	CMS	$E_{cm}^{pp} = 7$ TeV
10	SCHAEEL	09 ALEP	$E_{cm}^{pp} = 192\text{--}209$ GeV
11	ABAZOV	08k D0	$E_{cm}^{pp} = 1.96$ TeV
12	ABDALLAH	07c DLPH	$E_{cm}^{pp} = 183\text{--}208$ GeV
13	ABBIENDI	04c OPAL	
14	ACHARD	03D L3	

- 1 AAD 23CH measure ZZ production with the Z bosons decaying to electrons or muons. Analysing the angular information of the final-state four-lepton system, the following limits are derived at 95% C.L.: $-0.012 < f_4^Z < 0.012$, $-0.015 < f_4^\gamma < 0.015$.
- 2 SIRUNYAN 21q measure ZZ production where both Z bosons decay in the electron or muon channel. Analysing the four-lepton invariant mass distribution, the following limits are derived at 95% C.L. in units of 10^{-4} : $-6.6 < f_4^Z < 6.0$, $-5.5 < f_5^Z < 7.5$, $-7.8 < f_4^\gamma < 7.1$, $-6.8 < f_5^\gamma < 7.5$. This set of parameters is linearly related to a set of EFT parameters, resulting in the following limits at 95% C.L. in units of TeV^{-4} : $-2.3 < c_{BW}^4 < 2.5$, $-1.4 < c_{WW}^4 < 1.2$, $-1.4 < c_{BW}^4 < 1.3$, $-1.2 < c_{BB}^4 < 1.2$.
- 3 AABOUD 19AY study ZZ production in the $\ell\ell\nu\nu$ decay channel. Events with a pair of isolated high-transverse momentum charged leptons (electron pairs or muon pairs), and with large missing energy, are selected. In the data, 371 (416) di-electron (di-muon) events are found, with a total expected background of 128 ± 8 (143 ± 8) events. Analysing the transverse momentum distribution of the charged dilepton system above 150 GeV, the following 95% C.L. limits are derived in units of 10^{-3} : $-1.2 < f_4^\gamma < 1.2$, $-1.0 < f_4^Z < 1.0$, $-1.2 < f_5^\gamma < 1.2$, $-1.0 < f_5^Z < 1.0$.
- 4 AABOUD 18q study $pp \rightarrow ZZ$ events at $\sqrt{s} = 13$ TeV with $Z \rightarrow e^+e^-$ or $Z \rightarrow \mu^+\mu^-$. The number of events observed in the $4e$, $2e2\mu$, and 4μ channels is 249, 465, and 303 respectively. Analysing the p_T spectrum of the leading Z boson, the following

the following 95% C.L. limits are derived in units of 10^{-4} : $-1.8 < f_4^\gamma < 1.8$, $-1.5 < f_4^Z < 1.5$, $-1.8 < f_5^\gamma < 1.8$, $-1.5 < f_5^Z < 1.5$.

- 5 SIRUNYAN 18BT study $ppZZ$ events at $\sqrt{s} = 13$ TeV with $Z \rightarrow e^+e^-$ or $Z \rightarrow \mu^+\mu^-$. The number of events observed in the $4e$, $2e2\mu$, and 4μ channels is 220, 543 and 335 respectively. Analysing the 4-lepton invariant mass spectrum, the following 95% C.L. limits are derived in units of 10^{-3} : $-1.2 < f_4^\gamma < 1.3$, $-1.2 < f_4^Z < 1.0$, $-1.2 < f_5^\gamma < 1.3$, $-1.0 < f_5^Z < 1.3$.
- 6 KHACHATRYAN 15B study ZZ production in 8 TeV pp collisions. In the decay modes $ZZ \rightarrow 4e$, 4μ , $2e2\mu$, $54, 75, 148$ events are observed, with an expected background of 2.2 ± 0.9 , 1.2 ± 0.6 , and 2.4 ± 1.0 events, respectively. Analysing the 4-lepton invariant mass spectrum in the range from 110 GeV to 1200 GeV, the following 95% C.L. limits are obtained: $|f_4^Z| < 0.004$, $|f_5^Z| < 0.004$, $|f_4^\gamma| < 0.005$, $|f_5^\gamma| < 0.005$.
- 7 KHACHATRYAN 15BC use the cross section measurement of the final state $pp \rightarrow ZZ \rightarrow 2\ell 2\nu$ (ℓ being an electron or a muon) at 7 and 8 TeV to put limits on these triple gauge couplings. Effective mass of the charged lepton pair is required to be in the range 83.5–98.5 GeV and the dilepton $p_T > 45$ GeV. The reduced missing E_T is required to be > 65 GeV, which takes into account the fake missing E_T due to detector effects. The numbers of e^+e^- and $\mu^+\mu^-$ events selected are 35 and 40 at 7 TeV and 176 and 271 at 8 TeV respectively. The production cross sections so obtained are in agreement with SM predictions. The following 95% C.L. limits are set: $-0.0028 < f_4^Z < 0.0032$, $-0.0037 < f_4^\gamma < 0.0033$, $-0.0029 < f_5^Z < 0.0031$, $-0.0033 < f_5^\gamma < 0.0037$. Combining with previous results (KHACHATRYAN 15B and CHATRCHYAN 13B) which include 7 TeV and 8 TeV data on the final states $pp \rightarrow ZZ \rightarrow 2\ell 2\ell'$ where ℓ and ℓ' are an electron or a muon, the best limits are $-0.0022 < f_4^Z < 0.0026$, $-0.0029 < f_4^\gamma < 0.0026$, $-0.0023 < f_5^Z < 0.0023$, $-0.0026 < f_5^\gamma < 0.0027$.
- 8 AAD 13z study ZZ production in pp collisions at $\sqrt{s} = 7$ TeV. In the $ZZ \rightarrow \ell^+\ell^-\ell^+\ell^-$ final state they observe a total of 66 events with an expected background of 0.9 ± 1.3 . In the $ZZ \rightarrow \ell^+\ell^-\nu\nu$ final state they observe a total of 87 events with an expected background of 46.9 ± 5.2 . The limits on anomalous TGCs are determined using the observed and expected numbers of these ZZ events binned in p_T^Z . The 95% C.L. are as follows: for form factor scale $\Lambda = \infty$, $-0.015 < f_4^\gamma < 0.015$, $-0.013 < f_4^Z < 0.013$, $-0.016 < f_5^\gamma < 0.015$, $-0.013 < f_5^Z < 0.013$; for form factor scale $\Lambda = 3$ TeV, $-0.022 < f_4^\gamma < 0.023$, $-0.019 < f_4^Z < 0.019$, $-0.023 < f_5^\gamma < 0.023$, $-0.020 < f_5^Z < 0.019$.
- 9 CHATRCHYAN 13B study ZZ production in pp collisions and select 54 ZZ candidates in the Z decay channel with electrons or muons with an expected background of 1.4 ± 0.5 events. The resulting 95% C.L. ranges are: $-0.013 < f_4^\gamma < 0.015$, $-0.011 < f_4^Z < 0.012$, $-0.014 < f_5^\gamma < 0.014$, $-0.012 < f_5^Z < 0.012$.
- 10 Using data collected in the center of mass energy range 192–209 GeV, SCHAEEL 09 select 318 $e^+e^- \rightarrow ZZ$ events with 319.4 expected from the standard model. Using this data they derive the following 95% CL limits: $-0.321 < f_4^\gamma < 0.318$, $-0.534 < f_4^Z < 0.534$, $-0.724 < f_5^\gamma < 0.733$, $-1.194 < f_5^Z < 1.190$.
- 11 ABAZOV 08k search for ZZ and $Z\gamma^*$ events with $1 \text{ fb}^{-1} p\bar{p}$ data at $\sqrt{s} = 1.96$ TeV in $(e^+e^-)(e^+e^-)$, $(\mu^+\mu^-)(\mu^+\mu^-)$, $(e^+e^-)(\mu^+\mu^-)$ final states requiring the lepton pair masses to be > 30 GeV. They observe 1 event, which is consistent with an expected signal of 1.71 ± 0.15 events and a background of 0.13 ± 0.03 events. From this they derive the following limits, for a form factor (Λ) value of 1.2 TeV: $-0.28 < f_4^Z < 0.28$, $-0.31 < f_5^Z < 0.29$, $-0.26 < f_4^\gamma < 0.26$, $-0.30 < f_5^\gamma < 0.28$.
- 12 Using data collected at $\sqrt{s} = 183\text{--}208$ GeV, ABDALLAH 07c select 171 $e^+e^- \rightarrow ZZ$ events with $Z \rightarrow q\bar{q}$ or lepton pair (except an explicit τ pair), and 74 $e^+e^- \rightarrow Z\gamma^*$ events with a $q\bar{q}\mu^+\mu^-$ or $q\bar{q}e^+e^-$ signature, to derive 95% CL limits on f_i^γ . Each limit is derived with other parameters set to zero. They report: $-0.40 < f_4^Z < 0.42$, $-0.38 < f_5^Z < 0.62$, $-0.23 < f_4^\gamma < 0.25$, $-0.52 < f_5^\gamma < 0.48$.
- 13 ABBIENDI 04c study ZZ production in e^+e^- collisions in the C.M. energy range 190–209 GeV. They select 340 events with an expected background of 180 events. Including the ABBIENDI 00N data at 183 and 189 GeV (118 events with an expected background of 65 events) they report the following 95% CL limits: $-0.45 < f_4^Z < 0.58$, $-0.94 < f_5^Z < 0.25$, $-0.32 < f_4^\gamma < 0.33$, and $-0.71 < f_5^\gamma < 0.59$.
- 14 ACHARD 03D study Z-boson pair production in e^+e^- collisions in the C.M. energy range 200–209 GeV. They select 549 events with an expected background of 432 events. Including the ACCIARRI 99G and ACCIARRI 99O data (183 and 189 GeV respectively), 286 events with an expected background of 241 events) and the 192–202 GeV ACCIARRI 01I results (656 events, expected background of 512 events), they report the following 95% CL limits: $-0.48 \leq f_4^Z \leq 0.46$, $-0.36 \leq f_5^Z \leq 1.03$, $-0.28 \leq f_4^\gamma \leq 0.28$, and $-0.40 \leq f_5^\gamma \leq 0.47$.

ANOMALOUS W/Z QUARTIC COUPLINGS

Revised March 2024 by M.W. Grünewald (U. College Dublin) and A. Gurtu (CERN; TIFR Mumbai).

Quartic couplings, $WWZZ$, $WWZ\gamma$, $WW\gamma\gamma$, and $ZZ\gamma\gamma$, were studied at LEP and Tevatron at energies at which the Standard Model predicts negligible contributions to multiboson production. Thus, to parametrize limits on these couplings, an effective theory approach is adopted which supplements the

Gauge & Higgs Boson Particle Listings

Z

Standard Model Lagrangian with higher dimensional operators which include quartic couplings. The LEP collaborations chose the lowest dimensional representation of operators (dimension 6) which presumes the $SU(2) \times U(1)$ gauge symmetry is broken by means other than the conventional Higgs scalar doublet [1–3]. In this representation possible quartic couplings, a_0, a_c, a_n , are expressed in terms of the following dimension-6 operators [1,2];

$$\begin{aligned} L_6^0 &= -\frac{e^2}{16\Lambda^2} a_0 F^{\mu\nu} F_{\mu\nu} \vec{W}^\alpha \cdot \vec{W}_\alpha \\ L_6^c &= -\frac{e^2}{16\Lambda^2} a_c F^{\mu\alpha} F_{\mu\beta} \vec{W}^\beta \cdot \vec{W}_\alpha \\ L_6^n &= -i\frac{e^2}{16\Lambda^2} a_n \epsilon_{ijk} W_{\mu\alpha}^{(i)} W_{\nu}^{(j)} W^{(k)\alpha} F^{\mu\nu} \\ \tilde{L}_6^0 &= -\frac{e^2}{16\Lambda^2} \tilde{a}_0 F^{\mu\nu} \tilde{F}_{\mu\nu} \vec{W}^\alpha \cdot \vec{W}_\alpha \\ \tilde{L}_6^n &= -i\frac{e^2}{16\Lambda^2} \tilde{a}_n \epsilon_{ijk} W_{\mu\alpha}^{(i)} W_{\nu}^{(j)} W^{(k)\alpha} \tilde{F}^{\mu\nu} \end{aligned}$$

where F, W are photon and W fields, L_6^0 and L_6^c conserve C, P separately (\tilde{L}_6^0 conserves only C) and generate anomalous $W^+W^-\gamma\gamma$ and $ZZ\gamma\gamma$ couplings, L_6^n violates CP (\tilde{L}_6^n violates both C and P) and generates an anomalous $W^+W^-Z\gamma$ coupling, and Λ is an energy scale for new physics. For the $ZZ\gamma\gamma$ coupling the CP -violating term represented by L_6^n does not contribute. These couplings are assumed to be real and to vanish at tree level in the Standard Model.

Within the same framework as above, a more recent description of the quartic couplings [3] treats the anomalous parts of the $WW\gamma\gamma$ and $ZZ\gamma\gamma$ couplings separately, leading to two sets parametrized as a_0^V/Λ^2 and a_c^V/Λ^2 , where $V = W$ or Z .

With the discovery of a Higgs at the LHC in 2012, it is then useful to go to the next higher dimensional representation (dimension 8 operators) in which the gauge symmetry is broken by the conventional Higgs scalar doublet [3,4]. There are 14 operators which can contribute to the anomalous quartic coupling signal. Some of the operators have analogues in the dimension 6 scheme. The CMS collaboration, [5], have used this parametrization, in which the connections between the two schemes are also summarized:

$$\begin{aligned} \mathcal{L}_{AQGC} &= -\frac{e^2 a_0^W}{8 \Lambda^2} F_{\mu\nu} F^{\mu\nu} W^{+\alpha} W_a^- \\ &\quad -\frac{e^2 a_c^W}{16 \Lambda^2} F_{\mu\nu} F^{\mu\alpha} (W^{+\nu} W_a^- + W^{-\nu} W_a^+) \\ &\quad -e^2 g^2 \frac{\kappa_0^W}{\Lambda^2} F_{\mu\nu} Z^{\mu\nu} W^{+\alpha} W_a^- \\ &\quad -\frac{e^2 g^2 \kappa_c^W}{2 \Lambda^2} F_{\mu\nu} Z^{\mu\alpha} (W^{+\nu} W_a^- + W^{-\nu} W_a^+) \\ &\quad + \frac{f_{T,0}}{\Lambda^4} Tr[\widehat{W}_{\mu\nu} \widehat{W}^{\mu\nu}] \times Tr[\widehat{W}_{\alpha\beta} \widehat{W}^{\alpha\beta}] \end{aligned}$$

The energy scale of possible new physics is Λ , and $g = e/\sin(\theta_W)$, e being the unit electric charge and θ_W the Weinberg angle. The field tensors are described in [3,4].

The two dimension 6 operators a_0^W/Λ^2 and a_c^W/Λ^2 are associated with the $WW\gamma\gamma$ vertex. Among dimension 8 operators, κ_0^W/Λ^2 and κ_c^W/Λ^2 are associated with the $WWZ\gamma$ vertex, whereas the parameter $f_{T,0}/\Lambda^4$ contributes to both vertices. There is a relationship between these two dimension 6 parameters and the dimension 8 parameters $f_{M,i}/\Lambda^4$ as follows [3]:

$$\frac{a_0^W}{\Lambda^2} = -\frac{4M_W^2}{g^2} \frac{f_{M,0}}{\Lambda^4} - \frac{8M_W^2}{g'^2} \frac{f_{M,2}}{\Lambda^4}$$

$$\frac{a_c^W}{\Lambda^2} = -\frac{4M_W^2}{g^2} \frac{f_{M,1}}{\Lambda^4} - \frac{8M_W^2}{g'^2} \frac{f_{M,3}}{\Lambda^4}$$

where $g' = e/\cos(\theta_W)$ and M_W is the invariant mass of the W boson. This relation provides a translation between limits on dimension 6 operators $a_{0,c}^W$ and $f_{M,j}/\Lambda^4$. It is further required [4] that $f_{M,0} = 2f_{M,2}$ and $f_{M,1} = 2f_{M,3}$ which suppresses contributions to the $WWZ\gamma$ vertex. The complete set of Lagrangian contributions as presented in [4] corresponds to 19 anomalous couplings in total – $f_{S,i}$, $i = 1, 2$, $f_{M,i}$, $i = 0, \dots, 8$ and $f_{T,i}$, $i = 0, \dots, 9$ – each scaled by $1/\Lambda^4$.

Another approach to couplings is the so called K-matrix framework [7], in which the anomalous couplings can be expressed in terms of two parameters α_4 and α_5 , which account for all BSM effects.

The LHC collaborations have published couplings results based on various theoretical frameworks. It is hoped that the collaborations will agree to use at least one common set of parameters to express these limits to enable the reader to make a comparison, and to allow for a possible LHC combination.

References

1. G. Belanger and F. Boudjema, Phys. Lett. **B288**, 201 (1992).
2. J.W. Stirling and A. Werthenbach, Eur. Phys. J. **C14**, 103 (2000);
J.W. Stirling and A. Werthenbach, Phys. Lett. **B466**, 369 (1999);
A. Denner *et al.*, Eur. Phys. J. **C20**, 201 (2001);
G. Montagna *et al.*, Phys. Lett. **B515**, 197 (2001).
3. G. Belanger *et al.*, Eur. Phys. J. **C13**, 283 (2000).
4. O.J.P. Éboli, M.C. Gonzalez-Garcia, and S.M. Lietti, Phys. Rev. **D69**, 095005 (2004);
O.J.P. Éboli, M.C. Gonzalez-Garcia, and J.K. Mizukoshi, Phys. Rev. **D77**, 073005 (2006).
5. S. Chatrchyan *et al.*, Phys. Rev. **D90**, 032008 (2014);
S. Chatrchyan *et al.*, Phys. Rev. Lett. **114**, 051801 (2015).
6. G. Aad *et al.*, Phys. Rev. Lett. **113**, 141803 (2014).
7. A. Albateanu, W. Killian, and J. Reuter, JHEP **0811**, 010 (2008).

 $a_0/\Lambda^2, a_c/\Lambda^2$

Combining published and unpublished preliminary LEP results the following 95% CL intervals for the QGCs associated with the $ZZ\gamma\gamma$ vertex are derived (CERN-PH-EP/2005-051 or hep-ex/0511027):

$$\begin{aligned} -0.008 < a_0^Z/\Lambda^2 < +0.021 \\ -0.029 < a_c^Z/\Lambda^2 < +0.039 \end{aligned}$$

Anomalous Z quartic couplings have also been measured by the Tevatron and LHC experiments. As discussed in the review on "Anomalous W/Z quartic couplings," the coupling parameters in the Anomalous QGC Lagrangian may relate to processes involving only the W or only to the Z or to both. Thus, results on all other AQGCs are reported together in the W listings.

VALUE

DOCUMENT ID

TECN

••• We do not use the following data for averages, fits, limits, etc. •••

1	ABBIENDI	04L	OPAL
2	HEISTER	04A	ALEP
3	ACHARD	02G	L3

¹ABBIENDI 04L select $20 e^+ e^- \rightarrow \nu\bar{\nu}\gamma\gamma$ acoplanar events in the energy range 180–209 GeV and 176 $e^+ e^- \rightarrow q\bar{q}\gamma\gamma$ events in the energy range 130–209 GeV. These samples

are used to constrain possible anomalous $W^+W^-\gamma\gamma$ and $ZZ\gamma\gamma$ quartic couplings. Further combining with the $W^+W^-\gamma$ sample of **ABBIENDI 04b** the following one-parameter 95% CL limits are obtained: $-0.007 < a_0^Z/\Lambda^2 < 0.023 \text{ GeV}^{-2}$, $-0.029 < a_0^Z/\Lambda^2 < 0.029 \text{ GeV}^{-2}$, $-0.020 < a_0^W/\Lambda^2 < 0.020 \text{ GeV}^{-2}$, $-0.052 < a_C^W/\Lambda^2 < 0.037 \text{ GeV}^{-2}$.

² In the CM energy range 183 to 209 GeV **HEISTER 04a** select 30 $e^+e^- \rightarrow \nu\bar{\nu}\gamma\gamma$ events with two acoplanar, high energy and high transverse momentum photons. The photon-photon acoplanarity is required to be $> 5^\circ$, $E_{\gamma}/\sqrt{s} > 0.025$ (the more energetic photon having energy $> 0.2\sqrt{s}$), $p_{T,\gamma}/E_{\text{beam}} > 0.05$ and $|\cos\theta_\gamma| < 0.94$. A likelihood fit to the photon energy and recoil missing mass yields the following one-parameter 95% CL limits: $-0.012 < a_0^Z/\Lambda^2 < 0.019 \text{ GeV}^{-2}$, $-0.041 < a_0^Z/\Lambda^2 < 0.044 \text{ GeV}^{-2}$, $-0.060 < a_0^W/\Lambda^2 < 0.055 \text{ GeV}^{-2}$, $-0.099 < a_C^W/\Lambda^2 < 0.093 \text{ GeV}^{-2}$.

³ **ACHARD 02g** study $e^+e^- \rightarrow Z\gamma\gamma \rightarrow q\bar{q}\gamma\gamma$ events using data at center-of-mass energies from 200 to 209 GeV. The photons are required to be isolated, each with energy $> 5 \text{ GeV}$ and $|\cos\theta| < 0.97$, and the di-jet invariant mass to be compatible with that of the Z boson (74–111 GeV). Cuts on Z velocity ($\beta < 0.73$) and on the energy of the most energetic photon reduce the backgrounds due to non-resonant production of the $q\bar{q}\gamma\gamma$ state and due to ISR respectively, yielding a total of 40 candidate events of which 8.6 are expected to be due to background. The energy spectra of the least energetic photon are fitted for all ten center-of-mass energy values from 130 GeV to 209 GeV (as obtained adding to the present analysis 130–202 GeV data of **ACCIARRI 01e**, for a total of 137 events with an expected background of 34.1 events) to obtain the fitted values $a_0/\Lambda^2 = 0.00 \pm 0.02 \text{ GeV}^{-2}$ and $a_C/\Lambda^2 = 0.03 \pm 0.01 \text{ GeV}^{-2}$, where the other parameter is kept fixed to its Standard Model value (0). A simultaneous fit to both parameters yields the 95% CL limits $-0.02 \text{ GeV}^{-2} < a_0/\Lambda^2 < 0.03 \text{ GeV}^{-2}$ and $-0.07 \text{ GeV}^{-2} < a_C/\Lambda^2 < 0.05 \text{ GeV}^{-2}$.

Z REFERENCES

ABOUD 23A	JHEP 2312 158 (errat.)	M. Abooud et al.	(ATLAS Collab.)	HEISTER 04A	PL B602 31	A. Heister et al.	(ALEPH Collab.)
AAD 23Aq	PR D108 032015	G. Aad et al.	(ATLAS Collab.)	ABBIENDI 03P	PL B577 18	G. Abbiendi et al.	(OPAL Collab.)
AAD 23B5	PL B847 138292	G. Aad et al.	(ATLAS Collab.)	ABDALLAH 03H	PL B569 129	J. Abdallah et al.	(DELPHI Collab.)
AAD 23CD	EPJ C83 781	G. Aad et al.	(ATLAS Collab.)	ABDALLAH 03F	PL B576 29	J. Abdallah et al.	(DELPHI Collab.)
AAD 23CH	JHEP 2312 107	G. Aad et al.	(ATLAS Collab.)	ABE 03K	PRL 90 141804	K. Abe et al.	(SLD Collab.)
AAU 23AM	CP C47 093002	R. Aaij et al.	(LHCb Collab.)	ACHARD 03D	PL B572 133	P. Achard et al.	(L3 Collab.)
TUMASYAN 23E	PL B842 137563	A. Tumasyan et al.	(CMS Collab.)	ACHARD 03G	PL B577 109	P. Achard et al.	(L3 Collab.)
AALTONEN 22	SCI 376 170	T. Aaltonen et al.	(CDF Collab.)	ABBIENDI 02I	PL B546 29	G. Abbiendi et al.	(OPAL Collab.)
AAD 21A0	NATP 17 819	G. Aad et al.	(ATLAS Collab.)	ABE 02G	PRL 88 151801	K. Abe et al.	(SLD Collab.)
AAD 21Aq	JHEP 2107 005	G. Aad et al.	(ATLAS Collab.)	ACHARD 02G	PL B540 43	P. Achard et al.	(L3 Collab.)
AAD 21AV	PRL 127 271801	G. Aad et al.	(ATLAS Collab.)	HEISTER 02B	PL B526 34	A. Heister et al.	(ALEPH Collab.)
SIRUNYAN 21Q	EPJ C81 200	A. M. Sirunyan et al.	(CMS Collab.)	HEISTER 02C	PL B528 19	A. Heister et al.	(ALEPH Collab.)
JANOT 20	PL B803 135319	P. Janot, S. Jadach	(LHCb Collab.)	HEISTER 02H	EPJ C24 177	A. Heister et al.	(ALEPH Collab.)
VOUSINAS 20	PL B800 135068	G. Voutsinas et al.	(LHCb Collab.)	ABBIENDI 01A	EPJ C19 587	G. Abbiendi et al.	(OPAL Collab.)
ABOUD 19AY	JHEP 1910 127	M. Abooud et al.	(ATLAS Collab.)	ABBIENDI 01G	EPJ C18 447	G. Abbiendi et al.	(OPAL Collab.)
ABOUD 19N	JHEP 1904 048	M. Abooud et al.	(ATLAS Collab.)	ABBIENDI 01K	PL B516 1	G. Abbiendi et al.	(OPAL Collab.)
RAINBOLT 19	PR D99 013004	J.L. Rainbolt, M. Schmitt	(NWES)	ABBIENDI 01N	EPJ C20 445	G. Abbiendi et al.	(OPAL Collab.)
SIRUNYAN 19AJ	EPJ C79 94	A. M. Sirunyan et al.	(CMS Collab.)	ABBIENDI 01O	EPJ C21 1	G. Abbiendi et al.	(OPAL Collab.)
SIRUNYAN 19BR	PL B797 134811	A. M. Sirunyan et al.	(CMS Collab.)	ABE 01P	PRL 86 1162	K. Abe et al.	(SLD Collab.)
ABOUD 18AU	JHEP 1807 127	M. Abooud et al.	(ATLAS Collab.)	ACCIARRI 01E	PL B505 47	M. Acciarri et al.	(L3 Collab.)
Also	JHEP 2312 158 (errat.)	M. Abooud et al.	(ATLAS Collab.)	ACCIARRI 01I	PL B497 23	M. Acciarri et al.	(L3 Collab.)
ABOUD 18BL	PL B796 134	M. Abooud et al.	(ATLAS Collab.)	HEISTER 01I	EPJ C20 401	A. Heister et al.	(ALEPH Collab.)
ABOUD 18CM	PR D98 092010	M. Abooud et al.	(ATLAS Collab.)	HEISTER 01D	EPJ C22 201	A. Heister et al.	(ALEPH Collab.)
ABOUD 18Q	PR D97 032005	M. Abooud et al.	(ATLAS Collab.)	ABBIENDI 00N	PL B476 256	G. Abbiendi et al.	(OPAL Collab.)
AAU 18AR	JHEP 1809 159	R. Aaij et al.	(LHCb Collab.)	ABBIENDI,G 00C	EPJ C17 553	G. Abbiendi et al.	(OPAL Collab.)
ANDREEV 18A	EPJ C78 777	V. Andreev et al.	(HI Collab.)	ABE 00B	PRL 84 5945	K. Abe et al.	(SLD Collab.)
SIRUNYAN 18BT	EPJ C78 165	A. M. Sirunyan et al.	(CMS Collab.)	ABE 00D	PRL 85 5059	K. Abe et al.	(SLD Collab.)
SIRUNYAN 18DZ	PRL 121 141801	A. M. Sirunyan et al.	(CMS Collab.)	ABREU 000	EPJ C12 2225	P. Abreu et al.	(DELPHI Collab.)
ABOUD 17Q	EPJ C77 367	M. Abooud et al.	(ATLAS Collab.)	ABREU 00B	EPJ C14 513	P. Abreu et al.	(DELPHI Collab.)
ABOUD 16K	PRL 117 111802	M. Abooud et al.	(ATLAS Collab.)	ABREU 00F	EPJ C16 371	P. Abreu et al.	(DELPHI Collab.)
AAD 16L	EPJ C76 210	G. Aad et al.	(ATLAS Collab.)	ABREU 00P	PL B475 429	P. Abreu et al.	(DELPHI Collab.)
AAD 16Q	PR D93 112002	G. Aad et al.	(ATLAS Collab.)	ACCIARRI 000	EPJ C13 47	M. Acciarri et al.	(L3 Collab.)
ABRAMOWICZ 16A	PR D93 092002	H. Abramowicz et al.	(ATLAS Collab.)	ACCIARRI 00J	EPJ C16 1	M. Acciarri et al.	(L3 Collab.)
ABT 16	PR D94 052007	I. Abt et al.	(MPIM, OXF, HAMB, DESY)	ACCIARRI 00K	PL B479 79	M. Acciarri et al.	(L3 Collab.)
KHACHATRYAN 16AE	PL B760 448	V. Khachatryan et al.	(CMS Collab.)	ACCIARRI 00Q	PL B489 93	M. Acciarri et al.	(L3 Collab.)
KHACHATRYAN 16CC	PL B763 280	V. Khachatryan et al.	(CMS Collab.)	BARATE 00B	EPJ C16 597	R. Barate et al.	(ALEPH Collab.)
AAD 15BT	JHEP 1509 049	G. Aad et al.	(ATLAS Collab.)	BARATE 00C	EPJ C14 1	R. Barate et al.	(ALEPH Collab.)
AAD 15I	PRL 114 121801	G. Aad et al.	(ATLAS Collab.)	BARATE 000	EPJ C16 613	R. Barate et al.	(ALEPH Collab.)
KHACHATRYAN 15AC	JHEP 1504 164	V. Khachatryan et al.	(CMS Collab.)	ABBIENDI 99B	EPJ C8 217	G. Abbiendi et al.	(OPAL Collab.)
KHACHATRYAN 15B	PL B740 250	V. Khachatryan et al.	(CMS Collab.)	ABBIENDI 99I	PL B447 157	G. Abbiendi et al.	(OPAL Collab.)
KHACHATRYAN 15BC	EPJ C75 511	V. Khachatryan et al.	(CMS Collab.)	ABE 99E	PR D59 052001	K. Abe et al.	(SLD Collab.)
AAD 14AU	PR D90 072010	G. Aad et al.	(ATLAS Collab.)	ABE 99L	PRL 83 1902	K. Abe et al.	(SLD Collab.)
AAD 14N	PL 112 231806	G. Aad et al.	(ATLAS Collab.)	ABREU 99	EPJ C6 19	P. Abreu et al.	(DELPHI Collab.)
AALTONEN 14E	PRL 112 111803	T. Aaltonen et al.	(CDF Collab.)	ABREU 99B	EPJ C10 415	P. Abreu et al.	(DELPHI Collab.)
CHATRCHYAN 14AB	PR D89 092005	S. Chatrchyan et al.	(CMS Collab.)	ABREU 99J	PL B449 364	P. Abreu et al.	(DELPHI Collab.)
AAD 13AN	PR D87 112003	G. Aad et al.	(ATLAS Collab.)	ABREU 99U	PL B462 425	P. Abreu et al.	(DELPHI Collab.)
Also	PR D91 119901 (errat.)	G. Aad et al.	(ATLAS Collab.)	ABREU 99Y	EPJ C10 219	P. Abreu et al.	(DELPHI Collab.)
AAD 13Z	JHEP 1303 128	G. Aad et al.	(ATLAS Collab.)	ACCIARRI 99D	PL B448 152	M. Acciarri et al.	(L3 Collab.)
CHATRCHYAN 13B	JHEP 1301 063	S. Chatrchyan et al.	(CMS Collab.)	ACCIARRI 99F	PL B454 94	M. Acciarri et al.	(L3 Collab.)
CHATRCHYAN 13BI	JHEP 1310 164	S. Chatrchyan et al.	(CMS Collab.)	ACCIARRI 99G	PL B450 281	M. Acciarri et al.	(L3 Collab.)
SCHAEF 13A	PRPL 532 119	S. Schaefer et al.	(CMS Collab.)	ACCIARRI 99H	PL B465 363	M. Acciarri et al.	(L3 Collab.)
AAD 12BX	PL B717 49	G. Aad et al.	(ATLAS Collab.)	ABBOTT 98M	PR D57 3817	B. Abbott et al.	(DO Collab.)
ABAZOV 12S	PR D85 052001	V. M. Abazov et al.	(DO Collab.)	ABE 98D	PRL 80 660	K. Abe et al.	(SLD Collab.)
CHATRCHYAN 12BM	JHEP 1212 034	S. Chatrchyan et al.	(CMS Collab.)	ABE 98I	PRL 81 942	K. Abe et al.	(SLD Collab.)
AALTONEN 11S	PRL 107 051802	T. Aaltonen et al.	(CDF Collab.)	ABREU 98K	PL B423 194	P. Abreu et al.	(DELPHI Collab.)
ABAZOV 11D	PR D84 012007	V. M. Abazov et al.	(DO Collab.)	ABREU 98L	EPJ C5 585	P. Abreu et al.	(DELPHI Collab.)
CHATRCHYAN 11M	PL B701 535	S. Chatrchyan et al.	(CMS Collab.)	ACCIARRI 98G	PL B431 199	M. Acciarri et al.	(L3 Collab.)
ABAZOV 09L	PRL 102 201802	V. M. Abazov et al.	(DO Collab.)	ACCIARRI 98H	PL B429 387	M. Acciarri et al.	(L3 Collab.)
BEDDALL 09	PL B670 300	A. Beddall, A. Beddall, A. Bingul	(UGAZ)	ACCIARRI 98U	PL B439 225	M. Acciarri et al.	(L3 Collab.)
SCHAEF 09	JHEP 0904 124	S. Schaefer et al.	(ALEPH Collab.)	ACKERS TAFF 98A	EPJ C5 411	K. Ackerstaff et al.	(OPAL Collab.)
ABAZOV 08K	PRL 100 131801	V. M. Abazov et al.	(DO Collab.)	ACKERS TAFF 98E	EPJ C1 439	K. Ackerstaff et al.	(OPAL Collab.)
ABDALLAH 07C	EPJ C51 525	J. Abdallah et al.	(DELPHI Collab.)	ACKERS TAFF 98O	PL B464 157	K. Ackerstaff et al.	(OPAL Collab.)
ABDALLAH 06E	PL B639 179	J. Abdallah et al.	(DELPHI Collab.)	ACKERS TAFF 98Q	EPJ C4 19	K. Ackerstaff et al.	(OPAL Collab.)
AKTAS 06	PL B632 35	A. Aktas et al.	(HI Collab.)	BARATE 98T	PL B434 415	R. Barate et al.	(ALEPH Collab.)
LEP-SLC 06	PRPL 427 257	ALEPH, DELPHI, L3, OPAL, SLD and working groups	(ALEPH Collab.)	BARATE 98U	EPJ C4 557	R. Barate et al.	(ALEPH Collab.)
SCHAEF 06A	PL B639 192	J. Schaefer et al.	(DELPHI Collab.)	BARATE 98V	EPJ C5 205	R. Barate et al.	(ALEPH Collab.)
ABDALLAH 05C	EPJ C44 299	J. Abdallah et al.	(DELPHI Collab.)	ABE 97	PRL 78 17	K. Abe et al.	(SLD Collab.)
ABE 05	PRL 94 091801	K. Abe et al.	(SLD Collab.)	ABREU 97C	ZPHY C73 243	P. Abreu et al.	(DELPHI Collab.)
ABE 05F	PR D71 112004	K. Abe et al.	(SLD Collab.)	ABREU 97E	PL B398 207	P. Abreu et al.	(DELPHI Collab.)
ACOSTA 05M	PR D71 052002	D. Acosta et al.	(CDF Collab.)	ABREU 97F	PL B404 194	P. Abreu et al.	(DELPHI Collab.)
ABBIENDI 04B	PL B580 17	G. Abbiendi et al.	(OPAL Collab.)	ACCIARRI 97D	PL B393 465	M. Acciarri et al.	(L3 Collab.)
ABBIENDI 04C	EPJ C32 303	G. Abbiendi et al.	(OPAL Collab.)	ACCIARRI 97J	PL B407 351	M. Acciarri et al.	(L3 Collab.)
ABBIENDI 04E	PL B586 167	G. Abbiendi et al.	(OPAL Collab.)	ACCIARRI 97L	PL B407 369	M. Acciarri et al.	(L3 Collab.)
ABBIENDI 04G	EPJ C33 173	G. Abbiendi et al.	(OPAL Collab.)	ACCIARRI 97M	PL B413 167	M. Acciarri et al.	(L3 Collab.)
ABBIENDI 04I	PR D70 032005	G. Abbiendi et al.	(OPAL Collab.)	ACKERS TAFF 97N	ZPHY C74 413	K. Ackerstaff et al.	(OPAL Collab.)
ABDALLAH 04F	EPJ C34 1019	J. Abdallah et al.	(DELPHI Collab.)	ACKERS TAFF 97P	ZPHY C76 387	K. Ackerstaff et al.	(OPAL Collab.)
ABE 04C	PR D69 072003	K. Abe et al.	(SLD Collab.)	ACKERS TAFF 97W	ZPHY C76 425	K. Ackerstaff et al.	(OPAL Collab.)
ACHARD 04C	PL B585 42	P. Achard et al.	(L3 Collab.)	ALEXANDER 97C	ZPHY C73 379	G. Alexander et al.	(OPAL Collab.)
ACHARD 04H	PL B597 119	P. Achard et al.	(L3 Collab.)	ALEXANDER 97D	ZPHY C73 569	G. Alexander et al.	(OPAL Collab.)
				ALEXANDER 97E	ZPHY C73 587	G. Alexander et al.	(OPAL Collab.)
				BARATE 97F	PL B405 191	R. Barate et al.	(ALEPH Collab.)
				BARATE 97G	PL B401 150	R. Barate et al.	(ALEPH Collab.)
				BARATE 97H	PL B401 163	R. Barate et al.	(ALEPH Collab.)
				BARATE 97I	PL B402 213	R. Barate et al.	(ALEPH Collab.)
				BARATE 97J	ZPHY C74 451	R. Barate et al.	(ALEPH Collab.)
				ABREU 96R	ZPHY C72 31	P. Abreu et al.	(DELPHI Collab.)
				ABREU 96S	PL B389 405	P. Abreu et al.	(DELPHI Collab.)
				ABREU 96U	ZPHY C73 61	P. Abreu et al.	(DELPHI Collab.)
				ACCIARRI 96	PL B371 126	M. Acciarri et al.	(L3 Collab.)
				ADAM 96	ZPHY C69 561	W. Adam et al.	(DELPHI Collab.)
				ADAM 96B	ZPHY C70 371	W. Adam et al.	(DELPHI Collab.)
				ALEXANDER 96B	ZPHY C70 197	G. Alexander et al.	(OPAL Collab.)
				ALEXANDER 96F	PL B370 185	G. Alexander et al.	(OPAL Collab.)
				ALEXANDER 96N	PL B384 343	G. Alexander et al.	(OPAL Collab.)
				ALEXANDER 96R	ZPHY C72 1	G. Alexander et al.	(OPAL Collab.)
				BUSKULIC 96D	ZPHY C69 393	D. Buskulic et al.	(ALEPH Collab.)
				BUSKULIC 96H	ZPHY C69 379	D. Buskulic et al.	(ALEPH Collab.)
				BUSKULIC 96T	PL B384 449	D. Buskulic et	

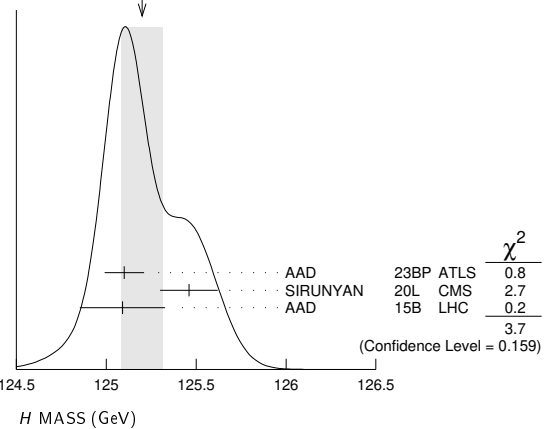
Gauge & Higgs Boson Particle Listings

Z, H

MIYABAYASHI	95	PL B347 171	K. Miyabayashi et al.	(TOPAZ Collab.)
ABE	94C	PRL 73 25	K. Abe et al.	(SLD Collab.)
ABREU	94B	PL B327 386	P. Abreu et al.	(DELPHI Collab.)
ABREU	94P	PL B341 109	P. Abreu et al.	(DELPHI Collab.)
AKERS	94P	ZPHY C63 181	R. Akers et al.	(OPAL Collab.)
BUSKULIC	94G	ZPHY C62 179	D. Buskulic et al.	(ALEPH Collab.)
BUSKULIC	94J	ZPHY C62 1	D. Buskulic et al.	(ALEPH Collab.)
VILAIN	94	PL B320 203	P. Vilain et al.	(CHARM II Collab.)
ABREU	93	PL B298 236	P. Abreu et al.	(DELPHI Collab.)
ABREU	93I	ZPHY C59 533	P. Abreu et al.	(DELPHI Collab.)
Also		ZPHY C65 709 (errata.)	P. Abreu et al.	(DELPHI Collab.)
ABREU	93L	PL B318 249	P. Abreu et al.	(DELPHI Collab.)
ACTON	93	PL B305 407	P.D. Acton et al.	(OPAL Collab.)
ACTON	93D	ZPHY C58 219	P.D. Acton et al.	(OPAL Collab.)
ACTON	93E	PL B311 391	P.D. Acton et al.	(OPAL Collab.)
ADRIANI	93	PL B301 136	O. Adriani et al.	(L3 Collab.)
ADRIANI	93I	PL B316 427	O. Adriani et al.	(L3 Collab.)
BUSKULIC	93L	PL B313 520	D. Buskulic et al.	(ALEPH Collab.)
NOVIKOV	93C	PL B298 453	V.A. Novikov, L.B. Okun, M.I. Vysotsky	(ITEP Collab.)
ABREU	92I	PL B277 371	P. Abreu et al.	(DELPHI Collab.)
ABREU	92M	PL B289 199	P. Abreu et al.	(DELPHI Collab.)
ACTON	92B	ZPHY C53 539	D.P. Acton et al.	(OPAL Collab.)
ACTON	92L	PL B294 436	P.D. Acton et al.	(OPAL Collab.)
ACTON	92N	PL B295 357	P.D. Acton et al.	(OPAL Collab.)
ADEVA	92	PL B275 209	B. Adeva et al.	(L3 Collab.)
ADRIANI	92D	PL B292 454	O. Adriani et al.	(L3 Collab.)
ALITTI	92B	PL B276 354	J. Alitti et al.	(UA2 Collab.)
BUSKULIC	92D	PL B292 210	D. Buskulic et al.	(ALEPH Collab.)
BUSKULIC	92E	PL B294 145	D. Buskulic et al.	(ALEPH Collab.)
DECAMP	92	PRL 216 253	D. Decamp et al.	(ALEPH Collab.)
ABE	91E	PRL 67 1502	F. Abe et al.	(CDF Collab.)
ABREU	91H	ZPHY C50 185	P. Abreu et al.	(DELPHI Collab.)
ACTON	91B	PL B273 338	D.P. Acton et al.	(OPAL Collab.)
ADACHI	91	PL B255 613	I. Adachi et al.	(TOPAZ Collab.)
ADEVA	91I	PL B259 199	B. Adeva et al.	(L3 Collab.)
AKRAWY	91F	PL B257 531	M.Z. Akrawy et al.	(OPAL Collab.)
DECAMP	91B	PL B259 377	D. Decamp et al.	(ALEPH Collab.)
DECAMP	91J	PL B266 218	D. Decamp et al.	(ALEPH Collab.)
JACOBSEN	91	PRL 67 3347	R.G. Jacobsen et al.	(Mark II Collab.)
SHIMONAKA	91	PL B268 457	A. Shimonaka et al.	(TOPAZ Collab.)
ABE	90I	ZPHY C48 13	K. Abe et al.	(VENUS Collab.)
ABRAMS	90	PRL 64 1334	G.S. Abrams et al.	(Mark II Collab.)
AKRAWY	90J	PL B246 285	M.Z. Akrawy et al.	(OPAL Collab.)
BEHREND	90D	ZPHY C47 333	H.J. Behrend et al.	(CELLO Collab.)
BRAUNSCH...	90	ZPHY C48 433	W. Braunschweig et al.	(TASSO Collab.)
ELSEN	90	ZPHY C46 349	E. Elsen et al.	(JADE Collab.)
HEGNER	90	ZPHY C46 547	S. Hegner et al.	(JADE Collab.)
STUART	90	PRL 64 983	D. Stuart et al.	(AMY Collab.)
ABE	89	PRL 62 613	F. Abe et al.	(CDF Collab.)
ABE	89C	PRL 63 720	F. Abe et al.	(CDF Collab.)
ABE	89L	PL B232 425	K. Abe et al.	(VENUS Collab.)
ABRAMS	89B	PRL 63 2173	G.S. Abrams et al.	(Mark II Collab.)
ABRAMS	89D	PRL 63 2780	G.S. Abrams et al.	(Mark II Collab.)
ALBAJAR	89	ZPHY C44 15	C. Albajar et al.	(UA1 Collab.)
BACALA	89	PL B218 112	A. Bacala et al.	(AMY Collab.)
BAND	89	PL B218 369	H.R. Band et al.	(MAC Collab.)
GREENSHAW	89	ZPHY C42 1	T. Greenshaw et al.	(JADE Collab.)
OULD-SAAD	89	ZPHY C44 567	F. Ould-Saada et al.	(JADE Collab.)
SAGAWA	89	PRL 63 2341	H. Sagawa et al.	(AMY Collab.)
ADACHI	88C	PL B208 319	I. Adachi et al.	(TOPAZ Collab.)
ADEVA	88	PR D38 2665	B. Adeva et al.	(Mark-J Collab.)
BRAUNSCH...	88D	ZPHY C40 163	W. Braunschweig et al.	(TASSO Collab.)
ANSARI	87	PL B186 440	R. Ansari et al.	(UA2 Collab.)
BEHREND	87C	PL B191 209	H.J. Behrend et al.	(CELLO Collab.)
BARTEL	86C	ZPHY C30 371	W. Bartel et al.	(JADE Collab.)
Also		ZPHY C26 507	W. Bartel et al.	(JADE Collab.)
Also		PL 108B 140	W. Bartel et al.	(JADE Collab.)
ASH	85	PRL 55 1831	W.W. Ash et al.	(MAC Collab.)
BARTEL	85F	PL 161B 188	W. Bartel et al.	(JADE Collab.)
DERRICK	85	PR D31 2352	M. Derrick et al.	(HRS Collab.)
FERNANDEZ	85A	PRL 54 1620	E. Fernandez et al.	(MAC Collab.)
LEVI	83	PRL 51 1941	M.E. Levi et al.	(Mark II Collab.)
BEHREND	82	PL 114B 282	H.J. Behrend et al.	(CELLO Collab.)
BRANDELIC	82C	PL 110B 173	R. Brandelik et al.	(TASSO Collab.)

125.22±0.11±0.09	9 AAD	23BU ATLS	pp, 7, 8, 13 TeV, $\gamma\gamma$
125.78±0.26	10 SIRUNYAN	20L CMS	pp, 13 TeV, $\gamma\gamma$
125.38±0.14	11 SIRUNYAN	20L CMS	pp, 7, 8, 13 TeV, $\gamma\gamma$, $ZZ^* \rightarrow 4\ell$
124.79±0.37	12 AABOUD	18BM ATLS	pp, 13 TeV, $ZZ^* \rightarrow 4\ell$
124.93±0.40	13 AABOUD	18BM ATLS	pp, 13 TeV, $\gamma\gamma$
124.86±0.27	3 AABOUD	18BM ATLS	pp, 13 TeV, $\gamma\gamma$, $ZZ^* \rightarrow 4\ell$
124.97±0.24	3,14 AABOUD	18BM ATLS	pp, 7, 8, 13 TeV, $\gamma\gamma$, $ZZ^* \rightarrow 4\ell$
125.26±0.20±0.08	15 SIRUNYAN	17AV CMS	pp, 13 TeV, $ZZ^* \rightarrow 4\ell$
125.07±0.25±0.14	4 AAD	15B LHC	pp, 7, 8 TeV, $\gamma\gamma$
125.15±0.37±0.15	4 AAD	15B LHC	pp, 7, 8 TeV, $ZZ^* \rightarrow 4\ell$
126.02±0.43±0.27	AAD	15B ATLS	pp, 7, 8 TeV, $\gamma\gamma$
124.51±0.52±0.04	AAD	15B ATLS	pp, 7, 8 TeV, $ZZ^* \rightarrow 4\ell$
125.59±0.42±0.17	AAD	15B CMS	pp, 7, 8 TeV, $ZZ^* \rightarrow 4\ell$
125.02±0.26±0.14	16 KHACHATRY...	15AM CMS	pp, 7, 8 TeV
125.36±0.37±0.18	3,17 AAD	14W ATLS	pp, 7, 8 TeV
125.98±0.42±0.28	17 AAD	14W ATLS	pp, 7, 8 TeV, $\gamma\gamma$
124.51±0.52±0.06	17 AAD	14W ATLS	pp, 7, 8 TeV, $ZZ^* \rightarrow 4\ell$
125.6±0.4±0.2	18 CHATRCHYAN14AA	CMS	pp, 7, 8 TeV, $ZZ^* \rightarrow 4\ell$
122 ± 7	19 CHATRCHYAN14K	CMS	pp, 7, 8 TeV, $\tau\tau$
124.70±0.31±0.15	20 KHACHATRY...14P	CMS	pp, 7, 8 TeV, $\gamma\gamma$
125.5±0.2±0.5	3,21 AAD	13AK ATLS	pp, 7, 8 TeV
126.8±0.2±0.7	21 AAD	13AK ATLS	pp, 7, 8 TeV, $\gamma\gamma$
124.3 +0.6 +0.5	21 AAD	13AK ATLS	pp, 7, 8 TeV, $ZZ^* \rightarrow 4\ell$
125.8±0.4±0.4	3,22 CHATRCHYAN13J	CMS	pp, 7, 8 TeV
126.2±0.6±0.2	22 CHATRCHYAN13J	CMS	pp, 7, 8 TeV, $ZZ^* \rightarrow 4\ell$
126.0±0.4±0.4	3,23 AAD	12AI ATLS	pp, 7, 8 TeV
125.3±0.4±0.5	3,24 CHATRCHYAN12N	CMS	pp, 7, 8 TeV

WEIGHTED AVERAGE
125.20±0.11 (Error scaled by 1.4)



H

was H^0

In the following H refers to the signal that has been discovered in the Higgs searches. Whereas the observed signal is labeled as a spin 0 particle and is called a Higgs Boson, the detailed properties of H and its role in the context of electroweak symmetry breaking need to be further clarified. These issues are addressed by the measurements listed below.

Concerning mass limits and cross section limits that have been obtained in the searches for neutral and charged Higgs bosons, see the sections "Searches for Neutral Higgs Bosons" and "Searches for Charged Higgs Bosons (H^\pm and $H^{\pm\pm}$)", respectively.

H MASS

VALUE (GeV)	DOCUMENT ID	TECN	COMMENT
125.20±0.11 OUR AVERAGE	Error includes scale factor of 1.4. See the ideogram below.		
125.10±0.11	1 AAD	23BP ATLS	pp, 13 TeV, $\gamma\gamma$, $ZZ^* \rightarrow 4\ell$
125.46±0.16	2 SIRUNYAN	20L CMS	pp, 13 TeV, $\gamma\gamma$, $ZZ^* \rightarrow 4\ell$
125.09±0.21±0.11	3,4 AAD	15B LHC	pp, 7, 8 TeV
• • • We do not use the following data for averages, fits, limits, etc. • • •			
124.99±0.18±0.04	5 AAD	23AU ATLS	pp, 13 TeV, $ZZ^* \rightarrow 4\ell$
124.94±0.17±0.03	6 AAD	23AU ATLS	pp, 7, 8, 13 TeV, $ZZ^* \rightarrow 4\ell$
125.11±0.11	7 AAD	23BP ATLS	pp, 7, 8, 13 TeV, $\gamma\gamma$, $ZZ^* \rightarrow 4\ell$
125.17±0.11±0.09	8 AAD	23BU ATLS	pp, 13 TeV, $\gamma\gamma$

- AAD 23BP combine 13 TeV results of $H \rightarrow \gamma\gamma$ (AAD 23BU) and $H \rightarrow ZZ^* \rightarrow 4\ell$ where $\ell = e, \mu$ (AAD 23AU) using 140 fb^{-1} of pp collision data. The result is $125.10 \pm 0.09(\text{stat}) \pm 0.07(\text{sys}) \text{ GeV}$.
- SIRUNYAN 20L result of $H \rightarrow \gamma\gamma$ is combined with that of $H \rightarrow ZZ^* \rightarrow 4\ell$ where $\ell = e, \mu$ (SIRUNYAN 17AV).
- Combined value from $\gamma\gamma$ and $ZZ^* \rightarrow 4\ell$ final states.
- ATLAS and CMS data are fitted simultaneously.
- AAD 23AU use 139 fb^{-1} of pp collisions at $E_{\text{cm}} = 13 \text{ TeV}$ with $H \rightarrow ZZ^* \rightarrow 4\ell$ where $\ell = e, \mu$.
- AAD 23AU combine 13 TeV results with 7 and 8 TeV results (AAD 14W).
- AAD 23BP combine 13 TeV results with 7 and 8 TeV results. The result is $125.11 \pm 0.09(\text{stat}) \pm 0.06(\text{sys}) \text{ GeV}$.
- AAD 23BU use 140 fb^{-1} of pp collisions at $E_{\text{cm}} = 13 \text{ TeV}$ with $H \rightarrow \gamma\gamma$.
- AAD 23BU combine 13 TeV results with 7 and 8 TeV results (AAD 15B).
- SIRUNYAN 20L use 35.9 fb^{-1} of pp collisions at $E_{\text{cm}} = 13 \text{ TeV}$ with $H \rightarrow \gamma\gamma$.
- SIRUNYAN 20L combine 13 TeV results with 7 and 8 TeV results (KHACHATRYAN 15AM).
- AABOUD 18BM use 36.1 fb^{-1} of pp collisions at $E_{\text{cm}} = 13 \text{ TeV}$ with $H \rightarrow ZZ^* \rightarrow 4\ell$ where $\ell = e, \mu$.
- AABOUD 18BM use 36.1 fb^{-1} of pp collisions at $E_{\text{cm}} = 13 \text{ TeV}$ with $H \rightarrow \gamma\gamma$.
- AABOUD 18BM combine 13 TeV results with 7 and 8 TeV results. Other combined results are summarized in their Fig. 4.
- SIRUNYAN 17AV use 35.9 fb^{-1} of pp collisions at $E_{\text{cm}} = 13 \text{ TeV}$ with $H \rightarrow ZZ^* \rightarrow 4\ell$ where $\ell = e, \mu$.
- KHACHATRYAN 15AM use up to 5.1 fb^{-1} of pp collisions at $E_{\text{cm}} = 7 \text{ TeV}$ and up to 19.7 fb^{-1} at $E_{\text{cm}} = 8 \text{ TeV}$.
- AAD 14W use 4.5 fb^{-1} of pp collisions at $E_{\text{cm}} = 7 \text{ TeV}$ and 20.3 fb^{-1} at 8 TeV .
- CHATRCHYAN 14AA use 5.1 fb^{-1} of pp collisions at $E_{\text{cm}} = 7 \text{ TeV}$ and 19.7 fb^{-1} at $E_{\text{cm}} = 8 \text{ TeV}$.
- CHATRCHYAN 14K use 4.9 fb^{-1} of pp collisions at $E_{\text{cm}} = 7 \text{ TeV}$ and 19.7 fb^{-1} at $E_{\text{cm}} = 8 \text{ TeV}$.

- 20 KHACHATRYAN 14P use 5.1 fb⁻¹ of pp collisions at $E_{\text{cm}} = 7$ TeV and 19.7 fb⁻¹ at $E_{\text{cm}} = 8$ TeV.
- 21 AAD 13AK use 4.7 fb⁻¹ of pp collisions at $E_{\text{cm}} = 7$ TeV and 20.7 fb⁻¹ at $E_{\text{cm}} = 8$ TeV. Superseded by AAD 14w.
- 22 CHATRCHYAN 13J use 5.1 fb⁻¹ of pp collisions at $E_{\text{cm}} = 7$ TeV and 12.2 fb⁻¹ at $E_{\text{cm}} = 8$ TeV.
- 23 AAD 12AI obtain results based on 4.6–4.8 fb⁻¹ of pp collisions at $E_{\text{cm}} = 7$ TeV and 5.8–5.9 fb⁻¹ at $E_{\text{cm}} = 8$ TeV. An excess of events over background with a local significance of 5.9 σ is observed at $m_H = 126$ GeV. See also AAD 12DA.
- 24 CHATRCHYAN 12N obtain results based on 4.9–5.1 fb⁻¹ of pp collisions at $E_{\text{cm}} = 7$ TeV and 5.1–5.3 fb⁻¹ at $E_{\text{cm}} = 8$ TeV. An excess of events over background with a local significance of 5.0 σ is observed at about $m_H = 125$ GeV. See also CHATRCHYAN 12BY and CHATRCHYAN 13Y.

H SPIN AND CP PROPERTIES

The observation of the signal in the $\gamma\gamma$ final state rules out the possibility that the discovered particle has spin 1, as a consequence of the Landau-Yang theorem. This argument relies on the assumptions that the decaying particle is an on-shell resonance and that the decay products are indeed two photons rather than two pairs of boosted photons, which each could in principle be misidentified as a single photon.

Concerning distinguishing the spin 0 hypothesis from a spin 2 hypothesis, some care has to be taken in modelling the latter in order to ensure that the discriminating power is actually based on the spin properties rather than on unphysical behavior that may affect the model of the spin 2 state.

Under the assumption that the observed signal consists of a single state rather than an overlap of more than one resonance, it is sufficient to discriminate between distinct hypotheses in the spin analyses. On the other hand, the determination of the CP properties is in general much more difficult since in principle the observed state could consist of any admixture of CP-even and CP-odd components. As a first step, the compatibility of the data with distinct hypotheses of pure CP-even and pure CP-odd states with different spin assignments has been investigated. In order to treat the case of a possible mixing of different CP states, certain cross section ratios are considered. Those cross section ratios need to be distinguished from the amount of mixing between a CP-even and a CP-odd state, as the cross section ratios depend in addition also on the coupling strengths of the CP-even and CP-odd components to the involved particles. A small relative coupling implies a small sensitivity of the corresponding cross section ratio to effects of CP mixing.

VALUE	DOCUMENT ID	TECN	COMMENT
• • •	We do not use the following data for averages, fits, limits, etc. • • •		
1	AAD	23AK ATLS	$H \rightarrow \tau\tau$, 13 TeV
2	AAD	23AN ATLS	$H \rightarrow \gamma\gamma$, VBF, 13 TeV
3	TUMASYAN	23AJ CMS	$H \rightarrow \tau\tau$, 13 TeV
4	TUMASYAN	23P CMS	$t\bar{t}H, H \rightarrow WW^*, \tau\tau$, 13 TeV
5	AAD	22V ATLS	$WW^* (\rightarrow e\nu\mu\nu) + 2j$, 13 TeV
6	TUMASYAN	22Y CMS	$H \rightarrow \tau\tau$, 13 TeV
7	AAD	20N ATLS	$H \rightarrow \tau\tau$, VBF, 13 TeV
8	AAD	20Z ATLS	$t\bar{t}H, H \rightarrow \gamma\gamma$, 13 TeV
9	SIRUNYAN	20AS CMS	$t\bar{t}H, H \rightarrow \gamma\gamma$, 13 TeV
10	SIRUNYAN	19BL CMS	$pp, 7, 8, 13$ TeV, $ZZ^*/ZZ \rightarrow 4\ell$
11	SIRUNYAN	19BZ CMS	$pp \rightarrow H + 2\text{jets}$ (VBF, ggF, VH), $H \rightarrow \tau\tau$, 13 TeV
12	AABOUD	18AJ ATLS	$H \rightarrow ZZ^* \rightarrow 4\ell$ ($\ell = e, \mu$), 13 TeV
13	SIRUNYAN	17AM CMS	$pp \rightarrow H + \geq 2j, H \rightarrow 4\ell$ ($\ell = e, \mu$)
14	AAD	16 ATLS	$H \rightarrow \gamma\gamma$
15	AAD	16BL ATLS	$pp \rightarrow HjjX$ (VBF), $H \rightarrow \tau\tau$, 8 TeV
16	KHACHATRYAN	16AB CMS	$pp \rightarrow WH, ZH, H \rightarrow b\bar{b}$, 8 TeV
17	AAD	15AX ATLS	$H \rightarrow WW^*$
18	AAD	15CI ATLS	$H \rightarrow ZZ^*, WW^*, \gamma\gamma$
19	AALTONEN	15 TEVA	$p\bar{p} \rightarrow WH, ZH, H \rightarrow b\bar{b}$
20	AALTONEN	15B CDF	$p\bar{p} \rightarrow WH, ZH, H \rightarrow b\bar{b}$
21	KHACHATRYAN	15Y CMS	$H \rightarrow 4\ell, WW^*, \gamma\gamma$
22	ABAZOV	14F D0	$p\bar{p} \rightarrow WH, ZH, H \rightarrow b\bar{b}$
23	CHATRCHYAN	14AA CMS	$H \rightarrow ZZ^*$
24	CHATRCHYAN	14G CMS	$H \rightarrow WW^*$
25	KHACHATRYAN	14P CMS	$H \rightarrow \gamma\gamma$
26	AAD	13AJ ATLS	$H \rightarrow \gamma\gamma, ZZ^* \rightarrow 4\ell, WW^* \rightarrow \ell\nu\ell\nu$
27	CHATRCHYAN	13J CMS	$H \rightarrow ZZ^* \rightarrow 4\ell$

- 1 AAD 23AK measure the CP structure of the τ Yukawa coupling using 139 fb⁻¹ of data at $E_{\text{cm}} = 13$ TeV. The CP-mixing angle α for τ Yukawa coupling is measured to be $9 \pm 16^\circ$. The data disfavour the pure CP-odd ($\alpha = 90^\circ$) at 3.4 σ .
- 2 AAD 23AN test CP invariance in H production via VBF using $H \rightarrow \gamma\gamma$ decay channel with 139 fb⁻¹ at $E_{\text{cm}} = 13$ TeV. By using the Optimal Observable method, the data constrain parameters describing the strength of the CP-odd component in the coupling between Higgs and W/Z in effective field theory bases: \tilde{d} in the HISZ basis and $C_{H\tilde{W}}$ in the Warsaw basis. The result is $-0.010 \leq \tilde{d} \leq 0.040$ and $-0.15 \leq C_{H\tilde{W}} \leq 0.67$ at 68% CL. See their Table I, which shows the result combined with $H \rightarrow \tau\tau$ (AAD 20N): $-0.012 \leq \tilde{d} \leq 0.030$ at 68% CL.
- 3 TUMASYAN 23AJ constrain anomalous couplings of the Higgs to vector bosons and fermions using $pp \rightarrow H \rightarrow \tau\tau$ at $E_{\text{cm}} = 13$ TeV with 138 fb⁻¹ data. The CP-violating parameter in gluon-fusion production f_{a3}^{ggH} and the effective mixing angle α_{Hff} are given in their Table VII with $H \rightarrow \tau\tau$ and f_{a3}^{ggH} in their Table X with $H \rightarrow \tau\tau$ and $H \rightarrow 4\ell$. Using the VBF production analysis, the CP-violating parameter f_{a3} and CP-conserving parameters $f_{a2}, f_{\Lambda 1}$ and $f_{\Lambda 1}^{Z\gamma}$ are given in their Table VIII with $H \rightarrow \tau\tau$ and Table IX with $H \rightarrow \tau\tau$ and $H \rightarrow 4\ell$. The CP-violating parameter $f_{CP}^{H\tilde{t}t}$ is constrained to be $0.03^{+0.17}_{-0.03}$ using $H \rightarrow \tau\tau, H \rightarrow 4\ell$ and $H \rightarrow \gamma\gamma$.

- 4 TUMASYAN 23P constrain $\tilde{\kappa}_t$ from $t\bar{t}H$ and tH decaying $H \rightarrow WW^*$ and $H \rightarrow \tau\tau$ (multiplepton decay mode) with 138 fb⁻¹ pp collision data at $E_{\text{cm}} = 13$ TeV. The $\tilde{\kappa}_t$ is constrained to be $|\tilde{\kappa}_t| \leq 1.4$ at 95% CL by fixing $\kappa_t = 1$ and other couplings (κ_V etc.) to the SM values, see their Table 6 (see their Fig. 9 for 2-dim contours). The fractional contribution of the CP-odd component $|f_{CP}^{H\tilde{t}t}|$ is constrained to (0.24, 0.81) at 68% CL with a best fit value of 0.59. The combination with other $t\bar{t}H$ decaying $H \rightarrow \gamma\gamma$ (SIRUNYAN 20AS) and $H \rightarrow 4\ell$ (SIRUNYAN 21AE) constraints to be $|\tilde{\kappa}_t| \leq 1.07$ at 95% CL and $|f_{CP}^{H\tilde{t}t}| < 0.55$ at 68% CL with a best fit value of 0.28.
- 5 AAD 22V measure the CP properties of the effective Higgs-gluon interaction using gluon fusion $H \rightarrow WW^* \rightarrow e\nu\mu\nu$ plus two jets with 36.1 fb⁻¹ of data at $E_{\text{cm}} = 13$ TeV. The measured tangent of the CP-mixing angle α is $0.0 \pm 0.4 \pm 0.3$ assuming the standard model HVV couplings. See their Fig. 6.
- 6 TUMASYAN 22Y measure the CP structure of the τ Yukawa coupling using 137 fb⁻¹ of data at $E_{\text{cm}} = 13$ TeV. The CP-mixing angle α for τ Yukawa coupling is measured to be $-1 \pm 19^\circ$. The data disfavour the pure CP-odd ($\alpha = 90^\circ$) at 3.0 σ .
- 7 AAD 20N test CP invariance in H production via VBF using $H \rightarrow \tau\tau$ decay channel with 36.1 fb⁻¹ at $E_{\text{cm}} = 13$ TeV. By using the Optimal Observable method, the data constrain a parameter \tilde{d} , which is for the strength of CP violation in an effective field theory, to be $-0.090 \leq \tilde{d} \leq 0.035$ at 68% CL (see their Fig. 6).
- 8 AAD 20Z exclude a CP-mixing angle $\alpha, |\alpha| > 43^\circ$ at 95% CL, where $\alpha = 0$ represents the Standard Model, in 139 fb⁻¹ of data at $E_{\text{cm}} = 13$ TeV. The pure CP-odd structure of the top Yukawa coupling ($\alpha = 90^\circ$) is excluded at 3.9 σ .
- 9 SIRUNYAN 20AS exclude the pure CP-odd structure of the top Yukawa coupling at 3.2 σ using $t\bar{t}H, H \rightarrow \gamma\gamma$ in 137 fb⁻¹ of data at $E_{\text{cm}} = 13$ TeV. The fractional contribution of the CP-odd component $f_{CP}^{H\tilde{t}t}$ is measured to be 0.00 ± 0.33 .
- 10 SIRUNYAN 19BL measure the anomalous HVV couplings from on-shell and off-shell production in the 4ℓ final state. Data of 80.2 fb⁻¹ at 13 TeV, 19.7 fb⁻¹ at 8 TeV, and 5.1 fb⁻¹ at 7 TeV are used. See their Tables VI and VII for anomalous HVV couplings of CP-violating and CP-conserving parameters with on- and off-shells.
- 11 SIRUNYAN 19BZ constrain anomalous HVV couplings of the Higgs boson with data of 35.9 fb⁻¹ at $E_{\text{cm}} = 13$ TeV using Higgs boson candidates with two jets produced in VBF, ggF, and VH that decay to $\tau\tau$. See their Table 2 and Fig. 10, which show 68% CL and 95% CL intervals. Combining those with the $H \rightarrow 4\ell$ (SIRUNYAN 19BL, on-shell scenario), results shown in their Tables 3, 4, and Fig. 11 are obtained. A CP-violating parameter is set to be $f_{a3}\cos(\phi_{a3}) = (0.00 \pm 0.27) \times 10^{-3}$ and CP-conserving parameters are $f_{a2}\cos(\phi_{a2}) = (0.08^{+1.04}_{-0.21}) \times 10^{-3}$, $f_{\Lambda 1}\cos(\phi_{\Lambda 1}) = (0.00^{+0.53}_{-0.09}) \times 10^{-3}$, and $f_{\Lambda 1}^{Z\gamma}\cos(\phi_{\Lambda 1}^{Z\gamma}) = (0.0^{+1.1}_{-1.3}) \times 10^{-3}$.
- 12 AABOUD 18AJ study the tensor structure of the Higgs boson couplings using an effective Lagrangian using 36.1 fb⁻¹ of pp collision data at $E_{\text{cm}} = 13$ TeV. Constraints are set on the non-Standard-Model CP-even and CP-odd couplings to Z bosons and on the CP-odd coupling to gluons. See their Figs. 9 and 10, and Tables 10 and 11.
- 13 SIRUNYAN 17AM constrain anomalous couplings of the Higgs boson with 5.1 fb⁻¹ of pp collisions at $E_{\text{cm}} = 7$ TeV, 19.7 fb⁻¹ at $E_{\text{cm}} = 8$ TeV, and 38.6 fb⁻¹ at $E_{\text{cm}} = 13$ TeV. See their Table 3 and Fig. 3, which show 68% CL and 95% CL intervals. A CP violation parameter f_{a3} is set to be $f_{a3}\cos(\phi_{a3}) = [-0.38, 0.46]$ at 95% CL ($\phi_{a3} = 0$ or π).
- 14 AAD 16 study $H \rightarrow \gamma\gamma$ with an effective Lagrangian including CP even and odd terms in 20.3 fb⁻¹ of pp collisions at $E_{\text{cm}} = 8$ TeV. The data is consistent with the expectations for the Higgs boson of the Standard Model. Limits on anomalous couplings are also given.
- 15 AAD 16BL study VBF $H \rightarrow \tau\tau$ with an effective Lagrangian including a CP odd term in 20.3 fb⁻¹ of pp collisions at $E_{\text{cm}} = 8$ TeV. The measurement is consistent with the expectation of the Standard Model. The CP-mixing parameter \tilde{d} (a dimensionless coupling $\tilde{d} = -(m_W^2/\Lambda^2)f_{\tilde{W}W}$) is constrained to the interval of $(-0.11, 0.05)$ at 68% CL under the assumption of $\tilde{d} = \tilde{d}_B$.
- 16 KHACHATRYAN 16AB search for anomalous pseudoscalar couplings of the Higgs boson to W and Z with 18.9 fb⁻¹ of pp collisions at $E_{\text{cm}} = 8$ TeV. See their Table 5 and Figs 5 and 6 for limits on possible anomalous pseudoscalar coupling parameters.
- 17 AAD 15AX compare the $J^{CP} = 0^+$ Standard Model assignment with other J^{CP} hypotheses in 20.3 fb⁻¹ of pp collisions at $E_{\text{cm}} = 8$ TeV, using the process $H \rightarrow WW^* \rightarrow e\nu\mu\nu$. 2^+ hypotheses are excluded at 84.5–99.4%CL, 0^- at 96.5%CL, 0^+ (field strength coupling) at 70.8%CL. See their Fig. 19 for limits on possible CP mixture parameters.
- 18 AAD 15CI compare the $J^{CP} = 0^+$ Standard Model assignment with other J^{CP} hypotheses in 4.5 fb⁻¹ of pp collisions at $E_{\text{cm}} = 7$ TeV and 20.3 fb⁻¹ at $E_{\text{cm}} = 8$ TeV, using the processes $H \rightarrow ZZ^* \rightarrow 4\ell, H \rightarrow \gamma\gamma$ and combine with AAD 15AX data. 0^+ (field strength coupling), 0^- and several 2^+ hypotheses are excluded at more than 99.9% CL. See their Tables 7–9 for limits on possible CP mixture parameters.
- 19 AALTONEN 15 combine AALTONEN 15B and ABAZOV 14F data. An upper limit of 0.36 of the Standard Model production rate at 95% CL is obtained both for a 0^- and a 2^+ state. Assuming the SM event rate, the $J^{CP} = 0^-$ (2^+) hypothesis is excluded at the 5.0 σ (4.9 σ) level.
- 20 AALTONEN 15B compare the $J^{CP} = 0^+$ Standard Model assignment with other J^{CP} hypotheses in 9.45 fb⁻¹ of $p\bar{p}$ collisions at $E_{\text{cm}} = 1.96$ TeV, using the processes $ZH \rightarrow \ell\ell b\bar{b}, WH \rightarrow \ell\nu b\bar{b}$, and $ZH \rightarrow \nu\nu b\bar{b}$. Bounds on the production rates of 0^- and 2^+ (graviton-like) states are set, see their tables II and III.
- 21 KHACHATRYAN 15Y compare the $J^{CP} = 0^+$ Standard Model assignment with other J^{CP} hypotheses in up to 5.1 fb⁻¹ of pp collisions at $E_{\text{cm}} = 7$ TeV and up to 19.7 fb⁻¹ at $E_{\text{cm}} = 8$ TeV, using the processes $H \rightarrow 4\ell, H \rightarrow WW^*$, and $H \rightarrow \gamma\gamma$. 0^- is excluded at 99.98% CL, and several 2^+ hypotheses are excluded at more than 99% CL. Spin 1 models are excluded at more than 99.999% CL in ZZ^* and WW^* modes. Limits on anomalous couplings and several cross section fractions, treating the case of CP-mixed states, are also given.
- 22 ABAZOV 14F compare the $J^{CP} = 0^+$ Standard Model assignment with $J^{CP} = 0^-$ and 2^+ (graviton-like coupling) hypotheses in up to 9.7 fb⁻¹ of $p\bar{p}$ collisions at $E_{\text{cm}} = 1.96$ TeV. They use kinematic correlations between the decay products of the vector boson and the Higgs boson in the final states $ZH \rightarrow \ell\ell b\bar{b}, WH \rightarrow \ell\nu b\bar{b}$, and $ZH \rightarrow$

Gauge & Higgs Boson Particle Listings

H

- $\nu\nu\bar{\nu}$. The 0^- (2^+) hypothesis is excluded at 97.6% CL (99.0% CL). In order to treat the case of a possible mixture of a 0^+ state with another J^{CP} state, the cross section fractions $f_X = \sigma_X / (\sigma_{0^+} + \sigma_X)$ are considered, where $X = 0^-, 2^+$. Values for f_{0^-} (f_{2^+}) above 0.80 (0.67) are excluded at 95% CL under the assumption that the total cross section is that of the SM Higgs boson.
- 23 CHATRCHYAN 14AA compare the $J^{CP} = 0^+$ Standard Model assignment with various J^{CP} hypotheses in 5.1 fb $^{-1}$ of pp collisions at $E_{cm} = 7$ TeV and 19.7 fb $^{-1}$ at $E_{cm} = 8$ TeV. $J^{CP} = 0^-$ and 1^\pm hypotheses are excluded at 99% CL, and several $J = 2$ hypotheses are excluded at 95% CL. In order to treat the case of a possible mixture of a 0^+ state with another J^{CP} state, the cross section fraction $f_{a3} = |a_3|^2 \sigma_3 / (|a_1|^2 \sigma_1 + |a_2|^2 \sigma_2 + |a_3|^2 \sigma_3)$ is considered, where the case $a_3 = 1, a_1 = a_2 = 0$ corresponds to a pure CP -odd state. Assuming $a_2 = 0$, a value for f_{a3} above 0.51 is excluded at 95% CL.
- 24 CHATRCHYAN 14G compare the $J^{CP} = 0^+$ Standard Model assignment with $J^{CP} = 0^-$ and 2^+ (graviton-like coupling) hypotheses in 4.9 fb $^{-1}$ of pp collisions at $E_{cm} = 7$ TeV and 19.4 fb $^{-1}$ at $E_{cm} = 8$ TeV. Varying the fraction of the production of the 2^+ state via gg and $q\bar{q}$, 2^+ hypotheses are disfavored at CL between 83.7 and 99.8%. The 0^- hypothesis is disfavored against 0^+ at the 65.3% CL.
- 25 KHACHATRYAN 14P compare the $J^{CP} = 0^+$ Standard Model assignment with a 2^+ (graviton-like coupling) hypothesis in 5.1 fb $^{-1}$ of pp collisions at $E_{cm} = 7$ TeV and 19.7 fb $^{-1}$ at $E_{cm} = 8$ TeV. Varying the fraction of the production of the 2^+ state via gg and $q\bar{q}$, 2^+ hypotheses are disfavored at CL between 71 and 94%.
- 26 AAD 13AJ compare the spin 0, CP -even hypothesis with specific alternative hypotheses of spin 0, CP -odd, spin 1, CP -even and CP -odd, and spin 2, CP -even models using the Higgs boson decays $H \rightarrow \gamma\gamma$, $H \rightarrow ZZ^* \rightarrow 4\ell$ and $H \rightarrow WW^* \rightarrow \ell\nu\ell\nu$ and combinations thereof. The data are compatible with the spin 0, CP -even hypothesis, while all other tested hypotheses are excluded at confidence levels above 97.8%.
- 27 CHATRCHYAN 13J study angular distributions of the lepton pairs in the ZZ^* channel where both Z bosons decay to e or μ pairs. Under the assumption that the observed particle has spin 0, the data are found to be consistent with the pure CP -even hypothesis, while the pure CP -odd hypothesis is disfavored.

H DECAY WIDTH

The total decay width for a light Higgs boson with a mass in the observed range is not expected to be directly observable at the LHC. For the case of the Standard Model the prediction for the total width is about 4 MeV, which is three orders of magnitude smaller than the experimental mass resolution. There is no indication from the results observed so far that the natural width is broadened by new physics effects to such an extent that it could be directly observable. Furthermore, as all LHC Higgs channels rely on the identification of Higgs decay products, the total Higgs width cannot be measured indirectly without additional assumptions. The different dependence of on-peak and off-peak contributions on the total width in Higgs decays to ZZ^* and interference effects between signal and background in Higgs decays to $\gamma\gamma$ can provide additional information in this context. Constraints on the total width from the combination of on-peak and off-peak contributions in Higgs decays to ZZ^* rely on the assumption of equal on- and off-shell effective couplings. Without an experimental determination of the total width or further theoretical assumptions, only ratios of couplings can be determined at the LHC rather than absolute values of couplings.

VALUE (MeV)	CL%	DOCUMENT ID	TECN	COMMENT
$3.7^{+1.9}_{-1.4}$				OUR AVERAGE
$4.5^{+3.3}_{-2.5}$	95	1 AAD	23BR ATLS	$pp, 13 \text{ TeV}, ZZ^*/ZZ \rightarrow 4\ell, ZZ \rightarrow 2\ell 2\nu$
$3.2^{+2.4}_{-1.7}$	95	2 TUMASYAN	22AM CMS	$pp, 13 \text{ TeV}, ZZ^*/ZZ \rightarrow 4\ell, ZZ \rightarrow 2\ell 2\nu$
$3.2^{+2.8}_{-2.2}$	95	3 SIRUNYAN	19BL CMS	$pp, 7, 8, 13 \text{ TeV}, ZZ^*/ZZ \rightarrow 4\ell$
< 14.4	95	4 AABOUD	18BP ATLS	$pp, 13 \text{ TeV}, ZZ \rightarrow 4\ell, 2\ell 2\nu$
< 1100	95	5 SIRUNYAN	17AV CMS	$pp, 13 \text{ TeV}, ZZ^* \rightarrow 4\ell$
< 26	95	6 KHACHATRYAN	16BA CMS	$pp, 7, 8 \text{ TeV}, WW^*$
< 13	95	7 KHACHATRYAN	16BA CMS	$pp, 7, 8 \text{ TeV}, ZZ^*(^*), WW^*$
< 22.7	95	8 AAD	15BE ATLS	$pp, 8 \text{ TeV}, ZZ^*(^*), WW^*$
< 1700	95	9 KHACHATRYAN	15AM CMS	$pp, 7, 8 \text{ TeV}$
> 3.5×10^{-9}	95	10 KHACHATRYAN	15BA CMS	$pp, 7, 8 \text{ TeV}$, flight distance
< 46	95	11 KHACHATRYAN	15BA CMS	$pp, 7, 8 \text{ TeV}, ZZ^*(^*) \rightarrow 4\ell$
< 5000	95	12 AAD	14W ATLS	$pp, 7, 8 \text{ TeV}, \gamma\gamma$
< 2600	95	12 AAD	14W ATLS	$pp, 7, 8 \text{ TeV}, ZZ^* \rightarrow 4\ell$
< 3400	95	13 CHATRCHYAN	14AA CMS	$pp, 7, 8 \text{ TeV}, ZZ^* \rightarrow 4\ell$
< 22	95	14 KHACHATRYAN	14D CMS	$pp, 7, 8 \text{ TeV}, ZZ^*(^*)$
< 2400	95	15 KHACHATRYAN	14P CMS	$pp, 7, 8 \text{ TeV}, \gamma\gamma$

1 AAD 23BR use 139 fb $^{-1}$ at $E_{cm} = 13$ TeV. The off-shell Higgs boson production in the $ZZ \rightarrow 4\ell$ and $ZZ \rightarrow 2\ell 2\nu$ decay channels and the on-shell production in the $ZZ^* \rightarrow 4\ell$ ($\ell = e, \mu$, AAD 20AQ) decay channels are used to measure the total width. The off-shell Higgs signal strength is measured to be $1.1^{+0.7}_{-0.6}$ assuming the same on-shell and off-shell coupling modifiers are used individually for gluon-fusion and for gauge-boson modes. The scenario of no off-shell contribution is excluded at 3.3 σ . Combining with the on-shell signal strength measurement, the total width normalized to its SM expectation Γ_H/Γ_H^{SM} is measured to be $1.1^{+0.7}_{-0.6}$ assuming the same on-shell and off-shell coupling modifiers are used individually for gluon-fusion and for gauge-boson modes. The observed upper limit on the total width is 10.5 MeV at 95% CL. See their Fig. 7.

- 2 TUMASYAN 22AM use up to 140 fb $^{-1}$ at $E_{cm} = 13$ TeV. The off-shell Higgs boson production in the $ZZ \rightarrow 4\ell$ and $ZZ \rightarrow 2\ell 2\nu$ decay channels and the on-shell production in the $ZZ^* \rightarrow 4\ell$ ($\ell = e, \mu$) decay channels are used to measure the total width. The off-shell Higgs signal strength is measured to be $0.62^{+0.68}_{-0.45}$ without the constraint on the ratio of the off-shell signal strengths for gluon-fusion and gauge-boson modes. The scenario of no off-shell contribution is excluded at 3.6 σ . The results are shown in their Table 1 with other constraint scenarios and the decay widths assuming the same coupling modifiers for on- and off-shell couplings (g_p and g_d in their notation). The measurement of anomalous HVV couplings is shown in their Extended Data Table 1 and Fig. 8.
- 3 SIRUNYAN 19BL measure the width and anomalous HVV couplings from on-shell and off-shell production in the 4ℓ final state. Data of 80.2 fb $^{-1}$ at 13 TeV, 19.7 fb $^{-1}$ at 8 TeV, and 5.1 fb $^{-1}$ at 7 TeV are used. The total width for the SM-like couplings is measured to be also [0.08, 9.16] MeV with 95% CL, assuming SM-like couplings for on- and off-shells (see their Table VIII). Constraints on the total width for anomalous HVV interaction cases are found in their Table IX. See their Table X for the Higgs boson signal strength in the off-shell region.
- 4 AABOUD 18BP use 36.1 fb $^{-1}$ at $E_{cm} = 13$ TeV. An observed upper limit on the off-shell Higgs signal strength of 3.8 is obtained at 95% CL using off-shell Higgs boson production in the $ZZ \rightarrow 4\ell$ and $ZZ \rightarrow 2\ell 2\nu$ decay channels ($\ell = e, \mu$). Combining with the on-shell signal strength measurements, the quoted upper limit on the Higgs boson total width is obtained, assuming the ratios of the relevant Higgs-boson couplings to the SM predictions are constant with energy from on-shell production to the high-mass range.
- 5 SIRUNYAN 17AV obtain an upper limit on the width from the $m_{4\ell}$ distribution in $ZZ^* \rightarrow 4\ell$ ($\ell = e, \mu$) decays. Data of 35.9 fb $^{-1}$ pp collisions at $E_{cm} = 13$ TeV is used. The expected limit is 1.60 GeV.
- 6 KHACHATRYAN 16BA derive constraints on the total width from comparing WW^* production via on-shell and off-shell H using 4.9 fb $^{-1}$ of pp collisions at $E_{cm} = 7$ TeV and 19.4 fb $^{-1}$ at 8 TeV.
- 7 KHACHATRYAN 16BA combine the WW^* result with $ZZ^*(^*)$ results of KHACHATRYAN 15BA and KHACHATRYAN 14D.
- 8 AAD 15BE derive constraints on the total width from comparing $ZZ^*(^*)$ and WW^* production via on-shell and off-shell H using 20.3 fb $^{-1}$ of pp collisions at $E_{cm} = 8$ TeV. The K factor for the background processes is assumed to be equal to that for the signal.
- 9 KHACHATRYAN 15AM combine $\gamma\gamma$ and $ZZ^* \rightarrow 4\ell$ results. The expected limit is 2.3 GeV.
- 10 KHACHATRYAN 15BA derive a lower limit on the total width from an upper limit on the decay flight distance $\tau < 1.9 \times 10^{-13}$ s. 5.1 fb $^{-1}$ of pp collisions at $E_{cm} = 7$ TeV and 19.7 fb $^{-1}$ at 8 TeV are used.
- 11 KHACHATRYAN 15BA derive constraints on the total width from comparing $ZZ^*(^*)$ production via on-shell and off-shell H with an unconstrained anomalous coupling. 4ℓ final states in 5.1 fb $^{-1}$ of pp collisions at $E_{cm} = 7$ TeV and 19.7 fb $^{-1}$ at $E_{cm} = 8$ TeV are used.
- 12 AAD 14W use 4.5 fb $^{-1}$ of pp collisions at $E_{cm} = 7$ TeV and 20.3 fb $^{-1}$ at 8 TeV. The expected limit is 6.2 GeV.
- 13 CHATRCHYAN 14AA use 5.1 fb $^{-1}$ of pp collisions at $E_{cm} = 7$ TeV and 19.7 fb $^{-1}$ at $E_{cm} = 8$ TeV. The expected limit is 2.8 GeV.
- 14 KHACHATRYAN 14D derive constraints on the total width from comparing $ZZ^*(^*)$ production via on-shell and off-shell H . 4ℓ and $\ell\nu\nu$ final states in 5.1 fb $^{-1}$ of pp collisions at $E_{cm} = 7$ TeV and 19.7 fb $^{-1}$ at $E_{cm} = 8$ TeV are used.
- 15 KHACHATRYAN 14P use 5.1 fb $^{-1}$ of pp collisions at $E_{cm} = 7$ TeV and 19.7 fb $^{-1}$ at $E_{cm} = 8$ TeV. The expected limit is 3.1 GeV.

H DECAY MODES

Mode	Fraction (Γ_i/Γ)	Confidence level
Γ_1 WW^*	(25.7 \pm 2.5) %	
Γ_2 ZZ^*	(2.80 \pm 0.30) %	
Γ_3 $\gamma\gamma$	(2.50 \pm 0.20) $\times 10^{-3}$	
Γ_4 $b\bar{b}$	(53 \pm 8) %	
Γ_5 e^+e^-	< 3.0	$\times 10^{-4}$ 95%
Γ_6 $\mu^+\mu^-$	(2.6 \pm 1.3) $\times 10^{-4}$	
Γ_7 $\tau^+\tau^-$	(6.0 $^{+0.8}_{-0.7}$) %	
Γ_8 $Z\gamma$	(3.4 \pm 1.1) $\times 10^{-3}$	
Γ_9 $Z\rho(770)$	< 1.21	% 95%
Γ_{10} $Z\phi(1020)$	< 3.6	$\times 10^{-3}$ 95%
Γ_{11} $Z\eta_c$		
Γ_{12} ZJ/ψ	< 1.9	$\times 10^{-3}$ 95%
Γ_{13} $Z\psi(2S)$	< 6.6	$\times 10^{-3}$ 95%
Γ_{14} $J/\psi\gamma$	< 2.0	$\times 10^{-4}$ 95%
Γ_{15} $J/\psi J/\psi$	< 3.8	$\times 10^{-4}$ 95%
Γ_{16} $\psi(2S)\gamma$	< 1.05	$\times 10^{-3}$ 95%
Γ_{17} $\psi(2S)J/\psi$	< 2.1	$\times 10^{-3}$ 95%
Γ_{18} $\psi(2S)\psi(2S)$	< 3.0	$\times 10^{-3}$ 95%
Γ_{19} $\Upsilon(1S)\gamma$	< 2.5	$\times 10^{-4}$ 95%
Γ_{20} $\Upsilon(1S)\Upsilon(1S)$	< 1.7	$\times 10^{-3}$ 95%
Γ_{21} $\Upsilon(2S)\gamma$	< 4.2	$\times 10^{-4}$ 95%
Γ_{22} $\Upsilon(3S)\gamma$	< 3.4	$\times 10^{-4}$ 95%
Γ_{23} $\Upsilon(nS)\Upsilon(mS)$	< 3.5	$\times 10^{-4}$ 95%
Γ_{24} $\rho(770)\gamma$	< 1.04	$\times 10^{-3}$ 95%
Γ_{25} $\omega(782)\gamma$	< 5.5	$\times 10^{-4}$ 95%
Γ_{26} $K^*(892)\gamma$	< 2.2	$\times 10^{-4}$ 95%
Γ_{27} $\phi(1020)\gamma$	< 5	$\times 10^{-4}$ 95%
Γ_{28} $e\mu$	LF < 4.4	$\times 10^{-5}$ 95%

See key on page 1171

Gauge & Higgs Boson Particle Listings

H

Γ_{29}	$e\tau$	LF	< 2.0	$\times 10^{-3}$	95%
Γ_{30}	$\mu\tau$	LF	< 1.5	$\times 10^{-3}$	95%
Γ_{31}	invisible		< 10.7	%	95%
Γ_{32}	γ invisible		< 2.9	%	95%

H BRANCHING RATIOS

$\Gamma(WW^*)/\Gamma_{\text{total}}$		Γ_1/Γ	
VALUE	DOCUMENT ID	TECN	COMMENT
0.257 ± 0.026 -0.024	¹ ATLAS	22 ATLS	pp, 13 TeV

¹ ATLAS 22 report combined results (see their Extended Data Table 1) using up to 139 fb⁻¹ of data at $E_{\text{cm}} = 13$ TeV, assuming $m_H = 125.09$ GeV. SM values for the production cross-sections are assumed. See their Fig. 2b.

$\Gamma(ZZ^*)/\Gamma_{\text{total}}$		Γ_2/Γ	
VALUE	DOCUMENT ID	TECN	COMMENT
0.028 ± 0.003	¹ ATLAS	22 ATLS	pp, 13 TeV

¹ ATLAS 22 report combined results (see their Extended Data Table 1) using up to 139 fb⁻¹ of data at $E_{\text{cm}} = 13$ TeV, assuming $m_H = 125.09$ GeV. SM values for the production cross-sections are assumed. See their Fig. 2b.

$\Gamma(\gamma\gamma)/\Gamma_{\text{total}}$		Γ_3/Γ	
VALUE	DOCUMENT ID	TECN	COMMENT
0.0025 ± 0.0002	¹ ATLAS	22 ATLS	pp, 13 TeV

¹ ATLAS 22 report combined results (see their Extended Data Table 1) using up to 139 fb⁻¹ of data at $E_{\text{cm}} = 13$ TeV, assuming $m_H = 125.09$ GeV. SM values for the production cross-sections are assumed. See their Fig. 2b.

$\Gamma(b\bar{b})/\Gamma_{\text{total}}$		Γ_4/Γ	
VALUE	DOCUMENT ID	TECN	COMMENT
0.53 ± 0.08	¹ ATLAS	22 ATLS	pp, 13 TeV

¹ ATLAS 22 report combined results (see their Extended Data Table 1) using up to 139 fb⁻¹ of data at $E_{\text{cm}} = 13$ TeV, assuming $m_H = 125.09$ GeV. SM values for the production cross-sections are assumed. See their Fig. 2b.

$\Gamma(e^+e^-)/\Gamma_{\text{total}}$		Γ_5/Γ		
VALUE	CL%	DOCUMENT ID	TECN	COMMENT
$< 3.0 \times 10^{-4}$	95	¹ TUMASYAN	23AU CMS	pp, 13 TeV
•••				We do not use the following data for averages, fits, limits, etc. •••
$< 3.6 \times 10^{-4}$	95	² AAD	20F ATLS	pp, 13 TeV
$< 1.9 \times 10^{-3}$	95	³ KHACHATRYAN..15H	CMS	pp, 7, 8 TeV

¹ TUMASYAN 23AU use 138 fb⁻¹ of pp collisions at $E_{\text{cm}} = 13$ TeV.
² AAD 20F use 139 fb⁻¹ of pp collisions at $E_{\text{cm}} = 13$ TeV. The best-fit value of the $H \rightarrow ee$ branching fraction is $(0.0 \pm 1.7 \pm 0.6) \times 10^{-4}$ for $m_H = 125$ GeV.
³ KHACHATRYAN 15H use 5.0 fb⁻¹ of pp collisions at $E_{\text{cm}} = 7$ TeV and 19.7 fb⁻¹ at 8 TeV.

$\Gamma(\mu^+\mu^-)/\Gamma_{\text{total}}$		Γ_6/Γ	
VALUE (units 10^{-4})	DOCUMENT ID	TECN	COMMENT
2.6 ± 1.3	¹ ATLAS	22 ATLS	pp, 13 TeV

¹ ATLAS 22 report combined results (see their Extended Data Table 1) using up to 139 fb⁻¹ of data at $E_{\text{cm}} = 13$ TeV, assuming $m_H = 125.09$ GeV. SM values for the production cross-sections are assumed. See their Fig. 2b.

$\Gamma(\tau^+\tau^-)/\Gamma_{\text{total}}$		Γ_7/Γ	
VALUE	DOCUMENT ID	TECN	COMMENT
0.060 ± 0.008 -0.007	¹ ATLAS	22 ATLS	pp, 13 TeV

¹ ATLAS 22 report combined results (see their Extended Data Table 1) using up to 139 fb⁻¹ of data at $E_{\text{cm}} = 13$ TeV, assuming $m_H = 125.09$ GeV. SM values for the production cross-sections are assumed. See their Fig. 2b.

$\Gamma(Z\gamma)/\Gamma_{\text{total}}$		Γ_8/Γ	
VALUE (units 10^{-3})	DOCUMENT ID	TECN	COMMENT
3.4 ± 1.1	¹ AAD	24D LHC	pp, 13 TeV
•••			We do not use the following data for averages, fits, limits, etc. •••
3.2 ± 1.5	² ATLAS	22 ATLS	pp, 13 TeV

¹ AAD 24d report combined results of ATLAS (AAD 20Ag) and CMS (TUMASYAN 23F). SM values for the production cross-sections are assumed.
² ATLAS 22 report combined results (see their Extended Data Table 1) using up to 139 fb⁻¹ of data at $E_{\text{cm}} = 13$ TeV, assuming $m_H = 125.09$ GeV. SM values for the production cross-sections are assumed. See their Fig. 2b.

$\Gamma(Z\rho(770))/\Gamma_{\text{total}}$		Γ_9/Γ		
VALUE	CL%	DOCUMENT ID	TECN	COMMENT
$< 1.21 \times 10^{-2}$	95	¹ SIRUNYAN	20BK CMS	pp, 13 TeV

¹ SIRUNYAN 20BK search for $H \rightarrow Z\rho$, $Z \rightarrow e^+e^-/\mu^+\mu^-$, $\rho \rightarrow \pi^+\pi^-$ with 137 fb⁻¹ of pp collision data at $E_{\text{cm}} = 13$ TeV. The quoted branching fraction is for the unpolarized decay. See their Table 3 for different polarizations.

$\Gamma(Z\phi(1020))/\Gamma_{\text{total}}$		Γ_{10}/Γ		
VALUE	CL%	DOCUMENT ID	TECN	COMMENT
$< 3.6 \times 10^{-3}$	95	¹ SIRUNYAN	20BK CMS	pp, 13 TeV

¹ SIRUNYAN 20BK search for $H \rightarrow Z\phi$, $Z \rightarrow e^+e^-/\mu^+\mu^-$, $\phi \rightarrow K^+K^-$ with 137 fb⁻¹ of pp collision data at $E_{\text{cm}} = 13$ TeV. The quoted branching fraction is for the unpolarized decay. See their Table 4 for different polarizations.

$\Gamma(Z\eta_c)/\Gamma_{\text{total}}$		Γ_{11}/Γ	
VALUE	DOCUMENT ID	TECN	COMMENT
•••			We do not use the following data for averages, fits, limits, etc. •••
	¹ AAD	20AE ATLS	pp, 13 TeV

¹ AAD 20AE search for $H \rightarrow Z\eta_c$ with two-leptons ($e^+e^-/\mu^+\mu^-$) plus jet events using 139 fb⁻¹ of pp collision data at $E_{\text{cm}} = 13$ TeV. The upper limit of $\sigma(pp \rightarrow H) \cdot \mathcal{B}(H \rightarrow Z\eta_c)$ is 110 pb at 95% CL.

$\Gamma(ZJ/\psi)/\Gamma_{\text{total}}$		Γ_{12}/Γ		
VALUE	CL%	DOCUMENT ID	TECN	COMMENT
$< 1.9 \times 10^{-3}$	95	¹ TUMASYAN	23c CMS	pp, 13 TeV
•••				We do not use the following data for averages, fits, limits, etc. •••
		² AAD	20AE ATLS	pp, 13 TeV

¹ TUMASYAN 23c search for $H \rightarrow ZJ/\psi$, $Z \rightarrow e^+e^-$ or $\mu^+\mu^-$, $J/\psi \rightarrow \mu^+\mu^-$ with 138 fb⁻¹ of pp collision data at $E_{\text{cm}} = 13$ TeV. The quoted value is for the Higgs decays for longitudinally polarized mesons. See their Table 1 for other cases.
² AAD 20AE search for $H \rightarrow ZJ/\psi$ with two-leptons ($e^+e^-/\mu^+\mu^-$) plus jet events using 139 fb⁻¹ of pp collision data at $E_{\text{cm}} = 13$ TeV. The upper limit of $\sigma(pp \rightarrow H) \cdot \mathcal{B}(H \rightarrow ZJ/\psi)$ is 100 pb at 95% CL.

$\Gamma(Z\psi(2S))/\Gamma_{\text{total}}$		Γ_{13}/Γ		
VALUE	CL%	DOCUMENT ID	TECN	COMMENT
$< 6.6 \times 10^{-3}$	95	¹ TUMASYAN	23c CMS	pp, 13 TeV

¹ TUMASYAN 23c search for $H \rightarrow Z\psi(2S)$, $Z \rightarrow e^+e^-$ or $\mu^+\mu^-$, $\psi(2S) \rightarrow \mu^+\mu^-$ with 138 fb⁻¹ of pp collision data at $E_{\text{cm}} = 13$ TeV. The quoted value is for the Higgs decays for longitudinally polarized mesons. See their Table 1 for other cases.

$\Gamma(J/\psi\gamma)/\Gamma_{\text{total}}$		Γ_{14}/Γ		
VALUE	CL%	DOCUMENT ID	TECN	COMMENT
$< 2.0 \times 10^{-4}$	95	¹ AAD	23CD ATLS	13 TeV, 138 fb ⁻¹
•••				We do not use the following data for averages, fits, limits, etc. •••
$< 7.6 \times 10^{-4}$	95	² SIRUNYAN	19AJ CMS	13 TeV, 35.9 fb ⁻¹
$< 3.5 \times 10^{-4}$	95	³ AABOUD	18BL ATLS	13 TeV, 36.1 fb ⁻¹
$< 1.5 \times 10^{-3}$	95	⁴ KHACHATRYAN..16B	CMS	8 TeV
$< 1.5 \times 10^{-3}$	95	⁵ AAD	15I ATLS	8 TeV

¹ AAD 23CD search for $H \rightarrow J/\psi\gamma$, $J/\psi \rightarrow \mu^+\mu^-$ with 138 fb⁻¹ of pp collision data at $E_{\text{cm}} = 13$ TeV. SM values for the production cross-sections are assumed.
² SIRUNYAN 19AJ search for $H \rightarrow J/\psi\gamma$, $J/\psi \rightarrow \mu^+\mu^-$ with 35.9 fb⁻¹ of pp collision data at $E_{\text{cm}} = 13$ TeV. The upper limit corresponds to 260 times the SM prediction and by combining the KHACHATRYAN 16B, it is 220 times the SM prediction.
³ AABOUD 18BL search for $H \rightarrow J/\psi\gamma$, $J/\psi \rightarrow \mu^+\mu^-$ with 36.1 fb⁻¹ of pp collision data at $E_{\text{cm}} = 13$ TeV.
⁴ KHACHATRYAN 16B use 19.7 fb⁻¹ of pp collision data at 8 TeV.
⁵ AAD 15I use 19.7 fb⁻¹ of pp collision data at 8 TeV.

$\Gamma(J/\psi J/\psi)/\Gamma_{\text{total}}$		Γ_{15}/Γ		
VALUE	CL%	DOCUMENT ID	TECN	COMMENT
$< 3.8 \times 10^{-4}$	95	¹ TUMASYAN	23c CMS	pp, 13 TeV
•••				We do not use the following data for averages, fits, limits, etc. •••
$< 1.8 \times 10^{-3}$	95	² SIRUNYAN	19BR CMS	pp at 13 TeV

¹ TUMASYAN 23c search for $H \rightarrow J/\psi J/\psi$, $J/\psi \rightarrow \mu^+\mu^-$ with 138 fb⁻¹ of pp collision data at $E_{\text{cm}} = 13$ TeV. The quoted value is for the Higgs decays for longitudinally polarized mesons. See their Table 1 for other cases.
² SIRUNYAN 19BR search for $H \rightarrow J/\psi J/\psi$, $J/\psi \rightarrow \mu^+\mu^-$ with 37.5 fb⁻¹ of pp collision data at $E_{\text{cm}} = 13$ TeV. J/ψ s from the Higgs decay are assumed to be unpolarized. For fully longitudinal (transverse) polarized J/ψ s, limits change by -22% ($+10\%$).

$\Gamma(\psi(2S)\gamma)/\Gamma_{\text{total}}$		Γ_{16}/Γ		
VALUE	CL%	DOCUMENT ID	TECN	COMMENT
$< 1.05 \times 10^{-3}$	95	¹ AAD	23CD ATLS	13 TeV, 138 fb ⁻¹
•••				We do not use the following data for averages, fits, limits, etc. •••
$< 2.0 \times 10^{-3}$	95	² AABOUD	18BL ATLS	13 TeV, 36.1 fb ⁻¹

¹ AAD 23CD search for $H \rightarrow \psi(2S)\gamma$, $\psi(2S) \rightarrow \mu^+\mu^-$ with 138 fb⁻¹ of pp collision data at $E_{\text{cm}} = 13$ TeV. SM values for the production cross-sections are assumed.
² AABOUD 18BL search for $H \rightarrow \psi(2S)\gamma$, $\psi(2S) \rightarrow \mu^+\mu^-$ with 36.1 fb⁻¹ of pp collision data at $E_{\text{cm}} = 13$ TeV.

$\Gamma(\psi(2S)J/\psi)/\Gamma_{\text{total}}$		Γ_{17}/Γ		
VALUE	CL%	DOCUMENT ID	TECN	COMMENT
$< 2.1 \times 10^{-3}$	95	¹ TUMASYAN	23c CMS	pp, 13 TeV

¹ TUMASYAN 23c search for $H \rightarrow \psi(2S)J/\psi$, $\psi(2S) \rightarrow \mu^+\mu^-$, $J/\psi \rightarrow \mu^+\mu^-$ with 138 fb⁻¹ of pp collision data at $E_{\text{cm}} = 13$ TeV. The quoted value is for the Higgs decays for longitudinally polarized mesons. See their Table 1 for other cases.

Gauge & Higgs Boson Particle Listings

H

 $\Gamma(\psi(2S)\psi(2S))/\Gamma_{\text{total}}$ Γ_{18}/Γ

VALUE	CL%	DOCUMENT ID	TECN	COMMENT
$<3.0 \times 10^{-3}$	95	1 TUMASYAN	23c CMS	pp, 13 TeV

¹TUMASYAN 23c search for $H \rightarrow \psi(2S)\psi(2S)$, $\psi(2S) \rightarrow \mu^+\mu^-$ with 138 fb⁻¹ of pp collision data at $E_{\text{cm}} = 13$ TeV. The quoted value is for the Higgs decays for longitudinally polarized mesons. See their Table 1 for other cases.

 $\Gamma(\Upsilon(1S)\gamma)/\Gamma_{\text{total}}$ Γ_{19}/Γ

VALUE	CL%	DOCUMENT ID	TECN	COMMENT
$<2.5 \times 10^{-4}$	95	1 AAD	23CD ATLS	13 TeV, 138 fb ⁻¹

••• We do not use the following data for averages, fits, limits, etc. •••

$<4.9 \times 10^{-4}$	95	2 AABOUD	18BL ATLS	13 TeV, 36.1 fb ⁻¹
$<1.3 \times 10^{-3}$	95	3 AAD	15i ATLS	8 TeV

¹AAD 23CD search for $H \rightarrow \Upsilon(1S)\gamma$, $\Upsilon(1S) \rightarrow \mu^+\mu^-$ with 138 fb⁻¹ of pp collision data at $E_{\text{cm}} = 13$ TeV. SM values for the production cross-sections are assumed.

²AABOUD 18BL search for $H \rightarrow \Upsilon(1S)\gamma$, $\Upsilon(1S) \rightarrow \mu^+\mu^-$ with 36.1 fb⁻¹ of pp collision data at $E_{\text{cm}} = 13$ TeV.

³AAD 15i use 19.7 fb⁻¹ of pp collision data at 8 TeV.

 $\Gamma(\Upsilon(1S)\Upsilon(1S))/\Gamma_{\text{total}}$ Γ_{20}/Γ

VALUE	CL%	DOCUMENT ID	TECN	COMMENT
$<1.7 \times 10^{-3}$	95	1 TUMASYAN	23c CMS	pp, 13 TeV

¹TUMASYAN 23c search for $H \rightarrow \Upsilon(1S)\Upsilon(1S)$, $\Upsilon(1S) \rightarrow \mu^+\mu^-$ with 138 fb⁻¹ of pp collision data at $E_{\text{cm}} = 13$ TeV. The quoted value is for the Higgs decays for longitudinally polarized mesons. See their Table 1 for other cases.

 $\Gamma(\Upsilon(2S)\gamma)/\Gamma_{\text{total}}$ Γ_{21}/Γ

VALUE	CL%	DOCUMENT ID	TECN	COMMENT
$<4.2 \times 10^{-4}$	95	1 AAD	23CD ATLS	13 TeV, 138 fb ⁻¹

••• We do not use the following data for averages, fits, limits, etc. •••

$<5.9 \times 10^{-4}$	95	2 AABOUD	18BL ATLS	13 TeV, 36.1 fb ⁻¹
$<1.9 \times 10^{-3}$	95	3 AAD	15i ATLS	8 TeV

¹AAD 23CD search for $H \rightarrow \Upsilon(2S)\gamma$, $\Upsilon(2S) \rightarrow \mu^+\mu^-$ with 138 fb⁻¹ of pp collision data at $E_{\text{cm}} = 13$ TeV. SM values for the production cross-sections are assumed.

²AABOUD 18BL search for $H \rightarrow \Upsilon(2S)\gamma$, $\Upsilon(2S) \rightarrow \mu^+\mu^-$ with 36.1 fb⁻¹ of pp collision data at $E_{\text{cm}} = 13$ TeV.

³AAD 15i use 19.7 fb⁻¹ of pp collision data at 8 TeV.

 $\Gamma(\Upsilon(3S)\gamma)/\Gamma_{\text{total}}$ Γ_{22}/Γ

VALUE	CL%	DOCUMENT ID	TECN	COMMENT
$<3.4 \times 10^{-4}$	95	1 AAD	23CD ATLS	13 TeV, 138 fb ⁻¹

••• We do not use the following data for averages, fits, limits, etc. •••

$<5.7 \times 10^{-4}$	95	2 AABOUD	18BL ATLS	13 TeV, 36.1 fb ⁻¹
$<1.3 \times 10^{-3}$	95	3 AAD	15i ATLS	8 TeV

¹AAD 23CD search for $H \rightarrow \Upsilon(3S)\gamma$, $\Upsilon(3S) \rightarrow \mu^+\mu^-$ with 138 fb⁻¹ of pp collision data at $E_{\text{cm}} = 13$ TeV. SM values for the production cross-sections are assumed.

²AABOUD 18BL search for $H \rightarrow \Upsilon(3S)\gamma$, $\Upsilon(3S) \rightarrow \mu^+\mu^-$ with 36.1 fb⁻¹ of pp collision data at $E_{\text{cm}} = 13$ TeV.

³AAD 15i use 19.7 fb⁻¹ of pp collision data at 8 TeV.

 $\Gamma(\Upsilon(nS)\Upsilon(mS))/\Gamma_{\text{total}}$ Γ_{23}/Γ

VALUE	CL%	DOCUMENT ID	TECN	COMMENT
$<3.5 \times 10^{-4}$	95	1 TUMASYAN	23c CMS	pp, 13 TeV

••• We do not use the following data for averages, fits, limits, etc. •••

$<1.4 \times 10^{-3}$	95	2 SIRUNYAN	19BR CMS	pp, 13 TeV
-----------------------	----	------------	----------	------------

¹TUMASYAN 23c search for $H \rightarrow \Upsilon(nS)\Upsilon(mS)$ with $\Upsilon(nS)$, $\Upsilon(mS) \rightarrow \mu^+\mu^-$ ($n, m = 1, 2, 3$) with 138 fb⁻¹ of pp collision data at $E_{\text{cm}} = 13$ TeV. The quoted value is for the Higgs decays for longitudinally polarized mesons. See their Table 1 for other cases.

²SIRUNYAN 19BR search for $H \rightarrow \Upsilon(nS)\Upsilon(mS)$ with $\Upsilon(nS)$, $\Upsilon(mS) \rightarrow \mu^+\mu^-$ ($n, m = 1, 2, 3$) for 37.5 fb⁻¹ of pp collision data at $E_{\text{cm}} = 13$ TeV. Υ s from the Higgs decay are assumed to be unpolarized. For fully longitudinal (transverse) polarized Υ s, limits change by -22% (+10%). The three Υ states selected in a mass range of 8.5-11 GeV are not distinguished.

 $\Gamma(\rho(770)\gamma)/\Gamma_{\text{total}}$ Γ_{24}/Γ

VALUE	CL%	DOCUMENT ID	TECN	COMMENT
$<1.04 \times 10^{-4}$	95	1 AABOUD	18AU ATLS	pp, 13 TeV

¹AABOUD 18AU use 35.6 fb⁻¹ of pp collision data at 13 TeV. See their erratum AABOUD 23A.

 $\Gamma(\omega(782)\gamma)/\Gamma_{\text{total}}$ Γ_{25}/Γ

VALUE	CL%	DOCUMENT ID	TECN	COMMENT
$<5.5 \times 10^{-4}$	95	1 AAD	23BS ATLS	pp, 13 TeV

¹AAD 23BS use 89.5 fb⁻¹ of pp collision data at 13 TeV.

 $\Gamma(K^*(892)\gamma)/\Gamma_{\text{total}}$ Γ_{26}/Γ

VALUE	CL%	DOCUMENT ID	TECN	COMMENT
$<2.2 \times 10^{-4}$	95	1 AAD	23BS ATLS	pp, 13 TeV

¹AAD 23BS use 134 fb⁻¹ of pp collision data at 13 TeV.

 $\Gamma(\phi(1020)\gamma)/\Gamma_{\text{total}}$ Γ_{27}/Γ

VALUE	CL%	DOCUMENT ID	TECN	COMMENT
$<5 \times 10^{-4}$	95	1 AABOUD	18AU ATLS	pp, 13 TeV

••• We do not use the following data for averages, fits, limits, etc. •••

$<1.4 \times 10^{-3}$	95	2 AABOUD	16K ATLS	pp, 13 TeV
-----------------------	----	----------	----------	------------

¹AABOUD 18AU use 35.6 fb⁻¹ of pp collision data at 13 TeV. See their erratum AABOUD 23A.

²AABOUD 16K use 2.7 fb⁻¹ of pp collision data at 13 TeV.

 $\Gamma(e\mu)/\Gamma_{\text{total}}$ Γ_{28}/Γ

VALUE	CL%	DOCUMENT ID	TECN	COMMENT
$<4.4 \times 10^{-5}$	95	1 HAYRAPETYAN...	23c CMS	pp, 13 TeV

••• We do not use the following data for averages, fits, limits, etc. •••

$<6.1 \times 10^{-5}$	95	2 AAD	20F ATLS	pp, 13 TeV
$<3.5 \times 10^{-4}$	95	3 KHACHATRYAN...	16CD CMS	pp, 8 TeV

¹HAYRAPETYAN 23c use 138 fb⁻¹ of pp collisions at $E_{\text{cm}} = 13$ TeV. The limit constrains the $Y_{e\mu}$ Yukawa coupling to $\sqrt{|Y_{e\mu}|^2 + |Y_{\mu e}|^2} < 1.9 \times 10^{-4}$ at 95% CL (see their Fig. 6).

²AAD 20F use 139 fb⁻¹ of pp collisions at $E_{\text{cm}} = 13$ TeV. The best-fit value of the $H \rightarrow e\mu$ branching fraction is $(0.4 \pm 2.9 \pm 0.3) \times 10^{-5}$ for $m_H = 125$ GeV.

³KHACHATRYAN 16CD search for $H \rightarrow e\mu$ in 19.7 fb⁻¹ of pp collisions at $E_{\text{cm}} = 8$ TeV. The limit constrains the $Y_{e\mu}$ Yukawa coupling to $\sqrt{|Y_{e\mu}|^2 + |Y_{\mu e}|^2} < 5.4 \times 10^{-4}$ at 95% CL (see their Fig. 6).

 $\Gamma(e\tau)/\Gamma_{\text{total}}$ Γ_{29}/Γ

VALUE	CL%	DOCUMENT ID	TECN	COMMENT
$<2.0 \times 10^{-3}$	95	1 AAD	23Q ATLS	pp, 13 TeV

••• We do not use the following data for averages, fits, limits, etc. •••

$<2.3 \times 10^{-3}$	95	2 AAD	23Q ATLS	pp, 13 TeV
$<2.2 \times 10^{-3}$	95	3 SIRUNYAN	21Z CMS	pp, 13 TeV
$<4.7 \times 10^{-3}$	95	4 AAD	20A ATLS	pp, 13 TeV
$<6.1 \times 10^{-3}$	95	5 SIRUNYAN	18BH CMS	pp, 13 TeV
$<10.4 \times 10^{-3}$	95	6 AAD	17 ATLS	pp, 8 TeV
$<6.9 \times 10^{-3}$	95	7 KHACHATRYAN...	16CD CMS	pp, 8 TeV

¹AAD 23Q search for $H \rightarrow e\tau$ in 138 fb⁻¹ of pp collisions at $E_{\text{cm}} = 13$ TeV. The result is obtained from a simultaneous fit of possible $H \rightarrow e\tau$ and $H \rightarrow \mu\tau$ signals (see their Figs. 13 and 14). The limit constrains the $Y_{e\tau}$ Yukawa coupling to $\sqrt{|Y_{e\tau}|^2 + |Y_{\tau e}|^2} < 1.3 \times 10^{-3}$ at 95% CL (see their Fig. 15).

²AAD 23Q search for $H \rightarrow e\tau$ in 138 fb⁻¹ of pp collisions at $E_{\text{cm}} = 13$ TeV. The limit constrains the $Y_{e\tau}$ Yukawa coupling to $\sqrt{|Y_{e\tau}|^2 + |Y_{\tau e}|^2} < 1.4 \times 10^{-3}$ at 95% CL (see their Fig. 12).

³SIRUNYAN 21Z search for $H \rightarrow e\tau$ in 137 fb⁻¹ of pp collisions at $E_{\text{cm}} = 13$ TeV. The limit constrains the $Y_{e\tau}$ Yukawa coupling to $\sqrt{|Y_{e\tau}|^2 + |Y_{\tau e}|^2} < 1.35 \times 10^{-3}$ at 95% CL (see their Fig. 8).

⁴AAD 20A search for $H \rightarrow e\tau$ in 36.1 fb⁻¹ of pp collisions at $E_{\text{cm}} = 13$ TeV. The limit constrains the $Y_{e\tau}$ Yukawa coupling to $\sqrt{|Y_{e\tau}|^2 + |Y_{\tau e}|^2} < 2.0 \times 10^{-3}$ at 95% CL (see their Fig. 5).

⁵SIRUNYAN 18BH search for $H \rightarrow e\tau$ in 35.9 fb⁻¹ of pp collisions at $E_{\text{cm}} = 13$ TeV. The limit constrains the $Y_{e\tau}$ Yukawa coupling to $\sqrt{|Y_{e\tau}|^2 + |Y_{\tau e}|^2} < 2.26 \times 10^{-3}$ at 95% CL (see their Fig. 10).

⁶AAD 17 search for $H \rightarrow e\tau$ in 20.3 fb⁻¹ of pp collisions at $E_{\text{cm}} = 8$ TeV.

⁷KHACHATRYAN 16CD search for $H \rightarrow e\tau$ in 19.7 fb⁻¹ of pp collisions at $E_{\text{cm}} = 8$ TeV. The limit constrains the $Y_{e\tau}$ Yukawa coupling to $\sqrt{|Y_{e\tau}|^2 + |Y_{\tau e}|^2} < 2.4 \times 10^{-3}$ at 95% CL (see their Fig. 6).

 $\Gamma(\mu\tau)/\Gamma_{\text{total}}$ Γ_{30}/Γ

VALUE	CL%	DOCUMENT ID	TECN	COMMENT
$<1.5 \times 10^{-3}$	95	1 SIRUNYAN	21Z CMS	pp, 13 TeV

••• We do not use the following data for averages, fits, limits, etc. •••

$<1.8 \times 10^{-3}$	95	2 AAD	23Q ATLS	pp, 13 TeV
$<1.7 \times 10^{-3}$	95	3 AAD	23Q ATLS	pp, 13 TeV
$<2.8 \times 10^{-3}$	95	4 AAD	20A ATLS	pp, 13 TeV
$<26 \times 10^{-2}$	95	5 AAIJ	18AMLHCB	pp, 8 TeV
$<2.5 \times 10^{-3}$	95	6 SIRUNYAN	18BH CMS	pp, 13 TeV
$<1.43 \times 10^{-2}$	95	7 AAD	17 ATLS	pp, 8 TeV
$<1.51 \times 10^{-2}$	95	8 KHACHATRYAN...	15Q CMS	pp, 8 TeV

¹SIRUNYAN 21Z search for $H \rightarrow \mu\tau$ in 137 fb⁻¹ of pp collisions at $E_{\text{cm}} = 13$ TeV. The limit constrains the $Y_{\mu\tau}$ Yukawa coupling to $\sqrt{|Y_{\mu\tau}|^2 + |Y_{\tau\mu}|^2} < 1.11 \times 10^{-3}$ at 95% CL (see their Fig. 8).

²AAD 23Q search for $H \rightarrow \mu\tau$ in 138 fb⁻¹ of pp collisions at $E_{\text{cm}} = 13$ TeV. The result is obtained from a simultaneous fit of possible $H \rightarrow e\tau$ and $H \rightarrow \mu\tau$ signals (see their Figs. 13 and 14). The limit constrains the $Y_{\mu\tau}$ Yukawa coupling to $\sqrt{|Y_{\mu\tau}|^2 + |Y_{\tau\mu}|^2} < 1.2 \times 10^{-3}$ at 95% CL (see their Fig. 15).

³AAD 23Q search for $H \rightarrow \mu\tau$ in 138 fb⁻¹ of pp collisions at $E_{\text{cm}} = 13$ TeV. The limit constrains the $Y_{\mu\tau}$ Yukawa coupling to $\sqrt{|Y_{\mu\tau}|^2 + |Y_{\tau\mu}|^2} < 1.2 \times 10^{-3}$ at 95% CL (see their Fig. 12).

⁴AAD 20A search for $H \rightarrow \mu\tau$ in 36.1 fb⁻¹ of pp collisions at $E_{\text{cm}} = 13$ TeV. The limit constrains the $Y_{\mu\tau}$ Yukawa coupling to $\sqrt{|Y_{\mu\tau}|^2 + |Y_{\tau\mu}|^2} < 1.5 \times 10^{-3}$ at 95% CL (see their Fig. 5).

⁵ AAIJ 18AM search for $H \rightarrow \mu\tau$ in 2.0 fb⁻¹ of pp collisions at $E_{\text{cm}} = 8$ TeV. The limit constrains the $Y_{\mu\tau}$ Yukawa coupling to $\sqrt{|Y_{\mu\tau}|^2 + |Y_{\tau\mu}|^2} < 1.7 \times 10^{-2}$ at 95% CL assuming SM production cross sections.

⁶ SIRUNYAN 18BH search for $H \rightarrow \mu\tau$ in 35.9 fb⁻¹ of pp collisions at $E_{\text{cm}} = 13$ TeV. The limit constrains the $Y_{\mu\tau}$ Yukawa coupling to $\sqrt{|Y_{\mu\tau}|^2 + |Y_{\tau\mu}|^2} < 1.43 \times 10^{-3}$ at 95% CL (see their Fig. 10).

⁷ AAD 17 search for $H \rightarrow \mu\tau$ in 20.3 fb⁻¹ of pp collisions at $E_{\text{cm}} = 8$ TeV.

⁸ KHACHATRYAN 15Q search for $H \rightarrow \mu\tau$ with τ decaying electronically or hadronically in 19.7 fb⁻¹ of pp collisions at $E_{\text{cm}} = 8$ TeV. The fit gives $B(H \rightarrow \mu\tau) = (0.84_{-0.39}^{+0.39})\%$ with a significance of 2.4 σ .

$\Gamma(\text{invisible})/\Gamma_{\text{total}}$ Γ_{31}/Γ

VALUE	CL%	DOCUMENT ID	TECN	COMMENT
<0.107	95	1 AAD	23A ATLS	$pp, 7, 8, 13$ TeV
••• We do not use the following data for averages, fits, limits, etc. •••				
<0.113	95	2 AAD	23A ATLS	$pp, 13$ TeV
<0.38	95	3 AAD	23AF ATLS	$pp \rightarrow t\bar{t}H, 13$ TeV
<0.54	95	4 TUMASYAN	23BA CMS	$pp \rightarrow q\bar{q}H, V(\rightarrow q\bar{q})H, 13$ TeV
<0.15	95	5 TUMASYAN	23BA CMS	$pp, 7, 8, 13$ TeV
<0.19	95	6 AAD	22D ATLS	$pp \rightarrow ZH, 13$ TeV
<0.145	95	7 AAD	22P ATLS	$pp \rightarrow qqH, 13$ TeV
<0.37	95	8 AAD	22S ATLS	$pp \rightarrow qqH\gamma, 13$ TeV
<0.13	95	9 ATLAS	22 ATLS	$pp, 13$ TeV
<0.16	95	10 CMS	22 CMS	$pp, 13$ TeV
<0.18	95	11 TUMASYAN	22G CMS	$pp \rightarrow qqH, 8, 13$ TeV
<0.18	95	12 TUMASYAN	22G CMS	$pp \rightarrow qqH, 13$ TeV
<0.34	95	13 AAD	21F ATLS	$pp, 13$ TeV
<0.29	95	14 SIRUNYAN	21A CMS	$pp \rightarrow ZH, 13$ TeV
<0.278	95	15 TUMASYAN	21D CMS	$pp, 13$ TeV, jet or $V(\rightarrow q\bar{q})$
<0.37	95	16 AABOUD	19AI ATLS	$pp \rightarrow qqH, 13$ TeV
<0.38	95	17 AABOUD	19AL ATLS	$pp, 13$ TeV
<0.26	95	18 AABOUD	19AL ATLS	$pp, 7, 8, 13$ TeV
<0.22	95	19 SIRUNYAN	19AT CMS	$pp, 13$ TeV
<0.33	95	20 SIRUNYAN	19Bo CMS	$pp \rightarrow qqH, 13$ TeV
<0.26	95	21 SIRUNYAN	19Bo CMS	$pp, 13$ TeV
<0.19	95	22 SIRUNYAN	19Bo CMS	$pp, 7, 8, 13$ TeV
<0.67	95	23 AABOUD	18 ATLS	$pp \rightarrow ZH, 13$ TeV
<0.83	95	24 AABOUD	18CA ATLS	$pp \rightarrow WH/ZH, W/Z \rightarrow jj, 13$ TeV
<0.40	95	25 SIRUNYAN	18BV CMS	$pp \rightarrow ZH, 13$ TeV
<0.53	95	26 SIRUNYAN	18S CMS	$pp, 13$ TeV, jet or $V(\rightarrow q\bar{q})$
<0.46	95	27 AABOUD	17BD ATLS	$pp \rightarrow H_j, qqH, 13$ TeV
<0.24	95	28 KHACHATRYAN	17F CMS	$pp, 7, 8, 13$ TeV
<0.28	95	29 AAD	16AF ATLS	$pp \rightarrow qqH, 8$ TeV
<0.34	95	30 AAD	16AN LHC	$pp, 7, 8$ TeV
<0.78	95	31 AAD	15BD ATLS	$pp \rightarrow WH/ZH, 8$ TeV
<0.25	95	32 AAD	15CX ATLS	$pp, 7, 8$ TeV
<0.75	95	33 AAD	14O ATLS	$pp \rightarrow ZH, 7, 8$ TeV
<0.58	95	34 CHATRCHYAN	14B CMS	$pp \rightarrow ZH, qqH$
<0.81	95	35 CHATRCHYAN	14B CMS	$pp \rightarrow ZH, 7, 8$ TeV
<0.65	95	36 CHATRCHYAN	14B CMS	$pp \rightarrow qqH, 8$ TeV

¹ AAD 23A report the combined results of 7, 8 (AAD 15CX) and 13 TeV assuming the Standard Model cross section ($m_H = 125$ GeV). See their Table 1 and Fig. 3.

² AAD 23A report the combined results using 139 fb⁻¹ of data at $E_{\text{cm}} = 13$ TeV, where H decaying to invisible final states in VBF (AAD 22P), $ZH, Z \rightarrow ee, \mu\mu$ (AAD 22D), $pp \rightarrow t\bar{t}H$ (AAD 23AF), VBF+ γ (AAD 22S) and gluon-fusion production with an energetic jet (AAD 21F) assuming the Standard Model cross section ($m_H = 125$ GeV). See their Table 1 and Fig. 3.

³ AAD 23AF search for $pp \rightarrow t\bar{t}H$ with H decaying to invisible final states using 139 fb⁻¹ of data. The quoted limit on the branching ratio is given for $m_H = 125$ GeV and assumes the Standard Model cross section. See their Table 3 for different decay topologies.

⁴ TUMASYAN 23BA search for H decaying to invisible final states produced in association with a $t\bar{t}$ or a V , which decay to a fully hadronic final state. 138 fb⁻¹ of data is used. The quoted limit on the branching ratio is given for $m_H = 125$ GeV and assumes the Standard Model cross section. See their Fig. 6 for the results of individual topologies.

⁵ TUMASYAN 23BA report the combined results of 7, 8, and 13 TeV assuming the Standard Model cross section ($m_H = 125$ GeV). They combine results from TUMASYAN 22G, SIRUNYAN 21A, SIRUNYAN 21B, TUMASYAN 21D, SIRUNYAN 20AH, KHACHATRYAN 17F, CHATRCHYAN 14B as shown in their Table 8. See their Fig. 7 and Table 9 for the results of individual topologies.

⁶ AAD 22D search for H decaying to invisible final states associated with a Z decaying $ee/\mu\mu$ using 139 fb⁻¹ at 13 TeV. The limit is obtained for $m_H = 125$ GeV and assuming the SM ZH production cross section. The branching ratio is obtained to be $(0.3 \pm 9.0)\%$.

⁷ AAD 22P search for $pp \rightarrow qqHX$ (VBF) with H decaying to invisible final states using 139 fb⁻¹ of data. The quoted limit on the branching ratio is given for $m_H = 125$ GeV and assumes the Standard Model cross section.

⁸ AAD 22S observe electroweak $Z(\rightarrow \nu\nu)\gamma+2$ jets production process with 139 fb⁻¹ of data. This result is applicable to search for $pp \rightarrow qqH\gamma X$ (VBF+ γ) with H decaying to invisible final states. The quoted limit on the branching ratio is given for $m_H = 125$ GeV and assumes the Standard Model cross section.

⁹ ATLAS 22 report the combined results using 139 fb⁻¹ of data at $E_{\text{cm}} = 13$ TeV, where H decaying to invisible final states in VBF (AAD 22P), and $ZH, Z \rightarrow ee, \mu\mu$ (AAD 22D), assuming $\kappa_V \leq 1$ and $B_{\text{undetected}} \geq 0$.

¹⁰ CMS 22 report the combined results using (a part of) 138 fb⁻¹ of data at $E_{\text{cm}} = 13$ TeV, where H decaying to invisible final states in VBF (SIRUNYAN 19Bo), associated with an energetic jet or a $V(\rightarrow q\bar{q})$ (TUMASYAN 21D), and $ZH, Z \rightarrow ee, \mu\mu$ (SIRUNYAN 21A) and assuming $\kappa_V \leq 1$ and $B_{\text{undetected}} \geq 0$.

¹¹ TUMASYAN 22G combine 13 TeV 101 fb⁻¹ results with 8 TeV (KHACHATRYAN 17F) and other 13 TeV (KHACHATRYAN 17F for 2015 and SIRUNYAN 19Bo for 2016) for H decaying to invisible final states with VBF topology. The quoted limit on the branching ratio is given for $m_H = 125.38$ GeV and assumes the Standard Model production rates. The branching ratio is obtained to be $0.086_{-0.052}^{+0.054}$. See their Figs. 11 and 12.

¹² TUMASYAN 22G search for $pp \rightarrow qqHX$ (VBF) with H decaying to invisible final states using 101 fb⁻¹ of data (2017 and 2018). The quoted limit on the branching ratio is given for $m_H = 125.38$ GeV and assumes the Standard Model cross section. See their Figs. 11 and 12.

¹³ AAD 21F search for an invisibly decaying Higgs boson with an energetic jet ($p_T > 150$ GeV) and missing transverse momentum (> 200 GeV) in 139 fb⁻¹ at $E_{\text{cm}} = 13$ TeV. The quoted limit on the branching ratio is given for $m_H = 125$ GeV.

¹⁴ SIRUNYAN 21A search for H decaying to invisible final states associated with a Z decaying $ee/\mu\mu$ using 137 fb⁻¹ at 13 TeV. The limit is obtained for $m_H = 125$ GeV and assuming the SM ZH production cross section.

¹⁵ TUMASYAN 21D search for H decaying to invisible final states associated with an energetic jet or a $V, V \rightarrow q\bar{q}$ using 101 fb⁻¹ at 13 TeV and the result is combined with SIRUNYAN 18S.

¹⁶ AABOUD 19AI search for $pp \rightarrow qqHX$ (VBF) with H decaying to invisible final states using 36.1 fb⁻¹ of data. The quoted limit on the branching ratio is given for $m_H = 125$ GeV and assumes the Standard Model rates for VBF and gluon-fusion production.

¹⁷ AABOUD 19AL combine results of H decaying to invisible final states with VBF(AABOUD 19AI), ZH , and WH productions (AABOUD 18, AABOUD 18CA), which use 36.1 fb⁻¹ of data at 13 TeV. The quoted limit is given for $m_H = 125$ GeV and assumes the Standard Model rates for gluon fusion, VBF, ZH , and WH productions.

¹⁸ AABOUD 19AL combine results of 7, 8 (AAD 15CX), and 13 TeV for H decaying to invisible final states.

¹⁹ SIRUNYAN 19AT perform a combined fit with visible decay using 35.9 fb⁻¹ of data at 13 TeV.

²⁰ SIRUNYAN 19Bo search for $pp \rightarrow qqHX$ (VBF) with H decaying to invisible final states using 35.9 fb⁻¹ of data. The quoted limit on the branching ratio is given for $m_H = 125.09$ GeV and assumes the Standard Model production rates.

²¹ SIRUNYAN 19Bo combine the VBF channel with results of other 13 TeV analyses: SIRUNYAN 18BV and SIRUNYAN 18S. The quoted limit on the branching ratio is given for $m_H = 125.09$ GeV and assumes the Standard Model production rates.

²² SIRUNYAN 19Bo combine 13 TeV 35.9 fb⁻¹ results with 7, 8, 13 TeV (KHACHATRYAN 17F) for H decaying to invisible final states. The quoted limit on the branching ratio is given for $m_H = 125.09$ GeV and assumes the Standard Model production rates. The branching ratio is obtained to be 0.05 ± 0.03 (stat) ± 0.07 (syst).

²³ AABOUD 18 search for $pp \rightarrow HZX, Z \rightarrow ee, \mu\mu$ with H decaying to invisible final states in 36.1 fb⁻¹ at $E_{\text{cm}} = 13$ TeV. The quoted limit on the branching ratio is given for $m_H = 125$ GeV and assumes the Standard Model rate for HZ production.

²⁴ AABOUD 18CA search for H decaying to invisible final states using WH, ZH and ZH productions, where W and Z hadronically decay. The data of 36.1 fb⁻¹ at $E_{\text{cm}} = 13$ TeV is used. The quoted limit assumes SM production cross sections with combining the contributions from WH, ZH, ggF and VBF production modes.

²⁵ SIRUNYAN 18BV search for H decaying to invisible final states associated with a $Z, Z \rightarrow \ell\ell$ using 35.9 fb⁻¹ at 13 TeV. The limit is obtained for $m_H = 125$ GeV and assuming the SM ZH production cross section.

²⁶ SIRUNYAN 18S search for H decaying to invisible final states associated with an energetic jet or a $V, V \rightarrow q\bar{q}$ using 35.9 fb⁻¹ at 13 TeV.

²⁷ AABOUD 17BD search for H decaying to invisible final states with ≥ 1 jet and VBF events using 3.2 fb⁻¹ of pp collisions at $E_{\text{cm}} = 13$ TeV. A cross-section ratio R^{miss} is used in the measurement. The quoted limit is given for $m_H = 125$ GeV.

²⁸ KHACHATRYAN 17F search for H decaying to invisible final states with gluon fusion, VBF, ZH , and WH productions using 2.3 fb⁻¹ of pp collisions at $E_{\text{cm}} = 13$ TeV, 19.7 fb⁻¹ at 8 TeV, and 5.1 fb⁻¹ at 7 TeV. The quoted limit is given for $m_H = 125$ GeV and assumes the Standard Model rates for gluon fusion, VBF, ZH , and WH productions.

²⁹ AAD 16AF search for $pp \rightarrow qqHX$ (VBF) with H decaying to invisible final states in 20.3 fb⁻¹ at $E_{\text{cm}} = 8$ TeV. The quoted limit on the branching ratio is given for $m_H = 125$ GeV and assumes the Standard Model rates for VBF and gluon-fusion production.

³⁰ AAD 16AN perform fits to the ATLAS and CMS data at $E_{\text{cm}} = 7$ and 8 TeV. The branching fraction of decays into BSM particles that are invisible or into undetected decay modes is measured for $m_0 = 125.09$ GeV.

³¹ AAD 15BD search for $pp \rightarrow HWX$ and $pp \rightarrow HZX$ with W or Z decaying hadronically and H decaying to invisible final states using data at $E_{\text{cm}} = 8$ TeV. The quoted limit is given for $m_H = 125$ GeV, assumes the Standard Model rates for the production processes and is based on a combination of the contributions from HW, HZ and the gluon-fusion process.

³² AAD 15CX search for H decaying to invisible final states with VBF, ZH , and WH productions using 20.3 fb⁻¹ at 8 TeV, and 4.7 fb⁻¹ at 7 TeV. The quoted limit is given for $m_H = 125.36$ GeV and assumes the Standard Model rates for gluon fusion, VBF, ZH , and WH productions. The upper limit is improved to 0.23 by adding the measured visible decay rates.

³³ AAD 14O search for $pp \rightarrow HZX, Z \rightarrow \ell\ell$, with H decaying to invisible final states in 4.5 fb⁻¹ at $E_{\text{cm}} = 7$ TeV and 20.3 fb⁻¹ at $E_{\text{cm}} = 8$ TeV. The quoted limit on the branching ratio is given for $m_H = 125.5$ GeV and assumes the Standard Model rate for HZ production.

³⁴ CHATRCHYAN 14B search for $pp \rightarrow HZX, Z \rightarrow \ell\ell$ and $Z \rightarrow b\bar{b}$, and also $pp \rightarrow qqHX$ with H decaying to invisible final states using data at $E_{\text{cm}} = 7$ and 8 TeV. The quoted limit on the branching ratio is obtained from a combination of the limits from HZ and qqH . It is given for $m_H = 125$ GeV and assumes the Standard Model rates for the two production processes.

³⁵ CHATRCHYAN 14B search for $pp \rightarrow HZX$ with H decaying to invisible final states and $Z \rightarrow \ell\ell$ in 4.9 fb⁻¹ at $E_{\text{cm}} = 7$ TeV and 19.7 fb⁻¹ at $E_{\text{cm}} = 8$ TeV, and also with $Z \rightarrow b\bar{b}$ in 18.9 fb⁻¹ at $E_{\text{cm}} = 8$ TeV. The quoted limit on the branching ratio is given for $m_H = 125$ GeV and assumes the Standard Model rate for HZ production.

³⁶ CHATRCHYAN 14B search for $pp \rightarrow qqHX$ (vector boson fusion) with H decaying to invisible final states in 19.5 fb⁻¹ at $E_{\text{cm}} = 8$ TeV. The quoted limit on the branching ratio is given for $m_H = 125$ GeV and assumes the Standard Model rate for qqH production.

Gauge & Higgs Boson Particle Listings

H

$\Gamma(\gamma\text{invisible})/\Gamma_{\text{total}}$					Γ_{32}/Γ
VALUE	CL%	DOCUMENT ID	TECN	COMMENT	
<0.029	95	1,2 SIRUNYAN	21L CMS	VBF, $HZ, H \rightarrow \gamma + \text{invisible}$, 13 TeV	
• • • We do not use the following data for averages, fits, limits, etc. • • •					
<0.035	95	1 SIRUNYAN	21L CMS	VBF, $H \rightarrow \gamma + \text{invisible}$, 13 TeV	
<0.046	95	3 SIRUNYAN	19CG CMS	$pp \rightarrow HZ, H \rightarrow \gamma + \text{invisible}, Z \rightarrow \ell\ell$, 13 TeV	
<p>¹ SIRUNYAN 21L search for H decaying to an invisible final state plus a γ in the VBF production using 130 fb^{-1} data at $E_{\text{cm}} = 13 \text{ TeV}$. The invisible state is called a dark photon. The quoted limit on the branching ratio is given for $m_H = 125 \text{ GeV}$ assuming the Standard Model rates.</p> <p>² The result of the VBF production is combined with the $pp \rightarrow HZ$ result (SIRUNYAN 19CG).</p> <p>³ SIRUNYAN 19CG search for $pp \rightarrow HZ, Z \rightarrow e\bar{e}, \mu\mu$ with H decaying to invisible final states plus a γ in 137 fb^{-1} at $E_{\text{cm}} = 13 \text{ TeV}$. The quoted limit on the branching ratio is given for $m_H = 125 \text{ GeV}$ assuming the Standard Model rate for HZ production and is obtained in the context of a theoretical model, where the undetected (invisible) particle is massless.</p>					

H SIGNAL STRENGTHS IN DIFFERENT CHANNELS

The H signal strength in a particular final state xx is given by the cross section times branching ratio in this channel normalized to the Standard Model (SM) value, $\sigma \cdot \text{B}(H \rightarrow xx) / (\sigma \cdot \text{B}(H \rightarrow xx))_{\text{SM}}$, for the specified mass value of H . For the SM predictions, see DITTMAYER 11, DITTMAYER 12, and HEINEMEYER 13A. Results for fiducial and differential cross sections are also listed below.

Combined Final States

VALUE		DOCUMENT ID	TECN	COMMENT
1.03 ± 0.04 OUR AVERAGE				
1.05 ± 0.06		1 ATLAS	22 ATLS	pp , 13 TeV
1.002 ± 0.057		2 CMS	22 CMS	pp , 13 TeV
1.09 ± 0.07 ± 0.04 ^{+0.08} _{-0.07}		3,4 AAD	16AN LHC	pp , 7, 8 TeV
1.44 ^{+0.59} _{-0.56}		5 AALTONEN	13M TEVA	$p\bar{p} \rightarrow HX$, 1.96 TeV
• • • We do not use the following data for averages, fits, limits, etc. • • •				
1.11 ^{+0.09} _{-0.08}		6 AAD	20 ATLS	pp , 13 TeV
1.17 ± 0.10		7 SIRUNYAN	19AT CMS	pp , 13 TeV
		8 SIRUNYAN	19BA CMS	pp , 13 TeV, differential cross sections
1.20 ± 0.10 ± 0.06 ^{+0.09} _{-0.08}		4 AAD	16AN ATLS	pp , 7, 8 TeV
0.97 ± 0.09 ± 0.05 ^{+0.08} _{-0.07}		4 AAD	16AN CMS	pp , 7, 8 TeV
1.18 ± 0.10 ± 0.07 ^{+0.08} _{-0.07}		9 AAD	16K ATLS	pp , 7, 8 TeV
0.75 ^{+0.28} _{-0.26} ± 0.13 ^{+0.08} _{-0.11} ± 0.05		9 AAD	16K ATLS	pp , 7 TeV
1.28 ± 0.11 ± 0.08 ^{+0.10} _{-0.07} ± 0.08		9 AAD	16K ATLS	pp , 8 TeV
		10 AAD	15P ATLS	pp , 8 TeV, cross section
1.00 ± 0.09 ± 0.07 ^{+0.08} _{-0.07}		11 KHACHATRYAN	15AM CMS	pp , 7, 8 TeV
1.33 ^{+0.14} _{-0.10} ± 0.15		12 AAD	13AK ATLS	pp , 7 and 8 TeV
1.54 ^{+0.77} _{-0.73}		13 AALTONEN	13L CDF	$p\bar{p} \rightarrow HX$, 1.96 TeV
1.40 ^{+0.92} _{-0.88}		14 ABAZOV	13L D0	$p\bar{p} \rightarrow HX$, 1.96 TeV
1.4 ± 0.3		15 AAD	12AI ATLS	$pp \rightarrow HX$, 7, 8 TeV
1.2 ± 0.4		15 AAD	12AI ATLS	$pp \rightarrow HX$, 7 TeV
1.5 ± 0.4		15 AAD	12AI ATLS	$pp \rightarrow HX$, 8 TeV
0.87 ± 0.23		16 CHATRCHYAN	12N CMS	$pp \rightarrow HX$, 7, 8 TeV

- ¹ ATLAS 22 report combined results (see their Extended Data Table 1) using up to 139 fb^{-1} of data at $E_{\text{cm}} = 13 \text{ TeV}$, assuming $m_H = 125.09 \text{ GeV}$. The Higgs production cross-sections, branching fractions and several ratios are found in their Figs. 2 and 3.
- ² CMS 22 report combined results (see their Extended Data Table 2) using 138 fb^{-1} of data at $E_{\text{cm}} = 13 \text{ TeV}$, assuming $m_H = 125.38 \text{ GeV}$. Signal strengths for production modes and decay channels are found in their Fig. 2.
- ³ AAD 16AN perform fits to the ATLAS and CMS data at $E_{\text{cm}} = 7$ and 8 TeV . The signal strengths for individual production processes are 1.03 ± 0.16 for gluon fusion, 1.18 ± 0.25 for vector boson fusion, 0.89 ± 0.40 for WH production, 0.79 ± 0.38 for ZH production, and 2.3 ± 0.6 for $t\bar{t}H$ production.
- ⁴ AAD 16AN: The uncertainties represent statistics, experimental systematics, and added in quadrature theory systematics on the background and on the signal. The quoted signal strengths are given for $m_H = 125.09 \text{ GeV}$. In the fit, relative branching ratios and relative production cross sections are fixed to those in the Standard Model.
- ⁵ AALTONEN 13M combine all Tevatron data from the CDF and D0 Collaborations with up to 10.0 fb^{-1} and 9.7 fb^{-1} , respectively, of $p\bar{p}$ collisions at $E_{\text{cm}} = 1.96 \text{ TeV}$. The quoted signal strength is given for $m_H = 125 \text{ GeV}$.
- ⁶ AAD 20 combine results of up to 79.8 fb^{-1} of data at $E_{\text{cm}} = 13 \text{ TeV}$, assuming $m_H = 125.09 \text{ GeV}$: $\gamma\gamma, ZZ^*, WW^*, \tau\tau, b\bar{b}, \mu\mu$, invisible, and off-shell analyses (see their Table I). The signal strengths for individual production processes are 1.04 ± 0.09 for gluon fusion, 1.21 ± 0.24 for vector boson fusion, 1.30 ± 0.40 for WH production, 1.05 ± 0.31 for ZH production, and 1.21 ± 0.26 for $t\bar{t}H+tH$ production (see their Fig. 2 and Table IV). Several results with the simplified template cross section and κ -frameworks

are presented: see their Figs. 9–11, Figs 20, 21 and Table VIII for stage-1 simplified template cross sections, their Figs. 12–17 and Tables X–XII for the κ -framework.

- ⁷ SIRUNYAN 19AT combine results of 35.9 fb^{-1} of data at $E_{\text{cm}} = 13 \text{ TeV}$, assuming $m_H = 125.09 \text{ GeV}$. The signal strengths for individual production processes are 1.22 ± 0.14 for gluon fusion, 0.73 ± 0.30 for vector boson fusion, 2.18 ± 0.58 for WH production, 0.87 ± 0.44 for ZH production, and 1.18 ± 0.30 for $t\bar{t}H$ production. Several results with the simplified template cross section and κ -frameworks are presented: see their Fig. 8 and Table 5 for stage-0 simplified template cross sections, their Figs. 9–18 and Tables 7–11 for the κ -framework.
- ⁸ SIRUNYAN 19BA measure differential cross sections for the Higgs boson transverse momentum, the number of jets, the rapidity of the Higgs boson and the transverse momentum of the leading jet using 35.9 fb^{-1} of data at $E_{\text{cm}} = 13 \text{ TeV}$ with $H \rightarrow \gamma\gamma, H \rightarrow ZZ^*$, and $H \rightarrow b\bar{b}$. The total cross section for Higgs boson production is measured to be $61.1 \pm 6.0 \pm 3.7 \text{ pb}$ using $H \rightarrow \gamma\gamma$ and $H \rightarrow ZZ^*$ channels. Several coupling measurements in the κ -framework are performed.
- ⁹ AAD 16K use up to 4.7 fb^{-1} of pp collisions at $E_{\text{cm}} = 7 \text{ TeV}$ and up to 20.3 fb^{-1} at $E_{\text{cm}} = 8 \text{ TeV}$. The third uncertainty in the measurement is theory systematics. The signal strengths for individual production modes are $1.23 \pm 0.14 \pm 0.09 \pm 0.16$ for gluon fusion, $1.23 \pm 0.28 \pm 0.13 \pm 0.11$ for vector boson fusion, $0.80 \pm 0.31 \pm 0.17 \pm 0.10$ for W/ZH production, and $1.81 \pm 0.52 \pm 0.58 \pm 0.31$ for $t\bar{t}H$ production. The quoted signal strengths are given for $m_H = 125.36 \text{ GeV}$.
- ¹⁰ AAD 15P measure total and differential cross sections of the process $pp \rightarrow HX$ at $E_{\text{cm}} = 8 \text{ TeV}$ with 20.3 fb^{-1} . $\gamma\gamma$ and 4ℓ final states are used. $\sigma(pp \rightarrow HX) = 33.0 \pm 5.3 \pm 1.6 \text{ pb}$ is given. See their Figs. 2 and 3 for data on differential cross sections.
- ¹¹ KHACHATRYAN 15AM use up to 5.1 fb^{-1} of pp collisions at $E_{\text{cm}} = 7 \text{ TeV}$ and up to 19.7 fb^{-1} at $E_{\text{cm}} = 8 \text{ TeV}$. The third uncertainty in the measurement is theory systematics. Fits to each production mode give the value of 0.85 ± 0.19 for gluon fusion, 1.16 ± 0.37 for vector boson fusion, 0.92 ± 0.38 for WH, ZH production, and 2.90 ± 1.08 for $t\bar{t}H$ production.
- ¹² AAD 13AK use 4.7 fb^{-1} of pp collisions at $E_{\text{cm}} = 7 \text{ TeV}$ and 20.7 fb^{-1} at $E_{\text{cm}} = 8 \text{ TeV}$. The combined signal strength is based on the $\gamma\gamma, ZZ^* \rightarrow 4\ell$, and $WW^* \rightarrow \ell\nu\ell\nu$ channels. The quoted signal strength is given for $m_H = 125.5 \text{ GeV}$. Reported statistical error value modified following private communication with the experiment.
- ¹³ AALTONEN 13L combine all CDF results with $9.45\text{--}10.0 \text{ fb}^{-1}$ of $p\bar{p}$ collisions at $E_{\text{cm}} = 1.96 \text{ TeV}$. The quoted signal strength is given for $m_H = 125 \text{ GeV}$.
- ¹⁴ ABAZOV 13L combine all D0 results with up to 9.7 fb^{-1} of $p\bar{p}$ collisions at $E_{\text{cm}} = 1.96 \text{ TeV}$. The quoted signal strength is given for $m_H = 125 \text{ GeV}$.
- ¹⁵ AAD 12AI obtain results based on $4.6\text{--}4.8 \text{ fb}^{-1}$ of pp collisions at $E_{\text{cm}} = 7 \text{ TeV}$ and $5.8\text{--}5.9 \text{ fb}^{-1}$ at $E_{\text{cm}} = 8 \text{ TeV}$. An excess of events over background with a local significance of 5.9σ is observed at $m_H = 126 \text{ GeV}$. The quoted signal strengths are given for $m_H = 126 \text{ GeV}$. See also AAD 12DA.
- ¹⁶ CHATRCHYAN 12N obtain results based on $4.9\text{--}5.1 \text{ fb}^{-1}$ of pp collisions at $E_{\text{cm}} = 7 \text{ TeV}$ and $5.1\text{--}5.3 \text{ fb}^{-1}$ at $E_{\text{cm}} = 8 \text{ TeV}$. An excess of events over background with a local significance of 5.0σ is observed at about $m_H = 125 \text{ GeV}$. The combined signal strength is based on the $\gamma\gamma, ZZ^*, WW^*, \tau^+\tau^-,$ and $b\bar{b}$ channels. The quoted signal strength is given for $m_H = 125.5 \text{ GeV}$. See also CHATRCHYAN 13X.

WW* Final State

VALUE	DOCUMENT ID	TECN	COMMENT
1.00 ± 0.08 OUR AVERAGE			
0.97 ± 0.09	1 CMS	22 CMS	pp , 13 TeV
1.09 ± 0.18 ± 0.16	2,3 AAD	16AN LHC	pp , 7, 8 TeV
0.94 ^{+0.85} _{-0.83}	4 AALTONEN	13M TEVA	$p\bar{p} \rightarrow HX$, 1.96 TeV
• • • We do not use the following data for averages, fits, limits, etc. • • •			
0.95 ^{+0.10} _{-0.09}	5 AAD	23AP ATLS	pp , 13 TeV, cross sections
	6 AAD	23BV ATLS	pp , 13 TeV, cross sections
	7,8 TUMASYAN	23W CMS	pp , 13 TeV
0.92 ^{+0.11} _{-0.10}	7,9,10 TUMASYAN	23W CMS	pp , 13 TeV
0.71 ^{+0.28} _{-0.25}	7,9,11 TUMASYAN	23W CMS	pp , 13 TeV
2.2 ± 0.6	7,9,12 TUMASYAN	23W CMS	pp , 13 TeV
2.0 ± 0.7	7,9,13 TUMASYAN	23W CMS	pp , 13 TeV
	7,14 TUMASYAN	23W CMS	pp , 13 TeV
0.5 ± 0.4 ^{+0.7} _{-0.6}	15 AAD	22V ATLS	$pp, WW^* (\rightarrow e\nu\nu\nu) + 2j$, 13 TeV
	16 AAD	22V ATLS	$pp, WW^* (\rightarrow e\nu\nu\nu) + 2j$, 13 TeV
	17 AABOUD	19F ATLS	pp , 13 TeV, cross sections
2.5 ^{+0.9} _{-0.8}	18 AAD	19A ATLS	$pp \rightarrow HW/HZ, H \rightarrow WW^*$, 13 TeV
1.28 ^{+0.17} _{-0.16}	19 SIRUNYAN	19AT CMS	pp , 13 TeV
1.28 ± 0.17	20 SIRUNYAN	19AX CMS	pp , 13 TeV
1.22 ^{+0.23} _{-0.21}	3 AAD	16AN ATLS	pp , 7, 8 TeV
0.90 ^{+0.23} _{-0.21}	3 AAD	16AN CMS	pp , 7, 8 TeV
	21 AAD	16AO ATLS	pp , 8 TeV, cross sections
1.18 ± 0.16 ± 0.17 ± 0.14	22 AAD	16K ATLS	pp , 7, 8 TeV
1.09 ^{+0.16} _{-0.15} ± 0.17 ± 0.14	23 AAD	15AA ATLS	pp , 7, 8 TeV

$3.0^{+1.3}_{-1.1}^{+1.0}_{-0.7}$	24 AAD	15AQ ATLS	$pp \rightarrow HW/ZX, 7, 8$ TeV
$1.16^{+0.16}_{-0.15}^{+0.18}_{-0.15}$	25 AAD	15AQ ATLS	$pp, 7, 8$ TeV
$0.72 \pm 0.12 \pm 0.10^{+0.12}_{-0.10}$	26 CHATRCHYAN14G	CMS	$pp, 7, 8$ TeV
$0.99^{+0.31}_{-0.28}$	27 AAD	13AK ATLS	$pp, 7$ and 8 TeV
$0.00^{+1.78}_{-0.00}$	28 AALTONEN	13L CDF	$p\bar{p} \rightarrow HX, 1.96$ TeV
$1.90^{+1.63}_{-1.52}$	29 ABAZOV	13L D0	$p\bar{p} \rightarrow HX, 1.96$ TeV
1.3 ± 0.5	30 AAD	12AI ATLS	$pp \rightarrow HX, 7, 8$ TeV
0.5 ± 0.6	30 AAD	12AI ATLS	$pp \rightarrow HX, 7$ TeV
1.9 ± 0.7	30 AAD	12AI ATLS	$pp \rightarrow HX, 8$ TeV
$0.60^{+0.42}_{-0.37}$	31 CHATRCHYAN12N	CMS	$pp \rightarrow HX, 7, 8$ TeV

- 1 CMS 22 report combined results (see their Extended Data Table 2) using up to 138 fb⁻¹ of data at $E_{\text{cm}} = 13$ TeV, assuming $m_H = 125.38$ GeV. See their Fig. 2 right.
- 2 AAD 16AN perform fits to the ATLAS and CMS data at $E_{\text{cm}} = 7$ and 8 TeV. The signal strengths for individual production processes are 0.84 ± 0.17 for gluon fusion, 1.2 ± 0.4 for vector boson fusion, $1.6^{+1.2}_{-1.0}$ for WH production, $5.9^{+2.6}_{-2.2}$ for ZH production, and $5.0^{+1.8}_{-1.7}$ for $t\bar{t}H$ production.
- 3 AAD 16AN: In the fit, relative production cross sections are fixed to those in the Standard Model. The quoted signal strength is given for $m_H = 125.09$ GeV.
- 4 AALTONEN 13M combine all Tevatron data from the CDF and D0 Collaborations with up to 10.0 fb⁻¹ and 9.7 fb⁻¹, respectively, of $p\bar{p}$ collisions at $E_{\text{cm}} = 1.96$ TeV. The quoted signal strength is given for $m_H = 125$ GeV.
- 5 AAD 23AP measure cross-sections times the $H \rightarrow WW^*$ branching fraction in the $H \rightarrow WW^* \rightarrow e\nu\mu\nu$ channel using 139 fb⁻¹ of pp collisions at $E_{\text{cm}} = 13$ TeV: $\sigma_{\text{ggF}} \times \text{B}(H \rightarrow WW^*) = 12.0 \pm 1.4$ pb, $\sigma_{\text{VBF}} \times \text{B}(H \rightarrow WW^*) = 0.75^{+0.19}_{-0.16}$ pb, and $\sigma_{\text{ggF}+\text{VBF}} \times \text{B}(H \rightarrow WW^*) = 12.3 \pm 1.3$ pb. The results are given for $m_H = 125.09$ GeV. Measured cross sections and ratios to the SM predictions in the reduced stage-1.2 (see their Fig. 5) simplified template cross section framework are shown in their Table VII and Fig. 15.
- 6 AAD 23BV measure fiducial total and differential cross sections of VBF process at $E_{\text{cm}} = 13$ TeV with 139 fb⁻¹ using $H \rightarrow WW^* \rightarrow e\nu\mu\nu$. The measured total fiducial cross section is $1.68 \pm 0.33(\text{stat}) \pm 0.23(\text{syst})$ fb in their fiducial region (Table II and Section V). See their Fig. 9 for the comparison with theory predictions. The fiducial differential cross sections are shown in their Figs. 11, 12, and 13. Wilson coefficients in the Warsaw basis at 95% confidence interval are measured; see their Table V and Fig. 16.
- 7 TUMASYAN 23W measure Higgs production rates with $H \rightarrow WW^*$ at $E_{\text{cm}} = 13$ TeV with 138 fb⁻¹ data. The quoted results are given for $m_H = 125.38$ GeV.
- 8 The quoted global signal strength is obtained assuming the relative ratios of different Higgs production modes fixed to the SM values.
- 9 The 4 signal strengths for gluon-fusion (ggF), VBF, WH and ZH modes are fit assuming $t\bar{t}H$ and $b\bar{b}H$ fixed to the SM values.
- 10 The quoted result is for ggF production mode.
- 11 The quoted result is for VBF production mode.
- 12 The quoted result is for WH production mode.
- 13 The quoted result is for ZH production mode.
- 14 Measured cross sections and ratios to the SM predictions in the reduced stage-1.2 (see their Fig. 17) simplified template cross section framework (6 ggF, 4 VBF, and 4 VH) are shown in their Table 18 and Fig. 26.
- 15 AAD 22V measure the signal strength for ggF+2jets with 36.1 fb⁻¹ data at 13 TeV.
- 16 AAD 22V probe the Higgs couplings to longitudinally and transversely polarized W and Z using VBF ($H \rightarrow WW^* \rightarrow e\nu\mu\nu$ plus two jets) with 36.1 fb⁻¹ of data at $E_{\text{cm}} = 13$ TeV. The ratios of the polarization-dependent couplings $g_{H V_L V_L}$ and $g_{H V_T V_T}$ to the Higgs- V coupling predicted by the SM, $a_L = g_{H V_L V_L} / g_{H V V}^{\text{SM}}$ and $a_T = g_{H V_T V_T} / g_{H V V}^{\text{SM}}$ are measured to be $0.91^{+0.10+0.09}_{-0.18-0.17}$ and $1.2 \pm 0.4^{+0.2}_{-0.3}$, respectively, assuming the standard Hgg coupling. These measurements are translated into pseudo-observables of κ_{VV} and ϵ_{VV} : $\kappa_{VV} = 0.91^{+0.10+0.09}_{-0.18-0.17}$ and $\epsilon_{VV} = 0.13^{+0.28+0.08}_{-0.20-0.10}$, where $\kappa_{VV} = 1$ and $\epsilon_{VV} = 0$ for the SM. See their Tables 9 and 10.
- 17 AABOUD 19F measure cross-sections times the $H \rightarrow WW^*$ branching fraction in the $H \rightarrow WW^* \rightarrow e\nu\mu\nu$ channel using 36.1 fb⁻¹ of pp collisions at $E_{\text{cm}} = 13$ TeV: $\sigma_{\text{ggF}} \times \text{B}(H \rightarrow WW^*) = 11.4^{+1.2+1.8}_{-1.1-1.7}$ pb and $\sigma_{\text{VBF}} \times \text{B}(H \rightarrow WW^*) = 0.50^{+0.24}_{-0.22} \pm 0.17$ pb.
- 18 AAD 19A use 36.1 fb⁻¹ data at 13 TeV. The cross section times branching fraction values are measured to be $0.67^{+0.31+0.18}_{-0.27-0.14}$ pb for $WH, H \rightarrow WW^*$ and $0.54^{+0.31+0.15}_{-0.24-0.07}$ pb for $ZH, H \rightarrow WW^*$.
- 19 SIRUNYAN 19AT perform a combine fit to 35.9 fb⁻¹ of data at $E_{\text{cm}} = 13$ TeV.
- 20 SIRUNYAN 19AX measure the signal strengths, cross sections and so on using gluon fusion, VBF and VH production processes with 35.9 fb⁻¹ of data. The quoted signal strength is given for $m_H = 125.09$ GeV. Signal strengths for each production process is found in their Fig. 9. Measured cross sections and ratios to the SM predictions in the stage-0 simplified template cross section framework are shown in their Fig. 10. $\kappa_F = 1.52^{+0.48}_{-0.41}$ and $\kappa_V = 1.10 \pm 0.08$ are obtained (see their Fig. 11 (right)).
- 21 AAD 16AO measure fiducial total and differential cross sections of gluon fusion process at $E_{\text{cm}} = 8$ TeV with 20.3 fb⁻¹ using $H \rightarrow WW^* \rightarrow e\nu\mu\nu$. The measured fiducial total cross section is 36.0 ± 9.7 fb in their fiducial region (Table 7). See their Fig. 6 for fiducial differential cross sections. The results are given for $m_H = 125$ GeV.
- 22 AAD 16K use up to 4.7 fb⁻¹ of pp collisions at $E_{\text{cm}} = 7$ TeV and up to 20.3 fb⁻¹ at $E_{\text{cm}} = 8$ TeV. The quoted signal strength is given for $m_H = 125.36$ GeV.
- 23 AAD 15AA use 4.5 fb⁻¹ of pp collisions at $E_{\text{cm}} = 7$ TeV and 20.3 fb⁻¹ at $E_{\text{cm}} = 8$ TeV. The signal strength for the gluon fusion and vector boson fusion mode is

- $1.02 \pm 0.19^{+0.22}_{-0.18}$ and $1.27^{+0.44+0.30}_{-0.40-0.21}$, respectively. The quoted signal strengths are given for $m_H = 125.36$ GeV.
- 24 AAD 15AQ use 4.5 fb⁻¹ of pp collisions at $E_{\text{cm}} = 7$ TeV and 20.3 fb⁻¹ at $E_{\text{cm}} = 8$ TeV. The quoted signal strength is given for $m_H = 125.36$ GeV.
- 25 AAD 15AQ combine their result on W/ZH production with the results of AAD 15AA (gluon fusion and vector boson fusion, slightly updated). The quoted signal strength is given for $m_H = 125.36$ GeV.
- 26 CHATRCHYAN 14G use 4.9 fb⁻¹ of pp collisions at $E_{\text{cm}} = 7$ TeV and 19.4 fb⁻¹ at $E_{\text{cm}} = 8$ TeV. The last uncertainty in the measurement is theory systematics. The quoted signal strength is given for $m_H = 125.6$ GeV.
- 27 AAD 13AK use 4.7 fb⁻¹ of pp collisions at $E_{\text{cm}} = 7$ TeV and 20.7 fb⁻¹ at $E_{\text{cm}} = 8$ TeV. The quoted signal strength is given for $m_H = 125.5$ GeV. Superseded by AAD 15AA.
- 28 AALTONEN 13L combine all CDF results with 9.45–10.0 fb⁻¹ of $p\bar{p}$ collisions at $E_{\text{cm}} = 1.96$ TeV. The quoted signal strength is given for $m_H = 125$ GeV.
- 29 ABAZOV 13I combine all D0 results with up to 9.7 fb⁻¹ of $p\bar{p}$ collisions at $E_{\text{cm}} = 1.96$ TeV. The quoted signal strength is given for $m_H = 125$ GeV.
- 30 AAD 12AI obtain results based on 4.7 fb⁻¹ of pp collisions at $E_{\text{cm}} = 7$ TeV and 5.8 fb⁻¹ at $E_{\text{cm}} = 8$ TeV. The quoted signal strengths are given for $m_H = 126$ GeV. See also AAD 12DA.
- 31 CHATRCHYAN 12N obtain results based on 4.9 fb⁻¹ of pp collisions at $E_{\text{cm}} = 7$ TeV and 5.1 fb⁻¹ at $E_{\text{cm}} = 8$ TeV. The quoted signal strength is given for $m_H = 125.5$ GeV. See also CHATRCHYAN 13Y.

ZZ* Final State

VALUE	CL%	DOCUMENT ID	TECN	COMMENT
1.02 ± 0.08 OUR AVERAGE				
$0.97^{+0.12}_{-0.11}$		1 CMS	22 CMS	$pp, 13$ TeV
1.01 ± 0.11		2,3 AAD	20AQ ATLS	$pp, 13$ TeV
$1.29^{+0.26}_{-0.23}$		4,5 AAD	16AN LHC	$pp, 7, 8$ TeV
• • • We do not use the following data for averages, fits, limits, etc. • • •				
		6 HAYRAPETYAN...23	CMS	$pp, 13$ TeV cross sections
		7 SIRUNYAN	21AE CMS	$pp, 13$ TeV, couplings
		8 SIRUNYAN	21s CMS	$pp, 13$ TeV
		2,9 AAD	20AQ ATLS	$pp, 13$ TeV
		10 AAD	20BA ATLS	$pp, 13$ TeV cross sections
<6.5	95	11 AABOUD	19N ATLS	$pp, 13$ TeV, off-shell
$1.06^{+0.19}_{-0.17}$		12 SIRUNYAN	19AT CMS	$pp, 13$ TeV
$1.28^{+0.21}_{-0.19}$		13 AABOUD	18AJ ATLS	$pp, 13$ TeV
<3.8	95	14 AABOUD	18BP ATLS	$pp, 13$ TeV, off-shell
$1.05^{+0.15+0.11}_{-0.14-0.09}$		15 SIRUNYAN	17AV CMS	$pp, 13$ TeV
$1.52^{+0.40}_{-0.34}$		5 AAD	16AN ATLS	$pp, 7, 8$ TeV
$1.04^{+0.32}_{-0.26}$		5 AAD	16AN CMS	$pp, 7, 8$ TeV
$1.46^{+0.35+0.19}_{-0.31-0.13}$		16 AAD	16K ATLS	$pp, 7, 8$ TeV
		17 KHACHATRYAN...16AR	CMS	$pp, 7, 8$ TeV cross sections
$1.44^{+0.34+0.21}_{-0.31-0.11}$		18 AAD	15F ATLS	$pp \rightarrow HX, 7, 8$ TeV
		19 AAD	14AR ATLS	$pp, 8$ TeV, cross sections
$0.93^{+0.26+0.13}_{-0.23-0.09}$		20 CHATRCHYAN14AA	CMS	$pp, 7, 8$ TeV
$1.43^{+0.40}_{-0.35}$		21 AAD	13AK ATLS	$pp, 7$ and 8 TeV
$0.80^{+0.35}_{-0.28}$		22 CHATRCHYAN13J	CMS	$pp \rightarrow HX, 7, 8$ TeV
1.2 ± 0.6		23 AAD	12AI ATLS	$pp \rightarrow HX, 7, 8$ TeV
1.4 ± 1.1		23 AAD	12AI ATLS	$pp \rightarrow HX, 7$ TeV
1.1 ± 0.8		23 AAD	12AI ATLS	$pp \rightarrow HX, 8$ TeV
$0.73^{+0.45}_{-0.33}$		24 CHATRCHYAN12N	CMS	$pp \rightarrow HX, 7, 8$ TeV

- 1 CMS 22 report combined results (see their Extended Data Table 2) using up to 138 fb⁻¹ of data at $E_{\text{cm}} = 13$ TeV, assuming $m_H = 125.38$ GeV. See their Fig. 2 right.
- 2 AAD 20AQ perform analyses using $H \rightarrow ZZ^* \rightarrow 4\ell$ ($\ell = e, \mu$) with data of 139 fb⁻¹ at $E_{\text{cm}} = 13$ TeV. Results are given for $m_H = 125$ GeV.
- 3 AAD 20AQ measured the inclusive cross section times branching ratio for $H \rightarrow ZZ^*$ decay ($|\eta(H)| < 2.5$) to be 1.34 ± 0.12 pb (with 1.33 ± 0.08 pb expected in the SM).
- 4 AAD 16AN perform fits to the ATLAS and CMS data at $E_{\text{cm}} = 7$ and 8 TeV. The signal strengths for individual production processes are $1.13^{+0.34}_{-0.31}$ for gluon fusion and $0.1^{+1.1}_{-0.6}$ for vector boson fusion.
- 5 AAD 16AN: In the fit, relative production cross sections are fixed to those in the Standard Model. The quoted signal strength is given for $m_H = 125.09$ GeV.
- 6 HAYRAPETYAN 23 measure the cross sections for $pp \rightarrow H \rightarrow ZZ^* \rightarrow 4\ell$ ($\ell = e, \mu$) using 138 fb⁻¹ at $E_{\text{cm}} = 13$ TeV. They give $\sigma = 2.73 \pm 0.22(\text{stat}) \pm 0.15(\text{syst})$ fb in their fiducial region (see their Section 5 and Table 2), where 2.86 ± 0.15 fb is expected in the Standard Model for $m_H = 125.38$ GeV. 26 differential and 6 double-differential cross sections are given; see their Figs. 6–23 and 24–25.
- 7 SIRUNYAN 21AE obtains constraints on anomalous couplings to vector bosons (W, Z , and gluon) and top quark using $H \rightarrow ZZ^* \rightarrow 4\ell$ ($\ell = e, \mu$) with data of 137 fb⁻¹ at $E_{\text{cm}} = 13$ TeV. Their Table 5 and Figs 14–17 show (effective) couplings to gluon and top with combining gluon fusion, $t\bar{t}H$ and tH production channels and the result of $t\bar{t}H, H \rightarrow \gamma\gamma$ (SIRUNYAN 20AS). Their Tables 6–9 and Figs 18–22 show couplings to W and Z for different assumptions and bases (Higgs and Warsaw).

Gauge & Higgs Boson Particle Listings

H

- ⁸ SIRUNYAN 21s measure cross sections with the $H \rightarrow ZZ^* \rightarrow 4\ell$ ($\ell = e, \mu$) channel using 137 fb^{-1} data at $E_{\text{cm}} = 13 \text{ TeV}$. Results are given for $m_H = 125.38 \text{ GeV}$. The signal strengths for individual production processes in their Table 4. Cross sections are given in their Table 6 and Fig. 14, which are based on the simplified template cross section framework (reduced stage-1.2).
- ⁹ AAD 20AQ present several results for the channel $H \rightarrow ZZ^* \rightarrow 4\ell$ ($\ell = e, \mu$) with the simplified template cross section with κ -frameworks and the effective field theory (EFT) approach; see their Table 8 and Fig. 10 for simplified template cross sections. $\kappa_V = 1.02 \pm 0.06$ and $\kappa_F = 0.88 \pm 0.16$ are obtained, see their Fig. 12 for the κ -framework. See their Tables 9 and 10 and Figs. 16–18 for the EFT-framework.
- ¹⁰ AAD 20BA measure the cross section for $pp \rightarrow H \rightarrow ZZ^* \rightarrow 4\ell$ ($\ell = e, \mu$) using 139 fb^{-1} at $E_{\text{cm}} = 13 \text{ TeV}$. They give $\sigma \cdot B = 3.28 \pm 0.30 \pm 0.11 \text{ fb}$ in their fiducial region, where $3.41 \pm 0.18 \text{ fb}$ is expected in the Standard Model for $m_H = 125 \text{ GeV}$. Various differential cross sections are also given; see their Figs. 19–39. Constraints on Yukawa couplings for bottom and charm quarks are given in their Table 9 and Fig. 41.
- ¹¹ AABOUD 19N measure the spectrum of the four-lepton invariant mass $m_{4\ell}$ ($\ell = e$ or μ) using 36.1 fb^{-1} of data at $E_{\text{cm}} = 13 \text{ TeV}$. The quoted signal strength upper limit is obtained from $180 \text{ GeV} < m_{4\ell} < 1200 \text{ GeV}$.
- ¹² SIRUNYAN 19AT perform a combine fit to 35.9 fb^{-1} of data at $E_{\text{cm}} = 13 \text{ TeV}$.
- ¹³ AABOUD 18AJ perform analyses using $H \rightarrow ZZ^* \rightarrow 4\ell$ ($\ell = e, \mu$) with data of 36.1 fb^{-1} at $E_{\text{cm}} = 13 \text{ TeV}$. Results are given for $m_H = 125.09 \text{ GeV}$. The inclusive cross section times branching ratio for $H \rightarrow ZZ^* \rightarrow 4\ell$ ($|\eta(H)| < 2.5$) is measured to be $1.73^{+0.26}_{-0.24} \text{ pb}$ (with $1.34^{+0.09}_{-0.09} \text{ pb}$ expected in the SM).
- ¹⁴ AABOUD 18BP measure an off-shell Higgs boson production using $ZZ \rightarrow 4\ell$ and $ZZ \rightarrow 2\ell 2\nu$ ($\ell = e, \mu$) decay channels with 36.1 fb^{-1} of data at $E_{\text{cm}} = 13 \text{ TeV}$. The quoted signal strength upper limit is obtained from a combination of these two channels, where $220 \text{ GeV} < m_{4\ell} < 2000 \text{ GeV}$ for $ZZ \rightarrow 4\ell$ and $250 \text{ GeV} < m_{\ell\ell}^{ZZ} < 2000 \text{ GeV}$ for $ZZ \rightarrow 2\ell 2\nu$ ($m_{\ell\ell}^{ZZ}$ is defined in their Section 5). See their Table 2 for each measurement.
- ¹⁵ SIRUNYAN 17AV use 35.9 fb^{-1} of pp collisions at $E_{\text{cm}} = 13 \text{ TeV}$. The quoted signal strength, obtained from the analysis of $H \rightarrow ZZ^* \rightarrow 4\ell$ ($\ell = e, \mu$) decays, is given in their Table 3. The fiducial and differential cross sections are shown in their Fig. 10.
- ¹⁶ AAD 16K use up to 4.7 fb^{-1} of pp collisions at $E_{\text{cm}} = 7 \text{ TeV}$ and up to 20.3 fb^{-1} at $E_{\text{cm}} = 8 \text{ TeV}$. The quoted signal strength is given for $m_H = 125.36 \text{ GeV}$.
- ¹⁷ KHACHATRYAN 16AR use data of 5.1 fb^{-1} at $E_{\text{cm}} = 7 \text{ TeV}$ and 19.7 fb^{-1} at 8 TeV . The fiducial cross sections for the production of 4 leptons via $H \rightarrow 4\ell$ decays are measured to be $0.56^{+0.67+0.21}_{-0.44-0.06} \text{ fb}$ at 7 TeV and $1.11^{+0.41+0.14}_{-0.35-0.10} \text{ fb}$ at 8 TeV in their fiducial region (Table 2). The differential cross sections at $E_{\text{cm}} = 8 \text{ TeV}$ are also shown in Figs. 4 and 5. The results are given for $m_H = 125 \text{ GeV}$.
- ¹⁸ AAD 15F use 4.5 fb^{-1} of pp collisions at $E_{\text{cm}} = 7 \text{ TeV}$ and 20.3 fb^{-1} at $E_{\text{cm}} = 8 \text{ TeV}$. The quoted signal strength is given for $m_H = 125.36 \text{ GeV}$. The signal strength for the gluon fusion production mode is $1.66^{+0.45+0.25}_{-0.41-0.15}$, while the signal strength for the vector boson fusion production mode is $0.26^{+1.60+0.36}_{-0.91-0.23}$.
- ¹⁹ AAD 14AR measure the cross section for $pp \rightarrow H \rightarrow ZZ^* \rightarrow 4\ell$ ($\ell = e, \mu$) using 20.3 fb^{-1} at $E_{\text{cm}} = 8 \text{ TeV}$. They give $\sigma \cdot B = 2.11^{+0.53}_{-0.47} \pm 0.08 \text{ fb}$ in their fiducial region, where $1.30 \pm 0.13 \text{ fb}$ is expected in the Standard Model for $m_H = 125.4 \text{ GeV}$. Various differential cross sections are also given; see their Fig. 2.
- ²⁰ CHATRCHYAN 14AA use 5.1 fb^{-1} of pp collisions at $E_{\text{cm}} = 7 \text{ TeV}$ and 19.7 fb^{-1} at $E_{\text{cm}} = 8 \text{ TeV}$. The quoted signal strength is given for $m_H = 125.6 \text{ GeV}$. The signal strength for the gluon fusion and $t\bar{t}H$ production mode is $0.80^{+0.46}_{-0.36}$, while the signal strength for the vector boson fusion and WH, ZH production mode is $1.7^{+2.2}_{-2.1}$.
- ²¹ AAD 13AK use 4.7 fb^{-1} of pp collisions at $E_{\text{cm}} = 7 \text{ TeV}$ and 20.7 fb^{-1} at $E_{\text{cm}} = 8 \text{ TeV}$. The quoted signal strength is given for $m_H = 125.5 \text{ GeV}$.
- ²² CHATRCHYAN 13J obtain results based on $ZZ \rightarrow 4\ell$ final states in 5.1 fb^{-1} of pp collisions at $E_{\text{cm}} = 7 \text{ TeV}$ and 12.2 fb^{-1} at $E_{\text{cm}} = 8 \text{ TeV}$. The quoted signal strength is given for $m_H = 125.8 \text{ GeV}$. Superseded by CHATRCHYAN 14AA.
- ²³ AAD 12AI obtain results based on $4.7\text{--}4.8 \text{ fb}^{-1}$ of pp collisions at $E_{\text{cm}} = 7 \text{ TeV}$ and 5.8 fb^{-1} at $E_{\text{cm}} = 8 \text{ TeV}$. The quoted signal strengths are given for $m_H = 126 \text{ GeV}$. See also AAD 12DA.
- ²⁴ CHATRCHYAN 12N obtain results based on $4.9\text{--}5.1 \text{ fb}^{-1}$ of pp collisions at $E_{\text{cm}} = 7 \text{ TeV}$ and $5.1\text{--}5.3 \text{ fb}^{-1}$ at $E_{\text{cm}} = 8 \text{ TeV}$. An excess of events over background with a local significance of 5.0σ is observed at about $m_H = 125 \text{ GeV}$. The quoted signal strengths are given for $m_H = 125.5 \text{ GeV}$. See also CHATRCHYAN 12BY and CHATRCHYAN 13Y.
- ⁴ AAD 16AN CMS $pp, 7, 8 \text{ TeV}$
- ¹³ KHACHATRYAN...16G CMS $pp, 8 \text{ TeV}$, diff. x-section
- ¹⁴ AAD 14BC ATLS $pp \rightarrow HX, 7, 8 \text{ TeV}$
- ¹⁵ AAD 14BJ ATLS $pp, 8 \text{ TeV}$, diff. x-section
- ¹⁶ KHACHATRYAN...14P CMS $pp, 7, 8 \text{ TeV}$
- ¹⁷ AAD 13AK ATLS $pp, 7$ and 8 TeV
- ¹⁸ AALTONEN 13L CDF $p\bar{p} \rightarrow HX, 1.96 \text{ TeV}$
- ¹⁹ ABAZOV 13L D0 $p\bar{p} \rightarrow HX, 1.96 \text{ TeV}$
- ²⁰ AAD 12AI ATLS $pp \rightarrow HX, 7, 8 \text{ TeV}$
- ²⁰ AAD 12AI ATLS $pp \rightarrow HX, 7 \text{ TeV}$
- ²⁰ AAD 12AI ATLS $pp \rightarrow HX, 8 \text{ TeV}$
- ²¹ CHATRCHYAN12N CMS $pp \rightarrow HX, 7, 8 \text{ TeV}$
- ¹ AAD 23Y use 139 fb^{-1} of pp collisions at $E_{\text{cm}} = 13 \text{ TeV}$. The quoted results are given for $m_H = 125.09 \text{ GeV}$ and $\Gamma_H = 4.07 \text{ MeV}$. Measured $\sigma \cdot B$ and ratios to the SM predictions for the different production modes are shown in their Table 9 and Fig. 9. Measured cross sections and ratios to the SM predictions in the reduced stage-1.2 (see their Fig. 11) simplified template cross section framework are shown in their Table 10 and Fig. 12. Wilson coefficients in the Warsaw basis (see their Table 11) at 95% CL are measured; see their Table 16 and Fig. 17.
- ² CMS 22 report combined results (see their Extended Data Table 2) using up to 138 fb^{-1} of data at $E_{\text{cm}} = 13 \text{ TeV}$, assuming $m_H = 125.38 \text{ GeV}$. See their Fig. 2 right.
- ³ AAD 16AN perform fits to the ATLAS and CMS data at $E_{\text{cm}} = 7$ and 8 TeV . The signal strengths for individual production processes are $1.10^{+0.23}_{-0.22}$ for gluon fusion, 1.3 ± 0.5 for vector boson fusion, $0.5^{+1.3}_{-1.2}$ for WH production, $0.5^{+3.0}_{-2.5}$ for ZH production, and $2.2^{+1.6}_{-1.3}$ for $t\bar{t}H$ production.
- ⁴ AAD 16AN: In the fit, relative production cross sections are fixed to those in the Standard Model. The quoted signal strength is given for $m_H = 125.09 \text{ GeV}$.
- ⁵ AALTONEN 13M combine all Tevatron data from the CDF and D0 Collaborations with up to 10.0 fb^{-1} and 9.7 fb^{-1} , respectively, of $p\bar{p}$ collisions at $E_{\text{cm}} = 1.96 \text{ TeV}$. The quoted signal strength is given for $m_H = 125 \text{ GeV}$.
- ⁶ TUMASYAN 23Q measure fiducial and differential cross sections at $E_{\text{cm}} = 13 \text{ TeV}$ with 137 fb^{-1} data. The quoted results are given for $m_H = 125.38 \text{ GeV}$. The inclusive fiducial $\sigma \cdot B$ is $73.4^{+5.4}_{-5.3}(\text{stat})^{+2.4}_{-2.2}(\text{syst}) \text{ fb}$ with their defined fiducial region (see their Section 7 and Table 2), where $75.4 \pm 4.1 \text{ fb}$ is expected in the Standard Model. See their Fig. 8 including other fiducial $\sigma \cdot B$ defined in their Table 3. Differential $\sigma \cdot B$ are shown in their Figs. 10–15. Double-differential $\sigma \cdot B$ are in their Figs. 16 and 17.
- ⁷ AAD 22m measure fiducial and differential cross sections of $pp \rightarrow H \rightarrow \gamma\gamma$ at $E_{\text{cm}} = 13 \text{ TeV}$ with 139 fb^{-1} data. The quoted results are given for $m_H = 125.09 \text{ GeV}$. The inclusive fiducial $\sigma \cdot B$ is $67 \pm 5 \pm 4 \text{ fb}$ with their defined fiducial region. Other fiducial $\sigma \cdot B$ are in their Table 3. Differential $\sigma \cdot B$ are shown in their Figs. 8–13, 15, 25–32, 36. Double-differential $\sigma \cdot B$ are in their Figs. 14, 33, 34. Modifications of the b - and c -quark Yukawa couplings to H, κ_b and κ_c at 95% CL are in their Table 6 and Fig. 18. Wilson coefficients at 95% CL are in their Table 7 and Fig. 21.
- ⁸ SIRUNYAN 21o measures cross sections and couplings with the $H \rightarrow \gamma\gamma$ channel using 137 fb^{-1} data at $E_{\text{cm}} = 13 \text{ TeV}$. Results are given for $m_H = 125.38 \text{ GeV}$. The signal strengths for individual production processes are given in their Fig. 16. Cross sections are given in their Tables 12 and 13 and Figs. 18 and 20, which are based on the simplified template cross section framework (reduced stage-1.2). Results in the κ -framework are given in their Fig. 22.
- ⁹ SIRUNYAN 19AT perform a combine fit to 35.9 fb^{-1} of data at $E_{\text{cm}} = 13 \text{ TeV}$.
- ¹⁰ SIRUNYAN 19L measure fiducial and differential cross sections of the process $pp \rightarrow H \rightarrow \gamma\gamma$ at $E_{\text{cm}} = 13 \text{ TeV}$ with 35.9 fb^{-1} . See their Figs. 4–11.
- ¹¹ AABOUD 18BO use 36.1 fb^{-1} of pp collisions at $E_{\text{cm}} = 13 \text{ TeV}$. The signal strengths for the individual production modes are: $0.81^{+0.19}_{-0.18}$ for gluon fusion, $2.0^{+0.6}_{-0.5}$ for vector boson fusion, $0.7^{+0.9}_{-0.8}$ for VH production ($V = W, Z$), and 0.5 ± 0.6 for $t\bar{t}H$ and tH production. Other measurements of cross sections and couplings are summarized in their Section 10. The quoted values are given for $m_H = 125.09 \text{ GeV}$.
- ¹² SIRUNYAN 18ps use 35.9 fb^{-1} of $pp \rightarrow H$ collisions with $H \rightarrow \gamma\gamma$ at $E_{\text{cm}} = 13 \text{ TeV}$. The Higgs mass is floated in the measurement of a signal strength. The result is $1.18^{+0.12}_{-0.11}(\text{stat.})^{+0.09}_{-0.07}(\text{syst.})^{+0.07}_{-0.06}(\text{theory})$, which is largely insensitive to the Higgs mass around 125 GeV .
- ¹³ KHACHATRYAN 16G measure fiducial and differential cross sections of the process $pp \rightarrow HX, H \rightarrow \gamma\gamma$ at $E_{\text{cm}} = 8 \text{ TeV}$ with 19.7 fb^{-1} . See their Figs. 4–6 and Table 1 for data.
- ¹⁴ AAD 14BC use 4.5 fb^{-1} of pp collisions at $E_{\text{cm}} = 7 \text{ TeV}$ and 20.3 fb^{-1} at $E_{\text{cm}} = 8 \text{ TeV}$. The last uncertainty in the measurement is theory systematics. The quoted signal strength is given for $m_H = 125.4 \text{ GeV}$. The signal strengths for the individual production modes are: 1.32 ± 0.38 for gluon fusion, 0.8 ± 0.7 for vector boson fusion, 1.0 ± 1.6 for WH production, $0.1^{+3.7}_{-0.1}$ for ZH production, and $1.6^{+2.7}_{-1.8}$ for $t\bar{t}H$ production.
- ¹⁵ AAD 14BJ measure fiducial and differential cross sections of the process $pp \rightarrow HX, H \rightarrow \gamma\gamma$ at $E_{\text{cm}} = 8 \text{ TeV}$ with 20.3 fb^{-1} . See their Table 3 and Figs. 3–12 for data.
- ¹⁶ KHACHATRYAN 14P use 5.1 fb^{-1} of pp collisions at $E_{\text{cm}} = 7 \text{ TeV}$ and 19.7 fb^{-1} at $E_{\text{cm}} = 8 \text{ TeV}$. The last uncertainty in the measurement is theory systematics. The quoted signal strength is given for $m_H = 124.7 \text{ GeV}$. The signal strength for the gluon fusion and $t\bar{t}H$ production mode is $1.13^{+0.37}_{-0.31}$, while the signal strength for the vector boson fusion and WH, ZH production mode is $1.16^{+0.63}_{-0.58}$.
- ¹⁷ AAD 13AK use 4.7 fb^{-1} of pp collisions at $E_{\text{cm}} = 7 \text{ TeV}$ and 20.7 fb^{-1} at $E_{\text{cm}} = 8 \text{ TeV}$. The quoted signal strength is given for $m_H = 125.5 \text{ GeV}$.
- ¹⁸ AALTONEN 13L combine all CDF results with $9.45\text{--}10.0 \text{ fb}^{-1}$ of $p\bar{p}$ collisions at $E_{\text{cm}} = 1.96 \text{ TeV}$. The quoted signal strength is given for $m_H = 125 \text{ GeV}$.
- ¹⁹ ABAZOV 13L combine all D0 results with up to 9.7 fb^{-1} of $p\bar{p}$ collisions at $E_{\text{cm}} = 1.96 \text{ TeV}$. The quoted signal strength is given for $m_H = 125 \text{ GeV}$.

 $\gamma\gamma$ Final State

VALUE	DOCUMENT ID	TECN	COMMENT
1.10±0.06 OUR AVERAGE			
$1.04^{+0.10}_{-0.09}$	1 AAD	23Y ATLS	$pp, 13 \text{ TeV}$
1.13 ± 0.09	2 CMS	22 CMS	$pp, 13 \text{ TeV}$
$1.14^{+0.19}_{-0.18}$	3,4 AAD	16AN LHC	$pp, 7, 8 \text{ TeV}$
$5.97^{+3.39}_{-3.12}$	5 AALTONEN	13M TEVA	$p\bar{p} \rightarrow HX, 1.96 \text{ TeV}$
• • • We do not use the following data for averages, fits, limits, etc. • • •			
1.12 ± 0.09	6 TUMASYAN	23Q CMS	$pp, 13 \text{ TeV}$, cross sections
$1.20^{+0.18}_{-0.14}$	7 AAD	22N ATLS	$pp, 13 \text{ TeV}$, diff. x-sections
$0.99^{+0.15}_{-0.14}$	8 SIRUNYAN	21O CMS	$pp, 13 \text{ TeV}$
$1.18^{+0.17}_{-0.14}$	9 SIRUNYAN	19AT CMS	$pp, 13 \text{ TeV}$
$1.14^{+0.27}_{-0.25}$	10 SIRUNYAN	19L CMS	$pp, 13 \text{ TeV}$, diff. x-section
	11 AABOUD	18BO ATLS	$pp, 13 \text{ TeV}$
	12 SIRUNYAN	18DS CMS	$pp, H \rightarrow \gamma\gamma, 13 \text{ TeV}$, floated m_H
	4 AAD	16AN ATLS	$pp, 7, 8 \text{ TeV}$

See key on page 1171

Gauge & Higgs Boson Particle Listings

H

- ²⁰ AAD 12A_l obtain results based on 4.8 fb^{-1} of pp collisions at $E_{\text{cm}} = 7 \text{ TeV}$ and 5.9 fb^{-1} at $E_{\text{cm}} = 8 \text{ TeV}$. The quoted signal strengths are given for $m_H = 126 \text{ GeV}$. See also AAD 12DA.
- ²¹ CHATRCHYAN 12N obtain results based on 5.1 fb^{-1} of pp collisions at $E_{\text{cm}} = 7 \text{ TeV}$ and 5.3 fb^{-1} at $E_{\text{cm}} = 8 \text{ TeV}$. The quoted signal strength is given for $m_H = 125.5 \text{ GeV}$. See also CHATRCHYAN 13Y.

 $c\bar{c}$ Final State

VALUE	CL%	DOCUMENT ID	TECN	COMMENT
< 14	95	¹ TUMASYAN 23AH CMS	$pp \rightarrow WH/ZH, 13 \text{ TeV}$	
$9.4^{+20.3}_{-19.9}$		² TUMASYAN 23AD CMS	$pp \rightarrow WH/ZH$ (boosted), 13 TeV	
< 47	95	² TUMASYAN 23AD CMS	$pp \rightarrow WH/ZH$ (boosted), 13 TeV	
$-9 \pm 10 \pm 11$		^{3,4} AAD 22W ATLS	$pp \rightarrow WH/ZH, 13 \text{ TeV}$	
$-9 \pm 10 \pm 11$		^{3,5} AAD 22W ATLS	$pp \rightarrow WH/ZH, 13 \text{ TeV}$	
< 26	95	³ AAD 22W ATLS	$pp \rightarrow WH/ZH, 13 \text{ TeV}$	
$37 \pm 17^{+11}_{-9}$		⁶ SIRUNYAN 20AE CMS	$pp, 13 \text{ TeV}$	
< 110	95	⁷ AABOUD 18M ATLS	$pp, 13 \text{ TeV}$	

¹ TUMASYAN 23AH search for $VH, H \rightarrow c\bar{c}$ ($V = W, Z$) using 138 fb^{-1} of pp collision data at $E_{\text{cm}} = 13 \text{ TeV}$. The upper limit on $\sigma(pp \rightarrow VH) \cdot \mathcal{B}(H \rightarrow c\bar{c})$ is 0.94 pb at 95% CL. See their Fig. 4. The quoted values are given for $m_H = 125.38 \text{ GeV}$.

² TUMASYAN 23AD search for Higgs produced with transverse momenta greater than 450 GeV and decaying to $c\bar{c}$ using 138 fb^{-1} of pp collision data at $E_{\text{cm}} = 13 \text{ TeV}$.

³ AAD 22W search for $VH, H \rightarrow c\bar{c}$ ($V = W, Z$) using 139 fb^{-1} of pp collision data at $E_{\text{cm}} = 13 \text{ TeV}$. The results are given for $m_H = 125 \text{ GeV}$.

⁴ The analysis of $VH, H \rightarrow c\bar{c}$ is combined with $VH, H \rightarrow b\bar{b}$ (AAD 21AB). The ratio $|\kappa_c/\kappa_b|$ is constrained to be less than 4.5 at 95% CL. See their Fig. 7.

⁵ The constraint on the charm Yukawa coupling modifier κ_c is measured to be $|\kappa_c| < 8.5$ at 95% CL. See their Fig. 4.

⁶ SIRUNYAN 20AE use 35.9 fb^{-1} at pp collisions at $E_{\text{cm}} = 13 \text{ TeV}$. The measured best fit value of $\sigma(pp \rightarrow VH) \cdot \mathcal{B}(H \rightarrow c\bar{c})$ is $2.40^{+1.12+0.65}_{-1.11-0.61}$ pb (equivalent to < 4.5 pb at 95% CL upper limit, i.e. 70 times the standard model), where V is $W \rightarrow \ell\nu$, $Z \rightarrow \ell\ell$, or $Z \rightarrow \nu\nu$ ($\ell = e, \mu$). The quoted values are given for $m_H = 125 \text{ GeV}$.

⁷ AABOUD 18M use 36.1 fb^{-1} at pp collisions at $E_{\text{cm}} = 13 \text{ TeV}$. The upper limit on $\sigma(pp \rightarrow ZH) \cdot \mathcal{B}(H \rightarrow c\bar{c})$ is 2.7 pb at 95% CL. This corresponds to 110 times the standard model. The quoted values are given for $m_H = 125 \text{ GeV}$.

 $b\bar{b}$ Final State

VALUE	DOCUMENT ID	TECN	COMMENT
0.99 ± 0.12 OUR AVERAGE			
$1.05^{+0.22}_{-0.21}$	¹ CMS 22 CMS	$pp, 13 \text{ TeV}$	
$1.02^{+0.12+0.14}_{-0.11-0.13}$	² AAD 21AB ATLS	$pp \rightarrow HW/HZ, H \rightarrow b\bar{b}$, 13 TeV, 139 fb^{-1}	
$0.95 \pm 0.32^{+0.20}_{-0.17}$	³ AAD 21AJ ATLS	VBF, $H \rightarrow b\bar{b}, pp$, 13 TeV, 126 fb^{-1}	
$0.70^{+0.29}_{-0.27}$	^{4,5} AAD 16AN LHC	$pp, 7, 8 \text{ TeV}$	
$1.59^{+0.69}_{-0.72}$	⁶ AALTONEN 13M TEVA	$p\bar{p} \rightarrow HX, 1.96 \text{ TeV}$	
0.8 ± 3.2	⁷ AAD 22X ATLS	boosted $H \rightarrow b\bar{b}, pp$, 13 TeV	
$0.95 \pm 0.18^{+0.19}_{-0.18}$	² AAD 21AB ATLS	$pp \rightarrow HW, H \rightarrow b\bar{b}$, 13 TeV, 139 fb^{-1}	
$1.08 \pm 0.17^{+0.18}_{-0.15}$	² AAD 21AB ATLS	$pp \rightarrow HZ, H \rightarrow b\bar{b}$, 13 TeV, 139 fb^{-1}	
$0.72^{+0.29+0.26}_{-0.28-0.22}$	⁸ AAD 21H ATLS	$pp \rightarrow HW/HZ, H \rightarrow b\bar{b}$, boosted W/Z , 13 TeV, 139 fb^{-1}	
1.3 ± 1.0	⁹ AAD 21M ATLS	VBF+ $\gamma, H \rightarrow b\bar{b}, pp$, 13 TeV, 132 fb^{-1}	
$3.7 \pm 1.2^{+0.11}_{-0.9}$	¹⁰ SIRUNYAN 20BL CMS	boosted $H \rightarrow b\bar{b}, pp$, 13 TeV	
1.12 ± 0.29	¹¹ AABOUD 19U ATLS	$pp \rightarrow VH, H \rightarrow b\bar{b}$, 13 TeV, cross sections	
$1.16^{+0.27}_{-0.25}$	¹² SIRUNYAN 19AT CMS	$pp, 13 \text{ TeV}$	
$0.98^{+0.22}_{-0.21}$	¹³ AABOUD 18BN ATLS	$pp \rightarrow HW/HZ, H \rightarrow b\bar{b}$, 13 TeV, 79.8 fb^{-1}	
1.01 ± 0.20	¹⁴ AABOUD 18BN ATLS	$pp \rightarrow HW/HZ, H \rightarrow b\bar{b}$, 7, 8, 13 TeV	
1.01 ± 0.20	¹⁵ AABOUD 18BN ATLS	$pp \rightarrow HX, \text{ggF}, \text{VBF}, VH, t\bar{t}H, 7, 8, 13 \text{ TeV}$	
$2.5^{+1.4}_{-1.3}$	^{16,17} AABOUD 18BQ ATLS	$pp \rightarrow HX, \text{VBF}, \text{ggF}, VH, t\bar{t}H, 13 \text{ TeV}$	
$3.0^{+1.7}_{-1.6}$	^{16,18} AABOUD 18BQ ATLS	$pp \rightarrow HX, \text{VBF}, 13 \text{ TeV}$	
$1.19^{+0.40}_{-0.38}$	¹⁹ AALTONEN 18C CDF	$p\bar{p} \rightarrow HX, 1.96 \text{ TeV}$	
$1.06^{+0.31}_{-0.29}$	²⁰ SIRUNYAN 18AE CMS	$pp \rightarrow HW/HZ, H \rightarrow b\bar{b}$, 13 TeV	
1.06 ± 0.26	²¹ SIRUNYAN 18AE CMS	$pp \rightarrow HW/HZ, H \rightarrow b\bar{b}$, 7, 8, 13 TeV	
1.06 ± 0.26	²² SIRUNYAN 18DB CMS	$pp \rightarrow HW/HZ, H \rightarrow b\bar{b}$, 13 TeV, 77.2 fb^{-1}	
1.01 ± 0.22	²³ SIRUNYAN 18DB CMS	$pp \rightarrow HW/HZ, H \rightarrow b\bar{b}$, 7, 8, 13 TeV	

• • • We do not use the following data for averages, fits, limits, etc. • • •

1.04 ± 0.20	²⁴ SIRUNYAN 18DB CMS	$pp \rightarrow HX, \text{ggF}, \text{VBF}, VH, t\bar{t}H, 7, 8, 13 \text{ TeV}$
$2.3^{+1.8}_{-1.6}$	²⁵ SIRUNYAN 18E CMS	$pp \rightarrow HX$, boosted, 13 TeV
$1.20^{+0.24+0.34}_{-0.23-0.28}$	²⁶ AABOUD 17BA ATLS	$pp \rightarrow HW/ZX, H \rightarrow b\bar{b}$, 13 TeV, 36.1 fb^{-1}
$0.90 \pm 0.18^{+0.21}_{-0.19}$	²⁷ AABOUD 17BA ATLS	$pp \rightarrow HW/ZX, H \rightarrow b\bar{b}$, 7, 8, 13 TeV
$-0.8 \pm 1.3^{+1.8}_{-1.9}$	²⁸ AABOUD 16X ATLS	$pp \rightarrow HX, \text{VBF}, 8 \text{ TeV}$
0.62 ± 0.37	⁵ AAD 16AN ATLS	$pp, 7, 8 \text{ TeV}$
$0.81^{+0.45}_{-0.43}$	⁵ AAD 16AN CMS	$pp, 7, 8 \text{ TeV}$
$0.63^{+0.31+0.24}_{-0.30-0.23}$	²⁹ AAD 16K ATLS	$pp, 7, 8 \text{ TeV}$
$0.52 \pm 0.32 \pm 0.24$	³⁰ AAD 15G ATLS	$pp \rightarrow HW/ZX, 7, 8 \text{ TeV}$
$2.8^{+1.6}_{-1.4}$	³¹ KHACHATRY...15Z CMS	$pp \rightarrow HX, \text{VBF}, 8 \text{ TeV}$
$1.03^{+0.44}_{-0.42}$	³² KHACHATRY...15Z CMS	$pp, 8 \text{ TeV}$, combined
1.0 ± 0.5	³³ CHATRCHYAN14AI CMS	$pp \rightarrow HW/ZX, 7, 8 \text{ TeV}$
$1.72^{+0.92}_{-0.87}$	³⁴ AALTONEN 13L CDF	$p\bar{p} \rightarrow HX, 1.96 \text{ TeV}$
$1.23^{+1.24}_{-1.17}$	³⁵ ABAZOV 13L D0	$p\bar{p} \rightarrow HX, 1.96 \text{ TeV}$
0.5 ± 2.2	³⁶ AAD 12AI ATLS	$pp \rightarrow HW/ZX, 7 \text{ TeV}$
	³⁷ AALTONEN 12T TEVA	$p\bar{p} \rightarrow HW/ZX, 1.96 \text{ TeV}$
$0.48^{+0.81}_{-0.70}$	³⁸ CHATRCHYAN12N CMS	$pp \rightarrow HW/ZX, 7, 8 \text{ TeV}$

¹ CMS 22 report combined results (see their Extended Data Table 2) using up to 138 fb^{-1} of data at $E_{\text{cm}} = 13 \text{ TeV}$, assuming $m_H = 125.38 \text{ GeV}$. See their Fig. 2 right.

² AAD 21AB search for $VH, H \rightarrow b\bar{b}$ ($V = W, Z$) using 139 fb^{-1} of pp collision data at $E_{\text{cm}} = 13 \text{ TeV}$. The results are given for $m_H = 125 \text{ GeV}$. Cross sections are given in their Table 13 and Fig. 7, which are based on the simplified template cross section framework (reduced stage-1.2). Wilson coefficients of the Warsaw-basis operators are given in their Fig. 9.

³ AAD 21AJ present measurements of $H \rightarrow b\bar{b}$ in the VBF production mode. The inclusive VBF cross sections with and without the branching ratio of $H \rightarrow b\bar{b}$ are $2.07 \pm 0.70^{+0.46}_{-0.37}$ fb and $3.56 \pm 1.21^{+0.80}_{-0.64}$ fb, respectively. The latter is obtained assuming the SM value of $\mathcal{B}(H \rightarrow b\bar{b}) = 0.5809$ and $m_H = 125 \text{ GeV}$.

⁴ AAD 16AN perform fits to the ATLAS and CMS data at $E_{\text{cm}} = 7$ and 8 TeV. The signal strengths for individual production processes are 1.0 ± 0.5 for WH production, 0.4 ± 0.4 for ZH production, and 1.1 ± 1.0 for $t\bar{t}H$ production.

⁵ AAD 16AN: In the fit, relative production cross sections are fixed to those in the Standard Model. The quoted signal strength is given for $m_H = 125.09 \text{ GeV}$.

⁶ AALTONEN 13M combine all Tevatron data from the CDF and D0 Collaborations with up to 10.0 fb^{-1} and 9.7 fb^{-1} , respectively, of $p\bar{p}$ collisions at $E_{\text{cm}} = 1.96 \text{ TeV}$. The quoted signal strength is given for $m_H = 125 \text{ GeV}$.

⁷ AAD 22X measure cross sections using a boosted $H \rightarrow b\bar{b}$ with large-radius jets. The data is 136 fb^{-1} of pp collisions at $E_{\text{cm}} = 13 \text{ TeV}$. All the results are given for $m_H = 125 \text{ GeV}$. The inclusive signal strength is given using data with a H candidate jet $p_{T(H)} > 250 \text{ GeV}$. The fiducial H production cross section ($p_{T(H)} > 450 \text{ GeV}$ and $|\eta(H)| < 2$) is < 115 fb (95% CL) and the upper limits for other four different $p_{T(H)}$ regions are shown in their Fig. 12. The measured fiducial H production cross section ($p_{T(H)} > 1 \text{ TeV}$) is $2.3 \pm 3.9(\text{stat}) \pm 1.3(\text{syst}) \pm 0.5(\text{theory})$ fb.

⁸ AAD 21H present measurements of $H \rightarrow b\bar{b}$ with a boosted vector boson ($p_{T(H)} > 250 \text{ GeV}$) using 139 fb^{-1} of pp collision data at $E_{\text{cm}} = 13 \text{ TeV}$. Cross sections are given in their Table 6 and Fig. 4, which are based on the simplified template cross section framework (reduced stage-1.2). Wilson coefficients of the Warsaw-basis operators are given in their Fig. 5.

⁹ AAD 21M search for VBF+ $\gamma, H \rightarrow b\bar{b}$ using 132 fb^{-1} of pp collision data at $E_{\text{cm}} = 13 \text{ TeV}$.

¹⁰ SIRUNYAN 20BL search for boosted $H \rightarrow b\bar{b}$ (a H candidate jet $p_{T(H)} > 450 \text{ GeV}$) using 137 fb^{-1} of pp collision data at $E_{\text{cm}} = 13 \text{ TeV}$. The quoted signal strength corresponds to a significance of 2.5 standard deviations and is given for $m_H = 125 \text{ GeV}$. A differential fiducial cross section as a function of Higgs boson $p_{T(H)}$ for ggF is shown in their Fig. 7, assuming the other production modes occur at the expected SM rates. The reported value is $3.7 \pm 1.2^{+0.8+0.8}_{-0.7-0.5}$ where the last uncertainty comes from theoretical modeling. We have combined the systematic uncertainties in quadrature.

¹¹ AABOUD 19U measure cross sections of $pp \rightarrow VH, H \rightarrow b\bar{b}$ production as a function of the gauge boson transverse momentum using data of 79.8 fb^{-1} . The kinematic fiducial volumes used is based on the simplified template cross section framework (reduced stage-1). See their Table 3 and Fig. 3.

¹² SIRUNYAN 19AT perform a combine fit to 35.9 fb^{-1} of data at $E_{\text{cm}} = 13 \text{ TeV}$.

¹³ AABOUD 18BN search for $VH, H \rightarrow b\bar{b}$ ($V = W, Z$) using 79.8 fb^{-1} of pp collision data at $E_{\text{cm}} = 13 \text{ TeV}$. The quoted signal strength corresponds to a significance of 4.9 standard deviations and is given for $m_H = 125 \text{ GeV}$.

¹⁴ AABOUD 18BN combine results of 79.8 fb^{-1} at $E_{\text{cm}} = 13 \text{ TeV}$ with results of VH at $E_{\text{cm}} = 7$ and 8 TeV.

¹⁵ AABOUD 18BN combine results of VH at $E_{\text{cm}} = 7, 8$ and 13 TeV with results of VBF (+gluon fusion) and $t\bar{t}H$ at $E_{\text{cm}} = 7, 8$, and 13 TeV to perform a search for the $H \rightarrow b\bar{b}$ decay. The quoted signal strength assumes a SM production strength and corresponds to a significance of 5.4 standard deviations.

¹⁶ AABOUD 18BQ search for $H \rightarrow b\bar{b}$ produced through vector-boson fusion (VBF) and VBF+ γ with 30.6 fb^{-1} pp collision data at $E_{\text{cm}} = 13 \text{ TeV}$. The quoted signal strength is given for $m_H = 125 \text{ GeV}$.

¹⁷ The signal strength is measured including all production modes (VBF, ggF, $VH, t\bar{t}H$).

¹⁸ The signal strength is measured for VBF-only and others (ggF, $VH, t\bar{t}H$) are constrained to Standard Model expectations with uncertainties described in their Section VIII B.

¹⁹ AALTONEN 18C use 5.4 fb^{-1} of $p\bar{p}$ collisions at $E_{\text{cm}} = 1.96 \text{ TeV}$. The upper limit at 95% CL on $p\bar{p} \rightarrow H \rightarrow b\bar{b}$ is 33 times the SM prediction, which corresponds to a cross section of 40.6 pb.

Gauge & Higgs Boson Particle Listings

H

- 20 SIRUNYAN 18AE use 35.9 fb⁻¹ of pp collision data at $E_{cm} = 13$ TeV. The quoted signal strength corresponds to 3.3 standard deviations and is given for $m_H = 125.09$ GeV.
- 21 SIRUNYAN 18AE combine the result of 35.9 fb⁻¹ at $E_{cm} = 13$ TeV with the results obtained from data of up to 5.1 fb⁻¹ at $E_{cm} = 7$ TeV and up to 18.9 fb⁻¹ at $E_{cm} = 8$ TeV (CHATRCHYAN 14AI and KHACHATRYAN 15Z). The quoted signal strength corresponds to 3.8 standard deviations and is given for $m_H = 125.09$ GeV.
- 22 SIRUNYAN 18DB search for $VH, H \rightarrow b\bar{b}$ ($V = W, Z$) using 77.2 fb⁻¹ of pp collision data at $E_{cm} = 13$ TeV. The quoted signal strength corresponds to a significance of 4.4 standard deviations and is given for $m_H = 125.09$ GeV.
- 23 SIRUNYAN 18DB combine the result of 77.2 fb⁻¹ at $E_{cm} = 13$ TeV with the results obtained from data of up to 5.1 fb⁻¹ at $E_{cm} = 7$ TeV and up to 18.9 fb⁻¹ at $E_{cm} = 8$ TeV. The quoted signal strength corresponds to a significance of 4.8 standard deviations and is given for $m_H = 125.09$ GeV.
- 24 SIRUNYAN 18DB combine results of 77.2 fb⁻¹ at $E_{cm} = 13$ TeV with results of gluon fusion (ggF), VBF and $t\bar{t}H$ at $E_{cm} = 7$ TeV, 8 TeV and 13 TeV to perform a search for the $H \rightarrow b\bar{b}$ decay. The quoted signal strength assumes a SM production strength and corresponds to a significance of 5.6 standard deviations and is given for $m_H = 125.09$ GeV.
- 25 SIRUNYAN 18E use 35.9 fb⁻¹ at $E_{cm} = 13$ TeV. The quoted signal strength is given for $m_H = 125$ GeV. They measure $\sigma \cdot B$ for gluon fusion production of $H \rightarrow b\bar{b}$ with $p_T > 450$ GeV, $|\eta| < 2.5$ to be $74 \pm 48^{+17}_{-10}$ fb.
- 26 AABOUD 17BA use 36.1 fb⁻¹ at $E_{cm} = 13$ TeV. The quoted signal strength is given for $m_H = 125$ GeV. They give $\sigma(WH) \cdot B(H \rightarrow b\bar{b}) = 1.08^{+0.54}_{-0.47}$ pb and $\sigma(ZH) \cdot B(H \rightarrow b\bar{b}) = 0.57^{+0.26}_{-0.23}$ pb.
- 27 AABOUD 17BA combine 7, 8 and 13 TeV analyses. The quoted signal strength is given for $m_H = 125$ GeV.
- 28 AABOUD 16X search for vector-boson fusion production of H decaying to $b\bar{b}$ in 20.2 fb⁻¹ of pp collisions at $E_{cm} = 8$ TeV. The quoted signal strength is given for $m_H = 125$ GeV.
- 29 AAD 16K use up to 4.7 fb⁻¹ of pp collisions at $E_{cm} = 7$ TeV and up to 20.3 fb⁻¹ at $E_{cm} = 8$ TeV. The quoted signal strength is given for $m_H = 125.36$ GeV.
- 30 AAD 15G use 4.7 fb⁻¹ of pp collisions at $E_{cm} = 7$ TeV and 20.3 fb⁻¹ at $E_{cm} = 8$ TeV. The quoted signal strength is given for $m_H = 125.36$ GeV.
- 31 KHACHATRYAN 15Z search for vector-boson fusion production of H decaying to $b\bar{b}$ in up to 19.8 fb⁻¹ of pp collisions at $E_{cm} = 8$ TeV. The quoted signal strength is given for $m_H = 125$ GeV.
- 32 KHACHATRYAN 15Z combined vector boson fusion, WH, ZH production, and $t\bar{t}H$ production results. The quoted signal strength is given for $m_H = 125$ GeV.
- 33 CHATRCHYAN 14AI use up to 5.1 fb⁻¹ of pp collisions at $E_{cm} = 7$ TeV and up to 18.9 fb⁻¹ at $E_{cm} = 8$ TeV. The quoted signal strength is given for $m_H = 125$ GeV. See also CHATRCHYAN 14AJ.
- 34 AALTONEN 13L combine all CDF results with 9.45–10.0 fb⁻¹ of $p\bar{p}$ collisions at $E_{cm} = 1.96$ TeV. The quoted signal strength is given for $m_H = 125$ GeV.
- 35 ABAZOV 13L combine all D0 results with up to 9.7 fb⁻¹ of $p\bar{p}$ collisions at $E_{cm} = 1.96$ TeV. The quoted signal strength is given for $m_H = 125$ GeV.
- 36 AAD 12AI obtain results based on 4.6–4.8 fb⁻¹ of pp collisions at $E_{cm} = 7$ TeV. The quoted signal strengths are given in their Fig. 10 for $m_H = 126$ GeV. See also Fig. 13 of AAD 12DA.
- 37 AALTONEN 12T combine AALTONEN 12Q, AALTONEN 12R, AALTONEN 12S, ABAZOV 12O, ABAZOV 12P, and ABAZOV 12K. An excess of events over background is observed which is most significant in the region $m_H = 120$ –135 GeV, with a local significance of up to 3.3 σ . The local significance at $m_H = 125$ GeV is 2.8 σ , which corresponds to $(\sigma(HW) + \sigma(HZ)) \cdot B(H \rightarrow b\bar{b}) = (0.23^{+0.09}_{-0.08})$ pb, compared to the Standard Model expectation at $m_H = 125$ GeV of 0.12 ± 0.01 pb. Superseded by AALTONEN 13M.
- 38 CHATRCHYAN 12W obtain results based on 5.0 fb⁻¹ of pp collisions at $E_{cm} = 7$ TeV and 5.1 fb⁻¹ at $E_{cm} = 8$ TeV. The quoted signal strength is given for $m_H = 125.5$ GeV. See also CHATRCHYAN 13Y.

 $\mu^+ \mu^-$ Final State

VALUE	CL%	DOCUMENT ID	TECN	COMMENT
1.21 ± 0.35 OUR AVERAGE				
1.21 ^{+0.45} _{-0.42}		1 CMS	22 CMS	pp , 13 TeV
1.2 ± 0.6		2 AAD	21 ATLS	pp , 13 TeV
• • • We do not use the following data for averages, fits, limits, etc. • • •				
1.19 ^{+0.40+0.15} _{-0.39-0.14}		3 SIRUNYAN	21c CMS	pp , 13 TeV
0.68 ^{+1.25} _{-1.24}		4 SIRUNYAN	19AT CMS	pp , 13 TeV
0.7 ± 1.0 ^{+0.2} _{-0.1}		5 SIRUNYAN	19E CMS	pp , 13 TeV, 35.9 fb ⁻¹
1.0 ± 1.0 ± 0.1		5 SIRUNYAN	19E CMS	pp , 7, 8, 13 TeV
-0.1 ± 1.4		6 AABOUD	17Y ATLS	pp , 7, 8, 13 TeV
-0.1 ± 1.5		6 AABOUD	17Y ATLS	pp , 13 TeV
0.1 ± 2.5		7 AAD	16AN LHC	pp , 7, 8 TeV
-0.6 ± 3.6		7 AAD	16AN ATLS	pp , 7, 8 TeV
0.9 ^{+3.6} _{-3.5}		7 AAD	16AN CMS	pp , 7, 8 TeV
< 7.4	95	8 KHACHATRYAN 15H	CMS	$pp \rightarrow HX$, 7, 8 TeV
< 7.0	95	9 AAD	14AS ATLS	$pp \rightarrow HX$, 7, 8 TeV

- 1 CMS 22 report combined results (see their Extended Data Table 2) using up to 138 fb⁻¹ of data at $E_{cm} = 13$ TeV, assuming $m_H = 125.38$ GeV. See their Fig. 2 right.
- 2 AAD 21 search for $H \rightarrow \mu^+ \mu^-$ using 139 fb⁻¹ of pp collision data at $E_{cm} = 13$ TeV. The quoted signal strength corresponds to a significance of 2.0 standard deviations and is given for $m_H = 125.09$ GeV. The upper limit on the cross section times branching fraction is 2.2 times the SM prediction at 95% CL, which corresponds to the branching fraction upper limit of 4.7×10^{-4} (assuming SM production cross sections).

- 3 SIRUNYAN 21 search for $H \rightarrow \mu^+ \mu^-$ using 137 fb⁻¹ of pp collision data at $E_{cm} = 13$ TeV. The quoted signal strength corresponds to a significance of 3.0 standard deviations and is given for $m_H = 125.38$ GeV.
- 4 SIRUNYAN 19AT perform a combine fit to 35.9 fb⁻¹ of data at $E_{cm} = 13$ TeV.
- 5 SIRUNYAN 19E search for $H \rightarrow \mu^+ \mu^-$ using 35.9 fb⁻¹ of pp collisions at $E_{cm} = 13$ TeV and combine with results of 7 TeV (5.0 fb⁻¹) and 8 TeV (19.7 fb⁻¹). The upper limit at 95% CL on the signal strength is 2.9, which corresponds to the SM Higgs boson branching fraction to a muon pair of 6.4×10^{-4} .
- 6 AABOUD 17Y use 36.1 fb⁻¹ of pp collisions at $E_{cm} = 13$ TeV, 20.3 fb⁻¹ at 8 TeV and 4.5 fb⁻¹ at 7 TeV. The quoted signal strength is given for $m_H = 125$ GeV.
- 7 AAD 16AN: In the fit, relative production cross sections are fixed to those in the Standard Model. The quoted signal strength is given for $m_H = 125.09$ GeV.
- 8 KHACHATRYAN 15H use 5.0 fb⁻¹ of pp collisions at $E_{cm} = 7$ TeV and 19.7 fb⁻¹ at 8 TeV. The quoted signal strength is given for $m_H = 125$ GeV.
- 9 AAD 14AS search for $H \rightarrow \mu^+ \mu^-$ in 4.5 fb⁻¹ of pp collisions at $E_{cm} = 7$ TeV and 20.3 fb⁻¹ at $E_{cm} = 8$ TeV. The quoted signal strength is given for $m_H = 125.5$ GeV.

 $\tau^+ \tau^-$ Final State

VALUE	DOCUMENT ID	TECN	COMMENT
0.91 ± 0.09 OUR AVERAGE			
0.85 ± 0.10	1 CMS	22 CMS	pp , 13 TeV
1.09 ^{+0.18+0.26+0.16} _{-0.17-0.22-0.11}	2 AABOUD	19AQ ATLS	pp , 13 TeV
1.11 ^{+0.24} _{-0.22}	3,4 AAD	16AN LHC	pp , 7, 8 TeV
1.68 ^{+2.28} _{-1.68}	5 AALTONEN	13M TEVA	$p\bar{p} \rightarrow HX$, 1.96 TeV
• • • We do not use the following data for averages, fits, limits, etc. • • •			
0.82 ^{+0.11} _{-0.10}	6,7 TUMASYAN	23Y CMS	pp , 13 TeV
0.67 ^{+0.20} _{-0.18}	6,8 TUMASYAN	23Y CMS	pp , 13 TeV
0.81 ^{+0.17} _{-0.16}	6,9 TUMASYAN	23Y CMS	pp , 13 TeV
1.79 ^{+0.47} _{-0.42}	6,10 TUMASYAN	23Y CMS	pp , 13 TeV
2.5 ^{+1.4} _{-1.3}	11 AAD	22Q ATLS	pp , 13 TeV
	12 TUMASYAN	22AJ CMS	pp , 13 TeV
	13 SIRUNYAN	19AF CMS	$pp \rightarrow HW/HZ, H \rightarrow \tau\tau$, 13 TeV
1.24 ^{+0.29} _{-0.27}	14 SIRUNYAN	19AF CMS	pp , 13 TeV
1.02 ^{+0.26} _{-0.24}	15 SIRUNYAN	19AT CMS	pp , 13 TeV
1.09 ^{+0.27} _{-0.26}	16 SIRUNYAN	18Y CMS	pp , 13 TeV
0.98 ± 0.18	17 SIRUNYAN	18Y CMS	pp , 7, 8, 13 TeV
2.3 ± 1.6	18 AAD	16AC ATLS	$pp \rightarrow HW/ZX$, 8 TeV
1.41 ^{+0.40} _{-0.36}	4 AAD	16AN ATLS	pp , 7, 8 TeV
0.89 ^{+0.30} _{-0.28}	4 AAD	16AN CMS	pp , 7, 8 TeV
1.44 ^{+0.30+0.29} _{-0.29-0.23}	19 AAD	16K ATLS	pp , 7, 8 TeV
1.43 ^{+0.27+0.32} _{-0.26-0.25 ± 0.09}	20 AAD	15AH ATLS	$pp \rightarrow HX$, 7, 8 TeV
0.78 ± 0.27	21 CHATRCHYAN 14K	CMS	$pp \rightarrow HX$, 7, 8 TeV
0.00 ^{+8.44} _{-0.00}	22 AALTONEN	13L CDF	$p\bar{p} \rightarrow HX$, 1.96 TeV
3.96 ^{+4.11} _{-3.38}	23 ABAZOV	13L D0	$p\bar{p} \rightarrow HX$, 1.96 TeV
0.4 ^{+1.6} _{-2.0}	24 AAD	12AI ATLS	$pp \rightarrow HX$, 7 TeV
0.09 ^{+0.76} _{-0.74}	25 CHATRCHYAN 12N	CMS	$pp \rightarrow HX$, 7, 8 TeV

- 1 CMS 22 report combined results (see their Extended Data Table 2) using up to 138 fb⁻¹ of data at $E_{cm} = 13$ TeV, assuming $m_H = 125.38$ GeV. See their Fig. 2 right.
- 2 AABOUD 19AQ use 36.1 fb⁻¹ of data. The first, second and third quoted errors are statistical, experimental systematic and theory systematic uncertainties, respectively. The quoted signal strength is given for $m_H = 125$ GeV and corresponds to 4.4 standard deviations. Combining with 7 TeV and 8 TeV results (AAD 15AH), the observed significance is 6.4 standard deviations. The cross sections in the $H \rightarrow \tau\tau$ decay channel ($m_H = 125$ GeV) are measured to $3.77^{+0.60}_{-0.59}$ (stat) ± 0.87 (syst) pb for the inclusive, $0.28 \pm 0.09^{+0.11}_{-0.09}$ pb for VBF, and $3.1 \pm 1.0^{+1.6}_{-1.3}$ pb for gluon-fusion production. See their Table XI for the cross sections in the framework of simplified template cross sections.
- 3 AAD 16AN perform fits to the ATLAS and CMS data at $E_{cm} = 7$ and 8 TeV. The signal strengths for individual production processes are 1.0 ± 0.6 for gluon fusion, 1.3 ± 0.4 for vector boson fusion, -1.4 ± 1.4 for WH production, $2.2^{+2.2}_{-1.8}$ for ZH production, and $-1.9^{+3.7}_{-3.3}$ for $t\bar{t}H$ production.
- 4 AAD 16AN: In the fit, relative production cross sections are fixed to those in the Standard Model. The quoted signal strength is given for $m_H = 125.09$ GeV.
- 5 AALTONEN 13M combine all Tevatron data from the CDF and D0 Collaborations with up to 10.0 fb⁻¹ and 9.7 fb⁻¹, respectively, of $p\bar{p}$ collisions at $E_{cm} = 1.96$ TeV. The quoted signal strength is given for $m_H = 125$ GeV.
- 6 TUMASYAN 23Y measure Higgs production with $pp \rightarrow H \rightarrow \tau\tau$ at $E_{cm} = 13$ TeV with 138 fb⁻¹ data. The quoted results are given for $m_H = 125.38$ GeV.
- 7 The inclusive $\sigma \cdot B$ is 2800^{+356}_{-335} fb (see their Figs. 10 and 14). See their Fig. 15 for the 68 % and 95 % CL contours in the $\kappa_V - \kappa_F$ plane.

⁸ The quoted result is for the stage-0 simplified template cross section (STXS) and the $\sigma_{ggF} \cdot B$ is 2030^{+598}_{-555} fb (see their Figs. 10 and 14). Measured cross sections and ratios to the SM predictions in the reduced stage-1.2 STXS (see their Fig. 1) are shown in their Table 9 and Figs. 12 and 14.

⁹ The quoted result is for the stage-0 STXS and the $\sigma_{VBF} \cdot B$ is $267^{+53.9}_{-52.6}$ fb (see their Figs. 10 and 14). Measured cross sections and ratios to the SM predictions in the reduced stage-1.2 STXS (see their Fig. 2) are shown in their Table 9 and Figs. 12, 14.

¹⁰ The quoted result is for the stage-0 STXS and the $\sigma_{VH} \cdot B$ is $79.0^{+20.5}_{-18.6}$ fb (see their Figs. 10 and 14). Measured cross sections and ratios to the SM predictions in the reduced stage-1.2 STXS (see their Fig. 3) are shown in their Table 9 and Figs. 12, 14.

¹¹ AAD 22q measure cross sections of $pp \rightarrow H \rightarrow \tau\tau$ at $E_{cm} = 13$ TeV with 139 fb⁻¹ data. The quoted results are given for $m_H = 125.09$ GeV and $|y(H)| < 2.5$ is required. The inclusive fiducial $\sigma \cdot B$ is $2.94 \pm 0.21^{+0.37}_{-0.32}$ pb. The fiducial $\sigma \cdot B$ for the four dominant production modes are $2.65 \pm 0.41^{+0.91}_{-0.67}$ pb for ggF, $0.197 \pm 0.028^{+0.032}_{-0.026}$ pb for VBF, $0.115 \pm 0.058^{+0.042}_{-0.040}$ pb for VH , $0.033 \pm 0.031^{+0.022}_{-0.017}$ pb for $t\bar{t}H$. Their cross sections using simplified template cross section framework (STXS) are given in their Fig. 14(a) and Table 15. The STXS bins (a reduced stage 1.2) are defined in their Fig. 1.

¹² TUMASYAN 22AJ measure cross sections with $pp \rightarrow H \rightarrow \tau\tau$ at $E_{cm} = 13$ TeV with 138 fb⁻¹ data. The fiducial inclusive $\sigma \cdot B$ is 426 ± 102 fb while 408 ± 27 fb is expected in the Standard Mode for $m_H = 125.38$ GeV. Three differential cross sections are given; see their Fig. 1.

¹³ SIRUNYAN 19AF use 35.9 fb⁻¹ of data. The quoted signal strength is given for $m_H = 125$ GeV and corresponds to 2.3 standard deviations.

¹⁴ SIRUNYAN 19AF use 35.9 fb⁻¹ of data. HW/Z channels are added with a few updates on gluon fusion and vector boson fusion with respect to SIRUNYAN 18Y. The quoted signal strength is given for $m_H = 125$ GeV and corresponds to 5.5 standard deviations. The signal strengths for the individual production modes are: $1.12^{+0.53}_{-0.50}$ for gluon fusion, $1.13^{+0.45}_{-0.42}$ for vector boson fusion, $3.39^{+1.68}_{-1.54}$ for WH and $1.23^{+1.62}_{-1.35}$ for ZH . See their Fig. 7 for other couplings (κ_V, κ_F).

¹⁵ SIRUNYAN 19AT perform a combine fit to 35.9 fb⁻¹ of data at $E_{cm} = 13$ TeV. This combination is based on SIRUNYAN 18Y.

¹⁶ SIRUNYAN 18Y use 35.9 fb⁻¹ of pp collisions at $E_{cm} = 13$ TeV. The quoted signal strength is given for $m_H = 125.09$ GeV and corresponds to 4.9 standard deviations.

¹⁷ SIRUNYAN 18Y combine the result of 35.9 fb⁻¹ at $E_{cm} = 13$ TeV with the results obtained from data of 4.9 fb⁻¹ at $E_{cm} = 7$ TeV and 19.7 fb⁻¹ at $E_{cm} = 8$ TeV (KHACHATRYAN 15AM). The quoted signal strength is given for $m_H = 125.09$ GeV and corresponds to 5.9 standard deviations.

¹⁸ AAD 16AC measure the signal strength with $pp \rightarrow HW/ZX$ processes using 20.3 fb⁻¹ of $E_{cm} = 8$ TeV. The quoted signal strength is given for $m_H = 125$ GeV.

¹⁹ AAD 16K use up to 4.7 fb⁻¹ of pp collisions at $E_{cm} = 7$ TeV and up to 20.3 fb⁻¹ at $E_{cm} = 8$ TeV. The quoted signal strength is given for $m_H = 125.36$ GeV.

²⁰ AAD 15AH use 4.5 fb⁻¹ of pp collisions at $E_{cm} = 7$ TeV and 20.3 fb⁻¹ at $E_{cm} = 8$ TeV. The third uncertainty in the measurement is theory systematics. The signal strength for the gluon fusion mode is $2.0 \pm 0.8^{+1.2}_{-0.8} \pm 0.3$ and that for vector boson fusion and W/ZH production modes is $1.24^{+0.49}_{-0.45} \pm 0.31 \pm 0.08$. The quoted signal strength is given for $m_H = 125.36$ GeV.

²¹ CHATRCHYAN 14K use 4.9 fb⁻¹ of pp collisions at $E_{cm} = 7$ TeV and 19.7 fb⁻¹ at $E_{cm} = 8$ TeV. The quoted signal strength is given for $m_H = 125$ GeV. See also CHATRCHYAN 14AJ.

²² AALTONEN 13L combine all CDF results with 9.45–10.0 fb⁻¹ of $p\bar{p}$ collisions at $E_{cm} = 1.96$ TeV. The quoted signal strength is given for $m_H = 125$ GeV.

²³ ABAZOV 13L combine all D0 results with up to 9.7 fb⁻¹ of $p\bar{p}$ collisions at $E_{cm} = 1.96$ TeV. The quoted signal strength is given for $m_H = 125$ GeV.

²⁴ AAD 12AI obtain results based on 4.7 fb⁻¹ of pp collisions at $E_{cm} = 7$ TeV. The quoted signal strengths are given in their Fig. 10 for $m_H = 126$ GeV. See also Fig. 13 of AAD 12DA.

²⁵ CHATRCHYAN 12N obtain results based on 4.9 fb⁻¹ of pp collisions at $E_{cm} = 7$ TeV and 5.1 fb⁻¹ at $E_{cm} = 8$ TeV. The quoted signal strength is given for $m_H = 125.5$ GeV. See also CHATRCHYAN 13Y.

Z γ Final State

VALUE	CL%	DOCUMENT ID	TECN	COMMENT
2.2 ± 0.7		1 AAD	24D LHC	pp , 13 TeV
• • • We do not use the following data for averages, fits, limits, etc. • • •				
2.4 ± 0.9		2 TUMASYAN	23F CMS	pp , 13 TeV
$2.59^{+1.07}_{-0.96}$		3 CMS	22 CMS	pp , 13 TeV
< 3.6	95	4 AAD	20AG ATLS	pp , 13 TeV
< 7.4	95	5 SIRUNYAN	18DQ CMS	pp , 13 TeV
< 6.6	95	6 AABOUD	17AW ATLS	pp , 13 TeV
< 11	95	7 AAD	14J ATLS	pp , 7, 8 TeV
< 9.5	95	8 CHATRCHYAN	13BK CMS	pp , 7, 8 TeV

¹ AAD 24D report combined results of ATLAS (AAD 20AG) and CMS (TUMASYAN 23F). The reported signal strength corresponds to a significance of 3.4 σ .

² TUMASYAN 23F search for $H \rightarrow Z\gamma, Z \rightarrow ee, \mu\mu$ in 138 fb⁻¹ of pp collisions at $E_{cm} = 13$ TeV, assuming $m_H = 125.38$ GeV. $\sigma(pp \rightarrow H) \cdot B(H \rightarrow Z\gamma)$ is measured to be 0.21 ± 0.08 pb. The ratio of branching fractions $B(H \rightarrow Z\gamma)/B(H \rightarrow \gamma\gamma)$ is measured to be $1.5^{+0.7}_{-0.6}$.

³ CMS 22 report combined results (see their Extended Data Table 2) using up to 138 fb⁻¹ of data at $E_{cm} = 13$ TeV, assuming $m_H = 125.38$ GeV. See their Fig. 2 right.

⁴ AAD 20AG search for $H \rightarrow Z\gamma, Z \rightarrow ee, \mu\mu$ in 139 fb⁻¹ of pp collisions at $E_{cm} = 13$ TeV. The signal strength is $2.0 \pm 0.9^{+0.4}_{-0.3}$ at $m_H = 125.09$ GeV, which corresponds to a significance of 2.2 σ . The upper limit of $\sigma(pp \rightarrow H) \cdot B(H \rightarrow Z\gamma)$ is 305 fb at 95% CL.

⁵ SIRUNYAN 18DQ search for $H \rightarrow Z\gamma, Z \rightarrow ee, \mu\mu$ in 35.9 fb⁻¹ of pp collisions at $E_{cm} = 13$ TeV. The quoted signal strength (see their Figs. 6 and 7) is given for $m_H = 125$ GeV.

⁶ AABOUD 17AW search for $H \rightarrow Z\gamma, Z \rightarrow ee, \mu\mu$ in 36.1 fb⁻¹ of pp collisions at $E_{cm} = 13$ TeV. The quoted signal strength is given for $m_H = 125.09$ GeV. The upper limit on the branching ratio of $H \rightarrow Z\gamma$ is 1.0% at 95% CL assuming the SM Higgs boson production.

⁷ AAD 14J search for $H \rightarrow Z\gamma \rightarrow \ell\ell\gamma$ in 4.5 fb⁻¹ of pp collisions at $E_{cm} = 7$ TeV and 20.3 fb⁻¹ at $E_{cm} = 8$ TeV. The quoted signal strength is given for $m_H = 125.5$ GeV.

⁸ CHATRCHYAN 13BK search for $H \rightarrow Z\gamma \rightarrow \ell\ell\gamma$ in 5.0 fb⁻¹ of pp collisions at $E_{cm} = 7$ TeV and 19.6 fb⁻¹ at $E_{cm} = 8$ TeV. A limit on cross section times branching ratio which corresponds to (4–25) times the expected Standard Model cross section is given in the range $m_H = 120$ –160 GeV at 95% CL. The quoted limit is given for $m_H = 125$ GeV, where 10 is expected for no signal.

$\gamma^* \gamma$ Final State

VALUE	CL%	DOCUMENT ID	TECN	COMMENT
1.5 ± 0.5 ± 0.2 ± 0.1		1 AAD	21I ATLS	pp , 13 TeV, $H \rightarrow \ell\ell\gamma$, 139 fb ⁻¹
• • • We do not use the following data for averages, fits, limits, etc. • • •				
< 4.0	95	2 SIRUNYAN	18DQ CMS	$pp \rightarrow HX$, 13 TeV, $H \rightarrow \gamma^* \gamma$
< 6.7	95	3 KHACHATRYAN	16B CMS	pp , 8 TeV, $ee\gamma, \mu\mu\gamma$
¹ AAD 21I search for $H \rightarrow \ell\ell\gamma$ ($\ell = e, \mu$) in 139 fb ⁻¹ of pp collisions at $E_{cm} = 13$ TeV. The mass of dilepton $m_{\ell\ell}$ is smaller than 30 GeV. This region is dominated by the decay through γ^* . The quoted signal strength corresponds to a significance of 3.2 standard deviations and is given for $m_H = 125.09$ GeV. The cross section times the branching ratio of $H \rightarrow \ell\ell\gamma$ for $m_{\ell\ell} < 30$ GeV is measured to be $8.7 \pm 2.7^{+0.7}_{-0.6}$ fb.				
² SIRUNYAN 18DQ search for $H \rightarrow \gamma^* \gamma, \gamma^* \rightarrow \mu\mu$ in 35.9 fb ⁻¹ of pp collisions at $E_{cm} = 13$ TeV. The mass of γ^* is smaller than 50 GeV except in J/ψ and Υ mass regions. The quoted signal strength (see their Figs. 6 and 7) is given for $m_H = 125$ GeV.				
³ KHACHATRYAN 16B search for $H \rightarrow \gamma^* \gamma \rightarrow e^+e^-\gamma$ and $\mu^+\mu^-\gamma$ (with $m(e^+e^-) < 3.5$ GeV and $m(\mu^+\mu^-) < 20$ GeV) in 19.7 fb ⁻¹ of pp collisions at $E_{cm} = 8$ TeV. See their Fig. 6 for limits on individual channels.				

Higgs couplings

Fermion coupling (κ_F)

VALUE	DOCUMENT ID	TECN	COMMENT
0.94 ± 0.05 OUR AVERAGE			
0.86 $^{+0.14}_{-0.11}$	1 TUMASYAN	23W CMS	pp , 13 TeV, $H \rightarrow WW^*$
0.95 ± 0.05	2 ATLAS	22 ATLS	pp , 13 TeV
• • • We do not use the following data for averages, fits, limits, etc. • • •			
1.00 $^{+0.16}_{-0.13}$	3 AAD	23Y ATLS	pp , 13 TeV, $H \rightarrow \gamma\gamma$
0.906	4 CMS	22 CMS	pp , 13 TeV
¹ TUMASYAN 23W measure Higgs production rates with $H \rightarrow WW^*$ at $E_{cm} = 13$ TeV with 138 fb ⁻¹ data, assuming $m_H = 125.38$ GeV. See their Fig. 25 for the 68% and 95% CL contours in the $\kappa_V - \kappa_F$ plane.			
² ATLAS 22 report combined results (see their Extended Data Table 1) using up to 139 fb ⁻¹ of data at $E_{cm} = 13$ TeV, assuming $m_H = 125.09$ GeV, $\kappa_V \geq 0$, and $\kappa_F \geq 0$ ($B_{inv} = B_{undetected} = 0$). See their Fig. 4.			
³ AAD 23Y measure Higgs production rates with $H \rightarrow \gamma\gamma$ at $E_{cm} = 13$ TeV with 139 fb ⁻¹ data, assuming $m_H = 125.09$ GeV. See their Fig. 23 for the 68% and 95% CL contours in the $\kappa_V - \kappa_F$ plane, where $\kappa_F > 0$ is assumed.			
⁴ CMS 22 report combined results (see their Extended Data Table 2) using up to 138 fb ⁻¹ of data at $E_{cm} = 13$ TeV, assuming $m_H = 125.38$ GeV. No uncertainty is given while their Fig. 3 left shows 68% and 95% CL contours.			

Gauge boson coupling (κ_V)

VALUE	DOCUMENT ID	TECN	COMMENT
1.023 ± 0.026 OUR AVERAGE			
0.99 ± 0.05	1 TUMASYAN	23W CMS	pp , 13 TeV, $H \rightarrow WW^*$
1.035 ± 0.031	2 ATLAS	22 ATLS	pp , 13 TeV
• • • We do not use the following data for averages, fits, limits, etc. • • •			
1.02 $^{+0.06}_{-0.05}$	3 AAD	23Y ATLS	pp , 13 TeV, $H \rightarrow \gamma\gamma$
1.014	4 CMS	22 CMS	pp , 13 TeV
¹ TUMASYAN 23W measure Higgs production rates with $H \rightarrow WW^*$ at $E_{cm} = 13$ TeV with 138 fb ⁻¹ data, assuming $m_H = 125.38$ GeV. See their Fig. 25 for the 68% and 95% CL contours in the $\kappa_V - \kappa_F$ plane.			
² ATLAS 22 report combined results (see their Extended Data Table 1) using up to 139 fb ⁻¹ of data at $E_{cm} = 13$ TeV, assuming $m_H = 125.09$ GeV, $\kappa_V \geq 0$, and $\kappa_F \geq 0$ ($B_{inv} = B_{undetected} = 0$). See their Fig. 4.			
³ AAD 23Y measure Higgs production rates with $H \rightarrow \gamma\gamma$ at $E_{cm} = 13$ TeV with 139 fb ⁻¹ data, assuming $m_H = 125.09$ GeV. See their Fig. 23 for the 68% and 95% CL contours in the $\kappa_V - \kappa_F$ plane, where $\kappa_F > 0$ is assumed.			
⁴ CMS 22 report combined results (see their Extended Data Table 2) using up to 138 fb ⁻¹ of data at $E_{cm} = 13$ TeV, assuming $m_H = 125.38$ GeV. See their Fig. 3 left.			

W boson coupling (κ_W)

VALUE	DOCUMENT ID	TECN	COMMENT
• • • We do not use the following data for averages, fits, limits, etc. • • •			
1.02 ± 0.05	1,2 ATLAS	22 ATLS	pp , 13 TeV
1.05 ± 0.06	1,3 ATLAS	22 ATLS	pp , 13 TeV
1.00 $^{+0.00}_{-0.02}$	1,4 ATLAS	22 ATLS	pp , 13 TeV
1.06 ± 0.07	5,6 CMS	22 CMS	pp , 13 TeV
1.02 ± 0.08	5,7 CMS	22 CMS	pp , 13 TeV

Gauge & Higgs Boson Particle Listings

H

- 1 ATLAS 22 report combined results (see their Extended Data Table 1) using up to 139 fb⁻¹ of data at $E_{\text{cm}} = 13$ TeV, assuming $m_H = 125.09$ GeV.
- 2 All modifiers(κ) > 0, and $\kappa_c = \kappa_t$ ($B_{\text{inv}} = B_{\text{undetected}} = 0$) are assumed. Only SM particles assume to contribute to the loop-induced processes. See their Fig. 5, which shows both $\kappa_c = \kappa_t$ and κ_c floating.
- 3 $B_{\text{inv}} = B_{\text{undetected}} = 0$ is assumed. Coupling strength modifiers including effective photon, $Z\gamma$ and gluon are measured. See their Fig. 6.
- 4 B_{inv} floating, $B_{\text{undetected}} \geq 0$, and $\kappa_V \leq 1$ are assumed. Coupling strength modifiers including effective photon, $Z\gamma$ and gluon are measured. See their Fig. 6.
- 5 CMS 22 report combined results (see their Extended Data Table 2) using up to 138 fb⁻¹ of data at $E_{\text{cm}} = 13$ TeV, assuming $m_H = 125.38$ GeV.
- 6 Only SM particles assume to contribute to the loop-induced processes. See their Fig. 3 right.
- 7 Coupling strength modifiers including effective photon, $Z\gamma$ and gluon are measured. See their Fig. 4 left.

Z boson coupling (κ_Z)

VALUE	DOCUMENT ID	TECN	COMMENT
••• We do not use the following data for averages, fits, limits, etc. •••			
$0.99^{+0.06}_{-0.05}$	1,2 ATLAS	22 ATLS	pp , 13 TeV
0.99 ± 0.06	1,3 ATLAS	22 ATLS	pp , 13 TeV
$0.98^{+0.02}_{-0.05}$	1,4 ATLAS	22 ATLS	pp , 13 TeV
1.04 ± 0.07	5,6 CMS	22 CMS	pp , 13 TeV
1.04 ± 0.07	5,7 CMS	22 CMS	pp , 13 TeV

- 1 ATLAS 22 report combined results (see their Extended Data Table 1) using up to 139 fb⁻¹ of data at $E_{\text{cm}} = 13$ TeV, assuming $m_H = 125.09$ GeV.
- 2 All modifiers(κ) > 0, and $\kappa_c = \kappa_t$ ($B_{\text{inv}} = B_{\text{undetected}} = 0$) are assumed. Only SM particles assume to contribute to the loop-induced processes. See their Fig. 5, which shows both $\kappa_c = \kappa_t$ and κ_c floating.
- 3 $B_{\text{inv}} = B_{\text{undetected}} = 0$ is assumed. Coupling strength modifiers including effective photon, $Z\gamma$ and gluon are measured. See their Fig. 6.
- 4 B_{inv} floating, $B_{\text{undetected}} \geq 0$, and $\kappa_V \leq 1$ are assumed. Coupling strength modifiers including effective photon, $Z\gamma$ and gluon are measured. See their Fig. 6.
- 5 CMS 22 report combined results (see their Extended Data Table 2) using up to 138 fb⁻¹ of data at $E_{\text{cm}} = 13$ TeV, assuming $m_H = 125.38$ GeV.
- 6 Only SM particles assume to contribute to the loop-induced processes. See their Fig. 3 right.
- 7 Coupling strength modifiers including effective photon, $Z\gamma$ and gluon are measured. See their Fig. 4 left.

top Yukawa coupling (κ_t)

VALUE	CL%	DOCUMENT ID	TECN	COMMENT
••• We do not use the following data for averages, fits, limits, etc. •••				
<1.8	95	1 AAD	23c ATLS	pp , 13 TeV
$0.87-1.20$	95	2 AAD	23y ATLS	pp , 13 TeV
$0.65-1.25$	95	3 AAD	23y ATLS	pp , 13 TeV
$-1.09 - 0.74$ or $0.77-1.3$	95	4 TUMASYAN	23P CMS	pp , 13 TeV
$0.86-1.26$		4,5 TUMASYAN	23P CMS	pp , 13 TeV
0.95 ± 0.07		6,7 ATLAS	22 ATLS	pp , 13 TeV
0.94 ± 0.11		6,8 ATLAS	22 ATLS	pp , 13 TeV
0.94 ± 0.11		6,9 ATLAS	22 ATLS	pp , 13 TeV
$0.95^{+0.07}_{-0.08}$		10,11 CMS	22 CMS	pp , 13 TeV
$1.01^{+0.11}_{-0.10}$		10,12 CMS	22 CMS	pp , 13 TeV
$-0.9 - 0.7$ or $0.7-1.1$	95	13 SIRUNYAN	21R CMS	pp , 13 TeV
<1.7	95	14 SIRUNYAN	20C CMS	pp , 13 TeV
<1.67	95	15 SIRUNYAN	19BY CMS	pp , 13 TeV
<2.1	95	16 SIRUNYAN	18BU CMS	pp , 13 TeV

- 1 AAD 23c measure the production of four top quarks with same-sign and multilepton final states with 140 fb⁻¹ pp collision data at $E_{\text{cm}} = 13$ TeV. The results constraint the ratio of the top quark Yukawa coupling y_t to its Standard Model value, yielding $|y_t/y_t^{\text{SM}}| < 1.8$ at 95% CL. See their Fig. 8 as a function of κ_t and CP -mixing angle.
- 2 AAD 23y constrain κ_t from Higgs production rates with $H \rightarrow \gamma\gamma$ with 139 fb⁻¹ pp collision data at $E_{\text{cm}} = 13$ TeV. The quoted result is obtained assuming the SM loop structure in $gg \rightarrow H$ and $H \rightarrow \gamma\gamma$. See their Fig. 14.
- 3 AAD 23y constrain κ_t from Higgs production rates with $H \rightarrow \gamma\gamma$ with 139 fb⁻¹ pp collision data at $E_{\text{cm}} = 13$ TeV. The quoted result is obtained assuming effective couplings κ_{gluon} and κ_γ for $gg \rightarrow H$ and $H \rightarrow \gamma\gamma$, respectively. See their Fig. 14.
- 4 TUMASYAN 23P constrain κ_t from $t\bar{t}H$ and tH decaying $H \rightarrow WW^*$ and $H \rightarrow \tau\tau$ (multilepton decay mode) with 138 fb⁻¹ pp collision data at $E_{\text{cm}} = 13$ TeV. The κ_t is obtained by fixing $\tilde{\kappa}_t = 0$ and other couplings (κ_V etc.) to the SM values. See their Fig. 9 for 2-dim contours and Table 6.
- 5 The quoted result is obtained by combining with other $t\bar{t}H$ decaying $H \rightarrow \gamma\gamma$ (SIRUNYAN 20As) and $H \rightarrow 4\ell$ (SIRUNYAN 21AE) and $\tilde{\kappa}_t = 0$. See their Fig. 12 for 2-dim contours and Table 7.
- 6 ATLAS 22 report combined results (see their Extended Data Table 1) using up to 139 fb⁻¹ of data at $E_{\text{cm}} = 13$ TeV, assuming $m_H = 125.09$ GeV.
- 7 All modifiers(κ) > 0, and $\kappa_c = \kappa_t$ ($B_{\text{inv}} = B_{\text{undetected}} = 0$) are assumed. Only SM particles assume to contribute to the loop-induced processes. See their Fig. 5, which shows both $\kappa_c = \kappa_t$ and κ_c floating.
- 8 $B_{\text{inv}} = B_{\text{undetected}} = 0$ is assumed. Coupling strength modifiers including effective photon, $Z\gamma$ and gluon are measured. See their Fig. 6.
- 9 B_{inv} floating, $B_{\text{undetected}} \geq 0$, and $\kappa_V \leq 1$ are assumed. Coupling strength modifiers including effective photon, $Z\gamma$ and gluon are measured. See their Fig. 6.
- 10 CMS 22 report combined results (see their Extended Data Table 2) using up to 138 fb⁻¹ of data at $E_{\text{cm}} = 13$ TeV, assuming $m_H = 125.38$ GeV.

- 11 Only SM particles assume to contribute to the loop-induced processes. See their Fig. 3 right.
- 12 Coupling strength modifiers including effective photon, $Z\gamma$ and gluon are measured. See their Fig. 4 left.
- 13 SIRUNYAN 21R constrain the ratio of the top quark Yukawa coupling y_t to its Standard Model value from $t\bar{t}H$ and tH production rates using 137 fb⁻¹ pp collision data at $E_{\text{cm}} = 13$ TeV. Assuming a SM Higgs couplings to τ 's, the joint interval $-0.9 < \kappa_t (=y_t/y_t^{\text{SM}}) < -0.7$ and $0.7 < \kappa_t < 1.1$ is obtained at 95% CL (see their Fig. 17).
- 14 SIRUNYAN 20c search for the production of four top quarks with same-sign and multilepton final states with 137 fb⁻¹ pp collision data at $E_{\text{cm}} = 13$ TeV. The results constraint the ratio of the top quark Yukawa coupling y_t to its Standard Model value by comparing to the central value of a theoretical prediction (see their Refs. [1-2]), yielding $|y_t/y_t^{\text{SM}}| < 1.7$ at 95% CL. See their Fig. 5.
- 15 SIRUNYAN 19By measure the top quark Yukawa coupling from $t\bar{t}$ kinematic distributions, the invariant mass of the top quark pair and the rapidity difference between t and \bar{t} , in the ℓ +jets final state with 35.8 fb⁻¹ pp collision data at $E_{\text{cm}} = 13$ TeV. The results constraint the ratio of the top quark Yukawa coupling to its the Standard Model to be $1.07^{+0.34}_{-0.43}$ with an upper limit of 1.67 at 95% CL (see their Table III).
- 16 SIRUNYAN 18BU search for the production of four top quarks with same-sign and multilepton final states with 35.9 fb⁻¹ pp collision data at $E_{\text{cm}} = 13$ TeV. The results constraint the ratio of the top quark Yukawa coupling y_t to its the Standard Model by comparing to the central value of a theoretical prediction (see their Ref. [16]), yielding $|y_t/y_t^{\text{SM}}| < 2.1$ at 95% CL.

bottom Yukawa coupling (κ_b)

VALUE	CL%	DOCUMENT ID	TECN	COMMENT
••• We do not use the following data for averages, fits, limits, etc. •••				
-1.09 to -0.86 OR 0.81 to 1.09	95	1 AAD	23c ATLS	pp , 13 TeV, $\gamma\gamma$, $ZZ^* \rightarrow 4\ell$ cross sections
-1.1 to 1.1	95	2 AAD	23cd ATLS	pp , 13 TeV, $H \rightarrow \tau(nS)\gamma$
		3 HAYRAPETY...23	CMS	pp , 13 TeV, $ZZ^* \rightarrow 4\ell$ cross sections
0.90 ± 0.11		4,5 ATLAS	22 ATLS	pp , 13 TeV
0.89 ± 0.11		4,6 ATLAS	22 ATLS	pp , 13 TeV
$0.82^{+0.09}_{-0.08}$		4,7 ATLAS	22 ATLS	pp , 13 TeV
$1.02^{+0.15}_{-0.17}$		8,9 CMS	22 CMS	pp , 13 TeV
$0.99^{+0.17}_{-0.16}$		8,10 CMS	22 CMS	pp , 13 TeV

- 1 AAD 23c combine results of $H \rightarrow \gamma\gamma$ and $H \rightarrow ZZ^* \rightarrow 4\ell$ ($\ell = e, \mu$) using 139 fb⁻¹ at $E_{\text{cm}} = 13$ TeV. The Higgs boson transverse momentum (p_T^H) distribution constrains κ_b and κ_c , assuming other couplings fixed to the SM values. The κ_b is obtained using the p_T^H shape and normalisation. Other cases are given in their Tables 6 and 7.
- 2 AAD 23cd search for $H \rightarrow \tau(nS)\gamma$, $\tau(nS) \rightarrow \mu^+\mu^-$ ($n=1,2,3$) with 138 fb⁻¹ of pp collision data at $E_{\text{cm}} = 13$ TeV. They interpret the $H \rightarrow \tau(nS)\gamma$ search to constraint the bottom Yukawa coupling by comparing to $H \rightarrow \gamma\gamma$. An observed 95% CL interval of $(-37, 40)$ is obtained for κ_b/κ_γ .
- 3 HAYRAPETYAN 23 measure the cross sections for $pp \rightarrow H \rightarrow ZZ^* \rightarrow 4\ell$ ($\ell = e, \mu$) using 138 fb⁻¹ at $E_{\text{cm}} = 13$ TeV. The κ_b is obtained from the p_T differential cross section of the ggF production employing the dependence of the branching fraction on κ_b and κ_c .
- 4 ATLAS 22 report combined results (see their Extended Data Table 1) using up to 139 fb⁻¹ of data at $E_{\text{cm}} = 13$ TeV, assuming $m_H = 125.09$ GeV.
- 5 All modifiers (κ) > 0, and $\kappa_c = \kappa_t$ ($B_{\text{inv}} = B_{\text{undetected}} = 0$) are assumed. Only SM particles assume to contribute to the loop-induced processes. See their Fig. 5, which shows both $\kappa_c = \kappa_t$ and κ_c floating.
- 6 $B_{\text{inv}} = B_{\text{undetected}} = 0$ is assumed. Coupling strength modifiers including effective photon, $Z\gamma$ and gluon are measured. See their Fig. 6.
- 7 B_{inv} floating, $B_{\text{undetected}} \geq 0$, and $\kappa_V \leq 1$ are assumed. Coupling strength modifiers including effective photon, $Z\gamma$ and gluon are measured. See their Fig. 6.
- 8 CMS 22 report combined results (see their Extended Data Table 2) using up to 138 fb⁻¹ of data at $E_{\text{cm}} = 13$ TeV, assuming $m_H = 125.38$ GeV.
- 9 Only SM particles assume to contribute to the loop-induced processes. See their Fig. 3 right.
- 10 Coupling strength modifiers including effective photon, $Z\gamma$ and gluon are measured. See their Fig. 4 left.

charm Yukawa coupling (κ_c)

VALUE	CL%	DOCUMENT ID	TECN	COMMENT
••• We do not use the following data for averages, fits, limits, etc. •••				
$ \kappa_c < 2.27$	95	1 AAD	23c ATLS	pp , 13 TeV, $\gamma\gamma$, $ZZ^* \rightarrow 4\ell$ cross sections
-5.3 to 5.2	95	2 AAD	23cd ATLS	pp , 13 TeV, $H \rightarrow J/\psi\gamma$
		3 HAYRAPETY...23	CMS	pp , 13 TeV, $ZZ^* \rightarrow 4\ell$ cross sections
$1.1 < \kappa_c < 5.5$	95	4 TUMASYAN	23AH CMS	$pp \rightarrow WH/ZH$, 13 TeV
$0.03^{+3.02}_{-0.03}$		5 ATLAS	22 ATLS	pp , 13 TeV

- 1 AAD 23c combine results of $H \rightarrow \gamma\gamma$ and $H \rightarrow ZZ^* \rightarrow 4\ell$ ($\ell = e, \mu$) using 139 fb⁻¹ at $E_{\text{cm}} = 13$ TeV. The Higgs boson transverse momentum (p_T^H) distribution constrains κ_b and κ_c , assuming other couplings fixed to the SM values. The κ_c is obtained using the p_T^H shape and normalisation. Other cases are given in their Tables 6 and 7. See their Table 8 for results combined with VH , $H \rightarrow b\bar{b}$ and $c\bar{c}$.
- 2 AAD 23cd search for $H \rightarrow J/\psi\gamma$, $J/\psi \rightarrow \mu^+\mu^-$ with 138 fb⁻¹ of pp collision data at $E_{\text{cm}} = 13$ TeV. They interpret the $H \rightarrow J/\psi\gamma$ search to constraint the charm Yukawa coupling by comparing to $H \rightarrow \gamma\gamma$. An observed 95% CL interval of $(-133, 175)$ is obtained for κ_c/κ_γ .

³ HAYRAPETYAN 23 measure the cross sections for $pp \rightarrow H \rightarrow ZZ^* \rightarrow 4\ell$ ($\ell = e, \mu$) using 138 fb⁻¹ at $E_{\text{cm}} = 13$ TeV. The κ_c is obtained from the p_T differential cross section of the ggF production employing the dependence of the branching fraction of κ_b and κ_c .

⁴ TUMASYAN 23AH search for $VH, H \rightarrow c\bar{c}$ ($V = W, Z$) using 138 fb⁻¹ of pp collision data at $E_{\text{cm}} = 13$ TeV. The quoted values are obtained from the measured signal strength in the κ -framework, where only the Higgs decay width for $H \rightarrow c\bar{c}$ is changed while assuming all the other decay widths and the production cross section to be SM ones. The quoted values are given for $m_H = 125.38$ GeV.

⁵ ATLAS 22 report combined results (see their Extended Data Table 1) using up to 139 fb⁻¹ of data at $E_{\text{cm}} = 13$ TeV, assuming $m_H = 125.09$ GeV, and all modifiers (κ) > 0 ($B_{\text{inv}} = B_{\text{undetected}} = 0$). Only SM particles assume to contribute to the loop-induced processes. See their Fig. 5, which shows both $\kappa_c = \kappa_t$ and κ_c floating.

tau Yukawa coupling (κ_τ)

VALUE	DOCUMENT ID	TECN	COMMENT
• • • We do not use the following data for averages, fits, limits, etc. • • •			
0.94 ± 0.07	1,2 ATLAS	22 ATLS	pp , 13 TeV
0.93 ± 0.07	1,3 ATLAS	22 ATLS	pp , 13 TeV
0.91 ^{+0.07} _{-0.06}	1,4 ATLAS	22 ATLS	pp , 13 TeV
0.93 ± 0.08	5,6 CMS	22 CMS	pp , 13 TeV
0.92 ± 0.08	5,7 CMS	22 CMS	pp , 13 TeV

¹ ATLAS 22 report combined results (see their Extended Data Table 1) using up to 139 fb⁻¹ of data at $E_{\text{cm}} = 13$ TeV, assuming $m_H = 125.09$ GeV.

² All modifiers (κ) > 0, and $\kappa_c = \kappa_t$ ($B_{\text{inv}} = B_{\text{undetected}} = 0$) are assumed. Only SM particles assume to contribute to the loop-induced processes. See their Fig. 5, which shows both $\kappa_c = \kappa_t$ and κ_c floating.

³ $B_{\text{inv}} = B_{\text{undetected}} = 0$ is assumed. Coupling strength modifiers including effective photon, $Z\gamma$ and gluon are measured. See their Fig. 6.

⁴ B_{inv} floating, $B_{\text{undetected}} \geq 0$, and $\kappa_V \leq 1$ are assumed. Coupling strength modifiers including effective photon, $Z\gamma$ and gluon are measured. See their Fig. 6.

⁵ CMS 22 report combined results (see their Extended Data Table 2) using up to 138 fb⁻¹ of data at $E_{\text{cm}} = 13$ TeV, assuming $m_H = 125.38$ GeV.

⁶ Only SM particles assume to contribute to the loop-induced processes. See their Fig. 3 right.

⁷ Coupling strength modifiers including effective photon, $Z\gamma$ and gluon are measured. See their Fig. 4 left.

muon Yukawa coupling (κ_μ)

VALUE	DOCUMENT ID	TECN	COMMENT
• • • We do not use the following data for averages, fits, limits, etc. • • •			
1.07 ^{+0.25} _{-0.31}	1,2 ATLAS	22 ATLS	pp , 13 TeV
1.06 ^{+0.25} _{-0.30}	1,3 ATLAS	22 ATLS	pp , 13 TeV
1.04 ^{+0.23} _{-0.30}	1,4 ATLAS	22 ATLS	pp , 13 TeV
1.12 ± 0.20	5,6 CMS	22 CMS	pp , 13 TeV
1.12 ^{+0.21} _{-0.22}	5,7 CMS	22 CMS	pp , 13 TeV

¹ ATLAS 22 report combined results (see their Extended Data Table 1) using up to 139 fb⁻¹ of data at $E_{\text{cm}} = 13$ TeV, assuming $m_H = 125.09$ GeV.

² All modifiers (κ) > 0, and $\kappa_c = \kappa_t$ ($B_{\text{inv}} = B_{\text{undetected}} = 0$) are assumed. Only SM particles assume to contribute to the loop-induced processes. See their Fig. 5, which shows both $\kappa_c = \kappa_t$ and κ_c floating.

³ $B_{\text{inv}} = B_{\text{undetected}} = 0$ is assumed. Coupling strength modifiers including effective photon, $Z\gamma$ and gluon are measured. See their Fig. 6.

⁴ B_{inv} floating, $B_{\text{undetected}} \geq 0$, and $\kappa_V \leq 1$ are assumed. Coupling strength modifiers including effective photon, $Z\gamma$ and gluon are measured. See their Fig. 6.

⁵ CMS 22 report combined results (see their Extended Data Table 2) using up to 138 fb⁻¹ of data at $E_{\text{cm}} = 13$ TeV, assuming $m_H = 125.38$ GeV.

⁶ Only SM particles assume to contribute to the loop-induced processes. See their Fig. 3 right.

⁷ Coupling strength modifiers including effective photon, $Z\gamma$ and gluon are measured. See their Fig. 4 left.

photon effective coupling (κ_γ)

VALUE	DOCUMENT ID	TECN	COMMENT
• • • We do not use the following data for averages, fits, limits, etc. • • •			
1.02 ^{+0.08} _{-0.07}	1 AAD	23Y ATLS	pp , 13 TeV
1.01 ± 0.06	2,3 ATLAS	22 ATLS	pp , 13 TeV
0.98 ± 0.05	2,4 ATLAS	22 ATLS	pp , 13 TeV
1.10 ± 0.08	5 CMS	22 CMS	pp , 13 TeV

¹ AAD 23Y constrain κ_γ from Higgs production rates with $H \rightarrow \gamma\gamma$ with 139 fb⁻¹ pp collision data at $E_{\text{cm}} = 13$ TeV. The quoted result is obtained assuming effective couplings κ_{gluon} and κ_γ for $gg \rightarrow H$ and $H \rightarrow \gamma\gamma$, respectively and other couplings fixed to the SM values. See their Fig. 15.

² ATLAS 22 report combined results (see their Extended Data Table 1) using up to 139 fb⁻¹ of data at $E_{\text{cm}} = 13$ TeV, assuming $m_H = 125.09$ GeV. Coupling strength modifiers including effective photon, $Z\gamma$ and gluon are measured. See their Fig. 6.

³ $B_{\text{inv}} = B_{\text{undetected}} = 0$ is assumed.

⁴ B_{inv} floating, $B_{\text{undetected}} \geq 0$, and $\kappa_V \leq 1$ are assumed.

⁵ CMS 22 report combined results (see their Extended Data Table 2) using up to 138 fb⁻¹ of data at $E_{\text{cm}} = 13$ TeV, assuming $m_H = 125.38$ GeV. Coupling strength modifiers including effective photon, $Z\gamma$ and gluon are measured. See their Fig. 4 left.

gluon effective coupling (κ_{gluon})

VALUE	DOCUMENT ID	TECN	COMMENT
• • • We do not use the following data for averages, fits, limits, etc. • • •			
1.01 ^{+0.11} _{-0.09}	1 AAD	23Y ATLS	pp , 13 TeV
0.95 ± 0.07	2,3 ATLAS	22 ATLS	pp , 13 TeV
0.94 ^{+0.07} _{-0.06}	2,4 ATLAS	22 ATLS	pp , 13 TeV
0.92 ± 0.08	5 CMS	22 CMS	pp , 13 TeV

¹ AAD 23Y constrain κ_{gluon} from Higgs production rates with $H \rightarrow \gamma\gamma$ with 139 fb⁻¹ pp collision data at $E_{\text{cm}} = 13$ TeV. The quoted result is obtained assuming effective couplings κ_{gluon} and κ_γ for $gg \rightarrow H$ and $H \rightarrow \gamma\gamma$, respectively and other couplings fixed to the SM values. See their Fig. 15.

² ATLAS 22 report combined results (see their Extended Data Table 1) using up to 139 fb⁻¹ of data at $E_{\text{cm}} = 13$ TeV, assuming $m_H = 125.09$ GeV. Coupling strength modifiers including effective photon, $Z\gamma$ and gluon are measured. See their Fig. 6.

³ $B_{\text{inv}} = B_{\text{undetected}} = 0$ is assumed.

⁴ B_{inv} floating, $B_{\text{undetected}} \geq 0$, and $\kappa_V \leq 1$ are assumed.

⁵ CMS 22 report combined results (see their Extended Data Table 2) using up to 138 fb⁻¹ of data at $E_{\text{cm}} = 13$ TeV, assuming $m_H = 125.38$ GeV. Coupling strength modifiers including effective photon, $Z\gamma$ and gluon are measured. See their Fig. 4 left.

$Z\gamma$ effective coupling ($\kappa_{Z\gamma}$)

VALUE	DOCUMENT ID	TECN	COMMENT
• • • We do not use the following data for averages, fits, limits, etc. • • •			
1.38 ^{+0.31} _{-0.37}	1,2 ATLAS	22 ATLS	pp , 13 TeV
1.35 ^{+0.29} _{-0.36}	1,3 ATLAS	22 ATLS	pp , 13 TeV
1.65 ^{+0.34} _{-0.37}	4 CMS	22 CMS	pp , 13 TeV

¹ ATLAS 22 report combined results (see their Extended Data Table 1) using up to 139 fb⁻¹ of data at $E_{\text{cm}} = 13$ TeV, assuming $m_H = 125.09$ GeV. Coupling strength modifiers including effective photon, $Z\gamma$ and gluon are measured. See their Fig. 6.

² $B_{\text{inv}} = B_{\text{undetected}} = 0$ is assumed.

³ B_{inv} floating, $B_{\text{undetected}} \geq 0$, and $\kappa_V \leq 1$ are assumed.

⁴ CMS 22 report combined results (see their Extended Data Table 2) using up to 138 fb⁻¹ of data at $E_{\text{cm}} = 13$ TeV, assuming $m_H = 125.38$ GeV. Coupling strength modifiers including effective photon, $Z\gamma$ and gluon are measured. See their Fig. 4 left.

OTHER H PRODUCTION PROPERTIES

$t\bar{t}H$ Production

Signal strength relative to the Standard Model cross section.			
VALUE	DOCUMENT ID	TECN	COMMENT
1.10 ± 0.18 OUR AVERAGE			
0.92 ± 0.19 ^{+0.17} _{-0.13}	1 SIRUNYAN	21R CMS	pp , 13 TeV, $H \rightarrow \tau\tau, WW^*, ZZ^*$
1.2 ± 0.3	2 AABOUD	18AC ATLS	pp , 13 TeV, $H \rightarrow b\bar{b}, \tau\tau, \gamma\gamma, WW^*, ZZ^*$
1.9 ± 0.8 ^{+0.8} _{-0.7}	3 AAD	16AN ATLS	pp , 7, 8 TeV
• • • We do not use the following data for averages, fits, limits, etc. • • •			
-0.27 ± 0.86 ^{+0.86} _{-0.83}	4 TUMASYAN	23AI ATLS	pp , 13 TeV, boosted $H \rightarrow b\bar{b}$
0.35 ± 0.36 ^{+0.36} _{-0.34}	5 AAD	22M ATLS	pp , 13 TeV, $H \rightarrow b\bar{b}$
1.43 ± 0.33 ± 0.21 ^{+0.33+0.21} _{-0.31-0.15}	6 AAD	20Z ATLS	pp , 13 TeV, $H \rightarrow \gamma\gamma$
1.38 ± 0.36 ^{+0.36} _{-0.29}	7 SIRUNYAN	20AS CMS	pp , 13 TeV, $H \rightarrow \gamma\gamma$
0.72 ± 0.24 ± 0.38 ^{+0.24+0.38} _{-0.24-0.38}	8 SIRUNYAN	19R CMS	pp , 13 TeV, $H \rightarrow b\bar{b}$
1.6 ± 0.5 ^{+0.5} _{-0.4}	9 AABOUD	18AC ATLS	pp , 13 TeV, $H \rightarrow \tau\tau, WW^*, ZZ^*$
	10 AABOUD	18BK ATLS	pp , 13 TeV, $H \rightarrow b\bar{b}, \tau\tau, \gamma\gamma, WW^*, ZZ^*$
0.84 ± 0.64 ^{+0.64} _{-0.61}	11 AABOUD	18T ATLS	pp , 13 TeV, $H \rightarrow b\bar{b}$
0.9 ± 1.5	12 SIRUNYAN	18BD CMS	pp , 13 TeV, $H \rightarrow b\bar{b}$
1.23 ± 0.45 ^{+0.45} _{-0.43}	13 SIRUNYAN	18BQ CMS	pp , 13 TeV, $H \rightarrow \tau\tau, WW^*, ZZ^*$
1.26 ± 0.31 ^{+0.31} _{-0.26}	14 SIRUNYAN	18L CMS	pp , 7, 8, 13 TeV, $H \rightarrow b\bar{b}, \tau\tau, \gamma\gamma, WW^*, ZZ^*$
1.7 ± 0.8	15 AAD	16AL ATLS	pp , 7, 8 TeV, $H \rightarrow b\bar{b}, \tau\tau, \gamma\gamma, WW^*$, and ZZ^*
2.3 ± 0.7 ^{+0.7} _{-0.6}	3,16 AAD	16AN LHC	pp , 7, 8 TeV
2.9 ± 1.0 ^{+1.0} _{-0.9}	3 AAD	16AN CMS	pp , 7, 8 TeV
1.81 ± 0.52 ± 0.58 ± 0.31 ^{+0.52+0.58+0.31} _{-0.50-0.55-0.12}	17 AAD	16K ATLS	pp , 7, 8 TeV
1.4 ± 2.1 ± 0.6 ^{+2.1+0.6} _{-1.4-0.3}	18 AAD	15 ATLS	pp , 7, 8 TeV
1.5 ± 1.1	19 AAD	15BC ATLS	pp , 8 TeV
2.1 ± 1.4 ^{+1.4} _{-1.2}	20 AAD	15T ATLS	pp , 8 TeV

Gauge & Higgs Boson Particle Listings

H

1.2 ^{+1.6} _{-1.5}	21	KHACHATRY...15AN CMS	pp , 8 TeV
2.8 ^{+1.0} _{-0.9}	22	KHACHATRY...14H CMS	pp , 7, 8 TeV
9.49 ^{+6.60} _{-6.28}	23	AALTONEN 13L CDF	$p\bar{p}$, 1.96 TeV
< 5.8 at 95% CL	24	CHATRCHYAN13x CMS	pp , 7, 8 TeV, $H \rightarrow b\bar{b}$
<p>1 SIRUNYAN 21R search for $t\bar{t}H$ in final states with electrons, muons and hadronically decaying τ leptons ($H \rightarrow WW^*, ZZ^*, \tau\tau$) with 137 fb⁻¹ of pp collision data at $E_{cm} = 13$ TeV. The quoted signal strength corresponds to a significance of 4.7 standard deviations and is given for $m_H = 125$ GeV.</p> <p>2 ABOUD 18AC combine results of $t\bar{t}H, H \rightarrow \tau\tau, WW^*(\rightarrow \ell\nu\ell\nu, \ell\nu q\bar{q}), ZZ^*(\rightarrow \ell\nu\nu, \ell\nu q\bar{q})$ with results of $t\bar{t}H, H \rightarrow b\bar{b}$ (AABOUD 18T), $\gamma\gamma$ (AABOUD 18B0), $ZZ^*(\rightarrow 4\ell)$ (AABOUD 18AJ) in 36.1 fb⁻¹ of pp collisions at $E_{cm} = 13$ TeV. The quoted signal strength is given for $m_H = 125$ GeV. See their Table 14.</p> <p>3 AAD 16AN: In the fit, relative branching ratios are fixed to those in the Standard Model. The quoted signal strength is given for $m_H = 125.09$ GeV.</p> <p>4 TUMASYAN 23AI measure boosted $H \rightarrow b\bar{b}$ ($p_T > 200$ GeV) in $t\bar{t}H$ production using 138 fb⁻¹ of data at $E_{cm} = 13$ TeV. The differential cross section for the Higgs p_T is shown in their Fig. 8 and Table V. Limits on eight Wilson coefficients at 68% and 95% CL are shown in their Fig. 10 and Table VI.</p> <p>5 AAD 22M measure $H \rightarrow b\bar{b}$ in $t\bar{t}H$ production using 139 fb⁻¹ of data at $E_{cm} = 13$ TeV. See their Fig. 14. The signal strengths and 95% CL cross section upper limits with simplified template cross section bins are given in their Figs. 18 and 19, respectively.</p> <p>6 AAD 20Z measure $\sigma_{t\bar{t}H} \cdot B(H \rightarrow \gamma\gamma)$ to be $1.64^{+0.38}_{-0.36-0.14}$ fb in 139 fb⁻¹ of data at $E_{cm} = 13$ TeV.</p> <p>7 SIRUNYAN 20AS measure $\sigma_{t\bar{t}H} \cdot B(H \rightarrow \gamma\gamma)$ to be $1.56^{+0.34}_{-0.32}$ fb in 137 fb⁻¹ of data at $E_{cm} = 13$ TeV.</p> <p>8 SIRUNYAN 19R search for $t\bar{t}H$ production with H decaying to $b\bar{b}$ in 35.9 fb⁻¹ of data at $E_{cm} = 13$ TeV. The quoted signal strength is given for $m_H = 125$ GeV.</p> <p>9 ABOUD 18AC search for $t\bar{t}H$ production with H decaying to $\tau\tau, WW^*(\rightarrow \ell\nu\ell\nu, \ell\nu q\bar{q}), ZZ^*(\rightarrow \ell\nu\nu, \ell\nu q\bar{q})$ in 36.1 fb⁻¹ of pp collisions at $E_{cm} = 13$ TeV. A significance of 5.8 standard deviations is observed for $m_H = 125.09$ GeV and its signal strength without the uncertainty of the $t\bar{t}H$ cross section is $1.32^{+0.28}_{-0.26}$. Combining with results of 7 and 8 TeV (AAD 16K), the significance is 6.3 standard deviations. Assuming Standard Model branching fractions, the total $t\bar{t}H$ production cross section at 13 TeV is measured to be $670 \pm 90^{+110}_{-100}$ fb.</p> <p>11 ABOUD 18T search for $t\bar{t}H$ production with H decaying to $b\bar{b}$ in 36.1 fb⁻¹ of pp collisions at $E_{cm} = 13$ TeV. The quoted signal strength is given for $m_H = 125$ GeV.</p> <p>12 SIRUNYAN 18BD search for $t\bar{t}H, H \rightarrow b\bar{b}$ in the all-jet final state with 35.9 fb⁻¹ pp collision data at $E_{cm} = 13$ TeV. The quoted signal strength is given for $m_H = 125$ GeV.</p> <p>13 SIRUNYAN 18BQ search for $t\bar{t}H$ in final states with electrons, muons and hadronically decaying τ leptons ($H \rightarrow WW^*, ZZ^*, \tau\tau$) with 35.9 fb⁻¹ of pp collision data at $E_{cm} = 13$ TeV. The quoted signal strength corresponds to a significance of 3.2 standard deviations and is given for $m_H = 125$ GeV.</p> <p>14 SIRUNYAN 18L use up to 5.1, 19.7 and 35.9 fb⁻¹ of pp collisions at $E_{cm} = 7, 8,$ and 13 TeV, respectively. The quoted signal strength corresponds to a significance of 5.2 standard deviations and is given for $m_H = 125.09$ GeV. H decay channels of $WW^*, ZZ^*, \gamma\gamma, \tau\tau$, and $b\bar{b}$ are used. See their Table 1 and Fig. 2 for results on individual channels.</p> <p>15 AAD 16AL search for $t\bar{t}H$ production with H decaying to $\gamma\gamma$ in 4.5 fb⁻¹ of pp collisions at $E_{cm} = 7$ TeV and $b\bar{b}, \tau\tau, \gamma\gamma, WW^*$, and ZZ^* in 20.3 fb⁻¹ at $E_{cm} = 8$ TeV. The quoted signal strength is given for $m_H = 125$ GeV. This paper combines the results of previous papers, and the new result of this paper only is: $\mu = 1.6 \pm 2.6$.</p> <p>16 AAD 16AN perform fits to the ATLAS and CMS data at $E_{cm} = 7$ and 8 TeV.</p> <p>17 AAD 16K use up to 4.7 fb⁻¹ of pp collisions at $E_{cm} = 7$ TeV and up to 20.3 fb⁻¹ at $E_{cm} = 8$ TeV. The third uncertainty in the measurement is theory systematics. The quoted signal strength is given for $m_H = 125.36$ GeV.</p> <p>18 AAD 15 search for $t\bar{t}H$ production with H decaying to $\gamma\gamma$ in 4.5 fb⁻¹ of pp collisions at $E_{cm} = 7$ TeV and 20.3 fb⁻¹ at $E_{cm} = 8$ TeV. The quoted result on the signal strength is equivalent to an upper limit of 6.7 at 95% CL and is given for $m_H = 125.4$ GeV.</p> <p>19 AAD 15BC search for $t\bar{t}H$ production with H decaying to $b\bar{b}$ in 20.3 fb⁻¹ of pp collisions at $E_{cm} = 8$ TeV. The corresponding upper limit is 3.4 at 95% CL. The quoted signal strength is given for $m_H = 125$ GeV.</p> <p>20 AAD 15T search for $t\bar{t}H$ production with H resulting in multilepton final states (mainly from $WW^*, \tau\tau, ZZ^*$) in 20.3 fb⁻¹ of pp collisions at $E_{cm} = 8$ TeV. The quoted result on the signal strength is given for $m_H = 125$ GeV and corresponds to an upper limit of 4.7 at 95% CL. The data sample is independent from AAD 15 and AAD 15BC.</p> <p>21 KHACHATRYAN 15AN search for $t\bar{t}H$ production with H decaying to $b\bar{b}$ in 19.5 fb⁻¹ of pp collisions at $E_{cm} = 8$ TeV. The quoted result on the signal strength is equivalent to an upper limit of 4.2 at 95% CL and is given for $m_H = 125$ GeV.</p> <p>22 KHACHATRYAN 14H search for $t\bar{t}H$ production with H decaying to $b\bar{b}, \tau\tau, \gamma\gamma, WW^*$, and ZZ^*, in 5.1 fb⁻¹ of pp collisions at $E_{cm} = 7$ TeV and 19.7 fb⁻¹ at $E_{cm} = 8$ TeV. The quoted signal strength is given for $m_H = 125.6$ GeV.</p> <p>23 AALTONEN 13L combine all CDF results with 9.45–10.0 fb⁻¹ of $p\bar{p}$ collisions at $E_{cm} = 1.96$ TeV. The quoted signal strength is given for $m_H = 125$ GeV.</p> <p>24 CHATRCHYAN 13x search for $t\bar{t}H$ production followed by $H \rightarrow b\bar{b}$, one top decaying to $\ell\nu$ and the other to either $\ell\nu$ or $q\bar{q}$ in 5.0 fb⁻¹ and 5.1 fb⁻¹ of pp collisions at $E_{cm} = 7$ and 8 TeV. A limit on cross section times branching ratio which corresponds to (4.0–8.6) times the expected Standard Model cross section is given for $m_H = 110$–140 GeV at 95% CL. The quoted limit is given for $m_H = 125$ GeV, where 5.2 is expected for no signal.</p>			

• • • We do not use the following data for averages, fits, limits, etc. • • •

<183	95	2 AAD	23AD ATLS	13 TeV, $VHH, HH \rightarrow b\bar{b}b\bar{b}$
< 5.4	95	3 AAD	23BK ATLS	13 TeV, $b\bar{b}b\bar{b}$
< 4.7	95	4 AAD	23Z ATLS	13 TeV, $b\bar{b}\tau\tau$
< 9.9	95	5 TUMASYAN	23AE CMS	13 TeV, $b\bar{b}b\bar{b}$
< 3.3	95	6.7 TUMASYAN	23D CMS	13 TeV, $b\bar{b}\tau\tau$
<124	95	6.8 TUMASYAN	23D CMS	13 TeV, $b\bar{b}\tau\tau$
< 32.4	95	9 TUMASYAN	23I CMS	13 TeV, $b\bar{b}ZZ^*$ ($ZZ^* \rightarrow 4\ell$)
< 21.3	95	10 TUMASYAN	23O CMS	13 TeV, WW^*WW^* , $WW^*\tau\tau, \tau\tau\tau\tau$
< 4.2	95	11 AAD	22Y ATLS	13 TeV, $\gamma\gamma b\bar{b}$
< 3.4	95	12 CMS	22 CMS	13 TeV, $b\bar{b}ZZ^*, b\bar{b}\gamma\gamma, b\bar{b}\tau\tau,$ $b\bar{b}b\bar{b}, \text{multilepton}$
< 3.9	95	13 TUMASYAN	22AN CMS	13 TeV, $b\bar{b}b\bar{b}$
< 7.7	95	14 SIRUNYAN	21K CMS	13 TeV, $\gamma\gamma b\bar{b}$
< 6.9	95	15 AAD	20C ATLS	13 TeV, $b\bar{b}\gamma\gamma, b\bar{b}\tau\tau, b\bar{b}b\bar{b},$ $b\bar{b}WW^*, WW^*\gamma\gamma,$ WW^*WW^*
< 40	95	16 AAD	20E ATLS	13 TeV, $HH \rightarrow b\bar{b}\ell\nu\ell\nu$
<840	95	17 AAD	20X ATLS	13 TeV, $VBF, b\bar{b}b\bar{b}$
<12.9	95	18 ABOUD	19A ATLS	13 TeV, $b\bar{b}b\bar{b}$
<300	95	19 ABOUD	19O ATLS	13 TeV, $b\bar{b}WW^*$
<160	95	20 ABOUD	19T ATLS	13 TeV, WW^*WW^*
< 24	95	21 SIRUNYAN	19 CMS	13 TeV, $\gamma\gamma b\bar{b}$
< 75	95	22 SIRUNYAN	19AB CMS	13 TeV, $b\bar{b}b\bar{b}$
< 22.2	95	23 SIRUNYAN	19BE CMS	13 TeV, $b\bar{b}\gamma\gamma, b\bar{b}\tau\tau, b\bar{b}b\bar{b},$ $b\bar{b}WW^*, b\bar{b}ZZ^*$
<179	95	24 SIRUNYAN	19H CMS	13 TeV, $b\bar{b}b\bar{b}$
<230	95	25 ABOUD	18BU ATLS	13 TeV, $\gamma\gamma WW^*$
< 12.7	95	26 ABOUD	18CQ ATLS	13 TeV, $b\bar{b}\tau\tau$
< 22	95	27 ABOUD	18CW ATLS	13 TeV, $\gamma\gamma b\bar{b}$
< 30	95	28 SIRUNYAN	18A CMS	13 TeV, $b\bar{b}\tau\tau$
< 79	95	29 SIRUNYAN	18F CMS	13 TeV, $b\bar{b}\ell\nu\ell\nu$
< 43	95	30 SIRUNYAN	17CN CMS	8 TeV, $b\bar{b}\tau\tau, \gamma\gamma b\bar{b}, b\bar{b}b\bar{b}$
<108	95	31 ABOUD	16I ATLS	13 TeV, $b\bar{b}b\bar{b}$
< 74	95	32 KHACHATRY...16BQ CMS	8 TeV, $\gamma\gamma b\bar{b}$	
< 70	95	33 AAD	15CE ATLS	8 TeV, $b\bar{b}b\bar{b}, b\bar{b}\tau\tau, \gamma\gamma b\bar{b},$ $\gamma\gamma WW$

- 1 AAD 23AT combine results from 126–139 fb⁻¹ of data at $E_{cm} = 13$ TeV for $pp \rightarrow HH \rightarrow b\bar{b}b\bar{b}$ (AAD 23BK), $b\bar{b}\tau\tau$ (AAD 23Z), and $b\bar{b}\gamma\gamma$ (AAD 22Y).
- 2 AAD 23AD search for non-resonant HH production in association with a vector boson using $HH \rightarrow b\bar{b}b\bar{b}$ with data of 139 fb⁻¹ at $E_{cm} = 13$ TeV. The vector boson decays leptonically ($W \rightarrow \ell\nu, Z \rightarrow \ell\ell, \nu\nu, \ell = e, \mu$).
- 3 AAD 23BK search for non-resonant HH production using $HH \rightarrow b\bar{b}b\bar{b}$ with data of 126 fb⁻¹ at $E_{cm} = 13$ TeV.
- 4 AAD 23Z search for non-resonant HH production using $HH \rightarrow b\bar{b}\tau\tau$ with data of 139 fb⁻¹ at $E_{cm} = 13$ TeV. The upper limit on the $pp \rightarrow HH$ production cross section at 95% CL is measured to be 140 fb, which corresponds to 4.7 times the SM prediction (see their Table 6).
- 5 TUMASYAN 23AE search for HH production using $HH \rightarrow b\bar{b}b\bar{b}$, where both $b\bar{b}$ pairs are highly boosted, with data of 138 fb⁻¹ at $E_{cm} = 13$ TeV.
- 6 TUMASYAN 23D search for non-resonant HH production using $HH \rightarrow b\bar{b}\tau\tau$ with data of 138 fb⁻¹ at $E_{cm} = 13$ TeV.
- 7 The upper limit on the $pp \rightarrow HH$ production cross section (gluon fusion and VBF) at 95% CL is measured to be 102 fb, which corresponds to 3.3 times the SM prediction (see their Table 2).
- 8 The upper limit on the VBF $pp \rightarrow HH$ production cross section at 95% CL is measured to be 212 fb, which corresponds to 124 times the SM prediction (see their Table 3).
- 9 TUMASYAN 23I search for non-resonant HH production using $HH \rightarrow b\bar{b}ZZ^*$ ($ZZ^* \rightarrow 4\ell, \ell = e, \mu$) with data of 138 fb⁻¹ at $E_{cm} = 13$ TeV.
- 10 TUMASYAN 23O search for non-resonant HH production using $HH \rightarrow WW^*WW^*, WW^*\tau\tau$, and $\tau\tau\tau\tau$ (multilepton) with data of 138 fb⁻¹ at $E_{cm} = 13$ TeV. See their Fig. 9 for different final states and these combination.
- 11 AAD 22Y search for non-resonant HH production using $HH \rightarrow \gamma\gamma b\bar{b}$ with data of 139 fb⁻¹ at $E_{cm} = 13$ TeV. The upper limit on the $pp \rightarrow HH$ production cross section at 95% CL is measured to be 130 fb, which corresponds to 4.2 times the SM prediction.
- 12 CMS 22 report combined results (see their Extended Data Table 2) using 138 fb⁻¹ of data at $E_{cm} = 13$ TeV. See their Fig. 5 (left) for different final states and these combination.
- 13 TUMASYAN 22AN search for non-resonant HH production using $HH \rightarrow b\bar{b}b\bar{b}$ with data of 138 fb⁻¹ at $E_{cm} = 13$ TeV. The upper limit on the $pp \rightarrow HH$ production cross section at 95% CL is measured to be 120 fb, which corresponds to 3.9 times the SM prediction.
- 14 SIRUNYAN 21K search for non-resonant HH production using $HH \rightarrow \gamma\gamma b\bar{b}$ with data of 137 fb⁻¹ at $E_{cm} = 13$ TeV. The upper limit on the $pp \rightarrow HH \rightarrow \gamma\gamma b\bar{b}$ production cross section at 95% CL is measured to be 0.67 fb, which corresponds to about 7.7 times the SM prediction.
- 15 AAD 20c combine results of up to 36.1 fb⁻¹ data at $E_{cm} = 13$ TeV for $pp \rightarrow HH \rightarrow b\bar{b}\gamma\gamma, b\bar{b}\tau\tau, b\bar{b}b\bar{b}, b\bar{b}WW^*, WW^*\gamma\gamma, WW^*WW^*$ (AABOUD 18CW, AABOUD 18CQ, AABOUD 19A, AABOUD 19O, AABOUD 18BU, and AABOUD 19T).
- 16 AAD 20E search non-resonant for HH production using $HH \rightarrow b\bar{b}\ell\nu\ell\nu$, where one of the Higgs bosons decays to $b\bar{b}$ and the other decays to either $WW^*, ZZ^*,$ or $\tau\tau$, with data of 139 fb⁻¹ at $E_{cm} = 13$ TeV. The upper limit on the $pp \rightarrow HH$ production cross section at 95% CL is measured to be 1.2 pb, which corresponds to about 40 times the SM prediction.
- 17 AAD 20X search for $HH \rightarrow b\bar{b}b\bar{b}$ process via VBF with data of 126 fb⁻¹ at $E_{cm} = 13$ TeV. The upper limit on the SM non-resonant HH production cross section is 1460 fb at 95% CL, which corresponds to 840 times the SM prediction.

HH Production Cross Section in pp Collisions

The HH production cross section relative to the SM prediction.

VALUE	CL%	DOCUMENT ID	TECN	COMMENT
< 2.4	95	1 AAD	23AT ATLS	13 TeV, $b\bar{b}b\bar{b}, b\bar{b}\tau\tau, b\bar{b}\gamma\gamma$

- 18 AABOUD 19A search for HH production using $HH \rightarrow b\bar{b}b\bar{b}$ with data of 36.1 fb^{-1} at $E_{\text{cm}} = 13 \text{ TeV}$. The upper limit on the $pp \rightarrow HH \rightarrow b\bar{b}b\bar{b}$ production cross section at 95% CL is measured to be 147 fb, which corresponds to about 12.9 times the SM prediction.
- 19 AABOUD 19o search for HH production using $HH \rightarrow b\bar{b}WW^*$ with data of 36.1 fb^{-1} at $E_{\text{cm}} = 13 \text{ TeV}$. The upper limit on the $pp \rightarrow HH$ production cross section at 95% CL is calculated to be 10 pb from the observed upper limit on the $pp \rightarrow HH \rightarrow b\bar{b}WW^*$ production cross section of 2.5 pb assuming the SM branching fractions. The former corresponds to about 300 times the SM prediction.
- 20 AABOUD 19T search for HH production using $HH \rightarrow WW^*WW^*$ with data of 36.1 fb^{-1} at $E_{\text{cm}} = 13 \text{ TeV}$. The upper limit on the $pp \rightarrow HH$ production cross section at 95% CL is measured to be 5.3 pb, which corresponds to about 160 times the SM prediction.
- 21 SIRUNYAN 19 search for HH production using $HH \rightarrow \gamma\gamma b\bar{b}$ with data of 35.9 fb^{-1} at $E_{\text{cm}} = 13 \text{ TeV}$. The upper limit on the $pp \rightarrow HH \rightarrow \gamma\gamma b\bar{b}$ production cross section at 95% CL is measured to be 2.0 fb, which corresponds to about 24 times the SM prediction.
- 22 SIRUNYAN 19AB search for HH production using $HH \rightarrow b\bar{b}b\bar{b}$, where 4 heavy flavor jets from two Higgs bosons are resolved, with data of 35.9 fb^{-1} at $E_{\text{cm}} = 13 \text{ TeV}$. The upper limit on the $pp \rightarrow HH \rightarrow b\bar{b}b\bar{b}$ production cross section at 95% CL is measured to be 847 fb, which corresponds to about 75 times the SM prediction.
- 23 SIRUNYAN 19BE combine results of 13 TeV 35.9 fb^{-1} data: SIRUNYAN 19, SIRUNYAN 18A, SIRUNYAN 19AB, SIRUNYAN 19H, and SIRUNYAN 18F.
- 24 SIRUNYAN 19H search for HH production using $HH \rightarrow b\bar{b}b\bar{b}$, where one of $b\bar{b}$ pairs is highly boosted and the other one is resolved, with data of 35.9 fb^{-1} at $E_{\text{cm}} = 13 \text{ TeV}$. The upper limit on the $pp \rightarrow HH \rightarrow b\bar{b}b\bar{b}$ production cross section at 95% CL is measured to be 1980 fb, which corresponds to about 179 times the SM prediction.
- 25 AABOUD 18BU search for HH production using $\gamma\gamma WW^*$ with the final state of $\gamma\gamma\ell\nu jj$ using data of 36.1 fb^{-1} at $E_{\text{cm}} = 13 \text{ TeV}$. The upper limit on the $pp \rightarrow HH$ production cross section at 95% CL is measured to be 7.7 pb, which corresponds to about 230 times the SM prediction. The upper limit on the $pp \rightarrow HH \rightarrow \gamma\gamma WW^*$ at 95% CL is measured to be 7.5 fb (see their Table 6).
- 26 AABOUD 18CQ search for HH production using $HH \rightarrow b\bar{b}\tau\tau$ with data of 36.1 fb^{-1} at $E_{\text{cm}} = 13 \text{ TeV}$. The upper limit on the $pp \rightarrow HH \rightarrow b\bar{b}\tau\tau$ production cross section at 95% CL is measured to be 30.9 fb, which corresponds to about 12.7 times the SM prediction.
- 27 AABOUD 18CW search for HH production using $HH \rightarrow \gamma\gamma b\bar{b}$ with data of 36.1 fb^{-1} at $E_{\text{cm}} = 13 \text{ TeV}$. The upper limit on the $pp \rightarrow HH$ production cross section at 95% CL is measured to be 0.73 pb, which corresponds to about 22 times the SM prediction.
- 28 SIRUNYAN 18A search for HH production using $HH \rightarrow b\bar{b}\tau\tau$ with data of 35.9 fb^{-1} at $E_{\text{cm}} = 13 \text{ TeV}$. The upper limit on the $gg \rightarrow HH \rightarrow b\bar{b}\tau\tau$ production cross section is measured to be 75.4 fb, which corresponds to about 30 times the SM prediction.
- 29 SIRUNYAN 18F search non-resonant for HH production using $HH \rightarrow b\bar{b}\ell\nu\ell\nu$, where $\ell\nu\ell\nu$ is either $WW \rightarrow \ell\nu\ell\nu$ or $ZZ \rightarrow \ell\nu\ell\nu$ ($\ell = e, \mu$ or a leptonically decaying τ), with data of 35.9 fb^{-1} at $E_{\text{cm}} = 13 \text{ TeV}$. The upper limit on the $HH \rightarrow b\bar{b}\ell\nu\ell\nu$ production cross section at 95% CL is measured to be 72 fb, which corresponds to about 79 times the SM prediction.
- 30 SIRUNYAN 17CN search for HH production using $HH \rightarrow b\bar{b}\tau\tau$ with data of 18.3 fb^{-1} at $E_{\text{cm}} = 8 \text{ TeV}$. Results are then combined with the published results of the $HH \rightarrow \gamma\gamma b\bar{b}$ and $HH \rightarrow b\bar{b}b\bar{b}$, which use data of up to 19.7 fb^{-1} at $E_{\text{cm}} = 8 \text{ TeV}$. The upper limit on the $gg \rightarrow HH$ production cross section is measured to be 0.59 pb from $b\bar{b}\tau\tau$, which corresponds to about 59 times the SM prediction (gluon fusion). The combined upper limit is 0.43 pb, which is about 43 times the SM prediction. The quoted values are given for $m_H = 125 \text{ GeV}$.
- 31 AABOUD 16I search for HH production using $HH \rightarrow b\bar{b}b\bar{b}$ with data of 3.2 fb^{-1} at $E_{\text{cm}} = 13 \text{ TeV}$. The upper limit on the $pp \rightarrow HH \rightarrow b\bar{b}b\bar{b}$ production cross section is measured to be 1.22 pb. This result corresponds to about 108 times the SM prediction (gluon fusion), which is $11.3^{+0.9}_{-1.0} \text{ fb}$ (NNLO+NNLL) including top quark mass effects. The quoted values are given for $m_H = 125 \text{ GeV}$.
- 32 KHACHATRYAN 16BQ search for HH production using $HH \rightarrow \gamma\gamma b\bar{b}$ with data of 19.7 fb^{-1} at $E_{\text{cm}} = 8 \text{ TeV}$. The upper limit on the $gg \rightarrow HH \rightarrow \gamma\gamma b\bar{b}$ production is measured to be 1.85 fb, which corresponds to about 74 times the SM prediction and is translated into 0.71 pb for $gg \rightarrow HH$ production cross section.
- 33 AAD 15CE search for HH production using $HH \rightarrow b\bar{b}\tau\tau$ and $HH \rightarrow \gamma\gamma WW$ with data of 20.3 fb^{-1} at $E_{\text{cm}} = 8 \text{ TeV}$. These results are then combined with the published results of the $HH \rightarrow \gamma\gamma b\bar{b}$ and $HH \rightarrow b\bar{b}b\bar{b}$, which use data of up to 20.3 fb^{-1} at $E_{\text{cm}} = 8 \text{ TeV}$. The upper limits on the $gg \rightarrow HH$ production cross section are measured to be 1.6 pb, 11.4 pb, 2.2 pb and 0.62 pb from $b\bar{b}\tau\tau, \gamma\gamma WW, \gamma\gamma b\bar{b}$ and $b\bar{b}b\bar{b}$, respectively. The combined upper limit is 0.69 pb, which corresponds to about 70 times the SM prediction. The quoted results are given for $m_H = 125.4 \text{ GeV}$. See their Table 4.
- 2.3 to 9.4 95 12 TUMASYAN 22AN CMS 13 TeV, $b\bar{b}b\bar{b}$
– 3.3 to 8.5 95 13 SIRUNYAN 21K CMS 13 TeV, $\gamma\gamma b\bar{b}$
– 5.0 to 12.0 95 14 AAD 20C ATLS 13 TeV, $b\bar{b}\gamma\gamma, b\bar{b}\tau\tau, b\bar{b}b\bar{b}, b\bar{b}WW^*, WW^*\gamma\gamma,$
 WW^*WW^*
– 11 to 17 95 15 SIRUNYAN 19 CMS 13 TeV, $\gamma\gamma b\bar{b}$
– 11.8 to 18.8 95 16 SIRUNYAN 19BE CMS 13 TeV, $b\bar{b}\gamma\gamma, b\bar{b}\tau\tau, b\bar{b}b\bar{b}, b\bar{b}WW^*, b\bar{b}ZZ^*$
– 8.2 to 13.2 95 17 AABOUD 18CWATLS 13 TeV, $\gamma\gamma b\bar{b}$
18 SIRUNYAN 18A CMS 13 TeV, $b\bar{b}\tau\tau$
– 17 to 22.5 95 19 KHACHATRYAN...16BQ CMS 8 TeV, $\gamma\gamma b\bar{b}$
- 1 AAD 23AD search for non-resonant HH production in association with a vector boson using $HH \rightarrow b\bar{b}b\bar{b}$ with data of 139 fb^{-1} at $E_{\text{cm}} = 13 \text{ TeV}$. The vector boson decays leptonically ($W \rightarrow \ell\nu, Z \rightarrow \ell\ell, \nu\nu, \ell = e, \mu$). The quoted κ_λ is measured assuming all other Higgs boson couplings are at their SM value.
- 2 AAD 23AT combine results from 126–139 fb^{-1} of data at $E_{\text{cm}} = 13 \text{ TeV}$ for $pp \rightarrow HH \rightarrow b\bar{b}b\bar{b}$ (AAD 23BK), $b\bar{b}\tau\tau$ (AAD 23Z), and $b\bar{b}\gamma\gamma$ (AAD 22Y). The quoted values are obtained from the profile likelihood scan as a function of κ_λ as shown in their Fig. 5(a). All other coupling modifiers are assumed to have their SM values.
- 3 AAD 23AT combine results from 126–139 fb^{-1} of data at $E_{\text{cm}} = 13 \text{ TeV}$ for $pp \rightarrow HH \rightarrow b\bar{b}b\bar{b}$ (AAD 23BK), $b\bar{b}\tau\tau$ (AAD 23Z), and $b\bar{b}\gamma\gamma$ (AAD 22Y) with single-Higgs boson analyses ($\gamma\gamma, ZZ^*, WW^*, \tau\tau, b\bar{b}$, see their Table 1). The quoted values are obtained from the profile likelihood scan as a function of κ_λ as shown in their Fig. 5(a), assuming that all other Higgs boson couplings are at their SM values. Results with other assumptions are shown in their Table 2.
- 4 AAD 23BK search for non-resonant HH production using $HH \rightarrow b\bar{b}b\bar{b}$ with data of 126 fb^{-1} at $E_{\text{cm}} = 13 \text{ TeV}$. The quoted values are obtained from the one-dimensional profile likelihood scan as a function of κ_λ . See their Fig. 12 (a). The $\mu_{\text{ggF}+VBF}$ measurement for different values of κ_λ constrains $-3.9 < \kappa_\lambda < 11.1$ at 95% CL as shown in their Fig. 10 (a). $\kappa_{2V} = \kappa_V = 1$ is assumed in both cases.
- 5 HAYRAPETIAN 23 measure the cross sections for $pp \rightarrow H \rightarrow ZZ^* \rightarrow 4\ell$ ($\ell = e, \mu$) using 138 fb^{-1} at $E_{\text{cm}} = 13 \text{ TeV}$.
- 6 TUMASYAN 23AE search for HH production using $HH \rightarrow b\bar{b}b\bar{b}$, where both $b\bar{b}$ pairs are highly boosted, with data of 138 fb^{-1} at $E_{\text{cm}} = 13 \text{ TeV}$. The quoted κ_λ is measured assuming all other Higgs boson couplings are at their SM values.
- 7 TUMASYAN 23D search for non-resonant HH production using $HH \rightarrow b\bar{b}\tau\tau$ with data of 138 fb^{-1} at $E_{\text{cm}} = 13 \text{ TeV}$. The quoted values are obtained from the upper limit on the HH production cross section times the $b\bar{b}\tau\tau$ branching fraction for different values of κ_λ . See their Fig. 8 (left). All other coupling modifiers are assumed to be 1. In addition, two-dimensional exclusion regions as a function of the κ_λ and κ_t couplings, with $\kappa_{2V} = \kappa_V = 1$, are shown in their Fig. 9 (left). The one-dimensional likelihood scan as a function of κ_λ is given in their Fig. 10 (left), from which a 95% confidence interval of $-1.77 < \kappa_\lambda < 8.73$ is extracted.
- 8 TUMASYAN 23AI search for non-resonant HH production using $HH \rightarrow b\bar{b}ZZ^*$ ($ZZ^* \rightarrow 4\ell, \ell = e, \mu$) with data of 138 fb^{-1} at $E_{\text{cm}} = 13 \text{ TeV}$. See their Fig. 4.
- 9 TUMASYAN 23O search for non-resonant HH production using $HH \rightarrow WW^*WW^*, WW^*\tau\tau$, and $\tau\tau\tau\tau$ (multilepton) with data of 138 fb^{-1} at $E_{\text{cm}} = 13 \text{ TeV}$. See their Fig. 10 for different final states and these combination. Limits are set on a variety of new-physics models using an effective field theory approach. See their Figs. 11, 12, and 13.
- 10 AAD 22Y search for non-resonant HH production using $HH \rightarrow \gamma\gamma b\bar{b}$ with data of 139 fb^{-1} at $E_{\text{cm}} = 13 \text{ TeV}$. The quoted κ_λ is obtained from their Fig. 12 where the theory uncertainties are not included while a negative log-likelihood scan vs. κ_λ is shown in their Fig. 13 with the theory uncertainties, which provides $\kappa_\lambda = 2.8^{+2.0}_{-2.2}$ for the 1σ confidence interval.
- 11 CMS 22 report combined results (see their Extended Data Table 2) using 138 fb^{-1} of data at $E_{\text{cm}} = 13 \text{ TeV}$. See their Fig. 6 (left).
- 12 TUMASYAN 22AN search for non-resonant HH production using $HH \rightarrow b\bar{b}b\bar{b}$ with data of 138 fb^{-1} at $E_{\text{cm}} = 13 \text{ TeV}$. The upper limit on the $pp \rightarrow HH$ production cross section at 95% CL is shown as a function of κ_λ in their Fig. 2 (top).
- 13 SIRUNYAN 21K search for non-resonant HH production using $HH \rightarrow \gamma\gamma b\bar{b}$ with data of 137 fb^{-1} at $E_{\text{cm}} = 13 \text{ TeV}$.
- 14 AAD 20C combine results of up to 36.1 fb^{-1} data at $E_{\text{cm}} = 13 \text{ TeV}$ for $pp \rightarrow HH \rightarrow b\bar{b}\gamma\gamma, b\bar{b}\tau\tau, b\bar{b}b\bar{b}, b\bar{b}WW^*, WW^*\gamma\gamma, WW^*WW^*$ (AABOUD 18CW, AABOUD 18CQ, AABOUD 19A, AABOUD 19o, AABOUD 18BU, and AABOUD 19T).
- 15 SIRUNYAN 19 search for HH production using $HH \rightarrow \gamma\gamma b\bar{b}$ with data of 35.9 fb^{-1} at $E_{\text{cm}} = 13 \text{ TeV}$. The quoted κ_λ is measured assuming all other Higgs boson couplings are at their SM value.
- 16 SIRUNYAN 19BE combine results of 13 TeV 35.9 fb^{-1} data: SIRUNYAN 19, SIRUNYAN 18A, SIRUNYAN 19AB, SIRUNYAN 19H, and SIRUNYAN 18F.
- 17 AABOUD 18CW search for HH production using $HH \rightarrow \gamma\gamma b\bar{b}$ with data of 36.1 fb^{-1} at $E_{\text{cm}} = 13 \text{ TeV}$. The quoted κ_λ is measured assuming all other Higgs boson couplings are at their SM value.
- 18 SIRUNYAN 18A search for HH production using $HH \rightarrow b\bar{b}\tau\tau$ with data of 35.9 fb^{-1} at $E_{\text{cm}} = 13 \text{ TeV}$. The upper limit on production cross section times branching fraction at 95% CL is shown as a function of κ_λ/κ_t in their Fig. 6 (top) where $\kappa_t = y_t / y_t^{\text{SM}}$ (top Yukawa coupling y_t).
- 19 KHACHATRYAN 16BQ search for HH production using $HH \rightarrow \gamma\gamma b\bar{b}$ with data of 19.7 fb^{-1} at $E_{\text{cm}} = 8 \text{ TeV}$.

Higgs trilinear self coupling modifier κ_λ

Signal strength relative to the SM prediction, $\kappa_\lambda = \lambda_{HHH} / \lambda_{HHH}^{\text{SM}}$.

VALUE	CL%	DOCUMENT ID	TECN	COMMENT
••• We do not use the following data for averages, fits, limits, etc. •••				
– 34.4 to 33.3	95	1 AAD	23AD ATLS	13 TeV, $VHH, HH \rightarrow b\bar{b}b\bar{b}$
– 0.6 to 6.6	95	2 AAD	23AT ATLS	13 TeV, $b\bar{b}b\bar{b}, b\bar{b}\tau\tau, b\bar{b}\gamma\gamma$
– 0.4 to 6.3	95	3 AAD	23AT ATLS	13 TeV, $b\bar{b}b\bar{b}, b\bar{b}\tau\tau, b\bar{b}\gamma\gamma$
– 3.5 to 11.3	95	4 AAD	23BK ATLS	13 TeV, $b\bar{b}b\bar{b}$
– 5.4 to 14.9	95	5 HAYRAPETY...23	CMS	13 TeV, $ZZ^* \rightarrow 4\ell$ cross sections
– 9.9 to 16.9	95	6 TUMASYAN	23AE CMS	13 TeV, $b\bar{b}b\bar{b}$
– 1.7 to 8.7	95	7 TUMASYAN	23D CMS	13 TeV, $b\bar{b}\tau\tau$
– 8.8 to 13.4	95	8 TUMASYAN	23I CMS	13 TeV, $b\bar{b}ZZ^* (ZZ^* \rightarrow 4\ell)$
– 6.9 to 11.1	95	9 TUMASYAN	23O CMS	13 TeV, $WW^*WW^*, WW^*\tau\tau, \tau\tau\tau\tau$
– 1.5 to 6.7	95	10 AAD	22Y ATLS	13 TeV, $\gamma\gamma b\bar{b}$
– 1.24 to 6.49	95	11 CMS	22 CMS	13 TeV, $b\bar{b}ZZ^*, b\bar{b}\gamma\gamma, b\bar{b}\tau\tau, b\bar{b}b\bar{b}, \text{multilepton}$

Higgs-gauge boson quartic coupling modifier κ_{2V}

Signal strength relative to the SM prediction, $\kappa_{2V} = \lambda_{VVHH} / \lambda_{VVHH}^{\text{SM}}$, $V = W, Z$.

VALUE	CL%	DOCUMENT ID	TECN	COMMENT
••• We do not use the following data for averages, fits, limits, etc. •••				
– 8.6 to 10.0	95	1 AAD	23AD ATLS	13 TeV, $VHH, HH \rightarrow b\bar{b}b\bar{b}$
0.1 to 2.0	95	2 AAD	23AT ATLS	13 TeV, $b\bar{b}b\bar{b}, b\bar{b}\tau\tau, b\bar{b}\gamma\gamma$
0.0 to 2.1	95	3 AAD	23BK ATLS	13 TeV, $b\bar{b}b\bar{b}$

Gauge & Higgs Boson Particle Listings

H

0.62 to 1.41	95	4 TUMASYAN	23AE CMS	13 TeV, $b\bar{b}b\bar{b}$
-0.4 to 2.6	95	5 TUMASYAN	23D CMS	13 TeV, $b\bar{b}\tau\tau$
0.67 to 1.38	95	6 CMS	22 CMS	13 TeV, $b\bar{b}ZZ^*$, $b\bar{b}\gamma\gamma$, $b\bar{b}\tau\tau$, $b\bar{b}b\bar{b}$, multilepton
-0.1 to 2.2	95	7 TUMASYAN	22AN CMS	13 TeV, $b\bar{b}b\bar{b}$
-1.3 to 3.5	95	8 SIRUNYAN	21K CMS	13 TeV, $\gamma\gamma b\bar{b}$
-0.43 to 2.56	95	9 AAD	20X ATLS	13 TeV, VBF, $b\bar{b}b\bar{b}$

- ¹ AAD 23AD search for non-resonant HH production in association with a vector boson using $HH \rightarrow b\bar{b}b\bar{b}$ with data of 139 fb⁻¹ at $E_{cm} = 13$ TeV. The vector boson decays leptonically ($W \rightarrow \ell\nu$, $Z \rightarrow \ell\ell$, $\nu\nu$, $\ell = e, \mu$). The constraints on κ_{2W} and κ_{2Z} are separately measured to be $-12.3 < \kappa_{2W} < 13.5$ and $-9.9 < \kappa_{2Z} < 11.3$ (95% CL). The quoted κ_{2V} ($V = W, Z$) is measured assuming all other Higgs boson couplings are at their SM value.
- ² AAD 23AT combine results from 126-139 fb⁻¹ of data at $E_{cm} = 13$ TeV for $pp \rightarrow HH \rightarrow b\bar{b}b\bar{b}$ (AAD 23BK), $b\bar{b}\tau\tau$ (AAD 23Z), and $b\bar{b}\gamma\gamma$ (AAD 22Y). The quoted values are obtained from the 95% CL VBF HH cross-section upper limit as a function of κ_{2V} as shown in their Fig. 4(b). All other coupling modifiers are assumed to have their SM values.
- ³ AAD 23BK search for non-resonant HH production using $HH \rightarrow b\bar{b}b\bar{b}$ with data of 126 fb⁻¹ at $E_{cm} = 13$ TeV. The quoted values are obtained from the one-dimensional profile likelihood scan as a function of κ_{2V} . See their Fig. 12 (b). The $\mu\nu BF$ measurement for different values of κ_{2V} constrains $-0.03 < \kappa_{2V} < 2.11$ at 95% CL as shown in their Fig. 10 (b). $\kappa_\lambda = \kappa_V = 1$ is assumed in both cases.
- ⁴ TUMASYAN 23AE search for HH production using $HH \rightarrow b\bar{b}b\bar{b}$, where both $b\bar{b}$ pairs are highly boosted, with data of 138 fb⁻¹ at $E_{cm} = 13$ TeV. The $\kappa_{2V} = 0$ is excluded at 6.3 σ assuming all other Higgs boson couplings are at their SM values.
- ⁵ TUMASYAN 23D search for non-resonant HH production using $HH \rightarrow b\bar{b}\tau\tau$ with data of 138 fb⁻¹ at $E_{cm} = 13$ TeV. The quoted values are obtained from the upper limits on the HH production cross section times the $b\bar{b}\tau\tau$ branching fraction for different values of κ_{2V} . See their Fig. 8 (right). All other coupling modifiers are assumed to be 1. In addition, two-dimensional exclusion regions as a function of the κ_{2V} and κ_V couplings, with $\kappa_\lambda = \kappa_t = 1$, are shown in their Fig. 9 (right). The one-dimensional likelihood scan as a function of κ_{2V} is given in their Fig. 10 (right), from which a 95% confidence interval of $-0.34 < \kappa_{2V} < 2.49$ is extracted.
- ⁶ CMS 22 report combined results (see their Extended Data Table 2) using 138 fb⁻¹ of data at $E_{cm} = 13$ TeV. See their Fig. 6 (right).
- ⁷ TUMASYAN 22AN search for non-resonant HH production using $HH \rightarrow b\bar{b}b\bar{b}$ with data of 138 fb⁻¹ at $E_{cm} = 13$ TeV. The upper limit on the $pp \rightarrow HH$ production cross section at 95% CL is shown as a function of κ_{2V} in their Fig. 2 (bottom).
- ⁸ SIRUNYAN 21K search for non-resonant HH production using $HH \rightarrow \gamma\gamma b\bar{b}$ with data of 137 fb⁻¹ at $E_{cm} = 13$ TeV.
- ⁹ AAD 20X search for $HH \rightarrow b\bar{b}b\bar{b}$ process via VBF with data of 126 fb⁻¹ at $E_{cm} = 13$ TeV.

tH production

VALUE	DOCUMENT ID	TECN	COMMENT
5.7 ± 2.7 ± 3.0	1 SIRUNYAN	21R CMS	pp, 13 TeV
• • • We do not use the following data for averages, fits, limits, etc. • • •	2 AAD	20Z ATLS	pp, 13 TeV
	3 SIRUNYAN	19BK CMS	pp, 13 TeV
	4 KHACHATRYAN	16AU CMS	pp, 8 TeV

- ¹ SIRUNYAN 21R search for tH in final states with electrons, muons and hadronically decaying τ leptons ($H \rightarrow WW^*, ZZ^*, \tau\tau$) with 137 fb⁻¹ of pp collision data at $E_{cm} = 13$ TeV. The quoted signal strength corresponds to a significance of 1.4 standard deviations and is given for $m_H = 125$ GeV.
- ² AAD 20Z search for the tH associated production using $H \rightarrow \gamma\gamma$ in 139 fb⁻¹ of data at $E_{cm} = 13$ TeV. An upper limit on its rate is set to be 12 times the Standard Model at 95% CL ($m_H = 125.09$ GeV).
- ³ SIRUNYAN 19BK search for the tH associated production using multilepton signatures ($H \rightarrow WW^*, H \rightarrow \tau\tau, H \rightarrow ZZ^*$) and signatures with a single lepton and a $b\bar{b}$ pair ($H \rightarrow b\bar{b}$) using 35.9 fb⁻¹ at $E_{cm} = 13$ TeV. Results are combined with $H \rightarrow \gamma\gamma$ (SIRUNYAN 18Ds). The observed 95% CL upper limit on the tH production cross section times $H \rightarrow WW^* + \tau\tau + ZZ^* + b\bar{b} + \gamma\gamma$ branching fraction is 1.94 pb (assuming SM tH production cross section). See their Table X and Fig. 14. The values outside the ranges of $[-0.9, -0.5]$ and $[1.0, 2.1]$ times the standard model top quark Yukawa coupling are excluded at 95% CL.
- ⁴ KHACHATRYAN 16AU search for the tH associated production in 19.7 fb⁻¹ at $E_{cm} = 8$ TeV. The 95% CL upper limits on the tH associated production cross section is measured to be 600-1000 fb depending on the assumed $\gamma\gamma$ branching ratios of the Higgs boson. The $\gamma\gamma$ branching ratio is varied to be by a factor of 0.5-3.0 of the Standard Model Higgs boson ($m_H = 125$ GeV). The results of the signal strengths for a negative Higgs-boson trilinear coupling are given. The results are given for $m_H = 125$ GeV.

H Production Cross Section in pp Collisions at $\sqrt{s} = 13$ TeVAssumes $m_H = 125$ GeV

VALUE (pb)	DOCUMENT ID	TECN	COMMENT
56.8 ± 3.4 OUR AVERAGE			
55.5 ± 4.0 3.8	1 AAD	23C ATLS	pp, 13 TeV, $\gamma\gamma, ZZ^* \rightarrow 4\ell$ ($\ell = e, \mu$)
61.1 ± 6.0 ± 3.7	2 SIRUNYAN	19BA CMS	pp, 13 TeV, $\gamma\gamma, ZZ^* \rightarrow 4\ell$ ($\ell = e, \mu$)
• • • We do not use the following data for averages, fits, limits, etc. • • •			
58 ± 4 ± 4	3 AAD	22N ATLS	pp, 13 TeV, $\gamma\gamma$
53.5 ± 4.9 ± 2.1	4 AAD	20BA ATLS	pp, 13 TeV, $ZZ^* \rightarrow 4\ell$ ($\ell = e, \mu$)
57.0 ± 6.0 + 4.0 5.9 - 3.3	5 AABOUD	18CG ATLS	pp, 13 TeV, $\gamma\gamma, ZZ^* \rightarrow 4\ell$ ($\ell = e, \mu$)

47.9 ^{+9.1} _{-8.6}	5 AABOUD	18CG ATLS	pp, 13 TeV, $\gamma\gamma$
68 ⁺¹¹ ₋₁₀	5 AABOUD	18CG ATLS	pp, 13 TeV, $ZZ^* \rightarrow 4\ell$ ($\ell = e, \mu$)
69 ⁺¹⁰ ₋₉ ± 5	6 AABOUD	17CO ATLS	pp, 13 TeV, $ZZ^* \rightarrow 4\ell$

- ¹ AAD 23C combine AAD 22N and AAD 20BA, where both use 139 fb⁻¹ of pp collisions at $E_{cm} = 13$ TeV. The Higgs production cross sections at $E_{cm} = 7$ and 8 TeV are obtained to be 34^{+11}_{-10} pb and $33.3^{+5.8}_{-5.4}$ pb, respectively. The quoted value is given for $m_H = 125.09$ GeV. The differential cross sections are given in their Figs. 3 and 4.
- ² SIRUNYAN 19BA use 35.9 fb⁻¹ of pp collisions at $E_{cm} = 13$ TeV.
- ³ AAD 22N use 139 fb⁻¹ of pp collisions at $E_{cm} = 13$ TeV. The quoted value is given for $m_H = 125.09$ GeV.
- ⁴ AAD 20BA use 139 fb⁻¹ of pp collisions at $E_{cm} = 13$ TeV with $H \rightarrow ZZ^* \rightarrow 4\ell$ where $\ell = e, \mu$. The quoted value is given for $m_H = 125$ GeV and assumes the Standard Model branching ratio.
- ⁵ AABOUD 18CG use 36.1 fb⁻¹ of pp collisions at $E_{cm} = 13$ TeV.
- ⁶ AABOUD 17CO use 36.1 fb⁻¹ of pp collisions at $E_{cm} = 13$ TeV with $H \rightarrow ZZ^* \rightarrow 4\ell$ where $\ell = e, \mu$ for $m_H = 125$ GeV. Differential cross sections for the Higgs boson transverse momentum, Higgs boson rapidity, and other related quantities are measured as shown in their Figs. 8 and 9.

H REFERENCES

AAD	24D	PRL 132 021803	G. Aad et al.	(ATLAS and CMS Collab.)
AABOUD	23A	JHEP 2312 158 (errat.)	M. Aaboud et al.	(ATLAS Collab.)
AAD	23A	PL B842 137963	G. Aad et al.	(ATLAS Collab.)
AAD	23AD	EPJ C83 519	G. Aad et al.	(ATLAS Collab.)
AAD	23AF	EPJ C83 503	G. Aad et al.	(ATLAS Collab.)
AAD	23AK	EPJ C83 563	G. Aad et al.	(ATLAS Collab.)
AAD	23AN	PRL 131 061802	G. Aad et al.	(ATLAS Collab.)
AAD	23AP	PR D108 032005	G. Aad et al.	(ATLAS Collab.)
AAD	23AT	PL B843 137745	G. Aad et al.	(ATLAS Collab.)
AAD	23AU	PL B843 137880	G. Aad et al.	(ATLAS Collab.)
AAD	23BC	EPJ C83 496	G. Aad et al.	(ATLAS Collab.)
AAD	23BK	PR D108 052003	G. Aad et al.	(ATLAS Collab.)
AAD	23BP	PRL 131 251802	G. Aad et al.	(ATLAS Collab.)
AAD	23BR	PL B846 138223	G. Aad et al.	(ATLAS Collab.)
AAD	23BS	PL B847 138292	G. Aad et al.	(ATLAS Collab.)
AAD	23BU	PL B847 138315	G. Aad et al.	(ATLAS Collab.)
AAD	23BV	PR D108 072003	G. Aad et al.	(ATLAS Collab.)
AAD	23C	JHEP 2305 028	G. Aad et al.	(ATLAS Collab.)
AAD	23CD	EPJ C83 781	G. Aad et al.	(ATLAS Collab.)
AAD	23Q	JHEP 2307 166	G. Aad et al.	(ATLAS Collab.)
AAD	23Y	JHEP 2307 088	G. Aad et al.	(ATLAS Collab.)
AAD	23Z	JHEP 2307 040	G. Aad et al.	(ATLAS Collab.)
AAD	HAYRAPETYAN...	23 JHEP 2308 040	A. Hayrapetyan et al.	(CMS Collab.)
AAD	HAYRAPETYAN...	23C PRL D108 072004	A. Hayrapetyan et al.	(CMS Collab.)
AAD	TUMASYAN	23AD PRL 131 041801	A. Tumasyan et al.	(CMS Collab.)
AAD	TUMASYAN	23AE PRL 131 041803	A. Tumasyan et al.	(CMS Collab.)
AAD	TUMASYAN	23AH PRL 131 061801	A. Tumasyan et al.	(CMS Collab.)
AAD	TUMASYAN	23AI PRL D108 032008	A. Tumasyan et al.	(CMS Collab.)
AAD	TUMASYAN	23AJ PRL D108 032013	A. Tumasyan et al.	(CMS Collab.)
AAD	TUMASYAN	23AU PL B846 137783	A. Tumasyan et al.	(CMS Collab.)
AAD	TUMASYAN	23BA EPJ C83 933	A. Tumasyan et al.	(CMS Collab.)
AAD	TUMASYAN	23C PL B842 137534	A. Tumasyan et al.	(CMS Collab.)
AAD	TUMASYAN	23D PL B842 137531	A. Tumasyan et al.	(CMS Collab.)
AAD	TUMASYAN	23F JHEP 2305 233	A. Tumasyan et al.	(CMS Collab.)
AAD	TUMASYAN	23I JHEP 2306 130	A. Tumasyan et al.	(CMS Collab.)
AAD	TUMASYAN	23J JHEP 2307 095	A. Tumasyan et al.	(CMS Collab.)
AAD	TUMASYAN	23P JHEP 2307 092	A. Tumasyan et al.	(CMS Collab.)
AAD	TUMASYAN	23Q JHEP 2307 091	A. Tumasyan et al.	(CMS Collab.)
AAD	TUMASYAN	23W EPJ C83 667	A. Tumasyan et al.	(CMS Collab.)
AAD	TUMASYAN	23Y EPJ C83 562	A. Tumasyan et al.	(CMS Collab.)
AAD	22D	PL B829 137066	G. Aad et al.	(ATLAS Collab.)
AAD	22M	JHEP 2206 097	G. Aad et al.	(ATLAS Collab.)
AAD	22N	JHEP 2208 027	G. Aad et al.	(ATLAS Collab.)
AAD	22P	JHEP 2208 104	G. Aad et al.	(ATLAS Collab.)
AAD	22Q	JHEP 2208 175	G. Aad et al.	(ATLAS Collab.)
AAD	22S	EPJ C82 105	G. Aad et al.	(ATLAS Collab.)
AAD	22V	EPJ C82 622	G. Aad et al.	(ATLAS Collab.)
AAD	22W	EPJ C82 717	G. Aad et al.	(ATLAS Collab.)
AAD	22X	PR D105 092003	G. Aad et al.	(ATLAS Collab.)
AAD	22Y	PR D106 052001	G. Aad et al.	(ATLAS Collab.)
AAD	ATLAS	22 NAT 607 52	ATLAS Collaboration	(ATLAS Collab.)
AAD	Also	NAT 612 E24 (errat.)	ATLAS Collaboration	(ATLAS Collab.)
AAD	CMS	22 NAT 607 60	CMS Collaboration	(CMS Collab.)
AAD	TUMASYAN	22AJ PRL 128 081805	A. Tumasyan et al.	(CMS Collab.)
AAD	TUMASYAN	22AM NATP 18 1329	A. Tumasyan et al.	(CMS Collab.)
AAD	TUMASYAN	22AN PRL 129 081802	A. Tumasyan et al.	(CMS Collab.)
AAD	TUMASYAN	22G PR D105 092007	A. Tumasyan et al.	(CMS Collab.)
AAD	TUMASYAN	22Y JHEP 2206 012	A. Tumasyan et al.	(CMS Collab.)
AAD	21	PL B812 135980	G. Aad et al.	(ATLAS Collab.)
AAD	21AB	EPJ C81 178	G. Aad et al.	(ATLAS Collab.)
AAD	21AJ	EPJ C81 537	G. Aad et al.	(ATLAS Collab.)
AAD	21F	PR D103 112006	G. Aad et al.	(ATLAS Collab.)
AAD	21H	PL B816 136204	G. Aad et al.	(ATLAS Collab.)
AAD	21I	PL B819 136412	G. Aad et al.	(ATLAS Collab.)
AAD	21M	JHEP 2103 268	G. Aad et al.	(ATLAS Collab.)
AAD	SIRUNYAN	21 PL B812 135992	A.M. Sirunyan et al.	(CMS Collab.)
AAD	SIRUNYAN	21A EPJ C81 13	A.M. Sirunyan et al.	(CMS Collab.)
AAD	Also	EPJ C81 333 (errat.)	A.M. Sirunyan et al.	(CMS Collab.)
AAD	SIRUNYAN	21AE PR D104 052004	A.M. Sirunyan et al.	(CMS Collab.)
AAD	SIRUNYAN	21B EPJ C81 3	A.M. Sirunyan et al.	(CMS Collab.)
AAD	SIRUNYAN	21C JHEP 2101 148	A.M. Sirunyan et al.	(CMS Collab.)
AAD	SIRUNYAN	21K JHEP 2103 257	A.M. Sirunyan et al.	(CMS Collab.)
AAD	SIRUNYAN	21L JHEP 2103 011	A.M. Sirunyan et al.	(CMS Collab.)
AAD	SIRUNYAN	21O JHEP 2107 027	A.M. Sirunyan et al.	(CMS Collab.)
AAD	SIRUNYAN	21R EPJ C81 378	A.M. Sirunyan et al.	(CMS Collab.)
AAD	SIRUNYAN	21S EPJ C81 488	A.M. Sirunyan et al.	(CMS Collab.)
AAD	SIRUNYAN	21Z PR D104 032013	A.M. Sirunyan et al.	(CMS Collab.)
AAD	TUMASYAN	21D JHEP 2111 153	A. Tumasyan et al.	(CMS Collab.)
AAD	20A	PR D101 012002	G. Aad et al.	(ATLAS Collab.)
AAD	20A	PL B800 135069	G. Aad et al.	(ATLAS Collab.)
AAD	20AE	PRL 125 221802	G. Aad et al.	(ATLAS Collab.)
AAD	20AG	PL B809 135754	G. Aad et al.	(ATLAS Collab.)
AAD	20AQ	EPJ C80 957	G. Aad et al.	(ATLAS Collab.)
AAD	Also	EPJ C81 29 (errat.)	G. Aad et al.	(ATLAS Collab.)
AAD	Also	EPJ C81 398 (errat.)	G. Aad et al.	(ATLAS Collab.)
AAD	20BA	EPJ C80 942	G. Aad et al.	(ATLAS Collab.)
AAD	20C	PL B800 135103	G. Aad et al.	(ATLAS Collab.)
AAD	20E	PL B801 135145	G. Aad et al.	(ATLAS Collab.)
AAD	20F	PL B801 135148	G. Aad et al.	(ATLAS Collab.)

See key on page 1171

Gauge & Higgs Boson Particle Listings
H, Neutral Higgs Bosons, Searches for

Table listing particle searches for Higgs bosons. Columns include experiment name (e.g., AAD, SIRUNYAN), publication details (year, journal, volume, page), and collaboration (e.g., ATLAS, CMS). The table is organized into two columns.

Neutral Higgs Bosons, Searches for

CONTENTS:

- Mass Limits for Neutral Higgs Bosons in Supersymmetric Models
- Mass Limits for heavy neutral Higgs bosons (H2, A0) in the MSSM
- Mass Limits for H10 (Higgs Boson) in Supersymmetric Models
Mass Limits for Neutral Higgs Bosons in Extended Higgs Models
- Mass Limits in General two-Higgs-doublet Models
- Mass Limits for H0 with Vanishing Yukawa Couplings
- Mass Limits for H0 Decaying to Invisible Final States
- Mass Limits for Light A0
- Other Mass Limits
Electroweak Constraints on the Standard Model Higgs Boson Mass

MASS LIMITS FOR NEUTRAL HIGGS BOSONS IN SUPERSYMMETRIC MODELS

The minimal supersymmetric model has two complex doublets of Higgs bosons. The resulting physical states are two scalars [H10 and H20, where we define mH10 < mH20], a pseudoscalar (A0), and a charged Higgs pair (H±). H10 and H20 are also called h and H in the literature. There are two free parameters in the Higgs sector which can be chosen to be mA0 and tanβ = v2/v1, the ratio of vacuum expectation values of the two Higgs doublets. Tree-level Higgs masses are constrained by the model to be mH10 ≤ mZ, mH20 ≥ mZ, mA0 ≥ mH10, and mH± ≥ mW. However, as described in the review on "Status of Higgs Boson Physics" in this Volume these relations are violated by radiative corrections.

The observed signal at about 125 GeV, see section "H", can be interpreted as one of the neutral Higgs bosons of supersymmetric models. Unless otherwise noted, we identify the lighter scalar H10 with the Higgs discovered at 125 GeV at the LHC (AAD 12A1, CHATRCHYAN 12N).

Unless otherwise noted, the experiments in e+e- collisions search for the processes e+e- -> H10 Z0 in the channels used for the Standard Model Higgs searches and e+e- -> H10 A0 in the final states b b b b and b b tau+ tau-. Unless otherwise stated, the following results assume no invisible H10 or A0 decays. Unless otherwise noted, the results are given in the mHmax scenario, CARENA 13.

In p p and p p collisions the experiments search for a variety of processes, as explicitly specified for each entry. Limits on A0 mass arise from these direct searches, as well as from the relations valid in the minimal supersymmetric model between mA0 and mH10. As discussed in the review on "Status of Higgs Boson Physics" in this Volume, these relations

Gauge & Higgs Boson Particle Listings

Neutral Higgs Bosons, Searches for

depend, via potentially large radiative corrections, on the mass of the t quark and on the supersymmetric parameters, in particular those of the stop sector. These indirect limits are weaker for larger t and \bar{t} masses. To include the radiative corrections to the Higgs masses, unless otherwise stated, the listed papers use theoretical predictions incorporating two-loop corrections and beyond (SLAVICH 21), and the results are given for the M_h^{125} benchmark scenario, see BAGNASCHI 19.

Mass Limits for heavy neutral Higgs bosons (H_2^0, A^0) in the MSSM

The limits rely on $pp \rightarrow H_2^0/A^0 \rightarrow \tau^+\tau^-$ and assume that H_2^0 and A^0 are (sufficiently) mass degenerate. The limits depend on $\tan\beta$.

VALUE (GeV)	CL%	DOCUMENT ID	TECN	COMMENT
> 835	95	1 TUMASYAN	23s CMS	$\tan\beta = 10$ GeV
>1240	95	1 TUMASYAN	23s CMS	$\tan\beta = 20$ GeV
>1605	95	1 TUMASYAN	23s CMS	$\tan\beta = 30$ GeV
>1820	95	1 TUMASYAN	23s CMS	$\tan\beta = 40$ GeV
>1950	95	1 TUMASYAN	23s CMS	$\tan\beta = 50$ GeV
>2062	95	1 TUMASYAN	23s CMS	$\tan\beta = 60$ GeV
>1121	95	2 AAD	20AA ATLS	$\tan\beta = 10$ GeV
>1475	95	2 AAD	20AA ATLS	$\tan\beta = 20$ GeV
>1677	95	2 AAD	20AA ATLS	$\tan\beta = 30$ GeV
>1826	95	2 AAD	20AA ATLS	$\tan\beta = 40$ GeV
>1937	95	2 AAD	20AA ATLS	$\tan\beta = 50$ GeV
>2033	95	2 AAD	20AA ATLS	$\tan\beta = 60$ GeV
> 377	95	10 AABOUD	18G ATLS	$\tan\beta = 10$ GeV
> 863	95	10 AABOUD	18G ATLS	$\tan\beta = 20$ GeV
>1157	95	10 AABOUD	18G ATLS	$\tan\beta = 30$ GeV
>1328	95	10 AABOUD	18G ATLS	$\tan\beta = 40$ GeV
>1483	95	10 AABOUD	18G ATLS	$\tan\beta = 50$ GeV
>1613	95	10 AABOUD	18G ATLS	$\tan\beta = 60$ GeV
> 389	95	13 SIRUNYAN	18CX CMS	$\tan\beta = 10$ GeV
> 832	95	13 SIRUNYAN	18CX CMS	$\tan\beta = 20$ GeV
>1148	95	13 SIRUNYAN	18CX CMS	$\tan\beta = 30$ GeV
>1341	95	13 SIRUNYAN	18CX CMS	$\tan\beta = 40$ GeV
>1496	95	13 SIRUNYAN	18CX CMS	$\tan\beta = 50$ GeV
>1613	95	13 SIRUNYAN	18CX CMS	$\tan\beta = 60$ GeV
		14 AABOUD	16AA ATLS	$A^0 \rightarrow \tau^+\tau^-$
		15 KHACHATRYAN...16A	CMS	$H_{1,2}^0/A^0 \rightarrow \mu^+\mu^-$
		16 KHACHATRYAN...16P	CMS	$H_2^0 \rightarrow H^0 H^0, A^0 \rightarrow Z H^0$
		17 KHACHATRYAN...15AY	CMS	$pp \rightarrow H_{1,2}^0/A^0 + b + X,$ $H_{1,2}^0/A^0 \rightarrow b\bar{b}$
		18 AAD	14AW ATLS	$pp \rightarrow H_{1,2}^0/A^0 + X,$ $H_{1,2}^0/A^0 \rightarrow \tau\tau$
		19 KHACHATRYAN...14M	CMS	$pp \rightarrow H_{1,2}^0/A^0 + X,$ $H_{1,2}^0/A^0 \rightarrow \tau\tau$
		20 AAD	13o ATLS	$pp \rightarrow H_{1,2}^0/A^0 + X,$ $H_{1,2}^0/A^0 \rightarrow \tau^+\tau^-,$ $\mu^+\mu^-$
		21 AAIJ	13T LHCb	$pp \rightarrow H_{1,2}^0/A^0 + X,$ $H_{1,2}^0/A^0 \rightarrow \tau^+\tau^-$
		22 CHATRCHYAN13AG	CMS	$pp \rightarrow H_{1,2}^0/A^0 + b + X,$ $H_{1,2}^0/A^0 \rightarrow b\bar{b}$
		23 AALTONEN	12AQ TEVA	$p\bar{p} \rightarrow H_{1,2}^0/A^0 + b + X,$ $H_{1,2}^0/A^0 \rightarrow b\bar{b}$
		24 AALTONEN	12X CDF	$p\bar{p} \rightarrow H_{1,2}^0/A^0 + b + X,$ $H_{1,2}^0/A^0 \rightarrow b\bar{b}$
		25 ABAZOV	12G D0	$p\bar{p} \rightarrow H_{1,2}^0/A^0 + X,$ $H_{1,2}^0/A^0 \rightarrow \tau^+\tau^-$
		26 CHATRCHYAN12K	CMS	$pp \rightarrow H_{1,2}^0/A^0 + X,$ $H_{1,2}^0/A^0 \rightarrow \tau^+\tau^-$
		27 ABAZOV	11K D0	$p\bar{p} \rightarrow H_{1,2}^0/A^0 + b + X,$ $H_{1,2}^0/A^0 \rightarrow b\bar{b}$
		28 ABAZOV	11W D0	$p\bar{p} \rightarrow H_{1,2}^0/A^0 + b + X,$ $H_{1,2}^0/A^0 \rightarrow \tau^+\tau^-$

• • • We do not use the following data for averages, fits, limits, etc. • • •

		29 AALTONEN	09AR CDF	$p\bar{p} \rightarrow H_{1,2}^0/A^0 + X,$ $H_{1,2}^0/A^0 \rightarrow \tau^+\tau^-$
> 90.4		30 ABDALLAH	08B DLPH	$E_{cm} \leq 209$ GeV
> 93.4	95	31 SCHAELE	06B LEP	$E_{cm} \leq 209$ GeV
		32 ACOSTA	05Q CDF	$p\bar{p} \rightarrow H_{1,2}^0/A^0 + X$
> 85.0	95	33,34 ABBIENDI	04M OPAL	$E_{cm} \leq 209$ GeV
		35 ABBIENDI	03G OPAL	$H_1^0 \rightarrow A^0 A^0$
> 86.5	95	33,36 ACHARD	02H L3	$E_{cm} \leq 209$ GeV, $\tan\beta > 0.4$
		37 AKEROYD	02 RVUE	
> 90.1	95	33,38 HEISTER	02 ALEP	$E_{cm} \leq 209$ GeV, $\tan\beta > 0.5$
		1 TUMASYAN	23s	search for production of $H_2^0/A^0 \rightarrow \tau^+\tau^-$ by gluon fusion and b -associated production using 138 fb^{-1} of pp collisions at $E_{cm} = 13$ TeV. See their Fig. 13 for excluded regions in the m_{A^0} - $\tan\beta$ plane in M_h^{125} and M_{hEFT}^{125} MSSM scenarios. In both scenarios $m_{A^0} < 350$ GeV is excluded at 95% CL.
		2 AAD	20AA	search for $H_2^0/A^0 \rightarrow \tau^+\tau^-$ produced by gluon fusion or b -associated production using 139 fb^{-1} of pp collisions at $E_{cm} = 13$ TeV. See their Fig. 2(c) for excluded region in the M_h^{125} scenario of MSSM. Values of $\tan\beta > 8$ (21) are excluded for $m_{A^0} = 1.0$ (1.5) TeV at 95% CL.
		3 AAD	20	combine measurements on H^0 production and decay using data taken in years 2015–2017 (up to 79.8 fb^{-1}) of pp collisions at $E_{cm} = 13$ TeV. See their Fig. 19 for excluded region in the hMSSM parameter space.
		4 AAD	20c	combine searches for a scalar resonance decaying to $H^0 H^0$ in 36.1 fb^{-1} of pp collisions at $E_{cm} = 13$ TeV from AABOUD 19A, AABOUD 19o, AABOUD 18cQ, AABOUD 19T, AABOUD 18cW, and AABOUD 18BU. See their Fig. 7(b) for the excluded region in the hMSSM parameter space.
		5 AAD	20L	search for b -associated production of H_2^0 decaying to $b\bar{b}$ in 27.8 fb^{-1} of pp collisions at $E_{cm} = 13$ TeV. See their Fig. 9 for excluded regions in hMSSM, $m_h^{\text{mod}+}$ and $m_h^{\text{mod}-}$ scenarios of MSSM.
		6 SIRUNYAN	20AC	search for gluon-fusion and b -associated production of A^0 decaying to $Z H^0$ in 35.9 fb^{-1} of pp collisions at $E_{cm} = 13$ TeV. See their Fig. 6 for excluded regions in the M_h^{125} and hMSSM scenarios of the MSSM.
		7 SIRUNYAN	20AF	search for $H_2^0/A^0 \rightarrow t\bar{t}$ with one or two charged leptons in the final state using kinematic variables in 35.9 fb^{-1} of pp collisions at $E_{cm} = 13$ TeV. See their Fig. 8 for excluded region in the hMSSM scenario of MSSM. Values of $\tan\beta$ below 1.0–1.5 are excluded for $m_{A^0} = 0.4$ –0.75 TeV at 95% CL.
		8 SIRUNYAN	20V	search for gluon-fusion and vector-boson-fusion production of H_2^0 decaying to $W^+ W^-$ in the final states $\ell\nu\ell\nu$ and $\ell\nu q\bar{q}$ in 35.9 fb^{-1} of pp collisions at $E_{cm} = 13$ TeV. See their Figs. 8 and 9 for excluded regions in various MSSM scenarios.
		9 SIRUNYAN	19CR	search for production of H_2^0/A^0 in gluon fusion and in association with a $b\bar{b}$ pair, decaying to $\mu^+\mu^-$ in 35.9 fb^{-1} of pp collisions at $E_{cm} = 13$ TeV. See their Fig. 5 for the excluded region in the MSSM parameter space in the $m_h^{\text{mod}+}$ and hMSSM scenarios.
		10 AABOUD	18G	search for production of $H_2^0/A^0 \rightarrow \tau^+\tau^-$ by gluon fusion and b -associated production in 36.1 fb^{-1} of pp collisions at $E_{cm} = 13$ TeV. See their Fig. 10 for excluded regions in the m_{A^0} - $\tan\beta$ plane in several MSSM scenarios.
		11 SIRUNYAN	18A	search for production of a scalar resonance decaying to $H^0 H^0 \rightarrow b\bar{b}\tau^+\tau^-$ in 35.9 fb^{-1} of pp collisions at $E_{cm} = 13$ TeV. See their Fig. 5 (lower) for excluded regions in the m_{A^0} - $\tan\beta$ plane in the hMSSM scenario.
		12 SIRUNYAN	18BP	search for production of $H_2^0/A^0 \rightarrow b\bar{b}$ by b -associated production in 35.7 fb^{-1} of pp collisions at $E_{cm} = 13$ TeV. See their Fig. 6 for the limits on cross section times branching ratio for $m_{H_2^0}, m_{A^0} = 0.3$ –1.3 TeV, and Fig. 7 for excluded regions in the m_{A^0} - $\tan(\beta)$ plane in several MSSM scenarios.
		13 SIRUNYAN	18CX	search for production of $H_{1,2}^0/A^0 \rightarrow \tau^+\tau^-$ by gluon fusion and b -associated production in 35.9 fb^{-1} of pp collisions at $E_{cm} = 13$ TeV. See their Fig. 9 for excluded regions in the m_{A^0} - $\tan(\beta)$ plane in several MSSM scenarios.
		14 AABOUD	16AA	search for production of a Higgs boson in gluon fusion and in association with a $b\bar{b}$ pair followed by the decay $A^0 \rightarrow \tau^+\tau^-$ in 3.2 fb^{-1} of pp collisions at $E_{cm} = 13$ TeV. See their Fig. 5(a, b) for limits on cross section times branching ratio for $m_{A^0} = 200$ –1200 GeV, and Fig. 5(c, d) for the excluded region in the MSSM parameter space in the $m_h^{\text{mod}+}$ and hMSSM scenarios.
		15 KHACHATRYAN	16A	search for production of a Higgs boson in gluon fusion and in association with a $b\bar{b}$ pair followed by the decay $H_{1,2}^0/A^0 \rightarrow \mu^+\mu^-$ in 5.1 fb^{-1} of pp collisions at $E_{cm} = 7$ TeV and 19.3 fb^{-1} at $E_{cm} = 8$ TeV. See their Fig. 7 for the excluded region in the MSSM parameter space in the $m_h^{\text{mod}+}$ benchmark scenario and Fig. 9 for limits on cross section times branching ratio.
		16 KHACHATRYAN	16P	search for gluon fusion production of an H_2^0 decaying to $H^0 H^0 \rightarrow b\bar{b}\tau^+\tau^-$ and an A^0 decaying to $Z H^0 \rightarrow \ell^+\ell^-\tau^+\tau^-$ in 19.7 fb^{-1} of pp collisions at $E_{cm} = 8$ TeV. See their Fig. 12 for excluded region in the $\tan\beta$ - $\cos(\beta-\alpha)$ plane for $m_{H_2^0}^0 = m_{A^0}$.
		17 KHACHATRYAN	15AY	search for production of a Higgs boson in association with a b quark in the decay $H_{1,2}^0/A^0 \rightarrow b\bar{b}$ in 19.7 fb^{-1} of pp collisions at $E_{cm} = 8$ TeV and combine with CHATRCHYAN 13AG 7 TeV data. See their Fig. 6 for the limits on cross section times branching ratio for $m_{A^0} = 100$ –900 GeV and Figs. 7–9 for the excluded region in the MSSM parameter space in various benchmark scenarios.
		18 AAD	14AW	search for production of a Higgs boson followed by the decay $H_{1,2}^0/A^0 \rightarrow \tau^+\tau^-$ in 19.5 – 20.3 fb^{-1} of pp collisions at $E_{cm} = 8$ TeV. See their Fig. 11 for the limits on cross section times branching ratio and their Figs. 9 and 10 for the excluded region in the MSSM parameter space. For $m_{A^0} = 140$ GeV, the region $\tan\beta > 5.4$ is excluded at 95% CL in the m_h^{max} scenario.

Gauge & Higgs Boson Particle Listings

Neutral Higgs Bosons, Searches for

- 19 KHACHATRYAN 14M search for production of a Higgs boson in gluon fusion and in association with a b quark followed by the decay $H_{1,2}^0/A^0 \rightarrow \tau^+\tau^-$ in 4.9 fb^{-1} of pp collisions at $E_{\text{cm}} = 7 \text{ TeV}$ and 19.7 fb^{-1} at $E_{\text{cm}} = 8 \text{ TeV}$. See their Figs. 7 and 8 for one- and two-dimensional limits on cross section times branching ratio and their Figs. 5 and 6 for the excluded region in the MSSM parameter space. For $m_{A^0} = 140 \text{ GeV}$, the region $\tan\beta > 3.8$ is excluded at 95% CL in the m_h^{max} scenario.
- 20 AAD 13o search for production of a Higgs boson in the decay $H_{1,2}^0/A^0 \rightarrow \tau^+\tau^-$ and $\mu^+\mu^-$ with $4.7\text{--}4.8 \text{ fb}^{-1}$ of pp collisions at $E_{\text{cm}} = 7 \text{ TeV}$. See their Fig. 6 for the excluded region in the MSSM parameter space and their Fig. 7 for the limits on cross section times branching ratio. For $m_{A^0} = 110\text{--}170 \text{ GeV}$, $\tan\beta \gtrsim 10$ is excluded, and for $\tan\beta = 50$, m_{A^0} below 470 GeV is excluded at 95% CL in the m_h^{max} scenario.
- 21 AAIJ 13T search for production of a Higgs boson in the forward region in the decay $H_{1,2}^0/A^0 \rightarrow \tau^+\tau^-$ in 1.0 fb^{-1} of pp collisions at $E_{\text{cm}} = 7 \text{ TeV}$. See their Fig. 2 for the limits on cross section times branching ratio and the excluded region in the MSSM parameter space.
- 22 CHATRCHYAN 13AG search for production of a Higgs boson in association with a b quark in the decay $H_{1,2}^0/A^0 \rightarrow b\bar{b}$ in $2.7\text{--}4.8 \text{ fb}^{-1}$ of pp collisions at $E_{\text{cm}} = 7 \text{ TeV}$. See their Fig. 6 for the excluded region in the MSSM parameter space and Fig. 5 for the limits on cross section times branching ratio. For $m_{A^0} = 90\text{--}350 \text{ GeV}$, upper bounds on $\tan\beta$ of $18\text{--}42$ at 95% CL are obtained in the m_h^{max} scenario with $\mu = +200 \text{ GeV}$.
- 23 AALTONEN 12AQ combine AALTONEN 12X and ABAZOV 11K. See their Table I and Fig. 1 for the limit on cross section times branching ratio and Fig. 2 for the excluded region in the MSSM parameter space.
- 24 AALTONEN 12X search for associated production of a Higgs boson and a b quark in the decay $H_{1,2}^0/A^0 \rightarrow b\bar{b}$, with 2.6 fb^{-1} of $p\bar{p}$ collisions at $E_{\text{cm}} = 1.96 \text{ TeV}$. See their Table III and Fig. 15 for the limit on cross section times branching ratio and Figs. 17, 18 for the excluded region in the MSSM parameter space.
- 25 ABAZOV 12G search for production of a Higgs boson in the decay $H_{1,2}^0/A^0 \rightarrow \tau^+\tau^-$ with 7.3 fb^{-1} of $p\bar{p}$ collisions at $E_{\text{cm}} = 1.96 \text{ TeV}$ and combine with ABAZOV 11W and ABAZOV 11K. See their Figs. 4, 5, and 6 for the excluded region in the MSSM parameter space. For $m_{A^0} = 90\text{--}180 \text{ GeV}$, $\tan\beta \gtrsim 30$ is excluded at 95% CL in the m_h^{max} scenario.
- 26 CHATRCHYAN 12K search for production of a Higgs boson in the decay $H_{1,2}^0/A^0 \rightarrow \tau^+\tau^-$ with 4.6 fb^{-1} of pp collisions at $E_{\text{cm}} = 7 \text{ TeV}$. See their Fig. 3 and Table 4 for the excluded region in the MSSM parameter space. For $m_{A^0} = 160 \text{ GeV}$, the region $\tan\beta > 7.1$ is excluded at 95% CL in the m_h^{max} scenario. Supersedes by KHACHATRYAN 14M.
- 27 ABAZOV 11K search for associated production of a Higgs boson and a b quark, followed by the decay $H_{1,2}^0/A^0 \rightarrow b\bar{b}$, in 5.2 fb^{-1} of $p\bar{p}$ collisions at $E_{\text{cm}} = 1.96 \text{ TeV}$. See their Fig. 5/ Table 2 for the limit on cross section times branching ratio and Fig. 6 for the excluded region in the MSSM parameter space for $\mu = -200 \text{ GeV}$.
- 28 ABAZOV 11W search for associated production of a Higgs boson and a b quark, followed by the decay $H_{1,2}^0/A^0 \rightarrow \tau\tau$, in 7.3 fb^{-1} of $p\bar{p}$ collisions at $E_{\text{cm}} = 1.96 \text{ TeV}$. See their Fig. 2 for the limit on cross section times branching ratio and for the excluded region in the MSSM parameter space.
- 29 AALTONEN 09AR search for Higgs bosons decaying to $\tau^+\tau^-$ in two doublet models in 1.8 fb^{-1} of $p\bar{p}$ collisions at $E_{\text{cm}} = 1.96 \text{ TeV}$. See their Fig. 2 for the limit on $\sigma \cdot \text{BR}(H_{1,2}^0/A^0 \rightarrow \tau^+\tau^-)$ for different Higgs masses, and see their Fig. 3 for the excluded region in the MSSM parameter space.
- 30 ABDALLAH 08B give limits in eight CP -conserving benchmark scenarios and some CP -violating scenarios. See paper for excluded regions for each scenario. Supersedes ABDALLAH 04.
- 31 SCHAEEL 06B make a combined analysis of the LEP data. The quoted limit is for the m_h^{max} scenario with $m_t = 174.3 \text{ GeV}$. In the CP -violating CPX scenario no lower bound on $m_{H_1^0}$ can be set at 95% CL. See paper for excluded regions in various scenarios. See Figs. 2-6 and Tabs. 14-21 for limits on $\sigma(ZH^0) \cdot \text{BR}(H^0 \rightarrow b\bar{b}, \tau^+\tau^-)$ and $\sigma(H_1^0 H_2^0) \cdot \text{BR}(H_1^0 H_2^0 \rightarrow b\bar{b}, \tau^+\tau^-)$.
- 32 ACOSTA 05q search for $H_{1,2}^0/A^0$ production in $p\bar{p}$ collisions at $E_{\text{cm}} = 1.8 \text{ TeV}$ with $H_{1,2}^0/A^0 \rightarrow \tau^+\tau^-$. At $m_{A^0} = 100 \text{ GeV}$, the obtained cross section upper limit is above theoretical expectation.
- 33 Search for $e^+e^- \rightarrow H_1^0 A^0$ in the final states $b\bar{b}b\bar{b}$ and $b\bar{b}\tau^+\tau^-$, and $e^+e^- \rightarrow H_1^0 Z$. Universal scalar mass of 1 TeV , $SU(2)$ gaugino mass of 200 GeV , and $\mu = -200 \text{ GeV}$ are assumed, and two-loop radiative corrections incorporated. The limits hold for $m_t = 175 \text{ GeV}$, and for the m_h^{max} scenario.
- 34 ABBIENDI 04M exclude $0.7 < \tan\beta < 1.9$, assuming $m_t = 174.3 \text{ GeV}$. Limits for other MSSM benchmark scenarios, as well as for CP violating cases, are also given.
- 35 ABBIENDI 03G search for $e^+e^- \rightarrow H_1^0 Z$ followed by $H_1^0 \rightarrow A^0 A^0$, $A^0 \rightarrow c\bar{c}, gg$, or $\tau^+\tau^-$. In the no-mixing scenario, the region $m_{H_1^0} = 45\text{--}85 \text{ GeV}$ and $m_{A^0} = 2\text{--}9.5 \text{ GeV}$ is excluded at 95% CL.
- 36 ACHARD 02H also search for the final state $H_1^0 Z \rightarrow 2A^0 q\bar{q}, A^0 \rightarrow q\bar{q}$. In addition, the MSSM parameter set in the "large- μ " and "no-mixing" scenarios are examined.
- 37 AKEROYD 02 examine the possibility of a light A^0 with $\tan\beta < 1$. Electroweak measurements are found to be inconsistent with such a scenario.
- 38 HEISTER 02 excludes the range $0.7 < \tan\beta < 2.3$. A wider range is excluded with different stop mixing assumptions. Updates BARATE 01C.

Mass Limits for H_1^0 (Higgs Boson) in Supersymmetric Models

VALUE (GeV)	CL%	DOCUMENT ID	TECN	COMMENT
>89.7		1 ABDALLAH	08B DLPH	$E_{\text{cm}} \leq 209 \text{ GeV}$
>92.8	95	2 SCHAEEL	06B LEP	$E_{\text{cm}} \leq 209 \text{ GeV}$
>84.5	95	3,4 ABBIENDI	04M OPAL	$E_{\text{cm}} \leq 209 \text{ GeV}$

- >86.0 95 3,5 ACHARD 02H L3 $E_{\text{cm}} \leq 209 \text{ GeV}, \tan\beta > 0.4$
 >89.8 95 3,6 HEISTER 02 ALEP $E_{\text{cm}} \leq 209 \text{ GeV}, \tan\beta > 0.5$

• • • We do not use the following data for averages, fits, limits, etc. • • •

$$7 \text{ AALTONEN } 12\text{AQ TEVA } p\bar{p} \rightarrow H_{1,2}^0/A^0 + b + X, \\ H_{1,2}^0/A^0 \rightarrow b\bar{b}$$

- 1 ABDALLAH 08B give limits in eight CP -conserving benchmark scenarios and some CP -violating scenarios. See paper for excluded regions for each scenario. Supersedes ABDALLAH 04.
- 2 SCHAEEL 06B make a combined analysis of the LEP data. The quoted limit is for the m_h^{max} scenario with $m_t = 174.3 \text{ GeV}$. In the CP -violating CPX scenario no lower bound on $m_{H_1^0}$ can be set at 95% CL. See paper for excluded regions in various scenarios. See Figs. 2-6 and Tabs. 14-21 for limits on $\sigma(ZH^0) \cdot \text{BR}(H^0 \rightarrow b\bar{b}, \tau^+\tau^-)$ and $\sigma(H_1^0 H_2^0) \cdot \text{BR}(H_1^0 H_2^0 \rightarrow b\bar{b}, \tau^+\tau^-)$.
- 3 Search for $e^+e^- \rightarrow H_1^0 A^0$ in the final states $b\bar{b}b\bar{b}$ and $b\bar{b}\tau^+\tau^-$, and $e^+e^- \rightarrow H_1^0 Z$. Universal scalar mass of 1 TeV , $SU(2)$ gaugino mass of 200 GeV , and $\mu = -200 \text{ GeV}$ are assumed, and two-loop radiative corrections incorporated. The limits hold for $m_t = 175 \text{ GeV}$, and for the m_h^{max} scenario.
- 4 ABBIENDI 04M exclude $0.7 < \tan\beta < 1.9$, assuming $m_t = 174.3 \text{ GeV}$. Limits for other MSSM benchmark scenarios, as well as for CP violating cases, are also given.
- 5 ACHARD 02H also search for the final state $H_1^0 Z \rightarrow 2A^0 q\bar{q}, A^0 \rightarrow q\bar{q}$. In addition, the MSSM parameter set in the "large- μ " and "no-mixing" scenarios are examined.
- 6 HEISTER 02 excludes the range $0.7 < \tan\beta < 2.3$. A wider range is excluded with different stop mixing assumptions. Updates BARATE 01C.
- 7 AALTONEN 12AQ combine AALTONEN 12X and ABAZOV 11K. See their Table I and Fig. 1 for the limit on cross section times branching ratio and Fig. 2 for the excluded region in the MSSM parameter space.

MASS LIMITS FOR NEUTRAL HIGGS BOSONS IN EXTENDED HIGGS MODELS

This Section covers models which do not fit into either the Standard Model or its simplest minimal Supersymmetric extension (MSSM), leading to anomalous production rates, or nonstandard final states and branching ratios. In particular, this Section covers limits which may apply to generic two-Higgs-doublet models (2HDM), or to special regions of the MSSM parameter space where decays to invisible particles or to photon pairs are dominant (see the review on "Status of Higgs Boson Physics"). Concerning the mass limits for H^0 and A^0 listed below, see the footnotes or the comment lines for details on the nature of the models to which the limits apply.

The observed signal at about 125 GeV , see section "H", can be interpreted as one of the neutral Higgs bosons of an extended Higgs sector.

Mass Limits in General two-Higgs-doublet Models

VALUE (GeV)	CL%	DOCUMENT ID	TECN	COMMENT
• • • We do not use the following data for averages, fits, limits, etc. • • •				
1	AAD	23AD ATLAS	$A^0 \rightarrow ZH_2^0, H_2^0 \rightarrow HH$	
2	AAD	23BG ATLAS	$t\bar{t}H_2^0/A^0$	
3	AAD	23O ATLAS	$A^0 \rightarrow ZH$	
4	AAD	21AF ATLAS	$H_2^0 \rightarrow ZZ$	
5	AAD	21AI ATLAS	$A^0 \rightarrow ZH_2^0$	
6	AAD	20 ATLAS	H^0 properties	
7	AAD	20L ATLAS	$H_2^0 \rightarrow b\bar{b}$	
8	SIRUNYAN	20AA CMS	$H_2^0 \rightarrow ZA^0$ or $A^0 \rightarrow ZH_2^0$	
9	SIRUNYAN	20Y CMS	$H_2^0 \rightarrow W^+W^-$	
10	SIRUNYAN	19AE CMS	$A^0 \rightarrow \tau^+\tau^-$	
11	SIRUNYAN	19AV CMS	$A^0 \rightarrow ZH^0$	
12	AABOUD	18AH ATLAS	$A^0 \rightarrow ZH_2^0$	
13	AABOUD	18AI ATLAS	$A^0 \rightarrow ZH^0$	
14	AABOUD	18BF ATLAS	$H_2^0 \rightarrow ZZ$	
15	AABOUD	18CE ATLAS	$p\bar{p} \rightarrow H_2^0/A^0 t\bar{t}, H_2^0/A^0 \rightarrow t\bar{t}$	
16	HALLER	18 RVUE	global fits	
17	SIRUNYAN	18BP CMS	$p\bar{p} \rightarrow H_2^0/A^0 + b + X, H_2^0/A^0 \rightarrow b\bar{b}$	
18	SIRUNYAN	18ED CMS	$A^0 \rightarrow ZH^0$	
19	AABOUD	17AN ATLAS	$H_2^0, A^0 \rightarrow t\bar{t}$	
20	SIRUNYAN	17AX CMS	$A^0 b\bar{b}, A^0 \rightarrow \mu^+\mu^-$	
21	AAD	16AX ATLAS	$H_2^0 \rightarrow ZZ$	
22	KHACHATRYAN..16P	CMS	$H_2^0 \rightarrow H^0 H^0, A^0 \rightarrow ZH^0$	
23	KHACHATRYAN..16W	CMS	$A^0 b\bar{b}, A^0 \rightarrow \tau^+\tau^-$	
24	KHACHATRYAN..16Z	CMS	$H_2^0 \rightarrow ZA^0$ or $A^0 \rightarrow ZH_2^0$	
25	AAD	15BK ATLAS	$H_2^0 \rightarrow H^0 H^0$	
26	AAD	15S ATLAS	$A^0 \rightarrow ZH^0$	
27	KHACHATRYAN..15BB	CMS	$H_2^0, A^0 \rightarrow \gamma\gamma$	
28	KHACHATRYAN..15N	CMS	$A^0 \rightarrow ZH^0$	
29	AAD	14M ATLAS	$H_2^0 \rightarrow H^\pm W^\mp \rightarrow H^0 W^\pm W^\mp, H^0 \rightarrow b\bar{b}$	
30	KHACHATRYAN..14Q	CMS	$H_2^0 \rightarrow H^0 H^0, A^0 \rightarrow ZH^0$	

Gauge & Higgs Boson Particle Listings

Neutral Higgs Bosons, Searches for

Search ID	Author	Year	Experiment	Search Description
31	AALTONEN	09AR	CDF	$p\bar{p} \rightarrow H_{1,2}^0/A^0 + X$, $H_{1,2}^0/A^0 \rightarrow \tau^+\tau^-$
none 1-55	95	32	ABBIENDI	05A OPAL H_1^0 , Type II model
>110.6	95	33	ABDALLAH	05D DLPH $H^0 \rightarrow 2$ jets
		34	ABDALLAH	04o DLPH $Z \rightarrow t\bar{t}H$
		35	ABDALLAH	04o DLPH $e^+e^- \rightarrow H^0 Z, H^0 A^0$
		36	ABBIENDI	02D OPAL $e^+e^- \rightarrow b\bar{b}H$
none 1-44	95	37	ABBIENDI	01E OPAL H_1^0 , Type-II model
> 68.0	95	38	ABBIENDI	99E OPAL $\tan\beta > 1$
		39	ABREU	95H DLPH $Z \rightarrow H^0 Z^*, H^0 A^0$
		40	PICH	92 RVUE Very light Higgs

1 AAD 23AD search for associated production of W/ZH_2^0 and gluon fusion production of A^0 decaying to ZH_2^0 , with the decay chain $H_2^0 \rightarrow HH \rightarrow b\bar{b}b\bar{b}$, using 139 fb⁻¹ of pp collisions at $E_{cm} = 13$ TeV. See their Figs. 12 and 13 for excluded regions in Type-I and lepton-specific 2HDMs.

2 AAD 23B search for production of H_2^0/A^0 in association with a $t\bar{t}$ pair, decaying to $t\bar{t}$, using 139 fb⁻¹ of pp collisions at $E_{cm} = 13$ TeV. See their Fig. 8 for excluded regions in the parameter space of the type II 2HDM.

3 AAD 23O search for production of an A^0 in gluon-gluon fusion and in association with a $b\bar{b}$, decaying to ZH in the final states $\nu\bar{\nu}b\bar{b}$ and $\ell^+\ell^-b\bar{b}$ using 139 fb⁻¹ of pp collisions at $E_{cm} = 13$ TeV. See their Figs. 12 and 13 for excluded regions in the parameter space in various 2HDMs.

4 AAD 21AF search for production of a heavy H_2^0 state decaying to ZZ in the final states $\ell^+\ell^-\ell^+\ell^-$ and $\ell^+\ell^-\nu\bar{\nu}$ in 139 fb⁻¹ of pp collisions at $E_{cm} = 13$ TeV. See their Figs. 6 and 7 for excluded parameter regions of the 2HDM Type I and II.

5 AAD 21AI search for production of an A^0 in gluon-gluon fusion and in association with a $b\bar{b}$, decaying to $ZH_2^0 \rightarrow \ell^+\ell^-b\bar{b}$ or $\ell^+\ell^-W^+W^-$ in 139 fb⁻¹ of pp collisions at $E_{cm} = 13$ TeV. See their Figs. 10 and 14 for excluded regions in the parameter space of various 2HDMs.

6 AAD 20 combine measurements on H^0 production and decay using data taken in years 2015-2017 (up to 79.8 fb⁻¹) of pp collisions at $E_{cm} = 13$ TeV. See their Fig. 18 for excluded regions in various 2HDMs.

7 AAD 20L search for b -associated production of H_2^0 decaying to $b\bar{b}$ in 27.8 fb⁻¹ of pp collisions at $E_{cm} = 13$ TeV. See their Figs. 10 and 11 for excluded regions in the flipped two Higgs doublet model.

8 SIRUNYAN 20AA search for $H_2^0 \rightarrow ZA^0, A^0 \rightarrow b\bar{b}$ or $A^0 \rightarrow ZH_2^0, H_2^0 \rightarrow b\bar{b}$ in 35.9 fb⁻¹ of pp collisions at $E_{cm} = 13$ TeV. See their Figs. 8 and 9 for excluded regions in the parameter space of Type-II two Higgs doublet model.

9 SIRUNYAN 20Y search for gluon-fusion and vector-boson-fusion production of H_2^0 decaying to W^+W^- in the final states $\ell\nu\ell\nu$ and $\ell\nu q\bar{q}$ in 35.9 fb⁻¹ of pp collisions at $E_{cm} = 13$ TeV. See their Fig. 7 for excluded regions in Type I and II two Higgs doublet models.

10 SIRUNYAN 19AE search for a pseudoscalar resonance produced in association with a $b\bar{b}$ pair, decaying to $\tau^+\tau^-$ in 35.9 fb⁻¹ of pp collisions at $E_{cm} = 13$ TeV. See their Fig. 4 for cross section limits for $m_{A^0} = 25-70$ GeV and comparison with some representative 2HDMs.

11 SIRUNYAN 19AV search for a scalar resonance produced by gluon fusion or b associated production, decaying to $ZH^0 \rightarrow \ell^+\ell^-b\bar{b}$ ($\ell = e, \mu$) or $\nu\bar{\nu}b\bar{b}$ in 35.9 fb⁻¹ of pp collisions at $E_{cm} = 13$ TeV. See their Figs. 6 and 7 for excluded regions in the parameter space of various 2HDMs.

12 AABOUD 18AH search for production of an A^0 in gluon-gluon fusion and in association with a $b\bar{b}$, decaying to $ZH_2^0 \rightarrow \ell^+\ell^-b\bar{b}$ in 36.1 fb⁻¹ of pp collisions at $E_{cm} = 13$ TeV. See their Fig. 6 for excluded regions in the parameter space of various 2HDMs.

13 AABOUD 18AI search for production of an A^0 in gluon-gluon fusion and in association with a $b\bar{b}$, decaying to ZH^0 in the final states $\nu\bar{\nu}b\bar{b}$ and $\ell^+\ell^-b\bar{b}$ in 36.1 fb⁻¹ of pp collisions at $E_{cm} = 13$ TeV. See their Figs. 7 and 8 for excluded regions in the parameter space in various 2HDMs.

14 AABOUD 18BF search for production of a heavy H_2^0 state decaying to ZZ in the final states $\ell^+\ell^-\ell^+\ell^-$ and $\ell^+\ell^-\nu\bar{\nu}$ in 36.1 fb⁻¹ of pp collisions at $E_{cm} = 13$ TeV. See their Figs. 8 and 9 for excluded parameter regions in 2HDM Type I and II.

15 AABOUD 18CE search for the process $pp \rightarrow H_2^0/A^0 t\bar{t}$ followed by the decay $H_2^0/A^0 \rightarrow t\bar{t}$ in 36.1 fb⁻¹ of pp collisions at $E_{cm} = 13$ TeV. See their Fig. 12 for limits on cross section times branching ratio, and for lower limits on $\tan\beta$ for $m_{H_2^0}, m_{A^0} = 0.4-1.0$ TeV in the 2HDM type II.

16 HALLER 18 perform global fits in the framework of two-Higgs-doublet models (type I, II, lepton specific, flipped). See their Fig. 8 for allowed parameter regions from fits to LHC H^0 measurements, Fig. 9 bottom and charm decays, Fig. 10 muon anomalous magnetic moment, Fig. 11 electroweak precision data, and Fig. 12 by combination of all data.

17 SIRUNYAN 18BP search for production of $H_2^0/A^0 \rightarrow b\bar{b}$ by b -associated production in 35.7 fb⁻¹ of pp collisions at $E_{cm} = 13$ TeV. See their Fig. 6 for the limits on cross section times branching ratio for $m_{H_2^0}, m_{A^0} = 0.3-1.3$ TeV, and Figs. 8 and 9 for excluded regions in the parameter space of type-II and flipped 2HDMs.

18 SIRUNYAN 18ED search for production of an A^0 in gluon-gluon fusion and in association with a $b\bar{b}$, decaying to ZH^0 in the final states $\nu\bar{\nu}b\bar{b}$ or $\ell^+\ell^-b\bar{b}$ in 35.9 fb⁻¹ of pp collisions at $E_{cm} = 13$ TeV. See their Fig. 9 for excluded regions in the parameter space in Type I and II 2HDMs.

19 AABOUD 17AN search for production of a heavy H_2^0 and/or A^0 decaying to $t\bar{t}$ in 20.3 fb⁻¹ of pp collisions at $E_{cm} = 8$ TeV. See their Fig. 3 and Table III for excluded parameter regions in Type II Two-Higgs-Doublet-Models.

20 SIRUNYAN 17AX search for $A^0 b\bar{b}$ production followed by the decay $A^0 \rightarrow \mu^+\mu^-$ in 19.7 fb⁻¹ of pp collisions at $E_{cm} = 8$ TeV. Limits are set in the range $m_{A^0} = 25-60$ GeV. See their Fig. 5 for upper limits on $\sigma(A^0 b\bar{b}) \cdot \mathcal{B}(A^0 \rightarrow \mu^+\mu^-)$.

21 AAD 16AX search for production of a heavy H^0 state decaying to ZZ in the final states $\ell^+\ell^-\ell^+\ell^-, \ell^+\ell^-\nu\bar{\nu}, \ell^+\ell^-q\bar{q}$, and $\nu\bar{\nu}q\bar{q}$ in 20.3 fb⁻¹ of pp collisions at $E_{cm} = 8$ TeV. See their Figs. 13 and 14 for excluded parameter regions in Type I and II models.

22	KHACHATRYAN	16P	search for gluon fusion production of an H_2^0 decaying to $H^0 H^0 \rightarrow b\bar{b}\tau^+\tau^-$ and an A^0 decaying to $ZH^0 \rightarrow \ell^+\ell^-\tau^+\tau^-$ in 19.7 fb ⁻¹ of pp collisions at $E_{cm} = 8$ TeV. See their Fig. 11 for limits on $\tan\beta$ for $m_{A^0} = 230-350$ GeV.
23	KHACHATRYAN	16W	search for $A^0 b\bar{b}$ production followed by the decay $A^0 \rightarrow \tau^+\tau^-$ in 19.7 fb ⁻¹ of pp collisions at $E_{cm} = 8$ TeV. See their Fig. 3 for upper limits on $\sigma(A^0 b\bar{b}) \cdot \mathcal{B}(A^0 \rightarrow \tau^+\tau^-)$.
24	KHACHATRYAN	16Z	search for $H_2^0 \rightarrow ZA^0$ followed by $A^0 \rightarrow b\bar{b}$ or $\tau^+\tau^-$, and $A^0 \rightarrow ZH_2^0$ followed by $H_2^0 \rightarrow b\bar{b}$ or $\tau^+\tau^-$, in 19.8 fb ⁻¹ of pp collisions at $E_{cm} = 8$ TeV. See their Fig. 4 for cross section limits and Fig. 5 for excluded region in the parameter space.
25	AAD	15BK	search for production of a heavy H_2^0 decaying to $H^0 H^0$ in the final state $b\bar{b}b\bar{b}$ in 19.5 fb ⁻¹ of pp collisions at $E_{cm} = 8$ TeV. See their Figs. 15-18 for excluded regions in the parameter space.
26	AAD	15S	search for production of A^0 decaying to $ZH^0 \rightarrow \ell^+\ell^-b\bar{b}, \nu\bar{\nu}b\bar{b}$ and $\ell^+\ell^-\tau^+\tau^-$ in 20.3 fb ⁻¹ of pp collisions at $E_{cm} = 8$ TeV. See their Figs. 4 and 5 for excluded regions in the parameter space.
27	KHACHATRYAN	15BB	search for $H_2^0, A^0 \rightarrow \gamma\gamma$ in 19.7 fb ⁻¹ of pp collisions at $E_{cm} = 8$ TeV. See their Fig. 10 for excluded regions in the two-Higgs-doublet model parameter space.
28	KHACHATRYAN	15N	search for production of A^0 decaying to $ZH^0 \rightarrow \ell^+\ell^-b\bar{b}$ in 19.7 fb ⁻¹ of pp collisions at $E_{cm} = 8$ TeV. See their Fig. 5 for excluded regions in the $\tan\beta - \cos(\beta - \alpha)$ plane for $m_{A^0} = 300$ GeV.
29	AAD	14M	search for the decay cascade $H_2^0 \rightarrow H^\pm W^\mp \rightarrow H^0 W^\pm W^\mp, H^0$ decaying to $b\bar{b}$ in 20.3 fb ⁻¹ of pp collisions at $E_{cm} = 8$ TeV. See their Table IV for limits in a two-Higgs-doublet model for $m_{H_2^0} = 325-1025$ GeV and $m_{H^\pm} = 225-825$ GeV.
30	KHACHATRYAN	14Q	search for $H_2^0 \rightarrow H^0 H^0$ and $A^0 \rightarrow ZH^0$ in 19.5 fb ⁻¹ of pp collisions at $E_{cm} = 8$ TeV. See their Figs. 4 and 5 for limits on cross section times branching ratio for $m_{H_2^0, A^0} = 260-360$ GeV and their Figs. 7-9 for limits in two-Higgs-doublet models.
31	AALTONEN	09AR	search for Higgs bosons decaying to $\tau^+\tau^-$ in two doublet models in 1.8 fb ⁻¹ of $p\bar{p}$ collisions at $E_{cm} = 1.96$ TeV. See their Fig. 2 for the limit on $\sigma \cdot \mathcal{B}(H_{1,2}^0/A^0 \rightarrow \tau^+\tau^-)$ for different Higgs masses, and see their Fig. 3 for the excluded region in the MSSM parameter space.
32	ABBIENDI	05A	search for $e^+e^- \rightarrow H_1^0/A^0$ in general Type-II two-doublet models, with decays $H_1^0/A^0 \rightarrow q\bar{q}, gg, \tau^+\tau^-,$ and $H_1^0/A^0 \rightarrow A^0 A^0$.
33	ABDALLAH	05D	search for $e^+e^- \rightarrow H^0 Z$ and $H^0 A^0$ with H^0, A^0 decaying to two jets of any flavor including gg . The limit is for SM $H^0 Z$ production cross section with $\mathcal{B}(H^0 \rightarrow jj) = 1$.
34	ABDALLAH	04o	search for $Z \rightarrow b\bar{b}H^0, b\bar{b}A^0, \tau^+\tau^-H^0$ and $\tau^+\tau^-A^0$ in the final states $4b, b\bar{b}\tau^+\tau^-$, and 4τ . See paper for limits on Yukawa couplings.
35	ABDALLAH	04o	search for $e^+e^- \rightarrow H^0 Z$ and $H^0 A^0$, with H^0, A^0 decaying to $b\bar{b}, \tau^+\tau^-$, or $H^0 \rightarrow A^0 A^0$ at $E_{cm} = 189-208$ GeV. See paper for limits on couplings.
36	ABBIENDI	02D	search for $Z \rightarrow b\bar{b}H_1^0$ and $b\bar{b}A^0$ with $H_1^0/A^0 \rightarrow \tau^+\tau^-$, in the range $4 < m_H < 12$ GeV. See their Fig. 8 for limits on the Yukawa coupling.
37	ABBIENDI	01E	search for neutral Higgs bosons in general Type-II two-doublet models, at $E_{cm} \leq 189$ GeV. In addition to usual final states, the decays $H_1^0, A^0 \rightarrow q\bar{q}, gg$ are searched for. See their Figs. 15,16 for excluded regions.
38	ABBIENDI	99E	search for $e^+e^- \rightarrow H^0 A^0$ and $H^0 Z$ at $E_{cm} = 183$ GeV. The limit is with $m_H = m_A$ in general two Higgs-doublet models. See their Fig. 18 for the exclusion limit in the $m_H - m_A$ plane. Updates the results of ACKERSTAFF 98s.
39			See Fig. 4 of ABREU 95H for the excluded region in the $m_{H^0} - m_{A^0}$ plane for general two-doublet models. For $\tan\beta > 1$, the region $m_{H^0} + m_{A^0} \lesssim 87$ GeV, $m_{H^0} < 47$ GeV is excluded at 95% CL.
40	PICH	92	analyse H^0 with $m_{H^0} < 2m_\mu$ in general two-doublet models. Excluded regions in the space of mass-mixing angles from LEP, beam dump, and π^\pm, η rare decays are shown in Figs. 3.4. The considered mass region is not totally excluded.

Mass Limits for H^0 with Vanishing Yukawa Couplings

These limits assume that H^0 couples to gauge bosons with the same strength as the Standard Model Higgs boson, but has no coupling to quarks and leptons (this is often referred to as "fermiophobic").

VALUE (GeV)	CL%	DOCUMENT ID	TECN	COMMENT
• • • We do not use the following data for averages, fits, limits, etc. • • •				
none 100-113	95	1 AALTONEN	13K CDF	$H^0 \rightarrow WW^*$
none 100-116	95	2 AALTONEN	13L CDF	$H^0 \rightarrow \gamma\gamma, WW^*, ZZ^*$
		3 AALTONEN	13M TEVA	$H^0 \rightarrow \gamma\gamma, WW^*, ZZ^*$
		4 ABAZOV	13G D0	$H^0 \rightarrow WW^*$
none 100-113	95	5 ABAZOV	13H D0	$H^0 \rightarrow \gamma\gamma$
		6 ABAZOV	13I D0	$H^0 \rightarrow WW^*$
		7 ABAZOV	13J D0	$H^0 \rightarrow WW^*, ZZ^*$
none 100-114	95	8 ABAZOV	13L D0	$H^0 \rightarrow \gamma\gamma, WW^*, ZZ^*$
none 110-147	95	9 CHATRCHYAN	13AL CMS	$H^0 \rightarrow \gamma\gamma$
none 110-118, 119.5-121	95	10 AAD	12N ATLS	$H^0 \rightarrow \gamma\gamma$
none 100-114	95	11 AALTONEN	12AN CDF	$H^0 \rightarrow \gamma\gamma$
none 110-194	95	12 CHATRCHYAN	12AO CMS	$H^0 \rightarrow \gamma\gamma, WW^*, ZZ^*$
none 70-106	95	13 AALTONEN	09AB CDF	$H^0 \rightarrow \gamma\gamma$
none 70-100	95	14 ABAZOV	08U D0	$H^0 \rightarrow \gamma\gamma$
>105.8	95	15 SCHAEF	07 ALEP	$e^+e^- \rightarrow H^0 Z, H^0 \rightarrow WW^*$
>104.1	95	16,17 ABDALLAH	04L DLPH	$e^+e^- \rightarrow H^0 Z, H^0 \rightarrow \gamma\gamma$
>107	95	18 ACHARD	03C L3	$H^0 \rightarrow WW^*, ZZ^*, \gamma\gamma$

Gauge & Higgs Boson Particle Listings

Neutral Higgs Bosons, Searches for

>105.5	95	16,19	ABBIENDI	02F	OPAL	$H^0 \rightarrow \gamma\gamma$
>105.4	95	20	ACHARD	02c	L3	$H^0 \rightarrow \gamma\gamma$
none 60–82	95	21	AFFOLDER	01H	CDF	$p\bar{p} \rightarrow H^0 W/Z, H^0 \rightarrow \gamma\gamma$
> 94.9	95	22	ACCIARRI	00s	L3	$e^+e^- \rightarrow H^0 Z, H^0 \rightarrow \gamma\gamma$
>100.7	95	23	BARATE	00L	ALEP	$e^+e^- \rightarrow H^0 Z, H^0 \rightarrow \gamma\gamma$
> 96.2	95	24	ABBIENDI	99o	OPAL	$e^+e^- \rightarrow H^0 Z, H^0 \rightarrow \gamma\gamma$
> 78.5	95	25	ABBOTT	99B	D0	$p\bar{p} \rightarrow H^0 W/Z, H^0 \rightarrow \gamma\gamma$
		26	ABREU	99P	DLPH	$e^+e^- \rightarrow H^0 \gamma$ and/or $H^0 \rightarrow \gamma\gamma$

- 1 AALTONEN 13K search for $H^0 \rightarrow WW^{(*)}$ in 9.7 fb^{-1} of $p\bar{p}$ collisions at $E_{\text{cm}} = 1.96 \text{ TeV}$. A limit on cross section times branching ratio which corresponds to (1.3–6.6) times the expected cross section is given in the range $m_{H^0} = 110\text{--}200 \text{ GeV}$ at 95% CL.
- 2 AALTONEN 13L combine all CDF searches with $9.45\text{--}10.0 \text{ fb}^{-1}$ of $p\bar{p}$ collisions at $E_{\text{cm}} = 1.96 \text{ TeV}$.
- 3 AALTONEN 13M combine all Tevatron data from the CDF and D0 Collaborations of $p\bar{p}$ collisions at $E_{\text{cm}} = 1.96 \text{ TeV}$.
- 4 ABAZOV 13G search for $H^0 \rightarrow WW^{(*)}$ in 9.7 fb^{-1} of $p\bar{p}$ collisions at $E_{\text{cm}} = 1.96 \text{ TeV}$. A limit on cross section times branching ratio which corresponds to (2–9) times the expected cross section is given for $m_{H^0} = 100\text{--}200 \text{ GeV}$ at 95% CL.
- 5 ABAZOV 13H search for $H^0 \rightarrow \gamma\gamma$ in 9.6 fb^{-1} of $p\bar{p}$ collisions at $E_{\text{cm}} = 1.96 \text{ TeV}$.
- 6 ABAZOV 13I search for H^0 production in the final state with one lepton and two or more jets plus missing E_T in 9.7 fb^{-1} of $p\bar{p}$ collisions at $E_{\text{cm}} = 1.96 \text{ TeV}$. The search is sensitive to WH^0, ZH^0 and vector-boson fusion Higgs production with $H^0 \rightarrow WW^{(*)}$. A limit on cross section times branching ratio which corresponds to (8–30) times the expected cross section is given in the range $m_{H^0} = 100\text{--}200 \text{ GeV}$ at 95% CL.
- 7 ABAZOV 13J search for H^0 production in the final states $e\mu, e\mu\mu, \mu\tau\tau$, and $e^\pm\mu^\pm$ in $8.6\text{--}9.7 \text{ fb}^{-1}$ of $p\bar{p}$ collisions at $E_{\text{cm}} = 1.96 \text{ TeV}$. The search is sensitive to WH^0, ZH^0 production with $H^0 \rightarrow WW^{(*)}, ZZ^{(*)}$, decaying to leptonic final states. A limit on cross section times branching ratio which corresponds to (2.4–13.0) times the expected cross section is given in the range $m_{H^0} = 100\text{--}200 \text{ GeV}$ at 95% CL.
- 8 ABAZOV 13L combine all D0 results with up to 9.7 fb^{-1} of $p\bar{p}$ collisions at $E_{\text{cm}} = 1.96 \text{ TeV}$.
- 9 CHATRCHYAN 13AL search for $H^0 \rightarrow \gamma\gamma$ in 5.1 fb^{-1} and 5.3 fb^{-1} of pp collisions at $E_{\text{cm}} = 7$ and 8 TeV .
- 10 AAD 12N search for $H^0 \rightarrow \gamma\gamma$ with 4.9 fb^{-1} of pp collisions at $E_{\text{cm}} = 7 \text{ TeV}$ in the mass range $m_{H^0} = 110\text{--}150 \text{ GeV}$.
- 11 AALTONEN 12AN search for $H^0 \rightarrow \gamma\gamma$ with 10 fb^{-1} of $p\bar{p}$ collisions at $E_{\text{cm}} = 1.96 \text{ TeV}$ in the mass range $m_{H^0} = 100\text{--}150 \text{ GeV}$.
- 12 CHATRCHYAN 12AO use data from CHATRCHYAN 12G, CHATRCHYAN 12E, CHATRCHYAN 12H, CHATRCHYAN 12I, CHATRCHYAN 12B, and CHATRCHYAN 12C.
- 13 AALTONEN 09AB search for $H^0 \rightarrow \gamma\gamma$ in 3.0 fb^{-1} of $p\bar{p}$ collisions at $E_{\text{cm}} = 1.96 \text{ TeV}$ in the mass range $m_{H^0} = 70\text{--}150 \text{ GeV}$. Associated $H^0 W, H^0 Z$ production and WW, ZZ fusion are considered.
- 14 ABAZOV 08U search for $H^0 \rightarrow \gamma\gamma$ in $p\bar{p}$ collisions at $E_{\text{cm}} = 1.96 \text{ TeV}$ in the mass range $m_{H^0} = 70\text{--}150 \text{ GeV}$. Associated $H^0 W, H^0 Z$ production and WW, ZZ fusion are considered. See their Tab. 1 for the limit on $\sigma \cdot B(H^0 \rightarrow \gamma\gamma)$, and see their Fig. 3 for the excluded region in the $m_{H^0} - B(H^0 \rightarrow \gamma\gamma)$ plane.
- 15 SCHAEEL 07 search for Higgs bosons in association with a fermion pair and decaying to WW^* . The limit is from this search and HEISTER 02L for a H^0 with SM production cross section.
- 16 Search for associated production of a $\gamma\gamma$ resonance with a Z boson, followed by $Z \rightarrow q\bar{q}, \ell^+\ell^-,$ or $\nu\bar{\nu}$, at $E_{\text{cm}} \leq 209 \text{ GeV}$. The limit is for a H^0 with SM production cross section.
- 17 Updates ABREU 01F.
- 18 ACHARD 03c search for $e^+e^- \rightarrow ZH^0$ followed by $H^0 \rightarrow WW^*$ or ZZ^* at $E_{\text{cm}} = 200\text{--}209 \text{ GeV}$ and combine with the ACHARD 02c result. The limit is for a H^0 with SM production cross section. For $B(H^0 \rightarrow WW^*) + B(H^0 \rightarrow ZZ^*) = 1, m_{H^0} > 108.1 \text{ GeV}$ is obtained. See Fig. 6 for the limits under different BR assumptions.
- 19 For $B(H^0 \rightarrow \gamma\gamma) = 1, m_{H^0} > 117 \text{ GeV}$ is obtained.
- 20 ACHARD 02c search for associated production of a $\gamma\gamma$ resonance with a Z boson, followed by $Z \rightarrow q\bar{q}, \ell^+\ell^-,$ or $\nu\bar{\nu}$, at $E_{\text{cm}} \leq 209 \text{ GeV}$. The limit is for a H^0 with SM production cross section. For $B(H^0 \rightarrow \gamma\gamma) = 1, m_{H^0} > 114 \text{ GeV}$ is obtained.
- 21 AFFOLDER 01H search for associated production of a $\gamma\gamma$ resonance and a W or Z (tagged by two jets, an isolated lepton, or missing E_T). The limit assumes Standard Model values for the production cross section and for the couplings of the H^0 to W and Z bosons. See their Fig. 11 for limits with $B(H^0 \rightarrow \gamma\gamma) < 1$.
- 22 ACCIARRI 00s search for associated production of a $\gamma\gamma$ resonance with a $q\bar{q}, \nu\bar{\nu}$, or $\ell^+\ell^-$ pair in e^+e^- collisions at $E_{\text{cm}} = 189 \text{ GeV}$. The limit is for a H^0 with SM production cross section. For $B(H^0 \rightarrow \gamma\gamma) = 1, m_{H^0} > 98 \text{ GeV}$ is obtained. See their Fig. 5 for limits on $B(H \rightarrow \gamma\gamma)\sigma(e^+e^- \rightarrow Hf\bar{f})/\sigma(e^+e^- \rightarrow Hf\bar{f})$ (SM).
- 23 BARATE 00L search for associated production of a $\gamma\gamma$ resonance with a $q\bar{q}, \nu\bar{\nu}$, or $\ell^+\ell^-$ pair in e^+e^- collisions at $E_{\text{cm}} = 88\text{--}202 \text{ GeV}$. The limit is for a H^0 with SM production cross section. For $B(H^0 \rightarrow \gamma\gamma) = 1, m_{H^0} > 109 \text{ GeV}$ is obtained. See their Fig. 3 for limits on $B(H \rightarrow \gamma\gamma)\sigma(e^+e^- \rightarrow Hf\bar{f})/\sigma(e^+e^- \rightarrow Hf\bar{f})$ (SM).
- 24 ABBIENDI 99o search for associated production of a $\gamma\gamma$ resonance with a $q\bar{q}, \nu\bar{\nu}$, or $\ell^+\ell^-$ pair in e^+e^- collisions at 189 GeV . The limit is for a H^0 with SM production cross section. See their Fig. 4 for limits on $\sigma(e^+e^- \rightarrow H^0 Z^0) \times B(H^0 \rightarrow \gamma\gamma) \times B(X^0 \rightarrow f\bar{f})$ for various masses. Updates the results of ACKERSTAFF 98v.
- 25 ABBOTT 99B search for associated production of a $\gamma\gamma$ resonance and a dijet pair. The limit assumes Standard Model values for the production cross section and for the couplings of the H^0 to W and Z bosons. Limits in the range of $\sigma(H^0 + Z/W) \cdot B(H^0 \rightarrow \gamma\gamma) = 0.80\text{--}0.34 \text{ pb}$ are obtained in the mass range $m_{H^0} = 65\text{--}150 \text{ GeV}$.
- 26 ABREU 99P search for $e^+e^- \rightarrow H^0 \gamma$ with $H^0 \rightarrow b\bar{b}$ or $\gamma\gamma$, and $e^+e^- \rightarrow H^0 q\bar{q}$ with $H^0 \rightarrow \gamma\gamma$. See their Fig. 4 for limits on $\sigma \times B$. Explicit limits within an effective interaction framework are also given.

Mass Limits for H^0 Decaying to Invisible Final States

These limits are for a neutral scalar H^0 which predominantly decays to invisible final states. Standard Model values are assumed for the couplings of H^0 to ordinary particles unless otherwise stated.

VALUE (GeV)	CL%	DOCUMENT ID	TECN	COMMENT
>108.2	95	1 AABOUD	19AI ATLS	W/Z fusion
		2 AAD	15BD ATLS	$p\bar{p} \rightarrow H^0 WX, H^0 ZX$
		3 AAD	15BH ATLS	jet + missing E_T
		4 AAD	14BA ATLS	secondary vertex
		5 AAD	14O ATLS	$p\bar{p} \rightarrow H^0 ZX$
		6 CHATRCHYAN	14B CMS	$p\bar{p} \rightarrow H^0 ZX, qqH^0 X$
		7 AAD	13AG ATLS	secondary vertex
		8 AAD	13AT ATLS	electron jets
		9 CHATRCHYAN	13BJ CMS	
		10 AAD	12AQ ATLS	secondary vertex
		11 AALTONEN	12AB CDF	secondary vertex
		12 AALTONEN	12U CDF	secondary vertex
		13 ABBIENDI	10 OPAL	
		14 ABBIENDI	07 OPAL	large width
		15 ACHARD	05 L3	
		15 ABDALLAH	04B DLPH	
		15 HEISTER	02 ALEP	$E_{\text{cm}} \leq 209 \text{ GeV}$
		15 BARATE	01C ALEP	$E_{\text{cm}} \leq 202 \text{ GeV}$
		16 ACCIARRI	00M L3	

- • • We do not use the following data for averages, fits, limits, etc. • • •
- 1 AABOUD 19AI search for $H^0_{1,2}$ production by vector boson fusion and decay to invisible final states in 36.1 fb^{-1} of pp collisions at $E_{\text{cm}} = 13 \text{ TeV}$. See their Fig. 6(b) for limits on cross section times branching ratios for $m_{H^0_{1,2}} = 0.1\text{--}3 \text{ TeV}$.
- 2 AAD 15BD search for $p\bar{p} \rightarrow H^0 WX$ and $p\bar{p} \rightarrow H^0 ZX$ with W or Z decaying hadronically and H^0 decaying to invisible final states in 20.3 fb^{-1} at $E_{\text{cm}} = 8 \text{ TeV}$. See their Fig. 6 for a limit on the cross section times branching ratio for $m_{H^0} = 115\text{--}300 \text{ GeV}$.
- 3 AAD 15BH search for events with a jet and missing E_T in 20.3 fb^{-1} of pp collisions at $E_{\text{cm}} = 8 \text{ TeV}$. Limits on $\sigma(H^0) B(H^0 \rightarrow \text{invisible}) < (44\text{--}10) \text{ pb}$ (95%CL) is given for $m_{H^0} = 115\text{--}300 \text{ GeV}$.
- 4 AAD 14BA search for H^0 production in the decay mode $H^0 \rightarrow X^0 X^0$, where X^0 is a long-lived particle which decays to collimated pairs of $e^+e^-, \mu^+\mu^-,$ or $\pi^+\pi^-$ plus invisible particles, in 20.3 fb^{-1} of pp collisions at $E_{\text{cm}} = 8 \text{ TeV}$. See their Figs. 15 and 16 for limits on cross section times branching ratio.
- 5 AAD 14O search for $p\bar{p} \rightarrow H^0 ZX, Z \rightarrow \ell\ell$, with H^0 decaying to invisible final states in 4.5 fb^{-1} at $E_{\text{cm}} = 7 \text{ TeV}$ and 20.3 fb^{-1} at $E_{\text{cm}} = 8 \text{ TeV}$. See their Fig. 3 for a limit on the cross section times branching ratio for $m_{H^0} = 110\text{--}400 \text{ GeV}$.
- 6 CHATRCHYAN 14B search for $p\bar{p} \rightarrow H^0 ZX, Z \rightarrow \ell\ell$ and $Z \rightarrow b\bar{b}$, and also $p\bar{p} \rightarrow qqH^0 X$ with H^0 decaying to invisible final states using data at $E_{\text{cm}} = 7$ and 8 TeV . See their Figs. 10, 11 for limits on the cross section times branching ratio for $m_{H^0} = 100\text{--}400 \text{ GeV}$.
- 7 AAD 13AG search for H^0 production in the decay mode $H^0 \rightarrow X^0 X^0$, where X^0 is a long-lived particle which decays to $\mu^+\mu^- X^0$, in 1.9 fb^{-1} of pp collisions at $E_{\text{cm}} = 7 \text{ TeV}$. See their Fig. 7 for limits on cross section times branching ratio.
- 8 AAD 13AT search for H^0 production in the decay $H^0 \rightarrow X^0 X^0$, where X^0 eventually decays to collimated e^+e^- pairs, in 2.04 fb^{-1} of pp collisions at $E_{\text{cm}} = 7 \text{ TeV}$. See their Fig. 3 for limits on cross section times branching ratio.
- 9 CHATRCHYAN 13BJ search for H^0 production in the decay chain $H^0 \rightarrow X^0 X^0, X^0 \rightarrow \mu^+\mu^- X^0$ in 5.3 fb^{-1} of pp collisions at $E_{\text{cm}} = 7 \text{ TeV}$. See their Fig. 2 for limits on cross section times branching ratio.
- 10 AAD 12AQ search for H^0 production in the decay mode $H^0 \rightarrow X^0 X^0$, where X^0 is a long-lived particle which decays mainly to $b\bar{b}$ in the muon detector, in 1.94 fb^{-1} of pp collisions at $E_{\text{cm}} = 7 \text{ TeV}$. See their Fig. 3 for limits on cross section times branching ratio for $m_{H^0} = 120, 140 \text{ GeV}, m_{X^0} = 20, 40 \text{ GeV}$ in the τ range of $0.5\text{--}35 \text{ ns}$.
- 11 AALTONEN 12AB search for H^0 production in the decay $H^0 \rightarrow X^0 X^0$, where X^0 eventually decays to clusters of collimated $\ell^+\ell^-$ pairs, in 5.1 fb^{-1} of $p\bar{p}$ collisions at $E_{\text{cm}} = 1.96 \text{ TeV}$. Cross section limits are provided for a benchmark MSSM model incorporating the parameters given in Table VI.
- 12 AALTONEN 12U search for H^0 production in the decay mode $H^0 \rightarrow X^0 X^0$, where X^0 is a long-lived particle with $\tau \approx 1 \text{ cm}$ which decays mainly to $b\bar{b}$, in 3.2 fb^{-1} of $p\bar{p}$ collisions at $E_{\text{cm}} = 1.96 \text{ TeV}$. See their Figs. 9 and 10 for limits on cross section times branching ratio for $m_{H^0} = (130\text{--}170) \text{ GeV}, m_{X^0} = 20, 40 \text{ GeV}$.
- 13 ABBIENDI 10 search for $e^+e^- \rightarrow H^0 Z$ with H^0 decaying invisibly. The limit assumes SM production cross section and $B(H^0 \rightarrow \text{invisible}) = 1$.
- 14 ABBIENDI 07 search for $e^+e^- \rightarrow H^0 Z$ with $Z \rightarrow q\bar{q}$ and H^0 decaying to invisible final states. The H^0 width is varied between 1 GeV and 3 TeV . A limit $\sigma \cdot B(H^0 \rightarrow \text{invisible}) < (0.07\text{--}0.57) \text{ pb}$ (95%CL) is obtained at $E_{\text{cm}} = 206 \text{ GeV}$ for $m_{H^0} = 60\text{--}114 \text{ GeV}$.
- 15 Search for $e^+e^- \rightarrow H^0 Z$ with H^0 decaying invisibly. The limit assumes SM production cross section and $B(H^0 \rightarrow \text{invisible}) = 1$.
- 16 ACCIARRI 00M search for $e^+e^- \rightarrow ZH^0$ with H^0 decaying invisibly at $E_{\text{cm}} = 183\text{--}189 \text{ GeV}$. The limit assumes SM production cross section and $B(H^0 \rightarrow \text{invisible}) = 1$. See their Fig. 6 for limits for smaller branching ratios.

Mass Limits for Light A^0

These limits are for a pseudoscalar A^0 in the mass range below $O(10) \text{ GeV}$.

VALUE (GeV)	DOCUMENT ID	TECN	COMMENT
• • •	• • •	• • •	• • •
1	ADACHI	23A BEL2	$\tau \rightarrow eA^0, \tau \rightarrow \mu A^0$
2	TUMASYAN	23AR CMS	$H \rightarrow A^0 A^0 \rightarrow 4\gamma$
3	ABLKIM	22H BES3	$J/\psi \rightarrow A^0 \gamma$

Gauge & Higgs Boson Particle Listings

Neutral Higgs Bosons, Searches for

4	JIA	22	BELL	$\Upsilon(1S) \rightarrow A^0 \gamma$
5	AAD	20AE	ATLS	$H^0 \rightarrow ZA^0$
6	AABOUD	18AP	ATLS	$H^0 \rightarrow A^0 A^0$
7	KHACHATRYAN	17AZ	CMS	$H^0 \rightarrow A^0 A^0$
8	ABLIKIM	16E	BES3	$J/\psi \rightarrow A^0 \gamma$
9	KHACHATRYAN	16F	CMS	$H^0 \rightarrow A^0 A^0$
10	LEES	15H	BABR	$\Upsilon(1S) \rightarrow A^0 \gamma$
11	LEES	13C	BABR	$\Upsilon(1S) \rightarrow A^0 \gamma$
12	LEES	13L	BABR	$\Upsilon(1S) \rightarrow A^0 \gamma$
13	LEES	13R	BABR	$\Upsilon(1S) \rightarrow A^0 \gamma$
14	ABLIKIM	12	BES3	$J/\psi \rightarrow A^0 \gamma$
15	CHATRCHYAN	12V	CMS	$A^0 \rightarrow \mu^+ \mu^-$
16	AALTONEN	11P	CDF	$t \rightarrow bH^+, H^+ \rightarrow W^+ A^0$
17,18	ABOUZAID	11A	KTEV	$K_L \rightarrow \pi^0 \pi^0 A^0, A^0 \rightarrow \mu^+ \mu^-$
19	DEL-AMO-SANCHEZ	11J	BABR	$\Upsilon(1S) \rightarrow A^0 \gamma$
20	LEES	11H	BABR	$\Upsilon(2S, 3S) \rightarrow A^0 \gamma$
21	ANDREAS	10	RVUE	
18,22	HYUN	10	BELL	$B^0 \rightarrow K^* A^0, A^0 \rightarrow \mu^+ \mu^-$
18,23	HYUN	10	BELL	$B^0 \rightarrow \rho^0 A^0, A^0 \rightarrow \mu^+ \mu^-$
24	AUBERT	09P	BABR	$\Upsilon(3S) \rightarrow A^0 \gamma$
25	AUBERT	09Z	BABR	$\Upsilon(2S) \rightarrow A^0 \gamma$
26	AUBERT	09Z	BABR	$\Upsilon(3S) \rightarrow A^0 \gamma$
18,27	TUNG	09	K391	$K_L \rightarrow \pi^0 \pi^0 A^0, A^0 \rightarrow \gamma \gamma$
28	LOVE	08	CLEO	$\Upsilon(1S) \rightarrow A^0 \gamma$
29	BESSION	07	CLEO	$\Upsilon(1S) \rightarrow \eta_b \gamma$
30	PARK	05	HYCP	$\Sigma^+ \rightarrow p A^0, A^0 \rightarrow \mu^+ \mu^-$
31	BALEST	95	CLE2	$\Upsilon(1S) \rightarrow A^0 \gamma$
32	ANTREASIAN	90C	CBAL	$\Upsilon(1S) \rightarrow A^0 \gamma$

- 1 ADACHI 23A search for flavor-changing τ decays $\tau \rightarrow eA^0$ and $\tau \rightarrow \mu A^0$, with A^0 invisible, using 62.8 fb^{-1} of e^+e^- collisions at $E_{\text{cm}} = 10.58 \text{ GeV}$. Limits on $B(\tau \rightarrow eA^0)/B(\tau \rightarrow e\nu\nu)$ in the range $1.1 \times 10^{-3} - 9.7 \times 10^{-3}$ (95% CL) and $B(\tau \rightarrow \mu A^0)/B(\tau \rightarrow \mu\nu\nu)$ in the range $0.7 \times 10^{-3} - 12.2 \times 10^{-3}$ (95% CL) are given for $m_{A^0} = 0-1.6 \text{ GeV}$. See their Fig. 2.
- 2 TUMASYAN 23AR search for the decay $H \rightarrow A^0 A^0$ with $A^0 \rightarrow \gamma\gamma$ (detected as a merged photonlike object) using 136 fb^{-1} of pp collisions at $E_{\text{cm}} = 13 \text{ TeV}$. Limits on $B(H \rightarrow A^0 A^0) \cdot B^2(A^0 \rightarrow \gamma\gamma)$ in the range $0.9 \times 10^{-3} - 3.3 \times 10^{-3}$ (95% CL) are given for $m_{A^0} = 0.1-1.2 \text{ GeV}$. See their Fig. 2.
- 3 ABLIKIM 22H search for the process $J/\psi \rightarrow A^0 \gamma$ with A^0 decaying to $\mu^+ \mu^-$ in $9 \times 10^9 J/\psi$ events and give limits on $B(J/\psi \rightarrow A^0 \gamma) \cdot B(A^0 \rightarrow \mu^+ \mu^-)$ in the range $1.2 \times 10^{-9} - 7.78 \times 10^{-7}$ (90% CL) for $0.212 \text{ GeV} \leq m_{A^0} \leq 3.0 \text{ GeV}$. See their Fig. 4.
- 4 JIA 22 search for the process $\Upsilon(2S) \rightarrow \Upsilon(1S) \pi^+ \pi^- \rightarrow A^0 \gamma \pi^+ \pi^-$ with A^0 decaying to $\tau^+ \tau^-$ or $\mu^+ \mu^-$ in $158 \times 10^6 \Upsilon(2S)$ events and give limits on $B(\Upsilon(1S) \rightarrow A^0 \gamma) \cdot B(A^0 \rightarrow \tau^+ \tau^-)$ in the range $3.8 \times 10^{-6} - 1.5 \times 10^{-4}$ (90% CL) for $m_{A^0} = 3.6-9.2 \text{ GeV}$, and $B(\Upsilon(1S) \rightarrow A^0 \gamma) \cdot B(A^0 \rightarrow \mu^+ \mu^-)$ in the range $3.1 \times 10^{-7} - 1.6 \times 10^{-5}$ (90% CL) for $m_{A^0} = 0.21-9.2 \text{ GeV}$. See their Fig. 4.
- 5 AAD 20AE search for the decay $H^0 \rightarrow ZA^0, Z \rightarrow \ell^+ \ell^-, A^0$ decaying hadronically ($A^0 \rightarrow gg$ or $s\bar{s}$), in 139 fb^{-1} of pp collisions at $E_{\text{cm}} = 13 \text{ TeV}$. Limit on the product of production cross section and the $H^0 \rightarrow ZA^0$ branching ratio in the range $17-340 \text{ pb}$ (95% CL) is given for $m_{A^0} = 0.5-4.0 \text{ GeV}$, see their Table 1.
- 6 AABOUD 18AP search for the decay $H^0 \rightarrow A^0 A^0 \rightarrow \mu^+ \mu^- \mu^+ \mu^-$ in 36.1 fb^{-1} of pp collisions at $E_{\text{cm}} = 13 \text{ TeV}$. See their Fig. 10(b) for limits on $B(H^0 \rightarrow A^0 A^0)$ in the range $m_{A^0} = 1-2.5, 4.5-8 \text{ GeV}$, assuming a type-II two-doublet plus singlet model with $\tan(\beta) = 5$.
- 7 KHACHATRYAN 17AZ search for the decay $H^0 \rightarrow A^0 A^0 \rightarrow \tau^+ \tau^- \tau^+ \tau^-, \mu^+ \mu^- b\bar{b}$, and $\mu^+ \mu^- \tau^+ \tau^-$ in 19.7 fb^{-1} of pp collisions at $E_{\text{cm}} = 8 \text{ TeV}$. See their Figs. 4, 5, and 6 for cross section limits in the range $m_{A^0} = 5-62.5 \text{ GeV}$. See also their Figs. 7, 8, and 9 for interpretation of the data in terms of models with two Higgs doublets and a singlet.
- 8 ABLIKIM 16E search for the process $J/\psi \rightarrow A^0 \gamma$ with A^0 decaying to $\mu^+ \mu^-$ and give limits on $B(J/\psi \rightarrow A^0 \gamma) \cdot B(A^0 \rightarrow \mu^+ \mu^-)$ in the range $2.8 \times 10^{-8} - 5.0 \times 10^{-6}$ (90% CL) for $0.212 \leq m_{A^0} \leq 3.0 \text{ GeV}$. See their Fig. 5.
- 9 KHACHATRYAN 16F search for the decay $H^0 \rightarrow A^0 A^0 \rightarrow \tau^+ \tau^- \tau^+ \tau^-$ in 19.7 fb^{-1} of pp collisions at $E_{\text{cm}} = 8 \text{ TeV}$. See their Fig. 8 for cross section limits for $m_{A^0} = 4-8 \text{ GeV}$.
- 10 LEES 15H search for the process $\Upsilon(2S) \rightarrow \Upsilon(1S) \pi^+ \pi^- \rightarrow A^0 \gamma \pi^+ \pi^-$ with A^0 decaying to $c\bar{c}$ and give limits on $B(\Upsilon(1S) \rightarrow A^0 \gamma) \cdot B(A^0 \rightarrow c\bar{c})$ in the range $7.4 \times 10^{-5} - 2.4 \times 10^{-3}$ (90% CL) for $4.00 \leq m_{A^0} \leq 8.95$ and $9.10 \leq m_{A^0} \leq 9.25 \text{ GeV}$. See their Fig. 6.
- 11 LEES 13C search for the process $\Upsilon(2S, 3S) \rightarrow \Upsilon(1S) \pi^+ \pi^- \rightarrow A^0 \gamma \pi^+ \pi^-$ with A^0 decaying to $\mu^+ \mu^-$ and give limits on $B(\Upsilon(1S) \rightarrow A^0 \gamma) \cdot B(A^0 \rightarrow \mu^+ \mu^-)$ in the range $(0.3-9.7) \times 10^{-6}$ (90% CL) for $0.212 \leq m_{A^0} \leq 9.20 \text{ GeV}$. See their Fig. 5(e) for limits on the $b-A^0$ Yukawa coupling derived by combining this result with AUBERT 09Z.
- 12 LEES 13L search for the process $\Upsilon(2S) \rightarrow \Upsilon(1S) \pi^+ \pi^- \rightarrow A^0 \gamma \pi^+ \pi^-$ with A^0 decaying to gg or $s\bar{s}$ and give limits on $B(\Upsilon(1S) \rightarrow A^0 \gamma) \cdot B(A^0 \rightarrow gg)$ between 1×10^{-6} and 2×10^{-2} (90% CL) for $0.5 \leq m_{A^0} \leq 9.0 \text{ GeV}$, and $B(\Upsilon(1S) \rightarrow A^0 \gamma) \cdot B(A^0 \rightarrow s\bar{s})$ between 4×10^{-6} and 1×10^{-3} (90% CL) for $1.5 \leq m_{A^0} \leq 9.0 \text{ GeV}$. See their Fig. 4.
- 13 LEES 13R search for the process $\Upsilon(2S) \rightarrow \Upsilon(1S) \pi^+ \pi^- \rightarrow A^0 \gamma \pi^+ \pi^-$ with A^0 decaying to $\tau^+ \tau^-$ and give limits on $B(\Upsilon(1S) \rightarrow A^0 \gamma) \cdot B(A^0 \rightarrow \tau^+ \tau^-)$ in the range $0.9-13 \times 10^{-5}$ (90% CL) for $3.6 \leq m_{A^0} \leq 9.2 \text{ GeV}$. See their Fig. 4 for limits on the $b-A^0$ Yukawa coupling derived by combining this result with AUBERT 09P.

- 14 ABLIKIM 12 searches for the process $\psi(3686) \rightarrow \pi\pi J/\psi, J/\psi \rightarrow A^0 \gamma$ with A^0 decaying to $\mu^+ \mu^-$. It gives mass dependent limits on $B(J/\psi \rightarrow A^0 \gamma) \cdot B(A^0 \rightarrow \mu^+ \mu^-)$ in the range $4 \times 10^{-7} - 2.1 \times 10^{-5}$ (90% C.L.) for $0.212 \leq m_{A^0} \leq 3.0 \text{ GeV}$. See their Fig. 2.
- 15 CHATRCHYAN 12V search for A^0 production in the decay $A^0 \rightarrow \mu^+ \mu^-$ with 1.3 fb^{-1} of pp collisions at $E_{\text{cm}} = 7 \text{ TeV}$. A limit on $\sigma(A^0) \cdot B(A^0 \rightarrow \mu^+ \mu^-)$ in the range $(1.5-7.5) \text{ pb}$ is given for $m_{A^0} = (5.5-8.7)$ and $(11.5-14) \text{ GeV}$ at 95% CL.
- 16 AALTONEN 11P search in 2.7 fb^{-1} of $p\bar{p}$ collisions at $E_{\text{cm}} = 1.96 \text{ TeV}$ for the decay chain $t \rightarrow bH^+, H^+ \rightarrow W^+ A^0, A^0 \rightarrow \tau^+ \tau^-$ with m_{A^0} between 4 and 9 GeV. See their Fig. 4 for limits on $B(t \rightarrow bH^+) \cdot B(H^+ \rightarrow W^+ A^0) \cdot B(A^0 \rightarrow \tau^+ \tau^-)$ for $90 < m_{H^+} < 160 \text{ GeV}$.
- 17 ABOUZAID 11A search for the decay chain $K_L \rightarrow \pi^0 \pi^0 A^0, A^0 \rightarrow \mu^+ \mu^-$ and give a limit $B(K_L \rightarrow \pi^0 \pi^0 A^0) \cdot B(A^0 \rightarrow \mu^+ \mu^-) < 1.0 \times 10^{-10}$ at 90% CL for $m_{A^0} = 214.3 \text{ MeV}$.
- 18 The search was motivated by PARK 05.
- 19 DEL-AMO-SANCHEZ 11J search for the process $\Upsilon(2S) \rightarrow \Upsilon(1S) \pi^+ \pi^- \rightarrow A^0 \gamma \pi^+ \pi^-$ with A^0 decaying to invisible final states. They give limits on $B(\Upsilon(1S) \rightarrow A^0 \gamma) \cdot B(A^0 \rightarrow \text{invisible})$ in the range $(1.9-4.5) \times 10^{-6}$ (90% CL) for $0 \leq m_{A^0} \leq 8.0 \text{ GeV}$, and $(2.7-37) \times 10^{-6}$ for $8.0 \leq m_{A^0} \leq 9.2 \text{ GeV}$.
- 20 LEES 11H search for the process $\Upsilon(2S, 3S) \rightarrow A^0 \gamma$ with A^0 decaying hadronically and give limits on $B(\Upsilon(2S, 3S) \rightarrow A^0 \gamma) \cdot B(A^0 \rightarrow \text{hadrons})$ in the range $1 \times 10^{-6} - 8 \times 10^{-5}$ (90% CL) for $0.3 < m_{A^0} < 7 \text{ GeV}$. The decay rates for $\Upsilon(2S)$ and $\Upsilon(3S)$ are assumed to be equal up to the phase space factor. See their Fig. 5.
- 21 ANDREAS 10 analyze constraints from rare decays and other processes on a light A^0 with $m_{A^0} < 2m_\mu$, and give limits on its coupling to fermions at the level of 10^{-4} times the Standard Model value.
- 22 HYUN 10 search for the decay chain $B^0 \rightarrow K^* A^0, A^0 \rightarrow \mu^+ \mu^-$ and give a limit on $B(B^0 \rightarrow K^* A^0) \cdot B(A^0 \rightarrow \mu^+ \mu^-)$ in the range $(2.26-5.53) \times 10^{-8}$ at 90% CL for $m_{A^0} = 212-300 \text{ MeV}$. The limit for $m_{A^0} = 214.3 \text{ MeV}$ is 2.26×10^{-8} .
- 23 HYUN 10 search for the decay chain $B^0 \rightarrow \rho^0 A^0, A^0 \rightarrow \mu^+ \mu^-$ and give a limit on $B(B^0 \rightarrow \rho^0 A^0) \cdot B(A^0 \rightarrow \mu^+ \mu^-)$ in the range $(1.73-4.51) \times 10^{-8}$ at 90% CL for $m_{A^0} = 212-300 \text{ MeV}$. The limit for $m_{A^0} = 214.3 \text{ MeV}$ is 1.73×10^{-8} .
- 24 AUBERT 09P search for the process $\Upsilon(3S) \rightarrow A^0 \gamma$ with $A^0 \rightarrow \tau^+ \tau^-$ for $4.03 < m_{A^0} < 9.52$ and $9.61 < m_{A^0} < 10.10 \text{ GeV}$, and give limits on $B(\Upsilon(3S) \rightarrow A^0 \gamma) \cdot B(A^0 \rightarrow \tau^+ \tau^-)$ in the range $(1.5-16) \times 10^{-5}$ (90% CL).
- 25 AUBERT 09Z search for the process $\Upsilon(2S) \rightarrow A^0 \gamma$ with $A^0 \rightarrow \mu^+ \mu^-$ for $0.212 < m_{A^0} < 9.3 \text{ GeV}$ and give limits on $B(\Upsilon(2S) \rightarrow A^0 \gamma) \cdot B(A^0 \rightarrow \mu^+ \mu^-)$ in the range $(0.3-8) \times 10^{-6}$ (90% CL).
- 26 AUBERT 09Z search for the process $\Upsilon(3S) \rightarrow A^0 \gamma$ with $A^0 \rightarrow \mu^+ \mu^-$ for $0.212 < m_{A^0} < 9.3 \text{ GeV}$ and give limits on $B(\Upsilon(3S) \rightarrow A^0 \gamma) \cdot B(A^0 \rightarrow \mu^+ \mu^-)$ in the range $(0.3-5) \times 10^{-6}$ (90% CL).
- 27 TUNG 09 search for the decay chain $K_L \rightarrow \pi^0 \pi^0 A^0, A^0 \rightarrow \gamma\gamma$ and give a limit on $B(K_L \rightarrow \pi^0 \pi^0 A^0) \cdot B(A^0 \rightarrow \gamma\gamma)$ in the range $(2.4-10.7) \times 10^{-7}$ at 90% CL for $m_{A^0} = 194.3-219.3 \text{ MeV}$. The limit for $m_{A^0} = 214.3 \text{ MeV}$ is 2.4×10^{-7} .
- 28 LOVE 08 search for the process $\Upsilon(1S) \rightarrow A^0 \gamma$ with $A^0 \rightarrow \mu^+ \mu^-$ (for $m_{A^0} < 2m_\tau$) and $A^0 \rightarrow \tau^+ \tau^-$. Limits on $B(\Upsilon(1S) \rightarrow A^0 \gamma) \cdot B(A^0 \rightarrow \ell^+ \ell^-)$ in the range $10^{-6} - 10^{-4}$ (90% CL) are given.
- 29 BESSION 07 give a limit $B(\Upsilon(1S) \rightarrow \eta_b \gamma) \cdot B(\eta_b \rightarrow \tau^+ \tau^-) < 0.27\%$ (95% CL), which constrains a possible A^0 exchange contribution to the η_b decay.
- 30 PARK 05 found three candidate events for $\Sigma^+ \rightarrow p \mu^+ \mu^-$ in the HyperCP experiment. Due to a narrow spread in dimuon mass, they hypothesize the events as a possible signal of a new boson. It can be interpreted as a neutral particle with $m_{A^0} = 214.3 \pm 0.5 \text{ MeV}$ and the branching fraction $B(\Sigma^+ \rightarrow p A^0) \cdot B(A^0 \rightarrow \mu^+ \mu^-) = (3.1^{+2.4}_{-1.9} \pm 1.5) \times 10^{-8}$.
- 31 BALEST 95 give limits $B(\Upsilon(1S) \rightarrow A^0 \gamma) ; 1.5 \times 10^{-5}$ at 90% CL for $m_{A^0} < 5 \text{ GeV}$. The limit becomes $< 10^{-4}$ for $m_{A^0} < 7.7 \text{ GeV}$.
- 32 ANTREASIAN 90C give limits $B(\Upsilon(1S) \rightarrow A^0 \gamma) ; 5.6 \times 10^{-5}$ at 90% CL for $m_{A^0} < 7.2 \text{ GeV}$. A^0 is assumed not to decay in the detector.

Other Mass Limits

We use a symbol H_1^0 if mass < 125 GeV or H_2^0 if mass > 125 GeV. The notation H is reserved for the 125 GeV particle.

VALUE (GeV)	CL%	DOCUMENT ID	TECN	COMMENT
•••	•••	•••	•••	•••
1	AAD	24A	ATLS	$H_1^0 \rightarrow Z\gamma$
2	AAD	23AD	ATLS	$H_2^0 \rightarrow HH$
3	AAD	23AD	ATLS	$A^0 \rightarrow ZH_1^0 \rightarrow ZHH$
4	AAD	23AJ	ATLS	$H^\pm \rightarrow W^\pm A^0$
5	AAD	23BD	ATLS	$t \rightarrow qH_{1,2}^0$
6	AAD	23BE	ATLS	$H_2^0 \rightarrow W^+ W^-$
7	AAD	23BG	ATLS	$t\bar{t}H_1^0/A^0$
8	AAD	23BW	ATLS	$A^0 t\bar{t}, A^0 \rightarrow \mu^+ \mu^-$
9	AAD	23BX	ATLS	$H \rightarrow \text{invisible } A^0$
10	AAD	23CA	ATLS	$H_3^0 \rightarrow H_1^0 H$
11	AAD	23CR	ATLS	flavor changing H_2^0
12	AAD	23O	ATLS	$A^0 \rightarrow ZH$
13	AAD	23R	ATLS	$A^0 \rightarrow \gamma\gamma$
14	AAD	23U	ATLS	$H_2^0 \rightarrow Z\gamma$
15	AAD	23Z	ATLS	$H_1^0 \rightarrow HH$
16	HAYRAPETY...	23C	CMS	$H_{1,2}^0 \rightarrow e\mu$
17	HAYRAPETY...	23G	CMS	$A^0 \rightarrow \mu^+ \mu^-$

See key on page 1171

Gauge & Higgs Boson Particle Listings
Neutral Higgs Bosons, Searches for

18	TUMASYAN	23	CMS	$H_3^0 \rightarrow H_{1,2}^0 H$	
19	TUMASYAN	23M	CMS	$H \rightarrow A^0 A^0$	
20	TUMASYAN	23o	CMS	$H_2^0 \rightarrow HH$	
21	TUMASYAN	23s	CMS	$H_{1,2}^0 \rightarrow \tau^+ \tau^-$	
22	AAD	22A	ATLS	$H \rightarrow A^0 A^0$	
23	AAD	22D	ATLS	$ZA^0, A^0 \rightarrow \text{invisible}$	
24	AAD	22F	ATLS	$H_2^0 \rightarrow HH$	
25	AAD	22i	ATLS	$H \rightarrow \tilde{\chi}_2^0 \tilde{\chi}_1^0, \tilde{\chi}_2^0 \rightarrow A^0 \tilde{\chi}_1^0,$ $A^0 \rightarrow b\bar{b}$	
26	AAD	22j	ATLS	$H \rightarrow ZA^0$	
27	AAD	22j	ATLS	$H \rightarrow A^0 A^0, H_1^0 H_1^0$	
28	AAD	22P	ATLS	$H_1^0, H_2^0 \rightarrow \text{invisible}$	
29	AAD	22Y	ATLS	$H_2^0 \rightarrow HH$	
30	ABRATENKO	22A	MCBN	$K^+ \rightarrow H_2^0 \pi^+$	
31	TUMASYAN	22AK	CMS	$H_3^0 \rightarrow H_1^0 H_1^0$	
32	TUMASYAN	22D	CMS	$H_2^0 \rightarrow W^+ W^-$	
33	AAD	21AF	ATLS	$H_2^0 \rightarrow ZZ$	
34	AAD	21AI	ATLS	$A^0 \rightarrow ZH_2^0$	
35	AAD	21AY	ATLS	$H_2^0 \rightarrow \gamma\gamma$	
36	AAD	21AZ	ATLS	$A_2^0 \rightarrow HA_1^0$	
37	AAD	21BB	ATLS	$A_2^0 \rightarrow HA_1^0$	
38	AAD	21BE	ATLS	$A_1^0 \rightarrow \text{invisible}$	
39	ABRATENKO	21	MCBN	$K^+ \rightarrow H_2^0 \pi^+$	
40	SIRUNYAN	21A	CMS	$H_2^0 \rightarrow ZA^0, A^0 \rightarrow \text{invisible}$	
41	TUMASYAN	21F	CMS	$H_3^0 \rightarrow HH_{1,2}^0$	
42	AAD	20AA	ATLS	$H_2^0/A^0 \rightarrow \tau^+ \tau^-$	
43	AAD	20AI	ATLS	$H \rightarrow A^0 A^0$	
44	AAD	20AO	ATLS	$H_2^0 \rightarrow HH$	
45	AAD	20C	ATLS	$H_2^0 \rightarrow HH$	
46	AAD	20L	ATLS	$H_2^0 \rightarrow b\bar{b}$	
47	AAD	20X	ATLS	$H_2^0 \rightarrow HH$	
48	AAIJ	20AL	LHCB	$A^0 \rightarrow \mu^+ \mu^-$	
49	SIRUNYAN	20	CMS	$H \rightarrow A^0 A^0$	
50	SIRUNYAN	20AA	CMS	$H_2^0 \rightarrow ZA^0$ or $A^0 \rightarrow ZH_2^0$	
51	SIRUNYAN	20AC	CMS	$A^0 \rightarrow ZH$	
52	SIRUNYAN	20AD	CMS	$H_2^0 \rightarrow \mu\tau, e\tau$	
53	SIRUNYAN	20AF	CMS	$H_2^0/A^0 \rightarrow t\bar{t}$	
54	SIRUNYAN	20AP	CMS	$H, H_2^0 \rightarrow A^0 A^0$	
55	SIRUNYAN	20Y	CMS	$H_2^0 \rightarrow W^+ W^-$	
56	SIRUNYAN	20Z	CMS	$t\bar{t}H_{1,2}^0$ or $t\bar{t}A^0, H_{1,2}^0/$ $A^0 \rightarrow e^+ e^-, \mu^+ \mu^-$	
57	AABOUD	19A	ATLS	$H_2^0 \rightarrow HH$	
58	AABOUD	19AG	ATLS	$H \rightarrow A^0 A^0$	
59	AABOUD	19o	ATLS	$H_2^0 \rightarrow HH$	
60	AABOUD	19T	ATLS	$H_2^0 \rightarrow HH$	
61	AABOUD	19v	ATLS	two doublet + pseudoscalar	
62	AABOUD	19Y	ATLS	$H_2^0 \rightarrow \mu^+ \mu^-$	
63	AALTONEN	19	CDF	$H_{1,2}^0 \rightarrow b\bar{b}$	
64	SIRUNYAN	19	CMS	$H_2^0 \rightarrow HH$	
65	SIRUNYAN	19AE	CMS	$A^0 \rightarrow \tau^+ \tau^-$	
66	SIRUNYAN	19AN	CMS	$A_2^0 \rightarrow HA_1^0$	
67	SIRUNYAN	19AV	CMS	$A^0 \rightarrow ZH$	
68	SIRUNYAN	19B	CMS	$H_{1,2}^0/A^0 \rightarrow b\bar{b}$	
69	SIRUNYAN	19BB	CMS	$H_1^0 \rightarrow \gamma\gamma$	
70	SIRUNYAN	19BD	CMS	$H \rightarrow A^0 A^0$	
71	SIRUNYAN	19BE	CMS	$H_2^0 \rightarrow HH$	
72	SIRUNYAN	19BQ	CMS	$H_{1,2}^0 \rightarrow A^0 A^0$	
73	SIRUNYAN	19CR	CMS	$H_2^0/A^0 \rightarrow \mu^+ \mu^-$	
74	SIRUNYAN	19H	CMS	$H_2^0 \rightarrow HH$	
75	AABOUD	18AA	ATLS	$H_2^0 \rightarrow Z\gamma$	
76	AABOUD	18AG	ATLS	$H \rightarrow A^0 A^0$	
77	AABOUD	18AH	ATLS	$A^0 \rightarrow ZH_2^0$	
78	AABOUD	18AI	ATLS	$A^0 \rightarrow ZH$	
79	AABOUD	18BF	ATLS	$H_2^0 \rightarrow ZZ$	
80	AABOUD	18BU	ATLS	$H_2^0 \rightarrow HH$	
81	AABOUD	18BX	ATLS	$H \rightarrow A^0 A^0$	
82	AABOUD	18CQ	ATLS	$H_2^0 \rightarrow HH$	
83	AABOUD	18F	ATLS	$H_2^0 \rightarrow W^+ W^-, ZZ$	
84	AAIJ	18AMLHCB	$H_{1,2}^0 \rightarrow \mu\tau$		
85	AAIJ	18AQ	LHCB	$A^0 \rightarrow \mu^+ \mu^-$	
86	AAIJ	18AQ	LHCB	$H \rightarrow A^0 A^0, A^0 \rightarrow \mu^+ \mu^-$	
87	SIRUNYAN	18AF	CMS	$H_2^0 \rightarrow HH$	
88	SIRUNYAN	18BA	CMS	$H_2^0 \rightarrow ZZ$	
89	SIRUNYAN	18CW	CMS	$H_2^0 \rightarrow HH$	
90	SIRUNYAN	18DK	CMS	$H_2^0 \rightarrow Z\gamma$	
91	SIRUNYAN	18DT	CMS	$H \rightarrow A^0 A^0$	
92	SIRUNYAN	18DU	CMS	$H_2^0 \rightarrow \gamma\gamma$	
93	SIRUNYAN	18ED	CMS	$A^0 \rightarrow ZH$	
94	SIRUNYAN	18EE	CMS	$H \rightarrow A^0 A^0$	
95	SIRUNYAN	18F	CMS	$pp, 13 \text{ TeV}, H_2^0 \rightarrow HH$	
96	AABOUD	17	ATLS	$H_2^0 \rightarrow Z\gamma$	
97	AABOUD	17AP	ATLS	$H_2^0 \rightarrow \gamma\gamma$	
98	AABOUD	17AW	ATLS	$H_2^0 \rightarrow Z\gamma$	
99	KHACHATRY...	17AZ	CMS	$H \rightarrow A^0 A^0$	
100	KHACHATRY...	17D	CMS	$pp, 8, 13 \text{ TeV}, H_2^0 \rightarrow Z\gamma$	
101	KHACHATRY...	17R	CMS	$H_2^0 \rightarrow \gamma\gamma$	
102	SIRUNYAN	17CN	CMS	$pp, 8 \text{ TeV}, H_2^0 \rightarrow HH$	
103	SIRUNYAN	17Y	CMS	$pp, 8, 13 \text{ TeV}, H_2^0 \rightarrow Z\gamma$	
104	AABOUD	16AB	ATLS	$H \rightarrow A^0 A^0$	
105	AABOUD	16AE	ATLS	$H_2^0 \rightarrow W^+ W^-, ZZ$	
106	AABOUD	16H	ATLS	$H_2^0 \rightarrow \gamma\gamma$	
107	AABOUD	16I	ATLS	$H_2^0 \rightarrow HH$	
108	AAD	16AX	ATLS	$H \rightarrow ZZ$	
109	AAD	16C	ATLS	$H \rightarrow W^+ W^-$	
110	AAD	16L	ATLS	$H \rightarrow A^0 A^0$	
111	AAD	16L	ATLS	$H_2^0 \rightarrow A^0 A^0$	
112	AALTONEN	16C	CDF	$H_1^0 H_1^0 \rightarrow H_1^0 H_1^0 W^*,$ $H_1^0 \rightarrow \gamma\gamma$	
113	KHACHATRY...	16BG	CMS	$H_2^0 \rightarrow HH$	
114	KHACHATRY...	16BQ	CMS	$pp, 8 \text{ TeV}, H_2^0 \rightarrow HH$	
115	KHACHATRY...	16F	CMS	$H \rightarrow H_1 H_1$	
116	KHACHATRY...	16M	CMS	$H_2^0 \rightarrow \gamma\gamma$	
117	KHACHATRY...	16P	CMS	$H_2^0 \rightarrow HH$	
118	KHACHATRY...	16P	CMS	$A^0 \rightarrow ZH$	
119	AAD	15BK	ATLS	$H_2^0 \rightarrow HH$	
120	AAD	15BZ	ATLS	$H \rightarrow A^0 A^0$	
121	AAD	15BZ	ATLS	$H_2^0 \rightarrow A^0 A^0$	
122	AAD	15CE	ATLS	$H_2^0 \rightarrow HH$	
123	AAD	15H	ATLS	$H_2^0 \rightarrow HH$	
124	AAD	15S	ATLS	$A^0 \rightarrow ZH$	
125	KHACHATRY...	15AW	CMS	$H_2^0 \rightarrow W^+ W^-, ZZ$	
126	KHACHATRY...	15BB	CMS	$H \rightarrow \gamma\gamma$	
127	KHACHATRY...	15N	CMS	$A^0 \rightarrow ZH$	
128	KHACHATRY...	15O	CMS	$A^0 \rightarrow ZH$	
129	KHACHATRY...	15R	CMS	$H_2^0 \rightarrow HH$	
130	AAD	14AP	ATLS	$H \rightarrow \gamma\gamma$	
131	AAD	14M	ATLS	$H_2^0 \rightarrow H^\pm W^\mp \rightarrow$ $HW^\pm W^\mp, H \rightarrow b\bar{b}$	
132	CHATRCHYAN	14G	CMS	$H \rightarrow WW^{(*)}$	
133	KHACHATRY...	14P	CMS	$H \rightarrow \gamma\gamma$	
134	AALTONEN	13P	CDF	$H^0 \rightarrow H^\pm W^\mp \rightarrow$ $HW^\pm W^\mp$	
135	CHATRCHYAN	13BJ	CMS	$H \rightarrow A^0 A^0$	
136	AALTONEN	11P	CDF	$t \rightarrow bH^+, H^+ \rightarrow W^+ A^0$	
137	ABBIENDI	10	OPAL	$H \rightarrow \tilde{\chi}_1^0 \tilde{\chi}_2^0$	
138	SCHAEI	10	ALEP	$H \rightarrow A^0 A^0$	
139	ABAZOV	09V	D0	$H \rightarrow A^0 A^0$	
140	ABBIENDI	05A	OPAL	A^0 , Type-II model	
141	ABBIENDI	04K	OPAL	$H \rightarrow 2 \text{ jets}$	
142	ABDALLAH	04	DLPH	HV couplings	
143	ACHARD	04B	L3	$H \rightarrow 2 \text{ jets}$	
144	ACHARD	04F	L3	Anomalous coupling	
145	ABBIENDI	03F	OPAL	$e^+ e^- \rightarrow HZ, H \rightarrow \text{any}$	
146	ABBIENDI	03G	OPAL	$H_2^0 \rightarrow A^0 A^0$	
147,148	HEISTER	02L	ALEP	$H_1^0 \rightarrow \gamma\gamma$	
149	HEISTER	02M	ALEP	$H \rightarrow 2 \text{ jets or } \tau^+ \tau^-$	
150	ABBIENDI	01E	OPAL	A^0 , Type-II model	
151	ACCIARRI	00R	L3	$e^+ e^- \rightarrow H\gamma$ and/or $H \rightarrow$ $\gamma\gamma$	
152	ACCIARRI	00R	L3	$e^+ e^- \rightarrow e^+ e^- H$	
153	GONZALEZ...	98B	RVUE	Anomalous coupling	
154	KRAWCZYK	97	RVUE	$(g-2)_\mu$	
155	ALEXANDER	96H	OPAL	$Z \rightarrow H\gamma$	

¹ AAD 24A search for the decay $H_2^0 \rightarrow Z\gamma$ with Z decaying to $e^+ e^-$ or $\mu^+ \mu^-$ using 140 fb^{-1} of pp collisions at $E_{\text{cm}} = 13 \text{ TeV}$. See their Fig. 4 for limits on production cross section times branching ratios for $m_{H_2^0} = 0.22\text{--}3.4 \text{ TeV}$.

² AAD 23AD search for associated production of W/ZH_2^0 with the decay chain $H_2^0 \rightarrow HH \rightarrow b\bar{b}b\bar{b}$ using 139 fb^{-1} of pp collisions at $E_{\text{cm}} = 13 \text{ TeV}$. See their Fig. 9 for limits on cross section times branching ratios for $m_{H_2^0} = 260\text{--}1000 \text{ GeV}$.

Gauge & Higgs Boson Particle Listings

Neutral Higgs Bosons, Searches for

- 3 AAD 23AD search for gluon fusion production of A^0 with the decay chain $A^0 \rightarrow ZH_2^0$, $H_2^0 \rightarrow HH \rightarrow b\bar{b}b\bar{b}$ using 139 fb^{-1} of pp collisions at $E_{\text{cm}} = 13 \text{ TeV}$. See their Fig. 10 for limits on cross section times branching ratios for $m_{A^0} = 350\text{--}800 \text{ GeV}$ and $m_{H_2^0} = 260\text{--}400 \text{ GeV}$.
- 4 AAD 23AJ search for production of H^\pm in association with a top quark, followed by $H^\pm \rightarrow W^\pm A^0$, $A^0 \rightarrow$ invisible, using 139 fb^{-1} of pp collisions at $E_{\text{cm}} = 13 \text{ TeV}$. See their Fig. 10 for excluded parameter regions of 2HDM + CP-odd singlet model.
- 5 AAD 23BD search for a top quark decaying to $qH_{1,2}^0$ ($q = u, c$), $H_{1,2}^0 \rightarrow b\bar{b}$, using 139 fb^{-1} of pp collisions at $E_{\text{cm}} = 13 \text{ TeV}$. See their Fig. 9 for limits on production cross section times branching ratios for $m_{H_{1,2}^0} = 20\text{--}160 \text{ GeV}$.
- 6 AAD 23BE search for associated production of $H_2^0 W$ and decay $H_2^0 \rightarrow W^+ W^-$ assuming the presence of higher dimensional $H_2^0 W^\pm W^\pm$ interactions, using 139 fb^{-1} of pp collisions at $E_{\text{cm}} = 13 \text{ TeV}$. See their Fig. 6 for excluded parameter region of higher dimensional operators, and Fig. 7 for limits on cross section times branching ratio for $m_{H_2^0} = 0.3\text{--}1.5 \text{ TeV}$.
- 7 AAD 23BG search for production of H_2^0/A^0 in association with a $t\bar{t}$ pair, decaying to $t\bar{t}$, using 139 fb^{-1} of pp collisions at $E_{\text{cm}} = 13 \text{ TeV}$. See their Fig. 7 for limits on cross section times branching ratios for $m_{H_2^0} = m_{A^0} = 0.4\text{--}1.0 \text{ TeV}$.
- 8 AAD 23BW search for A^0 production in association with a $t\bar{t}$ pair, decaying to $\mu^+ \mu^-$, using 139 fb^{-1} of pp collisions at $E_{\text{cm}} = 13 \text{ TeV}$. See their Fig. 5(a) for limits on production cross section times branching ratio for $m_{A^0} = 15\text{--}72 \text{ GeV}$.
- 9 AAD 23BX search for production of $H \rightarrow \tau^+ \tau^-$ with missing transverse momentum using 139 fb^{-1} of pp collisions at $E_{\text{cm}} = 13 \text{ TeV}$. See their Fig. 8 for interpretation of the data in terms of 2HDM + a model.
- 10 AAD 23CA search for production of H_3^0 decaying to $H_2^0 H$, $H_2^0 \rightarrow W^+ W^-$ or ZZ , and $H \rightarrow \tau^+ \tau^-$ using 140 fb^{-1} of pp collisions at $E_{\text{cm}} = 13 \text{ TeV}$. See their Figs. 4, 5 for limits on production cross section times branching ratios in the ranges $m_{H_3^0} = 0.5\text{--}1.5 \text{ TeV}$ and $m_{H_2^0} = 0.2\text{--}0.5 \text{ TeV}$.
- 11 AAD 23CR search for H_2^0 having flavor-violating couplings to tc or tu , produced in association with top quark(s), using 139 fb^{-1} of pp collisions at $E_{\text{cm}} = 13 \text{ TeV}$. See their Fig. 14 for limits on production cross section times branching ratios for $m_{H_2^0} = 0.2\text{--}1.5 \text{ TeV}$ with various assumptions on the flavor-changing couplings.
- 12 AAD 23o search for production of an A^0 in gluon-gluon fusion and in association with a $b\bar{b}$, decaying to ZH in the final states $\nu\bar{\nu}b\bar{b}$ and $\ell^+ \ell^- b\bar{b}$ using 139 fb^{-1} of pp collisions at $E_{\text{cm}} = 13 \text{ TeV}$. See their Fig. 9 for limits on cross section times branching ratio for $m_{A^0} = 0.22\text{--}2.0 \text{ TeV}$, and Fig. 11 for limits with both production components.
- 13 AAD 23R search for the decay $A^0 \rightarrow \gamma\gamma$ in 138 fb^{-1} of pp collisions at $E_{\text{cm}} = 13 \text{ TeV}$. See their Fig. 7 for limits on cross section times branching ratio for $m_{A^0} = 10\text{--}70 \text{ GeV}$.
- 14 AAD 23u search for the decay $H_2^0 \rightarrow Z\gamma$ with Z decaying hadronically in 139 fb^{-1} of pp collisions at $E_{\text{cm}} = 13 \text{ TeV}$. See their Fig. 8(a) for limits on production cross section times branching ratios for $m_{H_2^0} = 1.0\text{--}6.8 \text{ TeV}$.
- 15 AAD 23z search for the decay chain $H_2^0 \rightarrow HH \rightarrow b\bar{b}\tau^+\tau^-$ using 139 fb^{-1} of pp collisions at $E_{\text{cm}} = 13 \text{ TeV}$. See their Fig. 10 for limits on the product of production cross section times branching ratios for $m_{H_2^0} = 0.251\text{--}1.6 \text{ TeV}$.
- 16 HAYRAPETYAN 23c search for $H_{1,2}^0 \rightarrow e\mu$ using 138 fb^{-1} of pp collisions at $E_{\text{cm}} = 13 \text{ TeV}$. See their Fig. 7 for limits on production cross section times branching ratio for $m_{H_{1,2}^0} = 110\text{--}160 \text{ GeV}$.
- 17 HAYRAPETYAN 23g search for dimuon resonance in the mass range $1.1\text{--}2.6$ or $4.2\text{--}7.9 \text{ GeV}$ in 96.6 fb^{-1} of pp collisions at $E_{\text{cm}} = 13 \text{ TeV}$, in inclusive and high p_T selections. See their Fig. 5 for cross section times branching ratio limits and Fig. 7 for mixing angle limits in two Higgs doublet plus singlet model (at 90% CL).
- 18 TUMASYAN 23 search for production of H_3^0 decaying to $H_{1,2}^0 H \rightarrow b\bar{b}b\bar{b}$ using 138 fb^{-1} of pp collisions at $E_{\text{cm}} = 13 \text{ TeV}$. See their Fig. 4 for limits on production cross section times branching ratios for $m_{H_3^0} = 0.9\text{--}4.0 \text{ TeV}$ and $m_{H_{1,2}^0} = 60\text{--}600 \text{ GeV}$, and their interpretation in the NMSSM and the Two Real Singlet Model (TRSM).
- 19 TUMASYAN 23M search for the decay chain $H \rightarrow A^0 A^0 \rightarrow \gamma\gamma\gamma\gamma$ in 132 fb^{-1} of pp collisions at $E_{\text{cm}} = 13 \text{ TeV}$. See their Fig. 6 for limits on cross section times branching ratio in the range $m_{A^0} = 15\text{--}62 \text{ GeV}$.
- 20 TUMASYAN 23o search for $H_2^0 \rightarrow HH$, each H decaying to either WW^* or $\tau^+ \tau^-$ using 138 fb^{-1} of pp collisions at $E_{\text{cm}} = 13 \text{ TeV}$. See their Fig. 14 (upper) for limit on the product of production cross section times branching ratios for $m_{H_2^0} = 0.25\text{--}1.0 \text{ TeV}$.
- 21 TUMASYAN 23s search for gluon fusion and b -associated production of $H_{1,2}^0$ decaying to $\tau^+ \tau^-$ using 138 fb^{-1} of pp collisions at $E_{\text{cm}} = 13 \text{ TeV}$. See their Fig. 10 for limits on production cross section times branching ratios for $m_{H_{1,2}^0} = 0.06\text{--}3.5 \text{ TeV}$.
- 22 AAD 22A search for the decay chain $H \rightarrow A^0 A^0 \rightarrow \mu^+ \mu^- b\bar{b}$ in 139 fb^{-1} of pp collisions at $E_{\text{cm}} = 13 \text{ TeV}$. See their Fig. 9 for limits on the overall branching fraction in the range $m_{A^0} = 16\text{--}62 \text{ GeV}$. See also Fig. 11 for limits without assuming A^0 is pseudoscalar.
- 23 AAD 22d search for $Z A^0$ associate production with $Z \rightarrow \ell^+ \ell^-$, A^0 decaying invisibly, in 139 fb^{-1} of pp collisions at $E_{\text{cm}} = 13 \text{ TeV}$. See their Fig. 5 for excluded regions in the mass parameter space of two Higgs doublet plus singlet (2HDM+ A^0) model with a certain choice of the model parameters.
- 24 AAD 22f search for gluon fusion production of H_2^0 decaying to $HH \rightarrow b\bar{b}b\bar{b}$ using $126\text{--}139 \text{ fb}^{-1}$ of pp collisions at $E_{\text{cm}} = 13 \text{ TeV}$. $B(H \rightarrow b\bar{b}) = 0.582$ is assumed. See their Fig. 14 for limit on the product of production cross section times branching ratios for $m_{H_2^0} = 0.251\text{--}5.0 \text{ TeV}$.
- 25 AAD 22i search for ZH associate production with the decay chain $H \rightarrow \tilde{\chi}_2^0 \tilde{\chi}_1^0, \tilde{\chi}_2^0 \rightarrow A^0 \tilde{\chi}_1^0, A^0 \rightarrow b\bar{b}$, and $Z \rightarrow \ell^+ \ell^-$, in 139 fb^{-1} of pp collisions at $E_{\text{cm}} = 13 \text{ TeV}$. See their Figs. 3 and 4 for limits on the product of cross section times the branching ratios for $m_{A^0} = 20\text{--}65 \text{ GeV}$ with various choices of NMSSM model parameters.
- 26 AAD 22j search for the decay $H \rightarrow Z A^0$ with $A^0 \rightarrow \mu^+ \mu^-$ and $Z \rightarrow e^+ e^-$, $\mu^+ \mu^-$ in 139 fb^{-1} of pp collisions at $E_{\text{cm}} = 13 \text{ TeV}$ assuming SM gluon-gluon fusion production of the H . See their Fig. 17(b) for limits on the product of cross section times the branching ratios for $m_{A^0} = 15\text{--}30 \text{ GeV}$.
- 27 AAD 22j search for the decay $H \rightarrow A^0 A^0$ with $A^0 \rightarrow \mu^+ \mu^-$ in 139 fb^{-1} of pp collisions at $E_{\text{cm}} = 13 \text{ TeV}$ assuming SM gluon-gluon fusion production of the H in the range of $m_{A^0} = 1\text{--}60 \text{ GeV}$. See their Fig. 14(b) for limits on the product of cross section times the branching ratios for $m_{A^0} = 1.5\text{--}60 \text{ GeV}$ (excluding ψ and Υ regions). The limit also applies to the decay $H \rightarrow H_1^0 H_1^0$.
- 28 AAD 22p search for invisibly decaying H_1^0, H_2^0 produced by vector boson fusion in 139 fb^{-1} of pp collisions at $E_{\text{cm}} = 13 \text{ TeV}$. Limit on the product of cross section times branching ratio in the range $0.1\text{--}1 \text{ pb}$ (95% CL) is given for the mass range $0.05\text{--}2 \text{ TeV}$. See their Fig. 14.
- 29 AAD 22y search for gluon fusion production of H_2^0 decaying to $HH \rightarrow b\bar{b}\gamma\gamma$ in 139 fb^{-1} of pp collisions at $E_{\text{cm}} = 13 \text{ TeV}$. See their Fig. 15 for limit on the product of production cross section times branching ratios to HH for $m_{H_2^0} = 0.251\text{--}1.0 \text{ TeV}$.
- 30 ABRATENKO 22A search for a singlet scalar boson H_1^0 having a small mixing with the SM Higgs boson in the decay chain $K^+ \rightarrow H_1^0 \pi^+, H_1^0 \rightarrow \mu^+ \mu^-$ from data corresponding to 7.01×10^{20} protons on NuMI target. See their Fig. 13 (right) and Table V for limits on the SM Higgs component of H_1^0 for $m_{H_1^0} = 212\text{--}279 \text{ MeV}$.
- 31 TUMASYAN 22AK search for gluon-fusion production of H_3^0 decaying to $H_1^0 H_1^0 \rightarrow b\bar{b}b\bar{b}$ in 138 fb^{-1} of pp collisions at $E_{\text{cm}} = 13 \text{ TeV}$. See their Fig. 5 for limits on cross section times branching ratio for $m_{H_3^0} = 1\text{--}3 \text{ TeV}$, $m_{H_1^0} = 25\text{--}100 \text{ GeV}$.
- 32 TUMASYAN 22D search for production of an H_2^0 (denoted radion in the paper) in gluon fusion and vector boson fusion, decaying to $W^+ W^-$ in the final states $\ell\nu$ + hadrons, using 137 fb^{-1} of pp collisions at $E_{\text{cm}} = 13 \text{ TeV}$. See their Fig. 7 for limits on cross section times branching ratio for $m_{H_2^0} = 1.0\text{--}4.5 \text{ TeV}$.
- 33 AAD 21AF search for production of a heavy H_2^0 state decaying to ZZ in the final states $\ell^+ \ell^- \ell^+ \ell^-$ and $\ell^+ \ell^- \nu\bar{\nu}$ in 139 fb^{-1} of pp collisions at $E_{\text{cm}} = 13 \text{ TeV}$. See their Fig. 4 for upper limits on cross section times branching ratio for $m_{H_2^0} = 0.2\text{--}2.0 \text{ TeV}$ assuming ggF or VBF with narrow width approximation, and Fig. 5 for upper limits on cross section times branching ratio for $m_{H_2^0} = 0.4\text{--}2.0 \text{ TeV}$ assuming ggF, and with several assumptions on its width.
- 34 AAD 21AI search for production of an A^0 in gluon-gluon fusion and in association with a $b\bar{b}$, decaying to $ZH_2^0 \rightarrow \ell^+ \ell^- b\bar{b}$ or $\ell^+ \ell^- W^+ W^-$ in 139 fb^{-1} of pp collisions at $E_{\text{cm}} = 13 \text{ TeV}$. See their Figs. 9 and 13 for cross section limits for $m_{A^0} = 230\text{--}800 \text{ GeV}$ and $m_{H_2^0} = 130\text{--}700 \text{ GeV}$.
- 35 AAD 21AY search for production of a scalar resonance decaying to $\gamma\gamma$ in 139 fb^{-1} of pp collisions at $E_{\text{cm}} = 13 \text{ TeV}$. See their Fig. 5(a) for limits on fiducial cross section times branching ratio for $m_{H_2^0} = 0.16\text{--}3 \text{ TeV}$ with narrow width approximation, and Table 2 with several assumptions on the width.
- 36 AAD 21AZ search for production of A_2^0 decaying to HA_1^0 followed by $H \rightarrow \gamma\gamma, A_1^0 \rightarrow$ invisible in 139 fb^{-1} of pp collisions at $E_{\text{cm}} = 13 \text{ TeV}$. See their Figs. 10–12 for limits in terms of two-Higgs-doublet model plus singlet pseudoscalar and a fermionic Dark Matter particle.
- 37 AAD 21BB search for production of A_2^0 by gluon fusion or associated $A_2^0 b\bar{b}$ production, decaying to HA_1^0 followed by $H \rightarrow b\bar{b}, A_1^0 \rightarrow$ invisible in 139 fb^{-1} of pp collisions at $E_{\text{cm}} = 13 \text{ TeV}$. See their Fig. 8 for limits in terms of two-Higgs-doublet plus singlet pseudoscalar model.
- 38 AAD 21BE search for production of A_1^0 associated with a single top quark and either a light quark or a W boson, decaying to invisible final states, in 139 fb^{-1} of pp collisions at $E_{\text{cm}} = 13 \text{ TeV}$. See their Figs. 13–15 for limits in terms of two-Higgs-doublet model plus singlet pseudoscalar, which is assumed to decay to a pair of Dark Matter particles.
- 39 ABRATENKO 21 search for a singlet scalar boson H_1^0 having a small mixing with the SM Higgs boson in the decay chain $K^+ \rightarrow H_1^0 \pi^+, H_1^0 \rightarrow e^+ e^-$ from data corresponding to 1.93×10^{20} protons on NuMI target. See their Fig. 2 for limits on the SM Higgs component of H_1^0 for $m_{H_1^0} = 3\text{--}210 \text{ MeV}$.
- 40 SIRUNYAN 21A search for $H_2^0 \rightarrow Z A^0$ with $Z \rightarrow \ell^+ \ell^-$, A^0 decaying invisibly, in 137 fb^{-1} of pp collisions at $E_{\text{cm}} = 13 \text{ TeV}$. See their Fig. 8 for excluded regions in the mass parameter space of two Higgs doublet plus singlet model with a certain choice of the model parameters.
- 41 TUMASYAN 21F search for gluon fusion production of H_3^0 decaying to $HH_{1,2}^0 \rightarrow \tau^+ \tau^- b\bar{b}$ in 137 fb^{-1} of pp collisions at $E_{\text{cm}} = 13 \text{ TeV}$. See their Figs. 5 and 6 for limits on cross section times branching ratios for $m_{H_{1,2}^0} = 0.06\text{--}2.8 \text{ TeV}$ and $m_{H_3^0} = 0.24\text{--}3.0 \text{ TeV}$.
- 42 AAD 20AA search for $H_2^0/A^0 \rightarrow \tau^+ \tau^-$ produced by gluon fusion or b -associated production using 139 fb^{-1} of pp collisions at $E_{\text{cm}} = 13 \text{ TeV}$. See their Fig. 2(a), 2(b) for limits on the product of cross section and branching ratio for $m_{H_2^0}, m_{A^0} = 0.2\text{--}2.5 \text{ TeV}$.
- 43 AAD 20AI search for ZH production followed by the decay $H \rightarrow A^0 A^0 \rightarrow b\bar{b}b\bar{b}$ in 36 fb^{-1} of pp collisions at $E_{\text{cm}} = 13 \text{ TeV}$. The search looks for collimated $A^0 \rightarrow b\bar{b}$ decays and is complementary to AABOUD 18bx. See their Fig. 10 for limits on the product of production cross section and branching ratios in the range $m_{A^0} = 15\text{--}30 \text{ GeV}$.

See key on page 1171

Gauge & Higgs Boson Particle Listings

Neutral Higgs Bosons, Searches for

- 44 AAD 20A0 search for gluon fusion production of H_2^0 decaying to $HH \rightarrow \tau^+ \tau^- b \bar{b}$ (with hadronically decaying $\tau^+ \tau^-$) using 139 fb^{-1} of pp collisions at $E_{\text{cm}} = 13 \text{ TeV}$. Limit on the product of production cross section times branching ratios in the range 28–817 fb (95% CL) is given for $m_{A_0} = 1.0\text{--}3.0 \text{ TeV}$, see their Fig. 13.
- 45 AAD 20c combine searches for a scalar resonance decaying to HH in 36.1 fb^{-1} of pp collisions at $E_{\text{cm}} = 13 \text{ TeV}$ from AABOUD 19A, AABOUD 19O, AABOUD 18CQ, AABOUD 19T, AABOUD 18CW, and AABOUD 18BU. See their Fig. 5(a) for limits on cross section times branching ratio for $m_{H_2^0} = 0.26\text{--}3 \text{ TeV}$.
- 46 AAD 20L search for b -associated production of H_2^0 decaying to $b \bar{b}$ in 27.8 fb^{-1} of pp collisions at $E_{\text{cm}} = 13 \text{ TeV}$. See their Fig. 8 for limits on the product of cross section and branching ratio for $m_{H_2^0} = 0.45\text{--}1.4 \text{ TeV}$.
- 47 AAD 20x search for vector-boson-fusion production of H_2^0 decaying to HH using 126 fb^{-1} of pp collisions at $E_{\text{cm}} = 13 \text{ TeV}$. See their Fig. 5 for limits on the product of cross section and branching ratio for the assumptions of a narrow- and broad-width resonance.
- 48 AIJ 20AL search for dimuon resonance in the mass range $0.2\text{--}60 \text{ GeV}$ in 5.1 fb^{-1} of pp collisions at $E_{\text{cm}} = 13 \text{ TeV}$, in inclusive and b quark associated production. Displaced decays are searched for for masses below 3 GeV . See their Figs. 7–9 for cross section limits and Fig. 10 for limits for mixing angle in two Higgs doublet plus singlet model (at 90% CL).
- 49 SIRUNYAN 20 search for the decay $H \rightarrow A^0 A^0 \rightarrow \tau^+ \tau^- \tau^+ \tau^-$ or $\tau^+ \tau^- \mu^+ \mu^-$ in 35.9 fb^{-1} of pp collisions at $E_{\text{cm}} = 13 \text{ TeV}$. See their Fig. 10 for limits on the product of production cross section (normalized to the SM) and branching ratios in the range $m_{A_0} = 4\text{--}15 \text{ GeV}$.
- 50 SIRUNYAN 20AA search for $H_2^0 \rightarrow Z A^0$, $A^0 \rightarrow b \bar{b}$ or $A^0 \rightarrow Z H_2^0$, $H_2^0 \rightarrow b \bar{b}$ in 35.9 fb^{-1} of pp collisions at $E_{\text{cm}} = 13 \text{ TeV}$. See their Fig. 7 for limits on the product of cross section and branching ratio for $m_{H_2^0} = 0.12\text{--}1 \text{ TeV}$ and $m_{A_0} = 0.03\text{--}1 \text{ TeV}$.
- 51 SIRUNYAN 20AC search for gluon-fusion production of A^0 decaying to ZH in 35.9 fb^{-1} of pp collisions at $E_{\text{cm}} = 13 \text{ TeV}$. See their Fig. 5 for limits on the product of cross section and branching ratios for $m_{A_0} = 220\text{--}400 \text{ GeV}$.
- 52 SIRUNYAN 20AD search for lepton-flavor violating decays $H_2^0 \rightarrow \mu \tau$, $e \tau$ of gluon-fusion-produced H_2^0 in 35.9 fb^{-1} of pp collisions at $E_{\text{cm}} = 13 \text{ TeV}$. See their Fig. 5 (9) and Table 5 (6) for limits on production cross section times branching ratio for $m_{H_2^0} = 0.2\text{--}0.9 \text{ TeV}$ for the $\mu \tau$ ($e \tau$) final state.
- 53 SIRUNYAN 20AF search for $H_2^0/A^0 \rightarrow t \bar{t}$ with one or two charged leptons in the final state using kinematic variables in 35.9 fb^{-1} of pp collisions at $E_{\text{cm}} = 13 \text{ TeV}$. See their Figs. 5 and 6 for limits on top Yukawa coupling of H_2^0 and A^0 for $m_{H_2^0}$, $m_{A_0} = 0.4\text{--}0.75 \text{ TeV}$ for various width assumptions.
- 54 SIRUNYAN 20AP search for the decay H or $H_2^0 \rightarrow A^0 A^0 \rightarrow \mu^+ \mu^- \tau^+ \tau^-$ (for $m_{H_2^0} = 300 \text{ GeV}$) with boosted final-state topology in 35.9 fb^{-1} of pp collisions at $E_{\text{cm}} = 13 \text{ TeV}$. See their Fig. 7 for limits on the product of production cross section (normalized to the SM) and branching ratios in the range $m_{A_0} = 3.6\text{--}21 \text{ GeV}$, and Figs. 8 and 9 for its interpretation in terms of models with two Higgs doublets plus a singlet.
- 55 SIRUNYAN 20V search for gluon-fusion and vector-boson-fusion production of H_2^0 decaying to $W^+ W^-$ in the final states $l \nu l \nu$ and $l \nu q q$ in 35.9 fb^{-1} of pp collisions at $E_{\text{cm}} = 13 \text{ TeV}$. See their Fig. 6 for limits on the product of cross section and branching ratio for $m_{H_2^0} = 0.2\text{--}3 \text{ TeV}$.
- 56 SIRUNYAN 20Z search for $H_{1,2}^0$ or A^0 production in association with a $t \bar{t}$ pair, decaying to $e^+ e^-$ or $\mu^+ \mu^-$, in 137 fb^{-1} of pp collisions at $E_{\text{cm}} = 13 \text{ TeV}$. See their Fig. 12 for limits on production cross section times branching ratio for $m_{H_{1,2}^0}$, $m_{A_0} = 15\text{--}75 \text{ GeV}$ and $108\text{--}340 \text{ GeV}$.
- 57 AABOUD 19A search for a narrow scalar resonance decaying to $HH \rightarrow b \bar{b} b \bar{b}$ in $27.5\text{--}36.1 \text{ fb}^{-1}$ of pp collisions at $E_{\text{cm}} = 13 \text{ TeV}$. See their Fig. 9(a) for limits on cross section times branching ratios for $m_{H_2^0} = 0.26\text{--}3 \text{ TeV}$.
- 58 AABOUD 19AG search for the decay $H \rightarrow A^0 A^0 \rightarrow \mu^+ \mu^- b \bar{b}$ in 36.7 fb^{-1} of pp collisions at $E_{\text{cm}} = 13 \text{ TeV}$. See their Fig. 6(a) for limits on the product of production cross section (normalized to the SM) and branching ratios in the range $m_{A_0} = 20\text{--}60 \text{ GeV}$.
- 59 AABOUD 19O search for a scalar resonance decaying to $HH \rightarrow b \bar{b} W W^*$ in 36.1 fb^{-1} of pp collisions at $E_{\text{cm}} = 13 \text{ TeV}$. See their Fig. 12 (left) for limits on cross section times branching ratio for $m_{H_2^0} = 0.5\text{--}3 \text{ TeV}$.
- 60 AABOUD 19T search for a scalar resonance decaying to $HH \rightarrow W W^* W W^*$ in 36.1 fb^{-1} of pp collisions at $E_{\text{cm}} = 13 \text{ TeV}$. See their Fig. 3 for limits on cross section times branching ratio for $m_{H_2^0} = 260\text{--}500 \text{ GeV}$, assuming SM decay rates for the H .
- 61 AABOUD 19V combine published ATLAS data to constrain two-Higgs-doublet plus singlet pseudoscalar model with A_1^0 decaying to invisible final states. See their Fig. 19 for excluded parameter regions.
- 62 AABOUD 19Y search for a narrow scalar resonance produced by gluon fusion or b associated production, decaying to $\mu^+ \mu^-$ in 36.1 fb^{-1} of pp collisions at $E_{\text{cm}} = 13 \text{ TeV}$. See their Figs. 4 and 5(a) for cross section limits for $m_{H_2^0} = 0.2\text{--}1.0 \text{ TeV}$.
- 63 AALTONEN 19 search for b associated production of a scalar particle decaying to $b \bar{b}$ in 5.4 fb^{-1} of $p \bar{p}$ collisions at $E_{\text{cm}} = 1.96 \text{ TeV}$. See their Fig. 3 for limits on cross section times branching ratio for $m_{H_{1,2}^0} = 100\text{--}300 \text{ GeV}$.
- 64 SIRUNYAN 19 search for a narrow scalar resonance decaying to $HH \rightarrow \gamma \gamma b \bar{b}$ in 35.9 fb^{-1} of pp collisions at $E_{\text{cm}} = 13 \text{ TeV}$. See their Fig. 9 (left) for limits on cross section times branching ratios for $m_{H_2^0} = 260\text{--}900 \text{ GeV}$.
- 65 SIRUNYAN 19AE search for a scalar resonance produced in association with a $b \bar{b}$ pair, decaying to $\tau^+ \tau^-$ in 35.9 fb^{-1} of pp collisions at $E_{\text{cm}} = 13 \text{ TeV}$. See their Fig. 4 for cross section limits for $m_{A_0} = 25\text{--}70 \text{ GeV}$.
- 66 SIRUNYAN 19AN search for production of A_2^0 decaying to $H A_1^0$ followed by $H \rightarrow b \bar{b}$, $A_1^0 \rightarrow$ invisible in 35.9 fb^{-1} of pp collisions at $E_{\text{cm}} = 13 \text{ TeV}$, in the mass range $m_{A_2^0} = 0.2\text{--}1.6 \text{ TeV}$, $m_{A_1^0} = 0.15\text{--}0.5 \text{ TeV}$. See their Fig. 6 for limits in terms of two-Higgs-doublet plus singlet pseudoscalar model.
- 67 SIRUNYAN 19AV search for a scalar resonance produced by gluon fusion or b -associated production, decaying to $ZH \rightarrow \ell^+ \ell^- b \bar{b}$ ($\ell = e, \mu$) or $\nu \bar{\nu} b \bar{b}$ in 35.9 fb^{-1} of pp collisions at $E_{\text{cm}} = 13 \text{ TeV}$. See their Fig. 5 for cross section limits for $m_{A_0} = 0.22\text{--}1.0 \text{ TeV}$.
- 68 SIRUNYAN 19B search for gluon fusion production of narrow scalar resonance with large transverse momentum, decaying to $b \bar{b}$, in 35.9 fb^{-1} of pp collisions at $E_{\text{cm}} = 13 \text{ TeV}$. See their Figs. 7 and 8 for limits on cross section times branching ratio for the resonance mass of $50\text{--}350 \text{ GeV}$.
- 69 SIRUNYAN 19BB search for the decay $H_1^0 \rightarrow \gamma \gamma$ in 19.7 fb^{-1} of pp collisions at $E_{\text{cm}} = 8 \text{ TeV}$ and 35.9 fb^{-1} at $E_{\text{cm}} = 13 \text{ TeV}$. See their Figs. 4–6 for limits on cross section times branching ratio for $m_{H_1^0} = 80\text{--}110 \text{ GeV}$ (some results in Fig. 5 for $m_{H_1^0} = 70\text{--}110 \text{ GeV}$).
- 70 SIRUNYAN 19BD search for the decay $H \rightarrow A^0 A^0 \rightarrow \mu^+ \mu^- b \bar{b}$ in 35.9 fb^{-1} of pp collisions at $E_{\text{cm}} = 13 \text{ TeV}$. See their Fig. 5 for limits on the product of cross section times branching ratios in the range $m_{A_0} = 20\text{--}62.5 \text{ GeV}$. See also their Figs. 6 and 7 for interpretation of the data in terms of models with two Higgs doublets and a singlet.
- 71 SIRUNYAN 19BE combine searches for $H_2^0 \rightarrow HH$ in 35.9 fb^{-1} of pp collisions at $E_{\text{cm}} = 13 \text{ TeV}$ in various H decay modes, from SIRUNYAN 18A, SIRUNYAN 18AF, SIRUNYAN 18CW, SIRUNYAN 19, and SIRUNYAN 19H. See their Fig. 3 for limits on cross section times branching ratios for $m_{H_2^0} = 0.25\text{--}3 \text{ TeV}$.
- 72 SIRUNYAN 19BQ search for production of $H_{1,2}^0$ decaying to $A^0 A^0 \rightarrow \mu^+ \mu^- \mu^+ \mu^-$ in 35.9 fb^{-1} of pp collisions at $E_{\text{cm}} = 13 \text{ TeV}$. See their Fig. 2 for limits on cross section times branching ratio for $m_{H_{1,2}^0} = 90\text{--}150 \text{ GeV}$, $m_{A_0} = 0.25\text{--}3.55 \text{ GeV}$.
- 73 SIRUNYAN 19CR search for production of H_2^0/A^0 in gluon fusion and in association with a $b \bar{b}$ pair, decaying to $\mu^+ \mu^-$ in 35.9 fb^{-1} of pp collisions at $E_{\text{cm}} = 13 \text{ TeV}$. See their Fig. 6 for limits on cross section times branching ratio.
- 74 SIRUNYAN 19H search for a narrow scalar resonance decaying to $HH \rightarrow b \bar{b} b \bar{b}$ in 35.9 fb^{-1} of pp collisions at $E_{\text{cm}} = 13 \text{ TeV}$, where one $b \bar{b}$ pair is resolved and the other not. Limits on cross section times branching ratios for $m_{H_2^0} = 0.75\text{--}1.6 \text{ TeV}$ are obtained and combined with data from SIRUNYAN 18AF. See their Fig. 5 (right).
- 75 AABOUD 18AA search for production of a scalar resonance decaying to $Z \gamma$, with Z decaying hadronically, in 36.1 fb^{-1} of pp collisions at $E_{\text{cm}} = 13 \text{ TeV}$. See their Fig. 8(a) for limits on cross section times branching ratio for $m_{H_2^0} = 1.0\text{--}6.8 \text{ TeV}$.
- 76 AABOUD 18AG search for the decay $H \rightarrow A^0 A^0 \rightarrow \gamma \gamma g g$ in 36.7 fb^{-1} of pp collisions at $E_{\text{cm}} = 13 \text{ TeV}$. See their Fig. 2 and Table 6 for cross section limits in the range $m_{A_0} = 20\text{--}60 \text{ GeV}$.
- 77 AABOUD 18AH search for production of an A^0 in gluon-gluon fusion and in association with a $b \bar{b}$, decaying to $Z H_2^0 \rightarrow \ell^+ \ell^- b \bar{b}$ in 36.1 fb^{-1} of pp collisions at $E_{\text{cm}} = 13 \text{ TeV}$. See their Fig. 5 for cross section limits for $m_{A_0} = 230\text{--}800 \text{ GeV}$ and $m_{H_2^0} = 130\text{--}700 \text{ GeV}$.
- 78 AABOUD 18AI search for production of an A^0 in gluon-gluon fusion and in association with a $b \bar{b}$, decaying to ZH in the final states $\nu \bar{\nu} b \bar{b}$ and $\ell^+ \ell^- b \bar{b}$ in 36.1 fb^{-1} of pp collisions at $E_{\text{cm}} = 13 \text{ TeV}$. See their Fig. 6 for cross section limits for $m_{A_0} = 0.2\text{--}2 \text{ TeV}$. See also AABOUD 18CC.
- 79 AABOUD 18BF search for production of a heavy H_2^0 state decaying to ZZ in the final states $\ell^+ \ell^- \ell^+ \ell^-$ and $\ell^+ \ell^- \nu \bar{\nu}$ in 36.1 fb^{-1} of pp collisions at $E_{\text{cm}} = 13 \text{ TeV}$. See their Fig. 6 for upper limits on cross section times branching ratio for $m_{H_2^0} = 0.2\text{--}1.2 \text{ TeV}$ assuming ggF or VBF with the NWA. See their Fig. 7 for upper limits on cross section times branching ratio for $m_{H_2^0} = 0.4\text{--}1.0 \text{ TeV}$ assuming ggF, and with several assumptions on its width.
- 80 AABOUD 18BU search for a narrow scalar resonance decaying to $HH \rightarrow \gamma \gamma W W^*$ in 36.1 fb^{-1} of pp collisions at $E_{\text{cm}} = 13 \text{ TeV}$. See their Fig. 4 for limits on cross section times branching ratios for $m_{H_2^0} = 260\text{--}500 \text{ GeV}$.
- 81 AABOUD 18BX search for associated production of WH or ZH followed by the decay $H \rightarrow A^0 A^0 \rightarrow b \bar{b} b \bar{b}$ in 36.1 fb^{-1} of pp collisions at $E_{\text{cm}} = 13 \text{ TeV}$. See their Fig. 9 for limits on cross section times branching ratios for $m_{A_0} = 20\text{--}60 \text{ GeV}$. See also their Fig. 10 for the dependence of the limit on A^0 lifetime.
- 82 AABOUD 18CQ search for a narrow scalar resonance decaying to $HH \rightarrow b \bar{b} \tau^+ \tau^-$ in 36.1 fb^{-1} of pp collisions at $E_{\text{cm}} = 13 \text{ TeV}$. See their Fig. 2 (above) for limits on cross section times branching ratios for $m_{H_2^0} = 260\text{--}1000 \text{ GeV}$.
- 83 AABOUD 18F search for production of a narrow scalar resonance decaying to $W^+ W^-$ and ZZ , followed by hadronic decays of W and Z , in 36.7 fb^{-1} of pp collisions at $E_{\text{cm}} = 13 \text{ TeV}$. See their Fig. 5(c) for limits on cross section times branching ratio for $m_{H_2^0} = 1.2\text{--}3.0 \text{ TeV}$.
- 84 AIJ 18AM search for gluon-fusion production of $H_{1,2}^0$ decaying to $\mu \tau$ in 2 fb^{-1} of pp collisions at $E_{\text{cm}} = 8 \text{ TeV}$. See their Fig. 2 for limits on cross section times branching ratio for $m_{H_{1,2}^0} = 45\text{--}195 \text{ GeV}$.
- 85 AIJ 18AQ search for gluon-fusion production of a scalar particle A^0 decaying to $\mu^+ \mu^-$ in 1.99 fb^{-1} of pp collisions at $E_{\text{cm}} = 8 \text{ TeV}$ and 0.98 fb^{-1} at $E_{\text{cm}} = 7 \text{ TeV}$. See their Fig. 4 for limits on cross section times branching ratio for $m_{A_0} = 5.5\text{--}15 \text{ GeV}$ (using the $E_{\text{cm}} = 8 \text{ TeV}$ data set).
- 86 AIJ 18AQ search for the decay $H \rightarrow A^0 A^0$, with one of the A^0 decaying to $\mu^+ \mu^-$, in 1.99 fb^{-1} of pp collisions at $E_{\text{cm}} = 8 \text{ TeV}$ and 0.98 fb^{-1} at $E_{\text{cm}} = 7 \text{ TeV}$. See their Fig. 5 (right) for limits on the product of branching ratios for $m_{A_0} = 5.5\text{--}15 \text{ GeV}$ (using the $E_{\text{cm}} = 8 \text{ TeV}$ data set).
- 87 SIRUNYAN 18AF search for a narrow scalar resonance decaying to $HH \rightarrow b \bar{b} b \bar{b}$ in 35.9 fb^{-1} of pp collisions at $E_{\text{cm}} = 13 \text{ TeV}$, where both $b \bar{b}$ pairs are not resolved. See their Fig. 9 for limits on cross section times branching ratios for $m_{H_2^0} = 0.75\text{--}3 \text{ TeV}$.

Gauge & Higgs Boson Particle Listings

Neutral Higgs Bosons, Searches for

- 88 SIRUNYAN 18BA search for production of a heavy H_2^0 state decaying to ZZ in the final states $\ell^+\ell^-\ell^+\ell^-$, $\ell^+\ell^-q\bar{q}$, and $\ell^+\ell^-\nu\bar{\nu}$ in 35.9 fb^{-1} of pp collisions at $E_{\text{cm}} = 13 \text{ TeV}$. See their Figs. 10 and 11 for upper limits on cross section times branching ratio for $m_{H_2^0} = 0.13\text{--}3 \text{ TeV}$ with several assumptions on its width and on the fraction of Vector-Boson-Fusion of the total production cross section.
- 89 SIRUNYAN 18CW search for a narrow scalar resonance decaying to $HH \rightarrow b\bar{b}b\bar{b}$ in 35.9 fb^{-1} of pp collisions at $E_{\text{cm}} = 13 \text{ TeV}$, where both $b\bar{b}$ pairs are resolved. See their Fig. 9 for limits on cross section times branching ratios for $m_{H_2^0} = 260\text{--}1200 \text{ GeV}$.
- 90 SIRUNYAN 18DK search for production of a scalar resonance decaying to $Z\gamma$, with Z decaying to $\ell^+\ell^-$ or hadronically, in 35.9 fb^{-1} of pp collisions at $E_{\text{cm}} = 13 \text{ TeV}$. See their Fig. 7 for limits on cross section times branching ratio for $m_{H_2^0} = 0.35\text{--}4 \text{ TeV}$ for different assumptions on the width of the resonance.
- 91 SIRUNYAN 18DT search for the decay $H \rightarrow A^0 A^0 \rightarrow \tau^+\tau^-b\bar{b}$ in 35.9 fb^{-1} of pp collisions at $E_{\text{cm}} = 13 \text{ TeV}$. See their Fig. 7 for limits on the product of branching ratios in the range $m_{A^0} = 15\text{--}60 \text{ GeV}$. See also their Fig. 8 for interpretation of the data in terms of models with two Higgs doublets and a singlet.
- 92 SIRUNYAN 18DU search for production of a narrow scalar resonance decaying to $\gamma\gamma$ in 35.9 fb^{-1} (taken in 2016) of pp collisions at $E_{\text{cm}} = 13 \text{ TeV}$. See their Fig. 3 (right) for limits on cross section times branching ratio for $m_{H_2^0} = 0.5\text{--}5 \text{ TeV}$ for several values of its width-to-mass ratio.
- 93 SIRUNYAN 18ED search for production of an A^0 in gluon-gluon fusion and in association with a $b\bar{b}$, decaying to ZH in the final states $\nu\tau b\bar{b}$ or $\ell^+\ell^-b\bar{b}$ in 35.9 fb^{-1} of pp collisions at $E_{\text{cm}} = 13 \text{ TeV}$. See their Fig. 8 for cross section limits for $m_{A^0} = 0.8\text{--}2 \text{ TeV}$.
- 94 SIRUNYAN 18EE search for the decay $H \rightarrow A^0 A^0 \rightarrow \mu^+\mu^-\tau^+\tau^-$ in 35.9 fb^{-1} of pp collisions at $E_{\text{cm}} = 13 \text{ TeV}$. See their Fig. 4 for limits on the product of branching ratios in the range $m_{A^0} = 15\text{--}62.5 \text{ GeV}$, normalized to the SM production cross section. See also their Fig. 5 for interpretation of the data in terms of models with two Higgs doublets and a singlet.
- 95 SIRUNYAN 18F search for a narrow scalar resonance decaying to $HH \rightarrow WWb\bar{b}$ or $ZZb\bar{b}$ in the final state $\ell\ell\nu\nu b\bar{b}$ in 35.9 fb^{-1} of pp collisions at $E_{\text{cm}} = 13 \text{ TeV}$. See their Fig. 7 for limits on cross section times branching ratios for $m_{H_2^0} = 250\text{--}900 \text{ GeV}$.
- 96 ABOUD 17 search for production of a scalar resonance decaying to $Z\gamma$ in 3.2 fb^{-1} of pp collisions at $E_{\text{cm}} = 13 \text{ TeV}$. See their Fig. 4 for the limits on cross section times branching ratio for $m_{H_2^0} = 0.25\text{--}3.0 \text{ TeV}$.
- 97 ABOUD 17AP search for production of a scalar resonance decaying to $\gamma\gamma$ in 36.7 fb^{-1} of pp collisions at $E_{\text{cm}} = 13 \text{ TeV}$. See their Fig. 4(a) for limits on fiducial cross section times branching ratio for $m_{H_2^0} = 0.2\text{--}2.7 \text{ TeV}$ with narrow width approximation.
- 98 ABOUD 17AW search for production of a scalar resonance decaying to $Z\gamma$ in 36.1 fb^{-1} of pp collisions at $E_{\text{cm}} = 13 \text{ TeV}$. See their Fig. 7 for limits on cross section times branching ratio for $m_{H_2^0} = 0.25\text{--}2.4 \text{ TeV}$.
- 99 KHACHATRYAN 17AZ search for the decay $H \rightarrow A^0 A^0 \rightarrow \tau^+\tau^-\tau^+\tau^-$, $\mu^+\mu^-b\bar{b}$, and $\mu^+\mu^-\tau^+\tau^-$ in 19.7 fb^{-1} of pp collisions at $E_{\text{cm}} = 8 \text{ TeV}$. See their Figs. 4, 5, and 6 for cross section limits in the range $m_{A^0} = 5\text{--}62.5 \text{ GeV}$. See also their Figs. 7, 8, and 9 for interpretation of the data in terms of models with two Higgs doublets and a singlet.
- 100 KHACHATRYAN 17D search for production of a scalar resonance decaying to $Z\gamma$ in 19.7 fb^{-1} of pp collisions at $E_{\text{cm}} = 8 \text{ TeV}$ and 2.7 fb^{-1} at $E_{\text{cm}} = 13 \text{ TeV}$. See their Figs. 3 and 4 for the limits on cross section times branching ratio for $m_{H_2^0} = 0.2\text{--}2.0 \text{ TeV}$.
- 101 KHACHATRYAN 17R search for production of a narrow scalar resonance decaying to $\gamma\gamma$ in 12.9 fb^{-1} (taken in 2016) of pp collisions at $E_{\text{cm}} = 13 \text{ TeV}$. See their Fig. 2 for limits on cross section times branching ratio for $m_{H_2^0} = 0.5\text{--}4.5 \text{ TeV}$ for several values of its width-to-mass ratio. Limits from combination with KHACHATRYAN 16M are shown in their Figs. 4 and 6.
- 102 SIRUNYAN 17CN search for a narrow scalar resonance decaying to $HH \rightarrow b\bar{b}\tau^+\tau^-$ in 18.3 fb^{-1} of pp collisions at $E_{\text{cm}} = 8 \text{ TeV}$. See their Fig. 5 (above) and Table II for limits on the cross section times branching ratios for $m_{H_2^0} = 0.3\text{--}1 \text{ TeV}$, and Fig. 6 (above) and Table III for the corresponding limits by combining with data from KHACHATRYAN 16BQ and KHACHATRYAN 15R.
- 103 SIRUNYAN 17Y search for production of a scalar resonance decaying to $Z\gamma$ in 19.7 fb^{-1} of pp collisions at $E_{\text{cm}} = 8 \text{ TeV}$ and 2.7 fb^{-1} at $E_{\text{cm}} = 13 \text{ TeV}$. See their Figs. 3, 4 and Table 3 for limits on cross section times branching ratio for $m_{H_2^0} = 0.7\text{--}3.0 \text{ TeV}$, and Fig. 5 for the corresponding limits for $m_{H_2^0} = 0.2\text{--}3.0 \text{ TeV}$ from combination with KHACHATRYAN 17D data.
- 104 ABOUD 16AB search for associated production of WH with the decay $H \rightarrow A^0 A^0 \rightarrow b\bar{b}b\bar{b}$ in 3.2 fb^{-1} of pp collisions at $E_{\text{cm}} = 13 \text{ TeV}$. See their Fig. 8 for limits on cross section times branching ratios for $m_{A^0} = 20\text{--}60 \text{ GeV}$.
- 105 ABOUD 16AE search for production of a narrow scalar resonance decaying to W^+W^- and ZZ in 3.2 fb^{-1} of pp collisions at $E_{\text{cm}} = 13 \text{ TeV}$. See their Fig. 4 for limits on cross section times branching ratio for $m_{H_2^0} = 0.5\text{--}3 \text{ TeV}$.
- 106 ABOUD 16H search for production of a scalar resonance decaying to $\gamma\gamma$ in 3.2 fb^{-1} of pp collisions at $E_{\text{cm}} = 13 \text{ TeV}$. See their Fig. 12 for limits on cross section times branching ratio for $m_{H_2^0} = 0.2\text{--}2 \text{ TeV}$ with different assumptions on the width.
- 107 ABOUD 16I search for a narrow scalar resonance decaying to $HH \rightarrow b\bar{b}b\bar{b}$ in 3.2 fb^{-1} of pp collisions at $E_{\text{cm}} = 13 \text{ TeV}$. See their Fig. 10(c) for limits on cross section times branching ratios for $m_{H_2^0} = 0.5\text{--}3 \text{ TeV}$.
- 108 AAD 16AX search for production of a heavy H state decaying to ZZ in the final states $\ell^+\ell^-\ell^+\ell^-$, $\ell^+\ell^-\nu\bar{\nu}$, $\ell^+\ell^-q\bar{q}$, and $\nu\tau b\bar{b}$ in 20.3 fb^{-1} of pp collisions at $E_{\text{cm}} = 8 \text{ TeV}$. See their Fig. 12 for upper limits on $\sigma(H)B(H \rightarrow ZZ)$ for m_H ranging from 140 GeV to 1000 GeV .
- 109 AAD 16C search for production of a heavy H state decaying to W^+W^- in the final states $\ell\nu\ell\nu$ and $\ell\nu q\bar{q}$ in 20.3 fb^{-1} of pp collisions at $E_{\text{cm}} = 8 \text{ TeV}$. See their Figs. 12, 13, and 16 for upper limits on $\sigma(H)B(H \rightarrow W^+W^-)$ for m_H ranging from 300 GeV to 1000 or 1500 GeV with various assumptions on the total width of H .
- 110 AAD 16L search for the decay $H \rightarrow A^0 A^0 \rightarrow \gamma\gamma\gamma\gamma$ in 20.3 fb^{-1} of pp collisions at $E_{\text{cm}} = 8 \text{ TeV}$. See their Fig. 4 (upper right) for limits on cross section times branching ratios (normalized to the SM H cross section) for $m_{A^0} = 10\text{--}60 \text{ GeV}$.
- 111 AAD 16L search for the decay $H_2^0 \rightarrow A^0 A^0 \rightarrow \gamma\gamma\gamma\gamma$ in 20.3 fb^{-1} of pp collisions at $E_{\text{cm}} = 8 \text{ TeV}$. See their Fig. 4 (lower right) for limits on cross section times branching ratios for $m_{H_2^0} = 600 \text{ GeV}$ and $m_{A^0} = 10\text{--}245 \text{ GeV}$, and Table 5 for limits for $m_{H_2^0} = 300$ and 900 GeV .
- 112 AALTONEN 16C search for electroweak associated production of $H_1^0 H^\pm$ followed by the decays $H^\pm \rightarrow H_1^0 W^*$, $H_1^0 \rightarrow \gamma\gamma$ for $m_{H_1^0} = 10\text{--}105 \text{ GeV}$ and $m_{H^\pm} = 30\text{--}300 \text{ GeV}$. See their Fig. 3 for excluded parameter region in a two-doublet model in which H_1^0 has no direct decay to fermions.
- 113 KHACHATRYAN 16BG search for a narrow scalar resonance decaying to $HH \rightarrow b\bar{b}b\bar{b}$ in 19.7 fb^{-1} of pp collisions at $E_{\text{cm}} = 8 \text{ TeV}$. See their Fig. 6 for limits on the cross section times branching ratios for $m_{H_2^0} = 1.15\text{--}3 \text{ TeV}$.
- 114 KHACHATRYAN 16BQ search for a resonance decaying to $HH \rightarrow \gamma\gamma b\bar{b}$ in 19.7 fb^{-1} of pp collisions at $E_{\text{cm}} = 8 \text{ TeV}$. See their Fig. 9 for limits on the cross section times branching ratios for $m_{H_2^0} = 0.26\text{--}1.1 \text{ TeV}$.
- 115 KHACHATRYAN 16F search for the decay $H \rightarrow H_1^0 H_1^0 \rightarrow \tau^+\tau^-\tau^+\tau^-$ in 19.7 fb^{-1} of pp collisions at $E_{\text{cm}} = 8 \text{ TeV}$. See their Fig. 8 for cross section limits for $m_{H_1^0} = 4\text{--}8 \text{ GeV}$.
- 116 KHACHATRYAN 16M search for production of a narrow resonance decaying to $\gamma\gamma$ in 19.7 fb^{-1} of pp collisions at $E_{\text{cm}} = 8 \text{ TeV}$ and 3.3 fb^{-1} at $E_{\text{cm}} = 13 \text{ TeV}$. See their Fig. 3 (top) for limits on cross section times branching ratio for $m_{H_2^0} = 0.5\text{--}4 \text{ TeV}$.
- 117 KHACHATRYAN 16P search for gluon fusion production of an H_2^0 decaying to $HH \rightarrow b\bar{b}\tau^+\tau^-$ in 19.7 fb^{-1} of pp collisions at $E_{\text{cm}} = 8 \text{ TeV}$. See their Fig. 8 (lower right) for cross section limits for $m_{H_2^0} = 260\text{--}350 \text{ GeV}$.
- 118 KHACHATRYAN 16P search for gluon fusion production of an A^0 decaying to $ZH \rightarrow \ell^+\ell^-\tau^+\tau^-$ in 19.7 fb^{-1} of pp collisions at $E_{\text{cm}} = 8 \text{ TeV}$. See their Fig. 10 for cross section limits for $m_{H_2^0} = 220\text{--}350 \text{ GeV}$.
- 119 AAD 15BK search for production of a heavy H_2^0 decaying to HH in the final state $b\bar{b}b\bar{b}$ in 19.5 fb^{-1} of pp collisions at $E_{\text{cm}} = 8 \text{ TeV}$. See their Fig. 14(c) for $\sigma(H_2^0)B(H_2^0 \rightarrow HH)$ for $m_{H_2^0} = 500\text{--}1500 \text{ GeV}$ with $\Gamma_{H_2^0} = 1 \text{ GeV}$.
- 120 AAD 15BZ search for the decay $H \rightarrow A^0 A^0 \rightarrow \mu^+\mu^-\tau^+\tau^-$ ($m_H = 125 \text{ GeV}$) in 20.3 fb^{-1} of pp collisions at $E_{\text{cm}} = 8 \text{ TeV}$. See their Fig. 6 for limits on cross section times branching ratio for $m_{A^0} = 3.7\text{--}50 \text{ GeV}$.
- 121 AAD 15BZ search for a state H_2^0 via the decay $H_2^0 \rightarrow A^0 A^0 \rightarrow \mu^+\mu^-\tau^+\tau^-$ in 20.3 fb^{-1} of pp collisions at $E_{\text{cm}} = 8 \text{ TeV}$. See their Fig. 6 for limits on cross section times branching ratio for $m_{H_2^0} = 100\text{--}500 \text{ GeV}$ and $m_{A^0} = 5 \text{ GeV}$.
- 122 AAD 15CE search for production of a heavy H_2^0 decaying to HH in the final states $b\bar{b}\tau^+\tau^-$ and $\gamma\gamma WW^*$ in 20.3 fb^{-1} of pp collisions at $E_{\text{cm}} = 8 \text{ TeV}$ and combine with data from AAD 15H and AAD 15BK. A limit $\sigma(H_2^0)B(H_2^0 \rightarrow HH) < 2.1\text{--}0.011 \text{ pb}$ (95% CL) is given for $m_{H_2^0} = 260\text{--}1000 \text{ GeV}$. See their Fig. 6.
- 123 AAD 15H search for production of a heavy H_2^0 decaying to HH in the final state $\gamma\gamma b\bar{b}$ in 20.3 fb^{-1} of pp collisions at $E_{\text{cm}} = 8 \text{ TeV}$. A limit of $\sigma(H_2^0)B(H_2^0 \rightarrow HH) < 3.5\text{--}0.7 \text{ pb}$ is given for $m_{H_2^0} = 260\text{--}500 \text{ GeV}$ at 95% CL. See their Fig. 3.
- 124 AAD 15S search for production of A^0 decaying to $ZH \rightarrow \ell^+\ell^-b\bar{b}$, $\nu\tau b\bar{b}$ and $\ell^+\ell^-\tau^+\tau^-$ in 20.3 fb^{-1} of pp collisions at $E_{\text{cm}} = 8 \text{ TeV}$. See their Fig. 3 for cross section limits for $m_{A^0} = 200\text{--}1000 \text{ GeV}$.
- 125 KHACHATRYAN 15AW search for production of a heavy state H_2^0 of an electroweak singlet extension of the Standard Model via the decays of H_2^0 to W^+W^- and ZZ in up to 5.1 fb^{-1} of pp collisions at $E_{\text{cm}} = 7 \text{ TeV}$ and up to 19.7 fb^{-1} at $E_{\text{cm}} = 8 \text{ TeV}$ in the range $m_{H_2^0} = 145\text{--}1000 \text{ GeV}$. See their Figs. 8 and 9 for limits in the parameter space of the model.
- 126 KHACHATRYAN 15BB search for production of a resonance H decaying to $\gamma\gamma$ in 19.7 fb^{-1} of pp collisions at $E_{\text{cm}} = 8 \text{ TeV}$. See their Fig. 7 for limits on cross section times branching ratio for $m_H = 150\text{--}850 \text{ GeV}$.
- 127 KHACHATRYAN 15N search for production of A^0 decaying to $ZH \rightarrow \ell^+\ell^-b\bar{b}$ in 19.7 fb^{-1} of pp collisions at $E_{\text{cm}} = 8 \text{ TeV}$. See their Fig. 3 for limits on cross section times branching ratios for $m_{A^0} = 225\text{--}600 \text{ GeV}$.
- 128 KHACHATRYAN 15O search for production of a high-mass narrow resonance A^0 decaying to $ZH \rightarrow q\bar{q}\tau^+\tau^-$ in 19.7 fb^{-1} of pp collisions at $E_{\text{cm}} = 8 \text{ TeV}$. See their Fig. 6 for limits on cross section times branching ratios for $m_{A^0} = 800\text{--}2500 \text{ GeV}$.
- 129 KHACHATRYAN 15R search for a narrow scalar resonance decaying to $HH \rightarrow b\bar{b}b\bar{b}$ in 17.9 fb^{-1} of pp collisions at $E_{\text{cm}} = 8 \text{ TeV}$. See their Fig. 5 (top) for limits on cross section times branching ratios for $m_{H_2^0} = 0.27\text{--}1.1 \text{ TeV}$.
- 130 AAD 14AP search for a second H state decaying to $\gamma\gamma$ in addition to the state at about 125 GeV in 20.3 fb^{-1} of pp collisions at $E_{\text{cm}} = 8 \text{ TeV}$. See their Fig. 4 for limits on cross section times branching ratio for $m_H = 65\text{--}600 \text{ GeV}$.
- 131 AAD 14M search for the decay cascade $H_2^0 \rightarrow H^\pm W^\mp \rightarrow HW^\pm W^\mp$, H decaying to $b\bar{b}$ in 20.3 fb^{-1} of pp collisions at $E_{\text{cm}} = 8 \text{ TeV}$. See their Table III for limits on cross section times branching ratio for $m_{H_2^0} = 325\text{--}1025 \text{ GeV}$ and $m_{H^\pm} = 225\text{--}925 \text{ GeV}$.
- 132 CHATRCHYAN 14G search for a second H state decaying to WW^* in addition to the observed signal at about 125 GeV using 4.9 fb^{-1} of pp collisions at $E_{\text{cm}} = 7 \text{ TeV}$ and 19.4 fb^{-1} at $E_{\text{cm}} = 8 \text{ TeV}$. See their Fig. 21 (right) for cross section limits in the mass range $110\text{--}600 \text{ GeV}$.

See key on page 1171

Gauge & Higgs Boson Particle Listings

Neutral Higgs Bosons, Searches for

- 133 KHACHATRYAN 14P search for a second H state decaying to $\gamma\gamma$ in addition to the observed signal at about 125 GeV using 5.1 fb^{-1} of pp collisions at $E_{\text{cm}} = 7 \text{ TeV}$ and 19.7 fb^{-1} at $E_{\text{cm}} = 8 \text{ TeV}$. See their Figs. 27 and 28 for cross section limits in the mass range 110–150 GeV.
- 134 AALTONEN 13P search for production of a heavy Higgs boson $H^{0'}$ that decays into a charged Higgs boson H^{\pm} and a lighter Higgs boson H via the decay chain $H^{0'} \rightarrow H^{\pm} W^{\mp}, H^{\pm} \rightarrow W^{\pm} H, H \rightarrow b\bar{b}$ in the final state $\ell\nu$ plus 4 jets in 8.7 fb^{-1} of $p\bar{p}$ collisions at $E_{\text{cm}} = 1.96 \text{ TeV}$. See their Fig. 4 for limits on cross section times branching ratio in the $m_{H^{\pm}} - m_{H^{0'}}$ plane for $m_H = 126 \text{ GeV}$.
- 135 CHATRCHYAN 13BJ search for H production in the decay chain $H \rightarrow A^0 A^0, A^0 \rightarrow \mu^+ \mu^-$ in 5.3 fb^{-1} of pp collisions at $E_{\text{cm}} = 7 \text{ TeV}$. See their Fig. 2 for limits on cross section times branching ratio.
- 136 AALTONEN 11P search in 2.7 fb^{-1} of $p\bar{p}$ collisions at $E_{\text{cm}} = 1.96 \text{ TeV}$ for the decay chain $t \rightarrow bH^+, H^+ \rightarrow W^+ A^0, A^0 \rightarrow \tau^+ \tau^-$ with m_{A^0} between 4 and 9 GeV. See their Fig. 4 for limits on $B(t \rightarrow bH^+)$ for $90 < m_{H^+} < 160 \text{ GeV}$.
- 137 ABBIENDI 10 search for $e^+ e^- \rightarrow ZH$ with the decay chain $H \rightarrow \tilde{\chi}_1^0 \tilde{\chi}_2^0, \tilde{\chi}_2^0 \rightarrow \tilde{\chi}_1^0 + (\gamma \text{ or } Z^*)$, when $\tilde{\chi}_1^0$ and $\tilde{\chi}_2^0$ are nearly degenerate. For a mass difference of 2 (4) GeV, a lower limit on m_H of 108.4 (107.0) GeV (95% CL) is obtained for SM ZH cross section and $B(H \rightarrow \tilde{\chi}_1^0 \tilde{\chi}_2^0) = 1$.
- 138 SCHAEEL 10 search for the process $e^+ e^- \rightarrow HZ$ followed by the decay chain $H \rightarrow A^0 A^0 \rightarrow \tau^+ \tau^- \tau^+ \tau^-$ with $Z \rightarrow \ell^+ \ell^-, \nu\bar{\nu}$ at $E_{\text{cm}} = 183\text{--}209 \text{ GeV}$. For a HZZ coupling equal to the SM value, $B(H \rightarrow A^0 A^0) = B(A^0 \rightarrow \tau^+ \tau^-) = 1$, and $m_{A^0} = 4\text{--}10 \text{ GeV}$, m_H up to 107 GeV is excluded at 95% CL.
- 139 ABAZOV 09v search for H production followed by the decay chain $H \rightarrow A^0 A^0 \rightarrow \mu^+ \mu^- \mu^+ \mu^-$ or $\mu^+ \mu^- \tau^+ \tau^-$ in 4.2 fb^{-1} of $p\bar{p}$ collisions at $E_{\text{cm}} = 1.96 \text{ TeV}$. See their Fig. 3 for limits on $\sigma(H) \cdot B(H \rightarrow A^0 A^0)$ for $m_{A^0} = 3.6\text{--}19 \text{ GeV}$.
- 140 ABBIENDI 05A search for $e^+ e^- \rightarrow H_1^0 A^0$ in general Type-II two-doublet models, with decays $H_1^0, A^0 \rightarrow q\bar{q}, gg, \tau^+ \tau^-$, and $H_1^0 \rightarrow A^0 A^0$.
- 141 ABBIENDI 04k search for $e^+ e^- \rightarrow HZ$ with H decaying to two jets of any flavor including $g\bar{g}$. The limit is for SM production cross section with $B(H \rightarrow jj) = 1$.
- 142 ABDALLAH 04 consider the full combined LEP and LEP2 datasets to set limits on the Higgs coupling to W or Z bosons, assuming SM decays of the Higgs. Results in Fig. 26.
- 143 ACHARD 04B search for $e^+ e^- \rightarrow HZ$ with H decaying to $b\bar{b}, c\bar{c}$, or $g\bar{g}$. The limit is for SM production cross section with $B(H \rightarrow jj) = 1$.
- 144 ACHARD 04f search for H with anomalous coupling to gauge boson pairs in the processes $e^+ e^- \rightarrow H\gamma, e^+ e^- H, HZ$ with decays $H \rightarrow f\bar{f}, \gamma\gamma, Z\gamma$, and $W^* W$ at $E_{\text{cm}} = 189\text{--}209 \text{ GeV}$. See paper for limits.
- 145 ABBIENDI 03f search for $H \rightarrow$ anything in $e^+ e^- \rightarrow HZ$, using the recoil mass spectrum of $Z \rightarrow e^+ e^-$ or $\mu^+ \mu^-$. In addition, it searched for $Z \rightarrow \nu\bar{\nu}$ and $H \rightarrow e^+ e^-$ or photons. Scenarios with large width or continuum H mass distribution are considered. See their Figs. 11–14 for the results.
- 146 ABBIENDI 03g search for $e^+ e^- \rightarrow H_1^0 Z$ followed by $H_1^0 \rightarrow A^0 A^0, A^0 \rightarrow c\bar{c}, g\bar{g}$, or $\tau^+ \tau^-$ in the region $m_{H_1^0} = 45\text{--}86 \text{ GeV}$ and $m_{A^0} = 2\text{--}11 \text{ GeV}$. See their Fig. 7 for the limits.
- 147 Search for associated production of a $\gamma\gamma$ resonance with a Z boson, followed by $Z \rightarrow q\bar{q}, \ell^+ \ell^-$, or $\nu\bar{\nu}$, at $E_{\text{cm}} \leq 209 \text{ GeV}$. The limit is for a H with SM production cross section and $B(H \rightarrow f\bar{f})=0$ for all fermions f .
- 148 For $B(H \rightarrow \gamma\gamma)=1, m_H > 113.1 \text{ GeV}$ is obtained.
- 149 HEISTER 02M search for $e^+ e^- \rightarrow HZ$, assuming that H decays to $q\bar{q}, g\bar{g}$, or $\tau^+ \tau^-$ only. The limit assumes SM production cross section.
- 150 ABBIENDI 01E search for neutral Higgs bosons in general Type-II two-doublet models, at $E_{\text{cm}} \leq 189 \text{ GeV}$. In addition to usual final states, the decays $H_1^0, A^0 \rightarrow q\bar{q}, g\bar{g}$ are searched for. See their Figs. 15, 16 for excluded regions.
- 151 ACCIARRI 00r search for $e^+ e^- \rightarrow H\gamma$ with $H \rightarrow b\bar{b}, Z\gamma$, or $\gamma\gamma$. See their Fig. 3 for limits on $\sigma \cdot B$. Explicit limits within an effective interaction framework are also given, for which the Standard Model Higgs search results are used in addition.
- 152 ACCIARRI 00r search for the two-photon type processes $e^+ e^- \rightarrow e^+ e^- H$ with $H \rightarrow b\bar{b}$ or $\gamma\gamma$. See their Fig. 4 for limits on $\Gamma(H \rightarrow \gamma\gamma) \cdot B(H \rightarrow \gamma\gamma \text{ or } b\bar{b})$ for $m_H = 70\text{--}170 \text{ GeV}$.
- 153 GONZALEZ-GARCIA 98b use $D\bar{0}$ limit for $\gamma\gamma$ events with missing E_T in $p\bar{p}$ collisions (ABBOTT 98) to constrain possible ZH or WH production followed by unconventional $H \rightarrow \gamma\gamma$ decay which is induced by higher-dimensional operators. See their Figs. 1 and 2 for limits on the anomalous couplings.
- 154 KRAWCZYK 97 analyse the muon anomalous magnetic moment in a two-doublet Higgs model (with type II Yukawa couplings) assuming no $H_1^0 Z$ coupling and obtain $m_{H_1^0} \gtrsim 5 \text{ GeV}$ or $m_{A^0} \gtrsim 5 \text{ GeV}$ for $\tan\beta > 50$. Other Higgs bosons are assumed to be much heavier.
- 155 ALEXANDER 96h give $B(Z \rightarrow H\gamma) \times B(H \rightarrow q\bar{q}) < 1\text{--}4 \times 10^{-5}$ (95%CL) and $B(Z \rightarrow H\gamma) \times B(H \rightarrow b\bar{b}) < 0.7\text{--}2 \times 10^{-5}$ (95%CL) in the range $20 < m_H < 80 \text{ GeV}$.

91^{+31}_{-24}	4 ERLER	10A RVUE
129^{+74}_{-49}	5 LEP-SLC	06 RVUE

- 1 HALLER 18 make Standard Model fits to Z and neutral current parameters, m_t, m_W , and Γ_W measurements available in 2018. The direct mass measurement at the LHC is not used in the fit.
- 2 BAAK 12 make Standard Model fits to Z and neutral current parameters, m_t, m_W , and Γ_W measurements available in 2010 (using also preliminary data). The quoted result is obtained from a fit that does not include the limit from the direct Higgs searches. The result including direct search data from LEP2, the Tevatron and the LHC is $120^{+12}_{-5} \text{ GeV}$.
- 3 BAAK 12a make Standard Model fits to Z and neutral current parameters, m_t, m_W , and Γ_W measurements available in 2012 (using also preliminary data). The quoted result is obtained from a fit that does not include the measured mass value of the signal observed at the LHC and also no limits from direct Higgs searches.
- 4 ERLER 10A makes Standard Model fits to Z and neutral current parameters, m_t, m_W measurements available in 2009 (using also preliminary data). The quoted result is obtained from a fit that does not include the limits from the direct Higgs searches. With direct search data from LEP2 and Tevatron added to the fit, the 90% CL (99% CL) interval is 115–148 (114–197) GeV.
- 5 LEP-SLC 06 make Standard Model fits to Z parameters from LEP/SLC and m_t, m_W , and Γ_W measurements available in 2005 with $\Delta\alpha_{\text{had}}^{(5)}(m_Z) = 0.02758 \pm 0.00035$. The 95% CL limit is 285 GeV.

SEARCHES FOR NEUTRAL HIGGS BOSONS REFERENCES

AAD	24A	PL B848 138394	G. Aad et al.	(ATLAS Collab.)
AAD	23AD	EPJ C83 519	G. Aad et al.	(ATLAS Collab.)
AAD	23AJ	EPJ C83 603	G. Aad et al.	(ATLAS Collab.)
AAD	23BD	JHEP 2307 199	G. Aad et al.	(ATLAS Collab.)
AAD	23BE	JHEP 2307 200	G. Aad et al.	(ATLAS Collab.)
AAD	23BG	JHEP 2307 203	G. Aad et al.	(ATLAS Collab.)
AAD	23BW	PR D108 092007	G. Aad et al.	(ATLAS Collab.)
AAD	23BX	JHEP 2309 189	G. Aad et al.	(ATLAS Collab.)
AAD	23CA	JHEP 2310 009	G. Aad et al.	(ATLAS Collab.)
AAD	23CR	JHEP 2312 081	G. Aad et al.	(ATLAS Collab.)
AAD	23O	JHEP 2306 016	G. Aad et al.	(ATLAS Collab.)
AAD	23R	JHEP 2307 155	G. Aad et al.	(ATLAS Collab.)
AAD	23U	JHEP 2307 125	G. Aad et al.	(ATLAS Collab.)
AAD	23Z	JHEP 2307 040	G. Aad et al.	(ATLAS Collab.)
ADACHI	23A	PRL 130 181803	I. Adachi et al.	(BELLE II Collab.)
HAYRAPETYAN...	23C	PR D108 072004	A. Hayrapetyan et al.	(CMS Collab.)
HAYRAPETYAN...	23G	JHEP 2312 070	A. Hayrapetyan et al.	(CMS Collab.)
TUMASYAN	23	PL B642 137392	A. Tumasyan et al.	(CMS Collab.)
TUMASYAN	23AR	PRL 131 101801	A. Tumasyan et al.	(CMS Collab.)
TUMASYAN	23M	JHEP 2307 148	A. Tumasyan et al.	(CMS Collab.)
TUMASYAN	23O	JHEP 2307 095	A. Tumasyan et al.	(CMS Collab.)
TUMASYAN	23S	JHEP 2307 073	A. Tumasyan et al.	(CMS Collab.)
AAD	22A	PR D105 012006	G. Aad et al.	(ATLAS Collab.)
AAD	22F	PL B829 137066	G. Aad et al.	(ATLAS Collab.)
AAD	22D	PR D105 092002	G. Aad et al.	(ATLAS Collab.)
AAD	22J	JHEP 2201 063	G. Aad et al.	(ATLAS Collab.)
AAD	22J	JHEP 2203 041	G. Aad et al.	(ATLAS Collab.)
AAD	22P	JHEP 2208 104	G. Aad et al.	(ATLAS Collab.)
AAD	22Y	PR D106 052001	G. Aad et al.	(ATLAS Collab.)
ABLIKIM	22H	PR D105 012008	M. Ablikim et al.	(BESIII Collab.)
ABRATENKO	22A	PR D106 092006	P. Abratenko et al.	(MicroBooNE Collab.)
JIA	22	PRL 128 081804	S. Jia et al.	(BELLE Collab.)
TUMASYAN	22AK	PL B835 137566	A. Tumasyan et al.	(CMS Collab.)
TUMASYAN	22D	PR D105 032008	A. Tumasyan et al.	(CMS Collab.)
AAD	21AF	EPJ C81 332	G. Aad et al.	(ATLAS Collab.)
AAD	21AJ	EPJ C81 396	G. Aad et al.	(ATLAS Collab.)
AAD	21AY	PL B822 136651	G. Aad et al.	(ATLAS Collab.)
AAD	21AZ	JHEP 2110 013	G. Aad et al.	(ATLAS Collab.)
AAD	21BB	JHEP 2111 209	G. Aad et al.	(ATLAS Collab.)
AAD	21BE	EPJ C81 860	G. Aad et al.	(ATLAS Collab.)
ABRATENKO	21	PRL 127 151803	P. Abratenko et al.	(MicroBooNE Collab.)
SIRUNYAN	21A	EPJ C81 13	A.M. Sirunyan et al.	(CMS Collab.)
Also	EPJ	C81 333 (errat.)	A.M. Sirunyan et al.	(CMS Collab.)
SLAVICH	21	EPJ C81 450	P. Slavich et al.	(CMS Collab.)
TUMASYAN	21F	JHEP 2111 057	A. Tumasyan et al.	(CMS Collab.)
AAD	20	PR D101 012002	G. Aad et al.	(ATLAS Collab.)
AAD	20AA	PRL 125 051801	G. Aad et al.	(ATLAS Collab.)
AAD	20AE	PRL 125 221802	G. Aad et al.	(ATLAS Collab.)
AAD	20AI	PR D102 112006	G. Aad et al.	(ATLAS Collab.)
AAD	20AO	JHEP 2011 163	G. Aad et al.	(ATLAS Collab.)
AAD	20C	PL B800 135103	G. Aad et al.	(ATLAS Collab.)
AAD	20L	PR D102 032004	G. Aad et al.	(ATLAS Collab.)
AAD	20X	JHEP 2007 108	G. Aad et al.	(ATLAS Collab.)
Also	JHEP	2101 145 (errat.)	G. Aad et al.	(ATLAS Collab.)
Also	JHEP	2105 207 (errat.)	G. Aad et al.	(ATLAS Collab.)
AAJ	20AL	JHEP 2010 156	R. Aaij et al.	(LHCb Collab.)
SIRUNYAN	20	PL B800 135087	A.M. Sirunyan et al.	(CMS Collab.)
SIRUNYAN	20AA	JHEP 2003 055	A.M. Sirunyan et al.	(CMS Collab.)
SIRUNYAN	20AC	JHEP 2003 065	A.M. Sirunyan et al.	(CMS Collab.)
SIRUNYAN	20AD	JHEP 2003 103	A.M. Sirunyan et al.	(CMS Collab.)
SIRUNYAN	20AF	JHEP 2004 171	A.M. Sirunyan et al.	(CMS Collab.)
SIRUNYAN	20AP	JHEP 2008 139	A.M. Sirunyan et al.	(CMS Collab.)
SIRUNYAN	20AY	JHEP 2003 034	A.M. Sirunyan et al.	(CMS Collab.)
SIRUNYAN	20Z	JHEP 2003 051	A.M. Sirunyan et al.	(CMS Collab.)
AABOUD	19A	JHEP 1901 030	M. Aaboud et al.	(ATLAS Collab.)
AABOUD	19AG	PL B790 1	M. Aaboud et al.	(ATLAS Collab.)
AABOUD	19AI	PL B793 499	M. Aaboud et al.	(ATLAS Collab.)
AABOUD	19O	JHEP 1904 092	M. Aaboud et al.	(ATLAS Collab.)
AABOUD	19T	JHEP 1905 124	M. Aaboud et al.	(ATLAS Collab.)
AABOUD	19Y	JHEP 1905 142	M. Aaboud et al.	(ATLAS Collab.)
AABOUD	19V	JHEP 1907 117	M. Aaboud et al.	(ATLAS Collab.)
AALTONEN	19	PR D99 052001	T. Aaltonen et al.	(CDF Collab.)
BAGNASCHI	19	EPJ C79 617	E. Bagnaschi et al.	(ATLAS Collab.)
SIRUNYAN	19	PL B788 7	A.M. Sirunyan et al.	(CMS Collab.)
SIRUNYAN	19AE	JHEP 1905 210	A.M. Sirunyan et al.	(CMS Collab.)
SIRUNYAN	19AN	EPJ C79 280	A.M. Sirunyan et al.	(CMS Collab.)
SIRUNYAN	19AV	EPJ C79 564	A.M. Sirunyan et al.	(CMS Collab.)
SIRUNYAN	19B	PR D99 012005	A.M. Sirunyan et al.	(CMS Collab.)
SIRUNYAN	19BB	PL B793 320	A.M. Sirunyan et al.	(CMS Collab.)
SIRUNYAN	19BD	PL B795 398	A.M. Sirunyan et al.	(CMS Collab.)
SIRUNYAN	19BE	PRL 122 121803	A.M. Sirunyan et al.	(CMS Collab.)
SIRUNYAN	19BQ	PL B796 131	A.M. Sirunyan et al.	(CMS Collab.)
SIRUNYAN	19CR	PL B798 134992	A.M. Sirunyan et al.	(CMS Collab.)
SIRUNYAN	19H	JHEP 1901 040	A.M. Sirunyan et al.	(CMS Collab.)
AABOUD	18AA	PR D98 032015	M. Aaboud et al.	(ATLAS Collab.)
AABOUD	18AG	PL B782 750	M. Aaboud et al.	(ATLAS Collab.)
AABOUD	18AH	PL B783 392	M. Aaboud et al.	(ATLAS Collab.)

Electroweak Constraints on the Standard Model Higgs Boson Mass

Here we list constraints on the mass of the Higgs boson derived from fits to precision electroweak observables, assuming the minimal Standard Model with a doublet Higgs field and three generations of fermions.

VALUE (GeV)	DOCUMENT ID	TECN
90^{+21}_{-18}	1 HALLER	18 RVUE
• • • We do not use the following data for averages, fits, limits, etc. • • •		
91^{+30}_{-23}	2 BAAK	12 RVUE
94^{+25}_{-22}	3 BAAK	12A RVUE

Gauge & Higgs Boson Particle Listings

Neutral Higgs Bosons, Searches for, Charged Higgs Bosons (H^\pm and $H^{\pm\pm}$), Searches for

AABOUD	18AI	JHEP 1803 174	M. Aboud et al.	(ATLAS Collab.)	CHATRCHYAN	12V	PRL 109 121801	S. Chatrchyan et al.	(CMS Collab.)
	Also	JHEP 1811 015 (errat.)	M. Aboud et al.	(ATLAS Collab.)	AALTONEN	11P	PRL 107 031801	T. Aaltonen et al.	(CDF Collab.)
AABOUD	18AP	JHEP 1806 166	M. Aboud et al.	(ATLAS Collab.)	ABAZOV	11K	PL B698 97	V.M. Abazov et al.	(DO Collab.)
AABOUD	18BF	EPJ C78 293	M. Aboud et al.	(ATLAS Collab.)	ABAZOV	11W	PRL 107 121801	V.M. Abazov et al.	(DO Collab.)
AABOUD	18BU	EPJ C78 1007	M. Aboud et al.	(ATLAS Collab.)	ABOUZAID	11A	PRL 107 201803	E. Abouzaid et al.	(KTeV Collab.)
AABOUD	18BX	JHEP 1810 031	M. Aboud et al.	(ATLAS Collab.)	DEL-AMO-SA...	11J	PRL 107 021804	P. del Amo Sanchez et al.	(BABAR Collab.)
AABOUD	18CC	JHEP 1811 051 (errat.)	M. Aboud et al.	(ATLAS Collab.)	LEES	11H	PRL 107 221803	J.P. Lees et al.	(BABAR Collab.)
AABOUD	18CE	JHEP 1812 039	M. Aboud et al.	(ATLAS Collab.)	ABBIENDI	10	PL B682 381	G. Abbiendi et al.	(OPAL Collab.)
AABOUD	18CQ	PRL 121 191801	M. Aboud et al.	(ATLAS Collab.)	ANDREAS	10	JHEP 1008 003	S. Andreas et al.	(DESY)
AABOUD	18CW	JHEP 1811 040	M. Aboud et al.	(ATLAS Collab.)	ERLER	10A	PR D81 051301	J. Erler et al.	(UNAM)
AABOUD	18F	PL B777 91	M. Aboud et al.	(ATLAS Collab.)	HYUN	10	PRL 105 091801	H.J. Hyun et al.	(BELLE Collab.)
AABOUD	18G	JHEP 1801 055	M. Aboud et al.	(ATLAS Collab.)	SCHAEI	10	JHEP 1005 049	S. Schaei et al.	(ALEPH Collab.)
AAIJ	18AM	EPJ C78 1008	R. Aaij et al.	(LHCb Collab.)	AALTONEN	09AB	PRL 103 061803	T. Aaltonen et al.	(CDF Collab.)
AAIJ	18AQ	JHEP 1809 147	R. Aaij et al.	(LHCb Collab.)	AALTONEN	09AR	PRL 103 201801	T. Aaltonen et al.	(CDF Collab.)
HALLER	18	EPJ C78 675	J. Haller et al.	(Gfitter Group)	ABAZOV	09V	PRL 103 061801	V.M. Abazov et al.	(DO Collab.)
SIRUNYAN	18A	PL B778 101	A.M. Sirunyan et al.	(CMS Collab.)	AUBERT	09P	PRL 103 181801	B. Aubert et al.	(BABAR Collab.)
SIRUNYAN	18AF	PL B781 244	A.M. Sirunyan et al.	(CMS Collab.)	AUBERT	09Z	PRL 103 081803	B. Aubert et al.	(BABAR Collab.)
SIRUNYAN	18BA	JHEP 1806 127	A.M. Sirunyan et al.	(CMS Collab.)	TUNG	09	PRL 102 051802	Y.C. Tung et al.	(KEK E391a Collab.)
	Also	JHEP 1903 128 (errat.)	A.M. Sirunyan et al.	(CMS Collab.)	ABAZOV	08U	PRL 101 051801	V.M. Abazov et al.	(DO Collab.)
SIRUNYAN	18BP	JHEP 1808 113	A.M. Sirunyan et al.	(CMS Collab.)	ABDALLAH	08B	EPJ C54 1	J. Abdallah et al.	(DELPHI Collab.)
SIRUNYAN	18CW	JHEP 1808 152	A.M. Sirunyan et al.	(CMS Collab.)		Also	EPJ C56 165 (errat.)	J. Abdallah et al.	(DELPHI Collab.)
SIRUNYAN	18CX	JHEP 1809 007	A.M. Sirunyan et al.	(CMS Collab.)	LOVE	08	PRL 101 151802	W. Love et al.	(CLEO Collab.)
SIRUNYAN	18DK	JHEP 1809 148	A.M. Sirunyan et al.	(CMS Collab.)	ABBIENDI	07	EPJ C49 457	G. Abbiendi et al.	(OPAL Collab.)
SIRUNYAN	18DT	PL B785 462	A.M. Sirunyan et al.	(CMS Collab.)	BESSON	07	PRL 98 052002	D. Besson et al.	(CLEO Collab.)
SIRUNYAN	18DU	PR D98 092001	A.M. Sirunyan et al.	(CMS Collab.)	SCHAEI	07	EPJ C49 439	S. Schaei et al.	(ALEPH Collab.)
SIRUNYAN	18ED	JHEP 1811 172	A.M. Sirunyan et al.	(CMS Collab.)	LEP-SLC	06	PRPL 427 257	ALEPH, DELPHI, L3, OPAL, SLD and working groups	(LEP Collab.)
SIRUNYAN	18EE	JHEP 1811 018	A.M. Sirunyan et al.	(CMS Collab.)	SCHAEI	06B	EPJ C47 547	S. Schaei et al.	(LEP Collab.)
SIRUNYAN	18F	JHEP 1801 054	A.M. Sirunyan et al.	(CMS Collab.)	ABBIENDI	05A	EPJ C40 317	G. Abbiendi et al.	(OPAL Collab.)
AABOUD	17	PL B764 11	M. Aboud et al.	(ATLAS Collab.)	ABDALLAH	05D	EPJ C44 147	J. Abdallah et al.	(DELPHI Collab.)
AABOUD	17AN	PRL 119 191803	M. Aboud et al.	(ATLAS Collab.)	ACHARD	05	PL B609 35	P. Achard et al.	(L3 Collab.)
AABOUD	17AP	PL B775 105	M. Aboud et al.	(ATLAS Collab.)	ACOSTA	05Q	PR D72 072004	D. Acosta et al.	(CDF Collab.)
AABOUD	17AW	JHEP 1710 112	M. Aboud et al.	(ATLAS Collab.)	PARK	05	PRL 94 021801	H.K. Park et al.	(FNAL HyperCP Collab.)
KHACHATRY...	17AZ	JHEP 1710 076	V. Khachatryan et al.	(CMS Collab.)	ABBIENDI	04K	PL B597 11	G. Abbiendi et al.	(OPAL Collab.)
KHACHATRY...	17D	JHEP 1701 076	V. Khachatryan et al.	(CMS Collab.)	ABBIENDI	04M	EPJ C37 49	G. Abbiendi et al.	(OPAL Collab.)
KHACHATRY...	17R	PL B767 147	V. Khachatryan et al.	(CMS Collab.)	ABDALLAH	04	EPJ C32 145	J. Abdallah et al.	(DELPHI Collab.)
SIRUNYAN	17AX	JHEP 1711 010	A.M. Sirunyan et al.	(CMS Collab.)	ABDALLAH	04B	EPJ C32 475	J. Abdallah et al.	(DELPHI Collab.)
SIRUNYAN	17CN	PR D96 072004	A.M. Sirunyan et al.	(CMS Collab.)	ABDALLAH	04L	EPJ C35 313	J. Abdallah et al.	(DELPHI Collab.)
SIRUNYAN	17Y	PL B772 363	A.M. Sirunyan et al.	(CMS Collab.)	ABDALLAH	04O	EPJ C38 1	J. Abdallah et al.	(DELPHI Collab.)
AABOUD	16AA	EPJ C76 585	M. Aboud et al.	(ATLAS Collab.)	ACHARD	04F	PL B583 14	P. Achard et al.	(L3 Collab.)
AABOUD	16AB	EPJ C76 605	M. Aboud et al.	(ATLAS Collab.)	ACHARD	04B	PL B589 89	P. Achard et al.	(L3 Collab.)
AABOUD	16AE	JHEP 1609 173	M. Aboud et al.	(ATLAS Collab.)	ABBIENDI	03F	EPJ C27 311	G. Abbiendi et al.	(OPAL Collab.)
AABOUD	16H	JHEP 1609 001	M. Aboud et al.	(ATLAS Collab.)	ABBIENDI	03G	EPJ C27 483	G. Abbiendi et al.	(OPAL Collab.)
AABOUD	16I	PR D94 052002	M. Aboud et al.	(ATLAS Collab.)	ACHARD	03C	PL B568 191	P. Achard et al.	(L3 Collab.)
AAD	16AX	EPJ C76 45	G. Aad et al.	(ATLAS Collab.)	ABBIENDI	02D	EPJ C23 397	G. Abbiendi et al.	(OPAL Collab.)
AAD	16C	JHEP 1601 032	G. Aad et al.	(ATLAS Collab.)	ABBIENDI	02F	PL B544 44	G. Abbiendi et al.	(OPAL Collab.)
AAD	16L	EPJ C76 210	G. Aad et al.	(ATLAS Collab.)	ACHARD	02C	PL B534 28	P. Achard et al.	(L3 Collab.)
AALTONEN	16C	PR D93 112010	T. Aaltonen et al.	(CDF Collab.)	ACHARD	02H	PL B545 30	P. Achard et al.	(L3 Collab.)
ABLIKIM	16E	PR D93 052005	M. Ablikim et al.	(BESIII Collab.)	AKEROID	02	PR D66 037702	A.G. Akroyd et al.	(ALEPH Collab.)
KHACHATRY...	16A	PL B752 221	V. Khachatryan et al.	(CMS Collab.)	HEISTER	02	PL B526 191	A. Heister et al.	(ALEPH Collab.)
KHACHATRY...	16BG	EPJ C76 371	V. Khachatryan et al.	(CMS Collab.)	HEISTER	02M	PL B544 16	A. Heister et al.	(ALEPH Collab.)
KHACHATRY...	16BQ	PR D94 052012	V. Khachatryan et al.	(CMS Collab.)	HEISTER	02L	PL B544 25	A. Heister et al.	(ALEPH Collab.)
KHACHATRY...	16F	JHEP 1601 079	V. Khachatryan et al.	(CMS Collab.)	ABBIENDI	01E	EPJ C18 425	G. Abbiendi et al.	(OPAL Collab.)
KHACHATRY...	16M	PRL 117 051802	V. Khachatryan et al.	(CMS Collab.)	ABREU	01F	PL B507 89	P. Abreu et al.	(DELPHI Collab.)
KHACHATRY...	16P	PL B755 217	V. Khachatryan et al.	(CMS Collab.)	AFFOLDER	01H	PR D84 092002	T. Affolder et al.	(CDF Collab.)
KHACHATRY...	16W	PL B758 296	V. Khachatryan et al.	(CMS Collab.)	BARATE	01C	PL B439 53	R. Barate et al.	(ALEPH Collab.)
KHACHATRY...	16Z	PL B759 369	V. Khachatryan et al.	(CMS Collab.)	ACCARIARI	00M	PL B485 85	M. Acciarri et al.	(L3 Collab.)
AAD	15BD	EPJ C75 337	G. Aad et al.	(ATLAS Collab.)	ACCARIARI	00R	PL B489 102	M. Acciarri et al.	(L3 Collab.)
AAD	15BH	EPJ C75 299	G. Aad et al.	(ATLAS Collab.)	ACCARIARI	00S	PL B489 115	M. Acciarri et al.	(L3 Collab.)
	Also	EPJ C75 408 (errat.)	G. Aad et al.	(ATLAS Collab.)	BARATE	00L	PL B487 241	R. Barate et al.	(ALEPH Collab.)
AAD	15BK	EPJ C75 412	G. Aad et al.	(ATLAS Collab.)	ABBIENDI	99E	EPJ C7 407	G. Abbiendi et al.	(OPAL Collab.)
AAD	15BZ	PR D92 052002	G. Aad et al.	(ATLAS Collab.)	ABBIENDI	99O	PL B464 311	G. Abbiendi et al.	(OPAL Collab.)
AAD	15CE	PR D92 092004	G. Aad et al.	(ATLAS Collab.)	ABBOTT	99B	PRL 82 2244	B. Abbott et al.	(DO Collab.)
AAD	15H	PRL 114 081802	G. Aad et al.	(ATLAS Collab.)	ABREU	99P	PL B458 431	P. Abreu et al.	(DELPHI Collab.)
AAD	15S	PL B744 163	G. Aad et al.	(ATLAS Collab.)	ABBOTT	98	PRL 80 442	B. Abbott et al.	(DO Collab.)
KHACHATRY...	15AU	JHEP 1510 144	V. Khachatryan et al.	(CMS Collab.)	ACKERSTAFF	98S	EPJ C5 19	K. Ackerstaff et al.	(OPAL Collab.)
KHACHATRY...	15AY	JHEP 1511 071	V. Khachatryan et al.	(CMS Collab.)	ACKERSTAFF	98B	PL B437 218	K. Ackerstaff et al.	(OPAL Collab.)
KHACHATRY...	15BB	PL B750 494	V. Khachatryan et al.	(CMS Collab.)	GONZALEZ	98B	PR D57 7045	M.C. Gonzalez-Garcia, S.M. Lietti, S.F. Novaes	(WARS)
KHACHATRY...	15N	PL B748 221	V. Khachatryan et al.	(CMS Collab.)	KRAWCZYK	97	PR D55 6968	M. Krawczyk, J. Zochowski	(OPAL Collab.)
KHACHATRY...	15O	PL B748 255	V. Khachatryan et al.	(CMS Collab.)	ALEXANDER	96H	ZPHY C71 1	G. Alexander et al.	(DELPHI Collab.)
KHACHATRY...	15R	PL B749 560	V. Khachatryan et al.	(CMS Collab.)	ABREU	95H	ZPHY C67 69	P. Abreu et al.	(DELPHI Collab.)
LEES	15H	PR D91 071102	J.P. Lees et al.	(BABAR Collab.)	BALEST	95	PR D51 2053	R. Balest et al.	(CLEO Collab.)
AAD	14AP	PRL 113 171801	G. Aad et al.	(ATLAS Collab.)	PICH	92	NP B388 31	A. Pich, J. Prades, P. Yepes	(CERN, CPPM)
AAD	14AW	JHEP 1411 056	G. Aad et al.	(ATLAS Collab.)	ANTREASYAN	90C	PL B251 204	D. Antreasyan et al.	(Crystal Ball Collab.)
AAD	14BA	JHEP 1411 088	G. Aad et al.	(ATLAS Collab.)					
AAD	14M	PR D89 032002	G. Aad et al.	(ATLAS Collab.)					
AAD	14O	PRL 112 201802	G. Aad et al.	(ATLAS Collab.)					
CHATRCHYAN	14B	EPJ C74 2980	S. Chatrchyan et al.	(CMS Collab.)					
CHATRCHYAN	14G	JHEP 1401 096	S. Chatrchyan et al.	(CMS Collab.)					
KHACHATRY...	14M	JHEP 1410 160	V. Khachatryan et al.	(CMS Collab.)					
KHACHATRY...	14P	EPJ C74 3076	V. Khachatryan et al.	(CMS Collab.)					
KHACHATRY...	14Q	PR D90 112013	V. Khachatryan et al.	(CMS Collab.)					
AAD	13AG	PL B721 32	G. Aad et al.	(ATLAS Collab.)					
AAD	13AT	NJP 15 043009	G. Aad et al.	(ATLAS Collab.)					
AAD	13O	JHEP 1302 095	G. Aad et al.	(ATLAS Collab.)					
AAIJ	13T	JHEP 1305 132	R. Aaij et al.	(LHCb Collab.)					
AALTONEN	13K	PR D88 052012	T. Aaltonen et al.	(CDF Collab.)					
AALTONEN	13L	PR D88 052013	T. Aaltonen et al.	(CDF Collab.)					
AALTONEN	13M	PR D88 052014	T. Aaltonen et al.	(CDF and DO Collabs.)					
AALTONEN	13P	PRL 110 121801	T. Aaltonen et al.	(CDF Collab.)					
ABAZOV	13G	PR D88 052006	V.M. Abazov et al.	(DO Collab.)					
ABAZOV	13H	PR D88 052007	V.M. Abazov et al.	(DO Collab.)					
ABAZOV	13I	PR D88 052008	V.M. Abazov et al.	(DO Collab.)					
ABAZOV	13J	PR D88 052009	V.M. Abazov et al.	(DO Collab.)					
ABAZOV	13L	PR D88 052011	V.M. Abazov et al.	(DO Collab.)					
CARENA	13	EPJ C73 2552	M. Carena et al.	(CMS Collab.)					
CHATRCHYAN	13AG	PL B722 207	S. Chatrchyan et al.	(CMS Collab.)					
CHATRCHYAN	13AL	PL B725 36	S. Chatrchyan et al.	(CMS Collab.)					
CHATRCHYAN	13BJ	PL B726 564	S. Chatrchyan et al.	(CMS Collab.)					
LEES	13C	PR D87 031102	J.P. Lees et al.	(BABAR Collab.)					
LEES	13L	PR D88 031701	J.P. Lees et al.	(BABAR Collab.)					
LEES	13R	PR D88 071102	J.P. Lees et al.	(BABAR Collab.)					
AAD	12AI	PL B716 1	G. Aad et al.	(ATLAS Collab.)					
AAD	12AQ	PRL 108 251801	G. Aad et al.	(ATLAS Collab.)					
AAD	12N	EPJ C72 2157	G. Aad et al.	(ATLAS Collab.)					
AALTONEN	12AB	PR D85 092001	T. Aaltonen et al.	(CDF Collab.)					
AALTONEN	12AN	PL B717 173	T. Aaltonen et al.	(CDF Collab.)					
AALTONEN	12AQ	PR D86 091101	T. Aaltonen et al.	(CDF and DO Collabs.)					
AALTONEN	12U	PR D85 012007	T. Aaltonen et al.	(CDF Collab.)					
AALTONEN	12X	PR D85 032005	T. Aaltonen et al.	(CDF Collab.)					
ABAZOV	12G	PL B710 569	V.M. Abazov et al.	(DO Collab.)					
ABLIKIM	12	PR D85 092012	M. Ablikim et al.	(BESIII Collab.)					
BAAK	12	EPJ C72 2003	M. Baak et al.	(Gfitter Group)					
BAAK</									

See key on page 1171

Gauge & Higgs Boson Particle Listings

Charged Higgs Bosons (H^\pm and $H^{\pm\pm}$), Searches for

Searches in e^+e^- collisions at and above the Z pole have conclusively ruled out the existence of a charged Higgs in the region $m_{H^\pm} \lesssim 45$ GeV, and are meanwhile superseded by the searches in higher energy e^+e^- collisions at LEP. Results that are by now obsolete are therefore not included in this compilation, and can be found in a previous Edition (The European Physical Journal **C15** 1 (2000)) of this Review.

In the following, and unless otherwise stated, results from the LEP experiments (ALEPH, DELPHI, L3, and OPAL) are assumed to derive from the study of the $e^+e^- \rightarrow H^+H^-$ process. Limits from $b \rightarrow s\gamma$ decays are usually stronger in generic 2HDM models than in Supersymmetric models.

VALUE (GeV)	CL%	DOCUMENT ID	TECN	COMMENT
none 80–140	95	1 AAD	15AF ATLS	$t \rightarrow bH^+$
none 90–155	95	2 KHACHATRYAN	15AX CMS	$t \rightarrow bH^+, H^+ \rightarrow \tau^+\nu$
> 80	95	3 LEP	13 LEP	$e^+e^- \rightarrow H^+H^-, E_{cm} \leq 209\text{GeV}$
> 76.3	95	4 ABBIENDI	12 OPAL	$e^+e^- \rightarrow H^+H^-, E_{cm} \leq 209\text{GeV}$
> 74.4	95	ABDALLAH	04i DLPH	$E_{cm} \leq 209\text{ GeV}$
> 76.5	95	ACHARD	03E L3	$E_{cm} \leq 209\text{ GeV}$
> 79.3	95	HEISTER	02P ALEP	$E_{cm} \leq 209\text{ GeV}$
• • • We do not use the following data for averages, fits, limits, etc. • • •				
		5 AAD	23AH ATLS	$H^\pm \rightarrow W^\pm Z$
		6,7 AAD	23BB ATLS	$t \rightarrow bH^+, H^+ \rightarrow c\bar{b}$
		7,8 AAD	23BW ATLS	$t \rightarrow bH^+, H^+ \rightarrow W^+A^0, A^0 \rightarrow \mu^+\mu^-$
		9 TUMASYAN	23AV CMS	$H^\pm \rightarrow H_2^0 W^\pm$
		10 TUMASYAN	22B CMS	$H^\pm \rightarrow W^\pm \gamma$
		11 AAD	21V ATLS	$\bar{t}bH^+, H^+ \rightarrow t\bar{b}$
		12 SIRUNYAN	21W CMS	$H^+ \rightarrow W^+ Z$
		13 AAD	20W ATLS	$H^+ \rightarrow t\bar{b}$
		14 SIRUNYAN	20AO CMS	$H^+ \rightarrow t\bar{b}$
		15 SIRUNYAN	20AV CMS	$H^+ \rightarrow t\bar{b}$
		16 SIRUNYAN	20BE CMS	$t \rightarrow bH^+, H^+ \rightarrow c\bar{s}$
		17 SIRUNYAN	19AH CMS	$H^+ \rightarrow \tau^+\nu$
		18 SIRUNYAN	19BP CMS	$H^+ \rightarrow W^+ Z$
		19 SIRUNYAN	19CC CMS	$t \rightarrow bH^+, H^+ \rightarrow W^+A^0, A^0 \rightarrow \mu^+\mu^-$
		20 SIRUNYAN	19CQ CMS	$H^+ \rightarrow W^+ Z$
		21 AABOUD	18BW ATLS	$\bar{t}bH^+$ or $t \rightarrow bH^+, H^+ \rightarrow \tau^+\nu$
		22 AABOUD	18CD ATLS	$\bar{t}bH^+, H^+ \rightarrow t\bar{b}$
		23 AABOUD	18CH ATLS	$H^\pm \rightarrow W^\pm Z$
		24 HALLER	18 RVUE	$b \rightarrow s\gamma$
		25 SIRUNYAN	18DO CMS	$t \rightarrow bH^+, H^+ \rightarrow c\bar{b}$
		26 MISIAK	17 RVUE	$b \rightarrow s(d)\gamma$
		27 SIRUNYAN	17AE CMS	$H^\pm \rightarrow W^\pm Z$
		28 AABOUD	16A ATLS	$t(b)H^+, H^+ \rightarrow \tau^+\nu$
		29 AAD	16AJ ATLS	$t(b)H^+, H^+ \rightarrow t\bar{b}$
		30 AAD	16AJ ATLS	$qq \rightarrow H^+, H^+ \rightarrow t\bar{b}$
		31 AAD	15AF ATLS	tH^\pm
		32 AAD	15M ATLS	$H^\pm \rightarrow W^\pm Z$
		33 KHACHATRYAN	15AX CMS	$tH^+, H^+ \rightarrow t\bar{b}$
		34 KHACHATRYAN	15AX CMS	$tH^\pm, H^\pm \rightarrow \tau^\pm\nu$
		35 KHACHATRYAN	15BF CMS	$t \rightarrow bH^+, H^+ \rightarrow c\bar{s}$
		36 AAD	14M ATLS	$H_2^0 \rightarrow H^\pm W^\mp, H^0 \rightarrow b\bar{b}, H^0 W^\pm W^\mp, H^0 \rightarrow b\bar{b}$
		37 AALTONEN	14A CDF	$t \rightarrow b\tau\nu$
		38 AAD	13AC ATLS	$t \rightarrow bH^+$
		39 AAD	13V ATLS	$t \rightarrow bH^+, \text{lepton non-universality}$
		40 AAD	12BH ATLS	$t \rightarrow bH^+$
		41 CHATRCHYAN	12AA CMS	$t \rightarrow bH^+$
		42 AALTONEN	11P CDF	$t \rightarrow bH^+, H^+ \rightarrow W^+A^0$
> 316	95	43 DESCHAMPS	10 RVUE	Type II, flavor physics data
		44 AALTONEN	09AJ CDF	$t \rightarrow bH^+$
		45 ABZOV	09AC D0	$t \rightarrow bH^+$
		46 ABZOV	09AG D0	$t \rightarrow bH^+$
		47 ABZOV	09AI D0	$t \rightarrow bH^+$
		48 ABZOV	09P D0	$H^+ \rightarrow t\bar{b}$
		49 ABULENCIA	06E CDF	$t \rightarrow bH^+$
> 92.0	95	ABBIENDI	04 OPAL	$B(\tau\nu) = 1$
> 76.7	95	50 ABDALLAH	04i DLPH	Type I
		51 ABBIENDI	03 OPAL	$\tau \rightarrow \mu\nu, e\nu$
		52 ABZOV	02B D0	$t \rightarrow bH^+, H^+ \rightarrow \tau\nu$
		53 BORZUMATI	02 RVUE	
		54 ABBIENDI	01Q OPAL	$B \rightarrow \tau\nu, X$
		55 BARATE	01E ALEP	$B \rightarrow \tau\nu, \tau$
> 315	99	56 GAMBINO	01 RVUE	$b \rightarrow s\gamma$
		57 AFFOLDER	00i CDF	$t \rightarrow bH^+, H^+ \rightarrow \tau\nu$
> 59.5	95	ABBIENDI	99E OPAL	$E_{cm} \leq 183\text{ GeV}$
		58 ABBOTT	99E D0	$t \rightarrow bH^+$
		59 ACKERSTAFF	99D OPAL	$\tau \rightarrow e\nu, \mu\nu$
		60 ACCIARRI	97F L3	$B \rightarrow \tau\nu, \tau$
		61 AMMAR	97B CLEO	$\tau \rightarrow \mu\nu$

		62 COARASA	97 RVUE	$B \rightarrow \tau\nu, X$
		63 GUCHAIT	97 RVUE	$t \rightarrow bH^+, H^+ \rightarrow \tau\nu$
		64 MANGANO	97 RVUE	$B_u(c) \rightarrow \tau\nu, \tau$
		65 STAHL	97 RVUE	$\tau \rightarrow \mu\nu$
> 244	95	66 ALAM	95 CLE2	$b \rightarrow s\gamma$
		67 BUSKULIC	95 ALEP	$b \rightarrow \tau\nu, X$

- AAD 15AF search for $t\bar{t}$ production followed by $t \rightarrow bH^+, H^+ \rightarrow \tau^+\nu$ in 19.5 fb⁻¹ of pp collisions at $E_{cm} = 8$ TeV. Upper limits on $B(t \rightarrow bH^+)B(H^+ \rightarrow \tau\nu)$ between 2.3×10^{-3} and 1.3×10^{-2} (95% CL) are given for $m_{H^\pm} = 80\text{--}160$ GeV. See their Fig. 8 for the excluded regions in different benchmark scenarios of the MSSM. The region $m_{H^\pm} < 140$ GeV is excluded for $\tan\beta > 1$ in the considered scenarios.
- KHACHATRYAN 15AX search for $t\bar{t}$ production followed by $t \rightarrow bH^+, H^+ \rightarrow \tau^+\nu$ in 19.7 fb⁻¹ of pp collisions at $E_{cm} = 8$ TeV. Upper limits on $B(t \rightarrow bH^+)B(H^+ \rightarrow \tau\nu)$ between 1.2×10^{-2} and 1.5×10^{-3} (95% CL) are given for $m_{H^\pm} = 80\text{--}160$ GeV. See their Fig. 11 for the excluded regions in different benchmark scenarios of the MSSM. The region $m_{H^\pm} < 155$ GeV is excluded for $\tan\beta > 1$ in the considered scenarios.
- LEP 13 give a limit that refers to the Type II scenario. The limit for $B(H^+ \rightarrow \tau\nu) = 1$ is 94 GeV (95% CL), and for $B(H^+ \rightarrow c\bar{s}) = 1$ the region below 80.5 as well as the region 83–88 GeV is excluded (95% CL). LEP 13 also search for the decay mode $H^+ \rightarrow A^0 W^*$ with $A^0 \rightarrow b\bar{b}$, which is not negligible in Type I models. The limit in Type I models is 72.5 GeV (95% CL) if $m_{A^0} > 12$ GeV.
- ABBIENDI 12 also search for the decay mode $H^+ \rightarrow A^0 W^*$ with $A^0 \rightarrow b\bar{b}$.
- AAD 23AH search for vector boson fusion production of H^\pm decaying to $H^\pm \rightarrow W^\pm Z$ to $\ell^\pm\nu\ell^+\ell^-$ in 139 fb⁻¹ of pp collisions at $E_{cm} = 13$ TeV. See their Fig. 9 for limits on cross section times branching ratio in the Georgi-Machacek model for $m_{H^\pm} = 0.2\text{--}1.0$ TeV, and also for limits on the triplet vacuum expectation value fraction.
- AAD 23BB search for $t\bar{t}$ production followed by $t \rightarrow bH^+, H^+ \rightarrow c\bar{b}$ in 139 fb⁻¹ of pp collisions at $E_{cm} = 13$ TeV. See their Fig. 8 for limits on the product of branching ratios for $m_{H^\pm} = 60\text{--}160$ GeV.
- Charge conjugated states are also implied.
- AAD 23BW search for $t \rightarrow bH^+$ from pair produced top quarks, with the decay chain $H^+ \rightarrow W^+A^0, A^0 \rightarrow \mu^+\mu^-$ using 139 fb⁻¹ of pp collisions at $E_{cm} = 13$ TeV. See their Fig. 5(b)–(d) for limits on the product of branching ratios for $m_{H^\pm} = 120, 140, 160$ GeV, and $m_{A^0} = 15\text{--}72$ GeV.
- TUMASYAN 23AV search for production of H^\pm in association with a top quark, decaying to $H_2^0 W^\pm, H_2^0 \rightarrow \tau^+\tau^-$, using 138 fb⁻¹ of pp collisions at $E_{cm} = 13$ TeV. See their Fig. 9 for limits on production cross section times branching ratios for $m_{H^\pm} = 0.3\text{--}0.7$ TeV and $m_{H_2^0} = 0.2$ TeV.
- TUMASYAN 22B search for production of scalar resonance decaying to $W^\pm\gamma \rightarrow qq\gamma$ in 137 fb⁻¹ of pp collisions at $E_{cm} = 13$ TeV. See their Fig. 5 for limits on cross section times branching ratio for the mass range 0.7–6.0 TeV, assuming narrow width or $\Gamma/M = 0.05$.
- AAD 21V search for $\bar{t}bH^+$ associated production followed by $H^+ \rightarrow t\bar{b}$ in 139 fb⁻¹ of pp collisions at $E_{cm} = 13$ TeV. See their Fig. 6 for upper limits on cross section times branching ratio for $m_{H^\pm} = 0.2\text{--}2$ TeV. See also their Fig. 7 for the excluded region in the parameter space of the hMSSM and the following MSSM benchmark scenarios: $M_h^{125}, M_h^{125}(\tilde{\chi}), M_h^{125}(\tilde{\tau}), M_h^{125}(\text{alignment}), M_h^{125}(\text{CPV})$.
- SIRUNYAN 21W search for vector boson fusion production of H^+ decaying to $H^+ \rightarrow W^+ Z$ to $\ell^+\nu\ell^+\ell^-$ in 137 fb⁻¹ of pp collisions at $E_{cm} = 13$ TeV. See their Fig. 8 for limits on cross section times branching ratio for $m_{H^\pm} = 0.2\text{--}3.0$ TeV, and also for limits on the fraction of the triplet vev contribution to the W mass in the Georgi-Machacek model.
- AAD 20W search for dijet resonances in events with isolated leptons using 139 fb⁻¹ of pp collisions at $E_{cm} = 13$ TeV. As a byproduct, $H^+ \rightarrow t\bar{b}$ produced in association with $\bar{t}b$ is searched for. Limits on the product of cross section times branching ratio for $m_{H^\pm} = 0.6\text{--}2$ TeV are given in their Fig. 5(c).
- SIRUNYAN 20AO search for $H^+ \rightarrow t\bar{b}$ produced in association with $t(b)$ in all jet final states in 35.9 fb⁻¹ of pp collisions at $E_{cm} = 13$ TeV. See their Fig. 6 for limits on the product of cross section times branching ratio for $m_{H^\pm} = 0.2\text{--}3$ TeV. Limits for s -channel production are also given for $m_{H^\pm} = 0.8\text{--}3$ TeV. See also Fig. 7 for the corresponding limits in scenarios in the minimal supersymmetric standard model. Cross section limits from combined results with SIRUNYAN 20AV are given in Fig. 8.
- SIRUNYAN 20AV search for $H^+ \rightarrow t\bar{b}$ produced in association with $t(b)$ in final states with one or two leptons, in 35.9 fb⁻¹ of pp collisions at $E_{cm} = 13$ TeV. See their Fig. 5 for limits on the product of cross section times branching ratio for $m_{H^\pm} = 0.2\text{--}3$ TeV, and their Fig. 6 for the corresponding limits in scenarios in the minimal supersymmetric standard model.
- SIRUNYAN 20BE search for $t \rightarrow bH^+$ followed by the decay $H^+ \rightarrow c\bar{s}$ in pair produced top quark events using 35.9 fb⁻¹ of pp collisions at $E_{cm} = 13$ TeV. Limits on the branching ratio in the range 1.68–0.25% (95%CL) are given for $m_{H^\pm} = 80\text{--}160$ GeV, see their Fig. 4.
- SIRUNYAN 19AH search for H^+ in the decay of a pair-produced t quark, or in associated tH^+ or nonresonant $b\bar{b}H^+ W^-$ production, followed by $H^+ \rightarrow \tau^+\nu$, in 35.9 fb⁻¹ of pp collisions at $E_{cm} = 13$ TeV. Upper limits on cross section times branching ratio between 6 pb and 5 fb (95% CL) are given for $m_{H^\pm} = 80\text{--}3000$ GeV (including the non-resonant production near the top quark mass), see their Fig. 6 (left). See their Fig. 6 (right) for the excluded regions in the $m_h^{\text{mod-}}$ scenario of the MSSM.
- SIRUNYAN 19BP search for vector boson fusion production of H^+ decaying to $H^+ \rightarrow W^+ Z$ to $\ell^+\nu\ell^+\ell^-$ in 35.9 fb⁻¹ of pp collisions at $E_{cm} = 13$ TeV. See their Fig. 7 for limits on cross section times branching ratio for $m_{H^\pm} = 0.3\text{--}2.0$ TeV, and also for limits on the fraction of the triplet vev contribution to the W mass in the Georgi-Machacek model.
- SIRUNYAN 19CC search for $t \rightarrow bH^+$ from pair produced top quarks, with the decay chain $H^+ \rightarrow W^+A^0, A^0 \rightarrow \mu^+\mu^-$ in 35.9 fb⁻¹ of pp collisions at $E_{cm} = 13$ TeV. See their Fig. 2 for limits on the product of branching ratios for $m_{A^0} = 15\text{--}75$ GeV.

Gauge & Higgs Boson Particle Listings

Charged Higgs Bosons (H^\pm and $H^{\pm\pm}$), Searches for

- 20 SIRUNYAN 19CQ search for vector boson fusion production of H^+ decaying to $H^+ \rightarrow W^+ Z \rightarrow \ell^+ \nu q \bar{q}$ or $q \bar{q} \ell^+ \ell^-$ in 35.9 fb^{-1} of pp collisions at $E_{\text{cm}} = 13 \text{ TeV}$. See their Fig. 5 for limits on cross section times branching ratio for $m_{H^+} = 0.6\text{--}2.0 \text{ TeV}$, and also for limits on the triplet vacuum expectation value fraction in the Georgi-Machacek model.
- 21 AABOUD 18BW search for $\bar{t}bH^+$ associated production or the decay $t \rightarrow bH^+$, followed by $H^+ \rightarrow \tau^+ \nu$, in 36.1 fb^{-1} of pp collisions at $E_{\text{cm}} = 13 \text{ TeV}$. See their Fig. 8(a) for upper limits on cross section times branching ratio for $m_{H^+} = 90\text{--}2000 \text{ GeV}$, and Fig. 8(b) for limits on $B(t \rightarrow bH^+) B(H^+ \rightarrow \tau^+ \nu)$ for $m_{H^+} = 90\text{--}160 \text{ GeV}$. See also their Fig. 9 for the excluded region in the hMSSM parameter space.
- 22 AABOUD 18CD search for $\bar{t}bH^+$ associated production followed by $H^+ \rightarrow t\bar{b}$ in 36.1 fb^{-1} of pp collisions at $E_{\text{cm}} = 13 \text{ TeV}$. See their Fig. 8 for upper limits on cross section times branching ratio for $m_{H^+} = 0.2\text{--}2 \text{ TeV}$. See also their Fig. 9 for the excluded region in the parameter space of the $m_h^{\text{mod-}}$ and hMSSM scenarios of the MSSM. The theory predictions overlaid to the experimental limits to determine the excluded m_{H^+} range are shown without their respective uncertainty band.
- 23 AABOUD 18CH search for vector boson fusion production of H^\pm decaying to $H^\pm \rightarrow W^\pm Z \rightarrow \ell^\pm \nu \ell^+ \ell^-$ in 36.1 fb^{-1} of pp collisions at $E_{\text{cm}} = 13 \text{ TeV}$. See their Fig. 7 for limits on cross section times branching ratio for $m_{H^\pm} = 0.2\text{--}0.9 \text{ TeV}$, and also for limits on the triplet vacuum expectation value fraction in the Georgi-Machacek model.
- 24 HALLER 18 give 95% CL lower limits on m_{H^\pm} of 590 GeV in type II two Higgs doublet model from combined data (including an unpublished BELLE result) for $B(b \rightarrow s\gamma)$.
- 25 SIRUNYAN 18DO search for $t\bar{t}$ production followed by $t \rightarrow bH^+, H^+ \rightarrow c\bar{b}$ in 19.7 fb^{-1} of pp collisions at $E_{\text{cm}} = 8 \text{ TeV}$. See their Fig. 3 for upper limits on $B(t \rightarrow bH^+) B(H^+ \rightarrow c\bar{b})$ for $m_{H^+} = 90\text{--}150 \text{ GeV}$ assuming that $B(H^+ \rightarrow c\bar{b}) = 1$ and $B(t \rightarrow bH^+) + B(t \rightarrow bW^+) = 1$.
- 26 MISIAK 17 give 95% CL lower limits on m_{H^\pm} between 570 and 800 GeV in type II two Higgs doublet model from combined data (including an unpublished BELLE result) for $B(b \rightarrow s(d)\gamma)$.
- 27 SIRUNYAN 17AE search for vector boson fusion production of H^\pm decaying to $H^\pm \rightarrow W^\pm Z \rightarrow \ell^\pm \nu \ell^+ \ell^-$ in 15.2 fb^{-1} of pp collisions at $E_{\text{cm}} = 13 \text{ TeV}$. See their Fig. 3 for limits on cross section times branching ratio for $m_{H^\pm} = 0.2\text{--}2.0 \text{ TeV}$, and also for limits on the triplet vacuum expectation value fraction in the Georgi-Machacek model.
- 28 AABOUD 16A search for $t(b) H^\pm$ associated production followed by $H^\pm \rightarrow \tau^\pm \nu$ in 3.2 fb^{-1} of pp collisions at $E_{\text{cm}} = 13 \text{ TeV}$. Upper limits on $\sigma(t(b) H^\pm) B(H^\pm \rightarrow \tau^\pm \nu)$ between 1.9 pb and 15 fb (95% CL) are given for $m_{H^\pm} = 200\text{--}2000 \text{ GeV}$, see their Fig. 6. See their Fig. 7 for the excluded regions in the hMSSM scenario.
- 29 AAD 16AJ search for $t(b) H^\pm$ associated production followed by $H^\pm \rightarrow tb$ in 20.3 fb^{-1} of pp collisions at $E_{\text{cm}} = 8 \text{ TeV}$. See their Fig. 6 for upper limits on $\sigma(t(b) H^\pm) B(H^\pm \rightarrow tb)$ for $m_{H^\pm} = 200\text{--}600 \text{ GeV}$.
- 30 AAD 16AJ search for H^\pm production from quark-antiquark annihilation, followed by $H^\pm \rightarrow tb$, in 20.3 fb^{-1} of pp collisions at $E_{\text{cm}} = 8 \text{ TeV}$. See their Fig. 10 for upper limits on $\sigma(H^\pm) B(H^\pm \rightarrow tb)$ for $m_{H^\pm} = 400\text{--}3000 \text{ GeV}$.
- 31 AAD 15AF search for tH^\pm associated production followed by $H^\pm \rightarrow \tau^\pm \nu$ in 19.5 fb^{-1} of pp collisions at $E_{\text{cm}} = 8 \text{ TeV}$. Upper limits on $\sigma(tH^\pm) B(H^\pm \rightarrow \tau^\pm \nu)$ between 760 and 4.5 fb (95% CL) are given for $m_{H^\pm} = 180\text{--}1000 \text{ GeV}$. See their Fig. 8 for the excluded regions in different benchmark scenarios of the MSSM.
- 32 AAD 15M search for vector boson fusion production of H^\pm decaying to $H^\pm \rightarrow W^\pm Z \rightarrow q\bar{q}\ell^+\ell^-$ in 20.3 fb^{-1} of pp collisions at $E_{\text{cm}} = 8 \text{ TeV}$. See their Fig. 2 for limits on cross section times branching ratio for $m_{H^\pm} = 200\text{--}1000 \text{ GeV}$, and Fig. 3 for limits on the triplet vacuum expectation value fraction in the Georgi-Machacek model.
- 33 KHACHATRYAN 15AX search for tH^\pm associated production followed by $H^\pm \rightarrow tb$ in 19.7 fb^{-1} of pp collisions at $E_{\text{cm}} = 8 \text{ TeV}$. Upper limits on $\sigma(tH^\pm) B(H^\pm \rightarrow t\bar{b})$ between 2.0 and 0.13 pb (95% CL) are given for $m_{H^\pm} = 180\text{--}600 \text{ GeV}$. See their Fig. 11 for the excluded regions in different benchmark scenarios of the MSSM.
- 34 KHACHATRYAN 15AX search for tH^\pm associated production followed by $H^\pm \rightarrow \tau^\pm \nu$ in 19.7 fb^{-1} of pp collisions at $E_{\text{cm}} = 8 \text{ TeV}$. Upper limits on $\sigma(tH^\pm) B(H^\pm \rightarrow \tau^\pm \nu)$ between 380 and 25 fb (95% CL) are given for $m_{H^\pm} = 180\text{--}600 \text{ GeV}$. See their Fig. 11 for the excluded regions in different benchmark scenarios of the MSSM.
- 35 KHACHATRYAN 15BF search for $t\bar{t}$ production followed by $t \rightarrow bH^+, H^+ \rightarrow c\bar{s}$ in 19.7 fb^{-1} of pp collisions at $E_{\text{cm}} = 8 \text{ TeV}$. Upper limits on $B(t \rightarrow bH^+) B(H^+ \rightarrow c\bar{s})$ between 1.2×10^{-2} and 6.5×10^{-2} (95% CL) are given for $m_{H^+} = 90\text{--}160 \text{ GeV}$.
- 36 AAD 14M search for the decay cascade $H_2^0 \rightarrow H^\pm W^\mp \rightarrow H^0 W^\pm W^\mp, H^0$ decaying to $b\bar{b}$ in 20.3 fb^{-1} of pp collisions at $E_{\text{cm}} = 8 \text{ TeV}$. See their Table III for limits on cross section times branching ratio for $m_{H_2^0} = 325\text{--}1025 \text{ GeV}$ and $m_{H^\pm} = 225\text{--}925 \text{ GeV}$.
- 37 AALTONEN 14A measure $B(t \rightarrow b\tau\nu) = 0.096 \pm 0.028$ using 9 fb^{-1} of $p\bar{p}$ collisions at $E_{\text{cm}} = 1.96 \text{ TeV}$. For $m_{H^\pm} = 80\text{--}140 \text{ GeV}$, this measured value is translated to a limit $B(t \rightarrow bH^+) < 0.059$ at 95% CL assuming $B(H^+ \rightarrow \tau^+ \nu) = 1$.
- 38 AAD 13AC search for $t\bar{t}$ production followed by $t \rightarrow bH^+, H^+ \rightarrow c\bar{s}$ (flavor unidentified) in 4.7 fb^{-1} of pp collisions at $E_{\text{cm}} = 7 \text{ TeV}$. Upper limits on $B(t \rightarrow bH^+)$ between 0.05 and 0.01 (95%CL) are given for $m_{H^+} = 90\text{--}150 \text{ GeV}$ and $B(H^+ \rightarrow c\bar{s}) = 1$.
- 39 AAD 13V search for $t\bar{t}$ production followed by $t \rightarrow bH^+, H^+ \rightarrow \tau^+ \nu$ through violation of lepton universality with 4.6 fb^{-1} of pp collisions at $E_{\text{cm}} = 7 \text{ TeV}$. Upper limits on $B(t \rightarrow bH^+)$ between 0.032 and 0.044 (95% CL) are given for $m_{H^+} = 90\text{--}140 \text{ GeV}$ and $B(H^+ \rightarrow \tau^+ \nu) = 1$. By combining with AAD 12BH, the limits improve to 0.008 to 0.034 for $m_{H^+} = 90\text{--}160 \text{ GeV}$. See their Fig. 7 for the excluded region in the m_h^{max} scenario of the MSSM.
- 40 AAD 12BH search for $t\bar{t}$ production followed by $t \rightarrow bH^+, H^+ \rightarrow \tau^+ \nu$ with 4.6 fb^{-1} of pp collisions at $E_{\text{cm}} = 7 \text{ TeV}$. Upper limits on $B(t \rightarrow bH^+)$ between 0.01 and 0.05 (95% CL) are given for $m_{H^+} = 90\text{--}160 \text{ GeV}$ and $B(H^+ \rightarrow \tau^+ \nu) = 1$. See their Fig. 8 for the excluded region in the m_h^{max} scenario of the MSSM.
- 41 CHATRCHYAN 12AA search for $t\bar{t}$ production followed by $t \rightarrow bH^+, H^+ \rightarrow \tau^+ \nu$ with 2 fb^{-1} of pp collisions at $E_{\text{cm}} = 7 \text{ TeV}$. Upper limits on $B(t \rightarrow bH^+)$ between 0.019 and 0.041 (95% CL) are given for $m_{H^+} = 80\text{--}160 \text{ GeV}$ and $B(H^+ \rightarrow \tau^+ \nu) = 1$.
- 42 AALTONEN 11P search in 2.7 fb^{-1} of $p\bar{p}$ collisions at $E_{\text{cm}} = 1.96 \text{ TeV}$ for the decay chain $t \rightarrow bH^+, H^+ \rightarrow W^+ A^0, A^0 \rightarrow \tau^+ \tau^-$ with m_{A^0} between 4 and 9 GeV. See their Fig. 4 for limits on $B(t \rightarrow bH^+)$ for $90 < m_{H^+} < 160 \text{ GeV}$.
- 43 DESCHAMPS 10 make Type II two Higgs doublet model fits to weak leptonic and semileptonic decays, $b \rightarrow s\gamma, B, B_s$ mixings, and $Z \rightarrow b\bar{b}$. The limit holds irrespective of $\tan\beta$.
- 44 AALTONEN 09AJ search for $t \rightarrow bH^+, H^+ \rightarrow c\bar{s}$ in $t\bar{t}$ events in 2.2 fb^{-1} of $p\bar{p}$ collisions at $E_{\text{cm}} = 1.96 \text{ TeV}$. Upper limits on $B(t \rightarrow bH^+)$ between 0.08 and 0.32 (95% CL) are given for $m_{H^+} = 60\text{--}150 \text{ GeV}$ and $B(H^+ \rightarrow c\bar{s}) = 1$.
- 45 ABAZOV 09AC search for $t \rightarrow bH^+, H^+ \rightarrow \tau^+ \nu$ in $t\bar{t}$ events in 0.9 fb^{-1} of $p\bar{p}$ collisions at $E_{\text{cm}} = 1.96 \text{ TeV}$. Upper limits on $B(t \rightarrow bH^+)$ between 0.19 and 0.25 (95% CL) are given for $m_{H^+} = 80\text{--}155 \text{ GeV}$ and $B(H^+ \rightarrow \tau^+ \nu) = 1$. See their Fig. 4 for an excluded region in a MSSM scenario.
- 46 ABAZOV 09AG measure $t\bar{t}$ cross sections in final states with $\ell + \text{jets}$ ($\ell = e, \mu$), $\ell\ell$, and $\tau\ell$ in 1 fb^{-1} of $p\bar{p}$ collisions at $E_{\text{cm}} = 1.96 \text{ TeV}$, which constrains possible $t \rightarrow bH^+$ branching fractions. Upper limits (95% CL) on $B(t \rightarrow bH^+)$ between 0.15 and 0.40 (0.48 and 0.57) are given for $B(H^+ \rightarrow \tau^+ \nu) = 1$ ($B(H^+ \rightarrow c\bar{s}) = 1$) for $m_{H^+} = 80\text{--}155 \text{ GeV}$.
- 47 ABAZOV 09AI search for $t \rightarrow bH^+$ in $t\bar{t}$ events in 1 fb^{-1} of $p\bar{p}$ collisions at $E_{\text{cm}} = 1.96 \text{ TeV}$. Final states with $\ell + \text{jets}$ ($\ell = e, \mu$), $\ell\ell$, and $\tau\ell$ are examined. Upper limits on $B(t \rightarrow bH^+)$ (95% CL) between 0.15 and 0.19 (0.19 and 0.22) are given for $B(H^+ \rightarrow \tau^+ \nu) = 1$ ($B(H^+ \rightarrow c\bar{s}) = 1$) for $m_{H^+} = 80\text{--}155 \text{ GeV}$. For $B(H^+ \rightarrow \tau^+ \nu) = 1$ also a simultaneous extraction of $B(t \rightarrow bH^+)$ and the $t\bar{t}$ cross section is performed, yielding a limit on $B(t \rightarrow bH^+)$ between 0.12 and 0.26 for $m_{H^+} = 80\text{--}155 \text{ GeV}$. See their Figs. 5–8 for excluded regions in several MSSM scenarios.
- 48 ABAZOV 09P search for H^+ production by $q\bar{q}$ annihilation followed by $H^+ \rightarrow t\bar{b}$ decay in 0.9 fb^{-1} of $p\bar{p}$ collisions at $E_{\text{cm}} = 1.96 \text{ TeV}$. Cross section limits in several two-doublet models are given for $m_{H^+} = 180\text{--}300 \text{ GeV}$. A region with $20 \lesssim \tan\beta \lesssim 70$ is excluded (95% CL) for $180 \text{ GeV} \lesssim m_{H^+} \lesssim 184 \text{ GeV}$ in type-I models.
- 49 ABULENCIA 06E search for associated $H^0 W$ production in $p\bar{p}$ collisions at $E_{\text{cm}} = 1.96 \text{ TeV}$. A fit is made for $t\bar{t}$ production processes in dilepton, lepton + jets, and lepton + τ final states, with the decays $t \rightarrow W^+ b$ and $t \rightarrow H^+ b$ followed by $H^+ \rightarrow \tau^+ \nu, c\bar{s}, t^* \bar{b}$, or $W^+ H^0$. Within the MSSM the search is sensitive to the region $\tan\beta < 1$ or > 30 in the mass range $m_{H^\pm} = 80\text{--}160 \text{ GeV}$. See Fig. 2 for the excluded region in a certain MSSM scenario.
- 50 ABDALLAH 04 search for $e^+ e^- \rightarrow H^+ H^-$ with H^\pm decaying to $\tau\nu, cs$, or $W^* A^0$ in Type-I two-Higgs-doublet models.
- 51 ABBIENDI 03 give a limit $m_{H^\pm} > 1.28 \tan\beta \text{ GeV}$ (95%CL) in Type II two-doublet models.
- 52 ABAZOV 02B search for a charged Higgs boson in top decays with $H^+ \rightarrow \tau^+ \nu$ at $E_{\text{cm}} = 1.8 \text{ TeV}$. For $m_{H^+} = 75 \text{ GeV}$, the region $\tan\beta > 32.0$ is excluded at 95%CL. The excluded mass region extends to over 140 GeV for $\tan\beta$ values above 100.
- 53 BORZUMATI 02 point out that the decay modes such as $b\bar{b}W, A^0 W$, and supersymmetric ones can have substantial branching fractions in the mass range explored at LEP II and Tevatron.
- 54 ABBIENDI 01Q give a limit $\tan\beta/m_{H^\pm} < 0.53 \text{ GeV}^{-1}$ (95%CL) in Type II two-doublet models.
- 55 BARATE 01E give a limit $\tan\beta/m_{H^\pm} < 0.40 \text{ GeV}^{-1}$ (90% CL) in Type II two-doublet models. An independent measurement of $B \rightarrow \tau\nu X$ gives $\tan\beta/m_{H^\pm} < 0.49 \text{ GeV}^{-1}$ (90% CL).
- 56 GAMBINO 01 use the world average data in the summer of 2001 $B(b \rightarrow s\gamma) = (3.23 \pm 0.42) \times 10^{-4}$. The limit applies for Type-II two-doublet models.
- 57 AFFOLDER 00i search for a charged Higgs boson in top decays with $H^+ \rightarrow \tau^+ \nu$ in $p\bar{p}$ collisions at $E_{\text{cm}} = 1.8 \text{ TeV}$. The excluded mass region extends to over 120 GeV for $\tan\beta$ values above 100 and $B(\tau\nu) = 1$. If $B(t \rightarrow bH^+) \gtrsim 0.6$, m_{H^+} up to 160 GeV is excluded. Updates ABE 97L.
- 58 ABBOTT 99 search for a charged Higgs boson in top decays in $p\bar{p}$ collisions at $E_{\text{cm}} = 1.8 \text{ TeV}$, by comparing the observed $t\bar{t}$ cross section (extracted from the data assuming the dominant decay $t \rightarrow bW^+$) with theoretical expectation. The search is sensitive to regions of the domains $\tan\beta \lesssim 1, 50 < m_{H^\pm} (\text{GeV}) \lesssim 120$ and $\tan\beta \gtrsim 40, 50 < m_{H^\pm} (\text{GeV}) \lesssim 160$. See Fig. 3 for the details of the excluded region.
- 59 ACKERSTAFF 99D measure the Michel parameters ρ, ξ, η , and $\xi\delta$ in leptonic τ decays from $Z \rightarrow \tau\tau$. Assuming $e\text{--}\mu$ universality, the limit $m_{H^\pm} > 0.97 \tan\beta \text{ GeV}$ (95%CL) is obtained for two-doublet models in which only one doublet couples to leptons.
- 60 ACCIARRI 97F give a limit $m_{H^\pm} > 2.6 \tan\beta \text{ GeV}$ (90% CL) from their limit on the exclusive $B \rightarrow \tau\nu X$ branching ratio.
- 61 AMMAR 97B measure the Michel parameter ρ from $\tau \rightarrow e\nu\nu$ decays and assumes $e\text{--}\mu$ universality to extract the Michel η parameter from $\tau \rightarrow \mu\nu\nu$ decays. The measurement is translated to a lower limit on m_{H^\pm} in a two-doublet model $m_{H^\pm} > 0.97 \tan\beta \text{ GeV}$ (90% CL).
- 62 COARASA 97 reanalyzed the constraint on the $(m_{H^\pm}, \tan\beta)$ plane derived from the inclusive $B \rightarrow \tau\nu X$ branching ratio in GROSSMAN 95B and BUSKULIC 95. They show that the constraint is quite sensitive to supersymmetric one-loop effects.
- 63 GUCHAIT 97 studies the constraints on m_{H^\pm} set by Tevatron data on $\ell\tau$ final states in $t\bar{t} \rightarrow (Wb)(Hb), W \rightarrow \ell\nu, H \rightarrow \tau\nu$. See Fig. 2 for the excluded region.
- 64 MANGANO 97 reconsiders the limit in ACCIARRI 97F including the effect of the potentially large $B_c \rightarrow \tau\nu X$ background to $B_H \rightarrow \tau\nu X$ decays. Stronger limits are obtained.
- 65 STAHL 97 fit τ lifetime, leptonic branching ratios, and the Michel parameters and derive limit $m_{H^\pm} > 1.5 \tan\beta \text{ GeV}$ (90% CL) for a two-doublet model. See also STAHL 94.
- 66 ALAM 95 measure the inclusive $b \rightarrow s\gamma$ branching ratio at $T(4S)$ and give $B(b \rightarrow s\gamma) < 4.2 \times 10^{-4}$ (95% CL), which translates to the limit $m_{H^\pm} > [244 + 63/(\tan\beta)]^{1.3}$

See key on page 1171

Gauge & Higgs Boson Particle Listings

Charged Higgs Bosons (H^\pm and $H^{\pm\pm}$), Searches for

GeV in the Type II two-doublet model. Light supersymmetric particles can invalidate this bound.
 67 BUSKULIC 95 give a limit $m_{H^\pm} > 1.9 \tan\beta$ GeV (90% CL) for Type-II models from $b \rightarrow \tau\nu_\tau X$ branching ratio, as proposed in GROSSMAN 94.

H^\pm (charged Higgs) mass limits for $m_{H^\pm} > m(\text{top})$

Limits obtained at the LHC are given in the $m_{H^\pm}^{\text{mod-}}$ benchmark scenario, see CARENA 13, and depend on the $\tan\beta$ values.

VALUE (GeV)	CL%	DOCUMENT ID	TECN	COMMENT
> 181	95	1 AABOUD	18BWATLS	$\tan\beta = 10$
> 249	95	1 AABOUD	18BWATLS	$\tan\beta = 20$
> 390	95	1 AABOUD	18BWATLS	$\tan\beta = 30$
> 894	95	1 AABOUD	18BWATLS	$\tan\beta = 40$
> 1017	95	1 AABOUD	18BWATLS	$\tan\beta = 50$
> 1103	95	1 AABOUD	18BWATLS	$\tan\beta = 60$

1 AABOUD 18BW search for $\bar{t}bH^\pm$ associated production in 36.1 fb^{-1} of pp collisions at $E_{\text{cm}} = 13$ TeV. See also their Fig. 9 for the excluded region in the hMSSM parameter space.

$H^{\pm\pm}$ (doubly-charged Higgs boson) mass limits

This section covers searches for a doubly-charged Higgs boson with couplings to lepton pairs. Its weak isospin T_3 is thus restricted to two possibilities depending on lepton chiralities: $T_3(H^{\pm\pm}) = \pm 1$, with the coupling $g_{\ell\ell}$ to $\ell_L^- \ell_L^-$ and $\ell_R^+ \ell_R^+$ ("left-handed") and $T_3(H^{\pm\pm}) = 0$, with the coupling to $\ell_L^- \ell_R^+$ and $\ell_R^+ \ell_L^-$ ("right-handed"). These Higgs bosons appear in some left-right symmetric models based on the gauge group $SU(2)_L \times SU(2)_R \times U(1)$, the type-II seesaw model, and the Zee-Babu model. The two cases are listed separately in the following. Unless noted, one of the lepton flavor combinations is assumed to be dominant in the decay.

Limits for $H^{\pm\pm}$ with $T_3 = \pm 1$

VALUE (GeV)	CL%	DOCUMENT ID	TECN	COMMENT
> 1020	95	1 AAD	23AI ATLS	$\ell\ell$
> 220	95	2 AABOUD	19K ATLS	$W^\pm W^\pm$
> 768	95	3 AABOUD	18bC ATLS	ee
> 846	95	3 AABOUD	18bC ATLS	$\mu\mu$
> 468	95	4 AAD	15AG ATLS	$e\mu$
> 400	95	5 AAD	15AP ATLS	$e\tau$
> 400	95	5 AAD	15AP ATLS	$\mu\tau$
> 169	95	6 CHATRCHYAN 12AU	CMS	$\tau\tau$
> 300	95	6 CHATRCHYAN 12AU	CMS	$\mu\tau$
> 293	95	6 CHATRCHYAN 12AU	CMS	$e\tau$
> 395	95	6 CHATRCHYAN 12AU	CMS	$\mu\mu$
> 391	95	6 CHATRCHYAN 12AU	CMS	$e\mu$
> 382	95	6 CHATRCHYAN 12AU	CMS	ee
> 98.1	95	7 ABDALLAH 03	DLPH	$\tau\tau$
> 99.0	95	8 ABBIENDI 02c	OPAL	$\tau\tau$
• • • We do not use the following data for averages, fits, limits, etc. • • •				
> 350	95	9 AAD	21U ATLS	$W^\pm W^\pm$
> 230	95	10 AAD	21U ATLS	$H^{\pm\pm} H^\mp$ associated production, $H^{\pm\pm} \rightarrow W^\pm W^\pm, H^\pm \rightarrow W^\pm Z$
		11 SIRUNYAN	21W CMS	$W^\pm W^\pm$
		12 SIRUNYAN	19CQ CMS	$W^\pm W^\pm$
		13 SIRUNYAN	18CC CMS	$W^\pm W^\pm$
> 551	95	4 AAD	15AG ATLS	ee
> 516	95	4 AAD	15AG ATLS	$\mu\mu$
		14 KANEMURA 15	RVUE	$W^{(*)\pm} W^{(*)\pm}$
		15 KHACHATRYAN 15D	CMS	$W^\pm W^\pm$
		16 KANEMURA 14	RVUE	$W^{(*)\pm} W^{(*)\pm}$
> 330	95	17 AAD	13Y ATLS	$\mu\mu$
> 237	95	17 AAD	13Y ATLS	$\mu\tau$
> 355	95	18 AAD	12AY ATLS	$\mu\mu$
> 398	95	19 AAD	12CQ ATLS	$\mu\mu$
> 375	95	19 AAD	12CQ ATLS	$e\mu$
> 409	95	19 AAD	12CQ ATLS	ee
> 128	95	20 ABAZOV	12A D0	$\tau\tau$
> 144	95	20 ABAZOV	12A D0	$\mu\tau$
> 245	95	21 AALTONEN	11AF CDF	$\mu\mu$
> 210	95	21 AALTONEN	11AF CDF	$e\mu$
> 225	95	21 AALTONEN	11AF CDF	ee
> 114	95	22 AALTONEN	08AA CDF	$e\tau$
> 112	95	22 AALTONEN	08AA CDF	$\mu\tau$
> 168	95	23 ABAZOV	08V D0	$\mu\mu$
		24 AKTAS 06A	H1	single $H^{\pm\pm}$
> 133	95	25 ACOSTA 05L	CDF	stable
> 118.4	95	26 ABAZOV 04E	D0	$\mu\mu$
		27 ABBIENDI 03Q	OPAL	$E_{\text{cm}} \leq 209$ GeV, single $H^{\pm\pm}$
		28 GORDEEV 97	SPEC	muonium conversion
		29 ASAKA 95	THEO	

> 45.6	95	30 ACTON	92M OPAL
> 30.4	95	31 ACTON	92M OPAL
none 6.5–36.6	95	32 SWARTZ	90 MRK2

1 AAD 23AI search for $H^{++} H^{--}$ production using 139 fb^{-1} of pp collisions at $E_{\text{cm}} = 13$ TeV. Decay branching ratios $B(H^{++} \rightarrow \ell^+ \ell'^+)$ for the six flavor combinations are assumed to be equal, adding up to unity. If the $T_3 = 0$ states are degenerate with the $T_3 = \pm 1$ states, the limit becomes 1080 GeV.

2 AABOUD 19K search for pair production of $H^{++} H^{--}$ followed by the decay $H^{\pm\pm} \rightarrow W^\pm W^\pm$ in 36.1 fb^{-1} of pp collisions at $E_{\text{cm}} = 13$ TeV. The search is interpreted in a doublet-triplet extension of the scalar sector with a vev of 0.1 GeV, leading to $B(H^{\pm\pm} \rightarrow W^\pm W^\pm) = 1$. See their Fig. 5 for limits on the cross section for $m_{H^{++}}$ between 200 and 700 GeV.

3 See their Figs. 11(b) and 13 for limits with smaller branching ratios.

4 AAD 15AG search for $H^{++} H^{--}$ production in 20.3 fb^{-1} of pp collisions at $E_{\text{cm}} = 8$ TeV. The limit assumes 100% branching ratio to the specified final state. See their Fig. 5 for limits for arbitrary branching ratios.

5 AAD 15AP search for $H^{++} H^{--}$ production in 20.3 fb^{-1} of pp collisions at $E_{\text{cm}} = 8$ TeV. The limit assumes 100% branching ratio to the specified final state.

6 CHATRCHYAN 12AU search for $H^{++} H^{--}$ production with 4.9 fb^{-1} of pp collisions at $E_{\text{cm}} = 7$ TeV. The limit assumes 100% branching ratio to the specified final state. See their Table 6 for limits including associated $H^{++} H^{--}$ production or assuming different scenarios.

7 ABDALLAH 03 search for $H^{++} H^{--}$ pair production either followed by $H^{++} \rightarrow \tau^+ \tau^+$, or decaying outside the detector.

8 ABBIENDI 02c searches for pair production of $H^{++} H^{--}$, with $H^{\pm\pm} \rightarrow \ell^\pm \ell'^\pm$ ($\ell, \ell' = e, \mu, \tau$). The limit holds for $\ell = \ell' = \tau$, and becomes stronger for other combinations of leptonic final states. To ensure the decay within the detector, the limit only applies for $g(H\ell\ell) \gtrsim 10^{-7}$.

9 AAD 21U search for pair production of $H^{++} H^{--}$ followed by the decay $H^{\pm\pm} \rightarrow W^\pm W^\pm$ in 139 fb^{-1} of pp collisions at $E_{\text{cm}} = 13$ TeV. The search is interpreted in a triplet extension of the SM Higgs sector with a triplet vev of 0.1 GeV, leading to $B(H^{\pm\pm} \rightarrow W^\pm W^\pm) = 1$. See their Fig. 9(a) for limits on the cross section for $m_{H^{++}}$ between 200 and 600 GeV.

10 AAD 21U search for associated production of $H^{\pm\pm} H^\mp$ followed by the decays $H^{\pm\pm} \rightarrow W^\pm W^\pm, H^\pm \rightarrow W^\pm Z$ in 139 fb^{-1} of pp collisions at $E_{\text{cm}} = 13$ TeV. $H^{\pm\pm}$ and H^\pm are assumed to be degenerate in mass within 5 GeV. The search is interpreted in a triplet extension of the SM Higgs sector with a triplet vev of 0.1 GeV, leading to $B(H^{\pm\pm} \rightarrow W^\pm W^\pm) = 1$. See their Fig. 9(b) for limits on the cross section for $m_{H^{++}}$ between 200 and 600 GeV.

11 SIRUNYAN 21W search for vector boson fusion production of $H^{\pm\pm}$ decaying to $H^{\pm\pm} \rightarrow W^\pm W^\pm \rightarrow \ell^\pm \nu \ell'^\pm \nu$ in 137 fb^{-1} of pp collisions at $E_{\text{cm}} = 13$ TeV. See their Fig. 8 for limits on cross section times branching ratio for $m_{H^{++}}$ between 160 and 800 GeV.

12 SIRUNYAN 19CQ search for $H^{\pm\pm}$ production by vector boson fusion followed by the decay $H^{\pm\pm} \rightarrow W^\pm W^\pm \rightarrow qq\ell\nu$ in 35.9 fb^{-1} of pp collisions at $E_{\text{cm}} = 13$ TeV. See their Fig. 5 for limits on cross section times branching ratio for $m_{H^{\pm\pm}}$ between 0.6 and 2 TeV.

13 SIRUNYAN 18CC search for $H^{\pm\pm}$ production by vector boson fusion followed by the decay $H^{\pm\pm} \rightarrow W^\pm W^\pm$ in 35.9 fb^{-1} of pp collisions at $E_{\text{cm}} = 13$ TeV. See their Fig. 3 for limits on cross section times branching ratio for $m_{H^{\pm\pm}}$ between 200 and 1000 GeV.

14 KANEMURA 15 examine the case where H^{++} decays preferentially to $W^{(*)} W^{(*)}$ and estimate that a lower mass limit of ~ 84 GeV can be derived from the same-sign dilepton data of AAD 15AG if H^{++} decays with 100% branching ratio to $W^{(*)} W^{(*)}$.

15 KHACHATRYAN 15D search for $H^{\pm\pm}$ production by vector boson fusion followed by the decay $H^{\pm\pm} \rightarrow W^\pm W^\pm$ in 19.4 fb^{-1} of pp collisions at $E_{\text{cm}} = 8$ TeV. See their Fig. 4 for limits on cross section times branching ratio for $m_{H^{++}}$ between 160 and 800 GeV.

16 KANEMURA 14 examine the case where H^{++} decays preferentially to $W^{(*)} W^{(*)}$ and estimate that a lower mass limit of ~ 60 GeV can be derived from the same-sign dilepton data of AAD 12CY.

17 AAD 13Y search for $H^{++} H^{--}$ production in a generic search of events with three charged leptons in 4.6 fb^{-1} of pp collisions at $E_{\text{cm}} = 7$ TeV. The limit assumes 100% branching ratio to the specified final state.

18 AAD 12AY search for $H^{++} H^{--}$ production with 1.6 fb^{-1} of pp collisions at $E_{\text{cm}} = 7$ TeV. The limit assumes 100% branching ratio to the specified final state.

19 AAD 12CQ search for $H^{++} H^{--}$ production with 4.7 fb^{-1} of pp collisions at $E_{\text{cm}} = 7$ TeV. The limit assumes 100% branching ratio to the specified final state. See their Table 1 for limits assuming smaller branching ratios.

20 ABAZOV 12A search for $H^{++} H^{--}$ production in 7.0 fb^{-1} of $p\bar{p}$ collisions at $E_{\text{cm}} = 1.96$ TeV.

21 AALTONEN 11AF search for $H^{++} H^{--}$ production in 6.1 fb^{-1} of $p\bar{p}$ collisions at $E_{\text{cm}} = 1.96$ TeV. The limit assumes 100% branching ratio to the specified final state.

22 AALTONEN 08AA search for $H^{++} H^{--}$ production in $p\bar{p}$ collisions at $E_{\text{cm}} = 1.96$ TeV. The limit is updated in ABAZOV 12A.

23 ABAZOV 08V search for $H^{++} H^{--}$ production in $p\bar{p}$ collisions at $E_{\text{cm}} = 1.96$ TeV. The limit is for $B(H \rightarrow \mu\mu) = 1$. The limit is updated in ABAZOV 12A.

24 AKTAS 06A search for single $H^{\pm\pm}$ production in ep collisions at HERA. Assuming that H^{++} only couples to $e^+ \mu^+$ with $g_{e\mu} = 0.3$ (electromagnetic strength), a limit $m_{H^{++}} > 141$ GeV (95% CL) is derived. For the case where H^{++} couples to $e\tau$ only the limit is 112 GeV.

25 ACOSTA 05L search for $H^{++} H^{--}$ pair production in $p\bar{p}$ collisions. The limit is valid for $g_{\ell\ell} < 10^{-8}$ so that the Higgs decays outside the detector.

26 ABAZOV 04E search for $H^{++} H^{--}$ pair production in $H^{\pm\pm} \rightarrow \mu^\pm \mu^\pm$. The limit is valid for $g_{\mu\mu} \gtrsim 10^{-7}$.

27 ABBIENDI 03Q searches for single $H^{\pm\pm}$ via direct production in $e^+ e^- \rightarrow e^\mp H^{\pm\pm}$, and via t -channel exchange in $e^+ e^- \rightarrow e^+ e^-$. In the direct case, and assuming $B(H^{\pm\pm} \rightarrow \ell^\pm \ell^\pm) = 1$, a 95% CL limit on $h_{ee} < 0.071$ is set for $m_{H^{\pm\pm}} < 160$ GeV (see Fig. 6). In the second case, indirect limits on h_{ee} are set for $m_{H^{\pm\pm}} < 2$ TeV (see Fig. 8).

Gauge & Higgs Boson Particle Listings

Charged Higgs Bosons (H^\pm and $H^{\pm\pm}$), Searches for

- ²⁸ GORDEEV 97 search for muonium-antimuonium conversion and find $G_{M\overline{M}}/G_F < 0.14$ (90% CL), where $G_{M\overline{M}}$ is the lepton-flavor violating effective four-fermion coupling. This limit may be converted to $m_{H^{++}} > 210$ GeV if the Yukawa couplings of H^{++} to ee and $\mu\mu$ are as large as the weak gauge coupling. For similar limits on muonium-antimuonium conversion, see the muon Particle Listings.
- ²⁹ ASAKA 95 point out that H^{++} decays dominantly to four fermions in a large region of parameter space where the limit of ACTON 92M from the search of dilepton modes does not apply.
- ³⁰ ACTON 92M limit assumes $H^{\pm\pm} \rightarrow \ell^\pm \ell^\pm$ or $H^{\pm\pm}$ does not decay in the detector. Thus the region $g_{\ell\ell} \approx 10^{-7}$ is not excluded.
- ³¹ ACTON 92M from $\Delta\Gamma_Z < 40$ MeV.
- ³² SWARTZ 90 assume $H^{\pm\pm} \rightarrow \ell^\pm \ell^\pm$ (any flavor). The limits are valid for the Higgs-lepton coupling $g(H\ell\ell) \gtrsim 7.4 \times 10^{-7}/[m_H/\text{GeV}]^{1/2}$. The limits improve somewhat for ee and $\mu\mu$ decay modes.

Limits for $H^{\pm\pm}$ with $T_3 = 0$

VALUE (GeV)	CL%	DOCUMENT ID	TECN	COMMENT
>900	95	1 AAD	23AI ATLS	$\ell\ell$
> 58	95	2 AABOUD	18BC ATLS	ee
>723	95	2 AABOUD	18BC ATLS	$\mu\mu$
>402	95	3 AAD	15AG ATLS	$e\mu$
>290	95	4 AAD	15AP ATLS	$e\tau$
>290	95	4 AAD	15AP ATLS	$\mu\tau$
> 97.3	95	5 ABDALLAH	03 DLPH	$\tau\tau$
> 97.3	95	6 ACHARD	03F L3	$\tau\tau$
> 98.5	95	7 ABBIENDI	02C OPAL	$\tau\tau$
• • • We do not use the following data for averages, fits, limits, etc. • • •				
>374	95	3 AAD	15AG ATLS	ee
>438	95	3 AAD	15AG ATLS	$\mu\mu$
>251	95	8 AAD	12AY ATLS	$\mu\mu$
>306	95	9 AAD	12CQ ATLS	$\mu\mu$
>310	95	9 AAD	12CQ ATLS	$e\mu$
>322	95	9 AAD	12CQ ATLS	ee
>113	95	10 ABAZOV	12A D0	$\mu\tau$
>205	95	11 AALTONEN	11AF CDF	$\mu\mu$
>190	95	11 AALTONEN	11AF CDF	$e\mu$
>205	95	11 AALTONEN	11AF CDF	ee
>145	95	12 ABAZOV	08V D0	$\mu\mu$
		13 AKTAS	06A H1	single $H^{\pm\pm}$
>109	95	14 ACOSTA	05L CDF	stable
> 98.2	95	15 ABAZOV	04E D0	$\mu\mu$
		16 ABBIENDI	03Q OPAL	$E_{cm} \leq 209$ GeV, single $H^{\pm\pm}$
		17 GORDEEV	97 SPEC	muonium conversion
> 45.6	95	18 ACTON	92M OPAL	
> 25.5	95	19 ACTON	92M OPAL	
none 7.3–34.3	95	20 SWARTZ	90 MRK2	

- 1 AAD 23AI search for $H^{++}H^{--}$ production using 139 fb $^{-1}$ of pp collisions at $E_{cm} = 13$ TeV. Decay branching ratios $B(H^{++} \rightarrow \ell^+\ell^+)$ for the six flavor combinations are assumed to be equal, adding up to unity.
- 2 See their Figs. 12(b) and 14 for limits with smaller branching ratios.
- 3 AAD 15AG search for $H^{++}H^{--}$ production in 20.3 fb $^{-1}$ of pp collisions at $E_{cm} = 8$ TeV. The limit assumes 100% branching ratio to the specified final state. See their Fig. 5 for limits for arbitrary branching ratios.
- 4 AAD 15AP search for $H^{++}H^{--}$ production in 20.3 fb $^{-1}$ of pp collisions at $E_{cm} = 8$ TeV. The limit assumes 100% branching ratio to the specified final state.
- 5 ABDALLAH 03 search for $H^{++}H^{--}$ pair production either followed by $H^{++} \rightarrow \tau^+\tau^+$, or decaying outside the detector.
- 6 ACHARD 03F search for $e^+e^- \rightarrow H^{++}H^{--}$ with $H^{\pm\pm} \rightarrow \ell^\pm\ell^\pm$. The limit holds for $\ell = e, \mu, \tau$, and slightly different limits apply for other flavor combinations. The limit is valid for $g_{\ell\ell} \gtrsim 10^{-7}$.
- 7 ABBIENDI 02c searches for pair production of $H^{++}H^{--}$, with $H^{\pm\pm} \rightarrow \ell^\pm\ell^\pm$ ($\ell, \ell' = e, \mu, \tau$). the limit holds for $\ell = \ell' = \tau$, and becomes stronger for other combinations of leptonic final states. To ensure the decay within the detector, the limit only applies for $g(H\ell\ell) \gtrsim 10^{-7}$.
- 8 AAD 12AY search for $H^{++}H^{--}$ production with 1.6 fb $^{-1}$ of pp collisions at $E_{cm} = 7$ TeV. The limit assumes 100% branching ratio to the specified final state.
- 9 AAD 12CQ search for $H^{++}H^{--}$ production with 4.7 fb $^{-1}$ of pp collisions at $E_{cm} = 7$ TeV. The limit assumes 100% branching ratio to the specified final state. See their Table 1 for limits assuming smaller branching ratios.
- 10 ABAZOV 12A search for $H^{++}H^{--}$ production in 7.0 fb $^{-1}$ of $p\overline{p}$ collisions at $E_{cm} = 1.96$ TeV.
- 11 AALTONEN 11AF search for $H^{++}H^{--}$ production in 6.1 fb $^{-1}$ of $p\overline{p}$ collisions at $E_{cm} = 1.96$ TeV.
- 12 ABAZOV 08V search for $H^{++}H^{--}$ production in $p\overline{p}$ collisions at $E_{cm} = 1.96$ TeV. The limit is for $B(H \rightarrow \mu\mu) = 1$. The limit is updated in ABAZOV 12A.
- 13 AKTAS 06A search for single $H^{\pm\pm}$ production in ep collisions at HERA. Assuming that H^{++} only couples to $e^+\mu^+$ with $g_{e\mu} = 0.3$ (electromagnetic strength), a limit $m_{H^{++}} > 141$ GeV (95% CL) is derived. For the case where H^{++} couples to $e\tau$ only the limit is 112 GeV.
- 14 ACOSTA 05L search for $H^{++}H^{--}$ pair production in $p\overline{p}$ collisions. The limit is valid for $g_{\ell\ell} < 10^{-8}$ so that the Higgs decays outside the detector.
- 15 ABAZOV 04E search for $H^{++}H^{--}$ pair production in $H^{\pm\pm} \rightarrow \mu^\pm\mu^\pm$. The limit is valid for $g_{\mu\mu} \gtrsim 10^{-7}$.
- 16 ABBIENDI 03Q searches for single $H^{\pm\pm}$ via direct production in $e^+e^- \rightarrow e^\mp e^\mp H^{\pm\pm}$, and via t -channel exchange in $e^+e^- \rightarrow e^+e^-$. In the direct case, and assuming $B(H^{\pm\pm} \rightarrow \ell^\pm\ell^\pm) = 1$, a 95% CL limit on $h_{ee} < 0.071$ is set for $m_{H^{\pm\pm}} < 160$ GeV

(see Fig. 6). In the second case, indirect limits on h_{ee} are set for $m_{H^{\pm\pm}} < 2$ TeV (see Fig. 8).

- ¹⁷ GORDEEV 97 search for muonium-antimuonium conversion and find $G_{M\overline{M}}/G_F < 0.14$ (90% CL), where $G_{M\overline{M}}$ is the lepton-flavor violating effective four-fermion coupling. This limit may be converted to $m_{H^{++}} > 210$ GeV if the Yukawa couplings of H^{++} to ee and $\mu\mu$ are as large as the weak gauge coupling. For similar limits on muonium-antimuonium conversion, see the muon Particle Listings.
- ¹⁸ ACTON 92M limit assumes $H^{\pm\pm} \rightarrow \ell^\pm\ell^\pm$ or $H^{\pm\pm}$ does not decay in the detector. Thus the region $g_{\ell\ell} \approx 10^{-7}$ is not excluded.
- ¹⁹ ACTON 92M from $\Delta\Gamma_Z < 40$ MeV.
- ²⁰ SWARTZ 90 assume $H^{\pm\pm} \rightarrow \ell^\pm\ell^\pm$ (any flavor). The limits are valid for the Higgs-lepton coupling $g(H\ell\ell) \gtrsim 7.4 \times 10^{-7}/[m_H/\text{GeV}]^{1/2}$. The limits improve somewhat for ee and $\mu\mu$ decay modes.

H^\pm and $H^{\pm\pm}$ REFERENCES

AAD	23AH EPJ C83 633	G. Aad et al.	(ATLAS Collab.)
AAD	23AI EPJ C83 605	G. Aad et al.	(ATLAS Collab.)
AAD	23BB JHEP 2309 004	G. Aad et al.	(ATLAS Collab.)
AAD	23BW PR D108 092007	G. Aad et al.	(ATLAS Collab.)
TUMASYAN	23AV JHEP 2309 032	A. Tumasyan et al.	(CMS Collab.)
TUMASYAN	22B PL B826 136888	A. Tumasyan et al.	(CMS Collab.)
AAD	21U JHEP 2106 146	G. Aad et al.	(ATLAS Collab.)
AAD	21V JHEP 2106 145	G. Aad et al.	(ATLAS Collab.)
SIRUNYAN	21W EPJ C81 723	A.M. Sirunyan et al.	(CMS Collab.)
AAD	20W JHEP 2006 151	G. Aad et al.	(ATLAS Collab.)
SIRUNYAN	20XA JHEP 2007 126	A.M. Sirunyan et al.	(CMS Collab.)
SIRUNYAN	20AV JHEP 2001 096	A.M. Sirunyan et al.	(CMS Collab.)
SIRUNYAN	20BE PR D102 072001	A.M. Sirunyan et al.	(CMS Collab.)
AABOUD	19K EPJ C79 58	M. Aaboud et al.	(ATLAS Collab.)
SIRUNYAN	19AH JHEP 1907 142	A.M. Sirunyan et al.	(CMS Collab.)
SIRUNYAN	19BP PL B795 281	A.M. Sirunyan et al.	(CMS Collab.)
SIRUNYAN	19CC PRL 123 131802	A.M. Sirunyan et al.	(CMS Collab.)
SIRUNYAN	19CQ PL B798 134985	A.M. Sirunyan et al.	(CMS Collab.)
AABOUD	18BC EPJ C78 199	M. Aaboud et al.	(ATLAS Collab.)
AABOUD	18BW JHEP 1809 139	M. Aaboud et al.	(ATLAS Collab.)
AABOUD	18CD JHEP 1811 085	M. Aaboud et al.	(ATLAS Collab.)
AABOUD	18CH PL B787 68	M. Aaboud et al.	(ATLAS Collab.)
HALLER	18 EPJ C78 575	J. Haller et al.	(Gitter Group)
SIRUNYAN	18CC PRL 120 081801	A.M. Sirunyan et al.	(CMS Collab.)
SIRUNYAN	18DO JHEP 1811 115	A.M. Sirunyan et al.	(CMS Collab.)
MISIASK	17 EPJ C77 201	M. Misiak, M. Steinhauser	(CMS Collab.)
SIRUNYAN	17AE PRL 119 141802	A.M. Sirunyan et al.	(CMS Collab.)
AABOUD	16A PL B759 555	M. Aaboud et al.	(ATLAS Collab.)
AAD	16AJ JHEP 1603 127	G. Aad et al.	(ATLAS Collab.)
AAD	15AF JHEP 1503 088	G. Aad et al.	(ATLAS Collab.)
AAD	15AG JHEP 1503 041	G. Aad et al.	(ATLAS Collab.)
AAD	15AP JHEP 1508 138	G. Aad et al.	(ATLAS Collab.)
AAD	15M PRL 114 231801	G. Aad et al.	(ATLAS Collab.)
KANEMURA	15 PTEP 2015 051B02	S. Kanemura et al.	(CMS Collab.)
KHACHATRYAN	15AX JHEP 1511 016	V. Khachatryan et al.	(CMS Collab.)
KHACHATRYAN	15BF JHEP 1512 178	V. Khachatryan et al.	(CMS Collab.)
KHACHATRYAN	15D PRL 114 051801	V. Khachatryan et al.	(CMS Collab.)
AAD	14M PR D89 032002	G. Aad et al.	(ATLAS Collab.)
AALTONEN	14A PR D89 091101	T. Aaltonen et al.	(CDF Collab.)
KANEMURA	14 PR D90 115018	S. Kanemura et al.	(CMS Collab.)
AAD	13AC EPJ C73 2465	G. Aad et al.	(ATLAS Collab.)
AAD	13V JHEP 1303 076	G. Aad et al.	(ATLAS Collab.)
AAD	13Y PR D87 052002	G. Aad et al.	(ATLAS Collab.)
CARENA	13 EPJ C73 2552	M. Carena et al.	(LEP Collab.)
LEP	13 EPJ C73 2463	LEP Collab.	(ALEPH, DELPHI, L3, OPAL, LEP)
AAD	12AY PR D85 032004	G. Aad et al.	(ATLAS Collab.)
AAD	12BH JHEP 1206 039	G. Aad et al.	(ATLAS Collab.)
AAD	12CQ EPJ C72 2244	G. Aad et al.	(ATLAS Collab.)
AAD	12CY JHEP 1212 007	G. Aad et al.	(ATLAS Collab.)
ABAZOV	12A PRL 108 021801	V.M. Abazov et al.	(D0 Collab.)
ABBIENDI	12 EPJ C72 2076	G. Abbiendi et al.	(OPAL Collab.)
CHATRCHYAN	12AA JHEP 1207 143	S. Chatrchyan et al.	(CMS Collab.)
CHATRCHYAN	12AU EPJ C72 2189	S. Chatrchyan et al.	(CMS Collab.)
AALTONEN	11AF PRL 107 181801	T. Aaltonen et al.	(CDF Collab.)
AALTONEN	11P PRL 107 031801	T. Aaltonen et al.	(CDF Collab.)
O. DESCHAMPS	11 PR D82 073012	O. Deschamps et al.	(CLER, ORSAY, LAPP)
AALTONEN	09AJ PRL 103 101803	T. Aaltonen et al.	(CDF Collab.)
ABAZOV	09AC PR D80 051107	V.M. Abazov et al.	(D0 Collab.)
ABAZOV	09AG PR D80 071102	V.M. Abazov et al.	(D0 Collab.)
ABAZOV	09AI PL B682 278	V.M. Abazov et al.	(D0 Collab.)
ABAZOV	09P PRL 102 191802	V.M. Abazov et al.	(D0 Collab.)
AALTONEN	08AA PRL 101 121801	T. Aaltonen et al.	(CDF Collab.)
ABAZOV	08V PRL 101 071803	V.M. Abazov et al.	(D0 Collab.)
ABULENCIA	06E PRL 96 042003	A. Abulencia et al.	(CDF Collab.)
AKTAS	06A PL B638 432	A. Aktas et al.	(H1 Collab.)
ACOSTA	05L PRL 95 071801	D. Acosta et al.	(CDF Collab.)
ABAZOV	04E PRL 93 141801	V.M. Abazov et al.	(D0 Collab.)
ABBIENDI	04 EPJ C32 453	G. Abbiendi et al.	(OPAL Collab.)
ABDALLAH	04I EPJ C34 399	J. Abdallah et al.	(DELPHI Collab.)
ABBIENDI	03 PL B551 35	G. Abbiendi et al.	(OPAL Collab.)
ABBIENDI	03Q PL B577 93	G. Abbiendi et al.	(OPAL Collab.)
ABDALLAH	03 PL B552 127	J. Abdallah et al.	(DELPHI Collab.)
ACHARD	03E PL B575 208	P. Achard et al.	(L3 Collab.)
ACHARD	03F PL B576 18	P. Achard et al.	(L3 Collab.)
ABAZOV	02B PRL 88 151803	V.M. Abazov et al.	(D0 Collab.)
ABBIENDI	02C PL B526 221	G. Abbiendi et al.	(OPAL Collab.)
BORZUMATI	02 PL B549 170	F.M. Borzumati, A. Djouadi	(CMS Collab.)
HEISTER	02P PL B543 1	A. Heister et al.	(ALEPH Collab.)
ABBIENDI	01Q PL B520 1	G. Abbiendi et al.	(OPAL Collab.)
BARATE	01E EPJ C19 213	R. Barate et al.	(ALEPH Collab.)
GAMBINO	01 NP B611 338	P. Gambino, M. Misiak	(CMS Collab.)
AFFOLDER	00 PR D62 012004	T. Affolder et al.	(CDF Collab.)
PDG	00 EPJ C15 1	D.E. Groom et al.	(PDG Collab.)
ABBIENDI	99E EPJ C7 407	G. Abbiendi et al.	(OPAL Collab.)
ABBOTT	99E PRL 82 4975	B. Abbott et al.	(D0 Collab.)
ACKERSTAFF	99D EPJ C8 3	K. Ackerstaff et al.	(OPAL Collab.)
ABE	97L PRL 79 357	F. ABE et al.	(CDF Collab.)
ACCIARRI	97B PL B396 327	M. Acciarri et al.	(L3 Collab.)
AMMAR	97B PRL 78 4686	R. Ammar et al.	(CLEO Collab.)
COARASA	97 PL B406 337	J.A. Coarasa, R.A. Jimenez, J. Sola	(CMS Collab.)
GORDEEV	97 PAN 60 1164	V.A. Gordeev et al.	(PNPI)
GUCHAIT	97 PR D55 7263	M. Guchait, D.P. Roy	(TATA)
MANGANO	97 PL B410 299	M. Mangano, S. Slabospitsky	(CMS Collab.)
STAHL	97 ZPHY C74 73	A. Stahl, H. Voss	(BONN)
PDG	96 PR D54 1	R. M. Barnett et al.	(PDG Collab.)
ALAM	95 PRL 74 2885	M.S. Alam et al.	(CLEO Collab.)
ASAKA	95 PL B345 36	T. Asaka, K.I. Hikasa	(THOK)
BUSKULIC	95 PL B343 444	D. Buskulic et al.	(ALEPH Collab.)

See key on page 1171

Gauge & Higgs Boson Particle Listings
Charged Higgs Bosons (H± and H±±), Searches for, New Heavy Bosons

Table with 4 columns: Author, Year, Publication, and Contact Info. Includes GROSSMAN, STAHL, ACTON, SWARTZ, Y. Grossman, H. Haber, Y. Nir, A. Stahl, P.D. Acton et al., M.L. Swartz et al.

New Heavy Bosons (W', Z', leptoquarks, etc.), Searches for

We list here various limits on charged and neutral heavy vector bosons (other than W's and Z's), heavy scalar bosons (other than Higgs bosons), vector or scalar leptoquarks, and axiguons. The latest unpublished results are described in "W' Searches" and "Z' Searches" reviews. For recent searches on scalar bosons which could be identified as Higgs bosons, see the listings in the Higgs boson section.

CONTENTS:

- Mass Limits for W' (Heavy Charged Vector Boson Other Than W) in Hadron Collider Experiments
WR (Right-Handed W Boson) Mass Limits
Limit on WL-WR Mixing Angle c
Mass Limits for Z' (Heavy Neutral Vector Boson Other Than Z)
- Limits for Z'SM
- Limits for Z'LR
- Limits for Z'X
- Limits for Z'ij
- Limits for other Z'
- Searches for Z' with Lepton-Flavor-Violating decays
Indirect Constraints on Kaluza-Klein Gauge Bosons
Mass Limits for Leptoquarks from Pair Production
Mass Limits for Leptoquarks from Single Production
Indirect Limits for Leptoquarks
Mass Limits for Diquarks
Mass Limits for gA (axiguon) and Other Color-Octet Gauge Bosons
Mass Limits for Color-Octet Scalar Bosons
X0 (Heavy Boson) Searches in Z Decays
Mass Limits for a Heavy Neutral Boson Coupling to e+e-
Search for X0 Resonance in e+e- Collisions
Search for X0 Resonance in ep Collisions
Search for X0 Resonance in Two-Photon Process
Search for X0 Resonance in e+e- -> X0g
Search for X0 Resonance in Z -> fX0
Search for X0 Resonance in WX0 final state
Search for X0 Resonance in Quarkonium Decays

See the related review(s):

W'-Boson Searches

MASS LIMITS for W' (Heavy Charged Vector Boson Other Than W) in Hadron Collider Experiments

Couplings of W' to quarks and leptons are taken to be identical with those of W. The following limits are obtained from p-pbar or pp -> W'X with W' decaying to the mode indicated in the comments. New decay channels (e.g., W' -> WZ) are assumed to be suppressed. The most recent preliminary results can be found in the "W'-boson searches" review above.

Table with 5 columns: VALUE (GeV), CL%, DOCUMENT ID, TECN, COMMENT. Lists mass limits for W' decays to various particles like WZ, tb, ZX, WH, etc.

Main table listing experimental searches for W' bosons. Columns include search number, author, experiment, decay mode, and mass limit. Includes entries like 24 AABOUD 18AF ATLS W' -> tb, 25 AABOUD 18AI ATLS W' -> WH, etc.

••• We do not use the following data for averages, fits, limits, etc. •••

Gauge & Higgs Boson Particle Listings

New Heavy Bosons

none 200–760	95	102 AAD	12BB ATLS	$W' \rightarrow WZ$
		103 AAD	12CK ATLS	$W' \rightarrow \bar{t}q$
>2550	95	104 AAD	12CR ATLS	$W' \rightarrow e\nu, \mu\nu$
		105 AAD	12M ATLS	$W' \rightarrow N\ell \rightarrow \ell\ell jj$
		106 AALTONEN	12N CDF	$W' \rightarrow \bar{t}q$
none 200–1143	95	102 CHATRCHYAN12AF	CMS	$W' \rightarrow WZ$
		107 CHATRCHYAN12AR	CMS	$W' \rightarrow \bar{t}q$
		108 CHATRCHYAN12BG	CMS	$W' \rightarrow N\ell \rightarrow \ell\ell jj$
>1120	95	AALTONEN	11c CDF	$W' \rightarrow e\nu$
none 180–690	95	109 ABAZOV	11H D0	$W' \rightarrow WZ$
none 600–863	95	110 ABAZOV	11L D0	$W' \rightarrow tb$
none 285–516	95	111 AALTONEN	10N CDF	$W' \rightarrow WZ$
none 280–840	95	112 AALTONEN	09AC CDF	$W' \rightarrow q\bar{q}$
>1000	95	ABAZOV	08c D0	$W' \rightarrow e\nu$
none 300–800	95	ABAZOV	04c D0	$W' \rightarrow q\bar{q}$
none 225–536	95	113 ACOSTA	03B CDF	$W' \rightarrow tb$
none 200–480	95	114 AFFOLDER	02c CDF	$W' \rightarrow WZ$
> 786	95	115 AFFOLDER	01I CDF	$W' \rightarrow e\nu, \mu\nu$
none 300–420	95	116 ABE	97G CDF	$W' \rightarrow q\bar{q}$
> 720	95	117 ABACHI	96c D0	$W' \rightarrow e\nu$
> 610	95	118 ABACHI	95E D0	$W' \rightarrow e\nu, \tau\nu$
none 260–600	95	119 RIZZO	93 RVUE	$W' \rightarrow q\bar{q}$

- 1 AAD 23AH search for resonances produced through Drell-Yan and vector-boson-fusion processes in pp collisions at $\sqrt{s} = 13$ TeV. See their Fig. 7 and Fig. 8 for limits on $\sigma \cdot B$. The quoted limit is for heavy-vector-triplet W' with $g_V = 3$ produced mainly via Drell-Yan.
- 2 AAD 23CC search for resonances decaying to tb in pp collisions at $\sqrt{s} = 13$ TeV. The limit quoted above is for right-handed W' assuming a W' coupling equal to the SM W coupling. The limit becomes $M_{W'} > 4200$ GeV for left-handed W' . See their Figs. 12 and 13 for limits on $\sigma \cdot B$.
- 3 AAD 23L perform a generic search for resonances with events containing a Z decaying into e^+e^- or $\mu^+\mu^-$ in pp collisions at $\sqrt{s} = 13$ TeV. See their Figs. 6, 7, 8 for model independent limits on $\sigma \cdot B$ for Gaussian-shaped resonances. The limit above is for heavy-vector-triplet W' decaying to WZ with $g_V = 3$ as well as with $g_V = 1$.
- 4 AAD 23O search for resonances decaying to HW in pp collisions at $\sqrt{s} = 13$ TeV. The quoted limit is for heavy-vector-triplet W' with $g_V = 3$. The limit becomes $M_{W'} > 2950$ GeV for $g_V = 1$.
- 5 TUMASYAN 23AP search for resonances decaying to WZ in pp collisions at $\sqrt{s} = 13$ TeV. The limit quoted above is for heavy-vector-triplet W' with $g_V = 3$. The limit becomes $M_{W'} > 4.8$ TeV assuming $M_{W'} = M_{Z'}$ and combining $W' \rightarrow WZ, W' \rightarrow WH, Z' \rightarrow WW, Z' \rightarrow ZH$ channels.
- 6 TUMASYAN 23AP search for resonances decaying to WH in pp collisions at $\sqrt{s} = 13$ TeV. The limit quoted above is for heavy-vector-triplet W' with $g_V = 3$. The limit becomes $M_{W'} > 4.8$ TeV assuming $M_{W'} = M_{Z'}$ and combining $W' \rightarrow WZ, W' \rightarrow WH, Z' \rightarrow WW, Z' \rightarrow ZH$ channels.
- 7 TUMASYAN 23AW search for SSM W' resonance decaying to $\tau\nu$ in pp collisions at $\sqrt{s} = 13$ TeV. $W-W'$ interference and bosonic decays of W' are not included. See their Fig. 6 for limits on $\sigma \cdot B$.
- 8 TUMASYAN 22Ac search for W' with SM-like couplings in pp collisions at $\sqrt{s} = 13$ TeV. The diboson decays of W' are assumed to be suppressed. See their Fig. 5 for limits on $\sigma \cdot B$.
- 9 TUMASYAN 22D search for resonances produced through Drell-Yan and vector-boson-fusion processes in pp collisions at $\sqrt{s} = 13$ TeV. See their Fig. 8 for limits on $\sigma \cdot B$. The quoted limit is for heavy-vector-triplet W' with $g_V = 3$ produced mainly via Drell-Yan.
- 10 TUMASYAN 22J search for resonances produced through Drell-Yan and vector-boson-fusion processes in pp collisions at $\sqrt{s} = 13$ TeV. The quoted limit is for heavy-vector-triplet W' with $g_V = 3$, produced mainly via Drell-Yan. See their Fig. 9 for limits on $\sigma \cdot B$.
- 11 TUMASYAN 22R search for resonances decaying to WZ in pp collisions at $\sqrt{s} = 13$ TeV. The quoted limit is for heavy-vector-triplet W' produced mainly via Drell-Yan. See their Fig. 8 for limits on $\sigma \cdot B$.
- 12 SIRUNYAN 21Y search for resonances decaying to tb in pp collisions at $\sqrt{s} = 13$ TeV. See their Fig. 2 for limits on $\sigma \cdot B (W' \rightarrow tb)$.
- 13 AAD 20Aj search for resonances decaying to HW in pp collisions at $\sqrt{s} = 13$ TeV. The quoted limit is for heavy-vector-triplet W' with $g_V = 3$. The limit becomes $M_{W'} > 2900$ GeV for $g_V = 1$. See their Fig. 6 for limits on $\sigma \cdot B$.
- 14 AAD 20AT search for resonances decaying to WZ in pp collisions at $\sqrt{s} = 13$ TeV. The quoted limit is for heavy-vector-triplet W' with $g_V = 3$. The limit becomes $M_{W'} > 3900$ GeV for $g_V = 1$. See their Fig. 13 for limits on $\sigma \cdot B$.
- 15 AAD 20T search for W' with SM-like couplings in pp collisions at $\sqrt{s} = 13$ TeV. See their Fig. 4(c) for limits on the product of the cross section, acceptance, and branching fraction.
- 16 SIRUNYAN 20Ai limit is for W' with SM-like coupling using pp collisions at $\sqrt{s} = 13$ TeV.
- 17 SIRUNYAN 20q search for resonances decaying to WZ in pp collisions at $\sqrt{s} = 13$ TeV. The quoted limit is for heavy-vector-triplet W' with $g_V = 3$.
- 18 AABOUD 19E search for right-handed W' in pp collisions at $\sqrt{s} = 13$ TeV. See their Fig. 8 for limit on $\sigma \cdot B$.
- 19 AAD 19c search for W' with SM-like couplings in pp collisions at $\sqrt{s} = 13$ TeV. Bosonic decays and $W-W'$ interference are neglected. The limits on e and μ separately are 6.0 and 5.1 TeV respectively. See their Fig. 2 for limits on $\sigma \cdot B$.
- 20 AAD 19b search for resonances decaying to WZ in pp collisions at $\sqrt{s} = 13$ TeV. The quoted limit is for heavy-vector-triplet W' with $g_V = 3$. The limit becomes $M_{W'} > 3400$ GeV for $g_V = 1$. If we assume $M_{W'} = M_{Z'}$, the limit increases $M_{W'} > 3800$ GeV and $M_{W'} > 3500$ GeV for $g_V = 3$ and $g_V = 1$, respectively. See their Fig. 9 for limits on $\sigma \cdot B$.

- 21 SIRUNYAN 19AY limits shown for W' with SM-like coupling using pp collisions at $\sqrt{s} = 13$ TeV. $W-W'$ interference and bosonic decays of W' are not included. See their Fig. 5 for limits on $\sigma \cdot B$. Limits in the context of a nonuniversal gauge interaction are shown in Fig. 7. Model independent limits on $\sigma \cdot BA\epsilon$ can be seen in Fig. 8.
- 22 SIRUNYAN 19CP present a statistical combinations of searches for W' decaying to pairs of bosons or leptons in pp collisions at $\sqrt{s} = 13$ TeV. The quoted limit is for heavy-vector-triplet W' with $g_V = 3$. If we assume $M_{W'} = M_{Z'}$, the limit becomes $M_{W'} > 4500$ GeV for $g_V = 3$ and $M_{W'} > 5000$ GeV for $g_V = 1$. See their Figs. 2 and 3 for limits on $\sigma \cdot B$.
- 23 SIRUNYAN 19I search for resonances decaying to HW in pp collisions at $\sqrt{s} = 13$ TeV. The quoted limit is for heavy-vector-triplet W' with $g_V = 3$. The limit becomes $M_{W'} > 2800$ GeV if we assume $M_{W'} = M_{Z'}$.
- 24 AABOUD 18AF give the limit above for right-handed W' using pp collisions at $\sqrt{s} = 13$ TeV. These limits also exclude W bosons with left-handed couplings with masses below 2.9 TeV, at the 95% confidence level. $W' \rightarrow \ell\nu_R$ is assumed to be forbidden. See their Fig. 5 for limits on $\sigma \cdot B$ for both cases of left- and right-handed W' .
- 25 AABOUD 18Ai search for resonances decaying to HW in pp collisions at $\sqrt{s} = 13$ TeV. The quoted limit is for heavy-vector-triplet W' with $g_V = 3$. The limit becomes $M_{W'} > 2670$ GeV for $g_V = 1$. If we assume $M_{W'} = M_{Z'}$, the limit increases $M_{W'} > 2930$ GeV and $M_{W'} > 2800$ GeV for $g_V = 3$ and $g_V = 1$, respectively. See their Fig. 5 for limits on $\sigma \cdot B$.
- 26 AABOUD 18AK search for resonances decaying to WZ in pp collisions at $\sqrt{s} = 13$ TeV. The limit quoted above is for heavy-vector-triplet W' with $g_V = 3$. The limit becomes $M_{W'} > 2800$ GeV for $g_V = 1$.
- 27 AABOUD 18AL search for resonances decaying to WZ in pp collisions at $\sqrt{s} = 13$ TeV. The limit quoted above is for heavy-vector-triplet W' with $g_V = 3$. The limit becomes $M_{W'} > 2900$ GeV for $g_V = 1$.
- 28 AABOUD 18BG limit is for W' with SM-like couplings using pp collisions at $\sqrt{s} = 13$ TeV. Bosonic decays of W' and $W-W'$ interference are neglected. See Fig. 2 for limits on $\sigma \cdot B$.
- 29 AABOUD 18CH search for resonances decaying to WZ in pp collisions at $\sqrt{s} = 13$ TeV. The limit quoted above is for heavy-vector-triplet W' with $g_V = 3$. The limit becomes $M_{W'} > 2260$ GeV for $g_V = 1$.
- 30 AABOUD 18F search for resonances decaying to WZ in pp collisions at $\sqrt{s} = 13$ TeV. The quoted limit is for heavy-vector-triplet W' with $g_V = 3$. The limit becomes $M_{W'} > 3000$ GeV for $g_V = 1$. If we assume $M_{Z'} = M_{W'}$, the limit increases $M_{W'} > 3500$ GeV and $M_{W'} > 3100$ GeV for $g_V = 3$ and $g_V = 1$, respectively. See their Fig. 5 for limits on $\sigma \cdot B$.
- 31 AABOUD 18K limit is for W' with SM-like coupling using pp collisions at $\sqrt{s} = 13$ TeV. $W-W'$ interference and bosonic decays of W' are not included. See their Fig. 4 for limit on $\sigma \cdot B$.
- 32 SIRUNYAN 18I limit is for right-handed W' using pp collisions at $\sqrt{s} = 13$ TeV. $W' \rightarrow \ell\nu_R$ decay is assumed to be forbidden. The limit becomes $M_{W'} > 3.4$ TeV if $M_{\nu_R} \ll M_{W'}$. See their Fig. 5 for exclusion limits on W' models having both left- and right-handed couplings.
- 33 SIRUNYAN 18AX search for resonances decaying to WZ in pp collisions at $\sqrt{s} = 13$ TeV. The quoted limit is for heavy-vector-triplet W' with $g_V = 3$. See their Fig. 6 for limits on $\sigma \cdot B$.
- 34 SIRUNYAN 18AZ limit is derived for W' with SM-like coupling using pp collisions at $\sqrt{s} = 13$ TeV. No interference with SM W process is considered. The bosonic decays are assumed to be negligible. See their Fig. 6 for limits on $\sigma \cdot B$.
- 35 SIRUNYAN 18BK search for resonances decaying to WZ in pp collisions at $\sqrt{s} = 13$ TeV. The limit quoted above is for heavy-vector-triplet W' with $g_V = 3$. The limit becomes $M_{W'} > 3100$ GeV for $g_V = 1$.
- 36 SIRUNYAN 18Bo limit is for W' with SM-like coupling using pp collisions at $\sqrt{s} = 13$ TeV.
- 37 SIRUNYAN 18Dj search for resonances decaying to WZ in pp collisions at $\sqrt{s} = 13$ TeV. The limit quoted above is for heavy-vector-triplet W' with $g_V = 3$. The limit becomes $M_{W'} > 2270$ GeV for $g_V = 1$.
- 38 SIRUNYAN 18ED search for resonances decaying to HW in pp collisions at $\sqrt{s} = 13$ TeV. The limit above is for heavy-vector-triplet W' with $g_V = 3$. If we assume $M_{W'} = M_{Z'}$, the limit increases $M_{W'} > 2900$ GeV and $M_{W'} > 2800$ GeV for $g_V = 3$ and $g_V = 1$, respectively.
- 39 SIRUNYAN 18P give this limit for a heavy-vector-triplet W' with $g_V = 3$. If they assume $M_{Z'} = M_{W'}$, the limit increases to $M_{W'} > 3800$ GeV.
- 40 AABOUD 17AK search for a new resonance decaying to dijets in pp collisions at $\sqrt{s} = 13$ TeV. The limit above is for a W' boson having axial-vector SM couplings and decaying to quarks with 75% branching fraction.
- 41 AABOUD 17Ao search for resonances decaying to HW in pp collisions at $\sqrt{s} = 13$ TeV. The limit quoted above is for a W' in the heavy-vector-triplet model with $g_V = 3$. See their Fig. 4 for limits on $\sigma \cdot B$.
- 42 AABOUD 17B search for resonances decaying to HW ($H \rightarrow b\bar{b}, c\bar{c}; W \rightarrow \ell\nu$) in pp collisions at $\sqrt{s} = 13$ TeV. The quoted limit is for heavy-vector-triplet W' with $g_V = 3$. The limit becomes $M_{W'} > 1750$ GeV for $g_V = 1$. If we assume $M_{W'} = M_{Z'}$, the limit increases $M_{W'} > 2310$ GeV and $M_{W'} > 1730$ GeV for $g_V = 3$ and $g_V = 1$, respectively. See their Fig. 3 for limits on $\sigma \cdot B$.
- 43 KHACHATRYAN 17J search for right-handed W_R in pp collisions at $\sqrt{s} = 13$ TeV. W_R is assumed to decay into τ and hypothetical heavy neutrino N_τ , with N_τ decaying into τjj . The quoted limit is for $M_{N_\tau} = M_{W_R}/2$. The limit becomes $M_{W_R} > 2350$ GeV (1630 GeV) for $M_{W_R}/M_{N_\tau} = 0.8$ (0.2). See their Fig. 4 for excluded regions in the $M_{W_R}-M_{N_\tau}$ plane.
- 44 KHACHATRYAN 17w search for resonances decaying to dijets in pp collisions at $\sqrt{s} = 13$ TeV.
- 45 KHACHATRYAN 17z limit is for W' with SM-like coupling using pp collisions at $\sqrt{s} = 13$ TeV. The bosonic decays of W' and the interference with SM W process are neglected.
- 46 SIRUNYAN 17A search for resonances decaying to WZ with $WZ \rightarrow \ell\nu q\bar{q}, q\bar{q}q\bar{q}$ in pp collisions at $\sqrt{s} = 13$ TeV. The quoted limit is for heavy-vector-triplet W' with g_V

See key on page 1171

Gauge & Higgs Boson Particle Listings

New Heavy Bosons

- = 3. The limit becomes $M_{W'} > 2000$ GeV for $g_V = 1$. If we assume $M_{Z'} = M_{W'}$, the limit increases $M_{W'} > 2400$ GeV and $M_{W'} > 2300$ GeV for $g_V = 3$ and $g_V = 1$, respectively. See their Fig.6 for limits on $\sigma \cdot B$.
- 47 SIRUNYAN 17AK search for resonances decaying to WZ or HW in pp collisions at $\sqrt{s} = 8$ and 13 TeV. The quoted limit is for heavy-vector-triplet W' with $g_V = 3$. The limit becomes $M_{W'} > 2300$ GeV for $g_V = 1$. If we assume $M_{W'} = M_{Z'}$, the limit increases $M_{W'} > 2400$ GeV for both $g_V = 3$ and $g_V = 1$. See their Fig.1 and 2 for limits on $\sigma \cdot B$.
- 48 SIRUNYAN 17H search for right-handed W' in pp collisions at $\sqrt{s} = 13$ TeV. W' is assumed to decay into τ and a heavy neutrino N , with N decaying to $\tau q \bar{q}$. The limit above assumes $M_N = M_{W'}/2$.
- 49 SIRUNYAN 17I limit is for a right-handed W' using pp collisions at $\sqrt{s} = 13$ TeV. The limit becomes $M_{W'} > 2400$ GeV for $M_{\nu R} \ll M_{W'}$.
- 50 SIRUNYAN 17R search for resonances decaying to HW in pp collisions at $\sqrt{s} = 13$ TeV. The quoted limit is for heavy-vector-triplet W' with $g_V = 3$. Mass regions $M_{W'} < 2370$ GeV and $2870 < M_{W'} < 2970$ GeV are excluded for $g_V = 1$. If we assume $M_{Z'} = M_{W'}$, the excluded mass regions are $1000 < M_{W'} < 2500$ GeV and $2760 < M_{W'} < 3300$ GeV for $g_V = 3$; $1000 < M_{W'} < 2430$ GeV and $2810 < M_{W'} < 3130$ GeV for $g_V = 1$. See their Fig.5 for limits on $\sigma \cdot B$.
- 51 AABOUD 16AE search for resonances decaying to VV ($V = W$ or Z) in pp collisions at $\sqrt{s} = 13$ TeV. Results from $\nu\nu q\bar{q}$, $\nu\ell q\bar{q}$, $\ell\ell q\bar{q}$ and $qqq\bar{q}$ final states are combined. The quoted limit is for a heavy-vector-triplet W' with $g_V = 3$ and $M_{W'} = M_{Z'}$.
- 52 AABOUD 16V limit is for W' with SM-like coupling using pp collisions at $\sqrt{s} = 13$ TeV. The bosonic decays of W' and the interference with SM W process are neglected.
- 53 AAD 16R search for $W' \rightarrow WZ$ in pp collisions at $\sqrt{s} = 8$ TeV. $\ell\nu\ell'\ell'$, $\ell\ell q\bar{q}$, $\ell\nu q\bar{q}$, and all hadronic channels are combined. The quoted limit assumes $g_{W'WZ}/g_{WWZ} = (M_W/M_{W'})^2$.
- 54 AAD 16S search for a new resonance decaying to dijets in pp collisions at $\sqrt{s} = 13$ TeV. The limit quoted above is for a W' having SM-like couplings to quarks.
- 55 KHACHATRYAN 16AO limit is for a SM-like right-handed W' using pp collisions at $\sqrt{s} = 8$ TeV. The quoted limit combines $t \rightarrow q\bar{q}b$ and $t \rightarrow \ell\nu b$ events.
- 56 KHACHATRYAN 16AP search for a resonance decaying to HW in pp collisions at $\sqrt{s} = 8$ TeV. Both H and W are assumed to decay to fat jets. The quoted limit is for heavy-vector-triplet W' with $g_V = 3$.
- 57 KHACHATRYAN 16BD search for resonance decaying to HW in pp collisions at $\sqrt{s} = 8$ TeV. The quoted limit is for heavy-vector-triplet (HVT) W' with $g_V = 3$. The HVT model $m_{W'} = m_{Z'} > 1.8$ TeV is also obtained by combining $W'/Z' \rightarrow WH/ZH \rightarrow \ell\nu b\bar{b}$, $qq\tau\tau$, $qqb\bar{b}$, and $qqqqq\bar{q}$ channels.
- 58 KHACHATRYAN 16K search for resonances decaying to dijets in pp collisions at $\sqrt{s} = 13$ TeV.
- 59 KHACHATRYAN 16L search for resonances decaying to dijets in pp collisions at $\sqrt{s} = 8$ TeV with the data scouting technique, increasing the sensitivity to the low mass resonances.
- 60 KHACHATRYAN 16O limit is for W' having universal couplings. Interferences with the SM amplitudes are assumed to be absent.
- 61 AAD 15AU search for W' decaying into the WZ final state with $W \rightarrow q\bar{q}'$, $Z \rightarrow \ell^+\ell^-$ using pp collisions at $\sqrt{s} = 8$ TeV. The quoted limit assumes $g_{W'WZ}/g_{WWZ} = (M_W/M_{W'})^2$.
- 62 AAD 15AV limit is for a SM like right-handed W' using pp collisions at $\sqrt{s} = 8$ TeV. $W' \rightarrow \ell\nu$ decay is assumed to be forbidden.
- 63 AAD 15AZ search for W' decaying into the WZ final state with $W \rightarrow \ell\nu$, $Z \rightarrow q\bar{q}$ using pp collisions at $\sqrt{s} = 8$ TeV. The quoted limit assumes $g_{W'WZ}/g_{WWZ} = (M_W/M_{W'})^2$.
- 64 AAD 15CP search for W' decaying into the WZ final state with $W \rightarrow q\bar{q}$, $Z \rightarrow q\bar{q}$ using pp collisions at $\sqrt{s} = 8$ TeV. The quoted limit assumes $g_{W'WZ}/g_{WWZ} = (M_W/M_{W'})^2$.
- 65 AAD 15R limit is for a SM like right-handed W' using pp collisions at $\sqrt{s} = 8$ TeV. $W' \rightarrow \ell\nu$ decay is assumed to be forbidden.
- 66 AAD 15V search for new resonance decaying to dijets in pp collisions at $\sqrt{s} = 8$ TeV.
- 67 KHACHATRYAN 15C search for W' decaying via WZ to fully leptonic final states using pp collisions at $\sqrt{s}=8$ TeV. The quoted limit assumes $g_{W'WZ}/g_{WWZ} = M_W M_Z/M_{W'}^2$.
- 68 KHACHATRYAN 15T limit is for W' with SM-like coupling which interferes the SM W boson constructively using pp collisions at $\sqrt{s} = 8$ TeV. For W' without interference, the limit becomes > 3280 GeV.
- 69 KHACHATRYAN 14O search for right-handed W_R in pp collisions at $\sqrt{s} = 8$ TeV. W_R is assumed to decay into ℓ and hypothetical heavy neutrino N , with N decaying into $\ell j \bar{j}$. The quoted limit is for $M_{\nu eR} = M_{\nu \mu R} = M_{W_R}/2$. See their Fig. 3 and Fig. 5 for excluded regions in the $M_{W_R} - M_\nu$ plane.
- 70 AAD 23BF search for W' decaying to WZ' in pp collisions at $\sqrt{s} = 13$ TeV. The mass difference between W' and Z' is assumed to be 250 GeV. See their Fig. 9(a) for limits on $\sigma \cdot B$ as a function of $M_{W'}$.
- 71 AAD 23CG search for right-handed W_R in pp collisions at $\sqrt{s} = 13$ TeV. W_R is assumed to decay into ℓ and hypothetical heavy neutrino N , with N decaying into $\ell j \bar{j}$. See their Fig. 9 for limits in $m_N - m_{W_R}$ plane.
- 72 AAD 23CK search for a new resonance decaying to HX ($H \rightarrow b\bar{b}$, $X \rightarrow q\bar{q}'$) in pp collisions at $\sqrt{s} = 13$ TeV. See their Fig. 12 for limits on $\sigma \cdot B$.
- 73 AAD 23U search for a narrow charged vector boson decaying to $W\gamma$. See their Fig. 8(d) for the exclusion limit in $m_{W'} - \sigma \cdot B$ plane.
- 74 TUMASYAN 22 search for KK excited W decaying in cascade to three W via a scalar radion R . See their Fig. 4 for limits in $M_{W'} - M_R$ plane.
- 75 TUMASYAN 22AL search for resonances decaying to tB or bT with vector-like quarks B (T) subsequently decaying to bH or bZ (tH or tZ). See their Fig. 7 for limits on $\sigma \cdot B$.
- 76 TUMASYAN 22B search for a narrow charged vector boson decaying to $W\gamma$. See their Fig. 5 for limits on $\sigma \cdot B$.
- 77 TUMASYAN 22i search for KK excited W decaying in cascade to three W via a scalar radion R . See their Fig. 10 for limits in $M_{W'} - M_R$ plane.
- 78 TUMASYAN 22p search for right handed W_R in pp collisions at $\sqrt{s} = 13$ TeV. W_R is assumed to decay into ℓ and hypothetical heavy neutrino N , with N decaying to $\ell j \bar{j}$. See their Fig. 7 for excluded regions in $M_{W_R} - M_N$ plane.
- 79 AAD 20AD search for a narrow resonance decaying to a pair of large-radius-jets J_1 and J_2 employing a machine-learning procedure. See their Fig. 3 for limits on $\sigma \cdot B$ depending on assumptions about invariant masses for J_1 , J_2 , and $J_1 J_2$.
- 80 AAD 20W search for W' decaying to WZ' in pp collisions at $\sqrt{s} = 13$ TeV. See their Fig. 5(b) for limits on $\sigma \cdot B$ as a function of $m_{Z'}$. The $W' \rightarrow WZ'$ branching fraction was chosen to be 0.5 and the mass difference between the W' and Z' was set to 250 GeV.
- 81 AABOUD 19B search for right-handed W_R in pp collisions at $\sqrt{s} = 13$ TeV. W_R is assumed to decay into ℓ and hypothetical heavy neutrino N , with N decaying to $\ell j \bar{j}$. See their Figs. 7 and 8 for excluded regions in $M_{W_R} - M_N$ plane.
- 82 AABOUD 19BB search for right handed W_R in pp collisions at $\sqrt{s} = 13$ TeV. W_R is assumed to decay into ℓ and a boosted hypothetical heavy neutrino N , with N decaying to ℓ and a large radius jet $j = q\bar{q}$. See their Fig. 7 for excluded regions in $M_{W_R} - M_N$ plane.
- 83 SIRUNYAN 19v search for a new resonance decaying to a top quark and a heavy vector-like bottom partner B decaying to Hb (or a bottom quark and a heavy vector-like top partner T decaying to Ht) in pp collisions at $\sqrt{s} = 13$ TeV. See their Fig. 8 for limits on $\sigma \cdot B$.
- 84 AABOUD 18AA search for a narrow charged vector boson decaying to $W\gamma$. See their Fig. 9 for the exclusion limit in $M_{W'} - \sigma \cdot B$ plane.
- 85 AABOUD 18AD search for resonances decaying to HX ($H \rightarrow b\bar{b}$, $X \rightarrow q\bar{q}'$) in pp collisions at $\sqrt{s} = 13$ TeV. See their Figs. 3-5 for limits on $\sigma \cdot B$.
- 86 AABOUD 18CJ search for heavy-vector-triplet W' in pp collisions at $\sqrt{s} = 13$ TeV. The limit quoted above is for model with $g_V = 3$ assuming $M_{W'} = M_{Z'}$. The limit becomes $M_{W'} > 5500$ GeV for model with $g_V = 1$.
- 87 SIRUNYAN 18cv search for right-handed W_R in pp collisions at $\sqrt{s} = 13$ TeV. W_R is assumed to decay into ℓ and hypothetical heavy neutrino N , with N decaying to $\ell j \bar{j}$. The quoted limit is for $M_N = M_{W_R}/2$. See their Fig. 6 for excluded regions in the $M_{W_R} - M_N$ plane.
- 88 KHACHATRYAN 17U search for resonances decaying to HW ($H \rightarrow b\bar{b}$; $W \rightarrow \ell\nu$) in pp collisions at $\sqrt{s} = 13$ TeV. The limit on the heavy-vector-triplet model is $M_{Z'} = M_{W'} > 2$ TeV for $g_V = 3$, in which constraints from the $Z' \rightarrow HZ$ ($H \rightarrow b\bar{b}$; $Z \rightarrow \ell^+\ell^-$, $\nu\bar{\nu}$) are combined. See their Fig.3 and Fig.4 for limits on $\sigma \cdot B$.
- 89 AAD 15BB search for W' decaying into WH with $W \rightarrow \ell\nu$, $H \rightarrow b\bar{b}$. See their Fig. 4 for the exclusion limits in the heavy vector triplet benchmark model parameter space.
- 90 AALTONEN 15C limit is for a SM-like right-handed W' assuming $W' \rightarrow \ell\nu$ decays are forbidden, using $p\bar{p}$ collisions at $\sqrt{s}=1.96$ TeV. See their Fig. 3 for limit on $g_{W'}/g_W$.
- 91 KHACHATRYAN 15v search new resonance decaying to dijets in pp collisions at $\sqrt{s} = 8$ TeV.
- 92 AAD 14AT search for a narrow charged vector boson decaying to $W\gamma$. See their Fig. 3a for the exclusion limit in $m_{W'} - \sigma \cdot B$ plane.
- 93 AAD 14S search for W' decaying into the WZ final state with $W \rightarrow \ell\nu$, $Z \rightarrow \ell\ell$ using pp collisions at $\sqrt{s}=8$ TeV. The quoted limit assumes $g_{W'WZ}/g_{WWZ} = (M_W/M_{W'})^2$.
- 94 KHACHATRYAN 14 search for W' decaying into WZ final state with $W \rightarrow q\bar{q}$, $Z \rightarrow q\bar{q}$ using pp collisions at $\sqrt{s}=8$ TeV. The quoted limit assumes $g_{W'WZ}/g_{WWZ} = (M_W/M_{W'})^2$.
- 95 KHACHATRYAN 14A search for W' decaying into the WZ final state with $W \rightarrow \ell\nu$, $Z \rightarrow q\bar{q}$, or $W \rightarrow q\bar{q}$, $Z \rightarrow \ell\ell$. pp collisions data at $\sqrt{s}=8$ TeV are used for the search. See their Fig. 13 for the exclusion limit on the number of events in the mass-width plane.
- 96 AAD 13AO search for W' decaying into the WZ final state with $W \rightarrow \ell\nu$, $Z \rightarrow 2j$ using pp collisions at $\sqrt{s}=7$ TeV. The quoted limit assumes $g_{W'WZ}/g_{WWZ} = (M_W/M_{W'})^2$.
- 97 CHATRCHYAN 13AJ search for resonances decaying to WZ pair, using the hadronic decay modes of W and Z , in pp collisions at $\sqrt{s}=7$ TeV. See their Fig. 7 for the limit on the cross section.
- 98 CHATRCHYAN 13AQ limit is for W' with SM-like coupling which interferes with the SM W boson using pp collisions at $\sqrt{s}=7$ TeV.
- 99 CHATRCHYAN 13E limit is for W' with SM-like coupling which interferes with the SM W boson using pp collisions at $\sqrt{s}=7$ TeV. For W' with right-handed coupling, the bound becomes >1850 GeV (>1910 GeV) if W' decays to both leptons and quarks (only to quarks). If both left- and right-handed couplings are present, the limit becomes >1640 GeV.
- 100 CHATRCHYAN 13U search for W' decaying to the WZ final state, with W decaying into jets, in pp collisions at $\sqrt{s}=7$ TeV. The quoted limit assumes $g_{W'WZ}/g_{WWZ} = (M_W/M_{W'})^2$.
- 101 The AAD 12AV quoted limit is for a SM-like right-handed W' using pp collisions at $\sqrt{s}=7$ TeV. $W' \rightarrow \ell\nu$ decay is assumed to be forbidden.
- 102 AAD 12BB use pp collisions at $\sqrt{s}=7$ TeV. The quoted limit assumes $g_{W'WZ}/g_{WWZ} = (M_W/M_{W'})^2$.
- 103 AAD 12CK search for $pp \rightarrow tW'$, $W' \rightarrow \bar{t}q$ events in pp collisions. See their Fig. 5 for the limit on $\sigma \cdot B$.
- 104 AAD 12CR use pp collisions at $\sqrt{s}=7$ TeV.
- 105 AAD 12M search for right-handed W_R in pp collisions at $\sqrt{s} = 7$ TeV. W_R is assumed to decay into ℓ and hypothetical heavy neutrino N , with N decaying into $\ell j \bar{j}$. See their Fig. 4 for the limit in the $m_N - m_{W'}$ plane.
- 106 AALTONEN 12N search for $p\bar{p} \rightarrow tW'$, $W' \rightarrow \bar{t}d$ events in $p\bar{p}$ collisions. See their Fig. 3 for the limit on $\sigma \cdot B$.

Gauge & Higgs Boson Particle Listings

New Heavy Bosons

- ¹⁰⁷ CHATRCHYAN 12AR search for $pp \rightarrow tW', W' \rightarrow \bar{t}d$ events in pp collisions. See their Fig. 2 for the limit on $\sigma \cdot B$.
- ¹⁰⁸ CHATRCHYAN 12BG search for right-handed W_R in pp collisions $\sqrt{s} = 7$ TeV. W_R is assumed to decay into ℓ and hypothetical heavy neutrino N , with N decaying into ℓjj . See their Fig. 3 for the limit in the $m_N - m_{W'}$ plane.
- ¹⁰⁹ ABAZOV 11H use data from $p\bar{p}$ collisions at $\sqrt{s}=1.96$ TeV. The quoted limit is obtained assuming $W'WZ$ coupling strength is the same as the ordinary WWZ coupling strength in the Standard Model.
- ¹¹⁰ ABAZOV 11L limit is for W' with SM-like coupling which interferes with the SM W boson, using $p\bar{p}$ collisions at $\sqrt{s}=1.96$ TeV. For W' with right-handed coupling, the bound becomes >885 GeV (>890 GeV) if W' decays to both leptons and quarks (only to quarks). If both left- and right-handed couplings present, the limit becomes >916 GeV.
- ¹¹¹ AALTONEN 10N use $p\bar{p}$ collision data at $\sqrt{s}=1.96$ TeV. The quoted limit assumes $g_{W'WZ}/g_{WWZ} = (M_{W'}/M_W)^2$. See their Fig. 4 for limits in mass-coupling plane.
- ¹¹² AALTONEN 09AC search for new particle decaying to dijets using $p\bar{p}$ collisions at $\sqrt{s}=1.96$ TeV.
- ¹¹³ The ACOSTA 03B quoted limit is for $M_{W'} \gg M_{\nu_R}$, using $p\bar{p}$ collisions at $\sqrt{s}=1.8$ TeV. For $M_{W'} < M_{\nu_R}$, $M_{W'}$ between 225 and 566 GeV is excluded.
- ¹¹⁴ The quoted limit is obtained assuming $W'WZ$ coupling strength is the same as the ordinary WWZ coupling strength in the Standard Model, using $p\bar{p}$ collisions at $\sqrt{s}=1.8$ TeV. See their Fig. 2 for the limits on the production cross sections as a function of the W' width.
- ¹¹⁵ AFFOLDER 01i combine a new bound on $W' \rightarrow e\nu$ of 754 GeV, using $p\bar{p}$ collisions at $\sqrt{s}=1.8$ TeV, with the bound of ABE 00 on $W' \rightarrow \mu\nu$ to obtain quoted bound.
- ¹¹⁶ ABE 97G search for new particle decaying to dijets using $p\bar{p}$ collisions at $\sqrt{s}=1.8$ TeV.
- ¹¹⁷ For bounds on W_R with nonzero right-handed mass, see Fig. 5 from ABACHI 96C.
- ¹¹⁸ ABACHI 95E assume that the decay $W' \rightarrow WZ$ is suppressed and that the neutrino from W' decay is stable and has a mass significantly less $m_{W'}$.
- ¹¹⁹ RIZZO 93 analyses CDF limit on possible two-jet resonances. The limit is sensitive to the inclusion of the assumed K factor.

 W_R (Right-Handed W Boson) MASS LIMITS

Assuming a light right-handed neutrino, except for BEALL 82, LANGACKER 89B, and COLANGELO 91. $g_R = g_L$ assumed. [Limits in the section MASS LIMITS for W' below are also valid for W_R if $m_{\nu_R} \ll m_{W_R}$.] Some limits assume manifest left-right symmetry, i.e., the equality of left- and right Cabibbo-Kobayashi-Maskawa matrices. For a comprehensive review, see LANGACKER 89B. Limits on the $W_L - W_R$ mixing angle ζ are found in the next section. Values in brackets are from cosmological and astrophysical considerations and assume a light right-handed neutrino.

VALUE (GeV)	CL%	DOCUMENT ID	TECN	COMMENT
> 592	90	1 BUENO 11	TWST	μ decay
> 715	90	2 CZAKON 99	RVUE	Electroweak
• • • We do not use the following data for averages, fits, limits, etc. • • •				
> 235	90	3 PRIEELS 14	PIE3	μ decay
> 245	90	4 WAUTERS 10	CNTR	^{60}Co β decay
>2500		5 ZHANG 08	THEO	$m_{K_L^0} - m_{K_S^0}$
> 180	90	6 MELCONIAN 07	CNTR	^{37}K β^+ decay
> 290.7	90	7 SCHUMANN 07	CNTR	Polarized neutron decay
[> 3300]	95	8 CYBURT 05	COSM	Nucleosynthesis; light ν_R
> 310	90	9 THOMAS 01	CNTR	β^+ decay
> 137	95	10 ACKERSTAFF 99D	OPAL	τ decay
>1400	68	11 BARENBOIM 98	RVUE	Electroweak, Z-Z' mixing
> 549	68	12 BARENBOIM 97	RVUE	μ decay
> 220	95	13 STAHL 97	RVUE	τ decay
> 220	90	14 ALLET 96	CNTR	β^+ decay
> 281	90	15 KUZNETSOV 95	CNTR	Polarized neutron decay
> 282	90	16 KUZNETSOV 94B	CNTR	Polarized neutron decay
> 439	90	17 BHATTACH... 93	RVUE	Z-Z' mixing
> 250	90	18 SEVERIJNS 93	CNTR	β^+ decay
		19 IMAZATO 92	CNTR	K^+ decay
> 475	90	20 POLAK 92B	RVUE	μ decay
> 240	90	21 AQUINO 91	RVUE	Neutron decay
> 496	90	21 AQUINO 91	RVUE	Neutron and muon decay
> 700		22 COLANGELO 91	THEO	$m_{K_L^0} - m_{K_S^0}$
> 477	90	23 POLAK 91	RVUE	μ decay
[none 540-23000]		24 BARBIERI 89B	ASTR	SN 1987A; light ν_R
> 300	90	25 LANGACKER 89B	RVUE	General
> 160	90	26 BALKE 88	CNTR	$\mu \rightarrow e\nu\bar{\nu}$
> 406	90	27 JODIDIO 86	ELEC	Any ζ
> 482	90	27 JODIDIO 86	ELEC	$\zeta = 0$
> 800		MOHAPATRA 86	RVUE	$SU(2)_L \times SU(2)_R \times U(1)$
> 400	95	28 STOKER 85	ELEC	Any ζ
> 475	95	28 STOKER 85	ELEC	$\zeta < 0.041$
		29 BERGSMAN 83	CHRM	$\nu_\mu e \rightarrow \nu_\nu e$
> 380	90	30 CARR 83	ELEC	μ^+ decay
>1600		31 BEALL 82	THEO	$m_{K_L^0} - m_{K_S^0}$

¹ The quoted limit is for manifest left-right symmetric model.

² CZAKON 99 perform a simultaneous fit to charged and neutral sectors.

³ PRIEELS 14 limit is from $\mu^+ \rightarrow e^+ \nu\bar{\nu}$ decay parameter ξ'' , which is determined by the positron polarization measurement.

⁴ WAUTERS 10 limit is from a measurement of the asymmetry parameter of polarized ^{60}Co β decays. The listed limit assumes no mixing.

⁵ ZHANG 08 limit uses a lattice QCD calculation of the relevant hadronic matrix elements, while BEALL 82 limit used the vacuum saturation approximation.

⁶ MELCONIAN 07 measure the neutrino angular asymmetry in β^+ -decays of polarized ^{37}K , stored in a magneto-optical trap. Result is consistent with SM prediction and does not constrain the $W_L - W_R$ mixing angle appreciably.

⁷ SCHUMANN 07 limit is from measurements of the asymmetry $\langle \bar{p}_\nu \cdot \sigma_n \rangle$ in the β decay of polarized neutrons. Zero mixing is assumed.

⁸ CYBURT 05 limit follows by requiring that three light ν_R 's decouple when $T_{dec} > 140$ MeV. For different T_{dec} , the bound becomes $M_{W_R} > 3.3$ TeV ($T_{dec} / 140$ MeV) $^{3/4}$.

⁹ THOMAS 01 limit is from measurement of β^+ polarization in decay of polarized ^{12}N . The listed limit assumes no mixing.

¹⁰ ACKERSTAFF 99D limit is from τ decay parameters. Limit increase to 145 GeV for zero mixing.

¹¹ BARENBOIM 98 assumes minimal left-right model with Higgs of $SU(2)_R$ in $SU(2)_L$ doublet. For Higgs in $SU(2)_L$ triplet, $m_{W_R} > 1100$ GeV. Bound calculated from effect of corresponding Z_{LR} on electroweak data through Z-Z' mixing.

¹² The quoted limit is from μ decay parameters. BARENBOIM 97 also evaluate limit from $K_L - K_S$ mass difference.

¹³ STAHL 97 limit is from fit to τ -decay parameters.

¹⁴ ALLET 96 measured polarization-asymmetry correlation in ^{12}N β^+ decay. The listed limit assumes zero L-R mixing.

¹⁵ KUZNETSOV 95 limit is from measurements of the asymmetry $\langle \bar{p}_\nu \cdot \sigma_n \rangle$ in the β decay of polarized neutrons. Zero mixing assumed. See also KUZNETSOV 94B.

¹⁶ KUZNETSOV 94B limit is from measurements of the asymmetry $\langle \bar{p}_\nu \cdot \sigma_n \rangle$ in the β decay of polarized neutrons. Zero mixing assumed.

¹⁷ BHATTACHARYYA 93 uses Z-Z' mixing limit from LEP '90 data, assuming a specific Higgs sector of $SU(2)_L \times SU(2)_R \times U(1)$ gauge model. The limit is for $m_t = 200$ GeV and slightly improves for smaller m_t .

¹⁸ SEVERIJNS 93 measured polarization-asymmetry correlation in ^{107}In β^+ decay. The listed limit assumes zero L-R mixing. Value quoted here is from SEVERIJNS 94 erratum.

¹⁹ IMAZATO 92 measure positron asymmetry in $K^+ \rightarrow \mu^+ \nu_\mu$ decay and obtain $\xi_P \mu > 0.990$ (90% CL). If W_R couples to $u\bar{s}$ with full weak strength ($V_{us}^R = 1$), the result corresponds to $m_{W_R} > 653$ GeV. See their Fig. 4 for m_{W_R} limits for general $|V_{us}^R|^2 = 1 - |V_{ud}^R|^2$.

²⁰ POLAK 92B limit is from fit to muon decay parameters and is essentially determined by JODIDIO 86 data assuming $\zeta=0$. Supersedes POLAK 91.

²¹ AQUINO 91 limits obtained from neutron lifetime and asymmetries together with unitarity of the CKM matrix. Manifest left-right symmetry assumed. Stronger of the two limits also includes muon decay results.

²² COLANGELO 91 limit uses hadronic matrix elements evaluated by QCD sum rule and is less restrictive than BEALL 82 limit which uses vacuum saturation approximation. Manifest left-right symmetry assumed.

²³ POLAK 91 limit is from fit to muon decay parameters and is essentially determined by JODIDIO 86 data assuming $\zeta=0$. Supersedes by POLAK 92B.

²⁴ BARBIERI 89B limit holds for $m_{\nu_R} \leq 10$ MeV.

²⁵ LANGACKER 89B limit is for any ν_R mass (either Dirac or Majorana) and for a general class of right-handed quark mixing matrices.

²⁶ BALKE 88 limit is for $m_{\nu_{eR}} = 0$ and $m_{\nu_{\mu R}} \leq 50$ MeV. Limits come from precise measurements of the muon decay asymmetry as a function of the positron energy.

²⁷ JODIDIO 86 is the same TRIUMF experiment as STOKER 85 (and CARR 83); however, it uses a different technique. The results given here are combined results of the two techniques. The technique here involves precise measurement of the end-point e^+ spectrum in the decay of the highly polarized μ^+ .

²⁸ STOKER 85 is same TRIUMF experiment as CARR 83. Here they measure the decay e^+ spectrum asymmetry above 46 MeV/c using a muon-spin-rotation technique. Assumed a light right-handed neutrino. Quoted limits are from combining with CARR 83.

²⁹ BERGSMAN 83 set limit $m_{W_2}/m_{W_1} > 1.9$ at CL = 90%.

³⁰ CARR 83 is TRIUMF experiment with a highly polarized μ^+ beam. Looked for deviation from V-A at the high momentum end of the decay e^+ energy spectrum. Limit from previous world-average muon polarization parameter is $m_{W_R} > 240$ GeV. Assumes a light right-handed neutrino.

³¹ BEALL 82 limit is obtained assuming that W_R contribution to $K_L^0 - K_S^0$ mass difference is smaller than the standard one, neglecting the top quark contributions. Manifest left-right symmetry assumed.

Limit on $W_L - W_R$ Mixing Angle ζ

Lighter mass eigenstate $W_1 = W_L \cos \zeta - W_R \sin \zeta$. Light ν_R assumed unless noted. Values in brackets are from cosmological and astrophysical considerations.

VALUE	CL%	DOCUMENT ID	TECN	COMMENT
• • • We do not use the following data for averages, fits, limits, etc. • • •				
-0.020 to 0.017	90	BUENO 11	TWST	$\mu \rightarrow e\nu\bar{\nu}$
< 0.022	90	MACDONALD 08	TWST	$\mu \rightarrow e\nu\bar{\nu}$
< 0.12	95	1 ACKERSTAFF 99D	OPAL	τ decay
< 0.013	90	2 CZAKON 99	RVUE	Electroweak
< 0.0333		3 BARENBOIM 97	RVUE	μ decay
< 0.04	90	4 MISHRA 92	CCFR	νN scattering
-0.0006 to 0.0028	90	5 AQUINO 91	RVUE	
[none 0.00001-0.02]		6 BARBIERI 89B	ASTR	SN 1987A
< 0.040	90	7 JODIDIO 86	ELEC	μ decay
-0.056 to 0.040	90	7 JODIDIO 86	ELEC	μ decay

¹ ACKERSTAFF 99D limit is from τ decay parameters.

² CZAKON 99 perform a simultaneous fit to charged and neutral sectors.

³ The quoted limit is from μ decay parameters. BARENBOIM 97 also evaluate limit from $K_L - K_S$ mass difference.

⁴ MISHRA 92 limit is from the absence of extra large-x, large-y $\bar{\nu}_\mu N \rightarrow \bar{\nu}_\mu X$ events at Tevatron, assuming left-handed ν and right-handed $\bar{\nu}$ in the neutrino beam. The result gives $\zeta^2(1-2m_{W_2}^2/m_{W_1}^2) < 0.0015$. The limit is independent of ν_R mass.

See key on page 1171

Gauge & Higgs Boson Particle Listings
New Heavy Bosons

- ⁵ AQUINO 91 limits obtained from neutron lifetime and asymmetries together with unitarity of the CKM matrix. Manifest left-right asymmetry is assumed.
⁶ BARBIERI 89B limit holds for $m_{\nu R} \leq 10$ MeV.
⁷ First JODIDIO 86 result assumes $m_{W_R} = \infty$, second is for unconstrained m_{W_R} .

See the related review(s):
Z'-Boson Searches

MASS LIMITS for Z' (Heavy Neutral Vector Boson Other Than Z)

Limits for Z'_{SM}

Z'_{SM} is assumed to have couplings with quarks and leptons which are identical to those of Z, and decays only to known fermions. The most recent preliminary results can be found in the "Z'-boson searches" review above.

VALUE (GeV)	CL%	DOCUMENT ID	TECN	COMMENT
>5150 (CL = 95%) OUR LIMIT				
none 1800-2400	95	1 TUMASYAN 23AF CMS	pp; Z' _{SM} → b \bar{b}	
>4400	95	2 TUMASYAN 22AE CMS	pp; Z' _{SM} → e ⁺ e ⁻ , μ ⁺ μ ⁻	
>5150	95	3 SIRUNYAN 21N CMS	pp; Z' _{SM} → e ⁺ e ⁻ , μ ⁺ μ ⁻	
none 1133-2700	95	4 AAD 20T ATLS	pp, Z' _{SM} → b \bar{b}	
none 1800-2900, 3100-3300	95	5 SIRUNYAN 20AI CMS	pp; Z' _{SM} → q \bar{q}	
none 250-5100	95	6 AAD 19L ATLS	pp; Z' _{SM} → e ⁺ e ⁻ , μ ⁺ μ ⁻	
none 600-2000	95	7 AABOUD 18AB ATLS	pp; Z' _{SM} → b \bar{b}	
>2420	95	8 AABOUD 18G ATLS	pp; Z' _{SM} → τ ⁺ τ ⁻	
none 200-4500	95	9 SIRUNYAN 18BB CMS	pp; Z' _{SM} → e ⁺ e ⁻ , μ ⁺ μ ⁻	
none 600-2700	95	10 SIRUNYAN 18B0 CMS	pp; Z' _{SM} → q \bar{q}	
>4500	95	11 AABOUD 17AT ATLS	pp; Z' _{SM} → e ⁺ e ⁻ , μ ⁺ μ ⁻	
>2100	95	12 KHACHATRYAN...17H CMS	pp; Z' _{SM} → τ ⁺ τ ⁻	
>3370	95	13 KHACHATRYAN...17T CMS	pp; Z' _{SM} → e ⁺ e ⁻ , μ ⁺ μ ⁻	
none 600-2100, 2300-2600	95	14 KHACHATRYAN...17W CMS	pp; Z' _{SM} → q \bar{q}	
>3360	95	15 AABOUD 16U ATLS	pp; Z' _{SM} → e ⁺ e ⁻ , μ ⁺ μ ⁻	
>2900	95	16 KHACHATRYAN...15AE CMS	pp; Z' _{SM} → e ⁺ e ⁻ , μ ⁺ μ ⁻	
none 1200-1700	95	17 KHACHATRYAN...15V CMS	pp; Z' _{SM} → q \bar{q}	
>2900	95	18 AAD 14V ATLS	pp; Z' _{SM} → e ⁺ e ⁻ , μ ⁺ μ ⁻	
••• We do not use the following data for averages, fits, limits, etc. •••				
>1900	95	19 BOBOVNIKOV 18 RVUE	pp, Z' _{SM} → W ⁺ W ⁻	
>2020	95	20 AABOUD 16AA ATLS	pp; Z' _{SM} → τ ⁺ τ ⁻	
>1400	95	21 AAD 15AM ATLS	pp; Z' _{SM} → τ ⁺ τ ⁻	
>1470	95	22 AAD 13S ATLS	pp; Z' _{SM} → τ ⁺ τ ⁻	
>2590	95	23 CHATRCHYAN 13A CMS	pp; Z' _{SM} → q \bar{q}	
>2220	95	24 CHATRCHYAN 13AF CMS	pp; Z' _{SM} → e ⁺ e ⁻ , μ ⁺ μ ⁻	
>1400	95	25 AAD 12CC ATLS	pp; Z' _{SM} → e ⁺ e ⁻ , μ ⁺ μ ⁻	
>1071	95	26 CHATRCHYAN 120 CMS	pp; Z' _{SM} → τ ⁺ τ ⁻	
>1023	95	27 AALTONEN 11I CDF	p \bar{p} ; Z' _{SM} → μ ⁺ μ ⁻	
none 247-544	95	28 ABZOV 11A D0	p \bar{p} ; Z' _{SM} → e ⁺ e ⁻	
none 320-740	95	29 AALTONEN 10N CDF	Z' → WW	
> 963	95	30 AALTONEN 09AC CDF	Z' → q \bar{q}	
>1403	95	31 AALTONEN 09T CDF	p \bar{p} ; Z' _{SM} → e ⁺ e ⁻	
>1305	95	32 ERLER 09 RVUE	Electroweak	
> 399	95	33 ABDALLAH 06C DLPH	e ⁺ e ⁻	
none 400-640	95	34 ACOSTA 05R CDF	p \bar{p} ; Z' _{SM} → τ ⁺ τ ⁻	
>1018	95	35 ABZOV 04C D0	p \bar{p} ; Z' _{SM} → q \bar{q}	
> 670	95	36 ABBIENDI 04G OPAL	e ⁺ e ⁻	
>1500	95	37 ABZOV 01B D0	p \bar{p} ; Z' _{SM} → e ⁺ e ⁻	
> 710	95	38 CHEUNG 01B RVUE	Electroweak	
> 898	95	39 ABREU 00S DLPH	e ⁺ e ⁻	
> 809	95	40 BARATE 00I ALEP	e ⁺ e ⁻	
> 690	95	41 ERLER 99 RVUE	Electroweak	
> 398	95	42 ABE 97S CDF	p \bar{p} ; Z' _{SM} → e ⁺ e ⁻ , μ ⁺ μ ⁻	
> 237	90	43 VILAIN 94B CHM2	ν _μ e → ν _μ e and ν̄ _μ e → ν̄ _μ e	
none 260-600	95	44 ALITTI 93 UA2	p \bar{p} ; Z' _{SM} → q \bar{q}	
> 426	90	45 RIZZO 93 RVUE	p \bar{p} ; Z' _{SM} → q \bar{q}	
		46 ABE 90F VNS	e ⁺ e ⁻	

- ¹ TUMASYAN 23AF search for resonance decaying to b \bar{b} in pp collisions at $\sqrt{s} = 13$ TeV. See their Fig. 4 for limits on σ -B.
² TUMASYAN 22AE set limits on Z' from the measurements of the forward-backward asymmetry in e⁺e⁻ and μ⁺μ⁻ events in pp collisions at $\sqrt{s} = 13$ TeV. The quoted limit is for the sequential SM Z'. See their Fig. 6 for limits in mass-coupling plane.
³ SIRUNYAN 21N search for resonance decaying to e⁺e⁻, μ⁺μ⁻ in pp collisions at $\sqrt{s} = 13$ TeV.
⁴ AAD 20T search for resonances decaying to b \bar{b} in pp collisions at $\sqrt{s} = 13$ TeV. See their Fig. 7(b) for limits on the product of the cross section, acceptance, b-tagging efficiency, and branching fraction.
⁵ SIRUNYAN 20AI search for resonances decaying into dijets in pp collisions at $\sqrt{s} = 13$ TeV.
⁶ AAD 19L search for resonances decaying to e⁺e⁻ in pp collisions at $\sqrt{s} = 13$ TeV.
⁷ AABOUD 18AB search for resonances decaying to b \bar{b} in pp collisions at $\sqrt{s} = 13$ TeV.

- ⁸ AABOUD 18G search for resonances decaying to τ⁺τ⁻ in pp collisions at $\sqrt{s} = 13$ TeV.
⁹ SIRUNYAN 18BB search for resonances decaying to e⁺e⁻ in pp collisions at $\sqrt{s} = 13$ TeV. See their Fig.5 for limits on the Z' coupling strengths with light quarks.
¹⁰ SIRUNYAN 18B0 search for resonances decaying to dijets in pp collisions at $\sqrt{s} = 13$ TeV.
¹¹ AABOUD 17AT search for resonances decaying to e⁺e⁻ in pp collisions at $\sqrt{s} = 13$ TeV.
¹² KHACHATRYAN 17H search for resonances decaying to τ⁺τ⁻ in pp collisions at $\sqrt{s} = 13$ TeV.
¹³ KHACHATRYAN 17T search for resonances decaying to e⁺e⁻, μ⁺μ⁻ in pp collisions at $\sqrt{s} = 8, 13$ TeV.
¹⁴ KHACHATRYAN 17W search for resonances decaying to dijets in pp collisions at $\sqrt{s} = 13$ TeV.
¹⁵ AABOUD 16U search for resonances decaying to e⁺e⁻ in pp collisions at $\sqrt{s} = 13$ TeV.
¹⁶ KHACHATRYAN 15AE search for resonances decaying to e⁺e⁻, μ⁺μ⁻ in pp collisions at $\sqrt{s} = 8$ TeV.
¹⁷ KHACHATRYAN 15V search for resonances decaying to dijets in pp collisions at $\sqrt{s} = 8$ TeV.
¹⁸ AAD 14V search for resonances decaying to e⁺e⁻, μ⁺μ⁻ in pp collisions at $\sqrt{s} = 8$ TeV.
¹⁹ BOBOVNIKOV 18 use the ATLAS limits on $\sigma(pp \rightarrow Z')$ -B(Z' → W⁺W⁻) to constrain the Z-Z' mixing parameter ξ . See their Fig. 11 for limits in M_{Z'}- ξ plane.
²⁰ AABOUD 16AA search for resonances decaying to τ⁺τ⁻ in pp collisions at $\sqrt{s} = 13$ TeV.
²¹ AAD 15AM search for resonances decaying to τ⁺τ⁻ in pp collisions at $\sqrt{s} = 8$ TeV.
²² AAD 13S search for resonances decaying to τ⁺τ⁻ in pp collisions at $\sqrt{s} = 7$ TeV.
²³ CHATRCHYAN 13A use pp collisions at $\sqrt{s} = 7$ TeV.
²⁴ CHATRCHYAN 13AF search for resonances decaying to e⁺e⁻, μ⁺μ⁻ in pp collisions at $\sqrt{s} = 7$ TeV and 8 TeV.
²⁵ AAD 12CC search for resonances decaying to e⁺e⁻, μ⁺μ⁻ in pp collisions at $\sqrt{s} = 7$ TeV.
²⁶ CHATRCHYAN 120 search for resonances decaying to τ⁺τ⁻ in pp collisions at $\sqrt{s} = 7$ TeV.
²⁷ AALTONEN 11I search for resonances decaying to μ⁺μ⁻ in p \bar{p} collisions at $\sqrt{s} = 1.96$ TeV.
²⁸ ABZOV 11A, AALTONEN 09T, AALTONEN 07H, and ABULENCIA 06L search for resonances decaying to e⁺e⁻ in p \bar{p} collisions at $\sqrt{s} = 1.96$ TeV.
²⁹ The quoted limit assumes $g_{WWZ'}/g_{WWZ} = (M_W/M_{Z'})^2$. See their Fig. 4 for limits in mass-coupling plane.
³⁰ AALTONEN 09AC search for new particle decaying to dijets.
³¹ ERLER 09 give 95% CL limit on the Z-Z' mixing $-0.0026 < \theta < 0.0006$.
³² ABDALLAH 06C use data $\sqrt{s} = 130-207$ GeV.
³³ ACOSTA 05R search for resonances decaying to tau lepton pairs in p \bar{p} collisions at $\sqrt{s} = 1.96$ TeV.

- ³⁴ ABBIENDI 04G give 95% CL limit on Z-Z' mixing $-0.00422 < \theta < 0.00091$. $\sqrt{s} = 91$ to 207 GeV.
³⁵ ABZOV 01B search for resonances in p \bar{p} → e⁺e⁻ at $\sqrt{s} = 1.8$ TeV. They find $\sigma \cdot B(Z' \rightarrow ee) < 0.06$ pb for M_{Z'} > 500 GeV.
³⁶ CHEUNG 01B limit is derived from bounds on contact interactions in a global electroweak analysis.
³⁷ ABREU 00S uses LEP data at $\sqrt{s} = 90$ to 189 GeV.
³⁸ BARATE 00I search for deviations in cross section and asymmetries in e⁺e⁻ → fermions at $\sqrt{s} = 90$ to 183 GeV. Assume $\theta = 0$. Bounds in the mass-mixing plane are shown in their Figure 18.
³⁹ ERLER 99 give 90%CL limit on the Z-Z' mixing $-0.0041 < \theta < 0.0003$. $\rho_0 = 1$ is assumed.
⁴⁰ ABE 97S find $\sigma(Z') \times B(e^+e^-, \mu^+\mu^-) < 40$ fb for M_{Z'} > 600 GeV at $\sqrt{s} = 1.8$ TeV.
⁴¹ VILAIN 94B assume m_t = 150 GeV.
⁴² ALITTI 93 search for resonances in the two-jet invariant mass. The limit assumes B(Z' → q \bar{q}) = 0.7. See their Fig. 5 for limits in the m_{Z'}-B(q \bar{q}) plane.
⁴³ RIZZO 93 analyses CDF limit on possible two-jet resonances.
⁴⁴ ABE 90F use data for R, R_{ℓℓ}, and A_{ℓℓ}. They fix m_W = 80.49 ± 0.43 ± 0.24 GeV and m_Z = 91.13 ± 0.03 GeV.

Limits for Z_{LR}

Z_{LR} is the extra neutral boson in left-right symmetric models. $g_L = g_R$ is assumed unless noted. Values in parentheses assume stronger constraint on the Higgs sector, usually motivated by specific left-right symmetric models (see the Note on the W'). Values in brackets are from cosmological and astrophysical considerations and assume a light right-handed neutrino. Direct search bounds assume decays to Standard Model fermions only, unless noted.

VALUE (GeV)	CL%	DOCUMENT ID	TECN	COMMENT
>1162	95	1 DEL-AGUILA 10 RVUE	Electroweak	
> 630	95	2 ABE 97S CDF	p \bar{p} ; Z' _{LR} → e ⁺ e ⁻ , μ ⁺ μ ⁻	
••• We do not use the following data for averages, fits, limits, etc. •••				
		3 TUMASYAN 23BE CMS	pp; Z' _{LR} → N \bar{N} , N → ℓq \bar{q} '	
> 998	95	4 BOBOVNIKOV 18 RVUE	pp, Z' _{LR} → W ⁺ W ⁻	
> 600	95	5 ERLER 09 RVUE	Electroweak	
> 455	95	6 SCHAEEL 07A ALEP	e ⁺ e ⁻	
> 518	95	7 ABDALLAH 06C DLPH	e ⁺ e ⁻	
> 860	95	8 ABBIENDI 04G OPAL	e ⁺ e ⁻	
> 380	95	9 CHEUNG 01B RVUE	Electroweak	
> 436	95	10 ABREU 00S DLPH	e ⁺ e ⁻	
> 550	95	11 BARATE 00I ALEP	Repl. by SCHAEEL 07A	
		12 CHAY 00 RVUE	Electroweak	
		13 ERLER 00 RVUE	Cs	

Gauge & Higgs Boson Particle Listings

New Heavy Bosons

VALUE (GeV)	CL%	DOCUMENT ID	TECN	COMMENT
(> 1205)	90	13 CASALBUONI 99	RVUE	Cs
> 564	95	14 CZAKON 99	RVUE	Electroweak
(> 1673)	95	15 ERLER 99	RVUE	Electroweak
(> 1700)	68	16 ERLER 99	RVUE	Electroweak
> 244	95	17 BARENBOIM 98	RVUE	Electroweak
> 253	95	18 CONRAD 98	RVUE	$\nu_\mu N$ scattering
none 200-600	95	19 VILAIN 94B	CHM2	$\nu_\mu e \rightarrow \nu_\mu e$ and $\bar{\nu}_\mu e \rightarrow \bar{\nu}_\mu e$
[> 2000]		20 RIZZO 93	RVUE	$p\bar{p}; Z_{LR} \rightarrow q\bar{q}$
none 200-500		21 WALKER 91	COSM	Nucleosynthesis; light ν_R
none 350-2400		22 GRIFOLS 90	ASTR	SN 1987A; light ν_R
		23 BARBIERI 89B	ASTR	SN 1987A; light ν_R

- 1 DEL-AGUILA 10 give 95% CL limit on the Z-Z' mixing $-0.0012 < \theta < 0.0004$.
- 2 ABE 97s find $\sigma(Z') \times B(e^+e^-, \mu^+\mu^-) < 40$ fb for $m_{Z'} > 600$ GeV at $\sqrt{s} = 1.8$ TeV.
- 3 TUMASYAN 23BE search for pair production of heavy Majorana neutrinos via the decay of a Z' boson in a final state with $\ell^+\ell^-$ and at least two jets. For cases with $m_N = M_{Z'}/4$, their 95% CL limits are $M_{Z'} > 3.59$ TeV (> 4.10 TeV) in the dielectron (dimuon) channel. See their Fig. 5 for limits on $\sigma \cdot B$.
- 4 BOBOVNIKOV 18 use the ATLAS limits on $\sigma(pp \rightarrow Z') \cdot B(Z' \rightarrow W^+W^-)$ to constrain the Z-Z' mixing parameter ξ . See their Fig. 10 for limits in $M_{Z'} - \xi$ plane.
- 5 ERLER 09 give 95% CL limit on the Z-Z' mixing $-0.0013 < \theta < 0.0006$.
- 6 ABDALLAH 06c give 95% CL limit $|\theta| < 0.0028$. See their Fig. 14 for limit contours in the mass-mixing plane.
- 7 ABBIENDI 04c give 95% CL limit on Z-Z' mixing $-0.00098 < \theta < 0.00190$. See their Fig. 20 for the limit contour in the mass-mixing plane. $\sqrt{s} = 91$ to 207 GeV.
- 8 CHEUNG 01b limit is derived from bounds on contact interactions in a global electroweak analysis.
- 9 ABREU 00s give 95% CL limit on Z-Z' mixing $|\theta| < 0.0018$. See their Fig. 6 for the limit contour in the mass-mixing plane. $\sqrt{s} = 90$ to 189 GeV.
- 10 BARATE 00i search for deviations in cross section and asymmetries in $e^+e^- \rightarrow$ fermions at $\sqrt{s} = 90$ to 183 GeV. Assume $\theta = 0$. Bounds in the mass-mixing plane are shown in their Figure 18.
- 11 CHAY 00 also find $-0.0003 < \theta < 0.0019$. For g_R free, $m_{Z'} > 430$ GeV.
- 12 ERLER 00 discuss the possibility that a discrepancy between the observed and predicted values of $Q_W(\text{Cs})$ is due to the exchange of Z'. The data are better described in a certain class of the Z' models including Z_{LR} and Z_χ .
- 13 CASALBUONI 99 discuss the discrepancy between the observed and predicted values of $Q_W(\text{Cs})$. It is shown that the data are better described in a class of models including the Z_{LR} model.
- 14 CZAKON 99 perform a simultaneous fit to charged and neutral sectors. Assumes manifest left-right symmetric model. Finds $|\theta| < 0.0042$.
- 15 ERLER 99 give 90% CL limit on the Z-Z' mixing $-0.0009 < \theta < 0.0017$.
- 16 ERLER 99 assumes 2 Higgs doublets, transforming as 10 of SO(10), embedded in E_6 .
- 17 BARENBOIM 98 also gives 68% CL limits on the Z-Z' mixing $-0.0005 < \theta < 0.0033$. Assumes Higgs sector of minimal left-right model.
- 18 CONRAD 98 limit is from measurements at CCFR, assuming no Z-Z' mixing.
- 19 VILAIN 94b assume $m_t = 150$ GeV and $\theta = 0$. See Fig. 2 for limit contours in the mass-mixing plane.
- 20 RIZZO 93 analyses CDF limit on possible two-jet resonances.
- 21 GRIFOLS 90 limit holds for $m_{\nu_R} \lesssim 1$ MeV. A specific Higgs sector is assumed. See also GRIFOLS 90D, RIZZO 91.
- 22 BARBIERI 89b limit holds for $m_{\nu_R} \leq 10$ MeV. Bounds depend on assumed supernova core temperature.

Limits for Z_χ

Z_χ is the extra neutral boson in $\text{SO}(10) \rightarrow \text{SU}(5) \times \text{U}(1)_\chi$. $g_\chi = e/\cos\theta_W$ is assumed unless otherwise stated. We list limits with the assumption $\rho = 1$ but with no further constraints on the Higgs sector. Values in parentheses assume stronger constraint on the Higgs sector motivated by superstring models. Values in brackets are from cosmological and astrophysical considerations and assume a light right-handed neutrino.

VALUE (GeV)	CL%	DOCUMENT ID	TECN	COMMENT
>4800 (CL = 95%) OUR LIMIT				
none 250-4800	95	1 AAD 19L	ATLS	$p\bar{p}; Z'_\chi \rightarrow e^+e^-, \mu^+\mu^-$
>4100	95	2 AABOUD 17AT	ATLS	$p\bar{p}; Z'_\chi \rightarrow e^+e^-, \mu^+\mu^-$
• • • We do not use the following data for averages, fits, limits, etc. • • •				
>3050	95	3 BOBOVNIKOV 18	RVUE	$p\bar{p}; Z'_\chi \rightarrow W^+W^-$
>2620	95	4 AABOUD 16u	ATLS	$p\bar{p}; Z'_\chi \rightarrow e^+e^-, \mu^+\mu^-$
>1970	95	5 AAD 14v	ATLS	$p\bar{p}; Z'_\chi \rightarrow e^+e^-, \mu^+\mu^-$
> 930	95	6 AAD 12cc	ATLS	$p\bar{p}; Z'_\chi \rightarrow e^+e^-, \mu^+\mu^-$
> 903	95	7 AALTONEN 11i	CDF	$p\bar{p}; Z'_\chi \rightarrow \mu^+\mu^-$
>1022	95	8 ABAZOV 11A	D0	$p\bar{p}; Z'_\chi \rightarrow e^+e^-$
> 862	95	9 DEL-AGUILA 10	RVUE	Electroweak
> 892	95	10 AALTONEN 09v	CDF	Repl. by AALTONEN 11i
>1141	95	11 ERLER 09	RVUE	Electroweak
> 822	95	12 AALTONEN 07h	CDF	Repl. by AALTONEN 09t
> 680	95	13 SCHAEL 07A	ALEP	e^+e^-
> 545	95	14 ABDALLAH 06c	DLPH	e^+e^-
> 740	95	15 ABULENCIA 06L	CDF	Repl. by AALTONEN 07h
> 690	95	16 ABULENCIA 05A	CDF	$p\bar{p}; Z'_\chi \rightarrow e^+e^-, \mu^+\mu^-$
> 781	95	17 ABBIENDI 04g	OPAL	e^+e^-
>2100	95	18 BARGER 03b	COSM	Nucleosynthesis; light ν_R

VALUE (GeV)	CL%	DOCUMENT ID	TECN	COMMENT
> 680	95	16 CHEUNG 01b	RVUE	Electroweak
> 440	95	17 ABREU 00s	DLPH	e^+e^-
> 533	95	18 BARATE 00i	ALEP	Repl. by SCHAEL 07A
> 554	95	19 CHO 00	RVUE	Electroweak
		20 ERLER 00	RVUE	Cs
		21 ROSNER 00	RVUE	Cs
> 545	95	22 ERLER 99	RVUE	Electroweak
(> 1368)	95	23 ERLER 99	RVUE	Electroweak
> 215	95	24 CONRAD 98	RVUE	$\nu_\mu N$ scattering
> 595	95	25 ABE 97s	CDF	$p\bar{p}; Z'_\chi \rightarrow e^+e^-, \mu^+\mu^-$
> 190	95	26 ARIMA 97	VNS	Bhabha scattering
> 262	95	27 VILAIN 94B	CHM2	$\nu_\mu e \rightarrow \nu_\mu e; \bar{\nu}_\mu e \rightarrow \bar{\nu}_\mu e$
[>1470]		28 FARAGGI 91	COSM	Nucleosynthesis; light ν_R
> 231	90	29 ABE 90f	VNS	e^+e^-
[> 1140]		30 GONZALEZ... 90D	COSM	Nucleosynthesis; light ν_R
[> 2100]		31 GRIFOLS 90	ASTR	SN 1987A; light ν_R

- 1 AAD 19L search for resonances decaying to $\ell^+\ell^-$ in pp collisions at $\sqrt{s} = 13$ TeV.
- 2 AABOUD 17AT search for resonances decaying to $\ell^+\ell^-$ in pp collisions at $\sqrt{s} = 13$ TeV.
- 3 BOBOVNIKOV 18 use the ATLAS limits on $\sigma(pp \rightarrow Z') \cdot B(Z' \rightarrow W^+W^-)$ to constrain the Z-Z' mixing parameter ξ . See their Fig. 9 for limits in $M_{Z'} - \xi$ plane.
- 4 AABOUD 16u search for resonances decaying to $\ell^+\ell^-$ in pp collisions at $\sqrt{s} = 13$ TeV.
- 5 AAD 14v search for resonances decaying to $e^+e^-, \mu^+\mu^-$ in pp collisions at $\sqrt{s} = 8$ TeV.
- 6 AAD 12cc search for resonances decaying to $e^+e^-, \mu^+\mu^-$ in pp collisions at $\sqrt{s} = 7$ TeV.
- 7 AALTONEN 11i search for resonances decaying to $\mu^+\mu^-$ in $p\bar{p}$ collisions at $\sqrt{s} = 1.96$ TeV.
- 8 ABAZOV 11A, AALTONEN 09T, AALTONEN 07H, and ABULENCIA 06L search for resonances decaying to e^+e^- in $p\bar{p}$ collisions at $\sqrt{s} = 1.96$ TeV.
- 9 DEL-AGUILA 10 give 95% CL limit on the Z-Z' mixing $-0.0011 < \theta < 0.0007$.
- 10 AALTONEN 09v search for resonances decaying to $\mu^+\mu^-$ in $p\bar{p}$ collisions at $\sqrt{s} = 1.96$ TeV.
- 11 ERLER 09 give 95% CL limit on the Z-Z' mixing $-0.0016 < \theta < 0.0006$.
- 12 ABDALLAH 06c give 95% CL limit $|\theta| < 0.0031$. See their Fig. 14 for limit contours in the mass-mixing plane.
- 13 ABULENCIA 05A search for resonances decaying to electron or muon pairs in $p\bar{p}$ collisions at $\sqrt{s} = 1.96$ TeV.
- 14 ABBIENDI 04c give 95% CL limit on Z-Z' mixing $-0.00098 < \theta < 0.00194$. See their Fig. 20 for the limit contour in the mass-mixing plane. $\sqrt{s} = 91$ to 207 GeV.
- 15 BARGER 03b limit is from the nucleosynthesis bound on the effective number of light neutrino $\delta N_\nu < 1$. The quark-hadron transition temperature $T_C = 150$ MeV is assumed. The limit with $T_C = 400$ MeV is > 4300 GeV.
- 16 CHEUNG 01b limit is derived from bounds on contact interactions in a global electroweak analysis.
- 17 ABREU 00s give 95% CL limit on Z-Z' mixing $|\theta| < 0.0017$. See their Fig. 6 for the limit contour in the mass-mixing plane. $\sqrt{s} = 90$ to 189 GeV.
- 18 BARATE 00i search for deviations in cross section and asymmetries in $e^+e^- \rightarrow$ fermions at $\sqrt{s} = 90$ to 183 GeV. Assume $\theta = 0$. Bounds in the mass-mixing plane are shown in their Figure 18.
- 19 CHO 00 use various electroweak data to constrain Z' models assuming $m_H = 100$ GeV. See Fig. 3 for limits in the mass-mixing plane.
- 20 ERLER 00 discuss the possibility that a discrepancy between the observed and predicted values of $Q_W(\text{Cs})$ is due to the exchange of Z'. The data are better described in a certain class of the Z' models including Z_{LR} and Z_χ .
- 21 ROSNER 00 discusses the possibility that a discrepancy between the observed and predicted values of $Q_W(\text{Cs})$ is due to the exchange of Z'. The data are better described in a certain class of the Z' models including Z_χ .
- 22 ERLER 99 give 90% CL limit on the Z-Z' mixing $-0.0020 < \theta < 0.0015$.
- 23 ERLER 99 assumes 2 Higgs doublets, transforming as 10 of SO(10), embedded in E_6 .
- 24 CONRAD 98 limit is from measurements at CCFR, assuming no Z-Z' mixing.
- 25 ABE 97s find $\sigma(Z') \times B(e^+e^-, \mu^+\mu^-) < 40$ fb for $m_{Z'} > 600$ GeV at $\sqrt{s} = 1.8$ TeV.
- 26 Z-Z' mixing is assumed to be zero. $\sqrt{s} = 57.77$ GeV.
- 27 VILAIN 94b assume $m_t = 150$ GeV and $\theta = 0$. See Fig. 2 for limit contours in the mass-mixing plane.
- 28 FARAGGI 91 limit assumes the nucleosynthesis bound on the effective number of neutrinos $\Delta N_\nu < 0.5$ and is valid for $m_{\nu_R} < 1$ MeV.
- 29 ABE 90f use data for $R, R_{\ell\ell}$, and $A_{\ell\ell}$. ABE 90f fix $m_W = 80.49 \pm 0.43 \pm 0.24$ GeV and $m_Z = 91.13 \pm 0.03$ GeV.
- 30 Assumes the nucleosynthesis bound on the effective number of light neutrinos ($\delta N_\nu < 1$) and that ν_R is light ($\lesssim 1$ MeV).
- 31 GRIFOLS 90 limit holds for $m_{\nu_R} \lesssim 1$ MeV. See also GRIFOLS 90D, RIZZO 91.

Limits for Z_ψ

Z_ψ is the extra neutral boson in $E_6 \rightarrow \text{SO}(10) \times \text{U}(1)_\psi$. $g_\psi = e/\cos\theta_W$ is assumed unless otherwise stated. We list limits with the assumption $\rho = 1$ but with no further constraints on the Higgs sector. Values in brackets are from cosmological and astrophysical considerations and assume a light right-handed neutrino.

VALUE (GeV)	CL%	DOCUMENT ID	TECN	COMMENT
>4560 (CL = 95%) OUR LIMIT				
>4560	95	1 SIRUNYAN 21N	CMS	$p\bar{p}; Z'_\psi \rightarrow e^+e^-, \mu^+\mu^-$
none 250-4500	95	2 AAD 19L	ATLS	$p\bar{p}; Z'_\psi \rightarrow e^+e^-, \mu^+\mu^-$
none 200-3900	95	3 SIRUNYAN 18BB	CMS	$p\bar{p}; Z'_\psi \rightarrow e^+e^-, \mu^+\mu^-$
>3800	95	4 AABOUD 17AT	ATLS	$p\bar{p}; Z'_\psi \rightarrow e^+e^-, \mu^+\mu^-$
>2820	95	5 KHACHATRY...17T	CMS	$p\bar{p}; Z'_\psi \rightarrow e^+e^-, \mu^+\mu^-$
>1100	95	6 CHATRCHYAN 12o	CMS	$p\bar{p}; Z'_\psi \rightarrow \tau^+\tau^-$

• • • We do not use the following data for averages, fits, limits, etc. • • •

		7	BOBOVNIKOV 18	RVUE	$pp, Z'_\psi \rightarrow W^+ W^-$
>2740	95	8	AABOUD 16U	ATLS	$pp; Z'_\psi \rightarrow e^+ e^-, \mu^+ \mu^-$
>2570	95	9	KHACHATRYAN 15AE	CMS	$pp; Z'_\psi \rightarrow e^+ e^-, \mu^+ \mu^-$
>2510	95	10	AAD 14V	ATLS	$pp, Z'_\psi \rightarrow e^+ e^-, \mu^+ \mu^-$
>2260	95	11	CHATRCHYAN 13AF	CMS	$pp, Z'_\psi \rightarrow e^+ e^-, \mu^+ \mu^-$
>1790	95	12	AAD 12CC	ATLS	$pp, Z'_\psi \rightarrow e^+ e^-, \mu^+ \mu^-$
>2000	95	13	CHATRCHYAN 12M	CMS	Repl. by CHATRCHYAN 13AF
> 917	95	14	AALTONEN 11I	CDF	$p\bar{p}; Z'_\psi \rightarrow \mu^+ \mu^-$
> 891	95	15	ABAZOV 11A	D0	$p\bar{p}; Z'_\psi \rightarrow e^+ e^-$
> 476	95	16	DEL-AGUILA 10	RVUE	Electroweak
> 851	95	15	AALTONEN 09T	CDF	$p\bar{p}; Z'_\psi \rightarrow e^+ e^-$
> 878	95	17	AALTONEN 09V	CDF	Repl. by AALTONEN 11I
> 147	95	18	ERLER 09	RVUE	Electroweak
> 822	95	15	AALTONEN 07H	CDF	Repl. by AALTONEN 09T
> 410	95	95	SCHAEEL 07A	ALEP	$e^+ e^-$
> 475	95	19	ABDALLAH 06C	DLPH	$e^+ e^-$
> 725	95	15	ABULENCIA 06L	CDF	Repl. by AALTONEN 07H
> 675	95	20	ABULENCIA 05A	CDF	Repl. by AALTONEN 11I and AALTONEN 09T
> 366	95	21	ABBIENDI 04G	OPAL	$e^+ e^-$
> 600	95	22	BARGER 03B	COSM	Nucleosynthesis; light ν_R
> 350	95	23	ABREU 00S	DLPH	$e^+ e^-$
> 294	95	24	BARATE 00I	ALEP	Repl. by SCHAEEL 07A
> 137	95	25	CHO 00	RVUE	Electroweak
> 146	95	26	ERLER 99	RVUE	Electroweak
> 54	95	27	CONRAD 98	RVUE	$\nu_\mu N$ scattering
> 590	95	28	ABE 97S	CDF	$p\bar{p}; Z'_\psi \rightarrow e^+ e^-, \mu^+ \mu^-$
> 135	95	29	VILAIN 94B	CHM2	$\nu_\mu e \rightarrow \nu_\mu e; \bar{\nu}_\mu e \rightarrow \bar{\nu}_\mu e$
> 105	90	30	ABE 90F	VNS	$e^+ e^-$
[> 160]		31	GONZALEZ... 90D	COSM	Nucleosynthesis; light ν_R
[> 2000]		32	GRIFOLS 90D	ASTR	SN 1987A; light ν_R

- 1 SIRUNYAN 21N search for resonance decaying to $e^+ e^-, \mu^+ \mu^-$ in pp collisions at $\sqrt{s} = 13$ TeV.
- 2 AAD 19L search for resonances decaying to $\ell^+ \ell^-$ in pp collisions at $\sqrt{s} = 13$ TeV.
- 3 SIRUNYAN 18BB search for resonances decaying to $\ell^+ \ell^-$ in pp collisions at $\sqrt{s} = 13$ TeV.
- 4 AABOUD 17AT search for resonances decaying to $\ell^+ \ell^-$ in pp collisions at $\sqrt{s} = 13$ TeV.
- 5 KHACHATRYAN 17T search for resonances decaying to $e^+ e^-, \mu^+ \mu^-$ in pp collisions at $\sqrt{s} = 8, 13$ TeV.
- 6 CHATRCHYAN 12O search for resonances decaying to $\tau^+ \tau^-$ in pp collisions at $\sqrt{s} = 7$ TeV.
- 7 BOBOVNIKOV 18 use the ATLAS limits on $\sigma(pp \rightarrow Z')B(Z' \rightarrow W^+ W^-)$ to constrain the $Z-Z'$ mixing parameter ξ . See their Fig. 10 for limits in $M_{Z'} - \xi$ plane.
- 8 AABOUD 16U search for resonances decaying to $\ell^+ \ell^-$ in pp collisions at $\sqrt{s} = 13$ TeV.
- 9 KHACHATRYAN 15AE search for resonances decaying to $e^+ e^-, \mu^+ \mu^-$ in pp collisions at $\sqrt{s} = 8$ TeV.
- 10 AAD 14V search for resonances decaying to $e^+ e^-, \mu^+ \mu^-$ in pp collisions at $\sqrt{s} = 8$ TeV.
- 11 CHATRCHYAN 13AF search for resonances decaying to $e^+ e^-, \mu^+ \mu^-$ in pp collisions at $\sqrt{s} = 7$ TeV and 8 TeV.
- 12 AAD 12CC search for resonances decaying to $e^+ e^-, \mu^+ \mu^-$ in pp collisions at $\sqrt{s} = 7$ TeV.
- 13 CHATRCHYAN 12M search for resonances decaying to $e^+ e^-$ or $\mu^+ \mu^-$ in pp collisions at $\sqrt{s} = 7$ TeV.
- 14 AALTONEN 11I search for resonances decaying to $\mu^+ \mu^-$ in $p\bar{p}$ collisions at $\sqrt{s} = 1.96$ TeV.
- 15 ABAZOV 11A, AALTONEN 09T, AALTONEN 07H, and ABULENCIA 06L search for resonances decaying to $e^+ e^-$ in $p\bar{p}$ collisions at $\sqrt{s} = 1.96$ TeV.
- 16 DEL-AGUILA 10 give 95% CL limit on the $Z-Z'$ mixing $-0.0019 < \theta < 0.0007$.
- 17 AALTONEN 09V search for resonances decaying to $\mu^+ \mu^-$ in $p\bar{p}$ collisions at $\sqrt{s} = 1.96$ TeV.
- 18 ERLER 09 give 95% CL limit on the $Z-Z'$ mixing $-0.0018 < \theta < 0.0009$.
- 19 ABDALLAH 06C give 95% CL limit $|\theta| < 0.0027$. See their Fig. 14 for limit contours in the mass-mixing plane.
- 20 ABULENCIA 05A search for resonances decaying to electron or muon pairs in $p\bar{p}$ collisions at $\sqrt{s} = 1.96$ TeV.
- 21 ABBIENDI 04G give 95% CL limit on $Z-Z'$ mixing $-0.00129 < \theta < 0.00258$. See their Fig. 20 for the limit contour in the mass-mixing plane. $\sqrt{s} = 91$ to 207 GeV.
- 22 BARGER 03B limit is from the nucleosynthesis bound on the effective number of light neutrino $\delta N_\nu < 1$. The quark-hadron transition temperature $T_C = 150$ MeV is assumed. The limit with $T_C = 400$ MeV is > 1100 GeV.
- 23 ABREU 00S give 95% CL limit on $Z-Z'$ mixing $|\theta| < 0.0018$. See their Fig. 6 for the limit contour in the mass-mixing plane. $\sqrt{s} = 90$ to 189 GeV.
- 24 BARATE 00I search for deviations in cross section and asymmetries in $e^+ e^- \rightarrow$ fermions at $\sqrt{s} = 90$ to 183 GeV. Assume $\theta = 0$. Bounds in the mass-mixing plane are shown in their Figure 18.
- 25 CHO 00 use various electroweak data to constrain Z' models assuming $m_H = 100$ GeV. See Fig. 3 for limits in the mass-mixing plane.
- 26 ERLER 99 give 90% CL limit on the $Z-Z'$ mixing $-0.0013 < \theta < 0.0024$.
- 27 CONRAD 98 limit is from measurements at CCFR, assuming no $Z-Z'$ mixing.
- 28 ABE 97S find $\sigma(Z') \times B(e^+ e^-, \mu^+ \mu^-) < 40$ fb for $m_{Z'} > 600$ GeV at $\sqrt{s} = 1.8$ TeV.
- 29 VILAIN 94B assume $m_t = 150$ GeV and $\theta = 0$. See Fig. 2 for limit contours in the mass-mixing plane.

- 30 ABE 90F use data for $R, R_{\ell\ell}$, and $A_{\ell\ell}$. ABE 90F fix $m_W = 80.49 \pm 0.43 \pm 0.24$ GeV and $m_Z = 91.13 \pm 0.03$ GeV.
- 31 Assumes the nucleosynthesis bound on the effective number of light neutrinos ($\delta N_\nu < 1$) and that ν_R is light ($\lesssim 1$ MeV).
- 32 GRIFOLS 90D limit holds for $m_{\nu_R} \lesssim 1$ MeV. See also RIZZO 91.

Limits for Z_η

Z_η is the extra neutral boson in E_6 models, corresponding to $Q_\eta = \sqrt{3/8} Q_X - \sqrt{5/8} Q_\psi$. $g_\eta = e/\cos\theta_W$ is assumed unless otherwise stated. We list limits with the assumption $\rho = 1$ but with no further constraints on the Higgs sector. Values in parentheses assume stronger constraint on the Higgs sector motivated by superstring models. Values in brackets are from cosmological and astrophysical considerations and assume a light right-handed neutrino.

VALUE (GeV)	CL%	DOCUMENT ID	TECN	COMMENT
>3900	95	1	AABOUD 17AT	ATLS $pp; Z'_\eta \rightarrow e^+ e^-, \mu^+ \mu^-$
		• • • We do not use the following data for averages, fits, limits, etc. • • •		
		2	BOBOVNIKOV 18	RVUE $pp, Z'_\eta \rightarrow W^+ W^-$
>2810	95	3	AABOUD 16U	ATLS $pp; Z'_\eta \rightarrow e^+ e^-, \mu^+ \mu^-$
>1870	95	4	AAD 12CC	ATLS $pp, Z'_\eta \rightarrow e^+ e^-, \mu^+ \mu^-$
> 938	95	5	AALTONEN 11I	CDF $p\bar{p}; Z'_\eta \rightarrow \mu^+ \mu^-$
> 923	95	6	ABAZOV 11A	D0 $p\bar{p}; Z'_\eta \rightarrow e^+ e^-$
> 488	95	7	DEL-AGUILA 10	RVUE Electroweak
> 877	95	6	AALTONEN 09T	CDF $p\bar{p}; Z'_\eta \rightarrow e^+ e^-$
> 904	95	8	AALTONEN 09V	CDF Repl. by AALTONEN 11I
> 427	95	9	ERLER 09	RVUE Electroweak
> 891	95	6	AALTONEN 07H	CDF Repl. by AALTONEN 09T
> 350	95	95	SCHAEEL 07A	ALEP $e^+ e^-$
> 360	95	10	ABDALLAH 06C	DLPH $e^+ e^-$
> 745	95	6	ABULENCIA 06L	CDF Repl. by AALTONEN 07H
> 720	95	11	ABULENCIA 05A	CDF Repl. by AALTONEN 11I and AALTONEN 09T
> 515	95	12	ABBIENDI 04G	OPAL $e^+ e^-$
>1600	95	13	BARGER 03B	COSM Nucleosynthesis; light ν_R
> 310	95	14	ABREU 00S	DLPH $e^+ e^-$
> 329	95	15	BARATE 00I	ALEP Repl. by SCHAEEL 07A
> 619	95	16	CHO 00	RVUE Electroweak
> 365	95	17	ERLER 99	RVUE Electroweak
> 87	95	18	CONRAD 98	RVUE $\nu_\mu N$ scattering
> 620	95	19	ABE 97S	CDF $p\bar{p}; Z'_\eta \rightarrow e^+ e^-, \mu^+ \mu^-$
> 100	95	20	VILAIN 94B	CHM2 $\nu_\mu e \rightarrow \nu_\mu e; \bar{\nu}_\mu e \rightarrow \bar{\nu}_\mu e$
> 125	90	21	ABE 90F	VNS $e^+ e^-$
[> 820]		22	GONZALEZ... 90D	COSM Nucleosynthesis; light ν_R
[> 3300]		23	GRIFOLS 90	ASTR SN 1987A; light ν_R
[> 1040]		22	LOPEZ 90	COSM Nucleosynthesis; light ν_R

- 1 AABOUD 17AT search for resonances decaying to $\ell^+ \ell^-$ in pp collisions at $\sqrt{s} = 13$ TeV.
- 2 BOBOVNIKOV 18 use the ATLAS limits on $\sigma(pp \rightarrow Z')B(Z' \rightarrow W^+ W^-)$ to constrain the $Z-Z'$ mixing parameter ξ . See their Fig. 9 for limits in $M_{Z'} - \xi$ plane.
- 3 AABOUD 16U search for resonances decaying to $\ell^+ \ell^-$ in pp collisions at $\sqrt{s} = 13$ TeV.
- 4 AAD 12CC search for resonances decaying to $e^+ e^-, \mu^+ \mu^-$ in pp collisions at $\sqrt{s} = 7$ TeV.
- 5 AALTONEN 11I search for resonances decaying to $\mu^+ \mu^-$ in $p\bar{p}$ collisions at $\sqrt{s} = 1.96$ TeV.
- 6 ABAZOV 11A, AALTONEN 09T, AALTONEN 07H, and ABULENCIA 06L search for resonances decaying to $e^+ e^-$ in $p\bar{p}$ collisions at $\sqrt{s} = 1.96$ TeV.
- 7 DEL-AGUILA 10 give 95% CL limit on the $Z-Z'$ mixing $-0.0023 < \theta < 0.0027$.
- 8 AALTONEN 09V search for resonances decaying to $\mu^+ \mu^-$ in $p\bar{p}$ collisions at $\sqrt{s} = 1.96$ TeV.
- 9 ERLER 09 give 95% CL limit on the $Z-Z'$ mixing $-0.0047 < \theta < 0.0021$.
- 10 ABDALLAH 06C give 95% CL limit $|\theta| < 0.0092$. See their Fig. 14 for limit contours in the mass-mixing plane.
- 11 ABULENCIA 05A search for resonances decaying to electron or muon pairs in $p\bar{p}$ collisions at $\sqrt{s} = 1.96$ TeV.
- 12 ABBIENDI 04G give 95% CL limit on $Z-Z'$ mixing $-0.00447 < \theta < 0.00331$. See their Fig. 20 for the limit contour in the mass-mixing plane. $\sqrt{s} = 91$ to 207 GeV.
- 13 BARGER 03B limit is from the nucleosynthesis bound on the effective number of light neutrino $\delta N_\nu < 1$. The quark-hadron transition temperature $T_C = 150$ MeV is assumed. The limit with $T_C = 400$ MeV is > 3300 GeV.
- 14 ABREU 00S give 95% CL limit on $Z-Z'$ mixing $|\theta| < 0.0024$. See their Fig. 6 for the limit contour in the mass-mixing plane. $\sqrt{s} = 90$ to 189 GeV.
- 15 BARATE 00I search for deviations in cross section and asymmetries in $e^+ e^- \rightarrow$ fermions at $\sqrt{s} = 90$ to 183 GeV. Assume $\theta = 0$. Bounds in the mass-mixing plane are shown in their Figure 18.
- 16 CHO 00 use various electroweak data to constrain Z' models assuming $m_H = 100$ GeV. See Fig. 3 for limits in the mass-mixing plane.
- 17 ERLER 99 give 90% CL limit on the $Z-Z'$ mixing $-0.0062 < \theta < 0.0011$.
- 18 CONRAD 98 limit is from measurements at CCFR, assuming no $Z-Z'$ mixing.
- 19 ABE 97S find $\sigma(Z') \times B(e^+ e^-, \mu^+ \mu^-) < 40$ fb for $m_{Z'} > 600$ GeV at $\sqrt{s} = 1.8$ TeV.
- 20 VILAIN 94B assume $m_t = 150$ GeV and $\theta = 0$. See Fig. 2 for limit contours in the mass-mixing plane.
- 21 ABE 90F use data for $R, R_{\ell\ell}$, and $A_{\ell\ell}$. ABE 90F fix $m_W = 80.49 \pm 0.43 \pm 0.24$ GeV and $m_Z = 91.13 \pm 0.03$ GeV.
- 22 These authors claim that the nucleosynthesis bound on the effective number of light neutrinos ($\delta N_\nu < 1$) constrains Z' masses if ν_R is light ($\lesssim 1$ MeV).
- 23 GRIFOLS 90 limit holds for $m_{\nu_R} \lesssim 1$ MeV. See also GRIFOLS 90D, RIZZO 91.

Gauge & Higgs Boson Particle Listings

New Heavy Bosons

Limits for other Z'

VALUE (GeV)	CL%	DOCUMENT ID	TECN	COMMENT
none 300–3200	95	1 AAD	23O ATLS	$Z' \rightarrow ZH$
none 1800–2400	95	2 TUMASYAN	23AF CMS	$Z' \rightarrow b\bar{b}$
none 1300–3100, 3300–3500	95	3 TUMASYAN	23AP CMS	$Z' \rightarrow WW$
>3900	95	4 TUMASYAN	23AP CMS	$Z' \rightarrow ZH$
>4000	95	5 TUMASYAN	22D CMS	$Z' \rightarrow WW$
none 800–3700	95	6 SIRUNYAN	21X CMS	$Z' \rightarrow HZ$
>2650	95	7 AAD	20AJ ATLS	$Z' \rightarrow HZ$
>3900	95	8 AAD	20AM ATLS	$Z' \rightarrow t\bar{t}$
>3900	95	9 AAD	20AT ATLS	$Z' \rightarrow WW$
none 1200–3500	95	10 SIRUNYAN	20Q CMS	$Z' \rightarrow WW$
none 580–3100	95	11 AABOUD	19AS ATLS	$Z' \rightarrow t\bar{t}$
none 1300–3100	95	12 AAD	19D ATLS	$Z' \rightarrow WW$
>3800	95	13 SIRUNYAN	19AA CMS	$Z' \rightarrow t\bar{t}$
>3700	95	14 SIRUNYAN	19CP CMS	$Z' \rightarrow WW, HZ, \ell^+ \ell^-$
>1800	95	15 SIRUNYAN	19I CMS	$Z' \rightarrow HZ$
none 600–2100	95	16 AABOUD	18AB ATLS	$Z' \rightarrow b\bar{b}$
none 500–2830	95	17 AABOUD	18AI ATLS	$Z' \rightarrow HZ$
none 300–3000	95	18 AABOUD	18AK ATLS	$Z' \rightarrow WW$
>1300	95	19 AABOUD	18B ATLS	$Z' \rightarrow WW$
none 400–3000	95	20 AABOUD	18BI ATLS	$Z' \rightarrow t\bar{t}$
none 1200–2800	95	21 AABOUD	18F ATLS	$Z' \rightarrow WW$
>2300	95	22 SIRUNYAN	18ED CMS	$Z' \rightarrow HZ$
none 1200–2700	95	23 SIRUNYAN	18P CMS	$Z' \rightarrow WW$
>2900	95	24 AABOUD	17AK ATLS	$Z' \rightarrow q\bar{q}$
none 1100–2600	95	25 AABOUD	17AO ATLS	$Z' \rightarrow HZ$
>2300	95	26 SIRUNYAN	17AK CMS	$Z' \rightarrow WW, HZ$
>2500	95	27 SIRUNYAN	17Q CMS	$Z' \rightarrow t\bar{t}$
>1190	95	28 SIRUNYAN	17R CMS	$Z' \rightarrow HZ$
none 1210–2260	95	28 SIRUNYAN	17R CMS	$Z' \rightarrow HZ$
••• We do not use the following data for averages, fits, limits, etc. •••				
29 AAD	23BF ATLS	DM simplified Z'		
30 AAD	23W ATLS	dark Higgs Z'		
31 AAD	23X ATLS	$L_\mu - L_\tau$		
32 ADACHI	23B BEL2	$L_\mu - L_\tau$		
33 ADACHI	23F BEL2	$L_\mu - L_\tau$		
34 HAYRAPETY...	23D CMS	$Z' \rightarrow \mu^+ \mu^-$		
35 HAYRAPETY...	23G CMS	$Z' \rightarrow \mu^+ \mu^-$		
36 LI	23I ASTR	Stellar cooling		
37 MANZARI	23 ASTR	DM mediator Z'		
38 AAD	22 ATLS	$pp \rightarrow b\bar{b}Z' \rightarrow b\bar{b}b\bar{b}$		
39 AAD	22D ATLS	DM mediator Z'		
40 ANDREEV	22 CALO	electron beam dump		
41 BONET	22 HPGE	ν -nucleus scattering		
42 COLOMA	22 RVUE	ν -nucleus scattering		
43 COLOMA	22A RVUE	ν -e scattering		
44 CZANK	22 BELL	$e^+ e^- \rightarrow \mu^+ \mu^- Z' (\rightarrow \mu^+ \mu^-)$		
45 TUMASYAN	22AA CMS	$Z' \rightarrow SVJs$		
46 AAD	21AQ ATLS	$pp, \ell^+ \ell^- \ell^+ \ell^-$		
47 AAD	21AZ ATLS	DM mediator Z'		
48 AAD	21BB ATLS	$Z' \rightarrow AH$		
49 AAD	21D ATLS	dark Higgs Z'		
50 AAD	21K ATLS	$Z' \rightarrow \chi\chi$		
51 BURAS	21 RVUE	leptophilic Z'		
52 CADEDDU	21 RVUE	ν -nucleus scattering		
53 COLARES	21 HPGE	ν -nucleus scattering		
54 KRIBS	21 RVUE	$e p$ scattering		
55 TUMASYAN	21D CMS	$Z' \rightarrow \chi\chi$		
56 AAD	20AF ATLS	$Z' \rightarrow H\gamma$		
57 AAD	20T ATLS	DM simplified Z'		
58 AAD	20W ATLS	DM simplified Z'		
59 AAIJ	20AL LHCB	$Z' \rightarrow \mu^+ \mu^-$		
60 ADACHI	20 BEL2	$e^+ e^- \rightarrow \mu^+ \mu^- Z', e^\pm \mu^\mp Z'$		
61 SIRUNYAN	20AI CMS	$Z' \rightarrow q\bar{q}$		
62 SIRUNYAN	20AQ CMS	$Z' \rightarrow \mu^+ \mu^-$		
63 SIRUNYAN	20M CMS	$Z' \rightarrow q\bar{q}$		
64 AABOUD	19AJ ATLS	$Z' \rightarrow q\bar{q}$		
65 AABOUD	19D ATLS	$Z' \rightarrow q\bar{q}$		
66 AABOUD	19V ATLS	DM simplified Z'		
67 AAD	19L ATLS	$Z' \rightarrow e^+ e^-, \mu^+ \mu^-$		
68 LONG	19 RVUE	Electroweak		
69 PANDEY	19 RVUE	neutrino NSI		
70 SIRUNYAN	19AL CMS	$Z' \rightarrow t\bar{t}, T \rightarrow Ht, Zt, Wb$		
71 SIRUNYAN	19AN CMS	DM simplified Z'		
72 SIRUNYAN	19CB CMS	$Z' \rightarrow q\bar{q}$		
73 SIRUNYAN	19CD CMS	$Z' \rightarrow q\bar{q}$		
74 SIRUNYAN	19D CMS	$Z' \rightarrow H\gamma$		
75 AABOUD	18AA ATLS	$Z' \rightarrow H\gamma$		
>4500	95	76 AABOUD	18CJ ATLS	$Z' \rightarrow WW, HZ, \ell^+ \ell^-$
77 AABOUD	18N ATLS	$Z' \rightarrow q\bar{q}$		

78 AAIJ	18AQ LHCB	$Z' \rightarrow \mu^+ \mu^-$		
79 SIRUNYAN	18DR CMS	$Z' \rightarrow \mu^+ \mu^-$		
80 SIRUNYAN	18G CMS	$Z' \rightarrow q\bar{q}$		
81 SIRUNYAN	18I CMS	$Z' \rightarrow b\bar{b}$		
82 AABOUD	17B ATLS	$Z' \rightarrow HZ$	>1580	95
83 KHACHATRY...	17AX CMS	$Z' \rightarrow \ell\ell\ell$		
84 KHACHATRY...	17U CMS	$Z' \rightarrow HZ$		
85 SIRUNYAN	17A CMS	$Z' \rightarrow WW$	>1700	95
86 SIRUNYAN	17AP CMS	$Z' \rightarrow HA$		
87 SIRUNYAN	17T CMS	$Z' \rightarrow q\bar{q}$		
88 SIRUNYAN	17V CMS	$Z' \rightarrow Tt$		
89 AABOUD	16 ATLS	$Z' \rightarrow b\bar{b}$	none 1100–1500	95
90 AAD	16L ATLS	$Z' \rightarrow a\gamma, a \rightarrow \gamma\gamma$		
91 AAD	16S ATLS	$Z' \rightarrow q\bar{q}$	none 1500–2600	95
92 KHACHATRY...	16AF CMS	$Z' \rightarrow HZ$	none 1000–1100, none 1300–1500	95
93 KHACHATRY...	16E CMS	$Z' \rightarrow t\bar{t}$	>2400	95
94 AAD	15AO ATLS	$Z' \rightarrow t\bar{t}$		
95 AAD	15AT ATLS	monotop		
96 AAD	15CD ATLS	$H \rightarrow ZZ', Z'Z'; Z' \rightarrow \ell^+ \ell^-$		
97 KHACHATRY...	15F CMS	monotop		
98 KHACHATRY...	15O CMS	$Z' \rightarrow HZ$		
99 AAD	14AT ATLS	$Z' \rightarrow Z\gamma$		
100 KHACHATRY...	14A CMS	$Z' \rightarrow VV$		
101 MARTINEZ	14 RVUE	Electroweak		
102 AAD	13AQ ATLS	$Z' \rightarrow t\bar{t}$	none 500–1740	95
103 AAD	13G ATLS	$Z' \rightarrow t\bar{t}$	>1320 or 1000–1280	95
103 AALTONEN	13A CDF	$Z' \rightarrow t\bar{t}$	> 915	95
104 CHATRCHYAN	13AP CMS	$Z' \rightarrow t\bar{t}$	>1300	95
103 CHATRCHYAN	13BM CMS	$Z' \rightarrow t\bar{t}$	>2100	95
105 AAD	12BV ATLS	$Z' \rightarrow t\bar{t}$		
106 AAD	12K ATLS	$Z' \rightarrow t\bar{t}$		
107 AALTONEN	12AR CDF	Chromophilic		
108 AALTONEN	12N CDF	$Z' \rightarrow \bar{\tau}\nu$		
109 ABAZOV	12R D0	$Z' \rightarrow t\bar{t}$	> 835	95
110 CHATRCHYAN	12AI CMS	$Z' \rightarrow t\bar{t}$		
111 CHATRCHYAN	12AQ CMS	$Z' \rightarrow t\bar{t}$		
103 CHATRCHYAN	12BL CMS	$Z' \rightarrow t\bar{t}$	>1490	95
112 AALTONEN	11AD CDF	$Z' \rightarrow t\bar{t}$		
113 AALTONEN	11AE CDF	$Z' \rightarrow t\bar{t}$		
114 CHATRCHYAN	11O CMS	$pp \rightarrow tt$		
115 AALTONEN	08D CDF	$Z' \rightarrow t\bar{t}$		
115 AALTONEN	08Y CDF	$Z' \rightarrow t\bar{t}$		
115 ABAZOV	08AA D0	$Z' \rightarrow t\bar{t}$		
116 ABAZOV	04A D0	Repl. by ABAZOV 08AA		
117 BARGER	03B COSM	Nucleosynthesis; light ν_R		
118 CHO	00 RVUE	E_g -motivated		
119 CHO	98 RVUE	E_g -motivated		
120 ABE	97G CDF	$Z' \rightarrow q\bar{q}$		

1 AAD 23O search for resonances decaying to HZ in pp collisions at $\sqrt{s} = 13$ TeV. The quoted limit is for heavy-vector-triplet Z' with $g_V = 3$. The limit becomes $M_{Z'} > 2800$ GeV for $g_V = 1$.

2 TUMASYAN 23AF search for resonance decaying to $b\bar{b}$ in pp collisions at $\sqrt{s} = 13$ TeV. The limit quoted above is for heavy-vector-triplet Z' with $g_V = 1$. See their Fig. 4 for limits on σ_B .

3 TUMASYAN 23AP search for resonances decaying to WW in pp collisions at $\sqrt{s} = 13$ TeV. The limit quoted above is for heavy-vector-triplet Z' with $g_V = 3$. The limit becomes $M_{Z'} > 4.8$ TeV assuming $M_{W'} = M_{Z'}$ and combining $W' \rightarrow WZ, W' \rightarrow WH, Z' \rightarrow WW, Z' \rightarrow ZH$ channels.

4 TUMASYAN 23AP search for resonances decaying to ZH in pp collisions at $\sqrt{s} = 13$ TeV. The limit quoted above is for heavy-vector-triplet Z' with $g_V = 3$. The limit becomes $M_{Z'} > 4.8$ TeV assuming $M_{W'} = M_{Z'}$ and combining $W' \rightarrow WZ, W' \rightarrow WH, Z' \rightarrow WW, Z' \rightarrow ZH$ channels.

5 SIRUNYAN 22D search for resonances produced through Drell-Yan and vector-boson-fusion processes in pp collisions at $\sqrt{s} = 13$ TeV. See their Fig. 8 for limits on σ_B . The quoted limit is for heavy-vector-triplet W' with $g_V = 3$ produced mainly via Drell-Yan.

6 SIRUNYAN 21X search for resonances decaying to HZ in pp collisions at $\sqrt{s} = 13$ TeV. The limit quoted above is for heavy-vector-triplet Z' with $g_V = 3$. The limit becomes $M_{Z'} > 3500$ GeV for $g_V = 1$.

7 AAD 20AJ search for resonances decaying to HZ in pp collisions at $\sqrt{s} = 13$ TeV. The quoted limit is for heavy-vector-triplet Z' with $g_V = 3$. The limit becomes $M_{Z'} > 2200$ GeV for $g_V = 1$. See their Fig. 6 for limits on σ_B .

8 AAD 20AM search for a resonance decaying to $t\bar{t}$ in pp collisions at $\sqrt{s} = 13$ TeV. The quoted limit is for a leptophobic top-color Z' with $\Gamma_{Z'}/M_{Z'} = 0.01$. The limit becomes $M_{Z'} > 4700$ GeV for $\Gamma_{Z'}/M_{Z'} = 0.03$.

9 AAD 20AT search for resonances decaying to WW in pp collisions at $\sqrt{s} = 13$ TeV. The quoted limit is for heavy-vector-triplet Z' with $g_V = 3$. The limit becomes $M_{Z'} > 3500$ GeV for $g_V = 1$. See their Fig. 14 for limits on σ_B .

10 SIRUNYAN 20Q search for resonances decaying to WW in pp collisions at $\sqrt{s} = 13$ TeV. The quoted limit is for heavy-vector-triplet Z' with $g_V = 3$.

11 AABOUD 19AS search for a resonance decaying to $t\bar{t}$ in pp collisions at $\sqrt{s} = 13$ TeV. The quoted limit is for a top-color Z' with $\Gamma_{Z'}/M_{Z'} = 0.01$. Limits are also set on Z' masses in simplified Dark Matter models.

See key on page 1171

Gauge & Higgs Boson Particle Listings

New Heavy Bosons

- 12 AAD 19d search for resonances decaying to WW in pp collisions at $\sqrt{s} = 13$ TeV. The quoted limit is for heavy-vector-triplet Z' with $g_V = 3$. The limit becomes $M_{Z'} > 2900$ GeV for $g_V = 1$. If we assume $M_{Z'} = M_{W'}$, the limit increases $M_{Z'} > 3800$ GeV and $M_{Z'} > 3500$ GeV for $g_V = 3$ and $g_V = 1$, respectively. See their Fig. 9 for limits on $\sigma \cdot B$.
- 13 SIRUNYAN 19AA search for a resonance decaying to $t\bar{t}$ in pp collisions at $\sqrt{s} = 13$ TeV. The quoted limit is for a leptophobic top-color Z' with $\Gamma_{Z'}/M_{Z'} = 0.01$.
- 14 SIRUNYAN 19CP present a statistical combinations of searches for Z' decaying to pairs of bosons or leptons in pp collisions at $\sqrt{s} = 13$ TeV. The quoted limit is for heavy-vector-triplet Z' with $g_V = 3$. If we assume $M_{Z'} = M_{W'}$, the limit becomes $M_{Z'} > 4500$ GeV for $g_V = 3$ and $M_{Z'} > 5000$ GeV for $g_V = 1$. See their Figs. 2 and 3 for limits on $\sigma \cdot B$.
- 15 SIRUNYAN 19I search for resonances decaying to ZW in pp collisions at $\sqrt{s} = 13$ TeV. The quoted limit is for heavy-vector-triplet Z' with $g_V = 3$. The limit becomes $M_{Z'} > 2800$ GeV if we assume $M_{Z'} = M_{W'}$.
- 16 AABOUD 18AB search for resonances decaying to $b\bar{b}$ in pp collisions at $\sqrt{s} = 13$ TeV. The limit quoted above is for a leptophobic Z' with SM-like couplings to quarks. See their Fig. 6 for limits on $\sigma \cdot B$. Additional limits on a Z' axial-vector mediator in a simplified dark-matter model are shown in Fig. 7.
- 17 AABOUD 18AI search for resonances decaying to HZ in pp collisions at $\sqrt{s} = 13$ TeV. The quoted limit is for heavy-vector-triplet Z' with $g_V = 3$. The limit becomes $M_{Z'} > 2650$ GeV for $g_V = 1$. If we assume $M_{W'} = M_{Z'}$, the limit increases $M_{Z'} > 2930$ GeV and $M_{Z'} > 2800$ GeV for $g_V = 3$ and $g_V = 1$, respectively. See their Fig. 5 for limits on $\sigma \cdot B$.
- 18 AABOUD 18AK search for resonances decaying to WW in pp collisions at $\sqrt{s} = 13$ TeV. The limit quoted above is for heavy-vector-triplet Z' with $g_V = 3$. The limit becomes $M_{Z'} > 2750$ GeV for $g_V = 1$.
- 19 AABOUD 18B search for resonances decaying to WW in pp collisions at $\sqrt{s} = 13$ TeV. The quoted limit is for heavy-vector-triplet Z' with $g_V = 1$. See their Fig.11 for limits on $\sigma \cdot B$.
- 20 AABOUD 18BI search for a resonance decaying to $t\bar{t}$ in pp collisions at $\sqrt{s} = 13$ TeV. The quoted limit is for a top-color assisted $TC Z'$ with $\Gamma_{Z'}/M_{Z'} = 0.01$. The limits for wider resonances are available. See their Fig. 14 for limits on $\sigma \cdot B$.
- 21 AABOUD 18F search for resonances decaying to WW in pp collisions at $\sqrt{s} = 13$ TeV. The quoted limit is for heavy-vector-triplet Z' with $g_V = 3$. The limit becomes $M_{Z'} > 2200$ GeV for $g_V = 1$. If we assume $M_{Z'} = M_{W'}$, the limit increases $M_{Z'} > 3500$ GeV and $M_{Z'} > 3100$ GeV for $g_V = 3$ and $g_V = 1$, respectively. See their Fig.5 for limits on $\sigma \cdot B$.
- 22 SIRUNYAN 18ED search for resonances decaying to HZ in pp collisions at $\sqrt{s} = 13$ TeV. The limit above is for heavy-vector-triplet Z' with $g_V = 3$. If we assume $M_{Z'} = M_{W'}$, the limit increases $M_{Z'} > 2900$ GeV and $M_{Z'} > 2800$ GeV for $g_V = 3$ and $g_V = 1$, respectively.
- 23 SIRUNYAN 18P give this limit for a heavy-vector-triplet Z' with $g_V = 3$. If they assume $M_{Z'} = M_{W'}$, the limit increases to $M_{Z'} > 3800$ GeV.
- 24 AABOUD 17AK search for a new resonance decaying to dijets in pp collisions at $\sqrt{s} = 13$ TeV. The limit quoted above is for a leptophobic Z' boson having axial-vector coupling strength with quarks $g_q = 0.2$. The limit is 2100 GeV if $g_q = 0.1$.
- 25 AABOUD 17AO search for resonances decaying to HZ in pp collisions at $\sqrt{s} = 13$ TeV. The limit quoted above is for a Z' in the heavy-vector-triplet model with $g_V = 3$. See their Fig.4 for limits on $\sigma \cdot B$.
- 26 SIRUNYAN 17AK search for resonances decaying to WW or HZ in pp collisions at $\sqrt{s} = 8$ and 13 TeV. The quoted limit is for heavy-vector-triplet Z' with $g_V = 3$. The limit becomes $M_{Z'} > 2200$ GeV for $g_V = 1$. If we assume $M_{Z'} = M_{W'}$, the limit increases $M_{Z'} > 2400$ GeV for both $g_V = 3$ and $g_V = 1$. See their Fig.1 and 2 for limits on $\sigma \cdot B$.
- 27 SIRUNYAN 17Q search for a resonance decaying to $t\bar{t}$ in pp collisions at $\sqrt{s} = 13$ TeV. The limit quoted above is for a resonance with relative width $\Gamma_{Z'}/M_{Z'} = 0.01$. Limits for wider resonances are available. See their Fig.6 for limits on $\sigma \cdot B$.
- 28 SIRUNYAN 17R search for resonances decaying to HZ in pp collisions at $\sqrt{s} = 13$ TeV. The quoted limit is for heavy-vector-triplet Z' with $g_V = 3$. Mass regions $M_{Z'} < 1150$ GeV and 1250 GeV $< M_{Z'} < 1670$ GeV are excluded for $g_V = 1$. If we assume $M_{Z'} = M_{W'}$, the excluded mass regions are $1000 < M_{Z'} < 2500$ GeV and $2760 < M_{Z'} < 3300$ GeV for $g_V = 3$; $1000 < M_{Z'} < 2430$ GeV and $2810 < M_{Z'} < 3130$ GeV for $g_V = 1$. See their Fig.5 for limits on $\sigma \cdot B$.
- 29 AAD 23BF search for a Dark Matter (DM) simplified Z' produced in association with W in pp collisions at $\sqrt{s} = 13$ TeV. See their Fig. 9(c) for limits on $\sigma \cdot B$ as a function of $M_{Z'}$.
- 30 AAD 23W set limits on a dark Higgs model with a spin-1 mediator Z' and a dark Higgs s . Dark Higgs s is assumed to decay into WW . See their Fig. 9 for limits in $M_{Z'} - M_s$ plane.
- 31 AAD 23X set limits on $L_\mu - L_\tau$ of Z' using four-muon final states in pp collisions at $\sqrt{s} = 13$ TeV. See their Fig. 7 for limits in mass-coupling plane.
- 32 ADACHI 23B search for Z' produced in association with $\mu^+\mu^-$ and decaying invisibly in e^+e^- collisions at $\sqrt{s} = 10.58$ GeV. See their Fig. 3 and Fig. 4 for limits in mass-coupling plane.
- 33 ADACHI 23F search for resonances decaying to $\tau^+\tau^-$ in $\mu^+\mu^-\tau^+\tau^-$ events in e^+e^- collisions at $\sqrt{s} = 10.58$ GeV. See their Fig. 3 for limits on $\sigma \cdot B$.
- 34 HAYRAPETYAN 23D search for $\mu^+\mu^-$ resonance produced in association with one or more b -jets in pp collisions at $\sqrt{s} = 13$ TeV. See their Fig. 8 for limits in the mass-coupling plane of the $B_3 - L_2$ Z' model.
- 35 HAYRAPETYAN 23G search for spin-0 and spin-1 resonances decaying to $\mu^+\mu^-$ in pp collisions at $\sqrt{s} = 13$ TeV in the mass ranges of 1.1–2.6 GeV and 4.2–7.9 GeV. See their Fig. 5 for limits on $\sigma \cdot B$.
- 36 Li 23I limits on light Z' couplings are derived from the steller cooling bounds in the mass range of $10^4 - 10^6$ eV. See their Fig. 4 for limits on dark photon, $B-L$, $L_\mu - L_\tau$, and $L_e - L_\mu(\tau)$ models.
- 37 MANZARI 23 study supernova cooling induced by the emission of light dark fermions χ assumed to couple with leptons via a new massive vector boson Z' . See their Figs. 4 and 5 for limits in mass-coupling plane.
- 38 AAD 22 search for $b\bar{b}Z'$ productions in pp collisions at $\sqrt{s} = 13$ TeV. Z' is assumed to decay into $b\bar{b}$. See their Fig.4 for limits on $\sigma \cdot B$.
- 39 AAD 22b search for DM mediator Z' produced in association with a Z boson in pp collisions at $\sqrt{s} = 13$ TeV. Z' is assumed to decay invisibly $Z' \rightarrow \chi\chi$. See their Fig. 4 for limits in $M_{Z'} - M_\chi$ plane.
- 40 ANDREEV 22 search for missing energy in CERN NA64-e experiment. See their Fig. 7 for limits on couplings of $U(1)$ gauge $L_\mu - L_\tau$ Z' models, in the mass range of 1 MeV $< M_{Z'} < 600$ MeV with the kinetic $Z' - \gamma$ mixing being determined by μ and τ loops.
- 41 BONET 22 obtain limits on Z' coupling from ν -nucleus scattering data collected by the CONUS experiment at the nuclear power plant in Brokkdorf. See their Fig. 5 for limits in mass-coupling plane.
- 42 COLOMA 22 set limits on Z' coupling from ν -nucleus and ν -e scattering data collected by a Ge detector at the Dresden-II power reactor and the COHERENT experiment. See their Fig. 6 for limits in mass-coupling plane in the mass range of 1 keV $< M_{Z'} < 5$ GeV.
- 43 COLOMA 22A use Borexino Phase-II spectral data to constrain Z' couplings. See their Fig. 7 for limits in mass-coupling plane in the mass range of 10 keV $< M_{Z'} < 100$ MeV.
- 44 CZANK 22 search for Z' produced in association with $\mu^+\mu^-$ in e^+e^- collisions at and near T resonances. Z' is assumed to decay into $\mu^+\mu^-$. See their Fig. 8 for limits on Z' $\mu\mu$ couplings.
- 45 TUMASYAN 22AA search for Z' production in pp collisions at $\sqrt{s} = 13$ TeV. Z' is assumed to decay into two "semivisible" jets (SVJ), i.e., collimated mixtures of visible and invisible particles. See their Fig. 7 and 8 for limits on $\sigma \cdot B$.
- 46 AAD 21AQ limits are for a $B - L$ gauge boson model derived from their measurements on four-lepton differential cross sections. See their Fig. 13 for exclusion limits on the $B - L$ breaking Higgs boson mass.
- 47 AAD 21AZ search for DM mediator Z' produced in association with a SM Higgs boson in pp collisions at $\sqrt{s} = 13$ TeV. Z' is assumed to decay invisibly $Z' \rightarrow \chi\chi$. See their Fig. 7 for limits in $M_{Z'} - M_\chi$ plane.
- 48 AAD 21BB search for Z' productions in pp collisions at $\sqrt{s} = 13$ TeV. Z' is assumed to decay into a SM Higgs boson H and an invisible particle A . See their Fig.7 for limits in $M_{Z'} - M_A$ plane.
- 49 AAD 21D set limits on a dark Higgs model with a spin-1 mediator Z' and a scalar dark Higgs boson s . Dark Higgs s is assumed to decay into WW or ZZ . See their Fig.4 for limits in $M_{Z'} - M_s$ plane.
- 50 AAD 21K search for $\gamma + \cancel{E}_T$ events in pp collision at $\sqrt{s} = 13$ TeV. See their Fig. 5 for limits on Z' particle invisibly decaying to $\chi\chi$.
- 51 BURAS 21 performed global fit to leptophilic Z' models using a large number of observables.
- 52 CADEDDU 21 obtain limits on Z' coupling $g_{Z'}$ from coherent ν -nucleus scattering data collected by COHERENT experiment. For limits in the $M_{Z'} - g_{Z'}$ plane, see their Figures 3 and 4 for the universal Z' model and Figures 5 and 6 for the $B - L$ model.
- 53 COLARESI 21 obtain limits on Z' coupling from coherent ν -nucleus scattering data collected by a Ge detector at the Dresden-II power reactor. See their Fig.7 for limits in mass-coupling plane.
- 54 KRIBS 21 set decay-agnostic limits on kinetic mixing parameter between $U(1)_Y$ field and new heavy abelian vector boson (dark photon) field using the HERA ep collision data. See their Fig. 3 for limits in mass-mixing plane.
- 55 TUMASYAN 21D search for energetic jets + \cancel{E}_T events in pp collisions at $\sqrt{s} = 13$ TeV. Z' is assumed to decay into a pair of invisible particles $\chi\chi$. See their Fig. 7 for limits on signal strength in $M_{Z'} - M_\chi$ plane, and Fig. 8 for limits on signal strength in quark and dark matter coupling vs mediator mass.
- 56 AAD 20AF search for resonances decaying to $H\gamma$ in pp collisions at $\sqrt{s} = 13$ TeV. See their Fig. 1c for limits on $\sigma \cdot B$ for the mass range $0.7 < m_{Z'} < 4$ TeV.
- 57 AAD 20T search for Dark Matter mediator Z' decaying invisibly or decaying to $q\bar{q}$ in pp collisions at $\sqrt{s} = 13$ TeV. See their Fig. 5 for limits in $M_{Z'} - g_q$ plane from the inclusive category. See their Fig. 7(a) for limits on the product of the cross section, acceptance, b -tagging efficiency, and branching fraction from the 2 b -tag category.
- 58 AAD 20W search for a Dark Matter (DM) simplified model Z' produced in association with W in pp collisions at $\sqrt{s} = 13$ TeV. See their Fig. 5 for limits on Z' production cross section.
- 59 AAIJ 20AL search for spin-0 and spin-1 resonances decaying to $\mu^+\mu^-$ in pp collisions at $\sqrt{s} = 13$ TeV in the mass regions $M_{Z'} < 60$ GeV, with non-negligible widths considered above 20 GeV. See their Figs. 7, 8, and 9 for limits on $\sigma \cdot B$.
- 60 ADACHI 20 search for production of Z' in e^+e^- collisions. The Z' is assumed to decay invisibly. See their Fig. 3 and Fig. 5 for limits on Z' coupling and $\sigma(e^+e^- \rightarrow e^+\mu^-\bar{\nu}Z')$.
- 61 SIRUNYAN 20AI search for broad resonances decaying into dijets in pp collisions at $\sqrt{s} = 13$ TeV. See their Fig. 11 for exclusion limits in mass-coupling plane.
- 62 SIRUNYAN 20AQ search for a narrow resonance lighter than 200 GeV decaying to $\mu^+\mu^-$ in pp collisions at $\sqrt{s} = 13$ TeV. See their Fig. 3 for limits on Z' kinetic mixing coefficient.
- 63 SIRUNYAN 20M search for a narrow resonance with a mass between 350 and 700 GeV in pp collisions at $\sqrt{s} = 13$ TeV. See their Fig.3 for exclusion limits in mass-coupling plane.
- 64 AABOUD 19AJ search in pp collisions at $\sqrt{s} = 13$ TeV for a new resonance decaying to $q\bar{q}$ and produced in association with a high p_T photon. For a leptophobic axial-vector Z' in the mass region 250 GeV $< M_{Z'} < 950$ GeV, the Z' coupling with quarks g_q is constrained below 0.18. See their Fig.2 for limits in $M_{Z'} - g_q$ plane.
- 65 AABOUD 19D search in pp collisions at $\sqrt{s} = 13$ TeV for a new resonance decaying to $q\bar{q}$ and produced in association with a high- p_T photon or jet. For a leptophobic axial-vector Z' in the mass region 100 GeV $< M_{Z'} < 220$ GeV, the Z' coupling with quarks g_q is constrained below 0.23. See their Fig. 6 for limits in $M_{Z'} - g_q$ plane.
- 66 AABOUD 19V search for Dark Matter simplified Z' decaying invisibly or decaying to fermion pair in pp collisions at $\sqrt{s} = 13$ TeV.

Gauge & Higgs Boson Particle Listings

New Heavy Bosons

- 67 AAD 19L search for resonances decaying to $\ell^+ \ell^-$ in pp collisions at $\sqrt{s} = 13$ TeV. See their Fig. 4 for limits in the heavy vector triplet model couplings.
- 68 LONG 19 uses the weak charge data of Cesium and proton to constrain mass of Z' in the 3-3-1 models.
- 69 PANDEY 19 obtain limits on Z' induced neutrino non-standard interaction (NSI) parameter ϵ from LHC and IceCube data. See their Fig.2 for limits in $M_{Z'} - \epsilon$ plane, where $\epsilon = g_q g_\nu v^2 / (2 M_{Z'}^2)$.
- 70 SIRUNYAN 19AL search for a new resonance decaying to a top quark and a heavy vector-like top partner in pp collisions at $\sqrt{s} = 13$ TeV. See their Fig. 8 for limits on Z' production cross section.
- 71 SIRUNYAN 19AN search for a Dark Matter (DM) simplified model Z' decaying to HD DM in pp collisions at $\sqrt{s} = 13$ TeV. See their Fig. 7 for limits on the signal strength modifiers.
- 72 SIRUNYAN 19CB search in pp collisions at $\sqrt{s} = 13$ TeV for a new resonance decaying to $q\bar{q}$. For a leptophobic Z' in the mass region 50–300 GeV, the Z' coupling with quarks g'_q is constrained below 0.2. See their Figs. 4 and 5 for limits on g'_q in the mass range $50 < M_{Z'} < 450$ GeV.
- 73 SIRUNYAN 19CD search in pp collisions at $\sqrt{s}=13$ TeV for a leptophobic Z' produced in association of high p_T ISR photon and decaying to $q\bar{q}$. See their Fig. 2 for limits on the Z' coupling strength g'_q to $q\bar{q}$ in the mass range between 10 and 125 GeV.
- 74 SIRUNYAN 19D search for a narrow neutral vector resonance decaying to $H\gamma$. See their Fig. 3 for exclusion limit in $M_{Z'} - \sigma_B$ plane. Upper limits on the production of $H\gamma$ resonances are set as a function of the resonance mass in the range of 720–3250 GeV.
- 75 AABOUD 18AA search for a narrow neutral vector boson decaying to $H\gamma$. See their Fig. 10 for the exclusion limit in $M_{Z'} - \sigma_B$ plane.
- 76 AABOUD 18CJ search for heavy-vector-triplet Z' in pp collisions at $\sqrt{s} = 13$ TeV. The limit quoted above is for model with $g_V = 3$ assuming $M_{Z'} = M_{W'}$. The limit becomes $M_{Z'} > 5500$ GeV for model with $g_V = 1$.
- 77 AABOUD 18N search for a narrow resonance decaying to $q\bar{q}$ in pp collisions at $\sqrt{s} = 13$ TeV using trigger level analysis to improve the low mass region sensitivity. See their Fig. 5 for limits in the mass-coupling plane in the Z' mass range 450–1800 GeV.
- 78 AAIJ 18AQ search for spin-0 and spin-1 resonances decaying to $\mu^+ \mu^-$ in pp collisions at $\sqrt{s} = 7$ and 8 TeV in the mass region near 10 GeV. See their Figs. 4 and 5 for limits on σ_B .
- 79 SIRUNYAN 18DR searches for $\mu^+ \mu^-$ resonances produced in association with b -jets in the pp collision data with $\sqrt{s} = 8$ TeV and 13 TeV. An excess of events near $m_{\mu\mu} = 28$ GeV is observed in the 8 TeV data. See their Fig. 3 for the measured fiducial signal cross sections at $\sqrt{s} = 8$ TeV and the 95% CL upper limits at $\sqrt{s} = 13$ TeV.
- 80 SIRUNYAN 18G search for a new resonance decaying to dijets in pp collisions at $\sqrt{s} = 13$ TeV in the mass range 50–300 GeV. See their Fig.7 for limits in the mass-coupling plane.
- 81 SIRUNYAN 18I search for a narrow resonance decaying to $b\bar{b}$ in pp collisions at $\sqrt{s} = 8$ TeV using dedicated b -tagged dijet triggers to improve the sensitivity in the low mass region. See their Fig. 3 for limits on $\sigma \cdot B$ in the Z' mass range 325–1200 GeV.
- 82 AABOUD 17B search for resonances decaying to HZ ($H \rightarrow b\bar{b}, c\bar{c}, Z \rightarrow \ell^+ \ell^-, \nu\bar{\nu}$) in pp collisions at $\sqrt{s} = 13$ TeV. The quoted limit is for heavy-vector-triplet Z' with $g_V = 3$. The limit becomes $M_{Z'} > 1490$ GeV for $g_V = 1$. If we assume $M_{Z'} = M_{W'}$, the limit increases $M_{Z'} > 2310$ GeV and $M_{Z'} > 1730$ GeV for $g_V = 3$ and $g_V = 1$, respectively. See their Fig.3 for limits on $\sigma \cdot B$.
- 83 KHACHATRYAN 17AX search for lepto-phobic resonances decaying to four leptons in pp collisions at $\sqrt{s} = 8$ TeV.
- 84 KHACHATRYAN 17U search for resonances decaying to HZ ($H \rightarrow b\bar{b}, Z \rightarrow \ell^+ \ell^-, \nu\bar{\nu}$) in pp collisions at $\sqrt{s} = 13$ TeV. The limit on the heavy-vector-triplet model is $M_{Z'} = M_{W'} > 2$ TeV for $g_V = 3$, in which constraints from the $W' \rightarrow HW$ ($H \rightarrow b\bar{b}, W \rightarrow \ell\nu$) are combined. See their Fig.3 and Fig.4 for limits on $\sigma \cdot B$.
- 85 SIRUNYAN 17A search for resonances decaying to WW with $WW \rightarrow \ell\nu q\bar{q}, q\bar{q}q\bar{q}$ in pp collisions at $\sqrt{s} = 13$ TeV. The quoted limit is for heavy-vector-triplet Z' with $g_V = 3$. The limit becomes $M_{Z'} > 1600$ GeV for $g_V = 1$. If we assume $M_{Z'} = M_{W'}$, the limit increases $M_{Z'} > 2400$ GeV and $M_{Z'} > 2300$ GeV for $g_V = 3$ and $g_V = 1$, respectively. See their Fig.6 for limits on $\sigma \cdot B$.
- 86 SIRUNYAN 17AP search for resonances decaying into a SM-like Higgs scalar H and a light pseudo scalar A . A is assumed to decay invisibly. See their Fig.9 for limits on $\sigma \cdot B$.
- 87 SIRUNYAN 17T search for a new resonance decaying to dijets in pp collisions at $\sqrt{s} = 13$ TeV in the mass range 100–300 GeV. See their Fig.3 for limits in the mass-coupling plane.
- 88 SIRUNYAN 17V search for a new resonance decaying to a top quark and a heavy vector-like top partner T in pp collisions at $\sqrt{s} = 13$ TeV. See their table 5 for limits on the Z' production cross section for various values of $M_{Z'}$ and M_T in the range of $M_{Z'} = 1500$ –2500 GeV and $M_T = 700$ –1500 GeV.
- 89 AABOUD 16 search for a narrow resonance decaying into $b\bar{b}$ in pp collisions at $\sqrt{s} = 13$ TeV. The limit quoted above is for a leptophobic Z' with SM-like couplings to quarks. See their Fig.6 for limits on $\sigma \cdot B$.
- 90 AAD 16L search for $Z' \rightarrow a\gamma, a \rightarrow \gamma\gamma$ in pp collisions at $\sqrt{s} = 8$ TeV. See their Table 6 for limits on $\sigma \cdot B$.
- 91 AAD 16S search for a new resonance decaying to dijets in pp collisions at $\sqrt{s} = 13$ TeV. The limit quoted above is for a leptophobic Z' having coupling strength with quark $g_q = 0.3$ and is taken from their Figure 3.
- 92 KHACHATRYAN 16AP search for a resonance decaying to HZ in pp collisions at $\sqrt{s} = 8$ TeV. Both H and Z are assumed to decay to fat jets. The quoted limit is for heavy-vector-triplet Z' with $g_V = 3$.
- 93 KHACHATRYAN 16E search for a leptophobic top-color Z' decaying to $t\bar{t}$ using pp collisions at $\sqrt{s} = 8$ TeV. The quoted limit assumes that $\Gamma_{Z'}/m_{Z'} = 0.012$. Also $m_{Z'} < 2.9$ TeV is excluded for wider topcolor Z' with $\Gamma_{Z'}/m_{Z'} = 0.1$.
- 94 AAD 15AO search for narrow resonance decaying to $t\bar{t}$ using pp collisions at $\sqrt{s} = 8$ TeV. See Fig. 11 for limit on σ_B .
- 95 AAD 15AT search for monotop production plus large missing E_T events in pp collisions at $\sqrt{s} = 8$ TeV and give constraints on a Z' model having $Z' u\bar{t}$ coupling. Z' is assumed to decay invisibly. See their Fig. 6 for limits on $\sigma \cdot B$.
- 96 AAD 15CD search for decays of Higgs bosons to 4 ℓ states via Z' bosons, $H \rightarrow ZZ' \rightarrow 4\ell$ or $H \rightarrow Z'Z' \rightarrow 4\ell$. See Fig. 5 for the limit on the signal strength of the $H \rightarrow Z'Z' \rightarrow 4\ell$ process and Fig. 16 for the limit on $H \rightarrow Z'Z' \rightarrow 4\ell$.
- 97 KHACHATRYAN 15F search for monotop production plus large missing E_T events in pp collisions at $\sqrt{s} = 8$ TeV and give constraints on a Z' model having $Z' u\bar{t}$ coupling. Z' is assumed to decay invisibly. See Fig. 3 for limits on σ_B .
- 98 KHACHATRYAN 15O search for narrow Z' resonance decaying to ZH in pp collisions at $\sqrt{s} = 8$ TeV. See their Fig. 6 for limit on σ_B .
- 99 AAD 14AT search for a narrow neutral vector boson decaying to $Z\gamma$. See their Fig. 3b for the exclusion limit in $m_{Z'} - \sigma_B$ plane.
- 100 KHACHATRYAN 14A search for new resonance in the WW ($\ell\nu q\bar{q}$) and the ZZ ($\ell\ell q\bar{q}$) channels using pp collisions at $\sqrt{s}=8$ TeV. See their Fig.13 for the exclusion limit on the number of events in the mass-width plane.
- 101 MARTINEZ 14 use various electroweak data to constrain the Z' boson in the 3-3-1 models.
- 102 AAD 13AQ search for a leptophobic top-color Z' decaying to $t\bar{t}$. The quoted limit assumes that $\Gamma_{Z'}/m_{Z'} = 0.012$.
- 103 CHATRCHYAN 13BM search for top-color Z' decaying to $t\bar{t}$ using pp collisions at $\sqrt{s}=8$ TeV. The quoted limit is for $\Gamma_{Z'}/m_{Z'} = 0.012$.
- 104 CHATRCHYAN 13AP search for top-color leptophobic Z' decaying to $t\bar{t}$ using pp collisions at $\sqrt{s}=7$ TeV. The quoted limit is for $\Gamma_{Z'}/m_{Z'} = 0.012$.
- 105 AAD 12BV search for narrow resonance decaying to $t\bar{t}$ using pp collisions at $\sqrt{s}=7$ TeV. See their Fig. 7 for limit on $\sigma \cdot B$.
- 106 AAD 12K search for narrow resonance decaying to $t\bar{t}$ using pp collisions at $\sqrt{s}=7$ TeV. See their Fig. 5 for limit on $\sigma \cdot B$.
- 107 AALTONEN 12AR search for chromophilic Z' in $p\bar{p}$ collisions at $\sqrt{s} = 1.96$ TeV. See their Fig. 5 for limit on $\sigma \cdot B$.
- 108 AALTONEN 12N search for $p\bar{p} \rightarrow tZ', Z' \rightarrow T\bar{u}$ events in $p\bar{p}$ collisions. See their Fig. 3 for the limit on $\sigma \cdot B$.
- 109 ABAZOV 12R search for top-color Z' boson decaying exclusively to $t\bar{t}$. The quoted limit is for $\Gamma_{Z'}/m_{Z'} = 0.012$.
- 110 CHATRCHYAN 12A search for $pp \rightarrow t\bar{t}$ events and give constraints on a Z' model having $Z' t\bar{t}$ coupling. See their Fig. 4 for the limit in mass-coupling plane.
- 111 Search for resonance decaying to $t\bar{t}$. See their Fig. 6 for limit on $\sigma \cdot B$.
- 112 Search for narrow resonance decaying to $t\bar{t}$. See their Fig. 4 for limit on $\sigma \cdot B$.
- 113 Search for narrow resonance decaying to $t\bar{t}$. See their Fig. 3 for limit on $\sigma \cdot B$.
- 114 CHATRCHYAN 11O search for same-sign top production in pp collisions induced by a hypothetical FCNC Z' at $\sqrt{s} = 7$ TeV. See their Fig. 3 for limit in mass-coupling plane.
- 115 Search for narrow resonance decaying to $t\bar{t}$. See their Fig. 3 for limit on $\sigma \cdot B$.
- 116 Search for narrow resonance decaying to $t\bar{t}$. See their Fig. 2 for limit on $\sigma \cdot B$.
- 117 BARGER 03b use the nucleosynthesis bound on the effective number of light neutrino δN_{ν} . See their Figs.4–5 for limits in general E_6 motivated models.
- 118 CHO 00 use various electroweak data to constrain Z' models assuming $m_H=100$ GeV. See Fig. 2 for limits in general E_6 -motivated models.
- 119 CHO 98 study constraints on four-Fermi contact interactions obtained from low-energy electroweak experiments, assuming no Z - Z' mixing.
- 120 Search for Z' decaying to dijets at $\sqrt{s}=1.8$ TeV. For Z' with electromagnetic strength coupling, no bound is obtained.

Searches for Z' with Lepton-Flavor-Violating decays

The following limits are obtained from $p\bar{p}$ or $pp \rightarrow Z' X$ with Z' decaying to the mode indicated in the comments.

VALUE	DOCUMENT ID	TECN	COMMENT
• • •	We do not use the following data for averages, fits, limits, etc. • • •		
1	CABARCAS 24 RVUE	$Z' \rightarrow \mu\tau$	
2	AAD 23CB ATLS	$Z' \rightarrow e\mu, e\tau, \mu\tau$	
3	TUMASYAN 23H CMS	$Z' \rightarrow e\mu, e\tau, \mu\tau$	
4	AABOUD 18CM ATLS	$Z' \rightarrow e\mu, e\tau, \mu\tau$	
5	SIRUNYAN 18AT CMS	$Z' \rightarrow e\mu$	
6	AABOUD 16P ATLS	$Z' \rightarrow e\mu, e\tau, \mu\tau$	
7	KHACHATRYAN 16BE CMS	$Z' \rightarrow e\mu$	
8	AAD 15O ATLS	$Z' \rightarrow e\mu, e\tau, \mu\tau$	
9	AAD 11H ATLS	$Z' \rightarrow e\mu$	
10	AAD 11Z ATLS	$Z' \rightarrow e\mu$	
11	ABULENCIA 06M CDF	$Z' \rightarrow e\mu$	

- 1 CABARCAS 24 use constraints on the non-standard neutrino interactions reported by ANTARES and IceCube experiments to constrain Z' models with $\mu\tau$ coupling. See their Figs. 1 and 2 for limits in mass-coupling plane.
- 2 AAD 23CB search for a new particle with lepton-flavor violating decay in pp collisions at $\sqrt{s} = 13$ TeV. See their Figs.4, 5, and 6 for limits on $\sigma \cdot B$.
- 3 TUMASYAN 23H search for a new particle with lepton-flavor violating decay in pp collisions at $\sqrt{s} = 13$ TeV. See their Fig. 4 for limits on $\sigma \cdot B$.
- 4 AABOUD 18CM search for a new particle with lepton-flavor violating decay in pp collisions at $\sqrt{s} = 13$ TeV. See their Figs. 4, 5, and 6 for limits on $\sigma \cdot B$.
- 5 SIRUNYAN 18AT search for a narrow resonance Z' decaying into $e\mu$ in pp collisions at $\sqrt{s} = 13$ TeV. See their Fig.5 for limit on $\sigma \cdot B$ in the range of $600 \text{ GeV} < M_{Z'} < 5000$ GeV.
- 6 AABOUD 16P search for new particle with lepton flavor violating decay in pp collisions at $\sqrt{s} = 13$ TeV. See their Figs.2, 3, and 4 for limits on $\sigma \cdot B$.
- 7 KHACHATRYAN 16BE search for new particle Z' with lepton flavor violating decay in pp collisions at $\sqrt{s} = 8$ TeV in the range of $200 \text{ GeV} < M_{Z'} < 2000$ GeV. See their Fig.4 for limits on $\sigma \cdot B$ and their Table 5 for bounds on various masses.
- 8 AAD 15O search for new particle Z' with lepton flavor violating decay in pp collisions at $\sqrt{s} = 8$ TeV in the range of $500 \text{ GeV} < M_{Z'} < 3000$ GeV. See their Fig. 2 for limits on $\sigma \cdot B$.
- 9 AAD 11H search for new particle Z' with lepton flavor violating decay in pp collisions at $\sqrt{s} = 7$ TeV in the range of $700 \text{ GeV} < M_{Z'} < 1000$ GeV. See their Fig. 3 for limits on $\sigma \cdot B$.

See key on page 1171

Gauge & Higgs Boson Particle Listings

New Heavy Bosons

- ¹⁰AAD 11z search for new particle Z' with lepton flavor violating decay in pp collisions at $\sqrt{s} = 7$ TeV in the range $700 \text{ GeV} < M_{Z'} < 2000 \text{ GeV}$. See their Fig. 3 for limits on $\sigma \cdot B$.
- ¹¹ABULENCIA 06M search for new particle Z' with lepton flavor violating decay in $p\bar{p}$ collisions at $\sqrt{s} = 1.96$ TeV in the range of $100 \text{ GeV} < M_{Z'} < 800 \text{ GeV}$. See their Fig. 4 for limits in the mass-coupling plane.

Indirect Constraints on Kaluza-Klein Gauge Bosons

Bounds on a Kaluza-Klein excitation of the Z boson or photon in $d=1$ extra dimension. These bounds can also be interpreted as a lower bound on $1/R$, the size of the extra dimension. Unless otherwise stated, bounds assume all fermions live on a single brane and all gauge fields occupy the $4+d$ -dimensional bulk. See also the section on "Extra Dimensions" in the "Searches" Listings in this Review.

VALUE (TeV)	CL%	DOCUMENT ID	TECN	COMMENT
> 4.7		1 MUECK 02	RVUE	Electroweak
> 3.3	95	2 CORNET 00	RVUE	$e\nu q q'$
>5000		3 DELGADO 00	RVUE	$e\kappa$
> 2.6	95	4 DELGADO 00	RVUE	Electroweak
> 3.3	95	5 RIZZO 00	RVUE	Electroweak
> 2.9	95	6 MARIANO 99	RVUE	Electroweak
> 2.5	95	7 MASIP 99	RVUE	Electroweak
> 1.6	90	8 NATH 99	RVUE	Electroweak
> 3.4	95	9 STRUMIA 99	RVUE	Electroweak

- • • We do not use the following data for averages, fits, limits, etc. • • •
- > 4.7
- > 3.3
- >5000
- > 2.6
- > 3.3
- > 2.9
- > 2.5
- > 1.6
- > 3.4
- ¹MUECK 02 limit is 2σ and is from global electroweak fit ignoring correlations among observables. Higgs is assumed to be confined on the brane and its mass is fixed. For scenarios of bulk Higgs, of brane-SU(2)_L, bulk-U(1)_Y, and of bulk-SU(2)_L, brane-U(1)_Y, the corresponding limits are $> 4.6 \text{ TeV}$, $> 4.3 \text{ TeV}$ and $> 3.0 \text{ TeV}$, respectively.
- ²Bound is derived from limits on $e\nu q q'$ contact interaction, using data from HERA and the Tevatron.
- ³Bound holds only if first two generations of quarks lives on separate branes. If quark mixing is not complex, then bound lowers to 400 TeV from Δm_{κ} .
- ⁴See Figs. 1 and 2 of DELGADO 00 for several model variations. Special boundary conditions can be found which permit KK states down to 950 GeV and that agree with the measurement of $Q_{WW}(Cs)$. Quoted bound assumes all Higgs bosons confined to brane; placing one Higgs doublet in the bulk lowers bound to 2.3 TeV.
- ⁵Bound is derived from global electroweak analysis assuming the Higgs field is trapped on the matter brane. If the Higgs propagates in the bulk, the bound increases to 3.8 TeV.
- ⁶Bound is derived from global electroweak analysis but considering only presence of the KK W bosons.
- ⁷Global electroweak analysis used to obtain bound independent of position of Higgs on brane or in bulk.
- ⁸Bounds from effect of KK states on G_F , α , M_W , and M_Z . Hard cutoff at string scale determined using gauge coupling unification. Limits for $d=2,3,4$ rise to 3.5, 5.7, and 7.8 TeV.
- ⁹Bound obtained for Higgs confined to the matter brane with $m_H=500 \text{ GeV}$. For Higgs in the bulk, the bound increases to 3.5 TeV.

See the related review(s): Leptoquarks

MASS LIMITS for Leptoquarks from Pair Production

These limits rely only on the color or electroweak charge of the leptoquark.

VALUE (GeV)	CL%	DOCUMENT ID	TECN	COMMENT
>1300	95	1 AAD 23BJ	ATLS	Scalar LQ. $B(c\tau) = 1$
>1460	95	2 AAD 23CF	ATLS	Scalar LQ. $B(b\tau) = 1$
>1910	95	3 AAD 23CF	ATLS	Vector LQ. $\kappa = 1, B(b\tau) = 1$
>1460	95	4 AAD 23F	ATLS	Scalar LQ. $B(t\nu)=B(b\mu)=0.5$
>1440	95	5 AAD 23F	ATLS	Scalar LQ. $B(t\nu)=B(b\epsilon)=0.5$
>1370	95	6 AAD 23F	ATLS	Scalar LQ. $B(t\mu)=B(b\nu)=0.5$
>1390	95	7 AAD 23F	ATLS	Scalar LQ. $B(t\epsilon)=B(b\nu)=0.5$
>1980	95	8 AAD 23F	ATLS	Vector LQ. $\kappa = 1, B(t\nu) = B(b\mu) = 0.5$
>1900	95	9 AAD 23F	ATLS	Vector LQ. $\kappa = 1, B(t\nu) = B(b\epsilon) = 0.5$
>1340	95	10 TUMASYAN 22H	CMS	Scalar LQ. $B(t\epsilon) = 1$
>1420	95	11 TUMASYAN 22H	CMS	Scalar LQ. $B(t\mu) = 1$
>1120	95	12 TUMASYAN 22H	CMS	Scalar LQ. $B(t\tau) = 1$
>1480	95	13 AAD 21AG	ATLS	Scalar LQ. $B(t\epsilon) = 1$
>1470	95	14 AAD 21AG	ATLS	Scalar LQ. $B(t\mu) = 1$
>1190	95	15 AAD 21AW	ATLS	Scalar LQ. $B(b\tau) = 1$
>1030	95	16 AAD 21AW	ATLS	Scalar LQ. $B(t\tau) = 1$
>1760	95	17 AAD 21AW	ATLS	Vector LQ. $\kappa = 1, B(b\tau) = 1$
>1260	95	18 AAD 21s	ATLS	Scalar LQ. $B(b\nu) = 1$
>1430	95	19 AAD 21T	ATLS	Scalar LQ. $B(t\tau) = 1$
> 950	95	20 SIRUNYAN 21J	CMS	Scalar LQ. $B(t\tau)=B(b\nu)=0.5$
>1650	95	21 SIRUNYAN 21J	CMS	Vector LQ. $\kappa=1, B(t\nu) = B(b\tau) = 0.5$
>1800	95	22 AAD 20AK	ATLS	Scalar LQ. $B(eq) = 1$
>1700	95	23 AAD 20AK	ATLS	Scalar LQ. $B(\mu q) = 1$
>1240	95	24 AAD 20s	ATLS	Scalar LQ. $B(t\nu) = 1$
>1185	95	25 SIRUNYAN 20A	CMS	Scalar LQ. $B(\nu b) = 1$
>1140	95	26 SIRUNYAN 20A	CMS	Scalar LQ. $B(\nu t) = 1$
>1140	95	27 SIRUNYAN 20A	CMS	Scalar LQ. $B(\nu q) = 1$ with $q = u, d, s, c$
>1925	95	28 SIRUNYAN 20A	CMS	Vector LQ. $\kappa = 1, B(\nu b) = 1$
>1825	95	29 SIRUNYAN 20A	CMS	Vector LQ. $\kappa = 1, B(\nu t) = 1$

>1980	95	30 SIRUNYAN 20A	CMS	Vector LQ. $\kappa = 1, B(\nu q) = 1$ with $q = u, d, s, c$
>1400	95	31 AABOUD 19AX	ATLS	Scalar LQ. $B(eq) = 1$
>1560	95	32 AABOUD 19AX	ATLS	Scalar LQ. $B(\mu q) = 1$
>1000	95	33 AABOUD 19X	ATLS	Scalar LQ. $B(t\nu) = 1$
>1030	95	34 AABOUD 19X	ATLS	Scalar LQ. $B(b\tau) = 1$
> 970	95	35 AABOUD 19X	ATLS	Scalar LQ. $B(b\nu) = 1$
> 920	95	36 AABOUD 19X	ATLS	Scalar LQ. $B(t\tau) = 1$
>1530	95	37 SIRUNYAN 19BI	CMS	Scalar LQ. $B(\mu q)+B(\nu q) = 1$
>1435	95	38 SIRUNYAN 19BJ	CMS	Scalar LQ. $B(eq)+B(\nu q) = 1$
>1020	95	39 SIRUNYAN 19Y	CMS	Scalar LQ. $B(\tau b) = 1$
none 300-900	95	40 SIRUNYAN 18CZ	CMS	Scalar LQ. $B(\tau t) = 1$
>1420	95	41 SIRUNYAN 18EC	CMS	Scalar LQ. $B(\mu t) = 1$
>1190	95	42 SIRUNYAN 18EC	CMS	Vector LQ. μ, τ, ν, b
>1100	95	43 SIRUNYAN 18U	CMS	Scalar LQ. $B(\nu b) = 1$
> 980	95	44 SIRUNYAN 18U	CMS	Scalar LQ. $B(\nu q) = 1$ with $q = u, d, s, c$
>1020	95	45 SIRUNYAN 18U	CMS	Scalar LQ. $B(\nu t) = 1$
>1810	95	46 SIRUNYAN 18U	CMS	Vector LQ. $\kappa=1, LQ \rightarrow b\nu$
>1790	95	47 SIRUNYAN 18U	CMS	Vector LQ. $\kappa=1, LQ \rightarrow q\nu$ with $q = u, d, s, c$
>1780	95	48 SIRUNYAN 18U	CMS	Vector LQ. $\kappa=1, LQ \rightarrow t\nu$
> 740	95	49 KHACHATRY..17J	CMS	Scalar LQ. $B(\tau b) = 1$
> 850	95	50 SIRUNYAN 17H	CMS	Scalar LQ. $B(\tau b) = 1$
>1050	95	51 AAD 16G	ATLS	Scalar LQ. $B(eq) = 1$
>1000	95	52 AAD 16G	ATLS	Scalar LQ. $B(\mu q) = 1$
> 625	95	53 AAD 16G	ATLS	Scalar LQ. $B(\nu b) = 1$
none 200-640	95	54 AAD 16G	ATLS	Scalar LQ. $B(\nu t) = 1$
>1010	95	55 KHACHATRY..16AF	CMS	Scalar LQ. $B(eq) = 1$
>1080	95	56 KHACHATRY..16AF	CMS	Scalar LQ. $B(\mu q) = 1$
> 685	95	57 KHACHATRY..15AJ	CMS	Scalar LQ. $B(\tau t) = 1$
> 740	95	58 KHACHATRY..14T	CMS	Scalar LQ. $B(\tau b) = 1$
• • • We do not use the following data for averages, fits, limits, etc. • • •				
> 534	95	59 SIRUNYAN 19bc	CMS	Scalar LQ ($\rightarrow \mu q$) LQ ($\rightarrow X + DM$)
> 525	95	60 AAD 13AE	ATLS	Third generation
> 660	95	61 CHATRCHYAN13M	CMS	Third generation
> 685	95	62 AAD 12H	ATLS	First generation
> 830	95	63 AAD 12o	ATLS	Second generation
> 840	95	64 CHATRCHYAN12AG	CMS	First generation
> 450	95	65 CHATRCHYAN12AG	CMS	Second generation
> 376	95	66 CHATRCHYAN12Bo	CMS	Third generation
> 422	95	67 AAD 11D	ATLS	Superseded by AAD 12H
> 326	95	68 AAD 11D	ATLS	Superseded by AAD 12O
> 339	95	69 ABAZOV 11V	D0	First generation
> 384	95	70 CHATRCHYAN11N	CMS	Superseded by CHATRCHYAN 12AG
> 394	95	71 KHACHATRY..11D	CMS	Superseded by CHATRCHYAN 12AG
> 247	95	72 KHACHATRY..11E	CMS	Superseded by CHATRCHYAN 12AG
> 316	95	73 ABAZOV 10L	D0	Third generation
> 299	95	74 ABAZOV 09D	D0	Second generation
> 153	95	75 ABAZOV 09AF	D0	Superseded by ABAZOV 11V
> 205	95	76 AALTONEN 08P	CDF	Third generation
> 210	95	77 AALTONEN 08Z	CDF	Third generation
> 229	95	78 ABAZOV 08AD	D0	All generations
> 251	95	79 ABAZOV 08AN	D0	Third generation
> 136	95	80 ABAZOV 07J	D0	Superseded by ABAZOV 10L
> 226	95	81 ABAZOV 06A	D0	Superseded by ABAZOV 09
> 256	95	82 ABAZOV 06L	D0	Superseded by ABAZOV 08AD
> 117	95	83 ABULENCIA 06T	CDF	Second generation
> 236	95	84 ABAZOV 05H	D0	First generation
> 99	95	85 ACOSTA 05I	CDF	First generation
> 100	95	86 ACOSTA 05P	CDF	First generation
> 98	95	87 ABBIENDI 03R	OPAL	First generation
> 98	95	88 ABBIENDI 03R	OPAL	Second generation
> 98	95	89 ABBIENDI 03R	OPAL	Third generation
> 85.8	95	90 ABAZOV 02D	D0	All generations
> 85.5	95	91 ABAZOV 01D	D0	First generation
> 82.7	95	92 ABBIENDI 00M	OPAL	Superseded by ABBIENDI 03R
> 200	95	93 ABBIENDI 00M	OPAL	Superseded by ABBIENDI 03R
> 123	95	94 ABBIENDI 00M	OPAL	Superseded by ABBIENDI 03R
> 148	95	95 ABBOTT 00C	D0	Second generation
> 160	95	96 AFFOLDER 00K	CDF	Second generation
> 225	95	97 AFFOLDER 00K	CDF	Second generation
> 94	95	98 ABBOTT 99J	D0	Third generation
> 202	95	99 ABBOTT 98D	D0	First generation
> 242	95	100 ABE 98S	CDF	Second generation
> 99	95	101 GROSS-PILCH.98	98	First generation
> 213	95	102 ABE 97F	CDF	Third generation
> 45.5	95	103 ABE 97X	CDF	First generation
> 44.4	95	104 ABREU 93J	DLPH	First + second generation
> 44.5	95	105 ADRIANI 93M	L3	First generation
> 45	95	106 ADRIANI 93M	L3	Second generation
none 8.9-22.6	95	107 DECAMP 92	ALEP	Third generation
none 10.2-23.2	95	108 KIM 90	AMY	First generation
	95	109 KIM 90	AMY	Second generation

Gauge & Higgs Boson Particle Listings

New Heavy Bosons

none 5–20.8 95 103 BARTEL 87B JADE
 none 7–20.5 95 104 BEHREND 86B CELL

- 1 AAD 23B search for scalar leptoquarks decaying to $c\tau$ in pp collisions at $\sqrt{s} = 13$ TeV. See their Fig. 8 for exclusion limit on σ as function of M_{LQ} .
- 2 AAD 23C search for scalar and vector leptoquarks decaying to $b\tau$. The limit quoted above is for scalar leptoquark. See their Fig. 9 for limits on leptoquark pair production cross sections.
- 3 AAD 23C search for scalar and vector leptoquarks decaying to $b\tau$. The limit quoted above is for vector leptoquark with $\kappa = 1$. The limit becomes $M_{LQ} > 1650$ for vector leptoquark with $\kappa = 0$. See their Fig. 9 for limits on leptoquark pair production cross sections.
- 4 AAD 23F search for scalar leptoquarks decaying to $t\nu$ and $b\mu$ in pp collisions at $\sqrt{s} = 13$ TeV. See their Fig. 9 for exclusion contour in $B(b\mu) - M_{LQ}$ plane.
- 5 AAD 23F search for scalar leptoquarks decaying to $t\nu$ and $b\mu$ in pp collisions at $\sqrt{s} = 13$ TeV. See their Fig. 9 for exclusion contour in $B(b\mu) - M_{LQ}$ plane.
- 6 AAD 23F search for scalar leptoquarks decaying to $t\mu$ and $b\nu$ in pp collisions at $\sqrt{s} = 13$ TeV. See their Fig. 9 for exclusion contour in $B(t\mu) - M_{LQ}$ plane.
- 7 AAD 23F search for scalar leptoquarks decaying to $t\mu$ and $b\nu$ in pp collisions at $\sqrt{s} = 13$ TeV. See their Fig. 9 for exclusion contour in $B(t\mu) - M_{LQ}$ plane.
- 8 AAD 23F search for $\kappa = 1$ (YM coupling) vector leptoquarks decaying to $t\nu$ and $b\mu$ in pp collisions at $\sqrt{s} = 13$ TeV. If $\kappa = 0$ (minimal coupling) is assumed, the limit becomes $M_{LQ} > 1710$ GeV. See their Fig. 10 for exclusion contour in $B(b\mu) - M_{LQ}$ plane.
- 9 AAD 23F search for $\kappa = 1$ (YM coupling) vector leptoquarks decaying to $t\nu$ and $b\mu$ in pp collisions at $\sqrt{s} = 13$ TeV. If $\kappa = 0$ (minimal coupling) is assumed, the limit becomes $M_{LQ} > 1620$ GeV. See their Fig. 10 for exclusion contour in $B(b\mu) - M_{LQ}$ plane.
- 10 TUMASYAN 22H search for scalar leptoquarks decaying to $t\tau$. See their Fig. 27 for exclusion limit on leptoquark pair production cross section as function of M_{LQ} .
- 11 TUMASYAN 22H search for scalar leptoquarks decaying to $t\mu$. See their Fig. 27 for exclusion limit on leptoquark pair production cross section as function of M_{LQ} .
- 12 TUMASYAN 22H search for scalar leptoquarks decaying to $t\tau$. See their Fig. 27 for exclusion limit on leptoquark pair production cross section as function of M_{LQ} .
- 13 AAD 21AG search for scalar leptoquarks decaying to $t\mu$. See their Fig. 6 for exclusion limit on $B(t\mu)$ as function of M_{LQ} .
- 14 AAD 21AG search for scalar leptoquarks decaying to $t\mu$. See their Fig. 6 for exclusion limit on $B(t\mu)$ as function of M_{LQ} .
- 15 AAD 21AW search for scalar leptoquarks decaying to $b\tau$. See their Fig. 9 for exclusion contour in $B(b\tau) - M_{LQ}$ plane.
- 16 AAD 21AW search for scalar leptoquarks decaying to $t\tau$. See their Fig. 9 for exclusion contour in $B(t\tau) - M_{LQ}$ plane.
- 17 AAD 21AW search for $\kappa = 1$ vector leptoquarks decaying to $b\tau$. See their Fig. 10 for exclusion contour in $B(b\tau) - M_{LQ}$ plane and for limit on $\kappa = 0$ vector leptoquarks.
- 18 AAD 21s search for scalar leptoquarks decaying to $b\nu$ in pp collisions at $\sqrt{s} = 13$ TeV. The limit above assumes $B(b\nu) = 1$. For $B(b\nu) = 0.05$, the limit becomes 400 GeV.
- 19 AAD 21t search for scalar leptoquarks decaying to $t\tau$ in pp collisions at $\sqrt{s} = 13$ TeV. The limit above assumes $B(t\tau) = 1$. For $B(t\tau) = 0.5$, the limit becomes 1220 GeV. See their Fig. 15b for limits on $B(t\tau)$ as a function of leptoquark mass.
- 20 SIRUNYAN 21J search for scalar leptoquarks decaying to $t\tau$ and $b\nu$ in pp collisions at $\sqrt{s} = 13$ TeV.
- 21 SIRUNYAN 21J search for vector leptoquarks decaying to $t\nu$ and $b\tau$ in pp collisions at $\sqrt{s} = 13$ TeV. The limit quoted above assumes $\kappa = 1$. If we assume $\kappa = 0$, the limit becomes $M_{LQ} > 1290$ GeV.
- 22 AAD 20AK search for scalar leptoquarks decaying to $eq, eb, ec, \mu q, \mu b, \mu c$. The quoted limit assumes $B(eq) = 1$. See their Fig. 9 for limits on $B(eq), B(eb), B(ec), B(\mu q), B(\mu b), B(\mu c)$ as a function of leptoquark mass.
- 23 AAD 20AK search for scalar leptoquarks decaying to $eq, eb, ec, \mu q, \mu b, \mu c$. The quoted limit assumes $B(\mu q) = 1$. See their Fig. 9 for limits on $B(eq), B(eb), B(ec), B(\mu q), B(\mu b), B(\mu c)$ as a function of leptoquark mass.
- 24 AAD 20s search for scalar leptoquarks decaying to $t\nu$ in pp collisions at $\sqrt{s} = 13$ TeV.
- 25 SIRUNYAN 20A search for scalar and vector leptoquarks decaying to $t\nu, b\nu$, and $q\nu$ ($q = u, d, s, c$). The limit quoted above assumes scalar leptoquark with $B(\nu b) = 1$.
- 26 SIRUNYAN 20A search for scalar and vector leptoquarks decaying to $t\nu, b\nu$, and $q\nu$ ($q = u, d, s, c$). The limit quoted above assumes scalar leptoquark with $B(\nu t) = 1$.
- 27 SIRUNYAN 20A search for scalar and vector leptoquarks decaying to $t\nu, b\nu$, and $q\nu$ ($q = u, d, s, c$). The limit quoted above assumes scalar leptoquark with $B(\nu q) = 1$.
- 28 SIRUNYAN 20A search for scalar and vector leptoquarks decaying to $t\nu, b\nu$, and $q\nu$ ($q = u, d, s, c$). The limit quoted above assumes vector leptoquark with $B(\nu b) = 1$ and $\kappa = 1$. If we assume $\kappa = 0$, the limit becomes $M_{LQ} > 1560$ GeV.
- 29 SIRUNYAN 20A search for scalar and vector leptoquarks decaying to $t\nu, b\nu$, and $q\nu$ ($q = u, d, s, c$). The limit quoted above assumes vector leptoquark with $B(\nu t) = 1$ and $\kappa = 1$. If we assume $\kappa = 0$, the limit becomes $M_{LQ} > 1475$ GeV.
- 30 SIRUNYAN 20A search for scalar and vector leptoquarks decaying to $t\nu, b\nu$, and $q\nu$ ($q = u, d, s, c$). The limit quoted above assumes vector leptoquark with $B(\nu q) = 1$ and $\kappa = 1$. If we assume $\kappa = 0$, the limit becomes $M_{LQ} > 1560$ GeV.
- 31 AABOUD 19AX search for leptoquarks using $eejj$ events in pp collisions at $\sqrt{s} = 13$ TeV. The limit above assumes $B(eq) = 1$.
- 32 AABOUD 19AX search for leptoquarks using $\mu\mu jj$ events in pp collisions at $\sqrt{s} = 13$ TeV. The limit above assumes $B(\mu q) = 1$.
- 33 AABOUD 19X search for scalar leptoquarks decaying to $t\nu$ in pp collisions at $\sqrt{s} = 13$ TeV.
- 34 AABOUD 19X search for scalar leptoquarks decaying to $b\tau$ in pp collisions at $\sqrt{s} = 13$ TeV.
- 35 AABOUD 19X search for scalar leptoquarks decaying to $b\nu$ in pp collisions at $\sqrt{s} = 13$ TeV.
- 36 AABOUD 19X search for scalar leptoquarks decaying to $t\tau$ in pp collisions at $\sqrt{s} = 13$ TeV.
- 37 SIRUNYAN 19B search for a pair of scalar leptoquarks decaying to $\mu\mu jj$ and $\nu\nu jj$ final states in pp collisions at $\sqrt{s} = 13$ TeV. Limits are shown as a function of β where β is the branching fraction to a muon and a quark. For $\beta = 1.0$ (0.5) LQ masses up to 1530 (1285) GeV are excluded. See Fig. 9 for exclusion limits in the plane of β and LQ mass.
- 38 SIRUNYAN 19B search for a pair of scalar leptoquarks decaying to $eejj$ and $\nu\nu jj$ final states in pp collisions at $\sqrt{s} = 13$ TeV. Limits are shown as a function of the branching fraction β to an electron and a quark. For $\beta = 1.0$ (0.5) LQ masses up to 1435 (1270) GeV are excluded. See Fig. 9 for exclusion limits in the plane of β and LQ mass.
- 39 SIRUNYAN 19Y search for a pair of third generation scalar leptoquarks, each decaying to τ and a jet. Assuming $B(\tau b) = 1$, leptoquark masses below 1.02 TeV are excluded.
- 40 SIRUNYAN 18CZ search for scalar leptoquarks decaying to τt in pp collisions at $\sqrt{s} = 13$ TeV. The limit above assumes $B(\tau t) = 1$.
- 41 SIRUNYAN 18EC set limits for scalar and vector leptoquarks decaying to $\mu t, \tau t$, and νb . The limit quoted above assumes scalar leptoquark with $B(\mu t) = 1$.
- 42 SIRUNYAN 18EC set limits for scalar and vector leptoquarks decaying to $\mu t, \tau t$, and νb . The limit quoted above assumes vector leptoquark with all possible combinations of branching fractions to $\mu t, \tau t$, and νb .
- 43 SIRUNYAN 18U set limits for scalar and vector leptoquarks decaying to $t\nu, b\nu$, and $q\nu$. The limit quoted above assumes scalar leptoquark with $B(b\nu) = 1$. Vector leptoquarks with $\kappa = 1$ are excluded below masses of 1810 GeV.
- 44 SIRUNYAN 18U set limits for scalar and vector leptoquarks decaying to $t\nu, b\nu$, and $q\nu$. The limit quoted above assumes scalar leptoquark with $B(q\nu) = 1$. Vector leptoquarks with $\kappa = 1$ are excluded below masses of 1790 GeV.
- 45 SIRUNYAN 18U set limits for scalar and vector leptoquarks decaying to $t\nu, b\nu$, and $q\nu$. The limit quoted above assumes scalar leptoquark with $B(\nu t) = 1$. Vector leptoquarks with $\kappa = 1$ are excluded below masses of 1780 GeV.
- 46 SIRUNYAN 18U set limits for scalar and vector leptoquarks decaying to $t\nu, b\nu$, and $q\nu$. $\kappa = 1$ and $LQ \rightarrow b\nu$ are assumed.
- 47 SIRUNYAN 18U set limits for scalar and vector leptoquarks decaying to $t\nu, b\nu$, and $q\nu$. $\kappa = 1$ and $LQ \rightarrow q\nu$ with $q = u, d, s, c$ are assumed.
- 48 SIRUNYAN 18U set limits for scalar and vector leptoquarks decaying to $t\nu, b\nu$, and $q\nu$. $\kappa = 1$ and $LQ \rightarrow t\nu$ are assumed.
- 49 KHACHATRYAN 17J search for scalar leptoquarks decaying to τb using pp collisions at $\sqrt{s} = 13$ TeV. The limit above assumes $B(\tau b) = 1$.
- 50 SIRUNYAN 17H search for scalar leptoquarks using $\tau\tau bb$ events in pp collisions at $\sqrt{s} = 8$ TeV. The limit above assumes $B(\tau b) = 1$.
- 51 AAD 16c search for scalar leptoquarks using $eejj$ events in collisions at $\sqrt{s} = 8$ TeV. The limit above assumes $B(eq) = 1$.
- 52 AAD 16c search for scalar leptoquarks using $\mu\mu jj$ events in collisions at $\sqrt{s} = 8$ TeV. The limit above assumes $B(\mu q) = 1$.
- 53 AAD 16c search for scalar leptoquarks decaying to $b\nu$. The limit above assumes $B(b\nu) = 1$.
- 54 AAD 16c search for scalar leptoquarks decaying to $t\nu$. The limit above assumes $B(t\nu) = 1$.
- 55 KHACHATRYAN 16AF search for scalar leptoquarks using $eejj$ and $\nu\nu jj$ events in pp collisions at $\sqrt{s} = 8$ TeV. The limit above assumes $B(eq) = 1$. For $B(eq) = 0.5$, the limit becomes 850 GeV.
- 56 KHACHATRYAN 16AF search for scalar leptoquarks using $\mu\mu jj$ and $\nu\nu jj$ events in pp collisions at $\sqrt{s} = 8$ TeV. The limit above assumes $B(\mu q) = 1$. For $B(\mu q) = 0.5$, the limit becomes 760 GeV.
- 57 KHACHATRYAN 15AJ search for scalar leptoquarks using $\tau\tau tt$ events in pp collisions at $\sqrt{s} = 8$ TeV. The limit above assumes $B(\tau t) = 1$.
- 58 KHACHATRYAN 14T search for scalar leptoquarks decaying to τb using pp collisions at $\sqrt{s} = 8$ TeV. The limit above assumes $B(\tau b) = 1$. See their Fig. 5 for the exclusion limit as function of $B(\tau b)$.
- 59 SIRUNYAN 19BC search for scalar leptoquark (LQ) pair production in pp collisions at $\sqrt{s} = 13$ TeV. One LQ is assumed to decay to μq , while the other decays to dark matter pair and SM particles. See their Fig. 4 for limits in $M_{LQ} - M_{DM}$ plane.
- 60 AAD 13AE search for scalar leptoquarks using $\tau\tau bb$ events in pp collisions at $E_{cm} = 7$ TeV. The limit above assumes $B(\tau b) = 1$.
- 61 CHATRCHYAN 13M search for scalar and vector leptoquarks decaying to τb in pp collisions at $E_{cm} = 7$ TeV. The limit above is for scalar leptoquarks with $B(\tau b) = 1$.
- 62 AAD 12H search for scalar leptoquarks using $eejj$ and $\nu\nu jj$ events in pp collisions at $E_{cm} = 7$ TeV. The limit above assumes $B(eq) = 1$. For $B(eq) = 0.5$, the limit becomes 607 GeV.
- 63 AAD 12o search for scalar leptoquarks using $\mu\mu jj$ and $\nu\nu jj$ events in pp collisions at $E_{cm} = 7$ TeV. The limit above assumes $B(\mu q) = 1$. For $B(\mu q) = 0.5$, the limit becomes 594 GeV.
- 64 CHATRCHYAN 12AG search for scalar leptoquarks using $eejj$ and $\nu\nu jj$ events in pp collisions at $E_{cm} = 7$ TeV. The limit above assumes $B(eq) = 1$. For $B(eq) = 0.5$, the limit becomes 640 GeV.
- 65 CHATRCHYAN 12AG search for scalar leptoquarks using $\mu\mu jj$ and $\nu\nu jj$ events in pp collisions at $E_{cm} = 7$ TeV. The limit above assumes $B(\mu q) = 1$. For $B(\mu q) = 0.5$, the limit becomes 650 GeV.
- 66 CHATRCHYAN 12Bo search for scalar leptoquarks decaying to νb in pp collisions at $\sqrt{s} = 7$ TeV. The limit above assumes $B(\nu b) = 1$.
- 67 AAD 11D search for scalar leptoquarks using $eejj$ and $\nu\nu jj$ events in pp collisions at $E_{cm} = 7$ TeV. The limit above assumes $B(eq) = 1$. For $B(eq) = 0.5$, the limit becomes 319 GeV.
- 68 AAD 11D search for scalar leptoquarks using $\mu\mu jj$ and $\nu\nu jj$ events in pp collisions at $E_{cm} = 7$ TeV. The limit above assumes $B(\mu q) = 1$. For $B(\mu q) = 0.5$, the limit becomes 362 GeV.
- 69 ABAZOV 11V search for scalar leptoquarks using $\nu\nu jj$ events in $p\bar{p}$ collisions at $E_{cm} = 1.96$ TeV. The limit above assumes $B(eq) = 0.5$.
- 70 CHATRCHYAN 11N search for scalar leptoquarks using $\nu\nu jj$ events in pp collisions at $E_{cm} = 7$ TeV. The limit above assumes $B(eq) = 0.5$.
- 71 KHACHATRYAN 11D search for scalar leptoquarks using $eejj$ events in pp collisions at $E_{cm} = 7$ TeV. The limit above assumes $B(eq) = 1$.
- 72 KHACHATRYAN 11E search for scalar leptoquarks using $\mu\mu jj$ events in pp collisions at $E_{cm} = 7$ TeV. The limit above assumes $B(\mu q) = 1$.
- 73 ABAZOV 10L search for pair productions of scalar leptoquark state decaying to νb in $p\bar{p}$ collisions at $E_{cm} = 1.96$ TeV. The limit above assumes $B(\nu b) = 1$.
- 74 ABAZOV 09 search for scalar leptoquarks using $\mu\mu jj$ and $\nu\nu jj$ events in $p\bar{p}$ collisions at $E_{cm} = 1.96$ TeV. The limit above assumes $B(\mu q) = 1$. For $B(\mu q) = 0.5$, the limit becomes 270 GeV.
- 75 ABAZOV 09AF search for scalar leptoquarks using $eejj$ and $\nu\nu jj$ events in $p\bar{p}$ collisions at $E_{cm} = 1.96$ TeV. The limit above assumes $B(eq) = 1$. For $B(eq) = 0.5$ the bound becomes 284 GeV.
- 76 AALTONEN 08P search for vector leptoquarks using $\tau^+ \tau^- b\bar{b}$ events in $p\bar{p}$ collisions at $E_{cm} = 1.96$ TeV. Assuming Yang-Mills (minimal) couplings, the mass limit is > 317 GeV (251 GeV) at 95% CL for $B(\tau b) = 1$.

- 77 Search for pair production of scalar leptoquark state decaying to τb in $p\bar{p}$ collisions at $E_{cm} = 1.96$ TeV. The limit above assumes $B(\tau b) = 1$.
- 78 Search for scalar leptoquarks using $\nu\nu jj$ events in $p\bar{p}$ collisions at $E_{cm} = 1.96$ TeV. The limit above assumes $B(\nu q) = 1$.
- 79 ABAZOV 07J search for pair productions of scalar leptoquark state decaying to νb in $p\bar{p}$ collisions at $E_{cm} = 1.96$ TeV. The limit above assumes $B(\nu b) = 1$.
- 80 ABAZOV 06A search for scalar leptoquarks using $\mu\mu jj$ events in $p\bar{p}$ collisions at $E_{cm} = 1.8$ TeV and 1.96 TeV. The limit above assumes $B(\mu q) = 1$. For $B(\mu q) = 0.5$, the limit becomes 204 GeV.
- 81 ABAZOV 06L search for scalar leptoquarks using $\nu\nu jj$ events in $p\bar{p}$ collisions at $E_{cm} = 1.8$ TeV and at 1.96 TeV. The limit above assumes $B(\nu q) = 1$.
- 82 ABULENCIA 06T search for scalar leptoquarks using $\mu\mu jj$, $\mu\nu jj$, and $\nu\nu jj$ events in $p\bar{p}$ collisions at $E_{cm} = 1.96$ TeV. The quoted limit assumes $B(\mu q) = 1$. For $B(\mu q) = 0.5$ or 0.1, the bound becomes 208 GeV or 143 GeV, respectively. See their Fig. 4 for the exclusion limit as a function of $B(\mu q)$.
- 83 ABAZOV 05H search for scalar leptoquarks using $eejj$ and $e\nu jj$ events in $p\bar{p}$ collisions at $E_{cm} = 1.8$ TeV and 1.96 TeV. The limit above assumes $B(eq) = 1$. For $B(eq) = 0.5$ the bound becomes 234 GeV.
- 84 ACOSTA 05P search for scalar leptoquarks using $eejj$, $e\nu jj$ events in $p\bar{p}$ collisions at $E_{cm} = 1.96$ TeV. The limit above assumes $B(eq) = 1$. For $B(eq) = 0.5$ and 0.1, the bound becomes 205 GeV and 145 GeV, respectively.
- 85 ABBIENDI 03R search for scalar/vector leptoquarks in e^+e^- collisions at $\sqrt{s} = 189$ –209 GeV. The quoted limits are for charge $-4/3$ isospin 0 scalar-leptoquark with $B(\ell q) = 1$. See their table 12 for other cases.
- 86 ABAZOV 02 search for scalar leptoquarks using $\nu\nu jj$ events in $p\bar{p}$ collisions at $E_{cm}=1.8$ TeV. The bound holds for all leptoquark generations. Vector leptoquarks are likewise constrained to lie above 200 GeV.
- 87 ABAZOV 01D search for scalar leptoquarks using $e\nu jj$, $eejj$, and $\nu\nu jj$ events in $p\bar{p}$ collisions at $E_{cm}=1.8$ TeV. The limit above assumes $B(eq)=1$. For $B(eq)=0.5$ and 0, the bound becomes 204 and 79 GeV, respectively. Bounds for vector leptoquarks are also given. Supersedes ABBOTT 98E.
- 88 ABBIENDI 00M search for scalar/vector leptoquarks in e^+e^- collisions at $\sqrt{s}=183$ GeV. The quoted limits are for charge $-4/3$ isospin 0 scalar-leptoquarks with $B(\ell q)=1$. See their Table 8 and Figs. 6–9 for other cases.
- 89 ABBOTT 00c search for scalar leptoquarks using $\mu\mu jj$, $\mu\nu jj$, and $\nu\nu jj$ events in $p\bar{p}$ collisions at $E_{cm}=1.8$ TeV. The limit above assumes $B(\mu q)=1$. For $B(\mu q)=0.5$ and 0, the bound becomes 180 and 79 GeV respectively. Bounds for vector leptoquarks are also given.
- 90 AFFOLDER 00k search for scalar leptoquark using $\nu\nu cc$ events in $p\bar{p}$ collisions at $E_{cm}=1.8$ TeV. The quoted limit assumes $B(\nu c)=1$. Bounds for vector leptoquarks are also given.
- 91 AFFOLDER 00k search for scalar leptoquark using $\nu\nu bb$ events in $p\bar{p}$ collisions at $E_{cm}=1.8$ TeV. The quoted limit assumes $B(\nu b)=1$. Bounds for vector leptoquarks are also given.
- 92 ABBOTT 99j search for leptoquarks using $\mu\nu jj$ events in $p\bar{p}$ collisions at $E_{cm}=1.8$ TeV. The quoted limit is for a scalar leptoquark with $B(\mu q) = B(\nu q) = 0.5$. Limits on vector leptoquarks range from 240 to 290 GeV.
- 93 ABBOTT 98E search for scalar leptoquarks using $e\nu jj$, $eejj$, and $\nu\nu jj$ events in $p\bar{p}$ collisions at $E_{cm}=1.8$ TeV. The limit above assumes $B(eq)=1$. For $B(eq)=0.5$ and 0, the bound becomes 204 and 79 GeV, respectively.
- 94 ABBOTT 98j search for charge $-1/3$ third generation scalar and vector leptoquarks in $p\bar{p}$ collisions at $E_{cm} = 1.8$ TeV. The quoted limit is for scalar leptoquark with $B(\nu b)=1$.
- 95 ABE 98s search for scalar leptoquarks using $\mu\mu jj$ events in $p\bar{p}$ collisions at $E_{cm}=1.8$ TeV. The limit is for $B(\mu q) = 1$. For $B(\mu q)=B(\nu q)=0.5$, the limit is > 160 GeV.
- 96 GROSS-PILCHER 98 is the combined limit of the CDF and DØ Collaborations as determined by a joint CDF/DØ working group and reported in this FNAL Technical Memo. Original data published in ABE 97x and ABBOTT 98E.
- 97 ABE 97f search for third generation scalar and vector leptoquarks in $p\bar{p}$ collisions at $E_{cm} = 1.8$ TeV. The quoted limit is for scalar leptoquark with $B(\tau b) = 1$.
- 98 ABE 97x search for scalar leptoquarks using $eejj$ events in $p\bar{p}$ collisions at $E_{cm}=1.8$ TeV. The limit is for $B(eq)=1$.
- 99 Limit is for charge $-1/3$ isospin-0 leptoquark with $B(\ell q) = 2/3$.
- 100 First and second generation leptoquarks are assumed to be degenerate. The limit is slightly lower for each generation.
- 101 Limits are for charge $-1/3$, isospin-0 scalar leptoquarks decaying to $\ell^- q$ or νq with any branching ratio. See paper for limits for other charge-isospin assignments of leptoquarks.
- 102 KIM 90 assume pair production of charge 2/3 scalar-leptoquark via photon exchange. The decay of the first (second) generation leptoquark is assumed to be any mixture of $d e^+$ and $u \bar{p}$ ($s \mu^+$ and $c \bar{p}$). See paper for limits for specific branching ratios.
- 103 BARTEL 87b limit is valid when a pair of charge 2/3 spinless leptoquarks X is produced with point coupling, and when they decay under the constraint $B(X \rightarrow c \bar{\mu}) + B(X \rightarrow s \mu^+) = 1$.
- 104 BEHREND 86b assumed that a charge 2/3 spinless leptoquark, χ , decays either into $s \mu^+$ or $c \bar{\mu}$. $B(\chi \rightarrow s \mu^+) + B(\chi \rightarrow c \bar{\mu}) = 1$.

10	DEY	16	ICCB	$\nu q \rightarrow LQ \rightarrow \nu q$
11	AARON	11A	H1	Lepton-flavor violation
12	AARON	11B	H1	First generation
13	ABAZOV	07E	D0	Second generation
14	AKTAS	05B	H1	First generation
15	CHEKANOV	05A	ZEUS	Lepton-flavor violation
16	CHEKANOV	03B	ZEUS	First generation
17	ABBIENDI	02B	OPAL	First generation
18	CHEKANOV	02	ZEUS	Repl. by CHEKANOV 05A
19	ADLOFF	01c	H1	First generation
20	BREITWEG	01	ZEUS	First generation
21	BREITWEG	00E	ZEUS	First generation
22	ABREU	99G	DLPH	First generation
23	ADLOFF	99	H1	First generation
24	DERRICK	97	ZEUS	Lepton-flavor violation
25	DERRICK	93	ZEUS	First generation

- 1 AAD 23bz search for single production of charge 4/3 scalar leptoquarks decaying to $b\tau^-$, and charge 2/3 vector leptoquarks decaying to $\bar{b}\tau^-$ in pp collisions at $\sqrt{s} = 13$ TeV. The limit quoted above assumes a scalar leptoquark with $B(b\tau) = 1$ and the leptoquark coupling strength $\lambda = 1.0$. The limit becomes $M_{LQ} > 1530$ GeV for $\lambda = 2.5$.
- 2 SIRUNYAN 21J search for single production of charge $-1/3$ scalar leptoquarks decaying to $t\tau^-$ and $b\nu$, and charge 2/3 vector leptoquarks decaying to $t\nu$ and $b\tau^+$ in pp collisions at $\sqrt{s} = 13$ TeV. The limit quoted above assumes a scalar leptoquark with $B(\tau) = B(b\nu) = 0.5$ and the leptoquark coupling strength $\lambda = 1.5$. The limit becomes $M_{LQ} > 750$ GeV for $\lambda = 2.5$.
- 3 SIRUNYAN 18bJ search for single production of charge 2/3 scalar leptoquarks decaying to τb in pp collisions at $\sqrt{s} = 13$ TeV. The limit above assumes $B(\tau b) = 1$ and the leptoquark coupling strength $\lambda = 1$.
- 4 KHACHATRYAN 16AG search for single production of charge $\pm 1/3$ scalar leptoquarks using eej events in pp collisions at $\sqrt{s} = 8$ TeV. The limit above assumes $B(eq) = 1$ and the leptoquark coupling strength $\lambda = 1$.
- 5 KHACHATRYAN 16AG search for single production of charge $\pm 1/3$ scalar leptoquarks using $\mu\mu j$ events in pp collisions at $\sqrt{s} = 8$ TeV. The limit above assumes $B(\mu q) = 1$ and the leptoquark coupling strength $\lambda = 1$.
- 6 ABRAMOWICZ 12A limit is for a scalar, weak isoscalar, charge $-1/3$ leptoquark coupled with e_R . See their Figs. 12–17 and Table 4 for states with different quantum numbers.
- 7 Limit from single production in Z decay. The limit is for a leptoquark coupling of electromagnetic strength and assumes $B(\ell q) = 2/3$. The limit is 77 GeV if first and second leptoquarks are degenerate.
- 8 AAD 22E leptoquarks decaying both to ue^- and $c\mu^-$ are constrained from the comparison of the production cross sections for $e^+\mu^-$ and $e^-\mu^+$ in pp collisions at $\sqrt{s} = 13$ TeV. Scalar leptoquarks with $M_{LQ} < 1880$ GeV are excluded for $g^{eu} = g^{\mu c} = 1$.
- 9 TUMASYAN 21D search for energetic jets + E_T events in pp collisions at $\sqrt{s} = 13$ TeV. The branching fraction for the decay of the leptoquark into an electron neutrino and up quark is assumed to be 100% ($\beta = 0$). See their Fig. 12 for exclusion limits in mass-coupling plane.
- 10 DEY 16 use the 2010-2012 IceCube PeV energy data set to constrain the leptoquark production cross section through the $\nu q \rightarrow LQ \rightarrow \nu q$ process. See their Figure 4 for the exclusion limit in the mass-coupling plane.
- 11 AARON 11A search for various leptoquarks with lepton-flavor violating couplings. See their Figs. 2–3 and Tables 1–4 for detailed limits.
- 12 The quoted limit is for a scalar, weak isoscalar, charge $-1/3$ leptoquark coupled with e_R . See their Figs. 3–5 for limits on states with different quantum numbers.
- 13 ABAZOV 07E search for leptoquark single production through qg fusion process in $p\bar{p}$ collisions. See their Fig. 4 for exclusion plot in mass-coupling plane.
- 14 AKTAS 05B limit is for a scalar, weak isoscalar, charge $-1/3$ leptoquark coupled with e_R . See their Fig. 3 for limits on states with different quantum numbers.
- 15 CHEKANOV 05 search for various leptoquarks with lepton-flavor violating couplings. See their Figs. 6–7 and Tables 1–8 for detailed limits.
- 16 CHEKANOV 03B limit is for a scalar, weak isoscalar, charge $-1/3$ leptoquark coupled with e_R . See their Figs. 11–12 and Table 5 for limits on states with different quantum numbers.
- 17 For limits on states with different quantum numbers and the limits in the mass-coupling plane, see their Fig. 4 and Fig. 5.
- 18 CHEKANOV 02 search for various leptoquarks with lepton-flavor violating couplings. See their Figs. 6–7 and Tables 5–6 for detailed limits.
- 19 For limits on states with different quantum numbers and the limits in the mass-coupling plane, see their Fig. 3.
- 20 See their Fig. 14 for limits in the mass-coupling plane.
- 21 BREITWEG 00E search for $F=0$ leptoquarks in e^+p collisions. For limits in mass-coupling plane, see their Fig. 11.
- 22 ABREU 99G limit obtained from process $e\gamma \rightarrow LQ+q$. For limits on vector and scalar states with different quantum numbers and the limits in the coupling-mass plane, see their Fig. 4 and Table 2.
- 23 For limits on states with different quantum numbers and the limits in the mass-coupling plane, see their Fig. 13 and Fig. 14. ADLOFF 99 also search for leptoquarks with lepton-flavor violating couplings. ADLOFF 99 supersedes AID 96b.
- 24 DERRICK 97 search for various leptoquarks with lepton-flavor violating couplings. See their Figs. 5–8 and Table 1 for detailed limits.
- 25 DERRICK 93 search for single leptoquark production in ep collisions with the decay $e q$ and νq . The limit is for leptoquark coupling of electromagnetic strength and assumes $B(eq) = B(\nu q) = 1/2$. The limit for $B(eq) = 1$ is 176 GeV. For limits on states with different quantum numbers, see their Table 3.

MASS LIMITS for Leptoquarks from Single Production

These limits depend on the q - ℓ leptoquark coupling g_{LQ} . It is often assumed that $g_{LQ}^2/4\pi=1/137$. Limits shown are for a scalar, weak isoscalar, charge $-1/3$ leptoquark.

VALUE (GeV)	CL%	DOCUMENT ID	TECN	COMMENT
>1280	95	1 AAD 23bz ATLS	LQ	$LQ \rightarrow b\tau$
> 550	95	2 SIRUNYAN 21J CMS	Third generation	
none 150–740	95	3 SIRUNYAN 18bJ CMS	Third generation	
>1755	95	4 KHACHATRY..16AG CMS	First generation	
> 660	95	5 KHACHATRY..16AG CMS	Second generation	
> 304	95	6 ABRAMOWICZ12A ZEUS	First generation	
> 73	95	7 ABREU 93J DLPH	Second generation	

- • • We do not use the following data for averages, fits, limits, etc. • • •
- | | | | | |
|---|----------|-----|------|-------------------------------|
| 8 | AAD | 22E | ATLS | $LQ \rightarrow ue^-, c\mu^-$ |
| 9 | TUMASYAN | 21D | CMS | First generation |

Indirect Limits for Leptoquarks

VALUE (TeV)	CL%	DOCUMENT ID	TECN	COMMENT
• • • We do not use the following data for averages, fits, limits, etc. • • •				
1	CALABRESE	23	RVUE	ν -nucleus scattering
2	TUMASYAN	23AW	CMS	$q\bar{q}' \rightarrow \tau\nu$

Gauge & Higgs Boson Particle Listings

New Heavy Bosons

			3	TUMASYAN	23s	CMV	$pp \rightarrow \tau\tau$
			4	CRIVELLIN	21A	RVUE	First generation
			5	AEBISCHER	20	RVUE	B decays
			6	DEPPISCH	20	RVUE	$K \rightarrow \pi\nu\nu$
>	3.1	95	7	ABRAMOWICZ	19	ZEUS	First generation
			8	MANDAL	19	RVUE	τ, μ, e, K
			9	ZHANG	18A	RVUE	D decays
			10	BARRANCO	16	RVUE	D decays
			11	KUMAR	16	RVUE	neutral K mixing, rare K decays
			12	BESSAA	15	RVUE	$q\bar{q} \rightarrow e^+e^-$
>	14	95	13	SAHOO	15A	RVUE	$B_{s,d} \rightarrow \mu^+\mu^-$
			14	SAKAKI	13	RVUE	$B \rightarrow D^{(*)}\tau\bar{\nu}, B \rightarrow X_S\nu\bar{\nu}$
			15	KOSNIK	12	RVUE	$b \rightarrow s\ell^+\ell^-$
>	2.5	95	16	AARON	11C	H1	First generation
			17	DORSNER	11	RVUE	scalar, weak singlet, charge 4/3
			18	AKTAS	07A	H1	Lepton-flavor violation
>	0.49	95	19	SCHAEEL	07A	ALEP	$e^+e^- \rightarrow q\bar{q}$
			20	SMIRNOV	07	RVUE	$K \rightarrow e\mu, B \rightarrow e\tau$
			21	CHEKANOV	05A	ZEUS	Lepton-flavor violation
>	1.7	96	22	ADLOFF	03	H1	First generation
>	46	90	23	CHANG	03	BELL	Pati-Salam type
			24	CHEKANOV	02	ZEUS	Repl. by CHEKANOV 05A
>	1.7	95	25	CHEUNG	01B	RVUE	First generation
>	0.39	95	26	ACCIARRI	00P	L3	$e^+e^- \rightarrow q\bar{q}$
>	1.5	95	27	ADLOFF	00	H1	First generation
>	0.2	95	28	BARATE	00I	ALEP	Repl. by SCHAEEL 07A
			29	BARGER	00	RVUE	Cs
			30	GABRIELLI	00	RVUE	Lepton flavor violation
>	0.74	95	31	ZARNECKI	00	RVUE	S_1 leptoquark
			32	ABBIENDI	99	OPAL	
>	19.3	95	33	ABE	98V	CDF	$B_S \rightarrow e^\pm\mu^\mp$, Pati-Salam type
			34	ACCIARRI	98J	L3	$e^+e^- \rightarrow q\bar{q}$
			35	ACKERSTAFF	98V	OPAL	$e^+e^- \rightarrow q\bar{q}, e^+e^- \rightarrow b\bar{b}$
>	0.76	95	36	DEANDREA	97	RVUE	\bar{R}_2 leptoquark
			37	DERRICK	97	ZEUS	Lepton-flavor violation
			38	GROSSMAN	97	RVUE	$B \rightarrow \tau^+\tau^-(X)$
			39	JADACH	97	RVUE	$e^+e^- \rightarrow q\bar{q}$
>	1200		40	KUZNETSOV	95B	RVUE	Pati-Salam type
			41	MIZUKOSHI	95	RVUE	Third generation scalar leptoquark
>	0.3	95	42	BHATTACH...	94	RVUE	Spin-0 leptoquark coupled to $\bar{\nu}_R t_L$
			43	DAVIDSON	94	RVUE	
>	18		44	KUZNETSOV	94	RVUE	Pati-Salam type
>	0.43	95	45	LEURER	94	RVUE	First generation spin-1 leptoquark
>	0.44	95	46	MAHANTA	94	RVUE	First generation spin-0 leptoquark
			47	SHANKER	82	RVUE	P and T violation
>	1		48	SHANKER	82	RVUE	Nonchiral spin-0 leptoquark
>	125		49	SHANKER	82	RVUE	Nonchiral spin-1 leptoquark

1 CALABRESE 23 obtain limits on leptoquark coupling from coherent ν -nucleus scattering data collected by COHERENT experiment. See their Fig. 3 for limits in mass-coupling plane.

2 TUMASYAN 23AV search for $\tau\nu$ events mediated by t -channel leptoquark exchange in pp collisions at $\sqrt{s}=13$ TeV. See their Fig. 10 for limits in mass-coupling plane.

3 TUMASYAN 23s search for leptoquark induced $b\bar{b} \rightarrow \tau^+\tau^-$ process in pp collisions at $\sqrt{s}=13$ TeV. See their Fig. 12 for limits on a vector $b\tau$ leptoquark in mass-coupling plane.

4 CRIVELLIN 21A set limits on coupling strengths of scalar and vector leptoquarks using $K \rightarrow \pi\nu\nu, K \rightarrow \pi e^+e^-, K^0 - \bar{K}^0$ and $D^0 - \bar{D}^0$ mixings, and weak neutral current measurements. See their Fig. 2 and Fig. 3 for the limits in mass-coupling plane.

5 AEBISCHER 20 explain the B decay anomalies using four-fermion operator Wilson coefficients. See their Table 1. These Wilson coefficients may be generated by a U_1 vector leptoquark with U_1 transforming as $(3,1)_{2/3}$ under the SM gauge group. See their Figures 6, 7, 8 for the regions of the LQ parameter space which explains the B anomalies and avoids the indirect low energy constraints.

6 DEPPISCH 20 limits on the lepton-number-violating higher-dimensional-operators are derived from $K \rightarrow \pi\nu\nu$ in the standard model effective field theory. These higher-dimensional-operators may be induced from leptoquark-exchange diagrams.

7 ABRAMOWICZ 19 obtain a limit on $\lambda/M_{LQ} > 1.16 \text{ TeV}^{-1}$ for weak isospin triplet spin-0 leptoquark S_L^T . We obtain the limit quoted above by converting the limit on λ/M_{LQ} for S_L^T assuming $\lambda = \sqrt{4\pi}$. See their Table 5 for the limits of leptoquarks with different quantum numbers. These limits are derived from bounds of eq contact interactions.

8 MANDAL 19 give bounds on leptoquarks from τ -decays, leptonic dipole moments, lepton-flavor-violating processes, and K decays.

9 ZHANG 18A give bounds on leptoquark induced four-fermion interactions from $D \rightarrow K\ell\nu$. The authors inform us that the shape parameter of the vector form factor in both the abstract and the conclusions of ZHANG 18A should be $r_{+1} = 2.16 \pm 0.07$ rather than ± 0.07 . The numbers listed in their Table 7 are correct.

10 BARRANCO 16 give bounds on leptoquark induced four-fermion interactions from $D \rightarrow K\ell\nu$ and $D_S \rightarrow \ell\nu$.

11 KUMAR 16 gives bound on SU(2) singlet scalar leptoquark with charge $-1/3$ from $K^0 - \bar{K}^0$ mixing, $K \rightarrow \pi\nu\bar{\nu}, K_L^0 \rightarrow \mu^+\mu^-,$ and $K_L^0 \rightarrow \mu^\pm e^\mp$ decays.

12 BESSAA 15 obtain limit on leptoquark induced four-fermion interactions from the ATLAS and CMS limit on the $q\bar{q}e\bar{e}$ contact interactions.

13 SAHOO 15A obtain limit on leptoquark induced four-fermion interactions from $B_{s,d} \rightarrow \mu^+\mu^-$ for $\lambda \simeq O(1)$.

14 SAKAKI 13 explain the $B \rightarrow D^{(*)}\tau\bar{\nu}$ anomaly using Wilson coefficients of leptoquark-induced four-fermion operators.

15 KOSNIK 12 obtains limits on leptoquark induced four-fermion interactions from $b \rightarrow s\ell^+\ell^-$ decays.

16 AARON 11C limit is for weak isospin triplet spin-0 leptoquark at strong coupling $\lambda = \sqrt{4\pi}$. For the limits of leptoquarks with different quantum numbers, see their Table 3. Limits are derived from bounds of eq contact interactions.

17 DORSNER 11 give bounds on scalar, weak singlet, charge 4/3 leptoquark from K, B, τ decays, meson mixings, L $FV, g=2$ and $Z \rightarrow b\bar{b}$.

18 AKTAS 07A search for lepton-flavor violation in $e p$ collision. See their Tables 4–7 for limits on lepton-flavor violating four-fermion interactions induced by various leptoquarks.

19 SCHAEEL 07A limit is for the weak-isoscalar spin-0 left-handed leptoquark with the coupling of electromagnetic strength. For the limits of leptoquarks with different quantum numbers, see their Table 35.

20 SMIRNOV 07 obtains mass limits for the vector and scalar chiral leptoquark states from $K \rightarrow e\mu, B \rightarrow e\tau$ decays.

21 CHEKANOV 05 search for various leptoquarks with lepton-flavor violating couplings. See their Figs.6–10 and Tables 1–8 for detailed limits.

22 ADLOFF 03 limit is for the weak isospin triplet spin-0 leptoquark at strong coupling $\lambda = \sqrt{4\pi}$. For the limits of leptoquarks with different quantum numbers, see their Table 3. Limits are derived from bounds on $e^\pm q$ contact interactions.

23 The bound is derived from $B(B^0 \rightarrow e^\pm\mu^\mp) < 1.7 \times 10^{-7}$.

24 CHEKANOV 02 search for lepton-flavor violation in $e p$ collisions. See their Tables 1–4 for limits on lepton-flavor violating and four-fermion interactions induced by various leptoquarks.

25 CHEUNG 01B quoted limit is for a scalar, weak isoscalar, charge $-1/3$ leptoquark with a coupling of electromagnetic strength. The limit is derived from bounds on contact interactions in a global electroweak analysis. For the limits of leptoquarks with different quantum numbers, see Table 5.

26 ACCIARRI 00P limit is for the weak isoscalar spin-0 leptoquark with the coupling of electromagnetic strength. For the limits of leptoquarks with different quantum numbers, see their Table 4.

27 ADLOFF 00 limit is for the weak isospin triplet spin-0 leptoquark at strong coupling, $\lambda = \sqrt{4\pi}$. For the limits of leptoquarks with different quantum numbers, see their Table 2. ADLOFF 00 limits are from the Q^2 spectrum measurement of $e^+p \rightarrow e^+X$.

28 BARATE 00I search for deviations in cross section and jet-charge asymmetry in $e^+e^- \rightarrow \bar{q}q$ due to t -channel exchange of a leptoquark at $\sqrt{s}=130$ to 183 GeV. Limits for other scalar and vector leptoquarks are also given in their Table 22.

29 BARGER 00 explain the deviation of atomic parity violation in cesium atoms from prediction is explained by scalar leptoquark exchange.

30 GABRIELLI 00 calculate various process with lepton flavor violation in leptoquark models.

31 ZARNECKI 00 limit is derived from data of HERA, LEP, and Tevatron and from various low-energy data including atomic parity violation. Leptoquark coupling with electromagnetic strength is assumed.

32 ABBIENDI 99 limits are from $e^+e^- \rightarrow q\bar{q}$ cross section at 130–136, 161–172, 183 GeV. See their Fig. 8 and Fig. 9 for limits in mass-coupling plane.

33 ABE 98V quoted limit is from $B(B_S \rightarrow e^\pm\mu^\mp) < 8.2 \times 10^{-6}$. ABE 98V also obtain a similar limit on $M_{LQ} > 20.4$ TeV from $B(B_d \rightarrow e^\pm\mu^\mp) < 4.5 \times 10^{-6}$. Both bounds assume the non-canonical association of the b quark with electrons or muons under SU(4).

34 ACCIARRI 98J limit is from $e^+e^- \rightarrow q\bar{q}$ cross section at $\sqrt{s}=130$ –172 GeV which can be affected by the t - and u -channel exchanges of leptoquarks. See their Fig. 4 and Fig. 5 for limits in the mass-coupling plane.

35 ACKERSTAFF 98V limits are from $e^+e^- \rightarrow q\bar{q}$ and $e^+e^- \rightarrow b\bar{b}$ cross sections at $\sqrt{s}=130$ –172 GeV, which can be affected by the t - and u -channel exchanges of leptoquarks. See their Fig. 21 and Fig. 22 for limits of leptoquarks in mass-coupling plane.

36 DEANDREA 97 limit is for \bar{R}_2 leptoquark obtained from atomic parity violation (APV). The coupling of leptoquark is assumed to be electromagnetic strength. See Table 2 for limits of the four-fermion interactions induced by various scalar leptoquark exchange.

37 DEANDREA 97 combines APV limit and limits from Tevatron and HERA. See Fig. 1–4 for combined limits of leptoquark in mass-coupling plane.

38 DERRICK 97 search for lepton-flavor violation in $e p$ collision. See their Tables 2–5 for limits on lepton-flavor violating four-fermion interactions induced by various leptoquarks.

39 GROSSMAN 97 estimate the upper bounds on the branching fraction $B \rightarrow \tau^+\tau^-(X)$ from the absence of the B decay with large missing energy. These bounds can be used to constrain leptoquark induced four-fermion interactions.

40 JADACH 97 limit is from $e^+e^- \rightarrow q\bar{q}$ cross section at $\sqrt{s}=172.3$ GeV which can be affected by the t - and u -channel exchanges of leptoquarks. See their Fig. 1 for limits on vector leptoquarks in mass-coupling plane.

41 KUZNETSOV 95B use π, K, B, τ decays and μe conversion and give a list of bounds on the leptoquark mass and the fermion mixing matrix in the Pati-Salam model. The quoted limit is from $K_L \rightarrow \mu e$ decay assuming zero mixing.

42 MIZUKOSHI 95 calculate the one-loop radiative correction to the Z -physics parameters in various scalar leptoquark models. See their Fig. 4 for the exclusion plot of third generation leptoquark models in mass-coupling plane.

43 BHATTACHARYYA 94 limit is from one-loop radiative correction to the leptonic decay width of the Z . $m_H=250$ GeV, $\alpha_s(m_Z)=0.12, m_t=180$ GeV, and the electroweak strength of leptoquark coupling are assumed. For leptoquark coupled to $\bar{\nu}_L t_R, \bar{\nu}_L, \bar{\nu}_L$ and $\bar{\nu}_L$, see Fig. 2 in BHATTACHARYYA 94b erratum and Fig. 3.

44 DAVIDSON 94 gives an extensive list of the bounds on leptoquark-induced four-fermion interactions from π, K, D, B, μ, τ decays and meson mixings, etc. See Table 15 of DAVIDSON 94 for detail.

45 KUZNETSOV 94 gives mixing independent bound of the Pati-Salam leptoquark from the cosmological limit on $\pi^0 \rightarrow \bar{\nu}\nu$.

46 LEURER 94, LEURER 94b limits are obtained from atomic parity violation and apply to any chiral leptoquark which couples to the first generation with electromagnetic strength. For a nonchiral leptoquark, universality in $\pi_{\ell 2}$ decay provides a much more stringent bound.

47 MAHANTA 94 gives bounds of P - and T -violating scalar-leptoquark couplings from atomic and molecular experiments.

48 From $(\pi \rightarrow e\nu)/(\pi \rightarrow \mu\nu)$ ratio. SHANKER 82 assumes the leptoquark induced four-fermion coupling $4g^2/M^2 (\bar{\nu}_L u_R) (\bar{\nu}_L e_R)$ with $g=0.004$ for spin-0 leptoquark and $g^2/M^2 (\bar{\nu}_L e_L u_L) (\bar{\nu}_R \gamma^\mu e_R)$ with $g=0.6$ for spin-1 leptoquark.

Gauge & Higgs Boson Particle Listings

New Heavy Bosons

MASS LIMITS for Diquarks

VALUE (GeV)	CL%	DOCUMENT ID	TECN	COMMENT
>7200 (CL = 95%) OUR LIMIT				
none 600-7200	95	1 SIRUNYAN 18B0	CMS	E_6 diquark
none 600-6900	95	2 KHACHATRYAN...17W	CMS	E_6 diquark
none 1500-6000	95	3 KHACHATRYAN...16K	CMS	E_6 diquark
none 500-1600	95	4 KHACHATRYAN...16L	CMS	E_6 diquark
none 1200-4700	95	5 KHACHATRYAN...15V	CMS	E_6 diquark
• • • We do not use the following data for averages, fits, limits, etc. • • •				
>3750	95	6 CHATRCHYAN13A	CMS	E_6 diquark
none 1000-4280	95	7 CHATRCHYAN13AS	CMS	Superseded by KHACHATRYAN 15V
>3520	95	8 CHATRCHYAN11Y	CMS	Superseded by CHATRCHYAN 13A
none 970-1080, 1450-1600	95	9 KHACHATRYAN...10	CMS	Superseded by CHATRCHYAN 13A
none 290-630	95	10 AALTONEN 09AC	CDF	E_6 diquark
none 290-420	95	11 ABE 97G	CDF	E_6 diquark
none 15-31.7	95	12 ABREU 940	DLPH	SUSY E_6 diquark

1 SIRUNYAN 18B0 search for resonances decaying to dijets in pp collisions at $\sqrt{s} = 13$ TeV.
 2 KHACHATRYAN 17W search for resonances decaying to dijets in pp collisions at $\sqrt{s} = 13$ TeV.
 3 KHACHATRYAN 16K search for resonances decaying to dijets in pp collisions at $\sqrt{s} = 13$ TeV.
 4 KHACHATRYAN 16L search for resonances decaying to dijets in pp collisions at $\sqrt{s} = 8$ TeV with the data scouting technique, increasing the sensitivity to the low mass resonances.
 5 KHACHATRYAN 15V search for resonances decaying to dijets in pp collisions at $\sqrt{s} = 8$ TeV.
 6 CHATRCHYAN 13A search for new resonance decaying to dijets in pp collisions at $\sqrt{s} = 7$ TeV.
 7 CHATRCHYAN 13AS search for new resonance decaying to dijets in pp collisions at $\sqrt{s} = 8$ TeV.
 8 CHATRCHYAN 11Y search for new resonance decaying to dijets in pp collisions at $\sqrt{s} = 7$ TeV.
 9 KHACHATRYAN 10 search for new resonance decaying to dijets in pp collisions at $\sqrt{s} = 7$ TeV.
 10 AALTONEN 09AC search for new narrow resonance decaying to dijets.
 11 ABE 97G search for new particle decaying to dijets.
 12 ABREU 940 limit is from $e^+e^- \rightarrow \tau\bar{\nu}_s c$. Range extends up to 43 GeV if diquarks are degenerate in mass.

MASS LIMITS for g_A (axigluon) and Other Color-Octet Gauge Bosons

Axigluons are massive color-octet gauge bosons in chiral color models and have axial-vector coupling to quarks with the same coupling strength as gluons.

VALUE (GeV)	CL%	DOCUMENT ID	TECN	COMMENT
>6600 (CL = 95%) OUR LIMIT				
none 1800-6600	95	1 SIRUNYAN 20A1	CMS	$pp \rightarrow g_A X, g_A \rightarrow 2j$
none 600-6100	95	2 SIRUNYAN 18B0	CMS	$pp \rightarrow g_A X, g_A \rightarrow 2j$
none 600-5500	95	3 KHACHATRYAN...17W	CMS	$pp \rightarrow g_A X, g_A \rightarrow 2j$
none 1500-5100	95	4 KHACHATRYAN...16K	CMS	$pp \rightarrow g_A X, g_A \rightarrow 2j$
none 500-1600	95	5 KHACHATRYAN...16L	CMS	$pp \rightarrow g_A X, g_A \rightarrow 2j$
none 1300-3600	95	6 KHACHATRYAN...15V	CMS	$pp \rightarrow g_A X, g_A \rightarrow 2j$
• • • We do not use the following data for averages, fits, limits, etc. • • •				
>2800	95	7 KHACHATRYAN...17Y	CMS	$pp \rightarrow g_A g_A \rightarrow 8j$
		8 AAD 16W	ATLS	$pp \rightarrow g_A X, g_A \rightarrow b\bar{b}b\bar{b}$
		9 KHACHATRYAN...16E	CMS	$pp \rightarrow g_{KK} X, g_{KK} \rightarrow i\bar{i}$
		10 KHACHATRYAN...15AV	CMS	$pp \rightarrow \theta^0 \theta^0 \rightarrow b\bar{b}Zg$
		11 AALTONEN 13R	CDF	$p\bar{p} \rightarrow g_A X, g_A \rightarrow \sigma\sigma, \sigma \rightarrow 2j$
>3360	95	12 CHATRCHYAN13A	CMS	$pp \rightarrow g_A X, g_A \rightarrow 2j$
none 1000-3270	95	13 CHATRCHYAN13AS	CMS	Superseded by KHACHATRYAN 15V
none 250-740	95	14 CHATRCHYAN13AU	CMS	$pp \rightarrow 2g_A X, g_A \rightarrow 2j$
> 775	95	15 ABAZOV 12R	D0	$p\bar{p} \rightarrow g_A X, g_A \rightarrow t\bar{t}$
>2470	95	16 CHATRCHYAN11Y	CMS	Superseded by CHATRCHYAN 13A
none 1470-1520	95	17 AALTONEN 10L	CDF	$p\bar{p} \rightarrow g_A X, g_A \rightarrow t\bar{t}$
		18 KHACHATRYAN...10	CMS	Superseded by CHATRCHYAN 13A
none 260-1250	95	19 AALTONEN 09AC	CDF	$p\bar{p} \rightarrow g_A X, g_A \rightarrow 2j$
> 910	95	20 CHOUDHURY 07	RVUE	$p\bar{p} \rightarrow t\bar{t}X$
> 365	95	21 DONCHESKI 98	RVUE	$\Gamma(Z \rightarrow \text{hadron})$
none 200-980	95	22 ABE 97G	CDF	$p\bar{p} \rightarrow g_A X, g_A \rightarrow 2j$
none 200-870	95	23 ABE 95N	CDF	$p\bar{p} \rightarrow g_A X, g_A \rightarrow q\bar{q}$
none 240-640	95	24 ABE 93G	CDF	$p\bar{p} \rightarrow g_A X, g_A \rightarrow 2j$
> 50	95	25 CUYPERS 91	RVUE	$\sigma(e^+e^- \rightarrow \text{hadrons})$
none 120-210	95	26 ABE 90H	CDF	$p\bar{p} \rightarrow g_A X, g_A \rightarrow 2j$
> 29	95	27 ROBINETT 89	THEO	Partial-wave unitarity
none 150-310	95	28 ALBAJAR 88B	UA1	$p\bar{p} \rightarrow g_A X, g_A \rightarrow 2j$
> 20	95	29 BERGSTROM 88	RVUE	$p\bar{p} \rightarrow TX$ via $g_A g$
> 9	95	30 CUYPERS 88	RVUE	T decay
> 25	95	31 DONCHESKI 88B	RVUE	T decay

1 SIRUNYAN 20A1 search for resonances decaying into dijets in pp collisions at $\sqrt{s} = 13$ TeV.
 2 SIRUNYAN 18B0 search for resonances decaying to dijets in pp collisions at $\sqrt{s} = 13$ TeV.

- 3 KHACHATRYAN 17W search for resonances decaying to dijets in pp collisions at $\sqrt{s} = 13$ TeV.
 4 KHACHATRYAN 16K search for resonances decaying to dijets in pp collisions at $\sqrt{s} = 13$ TeV.
 5 KHACHATRYAN 16L search for resonances decaying to dijets in pp collisions at $\sqrt{s} = 8$ TeV with the data scouting technique, increasing the sensitivity to the low mass resonances.
 6 KHACHATRYAN 15V search for resonances decaying to dijets in pp collisions at $\sqrt{s} = 8$ TeV.
 7 KHACHATRYAN 17Y search for pair production of color-octet gauge boson g_A each decaying to $4j$ in pp collisions at $\sqrt{s} = 8$ TeV.
 8 AAD 16W search for a new resonance decaying to a pair of b and B_H in pp collisions at $\sqrt{s} = 8$ TeV. The vector-like quark B_H is assumed to decay to bH . See their Fig. 3 and Fig. 4 for limits on $\sigma \cdot B$.
 9 KHACHATRYAN 16E search for KK gluon decaying to $t\bar{t}$ in pp collisions at $\sqrt{s} = 8$ TeV.
 10 KHACHATRYAN 15AV search for pair productions of neutral color-octet weak-triplet scalar particles (θ^0), decaying to $b\bar{b}$, Zg or γg , in pp collisions at $\sqrt{s} = 8$ TeV. The θ^0 particle is often predicted in coloron (G' , color-octet gauge boson) models and appear in the pp collisions through $G' \rightarrow \theta^0 \theta^0$ decays. Assuming $B(\theta^0 \rightarrow b\bar{b}) = 0.5$, they give limits $m_{\theta^0} > 623$ GeV (426 GeV) for $m_{G'} = 2.3 m_{\theta^0}$ ($m_{G'} = 5 m_{\theta^0}$).
 11 AALTONEN 13R search for new resonance decaying to $\sigma\sigma$, with hypothetical strongly interacting σ particle subsequently decaying to 2 jets, in $p\bar{p}$ collisions at $\sqrt{s} = 1.96$ TeV, using data corresponding to an integrated luminosity of 6.6 fb^{-1} . For $50 \text{ GeV} < m_\sigma < m_{g_A}/2$, axigluons in mass range 150-400 GeV are excluded.
 12 CHATRCHYAN 13A search for new resonance decaying to dijets in pp collisions at $\sqrt{s} = 7$ TeV.
 13 CHATRCHYAN 13AS search for new resonance decaying to dijets in pp collisions at $\sqrt{s} = 8$ TeV.
 14 CHATRCHYAN 13AU search for the pair produced color-octet vector bosons decaying to $q\bar{q}$ pairs in pp collisions. The quoted limit is for $B(g_A \rightarrow q\bar{q}) = 1$.
 15 ABAZOV 12R search for massive color octet vector particle decaying to $t\bar{t}$. The quoted limit assumes g_A couplings with light quarks are suppressed by 0.2.
 16 CHATRCHYAN 11Y search for new resonance decaying to dijets in pp collisions at $\sqrt{s} = 7$ TeV.
 17 AALTONEN 10L search for massive color octet non-chiral vector particle decaying into $t\bar{t}$ pair with mass in the range $400 \text{ GeV} < M < 800 \text{ GeV}$. See their Fig. 6 for limit in the mass-coupling plane.
 18 KHACHATRYAN 10 search for new resonance decaying to dijets in pp collisions at $\sqrt{s} = 7$ TeV.
 19 AALTONEN 09AC search for new narrow resonance decaying to dijets.
 20 CHOUDHURY 07 limit is from the $t\bar{t}$ production cross section measured at CDF.
 21 DONCHESKI 98 compare α_s derived from low-energy data and that from $\Gamma(Z \rightarrow \text{hadrons})/\Gamma(Z \rightarrow \text{leptons})$.
 22 ABE 97G search for new particle decaying to dijets.
 23 ABE 95N assume axigluons decaying to quarks in the Standard Model only.
 24 ABE 93G assume $\Gamma(g_A) = N\alpha_s m_{g_A}/6$ with $N = 10$.
 25 CUYPERS 91 compare α_s measured in T decay and that from R at PEP/PETRA energies.
 26 ABE 90H assumes $\Gamma(g_A) = N\alpha_s m_{g_A}/6$ with $N = 5$ ($\Gamma(g_A) = 0.09 m_{g_A}$). For $N = 10$, the excluded region is reduced to 120-150 GeV.
 27 ROBINETT 89 result demands partial-wave unitarity of $J = 0$ $t\bar{t} \rightarrow t\bar{t}$ scattering amplitude and derives a limit $m_{g_A} > 0.5 m_t$. Assumes $m_t > 56$ GeV.
 28 ALBAJAR 88B result is from the nonobservation of a peak in two-jet invariant mass distribution. $\Gamma(g_A) < 0.4 m_{g_A}$ assumed. See also BAGGER 88.
 29 CUYPERS 88 requires $\Gamma(T \rightarrow g g_A) < \Gamma(T \rightarrow g g g)$. A similar result is obtained by DONCHESKI 88.
 30 DONCHESKI 88B requires $\Gamma(T \rightarrow g q\bar{q})/\Gamma(T \rightarrow g g g) < 0.25$, where the former decay proceeds via axigluon exchange. A more conservative estimate of < 0.5 leads to $m_{g_A} > 21$ GeV.

MASS LIMITS for Color-Octet Scalar Bosons

VALUE (GeV)	CL%	DOCUMENT ID	TECN	COMMENT
• • • We do not use the following data for averages, fits, limits, etc. • • •				
none 1800-3700	95	1 SIRUNYAN 20A1	CMS	$pp \rightarrow S_8 X, S_8 \rightarrow gg$
none 600-3400	95	2 SIRUNYAN 18B0	CMS	$pp \rightarrow S_8 X, S_8 \rightarrow gg$
		3 KHACHATRYAN...15AV	CMS	$pp \rightarrow \theta^0 \theta^0 \rightarrow b\bar{b}Zg$
none 150-287	95	4 AAD 13K	ATLS	$pp \rightarrow S_8 S_8 X, S_8 \rightarrow 2 \text{ jets}$

1 SIRUNYAN 20A1 search for resonances decaying into dijets in pp collisions at $\sqrt{s} = 13$ TeV. The limit above assumes S_{8gg} coupling $k_s^2 = 1/2$.
 2 SIRUNYAN 18B0 search for color octet scalar boson produced through gluon fusion process in pp collisions at $\sqrt{s} = 13$ TeV. The limit above assumes S_{8gg} coupling $k_s^2 = 1/2$.
 3 KHACHATRYAN 15AV search for pair productions of neutral color-octet weak-triplet scalar particles (θ^0), decaying to $b\bar{b}$, Zg or γg , in pp collisions at $\sqrt{s} = 8$ TeV. The θ^0 particle is often predicted in coloron (G' , color-octet gauge boson) models and appear in the pp collisions through $G' \rightarrow \theta^0 \theta^0$ decays. Assuming $B(\theta^0 \rightarrow b\bar{b}) = 0.5$, they give limits $m_{\theta^0} > 623$ GeV (426 GeV) for $m_{G'} = 2.3 m_{\theta^0}$ ($m_{G'} = 5 m_{\theta^0}$).
 4 AAD 13K search for pair production of color-octet scalar particles in pp collisions at $\sqrt{s} = 7$ TeV. Cross section limits are interpreted as mass limits on scalar partners of a Dirac gluino.

X^0 (Heavy Boson) Searches in Z Decays

Searches for radiative transition of Z to a lighter spin-0 state X^0 decaying to hadrons, a lepton pair, a photon pair, or invisible particles as shown in the comments. The limits are for the product of branching ratios.

VALUE	CL%	DOCUMENT ID	TECN	COMMENT
• • • We do not use the following data for averages, fits, limits, etc. • • •				
		1 RAINBOLT 19	RVUE	$X^0 \rightarrow \ell^+ \ell^-$
		2 SIRUNYAN 19AZ	CMS	$X^0 \rightarrow \mu^+ \mu^-$

Gauge & Higgs Boson Particle Listings

New Heavy Bosons

VALUE	CL%	DOCUMENT ID	TECN	COMMENT
		3 BARATE 98U ALEP	$X^0 \rightarrow \ell\bar{\ell}, q\bar{q}, gg, \gamma\gamma, \nu\bar{\nu}$	
		4 ACCIARRI 97Q L3	$X^0 \rightarrow$ invisible particle(s)	
		5 ACTON 93E OPAL	$X^0 \rightarrow \gamma\gamma$	
		6 ABREU 92D DLPH	$X^0 \rightarrow$ hadrons	
		7 ADRIANI 92F L3	$X^0 \rightarrow$ hadrons	
		8 ACTON 91 OPAL	$X^0 \rightarrow$ anything	
$<1.1 \times 10^{-4}$	95	9 ACTON 91B OPAL	$X^0 \rightarrow e^+e^-$	
$<9 \times 10^{-5}$	95	9 ACTON 91B OPAL	$X^0 \rightarrow \mu^+\mu^-$	
$<1.1 \times 10^{-4}$	95	9 ACTON 91B OPAL	$X^0 \rightarrow \tau^+\tau^-$	
$<2.8 \times 10^{-4}$	95	10 ADEVA 91D L3	$X^0 \rightarrow e^+e^-$	
$<2.3 \times 10^{-4}$	95	10 ADEVA 91D L3	$X^0 \rightarrow \mu^+\mu^-$	
$<4.7 \times 10^{-4}$	95	11 ADEVA 91D L3	$X^0 \rightarrow$ hadrons	
$<8 \times 10^{-4}$	95	12 AKRAWY 90J OPAL	$X^0 \rightarrow$ hadrons	

- 1 RAINBOLT 19 limits are from $B(Z \rightarrow \ell^+\ell^-\ell^+\ell^-)$. See their Figs. 5 and 6 for limits in mass-coupling plane.
- 2 SIRUANYAN 19AZ search for $pp \rightarrow Z \rightarrow X^0\mu^+\mu^- \rightarrow \mu^+\mu^-\mu^+\mu^-$ events in pp collisions at $\sqrt{s} = 13$ TeV. See their Fig. 5 for limits on $\sigma(pp \rightarrow X^0\mu^+\mu^-) \cdot B(X^0 \rightarrow \mu^+\mu^-)$.
- 3 BARATE 98U obtain limits on $B(Z \rightarrow \gamma X^0) \cdot B(X^0 \rightarrow \ell\bar{\ell}, q\bar{q}, gg, \gamma\gamma, \nu\bar{\nu})$. See their Fig. 17.
- 4 See Fig. 4 of ACCIARRI 97Q for the upper limit on $B(Z \rightarrow \gamma X^0; E_\gamma > E_{\min})$ as a function of E_{\min} .
- 5 ACTON 93E give $\sigma(e^+e^- \rightarrow X^0\gamma) \cdot B(X^0 \rightarrow \gamma\gamma) < 0.4$ pb (95%CL) for $m_{X^0} = 60 \pm 2.5$ GeV. If the process occurs via s -channel γ exchange, the limit translates to $\Gamma(X^0) \cdot B(X^0 \rightarrow \gamma\gamma)^2 < 20$ MeV for $m_{X^0} = 60 \pm 1$ GeV.
- 6 ABREU 92D give $\sigma_Z \cdot B(Z \rightarrow \gamma X^0) \cdot B(X^0 \rightarrow \text{hadrons}) < (3-10)$ pb for $m_{X^0} = 10-78$ GeV. A very similar limit is obtained for spin-1 X^0 .
- 7 ADRIANI 92F search for isolated γ in hadronic Z decays. The limit $\sigma_Z \cdot B(Z \rightarrow \gamma X^0) \cdot B(X^0 \rightarrow \text{hadrons}) < (2-10)$ pb (95%CL) is given for $m_{X^0} = 25-85$ GeV.
- 8 ACTON 91 searches for $Z \rightarrow Z^*X^0$, $Z^* \rightarrow e^+e^-, \mu^+\mu^-, \text{ or } \nu\bar{\nu}$. Excludes any new scalar X^0 with $m_{X^0} < 9.5$ GeV/c if it has the same coupling to ZZ^* as the MSM Higgs boson.
- 9 ACTON 91B limits are for $m_{X^0} = 60-85$ GeV.
- 10 ADEVA 91D limits are for $m_{X^0} = 30-89$ GeV.
- 11 ADEVA 91D limits are for $m_{X^0} = 30-86$ GeV.
- 12 AKRAWY 90J give $\Gamma(Z \rightarrow \gamma X^0) \cdot B(X^0 \rightarrow \text{hadrons}) < 1.9$ MeV (95%CL) for $m_{X^0} = 32-80$ GeV. We divide by $\Gamma(Z) = 2.5$ GeV to get product of branching ratios. For nonresonant transitions, the limit is $B(Z \rightarrow \gamma q\bar{q}) < 8.2$ MeV assuming three-body phase space distribution.

MASS LIMITS for a Heavy Neutral Boson Coupling to e^+e^-

VALUE (GeV)	CL%	DOCUMENT ID	TECN	COMMENT
none 55-61		1 ODAKA 89 VNS	$\Gamma(X^0 \rightarrow e^+e^-) \cdot B(X^0 \rightarrow \text{had.}) \gtrsim 0.2$ MeV	
>45	95	2 DERRICK 86 HRS	$\Gamma(X^0 \rightarrow e^+e^-) = 6$ MeV	
>46.6	95	3 ADEVA 85 MRKJ	$\Gamma(X^0 \rightarrow e^+e^-) = 10$ keV	
>48	95	3 ADEVA 85 MRKJ	$\Gamma(X^0 \rightarrow e^+e^-) = 4$ MeV	
		4 BERGER 85B PLUT		
none 39.8-45.5		5 ADEVA 84 MRKJ	$\Gamma(X^0 \rightarrow e^+e^-) = 10$ keV	
>47.8	95	5 ADEVA 84 MRKJ	$\Gamma(X^0 \rightarrow e^+e^-) = 4$ MeV	
none 39.8-45.2		5 BEHREND 84c CELL		
>47	95	5 BEHREND 84c CELL	$\Gamma(X^0 \rightarrow e^+e^-) = 4$ MeV	

- 1 ODAKA 89 looked for a narrow or wide scalar resonance in $e^+e^- \rightarrow$ hadrons at $E_{\text{cm}} = 55.0-60.8$ GeV.
- 2 DERRICK 86 found no deviation from the Standard Model Bhabha scattering at $E_{\text{cm}} = 29$ GeV and set limits on the possible scalar boson e^+e^- coupling. See their figure 4 for excluded region in the $\Gamma(X^0 \rightarrow e^+e^-) \cdot m_{X^0}$ plane. Electronic chiral invariance requires a parity doublet of X^0 , in which case the limit applies for $\Gamma(X^0 \rightarrow e^+e^-) = 3$ MeV.
- 3 ADEVA 85 first limit is from $2\gamma, \mu^+\mu^-,$ hadrons assuming X^0 is a scalar. Second limit is from e^+e^- channel. $E_{\text{cm}} = 40-47$ GeV. Supersedes ADEVA 84.
- 4 BERGER 85B looked for effect of spin-0 boson exchange in $e^+e^- \rightarrow e^+e^-$ and $\mu^+\mu^-$ at $E_{\text{cm}} = 34.7$ GeV. See Fig. 5 for excluded region in the $m_{X^0} - \Gamma(X^0)$ plane.
- 5 ADEVA 84 and BEHREND 84c have $E_{\text{cm}} = 39.8-45.5$ GeV. MARK-J searched X^0 in $e^+e^- \rightarrow$ hadrons, $2\gamma, \mu^+\mu^-, e^+e^-$ and CELLO in the same channels plus τ pair. No narrow or broad X^0 is found in the energy range. They also searched for the effect of X^0 with $m_X > E_{\text{cm}}$. The second limits are from Bhabha data and for spin-0 singlet. The same limits apply for $\Gamma(X^0 \rightarrow e^+e^-) = 2$ MeV if X^0 is a spin-0 doublet. The second limit of BEHREND 84c was read off from their figure 2. The original papers also list limits in other channels.

Search for X^0 Resonance in e^+e^- Collisions

The limit is for $\Gamma(X^0 \rightarrow e^+e^-) \cdot B(X^0 \rightarrow f)$, where f is the specified final state. Spin 0 is assumed for X^0 .

VALUE (keV)	CL%	DOCUMENT ID	TECN	COMMENT
$<10^3$	95	1 ABE 93c VNS	$\Gamma(ee)$	
$<(0.4-1.0)$	95	2 ABE 93c VNS	$f = \gamma\gamma$	

- • • We do not use the following data for averages, fits, limits, etc. • • •

$<(0.3-5)$	95	3,4 ABE	93D TOPZ	$f = \gamma\gamma$
$<(2-12)$	95	3,4 ABE	93D TOPZ	$f = \text{hadrons}$
$<(4-200)$	95	4,5 ABE	93D TOPZ	$f = ee$
$<(0.1-6)$	95	4,5 ABE	93D TOPZ	$f = \mu\mu$
$<(0.5-8)$	90	6 STERNER	93 AMY	$f = \gamma\gamma$

- 1 Limit is for $\Gamma(X^0 \rightarrow e^+e^-) m_{X^0} = 56-63.5$ GeV for $\Gamma(X^0) = 0.5$ GeV.
- 2 Limit is for $m_{X^0} = 56-61.5$ GeV and is valid for $\Gamma(X^0) \ll 100$ MeV. See their Fig. 5 for limits for $\Gamma = 1, 2$ GeV.
- 3 Limit is for $m_{X^0} = 57.2-60$ GeV.
- 4 Limit is valid for $\Gamma(X^0) \ll 100$ MeV. See paper for limits for $\Gamma = 1$ GeV and those for $J = 2$ resonances.
- 5 Limit is for $m_{X^0} = 56.6-60$ GeV.
- 6 STERNER 93 limit is for $m_{X^0} = 57-59.6$ GeV and is valid for $\Gamma(X^0) < 100$ MeV. See their Fig. 2 for limits for $\Gamma = 1, 3$ GeV.

Search for X^0 Resonance in $e\rho$ Collisions

VALUE	DOCUMENT ID	TECN	COMMENT
• • • We do not use the following data for averages, fits, limits, etc. • • •			
	1 CHEKANOV 02b ZEUS	$X \rightarrow jj$	

- 1 CHEKANOV 02b search for photoproduction of X decaying into dijets in $e\rho$ collisions. See their Fig. 5 for the limit on the photoproduction cross section.

Search for X^0 Resonance in $e^+e^- \rightarrow X^0\gamma$

VALUE (GeV)	DOCUMENT ID	TECN	COMMENT
• • • We do not use the following data for averages, fits, limits, etc. • • •			
	1 ABBIENDI 03D OPAL	$X^0 \rightarrow \gamma\gamma$	
	2 ABREU 00z DLPH	X^0 decaying invisibly	
	3 ADAM 96c DLPH	X^0 decaying invisibly	

- 1 ABBIENDI 03D measure the $e^+e^- \rightarrow \gamma\gamma\gamma$ cross section at $\sqrt{s}=181-209$ GeV. The upper bound on the production cross section, $\sigma(e^+e^- \rightarrow X^0\gamma)$ times the branching ratio for $X^0 \rightarrow \gamma\gamma$, is less than 0.03 pb at 95%CL for X^0 masses between 20 and 180 GeV. See their Fig. 9b for the limits in the mass-cross section plane.
- 2 ABREU 00z is from the single photon cross section at $\sqrt{s}=183, 189$ GeV. The production cross section upper limit is less than 0.3 pb for X^0 mass between 40 and 160 GeV. See their Fig. 4 for the limit in mass-cross section plane.
- 3 ADAM 96c is from the single photon production cross at $\sqrt{s}=130, 136$ GeV. The upper bound is less than 3 pb for X^0 masses between 60 and 130 GeV. See their Fig. 5 for the exact bound on the cross section $\sigma(e^+e^- \rightarrow \gamma X^0)$.

Search for X^0 Resonance in $Z \rightarrow f\bar{f}X^0$

The limit is for $B(Z \rightarrow f\bar{f}X^0) \cdot B(X^0 \rightarrow F)$ where f is a fermion and F is the specified final state. Spin 0 is assumed for X^0 .

VALUE	CL%	DOCUMENT ID	TECN	COMMENT
• • • We do not use the following data for averages, fits, limits, etc. • • •				
$<3.7 \times 10^{-6}$	95	1 ABREU 96T DLPH	$f=e, \mu, \tau; F=\gamma\gamma$	
		2 ABREU 96T DLPH	$f=\nu; F=\gamma\gamma$	
		3 ABREU 96T DLPH	$f=q; F=\gamma\gamma$	
$<6.8 \times 10^{-6}$	95	2 ACTON 93E OPAL	$f=e, \mu, \tau; F=\gamma\gamma$	
$<5.5 \times 10^{-6}$	95	2 ACTON 93E OPAL	$f=q; F=\gamma\gamma$	
$<3.1 \times 10^{-6}$	95	2 ACTON 93E OPAL	$f=\nu; F=\gamma\gamma$	
$<6.5 \times 10^{-6}$	95	2 ACTON 93E OPAL	$f=e, \mu; F=\ell\bar{\ell}, q\bar{q}, \nu\bar{\nu}$	
$<7.1 \times 10^{-6}$	95	2 BUSKULIC 93F ALEP	$f=e, \mu; F=\ell\bar{\ell}, q\bar{q}, \nu\bar{\nu}$	
		4 ADRIANI 92F L3	$f=q; F=\gamma\gamma$	

- 1 ABREU 96T obtain limit as a function of m_{X^0} . See their Fig. 6.
- 2 Limit is for m_{X^0} around 60 GeV.
- 3 ABREU 96T obtain limit as a function of m_{X^0} . See their Fig. 15.
- 4 ADRIANI 92F give $\sigma_Z \cdot B(Z \rightarrow q\bar{q}X^0) \cdot B(X^0 \rightarrow \gamma\gamma) < (0.75-1.5)$ pb (95%CL) for $m_{X^0} = 10-70$ GeV. The limit is 1 pb at 60 GeV.

Search for X^0 Resonance in WX^0 final state

VALUE (MeV)	DOCUMENT ID	TECN	COMMENT
• • • We do not use the following data for averages, fits, limits, etc. • • •			
	1 AALTONEN 13AA CDF	$X^0 \rightarrow jj$	
	2 CHATRCHYAN 12BR CMS	$X^0 \rightarrow jj$	
	3 ABAZOV 11i D0	$X^0 \rightarrow jj$	
	4 ABE 97W CDF	$X^0 \rightarrow b\bar{b}$	

- 1 AALTONEN 13AA search for X^0 production associated with W (or Z) in $p\bar{p}$ collisions at $E_{\text{cm}} = 1.96$ TeV. The upper limit on the cross section $\sigma(p\bar{p} \rightarrow WX^0)$ is 2.2 pb for $M_{X^0} = 145$ GeV.
- 2 CHATRCHYAN 12BR search for X^0 production associated with W in pp collisions at $E_{\text{cm}} = 7$ TeV. The upper limit on the cross section is 5.0 pb at 95% CL for $m_{X^0} = 150$ GeV.
- 3 ABAZOV 11i search for X^0 production associated with W in $p\bar{p}$ collisions at $E_{\text{cm}} = 1.96$ TeV. The 95% CL upper limit on the cross section ranges from 2.57 to 1.28 pb for X^0 mass between 110 and 170 GeV.
- 4 ABE 97W search for X^0 production associated with W in $p\bar{p}$ collisions at $E_{\text{cm}} = 1.8$ TeV. The 95%CL upper limit on the production cross section times the branching ratio

See key on page 1171

Gauge & Higgs Boson Particle Listings
New Heavy Bosons

for X0 -> b b-bar ranges from 14 to 19 pb for X0 mass between 70 and 120 GeV. See their Fig. 3 for upper limits of the production cross section as a function of m_X0.

Search for X0 Resonance in Quarkonium Decays

Limits are for branching ratios to modes shown. Spin 1 is assumed for X0.

Table with columns: VALUE, CL%, DOCUMENT ID, TECN, COMMENT. Includes entries like BALEST 95 CLE2 for gamma(15) -> X0 X0-bar.

Search for X0 Resonance in H(125) Decays

Spin 1 is assumed for X0. See neutral Higgs search listing for pseudoscalar X0.

Table with columns: VALUE, DOCUMENT ID, TECN, COMMENT. Includes entries like AAD 22j ATLS for X0 -> l+ l- and AABOUD 18AP ATLS for H(125) -> X0 X0-bar.

REFERENCES FOR Searches for New Heavy Bosons (W', Z', leptoquarks, etc.)

Extensive list of references for searches for new heavy bosons, including authors like Cabarcas, Aad, Aaboud, and various ATLAS and CMS publications.

Extensive list of references for gauge and Higgs boson particle listings, including authors like Aad, Aaboud, Aaij, and various ATLAS, CMS, and LHCb publications.

See key on page 1171

Gauge & Higgs Boson Particle Listings
New Heavy Bosons, Axions (A^0) and Other Very Light Bosons

Table listing particle decays and searches, including authors (e.g., Grossman, Stahl, Abachi), journal references (e.g., PR D55 2768), and experimental collaborations (e.g., REHO, CIT, CERN).

Table listing authors (e.g., Mikaelian, SATO, Vysotskii) and their associated experiments (e.g., ASTR, Standard Axion).

1 Lower bound from 5.5 MeV gamma-ray line from the sun.
2 Lower bound from requiring the red giants' stellar evolution not be disrupted by axion emission.

A^0 (Axion) and Other Light Boson (X^0) Searches in Hadron Decays
Limits are for branching ratios.

Table of branching ratios and search results for Axion (A^0) and other light bosons (X^0) in hadron decays, including columns for VALUE, CL%, DOCUMENT ID, TECN, and COMMENT.

Axions (A^0) and Other Very Light Bosons, Searches for

See the related review(s): Axions and Other Similar Particles

A^0 (Axion) MASS LIMITS from Astrophysics and Cosmology

These bounds depend on model-dependent assumptions (i.e. — on a combination of axion parameters).

Table listing mass limits for Axion (A^0) from astrophysics and cosmology, including columns for VALUE (MeV), DOCUMENT ID, TECN, and COMMENT.

1 ADACHI 23k quoted limit is for m_X0 approx 3 GeV, ctau_X0 = 1 cm, and the decay channel X0 -> e+e-. See their Fig. 2 for limits with different lifetimes and decay channels.
2 ADACHI 23k quoted limit is for m_X0 approx 2 GeV, ctau_X0 = 1 cm, and the decay channel X0 -> e+e-. See their Fig. 2 for limits with different lifetimes and decay channels.
3 CORTINA-GIL 23B limit extends over 10-170 MeV in mass. Quoted limit is at 155 MeV.

Gauge & Higgs Boson Particle Listings

Axions (A^0) and Other Very Light Bosons

- ⁴ LEES 22B quoted limit is for $m_{A^0} = 3.9$ GeV, assuming the promptly decaying axion. Limits of $O(10^{-7})$ are obtained for $m_{A^0} = 0.175\text{--}4.78$ GeV. See their Figs.3 and 4 for mass and lifetime dependent limits.
- ⁵ ABRATENKO 21 quoted limit is for $m_{X^0} = 150$ MeV and the lifetime $c\tau_{X^0} = 80$ m. See their Fig. 4 for the limits in the range of $m_{X^0} = 10\text{--}210$ MeV.
- ⁶ CORTINA-GIL 21 quoted limit is for $m_{X^0} = 370$ MeV. Limits from $O(10^{-5})$ and $O(10^{-6})$ are obtained for $m_{X^0} = 10\text{--}370$ MeV (see their Fig. 7).
- ⁷ CORTINA-GIL 21A quoted limit is for $m_{X^0} = 160\text{--}250$ MeV. Limits between 5×10^{-11} and 2×10^{-10} are obtained in the range of $m_{X^0} = 0\text{--}110$ and $154\text{--}260$ MeV, assuming stable or invisibly decaying X^0 . See their Fig. 4 for mass- and lifetime-dependent limits.
- ⁸ CORTINA-GIL 21C quoted limit is for $m_{X^0} = 130\text{--}140$ MeV, and limits of $9 \times 10^{-10}\text{--}6 \times 10^{-7}$ are obtained in the mass range of $m_{X^0} = 110\text{--}155$ MeV, assuming X^0 escapes detection. See their Fig. 6 for mass- and lifetime-dependent limits.
- ⁹ PARK 21 look for dark photons produced by decays of B^0 through off-shell Higgs-dark Higgs mixing. See their Fig. 5 for limits in the range of $m_{X^0} = 0.01\text{--}2.62$ GeV.
- ¹⁰ AHN 19 is an update of AHN 17 from a new data set. See their Fig. 4 for the limits in the range of $m_{X^0} = 0\text{--}250$ MeV.
- ¹¹ AAIJ 17AQ limit is for $\tau_{X^0} = 10$ ps. See their Fig. 4 for limits in the range of $m_{X^0} = 250\text{--}4700$ MeV and $\tau_{X^0} = 0.1\text{--}1000$ ps.
- ¹² AHN 17 limit as a function of m_{X^0} from 0 to 250 MeV is provided in their Fig. 5.
- ¹³ BATLEY 17 limit is for $m_{X^0} = 216$ MeV and $\tau_{X^0} \leq 10$ ps. See their Fig. 4(c) for limits in the range of $m_{X^0} = 211\text{--}354$ MeV and longer lifetimes.
- ¹⁴ WON 16 look for a vector boson coupled to baryon number. Derived limits on $\alpha' < 10^{-3}\text{--}10^{-2}$ for $m_{X^0} = 290\text{--}520$ MeV at 95% CL. See their Fig. 4 for mass-dependent limits.
- ¹⁵ AAIJ 15AZ limit is for $\tau_{X^0} = 10$ ps and $m_{X^0} = 214\text{--}4350$ MeV. See their Fig. 4 for mass- and lifetime-dependent limits.
- ¹⁶ ADLARSON 13 limits between 2.0×10^{-5} and 1.5×10^{-6} are obtained for $m_{X^0} = 20\text{--}100$ MeV (see their Fig. 8). Angular momentum conservation requires that X^0 has spin ≥ 1 .
- ¹⁷ BABUSCI 13B limit is for $B(\phi \rightarrow \eta X^0) \cdot B(X^0 \rightarrow e^+ e^-)$ and applies to $m_{X^0} = 410$ MeV. It is derived by analyzing $\eta \rightarrow \pi^0 a_0^0$ and $\pi^- \pi^+ \pi^0$. Limits between 1×10^{-6} and 2×10^{-8} are obtained for $m_{X^0} \leq 450$ MeV (see their Fig. 6).
- ¹⁸ ARCHILLI 12 analyzed $\eta \rightarrow \pi^+ \pi^- \pi^0$ decays. Derived limits on $\alpha'/\alpha < 2 \times 10^{-5}$ for $m_{X^0} = 50\text{--}420$ MeV at 90% CL. See their Fig. 8 for mass-dependent limits.
- ¹⁹ GNINENKO 12A limit is for $B(\pi^0 \rightarrow \gamma X^0) \cdot B(X^0 \rightarrow e^+ e^-)$ and applies for $m_{X^0} = 90$ MeV and $\tau_{X^0} \approx 1 \times 10^{-8}$ sec. Limits between 10^{-8} and 2×10^{-15} are obtained for $m_{X^0} = 3\text{--}120$ MeV and $\tau_{X^0} = 1 \times 10^{-11}\text{--}1$ sec. See their Fig. 3 for limits at different masses and lifetimes.
- ²⁰ GNINENKO 12B limit is for $B(\eta \rightarrow \gamma X^0) \cdot B(X^0 \rightarrow e^+ e^-)$ and applies for $m_{X^0} = 100$ MeV and $\tau_{X^0} \approx 6 \times 10^{-9}$ sec. Limits between 10^{-5} and 3×10^{-14} are obtained for $m_{X^0} \lesssim 550$ MeV and $\tau_{X^0} = 10^{-10}\text{--}10$ sec. See their Fig. 5 for limits at different mass and lifetime and for η' decays.
- ²¹ ADLER 04 limit applies for a mass near 180 MeV. For other masses in the range $m_{X^0} = 150\text{--}250$ MeV the limit is less restrictive, but still improves ADLER 02c and ATIYA 93B.
- ²² ANISIMOVSKY 04 bound is for $m_{X^0} = 0$.
- ²³ ADLER 02c bound is for $m_{X^0} < 60$ MeV. See Fig. 2 for limits at higher masses.
- ²⁴ The quoted limit is for $m_{X^0} = 0\text{--}80$ MeV. See their Fig. 5 for the limit at higher mass. The branching fraction limit assumes pure phase space decay distributions.
- ²⁵ ALTEGOER 98 looked for X^0 from π^0 decay which penetrate the shielding and convert to π^0 in the external Coulomb field of a nucleus.
- ²⁶ KITCHING 97 limit is for $B(K^+ \rightarrow \pi^+ X^0) \cdot B(X^0 \rightarrow \gamma\gamma)$ and applies for $m_{X^0} \approx 50$ MeV, $\tau_{X^0} < 10^{-10}$ s. Limits are provided for $0 < m_{X^0} < 100$ MeV, $\tau_{X^0} < 10^{-8}$ s.
- ²⁷ ADLER 96 looked for a peak in missing-mass distribution. This work is an update of ATIYA 93. The limit is for massless stable X^0 particles and extends to $m_{X^0} = 80$ MeV at the same level. See paper for dependence on finite lifetime.
- ²⁸ AMSLER 94b and AMSLER 96b looked for a peak in missing-mass distribution.
- ²⁹ MEIJERDREES 94 limit is based on inclusive photon spectrum and is independent of X^0 decay modes. It applies to $\tau(X^0) > 10^{-23}$ sec.
- ³⁰ ATIYA 93b looked for a peak in missing mass distribution. The bound applies for stable X^0 of $m_{X^0} = 150\text{--}250$ MeV, and the limit becomes stronger (10^{-8}) for $m_{X^0} = 180\text{--}240$ MeV.
- ³¹ NG 93 studied the production of X^0 via $\gamma\gamma \rightarrow \pi^0 \rightarrow \gamma X^0$ in the early universe at $T \approx 1$ MeV. The bound on extra neutrinos from nucleosynthesis $\Delta N_\nu < 0.3$ (WALKER 91) is employed. It applies to $m_{X^0} \ll 1$ MeV in order to be relativistic down to nucleosynthesis temperature. See paper for heavier X^0 .
- ³² ALLIEGRO 92 limit applies for $m_{X^0} = 150\text{--}340$ MeV and is the branching ratio times the decay probability. Limit is $< 1.5 \times 10^{-8}$ at 99% CL.
- ³³ ATIYA 92 looked for a peak in missing mass distribution. The limit applies to $m_{X^0} = 0\text{--}130$ MeV in the narrow resonance limit. See paper for the dependence on lifetime. Covariance requires X^0 to be a vector particle.
- ³⁴ BARABASH 92 is a beam dump experiment that searched for a light Higgs. Limits between 1×10^{-12} and 1×10^{-7} are obtained for $3 < m_{X^0} < 40$ MeV.
- ³⁵ Limits between 1×10^{-12} and 1 are obtained for $4 < m_{X^0} < 69$ MeV.
- ³⁶ Limits between 1×10^{-11} and 5×10^{-3} are obtained for $4 < m_{X^0} < 63$ MeV.
- ³⁷ Limits between 1×10^{-14} and 1 are obtained for $3 < m_{X^0} < 82$ MeV.
- ³⁸ MEIJERDREES 92 limit applies for $\tau_{X^0} = 10^{-23}\text{--}10^{-11}$ sec. Limits between 2×10^{-4} and 4×10^{-6} are obtained for $m_{X^0} = 25\text{--}120$ MeV. Angular momentum conservation requires that X^0 has spin ≥ 1 .

- ³⁹ ATIYA 90b limit is for $B(K^+ \rightarrow \pi^+ X^0) \cdot B(X^0 \rightarrow \gamma\gamma)$ and applies for $m_{X^0} = 50$ MeV, $\tau_{X^0} < 10^{-10}$ s. Limits are also provided for $0 < m_{X^0} < 100$ MeV, $\tau_{X^0} < 10^{-8}$ s.
- ⁴⁰ KORENCHENKO 87 limit assumes $m_{A^0} = 1.7$ MeV, $\tau_{A^0} \lesssim 10^{-12}$ s, and $B(A^0 \rightarrow e^+ e^-) = 1$.
- ⁴¹ EICHLER 86 looked for $\pi^+ \rightarrow e^+ \nu A^0$ followed by $A^0 \rightarrow e^+ e^-$. Limits on the branching fraction depend on the mass and lifetime of A^0 . The quoted limits are valid when $\tau(A^0) \gtrsim 3 \times 10^{-10}$ s if the decays are kinematically allowed.
- ⁴² YAMAZAKI 84 looked for a discrete line in $K^+ \rightarrow \pi^+ X$. Sensitive to wide mass range (5–300 MeV), independent of whether X decays promptly or not.
- ⁴³ ASANO 82 at KEK set limits for $B(K^+ \rightarrow \pi^+ X^0)$ for $m_{X^0} < 100$ MeV as $BR < 4 \times 10^{-8}$ for $\tau(X^0 \rightarrow n\gamma\text{'s}) > 1 \times 10^{-9}$ s, $BR < 1.4 \times 10^{-6}$ for $\tau < 1 \times 10^{-9}$ s.
- ⁴⁴ ASANO 81B is KEK experiment. Set $B(K^+ \rightarrow \pi^+ X^0) < 3.8 \times 10^{-8}$ at CL = 90%.
- ⁴⁵ ZHITNITSKII 79 argue that a heavy axion predicted by YANG 78 ($3 < m < 40$ MeV) contradicts experimental muon anomalous magnetic moments.

A^0 (Axion) Searches in Quarkonium Decays

Decay or transition of quarkonium. Limits are for branching ratio.

VALUE	CL%	DOCUMENT ID	TECN	COMMENT
• • • We do not use the following data for averages, fits, limits, etc. • • •				
$< 8.3 \times 10^{-8}$	95	1 ABLIKIM	23E BES3	$J/\psi \rightarrow A^0 \gamma (A^0 \rightarrow \gamma\gamma)$
$< 3.1 \times 10^{-7}$	90	2 JIA	22 BELL	$\Upsilon(1S) \rightarrow A^0 \gamma (A^0 \rightarrow \mu^+ \mu^-)$
$< 2.8 \times 10^{-8}$	90	3 ABLIKIM	16E BES3	$J/\psi \rightarrow A^0 \gamma (A^0 \rightarrow \mu^+ \mu^-)$
$< 4 \times 10^{-7}$	90	4 ABLIKIM	12 BES3	$J/\psi \rightarrow A^0 \gamma (A^0 \rightarrow \mu^+ \mu^-)$
$< 4.0 \times 10^{-5}$	90	5 ANTREASYAN	90C CBAL	$\Upsilon(1S) \rightarrow A^0 \gamma$
$< 5 \times 10^{-5}$	90	6 DRUZHININ	87 ND	$\phi \rightarrow A^0 \gamma (A^0 \rightarrow e^+ e^-)$
$< 2 \times 10^{-3}$	90	7 DRUZHININ	87 ND	$\phi \rightarrow A^0 \gamma (A^0 \rightarrow \gamma\gamma)$
$< 7 \times 10^{-6}$	90	8 DRUZHININ	87 ND	$\phi \rightarrow A^0 \gamma (A^0 \rightarrow \text{missing})$
$< 1.4 \times 10^{-5}$	90	9 EDWARDS	82 CBAL	$J/\psi \rightarrow A^0 \gamma$
1 ABLIKIM 23c obtained limits in the range of $8.3 \times 10^{-8}\text{--}1.8 \times 10^{-6}$ for 0.165 GeV $\leq m_{A^0} \leq 2.84$ GeV. See their Fig. 5 for mass-dependent limits.				
2 JIA 22 limits between $3.1 \times 10^{-7}\text{--}1.6 \times 10^{-5}$ were obtained for 0.22 GeV $< m_{A^0} < 9.2$ GeV. See their Fig. 4 for mass-dependent limits.				
3 ABLIKIM 16E limits between $2.8\text{--}495.3 \times 10^{-8}$ were obtained for 0.212 GeV $< m_{A^0} < 3.0$ GeV. See their Fig. 5 for mass-dependent limits.				
4 ABLIKIM 12 derived limits between $4 \times 10^{-7}\text{--}2.1 \times 10^{-5}$ for 0.212 GeV $< m_{A^0} < 3.0$ GeV. See their Fig. 2(c) for mass-dependent limits.				
5 ANTREASYAN 90c assume that A^0 does not decay in the detector.				
6 The first DRUZHININ 87 limit is valid when $\tau_{A^0}/m_{A^0} < 3 \times 10^{-13}$ s/MeV and $m_{A^0} < 20$ MeV.				
7 The second DRUZHININ 87 limit is valid when $\tau_{A^0}/m_{A^0} < 5 \times 10^{-13}$ s/MeV and $m_{A^0} < 20$ MeV.				
8 The third DRUZHININ 87 limit is valid when $\tau_{A^0}/m_{A^0} > 7 \times 10^{-12}$ s/MeV and $m_{A^0} < 200$ MeV.				
9 EDWARDS 82 looked for $J/\psi \rightarrow \gamma A^0$ decays by looking for events with a single γ [of energy $\sim 1/2$ the $J/\psi(1S)$ mass], plus nothing else in the detector. The limit is inconsistent with the axion interpretation of the FAISSNER 81B result.				

A^0 (Axion) Searches in Positronium Decays

Decay or transition of positronium. Limits are for branching ratio.

VALUE	CL%	DOCUMENT ID	TECN	COMMENT
• • • We do not use the following data for averages, fits, limits, etc. • • •				
$< 4.4 \times 10^{-5}$	90	1 BADERT...	02 CNTR	$o\text{-Ps} \rightarrow \gamma X_1 X_2, m_{X_1} + m_{X_2} \leq 900$ keV
$< 2 \times 10^{-4}$	90	MAENO	95 CNTR	$o\text{-Ps} \rightarrow A^0 \gamma, m_{A^0} = 850\text{--}1013$ keV
$< 3.0 \times 10^{-4}$	90	2 ASAI	94 CNTR	$o\text{-Ps} \rightarrow A^0 \gamma, m_{A^0} = 30\text{--}500$ keV
$< 2.8 \times 10^{-5}$	90	3 AKOPYAN	91 CNTR	$o\text{-Ps} \rightarrow A^0 \gamma (A^0 \rightarrow \gamma\gamma), m_{A^0} < 30$ keV
$< 1.1 \times 10^{-6}$	90	4 ASAI	91 CNTR	$o\text{-Ps} \rightarrow A^0 \gamma, m_{A^0} < 800$ keV
$< 3.8 \times 10^{-4}$	90	GNINENKO	90 CNTR	$o\text{-Ps} \rightarrow A^0 \gamma, m_{A^0} < 30$ keV
$< (1\text{--}5) \times 10^{-4}$	95	5 TSUCHIYAKI	90 CNTR	$o\text{-Ps} \rightarrow A^0 \gamma, m_{A^0} = 300\text{--}900$ keV
$< 6.4 \times 10^{-5}$	90	6 ORITO	89 CNTR	$o\text{-Ps} \rightarrow A^0 \gamma, m_{A^0} < 30$ keV
		7 AMALDI	85 CNTR	Ortho-positronium
		8 CARBONI	83 CNTR	Ortho-positronium
1 BADERTSCHER 02 looked for a three-body decay of ortho-positronium into a photon and two penetrating (neutral or milli-charged) particles.				
2 The ASAI 94 limit is based on inclusive photon spectrum and is independent of A^0 decay modes.				
3 The AKOPYAN 91 limit applies for a short-lived A^0 with $\tau_{A^0} < 10^{-13}$ m_{A^0} [keV]s.				
4 ASAI 91 limit translates to $g_{A^0 e^+ e^-}^2 / 4\pi < 1.1 \times 10^{-11}$ (90% CL) for $m_{A^0} < 800$ keV.				
5 The TSUCHIYAKI 90 limit is based on inclusive photon spectrum and is independent of A^0 decay modes.				
6 ORITO 89 limit translates to $g_{A^0 e^+ e^-}^2 / 4\pi < 6.2 \times 10^{-10}$. Somewhat more sensitive limits are obtained for larger m_{A^0} : $B < 7.6 \times 10^{-6}$ at 100 keV.				
7 AMALDI 85 set limits $B(A^0 \gamma) / B(\gamma\gamma) < (1\text{--}5) \times 10^{-6}$ for $m_{A^0} = 900\text{--}100$ keV which are about 1/10 of the CARBONI 83 limits.				
8 CARBONI 83 looked for ortho-positronium $\rightarrow A^0 \gamma$. Set limit for A^0 electron coupling squared, $g(eA^0)^2 / (4\pi) < 6 \times 10^{-10}\text{--}7 \times 10^{-9}$ for m_{A^0} from 150–900 keV (CL = 99.7%). This is about 1/10 of the bound from $g\text{--}2$ experiments.				

See key on page 1171

Gauge & Higgs Boson Particle Listings
Axions (A^0) and Other Very Light Bosons A^0 (Axion) Search in Photoproduction

VALUE	DOCUMENT ID	TECN	COMMENT
• • •	We do not use the following data for averages, fits, limits, etc. • • •		
	¹ ADHIKARI 22c	GLUX	$m_{A^0} = 180\text{--}480, 600\text{--}720$ MeV
	² BASSOMPIERRE... 95		$m_{A^0} = 1.8 \pm 0.2$ MeV
¹ ADHIKARI 22c	search for $A^0 \rightarrow \gamma\gamma$ and $A^0 \rightarrow \pi^+\pi^-\pi^0$ decays, and set limits of $f_{A^0} \lesssim 0.5\text{--}14$ GeV at 90% CL. See their Fig. 4 for mass-dependent limits.		
² BASSOMPIERRE 95	is an extension of BASSOMPIERRE 93. They looked for a peak in the invariant mass of e^+e^- pairs in the region $m_{e^+e^-} = 1.8 \pm 0.2$ MeV. They obtained bounds on the production rate A^0 for $\tau(A^0) = 10^{-18}\text{--}10^{-9}$ sec. They also found an excess of events in the range $m_{e^+e^-} = 2.1\text{--}3.5$ MeV.		

 A^0 (Axion) Production in Hadron Collisions

VALUE	CL%	DOCUMENT ID	TECN	COMMENT
• • •	We do not use the following data for averages, fits, limits, etc. • • •			
		¹ ACCIARRI 23	ARNT	$A^0 \rightarrow \mu^+\mu^-$
		² BERTUZZO 23	ARNT	$A^0 \rightarrow \mu^+\mu^-$
		³ AAD 22j	ATLS	$H \rightarrow A^0 A^0, ZA^0$ ($A^0 \rightarrow \mu^+\mu^-$)
		⁴ TUMASYAN 22AH	CMS	$H \rightarrow A^0 A^0, A^0 \rightarrow e^+e^-, \mu^+\mu^-$
		⁵ TUMASYAN 22R	CMS	$pp \rightarrow A^0 \rightarrow ZZ, ZH$
		⁶ AAD 21F	ATLS	Monojet + missing p_T
		⁷ AAD 21K	ATLS	Mono- γ + missing p_T
		⁸ AAD 21N	ATLS	$\gamma\gamma$ scatt. in Pb+Pb
		⁹ CARRA 21	ATLS	$pp \rightarrow A^0 \rightarrow WW, Z\gamma$
		¹⁰ AAIJ 20AL	LHCB	$pp \rightarrow X^0 \rightarrow \mu^+\mu^-$
		¹¹ GAVELA 20	CMS	$pp \rightarrow A^0 \rightarrow \gamma\gamma, ZZ$
		¹² SIRUNYAN 19BQ	CMS	$X^0 \rightarrow \mu^+\mu^-$
		¹³ JAIN 07	CNTR	$A^0 \rightarrow e^+e^-$
		¹⁴ AHMAD 97	SPEC	e^+ production
		¹⁵ LEINBERGER 97	SPEC	$A^0 \rightarrow e^+e^-$
		¹⁶ GANZ 96	SPEC	$A^0 \rightarrow e^+e^-$
		¹⁷ KAMEL 96	EMUL	^{32}S emulsion, $A^0 \rightarrow e^+e^-$
		¹⁸ BLUEMLEIN 92	BDMP	$A^0 NZ \rightarrow \ell^+ \ell^- NZ$
		¹⁹ MEIJERDREES 92	SPEC	$\pi^- p \rightarrow nA^0, A^0 \rightarrow e^+e^-$
		²⁰ BLUEMLEIN 91	BDMP	$A^0 \rightarrow e^+e^-, 2\gamma$
		²¹ FAISSNER 89	OSPK	Beam dump, $A^0 \rightarrow e^+e^-$
		²² DEBOER 88	RVUE	$A^0 \rightarrow e^+e^-$
		²³ EL-NADI 88	EMUL	$A^0 \rightarrow e^+e^-$
		²⁴ FAISSNER 88	OSPK	Beam dump, $A^0 \rightarrow 2\gamma$
		²⁵ BADIER 86	BDMP	$A^0 \rightarrow e^+e^-$
		²⁶ BERGSMA 85	CHRM	CERN beam dump
		²⁶ BERGSMA 85	CHRM	CERN beam dump
		²⁷ FAISSNER 83	OSPK	Beam dump, $A^0 \rightarrow 2\gamma$
		²⁸ FAISSNER 83B	RVUE	LAMPF beam dump
		²⁹ FRANK 83B	RVUE	LAMPF beam dump
		³⁰ HOFFMAN 83	CNTR	$\pi p \rightarrow nA^0$ ($A^0 \rightarrow e^+e^-$)
		³¹ FETSCHER 82	RVUE	See FAISSNER 81B
		³² FAISSNER 81	OSPK	CERN PS ν band
		³³ FAISSNER 81B	OSPK	Beam dump, $A^0 \rightarrow 2\gamma$
		³⁴ KIM 81	OSPK	26 GeV $pN \rightarrow A^0 X$
		³⁵ FAISSNER 80	OSPK	Beam dump, $A^0 \rightarrow e^+e^-$
$<1. \times 10^{-11}$	90	³⁶ JACQUES 80	HLBC	28 GeV protons
$<1. \times 10^{-13}$	90	³⁶ JACQUES 80	HLBC	Beam dump
		³⁷ SOUKAS 80	CALO	28 GeV p beam dump
		³⁸ BECHIS 79	CNTR	
$<1. \times 10^{-8}$	90	³⁹ COTEUS 79	OSPK	Beam dump
$<1. \times 10^{-3}$	95	⁴⁰ DISHAW 79	CALO	400 GeV pp
$<1. \times 10^{-8}$	90	⁴¹ ALIBRAN 78	HYBR	Beam dump
$<6. \times 10^{-9}$	95	⁴² ASRATYAN 78B	CALO	Beam dump
$<1.5 \times 10^{-8}$	90	⁴¹ BELLOTTI 78	HLBC	Beam dump
$<5.4 \times 10^{-14}$	90	⁴¹ BELLOTTI 78	HLBC	$m_{A^0}=1.5$ MeV
$<4.1 \times 10^{-9}$	90	⁴¹ BELLOTTI 78	HLBC	$m_{A^0}=1$ MeV
$<1. \times 10^{-8}$	90	⁴² BOSETTI 78B	HYBR	Beam dump
		⁴³ DONNELLY 78		
$<0.5 \times 10^{-8}$	90	⁴⁴ HANSL 78D	WIRE	Beam dump
		⁴⁵ MICELMAC... 78		
		⁴⁶ VYSOTSKII 78		

¹ACCIARRI 23 search for axions in the NuMI neutrino beam target, which are produced through mixings with mesons due to the coupling with gluons, and exclude f_{A^0} around tens of TeV for $m_{A^0} = 0.2\text{--}0.9$ GeV. They assume a slightly suppressed axion coupling to muons. See their Fig. 4 for the limits.

²BERTUZZO 23 employs an analysis analogous to ACCIARRI 23. They search for lepton-like axions primarily produced via $\tau \rightarrow \mu A^0$ and $\tau \rightarrow e A^0$, and exclude f_{A^0} around $1 \times 10^6\text{--}6 \times 10^7$ GeV for $m_{A^0} = 0.2\text{--}1.7$ GeV. See their Fig. 2 for the limits.

³AAD 22j set upper limits for the cross sections of $H \rightarrow A^0 A^0 \rightarrow 4\mu$ and $H \rightarrow ZA^0 \rightarrow 2E2\mu$. See their Figs. 14 and 17 for the respective mass-dependent limits.

⁴TUMASYAN 22AH set the limits of $O(10^{-6})$ with respect to the product of the branching fractions of $H \rightarrow A^0 A^0$ and $A^0 \rightarrow e^+e^-, \mu^+\mu^-$. They also derive limits on the effective axion couplings contributing to $H \rightarrow A^0 A^0$ and $H \rightarrow ZA^0$. See their Figs. 5 and 7 for the limits.

⁵TUMASYAN 22R is analogous to GAVELA 20, and set a limit on the products of the axion couplings to gluons and Z bosons as $G_{AZZ} G_{Agg} < 6.64 \times 10^{-7} \text{ GeV}^{-2}$ at 95% CL for $f_{A^0} = 3$ TeV and $m_{A^0} < 100$ GeV. Here we use $c_G^- = G_{Agg} f_{A^0}/4$ and $c_Z^- = G_{AZZ} f_{A^0}/4$ to translate their limits. They also set a limit on the product of the axion couplings to gluons and ZH. See their Fig. 9 for the f_{A^0} -dependent limits.

⁶AAD 21F look for axion production with an energetic jet and large missing p_T , and set a limit on the axion coupling to gluons, $c_G^-/f_{A^0} < 8 \times 10^{-6} \text{ GeV}^{-1}$ at 95% CL for $m_{A^0} = 1$ MeV. Using $c_G^- = \alpha_s/8\pi$, we interpret the limit as $f_{A^0} > 0.4$ TeV for $\alpha_s \approx 0.08$.

⁷AAD 21K look for axion production with an energetic photon and large missing p_T , and set a limit on the axion coupling to a Z boson and photon, $G_{AZ\gamma} < 5.1 \times 10^{-4} \text{ GeV}^{-1}$ at 95% CL for $m_{A^0} = 1$ MeV and assuming $G_{A\gamma\gamma} = 0$.

⁸AAD 21N look for axion production using the measurement of light-by-light scattering based on Pb+Pb collision data. They set the limit on the axion-photon coupling, $G_{A\gamma\gamma} < 5.3 \times 10^{-5}\text{--}3.4 \times 10^{-4} \text{ GeV}^{-1}$ at 95% CL for $m_{A^0} = 6\text{--}100$ GeV. Here we use $\Lambda_a = G_{A\gamma\gamma}^{-1}$ to translate their limits. See their Fig. 9 for mass-dependent limits.

⁹CARRA 21 is analogous to GAVELA 20, and they use the differential cross sections for WW and Z γ production measured with the ATLAS detector to set limits on the product of the axion couplings to gauge bosons as $G_{AWW} G_{Agg} < 6.2 \times 10^{-7} \text{ GeV}^{-2}$ and $G_{AZ\gamma} G_{Agg} < 3.7 \times 10^{-7} \text{ GeV}^{-2}$ at 95% CL for $m_{A^0} \lesssim 100$ GeV.

¹⁰AAIJ 20AL look for a light new boson decaying into a pair of muons using the LHCb data with an integrated luminosity of 5.1 fb $^{-1}$, and set limits on the cross section over a range of $m_{X^0} = 0.22\text{--}3$ and 20–60 GeV. See Figs. 8 and 9 for mass-dependent limits.

¹¹GAVELA 20 focus on the axion production as an s-channel off shell mediator, and use the Run 2 CMS public data to set limits on the product of the axion couplings to gluons and photons as well as Z bosons as $G_{A\gamma\gamma} G_{Agg} < 2.8 \times 10^{-7} \text{ GeV}^{-2}$ and $G_{AZZ} G_{Agg} < 9.8 \times 10^{-7} \text{ GeV}^{-2}$ for $m_{A^0} \lesssim 200$ GeV. See their Fig.3 for the limits.

¹²SIRUNYAN 19BQ look for the pair production of a new light boson decaying into a pair of muons, and set limits on the product of the production cross section times branching fraction to dimuons squared times acceptance over a range of $m_{X^0} = 0.25\text{--}8.5$ GeV. See the right panel of their Fig. 1 for mass-dependent limits.

¹³JAIN 07 claims evidence for $A^0 \rightarrow e^+e^-$ produced in 207Pb collision on nuclear emulsion (Ag/Br) for $m(A^0) = 7 \pm 1$ or 19 ± 1 MeV and $\tau(A^0) \leq 10^{-13}$ s.

¹⁴AHMAD 97 reports a result of APEX Collaboration which studied positron production in $^{238}\text{U}+^{232}\text{Th}$ and $^{238}\text{U}+^{181}\text{Ta}$ collisions, without requiring a coincident electron. No narrow lines were found for $250 < E_{e^+} < 750$ keV.

¹⁵LEINBERGER 97 (ORANGE Collaboration) at GSI looked for a narrow sum-energy e^+e^- line at ≈ 635 keV in $^{238}\text{U}+^{181}\text{Ta}$ collision. Limits on the production probability for a narrow sum-energy e^+e^- line are set. See their Table 2.

¹⁶GANZ 96 (EPOS II Collaboration) has placed upper bounds on the production cross section of e^+e^- pairs from $^{238}\text{U}+^{181}\text{Ta}$ and $^{238}\text{U}+^{232}\text{Th}$ collisions at GSI. See Table 2 for limits both for back-to-back and isotropic configurations of e^+e^- pairs. These limits rule out the existence of peaks in the e^+e^- sum-energy distribution, reported by an earlier version of this experiment.

¹⁷KAMEL 96 looked for e^+e^- pairs from the collision of ^{32}S (200 GeV/nucleon) and emulsion. No evidence of mass peaks is found in the region of sensitivity $m_{e^+e^-} > 2$ MeV.

¹⁸BLUEMLEIN 92 is a proton beam dump experiment at Serpukhov with a secondary target to induce Bethe-Heitler production of e^+e^- or $\mu^+\mu^-$ from the produce A^0 . See Fig. 5 for the excluded region in m_{A^0} -x plane. For the standard axion, $0.3 < x < 25$ is excluded at 95% CL. If combined with BLUEMLEIN 91, $0.008 < x < 32$ is excluded.

¹⁹MEIJERDREES 92 give $\Gamma(\pi^- p \rightarrow nA^0)/\Gamma(\pi^- p \rightarrow \text{all}) < 10^{-5}$ (90% CL) for $m_{A^0} = 100$ MeV, $\tau_{A^0} = 10^{-11}\text{--}10^{-23}$ sec. Limits ranging from 2.5×10^{-3} to 10^{-7} are given for $m_{A^0} = 25\text{--}136$ MeV.

²⁰BLUEMLEIN 91 is a proton beam dump experiment at Serpukhov. No candidate event for $A^0 \rightarrow e^+e^-, 2\gamma$ are found. Fig. 6 gives the excluded region in m_{A^0} -x plane ($x = \tan\beta = v_2/v_1$). Standard axion is excluded for $0.2 < m_{A^0} < 3.2$ MeV for most $x > 1$, 0.2–11 MeV for most $x < 1$.

²¹FAISSNER 89 searched for $A^0 \rightarrow e^+e^-$ in a proton beam dump experiment at SIN. No excess of events was observed over the background. A standard axion with mass $2m_e\text{--}20$ MeV is excluded. Lower limit on f_{A^0} of $\approx 10^4$ GeV is given for $m_{A^0} = 2m_e\text{--}20$ MeV.

²²DEBOER 88 reanalyze EL-NADI 88 data and claim evidence for three distinct states with mass $\sim 1.1, \sim 2.1, \text{ and } \sim 9$ MeV, lifetimes $10\text{--}16\text{--}10\text{--}15$ s decaying to e^+e^- and note the similarity of the data with those of a cosmic-ray experiment by Bristol group (B.M. Anand, Proc. of the Royal Society of London, Section A **A22** 183 (1953)). For a criticism see PERKINS 89, who suggests that the events are compatible with π^0 Dalitz decay. DEBOER 89B is a reply which contests the criticism.

²³EL-NADI 88 claim the existence of a neutral particle decaying into e^+e^- with mass 1.60 ± 0.59 MeV, lifetime $(0.15 \pm 0.01) \times 10^{-14}$ s, which is produced in heavy ion interactions with emulsion nuclei at ~ 4 GeV/c/nucleon.

²⁴FAISSNER 88 is a proton beam dump experiment at SIN. They found no candidate event for $A^0 \rightarrow \gamma\gamma$. A standard axion decaying to 2γ is excluded except for a region $x \approx 1$. Lower limit on f_{A^0} of $10^2\text{--}10^3$ GeV is given for $m_{A^0} = 0.1\text{--}1$ MeV.

²⁵BADIER 86 did not find long-lived A^0 in 300 GeV π^- Beam Dump Experiment that decays into e^+e^- in the mass range $m_{A^0} = (20\text{--}200)$ MeV, which excludes the A^0 decay constant $f(A^0)$ in the interval (60–600) GeV. See their figure 6 for excluded region on $f(A^0)\text{--}m_{A^0}$ plane.

²⁶BERGSMA 85 look for $A^0 \rightarrow 2\gamma, e^+e^-, \mu^+\mu^-$. First limit above is for $m_{A^0} = 1$ MeV; second is for 200 MeV. See their figure 4 for excluded region on $f_{A^0}\text{--}m_{A^0}$ plane.

Gauge & Higgs Boson Particle Listings

Axions (A^0) and Other Very Light Bosons

- where f_{A^0} is A^0 decay constant. For Peccei-Quinn PECCEI 77 A^0 , $m_{A^0} < 180$ keV and $\tau > 0.037$ s. (CL = 90%). For the axion of FAISSNER 81b at 250 keV, BERGSMAS 85 expect 15 events but observe zero.
- 27 FAISSNER 83 observed 19 $1-\gamma$ and 12 $2-\gamma$ events where a background of 4.8 and 2.3 respectively is expected. A small-angle peak is observed even if iron wall is set in front of the decay region.
- 28 FAISSNER 83b extrapolate SIN γ signal to LAMPF ν experimental condition. Resulting 370 γ 's are not at variance with LAMPF upper limit of 450 γ 's. Derived from LAMPF limit that $[d\sigma(A^0)/d\omega \text{ at } 90^\circ] m_{A^0} / \tau_{A^0} < 14 \times 10^{-35} \text{ cm}^2 \text{ sr}^{-1} \text{ MeV ms}^{-1}$. See comment on FRANK 83b.
- 29 FRANK 83b stress the importance of LAMPF data bins with negative net signal. By statistical analysis say that LAMPF and SIN-A0 are at variance when extrapolation by phase-space model is done. They find LAMPF upper limit is 248 not 450 γ 's. See comment on FAISSNER 83b.
- 30 HOFFMAN 83 set CL = 90% limit $d\sigma/dt \text{ B}(e^+e^-) < 3.5 \times 10^{-32} \text{ cm}^2/\text{GeV}^2$ for $140 < m_{A^0} < 160$ MeV. Limit assumes $\tau(A^0) < 10^{-9}$ s.
- 31 FETSCHER 82 reanalyzes SIN beam-dump data of FAISSNER 81. Claims no evidence for axion since $2-\gamma$ peak rate remarkably decreases if iron wall is set in front of the decay region.
- 32 FAISSNER 81 see excess μe events. Suggest axion interactions.
- 33 FAISSNER 81b is SIN 590 MeV proton beam dump. Observed 14.5 ± 5.0 events of 2γ decay of long-lived neutral penetrating particle with $m_{2\gamma} \lesssim 1$ MeV. Axion interpretation with $\eta-A^0$ mixing gives $m_{A^0} = 250 \pm 25$ keV, $\tau(2\gamma) = (7.3 \pm 3.7) \times 10^{-3}$ s from above rate. See critical remarks below in comments of FETSCHER 82, FAISSNER 83, FAISSNER 83b, FRANK 83b, and BERGSMAS 85. Also see in the next subsection ALEKSEEV 82b, CAVAINAC 83, and ANANEV 85.
- 34 KIM 81 analyzed 8 candidates for $A^0 \rightarrow 2\gamma$ obtained by Aachen-Padova experiment at CERN with 26 GeV protons on Be. Estimated axion mass is about 300 keV and lifetime is $(0.86 \sim 5.6) \times 10^{-3}$ s depending on models. Faisner (private communication), says axion production underestimated and mass overestimated. Correct value around 200 keV.
- 35 FAISSNER 80 is SIN beam dump experiment with 590 MeV protons looking for $A^0 \rightarrow e^+e^-$ decay. Assuming $A^0/m^0 = 5.5 \times 10^{-7}$, obtained decay rate limit $20/(A^0 \text{ mass}) \text{ MeV/s}$ (CL = 90%), which is about 10^{-7} below theory and interpreted as upper limit to $m_{A^0} < 2m_{e^-}$.
- 36 JACQUES 80 is a BNL beam dump experiment. First limit above comes from nonobservation of excess neutral-current-type events $[\sigma(\text{production})\sigma(\text{interaction}) < 7. \times 10^{-68} \text{ cm}^4, \text{ CL} = 90\%]$. Second limit is from nonobservation of axion decays into 2γ 's or e^+e^- , and for axion mass a few MeV.
- 37 SOUKAS 80 at BNL observed no excess of neutral-current-type events in beam dump.
- 38 BECHIS 79 looked for the axion production in low energy electron Bremsstrahlung and the subsequent decay into either 2γ or e^+e^- . No signal found. CL = 90% limits for model parameter(s) are given.
- 39 COTEUS 79 is a beam dump experiment at BNL.
- 40 DISHAW 79 is a calorimetric experiment and looks for low energy tail of energy distributions due to energy lost to weakly interacting particles.
- 41 BELLOTTI 78 first value comes from search for $A^0 \rightarrow e^+e^-$. Second value comes from search for $A^0 \rightarrow 2\gamma$, assuming mass $< 2m_{e^-}$. For any mass satisfying this, limit is above value $\times (\text{mass}^{-4})$. Third value uses data of PL 60B 401 and quotes $\sigma(\text{production})\sigma(\text{interaction}) < 10^{-67} \text{ cm}^4$.
- 42 BOSETTI 78b quotes $\sigma(\text{production})\sigma(\text{interaction}) < 2. \times 10^{-67} \text{ cm}^4$.
- 43 DONNELLY 78 examines data from reactor neutrino experiments of REINES 76 and GURR 74 as well as SLAC beam dump experiment. Evidence is negative.
- 44 MICELMACHER 78 finds no evidence of axion existence in reactor experiments of REINES 76 and GURR 74. (See reference under DONNELLY 78 below).
- 45 VYSOTSKI 78 derived lower limit for the axion mass 25 keV from luminosity of the sun and 200 keV from red supergiants.

A^0 (Axion) Searches in Reactor Experiments

VALUE	DOCUMENT ID	TECN	COMMENT
• • • We do not use the following data for averages, fits, limits, etc. • • •			
1	CHANG 07		Primakoff or Compton
2	ALTMANN 95	CNTR	Reactor; $A^0 \rightarrow e^+e^-$
3	KETOV 86	SPEC	Reactor; $A^0 \rightarrow \gamma\gamma$
4	KOCH 86	SPEC	Reactor; $A^0 \rightarrow \gamma\gamma$
5	DATAR 82	CNTR	Light water reactor
6	VUILLEUMIER 81	CNTR	Reactor; $A^0 \rightarrow 2\gamma$

- 1 CHANG 07 looked for monochromatic photons from Primakoff or Compton conversion of axions from the Kuo-Sheng reactor due to axion coupling to photon or electron, respectively. The search places model-independent limits on the products $G_{A\gamma\gamma} G_{ANN}$ and $G_{Aee} G_{ANN}$ for $m(A^0)$ less than the MeV range.
- 2 ALTMANN 95 looked for A^0 decaying into e^+e^- from the Bugey5 nuclear reactor. They obtain an upper limit on the A^0 production rate of $\omega(A^0)/\omega(\gamma) \times \text{B}(A^0 \rightarrow e^+e^-) < 10^{-16}$ for $m_{A^0} = 1.5$ MeV at 90% CL. The limit is weaker for heavier A^0 . In the case of a standard axion, this limit excludes a mass in the range $2m_e < m_{A^0} < 4.8$ MeV at 90% CL. See Fig. 5 of their paper for exclusion limits of axion-like resonances Z^0 in the (m_{χ^0}, f_{χ^0}) plane.
- 3 KETOV 86 searched for A^0 at the Rovno nuclear power plant. They found an upper limit on the A^0 production probability of $0.8 [100 \text{ keV}/m_{A^0}]^6 \times 10^{-6}$ per fission. In the standard axion model, this corresponds to $m_{A^0} > 150$ keV. Not valid for $m_{A^0} \gtrsim 1$ MeV.
- 4 KOCH 86 searched for $A^0 \rightarrow \gamma\gamma$ at nuclear power reactor Biblis A. They found an upper limit on the A^0 production rate of $\omega(A^0)/\omega(\gamma(M1)) < 1.5 \times 10^{-10}$ (CL=95%). Standard axion with $m_{A^0} = 250$ keV gives 10^{-5} for the ratio. Not valid for $m_{A^0} > 1022$ keV.

- 5 DATAR 82 looked for $A^0 \rightarrow 2\gamma$ in neutron capture ($np \rightarrow dA^0$) at Tarapur 500 MW reactor. Sensitive to sum of $l = 0$ and $l = 1$ amplitudes. With ZEHNDER 81 [$(l = 0) - (l = 1)$] result, assert nonexistence of standard A^0 .
- 6 VUILLEUMIER 81 is at Grenoble reactor. Set limit $m_{A^0} < 280$ keV.

A^0 (Axion) and Other Light Boson (X^0) Searches in Nuclear Transitions

Limits are for branching ratio.

VALUE	CL%	DOCUMENT ID	TECN	COMMENT
• • • We do not use the following data for averages, fits, limits, etc. • • •				
$< 8.89 \times 10^{-6}$	90	1 DERBIN 23	CNTR	M1 transition of ^{169}Tm
$< 8.5 \times 10^{-6}$	90	2 DERBIN 02	CNTR	^{125m}Te decay
		3 DEBOER 97c	RVUE	M1 transitions
$< 5.5 \times 10^{-10}$	95	4 TSUNODA 95	CNTR	^{252}Cf fission, $A^0 \rightarrow e^+e^-$
$< 1.2 \times 10^{-6}$	95	5 MINOWA 93	CNTR	$^{139}\text{La}^* \rightarrow ^{139}\text{La} A^0$
$< 2 \times 10^{-4}$	90	6 HICKS 92	CNTR	^{35}S decay, $A^0 \rightarrow \gamma\gamma$
$< 1.5 \times 10^{-9}$	95	7 ASANUMA 90	CNTR	^{241}Am decay
$< (0.4-10) \times 10^{-3}$	95	8 DEBOER 90	CNTR	$^8\text{Be}^* \rightarrow ^8\text{Be} A^0$, $^{16}\text{O}^* \rightarrow ^{16}\text{O} X^0$, $X^0 \rightarrow e^+e^-$
$< (0.2-1) \times 10^{-3}$	90	9 BINI 89	CNTR	$^{16}\text{O}^* \rightarrow ^{16}\text{O} X^0$, $X^0 \rightarrow e^+e^-$
		10 AVIGNONE 88	CNTR	$\text{Cu}^* \rightarrow \text{Cu} A^0 (A^0 \rightarrow 2\gamma)$, $A^0 e^- \rightarrow \gamma e, A^0 Z \rightarrow \gamma Z$
$< 1.5 \times 10^{-4}$	90	11 DATAR 88	CNTR	$^{12}\text{C}^* \rightarrow ^{12}\text{C} A^0$, $A^0 \rightarrow e^+e^-$
$< 5 \times 10^{-3}$	90	12 DEBOER 88c	CNTR	$^{16}\text{O}^* \rightarrow ^{16}\text{O} X^0$, $X^0 \rightarrow e^+e^-$
$< 3.4 \times 10^{-5}$	95	13 DOEHNER 88	SPEC	$^2\text{H}^*, A^0 \rightarrow e^+e^-$
$< 4 \times 10^{-4}$	95	14 SAVAGE 88	CNTR	Nuclear decay (isovector)
$< 3 \times 10^{-3}$	95	14 SAVAGE 88	CNTR	Nuclear decay (isoscalar)
$< 10.6 \times 10^{-2}$	90	15 HALLIN 86	SPEC	^6Li isovector decay
< 10.8	90	15 HALLIN 86	SPEC	^{10}B isoscalar decays
< 2.2	90	15 HALLIN 86	SPEC	^{14}N isoscalar decays
$< 4 \times 10^{-4}$	90	16 SAVAGE 86b	CNTR	$^{14}\text{N}^*$
		17 ANANEV 85	CNTR	$\text{Li}^*, \text{deut}^* A^0 \rightarrow 2\gamma$
		18 CAVAINAC 83	CNTR	$^{97}\text{Nb}^*, \text{deut}^* \text{ transition } A^0 \rightarrow 2\gamma$
		19 ALEKSEEV 82b	CNTR	$\text{Li}^*, \text{deut}^* \text{ transition } A^0 \rightarrow 2\gamma$
		20 LEHMANN 82	CNTR	$\text{Cu}^* \rightarrow \text{Cu} A^0 (A^0 \rightarrow 2\gamma)$
		21 ZEHNDER 82	CNTR	$\text{Li}^*, \text{Nb}^* \text{ decay, } n\text{-capt.}$
		22 ZEHNDER 81	CNTR	$\text{Ba}^* \rightarrow \text{Ba} A^0 (A^0 \rightarrow 2\gamma)$
		23 CALAPRICE 79		Carbon

- 1 DERBIN 23 use a thallium garnet bolometric detector to search for the 8.4 keV solar axion line emitted from the M1 nuclear transition of ^{169}Tm . Their limits are equivalent to an upper bound on the KSVZ and DFSZ axion masses of 141 eV and 244 eV, respectively.
- 2 DERBIN 02 looked for the axion emission in an M1 transition in ^{125m}Te decay. They looked for a possible presence of a shifted energy spectrum in gamma rays due to the undetected axion.
- 3 DEBOER 97c reanalyzed the existent data on Nuclear M1 transitions and find that a 9 MeV boson decaying into e^+e^- would explain the excess of events with large opening angles. See also DEBOER 01 for follow-up experiments.
- 4 TSUNODA 95 looked for axion emission when ^{252}Cf undergoes a spontaneous fission, with the axion decaying into e^+e^- . The bound is for $m_{A^0} = 40$ MeV. It improves to 2.5×10^{-5} for $m_{A^0} = 200$ MeV.
- 5 MINOWA 93 studied chain process, $^{139}\text{Ce} \rightarrow ^{139}\text{La}^*$ by electron capture and M1 transition of $^{139}\text{La}^*$ to the ground state. It does not assume decay modes of A^0 . The bound applies for $m_{A^0} < 166$ keV.
- 6 HICKS 92 bound is applicable for $\tau_{X^0} < 4 \times 10^{-11}$ sec.
- 7 The ASANUMA 90 limit is for the branching fraction of X^0 emission per ^{241}Am α decay and valid for $\tau_{X^0} < 3 \times 10^{-11}$ s.
- 8 The DEBOER 90 limit is for the branching ratio $^8\text{Be}^* (18.15 \text{ MeV}, 1^+) \rightarrow ^8\text{Be} A^0$, $A^0 \rightarrow e^+e^-$ for the mass range $m_{A^0} = 4-15$ MeV.
- 9 The BINI 89 limit is for the branching fraction of $^{16}\text{O}^* (6.05 \text{ MeV}, 0^+) \rightarrow ^{16}\text{O} X^0$, $X^0 \rightarrow e^+e^-$ for $m_{X^0} = 1.5-3.1$ MeV. $\tau_{X^0} \lesssim 10^{-11}$ s is assumed. The spin-parity of X^0 is restricted to 0^+ or 1^- .
- 10 AVIGNONE 88 looked for the 1115 keV transition $\text{C}^* \rightarrow \text{Cu} A^0$, either from $A^0 \rightarrow 2\gamma$ in-flight decay or from the secondary A^0 interactions by Compton and by Primakoff processes. Limits for axion parameters are obtained for $m_{A^0} < 1.1$ MeV.
- 11 DATAR 88 rule out light pseudoscalar particle emission through its decay $A^0 \rightarrow e^+e^-$ in the mass range 1.02-2.5 MeV and lifetime range $10^{-13}-10^{-8}$ s. The above limit is for $\tau = 5 \times 10^{-13}$ s and $m = 1.7$ MeV; see the paper for the τ - m dependence of the limit.
- 12 The limit is for the branching fraction of $^{16}\text{O}^* (6.05 \text{ MeV}, 0^+) \rightarrow ^{16}\text{O} X^0$, $X^0 \rightarrow e^+e^-$ against internal pair conversion for $m_{X^0} = 1.7$ MeV and $\tau_{X^0} < 10^{-11}$ s. Similar limits are obtained for $m_{X^0} = 1.3-3.2$ MeV. The spin parity of X^0 must be either 0^+ or 1^- . The limit at 1.7 MeV is translated into a limit for the X^0 -nucleon coupling constant: $g_{X^0 NN}^2/4\pi < 2.3 \times 10^{-9}$.
- 13 The DOEHNER 88 limit is for $m_{A^0} = 1.7$ MeV, $\tau(A^0) < 10^{-10}$ s. Limits less than 10^{-4} are obtained for $m_{A^0} = 1.2-2.2$ MeV.
- 14 SAVAGE 88 looked for A^0 that decays into e^+e^- in the decay of the 9.17 MeV $J^P = 2^+$ state in ^{14}N , 17.64 MeV state $J^P = 1^+$ in ^9Be , and the 18.15 MeV state $J^P = 1^+$ in ^8Be . This experiment constrains the isovector coupling of A^0 to hadrons, if m_{A^0}

See key on page 1171

Gauge & Higgs Boson Particle Listings

Axions (A^0) and Other Very Light Bosons

- $= (1.1 \rightarrow 2.2)$ MeV and the isoscalar coupling of A^0 to hadrons, if $m_{A^0} = (1.1 \rightarrow 2.6)$ MeV. Both limits are valid only if $\tau(A^0) \lesssim 1 \times 10^{-11}$ s.
- 15 Limits are for $\Gamma(A^0(1.8 \text{ MeV})/\Gamma(\pi M1))$; i.e., for 1.8 MeV axion emission normalized to the rate for internal emission of e^+e^- pairs. Valid for $\tau_{A^0} < 2 \times 10^{-11}$ s. ${}^6\text{Li}$ isovector decay data strongly disfavor PECCEI 86 model I, whereas the ${}^{10}\text{B}$ and ${}^{14}\text{N}$ isoscalar decay data strongly reject PECCEI 86 model II and III.
- 16 SAVAGE 86B looked for A^0 that decays into e^+e^- in the decay of the 9.17 MeV $J^P = 2^+$ state in ${}^{14}\text{N}$. Limit on the branching fraction is valid if $\tau_{A^0} \lesssim 1 \times 10^{-11}$ s for $m_{A^0} = (1.1-1.7)$ MeV. This experiment constrains the iso-vector coupling of A^0 to hadrons.
- 17 ANANEV 85 with IBR-2 pulsed reactor exclude standard A^0 at CL = 95% masses below 470 keV (Li^* decay) and below $2m_e$ for deuteron* decay.
- 18 CAVAINAC 83 at Bugey reactor exclude axion at any $m_{97}\text{Nb}^*$ decay and axion with m_{A^0} between 275 and 288 keV (deuteron* decay).
- 19 ALEKSEEV 82 with IBR-2 pulsed reactor exclude standard A^0 at CL = 95% mass-ranges $m_{A^0} < 400$ keV (Li^* decay) and $330 \text{ keV} < m_{A^0} < 2.2$ MeV. (deuteron* decay).
- 20 LEHMANN 82 obtained $A^0 \rightarrow 2\gamma$ rate $< 6.2 \times 10^{-5}/\text{s}$ (CL = 95%) excluding m_{A^0} between 100 and 1000 keV.
- 21 ZEHNDER 82 used Gosgen 2.8GW light-water reactor to check A^0 production. No 2γ peak in Li^* , Nb^* decay (both single p transition) nor in n capture (combined with previous Ba^* negative result) rules out standard A^0 . Set limit $m_{A^0} < 60$ keV for any A^0 .
- 22 ZEHNDER 81 looked for $\text{Ba}^* \rightarrow A^0\text{Ba}$ transition with $A^0 \rightarrow 2\gamma$. Obtained 2γ coincidence rate $< 2.2 \times 10^{-5}/\text{s}$ (CL = 95%) excluding $m_{A^0} > 160$ keV (or 200 keV depending on Higgs mixing). However, see BARROSO 81.
- 23 CALAPRICE 79 saw no axion emission from excited states of carbon. Sensitive to axion mass between 1 and 15 MeV.

A^0 (Axion) Limits from Its Electron Coupling

Limits are for $\tau(A^0 \rightarrow e^+e^-)$.

VALUE (s)	CL%	DOCUMENT ID	TECN	COMMENT
• • •				We do not use the following data for averages, fits, limits, etc. • • •
		1 ANDREEV 21	NA64	$eN \rightarrow eA^0N$ ($A^0 \rightarrow \text{invisible}$)
		2 ANDREEV 21B	NA64	$eN \rightarrow eA^0N$ ($A^0 \rightarrow ee$)
none 4×10^{-16} – 4.5×10^{-12}	90	3 BROSS 91	BDMP	$eN \rightarrow eA^0N$ ($A^0 \rightarrow ee$)
		4 GUO 90	BDMP	$eN \rightarrow eA^0N$ ($A^0 \rightarrow ee$)
		5 BJORKEN 88	CALO	$A \rightarrow e^+e^-$ or 2γ
none 1×10^{-14} – 1×10^{-10}	90	6 BLINOV 88	MD1	$ee \rightarrow eeA^0$ ($A^0 \rightarrow ee$)
none 1×10^{-14} – 1×10^{-11}	90	7 RIORDAN 87	BDMP	$eN \rightarrow eA^0N$ ($A^0 \rightarrow ee$)
none 6×10^{-14} – 9×10^{-11}	95	8 BROWN 86	BDMP	$eN \rightarrow eA^0N$ ($A^0 \rightarrow ee$)
none 3×10^{-13} – 1×10^{-7}	90	9 DAVIER 86	BDMP	$eN \rightarrow eA^0N$ ($A^0 \rightarrow ee$)
		10 KONAKA 86	BDMP	$eN \rightarrow eA^0N$ ($A^0 \rightarrow ee$)

- 1 ANDREEV 21 look for invisible decays of axions coupled to electrons, and set limits on $g_{Aee} < 4.6 \times 10^{-6}$ – 3.1×10^{-3} for $m_{A^0} = 10^{-3}$ –1 GeV. This limits the axion contribution to the electron g -2 to an order of magnitude less than the current experimental uncertainty. See their Figs. 3 and 4 for mass-dependent limits.
- 2 ANDREEV 21B set limits on g_{Aee} in the range of 6.3×10^{-6} – 1.6×10^{-3} for $m_{A^0} = 2$ –17 MeV at 90% CL. This excludes $6.6 \times 10^{-5} < g_{Aee} < 1 \times 10^{-4}$ at $m_{A^0} = 16.7$ MeV corresponding to the ATOMKI anomaly. See their Fig. 2 for mass-dependent limits.
- 3 The listed BROSS 91 limit is for $m_{A^0} = 1.14$ MeV. $B(A^0 \rightarrow e^+e^-) = 1$ assumed. Excluded domain in the τ_{A^0} - m_{A^0} plane extends up to $m_{A^0} \approx 7$ MeV (see Fig. 5). Combining with electron g -2 constraint, axions coupling only to e^+e^- ruled out for $m_{A^0} < 4.8$ MeV (90% CL).
- 4 GUO 90 use the same apparatus as BROWN 86 and improve the previous limit in the shorter lifetime region. Combined with g -2 constraint, axions coupling only to e^+e^- are ruled out for $m_{A^0} < 2.7$ MeV (90% CL).
- 5 BJORKEN 88 reports limits on axion parameters (f_A, m_A, τ_A) for $m_{A^0} < 200$ MeV from electron beam-dump experiment with production via Primakoff photoproduction, bremsstrahlung from electrons, and resonant annihilation of positrons on atomic electrons.
- 6 BLINOV 88 assume zero spin, $m = 1.8$ MeV and lifetime $< 5 \times 10^{-12}$ s and find $\Gamma(A^0 \rightarrow \gamma\gamma)B(A^0 \rightarrow e^+e^-) < 2$ eV (CL=90%).
- 7 Assumes $A^0\gamma\gamma$ coupling is small and hence Primakoff production is small. Their figure 2 shows limits on axions for $m_{A^0} < 15$ MeV.
- 8 Uses electrons in hadronic showers from an incident 800 GeV proton beam. Limits for $m_{A^0} < 15$ MeV are shown in their figure 3.
- 9 $m_{A^0} = 1.8$ MeV assumed. The excluded domain in the τ_{A^0} - m_{A^0} plane extends up to $m_{A^0} \approx 14$ MeV, see their figure 4.
- 10 The limits are obtained from their figure 3. Also given is the limit on the $A^0\gamma\gamma$ - $A^0e^+e^-$ coupling plane by assuming Primakoff production.

Search for A^0 (Axion) Resonance in Bhabha Scattering

The limit is for $\Gamma(A^0)[B(A^0 \rightarrow e^+e^-)]^2$.

VALUE (10^{-3} eV)	CL%	DOCUMENT ID	TECN	COMMENT
• • •				We do not use the following data for averages, fits, limits, etc. • • •
< 1.3	97	1 HALLIN 92	CNTR	$m_{A^0} = 1.75$ –1.88 MeV
none 0.0016–0.47	90	2 HENDERSON 92c	CNTR	$m_{A^0} = 1.5$ –1.86 MeV
< 2.0	90	3 WU 92	CNTR	$m_{A^0} = 1.56$ –1.86 MeV
< 0.013	95	TSERTOS 91	CNTR	$m_{A^0} = 1.832$ MeV
none 0.19–3.3	95	4 WIDMANN 91	CNTR	$m_{A^0} = 1.78$ –1.92 MeV
< 5	97	BAUER 90	CNTR	$m_{A^0} = 1.832$ MeV
none 0.09–1.5	95	5 JUDGE 90	CNTR	$m_{A^0} = 1.832$ MeV, elastic
< 1.9	97	6 TSERTOS 89	CNTR	$m_{A^0} = 1.82$ MeV
<(10–40)	97	6 TSERTOS 89	CNTR	$m_{A^0} = 1.51$ –1.65 MeV
<(1–2.5)	97	6 TSERTOS 89	CNTR	$m_{A^0} = 1.80$ –1.86 MeV
< 31	95	LORENZ 88	CNTR	$m_{A^0} = 1.646$ MeV
< 94	95	LORENZ 88	CNTR	$m_{A^0} = 1.726$ MeV
< 23	95	LORENZ 88	CNTR	$m_{A^0} = 1.782$ MeV
< 19	95	LORENZ 88	CNTR	$m_{A^0} = 1.837$ MeV
< 3.8	97	7 TSERTOS 88	CNTR	$m_{A^0} = 1.832$ MeV
		8 VANKLINKEN 88	CNTR	
		9 MAIER 87	CNTR	
<2500	90	MILLS 87	CNTR	$m_{A^0} = 1.8$ MeV
		10 VONWIMMER.87	CNTR	

- 1 HALLIN 92 quote limits on lifetime, 8×10^{-14} – 5×10^{-13} sec depending on mass, assuming $B(A^0 \rightarrow e^+e^-) = 100\%$. They say that TSERTOS 91 overstated their sensitivity by a factor of 3.
- 2 HENDERSON 92c exclude axion with lifetime $\tau_{A^0} = 1.4 \times 10^{-12}$ – 4.0×10^{-10} s, assuming $B(A^0 \rightarrow e^+e^-) = 100\%$. HENDERSON 92c also exclude a vector boson with $\tau = 1.4 \times 10^{-12}$ – 6.0×10^{-10} s.
- 3 WU 92 quote limits on lifetime $> 3.3 \times 10^{-13}$ s assuming $B(A^0 \rightarrow e^+e^-) = 100\%$. They say that TSERTOS 89 overestimate the limit by a factor of $\pi/2$. WU 92 also quote a bound for vector boson, $\tau > 8.2 \times 10^{-13}$ s.
- 4 WIDMANN 91 bound applies exclusively to the case $B(A^0 \rightarrow e^+e^-) = 1$, since the detection efficiency varies substantially as $\Gamma(A^0)_{\text{total}}$ changes. See their Fig. 6.
- 5 JUDGE 90 excludes an elastic pseudoscalar e^+e^- resonance for 4.5×10^{-13} s $< \tau(A^0) < 7.5 \times 10^{-12}$ s (95% CL) at $m_{A^0} = 1.832$ MeV. Comparable limits can be set for $m_{A^0} = 1.776$ –1.856 MeV.
- 6 See also TSERTOS 88B in references.
- 7 The upper limit listed in TSERTOS 88 is too large by a factor of 4. See TSERTOS 88B, footnote 3.
- 8 VANKLINKEN 88 looked for relatively long-lived resonance ($\tau = 10^{-10}$ – 10^{-12} s). The sensitivity is not sufficient to exclude such a narrow resonance.
- 9 MAIER 87 obtained limits $R\Gamma \lesssim 60$ eV (100 eV) at $m_{A^0} \approx 1.64$ MeV (1.83 MeV) for energy resolution $\Delta E_{\text{cm}} \approx 3$ keV, where R is the resonance cross section normalized to that of Bhabha scattering, and $\Gamma = \Gamma_{ee}^2/\Gamma_{\text{total}}$. For a discussion implying that $\Delta E_{\text{cm}} \approx 10$ keV, see TSERTOS 89.
- 10 VONWIMMERSPERG 87 measured Bhabha scattering for $E_{\text{cm}} = 1.37$ –1.86 MeV and found a possible peak at 1.73 with $\int \sigma dE_{\text{cm}} = 14.5 \pm 6.8$ keV-b. For a comment and a reply, see VANKLINKEN 88B and VONWIMMERSPERG 88. Also see CONNELL 88.

Search for A^0 (Axion) Resonance in $e^+e^- \rightarrow \gamma\gamma$

The limit is for $\Gamma(A^0 \rightarrow e^+e^-)\Gamma(A^0 \rightarrow \gamma\gamma)/\Gamma_{\text{total}}$

VALUE (10^{-3} eV)	CL%	DOCUMENT ID	TECN	COMMENT
• • •				We do not use the following data for averages, fits, limits, etc. • • •
< 0.18	95	VO 94	CNTR	$m_{A^0} = 1.1$ MeV
< 1.5	95	VO 94	CNTR	$m_{A^0} = 1.4$ MeV
<12	95	VO 94	CNTR	$m_{A^0} = 1.7$ MeV
< 6.6	95	1 TRZASKA 91	CNTR	$m_{A^0} = 1.8$ MeV
< 4.4	95	WIDMANN 91	CNTR	$m_{A^0} = 1.78$ –1.92 MeV
		2 FOX 89	CNTR	
< 0.11	95	3 MINOWA 89	CNTR	$m_{A^0} = 1.062$ MeV
<33	97	CONNELL 88	CNTR	$m_{A^0} = 1.580$ MeV
<42	97	CONNELL 88	CNTR	$m_{A^0} = 1.642$ MeV
<73	97	CONNELL 88	CNTR	$m_{A^0} = 1.782$ MeV
<79	97	CONNELL 88	CNTR	$m_{A^0} = 1.832$ MeV
		1 TRZASKA 91		also give limits in the range $(6.6-30) \times 10^{-3}$ eV (95%CL) for $m_{A^0} = 1.6$ –2.0 MeV.
		2 FOX 89		measured positron annihilation with an electron in the source material into two photons and found no signal at 1.062 MeV ($< 9 \times 10^{-5}$ of two-photon annihilation at rest).
		3		Similar limits are obtained for $m_{A^0} = 1.045$ –1.085 MeV.

Search for X^0 (Light Boson) Resonance in $e^+e^- \rightarrow \gamma\gamma\gamma$

The limit is for $\Gamma(X^0 \rightarrow e^+e^-)\Gamma(X^0 \rightarrow \gamma\gamma\gamma)/\Gamma_{\text{total}}$. C invariance forbids spin-0 X^0 coupling to both e^+e^- and $\gamma\gamma\gamma$.

VALUE (10^{-3} eV)	CL%	DOCUMENT ID	TECN	COMMENT
• • •				We do not use the following data for averages, fits, limits, etc. • • •
< 0.2	95	1 VO 94	CNTR	$m_{X^0} = 1.1$ –1.9 MeV
< 1.0	95	2 VO 94	CNTR	$m_{X^0} = 1.1$ MeV

Gauge & Higgs Boson Particle Listings

Axions (A^0) and Other Very Light Bosons

< 2.5	95	2 VO	94 CNTR	$m_{X^0}=1.4$ MeV
<120	95	2 VO	94 CNTR	$m_{X^0}=1.7$ MeV
< 3.8	95	3 SKALSEY	92 CNTR	$m_{X^0}=1.5$ MeV

¹ VO 94 looked for $X^0 \rightarrow \gamma\gamma\gamma$ decaying at rest. The precise limits depend on m_{X^0} . See Fig. 2(b) in paper.
² VO 94 looked for $X^0 \rightarrow \gamma\gamma\gamma$ decaying in flight.
³ SKALSEY 92 also give limits 4.3 for $m_{X^0} = 1.54$ and 7.5 for 1.64 MeV. The spin of X^0 is assumed to be one.

Light Boson (X^0) Search in Nonresonant e^+e^- Annihilation at Rest

Limits are for the ratio of $n\gamma + X^0$ production relative to $\gamma\gamma$.

VALUE (units 10^{-6})	CL%	DOCUMENT ID	TECN	COMMENT
• • •				We do not use the following data for averages, fits, limits, etc. • • •
< 4.2	90	1 MITSUI	96 CNTR	γX^0
< 4	68	2 SKALSEY	95 CNTR	γX^0
<40	68	3 SKALSEY	95 RVUE	γX^0
< 0.18	90	4 ADACHI	94 CNTR	$\gamma\gamma X^0, X^0 \rightarrow \gamma\gamma$
< 0.26	90	5 ADACHI	94 CNTR	$\gamma\gamma X^0, X^0 \rightarrow \gamma\gamma$
< 0.33	90	6 ADACHI	94 CNTR	$\gamma X^0, X^0 \rightarrow \gamma\gamma\gamma$

- ¹ MITSUI 96 looked for a monochromatic γ . The bound applies for a vector X^0 with $C=-1$ and $m_{X^0} < 200$ keV. They derive an upper bound on eX^0 coupling and hence on the branching ratio $B(\rho\text{-Ps} \rightarrow \gamma\gamma X^0) < 6.2 \times 10^{-6}$. The bounds weaken for heavier X^0 .
² SKALSEY 95 looked for a monochromatic γ without an accompanying γ in e^+e^- annihilation. The bound applies for scalar and vector X^0 with $C = -1$ and $m_{X^0} = 100\text{--}1000$ keV.
³ SKALSEY 95 reinterpreted the bound on γA^0 decay of ρ -Ps by ASA1 91 where 3% of delayed annihilations are not from 3S_1 states. The bound applies for scalar and vector X^0 with $C = -1$ and $m_{X^0} = 0\text{--}800$ keV.
⁴ ADACHI 94 looked for a peak in the $\gamma\gamma$ invariant mass distribution in $\gamma\gamma\gamma\gamma$ production from e^+e^- annihilation. The bound applies for $m_{X^0} = 70\text{--}800$ keV.
⁵ ADACHI 94 looked for a peak in the missing-mass mass distribution in $\gamma\gamma$ channel, using $\gamma\gamma\gamma\gamma$ production from e^+e^- annihilation. The bound applies for $m_{X^0} < 800$ keV.
⁶ ADACHI 94 looked for a peak in the missing mass distribution in $\gamma\gamma\gamma\gamma$ channel, using $\gamma\gamma\gamma\gamma$ production from e^+e^- annihilation. The bound applies for $m_{X^0} = 200\text{--}900$ keV.

Searches for Goldstone Bosons (X^0)

(Including Horizontal Bosons and Majorons.) Limits are for branching ratios.

VALUE	CL%	DOCUMENT ID	TECN	COMMENT
• • •				We do not use the following data for averages, fits, limits, etc. • • •
<4.3 $\times 10^{-6}$	90	1 ADACHI	23A BEL2	$\tau^- \rightarrow e^- X^0$, Familon
<5.2 $\times 10^{-8}$	90	2 ADACHI	23A BEL2	$\tau^- \rightarrow \mu^- X^0$, Familon
<9 $\times 10^{-6}$	90	3 FIORILLO	23 ASTR	Majoron, SN 1987A
<7 $\times 10^{-12}$	90	4 SANDNER	23 COSM	Majoron, CMB
<9 $\times 10^{-6}$	90	5 COLOMA	22A BORX	νe non-standard interactions
<3.3 $\times 10^{-2}$	95	6 AGUILAR-AR...	21A PIEN	$\pi \rightarrow \mu\nu X^0$, Majoron
<1.8 $\times 10^{-2}$	95	7 AGUILAR-AR...	21A PIEN	$\pi \rightarrow e\nu X^0$, Majoron
<6.4 $\times 10^{-9}$	90	8 AGUILAR-AR...	20 PIEN	$\mu^+ \rightarrow e^+ X^0$, Familon
<1.4 $\times 10^{-5}$	90	9 BALDINI	20 MEG	$\mu^+ \rightarrow e^+ X^0$ ($X^0 \rightarrow \gamma\gamma$), Familon
<1.1 $\times 10^{-9}$	90	10 BAYES	15 TWST	$\mu^+ \rightarrow e^+ X^0$, Familon
<5 $\times 10^{-6}$	90	11 LATTANZI	13 COSM	Majoron dark matter decay
<1.3 $\times 10^{-9}$	90	12 LESSA	07 RVUE	Meson, ℓ decays to Majoron
<3 $\times 10^{-4}$	90	13 FARZAN	03 ASTR	Majoron, SN cooling
<1 $\times 10^{-10}$	90	14 DIAZ	98 THEO	$H^0 \rightarrow X^0 X^0, A^0 \rightarrow X^0 X^0 X^0$, Majoron
<2.6 $\times 10^{-6}$	90	15 BOBRKOV	91	Electron quasi-magnetic interaction
<3 $\times 10^{-2}$	95	16 ALBRECHT	90E ARG	$\tau \rightarrow \mu X^0$, Familon
<1.8 $\times 10^{-2}$	95	16 ALBRECHT	90E ARG	$\tau \rightarrow e X^0$, Familon
<6.4 $\times 10^{-9}$	90	17 ATIYA	90 B787	$K^+ \rightarrow \pi^+ X^0$, Familon
<1.4 $\times 10^{-5}$	90	18 BALKE	88 CNTR	$\mu^+ \rightarrow e^+ X^0$, Familon
<1.1 $\times 10^{-9}$	90	19 BOLTON	88 CBOX	$\mu^+ \rightarrow e^+ X^0$, Familon
<5 $\times 10^{-6}$	90	20 CHANDA	88 ASTR	Sun, Majoron
<1.3 $\times 10^{-9}$	90	21 CHOI	88 ASTR	Majoron, SN 1987A
<3 $\times 10^{-4}$	90	22 PICCIOTTO	88 CNTR	$\pi \rightarrow e\nu X^0$, Majoron
<1 $\times 10^{-10}$	90	23 GOLDMAN	87 CNTR	$\mu \rightarrow e\gamma X^0$, Familon
<2.6 $\times 10^{-6}$	90	24 BRYMAN	86B RVUE	$\mu \rightarrow e X^0$, Familon
<1 $\times 10^{-10}$	90	25 EICHLER	86 SPEC	$\mu^+ \rightarrow e^+ X^0$, Familon
<2.6 $\times 10^{-6}$	90	26 JODIDIO	86 SPEC	$\mu^+ \rightarrow e^+ X^0$, Familon
		27 BALTRUSAITIS	85 MRK3	$\tau \rightarrow \ell X^0$, Familon
		28 DICUS	83 COSM	$\nu(\text{h}\nu) \rightarrow \nu(\text{light})X^0$

- ¹ ADACHI 23A set limits in the range of $1.1 \times 10^{-3}\text{--}9.7 \times 10^{-3}$ for $0 < m_{X^0} < 1.6$ GeV on $B(\tau^- \rightarrow e^- X^0)/B(\tau^- \rightarrow e^- \bar{\nu}_e \nu_\tau)$. See their Fig. 2 for mass-dependent limits.
² ADACHI 23A set limits in the range of $7 \times 10^{-4}\text{--}1.22 \times 10^{-2}$ for $0 < m_{X^0} < 1.6$ GeV on $B(\tau^- \rightarrow \mu^- X^0)/B(\tau^- \rightarrow \mu^- \bar{\nu}_\mu \nu_\tau)$. See their Fig. 2 for mass-dependent limits.

- ³ FIORILLO 23 used data from Kamiokande-II and IMB on the neutrino flux from SN1987A to constrain the universal neutrino Majoron Yukawa coupling, g . They set an upper limit of $g m_{X^0} \lesssim 10^{-9}$ MeV for Majoron masses $100 \text{ eV} \lesssim m_{X^0} \lesssim 100 \text{ MeV}$, using neutrino coalescence as production of Majorons which then decay back to neutrinos. See their Fig. 1 for the mass-dependent limits.
⁴ SANDNER 23 study Majoron production via neutrino inverse decay and use Planck data to constrain the neutrino Majoron Yukawa coupling to $g \lesssim 2 \times 10^{-13}\text{--}1 \times 10^{-12}$ for Majoron masses $m_{X^0} = 1\text{--}10$ eV. See their Fig. 1 for mass-dependent limits.
⁵ COLOMA 22A used the spectral data of Borexino Phase II to constrain the neutrino non-standard interaction with electrons mediated by a scalar or a pseudoscalar. Limits on the universal coupling to neutrinos and electrons between 2×10^{-6} and 10^{-4} are obtained for $m_{X^0} \lesssim 30\text{--}40$ MeV. See their Fig. 6 for mass-dependent limits.
⁶ AGUILAR-AREVALO 21A quoted limit applies to $m_{X^0} = 33.9$ MeV. Limits between 4.3×10^{-6} and 7.5×10^{-5} are obtained for $0 < m_{X^0} < 33.9$ MeV. The lifetime of X^0 is assumed to be long enough. See their Fig. 6 for mass-dependent limits.
⁷ AGUILAR-AREVALO 21A quoted limit applies to $m_{X^0} = 85$ MeV. Limits between 5.2×10^{-8} and 1.4×10^{-6} are obtained for $0 < m_{X^0} < 120$ MeV, which improve the limits of PICCIOTTO 88 by an order of magnitude. The lifetime of X^0 is assumed to be long enough. See their Fig. 4 for mass-dependent limits.
⁸ AGUILAR-AREVALO 20 obtained limits of order 10^{-5} for $m_{X^0} = 47.8\text{--}95.1$ MeV. The quoted limit applies to $m_{X^0} = 75$ MeV. See their Fig. 1 for mass-dependent limits.
⁹ BALDINI 20 obtained limits for $m_{X^0} = 20\text{--}45$ MeV and $\tau_{X^0} < 40$ ps, and supersedes BOLTON 88 for $m_{X^0} = 20\text{--}40$ MeV. See their Fig. 17 for mass-dependent limits.
¹⁰ BAYES 15 limits are the average over $m_{X^0} = 13\text{--}80$ MeV for the isotropic decay distribution of positrons. See their Fig. 4 and Table II for the mass-dependent limits as well as the dependence on the decay anisotropy. In particular, they find a limit $< 58 \times 10^{-6}$ at 90% CL for massless familons and for the same asymmetry as normal muon decay, a case not covered by JODIDIO 86.
¹¹ LATTANZI 13 use WMAP 9 year data as well as X-ray and γ -ray observations to derive limits on decaying majoron dark matter. A limit on the decay width $\Gamma(X^0 \rightarrow \nu\bar{\nu}) < 6.4 \times 10^{-19} \text{ s}^{-1}$ at 95% CL is found if majorons make up all of the dark matter.
¹² LESSA 07 consider decays of the form Meson $\rightarrow \ell\nu$ Majoron and $\ell \rightarrow \ell'\nu\bar{\nu}$ Majoron and use existing data to derive limits on the neutrino-Majoron Yukawa couplings $g_{\alpha\beta}$ ($\alpha, \beta = e, \mu, \tau$). Their best limits are $|g_{e\alpha}|^2 < 5.5 \times 10^{-6}$, $|g_{\mu\alpha}|^2 < 4.5 \times 10^{-5}$, $|g_{\tau\alpha}|^2 < 5.5 \times 10^{-2}$ at CL = 90%.
¹³ FARZAN 03 set limits on the neutrino Majoron Yukawa coupling, $|g_{e\alpha}| < 4 \times 10^{-7}$, by considering the SN cooling due to the massless Majoron emission via neutrino coalescence. They also exclude values around 10^{-5} for both $g_{e\mu}$ and $g_{\mu\mu}$ using the process $\nu\nu \rightarrow X^0 X^0$. See also their Figs. 3 and 4 for mass-dependent limits.
¹⁴ DIAZ 98 studied models of spontaneously broken lepton number with both singlet and triplet Higgses. They obtain limits on the parameter space from invisible decay $Z \rightarrow H^0 A^0 \rightarrow X^0 X^0 X^0 X^0$ and $e^+e^- \rightarrow Z H^0$ with $H^0 \rightarrow X^0 X^0$.
¹⁵ BOBRKOV 91 searched for anomalous magnetic interactions between polarized electrons expected from the exchange of a massless pseudoscalar boson (arion). A limit $x_e^2 < 2 \times 10^{-4}$ (95%CL) is found for the effective anomalous magneton parametrized as $x_e(G_F/8\pi\sqrt{2})^{1/2}$.
¹⁶ ALBRECHT 90E limits are for $B(\tau \rightarrow \ell X^0)/B(\tau \rightarrow \ell\nu\bar{\nu})$. Valid for $m_{X^0} < 100$ MeV. The limits rise to 7.1% (for μ), 5.0% (for e) for $m_{X^0} = 500$ MeV.
¹⁷ ATIYA 90 limit is for $m_{X^0} = 0$. The limit $B < 1 \times 10^{-8}$ holds for $m_{X^0} < 95$ MeV. For the reduction of the limit due to finite lifetime of X^0 , see their Fig. 3.
¹⁸ BALKE 88 limits are for $B(\mu^+ \rightarrow e^+ X^0)$. Valid for $m_{X^0} < 80$ MeV and $\tau_{X^0} > 10^{-8}$ sec.
¹⁹ BOLTON 88 limit corresponds to $F > 3.1 \times 10^9$ GeV, which does not depend on the chirality property of the coupling.
²⁰ CHANDA 88 find $\nu_T < 10$ MeV for the weak-triplet Higgs vacuum expectation value in Gelmini-Roncadelli model, and $\nu_S > 5.8 \times 10^6$ GeV in the singlet Majoron model.
²¹ CHOI 88 used the observed neutrino flux from the supernova SN 1987A to exclude the neutrino Majoron Yukawa coupling h in the range $2 \times 10^{-5} < h < 3 \times 10^{-4}$ for the interaction $L_{\text{int}} = \frac{1}{2} i h \bar{\psi}_\nu \gamma_5 \psi_\nu \phi_X$. For several families of neutrinos, the limit applies for $(\Sigma h_i^4)^{1/4}$.
²² PICCIOTTO 88 limit applies when $m_{X^0} < 55$ MeV and $\tau_{X^0} > 2$ ns, and it decreases to 4×10^{-7} at $m_{X^0} = 125$ MeV, beyond which no limit is obtained.
²³ GOLDMAN 87 limit corresponds to $F > 2.9 \times 10^9$ GeV for the family symmetry breaking scale from the Lagrangian $L_{\text{int}} = (1/F) \bar{\psi}_\mu \gamma^\mu (a + b\gamma_5) \psi_e \theta_\mu \phi_X$ with $a^2 + b^2 = 1$. This is not as sensitive as the limit $F > 9.9 \times 10^9$ GeV derived from the search for $\mu^+ \rightarrow e^+ X^0$ by JODIDIO 86, but does not depend on the chirality property of the coupling.
²⁴ Limits are for $\Gamma(\mu \rightarrow e X^0)/\Gamma(\mu \rightarrow e\nu\bar{\nu})$. Valid when $m_{X^0} = 0\text{--}93.4, 98.1\text{--}103.5$ MeV.
²⁵ EICHLER 86 looked for $\mu^+ \rightarrow e^+ X^0$ followed by $X^0 \rightarrow e^+ e^-$. Limits on the branching fraction depend on the mass and lifetime of X^0 . The quoted limits are valid when $\tau_{X^0} \lesssim 3 \times 10^{-10}$ s if the decays are kinematically allowed.
²⁶ JODIDIO 86 corresponds to $F > 9.9 \times 10^9$ GeV for the family symmetry breaking scale with the parity-conserving effective Lagrangian $L_{\text{int}} = (1/F) \bar{\psi}_\mu \gamma^\mu \psi_e \theta^\mu \phi_X$.
²⁷ BALTRUSAITIS 85 search for light Goldstone boson (X^0) of broken U(1). CL = 95% limits are $B(\tau \rightarrow \mu^+ X^0)/B(\tau \rightarrow \mu^+ \nu\bar{\nu}) < 0.125$ and $B(\tau \rightarrow e^+ X^0)/B(\tau \rightarrow e^+ \nu\bar{\nu}) < 0.04$. Inferred limit for the symmetry breaking scale is $m > 3000$ TeV.
²⁸ The primordial heavy neutrino must decay into ν and familon, f_A , early so that the red-shifted decay products are below critical density, see their table. In addition, $K \rightarrow \pi f_A$ and $\mu \rightarrow e f_A$ are unseen. Combining these excludes $m_{\text{heavy}\nu}$ between 5×10^{-5} and 5×10^{-4} MeV (μ decay) and $m_{\text{heavy}\nu}$ between 5×10^{-5} and 0.1 MeV (K -decay).

Gauge & Higgs Boson Particle Listings

Axions (A^0) and Other Very Light Bosons

Majoron Searches in Neutrinoless Double β Decay

Limits are for the half-life of neutrinoless $\beta\beta$ decay with a Majoron emission. No experiment currently claims any such evidence. Only the best or comparable limits for each isotope are reported.

$t_{1/2}$ (10^{21} yr)	CL% ISOTOPE	TRANSITION	METHOD	DOCUMENT ID
>7200	90 ¹²⁸ Te	CNTR		1 BERNATOW... 92
• • • We do not use the following data for averages, fits, limits, etc. • • •				
> 120	90 ⁸² Se	$0\nu 1\chi$	CUPID-0	2 AZZOLINI 23
> 640	90 ⁷⁶ Ge	$0\nu 1\chi$	GERDA	3 AGOSTINI 22
>4300	90 ¹³⁶ Xe	$0\nu 1\chi$	EXO-200	4 AL-KHARUSI 21
> 4.4	90 ¹⁰⁰ Mo	$0\nu 1\chi$	NEMO-3	5 ARNOLD 19
> 37	90 ⁸² Se	$0\nu 1\chi$	NEMO-3	6 ARNOLD 18
> 420	90 ⁷⁶ Ge	$0\nu 1\chi$	GERDA	7 AGOSTINI 15A
> 400	90 ¹⁰⁰ Mo	$0\nu 1\chi$	NEMO-3	8 ARNOLD 15
>1200	90 ¹³⁶ Xe	$0\nu 1\chi$	EXO-200	9 ALBERT 14A
>2600	90 ¹³⁶ Xe	$0\nu 1\chi$	KamLAND-Zen	10 GANDO 12
> 16	90 ¹³⁰ Te	$0\nu 1\chi$	NEMO-3	11 ARNOLD 11
> 1.9	90 ⁹⁶ Zr	$2\nu 1\chi$	NEMO-3	12 ARGYRIADES 10
> 1.52	90 ¹⁵⁰ Nd	$0\nu 1\chi$	NEMO-3	13 ARGYRIADES 09
> 27	90 ¹⁰⁰ Mo	$0\nu 1\chi$	NEMO-3	14 ARNOLD 06
> 15	90 ⁸² Se	$0\nu 1\chi$	NEMO-3	15 ARNOLD 06
> 14	90 ¹⁰⁰ Mo	$0\nu 1\chi$	NEMO-3	16 ARNOLD 04
> 12	90 ⁸² Se	$0\nu 1\chi$	NEMO-3	17 ARNOLD 04
> 2.2	90 ¹³⁰ Te	$0\nu 1\chi$	Cryog. det.	18 ARNABOLDI 03
> 0.9	90 ¹³⁰ Te	$0\nu 2\chi$	Cryog. det.	19 ARNABOLDI 03
> 8	90 ¹¹⁶ Cd	$0\nu 1\chi$	CdWO ₄ scint.	20 DANEVICH 03
> 0.8	90 ¹¹⁶ Cd	$0\nu 2\chi$	CdWO ₄ scint.	21 DANEVICH 03
> 500	90 ¹³⁶ Xe	$0\nu 1\chi$	Liquid Xe Scint.	22 BERNABEI 02D
> 5.8	90 ¹⁰⁰ Mo	$0\nu 1\chi$	ELEGANT V	23 FUSHIMI 02
> 0.32	90 ¹⁰⁰ Mo	$0\nu 1\chi$	Liq. Ar ioniz.	24 ASHITKOV 01
> 0.0035	90 ¹⁶⁰ Gd	$0\nu 1\chi$	¹⁶⁰ Gd ₂ SiO ₅ :Ce	25 DANEVICH 01
> 0.013	90 ¹⁶⁰ Gd	$0\nu 2\chi$	¹⁶⁰ Gd ₂ SiO ₅ :Ce	26 DANEVICH 01
> 2.3	90 ⁸² Se	$0\nu 1\chi$	NEMO 2	27 ARNOLD 00
> 0.31	90 ⁹⁶ Zr	$0\nu 1\chi$	NEMO 2	28 ARNOLD 00
> 0.63	90 ⁸² Se	$0\nu 2\chi$	NEMO 2	29 ARNOLD 00
> 0.063	90 ⁹⁶ Zr	$0\nu 2\chi$	NEMO 2	29 ARNOLD 00
> 0.16	90 ¹⁰⁰ Mo	$0\nu 2\chi$	NEMO 2	29 ARNOLD 00
> 2.4	90 ⁸² Se	$0\nu 1\chi$	NEMO 2	30 ARNOLD 98
> 7.2	90 ¹³⁶ Xe	$0\nu 2\chi$	TPC	31 LUESCHER 98
> 7.91	90 ⁷⁶ Ge		SPEC	32 GUENTHER 96
> 17	90 ⁷⁶ Ge		CNTR	BECK 93

- BERNATOWICZ 92 studied double- β decays of ¹²⁸Te and ¹³⁰Te, and found the ratio $\tau(^{130}\text{Te})/\tau(^{128}\text{Te}) = (3.52 \pm 0.11) \times 10^{-4}$ in agreement with relatively stable theoretical predictions. The bound is based on the requirement that Majoron-emitting decay cannot be larger than the observed double-beta rate of ¹²⁸Te of $(7.7 \pm 0.4) \times 10^{24}$ year. We calculated 90% CL limit as $(7.7-1.28 \times 0.4=7.2) \times 10^{24}$.
- AZZOLINI 23 use 9.95 kg-yr of data, collected by the CUPID-0 experiment, to place a limit on the single Majoron mode of the $0\nu\beta\beta$ decay of ⁸²Se. Various limits on modes involving the emission of multiple Majorons are given too. The resulting constraint on the Majoron-neutrino coupling constant is $g_{\nu\chi} < 1.8-4.4 \times 10^{-5}$. The range is due to the variability of the used nuclear matrix elements.
- AGOSTINI 22 use 32.8 kg-yr of GERDA phase 2 data to derive a limit of $g_{\nu\chi} < 1.8-4.4 \times 10^{-5}$ on the neutrino-Majoron coupling. The range reflects the author's evaluation of the spread of nuclear matrix elements.
- AL-KHARUSI 21 utilize the complete dataset of the EXO-200 experiment, corresponding to an exposure of 234 kg yr, to place a limit on the one Majoron mode of the neutrinoless double beta decay of ¹³⁶Xe. Several limits are reported, the one given here corresponds to a spectral index of 1, resulting in a limit of $g_{\nu\chi} < 0.4-0.9 \times 10^{-5}$ on the Majoron-neutrino coupling constant. The range reflects the spread of the nuclear matrix elements.
- ARNOLD 19 uses the NEMO-3 tracking calorimeter to determine limits for the Majoron emitting double beta decay, with spectral index $n = 3$. The limit corresponds to the range of the g_{ee} coupling of 0.013-0.035; depending on the nuclear matrix elements used.
- ARNOLD 18 use the NEMO-3 tracking detector. The limit corresponds to $\langle g_{ee} \rangle < 3.2-8.0 \times 10^{-5}$; the range corresponds to different nuclear matrix element calculations.
- AGOSTINI 15A analyze a 20.3 kg yr of data set of the GERDA calorimeter to determine $g_{\nu\chi} < 3.4-8.7 \times 10^{-5}$ on the Majoron-neutrino coupling constant. The range reflects the spread of the nuclear matrix elements.
- ARNOLD 15 use the NEMO-3 tracking calorimeter with 3.43 kg yr exposure to determine the limit on Majoron emission. The limit corresponds to $g_{\nu\chi} < 1.6-3.0 \times 10^{-4}$. The spread reflects different nuclear matrix elements. Supersedes ARNOLD 06.
- ALBERT 14A utilize 100 kg yr of exposure of the EXO-200 tracking calorimeter to place a limit on the $g_{\nu\chi} < 0.8-1.7 \times 10^{-5}$ on the Majoron-neutrino coupling constant. The range reflects the spread of the nuclear matrix elements.
- GANDO 12 use the KamLAND-Zen detector to obtain the limit on the $0\nu\chi$ decay with Majoron emission. It implies that the coupling constant $g_{\nu\chi} < 0.8-1.6 \times 10^{-5}$ depending on the nuclear matrix elements used.
- ARNOLD 11 use the NEMO-3 detector to obtain the reported limit on Majoron emission. It implies that the coupling constant $g_{\nu\chi} < 0.6-1.6 \times 10^{-4}$ depending on the nuclear matrix element used. Supersedes ARNABOLDI 03.
- ARGYRIADES 10 use the NEMO-3 tracking detector and ⁹⁶Zr to derive the reported limit. No limit for the Majoron electron coupling is given.
- ARGYRIADES 09 use ¹⁵⁰Nd data taken with the NEMO-3 tracking detector. The reported limit corresponds to $\langle g_{\nu\chi} \rangle < 1.7-3.0 \times 10^{-4}$ using a range of nuclear matrix elements that include the effect of nuclear deformation.

- ARNOLD 06 use ¹⁰⁰Mo data taken with the NEMO-3 tracking detector. The reported limit corresponds to $\langle g_{\nu\chi} \rangle < (0.4-1.8) \times 10^{-4}$ using a range of matrix element calculations. Supersedes by ARNOLD 15.
- NEMO-3 tracking calorimeter is used in ARNOLD 06. Reported half-life limit for ⁸²Se corresponds to $\langle g_{\nu\chi} \rangle < (0.66-1.9) \times 10^{-4}$ using a range of matrix element calculations. Supersedes ARNOLD 04.
- ARNOLD 04 use the NEMO-3 tracking detector. The limit corresponds to $\langle g_{\nu\chi} \rangle < (0.5-0.9)10^{-4}$ using the matrix elements of SIMKOVIC 99, STOICA 01 and CIVITARESE 03. Supersedes by ARNOLD 06.
- ARNOLD 04 use the NEMO-3 tracking detector. The limit corresponds to $\langle g_{\nu\chi} \rangle < (0.7-1.6)10^{-4}$ using the matrix elements of SIMKOVIC 99, STOICA 01 and CIVITARESE 03.
- Supersedes ALESSANDRELLO 00. Array of TeO₂ crystals in high resolution cryogenic calorimeter. Some enriched in ¹³⁰Te. Derive $\langle g_{\nu\chi} \rangle < 17-33 \times 10^{-5}$ depending on matrix element.
- Supersedes ALESSANDRELLO 00. Cryogenic calorimeter search.
- Limit for the $0\nu\chi$ decay with Majoron emission of ¹¹⁶Cd using enriched CdWO₄ scintillators. $\langle g_{\nu\chi} \rangle < 4.6-8.1 \times 10^{-5}$ depending on the matrix element. Supersedes DANEVICH 00.
- Limit for the $0\nu 2\chi$ decay of ¹¹⁶Cd. Supersedes DANEVICH 00.
- BERNABEI 02b obtain limit for $0\nu\chi$ decay with Majoron emission of ¹³⁶Xe using liquid Xe scintillation detector. They derive $\langle g_{\nu\chi} \rangle < 2.0-3.0 \times 10^{-5}$ with several nuclear matrix elements.
- Replaces TANAKA 93. FUSHIMI 02 derive half-life limit for the $0\nu\chi$ decay by means of tracking calorimeter ELEGANT V. Considering various matrix element calculations, a range of limits for the Majoron-neutrino coupling is given: $\langle g_{\nu\chi} \rangle < (6.3-360) \times 10^{-5}$.
- ASHITKOV 01 result for $0\nu\chi$ of ¹⁰⁰Mo is less stringent than ARNOLD 00.
- DANEVICH 01 obtain limit for the $0\nu\chi$ decay with Majoron emission of ¹⁶⁰Gd using Gd₂SiO₅:Ce crystal scintillators.
- DANEVICH 01 obtain limit for the $0\nu 2\chi$ decay with 2 Majoron emission of ¹⁶⁰Gd.
- ARNOLD 00 reports limit for the $0\nu\chi$ decay with Majoron emission derived from tracking calorimeter NEMO 2. Using ⁸²Se source: $\langle g_{\nu\chi} \rangle < 1.6 \times 10^{-4}$. Matrix element from GUENTHER 96.
- Using ⁹⁶Zr source: $\langle g_{\nu\chi} \rangle < 2.6 \times 10^{-4}$. Matrix element from ARNOLD 99.
- ARNOLD 00 reports limit for the $0\nu 2\chi$ decay with two Majoron emission derived from tracking calorimeter NEMO 2.
- ARNOLD 98 determine the limit for $0\nu\chi$ decay with Majoron emission of ⁸²Se using the NEMO-2 tracking detector. They derive $\langle g_{\nu\chi} \rangle < 2.3-4.3 \times 10^{-4}$ with several nuclear matrix elements.
- LUESCHER 98 report a limit for the 0ν decay with Majoron emission of ¹³⁶Xe using Xe TPC. This result is more stringent than BARABASH 89. Using the matrix elements of ENGEL 88, they obtain a limit on $\langle g_{\nu\chi} \rangle$ of 2.0×10^{-4} .
- See Table 1 in GUENTHER 96 for limits on the Majoron coupling in different models.

Invisible A^0 (Axion) MASS LIMITS from Astrophysics and Cosmology

$v_1 = v_2$ is usually assumed ($v_j =$ vacuum expectation values). For a review of these limits, see RAFFELT 91 and TURNER 90. In the comment lines below, D and K refer to DFSZ and KSVZ axion types, discussed in the above minireview.

VALUE (eV)	CL%	DOCUMENT ID	TECN	COMMENT
• • • We do not use the following data for averages, fits, limits, etc. • • •				
> 3.2 $\times 10^{-19}$	95	1 CHENG 23	ASTR	BH superradiance
<141	90	2 DELLA-MON... 23	ASTR	Ultralight DM soliton halo core
< 0.24	95	3 DERBIN 23	CNTR	K, solar axions
none $10^{-24}-5 \times 10^{-23}$	95	4 NOTARI 23	COSM	K, Hot dark matter
		5 ROGERS 23	COSM	Ultra-light axion DM
		6 SMARRA 23	EPTA	Ultralight DM mass limit
		7 XIA 23	ASTR	Fuzzy DM
		8 LAGUE 22	COSM	Ultralight axion DM
none $0.15-1.5 \times 10^{-12}$	95	9 YUAN 22A	ASTR	BH superradiance
> 1.4 $\times 10^{-21}$	95	10 BANIK 21	ASTR	Fuzzy DM
< 1.9 $\times 10^4$		11 BAUMHOLZ... 21	COSM	warm dark matter
		12 CROON 21	ASTR	SN 1987A, axion-muon coupling
		13 FUJIKURA 21	ASTR	Microlensing
		14 MARTINCA M... 21	ASTR	SN 1987A, A decay
		15 NG 21	ASTR	BH superradiance
none $1.3-2.7 \times 10^{-13}$		16 ROGERS 21	COSM	Lyman- α
> 2 $\times 10^{-20}$	95	17 TSUKADA 21	ASTR	BH superradiance
none $0.8-6.5 \times 10^{-13}$	95	18 IRSIC 20	COSM	Isocurvature fluctuations
> 2 $\times 10^{-17}$		19 PODDAR 20	ASTR	Compact binary systems
		20 SCHUTZ 20	COSM	Fuzzy DM
none $6.4-8.0 \times 10^{-13}$	95	21 SUN 20	ASTR	BH superradiance
none $2.9-4.6 \times 10^{-21}$		22 DAVOUDIASL 19	ASTR	BH superradiance
none $10^{-21}-6 \times 10^{-20}$		23 MARSH 19	ASTR	Fuzzy DM
none $1.1-4 \times 10^{-13}$	95	24 PALOMBA 19	ASTR	BH superradiance
< 0.06		25 CHANG 18	ASTR	K, SN 1987A
		26 PORAYKO 18	PPTA	Fuzzy DM
< 0.67	95	27 ARCHIDIACO... 13A	COSM	K, hot dark matter
none $0.7-3 \times 10^5$		28 CADAMURO 11	COSM	D abundance
<105	90	29 DERBIN 11A	CNTR	D, solar axion
		30 ANDRIAMON... 10	CAST	K, solar axions
< 0.72	95	31 HANNESTAD 10	COSM	K, hot dark matter
		32 ANDRIAMON... 09	CAST	K, solar axions
<191	90	33 DERBIN 09A	CNTR	K, solar axions

Gauge & Higgs Boson Particle Listings

Axions (A^0) and Other Very Light Bosons

<334	95	34	KEKEZ	09	HPGE	K, solar axions
< 1.02	95	35	HANNESTAD	08	COSM	K, hot dark matter
< 1.2	95	36	HANNESTAD	07	COSM	K, hot dark matter
< 0.42	95	37	MELCHIORRI	07A	COSM	K, hot dark matter
< 1.05	95	38	HANNESTAD	05A	COSM	K, hot dark matter
3 to 20		39	MORO	98	COSM	K, hot dark matter
< 0.007		40	BORISOV	97	ASTR	D, neutron star
< 4		41	KACHELRIESS	97	ASTR	D, neutron star cooling
<(0.5-6) × 10 ⁻³		42	KEIL	97	ASTR	SN 1987A
< 0.018		43	RAFFELT	95	ASTR	D, red giant
< 0.010		44	ALTHERR	94	ASTR	D, red giants, white dwarfs
		45	CHANG	93	ASTR	K, SN 1987A
< 0.01		WANG	92	ASTR	D, white dwarf	
< 0.03		WANG	92c	ASTR	D, C-O burning	
none 3-8		46	BERSHADY	91	ASTR	D, K, intergalactic light
< 10		47	KIM	91c	COSM	D, K, mass density of the universe, super-symmetry
		48	RAFFELT	91B	ASTR	D, K, SN 1987A
< 1 × 10 ⁻³		49	RESSELL	91	ASTR	K, intergalactic light
none 10 ⁻³ -3		BURROWS	90	ASTR	D, K, SN 1987A	
		50	ENGEL	90	ASTR	D, K, SN 1987A
< 0.02		51	RAFFELT	90D	ASTR	D, red giant
< 1 × 10 ⁻³		52	BURROWS	89	ASTR	D, K, SN 1987A
<(1.4-10) × 10 ⁻³		53	ERICSON	89	ASTR	D, K, SN 1987A
< 3.6 × 10 ⁻⁴		54	MAYLE	89	ASTR	D, K, SN 1987A
< 12		CHANDA	88	ASTR	D, Sun	
< 1 × 10 ⁻³		RAFFELT	88	ASTR	D, K, SN 1987A	
		55	RAFFELT	88B	ASTR	red giant
< 0.07		FRIEMAN	87	ASTR	D, red giant	
< 0.7		56	RAFFELT	87	ASTR	K, red giant
< 2-5		TURNER	87	COSM	K, thermal production	
< 0.01		57	DEARBORN	86	ASTR	D, red giant
< 0.06		RAFFELT	86	ASTR	D, red giant	
< 0.7		58	RAFFELT	86	ASTR	K, red giant
< 0.03		RAFFELT	86B	ASTR	D, white dwarf	
< 1		59	KAPLAN	85	ASTR	K, red giant
< 0.003-0.02		IWAMOTO	84	ASTR	D, K, neutron star	
> 1 × 10 ⁻⁵		ABBOTT	83	COSM	D, K, mass density of the universe	
> 1 × 10 ⁻⁵		DINE	83	COSM	D, K, mass density of the universe	
< 0.04		ELLIS	83B	ASTR	D, red giant	
> 1 × 10 ⁻⁵		PRESKILL	83	COSM	D, K, mass density of the universe	
< 0.1		BARROSO	82	ASTR	D, red giant	
< 1		60	FUKUGITA	82	ASTR	D, stellar cooling
< 0.07		FUKUGITA	82B	ASTR	D, red giant	

- 1 CHENG 23 employ an improved approximation of the boson cloud eigenfrequency to calculate the superradiance rate. They find that sensitivity depends on initial spin distribution and the merger timescale, and identify two preferred ranges for boson mass centered at 1.78×10^{-12} and 7.94×10^{-13} eV.
- 2 DELLA-MONICA 23 consider the solitonic core implied by ultralight scalar dark matter in the centre of the Milky Way and the effect its presence would have on the precisely tracked orbits of the stars orbiting our galaxy's central supermassive black hole, Sagittarius A*.
- 3 DERBIN 23 employ a thulium garnet crystal bolometer to search for the 8.4 keV solar axion line emitted from the M1 nuclear transition of thulium-169, ^{169}Tm . Mass bound applies to KSVZ axions, value for DFSZ is 244 eV.
- 4 NOTARI 23 improved the evaluation of axion production from pion scatterings by using pion-pion scattering data and incorporating the momentum dependence of the Boltzmann equation. The limit is based on the Planck 2018, BAO, and Pantheon SN Ia data.
- 5 ROGERS 23 use the CMB and BOSS galaxy-clustering data to set limits on the abundance of ultralight axion DM. They obtained $\Omega_{A^0} < 0.002$ for $m_{A^0} = 10^{-30}$ - 10^{-28} eV and set upper limits ranging from 0.002 to 0.07 for $m_{A^0} = 10^{-32}$ - 10^{-25} eV. See their Fig. 22 for mass-dependent limits.
- 6 SMARRA 23 is the European Pulsar Timing Array's constraint on the contribution of ultralight DM to the DM density in our local galactic neighbourhood. Ultralight DM cannot saturate the known DM density of 0.3 GeV/cc for masses inside this mass interval of $10^{-24.5}$ - 10^{-23} eV.
- 7 XIA 23 is analogous to PORAYKO 18 and use the Fermi-LAT pulsar timing array. They set a bound on the local density as $\rho_{A^0} \lesssim 8 \text{ GeV/cm}^3$ for $m_{A^0} \lesssim 10^{-23}$ eV at 95% CL, with weaker constraints up to 10^{-22} eV. See their Fig. 1 for the mass-dependent limits.
- 8 LAGUE 22 used the BOSS galaxy-clustering data to set limits on the abundance of ultralight axion dark matter. When combined with the CMB data, they obtained $\Omega_{A^0} h^2 < 0.004$ for $m_{A^0} = 10^{-31}$ - 10^{-26} eV. See their Figs. 1 and 15 for mass-dependent limits.
- 9 YUAN 22a use the data of Advanced LIGO and Advanced Virgo's first three observing runs to search for stochastic GW background produced by scalar bosonic clouds formed by the BH superradiant instability. They set the limit, taking into account all the unstable modes.
- 10 BANIK 21 use the subhalo mass function inferred from the analyses of the GD-1 and Pal 5 stellar streams. The limit is strengthened to 2.2×10^{-21} eV when adding dwarf satellite counts.
- 11 BAUMHOLZER 21 study the freeze-in production of axion dark matter through couplings to photons, and set the limit using Lyman- α forest data and the observed number of Milky Way subhalos.

- 12 CROON 21 study the supernova cooling effect of the axion-muon coupling, taking account of semi-Compton scattering and muon-proton bremsstrahlung, as well as the loop-induced axion-photon coupling, and exclude the range of $g_{A\mu\mu} \simeq 7 \times 10^{-3}$ - 2×10^{-10} for $m_{A^0} < 0.5$ GeV. See their Fig. 8 for mass-dependent limits.
- 13 FUJIKURA 21 use the EROS-2 survey and the Subaru HSC observation to set limits on spherically symmetric axion clumps, taking account of the finite lens and source size effects. $f_{A^0} \gtrsim 10^{12}$ GeV can be constrained depending on the fraction of the axion dark matter collapsed into clumps, and the clump densities. See their Figs. 7-10 for the limits.
- 14 MARTINCAMALICH 21 considered axion emission from a supernova core through the Λ hyperon decay, and set the limit on $B(\Lambda \rightarrow nA^0) \lesssim 8 \times 10^{-9}$, or equivalently, $f_{A^0}/c_{sd} \gtrsim 2.6 \times 10^9$ GeV in terms of the flavor-violating axion coupling to the down and strange quarks.
- 15 NG 21 use the binary black holes reported by LIGO and Virgo to determine the black hole spin distribution at formation and the scalar boson mass simultaneously, neglecting the boson self-interaction.
- 16 ROGERS 21 set the limit by using a framework involving Bayesian emulator optimization to accurately forward-model the Lyman- α flux power spectrum, and comparing this with small-scale data to constrain the predicted suppression of cosmic structure growth.
- 17 TSUKADA 21 look for a stochastic GW background produced by extragalactic BH-hidden photon cloud systems through the superradiant instability. They assume a uniform spin distribution at birth of isolated BHs from 0 to 1.
- 18 IRSIC 20 used the Lyman- α forest constraint on small-scale isocurvature perturbation to derive limits on the axion mass and decay constant, assuming that the axion makes up all dark matter in the post-inflationary scenario. See their Fig. 1 for other astrophysical limits as well as the limits on the case of the temperature-dependent axion mass.
- 19 PODDAR 20 used the observed decay in orbital period of four compact binary systems to derive a limit on the emission of axions with $m_{A^0} < 1 \times 10^{-19}$ eV, assuming they couple to nucleons and the strong CP phase vanishes at the potential minimum. They exclude $f_{A^0} \lesssim 10^{11}$ GeV for such axions.
- 20 SCHUTZ 20 set a limit on fuzzy dark matter based on the existing limits for warm dark matter derived from the inferred subhalo mass function.
- 21 SUN 20 look for quasimonochromatic gravitational waves emitted from boson clouds around the Cygnus X-1 black hole. The quoted limit assume the black hole age of 5×10^6 years. A mass range of 9.6 - 15.5×10^{-13} eV is disfavored when repeated induction of bosonova for string axions with decay constant $f_{A^0} \simeq 10^{15}$ GeV prevents the superradiance from being saturated.
- 22 DAVOUDIASL 19 used the observed data of M87* by the Event Horizon Telescope to set the limit. A mass range of 0.85 - 4.6×10^{-21} eV is disfavored for a spin-1 boson.
- 23 MARSH 19 considered heating of star clusters due to the stochastic oscillations of the core and granular quasiparticles in the outer halo. The limit was derived by requiring the survival of the old star cluster in Eridanus II, where the lower end is set by the validity of diffusion approximation. The effect of tidal stripping is also discussed for lower masses.
- 24 PALOMBA 19 used the LIGO O2 dataset to derive limits on nearly monochromatic gravitational waves emitted by boson clouds formed around a stellar-mass black hole. They exclude boson masses in a range of 1.1×10^{-13} and 4×10^{-13} eV for high initial black hole spin, and 1.2×10^{-13} and 1.8×10^{-13} eV for moderate spin. See their Figs. 2 and 3 for limits based on various values of black hole initial spin, boson cloud age, and distance.
- 25 CHANG 18 update axion bremsstrahlung emission rates in nucleon-nucleon collisions, shifting the excluded mass range to higher values. They rule out the hadronic axion with mass up to a few hundred eV, closing the hadronic axion window. See their Fig. 11 for results based on several different choices of the temperature and density profile of the proto-neutron star.
- 26 PORAYKO 18 look for time-dependent oscillations in the gravitational potential generated by ultralight scalar dark matter, and set a bound on its local density as $\rho_{A^0} \lesssim 6 \text{ GeV/cm}^3$ for $m_{A^0} \lesssim 10^{-23}$ eV at 95% CL. See their Fig. 4 for the limits.
- 27 ARCHIDIACONO 13A is analogous to HANNESTAD 05A. The limit is based on the CMB temperature power spectrum of the Planck data, the CMB polarization from the WMAP 9-year data, the matter power spectrum from SDSS-DR7, and the local Hubble parameter measurement by the Carnegie Hubble program.
- 28 CADAMURO 11 use the deuterium abundance to show that the m_{A^0} range 0.7 eV - 300 keV is excluded for axions, complementing HANNESTAD 10.
- 29 DERBIN 11A look for solar axions produced by Compton and bremsstrahlung processes, in the resonant excitation of ^{169}Tm , constraining the axion-electron \times axion-nucleon couplings.
- 30 ANDRIAMONJE 10 search for solar axions produced from ^7Li (478 keV) and $D(p,\gamma)^3\text{He}$ (5.5 MeV) nuclear transitions. They show limits on the axion-photon coupling for two reference values of the axion-nucleon coupling for $m_A < 100$ eV.
- 31 This is an update of HANNESTAD 08 including 7 years of WMAP data.
- 32 ANDRIAMONJE 09 look for solar axions produced from the thermally excited 14.4 keV level of ^{57}Fe . They show limits on the axion-nucleon \times axion-photon coupling assuming $m_A < 0.03$ eV.
- 33 DERBIN 09A look for Primakoff-produced solar axions in the resonant excitation of ^{169}Tm , constraining the axion-photon \times axion-nucleon couplings.
- 34 KEKEZ 09 look at axio-electric effect of solar axions in HPGE detectors. The one-loop axion-electron coupling for hadronic axions is used.
- 35 This is an update of HANNESTAD 07 including 5 years of WMAP data.
- 36 This is an update of HANNESTAD 05a with new cosmological data, notably WMAP (3 years) and baryon acoustic oscillations (BAO). Lyman- α data are left out, in contrast to HANNESTAD 05a and MELCHIORRI 07A, because it is argued that systematic errors are large. It uses Bayesian statistics and marginalizes over a possible neutrino hot dark matter component.
- 37 MELCHIORRI 07A is analogous to HANNESTAD 05a, with updated cosmological data, notably WMAP (3 years). Uses Bayesian statistics and marginalizes over a possible neutrino hot dark matter component. Leaving out Lyman- α data, a conservative limit is 1.4 eV.
- 38 HANNESTAD 05a puts an upper limit on the mass of hadronic axion because in this mass range it would have been thermalized and contribute to the hot dark matter component of the universe. The limit is based on the CMB anisotropy from WMAP, SDSS large scale structure, Lyman α , and the prior Hubble parameter from HST Key Project. A χ^2 statistic is used. Neutrinos are assumed not to contribute to hot dark matter.

See key on page 1171

Gauge & Higgs Boson Particle Listings

Axions (A^0) and Other Very Light Bosons

- ³⁹ MOROJ 98 points out that a KSVZ axion of this mass range (see CHANG 93) can be a viable hot dark matter of Universe, as long as the model-dependent $g_{A\gamma}$ is accidentally small enough as originally emphasized by KAPLAN 85; see Fig. 1.
- ⁴⁰ BORISOV 97 bound is on the axion-electron coupling $g_{ae} < 1 \times 10^{-13}$ from the photo-production of axions off of magnetic fields in the outer layers of neutron stars.
- ⁴¹ KACHELRIESS 97 bound is on the axion-electron coupling $g_{ae} < 1 \times 10^{-10}$ from the production of axions in strongly magnetized neutron stars. The authors also quote a stronger limit, $g_{ae} < 9 \times 10^{-13}$ which is strongly dependent on the strength of the magnetic field in white dwarfs.
- ⁴² KEIL 97 uses new measurements of the axial-vector coupling strength of nucleons, as well as a reanalysis of many-body effects and pion-emission processes in the core of the neutron star, to update limits on the invisible-axion mass.
- ⁴³ RAFFELT 95 reexamined the constraints on axion emission from red giants due to the axion-electron coupling. They improve on DEARBORN 86 by taking into proper account degeneracy effects in the bremsstrahlung rate. The limit comes from requiring the red giant core mass at helium ignition not to exceed its standard value by more than 5% (0.025 solar masses).
- ⁴⁴ ALTHERR 94 bound is on the axion-electron coupling $g_{ae} < 1.5 \times 10^{-13}$, from energy loss via axion emission.
- ⁴⁵ CHANG 93 updates ENGEL 90 bound with the Kaplan-Manohar ambiguity in $z=m_{\eta}/m_{\phi}$ (see the Note on the Quark Masses in the Quark Particle Listings). It leaves the window $f_A=3 \times 10^5-3 \times 10^6$ GeV open. The constraint from Big-Bang Nucleosynthesis is satisfied in this window as well.
- ⁴⁶ BERSHADY 91 searched for a line at wave length from 3100-8300 Å expected from 2γ decays of relic thermal axions in intergalactic light of three rich clusters of galaxies.
- ⁴⁷ KIM 91c argues that the bound from the mass density of the universe will change drastically for the supersymmetric models due to the entropy production of saxion (scalar component in the axionic chiral multiplet) decay. Note that it is an *upperbound* rather than a lowerbound.
- ⁴⁸ RAFFELT 91b argue that previous SN1987A bounds must be relaxed due to corrections to nucleon bremsstrahlung processes.
- ⁴⁹ RESSELL 91 uses absence of any intracuster line emission to set limit.
- ⁵⁰ ENGEL 90 rule out $10^{-10} \lesssim g_{AN} \lesssim 10^{-3}$, which for a hadronic axion with EMC motivated axion-nucleon couplings corresponds to $2.5 \times 10^{-3} \text{ eV} \lesssim m_{A^0} \lesssim 2.5 \times 10^4 \text{ eV}$. The constraint is loose in the middle of the range, i.e. for $g_{AN} \sim 10^{-6}$.
- ⁵¹ RAFFELT 90d is a re-analysis of DEARBORN 86.
- ⁵² The region $m_{A^0} \gtrsim 2 \text{ eV}$ is also allowed.
- ⁵³ ERICSON 89 considered various nuclear corrections to axion emission in a supernova core, and found a reduction of the previous limit (MAYLE 88) by a large factor.
- ⁵⁴ MAYLE 89 limit based on naive quark model couplings of axion to nucleons. Limit based on couplings motivated by EMC measurements is 2-4 times weaker. The limit from axion-electron coupling is weak: see HATSUDA 88b.
- ⁵⁵ RAFFELT 88b derives a limit for the energy generation rate by exotic processes in helium-burning stars $\epsilon < 100 \text{ erg g}^{-1} \text{ s}^{-1}$, which gives a firmer basis for the axion limits based on red giant cooling.
- ⁵⁶ RAFFELT 87 also gives a limit $g_{A\gamma} < 1 \times 10^{-10} \text{ GeV}^{-1}$.
- ⁵⁷ DEARBORN 86 also gives a limit $g_{A\gamma} < 1.4 \times 10^{-11} \text{ GeV}^{-1}$.
- ⁵⁸ RAFFELT 86 gives a limit $g_{A\gamma} < 1.1 \times 10^{-10} \text{ GeV}^{-1}$ from red giants and $< 2.4 \times 10^{-9} \text{ GeV}^{-1}$ from the sun.
- ⁵⁹ KAPLAN 85 says $m_{A^0} < 23 \text{ eV}$ is allowed for a special choice of model parameters.
- ⁶⁰ FUKUGITA 82 gives a limit $g_{A\gamma} < 2.3 \times 10^{-10} \text{ GeV}^{-1}$.

$<1.03 \times 10^{-35}$	95	19	ZHOU	22	ASTR	$m_{A^0} = 3.18-4.35 \mu\text{eV}$
$<2.8 \times 10^{-4}$	95	20	ADE	21	CMB	$m_{A^0} = 0.16-4.8 \times 10^{-20} \text{ eV}$
$<1.1 \times 10^{-41}$	90	21	ALESINI	21	QUAX	$m_{A^0} = 43 \mu\text{eV}$
$<1 \times 10^{-44}$	90	22	BARTRAM	21A	ADMX	$m_{A^0} = 3.3-4.2 \mu\text{eV}$
$<1.6 \times 10^{-29}$	95	23	DEVLIN	21	TRAP	$m_{A^0} = 2.7906-2.7914 \text{ neV}$
$<1.4 \times 10^{-23}$	95	24	GRAMOLIN	21	SHFT	$m_{A^0} = 0.012-12 \text{ neV}$
$<7 \times 10^{-43}$	90	25	KWON	21	CASK	$m_{A^0} = 10.7126-10.7186 \mu\text{eV}$
$<4.6 \times 10^{-40}$	95	26	MELCON	21	RADE	$m_{A^0} = 34.6738-34.6771 \mu\text{eV}$
$<3.5 \times 10^{-28}$	95	27	SALEMI	21	ABRA	$m_{A^0} = 0.41-8.27 \text{ neV}$
$<3 \times 10^{-3}$	95	28	THOMSON	21		$m_{A^0} = 7.44-19.38 \text{ neV}$
$<1 \times 10^{-2}$	95	28	THOMSON	21		$m_{A^0} = 74.4-74.5 \mu\text{eV}$
		29	YUAN	21	ASTR	$m_{A^0} = 10^{-20}-10^{-17} \text{ eV}$
$<1.9 \times 10^{-44}$	90	30	BRAINE	20	ADMX	$m_{A^0} = 2.81-3.31 \mu\text{eV}$
$<2 \times 10^{-35}$	90	31	CRISOSTO	20	SLIC	$m_{A^0} = 180.07-180.15 \text{ neV}$
$<4 \times 10^{-37}$	95	32	DARLING	20A	ASTR	$m_{A^0} = 4.2-165.6 \mu\text{eV}$
$<3.2 \times 10^{-36}$	95	33	FOSTER	20	ASTR	$m_{A^0} = 5-7, 10-11 \mu\text{eV}$
$<5.7 \times 10^{-41}$	90	34	JEONG	20	CASK	$m_{A^0} = 13.0-13.9 \mu\text{eV}$
		35	KENNEDY	20		$m_{S^0} = 10^{-19}-10^{-17} \text{ eV}$
$<4.8 \times 10^{-42}$	90	36	LEE	20A	CASK	$m_{A^0} = 6.62-6.82 \mu\text{eV}$
$<2.6 \times 10^{-39}$	95	37	ALESINI	19	QUAX	$m_{A^0} = 37.5 \mu\text{eV}$
$<6 \times 10^{-5}$		38	FUJITA	19	ASTR	$m_{A^0} < 10^{-21} \text{ eV}$
$<2 \times 10^{-27}$	95	39	OUELLET	19A	ABRA	$m_{A^0} = 0.31-8.3 \text{ neV}$
$<7.3 \times 10^{-40}$	90	40	BOUTAN	18	ADMX	$m_{A^0} = 17.38-17.57 \mu\text{eV}$
$<1.8 \times 10^{-39}$	90	40	BOUTAN	18	ADMX	$m_{A^0} = 21.03-23.98 \mu\text{eV}$
$<3.4 \times 10^{-39}$	90	40	BOUTAN	18	ADMX	$m_{A^0} = 29.67-29.79 \mu\text{eV}$
$<1.4 \times 10^{-44}$	90	41	DU	18	ADMX	$m_{A^0} = 2.66-2.81 \mu\text{eV}$
$<2.87 \times 10^{-42}$	90	42	ZHONG	18	HYST	$m_{A^0} = 23.15-24 \mu\text{eV}$
		43	BRANCA	17	AURG	$m_{S^0} = 3.5-3.9 \text{ peV}$
$<3 \times 10^{-42}$	90	44	BRUBAKER	17	HYST	$m_{A^0} = 23.55-24.0 \mu\text{eV}$
$<1.0 \times 10^{-29}$	95	45	CHOI	17	CASK	$m_{A^0} = 24.7-29.1 \mu\text{eV}$
$<5.9 \times 10^{-36}$	90	46	MCALLISTER	17	ORGN	at $m_{A^0} = 110 \mu\text{eV}$
$<8.6 \times 10^{-42}$	90	47	HOSKINS	16	ADMX	$m_{A^0} = 3.36-3.52 \text{ or } 3.55-3.69 \mu\text{eV}$
		48	BECK	13		$m_{A^0} = 0.11 \text{ meV}$
$<3.5 \times 10^{-43}$		49	HOSKINS	11	ADMX	$m_{A^0} = 3.3-3.69 \times 10^{-6} \text{ eV}$
$<2.9 \times 10^{-43}$	90	50	ASZTALOS	10	ADMX	$m_{A^0} = 3.34-3.53 \times 10^{-6} \text{ eV}$
$<1.9 \times 10^{-43}$	97.7	51	DUFFY	06	ADMX	$m_{A^0} = 1.98-2.17 \times 10^{-6} \text{ eV}$
$<5.5 \times 10^{-43}$	90	52	ASZTALOS	04	ADMX	$m_{A^0} = 1.9-3.3 \times 10^{-6} \text{ eV}$
		53	KIM	98	THEO	
$<2 \times 10^{-41}$		54	HAGMANN	90	CNTR	$m_{A^0} = (5.4-5.9)10^{-6} \text{ eV}$
$<6.3 \times 10^{-42}$	95	55	WUENSCH	89	CNTR	$m_{A^0} = (4.5-10.2)10^{-6} \text{ eV}$
$<5.4 \times 10^{-41}$	95	55	WUENSCH	89	CNTR	$m_{A^0} = (11.3-16.3)10^{-6} \text{ eV}$

Search for Relic Invisible Axions

Limits are for the dimensionless quantity $[G_{A\gamma\gamma}/m_{A^0}]^2 \rho_A$ where $G_{A\gamma\gamma}$ denotes the axion two-photon coupling, $L_{\text{int}} = -\frac{G_{A\gamma\gamma}}{4} \phi_A F_{\mu\nu} \tilde{F}^{\mu\nu} = G_{A\gamma\gamma} \phi_A \mathbf{E} \cdot \mathbf{B}$, and ρ_A is the axion energy density near the earth, unless otherwise stated. Notice that for QCD axions $G_{A\gamma\gamma}/m_{A^0}$ does not depend on m_{A^0} . For the reference values $m_{A^0} = 1 \mu\text{eV}$, $G_{A\gamma\gamma} = 3.9 \times 10^{-16} \text{ GeV}^{-1}$ (that would apply to KSVZ axions at that mass), and $\rho_A = 300 \text{ MeV}/\text{cm}^3$ one finds $[G_{A\gamma\gamma}/m_{A^0}]^2 \rho_A = 3.5 \times 10^{-43}$.

VALUE	CL%	DOCUMENT ID	TECN	COMMENT
$<1.3 \times 10^{-3}$	95	1 ADACHI	23D	CMB $m_{A^0} = 0.096-2.2 \times 10^{-20} \text{ eV}$
$<7.5 \times 10^{-43}$	90	2 DI-VORA	23	QUAX $m_{A^0} = 42.8178-42.8190 \mu\text{eV}$
$<2.3 \times 10^{-42}$	90	3 JEWELL	23	HYST $m_{A^0} = 18.44-18.71 \mu\text{eV}$
$<2.0 \times 10^{-42}$	90	4 JEWELL	23	HYST $m_{A^0} = 16.96-17.12, 17.14-17.28 \mu\text{eV}$
$<2.5 \times 10^{-42}$	90	5 KIM	23	CASK $m_{A^0} = 9.39-9.51 \mu\text{eV}$
$<3.0 \times 10^{-4}$	95	6 OSHIMA	23	DANC $m_{A^0} = 4.1 \times 10^{-16}-2.0 \times 10^{-12} \text{ eV}$
$<2.56 \times 10^{-24}$	95	7 THOMSON	23	UPLD $m_{A^0} = 1.12-1.20 \mu\text{eV}$
$<6.09 \times 10^{-43}$	90	8 YANG	23	CAPP $m_{A^0} = 19.883-19.926 \mu\text{eV}$
$<6.6 \times 10^{-44}$	90	9 YI	23	CASK $m_{A^0} = 4.51-4.59 \mu\text{eV}$
$<6.6 \times 10^{-44}$	90	10 YI	23A	CASK $m_{A^0} = 4.51-4.59 \mu\text{eV}$
$<4.7 \times 10^{-5}$	95	11 ADE	22	CMB $m_{A^0} = 0.16-4.8 \times 10^{-20} \text{ eV}$
$<1.0 \times 10^{-41}$	90	12 ALESINI	22	QUAX $m_{A^0} = 42.8210-42.8223 \mu\text{eV}$
$<7 \times 10^{-33}$	95	13 BATTYE	22	ASTR $m_{A^0} = 4.2-60 \mu\text{eV}$
$<5.8 \times 10^{-41}$	95	14 CHANG	22	TASE $m_{A^0} = 19.4687-19.8436 \mu\text{eV}$
$<3.2 \times 10^{-6}$	95	15 FERGUSON	22	CMB $m_{A^0} = 0.047-4.7 \times 10^{-20} \text{ eV}$
$<8.4 \times 10^{-43}$	90	16 LEE	22	CASK $m_{A^0} = 19.764-19.890 \mu\text{eV}$
$<4.9 \times 10^{-39}$	95	17 QUISKAMP	22	ORGN $m_{A^0} = 63.2-67.1 \mu\text{eV}$
$<3.6 \times 10^{-43}$	90	18 YOON	22	CASK $m_{A^0} = 19.764-19.890 \mu\text{eV}$

- ¹ ADACHI 23D is analogous to ADE 21. They used POLARBEAR data, and take account of a stochastic local axion field amplitude with the time-averaged local axion density $\rho_A = 0.3 \text{ GeV}/\text{cm}^3$. Limits are set at $G_{A\gamma\gamma} < 2.4 \times 10^{-11} \text{ GeV}^{-1}$ ($m_{A^0}/10^{-21} \text{ eV}$), which is 2.2 times larger than the deterministic case. See Fig. 5 for mass-dependent limits.
- ² DI-VORA 23 searches for axions in a narrow mass window using an 8T haloscope and a travelling wave parametric amplifier to achieve noise close to the quantum limit. This is an improvement on their previous scan at the same mass, ALESINI 21. See Fig. 7 for mass-dependent limits and a comparison.
- ³ JEWELL 23 is an update of BRUBAKER 17. See their Fig. 11 for the mass-dependent limits.
- ⁴ JEWELL 23 correct an underestimation of intermediate frequency noise in BACKES 21. See their Fig. 11 for the mass-dependent limits.
- ⁵ KIM 23 is an update of KWON 21 on the CAPP-PACE experiment. See their Fig. 4 for mass-dependent limits.
- ⁶ OSHIMA 23 report first limits from the DANCE experiment. This experiment is based on a novel bow-tie cavity design that searches for the oscillating rotation of polarised laser light driven by the DM axion-photon mixing at low frequencies. See their Fig. 6 for mass-dependent limits.
- ⁷ THOMSON 23 used an AC microwave cavity to search for dark matter axions. The axion signal is resonantly enhanced when the axion mass matches the difference between a cavity which is pumped with power and another resonant mode close in frequency that is used to read out the signal. See their Fig. 7 for the mass-dependent limits.
- ⁸ YANG 23 extends the first phase of CAPP 18T to KSVZ axions between 4.8077 and 4.8181 GHz. They used an 18T high-temperature superconducting magnet haloscope. See their Fig. 5 for mass-dependent limits. Quoted value is for their limit derived with a Bayesian method.
- ⁹ YI 23 is analogous to LEE 20A, using the CAPP-12TB haloscope. See their Fig. 4 for mass-dependent limits.
- ¹⁰ YI 23A used the same data as YI 23, but instead of the standard halo model, they searched for axion dark matter in the Sagittarius tidal stream with a velocity $v = 300 \text{ km}/\text{sec}$ and a velocity dispersion $\delta v = 20 \text{ km}/\text{sec}$. See their Fig. 4 for mass-dependent limits.
- ¹¹ ADE 22 is an update of ADE 21 based on the expanded data of the 2012-2015 observing seasons. See their Fig. 3 for mass-dependent limits over the extended mass range $1 \times 10^{-23}-6 \times 10^{-19} \text{ eV}$.
- ¹² ALESINI 22 is an update of ALESINI 21, using the TM030 mode of the cylindrical dielectric cavity. See their Fig. 8 for mass-dependent limits.

Gauge & Higgs Boson Particle Listings

Axions (A^0) and Other Very Light Bosons

- 13 BATTYE 22 is analogous to DARLING 20A, and use plasma ray tracing technique to analyze the propagation of radio photons converted from axion dark matter in the magnetosphere of PSR J1745-2900. The quoted limit assumes $\rho_A = 6.5 \times 10^4 \text{ GeV/cm}^3$ in the vicinity of the magnetar. See their Fig. 1 for mass-dependent limits.
- 14 CHANG 22 used a microwave cavity detector to search for dark matter axions. See Fig. 3 for the mass-dependent limits.
- 15 FERGUSON 22 is analogous to ADE 21. They use the data of the SPT-3G's 2019 observing season. See their Fig. 5 for mass-dependent limits over the extended mass range $0.047\text{--}9.5 \times 10^{-20} \text{ eV}$.
- 16 LEE 22 is analogous to LEE 20A. They used an 18T high-temperature superconducting magnet haloscope. See their Fig. 5 for mass-dependent limits.
- 17 QUICKAMP 22 is a 15.28 to 16.23 GHz microwave cavity haloscope with 11.5 T B-field. See Fig. 4 for mass-dependent limits.
- 18 YOON 22 analyzed the data from LEE 22 and changed from a frequentist to a Bayesian method to set limits. See their Fig. 27 for mass-dependent limits.
- 19 ZHOU 22 is analogous to DARLING 20A, and they use the data from the MeerKAT radio telescope's observation of the neutron star J0806.4-4123, which is 250 pc from Earth. See their Fig.3 for mass-dependent limits.
- 20 ADE 21 looks for a time-variable global rotation of the CMB polarization induced by the harmonic oscillations of local axion-like dark matter and uses data from the 2012 observing season of the Keck Array, part of the BICEP program. The limits get 25% weaker for $m_{A^0} = 4.8 \times 10^{-20}\text{--}5.7 \times 10^{-19} \text{ eV}$. See their Eq. (80) and Fig. 6 for mass-dependent limits.
- 21 ALESINI 21 is an update of ALESINI 19. See their Figs. 5 and 6 for the mass-dependent limits.
- 22 BARTRAM 21A is analogous to DU 18. See their Fig.4 for mass-dependent limits.
- 23 DEVLIN 21 use the superconducting resonant detection circuit of a cryogenic Penning trap with a single antiproton. See their Fig. 3 for mass-dependent limits.
- 24 GRAMOLIN 21 use two detection channels, each consisting of two stacked toroids to look for the axion-induced oscillating magnetic field. The quoted limit applies at $m_{A^0} = 0.02 \text{ neV}$. See their Fig. 4 for mass-dependent limits.
- 25 KWON 21 is analogous to LEE 20A. They also obtain weaker limits in the range of $m_{A^0} = 10.16\text{--}11.37 \mu\text{eV}$. See their Fig. 4 for mass-dependent limits.
- 26 MELCON 21 use a radio frequency cavity consisting of 5 sub-cavities coupled by inductive irises installed inside the CAST dipole magnet to look for higher axion masses. See their Fig. 9 for mass-dependent limits.
- 27 SALEM 21 is an update of OUELLET 19A. See their Fig. 4 for mass-dependent limits.
- 28 THOMSON 21 use a resonant cavity supporting two spatially overlapping microwave modes, which is sensitive to the axion mass corresponding to the sum or difference of the two resonant frequencies. The original limit was retracted due to a sign error. See their Fig. 2 in the erratum for the corrected limits.
- 29 YUAN 21 use polarimetric observations of Sgr A* taken by the Event Horizon Telescope to search for periodic oscillation of the polarization induced by axion dark matter, assuming a solitonic core near the Galactic center. They obtained limits in the range of $G_{A\gamma\gamma} = 8 \times 10^{-13}\text{--}3 \times 10^{-11} \text{ GeV}^{-1}$.
- 30 BRAINE 20 is analogous to DU 18. See Fig. 4 for their mass-dependent limits.
- 31 CRISOSTO 20 used a resonant LC circuit to look for lighter axion dark matter. They obtained a similar, slightly weaker limit for $m_{A^0} = 174.98\text{--}175.19$ and $177.34\text{--}177.38 \text{ neV}$. See their Fig. 4 for mass-dependent limits.
- 32 DARLING 20A use VLA data to look for radio-frequency radiation converted from axion dark matter in the magnetosphere of the Galactic Center magnetar PSR J1745-2900. They extended the results of DARLING 20, which used only data with the highest angular resolution, by adding sub-optimal data. They use $\rho_A = 6.5 \times 10^4 \text{ GeV/cm}^3$ in the vicinity of the magnetar. See their Fig. 2 for mass-dependent limits.
- 33 FOSTER 20 look for radio-frequency radiation converted from axion dark matter in the magnetic field around neutron stars. They use the observed data of isolated local neutron stars and in the Galactic center. The quoted limit applies to $m_{A^0} \simeq 7 \mu\text{eV}$. See their Fig. 2 for mass-dependent limits.
- 34 JEONG 20 is analogous to LEE 20A, and they use a double-cell cavity to look for axions with mass $> 10 \mu\text{eV}$. See their Fig. 5 for mass-dependent limits.
- 35 KENNEDY 20 is analogous to BRANCA 17, and they compare the frequency ratios of the Si cavity measured by a Sr optical lattice clock and by a H maser. Assuming the local density of moduli dark matter, $\rho_S = 0.3 \text{ GeV/cm}^3$, they obtain a limit $G_{S\gamma\gamma} < 5.8 \times 10^{-24} \text{ GeV}^{-1}$ at $m_{S^0} = 2 \times 10^{-19} \text{ eV}$. See their Fig. 2 for mass-dependent limits as well as limits on the modulus coupling to electrons.
- 36 LEE 20A used a microwave cavity detector at the IBS/CAPP to search for dark matter axions. See Fig. 3 for the mass-dependent limits.
- 37 ALESINI 19 used a superconducting resonant cavity made of NbTi to increase the quality factor. The limit applies to a mass range of 0.2 neV around $m_{A^0} = 37.5 \mu\text{eV}$.
- 38 FUJITA 19 look for photon birefringence under the oscillating axion background using the polarimetric imaging observation of a protoplanetary disk, AB Aur. See their Fig. 2 for a more conservative limit taking account of possible systematic effects.
- 39 OUELLET 19A look for the axion-induced oscillating magnetic field generated by a toroidal magnetic field. The quoted limit applies at $m_{A^0} = 8 \text{ neV}$. See their Fig. 3 for the mass-dependent limits.
- 40 BOUTAN 18 use a small high frequency cavity installed above the main ADMX cavity to look for heavier axion dark matter. See their Fig. 4 for mass-dependent limits.
- 41 DU 18 is analogous to DUFFY 06. They upgraded a dilution refrigerator to reduce the system noise. The quoted limit is around $m_{A^0} = 2.69 \mu\text{eV}$ for the boosted Maxwellian axion line shape. See Fig. 4 for their mass-dependent limits.
- 42 ZHONG 18 is analogous to BRUBAKER 17. The quoted limit applies at $m_{A^0} = 23.76 \mu\text{eV}$. See Fig. 4 for their mass-dependent limits.
- 43 BRANCA 17 look for modulations of the fine-structure constant and the electron mass due to moduli dark matter by using the cryogenic resonant-mass AURIGA detector. The limit on the assumed dilatonic coupling implies $G_{S\gamma\gamma} < 1.5 \times 10^{-24} \text{ GeV}^{-1}$ for the scalar to two-photon coupling. See Fig. 5 for the mass-dependent limits.
- 44 BRUBAKER 17 used a microwave cavity detector at the Yale Wright Laboratory to search for dark matter axions. See Fig. 3 for the mass-dependent limits.
- 45 CHOI 17 used a microwave cavity detector with toroidal geometry. See Fig. 4 for their mass-dependent limits.
- 46 MCALLISTER 17 used a high-frequency microwave cavity haloscope at 26.6 GHz in a 7 T magnetic field. See Fig. 4 for mass-dependent limits.

- 47 HOSKINS 16 is analogous to DUFFY 06. See Fig. 12 for mass-dependent limits in terms of the local dark matter density.
- 48 BECK 13 argues that dark-matter axions passing through Earth may generate a small observable signal in resonant S/N/S Josephson junctions. A measurement by HOFFMANN 04 [Physical Review **B70** 180503 (2004)] is interpreted in terms of subdominant dark matter axions with $m_{A^0} = 0.11 \text{ meV}$.
- 49 HOSKINS 11 is analogous to DUFFY 06. See Fig. 4 for the mass-dependent limit in terms of the local density.
- 50 ASZTALOS 10 used the upgraded detector of ASZTALOS 04 to search for halo axions. See their Fig. 5 for the m_{A^0} dependence of the limit.
- 51 DUFFY 06 used the upgraded detector of ASZTALOS 04, while assuming a smaller velocity dispersion than the isothermal model as in Eq. (8) of their paper. See Fig. 10 of their paper on the axion mass dependence of the limit.
- 52 ASZTALOS 04 looked for a conversion of halo axions to microwave photons in magnetic field. At 90% CL, the KSVZ axion cannot have a local halo density more than 0.45 GeV/cm^3 in the quoted mass range. See Fig. 7 of their paper on the axion mass dependence of the limit.
- 53 KIM 98 calculated the axion-to-photon couplings for various axion models and compared them to the HAGMANN 90 bounds. This analysis demonstrates a strong model dependence of $G_{A\gamma\gamma}$ and hence the bound from relic axion search.
- 54 HAGMANN 90 experiment is based on the proposal of SIKIVIE 83.
- 55 WUENSCH 89 looks for condensed axions near the earth that could be converted to photons in the presence of an intense electromagnetic field via the Primakoff effect, following the proposal of SIKIVIE 83. The theoretical prediction with $[G_{A\gamma\gamma}/m_{A^0}]^2 = 2 \times 10^{-14} \text{ MeV}^{-4}$ (the three generation DFSZ model) and $\rho_A = 300 \text{ MeV/cm}^3$ that makes up galactic halos gives $(G_{A\gamma\gamma}/m_{A^0})^2 \rho_A = 4 \times 10^{-44}$. Note that our definition of $G_{A\gamma\gamma}$ is $(1/4\pi)$ smaller than that of WUENSCH 89.

Invisible A^0 (Axion) Limits from Photon Coupling

Limits are for the modulus of the axion-two-photon coupling $G_{A\gamma\gamma}$ defined by $L = -G_{A\gamma\gamma} \phi_A \mathbf{E} \cdot \mathbf{B}$. For scalars S^0 the limit is on the coupling constant in $L = G_{S\gamma\gamma} \phi_S (\mathbf{E}^2 - \mathbf{B}^2)$. The relation between $G_{A\gamma\gamma}$ and m_{A^0} is not used unless stated otherwise, i.e., many of these bounds apply to low-mass axion-like particles (ALPs), not to QCD axions.

VALUE (GeV^{-1})	CL%	DOCUMENT ID	TECN	COMMENT
$< 3 \times 10^{-11}$	95	1 PANT	24	ASTR $m_{A^0} = 0.3\text{--}1 \text{ neV}$
$< 5.5 \times 10^{-11}$	95	2 BATTYE	23	DM $m_{A^0} = 3.9\text{--}4.7 \mu\text{eV}$
$< 2 \times 10^{-13}$	95	3 BEAUFORT	23	ASTR $m_{A^0} = 3\text{--}38 \text{ keV}$
$< 2 \times 10^{-12}$	99	4 BERNAL	23	COSM $m_{A^0} = 8\text{--}25 \text{ eV}$
$< 4 \times 10^{-14}$	99	5 CAPOZZI	23	COSM $m_{A^0} = 30\text{--}800 \text{ eV}$
$< 1.3 \times 10^{-7}$	95	6 CAPOZZI	23A	DUMP $m_{A^0} = 10^3\text{--}2 \times 10^8 \text{ eV}$
$< 5 \times 10^{-12}$	95	7 DAVIES	23	ASTR $m_{A^0} = 5\text{--}200 \text{ neV}$
$< 1.7 \times 10^{-10}$	95	8 DIAMOND	23	ASTR $m_{A^0} = 2\text{--}56 \text{ MeV}$
$< 6 \times 10^{-29}$	95	9 FILZINGER	23	Dilaton-like dark matter
$< 4.5 \times 10^{-12}$	95	10 HOOFF	23	ASTR $m_{A^0} = 4 \times 10^{-10} \text{ eV}$
$< 3 \times 10^{-12}$	95	11 HOOFF	23	ASTR $m_{A^0} = 60 \text{ MeV}$
$< 2.7 \times 10^{-11}$	99.7	12 JACOBSEN	23	ASTR $m_{A^0} < 3 \times 10^{-7} \text{ eV}$
$< 2 \times 10^{-11}$	99	13 LI	23H	ASTR $m_{A^0} = 1\text{--}100 \text{ neV}$
$< 3.0 \times 10^{-12}$	95	14 NOORDHUIS	23	ASTR $m_{A^0} = 10^{-9}\text{--}10^{-5} \text{ eV}$
$< 5 \times 10^{-11}$	95	15 PANT	23	ASTR $m_{A^0} = 0.1\text{--}1000 \text{ neV}$
$< 5 \times 10^{-26}$	95	16 SHERRILL	23	DM Dilaton-like dark matter
$< 8 \times 10^{-9}$	95	17 SULAI	23	DM $m_{A^0} = 0.25\text{--}2 \times 10^{-14} \text{ eV}$
$< 7.9 \times 10^{-12}$		18 YAO	23	ASTR $m_{A^0} \lesssim 10^{-13} \text{ eV}$
$< 3.8 \times 10^{-22}$	95	19 ZHANG	23A	Dilaton-like dark matter
$< 5 \times 10^{-10}$	90	20 APRILE	22B	XENT Solar axions
$< 1.45 \times 10^{-9}$	95	21 ARNQUIST	22	MAJD $m_{A^0} < 100 \text{ eV}$
$< 7 \times 10^{-11}$	95	22 ARZA	22	DM $m_{A^0} = 0.2\text{--}7 \times 10^{-17} \text{ eV}$
$3\text{--}6 \times 10^{-11}$	95	23 BERNAL	22	COSM $m_{A^0} = 8\text{--}20 \text{ eV}$
$< 3.76 \times 10^{-11}$	95	24 CALORE	22	ASTR $m_{A^0} < 10^{-11} \text{ eV}$
$< 2 \times 10^{-10}$		25 CAPUTO	22	ASTR $m_{A^0} = 1\text{--}500 \text{ MeV}$
$< 3 \times 10^{-14}$	95	26 CASTILLO	22	ASTR $m_{A^0} = 3 \times 10^{-23} \text{ eV}$
$< 6 \times 10^{-12}$	90	27 DEROCCO	22	ASTR $m_{A^0} = 5\text{--}30 \text{ keV}$
$< 5.4 \times 10^{-12}$	95	28 DESSERT	22A	ASTR $m_{A^0} \lesssim 3 \times 10^{-7} \text{ eV}$
$< 2.1 \times 10^{-11}$	95	29 ECKNER	22	ASTR $m_{A^0} < 2 \times 10^{-7} \text{ eV}$
$< 1 \times 10^{-11}$	95	30 FOSTER	22	ASTR $m_{A^0} = 16.5\text{--}32.5 \mu\text{eV}$
$< 1.14 \times 10^{-5}$	95	31 KIRITA	22	SAPH $m_{A^0} = 0.5\text{--}500 \text{ meV}$
$< 2 \times 10^{-16}$		32 LANGHOFF	22	COSM $m_{A^0} = 0.1\text{--}3 \times 10^4 \text{ keV}$
$< 6 \times 10^{-12}$	95	33 LI	22	ASTR $m_{A^0} = 0.2\text{--}20 \text{ neV}$
$< 1.3 \times 10^{-11}$	95	34 LI	22C	ASTR $m_{A^0} = 8\text{--}200 \text{ neV}$
$< 1 \times 10^{-5}$		35 LUCENTE	22	ASTR $m_{A^0} \lesssim 0.4 \text{ MeV}$
$< 9.2 \times 10^{-11}$	95	36 BASU	21	ASTR $m_{A^0} = 3.6 \times 10^{-21} \text{ eV}$
$< 1.8 \times 10^{-10}$	95	37 BI	21	ASTR $m_{A^0} = 2\text{--}6 \times 10^{-7} \text{ eV}$
$< 1.6 \times 10^{-10}$	95	38 DOLAN	21A	ASTR $m_{A^0} = 1\text{--}570 \text{ keV}$
$< 5 \times 10^{-11}$	95	39 GUO	21	ASTR $m_{A^0} = 8\text{--}23 \text{ neV}$
$< 1.2 \times 10^{-4}$	95	40 HOMMA	21	SAPH $m_{A^0} = 0.4\text{--}600 \text{ meV}$
$< 1.2 \times 10^{-11}$	95	41 LI	21B	ASTR $m_{A^0} = 0.5\text{--}500 \text{ neV}$
		42 LLOYD	21	ASTR Magnetars
$< 1 \times 10^{-13}$	95	43 REGIS	21	ASTR $m_{A^0} = 2.7\text{--}5.3 \text{ eV}$

See key on page 1171

Gauge & Higgs Boson Particle Listings
Axions (A^0) and Other Very Light Bosons

$<1.8 \times 10^{-11}$	95	44	XIAO	21	ASTR	$m_{A^0} < 3.5 \times 10^{-11}$ eV	$<1.5 \times 10^{-4}$	90	119	ASTIER	00B	NOMD	$m_{A^0} < 40$ eV
$<7 \times 10^{-4}$	95	45	ABUDINEN	20	BEL2	$m_{A^0} = 0.2\text{--}1$ GeV			120	MASSO	00	THEO	induced γ coupling
$<2 \times 10^{-4}$	90	46	BANERJEE	20A	NA64	$m_{A^0} < 55$ MeV	$<2.7 \times 10^{-9}$	95	121	AVIGNONE	98	SLAX	$m_{A^0} < 1$ keV
$<1.0 \times 10^{-11}$	95	47	BUEHLER	20	ASTR	$m_{A^0} < 3$ neV	$<6.0 \times 10^{-10}$	95	122	MORIYAMA	98		$m_{A^0} < 0.03$ eV
$<5 \times 10^{-10}$		48	CALORE	20	ASTR	$m_{A^0} \lesssim 10^{-11}$ eV	$<3.6 \times 10^{-7}$	95	123	CAMERON	93		$m_{A^0} < 10^{-3}$ eV, optical rotation
$2\text{--}4 \times 10^{-10}$	95	49	CARENZA	20	ASTR	Globular clusters	$<6.7 \times 10^{-7}$	95	124	CAMERON	93		$m_{A^0} < 10^{-3}$ eV, photon regeneration
		50	DENT	20A	ASTR	Solar axions							
		51	DEPTA	20	COSM	Axion-like particles							
$<3.6 \times 10^{-12}$	95	52	DESSERT	20A	ASTR	$m_{A^0} < 5 \times 10^{-11}$ eV	$<3.6 \times 10^{-9}$	99.7	125	LAZARUS	92		$m_{A^0} < 0.03$ eV
		53	ESTEBAN	20	ANIT	Axion-like particles	$<7.7 \times 10^{-9}$	99.7	125	LAZARUS	92		$m_{A^0} = 0.03\text{--}0.11$ eV
$4\text{--}6 \times 10^{-10}$	90	54	GAO	20	ASTR	Solar axions	$<7.7 \times 10^{-7}$	99	126	RUOSO	92		$m_{A^0} < 10^{-3}$ eV
$<2.8 \times 10^{-11}$	95	55	KOROCHKIN	20	ASTR	$m_{A^0} = 25$ eV	$<2.5 \times 10^{-6}$		127	SEMERTZIDIS	90		$m_{A^0} < 7 \times 10^{-4}$ eV
none $6.0 \times 10^{-9}\text{--}1.3 \times 10^{-5}$		56	LUCENTE	20A	ASTR	$m_{A^0} < 270$ MeV							
$<2.6 \times 10^{-11}$	95	57	MEYER	20	FLAT	$m_{A^0} < 3 \times 10^{-10}$ eV							1 PANT 24 searches for the imprint of axion-photon oscillations in the very-high-energy gamma-ray spectrum of the quasar QSO B1420+326 observed by the MAGIC telescope. Three small disconnected regions of mass-coupling parameter space below 1 neV are ruled out. See Fig. 4 for the limits.
$<8.4 \times 10^{-8}$	99	58	YAMAMOTO	20	COSM	$m_{A^0} < 4 \times 10^{-6}$ eV							2 BATTYE 23 look for dark-matter axions falling into pulsar magnetospheres and converting into narrow radio lines. Unlike the earlier FOSTER 22 they search for evidence of conversion in the time-domain signal of a single pulsar, using 1 hour of MeerKAT data on the pulsar PSR J2144-3933. The quoted limit applies to an assumed magnetic field of 2×10^{12} G and a dark matter density of 0.45 GeV/cm ³ .
$<1 \times 10^{-3}$	95	59	ALONI	19	PRMX	$m_{A^0} = 0.16$ GeV							3 BEAUFORT 23 extends DEROCO 22 who searched for the X-ray decay of axions that build up in the gravitational well of the Sun over its lifetime, the 'solar basin'. They use data from NuSTAR and SpHinx telescopes and extends the previous study by accounting for the axion production via photon coalescence.
$<1.4 \times 10^{-14}$	95	60	CAPUTO	19	ASTR	$m_{A^0} < 5 \times 10^{-24}$ eV							4 BERNAL 23 use gamma-ray data from 739 blazars observed by FermiLAT and 38 blazars by Cherenkov observatories. They estimate optical depth, subtract the astrophysical component, and attribute the residual to axion two-photon decay. The quoted limit is for $m_{A^0} \approx 25$ eV. See their Fig. 3 for the mass-dependent limits.
$<9.6 \times 10^{-14}$	95	61	FEDDERKE	19	CMB	$m_{A^0} = 10^{-22}$ eV							5 CAPOZZI 23 use Planck CMB and Lyman-alpha observations to set limits on early energy injection by decaying dark matter axions that would affect CMB anisotropies and the reionisation history of the Universe. The quoted limit applies to $m_{A^0} = 100$ eV and the reionization model of Fauchere-Giguere. See Fig.4 for mass-dependent constraints from different reionization models.
$<7 \times 10^{-13}$	95	62	IVANOV	19	ASTR	$m_{A^0} = 5 \times 10^{-23}$ eV							6 CAPOZZI 23A search for axions produced in electromagnetic showers in proton beam dumps and fixed target experiments. In this case, they reinterpret MiniBoone data. Quoted limit applies at 100 MeV but the limit does not extend to arbitrarily large couplings. See Fig. 7 for mass-dependent limits.
$<4 \times 10^{-11}$	95	63	LIANG	19	ASTR	$m_{A^0} = 1.2 \times 10^{-7}$ eV							7 DAVIES 23 is analogous to AJELLO 16, and use the Fermi-LAT data from three quasars (3C454.3, CTA 102, and 3C279), considering the blazar jets as the regions where the axion-photon oscillations occur. See Fig. 8 for the mass-dependent limits.
		64	FORTIN	18	ASTR	Axion-like particles							8 DIAMOND 23 demonstrate that a window of decaying 10-MeV-mass ALP parameter space previously thought to be excluded by the lack of gamma-ray emission from the SN 1987A explosion is actually unconstrained because of the formation of a fireball that would prevent decay photons from escaping. They nevertheless re-exclude this window by considering the non-detection of the sub-MeV emission by the Pioneer Venus Orbiter. The quoted limit is at $m_{A^0} = 56$ MeV. See their Fig. 2 for mass-dependent limits.
$<3 \times 10^{-12}$		65	JAECKEL	18	ASTR	$m_{A^0} = 30\text{--}100$ MeV							9 FILZINGER 23 searched for oscillations in the fine structure constant induced by dilaton-like dark matter by measuring the frequency ratio between the E3 and E2 transitions of $^{171}\text{Yb}^+$. They assume the local dark matter density $\rho_S = 0.4$ GeV/cm ³ . The quoted limit is set at $m_{S^0} \approx 4 \times 10^{-23}$ eV. See their Fig. 4 for the limits over $m_{S^0} = 1 \times 10^{-24}\text{--}1 \times 10^{-17}$ eV.
$<5.0 \times 10^{-3}$	90	66	YAMAJI	18	LSW	$m_{A^0} = 46\text{--}1020$ eV							10 HOOFF 23 consider axions emitted from SN1987A converting to gamma rays in Galactic magnetic fields, using temporal information of the Solar Maximum Mission data. They set a limit $G_{A\gamma\gamma} \lesssim 5 \times 10^{-12}$ for masses $m_{A^0} \lesssim 2 \times 10^{-10}$ eV. See left panel in Fig. 3 for mass-dependent limits.
$<1 \times 10^{-11}$	99.9	67	ZHANG	18	ASTR	$m_{A^0} = 0.6\text{--}4$ neV							11 HOOFF 23 look for gamma rays resulting from the decay of axions produced from SN1987A, using the Solar Maximum Mission data. See right panel in Fig. 3 for mass-dependent limits.
		68	ADE	17	CMB	Axion-like particles							12 JACOBSEN 23 search for the imprints of axion-photon mixing on the TeV spectra of several blazars using data from the HAWC air shower detector.
$<6.6 \times 10^{-11}$	95	69	ANASTASSO...	17	CAST	$m_{A^0} < 0.02$ eV							13 LI 23h look for gamma-ray spectral irregularities induced by axion-photon oscillations from AGN VER J0521+211, using the Fermi-LAT and VERITAS data. See their Fig. 4 for mass-dependent limits.
		70	DOLAN	17	RVUE	Axion-like particles							14 NOORDHUIS 23 places strong constraints on the axion-photon coupling over a broad mass window using the fact that the polar cap regions of pulsars can generate a population of axions, which would then convert into an observable outgoing radio flux in the presence of the neutron star's B-field. They search for this signal in 27 pulsars and set mass-dependent limits shown in their Fig. 2.
$<2.51 \times 10^{-4}$	95	71	INADA	17	LSW	$m_{A^0} < 0.1$ eV							15 PANT 23 study the effect of axion-photon oscillations on the gamma-ray spectrum from the extragalactic neutrino source, TXS 0506+056. The quoted limit is at $m_{A^0} \approx 2.7 \times 10^{-7}$ eV. See their Fig. 2 for mass-dependent limits.
$>1.5 \times 10^{-11}$	95	72	KOHHI	17	ASTR	$m_{A^0} = 0.7\text{--}50$ neV							16 SHERRILL 23 search for scalar dilaton-like dark matter via oscillations in the fundamental constants. Their most competitive constraint is on the scalar photon coupling (Fig. 6, upper panel) that affects the fine-structure constant, which they extract using an optical-to-optical clock comparison between $^{171}\text{Yb}^+$ and ^{87}Sr . Quoted limit applies at the smallest mass in their search window for this case of 10^{-20} eV.
$<2.6 \times 10^{-12}$	95	73	MARSH	17	ASTR	$m_{A^0} \leq 10^{-13}$ eV							17 SULAI 23 looked for ultralight axion dark matter using the "Earth as a transducer" concept over the 0.5 to 5 Hz frequency range. They situate several magnetometers at magnetically quiet places and search for spatially-correlated magnetic field patterns induced by axion dark matter interacting in the effective cavity formed between the Earth's surface and the ionosphere. See their Fig. 12 for mass-dependent limits in context. This limit extends to higher-frequencies than their previous limit using archival geomagnetic field data collected by the SuperMAG collaboration, see ARZA 22
$<6 \times 10^{-13}$	95	74	TIWARI	17	COSM	$m_{A^0} \leq 10^{-15}$ eV							18 YAO 23 study an optical circular polarization in blazars induced by the axion-photon mixing. The quoted limit assumes the transverse magnetic field at the jet's emission site, with $B_T = 1$ G, and this limit inversely scales with B_T . See their Fig. 3 for the limits' dependence on B_T and electron density.
$<5 \times 10^{-12}$	95	75	AJELLO	16	COSM	$m_{A^0} = 0.5\text{--}5$ neV							
$<1.2 \times 10^{-7}$	95	76	DELLA-VALLE	16	LASR	$m_{A^0} = 1.3$ meV							
$<7.2 \times 10^{-8}$	95	77	DELLA-VALLE	16	LASR	$m_{A^0} < 0.5$ meV							
$<8 \times 10^{-4}$	95	78	JAECKEL	16	ALPS	$m_{A^0} = 0.1\text{--}100$ GeV							
$<6 \times 10^{-21}$	95	79	LEEFER	16	ALPS	$m_{S^0} < 10^{-18}$ eV							
		80	ANASTASSO...	15	CAST	Chameleons							
$<1.47 \times 10^{-10}$	95	81	ARIK	15	CAST	$m_{A^0} = 0.39\text{--}0.42$ eV							
$<3.5 \times 10^{-8}$	95	82	BALLOU	15	LSW	$m_{A^0} < 2 \times 10^{-4}$ eV							
		83	BRAX	15	ASTR	$m_{S^0} < 4 \times 10^{-12}$ eV							
$<5.42 \times 10^{-4}$	95	84	HASEBE	15	LASR	$m_{A^0} = 0.15$ eV							
		85	MILLEA	15	COSM	Axion-like particles							
		86	VANTILBURG	15	ASTR	Dilaton-like dark matter							
$<4.1 \times 10^{-10}$	99.7	87	VINYOLES	15	ASTR	$m_{A^0} = 0.6\text{--}185$ eV							
$<3.3 \times 10^{-10}$	95	88	ARIK	14	CAST	$m_{A^0} = 0.64\text{--}1.17$ eV							
$<6.6 \times 10^{-11}$	95	89	AYALA	14	ASTR	Globular clusters							
$<1.4 \times 10^{-7}$	95	90	DELLA-VALLE	14	LASR	$m_{A^0} = 1$ meV							
		91	EJLLI	14	COSM	$m_{A^0} = 2.66\text{--}48.8$ μ eV							
$<8 \times 10^{-8}$	95	92	PUGNAT	14	LSW	$m_{A^0} < 0.3$ meV							
$<1 \times 10^{-11}$	95	93	REESMAN	14	ASTR	$m_{A^0} < 1 \times 10^{-10}$ eV							
$<2.1 \times 10^{-11}$	95	94	ABRAMOWSKI13A	IACT		$m_{A^0} = 15\text{--}60$ neV							
$<2.15 \times 10^{-9}$	95	95	ARMENGAUD	13	EDEL	$m_{A^0} < 200$ eV							
$<4.5 \times 10^{-8}$	95	96	BETZ	13	LSW	$m_{A^0} = 7.2 \times 10^{-6}$ eV							
$<8 \times 10^{-11}$	95	97	FRIEDLAND	13	ASTR	Red giants							
$>2 \times 10^{-11}$	95	98	MEYER	13	ASTR	$m_{A^0} < 1 \times 10^{-7}$ eV							
$<8.3 \times 10^{-12}$	95	99	WOUTERS	13	ASTR	$m_{A^0} < 7 \times 10^{-12}$ eV							
		100	CADAMURO	12	COSM	Axion-like particles							
$<2.5 \times 10^{-13}$	95	101	PAYEZ	12	ASTR	$m_{A^0} < 4.2 \times 10^{-14}$ eV							
$<2.3 \times 10^{-10}$	95	102	ARIK	11	CAST	$m_{A^0} = 0.39\text{--}0.64$ eV							
$<6.5 \times 10^{-8}$	95	103	EHRET	10	ALPS	$m_{A^0} < 0.7$ meV							
$<2.4 \times 10^{-9}$	95	104	AHMED	09A	CDMS	$m_{A^0} < 100$ eV							
$<1.2\text{--}2.8 \times 10^{-10}$	95	105	ARIK	09	CAST	$m_{A^0} = 0.02\text{--}0.39$ eV							
		106	CHOU	09		Chameleons							
$<7 \times 10^{-10}$		107	GONDOLO	09	ASTR	$m_{A^0} < \text{few keV}$							
$<1.3 \times 10^{-6}$	95	108	AFANA SEV	08		$m_{S^0} < 1$ meV							
$<3.5 \times 10^{-7}$	99.7	109	CHOU	08		$m_{A^0} < 0.5$ meV							
$<1.1 \times 10^{-6}$	99.7	110	FOUCHE	08		$m_{A^0} < 1$ meV							
$<5.6\text{--}13.4 \times 10^{-10}$	95	111	INOUE	08		$m_{A^0} = 0.84\text{--}1.00$ eV							
$<5 \times 10^{-7}$		112	ZAVATTINI	08		$m_{A^0} < 1$ meV							
$<8.8 \times 10^{-11}$	95	113	ANDRIAMON...07	CAST		$m_{A^0} < 0.02$ eV							
$<1.25 \times 10^{-6}$	95	114	ROBILLIARD	07		$m_{A^0} < 1$ meV							
$2\text{--}5 \times 10^{-6}$		115	ZAVATTINI	06		$m_{A^0} = 1\text{--}1.5$ meV							
$<1.1 \times 10^{-9}$	95	116	INOUE	02		$m_{A^0} = 0.05\text{--}0.27$ eV							
$<2.78 \times 10^{-9}$	95	117	MORALES	02B		$m_{A^0} < 1$ keV							
$<1.7 \times 10^{-9}$	90	118	BERNABEI	01B		$m_{A^0} < 100$ eV							

Gauge & Higgs Boson Particle Listings

Axions (A^0) and Other Very Light Bosons

- 19 ZHANG 23A searched for oscillations in the fine structure constant induced by dilaton-like dark matter by measuring the frequencies of a hyperfine-structure transition in ^{87}Rb and an electronic transition in ^{164}Dy , and by comparing them with that of a quartz oscillator. They assume the local dark matter density $\rho_S \simeq 0.4 \text{ GeV}/\text{cm}^3$. The quoted limit is set at $m_{S0} \simeq 1 \times 10^{-17} \text{ eV}$. See their Fig. 3 for the limits over $m_{S0} = 1 \times 10^{-17} - 8.3 \times 10^{-13} \text{ eV}$.
- 20 APRILE 22B is an update of APRILE 20 based on a similar solar axion modeling to DENT 20A and GAO 20. They exclude the XENONIT excess found in APRILE 20. The quoted limit holds for small g_{Aee} . See Fig. 6 for correlation between $G_{A\gamma\gamma}$ and g_{Aee} .
- 21 ARQUIST 22 is analogous to AVIGNONE 98, and supersedes ANASTASSOPOULOS 17 for $m_{A0} \gtrsim 1.2 \text{ eV}$.
- 22 ARZA 22 search for low-mass axions as dark matter using the Earth as a transducer for axion-photon conversion. The concept works because the region between the Earth and the ionosphere forms an insulating cavity that parametrically enhances the axion signal by the radius of the Earth. The result is an oscillating and spatially correlated magnetic field induced via the interaction between axion dark matter and the geomagnetic field, which they searched for using archival magnetometer field data over 20 years compiled by the SuperMAG collaboration. Quoted limit applies for masses $3-4 \times 10^{-17} \text{ eV}$, see Fig. 1 for mass-dependent limits.
- 23 BERNAL 22 explored the possibility that the excess in the cosmic optical background measured by New Horizons Long Range Reconnaissance Imager was due to axion dark matter decaying into monoenergetic photons. See their Fig. 2 for the axion-photon coupling to explain the excess.
- 24 CALORE 22 update CALORE 20 by evaluating axion fluxes from progenitors of various masses and performing a template-based analysis using 12 years of Fermi-LAT data in the energy range from 50 MeV to 500 GeV. See their Fig. 10 for mass-dependent limits.
- 25 CAPUTO 22 study the effect of energy deposition by radiative decay of axions produced via the Primakoff process and photon coalescence in the supernova core, and set the limits by the radiative energy deposition $< 10^{50} \text{ erg}$ and progenitor radius $= 5 \times 10^{13} \text{ cm}$. The quoted limit is at $m_{A0} = 150 \text{ MeV}$. See their Fig. 2 for mass-dependent limits.
- 26 CASTILLO 22 update CAPUTO 19 using the polarization measurements of the Crab Pulsar by the QUIJOTE MFI instrument and 20 Galactic pulsars from the PPTA project. See their Table 1 for the assumed local axion energy density ρ_A for each pulsar and their Fig. 7 for the mass-dependent limits in the range of $3 \times 10^{-23} \text{ eV} \leq m_{A0} \leq 10^{-19} \text{ eV}$.
- 27 DEROCO 22 uses the NuSTAR data to search for monochromatic X-ray lines produced by the decay of solar axions trapped on bound orbits. The quoted limit applies to $m_{A0} \simeq 9 \text{ keV}$. They also derive limits in the plane of g_{Aee} and $G_{A\gamma\gamma}$. See their Figs. 2 and 4 for mass-dependent limits.
- 28 DESSERT 22A look for an axion-induced linear polarization using data from multiple magnetic white dwarf stars. See their Figs. 1 and 8 for the mass-dependent limits.
- 29 ECKNER 22 set limits by using sub-PeV diffuse gamma-ray data from HAWC and Tibet AS γ by assuming that gamma rays produced simultaneously with high-energy neutrinos from extragalactic sources suggested by IceCube are converted to axions in the magnetic field at the source and reconverted to gamma rays in the Galactic magnetic field. See their Fig. 4 for mass-dependent limits.
- 30 FOSTER 22 is an update of FOSTER 20 in the list of limits on relic invisible axions. They search for axion-photon transitions generated by neutron stars in the Galactic center region. They use improved population models of the Galactic center neutron stars and a Navarro-Frenk-White (NFW) model of the galactic dark matter distribution. The quoted limit applies to $m_{A0} \simeq 17-25 \mu\text{eV}$. See their Fig. 1 for mass-dependent limits.
- 31 KIRITA 22 update HOMMA 21 by increasing the laser energy and developing a background discrimination method using the beam cross-section dependence of the background originated from optical elements. The quoted limits applies to $m_{A0} = 0.18 \text{ eV}$. See their Fig. 11 for mass-dependent limits.
- 32 LANGHOFF 22 set limits by considering the freeze-in production of axions coupled only to photons. The quoted limit applies to $m_{A0} = 2 \text{ MeV}$ for the reheating temperature equal to 5 MeV. See their Fig. 1 for mass-dependent limits.
- 33 LI 22 is analogous to LI 21B, and use the spectra of the blazar FSRQ 4C+21.35 measured by MAGIC, VERITAS, and Fermi-LAT. The quoted limit applies to $m_{A0} \simeq 8 \times 10^{-10} \text{ eV}$. See their Fig. 1 for mass-dependent limits.
- 34 LI 22C is analogous to LI 21B, and use the spectra of the blazars Mrk 421 and PG 1553+113 measured by MAGIC and Fermi-LAT. The quoted limit applies to $m_{A0} \simeq 1 \times 10^{-8} \text{ eV}$. See their Fig. 4 for mass-dependent limits.
- 35 LUCENTE 22 developed a method to correctly incorporate the effects of axions decaying into photons inside the core of horizontal-branch stars. They update AXENZA 20 by evaluating axion energy transfer in the range of axion mean free path where the diffusive energy transport and free streaming approximations are not applicable. See their Fig. 1 for the limits.
- 36 BASU 21 searched for birefringence induced by axion dark matter using multiple images of the polarized source in the strongly gravitationally lensed system CLASS B1152+199. They assume the axion makes up all dark matter, and used the axion density in the emitting region, $\rho_A = 20 \text{ GeV}/\text{cm}^3$. Limits between $9.2 \times 10^{-11} - 7.7 \times 10^{-8} \text{ GeV}^{-1}$ are obtained for $m_{A0} = 3.6 \times 10^{-21} - 4.6 \times 10^{-18} \text{ eV}$. See their Fig. 2 for mass-dependent limits.
- 37 BI 21 look for the gamma-ray spectral distortions induced by axion-photon oscillations in the presence of the Galactic magnetic field, using the measurements of sub-PeV gamma-rays from the Crab Nebula by the Tibet AS γ and HAWC experiments, together with MAGIC and HEGRA gamma-ray data. See their Fig. 3 for mass-dependent limits.
- 38 DOLAN 21A study the effect of axion production on the evolution of asymptotic giant branch stars, and use the white-dwarf initial-final mass relation to set the limits. See their Fig. 1 for mass-dependent limits.
- 39 GUO 21 is analogous to AJELLO 16, and use the Fermi-LAT and H.E.S.S. II measurements of PG 1553+113 and PKS 2155-304. See their Fig. 6 for mass-dependent limits.
- 40 HOMMA 21 look for the production of axion resonance states and their subsequent stimulated decays by combining linearly polarized creation laser pulses and circularly polarized inducing laser pulses. The quoted limit is at $m_{A0} \simeq 0.178 \text{ eV}$. See their Fig. 14 for mass-dependent limits.
- 41 LI 21B is analogous to AJELLO 16, and use the spectra of the blazar Mrk 421 measured by ARGO-YBJ and Fermi-LAT. They consider ALP-photon mixing in the magnetic fields of both the blazar jet and the Galaxy. The quoted limit applies to $m_{A0} \simeq 1 \times 10^{-9} \text{ eV}$. See their Fig. 5 for mass-dependent limits.
- 42 LLOYD 21 is analogous to FORTIN 18, and set limits on the product of the axion couplings to photons and nucleons as $g_{ANN} G_{A\gamma\gamma} \lesssim 4.6 \times 10^{-19} \text{ GeV}^{-1}$ for $m_{A0} \lesssim 10^{-5} \text{ eV}$ by using the quiescent soft gamma-ray flux upper limits in five magnetars. We use $g_{ANN} = G_{AN} 2m_N$ to translate their limits. See their Table II and Fig. 3 for the limits.
- 43 REGIS 21 look for monochromatic photons from axion decay, using the MUSE spectroscopic data on the Leo T dwarf spheroidal galaxy. They assume that axions make up all of dark matter and use the integrated dark matter density along the line of sight determined by observations.
- 44 XIAO 21 use X-ray data from Betelgeuse to look for signals from axions produced in the stellar core that were converted to X-rays by the Galactic magnetic field. See their Fig. 1 for the mass-dependent limit.
- 45 ABUDINEN 20 look for the process $e^+e^- \rightarrow \gamma A^0$ ($A^0 \rightarrow \gamma\gamma$) and set upper limits of around 10^{-3} over the mass range. The quoted limit is at $m_{A0} = 0.3 \text{ GeV}$. See their Fig. 5 for mass dependent limits.
- 46 BANERJEE 20A look for axions produced from high-energy bremsstrahlung photons through the Primakoff effect with the electric field of the target nuclei. They exclude $G_{A\gamma\gamma} = 2 \times 10^{-4} - 5 \times 10^{-2} \text{ GeV}^{-1}$ for $m_{A0} < 55 \text{ MeV}$. See their Fig. 5 for mass-dependent limits.
- 47 BUEHLER 20 look for the γ -ray transparency due to axion-photon oscillations using high-energy photon events from 79 sources in the Second Fermi-LAT Catalog of High-Energy Sources. The quoted limit is for the intergalactic magnetic field strength and coherence length of $B = 1 \text{ nG}$ and $s = 1 \text{ Mpc}$. See their Figs. 4 and 5 for mass-dependent limits and for different magnetic-field parameters.
- 48 CALORE 20 use the isotropic diffuse γ -ray background measured by the Fermi-LAT to constrain the γ -ray flux converted in the Galactic magnetic field from axions produced from past core-collapse supernovae. They also derive a limit on a heavier axion with $m_{A0} \gtrsim \text{keV}$ decaying into two photons of $G_{A\gamma\gamma} \lesssim 5 \times 10^{-11} \text{ GeV}^{-1}$ for $m_{A0} = 5 \text{ keV}$. See their Figs. 5 and 7 for the limits as well as limits in the presence of axion-nucleon couplings.
- 49 AXENZA 20 extend the globular cluster bound of AYALA 14 to heavier masses ($m_{A0} \leq$ a few 100 keV) by taking account of the coalescence process $\gamma + \gamma \rightarrow A^0$ as well as the decay of the ALP inside the stellar core. See their Fig. 4 for mass-dependent limits.
- 50 DENT 20A is analogous to GAO 20. The quoted limit is from their arXiv:2006.15118v3 (v2 is their published version), using the relativistic Hartree-Fock form factor. The limit is up to two times weaker than the published one. See Fig. 4 in their arXiv version 3 for the correlation between $G_{A\gamma\gamma}$ and g_{Aee} corresponding to the excess reported in APRILE 20.
- 51 DEPTA 20 correct the underestimated D abundance in MILLEA 15, and derive robust cosmological bounds by allowing the reheating temperature, N_{eff} , and neutrino chemical potential to vary. See their Fig. 6 for mass-dependent limits.
- 52 DESSERT 20A use the NuSTAR data of the Quintuplet and Westerlund 1 super star clusters to look for X-rays converted in the Galactic magnetic field from the axions produced in stellar cores. See their Fig. 3 for the mass-dependent limits.
- 53 ESTEBAN 20 show that the two anomalous ANITA events can be explained by the reflected radio pulses that are resonantly produced in the ionosphere via axion-photon conversion for $m_{A0} \lesssim 1 \times 10^{-7} \text{ eV}$, if an axion clump passes the Earth about once a month. See their Fig. 5 for the region consistent with this interpretation for different values of the axion density inside the clumps.
- 54 GAO 20 correct the limit of APRILE 20 by including inverse Primakoff scattering in the XENONIT detector. The quoted limit is from their arXiv:2006.14598v4 (v3 is their published version), taking account of the atomic form factor of Xe as pointed out in ABE 201. The limit is weaker by a factor of 1.5-2 than the published one. See Fig. 3 in their arXiv version 4 for correlation between $G_{A\gamma\gamma}$ and g_{Aee} corresponding to the excess reported in APRILE 20.
- 55 KOROCHKIN 20 assume the axion makes up all dark matter, and look for a dip in the observed gamma-ray spectrum of the blazar 1ES 1218+304 by Fermi/LAT and VERITAS due to the extragalactic background light produced by the axion decay. Their analysis favors nonzero axion-induced absorption with $G_{A\gamma\gamma} = 3 \times 10^{-11} - 2 \times 10^{-10} \text{ GeV}^{-1}$ over a range of $m_{A0} = 2-18 \text{ eV}$. See their Fig. 1 for mass-dependent limits between $0.25 < m_{A0} < 25 \text{ eV}$.
- 56 LUCENTE 20A study the SN 1987A energy-loss argument on the axion-like particle production. In addition to the Primakoff process, they take account of photon coalescence as well as gravitational trapping that become relevant at $m_{A0} > 100 \text{ MeV}$. See their Fig. 12 for the mass-dependent limit.
- 57 MEYER 20 look for prompt γ -rays converted in the Galactic magnetic fields from axions produced via the Primakoff process in a sample of 20 extragalactic core-collapse supernovae. The limits assume a progenitor mass of 10 times the solar mass and certain models for the optical emission and the galactic magnetic field. See their Figs. 2 and 6 in the erratum for mass- and model-dependent limits.
- 58 YAMAMOTO 20 look for X-ray photons converted by the Earth's magnetic field from the axions produced by the two-body decay of dark matter, and set the limits by using the Suzaku data. The quoted limit is for the monochromatic X-ray line from the galactic dark matter with lifetime $\tau = 4.32 \times 10^{17} \text{ sec}$. They also derive limits on the continuum spectrum from the extragalactic component. See their Fig. 7 for the limits.
- 59 ALONI 19 used the data collected by the PRIMEX experiment to derive a limit based on a data-driven method. See their Fig. 2 for mass-dependent limits.
- 60 CAPUTO 19 look for an oscillating variation of the polarization angle of the pulsar J0437-4715, where they assume the local axion energy density $\rho_A = 0.3 \text{ GeV}/\text{cm}^3$. See their Fig. 2 for mass-dependent limits for $5 \times 10^{-24} \text{ eV} \leq m_{A0} \leq 2 \times 10^{-19} \text{ eV}$.
- 61 FEDDERKE 19 look for a uniform reduction of the CMB polarization at large scales, which is induced by the oscillating axion background during CMB decoupling. The quoted limit is based on the assumption that axions make up all of the dark matter. See their Fig. 3 for mass-dependent limits for $m_{A0} = 10^{-22} - 10^{-19} \text{ eV}$.
- 62 IVANOV 19 look for the axion-induced periodic changes in the polarization angle of parsec-scale jets in active galactic nuclei observed by the MOJAVE program, where they use the axion energy density $\rho_A = 20 \text{ GeV}/\text{cm}^3$. See their Fig. 6 for mass-dependent limits for $5 \times 10^{-23} \text{ eV} \leq m_{A0} \leq 1.2 \times 10^{-21} \text{ eV}$.
- 63 LIANG 19 look for spectral irregularities in the spectrum of 10 bright H.E.S.S. sources in the Galactic plane, assuming photon-ALP mixing in the Galactic magnetic fields. See their Fig. 2 for mass-dependent limits with different Galactic magnetic field models.

See key on page 1171

Gauge & Higgs Boson Particle Listings Axions (A^0) and Other Very Light Bosons

- ⁶⁴FORTIN 18 studied the conversion of axion-like particles produced in the core of a magnetar to hard X-rays in the magnetosphere. See their Fig. 5 for mass-dependent limits with different values of the magnetar core temperature.
- ⁶⁵JAECKEL 18 study axions produced through the Primakoff process from SN 1987A, which subsequently decay into photon pairs. See their Fig. 1 for the mass-dependent limits in the range of $m_{A^0} = 0.01\text{--}100$ MeV.
- ⁶⁶YAMAJI 18 search for axions with an x-ray LSW at Spring-8, using the Laue-case conversion in a silicon crystal. They also obtain $G_{A\gamma\gamma} < 4.2 \times 10^{-3} \text{ GeV}^{-1}$ for $m_{A^0} < 10$ eV. See their Fig. 5 for mass-dependent limits.
- ⁶⁷ZHANG 18 look for spectral irregularities in the spectrum of PKS 2155-304 measured by Fermi LAT, assuming photon-ALP mixing in the intercluster and Galactic magnetic fields. See their Figs. 2 and 3 for mass-dependent limits with different values of the intercluster magnetic field parameters.
- ⁶⁸ADE 17 look for cosmic birefringence from axion-like particles using CMB polarization data taken by the BICEP2 and Keck Array experiments. They set a limit $G_{A\gamma\gamma} H_I < 7.2 \times 10^{-2}$ at 95%CL for $m_{A^0} < 10^{-28}$ eV, where H_I is the Hubble parameter during inflation.
- ⁶⁹ANASTASSOPOULOS 17 looked for solar axions by the CAST axion helioscope in the vacuum phase, and supersedes ANDRIAMONJE 07.
- ⁷⁰DOLAN 17 update existing limits on $G_{A\gamma\gamma}$ for axion-like particles. The limits from the proton beam dump experiments in their Fig. 2 contained an error, and the corrected version is shown in Fig. 1 of DOLAN 21.
- ⁷¹INADA 17 search for axions with an x-ray LSW at Spring-8. See their Fig. 4 for mass-dependent limits.
- ⁷²KOHR1 17 attributed to axion-photon oscillations the excess of cosmic infrared background observed by the CIBER experiment. See their Fig. 5 for the region preferred by their scenario.
- ⁷³MARSH 17 is similar to WOUTERS 13, using Chandra observations of M87. See their Fig. 6 for mass-dependent limits.
- ⁷⁴TIWARI 17 use observed limits of the cosmic distance-duality relation to constrain the photon-ALP mixing based on 3D simulations of the magnetic field configuration. The quoted value is for the averaged magnetic field of 1nG with a coherent length of 1 Mpc. See their Fig. 5 for mass-dependent limits.
- ⁷⁵AJELLO 16 look for irregularities in the energy spectrum of the NGC1275 measured by Fermi LAT, assuming photon-ALP mixing in the intra-cluster and Galactic magnetic fields. See their Fig. 2 for mass-dependent limits.
- ⁷⁶DELLA-VALLE 16 look for the birefringence induced by axion-like particles. See their Fig. 14 for mass-dependent limits.
- ⁷⁷DELLA-VALLE 16 look for the dichroism induced by axion-like particles. See their Fig. 14 for mass-dependent limits.
- ⁷⁸JAECKEL 16 use the LEP data of $Z \rightarrow 2\gamma$ and $Z \rightarrow 3\gamma$ to constrain the ALP production via $e^+e^- \rightarrow Z \rightarrow A^0\gamma (A^0 \rightarrow \gamma\gamma)$, assuming the ALP coupling with two hypercharge bosons. See their Fig. 4 for mass-dependent limits.
- ⁷⁹LEEFER 16 derived limits by using radio-frequency spectroscopy of dysprosium and atomic clock measurements. See their Fig. 1 for mass-dependent limits as well as limits on Yukawa-type couplings of the scalar to the electron and nucleons.
- ⁸⁰ANASTASSOPOULOS 15 search for solar chameleons with CAST and derived limits on the chameleon coupling to photons and matter. See their Fig. 12 for the exclusion region.
- ⁸¹ARIK 15 is analogous to ARIK 09, and search for solar axions for m_{A^0} around 0.2 and 0.4 eV. See their Figs. 1 and 3 for the mass-dependent limits.
- ⁸²Based on OSQAR photon regeneration experiment. See their Fig. 6 for mass-dependent limits on scalar and pseudoscalar bosons.
- ⁸³BRAX 15 derived limits on conformal and disformal couplings of a scalar to photons by searching for a chaotic absorption pattern in the X-ray and UV bands of the Hydra A galaxy cluster and a BL lac object, respectively. See their Fig. 8.
- ⁸⁴HASEBE 15 look for an axion via a four-wave mixing process at quasi-parallel colliding laser beams. They also derived limits on a scalar coupling to photons $G_{S\gamma\gamma} < 2.62 \times 10^{-4} \text{ GeV}^{-1}$ at $m_{S^0} = 0.15$ eV. See their Figs. 11 and 12 for mass-dependent limits.
- ⁸⁵MILLEA 15 is similar to CADAMURO 12, including the Planck data and the latest inferences of primordial deuterium abundance. See their Fig. 3 for mass-dependent limits.
- ⁸⁶VANTILBURG 15 look for harmonic variations in the dysprosium transition frequency data, induced by coherent oscillations of the fine-structure constant due to dilaton-like dark matter, and set the limits, $G_{S\gamma\gamma} < 6 \times 10^{-27} \text{ GeV}^{-1}$ at $m_{S^0} = 6 \times 10^{-23}$ eV. See their Fig. 4 for mass-dependent limits between $1 \times 10^{-24} < m_{S^0} < 1 \times 10^{-15}$ eV.
- ⁸⁷VINOLES 15 performed a global fit analysis based on helioseismology and solar neutrino observations. See their Fig. 9.
- ⁸⁸ARIK 14 is similar to ARIK 11. See their Fig. 2 for mass-dependent limits.
- ⁸⁹AYALA 14 derived the limit from the helium-burning lifetime of horizontal-branch stars based on number counts in globular clusters.
- ⁹⁰DELLA-VALLE 14 use the new PVLAS apparatus to set a limit on vacuum magnetic birefringence induced by axion-like particles. See their Fig. 6 for the mass-dependent limits.
- ⁹¹EJLI 14 set limits on a product of primordial magnetic field and the axion mass using CMB distortion induced by resonant axion production from CMB photons. See their Fig. 1 for limits applying specifically to the DFSZ and KSVZ axion models.
- ⁹²PUGNAT 14 is analogous to EHRET 10. See their Fig. 5 for mass-dependent limits on scalar and pseudoscalar bosons.
- ⁹³REESMAN 14 derive limits by requiring effects of axion-photon interconversion on gamma-ray spectra from distant blazars to be no larger than errors in the best-fit optical depth based on a certain extragalactic background light model. See their Fig. 5 for mass-dependent limits.
- ⁹⁴ABRAMOWSKI 13a look for irregularities in the energy spectrum of the BL Lac object PKS 2155-304 measured by H.E.S.S. The limits depend on assumed magnetic field around the source. See their Fig. 7 for mass-dependent limits.
- ⁹⁵ARMENGAUD 13 is analogous to AVIGNONE 98. See Fig. 6 for the limit.
- ⁹⁶BETZ 13 performed a microwave-based light shining through the wall experiment. See their Fig. 13 for mass-dependent limits.
- ⁹⁷FRIEDLAND 13 derived the limit by considering blue-loop suppression of the evolution of red giants with 7-12 solar masses.
- ⁹⁸MEYER 13 attributed to axion-photon oscillations the observed excess of very high-energy γ -rays with respect to predictions based on extragalactic background light models. See their Fig.4 for mass-dependent lower limits for various magnetic field configurations.
- ⁹⁹WOUTERS 13 look for irregularities in the X-ray spectrum of the Hydra cluster observed by Chandra. See their Fig. 4 for mass-dependent limits.
- ¹⁰⁰CADAMURO 12 derived cosmological limits on $G_{A\gamma\gamma}$ for axion-like particles. See their Fig. 1 for mass-dependent limits.
- ¹⁰¹PAYEZ 12 derive limits from polarization measurements of quasar light (see their Fig. 3). The limits depend on assumed magnetic field strength in galaxy clusters. The limits depend on assumed magnetic field and electron density in the local galaxy supercluster.
- ¹⁰²ARIK 11 search for solar axions using ^3He buffer gas in CAST, continuing from the ^4He version of ARIK 09. See Fig. 2 for the exact mass-dependent limits.
- ¹⁰³ALPS is a photon regeneration experiment. See their Fig. 4 for mass-dependent limits on scalar and pseudoscalar bosons.
- ¹⁰⁴AHMED 09a is analogous to AVIGNONE 98.
- ¹⁰⁵ARIK 09 is the ^4He filling version of the CAST axion helioscope in analogy to INOUE 02 and INOUE 08. See their Fig. 7 for mass-dependent limits.
- ¹⁰⁶CHOU 09 use the GammeV apparatus in the afterglow mode to search for chameleons, (pseudo)scalar bosons with a mass depending on the environment. For pseudoscalars they exclude at 3 σ the range $2.6 \times 10^{-7} \text{ GeV}^{-1} < G_{A\gamma\gamma} < 4.2 \times 10^{-6} \text{ GeV}^{-1}$ for vacuum m_{A^0} roughly below 6 meV for density scaling index exceeding 0.8.
- ¹⁰⁷GONDOL0 09 use the all-flavor measured solar neutrino flux to constrain solar interior temperature and thus energy losses.
- ¹⁰⁸LIPSS photon regeneration experiment, assuming scalar particle S^0 . See Fig. 4 for mass-dependent limits.
- ¹⁰⁹CHOU 08 perform a variable-baseline photon regeneration experiment. See their Fig. 3 for mass-dependent limits. Excludes the PVLAS result of ZAVATTINI 06.
- ¹¹⁰FOUCHE 08 is an update of ROBILLIARD 07. See their Fig. 12 for mass-dependent limits.
- ¹¹¹INOUE 08 is an extension of INOUE 02 to larger axion masses, using the Tokyo axion helioscope. See their Fig. 4 for mass-dependent limits.
- ¹¹²ZAVATTINI 08 is an upgrade of ZAVATTINI 06, see their Fig. 8 for mass-dependent limits. They now exclude the parameter range where ZAVATTINI 06 had seen a positive signature.
- ¹¹³ANDRIAMONJE 07 looked for Primakoff conversion of solar axions in 9T superconducting magnet into X-rays. Supersedes ZIOUTAS 05.
- ¹¹⁴ROBILLIARD 07 perform a photon regeneration experiment with a pulsed laser and pulsed magnetic field. See their Fig. 4 for mass-dependent limits. Excludes the PVLAS result of ZAVATTINI 06 with a CL exceeding 99.9%.
- ¹¹⁵ZAVATTINI 06 propagate a laser beam in a magnetic field and observe dichroism and birefringence effects that could be attributed to an axion-like particle. This result is now excluded by ROBILLIARD 07, ZAVATTINI 08, and CHOU 08.
- ¹¹⁶INOUE 02 looked for Primakoff conversion of solar axions in 4T superconducting magnet into X ray.
- ¹¹⁷MORALES 02b looked for the coherent conversion of solar axions to photons via the Primakoff effect in Germanium detector.
- ¹¹⁸BERNABE 01b looked for Primakoff coherent conversion of solar axions into photons via Bragg scattering in NaI crystal in DAMA dark matter detector.
- ¹¹⁹ASTIER 00b looked for production of axions from the interaction of high-energy photons with the horn magnetic field and their subsequent re-conversion to photons via the interaction with the NOMAD dipole magnetic field.
- ¹²⁰MASSO 00 studied limits on axion-photon coupling using the induced axion-photon coupling through the proton loop and CAMERON 93 bound on the axion-photon coupling using optical rotation. They obtained the bound $g_{p\bar{p}\gamma}^2/4\pi < 1.7 \times 10^{-9}$ for the coupling $g_{p\bar{p}\gamma}^2/4\pi$.
- ¹²¹AVIGNONE 98 result is based on the coherent conversion of solar axions to photons via the Primakoff effect in a single crystal germanium detector.
- ¹²²Based on the conversion of solar axions to X-rays in a strong laboratory magnetic field.
- ¹²³Experiment based on proposal by MAIANI 86.
- ¹²⁴Experiment based on proposal by VANBIBBER 87.
- ¹²⁵LAZARUS 92 experiment is based on proposal found in VANBIBBER 89.
- ¹²⁶RUOSO 92 experiment is based on the proposal by VANBIBBER 87.
- ¹²⁷SEMERTZIDIS 90 experiment is based on the proposal of MAIANI 86. The limit is obtained by taking the noise amplitude as the upper limit. Limits extend to $m_{A^0} = 4 \times 10^{-3}$ where $G_{A\gamma\gamma} < 1 \times 10^{-4} \text{ GeV}^{-1}$.

Limit on Invisible A^0 (Axion) Electron Coupling

The limit is for $g_{Aee} \phi_A \bar{e}(i\gamma_5)e$, or equivalently, the dipole-dipole potential

$$-\frac{g_{Aee}^2}{16\pi m_{A^0}^2} ((\boldsymbol{\sigma}_1 \cdot \boldsymbol{\sigma}_2) - 3(\boldsymbol{\sigma}_1 \cdot \mathbf{n})(\boldsymbol{\sigma}_2 \cdot \mathbf{n}))/r^3 \text{ where } \mathbf{n} = \mathbf{r}/r \text{ and the sign of the potential was corrected based on DAIDO 17.}$$

VALUE	CL%	DOCUMENT ID	TEC	COMMENT
●●● We do not use the following data for averages, fits, limits, etc. ●●●				
$< 2.35 \times 10^{-12}$	90	¹ AALBERS	23A LZ	Solar axions
$< 1.3 \times 10^{-14}$	90	² AALBERS	23A LZ	$m_{A^0} = 1\text{--}17$ keV
$< 1.61 \times 10^{-11}$	90	³ ADHIKARI	23C C100	Solar axions
$< 6 \times 10^{-13}$	90	⁴ ADHIKARI	23A C100	$m_{A^0} = 10\text{--}1000$ keV
$< 8 \times 10^{-14}$	90	⁵ AGNES	23A DS50	$m_{A^0} = 0.03\text{--}20$ keV
		⁶ APRILE	23B XE1T	Neutron star merger
$< 3 \times 10^{-9}$	95	⁷ CAPOZZI	23A DUMP	$m_{A^0} = 10^4\text{--}2 \times 10^7$ eV
$< 6 \times 10^{-15}$		⁸ WADEKAR	23A ASTR	$m_{A^0} = 100$ keV
$< 4 \times 10^{-12}$	90	⁹ APRILE	22 XE1T	$m_{A^0} = 0.01\text{--}0.4$ keV
$< 9 \times 10^{-15}$	90	¹⁰ APRILE	22B XENT	$m_{A^0} = 1\text{--}39, 44\text{--}140$ keV
$< 2 \times 10^{-12}$	90	¹¹ APRILE	22B XENT	Solar axions
		¹² DESSERT	22A ASTR	Magnetic white dwarf
$< 2.6 \times 10^{-6}$	95	¹³ IKEDA	22	$m_{A^0} = 33.117\text{--}33.130$ μeV
$< 2.5 \times 10^{-18}$		¹⁴ LANGHOFF	22 COSM	$m_{A^0} = 20\text{--}3 \times 10^4$ keV

Gauge & Higgs Boson Particle Listings

Axions (A^0) and Other Very Light Bosons

	15	WANG	22c	$m_{A^0} \leq 0.47$ MeV	
	16	XIAO	22	ASTR Betelgeuse	
	17	CALORE	21	ASTR Core-collapse SNe	
$<2.5 \times 10^{-10}$		18	LUCENTE	21	ASTR SN 1987A
$<5.1 \times 10^{-12}$	90	19	AGOSTINI	20	HPGE $m_{A^0} = 0.06\text{--}1$ MeV
$<1 \times 10^{-9}$	90	20	AMARAL	20	SCDM $m_{A^0} = 1.2\text{--}50$ eV
$<2 \times 10^{-14}$	90	21	APRILE	20	XE1T $m_{A^0} = 1$ keV
$2.6\text{--}3.7 \times 10^{-12}$	90	22	APRILE	20	XE1T Solar axions
$<6 \times 10^{-13}$	90	23	ARALIS	20	SCDM $m_{A^0} = 0.04\text{--}500$ keV
$<1.3 \times 10^{-13}$	95	24	CAPOZZI	20	ASTR Tip of the Red Giant Branch
$<1.7 \times 10^{-11}$	95	25	CRESCINI	20	QUAX $m_{A^0} = 42.4\text{--}43.1$ μ eV
$<1.8 \times 10^{-9}$		26	GHOSH	20A	COSM $m_{A^0} \lesssim 0.5$ MeV
$<1.48 \times 10^{-13}$	95	27	STRANIERO	20	ASTR Tip of the Red Giant Branch
$<2.48 \times 10^{-11}$	90	28	WANG	20A	CDEX Solar axions
$<4 \times 10^{-13}$	90	29	WANG	20A	CDEX $m_{A^0} = 1.5$ keV
$<1.7 \times 10^{-11}$	90	30	ADHIKARI	19B	C100 Solar axions
$<2.3 \times 10^{-14}$	90	31	APRILE	19D	XE1T $m_{A^0} = 0.186\text{--}1$ keV
		32	DESSERT	19	ASTR Magnetic white dwarf
$<2.6 \times 10^{-10}$	95	33	TERRANO	19	Torsion pendulum
$<1.5 \times 10^{-13}$	90	34	ABE	18F	XMAS $m_{A^0} = 40\text{--}120$ keV
$<1.1 \times 10^{-11}$	90	35	ARMENGAUD	18	EDE3 Solar axions
$<4 \times 10^{-13}$	90	36	ARMENGAUD	18	EDE3 $m_{A^0} = 0.8\text{--}500$ keV
$<4.9 \times 10^{-10}$	95	37	CRESCINI	18	QUAX $m_{A^0} = 58$ μ eV
		38	FICEK	18	THEO $m_{A^0} < 10$ keV
$<4.5 \times 10^{-13}$	90	39	ABGRALL	17	HPGE $m_{A^0} = 11.8$ keV
$<3.5 \times 10^{-12}$	90	40	AKERIB	17B	LUX Solar axions
$<4.2 \times 10^{-13}$	90	41	AKERIB	17B	LUX $m_{A^0} = 1\text{--}16$ keV
$<2.3 \times 10^{-13}$	90	42	APRILE	17B	X100 $m_{A^0} = 6$ keV
$<4 \times 10^{-4}$	90	43	FICEK	17	THEO $m_{A^0} < 1$ keV
$<4.35 \times 10^{-12}$	90	44	FU	17A	PNDX Solar axions
$<4.3 \times 10^{-14}$	90	45	FU	17A	PNDX $m_{A^0} = 2$ keV
$<5 \times 10^{-13}$	90	46	LIU	17A	CDEX $m_{A^0} = 13$ keV
$<2.5 \times 10^{-11}$	90	47	LIU	17A	CDEX Solar axions
<0.15	95	48	LUO	17	$m_{A^0} = 300$ eV
$<3.3 \times 10^{-13}$	68	49	BATTICH	16	ASTR White dwarf cooling
$<7 \times 10^{-13}$		50	CORSICO	16	ASTR White dwarf cooling
$<1.39 \times 10^{-11}$	90	51	YOON	16	KIMS Solar axions
$<7.4 \times 10^{-9}$	95	52	TERRANO	15	$m_{A^0} < 30$ μ eV
$<8 \times 10^{-13}$	90	53	ABE	14F	XMAS $m_{A^0} = 60$ keV
$<7.7 \times 10^{-12}$	90	54	APRILE	14B	X100 Solar axions
		55	APRILE	14B	X100 $m_{A^0} = 5\text{--}7$ keV
$< 0.96\text{--}8.2 \times 10^{-8}$	90	56	DERBIN	14	CNTR $m_{A^0} = 0.1\text{--}1$ MeV
$<2.8 \times 10^{-13}$	99	57	MILLER-BER...	14	ASTR White dwarf cooling
$<5.4 \times 10^{-11}$	90	58	ABE	13D	XMAS Solar axions
$<1.07 \times 10^{-12}$	90	59	ARMENGAUD	13	EDEL $m_{A^0} = 12.5$ keV
$<2.59 \times 10^{-11}$	90	60	ARMENGAUD	13	EDEL Solar axions
		61	BARTH	13	CAST Solar axions
$< 1.4\text{--}9.7 \times 10^{-7}$	90	62	DERBIN	13	CNTR $m_{A^0} = 0.1\text{--}1$ MeV
$<1.5 \times 10^{-8}$	68	63	HECKEL	13	$m_{A^0} \leq 0.1$ μ eV
$<4.3 \times 10^{-13}$	95	64	VIAUX	13A	ASTR Low-mass red giants
$<7 \times 10^{-13}$	95	65	CORSICO	12	ASTR White dwarf cooling
$<2.2 \times 10^{-10}$	90	66	DERBIN	12	CNTR Solar axions
$< 0.02\text{--}1 \times 10^{-10}$	90	67	AALSETH	11	CNTR $m_{A^0} = 0.3\text{--}8$ keV
$<1.4 \times 10^{-12}$	90	68	AHMED	09A	CDMS $m_{A^0} = 2.5$ keV
$<4 \times 10^{-9}$		69	DAVOUDIASEL	09	ASTR Earth cooling
$<2.7 \times 10^{-8}$	66	70	NI	94	Induced magnetism
		70	CHUI	93	Induced magnetism
$<3.6 \times 10^{-7}$	66	71	PAN	92	Torsion pendulum
$<2.9 \times 10^{-8}$	95	70	BOBRAKOV	91	Induced magnetism
$<1.9 \times 10^{-6}$	66	72	WINELAND	91	NMR
$<7 \times 10^{-7}$	66	71	RITTER	90	Torsion pendulum
$<6.6 \times 10^{-8}$	95	70	VOROBYOV	88	Induced magnetism

¹ AALBERS 23A look for solar axions from the ABC processes. See their Fig. 6 for the limits.

² AALBERS 23A look for absorption of axion dark matter. The quoted limit is for $m_{A^0} \simeq 1.4$ keV. The local density $\rho_A = 0.3$ GeV/cm³ is assumed. See their Fig. 7 for mass-dependent limits.

³ ADHIKARI 23 is an update of ADHIKARI 19B.

⁴ ADHIKARI 23A look for absorption and Compton-like processes of axion dark matter. The quoted limit is for $m_{A^0} \simeq 37$ keV. See their Fig. 4 for mass-dependent limits.

⁵ AGNES 23A look for absorption of axion dark matter. The quoted limit is for $m_{A^0} \simeq 0.25$ keV. The local density $\rho_A = 0.3$ GeV/cm³ is assumed. See their Fig. 2 for mass-dependent limits.

⁶ APRILE 23B look for an absorption signal of axions within ± 500 seconds of the GW signals, including the neutron star merger GW170817. They set a 90% CL upper limit on the product of coincident fluence and cross section of axions to be less than $10\text{--}29$ cm²/cm² in the recoil energy range of 5.5–210 keV_{ee}.

⁷ CAPOZZI 23A search for axions produced in electromagnetic showers in proton beam dumps and fixed target experiments. In this case, they reinterpret MiniBoone data. Quoted limit applies at 1 MeV. See Fig. 8 for mass-dependent limits.

⁸ WADEKAR 23 use the Leo T dwarf galaxy's interstellar medium to derive limits, requiring the heating rate from axion dark matter absorption into hydrogen atoms and two-photon decay to be less than the astrophysical cooling rate. See Fig. 2 for limits over $m_{A^0} = 1\text{--}100$ keV, which loosen for lighter masses.

⁹ APRILE 22 extend APRILE 19D to lower masses by removing the background of ionization signals correlated with high-energy events. The quoted limit applies to $m_{A^0} = 0.1$ keV. See their Fig. 15 for mass-dependent limits.

¹⁰ APRILE 22B is an update of APRILE 20, and set the limit, $g_{Aee} \lesssim 9 \times 10^{-15}\text{--}3 \times 10^{-13}$. The quoted limit applies to $m_{A^0} = 2$ keV. They exclude the XENON1T excess found in APRILE 20. See their Fig. 6 for mass-dependent limits.

¹¹ APRILE 22B is an update of APRILE 20. They exclude the XENON1T excess found in APRILE 20. The quoted limit holds for small $G_{A\gamma\gamma}$. See their Fig. 6 for correlation between g_{Aee} and $G_{A\gamma\gamma}$.

¹² DESSERT 22 is an update of DESSERT 19. They used the Chandra observation of the magnetic white dwarf RE J0317-853 to look for converted X-rays in the magnetosphere from axions produced in the core through electron bremsstrahlung. They obtained the limit, $g_{Aee} \cdot G_{A\gamma\gamma} < 1.3 \times 10^{-25}$ GeV⁻¹ at 95% CL for $m_{A^0} \lesssim 10^{-5}$ eV. See their Fig. 1 for mass-dependent limits.

¹³ IKEDA 22 look for magnons excited by dark matter axions, using data taken with a hybrid quantum system consisting of a superconducting qubit and a spherical ferromagnetic crystal. The quoted limit assumes the local dark matter density $\rho_A = 0.45$ GeV/cm³ and the velocity $v = 220$ km/sec. See their Fig. 4 for the limits.

¹⁴ LANGHOFF 22 set limits by considering the freeze-in production of axions coupled to electrons without anomalous coupling to photons. The quoted limit applies to $m_{A^0} = 15$ MeV for the reheating temperature equal to 5 MeV. See their Fig. 2 for mass-dependent limits.

¹⁵ WANG 22c use the spin-amplifier based on hyperpolarized ¹²⁹Xe to set limits on the product of the axion couplings to electrons and nucleons as $g_{Aee} g_{ANN} < 4 \times 10^2$ (95 % CL) at $m_{A^0} = 0.1$ meV. Here g_{ANN} is the dimensionless axion-neutron coupling. See their Fig. 4 for the mass-dependent limits.

¹⁶ XIAO 22 extend XIAO 21 in the list of photon coupling limits by including the production of axions from Compton and bremsstrahlung processes, and set limits on the product of the axion couplings to electrons and photons as $G_{A\gamma\gamma} g_{Aee} < 0.4\text{--}2.8 \times 10^{-24}$ GeV⁻¹ (95 % CL) for $m_{A^0} < 3.5 \times 10^{-11}$ eV. See their Fig. 5 for the limits. They are comparable to those of DESSERT 19 and more restrictive than the CAST bounds of BARTH 13.

¹⁷ CALORE 21 consider the production of axions from Galactic and extragalactic SNe via nucleon-nucleon bremsstrahlung and their subsequent decay into electron-positron pairs, and exclude the range of $g_{Aee} \simeq 10^{-19}\text{--}10^{-11}$ at $g_{APP} = 10^{-9}$ for $m_{A^0} = 3\text{--}30$ MeV. See their Fig. 7 for the limits.

¹⁸ LUCENTE 21 study the axion production in a supernova via electron-proton bremsstrahlung and electron-positron fusion, and exclude the range of $g_{Aee} \simeq 10^{-10}\text{--}10^{-8}$ for $m_{A^0} = 1\text{--}160$ MeV. The quoted limit is at $m_{A^0} = 120$ MeV. See their Fig. 12 for the mass-dependent limits.

¹⁹ AGOSTINI 20 is analogous to AHMED 09A. The quoted limit applies to $m_{A^0} = 150$ keV. Their limits in their Fig. 3 were later found to be incorrect due to an error of their Eqs. (1) and (2). See Fig. 3 in AGOSTINI 22A for the corrected limits.

²⁰ AMARAL 20 use a second-generation SuperCDMS high-voltage eV-resolution detector to set limits on dark-matter axion absorption. The quoted limit is for $m_{A^0} \simeq 17$ eV. The local density $\rho_A = 0.3$ GeV/cm³ is assumed. See their Fig. 3 for mass-dependent limits.

²¹ APRILE 20 is an update of APRILE 17B where they look for an absorption signal of axion dark matter. They obtained the limit, $g_{Aee} \lesssim 2 \times 10^{-14}\text{--}1 \times 10^{-12}$ at 90% CL for $m_{A^0} = 1\text{--}200$ keV. They also found an excess over known backgrounds, which favors the mass $m_{A^0} = 2.3 \pm 0.2$ keV with a 3 σ significance. See their Fig. 10 for mass-dependent limits.

²² APRILE 20 look for solar axions from the ABC interactions, the Primakoff conversion, and the 14.4 keV M1 transition of ⁵⁷Fe, and set limits on g_{Aee} , $G_{A\gamma\gamma}$, g_{ANN} , and their products. An excess is observed at low energies between 2 and 3 keV. See their Fig. 8 for correlation between the couplings. The quoted limit applies to the case of vanishing $G_{A\gamma\gamma}$ and g_{ANN} .

²³ ARALIS 20 is analogous to AHMED 09A. The quoted limit applies to $m_{A^0} = 0.3$ keV. The limits at masses above 3 keV in their Fig. 9 was later found to be incorrect due to an error in their analysis. See Fig. 2 in ARALIS 21 for the corrected limits.

²⁴ CAPOZZI 20 obtains a limit on the axion-electron coupling from the brightness of the tip of the red-giant branch in ω Centauri. A similar limit of $< 1.6 \times 10^{-13}$ is obtained in NGC 4258.

²⁵ CRESCINI 20 is an update of CRESCINI 18. They assume a local axion dark matter density, $\rho_A = 0.3$ GeV/cm³. See their Fig. 4 for the limits.

²⁶ GHOSH 20A study thermal production of axion via coupling to leptons in the early universe and estimate its contribution to ΔN_{eff} . The quoted limit is for $\Delta N_{\text{eff}} < 0.5$. See their Fig. 7 for their mass-dependent limits.

²⁷ STRANIERO 20 is analogous to CAPOZZI 20, with 22 galactic globular clusters used to derive the limit.

²⁸ WANG 20A is an update of LIU 17A. See their Fig. 9.

²⁹ WANG 20A is an update of LIU 17A. They assume a local axion dark matter density, $\rho_A = 0.3$ GeV/cm³. See their Fig. 10 for limits between $0.185 < m_{A^0} < 10$ keV.

³⁰ ADHIKARI 19B is analogous to LIU 17A.

³¹ APRILE 19D is analogous to APRILE 17B, but they use only ionization signals. The quoted limit applies to $m_{A^0} = 0.7$ keV. See their Fig. 5(e) for mass-dependent limits.

³² DESSERT 19 used the Suzaku observations of a magnetic white dwarf (RE J0317-853) to look for X-ray signatures converted from axions in the surrounding magnetic fields. They obtained the limit, $g_{Aee} \cdot G_{A\gamma\gamma} < 1.6 \times 10^{-24}$ GeV⁻¹ at 95% CL for $m_{A^0} \lesssim 10^{-5}$ eV. See their Fig. 2 for mass-dependent limits.

³³ TERRANO 19 look for the axion-induced oscillating magnetic field acting on the electron spin, using data taken with a rotating torsion pendulum containing polarized electrons.

See key on page 1171

Gauge & Higgs Boson Particle Listings

Axions (A^0) and Other Very Light Bosons

Reference	Technique	Limit	Technique	Limit	Reference	Technique	Limit	Reference	Technique	Limit
		< 0.016	95	4	BUSCHMANN	22	ASTR	Neutron star cooling		
		< 320	90	5	GAVRILYUK	22	CNTR	Solar axion		
				6	SCHULTHESS	22		Neutron EDM		
				7	AYBAS	21	CASP	Nucleon EDM		
				8	BHUSAL	21		Solar axion		
				9	JIANG	21	NMR	Axion dark matter		
				10	ROUSSY	21		Molecular EDM		
				11	ZHANG	21B	ASTR	Neutron star inspiral		
		< 24	90	12	ABDELHAME	20	CNTR	Solar axion		
				13	ABDELHAME	20	CNTR	Solar axion		
				14	APRILE	20	XE1T	Solar axion		
				15	KLIMCHITSK	20		Casimir effect		
		< 7.3	90	16	WANG	20A	CDEX	Solar axion		
		< 0.03		17	LEINSON	19	ASTR	Neutron star cooling		
		$< 9.6 \times 10^{-3}$	95	18	LLOYD	19	ASTR	γ -rays from NS		
				19	SMORRA	19		\bar{p} g-factor		
				20	WU	19	NMR	Axion dark matter		
		< 65	95	21	AKHMATOV	18	CNTR	Solar axion		
		< 6.6	90	22	ARMENGAUD	18	EDE3	Solar axion		
		< 0.085	90	23	BEZNOGOV	18	ASTR	Neutron star cooling		
		< 12.7	95	24	GAVRILYUK	18	CNTR	Solar axion		
		< 0.01		25	HAMAGUCHI	18	ASTR	Neutron star cooling		
				26	ABEL	17		Neutron EDM		
		< 93	90	27	ABGRALL	17	HPGE	Solar axion		
		< 4	90	28	FU	17A	PNDX	Solar axion		
				29	KLIMCHITSK	17A		Casimir effect		
		< 177	90	30	LIU	17A	CDEX	Solar axion		
		< 0.079	95	31	BERENJI	16	ASTR	γ -rays from NS		
		< 100	95	32	GAVRILYUK	15	CNTR	Solar axion		
				33	KLIMCHITSK	15		Casimir-less		
				34	BEZERRA	14		Casimir effect		
				35	BEZERRA	14A		Casimir effect		
				36	BEZERRA	14B		Casimir effect		
				37	BEZERRA	14C		Casimir effect		
				38	BLUM	14	COSM	^4He abundance		
		< 250	95	39	LEINSON	14	ASTR	Neutron star cooling		
		< 155	90	40	ALESSANDRIA	13	CNTR	Solar axion		
		$< 8.6 \times 10^3$	90	41	ARMENGAUD	13	EDEL	Solar axion		
		$< 1.4 \times 10^4$	90	42	BELLI	12	CNTR	Solar axion		
		< 145	95	43	BELLINI	12B	BORX	Solar axion		
				44	DERBIN	11	CNTR	Solar axion		
				45	BELLINI	08	CNTR	Solar axion		
				46	ADELBERGER	07		Test of Newton's law		
1	LELLA	24						update constraints on the axion-proton coupling from supernova 1987A based on the SN cooling argument (including a treatment of the trapping regime) as well as the non-observation of any coincident axion-induced events in the Kamiokande II neutrino detector. They exclude QCD axion models above 0.01 eV, and axion-like particles in a window that extends up to 300 MeV. See their Fig. 3 for mass-dependent limits.		
2	KARANTH	23						utilized an in-plane polarized deuteron beam in a storage ring to constrain the axion-induced oscillating EDM of the deuteron for $m_{A^0} = 0.496\text{--}0.502$ neV. Assuming axions account for all dark matter with $\rho_A \simeq 0.55$ GeV/cm ³ , they derived constraints on axion couplings to the deuteron EDM operator, gluons, and the deuteron spin. For detailed limits, see their Figs. 19–21.		
3	LEE	23						analyzed data from a K– ³ He comagnetometer, accounting for stochastic effects, to limit the axion-neutron coupling $g_{Ann} < 2.4 \times 10^{-10}$ GeV ⁻¹ at 95% CL for $m_{A^0} = 0.4\text{--}4$ feV. They assumed axions form all dark matter with a density of 0.3 GeV/cm ³ . See their Fig. 5 for the limits.		
4	BUSCHMANN	22						studied the axion emission from five neutron stars with ages $\sim 10^5\text{--}10^6$ years, comparing the simulation with axions to age and luminosity measurements. The mass bound assumes the KSVZ axion model with $C_p = -0.47$ and $C_n = -0.02$. See their Fig. 3 for the limits on the DFSZ axion model.		
5	GAVRILYUK	22						look for solar axions from the ABC interactions with the experimental setup similar to GAVRILYUK 15. The mass bound assumes the KSVZ axion model, $S = 0.5$, and $m_H/m_d = 0.56$.		
6	SCHULTHESS	22						look for a time-oscillating neutron EDM caused by the coupling between axion dark matter and gluons, using a Ramsey-type apparatus for a cold neutron beam. See their Fig. 4 for limits in the range of $m_{A^0} = 10^{-19}\text{--}4 \times 10^{-12}$ eV.		
7	AYBAS	21						limits the axion couplings to the nucleon EDM and the nucleons as $g_{AN\gamma} < 9.5 \times 10^{-4}$ GeV ⁻² and $g_{ANN}/2m_N < 0.28$ GeV ⁻¹ (95% CL) for $m_{A^0} = 162\text{--}166$ neV, based on a measurement of ²⁰⁷ Pb solid-state NMR in a polarized ferroelectric crystal. Here m_N is the nucleon mass and g_{ANN} is the dimensionless axion-nucleon coupling. They assume that axions make up all the dark matter with $\rho_A \simeq 0.46$ GeV/cm ³ . See their Fig. 3 for the limits.		
8	BHUSAL	21						looked for 5.5 MeV solar axions produced by $pd \rightarrow ^3\text{He} A^0$ through the axion-induced dissociation of deuterons by using SNO data, and set a limit on the isovector axion-nucleon coupling, $ g_{a,N}^3 < 2 \times 10^{-5}$ GeV ⁻¹ , which is equivalent to $ g_{Ann} - g_{App} < 4 \times 10^{-5}$ in terms of the dimensionless axion-nucleon couplings.		
9	JIANG	21						use the spin-amplifier based on hyperpolarized ¹²⁹ Xe gas to set limits on the axion couplings to nucleons as $g_{ANN}/2m_N < 3.2 \times 10^{-9}$ GeV ⁻¹ (95% CL) at $m_{A^0} = 52.94$ feV, and comparable limits in the mass range of 8.3–744 feV. Here m_N is the nucleon mass and g_{ANN} is the dimensionless axion-nucleon coupling. They assume that axions make up all the dark matter with $\rho_A \simeq 0.4$ GeV/cm ³ . See their Fig. 4b for the limits.		
10	ROUSSY	21						look for a time-oscillating EDM of molecular ions HFF ⁺ induced by axion dark matter couplings to gluons. See their Fig. 3 for limits in the range of $m_{A^0} = 10^{-22}\text{--}10^{-15}$ eV.		

Invisible A^0 (Axion) Limits from Nucleon Coupling

Limits are for the axion mass in eV.

VALUE (eV)	CL%	DOCUMENT ID	TECN	COMMENT
< 0.01	95	1 LELLA	24	ASTR SN1987A
		2 KARANTH	23	Deuteron EDM
		3 LEE	23	Axion dark matter

••• We do not use the following data for averages, fits, limits, etc. •••

Gauge & Higgs Boson Particle Listings

Axions (A^0) and Other Very Light Bosons

- 11** ZHANG 21B use the gravitational waves from the binary neutron star inspiral GW170817 to look for a type of axion whose mass is suppressed due to cancellation with additional contributions. They exclude $1.6 \times 10^{16} < f_A < 10^{18}$ GeV at 3σ for $m_{A^0} \lesssim 10^{-13}$ eV. See their Fig. 1 for mass-dependent limits.
- 12** ABDELHAMEED 20 look for the resonant excitation of ^{169}Tm (8.41 keV) by solar axions produced via the Primakoff effect. The mass bound assumes the KSVZ axion model, $S = 0.5$, and $m_U/m_d = 0.56$. They set a limit on the product of axion couplings to photons and nucleons as $G_{A\gamma\gamma} \cdot g_{A\text{pp}} < 1.44 \times 10^{-14}$ GeV $^{-1}$ (90% CL).
- 13** ABDELHAMEED 20 look for the resonant excitation of ^{169}Tm (8.41 keV) by solar axions produced via the axion-electron coupling. They set a limit on the product of axion couplings to electrons and nucleons as $g_{Aee} \cdot g_{A\text{pp}} < 2.81 \times 10^{-16}$ (90% CL).
- 14** APRILE 20 look for solar axions from the ABC interactions, the Primakoff conversion, and the 14.4 keV M1 transition of ^{57}Fe . An excess is observed at low energies between 2 and 3 keV. See their Fig. 8 for correlation between the couplings.
- 15** KLIMCHITSKAYA 20 use the measurement of the Casimir force between a Au-coated microsphere and a SiC plate to constrain the force due to two-axion exchange for $17.8 < m_{A^0} < 100$ eV. See their Fig. 2 for mass-dependent limits.
- 16** WANG 20A is an update of LIU 17A. The limit assumes the DFSZ axion. See their Fig. 7 for the limit on product of axion couplings to electrons and nucleons.
- 17** LEINSON 19 is analogous to BEZNOGOV 18, but estimating the axion luminosity based on the Tolman's analytic solution to the Einstein equations of spherical fluids in hydrostatic equilibrium. The dimensionless axion-neutron coupling is constrained as $g_{Ann} < 1.0 \times 10^{-10}$.
- 18** LLOYD 19 is analogous to BERENJI 16. They highlight that the limit obtained with this technique strongly depends on the assumed NS core temperature.
- 19** SMORRA 19 look for spin-precession effects from ultra-light axion dark matter in the \bar{p} spin-flip resonance data. Assuming $\rho_A = 0.4$ GeV/cm 3 , they constrain the dimensionless axion-antiproton coupling as $g_{A\bar{p}p} < 2-9$ at 95% CL for $m_{A^0} = 2 \times 10^{-23}-4 \times 10^{-17}$ eV. See the right panel of their Fig. 3.
- 20** WU 19 look for axion-induced time-oscillating features of the NMR spectrum of acetonitrile- $2,13\text{C}$. Assuming $C_p = C_n$ and $\rho_A = 0.4$ GeV/cm 3 , they constrain the dimensionless axion-nucleon coupling as $g_{ANN} < 6 \times 10^{-5}$ for $m_{A^0} = 10^{-21}-1.3 \times 10^{-17}$ eV. Note that the limits for $m_{A^0} < 10^{-21}$ eV in their Fig. 3(a) should be weaker than those for heavier masses. See ADELBERGER 19 and WU 19c on this issue.
- 21** AKHMATOV 18 is an update of GAVRILYUK 15.
- 22** ARMENGAUD 18 is analogous to ALESSANDRIA 13. The quoted limit assumes the DFSZ axion model. See their Fig. 4 for the limit on product of axion couplings to electrons and nucleons.
- 23** BEZNOGOV 18 constrain the axion-neutron coupling by assuming that thermal evolution of the hot neutron star HESS J1731-347 is dominated by the lowest possible neutrino emission. The quoted limit assumes the KSVZ axion with the effective Peccei-Quinn charge of the neutron $C_n = -0.02$. The dimensionless axion-neutron coupling is constrained as $g_{Ann} < 2.8 \times 10^{-10}$.
- 24** GAVRILYUK 18 look for the resonant excitation of ^{83}Kr (9.4 keV) by solar axions produced via the Primakoff effect. The mass bound assumes $m_U/m_d = 0.56$ and $S = 0.5$.
- 25** HAMAGUCHI 18 studied the axion emission from the neutron star in Cassiopeia A based on the minimal cooling scenario which explains the observed rapid cooling rate. The quoted limit corresponds to $f_A > 5 \times 10^8$ GeV obtained for the KSVZ axion with $C_p = -0.47$ and $C_n = -0.02$.
- 26** ABEL 17 look for a time-oscillating neutron EDM and an axion-wind spin-precession effect respectively induced by axion dark matter couplings to gluons and nucleons. See their Fig. 4 for limits in the range of $m_{A^0} = 10^{-24}-10^{-17}$ eV.
- 27** ABGRALL 17 limit assumes the hadronic axion model used in ALESSANDRIA 13. See their Fig. 4 for the limit on product of axion couplings to electrons and nucleons.
- 28** FU 17A look for the 14.4 keV ^{57}Fe solar axions. The limit assumes the DFSZ axion model. See their Fig. 3 for mass-dependent limits on the axion-electron coupling. Notice that in this figure the DFSZ and KSVZ lines should be interchanged.
- 29** KLIMCHITSKAYA 17A use the differential measurement of the Casimir force between a Ni-coated sphere and Au and Ni sectors of the structured disc to constrain the axion coupling to nucleons for $2.61 \text{ meV} < m_{A^0} < 0.9$ eV. See their Figs. 1 and 2 for mass dependent limits.
- 30** LIU 17 is analogous to ALESSANDRIA 13. The limit assumes the hadronic axion model. See their Fig. 6(b) for the limit on product of axion couplings to electrons and nucleons.
- 31** BERENJI 16 used the Fermi LAT observations of neutron stars to look for photons from axion decay. They assume the effective Peccei-Quinn charge of the neutron $C_n = 0.1$ and a neutron-star core temperature of 20 MeV.
- 32** GAVRILYUK 15 look for solar axions emitted by the M1 transition of ^{83}Kr (9.4 keV). The mass bound assumes $m_U/m_d = 0.56$ and $S = 0.5$.
- 33** KLIMCHITSKAYA 15 use the measurement of differential forces between a test mass and rotating source masses of Au and Si to constrain the force due to two-axion exchange for $1.7 \times 10^{-3} < m_{A^0} < 0.9$ eV. See their Figs. 1 and 2 for mass dependent limits.
- 34** BEZERRA 14 use the measurement of the thermal Casimir-Polder force between a Bose-Einstein condensate of ^{87}Rb atoms and a SiO_2 plate to constrain the force mediated by exchange of two pseudoscalars for $0.1 \text{ meV} < m_{A^0} < 0.3$ eV. See their Fig. 2 for the mass-dependent limit on pseudoscalar coupling to nucleons.
- 35** BEZERRA 14A is analogous to BEZERRA 14. They use the measurement of the Casimir pressure between two Au-coated plates to constrain pseudoscalar coupling to nucleons for $1 \times 10^{-3} \text{ eV} < m_{A^0} < 15$ eV. See their Figs. 1 and 2 for the mass-dependent limit.
- 36** BEZERRA 14B is analogous to BEZERRA 14. BEZERRA 14B use the measurement of the normal and lateral Casimir forces between sinusoidally corrugated surfaces of a sphere and a plate to constrain pseudoscalar coupling to nucleons for $1 \text{ eV} < m_{A^0} < 20$ eV. See their Figs. 1-3 for mass-dependent limits.
- 37** BEZERRA 14c is analogous to BEZERRA 14. They use the measurement of the gradient of the Casimir force between Au- and Ni-coated surfaces of a sphere and a plate to constrain pseudoscalar coupling to nucleons for $3 \times 10^{-5} \text{ eV} < m_{A^0} < 1$ eV. See their Figs. 1, 3, and 4 for the mass-dependent limits.

- 38** BLUM 14 studied effects of an oscillating strong CP phase induced by axion dark matter on the primordial ^4He abundance. See their Fig. 1 for mass-dependent limits.
- 39** LEINSON 14 attributes the excessive cooling rate of the neutron star in Cassiopeia A to axion emission from the superfluid core, and found $C_n^2 m_{A^0}^2 \simeq 5.7 \times 10^{-6} \text{ eV}^2$, where C_n is the effective Peccei-Quinn charge of the neutron.
- 40** ALESSANDRIA 13 used the CUORE experiment to look for 14.4 keV solar axions produced from the M1 transition of thermally excited ^{57}Fe nuclei in the solar core, using the axio-electric effect. The limit assumes the hadronic axion model. See their Fig. 4 for the limit on product of axion couplings to electrons and nucleons.
- 41** ARMENGAUD 13 is analogous to ALESSANDRIA 13. The limit assumes the hadronic axion model. See their Fig. 8 for the limit on product of axion couplings to electrons and nucleons.
- 42** BELLINI 12 looked for solar axions emitted by the M1 transition of $^7\text{Li}^*$ (478 keV) after the electron capture of ^7Be , using the resonant excitation ^7Li in the LiF crystal. The mass bound assumes $m_U/m_d = 0.55$, $m_U/m_S = 0.029$, and the flavor-singlet axial vector matrix element $S = 0.4$.
- 43** BELLINI 12b looked for 5.5 MeV solar axions produced in the $p\bar{d} \rightarrow ^3\text{He} A^0$. The limit assumes the hadronic axion model. See their Figs. 6 and 7 for mass-dependent limits on product of axion couplings to photons, electrons, and nucleons.
- 44** DERBIN 11 looked for solar axions emitted by the M1 transition of thermally excited ^{57}Fe nuclei in the Sun, using their possible resonant capture on ^{57}Fe in the laboratory. The mass bound assumes $m_U/m_d = 0.56$ and the flavor-singlet axial vector matrix element $S = 3F - D \simeq 0.5$.
- 45** BELLINI 08 consider solar axions emitted in the M1 transition of $^7\text{Li}^*$ (478 keV) and look for a peak at 478 keV in the energy spectra of the Counting Test Facility (CTF), a Borexino prototype. For $m_{A^0} < 450$ keV they find mass-dependent limits on products of axion couplings to photons, electrons, and nucleons.
- 46** ADELBERGER 07 use precision tests of Newton's law to constrain a force contribution from the exchange of two pseudoscalars. See their Fig. 5 for limits on the pseudoscalar coupling to nucleons, relevant for m_{A^0} below about 1 meV.

Axion Limits from T -violating Medium-Range Forces

The limit is for the coupling $g = g_p g_s$ in a T -violating potential between nucleons,

nucleon and electron, or electrons of the form $V = \frac{g\hbar^2}{8\pi m_p} (\boldsymbol{\sigma} \cdot \boldsymbol{\tau}) \left(\frac{1}{r^2} + \frac{1}{\lambda r} \right) e^{-r/\lambda}$, where g_s and g_p are dimensionless scalar and pseudoscalar coupling constants, m_p is the fermion mass with the pseudoscalar coupling (whereas the mass m_s of the fermion with the scalar coupling does not explicitly appear), and $\lambda = \hbar/(m_A c)$ is the range of the force.

VALUE	DOCUMENT ID	TECN	COMMENT
• • •	We do not use the following data for averages, fits, limits, etc. • • •		
1	AYRES	23	EDM ultracold neutrons
2	PODDAR	23	ASTR solar system
3	ZHANG	23	NMR polarized ^{129}Xe and ^{131}Xe
4	CRESCINI	22	SQID paramagnetic GSO crystal
5	FENG	22	NMR polarized ^{129}Xe and ^{131}Xe
6	AFACH	21	GNME Optical magnetometers
7	DZUBA	18	THEO atomic EDM
8	STADNIK	18	THEO atomic and molecular EDMs
9	CRESCINI	17	SQID paramagnetic GSO crystal
10	AFACH	15	ultracold neutrons
11	STADNIK	15	THEO nucleon spin contributions for nuclei
12	TERRANO	15	torsion pendulum
13	BULATOWICZ	13	NMR polarized ^{129}Xe and ^{131}Xe
14	CHU	13	polarized ^3He
15	TULLNEY	13	SQID polarized ^3He and ^{129}Xe
16	RAFFELT	12	stellar energy loss
17	HOEDL	11	torsion pendulum
18	PETUKHOV	10	polarized ^3He
19	SEREBROV	10	ultracold neutrons
20	IGNATOVICH	09	RVUE ultracold neutrons
21	SEREBROV	09	RVUE ultracold neutrons
22	BAESSLER	07	ultracold neutrons
23	HECKEL	06	torsion pendulum
24	NI	99	paramagnetic Tb F $_3$
25	POSPELOV	98	THEO neutron EDM
26	YUJIN	96	
27	RITTER	93	torsion pendulum
28	VENEMA	92	nuclear spin-precession frequencies
29	WINELAND	91	NMR
1	AYRES	23	at PSI use their neutron EDM setup to look for a mm to micron-range spin-dependent force between ultracold spin-polarized neutrons stored in vacuum and the unpolarised nucleons in the surrounding apparatus. They constrain a nucleon-neutron monopole-dipole interaction parameterised by the coupling $g_s^N g_p^N$. They set a limit of $g_s^N g_p^N < 10^{-20}$ (95% CL) for a 1 meV mass axion, see Fig. 6.
2	PODDAR	23	search for long-range monopole-dipole forces between the polarized population of electrons inside the Earth and the unpolarised nucleons in the Sun, which would affect the precession of orbital perihelion. However, the most competitive limit is obtained by combining the monopole-monopole force constraints on g_s^N from planetary precession with the strongest stellar bound on the pseudoscalar electron coupling (g_p^e), shown in Fig. 5.
3	ZHANG	23	look for changes of the ratio of precession frequencies between ^{129}Xe and ^{131}Xe as the bias field is flipped in Earth's gravitational field after Earth rotation effect is subtracted. They find $g_p^N g_s^N < 1 \times 10^{-26}-3.7 \times 10^{-36}$ for $\lambda = 0.3-1 \times 10^{10}$ m. See their Fig. 4 for limits as a function of λ .

4 CRESCINI 22 is an update of CRESCINI 17, and find $g_p^e g_s^N \leq 5.7 \times 10^{-32}$ and $g_p^e g_s^e \leq 1.6 \times 10^{-31}$ for $\lambda \gtrsim 10$ cm at 95% CL. See their Fig. 4 for limits as a function of λ .	< 4	$\times 10^{-6}$	90	1 ABREU	24	FASR	$m_{\gamma\gamma} \simeq 50$ MeV
5 FENG 22 look for changes of the ratio of precession frequencies between ^{129}Xe and ^{131}Xe when a BGO crystal is positioned near the atomic cell. They find $g_p^n g_s^N < 2 \times 10^{-20} - 3 \times 10^{-24}$ for $\lambda = 0.11-0.55$ mm. See their Fig. 4 for limits as a function of λ .	< 1	$\times 10^{-3}$	90	2 AAD	23b	ATLS	$m_{\gamma\gamma} = 5-40$ GeV
6 AFACH 21 look for axion domain walls coupled to atomic spins by using the global network of optical magnetometers. Assuming that the axion domain walls make up all dark matter, they exclude the effective decay constant below 4×10^5 GeV for m_{A^0} in the range of $10^{-15}-10^{-11}$ eV. See their Fig. 4 for the mass-dependent limits.	< 1.3	$\times 10^{-8}$	90	3 AAD	23i	ATLS	$m_{\gamma\gamma} = 0.017-15$ GeV
7 DZUBA 18 used atomic EDM measurements to derive limits on the product of the pseudoscalar coupling to nucleon and the scalar coupling to electron, which improved on the laboratory bounds for $m_{A^0} > 0.01$ eV. See their Fig. 1 for mass-dependent limits.	< 1	$\times 10^{-16}$	90	4 AAD	23t	ATLS	$m_{\gamma\gamma} \lesssim 40$ GeV
8 STADNIK 18 used atomic and molecular EDM experiments to derive limits on the product of the pseudoscalar couplings to electron and the scalar coupling to nucleon and electron. See their Fig. 2 for mass-dependent limits, which improved on the laboratory bounds for $m_{A^0} > 0.01$ eV.	< 1.6	$\times 10^{-3}$	90	5 AALBERS	23a	LZ	$m_{\gamma\gamma} = 4.1-17$ keV
9 CRESCINI 17 use the QUAX- $g_p g_s$ experiment to look for variation of a paramagnetic GSO crystal magnetization when rotating lead disks are positioned near the crystal, and find $g = g_p^e g_s^N < 4.3 \times 10^{-30}$ for $\lambda = 0.1-0.2$ m at 95% CL. See their Fig. 6 for limits as a function of λ .	< 6	$\times 10^{-14}$	90	6 ABLIKIM	23af	BES3	$m_{\gamma\gamma} = 1.5-2.9$ GeV
10 AFACH 15 look for a change of spin precession frequency of ultracold neutrons when a magnetic field with opposite directions is applied, and find $g < 2.2 \times 10^{-27}$ (m/ λ) ² at 95% CL for $1 \mu\text{m} < \lambda < 5$ mm. See their Fig. 3 for their limits.	< 2.1	$\times 10^{-3}$	95	7 ABUDINEN	23b	BEL2	$m_{\gamma\gamma} = 4-9.7$ GeV
11 STADNIK 15 studied proton and neutron spin contributions for nuclei and derive the limits $g < 10^{-28}-10^{-23}$ for $\lambda > 3 \times 10^{-4}$ m using the data of TULLNEY 13. See their Figs. 1 and 2 for λ -dependent limits.	< 1.1	$\times 10^{-16}$	90	8 ADHIKARI	23	C100	$m_{\gamma\gamma} = 215$ eV
12 TERRANO 15 used a torsion pendulum and rotating attractor, and derived a restrictive limit on the product of the pseudoscalar coupling to electron and the scalar coupling to nucleons, $g < 9 \times 10^{-29} - 5 \times 10^{-26}$ for $m_{A^0} < 1.5-400 \mu\text{eV}$. See their Fig. 5 for mass-dependent limits.	< 2	$\times 10^{-7}$	90	9 ADHIKARI	23a	C100	$m_{\gamma\gamma} = 10-1000$ keV
13 BULATOWICZ 13 looked for NMR frequency shifts in polarized ^{129}Xe and ^{131}Xe when a zirconia rod is positioned near the NMR cell, and find $g < 1 \times 10^{-19} - 1 \times 10^{-24}$ for $\lambda = 0.01-1$ cm. See their Fig. 4 for their limits.	< 2.2	$\times 10^{-3}$	90	10 ADRIAN	23	HPS	$m_{\gamma\gamma} = 19-81$ MeV
14 CHU 13 look for a shift of the spin precession frequency of polarized ^3He in the presence of an unpolarized mass, in analogy to YODIN 96. See Fig. 3 for limits on g in the approximate m_{A^0} range 0.02-2 MeV.	< 3	$\times 10^{-11}$	95	11 AGNES	23a	D550	$m_{\gamma\gamma} = 0.03-20$ keV
15 TULLNEY 13 look for a shift of the precession frequency difference between the colocated ^3He and ^{129}Xe in the presence an unpolarized mass, and derive limits $g < 3 \times 10^{-29} - 2 \times 10^{-22}$ for $\lambda > 3 \times 10^{-4}$ m. See their Fig. 3 for λ -dependent limits.	< 2	$\times 10^{-15}$	90	12 AN	23a		$m_{\gamma\gamma} = 4.1-6.2 \mu\text{eV}$
16 RAFFELT 12 show that the pseudoscalar couplings to electron and nucleon and the scalar coupling to nucleon are individually constrained by stellar energy-loss arguments and searches for anomalous monopole-monopole forces, together providing restrictive constraints on g . See their Figs. 2 and 3 for results.	< 2.2	$\times 10^{-3}$	90	13 ANDREEV	23	NA64	$m_{\gamma\gamma} = 10^{-3}-1.5$ GeV
17 HOEDL 11 use a novel torsion pendulum to study the force by the polarized electrons of an external magnet. In their Fig. 3 they show restrictive limits on g in the approximate m_{A^0} range 0.03-10 MeV.	< 3	$\times 10^{-11}$	95	14 BAJJALI	23	BRAS	$m_{\gamma\gamma} = 49.63-74.44 \mu\text{eV}$
18 PETUKHOV 10 use spin relaxation of polarized ^3He and find $g < 3 \times 10^{-23}$ (cm/ λ) ² at 95% CL for the force range $\lambda = 10^{-4}-1$ cm.	< 2	$\times 10^{-7}$	90	15 CORTINA-GIL	23c	NA62	$m_{\gamma\gamma} = 10-700$ MeV
19 SEREBROV 10 use spin precession of ultracold neutrons close to bulk matter and find $g < 2 \times 10^{-21}$ (cm/ λ) ² at 95% CL for the force range $\lambda = 10^{-4}-1$ cm.	< 2.2	$\times 10^{-3}$	90	16 HAYRAPETY...	23g	CMS	$m_{\gamma\gamma} = 1.1-7.9$ GeV
20 IGNATOVICH 09 use data on depolarization of ultracold neutrons in material traps. They show λ -dependent limits in their Fig. 1.	< 2	$\times 10^{-11}$	95	17 KOTAKA	23	DORR	$m_{\gamma\gamma} = 74-110 \mu\text{eV}$
21 SEREBROV 09 uses data on depolarization of ultracold neutrons stored in material traps and finds $g < 2.96 \times 10^{-21}$ (cm/ λ) ² for the force range $\lambda = 10^{-3}-1$ cm and $g < 3.9 \times 10^{-22}$ (cm/ λ) ² for $\lambda = 10^{-4}-10^{-3}$ cm, each time at 95% CL, significantly improving on BAESSLER 07.	< 2	$\times 10^{-15}$	90	18 LI	23i	ASTR	$m_{\gamma\gamma} = 10^{-3}-10^5$ eV
22 BAESSLER 07 use the observation of quantum states of ultracold neutrons in the Earth's gravitational field to constrain g for an interaction range $1 \mu\text{m}$ -a few mm. See their Fig. 3 for results.	< 2.2	$\times 10^{-3}$	90	19 RAMANATH...	23	QULP	$m_{\gamma\gamma} = 19.7-30.5 \mu\text{eV}$
23 HECKEL 06 studied the influence of unpolarized bulk matter, including the laboratory's surroundings or the Sun, on a torsion pendulum containing about 9×10^{22} polarized electrons. See their Fig. 4 for limits on g as a function of interaction range.	< 2.2	$\times 10^{-3}$	90	20 ROMANENKO	23	LSW	$m_{\gamma\gamma} = 0.21-5.7 \mu\text{eV}$
24 NI 99 searched for a T -violating medium-range force acting on paramagnetic Tb F_3 salt. See their Fig. 1 for the result.	< 2	$\times 10^{-15}$	90	21 XIA	23	ASTR	$m_{\gamma\gamma} \lesssim 10^{-23}$ eV
25 POSPELOV 98 studied the possible contribution of T -violating Medium-Range Force to the neutron electric dipole moment, which is possible when axion interactions violate CP. The size of the force among nucleons must be smaller than gravity by a factor of 2×10^{-10} (1 cm/ λ_A), where $\lambda_A = h/m_A c$.	< 2	$\times 10^{-15}$	90	22 AAD	22j	ATLS	$m_{\gamma\gamma} = 1-60$ GeV
26 YODIN 96 compared the precession frequencies of atomic ^{199}Hg and Cs when a large mass is positioned near the cells, relative to an applied magnetic field. See Fig. 3 for their limits.	< 2	$\times 10^{-17}$	90	23 AAD	22s	ATLS	$m_{\gamma\gamma} \lesssim 10$ GeV
27 RITTER 93 studied the influence of bulk mass with polarized electrons on an unpolarized torsion pendulum, providing limits in the interaction range from 1 to 100 cm.	< 2	$\times 10^{-2}$	90	24 APRILE	22	XE1T	$m_{\gamma\gamma} = 0.9$ keV
28 VENEMA 92 looked for an effect of Earth's gravity on nuclear spin-precession frequencies of ^{199}Hg and ^{201}Hg atoms.	< 2	$\times 10^{-15}$	90	25 APRILE	22	XE1T	$m_{\gamma\gamma} = 0.01-0.4$ keV
29 WINELAND 91 looked for an effect of bulk matter with aligned electron spins on atomic hyperfine resonances in stored $^9\text{Be}^+$ ions using nuclear magnetic resonance.	< 2	$\times 10^{-2}$	90	26 APRILE	22b	XENT	$m_{\gamma\gamma} = 1-39,44-140$ keV
	< 1	$\times 10^{-9}$	95	27 BATTAGLIERI	22	BDMP	$m_{\gamma\gamma} = 3-100$ MeV
	(4.6 \pm 0.5 \pm 0.4)	$\times 10^{-15}$	68	28 BOLTON	22	ASTR	$m_{\gamma\gamma} = (8.4 \pm 0.6) \times 10^{-14}$ eV
	< 1	$\times 10^{-13}$	90	29 CERVANTES	22	ORPH	$m_{\gamma\gamma} = 65.5-69.3 \mu\text{eV}$
	< 1	$\times 10^{-12}$	90	30 CHILES	22		$m_{\gamma\gamma} = 0.7-0.8$ eV
	< 8.7	$\times 10^{-11}$	95	31 HOCHBERG	22	SNSP	$m_{\gamma\gamma} = 0.73-30$ eV
	< 7.97	$\times 10^{-9}$	95	32 LEES	22	BABR	$m_{\gamma\gamma} = 1 \times 10^{-3}-3.16$ GeV
	< 6.86	$\times 10^{-11}$	90	33 LU	22	ASTR	$m_{\gamma\gamma} \lesssim 3 \times 10^{-5}$ eV
	< 3	$\times 10^{-2}$	95	34 MANENTI	22	MDHI	$m_{\gamma\gamma} = 1.61$ eV
	< 8	$\times 10^{-6}$	90	35 THOMAS	22		$m_{\gamma\gamma} = 1-80$ GeV
	< 2.3	$\times 10^{-4}$	90	36 TUMASYAN	22ah	CMS	$m_{\gamma\gamma} = 4-62.5$ GeV
	< 1.6	$\times 10^{-4}$	95	37 TUMASYAN	22n	CMS	$m_{\gamma\gamma} = 0.6-49$ GeV
	< 3	$\times 10^{-5}$	90	38 WU	22a	PPTA	$m_{\gamma\gamma} \lesssim 10^{-23}$ eV
	< 1.68	$\times 10^{-15}$	90	39 ANDREEV	21	NA64	$m_{\gamma\gamma} = 1 \times 10^{-3}-1$ GeV
	< 2	$\times 10^{-16}$	90	40 ANDREEV	21a	NA64	$m_{\gamma\gamma} = 0.1-0.35$ GeV
	< 1.8	$\times 10^{-13}$	90	41 BI	21	ASTR	$m_{\gamma\gamma} = 0.03-0.06$ eV
	< 3	$\times 10^{-12}$	95	42 CAZZANIGA	21	NA64	$m_{\gamma\gamma} = 10-390$ MeV
	< 2	$\times 10^{-2}$	95	43 DIXIT	21	CNTR	$m_{\gamma\gamma} = 24.86 \mu\text{eV}$
	< 1	$\times 10^{-4}$	90	44 GHOSH	21	RVUE	$m_{\gamma\gamma} = 2-30 \mu\text{eV}$
	< 1.6	$\times 10^{-14}$	90	45 GODFREY	21		$m_{\gamma\gamma} = 0.2637-0.2648 \mu\text{eV}$
	< 1.2	$\times 10^{-14}$	90	46 KOPYLOV	21a	CNTR	$m_{\gamma\gamma} = 9-40$ eV
	< 6.72	$\times 10^{-13}$	95	47 KRIBS	21		$m_{\gamma\gamma} \lesssim 10$ GeV
	< 1	$\times 10^{-16}$	90	48 SCHMIDT	21	THEO	$m_{\gamma\gamma} < 0.6$ GeV
	< 9	$\times 10^{-16}$	90	49 TSAI	21	BDMP	$m_{\gamma\gamma} = 0.78$ GeV
	< 3	$\times 10^{-5}$	90	50 AAJ	20c	LHCB	$m_{\gamma\gamma} = 21.4$ MeV
	< 7	$\times 10^{-14}$	90	51 AAJ	20c	LHCB	$m_{\gamma\gamma} = 218-315$ MeV
	< 8.2	$\times 10^{-5}$	90	52 ABLIKIM	20ab	BES3	$m_{\gamma\gamma} = 0.2-2.1$ GeV
	< 7	$\times 10^{-15}$	90	53 AGOSTINI	20	HPGE	$m_{\gamma\gamma} = 60$ keV - 1 MeV
	< 7	$\times 10^{-15}$	90	54 AMARAL	20	SCDM	$m_{\gamma\gamma} = 1.2-50$ eV
	< 1.2	$\times 10^{-14}$	90	55 AN	20	XE1T	$m_{\gamma\gamma} = 200$ eV
	< 6.72	$\times 10^{-13}$	95	56 ANDRIANAV...	20	FUNK	$m_{\gamma\gamma} = 1.95-8.55$ eV
	< 1	$\times 10^{-16}$	90	57 APRILE	20	XE1T	$m_{\gamma\gamma} = 1-200$ keV
	< 9	$\times 10^{-16}$	90	58 ARALIS	20	SCDM	$m_{\gamma\gamma} = 0.04-500$ keV
	< 3	$\times 10^{-5}$	90	59 ARGUELLES	20	THEO	$m_{\gamma\gamma} = 0.01$ GeV
	< 7	$\times 10^{-14}$	90	60 ARNAUD	20	EDEL	$m_{\gamma\gamma} = 1-40$ eV
	< 8.2	$\times 10^{-5}$	90	61 BANERJEE	20	NA64	$m_{\gamma\gamma} = 1.5-24$ MeV
	< 7	$\times 10^{-15}$	90	62 BARAK	20	SENS	$m_{\gamma\gamma} = 1.2-12.8$ eV
	< 7	$\times 10^{-15}$	90	63 KRASNIKOV	20	RVUE	$m_{\gamma\gamma} = 16.7$ MeV

Hidden Photons: Kinetic Mixing Parameter Limits

Limits are on the kinetic mixing parameter χ which is defined by the Lagrangian

$$L = -\frac{1}{4} F_{\mu\nu} F^{\mu\nu} - \frac{1}{4} F'_{\mu\nu} F'^{\mu\nu} - \frac{\chi}{2} F_{\mu\nu} F'^{\mu\nu} + \frac{m^2}{2} A'_\mu A'^\mu,$$

where A_μ and A'_μ are the photon and hidden-photon fields with field strengths $F_{\mu\nu}$ and $F'_{\mu\nu}$, respectively, and $m_{\gamma'}$ is the hidden-photon mass.

VALUE	CL%	DOCUMENT ID	TECN	COMMENT
-------	-----	-------------	------	---------

• • • We do not use the following data for averages, fits, limits, etc. • • •

Gauge & Higgs Boson Particle Listings

Axions (A^0) and Other Very Light Bosons

< 1.4	$\times 10^{-14}$	90	64 SHE	20	CDEX	$m_{\gamma\prime} = 10\text{--}300$ eV
< 1.3	$\times 10^{-15}$	90	65 SHE	20	CDEX	$m_{\gamma\prime} = 0.1\text{--}4$ keV
< 1	$\times 10^{-3}$	90	66 SIRUNYAN	20aQ	CMS	$m_{\gamma\prime} = 11.5\text{--}75$ GeV, 110–200 GeV
< 4.3	$\times 10^{-10}$	95	67 TOMITA	20		$m_{\gamma\prime} =$ 115.79–115.85 μeV
< 9	$\times 10^{-16}$	90	68 WANG	20A	CDEX	$m_{\gamma\prime} = 0.185\text{--}10$ keV
< 6	$\times 10^{-3}$	90	69 AABOUD	19G	ATLS	$m_{\gamma\prime} = 20\text{--}60$ GeV
< 3.4	$\times 10^{-3}$	90	70 ABLIKIM	19A	BES3	$m_{\gamma\prime} = 0.01\text{--}2.4$ GeV
< 8	$\times 10^{-15}$	90	71 ABLIKIM	19H	BES3	$m_{\gamma\prime} = 0.1\text{--}2.1$ GeV
< 8	$\times 10^{-15}$	90	72 AGUILAR-AR...	19A	DAMC	$m_{\gamma\prime} = 1.2\text{--}30$ eV
< 9	$\times 10^{-17}$	90	73 APRILE	19D	XE1T	$m_{\gamma\prime} = 0.186\text{--}5$ keV
< 7.5	$\times 10^{-6}$	90	74 BANERJEE	19	NA64	$m_{\gamma\prime} = 1\text{--}200$ MeV
< 2	$\times 10^{-11}$		75 BHOONAH	19	ASTR	$m_{\gamma\prime} = 10^{-22}\text{--}10^{-10}$ eV
< 5	$\times 10^{-12}$	95	76 BRUN	19	SHUK	$m_{\gamma\prime} = 20.8\text{--}28.3$ μeV
< 4.4	$\times 10^{-4}$	90	77 CORTINA-GIL	19	NA62	$m_{\gamma\prime} = 60\text{--}110$ MeV
< 3	$\times 10^{-5}$	95	78 DANILOV	19	TEXO	$m_{\gamma\prime} = 20$ eV - 1 MeV
< 6	$\times 10^{-9}$	95	79 HOCHBERG	19		$m_{\gamma\prime} = 0.8\text{--}4$ eV
< 1	$\times 10^{-11}$	95	80 KOPYLOV	19	CNTR	$m_{\gamma\prime} = 9\text{--}40$ eV
< 1.5	$\times 10^{-9}$		81 KOVETZ	19	COSM	$m_{\gamma\prime} = 10^{-23}\text{--}10^{-13}$ eV
< 3	$\times 10^{-14}$	95	82 NGUYEN	19	WDMX	$m_{\gamma\prime} = 6$ neV - 2.07 μeV
< 4.5	$\times 10^{-14}$	90	83 ABE	18F	XMAS	$m_{\gamma\prime} = 40\text{--}120$ keV
< 2.5	$\times 10^{-3}$	95	84 ADRIAN	18	HPS	$m_{\gamma\prime} = 19\text{--}81$ MeV
< 4.4	$\times 10^{-4}$	90	85 ANASTASI	18B	KLOE	$m_{\gamma\prime} = 519\text{--}987$ MeV
< 4	$\times 10^{-15}$	90	86 ARMENGAUD	18	EDE3	$m_{\gamma\prime} = 0.8\text{--}500$ keV
< 1.8	$\times 10^{-5}$	90	87 BANERJEE	18	NA64	$m_{\gamma\prime} = 1\text{--}23$ MeV
< 1	$\times 10^{-8}$	90	88 BANERJEE	18A	NA64	$m_{\gamma\prime} = 1\text{--}100$ MeV
< 3.1	$\times 10^{-14}$	90	89 KNIRCK	18		$m_{\gamma\prime} = 0.67\text{--}0.92$ meV
< 6	$\times 10^{-4}$	90	90 ABGRALL	17	HPGE	$m_{\gamma\prime} = 11.8$ keV
< 7	$\times 10^{-15}$	90	91 ABLIKIM	17AA	BES3	$m_{\gamma\prime} = 1.5\text{--}3.4$ GeV
< 1.2	$\times 10^{-4}$	90	92 ANGLOHER	17	CRES	$m_{\gamma\prime} = 0.3\text{--}0.7$ keV
< 2	$\times 10^{-11}$		93 BANERJEE	17	NA64	$m_{\gamma\prime} = 0.002\text{--}0.4$ GeV
< 4.5	$\times 10^{-3}$	90	94 CHANG	17	ASTR	$m_{\gamma\prime} = 15$ MeV
< 4	$\times 10^{-4}$	90	95 DUBININA	17	EMUL	$m_{\gamma\prime} = 1.1\text{--}24$ MeV
< 4.4	$\times 10^{-4}$	90	96 LEES	17E	BABR	$m_{\gamma\prime} = 4.7$ GeV
< 1.7	$\times 10^{-6}$	95	97 AAD	16AG	ATLS	$m_{\gamma\prime} = 0.1\text{--}2$ GeV
< 4	$\times 10^{-2}$	95	98 ANASTASI	16	KLOE	$m_{\gamma\prime} = 527\text{--}987$ MeV
< 1.4	$\times 10^{-3}$	90	99 KHACHATRY...	16	CMS	$m_{\gamma\prime} = 2$ GeV
< 1.7	$\times 10^{-3}$	90	100 AAD	15CD	ATLS	$m_{\gamma\prime} = 15\text{--}55$ GeV
< 4.2	$\times 10^{-4}$	90	101 ADARE	15		$m_{\gamma\prime} = 30\text{--}90$ MeV
< 3	$\times 10^{-13}$		102 AN	15A		$m_{\gamma\prime} = 12$ eV - 40 keV
< 6	$\times 10^{-12}$		103 ANASTASI	15	KLOE	$m_{\gamma\prime} = 2m_{\mu} - 1$ GeV
< 2	$\times 10^{-13}$		104 ANASTASI	15A	KLOE	$m_{\gamma\prime} = 5\text{--}320$ MeV
< 9.0	$\times 10^{-4}$	90	105 BATLEY	15A	NA48	$m_{\gamma\prime} = 36$ MeV
< 2.3	$\times 10^{-13}$	99.7	106 JAEGLE	15A	BELL	$m_{\gamma\prime} = 0.1\text{--}3.5$ GeV
< 2	$\times 10^{-13}$		107 KAZANAS	15	ASTR	$m_{\gamma\prime} = 2m_e - 100$ MeV
< 1.8	$\times 10^{-3}$	90	108 SUZUKI	15		$m_{\gamma\prime} = 1.9\text{--}4.3$ eV
< 9.0	$\times 10^{-4}$	90	109 VINYOLES	15	ASTR	$m_{\gamma\prime} = 8$ eV
< 3	$\times 10^{-18}$		110 ABE	14F	XMAS	$m_{\gamma\prime} = 40\text{--}120$ keV
< 3.5	$\times 10^{-4}$	90	111 AGAKISHIEV	14	HDES	$m_{\gamma\prime} = 63$ MeV
< 9	$\times 10^{-4}$	95	112 BABUSCI	14	KLOE	$m_{\gamma\prime} = 969$ MeV
< 3	$\times 10^{-15}$		113 BATELL	14	BDMP	$m_{\gamma\prime} = 10^{-3}\text{--}1$ GeV
< 7	$\times 10^{-14}$		114 BLUEMLEIN	14	BDMP	$m_{\gamma\prime} = 0.6$ GeV
< 8	$\times 10^{-4}$		115 FRADETTE	14	COSM	$m_{\gamma\prime} = 50\text{--}300$ MeV
< 2	$\times 10^{-3}$	90	116 LEES	14J	BABR	$m_{\gamma\prime} = 0.2$ GeV
< 2.2	$\times 10^{-13}$		117 MERKEL	14	A1	$m_{\gamma\prime} = 40\text{--}300$ MeV
< 8.06	$\times 10^{-5}$	95	118 AN	13B	ASTR	$m_{\gamma\prime} = 2$ keV
< 2	$\times 10^{-10}$	95	119 AN	13C	XE10	$m_{\gamma\prime} = 100$ eV
< 2	$\times 10^{-7}$		120 DIAMOND	13	BDMP	$m_{\gamma\prime} = 30\text{--}250$ MeV
< 2	$\times 10^{-3}$	90	121 GNINENKO	13	BDMP	$m_{\gamma\prime} = 25\text{--}120$ MeV
< 2	$\times 10^{-13}$		122 HORVAT	13	HPGE	$m_{\gamma\prime} = 230$ eV
< 8.06	$\times 10^{-5}$	95	123 INADA	13	LSW	$m_{\gamma\prime} = 0.04$ eV–26 keV
< 2	$\times 10^{-10}$	95	124 MIZUMOTO	13		$m_{\gamma\prime} = 1$ eV
< 1.7	$\times 10^{-7}$		125 PARKER	13	LSW	$m_{\gamma\prime} = 53$ μeV

< 5.32	$\times 10^{-15}$		126 PARKER	13		$m_{\gamma\prime} = 53$ μeV
< 1	$\times 10^{-15}$		127 REDONDO	13	ASTR	$m_{\gamma\prime} = 2$ keV
< 8	$\times 10^{-8}$	90	128 GNINENKO	12A	BDMP	$m_{\gamma\prime} = 1\text{--}135$ MeV
< 1	$\times 10^{-7}$	90	129 GNINENKO	12B	CHRM	$m_{\gamma\prime} = 1\text{--}500$ MeV
< 1	$\times 10^{-3}$	90	130 ABRAHAMY...	11		$m_{\gamma\prime} = 175\text{--}250$ MeV
< 9	$\times 10^{-8}$	95	131 BLUEMLEIN	11	BDMP	$m_{\gamma\prime} = 70$ MeV
< 1	$\times 10^{-7}$		132 BJORKEN	09	BDMP	$m_{\gamma\prime} = 2\text{--}400$ MeV
< 5	$\times 10^{-9}$		133 BJORKEN	09	ASTR	$m_{\gamma\prime} = 2\text{--}50$ MeV

- 1 ABREU 24 look for hidden photons produced from the pp collision in the decay channel $\gamma' \rightarrow e^+e^-$, and exclude at 90% CL the region of $\chi = 4 \times 10^{-6}\text{--}2 \times 10^{-4}$ and $m_{\gamma\prime} = 10\text{--}80$ MeV, with the newly excluded region near the higher values of χ . See their Fig. 7 for mass-dependent limits.
- 2 AAD 23B0 look for rare decays of the Z boson, $Z \rightarrow \gamma' + H'$, with dark Higgs decaying into a pair of hidden photons, assuming that at least two of the hidden photons decay into e^+e^- or $\mu^+\mu^-$. The quoted limit assumes the hidden fine structure constant $\alpha_D = 0.1$ and the dark Higgs mass ranging 20 to 70 GeV. See their Fig. 5 for the mass-dependent limits.
- 3 AAD 23I look for exotic decays of the SM-like Higgs boson, $H \rightarrow \gamma'\gamma'$ with hidden photons decaying into displaced lepton or light quark pairs, and set limits on the kinetic mixing within $1 \times 10^{-4}\text{--}1 \times 10^{-8}$ for the given mass range. The quoted limit is for $m_{\gamma\prime} \approx 13$ GeV with a branching fraction of 0.1 for the Higgs decaying into hidden photon pairs. See their Fig. 13 for the mass-dependent limits.
- 4 AAD 23T is analogous to AAD 22s, but using the ZH production mode, and set the upper limit on the branching ratio $B(H \rightarrow \gamma\gamma')$ within 0.0219–0.0252 (95% CL).
- 5 AALBERS 23A look for an absorption of hidden photon dark matter. The quoted limit is for $m_{\gamma\prime} = 1.4$ keV. The local density $\rho_{\gamma\prime} = 0.3$ GeV/cm³ is assumed. See their Fig. 7 for mass-dependent limits.
- 6 ABLIKIM 23AF look for invisible decays of hidden photons produced in the reaction $e^+e^- \rightarrow \gamma\gamma'$. They set limits within the $1.6 \times 10^{-3}\text{--}5.7 \times 10^{-3}$. See their Fig. 3 for mass-dependent limits.
- 7 ABUDINEN 23B look for hidden photons in the dark Higgsstrahlung process, $e^+e^- \rightarrow \gamma' H'$ ($\gamma' \rightarrow \mu^+\mu^-$) with H' being invisible. They set upper limits on the product of the kinetic mixing and the hidden gauge coupling, $\chi^2 \cdot \alpha_D$, in the range of $1.7 \times 10^{-8}\text{--}2 \times 10^{-6}$ at 90% CL for a 1 GeV dark Higgs mass. See their Fig. 3 for the mass-dependent limits.
- 8 ADHIKARI 23 look for the annual modulation signal induced by solar flux of hidden photons. See their Fig. 10 for mass-dependent limits.
- 9 ADHIKARI 23A look for absorption and Compton-like processes of hidden photon dark matter. The quoted limit is for $m_{\gamma\prime} \approx 12$ keV. Limits between $6 \times 10^{-14}\text{--}3 \times 10^{-11}$ are obtained. See their Fig. 4 for mass-dependent limits.
- 10 ADRIAN 23 is an update of ADRIAN 18, and use the data from the 2016 engineering run at 2.3 GeV. The quoted limit is at $m_{\gamma\prime} \approx 74$ MeV. See their Fig. 28 for the mass-dependent limits.
- 11 AGNES 23A look for an absorption of hidden photon dark matter. The quoted limit is for $m_{\gamma\prime} = 0.03$ keV. The local density $\rho_{\gamma\prime} = 0.3$ GeV/cm³ is assumed. See their Fig. 2 for mass-dependent limits.
- 12 AN 23A look for absorption of hidden photon dark matter at radio telescopes, setting limits based on data from the FAST telescope. The local density $\rho_{\gamma\prime} = 0.3$ GeV/cm³ is assumed. See their Fig. 1 for mass-dependent limits.
- 13 ANDREEV 23 is an update of ANDREEV 21 and ANDREEV 21A. The quoted limit applies to $m_{\gamma\prime} = 1$ MeV. See their Fig. 3 for mass-dependent limits.
- 14 BAJJALI 23 look for hidden photon dark matter by using a 12–18 GHz dish antenna at U. Hamburg that is sensitive to vertically aligned hidden photon polarizations. They assume a local density of $\rho_{\gamma\prime} = 0.3$ GeV/cm³. See their Figure 12 for mass-dependent limits in the range of $m_{\gamma\prime} = 50\text{--}75$ μeV under the assumption of randomly aligned hidden photon polarizations, defined as "1 sigma sensitivity". The run is labelled BRASS-p.
- 15 CORTINA-GIL 23c NA62 beam dump experiment searches for hidden photons decaying to $\mu^+\mu^-$, extending their previous search CORTINA-GIL 19. The quoted limit applies at 300 MeV but does not extend to arbitrarily large kinetic mixing parameters. See Fig. 4 for mass-dependent limits.
- 16 HAYRAPETYAN 23G search for kinetically mixed hidden photons in proton-proton collisions at the LHC that would generate a narrow peak in the mass spectrum of dimuon events. The mass window between 2.6 and 4.2 GeV is left unconstrained to avoid J/ψ and $\psi(2S)$ resonances. Mass dependent limits given in their Fig. 6.
- 17 KOTAKA 23 is an update of TOMITA 20, and set limits $\chi_1 < 0.3\text{--}2 \times 10^{-10}$ for the quoted mass range. The local density $\rho_{\gamma\prime} = 0.39$ GeV/cm³ is assumed. See their Fig. 5 for mass-dependent limits.
- 18 LI 23I set cooling bounds on the emission of hidden photons from the Sun, red giant, and horizontal branch stars, including emission of both the transverse and longitudinal modes. Cooling bounds are computed assuming a static model as opposed to considering the impact on stellar evolution. The result is comparable to earlier estimates of the same bound e.g. REDONDO 13. Limit applies at the most constraining mass around 200 eV for the solar bound.
- 19 RAMANATHAN 23 look for hidden photon dark matter using a gold-plated copper dish antenna cooled to 20 mK. The local density $\rho_{\gamma\prime} = 0.45$ GeV/cm³ is assumed. Limits between 7.9×10^{-13} and 3.81×10^{-12} are obtained. See their Fig. 5 for mass-dependent limits.
- 20 ROMANENKO 23 employed two superconducting radio frequency cavities with a high quality factor, optimized for detecting the longitudinal polarization of the hidden photon. The quoted limit is set at $m_{\gamma\prime} \approx 5$ μeV . See their Fig. 4 for the mass-dependent limits.
- 21 XIA 23 is analogous to WU 22A and use the Fermi-LAT pulsar timing array. They set a bound on the local density as $\rho_{\gamma\prime} \lesssim 7$ GeV/cm³ for $m_{\gamma\prime} \lesssim 10^{-23}$ eV at 95% CL, with weaker constraints up to 10^{-22} eV. See their Fig. 1 for the mass-dependent limits.

See key on page 1171

Gauge & Higgs Boson Particle Listings Axions (A^0) and Other Very Light Bosons

- 22 AAD 22i look for exotic decays of the SM-like Higgs boson, $H \rightarrow \gamma' \gamma' \rightarrow 4\ell$ and $H \rightarrow Z \gamma' \rightarrow 4\ell$, and set limits on the kinetic mixing and the Higgs portal coupling. See their Figs. 19 and 20 for the mass-dependent limits.
- 23 AAD 22s look for decays of a Higgs boson into γ and γ' using the VBF production mode, and set the upper limit on the branching ratio at 0.018 (95% CL) for the 125 GeV Higgs boson. For the quoted mass range, the signal acceptance changes by less than 1%.
- 24 APRILE 22 is analogous to AN 20, and set limits $\chi < 3 \times 10^{-13}$ (eV/ $m_{\gamma'}$) for $m_{\gamma'} < 3$ eV (90% C.L.). For $m_{\gamma'} > 3$ eV, see their Fig. 16 for mass-dependent limits.
- 25 APRILE 22 extend APRILE 19 to lower masses by removing the background of ionization signals correlated with high-energy events. The quoted limit applies to $m_{\gamma'} = 0.09$ keV. See their Fig. 15 for mass-dependent limits.
- 26 APRILE 22b is an update of APRILE 20, and set limits $\chi \lesssim 5 \times 10^{-17} - 2 \times 10^{-13}$. The quoted limit applies to $m_{\gamma'} = 1$ keV. They exclude the XENONIT excess found in APRILE 20. See their Fig. 6 for mass-dependent limits.
- 27 BATTAGLIERI 22 is analogous to BATELL 14, and derived limits from the electron beam dump experiment at Jefferson Lab (BDX-MINI). Limits at the level of $7 \times 10^{-5} - 1 \times 10^{-2}$ are obtained for the dark matter mass $m_{\gamma'}/3$ and the hidden gauge coupling $\alpha_D = 0.1$. See their Fig. 11.
- 28 BOLTON 22 use the Ly- α forest at $z \simeq 0.1$ as a calorimeter for heating in the intergalactic medium by the resonant conversion of hidden photon dark matter to photons, which is assumed to be responsible for the tension between the predicted and observed Ly- α absorption linewidths.
- 29 CERVANTES 22 use a dielectrically loaded Fabry-Perot open cavity to look for hidden photon dark matter. The local density $\rho_{\gamma'} = 0.45$ GeV/cm³ is assumed. See their Fig. 5 for mass-dependent limits.
- 30 CHILES 22 look for hidden photon dark matter by using a layered dielectric target and a superconducting nanowire single-photon detector. The local density $\rho_{\gamma'} = 0.4$ GeV/cm³ is assumed. See their Fig. 4 for mass-dependent limits.
- 31 HOCHBERG 22 update HOCHBERG 19. The quoted limit applies to $m_{A^0} \simeq 11$ eV. See their Fig. 5 for mass-dependent limits.
- 32 LEES 22 look for a hidden fermion-fermion bound state decaying into three hidden photons, which subsequently decay into e^+e^- , $\mu^+\mu^-$, or $\pi^+\pi^-$. For the bound-state mass in the range of 0.05–9.5 GeV, limits at the level of $5 \times 10^{-5} - 1 \times 10^{-3}$ are obtained. See their Fig. 6 for mass-dependent limits.
- 33 LU 22 derive the limit by studying the effect of photons oscillating into hidden photons on the surface luminosity of the neutron star RX J1856.6-3754.
- 34 MARENTI 22 look for hidden photon dark matter by using a multilayer dielectric haloscope. Limits between 6.86×10^{-11} and 5×10^{-8} are obtained for $m_{\gamma'} \simeq 1.1-3.1$ eV. See their Fig. 11 for mass-dependent limits.
- 35 THOMAS 22 improved KRIBS 21 by taking account of the changes in the parton distribution functions due to the inclusion of hidden photons. The quoted limit is at $m_{\gamma'} \simeq 4$ GeV. Limits in the range of $3 \times 10^{-2} - 9 \times 10^{-2}$ are obtained for $m_{\gamma'} = 1-80$ GeV. See their Fig. 1 for the limits.
- 36 TUMASYAN 22AH look for exotic decays of the SM-like Higgs boson, $H \rightarrow Z \gamma' \rightarrow 4\ell$, and set limits on the Higgs portal coupling. See their Fig. 6 for the limits.
- 37 TUMASYAN 22N look for exotic decays of the SM-like Higgs boson, $H \rightarrow \gamma' \gamma' (\gamma' \rightarrow \mu^+ \mu^-)$, and set limits on the branching fraction product. See their Fig. 7 for mass- and lifetime-dependent limits.
- 38 WU 22A look for direction-dependent oscillations in the gravitational potential generated by ultralight hidden photon dark matter, and set a bound on its local density as $\rho_{\gamma'} \lesssim 5$ GeV/cm³ for $m_{\gamma'} \lesssim 10^{-23}$ eV at 95% CL.
- 39 ANDREEV 21 is analogous to BANERJEE 18A. The quoted limit applies to $m_{\gamma'} = 1$ MeV. See their Fig. 3 for mass-dependent limits.
- 40 ANDREEV 21A extends the limits of BANERJEE 19 by taking account of production through the resonant annihilation of secondary positrons with atomic electrons. The quoted limit is at $m_{\gamma'} = 0.23$ GeV, assuming the fermion dark matter of mass $m_{\gamma'}/3$ and the hidden gauge coupling $\alpha_D = 0.1$. See their Fig. 3 for mass-dependent limits.
- 41 BI 21 look for the gamma-ray spectral attenuation due to scattering with hidden photons constituting all dark matter, using the measurements of sub-PeV gamma-rays from the Crab Nebula by the Tibet AS γ and HAWC experiments, together with MAGIC and HEGRA gamma-ray data. See their Fig. 4 for mass-dependent limits.
- 42 CAZZANIGA 21 look for semi-visible decays of hidden photons, $\gamma' \rightarrow \chi_1 \chi_2 (\chi_2 \rightarrow \chi_1 e^+ e^-)$, where χ_1 and χ_2 are hidden fermions. They exclude $3 \times 10^{-5} \lesssim \chi \lesssim 2 \times 10^{-2}$ assuming the hidden gauge coupling $\alpha_D = 0.1$, and the fermion masses $m_{\chi_1} = m_{\gamma'}/3$, $(m_{\chi_2} - m_{\chi_1})/m_{\chi_1} = 0.4$. See their Fig. 4 for mass-dependent limits.
- 43 DIXIT 21 look for hidden photon dark matter by using a superconducting transmon qubit dispersively coupled to a high Q storage cavity. The local density $\rho_{\gamma'} = 0.4$ GeV/cm³ is assumed. See their Fig. 4 for mass-dependent limits.
- 44 GHOSH 21 use existing haloscope axion search limits to set limits on hidden photon dark matter, considering the polarization of hidden photons. The quoted limit is at $m_{\gamma'} \simeq 3$ μ eV. See their Fig. 1 for mass-dependent limits.
- 45 GODFREY 21 look for hidden photon dark matter by using a wideband antenna, and set 5σ limits on χ . The local density $\rho_{\gamma'} = 0.38$ GeV/cm³ is assumed. See their updated Fig. 12 in arXiv:2101.02805v4 for mass-dependent limits in the range of $m_{\gamma'} = 0.207-1.24$ μ eV.
- 46 KOPYLOV 21A is an update of KOPYLOV 19, but use Ne gas instead of Ar. The quoted limit applies to $m_{\gamma'} = 12$ eV. See their Fig. 4 for mass-dependent limits.
- 47 KRIBS 21 used the HERA data on neutral current deep inelastic $e p$ scattering to derive the limits, which become weaker for heavier masses. See their Fig. 3 for mass-dependent limits.
- 48 SCHMIDT 21 use the microscopic Parton-Hadron-String Dynamics approach to extract limits by comparing the theoretically calculated dilepton spectra with the HADES data on the search for $\gamma' \rightarrow e^+ e^-$. See their Fig. 5 for the mass-dependent limits for various allowed surplus of the hidden photon contribution over the standard model yield.
- 49 TSAI 21 update the limits from the CHARM and NuCal experiments, taking account of additional production channels from proton bremsstrahlung and η meson decays, respectively. Limits between 3×10^{-8} and 1×10^{-4} are obtained for $0.01 < m_{\gamma'} < 0.8$ GeV (see their Fig. 1).
- 50 AAIJ 20c look for hidden photons produced from the pp collision in the decay channel $\gamma' \rightarrow \mu^+ \mu^-$. For prompt decaying hidden photons, limits at the level of $10^{-4}-10^{-3}$ are obtained for $m_{\gamma'} = 0.214-30$ GeV. See their Fig. 2 for mass-dependent limits.
- 51 AAIJ 20c look for hidden photons produced from the pp collision in the decay channel $\gamma' \rightarrow \mu^+ \mu^-$. For hidden photons with lifetimes of order ps, limits at the level of 10^{-5} are obtained for $m_{\gamma'} = 218-315$ MeV. See their Fig. 4 for mass-dependent limits.
- 52 ABLIKIM 20AB search for $J/\psi \rightarrow \eta' \gamma' (\gamma' \rightarrow \gamma \pi^0)$, and set the upper limit on the product branching fraction of order 10^{-7} . See their Fig. 7 for mass-dependent limits.
- 53 AGOSTINI 20 is analogous to ABE 14F. The quoted limit applies to $m_{\gamma'} = 150$ keV. The local density $\rho_{\gamma'} = 0.3$ GeV/cm³ is assumed. Their limits in their Fig. 3 were later found to be incorrect due to an error of their Eqs. (1) and (2). See Fig. 3 in AGOSTINI 22A for the corrected limits.
- 54 AMARAL 20 use a second-generation SuperCDMS high-voltage eV-resolution detector to set limits on dark-matter hidden photon absorption. The quoted limit is for $m_{\gamma'} \simeq 17$ eV. The local density $\rho_{\gamma'} = 0.3$ GeV/cm³ is assumed. See their Fig. 3 for mass-dependent limits.
- 55 AN 20 updates the direct detection limit of AN 13C on solar flux of hidden photons; $\chi < 1.6 \times 10^{-12}$ (eV/ $m_{\gamma'}$) for $m_{\gamma'} < 6$ eV (90% C.L.). For $m_{\gamma'} > 6$ eV, see their Fig. 1 for mass-dependent limits.
- 56 ANDRIANAVALOMAEFA 20 is analogous to SUZUKI 15, but uses a mirror that is about one order of magnitude larger than in similar studies in the past. Limits at the level of 10^{-12} are obtained for $m_{\gamma'} = 2.5-7$ eV. See their Fig. 23 and Table III for mass-dependent limits.
- 57 APRILE 20 is analogous to ABE 14F, and set limits $\chi \lesssim 10^{-16}-10^{-12}$. The quoted limit applies to $m_{\gamma'} = 1$ keV. They also found an excess over known backgrounds, which favors the mass $m_{\gamma'} = 2.3 \pm 0.2$ keV with a 3σ significance. See their Fig. 10 for mass-dependent limits.
- 58 ARALIS 20 is analogous to ABE 14F. The quoted limit applies to $m_{\gamma'} = 0.1$ keV. The local density $\rho_{\gamma'} = 0.3$ GeV/cm³ is assumed. The limits at masses above 3 keV in their Fig. 10 was later found to be incorrect due to an error in their analysis. See Fig. 3 in ARALIS 21 for the corrected limits.
- 59 ARGUELLES 20 examine hidden-photon production in atmospheric cosmic-ray showers and its decay in IceCube and Super-Kamiokande. The quoted limit assumes a lifetime of $\tau = 0.1$ km. See their Fig. 16 for mass- and lifetime-dependent limits.
- 60 ARNAUD 20 look for the absorption signal of hidden photon dark matter in a Ge detector. The quoted limit applies to $m_{\gamma'} \simeq 9$ eV. The local density $\rho_{\gamma'} = 0.3$ GeV/cm³ is assumed. See their Fig. 3 for mass-dependent limits.
- 61 BANERJEE 20 is an update of BANERJEE 18. They exclude $8.2 \times 10^{-5} \lesssim \chi \lesssim 1 \times 10^{-2}$ for $m_{\gamma'} = 1.5-24$ MeV. In particular, they exclude $\chi = 1.2 \times 10^{-4} - 6.8 \times 10^{-4}$ for the 16.7 MeV gauge boson. See their Fig. 5 for mass-dependent limits.
- 62 BARAK 20 is analogous to AGUILAR-AREVALO 19A, and look for hidden photon dark matter by using the Skipper CCD. The quoted limit applies to $m_{\gamma'} = 12.8$ eV. See their Fig. 4 for mass-dependent limits.
- 63 KRASNINKOV 20 showed that the limit of BANERJEE 20 combined with the measured anomalous magnetic moment of the electron exclude the 16.7 MeV gauge boson suggested by the ATOMKI (KRASZNAHORKAY 16) experiment if it has pure vector or axial-vector interactions.
- 64 SHE 20 look for solar hidden photons. The quoted limit applies to $m_{\gamma'} = 180$ eV. See their Fig. 4 for mass-dependent limits.
- 65 SHE 20 look for hidden photon dark matter and set limits $\chi < 1.3 \times 10^{-15} - 2.8 \times 10^{-14}$ for the quoted mass range. The local density $\rho_{\gamma'} = 0.3$ GeV/cm³ is assumed. See their Fig. 6 for mass-dependent limits.
- 66 SIRUNYAN 20AQ look for a narrow resonance decaying into a pair of muons. For $m_{\gamma'} < 45$ GeV, they use dedicated high-rate dimuon triggers to reduce the muon transverse momentum thresholds. The quoted limit applies to $m_{\gamma'} = 50$ GeV, and limits of order 10^{-3} are obtained for the quoted mass range. See their Fig. 3 for mass-dependent limits.
- 67 TOMITA 20 look for hidden photon dark matter using a planar metal plate and cryogenic receiver and set limits $\chi < 1.8-4.3 \times 10^{-10}$ for the quoted mass range. The local density $\rho_{\gamma'} = 0.39$ GeV/cm³ is assumed. See their Fig. 7 for mass-dependent limits.
- 68 WANG 20A is analogous to ABE 14F. The quoted limit applies to $m_{\gamma'} = 185$ eV. The local density $\rho_{\gamma'} = 0.3$ GeV/cm³ is assumed. See their Fig. 11 for mass-dependent limits.
- 69 AABOUD 19G look for $h \rightarrow \gamma' \gamma' (\gamma' \rightarrow \mu^+ \mu^-)$ and exclude a kinetic mixing around $10^{-9}-10^{-8}$ for $B(h \rightarrow \gamma' \gamma') = 0.01$ and 0.1. See their Fig. 9 for mass-dependent limits.
- 70 ABLIKIM 19A look for $J/\psi \rightarrow \gamma' \eta (\gamma' \rightarrow e^+ e^-)$. Limits between 6×10^{-3} and 5×10^{-2} are obtained (see their Fig. 8).
- 71 ABLIKIM 19H look for $J/\psi \rightarrow \gamma' \eta' (\gamma' \rightarrow e^+ e^-)$. Limits between 3.4×10^{-3} and 2.6×10^{-2} are obtained. See their Fig. 5 for mass-dependent limits.
- 72 AGUILAR-AREVALO 19A look for the absorption signal of hidden photon dark matter by using a CCD. The quoted limit applies to $m_{\gamma'} = 17$ eV. The local density $\rho_{\gamma'} = 0.3$ GeV/cm³ is assumed. See their Fig. 4 for mass-dependent limits.
- 73 APRILE 19D is analogous to ABE 14F. The quoted limit applies to $m_{\gamma'} = 0.7$ keV. See their Fig. 5(f) for mass-dependent limits.
- 74 BANERJEE 19 is an update of BANERJEE 18A. The quoted limit is at $m_{\gamma'} = 1$ MeV. See their Fig. 3 for mass-dependent limits.

Gauge & Higgs Boson Particle Listings

Axions (A^0) and Other Very Light Bosons

- ⁷⁵ BHOONAH 19 examine heating of Galactic Center gas clouds by hidden photon dark matter. The quoted limit applies to $m_{\gamma'} \simeq 10^{-12}$ eV. See their Fig. 2 for mass-dependent limits.
- ⁷⁶ BRUN 19 is analogous to SUZUKI 15. The limit is derived under an assumption that hidden photons constitute the local dark matter density $\rho_{\gamma'} = 0.3 \text{ GeV}/\text{cm}^3$.
- ⁷⁷ CORTINA-GIL 19 look for an invisible hidden photon in the reaction $K^+ \rightarrow \pi^+ \pi^0 (\pi^0 \rightarrow \gamma\gamma')$. The quoted limit applies to $m_{\gamma'} = 62.5\text{--}65 \text{ MeV}$. See their Figs. 6 and 7 for mass-dependent limits.
- ⁷⁸ DANILOV 19 examined the hidden photon production in nuclear reactors, correctly taking account of the effective photon mass in the reactor and detector. The limit gets weaker for $m_{\gamma'}$ less than the effective photon mass in proportion to $1/m_{\gamma'}^2$. See their Fig. 1 for mass-dependent limits.
- ⁷⁹ HOCHBERG 19 look for the absorption signal of hidden photon dark matter by using superconducting-nanowire single-photon detectors. The quoted limit applies to $m_{\gamma'} \simeq 1 \text{ eV}$. The local density $\rho_{\gamma'} = 0.3 \text{ GeV}/\text{cm}^3$ is assumed. See their Fig. 4 for mass-dependent limits.
- ⁸⁰ KOPYLOV 19 look for hidden-photon dark matter using a counter with an aluminum cathode and derive limits assuming it constitute all the local dark matter. The quoted limit applies to $m_{\gamma'} = 12 \text{ eV}$. See their Fig. 7 for mass-dependent limits.
- ⁸¹ KOVETZ 19 examine heating of the early Universe plasma by hidden photon dark matter, and derive the limits by requiring that the cosmic mean 21 cm brightness temperature relative to the CMB temperature satisfy $T_{21} > -100 \text{ mK}$. The quoted limit applies to $m_{\gamma'} \simeq 2 \times 10^{-14} \text{ eV}$. See their Fig. 3 for mass-dependent limits.
- ⁸² NGUYEN 19 look for hidden photon dark matter with a resonant cavity, and set limits $\sim 10^{-12}$ for $m_{\gamma'} = 0.2\text{--}2.07 \mu\text{eV}$. The quoted limit applies to $m_{\gamma'} = 1.3 \mu\text{eV}$. The local density $\rho_{\gamma'} = 0.3 \text{ GeV}/\text{cm}^3$ is assumed. See their Fig. 19 for mass-dependent limits.
- ⁸³ ABE 18f is an update of ABE 14f. The quoted limit applies to $m_{\gamma'} \simeq 40 \text{ keV}$. See their Fig. 5 for mass-dependent limits.
- ⁸⁴ ADRIAN 18 look for a hidden photon resonance in the reaction $e^- Z \rightarrow e^- Z \gamma' (\gamma' \rightarrow e^+ e^-)$. The quoted limit applies to $m_{\gamma'} = 40 \text{ MeV}$. See their Fig. 4 for mass-dependent limits.
- ⁸⁵ ANASTASI 18b look for a hidden photon resonance in the reaction $e^+ e^- \rightarrow \gamma \gamma' (\gamma' \rightarrow \mu^+ \mu^-)$. The quoted limit is obtained by combining the result of ANASTASI 16 and it applies to $m_{\gamma'} \simeq 519\text{--}987 \text{ MeV}$. See their Fig. 9 for mass-dependent limits.
- ⁸⁶ ARMENGAUD 18 is analogous to ABE 14f. The quoted limits applies to $m_{\gamma'} = 1.6 \text{ keV}$. See the right panel of Fig. 5 for mass-dependent limits.
- ⁸⁷ BANERJEE 18 look for hidden photons produced in the reaction $e^- Z \rightarrow e^- Z \gamma' (\gamma' \rightarrow e^+ e^-)$, and exclude $9.2 \times 10^{-5} \lesssim \chi \lesssim 1 \times 10^{-2}$ for $m_{\gamma'} = 1\text{--}23 \text{ MeV}$. They also set a limit on the electron coupling to a 16.7 MeV gauge boson suggested by the ATOMKI (KRASZNAHORKAY 16) experiment. See their Fig. 3 for mass-dependent limits.
- ⁸⁸ BANERJEE 18a look for invisible decays of hidden photons produced in the reaction $e^- Z \rightarrow e^- Z \gamma'$. The quoted limit is at $m_{\gamma'} = 1 \text{ MeV}$. See their Fig. 15 for mass-dependent limits.
- ⁸⁹ KNIRCK 18 is analogous to SUZUKI 15. See their Fig. 5 for mass-dependent limits.
- ⁹⁰ ABRGALL 17 is analogous to ABE 14f using the MAJORANA DEMONSTRATOR. See their Fig. 3 for limits between $6 \text{ keV} < m_{\gamma'} < 97 \text{ keV}$.
- ⁹¹ ABLIKIM 17AA look for $e^+ e^- \rightarrow \gamma \gamma' (\gamma' \rightarrow e^+ e^- \text{ or } \mu^+ \mu^-)$. Limits between 10^{-3} and 10^{-4} are obtained (see their Fig. 3).
- ⁹² ANGLÖHER 17 is analogous to ABE 14f. The quoted limit is at $m_{\gamma'} = 0.7 \text{ keV}$. See their Fig. 8 for mass-dependent limits.
- ⁹³ BANERJEE 17 look for invisible decays of hidden photons produced in the reaction $e^- Z \rightarrow e^- Z \gamma'$. The quoted limit applies to $m_{\gamma'} = 2 \text{ MeV}$. See their Fig. 3 for mass-dependent limits.
- ⁹⁴ CHANG 17 examine the hidden photon emission from SN1987A, including the effects of finite temperature and density on χ and obtain limits $\chi (m_{\gamma'}/\text{MeV}) \lesssim 3 \times 10^{-9}$ for $m_{\gamma'} < 15 \text{ MeV}$ and $\chi \lesssim 10^{-9}$ for $m_{\gamma'} = 15\text{--}120 \text{ MeV}$.
- ⁹⁵ DUBININA 17 look for $\mu^+ \rightarrow e^+ \bar{\nu}_\mu \nu_e \gamma' (\gamma' \rightarrow e^+ e^-)$ in a nuclear photoemulsion. The quoted limit applies to $m_{\gamma'} = 1.1 \text{ MeV}$. Limits between 4.5×10^{-3} and 10^{-2} are obtained (see their Fig. 3).
- ⁹⁶ LEES 17E look for invisible decays of hidden photons produced in the reaction $e^+ e^- \rightarrow \gamma \gamma'$. See their Fig. 5 for limits in the mass range $m_{\gamma'} \leq 8 \text{ GeV}$.
- ⁹⁷ AAD 16AG look for hidden photons promptly decaying into collimated electrons and/or muons, assuming that they are produced in the cascade decays of squarks or the Higgs boson. See their Fig. 10 and Fig.13 for their limits on the cross section times branching fractions.
- ⁹⁸ ANASTASI 16 look for the decay $\gamma' \rightarrow \pi^+ \pi^-$ in the reaction $e^+ e^- \rightarrow \gamma \gamma'$. Limits between 4.3×10^{-3} and 4.4×10^{-4} are obtained for $527 < m_{\gamma'} < 987 \text{ MeV}$ (see their Fig. 9).
- ⁹⁹ KHACHATRYAN 16 look for $\gamma' \rightarrow \mu^+ \mu^-$ in a dark SUSY scenario where the SM-like Higgs boson decays into a pair of the visible lightest neutralinos with mass 10 GeV, both of which decay into γ' and a hidden neutralino with mass 1 GeV. See the right panel in their Fig. 2.
- ¹⁰⁰ AAD 15cd look for $H \rightarrow Z \gamma' \rightarrow 4\ell$ with the ATLAS detector at LHC and find $\chi < 4\text{--}17 \times 10^{-2}$ for $m_{\gamma'} = 15\text{--}55 \text{ GeV}$. See their Fig. 6.
- ¹⁰¹ ADARE 15 look for a hidden photon in $\pi^0, \eta^0 \rightarrow \gamma e^+ e^-$ at the PHENIX experiment. See their Fig. 4 for mass-dependent limits.
- ¹⁰² AN 15A derived limits from the absence of ionization signals in the XENON10 and XENON100 experiments, assuming hidden photons constitute all the local dark matter. Their best limit is $\chi < 1.3 \times 10^{-10}$ at $m_{\gamma'} = 18 \text{ eV}$. See their Fig. 1 for mass-dependent limits.
- ¹⁰³ ANASTASI 15 look for a production of a hidden photon and a hidden Higgs boson with the KLOE detector at DAΦNE, where the hidden photon decays into a pair of muons and the hidden Higgs boson lighter than $m_{\gamma'}$ escape detection. See their Figs. 6 and 7 for mass-dependent limits on a product of the hidden fine structure constant and the kinetic mixing.
- ¹⁰⁴ ANASTASI 15A look for the decay $\gamma' \rightarrow e^+ e^-$ in the reaction $e^+ e^- \rightarrow e^+ e^- \gamma'$. Limits between 1.7×10^{-3} and 1×10^{-2} are obtained for $m_{\gamma'} = 5\text{--}320 \text{ MeV}$ (see their Fig. 7).
- ¹⁰⁵ BATLEY 15A look for $\pi^0 \rightarrow \gamma \gamma' (\gamma' \rightarrow e^+ e^-)$ at the NA48/2 experiment. Limits between 4.2×10^{-4} and 8.8×10^{-3} are obtained for $m_{\gamma'} = 9\text{--}120 \text{ MeV}$ (see their Fig. 4).
- ¹⁰⁶ JAEGLER 15 look for the decay $\gamma' \rightarrow e^+ e^-, \mu^+ \mu^-, \text{ or } \pi^+ \pi^-$ in the dark Higgsstrahlung channel, $e^+ e^- \rightarrow \gamma' H' (H' \rightarrow \gamma \gamma')$ at the BELLE experiment. They set limits on a product of the branching fraction and the Born cross section as well as a product of the hidden fine structure constant and the kinetic mixing. See their Figs. 3 and 4.
- ¹⁰⁷ KAZANAS 15 set limits by studying the decay of hidden photons $\gamma' \rightarrow e^+ e^-$ inside and near the progenitor star of SN1987A. See their Fig. 6 for mass-dependent limits.
- ¹⁰⁸ SUZUKI 15 looked for hidden-photon dark matter with a dish antenna and derived limits assuming they constitute all the local dark matter. Their limits are $\chi < 6 \times 10^{-12}$ for $m_{\gamma'} = 1.9\text{--}4.3 \text{ eV}$. See their Fig. 7 for mass-dependent limits.
- ¹⁰⁹ VINYOLETS 15 performed a global fit analysis based on helioseismology and solar neutrino observations, and set the limits $\chi m_{\gamma'} < 1.8 \times 10^{-12} \text{ eV}$ for $m_{\gamma'} = 3 \times 10^{-5}\text{--}8 \text{ eV}$. See their Fig. 11.
- ¹¹⁰ ABE 14f look for the photoelectric-like interaction in the XMASS detector assuming the hidden photon constitutes all the local dark matter. Limits between 2×10^{-13} and 1×10^{-12} are obtained, where the relation $\chi^2 = \alpha'/\alpha$ is used to translate the original bound on the ratio of the hidden and EM fine-structure constants. See their Fig. 3 for mass-dependent limits.
- ¹¹¹ AGA KISHIEV 14 look for hidden photons $\gamma' \rightarrow e^+ e^-$ at the HADES experiment, and set limits on χ for $m_{\gamma'} = 0.02\text{--}0.6 \text{ GeV}$. See their Fig. 5 for mass-dependent limits.
- ¹¹² BABUSCI 14 look for the decay $\gamma' \rightarrow \mu^+ \mu^-$ in the reaction $e^+ e^- \rightarrow \mu^+ \mu^- \gamma'$. Limits between 4×10^{-3} and 9.0×10^{-4} are obtained for $520 \text{ MeV} < m_{\gamma'} < 980 \text{ MeV}$ (see their Fig. 7).
- ¹¹³ BATELL 14 derived limits from the electron beam dump experiment at SLAC (E-137) by searching for events with recoil electrons by sub-GeV dark matter produced from the decay of the hidden photon. Limits at the level of $10^{-4}\text{--}10^{-1}$ are obtained for $m_{\gamma'} = 10^{-3}\text{--}1 \text{ GeV}$, depending on the dark matter mass and the hidden gauge coupling (see their Fig. 2).
- ¹¹⁴ BLUEMLEIN 14 analyzed the beam dump data taken at the U-70 accelerator to look for γ' -bremsstrahlung and the subsequent decay into muon pairs and hadrons. See their Fig. 4 for mass-dependent excluded region.
- ¹¹⁵ FRADETTE 14 studied effects of decay of relic hidden photons on BBN and CMB to set constraints on very small values of the kinetic mixing. See their Figs. 4 and 7 for mass-dependent excluded regions.
- ¹¹⁶ LEES 14i look for hidden photons in the reaction $e^+ e^- \rightarrow \gamma \gamma' (\gamma' \rightarrow e^+ e^-, \mu^+ \mu^-)$. Limits at the level of $10^{-4}\text{--}10^{-3}$ are obtained for $0.02 \text{ GeV} < m_{\gamma'} < 10.2 \text{ GeV}$. See their Fig. 4 for mass-dependent limits.
- ¹¹⁷ MERKEL 14 look for $\gamma' \rightarrow e^+ e^-$ at the A1 experiment at the Mainz Microtron (MAMI). See their Fig. 3 for mass-dependent limits.
- ¹¹⁸ AN 13B examined the stellar production of hidden photons, correcting an important error of the production rate of the longitudinal mode which now dominates. See their Fig. 2 for mass-dependent limits based on solar energy loss.
- ¹¹⁹ AN 13C use the solar flux of hidden photons to set a limit on the atomic ionization rate in the XENON10 experiment. They find $\chi m_{\gamma'} < 3 \times 10^{-12} \text{ eV}$ for $m_{\gamma'} < 1 \text{ eV}$. See their Fig. 2 for mass-dependent limits.
- ¹²⁰ DIAMOND 13 analyzed the beam dump data taken at the SLAC millicharge experiment to constrain a hidden photon invisibly decaying into lighter long-lived particles, which undergo elastic scattering off nuclei in the detector. Limits between $8 \times 10^{-4}\text{--}2 \times 10^{-2}$ are obtained. The quoted limit is applied when the dark gauge coupling is set equal to the electromagnetic coupling. See their Fig.4 for mass-dependent limits.
- ¹²¹ GNINENKO 13 used the data taken at the SINDRUM experiment to constrain the decay, $\pi^0 \rightarrow \gamma \gamma' (\gamma' \rightarrow e^+ e^-)$ to derive limits. See their Fig. 2 for their mass-dependent excluded region.
- ¹²² HORVAT 13 look for hidden-photo-electric effect in HPGe detectors induced by solar hidden photons. See their Fig. 3 for mass-dependent limits.
- ¹²³ INADA 13 search for hidden photons using an intense X-ray beamline at SPring-8. See their Fig. 4 for mass-dependent limits.
- ¹²⁴ MIZUMOTO 13 look for solar hidden photons. See their Fig. 5 for mass-dependent limits.
- ¹²⁵ PARKER 13 look for hidden photons using a cryogenic resonant microwave cavity. See their Fig.5 for mass-dependent limits.
- ¹²⁶ PARKER 13 derived a limit for the hidden photon CDM with a randomly oriented hidden photon field.
- ¹²⁷ REDONDO 13 examined the solar emission of hidden photons including the enhancement factor for the longitudinal mode pointed out by AN 13B, and also updated stellar-energy loss arguments. See their Fig.3 for mass-dependent limits, including a review of the currently best limits from other arguments.
- ¹²⁸ GNINENKO 12a obtained bounds on $B(\pi^0 \rightarrow \gamma \gamma') \cdot B(\gamma' \rightarrow e^+ e^-)$ from the NOMAD and PS191 neutrino experiments, and derived limits between $8 \times 10^{-8}\text{--}2 \times 10^{-4}$. See their Fig.4 for mass-dependent excluded regions.
- ¹²⁹ GNINENKO 12b used the data taken at the CHARM experiment to constrain the decay, $\eta(\eta') \rightarrow \gamma \gamma' (\gamma' \rightarrow e^+ e^-)$, and derived limits between $1 \times 10^{-7}\text{--}1 \times 10^{-4}$. See their Fig.4 for mass-dependent excluded region.
- ¹³⁰ ABRAHAMYAN 11 look for $\gamma' \rightarrow e^+ e^-$ in the electron-nucleon fixed-target experiment at the Jefferson Laboratory (APEX). See their Fig. 5 for mass-dependent limits.
- ¹³¹ BLUEMLEIN 11 analyzed the beam dump data taken at the U-70 accelerator to look for $\pi^0 \rightarrow \gamma \gamma' (\gamma' \rightarrow e^+ e^-)$. See their Fig. 5 for mass-dependent limits.
- ¹³² BJORKEN 09 analyzed the beam dump data taken at E137, E141, and E774 to constrain a hidden photon produced by bremsstrahlung, subsequently decaying into $e^+ e^-$, and

See key on page 1171

Gauge & Higgs Boson Particle Listings
Axions (A^0) and Other Very Light Bosons

Table with columns for author names, experiment codes, and particle names. Includes entries for DERBIN, GONDOLO, IGNATOVICH, KEKEZ, SEREBROV, AFANASEV, BELLINI, CHOU, FOUICHE, HANNESSTAD, INOUE, ZAVATTINI, ADELBERGER, ANDRIAMON, BAESSLER, CHANG, HANNESSTAD, JAIN, LESSA, MELCHIORRI, ROBILIARD, ARNOLD, DUFFY, HECKEL, ZAVATTINI, HANNESSTAD, ZIOUTAS, ADLER, ANISIMOVSK..., ARNOLD, ASZTALOS, HOFFMANN, ARNOLD, CIVITARESE, DANEVICH, FARZAN, ADLER, BERNABEI, DERBIN, FUSHIMI, INOUE, MORALES, ADLER, AMMAR, ASHITKOV, BERNABEI, DANEVICH, DEBOER, STOICA, ALESSAND..., ARNOLD, ASTIER, DANEVICH, MASSO, ARNOLD, NI, SIMKOVIC, ALTEGOER, ARNOLD, AVIGNONE, DIAZ, KIM, LUESCHER, MORIYAMA, MORI, POSPELOV, AHMAD, BORISOV, DEBOER, KACHELRIESS, KEIL, KITCHING, LEINBERGER, ADLER, AMSLER, GANZ, GUENTHER, KAMEL, MITSUI, YOUNDIN, ALTMANN, BASSOMPIE..., MAENO, RAFFELT, SKALSEY, TSUNODA, ADACHI, ALTHERR, AMSLER, ASAI, MEIJERDREES, NI, VO, ATIYA, ATIYA, BASSOMPIE..., BECK, CAMERON, CHANG, CHUI, MINOWA, NG, RITTER, TANAKA, ALLIEGRO, ATIYA, BARABASH, BERNATOW..., BLUEMLEIN, HALLIN, HENDERSO..., HICKS, LAZARUS, MEIJERDREES, PAN, RUOSO, SKALSEY, VENEMA, WANG, WANG, WU, AKOPYAN, ASAI, BERSHADY, BLUEMLEIN, BOBRAKOV, BROSS, KIM, RAFFELT, RAFFELT, RESELL, TRZASKA, TSERTOS, WALKER, WIDMANN, WINELAND, ALBRECHT, ANTREASYAN, ASANUMA, ATIYA, ATIYA, BAUER, BURROWS, DEBOER, ENDEL, GNINENKO, GUO, HAGMANN, HAGMANN, JUDGE, RAFFELT, RITTER, SEMERTZIDIS, TSUCHIAKI, TURNER, BARABASH, BINI, BURROWS, DEBOER, ERICSON, FAISSNER, FOX, MAYLE, MINOWA, ORITO, PERKINS, TSERTOS, VANBIBBER, WUENSCH, WUENSCH, AVIGNONE, BALK, BJORKEN, BLINOV, BOLTON, CHANDA, CHOI, CONNELL, DATAR, DEBOER, DEBOER, DOEHRER, EL-NADI, ENGEL, FAISSNER, HATSUDA, LORENZ, MAYLE, PICCIOTTO, RAFFELT, RAFFELT, SAVAGE, TSERTOS, VANBIBBER, VANKLINKEN, VANKLINKEN, VONWIMMER..., VOROBYOV, DRUZHININ, FRIEMAN, GOLDMAN, KORENCHEN..., MAIER, MILLS, RAFFELT, RIORDAN, TURNER, VANBIBBER, VONWIMMER..., BADIER, BROWN, BRYMAN, DAVIER, DEARBORN, EICHLER, HALLIN, JODIDIO, KETOV, KOCH, KONAKA, MAIANI, PECCERI, RAFFELT, RAFFELT, SAVAGE, AMALDI, ANANEV, B.J. Venema et al., J. Wang, J. Wang, X.Y. Wu et al., M.V. Akopyan et al., S. Asai et al., M.A. Bershad, M.T. Ressell, M.S. Turner, J. Bluemel et al., V.F. Bobrov et al., A.D. Bross et al., J.E. Kim, G.G. Raffelt, G. Raffelt, D. Seckel, M.T. Ressell, W.H. Trzaska et al., H. Tsertos et al., T.P. Walker et al., E. Widmann et al., D.J. Wineland et al., H. Albrecht et al., D. Antreasyan et al., T. Asanuma et al., M.S. Atiya et al., M.S. Atiya et al., W. Bauer et al., A. Burrows, M.T. Ressell, M.S. Turner, F.W.N. de Boer, J. Lehmann, J. Steyart, J. Engel, D. Seckel, A.C. Hayes, S.M. Gninenko et al., R. Guo et al., C. Haggmann et al., S.M. Judge et al., G.G. Raffelt, R.C. Ritter et al., Y.K. Semertzidis et al., M. Tsuchiaki et al., M.S. Turner, A.S. Barabash et al., M. Bini et al., A. Burrows, M.S. Turner, R.P. Brinkmann, M.S. Turner, F.W.N. de Boer, R. van Dantzig, T.E.O. Ericson, J.F. Mathiot, H. Faissner et al., J.D. Fox et al., R. Mayle et al., H. Minowa et al., S. Orto et al., D.H. Perkins, H. Tsertos et al., K. von Bibber et al., W.U. Wuensch et al., S. de Panfilis et al., F.T. Avignone et al., B. Balke et al., J.D. Bjorken et al., A.E. Blinov et al., R.D. Bolton et al., R.D. Bolton et al., D. Gronick et al., R. Chanda, J.F. Nieves, P.B. Pal, K. Choi et al., S.H. Connell et al., V.M. Datar et al., F.W.N. de Boer, R. van Dantzig, F.W.N. de Boer, R. van Dantzig, D.H. Perkins, F.W.N. de Boer, R. van Dantzig, J. Doehrer et al., M. el Nadi, O.E. Badawy, J. Engel, P. Vogel, M.R. Zimbauer, H. Faissner et al., T. Hatsuda, M. Yoshimura, E. Lorenz et al., R. Mayle et al., C.E. Picciotto et al., G. Raffelt, D. Seckel, G.G. Raffelt, D.S.P. Dearborn, M.J. Savage, B.W. Filippone, L.W. Mitchell, A. Tsertos et al., A. Tsertos et al., J. van Klinken et al., J. van Klinken, U. von Wimmersperg et al., P.V. Vorobyov, Y.I. Gitars, V.P. Druzhinin et al., J.A. Frieman, S. Dimopoulos, M.S. Turner, T. Goldman et al., S.M. Korenchenko et al., K. Maier et al., A.P. Mills, J. Levy, G.G. Raffelt, D.S.P. Dearborn, E.M. Riordan et al., M.S. Turner, K. von Bibber et al., U. von Wimmersperg et al., J. Badier et al., C.N. Brown et al., D.J. Bryman, E.T.H. Clifford, M. Davier, J. Jeanjean, H. Nguyen Ngoc, D.S.P. Dearborn, D.N. Schramm, G. Steigman, R.A. Eickler et al., A.L. Hallin et al., A. Jodidio et al., A. Jodidio et al., S.N. Ketov et al., H.R. Koch, O.W.B. Schult, A. Konaka et al., L. Maiani, R. Petronzio, E. Zavattini, R.D. Peccei, T.T. Wu, T. Yanagida, G.G. Raffelt, G.G. Raffelt, M.J. Savage et al., U. Amaldi et al., V.D. Ananev et al., (ILL), (ILL), (BNL, YALE, CUNY), (INRM), (ICEPP), (CHIC+), (BERL, BUDA, JINR+), (PNPI), (FNAL, ILL), (SEOUL), (MPIM), (Graflet, D. Seckel), (CHIC, FNAL), (TAMU), (ILLG, GS), (HSCA, OSU, CHIC+), (STUT, GSI, STUFM), (NBS), (ARGUS Collab.), (Crystal Ball Collab.), (TOKY), (BNL E787 Collab.), (BNL E787 Collab.), (STUT, VILL, GS), (ARIZ+), (LOUV), (BART, LANL), (INRM), (CASE+), (FLOR), (ILLG, GS), (MPIM), (UVA), (ROCH, BNL, FNAL+), (ICEPP), (FNAL), (ITEP, INRM), (FIRZ, CERN, AARH), (BRINKMANN), (FNAL), (ANIK), (CERN, IPN), (AAACH3, BERL, PSI), (FSU), (LLL, CERN, MINN, FNAL+), (LLL, CERN, MINN, FNAL+), (ICEPP), (ICEPP), (OXF), (GSI, ILLG), (ROCH, TAMU, LBL), (ROCH, BNL, FNAL), (ROCH, BNL, FNAL), (PRIN, SCUC, ORNL+), (LBL, UCB, COLA, NWES+), (FNAL, SLAC, VPI), (NOVO), (LANL, STAN, CHIC+), (LANL, STAN, CHIC+), (CHIC, LANL, STAN+), (UMD, UPRA+), (JHU), (WITW), (IPN), (ANIK), (ANIK), (OXF), (ANIK), (HEIDP, ANL, ILLG), (CAIR), (AAACH3, BERL, SIN), (KEK), (MPIM, PSI), (LLL, CERN, MINN, FNAL+), (TRIU, CNRC), (UCB, LBL, UCSC), (UCB, LLL), (CIT), (GSI, ILLG), (GSI, ILLG), (GRON, GSI), (GRON), (BNL), (NOVO), (NOVO), (SLAC+), (LANL, CHIC, STAN+), (JINR), (STUT, GSI), (BELL), (LLL, UCB), (ROCH, CIT+), (FNAL, EFI), (LLL, CIT, MIT+), (WITW), (NA3 Collab.), (FNAL, WASH, KYOT+), (TRIU), (LAI), (GSI, ILLG), (LLA), (LLA), (SINDRUM Collab.), (PRIN), (LBL, NWES, TRIU), (LBL, NWES, TRIU), (KIAE), (JHU), (KYOT, KEK), (CERN), (DESY), (MPIM), (MPIM), (CIT), (CERN), (JINR)

Gauge & Higgs Boson Particle Listings

Axions (A^0) and Other Very Light Bosons

BALTRUSAITIS...	85	PRL 55 1842	R. M. Baltrusaitis <i>et al.</i>	(Mark III Collab.)	VUILLEUMIER	81	PL 101B 341	J.L. Vuilleumier <i>et al.</i>	(CIT, MUNI)
BERGSMÄ	85	PL 157B 458	F. Bergsma <i>et al.</i>	(CHARM Collab.)	ZEHNDER	80	PL 104B 494	A. Zehnder	(ETH)
KAPLAN	85	NP B260 215	D.B. Kaplan	(HARV)	FAISSNER	81	PL 96B 201	H. Faissner <i>et al.</i>	(AACH3)
IWAMOTO	84	PRL 53 1198	N. Iwamoto	(UCSB, WUSL)	JACQUES	80	PR D21 1206	P.F. Jacques <i>et al.</i>	(RUTG, STEV, COLU)
YAMAZAKI	84	PRL 52 1089	T. Yamazaki <i>et al.</i>	(INUS, KEK)	SOUKAS	80	PRL 44 564	A. Soukas <i>et al.</i>	(BNL, HARV, ORNL, PENN)
ABBOTT	83	PL 120B 133	L.F. Abbott, P. Sikivie	(BRAN, FLOR)	BECHIS	79	PRL 42 1511	D.J. Bechis <i>et al.</i>	(UMD, COLU, AFRR)
CARBONI	83	PL 123B 349	G. Carbone, W. Dahme	(CERN, MUNI)	CALAPRICE	79	PR D20 2708	F.P. Calaprice <i>et al.</i>	(PRIN)
CAVAIGNAC	83	PL 121B 193	J.F. Cavaignac <i>et al.</i>	(ISNG, LAPP)	COTEUS	79	PRL 42 1438	P. Coteus <i>et al.</i>	(COLU, ILL, BNL)
DICUS	83	PR D28 1778	D.A. Dicus, V.L. Teplitz	(TEXA, UMD)	DISHAW	79	PL 85B 142	J.P. Dishaw <i>et al.</i>	(SLAC, CIT)
DINE	83	PL 120B 137	M. Dine, W. Fischer	(IAS, PENN)	ZHITNITSKII	79	SJNP 29 517	A.R. Zhitnitsky, Y.I. Skovpen	(NOVO)
ELLIS	83B	NP B223 252	J. Ellis, K.A. Olive	(CERN)			Translated from YAF 29 1001.		
FAISSNER	83	PR D28 1198	H. Faissner <i>et al.</i>	(AACH)	ALIBRAN	78	PL 74B 134	P. Alibrand <i>et al.</i>	(Gargamelle Collab.)
FAISSNER	83B	PR D28 1787	H. Faissner <i>et al.</i>	(AACH3)	ASRATYAN	78B	PL 79B 497	A.E. Asratyan <i>et al.</i>	(ITEP, SERP)
FRANK	83B	PR D28 1790	J.S. Frank <i>et al.</i>	(LANL, YALE, LBL+)	BELLOTTI	78	PL 76B 223	E. Bellotti, E. Fiorini, L. Zanotti	(MILA)
HOFFMAN	83	PR D28 660	C.M. Hoffman <i>et al.</i>	(LANL, ARZS)	BOSETTI	78B	PL 74B 143	P.C. Bosetti <i>et al.</i>	(BEBC Collab.)
PRESKILL	83	PL 120B 127	J. Preskill, M.B. Wise, F. Wilczek	(HARV, UCSBT)	DICUS	78C	PR D18 1829	D.A. Dicus <i>et al.</i>	(TEXA, VPI, STAN)
SIKIVIE	83	PRL 51 1415	P. Sikivie	(FLOR)	DONNELLY	78	PR D18 1607	T.W. Donnelly <i>et al.</i>	(STAN)
		PRL 52 695 (errat.)	P. Sikivie	(FLOR)			PRL 37 315	F. Reines, H.S. Gurr, H.W. Sobel	(UCI)
ALEKSEEV	82	JETP 55 591	E.A. Alekseeva <i>et al.</i>	(KIAE)			PRL 33 179	H.S. Gurr, F. Reines, H.W. Sobel	(UCI)
		Translated from ZETF 82 1007.	G.D. Alekseev <i>et al.</i>	(MOSU, JINR)	HANSL	78D	PL 74B 139	T. Hansl <i>et al.</i>	(CDHS Collab.)
ALEKSEEV	82B	JETPL 36 116			MICELMAC...	78	LNC 21 441	G.V. Mitselmakher, B. Pontecorvo	(JINR)
		Translated from ZETFP 36 94.			MIKAEIAN	78	PR D18 3605	K.O. Mikaelian	(FNAL, NWES)
ASANO	82	PL 113B 195	Y. Asano <i>et al.</i>	(KEK, TOKY, INUS, OSAK)	SATO	78	PTP 60 1942	K. Sato	(KYOT)
BARROSO	82	PL 116B 247	A. Barroso, G.C. Branco	(LSB)	VYSOTSKII	78	JETPL 27 502	M.I. Vysotsky <i>et al.</i>	(ASCI)
DATAR	82	PL 114B 63	V.M. Datar <i>et al.</i>	(BHAB)			Translated from ZETFP 27 533.		
EDWARDS	82	PRL 48 903	C. Edwards <i>et al.</i>	(Crystal Ball Collab.)	YANG	78	PRL 41 523	T.C. Yang	(MASA)
FETSCHER	82	JP G8 L147	W. Fetscher	(ETH)	PECCER	77	PR D16 1791	R.D. Peccer, H.R. Quinn	(STAN, SLAC)
FUKUGITA	82	PRL 48 1522	M. Fukugita, S. Watamura, M. Yoshimura	(KEK)			PRL 38 1440	R.D. Peccer, H.R. Quinn	(STAN, SLAC)
FUKUGITA	82B	PR D26 1840	M. Fukugita, S. Watamura, M. Yoshimura	(KEK)	REINES	76	PRL 37 315	F. Reines, H.S. Gurr, H.W. Sobel	(UCI)
LEHMANN	82	PL 115B 270	P. Lehmann <i>et al.</i>	(SACL)	GURR	74	PR 33 179	H.S. Gurr, F. Reines, H.W. Sobel	(UCI)
RAFFELT	82	PL 119B 323	G. Raffelt, L. Stodolsky	(MPIM)	ANAND	53	PRSL A22 183	B.M. Anand	
ZEHNDER	82	PL 110B 419	A. Zehnder, K. Gabathuler, J.L. Vuilleumier	(ETH+)					
ASANO	81B	PL 107B 159	Y. Asano <i>et al.</i>	(KEK, TOKY, INUS, OSAK)					
BARROSO	81	PL 106B 91	A. Barroso, N.C. Mukhopadhyay	(SIN)					
FAISSNER	81	ZPHY C10 95	H. Faissner <i>et al.</i>	(AACH3)					
FAISSNER	81B	PL 103B 234	H. Faissner <i>et al.</i>	(AACH3)					
KIM	81	PL 105B 55	B.R. Kim, C. Stamm	(AACH3)					

OTHER RELATED PAPERS

SREDNICKI	85	NP B260 689	M. Srednicki	(UCSB)
BARDEEN	78	PL 74B 229	W.A. Bardeen, S.-H.H. Tye	(FNAL)

LEPTONS

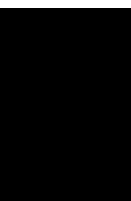
e	1297
μ	1298
τ	1303
Heavy Charged Lepton Searches	1331
Neutrino Properties	1332
Number of Neutrino Types	1341
Double- β Decay	1343
Neutrino Mixing	1348
Heavy Neutral Leptons, Searches for	1367

Notes in the Listings

Neutrino properties (rev.)	1332
Sum of neutrino masses (rev.)	1335
Number of light neutrino types from collider experiments	1341
Neutrinoless double- β decay	1343

Related Reviews in Volume 1

56. Muon anomalous magnetic moment (rev.)	822
57. Muon decay parameters (rev.)	826
58. τ branching fractions (rev.)	829
59. τ -lepton decay parameters (rev.)	832





See key on page 1171

Lepton Particle Listings

e

LEPTONS

e

$$J = \frac{1}{2}$$

e MASS (atomic mass units u)

The primary determination of an electron's mass comes from measuring the ratio of the mass to that of a nucleus, so that the result is obtained in u (atomic mass units). The conversion factor to MeV is more uncertain than the mass of the electron in u; indeed, the recent improvements in the mass determination are not evident when the result is given in MeV. In this datablock we give the result in u, and in the following datablock in MeV.

VALUE (10 ⁻⁶ u)	DOCUMENT ID	TECN	COMMENT
548.579909065 ± 0.000000016	TIESINGA 21	RVUE	2018 CODATA value
• • • We do not use the following data for averages, fits, limits, etc. • • •			
548.579909070 ± 0.000000016	MOHR 16	RVUE	2014 CODATA value
548.57990946 ± 0.000000022	MOHR 12	RVUE	2010 CODATA value
548.57990943 ± 0.000000023	MOHR 08	RVUE	2006 CODATA value
548.57990945 ± 0.000000024	MOHR 05	RVUE	2002 CODATA value
548.5799092 ± 0.00000004	¹ BEIER 02	CNTR	Penning trap
548.5799110 ± 0.00000012	MOHR 99	RVUE	1998 CODATA value
548.5799111 ± 0.00000012	² FARNHAM 95	CNTR	Penning trap
548.579903 ± 0.0000013	COHEN 87	RVUE	1986 CODATA value

¹BEIER 02 compares Larmor frequency of the electron bound in a ¹²C⁵⁺ ion with the cyclotron frequency of a single trapped ¹²C⁵⁺ ion.
²FARNHAM 95 compares cyclotron frequency of trapped electrons with that of a single trapped ¹²C⁶⁺ ion.

e MASS

The mass is known more precisely in u (atomic mass units) than in MeV. The conversion is: 1 u = 931.494 102 42(28) MeV/c² (2018 CODATA value, TIESINGA 21). The conversion error dominates the uncertainty of the masses given below.

VALUE (MeV)	DOCUMENT ID	TECN	COMMENT
0.51099895000 ± 0.00000000015	TIESINGA 21	RVUE	2018 CODATA value
• • • We do not use the following data for averages, fits, limits, etc. • • •			
0.5109989461 ± 0.0000000031	MOHR 16	RVUE	2014 CODATA value
0.510998928 ± 0.000000011	MOHR 12	RVUE	2010 CODATA value
0.510998910 ± 0.000000013	MOHR 08	RVUE	2006 CODATA value
0.510998918 ± 0.000000044	MOHR 05	RVUE	2002 CODATA value
0.510998901 ± 0.000000020	^{1,2} BEIER 02	CNTR	Penning trap
0.510998902 ± 0.000000021	MOHR 99	RVUE	1998 CODATA value
0.510998903 ± 0.000000020	^{1,3} FARNHAM 95	CNTR	Penning trap
0.510998895 ± 0.000000024	¹ COHEN 87	RVUE	1986 CODATA value
0.5110034 ± 0.0000014	COHEN 73	RVUE	1973 CODATA value

¹Converted to MeV using the 1998 CODATA value of the conversion constant, 931.494013 ± 0.000037 MeV/u.
²BEIER 02 compares Larmor frequency of the electron bound in a ¹²C⁵⁺ ion with the cyclotron frequency of a single trapped ¹²C⁵⁺ ion.
³FARNHAM 95 compares cyclotron frequency of trapped electrons with that of a single trapped ¹²C⁶⁺ ion.

$$(m_{e^+} - m_{e^-}) / m_{average}$$

A test of CPT invariance.

VALUE	CL%	DOCUMENT ID	TECN	COMMENT
< 8 × 10⁻⁹	90	¹ FEE 93	CNTR	Positronium spectroscopy
• • • We do not use the following data for averages, fits, limits, etc. • • •				
< 4 × 10 ⁻²³	90	² DOLGOV 14		From photon mass limit
< 4 × 10 ⁻⁸	90	CHU 84	CNTR	Positronium spectroscopy

¹FEE 93 value is obtained under the assumption that the positronium Rydberg constant is exactly half the hydrogen one.
²DOLGOV 14 result is obtained under the assumption that any mass difference between electron and positron would lead to a non-zero photon mass. The PDG 12 limit of 1 × 10⁻¹⁸ eV on the photon mass is in turn used to derive the value quoted here.

$$|q_{e^+} + q_{e^-}|/e$$

A test of CPT invariance. See also similar tests involving the proton.

VALUE	DOCUMENT ID	TECN	COMMENT
< 4 × 10⁻⁸	¹ HUGHES 92	RVUE	
• • • We do not use the following data for averages, fits, limits, etc. • • •			
< 2 × 10 ⁻¹⁸	² SCHAEFER 95	THEO	Vacuum polarization
< 1 × 10 ⁻¹⁸	³ MUELLER 92	THEO	Vacuum polarization

¹HUGHES 92 uses recent measurements of Rydberg-energy and cyclotron-frequency ratios.
²SCHAEFER 95 removes model dependency of MUELLER 92.
³MUELLER 92 argues that an inequality of the charge magnitudes would, through higher-order vacuum polarization, contribute to the net charge of atoms.

e MAGNETIC MOMENT ANOMALY

$$\mu_e/\mu_B - 1 = (g-2)/2$$

VALUE (units 10 ⁻⁶)	DOCUMENT ID	TECN	CHG	COMMENT
1159.65218062 ± 0.00000012	OUR AVERAGE			
1159.65218059 ± 0.00000013	¹ FAN 23	MRS		Single electron
1159.65218073 ± 0.00000028	HANNEKE 08	MRS		Single electron
1159.6521884 ± 0.00000043	VANDYCK 87	MRS	-	Single electron
• • • We do not use the following data for averages, fits, limits, etc. • • •				
1159.65218128 ± 0.00000018	TIESINGA 21	RVUE		2018 CODATA value
1159.65218091 ± 0.00000026	MOHR 16	RVUE		2014 CODATA value
1159.65218076 ± 0.00000027	MOHR 12	RVUE		2010 CODATA value
1159.65218111 ± 0.00000074	² MOHR 08	RVUE		2006 CODATA value
1159.65218085 ± 0.00000076	³ ODOM 06	MRS	-	Single electron
1159.6521859 ± 0.00000038	MOHR 05	RVUE		2002 CODATA value
1159.6521869 ± 0.00000041	MOHR 99	RVUE		1998 CODATA value
1159.652193 ± 0.0000010	COHEN 87	RVUE		1986 CODATA value
1159.6521879 ± 0.00000043	⁴ VANDYCK 87	MRS	+	Single positron

¹FAN 23 report the most accurate measurement of the electron magnetic moment. A one-electron quantum cyclotron is used. We do not propagate at the moment this measurement to the fine structure and other physical constants. When discrepancies in the independent determinations of alpha are resolved, the new measurement uncertainty of 0.13 ppt is available for precise tests for BSM physics.
²MOHR 08 average is dominated by ODOM 06.
³Superseded by HANNEKE 08 per private communication with Gerald Gabrielse.
⁴This VANDYCK 87 result is for a positron. We do not take it into account for the average to avoid the assumption of CPT invariance.

$$(g_{e^+} - g_{e^-}) / g_{average}$$

A test of CPT invariance.

VALUE (units 10 ⁻¹²)	CL%	DOCUMENT ID	TECN	COMMENT
- 0.5 ± 2.1		¹ VANDYCK 87	MRS	Penning trap
• • • We do not use the following data for averages, fits, limits, etc. • • •				
< 12	95	² VASSERMAN 87	CNTR	Assumes $m_{e^+} = m_{e^-}$
22 ± 64		SCHWINBERG 81	MRS	Penning trap

¹VANDYCK 87 measured $(g_-/g_+) - 1$ and we converted it.
²VASSERMAN 87 measured $(g_+ - g_-)/(g-2)$. We multiplied by $(g-2)/g = 1.2 \times 10^{-3}$.

e ELECTRIC DIPOLE MOMENT (d)

A nonzero value is forbidden by both T invariance and P invariance.

VALUE (10 ⁻²⁸ ecm)	CL%	DOCUMENT ID	TECN	COMMENT
< 0.041	90	¹ ROUSSY 23	ESR	electrons in intramolecular electric field
• • • We do not use the following data for averages, fits, limits, etc. • • •				
< 0.11	90	² ANDREEV 18	CNTR	ThO molecules
< 1.3	90	³ CAIRNCROSS 17	ESR	¹⁸⁰ Hf ¹⁹ F molecules
- 5570 ± 7980 ± 120		KIM 15	CNTR	Gd ₃ Ga ₅ O ₁₂ molecules
< 0.87	90	⁴ BARON 14	CNTR	ThO molecules
< 6050	90	⁵ ECKEL 12	CNTR	Eu _{0.5} Ba _{0.5} TiO ₃ molecules
< 10.5	90	⁶ HUDSON 11	NMR	YbF molecules
6.9 ± 7.4		REGAN 02	MRS	205Tl beams
18 ± 12 ± 10		⁷ COMMINS 94	MRS	205Tl beams
- 27 ± 83		⁷ ABDULLAH 90	MRS	205Tl beams
- 1400 ± 2400		CHO 89	NMR	TlF molecules
- 150 ± 550 ± 150		MURTHY 89		Cs, no B field
- 5000 ± 11000		LAMOREAUX 87	NMR	¹⁹⁹ Hg
19000 ± 34000	90	SANDARS 75	MRS	Thallium
7000 ± 22000	90	PLAYER 70	MRS	Xenon
< 30000	90	WEISSKOPF 68	MRS	Cesium

¹ROUSSY 23 gives a measurement corresponding to this limit as $(-1.3 \pm 2.0 \pm 0.6) \times 10^{-30}$ ecm.
²ANDREEV 18 gives a measurement corresponding to this limit as $(4.3 \pm 3.1 \pm 2.6) \times 10^{-30}$ ecm.
³CAIRNCROSS 17 gives a measurement corresponding to this limit as $(0.09 \pm 0.77 \pm 0.17) \times 10^{-28}$ ecm.
⁴BARON 14 gives a measurement corresponding to this limit as $(-0.21 \pm 0.37 \pm 0.25) \times 10^{-28}$ ecm.
⁵ECKEL 12 gives a measurement corresponding to this limit as $(-1.07 \pm 3.06 \pm 1.74) \times 10^{-25}$ ecm.
⁶HUDSON 11 gives a measurement corresponding to this limit as $(-2.4 \pm 5.7 \pm 1.5) \times 10^{-28}$ ecm.
⁷ABDULLAH 90, COMMINS 94, and REGAN 02 use the relativistic enhancement of a valence electron's electric dipole moment in a high-Z atom.

Lepton Particle Listings

e, μ

e^- MEAN LIFE / BRANCHING FRACTION

A test of charge conservation. See the "Note on Testing Charge Conservation and the Pauli Exclusion Principle" following this section in our 1992 edition (Physical Review **D45** S1 (1992), p. VI.10).

Most of these experiments are one of three kinds: Attempts to observe (a) the 255.5 keV gamma ray produced in $e^- \rightarrow \nu_e \gamma$, (b) the (K) shell x-ray produced when an electron decays without additional energy deposit, e.g., $e^- \rightarrow \nu_e \bar{\nu}_e \nu_e$ ("disappearance" experiments), and (c) nuclear de-excitation gamma rays after the electron disappears from an atomic shell and the nucleus is left in an excited state. The last can include both weak boson and photon mediating processes. We use the best $e^- \rightarrow \nu_e \gamma$ limit for the Summary Tables.

Note that we use the mean life rather than the half life, which is often reported.

$e^- \rightarrow \nu_e \gamma$ and astrophysical limits

VALUE (yr)	CL%	DOCUMENT ID	TECN	COMMENT
$>6.6 \times 10^{28}$	90	AGOSTINI 15B	BORX	$e^- \rightarrow \nu \gamma$
$>1.22 \times 10^{26}$	68	¹ KLAPDOR-K... 07	CNTR	$e^- \rightarrow \nu \gamma$
$>4.6 \times 10^{26}$	90	BACK 02	BORX	$e^- \rightarrow \nu \gamma$
$>3.4 \times 10^{26}$	68	BELLI 00B	DAMA	$e^- \rightarrow \nu \gamma$, liquid Xe
$>3.7 \times 10^{25}$	68	AHARONOV 95B	CNTR	$e^- \rightarrow \nu \gamma$
$>2.35 \times 10^{25}$	68	BALYSH 93	CNTR	$e^- \rightarrow \nu \gamma$, ⁷⁶ Ge detector
$>1.5 \times 10^{25}$	68	AVIGNONE 86	CNTR	$e^- \rightarrow \nu \gamma$
$>1 \times 10^{39}$		² ORITO 85	ASTR	Astrophysical argument
$>3 \times 10^{23}$	68	BELLOTTI 83B	CNTR	$e^- \rightarrow \nu \gamma$

¹ The authors of A. Derbin et al, arXiv:0704.2047v1 argue that this limit is overestimated by at least a factor of 5.

² ORITO 85 assumes that electromagnetic forces extend out to large enough distances and that the age of our galaxy is 10^{10} years.

Disappearance and nuclear-de-excitation experiments

VALUE (yr)	CL%	DOCUMENT ID	TECN	COMMENT
$>6.4 \times 10^{24}$	68	¹ BELLI 99B	DAMA	De-excitation of ¹²⁹ Xe
$>1.2 \times 10^{24}$	90	ABGRALL 17	HPGE	Ge K-shell disappearance
$>4.2 \times 10^{24}$	68	BELLI 99	DAMA	Iodine L-shell disappearance
$>2.4 \times 10^{23}$	90	² BELLI 99B	DAMA	De-excitation of ¹²⁷ I (in Nal)
$>4.3 \times 10^{23}$	68	AHARONOV 95B	CNTR	Ge K-shell disappearance
$>2.7 \times 10^{23}$	68	REUSSER 91	CNTR	Ge K-shell disappearance
$>2 \times 10^{22}$	68	BELLOTTI 83B	CNTR	Ge K-shell disappearance

¹ BELLI 99B limit on charge nonconserving e^- capture involving excitation of the 236.1 keV nuclear state of ¹²⁹Xe; the 90% CL limit is 3.7×10^{24} yr. Less stringent limits for other states are also given.

² BELLI 99B limit on charge nonconserving e^- capture involving excitation of the 57.6 keV nuclear state of ¹²⁷I. Less stringent limits for the other states and for the state of ²³Na are also given.

LIMITS ON LEPTON-FLAVOR VIOLATION IN PRODUCTION

Forbidden by lepton family number conservation.

This section was added for the 2008 edition of this Review and is not complete. For a list of further measurements see references in the papers listed below.

$\sigma(e^+ e^- \rightarrow e^\pm \tau^\mp) / \sigma(e^+ e^- \rightarrow \mu^\pm \mu^-)$

VALUE	CL%	DOCUMENT ID	TECN	COMMENT
$<8.9 \times 10^{-6}$	95	AUBERT 07P	BABR	$e^+ e^-$ at $E_{cm} = 10.58$ GeV
$<1.8 \times 10^{-3}$	95	GOMEZ-CAD... 91	MRK2	$e^+ e^-$ at $E_{cm} = 29$ GeV

$\sigma(e^+ e^- \rightarrow \mu^\pm \tau^\mp) / \sigma(e^+ e^- \rightarrow \mu^\pm \mu^-)$

VALUE	CL%	DOCUMENT ID	TECN	COMMENT
$<4.0 \times 10^{-6}$	95	AUBERT 07P	BABR	$e^+ e^-$ at $E_{cm} = 10.58$ GeV
$<6.1 \times 10^{-3}$	95	GOMEZ-CAD... 91	MRK2	$e^+ e^-$ at $E_{cm} = 29$ GeV

e REFERENCES

FAN 23 PRL 130 071801	X. Fan et al.	(HARV, NWES)
ROUSSY 23 SCI 381 46	T.S. Roussy et al.	(COLO)
TIESINGA 21 RMP 93 025010	E. Tiesinga et al.	(NIST)
ANDREEV 18 NAT 562 355	V. Andreev et al.	(ACME Collab.)
ABGRALL 17 PRL 118 161801	N. Abgrall et al.	(MAJORANA Collab.)
CAIRN CROSS 17 PRL 119 153001	W.B. Cairncross et al.	(NIST, COLO)
MOHR 16 RMP 88 035009	P.J. Mohr, D.B. Newell, B.N. Taylor	(NIST)
AGOSTINI 15B PRL 115 231802	M. Agostini et al.	(Borexino Collab.)
KIM 15 PR D91 102004	Y.J. Kim et al.	(IND, YALE, LANL)
BARON 14 SCI 343 269	J. Baron et al.	(ACME Collab.)
DOLGOV 14 PL B732 244	A.D. Dolgov, V.A. Novikov	
ECKEL 12 PRL 109 193003	S. Eckel, A.O. Sushkov, S.K. Lamoreaux	(YALE)
MOHR 12 RMP 84 1527	P.J. Mohr, B.N. Taylor, D.B. Newell	(NIST)
PDG 12 PR D86 010001	J. Beringer et al.	(PDG Collab.)
HUDSON 11 NAT 473 493	J.J. Hudson et al.	(LOIC)
HANNEKE 08 PRL 100 120801	D. Hanneke, S. Fogwell, G. Gabrielse	(HARV)

MOHR 08 RMP 80 633	P.J. Mohr, B.N. Taylor, D.B. Newell	(NIST)
AUBERT 07P PR D75 031103	B. Aubert et al.	(BABAR Collab.)
KLAPDOR-K... 07 PL B644 109	H.V. Klapdor-Kleingrothaus, I.V. Krivosheina, I.V. Titkova	(HARV)
ODOM 06 PRL 97 030801	B. Odom et al.	(NIST)
MOHR 05 RMP 77 1	P.J. Mohr, B.N. Taylor	(NIST)
BACK 02 PL B525 29	H.O. Back et al.	(Borexino/SASSO Collab.)
BEIER 02 PRL 88 011603	T. Beier et al.	
REGAN 02 PRL 88 071805	B.C. Regan et al.	(DAMA Collab.)
BELLI 00B PR D51 117301	P. Belli et al.	(DAMA Collab.)
BELLI 99 PL B460 236	P. Belli et al.	(DAMA Collab.)
BELLI 99B PL B465 315	P. Belli et al.	(DAMA Collab.)
BELLI 99D PR C60 065501	P. Belli et al.	(DAMA Collab.)
MOHR 99 JPCRD 28 1713	P.J. Mohr, B.N. Taylor	(NIST)
Also RMP 72 351	P.J. Mohr, B.N. Taylor	(NIST)
AHARONOV 95B PR D52 3785	Y. Aharonov et al.	(SCUC, PNL, ZARA+)
Also PL B353 168	Y. Aharonov et al.	(SCUC, PNL, ZARA+)
FARNHAM 95 PRL 75 3598	D.L. Farnham, R.S. van Dyck, P.B. Schwinberg	(WASH)
SCHAEFER 95 PR A51 838	A. Schaefer, J. Reinhardt	(FRAN)
COMMINS 94 PR A50 2360	E.D. Commins et al.	
BALYSH 93 PL B298 278	A. Balysh et al.	(KIAE, MPIK, SASSO)
FEI 93 PR A48 192	M.S. Fei et al.	
HUGHES 92 PRL 69 578	R.J. Hughes, B.J. Deutch	(LANL, AARH)
MUELLER 92 PRL 69 3432	B. Muller, M.H. Thoma	(DUKE)
PDG 92 PR D45 51	K. Hikasa et al.	(KEK, LBL, BOST+)
GOMEZ-CAD... 91 PRL 66 1007	J.J. Gomez-Cadenas et al.	(SLAC MARK-2 Collab.)
REUSSER 91 PL B255 143	D. Reusser et al.	(NEUC, CIT, PSI)
ABDULLAH 90 PRL 65 2347	K. Abdullah et al.	(LBL, UCB)
CHO 89 PRL 63 2559	D. Cho, K. Sangster, E.A. Hinds	(YALE)
MURTHY 89 PRL 63 965	S.A. Murthy et al.	(AMHT)
COHEN 87 RMP 59 1121	E.R. Cohen, B.N. Taylor	(RISC, NBS)
LAMOREAUX 87 PRL 59 2275	S.K. Lamoreaux et al.	(WASH)
VANDYCK 87 PRL 59 26	R.S. van Dyck, P.B. Schwinberg, H.G. Dehmelt	(WASH)
VASSERMAN 87 PL B198 302	I.B. Vasserman et al.	(NOVO)
Also PL B187 172	I.B. Vasserman et al.	(NOVO)
AVIGNONE 86 PR D34 97	F.T. Avignone et al.	(PNL, SCUC)
ORITO 85 PRL 54 2457	S. Orto, M. Yoshimura	(TOKY, KEK)
CHU 84 PRL 52 1689	S. Chu, A.P. Mills, J.L. Hall	(BELL, NBS, COLO)
BELLOTTI 83B PL 124B 435	E. Bellotti et al.	(MILA)
SCHWINBERG 81 PRL 47 1679	P.B. Schwinberg, R.S. van Dyck, H.G. Dehmelt	(WASH)
SANDARS 75 PR A11 475	P.G.H. Sandars, D.M. Sternheimer	(OXF, BNL)
COHEN 73 JPCRD 2 664	E.R. Cohen, B.N. Taylor	(RISC, NBS)
PLAYER 70 JP B3 1620	M.A. Player, P.G.H. Sandars	(OXF)
WEISSKOPF 68 PRL 21 1645	M.C. Weisskopf et al.	(BRAN)

μ

$$J = \frac{1}{2}$$

μ MASS (atomic mass units u)

The muon's mass is obtained from the muon-electron mass ratio as determined from the measurement of Zeeman transition frequencies in muonium ($\mu^+ e^-$ atom). Since the electron's mass is most accurately known in u, the muon's mass is also most accurately known in u. The conversion factor to MeV has approximately the same relative uncertainty as the mass of the muon in u. In this datablock we give the result in u, and in the following datablock in MeV.

VALUE (u)	DOCUMENT ID	TECN	COMMENT
$0.1134289259 \pm 0.000000025$	TIESINGA 21	RVUE	2018 CODATA value
$0.1134289257 \pm 0.000000025$	MOHR 16	RVUE	2014 CODATA value
$0.1134289267 \pm 0.000000029$	MOHR 12	RVUE	2010 CODATA value
$0.1134289256 \pm 0.000000029$	MOHR 08	RVUE	2006 CODATA value
$0.1134289264 \pm 0.000000030$	MOHR 05	RVUE	2002 CODATA value
$0.1134289168 \pm 0.000000034$	¹ MOHR 99	RVUE	1998 CODATA value
$0.113428913 \pm 0.000000017$	² COHEN 87	RVUE	1986 CODATA value

¹ MOHR 99 make use of other 1998 CODATA entries below.
² COHEN 87 make use of other 1986 CODATA entries below.

μ MASS

The mass is known more precisely in u (atomic mass units) than in MeV. The conversion is: $1 \text{ u} = 931.494 102 42(28) \text{ MeV}/c^2$ (2018 CODATA value, TIESINGA 21). The conversion error contributes significantly to the uncertainty of the masses given below.

VALUE (MeV)	DOCUMENT ID	TECN	CHG	COMMENT
$105.6583755 \pm 0.0000023$	TIESINGA 21	RVUE		2018 CODATA value
$105.6583745 \pm 0.0000024$	MOHR 16	RVUE		2014 CODATA value
$105.6583715 \pm 0.0000035$	MOHR 12	RVUE		2010 CODATA value
$105.6583668 \pm 0.0000038$	MOHR 08	RVUE		2006 CODATA value
$105.6583692 \pm 0.0000094$	MOHR 05	RVUE		2002 CODATA value
$105.6583568 \pm 0.0000052$	MOHR 99	RVUE		1998 CODATA value
105.658353 ± 0.000016	¹ COHEN 87	RVUE		1986 CODATA value
105.658386 ± 0.000044	² MARIAM 82	CNTR +		
105.65836 ± 0.00026	³ CROWE 72	CNTR		
105.65865 ± 0.00044	⁴ CRANE 71	CNTR		

¹ Converted to MeV using the 1998 CODATA value of the conversion constant, $931.494013 \pm 0.000037 \text{ MeV}/u$.
² MARIAM 82 give $m_\mu/m_e = 206.768259(62)$.
³ CROWE 72 give $m_\mu/m_e = 206.7682(5)$.
⁴ CRANE 71 give $m_\mu/m_e = 206.76878(85)$.

μ MEAN LIFE τ

Measurements with an error $> 0.001 \times 10^{-6}$ s have been omitted.

VALUE (10^{-6} s)	DOCUMENT ID	TECN	CHG	COMMENT
2.1969811 ± 0.0000022 OUR AVERAGE				
2.1969803 ± 0.0000021 ± 0.0000007 ¹	TISHCHENKO 13	CNTR	+	Surface μ^+ at PSI
2.197083 ± 0.000032 ± 0.000015	BARCZYK 08	CNTR	+	Muons from π^+ decay at rest
2.197013 ± 0.000021 ± 0.000011	CHITWOOD 07	CNTR	+	Surface μ^+ at PSI
2.197078 ± 0.000073	BARDIN 84	CNTR	+	
2.197025 ± 0.000155	BARDIN 84	CNTR	-	
2.19695 ± 0.00006	GIOVANNETTI 84	CNTR	+	
2.19711 ± 0.00008	BALANDIN 74	CNTR	+	
2.1973 ± 0.0003	DUCLOS 73	CNTR	+	
• • • We do not use the following data for averages, fits, limits, etc. • • •				
2.1969803 ± 0.0000022	WEBBER 11	CNTR	+	Surface μ^+ at PSI

¹ TISHCHENKO 13 uses 1.6×10^{12} μ^+ events and supersedes WEBBER 11.

$\tau_{\mu^+}/\tau_{\mu^-}$ MEAN LIFE RATIO

A test of CPT invariance.

VALUE	DOCUMENT ID	TECN	COMMENT
1.000024 ± 0.000078	BARDIN 84	CNTR	
• • • We do not use the following data for averages, fits, limits, etc. • • •			
1.0008 ± 0.0010	BAILEY 79	CNTR	Storage ring
1.000 ± 0.001	MEYER 63	CNTR	Mean life μ^+ / μ^-

$(\tau_{\mu^+} - \tau_{\mu^-}) / \tau_{\text{average}}$

A test of CPT invariance. Calculated from the mean-life ratio, above.

VALUE	DOCUMENT ID
$(2 \pm 8) \times 10^{-5}$ OUR EVALUATION	

μ/p MAGNETIC MOMENT RATIO

This ratio is used to obtain a precise value of the muon mass and to reduce experimental muon Larmor frequency measurements to the muon magnetic moment anomaly. Measurements with an error > 0.00001 have been omitted. By convention, the minus sign on this ratio is omitted. CODATA values were fitted using their selection of data, plus other data from multiparameter fits.

VALUE	DOCUMENT ID	TECN	CHG	COMMENT
3.183345142 ± 0.000000071	TIESINGA 21	RVUE		2018 CODATA value
• • • We do not use the following data for averages, fits, limits, etc. • • •				
3.183345142 ± 0.000000071	MOHR 16	RVUE		2014 CODATA value
3.183345107 ± 0.000000084	MOHR 12	RVUE		2010 CODATA value
3.183345137 ± 0.000000085	MOHR 08	RVUE		2006 CODATA value
3.183345118 ± 0.000000089	MOHR 05	RVUE		2002 CODATA value
3.18334513 ± 0.000000039	LIU 99	CNTR	+	HFS in muonium
3.18334539 ± 0.000000010	MOHR 99	RVUE		1998 CODATA value
3.18334547 ± 0.000000047	COHEN 87	RVUE		1986 CODATA value
3.1833441 ± 0.0000017	KLEMP T 82	CNTR	+	Precession strob
3.1833461 ± 0.0000011	MARIAM 82	CNTR	+	HFS splitting
3.1833448 ± 0.0000029	CAMANI 78	CNTR	+	See KLEMP T 82
3.1833403 ± 0.0000044	CASPERSON 77	CNTR	+	HFS splitting
3.1833402 ± 0.0000072	COHEN 73	RVUE		1973 CODATA value
3.1833467 ± 0.0000082	CROWE 72	CNTR	+	Precession phase

See the related review(s):
Muon Anomalous Magnetic Moment

μ MAGNETIC MOMENT ANOMALY

The parity-violating decay of muons in a storage ring is observed. The difference frequency ω_3 between the muon spin precession and the orbital angular frequency ($e/m_\mu c \langle B \rangle$) is measured, as is the free proton NMR frequency ω_p , thus determining the ratio $R = \omega_3 / \omega_p$. Given the magnetic moment ratio $\lambda = \mu_\mu / \mu_p$ (from hyperfine structure in muonium), $(g-2)/2 = R / (\lambda - R)$.

$\mu_\mu / (e\hbar/2m_\mu) - 1 = (g_\mu - 2)/2$

VALUE (units 10^{-10})	DOCUMENT ID	TECN	CHG	COMMENT
11659205.9 ± 2.2	¹ AGUILLARD 23	MUG2	±	Combined FNAL and BNL values
• • • We do not use the following data for averages, fits, limits, etc. • • •				
11659205.5 ± 2.4	² AGUILLARD 23	MUG2	+	Storage ring
11659204.0 ± 5.4	ABI 21	MUG2	+	Storage ring
11659206.1 ± 4.1	³ ABI 21	MUG2	±	Combined FNAL and BNL values
11659208.0 ± 5.4 ± 3.3	BENNETT 06	MUG2	±	Average μ^+ and μ^-

11659208 ± 6	BENNETT 04	MUG2	±	Average μ^+ and μ^-
11659214 ± 8 ± 3	BENNETT 04	MUG2	-	Storage ring
11659203 ± 6 ± 5	BENNETT 04	MUG2	+	Storage ring
11659204 ± 7 ± 5	BENNETT 02	MUG2	+	Storage ring
11659202 ± 14 ± 6	BROWN 01	MUG2	+	Storage ring
11659191 ± 59	BROWN 00	MUG2	+	
11659100 ± 110	⁴ BAILEY 79	CNTR	+	Storage ring
11659360 ± 120	⁴ BAILEY 79	CNTR	-	Storage ring
11659230 ± 85	⁴ BAILEY 79	CNTR	±	Storage ring
11620000 ± 5000	CHARPAK 62	CNTR	+	

¹ AGUILLARD 23 combined their value with the previous independent BNL measurement of BENNETT 06.

² This AGUILLARD 23 value is the combination of all 2018, 2019 and 2020 data, including the ABI 21 value. The new FNAL 2019 and 2020 data alone combined yield $(11659205.7 \pm 2.5) \times 10^{-10}$.

³ ABI 21 combined their value with the previous independent BNL measurement of BENNETT 06. ABI 21 also report that the difference of this combination with the standard model value of $(11659181.0 \pm 4.3) \times 10^{-10}$ (AOYAMA 20) has a significance of 4.2σ .

⁴ BAILEY 79 values recalculated by HUGHES 99 using the COHEN 87 μ/p magnetic moment. The improved MOHR 99 value does not change the result.

$(g_{\mu^+} - g_{\mu^-}) / g_{\text{average}}$

A test of CPT invariance.

VALUE (units 10^{-8})	DOCUMENT ID	TECN
-0.11 ± 0.12	BENNETT 04	MUG2
• • • We do not use the following data for averages, fits, limits, etc. • • •		
-2.6 ± 1.6	BAILEY 79	CNTR

μ ELECTRIC DIPOLE MOMENT (d)

A nonzero value is forbidden by both T invariance and P invariance.

VALUE (10^{-19} ecm)	CL%	DOCUMENT ID	TECN	CHG	COMMENT
< 1.8	95	¹ BENNETT 09	MUG2	±	Storage ring
• • • We do not use the following data for averages, fits, limits, etc. • • •					
< 0.19	90	² EMA 22			theory limit
-0.1 ± 1.0		³ BENNETT 09	MUG2	+	Storage ring
-0.1 ± 0.7		⁴ BENNETT 09	MUG2	-	Storage ring
-3.7 ± 3.4		⁵ BAILEY 78	CNTR	±	Storage ring
8.6 ± 4.5		BAILEY 78	CNTR	+	Storage ring
0.8 ± 4.3		BAILEY 78	CNTR	-	Storage ring

¹ This is the combination of the two BENNETT 09 measurements quoted here separately for μ^+ and μ^- . The result is also presented as a measurement of $(0.0 \pm 0.9) \times 10^{-19}$ e cm.

² EMA 22 determine indirect constraints on $|\mu_{EDM}^\mu|$ from EDM measurements performed on heavy atoms and molecules, based on the muon-loop induced light-by-light CP-odd amplitude.

³ Also reported as the limit of $|d(\mu^+)| < 2.1 \times 10^{-19}$ e cm at 95% CL.

⁴ Also reported as the limit of $|d(\mu^-)| < 1.5 \times 10^{-19}$ e cm at 95% CL.

⁵ This is the combination of the two BAILEY 78 results quoted here separately for μ^+ and μ^- . BAILEY 78 uses the convention $d = 1/2 \cdot (d_{\mu^+} - d_{\mu^-})$ and reports 3.7 ± 3.4 . We convert their result to use the same convention as BENNETT 09.

MUON-ELECTRON CHARGE RATIO ANOMALY $q_{\mu^+}/q_{e^-} - 1$

VALUE	DOCUMENT ID	TECN	CHG	COMMENT
$(1.1 \pm 2.1) \times 10^{-9}$	¹ MEYER 00	CNTR	+	1s-2s muonium interval

¹ MEYER 00 measure the 1s-2s muonium interval, and then interpret the result in terms of muon-electron charge ratio q_{μ^+}/q_{e^-} .

μ^- DECAY MODES

μ^+ modes are charge conjugates of the modes below.

Mode	Fraction (Γ_i/Γ)	Confidence level
Γ_1 $e^- \bar{\nu}_e \nu_\mu$	$\approx 100\%$	
Γ_2 $e^- \bar{\nu}_e \nu_\mu \gamma$	[a] $(6.0 \pm 0.5) \times 10^{-8}$	
Γ_3 $e^- \bar{\nu}_e \nu_\mu e^+ e^-$	[b] $(3.4 \pm 0.4) \times 10^{-5}$	

Lepton Family number (LF) violating modes

Γ_4 $e^- \nu_e \bar{\nu}_\mu$	LF [c] < 1.2	%	90%
Γ_5 $e^- \gamma$	LF	< 4.2	$\times 10^{-13}$
Γ_6 $e^- e^+ e^-$	LF	< 1.0	$\times 10^{-12}$
Γ_7 $e^- 2\gamma$	LF	< 7.2	$\times 10^{-11}$

[a] This only includes events with energy of $e > 45$ MeV and energy of $\gamma > 40$ MeV. Since the $e^- \bar{\nu}_e \nu_\mu$ and $e^- \bar{\nu}_e \nu_\mu \gamma$ modes cannot be clearly separated, we regard the latter mode as a subset of the former.

[b] See the Particle Listings below for the energy limits used in this measurement.

[c] A test of additive vs. multiplicative lepton family number conservation.

Lepton Particle Listings

 μ μ^- BRANCHING RATIOS $\Gamma(e^- \bar{\nu}_e \nu_\mu \gamma) / \Gamma_{\text{total}}$ Γ_2 / Γ

VALUE	EVTs	DOCUMENT ID	TECN	CHG	COMMENT
$(6.03 \pm 0.14 \pm 0.53) \times 10^{-8}$	13k	¹ BALDINI	16A	SPEC	γ KE > 40 MeV
••• We do not use the following data for averages, fits, limits, etc. •••					
$(3.3 \pm 1.3) \times 10^{-3}$	862	BOGART	67	CNTR	γ KE > 14.5 MeV
$(1.4 \pm 0.4) \times 10^{-2}$		CRITTENDEN	61	CNTR	γ KE > 20 MeV
		CRITTENDEN	61	CNTR	γ KE > 10 MeV
	27	ASHKIN	59	CNTR	

¹BALDINI 16 measurement refers to $\mu^+ \rightarrow e^+ \nu \bar{\nu} \gamma$ decay and requires energy of $e^+ > 45$ MeV and energy $\gamma > 40$ MeV.

 $\Gamma(e^- \bar{\nu}_e \nu_\mu e^+) / \Gamma_{\text{total}}$ Γ_3 / Γ

VALUE (units 10^{-5})	EVTs	DOCUMENT ID	TECN	CHG	COMMENT
$3.4 \pm 0.2 \pm 0.3$	7443	¹ BERTL	85	SPEC	+ SINDRUM
••• We do not use the following data for averages, fits, limits, etc. •••					
2.2 ± 1.5	7	² CRITTENDEN	61	HLBC	+ $E(e^+ e^-) > 10$ MeV
2	1	³ GUREVICH	60	EMUL	+
1.5 ± 1.0	3	⁴ LEE	59	HBC	+

¹BERTL 85 has transverse momentum cut $p_T > 17$ MeV/c. Systematic error was increased by us.

²CRITTENDEN 61 count only those decays where total energy of either (e^+ , e^-) combination is > 10 MeV.

³GUREVICH 60 interpret their event as either virtual or real photon conversion. e^+ and e^- energies not measured.

⁴In the three LEE 59 events, the sum of energies $E(e^+) + E(e^-) + E(e^+)$ was 51 MeV, 55 MeV, and 33 MeV.

 $\Gamma(e^- \nu_e \bar{\nu}_\mu) / \Gamma_{\text{total}}$ Γ_4 / Γ

Forbidden by the additive conservation law for lepton family number. A multiplicative law predicts this branching ratio to be 1/2. For a review see NEMETHY 81.

VALUE	CL%	DOCUMENT ID	TECN	CHG	COMMENT
< 0.012	90	¹ FREEDMAN	93	CNTR	+ ν oscillation search
••• We do not use the following data for averages, fits, limits, etc. •••					
< 0.018	90	KRAKAUER	91B	CALO	+
< 0.05	90	² BERGSMA	83	CALO	$\bar{\nu}_\mu e \rightarrow \mu^- \bar{\nu}_e$
< 0.09	90	JONKER	80	CALO	See BERGSMA 83
-0.001 ± 0.061		WILLIS	80	CNTR	+
0.13 ± 0.15		BLIETSCHAU	78	HLBC	\pm Avg. of 4 values
< 0.25	90	EICHTEN	73	HLBC	+

¹FREEDMAN 93 limit on $\bar{\nu}_e$ observation is here interpreted as a limit on lepton family number violation.

²BERGSMA 83 gives a limit on the inverse muon decay cross-section ratio $\sigma(\bar{\nu}_\mu e^- \rightarrow \mu^- \bar{\nu}_e) / \sigma(\nu_\mu e^- \rightarrow \mu^- \nu_e)$, which is essentially equivalent to $\Gamma(e^- \nu_e \bar{\nu}_\mu) / \Gamma_{\text{total}}$ for small values like that quoted.

 $\Gamma(e^- \gamma) / \Gamma_{\text{total}}$ Γ_5 / Γ

Forbidden by lepton family number conservation.

VALUE (units 10^{-11})	CL%	DOCUMENT ID	TECN	CHG	COMMENT
< 0.042	90	BALDINI	16	SPEC	+ MEG at PSI
••• We do not use the following data for averages, fits, limits, etc. •••					
< 0.057	90	ADAM	13B	SPEC	+ MEG at PSI
< 0.24	90	ADAM	11	SPEC	+ MEG at PSI
< 2.8	90	ADAM	10	SPEC	+ MEG at PSI
< 1.2	90	AHMED	02	SPEC	+ MEGA
< 1.2	90	BROOKS	99	SPEC	+ LAMPF
< 4.9	90	BOLTON	88	CBOX	+ LAMPF
< 100	90	AZUELOS	83	CNTR	+ TRIUMF
< 17	90	KINNISON	82	SPEC	+ LAMPF
< 100	90	SCHAAF	80	ELEC	+ SIN

 $\Gamma(e^- e^+ e^-) / \Gamma_{\text{total}}$ Γ_6 / Γ

Forbidden by lepton family number conservation.

VALUE (units 10^{-12})	CL%	DOCUMENT ID	TECN	CHG	COMMENT
< 1.0	90	¹ BELLEGARDT	88	SPEC	+ SINDRUM
••• We do not use the following data for averages, fits, limits, etc. •••					
< 36	90	BARANOV	91	SPEC	+ ARES
< 35	90	BOLTON	88	CBOX	+ LAMPF
< 2.4	90	¹ BERTL	85	SPEC	+ SINDRUM
< 160	90	¹ BERTL	84	SPEC	+ SINDRUM
< 130	90	¹ BOLTON	84	CNTR	+ LAMPF

¹These experiments assume a constant matrix element.

 $\Gamma(e^- 2\gamma) / \Gamma_{\text{total}}$ Γ_7 / Γ

Forbidden by lepton family number conservation.

VALUE (units 10^{-11})	CL%	DOCUMENT ID	TECN	CHG	COMMENT
< 7.2	90	BOLTON	88	CBOX	+ LAMPF
••• We do not use the following data for averages, fits, limits, etc. •••					
< 1	90	¹ BALDINI	20	MEG	PSI
< 840	90	² AZUELOS	83	CNTR	+ TRIUMF
< 5000	90	³ BOWMAN	78	CNTR	DEPOMMIER 77 data

¹BALDINI 20 uses 7.5×10^{14} stopped muons to obtain limits on $\mu \rightarrow eX$ decay mediated by a new light particle X with lifetimes < 40 ps, which decays to $\gamma\gamma$ for X -mass ranges 20–45 MeV. The limit of the order $< 10^{-11}$ at 90% CL is for the mass range 20–30 MeV.

²AZUELOS 83 uses the phase space distribution of BOWMAN 78.

³BOWMAN 78 assumes an interaction Lagrangian local on the scale of the inverse μ mass.

LIMIT ON $\mu^- \rightarrow e^-$ CONVERSION

Forbidden by lepton family number conservation.

 $\sigma(\mu^- {}^{32}\text{S} \rightarrow e^- {}^{32}\text{S}) / \sigma(\mu^- {}^{32}\text{S} \rightarrow \nu_\mu {}^{32}\text{P}^*)$

VALUE	CL%	DOCUMENT ID	TECN	COMMENT
$< 7 \times 10^{-11}$	90	BADERT...	80	STRC SIN
••• We do not use the following data for averages, fits, limits, etc. •••				
$< 4 \times 10^{-10}$	90	BADERT...	77	STRC SIN

 $\sigma(\mu^- \text{Cu} \rightarrow e^- \text{Cu}) / \sigma(\mu^- \text{Cu} \rightarrow \text{capture})$

VALUE	CL%	DOCUMENT ID	TECN	COMMENT
$< 1.6 \times 10^{-8}$	90	BRYMAN	72	SPEC

 $\sigma(\mu^- \text{Ti} \rightarrow e^- \text{Ti}) / \sigma(\mu^- \text{Ti} \rightarrow \text{capture})$

VALUE	CL%	DOCUMENT ID	TECN	COMMENT
$< 4.3 \times 10^{-12}$	90	¹ DOHMEN	93	SPEC SINDRUM II
••• We do not use the following data for averages, fits, limits, etc. •••				
$< 4.6 \times 10^{-12}$	90	AHMAD	88	TPC TRIUMF
$< 1.6 \times 10^{-11}$	90	BRYMAN	85	TPC TRIUMF

¹DOHMEN 93 assumes $\mu^- \rightarrow e^-$ conversion leaves the nucleus in its ground state, a process enhanced by coherence and expected to dominate.

 $\sigma(\mu^- \text{Pb} \rightarrow e^- \text{Pb}) / \sigma(\mu^- \text{Pb} \rightarrow \text{capture})$

VALUE	CL%	DOCUMENT ID	TECN	COMMENT
$< 4.6 \times 10^{-11}$	90	HONECKER	96	SPEC SINDRUM II
••• We do not use the following data for averages, fits, limits, etc. •••				
$< 4.9 \times 10^{-10}$	90	AHMAD	88	TPC TRIUMF

 $\sigma(\mu^- \text{Au} \rightarrow e^- \text{Au}) / \sigma(\mu^- \text{Au} \rightarrow \text{capture})$

VALUE	CL%	DOCUMENT ID	TECN	CHG	COMMENT
$< 7 \times 10^{-13}$	90	BERTL	06	SPEC	– SINDRUM II

LIMIT ON $\mu^- \rightarrow e^+$ CONVERSION

Forbidden by total lepton number conservation.

 $\sigma(\mu^- {}^{32}\text{S} \rightarrow e^+ {}^{32}\text{Si}^*) / \sigma(\mu^- {}^{32}\text{S} \rightarrow \nu_\mu {}^{32}\text{P}^*)$

VALUE	CL%	DOCUMENT ID	TECN	COMMENT
$< 9 \times 10^{-10}$	90	BADERT...	80	STRC SIN
••• We do not use the following data for averages, fits, limits, etc. •••				
$< 1.5 \times 10^{-9}$	90	BADERT...	78	STRC SIN

 $\sigma(\mu^- {}^{127}\text{I} \rightarrow e^+ {}^{127}\text{Sb}^*) / \sigma(\mu^- {}^{127}\text{I} \rightarrow \text{anything})$

VALUE	CL%	DOCUMENT ID	TECN	COMMENT
$< 3 \times 10^{-10}$	90	¹ ABELA	80	CNTR Radiochemical tech.

¹ABELA 80 is upper limit for $\mu^- e^+$ conversion leading to particle-stable states of ${}^{127}\text{Sb}$. Limit for total conversion rate is higher by a factor less than 4 (G. Backenstoss, private communication).

 $\sigma(\mu^- \text{Cu} \rightarrow e^+ \text{Co}) / \sigma(\mu^- \text{Cu} \rightarrow \nu_\mu \text{Ni})$

VALUE	CL%	DOCUMENT ID	TECN	COMMENT
$< 2.6 \times 10^{-8}$	90	BRYMAN	72	SPEC
$< 2.2 \times 10^{-7}$	90	CONFORTO	62	OSPK

 $\sigma(\mu^- \text{Ti} \rightarrow e^+ \text{Ca}) / \sigma(\mu^- \text{Ti} \rightarrow \text{capture})$

VALUE	CL%	EVTs	DOCUMENT ID	TECN	CHG	COMMENT
$< 3.6 \times 10^{-11}$	90	1	^{1,2} KAULARD	98	SPEC	– SINDRUM II
••• We do not use the following data for averages, fits, limits, etc. •••						
$< 1.7 \times 10^{-12}$	90	1	^{2,3} KAULARD	98	SPEC	– SINDRUM II
$< 4.3 \times 10^{-12}$	90		³ DOHMEN	93	SPEC	SINDRUM II
$< 8.9 \times 10^{-11}$	90		¹ DOHMEN	93	SPEC	SINDRUM II
$< 1.7 \times 10^{-10}$	90		⁴ AHMAD	88	TPC	TRIUMF

¹This limit assumes a giant resonance excitation of the daughter Ca nucleus (mean energy and width both 20 MeV).

²KAULARD 98 obtained these same limits using the unified classical analysis of FELDMAN 98.

³This limit assumes the daughter Ca nucleus is left in the ground state. However, the probability of this is unknown.

⁴Assuming a giant-resonance-excitation model.

LIMIT ON MUONIUM \rightarrow ANTIMUONIUM CONVERSION

Forbidden by lepton family number conservation.

$R_g = G_C / G_F$

The effective Lagrangian for the $\mu^+ e^- \rightarrow \mu^- e^+$ conversion is assumed to be

$\mathcal{L} = 2^{-1/2} G_C [\bar{\psi}_\mu \gamma_\lambda (1 - \gamma_5) \psi_e] [\bar{\psi}_\mu \gamma_\lambda (1 - \gamma_5) \psi_e] + \text{h.c.}$

The experimental result is then an upper limit on G_C/G_F , where G_F is the Fermi coupling constant.

VALUE	CL%	EVTS	DOCUMENT ID	TECN	CHG	COMMENT
< 0.0030	90	1	1 WILLMANN	99	SPEC +	μ^+ at 26 GeV/c
< 0.14	90	1	2 GORDEEV	97	SPEC +	JINR phasotron
< 0.018	90	0	3 ABELA	96	SPEC +	μ^+ at 24 MeV
< 6.9	90		NI	93	CBOX	LAMPF
< 0.16	90		MATTHIAS	91	SPEC	LAMPF
< 0.29	90		HUBER	90b	CNTR	TRIUMF
<20	95		BEER	86	CNTR	TRIUMF
<42	95		MARSHALL	82	CNTR	

- • • We do not use the following data for averages, fits, limits, etc. • • •
- 1 WILLMANN 99 quote both probability $P_{MM} < 8.3 \times 10^{-11}$ at 90%CL in a 0.1 T field and $R_g = G_C/G_F$.
- 2 GORDEEV 97 quote limits on both $f = G_{MM}/G_F$ and the probability $W_{MM} < 4.7 \times 10^{-7}$ (90% CL).
- 3 ABELA 96 quote both probability $P_{MM} < 8 \times 10^{-9}$ at 90% CL and $R_g = G_C/G_F$.

See the related review(s):
Muon Decay Parameters

μ DECAY PARAMETERS

ρ PARAMETER

(V-A) theory predicts $\rho = 0.75$.

VALUE	CL%	EVTS	DOCUMENT ID	TECN	CHG	COMMENT
0.74979 ± 0.00026 OUR AVERAGE						
0.74977 ± 0.00012 ± 0.00023			1 BAYES	11	TWST +	Surface μ^+
0.7518 ± 0.0026			DERENZO	69	RVUE	
0.75014 ± 0.00017 ± 0.00045			2 MACDONALD	08	TWST +	Surface μ^+
0.75080 ± 0.00032 ± 0.00100	6G		3 MUSSER	05	TWST +	Surface μ^+
0.72 ± 0.06 ± 0.08			AMORUSO	04	ICAR	Liquid Ar TPC
0.762 ± 0.008		170k	4 FRYBERGER	68	ASPK +	25-53 MeV e^+
0.760 ± 0.009		280k	4 SHERWOOD	67	ASPK +	25-53 MeV e^+
0.7503 ± 0.0026		800k	4 PEOPLES	66	ASPK +	20-53 MeV e^+

- • • We do not use the following data for averages, fits, limits, etc. • • •
- 1 The quoted systematic error includes a contribution of 0.00013 (added in quadrature) from uncertainties on radiative corrections and on the Michel parameter η .
- 2 The quoted systematic error includes a contribution of 0.00011 (added in quadrature) from the dependence on the Michel parameter η .
- 3 The quoted systematic error includes a contribution of 0.00023 (added in quadrature) from the dependence on the Michel parameter η .
- 4 η constrained = 0. These values incorporated into a two parameter fit to ρ and η by DERENZO 69.

η PARAMETER

(V-A) theory predicts $\eta = 0$.

VALUE	CL%	EVTS	DOCUMENT ID	TECN	CHG	COMMENT
0.057 ± 0.034 OUR AVERAGE						
0.071 ± 0.037 ± 0.005		30M	DANNEBERG	05	CNTR +	7-53 MeV e^+
0.011 ± 0.081 ± 0.026		5.3M	1 BURKARD	85b	CNTR +	9-53 MeV e^+
-0.12 ± 0.21		6346	DERENZO	69	HBC +	1.6-6.8 MeV e^+
-0.0021 ± 0.0070 ± 0.0010		30M	2 DANNEBERG	05	CNTR +	7-53 MeV e^+
-0.012 ± 0.015 ± 0.003		5.3M	2 BURKARD	85b	CNTR +	9-53 MeV e^+
-0.007 ± 0.013		5.3M	3 BURKARD	85b	FIT +	9-53 MeV e^+
-0.7 ± 0.5		170k	4 FRYBERGER	68	ASPK +	25-53 MeV e^+
-0.7 ± 0.6		280k	4 SHERWOOD	67	ASPK +	25-53 MeV e^+
0.05 ± 0.5		800k	4 PEOPLES	66	ASPK +	20-53 MeV e^+
-2.0 ± 0.9		9213	5 PLANO	60	HBC +	Whole spectrum

- • • We do not use the following data for averages, fits, limits, etc. • • •
- 1 Previously we used the global fit result from BURKARD 85b in OUR AVERAGE, we now only include their actual measurement.
- 2 $\alpha = \alpha' = 0$ assumed.
- 3 Global fit to all measured parameters. The fit correlation coefficients are given in BURKARD 85b.
- 4 ρ constrained = 0.75.
- 5 Two parameter fit to ρ and η ; PLANO 60 discounts value for η .

δ PARAMETER

(V-A) theory predicts $\delta = 0.75$.

VALUE	CL%	EVTS	DOCUMENT ID	TECN	CHG	COMMENT
0.75047 ± 0.00034 OUR AVERAGE						
0.75049 ± 0.00021 ± 0.00027			1 BAYES	11	TWST +	Surface μ^+
0.7486 ± 0.0026 ± 0.0028			2 BALKE	88	SPEC +	Surface μ^+

- • • We do not use the following data for averages, fits, limits, etc. • • •

0.75067 ± 0.00030 ± 0.00067			MACDONALD	08	TWST +	Surface μ^+
0.74964 ± 0.00066 ± 0.00112	6G		GAPONENKO	05	TWST +	Surface μ^+
0.752 ± 0.009		490k	3 VOSSLER	69		
0.782 ± 0.031			FRYBERGER	68	ASPK +	25-53 MeV e^+
0.78 ± 0.05		8354	KRUGER	61		
			PLANO	60	HBC +	Whole spectrum

- 1 The quoted systematic error includes a contribution of 0.00006 (added in quadrature) from uncertainties on radiative corrections and on the Michel parameter η .
- 2 BALKE 88 uses $\rho = 0.752 \pm 0.003$.
- 3 VOSSLER 69 has measured the asymmetry below 10 MeV. See comments about radiative corrections in VOSSLER 69.

[(ξ PARAMETER) \times (μ LONGITUDINAL POLARIZATION)]

(V-A) theory predicts $\xi = 1$, longitudinal polarization = 1.

VALUE	CL%	EVTS	DOCUMENT ID	TECN	CHG	COMMENT
1.0009 ± 0.0016 OUR AVERAGE						
1.00084 ± 0.00029 ± 0.00165			BUENO	11	TWST	Surface μ^+ beam
1.0027 ± 0.0079 ± 0.0030			BELTRAMI	87	CNTR	SIN, π decay in flight
1.0003 ± 0.0006 ± 0.0038			JAMIESON	06	TWST +	surface μ^+ beam
1.0013 ± 0.0030 ± 0.0053			1 IMAZATO	92	SPEC +	$K^+ \rightarrow \mu^+ \nu_\mu$
0.975 ± 0.015			AKHMANOV	68	EMUL	140 kG
0.975 ± 0.030			GUREVICH	64	EMUL	See AKHMANOV 68
0.903 ± 0.027			2 ALI-ZADE	61	EMUL +	27 kG
0.93 ± 0.06			PLANO	60	HBC +	8.8 kG
0.97 ± 0.05			BARDON	59	CNTR	Bromoform target

- • • We do not use the following data for averages, fits, limits, etc. • • •
- 1 The corresponding 90% confidence limit from IMAZATO 92 is $|\xi P_\mu| > 0.990$. This measurement is of K^+ decay, not π^+ decay, so we do not include it in an average, nor do we yet set up a separate data block for K results.
- 2 Depolarization by medium not known sufficiently well.

$\xi \times (\mu$ LONGITUDINAL POLARIZATION) $\times \delta / \rho$

VALUE	CL%	EVTS	DOCUMENT ID	TECN	CHG	COMMENT
1.00179 ± 0.00156 OUR AVERAGE						
1.00179 ± 0.00156 ± 0.00071			1 BAYES	11	TWST +	Surface μ^+ beam
>0.99682	90		2 JODIDIO	86	SPEC +	TRIUMF
>0.9966	90		3 STOKER	85	SPEC +	μ -spin rotation
>0.9959	90		CARR	83	SPEC +	11 kG

- • • We do not use the following data for averages, fits, limits, etc. • • •
- 1 BAYES 11 obtains the limit > 0.99909 (90% CL) with the constraint that $\xi \times (\mu$ LONGITUDINAL POLARIZATION) $\times \delta / \rho \leq 1.0$.
- 2 JODIDIO 86 includes data from CARR 83 and STOKER 85. The value here is from the erratum.
- 3 STOKER 85 find $(\xi P_\mu \delta / \rho) > 0.9955$ and > 0.9966 , where the first limit is from new μ spin-rotation data and the second is from combination with CARR 83 data. In V-A theory, $(\delta / \rho) = 1.0$.

$\xi' =$ LONGITUDINAL POLARIZATION OF e^+

(V-A) theory predicts the longitudinal polarization = ± 1 for e^\pm , respectively. We have flipped the sign for e^- so our programs can average.

VALUE	CL%	EVTS	DOCUMENT ID	TECN	CHG	COMMENT
1.00 ± 0.04 OUR AVERAGE						
0.998 ± 0.045		1M	BURKARD	85	CNTR +	Bhabha + annihil
0.89 ± 0.28		29k	SCHWARTZ	67	OSPK -	Moller scattering
0.94 ± 0.38			BLOOM	64	CNTR +	Brems. transmiss.
1.04 ± 0.18			DUCLOS	64	CNTR +	Bhabha scattering
1.05 ± 0.30			BUHLER	63	CNTR +	Annihilation

ξ'' PARAMETER

VALUE	CL%	EVTS	DOCUMENT ID	TECN	CHG	COMMENT
0.98 ± 0.04 OUR AVERAGE						
0.981 ± 0.045 ± 0.003		3.87M	PRIEELS	14	CNTR +	Bhabha + annihil
0.65 ± 0.36		326k	1 BURKARD	85	CNTR +	Bhabha + annihil

- 1 BURKARD 85 measure $(\xi'' - \xi \xi') / \xi$ and ξ' and set $\xi = 1$.

TRANSVERSE e^+ POLARIZATION IN PLANE OF μ SPIN, e^+ MOMENTUM

VALUE (units 10^{-3})	CL%	EVTS	DOCUMENT ID	TECN	CHG	COMMENT
7 ± 8 OUR AVERAGE						
6.3 ± 7.7 ± 3.4		30M	DANNEBERG	05	CNTR +	7-53 MeV e^+
16 ± 21 ± 10		5.3M	BURKARD	85b	CNTR +	Annihil 9-53 MeV

TRANSVERSE e^+ POLARIZATION NORMAL TO PLANE OF μ SPIN, e^+ MOMENTUM

Zero if T invariance holds.

VALUE (units 10^{-3})	CL%	EVTS	DOCUMENT ID	TECN	CHG	COMMENT
-2 ± 8 OUR AVERAGE						
-3.7 ± 7.7 ± 3.4		30M	DANNEBERG	05	CNTR +	7-53 MeV e^+
7 ± 22 ± 7		5.3M	BURKARD	85b	CNTR +	Annihil 9-53 MeV

Lepton Particle Listings

μ

α/A

VALUE (units 10^{-3})	EVTS	DOCUMENT ID	TECN	CHG	COMMENT
0.4 ± 4.3		¹ BURKARD	85B	FIT	
••• We do not use the following data for averages, fits, limits, etc. •••					
15 ± 50 ± 14	5.3M	BURKARD	85B	CNTR +	9–53 MeV e ⁺
¹ Global fit to all measured parameters. Correlation coefficients are given in BURKARD 85B.					

α'/A

Zero if T invariance holds.

VALUE (units 10^{-3})	EVTS	DOCUMENT ID	TECN	CHG	COMMENT
-10 ± 20 OUR AVERAGE					
-3.4 ± 21.3 ± 4.9	30M	DANNEBERG	05	CNTR +	7–53 MeV e ⁺
-47 ± 50 ± 14	5.3M	¹ BURKARD	85B	CNTR +	9–53 MeV e ⁺
••• We do not use the following data for averages, fits, limits, etc. •••					
-0.2 ± 4.3		² BURKARD	85B	FIT	
¹ Previously we used the global fit result from BURKARD 85B in OUR AVERAGE, we now only include their actual measurement. BURKARD 85B measure e ⁺ polarizations P_{T_1} and P_{T_2} versus e ⁺ energy.					
² Global fit to all measured parameters. The fit correlation coefficients are given in BURKARD 85B.					

β/A

VALUE (units 10^{-3})	EVTS	DOCUMENT ID	TECN	CHG	COMMENT
3.9 ± 6.2		¹ BURKARD	85B	FIT	
••• We do not use the following data for averages, fits, limits, etc. •••					
2 ± 17 ± 6	5.3M	BURKARD	85B	CNTR +	9–53 MeV e ⁺
¹ Global fit to all measured parameters. The fit correlation coefficients are given in BURKARD 85B.					

β'/A

Zero if T invariance holds.

VALUE (units 10^{-3})	EVTS	DOCUMENT ID	TECN	CHG	COMMENT
2 ± 7 OUR AVERAGE					
-0.5 ± 7.8 ± 1.8	30M	DANNEBERG	05	CNTR +	7–53 MeV e ⁺
17 ± 17 ± 6	5.3M	¹ BURKARD	85B	CNTR +	9–53 MeV e ⁺
••• We do not use the following data for averages, fits, limits, etc. •••					
-1.3 ± 3.5 ± 0.6	30M	² DANNEBERG	05	CNTR +	7–53 MeV e ⁺
1.5 ± 6.3		³ BURKARD	85B	FIT	
¹ Previously we used the global fit result from BURKARD 85B in OUR AVERAGE, we now only include their actual measurement. BURKARD 85B measure e ⁺ polarizations P_{T_1} and P_{T_2} versus e ⁺ energy.					
² $\alpha = \alpha' = 0$ assumed.					
³ Global fit to all measured parameters. The fit correlation coefficients are given in BURKARD 85B.					

a/A

This comes from an alternative parameterization to that used in the Summary Table (see the "Note on Muon Decay Parameters" above).

VALUE (units 10^{-3})	CL%	DOCUMENT ID	TECN	COMMENT
<15.9	90	¹ BURKARD	85B	FIT
¹ Global fit to all measured parameters. Correlation coefficients are given in BURKARD 85B.				

a'/A

This comes from an alternative parameterization to that used in the Summary Table (see the "Note on Muon Decay Parameters" above).

VALUE (units 10^{-3})	DOCUMENT ID	TECN	COMMENT
••• We do not use the following data for averages, fits, limits, etc. •••			
5.3 ± 4.1	¹ BURKARD	85B	FIT
¹ Global fit to all measured parameters. Correlation coefficients are given in BURKARD 85B.			

$(b'+b)/A$

This comes from an alternative parameterization to that used in the Summary Table (see the "Note on Muon Decay Parameters" above).

VALUE (units 10^{-3})	CL%	DOCUMENT ID	TECN	COMMENT
<1.0	90	¹ BURKARD	85B	FIT
¹ Global fit to all measured parameters. Correlation coefficients are given in BURKARD 85B.				

c/A

This comes from an alternative parameterization to that used in the Summary Table (see the "Note on Muon Decay Parameters" above).

VALUE (units 10^{-3})	CL%	DOCUMENT ID	TECN	COMMENT
<6.4	90	¹ BURKARD	85B	FIT
¹ Global fit to all measured parameters. Correlation coefficients are given in BURKARD 85B.				

c'/A

This comes from an alternative parameterization to that used in the Summary Table (see the "Note on Muon Decay Parameters" above).

VALUE (units 10^{-3})	DOCUMENT ID	TECN	COMMENT
••• We do not use the following data for averages, fits, limits, etc. •••			
3.5 ± 2.0	¹ BURKARD	85B	FIT
¹ Global fit to all measured parameters. Correlation coefficients are given in BURKARD 85B.			

$\overline{\eta}$ PARAMETER

($V-A$) theory predicts $\overline{\eta} = 0$. $\overline{\eta}$ affects spectrum of radiative muon decay.

VALUE	DOCUMENT ID	TECN	CHG	COMMENT
0.02 ± 0.08 OUR AVERAGE				
-0.014 ± 0.090	EICHENBER...	84	ELEC +	ρ free
+0.09 ± 0.14	BOGART	67	CNTR +	
••• We do not use the following data for averages, fits, limits, etc. •••				
-0.035 ± 0.098	EICHENBER...	84	ELEC +	$\rho = 0.75$ assumed

μ REFERENCES

AGUILLARD	23	PRL 131 161802	D.P. Aguiard et al.	(Muon g-2 Collab.)
EMA	22	PRL 128 131803	Y. Ema, T. Gao, M. Pospelov	(DESY, MINN)
ABI	21	PRL 126 141801	E. Abi et al.	(Muon g-2 Collab.)
TIESINGA	21	RMP 93 025010	E. Tiesinga et al.	(NIST)
AOYAMA	20	PRPL 887 1	T. Aoyama et al.	
BALDINI	20	EPJ C80 858	A.M. Baldini et al.	(MEG Collab.)
BALDINI	16	EPJ C76 434	A.M. Baldini et al.	(MEG Collab.)
BALDINI	16A	EPJ C76 108	A.M. Baldini et al.	(MEG Collab.)
MOHR	16	RMP 88 035009	P.J. Mohr, D.B. Newell, B.N. Taylor	(NIST)
PRIEELS	14	PR D90 112003	R. Prieels et al.	(LOUV, ETH, PSI+)
ADAM	13B	PRL 110 201801	J. Adam et al.	(MEG Collab.)
TISHCHENKO	13	PR D87 052003	V. Tishchenko et al.	(MuLan Collab.)
MOHR	12	RMP 84 1527	P.J. Mohr, B.N. Taylor, D.B. Newell	(NIST)
ADAM	11	PRL 107 171801	J. Adam et al.	(MEG Collab.)
BAYES	11	PRL 106 041804	R. Bayes et al.	(TWIST Collab.)
Also		PR D85 092013	A. Hillairet et al.	(TWIST Collab.)
BUENO	11	PR D84 032005	J.F. Bueno et al.	(TWIST Collab.)
Also		PR D85 039908 (err.)	J.F. Bueno et al.	(TWIST Collab.)
WEBBER	11	PRL 106 041803	D.M. Webber et al.	(MuLan Collab.)
Also		PRL 106 079901 (err.)	D.M. Webber et al.	(MuLan Collab.)
ADAM	10	NP B834 1	J. Adam et al.	(MEG Collab.)
BENNETT	09	PR D80 052008	G.W. Bennett et al.	(MUG-2 Collab.)
BARCZYK	08	PL B663 172	A. Barczyk et al.	(FAST Collab.)
MACDONALD	08	PR D78 032010	R.P. MacDonald et al.	(TWIST Collab.)
MOHR	08	RMP 80 633	P.J. Mohr, B.N. Taylor, D.B. Newell	(NIST)
CHITWOOD	07	PRL 99 032001	D.B. Chitwood et al.	(MULAN Collab.)
BENNETT	06	PR D73 072003	G.W. Bennett et al.	(MUG-2 Collab.)
BERTL	06	EPJ C47 337	W. Bertl et al.	(SINDRUM II Collab.)
JAMIESON	06	PR D74 072007	B. Jamieson et al.	(TWIST Collab.)
DANNEBERG	05	PRL 94 021802	N. Danneberg et al.	(ETH, JAGL, PSI+)
GAPONENKO	05	PR D71 071101	A. Gaponenko et al.	(TWIST Collab.)
MOHR	05	RMP 77 1	P.J. Mohr, B.N. Taylor	(NIST)
MUSSER	05	PRL 94 101805	J.R. Musser et al.	(TWIST Collab.)
AMORUSO	04	EPJ C33 233	S. Amoroso et al.	(ICARUS Collab.)
BENNETT	04	PRL 92 161802	G.W. Bennett et al.	(Muon(g-2) Collab.)
AHMED	02	PR D65 112002	M. Ahmed et al.	(MEG Collab.)
BENNETT	02	PRL 89 101804	G.W. Bennett et al.	(Muon(g-2) Collab.)
BROWN	01	PRL 86 2227 1	H.N. Brown et al.	(Muon(g-2) Collab.)
BROWN	00	PR D62 091101	H.N. Brown et al.	(BNL/G-2 Collab.)
MEYER	00	PRL 84 1136	V. Meyer et al.	
BROOKS	99	PRL 83 1521	M.L. Brooks et al.	(MEGA/LAMPF Collab.)
HUGHES	99	RMP 71 5133	V.W. Hughes, T. Kinoshita	
LIU	99	PRL 82 711	W. Liu et al.	(LAMPF Collab.)
MOHR	99	JPCRD 28 1713	P.J. Mohr, B.N. Taylor	(NIST)
Also		RMP 72 351	P.J. Mohr, B.N. Taylor	(NIST)
WILLMANN	99	PRL 82 49	L. Willmann et al.	
FELDMAN	97	PR D57 3873	G.J. Feldman, R.D. Cousins	
KAULARD	96	PL B422 334	J. Kaulard et al.	(SINDRUM-II Collab.)
GORDEV	97	PAN 60 1164	V.A. Gordeev et al.	(PNPI)
Translated from YAF 60 1291.				
ABELA	96	PRL 77 1950	R. Abela et al.	(PSI, ZURI, HEIDH, TBI+)
HONECKER	96	PRL 76 200	W. Honecker et al.	(SINDRUM II Collab.)
DOHMEN	93	PL B317 631	C. Dohmen et al.	(PSI SINDRUM-II Collab.)
FREEDMAN	93	PR D47 811	S.J. Freedman et al.	(LAMPF E645 Collab.)
NI	93	PR D48 1376	B. Ni et al.	(LAMPF Crystal-Box Collab.)
IMAZATO	92	PRL 69 877	J. Imazato et al.	(KEK, INUS, TOKY+)
BARANOV	91	SJNP 53 802	V.A. Baranov et al.	(JINR)
Translated from YAF 53 1302.				
KRAKAUER	91B	PL B263 534	D.A. Krakauer et al.	(UMD, UCI, LANL)
MATTHIAS	91	PRL 66 2716	B.E. Matthias et al.	(YALE, HEIDP, WILL+)
Also		PRL 67 932 (err.)	B.E. Matthias et al.	(YALE, HEIDP, WILL+)
HUBER	90B	PR D41 2709	T.M. Huber et al.	(WYOM, VICT, ARIZ+)
AHMAD	88	PR D38 2102	S. Ahmad et al.	(TRIUM, VICT, VPI, BRCO+)
Also		PRL 59 970	S. Ahmad et al.	(TRIUM, VPI, VICT, BRCO+)
BALKE	88	PR D37 587	B. Balke et al.	(LBL, UCB, COLO, NWES+)
BELLEGARDT	88	NP B219 1	U. Bellgardt et al.	(SINDRUM Collab.)
BOLTON	88	PR D38 2077	R.D. Bolton et al.	(LANL, STAN, CHIC+)
Also		PRL 56 2461	R.D. Bolton et al.	(LANL, STAN, CHIC+)
Also		PRL 57 3241	D. Grosnick et al.	(CHIC, LANL, STAN+)
BELTRAMI	87	PL B194 326	I. Beltrami et al.	(ETH, SIN, MAINZ)
COHEN	87	RMP 59 1121	E.R. Cohen, B.N. Taylor	(RISC, NBS)
BEER	86	PRL 57 671	G.A. Beer et al.	(VICT, TRIUM, WYOM)
JODIDIO	86	PR D34 1967	A. Jodidio et al.	(LBL, NWES, TRIUM)
Also		PR D37 237 (err.)	A. Jodidio et al.	(LBL, NWES, TRIUM)
BERTL	85	NP B260 1	W. Bertl et al.	(SINDRUM Collab.)
BRYMAN	85	PRL 55 465	D.A. Bryman et al.	(TRIUM, CNRC, BRCO+)
BURKARD	85	PL 150B 242	H. Burkhardt et al.	(ETH, SIN, MAINZ)
BURKARD	85B	PL 150B 343	H. Burkhardt et al.	(ETH, SIN, MAINZ)
Also		PR D24 2004	F. Corvieve et al.	(ETH, SIN, MAINZ)
Also		PL 129B 260	F. Corvieve et al.	(ETH, SIN, MAINZ)
STOKER	85	PRL 54 1887	D.P. Stoker et al.	(LBL, NWES, TRIUM)
BARDIN	84	PL 137B 135	G. Bardin et al.	(SACL, CERN, BGN, FRI)
BERTL	84	PL 140B 299	W. Bertl et al.	(SINDRUM Collab.)
BOLTON	84	PRL 53 1415	R.D. Bolton et al.	(LANL, CHIC, STAN+)
EICHENBER...	84	NP A412 523	W. Eichenberger, R. Engfer, A. van der Schaff	
GIOVANNETTI	84	PR D29 343	K.L. Giovanetti et al.	(WILL)
AZUELOS	83	PRL 51 164	G. Azuelos et al.	(MONT, TRIUM, BRCO)
Also		PRL 39 1113	P. Depommier et al.	(MONT, BRCO, TRIUM)
BERGSMAS	83	PL 122B 465	F. Bergsma et al.	(CHARM Collab.)
CARR	83	PRL 51 627	J. Carr et al.	(LBL, NWES, TRIUM)
KINNISON	82	PR D25 2846	W.W. Kinnison et al.	(EFI, STAN, LANL)
Also		PRL 42 556	J.D. Bowman et al.	(LASL, EFI, STAN)

See key on page 1171

Lepton Particle Listings

μ, τ

NAME	EXPT	REF	TECN	COMMENT
KLEMP	82	PR D25 652		E. Klempt et al. (MAINZ, ETH)
MARIAM	82	PRL 49 993		F.G. Mariani et al. (YALE, HEIDH, BERN)
MARSHALL	82	PR D25 1174		G.M. Marshall et al. (BRCO)
NEMETHY	81	CNPP 10 147		P. Nemethy, V.W. Hughes (LBL, YALE)
ABELA	80	PL 95B 318		R. Abela et al. (BASL, KARLK, KARLE)
BADERT...	80	LNC 28 401		A. Badertscher et al. (BERN)
JONKER	80	NP A377 406		A. Badertscher et al. (BERN)
SCHAAF	80	NP 93B 203		M. Jonker et al. (CHARM Collab.)
Willis	80	NP A340 249		A. van der Schaaf et al. (ZURI, ETH+)
Willis	80	PL 72B 183		H.P. Povel et al. (ZURI, ETH, SIN)
Willis	80	PRL 44 522		S.E. Willis et al. (YALE, LBL, LASL+)
Bailey	79	PRL 45 1370		S.E. Willis et al. (YALE, LBL, LASL+)
BADERT...	79	NP B150 1		J.M. Bailey (CERN, DARE, MAINZ)
BADERT...	78	PL 79B 371		A. Badertscher et al. (BERN)
Bailey	78	JP G4 345		J.M. Bailey (DARE, BERN, SHEF, MAINZ, RMCS+)
Blietschau	78	NP B150 1		J.M. Bailey (CERN, DARE, MAINZ)
Blietschau	78	NP B133 205		J. Blietschau et al. (Gargamelle Collab.)
Bowman	78	PRL 41 442		J.D. Bowman et al. (LASL, IAS, CMU+)
CAMANI	78	PL 77B 326		M. Camani et al. (ETH, MAINZ)
BADERT...	77	PRL 39 1385		A. Badertscher et al. (BERN)
CASPERSON	77	PRL 38 956		D.E. Casperson et al. (BERN, HEIDH, LASL+)
DEPOMMIER	77	PRL 39 1113		P. Depommier et al. (MONT, BRCO, TRIU+)
BALANDIN	74	JETP 40 811		M.P. Balandin et al. (JINR)
COHEN	73	JPCRD 2 664		E.R. Cohen, B.N. Taylor (RISC, NBS)
DUCLOS	73	PL 47B 491		J. Duclos, A. Magnon, J. Picard (SACL)
EICHTEN	73	PL 46B 281		T. Eichten et al. (Gargamelle Collab.)
BRYMAN	72	PRL 28 1469		D.A. Bryman et al. (VPI)
CROWE	72	PR D5 2145		K.M. Crowe et al. (LBL, WASH)
CRANE	71	PRL 27 474		T. Crane et al. (YALE)
DERENZO	69	PR 181 1854		S.E. Derenzo (EFI)
VOSSLER	69	NC 63A 423		C. Vossler (EFI)
AKHMANOV	68	SJNP 6 230		V.V. Akhmanov et al. (KIAE)
Fryberger	68	PR 166 1379		D. Fryberger (EFI)
BOGART	67	PR 156 1405		E. Bogart et al. (COLU)
SCHWARTZ	67	PR 162 1306		D.M. Schwartz (EFI)
SHERWOOD	67	PR 156 1475		B.A. Sherwood (EFI)
PEOPLES	66	Nevis 147 unpub.		J. Peoples (COLU)
BLOOM	64	PL 8 87		S. Bloom et al. (CERN)
DUCLOS	64	PL 9 62		J. Duclos et al. (CERN)
GUREVICH	64	PL 11 185		I.I. Gurevich et al. (KIAE)
BUHLER	63	PL 7 368		A. Buhler-Broglin et al. (CERN)
MEYER	63	PR 132 2693		S.L. Meyer et al. (COLU)
CHARPAK	62	PL 1 16		G. Charpak et al. (CERN)
CONFORTO	62	NC 26 261		G. Conforto et al. (INFN, ROMA, CERN)
ALI-ZADE	61	JETP 13 313		S.A. Ali-Zade, I.I. Gurevich, B.A. Nikolsky
CRITTENDEN	61	Translated from ZETF 40 452		R.R. Crittenden, W.D. Walker, J. Ballam (WIS C+)
KRUGER	61	PR 121 1823		H. Kruger (LRL)
GUREVICH	60	UCRL 9322 unpub.		H. Kruger (LRL)
PLANO	60	JETP 10 225		I.I. Gurevich, B.A. Nikolsky, L.V. Surkova (ITEP)
ASHKIN	59	PR 119 1400		R.J. Plano (COLU)
BARDON	59	NC 14 1266		J. Ashkin et al. (CERN)
LEE	59	PRL 2 56		M. Bardon, D. Berley, L.M. Lederman (COLU)
LEE	59	PRL 3 55		J. Lee, N.P. Samios (COLU)

τ

$J = \frac{1}{2}$

τ discovery paper was PERL 75. $e^+e^- \rightarrow \tau^+\tau^-$ cross-section threshold behavior and magnitude are consistent with pointlike spin-1/2 Dirac particle. BRANDELIK 78 ruled out pointlike spin-0 or spin-1 particle. FELDMAN 78 ruled out $J = 3/2$. KIRKBY 79 also ruled out $J = \text{integer}$, $J = 3/2$.

τ MASS

VALUE (MeV)	EVTS	DOCUMENT ID	TECN	COMMENT
1776.93 ± 0.09 OUR AVERAGE				
1777.09 ± 0.08 ± 0.11	175 M	¹ ADACHI	23c BELL	190 fb ⁻¹ , $E_{cm}^{ee} = 10.6$ GeV
1776.69 ^{+0.17} / _{-0.19} ± 0.15		² ANASHIN	23A KEDR	(6.7+ 8.5) pb ⁻¹ , $E_{cm}^{ee} = 3.54-3.78$ GeV
1776.91 ± 0.12 ^{+0.10} / _{-0.13}	1171	³ ABLIKIM	14D BES3	23.3 pb ⁻¹ , $E_{cm}^{ee} = 3.54-3.60$ GeV
1776.68 ± 0.12 ± 0.41	682k	¹ AUBERT	09AK BABR	423 fb ⁻¹ , $E_{cm}^{ee} = 10.6$ GeV
1776.61 ± 0.13 ± 0.35		¹ BELOUS	07 BELL	414 fb ⁻¹ , $E_{cm}^{ee} = 10.6$ GeV
1775.1 ± 1.6 ± 1.0	13.3k	⁴ ABBIENDI	00A OPAL	1990-1995 LEP runs
1778.2 ± 0.8 ± 1.2		ANASTASSOV	97 CLEO	$E_{cm}^{ee} = 10.6$ GeV
1776.96 ^{+0.18} / _{-0.21} ± 0.25 ± 0.17	65	⁵ BAI	96 BES	$E_{cm}^{ee} = 3.54-3.57$ GeV
1776.3 ± 2.4 ± 1.4	11k	⁶ ALBRECHT	92M ARG	$E_{cm}^{ee} = 9.4-10.6$ GeV
1783 ⁺³ / ₋₄	692	⁷ BACINO	78B DLCO	$E_{cm}^{ee} = 3.1-7.6$ GeV

••• We do not use the following data for averages, fits, limits, etc. •••

¹ ADACHI 23c, AUBERT 09AK and BELOUS 07 fit τ pseudomass spectrum in $\tau \rightarrow \pi^+\pi^-\nu_\tau$ decays. Result assumes $m_{\nu_\tau} = 0$.

² Previously also reported LEVICHEV 14. Superseeds ANASHIN 07.

³ ABLIKIM 14D fit $\sigma(e^+e^- \rightarrow \tau^+\tau^-)$ at different energies near threshold.

⁴ ABBIENDI 00A fit τ pseudomass spectrum in $\tau \rightarrow \pi^\pm \leq 2\pi^0 \nu_\tau$ and $\tau \rightarrow \pi^\pm \pi^+ \pi^- \leq 1\pi^0 \nu_\tau$ decays. Result assumes $m_{\nu_\tau} = 0$.

⁵ BAI 96 fit $\sigma(e^+e^- \rightarrow \tau^+\tau^-)$ at different energies near threshold.

⁶ ALBRECHT 92M fit τ pseudomass spectrum in $\tau^- \rightarrow 2\pi^-\pi^+ \nu_\tau$ decays. Result assumes $m_{\nu_\tau} = 0$.

⁷ BACINO 78B value comes from $e^\pm X \bar{X}$ threshold. Published mass 1782 MeV increased by 1 MeV using the high precision $\psi(2S)$ mass measurement of ZHOLENTZ 80 to eliminate the absolute SPEAR energy calibration uncertainty.

⁸ BALEST 93 fit spectra of minimum kinematically allowed τ mass in events of the type $e^+e^- \rightarrow \tau^+\tau^- \rightarrow (\pi^+ n \pi^0 \nu_\tau)(\pi^- m \pi^0 \nu_\tau)$ $n \leq 2, m \leq 2, 1 \leq n+m \leq 3$. If $m_{\nu_\tau} \neq 0$, result increases by $(m_{\nu_\tau}^2 / 1100 \text{ MeV})$.

⁹ BAI 92 fit $\sigma(e^+e^- \rightarrow \tau^+\tau^-)$ near threshold using $e\mu$ events.

$(m_{\tau^+} - m_{\tau^-}) / m_{\text{average}}$

A test of CPT invariance.

VALUE	CL%	DOCUMENT ID	TECN	COMMENT
< 2.8 × 10⁻⁴	90	BELOUS	07 BELL	414 fb ⁻¹ , $E_{cm}^{ee} = 10.6$ GeV
••• We do not use the following data for averages, fits, limits, etc. •••				
< 5.5 × 10 ⁻⁴	90	¹ AUBERT	09AK BABR	423 fb ⁻¹ , $E_{cm}^{ee} = 10.6$ GeV
< 3.0 × 10 ⁻³	90	ABBIENDI	00A OPAL	1990-1995 LEP runs
¹ AUBERT 09AK quote both the listed upper limit and $(m_{\tau^+} - m_{\tau^-}) / m_{\text{average}} = (-3.4 \pm 1.3 \pm 0.3) \times 10^{-4}$.				

τ MEAN LIFE

VALUE (10 ⁻¹⁵ s)	EVTS	DOCUMENT ID	TECN	COMMENT
290.3 ± 0.5 OUR AVERAGE				
290.17 ± 0.53 ± 0.33	1.1M	BELOUS	14 BELL	711 fb ⁻¹ , $E_{cm}^{ee} = 10.6$ GeV
290.9 ± 1.4 ± 1.0		ABDALLAH	04T DLPH	1991-1995 LEP runs
293.2 ± 2.0 ± 1.5		ACCIARRI	00B L3	1991-1995 LEP runs
290.1 ± 1.5 ± 1.1		BARATE	97R ALEP	1989-1994 LEP runs
289.2 ± 1.7 ± 1.2		ALEXANDER	96E OPAL	1990-1994 LEP runs
289.0 ± 2.8 ± 4.0	57.4k	BALEST	96 CLEO	$E_{cm}^{ee} = 10.6$ GeV
••• We do not use the following data for averages, fits, limits, etc. •••				
291.2 ± 2.0 ± 1.2		BARATE	97I ALEP	Repl. by BARATE 97R
291.4 ± 3.0		ABREU	96B DLPH	Repl. by ABDALLAH 04T
290.1 ± 4.0	34k	ACCIARRI	96K L3	Repl. by ACCIARRI 00B
297 ± 9 ± 5	1671	ABE	95Y SLD	1992-1993 SLC runs
304 ± 14 ± 7	4100	BATTLE	92 CLEO	$E_{cm}^{ee} = 10.6$ GeV
301 ± 29	3780	KLEINWORT	89 JADE	$E_{cm}^{ee} = 35-46$ GeV
288 ± 16 ± 17	807	AMIDEI	88 MRK2	$E_{cm}^{ee} = 29$ GeV
306 ± 20 ± 14	695	BRAUNSCH...	88C TASS	$E_{cm}^{ee} = 36$ GeV
299 ± 15 ± 10	1311	ABACHI	87C HRS	$E_{cm}^{ee} = 29$ GeV
295 ± 14 ± 11	5696	ALBRECHT	87P ARG	$E_{cm}^{ee} = 9.3-10.6$ GeV
309 ± 17 ± 7	3788	BAND	87B MAC	$E_{cm}^{ee} = 29$ GeV
325 ± 14 ± 18	8470	BEBEK	87C CLEO	$E_{cm}^{ee} = 10.5$ GeV
460 ± 190	102	FELDMAN	82 MRK2	$E_{cm}^{ee} = 29$ GeV

$(\tau_{\tau^+} - \tau_{\tau^-}) / \tau_{\text{average}}$

Test of CPT invariance.

VALUE	CL%	DOCUMENT ID	TECN	COMMENT
< 7.0 × 10⁻³	90	¹ BELOUS	14 BELL	711 fb ⁻¹ , $E_{cm}^{ee} = 10.6$ GeV
¹ BELOUS 14 quote limit on the absolute value of the relative lifetime difference.				

τ MAGNETIC MOMENT ANOMALY

The g_2 dependence is expected to be small providing no thresholds are nearby.

$\mu_\tau / (e\hbar/2m_\tau) - 1 = (g_\tau - 2)/2$

For a theoretical calculation $[(g_\tau - 2)/2 = 117721(5) \times 10^{-8}]$, see EIDELMAN 07.

VALUE	CL%	DOCUMENT ID	TECN	COMMENT
-0.057 to 0.024	95	¹ AAD	23BMATLS	$\gamma\gamma \rightarrow \tau^+\tau^-$, Pb-Pb
••• We do not use the following data for averages, fits, limits, etc. •••				
-0.041 ^{+0.012} / _{-0.009}	1,2	AAD	23BMATLS	$\gamma\gamma \rightarrow \tau^+\tau^-$, Pb-Pb
0.001 ^{+0.055} / _{-0.089}	2,3	TUMASYAN	23As CMS	$\gamma\gamma \rightarrow \tau^+\tau^-$, Pb-Pb
-0.018 ± 0.017	2,4	ABDALLAH	04k DLPH	$e^+e^- \rightarrow e^+e^-\tau^+\tau^-$
< 0.107	95	⁵ ACHARD	04c L3	$e^+e^- \rightarrow e^+e^-\tau^+\tau^-$
-0.007 to 0.005	95	⁶ GONZALEZ-S.	00 RVUE	$e^+e^- \rightarrow \tau^+\tau^-$ and $W \rightarrow \tau\nu_\tau$
-0.052 to 0.058	95	⁷ ACCIARRI	98E L3	1991-1995 LEP runs
-0.068 to 0.065	95	⁸ ACKERSTAFF	98N OPAL	1990-1995 LEP runs
-0.004 to 0.006	95	⁹ ESCRIBANO	97 RVUE	$Z \rightarrow \tau^+\tau^-$ at LEP
< 0.01	95	¹⁰ ESCRIBANO	93 RVUE	$Z \rightarrow \tau^+\tau^-$ at LEP
< 0.12	90	GRIFOLS	91 RVUE	$Z \rightarrow \tau\tau\gamma$ at LEP
< 0.023	95	¹¹ SILVERMAN	83 RVUE	$e^+e^- \rightarrow \tau^+\tau^-$ at PETRA
¹ AAD 23BM measurement is derived from $\gamma\gamma \rightarrow \tau^+\tau^-$ total cross-section from 1.44 nb ⁻¹ LHC Pb-Pb collisions at $\sqrt{s_{NN}} = 5.02$ TeV. Authors report both the measured value and the corresponding 95% CL limit.				

Lepton Particle Listings

 τ

² Measurement ill-suited for a standard average because its likelihood appears to be remarkably non-Gaussian and asymmetric according to the model-dependent extraction procedure and the reported 95% CL limits.

³ TUMASYAN 23As measurement is derived from $\gamma\gamma \rightarrow \tau^+\tau^-$ total cross-section from 404 μb^{-1} LHC Pb-Pb collisions at $\sqrt{s_{NN}} = 5.02$ TeV.

⁴ ABDALLAH 04k measurement is derived from $e^+e^- \rightarrow e^+e^-\tau^+\tau^-$ total cross-section measurements at \sqrt{s} between 183 and 208 GeV. In addition to the measurement, the authors also quote 95% CL limits of > -0.052 and < 0.013 .

⁵ ACHARD 04G limit is derived from $e^+e^- \rightarrow e^+e^-\tau^+\tau^-$ total cross-section measurements at \sqrt{s} between 189 and 206 GeV, and is on the absolute value of the magnetic moment anomaly.

⁶ GONZALEZ-SPRINBERG 00 use data on tau lepton production at LEP1, SLC, and LEP2, and data from colliders and LEP2 to determine limits. Assume imaginary component is zero.

⁷ ACCIARRI 98E use $Z \rightarrow \tau^+\tau^- \gamma$ events. In addition to the limits, the authors also quote a value of $0.004 \pm 0.027 \pm 0.023$.

⁸ ACKERSTAFF 98N use $Z \rightarrow \tau^+\tau^- \gamma$ events. The limit applies to an average of the form factor for off-shell τ 's having p^2 ranging from m_τ^2 to $(M_Z - m_\tau)^2$.

⁹ ESCRIBANO 97 use preliminary experimental results.

¹⁰ ESCRIBANO 93 limit derived from $\Gamma(Z \rightarrow \tau^+\tau^-)$, and is on the absolute value of the magnetic moment anomaly.

¹¹ SILVERMAN 83 limit is derived from $e^+e^- \rightarrow \tau^+\tau^-$ total cross-section measurements for q^2 up to $(37 \text{ GeV})^2$.

 τ ELECTRIC DIPOLE MOMENT (d_τ)

A nonzero value is forbidden by both T invariance and P invariance.

The q^2 dependence is expected to be small providing no thresholds are nearby.

 $\text{Re}(d_\tau)$

VALUE (10^{-16} ecm)	CL%	DOCUMENT ID	TECN	COMMENT
- 0.185 to 0.061	95	¹ INAMI	22 BELL	$E_{\text{cm}}^{\text{ee}} = 10.6$ GeV
• • • We do not use the following data for averages, fits, limits, etc. • • •				
< 2.3	90	² GROZIN	09A RVUE	From e EDM limit
< 3.7	95	³ ABDALLAH	04k DLPH	$e^+e^- \rightarrow e^+e^-\tau^+\tau^-$ at LEP2
< 11.4	95	⁴ ACHARD	04G L3	$e^+e^- \rightarrow e^+e^-\tau^+\tau^-$ at LEP2
- 0.22 to 0.45	95	⁵ INAMI	03 BELL	$E_{\text{cm}}^{\text{ee}} = 10.6$ GeV
< 4.6	95	⁶ ALBRECHT	00 ARG	$E_{\text{cm}}^{\text{ee}} = 10.4$ GeV
> -3.1 and < 3.1	95	⁷ ACCIARRI	98E L3	1991-1995 LEP runs
> -3.8 and < 3.6	95	⁷ ACKERSTAFF	98N OPAL	1990-1995 LEP runs
< 0.11	95	^{8,9} ESCRIBANO	97 RVUE	$Z \rightarrow \tau^+\tau^-$ at LEP
< 0.5	95	¹⁰ ESCRIBANO	93 RVUE	$Z \rightarrow \tau^+\tau^-$ at LEP
< 7	90	GRIFOLS	91 RVUE	$Z \rightarrow \tau\tau\gamma$ at LEP
< 1.6	90	DELAGUILA	90 RVUE	$e^+e^- \rightarrow \tau^+\tau^-$ $E_{\text{cm}}^{\text{ee}} = 35$ GeV

¹ INAMI 22 use $e^+e^- \rightarrow \tau^+\tau^-$ events from 833 fb^{-1} of data. Also report a measurement of $\text{Re}(d_\tau) = (-0.62 \pm 0.63) \times 10^{-17}$ ecm.

² GROZIN 09A calculate the contribution to the electron electric dipole moment from the τ electric dipole moment appearing in loops, which is $\Delta d_e = 6.9 \times 10^{-12} d_\tau$. Dividing the REGAN 02 upper limit $|d_e| \leq 1.6 \times 10^{-27}$ ecm at CL=90% by 6.9×10^{-12} gives this limit.

³ ABDALLAH 04k limit is derived from $e^+e^- \rightarrow e^+e^-\tau^+\tau^-$ total cross-section measurements at \sqrt{s} between 183 and 208 GeV and is on the absolute value of d_τ .

⁴ ACHARD 04G limit is derived from $e^+e^- \rightarrow e^+e^-\tau^+\tau^-$ total cross-section measurements at \sqrt{s} between 189 and 206 GeV, and is on the absolute value of d_τ .

⁵ INAMI 03 use $e^+e^- \rightarrow \tau^+\tau^-$ events.

⁶ ALBRECHT 00 use $e^+e^- \rightarrow \tau^+\tau^-$ events. Limit is on the absolute value of $\text{Re}(d_\tau)$.

⁷ ACKERSTAFF 98N use $Z \rightarrow \tau^+\tau^- \gamma$ events. The limit applies to an average of the form factor for off-shell τ 's having p^2 ranging from m_τ^2 to $(M_Z - m_\tau)^2$.

⁸ ESCRIBANO 97 derive the relationship $|d_\tau| = \cot \theta_W |d_\tau^W|$ using effective Lagrangian methods, and use a conference result $|d_\tau^W| < 5.8 \times 10^{-18}$ ecm at 95% CL (L. Silvestris, ICHEP96) to obtain this result.

⁹ ESCRIBANO 97 use preliminary experimental results.

¹⁰ ESCRIBANO 93 limit derived from $\Gamma(Z \rightarrow \tau^+\tau^-)$, and is on the absolute value of the electric dipole moment.

 $\text{Im}(d_\tau)$

VALUE (10^{-16} ecm)	CL%	DOCUMENT ID	TECN	COMMENT
- 0.103 to 0.023	95	¹ INAMI	22 BELL	$E_{\text{cm}}^{\text{ee}} = 10.6$ GeV
• • • We do not use the following data for averages, fits, limits, etc. • • •				
- 0.25 to 0.008	95	² INAMI	03 BELL	$E_{\text{cm}}^{\text{ee}} = 10.6$ GeV
< 1.8	95	³ ALBRECHT	00 ARG	$E_{\text{cm}}^{\text{ee}} = 10.4$ GeV

¹ INAMI 22 use $e^+e^- \rightarrow \tau^+\tau^-$ events from 833 fb^{-1} of data. Also report a measurement of $\text{Im}(d_\tau) = (-0.40 \pm 0.32) \times 10^{-17}$ ecm.

² INAMI 03 use $e^+e^- \rightarrow \tau^+\tau^-$ events.

³ ALBRECHT 00 use $e^+e^- \rightarrow \tau^+\tau^-$ events. Limit is on the absolute value of $\text{Im}(d_\tau)$.

 τ WEAK DIPOLE MOMENT (d_τ^W)

A nonzero value is forbidden by CP invariance.

The q^2 dependence is expected to be small providing no thresholds are nearby.

 $\text{Re}(d_\tau^W)$

VALUE (10^{-17} ecm)	CL%	DOCUMENT ID	TECN	COMMENT
< 0.50	95	¹ HEISTER	03F ALEP	1990-1995 LEP runs
• • • We do not use the following data for averages, fits, limits, etc. • • •				
< 3.0	90	¹ ACCIARRI	98C L3	1991-1995 LEP runs
< 0.56	95	ACKERSTAFF	97L OPAL	1991-1995 LEP runs
< 0.78	95	² AKERS	95F OPAL	Repl. by ACKERSTAFF 97L
< 1.5	95	² BUSKULIC	95C ALEP	Repl. by HEISTER 03F
< 7.0	95	² ACTON	92F OPAL	$Z \rightarrow \tau^+\tau^-$ at LEP
< 3.7	95	² BUSKULIC	92J ALEP	Repl. by BUSKULIC 95C

¹ Limit is on the absolute value of the real part of the weak dipole moment.

² Limit is on the absolute value of the real part of the weak dipole moment, and applies for $q^2 = m_Z^2$.

 $\text{Im}(d_\tau^W)$

VALUE (10^{-17} ecm)	CL%	DOCUMENT ID	TECN	COMMENT
< 1.1	95	¹ HEISTER	03F ALEP	1990-1995 LEP runs
• • • We do not use the following data for averages, fits, limits, etc. • • •				
< 1.5	95	ACKERSTAFF	97L OPAL	1991-1995 LEP runs
< 4.5	95	² AKERS	95F OPAL	Repl. by ACKERSTAFF 97L

¹ HEISTER 03F limit is on the absolute value of the imaginary part of the weak dipole moment.

² Limit is on the absolute value of the imaginary part of the weak dipole moment, and applies for $q^2 = m_Z^2$.

 τ WEAK ANOMALOUS MAGNETIC DIPOLE MOMENT (α_τ^W)

Electroweak radiative corrections are expected to contribute at the 10^{-6} level. See BERNABEU 95.

The q^2 dependence is expected to be small providing no thresholds are nearby.

 $\text{Re}(\alpha_\tau^W)$

VALUE	CL%	DOCUMENT ID	TECN	COMMENT
< 1.1×10^{-3}	95	¹ HEISTER	03F ALEP	1990-1995 LEP runs
• • • We do not use the following data for averages, fits, limits, etc. • • •				
> -0.0024 and < 0.0025	95	² GONZALEZ-S...	00 RVUE	$e^+e^- \rightarrow \tau^+\tau^-$ and $W \rightarrow \tau\nu_\tau$
< 4.5×10^{-3}	90	¹ ACCIARRI	98C L3	1991-1995 LEP runs

¹ Limit is on the absolute value of the real part of the weak anomalous magnetic dipole moment.

² GONZALEZ-SPRINBERG 00 use data on tau lepton production at LEP1, SLC, and LEP2, and data from colliders and LEP2 to determine limits. Assume imaginary component is zero.

 $\text{Im}(\alpha_\tau^W)$

VALUE	CL%	DOCUMENT ID	TECN	COMMENT
< 2.7×10^{-3}	95	¹ HEISTER	03F ALEP	1990-1995 LEP runs
• • • We do not use the following data for averages, fits, limits, etc. • • •				
< 9.9×10^{-3}	90	¹ ACCIARRI	98C L3	1991-1995 LEP runs

¹ Limit is on the absolute value of the imaginary part of the weak anomalous magnetic dipole moment.

 τ^- DECAY MODES

τ^- modes are charge conjugates of the modes below. " h^\pm " stands for π^\pm or K^\pm . " e " stands for e or μ . "Neutrals" stands for γ 's and/or π^0 's.

Mode	Fraction (Γ_i/Γ)	Scale factor/ Confidence level
------	--------------------------------	-----------------------------------

Modes with one charged particle

Γ_1	particle $^- \geq 0$ neutrals $\geq 0K^0\nu_\tau$ ("1-prong")	(85.24 \pm 0.06) %
Γ_2	particle $^- \geq 0$ neutrals $\geq 0K^0_L\nu_\tau$	(84.58 \pm 0.06) %
Γ_3	$\mu^- \bar{\nu}_\mu \nu_\tau$	[a] (17.39 \pm 0.04) %
Γ_4	$\mu^- \bar{\nu}_\mu \nu_\tau \gamma$	[b] (3.67 \pm 0.08) $\times 10^{-3}$
Γ_5	$e^- \bar{\nu}_e \nu_\tau$	[a] (17.82 \pm 0.04) %
Γ_6	$e^- \bar{\nu}_e \nu_\tau \gamma$	[b] (1.83 \pm 0.05) %
Γ_7	$h^- \geq 0K^0_L \nu_\tau$	(12.03 \pm 0.05) %
Γ_8	$h^- \nu_\tau$	(11.51 \pm 0.05) %

Γ ₉	$\pi^- \nu_\tau$	[a]	(10.82 ± 0.05) %	Γ ₇₂	$h^- h^- h^+ \geq 1\pi^0 \nu_\tau$ (ex. K^0)	(5.09 ± 0.05) %	
Γ ₁₀	$K^- \nu_\tau$	[a]	(6.96 ± 0.10) × 10 ⁻³	Γ ₇₃	$h^- h^- h^+ \pi^0 \nu_\tau$	(4.76 ± 0.05) %	
Γ ₁₁	$h^- \geq 1$ neutrals ν_τ		(37.00 ± 0.09) %	Γ ₇₄	$h^- h^- h^+ \pi^0 \nu_\tau$ (ex. K^0)	(4.57 ± 0.05) %	
Γ ₁₂	$h^- \geq 1\pi^0 \nu_\tau$ (ex. K^0)		(36.50 ± 0.09) %	Γ ₇₅	$h^- h^- h^+ \pi^0 \nu_\tau$ (ex. K^0, ω)	(2.79 ± 0.07) %	
Γ ₁₃	$h^- \pi^0 \nu_\tau$		(25.93 ± 0.09) %	Γ ₇₆	$\pi^- \pi^+ \pi^- \pi^0 \nu_\tau$	(4.62 ± 0.05) %	
Γ ₁₄	$\pi^- \pi^0 \nu_\tau$	[a]	(25.49 ± 0.09) %	Γ ₇₇	$\pi^- \pi^+ \pi^- \pi^0 \nu_\tau$ (ex. K^0)	(4.49 ± 0.05) %	
Γ ₁₅	$\pi^- \pi^0$ non- $\rho(770) \nu_\tau$		(3.0 ± 3.2) × 10 ⁻³	Γ ₇₈	$\pi^- \pi^+ \pi^- \pi^0 \nu_\tau$ (ex. K^0, ω)	[a] (2.74 ± 0.07) %	
Γ ₁₆	$K^- \pi^0 \nu_\tau$	[a]	(4.33 ± 0.15) × 10 ⁻³	Γ ₇₉	$h^- \rho \pi^0 \nu_\tau$		
Γ ₁₇	$h^- \geq 2\pi^0 \nu_\tau$		(10.81 ± 0.09) %	Γ ₈₀	$h^- \rho^+ h^- \nu_\tau$		
Γ ₁₈	$h^- 2\pi^0 \nu_\tau$		(9.48 ± 0.10) %	Γ ₈₁	$h^- \rho^- h^+ \nu_\tau$		
Γ ₁₉	$h^- 2\pi^0 \nu_\tau$ (ex. K^0)		(9.32 ± 0.10) %	Γ ₈₂	$h^- h^+ \geq 2\pi^0 \nu_\tau$ (ex. K^0)	(5.17 ± 0.31) × 10 ⁻³	
Γ ₂₀	$\pi^- 2\pi^0 \nu_\tau$ (ex. K^0)	[a]	(9.26 ± 0.10) %	Γ ₈₃	$h^- h^- h^+ 2\pi^0 \nu_\tau$	(5.05 ± 0.31) × 10 ⁻³	
Γ ₂₁	$\pi^- 2\pi^0 \nu_\tau$ (ex. K^0), scalar	< 9	× 10 ⁻³	CL=95%	Γ ₈₄	$h^- h^- h^+ 2\pi^0 \nu_\tau$ (ex. K^0)	(4.95 ± 0.31) × 10 ⁻³
Γ ₂₂	$\pi^- 2\pi^0 \nu_\tau$ (ex. K^0), vector	< 7	× 10 ⁻³	CL=95%	Γ ₈₅	$h^- h^- h^+ 2\pi^0 \nu_\tau$ (ex. K^0, ω, η)	[a] (10 ± 4) × 10 ⁻⁴
Γ ₂₃	$K^- 2\pi^0 \nu_\tau$ (ex. K^0)	[a]	(6.5 ± 2.2) × 10 ⁻⁴	Γ ₈₆	$h^- h^- h^+ 3\pi^0 \nu_\tau$	(2.13 ± 0.30) × 10 ⁻⁴	
Γ ₂₄	$h^- \geq 3\pi^0 \nu_\tau$		(1.34 ± 0.07) %	Γ ₈₇	$2\pi^- \pi^+ 3\pi^0 \nu_\tau$ (ex. K^0)	(1.94 ± 0.30) × 10 ⁻⁴	
Γ ₂₅	$h^- \geq 3\pi^0 \nu_\tau$ (ex. K^0)		(1.25 ± 0.07) %	Γ ₈₈	$2\pi^- \pi^+ 3\pi^0 \nu_\tau$ (ex. $K^0, \eta, f_1(1285)$)	(1.7 ± 0.4) × 10 ⁻⁴	
Γ ₂₆	$h^- 3\pi^0 \nu_\tau$		(1.18 ± 0.07) %	Γ ₈₉	$2\pi^- \pi^+ 3\pi^0 \nu_\tau$ (ex. $K^0, \eta, \omega, f_1(1285)$)	[a] (1.4 ± 2.7) × 10 ⁻⁵	
Γ ₂₇	$\pi^- 3\pi^0 \nu_\tau$ (ex. K^0)	[a]	(1.04 ± 0.07) %	Γ ₉₀	$K^- h^+ h^- \geq 0$ neutrals ν_τ	(6.29 ± 0.14) × 10 ⁻³	
Γ ₂₈	$K^- 3\pi^0 \nu_\tau$ (ex. K^0, η)	[a]	(4.8 ± 2.1) × 10 ⁻⁴	Γ ₉₁	$K^- h^+ \pi^- \nu_\tau$ (ex. K^0)	(4.37 ± 0.07) × 10 ⁻³	
Γ ₂₉	$h^- 4\pi^0 \nu_\tau$ (ex. K^0)		(1.6 ± 0.4) × 10 ⁻³	Γ ₉₂	$K^- h^+ \pi^- \pi^0 \nu_\tau$ (ex. K^0)	(8.6 ± 1.2) × 10 ⁻⁴	
Γ ₃₀	$h^- 4\pi^0 \nu_\tau$ (ex. K^0, η)	[a]	(1.1 ± 0.4) × 10 ⁻³	Γ ₉₃	$K^- \pi^+ \pi^- \geq 0$ neutrals ν_τ	(4.77 ± 0.14) × 10 ⁻³	
Γ ₃₁	$a_1(1260) \nu_\tau \rightarrow \pi^- \gamma \nu_\tau$		(4.0 ± 1.5) × 10 ⁻⁴	Γ ₉₄	$K^- \pi^+ \pi^- \geq 0\pi^0 \nu_\tau$ (ex. K^0)	(3.73 ± 0.13) × 10 ⁻³	
Γ ₃₂	$K^- \geq 0\pi^0 \geq 0K^0 \geq 0\gamma \nu_\tau$		(1.552 ± 0.029) %	Γ ₉₅	$K^- \pi^+ \pi^- \nu_\tau$	(3.45 ± 0.07) × 10 ⁻³	
Γ ₃₃	$K^- \geq 1(\pi^0 \text{ or } K^0 \text{ or } \gamma) \nu_\tau$		(8.59 ± 0.28) × 10 ⁻³	Γ ₉₆	$K^- \pi^+ \pi^- \nu_\tau$ (ex. K^0)	(2.93 ± 0.07) × 10 ⁻³	
Modes with K^0's				Γ ₉₇	$K^- \pi^+ \pi^- \nu_\tau$ (ex. K^0, ω)	[a] (2.93 ± 0.07) × 10 ⁻³	
Γ ₃₄	K_S^0 (particles) ν_τ		(9.43 ± 0.28) × 10 ⁻³	Γ ₉₈	$K^- \rho^0 \nu_\tau \rightarrow K^- \pi^+ \pi^- \nu_\tau$	(1.4 ± 0.5) × 10 ⁻³	
Γ ₃₅	$h^- \bar{K}^0 \nu_\tau$		(9.87 ± 0.14) × 10 ⁻³	Γ ₉₉	$K^- \pi^+ \pi^- \pi^0 \nu_\tau$	(1.31 ± 0.12) × 10 ⁻³	
Γ ₃₆	$\pi^- \bar{K}^0 \nu_\tau$	[a]	(8.38 ± 0.14) × 10 ⁻³	Γ ₁₀₀	$K^- \pi^+ \pi^- \pi^0 \nu_\tau$ (ex. K^0)	(7.9 ± 1.2) × 10 ⁻⁴	
Γ ₃₇	$\pi^- \bar{K}^0$ (non- $K^*(892)^- \nu_\tau$)	[a]	(5.4 ± 2.1) × 10 ⁻⁴	Γ ₁₀₁	$K^- \pi^+ \pi^- \pi^0 \nu_\tau$ (ex. K^0, η)	(7.6 ± 1.2) × 10 ⁻⁴	
Γ ₃₈	$K^- K^0 \nu_\tau$	[a]	(1.486 ± 0.034) × 10 ⁻³	Γ ₁₀₂	$K^- \pi^+ \pi^- \pi^0 \nu_\tau$ (ex. K^0, ω)	(3.7 ± 0.9) × 10 ⁻⁴	
Γ ₃₉	$K^- K^0 \geq 0\pi^0 \nu_\tau$		(2.99 ± 0.07) × 10 ⁻³	Γ ₁₀₃	$K^- \pi^+ \pi^- \pi^0 \nu_\tau$ (ex. K^0, ω, η)	[a] (3.9 ± 1.4) × 10 ⁻⁴	
Γ ₄₀	$h^- \bar{K}^0 \pi^0 \nu_\tau$		(5.32 ± 0.13) × 10 ⁻³	Γ ₁₀₄	$K^- \pi^+ K^- \geq 0$ neut. ν_τ	< 9 × 10 ⁻⁴ CL=95%	
Γ ₄₁	$\pi^- \bar{K}^0 \pi^0 \nu_\tau$	[a]	(3.82 ± 0.13) × 10 ⁻³	Γ ₁₀₅	$K^- K^+ \pi^- \geq 0$ neut. ν_τ	(1.496 ± 0.033) × 10 ⁻³	
Γ ₄₂	$\bar{K}^0 \rho^- \nu_\tau$		(2.2 ± 0.5) × 10 ⁻³	Γ ₁₀₆	$K^- K^+ \pi^- \nu_\tau$	[a] (1.435 ± 0.027) × 10 ⁻³	
Γ ₄₃	$K^- K^0 \pi^0 \nu_\tau$	[a]	(1.50 ± 0.07) × 10 ⁻³	Γ ₁₀₇	$K^- K^+ \pi^- \pi^0 \nu_\tau$	[a] (6.1 ± 1.8) × 10 ⁻⁵	
Γ ₄₄	$\pi^- \bar{K}^0 \geq 1\pi^0 \nu_\tau$		(4.08 ± 0.25) × 10 ⁻³	Γ ₁₀₈	$K^- K^+ K^- \nu_\tau$	(2.2 ± 0.8) × 10 ⁻⁵	
Γ ₄₅	$\pi^- \bar{K}^0 \pi^0 \pi^0 \nu_\tau$ (ex. K^0)	[a]	(2.6 ± 2.3) × 10 ⁻⁴	Γ ₁₀₉	$K^- K^+ K^- \nu_\tau$ (ex. ϕ)	< 2.5 × 10 ⁻⁶ S=5.4 CL=90%	
Γ ₄₆	$K^- K^0 \pi^0 \pi^0 \nu_\tau$	< 1.6	× 10 ⁻⁴	CL=95%	Γ ₁₁₀	$K^- K^+ K^- \pi^0 \nu_\tau$	< 4.8 × 10 ⁻⁶ CL=90%
Γ ₄₇	$\pi^- K^0 \bar{K}^0 \nu_\tau$		(1.55 ± 0.24) × 10 ⁻³	Γ ₁₁₁	$\pi^- K^+ \pi^- \geq 0$ neut. ν_τ	< 2.5 × 10 ⁻³ CL=95%	
Γ ₄₈	$\pi^- K_S^0 K_S^0 \nu_\tau$	[a]	(2.35 ± 0.06) × 10 ⁻⁴	Γ ₁₁₂	$e^- e^- e^+ \bar{\nu}_e \nu_\tau$	(2.8 ± 1.5) × 10 ⁻⁵	
Γ ₄₉	$\pi^- K_S^0 K_L^0 \nu_\tau$	[a]	(1.08 ± 0.24) × 10 ⁻³	Γ ₁₁₃	$\mu^- e^- e^+ \bar{\nu}_\mu \nu_\tau$	< 3.2 × 10 ⁻⁵ CL=90%	
Γ ₅₀	$\pi^- K_L^0 K_L^0 \nu_\tau$		(2.35 ± 0.06) × 10 ⁻⁴	Γ ₁₁₄	$\pi^- e^- e^+ \nu_\tau$	seen	
Γ ₅₁	$\pi^- K^0 \bar{K}^0 \pi^0 \nu_\tau$		(3.6 ± 1.2) × 10 ⁻⁴	Γ ₁₁₅	$\pi^- \mu^- \mu^+ \nu_\tau$	< 1.14 × 10 ⁻⁵ CL=90%	
Γ ₅₂	$\pi^- K_S^0 K_S^0 \pi^0 \nu_\tau$	[a]	(1.82 ± 0.21) × 10 ⁻⁵	Modes with five charged particles			
Γ ₅₃	$K^* K^0 \pi^0 \nu_\tau \rightarrow \pi^- K_S^0 K_S^0 \pi^0 \nu_\tau$		(1.08 ± 0.21) × 10 ⁻⁵	Γ ₁₁₆	$3h^- 2h^+ \geq 0$ neutrals ν_τ (ex. $K_S^0 \rightarrow \pi^- \pi^+$) ("5-prong")	(9.9 ± 0.4) × 10 ⁻⁴	
Γ ₅₄	$f_1(1285) \pi^- \nu_\tau \rightarrow \pi^- K_S^0 K_S^0 \pi^0 \nu_\tau$		(6.8 ± 1.5) × 10 ⁻⁶	Γ ₁₁₇	$3h^- 2h^+ \nu_\tau$ (ex. K^0)	(8.29 ± 0.31) × 10 ⁻⁴	
Γ ₅₅	$f_1(1420) \pi^- \nu_\tau \rightarrow \pi^- K_S^0 K_S^0 \pi^0 \nu_\tau$		(2.4 ± 0.8) × 10 ⁻⁶	Γ ₁₁₈	$3\pi^- 2\pi^+ \nu_\tau$ (ex. K^0, ω)	(8.27 ± 0.31) × 10 ⁻⁴	
Γ ₅₆	$\pi^- K_S^0 K_L^0 \pi^0 \nu_\tau$	[a]	(3.2 ± 1.2) × 10 ⁻⁴	Γ ₁₁₉	$3\pi^- 2\pi^+ \nu_\tau$ (ex. $K^0, \omega, f_1(1285)$)	[a] (7.75 ± 0.30) × 10 ⁻⁴	
Γ ₅₇	$\pi^- K_L^0 K_L^0 \pi^0 \nu_\tau$		(1.82 ± 0.21) × 10 ⁻⁵	Γ ₁₂₀	$K^- 2\pi^- 2\pi^+ \nu_\tau$ (ex. K^0)	[a] (6 ± 12) × 10 ⁻⁷	
Γ ₅₈	$K^- K_S^0 K_S^0 \nu_\tau$	< 6.3	× 10 ⁻⁷	CL=90%	Γ ₁₂₁	$K^+ 3\pi^- \pi^+ \nu_\tau$	< 5.0 × 10 ⁻⁶ CL=90%
Γ ₅₉	$K^- K_S^0 K_S^0 \pi^0 \nu_\tau$	< 4.0	× 10 ⁻⁷	CL=90%	Γ ₁₂₂	$K^+ K^- 2\pi^- \pi^+ \nu_\tau$	< 4.5 × 10 ⁻⁷ CL=90%
Γ ₆₀	$K^0 h^+ h^- h^- \geq 0$ neutrals ν_τ	< 1.7	× 10 ⁻³	CL=95%	Γ ₁₂₃	$3h^- 2h^+ \pi^0 \nu_\tau$ (ex. K^0)	(1.65 ± 0.11) × 10 ⁻⁴
Γ ₆₁	$K^0 h^+ h^- h^- \nu_\tau$	[a]	(2.5 ± 2.0) × 10 ⁻⁴	Γ ₁₂₄	$3\pi^- 2\pi^+ \pi^0 \nu_\tau$ (ex. K^0)	(1.64 ± 0.11) × 10 ⁻⁴	
Modes with three charged particles				Γ ₁₂₅	$3\pi^- 2\pi^+ \pi^0 \nu_\tau$ (ex. $K^0, \eta, f_1(1285)$)	(1.11 ± 0.10) × 10 ⁻⁴	
Γ ₆₂	$h^- h^- h^+ \geq 0$ neutrals $\geq 0K_L^0 \nu_\tau$		(15.20 ± 0.06) %	Γ ₁₂₆	$3\pi^- 2\pi^+ \pi^0 \nu_\tau$ (ex. $K^0, \eta, \omega, f_1(1285)$)	[a] (3.8 ± 0.9) × 10 ⁻⁵	
Γ ₆₃	$h^- h^- h^+ \geq 0$ neutrals ν_τ (ex. $K_S^0 \rightarrow \pi^+ \pi^-$) ("3-prong")		(14.55 ± 0.06) %	Γ ₁₂₇	$K^- 2\pi^- 2\pi^+ \pi^0 \nu_\tau$ (ex. K^0)	[a] (1.1 ± 0.6) × 10 ⁻⁶	
Γ ₆₄	$h^- h^- h^+ \nu_\tau$		(9.80 ± 0.05) %	Γ ₁₂₈	$K^+ 3\pi^- \pi^+ \pi^0 \nu_\tau$	< 8 × 10 ⁻⁷ CL=90%	
Γ ₆₅	$h^- h^- h^+ \nu_\tau$ (ex. K^0)		(9.46 ± 0.05) %	Γ ₁₂₉	$3h^- 2h^+ 2\pi^0 \nu_\tau$	< 3.4 × 10 ⁻⁶ CL=90%	
Γ ₆₆	$h^- h^- h^+ \nu_\tau$ (ex. K^0, ω)		(9.43 ± 0.05) %	Miscellaneous other allowed modes			
Γ ₆₇	$\pi^- \pi^+ \pi^- \nu_\tau$		(9.31 ± 0.05) %	Γ ₁₃₀	$(5\pi^-) \nu_\tau$	(7.8 ± 0.5) × 10 ⁻³	
Γ ₆₈	$\pi^- \pi^+ \pi^- \nu_\tau$ (ex. K^0)		(9.02 ± 0.05) %	Γ ₁₃₁	$4h^- 3h^+ \geq 0$ neutrals ν_τ ("7-prong")	< 3.0 × 10 ⁻⁷ CL=90%	
Γ ₆₉	$\pi^- \pi^+ \pi^- \nu_\tau$ (ex. K^0), non-axial vector	< 2.4	%	CL=95%	Γ ₁₃₂	$4h^- 3h^+ \nu_\tau$	< 4.3 × 10 ⁻⁷ CL=90%
Γ ₇₀	$\pi^- \pi^+ \pi^- \nu_\tau$ (ex. K^0, ω)	[a]	(8.99 ± 0.05) %	Γ ₁₃₃	$4h^- 3h^+ \pi^0 \nu_\tau$	< 2.5 × 10 ⁻⁷ CL=90%	
Γ ₇₁	$h^- h^- h^+ \geq 1$ neutrals ν_τ		(5.29 ± 0.05) %				

Lepton Particle Listings

 τ

Γ_{134}	$X^-(S=-1)\nu_\tau$	(2.92 ± 0.04) %		Γ_{195}	$\mu^-\eta$	LF	< 6.5	$\times 10^{-8}$	CL=90%
Γ_{135}	$K^*(892)^-\geq 0$ neutrals $\geq 0K^0_1\nu_\tau$	(1.42 ± 0.18) %	S=1.4	Γ_{196}	$e^-\rho^0$	LF	< 2.2	$\times 10^{-8}$	CL=90%
Γ_{136}	$K^*(892)^-\nu_\tau$	(1.20 ± 0.07) %	S=1.8	Γ_{197}	$\mu^-\rho^0$	LF	< 1.7	$\times 10^{-8}$	CL=90%
Γ_{137}	$K^*(892)^-\nu_\tau \rightarrow \pi^-\bar{K}^0\nu_\tau$	(7.82 ± 0.26) $\times 10^{-3}$		Γ_{198}	$e^-\omega$	LF	< 2.4	$\times 10^{-8}$	CL=90%
Γ_{138}	$K^*(892)^0K^-\geq 0$ neutrals ν_τ	(3.2 ± 1.4) $\times 10^{-3}$		Γ_{199}	$\mu^-\omega$	LF	< 3.9	$\times 10^{-8}$	CL=90%
Γ_{139}	$K^*(892)^0K^-\nu_\tau$	(2.1 ± 0.4) $\times 10^{-3}$		Γ_{200}	$e^-K^*(892)^0$	LF	< 1.9	$\times 10^{-8}$	CL=90%
Γ_{140}	$\bar{K}^*(892)^0\pi^-\geq 0$ neutrals ν_τ	(3.8 ± 1.7) $\times 10^{-3}$		Γ_{201}	$\mu^-K^*(892)^0$	LF	< 2.9	$\times 10^{-8}$	CL=90%
Γ_{141}	$\bar{K}^*(892)^0\pi^-\nu_\tau$	(2.2 ± 0.5) $\times 10^{-3}$		Γ_{202}	$e^-\bar{K}^*(892)^0$	LF	< 1.7	$\times 10^{-8}$	CL=90%
Γ_{142}	$(\bar{K}^*(892)\pi)^-\nu_\tau \rightarrow \pi^-\bar{K}^0\pi^0\nu_\tau$	(1.0 ± 0.4) $\times 10^{-3}$		Γ_{203}	$\mu^-\bar{K}^*(892)^0$	LF	< 4.3	$\times 10^{-8}$	CL=90%
Γ_{143}	$K_1(1270)^-\nu_\tau$	(4.7 ± 1.1) $\times 10^{-3}$		Γ_{204}	$e^-\eta'(958)$	LF	< 1.6	$\times 10^{-7}$	CL=90%
Γ_{144}	$K_1(1400)^-\nu_\tau$	(1.7 ± 2.6) $\times 10^{-3}$	S=1.7	Γ_{205}	$\mu^-\eta'(958)$	LF	< 1.3	$\times 10^{-7}$	CL=90%
Γ_{145}	$K^*(1410)^-\nu_\tau$	(1.5 ± 1.4) $\times 10^{-3}$		Γ_{206}	$e^-f_0(980) \rightarrow e^-\pi^+\pi^-$	LF	< 3.2	$\times 10^{-8}$	CL=90%
Γ_{146}	$K^*_0(1430)^-\nu_\tau$	< 5	$\times 10^{-4}$ CL=95%	Γ_{207}	$\mu^-f_0(980) \rightarrow \mu^-\pi^+\pi^-$	LF	< 3.4	$\times 10^{-8}$	CL=90%
Γ_{147}	$K^*_2(1430)^-\nu_\tau$	< 3	$\times 10^{-3}$ CL=95%	Γ_{208}	$e^-\phi$	LF	< 2.0	$\times 10^{-8}$	CL=90%
Γ_{148}	$a_0(980)^-\geq 0$ neutrals ν_τ			Γ_{209}	$\mu^-\phi$	LF	< 2.3	$\times 10^{-8}$	CL=90%
Γ_{149}	$\eta\pi^-\nu_\tau$	< 9.9	$\times 10^{-5}$ CL=95%	Γ_{210}	$e^-e^+e^-$	LF	< 2.7	$\times 10^{-8}$	CL=90%
Γ_{150}	$\eta\pi^-\pi^0\nu_\tau$	[a] (1.39 ± 0.07) $\times 10^{-3}$		Γ_{211}	$e^-\mu^+\mu^-$	LF	< 2.7	$\times 10^{-8}$	CL=90%
Γ_{151}	$\eta\pi^-\pi^0\pi^0\nu_\tau$	[a] (1.9 ± 0.4) $\times 10^{-4}$		Γ_{212}	$e^+\mu^-\mu^-$	LF	< 1.7	$\times 10^{-8}$	CL=90%
Γ_{152}	$\eta K^-\nu_\tau$	[a] (1.55 ± 0.08) $\times 10^{-4}$		Γ_{213}	$\mu^-e^+e^-$	LF	< 1.8	$\times 10^{-8}$	CL=90%
Γ_{153}	$\eta K^*(892)^-\nu_\tau$	(1.38 ± 0.15) $\times 10^{-4}$		Γ_{214}	$\mu^+e^-e^-$	LF	< 1.5	$\times 10^{-8}$	CL=90%
Γ_{154}	$\eta K^-\pi^0\nu_\tau$	[a] (4.8 ± 1.2) $\times 10^{-5}$		Γ_{215}	$\mu^-\mu^+\mu^-$	LF	< 2.1	$\times 10^{-8}$	CL=90%
Γ_{155}	$\eta K^-\pi^0$ (non- $K^*(892)$) ν_τ	< 3.5	$\times 10^{-5}$ CL=90%	Γ_{216}	$e^-\pi^+\pi^-$	LF	< 2.3	$\times 10^{-8}$	CL=90%
Γ_{156}	$\eta\bar{K}^0\pi^-\nu_\tau$	[a] (9.4 ± 1.5) $\times 10^{-5}$		Γ_{217}	$e^+\pi^-\pi^-$	L	< 2.0	$\times 10^{-8}$	CL=90%
Γ_{157}	$\eta\bar{K}^0\pi^-\pi^0\nu_\tau$	< 5.0	$\times 10^{-5}$ CL=90%	Γ_{218}	$\mu^-\pi^+\pi^-$	LF	< 2.1	$\times 10^{-8}$	CL=90%
Γ_{158}	$\eta K^-K^0\nu_\tau$	< 9.0	$\times 10^{-6}$ CL=90%	Γ_{219}	$\mu^+\pi^-\pi^-$	L	< 3.9	$\times 10^{-8}$	CL=90%
Γ_{159}	$\eta\pi^+\pi^-\pi^-\geq 0$ neutrals ν_τ	< 3	$\times 10^{-3}$ CL=90%	Γ_{220}	$e^-\pi^+K^-$	LF	< 3.7	$\times 10^{-8}$	CL=90%
Γ_{160}	$\eta\pi^-\pi^+\pi^-\nu_\tau$ (ex. K^0)	[a] (2.20 ± 0.13) $\times 10^{-4}$		Γ_{221}	$e^-\pi^-K^+$	LF	< 3.1	$\times 10^{-8}$	CL=90%
Γ_{161}	$\eta\pi^-\pi^+\pi^-\nu_\tau$ (ex. $K^0, f_1(1285)$)	(9.9 ± 1.6) $\times 10^{-5}$		Γ_{222}	$e^+\pi^-K^-$	L	< 3.2	$\times 10^{-8}$	CL=90%
Γ_{162}	$\eta a_1(1260)^-\nu_\tau \rightarrow \eta\pi^-\rho^0\nu_\tau$	< 3.9	$\times 10^{-4}$ CL=90%	Γ_{223}	$e^-K^0_S K^0_S$	LF	< 7.1	$\times 10^{-8}$	CL=90%
Γ_{163}	$\eta\eta\pi^-\nu_\tau$	< 7.4	$\times 10^{-6}$ CL=90%	Γ_{224}	$e^-K^+K^-$	LF	< 3.4	$\times 10^{-8}$	CL=90%
Γ_{164}	$\eta\eta\pi^-\pi^0\nu_\tau$	< 2.0	$\times 10^{-4}$ CL=95%	Γ_{225}	$e^+K^-K^-$	L	< 3.3	$\times 10^{-8}$	CL=90%
Γ_{165}	$\eta\eta K^-\nu_\tau$	< 3.0	$\times 10^{-6}$ CL=90%	Γ_{226}	$\mu^-\pi^+K^-$	LF	< 8.6	$\times 10^{-8}$	CL=90%
Γ_{166}	$\eta'(958)\pi^-\nu_\tau$	< 4.0	$\times 10^{-6}$ CL=90%	Γ_{227}	$\mu^-\pi^-K^+$	LF	< 4.5	$\times 10^{-8}$	CL=90%
Γ_{167}	$\eta'(958)\pi^-\pi^0\nu_\tau$	< 1.2	$\times 10^{-5}$ CL=90%	Γ_{228}	$\mu^+\pi^-K^-$	L	< 4.8	$\times 10^{-8}$	CL=90%
Γ_{168}	$\eta'(958)K^-\nu_\tau$	< 2.4	$\times 10^{-6}$ CL=90%	Γ_{229}	$\mu^-K^0_S K^0_S$	LF	< 8.0	$\times 10^{-8}$	CL=90%
Γ_{169}	$\phi\pi^-\nu_\tau$	(3.4 ± 0.6) $\times 10^{-5}$		Γ_{230}	$\mu^-K^+K^-$	LF	< 4.4	$\times 10^{-8}$	CL=90%
Γ_{170}	$\phi K^-\nu_\tau$	[a] (4.4 ± 1.6) $\times 10^{-5}$		Γ_{231}	$\mu^+K^-K^-$	L	< 4.7	$\times 10^{-8}$	CL=90%
Γ_{171}	$f_1(1285)\pi^-\nu_\tau$	(3.9 ± 0.5) $\times 10^{-4}$	S=1.9	Γ_{232}	$e^-\pi^0\pi^0$	LF	< 6.5	$\times 10^{-6}$	CL=90%
Γ_{172}	$f_1(1285)\pi^-\nu_\tau \rightarrow \eta\pi^-\pi^+\pi^-\nu_\tau$	(1.18 ± 0.07) $\times 10^{-4}$	S=1.3	Γ_{233}	$\mu^-\pi^0\pi^0$	LF	< 1.4	$\times 10^{-5}$	CL=90%
Γ_{173}	$f_1(1285)\pi^-\nu_\tau \rightarrow 3\pi^-2\pi^+\nu_\tau$	[a] (5.2 ± 0.4) $\times 10^{-5}$		Γ_{234}	$e^-\eta\eta$	LF	< 3.5	$\times 10^{-5}$	CL=90%
Γ_{174}	$\pi(1300)^-\nu_\tau \rightarrow (\rho\pi)^-\nu_\tau \rightarrow (3\pi)^-\nu_\tau$	< 1.0	$\times 10^{-4}$ CL=90%	Γ_{235}	$\mu^-\eta\eta$	LF	< 6.0	$\times 10^{-5}$	CL=90%
Γ_{175}	$\pi(1300)^-\nu_\tau \rightarrow ((\pi\pi)_{S\text{-wave}}\pi)^-\nu_\tau \rightarrow (3\pi)^-\nu_\tau$	< 1.9	$\times 10^{-4}$ CL=90%	Γ_{236}	$e^-\pi^0\eta$	LF	< 2.4	$\times 10^{-5}$	CL=90%
Γ_{176}	$h^-\omega \geq 0$ neutrals ν_τ	(2.40 ± 0.08) %		Γ_{237}	$\mu^-\pi^0\eta$	LF	< 2.2	$\times 10^{-5}$	CL=90%
Γ_{177}	$h^-\omega\nu_\tau$	(1.99 ± 0.06) %		Γ_{238}	ρe^-e^-	L,B	< 3.0	$\times 10^{-8}$	CL=90%
Γ_{178}	$\pi^-\omega\nu_\tau$	[a] (1.95 ± 0.06) %		Γ_{239}	$\bar{\rho} e^+e^-$	L,B	< 3.0	$\times 10^{-8}$	CL=90%
Γ_{179}	$K^-\omega\nu_\tau$	[a] (4.1 ± 0.9) $\times 10^{-4}$		Γ_{240}	$\bar{\rho} e^+\mu^-$	L,B	< 2.0	$\times 10^{-8}$	CL=90%
Γ_{180}	$h^-\omega\pi^0\nu_\tau$	[a] (4.1 ± 0.4) $\times 10^{-3}$		Γ_{241}	$\bar{\rho} e^-\mu^+$	L,B	< 1.8	$\times 10^{-8}$	CL=90%
Γ_{181}	$h^-\omega 2\pi^0\nu_\tau$	(1.4 ± 0.5) $\times 10^{-4}$		Γ_{242}	$\rho\mu^-\mu^-$	L,B	< 4.0	$\times 10^{-8}$	CL=90%
Γ_{182}	$\pi^-\omega 2\pi^0\nu_\tau$	[a] (7.2 ± 1.6) $\times 10^{-5}$		Γ_{243}	$\bar{\rho}\mu^+\mu^-$	L,B	< 1.8	$\times 10^{-8}$	CL=90%
Γ_{183}	$h^-2\omega\nu_\tau$	< 5.4	$\times 10^{-7}$ CL=90%	Γ_{244}	$\bar{\rho}\gamma$	L,B	< 3.5	$\times 10^{-6}$	CL=90%
Γ_{184}	$2h^-h^+\omega\nu_\tau$	(1.20 ± 0.22) $\times 10^{-4}$		Γ_{245}	$\bar{\rho}\pi^0$	L,B	< 1.5	$\times 10^{-5}$	CL=90%
Γ_{185}	$2\pi^-\pi^+\omega\nu_\tau$ (ex. K^0)	[a] (8.4 ± 0.6) $\times 10^{-5}$		Γ_{246}	$\bar{\rho} 2\pi^0$	L,B	< 3.3	$\times 10^{-5}$	CL=90%
				Γ_{247}	$\bar{\rho}\eta$	L,B	< 8.9	$\times 10^{-6}$	CL=90%
				Γ_{248}	$\bar{\rho}\pi^0\eta$	L,B	< 2.7	$\times 10^{-5}$	CL=90%
				Γ_{249}	$\Lambda\pi^-$	L,B	< 7.2	$\times 10^{-8}$	CL=90%
				Γ_{250}	$\Lambda\pi^-$	L,B	< 1.4	$\times 10^{-7}$	CL=90%
				Γ_{251}	e^- light boson	LF	< 9	$\times 10^{-4}$	CL=95%
				Γ_{252}	μ^- light boson	LF	< 6	$\times 10^{-4}$	CL=95%

[a] Basis mode for the τ .

[b] See the Particle Listings below for the energy limits used in this measurement.

L means lepton number violation (e.g. $\tau^- \rightarrow e^+\pi^-\pi^-$). Following common usage, LF means lepton family violation and not lepton number violation (e.g. $\tau^- \rightarrow e^-\pi^+\pi^-$). B means baryon number violation.

Γ_{186}	$e^-\gamma$	LF	< 3.3	$\times 10^{-8}$	CL=90%
Γ_{187}	$e^-\gamma\gamma$	LF	< 2.5	$\times 10^{-4}$	CL=90%
Γ_{188}	$\mu^-\gamma$	LF	< 4.2	$\times 10^{-8}$	CL=90%
Γ_{189}	$\mu^-\gamma\gamma$	LF	< 5.8	$\times 10^{-4}$	CL=90%
Γ_{190}	$e^-\pi^0$	LF	< 8.0	$\times 10^{-8}$	CL=90%
Γ_{191}	$\mu^-\pi^0$	LF	< 1.1	$\times 10^{-7}$	CL=90%
Γ_{192}	$e^-K^0_S$	LF	< 2.6	$\times 10^{-8}$	CL=90%
Γ_{193}	$\mu^-K^0_S$	LF	< 2.3	$\times 10^{-8}$	CL=90%
Γ_{194}	$e^-\eta$	LF	< 9.2	$\times 10^{-8}$	CL=90%

CONSTRAINED FIT INFORMATION

An overall fit to 85 branching ratios uses 170 measurements and one constraint to determine 46 parameters. The overall fit has a $\chi^2 = 135.0$ for 125 degrees of freedom.

The following off-diagonal array elements are the correlation coefficients $\langle \delta x_i \delta x_j \rangle / (\delta x_i \delta x_j)$, in percent, from the fit to the branching fractions, $x_i \equiv \Gamma_i / \Gamma_{\text{total}}$. The fit constrains the x_i whose labels appear in this array to sum to one.

Table of correlation coefficients for parameters x5, x9, x10, x14, x16, x20, x23, x27, x28, x30, x36, x38, x41, x43, x45, x48, x49, x52, x56, x61, x70, x78, x85, x89, x97, x103, x106, x107, x119, x120, x126, x127, x150, x151, x152, x154, x156, x160, x170, x173, x178, x179, x180, x182, x185. Includes column labels x3, x5, x9, x10, x14, x16, x20, x23, x27, x28.

Table of correlation coefficients for parameters x36, x38, x41, x43, x45, x48, x49, x52, x56, x61, x70, x78, x85, x89, x97, x103, x106, x107, x119, x120, x126, x127, x150, x151, x152, x154, x156, x160, x170, x173, x178, x179, x180, x182, x185. Includes column labels x30, x36, x38, x41, x43, x45, x48, x49, x52, x56.

Table of correlation coefficients for parameters x70, x78, x85, x89, x97, x103, x106, x107, x119, x120, x126, x127, x150, x151, x152, x154, x156, x160, x170, x173, x178, x179, x180, x182, x185. Includes column labels x61, x70, x78, x85, x89, x97, x103, x106, x107, x119.

Lepton Particle Listings

τ

x_{126}	0									
x_{127}	0	-1								
x_{150}	0	0	0							
x_{151}	0	2	0	0						
x_{152}	0	0	0	4	0					
x_{154}	0	0	0	1	0	1				
x_{156}	0	0	0	2	-1	1	0			
x_{160}	-1	3	-1	0	25	0	0	0		
x_{170}	0	0	0	0	0	0	0	0	0	
x_{173}	-1	1	0	0	4	0	0	0	20	0
x_{178}	0	0	0	0	0	0	0	0	0	0
x_{179}	0	0	0	0	0	0	0	0	0	0
x_{180}	0	0	0	0	0	0	0	0	0	0
x_{182}	0	2	0	0	10	0	0	-1	20	0
x_{185}	-1	-2	-1	0	17	0	0	0	38	0

x_{178}	0									
x_{179}	0	-14								
x_{180}	0	-4	0							
x_{182}	3	0	0	0						
x_{185}	17	0	0	0	14					

See the related review(s):
 τ Branching Fractions

$$\frac{\Gamma(\tau^+) - \Gamma(\tau^-)}{\Gamma(\tau^+) + \Gamma(\tau^-)}$$

$\tau^\pm \rightarrow \pi^\pm K_S^0 \nu_\tau$ (RATE DIFFERENCE) / (RATE SUM)

VALUE (%)	DOCUMENT ID	TECN	COMMENT
-0.36 ± 0.23 ± 0.11	LEES	12M BABR	476 fb ⁻¹ E _{cm} ^{ee} = 10.6 GeV

τ^- BRANCHING RATIOS

$$\Gamma(\text{particle}^- \geq 0 \text{ neutrals} \geq 0 K_S^0 \nu_\tau \text{ ("1-prong")}) / \Gamma_{\text{total}} \quad \Gamma_1 / \Gamma$$

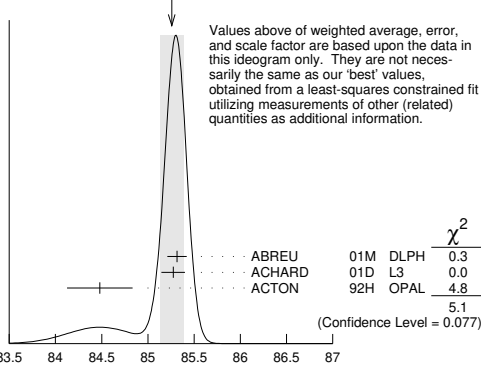
$$\Gamma_1 / \Gamma = \Gamma_3 + \Gamma_5 + \Gamma_9 + \Gamma_{10} + \Gamma_{14} + \Gamma_{16} + \Gamma_{20} + \Gamma_{23} + \Gamma_{27} + \Gamma_{28} + \Gamma_{30} + \Gamma_{36} + \Gamma_{38} + \Gamma_{41} + \Gamma_{43} + \Gamma_{45} + \Gamma_{48} + \Gamma_{49} + \Gamma_{50} + \Gamma_{52} + \Gamma_{56} + \Gamma_{57} + 0.7196\Gamma_{150} + 0.7196\Gamma_{152} + 0.7196\Gamma_{154} + 0.7196\Gamma_{156} + 0.339\Gamma_{170} + 0.0835\Gamma_{178} + 0.0835\Gamma_{179} + 0.0835\Gamma_{180} / \Gamma$$

The charged particle here can be e, μ , or hadron. In many analyses, the sum of the topological branching fractions (1, 3, and 5 prongs) is constrained to be unity. Since the 5-prong fraction is very small, the measured 1-prong and 3-prong fractions are highly correlated and cannot be treated as independent quantities in our overall fit. We arbitrarily choose to use the 3-prong fraction in our fit, and leave the 1-prong fraction out. We do, however, use these 1-prong measurements in our average below.

VALUE (%)	EVTS	DOCUMENT ID	TECN	COMMENT
85.24 ± 0.06 OUR FIT		(Produced by HFLAV)		
85.26 ± 0.13 OUR AVERAGE		Error includes scale factor of 1.6. See the ideogram below.		

- • • We use the following data for averages but not for fits. • • •
- 85.316 ± 0.093 ± 0.049 78k ¹ ABREU 01M DLPH 1992-1995 LEP runs
- 85.274 ± 0.105 ± 0.073 ² ACHARD 01D L3 1992-1995 LEP runs
- 84.48 ± 0.27 ± 0.23 ACTON 92H OPAL 1990-1991 LEP runs
- • • We do not use the following data for averages, fits, limits, etc. • • •
- 85.45 ^{+0.69}/_{-0.73} ± 0.65 DECAMP 92C ALEP Repl. by SCHAEEL 05c

WEIGHTED AVERAGE
 85.26 ± 0.13 (Error scaled by 1.6)



$$\Gamma(\text{particle}^- \geq 0 \text{ neutrals} \geq 0 K_S^0 \nu_\tau \text{ ("1-prong")}) / \Gamma_{\text{total}} (\%)$$

¹ The correlation coefficients between this measurement and the ABREU 01M measurements of $B(\tau \rightarrow 3\text{-prong})$ and $B(\tau \rightarrow 5\text{-prong})$ are -0.98 and -0.08 respectively.

² The correlation coefficients between this measurement and the ACHARD 01D measurements of $B(\tau \rightarrow 3\text{-prong})$ and $B(\tau \rightarrow 5\text{-prong})$ are -0.978 and -0.082 respectively.

$$\Gamma(\text{particle}^- \geq 0 \text{ neutrals} \geq 0 K_L^0 \nu_\tau) / \Gamma_{\text{total}} \quad \Gamma_2 / \Gamma$$

$$\Gamma_2 / \Gamma = \Gamma_3 + \Gamma_5 + \Gamma_9 + \Gamma_{10} + \Gamma_{14} + \Gamma_{16} + \Gamma_{20} + \Gamma_{23} + \Gamma_{27} + \Gamma_{28} + \Gamma_{30} + 0.6534\Gamma_{36} + 0.6534\Gamma_{38} + 0.6534\Gamma_{41} + 0.6534\Gamma_{43} + 0.6534\Gamma_{45} + 0.0942\Gamma_{48} + 0.3069\Gamma_{49} + \Gamma_{50} + 0.0942\Gamma_{52} + 0.3069\Gamma_{56} + \Gamma_{57} + 0.7196\Gamma_{150} + 0.7196\Gamma_{152} + 0.7196\Gamma_{154} + 0.4702\Gamma_{156} + 0.1049\Gamma_{170} + 0.0835\Gamma_{178} + 0.0835\Gamma_{179} + 0.0835\Gamma_{180} / \Gamma$$

VALUE (%)	EVTS	DOCUMENT ID	TECN	COMMENT
84.58 ± 0.06 OUR FIT		(Produced by HFLAV)		
85.1 ± 0.4 OUR AVERAGE				

- • • We use the following data for averages but not for fits. • • •
- 85.6 ± 0.6 ± 0.3 3300 ¹ ADEVA 91F L3 E_{cm}^{ee} = 88.3-94.3 GeV
- 84.9 ± 0.4 ± 0.3 BEHREND 89B CELL E_{cm}^{ee} = 14-47 GeV
- 84.7 ± 0.8 ± 0.6 ² AIHARA 87B TPC E_{cm}^{ee} = 29 GeV
- • • We do not use the following data for averages, fits, limits, etc. • • •
- 86.4 ± 0.3 ± 0.3 ABACHI 89B HRS E_{cm}^{ee} = 29 GeV
- 87.1 ± 1.0 ± 0.7 ³ BURCHAT 87 MRK2 E_{cm}^{ee} = 29 GeV
- 87.2 ± 0.5 ± 0.8 SCHMIDKE 86 MRK2 E_{cm}^{ee} = 29 GeV
- 84.7 ± 1.1 ^{+1.6}/_{-1.3} 169 ⁴ ALTHOFF 85 TASS E_{cm}^{ee} = 34.5 GeV
- 86.1 ± 0.5 ± 0.9 BARTEL 85F JADE E_{cm}^{ee} = 34.6 GeV
- 87.8 ± 1.3 ± 3.9 ⁵ BERGER 85 PLUT E_{cm}^{ee} = 34.6 GeV
- 86.7 ± 0.3 ± 0.6 FERNADEZ 85 MAC E_{cm}^{ee} = 29 GeV

¹ Not independent of ADEVA 91F $\Gamma(h^- h^- h^+ \geq 0 \text{ neutrals} \geq 0 K_L^0 \nu_\tau) / \Gamma_{\text{total}}$ value.
² Not independent of AIHARA 87B $\Gamma(\mu^- \bar{\nu}_\mu \nu_\tau) / \Gamma_{\text{total}}$, $\Gamma(e^- \bar{\nu}_e \nu_\tau) / \Gamma_{\text{total}}$, and $\Gamma(h^- \geq 0 \text{ neutrals} \geq 0 K_L^0 \nu_\tau) / \Gamma_{\text{total}}$ values.
³ Not independent of SCHMIDKE 86 value (also not independent of BURCHAT 87 value for $\Gamma(h^- h^- h^+ \geq 0 \text{ neutrals} \geq 0 K_L^0 \nu_\tau) / \Gamma_{\text{total}}$.
⁴ Not independent of ALTHOFF 85 $\Gamma(\mu^- \bar{\nu}_\mu \nu_\tau) / \Gamma_{\text{total}}$, $\Gamma(e^- \bar{\nu}_e \nu_\tau) / \Gamma_{\text{total}}$, $\Gamma(h^- \geq 0 \text{ neutrals} \geq 0 K_L^0 \nu_\tau) / \Gamma_{\text{total}}$, and $\Gamma(h^- h^- h^+ \geq 0 \text{ neutrals} \geq 0 K_L^0 \nu_\tau) / \Gamma_{\text{total}}$ values.
⁵ Not independent of (1-prong + 0 π^0) and (1-prong + $\geq 1\pi^0$) values.

$$\Gamma(\mu^- \bar{\nu}_\mu \nu_\tau) / \Gamma_{\text{total}} \quad \Gamma_3 / \Gamma$$

To minimize the effect of experiments with large systematic errors, we exclude experiments which together would contribute 5% of the weight in the average.

VALUE (%)	EVTS	DOCUMENT ID	TECN	COMMENT
17.39 ± 0.04 OUR FIT		(Produced by HFLAV)		
17.33 ± 0.05 OUR AVERAGE				

- 17.319 ± 0.070 ± 0.032 54k ¹ SCHAEEL 05c ALEP 1991-1995 LEP runs
- 17.34 ± 0.09 ± 0.06 31.4k ABBIENDI 03 OPAL 1990-1995 LEP runs
- 17.342 ± 0.110 ± 0.067 21.5k ² ACCIARRI 01F L3 1991-1995 LEP runs
- 17.325 ± 0.095 ± 0.077 27.7k ABREU 99X DLPH 1991-1995 LEP runs
- • • We use the following data for averages but not for fits. • • •
- 17.37 ± 0.08 ± 0.18 ³ ANASTASSOV 97 CLEO E_{cm}^{ee} = 10.6 GeV
- • • We do not use the following data for averages, fits, limits, etc. • • •
- 17.31 ± 0.11 ± 0.05 20.7k BUSKULIC 96c ALEP Repl. by SCHAEEL 05c
- 17.02 ± 0.19 ± 0.24 6586 ABREU 95T DLPH Repl. by ABREU 99X
- 17.36 ± 0.27 7941 AKERS 95I OPAL Repl. by ABBIENDI 03
- 17.6 ± 0.4 ± 0.4 2148 ADRIANI 93M L3 Repl. by ACCIARRI 01F
- 17.4 ± 0.3 ± 0.5 ⁴ ALBRECHT 93G ARG E_{cm}^{ee} = 9.4-10.6 GeV
- 17.35 ± 0.41 ± 0.37 DECAMP 92C ALEP 1989-1990 LEP runs
- 17.7 ± 0.8 ± 0.4 568 BEHREND 90 CELL E_{cm}^{ee} = 35 GeV
- 17.4 ± 1.0 2197 ADEVA 88 MRKJ E_{cm}^{ee} = 14-16 GeV
- 17.7 ± 1.2 ± 0.7 AIHARA 87B TPC E_{cm}^{ee} = 29 GeV
- 18.3 ± 0.9 ± 0.8 BURCHAT 87 MRK2 E_{cm}^{ee} = 29 GeV
- 18.6 ± 0.8 ± 0.7 558 ⁵ BARTEL 86D JADE E_{cm}^{ee} = 34.6 GeV
- 12.9 ± 1.7 ^{+0.7}/_{-0.5} ALTHOFF 85 TASS E_{cm}^{ee} = 34.5 GeV
- 18.0 ± 0.9 ± 0.5 473 ⁵ ASH 85B MAC E_{cm}^{ee} = 29 GeV
- 18.0 ± 1.0 ± 0.6 ⁶ BALTRUSAIT...85 MRK3 E_{cm}^{ee} = 3.77 GeV
- 19.4 ± 1.6 ± 1.7 153 BERGER 85 PLUT E_{cm}^{ee} = 34.6 GeV
- 17.6 ± 2.6 ± 2.1 47 BEHREND 83c CELL E_{cm}^{ee} = 34 GeV
- 17.8 ± 2.0 ± 1.8 BERGER 81B PLUT E_{cm}^{ee} = 9-32 GeV

¹ See footnote to SCHAEEL 05c $\Gamma(\tau^- \rightarrow e^- \bar{\nu}_e \nu_\tau) / \Gamma_{\text{total}}$ measurement for correlations with other measurements.
² The correlation coefficient between this measurement and the ACCIARRI 01F measurement of $B(\tau^- \rightarrow e^- \bar{\nu}_e \nu_\tau)$ is 0.08.
³ The correlation coefficients between this measurement and the ANASTASSOV 97 measurements of $B(e \bar{\nu}_e \nu_\tau)$, $B(\mu \bar{\nu}_\mu \nu_\tau) / B(e \bar{\nu}_e \nu_\tau)$, $B(h^- \nu_\tau)$, and $B(h^- \nu_\tau) / B(e \bar{\nu}_e \nu_\tau)$ are 0.50, 0.58, 0.50, and 0.08 respectively.
⁴ Not independent of ALBRECHT 92D $\Gamma(\mu^- \bar{\nu}_\mu \nu_\tau) / \Gamma_{\text{total}}$ and ALBRECHT 93G $\Gamma(\mu^- \bar{\nu}_\mu \nu_\tau) \times \Gamma(e^- \bar{\nu}_e \nu_\tau) / \Gamma_{\text{total}}^2$ values.
⁵ Modified using $B(e^- \bar{\nu}_e \nu_\tau) / B(\text{"1 prong"})$ and $B(\text{"1 prong"})$, = 0.855.
⁶ Error correlated with BALTRUSAITIS 85 $e \nu \bar{\nu}$ value.

$\Gamma(\mu^- \bar{\nu}_\mu \nu_\tau \gamma) / \Gamma_{\text{total}}$ Γ_4 / Γ

VALUE (%)	EVTS	DOCUMENT ID	TECN	COMMENT
0.367 ± 0.008 OUR AVERAGE				
0.363 ± 0.002 ± 0.015	22k	¹ SHIMIZU	18A BELL	711 fb ⁻¹ E _{cm} ^{ee} = 10.6 GeV
0.369 ± 0.003 ± 0.010	16k	² LEES	15G BABR	431 fb ⁻¹ E _{cm} ^{ee} = 10.6 GeV
0.361 ± 0.016 ± 0.035		³ BERGFELD	00 CLEO	E _{cm} ^{ee} = 10.6 GeV
0.30 ± 0.04 ± 0.05	116	⁴ ALEXANDER	96S OPAL	1991-1994 LEP runs
0.23 ± 0.10	10	⁵ WU	90 MRK2	E _{cm} ^{ee} = 29 GeV

• • • We do not use the following data for averages, fits, limits, etc. • • •

¹ SHIMIZU 18A impose requirements on detected γ 's corresponding to a τ -rest-frame energy cutoff $E_\gamma^* > 10$ MeV.

² LEES 15G impose requirements on detected γ 's corresponding to a τ -rest-frame energy cutoff $E_\gamma^* > 10$ MeV.

³ BERGFELD 00 impose requirements on detected γ 's corresponding to a τ -rest-frame energy cutoff $E_\gamma^* > 10$ MeV. For $E_\gamma^* > 20$ MeV, they quote $(3.04 \pm 0.14 \pm 0.30) \times 10^{-3}$.

⁴ ALEXANDER 96S impose requirements on detected γ 's corresponding to a τ -rest-frame energy cutoff $E_\gamma > 20$ MeV.

⁵ WU 90 reports $\Gamma(\mu^- \bar{\nu}_\mu \nu_\tau \gamma) / \Gamma(\mu^- \bar{\nu}_\mu \nu_\tau) = 0.013 \pm 0.006$, which is converted to $\Gamma(\mu^- \bar{\nu}_\mu \nu_\tau \gamma) / \Gamma_{\text{total}}$ using $\Gamma(\mu^- \bar{\nu}_\mu \nu_\tau \gamma) / \Gamma_{\text{total}} = 17.35\%$. Requirements on detected γ 's correspond to a τ rest frame energy cutoff $E_\gamma > 37$ MeV.

$\Gamma(e^- \bar{\nu}_e \nu_\tau) / \Gamma_{\text{total}}$ Γ_5 / Γ

To minimize the effect of experiments with large systematic errors, we exclude experiments which together would contribute 5% of the weight in the average.

VALUE (%)	EVTS	DOCUMENT ID	TECN	COMMENT
17.82 ± 0.04 OUR FIT (Produced by HFLAV)				
17.82 ± 0.05 OUR AVERAGE				
17.837 ± 0.072 ± 0.036	56k	¹ SCHAEEL	05c ALEP	1991-1995 LEP runs
17.806 ± 0.104 ± 0.076	24.7k	² ACCIARRI	01F L3	1991-1995 LEP runs
17.81 ± 0.09 ± 0.06	33.1k	ABBIENDI	99H OPAL	1991-1995 LEP runs
17.877 ± 0.109 ± 0.110	23.3k	ABREU	99X DLPH	1991-1995 LEP runs
17.76 ± 0.06 ± 0.17		³ ANASTASSOV	97 CLEO	E _{cm} ^{ee} = 10.6 GeV
• • • We do not use the following data for averages, fits, limits, etc. • • •				
17.78 ± 0.10 ± 0.09	25.3k	ALEXANDER	96D OPAL	Repl. by ABBI-ENDDI 99H
17.79 ± 0.12 ± 0.06	20.6k	BUSKULIC	96c ALEP	Repl. by SCHAEEL 05c
17.51 ± 0.23 ± 0.31	5059	ABREU	95T DLPH	Repl. by ABREU 99X
17.9 ± 0.4 ± 0.4	2892	ADRIANI	93M L3	Repl. by ACCIARRI 01F
17.5 ± 0.3 ± 0.5		⁴ ALBRECHT	93G ARG	E _{cm} ^{ee} = 9.4-10.6 GeV
17.97 ± 0.14 ± 0.23	3970	AKERIB	92 CLEO	Repl. by ANA-S-TASSOV 97
19.1 ± 0.4 ± 0.6	2960	⁵ AMMAR	92 CLEO	E _{cm} ^{ee} = 10.5-10.9 GeV
18.09 ± 0.45 ± 0.45		DECAMP	92c ALEP	Repl. by SCHAEEL 05c
17.0 ± 0.5 ± 0.6	1.7k	ABACHI	90 HRS	E _{cm} ^{ee} = 29 GeV
18.4 ± 0.8 ± 0.4	644	BEHREND	90 CELL	E _{cm} ^{ee} = 35 GeV
16.3 ± 0.3 ± 3.2		JANSEN	89 CBAL	E _{cm} ^{ee} = 9.4-10.6 GeV
18.4 ± 1.2 ± 1.0		AIHARA	87B TPC	E _{cm} ^{ee} = 29 GeV
19.1 ± 0.8 ± 1.1		BURCHAT	87 MRK2	E _{cm} ^{ee} = 29 GeV
16.8 ± 0.7 ± 0.9	515	⁵ BARTEL	86D JADE	E _{cm} ^{ee} = 34.6 GeV
20.4 ± 3.0 ^{+1.4} / _{-0.9}		ALTHOFF	85 TASS	E _{cm} ^{ee} = 34.5 GeV
17.8 ± 0.9 ± 0.6	390	⁵ ASH	85B MAC	E _{cm} ^{ee} = 29 GeV
18.2 ± 0.7 ± 0.5		⁶ BALTRUSAITIS	85 MRK3	E _{cm} ^{ee} = 3.77 GeV
13.0 ± 1.9 ± 2.9		BERGER	85 PLUT	E _{cm} ^{ee} = 34.6 GeV
18.3 ± 2.4 ± 1.9	60	BEHREND	83c CELL	E _{cm} ^{ee} = 34 GeV
16.0 ± 1.3	459	⁷ BACINO	78B DLCO	E _{cm} ^{ee} = 3.1-7.4 GeV

¹ Correlation matrix for SCHAEEL 05c branching fractions, in percent:

(1) $\Gamma(\tau^- \rightarrow e^- \bar{\nu}_e \nu_\tau) / \Gamma_{\text{total}}$

(2) $\Gamma(\tau^- \rightarrow \mu^- \bar{\nu}_\mu \nu_\tau) / \Gamma_{\text{total}}$

(3) $\Gamma(\tau^- \rightarrow \pi^- \nu_\tau) / \Gamma_{\text{total}}$

(4) $\Gamma(\tau^- \rightarrow \pi^- \pi^0 \nu_\tau) / \Gamma_{\text{total}}$

(5) $\Gamma(\tau^- \rightarrow \pi^- 2\pi^0 \nu_\tau \text{ (ex. } K^0)) / \Gamma_{\text{total}}$

(6) $\Gamma(\tau^- \rightarrow \pi^- 3\pi^0 \nu_\tau \text{ (ex. } K^0)) / \Gamma_{\text{total}}$

(7) $\Gamma(\tau^- \rightarrow h^- 4\pi^0 \nu_\tau \text{ (ex. } K^0, \eta)) / \Gamma_{\text{total}}$

(8) $\Gamma(\tau^- \rightarrow \pi^- \pi^+ \pi^- \nu_\tau \text{ (ex. } K^0, \omega)) / \Gamma_{\text{total}}$

(9) $\Gamma(\tau^- \rightarrow \pi^- \pi^+ \pi^- \pi^0 \nu_\tau \text{ (ex. } K^0)) / \Gamma_{\text{total}}$

(10) $\Gamma(\tau^- \rightarrow h^- h^- h^+ 2\pi^0 \nu_\tau \text{ (ex. } K^0)) / \Gamma_{\text{total}}$

(11) $\Gamma(\tau^- \rightarrow h^- h^- h^+ 3\pi^0 \nu_\tau) / \Gamma_{\text{total}}$

(12) $\Gamma(\tau^- \rightarrow 3h^- 2h^+ \nu_\tau \text{ (ex. } K^0)) / \Gamma_{\text{total}}$

(13) $\Gamma(\tau^- \rightarrow 3h^- 2h^+ \pi^0 \nu_\tau \text{ (ex. } K^0)) / \Gamma_{\text{total}}$

(1) (2) (3) (4) (5) (6) (7) (8) (9) (10) (11) (12)

(2) -20

(3) -9 -6

(4) -16 -12 2

(5) -5 -5 -17 -37

(6) 0 -4 -15 2 -27

(7) -2 -4 -24 -15 20 -47

(8) -14 -9 15 -5 -17 -14 -8

(9)	-13	-12	-25	-30	4	-2	16	-15				
(10)	0	-2	-23	-14	4	10	13	-6	-17			
(11)	1	0	-5	1	4	6	0	-9	-2	-11		
(12)	0	1	9	4	-8	-4	-6	9	-5	-4	-2	
(13)	1	-4	-3	-5	3	2	-4	-3	-1	4	1	-24

² The correlation coefficient between this measurement and the ACCIARRI 01F measurement of $B(\tau^- \rightarrow \mu^- \bar{\nu}_\mu \nu_\tau)$ is 0.08.

³ The correlation coefficients between this measurement and the ANASTASSOV 97 measurements of $B(\mu^- \bar{\nu}_\mu \nu_\tau)$, $B(\mu^- \bar{\nu}_\mu \nu_\tau) / B(e^- \bar{\nu}_e \nu_\tau)$, $B(h^- \nu_\tau)$, and $B(h^- \nu_\tau) / B(e^- \bar{\nu}_e \nu_\tau)$ are 0.50, -0.42, 0.48, and -0.39 respectively.

⁴ Not independent of ALBRECHT 92D $\Gamma(\mu^- \bar{\nu}_\mu \nu_\tau) / \Gamma(e^- \bar{\nu}_e \nu_\tau)$ and ALBRECHT 93G $\Gamma(\mu^- \bar{\nu}_\mu \nu_\tau) \times \Gamma(e^- \bar{\nu}_e \nu_\tau) / \Gamma_{\text{total}}^2$ values.

⁵ Modified using $B(e^- \bar{\nu}_e \nu_\tau) / B(\text{"1 prong"})$ and $B(\text{"1 prong"}) = 0.855$.

⁶ Error correlated with BALTRUSAITIS 85 $\Gamma(\mu^- \bar{\nu}_\mu \nu_\tau) / \Gamma_{\text{total}}$.

⁷ BACINO 78B value comes from fit to events with e^\pm and one other nonelectron charged prong.

$\Gamma(\mu^- \bar{\nu}_\mu \nu_\tau) / \Gamma(e^- \bar{\nu}_e \nu_\tau)$ Γ_3 / Γ_5

Standard Model prediction including mass effects is 0.9726.

VALUE (units 10 ⁻²)	EVTS	DOCUMENT ID	TECN	COMMENT
97.62 ± 0.28 OUR FIT (Produced by HFLAV)				
97.9 ± 0.4 OUR AVERAGE				
97.96 ± 0.16 ± 0.36	731k	¹ AUBERT	10F BABR	467 fb ⁻¹ E _{cm} ^{ee} = 10.6 GeV
97.77 ± 0.63 ± 0.87		² ANASTASSOV	97 CLEO	E _{cm} ^{ee} = 10.6 GeV
99.7 ± 3.5 ± 4.0		ALBRECHT	92D ARG	E _{cm} ^{ee} = 9.4-10.6 GeV

¹ Correlation matrix for AUBERT 10F branching fractions:

(1) $\Gamma(\tau^- \rightarrow \mu^- \bar{\nu}_\mu \nu_\tau) / \Gamma(\tau^- \rightarrow e^- \bar{\nu}_e \nu_\tau)$

(2) $\Gamma(\tau^- \rightarrow \pi^- \nu_\tau) / \Gamma(\tau^- \rightarrow e^- \bar{\nu}_e \nu_\tau)$

(3) $\Gamma(\tau^- \rightarrow K^- \nu_\tau) / \Gamma(\tau^- \rightarrow e^- \bar{\nu}_e \nu_\tau)$

(1) (2)

(2) 0.25

(3) 0.12 0.33

² The correlation coefficients between this measurement and the ANASTASSOV 97 measurements of $B(\mu^- \bar{\nu}_\mu \nu_\tau)$, $B(e^- \bar{\nu}_e \nu_\tau)$, $B(h^- \nu_\tau)$, and $B(h^- \nu_\tau) / B(e^- \bar{\nu}_e \nu_\tau)$ are 0.58, -0.42, 0.07, and 0.45 respectively.

$\Gamma(e^- \bar{\nu}_e \nu_\tau \gamma) / \Gamma_{\text{total}}$ Γ_6 / Γ

VALUE (%)	EVTS	DOCUMENT ID	TECN	COMMENT
1.83 ± 0.05 OUR AVERAGE				
1.79 ± 0.02 ± 0.10	12k	¹ SHIMIZU	18A BELL	711 fb ⁻¹ E _{cm} ^{ee} = 10.6 GeV
1.847 ± 0.015 ± 0.052	18k	² LEES	15G BABR	431 fb ⁻¹ E _{cm} ^{ee} = 10.6 GeV
1.75 ± 0.06 ± 0.17		³ BERGFELD	00 CLEO	E _{cm} ^{ee} = 10.6 GeV

¹ SHIMIZU 18A impose requirements on detected γ 's corresponding to a τ -rest-frame energy cutoff $E_\gamma^* > 10$ MeV.

² LEES 15G impose requirements on detected γ 's corresponding to a τ -rest-frame energy cutoff $E_\gamma^* > 10$ MeV.

³ BERGFELD 00 impose requirements on detected γ 's corresponding to a τ -rest-frame energy cutoff $E_\gamma^* > 10$ MeV.

$\Gamma(h^- \geq 0 K_L^0 \nu_\tau) / \Gamma_{\text{total}}$ Γ_7 / Γ

$\Gamma_7 / \Gamma = (\Gamma_9 + \Gamma_{10} + \frac{1}{2} \Gamma_{36} + \frac{1}{2} \Gamma_{38} + \Gamma_{50}) / \Gamma$

VALUE (%)	EVTS	DOCUMENT ID	TECN	COMMENT
12.03 ± 0.05 OUR FIT (Produced by HFLAV)				
12.2 ± 0.4 OUR AVERAGE				
12.47 ± 0.26 ± 0.43	2967	¹ ACCIARRI	95 L3	1992 LEP run
12.4 ± 0.7 ± 0.7	283	² ABREU	92N DLPH	1990 LEP run
12.1 ± 0.7 ± 0.5	309	ALEXANDER	91D OPAL	1990 LEP run
• • • We use the following data for averages but not for fits. • • •				
11.3 ± 0.5 ± 0.8	798	³ FORD	87 MAC	E _{cm} ^{ee} = 29 GeV
• • • We do not use the following data for averages, fits, limits, etc. • • •				
12.44 ± 0.11 ± 0.11	15k	⁴ BUSKULIC	96 ALEP	Repl. by SCHAEEL 05c
11.7 ± 0.6 ± 0.8		⁵ ALBRECHT	92D ARG	E _{cm} ^{ee} = 9.4-10.6 GeV
12.98 ± 0.44 ± 0.33		⁶ DECAMP	92c ALEP	Repl. by SCHAEEL 05c
12.3 ± 0.9 ± 0.5	1338	BEHREND	90 CELL	E _{cm} ^{ee} = 35 GeV
11.1 ± 1.1 ± 1.4		⁷ BURCHAT	87 MRK2	E _{cm} ^{ee} = 29 GeV
12.3 ± 0.6 ± 1.1	328	⁸ BARTEL	86D JADE	E _{cm} ^{ee} = 34.6 GeV
13.0 ± 2.0 ± 4.0		BERGER	85 PLUT	E _{cm} ^{ee} = 34.6 GeV
11.2 ± 1.7 ± 1.2	34	⁹ BEHREND	83c CELL	E _{cm} ^{ee} = 34 GeV

¹ ACCIARRI 95 with 0.65% added to remove their correction for $\pi^- K_L^0$ backgrounds.

² ABREU 92N with 0.5% added to remove their correction for $K^*(892)^-$ backgrounds.

³ FORD 87 result for $B(\pi^- \nu_\tau)$ with 0.67% added to remove their K^- correction and adjusted for 1992 B("1 prong").

⁴ BUSKULIC 96 quote $11.78 \pm 0.11 \pm 0.13$ We add 0.66 to undo their correction for unseen K_L^0 and modify the systematic error accordingly.

⁵ Not independent of ALBRECHT 92D $\Gamma(\mu^- \bar{\nu}_\mu \nu_\tau) / \Gamma(e^- \bar{\nu}_e \nu_\tau)$, $\Gamma(\mu^- \bar{\nu}_\mu \nu_\tau) \times \Gamma(e^- \bar{\nu}_e \nu_\tau)$, and $\Gamma(h^- \geq 0 K_L^0 \nu_\tau) / \Gamma(e^- \bar{\nu}_e \nu_\tau)$ values.

⁶ DECAMP 92c quote $B(h^- \geq 0 K_L^0 \nu_\tau) = 13.32 \pm 0.44 \pm 0.33$. We subtract 0.35 to correct for their inclusion of the K_S^0 decays.

Lepton Particle Listings

τ

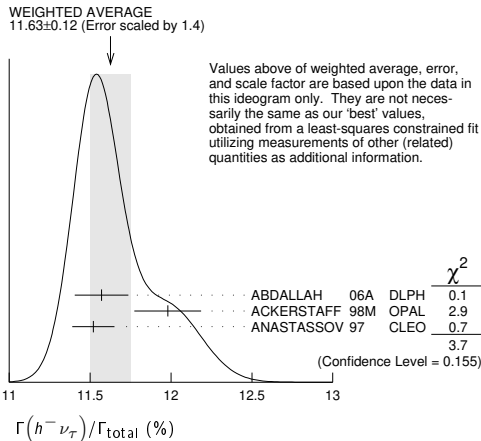
- ⁷ BURCHAT 87 with 1.1% added to remove their correction for K^- and $K^*(892)^-$ backgrounds.
- ⁸ BARTEL 86d result for $B(\pi^- \nu_\tau)$ with 0.59% added to remove their K^- correction and adjusted for 1992 B("1 prong").
- ⁹ BEHREND 83c quote $B(\pi^- \nu_\tau) = 9.9 \pm 1.7 \pm 1.3$ after subtracting 1.3 ± 0.5 to correct for $B(K^- \nu_\tau)$.

$\Gamma(h^- \nu_\tau)/\Gamma_{\text{total}}$		$\Gamma_8/\Gamma = (\Gamma_9 + \Gamma_{10})/\Gamma$			
VALUE (%)	EVTS	DOCUMENT ID	TECN	COMMENT	
11.51 ± 0.05 OUR FIT		(Produced by HFLAV)			
11.63 ± 0.12 OUR AVERAGE		Error includes scale factor of 1.4. See the ideogram below.			
11.571 ± 0.120 ± 0.114	19k	¹ ABDALLAH 06A DLPH	1992-1995 LEP runs		
11.98 ± 0.13 ± 0.16		ACKERSTAFF 98M OPAL	1991-1995 LEP runs		
11.52 ± 0.05 ± 0.12		² ANASTASSOV 97 CLEO	$E_{\text{cm}}^{\text{e}} = 10.6$ GeV		

¹ Correlation matrix for ABDALLAH 06A branching fractions, in percent:

(1) $\Gamma(\tau^- \rightarrow h^- \nu_\tau)/\Gamma_{\text{total}}$	(2)	(3)	(4)	(5)	(6)	(7)	(8)	(9)	(10)
(2) -34									
(3) -47 56									
(4) 6 -66 15									
(5) -6 38 11 -86									
(6) -7 -8 15 0 -2									
(7) -2 -1 -5 -3 3 -53									
(8) -4 -4 -13 -4 -2 -56 75									
(9) -1 -1 -4 3 -6 26 -78 -16									
(10) -1 -1 1 0 0 -2 -3 -1 3									
(11) 0 0 0 0 0 1 0 -5 5 -57									

² The correlation coefficients between this measurement and the ANASTASSOV 97 measurements of $B(\mu \bar{\nu}_\mu \nu_\tau)$, $B(e \bar{\nu}_e \nu_\tau)$, $B(\mu \bar{\nu}_\mu \nu_\tau)/B(e \bar{\nu}_e \nu_\tau)$, and $B(h^- \nu_\tau)/B(e \bar{\nu}_e \nu_\tau)$ are 0.50, 0.48, 0.07, and 0.63 respectively.



$\Gamma(h^- \nu_\tau)/\Gamma(e^- \bar{\nu}_e \nu_\tau)$		$\Gamma_8/\Gamma_5 = (\Gamma_9 + \Gamma_{10})/\Gamma_5$			
VALUE (units 10^{-2})	EVTS	DOCUMENT ID	TECN	COMMENT	
64.61 ± 0.33 OUR FIT		(Produced by HFLAV)			
64.0 ± 0.7 OUR AVERAGE		Error includes scale factor of 1.6.			
63.33 ± 0.14 ± 0.61	394k	¹ AUBERT 10F BABR	467 fb ⁻¹ $E_{\text{cm}}^{\text{e}} = 10.6$ GeV		
64.84 ± 0.41 ± 0.60		² ANASTASSOV 97 CLEO	$E_{\text{cm}}^{\text{e}} = 10.6$ GeV		

- ¹ Not independent of AUBERT 10F $\Gamma(\tau^- \rightarrow \pi^- \nu_\tau)/\Gamma(\tau^- \rightarrow e^- \bar{\nu}_e \nu_\tau)$ and $\Gamma(\tau^- \rightarrow K^- \nu_\tau)/\Gamma(\tau^- \rightarrow e^- \bar{\nu}_e \nu_\tau)$.
- ² The correlation coefficients between this measurement and the ANASTASSOV 97 measurements of $B(\mu \bar{\nu}_\mu \nu_\tau)$, $B(e \bar{\nu}_e \nu_\tau)$, $B(\mu \bar{\nu}_\mu \nu_\tau)/B(e \bar{\nu}_e \nu_\tau)$, and $B(h^- \nu_\tau)$ are 0.08, -0.39, 0.45, and 0.63 respectively.

$\Gamma(\pi^- \nu_\tau)/\Gamma_{\text{total}}$		Γ_9/Γ			
VALUE (%)	EVTS	DOCUMENT ID	TECN	COMMENT	
10.82 ± 0.05 OUR FIT		(Produced by HFLAV)			
10.828 ± 0.070 ± 0.078	38k	¹ SCHAEEL 05c ALEP	1991-1995 LEP runs		

- • • We do not use the following data for averages, fits, limits, etc. • • •
- 11.06 ± 0.11 ± 0.14 ² BUSKULIC 96 ALEP Repl. by SCHAEEL 05c
- 11.7 ± 0.4 ± 1.8 1138 BLOCKER 82b MRK2 $E_{\text{cm}}^{\text{e}} = 3.5-6.7$ GeV

- ¹ See footnote to SCHAEEL 05c $\Gamma(\tau^- \rightarrow e^- \bar{\nu}_e \nu_\tau)/\Gamma_{\text{total}}$ measurement for correlations with other measurements.
- ² Not independent of BUSKULIC 96 $B(h^- \nu_\tau)$ and $B(K^- \nu_\tau)$ values.

$\Gamma(\pi^- \nu_\tau)/\Gamma(e^- \bar{\nu}_e \nu_\tau)$		Γ_9/Γ_5			
VALUE (units 10^{-2})	EVTS	DOCUMENT ID	TECN	COMMENT	
60.71 ± 0.32 OUR FIT		(Produced by HFLAV)			
59.45 ± 0.14 ± 0.61	369k	¹ AUBERT 10F BABR	467 fb ⁻¹ $E_{\text{cm}}^{\text{e}} = 10.6$ GeV		

- ¹ See footnote to AUBERT 10F $\Gamma(\tau^- \rightarrow \mu^- \bar{\nu}_\mu \nu_\tau)/\Gamma(\tau^- \rightarrow e^- \bar{\nu}_e \nu_\tau)$ for correlations with other measurements.

$\Gamma(K^- \nu_\tau)/\Gamma_{\text{total}}$		Γ_{10}/Γ			
VALUE (%)	EVTS	DOCUMENT ID	TECN	COMMENT	
0.696 ± 0.010 OUR FIT		(Produced by HFLAV)			
0.685 ± 0.023 OUR AVERAGE					
0.658 ± 0.027 ± 0.029		¹ ABBIENDI 01J OPAL	1990-1995 LEP runs		
0.696 ± 0.025 ± 0.014	2032	BARATE 99k ALEP	1991-1995 LEP runs		
0.85 ± 0.18	27	ABREU 94k DLPH	LEP 1992 Z data		
0.66 ± 0.07 ± 0.09	99	BATTLE 94 CLEO	$E_{\text{cm}}^{\text{e}} \approx 10.6$ GeV		

- • • We do not use the following data for averages, fits, limits, etc. • • •

0.72 ± 0.04 ± 0.04	728	BUSKULIC 96 ALEP	Repl. by BARATE 99k		
0.59 ± 0.18	16	MILLS 84 DLCO	$E_{\text{cm}}^{\text{e}} = 29$ GeV		
1.3 ± 0.5	15	BLOCKER 82b MRK2	$E_{\text{cm}}^{\text{e}} = 3.9-6.7$ GeV		

- ¹ The correlation coefficient between this measurement and the ABBIENDI 01J $B(\tau^- \rightarrow K^- \geq 0\pi^0 \geq 0K^0 \geq 0\gamma \nu_\tau)$ is 0.60.

$\Gamma(K^- \nu_\tau)/\Gamma(e^- \bar{\nu}_e \nu_\tau)$		Γ_{10}/Γ_5			
VALUE (units 10^{-2})	EVTS	DOCUMENT ID	TECN	COMMENT	
3.91 ± 0.05 OUR FIT		(Produced by HFLAV)			
3.882 ± 0.032 ± 0.057	25k	¹ AUBERT 10F BABR	467 fb ⁻¹ $E_{\text{cm}}^{\text{e}} = 10.6$ GeV		

- ¹ See footnote to AUBERT 10F $\Gamma(\tau^- \rightarrow \mu^- \bar{\nu}_\mu \nu_\tau)/\Gamma(\tau^- \rightarrow e^- \bar{\nu}_e \nu_\tau)$ for correlations with other measurements.

$\Gamma(K^- \nu_\tau)/\Gamma(\pi^- \nu_\tau)$		Γ_{10}/Γ_9			
VALUE (units 10^{-2})	EVTS	DOCUMENT ID	TECN	COMMENT	
6.44 ± 0.09 OUR FIT		(Produced by HFLAV)			

- • • We use the following data for averages but not for fits. • • •
- 6.531 ± 0.056 ± 0.093** ¹ AUBERT 10F BABR 467 fb⁻¹ $E_{\text{cm}}^{\text{e}} = 10.6$ GeV
- ¹ Not independent of AUBERT 10F $\Gamma(\tau^- \rightarrow \pi^- \nu_\tau)/\Gamma(\tau^- \rightarrow e^- \bar{\nu}_e \nu_\tau)$ and $\Gamma(\tau^- \rightarrow K^- \nu_\tau)/\Gamma(\tau^- \rightarrow e^- \bar{\nu}_e \nu_\tau)$.

$\Gamma(h^- \geq 1 \text{ neutrals } \nu_\tau)/\Gamma_{\text{total}}$		Γ_{11}/Γ			
VALUE (%)	EVTS	DOCUMENT ID	TECN	COMMENT	
37.00 ± 0.09 OUR FIT		(Produced by HFLAV)			

$$\Gamma_{11}/\Gamma = (\Gamma_{14} + \Gamma_{16} + \Gamma_{20} + \Gamma_{23} + \Gamma_{27} + \Gamma_{28} + \Gamma_{30} + 0.15344\Gamma_{36} + 0.15344\Gamma_{38} + 0.15344\Gamma_{41} + 0.15344\Gamma_{43} + 0.0942\Gamma_{48} + 0.0942\Gamma_{52} + 0.7196\Gamma_{150} + 0.7196\Gamma_{152} + 0.7196\Gamma_{154} + 0.1107\Gamma_{156} + 0.0835\Gamma_{178} + 0.0835\Gamma_{179} + 0.0835\Gamma_{180})/\Gamma$$

36.14 ± 0.33 ± 0.58		¹ AKERS 94E OPAL	1991-1992 LEP runs		
38.4 ± 1.2 ± 1.0		² BURCHAT 87 MRK2	$E_{\text{cm}}^{\text{e}} = 29$ GeV		
42.7 ± 2.0 ± 2.9		BERGER 85 PLUT	$E_{\text{cm}}^{\text{e}} = 34.6$ GeV		

- • • We do not use the following data for averages, fits, limits, etc. • • •
- ¹ Not independent of ACKERSTAFF 98M $B(h^- \pi^0 \nu_\tau)$ and $B(h^- \geq 2\pi^0 \nu_\tau)$ values.
- ² BURCHAT 87 quote for $B(\pi^\pm \geq 1 \text{ neutral } \nu_\tau) = 0.378 \pm 0.012 \pm 0.010$. We add 0.006 to account for contribution from $(K^{*-} \nu_\tau)$ which they fixed at BR = 0.013.

$\Gamma(h^- \geq 1\pi^0 \nu_\tau \text{ (ex. } K^0))/\Gamma_{\text{total}}$		Γ_{12}/Γ			
VALUE (%)	EVTS	DOCUMENT ID	TECN	COMMENT	
36.50 ± 0.09 OUR FIT		(Produced by HFLAV)			

$$\Gamma_{12}/\Gamma = (\Gamma_{14} + \Gamma_{16} + \Gamma_{20} + \Gamma_{23} + \Gamma_{27} + \Gamma_{28} + \Gamma_{30} + 0.3257\Gamma_{150} + 0.3257\Gamma_{152} + 0.3257\Gamma_{154})/\Gamma$$

- • • We use the following data for averages but not for fits. • • •
- 36.641 ± 0.155 ± 0.127** 45k ¹ ABDALLAH 06A DLPH 1992-1995 LEP runs
- ¹ See footnote to ABDALLAH 06A $\Gamma(\tau^- \rightarrow h^- \nu_\tau)/\Gamma_{\text{total}}$ measurement for correlations with other measurements.

$\Gamma(h^- \pi^0 \nu_\tau)/\Gamma_{\text{total}}$		$\Gamma_{13}/\Gamma = (\Gamma_{14} + \Gamma_{16})/\Gamma$			
VALUE (%)	EVTS	DOCUMENT ID	TECN	COMMENT	
25.93 ± 0.09 OUR FIT		(Produced by HFLAV)			
25.73 ± 0.16 OUR AVERAGE					
25.67 ± 0.01 ± 0.39	5.4M	FUJIKAWA 08 BELL	72 fb ⁻¹ $E_{\text{cm}}^{\text{e}} = 10.6$ GeV		
25.740 ± 0.201 ± 0.138	35k	¹ ABDALLAH 06A DLPH	1992-1995 LEP runs		
25.89 ± 0.17 ± 0.29		ACKERSTAFF 98M OPAL	1991-1995 LEP runs		
25.05 ± 0.35 ± 0.50	6613	ACCIARRI 95 L3	1992 LEP run		
25.87 ± 0.12 ± 0.42	51k	² ARTUSO 94 CLEO	$E_{\text{cm}}^{\text{e}} = 10.6$ GeV		

- • • We do not use the following data for averages, fits, limits, etc. • • •

25.76 ± 0.15 ± 0.13	31k	BUSKULIC	96	ALEP	Repl. by SCHAEL 05c
25.98 ± 0.36 ± 0.52		³ AKERS	94E	OPAL	Repl. by ACKER-STAFF 98M
22.9 ± 0.8 ± 1.3	283	⁴ ABREU	92N	DLPH	$E_{cm}^{ee} = 88.2-94.2$ GeV
23.1 ± 0.4 ± 0.9	1249	⁵ ALBRECHT	92Q	ARG	$E_{cm}^{ee} = 10$ GeV
25.02 ± 0.64 ± 0.88	1849	DECAMP	92C	ALEP	1989-1990 LEP runs
22.0 ± 0.8 ± 1.9	779	ANTREASIAN	91	CBAL	$E_{cm}^{ee} = 9.4-10.6$ GeV
22.6 ± 1.5 ± 0.7	1101	BEHREND	90	CELL	$E_{cm}^{ee} = 35$ GeV
23.1 ± 1.9 ± 1.6		BEHREND	84	CELL	$E_{cm}^{ee} = 14,22$ GeV

- See footnote to ABDALLAH 06A $\Gamma(\tau^- \rightarrow h^- \nu_\tau)/\Gamma_{total}$ measurement for correlations with other measurements.
- ARTUSO 94 reports the combined result from three independent methods, one of which (23% of the $\tau^- \rightarrow h^- \pi^0 \nu_\tau$) is normalized to the inclusive one-prong branching fraction, taken as 0.854 ± 0.004 . Renormalization to the present value causes negligible change.
- AKERS 94E quote $(26.25 \pm 0.36 \pm 0.52) \times 10^{-2}$; we subtract 0.27% from their number to correct for $\tau^- \rightarrow h^- K_L^0 \nu_\tau$.
- ABREU 92N with 0.5% added to remove their correction for $K^*(892)^-$ backgrounds.
- ALBRECHT 92Q with 0.5% added to remove their correction for $\tau^- \rightarrow K^*(892)^- \nu_\tau$ background.

$\Gamma(\pi^- \pi^0 \nu_\tau)/\Gamma_{total}$ Γ_{14}/Γ

VALUE (%)	EVTS	DOCUMENT ID	TECN	COMMENT
25.49 ± 0.09 OUR FIT		(Produced by HFLAV)		
25.46 ± 0.12 OUR AVERAGE				
25.471 ± 0.097 ± 0.085	81k	¹ SCHAEL	05c	ALEP 1991-1995 LEP runs
• • • We use the following data for averages but not for fits. • • •				
25.36 ± 0.44		² ARTUSO	94	CLEO $E_{cm}^{ee} = 10.6$ GeV
• • • We do not use the following data for averages, fits, limits, etc. • • •				
25.30 ± 0.15 ± 0.13		³ BUSKULIC	96	ALEP Repl. by SCHAEL 05c
21.5 ± 0.4 ± 1.9	4400	^{4,5} ALBRECHT	88L	ARG $E_{cm}^{ee} = 10$ GeV
23.0 ± 1.3 ± 1.7	582	ADLER	87B	MRK3 $E_{cm}^{ee} = 3.77$ GeV
25.8 ± 1.7 ± 2.5		⁶ BURCHAT	87	MRK2 $E_{cm}^{ee} = 29$ GeV
22.3 ± 0.6 ± 1.4	629	⁵ YELTON	86	MRK2 $E_{cm}^{ee} = 29$ GeV

- See footnote to SCHAEL 05c $\Gamma(\tau^- \rightarrow e^- \bar{\nu}_e \nu_\tau)/\Gamma_{total}$ measurement for correlations with other measurements.
- Not independent of ARTUSO 94 $B(h^- \pi^0 \nu_\tau)$ and BATTLE 94 $B(K^- \pi^0 \nu_\tau)$ values.
- Not independent of BUSKULIC 96 $B(h^- \pi^0 \nu_\tau)$ and $B(K^- \pi^0 \nu_\tau)$ values.
- The authors divide by $(\Gamma_3 + \Gamma_5 + \Gamma_9 + \Gamma_{10})/\Gamma = 0.467$ to obtain this result.
- Experiment had no hadron identification. Kaon corrections were made, but insufficient information is given to permit their removal.
- BURCHAT 87 value is not independent of YELTON 86 value. Nonresonant decays included.

$\Gamma(\pi^- \pi^0 \text{non-}\rho(770)\nu_\tau)/\Gamma_{total}$ Γ_{15}/Γ

VALUE (%)	DOCUMENT ID	TECN	COMMENT
0.3 ± 0.1 ± 0.3	¹ BEHREND 84	CELL	$E_{cm}^{ee} = 14,22$ GeV

- BEHREND 84 assume a flat nonresonant mass distribution down to the $\rho(770)$ mass, using events with mass above 1300 to set the level.

$\Gamma(K^- \pi^0 \nu_\tau)/\Gamma_{total}$ Γ_{16}/Γ

VALUE (%)	EVTS	DOCUMENT ID	TECN	COMMENT
0.433 ± 0.015 OUR FIT		(Produced by HFLAV)		
0.426 ± 0.016 OUR AVERAGE				
0.416 ± 0.003 ± 0.018	78k	AUBERT	07AP	BABR 230 fb^{-1} $E_{cm}^{ee} = 10.6$ GeV
0.471 ± 0.059 ± 0.023	360	ABBIENDI	04J	OPAL 1991-1995 LEP runs
0.444 ± 0.026 ± 0.024	923	BARATE	99K	ALEP 1991-1995 LEP runs
0.51 ± 0.10 ± 0.07	37	BATTLE	94	CLEO $E_{cm}^{ee} \approx 10.6$ GeV
• • • We do not use the following data for averages, fits, limits, etc. • • •				
0.52 ± 0.04 ± 0.05	395	BUSKULIC	96	ALEP Repl. by BARATE 99k

$\Gamma(h^- \geq 2\pi^0 \nu_\tau)/\Gamma_{total}$ Γ_{17}/Γ

$\Gamma_{17}/\Gamma = (\Gamma_{20} + \Gamma_{23} + \Gamma_{27} + \Gamma_{28} + \Gamma_{30} + 0.15344\Gamma_{36} + 0.15344\Gamma_{38} + 0.15344\Gamma_{41} + 0.15344\Gamma_{43} + 0.09419\Gamma_{48} + 0.0942\Gamma_{52} + 0.3257\Gamma_{150} + 0.3257\Gamma_{152} + 0.3257\Gamma_{154})/\Gamma$

VALUE (%)	EVTS	DOCUMENT ID	TECN	COMMENT
10.81 ± 0.09 OUR FIT		(Produced by HFLAV)		
9.91 ± 0.31 ± 0.27		ACKERSTAFF 98M	OPAL	1991-1995 LEP runs
• • • We do not use the following data for averages, fits, limits, etc. • • •				
9.89 ± 0.34 ± 0.55		¹ AKERS	94E	OPAL Repl. by ACKER-STAFF 98M
14.0 ± 1.2 ± 0.6	938	² BEHREND	90	CELL $E_{cm}^{ee} = 35$ GeV
12.0 ± 1.4 ± 2.5		³ BURCHAT	87	MRK2 $E_{cm}^{ee} = 29$ GeV
13.9 ± 2.0 $\pm \frac{1.9}{-2.2}$		⁴ AIHARA	86E	TPC $E_{cm}^{ee} = 29$ GeV

- AKERS 94E not independent of AKERS 94E $B(h^- \geq 1\pi^0 \nu_\tau)$ and $B(h^- \pi^0 \nu_\tau)$ measurements.
- No independent of BEHREND 90 $\Gamma(h^- 2\pi^0 \nu_\tau \text{ (ex. } K^0))$ and $\Gamma(h^- \geq 3\pi^0 \nu_\tau)$.
- Error correlated with BURCHAT 87 $\Gamma(\rho^- \nu_e)/\Gamma(\text{total})$ value.
- AIHARA 86E (TPC) quote $B(2\pi^0 \pi^- \nu_\tau) + 1.6B(3\pi^0 \pi^- \nu_\tau) + 1.1B(\pi^0 \eta \pi^- \nu_\tau)$.

$\Gamma(h^- 2\pi^0 \nu_\tau)/\Gamma_{total}$ Γ_{18}/Γ

$\Gamma_{18}/\Gamma = (\Gamma_{20} + \Gamma_{23} + 0.15344\Gamma_{36} + 0.15344\Gamma_{38})/\Gamma$

VALUE (%)	EVTS	DOCUMENT ID	TECN	COMMENT
9.48 ± 0.10 OUR FIT		(Produced by HFLAV)		
• • • We do not use the following data for averages, fits, limits, etc. • • •				
9.48 ± 0.13 ± 0.10	12k	¹ BUSKULIC	96	ALEP Repl. by SCHAEL 05c
¹ BUSKULIC 96 quote $9.29 \pm 0.13 \pm 0.10$. We add 0.19 to undo their correction for $\tau^- \rightarrow h^- K^0 \nu_\tau$.				

• • • We do not use the following data for averages, fits, limits, etc. • • •

$\Gamma(h^- 2\pi^0 \nu_\tau \text{ (ex. } K^0))/\Gamma_{total}$ Γ_{19}/Γ

$\Gamma_{19}/\Gamma = (\Gamma_{20} + \Gamma_{23})/\Gamma$

VALUE (%)	EVTS	DOCUMENT ID	TECN	COMMENT
9.32 ± 0.10 OUR FIT		(Produced by HFLAV)		
9.17 ± 0.27 OUR AVERAGE				
9.498 ± 0.320 ± 0.275	9.5k	¹ ABDALLAH	06A	DLPH 1992-1995 LEP runs
8.88 ± 0.37 ± 0.42	1060	ACCIARRI	95	L3 1992 LEP run

• • • We use the following data for averages but not for fits. • • •

8.96 ± 0.16 ± 0.44		² PROCARIO	93	CLEO $E_{cm}^{ee} \approx 10.6$ GeV
• • • We do not use the following data for averages, fits, limits, etc. • • •				
10.38 ± 0.66 ± 0.82	809	³ DECAMP	92C	ALEP Repl. by SCHAEL 05c
5.7 ± 0.5 $\pm \frac{1.7}{-1.0}$	133	⁴ ANTREASIAN	91	CBAL $E_{cm}^{ee} = 9.4-10.6$ GeV
10.0 ± 1.5 ± 1.1	333	⁵ BEHREND	90	CELL $E_{cm}^{ee} = 35$ GeV
8.7 ± 0.4 ± 1.1	815	⁶ BAND	87	MAC $E_{cm}^{ee} = 29$ GeV
6.2 ± 0.6 ± 1.2		⁷ GAN	87	MRK2 $E_{cm}^{ee} = 29$ GeV
6.0 ± 3.0 ± 1.8		BEHREND	84	CELL $E_{cm}^{ee} = 14,22$ GeV

- See footnote to ABDALLAH 06A $\Gamma(\tau^- \rightarrow h^- \nu_\tau)/\Gamma_{total}$ measurement for correlations with other measurements.
- PROCARIO 93 entry is obtained from $B(h^- 2\pi^0 \nu_\tau)/B(h^- \pi^0 \nu_\tau)$ using ARTUSO 94 result for $B(h^- \pi^0 \nu_\tau)$.
- We subtract 0.0015 to account for $\tau^- \rightarrow K^*(892)^- \nu_\tau$ contribution.
- ANTREASIAN 91 subtract 0.001 to account for the $\tau^- \rightarrow K^*(892)^- \nu_\tau$ contribution.
- BEHREND 90 subtract 0.002 to account for the $\tau^- \rightarrow K^*(892)^- \nu_\tau$ contribution.
- BAND 87 assume $B(\pi^- 3\pi^0 \nu_\tau) = 0.01$ and $B(\pi^- \pi^0 \eta \nu_\tau) = 0.005$.
- GAN 87 analysis use photon multiplicity distribution.

$\Gamma(h^- 2\pi^0 \nu_\tau \text{ (ex. } K^0))/\Gamma(h^- \pi^0 \nu_\tau)$ Γ_{19}/Γ_{13}

$\Gamma_{19}/\Gamma_{13} = (\Gamma_{20} + \Gamma_{23})/(\Gamma_{14} + \Gamma_{16})$

VALUE (units 10^{-2})	DOCUMENT ID	TECN	COMMENT
36.0 ± 0.4 OUR FIT		(Produced by HFLAV)	
34.2 ± 0.6 ± 1.6			
¹ PROCARIO 93 quote $0.345 \pm 0.006 \pm 0.016$ after correction for 2 kaon backgrounds assuming $B(K^{*-} \nu_\tau) = 1.42 \pm 0.18\%$ and $B(h^- K^0 \pi^0 \nu_\tau) = 0.48 \pm 0.48\%$. We multiply by 0.990 ± 0.010 to remove these corrections to $B(h^- \pi^0 \nu_\tau)$.			

• • • We do not use the following data for averages, fits, limits, etc. • • •

$\Gamma(\pi^- 2\pi^0 \nu_\tau \text{ (ex. } K^0))/\Gamma_{total}$ Γ_{20}/Γ

VALUE (%)	EVTS	DOCUMENT ID	TECN	COMMENT
9.26 ± 0.10 OUR FIT		(Produced by HFLAV)		
9.239 ± 0.086 ± 0.090	31k	¹ SCHAEL	05c	ALEP 1991-1995 LEP runs
• • • We do not use the following data for averages, fits, limits, etc. • • •				
9.21 ± 0.13 ± 0.11		² BUSKULIC	96	ALEP Repl. by SCHAEL 05c

- See footnote to SCHAEL 05c $\Gamma(\tau^- \rightarrow e^- \bar{\nu}_e \nu_\tau)/\Gamma_{total}$ measurement for correlations with other measurements.
- Not independent of BUSKULIC 96 $B(h^- 2\pi^0 \nu_\tau \text{ (ex. } K^0))$ and $B(K^- 2\pi^0 \nu_\tau \text{ (ex. } K^0))$ values.

$\Gamma(\pi^- 2\pi^0 \nu_\tau \text{ (ex. } K^0, \text{ scalar)})/\Gamma(\pi^- 2\pi^0 \nu_\tau \text{ (ex. } K^0))$ Γ_{21}/Γ_{20}

VALUE	CL%	DOCUMENT ID	TECN	COMMENT
<0.094	95	¹ BROWDER	00	CLEO 4.7 fb^{-1} $E_{cm}^{ee} = 10.6$ GeV

- Model-independent limit from structure function analysis on contribution to $B(\tau^- \rightarrow \pi^- 2\pi^0 \nu_\tau \text{ (ex. } K^0))$ from scalars.

$\Gamma(\pi^- 2\pi^0 \nu_\tau \text{ (ex. } K^0, \text{ vector)})/\Gamma(\pi^- 2\pi^0 \nu_\tau \text{ (ex. } K^0))$ Γ_{22}/Γ_{20}

VALUE	CL%	DOCUMENT ID	TECN	COMMENT
<0.073	95	¹ BROWDER	00	CLEO 4.7 fb^{-1} $E_{cm}^{ee} = 10.6$ GeV

- Model-independent limit from structure function analysis on contribution to $B(\tau^- \rightarrow \pi^- 2\pi^0 \nu_\tau \text{ (ex. } K^0))$ from vectors.

$\Gamma(K^- 2\pi^0 \nu_\tau \text{ (ex. } K^0))/\Gamma_{total}$ Γ_{23}/Γ

VALUE (units 10^{-4})	EVTS	DOCUMENT ID	TECN	COMMENT
5.8 ± 2.2 OUR FIT		(Produced by HFLAV)		
5.8 ± 2.4 OUR AVERAGE				
5.6 ± 2.0 ± 1.5	131	BARATE	99K	ALEP 1991-1995 LEP runs
9 ± 10 ± 3	3	¹ BATTLE	94	CLEO $E_{cm}^{ee} \approx 10.6$ GeV

• • • We do not use the following data for averages, fits, limits, etc. • • •

8 ± 2 ± 2	59	BUSKULIC	96	ALEP Repl. by BARATE 99k
¹ BATTLE 94 quote $(14 \pm 10 \pm 3) \times 10^{-4}$ or $< 30 \times 10^{-4}$ at 90% CL. We subtract $(5 \pm 2) \times 10^{-4}$ to account for $\tau^- \rightarrow K^-(K^0 \rightarrow \pi^0 \pi^0) \nu_\tau$ background.				

Lepton Particle Listings

 τ

$$\Gamma(h^- \geq 3\pi^0 \nu_\tau) / \Gamma_{\text{total}} \quad \Gamma_{24} / \Gamma$$

$$\Gamma_{24} / \Gamma = (\Gamma_{27} + \Gamma_{28} + \Gamma_{30} + 0.15344\Gamma_{41} + 0.15344\Gamma_{43} + 0.0942\Gamma_{48} + 0.0942\Gamma_{52} + 0.3257\Gamma_{150} + 0.3257\Gamma_{152} + 0.3257\Gamma_{154} + 0.0501\Gamma_{156}) / \Gamma$$

VALUE (%)	EVTS	DOCUMENT ID	TECN	COMMENT
1.34 ± 0.07 OUR FIT		(Produced by HFLAV)		
• • • We do not use the following data for averages, fits, limits, etc. • • •				
1.53 ± 0.40 ± 0.46	186	DECAMP	92c ALEP	Repl. by SCHAEEL 05c
3.2 ± 1.0 ± 1.0		BEHREND	90 CELL	$E_{\text{cm}}^{\text{ee}} = 35$ GeV

$$\Gamma(h^- \geq 3\pi^0 \nu_\tau \text{ (ex. } K^0)) / \Gamma_{\text{total}} \quad \Gamma_{25} / \Gamma$$

$$\Gamma_{25} / \Gamma = (\Gamma_{27} + \Gamma_{28} + \Gamma_{30} + 0.3257\Gamma_{150} + 0.3257\Gamma_{152} + 0.3257\Gamma_{154}) / \Gamma$$

VALUE (%)	EVTS	DOCUMENT ID	TECN	COMMENT
1.25 ± 0.07 OUR FIT		(Produced by HFLAV)		
1.403 ± 0.214 ± 0.224	1.1k	¹ ABDALLAH	06A DLPH	1992–1995 LEP runs
¹ See footnote to ABDALLAH 06A $\Gamma(\tau^- \rightarrow h^- \nu_\tau) / \Gamma_{\text{total}}$ measurement for correlations with other measurements.				

$$\Gamma(h^- 3\pi^0 \nu_\tau) / \Gamma_{\text{total}} \quad \Gamma_{26} / \Gamma$$

$$\Gamma_{26} / \Gamma = (\Gamma_{27} + \Gamma_{28} + 0.15344\Gamma_{41} + 0.15344\Gamma_{43} + 0.3257\Gamma_{152}) / \Gamma$$

VALUE (%)	EVTS	DOCUMENT ID	TECN	COMMENT
1.18 ± 0.07 OUR FIT		(Produced by HFLAV)		
1.21 ± 0.17 OUR AVERAGE		Error includes scale factor of 1.2.		
1.70 ± 0.24 ± 0.38	293	ACCIARRI	95 L3	1992 LEP run
• • • We use the following data for averages but not for fits. • • •				
1.15 ± 0.08 ± 0.13		¹ PROCARIO	93 CLEO	$E_{\text{cm}}^{\text{ee}} \approx 10.6$ GeV
• • • We do not use the following data for averages, fits, limits, etc. • • •				
1.24 ± 0.09 ± 0.11	2.3k	² BUSKULIC	96 ALEP	Repl. by SCHAEEL 05c
0.0 +1.4 -0.1 +1.1 -0.1		³ GAN	87 MRK2	$E_{\text{cm}}^{\text{ee}} = 29$ GeV

¹ PROCARIO 93 entry is obtained from $B(h^- 3\pi^0 \nu_\tau) / B(h^- \pi^0 \nu_\tau)$ using ARTUSO 94 result for $B(h^- \pi^0 \nu_\tau)$.

² BUSKULIC 96 quote $B(h^- 3\pi^0 \nu_\tau \text{ (ex. } K^0)) = 1.17 \pm 0.09 \pm 0.11$. We add 0.07 to remove their correction for K^0 backgrounds.

³ Highly correlated with GAN 87 $\Gamma(\eta \pi^- \pi^0 \nu_\tau) / \Gamma_{\text{total}}$ value. Authors quote $B(\pi^\pm 3\pi^0 \nu_\tau) + 0.67B(\pi^\pm \eta \pi^0 \nu_\tau) = 0.047 \pm 0.010 \pm 0.011$.

$$\Gamma(h^- 3\pi^0 \nu_\tau) / \Gamma(h^- \pi^0 \nu_\tau) \quad \Gamma_{26} / \Gamma_{13}$$

$$\Gamma_{26} / \Gamma_{13} = (\Gamma_{27} + \Gamma_{28} + 0.15344\Gamma_{41} + 0.15344\Gamma_{43} + 0.3257\Gamma_{152}) / (\Gamma_{14} + \Gamma_{16})$$

VALUE (units 10^{-2})	DOCUMENT ID	TECN	COMMENT
4.54 ± 0.28 OUR FIT	(Produced by HFLAV)		
4.4 ± 0.3 ± 0.5	¹ PROCARIO	93 CLEO	$E_{\text{cm}}^{\text{ee}} \approx 10.6$ GeV

¹ PROCARIO 93 quote $0.041 \pm 0.003 \pm 0.005$ after correction for 2 kaon backgrounds assuming $B(K^* \nu_\tau) = 1.42 \pm 0.18\%$ and $B(h^- K^0 \pi^0 \nu_\tau) = 0.48 \pm 0.48\%$. We add 0.003 ± 0.003 and multiply the sum by 0.990 ± 0.010 to remove these corrections.

$$\Gamma(\pi^- 3\pi^0 \nu_\tau \text{ (ex. } K^0)) / \Gamma_{\text{total}} \quad \Gamma_{27} / \Gamma$$

VALUE (%)	EVTS	DOCUMENT ID	TECN	COMMENT
1.04 ± 0.07 OUR FIT		(Produced by HFLAV)		
0.977 ± 0.069 ± 0.058	6.1k	¹ SCHAEEL	05c ALEP	1991–1995 LEP runs

¹ See footnote to SCHAEEL 05c $\Gamma(\tau^- \rightarrow e^- \bar{\nu}_e \nu_\tau) / \Gamma_{\text{total}}$ measurement for correlations with other measurements.

$$\Gamma(K^- 3\pi^0 \nu_\tau \text{ (ex. } K^0, \eta)) / \Gamma_{\text{total}} \quad \Gamma_{28} / \Gamma$$

VALUE (units 10^{-4})	EVTS	DOCUMENT ID	TECN	COMMENT
4.8 ± 2.1 OUR FIT		(Produced by HFLAV)		
3.7 ± 2.1 ± 1.1	22	BARATE	99k ALEP	1991–1995 LEP runs
• • • We do not use the following data for averages, fits, limits, etc. • • •				
5 ± 13		¹ BUSKULIC	94e ALEP	Repl. by BARATE 99k

¹ BUSKULIC 94e quote $B(K^- \geq 0\pi^0 \geq 0K^0 \nu_\tau) - [B(K^- \nu_\tau) + B(K^- \pi^0 \nu_\tau) + B(K^- K^0 \nu_\tau) + B(K^- \pi^0 \pi^0 \nu_\tau) + B(K^- \pi^0 K^0 \nu_\tau)] = (5 \pm 13) \times 10^{-4}$ accounting for common systematic errors in BUSKULIC 94e and BUSKULIC 94f measurements of these modes. We assume $B(K^- \geq 2K^0 \nu_\tau)$ and $B(K^- \geq 4\pi^0 \nu_\tau)$ are negligible.

$$\Gamma(h^- 4\pi^0 \nu_\tau \text{ (ex. } K^0)) / \Gamma_{\text{total}} \quad \Gamma_{29} / \Gamma$$

$$\Gamma_{29} / \Gamma = (\Gamma_{30} + 0.3257\Gamma_{150} + 0.3257\Gamma_{154}) / \Gamma$$

VALUE (%)	EVTS	DOCUMENT ID	TECN	COMMENT
0.16 ± 0.04 OUR FIT		(Produced by HFLAV)		
0.16 ± 0.05 ± 0.05		¹ PROCARIO	93 CLEO	$E_{\text{cm}}^{\text{ee}} \approx 10.6$ GeV
• • • We do not use the following data for averages, fits, limits, etc. • • •				
0.16 ± 0.04 ± 0.09	232	² BUSKULIC	96 ALEP	Repl. by SCHAEEL 05c

¹ PROCARIO 93 quotes $B(h^- 4\pi^0 \nu_\tau) / B(h^- \pi^0 \nu_\tau) = 0.006 \pm 0.002 \pm 0.002$. We multiply by the ARTUSO 94 result for $B(h^- \pi^0 \nu_\tau)$ to obtain $B(h^- 4\pi^0 \nu_\tau)$. PROCARIO 93 assume $B(h^- \geq 5\pi^0 \nu_\tau)$ is small and do not correct for it.

² BUSKULIC 96 quote result for $\tau^- \rightarrow h^- \geq 4\pi^0 \nu_\tau$. We assume $B(h^- \geq 5\pi^0 \nu_\tau)$ is negligible.

$$\Gamma(h^- 4\pi^0 \nu_\tau \text{ (ex. } K^0, \eta)) / \Gamma_{\text{total}} \quad \Gamma_{30} / \Gamma$$

VALUE (%)	EVTS	DOCUMENT ID	TECN	COMMENT
0.11 ± 0.04 OUR FIT		(Produced by HFLAV)		
0.112 ± 0.037 ± 0.035	957	¹ SCHAEEL	05c ALEP	1991–1995 LEP runs

¹ See footnote to SCHAEEL 05c $\Gamma(\tau^- \rightarrow e^- \bar{\nu}_e \nu_\tau) / \Gamma_{\text{total}}$ measurement for correlations with other measurements.

$$\Gamma(a_1(1260) \nu_\tau \rightarrow \pi^- \gamma \nu_\tau) / \Gamma_{\text{total}} \quad \Gamma_{31} / \Gamma = (0.0022\Gamma_{20} + 0.0022\Gamma_{70}) / \Gamma$$

In the fit, $\Gamma(\tau^- \rightarrow a_1(1260) \nu_\tau \rightarrow \pi^- \gamma \nu_\tau) / \Gamma_{\text{total}}$ is set equal to $(\Gamma(\tau^- \rightarrow \pi^- 2\pi^0 \nu_\tau \text{ (ex. } K^0)) + \Gamma(\tau^- \rightarrow \pi^- \pi^+ \pi^- \nu_\tau \text{ (ex. } K^0, \omega)) / \Gamma_{\text{total}}) \times B(a_1(1260) \rightarrow \pi^- \gamma) / (1 - B(a_1(1260) \rightarrow \pi^- \gamma))$ and $B(a_1(1260) \rightarrow \pi^- \gamma) = \Gamma(a_1(1260) \rightarrow \pi^- \gamma) / \Gamma_{\text{total}}$ is a nuisance fit variable with a χ^2 term corresponding to its estimate in reference SCHAEEL 05c.

VALUE (units 10^{-4})	DOCUMENT ID
4.0 ± 1.5 OUR FIT	(Produced by HFLAV)

$$\Gamma(K^- \geq 0\pi^0 \geq 0K^0 \geq 0\gamma \nu_\tau) / \Gamma_{\text{total}} \quad \Gamma_{32} / \Gamma$$

$$\Gamma_{32} / \Gamma = (\Gamma_{10} + \Gamma_{16} + \Gamma_{23} + \Gamma_{28} + \Gamma_{38} + \Gamma_{43} + 0.7196\Gamma_{152} + 0.1049\Gamma_{170}) / \Gamma$$

VALUE (%)	EVTS	DOCUMENT ID	TECN	COMMENT
1.552 ± 0.029 OUR FIT		(Produced by HFLAV)		
1.53 ± 0.04 OUR AVERAGE				
1.528 ± 0.039 ± 0.040		¹ ABBIENDI	01J OPAL	1990–1995 LEP runs
1.54 ± 0.24		ABREU	94K DLPH	LEP 1992 Z data
1.70 ± 0.12 ± 0.19	202	² BATTLE	94 CLEO	$E_{\text{cm}}^{\text{ee}} \approx 10.6$ GeV
• • • We use the following data for averages but not for fits. • • •				
1.520 ± 0.040 ± 0.041	4006	³ BARATE	99k ALEP	1991–1995 LEP runs
• • • We do not use the following data for averages, fits, limits, etc. • • •				
1.70 ± 0.05 ± 0.06	1610	⁴ BUSKULIC	96 ALEP	Repl. by BARATE 99k
1.6 ± 0.4 ± 0.2	35	AIHARA	87B TPC	$E_{\text{cm}}^{\text{ee}} = 29$ GeV
1.71 ± 0.29	53	MILLS	84 DLCO	$E_{\text{cm}}^{\text{ee}} = 29$ GeV

¹ The correlation coefficient between this measurement and the ABBIENDI 01J $B(\tau^- \rightarrow K^- \nu_\tau)$ is 0.60.

² BATTLE 94 quote $1.60 \pm 0.12 \pm 0.19$. We add 0.10 ± 0.02 to correct for their rejection of $K_S^0 \rightarrow \pi^+ \pi^-$ decays.

³ Not independent of BARATE 99k $B(K^- \nu_\tau)$, $B(K^- \pi^0 \nu_\tau)$, $B(K^- 2\pi^0 \nu_\tau \text{ (ex. } K^0))$, $B(K^- 3\pi^0 \nu_\tau \text{ (ex. } K^0))$, $B(K^- K^0 \nu_\tau)$, and $B(K^- K^0 \pi^0 \nu_\tau)$ values.

⁴ Not independent of BUSKULIC 96 $B(K^- \nu_\tau)$, $B(K^- \pi^0 \nu_\tau)$, $B(K^- 2\pi^0 \nu_\tau)$, $B(K^- K^0 \nu_\tau)$, and $B(K^- K^0 \pi^0 \nu_\tau)$ values.

$$\Gamma(K^- \geq 1(\pi^0 \text{ or } K^0 \text{ or } \gamma) \nu_\tau) / \Gamma_{\text{total}} \quad \Gamma_{33} / \Gamma$$

$$\Gamma_{33} / \Gamma = (\Gamma_{16} + \Gamma_{23} + \Gamma_{28} + \Gamma_{38} + \Gamma_{43} + 0.7196\Gamma_{152} + 0.7196\Gamma_{154} + 0.1049\Gamma_{170}) / \Gamma$$

VALUE (%)	EVTS	DOCUMENT ID	TECN	COMMENT
0.859 ± 0.028 OUR FIT		(Produced by HFLAV)		
0.86 ± 0.05 OUR AVERAGE				

• • • We use the following data for averages but not for fits. • • •				
0.869 ± 0.031 ± 0.034		¹ ABBIENDI	01J OPAL	1990–1995 LEP runs
0.69 ± 0.25		² ABREU	94K DLPH	LEP 1992 Z data
• • • We do not use the following data for averages, fits, limits, etc. • • •				
1.2 ± 0.5 +0.2 -0.4	9	AIHARA	87B TPC	$E_{\text{cm}}^{\text{ee}} = 29$ GeV

¹ Not independent of ABBIENDI 01J $B(\tau^- \rightarrow K^- \nu_\tau)$ and $B(\tau^- \rightarrow K^- \geq 0\pi^0 \geq 0K^0 \geq 0\gamma \nu_\tau)$ values.

² Not independent of ABREU 94k $B(K^- \nu_\tau)$ and $B(K^- \geq 0$ neutrals $\nu_\tau)$ measurements.

$$\Gamma(K_S^0 \text{ (particles)} \nu_\tau) / \Gamma_{\text{total}} \quad \Gamma_{34} / \Gamma$$

$$\Gamma_{34} / \Gamma = (\frac{1}{2}\Gamma_{36} + \frac{1}{2}\Gamma_{38} + \frac{1}{2}\Gamma_{41} + \frac{1}{2}\Gamma_{43} + \frac{1}{2}\Gamma_{45} + \Gamma_{48} + \Gamma_{49} + \Gamma_{52} + \Gamma_{56} + 0.3598\Gamma_{156} + 0.3399\Gamma_{170}) / \Gamma$$

VALUE (%)	EVTS	DOCUMENT ID	TECN	COMMENT
0.943 ± 0.028 OUR FIT		(Produced by HFLAV)		
0.918 ± 0.015 OUR AVERAGE				
0.970 ± 0.058 ± 0.062	929	BARATE	98E ALEP	1991–1995 LEP runs
0.97 ± 0.09 ± 0.06	141	AKERS	94G OPAL	$E_{\text{cm}}^{\text{ee}} = 88$ –94 GeV

• • • We use the following data for averages but not for fits. • • •

0.915 ± 0.001 ± 0.015 398k ¹ RYU 14 BELL 669 fb⁻¹ $E_{\text{cm}}^{\text{ee}} = 10.6$ GeV

¹ Not independent of RYU 14 measurements of $B(\tau^- \rightarrow \pi^- \bar{K}^0 \nu_\tau)$, $B(\tau^- \rightarrow K^- K^0 \nu_\tau)$, $B(\tau^- \rightarrow \pi^- \bar{K}^0 \pi^0 \nu_\tau)$, $B(\tau^- \rightarrow K^- K^0 \pi^0 \nu_\tau)$, $B(\tau^- \rightarrow \pi^- K_S^0 K_S^0 \nu_\tau)$, and $B(\tau^- \rightarrow \pi^- K_S^0 K_S^0 \pi^0 \nu_\tau)$.

$$\Gamma(h^- \bar{K}^0 \nu_\tau) / \Gamma_{\text{total}} \quad \Gamma_{35} / \Gamma = (\Gamma_{36} + \Gamma_{38}) / \Gamma$$

VALUE (%)	EVTS	DOCUMENT ID	TECN	COMMENT
0.987 ± 0.014 OUR FIT		(Produced by HFLAV)		
0.90 ± 0.07 OUR AVERAGE				
0.855 ± 0.036 ± 0.073	1242	COAN	96 CLEO	$E_{\text{cm}}^{\text{ee}} \approx 10.6$ GeV
• • • We use the following data for averages but not for fits. • • •				
1.01 ± 0.11 ± 0.07	555	¹ BARATE	98E ALEP	1991–1995 LEP runs

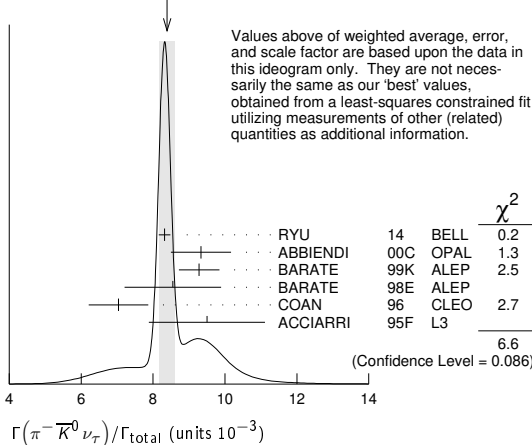
¹ Not independent of BARATE 98E $B(\tau^- \rightarrow \pi^- \bar{K}^0 \nu_\tau)$ and $B(\tau^- \rightarrow K^- K^0 \nu_\tau)$ values.

$\Gamma(\pi^- \bar{K}^0 \nu_\tau) / \Gamma_{\text{total}}$ Γ_{36} / Γ

VALUE (units 10^{-3})	EVTS	DOCUMENT ID	TECN	COMMENT
8.38 ± 0.14 OUR FIT	(Produced by HFLAV)			
8.39 ± 0.22 OUR AVERAGE	Error includes scale factor of 1.5. See the ideogram below.			
8.32 ± 0.02 ± 0.16	158k	¹ RYU	14 BELL	669 fb ⁻¹ $E_{\text{cm}}^{\text{e}^+e^-} = 10.6$ GeV
9.33 ± 0.68 ± 0.49	377	ABBIENDI	00c OPAL	1991–1995 LEP runs
9.28 ± 0.45 ± 0.34	937	² BARATE	99k ALEP	1991–1995 LEP runs
9.5 ± 1.5 ± 0.6		³ ACCIARRI	95F L3	1991–1993 LEP runs
• • • We use the following data for averages but not for fits. • • •				
8.55 ± 1.17 ± 0.66	509	⁴ BARATE	98E ALEP	1991–1995 LEP runs
7.04 ± 0.41 ± 0.72		⁵ COAN	96 CLEO	$E_{\text{cm}}^{\text{e}^+e^-} \approx 10.6$ GeV
• • • We do not use the following data for averages, fits, limits, etc. • • •				
8.08 ± 0.04 ± 0.26	53k	EPIFANOV	07 BELL	Repl. by RYU 14
7.9 ± 1.0 ± 0.9	98	⁶ BUSKULIC	96 ALEP	Repl. by BARATE 99k

- RYU 14 reconstruct K^0 's using $K_S^0 \rightarrow \pi^+ \pi^-$ decays.
- BARATE 99k measure K^0 's by detecting K_L^0 's in their hadron calorimeter.
- ACCIARRI 95F do not identify π^- / K^- and assume $B(K^- K^0 \nu_\tau) = (0.29 \pm 0.12)\%$.
- BARATE 98E reconstruct K^0 's using $K_S^0 \rightarrow \pi^+ \pi^-$ decays. Not independent of BARATE 98E $B(K^0 \text{ particles} - \nu_\tau)$ value.
- Not independent of COAN 96 $B(h^- K^0 \nu_\tau)$ and $B(K^- K^0 \nu_\tau)$ measurements.
- BUSKULIC 96 measure K^0 's by detecting K_L^0 's in their hadron calorimeter.

WEIGHTED AVERAGE
8.39 ± 0.22 (Error scaled by 1.5)



$\Gamma(\pi^- \bar{K}^0 (\text{non-} K^*(892)^-) \nu_\tau) / \Gamma_{\text{total}}$ Γ_{37} / Γ

VALUE (units 10^{-4})	CL%	DOCUMENT ID	TECN	COMMENT
5.4 ± 2.1		¹ EPIFANOV	07 BELL	351 fb ⁻¹ $E_{\text{cm}}^{\text{e}^+e^-} = 10.6$ GeV
• • • We do not use the following data for averages, fits, limits, etc. • • •				
<17	95	ACCIARRI	95F L3	1991–1993 LEP runs
¹ EPIFANOV 07 quote $B(\tau^- \rightarrow K^*(892)^- \nu_\tau) B(K^*(892)^- \rightarrow K_S^0 \pi^-) / B(\tau^- \rightarrow K_S^0 \pi^- \nu_\tau) = 0.933 \pm 0.027$. We multiply their $B(\tau^- \rightarrow \bar{K}^0 \pi^- \nu_\tau)$ by $[1 - (0.933 \pm 0.027)]$ to obtain this result.				

$\Gamma(K^- K^0 \nu_\tau) / \Gamma_{\text{total}}$ Γ_{38} / Γ

VALUE (units 10^{-4})	EVTS	DOCUMENT ID	TECN	COMMENT
14.86 ± 0.34 OUR FIT	(Produced by HFLAV)			
14.83 ± 0.35 OUR AVERAGE				
14.78 ± 0.22 ± 0.40	29k	¹ LEES	18b BABR	468 fb ⁻¹ $E_{\text{cm}}^{\text{e}^+e^-} = 10.6$ GeV
14.80 ± 0.14 ± 0.54	33k	² RYU	14 BELL	669 fb ⁻¹ $E_{\text{cm}}^{\text{e}^+e^-} = 10.6$ GeV
16.2 ± 2.1 ± 1.1	150	³ BARATE	99k ALEP	1991–1995 LEP runs
15.8 ± 4.2 ± 1.7	46	⁴ BARATE	98E ALEP	1991–1995 LEP runs
15.1 ± 2.1 ± 2.2	111	COAN	96 CLEO	$E_{\text{cm}}^{\text{e}^+e^-} \approx 10.6$ GeV
• • • We do not use the following data for averages, fits, limits, etc. • • •				
26 ± 9 ± 2	13	⁵ BUSKULIC	96 ALEP	Repl. by BARATE 99k

- LEES 18b reconstructs K_S^0 's using $K_S^0 \rightarrow \pi^+ \pi^-$ decays.
- RYU 14 reconstruct K^0 's using $K_S^0 \rightarrow \pi^+ \pi^-$ decays.
- BARATE 99k measure K^0 's by detecting K_L^0 's in their hadron calorimeter.
- BARATE 98E reconstruct K^0 's using $K_S^0 \rightarrow \pi^+ \pi^-$ decays.
- BUSKULIC 96 measure K^0 's by detecting K_L^0 's in their hadron calorimeter.

$\Gamma(K^- K^0 \geq 0 \pi^0 \nu_\tau) / \Gamma_{\text{total}}$ $\Gamma_{39} / \Gamma = (\Gamma_{38} + \Gamma_{43}) / \Gamma$

VALUE (%)	EVTS	DOCUMENT ID	TECN	COMMENT
0.299 ± 0.007 OUR FIT	(Produced by HFLAV)			
0.330 ± 0.055 ± 0.039	124	ABBIENDI	00c OPAL	1991–1995 LEP runs

$\Gamma(h^- \bar{K}^0 \pi^0 \nu_\tau) / \Gamma_{\text{total}}$ $\Gamma_{40} / \Gamma = (\Gamma_{41} + \Gamma_{43}) / \Gamma$

VALUE (%)	EVTS	DOCUMENT ID	TECN	COMMENT
0.532 ± 0.013 OUR FIT	(Produced by HFLAV)			
0.50 ± 0.06 OUR AVERAGE	Error includes scale factor of 1.2.			
0.562 ± 0.050 ± 0.048	264	COAN	96 CLEO	$E_{\text{cm}}^{\text{e}^+e^-} \approx 10.6$ GeV
• • • We use the following data for averages but not for fits. • • •				
0.446 ± 0.052 ± 0.046	157	¹ BARATE	98E ALEP	1991–1995 LEP runs
¹ Not independent of BARATE 98E $B(\tau^- \rightarrow \pi^- \bar{K}^0 \pi^0 \nu_\tau)$ and $B(\tau^- \rightarrow K^- K^0 \pi^0 \nu_\tau)$ values.				

$\Gamma(\pi^- \bar{K}^0 \pi^0 \nu_\tau) / \Gamma_{\text{total}}$ Γ_{41} / Γ

VALUE (%)	EVTS	DOCUMENT ID	TECN	COMMENT
0.382 ± 0.013 OUR FIT	(Produced by HFLAV)			
0.383 ± 0.014 OUR AVERAGE				
0.386 ± 0.004 ± 0.014	27k	¹ RYU	14 BELL	669 fb ⁻¹ $E_{\text{cm}}^{\text{e}^+e^-} = 10.6$ GeV
0.347 ± 0.053 ± 0.037	299	² BARATE	99k ALEP	1991–1995 LEP runs
0.294 ± 0.073 ± 0.037	142	³ BARATE	98E ALEP	1991–1995 LEP runs
0.41 ± 0.12 ± 0.03		⁴ ACCIARRI	95F L3	1991–1993 LEP runs
• • • We use the following data for averages but not for fits. • • •				
0.417 ± 0.058 ± 0.044		⁵ COAN	96 CLEO	$E_{\text{cm}}^{\text{e}^+e^-} \approx 10.6$ GeV
• • • We do not use the following data for averages, fits, limits, etc. • • •				
0.32 ± 0.11 ± 0.05	23	⁶ BUSKULIC	96 ALEP	Repl. by BARATE 99k

- RYU 14 reconstruct K^0 's using $K_S^0 \rightarrow \pi^+ \pi^-$ decays.
- BARATE 99k measure K^0 's by detecting K_L^0 's in their hadron calorimeter.
- BARATE 98E reconstruct K^0 's using $K_S^0 \rightarrow \pi^+ \pi^-$ decays.
- ACCIARRI 95F do not identify π^- / K^- and assume $B(K^- K^0 \pi^0 \nu_\tau) = (0.05 \pm 0.05)\%$.
- Not independent of COAN 96 $B(h^- K^0 \pi^0 \nu_\tau)$ and $B(K^- K^0 \pi^0 \nu_\tau)$ measurements.
- BUSKULIC 96 measure K^0 's by detecting K_L^0 's in their hadron calorimeter.

$\Gamma(\bar{K}^0 \rho^- \nu_\tau) / \Gamma_{\text{total}}$ Γ_{42} / Γ

VALUE (%)	DOCUMENT ID	TECN	COMMENT
0.22 ± 0.05 OUR AVERAGE			
0.250 ± 0.057 ± 0.044	¹ BARATE	99k ALEP	1991–1995 LEP runs
0.188 ± 0.054 ± 0.038	² BARATE	98E ALEP	1991–1995 LEP runs

- BARATE 99k measure K^0 's by detecting K_L^0 's in hadron calorimeter. They determine the $\bar{K}^0 \rho^-$ fraction in $\tau^- \rightarrow \pi^- \bar{K}^0 \pi^0 \nu_\tau$ decays to be $(0.72 \pm 0.12 \pm 0.10)$ and multiply their $B(\pi^- \bar{K}^0 \pi^0 \nu_\tau)$ measurement by this fraction to obtain the quoted result.
- BARATE 98E reconstruct K^0 's using $K_S^0 \rightarrow \pi^+ \pi^-$ decays. They determine the $\bar{K}^0 \rho^-$ fraction in $\tau^- \rightarrow \pi^- \bar{K}^0 \pi^0 \nu_\tau$ decays to be $(0.64 \pm 0.09 \pm 0.10)$ and multiply their $B(\pi^- \bar{K}^0 \pi^0 \nu_\tau)$ measurement by this fraction to obtain the quoted result.

$\Gamma(K^- K^0 \pi^0 \nu_\tau) / \Gamma_{\text{total}}$ Γ_{43} / Γ

VALUE (units 10^{-4})	EVTS	DOCUMENT ID	TECN	COMMENT
15.0 ± 0.7 OUR FIT	(Produced by HFLAV)			
14.9 ± 0.7 OUR AVERAGE				
14.96 ± 0.20 ± 0.74	8.3k	¹ RYU	14 BELL	669 fb ⁻¹ $E_{\text{cm}}^{\text{e}^+e^-} = 10.6$ GeV
14.3 ± 2.5 ± 1.5	78	² BARATE	99k ALEP	1991–1995 LEP runs
15.2 ± 7.6 ± 2.1	15	³ BARATE	98E ALEP	1991–1995 LEP runs
14.5 ± 3.6 ± 2.0	32	COAN	96 CLEO	$E_{\text{cm}}^{\text{e}^+e^-} \approx 10.6$ GeV

- RYU 14 reconstruct K^0 's using $K_S^0 \rightarrow \pi^+ \pi^-$ decays.
- BARATE 99k measure K^0 's by detecting K_L^0 's in their hadron calorimeter.
- BARATE 98E reconstruct K^0 's using $K_S^0 \rightarrow \pi^+ \pi^-$ decays.
- BUSKULIC 96 measure K^0 's by detecting K_L^0 's in their hadron calorimeter.

$\Gamma(\pi^- \bar{K}^0 \geq 1 \pi^0 \nu_\tau) / \Gamma_{\text{total}}$ $\Gamma_{44} / \Gamma = (\Gamma_{41} + \Gamma_{45}) / \Gamma$

VALUE (%)	EVTS	DOCUMENT ID	TECN	COMMENT
0.408 ± 0.025 OUR FIT	(Produced by HFLAV)			
0.324 ± 0.074 ± 0.066	148	ABBIENDI	00c OPAL	1991–1995 LEP runs

$\Gamma(\pi^- \bar{K}^0 \pi^0 \pi^0 \nu_\tau (\text{ex. } K^0)) / \Gamma_{\text{total}}$ Γ_{45} / Γ

VALUE (units 10^{-3})	CL%	EVTS	DOCUMENT ID	TECN	COMMENT
0.26 ± 0.23 OUR FIT	(Produced by HFLAV)				
0.26 ± 0.24					
• • • We do not use the following data for averages, fits, limits, etc. • • •					
<0.66	95	17	² BARATE	99k ALEP	1991–1995 LEP runs
0.58 ± 0.33 ± 0.14		5	³ BARATE	98E ALEP	1991–1995 LEP runs
¹ BARATE 99k combine the BARATE 98E and BARATE 99k measurements to obtain this value.					
² BARATE 99k measure K^0 's by detecting K_L^0 's in their hadron calorimeter.					
³ BARATE 98E reconstruct K^0 's using $K_S^0 \rightarrow \pi^+ \pi^-$ decays.					

$\Gamma(K^- K^0 \pi^0 \pi^0 \nu_\tau) / \Gamma_{\text{total}}$ Γ_{46} / Γ

VALUE	CL%	DOCUMENT ID	TECN	COMMENT
<0.16 × 10⁻³		¹ BARATE	99R ALEP	1991–1995 LEP runs
• • • We do not use the following data for averages, fits, limits, etc. • • •				
<0.18 × 10 ⁻³	95	² BARATE	99k ALEP	1991–1995 LEP runs
<0.39 × 10 ⁻³	95	³ BARATE	98E ALEP	1991–1995 LEP runs
¹ BARATE 99R combine the BARATE 98E and BARATE 99k bounds to obtain this value.				
² BARATE 99k measure K^0 's by detecting K_L^0 's in hadron calorimeter.				
³ BARATE 98E reconstruct K^0 's by using $K_S^0 \rightarrow \pi^+ \pi^-$ decays.				

Lepton Particle Listings

T

$\Gamma(\pi^- K^0 \bar{K}^0 \nu_\tau)/\Gamma_{total}$ $\Gamma_{47}/\Gamma = (\Gamma_{48} + \Gamma_{49} + \Gamma_{50})/\Gamma$

VALUE (%)	EVTS	DOCUMENT ID	TECN	COMMENT
0.155 ± 0.024 OUR FIT	(Produced by HFLAV)			

- • • We use the following data for averages but not for fits. • • •
- 0.153 ± 0.030 ± 0.016** 74 1 BARATE 98E ALEP 1991–1995 LEP runs
- • • We do not use the following data for averages, fits, limits, etc. • • •
- 0.31 ± 0.12 ± 0.04 2 ACCIARRI 95F L3 1991–1993 LEP runs
- 1 BARATE 98E obtain this value by adding twice their $B(\pi^- K_S^0 K_L^0 \nu_\tau)$ value to their $B(\pi^- K_S^0 K_L^0 \nu_\tau)$ value.
- 2 ACCIARRI 95F assume $B(\pi^- K_S^0 K_S^0 \nu) = B(\pi^- K_S^0 K_L^0 \nu) = 1/2B(\pi^- K_S^0 K_L^0 \nu)$.

$\Gamma(\pi^- K_S^0 K_S^0 \nu_\tau)/\Gamma_{total}$ Γ_{48}/Γ

VALUE (units 10^{-4})	EVTS	DOCUMENT ID	TECN	COMMENT
2.35 ± 0.06 OUR FIT	(Produced by HFLAV)			
2.32 ± 0.06 OUR AVERAGE				

2.33 ± 0.03 ± 0.09	6.7k	RYU	14	BELL	669 fb ⁻¹	$E_{cm}^{ee} = 10.6$ GeV
2.31 ± 0.04 ± 0.08	5.0k	1 LEES	12Y	BABR	468 fb ⁻¹	$E_{cm}^{ee} = 10.6$ GeV
2.6 ± 1.0 ± 0.5	6	BARATE	98E	ALEP	1991–1995	LEP runs
2.3 ± 0.5 ± 0.3	42	COAN	96	CLEO		$E_{cm}^{ee} \approx 10.6$ GeV

1 The correlation coefficient between this measurement and the LEES 12Y $\Gamma(\tau^- \rightarrow \pi^- K_S^0 K_S^0 \nu_\tau)/\Gamma_{total}$ one is 0.0828.

$\Gamma(\pi^- K_S^0 K_L^0 \nu_\tau)/\Gamma_{total}$ Γ_{49}/Γ

VALUE (units 10^{-4})	EVTS	DOCUMENT ID	TECN	COMMENT		
10.8 ± 2.4 OUR FIT	(Produced by HFLAV)					
10.1 ± 2.3 ± 1.3	68	BARATE	98E	ALEP	1991–1995	LEP runs

$\Gamma(\pi^- K_L^0 K_L^0 \nu_\tau)/\Gamma_{total}$ $\Gamma_{50}/\Gamma = \Gamma_{48}/\Gamma$

VALUE (units 10^{-4})	DOCUMENT ID	TECN	COMMENT
2.35 ± 0.06 OUR FIT	(Produced by HFLAV)		

$\Gamma(\pi^- K^0 \bar{K}^0 \pi^0 \nu_\tau)/\Gamma_{total}$ $\Gamma_{51}/\Gamma = (\Gamma_{52} + \Gamma_{56} + \Gamma_{57})/\Gamma$

VALUE (units 10^{-4})	DOCUMENT ID	TECN	COMMENT
3.6 ± 1.2 OUR FIT	(Produced by HFLAV)		

- • • We use the following data for averages but not for fits. • • •
- 3.1 ± 2.3** 1 BARATE 99R ALEP 1991–1995 LEP runs
- 1 BARATE 99R combine BARATE 98E $\Gamma(\pi^- K_S^0 K_S^0 \pi^0 \nu_\tau)/\Gamma_{total}$ and $\Gamma(\pi^- K_S^0 K_L^0 \pi^0 \nu_\tau)/\Gamma_{total}$ measurements to obtain this value.

$\Gamma(\pi^- K_S^0 K_S^0 \pi^0 \nu_\tau)/\Gamma_{total}$ Γ_{52}/Γ

VALUE (units 10^{-5})	CL%	EVTS	DOCUMENT ID	TECN	COMMENT
1.82 ± 0.21 OUR FIT		(Produced by HFLAV)			
1.80 ± 0.21 OUR AVERAGE					

2.00 ± 0.22 ± 0.20	303	RYU	14	BELL	669 fb ⁻¹	$E_{cm}^{ee} = 10.6$ GeV
1.60 ± 0.20 ± 0.22	409	1 LEES	12Y	BABR	468 fb ⁻¹	$E_{cm}^{ee} = 10.6$ GeV

• • • We do not use the following data for averages, fits, limits, etc. • • •

<20 95 BARATE 98E ALEP 1991–1995 LEP runs

1 The correlation coefficient between this measurement and the LEES 12Y $\Gamma(\tau^- \rightarrow \pi^- K_S^0 K_S^0 \nu_\tau)/\Gamma_{total}$ one is 0.0828.

$\Gamma(K^+ K^0 \pi^0 \nu_\tau \rightarrow \pi^- K_S^0 K_S^0 \pi^0 \nu_\tau)/\Gamma_{total}$ Γ_{53}/Γ

VALUE (units 10^{-6})	DOCUMENT ID	TECN	COMMENT		
10.8 ± 1.4 ± 1.5	RYU	14	BELL	669 fb ⁻¹	$E_{cm}^{ee} = 10.6$ GeV

$\Gamma(f_1(1285)\pi^- \nu_\tau \rightarrow \pi^- K_S^0 K_S^0 \pi^0 \nu_\tau)/\Gamma_{total}$ Γ_{54}/Γ

VALUE (units 10^{-6})	DOCUMENT ID	TECN	COMMENT		
6.8 ± 1.3 ± 0.7	RYU	14	BELL	669 fb ⁻¹	$E_{cm}^{ee} = 10.6$ GeV

$\Gamma(f_1(1420)\pi^- \nu_\tau \rightarrow \pi^- K_S^0 K_S^0 \pi^0 \nu_\tau)/\Gamma_{total}$ Γ_{55}/Γ

VALUE (units 10^{-6})	DOCUMENT ID	TECN	COMMENT		
2.4 ± 0.5 ± 0.6	RYU	14	BELL	669 fb ⁻¹	$E_{cm}^{ee} = 10.6$ GeV

$\Gamma(\pi^- K_S^0 K_L^0 \pi^0 \nu_\tau)/\Gamma_{total}$ Γ_{56}/Γ

VALUE (units 10^{-4})	EVTS	DOCUMENT ID	TECN	COMMENT		
3.2 ± 1.2 OUR FIT	(Produced by HFLAV)					
3.1 ± 1.1 ± 0.5	11	BARATE	98E	ALEP	1991–1995	LEP runs

$\Gamma(\pi^- K_L^0 K_L^0 \pi^0 \nu_\tau)/\Gamma_{total}$ $\Gamma_{57}/\Gamma = \Gamma_{52}/\Gamma$

VALUE (units 10^{-5})	DOCUMENT ID	TECN	COMMENT
1.82 ± 0.21 OUR FIT	(Produced by HFLAV)		

$\Gamma(K^- K_S^0 K_S^0 \nu_\tau)/\Gamma_{total}$ Γ_{58}/Γ

VALUE	CL%	DOCUMENT ID	TECN	COMMENT		
<6.3 × 10⁻⁷	90	LEES	12Y	BABR	468 fb ⁻¹	$E_{cm}^{ee} = 10.6$ GeV

$\Gamma(K^- K_S^0 K_S^0 \pi^0 \nu_\tau)/\Gamma_{total}$ Γ_{59}/Γ

VALUE	CL%	DOCUMENT ID	TECN	COMMENT		
<4.0 × 10⁻⁷	90	LEES	12Y	BABR	468 fb ⁻¹	$E_{cm}^{ee} = 10.6$ GeV

$\Gamma(K^0 h^+ h^- h^- \geq 0 \text{ neutrals } \nu_\tau)/\Gamma_{total}$ Γ_{60}/Γ

VALUE (%)	CL%	DOCUMENT ID	TECN	COMMENT	
<0.17	95	TSCHIRHART	88	HRS	$E_{cm}^{ee} = 29$ GeV

- • • We do not use the following data for averages, fits, limits, etc. • • •

<0.27	90	BELTRAMI	85	HRS	$E_{cm}^{ee} = 29$ GeV
-------	----	----------	----	-----	------------------------

$\Gamma(K^0 h^+ h^- h^- \nu_\tau)/\Gamma_{total}$ Γ_{61}/Γ

VALUE (units 10^{-4})	EVTS	DOCUMENT ID	TECN	COMMENT		
2.5 ± 2.0 OUR FIT	(Produced by HFLAV)					
2.3 ± 1.9 ± 0.7	6	1 BARATE	98E	ALEP	1991–1995	LEP runs

1 BARATE 98E reconstruct K^0 's using $K_S^0 \rightarrow \pi^+ \pi^-$ decays.

$\Gamma(h^- h^- h^+ \geq 0 \text{ neutrals } \geq 0 K^0 \nu_\tau)/\Gamma_{total}$ Γ_{62}/Γ

VALUE (%)	EVTS	DOCUMENT ID	TECN	COMMENT
15.20 ± 0.06 OUR FIT	(Produced by HFLAV)			
14.8 ± 0.4 OUR AVERAGE				

14.4 ± 0.6 ± 0.3		ADEVA	91F	L3	$E_{cm}^{ee} = 88.3\text{--}94.3$ GeV
15.0 ± 0.4 ± 0.3		BEHREND	89B	CELL	$E_{cm}^{ee} = 14\text{--}47$ GeV
15.1 ± 0.8 ± 0.6		AIHARA	87B	TPC	$E_{cm}^{ee} = 29$ GeV

- • • We do not use the following data for averages, fits, limits, etc. • • •

13.5 ± 0.3 ± 0.3		ABACHI	89B	HRS	$E_{cm}^{ee} = 29$ GeV
12.8 ± 1.0 ± 0.7		1 BURCHAT	87	MRK2	$E_{cm}^{ee} = 29$ GeV
12.1 ± 0.5 ± 1.2		RUCKSTUHL	86	DLCO	$E_{cm}^{ee} = 29$ GeV
12.8 ± 0.5 ± 0.8	1420	SCHMIDKE	86	MRK2	$E_{cm}^{ee} = 29$ GeV
15.3 ± 1.1 ± 1.3	367	ALTHOFF	85	TASS	$E_{cm}^{ee} = 34.5$ GeV
13.6 ± 0.5 ± 0.8		BARTEL	85F	JADE	$E_{cm}^{ee} = 34.6$ GeV
12.2 ± 1.3 ± 3.9		2 BERGER	85	PLUT	$E_{cm}^{ee} = 34.6$ GeV
13.3 ± 0.3 ± 0.6		FERNANDEZ	85	MAC	$E_{cm}^{ee} = 29$ GeV
24 ± 6	35	BRANDELIK	80	TASS	$E_{cm}^{ee} = 30$ GeV
32 ± 5	692	3 BACINO	78B	DLCO	$E_{cm}^{ee} = 3.1\text{--}7.4$ GeV
35 ± 11		3 BRANDELIK	78	DASP	Assumes $V\text{--}A$ decay
18 ± 6.5	33	3 JAROS	78	LGW	$E_{cm}^{ee} > 6$ GeV

- 1 BURCHAT 87 value is not independent of SCHMIDKE 86 value.
- 2 Not independent of BERGER 85 $\Gamma(\mu^- \bar{\nu}_\mu \nu_\tau)/\Gamma_{total}$, $\Gamma(e^- \bar{\nu}_e \nu_\tau)/\Gamma_{total}$, $\Gamma(h^- \geq 1 \text{ neutrals } \nu_\tau)/\Gamma_{total}$, and $\Gamma(h^- \geq 0 K^0 \nu_\tau)/\Gamma_{total}$, and therefore not used in the fit.
- 3 Low energy experiments are not in average or fit because the systematic errors in background subtraction are judged to be large.

$\Gamma(h^- h^- h^+ \geq 0 \text{ neutrals } \nu_\tau \text{ (ex. } K_S^0 \rightarrow \pi^+ \pi^- \text{)} (*3\text{-prong}))/\Gamma_{total}$ Γ_{63}/Γ

VALUE (%)	EVTS	DOCUMENT ID	TECN	COMMENT
14.55 ± 0.06 OUR FIT	(Produced by HFLAV)			
14.61 ± 0.06 OUR AVERAGE				

14.56 ± 0.105 ± 0.076		1 ACHARD	01D	L3	1992–1995	LEP runs
14.96 ± 0.09 ± 0.22	10.4k	AKERS	95Y	OPAL	1991–1994	LEP runs

- • • We use the following data for averages but not for fits. • • •

14.652 ± 0.067 ± 0.086		SCHAEEL	05c	ALEP	1991–1995	LEP runs
14.569 ± 0.093 ± 0.048	23k	2 ABREU	01M	DLPH	1992–1995	LEP runs
14.22 ± 0.10 ± 0.37		3 BALEST	95c	CLEO	$E_{cm}^{ee} \approx 10.6$ GeV	

- • • We do not use the following data for averages, fits, limits, etc. • • •

15.26 ± 0.26 ± 0.22		ACTON	92H	OPAL	Repl. by AKERS 95Y	
13.3 ± 0.3 ± 0.8		4 ALBRECHT	92D	ARG	$E_{cm}^{ee} = 9.4\text{--}10.6$ GeV	
14.35 ± 0.40 ± 0.24		DECAMP	92C	ALEP	1989–1990	LEP runs

1 The correlation coefficients between this measurement and the ACHARD 01D measurements of $B(\tau \rightarrow \text{"1-prong"})$ and $B(\tau \rightarrow \text{"5-prong"})$ are -0.978 and -0.19 respectively.

2 The correlation coefficients between this measurement and the ABREU 01M measurements of $B(\tau \rightarrow 1\text{-prong})$ and $B(\tau \rightarrow 5\text{-prong})$ are -0.98 and -0.08 respectively.

3 Not independent of BALEST 95c $B(h^- h^- h^+ \nu_\tau)$ and $B(h^- h^- h^+ \pi^0 \nu_\tau)$ values, and BORTOLETTO 93 B($h^- h^- h^+ 2\pi^0 \nu_\tau$)/ $B(h^- h^- h^+ \geq 0 \text{ neutrals } \nu_\tau)$ value.

4 This ALBRECHT 92D value is not independent of their $\Gamma(\mu^- \bar{\nu}_\mu \nu_\tau)/\Gamma_{total}$ value.

$\Gamma(h^- h^- h^+ \nu_\tau)/\Gamma_{total}$ Γ_{64}/Γ

VALUE (%)	EVTS	DOCUMENT ID	TECN	COMMENT
9.80 ± 0.05 OUR FIT	(Produced by HFLAV)			

- • • We use the following data for averages but not for fits. • • •

7.6 ± 0.1 ± 0.5	7.5k	1 ALBRECHT	96E	ARG	$E_{cm}^{ee} = 9.4\text{--}10.6$ GeV
------------------------	------	------------	-----	-----	--------------------------------------

• • • We do not use the following data for averages, fits, limits, etc. • • •

9.92 ± 0.10 ± 0.09	11.2k	2	BUSKULIC	96	ALEP	Repl. by SCHAEEL 05c
9.49 ± 0.36 ± 0.63			DECAMP	92c	ALEP	Repl. by SCHAEEL 05c
8.7 ± 0.7 ± 0.3	694	3	BEHREND	90	CELL	$E_{cm}^{ee} = 35$ GeV
7.0 ± 0.3 ± 0.7	1566	4	BAND	87	MAC	$E_{cm}^{ee} = 29$ GeV
6.7 ± 0.8 ± 0.9		5	BURCHAT	87	MRK2	$E_{cm}^{ee} = 29$ GeV
6.4 ± 0.4 ± 0.9		6	RUCKSTUHL	86	DLCO	$E_{cm}^{ee} = 29$ GeV
7.8 ± 0.5 ± 0.8	890		SCHMIDKE	86	MRK2	$E_{cm}^{ee} = 29$ GeV
8.4 ± 0.4 ± 0.7	1255	6	FERNANDEZ	85	MAC	$E_{cm}^{ee} = 29$ GeV
9.7 ± 2.0 ± 1.3			BEHREND	84	CELL	$E_{cm}^{ee} = 14.22$ GeV

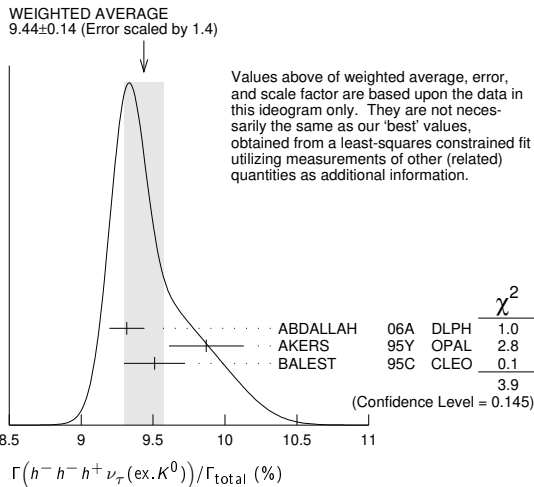
- 1 ALBRECHT 96E not independent of ALBRECHT 93c $\Gamma(h^-h^-h^+\nu_\tau(\text{ex. } K^0)) / \Gamma(\text{particle}^- \geq 0 \text{ neutrals} \geq 0 K_L^0 \nu_\tau) / \Gamma_{\text{total}}$ value.
- 2 BUSKULIC 96 quote $B(h^-h^-h^+\nu_\tau(\text{ex. } K^0)) = 9.50 \pm 0.10 \pm 0.11$. We add 0.42 to remove their K^0 correction and reduce the systematic error accordingly.
- 3 BEHREND 90 subtract 0.3% to account for the $\tau^- \rightarrow K^*(892)^-\nu_\tau$ contribution to measured events.
- 4 BAND 87 subtract for charged kaon modes; not independent of FERNANDEZ 85 value.
- 5 BURCHAT 87 value is not independent of SCHMIDKE 86 value.
- 6 Value obtained by multiplying paper's $R = B(h^-h^-h^+\nu_\tau)/B(3\text{-prong})$ by $B(3\text{-prong}) = 0.143$ and subtracting 0.3% for $K^*(892)$ background.

$\Gamma(h^-h^-h^+\nu_\tau(\text{ex. } K^0)) / \Gamma_{\text{total}}$ Γ_{65} / Γ

$\Gamma_{65} / \Gamma = (\Gamma_{70} + \Gamma_{97} + \Gamma_{106} + 0.491\Gamma_{170} + 0.0153\Gamma_{178} + 0.0153\Gamma_{179}) / \Gamma$

VALUE (%)	EVTS	DOCUMENT ID	TECN	COMMENT
9.46 ± 0.05 OUR FIT				(Produced by HFLAV)
9.44 ± 0.14 OUR AVERAGE				Error includes scale factor of 1.4. See the ideogram below.
9.317 ± 0.090 ± 0.082	12.2k	1 ABDALLAH	06A DLPH	1992-1995 LEP runs
9.51 ± 0.07 ± 0.20	37.7k	BALEST	95c CLEO	$E_{cm}^{ee} \approx 10.6$ GeV

- • • We use the following data for averages but not for fits. • • •
- 9.87 ± 0.10 ± 0.24 2 AKERS 95Y OPAL 1991-1994 LEP runs
- • • We do not use the following data for averages, fits, limits, etc. • • •
- 9.50 ± 0.10 ± 0.11 11.2k 3 BUSKULIC 96 ALEP Repl. by SCHAEEL 05c
- 1 See footnote to ABDALLAH 06A $\Gamma(\tau^- \rightarrow h^- \nu_\tau) / \Gamma_{\text{total}}$ measurement for correlations with other measurements.
- 2 Not independent of AKERS 95Y $B(h^-h^-h^+ \geq 0 \text{ neutrals } \nu_\tau(\text{ex. } K_S^0 \rightarrow \pi^+\pi^-))$ and $B(h^-h^-h^+\nu_\tau(\text{ex. } K^0)) / B(h^-h^-h^+ \geq 0 \text{ neutrals } \nu_\tau(\text{ex. } K_S^0 \rightarrow \pi^+\pi^-))$ values.
- 3 Not independent of BUSKULIC 96 $B(h^-h^-h^+\nu_\tau)$ value.



$\Gamma(h^-h^-h^+\nu_\tau(\text{ex. } K^0)) / \Gamma(h^-h^-h^+ \geq 0 \text{ neutrals } \nu_\tau(\text{ex. } K_S^0 \rightarrow \pi^+\pi^-))$ $\Gamma_{65} / \Gamma_{63}$

(“3-prong”)

$\Gamma_{65} / \Gamma_{63} = (\Gamma_{70} + \Gamma_{97} + \Gamma_{106} + 0.491\Gamma_{170} + 0.0153\Gamma_{178} + 0.0153\Gamma_{179}) / ((0.4247\Gamma_{52} + \Gamma_{70} + \Gamma_{78} + \Gamma_{85} + \Gamma_{89} + \Gamma_{97} + \Gamma_{103} + \Gamma_{106} + \Gamma_{107} + 0.2804\Gamma_{150} + 0.2302\Gamma_{151} + 0.2804\Gamma_{152} + 0.2804\Gamma_{154} + 0.1131\Gamma_{156} + 0.3257\Gamma_{160} + 0.491\Gamma_{170} + 0.9078\Gamma_{178} + 0.9078\Gamma_{179} + 0.9078\Gamma_{180} + 0.892\Gamma_{182}))$

VALUE (units 10^{-2})	DOCUMENT ID	TECN	COMMENT
64.98 ± 0.31 OUR FIT			(Produced by HFLAV)
66.0 ± 0.4 ± 1.4	AKERS	95Y OPAL	1991-1994 LEP runs

$\Gamma(h^-h^-h^+\nu_\tau(\text{ex. } K^0, \omega)) / \Gamma_{\text{total}}$ Γ_{66} / Γ

$\Gamma_{66} / \Gamma = (\Gamma_{70} + \Gamma_{97} + \Gamma_{106} + 0.491\Gamma_{170}) / \Gamma$

VALUE (%)	DOCUMENT ID
9.43 ± 0.05 OUR FIT	(Produced by HFLAV)

$\Gamma(\pi^-\pi^+\pi^-\nu_\tau) / \Gamma_{\text{total}}$ $\Gamma_{67} / \Gamma = (0.34598\Gamma_{36} + \Gamma_{70} + 0.0153\Gamma_{178}) / \Gamma$

VALUE (%)	DOCUMENT ID
9.31 ± 0.05 OUR FIT	(Produced by HFLAV)

$\Gamma(\pi^-\pi^+\pi^-\nu_\tau(\text{ex. } K^0)) / \Gamma_{\text{total}}$ $\Gamma_{68} / \Gamma = (\Gamma_{70} + 0.0153\Gamma_{178}) / \Gamma$

VALUE (%)	EVTS	DOCUMENT ID	TECN	COMMENT
9.02 ± 0.05 OUR FIT				(Produced by HFLAV)
8.77 ± 0.13 OUR AVERAGE				Error includes scale factor of 1.1.
8.42 ± 0.00 ± 0.26	8.9M	1 LEE	10	BELL 666 fb^{-1} $E_{cm}^{ee} = 10.6$ GeV
8.83 ± 0.01 ± 0.13	1.6M	2 AUBERT	08	BABR 342 fb^{-1} $E_{cm}^{ee} = 10.6$ GeV
9.13 ± 0.05 ± 0.46	43k	3 BRIERE	03	CLE3 $E_{cm}^{ee} = 10.6$ GeV

- 1 Quoted statistical error is 0.003%. Correlation matrix for LEE 10 branching fractions:
- | | | | |
|---|-----|--------|--------------|
| (1) $\Gamma(\tau^- \rightarrow \pi^-\pi^+\pi^-\nu_\tau(\text{ex. } K^0)) / \Gamma_{\text{total}}$ | (1) | (2) | (3) |
| (2) $\Gamma(\tau^- \rightarrow K^-\pi^+\pi^-\nu_\tau(\text{ex. } K^0)) / \Gamma_{\text{total}}$ | (2) | 0.175 | |
| (3) $\Gamma(\tau^- \rightarrow K^-\pi^+\pi^-\nu_\tau(\text{ex. } K^0)) / \Gamma_{\text{total}}$ | (3) | 0.049 | 0.080 |
| (4) $\Gamma(\tau^- \rightarrow K^-\pi^+\pi^-\nu_\tau(\text{ex. } K^0)) / \Gamma_{\text{total}}$ | (4) | -0.053 | 0.035 -0.008 |
- 2 Correlation matrix for AUBERT 08 branching fractions:
- | | | | |
|---|-----|-------|-------------|
| (1) $\Gamma(\tau^- \rightarrow \pi^-\pi^+\pi^-\nu_\tau(\text{ex. } K^0)) / \Gamma_{\text{total}}$ | (1) | (2) | (3) |
| (2) $\Gamma(\tau^- \rightarrow K^-\pi^+\pi^-\nu_\tau(\text{ex. } K^0)) / \Gamma_{\text{total}}$ | (2) | 0.544 | |
| (3) $\Gamma(\tau^- \rightarrow K^-\pi^+\pi^-\nu_\tau(\text{ex. } K^0)) / \Gamma_{\text{total}}$ | (3) | 0.390 | 0.177 |
| (4) $\Gamma(\tau^- \rightarrow K^-\pi^+\pi^-\nu_\tau(\text{ex. } K^0)) / \Gamma_{\text{total}}$ | (4) | 0.031 | 0.093 0.087 |
- 3 47% correlated with BRIERE 03 $\tau^- \rightarrow K^-\pi^+\pi^-\nu_\tau$ and 71% correlated with $\tau^- \rightarrow K^-K^+\pi^-\nu_\tau$ because of a common 5% normalization error.

$\Gamma(\pi^-\pi^+\pi^-\nu_\tau(\text{ex. } K^0), \text{non-axial vector}) / \Gamma(\pi^-\pi^+\pi^-\nu_\tau(\text{ex. } K^0))$ $\Gamma_{69} / \Gamma_{68}$

$\Gamma_{69} / \Gamma_{68} = \Gamma_{69} / (\Gamma_{70} + 0.0153\Gamma_{177})$

VALUE	CL%	DOCUMENT ID	TECN	COMMENT
< 0.261	95	1 ACKERSTAFF 97R	OPAL	1992-1994 LEP runs

1 Model-independent limit from structure function analysis on contribution to $B(\tau^- \rightarrow \pi^-\pi^+\pi^-\nu_\tau(\text{ex. } K^0))$ from non-axial vectors.

$\Gamma(\pi^-\pi^+\pi^-\nu_\tau(\text{ex. } K^0, \omega)) / \Gamma_{\text{total}}$ Γ_{70} / Γ

VALUE (%)	EVTS	DOCUMENT ID	TECN	COMMENT
8.99 ± 0.05 OUR FIT				(Produced by HFLAV)
9.041 ± 0.060 ± 0.076	29k	1 SCHAEEL	05c ALEP	1991-1995 LEP runs

1 See footnote to SCHAEEL 05c $\Gamma(\tau^- \rightarrow e^-\bar{\nu}_e\nu_\tau) / \Gamma_{\text{total}}$ measurement for correlations with other measurements.

$\Gamma(h^-h^-h^+ \geq 1 \text{ neutrals } \nu_\tau) / \Gamma_{\text{total}}$ Γ_{71} / Γ

$\Gamma_{71} / \Gamma = (0.34598\Gamma_{41} + 0.34598\Gamma_{43} + 0.4247\Gamma_{48} + 0.4247\Gamma_{52} + \Gamma_{78} + \Gamma_{85} + \Gamma_{86} + \Gamma_{103} + \Gamma_{107} + 0.2804\Gamma_{150} + 0.2804\Gamma_{152} + 0.2804\Gamma_{154} + 0.2926\Gamma_{156} + 0.892\Gamma_{178} + 0.892\Gamma_{179} + 0.9078\Gamma_{180}) / \Gamma$

VALUE (%)	EVTS	DOCUMENT ID	TECN	COMMENT
5.29 ± 0.05 OUR FIT				(Produced by HFLAV)
5.6 ± 0.7 ± 0.3	352	1 BEHREND	90	CELL $E_{cm}^{ee} = 35$ GeV
4.2 ± 0.5 ± 0.9	203	2 ALBRECHT	87L	ARG $E_{cm}^{ee} = 10$ GeV
6.1 ± 0.8 ± 0.9		3 BURCHAT	87	MRK2 $E_{cm}^{ee} = 29$ GeV
7.6 ± 0.4 ± 0.9		4,5 RUCKSTUHL	86	DLCO $E_{cm}^{ee} = 29$ GeV
4.7 ± 0.5 ± 0.8	530	6 SCHMIDKE	86	MRK2 $E_{cm}^{ee} = 29$ GeV
5.6 ± 0.4 ± 0.7		5 FERNANDEZ	85	MAC $E_{cm}^{ee} = 29$ GeV
6.2 ± 2.3 ± 1.7		BEHREND	84	CELL $E_{cm}^{ee} = 14.22$ GeV

- 1 BEHREND 90 value is not independent of BEHREND 90 $B(3h\nu_\tau \geq 1 \text{ neutrals}) + B(5\text{-prong})$.
- 2 ALBRECHT 87L measure the product of branching ratios $B(3\pi^{\pm 0}\nu_\tau) B((e\bar{\nu}_0\mu\bar{\nu}_0\pi^0\text{ or } \rho)\nu_\tau) = 0.029$ and use the PDG 86 values for the second branching ratio which sum to 0.69 ± 0.03 to get the quoted value.
- 3 BURCHAT 87 value is not independent of SCHMIDKE 86 value.
- 4 Contributions from kaons and from $>1\pi^0$ are subtracted. Not independent of (3-prong + $0\pi^0$) and (3-prong + $\geq 0\pi^0$) values.
- 5 Value obtained using paper's $R = B(h^-h^-h^+\nu_\tau) / B(3\text{-prong})$ and current $B(3\text{-prong}) = 0.143$.
- 6 Not independent of SCHMIDKE 86 $h^-h^-h^+\nu_\tau$ and $h^-h^-h^+ (\geq 0\pi^0)\nu_\tau$ values.

$\Gamma(h^-h^-h^+ \geq 1\pi^0\nu_\tau(\text{ex. } K^0)) / \Gamma_{\text{total}}$ Γ_{72} / Γ

$\Gamma_{72} / \Gamma = (\Gamma_{78} + \Gamma_{85} + \Gamma_{86} + \Gamma_{103} + \Gamma_{107} + 0.2302\Gamma_{150} + 0.2302\Gamma_{152} + 0.2302\Gamma_{154} + 0.892\Gamma_{178} + 0.892\Gamma_{179} + 0.9078\Gamma_{180}) / \Gamma$

VALUE (%)	EVTS	DOCUMENT ID	TECN	COMMENT
5.09 ± 0.05 OUR FIT				(Produced by HFLAV)
5.10 ± 0.12 OUR AVERAGE				

- • • We use the following data for averages but not for fits. • • •
- 5.106 ± 0.083 ± 0.103 10.1k 1 ABDALLAH 06A DLPH 1992-1995 LEP runs
- 5.09 ± 0.10 ± 0.23 2 AKERS 95Y OPAL 1991-1994 LEP runs

Lepton Particle Listings

 τ

• • • We do not use the following data for averages, fits, limits, etc. • • •
 4.95 ± 0.29 ± 0.65 570 DECAMP 92c ALEP Repl. by SCHAELE 05c

¹ See footnote to ABDALLAH 06A $\Gamma(\tau^- \rightarrow h^- \nu_\tau)/\Gamma_{\text{total}}$ measurement for correlations with other measurements.

² Not independent of AKERS 95V $B(h^- h^- h^+ \geq 0 \text{ neutrals } \nu_\tau \text{ (ex. } K_S^0 \rightarrow \pi^+ \pi^-))$ and $B(h^- h^- h^+ \geq 0 \text{ neutrals } \nu_\tau \text{ (ex. } K_S^0)) / B(h^- h^- h^+ \geq 0 \text{ neutrals } \nu_\tau \text{ (ex. } K_S^0 \rightarrow \pi^+ \pi^-))$ values.

$\Gamma(h^- h^- h^+ \pi^0 \nu_\tau) / \Gamma_{\text{total}}$ Γ_{73} / Γ
 $\Gamma_{73} / \Gamma = (0.34598\Gamma_{41} + 0.34598\Gamma_{43} + \Gamma_{78} + \Gamma_{103} + \Gamma_{107} + 0.2302\Gamma_{152} + 0.892\Gamma_{178} + 0.892\Gamma_{179} + 0.0153\Gamma_{180}) / \Gamma$

VALUE (%)	EVTS	DOCUMENT ID	TECN	COMMENT
4.76 ± 0.05 OUR FIT		(Produced by HFLAV)		

• • • We do not use the following data for averages, fits, limits, etc. • • •
 4.45 ± 0.09 ± 0.07 6.1k ¹BUSKULIC 96 ALEP Repl. by SCHAELE 05c

¹BUSKULIC 96 quote $B(h^- h^- h^+ \pi^0 \nu_\tau \text{ (ex. } K^0)) = 4.30 \pm 0.09 \pm 0.09$. We add 0.15 to remove their K^0 correction and reduce the systematic error accordingly.

$\Gamma(h^- h^- h^+ \pi^0 \nu_\tau \text{ (ex. } K^0)) / \Gamma_{\text{total}}$ Γ_{74} / Γ
 $\Gamma_{74} / \Gamma = (\Gamma_{78} + \Gamma_{103} + \Gamma_{107} + 0.2302\Gamma_{152} + 0.892\Gamma_{178} + 0.892\Gamma_{179} + 0.0153\Gamma_{180}) / \Gamma$

VALUE (%)	EVTS	DOCUMENT ID	TECN	COMMENT
4.57 ± 0.05 OUR FIT		(Produced by HFLAV)		

4.45 ± 0.14 OUR AVERAGE Error includes scale factor of 1.2.
 4.545 ± 0.106 ± 0.103 8.9k ¹ABDALLAH 06A DLPH 1992–1995 LEP runs
 4.23 ± 0.06 ± 0.22 7.2k BALEST 95c CLEO $E_{\text{cm}}^{ee} \approx 10.6 \text{ GeV}$

¹ See footnote to ABDALLAH 06A $\Gamma(\tau^- \rightarrow h^- \nu_\tau)/\Gamma_{\text{total}}$ measurement for correlations with other measurements.

$\Gamma(h^- h^- h^+ \pi^0 \nu_\tau \text{ (ex. } K^0, \omega)) / \Gamma_{\text{total}}$ $\Gamma_{75} / \Gamma = (\Gamma_{78} + \Gamma_{103} + \Gamma_{107} + 0.2302\Gamma_{152}) / \Gamma$

VALUE (%)	EVTS	DOCUMENT ID	TECN	COMMENT
2.79 ± 0.07 OUR FIT		(Produced by HFLAV)		

$\Gamma(\pi^- \pi^+ \pi^- \pi^0 \nu_\tau) / \Gamma_{\text{total}}$ Γ_{76} / Γ
 $\Gamma_{76} / \Gamma = (0.34598\Gamma_{41} + \Gamma_{78} + 0.892\Gamma_{178} + 0.0153\Gamma_{180}) / \Gamma$

VALUE (%)	EVTS	DOCUMENT ID	TECN	COMMENT
4.62 ± 0.05 OUR FIT		(Produced by HFLAV)		

$\Gamma(\pi^- \pi^+ \pi^- \pi^0 \nu_\tau \text{ (ex. } K^0)) / \Gamma_{\text{total}}$ Γ_{77} / Γ
 $\Gamma_{77} / \Gamma = (\Gamma_{78} + 0.892\Gamma_{178} + 0.0153\Gamma_{180}) / \Gamma$

VALUE (%)	EVTS	DOCUMENT ID	TECN	COMMENT
4.49 ± 0.05 OUR FIT		(Produced by HFLAV)		

4.55 ± 0.13 OUR AVERAGE Error includes scale factor of 1.6.
 4.598 ± 0.057 ± 0.064 16k ¹SCHAELE 05c ALEP 1991–1995 LEP runs
 4.19 ± 0.10 ± 0.21 ²EDWARDS 00A CLEO 4.7 fb⁻¹ $E_{\text{cm}}^{ee} = 10.6 \text{ GeV}$

¹SCHAELE 05c quote $(4.590 \pm 0.057 \pm 0.064)\%$. We add 0.008% to remove their correction for $\tau^- \rightarrow \pi^- \pi^0 \omega \nu_\tau \rightarrow \pi^- \pi^0 \pi^+ \pi^- \nu_\tau$ decays. See footnote to SCHAELE 05c $\Gamma(\tau^- \rightarrow e^- \bar{\nu}_e \nu_\tau) / \Gamma_{\text{total}}$ measurement for correlations with other measurements.

²EDWARDS 00A quote $(4.19 \pm 0.10) \times 10^{-2}$ with a 5% systematic error.

$\Gamma(\pi^- \pi^+ \pi^- \pi^0 \nu_\tau \text{ (ex. } K^0, \omega)) / \Gamma_{\text{total}}$ Γ_{78} / Γ

VALUE (%)	EVTS	DOCUMENT ID	TECN	COMMENT
2.74 ± 0.07 OUR FIT		(Produced by HFLAV)		

$\Gamma(h^- \rho^0 \nu_\tau) / \Gamma(h^- h^- h^+ \pi^0 \nu_\tau)$ $\Gamma_{79} / \Gamma_{73}$

VALUE	EVTS	DOCUMENT ID	TECN	COMMENT
0.30 ± 0.04 ± 0.02	393	ALBRECHT 91D ARG		$E_{\text{cm}}^{ee} = 9.4\text{--}10.6 \text{ GeV}$

$\Gamma(h^- \rho^+ h^- \nu_\tau) / \Gamma(h^- h^- h^+ \pi^0 \nu_\tau)$ $\Gamma_{80} / \Gamma_{73}$

VALUE	EVTS	DOCUMENT ID	TECN	COMMENT
0.10 ± 0.03 ± 0.04	142	ALBRECHT 91D ARG		$E_{\text{cm}}^{ee} = 9.4\text{--}10.6 \text{ GeV}$

$\Gamma(h^- \rho^- h^+ \nu_\tau) / \Gamma(h^- h^- h^+ \pi^0 \nu_\tau)$ $\Gamma_{81} / \Gamma_{73}$

VALUE	EVTS	DOCUMENT ID	TECN	COMMENT
0.26 ± 0.05 ± 0.01	370	ALBRECHT 91D ARG		$E_{\text{cm}}^{ee} = 9.4\text{--}10.6 \text{ GeV}$

$\Gamma(h^- h^- h^+ \geq 2\pi^0 \nu_\tau \text{ (ex. } K^0)) / \Gamma_{\text{total}}$ Γ_{82} / Γ
 $\Gamma_{82} / \Gamma = (\Gamma_{85} + \Gamma_{86} + 0.2302\Gamma_{150} + 0.2302\Gamma_{154} + 0.892\Gamma_{180}) / \Gamma$

VALUE (%)	EVTS	DOCUMENT ID	TECN	COMMENT
0.517 ± 0.031 OUR FIT		(Produced by HFLAV)		

0.561 ± 0.068 ± 0.095 1.3k ¹ABDALLAH 06A DLPH 1992–1995 LEP runs

¹ See footnote to ABDALLAH 06A $\Gamma(\tau^- \rightarrow h^- \nu_\tau) / \Gamma_{\text{total}}$ measurement for correlations with other measurements.

$\Gamma(h^- h^- h^+ 2\pi^0 \nu_\tau) / \Gamma_{\text{total}}$ Γ_{83} / Γ
 $\Gamma_{83} / \Gamma = (0.4247\Gamma_{48} + \Gamma_{85} + 0.2302\Gamma_{150} + 0.2302\Gamma_{154} + 0.892\Gamma_{180}) / \Gamma$

VALUE (%)	EVTS	DOCUMENT ID	TECN	COMMENT
0.505 ± 0.031 OUR FIT		(Produced by HFLAV)		

$\Gamma(h^- h^- h^+ 2\pi^0 \nu_\tau \text{ (ex. } K^0)) / \Gamma_{\text{total}}$ Γ_{84} / Γ
 $\Gamma_{84} / \Gamma = (\Gamma_{85} + 0.2302\Gamma_{150} + 0.2302\Gamma_{154} + 0.892\Gamma_{180}) / \Gamma$

VALUE (%)	EVTS	DOCUMENT ID	TECN	COMMENT
0.495 ± 0.031 OUR FIT		(Produced by HFLAV)		

0.435 ± 0.030 ± 0.035 2.6k ¹SCHAELE 05c ALEP 1991–1995 LEP runs

• • • We do not use the following data for averages, fits, limits, etc. • • •
 0.50 ± 0.07 ± 0.07 1.8k BUSKULIC 96 ALEP Repl. by SCHAELE 05c

¹SCHAELE 05c quote $(0.392 \pm 0.030 \pm 0.035)\%$. We add 0.043% to remove their correction for $\tau^- \rightarrow \pi^- \eta \pi^0 \nu_\tau \rightarrow \pi^- \pi^+ \pi^- 2\pi^0 \nu_\tau$ and $\tau^- \rightarrow K^*(892)^- \eta \nu_\tau \rightarrow K^- \pi^+ \pi^- 2\pi^0 \nu_\tau$ decays. See footnote to SCHAELE 05c $\Gamma(\tau^- \rightarrow e^- \bar{\nu}_e \nu_\tau) / \Gamma_{\text{total}}$ measurement for correlations with other measurements.

$\Gamma(h^- h^- h^+ 2\pi^0 \nu_\tau \text{ (ex. } K^0)) / \Gamma(h^- h^- h^+ \geq 0 \text{ neutrals } \nu_\tau)$ $\Gamma_{84} / \Gamma_{62}$
 $\Gamma_{84} / \Gamma_{62} = (\Gamma_{85} + 0.2302\Gamma_{150} + 0.2302\Gamma_{154} + 0.892\Gamma_{180}) / (0.34598\Gamma_{36} + 0.34598\Gamma_{38} + 0.34598\Gamma_{41} + 0.34598\Gamma_{43} + 0.4247\Gamma_{48} + 0.692\Gamma_{49} + 0.8494\Gamma_{52} + 0.692\Gamma_{56} + 0.6534\Gamma_{61} + \Gamma_{70} + \Gamma_{78} + \Gamma_{85} + \Gamma_{89} + \Gamma_{97} + \Gamma_{103} + \Gamma_{106} + \Gamma_{107} + 0.2804\Gamma_{150} + 0.2302\Gamma_{151} + 0.2804\Gamma_{152} + 0.2804\Gamma_{154} + 0.3759\Gamma_{156} + 0.3257\Gamma_{160} + 0.7259\Gamma_{170} + 0.9078\Gamma_{178} + 0.9078\Gamma_{179} + 0.9078\Gamma_{180} + 0.892\Gamma_{182})$

VALUE (units 10 ⁻²)	EVTS	DOCUMENT ID	TECN	COMMENT
3.26 ± 0.20 OUR FIT		(Produced by HFLAV)		

3.4 ± 0.2 ± 0.3 668 BORTOLETTO93 CLEO $E_{\text{cm}}^{ee} \approx 10.6 \text{ GeV}$

$\Gamma(h^- h^- h^+ 2\pi^0 \nu_\tau \text{ (ex. } K^0, \omega, \eta)) / \Gamma_{\text{total}}$ Γ_{85} / Γ

VALUE (units 10 ⁻⁴)	DOCUMENT ID	TECN	COMMENT
10 ± 4 OUR FIT	(Produced by HFLAV)		

$\Gamma(h^- h^- h^+ 3\pi^0 \nu_\tau) / \Gamma_{\text{total}}$ $\Gamma_{86} / \Gamma = (0.4247\Gamma_{52} + \Gamma_{87} + 0.1131\Gamma_{156}) / \Gamma$

VALUE (units 10 ⁻⁴)	CL%	EVTS	DOCUMENT ID	TECN	COMMENT
2.13 ± 0.30 OUR FIT			(Produced by HFLAV)		

2.2 ± 0.3 ± 0.4 139 ANASTASSOV 01 CLEO $E_{\text{cm}}^{ee} = 10.6 \text{ GeV}$

• • • We do not use the following data for averages, fits, limits, etc. • • •

< 4.9 95 SCHAELE 05c ALEP 1991–1995 LEP runs

2.85 ± 0.56 ± 0.51 57 ANDERSON 97 CLEO Repl. by ANASTASSOV 01

11 ± 4 ± 5 440 ¹BUSKULIC 96 ALEP Repl. by SCHAELE 05c

¹BUSKULIC 96 state their measurement is for $B(h^- h^- h^+ \geq 3\pi^0 \nu_\tau)$. We assume that $B(h^- h^- h^+ \geq 4\pi^0 \nu_\tau)$ is very small.

$\Gamma(2\pi^- \pi^+ 3\pi^0 \nu_\tau \text{ (ex. } K^0)) / \Gamma_{\text{total}}$ Γ_{87} / Γ
 $\Gamma_{87} / \Gamma = (\Gamma_{89} + 0.2302\Gamma_{151} + 0.3257\Gamma_{160} + 0.892\Gamma_{182}) / \Gamma$

VALUE (units 10 ⁻⁴)	DOCUMENT ID	TECN	COMMENT
1.94 ± 0.30 OUR FIT	(Produced by HFLAV)		

• • • We use the following data for averages but not for fits. • • •
2.07 ± 0.18 ± 0.37 ¹LEES 12x BABR 468 fb⁻¹ $E_{\text{cm}}^{ee} = 10.6 \text{ GeV}$

¹Not independent of LEES 12x $\Gamma(\tau^- \rightarrow \eta \pi^- \pi^+ \pi^- \nu_\tau \text{ (ex. } K^0)) / \Gamma$, $\Gamma(\tau^- \rightarrow \eta \pi^- \pi^0 \pi^0 \nu_\tau) / \Gamma$, $\Gamma(\tau^- \rightarrow \pi^- \omega 2\pi^0 \nu_\tau) / \Gamma$, and $\Gamma(\tau^- \rightarrow f_1(1285) \pi^- \nu_\tau \rightarrow \eta \pi^- \pi^+ \pi^- \nu_\tau) / \Gamma$ values.

$\Gamma(2\pi^- \pi^+ 3\pi^0 \nu_\tau \text{ (ex. } K^0, \eta, f_1(1285))) / \Gamma_{\text{total}}$ Γ_{88} / Γ

VALUE (units 10 ⁻⁴)	DOCUMENT ID	TECN	COMMENT
1.69 ± 0.08 ± 0.43	LEES 12x BABR 468 fb ⁻¹		$E_{\text{cm}}^{ee} = 10.6 \text{ GeV}$

$\Gamma(2\pi^- \pi^+ 3\pi^0 \nu_\tau \text{ (ex. } K^0, \eta, \omega, f_1(1285))) / \Gamma_{\text{total}}$ Γ_{89} / Γ

VALUE (units 10 ⁻⁵)	DOCUMENT ID	TECN	COMMENT
1.4 ± 2.7 OUR FIT	(Produced by HFLAV)		

1.0 ± 0.8 ± 3.0 ¹LEES 12x BABR 468 fb⁻¹ $E_{\text{cm}}^{ee} = 10.6 \text{ GeV}$

¹LEES 12x measurement corresponds to the lower limit of $< 5.8 \times 10^{-5}$ at 90% CL.

$\Gamma(K^- h^+ h^- \geq 0 \text{ neutrals } \nu_\tau) / \Gamma_{\text{total}}$ Γ_{90} / Γ
 $\Gamma_{90} / \Gamma = (0.34598\Gamma_{38} + 0.34598\Gamma_{43} + \Gamma_{97} + \Gamma_{103} + \Gamma_{106} + \Gamma_{107} + 0.2804\Gamma_{152} + 0.491\Gamma_{170} + 0.9078\Gamma_{179}) / \Gamma$

VALUE (%)	CL%	DOCUMENT ID	TECN	COMMENT
0.629 ± 0.014 OUR FIT		(Produced by HFLAV)		

< 0.6 90 AIHARA 84c TPC $E_{\text{cm}}^{ee} = 29 \text{ GeV}$

$\Gamma(K^- h^+ \pi^- \nu_\tau \text{ (ex. } K^0)) / \Gamma_{\text{total}}$ $\Gamma_{91} / \Gamma = (\Gamma_{97} + \Gamma_{106} + 0.0153\Gamma_{179}) / \Gamma$

VALUE (%)	DOCUMENT ID	TECN	COMMENT
0.437 ± 0.007 OUR FIT	(Produced by HFLAV)		

$\Gamma(K^- h^+ \pi^- \nu_\tau \text{ (ex. } K^0)) / \Gamma(\pi^- \pi^+ \pi^- \nu_\tau \text{ (ex. } K^0))$ $\Gamma_{91} / \Gamma_{68}$
 $\Gamma_{91} / \Gamma_{68} = (\Gamma_{97} + \Gamma_{106} + 0.0153\Gamma_{179}) / (\Gamma_{70} + 0.0153\Gamma_{178})$

VALUE (%)	EVTS	DOCUMENT ID	TECN	COMMENT
4.84 ± 0.08 OUR FIT		(Produced by HFLAV)		

5.44 ± 0.21 ± 0.53 7.9k RICHICHI 99 CLEO $E_{\text{cm}}^{ee} = 10.6 \text{ GeV}$

$\Gamma(K^- h^+ \pi^- \pi^0 \nu_\tau \text{ (ex. } K^0)) / \Gamma_{\text{total}}$ Γ_{92} / Γ
 $\Gamma_{92} / \Gamma = (\Gamma_{103} + \Gamma_{107} + 0.2302\Gamma_{152} + 0.892\Gamma_{179}) / \Gamma$

VALUE (units 10 ⁻⁴)	DOCUMENT ID	TECN	COMMENT
8.6 ± 1.2 OUR FIT	(Produced by HFLAV)		

$$\Gamma(K^- h^+ \pi^- \pi^0 \nu_\tau(\text{ex. } K^0))/\Gamma(\pi^- \pi^+ \pi^- \pi^0 \nu_\tau(\text{ex. } K^0)) \quad \Gamma_{92}/\Gamma_{77}$$

$$\Gamma_{92}/\Gamma_{77} = (\Gamma_{103} + \Gamma_{107} + 0.2302\Gamma_{152} + 0.892\Gamma_{179})/(\Gamma_{78} + 0.892\Gamma_{178} + 0.0153\Gamma_{180})$$

VALUE (%)	EVTS	DOCUMENT ID	TECN	COMMENT
1.91 ± 0.26 OUR FIT	(Produced by HFLAV)			
2.61 ± 0.45 ± 0.42	719	RICHICHI	99	CLEO $E_{cm}^{ee} = 10.6$ GeV

$$\Gamma(K^- \pi^+ \pi^- \geq 0 \text{ neutrals } \nu_\tau)/\Gamma_{\text{total}} \quad \Gamma_{93}/\Gamma$$

$$\Gamma_{93}/\Gamma = (0.34598\Gamma_{38} + 0.34598\Gamma_{43} + \Gamma_{97} + \Gamma_{103} + 0.2804\Gamma_{152} + 0.9078\Gamma_{179})/\Gamma$$

VALUE (%)	EVTS	DOCUMENT ID	TECN	COMMENT
0.477 ± 0.014 OUR FIT	(Produced by HFLAV)			

0.58 ± 0.15 ± 0.12	20	¹ BAUER	94	TPC $E_{cm}^{ee} = 29$ GeV
• • •				We do not use the following data for averages, fits, limits, etc. • • •
0.22 +0.16 -0.13 ± 0.05	9	² MILLS	85	DLCO $E_{cm}^{ee} = 29$ GeV

¹ We multiply 0.58% by 0.20, the relative systematic error quoted by BAUER 94, to obtain the systematic error.
² Error correlated with MILLS 85 ($K K \pi \nu$) value. We multiply 0.22% by 0.23, the relative systematic error quoted by MILLS 85, to obtain the systematic error.

$$\Gamma(K^- \pi^+ \pi^- \geq 0 \pi^0 \nu_\tau(\text{ex. } K^0))/\Gamma_{\text{total}} \quad \Gamma_{94}/\Gamma$$

$$\Gamma_{94}/\Gamma = (\Gamma_{97} + \Gamma_{103} + 0.2302\Gamma_{152} + 0.9078\Gamma_{179})/\Gamma$$

VALUE (%)	DOCUMENT ID	TECN	COMMENT
0.373 ± 0.013 OUR FIT	(Produced by HFLAV)		
0.30 ± 0.05 OUR AVERAGE			

• • •				We use the following data for averages but not for fits. • • •
0.343 ± 0.073 ± 0.031		ABBIENDI	00D	OPAL 1990–1995 LEP runs
0.275 ± 0.064		¹ BARATE	98	ALEP 1991–1995 LEP runs
• • •				We use the following data for averages but not for fits. • • •
• • •				We do not use the following data for averages, fits, limits, etc. • • •

¹ Not independent of BARATE 98 $\Gamma(\tau^- \rightarrow K^- \pi^+ \pi^- \nu_\tau)/\Gamma_{\text{total}}$ and $\Gamma(\tau^- \rightarrow K^- \pi^+ \pi^- \pi^0 \nu_\tau)/\Gamma_{\text{total}}$ values.

$$\Gamma(K^- \pi^+ \pi^- \nu_\tau)/\Gamma_{\text{total}} \quad \Gamma_{95}/\Gamma = (0.34598\Gamma_{38} + \Gamma_{97} + 0.0153\Gamma_{179})/\Gamma$$

VALUE (%)	DOCUMENT ID	TECN	COMMENT
0.345 ± 0.007 OUR FIT	(Produced by HFLAV)		

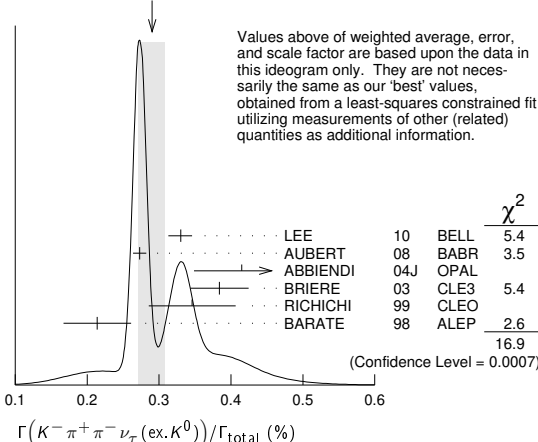
$$\Gamma(K^- \pi^+ \pi^- \nu_\tau(\text{ex. } K^0))/\Gamma_{\text{total}} \quad \Gamma_{96}/\Gamma = (\Gamma_{97} + 0.0153\Gamma_{179})/\Gamma$$

VALUE (%)	EVTS	DOCUMENT ID	TECN	COMMENT
0.293 ± 0.017 OUR FIT	(Produced by HFLAV)			
0.290 ± 0.018 OUR AVERAGE	Error includes scale factor of 2.4. See the ideogram below.			

0.330 ± 0.001 ± 0.016 -0.017	794k	¹ LEE	10	BELL 666 fb ⁻¹ $E_{cm}^{ee} = 10.6$ GeV
0.273 ± 0.002 ± 0.009	70k	² AUBERT	08	BABR 342 fb ⁻¹ $E_{cm}^{ee} = 10.6$ GeV
0.415 ± 0.053 ± 0.040	269	ABBIENDI	04J	OPAL 1991–1995 LEP runs
0.384 ± 0.014 ± 0.038	3.5k	³ BRIERE	03	CLE3 $E_{cm}^{ee} = 10.6$ GeV
0.214 ± 0.037 ± 0.029		BARATE	98	ALEP 1991–1995 LEP runs
• • •				We use the following data for averages but not for fits. • • •
0.346 ± 0.023 ± 0.056	158	⁴ RICHICHI	99	CLEO $E_{cm}^{ee} = 10.6$ GeV
• • •				We do not use the following data for averages, fits, limits, etc. • • •
0.360 ± 0.082 ± 0.048		ABBIENDI	00D	OPAL 1990–1995 LEP runs

¹ See footnote to LEE 10 $\Gamma(\tau^- \rightarrow \pi^- \pi^+ \pi^- \nu_\tau(\text{ex. } K^0))/\Gamma_{\text{total}}$ measurement for correlations with other measurements. Not independent of LEE 10 $\Gamma(\tau^- \rightarrow K^- \pi^+ \pi^- \nu_\tau(\text{ex. } K^0))/\Gamma(\tau^- \rightarrow \pi^- \pi^+ \pi^- \nu_\tau(\text{ex. } K^0))$ value.
² See footnote to AUBERT 08 $\Gamma(\tau^- \rightarrow \pi^- \pi^+ \pi^- \nu_\tau(\text{ex. } K^0))/\Gamma_{\text{total}}$ measurement for correlations with other measurements.
³ 47% correlated with BRIERE 03 $\tau^- \rightarrow \pi^- \pi^+ \pi^- \nu_\tau$ and 34% correlated with $\tau^- \rightarrow K^- K^+ \pi^- \nu_\tau$ because of a common 5% normalization error.
⁴ Not independent of RICHICHI 99 $\Gamma(\tau^- \rightarrow K^- h^+ \pi^- \nu_\tau(\text{ex. } K^0))/\Gamma(\tau^- \rightarrow \pi^- \pi^+ \pi^- \nu_\tau(\text{ex. } K^0))$, $\Gamma(\tau^- \rightarrow K^- K^+ \pi^- \nu_\tau)/\Gamma(\tau^- \rightarrow \pi^- \pi^+ \pi^- \nu_\tau(\text{ex. } K^0))$ and BALEST 95c $\Gamma(\tau^- \rightarrow h^- h^- h^+ \nu_\tau(\text{ex. } K^0))/\Gamma_{\text{total}}$ values.

WEIGHTED AVERAGE
 0.290 ± 0.018 (Error scaled by 2.4)



$$\Gamma(K^- \pi^+ \pi^- \nu_\tau(\text{ex. } K^0))/\Gamma(\pi^- \pi^+ \pi^- \nu_\tau(\text{ex. } K^0)) \quad \Gamma_{96}/\Gamma_{68}$$

$$\Gamma_{96}/\Gamma_{68} = (\Gamma_{97} + 0.0153\Gamma_{179})/(\Gamma_{70} + 0.0153\Gamma_{178})$$

VALUE (units 10 ⁻²)	EVTS	DOCUMENT ID	TECN	COMMENT
3.25 ± 0.07 OUR FIT	(Produced by HFLAV)			

• • • We use the following data for averages but not for fits. • • •
3.92 ± 0.02 ± 0.15 -0.16 794k ¹LEE 10 BELL 666 fb⁻¹ $E_{cm}^{ee} = 10.6$ GeV
¹ Not independent of LEE 10 $\Gamma(\tau^- \rightarrow K^- \pi^+ \pi^- \nu_\tau(\text{ex. } K^0))/\Gamma_{\text{total}}$ and $\Gamma(\tau^- \rightarrow \pi^- \pi^+ \pi^- \nu_\tau(\text{ex. } K^0))/\Gamma_{\text{total}}$ values.

$$\Gamma(K^- \pi^+ \pi^- \nu_\tau(\text{ex. } K^0, \omega))/\Gamma_{\text{total}} \quad \Gamma_{97}/\Gamma$$

VALUE (units 10 ⁻³)	DOCUMENT ID	TECN	COMMENT
2.93 ± 0.07 OUR FIT	(Produced by HFLAV)		

$$\Gamma(K^- \rho^0 \nu_\tau \rightarrow K^- \pi^+ \pi^- \nu_\tau)/\Gamma(K^- \pi^+ \pi^- \nu_\tau(\text{ex. } K^0)) \quad \Gamma_{98}/\Gamma_{96}$$

VALUE	DOCUMENT ID	TECN	COMMENT
0.48 ± 0.14 ± 0.10	¹ ASNER 00B	CLEO	$E_{cm}^{ee} = 10.6$ GeV

• • • We do not use the following data for averages, fits, limits, etc. • • •
 0.39 ± 0.14 ²BARATE 99R ALEP 1991–1995 LEP runs
¹ ASNER 00B assume $\tau^- \rightarrow K^- \pi^+ \pi^- \nu_\tau(\text{ex. } K^0)$ decays proceed only through $K \rho$ and $K^* \pi$ intermediate states. They assume the resonance structure of $\tau^- \rightarrow K^- \pi^+ \pi^- \nu_\tau(\text{ex. } K^0)$ decays is dominated by $K_1(1270)^-$ and $K_1(1400)^-$ resonances, and assume $B(K_1(1270) \rightarrow K^*(892)\pi) = (16 \pm 5)\%$, $B(K_1(1270) \rightarrow K \rho) = (42 \pm 6)\%$, and $B(K_1(1400) \rightarrow K \rho) = 0$.
² BARATE 99R assume $\tau^- \rightarrow K^- \pi^+ \pi^- \nu_\tau(\text{ex. } K^0)$ decays proceed only through $K \rho$ and $K^* \pi$ intermediate states. The quoted error is statistical only.

$$\Gamma(K^- \pi^+ \pi^- \pi^0 \nu_\tau)/\Gamma_{\text{total}} \quad \Gamma_{99}/\Gamma$$

$$\Gamma_{99}/\Gamma = (0.34598\Gamma_{43} + \Gamma_{103} + 0.2302\Gamma_{152} + 0.892\Gamma_{179})/\Gamma$$

VALUE (units 10 ⁻⁴)	DOCUMENT ID	TECN	COMMENT
13.1 ± 1.2 OUR FIT	(Produced by HFLAV)		

$$\Gamma(K^- \pi^+ \pi^- \pi^0 \nu_\tau(\text{ex. } K^0))/\Gamma_{\text{total}} \quad \Gamma_{100}/\Gamma$$

$$\Gamma_{100}/\Gamma = (\Gamma_{103} + 0.2302\Gamma_{152} + 0.892\Gamma_{179})/\Gamma$$

VALUE (units 10 ⁻⁴)	CL%	DOCUMENT ID	TECN	COMMENT
7.9 ± 1.2 OUR FIT	(Produced by HFLAV)			
7.3 ± 1.2 OUR AVERAGE				

7.4 ± 0.8 ± 1.1		¹ ARMS 05	CLE3	7.6 fb ⁻¹ , $E_{cm}^{ee} = 10.6$ GeV	
6.1 ± 3.9 ± 1.8		BARATE	98	ALEP 1991–1995 LEP runs	
• • •				We use the following data for averages but not for fits. • • •	
7.5 ± 2.6 ± 1.8		² RICHICHI	99	CLEO $E_{cm}^{ee} = 10.6$ GeV	
• • •				We do not use the following data for averages, fits, limits, etc. • • •	
<17		95	ABBIENDI	00D	OPAL 1990–1995 LEP runs

¹ Not independent of ARMS 05 $\Gamma(\tau^- \rightarrow K^- \pi^+ \pi^- \pi^0 \nu_\tau(\text{ex. } K^0, \omega))/\Gamma_{\text{total}}$ and $\Gamma(\tau^- \rightarrow K^- \omega \nu_\tau)/\Gamma_{\text{total}}$ values.
² Not independent of RICHICHI 99 $\Gamma(\tau^- \rightarrow K^- h^+ \pi^- \nu_\tau(\text{ex. } K^0))/\Gamma(\tau^- \rightarrow \pi^- \pi^+ \pi^- \nu_\tau(\text{ex. } K^0))$, $\Gamma(\tau^- \rightarrow K^- K^+ \pi^- \nu_\tau)/\Gamma(\tau^- \rightarrow \pi^- \pi^+ \pi^- \nu_\tau(\text{ex. } K^0))$ and BALEST 95c $\Gamma(\tau^- \rightarrow h^- h^- h^+ \nu_\tau(\text{ex. } K^0))/\Gamma_{\text{total}}$ values.

$$\Gamma(K^- \pi^+ \pi^- \pi^0 \nu_\tau(\text{ex. } K^0, \eta))/\Gamma_{\text{total}} \quad \Gamma_{101}/\Gamma = (\Gamma_{103} + 0.892\Gamma_{179})/\Gamma$$

VALUE (units 10 ⁻⁴)	DOCUMENT ID	TECN	COMMENT
7.6 ± 1.2 OUR FIT	(Produced by HFLAV)		

$$\Gamma(K^- \pi^+ \pi^- \pi^0 \nu_\tau(\text{ex. } K^0, \omega))/\Gamma_{\text{total}} \quad \Gamma_{102}/\Gamma$$

VALUE (units 10 ⁻⁴)	EVTS	DOCUMENT ID	TECN	COMMENT
3.7 ± 0.5 ± 0.8	833	ARMS	05	CLE3 7.6 fb ⁻¹ , $E_{cm}^{ee} = 10.6$ GeV

$$\Gamma(K^- \pi^+ \pi^- \pi^0 \nu_\tau(\text{ex. } K^0, \omega, \eta))/\Gamma_{\text{total}} \quad \Gamma_{103}/\Gamma$$

VALUE (units 10 ⁻⁴)	DOCUMENT ID	TECN	COMMENT
3.9 ± 1.4 OUR FIT	(Produced by HFLAV)		

$$\Gamma(K^- \pi^+ K^- \geq 0 \text{ neut. } \nu_\tau)/\Gamma_{\text{total}} \quad \Gamma_{104}/\Gamma$$

VALUE (%)	CL%	DOCUMENT ID	TECN	COMMENT
<0.09	95	BAUER	94	TPC $E_{cm}^{ee} = 29$ GeV

$$\Gamma(K^- K^+ \pi^- \geq 0 \text{ neut. } \nu_\tau)/\Gamma_{\text{total}} \quad \Gamma_{105}/\Gamma = (\Gamma_{106} + \Gamma_{107})/\Gamma$$

VALUE (%)	EVTS	DOCUMENT ID	TECN	COMMENT
0.1496 ± 0.0033 OUR FIT	(Produced by HFLAV)			
0.203 ± 0.031 OUR AVERAGE				

0.159 ± 0.053 ± 0.020		ABBIENDI	00D	OPAL 1990–1995 LEP runs
0.15 +0.09 -0.07 ± 0.03	4	¹ BAUER	94	TPC $E_{cm}^{ee} = 29$ GeV
• • •				We use the following data for averages but not for fits. • • •
0.238 ± 0.042		² BARATE	98	ALEP 1991–1995 LEP runs

¹ We multiply 0.15% by 0.20, the relative systematic error quoted by BAUER 94, to obtain the systematic error.
² Not independent of BARATE 98 $\Gamma(\tau^- \rightarrow K^- K^+ \pi^- \nu_\tau)/\Gamma_{\text{total}}$ and $\Gamma(\tau^- \rightarrow K^- K^+ \pi^- \pi^0 \nu_\tau)/\Gamma_{\text{total}}$ values.

Lepton Particle Listings

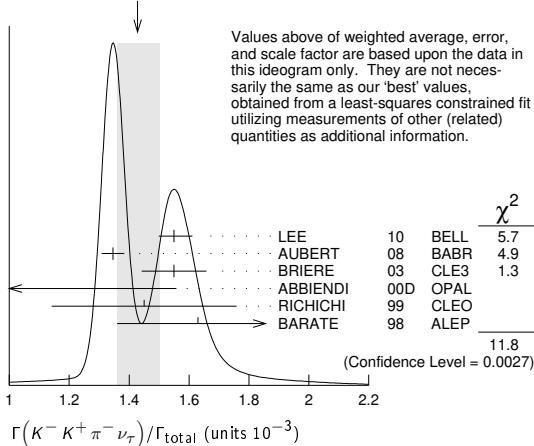
τ

$\Gamma(K^- K^+ \pi^- \nu_\tau)/\Gamma_{\text{total}}$ Γ_{106}/Γ

VALUE (units 10^{-3})	EVTS	DOCUMENT ID	TECN	COMMENT
1.435 ± 0.027 OUR FIT	(Produced by HFLAV)			
1.43 ± 0.07 OUR AVERAGE	Error includes scale factor of 2.4. See the ideogram below.			
1.55 ± 0.01 ± 0.06 -0.05	108k	¹ LEE	10 BELL	666 fb ⁻¹ $E_{\text{cm}}^{\text{ee}} = 10.6$ GeV
1.346 ± 0.010 ± 0.036	18k	² AUBERT	08 BABR	342 fb ⁻¹ $E_{\text{cm}}^{\text{ee}} = 10.6$ GeV
1.55 ± 0.06 ± 0.09	932	³ BRIERE	03 CLE3	$E_{\text{cm}}^{\text{ee}} = 10.6$ GeV
1.63 ± 0.21 ± 0.17		BARATE	98 ALEP	1991–1995 LEP runs
••• We use the following data for averages but not for fits. •••				
0.87 ± 0.56 ± 0.40		ABBIENDI	00D OPAL	1990–1995 LEP runs
1.45 ± 0.13 ± 0.28	2.3k	⁴ RICHICHI	99 CLEO	$E_{\text{cm}}^{\text{ee}} = 10.6$ GeV
••• We do not use the following data for averages, fits, limits, etc. •••				
2.2 ± 1.7 -1.1	± 0.5	⁵ MILLS	85 DLCO	$E_{\text{cm}}^{\text{ee}} = 29$ GeV

- See footnote to LEE 10 $\Gamma(\tau^- \rightarrow \pi^- \pi^+ \pi^- \nu_\tau(\text{ex. } K^0))/\Gamma_{\text{total}}$ measurement for correlations with other measurements. Not independent of LEE 10 $\Gamma(\tau^- \rightarrow K^- K^+ \pi^- \nu_\tau)/\Gamma(\tau^- \rightarrow \pi^- \pi^+ \pi^- \nu_\tau(\text{ex. } K^0))$ value.
- See footnote to AUBERT 08 $\Gamma(\tau^- \rightarrow \pi^- \pi^+ \pi^- \nu_\tau(\text{ex. } K^0))/\Gamma_{\text{total}}$ measurement for correlations with other measurements.
- 71% correlated with BRIERE 03 $\tau^- \rightarrow \pi^- \pi^+ \pi^- \nu_\tau$ and 34% correlated with $\tau^- \rightarrow K^- \pi^+ \pi^- \nu_\tau$ because of a common 5% normalization error.
- Not independent of RICHICHI 99 $\Gamma(\tau^- \rightarrow K^- K^+ \pi^- \nu_\tau)/\Gamma(\tau^- \rightarrow \pi^- \pi^+ \pi^- \nu_\tau(\text{ex. } K^0))$ and BALEST 95c $\Gamma(\tau^- \rightarrow h^- h^+ h^+ \nu_\tau(\text{ex. } K^0))/\Gamma_{\text{total}}$ values.
- Error correlated with MILLS 85 ($K\pi\pi^0\nu$) value. We multiply 0.22% by 0.23, the relative systematic error quoted by MILLS 85, to obtain the systematic error.

WEIGHTED AVERAGE
1.43±0.07 (Error scaled by 2.4)



Values above of weighted average, error, and scale factor are based upon the data in this ideogram only. They are not necessarily the same as our 'best' values, obtained from a least-squares constrained fit utilizing measurements of other (related) quantities as additional information.

$\Gamma(K^- K^+ K^- \nu_\tau)/\Gamma_{\text{total}}$ $\Gamma_{108}/\Gamma = 0.491\Gamma_{170}/\Gamma$

VALUE (units 10^{-5})	CL%	EVTS	DOCUMENT ID	TECN	COMMENT
2.2 ± 0.8 OUR FIT					Error includes scale factor of 5.4. (Produced by HFLAV)
2.1 ± 0.8 OUR AVERAGE					Error includes scale factor of 5.4.
3.29 ± 0.17 ± 0.19 -0.20	3.2k	¹ LEE	10 BELL	666 fb ⁻¹ $E_{\text{cm}}^{\text{ee}} = 10.6$ GeV	
1.58 ± 0.13 ± 0.12	275	² AUBERT	08 BABR	342 fb ⁻¹ $E_{\text{cm}}^{\text{ee}} = 10.6$ GeV	
••• We do not use the following data for averages, fits, limits, etc. •••					
< 3.7	90	BRIERE	03 CLE3	$E_{\text{cm}}^{\text{ee}} = 10.6$ GeV	
< 19	90	BARATE	98 ALEP	1991–1995 LEP runs	
¹ See footnote to LEE 10 $\Gamma(\tau^- \rightarrow \pi^- \pi^+ \pi^- \nu_\tau(\text{ex. } K^0))/\Gamma_{\text{total}}$ measurement for correlations with other measurements. Not independent of LEE 10 $\Gamma(\tau^- \rightarrow K^- K^+ K^- \nu_\tau)/\Gamma(\tau^- \rightarrow \pi^- \pi^+ \pi^- \nu_\tau(\text{ex. } K^0))$ value.					
² See footnote to AUBERT 08 $\Gamma(\tau^- \rightarrow \pi^- \pi^+ \pi^- \nu_\tau(\text{ex. } K^0))/\Gamma_{\text{total}}$ measurement for correlations with other measurements.					

$\Gamma(K^- K^+ K^- \nu_\tau)/\Gamma(\pi^- \pi^+ \pi^- \nu_\tau(\text{ex. } K^0))$ Γ_{108}/Γ_{68}

VALUE (units 10^{-4})	EVTS	DOCUMENT ID	TECN	COMMENT
3.90 ± 0.02 ± 0.22 -0.23	3.2k	¹ LEE	10 BELL	666 fb ⁻¹ $E_{\text{cm}}^{\text{ee}} = 10.6$ GeV
¹ Not independent of LEE 10 $\Gamma(\tau^- \rightarrow K^- K^+ K^- \nu_\tau)/\Gamma_{\text{total}}$ and $\Gamma(\tau^- \rightarrow \pi^- \pi^+ \pi^- \nu_\tau(\text{ex. } K^0))/\Gamma_{\text{total}}$ values.				

$\Gamma(K^- K^+ K^- \nu_\tau(\text{ex. } \phi))/\Gamma_{\text{total}}$ Γ_{109}/Γ

VALUE	CL%	DOCUMENT ID	TECN	COMMENT
< 2.5 × 10⁻⁶		90	AUBERT	08 BABR 342 fb ⁻¹ $E_{\text{cm}}^{\text{ee}} = 10.6$ GeV

$\Gamma(K^- K^+ K^- \pi^0 \nu_\tau)/\Gamma_{\text{total}}$ Γ_{110}/Γ

VALUE	CL%	DOCUMENT ID	TECN	COMMENT
< 4.8 × 10⁻⁶	90	ARMS	05 CLE3	7.6 fb ⁻¹ , $E_{\text{cm}}^{\text{ee}} = 10.6$ GeV

$\Gamma(\pi^- K^+ \pi^- \geq 0 \text{ neut. } \nu_\tau)/\Gamma_{\text{total}}$ Γ_{111}/Γ

VALUE (%)	CL%	DOCUMENT ID	TECN	COMMENT
< 0.25	95	BAUER	94 TPC	$E_{\text{cm}}^{\text{ee}} = 29$ GeV

$\Gamma(e^- e^- e^+ \bar{\nu}_e \nu_\tau)/\Gamma_{\text{total}}$ Γ_{112}/Γ

VALUE (units 10^{-5})	EVTS	DOCUMENT ID	TECN	COMMENT
2.8 ± 1.4 ± 0.4	5	ALAM	96 CLEO	$E_{\text{cm}}^{\text{ee}} = 10.6$ GeV

$\Gamma(\mu^- e^- e^+ \bar{\nu}_\mu \nu_\tau)/\Gamma_{\text{total}}$ Γ_{113}/Γ

VALUE (units 10^{-5})	CL%	DOCUMENT ID	TECN	COMMENT
< 3.2	90	ALAM	96 CLEO	$E_{\text{cm}}^{\text{ee}} = 10.6$ GeV

$\Gamma(\pi^- e^- e^+ \nu_\tau)/\Gamma_{\text{total}}$ Γ_{114}/Γ

VALUE (units 10^{-5})	EVTS	DOCUMENT ID	TECN	COMMENT
seen	400	¹ JIN	19 BELL	562 fb ⁻¹ , $E_{\text{cm}}^{\text{ee}} = 10.6$ GeV
••• We do not use the following data for averages, fits, limits, etc. •••				
1.46 ± 0.13 ± 0.21	400	¹ JIN	19 BELL	axial-vector, 562 fb ⁻¹ , $E_{\text{cm}}^{\text{ee}} = 10.6$ GeV
3.01 ± 0.27 ± 0.43	400	¹ JIN	19 BELL	vector, 562 fb ⁻¹ , $E_{\text{cm}}^{\text{ee}} = 10.6$ GeV
¹ JIN 19 measures $B(\tau^- \rightarrow \pi^- e^- e^+ \nu_\tau(m_{\pi^- e^- e^+} > 1.05 \text{ GeV}/c^2)) = (5.90 \pm 0.53 \pm 0.86) \times 10^{-6}$, which is only sensitive to the structure-dependent contribution, and assumes that the decay proceeds with either a pure axial-vector current or a pure vector current to obtain the two respective branching fraction measurements for this mode, which are 100% correlated.				

$\Gamma(\pi^- \mu^- \mu^+ \nu_\tau)/\Gamma_{\text{total}}$ Γ_{115}/Γ

VALUE	CL%	DOCUMENT ID	TECN	COMMENT
< 1.14 × 10⁻⁵	90	JIN	19 BELL	562 fb ⁻¹ , $E_{\text{cm}}^{\text{ee}} = 10.6$ GeV

$\Gamma(3h^- 2h^+ \geq 0 \text{ neutrals } \nu_\tau(\text{ex. } K_S^0 \rightarrow \pi^- \pi^+)(\text{"5-prong"}))/\Gamma_{\text{total}}$ Γ_{116}/Γ

VALUE (%)	EVTS	DOCUMENT ID	TECN	COMMENT
0.099 ± 0.004 OUR FIT	(Produced by HFLAV)			
0.107 ± 0.007 OUR AVERAGE	Error includes scale factor of 1.1.			
0.170 ± 0.022 ± 0.026		¹ ACHARD	01D L3	1992–1995 LEP runs
0.097 ± 0.005 ± 0.011	419	GIBAUT	94B CLEO	$E_{\text{cm}}^{\text{ee}} = 10.6$ GeV
0.102 ± 0.029	13	BYLSMA	87 HRS	$E_{\text{cm}}^{\text{ee}} = 29$ GeV
••• We use the following data for averages but not for fits. •••				
0.093 ± 0.009 ± 0.012		SCHAEL	05c ALEP	1991–1995 LEP runs
0.115 ± 0.013 ± 0.006	112	² ABREU	01M DLPH	1992–1995 LEP runs
0.119 ± 0.013 ± 0.008	119	³ ACKERSTAFF	99e OPAL	1991–1995 LEP runs
••• We do not use the following data for averages, fits, limits, etc. •••				
0.26 ± 0.06 ± 0.05		ACTION	92H OPAL	$E_{\text{cm}}^{\text{ee}} = 88.2\text{--}94.2$ GeV
0.10 ± 0.05 ± 0.03 -0.04		DECAMP	92c ALEP	1989–1990 LEP runs
0.16 ± 0.13 ± 0.04		BEHREND	89B CELL	$E_{\text{cm}}^{\text{ee}} = 14\text{--}47$ GeV
0.3 ± 0.1 ± 0.2		BARTEL	85F JADE	$E_{\text{cm}}^{\text{ee}} = 34.6$ GeV
0.13 ± 0.04	10	BELTRAMI	85 HRS	Repl. by BYLSMA 87

$\Gamma(K^- K^+ \pi^- \nu_\tau)/\Gamma(\pi^- \pi^+ \pi^- \nu_\tau(\text{ex. } K^0))$ Γ_{106}/Γ_{68}

VALUE (%)	EVTS	DOCUMENT ID	TECN	COMMENT
1.592 ± 0.030 OUR FIT	(Produced by HFLAV)			
1.83 ± 0.05 OUR AVERAGE				
1.60 ± 0.15 ± 0.30	2.3k	RICHICHI	99 CLEO	$E_{\text{cm}}^{\text{ee}} = 10.6$ GeV
••• We use the following data for averages but not for fits. •••				
1.84 ± 0.01 ± 0.05	108k	¹ LEE	10 BELL	666 fb ⁻¹ $E_{\text{cm}}^{\text{ee}} = 10.6$ GeV
¹ Not independent of LEE 10 $\Gamma(\tau^- \rightarrow K^- K^+ \pi^- \nu_\tau)/\Gamma_{\text{total}}$ and $\Gamma(\tau^- \rightarrow \pi^- \pi^+ \pi^- \nu_\tau(\text{ex. } K^0))/\Gamma_{\text{total}}$ values.				

$\Gamma(K^- K^+ \pi^- \pi^0 \nu_\tau)/\Gamma_{\text{total}}$ Γ_{107}/Γ

VALUE (units 10^{-4})	CL%	EVTS	DOCUMENT ID	TECN	COMMENT
0.61 ± 0.18 OUR FIT					(Produced by HFLAV)
0.60 ± 0.18 OUR AVERAGE					
0.55 ± 0.14 ± 0.12	48	ARMS	05 CLE3	7.6 fb ⁻¹ , $E_{\text{cm}}^{\text{ee}} = 10.6$ GeV	
7.5 ± 2.9 ± 1.5		BARATE	98 ALEP	1991–1995 LEP runs	
••• We use the following data for averages but not for fits. •••					
3.3 ± 1.8 ± 0.7	158	¹ RICHICHI	99 CLEO	$E_{\text{cm}}^{\text{ee}} = 10.6$ GeV	
••• We do not use the following data for averages, fits, limits, etc. •••					
< 27	95	ABBIENDI	00D OPAL	1990–1995 LEP runs	

- Not independent of RICHICHI 99 $\Gamma(\tau^- \rightarrow K^- K^+ \pi^- \nu_\tau)/\Gamma(\tau^- \rightarrow \pi^- \pi^+ \pi^- \nu_\tau(\text{ex. } K^0))$ and BALEST 95c $\Gamma(\tau^- \rightarrow h^- h^+ h^+ \nu_\tau(\text{ex. } K^0))/\Gamma_{\text{total}}$ values.

$\Gamma(K^- K^+ \pi^- \pi^0 \nu_\tau)/\Gamma(\pi^- \pi^+ \pi^- \pi^0 \nu_\tau(\text{ex. } K^0))$ Γ_{107}/Γ_{77}

VALUE (%)	EVTS	DOCUMENT ID	TECN	COMMENT
0.14 ± 0.04 OUR FIT	(Produced by HFLAV)			
0.79 ± 0.44 ± 0.16	158	¹ RICHICHI	99 CLEO	$E_{\text{cm}}^{\text{ee}} = 10.6$ GeV
¹ RICHICHI 99 also quote a 95%CL upper limit of 0.0157 for this measurement.				

See key on page 1171

Lepton Particle Listings

T

0.16 ± 0.08 ± 0.04	4	BURCHAT	85	MRK2	$E_{cm}^{ee} = 29$ GeV
1.0 ± 0.4	10	BEHREND	82	CELL	Repl. by BEHREND 89b

¹ The correlation coefficients between this measurement and the ACHARD 01D measurements of $B(\tau \rightarrow \text{"1-prong"})$ and $B(\tau \rightarrow \text{"3-prong"})$ are -0.082 and -0.19 respectively.
² The correlation coefficients between this measurement and the ABREU 01M measurements of $B(\tau \rightarrow \text{1-prong})$ and $B(\tau \rightarrow \text{3-prong})$ are -0.08 and -0.08 respectively.
³ Not independent of ACKERSTAFF 99E $B(\tau^- \rightarrow 3h^- 2h^+ \nu_\tau(\text{ex. } K^0))$ and $B(\tau^- \rightarrow 3h^- 2h^+ \pi^0 \nu_\tau(\text{ex. } K^0))$ measurements.

$\Gamma(3h^- 2h^+ \nu_\tau(\text{ex. } K^0))/\Gamma_{\text{total}}$ $\Gamma_{117}/\Gamma = (\Gamma_{118} + \Gamma_{120} + 0.0153\Gamma_{185})/\Gamma$

VALUE (units 10^{-4})	EVTS	DOCUMENT ID	TECN	COMMENT
8.29 ± 0.31 OUR FIT		(Produced by HFLAV)		
8.32 ± 0.35 OUR AVERAGE				
9.7 ± 1.5 ± 0.5	96	¹ ABDALLAH	06A	DLPH 1992-1995 LEP runs
7.2 ± 0.9 ± 1.2	165	² SCHAEEL	05c	ALEP 1991-1995 LEP runs
9.1 ± 1.4 ± 0.6	97	ACKERSTAFF	99E	OPAL 1991-1995 LEP runs
7.7 ± 0.5 ± 0.9	295	GIBAUT	94B	CLEO $E_{cm}^{ee} = 10.6$ GeV
6.4 ± 2.3 ± 1.0	12	ALBRECHT	88B	ARG $E_{cm}^{ee} = 10$ GeV
5.1 ± 2.0	7	BYLSMA	87	HRS $E_{cm}^{ee} = 29$ GeV

• • • We use the following data for averages but not for fits. • • •
 8.56 ± 0.05 ± 0.42 34k AUBERT,B 05W BABR 232 fb⁻¹, $E_{cm}^{ee} = 10.6$ GeV
 • • • We do not use the following data for averages, fits, limits, etc. • • •
 8.0 ± 1.1 ± 1.3 58 BUSKULIC 96 ALEP Repl. by SCHAEEL 05c
 6.7 ± 3.0 5 ³ BELTRAMI 85 HRS Repl. by BYLSMA 87
¹ See footnote to ABDALLAH 06A $\Gamma(\tau^- \rightarrow h^- \nu_\tau)/\Gamma_{\text{total}}$ measurement for correlations with other measurements.
² See footnote to SCHAEEL 05c $\Gamma(\tau^- \rightarrow e^- \bar{\nu}_e \nu_\tau)/\Gamma_{\text{total}}$ measurement for correlations with other measurements.
³ The error quoted is statistical only.

$\Gamma(3\pi^- 2\pi^+ \nu_\tau(\text{ex. } K^0, \omega))/\Gamma_{\text{total}}$ $\Gamma_{118}/\Gamma = (\Gamma_{119} + \Gamma_{173})/\Gamma$

VALUE (units 10^{-4})	DOCUMENT ID	TECN	COMMENT
8.27 ± 0.31 OUR FIT	(Produced by HFLAV)		
8.33 ± 0.04 ± 0.43	¹ LEES	12X	BABR 468 fb ⁻¹ , $E_{cm}^{ee} = 10.6$ GeV

¹ Not independent of LEES 12X $\Gamma(\tau^- \rightarrow f_1(1285) \pi^- \nu_\tau \rightarrow 3\pi^- 2\pi^+ \nu_\tau)/\Gamma$ and $\Gamma(\tau^- \rightarrow 3\pi^- 2\pi^+ \nu_\tau(\text{ex. } K^0, \omega, f_1(1285)))/\Gamma$ values.

$\Gamma(3\pi^- 2\pi^+ \nu_\tau(\text{ex. } K^0, \omega, f_1(1285)))/\Gamma_{\text{total}}$ Γ_{119}/Γ

VALUE (units 10^{-4})	EVTS	DOCUMENT ID	TECN	COMMENT
7.75 ± 0.30 OUR FIT	(Produced by HFLAV)			
7.68 ± 0.04 ± 0.40	69k	LEES	12X	BABR 468 fb ⁻¹ , $E_{cm}^{ee} = 10.6$ GeV

$\Gamma(K^- 2\pi^- 2\pi^+ \nu_\tau(\text{ex. } K^0))/\Gamma_{\text{total}}$ Γ_{120}/Γ

VALUE (units 10^{-6})	DOCUMENT ID	TECN	COMMENT
0.6 ± 1.2 OUR FIT	(Produced by HFLAV)		
0.6 ± 0.5 ± 1.1	¹ LEES	12X	BABR 468 fb ⁻¹ , $E_{cm}^{ee} = 10.6$ GeV

¹ LEES 12X measurement corresponds to the lower limit of $< 2.4 \times 10^{-6}$ at 90% CL.

$\Gamma(K^+ 3\pi^- \pi^+ \nu_\tau)/\Gamma_{\text{total}}$ Γ_{121}/Γ

VALUE	CL%	DOCUMENT ID	TECN	COMMENT
< 5.0 × 10⁻⁶	90	LEES	12X	BABR 468 fb ⁻¹ , $E_{cm}^{ee} = 10.6$ GeV

$\Gamma(K^+ K^- 2\pi^- \pi^+ \nu_\tau)/\Gamma_{\text{total}}$ Γ_{122}/Γ

VALUE	CL%	DOCUMENT ID	TECN	COMMENT
< 4.5 × 10⁻⁷	90	LEES	12X	BABR 468 fb ⁻¹ , $E_{cm}^{ee} = 10.6$ GeV

$\Gamma(3h^- 2h^+ \pi^0 \nu_\tau(\text{ex. } K^0))/\Gamma_{\text{total}}$ $\Gamma_{123}/\Gamma = (\Gamma_{124} + \Gamma_{127})/\Gamma$

VALUE (units 10^{-4})	EVTS	DOCUMENT ID	TECN	COMMENT
1.65 ± 0.11 OUR FIT	(Produced by HFLAV)			
1.74 ± 0.27 OUR AVERAGE				
1.6 ± 1.2 ± 0.6	13	¹ ABDALLAH	06A	DLPH 1992-1995 LEP runs
2.1 ± 0.7 ± 0.9	95	² SCHAEEL	05c	ALEP 1991-1995 LEP runs
1.7 ± 0.2 ± 0.2	231	ANASTASSOV	01	CLEO $E_{cm}^{ee} = 10.6$ GeV
2.7 ± 1.8 ± 0.9	23	ACKERSTAFF	99E	OPAL 1991-1995 LEP runs
• • • We do not use the following data for averages, fits, limits, etc. • • •				
1.8 ± 0.7 ± 1.2	18	BUSKULIC	96	ALEP Repl. by SCHAEEL 05c
1.9 ± 0.4 ± 0.4	31	GIBAUT	94B	CLEO Repl. by ANASTASSOV 01
5.1 ± 2.2	6	BYLSMA	87	HRS $E_{cm}^{ee} = 29$ GeV
6.7 ± 3.0	5	³ BELTRAMI	85	HRS Repl. by BYLSMA 87

¹ See footnote to ABDALLAH 06A $\Gamma(\tau^- \rightarrow h^- \nu_\tau)/\Gamma_{\text{total}}$ measurement for correlations with other measurements.
² SCHAEEL 05c quote $(1.4 \pm 0.7 \pm 0.9) \times 10^{-4}$. We add 0.7×10^{-4} to remove their correction for $\tau^- \rightarrow \eta \pi^- \pi^+ \pi^- \nu_\tau \rightarrow 3\pi^- 2\pi^+ \pi^0 \nu_\tau$ and $\tau^- \rightarrow K^*(892) \eta \nu_\tau \rightarrow 3\pi^- 2\pi^+ \pi^0 \nu_\tau$ decays. See footnote to SCHAEEL 05c $\Gamma(\tau^- \rightarrow e^- \bar{\nu}_e \nu_\tau)/\Gamma_{\text{total}}$ measurement for correlations with other measurements.
³ The error quoted is statistical only.

$\Gamma(3\pi^- 2\pi^+ \pi^0 \nu_\tau(\text{ex. } K^0))/\Gamma_{\text{total}}$ $\Gamma_{124}/\Gamma = (\Gamma_{126} + 0.2302\Gamma_{160} + 0.892\Gamma_{185})/\Gamma$

VALUE (units 10^{-4})	DOCUMENT ID	TECN	COMMENT
1.64 ± 0.11 OUR FIT	(Produced by HFLAV)		
• • • We use the following data for averages but not for fits. • • •			
1.65 ± 0.05 ± 0.09	¹ LEES	12X	BABR 468 fb ⁻¹ , $E_{cm}^{ee} = 10.6$ GeV

¹ Not independent of LEES 12X measurements of $\Gamma(\tau^- \rightarrow 2\pi^- \pi^+ \omega \nu_\tau(\text{ex. } K^0))/\Gamma$, $\Gamma(\tau^- \rightarrow \eta \pi^- \pi^+ \pi^- \nu_\tau(\text{ex. } K^0))/\Gamma$, and $\Gamma(\tau^- \rightarrow 3\pi^- 2\pi^+ \pi^0 \nu_\tau(\text{ex. } K^0, \eta, \omega, f_1(1285)))/\Gamma$.

$\Gamma(3\pi^- 2\pi^+ \pi^0 \nu_\tau(\text{ex. } K^0, \eta, f_1(1285)))/\Gamma_{\text{total}}$ Γ_{125}/Γ

VALUE (units 10^{-4})	DOCUMENT ID	TECN	COMMENT
1.11 ± 0.04 ± 0.09	¹ LEES	12X	BABR 468 fb ⁻¹ , $E_{cm}^{ee} = 10.6$ GeV

¹ Not independent of LEES 12X $\Gamma(\tau^- \rightarrow 2\pi^- \pi^+ \omega \nu_\tau(\text{ex. } K^0))/\Gamma$ and $\Gamma(\tau^- \rightarrow 3\pi^- 2\pi^+ \pi^0 \nu_\tau(\text{ex. } K^0, \eta, \omega, f_1(1285)))/\Gamma$ values.

$\Gamma(3\pi^- 2\pi^+ \pi^0 \nu_\tau(\text{ex. } K^0, \eta, \omega, f_1(1285)))/\Gamma_{\text{total}}$ Γ_{126}/Γ

VALUE (units 10^{-4})	EVTS	DOCUMENT ID	TECN	COMMENT
0.38 ± 0.09 OUR FIT	(Produced by HFLAV)			
0.36 ± 0.03 ± 0.09	7.3k	LEES	12X	BABR 468 fb ⁻¹ , $E_{cm}^{ee} = 10.6$ GeV

$\Gamma(K^- 2\pi^- 2\pi^+ \pi^0 \nu_\tau(\text{ex. } K^0))/\Gamma_{\text{total}}$ Γ_{127}/Γ

VALUE (units 10^{-6})	DOCUMENT ID	TECN	COMMENT
1.1 ± 0.6 OUR FIT	(Produced by HFLAV)		
1.1 ± 0.4 ± 0.4	¹ LEES	12X	BABR 468 fb ⁻¹ , $E_{cm}^{ee} = 10.6$ GeV

¹ LEES 12X measurement corresponds to the lower limit of $< 1.9 \times 10^{-6}$ at 90% CL.

$\Gamma(K^+ 3\pi^- \pi^+ \pi^0 \nu_\tau)/\Gamma_{\text{total}}$ Γ_{128}/Γ

VALUE	CL%	DOCUMENT ID	TECN	COMMENT
< 8 × 10⁻⁷	90	LEES	12X	BABR 468 fb ⁻¹ , $E_{cm}^{ee} = 10.6$ GeV

$\Gamma(3h^- 2h^+ 2\pi^0 \nu_\tau)/\Gamma_{\text{total}}$ Γ_{129}/Γ

VALUE	CL%	DOCUMENT ID	TECN	COMMENT
< 3.4 × 10⁻⁶	90	AUBERT,B	06	BABR 232 fb ⁻¹ , $E_{cm}^{ee} = 10.6$ GeV
• • • We do not use the following data for averages, fits, limits, etc. • • •				
< 1.1 × 10⁻⁴	90	GIBAUT	94B	CLEO $E_{cm}^{ee} = 10.6$ GeV

$\Gamma((5\pi^-) \nu_\tau)/\Gamma_{\text{total}}$ $\Gamma_{130}/\Gamma = (\Gamma_{30} + \frac{1}{2}\Gamma_{45} + \Gamma_{48} + \frac{1}{2}\Gamma_{61} + \Gamma_{85} + \Gamma_{117} + 0.5559\Gamma_{150} + 0.892\Gamma_{180})/\Gamma$

VALUE (%)	DOCUMENT ID	TECN	COMMENT
0.78 ± 0.05 OUR FIT	(Produced by HFLAV)		
• • • We use the following data for averages but not for fits. • • •			
0.61 ± 0.06 ± 0.08	¹ GIBAUT	94B	CLEO $E_{cm}^{ee} = 10.6$ GeV

¹ Not independent of GIBAUT 94B $B(3h^- 2h^+ \nu_\tau)$, PROCARIO 93 $B(h^- 4\pi^0 \nu_\tau)$, and BORTOLETTO 93 $B(2h^- h^+ 2\pi^0 \nu_\tau)/B(\text{"3prong"})$ measurements. Result is corrected for η contributions.

$\Gamma(4h^- 3h^+ \geq 0 \text{ neutrals } \nu_\tau(\text{"7-prong"}))/\Gamma_{\text{total}}$ Γ_{131}/Γ

VALUE	CL%	DOCUMENT ID	TECN	COMMENT
< 3.0 × 10⁻⁷	90	AUBERT,B	05F	BABR 232 fb ⁻¹ , $E_{cm}^{ee} = 10.6$ GeV
• • • We do not use the following data for averages, fits, limits, etc. • • •				
< 1.8 × 10⁻⁵	95	ACKERSTAFF	97J	OPAL 1990-1995 LEP runs
< 2.4 × 10⁻⁶	90	EDWARDS	97B	CLEO $E_{cm}^{ee} = 10.6$ GeV
< 2.9 × 10⁻⁴	90	BYLSMA	87	HRS $E_{cm}^{ee} = 29$ GeV

$\Gamma(4h^- 3h^+ \nu_\tau)/\Gamma_{\text{total}}$ Γ_{132}/Γ

VALUE	CL%	DOCUMENT ID	TECN	COMMENT
< 4.3 × 10⁻⁷	90	AUBERT,B	05F	BABR 232 fb ⁻¹ , $E_{cm}^{ee} = 10.6$ GeV

$\Gamma(4h^- 3h^+ \pi^0 \nu_\tau)/\Gamma_{\text{total}}$ Γ_{133}/Γ

VALUE	CL%	DOCUMENT ID	TECN	COMMENT
< 2.5 × 10⁻⁷	90	AUBERT,B	05F	BABR 232 fb ⁻¹ , $E_{cm}^{ee} = 10.6$ GeV

$\Gamma(X^-(S=-1) \nu_\tau)/\Gamma_{\text{total}}$ $\Gamma_{134}/\Gamma = (\Gamma_{10} + \Gamma_{16} + \Gamma_{23} + \Gamma_{28} + \Gamma_{36} + \Gamma_{41} + \Gamma_{45} + \Gamma_{61} + \Gamma_{97} + \Gamma_{103} + \Gamma_{120} + \Gamma_{127} + \Gamma_{152} + \Gamma_{154} + \Gamma_{156} + 0.8312\Gamma_{170} + \Gamma_{179})/\Gamma$

VALUE (%)	DOCUMENT ID	TECN	COMMENT
2.92 ± 0.04 OUR FIT	(Produced by HFLAV)		
• • • We use the following data for averages but not for fits. • • •			
2.87 ± 0.12	¹ BARATE	99R	ALEP 1991-1995 LEP runs

¹ BARATE 99R perform a combined analysis of all ALEPH LEP 1 data on τ branching fraction measurements for decay modes having total strangeness equal to -1 .

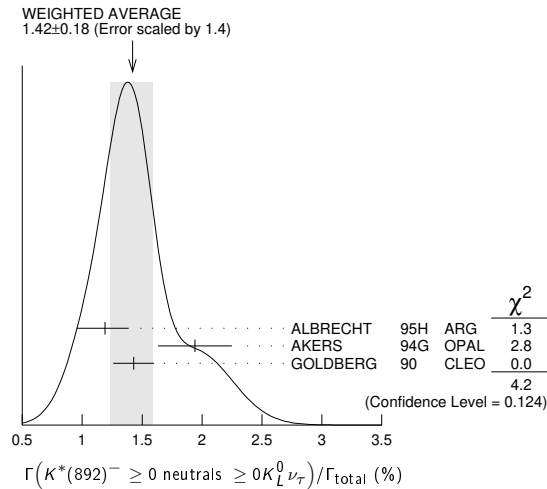
Lepton Particle Listings

 τ $\Gamma(K^*(892)^- \geq 0 \text{ neutrals} \geq 0 K_L^0 \nu_\tau) / \Gamma_{\text{total}}$ Γ_{135}/Γ

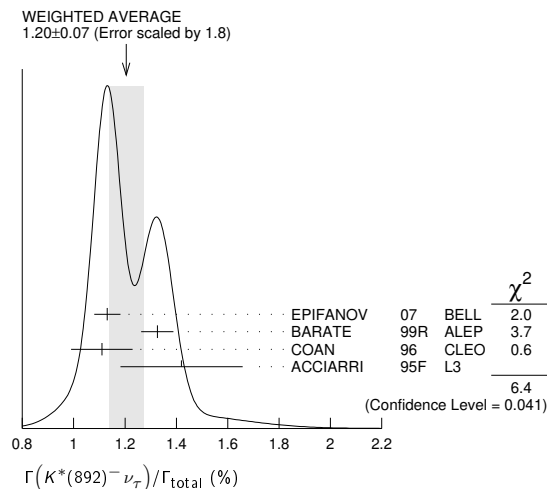
VALUE (%)	EVTS	DOCUMENT ID	TECN	COMMENT
1.42 ± 0.18 OUR AVERAGE	Error includes scale factor of 1.4. See the ideogram below.			
1.19 ± 0.15 +0.13 -0.18	104	ALBRECHT	95H ARG	$E_{\text{cm}}^{\text{ee}} = 9.4\text{--}10.6$ GeV
1.94 ± 0.27 ± 0.15	74	1 AKERS	94G OPAL	$E_{\text{cm}}^{\text{ee}} = 88\text{--}94$ GeV
1.43 ± 0.11 ± 0.13	475	2 GOLDBERG	90 CLEO	$E_{\text{cm}}^{\text{ee}} = 9.4\text{--}10.9$ GeV

¹ AKERS 94G reject events in which a K_S^0 accompanies the $K^*(892)^-$. We do not correct for them.

² GOLDBERG 90 estimates that 10% of observed $K^*(892)^-$ are accompanied by a π^0 .

 $\Gamma(K^*(892)^- \nu_\tau) / \Gamma_{\text{total}}$ Γ_{136}/Γ

VALUE (%)	EVTS	DOCUMENT ID	TECN	COMMENT
1.20 ± 0.07 OUR AVERAGE	Error includes scale factor of 1.8. See the ideogram below.			
1.131 ± 0.006 ± 0.051	49k	1 EPIFANOV	07 BELL	$351 \text{ fb}^{-1} E_{\text{cm}}^{\text{ee}} = 10.6$ GeV
1.326 ± 0.063		BARATE	99R ALEP	1991–1995 LEP runs
1.11 ± 0.12		2 COAN	96 CLEO	$E_{\text{cm}}^{\text{ee}} \approx 10.6$ GeV
1.42 ± 0.22 ± 0.09		3 ACCIARRI	95F L3	1991–1993 LEP runs
• • • We do not use the following data for averages, fits, limits, etc. • • •				
1.39 ± 0.09 ± 0.10		4 BUSKULIC	96 ALEP	Repl. by BARATE 99R
1.45 ± 0.13 ± 0.11	273	5 BUSKULIC	94F ALEP	Repl. by BUSKULIC 96
1.23 ± 0.21 +0.11 -0.21	54	6 ALBRECHT	88L ARG	$E_{\text{cm}}^{\text{ee}} = 10$ GeV
1.9 ± 0.3 ± 0.4	44	7 TSCHIRHART	88 HRS	$E_{\text{cm}}^{\text{ee}} = 29$ GeV
1.5 ± 0.4 ± 0.4	15	8 AIHARA	87C TPC	$E_{\text{cm}}^{\text{ee}} = 29$ GeV
1.3 ± 0.3 ± 0.3	31	YELTON	86 MRK2	$E_{\text{cm}}^{\text{ee}} = 29$ GeV
1.7 ± 0.7	11	DORFAN	81 MRK2	$E_{\text{cm}}^{\text{ee}} = 4.2\text{--}6.7$ GeV



¹ EPIFANOV 07 quote $B(\tau^- \rightarrow K^*(892)^- \nu_\tau) B(K^*(892)^- \rightarrow K_S^0 \pi^-) = (3.77 \pm 0.02(\text{stat}) \pm 0.12(\text{syst}) \pm 0.12(\text{mod})) \times 10^{-3}$. We add the systematic and model uncertainties in quadrature and divide by $B(K^*(892)^- \rightarrow K_S^0 \pi^-) = 0.3333$.

² Not independent of COAN 96 $B(\pi^- \bar{K}^0 \nu_\tau)$ and BATTLE 94 $B(K^- \pi^0 \nu_\tau)$ measurements. $K\pi$ final states are consistent with and assumed to originate from $K^*(892)^-$ production.

³ This result is obtained from their $B(\pi^- \bar{K}^0 \nu_\tau)$ assuming all those decays originate in $K^*(892)^-$ decays.

⁴ Not independent of BUSKULIC 96 $B(\pi^- \bar{K}^0 \nu_\tau)$ and $B(K^- \pi^0 \nu_\tau)$ measurements.

⁵ BUSKULIC 94F obtain this result from BUSKULIC 94F $B(\bar{K}^0 \pi^- \nu_\tau)$ and BUSKULIC 94E $B(K^- \pi^0 \nu_\tau)$ assuming all of those decays originate in $K^*(892)^-$ decays.

⁶ The authors divide by $\Gamma_2/\Gamma = 0.865$ to obtain this result.

⁷ Not independent of TSCHIRHART 88 $\Gamma(\tau^- \rightarrow h^- \bar{K}^0 \geq 0 \text{ neutrals} \geq 0 K_L^0 \nu_\tau) / \Gamma$.

⁸ Decay π^- identified in this experiment, is assumed in the others.

 $\Gamma(K^*(892)^- \nu_\tau) / \Gamma(\pi^- \pi^0 \nu_\tau)$ Γ_{136}/Γ_{14}

VALUE	DOCUMENT ID	TECN	COMMENT
0.075 ± 0.027	1 ABREU	94K DLPH	LEP 1992 Z data
¹ ABREU 94k quote $B(\tau^- \rightarrow K^*(892)^- \nu_\tau) B(K^*(892)^- \rightarrow K^- \pi^0) / B(\tau^- \rightarrow \rho^- \nu_\tau) = 0.025 \pm 0.009$. We divide by $B(K^*(892)^- \rightarrow K^- \pi^0) = 0.333$ to obtain this result.			

 $\Gamma(K^*(892)^- \nu_\tau \rightarrow \pi^- \bar{K}^0 \nu_\tau) / \Gamma(\pi^- \bar{K}^0 \nu_\tau)$ Γ_{137}/Γ_{36}

VALUE	EVTS	DOCUMENT ID	TECN	COMMENT
0.933 ± 0.027	49k	EPIFANOV	07 BELL	$351 \text{ fb}^{-1} E_{\text{cm}}^{\text{ee}} = 10.6$ GeV

 $\Gamma(K^*(892)^0 K^- \geq 0 \text{ neutrals} \nu_\tau) / \Gamma_{\text{total}}$ Γ_{138}/Γ

VALUE (%)	EVTS	DOCUMENT ID	TECN	COMMENT
0.32 ± 0.08 ± 0.12	119	GOLDBERG	90 CLEO	$E_{\text{cm}}^{\text{ee}} = 9.4\text{--}10.9$ GeV

 $\Gamma(K^*(892)^0 K^- \nu_\tau) / \Gamma_{\text{total}}$ Γ_{139}/Γ

VALUE (%)	EVTS	DOCUMENT ID	TECN	COMMENT
0.21 ± 0.04 OUR AVERAGE				
0.213 ± 0.048		1 BARATE	98 ALEP	1991–1995 LEP runs
0.20 ± 0.05 ± 0.04	47	ALBRECHT	95H ARG	$E_{\text{cm}}^{\text{ee}} = 9.4\text{--}10.6$ GeV

¹ BARATE 98 measure the $K^- (\rho^0 \rightarrow \pi^+ \pi^-)$ fraction in $\tau^- \rightarrow K^- \pi^+ \pi^- \nu_\tau$ decays to be $(35 \pm 11)\%$ and derive this result from their measurement of $\Gamma(\tau^- \rightarrow K^- \pi^+ \pi^- \nu_\tau) / \Gamma_{\text{total}}$ assuming the intermediate states are all $K^- \rho^-$ and $K^- K^*(892)^0$.

 $\Gamma(\bar{K}^*(892)^0 \pi^- \geq 0 \text{ neutrals} \nu_\tau) / \Gamma_{\text{total}}$ Γ_{140}/Γ

VALUE (%)	EVTS	DOCUMENT ID	TECN	COMMENT
0.38 ± 0.11 ± 0.13	105	GOLDBERG	90 CLEO	$E_{\text{cm}}^{\text{ee}} = 9.4\text{--}10.9$ GeV

 $\Gamma(\bar{K}^*(892)^0 \pi^- \nu_\tau) / \Gamma_{\text{total}}$ Γ_{141}/Γ

VALUE (%)	EVTS	DOCUMENT ID	TECN	COMMENT
0.22 ± 0.05 OUR AVERAGE				
0.209 ± 0.058		1 BARATE	98 ALEP	1991–1995 LEP runs
0.25 ± 0.10 ± 0.05	27	ALBRECHT	95H ARG	$E_{\text{cm}}^{\text{ee}} = 9.4\text{--}10.6$ GeV

¹ BARATE 98 measure the $K^- K^*(892)^0$ fraction in $\tau^- \rightarrow K^- K^+ \pi^- \nu_\tau$ decays to be $(87 \pm 13)\%$ and derive this result from their measurement of $\Gamma(\tau^- \rightarrow K^- K^+ \pi^- \nu_\tau) / \Gamma_{\text{total}}$.

 $\Gamma((\bar{K}^*(892)^0 \pi^-) \nu_\tau \rightarrow \pi^- \bar{K}^0 \pi^0 \nu_\tau) / \Gamma_{\text{total}}$ Γ_{142}/Γ

VALUE (%)	DOCUMENT ID	TECN	COMMENT
0.10 ± 0.04 OUR AVERAGE			
0.097 ± 0.044 ± 0.036	1 BARATE	99k ALEP	1991–1995 LEP runs
0.106 ± 0.037 ± 0.032	2 BARATE	98E ALEP	1991–1995 LEP runs

¹ BARATE 99k measure K^0 's by detecting K_S^0 's in their hadron calorimeter. They determine the $\bar{K}^0 \rho^-$ fraction in $\tau^- \rightarrow \pi^- \bar{K}^0 \pi^0 \nu_\tau$ decays to be $(0.72 \pm 0.12 \pm 0.10)$ and multiply their $B(\pi^- \bar{K}^0 \pi^0 \nu_\tau)$ measurement by one minus this fraction to obtain the quoted result.

² BARATE 98E reconstruct K^0 's using $K_S^0 \rightarrow \pi^+ \pi^-$ decays. They determine the $\bar{K}^0 \rho^-$ fraction in $\tau^- \rightarrow \pi^- \bar{K}^0 \pi^0 \nu_\tau$ decays to be $(0.64 \pm 0.09 \pm 0.10)$ and multiply their $B(\pi^- \bar{K}^0 \pi^0 \nu_\tau)$ measurement by one minus this fraction to obtain the quoted result.

 $\Gamma(K_1(1270)^- \nu_\tau) / \Gamma_{\text{total}}$ Γ_{143}/Γ

VALUE (%)	EVTS	DOCUMENT ID	TECN	COMMENT
0.47 ± 0.11 OUR AVERAGE				
0.48 ± 0.11		BARATE	99R ALEP	1991–1995 LEP runs
0.41 +0.41 -0.35 ± 0.10	5	1 BAUER	94 TPC	$E_{\text{cm}}^{\text{ee}} = 29$ GeV

¹ We multiply 0.41% by 0.25, the relative systematic error quoted by BAUER 94, to obtain the systematic error.

 $\Gamma(K_1(1400)^- \nu_\tau) / \Gamma_{\text{total}}$ Γ_{144}/Γ

VALUE (%)	EVTS	DOCUMENT ID	TECN	COMMENT
0.17 ± 0.26 OUR AVERAGE	Error includes scale factor of 1.7.			
0.05 ± 0.17		BARATE	99R ALEP	1991–1995 LEP runs
0.76 +0.40 -0.33 ± 0.20	11	1 BAUER	94 TPC	$E_{\text{cm}}^{\text{ee}} = 29$ GeV

¹ We multiply 0.76% by 0.25, the relative systematic error quoted by BAUER 94, to obtain the systematic error.

 $\Gamma(K_1(1270)^- \nu_\tau) + \Gamma(K_1(1400)^- \nu_\tau) / \Gamma_{\text{total}}$ $(\Gamma_{143} + \Gamma_{144}) / \Gamma$

VALUE (%)	EVTS	DOCUMENT ID	TECN	COMMENT
1.17 +0.41 -0.37 ± 0.29	16	1 BAUER	94 TPC	$E_{\text{cm}}^{\text{ee}} = 29$ GeV

¹ We multiply 1.17% by 0.25, the relative systematic error quoted by BAUER 94, to obtain the systematic error. Not independent of BAUER 94 $B(K_1(1270)^- \nu_\tau)$ and BAUER 94 $B(K_1(1400)^- \nu_\tau)$ measurements.

$\Gamma(K_1(1270)^-\nu_\tau)/[\Gamma(K_1(1270)^-\nu_\tau) + \Gamma(K_1(1400)^-\nu_\tau)] \quad \Gamma_{143}/(\Gamma_{143} + \Gamma_{144})$

VALUE	DOCUMENT ID	TECN	COMMENT
0.69 ± 0.15 OUR AVERAGE			
0.71 ± 0.16 ± 0.11	¹ ABBIENDI	00D OPAL	1990-1995 LEP runs
0.66 ± 0.19 ± 0.13	² ASNER	00B CLEO	$E_{cm}^{ee} = 10.6$ GeV

¹ ABBIENDI 00D assume the resonance structure of $\tau^- \rightarrow K^- \pi^+ \pi^- \nu_\tau$ decays is dominated by the $K_1(1270)^-$ and $K_1(1400)^-$ resonances.

² ASNER 00B assume the resonance structure of $\tau^- \rightarrow K^- \pi^+ \pi^- \nu_\tau$ (ex. K^0) decays is dominated by $K_1(1270)^-$ and $K_1(1400)^-$ resonances.

 $\Gamma(K^*(1410)^-\nu_\tau)/\Gamma_{total} \quad \Gamma_{145}/\Gamma$

VALUE (units 10^{-3})	DOCUMENT ID	TECN	COMMENT
1.5 ± 1.4	BARATE	99R ALEP	1991-1995 LEP runs

 $\Gamma(K_0^*(1430)^-\nu_\tau)/\Gamma_{total} \quad \Gamma_{146}/\Gamma$

VALUE (units 10^{-3})	CL%	DOCUMENT ID	TECN	COMMENT
< 0.5	95	BARATE	99R ALEP	1991-1995 LEP runs

 $\Gamma(K_2^*(1430)^-\nu_\tau)/\Gamma_{total} \quad \Gamma_{147}/\Gamma$

VALUE (%)	CL%	EVTS	DOCUMENT ID	TECN	COMMENT
< 0.3	95		TSCHIRHART	88 HRS	$E_{cm}^{ee} = 29$ GeV
• • • We do not use the following data for averages, fits, limits, etc. • • •					
< 0.33	95		¹ ACCIARRI	95F L3	1991-1993 LEP runs
< 0.9	95	0	DORFAN	81 MRK2	$E_{cm}^{ee} = 4.2-6.7$ GeV

¹ ACCIARRI 95F quote $B(\tau^- \rightarrow K^*(1430)^- \rightarrow \pi^- \bar{K}^0 \nu_\tau) < 0.11\%$. We divide by $B(K^*(1430)^- \rightarrow \pi^- \bar{K}^0) = 0.33$ to obtain the limit shown.

 $\Gamma(a_0(980)^- \geq 0 \text{ neutrals } \nu_\tau)/\Gamma_{total} \times B(a_0(980)^- \rightarrow K^0 K^-) \quad \Gamma_{148}/\Gamma \times B$

VALUE (units 10^{-4})	CL%	DOCUMENT ID	TECN	COMMENT
< 2.8	90	GOLDBERG	90 CLEO	$E_{cm}^{ee} = 9.4-10.9$ GeV

 $\Gamma(\eta \pi^- \nu_\tau)/\Gamma_{total} \quad \Gamma_{149}/\Gamma$

VALUE (units 10^{-3})	CL%	EVTS	DOCUMENT ID	TECN	COMMENT
< 0.99	95		¹ DEL-AMO-SA..11E	BABR	$470 \text{ fb}^{-1} E_{cm}^{ee} = 10.6$ GeV
• • • We do not use the following data for averages, fits, limits, etc. • • •					
< 6.2	95		BUSKULIC	97C ALEP	1991-1994 LEP runs
< 1.4	95	0	BARTELT	96 CLEO	$E_{cm}^{ee} \approx 10.6$ GeV
< 3.4	95		ARTUSO	92 CLEO	$E_{cm}^{ee} \approx 10.6$ GeV
< 90	95		ALBRECHT	88M ARG	$E_{cm}^{ee} \approx 10$ GeV
< 140	90		BEHREND	88 CELL	$E_{cm}^{ee} = 14-46.8$ GeV
< 180	95		BARINGER	87 CLEO	$E_{cm}^{ee} = 10.5$ GeV
< 250	90	0	COFFMAN	87 MRK3	$E_{cm}^{ee} = 3.77$ GeV
510 ± 100 ± 120	65		DERRICK	87 HRS	$E_{cm}^{ee} = 29$ GeV
< 100	95		GAN	87B MRK2	$E_{cm}^{ee} = 29$ GeV

¹ DEL-AMO-SANCHEZ 11E also quote $B(\tau^- \rightarrow \eta \pi^- \nu_\tau) = (3.4 \pm 3.4 \pm 2.1) \times 10^{-5}$.

 $\Gamma(\eta \pi^- \pi^0 \nu_\tau)/\Gamma_{total} \quad \Gamma_{150}/\Gamma$

VALUE (units 10^{-3})	CL%	EVTS	DOCUMENT ID	TECN	COMMENT
1.39 ± 0.07 OUR FIT					(Produced by HFLAV)
1.38 ± 0.09 OUR AVERAGE					Error includes scale factor of 1.2.
1.35 ± 0.03 ± 0.07	6.0k		INAMI	09 BELL	$490 \text{ fb}^{-1} E_{cm}^{ee} = 10.6$ GeV
1.8 ± 0.4 ± 0.2			BUSKULIC	97C ALEP	1991-1994 LEP runs
1.7 ± 0.2 ± 0.2	125		ARTUSO	92 CLEO	$E_{cm}^{ee} \approx 10.6$ GeV
• • • We do not use the following data for averages, fits, limits, etc. • • •					
< 11.0	95		ALBRECHT	88M ARG	$E_{cm}^{ee} \approx 10$ GeV
< 21.0	95		BARINGER	87 CLEO	$E_{cm}^{ee} = 10.5$ GeV
42.0 $\begin{smallmatrix} + 7.0 \\ - 12.0 \end{smallmatrix}$ ± 16.0			¹ GAN	87 MRK2	$E_{cm}^{ee} = 29$ GeV

¹ Highly correlated with GAN 87 $\Gamma(\pi^- \pi^0 \nu_\tau)/\Gamma_{total}$ value.

 $\Gamma(\eta \pi^- \pi^0 \pi^0 \nu_\tau)/\Gamma_{total} \quad \Gamma_{151}/\Gamma$

VALUE (units 10^{-4})	CL%	EVTS	DOCUMENT ID	TECN	COMMENT
1.9 ± 0.4 OUR FIT					(Produced by HFLAV)
1.81 ± 0.31 OUR AVERAGE					
2.01 ± 0.34 ± 0.22	381		LEES	12X BABR	$468 \text{ fb}^{-1} E_{cm}^{ee} = 10.6$ GeV
• • • We use the following data for averages but not for fits. • • •					
1.5 ± 0.5	30		¹ ANASTASSOV	01 CLEO	$E_{cm}^{ee} = 10.6$ GeV
• • • We do not use the following data for averages, fits, limits, etc. • • •					
1.4 ± 0.6 ± 0.3	15		² BERGFELD	97 CLEO	Repl. by ANASTASSOV 01
< 4.3	95		ARTUSO	92 CLEO	$E_{cm}^{ee} \approx 10.6$ GeV
< 120	95		ALBRECHT	88M ARG	$E_{cm}^{ee} \approx 10$ GeV

¹ Weighted average of BERGFELD 97 and ANASTASSOV 01 value of $(1.5 \pm 0.6 \pm 0.3) \times 10^{-4}$ obtained using η 's reconstructed from $\eta \rightarrow \pi^+ \pi^- \pi^0$ decays.

² BERGFELD 97 reconstruct η 's using $\eta \rightarrow \gamma \gamma$ decays.

 $\Gamma(\eta K^- \nu_\tau)/\Gamma_{total} \quad \Gamma_{152}/\Gamma$

VALUE (units 10^{-4})	CL%	EVTS	DOCUMENT ID	TECN	COMMENT
1.55 ± 0.08 OUR FIT					(Produced by HFLAV)
1.54 ± 0.08 OUR AVERAGE					
1.42 ± 0.11 ± 0.07	690		DEL-AMO-SA..11E	BABR	$470 \text{ fb}^{-1} E_{cm}^{ee} = 10.6$ GeV
1.58 ± 0.05 ± 0.09	1.6k		INAMI	09 BELL	$490 \text{ fb}^{-1} E_{cm}^{ee} = 10.6$ GeV
2.9 $\begin{smallmatrix} + 1.3 \\ - 1.2 \end{smallmatrix}$ ± 0.7			BUSKULIC	97C ALEP	1991-1994 LEP runs
2.6 ± 0.5 ± 0.5	85		BARTELT	96 CLEO	$E_{cm}^{ee} \approx 10.6$ GeV
• • • We do not use the following data for averages, fits, limits, etc. • • •					
< 4.7	95		ARTUSO	92 CLEO	$E_{cm}^{ee} \approx 10.6$ GeV

 $\Gamma(\eta K^*(892)^-\nu_\tau)/\Gamma_{total} \quad \Gamma_{153}/\Gamma$

VALUE (units 10^{-4})	EVTS	DOCUMENT ID	TECN	COMMENT
1.38 ± 0.15 OUR AVERAGE				
1.34 ± 0.12 ± 0.09	245	¹ INAMI	09 BELL	$490 \text{ fb}^{-1} E_{cm}^{ee} = 10.6$ GeV
2.90 ± 0.80 ± 0.42	25	BISHAI	99 CLEO	$E_{cm}^{ee} = 10.6$ GeV

¹ Not independent of INAMI 09 $B(\tau^- \rightarrow \eta K^- \pi^0 \nu_\tau)$ and $B(\tau^- \rightarrow \eta \bar{K}^0 \pi^- \nu_\tau)$ values.

 $\Gamma(\eta K^- \pi^0 \nu_\tau)/\Gamma_{total} \quad \Gamma_{154}/\Gamma$

VALUE (units 10^{-4})	EVTS	DOCUMENT ID	TECN	COMMENT
0.48 ± 0.12 OUR FIT				(Produced by HFLAV)
0.48 ± 0.12 OUR AVERAGE				
0.46 ± 0.11 ± 0.04	270	INAMI	09 BELL	$490 \text{ fb}^{-1} E_{cm}^{ee} = 10.6$ GeV
1.77 ± 0.56 ± 0.71	36	BISHAI	99 CLEO	$E_{cm}^{ee} = 10.6$ GeV

 $\Gamma(\eta K^- \pi^0 (\text{non-}K^*(892))\nu_\tau)/\Gamma_{total} \quad \Gamma_{155}/\Gamma$

VALUE	CL%	DOCUMENT ID	TECN	COMMENT
< 3.5 × 10⁻⁵	90	INAMI	09 BELL	$490 \text{ fb}^{-1} E_{cm}^{ee} = 10.6$ GeV

 $\Gamma(\eta \bar{K}^0 \pi^- \nu_\tau)/\Gamma_{total} \quad \Gamma_{156}/\Gamma$

VALUE (units 10^{-4})	EVTS	DOCUMENT ID	TECN	COMMENT
0.94 ± 0.15 OUR FIT				(Produced by HFLAV)
0.93 ± 0.15 OUR AVERAGE				
0.88 ± 0.14 ± 0.06	161	¹ INAMI	09 BELL	$490 \text{ fb}^{-1} E_{cm}^{ee} = 10.6$ GeV
2.20 ± 0.70 ± 0.22	15	² BISHAI	99 CLEO	$E_{cm}^{ee} = 10.6$ GeV

¹ We multiply the INAMI 09 measurement $B(\tau^- \rightarrow \eta K_S^0 \pi^- \nu_\tau) = (0.44 \pm 0.07 \pm 0.03) \times 10^{-4}$ by 2 to obtain the listed value.

² We multiply the BISHAI 99 measurement $B(\tau^- \rightarrow \eta K_S^0 \pi^- \nu_\tau) = (1.10 \pm 0.35 \pm 0.11) \times 10^{-4}$ by 2 to obtain the listed value.

 $\Gamma(\eta \bar{K}^0 \pi^- \pi^0 \nu_\tau)/\Gamma_{total} \quad \Gamma_{157}/\Gamma$

VALUE	CL%	DOCUMENT ID	TECN	COMMENT
< 5.0 × 10⁻⁵	90	¹ INAMI	09 BELL	$490 \text{ fb}^{-1} E_{cm}^{ee} = 10.6$ GeV

¹ We multiply the INAMI 09 measurement $B(\tau^- \rightarrow \eta K_S^0 \pi^- \pi^0 \nu_\tau) < 2.5 \times 10^{-5}$ by 2 to obtain the listed value.

 $\Gamma(\eta K^- K^0 \nu_\tau)/\Gamma_{total} \quad \Gamma_{158}/\Gamma$

VALUE	CL%	DOCUMENT ID	TECN	COMMENT
< 9.0 × 10⁻⁶	90	¹ INAMI	09 BELL	$490 \text{ fb}^{-1} E_{cm}^{ee} = 10.6$ GeV

¹ We multiply the INAMI 09 measurement $B(\tau^- \rightarrow \eta K^- K_S^0 \nu_\tau) < 4.5 \times 10^{-6}$ by 2 to obtain the listed value.

 $\Gamma(\eta \pi^+ \pi^- \pi^- \geq 0 \text{ neutrals } \nu_\tau)/\Gamma_{total} \quad \Gamma_{159}/\Gamma$

VALUE (%)	CL%	DOCUMENT ID	TECN	COMMENT
< 0.3	90	ABACHI	87B HRS	$E_{cm}^{ee} = 29$ GeV

 $\Gamma(\eta \pi^- \pi^+ \pi^- \nu_\tau (\text{ex. } K^0))/\Gamma_{total} \quad \Gamma_{160}/\Gamma$

VALUE (units 10^{-4})	EVTS	DOCUMENT ID	TECN	COMMENT
2.20 ± 0.13 OUR FIT				(Produced by HFLAV)
2.23 ± 0.12 OUR AVERAGE				
2.10 ± 0.09 ± 0.13	2.9k	¹ LEES	12X BABR	$\eta \rightarrow \gamma \gamma$
2.37 ± 0.12 ± 0.18	1.4k	¹ LEES	12X BABR	$\eta \rightarrow \pi^+ \pi^- \pi^0$
2.54 ± 0.27 ± 0.25	315	¹ LEES	12X BABR	$\eta \rightarrow 3\pi^0$
• • • We use the following data for averages but not for fits. • • •				
2.3 ± 0.5	170	² ANASTASSOV	01 CLEO	$E_{cm}^{ee} = 10.6$ GeV
• • • We do not use the following data for averages, fits, limits, etc. • • •				
1.60 ± 0.05 ± 0.11	1.8 k	AUBERT	08AE BABR	Repl. by LEES 12X
3.4 $\begin{smallmatrix} + 0.6 \\ - 0.5 \end{smallmatrix}$ ± 0.6	89	³ BERGFELD	97 CLEO	Repl. by ANASTASSOV 01

¹ LEES 12X uses 468 fb^{-1} of data taken at $E_{cm}^{ee} = 10.6$ GeV. It gives the average of the three measurements listed here as $(2.25 \pm 0.07 \pm 0.12) \times 10^{-4}$.

² Weighted average of BERGFELD 97 and ANASTASSOV 01 measurements using η 's reconstructed from $\eta \rightarrow \pi^+ \pi^- \pi^0$ and $\eta \rightarrow 3\pi^0$ decays.

³ BERGFELD 97 reconstruct η 's using $\eta \rightarrow \gamma \gamma$ and $\eta \rightarrow 3\pi^0$ decays.

Lepton Particle Listings

 τ $\Gamma(\eta\pi^-\pi^+\pi^-\nu_\tau(\text{ex. } K^0, f_1(1285)))/\Gamma_{\text{total}}$ Γ_{161}/Γ

VALUE (units 10^{-4})	CL%	DOCUMENT ID	TECN	COMMENT
0.99 ± 0.09 ± 0.13		¹ LEES	12X BABR	$468 \text{ fb}^{-1} E_{\text{cm}}^{\text{ee}} = 10.6 \text{ GeV}$

¹ LEES 12X obtain this result by subtracting their $B(\tau^- \rightarrow f_1(1285)\pi^-\nu_\tau \rightarrow \eta\pi^-\pi^+\pi^-\nu_\tau)$ measurement from their $B(\tau^- \rightarrow \eta\pi^-\pi^+\pi^-\nu_\tau(\text{ex. } K^0))$ measurement.

 $\Gamma(\eta a_1(1260)^-\nu_\tau \rightarrow \eta\pi^-\rho^0\nu_\tau)/\Gamma_{\text{total}}$ Γ_{162}/Γ

VALUE	CL%	DOCUMENT ID	TECN	COMMENT
< 3.9 × 10⁻⁴	90	BERGFELD	97 CLEO	$E_{\text{cm}}^{\text{ee}} = 10.6 \text{ GeV}$

 $\Gamma(\eta\eta\pi^-\nu_\tau)/\Gamma_{\text{total}}$ Γ_{163}/Γ

VALUE	CL%	DOCUMENT ID	TECN	COMMENT
< 7.4 × 10⁻⁶	90	INAMI	09 BELL	$490 \text{ fb}^{-1} E_{\text{cm}}^{\text{ee}} = 10.6 \text{ GeV}$

• • • We do not use the following data for averages, fits, limits, etc. • • •
 < 1.1 × 10⁻⁴ 95 ARTUSO 92 CLEO $E_{\text{cm}}^{\text{ee}} \approx 10.6 \text{ GeV}$
 < 8.3 × 10⁻³ 95 ALBRECHT 88M ARG $E_{\text{cm}}^{\text{ee}} \approx 10 \text{ GeV}$

 $\Gamma(\eta\eta\pi^-\pi^0\nu_\tau)/\Gamma_{\text{total}}$ Γ_{164}/Γ

VALUE (units 10^{-4})	CL%	DOCUMENT ID	TECN	COMMENT
< 2.0	95	ARTUSO	92 CLEO	$E_{\text{cm}}^{\text{ee}} \approx 10.6 \text{ GeV}$

• • • We do not use the following data for averages, fits, limits, etc. • • •
 < 90 95 ALBRECHT 88M ARG $E_{\text{cm}}^{\text{ee}} \approx 10 \text{ GeV}$

 $\Gamma(\eta\eta K^-\nu_\tau)/\Gamma_{\text{total}}$ Γ_{165}/Γ

VALUE	CL%	DOCUMENT ID	TECN	COMMENT
< 3.0 × 10⁻⁶	90	INAMI	09 BELL	$490 \text{ fb}^{-1} E_{\text{cm}}^{\text{ee}} = 10.6 \text{ GeV}$

 $\Gamma(\eta'(958)\pi^-\nu_\tau)/\Gamma_{\text{total}}$ Γ_{166}/Γ

VALUE	CL%	DOCUMENT ID	TECN	COMMENT
< 4.0 × 10⁻⁶	90	LEES	12X BABR	$468 \text{ fb}^{-1} E_{\text{cm}}^{\text{ee}} = 10.6 \text{ GeV}$

• • • We do not use the following data for averages, fits, limits, etc. • • •
 < 7.2 × 10⁻⁶ 90 AUBERT 08AE BABR $384 \text{ fb}^{-1}, E_{\text{cm}}^{\text{ee}} = 10.6 \text{ GeV}$
 < 7.4 × 10⁻⁵ 90 BERGFELD 97 CLEO $E_{\text{cm}}^{\text{ee}} = 10.6 \text{ GeV}$

 $\Gamma(\eta'(958)\pi^-\pi^0\nu_\tau)/\Gamma_{\text{total}}$ Γ_{167}/Γ

VALUE	CL%	DOCUMENT ID	TECN	COMMENT
< 1.2 × 10⁻⁵	90	LEES	12X BABR	$468 \text{ fb}^{-1} E_{\text{cm}}^{\text{ee}} = 10.6 \text{ GeV}$

• • • We do not use the following data for averages, fits, limits, etc. • • •
 < 8.0 × 10⁻⁵ 90 BERGFELD 97 CLEO $E_{\text{cm}}^{\text{ee}} = 10.6 \text{ GeV}$

 $\Gamma(\eta'(958)K^-\nu_\tau)/\Gamma_{\text{total}}$ Γ_{168}/Γ

VALUE	CL%	DOCUMENT ID	TECN	COMMENT
< 2.4 × 10⁻⁶	90	LEES	12X BABR	$468 \text{ fb}^{-1} E_{\text{cm}}^{\text{ee}} = 10.6 \text{ GeV}$

 $\Gamma(\phi\pi^-\nu_\tau)/\Gamma_{\text{total}}$ Γ_{169}/Γ

VALUE (units 10^{-5})	CL%	EVTS	DOCUMENT ID	TECN	COMMENT
3.42 ± 0.55 ± 0.25		344	AUBERT	08 BABR	$342 \text{ fb}^{-1} E_{\text{cm}}^{\text{ee}} = 10.6 \text{ GeV}$

• • • We do not use the following data for averages, fits, limits, etc. • • •
 < 20 90 ¹ AVERY 97 CLEO $E_{\text{cm}}^{\text{ee}} = 10.6 \text{ GeV}$
 < 35 90 ALBRECHT 95H ARG $E_{\text{cm}}^{\text{ee}} = 9.4\text{--}10.6 \text{ GeV}$

¹ AVERY 97 limit varies from $(1.2\text{--}2.0) \times 10^{-4}$ depending on decay model assumptions.

 $\Gamma(\phi K^-\nu_\tau)/\Gamma_{\text{total}}$ Γ_{170}/Γ

VALUE (units 10^{-5})	CL%	EVTS	DOCUMENT ID	TECN	COMMENT
4.4 ± 1.6 OUR FIT			(Produced by HFLAV)		
3.70 ± 0.33 OUR AVERAGE			Error includes scale factor of 1.3.		

• • • We use the following data for averages but not for fits. • • •
 3.39 ± 0.20 ± 0.28 274 AUBERT 08 BABR $342 \text{ fb}^{-1} E_{\text{cm}}^{\text{ee}} = 10.6 \text{ GeV}$
 4.05 ± 0.25 ± 0.26 551 INAMI 06 BELL $401 \text{ fb}^{-1} E_{\text{cm}}^{\text{ee}} = 10.6 \text{ GeV}$

• • • We do not use the following data for averages, fits, limits, etc. • • •
 < 6.7 90 ¹ AVERY 97 CLEO $E_{\text{cm}}^{\text{ee}} = 10.6 \text{ GeV}$

¹ AVERY 97 limit varies from $(5.4\text{--}6.7) \times 10^{-5}$ depending on decay model assumptions.

 $\Gamma(f_1(1285)\pi^-\nu_\tau)/\Gamma_{\text{total}}$ Γ_{171}/Γ

VALUE (units 10^{-4})	EVTS	DOCUMENT ID	TECN	COMMENT
3.9 ± 0.5 OUR AVERAGE		Error includes scale factor of 1.9.		
4.73 ± 0.28 ± 0.45	3.7k	¹ LEES	12X BABR	$468 \text{ fb}^{-1} E_{\text{cm}}^{\text{ee}} = 10.6 \text{ GeV}$
3.60 ± 0.18 ± 0.23	2.5k	² LEES	12X BABR	$468 \text{ fb}^{-1} E_{\text{cm}}^{\text{ee}} = 10.6 \text{ GeV}$

• • • We do not use the following data for averages, fits, limits, etc. • • •
 3.19 ± 0.18 ± 1.00 1.3 k ³ AUBERT 08AE BABR Repl. by LEES 12X
 3.9 ± 0.7 ± 0.5 1.4 k ⁴ AUBERT,B 05W BABR Repl. by LEES 12X
 5.8 $^{+1.4}_{-1.3} \pm 1.8$ 54 ⁵ BERGFELD 97 CLEO $E_{\text{cm}}^{\text{ee}} = 10.6 \text{ GeV}$

¹ LEES 12X obtain this value by dividing their $B(\tau^- \rightarrow f_1(1285)\pi^-\nu_\tau \rightarrow 3\pi^-2\pi^+\nu_\tau)$ measurement by the PDG 12 value of $B(f_1(1285) \rightarrow 2\pi^+2\pi^-) = 0.111^{+0.007}_{-0.006}$.

² LEES 12X obtain this value by dividing their $B(\tau^- \rightarrow f_1(1285)\pi^-\nu_\tau \rightarrow \eta\pi^-\pi^+\pi^-\nu_\tau)$ measurement by 2/3 of the PDG 12 value of $B(f_1(1285) \rightarrow \eta\pi\pi) = 0.524^{+0.019}_{-0.021}$.

³ AUBERT 08AE obtain this value by dividing their $B(\tau^- \rightarrow f_1(1285)\pi^-\nu_\tau \rightarrow \eta\pi^-\pi^+\pi^-\nu_\tau)$ measurement by the PDG 06 value of $B(f_1(1285) \rightarrow \eta\pi^-\pi^+) = 0.35 \pm 0.11$. The quote $(3.19 \pm 0.18 \pm 0.16 \pm 0.99) \times 10^{-4}$ where the final error is due to the uncertainty on $B(f_1(1285) \rightarrow \eta\pi^-\pi^+)$. We combine the two systematic errors in quadrature.

⁴ AUBERT,B 05W use the $f_1(1285) \rightarrow 2\pi^+2\pi^-$ decay mode and the PDG 04 value of $B(f_1(1285) \rightarrow 2\pi^+2\pi^-) = 0.110^{+0.007}_{-0.006}$.

⁵ BERGFELD 97 use the $f_1(1285) \rightarrow \eta\pi^+\pi^-$ decay mode.

 $\Gamma(f_1(1285)\pi^-\nu_\tau \rightarrow \eta\pi^-\pi^+\pi^-\nu_\tau)/\Gamma_{\text{total}}$ Γ_{172}/Γ

VALUE (units 10^{-4})	EVTS	DOCUMENT ID	TECN	COMMENT
1.18 ± 0.07 OUR AVERAGE		Error includes scale factor of 1.3.		
1.26 ± 0.06 ± 0.06	2.5k	LEES	12X BABR	$468 \text{ fb}^{-1} E_{\text{cm}}^{\text{ee}} = 10.6 \text{ GeV}$
1.11 ± 0.06 ± 0.05	1.3 k	AUBERT	08AE BABR	$384 \text{ fb}^{-1}, E_{\text{cm}}^{\text{ee}} = 10.6 \text{ GeV}$

• • • We do not use the following data for averages, fits, limits, etc. • • •

 $\Gamma(f_1(1285)\pi^-\nu_\tau \rightarrow \eta\pi^-\pi^+\pi^-\nu_\tau)/\Gamma(\eta\pi^-\pi^+\pi^-\nu_\tau(\text{ex. } K^0))$ $\Gamma_{172}/\Gamma_{160}$

VALUE	DOCUMENT ID	TECN	COMMENT
0.69 ± 0.01 ± 0.05	¹ AUBERT	08AE BABR	$384 \text{ fb}^{-1}, E_{\text{cm}}^{\text{ee}} = 10.6 \text{ GeV}$

• • • We do not use the following data for averages, fits, limits, etc. • • •
 0.55 ± 0.14 BERGFELD 97 CLEO $E_{\text{cm}}^{\text{ee}} = 10.6 \text{ GeV}$

¹ Not independent of AUBERT 08AE $B(\tau^- \rightarrow f_1(1285)\pi^-\nu_\tau \rightarrow \eta\pi^-\pi^+\pi^-\nu_\tau)$ and $B(\tau^- \rightarrow \eta\pi^-\pi^+\pi^-\nu_\tau(\text{ex. } K^0))$ values.

 $\Gamma(f_1(1285)\pi^-\nu_\tau \rightarrow 3\pi^-2\pi^+\nu_\tau)/\Gamma_{\text{total}}$ Γ_{173}/Γ

VALUE (units 10^{-4})	EVTS	DOCUMENT ID	TECN	COMMENT
0.52 ± 0.04 OUR FIT		(Produced by HFLAV)		
0.520 ± 0.031 ± 0.037	3.7k	LEES	12X BABR	$468 \text{ fb}^{-1} E_{\text{cm}}^{\text{ee}} = 10.6 \text{ GeV}$

 $\Gamma(\pi(1300)^-\nu_\tau \rightarrow (\rho\pi)^-\nu_\tau \rightarrow (3\pi)^-\nu_\tau)/\Gamma_{\text{total}}$ Γ_{174}/Γ

VALUE	CL%	DOCUMENT ID	TECN	COMMENT
< 1.0 × 10⁻⁴	90	ASNER	00 CLEO	$E_{\text{cm}}^{\text{ee}} = 10.6 \text{ GeV}$

 $\Gamma(\pi(1300)^-\nu_\tau \rightarrow ((\pi\pi)S\text{-wave})\pi^-\nu_\tau \rightarrow (3\pi)^-\nu_\tau)/\Gamma_{\text{total}}$ Γ_{175}/Γ

VALUE	CL%	DOCUMENT ID	TECN	COMMENT
< 1.9 × 10⁻⁴	90	ASNER	00 CLEO	$E_{\text{cm}}^{\text{ee}} = 10.6 \text{ GeV}$

 $\Gamma(h^-\omega \geq 0 \text{ neutrals } \nu_\tau)/\Gamma_{\text{total}}$ Γ_{176}/Γ

VALUE (%)	EVTS	DOCUMENT ID	TECN	COMMENT
2.40 ± 0.08 OUR FIT		(Produced by HFLAV)		
1.65 ± 0.3 ± 0.2	1513	ALBRECHT	88M ARG	$E_{\text{cm}}^{\text{ee}} \approx 10 \text{ GeV}$

• • • We use the following data for averages but not for fits. • • •

 $\Gamma(h^-\omega\nu_\tau)/\Gamma_{\text{total}}$ $\Gamma_{177}/\Gamma = (\Gamma_{178} + \Gamma_{179})/\Gamma$

VALUE (%)	EVTS	DOCUMENT ID	TECN	COMMENT
1.99 ± 0.06 OUR FIT		(Produced by HFLAV)		
1.92 ± 0.07 OUR AVERAGE				
1.91 ± 0.07 ± 0.06	5803	BUSKULIC	97C ALEP	1991–1994 LEP runs
1.60 ± 0.27 ± 0.41	139	BARINGER	87 CLEO	$E_{\text{cm}}^{\text{ee}} = 10.5 \text{ GeV}$

• • • We use the following data for averages but not for fits. • • •
 1.95 ± 0.07 ± 0.11 2223 ¹ BALEST 95C CLEO $E_{\text{cm}}^{\text{ee}} \approx 10.6 \text{ GeV}$

¹ Not independent of BALEST 95C $B(\tau^- \rightarrow h^-\omega\nu_\tau)/B(\tau^- \rightarrow h^-h^+h^+\pi^0\nu_\tau)$ value.

 $[\Gamma(\pi^-\omega\nu_\tau) + \Gamma(K^-\omega\nu_\tau)]/\Gamma(h^-h^+h^+\pi^0\nu_\tau(\text{ex. } K^0))$ $(\Gamma_{178} + \Gamma_{179})/\Gamma_{74}$

VALUE (%)	EVTS	DOCUMENT ID	TECN	COMMENT
43.5 ± 1.4 OUR FIT		(Produced by HFLAV)		
45.3 ± 1.9 OUR AVERAGE				
43.1 ± 3.3	2350	¹ BUSKULIC	96 ALEP	LEP 1991–1993 data
46.4 ± 1.6 ± 1.7	2223	² BALEST	95C CLEO	$E_{\text{cm}}^{\text{ee}} \approx 10.6 \text{ GeV}$

• • • We do not use the following data for averages, fits, limits, etc. • • •
 37 ± 5 ± 2 458 ³ ALBRECHT 91D ARG $E_{\text{cm}}^{\text{ee}} = 9.4\text{--}10.6 \text{ GeV}$

¹ BUSKULIC 96 quote the fraction of $\tau \rightarrow h^-h^+h^+\pi^0\nu_\tau(\text{ex. } K^0)$ decays which originate in a $h^-\omega$ final state = 0.383 ± 0.029 . We divide this by the $\omega(782) \rightarrow \pi^+\pi^-\pi^0$ branching fraction (0.888).

² BALEST 95C quote the fraction of $\tau^- \rightarrow h^-h^+h^+\pi^0\nu_\tau(\text{ex. } K^0)$ decays which originate in a $h^-\omega$ final state equals $0.412 \pm 0.014 \pm 0.015$. We divide this by the $\omega(782) \rightarrow \pi^+\pi^-\pi^0$ branching fraction (0.888).

³ ALBRECHT 91D quote the fraction of $\tau^- \rightarrow h^-h^+h^+\pi^0\nu_\tau$ decays which originate in a $\pi^-\omega$ final state equals $0.33 \pm 0.04 \pm 0.02$. We divide this by the $\omega(782) \rightarrow \pi^+\pi^-\pi^0$ branching fraction (0.888).

 $\Gamma(\pi^-\omega\nu_\tau)/\Gamma_{\text{total}}$ Γ_{178}/Γ

VALUE (%)	DOCUMENT ID
1.95 ± 0.06 OUR FIT	(Produced by HFLAV)

$\Gamma(K^- \omega \nu_\tau)/\Gamma_{total}$ Γ_{179}/Γ

VALUE (units 10^{-4})	EVTS	DOCUMENT ID	TECN	COMMENT
4.1 ± 0.9 OUR FIT	(Produced by HFLAV)			
$4.1 \pm 0.6 \pm 0.7$	500	ARMS	05	CLE3 7.6 fb $^{-1}$, $E_{cm}^{ee} = 10.6$ GeV

$\Gamma(h^- \omega \pi^0 \nu_\tau)/\Gamma_{total}$ Γ_{180}/Γ

VALUE (%)	EVTS	DOCUMENT ID	TECN	COMMENT
0.41 ± 0.04 OUR FIT	(Produced by HFLAV)			
$0.43 \pm 0.06 \pm 0.05$	7283	BUSKULIC	97c	ALEP 1991–1994 LEP runs

$\Gamma(h^- \omega \pi^0 \nu_\tau)/\Gamma(h^- h^- h^+ \geq 0 \text{ neutrals} \geq 0 K_L^0 \nu_\tau)$ Γ_{180}/Γ_{62}

$\Gamma_{180}/\Gamma_{62} = \Gamma_{180}/(0.34598\Gamma_{36} + 0.34598\Gamma_{38} + 0.34598\Gamma_{41} + 0.34598\Gamma_{43} + 0.4247\Gamma_{48} + 0.6920\Gamma_{49} + 0.8494\Gamma_{52} + 0.6920\Gamma_{56} + 0.6534\Gamma_{61} + \Gamma_{70} + \Gamma_{78} + \Gamma_{85} + \Gamma_{89} + \Gamma_{97} + \Gamma_{103} + \Gamma_{106} + \Gamma_{107} + 0.2804\Gamma_{150} + 0.2302\Gamma_{151} + 0.2804\Gamma_{152} + 0.2804\Gamma_{154} + 0.3759\Gamma_{156} + 0.3257\Gamma_{160} + 0.7259\Gamma_{170} + 0.9078\Gamma_{178} + 0.9078\Gamma_{179} + 0.9078\Gamma_{180} + 0.892\Gamma_{182})$

VALUE	EVTS	DOCUMENT ID	TECN	COMMENT
$(2.69 \pm 0.28) \times 10^{-2}$ OUR FIT	(Produced by HFLAV)			

• • • We use the following data for averages but not for fits. • • •

$0.028 \pm 0.003 \pm 0.003$ 430 ¹BORTOLETTO 93 CLEO $E_{cm}^{ee} \approx 10.6$ GeV

¹Not independent of BORTOLETTO 93 $\Gamma(\tau^- \rightarrow h^- \omega \pi^0 \nu_\tau)/\Gamma(\tau^- \rightarrow h^- h^- h^+ 2\pi^0 \nu_\tau \text{ (ex. } K^0))$ value.

$\Gamma(h^- \omega \pi^0 \nu_\tau)/\Gamma(h^- h^- h^+ 2\pi^0 \nu_\tau \text{ (ex. } K^0))$ Γ_{180}/Γ_{84}

$\Gamma_{180}/\Gamma_{84} = \Gamma_{180}/(\Gamma_{85} + 0.2302\Gamma_{150} + 0.2302\Gamma_{154} + 0.892\Gamma_{180})$

VALUE (units 10^{-2})	DOCUMENT ID	TECN	COMMENT
82 ± 8 OUR FIT	(Produced by HFLAV)		
$81 \pm 6 \pm 6$	BORTOLETTO 93	CLEO	$E_{cm}^{ee} \approx 10.6$ GeV

$\Gamma(h^- \omega 2\pi^0 \nu_\tau)/\Gamma_{total}$ Γ_{181}/Γ

VALUE (units 10^{-4})	EVTS	DOCUMENT ID	TECN	COMMENT
$1.4 \pm 0.4 \pm 0.3$	53	ANASTASSOV 01	CLEO	$E_{cm}^{ee} = 10.6$ GeV
• • • We do not use the following data for averages, fits, limits, etc. • • •				
$1.89^{+0.74}_{-0.67} \pm 0.40$	19	ANDERSON 97	CLEO	Repl. by ANASTASSOV 01

$\Gamma(\pi^- \omega 2\pi^0 \nu_\tau)/\Gamma_{total}$ Γ_{182}/Γ

VALUE (units 10^{-4})	EVTS	DOCUMENT ID	TECN	COMMENT
0.72 ± 0.16 OUR FIT	(Produced by HFLAV)			
$0.73 \pm 0.12 \pm 0.12$	1.1k	LEES	12x	BABR 468 fb $^{-1}$ $E_{cm}^{ee} = 10.6$ GeV

$\Gamma(h^- 2\omega \nu_\tau)/\Gamma_{total}$ Γ_{183}/Γ

VALUE	CL%	DOCUMENT ID	TECN	COMMENT
$< 5.4 \times 10^{-7}$	90	AUBERT, B	06	BABR 232 fb $^{-1}$ $E_{cm}^{ee} = 10.6$ GeV

$\Gamma(2h^- h^+ \omega \nu_\tau)/\Gamma_{total}$ Γ_{184}/Γ

VALUE (units 10^{-4})	EVTS	DOCUMENT ID	TECN	COMMENT
$1.2 \pm 0.2 \pm 0.1$	110	ANASTASSOV 01	CLEO	$E_{cm}^{ee} = 10.6$ GeV

$\Gamma(2\pi^- \pi^+ \omega \nu_\tau \text{ (ex. } K^0))/\Gamma_{total}$ Γ_{185}/Γ

VALUE (units 10^{-4})	EVTS	DOCUMENT ID	TECN	COMMENT
0.84 ± 0.06 OUR FIT	(Produced by HFLAV)			
$0.84 \pm 0.04 \pm 0.06$	2.4k	LEES	12x	BABR 468 fb $^{-1}$ $E_{cm}^{ee} = 10.6$ GeV

$\Gamma(e^- \gamma)/\Gamma_{total}$ Γ_{186}/Γ

Test of lepton family number conservation.

VALUE	CL%	DOCUMENT ID	TECN	COMMENT
$< 3.3 \times 10^{-8}$	90	AUBERT	10b	BABR 516 fb $^{-1}$, $E_{cm}^{ee} = 10.6$ GeV
• • • We do not use the following data for averages, fits, limits, etc. • • •				
$< 5.6 \times 10^{-8}$	90	UNO	21	BELL 988 fb $^{-1}$, $E_{cm}^{ee} = 10.6$ GeV
$< 1.2 \times 10^{-7}$	90	HAYASAKA	08	BELL 535 fb $^{-1}$, $E_{cm}^{ee} = 10.6$ GeV
$< 1.1 \times 10^{-7}$	90	AUBERT	06c	BABR 232 fb $^{-1}$, $E_{cm}^{ee} = 10.6$ GeV
$< 3.9 \times 10^{-7}$	90	HAYASAKA	05	BELL 86.7 fb $^{-1}$, $E_{cm}^{ee} = 10.6$ GeV
$< 2.7 \times 10^{-6}$	90	EDWARDS	97	CLEO
$< 1.1 \times 10^{-4}$	90	ABREU	95u	DLPH 1990–1993 LEP runs
$< 1.2 \times 10^{-4}$	90	ALBRECHT	92k	ARG $E_{cm}^{ee} = 10$ GeV
$< 2.0 \times 10^{-4}$	90	KEH	88	CBAL $E_{cm}^{ee} = 10$ GeV
$< 6.4 \times 10^{-4}$	90	HAYES	82	MRK2 $E_{cm}^{ee} = 3.8\text{--}6.8$ GeV

$\Gamma(e^- \gamma \gamma)/\Gamma_{total}$ Γ_{187}/Γ

VALUE	CL%	DOCUMENT ID	TECN	COMMENT
$< 2.5 \times 10^{-4}$	90	¹ BRYMAN	21	RVUE 516 fb $^{-1}$, $E_{cm}^{ee} = 10.6$ GeV

¹BRYMAN 21 reinterprets the upper limit result on $B(\tau^- \rightarrow e^- \gamma)$ and $B(\tau^- \rightarrow \mu^- \gamma)$ by AUBERT 10b, estimating with a simulation the efficiency for this decay mode to be detected as the corresponding AUBERT 10b decay mode.

$\Gamma(\mu^- \gamma)/\Gamma_{total}$ Γ_{188}/Γ

Test of lepton family number conservation.

VALUE	CL%	DOCUMENT ID	TECN	COMMENT
$< 4.2 \times 10^{-8}$	90	UNO	21	BELL 988 fb $^{-1}$, $E_{cm}^{ee} = 10.6$ GeV
• • • We do not use the following data for averages, fits, limits, etc. • • •				
$< 4.4 \times 10^{-8}$	90	AUBERT	10b	BABR 516 fb $^{-1}$, $E_{cm}^{ee} = 10.6$ GeV
$< 4.5 \times 10^{-8}$	90	HAYASAKA	08	BELL 535 fb $^{-1}$, $E_{cm}^{ee} = 10.6$ GeV
$< 6.8 \times 10^{-8}$	90	AUBERT, B	05a	BABR 232 fb $^{-1}$, $E_{cm}^{ee} = 10.6$ GeV
$< 3.1 \times 10^{-7}$	90	ABE	04b	BELL 86.3 fb $^{-1}$, $E_{cm}^{ee} = 10.6$ GeV
$< 1.1 \times 10^{-6}$	90	AHMED	00	CLEO $E_{cm}^{ee} = 10.6$ GeV
$< 3.0 \times 10^{-6}$	90	EDWARDS	97	CLEO
$< 6.2 \times 10^{-5}$	90	ABREU	95u	DLPH 1990–1993 LEP runs
$< 0.42 \times 10^{-5}$	90	BEAN	93	CLEO $E_{cm}^{ee} = 10.6$ GeV
$< 3.4 \times 10^{-5}$	90	ALBRECHT	92k	ARG $E_{cm}^{ee} = 10$ GeV
$< 55 \times 10^{-5}$	90	HAYES	82	MRK2 $E_{cm}^{ee} = 3.8\text{--}6.8$ GeV

$\Gamma(\mu^- \gamma \gamma)/\Gamma_{total}$ Γ_{189}/Γ

VALUE	CL%	DOCUMENT ID	TECN	COMMENT
$< 5.8 \times 10^{-4}$	90	¹ BRYMAN	21	RVUE 516 fb $^{-1}$, $E_{cm}^{ee} = 10.6$ GeV

¹BRYMAN 21 reinterprets the upper limit result on $B(\tau^- \rightarrow e^- \gamma)$ and $B(\tau^- \rightarrow \mu^- \gamma)$ by AUBERT 10b, estimating with a simulation the efficiency for this decay mode to be detected as the corresponding AUBERT 10b decay mode.

$\Gamma(e^- \pi^0)/\Gamma_{total}$ Γ_{190}/Γ

Test of lepton family number conservation.

VALUE	CL%	DOCUMENT ID	TECN	COMMENT
$< 8.0 \times 10^{-8}$	90	MIYAZAKI	07	BELL 401 fb $^{-1}$, $E_{cm}^{ee} = 10.6$ GeV
• • • We do not use the following data for averages, fits, limits, etc. • • •				
$< 1.3 \times 10^{-7}$	90	AUBERT	07i	BABR 339 fb $^{-1}$, $E_{cm}^{ee} = 10.6$ GeV
$< 1.9 \times 10^{-7}$	90	ENARI	05	BELL 154 fb $^{-1}$, $E_{cm}^{ee} = 10.6$ GeV
$< 3.7 \times 10^{-6}$	90	BONVICINI	97	CLEO $E_{cm}^{ee} = 10.6$ GeV
$< 17 \times 10^{-5}$	90	ALBRECHT	92k	ARG $E_{cm}^{ee} = 10$ GeV
$< 14 \times 10^{-5}$	90	KEH	88	CBAL $E_{cm}^{ee} = 10$ GeV
$< 210 \times 10^{-5}$	90	HAYES	82	MRK2 $E_{cm}^{ee} = 3.8\text{--}6.8$ GeV

$\Gamma(\mu^- \pi^0)/\Gamma_{total}$ Γ_{191}/Γ

Test of lepton family number conservation.

VALUE	CL%	DOCUMENT ID	TECN	COMMENT
$< 1.1 \times 10^{-7}$	90	AUBERT	07i	BABR 339 fb $^{-1}$, $E_{cm}^{ee} = 10.6$ GeV
• • • We do not use the following data for averages, fits, limits, etc. • • •				
$< 1.2 \times 10^{-7}$	90	MIYAZAKI	07	BELL 401 fb $^{-1}$, $E_{cm}^{ee} = 10.6$ GeV
$< 4.1 \times 10^{-7}$	90	ENARI	05	BELL 154 fb $^{-1}$, $E_{cm}^{ee} = 10.6$ GeV
$< 4.0 \times 10^{-6}$	90	BONVICINI	97	CLEO $E_{cm}^{ee} = 10.6$ GeV
$< 4.4 \times 10^{-5}$	90	ALBRECHT	92k	ARG $E_{cm}^{ee} = 10$ GeV
$< 82 \times 10^{-5}$	90	HAYES	82	MRK2 $E_{cm}^{ee} = 3.8\text{--}6.8$ GeV

$\Gamma(e^- K_S^0)/\Gamma_{total}$ Γ_{192}/Γ

Test of lepton family number conservation.

VALUE	CL%	DOCUMENT ID	TECN	COMMENT
$< 2.6 \times 10^{-8}$	90	MIYAZAKI	10a	BELL 671 fb $^{-1}$ $E_{cm}^{ee} = 10.6$ GeV
• • • We do not use the following data for averages, fits, limits, etc. • • •				
$< 3.3 \times 10^{-8}$	90	AUBERT	09d	BABR 469 fb $^{-1}$ $E_{cm}^{ee} = 10.6$ GeV
$< 5.6 \times 10^{-8}$	90	MIYAZAKI	06a	BELL 281 fb $^{-1}$ $E_{cm}^{ee} = 10.6$ GeV
$< 9.1 \times 10^{-7}$	90	CHEN	02c	CLEO $E_{cm}^{ee} = 10.6$ GeV
$< 1.3 \times 10^{-3}$	90	HAYES	82	MRK2 $E_{cm}^{ee} = 3.8\text{--}6.8$ GeV

$\Gamma(\mu^- K_S^0)/\Gamma_{total}$ Γ_{193}/Γ

Test of lepton family number conservation.

VALUE	CL%	DOCUMENT ID	TECN	COMMENT
$< 2.3 \times 10^{-8}$	90	MIYAZAKI	10a	BELL 671 fb $^{-1}$ $E_{cm}^{ee} = 10.6$ GeV
• • • We do not use the following data for averages, fits, limits, etc. • • •				
$< 4.0 \times 10^{-8}$	90	AUBERT	09d	BABR 469 fb $^{-1}$ $E_{cm}^{ee} = 10.6$ GeV
$< 4.9 \times 10^{-8}$	90	MIYAZAKI	06a	BELL 281 fb $^{-1}$ $E_{cm}^{ee} = 10.6$ GeV
$< 9.5 \times 10^{-7}$	90	CHEN	02c	CLEO $E_{cm}^{ee} = 10.6$ GeV
$< 1.0 \times 10^{-3}$	90	HAYES	82	MRK2 $E_{cm}^{ee} = 3.8\text{--}6.8$ GeV

$\Gamma(e^- \eta)/\Gamma_{total}$ Γ_{194}/Γ

Test of lepton family number conservation.

VALUE	CL%	DOCUMENT ID	TECN	COMMENT
$< 9.2 \times 10^{-8}$	90	MIYAZAKI	07	BELL 401 fb $^{-1}$, $E_{cm}^{ee} = 10.6$ GeV
• • • We do not use the following data for averages, fits, limits, etc. • • •				
$< 1.6 \times 10^{-7}$	90	AUBERT	07i	BABR 339 fb $^{-1}$, $E_{cm}^{ee} = 10.6$ GeV
$< 2.4 \times 10^{-7}$	90	ENARI	05	BELL 154 fb $^{-1}$, $E_{cm}^{ee} = 10.6$ GeV
$< 8.2 \times 10^{-6}$	90	BONVICINI	97	CLEO $E_{cm}^{ee} = 10.6$ GeV
$< 6.3 \times 10^{-5}$	90	ALBRECHT	92k	ARG $E_{cm}^{ee} = 10$ GeV
$< 24 \times 10^{-5}$	90	KEH	88	CBAL $E_{cm}^{ee} = 10$ GeV

$\Gamma(\mu^- \phi)/\Gamma_{total}$
Test of lepton family number conservation.

VALUE	CL%	DOCUMENT ID	TECN	COMMENT
$<2.3 \times 10^{-8}$	90	¹ TSUZUKI	23 BELL	$980 \text{ fb}^{-1} E_{cm}^{ee} = 10.6 \text{ GeV}$
$<8.4 \times 10^{-8}$	90	MIYAZAKI	11 BELL	$854 \text{ fb}^{-1} E_{cm}^{ee} = 10.6 \text{ GeV}$
$<1.9 \times 10^{-7}$	90	AUBERT	09W BABR	$451 \text{ fb}^{-1} E_{cm}^{ee} = 10.6 \text{ GeV}$
$<1.3 \times 10^{-7}$	90	NISHIO	08 BELL	$543 \text{ fb}^{-1} E_{cm}^{ee} = 10.6 \text{ GeV}$
$<7.7 \times 10^{-7}$	90	YUSA	06 BELL	$158 \text{ fb}^{-1} E_{cm}^{ee} = 10.6 \text{ GeV}$
$<7.0 \times 10^{-6}$	90	BLISS	98 CLEO	$E_{cm}^{ee} = 10.6 \text{ GeV}$

$\Gamma(e^- e^+ e^-)/\Gamma_{total}$
Test of lepton family number conservation.

VALUE	CL%	DOCUMENT ID	TECN	COMMENT
$< 2.7 \times 10^{-8}$	90	HAYASAKA	10 BELL	$782 \text{ fb}^{-1} E_{cm}^{ee} = 10.6 \text{ GeV}$
$< 2.9 \times 10^{-8}$	90	LEES	10A BABR	$468 \text{ fb}^{-1} E_{cm}^{ee} = 10.6 \text{ GeV}$
$< 3.6 \times 10^{-8}$	90	MIYAZAKI	08 BELL	$535 \text{ fb}^{-1} E_{cm}^{ee} = 10.6 \text{ GeV}$
$< 4.3 \times 10^{-8}$	90	AUBERT	07BK BABR	$376 \text{ fb}^{-1} E_{cm}^{ee} = 10.6 \text{ GeV}$
$< 2.0 \times 10^{-7}$	90	AUBERT	04J BABR	$91.5 \text{ fb}^{-1} E_{cm}^{ee} = 10.6 \text{ GeV}$
$< 3.5 \times 10^{-7}$	90	YUSA	04J BELL	$87.1 \text{ fb}^{-1} E_{cm}^{ee} = 10.6 \text{ GeV}$
$< 2.9 \times 10^{-6}$	90	BLISS	98 CLEO	$E_{cm}^{ee} = 10.6 \text{ GeV}$
$< 0.33 \times 10^{-5}$	90	¹ BARTELT	94 CLEO	Repl. by BLISS 98
$< 1.3 \times 10^{-5}$	90	ALBRECHT	92K ARG	$E_{cm}^{ee} = 10 \text{ GeV}$
$< 2.7 \times 10^{-5}$	90	BOWCOCK	90 CLEO	$E_{cm}^{ee} = 10.4-10.9$
$<40 \times 10^{-5}$	90	HAYES	82 MRK2	$E_{cm}^{ee} = 3.8-6.8 \text{ GeV}$

$\Gamma(e^- \mu^+ \mu^-)/\Gamma_{total}$
Test of lepton family number conservation.

VALUE	CL%	DOCUMENT ID	TECN	COMMENT
$< 2.7 \times 10^{-8}$	90	HAYASAKA	10 BELL	$782 \text{ fb}^{-1} E_{cm}^{ee} = 10.6 \text{ GeV}$
$< 3.2 \times 10^{-8}$	90	LEES	10A BABR	$468 \text{ fb}^{-1} E_{cm}^{ee} = 10.6 \text{ GeV}$
$< 4.1 \times 10^{-8}$	90	MIYAZAKI	08 BELL	$535 \text{ fb}^{-1} E_{cm}^{ee} = 10.6 \text{ GeV}$
$< 3.7 \times 10^{-8}$	90	AUBERT	07BK BABR	$376 \text{ fb}^{-1} E_{cm}^{ee} = 10.6 \text{ GeV}$
$< 3.3 \times 10^{-7}$	90	AUBERT	04J BABR	$91.5 \text{ fb}^{-1} E_{cm}^{ee} = 10.6 \text{ GeV}$
$< 2.0 \times 10^{-7}$	90	YUSA	04J BELL	$87.1 \text{ fb}^{-1} E_{cm}^{ee} = 10.6 \text{ GeV}$
$< 1.8 \times 10^{-6}$	90	BLISS	98 CLEO	$E_{cm}^{ee} = 10.6 \text{ GeV}$
$< 0.36 \times 10^{-5}$	90	¹ BARTELT	94 CLEO	Repl. by BLISS 98
$< 1.9 \times 10^{-5}$	90	ALBRECHT	92K ARG	$E_{cm}^{ee} = 10 \text{ GeV}$
$< 2.7 \times 10^{-5}$	90	BOWCOCK	90 CLEO	$E_{cm}^{ee} = 10.4-10.9$
$<33 \times 10^{-5}$	90	HAYES	82 MRK2	$E_{cm}^{ee} = 3.8-6.8 \text{ GeV}$

$\Gamma(e^+ \mu^- \mu^-)/\Gamma_{total}$
Test of lepton family number conservation.

VALUE	CL%	DOCUMENT ID	TECN	COMMENT
$<1.7 \times 10^{-8}$	90	HAYASAKA	10 BELL	$782 \text{ fb}^{-1} E_{cm}^{ee} = 10.6 \text{ GeV}$
$<2.6 \times 10^{-8}$	90	LEES	10A BABR	$468 \text{ fb}^{-1} E_{cm}^{ee} = 10.6 \text{ GeV}$
$<2.3 \times 10^{-8}$	90	MIYAZAKI	08 BELL	$535 \text{ fb}^{-1} E_{cm}^{ee} = 10.6 \text{ GeV}$
$<5.6 \times 10^{-8}$	90	AUBERT	07BK BABR	$376 \text{ fb}^{-1} E_{cm}^{ee} = 10.6 \text{ GeV}$
$<1.3 \times 10^{-7}$	90	AUBERT	04J BABR	$91.5 \text{ fb}^{-1} E_{cm}^{ee} = 10.6 \text{ GeV}$
$<2.0 \times 10^{-7}$	90	YUSA	04 BELL	$87.1 \text{ fb}^{-1} E_{cm}^{ee} = 10.6 \text{ GeV}$
$<1.5 \times 10^{-6}$	90	BLISS	98 CLEO	$E_{cm}^{ee} = 10.6 \text{ GeV}$
$<0.35 \times 10^{-5}$	90	¹ BARTELT	94 CLEO	Repl. by BLISS 98
$<1.8 \times 10^{-5}$	90	ALBRECHT	92K ARG	$E_{cm}^{ee} = 10 \text{ GeV}$
$<1.6 \times 10^{-5}$	90	BOWCOCK	90 CLEO	$E_{cm}^{ee} = 10.4-10.9$

$\Gamma(\mu^- e^+ e^-)/\Gamma_{total}$
Test of lepton family number conservation.

VALUE	CL%	DOCUMENT ID	TECN	COMMENT
$< 1.8 \times 10^{-8}$	90	HAYASAKA	10 BELL	$782 \text{ fb}^{-1} E_{cm}^{ee} = 10.6 \text{ GeV}$
$< 2.2 \times 10^{-8}$	90	LEES	10A BABR	$468 \text{ fb}^{-1} E_{cm}^{ee} = 10.6 \text{ GeV}$
$< 2.7 \times 10^{-8}$	90	MIYAZAKI	08 BELL	$535 \text{ fb}^{-1} E_{cm}^{ee} = 10.6 \text{ GeV}$
$< 8.0 \times 10^{-8}$	90	AUBERT	07BK BABR	$376 \text{ fb}^{-1} E_{cm}^{ee} = 10.6 \text{ GeV}$
$< 2.7 \times 10^{-7}$	90	AUBERT	04J BABR	$91.5 \text{ fb}^{-1} E_{cm}^{ee} = 10.6 \text{ GeV}$
$< 1.9 \times 10^{-7}$	90	YUSA	04 BELL	$87.1 \text{ fb}^{-1} E_{cm}^{ee} = 10.6 \text{ GeV}$
$< 1.7 \times 10^{-6}$	90	BLISS	98 CLEO	$E_{cm}^{ee} = 10.6 \text{ GeV}$
$< 0.34 \times 10^{-5}$	90	¹ BARTELT	94 CLEO	Repl. by BLISS 98
$< 1.4 \times 10^{-5}$	90	ALBRECHT	92K ARG	$E_{cm}^{ee} = 10 \text{ GeV}$
$< 2.7 \times 10^{-5}$	90	BOWCOCK	90 CLEO	$E_{cm}^{ee} = 10.4-10.9$
$<44 \times 10^{-5}$	90	HAYES	82 MRK2	$E_{cm}^{ee} = 3.8-6.8 \text{ GeV}$

$\Gamma(\mu^+ e^- e^-)/\Gamma_{total}$
Test of lepton family number conservation.

VALUE	CL%	DOCUMENT ID	TECN	COMMENT
$<1.5 \times 10^{-8}$	90	HAYASAKA	10 BELL	$782 \text{ fb}^{-1} E_{cm}^{ee} = 10.6 \text{ GeV}$
$<1.8 \times 10^{-8}$	90	LEES	10A BABR	$468 \text{ fb}^{-1} E_{cm}^{ee} = 10.6 \text{ GeV}$
$<2.0 \times 10^{-8}$	90	MIYAZAKI	08 BELL	$535 \text{ fb}^{-1} E_{cm}^{ee} = 10.6 \text{ GeV}$
$<5.8 \times 10^{-8}$	90	AUBERT	07BK BABR	$376 \text{ fb}^{-1} E_{cm}^{ee} = 10.6 \text{ GeV}$
$<1.1 \times 10^{-7}$	90	AUBERT	04J BABR	$91.5 \text{ fb}^{-1} E_{cm}^{ee} = 10.6 \text{ GeV}$
$<2.0 \times 10^{-7}$	90	YUSA	04 BELL	$87.1 \text{ fb}^{-1} E_{cm}^{ee} = 10.6 \text{ GeV}$
$<1.5 \times 10^{-6}$	90	BLISS	98 CLEO	$E_{cm}^{ee} = 10.6 \text{ GeV}$
$<0.34 \times 10^{-5}$	90	¹ BARTELT	94 CLEO	Repl. by BLISS 98
$<1.4 \times 10^{-5}$	90	ALBRECHT	92K ARG	$E_{cm}^{ee} = 10 \text{ GeV}$
$<1.6 \times 10^{-5}$	90	BOWCOCK	90 CLEO	$E_{cm}^{ee} = 10.4-10.9$

$\Gamma(\mu^- \mu^+ \mu^-)/\Gamma_{total}$
Test of lepton family number conservation.

VALUE	CL%	DOCUMENT ID	TECN	COMMENT
$< 2.1 \times 10^{-8}$	90	HAYASAKA	10 BELL	$782 \text{ fb}^{-1} E_{cm}^{ee} = 10.6 \text{ GeV}$
$< 8.0 \times 10^{-8}$	90	SIRUNYAN	21D CMS	$33.2 \text{ fb}^{-1}, pp$ at 13 TeV
$< 3.8 \times 10^{-7}$	90	AAD	16BA ATLS	$20.3 \text{ fb}^{-1}, pp$ at 8 TeV
$< 4.6 \times 10^{-8}$	90	AAIJ	15AI LHCb	$3.0 \text{ fb}^{-1}, pp$ at 7, 8 TeV
$< 8.0 \times 10^{-8}$	90	¹ AAIJ	13AH LHCb	$1.0 \text{ fb}^{-1}, pp$ at 7 TeV
$< 3.3 \times 10^{-8}$	90	LEES	10A BABR	$468 \text{ fb}^{-1} E_{cm}^{ee} = 10.6 \text{ GeV}$
$< 3.2 \times 10^{-8}$	90	MIYAZAKI	08 BELL	$535 \text{ fb}^{-1} E_{cm}^{ee} = 10.6 \text{ GeV}$
$< 5.3 \times 10^{-8}$	90	AUBERT	07BK BABR	$376 \text{ fb}^{-1} E_{cm}^{ee} = 10.6 \text{ GeV}$
$< 1.9 \times 10^{-7}$	90	AUBERT	04J BABR	$91.5 \text{ fb}^{-1} E_{cm}^{ee} = 10.6 \text{ GeV}$
$< 2.0 \times 10^{-7}$	90	YUSA	04 BELL	$87.1 \text{ fb}^{-1} E_{cm}^{ee} = 10.6 \text{ GeV}$
$< 1.9 \times 10^{-6}$	90	BLISS	98 CLEO	$E_{cm}^{ee} = 10.6 \text{ GeV}$
$< 0.43 \times 10^{-5}$	90	² BARTELT	94 CLEO	Repl. by BLISS 98
$< 1.9 \times 10^{-5}$	90	ALBRECHT	92K ARG	$E_{cm}^{ee} = 10 \text{ GeV}$
$< 1.7 \times 10^{-5}$	90	BOWCOCK	90 CLEO	$E_{cm}^{ee} = 10.4-10.9$
$<49 \times 10^{-5}$	90	HAYES	82 MRK2	$E_{cm}^{ee} = 3.8-6.8 \text{ GeV}$

$\Gamma(e^- \pi^+ \pi^-)/\Gamma_{total}$
Test of lepton family number conservation.

VALUE	CL%	DOCUMENT ID	TECN	COMMENT
$<2.3 \times 10^{-8}$	90	MIYAZAKI	13 BELL	$854 \text{ fb}^{-1} E_{cm}^{ee} = 10.6 \text{ GeV}$
$<4.4 \times 10^{-8}$	90	MIYAZAKI	10 BELL	Repl. by MIYAZAKI 13
$<7.3 \times 10^{-7}$	90	YUSA	06 BELL	$158 \text{ fb}^{-1} E_{cm}^{ee} = 10.6 \text{ GeV}$
$<1.2 \times 10^{-7}$	90	AUBERT, BE	05D BABR	$221 \text{ fb}^{-1}, E_{cm}^{ee} = 10.6 \text{ GeV}$
$<2.2 \times 10^{-6}$	90	BLISS	98 CLEO	$E_{cm}^{ee} = 10.6 \text{ GeV}$
$<4.4 \times 10^{-6}$	90	¹ BARTELT	94 CLEO	Repl. by BLISS 98
$<2.7 \times 10^{-5}$	90	ALBRECHT	92K ARG	$E_{cm}^{ee} = 10 \text{ GeV}$
$<6.0 \times 10^{-5}$	90	BOWCOCK	90 CLEO	$E_{cm}^{ee} = 10.4-10.9$

$\Gamma(e^+ \pi^+ \pi^-)/\Gamma_{total}$
Test of lepton number conservation.

VALUE	CL%	DOCUMENT ID	TECN	COMMENT
$<2.0 \times 10^{-8}$	90	MIYAZAKI	13 BELL	$854 \text{ fb}^{-1} E_{cm}^{ee} = 10.6 \text{ GeV}$
$<8.8 \times 10^{-8}$	90	MIYAZAKI	10 BELL	Repl. by MIYAZAKI 13
$<2.0 \times 10^{-7}$	90	YUSA	06 BELL	$158 \text{ fb}^{-1} E_{cm}^{ee} = 10.6 \text{ GeV}$
$<2.7 \times 10^{-7}$	90	AUBERT, BE	05D BABR	$221 \text{ fb}^{-1}, E_{cm}^{ee} = 10.6 \text{ GeV}$
$<1.9 \times 10^{-6}$	90	BLISS	98 CLEO	$E_{cm}^{ee} = 10.6 \text{ GeV}$
$<4.4 \times 10^{-6}$	90	¹ BARTELT	94 CLEO	Repl. by BLISS 98
$<1.8 \times 10^{-5}$	90	ALBRECHT	92K ARG	$E_{cm}^{ee} = 10 \text{ GeV}$
$<1.7 \times 10^{-5}$	90	BOWCOCK	90 CLEO	$E_{cm}^{ee} = 10.4-10.9$

$\Gamma(\mu^- \pi^+ \pi^-)/\Gamma_{total}$
Test of lepton family number conservation.

VALUE	CL%	DOCUMENT ID	TECN	COMMENT
$<2.1 \times 10^{-8}$	90	MIYAZAKI	13 BELL	$854 \text{ fb}^{-1} E_{cm}^{ee} = 10.6 \text{ GeV}$
$<3.3 \times 10^{-8}$	90	MIYAZAKI	10 BELL	Repl. by MIYAZAKI 13
$<4.8 \times 10^{-7}$	90	YUSA	06 BELL	$158 \text{ fb}^{-1} E_{cm}^{ee} = 10.6 \text{ GeV}$
$<2.9 \times 10^{-7}$	90	AUBERT, BE	05D BABR	$221 \text{ fb}^{-1}, E_{cm}^{ee} = 10.6 \text{ GeV}$
$<8.2 \times 10^{-6}$	90	BLISS	98 CLEO	$E_{cm}^{ee} = 10.6 \text{ GeV}$
$<7.4 \times 10^{-6}$	90	¹ BARTELT	94 CLEO	Repl. by BLISS 98
$<3.6 \times 10^{-5}$	90	ALBRECHT	92K ARG	$E_{cm}^{ee} = 10 \text{ GeV}$
$<3.9 \times 10^{-5}$	90	BOWCOCK	90 CLEO	$E_{cm}^{ee} = 10.4-10.9$

• • • We do not use the following data for averages, fits, limits, etc. • • •

• • • We do not use the following data for averages, fits, limits, etc. • • •

¹ Supersedes MIYAZAKI 11.

¹ BARTELT 94 assume phase space decays.

¹ BARTELT 94 assume phase space decays.

¹ Repl. by AAIJ 15AI.

² BARTELT 94 assume phase space decays.

¹ BARTELT 94 assume phase space decays.

¹ BARTELT 94 assume phase space decays.

¹ BARTELT 94 assume phase space decays.

¹ BARTELT 94 assume phase space decays.

¹ BARTELT 94 assume phase space decays.

¹ BARTELT 94 assume phase space decays.

$\Gamma(\mu^- \eta \eta) / \Gamma_{\text{total}}$
Test of lepton family number conservation.

VALUE	CL%	DOCUMENT ID	TECN	COMMENT
$< 6.0 \times 10^{-6}$	90	BONVICINI 97	CLEO	$E_{\text{cm}}^{\text{ee}} = 10.6 \text{ GeV}$

Γ_{235} / Γ

$\Gamma(e^- \text{light boson}) / \Gamma(e^- \bar{\nu}_e \nu_\tau)$
Test of lepton family number conservation.

VALUE	CL%	DOCUMENT ID	TECN	COMMENT
$< 5.3 \times 10^{-3}$	95	¹ ADACHI 23A	BELL	$E_{\text{cm}}^{\text{ee}} = 10.58 \text{ GeV}$

Γ_{251} / Γ_5

$\Gamma(e^- \pi^0 \eta) / \Gamma_{\text{total}}$
Test of lepton family number conservation.

VALUE	CL%	DOCUMENT ID	TECN	COMMENT
$< 24 \times 10^{-6}$	90	BONVICINI 97	CLEO	$E_{\text{cm}}^{\text{ee}} = 10.6 \text{ GeV}$

Γ_{236} / Γ

• • • We do not use the following data for averages, fits, limits, etc. • • •

< 0.008	95	² BRYMAN 21	RVUE	
< 0.015	95	³ ALBRECHT 95G	ARG	$E_{\text{cm}}^{\text{ee}} = 9.4\text{--}10.6 \text{ GeV}$
< 0.018	95	⁴ ALBRECHT 90E	ARG	$E_{\text{cm}}^{\text{ee}} = 9.4\text{--}10.6 \text{ GeV}$
< 0.040	95	⁵ BALTRUSAITIS...85	MRK3	$E_{\text{cm}}^{\text{ee}} = 3.77 \text{ GeV}$

$\Gamma(\mu^- \pi^0 \eta) / \Gamma_{\text{total}}$
Test of lepton family number conservation.

VALUE	CL%	DOCUMENT ID	TECN	COMMENT
$< 22 \times 10^{-6}$	90	BONVICINI 97	CLEO	$E_{\text{cm}}^{\text{ee}} = 10.6 \text{ GeV}$

Γ_{237} / Γ

¹ ADACHI 23A limit holds for bosons with mass $\equiv 0.0 \text{ GeV}$. The limit rises to 9.7×10^{-3} for a mass of 1.0 GeV, then falls to 1.1×10^{-3} at the upper mass limit of 1.6 GeV.
² BRYMAN 21 reports indirect limits obtained from the consistency of the world averages of $B(\tau^- \rightarrow e^- \bar{\nu}_e \nu_\tau)$ and $B(\tau^- \rightarrow \mu^- \bar{\nu}_\mu \nu_\tau)$ with their Standard Model predictions, without a simulation of the efficiency as a function of the X mass for the searched decay modes to be detected as the corresponding Standard Model decay modes.
³ ALBRECHT 95G limit holds for bosons with mass $< 0.4 \text{ GeV}$. The limit rises to 0.036 for a mass of 1.0 GeV, then falls to 0.006 at the upper mass limit of 1.6 GeV.
⁴ ALBRECHT 90E limit applies for spinless boson with mass $< 100 \text{ MeV}$, and rises to 0.050 for mass = 500 MeV.
⁵ BALTRUSAITIS 85 limit applies for spinless boson with mass $< 100 \text{ MeV}$.

$\Gamma(\rho e^- e^-) / \Gamma_{\text{total}}$

VALUE	CL%	DOCUMENT ID	TECN	COMMENT
$< 3.0 \times 10^{-8}$	90	SAHOO 20	BELL	921 fb^{-1} , $E_{\text{cm}}^{\text{ee}} = 10.6 \text{ GeV}$

Γ_{238} / Γ

$\Gamma(\mu^- \text{light boson}) / \Gamma(e^- \bar{\nu}_e \nu_\tau)$
Test of lepton family number conservation.

VALUE	CL%	DOCUMENT ID	TECN	COMMENT
$< 3.4 \times 10^{-3}$	95	¹ ADACHI 23A	BELL	$E_{\text{cm}}^{\text{ee}} = 10.58 \text{ GeV}$

Γ_{252} / Γ_5

$\Gamma(\bar{p} e^+ e^-) / \Gamma_{\text{total}}$

VALUE	CL%	DOCUMENT ID	TECN	COMMENT
$< 3.0 \times 10^{-8}$	90	SAHOO 20	BELL	921 fb^{-1} , $E_{\text{cm}}^{\text{ee}} = 10.6 \text{ GeV}$

Γ_{239} / Γ

• • • We do not use the following data for averages, fits, limits, etc. • • •

< 0.011	95	² BRYMAN 21	RVUE	
< 0.026	95	³ ALBRECHT 95G	ARG	$E_{\text{cm}}^{\text{ee}} = 9.4\text{--}10.6 \text{ GeV}$
< 0.033	95	⁴ ALBRECHT 90E	ARG	$E_{\text{cm}}^{\text{ee}} = 9.4\text{--}10.6 \text{ GeV}$
< 0.125	95	⁵ BALTRUSAITIS...85	MRK3	$E_{\text{cm}}^{\text{ee}} = 3.77 \text{ GeV}$

$\Gamma(\bar{p} e^+ \mu^-) / \Gamma_{\text{total}}$

VALUE	CL%	DOCUMENT ID	TECN	COMMENT
$< 2.0 \times 10^{-8}$	90	SAHOO 20	BELL	921 fb^{-1} , $E_{\text{cm}}^{\text{ee}} = 10.6 \text{ GeV}$

Γ_{240} / Γ

¹ ADACHI 23A limit holds for bosons with mass $\equiv 0.0 \text{ GeV}$. The limit rises to 12.2×10^{-3} for a mass of 1.0 GeV, then falls to 0.7×10^{-3} at the upper mass limit of 1.6 GeV.
² BRYMAN 21 reports indirect limits obtained from the consistency of the world averages of $B(\tau^- \rightarrow e^- \bar{\nu}_e \nu_\tau)$ and $B(\tau^- \rightarrow \mu^- \bar{\nu}_\mu \nu_\tau)$ with their Standard Model predictions, without a simulation of the efficiency as a function of the X mass for the searched decay modes to be detected as the corresponding Standard Model decay modes.
³ ALBRECHT 95G limit holds for bosons with mass $< 1.3 \text{ GeV}$. The limit rises to 0.034 for a mass of 1.4 GeV, then falls to 0.003 at the upper mass limit of 1.6 GeV.
⁴ ALBRECHT 90E limit applies for spinless boson with mass $< 100 \text{ MeV}$, and rises to 0.071 for mass = 500 MeV.
⁵ BALTRUSAITIS 85 limit applies for spinless boson with mass $< 100 \text{ MeV}$.

$\Gamma(\bar{p} e^- \mu^+) / \Gamma_{\text{total}}$

VALUE	CL%	DOCUMENT ID	TECN	COMMENT
$< 1.8 \times 10^{-8}$	90	SAHOO 20	BELL	921 fb^{-1} , $E_{\text{cm}}^{\text{ee}} = 10.6 \text{ GeV}$

Γ_{241} / Γ

$\Gamma(\rho \mu^- \mu^-) / \Gamma_{\text{total}}$

VALUE	CL%	DOCUMENT ID	TECN	COMMENT
$< 4.0 \times 10^{-8}$	90	SAHOO 20	BELL	921 fb^{-1} , $E_{\text{cm}}^{\text{ee}} = 10.6 \text{ GeV}$

Γ_{242} / Γ

• • • We do not use the following data for averages, fits, limits, etc. • • •

$\Gamma(\bar{p} \mu^+ \mu^-) / \Gamma_{\text{total}}$

VALUE	CL%	DOCUMENT ID	TECN	COMMENT
$< 4.4 \times 10^{-7}$	90	AAIJ 13AH	LHCB	1.0 fb^{-1} , $p\bar{p}$ at 7 TeV

Γ_{243} / Γ

• • • We do not use the following data for averages, fits, limits, etc. • • •

$\Gamma(\bar{p} \gamma) / \Gamma_{\text{total}}$
Test of lepton number and baryon number conservation.

VALUE	CL%	DOCUMENT ID	TECN	COMMENT
$< 3.5 \times 10^{-6}$	90	GODANG 99	CLEO	$E_{\text{cm}}^{\text{ee}} = 10.6 \text{ GeV}$

Γ_{244} / Γ

• • • We do not use the following data for averages, fits, limits, etc. • • •

$\Gamma(\bar{p} \pi^0) / \Gamma_{\text{total}}$
Test of lepton number and baryon number conservation.

VALUE	CL%	DOCUMENT ID	TECN	COMMENT
$< 29 \times 10^{-5}$	90	ALBRECHT 92K	ARG	$E_{\text{cm}}^{\text{ee}} = 10 \text{ GeV}$

Γ_{245} / Γ

$\Gamma(\bar{p} \pi^0) / \Gamma_{\text{total}}$
Test of lepton number and baryon number conservation.

VALUE	CL%	DOCUMENT ID	TECN	COMMENT
$< 15 \times 10^{-6}$	90	GODANG 99	CLEO	$E_{\text{cm}}^{\text{ee}} = 10.6 \text{ GeV}$

Γ_{245} / Γ

• • • We do not use the following data for averages, fits, limits, etc. • • •

$< 66 \times 10^{-5}$	90	ALBRECHT 92K	ARG	$E_{\text{cm}}^{\text{ee}} = 10 \text{ GeV}$
-----------------------	----	--------------	-----	--

$\Gamma(\bar{p} 2\pi^0) / \Gamma_{\text{total}}$
Test of lepton number and baryon number conservation.

VALUE	CL%	DOCUMENT ID	TECN	COMMENT
$< 33 \times 10^{-6}$	90	GODANG 99	CLEO	$E_{\text{cm}}^{\text{ee}} = 10.6 \text{ GeV}$

Γ_{246} / Γ

$\Gamma(\bar{p} \eta) / \Gamma_{\text{total}}$
Test of lepton number and baryon number conservation.

VALUE	CL%	DOCUMENT ID	TECN	COMMENT
$< 8.9 \times 10^{-6}$	90	GODANG 99	CLEO	$E_{\text{cm}}^{\text{ee}} = 10.6 \text{ GeV}$

Γ_{247} / Γ

• • • We do not use the following data for averages, fits, limits, etc. • • •

$< 130 \times 10^{-5}$	90	ALBRECHT 92K	ARG	$E_{\text{cm}}^{\text{ee}} = 10 \text{ GeV}$
------------------------	----	--------------	-----	--

$\Gamma(\bar{p} \pi^0 \eta) / \Gamma_{\text{total}}$
Test of lepton number and baryon number conservation.

VALUE	CL%	DOCUMENT ID	TECN	COMMENT
$< 27 \times 10^{-6}$	90	GODANG 99	CLEO	$E_{\text{cm}}^{\text{ee}} = 10.6 \text{ GeV}$

Γ_{248} / Γ

$\Gamma(\Lambda \pi^-) / \Gamma_{\text{total}}$
Test of lepton number and baryon number conservation.

VALUE	CL%	DOCUMENT ID	TECN	COMMENT
$< 0.72 \times 10^{-7}$	90	MIYAZAKI 06	BELL	154 fb^{-1} , $E_{\text{cm}}^{\text{ee}} = 10.6 \text{ GeV}$

Γ_{249} / Γ

$\Gamma(\bar{\Lambda} \pi^-) / \Gamma_{\text{total}}$
Test of lepton number and baryon number conservation.

VALUE	CL%	DOCUMENT ID	TECN	COMMENT
$< 1.4 \times 10^{-7}$	90	MIYAZAKI 06	BELL	154 fb^{-1} , $E_{\text{cm}}^{\text{ee}} = 10.6 \text{ GeV}$

Γ_{250} / Γ

τ -DECAY PARAMETERS

See the related review(s):

τ -Lepton Decay Parameters

$\rho(e \text{ or } \mu)$ PARAMETER

(V-A) theory predicts $\rho = 0.75$.

VALUE	EVTS	DOCUMENT ID	TECN	COMMENT
0.745 ± 0.008 OUR FIT				
0.749 ± 0.008 OUR AVERAGE				
0.742 ± 0.014 ± 0.006	81k	HEISTER	01E ALEP	1991–1995 LEP runs
0.775 ± 0.023 ± 0.020	36k	ABREU	00L DLPH	1992–1995 runs
0.781 ± 0.028 ± 0.018	46k	ACKERSTAFF	99D OPAL	1990–1995 LEP runs
0.762 ± 0.035	54k	ACCIARRI	98R L3	1991–1995 LEP runs
0.731 ± 0.031		¹ ALBRECHT 98	ARG	$E_{\text{cm}}^{\text{ee}} = 9.5\text{--}10.6 \text{ GeV}$
0.72 ± 0.09 ± 0.03		² ABE 97o	SLD	1993–1995 SLC runs
0.747 ± 0.010 ± 0.006	55k	ALEXANDER	97F CLEO	$E_{\text{cm}}^{\text{ee}} = 10.6 \text{ GeV}$
0.79 ± 0.10 ± 0.10	3732	FORD	87B MAC	$E_{\text{cm}}^{\text{ee}} = 29 \text{ GeV}$
0.71 ± 0.09 ± 0.03	1426	BEHRENDIS	85C CLEO	$e^+ e^-$ near $\Upsilon(4S)$
• • • We do not use the following data for averages, fits, limits, etc. • • •				
0.735 ± 0.013 ± 0.008	31k	AMMAR	97B CLEO	Repl. by ALEXANDER 97F
0.794 ± 0.039 ± 0.031	18k	ACCIARRI	96H L3	Repl. by ACCIARRI 98R
0.732 ± 0.034 ± 0.020	8.2k	³ ALBRECHT 95	ARG	$E_{\text{cm}}^{\text{ee}} = 9.5\text{--}10.6 \text{ GeV}$
0.738 ± 0.038		⁴ ALBRECHT 95c	ARG	Repl. by ALBRECHT 98
0.751 ± 0.039 ± 0.022		BUSKULIC	95D ALEP	Repl. by HEISTER 01E
0.742 ± 0.035 ± 0.020	8000	ALBRECHT	90E ARG	$E_{\text{cm}}^{\text{ee}} = 9.4\text{--}10.6 \text{ GeV}$

¹ Combined fit to ARGUS tau decay parameter measurements in ALBRECHT 98, ALBRECHT 95c, ALBRECHT 93g, and ALBRECHT 94E. ALBRECHT 98 use tau pair events of the type $\tau^- \tau^+ \rightarrow (\ell^- \bar{\nu}_\ell \nu_\tau)(\pi^+ \pi^0 \bar{\nu}_\tau)$, and their charged conjugates.
² ABE 97o assume $\eta = 0$ in their fit. Letting η vary in the fit gives a ρ value of $0.69 \pm 0.13 \pm 0.05$.
³ Value is from a simultaneous fit for the ρ and η decay parameters to the lepton energy spectrum. Not independent of ALBRECHT 90E $\rho(e \text{ or } \mu)$ value which assumes $\eta = 0$. Result is strongly correlated with ALBRECHT 95c.
⁴ Combined fit to ARGUS tau decay parameter measurements in ALBRECHT 95c, ALBRECHT 93g, and ALBRECHT 94E.

$\rho(e)$ PARAMETER

(V-A) theory predicts $\rho = 0.75$.

VALUE	EVTS	DOCUMENT ID	TECN	COMMENT
0.747 ± 0.010 OUR FIT				
0.744 ± 0.010 OUR AVERAGE				
0.747 ± 0.019 ± 0.014	44k	HEISTER	01E ALEP	1991–1995 LEP runs
0.744 ± 0.036 ± 0.037	17k	ABREU	00L DLPH	1992–1995 runs
0.779 ± 0.047 ± 0.029	25k	ACKERSTAFF	99D OPAL	1990–1995 LEP runs
0.68 ± 0.04 ± 0.07		¹ ALBRECHT 98	ARG	$E_{\text{cm}}^{\text{ee}} = 9.5\text{--}10.6 \text{ GeV}$

Lepton Particle Listings

 τ

0.71 ± 0.14 ± 0.05	ABE	97o	SLD	1993–1995 SLC runs
0.747 ± 0.012 ± 0.004	34k	ALEXANDER	97F	CLEO $E_{cm}^{ee} = 10.6$ GeV
0.735 ± 0.036 ± 0.020	4.7k	² ALBRECHT	95	ARG $E_{cm}^{ee} = 9.5–10.6$ GeV
0.79 ± 0.08 ± 0.06	3230	³ ALBRECHT	93G	ARG $E_{cm}^{ee} = 9.4–10.6$ GeV
0.64 ± 0.06 ± 0.07	2753	JANSSEN	89	CBAL $E_{cm}^{ee} = 9.4–10.6$ GeV
0.62 ± 0.17 ± 0.14	1823	FORD	87B	MAC $E_{cm}^{ee} = 29$ GeV
0.60 ± 0.13	699	BEHREND	85	CLEO e^+e^- near $\Upsilon(4S)$
0.72 ± 0.10 ± 0.11	594	BACINO	79B	DLCO $E_{cm}^{ee} = 3.5–7.4$ GeV
• • •	We do not use the following data for averages, fits, limits, etc.	• • •		
0.732 ± 0.014 ± 0.009	19k	AMMAR	97B	CLEO Repl. by ALEXANDER 97F
0.793 ± 0.050 ± 0.025		BUSKULIC	95D	ALEP Repl. by HEISTER 01E
0.747 ± 0.045 ± 0.028	5106	ALBRECHT	90E	ARG Repl. by ALBRECHT 95

¹ALBRECHT 98 use tau pair events of the type $\tau^- \tau^+ \rightarrow (\ell^- \bar{\nu}_\ell \nu_\tau)(\pi^+ \pi^0 \bar{\nu}_\tau)$, and their charged conjugates.

²ALBRECHT 95 use tau pair events of the type $\tau^- \tau^+ \rightarrow (\ell^- \bar{\nu}_\ell \nu_\tau)(h^+ h^- h^+ \pi^0 \bar{\nu}_\tau)$ and their charged conjugates.

³ALBRECHT 93G use tau pair events of the type $\tau^- \tau^+ \rightarrow (\mu^- \bar{\nu}_\mu \nu_\tau)(e^+ \nu_e \bar{\nu}_\tau)$ and their charged conjugates.

 $\rho(\mu)$ PARAMETER(V–A) theory predicts $\rho = 0.75$.

VALUE	EVTS	DOCUMENT ID	TECN	COMMENT
0.763 ± 0.020 OUR FIT				
0.770 ± 0.022 OUR AVERAGE				
0.776 ± 0.045 ± 0.019	46k	HEISTER	01E	ALEP 1991–1995 LEP runs
0.999 ± 0.098 ± 0.045	22k	ABREU	00L	DLPH 1992–1995 runs
0.777 ± 0.044 ± 0.016	27k	ACKERSTAFF	99D	OPAL 1990–1995 LEP runs
0.69 ± 0.06 ± 0.06		¹ ALBRECHT	98	ARG $E_{cm}^{ee} = 9.5–10.6$ GeV
0.54 ± 0.28 ± 0.14		ABE	97o	SLD 1993–1995 SLC runs
0.750 ± 0.017 ± 0.045	22k	ALEXANDER	97F	CLEO $E_{cm}^{ee} = 10.6$ GeV
0.76 ± 0.07 ± 0.08	3230	ALBRECHT	93G	ARG $E_{cm}^{ee} = 9.4–10.6$ GeV
0.734 ± 0.055 ± 0.027	3041	ALBRECHT	90E	ARG $E_{cm}^{ee} = 9.4–10.6$ GeV
0.89 ± 0.14 ± 0.08	1909	FORD	87B	MAC $E_{cm}^{ee} = 29$ GeV
0.81 ± 0.13	727	BEHREND	85	CLEO e^+e^- near $\Upsilon(4S)$
• • •	We do not use the following data for averages, fits, limits, etc.	• • •		
0.747 ± 0.048 ± 0.044	13k	AMMAR	97B	CLEO Repl. by ALEXANDER 97F
0.693 ± 0.057 ± 0.028		BUSKULIC	95D	ALEP Repl. by HEISTER 01E

¹ALBRECHT 98 use tau pair events of the type $\tau^- \tau^+ \rightarrow (\ell^- \bar{\nu}_\ell \nu_\tau)(\pi^+ \pi^0 \bar{\nu}_\tau)$, and their charged conjugates.

 $\xi(e \text{ or } \mu)$ PARAMETER(V–A) theory predicts $\xi = 1$.

VALUE	EVTS	DOCUMENT ID	TECN	COMMENT
0.985 ± 0.030 OUR FIT				
0.981 ± 0.031 OUR AVERAGE				
0.986 ± 0.068 ± 0.031	81k	HEISTER	01E	ALEP 1991–1995 LEP runs
0.929 ± 0.070 ± 0.030	36k	ABREU	00L	DLPH 1992–1995 runs
0.98 ± 0.22 ± 0.10	46k	ACKERSTAFF	99D	OPAL 1990–1995 LEP runs
0.70 ± 0.16	54k	ACCIARRI	98R	L3 1991–1995 LEP runs
1.03 ± 0.11		¹ ALBRECHT	98	ARG $E_{cm}^{ee} = 9.5–10.6$ GeV
1.05 ± 0.35 ± 0.04		² ABE	97o	SLD 1993–1995 SLC runs
1.007 ± 0.040 ± 0.015	55k	ALEXANDER	97F	CLEO $E_{cm}^{ee} = 10.6$ GeV
• • •	We do not use the following data for averages, fits, limits, etc.	• • •		
0.94 ± 0.21 ± 0.07	18k	ACCIARRI	96H	L3 Repl. by ACCIARRI 98R
0.97 ± 0.14		³ ALBRECHT	95C	ARG Repl. by ALBRECHT 98
1.18 ± 0.15 ± 0.16		BUSKULIC	95D	ALEP Repl. by HEISTER 01E
0.90 ± 0.15 ± 0.10	3230	⁴ ALBRECHT	93G	ARG $E_{cm}^{ee} = 9.4–10.6$ GeV

¹Combined fit to ARGUS tau decay parameter measurements in ALBRECHT 98, ALBRECHT 95c, ALBRECHT 93G, and ALBRECHT 94E. ALBRECHT 98 use tau pair events of the type $\tau^- \tau^+ \rightarrow (\ell^- \bar{\nu}_\ell \nu_\tau)(\pi^+ \pi^0 \bar{\nu}_\tau)$, and their charged conjugates.

²ABE 97o assume $\eta = 0$ in their fit. Letting η vary in the fit gives a ξ value of $1.02 \pm 0.36 \pm 0.05$.

³Combined fit to ARGUS tau decay parameter measurements in ALBRECHT 95c, ALBRECHT 93G, and ALBRECHT 94E. ALBRECHT 95c uses events of the type $\tau^- \tau^+ \rightarrow (\ell^- \bar{\nu}_\ell \nu_\tau)(h^+ h^- h^+ \pi^0 \bar{\nu}_\tau)$ and their charged conjugates.

⁴ALBRECHT 93G measurement determines $|\xi|$ for the case $\xi(e) = \xi(\mu)$, but the authors point out that other LEP experiments determine the sign to be positive.

 $\xi(e)$ PARAMETER(V–A) theory predicts $\xi = 1$.

VALUE	EVTS	DOCUMENT ID	TECN	COMMENT
0.994 ± 0.040 OUR FIT				
1.00 ± 0.04 OUR AVERAGE				
1.011 ± 0.094 ± 0.038	44k	HEISTER	01E	ALEP 1991–1995 LEP runs
1.01 ± 0.12 ± 0.05	17k	ABREU	00L	DLPH 1992–1995 runs
1.13 ± 0.39 ± 0.14	25k	ACKERSTAFF	99D	OPAL 1990–1995 LEP runs
1.11 ± 0.20 ± 0.08		¹ ALBRECHT	98	ARG $E_{cm}^{ee} = 9.5–10.6$ GeV
1.16 ± 0.52 ± 0.06		ABE	97o	SLD 1993–1995 SLC runs
0.979 ± 0.048 ± 0.016	34k	ALEXANDER	97F	CLEO $E_{cm}^{ee} = 10.6$ GeV
• • •	We do not use the following data for averages, fits, limits, etc.	• • •		
1.03 ± 0.23 ± 0.09		BUSKULIC	95D	ALEP Repl. by HEISTER 01E
¹ ALBRECHT 98 use tau pair events of the type $\tau^- \tau^+ \rightarrow (\ell^- \bar{\nu}_\ell \nu_\tau)(\pi^+ \pi^0 \bar{\nu}_\tau)$, and their charged conjugates.				

 $\xi(\mu)$ PARAMETER(V–A) theory predicts $\xi = 1$.

VALUE	EVTS	DOCUMENT ID	TECN	COMMENT
1.030 ± 0.059 OUR FIT				
1.06 ± 0.06 OUR AVERAGE				
1.030 ± 0.120 ± 0.050	46k	HEISTER	01E	ALEP 1991–1995 LEP runs
1.16 ± 0.19 ± 0.06	22k	ABREU	00L	DLPH 1992–1995 runs
0.79 ± 0.41 ± 0.09	27k	ACKERSTAFF	99D	OPAL 1990–1995 LEP runs
1.26 ± 0.27 ± 0.14		¹ ALBRECHT	98	ARG $E_{cm}^{ee} = 9.5–10.6$ GeV
0.75 ± 0.50 ± 0.14		ABE	97o	SLD 1993–1995 SLC runs
1.054 ± 0.069 ± 0.047	22k	ALEXANDER	97F	CLEO $E_{cm}^{ee} = 10.6$ GeV
• • •	We do not use the following data for averages, fits, limits, etc.	• • •		
1.23 ± 0.22 ± 0.10		BUSKULIC	95D	ALEP Repl. by HEISTER 01E

¹ALBRECHT 98 use tau pair events of the type $\tau^- \tau^+ \rightarrow (\ell^- \bar{\nu}_\ell \nu_\tau)(\pi^+ \pi^0 \bar{\nu}_\tau)$, and their charged conjugates.

 $\eta(e \text{ or } \mu)$ PARAMETER(V–A) theory predicts $\eta = 0$.

VALUE	EVTS	DOCUMENT ID	TECN	COMMENT
0.013 ± 0.020 OUR FIT				
0.015 ± 0.021 OUR AVERAGE				
0.012 ± 0.026 ± 0.004	81k	HEISTER	01E	ALEP 1991–1995 LEP runs
–0.005 ± 0.036 ± 0.037		ABREU	00L	DLPH 1992–1995 runs
0.027 ± 0.055 ± 0.005	46k	ACKERSTAFF	99D	OPAL 1990–1995 LEP runs
0.27 ± 0.14	54k	ACCIARRI	98R	L3 1991–1995 LEP runs
–0.13 ± 0.47 ± 0.15		ABE	97o	SLD 1993–1995 SLC runs
–0.015 ± 0.061 ± 0.062	31k	AMMAR	97B	CLEO $E_{cm}^{ee} = 10.6$ GeV
0.03 ± 0.18 ± 0.12	8.2k	ALBRECHT	95	ARG $E_{cm}^{ee} = 9.5–10.6$ GeV
• • •	We do not use the following data for averages, fits, limits, etc.	• • •		
0.25 ± 0.17 ± 0.11	18k	ACCIARRI	96H	L3 Repl. by ACCIARRI 98R
–0.04 ± 0.15 ± 0.11		BUSKULIC	95D	ALEP Repl. by HEISTER 01E

 $\eta(\mu)$ PARAMETER(V–A) theory predicts $\eta = 0$.

VALUE	EVTS	DOCUMENT ID	TECN	COMMENT
0.094 ± 0.073 OUR FIT				
0.17 ± 0.15 OUR AVERAGE				Error includes scale factor of 1.2.
0.160 ± 0.150 ± 0.060	46k	HEISTER	01E	ALEP 1991–1995 LEP runs
0.72 ± 0.32 ± 0.15		ABREU	00L	DLPH 1992–1995 runs
–0.59 ± 0.82 ± 0.45		¹ ABE	97o	SLD 1993–1995 SLC runs
0.010 ± 0.149 ± 0.171	13k	² AMMAR	97B	CLEO $E_{cm}^{ee} = 10.6$ GeV
• • •	We do not use the following data for averages, fits, limits, etc.	• • •		
0.010 ± 0.065 ± 0.001	27k	³ ACKERSTAFF	99D	OPAL 1990–1995 LEP runs
–0.24 ± 0.23 ± 0.18		BUSKULIC	95D	ALEP Repl. by HEISTER 01E

¹Highly correlated (corr. = 0.92) with ABE 97o $\rho(\mu)$ measurement.

²Highly correlated (corr. = 0.949) with AMMAR 97B $\rho(\mu)$ value.

³ACKERSTAFF 99D result is dominated by a constraint on η from the OPAL measurements of the τ lifetime and $B(\tau^- \rightarrow \mu^- \bar{\nu}_\mu \nu_\tau)$ assuming lepton universality for the total coupling strength.

 $(\delta\xi)(e \text{ or } \mu)$ PARAMETER(V–A) theory predicts $(\delta\xi) = 0.75$.

VALUE	EVTS	DOCUMENT ID	TECN	COMMENT
0.746 ± 0.021 OUR FIT				
0.744 ± 0.022 OUR AVERAGE				
0.776 ± 0.045 ± 0.024	81k	HEISTER	01E	ALEP 1991–1995 LEP runs
0.779 ± 0.070 ± 0.028	36k	ABREU	00L	DLPH 1992–1995 runs
0.65 ± 0.14 ± 0.07	46k	ACKERSTAFF	99D	OPAL 1990–1995 LEP runs
0.70 ± 0.11	54k	ACCIARRI	98R	L3 1991–1995 LEP runs
0.63 ± 0.09		¹ ALBRECHT	98	ARG $E_{cm}^{ee} = 9.5–10.6$ GeV
0.88 ± 0.27 ± 0.04		² ABE	97o	SLD 1993–1995 SLC runs
0.745 ± 0.026 ± 0.009	55k	ALEXANDER	97F	CLEO $E_{cm}^{ee} = 10.6$ GeV
• • •	We do not use the following data for averages, fits, limits, etc.	• • •		
0.81 ± 0.14 ± 0.06	18k	ACCIARRI	96H	L3 Repl. by ACCIARRI 98R
0.65 ± 0.12		³ ALBRECHT	95C	ARG Repl. by ALBRECHT 98
0.88 ± 0.11 ± 0.07		BUSKULIC	95D	ALEP Repl. by HEISTER 01E

¹Combined fit to ARGUS tau decay parameter measurements in ALBRECHT 98, ALBRECHT 95c, ALBRECHT 93G, and ALBRECHT 94E. ALBRECHT 98 use tau pair events of the type $\tau^- \tau^+ \rightarrow (\ell^- \bar{\nu}_\ell \nu_\tau)(\pi^+ \pi^0 \bar{\nu}_\tau)$, and their charged conjugates.

²ABE 97o assume $\eta = 0$ in their fit. Letting η vary in the fit gives a $(\delta\xi)$ value of $0.87 \pm 0.27 \pm 0.04$.

³Combined fit to ARGUS tau decay parameter measurements in ALBRECHT 95c, ALBRECHT 93G, and ALBRECHT 94E. ALBRECHT 95c uses events of the type $\tau^- \tau^+ \rightarrow (\ell^- \bar{\nu}_\ell \nu_\tau)(h^+ h^- h^+ \pi^0 \bar{\nu}_\tau)$ and their charged conjugates.

 $(\delta\xi)(e)$ PARAMETER(V–A) theory predicts $(\delta\xi) = 0.75$.

VALUE	EVTS	DOCUMENT ID	TECN	COMMENT
0.734 ± 0.028 OUR FIT				
0.731 ± 0.029 OUR AVERAGE				
0.778 ± 0.066 ± 0.024	44k	HEISTER	01E	ALEP 1991–1995 LEP runs
0.85 ± 0.12 ± 0.04	17k	ABREU	00L	DLPH 1992–1995 runs
0.72 ± 0.31 ± 0.14	25k	ACKERSTAFF	99D	OPAL 1990–1995 LEP runs
0.56 ± 0.14 ± 0.06		¹ ALBRECHT	98	ARG $E_{cm}^{ee} = 9.5–10.6$ GeV
0.85 ± 0.43 ± 0.08		ABE	97o	SLD 1993–1995 SLC runs
0.720 ± 0.032 ± 0.010	34k	ALEXANDER	97F	CLEO $E_{cm}^{ee} = 10.6$ GeV

• • • We do not use the following data for averages, fits, limits, etc. • • •
 1.11 ± 0.17 ± 0.07 BUSKULIC 95D ALEP Repl. by HEISTER 01E
¹ALBRECHT 98 use tau pair events of the type $\tau^- \tau^+ \rightarrow (\ell^- \bar{\nu}_\ell \nu_\tau)(\pi^+ \pi^0 \bar{\nu}_\tau)$, and their charged conjugates.

($\delta\xi$)(μ) PARAMETER

(V-A) theory predicts ($\delta\xi$) = 0.75.

VALUE	EVTs	DOCUMENT ID	TECN	COMMENT
0.778 ± 0.037 OUR FIT				
0.79 ± 0.04 OUR AVERAGE				
0.786 ± 0.066 ± 0.028	46k	HEISTER 01E	ALEP	1991-1995 LEP runs
0.86 ± 0.13 ± 0.04	22k	ABREU 00L	DLPH	1992-1995 runs
0.63 ± 0.23 ± 0.05	27k	ACKERSTAFF 99D	OPAL	1990-1995 LEP runs
0.73 ± 0.18 ± 0.10		¹ ALBRECHT 98	ARG	$E_{cm}^{ee} = 9.5-10.6$ GeV
0.82 ± 0.32 ± 0.07		ABE 97O	SLD	1993-1995 SLC runs
0.786 ± 0.041 ± 0.032	22k	ALEXANDER 97F	CLEO	$E_{cm}^{ee} = 10.6$ GeV

• • • We do not use the following data for averages, fits, limits, etc. • • •
 0.71 ± 0.14 ± 0.06 BUSKULIC 95D ALEP Repl. by HEISTER 01E
¹ALBRECHT 98 use tau pair events of the type $\tau^- \tau^+ \rightarrow (\ell^- \bar{\nu}_\ell \nu_\tau)(\pi^+ \pi^0 \bar{\nu}_\tau)$, and their charged conjugates.

(ξ)(π) PARAMETER

(V-A) theory predicts (ξ)(π) = 1.

VALUE	EVTs	DOCUMENT ID	TECN	COMMENT
0.993 ± 0.022 OUR FIT				
0.994 ± 0.023 OUR AVERAGE				
0.994 ± 0.020 ± 0.014	27k	HEISTER 01E	ALEP	1991-1995 LEP runs
0.81 ± 0.17 ± 0.02		ABE 97O	SLD	1993-1995 SLC runs
1.03 ± 0.06 ± 0.04	2.0k	COAN 97	CLEO	$E_{cm}^{ee} = 10.6$ GeV

• • • We do not use the following data for averages, fits, limits, etc. • • •
 0.987 ± 0.057 ± 0.027 BUSKULIC 95D ALEP Repl. by HEISTER 01E
 0.95 ± 0.11 ± 0.05 ¹BUSKULIC 94D ALEP 1990+1991 LEP run
¹Superseded by BUSKULIC 95D.

(ξ)(ρ) PARAMETER

(V-A) theory predicts (ξ)(ρ) = 1.

VALUE	EVTs	DOCUMENT ID	TECN	COMMENT
0.994 ± 0.008 OUR FIT				
0.994 ± 0.009 OUR AVERAGE				
0.987 ± 0.012 ± 0.011	59k	HEISTER 01E	ALEP	1991-1995 LEP runs
0.99 ± 0.12 ± 0.04		ABE 97O	SLD	1993-1995 SLC runs
0.995 ± 0.010 ± 0.003	66k	ALEXANDER 97F	CLEO	$E_{cm}^{ee} = 10.6$ GeV
1.022 ± 0.028 ± 0.030	1.7k	¹ ALBRECHT 94E	ARG	$E_{cm}^{ee} = 9.4-10.6$ GeV

• • • We do not use the following data for averages, fits, limits, etc. • • •
 1.045 ± 0.058 ± 0.032 BUSKULIC 95D ALEP Repl. by HEISTER 01E
 1.03 ± 0.11 ± 0.05 ²BUSKULIC 94D ALEP 1990+1991 LEP run
¹ALBRECHT 94E measure the square of this quantity and use the sign determined by ALBRECHT 90I to obtain the quoted result.
²Superseded by BUSKULIC 95D.

(ξ)(a_1) PARAMETER

(V-A) theory predicts (ξ)(a_1) = 1.

VALUE	EVTs	DOCUMENT ID	TECN	COMMENT
1.001 ± 0.027 OUR FIT				
1.002 ± 0.028 OUR AVERAGE				
1.000 ± 0.016 ± 0.024	35k	¹ HEISTER 01E	ALEP	1991-1995 LEP runs
1.02 ± 0.13 ± 0.03	17.2k	ASNER 00	CLEO	$E_{cm}^{ee} = 10.6$ GeV
1.29 ± 0.26 ± 0.11	7.4k	² ACKERSTAFF 97R	OPAL	1992-1994 LEP runs
0.85 ^{+0.15} _{-0.17} ± 0.05		ALBRECHT 95C	ARG	$E_{cm}^{ee} = 9.5-10.6$ GeV
1.25 ± 0.23 ^{+0.15} _{-0.08}	7.5k	ALBRECHT 93C	ARG	$E_{cm}^{ee} = 9.4-10.6$ GeV

• • • We do not use the following data for averages, fits, limits, etc. • • •
 1.08 ^{+0.46} _{-0.41} ^{-0.25} 2.6k ³AKERS 95P OPAL Repl. by ACKERSTAFF 97R
 0.937 ± 0.116 ± 0.064 BUSKULIC 95D ALEP Repl. by HEISTER 01E
¹HEISTER 01E quote $1.000 \pm 0.016 \pm 0.013 \pm 0.020$ where the errors are statistical, systematic, and an uncertainty due to the final state model. We combine the systematic error and model uncertainty.
²ACKERSTAFF 97R obtain this result with a model independent fit to the hadronic structure functions. Fitting with the model of Kuhn and Santamaria (ZPHY **C48**, 445 (1990)) gives $0.87 \pm 0.16 \pm 0.04$, and with the model of Isgur *et al.* (PR **D39**, 1357 (1989)) they obtain $1.20 \pm 0.21 \pm 0.14$.
³AKERS 95P obtain this result with a model independent fit to the hadronic structure functions. Fitting with the model of Kuhn and Santamaria (ZPHY **C48**, 445 (1990)) gives $0.87 \pm 0.27 ^{+0.05} _{-0.06}$, and with the model of Isgur *et al.* (PR **D39**, 1357 (1989)) they obtain $1.10 \pm 0.31 ^{+0.13} _{-0.14}$.

(ξ)(all hadronic modes) PARAMETER

(V-A) theory predicts (ξ) = 1.

VALUE	EVTs	DOCUMENT ID	TECN	COMMENT
0.995 ± 0.007 OUR FIT				
0.997 ± 0.007 OUR AVERAGE				
0.992 ± 0.007 ± 0.008	102k	¹ HEISTER 01E	ALEP	1991-1995 LEP runs
0.997 ± 0.027 ± 0.011	39k	² ABREU 00L	DLPH	1992-1995 runs
1.02 ± 0.13 ± 0.03	17.2k	³ ASNER 00	CLEO	$E_{cm}^{ee} = 10.6$ GeV
1.032 ± 0.031	37k	⁴ ACCIARRI 98R	L3	1991-1995 LEP runs
0.93 ± 0.10 ± 0.04		ABE 97O	SLD	1993-1995 SLC runs

1.29 ± 0.26 ± 0.11	7.4k	⁵ ACKERSTAFF 97R	OPAL	1992-1994 LEP runs
0.995 ± 0.010 ± 0.003	66k	⁶ ALEXANDER 97F	CLEO	$E_{cm}^{ee} = 10.6$ GeV
1.03 ± 0.06 ± 0.04	2.0k	⁷ COAN 97	CLEO	$E_{cm}^{ee} = 10.6$ GeV
1.017 ± 0.039		⁸ ALBRECHT 95C	ARG	$E_{cm}^{ee} = 9.5-10.6$ GeV
1.25 ± 0.23 ^{+0.15} _{-0.08}	7.5k	⁹ ALBRECHT 93C	ARG	$E_{cm}^{ee} = 9.4-10.6$ GeV

• • • We do not use the following data for averages, fits, limits, etc. • • •
 0.970 ± 0.053 ± 0.011 14k ¹⁰ACCIARRI 96H L3 Repl. by ACCIARRI 98R
 1.08 ^{+0.46} _{-0.41} ^{+0.14} _{-0.25} 2.6k ¹¹AKERS 95P OPAL Repl. by ACKERSTAFF 97R
 1.006 ± 0.032 ± 0.019 ¹²BUSKULIC 95D ALEP Repl. by HEISTER 01E
 1.022 ± 0.028 ± 0.030 1.7k ¹³ALBRECHT 94E ARG $E_{cm}^{ee} = 9.4-10.6$ GeV
 0.99 ± 0.07 ± 0.04 ¹⁴BUSKULIC 94D ALEP 1990+1991 LEP run
 1.14 ± 0.34 ^{+0.34} _{-0.17} 3.9k ⁹ALBRECHT 90I ARG Repl. by ALBRECHT 93C

¹HEISTER 01E quote $0.992 \pm 0.007 \pm 0.006 \pm 0.005$ where the errors are statistical, systematic, and an uncertainty due to the final state model. We combine the systematic error and model uncertainty. They use $\tau \rightarrow \pi \nu_\tau$, $\tau \rightarrow K \nu_\tau$, $\tau \rightarrow \rho \nu_\tau$, and $\tau \rightarrow a_1 \nu_\tau$ decays.
²ABREU 00L use $\tau^- \rightarrow h^- \geq 0\pi^0 \nu_\tau$ decays.
³ASNER 00 use $\tau^- \rightarrow \pi^- 2\pi^0 \nu_\tau$ decays.
⁴ACCIARRI 98R use $\tau \rightarrow \pi \nu_\tau$, $\tau \rightarrow K \nu_\tau$, and $\tau \rightarrow \rho \nu_\tau$ decays.
⁵ACKERSTAFF 97R use $\tau \rightarrow a_1 \nu_\tau$ decays.
⁶ALEXANDER 97F use $\tau \rightarrow \rho \nu_\tau$ decays.
⁷COAN 97 use $h^+ h^-$ energy correlations.
⁸Combined fit to ARGUS tau decay parameter measurements in ALBRECHT 95C, ALBRECHT 93G, and ALBRECHT 94E.
⁹Uses $\tau \rightarrow a_1 \nu_\tau$ decays. Replaced by ALBRECHT 95C.
¹⁰ACCIARRI 96H use $\tau \rightarrow \pi \nu_\tau$, $\tau \rightarrow K \nu_\tau$, and $\tau \rightarrow \rho \nu_\tau$ decays.
¹¹AKERS 95P use $\tau \rightarrow a_1 \nu_\tau$ decays.
¹²BUSKULIC 95D use $\tau \rightarrow \pi \nu_\tau$, $\tau \rightarrow \rho \nu_\tau$, and $\tau \rightarrow a_1 \nu_\tau$ decays.
¹³ALBRECHT 94E measure the square of this quantity and use the sign determined by ALBRECHT 90I to obtain the quoted result. Uses $\tau \rightarrow a_1 \nu_\tau$ decays. Replaced by ALBRECHT 95C.
¹⁴BUSKULIC 94D use $\tau \rightarrow \pi \nu_\tau$ and $\tau \rightarrow \rho \nu_\tau$ decays. Superseded by BUSKULIC 95D.

(ξ')(μ) PARAMETER

(V-A) theory predicts (ξ') = 1.

VALUE	EVTs	DOCUMENT ID	TECN	COMMENT
0.22 ± 0.94 ± 0.42	165	BODROV 23	BELL	$E_{cm}^{ee} = 10.6$ GeV

(η)(μ) PARAMETER

(V-A) theory predicts (η)(μ) = 0.

VALUE	EVTs	DOCUMENT ID	TECN	COMMENT
-1.3 ± 1.5 ± 0.8	71k	¹ SHIMIZU 18A	BELL	$\tau^- \rightarrow \nu_\tau \mu^- \bar{\nu}_\mu \gamma$

¹SHIMIZU 18A measurement procedure fits a distribution affected by $\bar{\eta}(\mu)$, $\xi\kappa(\mu)$ and $\eta''(\mu)$, floating $\bar{\eta}(\mu)$ and $\xi\kappa(\mu)$ and fixing $\eta''(\mu) = 0$. The contribution of $\eta''(\mu)$ is suppressed by m_μ/m_τ .

($\xi\kappa$)(e or μ) PARAMETER

(V-A) theory predicts ($\xi\kappa$)(e or μ) = 0.

VALUE	EVTs	DOCUMENT ID	TECN	COMMENT
0.5 ± 0.4 ± 0.2	149k	^{1,2} SHIMIZU 18A	BELL	$\tau^- \rightarrow \nu_\tau e^- \bar{\nu}_e \gamma$ and $\tau^- \rightarrow \nu_\tau \mu^- \bar{\nu}_\mu \gamma$

¹SHIMIZU 18A measurement procedure fits a distribution of radiative tau decays into both electrons and muons affected by $\bar{\eta}(e \text{ or } \mu)$, $\xi\kappa(e \text{ or } \mu)$ and $\eta''(e \text{ or } \mu)$, floating $\bar{\eta}(e \text{ or } \mu)$ and $\xi\kappa(e \text{ or } \mu)$ and fixing $\eta''(e \text{ or } \mu) = 0$. The contribution of $\eta''(e \text{ or } \mu)$ is suppressed by m_e/m_τ for tau decaying to electrons and by m_μ/m_τ for tau decaying to muons.
²Error correlated with SHIMIZU 18A ($\xi\kappa$)(e) and ($\xi\kappa$)(μ) values.

($\xi\kappa$)(e) PARAMETER

(V-A) theory predicts ($\xi\kappa$)(e) = 0.

VALUE	EVTs	DOCUMENT ID	TECN	COMMENT
-0.4 ± 0.8 ± 0.9	78k	^{1,2} SHIMIZU 18A	BELL	$\tau^- \rightarrow \nu_\tau e^- \bar{\nu}_e \gamma$

¹SHIMIZU 18A measurement procedure fits a distribution affected by $\bar{\eta}(e)$, ($\xi\kappa$)(e) and $\eta''(e)$, floating ($\xi\kappa$)(e) and fixing $\bar{\eta}(e) = 0$ and $\eta''(e) = 0$. The contribution of $\eta''(e)$ is suppressed by m_e/m_τ .
²Error correlated with SHIMIZU 18A ($\xi\kappa$)(e or μ) value.

($\xi\kappa$)(μ) PARAMETER

(V-A) theory predicts ($\xi\kappa$)(μ) = 0.

VALUE	EVTs	DOCUMENT ID	TECN	COMMENT
0.8 ± 0.5 ± 0.3	71k	^{1,2} SHIMIZU 18A	BELL	$\tau^- \rightarrow \nu_\tau \mu^- \bar{\nu}_\mu \gamma$

¹SHIMIZU 18A measurement procedure fits a distribution affected by $\bar{\eta}(\mu)$, $\xi\kappa(\mu)$ and $\eta''(\mu)$, floating $\bar{\eta}(\mu)$ and $\xi\kappa(\mu)$ and fixing $\eta''(\mu) = 0$. The contribution of $\eta''(\mu)$ is suppressed by m_μ/m_τ .
²Error correlated with SHIMIZU 18A ($\xi\kappa$)(e or μ) value.

REFERENCES

AAD	23BM PRL 131 151802	G. Aad <i>et al.</i>	(ATLAS Collab.)
ADACHI	23A PRL 130 181803	I. Adachi <i>et al.</i>	(BELLE II Collab.)
ADACHI	23C PR D108 032006	I. Adachi <i>et al.</i>	(BELLE II Collab.)
ANASHIN	23A PPN 54 185	V.V. Anashin <i>et al.</i>	(VEPP-4M KEDR Collab.)
BODROV	23 PRL 131 021801	D. Bodrov <i>et al.</i>	(BELLE Collab.)
ABO	PR D108 032003	D. Bodrov <i>et al.</i>	(BELLE Collab.)
TSUZUKI	JHEP 2306 118	N. Tsuzuki <i>et al.</i>	(BELLE Collab.)

Lepton Particle Listings

τ , Heavy Charged Lepton Searches

BEBEK	87C	PR D36 690	C. Bebek <i>et al.</i>	(CLEO Collab.)
BURCHAT	87	PR D35 27	P.R. Burchat <i>et al.</i>	(Mark II Collab.)
BYLSMA	87	PR D35 2269	B.G. Bylsma <i>et al.</i>	(HRS Collab.)
COFFMAN	87	PR D36 2185	D.M. Coffman <i>et al.</i>	(Mark III Collab.)
DERRICK	87	PL B189 260	M. Derrick <i>et al.</i>	(HRS Collab.)
FORD	87	PR D35 408	W.T. Ford <i>et al.</i>	(MAC Collab.)
FORD	87B	PR D36 1971	W.T. Ford <i>et al.</i>	(MAC Collab.)
GAN	87	PRL 59 411	K.K. Gan <i>et al.</i>	(Mark II Collab.)
GAN	87B	PL B197 561	K.K. Gan <i>et al.</i>	(Mark II Collab.)
AIHARA	86E	PRL 57 1836	H. Aihara <i>et al.</i>	(TPC Collab.)
BARTEL	86D	PL B182 216	W. Bartel <i>et al.</i>	(JADE Collab.)
PDG	86	PL 170B 1	M. Aguilar-Benitez <i>et al.</i>	(CERN, CIT+)
RUCKSTUHL	86	PRL 56 2132	W. Ruckstuhl <i>et al.</i>	(DELCO Collab.)
SCHMIDKE	86	PRL 57 527	W.B. Schmidke <i>et al.</i>	(Mark II Collab.)
YELTON	86	PRL 56 812	J.M. Yelton <i>et al.</i>	(Mark II Collab.)
ALTHOFF	85	ZPHY C26 521	M. Althoff <i>et al.</i>	(TASSO Collab.)
ASH	85B	PRL 55 2118	W.W. Ash <i>et al.</i>	(MAC Collab.)
BALTRUSAITIS	85	PRL 55 1842	R.M. Baltrusaitis <i>et al.</i>	(Mark III Collab.)
BARTEL	85F	PL 161B 188	W. Bartel <i>et al.</i>	(JADE Collab.)
BEHREND	85	PR D32 2469	S. Behrend <i>et al.</i>	(CLEO Collab.)
BELTRAMI	85	PRL 54 1775	I. Beltrami <i>et al.</i>	(HRS Collab.)
BERGER	85	ZPHY C28 1	C. Berger <i>et al.</i>	(PLUTO Collab.)
BURCHAT	85	PRL 54 2489	P.R. Burchat <i>et al.</i>	(Mark II Collab.)
FERNANDEZ	85	PRL 54 1624	E. Fernandez <i>et al.</i>	(MAC Collab.)
MILLS	85	PRL 54 624	G.B. Mills <i>et al.</i>	(DELCO Collab.)
AIHARA	84C	PR D30 2436	H. Aihara <i>et al.</i>	(TPC Collab.)
BEHREND	84	ZPHY C23 103	H.J. Behrend <i>et al.</i>	(CELLO Collab.)
MILLS	84	PRL 52 1944	G.B. Mills <i>et al.</i>	(DELCO Collab.)
BEHREND	83C	PL 127B 270	H.J. Behrend <i>et al.</i>	(CELLO Collab.)
SILVERMAN	83	PR D27 1196	D.J. Silverman, G.L. Shaw	(UCI)
BEHREND	82	PL 114B 202	H.J. Behrend <i>et al.</i>	(CLEO Collab.)
BLOCKER	82B	PRL 48 1586	C.A. Blocker <i>et al.</i>	(Mark II Collab.)
BLOCKER	82D	PL 109B 119	C.A. Blocker <i>et al.</i>	(Mark II Collab.)
FELDMAN	82	PRL 48 66	G.J. Feldman <i>et al.</i>	(Mark II Collab.)
HAYES	82	PR D25 2869	K.G. Hayes <i>et al.</i>	(Mark II Collab.)
BERGER	81B	PL 99B 489	C. Berger <i>et al.</i>	(PLUTO Collab.)
DORFAN	81	PRL 46 215	J.M. Dorfan <i>et al.</i>	(Mark II Collab.)
BRANDELIK	80	PL 92B 199	R. Brandelik <i>et al.</i>	(TASSO Collab.)
ZHOULENTZ	80	PL 96B 214	A.A. Zhoulents <i>et al.</i>	(NOVO)
		SJNP 34 814	A.A. Zhoulents <i>et al.</i>	(NOVO)
		Translated from YAF 34 147L		
BACINO	79B	PRL 42 749	W.J. Bacino <i>et al.</i>	(DELCO Collab.)
KIRKBY	79	SLAC-PUB-2419	J. Kirkby	(SLAC)
		Batavia Lepton Photon Conference.		
BACINO	78B	PRL 41 13	W.J. Bacino <i>et al.</i>	(DELCO Collab.)
		Also Tokyo Conf. 249	J. Kirz	(STON)
		Also PL 96B 214	A.A. Zhoulents <i>et al.</i>	(NOVO)
BRANDELIK	78	PL 73B 109	R. Brandelik <i>et al.</i>	(DASP Collab.)
FELDMAN	78	Tokyo Conf. 777	G.J. Feldman	(SLAC)
JAROS	78	PRL 40 1120	J. Jaros <i>et al.</i>	(LWG Collab.)
PERL	75	PRL 35 1489	M.L. Perl <i>et al.</i>	(LBL, SLAC)

OTHER RELATED PAPERS

DAVIER	06	RMP 78 1043	M. Davier, A. Hocker, Z. Zhang	(LALO, PARIN+)
RAHAL-CAL...	98	JMP A13 695	G. Rahal-Callot	(ETH)
GENTILE	96	PRL 274 287	S. Gentile, M. Pohl	(ROMA)
WEINSTEIN	93	ARNPS 43 457	A.J. Weinstein, R. Stroynowski	(CT, SIMU)
PERL	92	RPP 55 653	M.L. Perl	(SLAC)
PICH	90	MPL A5 1995	A. Pich	(VALE)
BARISH	88	PRPL 157 1	B.C. Barish, R. Stroynowski	(CIT)
GAN	88	JMP A3 531	K.K. Gan, M.L. Perl	(SLAC)
HAYES	88	PR D38 3351	K.G. Hayes, M.L. Perl	(SLAC)
PERL	80	ARNPS 30 299	M.L. Perl	(SLAC)

Heavy Charged Lepton Searches

Charged Heavy Lepton MASS LIMITS

Sequential Charged Heavy Lepton (L^\pm) MASS LIMITS

These experiments assumed that a fourth generation L^\pm decayed to a fourth generation ν_L (or L^0) where ν_L was stable, or that L^\pm decays to a light ν_L via mixing.

See the "Quark and Lepton Compositeness, Searches for" Listings for limits on radiatively decaying excited leptons, i.e. $L^{*0} \rightarrow \ell\gamma$. See the "WIMPs and other Particle Searches" section for heavy charged particle search limits in which the charged particle could be a lepton.

VALUE (GeV)	CL%	DOCUMENT ID	TECN	COMMENT
>100.8	95	ACHARD 01B L3		Decay to νW
>101.9	95	ACHARD 01B L3		$m_L - m_{L^0} > 15$ GeV
••• We do not use the following data for averages, fits, limits, etc. •••				
> 81.5	95	ACKERSTAFF 98c OPAL		Assumed $m_{L^\pm} - m_{L^0} > 8.4$ GeV
> 80.2	95	ACKERSTAFF 98c OPAL		$m_{L^0} > m_{L^\pm}$ and $L^\pm \rightarrow \nu W$
< 48 or > 61	95	¹ ACCIARRI 96G L3		
> 63.9	95	ALEXANDER 96P OPAL		Decay to massless ν 's
> 63.5	95	BUSKULIC 96s ALEP		$m_L - m_{L^0} > 7$ GeV
> 65	95	BUSKULIC 96s ALEP		Decay to massless ν 's
none 10-225		² AHMED 94 CNTR		H1 Collab. at HERA
none 12.6-29.6	95	KIM 91B AMY		Massless ν assumed
> 44.3	95	A KRAWY 90G OPAL		
none 0.5-10	95	³ RILES 90 MRK2		For $(m_{L^0} - m_{L^+}) > 0.25-0.4$ GeV
> 8	95	⁴ STOKER 89 MRK2		For $(m_{L^+} - m_{L^0}) = 0.4$ GeV
> 12	95	⁴ STOKER 89 MRK2		For $m_{L^0} = 0.9$ GeV
none 18.4-27.6	95	⁵ ABE 88 VNS		
> 25.5	95	⁶ ADACHI 88B TOPZ		
none 1.5-22.0	95	BEHREND 88C CELL		
> 41	90	⁷ ALBAJAR 87B UA1		

> 22.5	95	⁸ ADEVA 85 MRKJ		
> 18.0	95	⁹ BARTEL 83 JADE		
none 4-14.5	95	¹⁰ BERGER 81B PLUT		
> 15.5	95	¹¹ BRANDELIK 81 TASS		
> 13.		¹² AZIMOV 80		
> 16.	95	¹³ BARBER 80B CNTR		
> 0.490		¹⁴ ROTHE 69 RVUE		

- ACCIARRI 96G assumes LEP result that the associated neutral heavy lepton mass > 40 GeV.
- The AHMED 94 limits are from a search for neutral and charged sequential heavy leptons at HERA via the decay channels $L^- \rightarrow e\gamma$, $L^- \rightarrow \nu W^-$, $L^- \rightarrow eZ$; and $L^0 \rightarrow \nu\gamma$, $L^0 \rightarrow e^- W^+$, $L^- \rightarrow \nu Z$, where the W decays to $\ell\nu_\ell$, or to jets, and Z decays to $\ell^+ \ell^-$ or jets.
- RILES 90 limits were the result of a special analysis of the data in the case where the mass difference $m_{L^-} - m_{L^0}$ was allowed to be quite small, where L^0 denotes the neutrino into which the sequential charged lepton decays. With a slightly reduced m_{L^\pm} range, the mass difference extends to about 4 GeV.
- STOKER 89 (Mark II at PEP) gives bounds on charged heavy lepton (L^+) mass for the generalized case in which the corresponding neutral heavy lepton (L^0) in the SU(2) doublet is not of negligible mass.
- ABE 88 search for L^+ and $L^- \rightarrow$ hadrons looking for acoplanar jets. The bound is valid for $m_\nu < 10$ GeV.
- ADACHI 88B search for hadronic decays giving acoplanar events with large missing energy. $E_{cm}^{ee} = 52$ GeV.
- Assumes associated neutrino is approximately massless.
- ADEVA 85 analyze one-isolated-muon data and sensitive to $\tau < 10$ nanosec. Assume $B(\text{lepton}) = 0.30$. $E_{cm} = 40-47$ GeV.
- BARTEL 83 limit is from PETRA e^+e^- experiment with average $E_{cm} = 34.2$ GeV.
- BERGER 81B is DESY DORIS and PETRA experiment. Looking for $e^+e^- \rightarrow L^+L^-$.
- BRANDELIK 81 is DESY-PETRA experiment. Looking for $e^+e^- \rightarrow L^+L^-$.
- AZIMOV 80 estimated probabilities for $M + N$ type events in $e^+e^- \rightarrow L^+L^-$ deducing semi-hadronic decay multiplicities of L from e^+e^- annihilation data at $E_{cm} = (2/3)m_L$. Obtained above limit comparing these with e^+e^- data (BRANDELIK 80).
- BARBER 80B looked for $e^+e^- \rightarrow L^+L^-$, $L \rightarrow \nu^+ X$ with MARK-J at DESY-PETRA.
- ROTHE 69 examines previous data on μ pair production and π and K decays.

Stable Charged Heavy Lepton (L^\pm) MASS LIMITS

VALUE (GeV)	CL%	DOCUMENT ID	TECN
>102.6	95	ACHARD 01B L3	
••• We do not use the following data for averages, fits, limits, etc. •••			
> 28.2	95	¹⁵ ADACHI 90c TOPZ	
none 18.5-42.8	95	AKRAWY 90a OPAL	
> 26.5	95	DECAMP 90f ALEP	
none $m_\mu - 36.3$	95	SODERSTROM90 MRK2	

¹⁵ ADACHI 90c put lower limits on the mass of stable charged particles with electric charge Q satisfying $2/3 < Q/e < 4/3$ and with spin 0 or 1/2. We list here the special case for a stable charged heavy lepton.

Charged Long-Lived Heavy Lepton MASS LIMITS

VALUE (GeV)	CL%	DOCUMENT ID	TECN	CHG	COMMENT
••• We do not use the following data for averages, fits, limits, etc. •••					
>574	95	CHATRCHYAN13AB CMS			Leptons singlet model
>102.0	95	ABBIENDI 03L OPAL			pair produced in e^+e^-
> 0.1		¹⁶ ANSORGE 73B HBC			Long-lived
none 0.55-4.5		¹⁷ BUSHNIN 73 CNTR			Long-lived
none 0.2-0.92		¹⁸ BARNA 68 CNTR			Long-lived
none 0.97-1.03		¹⁸ BARNA 68 CNTR			Long-lived

- ANSORGE 73B looks for electron pair production and electron-like Bremsstrahlung.
- BUSHNIN 73 is SERPUKHOV 70 GeV p experiment. Masses assume mean life above 7×10^{-10} and 3×10^{-8} respectively. Calculated from cross section (see "Charged Quasi-Stable Lepton Production Differential Cross Section" below) and 30 GeV muon pair production data.
- BARNA 68 is SLAC photoproduction experiment.

Doubly-Charged Heavy Lepton MASS LIMITS

VALUE (GeV)	CL%	DOCUMENT ID	TECN	CHG
••• We do not use the following data for averages, fits, limits, etc. •••				
none 1-9 GeV	90	¹⁹ CLARK 81 SPEC		++
¹⁹ CLARK 81 is FNAL experiment with 209 GeV muons. Bounds apply to μp which couples with full weak strength to muon. See also section on "Doubly-Charged Lepton Production Cross Section."				

Doubly-Charged Lepton Production Cross Section (μN Scattering)

VALUE (cm ²)	EVTS	DOCUMENT ID	TECN	CHG
••• We do not use the following data for averages, fits, limits, etc. •••				
< $6. \times 10^{-38}$	0	²⁰ CLARK 81 SPEC		++
²⁰ CLARK 81 is FNAL experiment with 209 GeV muon. Looked for $\mu^+ X$, $\bar{\mu}^0 X$, $\bar{\mu}^0 \rightarrow \mu^+ \mu^- \bar{\nu}_\mu$ and $\mu^+ n \rightarrow \mu^+ X$, $\mu^+ p \rightarrow 2\mu^+ \nu_\mu$. Above limits are for $\sigma \times BR$ taken from their mass-dependence plot figure 2.				

Lepton Particle Listings

Heavy Charged Lepton Searches, Neutrino Properties

REFERENCES FOR Heavy Charged Lepton Searches

CHATRCHYAN	13AB	JHEP 1307 122	S. Chatrchyan et al.	(CMS Collab.)
Also		JHEP 2211 149 (errat.)	S. Chatrchyan et al.	(CMS Collab.)
ABBIENDI	03L	PL B572 8	G. Abbiendi et al.	(OPAL Collab.)
ACHARD	01B	PL B517 75	P. Achard et al.	(L3 Collab.)
ACKERSTAFF	98C	EPJ C1 45	K. Ackerstaff et al.	(OPAL Collab.)
ACCIARRI	96G	PL B377 304	M. Acciarri et al.	(L3 Collab.)
ALEXANDER	96P	PL B385 433	G. Alexander et al.	(OPAL Collab.)
BUSKULIC	96S	PL B384 439	D. Buskulic et al.	(ALEPH Collab.)
AHMED	94	PL B340 205	T. Ahmed et al.	(HI Collab.)
KIM	91B	UJMP A6 2583	G.N. Kim et al.	(AMY Collab.)
ADACHI	90C	PL B244 352	I. Adachi et al.	(TOPAZ Collab.)
AKRAWY	90G	PL B240 250	M.Z. Akrawy et al.	(OPAL Collab.)
AKRAWY	90O	PL B252 290	M.Z. Akrawy et al.	(OPAL Collab.)
DECAMP	90F	PL B236 511	D. Decamp et al.	(ALEPH Collab.)
RILES	90	PR D42 1	K. Riles et al.	(Mark II Collab.)
SODERSTROM	90	PR L64 2980	E. Soderstrom et al.	(Mark II Collab.)
STOKER	89	PR D39 1811	D.P. Stoker et al.	(Mark II Collab.)
ABE	88	PR L61 915	K. Abe et al.	(VENUS Collab.)
ADACHI	88B	PR D37 1339	I. Adachi et al.	(TOPAZ Collab.)
BEHREND	88C	ZPHY C41 7	H.J. Behrend et al.	(CELLO Collab.)
ALBAJAR	87B	PL B185 241	C. Albajar et al.	(UA1 Collab.)
ADEVA	85	PL B152B 439	B. Adeva et al.	(Mark-J Collab.)
Also		PRPL 109 131	B. Adeva et al.	(Mark-J Collab.)
BARTEL	83	PL B123B 353	W. Bartel et al.	(JADE Collab.)
BERGER	81B	PL B98 489	R. Berger et al.	(PLUTO Collab.)
BRANDELIK	81	PL B98 163	R. Brandelik et al.	(TASSO Collab.)
CLARK	81	PR L46 299	A.R. Clark et al.	(Mark II Collab.)
Also		PR D25 2762	W.H. Smith et al.	(UCB, LBL, FNAL+)
AZIMOV	80	JETPL 32 664	Y.I. Azimov, V.A. Khoze	(LBL, FNAL, PRIN)
Also		Translated from ZETFP 32 677		(PNPI)
BARBER	80B	PR L45 1904	D.P. Barber et al.	(Mark-J Collab.)
BRANDELIK	80	PL B98 199	R. Brandelik et al.	(TASSO Collab.)
ANSORGE	73B	PR D7 26	R.E. Ansorge et al.	(CAVE)
BUSHNIN	73	NP B58 476	Y.B. Bushnin et al.	(SERP)
Also		PL B42B 136	S.V. Golovkin et al.	(SERP)
ROTHE	69	NP B10 241	K.W. Rothe, A.M. Wolsky	(PENN)
BARNA	68	PR L73 1391	A. Barna et al.	(SLAC, STAN)

OTHER RELATED PAPERS

PERL	81	SLAC-PUB-2752	M.L. Perl	(SLAC)
Physics in		Collision Conference.		

Neutrino Properties

NEUTRINO PROPERTIES

Revised July 2023 by P. Vogel (Caltech) and A. Piepke (University of Alabama).

The Neutrino Properties Listings concern measurements of various properties of neutrinos. Nearly all of the measurements, so far only limits, actually concern superpositions of the mass eigenstates ν_i , which are in turn related to the weak eigenstates ν_ℓ , via the neutrino mixing matrix

$$|\nu_\ell\rangle = \sum_i U_{\ell i} |\nu_i\rangle.$$

In the analogous case of quark mixing via the CKM matrix, the smallness of the off-diagonal terms (small mixing angles) permits a “dominant eigenstate” approximation. However, the results of neutrino oscillation searches show that the mixing matrix contains two large mixing angles and a third angle that is not exceedingly small. We cannot therefore associate any particular state $|\nu_i\rangle$ with any particular lepton label e, μ or τ . Nevertheless, note that in the standard labeling the $|\nu_1\rangle$ has the largest $|\nu_e\rangle$ component ($\sim 2/3$), $|\nu_2\rangle$ contains $\sim 1/3$ of the $|\nu_e\rangle$ component and $|\nu_3\rangle$ contains only a small $\sim 2.5\%$ $|\nu_e\rangle$ component.

Neutrinos are produced in weak decays with a definite lepton flavor, and are typically detected by the charged current weak interaction again associated with a specific lepton flavor. Hence, the listings for the neutrino mass that follow are separated into the three associated charged lepton categories. Other properties (mean lifetime, magnetic moment, charge and

charge radius) are no longer separated this way. If needed, the associated lepton flavor is reported in the footnotes.

Measured quantities (mass-squared, magnetic moments, mean lifetimes, etc.) all depend upon the mixing parameters $|U_{\ell i}|^2$, but to some extent also on experimental conditions (e.g., on energy resolution). Many of these observables, in particular mass-squared, cannot distinguish between Dirac and Majorana neutrinos and are unaffected by CP phases.

Direct neutrino mass measurements are usually based on the analysis of the kinematics of charged particles (leptons, pions) emitted together with neutrinos (flavor states) in various weak decays. The most sensitive neutrino mass measurement to date, involving electron type antineutrinos, is based on fitting the shape of the beta spectrum. The quantity $m_{\nu_e}^{2(eff)} = \sum_i |U_{ei}|^2 m_{\nu_i}^2$ is determined or constrained, where the sum is over all mass eigenvalues m_{ν_i} that are too close together to be resolved experimentally. (The quantity $m_{\nu_e}^{eff} \equiv \sqrt{m_{\nu_e}^{2(eff)}}$ is often denoted $\langle m_\beta \rangle$ in the literature.) If the energy resolution is better than $\Delta m_{ij}^2 \equiv m_{\nu_i}^2 - m_{\nu_j}^2$, the corresponding heavier m_{ν_i} and mixing parameter could be determined by fitting the resulting spectral anomaly (step or kink).

The dependence of m_{ν_e} on the mass of the lightest neutrino is shown in Fig. 14.11 of the *Neutrino Masses, Mixing, and Oscillations* review. In the case of inverted ordering there is a minimum possible value of $m_{\nu_e}^{eff}$, approximately $\sqrt{(\Delta m_{32}^2)} \sim 50$ meV. If $m_{\nu_e}^{eff}$ is found to be larger than this value, it is impossible, based on this information only, to decide which ordering is realized in nature. On the other hand, if the $m_{\nu_e}^{eff}$ is less than ~ 50 meV, only the normal mass ordering is possible.

A limit on $m_{\nu_e}^{2(eff)}$ implies an upper limit on the minimum value m_{min}^2 of $m_{\nu_i}^2$, independent of the mixing parameters U_{ei} : $m_{min}^2 \leq m_{\nu_e}^{2(eff)}$. However, if and when the value of $m_{\nu_e}^{2(eff)}$ is determined then its combination with the results derived from neutrino oscillations that give us the values of the neutrino mass-squared differences $\Delta m_{ij}^2 \equiv m_i^2 - m_j^2$, including eventually also their signs, and the mixing parameters $|U_{ei}|^2$, the individual neutrino mass squares $m_{\nu_j}^2 = m_{\nu_e}^{2(eff)} - \sum_i |U_{ei}|^2 \Delta m_{ij}^2$ can be determined.

So far solar, reactor, atmospheric and accelerator neutrino oscillation experiments can be consistently described using three active neutrino flavors, i.e. two mass splittings and three mixing angles. However, several experiments with radioactive sources, reactors, and accelerators imply the possible existence of one or more non-interacting, i.e. sterile, neutrino species that might be observable since they couple, albeit weakly, to the flavor neutrinos $|\nu_l\rangle$. In that case, the neutrino mixing matrix would be $n \times n$ unitary matrix with $n > 3$.

Combined three neutrino analyses determine the squared mass differences and all three mixing angles to within reasonable accuracy. For given $|\Delta m_{ij}^2|$ a limit on $m_{\nu_e}^{2(eff)}$ from beta decay defines an upper limit on the maximum value m_{max} of m_{ν_i} : $m_{max}^2 \leq m_{\nu_e}^{2(eff)} + \sum_{i < j} |\Delta m_{ij}^2|$. The analysis of the low energy

See key on page 1171

Lepton Particle Listings

Neutrino Properties

beta decay of tritium, combined with the oscillation results, thus limits *all* active neutrino masses. Traditionally, experimental neutrino mass limits obtained from pion decay $\pi^+ \rightarrow \mu^+ + \nu_\mu$ or the shape of the spectrum of decay products of the τ lepton did not distinguish between flavor and mass eigenstates. These results are reported as limits of the μ and τ based neutrino mass. After the determination of the $|\Delta m_{ij}^2|$'s and the mixing angles θ_{ij} , the corresponding neutrino mass limits are no longer competitive with those derived from low energy beta decays.

The spread of arrival times of the neutrinos from SN1987A, coupled with the measured neutrino energies, provided a time-of-flight limit on a quantity similar to $\langle m_\beta \rangle \equiv \sqrt{m_{\nu_e}^{2(eff)}}$. This statement, clothed in various degrees of sophistication, has been the basis for a very large number of papers. The resulting limits, however, are no longer comparable with the limits from tritium beta decay.

Constraint, or eventually a value, of the sum of the neutrino masses m_{tot} can be determined from the analysis of the cosmic microwave background anisotropy, combined with the galaxy redshift surveys and other data. These limits are reported in a separate table (Sum of Neutrino Masses, m_{tot}). Obviously, m_{tot} represents an upper limit for all m_i values. Note that many reported m_{tot} limits are considerably more stringent than the listed $m_{\nu_e}^{eff}$ limits. Discussion concerning the model dependence of the m_{tot} limit is continuing.

$\bar{\nu}$ MASS (electron based)

Those limits given below are for the square root of $m_{\nu_e}^{2(eff)} \equiv \sum_i |U_{ei}|^2 m_{\nu_i}^2$. Limits that come from the kinematics of ${}^3\text{H} \beta^- \bar{\nu}$ decay are the square roots of the limits for $m_{\nu_e}^{2(eff)}$. Obtained from the measurements reported in the Listings for " $\bar{\nu}$ Mass Squared," below.

VALUE (eV)	CL%	DOCUMENT ID	TECN	COMMENT
< 0.8	90	1 AKER	22	SPEC ${}^3\text{H} \beta$ decay
• • • We do not use the following data for averages, fits, limits, etc. • • •				
<155	90	2 ESFAHANI	23	CRES ${}^3\text{H} \beta$ decay
< 1.1	90	3 AKER	19	SPEC ${}^3\text{H} \beta$ decay
< 2.05	95	4 ASEEV	11	SPEC ${}^3\text{H} \beta$ decay
< 5.8	95	5 PAGLIAROLI	10	ASTR SN1987A
< 2.3	95	6 KRAUS	05	SPEC ${}^3\text{H} \beta$ decay
< 21.7	90	7 ARNABOLDI	03A	BOLO ${}^{187}\text{Re} \beta$ decay
< 5.7	95	8 LOREDO	02	ASTR SN1987A
< 2.5	95	9 LOBASHEV	99	SPEC ${}^3\text{H} \beta$ decay
< 2.8	95	10 WEINHEIMER	99	SPEC ${}^3\text{H} \beta$ decay
< 4.35	95	11 BELESEV	95	SPEC ${}^3\text{H} \beta$ decay
< 12.4	95	12 CHING	95	SPEC ${}^3\text{H} \beta$ decay
< 92	95	13 HIDDEMANN	95	SPEC ${}^3\text{H} \beta$ decay
15 \pm^{+32}_{-15}		HIDDEMANN	95	SPEC ${}^3\text{H} \beta$ decay
< 19.6	95	KERNAN	95	ASTR SN 1987A
< 7.0	95	14 STOEFFL	95	SPEC ${}^3\text{H} \beta$ decay
< 7.2	95	15 WEINHEIMER	93	SPEC ${}^3\text{H} \beta$ decay
< 11.7	95	16 HOLZSCHUH	92B	SPEC ${}^3\text{H} \beta$ decay
< 13.1	95	17 KAWAKAMI	91	SPEC ${}^3\text{H} \beta$ decay
< 9.3	95	18 ROBERTSON	91	SPEC ${}^3\text{H} \beta$ decay
< 14	95	AVIGNONE	90	ASTR SN 1987A
< 16		SPERGEL	88	ASTR SN 1987A
17 to 40		19 BORIS	87	SPEC ${}^3\text{H} \beta$ decay

1 AKER 22 derive an upper limit on the kinematical neutrino mass using Tritium β -decay and the KATRIN spectrometer. The constraint is based on combining the first two science runs. Supersedes AKER 19.

2 ESFAHANI 23 report the first continuous-spectrum measurement of ${}^3\text{H} \beta$ decay, using cyclotron radiation emission spectroscopy (CRES) and a small demonstration detector. The energy resolution at the endpoint is demonstrated using ${}^{83m}\text{Kr}$ and a kinematical neutrino mass limit derived from the spectral shape. A frequentist analysis obtained a limit of <15.2 eV.

- 3 AKER 19 report a neutrino mass limit, derived from the first month of data collected by the KATRIN tritium endpoint experiment. The analysis of the electron kinematics shows no evidence for neutrino mass. The quoted result is based on a frequentist analysis of the data following the method described in LOKHOV 15. Using the method of Feldman and Cousins, the derived upper limit is < 0.8 eV at 90% C.L. Superseded by AKER 22.
- 4 ASEEV 11 report the analysis of the entire beta endpoint data, taken with the Troitsk integrating electrostatic spectrometer between 1997 and 2002 (some of the earlier runs were rejected), using a windowless gaseous tritium source. The fitted value of m_ν , based on the method of Feldman and Cousins, is obtained from the upper limit of the fit for m_ν^2 . Previous analysis problems were resolved by careful monitoring of the tritium gas column density. Supersedes LOBASHEV 99 and BELESEV 95.
- 5 PAGLIAROLI 10 is critical of the likelihood method used by LOREDO 02.
- 6 KRAUS 05 is a continuation of the work reported in WEINHEIMER 99. This result represents the final analysis of data taken from 1997 to 2001. Various sources of systematic uncertainties have been identified and quantified. The background has been reduced compared to the initial running period. A spectral anomaly at the endpoint, reported in LOBASHEV 99, was not observed.
- 7 ARNABOLDI 03A *et al.* report kinematical neutrino mass limit using β -decay of ${}^{187}\text{Re}$. Bolometric AgReO₄ micro-calorimeters are used. Mass bound is substantially weaker than those derived from tritium β -decays but has different systematic uncertainties.
- 8 LOREDO 02 updates LOREDO 89.
- 9 LOBASHEV 99 report a new measurement which continues the work reported in BELESEV 95. This limit depends on phenomenological fit parameters used to derive their best fit to m_ν^2 , making unambiguous interpretation difficult. See the footnote under " $\bar{\nu}$ Mass Squared."
- 10 WEINHEIMER 99 presents two analyses which exclude the spectral anomaly and result in an acceptable m_ν^2 . We report the most conservative limit, but the other is nearly the same. See the footnote under " $\bar{\nu}$ Mass Squared."
- 11 BELESEV 95 (Moscow) use an integral electrostatic spectrometer with adiabatic magnetic collimation and a gaseous tritium source. A fit to a normal Kurie plot above 18300-18350 eV (to avoid a low-energy anomaly) plus a monochromatic line 7-15 eV below the endpoint yields $m_\nu^2 = -4.1 \pm 10.9$ eV², leading to this Bayesian limit.
- 12 CHING 95 quotes results previously given by SUN 93; no experimental details are given. A possible explanation for consistently negative values of m_ν^2 is given.
- 13 HIDDEMANN 95 (Munich) experiment uses atomic tritium embedded in a metal-dioxide lattice. Bayesian limit calculated from the weighted mean $m_\nu^2 = 221 \pm 4244$ eV² from the two runs listed below.
- 14 STOEFFL 95 (LLNL) result is the Bayesian limit obtained from the m_ν^2 errors given below but with m_ν^2 set equal to 0. The anomalous endpoint accumulation leads to a value of m_ν^2 which is negative by more than 5 standard deviations.
- 15 WEINHEIMER 93 (Mainz) is a measurement of the endpoint of the tritium β spectrum using an electrostatic spectrometer with a magnetic guiding field. The source is molecular tritium frozen onto an aluminum substrate.
- 16 HOLZSCHUH 92b (Zurich) result is obtained from the measurement $m_\nu^2 = -24 \pm 48 \pm 61$ (1 σ errors), in eV², using the PDG prescription for conversion to a limit in m_ν .
- 17 KAWAKAMI 91 (Tokyo) experiment uses tritium-labeled arachidic acid. This result is the Bayesian limit obtained from the m_ν^2 limit with the errors combined in quadrature. This was also done in ROBERTSON 91, although the authors report a different procedure.
- 18 ROBERTSON 91 (LANL) experiment uses gaseous molecular tritium. The result is in strong disagreement with the earlier claims by the ITEP group [LUBIMOV 80, BORIS 87 (+BORIS 88 erratum)] that m_ν lies between 17 and 40 eV. However, the probability of a positive m^2 is only 3% if statistical and systematic error are combined in quadrature.
- 19 See also comment in BORIS 87B and erratum in BORIS 88.

$\bar{\nu}$ MASS SQUARED (electron based)

Given troubling systematics which result in improbably negative estimates of $m_{\nu_e}^{2(eff)} \equiv \sum_i |U_{ei}|^2 m_{\nu_i}^2$, in many experiments, we use only KRAUS 05, LOBASHEV 99, and AKER 22 for our average.

VALUE (eV ²)	DOCUMENT ID	TECN	COMMENT
0.08 ± 0.30 OUR AVERAGE			
0.1 ± 0.3	1 AKER	22	SPEC ${}^3\text{H} \beta$ decay
- 0.67 ± 2.53	2 ASEEV	11	SPEC ${}^3\text{H} \beta$ decay
- 0.6 ± 2.2 ± 2.1	3 KRAUS	05	SPEC ${}^3\text{H} \beta$ decay
• • • We do not use the following data for averages, fits, limits, etc. • • •			
- 1.0 ± 0.9	4 AKER	19	SPEC ${}^3\text{H} \beta$ decay
- 1.9 ± 3.4 ± 2.2	5 LOBASHEV	99	SPEC ${}^3\text{H} \beta$ decay
- 3.7 ± 5.3 ± 2.1	6 WEINHEIMER	99	SPEC ${}^3\text{H} \beta$ decay
- 22 ± 4.8	7 BELESEV	95	SPEC ${}^3\text{H} \beta$ decay
129 ± 6010	8 HIDDEMANN	95	SPEC ${}^3\text{H} \beta$ decay
313 ± 5994	8 HIDDEMANN	95	SPEC ${}^3\text{H} \beta$ decay
-130 ± 20 ± 15	9 STOEFFL	95	SPEC ${}^3\text{H} \beta$ decay
- 31 ± 75 ± 48	10 SUN	93	SPEC ${}^3\text{H} \beta$ decay
- 39 ± 34 ± 15	11 WEINHEIMER	93	SPEC ${}^3\text{H} \beta$ decay
- 24 ± 48 ± 61	12 HOLZSCHUH	92B	SPEC ${}^3\text{H} \beta$ decay
- 65 ± 85 ± 65	13 KAWAKAMI	91	SPEC ${}^3\text{H} \beta$ decay
-147 ± 68 ± 41	14 ROBERTSON	91	SPEC ${}^3\text{H} \beta$ decay

1 AKER 22 report results from the analysis of the Tritium β spectrum using the combined data set collected by the KATRIN experiment in the first two science runs. Supersedes AKER 19.

Lepton Particle Listings

Neutrino Properties

- ² ASEEV 11 report the analysis of the entire beta endpoint data, taken with the Troitsk integrating electrostatic spectrometer between 1997 and 2002, using a windowless gaseous tritium source. The analysis does not use the two additional fit parameters (see LOBASHEV 99) for a step-like structure near the endpoint. Using only the runs where the tritium gas column density was carefully monitored the need for such parameters was eliminated. Supersedes LOBASHEV 99 and BELESEV 95.
- ³ KRAUS 05 is a continuation of the work reported in WEINHEIMER 99. This result represents the final analysis of data taken from 1997 to 2001. Problems with significantly negative squared neutrino masses, observed in some earlier experiments, have been resolved in this work.
- ⁴ AKER 19 use the first month of data collected by the KATRIN experiment to determine m_{ν}^2 . The result is consistent with a neutrino mass of zero and is used to place a limit on m_{ν} . Superseded by AKER 22.
- ⁵ LOBASHEV 99 report a new measurement which continues the work reported in BELESEV 95. The data were corrected for electron trapping effects in the source, eliminating the dependence of the fitted neutrino mass on the fit interval. The analysis assuming a pure beta spectrum yields significantly negative fitted $m_{\nu}^2 \approx -(20-10) \text{ eV}^2$. This problem is attributed to a discrete spectral anomaly of about 6×10^{-11} intensity with a time-dependent energy of 5–15 eV below the endpoint. The data analysis accounts for this anomaly by introducing two extra phenomenological fit parameters resulting in a best fit of $m_{\nu}^2 = -1.9 \pm 3.4 \pm 2.2 \text{ eV}^2$ which is used to derive a neutrino mass limit. However, the introduction of phenomenological fit parameters which are correlated with the derived m_{ν}^2 limit makes unambiguous interpretation of this result difficult.
- ⁶ WEINHEIMER 99 is a continuation of the work reported in WEINHEIMER 93. Using a lower temperature of the frozen tritium source eliminated the dewetting of the T_2 film, which introduced a dependence of the fitted neutrino mass on the fit interval in the earlier work. An indication for a spectral anomaly reported in LOBASHEV 99 has been seen, but its time dependence does not agree with LOBASHEV 99. Two analyses, which exclude the spectral anomaly either by choice of the analysis interval or by using a particular data set which does not exhibit the anomaly, result in acceptable m_{ν}^2 fits and are used to derive the neutrino mass limit published by the authors. We list the most conservative of the two.
- ⁷ BELESEV 95 (Moscow) use an integral electrostatic spectrometer with adiabatic magnetic collimation and a gaseous tritium source. This value comes from a fit to a normal Kurie plot above 18300–18350 eV (to avoid a low-energy anomaly), including the effects of an apparent peak 7–15 eV below the endpoint.
- ⁸ HIDDEMANN 95 (Munich) experiment uses atomic tritium embedded in a metal-dioxide lattice. They quote measurements from two data sets.
- ⁹ STOEFFL 95 (LLNL) uses a gaseous source of molecular tritium. An anomalous pileup of events at the endpoint leads to the negative value for m_{ν}^2 . The authors acknowledge that “the negative value for the best fit of m_{ν}^2 has no physical meaning” and discuss possible explanations for this effect.
- ¹⁰ SUN 93 uses a tritiated hydrocarbon source. See also CHING 95.
- ¹¹ WEINHEIMER 93 (Mainz) is a measurement of the endpoint of the tritium β spectrum using an electrostatic spectrometer with a magnetic guiding field. The source is molecular tritium frozen onto an aluminum substrate.
- ¹² HOLZSCHUH 92B (Zurich) source is a monolayer of tritiated hydrocarbon.
- ¹³ KAWAKAMI 91 (Tokyo) experiment uses tritium-labeled arachidic acid.
- ¹⁴ ROBERTSON 91 (LANL) experiment uses gaseous molecular tritium. The result is in strong disagreement with the earlier claims by the ITEP group [LUBIMOV 80, BORIS 87 (+ BORIS 88 erratum)] that m_{ν} lies between 17 and 40 eV. However, the probability of a positive m_{ν}^2 is only 3% if statistical and systematic error are combined in quadrature.

ν MASS (electron based)

These are measurement of m_{ν} (in contrast to m_{τ} , given above). The masses can be different for a Dirac neutrino in the absence of *CPT* invariance. The possible distinction between ν and $\bar{\nu}$ properties is usually ignored elsewhere in these Listings.

VALUE (eV)	CL%	DOCUMENT ID	TECN	COMMENT
<460	68	YASUMI 94	CNTR	¹⁶³ Ho decay
<225	95	SPRINGER 87	CNTR	¹⁶³ Ho decay

ν MASS (muon based)

Limits given below are for the square root of $m_{\nu_{\mu}}^{2(\text{eff})} \equiv \sum_i |U_{\tau i}|^2 m_{\nu_i}^2$.

In some of the COSM papers listed below, the authors did not distinguish between weak and mass eigenstates.

OUR EVALUATION is based on OUR AVERAGE for the π^{\pm} mass and the ASSAMAGAN 96 value for the muon momentum for the π^{\pm} decay at rest. The limit is calculated using the unified classical analysis of FELDMAN 98 for a Gaussian distribution near a physical boundary. WARNING: since $m_{\nu_{\mu}}^{2(\text{eff})}$ is calculated from the differences of large numbers, it and the corresponding limits are extraordinarily sensitive to small changes in the pion mass, the decay muon momentum, and their errors. For example, the limits obtained using JECKELMANN 94, LENZ 98, and the weighted averages are 0.15, 0.29, and 0.19 MeV, respectively.

VALUE (MeV)	CL%	DOCUMENT ID	TECN	COMMENT
<0.19 (CL = 90%) OUR EVALUATION				
<0.17	90	1 ASSAMAGAN 96	SPEC	$m_{\nu}^2 = -0.016 \pm 0.023$

• • • We do not use the following data for averages, fits, limits, etc. • • •

<0.15		² DOLGOV 95	COSM	Nucleosynthesis
<0.48		³ ENQVIST 93	COSM	Nucleosynthesis
<0.3		⁴ FULLER 91	COSM	Nucleosynthesis
<0.42		⁴ LAM 91	COSM	Nucleosynthesis
<0.50	90	⁵ ANDERHUB 82	SPEC	$m_{\nu}^2 = -0.14 \pm 0.20$
<0.65	90	CLARK 74	ASPK	$K_{\mu 3}$ decay

¹ ASSAMAGAN 96 measurement of ρ_{μ} from $\pi^+ \rightarrow \mu^+ \nu$ at rest combined with JECKELMANN 94 Solution B pion mass yields $m_{\nu}^2 = -0.016 \pm 0.023$ with corresponding Bayesian limit listed above. If Solution A is used, $m_{\nu}^2 = -0.143 \pm 0.024 \text{ MeV}^2$. Replaces ASSAMAGAN 94.

² DOLGOV 95 removes earlier assumptions (DOLGOV 93) about thermal equilibrium below T_{QCD} for wrong-helicity Dirac neutrinos (ENQVIST 93, FULLER 91) to set more stringent limits.

³ ENQVIST 93 bases limit on the fact that thermalized wrong-helicity Dirac neutrinos would speed up expansion of early universe, thus reducing the primordial abundance. FULLER 91 exploits the same mechanism but in the older calculation obtains a larger production rate for these states, and hence a lower limit. Neutrino lifetime assumed to exceed nucleosynthesis time, $\sim 1 \text{ s}$.

⁴ Assumes neutrino lifetime $> 1 \text{ s}$. For Dirac neutrinos only. See also ENQVIST 93.

⁵ ANDERHUB 82 kinematics is insensitive to the pion mass.

ν MASS (tau based)

The limits given below are the square roots of limits for $m_{\nu_{\tau}}^{2(\text{eff})} \equiv \sum_i |U_{\tau i}|^2 m_{\nu_i}^2$.

In some of the ASTR and COSM papers listed below, the authors did not distinguish between weak and mass eigenstates.

VALUE (MeV)	CL%	EVTS	DOCUMENT ID	TECN	COMMENT
< 18.2	95		¹ BARATE 98F	ALEP	1991–1995 LEP runs

• • • We do not use the following data for averages, fits, limits, etc. • • •

< 28	95		² ATHANAS 00	CLEO	$E_{\text{cm}}^{\text{eff}} = 10.6 \text{ GeV}$
< 27.6	95		³ ACKERSTAFF 98T	OPAL	1990–1995 LEP runs
< 30	95	473	⁴ AMMAR 98	CLEO	$E_{\text{cm}}^{\text{eff}} = 10.6 \text{ GeV}$
< 60	95		⁵ ANASTASSOV 97	CLEO	$E_{\text{cm}}^{\text{eff}} = 10.6 \text{ GeV}$
< 0.37 or > 22			⁶ FIELDS 97	COSM	Nucleosynthesis
< 68	95		⁷ SWAIN 97	THEO	$m_{\tau}, \tau_{\tau}, \tau$ partial widths
< 29.9	95		⁸ ALEXANDER 96M	OPAL	1990–1994 LEP runs
< 149			⁹ BOTTINO 96	THEO	π, μ, τ leptonic decays
< 1 or > 25			¹⁰ HANNESTAD 96C	COSM	Nucleosynthesis
< 71	95		¹¹ SOBIE 96	THEO	$m_{\tau}, \tau_{\tau}, B(\tau^- \rightarrow e^- \bar{\nu}_e \nu_{\tau})$
< 24	95	25	¹² BUSKULIC 95H	ALEP	1991–1993 LEP runs
< 0.19			¹³ DOLGOV 95	COSM	Nucleosynthesis
< 3			¹⁴ SIGL 95	ASTR	SN 1987A
< 0.4 or > 30			¹⁵ DODELSON 94	COSM	Nucleosynthesis
< 0.1 or > 50			¹⁶ KAWASAKI 94	COSM	Nucleosynthesis
155–225			¹⁷ PERES 94	THEO	π, K, μ, τ weak decays
< 32.6	95	113	¹⁸ CINABRO 93	CLEO	$E_{\text{cm}}^{\text{eff}} \approx 10.6 \text{ GeV}$
< 0.3 or > 35			¹⁹ DOLGOV 93	COSM	Nucleosynthesis
< 0.74			²⁰ ENQVIST 93	COSM	Nucleosynthesis
< 31	95	19	²¹ ALBRECHT 92M	ARG	$E_{\text{cm}}^{\text{eff}} = 9.4\text{--}10.6 \text{ GeV}$
< 0.3			²² FULLER 91	COSM	Nucleosynthesis
< 0.5 or > 25			²³ KOLB 91	COSM	Nucleosynthesis
< 0.42			²² LAM 91	COSM	Nucleosynthesis

¹ BARATE 98F result based on kinematics of $2939 \tau^- \rightarrow 2\pi^- \pi^+ \nu_{\tau}$ and $52 \tau^- \rightarrow 3\pi^- 2\pi^+ (\pi^0) \nu_{\tau}$ decays. If possible 2.5% excited a_1 decay is included in 3-prong sample analysis, limit increases to 19.2 MeV.

² ATHANAS 00 bound comes from analysis of $\tau^- \rightarrow \pi^- \pi^+ \pi^- \pi^0 \nu_{\tau}$ decays.

³ ACKERSTAFF 98T use $\tau^- \rightarrow 5\pi^{\pm} \nu_{\tau}$ decays to obtain a limit of 43.2 MeV (95%CL). They combine this with ALEXANDER 96M value using $\tau^- \rightarrow 3h^{\pm} \nu_{\tau}$ decays to obtain quoted limit.

⁴ AMMAR 98 limit comes from analysis of $\tau^- \rightarrow 3\pi^- 2\pi^+ \nu_{\tau}$ and $\tau^- \rightarrow 2\pi^- \pi^+ 2\pi^0 \nu_{\tau}$ decay modes.

⁵ ANASTASSOV 97 derive limit by comparing their m_{τ} measurement (which depends on $m_{\nu_{\tau}}$) to BAI 96 m_{τ} threshold measurement.

⁶ FIELDS 97 limit for a Dirac neutrino. For a Majorana neutrino the mass region < 0.93 or $> 31 \text{ MeV}$ is excluded. These bounds assume $N_{\nu} < 4$ from nucleosynthesis; a wider excluded region occurs with a smaller N_{ν} upper limit.

⁷ SWAIN 97 derive their limit from the Standard Model relationships between the tau mass, lifetime, branching fractions for $\tau^- \rightarrow e^- \bar{\nu}_e \nu_{\tau}, \tau^- \rightarrow \mu^- \bar{\nu}_{\mu} \nu_{\tau}, \tau^- \rightarrow \pi^- \nu_{\tau}$, and $\tau^- \rightarrow K^- \nu_{\tau}$, and the muon mass and lifetime by assuming lepton universality and using world average values. Limit is reduced to 48 MeV when the CLEO τ mass measurement (BALEST 93) is included; see CLEO's more recent $m_{\nu_{\tau}}$ limit (ANASTASSOV 97).

Consideration of mixing with a fourth generation heavy neutrino yields $\sin^2 \theta_L < 0.016$ (95%CL).

See key on page 1171

Lepton Particle Listings

Neutrino Properties

- ⁸ALEXANDER 96M bound comes from analyses of $\tau^- \rightarrow 3\pi^- 2\pi^+ \nu_\tau$ and $\tau^- \rightarrow h^- h^- h^+ \nu_\tau$ decays.
- ⁹BOTTINO 96 assumes three generations of neutrinos with mixing, finds consistency with massless neutrinos with no mixing based on 1995 data for masses, lifetimes, and leptonic partial widths.
- ¹⁰HANNESTAD 96c limit is on the mass of a Majorana neutrino. This bound assumes $N_\nu < 4$ from nucleosynthesis. A wider excluded region occurs with a smaller N_ν upper limit. This paper is the corrected version of HANNESTAD 96; see the erratum: HANNESTAD 96b.
- ¹¹SOBIE 96 derive their limit from the Standard Model relationship between the tau mass, lifetime, and leptonic branching fraction, and the muon mass and lifetime, by assuming lepton universality and using world average values.
- ¹²BUSKULIC 95H bound comes from a two-dimensional fit of the visible energy and invariant mass distribution of $\tau \rightarrow 5\pi(\pi^0)\nu_\tau$ decays. Replaced by BARATE 98f.
- ¹³DOLGOV 95 removes earlier assumptions (DOLGOV 93) about thermal equilibrium below T_{QCD} for wrong-helicity Dirac neutrinos (ENQVIST 93, FULLER 91) to set more stringent limits. DOLGOV 96 argues that a possible window near 20 MeV is excluded.
- ¹⁴SIGL 95 exclude massive Dirac or Majorana neutrinos with lifetimes between 10^{-3} and 10^8 seconds if the decay products are predominantly γ or e^+e^- .
- ¹⁵DODELSON 94 calculate constraints on ν_τ mass and lifetime from nucleosynthesis for 4 generic decay modes. Limits depend strongly on decay mode. Quoted limit is valid for all decay modes of Majorana neutrinos with lifetime greater than about 300s. For Dirac neutrinos limits change to < 0.3 or > 33 .
- ¹⁶KAWASAKI 94 excluded region is for Majorana neutrino with lifetime > 1000 s. Other limits are given as a function of ν_τ lifetime for decays of the type $\nu_\tau \rightarrow \nu_\mu \phi$ where ϕ is a Nambu-Goldstone boson.
- ¹⁷PERES 94 used PDG 92 values for parameters to obtain a value consistent with mixing. Reexamination by BOTTINO 96 which included radiative corrections and 1995 PDG parameters resulted in two allowed regions, $m_3 < 70$ MeV and 140 MeV $m_3 < 149$ MeV.
- ¹⁸CINABRO 93 bound comes from analysis of $\tau^- \rightarrow 3\pi^- 2\pi^+ \nu_\tau$ and $\tau^- \rightarrow 2\pi^- \pi^+ 2\pi^0 \nu_\tau$ decay modes.
- ¹⁹DOLGOV 93 assumes neutrino lifetime > 100 s. For Majorana neutrinos, the low mass limit is 0.5 MeV. KAWANO 92 points out that these bounds can be overcome for a Dirac neutrino if it possesses a magnetic moment. See also DOLGOV 96.
- ²⁰ENQVIST 93 bases limit on the fact that thermalized wrong-helicity Dirac neutrinos would speed up expansion of early universe, thus reducing the primordial abundance. FULLER 91 exploits the same mechanism but in the older calculation obtains a larger production rate for these states, and hence a lower limit. Neutrino lifetime assumed to exceed nucleosynthesis time, ~ 1 s.
- ²¹ALBRECHT 92M reports measurement of a slightly lower τ mass, which has the effect of reducing the ν_τ mass reported in ALBRECHT 88B. Bound is from analysis of $\tau^- \rightarrow 3\pi^- 2\pi^+ \nu_\tau$ mode.
- ²²Assumes neutrino lifetime > 1 s. For Dirac neutrinos. See also ENQVIST 93.
- ²³KOLB 91 exclusion region is for Dirac neutrino with lifetime > 1 s; other limits are given.

Revised August 2023 by K.A. Olive (University of Minnesota).

Neutrinos decouple from thermal equilibrium in the early universe at temperatures $\mathcal{O}(1)$ MeV. The limits on low mass ($m_\nu \lesssim 1$ MeV) neutrinos apply to m_{tot} given by

$$m_{\text{tot}} = \sum_\nu m_\nu .$$

Stable neutrinos in this mass range decouple from the thermal bath while still relativistic and make a contribution to the total energy density of the Universe which is given by

$$\rho_\nu = m_{\text{tot}} n_\nu \simeq m_{\text{tot}} (3/11) (3.045/3)^{3/4} n_\gamma ,$$

where the factor $3/11$ is the ratio of (light) neutrinos to photons and the factor $(3.045/3)^{3/4}$ corrects for the fact that the effective number of neutrinos in the standard model is 3.045 when taking into account e^+e^- annihilation during neutrino decoupling. Writing $\Omega_\nu = \rho_\nu/\rho_c$, where ρ_c is the critical energy density of the Universe, and using $n_\gamma = 410.7 \text{ cm}^{-3}$, we have

$$\Omega_\nu h^2 \simeq m_{\text{tot}} / (93 \text{ eV}) .$$

While an upper limit to the matter density of $\Omega_m h^2 < 0.12$ would constrain $m_{\text{tot}} < 11$ eV, much stronger constraints are obtained from the observations of the CMB, combined with

lensing and baryon acoustic oscillations data. These combine to give an upper limit of around 0.12 eV, and may, in the near future, be able to provide a lower bound on the sum of the neutrino masses. The current lower bound of $m_{\text{tot}} > 0.06$ eV implies a lower limit of $\Omega_\nu h^2 > 6 \times 10^{-4}$. See our review on "Neutrinos in Cosmology" for more details.

SUM OF THE NEUTRINO MASSES, m_{tot}

This is a sum of the neutrino masses, m_{tot} , as defined in the above note, of effectively stable neutrinos, i.e. those with mean lifetimes on cosmological scales. When necessary, we have generalized the results reported so they apply to m_{tot} . For other limits, see SZALAY 76, VYSOTSKY 77, BERNSTEIN 81, FREESE 84, SCHRAMM 84, and COWSIK 85. For more information see a note on "Neutrinos in Cosmology" in this Review.

VALUE (eV)	CL%	DOCUMENT ID	TECN	COMMENT
• • • We do not use the following data for averages, fits, limits, etc. • • •				
< 0.082	95	¹ BRIEDEN 22	COSM	BOSS, eBOSS, and CMB
< 0.116	95	² KUMAR 22	COSM	BOSS and CMB
< 0.14	95	³ TANSERI 22	COSM	BOSS and CMB
< 0.13	95	⁴ ABBOTT 21A	COSM	DES and Planck
< 0.12	95	⁵ ALAM 21	COSM	
< 0.09	95	⁶ DI-VALENT... 21	COSM	
< 0.16	95	⁷ GARNY 21	COSM	
< 0.06-0.14	95	⁸ STOCKER 21	COSM	Normal mass ordering
< 0.12	95	⁹ AGHANIM 20	COSM	
< 0.15	95	¹⁰ CHOUDHURY 20	COSM	Normal mass hierarchy
< 0.16	95	¹¹ IVANOV 20	COSM	Planck and BOSS
< 0.11	95	¹² PALANQUE... 20	COSM	Lyman alpha and CMB
< 0.26	95	¹³ LOUREIRO 19	COSM	
< 0.18	95	¹⁴ UPADHYE 19	COSM	BOSS and CMB
< 0.152	95	¹⁵ CHOUDHURY 18	COSM	
0.064 \pm 0.061 -0.005	95	¹⁶ SIMPSON 17	COSM	
< 0.14	95	¹⁷ YECHE 17	COSM	BOSS and XQ-100
< 0.0926	90	¹⁸ DIVALENTINO 16	COSM	
< 0.18	95	¹⁹ HUANG 16	COSM	Normal mass hierarchy
< 0.14	95	²⁰ ROSSI 15	COSM	
< 0.23	95	²¹ ADE 14	COSM	Planck
0.320 \pm 0.081		²² BATTYE 14	COSM	
0.35 \pm 0.10		²³ BEUTLER 14	COSM	BOSS
0.22 \pm 0.09 -0.10		²⁴ COSTANZI 14	COSM	
0.32 \pm 0.11		²⁵ HOU 14	COSM	
< 0.26	95	²⁶ LEISTEDT 14	COSM	
< 0.18	95	²⁷ RIEMER-SOR... 14	COSM	
< 0.24	68	²⁸ MORESCO 12	COSM	
< 0.29	95	²⁹ XIA 12	COSM	
< 0.81	95	³⁰ SAITO 11	COSM	SDSS
< 0.44	95	³¹ HANNESTAD 10	COSM	
< 0.6	95	³² SEKIGUCHI 10	COSM	
< 0.28	95	³³ THOMAS 10	COSM	
< 1.1		³⁴ ICHIKI 09	COSM	
< 1.3	95	³⁵ KOMATSU 09	COSM	WMAP
< 1.2		³⁶ TERENO 09	COSM	
< 0.33		³⁷ VIKHLININ 09	COSM	
< 0.28		³⁸ BERNARDIS 08	COSM	
< 0.17-2.3		³⁹ FOGLI 07	COSM	
< 0.42	95	⁴⁰ KRISTIANSEN 07	COSM	
< 0.63-2.2		⁴¹ ZUNCKEL 07	COSM	
< 0.24	95	⁴² CIRELLI 06	COSM	
< 0.62	95	⁴³ HANNESTAD 06	COSM	
< 1.2		⁴⁴ SANCHEZ 06	COSM	
< 0.17	95	⁴² SELJAK 06	COSM	
< 2.0	95	⁴⁵ ICHIKAWA 05	COSM	
< 0.75		⁴⁶ BARGER 04	COSM	
< 1.0		⁴⁷ CROTTY 04	COSM	
< 0.7		⁴⁸ SPERGEL 03	COSM	WMAP
< 0.9		⁴⁹ LEWIS 02	COSM	
< 4.2		⁵⁰ WANG 02	COSM	CMB
< 2.7		⁵¹ FUKUGITA 00	COSM	
< 5.5		⁵² CROFT 99	ASTR	Ly α power spec
<180		SZALAY 74	COSM	
<132		COWSIK 72	COSM	
<280		MARX 72	COSM	
<400		GERSHTEIN 66	COSM	

¹BRIEDEN 22 combines redshift-space distortions and the shape of the matter power spectrum from BOSS and eBOSS data together with Planck CMB data. Absent the CMB data, the limit is 0.40 eV.

²KUMAR 22 combine the reconstructed galaxy power spectrum from BOSS data with Planck CMB data.

³TANSERI 22 combines BOSS galaxy clustering data with measurements of CMB data. Updates VAGNOZZI 17.

Lepton Particle Listings

Neutrino Properties

- ⁴ ABBOTT 21A combines Dark Energy Survey (DES) year 3 results with Planck CMB lensing measurements.
- ⁵ ALAM 21 limit on the sum of neutrino masses by the eBOSS collaboration is based on galaxy, quasar, and Lyman- α 3D clustering data combined with Planck temperature and polarization CMB and supernovae data.
- ⁶ DI-VALENTINO 21 combines CMB temperature and polarization, SNIa luminosity distances and baryon acoustic oscillations data.
- ⁷ GARNY 21 employs a model for the Lyman- α flux power spectrum to set a limit using BOSS data. When combined with Planck CMB temperature and polarization data, a 95% CL range 0.10–0.13 eV is found.
- ⁸ STOCKER 21 use terrestrial and cosmological experiments to set a 95% CL range on the sum of neutrino masses of 0.058–0.139 eV for normal ordering and 0.098–0.174 eV for inverse ordering. They also set an upper limit of 0.037 eV (NO) and 0.042 eV (IO) for the lightest neutrino mass.
- ⁹ AGHANIM 20 limit on the sum of neutrino masses from Planck data combined with lensing and baryon acoustic oscillations (BAO). Without BAO, the limit relaxes to <0.24 eV. Several other limits are quoted based on different combinations of data.
- ¹⁰ CHOUDHURY 20 combines 2018 Planck CMB temperature and polarization data plus lensing, together with baryon acoustic oscillation data from BOSS, MGS, and 6dFGS. Assumes Λ CDM model. The upper limit is 0.17 eV for the inverted hierarchy, and 0.12 eV for degenerate neutrinos. Limits are also derived for extended cosmological models.
- ¹¹ IVANOV 20 combines 2018 Planck CMB data with baryon acoustic oscillation data from BOSS. This study is based on a full-shape likelihood for the redshift-space galaxy power spectrum of the BOSS data.
- ¹² PALANQUE-DELABROUILLE 20 combine Lyman alpha and Planck temperature and polarization data. Limit improves to 0.09 eV when CMB lensing and baryon acoustic oscillation data are included.
- ¹³ LOUREIRO 19 combines data from large scale structure, cosmic microwave background, type Ia supernovae and big bang nucleosynthesis using physically motivated neutrino mass models.
- ¹⁴ UPADHYE 19 uses the shape of the BOSS redshift-space galaxy power spectrum in combination with the CMB, and supernovae data. Limit weakens to <0.54 eV if the dark energy equation of state is allowed to vary.
- ¹⁵ CHOUDHURY 18 combines 2015 Planck CMB temperature data, information from the optical depth to reionization from Planck 2016 intermediate results together with baryon acoustic oscillation data from BOSS, MGS, and 6dFGS as well as supernovae Type Ia data from the Pantheon Sample. The limit is strengthened to 0.118 eV when high- l CMB polarization data is also included.
- ¹⁶ SIMPSON 17 uses a combination of laboratory and cosmological measurements to determine the light neutrino masses and argue that there is strong evidence for the normal mass ordering.
- ¹⁷ Constrains the total mass of neutrinos using the Lyman- α forest power spectrum with BOSS (mid-resolution), XQ-100 (high-resolution) and CMB. Without the CMB data, the limit relaxes to 0.8 eV. Supersedes PALANQUE-DELABROUILLE 15A.
- ¹⁸ Constrains the total mass of neutrinos from Planck CMB data combined with baryon acoustic oscillation and Planck cluster data.
- ¹⁹ Constrains the total mass of neutrinos from BAO data from SDSS-II/BOSS combined with CMB data from Planck. Limit quoted for normal mass hierarchy. The limit for the inverted mass hierarchy is 0.20 eV and for the degenerate mass hierarchy it is 0.15 eV.
- ²⁰ ROSSI 15 sets limits on the sum of neutrino masses using BOSS Lyman alpha forest data combined with Planck CMB data and baryon acoustic oscillations.
- ²¹ Constrains the total mass of neutrinos from Planck CMB data along with WMAP polarization, high l , and BAO data.
- ²² Finite neutrino mass fit to resolve discrepancy between CMB and lensing measurements.
- ²³ Fit to the total mass of neutrinos from BOSS data along with WMAP CMB data and data from other BAO constraints and weak lensing.
- ²⁴ Fit to the total mass of neutrinos from Planck CMB data along with BAO.
- ²⁵ Fit based on the SPT-SZ survey combined with CMB, BAO, and H_0 data.
- ²⁶ Constrains the total mass of neutrinos (marginalizing over the effective number of neutrino species) from CMB, CMB lensing, BAO, and galaxy clustering data.
- ²⁷ Constrains the total mass of neutrinos from Planck CMB data combined with baryon acoustic oscillation data from BOSS, 6dFGS, SDSS, WiggleZ data on the galaxy power spectrum, and HST data on the Hubble parameter. The limit is increased to 0.25 eV if a lower bound to the sum of neutrino masses of 0.04 eV is assumed.
- ²⁸ Constrains the total mass of neutrinos from observational Hubble parameter data with seven-year WMAP data and the most recent estimate of H_0 .
- ²⁹ Constrains the total mass of neutrinos from the CFHTLS combined with seven-year WMAP data and a prior on the Hubble parameter. Limit is relaxed to 0.41 eV when small scales affected by non-linearities are removed.
- ³⁰ Constrains the total mass of neutrinos from the Sloan Digital Sky Survey and the five-year WMAP data.
- ³¹ Constrains the total mass of neutrinos from the 7-year WMAP data including SDSS and HST data. Limit relaxes to 1.19 eV when CMB data is used alone. Supersedes HANNESTAD 06.
- ³² Constrains the total mass of neutrinos from a combination of CMB data, a recent measurement of H_0 (SHOES), and baryon acoustic oscillation data from SDSS.
- ³³ Constrains the total mass of neutrinos from SDSS MegaZ LRG DR7 galaxy clustering data combined with CMB, HST, supernovae and baryon acoustic oscillation data. Limit relaxes to 0.47 eV when the equation of state parameter, $w \neq -1$.
- ³⁴ Constrains the total mass of neutrinos from weak lensing measurements when combined with CMB. Limit improves to 0.54 eV when supernovae and baryon acoustic oscillation observations are included. Assumes Λ CDM model.
- ³⁵ Constrains the total mass of neutrinos from five-year WMAP data. Limit improves to 0.67 eV when supernovae and baryon acoustic oscillation observations are included. Limits quoted assume the Λ CDM model. Supersedes SPERGEL 07.

- ³⁶ Constrains the total mass of neutrinos from weak lensing measurements when combined with CMB. Limit improves to $0.03 < \Sigma m_\nu < 0.54$ eV when supernovae and baryon acoustic oscillation observations are included. The slight preference for massive neutrinos at the two-sigma level disappears when systematic errors are taken into account. Assumes Λ CDM model.
- ³⁷ Constrains the total mass of neutrinos from recent Chandra X-ray observations of galaxy clusters when combined with CMB, supernovae, and baryon acoustic oscillation measurements. Assumes flat universe and constant dark-energy equation of state, w .
- ³⁸ Constrains the total mass of neutrinos from recent CMB and SOSS LRG power spectrum data along with bias mass relations from SDSS, DEEP2, and Lyman-Break Galaxies. It assumes Λ CDM model. Limit degrades to 0.59 eV in a more general w CDM model.
- ³⁹ Constrains the total mass of neutrinos from neutrino oscillation experiments and cosmological data. The most conservative limit uses only WMAP three-year data, while the most stringent limit includes CMB, large-scale structure, supernova, and Lyman-alpha data.
- ⁴⁰ Constrains the total mass of neutrinos from recent CMB, large scale structure, SNIa, and baryon acoustic oscillation data. The limit relaxes to 1.75 when WMAP data alone is used with no prior. Paper shows results with several combinations of data sets. Supersedes KRISTIANSEN 06.
- ⁴¹ Constrains the total mass of neutrinos from the CMB and the large scale structure data. The most conservative limit is obtained when generic initial conditions are allowed.
- ⁴² Constrains the total mass of neutrinos from recent CMB, large scale structure, Lyman-alpha forest, and SNIa data.
- ⁴³ Constrains the total mass of neutrinos from recent CMB and large scale structure data. See also GOOBAR 06. Superseded by HANNESTAD 10.
- ⁴⁴ Constrains the total mass of neutrinos from the CMB and the final 2dF Galaxy Redshift Survey.
- ⁴⁵ Constrains the total mass of neutrinos from the CMB experiments alone, assuming Λ CDM Universe. FUKUGITA 06 show that this result is unchanged by the 3-year WMAP data.
- ⁴⁶ Constrains the total mass of neutrinos from the power spectrum of fluctuations derived from the Sloan Digital Sky Survey and the 2dF galaxy redshift survey, WMAP and 27 other CMB experiments and measurements by the HST Key project.
- ⁴⁷ Constrains the total mass of neutrinos from the power spectrum of fluctuations derived from the Sloan Digital Sky Survey, the 2dF galaxy redshift survey, WMAP and ACBAR. The limit is strengthened to 0.6 eV when measurements by the HST Key project and supernovae data are included.
- ⁴⁸ Constrains the fractional contribution of neutrinos to the total matter density in the Universe from WMAP data combined with other CMB measurements, the 2dFGRS data, and Lyman α data. The limit does not noticeably change if the Lyman α data are not used.
- ⁴⁹ LEWIS 02 constrains the total mass of neutrinos from the power spectrum of fluctuations derived from the CMB, HST Key project, 2dF galaxy redshift survey, supernovae type Ia, and BBN.
- ⁵⁰ WANG 02 constrains the total mass of neutrinos from the power spectrum of fluctuations derived from the CMB and other cosmological data sets such as galaxy clustering and the Lyman α forest.
- ⁵¹ FUKUGITA 00 is a limit on neutrino masses from structure formation. The constraint is based on the clustering scale σ_8 and the COBE normalization and leads to a conservative limit of 0.9 eV assuming 3 nearly degenerate neutrinos. The quoted limit is on the sum of the light neutrino masses.
- ⁵² CROFT 99 result based on the power spectrum of the Ly α forest. If $\Omega_{\text{matter}} < 0.5$, the limit is improved to $m_\nu < 2.4 (\Omega_{\text{matter}}/0.17-1)$ eV.

Limits on MASSES of Light Stable Right-Handed ν (with necessarily suppressed interaction strengths)

VALUE (eV)	DOCUMENT ID	TECN	COMMENT
------------	-------------	------	---------

• • • We do not use the following data for averages, fits, limits, etc. • • •

$<100-200$	¹ OLIVE	82	COSM Dirac ν
$<200-2000$	¹ OLIVE	82	COSM Majorana ν

¹ Depending on interaction strength G_R where $G_R < G_F$.

Limits on MASSES of Heavy Stable Right-Handed ν (with necessarily suppressed interaction strengths)

VALUE (GeV)	DOCUMENT ID	TECN	COMMENT
-------------	-------------	------	---------

• • • We do not use the following data for averages, fits, limits, etc. • • •

>10	¹ OLIVE	82	COSM $G_R/G_F < 0.1$
>100	¹ OLIVE	82	COSM $G_R/G_F < 0.01$

¹ These results apply to heavy Majorana neutrinos and are summarized by the equation: $m_\nu > 1.2 \text{ GeV } (G_F/G_R)$. The bound saturates, and if G_R is too small no mass range is allowed.

ν CHARGE

e = electron charge is the unit of values listed below.

VALUE (e)	CL%	DOCUMENT ID	TECN	COMMENT
-----------	-----	-------------	------	---------

• • • We do not use the following data for averages, fits, limits, etc. • • •

$<2.24 \times 10^{-13}$	90	² AALBERS	23A	LZ Solar ν spectrum
$<1.5 \times 10^{-13}$	90	³ ATZORI-COR...23	FIT	solar neutrinos

See key on page 1171

Lepton Particle Listings

Neutrino Properties

$<3.3 \times 10^{-12}$	90	4 BONET	22A CONU	nuclear reactor
$<5.4 \times 10^{-12}$	90	5 ABE	20E XMAS	solar neutrinos
$1.7-2.3 \times 10^{-12}$	68	6 KHAN	20	spectral fit of XENON1T
$<3 \times 10^{-8}$	95	7 DELLA-VALLE	16 LASR	magnetic dichroism
$<2.1 \times 10^{-12}$	90	8 CHEN	14A TEXO	nuclear reactor
$<1.5 \times 10^{-12}$	90	9 STUDENIKIN	14	nuclear reactor
$<3.7 \times 10^{-12}$	90	10 GNINENKO	07 RVUE	nuclear reactor
$<2 \times 10^{-14}$		11 RAFFELT	99 ASTR	red giant luminosity
$<6 \times 10^{-14}$		12 RAFFELT	99 ASTR	solar cooling
$<4 \times 10^{-4}$		13 BABU	94 RVUE	BECB beam dump
$<3 \times 10^{-4}$		14 DAVIDSON	91 RVUE	SLAC e^- beam dump
$<2 \times 10^{-15}$		15 BARBIELLINI	87 ASTR	SN 1987A
$<1 \times 10^{-13}$		16 BERNSTEIN	63 ASTR	solar energy losses

- CAPRINI 05 limit derived from the lack of a charge asymmetry in the universe. Limit assumes that charge asymmetries between particles are not anti-correlated.
- AALBERS 23A utilize the first 60 days of data collected by the LZ dark matter search to place a limit on the electric charge of solar neutrinos. Low energy electron-recoil events are utilized. This LZ-collaboration analysis supersedes that of the external authors in ATZORI-CORONA 23 because of a more complete treatment of experiment uncertainties.
- ATZORI-CORONA 23 use LUX-ZEPLIN dark matter search data published by AALBERS 23 to place a limit on neutrino millicharge.
- BONET 22A use data collected by four low-threshold Ge detectors, placed 17.1 m from one of the cores of the nuclear reactors at Brokdorf to derive this limit. A spectral analysis is performed on reactor on and off data.
- ABE 20E obtains this result by assuming that the low-energy excess events in the XMAS detector are produced by neutrino millicharge which is common for all three neutrino flavors.
- KHAN 20 performed a constrained spectral fit analysis of the excess observed in the electron recoil energy spectrum by the XENON1T experiment. This range of neutrino millicharge values is one of the possible interpretations of these excess events. For the individual flavor constraints at 90% C.L. see the original reference.
- DELLA-VALLE 16 obtain a limit on the charge of neutrinos valid for masses of less than 10 MeV. For heavier neutrinos the limit increases as a power of mass, reaching $10^{-6} e$ for $m = 100$ MeV.
- CHEN 14A use the Multi-Configuration RHPA method to analyze reactor $\bar{\nu}_e$ scattering on Ge atoms with 300 eV recoil energy threshold to obtain this limit.
- STUDENIKIN 14 uses the limit on μ_{ν} from BEDA 13 and the 2.8 keV threshold of the electron recoil energy to obtain this limit.
- GNINENKO 07 use limit on $\bar{\nu}_e$ magnetic moment from LI 03b to derive this result. The limit is considerably weaker than the limits on the charge of ν_e and $\bar{\nu}_e$ from various astrophysics considerations.
- This RAFFELT 99 limit applies to all neutrino flavors which are light enough (<5 keV) to be emitted from globular-cluster red giants.
- This RAFFELT 99 limit is derived from the helioseismological limit on a new energy-loss channel of the Sun, and applies to all neutrino flavors which are light enough (<1 keV) to be emitted from the sun.
- BABU 94 use COOPER-SARKAR 92 limit on ν magnetic moment to derive quoted result. It applies to ν_τ .
- DAVIDSON 91 use data from early SLAC electron beam dump experiment to derive charge limit as a function of neutrino mass. It applies to ν_τ .
- Exact BARBIELLINI 87 limit depends on assumptions about the intergalactic or galactic magnetic fields and about the direct distance and time through the field. It applies to ν_e .
- The limit applies to all flavors.

$6-26 \times 10^9$	95	7 ESCUDERO	19 COSM	Invisible decay $m_{\nu} \geq 0.05$ eV
$> 10^5 - 10^{10}$	95	8 CECCHINI	11 ASTR	$\nu_2 \rightarrow \nu_1$ radiative decay
		9 MIRIZZI	07 CMB	radiative decay
		10 MIRIZZI	07 CIB	radiative decay
		11 WONG	07 CNTR	Reactor $\bar{\nu}_e$
> 0.11	90	12 XIN	05 CNTR	Reactor ν_e
		13 XIN	05 CNTR	Reactor ν_e
> 0.004	90	14 AHARMIM	04 SNO	quasidegen. ν masses
$> 4.4 \times 10^{-5}$	90	14 AHARMIM	04 SNO	hierarchical ν masses
$\gtrsim 100$	95	15 CECCHINI	04 ASTR	Radiative decay for ν mass > 0.01 eV
> 0.067	90	16 EGUCHI	04 KLND	quasidegen. ν masses
$> 1.1 \times 10^{-3}$	90	16 EGUCHI	04 KLND	hierarchical ν masses
$> 8.7 \times 10^{-5}$	99	17 BANDYOPA...	03 FIT	nonradiative decay
≥ 4200	90	18 DERBIN	02B CNTR	Solar $p\bar{p}$ and Be ν
$> 2.8 \times 10^{-5}$	99	19 JOSHIPURA	02B FIT	nonradiative decay
		20 DOLGOV	99 COSM	
		21 BILLER	98 ASTR	$m_{\nu} = 0.05-1$ eV
$> 2.8 \times 10^{15}$	22,23	22,23 BLUDMAN	92 ASTR	$m_{\nu} < 50$ eV
none $10^{-12} - 5 \times 10^4$	24	24 DODELSON	92 ASTR	$m_{\nu} = 1-300$ keV
$< 10^{-12}$ or $> 5 \times 10^4$	24	24 DODELSON	92 ASTR	$m_{\nu} = 1-300$ keV
		25 GRANEK	91 COSM	Decaying L^0
> 6.4	90	26 KRAKAUER	91 CNTR	ν_e at LAMPF
$> 1.1 \times 10^{15}$		27 WALKER	90 ASTR	$m_{\nu} = 0.03 - \sim 2$ MeV
$> 6.3 \times 10^{15}$	23,28	23,28 CHUPP	89 ASTR	$m_{\nu} < 20$ eV
$> 1.7 \times 10^{15}$	23	23 KOLB	89 ASTR	$m_{\nu} < 20$ eV
		29 RAFFELT	89 RVUE	$\bar{\nu}$ (Dirac, Majorana)
		30 RAFFELT	89B ASTR	
		31 VONFEILIT...	88 ASTR	
$> 8.3 \times 10^{14}$		32 OBERAUER	87	$\bar{\nu}_R$ (Dirac)
> 22	68	32 OBERAUER	87	$\bar{\nu}$ (Majorana)
> 38	68	32 OBERAUER	87	$\bar{\nu}_L$ (Dirac)
> 59	68	32 OBERAUER	87	$\bar{\nu}_L$ (Dirac)
> 30	68	KETOV	86 CNTR	$\bar{\nu}$ (Dirac)
> 20	68	KETOV	86 CNTR	$\bar{\nu}$ (Majorana)
		33 BINETRUY	84 COSM	$m_{\nu} \sim 1$ MeV
> 0.11	90	34 FRANK	81 CNTR	$\nu\bar{\nu}$ LAMPF
$> 2 \times 10^{21}$		35 STECKER	80 ASTR	$m_{\nu} = 10-100$ eV
$> 1.0 \times 10^{-2}$	90	34 BLIETSCHAU	78 HLBC	ν_μ , CERN GGM
$> 1.7 \times 10^{-2}$	90	34 BLIETSCHAU	78 HLBC	$\bar{\nu}_\mu$, CERN GGM
$< 3 \times 10^{-11}$		36 FALK	78 ASTR	$m_{\nu} < 10$ MeV
$> 2.2 \times 10^{-3}$	90	34 BARNES	77 DBC	ν , ANL 12-ft
		37 COWSIK	77 ASTR	
$> 3. \times 10^{-3}$	90	34 BELLOTTI	76 HLBC	ν , CERN GGM
$> 1.3 \times 10^{-2}$	90	34 BELLOTTI	76 HLBC	$\bar{\nu}$, CERN GGM

- KRAKAUER 91 quotes the limit $\tau/m_{\nu_1} > (0.75a^2 + 21.65a + 26.3) s/eV$, where a is a parameter describing the asymmetry in the neutrino decay defined as $dN_{\nu_1}/dcos\theta = (1/2)(1 + a\cos\theta)$. The parameter $a = 0$ for a Majorana neutrino, but can vary from -1 to 1 for a Dirac neutrino. The bound given by the authors is the most conservative (which applies for $a = -1$).
- RAFFELT 85 limit on the radiative decay is from solar x- and γ -ray fluxes. Limit depends on ν flux from $p\bar{p}$, now established from GALLEX and SAGE to be > 0.5 of expectation.
- REINES 74 looked for ν of nonzero mass decaying radiatively to a neutral of lesser mass $+\gamma$. Used liquid scintillator detector near fission reactor. Finds lab lifetime 6×10^7 s or more. Above value of (mean life)/mass assumes average effective neutrino energy of 0.2 MeV. To obtain the limit 6×10^7 s REINES 74 assumed that the full $\bar{\nu}_e$ reactor flux could be responsible for yielding decays with photon energies in the interval 0.1 MeV - 0.5 MeV. This represents some overestimate so their lower limit is an over-estimate of the lab lifetime (VOGEL 84). If so, OBERAUER 87 may be comparable or better.
- IVANEZ-BALLESTROS 23 reports a limit on the lifetime-to-mass ratio of the mass eigenstates ν_1 and ν_2 for inverted mass ordering. No limit was obtained in the case of normal mass ordering.
- AHARMIM 19 quotes the limit τ/m_{ν_2} for invisible nonradiative decay of ν_2 . They obtained this result by analyzing the entire SNO dataset, allowing for the decay of ν_2 which would cause an energy-dependent distortion of the survival probability of electron-type solar neutrinos.
- AHARMIM 19 quotes the limit τ/m_{ν_2} for invisible nonradiative decay of ν_2 . They obtained this result by combining the τ/m_{ν_2} measurements from SNO and other solar neutrino experiments (Super-Kamiokande, KamLAND, and Borexino 8B results; Borexino and KamLAND 7Be results; the combined gallium interaction rate from GNO, GALLEX, and SAGE; and the chlorine interaction rate from Homestake). The quoted limit at 99% CL is $> 1.04 \times 10^{-3}$.
- ESCUDERO 19 sets limits on invisible neutrino decays using Planck 2018 data of $\tau > 1.3-0.3 \times 10^9$ s at 95% C.L. Values in the range $\tau = 2-16 \times 10^9$ s are preferred at 95% C.L. when Planck polarization data is included. Limits scale as $(m_{\nu}/0.05 \text{ eV})^3$.
- CECCHINI 11 search for radiative decays of solar neutrinos into visible photons during the 2006 total solar eclipse. The range of (mean life)/mass values corresponds to a range of ν_1 masses between 10^{-4} and 0.1 eV.
- MIRIZZI 07 determine a limit on the neutrino radiative decay from analysis of the maximum allowed distortion of the CMB spectrum as measured by the COBE/FIRAS. For the decay $\nu_2 \rightarrow \nu_1$ the lifetime limit is $\lesssim 4 \times 10^{20}$ s for $m_{min} \lesssim 0.14$ eV. For transition with the $|\Delta m_{31}|$ mass difference the lifetime limit is $\sim 2 \times 10^{19}$ s for $m_{min} \lesssim 0.14$ eV and $\sim 5 \times 10^{20}$ s for $m_{min} \gtrsim 0.14$ eV.

ν (MEAN LIFE) / MASS

Measures $[\sum |U_{\ell j}|^2 \Gamma_j m_j]^{-1}$, where the sum is over mass eigenstates which cannot be resolved experimentally. Some of the limits constrain the radiative decay and are based on the limit of the corresponding photon flux. Other apply to the decay of a heavier neutrino into the lighter one and a Majoron or other invisible particle. Many of these limits apply to any ν within the indicated mass range.

Limits on the radiative decay are either directly based on the limits of the corresponding photon flux, or are derived from the limits on the neutrino magnetic moments. In the later case the transition rate for $\nu_i \rightarrow \nu_j + \gamma$

$$\text{is constrained by } \Gamma_{ij} = \frac{1}{\tau_{ij}} = \frac{(m_i^2 - m_j^2)^3}{m_i^2} \mu_{ij}^2 \text{ where } \mu_{ij} \text{ is the neutrino}$$

transition moment in the mass eigenstates basis. Typically, the limits on lifetime based on the magnetic moments are many orders of magnitude more restrictive than limits based on the nonobservation of photons.

VALUE (s/eV)	CL%	DOCUMENT ID	TECN	COMMENT
> 15.4	90	1 KRAKAUER	91 CNTR	$\nu_\mu, \bar{\nu}_\mu$ at LAMPF
$> 7 \times 10^9$		2 RAFFELT	85 ASTR	
> 300	90	3 REINES	74 CNTR	$\bar{\nu}_e$
● ● ● We do not use the following data for averages, fits, limits, etc. ● ● ●				
$> 1.2 \times 10^5$	90	4 IVANEZ-BAL...	23 ASTR	SN1987A, nonradiative decay
$> 8.08 \times 10^{-5}$	90	5 AHARMIM	19 SNO	ν_2 invisible nonradiative decay
$> 1.92 \times 10^{-3}$	90	6 AHARMIM	19 FIT	ν_2 invisible nonradiative decay

Lepton Particle Listings

Neutrino Properties

- ¹⁰ MIRIZZI 07 determine a limit on the neutrino radiative decay from analysis of the cosmic infrared background (CIB) using the Spitzer Observatory data. For transition with the $|\Delta m_{31}|$ mass difference they obtain the lifetime limit $\sim 10^{20}$ s for $m_{\min} \lesssim 0.14$ eV.
- ¹¹ WONG 07 use their limit on the neutrino magnetic moment together with the assumed experimental value of $\Delta m_{13}^2 \sim 2 \times 10^{-3}$ eV² to obtain $\tau_{13}/m_1^3 > 3.2 \times 10^{27}$ s/eV³ for the radiative decay in the case of the inverted mass hierarchy. Similarly to RAFFELT 89 this limit can be violated if electric and magnetic moments are equal to each other. Analogous, but numerically somewhat different limits are obtained for τ_{23} and τ_{21} .
- ¹² XIN 05 search for the γ from radiative decay of ν_e produced by the electron capture on ⁵¹Cr. No events were seen and the limit on τ/m_ν was derived. This is a weaker limit on the decay of ν_e than KRAKAUER 91.
- ¹³ XIN 05 use their limit on the neutrino magnetic moment of ν_e together with the assumed experimental value of $\Delta m_{13}^2 \sim 2 \times 10^{-3}$ eV² to obtain $\tau_{13}/m_1^3 > 1 \times 10^{23}$ s/eV³ for the radiative decay in the case of the inverted mass hierarchy. Similarly to RAFFELT 89 this limit can be violated if electric and magnetic moments are equal to each other. Analogous, but numerically somewhat different limits are obtained for τ_{23} and τ_{21} . Again, this limit is specific for ν_e .
- ¹⁴ AHARMIM 04 obtained these results from the solar $\bar{\nu}_e$ flux limit set by the SNO measurement assuming ν_2 decay through nonradiative process $\nu_2 \rightarrow \bar{\nu}_1 X$, where X is a Majoron or other invisible particle. Limits are given for the cases of quasidegenerate and hierarchical neutrino masses.
- ¹⁵ CECCHINI 04 obtained this bound through the observations performed on the occasion of the 21 June 2001 total solar eclipse, looking for visible photons from radiative decays of solar neutrinos. Limit is a τ/m_{ν_2} in $\nu_2 \rightarrow \nu_1 \gamma$. Limit ranges from ~ 100 to 10^7 s/eV for $0.01 < m_{\nu_1} < 0.1$ eV.
- ¹⁶ EGUCHI 04 obtained these results from the solar $\bar{\nu}_e$ flux limit set by the KamLAND measurement assuming ν_2 decay through nonradiative process $\nu_2 \rightarrow \bar{\nu}_1 X$, where X is a Majoron or other invisible particle. Limits are given for the cases of quasidegenerate and hierarchical neutrino masses.
- ¹⁷ The ratio of the lifetime over the mass derived by BANDYOPADHYAY 03 is for ν_2 . They obtained this result using the following solar-neutrino data: total rates measured in Cl and Ga experiments, the Super-Kamiokande's zenith-angle spectra, and SNO's day and night spectra. They assumed that ν_1 is the lowest mass, stable or nearly stable neutrino state and ν_2 decays through nonradiative Majoron emission process, $\nu_2 \rightarrow \bar{\nu}_1 + J$, or through nonradiative process with all the final state particles being sterile. The best fit is obtained in the region of the LMA solution.
- ¹⁸ DERBIN 02B (also BACK 03B) obtained this bound for the radiative decay from the results of background measurements with Counting Test Facility (the prototype of the Borexino detector). The laboratory gamma spectrum is given as $dN_\gamma/d\cos\theta = (1/2)(1 + \alpha\cos\theta)$ with $\alpha=0$ for a Majorana neutrino, and α varying to -1 to 1 for a Dirac neutrino. The listed bound is for the case of $\alpha=0$. The most conservative bound 1.5×10^{13} s eV⁻¹ is obtained for the case of $\alpha=-1$.
- ¹⁹ The ratio of the lifetime over the mass derived by JOSHIPURA 02B is for ν_2 . They obtained this result from the total rates measured in all solar neutrino experiments. They assumed that ν_1 is the lowest mass, stable or nearly stable neutrino state and ν_2 decays through nonradiative process like Majoron emission decay, $\nu_2 \rightarrow \nu'_1 + J$ where ν'_1 state is sterile. The exact limit depends on the specific solution of the solar neutrino problem. The quoted limit is for the LMA solution.
- ²⁰ DOLGOV 99 places limits in the (Majorana) τ -associated ν mass-lifetime plane based on nucleosynthesis. Results would be considerably modified if neutrino oscillations exist.
- ²¹ BILLER 98 use the observed TeV γ -ray spectra to set limits on the mean life of any radiatively decaying neutrino between 0.05 and 1 eV. Curve shows $\tau_\nu/B_\gamma > 0.15 \times 10^{21}$ s at 0.05 eV, $> 1.2 \times 10^{21}$ s at 0.17 eV, $> 3 \times 10^{21}$ s at 1 eV, where B_γ is the branching ratio to photons.
- ²² BLUDMAN 92 sets additional limits by this method for higher mass ranges. Cosmological limits are also obtained.
- ²³ Limit on the radiative decay based on nonobservation of γ 's in coincidence with ν 's from SN 1987A.
- ²⁴ DODELSON 92 range is for wrong-helicity keV mass Dirac ν 's from the core of neutron star in SN 1987A decaying to ν 's that would have interacted in KAM2 or IMB detectors.
- ²⁵ GRANEK 91 considers heavy neutrino decays to $\gamma\nu_L$ and $3\nu_L$, where $m_{\nu_L} < 100$ keV. Lifetime is calculated as a function of heavy neutrino mass, branching ratio into $\gamma\nu_L$, and m_{ν_L} .
- ²⁶ KRAKAUER 91 quotes the limit for ν_e , $\tau/m_\nu > (0.3a^2 + 9.8a + 15.9)$ s/eV, where a is a parameter describing the asymmetry in the radiative neutrino decay defined as $dN_\gamma/d\cos\theta = (1/2)(1 + a\cos\theta)$ $a=0$ for a Majorana neutrino, but can vary from -1 to 1 for a Dirac neutrino. The bound given by the authors is the most conservative (which applies for $a = -1$).
- ²⁷ WALKER 90 uses SN 1987A γ flux limits after 289 days.
- ²⁸ CHUPP 89 should be multiplied by a branching ratio (about 1) and a detection efficiency (about 1/4), and pertains to radiative decay of any neutrino to a lighter or sterile neutrino.
- ²⁹ RAFFELT 89 uses KYULDJIEV 84 to obtain $\tau m^3 > 3 \times 10^{18}$ s eV³ (based on $\bar{\nu}_e e^-$ cross sections). The bound for the radiative decay is not valid if electric and magnetic transition moments are equal for Dirac neutrinos.
- ³⁰ RAFFELT 89B analyze stellar evolution and exclude the region $3 \times 10^{12} < \tau m^3 < 3 \times 10^{21}$ s eV³.
- ³¹ Model-dependent theoretical analysis of SN 1987A neutrinos. Quoted limit is for $[\sum_j |U_{\ell j}|^2 \Gamma_j m_j]^{-1}$, where $\ell = \mu, \tau$. Limit is 3.3×10^{14} s/eV for $\ell = e$.
- ³² OBERAUER 87 looks for photons and e^+e^- pairs from radiative decays of reactor neutrinos.

³³ BINETRUY 84 finds $\tau < 10^8$ s for neutrinos in a radiation-dominated universe.

³⁴ These experiments look for $\nu_k \rightarrow \nu_j \gamma$ or $\bar{\nu}_k \rightarrow \bar{\nu}_j \gamma$.

³⁵ STECKER 80 limit based on UV background; result given is $\tau > 4 \times 10^{22}$ s at $m_\nu = 20$ eV.

³⁶ FALK 78 finds lifetime constraints based on supernova energetics.

³⁷ COWSIK 77 considers variety of scenarios. For neutrinos produced in the big bang, present limits on optical photon flux require $\tau > 10^{23}$ s for $m_\nu \sim 1$ eV. See also COWSIK 79 and GOLDMAN 79.

 ν MAGNETIC MOMENT

The coupling of neutrinos to an electromagnetic field is characterized by a 3×3 matrix λ of the magnetic (μ) and electric (d) dipole moments ($\lambda = \mu - id$). For Majorana neutrinos the matrix λ is antisymmetric and only transition moments are allowed, while for Dirac neutrinos λ is a general 3×3 matrix. In the standard electroweak theory extended to include neutrino masses (see FUJIKAWA 80) $\mu_\nu = 3eG_F m_\nu / (8\pi^2 \sqrt{2}) = 3.2 \times 10^{-19} (m_\nu / \text{eV}) \mu_B$, i.e. it is unobservably small given the known small neutrino masses. In more general models there is no longer a proportionality between neutrino mass and its magnetic moment, even though only massive neutrinos have nonvanishing magnetic moments without fine tuning.

Laboratory bounds on λ are obtained via elastic ν - e scattering, where the scattered neutrino is not observed. The combinations of matrix elements of λ that are constrained by various experiments depend on the initial neutrino flavor and on its propagation between source and detector (e.g., solar ν_e and reactor $\bar{\nu}_e$ do not constrain the same combinations). The listings below therefore identify the initial neutrino flavor.

Other limits, e.g. from various stellar cooling processes, apply to all neutrino flavors. Analogous flavor independent, but weaker, limits are obtained from the analysis of $e^+e^- \rightarrow \nu\bar{\nu}\gamma$ collider experiments.

VALUE ($10^{-10} \mu_B$)	CL%	DOCUMENT ID	TECN	COMMENT
< 0.064	90	¹ APRILE	22B	XENT Solar ν spectrum
< 0.29	90	² BEDA	13	CNTR Reactor $\bar{\nu}_e$
< 6.8	90	³ AUERBACH	01	LSND $\nu_e e, \nu_\mu e$ scattering
< 3900	90	⁴ SCHWIENHO...	01	DONU $\nu_\tau e^- \rightarrow \nu_\tau e^-$
••• We do not use the following data for averages, fits, limits, etc. •••				
< 0.136	90	⁵ AALBERS	23A	LZ Solar ν spectrum
< 0.11	90	⁶ ATZORI-COR..	23	FIT Solar ν spectrum
< 0.75	90	⁷ BONET	22A	CONU Reactor $\bar{\nu}_e$
< 2.8	90	⁸ COLOMA	22	CNTR Reactor $\bar{\nu}_e$
< 1.8	90	⁹ ABE	20E	XMAS Solar ν spectrum
0.14-0.29	90	¹⁰ APRILE	20	XE1T Solar ν spectrum
< 0.012	95	¹¹ CAPOZZI	20	ASTR Tip of the Red-Giant Branch
0.2-0.4	68	¹² KHAN	20	Spectral fit of XENON1T
< 0.28	90	¹³ AGOSTINI	17A	BORX Solar ν spectrum
< 0.022	90	¹⁴ ARCEO-DIAZ	15	ASTR Red giants
< 0.1	95	¹⁵ CORSICO	14	ASTR
< 0.05	95	¹⁶ MILLER-BER...	14B	ASTR
< 0.045	95	¹⁷ VIAUX	13A	ASTR Globular cluster M5
< 0.32	90	¹⁸ BEDA	10	CNTR Reactor $\bar{\nu}_e$
< 2.2	90	¹⁹ DENIZ	10	TEXO Reactor $\bar{\nu}_e$
< 0.011-0.027		²⁰ KUZNETSOV	09	ASTR $\nu_L \rightarrow \nu_R$ in SN1987A
< 0.54	90	²¹ ARPESELLA	08A	BORX Solar ν spectrum
< 0.58	90	²² BEDA	07	CNTR Reactor $\bar{\nu}_e$
< 0.74	90	²³ WONG	07	CNTR Reactor $\bar{\nu}_e$
< 0.9	90	²⁴ DARAKTCH...	05	Reactor $\bar{\nu}_e$
< 130	90	²⁵ XIN	05	CNTR Reactor ν_e
< 37	95	²⁶ GRIFOLS	04	FIT Solar $\bar{\nu}_e \nu$ (SNO NC)
< 3.6	90	²⁷ LIU	04	SKAM Solar ν spectrum
< 1.1	90	²⁸ LIU	04	SKAM Solar ν spectrum (LMA region)
< 5.5	90	²⁹ BACK	03B	CNTR Solar $p\bar{p}$ and $\text{Be } \nu$
< 1.0	90	³⁰ DARAKTCH...	03	Reactor $\bar{\nu}_e$
< 1.3	90	³¹ LI	03B	CNTR Reactor $\bar{\nu}_e$
< 2	90	³² GRIMUS	02	FIT solar + reactor (Majorana ν)
< 80000	90	³³ TANIMOTO	00	RVUE $e^+ e^- \rightarrow \nu\bar{\nu}\gamma$
< 0.01-0.04		³⁴ AYALA	99	ASTR $\nu_L \rightarrow \nu_R$ in SN1987A
< 1.5	90	³⁵ BEACOM	99	SKAM Solar ν spectrum
< 0.03		³⁶ RAFFELT	99	ASTR Red giant luminosity
< 4		³⁷ RAFFELT	99	ASTR Solar cooling
< 44000	90	³⁸ ABREU	97J	DLPH $e^+ e^- \rightarrow \nu\bar{\nu}\gamma$ at LEP
< 33000	90	³⁸ ACCIARRI	97Q	L3 $e^+ e^- \rightarrow \nu\bar{\nu}\gamma$ at LEP
< 0.62		³⁹ ELMFORS	97	COSM Depolarization in early universe plasma
< 27000	95	⁴⁰ ESCRIBANO	97	RVUE $\Gamma(Z \rightarrow \nu\nu)$ at LEP
< 30	90	⁴⁰ VILAIN	95B	CHM2 $\nu_\mu e^- \rightarrow \nu_\mu e$
< 55000	90	⁴⁰ GOULD	94	RVUE $e^+ e^- \rightarrow \nu\bar{\nu}\gamma$ at LEP
< 1.9	95	⁴¹ DERBIN	93	CNTR Reactor $\bar{\nu}_e \rightarrow \bar{\nu}_e$

See key on page 1171

Lepton Particle Listings

Neutrino Properties

< 5400	90	42	COOPER...	92	BEBC	$\nu_e e^- \rightarrow \nu_e e^-$
< 2.4	90	43	VIDYAKIN	92	CNTR	Reactor $\bar{\nu}_e \rightarrow \bar{\nu}_e$
< 56000	90		DESHPANDE	91	RVUE	$e^+ e^- \rightarrow \nu \bar{\nu} \gamma$
< 100	95	44	DORENBOS...	91	CHRM	$\nu_\mu e \rightarrow \nu_\mu e$
< 8.5	90		AHRENS	90	CNTR	$\nu_\mu e \rightarrow \nu_\mu e$
< 10.8	90	45	KRAKAUER	90	CNTR	LAMPF $\nu_e \rightarrow \nu_e$
< 7.4	90	45	KRAKAUER	90	CNTR	LAMPF ($\nu_\mu, \bar{\nu}_\mu$) e elast.
< 0.02		46	RAFFELT	90	ASTR	Red giant luminosity
< 0.1		47	RAFFELT	89b	ASTR	Cooling helium stars
		48	FUKUGITA	88	COSM	Primordial magn. fields
< 40000	90	49	GROTCH	88	RVUE	$e^+ e^- \rightarrow \nu \bar{\nu} \gamma$
< 3		47	RAFFELT	88b	ASTR	He burning stars
< 0.11		47	FUKUGITA	87	ASTR	Cooling helium stars
< 0.0006		50	NUSSINOV	87	ASTR	Cosmic EM backgrounds
< 0.1-0.2			MORGAN	81	COSM	^4He abundance
< 0.85			BEG	78	ASTR	Stellar plasmons
< 0.6		51	SUTHERLAND	76	ASTR	Red giants + degenerate dwarfs
< 81		52	KIM	74	RVUE	$\bar{\nu}_\mu e \rightarrow \bar{\nu}_\mu e$
< 1			BERNSTEIN	63	ASTR	Solar cooling
< 14			COWAN	57	CNTR	Reactor $\bar{\nu}$

- 1 APRILE 22b use data collected with the XENONnT dark matter detector to place a limit on an enhanced magnetic moment of solar neutrinos. Supersedes APRILE 20.
- 2 BEDA 13 report $\bar{\nu}_e e^-$ scattering results, using the Kalinin Nuclear Power Plant and a shielded Ge detector. The recoil electron spectrum is analyzed between 2.5 and 55 keV. Supersedes BEDA 07. Supersedes BEDA 10. This is the most stringent limit on the magnetic moment of reactor $\bar{\nu}_e$.
- 3 AUERBACH 01 limit is based on the LSND ν_e and ν_μ electron scattering measurements. The limit is slightly more stringent than KRAKAUER 90.
- 4 SCHWIENHORST 01 quote an experimental sensitivity of 4.9×10^{-7} .
- 5 AALBERS 23a utilize the first 60 days of data collected by the LZ dark matter search to place a limit on the magnetic moment of solar neutrinos. Low energy electron-recoil events are utilized. This LZ-collaboration analysis supersedes that of the external authors in ATZORI-CORONA 23 because of a more complete treatment of experiment uncertainties.
- 6 ATZORI-CORONA 23 use LUX-ZEPLIN dark matter search data published by AALBERS 23 to place a limit on an enhanced magnetic moment of solar neutrinos.
- 7 BONET 22a use data collected by four low-threshold Ge detectors, placed 17.1 m from one of the cores of the nuclear reactors at Brokdorf to derive this limit. A spectral analysis is performed on reactor on and off data.
- 8 COLOMA 22 present a re-analysis of data taken by the COHERENT and Dresden-II experiments. The combination of both experiments is used to place a limit on the magnetic moment of electron-type neutrinos. The presented value is one-sided limit as recommended by the authors; the two-sided limit is $< 3.2 \times 10^{-10} \mu_B$ at 90% C.L. Results based on Fe and Yb quenching models are reported in the paper. The authors are not part of either collaboration.
- 9 ABE 20e observed an excess of low-energy events in the XMASS detector, which could be interpreted as a signal produced by a neutrino magnetic moment with this magnitude.
- 10 APRILE 20 observed an excess of low-energy events in the XENON1T detector, which could be interpreted as a signal produced by a neutrino magnetic moment with this magnitude.
- 11 CAPOZZI 20 obtains a limit on the neutrino dipole moment from the brightness of the tip of the red-giant branch in ω Centauri. A similar limit of $\mu_\nu < 1.5 \times 10^{-12} \mu_B$ is obtained in NGC 4258.
- 12 KHAN 20 performed a constrained spectral fit analysis of the excess observed in the electron recoil energy spectrum by the XENON1T experiment. This range of the μ_B values is one of the possible interpretations of these excess events. For the individual flavor constraints at 90% C.L. see the original reference.
- 13 AGOSTINI 17a obtained this limit using the shape of the recoil electron energy spectrum from the Borexino Phase-II 1291.5 live days of solar neutrino data and the constraints on the sum of the solar neutrino fluxes from the radiochemical gallium experiments SAGE, Gallex, and GNO. Without radiochemical constraints, the 90% C.L. limit of $< 4.0 \times 10^{-11} \mu_B$ is obtained.
- 14 ARCEO-DIAZ 15 constrains the neutrino magnetic moment from observation of the tip of the red giant branch in the globular cluster ω -Centauri.
- 15 CORSICO 14 constrains the neutrino magnetic moment from observations of white dwarf pulsations.
- 16 MILLER-BERTOLAMI 14b constrains the neutrino magnetic moment from observations of the white dwarf luminosity function of the Galactic disk.
- 17 VIAUX 13a constrains the neutrino magnetic moment from observations of the globular cluster M5.
- 18 BEDA 10 report $\bar{\nu}_e e^-$ scattering results, using the Kalinin Nuclear Power Plant and a shielded Ge detector. The recoil electron spectrum is analyzed between 2.9 and 45 keV. Supersedes BEDA 07. Superseded by BEDA 13.
- 19 DENIZ 10 observe reactor $\bar{\nu}_e$ scattering with recoil kinetic energies 3-8 MeV using Cs(I) detectors. The observed rate and spectral shape are consistent with the Standard Model prediction, leading to the reported constraint on $\bar{\nu}_e$ magnetic moment.
- 20 KUZNETSOV 09 obtain a limit on the flavor averaged magnetic moment of Dirac neutrinos from the time averaged neutrino signal of SN1987A. Improves and supersedes the analysis of BARBIERI 88 and AYALA 99.
- 21 ARPESELLA 08a obtained this limit using the shape of the recoil electron energy spectrum from the Borexino 192 live days of solar neutrino data.
- 22 BEDA 07 performed search for electromagnetic $\bar{\nu}_e$ -e scattering at Kalininskaya nuclear reactor. A Ge detector with active and passive shield was used and the electron recoil spectrum between 3.0 and 61.3 keV analyzed. Superseded by BEDA 10.

- 23 WONG 07 performed search for non-standard $\bar{\nu}_e$ -e scattering at the Kuo-Sheng nuclear reactor. Ge detector equipped with active anti-Compton shield is used. Most stringent laboratory limit on magnetic moment of reactor $\bar{\nu}_e$. Supersedes LI 03b.
- 24 DARAKTCHIEVA 05 present the final analysis of the search for non-standard $\bar{\nu}_e$ -e scattering component at Bugey nuclear reactor. Full kinematical event reconstruction of both the kinetic energy above 700 keV and scattering angle of the recoil electron, by use of TPC. Most stringent laboratory limit on magnetic moment. Supersedes DARAKTCHIEVA 03.
- 25 XIN 05 evaluated the ν_e flux at the Kuo-Sheng nuclear reactor and searched for non-standard ν_e -e scattering. Ge detector equipped with active anti-Compton shield was used. This laboratory limit on magnetic moment is considerably less stringent than the limits for reactor $\bar{\nu}_e$, but is specific to ν_e .
- 26 GRIFOLS 04 obtained this bound using the SNO data of the solar ^8B neutrino flux measured with deuteron breakup. This bound applies to $\mu_{\text{eff}} = (\mu_{21}^2 + \mu_{22}^2 + \mu_{23}^2)^{1/2}$.
- 27 LIU 04 obtained this limit using the shape of the recoil electron energy spectrum from the Super-Kamiokande-I 1496 days of solar neutrino data. Neutrinos are assumed to have only diagonal magnetic moments, $\mu_{\nu 1} = \mu_{\nu 2}$. This limit corresponds to the oscillation parameters in the vacuum oscillation region.
- 28 LIU 04 obtained this limit using the shape of the recoil electron energy spectrum from the Super-Kamiokande-I 1496 live-day solar neutrino data, by limiting the oscillation parameter region in the LMA region allowed by solar neutrino experiments plus KamLAND. $\mu_{\nu 1} = \mu_{\nu 2}$ is assumed. In the LMA region, the same limit would be obtained even if neutrinos have off-diagonal magnetic moments.
- 29 BACK 03b obtained this bound from the results of background measurements with Counting Test Facility (the prototype of the Borexino detector). Standard Solar Model flux was assumed. This μ_ν can be different from the reactor μ_ν in certain oscillation scenarios (see BEACOM 99).
- 30 DARAKTCHIEVA 03 searched for non-standard $\bar{\nu}_e$ -e scattering component at Bugey nuclear reactor. Full kinematical event reconstruction by use of TPC. Superseded by DARAKTCHIEVA 05.
- 31 LI 03b used Ge detector in active shield near nuclear reactor to test for nonstandard $\bar{\nu}_e$ -e scattering.
- 32 GRIMOUS 02 obtain stringent bounds on all Majorana neutrino transition moments from a simultaneous fit of LMA-MSW oscillation parameters and transition moments to global solar neutrino data + reactor data. Using only solar neutrino data, a 90% CL bound of $6.3 \times 10^{-10} \mu_B$ is obtained.
- 33 TANIMOTO 00 combined $e^+ e^- \rightarrow \nu \bar{\nu} \gamma$ data from VENUS, TOPAZ, and AMY.
- 34 AYALA 99 improves the limit of BARBIERI 88.
- 35 BEACOM 99 obtain the limit using the shape, but not the absolute magnitude which is affected by oscillations, of the solar neutrino spectrum obtained by Superkamiokande (825 days). This μ_ν can be different from the reactor μ_ν in certain oscillation scenarios.
- 36 RAFFELT 99 is an update of RAFFELT 90. This limit applies to all neutrino flavors which are light enough (< 5 keV) to be emitted from globular-cluster red giants. This limit pertains equally to electric dipole moments and magnetic transition moments, and it applies to both Dirac and Majorana neutrinos.
- 37 RAFFELT 99 is essentially an update of BERNSTEIN 63, but is derived from the helioseismological limit on a new energy-loss channel of the Sun. This limit applies to all neutrino flavors which are light enough (< 1 keV) to be emitted from the Sun. This limit pertains equally to electric dipole and magnetic transition moments, and it applies to both Dirac and Majorana neutrinos.
- 38 ACCIARRI 97q result applies to both direct and transition magnetic moments and for $q^2=0$.
- 39 ELMFORS 97 calculate the rate of depolarization in a plasma for neutrinos with a magnetic moment and use the constraints from a big-bang nucleosynthesis on additional degrees of freedom.
- 40 Applies to absolute value of magnetic moment.
- 41 DERBIN 93 determine the cross section for 0.6-2.0 MeV electron energy as $(1.28 \pm 0.63) \times \sigma_{\text{weak}}$. However, the (reactor on - reactor off)/(reactor off) is only $\sim 1/100$.
- 42 COOPER-SARKAR 92 assume $f_{D_S}/f_\pi = 2$ and D_S, \bar{D}_S production cross section = $2.6 \mu\text{b}$ to calculate ν flux.
- 43 VIDYAKIN 92 limit is from a $e\bar{\nu}_e$ elastic scattering experiment. No experimental details are given except for the cross section from which this limit is derived. Signal/noise was 1/10. The limit uses $\sin^2 \theta_W = 0.23$ as input.
- 44 DORENBOSCH 91 corrects an incorrect statement in DORENBOSCH 89 that the ν magnetic moment is $< 1 \times 10^{-9}$ at the 95%CL. DORENBOSCH 89 measures both $\nu_\mu e$ and $\bar{\nu}_e$ elastic scattering and assume $\mu(\nu) = \mu(\bar{\nu})$.
- 45 KRAKAUER 90 experiment fully reported in ALLEN 93.
- 46 RAFFELT 90 limit applies for a diagonal magnetic moment of a Dirac neutrino, or for a transition magnetic moment of a Majorana neutrino. In the latter case, the same analysis gives $< 1.4 \times 10^{-12}$. Limit at 95%CL obtained from δM_C .
- 47 Significant dependence on details of stellar models.
- 48 FUKUGITA 88 find magnetic dipole moments of any two neutrino species are bounded by $\mu < 10^{-16} [10^{-9} G/B_0]$ where B_0 is the present-day intergalactic field strength.
- 49 GROTCH 88 combined data from MAC, ASP, CELLO, and Mark J.
- 50 For $m_\nu = 8-200$ eV. NUSSINOV 87 examines transition magnetic moments for $\nu_\mu \rightarrow \nu_e$ and obtain $< 3 \times 10^{-15}$ for $m_\nu > 16$ eV and $< 6 \times 10^{-14}$ for $m_\nu > 4$ eV.
- 51 We obtain above limit from SUTHERLAND 76 using their limit $f < 1/3$.
- 52 KIM 74 is a theoretical analysis of $\bar{\nu}_\mu$ reaction data.

Lepton Particle Listings

Neutrino Properties

NEUTRINO CHARGE RADIUS SQUARED

We report limits on the so-called neutrino charge radius squared. While the straight-forward definition of a neutrino charge radius has been proven to be gauge-dependent and, hence, unphysical (LEE 77c), there have been recent attempts to define a physically observable neutrino charge radius (BERNABEU 00, BERNABEU 02). The issue is still controversial (FUJIKAWA 03, BERNABEU 03). A more general interpretation of the experimental results is that they are limits on certain nonstandard contributions to neutrino scattering.

VALUE (10^{-32} cm^2)	CL%	DOCUMENT ID	TECN	COMMENT
- 2.1 to 3.3	90	¹ DENIZ	10 TEXO	Reactor $\bar{\nu}_e e$
-27.5 to 3	90	² CAEDDU	18	ν_μ coherent scat. on CsI
- 0.53 to 0.68	90	³ HIRSCH	03	$\nu_\mu e$ scat.
- 8.2 to 9.9	90	⁴ HIRSCH	03	anomalous $e^+ e^- \rightarrow \nu \bar{\nu}$
- 2.97 to 4.14	90	⁵ AUERBACH	01 LNSD	$\nu_e e \rightarrow \nu_e e$
- 0.6 to 0.6	90	VILAIN	95b CHM2	$\nu_\mu e$ elastic scat.
0.9 ± 2.7		ALLEN	93 CNTR	LAMPF $\nu e \rightarrow \nu e$
< 2.3	95	MOURAO	92 ASTR	HOME/KAM2 ν rates
< 7.3	90	⁶ VIDYAKIN	92 CNTR	Reactor $\bar{\nu} e \rightarrow \bar{\nu} e$
1.1 ± 2.3		ALLEN	91 CNTR	Repl. by ALLEN 93
- 1.1 ± 1.0		⁷ AHRENS	90 CNTR	$\nu_\mu e$ elastic scat.
- 0.3 ± 1.5		⁸ DORENBOS...	89 CHRM	$\nu_\mu e$ elastic scat.
		GRIFOLS	89b ASTR	SN 1987A

- ¹DENIZ 10 observe reactor $\bar{\nu}_e e$ scattering with recoil kinetic energies 3–8 MeV using CsI(Tl) detectors. The observed rate and spectral shape are consistent with the Standard Model prediction, leading to the reported constraint on $\bar{\nu}_e$ charge radius.
- ²CAEDDU 18 use the data of the COHERENT experiment, AKIMOV 18. The limit is $\langle r_{\nu_\mu}^2 \rangle$ obtained from the time-dependent data. Weaker limits were obtained for charge radii of ν_e and for transition charge radii. The published value was divided by 2 to conform to the convention of this table.
- ³Based on analysis of CCFR 98 results. Limit is on $\langle r_{\nu_\mu}^2 \rangle$ and $\langle r_{\nu_e}^2 \rangle$. The CHARM II and E734 at BNL results are reanalyzed, and weaker bounds on the charge radius squared than previously published are obtained. The NuTeV result is discussed; when tentatively interpreted as ν_μ charge radius it implies $\langle r_{\nu_\mu}^2 \rangle$ and $\langle r_{\nu_e}^2 \rangle$ = $(4.20 \pm 1.64) \times 10^{-33} \text{ cm}^2$.
- ⁴Results of LEP-2 are interpreted as limits on the axial-vector charge radius squared of a Majorana ν_τ . Slightly weaker limits for both vector and axial-vector charge radius squared are obtained for the Dirac case, and somewhat weaker limits are obtained from the analysis of lower energy data (LEP-1.5 and TRISTAN).
- ⁵AUERBACH 01 measure $\nu_e e$ elastic scattering with LNSD detector. The cross section agrees with the Standard Model expectation, including the charge and neutral current interference. The 90% CL applies to the range shown.
- ⁶VIDYAKIN 92 limit is from a $e\bar{\nu}$ elastic scattering experiment. No experimental details are given except for the cross section from which this limit is derived. Signal/noise was 1/10. The limit uses $\sin^2 \theta_W = 0.23$ as input.
- ⁷Result is obtained from reanalysis given in ALLEN 91, followed by our reduction to obtain 1 σ errors.
- ⁸GRIFOLS 89b sets a limit of $\langle r^2 \rangle < 0.2 \times 10^{-32} \text{ cm}^2$ for right-handed neutrinos.

HUANG 16 EPJ C76 489
ARCEO-DIAZ 15 ASP 70 1
LOKHOV 15 PPN 46 347
Translated from FECAV 46 3.
PALANQUE... 15A JCAP 1511 011
ROSSI 15 PR D92 063505
ADE 14 AA 571 A16
BATTYE 14 PRL 112 051303
BEUTLER 14 MNRAS 444 3501
CHEN 14A PR D95 011301
CORSICO 14 JCAP 1408 054
COSTANZI 14 JCAP 1410 081
HOU 14 APJ 782 74
LEISTEDT 14 PRL 113 041301
MILLER-BER... 14B AA 562 A123
RIEMER-SOR... 14 PR D89 103505
STUDENIKIN 14 EPL 107 21001
BEDA 13 PPNL 10 139
VIAUX 13A PRL 111 231301
MORESCO 12 JCAP 1207 053
XIA 12 JCAP 1206 010
ASEEV 11 PR D84 112003
CECCHINI 11 ASP 34 486
SAITO 11 PR D83 043529
BEDA 10 PPNL 7 406
DENIZ 10 PR D81 072001
HANNESTAD 10 JCAP 1008 001
PAGLIAROLI 10 ASP 33 287
SEKIGUCHI 10 JCAP 1003 015
THOMAS 10 PRL 105 031301
ICHIKI 09 PR D79 023520
KOMATSU 09 APJS 180 330
KUZNETSOV 09 IJMP A24 5977
TERENO 09 AA 500 557
VIKHLININ 09 APJ 692 1060
ARPESELLA 08A PRL 101 091302
BERNARDIS 08 PR D78 083535
BEDA 07 PAN 70 1873
Translated from YAF 70 1925.
FOGLI 07 PR D75 053001
GNINENKO 07 PR D75 075014
KRISTIANSEN 07 PR D75 083510
MIRIZZI 07 PR D76 053007
SPERDEL 07 APJS 170 377
WONG 07 PR D75 012001
ZUNCKEL 07 JCAP 0708 004
CIRELLI 06 JCAP 0612 013
FUKUGITA 06 PR D74 027302
GOOBAR 06 JCAP 0606 019
HANNESTAD 06 JCAP 0611 016
KRISTIANSEN 06 PR D74 123005
SANCHEZ 06 MNRAS 366 189
SELJAK 06 JCAP 0610 014
CAPRINI 05 JCAP 0502 006
DARAKTCH... 05 PL B615 153
ICHIKAWA 05 PR D71 043001
KRAUS 05 EPJ C40 447
XIN 05 PR D72 021006
AHARMM 04 PR D70 093014
BARGER 04 PL B595 55
CECCHINI 04 ASP 21 183
CROTTY 04 PR D69 123007
EGUCHI 04 PRL 92 071301
GRIFOLS 04 PL B587 184
LIU 04 PRL 93 021802
ARNABOLDI 03A PRL 91 161802
BACK 03B PL B563 35
BANDYOPA... 03 PL B555 33
BERNABEU 03 hep-ph/0303202
DARAKTCH... 03 PL B564 190
FUJIKAWA 03 hep-ph/0303188
HIRSCH 03 PR D67 033005
LI 03B PRL 90 131802
SPERDEL 03 APJS 148 175
BERNABEU 02 PRL 89 101802
Also PRL 89 229902 (err.)
DERBIN 02B JETPL 76 409
Translated from ZETFP 76 483.
GRIMUS 02 NP B648 376
W. Grimus et al.
JOSHIPURA 02B PR D66 113008
LEWIS 02 PR D66 103511
LOREDO 02 PR D65 063002
WANG 02 PR D65 123001
AUERBACH 01 PR D63 112001
SCHWIENHOR... 01 PL B513 23
ATHANAS 00 PR D61 052002
BERNABEU 00 PR D62 113012
FUKUGITA 00 PRL 84 1082
TANIMOTO 00 PL B478 1
AYALA 99 PR D59 111901
BEACOM 99 PRL 83 5222
CROFF 99 PRL 83 1032
DOLGOV 99 NP B548 385
LOBASHEV 99 PR B450 227
RAFFELT 99 PR PRL 320 319
WEINHIMER 99 PR B460 219
ACKERSTAFF 98 EPJ C5 229
AMMAR 98 PL B431 209
BARATE 98 EPJ C2 395
BILLER 98 PRL 80 2992
FELDMAN 98 PR D57 3873
LENZ 98 PL B416 50
ABREU 97B ZPHY C74 577
ACCIARRI 97Q PRL B412 201
ANASTASSOV 97 PR D55 2559
Also PR D58 119903 (err.)
ELMFORS 97 NP B503 3
ESCRIBANO 97 PL B395 369
FIELDS 97 ASP 6 169
SWAIN 97 PR D55 1
ALEXANDER 96M ZPHY C72 231
ASSAMAGAN 96 PR D53 6065
BAI 96 PR D53 20
BOTTINO 96 PR D53 6361
DOLGOV 96 PL B383 193
HANNESTAD 96 PRL 76 2848
HANNESTAD 96B PRL 77 5148 (err.)
HANNESTAD 96C PR D54 7894
SOBIE 96 ZPHY C70 383
BELESEV 95 PL B350 263
BUSKULIC 95 PL B349 585
Q.-G. Huang, K. Wang, S. Wang
S. Arceo-Diaz et al.
A.V. Lokhov, F.V. Tkachov
N. Palanque-Delabrouille et al.
G. Rossi et al.
P.A.R. Ade et al. (Planck Collab.)
R.A. Battye, A. Moss (MCHS, NOTT)
F. Beutler et al. (BOSS Collab.)
J.-W. Chen et al. (TEXONO Collab.)
A.H. Corsico
M. Costanzi et al.
Z. Hou et al. (TRST, TRSTI)
B. Leistedt, H.V. Peiris, L. Verde
M.M. Miller Bertolami (MPIG, LAPL)
S. Riemer-Sorensen, D. Parkinson, T.M. Davis
A.I. Studenikin
A.G. Beda et al. (GEMMA Collab.)
N. Viaux et al.
M. Moresco et al.
J.-Q. Xia et al.
Y.N. Assev et al.
S. Cecchini et al.
S. Saito, M. Takada, A. Taruya
A.G. Beda et al. (GEMMA Collab.)
M. Deniz et al. (TEXONO Collab.)
S. Hannestad et al.
G. Pagliaroli, F. Rossi-Torres, E. Vissani (INFN+)
T. Sekiguchi et al.
S.A. Thomas, F.B. Abdalla, O. Lahav
K. Ichiki, M. Takada, T. Takahashi
E. Komatsu et al.
A.V. Kuznetsov, N.V. Mikheev, A.A. Okrugin (YARO)
I. Tereno et al.
A. Vikhlinin et al.
C. Arpessella et al. (Borexino Collab.)
F. De Bernardis et al.
A.G. Beda et al.
G.L. Fogli et al.
S.N. Gninenko, N.V. Krasnikov, A. Rubbia
J. Kristiansen, O. Elgaroy, H. Dahle
A. Mirizzi, D. Montanino, P.D. Serpico
D.N. Spergel et al. (TEXONO Collab.)
H.T. Wong et al.
C. Zunckel, P. Ferreira
M. Cirelli et al.
M. Fukugita et al.
A. Goobar et al.
S. Hannestad, G. Raffelt
J. Kristiansen, O. Elgaroy, H. Eriksen
A.G. Sanchez et al.
U. Seljak, A. Slosar, P. McDonald
C. Caprini, P.G. Ferreira (GEVA, OXFPT)
Z. Darakchieva et al. (MUNU Collab.)
K. Ichikawa, M. Fukugita, M. Kawasaki (ICRR)
Ch. Xin et al. (TEXONO Collab.)
B. Aharim et al. (SNO Collab.)
V. Barger, D. Marfatia, A. Tregre (BGN+)
P. Crotty, J. Lesgourgues, S. Pastor
K. Eguchi et al. (KamLAND Collab.)
J.A. Grifols, E. Masso, S. Mohanty (BARC, AHMED)
D.W. Liu et al. (Super-Kamiokande Collab.)
C. Arnaboldi et al. (Borexino Collab.)
H.O. Back et al. (SAHA+)
A. Bandyopadhyay, S. Choubey, S. Goswami
J. Bernabeu, J. Papavassiliou, J. Vidal
Z. Darakchieva et al. (MUNU Collab.)
K. Fujikawa, R. Shrock
M. Hirsch, E. Nardi, D. Restrepo
H.B. Li et al. (TEXONO Collab.)
D.N. Spergel et al.
J. Bernabeu, J. Papavassiliou, J. Vidal
J. Bernabeu, J. Papavassiliou, J. Vidal
A.V. Derbin, O.Ju. Smirnov
W. Grimus et al.
A.S. Joshupura, E. Masso, S. Mohanty
A. Lewis, S. Bridle
T.J. Loredo, D.Q. Lamb
X. Wang, M. Tegmark, M. Zaldarriaga
L.B. Auerbach et al. (LNSD Collab.)
R. Schwienhorst et al. (DONUT Collab.)
M. Athanas et al. (CLEO Collab.)
J. Bernabeu et al.
M. Fukugita, G.C. Liu, N. Sugiyama
N. Tanimoto et al.
A. Ayala, J.C. D'Olivo, M. Torres
J.F. Beacom, P. Vogel
R.A.C. Croft, W. Hu, R. Dave
A.D. Dolgov et al.
V.M. Lobashev et al.
G.G. Raffelt
Ch. Weinheimer et al.
K. Ackersstaff et al. (OPAL Collab.)
R. Ammar et al. (CLEO Collab.)
R. Barate et al. (ALEPH Collab.)
S.D. Biller et al. (WHIPPLe Collab.)
G.J. Feldman, R.D. Cousins
S. Lenz et al.
P. Abreu et al. (DELPHI Collab.)
M. Acciari et al. (LS Collab.)
A. Anastassov et al. (CLEO Collab.)
A. Anastassov et al. (CLEO Collab.)
P. Elmfors et al.
R. Escribano, E. Masso (BARC, PARIT)
B.D. Fields, K. Kainulainen, K.A. Olive (NDAM+)
J. Swain, L. Taylor (NEAS)
G. Alexander et al. (OPAL Collab.)
K.A. Assamagan et al. (PSI, ZUR, VILL+)
J.Z. Bai et al. (BES Collab.)
A. Bottino et al.
A.D. Dolgov, S. Pastor, J.W.F. Valle (IFIC, VALE)
S. Hannestad, J. Madsen (AARH)
S. Hannestad, J. Madsen (AARH)
S. Hannestad, J. Madsen (AARH)
R.J. Sobie, R.K. Keeler, I. Lawson (VICT)
A.I. Belevsev et al. (INRM, KIAE)
D. Buskulic et al. (ALEPH Collab.)

REFERENCES FOR Neutrino Properties

AALBERS 23 PRL 131 041002
AALBERS 23A PR D108 072006
ATZORI-COR... 23 PR D107 053001
ESFAHANI 23 PRL 131 102502
IVANEZ-BAL... 23 PL B847 138252
AKER 22 NATP 18 160
APRILE 22B PRL 129 161805
BONET 22A EPJ C82 813
BRIEDEN 22 JCAP 2208 024
COLOMA 22 JHEP 2205 037
KUMAR 22 JCAP 2209 060
TANSEERI 22 JHEAP 36 1
ABBOTT 21A PR D105 023520
ALAM 21 PR D103 083533
DI-VALENT... 21 PR D104 083504
GARNY 21 JCAP 2103 049
STOCKER 21 PR D103 123508
ABE 20E PL B809 135741
AGHANIM 20 AA 641 A6
APRILE 20 PR D102 072004
CAPOZZI 20 PR D102 083007
CHOUDHURY 20 JCAP 2007 037
IVANOV 20 PR D101 083504
KHAN 20 PL B809 135782
PALANQUE... 20 JCAP 2004 038
AHARMM 19 PR D99 032013
AKER 19 PRL 123 221802
Also PR D104 012005
ESCUERO 19 PR D100 103531
LOUREIRO 19 PRL 123 081301
APRILE 19 JCAP 1905 041
CAPOZZI 19 PR D102 083007
AKIMOV 18 arXiv:1804.09459
CAEDDU 18 PR D98 113010
Also PR D101 059902 (err.)
CHOUDHURY 18 JCAP 1809 017
AGOSTINI 17A PR D96 091103
SIMPSON 17 JCAP 1706 029
VAGNOZZI 17 PR D96 123503
YECHÉ 17 JCAP 1706 047
DELLA-VALLE 16 EPJ C76 24
DIVALENTINO 16 PR D93 083527
J. Aalbers et al. (LZ Collab.)
J. Aalbers et al. (LZ Collab.)
M. Atzori Corona et al. (CAGL, CAGLI)
A.A. Esfahani et al. (Project 8 Collab.)
P. Ivanez-Ballesteros, M.C. Volpe (CNRS, UPCIT)
M. Aker et al. (KATRIN Collab.)
E. Aprile et al. (XENONnT Collab.)
H. Bonet et al. (CONUS Collab.)
S. Brieden, Hector Gil-Marin, Licia Verde (IFT, OSU, STON, ICREA+)
P. Coloma et al.
S. Kumar, R. Nunes, P.Yadav
I. Tanseri et al.
T.C.M. Abbott et al. (DES Collab.)
S. Alam et al. (eBOSS Collab.)
E. Di Valentino, S. Gariazzo, O. Mena (DURH+)
P. Stocker et al. (GAMBIT Collab.)
K. Abe et al. (XMASS Collab.)
N. Aghanim et al. (Planck Collab.)
E. Aprile et al. (XENON Collab.)
F. Capozzi, G. Raffelt (MFM)
S.R. Choudhury, S. Hannestad (ITB, AARH)
M.M. Ivanov, M. Simonovic, M. Zaldarriaga (NYU+)
N.N. Khan (MPIK)
N. Palanque-Delabrouille et al. (SACL+)
B. Aharim et al. (SNO Collab.)
M. Aker et al. (KATRIN Collab.)
M. Aker et al. (KATRIN Collab.)
M. Escudero, M. Fairbairn (LOK)
A. Loureiro et al.
A. Upadhye (WMIC)
D. Akimov et al. (COHERENT Collab.)
M. Cadeddu et al.
M. Cadeddu et al.
S.R. Choudhury, S. Choubey
M. Agostini et al. (Borexino Collab.)
F. Simpson et al. (BARC)
S. Vagnozzi et al.
C. Yeché et al.
F. Della Valle et al. (PVLAS Collab.)
E. Di Valentino et al.

Lepton Particle Listings

Neutrino Properties, Number of Neutrino Types

Number of Neutrino Types

The neutrinos referred to in this section are those of the Standard $SU(2) \times U(1)$ Electroweak Model possibly extended to allow nonzero neutrino masses. Light neutrinos are those with $m < m_Z/2$. The limits are on the number of neutrino mass eigenstates, including ν_1 , ν_2 , and ν_3 .

THE NUMBER OF LIGHT NEUTRINO TYPES FROM COLLIDER EXPERIMENTS

Revised June 2020 by C.-J. Lin (LBNL). Written by D. Karlen (University of Victoria and TRIUMF).

The most precise measurements of the number of light neutrino types, N_ν , come from studies of Z production in e^+e^- collisions. The invisible partial width, Γ_{inv} , is determined by subtracting the measured visible partial widths, corresponding to Z decays into quarks and charged leptons, from the total Z width. The invisible width is assumed to be due to N_ν light neutrino species each contributing the neutrino partial width Γ_ν as given by the Standard Model. In order to reduce the model dependence, the Standard Model value for the ratio of the neutrino to charged leptonic partial widths, $(\Gamma_\nu/\Gamma_\ell)_{\text{SM}} = 1.991 \pm 0.001$, is used instead of $(\Gamma_\nu)_{\text{SM}}$ to determine the number of light neutrino types:

$$N_\nu = \frac{\Gamma_{\text{inv}}}{\Gamma_\ell} \left(\frac{\Gamma_\ell}{\Gamma_\nu} \right)_{\text{SM}}. \quad (1)$$

The combined result from the four LEP experiments is $N_\nu = 2.984 \pm 0.008$ [1]. Recent analyses applied corrections to the LEP result [1] by including the effect of correlated luminosity systematics and also using an improved Bhabha cross section calculation [2,3] to obtain $N_\nu = 2.9963 \pm 0.0074$.

In the past, when only small samples of Z decays had been recorded by the LEP experiments and by the Mark II at SLC, the uncertainty in N_ν was reduced by using Standard Model fits to the measured hadronic cross sections at several center-of-mass energies near the Z resonance. Since this method is much more dependent on the Standard Model, the approach described above is favored.

Before SLC and LEP, limits on the number of neutrino generations were placed by experiments at lower-energy e^+e^- colliders by measuring the cross section of the process $e^+e^- \rightarrow \nu\bar{\nu}\gamma$. The ASP, CELLO, MAC, MARK J, and VENUS experiments observed a total of 3.9 events above background [4], leading to a 95% CL limit of $N_\nu < 4.8$. This process has a much larger cross section at center-of-mass energies near the Z mass and has been measured at LEP by the ALEPH, DELPHI, L3, and OPAL experiments [5]. These experiments have observed several thousand such events, and the combined result is $N_\nu = 3.00 \pm 0.08$. The same process has also been measured by the LEP experiments at much higher center-of-mass energies, between 130 and 208 GeV, in searches for new physics [6]. Combined with the lower energy data, the result is $N_\nu = 2.92 \pm 0.05$.

Experiments at $p\bar{p}$ colliders also placed limits on N_ν by determining the total Z width from the observed ratio of

CHING	95	JMP A10 2841	C.R. Ching et al. (CST, BEJT, CIAE)
DOLGOV	95	PR D51 4129	A.D. Dolgov, K. Kainulainen, I.Z. Rothstein (MICH+)
HIDDEMANN	95	JP G21 639	K.H. Hidemann, H. Daniel, O. Schwentker (TUM)
KERNAN	95	NP B437 243	P.J. Kernan, L.M. Krauss (CASE)
SIGL	95	PR D51 1499	G. Sigl, M.S. Turner (FNAL, EFI)
STOEHL	95	PRL 75 3237	W. Stoehl, D.J. Decman (LNL)
VILAIN	95B	PL B345 115	P. Vilain et al. (CHARM II Collab.)
ASSAMAGAN	94	PL B335 231	K.A. Assamagan et al. (PSI, ZUR1, VILL+)
BABU	94	PL B321 140	K.S. Babu, T.M. Gould, I.Z. Rothstein (BART+)
DODELSON	94	PR D49 5068	S. Dodelson, G. Gyuk, M.S. Turner (FNAL, CHIC+)
GOULD	94	PL B333 545	T.M. Gould, I.Z. Rothstein (JHU, MICH)
JECKELMANN	94	PL B335 326	B. Jeckelmann, P.F.A. Goudsmit, H.J. Leisi (WABRN+)
KAWASAKI	94	NP B419 105	M. Kawasaki et al. (OSU)
PERES	94	PR D50 513	O.L.G. Peres, V. Pleitez, R. Zukanovich Funchal
YASUMI	94	PL B334 229	S. Yasumi et al. (KEK, TSUK, KYOT+)
ALLEN	93	PR D47 11	R.C. Allen et al. (UCI, LANL, ANL+)
BALEST	93	PR D47 3671	R. Balest et al. (CLEO Collab.)
CINABRO	93	PRL 70 3700	D. Cinabro et al. (CLEO Collab.)
DERBIN	93	JETPL 57 768	A.V. Derbin et al. (PNPI)
Translated from ZETFP 57 755			
DOLGOV	93	PRL 71 476	A.D. Dolgov, I.Z. Rothstein (MICH)
ENQVIST	93	PL B301 376	K. Enqvist, H. Uibo (MORD)
SUN	93	CJNP 15 261	H.C. Sun et al. (CIAE, CST, BEJT)
WEINHEIMER	93	PL B300 210	C. Weinheimer et al. (MAINZ)
ALBRECHT	92M	PL B292 221	H. Albrecht et al. (ARGUS Collab.)
BLUDMAN	92	PR D45 4720	S.A. Bludman (CFPA)
COOPER...	92	PL B280 153	A.M. Cooper-Sarkar et al. (BEBC WA66 Collab.)
DODELSON	92	PRL 68 2572	S. Dodelson, J.A. Frieman, M.S. Turner (FNAL+)
HOLZSCHUH	92B	PL B287 381	E. Holzschuh, M. Fritsch, W. Kundig (ZUR1)
KAWANO	92	PL B275 487	L.H. Kawano et al. (CIT, UCSD, LLL+)
MOURAO	92	PL B285 364	A.M. Mourao, J. Pulido, J.P. Ralston (LSB, LSBT+)
PDG	92	PR D45 51	K. Hikasa et al. (KEK, LBL, BOST+)
VIDYAKIN	92	JETPL 55 206	A.V. Vidyakin et al. (KIAE)
Translated from ZETFP 55 212			
ALLEN	91	PR D43 1	R.C. Allen et al. (UCI, LANL, UMD)
DAVIDSON	91	PR D43 2314	S. Davidson, B.A. Campbell, D. Bailey (ALBE+)
DESHPANDE	91	PR D43 943	N.G. Deshpande, K.V.L. Sarma (OREG, TATA)
DORENBOSCH...	91	ZPHY C51 142 (err.)	J. Dorenbosch et al. (CHARM Collab.)
FULLER	91	PR D43 3136	G.M. Fuller, R.A. Malaney (UCSD)
GRANEK	91	JMP A6 2387	H. GraneK, B.H.J. McKellar (MELB)
KAWAKAMI	91	PL B256 105	H. Kawakami et al. (INUS, TOHOK, TINT+)
KOLB	91	PRL 67 533	E.W. Kolb et al. (FNAL, CHIC)
KRAKAUER	91	PR D44 6	D.A. Krakauer et al. (LAMPF E225 Collab.)
LAM	91	PR D44 3345	W.P. Lam, K.W. Ng (AST)
ROBERTSON	91	PRL 67 957	R.G.H. Robertson et al. (LASL, LLL)
AHRENS	90	PR D41 3297	L.A. Ahrens et al. (BNL, BROW, HIRO+)
AVIGNONE	90	PR D41 682	F.T. Avignone, J.L. Collar (SCC)
KRAKAUER	90	PL B252 177	D.A. Krakauer et al. (LAMPF E225 Collab.)
RAFFELT	90	PRL 64 2856	G.G. Raffelt (MPIM)
WALKER	90	PR D41 689	T.P. Walker (HARV)
CHUPP	89	PRL 62 505	E.L. Chupp, W.T. Vestrand, C. Reppin (UNH, MPIM)
DORENBOSCH...	89	ZPHY C41 567	J. Dorenbosch et al. (CHARM Collab.)
GRIFOLS	89B	PR D40 3819	J.A. Grifols, E. Masso (BARC)
KOLB	89	PRL 62 509	E.W. Kolb, M.S. Turner (CHIC, FNAL)
LOREDO	89	ANYAS 571 601	T.J. Loredo, D.Q. Lamb (CHIC)
RAFFELT	89	PR D39 2066	G.G. Raffelt (PRIN, UCB)
RAFFELT	89B	APJ 336 61	G. Raffelt, D. Dearborn, J. Silk (UCB, LLL)
ALBRECHT	88B	PL B202 149	H. Albrecht et al. (ARGUS Collab.)
BARBIERI	88	PRL 61 27	R. Barbieri, R.N. Mohapatra (PISA, UMD)
BORIS	88	PRL 61 245 (err.)	S.D. Boris et al. (ITEP, ASCI)
FUKUGITA	88	PRL 60 879	M. Fukugita et al. (KYOTU, MPIM, UCB)
GROTCH	88	ZPHY C39 553	H. Grotch, R.W. Robinett (PSU)
RAFFELT	88B	PR D37 549	G.G. Raffelt, D.S.P. Dearborn (UCB, LLL)
SPERGEL	88	PL B200 366	D.N. Spergel, J.N. Bahcall (IAS)
VONFEILITZ...	88	PL B200 580	F. von Feilitzsch, L. Oberauer (TUM)
BARBIELLINI	87	NAT 329 21	G. Barbilini, G. Cocconi (CERN)
BORIS	87	PRL 58 2019	S.D. Boris et al. (ITEP, ASCI)
Also		PRL 61 245 (err.)	S.D. Boris et al. (ITEP, ASCI)
BORIS	87B	JETPL 45 333	S.D. Boris et al. (ITEP)
Translated from ZETFP 45 267			
FUKUGITA	87	PR D36 3817	M. Fukugita, S. Yazaki (KYOTU, TOKY)
NUSSINOV	87	PR D36 2278	S. Nussinov, Y. Rephaeli (TELA)
OBERAUER	87	PL B198 113	L.F. Oberauer, F. von Feilitzsch, R.L. Mossbauer (FNAL, BART)
SPRINGER	87	PR A35 679	P.T. Springer et al. (LNL)
KETOV	86	JETPL 44 146	S.N. Ketov et al. (KIAE)
Translated from ZETFP 44 114			
COWSIK	85	PL 151B 62	R. Cowzik (TATA)
RAFFELT	85	PR D31 3002	G.G. Raffelt (MPIM)
BINETRUY	84	PL 134B 174	P. Binetruy, G. Girardi, P. Salati (LAPP)
FREESE	84	NP B233 167	K. Freese, D.N. Schramm (CHIC, FNAL)
KYULDJIEV	84	NP B243 387	A.V. Kyuldjiev (SOFI)
SCHRAMM	84	PL 141B 337	D.N. Schramm, G. Steigman (FNAL, BART)
VOGEL	84	PR D30 1505	P. Vogel (LASL)
ANDERHUB	82	PL 114B 76	H.B. Anderhub et al. (ETH, SIN)
OLIVE	82	PR D25 213	K.A. Olive, M.S. Turner (CHIC, UCSB)
BERNSTEIN	81	PL 101B 39	J. Bernstein, G. Feinberg (STEVE, COLU)
FRANK	81	PR D24 2001	J.S. Frank et al. (LASL, YALE, MIT+)
MORGAN	81	PL 102B 247	J.A. Morgan (SUSS)
FUJIKAWA	80	PRL 45 963	K. Fujikawa, R. Shrock (STON)
LUBIMOV	80	PL 94B 266	V.A. Lyubimov et al. (ITEP)
STECKER	80	PRL 45 1460	F.W. Stecker (NASA)
COWSIK	79	PR D19 2219	R. Cowzik (TATA)
GOLDMAN	79	PR D19 2215	T. Goldman, G.J. Stephenson (LASL)
BEG	78	PR D17 1395	M.A.B. Beg, W.J. Marciano, M. Ruderman (ROCK+)
BLITZSCHAU	78	NP B133 205	J. Blitschrau et al. (Gangamele Collab.)
FALK	77	PL 79B 511	S.W. Falk, D.N. Schramm (CHIC)
BARNES	77	PRL 38 1049	V.E. Barnes et al. (PURD, ANL)
COWSIK	77	PRL 39 784	R. Cowzik (MPIM, TATA)
LEE	77C	PR D16 1444	B.W. Lee, R.E. Shrock (STON)
VYSOTSKY	77	JETPL 26 188	M.I. Vysofsky, A.D. Dolgov, Y.B. Zeldovich (ITEP)
Translated from ZETFP 26 200			
BELLOTTI	76	LNC 17 553	E. Bellotti et al. (MILA)
SUTHERLAND	76	PR D13 2700	P. Sutherland et al. (PENN, COLU, NYU)
SZALAY	76	AA 49 437	A.S. Szalay, G. Marx (EOTV)
CLARK	74	PR D9 533	A.R. Clark et al. (LBL)
KIM	74	PR D9 3050	J.E. Kim, V.S. Mathur, S. Okubo (ROCH)
REINES	74	PRL 32 180	F. Reines, H.W. Sobel, H.S. Gurr (UCI)
SZALAY	74	APAH 35 8	A.S. Szalay, G. Marx (EOTV)
COWSIK	72	PRL 29 669	R. Cowzik, J. McClelland (UCB)
MARX	72	Nu Conf. Budapest	G. Marx, A.S. Szalay (EOTV)
GERSHTEIN	66	JETPL 4 120	S.S. Gershtein, Y.B. Zeldovich (KIAM)
Translated from ZETFP 4 189			
BERNSTEIN	63	PR 132 1227	J. Bernstein, M. Ruderman, G. Feinberg (NYU+)
COWAN	57	PR 107 528	C.L. Cowan, F. Reines (LANL)

Lepton Particle Listings

Number of Neutrino Types

$W^\pm \rightarrow \ell^\pm \nu$ to $Z \rightarrow \ell^+ \ell^-$ events [7]. This involved a calculation that assumed Standard Model values for the total W width and the ratio of W and Z leptonic partial widths, and used an estimate of the ratio of Z to W production cross sections. Now that the Z width is very precisely known from the LEP experiments, the approach is now one of those used to determine the W width.

References

1. ALEPH, DELPHI, L3, OPAL, and SLD Collaborations, and LEP Electroweak Working Group, and SLD Electroweak Group, and SLD Heavy Flavour Group, Phys. Reports **427**, 257 (2006).
2. P. Janot and S. Jadach, Phys. Lett. **B803**, 135319 (2020).
3. G. Voutsinas *et al.*, Phys. Lett. **B800**, 135068 (2020).
4. VENUS: K. Abe *et al.*, Phys. Lett. **B232**, 431 (1989); ASP: C. Hearty *et al.*, Phys. Rev. **D39**, 3207 (1989); CELLO: H.J. Behrend *et al.*, Phys. Lett. **B215**, 186 (1988); MAC: W.T. Ford *et al.*, Phys. Rev. **D33**, 3472 (1986); MARK J: H. Wu, Ph.D. Thesis, Univ. Hamburg (1986).
5. L3: M. Acciarri *et al.*, Phys. Lett. **B431**, 199 (1998); DELPHI: P. Abreu *et al.*, Z. Phys. **C74**, 577 (1997); OPAL: R. Akers *et al.*, Z. Phys. **C65**, 47 (1995); ALEPH: D. Buskulic *et al.*, Phys. Lett. **B313**, 520 (1993).
6. DELPHI: J. Abdallah *et al.*, Eur. Phys. J. **C38**, 395 (2005); L3: P. Achard *et al.*, Phys. Lett. **B587**, 16 (2004); ALEPH: A. Heister *et al.*, Eur. Phys. J. **C28**, 1 (2003); OPAL: G. Abbiendi *et al.*, Eur. Phys. J. **C18**, 253 (2000).
7. UA1: C. Albajar *et al.*, Phys. Lett. **B198**, 271 (1987); UA2: R. Ansari *et al.*, Phys. Lett. **B186**, 440 (1987).

Number from $e^+ e^-$ Colliders

Number of Light ν Types

VALUE	DOCUMENT ID	TECN
2.9963 ± 0.0074	1 JANOT	20

• • • We do not use the following data for averages, fits, limits, etc. • • •

2.9918 ± 0.0081	2 VOUTSINAS	20
2.9840 ± 0.0082	3 LEP-SLC	06 RVUE
3.00 ± 0.05	4 LEP	92 RVUE

¹ JANOT 20 applies a correction to LEP-SLC 06 using an updated Bhabha cross section calculation. This result also includes a correction to account for correlated luminosity bias as presented in VOUTSINAS 20.

² VOUTSINAS 20 applies a correction to LEP-SLC 06 to account for correlated luminosity bias.

³ Combined fit from ALEPH, DELPHI, L3 and OPAL Experiments.

⁴ Simultaneous fits to all measured cross section data from all four LEP experiments.

Number of Light ν Types from Direct Measurement of Invisible Z Width

In the following, the invisible Z width is obtained from studies of single-photon events from the reaction $e^+ e^- \rightarrow \nu \bar{\nu} \gamma$. All are obtained from LEP runs in the $E_{CM}^{e^+ e^-}$ range 88–209 GeV.

VALUE	DOCUMENT ID	TECN	COMMENT
2.92 ± 0.05 OUR AVERAGE	Error	includes scale factor of 1.2.	
2.84 ± 0.10 ± 0.14	ABDALLAH	05B DLPH	$\sqrt{s} = 180\text{--}209$ GeV
2.98 ± 0.05 ± 0.04	ACHARD	04E L3	1990–2000 LEP runs
2.86 ± 0.09	HEISTER	03C ALEP	$\sqrt{s} = 189\text{--}209$ GeV
2.69 ± 0.13 ± 0.11	ABBIENDI,G	00D OPAL	1998 LEP run
2.89 ± 0.32 ± 0.19	ABREU	97J DLPH	1993–1994 LEP runs
3.23 ± 0.16 ± 0.10	AKERS	95C OPAL	1990–1992 LEP runs
2.68 ± 0.20 ± 0.20	BUSKULIC	93L ALEP	1990–1991 LEP runs

• • • We do not use the following data for averages, fits, limits, etc. • • •

2.84 ± 0.15 ± 0.14	ABREU	00Z DLPH	1997–1998 LEP runs
3.01 ± 0.08	ACCIARRI	99R L3	1991–1998 LEP runs
3.1 ± 0.6 ± 0.1	ADAM	96C DLPH	$\sqrt{s} = 130, 136$ GeV

Limits from Astrophysics and Cosmology

Effective Number of Light ν Types

"Light" means here with a mass $<$ about 1 MeV. The quoted values correspond to N_{eff} , where $N_{\text{eff}} = 3.045$ in the Standard Model with $N_\nu = 3$. See also reviews on "Big-Bang Nucleosynthesis" and "Neutrinos in Cosmology."

VALUE	CL%	DOCUMENT ID	TECN	COMMENT
• • •				We do not use the following data for averages, fits, limits, etc. • • •
3.12 ± 0.38	95	1 BRIEDEN	22 COSM	BOSS, eBOSS, CMB
2.90 ± 0.15	68	2 KUMAR	22 COSM	BOSS + CMB
2.89 ± 0.14	68	3 YEH	22 COSM	BBN + CMB
2.99 ± 0.17	68	4 AGHANIM	20 COSM	
2.84 ± 0.15	68	5 FIELDS	20 COSM	BBN
2.88 ± 0.17	68	6 IVANOV	20 COSM	Planck and BOSS
2.3–3.2	95	7 VERDE	17 COSM	
2.88 ± 0.16	68	8 CYBURT	16 COSM	BBN
2.88 ± 0.20	95	9 ROSSI	15 COSM	
3.3 ± 0.5	95	10 ADE	14 COSM	Planck
3.78 $^{+0.31}_{-0.30}$		11 COSTANZI	14 COSM	
3.29 ± 0.31		12 HOU	14 COSM	
< 3.80	95	13 LEISTEDT	14 COSM	
< 4.10	95	14 MORESCO	12 COSM	
< 5.79	95	15 XIA	12 COSM	
< 4.08	95	MANGANO	11 COSM	BBN
0.9–8.2		16 ICHIKAWA	07 COSM	
3–7	95	17 CIRELLI	06 COSM	
2.7–4.6	95	18 HANNESTAD	06 COSM	
3.6–7.4	95	17 SELJAK	06 COSM	
< 4.4		19 CYBURT	05 COSM	
< 3.3		20 BARGER	03C COSM	
1.4–6.8		21 CROTTY	03 COSM	
1.9–6.6		21 PIERPAOLI	03 COSM	
2–4		LISI	99 COSM	BBN
< 4.3		OLIVE	99 COSM	BBN
< 4.9		COPI	97	Cosmology
< 3.6		HATA	97B	High D/H quasar abs.
< 4.0		OLIVE	97	BBN; high ^4He and ^7Li
< 4.7		CARDALL	96B	COSM High D/H quasar abs.
< 3.9		FIELDS	96	COSM BBN; high ^4He and ^7Li
< 4.5		KERNAN	96	COSM High D/H quasar abs.
< 3.6		OLIVE	95	BBN; ≥ 3 massless ν
< 3.3		WALKER	91	Cosmology
< 3.4		OLIVE	90	Cosmology
< 4		YANG	84	Cosmology
< 4		YANG	79	Cosmology
< 7		STEIGMAN	77	Cosmology
< 4		PEEBLES	71	Cosmology
< 16		22 SHVARTSMAN	69	Cosmology
		HOYLE	64	Cosmology

¹ BRIEDEN 22 combines large scale structure data from BOSS and eBOSS including the shape of the matter power spectrum with Planck CMB data.

² KUMAR 22 combine the reconstructed galaxy power spectrum from BOSS data with Planck CMB data.

³ YEH 22 combines Planck 2018 CMB data with BBN and observations of deuterium and Helium-4. Supersedes FIELDS 20.

⁴ AGHANIM 20 best fit on number of neutrino types is based on Planck data combined with lensing and baryon acoustic oscillations (BAO). Without BAO, they find $2.89^{+0.18}_{-0.19}$. Several other values are quoted using different combinations of data.

⁵ FIELDS 20 combines Planck 2018 CMB data with BBN and observations of deuterium and Helium-4.

⁶ IVANOV 20 combines 2018 Planck CMB data with baryon acoustic oscillation data from BOSS. This study is based on a full-shape likelihood for the redshift-space galaxy power spectrum of the BOSS data.

⁷ Uses Planck Data combined with an independent standard measure of distance to the sound horizon to set a limit on the total number of neutrinos. Only CMB and early-time information are used.

⁸ CYBURT 16 combines Planck 2015 CMB data with BBN and observations of deuterium and Helium-4.

⁹ ROSSI 15 sets limits on the number of neutrino types using BOSS Lyman alpha forest data combined with Planck CMB data and baryon acoustic oscillations.

¹⁰ Fit to the number of neutrino degrees of freedom from Planck CMB data along with WMAP polarization, high L, and BAO data.

¹¹ Fit to the number of neutrinos degrees of freedom from Planck CMB data along with BAO, shear and cluster data.

¹² Fit based on the SPT-SZ survey combined with CMB, BAO, and H_0 data.

¹³ Constrains the number of neutrino degrees of freedom (marginalizing over the total mass) from CMB, CMB lensing, BAO, and galaxy clustering data.

¹⁴ Limit on the number of light neutrino types from observational Hubble parameter data with seven-year WMAP data, SPT, and the most recent estimate of H_0 . Best fit is 3.45 ± 0.65 .

¹⁵ Limit on the number of light neutrino types from the CFHTLS combined with seven-year WMAP data and a prior on the Hubble parameter. Best fit is $4.17^{+1.62}_{-1.26}$. Limit is relaxed to $3.98^{+2.02}_{-1.20}$ when small scales affected by non-linearities are removed.

See key on page 1171

Lepton Particle Listings

Number of Neutrino Types, Double-β Decay

- ¹⁶ Constrains the number of neutrino types from recent CMB and large scale structure data. No priors on other cosmological parameters are used.
- ¹⁷ Constrains the number of neutrino types from recent CMB, large scale structure, Lyman-alpha forest, and SNIa data. The slight preference for $N_\nu > 3$ comes mostly from the Lyman-alpha forest data.
- ¹⁸ Constrains the number of neutrino types from recent CMB and large scale structure data. See also HAMANN 07.
- ¹⁹ Limit on the number of neutrino types based on ⁴He and D/H abundance assuming a baryon density fixed to the WMAP data. Limit relaxes to 4.6 if D/H is not used or to 5.8 if only D/H and the CMB are used. See also CYBURT 01 and CYBURT 03.
- ²⁰ Limit on the number of neutrino types based on combination of WMAP data and big-bang nucleosynthesis. The limit from WMAP data alone is 8.3. See also KNELLER 01. $N_\nu \geq 3$ is assumed to compute the limit.
- ²¹ 95% confidence level range on the number of neutrino flavors from WMAP data combined with other CMB measurements, the 2dfGRS data, and HST data.
- ²² SHVARTSMAN 69 limit inferred from his equations.

Number Coupling with Less Than Full Weak Strength

VALUE	DOCUMENT ID	TECN
-------	-------------	------

• • • We do not use the following data for averages, fits, limits, etc. • • •

<20	¹ OLIVE	81c COSM
<20	¹ STEIGMAN	79 COSM

¹ Limit varies with strength of coupling. See also WALKER 91.

REFERENCES FOR Limits on Number of Neutrino Types

BRIEDEN	22	JCAP 2208 024	S. Brieden, Hector Gil-Marín, Licia Verde
KUMAR	22	JCAP 2209 060	S. Kumar, R. Nunes, P.Yadav
YEH	22	JCAP 2210 046	T.-H. Yeh et al. (ILL, MINN)
AGHANIM	20	AA 641 A6	N. Aghanim et al. (Planck Collab.)
FIELDS	20	JCAP 2003 010	B. Fields et al. (ILL, MINN)
		JCAP 2011 E02 (errat.)	B. Fields et al. (ILL, MINN)
IVANOV	20	PR D101 083504	M.M. Ivanov, M. Simonovic, M. Zdravkovic (NYU,+)
JANOT	20	PL B803 135319	P. Janot, S. Jadach (CERN, CRAC)
VOUSINAS	20	PL B800 135068	G. Voutsinas et al. (CERN, BOHR)
VERDE	17	JCAP 1704 023	L. Verde et al.
CYBURT	16	RMP 88 015004	R.H. Cyburt et al. (MSU, ILL, MINN)
ROSSI	15	PR D92 063505	G. Rossi et al.
ADE	14	AA 571 A16	P.A.R. Ade et al. (Planck Collab.)
COSTANZI	14	JCAP 1410 081	M. Costanzi et al. (TRST, TRSTI)
HOU	14	APJ 782 74	Z. Hou et al.
LEISTEDT	14	PRL 113 041301	B. Leistedt, H.V. Peiris, L. Verde
MORESCO	12	JCAP 1207 053	M. Moresco et al.
XIA	12	JCAP 1206 010	J.-Q. Xia et al.
MANGANO	11	PL B701 296	G. Mangano, P. Serpico
HAMANN	07	JCAP 0708 021	J. Hamann et al.
ICHIKAWA	07	JCAP 0705 007	K. Ichikawa, M. Kawasaki, F. Takahashi
CIRELLI	06	JCAP 0612 013	M. Cirelli et al.
HANMESTAD	06	JCAP 0611 016	S. Hanmestad, G. Raffelt
LEP-SLC	06	PRPL 427 257	ALEPH, DELPHI, L3, OPAL, SLD and working groups
SELJAK	06	JCAP 0610 014	U. Seljak, A. Slosar, P. McDonald
ABDALLAH	05B	EPJ C38 395	J. Abdallah et al. (DELPHI Collab.)
CYBURT	05	ASP 23 313	R.H. Cyburt et al.
ACHARD	04E	PL B587 16	P. Achard et al. (L3 Collab.)
BARGER	03C	PL B566 8	V. Barger et al.
CROTTY	03	PR D67 123005	P. Crotty, J. Lesgourgues, S. Pastor
CYBURT	03	PL B567 227	R.H. Cyburt, B.D. Fields, K.A. Olive
HEISTER	03C	EPJ C28 1	A. Heister et al. (ALEPH Collab.)
PIERPAOLI	03	MNRAS 342 L63	E. Pierpaoli
CYBURT	01	ASP 17 87	R.H. Cyburt, B.D. Fields, K.A. Olive
KNELLER	01	PR D64 123506	J.P. Kneller et al.
ABBIENDI,G	00D	EPJ C18 253	G. Abbiendi et al. (OPAL Collab.)
ABREU	00Z	EPJ C17 53	P. Abreu et al. (DELPHI Collab.)
ACCIARRI	99R	PL B470 268	M. Acciarri et al. (L3 Collab.)
LISI	99	PR D59 123520	E. Lisi, S. Sarkar, F.L. Villante
OLIVE	99	ASP 11 403	K.A. Olive, D. Thomas
ABREU	97J	ZPHY C74 577	P. Abreu et al. (DELPHI Collab.)
COPI	97	PR D55 3389	C.J. Copi, D.N. Schramm, M.S. Turner (CHIC)
HATA	97B	PR D55 540	N. Hata et al. (OSU, PENN)
OLIVE	97	ASP 7 27	K.A. Olive, D. Thomas (MINN, FLOR)
ADAM	96C	PL B300 471	W. Adam et al. (DELPHI Collab.)
CARDALL	96B	APJ 472 435	C.Y. Cardall, G.M. Fuller (UCSD)
FIELDS	96	New Ast 1 77	B.D. Fields et al. (NDAM, CERN, MINN,+)
KERNAN	96	PR D54 3681	P.S. Kernan, S. Sarkar (CASE, OXFTP)
AKERS	95C	ZPHY C65 47	R. Akers et al. (OPAL Collab.)
OLIVE	95	PL B354 357	K.A. Olive, G. Steigman (MINN, OSU)
BUSKULIC	93L	PL B313 520	D. Buskulic et al. (ALEPH Collab.)
LEP	92	PL B276 247	LEP Collabs. (LEP, ALEPH, DELPHI, L3, OPAL)
WALKER	91	APJ 376 51	T.P. Walker et al. (HSCA, OSU, CHIC+)
OLIVE	90	PL B236 454	K.A. Olive et al. (MINN, CHIC, OSU+)
YANG	84	APJ 281 493	J. Yang et al. (CHIC, BART)
OLIVE	83C	NP B380 497	K.A. Olive, D.N. Schramm, G. Steigman (CHIC+)
STEIGMAN	79	PRL 43 239	G. Steigman, K.A. Olive, D.N. Schramm (BART+)
YANG	79	APJ 227 697	J. Yang et al. (CHIC, YALE, UVA)
STEIGMAN	77	PL 66B 202	G. Steigman, D.N. Schramm, J.E. Gunn (YALE, CHIC+)
PEEBLES	71	Physical Cosmology	P.Z. Peebles (PRIN)
		Princeton Univ. Press (1971)	
SHVARTSMAN	69	JETPL 9 184	V.F. Shvartsman (MOSU)
		Translated from ZETFP 9 315.	
HOYLE	64	NAT 203 1108	F. Hoyle, R.J. Tayler (CAMB)

Observation of neutrinoless double-beta ($0\nu\beta\beta$) decay would signal violation of total lepton number conservation. The process can be mediated by an exchange of a light Majorana neutrino, or by an exchange of other particles. However, the existence of $0\nu\beta\beta$ -decay requires a nonvanishing Majorana neutrino mass, no matter what the actual mechanism is. As long as only a limit on the lifetime is available, limits on the effective Majorana neutrino mass, on the lepton-number violating right-handed current or other possible mechanisms mediating $0\nu\beta\beta$ decay can be obtained, independently of the actual mechanism, by assuming that one of these “new physics” possibilities dominates. These limits are listed in the Double-β Decay Listings of the experimental measurements.

In the following we assume that the exchange of light Majorana neutrinos ($m_{\nu_i} \leq 10$ MeV) contributes dominantly to the decay rate. Besides a dependence on the phase space ($G^{0\nu}$) and the nuclear matrix element ($M^{0\nu}$), the observable $0\nu\beta\beta$ -decay rate is proportional then to the square of the effective Majorana mass m_{ee} , $(T_{1/2}^{0\nu})^{-1} = G^{0\nu} \cdot |M^{0\nu}|^2 \cdot m_{ee}^2$, with $m_{ee}^2 = |\sum_i U_{ei}^2 m_{\nu_i}|^2$. The sum contains, in general, complex CP-phases in U_{ei}^2 , i.e., cancellations may occur. For three neutrino flavors there are two physical phases for Majorana neutrinos (η_1, η_2) and one for Dirac neutrinos (δ_{CP}). The relevant Majorana phases affect only processes to which lepton-number changing amplitudes contribute. Given the general 3×3 mixing matrix for Majorana neutrinos, one can construct other analogous lepton number violating quantities, $m_{\ell\ell'} = \sum_i U_{ei} U_{\ell'i} m_{\nu_i}$ (ℓ or $\ell' \neq e$). However, these are currently much less constrained than m_{ee} .

Nuclear structure calculations are needed to deduce m_{ee} from the decay rate. While $G^{0\nu}$ can be calculated accurately, the computation of $M^{0\nu}$ is subject to uncertainty. Comparing different nuclear model evaluations indicates a factor ~ 2 - 3 spread in the calculated nuclear matrix elements. Nuclear structure calculation consistently overestimate Gamow-Teller (axial current) matrix elements. This inability of the nuclear models to reproduce Gamow-Teller decay rates is often parametrized in form of a modified coupling constant g_A . Many nuclear theorists interpret this shortcoming as evidence that important physics is missing in the modeling of weak nuclear transitions. It is not clear how these observed uncertainties impact $0\nu\beta\beta$ -matrix elements. Nevertheless, this constitutes an additional element of uncertainty. Recent work, [1] shows how the discrepancy between experimental and theoretical axial current matrix elements might be resolved. However, application of this approach to the $0\nu\beta\beta$ decay remains to be accomplished. The particle physics quantities to be determined are thus nuclear model-dependent, so the half-life measurements are listed first. Where possible, we reference the nuclear matrix elements used in the subsequent analysis. Since rates for the conventional $2\nu\beta\beta$ decay serve to constrain the nuclear theory models, results for this process are also given.

Double-β Decay

OMITTED FROM SUMMARY TABLE

NEUTRINOLESS DOUBLE-β DECAY

Revised August 2019 by A. Piepke (University of Alabama) and P. Vogel (Caltech) .

Lepton Particle Listings

Double- β Decay

Oscillation experiments utilizing atmospheric, accelerator, solar, and reactor produced neutrinos and anti-neutrinos show that at least some neutrinos are massive. However, so far the inverted mass ordering (i.e., whether $\Delta m_{31}^2 < 0$) is disfavored only by 2-3 σ compared to the normal mass ordering (when $\Delta m_{31}^2 > 0$), while the absolute neutrino mass values or the properties of neutrinos under CPT-conjugation (Dirac or Majorana) remain undetermined. All confirmed oscillation experiments can be consistently described using three interacting neutrino species with two mass splittings and three mixing angles. (For values of the mixing angles and mass square differences see the corresponding tables.)

Based on the 3-neutrino analysis:

$m_{ee}^2 = |\cos^2 \theta_{13} \cos^2 \theta_{12} m_1 + e^{2i(\eta_2 - \eta_1)} \cos^2 \theta_{13} \sin^2 \theta_{12} m_2 + e^{-2i(\eta_1 + \delta_{CP})} \sin^2 \theta_{13} m_3|^2$, valid for both mass orderings. Given the present knowledge of the neutrino oscillation parameters one can derive a relation between the effective Majorana mass and the mass of the lightest neutrino, as illustrated in Figure 14.11 in the Neutrino Masses, Mixing and Oscillations review. The three mass orderings allowed by the oscillation data: normal ($m_1 < m_2 \ll m_3$), inverted ($m_3 \ll m_1 < m_2$), and degenerate ($m_1 \approx m_2 \approx m_3$), result in different projections. The width of the colored bands reflects the uncertainty introduced by the unknown Majorana and Dirac phases as well as the experimental errors of the oscillation parameters. The latter causes only minor broadening of the bands. Because of the overlap of the different mass scenarios, a measurement of m_{ee} would not reveal which mass ordering is applicable, provided the value of m_{ee} is in the overlapping range.

Analogous plots depict the relation of m_{ee} with the summed neutrino mass $m_{tot} = m_1 + m_2 + m_3$, constrained by observational cosmology, and m_{ee} as a function of the average mass $m_{\nu_e}^{eff} = [\sum |U_{ei}|^2 m_{\nu_i}^2]^{1/2}$ determined through the analysis of the electron energy distribution in low energy beta decays. (See Fig. 1 of [2].) The oscillation data thus allow to test whether observed values of m_{ee} and m_{tot} or $m_{\nu_e}^{eff}$ are consistent within the 3 neutrino framework. The rather large intrinsic width of the $\beta\beta$ -decay constraints essentially does not allow to positively identify the mass ordering, and thus the sign of Δm_{31}^2 , even in combination with these other observables. Naturally, if a value of $0 < m_{ee} \leq 0.01$ eV is ever established, then the normal mass ordering becomes the only possible scenario.

It should be noted that systematic uncertainties of the nuclear matrix elements and possible quenching of the axial current matrix elements are sometimes not folded into the mass limits reported by $\beta\beta$ -decay experiments. Taking this additional uncertainty into account would further widen the projections. The plots are based on a 3-neutrino analysis. If it turns out that additional, i.e. sterile light neutrinos exist, the allowed regions would be modified substantially.

If neutrinoless double-beta decay is observed, it will be possible to fix a range of absolute values of the masses m_{ν_i} . Unlike the direct neutrino mass measurements, however, a limit

on m_{ee} does not allow one to constrain the individual mass values m_{ν_i} even when the mass differences Δm_{ij}^2 are known.

Neutrino oscillation data imply the existence of a lower limit ~ 0.014 eV for the Majorana neutrino mass for the inverted mass ordering pattern, while m_{ee} could, by fine tuning, vanish in the case of the normal mass ordering. Several new double-beta searches have been proposed to probe the interesting m_{ee} mass range, with the prospect of full coverage of the inverted mass ordering region within the next decade.

The $0\nu\beta\beta$ decay mechanism discussed so far is not the only way in which the decay can occur. Numerous other possible scenarios have been proposed, however, all of them requiring new physics. It will be a challenging task to decide which mechanism was responsible once $0\nu\beta\beta$ decay is observed. LHC experiments may reveal corresponding signatures for new physics of lepton number violation. If lepton-number violating right-handed weak current interactions exist, its strength can be characterized by the phenomenological coupling constants η and λ (η describes the coupling between the right-handed lepton current and left-handed quark current while λ describes the coupling when both currents are right-handed). The $0\nu\beta\beta$ decay rate then depends on $\langle \eta \rangle = \eta \sum_i U_{ei} V_{ei}$ and $\langle \lambda \rangle = \lambda \sum_i U_{ei} V_{ei}$ that vanish for massless or unmixed neutrinos (V_{ij} is a matrix analogous to U_{ij} but describing the mixing with the hypothetical right-handed neutrinos). The observation of the single electron spectra could, in principle, allow to distinguish this mechanism of $0\nu\beta\beta$ from the light Majorana neutrino exchange driven mode. The limits on $\langle \eta \rangle$ and $\langle \lambda \rangle$ are listed in a separate table. The reader is cautioned that a number of earlier experiments did not distinguish between η and λ . In addition, see the section on Majoron searches for additional limits set by these experiments.

References

1. P. Gysbers *et al.*, Nature Phys. **15**, 5 (2019); [arXiv:1903.00047].
2. M.J. Dolinski, A.W.P. Poon and W. Rodejohann, Ann. Rev. Nucl. Part. Sci. **49**, 219 (2019); [arXiv:1902.04097].

Half-life 0ν double- β decay

In most cases the transitions $(Z,A) \rightarrow (Z+2,A) + 2e^-$ to the 0^+ ground state of the final nucleus are listed. We also list transitions that decrease the nuclear charge ($2e^+$, e^+ CC and double EC) and transitions to an excited state of the final nucleus (0^+_i , 2^+ , and 2^+_i). In the following Listings only the best or comparable limits for the half-lives of each transition are reported and only those with about $T_{1/2} > 10^{23}$ years that are relevant for particle physics.

$T_{1/2}(10^{23} \text{ yr})$	CL%	ISOTOPE	TRANSITION	METHOD	DOCUMENT ID
• • • We do not use the following data for averages, fits, limits, etc. • • •					
>2300	90	^{136}Xe		KamLAND-Zen	1 ABE 23
> 830	90	^{76}Ge		MAJORANA	2 ARNQUIST 23
> 2.1	90	^{100}Mo	g.s. $\rightarrow 2^+_1$	CUPID-Mo	3 AUGIER 23
> 1.2	90	^{100}Mo	g.s. $\rightarrow 0^+_1$	CUPID-Mo	3 AUGIER 23
> 13	90	^{136}Xe		NEXT	4 NOVELLA 23
> 220	90	^{130}Te		CUORE	5 ADAMS 22A
> 36	90	^{128}Te		CUORE	6 ADAMS 22B

> 12	90	¹³⁶ Xe	XENON1T	7 APRILE	22A
> 18	90	¹⁰⁰ Mo	CUPID-Mo	8 AUGIER	22
> 46	90	⁸² Se	CUPID-0	9 AZZOLINI	22
> 1.8	90	⁸² Se	g.s. → 0 ₁ ⁺	10 AZZOLINI	22
> 3.0	90	⁸² Se	g.s. → 2 ₁ ⁺	11 AZZOLINI	22
> 3.2	90	⁸² Se	g.s. → 2 ₂ ⁺	12 AZZOLINI	22
> 59	90	¹³⁰ Te	g.s. → 0 ₁ ⁺	13 ADAMS	21A
> 15	90	¹⁰⁰ Mo	CUPID-Mo	14 ARMENGAUD	21
> 39.9	90	⁷⁶ Ge	g.s. → 0 ₁ ⁺	15 ARNQUIST	21
> 21.2	90	⁷⁶ Ge	g.s. → 2 ₁ ⁺	16 ARNQUIST	21
> 9.7	90	⁷⁶ Ge	g.s. → 2 ₂ ⁺	17 ARNQUIST	21
> 320	90	¹³⁰ Te	CUORE	18 ADAMS	20A
>1800	90	⁷⁶ Ge	GERDA	19 AGOSTINI	20B
> 14	90	¹³⁰ Te	g.s. → 0 ₁ ⁺	20 ALDUINO	19
> 0.95	90	¹⁰⁰ Mo	AMoRE	21 ALENKOV	19
> 350	90	¹³⁶ Xe	EXO-200	22 ANTON	19
> 2.4	90	¹³⁶ Xe	PANDAX-II	23 NI	19
> 150	90	¹³⁰ Te	CUORE	24 ALDUINO	18
> 2.5	90	⁸² Se	NEMO-3	25 ARNOLD	18
> 2.2	90	¹¹⁶ Cd	AURORA	26 BARABASH	18
> 1.1	90	¹³⁴ Xe	EXO-200	27 ALBERT	17C
> 1	90	¹¹⁶ Cd	NEMO-3	28 ARNOLD	17
> 40	90	¹³⁰ Te	CUORICINO	29 ALDUINO	16
> 260	90	¹³⁶ Xe	g.s. → 2 ₁ ⁺	30 ASAKURA	16
> 260	90	¹³⁶ Xe	g.s. → 2 ₂ ⁺	31 ASAKURA	16
> 240	90	¹³⁶ Xe	g.s. → 0 ₁ ⁺	32 ASAKURA	16
> 11	90	¹⁰⁰ Mo	NEMO-3	33 ARNOLD	15
> 9.4	90	¹³⁰ Te	g.s. → 0 ₁ ⁺	34 ANDREOTTI	12
> 0.58	90	⁴⁸ Ca	CaF ₂ scint.	35 UMEHARA	08
> 0.89	90	¹⁰⁰ Mo	g.s. → 0 ₁ ⁺	36 ARNOLD	07
> 1.6	90	¹⁰⁰ Mo	g.s. → 2 ₁ ⁺	37 ARNOLD	07
> 1.1	90	¹²⁸ Te	Cryog. det.	38 ARNABOLDI	03
> 1.7	90	¹¹⁶ Cd	¹¹⁶ CdWO ₄ scint.	39 DANEVICH	03
> 157	90	⁷⁶ Ge	Enriched HPGe	40 AALSETH	02B

- 1 ABE 23 use the combined data set of the KamLAND-Zen 400 and 800 experiments, utilizing 745 kg of isotopically enriched xenon (90.9% ¹³⁶Xe), dissolved in liquid scintillator and an exposure of 970 kg-yr of ¹³⁶Xe, to derive this limit on 0νββ decay. A half-life sensitivity of 1.5 × 10²⁶ yr is reported.
- 2 ARNQUIST 23 use the final data set of the MAJORANA DEMONSTRATOR experiment, operating enriched in ⁷⁶Ge detectors, to set this limit on the 0νββ half-life of ⁷⁶Ge. The exposure is 64.5 kg-yr. A median sensitivity of 8.1 × 10²⁵ yr is reported.
- 3 AUGIER 23 utilize the complete data, set collected by the CUPID-Mo bolometric calorimeter with particle ID and located at the LSM, to study various double beta decays of ¹⁰⁰Mo to excited states of the daughter nucleus. An exposure of 1.47 kg-yr of ¹⁰⁰Mo is available.
- 4 NOVELLA 23 use data collected by the NEXT-White experiment to limit the 0νββ half-life of ¹³⁶Xe. The experiment contains 3.5 kg of enriched Xe and is based on a high-pressure gas TPC. Two different limits are reported, based on different data analysis approaches, > 5.5 × 10²³ yr and > 13 × 10²³ yr.
- 5 ADAMS 22A use the CUORE TeO₂ experiment with an exposure of 288.8 kg-yr of ¹³⁰Te to place a limit on its 0νββ decay. The median sensitivity is reported as 280 × 10²³ yr. Supersedes ADAMS 20A.
- 6 ADAMS 22B use the CUORE bolometric calorimeter to place a limit on the 0νββ decay half-life of ¹²⁸Te.
- 7 APRILE 22A use 36.16 kg yr of ¹³⁶Xe exposure of the XENON1T not enriched detector to establish the stated limit.
- 8 AUGIER 22 use the final data set of the CUPID-Mo cryogenic calorimeter, utilizing enriched Li₂¹⁰⁰MoO₄ and an isotope exposure of 1.47 kg-y, to place a limit on the 0νββ decay half-life.
- 9 AZZOLINI 22 use the CUPID-0 scintillating cryogenic bolometer to set a limit on the 0νββ half-life of ⁸²Se. The analyzed isotope exposure is 8.82 kg-yr. A median sensitivity of 7 × 10²⁴ yr is reported. Supersedes AZZOLINI 19.
- 10 AZZOLINI 22 use CUPID-0 data with an isotope exposure of 8.82 kg-yr to set a limit on the 0νββ decay to the first excited 0⁺ state.
- 11 AZZOLINI 22 use CUPID-0 data with an isotope exposure of 8.82 kg-yr to set a limit on the 0νββ decay to the first excited 2⁺ state.
- 12 AZZOLINI 22 use CUPID-0 data with an isotope exposure of 8.82 kg-yr to set a limit on the 0νββ decay to the second excited 2⁺ state.
- 13 ADAMS 21A et al. used 101.76 kg yr of ¹³⁰Te exposure of the CUORE (LNGS) bolometric detector to place a limit on the decay to the first excited state of ¹³⁰Xe, superseding ALDUINO 19 as the most restrictive bound on this particular decay.
- 14 ARMENGAUD 21 use the CUPID-Mo 4.2 kg array of enriched Li₂¹⁰⁰MoO₄ scintillating bolometers, with 1.17 kg-yr exposure, to set this limit.
- 15 ARNQUIST 21 use the MAJORANA demonstrator to set this limit for the 0νββ decay to the first excited 0⁺ state, with a 41.9 kg yr isotopic exposure. The median sensitivity is 39.9 × 10²³ yr.
- 16 ARNQUIST 21 use the MAJORANA demonstrator to set this limit for the 0νββ decay to the first excited 2⁺ state, with a 41.9 kg yr isotopic exposure. The median sensitivity is 21.2 × 10²³ yr.

- 17 ARNQUIST 21 use the MAJORANA demonstrator to set this limit for the 0νββ decay to the second excited 2⁺ state, with a 41.9 kg yr isotopic exposure. The median sensitivity is 18.6 × 10²³ yr.
- 18 ADAMS 20A use the CUORE detector to search for the 0νββ decay of ¹³⁰Te. The exposure was 372.5 kg-yr of TeO₂ corresponding to 103.6 kg-yr of ¹³⁰Te. The exclusion sensitivity is 1.7 × 10²⁵ yr. Supersedes ALDUINO 18.
- 19 AGOSTINI 20B present the final data set of the GERDA experiment, searching for 0νββ decay of ⁷⁶Ge with isotopically enriched, high resolution Ge detectors. A final exposure of 127.2 kg-yr is reported. The experiment reports the lowest background and longest half life limit ever achieved by any double beta decay experiment. The reported experiment sensitivity equals the limit. Supersedes AGOSTINI 19.
- 20 ALDUINO 19 use the combined data of the CUORICINO and CUORE-0 experiments to place a lower limit on the half life of the 0νββ decay of ¹³⁰Te to the first excited 0⁺ state of ¹³⁰Xe. Supersedes ANDREOTTI 12.
- 21 ALENKOV 19 report the 0νββ decay half-life limit based on the 5.21 kg-d exposure of ¹⁰⁰Mo, of a cryogenic dual heat and light detector in the Yangyang underground laboratory. The median sensitivity is 1.1 × 10²³ years.
- 22 ANTON 19 uses the complete dataset of the EXO-200 detector to search for the 0νββ decay. The exposure is 234.1 kg yr. The median sensitivity is 5.0 × 10²⁵ yr. Supersedes ALBERT 18 and ALBERT 14b.
- 23 NI 19 use the PandaX-II dual phase TPC at CJPL to search for the 0νββ decay of ¹³⁶Xe. The half-life limit 2.4 × 10²³ yr is obtained from 22.2 kg yr exposure with a sensitivity of 1.9 × 10²³ yr.
- 24 ALDUINO 18 uses the CUORE detector to search for the 0νββ decay of ¹³⁰Te. The exposure is 86.3 kg-year of natural TeO₂ corresponding to 24.0 kg-year for ¹³⁰Te. The median sensitivity is 0.7 × 10²⁵ yr. The limit is obtained combining the new data from CUORE with those of CUORE0 (9.8 kg-year of ¹³⁰Te) and Cuoricino (19.8 kg-year of ¹³⁰Te).
- 25 ARNOLD 18 use the NEMO-3 tracking detector to place a limit on the 0νββ decay of ⁸²Se. This is a slightly weaker limit than in BARABASH 11A, using the same detector. Supersedes ARNOLD 05A.
- 26 BARABASH 18 use 1.162 kg of ¹¹⁶CdWO₄ scintillating crystals to obtain this limit. Supersedes DANEVICH 03 with analogous source and is more sensitive than ARNOLD 17.
- 27 ALBERT 17C uses the EXO-200 detector that contains 19.098 ± 0.014% admixture of ¹³⁴Xe to search for the 0ν and 2νββ decay modes. The exposure is 29.6 kg-year. The median sensitivity is 1.9 × 10²¹ years.
- 28 ARNOLD 17 use the NEMO-3 tracking calorimeter, containing 410 g of enriched ¹¹⁶Cd exposed for 5.26 yr, to determine the half-life limit. Supersedes BARABASH 11A.
- 29 ALDUINO 16 report result obtained with 9.8 kg-y of data collected with the CUORE-0 bolometer, combined with data from the CUORICINO. Supersedes ALFONSO 15.
- 30 ASAKURA 16 use the KamLAND-Zen liquid scintillator calorimeter (¹³⁶Xe 89.5 kg yr) to place a limit on the 0νββ-decay into the first excited state of the daughter nuclide.
- 31 ASAKURA 16 use the KamLAND-Zen liquid scintillator calorimeter (¹³⁶Xe 89.5 kg yr) to place a limit on the 0νββ-decay into the second excited state of the daughter nuclide.
- 32 ASAKURA 16 use the KamLAND-Zen liquid scintillator calorimeter (¹³⁶Xe 89.5 kg yr) to place a limit on the 0νββ-decay into the third excited state of the daughter nuclide.
- 33 ARNOLD 15 use the NEMO-3 tracking calorimeter with 34.3 kg yr exposure to determine the limit of 0νββ-half life of ¹⁰⁰Mo. Supersedes ARNOLD 2005A and BARABASH 11A.
- 34 ANDREOTTI 12 use high resolution TeO₂ bolometric calorimeter to search for the 0νββ decay of ¹³⁰Te leading to the excited 0₁⁺ state at 1793.5 keV.
- 35 UMEHARA 08 use CaF₂ scintillation calorimeter to search for double beta decay of ⁴⁸Ca. Limit is significantly more stringent than quoted sensitivity: 18 × 10²¹ years.
- 36 Limit on 0ν-decay to the first excited 0₁⁺-state of daughter nucleus using NEMO-3 tracking calorimeter. Supersedes DASSIE 95.
- 37 Limit on 0ν-decay to the first excited 2⁺-state of daughter nucleus using NEMO-3 tracking calorimeter.
- 38 Supersedes ALESSANDRELLO 00. Array of TeO₂ crystals in high resolution cryogenic calorimeter. Some enriched in ¹²⁸Te. Ground state to ground state decay.
- 39 Limit on 0νββ decay of ¹¹⁶Cd using enriched CdWO₄ scintillators. Supersedes DANEVICH 00.
- 40 AALSETH 02B limit is based on 117 mol-yr of data using enriched Ge detectors. Background reduction by means of pulse shape analysis is applied to part of the data set. Reported limit is slightly less restrictive than that in KLAPDOR-KLEINGROTHAUS 01 However, it excludes part of the allowed half-life range reported in KLAPDOR-KLEINGROTHAUS 01B for the same nuclide. The analysis has been criticized in KLAPDOR-KLEINGROTHAUS 04B. The criticism was addressed and disputed in AALSETH 04.

Half-life measurements of the two-neutrino double-β decay

The measured half-life values for the transitions (Z,A) → (Z+2,A) + 2e⁻ + 2ν̄_e to the 0⁺ ground state of the final nucleus are listed. We also list the transitions to an excited state of the final nucleus (0_i⁺, etc.). We report only the measurements with the smallest (or comparable) uncertainty for each transition.

t _{1/2} (10 ²⁰ yr)	ISOTOPE	TRANSITION	METHOD	DOCUMENT ID
• • •	We do not use the following data for averages, fits, limits, etc. • • •			
20.22 ± 0.18 ± 0.38	⁷⁶ Ge		GERDA	1 AGOSTINI 23
1.11 + 0.19 + 0.17 - 0.14 - 0.15	¹⁵⁰ Nd 0 ⁺ → 0 ₁ ⁺		NEMO-3	2 AGUERRE 23

Lepton Particle Listings

Double- β Decay

7.5	± 0.8	± 0.4 -0.3	^{100}Mo	$0^+ \rightarrow 0^+$	CUPID-Mo	3	AUGIER	23
0.0707	± 0.0002	± 0.0011	^{100}Mo		CUPID-Mo	4	AUGIER	23A
0.869	± 0.005	± 0.009 -0.006	^{82}Se		CUPID-0	5	AZZOLINI	23A
21.6	± 6.2 -4.0	± 4.0 -2.9	^{136}Xe		NEXT	6	NOVELLA	23
21900	± 700		^{128}Te		CUORE	7	ADAMS	22B
110	± 20	± 10	^{124}Xe		XENONIT	8	APRILE	22A
118	± 13	± 14	^{124}Xe		XENONnT	9	APRILE	22B
23.4	± 0.8 -4.6	± 3.0 -1.7	^{136}Xe		NEXT	10	NOVELLA	22
8.76	± 0.09 -0.07	± 0.14 -0.17	^{130}Te		CUORE	11	ADAMS	21
180	± 50	± 10	^{124}Xe	$2\nu\text{DEC}$	XENONIT	12	APRILE	19E
0.0680	± 0.0001	± 0.0038 -0.0040	^{100}Mo		NEMO-3	13	ARNOLD	19
0.939	± 0.017	± 0.058	^{82}Se		NEMO-3	14	ARNOLD	18
0.263	± 0.011 -0.012		^{116}Cd		AURORA	15	BARABASH	18
> 0.87			^{134}Xe		EXO-200	16	ALBERT	17C
8.2	± 0.2	± 0.6	^{130}Te		CUORE-0	17	ALDUINO	17
0.274	± 0.004	± 0.018	^{116}Cd		NEMO-3	18	ARNOLD	17
0.64	± 0.07 -0.06	± 0.12 -0.09	^{48}Ca		NEMO-3	19	ARNOLD	16
0.0934	± 0.0022	± 0.0062 -0.0060	^{150}Nd		NEMO-3	20	ARNOLD	16A
19.26	± 0.94		^{76}Ge		GERDA	21	AGOSTINI	15A
0.0693	± 0.0004		^{100}Mo		NEMO-3	22	ARNOLD	15
21.65	± 0.16	± 0.59	^{136}Xe		EXO-200	23	ALBERT	14
92	± 55 -26	± 13	^{78}Kr		BAKSAN	24	GAVRILYAK	13
23.8	± 0.2	± 1.4	^{136}Xe		KamLAND-Z	25	GANDO	12A
7.0	± 0.9	± 1.1	^{130}Te		NEMO-3	26	ARNOLD	11
0.235	± 0.014	± 0.016	^{96}Zr		NEMO-3	27	ARGYRIADES	10
6.9	± 1.0 -0.8	± 0.7	^{100}Mo	$0^+ \rightarrow 0^+$	Ge coinc.	28	BELLI	10
5.7	± 1.3 -0.9	± 0.8	^{100}Mo	$0^+ \rightarrow 0^+$	NEMO-3	29	ARNOLD	07
0.96	± 0.03	± 0.10	^{82}Se		NEMO-3	30	ARNOLD	05A
0.29	± 0.04 -0.03		^{116}Cd		CdWO ₄ sc.	31	DANEVICH	03

- 1 AGOSTINI 23 report an updated value for the $2\nu\beta\beta$ half-life of ^{76}Ge ; the final result of the GERDA Phase II experiment. A subset of the data, corresponding to an exposure of 11.8 kg-yr, is utilized. This is one of the most precise measurements of $2\nu\beta\beta$ decay reported in the literature. An effective nuclear matrix element of 0.101 ± 0.001 is derived from this result.
- 2 AGUERRE 23 report the results of a 5.25 yr search for the $2\nu\beta\beta$ decay to the excited $0^+ \rightarrow 0^+$ state of the daughter nucleus, using the NEMO-3 tracking calorimeter. 36.6 g of ^{150}Nd isotope were available for the measurement of this decay rate.
- 3 AUGIER 23 utilize the complete data, set collected by the CUPID-Mo bolometric calorimeter with particle ID and located at the LSM, to measure the ^{100}Mo $2\nu\beta\beta$ half-life to excited 0^+ state of the daughter nucleus. An exposure of 1.47 kg-yr of ^{100}Mo is available.
- 4 AUGIER 23A use full data set collected by the CUPID-Mo experiment to derive an improved $2\nu\beta\beta$ g.s. to g.s. half-life of ^{100}Mo . An exposure of 1.48 kg-yr of ^{100}Mo is utilized. Supersedes ARMENGAUD 20.
- 5 AZZOLINI 23A report an improved measurement of the $2\nu\beta\beta$ decay with an exposure of 8.82 kg-yr of ^{82}Se , collected with the CUPID-0 detector. Supersedes AZZOLINI 19B.
- 6 NOVELLA 23 used the NEXT-White experiment, with a fiducial mass of 3.5 kg of enriched xenon, to measure the $2\nu\beta\beta$ g.s. to g.s. half-life of ^{136}Xe . The experiment is based on a high-pressure gas TPC. Supersedes NOVELLA 22.
- 7 ADAMS 22B derive the $2\nu\beta\beta$ half-life of ^{128}Te from data of the CUORE bolometric calorimeter and the half-life ratio for $^{130}\text{Te} / ^{128}\text{Te}$ reported in BERNATOWICZ 92.
- 8 APRILE 22A report an improved ^{124}Xe $2\nu\text{DEC}$ half-life measurement for ^{124}Xe , using data collected by the XENONIT detector with an isotopically not enriched Xe target. The analyzed ^{124}Xe exposure is 0.87 kg-yr. The statistical significance of the signal is 7.0 sigma. The stated half-life considers captures from the K shell up to the N5 shell. This result supersedes APRILE 19E, which exclusively considered captures from the K shell.
- 9 APRILE 22B use data collected by the XENONnT dark matter experiment to derive an improved ^{124}Xe $2\nu\text{DEC}$ half-life measurement for ^{124}Xe . This result supersedes APRILE 22A.
- 10 NOVELLA 22 report on a high-pressure gas TPC at Canfranc underground laboratory, filled with 3.5 kg (fiducial) xenon gas, used to measure the $2\nu\beta\beta$ decay of ^{136}Xe . Topological track reconstruction is utilized in the data analysis. The measurement is based on comparing runs with isotopically enriched and depleted xenon. Other measurements with smaller error exist.
- 11 ADAMS 21 use 102.7 kg yr of ^{130}Te exposure, collected by the CUORE bolometric detector at LNGS, to perform a measurement of the $2\nu\beta\beta$ decay of ^{130}Te . The dataset is more than 10-times that collected by the CUORE-0 experiment. The result has been revised in ADAMS 23A. Supersedes ALDUINO 17.
- 12 APRILE 19E report first measurement of two-neutrino double electron capture in ^{124}Xe using the XENONIT detector with a 0.73 t-yr exposure. An excess of 126 ± 29 events is observed at 64.3 ± 0.6 keV decay energy, corresponding to $\sqrt{\Delta\chi^2} = 4.4$ with respect to the background-only hypothesis.
- 13 ARNOLD 19 use the NEMO-3 tracking calorimeter with 34.3 kg y exposure to determine the $2\nu\beta\beta$ half-life of ^{100}Mo . Supersedes ARNOLD 15.

- 14 ARNOLD 18 use the NEMO-3 tracking detector to determine the $2\nu\beta\beta$ half-life of ^{82}Se . 0.93 kg of ^{82}Se was observed for 5.25 y. The half-life value was obtained based on the single-state-dominance (SSD) hypothesis, preferred in this case by about 2σ . Supersedes ARNOLD 05A.
- 15 BARABASH 18 use 1.162 kg of $^{116}\text{CdWO}_4$ scintillating crystals to obtain this value. Supersedes DANEVICH 03 with analogous source and agrees with ARNOLD 17 with the NEMO-3 detector.
- 16 ALBERT 17C uses the EXO-200 detector that contains $19.098 \pm 0.014\%$ admixture of ^{134}Xe to search for the $2\nu\beta\beta$ decay mode. The exposure is 29.6 kg-year. The median sensitivity is 1.2×10^{21} years.
- 17 ALDUINO 17 use the CUORE-0 detector containing 10.8 kg of ^{130}Te in 52 crystals of TeO_2 . The exposure was 9.3 kg yr of ^{130}Te . This is a more accurate rate determination than in ARNOLD 11 and BARABASH 11A.
- 18 ARNOLD 17 use the NEMO-3 tracking calorimeter, containing 410 grams of enriched ^{116}Cd exposed for 5.26 years, to determine the half-life value.
- 19 ARNOLD 16 use the NEMO-3 detector and a source of 6.99 g of ^{48}Ca . The half-life is based on 36.7 g year exposure. It is consistent, although somewhat longer, than the previous determinations of the half-life. Supersedes BARABASH 11A.
- 20 ARNOLD 16A use the NEMO-3 tracking calorimeter, containing 36.6 g of ^{150}Nd exposed for 1918.5 days, to determine the half-life. Supersedes ARGYRIADES 09.
- 21 AGOSTINI 15A use 17.9 kg yr exposure of the GERDA calorimeter to derive an improved measurement of the $2\nu\beta\beta$ decay half life of ^{76}Ge .
- 22 ARNOLD 15 use the NEMO-3 tracking calorimeter with 34.3 kg yr exposure to determine the $2\nu\beta\beta$ -half life of ^{100}Mo . Supersedes ARNOLD 05A and ARNOLD 04.
- 23 ALBERT 14 use the EXO-200 tracking detector for a re-measurement of the $2\nu\beta\beta$ -half life of ^{136}Xe . A nuclear matrix element of $0.0218 \pm 0.0003 \text{ MeV}^{-1}$ is derived from this data. Supersedes ACKERMAN 11.
- 24 GAVRILYAK 13 use a proportional counter filled with Kr gas to search for the $2\nu 2K$ decay of ^{78}Kr . Data with the enriched and depleted Kr were used to determine signal and background. A 2.5σ excess of events obtained with the enriched sample is interpreted as an indication for the presence of this decay.
- 25 GANDO 12A use a modification of the existing KamLAND detector. The $\beta\beta$ decay source/detector is 13 tons of enriched ^{136}Xe -loaded scintillator contained in an inner balloon. The $2\nu\beta\beta$ decay rate is derived from the fit to the spectrum between 0.5 and 4.8 MeV. This result is in agreement with ACKERMAN 11.
- 26 ARNOLD 11 use enriched ^{130}Te in the NEMO-3 detector to measure the $2\nu\beta\beta$ decay rate. This result is in agreement with, but more accurate than ARNOLDI 03.
- 27 ARGYRIADES 10 use 9.4 ± 0.2 g of ^{96}Zr in NEMO-3 detector and identify its $2\nu\beta\beta$ decay. The result is in agreement and supersedes ARNOLD 99.
- 28 BELLI 10 use enriched ^{100}Mo with 4 HP Ge detectors to record the 590.8 and 539.5 keV γ rays from the decay of the 0^+ state in ^{100}Ru both in singles and coincidences. This result confirms the measurement of KIDD 09 and ARNOLD 07 and supersedes them.
- 29 First exclusive measurement of 2ν -decay to the first excited 0^+ -state of daughter nucleus. ARNOLD 07 use the NEMO-3 tracking calorimeter to detect all particles emitted in decay. Result agrees with the inclusive ($0\nu + 2\nu$) measurement of DEBRAECKELEER 01.
- 30 ARNOLD 05A use the NEMO-3 tracking detector to determine the $2\nu\beta\beta$ half-life of ^{82}Se with high statistics and low background (389 days of data taking). Supersedes ARNOLD 04.
- 31 DANEVICH 03 is calorimetric measurement of $2\nu\beta\beta$ ground state decay of ^{116}Cd using enriched CdWO_4 scintillators. Agrees with EJIRI 95 and ARNOLD 96. Supersedes DANEVICH 00.

$\langle m_{ee} \rangle$, The Effective Weighted Sum of Majorana Neutrino Masses Contributing to Neutrinoless Double- β Decay

$\langle m_{ee} \rangle = |\sum U_{ei}^2 m_{\nu_i}|$, $i = 1, 2, 3$. It is assumed that ν_i are Majorana particles and that the transition is dominated by the known (light) neutrinos. Note that U_{ei}^2 and not $|U_{ei}|^2$ occur in the sum, and that consequently cancellations are possible. The experiments obtain the limits on $\langle m_{ee} \rangle$ from the measured ones on $T_{1/2}$ using a range of nuclear matrix elements (NME), which is reflected in the spread of $\langle m_{ee} \rangle$. Different experiments may choose different NME. All assume $g_A = 1.27$. In the following Listings, only the best or comparable limits for each isotope are reported. When not mentioned explicitly the transition is between ground states, but transitions between excited states are also reported.

VALUE (eV)	ISOTOPE	METHOD	DOCUMENT ID
•••	We do not use the following data for averages, fits, limits, etc. •••		
< 0.036–0.156	^{136}Xe	KamLAND-Zen	1 ABE 23
< 0.113–0.269	^{76}Ge	MAJORANA	2 ARNQUIST 23
< 0.48–3.19	^{136}Xe	NEXT	3 NOVELLA 23
< 0.09–0.305	^{130}Te	CUORE	4 ADAMS 22A
< 0.8–2.5	^{136}Xe	XENONIT	5 APRILE 22A
< 0.28–0.49	^{100}Mo	CUPID-Mo	6 AUGIER 22
< 0.263–0.545	^{82}Se	CUPID-0	7 AZZOLINI 22
< 0.31–0.54	^{100}Mo	CUPID-Mo	8 ARMENGAUD 21
< 0.075–0.35	^{130}Te	CUORE	9 ADAMS 20A
< 0.079–0.180	^{76}Ge	GERDA	10 AGOSTINI 20B
< 1.2–2.1	^{100}Mo	AMoRE	11 ALENKOV 19
< 0.093–0.286	^{136}Xe	EXO-200	12 ANTON 19
< 1.3–3.5	^{136}Xe	PANDAX-II	13 NI 19

< 0.11-0.52	¹³⁰ Te	CUORE	¹⁴ ALDUINO	18
< 1.2-3.0	⁸² Se	NEMO-3	¹⁵ ARNOLD	18
< 1.0-1.7	¹¹⁶ Cd	AURORA	¹⁶ BARABASH	18
< 1.4-2.5	¹¹⁶ Cd	NEMO-3	¹⁷ ARNOLD	17
< 0.27-0.76	¹³⁰ Te	CUORICINO	¹⁸ ALDUINO	16
< 1.6-5.3	¹⁵⁰ Nd	NEMO-3	¹⁹ ARNOLD	16A
< 0.33-0.62	¹⁰⁰ Mo	NEMO-3	²⁰ ARNOLD	15
< 7.2-19.5	⁹⁶ Zr	NEMO-3	²¹ ARGYRIADES	10
< 3.5-22	⁴⁸ Ca	CaF ₂ scint.	²² UMEHARA	08
< 1.5-1.7	¹¹⁶ Cd	¹¹⁶ CdWO ₄ scint.	²³ DANEVICH	03

$\langle \lambda \rangle$ (10 ⁻⁶)	CL%	$\langle \eta \rangle$ (10 ⁻⁸)	CL%	ISOTOPE	METHOD	DOCUMENT ID
• • • We do not use the following data for averages, fits, limits, etc. • • •						
< 2.2-2.6	90	< 1.7-2.1	90	⁸² Se	NEMO-3	¹ ARNOLD 18
< 1.8-22	90	< 1.6-21	90	¹¹⁶ Cd	AURORA	² BARABASH 18
< 0.9-1.3	90	< 0.5-0.8	90	¹⁰⁰ Mo	NEMO-3	³ ARNOLD 14
< 120	90			¹⁰⁰ Mo	0 ⁺ → 2 ⁺	⁴ ARNOLD 07
0.692 ^{+0.058} _{-0.056}	68	0.305 ^{+0.026} _{-0.025}	68	⁷⁶ Ge	Enriched HPGe	⁵ KLAPDOR-K...06A
< 2.5	90			¹⁰⁰ Mo	0 ν , NEMO-3	⁶ ARNOLD 05A
< 3.8	90			⁸² Se	0 ν , NEMO-3	⁷ ARNOLD 05A
< 1.5-2.0	90			¹⁰⁰ Mo	0 ν , NEMO-3	⁸ ARNOLD 04
< 3.2-3.8	90			⁸² Se	0 ν , NEMO-3	⁹ ARNOLD 04
< 1.6-2.4	90	< 0.9-5.3	90	¹³⁰ Te	Cryog. det.	¹⁰ ARNABOLDI 03
< 2.2	90	< 2.5	90	¹¹⁶ Cd	¹¹⁶ CdWO ₄ scint.	¹¹ DANEVICH 03
< 3.2-4.7	90	< 2.4-2.7	90	¹⁰⁰ Mo	ELEGANT V	¹² EJIRI 01
< 1.1	90	< 0.64	90	⁷⁶ Ge	Enriched HPGe	¹³ GUENTHER 97
< 4.4	90	< 2.3	90	¹³⁶ Xe	TPC	¹⁴ VUILLEUMIER 93
		< 5.3		¹²⁸ Te	Geochem	¹⁵ BERNATOW... 92

- ABE 23 utilize 745 kg of ¹³⁶Xe isotope exposure from the combined data set of the KamLAND-Zen 400 and 800 to derive a limit on $\langle m_{\beta\beta} \rangle$. The range reflects the author's assessment of the variability of the theoretically calculated nuclear matrix elements.
- ARNQUIST 23 use the final data set of the MAJORANA DEMONSTRATOR experiment, with 64.5 kg-yr of isotope exposure, to derive an upper limit for $\langle m_{\beta\beta} \rangle$. The range reflects the author's assessment of the variability of the theoretically calculated nuclear matrix elements.
- NOVELLA 23 use data collected with the NEXT-White experiment to derive a range of upper limits for $\langle m_{\beta\beta} \rangle$. The range reflects the author's assessment of the variability of the theoretically calculated nuclear matrix elements and both half-life limits stated in NOVELLA 23.
- ADAMS 22A use 1038.4 kg-yr of TeO₂ exposure collected by the CUORE experiment to determine this range of limits. The range reflects the uncertainty of nuclear matrix element calculations needed for the conversion of half-life to neutrino mass.
- APRILE 22A use data taken with the XENONIT detector to limit the Majorana neutrino mass. 36.16 kg-yr of ¹³⁶Xe exposure were utilized. The reported range of limits is due to uncertainties in the nuclear matrix elements.
- AUGIER 22 use the final data set of the CUPID-Mo cryogenic calorimeter with an isotope exposure of 1.47 kg-y to derive a range of neutrino mass limits. The range reflects the authors' estimate of the spread of nuclear matrix element calculations.
- AZZOLINI 22 use 8.82 kg-yr of isotopic exposure of the CPID-0 scintillating cryogenic bolometer to set this range of neutrino mass limits. The range reflects the authors' estimate of the spread of nuclear matrix element calculations.
- ARMENGAUD 21 use the CUPID-Mo demonstrator, with 1.17 kg-yr exposure of ¹⁰⁰Mo, to set this limit. The range reflects the estimated uncertainty of the calculated nuclear matrix elements.
- ADAMS 20A use the data of CUORE (372.5 kg-yr exposure of TeO₂) to obtain this limit.
- AGOSTINI 20B use the final data set of the GERDA experiment, representing an exposure of 127.2 kg yr to derive an upper limit for $\langle m_{\beta\beta} \rangle$. Isotopically enriched Ge detectors were used. The range reflects the variability of the theoretically calculated nuclear matrix elements. Supersedes AGOSTINI 19.
- ALENKOV 19 report the range of the effective masses $\langle m_{\beta\beta} \rangle$ corresponding to the 0 ν $\beta\beta$ decay half-life limit. It is based on the 52.1 kg-d exposure of ¹⁰⁰Mo, in the Yangyang underground laboratory. The median sensitivity is 1.1 × 10²³ years. The range of $\langle m_{\beta\beta} \rangle$ reflects the uncertainty of nuclear matrix elements.
- ANTON 19 uses the complete dataset of the EXO-200 experiment to obtain these limits. The spread reflect the uncertainty in the nuclear matrix elements. Supersedes ALBERT 18 and ALBERT 14b.
- NI 19 use the PandaX-II dual phase TPC at CJPL to search for the 0 ν $\beta\beta$ decay of ¹³⁶Xe with 22.2 kg yr exposure. The range in the $m_{\beta\beta}$ limit of 1.3-3.5 eV reflects the range of the calculated nuclear matrix elements. The sensitivity is 1.9 × 10²³ yr.
- ALDUINO 18 use the combined data of CUORE, CUORE0, and Cuoricino to obtain this limit.
- ARNOLD 18 use the NEMO-3 tracking detector to constrain the 0 ν $\beta\beta$ decay of ⁸²Se. The limit on $\langle m_{\beta\beta} \rangle$ is obtained assuming light neutrino exchange; the range reflects different calculations of the nuclear matrix elements. This is a somewhat weaker limit than in BARABASH 11A using the same detector.
- BARABASH 18 use 1.162 kg of ¹¹⁶CdWO₄ scintillating crystals to obtain these limits. The spread reflects the estimated uncertainty in the nuclear matrix element. Supersedes DANEVICH 03.
- ARNOLD 17 utilize NEMO-3 data, taken with enriched ¹¹⁶Cd to limit the effective Majorana neutrino mass. The reported range results from the use of different nuclear matrix elements. Supersedes BARABASH 11A.
- ALDUINO 16 place a limit on the effective Majorana neutrino mass using the combined data of the CUORE-0 and CUORICINO experiments. The range reflects the authors' evaluation of the variability of the nuclear matrix elements. Supersedes ALFONSO 15.
- ARNOLD 16A limit is derived from data taken with the NEMO-3 detector and ¹⁵⁰Nd. A range of nuclear matrix elements that include the effect of nuclear deformation have been used. Supersedes ARGYRIADES 09.
- ARNOLD 15 use the NEMO-3 tracking calorimeter with 34.3 kg yr exposure to determine the neutrino mass limit based on the 0 ν $\beta\beta$ -half life of ¹⁰⁰Mo. The spread range reflects different nuclear matrix elements. Supersedes ARNOLD 14 and BARABASH 11A.
- ARGYRIADES 10 use ⁹⁶Zr and the NEMO-3 tracking detector to obtain the reported mass limit. The range reflects the fluctuation of the nuclear matrix elements considered.
- Limit was obtained using CaF₂ scintillation calorimeter to search for double beta decay of ⁴⁸Ca. Reported range of limits reflects spread of QRPA and SM matrix element calculations used. Supersedes OGAWA 04.
- Limit for $\langle m_{\nu} \rangle$ is based on the nuclear matrix elements of STAUDT 90 and ARNOLD 96. Supersedes DANEVICH 00.

Limits on Lepton-Number Violating (V+A) Current Admixture

For reasons given in the discussion at the beginning of this section, we list only results from 1989 and later. $\langle \lambda \rangle = \lambda \sum U_{ej} V_{ej}$ and $\langle \eta \rangle = \eta \sum U_{ej} V_{ej}$, where the sum is over the number of neutrino generations. This sum vanishes for massless or unmixed neutrinos. In the following Listings, only best or comparable limits or lifetimes for each isotope are reported.

- ARNOLD 18 use the NEMO03 tracking detector, with 0.93 kg of ⁸²Se mass and 5.25 y exposure to obtain the limits for the hypothetical right-handed currents. Supersedes ARNOLD 05A.
- BARABASH 18 use 1.162 kg of ¹¹⁶CdWO₄ scintillating crystals to obtain this limits for the hypothetical right-handed currents in the 0 ν $\beta\beta$ decay of ¹¹⁶Cd.
- ARNOLD 14 is based on 34.7 kg yr of exposure of the NEMO-3 tracking calorimeter. The reported range limit on $\langle \lambda \rangle$ and $\langle \eta \rangle$ reflects the nuclear matrix element uncertainty in ¹⁰⁰Mo.
- ARNOLD 07 use NEMO-3 half life limit for 0 ν -decay of ¹⁰⁰Mo to the first excited 2⁺-state of daughter nucleus to limit the right-right handed admixture of weak currents $\langle \lambda \rangle$. This limit is not competitive when compared to the decay to the ground state.
- Re-analysis of data originally published in KLAPDOR-KLEINGROTHAUS 04A. Modified pulse shape analysis leads the authors to claim 6 σ statistical evidence for observation of 0 ν -decay. Authors use matrix element of MUTO 89 to determine $\langle \lambda \rangle$ and $\langle \eta \rangle$. Uncertainty of nuclear matrix element is not reflected in stated errors.
- ARNOLD 05A derive limit for $\langle \lambda \rangle$ based on ¹⁰⁰Mo data collected with NEMO-3 detector. No limit for $\langle \eta \rangle$ is given. Supersedes ARNOLD 04.
- ARNOLD 05A derive limit for $\langle \lambda \rangle$ based on ⁸²Se data collected with NEMO-3 detector. No limit for $\langle \eta \rangle$ is given. Supersedes ARNOLD 04.
- ARNOLD 04 use the matrix elements of SUHONEN 94 to obtain a limit for $\langle \lambda \rangle$, no limit for $\langle \eta \rangle$ is given. This limit is more stringent than the limit in EJIRI 01 for the same nucleus.
- ARNOLD 04 use the matrix elements of TOMODA 91 and SUHONEN 91 to obtain a limit for $\langle \lambda \rangle$, no limit for $\langle \eta \rangle$ is given.
- Supersedes ALESSANDRELLO 00. Cryogenic calorimeter search. Reported a range reflecting uncertainty in nuclear matrix element calculations.
- Limits for $\langle \lambda \rangle$ and $\langle \eta \rangle$ are based on nuclear matrix elements of STAUDT 90. Supersedes DANEVICH 00.
- The range of the reported $\langle \lambda \rangle$ and $\langle \eta \rangle$ values reflects the spread of the nuclear matrix elements. On axis value assuming $\langle m_{\nu} \rangle = 0$ and $\langle \lambda \rangle = \langle \eta \rangle = 0$, respectively.
- GUENTHER 97 limits use the matrix elements of STAUDT 90. Supersedes BALYSH 95 and BALYSH 92.
- VUILLEUMIER 93 uses the matrix elements of MUTO 89. Based on a half-life limit 2.6 × 10²³ y at 90%CL.
- BERNATOWICZ 92 takes the measured geochemical decay width as a limit on the 0 ν width, and uses the SUHONEN 91 coefficients to obtain the least restrictive limit on η . Further details of the experiment are given in BERNATOWICZ 93.

Double-β Decay REFERENCES

ABE	23	PRL 130 051801	S. Abe et al.	(KamLAND-Zen Collab.)
ADAMS	23A	PRL 131 249902 (errat.)	D.Q. Adams et al.	(CUORE Collab.)
AGOSTINI	23	PRL 131 142501	M. Agostini et al.	(GERDA Collab.)
AGUIERRE	23	EPJ C03 1117	X. Aguierre et al.	(NEMO-3 Collab.)
ARNQUIST	23	PRL 130 062501	I.J. Arnuquist et al.	(MAJORANA Collab.)
AUGIER	23	PR C107 025503	C. Augier et al.	(CUPID-Mo Collab.)
AUGIER	23A	PRL 131 162501	C. Augier et al.	(CUPID-Mo Collab.)
AZZOLINI	23A	PRL 131 222501	O. Azzolini et al.	(CUPID-0 Collab.)
NOVELLA	23	JHEP 2309 190	P. Novella et al.	(NEXT Collab.)
ADAMS	22A	NAT 604 53	D.Q. Adams et al.	(CUORE Collab.)
ADAMS	22B	PRL 129 222501	D.Q. Adams et al.	(CUORE Collab.)
APRILE	22A	PR C106 024328	E. Aprile et al.	(XENONIT Collab.)
APRILE	22B	PRL 129 161805	E. Aprile et al.	(XENONIT Collab.)
AUGIER	22	EPJ C82 1033	C. Augier et al.	(CUPID-Mo Collab.)
AZZOLINI	22	PRL 129 111801	O. Azzolini et al.	(CUPID-0 Collab.)
NOVELLA	22	PR C105 055501	P. Novella et al.	(NEXT Collab.)
ADAMS	21	PRL 126 171801	D.Q. Adams et al.	(CUORE Collab.)
Also		PRL 131 249902 (errat.)	D.Q. Adams et al.	(CUORE Collab.)
ADAMS	21A	EPJ C81 567	D.Q. Adams et al.	(CUORE Collab.)
ARMENGAUD	21	PRL 126 181802	E. Armengaud et al.	(CUPID-Mo Collab.)
ARNQUIST	21	PR C103 015501	I.J. Arnuquist et al.	(MAJORANA Collab.)
ADAMS	20A	PRL 124 122501	D.Q. Adams et al.	(CUORE Collab.)
AGOSTINI	20B	PRL 125 252502	M. Agostini et al.	(GERDA Collab.)
ARMENGAUD	20	EPJ C80 674	E. Armengaud et al.	(CUPID-Mo Collab.)
AGOSTINI	19	SCI 365 1445	M. Agostini et al.	(GERDA Collab.)
ALDUINO	19	EPJ C79 795	C. Alduino et al.	(CUORE Collab.)
ALENKOV	19	EPJ C79 791	V. Alenkov et al.	(AMORE Collab.)
ANTON	19	PRL 123 161802	G. Anton et al.	(EXO-200 Collab.)
APRILE	19E	NAT 568 532	E. Aprile et al.	(XENONIT Collab.)
ARNOLD	19	EPJ C79 440	R. Arnold et al.	(NEMO-3 Collab.)
AZZOLINI	19	PRL 123 032501	O. Azzolini et al.	(CUPID-0 Collab.)
AZZOLINI	19B	PRL 123 262501	O. Azzolini et al.	(CUPID-0 Collab.)
NI	19	CP C43 113001	K. Ni et al.	(PandaX-II Collab.)

Lepton Particle Listings

Double- β Decay, Neutrino Mixing

ALBERT	18	PRL 120 072701	J.B. Albert et al.	(EXO-200 Collab.)
ALDUINO	18	PRL 120 132501	C. Alduino et al.	(CUORE Collab.)
ARNOLD	18	EPJ C78 821	R. Arnold et al.	(NEMO-3 Collab.)
BARABASH	18	PR D98 092007	A.S. Barabash et al.	(AURORA Collab.)
ALBERT	17C	PR D96 092001	J.B. Albert et al.	(EXO-200 Collab.)
ALDUINO	17	EPJ C77 13	C. Alduino et al.	(CUORE Collab.)
ARNOLD	17	PR D95 012007	R. Arnold et al.	(NEMO-3 Collab.)
ALDUINO	16	PR C93 045503	C. Alduino et al.	(CUORE Collab.)
ARNOLD	16	PR D93 112008	R. Arnold et al.	(NEMO-3 Collab.)
ARNOLD	16A	PR D94 072003	R. Arnold et al.	(NEMO-3 Collab.)
ASAKURA	16	NP A946 171	K. Asakura et al.	(KamLAND-Zen Collab.)
AGOSTINI	15A	EPJ C75 416	M. Agostini et al.	(GERDA Collab.)
ALFONSO	15	PRL 115 102502	K. Alfonso et al.	(CUORE Collab.)
ARNOLD	15	PR D92 072011	R. Arnold et al.	(NEMO-3 Collab.)
ALBERT	14	PR C89 015502	J. Albert et al.	(EXO-200 Collab.)
ALBERT	14B	NAT 510 229	J.B. Albert et al.	(EXO-200 Collab.)
ARNOLD	14	PR D89 111101	R. Arnold et al.	(NEMO-3 Collab.)
GAVRILYAK	13	PR C87 035501	Yu.M. Gavriluyak et al.	(CUORICINO Collab.)
ANDREOTTI	12	PR C85 045503	E. Andreotti et al.	(KamLAND-Zen Collab.)
GANDO	12A	PR C85 045504	A. Gando et al.	(EXO Collab.)
ACKERMAN	11	PRL 107 212501	N. Ackerman et al.	(EXO Collab.)
ARNOLD	11	PRL 107 062504	R. Arnold et al.	(NEMO-3 Collab.)
BARABASH	11A	PAN 74 312	A.S. Barabash et al.	(NEMO-3 Collab.)
Translated from YAF 74 330.				
ARGYRIADES	10	NP A847 168	J. Argyriades et al.	(NEMO-3 Collab.)
BELLI	10	NP A846 143	P. Belli et al.	(DAMA-INR Collab.)
ARGYRIADES	09	PR C80 032501	J. Argyriades et al.	(NEMO-3 Collab.)
KIDD	09	NP A821 251	M. Kidd et al.	
UMEHARA	08	PR C78 058501	S. Umehara et al.	
ARNOLD	07	NP A781 209	R. Arnold et al.	(NEMO-3 Collab.)
KLAPDOR-K...	06A	MPL A21 1547	H.V. Klapdor-Kleingrothaus, I.V. Krivosheina	
ARNOLD	05A	PRL 95 102302	R. Arnold et al.	(NEMO-3 Collab.)
AALSETH	04	PR D70 078302	C.E. Aalseth et al.	
ARNOLD	04	JETPL 80 377	R. Arnold et al.	(NEMO-3 Collab.)
Translated from ZETFP 80 429.				
KLAPDOR-K...	04A	PL B586 198	H.V. Klapdor-Kleingrothaus et al.	
KLAPDOR-K...	04B	PR D70 078301	H.V. Klapdor-Kleingrothaus, A. Dietz, I.V. Krivosheina	
OGAWA	04	NP A730 215	I. Ogawa et al.	
ARNABOLDI	03	PL B557 167	C. Arnaboldi et al.	
DANEVICH	03	PR C68 035501	F.A. Danevich et al.	
AALSETH	02B	PR D65 092007	C.E. Aalseth et al.	(IGEX Collab.)
DEBRAECKEL...	01	PRL 86 3510	L. De Braeckeleer et al.	
EJIRI	01	PR C63 065501	H. Ejiri et al.	
KLAPDOR-K...	01	EPJ A12 147	H.V. Klapdor-Kleingrothaus et al.	
KLAPDOR-K...	01B	MPL A16 2409	H.V. Klapdor-Kleingrothaus et al.	
ALESSANDRI...	00	PL B486 13	A. Alessandri et al.	
DANEVICH	00	PR C62 045501	F.A. Danevich et al.	
ARNOLD	99	NP A658 299	R. Arnold et al.	(NEMO Collab.)
GUNTHER	97	PR D55 54	M. Gunther et al.	(Heidelberg-Moscow Collab.)
ARNOLD	96	ZPHY C72 239	R. Arnold et al.	(BCEEN, CAEN, JINR+)
BALYSH	95	PL B356 450	A. Balysh et al.	(Heidelberg-Moscow Collab.)
DASSIE	95	PR D51 2090	D. Dassie et al.	(NEMO Collab.)
EJIRI	95	JPSJ 64 339	H. Ejiri et al.	(OSAK, KIEV)
SUHONEN	94	PR C49 3055	J. Suhonen, O. Civitarese	
BERNATOW...	93	PR C47 806	T. Bernatowicz et al.	(WUSL, TATA)
VUILLEUMIER	93	PR D48 1009	J.C. Vuilleumier et al.	(NEUC, CIT, VILL)
BALYSH	92	PL B283 32	A. Balysh et al.	(MPIK, KIAE, SASSO)
BERNATOW...	92	PRL 69 2341	T. Bernatowicz et al.	(WUSL, TATA)
SUHONEN	91	NP A535 509	J. Suhonen, S.B. Khadikar, A. Faessler	(JYV+)
TOMODA	91	RPP 54 53	T. Tomoda	
STAUDT	90	EPL 13 31	A. Staudt, K. Muto, H.V. Klapdor-Kleingrothaus	
MUTO	89	ZPHY A334 187	K. Muto, E. Bender, H.V. Klapdor	(TINT, MPIK)

Neutrino Mixing

With the possible exceptions of "short-baseline anomalies," such as LSND, all neutrino data can be described within the framework of a 3×3 mixing matrix between the mass eigenstates ν_1 , ν_2 , and ν_3 , leading to the flavor eigenstates ν_e , ν_μ , and ν_τ , as described in the review "Neutrino masses, mixing and oscillations."

The Listings are divided in the following sections:

(A) Neutrino fluxes and event ratios: shows measurements which correspond to various oscillation tests for Accelerator, Reactor, Atmospheric, and Solar neutrino experiments. Typically, ratios involve a measurement in a realm sensitive to oscillations compared to one for which no oscillation effect is expected.

(B) Neutrino mixing parameters: shows measurements of $\sin^2(\theta_{12})$, $\sin^2(\theta_{23})$, $\sin^2(\theta_{13})$, Δm_{21}^2 , Δm_{32}^2 , and δ_{CP} as extracted from the measured data in the quoted publications in the frame of the three-neutrino mixing scheme. The quoted averages are not the result of a global fit, as in the review "Neutrino masses, mixing, and oscillations," and, as a consequence, might slightly differ from them. In some cases, measurements depend on the mass order (normal when $\Delta m_{32}^2 > 0$ or inverted

when $\Delta m_{32}^2 < 0$) or octant of θ_{23} (lower when $\theta_{23} < 45^\circ$ or upper when $\theta_{23} > 45^\circ$).

(C) Other neutrino mixing results:

The LSND anomaly [AGUILAR 01], reported a signal which is consistent with $\bar{\nu}_\mu \rightarrow \bar{\nu}_e$ oscillations. In a three neutrino framework, this would be a measurement of θ_{12} and Δm_{21}^2 . This does not appear to be consistent with the interpretation of other neutrino data. It has been interpreted as evidence for a 4th "sterile" neutrino. The following listings include results which might be relevant towards understanding this observation. They include searches for $\nu_\mu \rightarrow \nu_e$, $\bar{\nu}_\mu \rightarrow \bar{\nu}_e$, sterile neutrino oscillations, and others.

(A) Neutrino fluxes and event ratios

Events (observed/expected) from accelerator ν_μ experiments.

Some neutrino oscillation experiments compare the flux in two or more detectors. This is usually quoted as the ratio of the event rate in the far detector to the expected rate based on an extrapolation from the near detector in the absence of oscillations.

VALUE	DOCUMENT ID	TECN	COMMENT
• • • We do not use the following data for averages, fits, limits, etc. • • •			
1.01 ± 0.10	¹ ABE	14B T2K	ν_e rate in T2K near detect.
0.71 ± 0.08	² AHN	06A K2K	K2K to Super-K
0.64 ± 0.05	³ MICHAEL	06 MINS	All charged current events
0.71 ± 0.08 - 0.09	⁴ ALIU	05 K2K	KEK to Super-K
0.70 ± 0.10 - 0.11	⁵ AHN	03 K2K	KEK to Super-K

¹ The rate of ν_e from μ decay was measured to be 0.68 ± 0.30 compared to the predicted flux. From K decay 1.10 ± 0.14 compared to the predicted flux.

² Based on the observation of 112 events when 158.1 ± 9.2 were expected without oscillations. Including not only the number of events but also the shape of the energy distribution, the evidence for oscillation is at the level of about 4.3σ . Supersedes ALIU 05.

³ This ratio is based on the observation of 215 events compared to an expectation of 336 ± 14 without oscillations. See also ADAMSON 08.

⁴ This ratio is based on the observation of 107 events at the far detector 250 km away from KEK, and an expectation of 151 ± 12 .

⁵ This ratio is based on the observation of 56 events with an expectation of 80.1 ± 6.2 .

Events (observed/expected) from reactor $\bar{\nu}_e$ experiments.

The quoted values are the ratios of the measured reactor $\bar{\nu}_e$ event rate at the quoted distances, and the rate expected without oscillations. The expected rate is based on the experimental data for the most significant reactor fuels (^{235}U , ^{239}Pu , ^{241}Pu) and on calculations for ^{238}U .

A recent re-evaluation of the spectral conversion of electron to $\bar{\nu}_e$ in MUELLER 11 results in an upward shift of the reactor $\bar{\nu}_e$ spectrum by 3% and, thus, might require revisions to the ratios listed in this table.

VALUE	DOCUMENT ID	TECN	COMMENT
• • • We do not use the following data for averages, fits, limits, etc. • • •			
$0.948 \pm 0.008 \pm 0.033$	¹ ALMAZAN	20 RHF	RHF reactor at ILL
0.952 ± 0.027	² ADEY	19 DAYA	DayaBay, Ling Ao/Ao II reactors
	³ AN	16 DAYA	DayaBay, Ling Ao/Ao II reactors
$1.08 \pm 0.21 \pm 0.16$	⁴ DENIZ	10 TEXO	Kuo-Sheng reactor, 28 m
$0.658 \pm 0.044 \pm 0.047$	⁵ ARAKI	05 KLND	Japanese react. ~180 km
$0.611 \pm 0.085 \pm 0.041$	⁶ EGUCHI	03 KLND	Japanese react. ~180 km
$1.01 \pm 0.024 \pm 0.053$	⁷ BOEHM	01	Palo Verde react. 0.75-0.89 km
$1.01 \pm 0.028 \pm 0.027$	⁸ APOLLONIO	99 CHOZ	Chooz reactors 1 km
$0.987 \pm 0.006 \pm 0.037$	⁹ GREENWOOD	96	Savannah River, 18.2 m
$0.988 \pm 0.004 \pm 0.05$	ACHKAR	95 CNTR	Bugey reactor, 15 m
$0.994 \pm 0.010 \pm 0.05$	ACHKAR	95 CNTR	Bugey reactor, 40 m
$0.915 \pm 0.132 \pm 0.05$	ACHKAR	95 CNTR	Bugey reactor, 95 m
$0.987 \pm 0.014 \pm 0.027$	¹⁰ DECLAIS	94 CNTR	Bugey reactor, 15 m
$0.985 \pm 0.018 \pm 0.034$	KUVSHIN...	91 CNTR	Rovno reactor
$1.05 \pm 0.02 \pm 0.05$	VUILLEUMIER	82	Gösgen reactor
$0.955 \pm 0.035 \pm 0.110$	¹¹ KWON	81	$\bar{\nu}_e p \rightarrow e^+ n$
0.89 ± 0.15	¹¹ BOEHM	80	$\bar{\nu}_e p \rightarrow e^+ n$

¹ ALMAZAN 20 use the RHF research reactor at ILL to compare their measured anti-neutrino event rate to the calculation by HUBER 11. Reported $0.948 \pm 0.008 \pm 0.023 \pm 0.023$ measurement with uncertainties from statistics, systematic, and model. Note that this result is obtained for highly enriched ^{235}U reactor fuel while most other reactor experiments utilize a low-enrichment mix of fissile nuclides.

- ² ADEY 19 present a re-analysis of 1230 days of Daya Bay near detector data with reduced systematic uncertainties on the neutron detection efficiency. Note that ADEY 19 report the measured to predicted antineutrino ratio using the reactor model of MUELLER 11 (Huber-Mueller model). The ratio using the older ILL-Vogel model is $1.001 \pm 0.015 \pm 0.027$.
- ³ AN 16 use 217 days of data (338k events) to determine the neutrino flux ratio relative to the prediction of Mueller-Huber and ILL-Vogel models (see AN 16 for details). The reported flux ratios were corrected for θ_{13} oscillation effect. The flux measurement is consistent with results from previous short-baseline reactor experiments. The measured inverse beta decay yield is $(1.55 \pm 0.04) \times 10^{-18} \text{ cm}^2/(\text{GW day})$ or $\sigma_f = (5.92 \pm 0.14) \times 10^{-43} \text{ cm}^2/\text{fission}$. About 4σ excess of events was observed in the 4–6 MeV prompt energy region.
- ⁴ DENIZ 10 observe reactor $\bar{\nu}_e$ scattering with recoil kinetic energies 3–8 MeV using CsI(Tl) detectors. The observed rate is consistent with the Standard Model prediction, leading to a constraint on $\sin^2\theta_{\text{WV}} = 0.251 \pm 0.031(\text{stat}) \pm 0.024(\text{sys})$.
- ⁵ Updated result of KamLAND, including the data used in EGUCHI 03. Note that the survival probabilities for different periods are not directly comparable because the effective baseline varies with power output of the reactor sources involved, and there were large variations in the reactor power production in Japan in 2003.
- ⁶ EGUCHI 03 observe reactor neutrino disappearance at $\sim 180 \text{ km}$ baseline to various Japanese nuclear power reactors.
- ⁷ BOEHM 01 search for neutrino oscillations at 0.75 and 0.89 km distance from the Palo Verde reactors.
- ⁸ APOLLONIO 99, APOLLONIO 98 search for neutrino oscillations at 1.1 km fixed distance from Chooz reactors. They use $\bar{\nu}_e p \rightarrow e^+ n$ in Gd-loaded scintillator target. APOLLONIO 99 supersedes APOLLONIO 98. See also APOLLONIO 03 for detailed description.
- ⁹ GREENWOOD 96 search for neutrino oscillations at 18 m and 24 m from the reactor at Savannah River.
- ¹⁰ DECLAIS 94 result based on integral measurement of neutrons only. Result is ratio of measured cross section to that expected in standard V-A theory. Replaced by ACHKAR 95.
- ¹¹ KWON 81 represents an analysis of a larger set of data from the same experiment as BOEHM 80.

Atmospheric neutrinos

Neutrinos and antineutrinos produced in the atmosphere induce μ -like and e -like events in underground detectors. The ratio of the numbers of the two kinds of events is defined as μ/e . It has the advantage that systematic effects, such as flux uncertainty, tend to cancel, for both experimental and theoretical values of the ratio. The “ratio of the ratios” of experimental to theoretical μ/e , $R(\mu/e)$, or that of experimental to theoretical μ/total , $R(\mu/\text{total})$ with $\text{total} = \mu + e$, is reported below. If the actual value is not unity, the value obtained in a given experiment may depend on the experimental conditions. In addition, the measured “up-down asymmetry” for μ ($N_{\text{up}}(\mu)/N_{\text{down}}(\mu)$) or e ($N_{\text{up}}(e)/N_{\text{down}}(e)$) is reported. The expected “up-down asymmetry” is nearly unity if there is no neutrino oscillation.

$R(\mu/e) = (\text{Measured Ratio } \mu/e) / (\text{Expected Ratio } \mu/e)$

VALUE	DOCUMENT ID	TECN	COMMENT
• • • We do not use the following data for averages, fits, limits, etc. • • •			
$0.658 \pm 0.016 \pm 0.035$	1 ASHIE	05	SKAM sub-GeV
$0.702 \pm 0.032 \pm 0.101$ -0.030	2 ASHIE	05	SKAM multi-GeV
$0.69 \pm 0.10 \pm 0.06$	3 SANCHEZ	03	SOU2 Calorimeter raw data
$1.00 \pm 0.15 \pm 0.08$	4 FUKUDA	96B	KAMI Water Cherenkov
$0.60 \pm 0.06 \pm 0.05$ -0.05	5 DAUM	95	FREJ Calorimeter
$0.57 \pm 0.08 \pm 0.07$ -0.07	6 FUKUDA	94	KAMI sub-GeV
	7 FUKUDA	94	KAMI multi-GeV
	8 BECKER-SZ...	92B	IMB Water Cherenkov

- ¹ ASHIE 05 results are based on an exposure of 92 kton yr during the complete Super-Kamiokande I running period. The analyzed data sample consists of fully-contained single-ring e -like events with $0.1 \text{ GeV}/c < p_e$ and μ -like events $0.2 \text{ GeV}/c < p_\mu$, both having a visible energy $< 1.33 \text{ GeV}$. These criteria match the definition used by FUKUDA 94.
- ² ASHIE 05 results are based on an exposure of 92 kton yr during the complete Super-Kamiokande I running period. The analyzed data sample consists of fully-contained single-ring events with visible energy $> 1.33 \text{ GeV}$ and partially-contained events. All partially-contained events are classified as μ -like.
- ³ SANCHEZ 03 result is based on an exposure of 5.9 kton yr, and updates ALLISON 99 result. The analyzed data sample consists of fully-contained e -flavor and μ -flavor events having lepton momentum $> 0.3 \text{ GeV}/c$.
- ⁴ FUKUDA 96B studied neutron background in the atmospheric neutrino sample observed in the Kamiokande detector. No evidence for the background contamination was found.
- ⁵ DAUM 95 results are based on an exposure of 2.0 kton yr which includes the data used by BERGER 90B. This ratio is for the contained and semicontained events. DAUM 95 also report $R(\mu/e) = 0.99 \pm 0.13 \pm 0.08$ for the total neutrino induced data sample which includes upward going stopping muons and horizontal muons in addition to the contained and semicontained events.
- ⁶ FUKUDA 94 result is based on an exposure of 7.7 kton yr and updates the HIRATA 92 result. The analyzed data sample consists of fully-contained e -like events with $0.1 < p_e < 1.33 \text{ GeV}/c$ and fully-contained μ -like events with $0.2 < p_\mu < 1.5 \text{ GeV}/c$.

- ⁷ FUKUDA 94 analyzed the data sample consisting of fully contained events with visible energy $> 1.33 \text{ GeV}$ and partially contained μ -like events.
- ⁸ BECKER-SZENDY 92B reports the fraction of nonshowering events (mostly muons from atmospheric neutrinos) as $0.36 \pm 0.02 \pm 0.02$, as compared with expected fraction $0.51 \pm 0.01 \pm 0.05$. After cutting the energy range to the Kamiokande limits, BEIER 92 finds $R(\mu/e)$ very close to the Kamiokande value.

$R(\nu_\mu) = (\text{Measured Flux of } \nu_\mu) / (\text{Expected Flux of } \nu_\mu)$

VALUE	DOCUMENT ID	TECN	COMMENT
• • • We do not use the following data for averages, fits, limits, etc. • • •			
0.84 ± 0.12	1 ADAMSON	06	MINS MINOS atmospheric
$0.72 \pm 0.026 \pm 0.13$	2 AMBROSIO	01	MCRO upward through-going
$0.57 \pm 0.05 \pm 0.15$	3 AMBROSIO	00	MCRO upgoing partially contained
$0.71 \pm 0.05 \pm 0.19$	4 AMBROSIO	00	MCRO downgoing partially contained + upgoing stopping
$0.74 \pm 0.036 \pm 0.046$	5 AMBROSIO	98	MCRO Streamer tubes
	6 CASPER	91	IMB Water Cherenkov
	7 AGLIETTA	89	NUSX
0.95 ± 0.22	8 BOLIEV	81	Baksan
0.62 ± 0.17	CROUCH	78	Case Western/UCI

- ¹ ADAMSON 06 uses a measurement of 107 total neutrinos compared to an expected rate of 127 ± 13 without oscillations.
- ² AMBROSIO 01 result is based on the upward through-going muon tracks with $E_\mu > 1 \text{ GeV}$. The data came from three different detector configurations, but the statistics is largely dominated by the full detector run, from May 1994 to December 2000. The total live time, normalized to the full detector configuration, is 6.17 years. The first error is the statistical error, the second is the systematic error, dominated by the theoretical error in the predicted flux.
- ³ AMBROSIO 00 result is based on the upgoing partially contained event sample. It came from 4.1 live years of data taking with the full detector, from April 1994 to February 1999. The average energy of atmospheric muon neutrinos corresponding to this sample is 4 GeV. The first error is statistical, the second is the systematic error, dominated by the 25% theoretical error in the rate (20% in the flux and 15% in the cross section, added in quadrature). Within statistics, the observed deficit is uniform over the zenith angle.
- ⁴ AMBROSIO 00 result is based on the combined samples of downgoing partially contained events and upgoing stopping events. These two subsamples could not be distinguished due to the lack of timing information. The result came from 4.1 live years of data taking with the full detector, from April 1994 to February 1999. The average energy of atmospheric muon neutrinos corresponding to this sample is 4 GeV. The first error is statistical, the second is the systematic error, dominated by the 25% theoretical error in the rate (20% in the flux and 15% in the cross section, added in quadrature). Within statistics, the observed deficit is uniform over the zenith angle.
- ⁵ AMBROSIO 98 result is for all nadir angles and updates AHLEN 95 result. The lower cutoff on the muon energy is 1 GeV. In addition to the statistical and systematic errors, there is a Monte Carlo flux error (theoretical error) of ± 0.13 . With a neutrino oscillation hypothesis, the fit either to the flux or zenith distribution independently yields $\sin^2 2\theta = 1.0$ and $\Delta(m^2) \sim$ a few times 10^{-3} eV^2 . However, the fit to the observed zenith distribution gives a maximum probability for χ^2 of only 5% for the best oscillation hypothesis.
- ⁶ CASPER 91 correlates showering/nonshowering signature of single-ring events with parent atmospheric-neutrino flavor. They find nonshowering ($\approx \nu_\mu$ induced) fraction is $0.41 \pm 0.03 \pm 0.02$, as compared with expected 0.51 ± 0.05 (syst).
- ⁷ AGLIETTA 89 finds no evidence for any anomaly in the neutrino flux. They define $\rho = (\text{measured number of } \nu_e\text{'s})/(\text{measured number of } \nu_\mu\text{'s})$. They report $\rho(\text{measured}) = \rho(\text{expected}) = 0.96 \pm 0.32$
 -0.28 .
- ⁸ From this data BOLIEV 81 obtain the limit $\Delta(m^2) \leq 6 \times 10^{-3} \text{ eV}^2$ for maximal mixing, $\nu_\mu \leftrightarrow \nu_\mu$ type oscillation.

$R(\mu/\text{total}) = (\text{Measured Ratio } \mu/\text{total}) / (\text{Expected Ratio } \mu/\text{total})$

VALUE	DOCUMENT ID	TECN	COMMENT
• • • We do not use the following data for averages, fits, limits, etc. • • •			
$1.1 \pm 0.07 \pm 0.11$ -0.12	1 CLARK	97	IMB multi-GeV

- ¹ CLARK 97 obtained this result by an analysis of fully contained and partially contained events in the IMB water-Cherenkov detector with visible energy $> 0.95 \text{ GeV}$.

$N_{\text{up}}(\mu)/N_{\text{down}}(\mu)$

VALUE	DOCUMENT ID	TECN	COMMENT
• • • We do not use the following data for averages, fits, limits, etc. • • •			
0.71 ± 0.06	1 ADAMSON	12B	MINS contained-vertex muons
$0.551 \pm 0.035 \pm 0.004$ -0.033	2 ASHIE	05	SKAM multi-GeV

- ¹ ADAMSON 12B reports the atmospheric neutrino results obtained with MINOS far detector in 2,553 live days (an exposure of 37.9 kton-yr). This result is obtained with a sample of high resolution contained-vertex muons. The quoted error is statistical only.
- ² ASHIE 05 results are based on an exposure of 92 kton yr during the complete Super-Kamiokande I running period. The analyzed data sample consists of fully-contained single-ring μ -like events with visible energy $> 1.33 \text{ GeV}$ and partially-contained events. All partially-contained events are classified as μ -like. Upward-going events are those with $-1 < \cos(\text{zenith angle}) < -0.2$ and downward-going events are those with $0.2 < \cos(\text{zenith angle}) < 1$. The μ -like up-down ratio for the multi-GeV data deviates from 1 (the expectation for no atmospheric ν_μ oscillations) by more than 12 standard deviations.

Lepton Particle Listings

Neutrino Mixing

$N_{up}(e)/N_{down}(e)$

VALUE	DOCUMENT ID	TECN	COMMENT
-------	-------------	------	---------

• • • We do not use the following data for averages, fits, limits, etc. • • •

$0.961^{+0.086}_{-0.079} \pm 0.016$	¹ ASHIE	05	SKAM multi-GeV
-------------------------------------	--------------------	----	----------------

¹ ASHIE 05 results are based on an exposure of 92 kton yr during the complete Super-Kamiokande I running period. The analyzed data sample consists of fully-contained single-ring e -like events with visible energy > 1.33 GeV. Upward-going events are those with $-1 < \cos(\text{zenith angle}) < -0.2$ and downward-going events are those with $0.2 < \cos(\text{zenith angle}) < 1$. The e -like up-down ratio for the multi-GeV data is consistent with 1 (the expectation for no atmospheric ν_e oscillations).

$R(\text{up/down}; \mu) = (\text{Measured up/down}; \mu) / (\text{Expected up/down}; \mu)$

VALUE	DOCUMENT ID	TECN	COMMENT
-------	-------------	------	---------

• • • We do not use the following data for averages, fits, limits, etc. • • •

$0.62 \pm 0.05 \pm 0.02$	¹ ADAMSON	12B	MINS contained-vertex muons
$0.62^{+0.19}_{-0.14} \pm 0.02$	² ADAMSON	06	MINS atmospheric ν with far detector

¹ ADAMSON 12B reports the atmospheric neutrino results obtained with MINOS far detector in 2,553 live days (an exposure of 37.9 kton-yr). This result is obtained with a sample of high resolution contained-vertex muons. The expected ratio is calculated with no neutrino oscillation.

² ADAMSON 06 result is obtained with the MINOS far detector with an exposure of 4.54 kton yr. The expected ratio is calculated with no neutrino oscillation.

$N(\mu^+)/N(\mu^-)$

VALUE	DOCUMENT ID	TECN	COMMENT
-------	-------------	------	---------

• • • We do not use the following data for averages, fits, limits, etc. • • •

$0.46^{+0.05}_{-0.04}$	^{1,2} ADAMSON	12B	MINS contained-vertex muons
$0.63^{+0.09}_{-0.08}$	^{1,3} ADAMSON	12B	MINS ν -induced rock-muons

¹ ADAMSON 12B reports the atmospheric neutrino results obtained with MINOS far detector in 2,553 live days (an exposure of 37.9 kton-yr). The muon charge ratio $N(\mu^+)/N(\mu^-)$ represents the $\overline{\nu}_\mu/\nu_\mu$ ratio.

² This result is obtained with a charge-separated sample of high resolution contained-vertex muons. The quoted error is statistical only.

³ This result is obtained with a charge-separated sample of high resolution neutrino-induced rock-muons. The quoted error is statistical only.

$R(\mu^+/\mu^-) = (\text{Measured } N(\mu^+)/N(\mu^-)) / (\text{Expected } N(\mu^+)/N(\mu^-))$

VALUE	DOCUMENT ID	TECN	COMMENT
-------	-------------	------	---------

• • • We do not use the following data for averages, fits, limits, etc. • • •

$0.93 \pm 0.09 \pm 0.09$	^{1,2} ADAMSON	12B	MINS contained-vertex muons
$1.29^{+0.19}_{-0.17} \pm 0.16$	^{1,3} ADAMSON	12B	MINS ν -induced rock-muons
$1.03 \pm 0.08 \pm 0.08$	^{1,4} ADAMSON	12B	MINS contained
$1.39^{+0.35+0.08}_{-0.46-0.14}$	⁵ ADAMSON	07	MINS Upward and horizontal μ with far detector
$0.96^{+0.38}_{-0.27} \pm 0.15$	⁶ ADAMSON	06	MINS atmospheric ν with far detector

¹ ADAMSON 12B reports the atmospheric neutrino results obtained with MINOS far detector in 2,553 live days (an exposure of 37.9 kton-yr). The muon charge ratio $N(\mu^+)/N(\mu^-)$ represents the $\overline{\nu}_\mu/\nu_\mu$ ratio. As far as the same oscillation parameters are used for ν_s and $\overline{\nu}_s$, the expected $\overline{\nu}_\mu/\nu_\mu$ ratio is almost entirely independent of any input oscillations.

² This result is obtained with a charge-separated sample of high resolution contained-vertex muons.

³ This result is obtained with a charge-separated sample of high resolution neutrino-induced rock-muons.

⁴ The charge-separated samples of high resolution contained-vertex muons and neutrino-induced rock-muons are combined to obtain this result which is consistent with unity.

⁵ ADAMSON 07 result is obtained with the MINOS far detector in 854.24 live days, based on neutrino-induced upward-going and horizontal muons. This result is consistent with CPT conservation.

⁶ ADAMSON 06 result is obtained with the MINOS far detector with an exposure of 4.54 kton yr, based on contained events. The expected ratio is calculated by assuming the same oscillation parameters for neutrinos and antineutrinos.

Solar neutrinos

Solar neutrinos are produced by thermonuclear fusion reactions in the Sun. Radiochemical experiments measure particular combinations of fluxes from various neutrino-producing reactions, whereas water-Cherenkov experiments mainly measure a flux of neutrinos from decay of ^8B . Solar neutrino fluxes are composed of all active neutrino species, ν_e , ν_μ , and ν_τ . In addition, some other mechanisms may cause antineutrino components in solar neutrino fluxes. Each measurement method is sensitive to a particular component or a combination of components of solar neutrino fluxes.

ν_e Capture Rates from Radiochemical Experiments

1 SNU (Solar Neutrino Unit) = 10^{-36} captures per atom per second.

VALUE (SNU)	DOCUMENT ID	TECN	COMMENT
-------------	-------------	------	---------

• • • We do not use the following data for averages, fits, limits, etc. • • •

$73.4^{+6.1+3.7}_{-6.0-4.1}$	¹ KAETHER	10	GALX reanalysis
$67.6 \pm 4.0 \pm 3.2$	² KAETHER	10	GNO+GALX reanalysis combined
$65.4^{+3.1+2.6}_{-3.0-2.8}$	³ ABDURASHI...	09	SAGE $^{71}\text{Ga} \rightarrow ^{71}\text{Ge}$
$62.9^{+5.5}_{-5.3} \pm 2.5$	⁴ ALTMANN	05	GNO $^{71}\text{Ga} \rightarrow ^{71}\text{Ge}$
$69.3 \pm 4.1 \pm 3.6$	⁵ ALTMANN	05	GNO GNO + GALX combined
$77.5 \pm 6.2^{+4.3}_{-4.7}$	⁶ HAMPEL	99	GALX $^{71}\text{Ga} \rightarrow ^{71}\text{Ge}$
$2.56 \pm 0.16 \pm 0.16$	⁷ CLEVELAND	98	HOME $^{37}\text{Cl} \rightarrow ^{37}\text{Ar}$

¹ KAETHER 10 reports the reanalysis results of a complete GALLEX data (GALLEX I+II+III+IV, reported in HAMPEL 99) based on the event selection with a new pulse shape analysis, which provides a better background reduction than the rise time analysis adopted in HAMPEL 99.

² Combined result of GALLEX I+II+III+IV reanalysis and GNO I+II+III (ALTMANN 05).

³ ABDURASHITOV 09 reports a combined analysis of 168 extractions of the SAGE solar neutrino experiment during the period January 1990 through December 2007, and updates the ABDURASHITOV 02 result. The data are consistent with the assumption that the solar neutrino production rate is constant in time. Note that a $\sim 15\%$ systematic uncertainty in the overall normalization may be added to the ABDURASHITOV 09 result, because calibration experiments for gallium solar neutrino measurements using intense ^{51}Cr (twice by GALLEX and once by SAGE) and ^{37}Ar (by SAGE) result in an average ratio of 0.87 ± 0.05 of the observed to calculated rates.

⁴ ALTMANN 05 reports the complete result from the GNO solar neutrino experiment (GNO I+II+III), which is the successor project of GALLEX. Experimental technique of GNO is essentially the same as that of GALLEX. The run data cover the period 20 May 1998 through 9 April 2003.

⁵ Combined result of GALLEX I+II+III+IV (HAMPEL 99) and GNO I+II+III.

⁶ HAMPEL 99 report the combined result for GALLEX I+II+III+IV (65 runs in total), which update the HAMPEL 96 result. The GALLEX IV result (12 runs) is $118.4 \pm 17.8 \pm 6.6$ SNU. (HAMPEL 99 discuss the consistency of partial results with the mean.) The GALLEX experimental program has been completed with these runs. The total run data cover the period 14 May 1991 through 23 January 1997. A total of 300 ^{71}Ge events were observed. Note that a $\sim 15\%$ systematic uncertainty in the overall normalization may be added to the HAMPEL 99 result, because calibration experiments for gallium solar neutrino measurements using intense ^{51}Cr (twice by GALLEX and once by SAGE) and ^{37}Ar (by SAGE) result in an average ratio of 0.87 ± 0.05 of the observed to calculated rates.

⁷ CLEVELAND 98 is a detailed report of the ^{37}Cl experiment at the Homestake Mine. The average solar neutrino-induced ^{37}Ar production rate from 108 runs between 1970 and 1994 updates the DAVIS 89 result.

$\Phi_{ES} (^8\text{B})$

^8B solar-neutrino flux measured via ν_e elastic scattering. This process is sensitive to all active neutrino flavors, but with reduced sensitivity to ν_μ , ν_τ due to the cross-section difference, $\sigma(\nu_{\mu,\tau} e) \sim 0.16\sigma(\nu_e e)$. If the ^8B solar-neutrino flux involves nonelectron flavor active neutrinos, their contribution to the flux is ~ 0.16 times of ν_e .

VALUE ($10^6 \text{ cm}^{-2}\text{s}^{-1}$)	DOCUMENT ID	TECN	COMMENT
---	-------------	------	---------

• • • We do not use the following data for averages, fits, limits, etc. • • •

$2.57^{+0.17+0.07}_{-0.18-0.07}$	¹ AGOSTINI	20A	BORX average flux
$2.53^{+0.31+0.13}_{-0.28-0.10}$	² ANDERSON	19	SNO+ Water phase; average flux
$2.57^{+0.17+0.07}_{-0.18-0.07}$	³ AGOSTINI	18B	BORX average flux
$2.345 \pm 0.014 \pm 0.036$	⁴ ABE	16C	SKAM SK-I+II+III+IV average flux
$2.308 \pm 0.020^{+0.039}_{-0.040}$	⁵ ABE	16C	SKAM SK-IV average flux
$2.250^{+0.030}_{-0.029} \pm 0.038$	⁵ ABE	16C	SKAM SK-IV day flux
$2.364 \pm 0.029 \pm 0.040$	⁵ ABE	16C	SKAM SK-IV night flux
$2.404 \pm 0.039 \pm 0.053$	⁶ ABE	16C	SKAM SK-III average flux
$2.41 \pm 0.05^{+0.16}_{-0.15}$	⁷ ABE	11	SKAM SK-II average flux
$2.38 \pm 0.02 \pm 0.08$	⁸ ABE	11	SKAM SK-I average flux
$2.77 \pm 0.26 \pm 0.32$	⁹ ABE	11B	KLND average flux
$2.4 \pm 0.4 \pm 0.1$	¹⁰ BELLINI	10A	BORX average flux
$1.77^{+0.24+0.09}_{-0.21-0.10}$	¹¹ AHARMIM	08	SNO Phase III
$2.38 \pm 0.05^{+0.16}_{-0.15}$	¹² CRAVENS	08	SKAM average flux
$2.35 \pm 0.02 \pm 0.08$	¹³ HOSAKA	06	SKAM average flux
$2.35 \pm 0.22 \pm 0.15$	¹⁴ AHARMIM	05A	SNO Salty D_2O ; ^8B shape not constrained
$2.34 \pm 0.23^{+0.15}_{-0.14}$	¹⁴ AHARMIM	05A	SNO Salty D_2O ; ^8B shape constrained
$2.39^{+0.24}_{-0.23} \pm 0.12$	¹⁵ AHMAD	02	SNO average flux
$2.39 \pm 0.34^{+0.16}_{-0.14}$	¹⁶ AHMAD	01	SNO average flux

See key on page 1171

Lepton Particle Listings

Neutrino Mixing

2.80 ± 0.19 ± 0.33	¹⁷ FUKUDA	96	KAMI	average flux
2.70 ± 0.27	¹⁷ FUKUDA	96	KAMI	day flux
2.87 +0.27 -0.26	¹⁷ FUKUDA	96	KAMI	night flux

- AGOSTINI 20A obtained this result from the $\nu_e e$ elastic scattering rate over the period between January 2008 and December 2016. Uses the same data as AGOSTINI 18B, but the analysis technique is significantly improved.
- ANDERSON 19 reports this result from the $\nu_e e$ elastic scattering rate using a 69.2 kton-day (or 114.7 days) of exposure from May through December, 2017 during the SNO+ detector's water commissioning phase. The events over the reconstructed electron kinetic energy range of 5–15 MeV were analyzed.
- AGOSTINI 18B obtained this result from the $\nu_e e$ elastic scattering rate over the period between January 2008 and December 2016.
- ABE 16c reports the combined results of the four phases of the Super-Kamiokande average flux measurements. Here the revised Super-Kamiokande-III result is used.
- ABE 16c reports the Super-Kamiokande-IV results for 1664 live days from September 2008 to February 2014. The analysis threshold is total electron energy of 4.0 MeV.
- ABE 16c revised the Super-Kamiokande-III average flux value reported in ABE 11. Super-Kamiokande-III results are for 548 live days from August 4, 2006 to August 18, 2008. The analysis threshold is 5.0 MeV, but the event sample in the 5.0–6.5 MeV total electron energy range has a total live time of 298 days.
- ABE 11 recalculated the Super-Kamiokande-II results using ⁸B spectrum of WINTER 06A.
- ABE 11 recalculated the Super-Kamiokande-I results using ⁸B spectrum of WINTER 06A.
- ABE 11B use a 123 kton-day exposure of the KamLAND liquid scintillation detector to measure the ⁸B solar neutrino flux. They utilize $\nu - e$ elastic scattering above a reconstructed-energy threshold of 5.5 MeV, corresponding to 5 MeV electron recoil energy. 299 electron recoil candidate events are reported, of which 157 ± 23.6 are assigned to background.
- BELLINI 10A reports the Borexino result with 3 MeV energy threshold for scattered electrons. The data correspond to 345.3 live days with a target mass of 100 t, between July 15, 2007 and August 23, 2009.
- AHARMIM 08 reports the results from SNO Phase III measurement using an array of ³He proportional counters to measure the rate of NC interactions in heavy water, over the period between November 27, 2004 and November 28, 2006, corresponding to 385.17 live days. A simultaneous fit was made for the number of NC events detected by the proportional counters and the numbers of NC, CC, and ES events detected by the PMTs, where the spectral distributions of the ES and CC events were not constrained to the ⁸B shape.
- CRAVENS 08 reports the Super-Kamiokande-II results for 791 live days from December 2002 to October 2005. The photocathode coverage of the detector is 19% (reduced from 40% of that of Super-Kamiokande-I due to an accident in 2001). The analysis threshold for the average flux is 7 MeV.
- HOSAKA 06 reports the final results for 1496 live days with Super-Kamiokande-I between May 31, 1996 and July 15, 2001, and replace FUKUDA 02 results. The analysis threshold is 5 MeV except for the first 280 live days (6.5 MeV).
- AHARMIM 05A measurements were made with dissolved NaCl (0.195% by weight) in heavy water over the period between July 26, 2001 and August 28, 2003, corresponding to 391.4 live days, and update AHMED 04A. The CC, ES, and NC events were statistically separated. In one method, the ⁸B energy spectrum was not constrained. In the other method, the constraint of an undistorted ⁸B energy spectrum was added for comparison with AHMAD 02 results.
- AHMAD 02 reports the ⁸B solar-neutrino flux measured via νe elastic scattering above the kinetic energy threshold of 5 MeV. The data correspond to 306.4 live days with SNO between November 2, 1999 and May 28, 2001, and updates AHMAD 01 results.
- AHMAD 01 reports the ⁸B solar-neutrino flux measured via νe elastic scattering above the kinetic energy threshold of 6.75 MeV. The data correspond to 241 live days with SNO between November 2, 1999 and January 15, 2001.
- FUKUDA 96 results are for a total of 2079 live days with Kamiokande II and III from January 1987 through February 1995, covering the entire solar cycle 22, with threshold $E_e > 9.3$ MeV (first 449 days), > 7.5 MeV (middle 794 days), and > 7.0 MeV (last 836 days). These results update the HIRATA 90 result for the average ⁸B solar-neutrino flux and HIRATA 91 result for the day-night variation in the ⁸B solar-neutrino flux. The total data sample was also analyzed for short-term variations: within experimental errors, no strong correlation of the solar-neutrino flux with the sunspot numbers was found.

ϕ_{CC} (⁸B)

⁸B solar-neutrino flux measured with charged-current reaction which is sensitive exclusively to ν_e .

VALUE ($10^6 \text{ cm}^{-2} \text{ s}^{-1}$)	DOCUMENT ID	TECN	COMMENT
• • • We do not use the following data for averages, fits, limits, etc. • • •			
1.67 +0.05 +0.07 -0.04 -0.08	1 AHARMIM	08	SNO Phase III
1.68 ± 0.06 ± 0.08 -0.09	2 AHARMIM	05A	SNO Salty D ₂ O; ⁸ B shape not const.
1.72 ± 0.05 ± 0.11	2 AHARMIM	05A	SNO Salty D ₂ O; ⁸ B shape constrained
1.76 +0.06 ± 0.09 -0.05	3 AHMAD	02	SNO average flux
1.75 ± 0.07 ± 0.12 ± 0.05 -0.11	4 AHMAD	01	SNO average flux

- AHARMIM 08 reports the results from SNO Phase III measurement using an array of ³He proportional counters to measure the rate of NC interactions in heavy water, over the period between November 27, 2004 and November 28, 2006, corresponding to 385.17 live days. A simultaneous fit was made for the number of NC events detected by the proportional counters and the numbers of NC, CC, and ES events detected by the PMTs,

where the spectral distributions of the ES and CC events were not constrained to the ⁸B shape.

- AHARMIM 05A measurements were made with dissolved NaCl (0.195% by weight) in heavy water over the period between July 26, 2001 and August 28, 2003, corresponding to 391.4 live days, and update AHMED 04A. The CC, ES, and NC events were statistically separated. In one method, the ⁸B energy spectrum was not constrained. In the other method, the constraint of an undistorted ⁸B energy spectrum was added for comparison with AHMAD 02 results.
- AHMAD 02 reports the ⁸B solar-neutrino flux measured with charged-current reaction on deuterium, $\nu_e d \rightarrow pp e^-$, above the kinetic energy threshold of 5 MeV. The data correspond to 306.4 live days with SNO between November 2, 1999 and May 28, 2001, and updates AHMAD 01 results. The complete description of the SNO Phase I data set is given in AHARMIM 07.
- AHMAD 01 reports the first SNO result of the ⁸B solar-neutrino flux measured with the charged-current reaction on deuterium, $\nu_e d \rightarrow pp e^-$, above the kinetic energy threshold of 6.75 MeV. The data correspond to 241 live days with SNO between November 2, 1999 and January 15, 2001.

ϕ_{NC} (⁸B)

⁸B solar neutrino flux measured with neutral-current reaction, which is equally sensitive to $\nu_e, \nu_\mu,$ and ν_τ .

VALUE ($10^6 \text{ cm}^{-2} \text{ s}^{-1}$)	CL%	DOCUMENT ID	TECN	COMMENT
• • • We do not use the following data for averages, fits, limits, etc. • • •				
<9.0	90	1 MA	23A	PNDX CE ν NS, liquid Xe detector
5.25 ± 0.16 +0.11 -0.13		2 AHARMIM	13	SNO All three phases combined
5.140 +0.160 +0.132 -0.158 -0.117		3 AHARMIM	10	SNO Phase I+II, low threshold
5.54 +0.33 +0.36 -0.31 -0.34		4 AHARMIM	08	SNO Phase III, prop. counter + PMT
4.94 ± 0.21 +0.38 -0.34		5 AHARMIM	05A	SNO Salty D ₂ O; ⁸ B shape not const.
4.81 ± 0.19 +0.28 -0.27		5 AHARMIM	05A	SNO Salty D ₂ O; ⁸ B shape constrained
5.09 +0.44 +0.46 -0.43 -0.43		6 AHMAD	02	SNO average flux; ⁸ B shape const.
6.42 ± 1.57 +0.55 -0.58		6 AHMAD	02	SNO average flux; ⁸ B shape not const.

- MA 23A searched for ⁸B solar neutrinos elastically scattered off xenon nuclei in the commissioning phase of the PANDAX-4T experiment with an effective exposure of 0.48 ton-yr. This experiment is dedicated to dark matter direct search using a dual-phase xenon TPC with a sensitive volume of 3.7 tons of liquid Xe.
- AHARMIM 13 obtained this result from a combined analysis of the data from all three phases, SNO-I, II, and III. The measurement of the ⁸B flux mostly comes from the NC signal, however, CC contribution is included in the fit.
- AHARMIM 10 reports this result from a joint analysis of SNO Phase I+II data with the "effective electron kinetic energy" threshold of 3.5 MeV. This result is obtained with a "binned-histogram unconstrained fit" where binned probability distribution functions of the neutrino signal observables were used without any model constraints on the shape of the neutrino spectrum.
- AHARMIM 08 reports the results from SNO Phase III measurement using an array of ³He proportional counters to measure the rate of NC interactions in heavy water, over the period between November 27, 2004 and November 28, 2006, corresponding to 385.17 live days. A simultaneous fit was made for the number of NC events detected by the proportional counters and the numbers of NC, CC, and ES events detected by the PMTs, where the spectral distributions of the ES and CC events were not constrained to the ⁸B shape.
- AHARMIM 05A measurements were made with dissolved NaCl (0.195% by weight) in heavy water over the period between July 26, 2001 and August 28, 2003, corresponding to 391.4 live days, and update AHMED 04A. The CC, ES, and NC events were statistically separated. In one method, the ⁸B energy spectrum was not constrained. In the other method, the constraint of an undistorted ⁸B energy spectrum was added for comparison with AHMAD 02 results.
- AHMAD 02 reports the first SNO result of the ⁸B solar-neutrino flux measured with the neutral-current reaction on deuterium, $\nu_e d \rightarrow np \nu_e$, above the neutral-current reaction threshold of 2.2 MeV. The data correspond to 306.4 live days with SNO between November 2, 1999 and May 28, 2001. The complete description of the SNO Phase I data set is given in AHARMIM 07.

$\phi_{\nu_\mu + \nu_\tau}$ (⁸B)

Nonelectron-flavor active neutrino component (ν_μ and ν_τ) in the ⁸B solar-neutrino flux.

VALUE ($10^6 \text{ cm}^{-2} \text{ s}^{-1}$)	DOCUMENT ID	TECN	COMMENT
• • • We do not use the following data for averages, fits, limits, etc. • • •			
3.26 ± 0.25 +0.40 -0.35	1 AHARMIM	05A	SNO From $\phi_{NC}, \phi_{CC},$ and ϕ_{ES} ; ⁸ B shape not const.
3.09 ± 0.22 +0.30 -0.27	1 AHARMIM	05A	SNO From $\phi_{NC}, \phi_{CC},$ and ϕ_{ES} ; ⁸ B shape constrained
3.41 ± 0.45 +0.48 -0.45	2 AHMAD	02	SNO From $\phi_{NC}, \phi_{CC},$ and ϕ_{ES}
3.69 ± 1.13	3 AHMAD	01	SNO Derived from SNO+SuperKam, water Cherenkov

- AHARMIM 05A measurements were made with dissolved NaCl (0.195% by weight) in heavy water over the period between July 26, 2001 and August 28, 2003, corresponding

Lepton Particle Listings

Neutrino Mixing

to 391.4 live days, and update AHMED 04A. The CC, ES, and NC events were statistically separated. In one method, the ^8B energy spectrum was not constrained. In the other method, the constraint of an undistorted ^8B energy spectrum was added for comparison with AHMAD 02 results.

²AHMAD 02 deduced the nonelectron-flavor active neutrino component (ν_μ and ν_τ) in the ^8B solar-neutrino flux, by combining the charged-current result, the ν_e elastic-scattering result and the neutral-current result. The complete description of the SNO Phase I data set is given in AHARMIM 07.

³AHMAD 01 deduced the nonelectron-flavor active neutrino component (ν_μ and ν_τ) in the ^8B solar-neutrino flux, by combining the SNO charged-current result (AHMAD 01) and the Super-Kamiokande ν_e elastic-scattering result (FUKUDA 01).

Total Flux of Active pp Solar Neutrinos

Total flux of active neutrinos (ν_e, ν_μ, ν_τ).

VALUE ($10^{10} \text{ cm}^{-2} \text{ s}^{-1}$)	DOCUMENT ID	TECN	COMMENT
--	-------------	------	---------

• • • We do not use the following data for averages, fits, limits, etc. • • •

$6.1 \pm 0.5 \pm_{-0.5}^{+0.3}$	¹ AGOSTINI	18B	BORX $\nu_e e$ scattering rate
---------------------------------	-----------------------	-----	--------------------------------

¹AGOSTINI 18B obtained this result from the measured $\nu_e e$ elastic scattering rate over the period between December 2011 and May 2016, assuming the MSW-LMA oscillation parameters derived by ESTEBAN 17. Assuming a high-metallicity standard solar model, the electron neutrino survival probability for the pp solar neutrino is calculated to be 0.57 ± 0.09 .

Total Flux of Active ^7Be Solar Neutrinos

Total flux of active neutrinos (ν_e, ν_μ, ν_τ).

VALUE ($10^9 \text{ cm}^{-2} \text{ s}^{-1}$)	DOCUMENT ID	TECN	COMMENT
---	-------------	------	---------

• • • We do not use the following data for averages, fits, limits, etc. • • •

$4.99 \pm 0.11 \pm_{-0.08}^{+0.06}$	¹ AGOSTINI	18B	BORX $\nu_e e$ scattering rate
-------------------------------------	-----------------------	-----	--------------------------------

¹AGOSTINI 18B obtained this result from the measured $\nu_e e$ elastic scattering rate over the period between December 2011 and May 2016, assuming the MSW-LMA oscillation parameters derived by ESTEBAN 17. Assuming a high-metallicity standard solar model, the electron neutrino survival probability for the ^7Be solar neutrino is calculated to be 0.53 ± 0.05 .

Total Flux of Active pep Solar Neutrinos

Total flux of active neutrinos (ν_e, ν_μ, ν_τ).

VALUE ($10^8 \text{ cm}^{-2} \text{ s}^{-1}$)	DOCUMENT ID	TECN	COMMENT
---	-------------	------	---------

• • • We do not use the following data for averages, fits, limits, etc. • • •

$1.27 \pm 0.19 \pm_{-0.12}^{+0.08}$	¹ AGOSTINI	18B	BORX $\nu_e e$ scattering rate
-------------------------------------	-----------------------	-----	--------------------------------

¹AGOSTINI 18B obtained this result from the measured $\nu_e e$ elastic scattering rate over the period between December 2011 and May 2016, assuming the MSW-LMA oscillation parameters derived by ESTEBAN 17 and a high-metallicity standard solar model. The electron neutrino survival probability for the pep solar neutrino is calculated to be 0.43 ± 0.11 .

Total Flux of Active ^8B Solar Neutrinos

Total flux of active neutrinos (ν_e, ν_μ, ν_τ).

VALUE ($10^6 \text{ cm}^{-2} \text{ s}^{-1}$)	DOCUMENT ID	TECN	COMMENT
---	-------------	------	---------

• • • We do not use the following data for averages, fits, limits, etc. • • •

$5.95 \pm_{-0.71}^{+0.75} \pm_{-0.30}^{+0.28}$	¹ ANDERSON	19	SNO+ Water phase; $\nu_e e$ scattering rate
--	-----------------------	----	---

$5.68 \pm_{-0.41}^{+0.39} \pm_{-0.03}^{+0.03}$	² AGOSTINI	18B	BORX From $\nu_e e$ scattering rate
--	-----------------------	-----	-------------------------------------

$5.25 \pm_{-0.13}^{+0.16} \pm_{-0.13}^{+0.11}$	³ AHARMIM	13	SNO All three phases combined
--	----------------------	----	-------------------------------

$5.046 \pm_{-0.152}^{+0.159} \pm_{-0.123}^{+0.107}$	⁴ AHARMIM	10	SNO From ϕ_{NC} in Phase I+II, low threshold
---	----------------------	----	---

$5.54 \pm_{-0.31}^{+0.33} \pm_{-0.34}^{+0.36}$	⁵ AHARMIM	08	SNO ϕ_{NC} in Phase III
--	----------------------	----	------------------------------

$4.94 \pm_{-0.34}^{+0.21} \pm_{-0.34}^{+0.38}$	⁶ AHARMIM	05A	SNO From ϕ_{NC} ; ^8B shape not const.
--	----------------------	-----	--

$4.81 \pm_{-0.27}^{+0.19} \pm_{-0.27}^{+0.28}$	⁶ AHARMIM	05A	SNO From ϕ_{NC} ; ^8B shape constrained
--	----------------------	-----	---

$5.09 \pm_{-0.43}^{+0.44} \pm_{-0.43}^{+0.46}$	⁷ AHMAD	02	SNO Direct measurement from ϕ_{NC}
--	--------------------	----	---

$5.44 \pm_{-0.99}^{+0.99}$	⁸ AHMAD	01	Derived from SNO+SuperKam, water Cherenkov
----------------------------	--------------------	----	--

¹ANDERSON 19 reports this result from the measured $\nu_e e$ elastic scattering rate using a 69.2 kton-day (or 114.7 days) of exposure from May through December, 2017 during the SNO+ detector's water commissioning phase, assuming the neutrino mixing parameters given in PDG 16 and a standard solar model given in BAHCALL 05.

²AGOSTINI 18B obtained this result from the measured $\nu_e e$ elastic scattering rate over the period between January 2008 and December 2016, assuming the MSW-LMA oscillation parameters derived by ESTEBAN 17. Assuming a high-metallicity standard solar model, the electron neutrino survival probability for the ^8B solar neutrino is calculated to be 0.37 ± 0.08 .

³AHARMIM 13 obtained this result from a combined analysis of the data from all three phases, SNO-I, II, and III. The measurement of the ^8B flux mostly comes from the NC signal, however, CC contribution is included in the fit.

⁴AHARMIM 10 reports this result from a joint analysis of SNO Phase I+II data with the "effective electron kinetic energy" threshold of 3.5 MeV. This result is obtained with the assumption of unitarity, which relates the NC, CC, and ES rates. The data were fit with the free parameters directly describing the total ^8B neutrino flux and the energy-dependent ν_e survival probability.

⁵AHARMIM 08 reports the results from SNO Phase III measurement using an array of ³He proportional counters to measure the rate of NC interactions in heavy water, over the period between November 27, 2004 and November 28, 2006, corresponding to 385.17 live days. A simultaneous fit was made for the number of NC events detected by the proportional counters and the numbers of NC, CC, and ES events detected by the PMTs, where the spectral distributions of the ES and CC events were not constrained to the ^8B shape.

⁶AHARMIM 05A measurements were made with dissolved NaCl (0.195% by weight) in heavy water over the period between July 26, 2001 and August 28, 2003, corresponding to 391.4 live days, and update AHMED 04A. The CC, ES, and NC events were statistically separated. In one method, the ^8B energy spectrum was not constrained. In the other method, the constraint of an undistorted ^8B energy spectrum was added for comparison with AHMAD 02 results.

⁷AHMAD 02 determined the total flux of active ^8B solar neutrinos by directly measuring the neutral-current reaction, $\nu_e d \rightarrow np\nu_e$, which is equally sensitive to ν_e, ν_μ , and ν_τ . The complete description of the SNO Phase I data set is given in AHARMIM 07.

⁸AHMAD 01 deduced the total flux of active ^8B solar neutrinos by combining the SNO charged-current result (AHMAD 01) and the Super-Kamiokande ν_e elastic-scattering result (FUKUDA 01).

Total Flux of Active CNO Solar Neutrinos

Total flux of active neutrinos (ν_e, ν_μ, ν_τ).

VALUE ($10^8 \text{ cm}^{-2} \text{ s}^{-1}$)	CL%	DOCUMENT ID	TECN	COMMENT
---	-----	-------------	------	---------

• • • We do not use the following data for averages, fits, limits, etc. • • •

$6.7 \pm_{-0.8}^{+1.2}$		¹ BASILICO	23	BORX $\nu_e e$ directional + spectral information
-------------------------	--	-----------------------	----	---

$6.6 \pm_{-0.9}^{+2.0}$		² APPEL	22	BORX $\nu_e e$ scattering rate
-------------------------	--	--------------------	----	--------------------------------

$7.0 \pm_{-2.0}^{+3.0}$		³ AGOSTINI	20D	BORX $\nu_e e$ scattering rate
-------------------------	--	-----------------------	-----	--------------------------------

<7.9	95	⁴ AGOSTINI	18B	BORX $\nu_e e$ scattering rate
--------	----	-----------------------	-----	--------------------------------

¹BASILICO 23 obtained this result by combining the newly developed Correlated Integrated Directionality (CID)-based CNO result obtained by using the complete Borexino data-taking period from 2007 to 2021, with a spectral fit of the Phase-III dataset (from July 2016 to October 2021, characterized by a thermally stable detector). Note that the directional information is independent from the spectral information on which the previous CNO solar neutrino measurements by Borexino were based. Neutrino flavor conversion was taken into account.

²APPEL 22 obtained this result from the measured $\nu_e e$ elastic scattering rate over the period between January 2017 and October 2021, assuming the MSW-LMA oscillation parameters derived by ESTEBAN 20A. The exposure corresponding to this data is 1431.6 days \times 71.3 tons.

³AGOSTINI 20D obtained this result from the measured $\nu_e e$ elastic scattering rate over the period between July 2016 to February 2020, assuming the MSW-LMA oscillation parameters derived by CAPOZZI 18.

⁴AGOSTINI 18B obtained this result from an upper limit of the $\nu_e e$ elastic scattering rate for the CNO neutrinos over the period between December 2011 and May 2016, assuming the MSW-LMA oscillation parameters derived by ESTEBAN 17.

Total Flux of Active hep Solar Neutrinos

Total flux of active neutrinos (ν_e, ν_μ, ν_τ).

VALUE ($10^5 \text{ cm}^{-2} \text{ s}^{-1}$)	CL%	DOCUMENT ID	TECN	COMMENT
---	-----	-------------	------	---------

• • • We do not use the following data for averages, fits, limits, etc. • • •

<1.8	90	¹ AGOSTINI	20A	BORX $\nu_e e$ scattering and $^{12}\text{C}(\nu, \nu')^{12}\text{C}^*$
--------	----	-----------------------	-----	---

<0.3	90	² AHARMIM	20	SNO CC, NC, $\nu_e e$ scattering
--------	----	----------------------	----	----------------------------------

<2.2	90	³ AGOSTINI	18B	BORX $\nu_e e$ scattering rate
--------	----	-----------------------	-----	--------------------------------

¹AGOSTINI 20A obtained this result from an upper limit of the $\nu_e e$ elastic scattering rate and NC-mediated inelastic scattering on carbon nuclei with 15.1 MeV deexcitation γ -ray for the hep neutrino. The dataset corresponds to an effective exposure of 0.745 kt-yr from November 2009 to October 2017. A FADC DAQ system, optimized for the acquisition of high-energy events was used for data collection. The MSW-LMA oscillation parameters derived by ESTEBAN 17 were assumed.

²AHARMIM 20 uses the entire SNO dataset, corresponding to 2.47 kton-yrs of exposure after fiducialization. With the D_2O target, SNO was sensitive to charged current, neutral current, and elastic scattering channels.

³AGOSTINI 18B obtained this result from an upper limit of the $\nu_e e$ elastic scattering rate for the hep neutrino using the dataset corresponding to an exposure of 0.8 kt-yr and assuming the MSW-LMA oscillation parameters derived by ESTEBAN 17.

Day-Night Asymmetry (^8B)

$A = (\phi_{\text{night}} - \phi_{\text{day}}) / \phi_{\text{average}}$

VALUE	DOCUMENT ID	TECN	COMMENT
-------	-------------	------	---------

$0.033 \pm 0.010 \pm 0.005$	¹ ABE	16C	SKAM SK combined; Based on ϕ_{ES}
-----------------------------	------------------	-----	--

• • • We do not use the following data for averages, fits, limits, etc. • • •

$0.036 \pm 0.016 \pm 0.006$	² ABE	16C	SKAM SK-IV; Based on ϕ_{ES}
-----------------------------	------------------	-----	----------------------------------

$0.032 \pm 0.011 \pm 0.005$	³ RENSHAW	14	SKAM Based on ϕ_{ES}
-----------------------------	----------------------	----	---------------------------

$0.063 \pm 0.042 \pm 0.037$	⁴ CRAVENS	08	SKAM Based on ϕ_{ES}
-----------------------------	----------------------	----	---------------------------

See key on page 1171

Lepton Particle Listings

Neutrino Mixing

$0.021 \pm 0.020 \pm^{+0.012}_{-0.013}$	⁵ HOSAKA	06	SKAM	Based on ϕ_{ES}
$0.017 \pm 0.016 \pm^{+0.012}_{-0.013}$	⁶ HOSAKA	06	SKAM	Fitted in the LMA region
$-0.056 \pm 0.074 \pm 0.053$	⁷ AHARMIM	05A	SNO	From salty SNO ϕ_{CC}
$-0.037 \pm 0.063 \pm 0.032$	⁷ AHARMIM	05A	SNO	From salty SNO ϕ_{CC} ; const. of no ϕ_{NC} asymmetry
$0.14 \pm 0.063 \pm^{+0.015}_{-0.014}$	⁸ AHMAD	02B	SNO	Derived from SNO ϕ_{CC}
$0.07 \pm 0.049 \pm^{+0.013}_{-0.012}$	⁹ AHMAD	02B	SNO	Const. of no ϕ_{NC} asymmetry

- ¹ ABE 16c reports the combined day-night flux asymmetry results of the four phases of the Super-Kamiokande measurements. Amplitude fit method is used. See footnote to RENSHAW 14.
- ² ABE 16c reports the Super-Kamiokande-IV results for 1664 live days from September 2008 to February 2014. The analysis threshold for day-night flux asymmetry is recoil electron energy of 4.49 MeV (total electron energy of 5.0 MeV). Amplitude fit method is used. See footnote to RENSHAW 14.
- ³ RENSHAW 14 obtains this result by using the "amplitude fit" introduced in SMY 04. The data from the Super-Kamiokande(SK)-I, -II, -III, and 1306 live days of the SK-IV measurements are used. The analysis threshold is recoil-electron kinetic energy of 4.5 MeV for SK-I, and SK-IV except for 250 live days in SK-III (6.0 MeV). The analysis threshold for SK-I and SK-II is the same as in the previous reports. (Note that in the previous SK solar-neutrino results, the analysis threshold is quoted as recoil-electron total energy.) This day-night asymmetry result is consistent with neutrino oscillations for $4 \times 10^{-5} \text{ eV}^2 < \Delta m_{21}^2 < 7 \times 10^{-5} \text{ eV}^2$ and large mixing values of θ_{12} at the 68% CL.
- ⁴ CRAVENS 08 reports the Super-Kamiokande-II results for 791 live days from December 2002 to October 2005. The photocathode coverage of the detector is 19% (reduced from 40% of that of Super-Kamiokande-I due to an accident in 2001). The analysis threshold for the day and night fluxes is 7.5 MeV except for the first 159 live days (8.0 MeV).
- ⁵ HOSAKA 06 reports the final results for 1496 live days with Super-Kamiokande-I between May 31, 1996 and July 15, 2001, and replace FUKUDA 02 results. The analysis threshold is 5 MeV except for the first 280 live days (6.5 MeV).
- ⁶ This result with reduced statistical uncertainty is obtained by assuming two-neutrino oscillations within the LMA (large mixing angle) region and by fitting the time variation of the solar neutrino flux measured via ν_e elastic scattering to the variations expected from neutrino oscillations. For details, see SMY 04. There is an additional small systematic error of ± 0.0004 coming from uncertainty of oscillation parameters.
- ⁷ AHARMIM 05a measurements were made with dissolved NaCl (0.195% by weight) in heavy water over the period between July 26, 2001 and August 28, 2003, with 176.5 days of the live time recorded during the day and 214.9 days during the night. This result is obtained with the spectral distribution of the CC events not constrained to the ⁸B shape.
- ⁸ AHMAD 02b results are based on the charged-current interactions recorded between November 2, 1999 and May 28, 2001, with the day and night live times of 128.5 and 177.9 days, respectively. The complete description of the SNO Phase I data set is given in AHARMIM 07.
- ⁹ AHMAD 02b results are derived from the charged-current interactions, neutral-current interactions, and ν_e elastic scattering, with the total flux of active neutrinos constrained to have no asymmetry. The data were recorded between November 2, 1999 and May 28, 2001, with the day and night live times of 128.5 and 177.9 days, respectively. The complete description of the SNO Phase I data set is given in AHARMIM 07.

ϕ_{ES} (⁷Be)

⁷Be solar-neutrino flux measured via ν_e elastic scattering. This process is sensitive to all active neutrino flavors, but with reduced sensitivity to ν_{μ}, ν_{τ} due to the cross-section difference, $\sigma(\nu_{\mu,\tau} e) \sim 0.2 \sigma(\nu_e e)$. If the ⁷Be solar-neutrino flux involves non-electron flavor active neutrinos, their contribution to the flux is ~ 0.2 times that of ν_e .

VALUE ($10^8 \text{ cm}^{-2} \text{ s}^{-1}$)	DOCUMENT ID	TECN	COMMENT
3.26 ± 0.52	¹ GANDO	15	KLND average flux
3.10 ± 0.15	² BELLINI	11A	BORX average flux

- ¹ GANDO 15 uses 165.4 kton-day exposure of the KamLAND liquid scintillator detector to measure the 862 keV ⁷Be solar neutrino flux via $\nu - e$ elastic scattering
- ² BELLINI 11A reports the ⁷Be solar neutrino flux measured via $\nu - e$ elastic scattering. The data correspond to 740.7 live days between May 16, 2007 and May 8, 2010, and also correspond to 153.6 ton-year fiducial exposure. BELLINI 11A measured the 862 keV ⁷Be solar neutrino flux, which is an 89.6% branch of the ⁷Be solar neutrino flux, to be $(2.78 \pm 0.13) \times 10^9 \text{ cm}^{-2} \text{ s}^{-1}$. Supersedes ARPESELLA 08A.

ϕ_{ES} (*pep*)

pep solar-neutrino flux measured via ν_e elastic scattering. This process is sensitive to all active neutrino flavors, but with reduced sensitivity to ν_{μ}, ν_{τ} due to the cross section difference, $\sigma(\nu_{\mu,\tau} e) \sim 0.2 \sigma(\nu_e e)$. If the *pep* solar-neutrino flux involves non-electron flavor active neutrinos, their contribution to the flux is ~ 0.2 times that of ν_e .

VALUE ($10^8 \text{ cm}^{-2} \text{ s}^{-1}$)	DOCUMENT ID	TECN	COMMENT
1.0 ± 0.2	¹ BELLINI	12A	BORX average flux

- ¹ BELLINI 12A reports 1.44 MeV *pep* solar-neutrino flux measured via ν_e elastic scattering. The data were collected between January 13, 2008 and May 9, 2010, corresponding to 20,409 ton-day fiducial exposure. The listed flux value is calculated from the observed rate of *pep* solar neutrino interactions in Borexino $(3.1 \pm 0.6 \pm 0.3 \text{ counts}/(\text{day} \cdot 100$

ton)) and the corresponding rate expected for no neutrino flavor oscillations $(4.47 \pm 0.05 \text{ counts}/(\text{day} \cdot 100 \text{ ton}))$, using the SSM prediction for the *pep* solar neutrino flux of $(1.441 \pm 0.012) \times 10^8 \text{ cm}^{-2} \text{ s}^{-1}$.

ϕ_{ES} (CNO)

CNO solar-neutrino flux measured via ν_e elastic scattering. This process is sensitive to all active neutrino flavors, but with reduced sensitivity to ν_{μ}, ν_{τ} due to the cross section difference, $\sigma(\nu_{\mu,\tau} e) \sim 0.2 \sigma(\nu_e e)$. If the CNO solar-neutrino flux involves non-electron flavor active neutrinos, their contribution to the flux is ~ 0.2 times that of ν_e .

VALUE ($10^8 \text{ cm}^{-2} \text{ s}^{-1}$)	CL%	DOCUMENT ID	TECN	COMMENT
< 7.7	90	¹ BELLINI	12A	BORX MSW-LMA solution assumed

- ¹ BELLINI 12A reports an upper limit of the CNO solar neutrino flux measured via ν_e elastic scattering. The data were collected between January 13, 2008 and May 9, 2010, corresponding to 20,409 ton-day fiducial exposure.

ϕ_{ES} (*pp*)

pp solar-neutrino flux measured via ν_e elastic scattering. This process is sensitive to all active neutrino flavors, but with reduced sensitivity to ν_{μ}, ν_{τ} due to the cross section difference, $\sigma(\nu_{\mu,\tau} e) \sim 0.3 \sigma(\nu_e e)$. If the *pp* solar-neutrino flux involves non-electron flavor active neutrinos, their contribution to the flux is ~ 0.3 times of ν_e .

VALUE ($10^{10} \text{ cm}^{-2} \text{ s}^{-1}$)	DOCUMENT ID	TECN	COMMENT
4.4 ± 0.5	¹ BELLINI	14A	BORX average flux

- ¹ BELLINI 14A reports *pp* solar-neutrino flux measured via ν_e elastic scattering. The data were collected between January 2012 and May 2013, corresponding to 408 days of data. The *pp* neutrino interaction rate in Borexino is measured to be $144 \pm 13 \pm 10 \text{ counts}/(\text{day} \cdot 100 \text{ ton})$ by fitting the measured energy spectrum of events in the 165–590 keV recoil electron kinetic energy window with the expected signal + background spectrum. The listed flux value $\phi_{ES}(\text{pp})$ is calculated from the observed rate and the number of $(3.307 \pm 0.003) \times 10^{31}$ electrons for 100 tons of the Borexino scintillator, and the $\nu_e e$ integrated cross section over the *pp* neutrino spectrum, $\sigma(\nu_e e) = 11.38 \times 10^{-46} \text{ cm}^2$.

ϕ_{CC} (*pp*)

pp solar-neutrino flux measured with charged-current reaction which is sensitive exclusively to ν_e .

VALUE ($10^{10} \text{ cm}^{-2} \text{ s}^{-1}$)	DOCUMENT ID	TECN	COMMENT
3.38 ± 0.47	¹ ABDURASHI...	09	FIT Fit existing solar- ν data

- ¹ ABDURASHITOV 09 reports the *pp* solar-neutrino flux derived from the Ga solar neutrino capture rate by subtracting contributions from ⁸B, ⁷Be, *pep* and CNO solar neutrino fluxes determined by other solar neutrino experiments as well as neutrino oscillation parameters determined from available world neutrino oscillation data.

ϕ_{ES} (*hep*)

hep solar-neutrino flux measured via ν_e elastic scattering. This process is sensitive to all active neutrino flavors, but with reduced sensitivity to ν_{μ}, ν_{τ} due to the cross-section difference, $\sigma(\nu_{\mu,\tau} e) \sim 0.16 \sigma(\nu_e e)$. If the *hep* solar-neutrino flux involves non-electron flavor active neutrinos, their contribution to the flux is ~ 0.16 times of ν_e .

VALUE ($10^3 \text{ cm}^{-2} \text{ s}^{-1}$)	CL%	DOCUMENT ID	TECN
< 73	90	¹ HOSAKA	06 SKAM

- ¹ HOSAKA 06 result is obtained from the recoil electron energy window of 18–21 MeV, and updates FUKUDA 01 result.

ϕ_{ν_e} (⁸B)

Searches are made for electron antineutrino flux from the Sun. Flux limits listed here are derived relative to the BS05(OP) Standard Solar Model ⁸B solar neutrino flux $(5.69 \times 10^6 \text{ cm}^{-2} \text{ s}^{-1})$, with an assumption that solar $\bar{\nu}_e$ s follow an unoscillated ⁸B neutrino spectrum.

VALUE (%)	CL%	DOCUMENT ID	TECN	COMMENT
< 0.072	90	¹ AGOSTINI	21	BORX $E_{\bar{\nu}_e} > 1.8 \text{ MeV}$
< 0.013	90	² BELLINI	11	BORX $E_{\bar{\nu}_e} > 1.8 \text{ MeV}$
< 1.9	90	³ BALATA	06	CNTR $1.8 < E_{\bar{\nu}_e} < 20.0 \text{ MeV}$
< 0.72	90	AHARMIM	04	SNO $4.0 < E_{\bar{\nu}_e} < 14.8 \text{ MeV}$
< 0.022	90	EGUCHI	04	KLND $8.3 < E_{\bar{\nu}_e} < 14.8 \text{ MeV}$
< 0.7	90	GANDO	03	SKAM $8.0 < E_{\bar{\nu}_e} < 20.0 \text{ MeV}$
< 1.7	90	AGLIETTA	96	LSD $7 < E_{\bar{\nu}_e} < 17 \text{ MeV}$

- ¹ AGOSTINI 21 derived this result relative to the Standard Solar Model ⁸B solar neutrino flux, under an assumption of high solar metallicity, of $5.46 (1 \pm 0.12) \times 10^6 \text{ cm}^{-2} \text{ s}^{-1}$ (see VINYOLETS 17).

- ² Superseded by AGOSTINI 21.

Lepton Particle Listings

Neutrino Mixing

³ BALATA 06 obtained this result from the search for $\bar{\nu}_e$ interactions with Counting Test Facility (the prototype of the Borexino detector).

(B) Three-neutrino mixing parameters

$\sin^2(\theta_{12})$

If an experiment reports $\sin^2(2\theta_{12})$ we convert the value to $\sin^2(\theta_{12})$.

VALUE	DOCUMENT ID	TECN	COMMENT
$0.307^{+0.013}_{-0.012}$	¹ ABE	16C FIT	KamLAND+global solar; 3ν
• • • We do not use the following data for averages, fits, limits, etc. • • •			
0.318 ± 0.016	² SALAS	21 FIT	global fit
0.304 ± 0.012	³ ESTEBAN	20A FIT	Global fit
$0.320^{+0.020}_{-0.016}$	DE-SALAS	18 FIT	Global fit
0.310 ± 0.014	⁴ ABE	16C FIT	SKAM+SNO; 3ν
$0.334^{+0.027}_{-0.023}$	⁵ ABE	16C FIT	SK-I+II+III+IV; 3ν
$0.327^{+0.026}_{-0.031}$	⁶ ABE	16C FIT	SK-IV; 3ν
0.323 ± 0.016	⁷ FORERO	14 FIT	3ν
$0.304^{+0.013}_{-0.012}$	⁸ GONZALEZ...	14 FIT	Either mass ordering; global fit
$0.299^{+0.014}_{-0.014}$	^{9,10} AHARMIM	13 FIT	global solar; 2ν
$0.307^{+0.016}_{-0.013}$	^{10,11} AHARMIM	13 FIT	global solar; 3ν
$0.304^{+0.022}_{-0.018}$	^{10,12} AHARMIM	13 FIT	KamLAND + global solar; 3ν
$0.304^{+0.014}_{-0.013}$	¹³ GANDO	13 FIT	KamLAND + global solar + SBL + accelerator; 3ν
$0.304^{+0.014}_{-0.013}$	¹⁴ GANDO	13 FIT	KamLAND + global solar; 3ν
$0.325^{+0.039}_{-0.039}$	¹⁵ GANDO	13 FIT	KamLAND; 3ν
$0.30^{+0.02}_{-0.01}$	¹⁶ ABE	11 FIT	KamLAND + global solar; 2ν
$0.30^{+0.02}_{-0.01}$	¹⁷ ABE	11 FIT	global solar; 2ν
$0.31^{+0.03}_{-0.02}$	¹⁸ ABE	11 FIT	KamLAND + global solar; 3ν
$0.31^{+0.03}_{-0.03}$	¹⁹ ABE	11 FIT	global solar; 3ν
$0.314^{+0.015}_{-0.012}$	²⁰ BELLINI	11A FIT	KamLAND + global solar; 2ν
$0.319^{+0.017}_{-0.015}$	²¹ BELLINI	11A FIT	global solar; 2ν
$0.311^{+0.016}_{-0.016}$	²² GANDO	11 FIT	KamLAND + solar; 3ν
$0.304^{+0.046}_{-0.042}$	²³ GANDO	11 FIT	KamLAND; 3ν
$0.314^{+0.018}_{-0.014}$	^{24,25} AHARMIM	10 FIT	KamLAND + global solar; 2ν
$0.314^{+0.017}_{-0.020}$	^{24,26} AHARMIM	10 FIT	global solar; 2ν
$0.319^{+0.019}_{-0.016}$	^{24,27} AHARMIM	10 FIT	KamLAND + global solar; 3ν
$0.319^{+0.023}_{-0.024}$	^{24,28} AHARMIM	10 FIT	global solar; 3ν
$0.36^{+0.05}_{-0.04}$	²⁹ ABE	08A FIT	KamLAND
0.32 ± 0.03	³⁰ ABE	08A FIT	KamLAND + global fit
0.32 ± 0.02	³¹ AHARMIM	08 FIT	KamLAND + global solar
$0.31^{+0.04}_{-0.04}$	³² HOSAKA	06 FIT	KamLAND + global solar
$0.31^{+0.04}_{-0.03}$	³³ HOSAKA	06 FIT	SKAM+SNO+KamLAND
$0.31^{+0.03}_{-0.04}$	³⁴ HOSAKA	06 FIT	SKAM+SNO
$0.31^{+0.02}_{-0.03}$	³⁵ AHARMIM	05A FIT	KamLAND + global solar
$0.25-0.39$	³⁶ AHARMIM	05A FIT	global solar
0.29 ± 0.03	³⁷ ARAKI	05 FIT	KamLAND + global solar
$0.29^{+0.03}_{-0.02}$	³⁸ AHMED	04A FIT	KamLAND + global solar
$0.23-0.37$	³⁹ AHMED	04A FIT	global solar
$0.31^{+0.04}_{-0.04}$	⁴⁰ SMY	04 FIT	KamLAND + global solar
$0.29^{+0.04}_{-0.04}$	⁴¹ SMY	04 FIT	global solar
$0.32^{+0.06}_{-0.05}$	⁴² SMY	04 FIT	SKAM + SNO
$0.19-0.33$	⁴³ AHMAD	02B FIT	global solar
$0.19-0.39$	⁴⁴ FUKUDA	02 FIT	global solar

¹ ABE 16c obtained this result by a three-neutrino oscillation analysis, with a constraint of $\sin^2(\theta_{13}) = 0.0219 \pm 0.0014$ coming from reactor neutrino experiments, using all solar data and KamLAND data. *CPT* invariance is assumed.

² SALAS 21 reports results of a global fit to neutrino oscillation data available at the time of the Neutrino 2020 conference.

³ ESTEBAN 20A reports results of a global fit to neutrino oscillation data available at the time of the Neutrino2020 conference.

⁴ ABE 16c obtained this result by a three-neutrino oscillation analysis, with a constraint of $\sin^2(\theta_{13}) = 0.0219 \pm 0.0014$ coming from reactor neutrino experiments, using Super-Kamiokande (I+II+III+IV) and SNO data.

⁵ ABE 16c obtained this result by a three-neutrino oscillation analysis, with a constraint of $\sin^2(\theta_{13}) = 0.0219 \pm 0.0014$ coming from reactor neutrino experiments, by combining the four phases of the Super-Kamiokande solar data.

⁶ ABE 16c obtained this result by a three-neutrino oscillation analysis, with a constraint of $\sin^2(\theta_{13}) = 0.0219 \pm 0.0014$ coming from reactor neutrino experiments, using the Super-Kamiokande-IV data.

⁷ FORERO 14 performs a global fit to neutrino oscillations using solar, reactor, long-baseline accelerator, and atmospheric neutrino data.

⁸ GONZALEZ-GARCIA 14 result comes from a frequentist global fit. The corresponding Bayesian global fit to the same data results are reported in BERGSTROM 15 as $0.304^{+0.013}_{-0.012}$ for normal and $0.305^{+0.012}_{-0.013}$ for inverted mass ordering.

⁹ AHARMIM 13 obtained this result by a two-neutrino oscillation analysis using global solar neutrino data.

¹⁰ AHARMIM 13 global solar neutrino data include SNO's all-phases-combined analysis results on the total active ^8B neutrino flux and energy-dependent ν_e survival probability parameters, measurements of Cl (CLEVELAND 98), Ga (ABDURASHITOV 09 which contains combined analysis with GNO (ALTMANN 05 and Ph.D. thesis of F. Kaether)), and ^7Be (BELLINI 11A) rates, and ^8B solar-neutrino recoil electron measurements of SK-I (HOSAKA 06) zenith, SK-II (CRAVENS 08) and SK-III (ABE 11) day/night spectra, and Borexino (BELLINI 10A) spectra.

¹¹ AHARMIM 13 obtained this result by a three-neutrino oscillation analysis with the value of Δm_{32}^2 fixed to $2.45 \times 10^{-3} \text{ eV}^2$, using global solar neutrino data.

¹² AHARMIM 13 obtained this result by a three-neutrino oscillation analysis with the value of Δm_{32}^2 fixed to $2.45 \times 10^{-3} \text{ eV}^2$, using global solar neutrino and KamLAND (GANDO 11) data. *CPT* invariance is assumed.

¹³ GANDO 13 obtained this result by a three-neutrino oscillation analysis using KamLAND, global solar neutrino, short-baseline (SBL) reactor, and accelerator data, assuming *CPT* invariance. Supersedes GANDO 11.

¹⁴ GANDO 13 obtained this result by a three-neutrino oscillation analysis using KamLAND and global solar neutrino data, assuming *CPT* invariance. Supersedes GANDO 11.

¹⁵ GANDO 13 obtained this result by a three-neutrino oscillation analysis using KamLAND data. Supersedes GANDO 11.

¹⁶ ABE 11 obtained this result by a two-neutrino oscillation analysis using solar neutrino data including Super-Kamiokande, SNO, Borexino (ARPESELLA 08A), Homestake, GALLEX/GNO, SAGE, and KamLAND data. *CPT* invariance is assumed.

¹⁷ ABE 11 obtained this result by a two-neutrino oscillation analysis using solar neutrino data including Super-Kamiokande, SNO, Borexino (ARPESELLA 08A), Homestake, GALLEX/GNO, and SAGE data.

¹⁸ ABE 11 obtained this result by a three-neutrino oscillation analysis with the value of Δm_{32}^2 fixed to $2.4 \times 10^{-3} \text{ eV}^2$, using solar neutrino data including Super-Kamiokande, SNO, Borexino (ARPESELLA 08A), Homestake, GALLEX/GNO, SAGE, and KamLAND data. The normal neutrino mass ordering and *CPT* invariance are assumed.

¹⁹ ABE 11 obtained this result by a three-neutrino oscillation analysis with the value of Δm_{32}^2 fixed to $2.4 \times 10^{-3} \text{ eV}^2$, using solar neutrino data including Super-Kamiokande, SNO, Borexino (ARPESELLA 08A), Homestake, and GALLEX/GNO data. The normal neutrino mass ordering is assumed.

²⁰ BELLINI 11A obtained this result by a two-neutrino oscillation analysis using KamLAND, Homestake, SAGE, Gallex, GNO, Kamiokande, Super-Kamiokande, SNO, and Borexino (BELLINI 11A) data and the SSM flux prediction in SERENELLI 11 (Astrophysical Journal **743** 24 (2011)) with the exception that the ^8B flux was left free. *CPT* invariance is assumed.

²¹ BELLINI 11A obtained this result by a two-neutrino oscillation analysis using Homestake, SAGE, Gallex, GNO, Kamiokande, Super-Kamiokande, SNO, and Borexino (BELLINI 11A) data and the SSM flux prediction in SERENELLI 11 (Astrophysical Journal **743** 24 (2011)) with the exception that the ^8B flux was left free.

²² GANDO 11 obtain this result with three-neutrino fit using the KamLAND + solar data. Superseded by GANDO 13.

²³ GANDO 11 obtain this result with three-neutrino fit using the KamLAND data only. Superseded by GANDO 13.

²⁴ AHARMIM 10 global solar neutrino data include SNO's low-energy-threshold analysis survival probability day/night curves, SNO Phase III integral rates (AHARMIM 08), Cl (CLEVELAND 98), SAGE (ABDURASHITOV 09), Gallex/GNO (HAMPEL 99, ALTMANN 05), Borexino (ARPESELLA 08A), SK-I zenith (HOSAKA 06), and SK-II day/night spectra (CRAVENS 08).

²⁵ AHARMIM 10 obtained this result by a two-neutrino oscillation analysis using global solar neutrino data and KamLAND data (ABE 08A). *CPT* invariance is assumed.

²⁶ AHARMIM 10 obtained this result by a two-neutrino oscillation analysis using global solar neutrino data.

²⁷ AHARMIM 10 obtained this result by a three-neutrino oscillation analysis with the value of Δm_{31}^2 fixed to $2.3 \times 10^{-3} \text{ eV}^2$, using global solar neutrino data and KamLAND data (ABE 08A). *CPT* invariance is assumed.

²⁸ AHARMIM 10 obtained this result by a three-neutrino oscillation analysis with the value of Δm_{31}^2 fixed to $2.3 \times 10^{-3} \text{ eV}^2$, using global solar neutrino data.

²⁹ ABE 08A obtained this result by a rate + shape + time combined geoneutrino and reactor two-neutrino fit for Δm_{21}^2 and $\tan^2\theta_{12}$, using KamLAND data only. Superseded by GANDO 11.

³⁰ ABE 08A obtained this result by means of a two-neutrino fit using KamLAND, Homestake, SAGE, GALLEX, GNO, SK (zenith angle and E-spectrum), the SNO χ^2 -map, and solar flux data. *CPT* invariance is assumed. Superseded by GANDO 11.

See key on page 1171

Lepton Particle Listings

Neutrino Mixing

- ³¹ The result given by AHARMIM 08 is $\theta = (34.4^{+1.3}_{-1.2})^\circ$. This result is obtained by a two-neutrino oscillation analysis using solar neutrino data including those of Borexino (ARPESELLA 08A) and Super-Kamiokande-I (HOSAKA 06), and KamLAND data (ABE 08A). *CPT* invariance is assumed.
- ³² HOSAKA 06 obtained this result by a two-neutrino oscillation analysis using SK ν_e data, CC data from other solar neutrino experiments, and KamLAND data (ARAKI 05). *CPT* invariance is assumed.
- ³³ HOSAKA 06 obtained this result by a two-neutrino oscillation analysis using the data from Super-Kamiokande, SNO (AHMAD 02 and AHMAD 02B), and KamLAND (ARAKI 05) experiments. *CPT* invariance is assumed.
- ³⁴ HOSAKA 06 obtained this result by a two-neutrino oscillation analysis using the Super-Kamiokande and SNO (AHMAD 02 and AHMAD 02B) solar neutrino data.
- ³⁵ The result given by AHARMIM 05A is $\theta = (33.9 \pm 1.6)^\circ$. This result is obtained by a two-neutrino oscillation analysis using SNO pure deuterium and salt phase data, SK ν_e data, CI and Ga CC data, and KamLAND data (ARAKI 05). *CPT* invariance is assumed. AHARMIM 05A also quotes $\theta = (33.9^{+2.4}_{-2.2})^\circ$ as the error enveloping the 68% CL two-dimensional region. This translates into $\sin^2 2\theta = 0.86^{+0.05}_{-0.06}$.
- ³⁶ AHARMIM 05A obtained this result by a two-neutrino oscillation analysis using the data from all solar neutrino experiments. The listed range of the parameter envelops the 95% CL two-dimensional region shown in figure 35a of AHARMIM 05A. AHARMIM 05A also quotes $\tan^2 \theta = 0.45^{+0.09}_{-0.08}$ as the error enveloping the 68% CL two-dimensional region. This translates into $\sin^2 2\theta = 0.86^{+0.05}_{-0.07}$.
- ³⁷ ARAKI 05 obtained this result by a two-neutrino oscillation analysis using KamLAND and solar neutrino data. *CPT* invariance is assumed. The 1σ error shown here is translated from the number provided by the KamLAND collaboration, $\tan^2 \theta = 0.40^{+0.07}_{-0.05}$. The corresponding number quoted in ARAKI 05 is $\tan^2 \theta = 0.40^{+0.10}_{-0.07}$ ($\sin^2 2\theta = 0.82 \pm 0.07$), which envelops the 68% CL two-dimensional region.
- ³⁸ The result given by AHMED 04A is $\theta = (32.5^{+1.7}_{-1.6})^\circ$. This result is obtained by a two-neutrino oscillation analysis using solar neutrino and KamLAND data (EGUCHI 03). *CPT* invariance is assumed. AHMED 04A also quotes $\theta = (32.5^{+2.4}_{-2.3})^\circ$ as the error enveloping the 68% CL two-dimensional region. This translates into $\sin^2 2\theta = 0.82 \pm 0.06$.
- ³⁹ AHMED 04A obtained this result by a two-neutrino oscillation analysis using the data from all solar neutrino experiments. The listed range of the parameter envelops the 95% CL two-dimensional region shown in Fig. 5(a) of AHMED 04A. The best-fit point is $\Delta(m^2) = 6.5 \times 10^{-5} \text{ eV}^2$, $\tan^2 \theta = 0.40$ ($\sin^2 2\theta = 0.82$).
- ⁴⁰ The result given by SMY 04 is $\tan^2 \theta = 0.44 \pm 0.08$. This result is obtained by a two-neutrino oscillation analysis using solar neutrino and KamLAND data (IANNI 03). *CPT* invariance is assumed.
- ⁴¹ SMY 04 obtained this result by a two-neutrino oscillation analysis using the data from all solar neutrino experiments. The 1σ errors are read from Fig. 6(a) of SMY 04.
- ⁴² SMY 04 obtained this result by a two-neutrino oscillation analysis using the Super-Kamiokande and SNO (AHMAD 02 and AHMAD 02B) solar neutrino data. The 1σ errors are read from Fig. 6(a) of SMY 04.
- ⁴³ AHMAD 02B obtained this result by a two-neutrino oscillation analysis using the data from all solar neutrino experiments. The listed range of the parameter envelops the 95% CL two-dimensional region shown in Fig. 4(b) of AHMAD 02B. The best fit point is $\Delta(m^2) = 5.0 \times 10^{-5} \text{ eV}^2$ and $\tan\theta = 0.34$ ($\sin^2 2\theta = 0.76$).
- ⁴⁴ FUKUDA 02 obtained this result by a two-neutrino oscillation analysis using the data from all solar neutrino experiments. The listed range of the parameter envelops the 95% CL two-dimensional region shown in Fig. 4 of FUKUDA 02. The best fit point is $\Delta(m^2) = 6.9 \times 10^{-5} \text{ eV}^2$ and $\tan^2 \theta = 0.38$ ($\sin^2 2\theta = 0.80$).

Δm_{21}^2

VALUE (10^{-5} eV^2)	DOCUMENT ID	TECN	COMMENT
7.53 ± 0.18	1 GANDO	13 FIT	KamLAND + global solar + SBL + accelerator: 3ν
$7.50^{+0.22}_{-0.20}$	2 SALAS	21 FIT	global fit
$7.42^{+0.21}_{-0.20}$	3 ESTEBAN	20A FIT	Global fit
$7.55^{+0.20}_{-0.16}$	DE-SALAS	18 FIT	Global fit
$7.49^{+0.19}_{-0.18}$	4 ABE	16c FIT	KamLAND+global solar; 3ν
$4.8^{+1.3}_{-0.6}$	5 ABE	16c FIT	SKAM+SNO; 3ν
$4.8^{+1.5}_{-0.8}$	6 ABE	16c FIT	SK-I+II+III+IV; 3ν
$3.2^{+2.8}_{-0.2}$	7 ABE	16c FIT	SK-IV; 3ν
$7.6^{+0.19}_{-0.18}$	8 FORERO	14 FIT	3ν
$7.50^{+0.19}_{-0.17}$	9 GONZALEZ...	14 FIT	Either mass ordering; global fit
$5.13^{+1.29}_{-0.96}$	10,11 AHARMIM	13 FIT	global solar: 2ν
$5.13^{+1.49}_{-0.98}$	11,12 AHARMIM	13 FIT	global solar: 3ν
$7.46^{+0.20}_{-0.19}$	11,13 AHARMIM	13 FIT	KamLAND + global solar: 3ν
$7.53^{+0.19}_{-0.18}$	14 GANDO	13 FIT	KamLAND + global solar: 3ν
$7.54^{+0.19}_{-0.18}$	15 GANDO	13 FIT	KamLAND: 3ν
7.6 ± 0.2	16 ABE	11 FIT	KamLAND + global solar: 2ν

• • • We do not use the following data for averages, fits, limits, etc. • • •

$6.2^{+1.1}_{-1.9}$	17 ABE	11 FIT	global solar: 2ν
7.7 ± 0.3	18 ABE	11 FIT	KamLAND + global solar: 3ν
$6.0^{+2.2}_{-2.5}$	19 ABE	11 FIT	global solar: 3ν
$7.50^{+0.16}_{-0.24}$	20 BELLINI	11A FIT	KamLAND + global solar: 2ν
$5.2^{+1.5}_{-0.9}$	21 BELLINI	11A FIT	global solar: 2ν
$7.50^{+0.19}_{-0.20}$	22 GANDO	11 FIT	KamLAND + solar: 3ν
7.49 ± 0.20	23 GANDO	11 FIT	KamLAND: 3ν
$7.59^{+0.20}_{-0.21}$	24,25 AHARMIM	10 FIT	KamLAND + global solar: 2ν
$5.89^{+2.13}_{-2.16}$	24,26 AHARMIM	10 FIT	global solar: 2ν
7.59 ± 0.21	24,27 AHARMIM	10 FIT	KamLAND + global solar: 3ν
$6.31^{+2.49}_{-2.58}$	24,28 AHARMIM	10 FIT	global solar: 3ν
$7.58^{+0.14}_{-0.13} \pm 0.15$	29 ABE	08A FIT	KamLAND
7.59 ± 0.21	30 ABE	08A FIT	KamLAND + global solar
$7.59^{+0.19}_{-0.21}$	31 AHARMIM	08 FIT	KamLAND + global solar
8.0 ± 0.3	32 HOSAKA	06 FIT	KamLAND + global solar
8.0 ± 0.3	33 HOSAKA	06 FIT	SKAM+SNO+KamLAND
$6.3^{+3.7}_{-1.5}$	34 HOSAKA	06 FIT	SKAM+SNO
5-12	35 HOSAKA	06 FIT	SKAM day/night in the LMA region
$8.0^{+0.4}_{-0.3}$	36 AHARMIM	05A FIT	KamLAND + global solar LMA
3.3-14.4	37 AHARMIM	05A FIT	global solar
$7.9^{+0.4}_{-0.3}$	38 ARAKI	05 FIT	KamLAND + global solar
$7.1^{+1.0}_{-0.3}$	39 AHMED	04A FIT	KamLAND + global solar
3.2-13.7	40 AHMED	04A FIT	global solar
$7.1^{+0.6}_{-0.5}$	41 SMY	04 FIT	KamLAND + global solar
$6.0^{+1.7}_{-1.6}$	42 SMY	04 FIT	global solar
$6.0^{+2.5}_{-1.6}$	43 SMY	04 FIT	SKAM + SNO
2.8-12.0	44 AHMAD	02B FIT	global solar
3.2-19.1	45 FUKUDA	02 FIT	global solar

- ¹ GANDO 13 obtained this result by a three-neutrino oscillation analysis using KamLAND, global solar neutrino, short-baseline (SBL) reactor, and accelerator data, assuming *CPT* invariance. Supersedes GANDO 11.
- ² SALAS 21 reports results of a global fit to neutrino oscillation data available at the time of the Neutrino 2020 conference.
- ³ ESTEBAN 20A reports results of a global fit to neutrino oscillation data available at the time of the Neutrino2020 conference.
- ⁴ ABE 16c obtained this result by a three-neutrino oscillation analysis, with a constraint of $\sin^2(\theta_{13}) = 0.0219 \pm 0.0014$ coming from reactor neutrino experiments, using all solar data and KamLAND data. *CPT* invariance is assumed.
- ⁵ ABE 16c obtained this result by a three-neutrino oscillation analysis, with a constraint of $\sin^2(\theta_{13}) = 0.0219 \pm 0.0014$ coming from reactor neutrino experiments, using Super-Kamiokande (I+II+III+IV) and SNO data.
- ⁶ ABE 16c obtained this result by a three-neutrino oscillation analysis, with a constraint of $\sin^2(\theta_{13}) = 0.0219 \pm 0.0014$ coming from reactor neutrino experiments, by combining the four phases of the Super-Kamiokande solar data.
- ⁷ ABE 16c obtained this result by a three-neutrino oscillation analysis, with a constraint of $\sin^2(\theta_{13}) = 0.0219 \pm 0.0014$ coming from reactor neutrino experiments, using the Super-Kamiokande-IV data.
- ⁸ FORERO 14 performs a global fit to Δm_{21}^2 using solar, reactor, long-baseline accelerator, and atmospheric neutrino data.
- ⁹ GONZALEZ-GARCIA 14 result comes from a frequentist global fit. The corresponding Bayesian global fit to the same data results are reported in BERGSTROM 15 as $(7.50^{+0.19}_{-0.17}) \times 10^{-5} \text{ eV}^2$ for normal and $(7.50^{+0.18}_{-0.17}) \times 10^{-5} \text{ eV}^2$ for inverted mass ordering.
- ¹⁰ AHARMIM 13 obtained this result by a two-neutrino oscillation analysis using global solar neutrino data.
- ¹¹ AHARMIM 13 global solar neutrino data include SNO's all-phases-combined analysis results on the total active ^8B neutrino flux and energy-dependent ν_e survival probability parameters, measurements of Cl (CLEVELAND 98), Ga (ABDURASHITOV 09 which contains combined analysis with GNO (ALTMANN 05 and Ph.D. thesis of F. Kaether)), and ^7Be (BELLINI 11A) rates, and ^8B solar-neutrino recoil electron measurements of SK-I (HOSAKA 06) zenith, SK-II (CRAVENS 08), and SK-III (ABE 11) day/night spectra, and Borexino (BELLINI 10A) spectra.
- ¹² AHARMIM 13 obtained this result by a three-neutrino oscillation analysis with the value of Δm_{31}^2 fixed to $2.45 \times 10^{-3} \text{ eV}^2$, using global solar neutrino data.
- ¹³ AHARMIM 13 obtained this result by a three-neutrino oscillation analysis with the value of Δm_{31}^2 fixed to $2.45 \times 10^{-3} \text{ eV}^2$, using global solar neutrino and KamLAND data (GANDO 11). *CPT* invariance is assumed.
- ¹⁴ GANDO 13 obtained this result by a three-neutrino oscillation analysis using KamLAND and global solar neutrino data, assuming *CPT* invariance. Supersedes GANDO 11.
- ¹⁵ GANDO 13 obtained this result by a three-neutrino oscillation analysis using KamLAND data. Supersedes GANDO 11.

Lepton Particle Listings

Neutrino Mixing

- ¹⁶ ABE 11 obtained this result by a two-neutrino oscillation analysis using solar neutrino data including Super-Kamiokande, SNO, Borexino (ARPESELLA 08A), Homestake, GALLEX/GNO, SAGE, and KamLAND data. *CPT* invariance is assumed.
- ¹⁷ ABE 11 obtained this result by a two-neutrino oscillation analysis using solar neutrino data including Super-Kamiokande, SNO, Borexino (ARPESELLA 08A), Homestake, GALLEX/GNO, and SAGE data.
- ¹⁸ ABE 11 obtained this result by a three-neutrino oscillation analysis with the value of Δm_{32}^2 fixed to $2.4 \times 10^{-3} \text{ eV}^2$, using solar neutrino data including Super-Kamiokande, SNO, Borexino (ARPESELLA 08A), Homestake, GALLEX/GNO, SAGE, and KamLAND data. The normal neutrino mass ordering and *CPT* invariance are assumed.
- ¹⁹ ABE 11 obtained this result by a three-neutrino oscillation analysis with the value of Δm_{32}^2 fixed to $2.4 \times 10^{-3} \text{ eV}^2$, using solar neutrino data including Super-Kamiokande, SNO, Borexino (ARPESELLA 08A), Homestake, and GALLEX/GNO data. The normal neutrino mass ordering is assumed.
- ²⁰ BELLINI 11A obtained this result by a two-neutrino oscillation analysis using KamLAND, Homestake, SAGE, Gallex, GNO, Kamiokande, Super-Kamiokande, SNO, and Borexino (BELLINI 11A) data and the SSM flux prediction in SERENELLI 11 (Astrophysical Journal **743** 24 (2011)) with the exception that the ^8B flux was left free. *CPT* invariance is assumed.
- ²¹ BELLINI 11A obtained this result by a two-neutrino oscillation analysis using Homestake, SAGE, Gallex, GNO, Kamiokande, Super-Kamiokande, SNO, and Borexino (BELLINI 11A) data and the SSM flux prediction in SERENELLI 11 (Astrophysical Journal **743** 24 (2011)) with the exception that the ^8B flux was left free.
- ²² GANDU 11 obtain this result with three-neutrino fit using the KamLAND + solar data. Superseded by GANDU 13.
- ²³ GANDU 11 obtain this result with three-neutrino fit using the KamLAND data only. Supersedes ABE 08A.
- ²⁴ AHARMIM 10 global solar neutrino data include SNO's low-energy-threshold analysis survival probability day/night curves, SNO Phase III integral rates (AHARMIM 08), CI (CLEVELAND 98), SAGE (ABDURASHITOV 09), Gallex/GNO (HAMPEL 99, ALTMANN 05), Borexino (ARPESELLA 08A), SK-I zenith (HOSAKA 06), and SK-II day/night spectra (CRAVENS 08).
- ²⁵ AHARMIM 10 obtained this result by a two-neutrino oscillation analysis using global solar neutrino data and KamLAND data (ABE 08A). *CPT* invariance is assumed.
- ²⁶ AHARMIM 10 obtained this result by a two-neutrino oscillation analysis using global solar neutrino data.
- ²⁷ AHARMIM 10 obtained this result by a three-neutrino oscillation analysis with the value of Δm_{31}^2 fixed to $2.3 \times 10^{-3} \text{ eV}^2$, using global solar neutrino data and KamLAND data (ABE 08A). *CPT* invariance is assumed.
- ²⁸ AHARMIM 10 obtained this result by a three-neutrino oscillation analysis with the value of Δm_{31}^2 fixed to $2.3 \times 10^{-3} \text{ eV}^2$, using global solar neutrino data.
- ²⁹ ABE 08A obtained this result by a rate + shape + time combined geoneutrino and reactor two-neutrino fit for Δm_{21}^2 and $\tan^2 \theta_{12}$, using KamLAND data only. Superseded by GANDU 11.
- ³⁰ ABE 08A obtained this result by means of a two-neutrino fit using KamLAND, Homestake, SAGE, GALLEX, GNO, SK (zenith angle and E-spectrum), the SNO χ^2 -map, and solar flux data. *CPT* invariance is assumed. Superseded by GANDU 11.
- ³¹ AHARMIM 08 obtained this result by a two-neutrino oscillation analysis using all solar neutrino data including those of Borexino (ARPESELLA 08A) and Super-Kamiokande-I (HOSAKA 06), and KamLAND data (ABE 08A). *CPT* invariance is assumed.
- ³² HOSAKA 06 obtained this result by a two-neutrino oscillation analysis using solar neutrino and KamLAND data (ARAKI 05). *CPT* invariance is assumed.
- ³³ HOSAKA 06 obtained this result by a two-neutrino oscillation analysis using the data from Super-Kamiokande, SNO (AHMAD 02 and AHMAD 02B), and KamLAND (ARAKI 05) experiments. *CPT* invariance is assumed.
- ³⁴ HOSAKA 06 obtained this result by a two-neutrino oscillation analysis using the Super-Kamiokande and SNO (AHMAD 02 and AHMAD 02B) solar neutrino data.
- ³⁵ HOSAKA 06 obtained this result from the consistency between the observed and expected day-night flux asymmetry amplitude. The listed 68% CL range is derived from the 1σ boundary of the amplitude fit to the data. Oscillation parameters are constrained to be in the LMA region. The mixing angle is fixed at $\tan^2 \theta = 0.44$ because the fit depends only very weakly on it.
- ³⁶ AHARMIM 05A obtained this result by a two-neutrino oscillation analysis using solar neutrino and KamLAND data (ARAKI 05). *CPT* invariance is assumed. AHARMIM 05A also quotes $\Delta(m^2) = (8.0^{+0.6}_{-0.4}) \times 10^{-5} \text{ eV}^2$ as the error enveloping the 68% CL two-dimensional region.
- ³⁷ AHARMIM 05A obtained this result by a two-neutrino oscillation analysis using the data from all solar neutrino experiments. The listed range of the parameter envelops the 95% CL two-dimensional region shown in figure 35a of AHARMIM 05A. AHARMIM 05A also quotes $\Delta(m^2) = (6.5^{+4.4}_{-2.3}) \times 10^{-5} \text{ eV}^2$ as the error enveloping the 68% CL two-dimensional region.
- ³⁸ ARAKI 05 obtained this result by a two-neutrino oscillation analysis using KamLAND and solar neutrino data. *CPT* invariance is assumed. The 1σ error shown here is provided by the KamLAND collaboration. The error quoted in ARAKI 05, $\Delta(m^2) = (7.9^{+0.6}_{-0.5}) \times 10^{-5}$, envelops the 68% CL two-dimensional region.
- ³⁹ AHMED 04A obtained this result by a two-neutrino oscillation analysis using solar neutrino and KamLAND data (EGUCHI 03). *CPT* invariance is assumed. AHMED 04A also quotes $\Delta(m^2) = (7.1^{+1.2}_{-0.6}) \times 10^{-5} \text{ eV}^2$ as the error enveloping the 68% CL two-dimensional region.
- ⁴⁰ AHMED 04A obtained this result by a two-neutrino oscillation analysis using the data from all solar neutrino experiments. The listed range of the parameter envelops the 95% CL two-dimensional region shown in Fig. 5(a) of AHMED 04A. The best-fit point is $\Delta(m^2) = 6.5 \times 10^{-5} \text{ eV}^2$, $\tan^2 \theta = 0.40$ ($\sin^2 2\theta = 0.82$).

- ⁴¹ SMY 04 obtained this result by a two-neutrino oscillation analysis using solar neutrino and KamLAND data (IANNI 03). *CPT* invariance is assumed.
- ⁴² SMY 04 obtained this result by a two-neutrino oscillation analysis using the data from all solar neutrino experiments. The 1σ errors are read from Fig. 6(a) of SMY 04.
- ⁴³ SMY 04 obtained this result by a two-neutrino oscillation analysis using the Super-Kamiokande and SNO (AHMAD 02 and AHMAD 02B) solar neutrino data. The 1σ errors are read from Fig. 6(a) of SMY 04.
- ⁴⁴ AHMAD 02B obtained this result by a two-neutrino oscillation analysis using the data from all solar neutrino experiments. The listed range of the parameter envelops the 95% CL two-dimensional region shown in Fig. 4(b) of AHMAD 02B. The best fit point is $\Delta(m^2) = 5.0 \times 10^{-5} \text{ eV}^2$ and $\tan \theta = 0.34$ ($\sin^2 2\theta = 0.76$).
- ⁴⁵ FUKUDA 02 obtained this result by a two-neutrino oscillation analysis using the data from all solar neutrino experiments. The listed range of the parameter envelops the 95% CL two-dimensional region shown in Fig. 4 of FUKUDA 02. The best fit point is $\Delta(m^2) = 6.9 \times 10^{-5} \text{ eV}^2$ and $\tan^2 \theta = 0.38$ ($\sin^2 2\theta = 0.80$).

$\sin^2(\theta_{23})$

The reported limits below correspond to the projection onto the $\sin^2(\theta_{23})$ axis of the 90% CL contours in the $\sin^2(\theta_{23}) - \Delta m_{32}^2$ plane presented by the authors. Unless otherwise specified, the limits are 90% CL and the reported uncertainties are 68% CL.

If an experiment reports $\sin^2(2\theta_{23})$ we convert the value to $\sin^2(\theta_{23})$.

VALUE	DOCUMENT ID	TECN	COMMENT
$0.553^{+0.016}_{-0.024}$	OUR FIT		Error includes scale factor of 1.1. Assuming inverted mass ordering
$0.558^{+0.015}_{-0.021}$	OUR FIT		Assuming normal mass ordering
0.51 ± 0.05	1 ABBASI	23 ICCB	Normal mass ordering
$0.561^{+0.021}_{-0.032}$	2 ABE	23F T2K	Normal mass ordering
$0.563^{+0.017}_{-0.032}$	2 ABE	23F T2K	Inverted mass ordering
$0.57^{+0.03}_{-0.04}$	3 ACERO	22 NOVA	Normal mass ordering; octant II for θ_{23}
0.56 ± 0.04	3 ACERO	22 NOVA	Inverted mass ordering; octant II for θ_{23}
$0.43^{+0.20}_{-0.04}$	4 ADAMSON	20A MINS	Normal mass ordering
$0.42^{+0.07}_{-0.03}$	4 ADAMSON	20A MINS	Inverted mass ordering
$0.588^{+0.031}_{-0.064}$	5 ABE	18B SKAM	Normal mass ordering, θ_{13} constrained
$0.575^{+0.036}_{-0.073}$	5 ABE	18B SKAM	Inverted mass ordering, θ_{13} constrained
• • • We do not use the following data for averages, fits, limits, etc. • • •			
$0.47^{+0.11}_{-0.02}$	6 ABE	23D T2K	ν_μ disappearance
$0.45^{+0.16}_{-0.04}$	6 ABE	23D T2K	$\bar{\nu}_\mu$ disappearance
$0.51^{+0.06}_{-0.07}$	7 ABE	21A T2K	ν_μ disappearance
$0.43^{+0.21}_{-0.05}$	7 ABE	21A T2K	$\bar{\nu}_\mu$ disappearance
0.574 ± 0.014	8 SALAS	21 FIT	Normal mass ordering, global fit
$0.578^{+0.010}_{-0.017}$	8 SALAS	21 FIT	Inverted mass ordering, global fit
0.455	9 AARTSEN	20 ICCB	For both mass orderings
$0.53^{+0.03}_{-0.04}$	10 ABE	20F T2K	Both mass orderings
$0.573^{+0.016}_{-0.020}$	11 ESTEBAN	20A FIT	Normal mass ordering, global fit
$0.575^{+0.016}_{-0.019}$	11 ESTEBAN	20A FIT	Inverted mass ordering, global fit
$0.58^{+0.04}_{-0.13}$	12 AARTSEN	19c ICCB	
$0.56^{+0.04}_{-0.03}$	13 ACERO	19 NOVA	Normal mass order; octant II for θ_{23}
$0.48^{+0.04}_{-0.03}$	13,14 ACERO	19 NOVA	Normal mass order; octant I for θ_{23}
$0.56^{+0.04}_{-0.03}$	13,14 ACERO	19 NOVA	Inverted mass order; octant II for θ_{23}
$0.47^{+0.04}_{-0.03}$	13,14 ACERO	19 NOVA	Inverted mass order; octant I for θ_{23}
$0.49^{+0.30}_{-0.28}$	AGAFONOVA	19 OPER	
$0.50^{+0.20}_{-0.19}$	15 ALBERT	19 ANTR	Atmospheric ν , deep sea telescope
$0.51^{+0.07}_{-0.09}$	16 AARTSEN	18A ICCB	Normal mass ordering
$0.587^{+0.036}_{-0.069}$	17 ABE	18B SKAM	3ν osc: normal mass ordering, θ_{13} free
$0.551^{+0.044}_{-0.075}$	17 ABE	18B SKAM	3ν osc: inverted mass ordering, θ_{13} free
$0.526^{+0.032}_{-0.036}$	18 ABE	18G T2K	Normal mass ordering, θ_{13} constrained
$0.530^{+0.030}_{-0.034}$	18 ABE	18G T2K	Inverted mass ordering, θ_{13} constrained
0.56 ± 0.04	19 ACERO	18 NOVA	Normal mass order; octant II for θ_{23}
0.47 ± 0.04	19 ACERO	18 NOVA	Normal mass order; octant I for θ_{23}
$0.547^{+0.020}_{-0.030}$	DE-SALAS	18 FIT	Normal mass ordering, global fit

See key on page 1171

Lepton Particle Listings
Neutrino Mixing

0.551 ^{+0.018} _{-0.030}	DE-SALAS	18	FIT	Inverted mass order, global fit	4	ADAMSON 20A uses the complete dataset from MINOS and MINOS+ experiments. The data were collected using a total exposure of 23.76 × 10 ²⁰ protons on target and 60.75 kton-yr exposure to atmospheric neutrinos. Supersedes ADAMSON 14.
0.532 ^{+0.061} _{-0.087}	20 ABE	17A	T2K	Normal mass ordering	5	ABE 18b uses 328 kton-years of Super-Kamiokande I-IV atmospheric neutrino data to obtain this result. The fit is performed over the three parameters, Δm_{32}^2 , $\sin^2(\theta_{23})$, and δ , while the solar parameters and $\sin^2(\theta_{13})$ are fixed to $\Delta m_{21}^2 = (7.53 \pm 0.18) \times 10^{-5} \text{ eV}^2$, $\sin^2(\theta_{12}) = 0.304 \pm 0.014$, and $\sin^2(\theta_{13}) = 0.0219 \pm 0.0012$.
0.534 ^{+0.061} _{-0.087}	20 ABE	17A	T2K	Inverted mass ordering	6	ABE 23d uses the same dataset as ABE 23f. The measurement of $\sin^2(\theta_{23})$ is performed independently for ν_μ and $\bar{\nu}_\mu$.
0.51 ^{+0.08} _{-0.07}	ABE	17C	T2K	Normal mass ordering with neutrinos	7	ABE 21a results are based on 1.49×10^{21} POT in neutrino mode and 1.64×10^{21} POT in antineutrino mode.
0.42 ^{+0.25} _{-0.07}	ABE	17C	T2K	Normal mass ordering with antineutrinos	8	SALAS 21 reports results of a global fit to neutrino oscillation data available at the time of the Neutrino 2020 conference.
0.52 ^{+0.075} _{-0.09}	ABE	17C	T2K	normal mass ordering with neutrinos and antineutrinos	9	AARTSEN 20 uses the data taken between May 2012 and April 2014 with the low-energy subdetector DeepCore of the IceCube neutrino telescope. The reconstructed energy range is between 4 (5) and 90 (80) GeV for the main (confirmatory) analysis. Though the observed best-fit is in the lower octant for both mass orderings, a substantial range of $\sin^2(\theta_{23}) > 0.5$ is still compatible with the observed data for both mass orderings.
0.55 ^{+0.05} _{-0.09}	20 ABE	17F	T2K	Normal mass ordering	10	ABE 20f results are based on data collected between 2009 and 2018 in (anti)neutrino mode and include a neutrino beam exposure of 1.49×10^{21} (1.64×10^{21}) protons on target. Supersedes ABE 18g.
0.55 ^{+0.05} _{-0.08}	20 ABE	17F	T2K	Inverted mass ordering	11	ESTEBAN 20A reports results of a global fit to neutrino oscillation data available at the time of the Neutrino2020 conference.
0.404 ^{+0.022} _{-0.030}	21 ADAMSON	17A	NOVA	Normal mass ordering; octant I for θ_{23}	12	AARTSEN 19c uses three years (April 2012 – May 2015) of neutrino data from full sky with reconstructed energies between 5.6 and 56 GeV, measured with the low-energy subdetector DeepCore of the IceCube neutrino telescope. AARTSEN 19c adopts looser event selection criteria to prioritize the efficiency of selecting neutrino events, different from tighter event selection criteria which closely follow the criteria used by AARTSEN 18a to measure the ν_μ disappearance.
0.624 ^{+0.022} _{-0.030}	21 ADAMSON	17A	NOVA	Normal mass ordering; octant II for θ_{23}	13	ACERO 19 is based on a sample size of 12.33×10^{20} protons on target. The fit combines both antineutrino and neutrino data to extract the oscillation parameters. The results favor the normal mass ordering by 1.9σ and θ_{23} values in octant II by 1.6σ . Supersedes ACERO 18.
0.398 ^{+0.030} _{-0.022}	21 ADAMSON	17A	NOVA	Inverted mass ordering; octant I for θ_{23}	14	Errors are from normal mass ordering and θ_{13} octant II fits.
0.618 ^{+0.022} _{-0.030}	21 ADAMSON	17A	NOVA	Inverted mass ordering; octant II for θ_{23}	15	ALBERT 19 measured the oscillation parameters of atmospheric neutrinos with the ANTARES deep sea neutrino telescope using the data taken from 2007 to 2016 (2830 days of total live time). Supersedes ADRIAN-MARTINEZ 12.
0.45 ^{+0.19} _{-0.07}	22 ABE	16D	T2K	3ν osc; normal mass ordering; $\bar{\nu}$ beam	16	ADAMSON 18a uses three years (April 2012 – May 2015) of neutrino data from full sky with reconstructed energies between 5.6 and 56 GeV, measured with the low-energy subdetector DeepCore of the IceCube neutrino telescope. AARTSEN 18a also reports the best fit result for the inverted mass ordering as $\Delta m_{32}^2 = -2.32 \times 10^{-3} \text{ eV}^2$ and $\sin^2(\theta_{23}) = 0.51$. Uncertainties for the inverted mass ordering fits were not provided. Supersedes AARTSEN 15a.
0.38 to 0.65	23 ADAMSON	16A	NOVA	normal mass ordering	17	ABE 18b uses 328 kton-years of Super-Kamiokande I-IV atmospheric neutrino data to obtain this result. The fit is performed over the four parameters, Δm_{32}^2 , $\sin^2\theta_{23}$, $\sin^2\theta_{13}$, and δ , while the solar parameters are fixed to $\Delta m_{21}^2 = (7.53 \pm 0.18) \times 10^{-5} \text{ eV}^2$ and $\sin^2\theta_{12} = 0.304 \pm 0.014$.
0.37 to 0.64	23 ADAMSON	16A	NOVA	Inverted mass ordering	18	ABE 18g data prefers normal mass ordering is with a posterior probability of 87%. Supersedes ABE 17f.
0.53 ^{+0.09} _{-0.12}	24 AARTSEN	15A	ICCB	Normal mass ordering	19	ACERO 18 performs a joint fit to the data for ν_μ disappearance and ν_e appearance. The overall best fit favors normal mass ordering and θ_{23} in octant II. No 1σ confidence intervals are presented for the inverted mass ordering scenarios. Superseded by ACERO 19.
0.51 ^{+0.09} _{-0.11}	24 AARTSEN	15A	ICCB	Inverted mass ordering	20	Errors are from the projections of the 68% contour on 2D plot of Δm^2 versus $\sin^2(\theta_{23})$. ABE 17f supersedes ABE 17a. Superseded by ABE 18g.
0.514 ^{+0.055} _{-0.056}	25 ABE	14	T2K	3ν osc.; normal mass ordering	21	Superseded by ACERO 18.
0.511 \pm 0.055	25 ABE	14	T2K	3ν osc.; inverted mass ordering	22	ABE 16d reports oscillation results using $\bar{\nu}_\mu$ disappearance in an off-axis beam.
0.41 ^{+0.23} _{-0.06}	26 ADAMSON	14	MINS	Normal mass ordering	23	ADAMSON 16a obtains $\sin^2(\theta_{23})$ in the 68% C.L. range [0.38, 0.65] ([0.37, 0.64]), with two statistically degenerate best-fit values of 0.44 and 0.59 (0.44 and 0.59) for normal (inverted) mass ordering. Superseded by ADAMSON 17a.
0.41 ^{+0.26} _{-0.07}	26 ADAMSON	14	MINS	Inverted mass ordering	24	AARTSEN 15a obtains this result by a three-neutrino oscillation analysis using 10–100 GeV muon neutrino sample from a total of 953 days of measurement with the low-energy subdetector DeepCore of the IceCube neutrino telescope. Superseded by AARTSEN 18a.
0.567 ^{+0.032} _{-0.128}	27 FORERO	14	FIT	Normal mass ordering	25	ABE 14 results are based on ν_μ disappearance using three-neutrino oscillation fit. The confidence intervals are derived from one dimensional profiled likelihoods. Superseded by ABE 17a.
0.573 ^{+0.025} _{-0.043}	27 FORERO	14	FIT	Inverted mass ordering	26	ADAMSON 14 uses a complete set of accelerator and atmospheric data. The analysis combines the ν_μ disappearance and ν_e appearance data using three-neutrino oscillation fit. The fit results are obtained for normal and inverted mass ordering assumptions. The best fit is for first θ_{23} octant and inverted mass ordering.
0.452 ^{+0.052} _{-0.028}	28 GONZALEZ...	14	FIT	Normal mass ordering; global fit	27	FORERO 14 performs a global fit to neutrino oscillations using solar, reactor, long-baseline accelerator, and atmospheric neutrino data.
0.579 ^{+0.025} _{-0.037}	28 GONZALEZ...	14	FIT	Inverted mass ordering; global fit	28	GONZALEZ-GARCIA 14 result comes from a frequentist global fit. The corresponding Bayesian global fit to the same data results are reported in BERGSTROM 15 as 68% CL intervals of 0.433–0.496 or 0.530–0.594 for normal and 0.514–0.612 for inverted mass ordering.
0.24 to 0.76	29 AARTSEN	13b	ICCB	DeepCore, 2ν oscillation	29	AARTSEN 13b obtained this result by a two-neutrino oscillation analysis using 20–100 GeV muon neutrino sample from a total of 318.9 days of live-time measurement with the low-energy subdetector DeepCore of the IceCube neutrino telescope.
0.514 \pm 0.082	30 ABE	13g	T2K	3ν osc.; normal mass ordering	30	The best fit value is $\sin^2(\theta_{23}) = 0.514 \pm 0.082$. Superseded by ABE 14.
0.388 ^{+0.051} _{-0.053}	31 ADAMSON	13b	MINS	Beam + Atmospheric; identical ν & $\bar{\nu}$	31	ADAMSON 13b obtained this result from ν_μ and $\bar{\nu}_\mu$ disappearance using ν_μ (10.71 × 10 ²⁰ POT) and $\bar{\nu}_\mu$ (3.36 × 10 ²⁰ POT) beams, and atmospheric (37.88kton-years) data
0.3 to 0.7	32 ABE	12A	T2K	Off-axis beam		
0.28 to 0.72	33 ADAMSON	12	MINS	$\bar{\nu}$ beam		
0.25 to 0.75	34,35 ADAMSON	12b	MINS	MINOS atmospheric		
0.27 to 0.73	34,36 ADAMSON	12b	MINS	MINOS pure atmospheric ν		
0.21 to 0.79	34,36 ADAMSON	12b	MINS	MINOS pure atmospheric $\bar{\nu}$		
0.15 to 0.85	37 ADRIAN-MAR.	12	ANTR	Atmospheric ν with deep see telescope		
0.39 to 0.61	38 ABE	11c	SKAM	Super-Kamiokande		
0.34 to 0.66	ADAMSON	11	MINS	2ν osc.; maximal mixing		
0.31 ^{+0.10} _{-0.07}	39 ADAMSON	11b	MINS	$\bar{\nu}$ beam		
0.41 to 0.59	40 WENDELL	10	SKAM	3ν osc. with solar terms; $\theta_{13}=0$		
0.39 to 0.61	41 WENDELL	10	SKAM	3ν osc.; normal mass ordering		
0.37 to 0.63	42 WENDELL	10	SKAM	3ν osc.; inverted mass ordering		
0.31 to 0.69	ADAMSON	08A	MINS	MINOS		
0.05 to 0.95	43 ADAMSON	06	MINS	Atmospheric ν with far detector		
0.18 to 0.82	44 AHN	06A	K2K	KEK to Super-K		
0.23 to 0.77	45 MICHAEL	06	MINS	MINOS		
0.18 to 0.82	46 ALIU	05	K2K	KEK to Super-K		
0.18 to 0.82	47 ALLISON	05	SOU2			
0.36 to 0.64	48 ASHIE	05	SKAM	Super-Kamiokande		
0.28 to 0.72	49 AMBROSIO	04	MCRO	MACRO		
0.34 to 0.66	50 ASHIE	04	SKAM	L/E distribution		
0.08 to 0.92	51 AHN	03	K2K	KEK to Super-K		
0.13 to 0.87	52 AMBROSIO	03	MCRO	MACRO		
0.26 to 0.74	53 AMBROSIO	03	MCRO	MACRO		
0.15 to 0.85	54 SANCHEZ	03	SOU2	Soudan-2 Atmospheric		
0.28 to 0.72	55 AMBROSIO	01	MCRO	Upward μ		
0.29 to 0.71	56 AMBROSIO	01	MCRO	Upward μ		
0.13 to 0.87	57 FUKUDA	99c	SKAM	Upward μ		
0.23 to 0.77	58 FUKUDA	99d	SKAM	Upward μ		
0.08 to 0.92	59 FUKUDA	99d	SKAM	Stop μ / through		
0.29 to 0.71	60 FUKUDA	98c	SKAM	Super-Kamiokande		
0.08 to 0.92	61 HATAKEYAMA	98	KAMI	Kamiokande		
0.24 to 0.76	62 HATAKEYAMA	98	KAMI	Kamiokande		
0.20 to 0.80	63 FUKUDA	94	KAMI	Kamiokande		

¹ABBASI 23 uses atmospheric neutrino data measured between 2011 and 2019 with the low-energy subdetector DeepCore of the IceCube neutrino telescope. Supersedes AARTSEN 18a.

²ABE 23f results are based on data collected between 2010 and 2020 in (anti)neutrino mode and include a neutrino beam exposure of 1.97×10^{21} (1.63×10^{21}) protons on target. Supersedes ABE 20f.

³ACERO 22 uses data from Jun 29, 2016 to Feb 26, 2019 (12.5×10^{20} POT) and Feb 6, 2014 to Mar 20, 2020 (13.6×10^{20} POT). Best fit for octant I (lower octant) is 0.46 for both normal and inverted mass orderings. Supersedes ACERO 19.

Lepton Particle Listings

Neutrino Mixing

- from MINOS. The fit assumed two-flavor neutrino hypothesis and identical ν_μ and $\bar{\nu}_\mu$ oscillation parameters. Superseded by ADAMSON 14.
- ³² ABE 12A obtained this result by a two-neutrino oscillation analysis. The best-fit point is $\sin^2(2\theta_{23}) = 0.98$.
- ³³ ADAMSON 12 is a two-neutrino oscillation analysis using antineutrinos. The best fit value is $\sin^2(2\theta_{23}) = 0.95^{+0.10}_{-0.11} \pm 0.01$.
- ³⁴ ADAMSON 12B obtained this result by a two-neutrino oscillation analysis of the L/E distribution using 37.9 kton-yr atmospheric neutrino data with the MINOS far detector.
- ³⁵ The best fit point is $\Delta m^2 = 0.0019 \text{ eV}^2$ and $\sin^2 2\theta = 0.99$. The 90% single-parameter confidence interval at the best fit point is $\sin^2 2\theta > 0.86$.
- ³⁶ The data are separated into pure samples of ν_s and $\bar{\nu}_s$, and separate oscillation parameters for ν_s and $\bar{\nu}_s$ are fit to the data. The best fit point is $(\Delta m^2, \sin^2 2\theta) = (0.0022 \text{ eV}^2, 0.99)$ and $(\Delta \bar{m}^2, \sin^2 2\bar{\theta}) = (0.0016 \text{ eV}^2, 1.00)$. The quoted result is taken from the 90% C.L. contour in the $(\Delta m^2, \sin^2 2\theta)$ plane obtained by minimizing the four parameter log-likelihood function with respect to the other oscillation parameters.
- ³⁷ ADRIAN-MARTINEZ 12 measured the oscillation parameters of atmospheric neutrinos with the ANTARES deep sea neutrino telescope using the data taken from 2007 to 2010 (863 days of total live time). Superseded by ALBERT 19.
- ³⁸ ABE 11c obtained this result by a two-neutrino oscillation analysis using the Super-Kamiokande-I+II+III atmospheric neutrino data. ABE 11c also reported results under a two-neutrino disappearance model with separate mixing parameters between ν and $\bar{\nu}$, and obtained $\sin^2 2\theta > 0.93$ for ν and $\sin^2 2\theta > 0.83$ for $\bar{\nu}$ at 90% C.L.
- ³⁹ ADAMSON 11b obtained this result by a two-neutrino oscillation analysis of antineutrinos in an antineutrino enhanced beam with 1.71×10^{20} protons on target. This result is consistent with the neutrino measurements of ADAMSON 11 at 2% C.L.
- ⁴⁰ WENDELL 10 obtained this result ($\sin^2 \theta_{23} = 0.407\text{--}0.583$) by a three-neutrino oscillation analysis using the Super-Kamiokande-I+II+III atmospheric neutrino data, assuming $\theta_{13} = 0$ but including the solar oscillation parameters Δm_{21}^2 and $\sin^2 \theta_{12}$ in the fit.
- ⁴¹ WENDELL 10 obtained this result ($\sin^2 \theta_{23} = 0.43\text{--}0.61$) by a three-neutrino oscillation analysis with one mass scale dominance ($\Delta m_{21}^2 = 0$) using the Super-Kamiokande-I+II+III atmospheric neutrino data, and updates the HOSAKA 06A result.
- ⁴² WENDELL 10 obtained this result ($\sin^2 \theta_{23} = 0.44\text{--}0.63$) by a three-neutrino oscillation analysis with one mass scale dominance ($\Delta m_{21}^2 = 0$) using the Super-Kamiokande-I+II+III atmospheric neutrino data, and updates the HOSAKA 06A result.
- ⁴³ ADAMSON 06 obtained this result by a two-neutrino oscillation analysis of the L/E distribution using 4.54 kton yr atmospheric neutrino data with the MINOS far detector.
- ⁴⁴ Supersedes ALIU 05.
- ⁴⁵ MICHAEL 06 best fit is for maximal mixing. See also ADAMSON 08.
- ⁴⁶ The best fit is for maximal mixing.
- ⁴⁷ ALLISON 05 result is based upon atmospheric neutrino interactions including upward-stopping muons, with an exposure of 5.9 kton yr. From a two-flavor oscillation analysis the best-fit point is $\Delta m^2 = 0.0017 \text{ eV}^2$ and $\sin^2(2\theta) = 0.97$.
- ⁴⁸ ASHIE 05 obtained this result by a two-neutrino oscillation analysis using 92 kton yr atmospheric neutrino data from the complete Super-Kamiokande I running period.
- ⁴⁹ AMBROSIO 04 obtained this result, without using the absolute normalization of the neutrino flux, by combining the angular distribution of upward through-going muon tracks with $E_\mu > 1 \text{ GeV}$, N_{low} and N_{high} , and the numbers of InDown + UpStop and InUp events. Here, N_{low} and N_{high} are the number of events with reconstructed neutrino energies $< 30 \text{ GeV}$ and $> 130 \text{ GeV}$, respectively. InDown and InUp represent events with downward and upward-going tracks starting inside the detector due to neutrino interactions, while UpStop represents entering upward-going tracks which stop in the detector. The best fit is for maximal mixing.
- ⁵⁰ ASHIE 04 obtained this result from the $L(\text{flight length})/E(\text{estimated neutrino energy})$ distribution of ν_μ disappearance probability, using the Super-Kamiokande-I 1489 live-day atmospheric neutrino data.
- ⁵¹ There are several islands of allowed region from this K2K analysis, extending to high values of Δm^2 . We only include the one that overlaps atmospheric neutrino analyses. The best fit is for maximal mixing.
- ⁵² AMBROSIO 03 obtained this result on the basis of the ratio $R = N_{low}/N_{high}$, where N_{low} and N_{high} are the number of upward through-going muon events with reconstructed neutrino energy $< 30 \text{ GeV}$ and $> 130 \text{ GeV}$, respectively. The data came from the full detector run started in 1994. The method of FELDMAN 98 is used to obtain the limits.
- ⁵³ AMBROSIO 03 obtained this result by using the ratio R and the angular distribution of the upward through-going muons. R is given in the previous note and the angular distribution is reported in AMBROSIO 01. The method of FELDMAN 98 is used to obtain the limits. The best fit is to maximal mixing.
- ⁵⁴ SANCHEZ 03 is based on an exposure of 5.9 kton yr. The result is obtained using a likelihood analysis of the neutrino L/E distribution for a selection μ flavor sample while the e -flavor sample provides flux normalization. The method of FELDMAN 98 is used to obtain the allowed region. The best fit is $\sin^2(2\theta) = 0.97$.
- ⁵⁵ AMBROSIO 01 result is based on the angular distribution of upward through-going muon tracks with $E_\mu > 1 \text{ GeV}$. The data came from three different detector configurations, but the statistics is largely dominated by the full detector run, from May 1994 to December 2000. The total live time, normalized to the full detector configuration is 6.17 years. The best fit is obtained outside the physical region. The method of FELDMAN 98 is used to obtain the limits. The best fit is for maximal mixing.
- ⁵⁶ AMBROSIO 01 result is based on the angular distribution and normalization of upward through-going muon tracks with $E_\mu > 1 \text{ GeV}$. See the previous footnote.
- ⁵⁷ FUKUDA 99c obtained this result from a total of 537 live days of upward through-going muon data in Super-Kamiokande between April 1996 to January 1998. With a threshold

of $E_\mu > 1.6 \text{ GeV}$, the observed flux is $(1.74 \pm 0.07 \pm 0.02) \times 10^{-13} \text{ cm}^{-2} \text{ s}^{-1} \text{ sr}^{-1}$. The best fit is $\sin^2(2\theta) = 0.95$.

- ⁵⁸ FUKUDA 99D obtained this result from a simultaneous fitting to zenith angle distributions of upward-stopping and through-going muons. The flux of upward-stopping muons of minimum energy of 1.6 GeV measured between April 1996 and January 1998 is $(0.39 \pm 0.04 \pm 0.02) \times 10^{-13} \text{ cm}^{-2} \text{ s}^{-1} \text{ sr}^{-1}$. This is compared to the expected flux of $(0.73 \pm 0.16 \text{ (theoretical error)}) \times 10^{-13} \text{ cm}^{-2} \text{ s}^{-1} \text{ sr}^{-1}$. The best fit is to maximal mixing.
- ⁵⁹ FUKUDA 99D obtained this result from the zenith dependence of the upward-stopping/through-going flux ratio. The best fit is to maximal mixing.
- ⁶⁰ FUKUDA 98c obtained this result by an analysis of 33.0 kton yr atmospheric neutrino data. The best fit is for maximal mixing.
- ⁶¹ HATAKEYAMA 98 obtained this result from a total of 2456 live days of upward-going muon data in Kamiokande between December 1985 and May 1995. With a threshold of $E_\mu > 1.6 \text{ GeV}$, the observed flux of upward through-going muons is $(1.94 \pm 0.10^{+0.07}_{-0.06}) \times 10^{-13} \text{ cm}^{-2} \text{ s}^{-1} \text{ sr}^{-1}$. This is compared to the expected flux of $(2.46 \pm 0.54 \text{ (theoretical error)}) \times 10^{-13} \text{ cm}^{-2} \text{ s}^{-1} \text{ sr}^{-1}$. The best fit is for maximal mixing.
- ⁶² HATAKEYAMA 98 obtained this result from a combined analysis of Kamiokande contained events (FUKUDA 94) and upward going muon events. The best fit is $\sin^2(2\theta) = 0.95$.
- ⁶³ FUKUDA 94 obtained the result by a combined analysis of sub- and multi-GeV atmospheric neutrino events in Kamiokande. The best fit is for maximal mixing.

Δm_{32}^2

The sign of Δm_{32}^2 is not known at this time. If given, values are shown separately for the normal and inverted mass ordering. Unless otherwise specified, the ranges below correspond to the projection onto the Δm_{32}^2 axis of the 90% CL contours in the $\sin^2(2\theta_{23}) - \Delta m_{32}^2$ plane presented by the authors. If uncertainties are reported with the value, they correspond to one standard deviation uncertainty.

VALUE (10^{-3} eV^2)	DOCUMENT ID	TECN	COMMENT
-2.529 ± 0.029 OUR FIT	Assuming inverted ordering		
2.455 ± 0.028 OUR FIT	Assuming normal ordering		
2.41 ± 0.07	¹ ABBASI	23 ICCB	Normal mass ordering
$2.494^{+0.041}_{-0.058}$	² ABE	23F T2K	Normal mass ordering, θ_{13} constrained
$-2.54^{+0.042}_{-0.056}$	^{2,3} ABE	23F T2K	Inverted mass ordering, θ_{13} constrained
2.47 ± 0.06	⁴ AN	23 DAYA	Normal mass ordering
-2.57 ± 0.06	⁴ AN	23 DAYA	Inverted mass ordering
2.41 ± 0.07	⁵ ACERO	22 NOVA	Normal mass ordering, octant II for θ_{23} , θ_{13} constrained
-2.45 ± 0.07	⁵ ACERO	22 NOVA	Inverted mass ordering, octant II for θ_{23} , θ_{13} constrained
$2.40^{+0.08}_{-0.09}$	⁶ ADAMSON	20A MINS	Accel., atmospheric, normal mass ordering
$-2.45^{+0.08}_{-0.07}$	⁶ ADAMSON	20A MINS	Accel., atmospheric, inverted mass ordering
$2.50^{+0.13}_{-0.20}$	⁷ ABE	18B SKAM	Normal mass ordering, θ_{13} constrained
$-2.58^{+0.08}_{-0.37}$	⁷ ABE	18B SKAM	Inverted mass ordering, θ_{13} constrained
2.63 ± 0.14	⁸ BAK	18 RENO	Normal mass ordering
-2.73 ± 0.14	⁸ BAK	18 RENO	Inverted mass ordering
• • • We do not use the following data for averages, fits, limits, etc. • • •			
$2.48^{+0.05}_{-0.06}$	⁹ ABE	23D T2K	ν_μ disappearance
$2.53^{+0.10}_{-0.11}$	⁹ ABE	23D T2K	$\bar{\nu}_\mu$ disappearance
$2.47^{+0.08}_{-0.09}$	¹⁰ ABE	21A T2K	ν_μ disappearance
$2.50^{+0.18}_{-0.13}$	¹⁰ ABE	21A T2K	$\bar{\nu}_\mu$ disappearance
2.45 ± 0.07	¹¹ ABE	20F T2K	Normal mass ordering, θ_{13} constrained
-2.51 ± 0.07	^{11,12} ABE	20F T2K	Inverted mass ordering, θ_{13} constrained
$2.517^{+0.026}_{-0.028}$	¹³ ESTEBAN	20A FIT	Normal mass ordering, global fit
$-2.498^{+0.028}_{-0.028}$	¹³ ESTEBAN	20A FIT	Inverted mass ordering, global fit
$2.55^{+0.12}_{-0.11}$	¹⁴ AARTSEN	19c ICCB	
$2.48^{+0.11}_{-0.06}$	¹⁵ ACERO	19 NOVA	Normal mass ordering, octant II for θ_{23}
$-2.54^{+0.06}_{-0.11}$	¹⁵ ACERO	19 NOVA	Inverted mass ordering, octant II for θ_{23}
< 4.1 at 90% CL	AGAFONOVA	19 OPER	
$2.0^{+0.4}_{-0.3}$	¹⁶ ALBERT	19 ANTR	Atmospheric ν , deep sea telescope
$2.31^{+0.11}_{-0.13}$	¹⁷ AARTSEN	18A ICCB	Normal mass ordering
$2.50^{+0.13}_{-0.31}$	¹⁸ ABE	18B SKAM	3ν osc: normal mass ordering, θ_{13} free

See key on page 1171

Lepton Particle Listings

Neutrino Mixing

-2.28 ^{+0.33} _{-0.13}	18 ABE	18B SKAM	3ν osc: inverted mass ordering, θ ₁₃ free	0.07-50	54 ADAMSON	06 MINS	atmospheric ν with far detector
2.463 ^{+0.071} _{-0.070}	19 ABE	18G T2K	Normal mass ordering, θ ₁₃ constrained	1.9-4.0	55,56 AHN	06A K2K	KEK to Super-K
-2.507 ± 0.070	19,20 ABE	18G T2K	Inverted mass ordering, θ ₁₃ constrained	2.2-3.8	57 MICHAEL	06 MINS	MINOS
2.44 ^{+0.08} _{-0.07}	21 ACERO	18 NOVA	Normal mass order, octant II for θ ₂₃	1.9-3.6	55 ALIU	05 K2K	KEK to Super-K
2.45 ^{+0.07} _{-0.08}	21,22 ACERO	18 NOVA	Normal mass order; octant I for θ ₂₃	0.3-12	58 ALLISON	05 SOU2	
2.471 ^{+0.068} _{-0.070}	23 ADEY	18A DAYA	Normal mass ordering	1.5-3.4	59 ASHIE	05 SKAM	atmospheric neutrino
-2.575 ^{+0.068} _{-0.070}	23 ADEY	18A DAYA	Inverted mass ordering	0.6-8.0	60 AMBROSIO	04 MCRO	MACRO
2.7 ^{+0.7} _{-0.6}	24 AGAFONOVA	18 OPER	OPERA ν _τ appearance	1.9 to 3.0	61 ASHIE	04 SKAM	L/E distribution
2.42 ± 0.03	DE-SALAS	18 FIT	Normal mass ordering, global fit	1.5-3.9	62 AHN	03 K2K	KEK to Super-K
-2.50 ^{+0.03} _{-0.04}	DE-SALAS	18 FIT	Inverted mass order, global fit	0.25-9.0	63 AMBROSIO	03 MCRO	MACRO
2.57 ^{+0.21} _{-0.23}	25 SEO	18 RENO	Normal mass ordering	0.6-7.0	64 AMBROSIO	03 MCRO	MACRO
-2.67 ^{+0.23} _{-0.21}	25 SEO	18 RENO	Inverted mass ordering	0.15-15	65 SANCHEZ	03 SOU2	Soudan-2 Atmospheric
2.53 ^{+0.15} _{-0.13}	ABE	17C T2K	Normal mass ordering with neutrinos	0.6-15	66 AMBROSIO	01 MCRO	upward μ
2.55 ^{+0.33} _{-0.27}	ABE	17C T2K	Normal mass ordering with antineutrinos	1.0-6.0	67 AMBROSIO	01 MCRO	upward μ
2.55 ^{+0.08} _{-0.08}	ABE	17C T2K	Normal mass ordering with neutrinos and antineutrinos	1.0-50	68 FUKUDA	99c SKAM	upward μ
-2.63 ^{+0.08} _{-0.08}	ABE	17C T2K	Inverted mass ordering with neutrinos and antineutrinos	1.5-15.0	69 FUKUDA	99D SKAM	upward μ
2.54 ± 0.08	26 ABE	17F T2K	Normal mass ordering; ν+ν̄	0.7-18	70 FUKUDA	99D SKAM	stop μ / through
-2.51 ± 0.08	26 ABE	17F T2K	Inverted mass ordering; ν+ν̄	0.5-6.0	71 FUKUDA	98C SKAM	Super-Kamiokande
2.67 ± 0.11	27 ADAMSON	17A NOVA	3ν osc; normal mass ordering	0.55-50	72 HATAKEYAMA	98 KAMI	Kamiokande
-2.72 ± 0.11	27 ADAMSON	17A NOVA	3ν osc; inverted mass ordering	4-23	73 HATAKEYAMA	98 KAMI	Kamiokande
2.45 ± 0.06 ± 0.06	28 AN	17A DAYA	Normal mass ordering	5-25	74 FUKUDA	94 KAMI	Kamiokande
-2.56 ± 0.06 ± 0.06	28 AN	17A DAYA	Inverted mass ordering				
2.51 ^{+0.29} _{-0.25}	29 ABE	16D T2K	3ν osc.; normal mass ordering; ν̄ beam				
2.52 ^{+0.20} _{-0.18}	30 ADAMSON	16A NOVA	3ν osc; normal mass ordering				
-2.56 ± 0.19	30 ADAMSON	16A NOVA	3ν osc; inverted mass ordering				
2.56 ^{+0.21} _{-0.23}	31 CHOI	16 RENO	3ν osc; normal mass ordering				
-2.69 ^{+0.23} _{-0.21}	31 CHOI	16 RENO	3ν osc; inverted mass ordering				
2.72 ^{+0.19} _{-0.20}	32 AARTSEN	15A ICCB	Normal mass ordering				
-2.73 ^{+0.21} _{-0.18}	32 AARTSEN	15A ICCB	Inverted mass ordering				
2.0-5.0	33 AGAFONOVA	15A OPER	90% CL, 5 events				
2.37 ± 0.11	34 AN	15 DAYA	3ν osc.; normal mass ordering				
-2.47 ± 0.11	34 AN	15 DAYA	3ν osc.; inverted mass ordering				
2.51 ± 0.10	35 ABE	14 T2K	3ν osc.; normal mass ordering				
-2.56 ± 0.10	35 ABE	14 T2K	3ν osc.; inverted mass ordering				
2.37 ± 0.09	36 ADAMSON	14 MINS	Accel., atmospheric, normal mass ordering				
-2.41 ^{+0.09} _{-0.12}	36 ADAMSON	14 MINS	Accel., atmospheric, inverted mass ordering				
2.54 ^{+0.19} _{-0.20}	37 AN	14 DAYA	3ν osc.; normal mass ordering				
-2.64 ^{+0.20} _{-0.19}	37 AN	14 DAYA	3ν osc.; inverted mass ordering				
2.48 ^{+0.05} _{-0.07}	38 FORERO	14 FIT	3ν; normal mass ordering				
-2.38 ^{+0.06} _{-0.05}	38 FORERO	14 FIT	3ν; inverted mass ordering				
2.457 ± 0.047	39,40 GONZALEZ...	14 FIT	Normal mass ordering; global fit				
-2.449 ^{+0.047} _{-0.048}	39 GONZALEZ...	14 FIT	Inverted mass ordering; global fit				
2.3 ^{+0.6} _{-0.5}	41 AARTSEN	13B ICCB	DeepCore, 2ν oscillation				
2.44 ^{+0.17} _{-0.15}	42 ABE	13G T2K	3ν osc.; normal mass ordering				
2.41 ^{+0.09} _{-0.10}	43 ADAMSON	13B MINS	2ν osc.; beam + atmospheric; identical ν & ν̄				
2.2-3.1	44 ABE	12A T2K	off-axis beam				
2.62 ^{+0.31} _{-0.28} ± 0.09	45 ADAMSON	12 MINS	ν̄ beam				
1.35-2.55	46,47 ADAMSON	12B MINS	MINOS atmospheric				
1.4-5.6	46,48 ADAMSON	12B MINS	MINOS pure atmospheric ν				
0.9-2.5	46,48 ADAMSON	12B MINS	MINOS pure atmospheric ν̄				
1.8-5.0	49 ADRIAN-MAR.12	ANTR	Atmospheric ν with deep sea telescope				
1.3-4.0	50 ABE	11C SKAM	atmospheric ν̄				
2.32 ^{+0.12} _{-0.08}	ADAMSON	11 MINS	2ν oscillation; maximal mixing				
3.36 ^{+0.46} _{-0.40}	51 ADAMSON	11B MINS	ν̄ beam				
< 3.37	52 ADAMSON	11C MINS	MINOS				
1.9-2.6	53 WENDELL	10 SKAM	3ν osc.; normal mass ordering				
-1.7- - 2.7	53 WENDELL	10 SKAM	3ν osc.; inverted mass ordering				
2.43 ± 0.13	ADAMSON	08A MINS	MINOS				

¹ ABBASI 23 uses atmospheric neutrino data measured between 2011 and 2019 with the low-energy subdetector DeepCore of the IceCube neutrino telescope. Supersedes AARTSEN 18A.

² ABE 23F results are based on data collected between 2010 and 2020 in (anti)neutrino mode and include a neutrino beam exposure of 1.97×10^{21} (1.63×10^{21}) protons on target. Supersedes ABE 20F.

³ ABE 23F reports $\Delta m_{13}^2 = (2.463 \pm 0.042 \pm 0.056) \times 10^{-3} \text{ eV}^2$ for inverted mass ordering. We convert to Δm_{32}^2 using PDG 23 value of $\Delta m_{21}^2 = (7.53 \pm 0.18) \times 10^{-5} \text{ eV}^2$.

⁴ AN 23 reports results derived from the complete data set collected by the Daya-Bay experiment, corresponding to 3158 days of operation, resulting in 5.55×10^6 $\bar{\nu}_e$ candidate events. Solar oscillation parameters are fixed in the analysis to $\sin^2(\theta_{12}) = 0.307 \pm 0.013$, $\Delta m_{21}^2 = (7.53 \pm 0.18) \times 10^{-5} \text{ eV}^2$ from PDG 20. Supersedes ACERO 18A.

⁵ ACERO 22 uses data from Jun 29, 2016 to Feb 26, 2019 (12.5×10^{20} POT) and Feb 6, 2014 to Mar 20, 2020 (13.6×10^{20} POT). For normal mass ordering and θ_{23} octant I (lower octant), best fit is 0.00239 eV^2 ; for inverted mass ordering and octant I, best fit is -0.00244 eV^2 . Supersedes ACERO 19.

⁶ ADAMSON 20A uses the complete dataset from MINOS and MINOS+ experiments. The data were collected using a total exposure of 23.76×10^{20} protons on target and 60.75 kton-yr exposure to atmospheric neutrinos. Supersedes ADAMSON 14.

⁷ ABE 18B uses 328 kton-years of Super-Kamiokande I-IV atmospheric neutrino data to obtain this result. The fit is performed over the three parameters, Δm_{32}^2 , $\sin^2(\theta_{23})$, and δ , while the solar parameters and $\sin^2(\theta_{13})$ are fixed to $\Delta m_{21}^2 = (7.53 \pm 0.18) \times 10^{-5} \text{ eV}^2$, $\sin^2(\theta_{12}) = 0.304 \pm 0.014$, and $\sin^2(\theta_{13}) = 0.0219 \pm 0.0012$.

⁸ BAK 18 reports results of the RENO experiment using about 2200 live-days of data taken with detectors placed at 410.6 and 1445.7 m from reactors of the Hanbit Nuclear Power Plant. We convert the results to Δm_{32}^2 using the PDG 18 values of $\sin^2\theta_{12} = 0.307 \pm 0.013$ and $\Delta m_{21}^2 = (7.53 \pm 0.18) \times 10^{-5} \text{ eV}^2$. Supersedes SEO 18.

⁹ ABE 23D uses the same dataset as ABE 23F. The measurement of Δm_{32}^2 is performed independently for ν_μ and $\bar{\nu}_\mu$.

¹⁰ ABE 21A results are based on 1.49×10^{21} POT in neutrino mode and 1.64×10^{21} POT in antineutrino mode.

¹¹ ABE 20F results are based on data collected between 2009 and 2018 in (anti)neutrino mode and include a neutrino beam exposure of 1.49×10^{21} (1.64×10^{21}) protons on target. Supersedes ABE 18G.

¹² ABE 20F reports $\Delta m_{13}^2 = (2.43 \pm 0.07) \times 10^{-3} \text{ eV}^2$ for inverted mass ordering. We convert to Δm_{32}^2 using PDG 20 value of $\Delta m_{21}^2 = (7.53 \pm 0.18) \times 10^{-5} \text{ eV}^2$.

¹³ ESTEBAN 20A reports results of a global fit to neutrino oscillation data available at the time of the Neutrino2020 conference.

¹⁴ AARTSEN 19c uses three years (April 2012 - May 2015) of neutrino data from full sky with reconstructed energies between 5.6 and 56 GeV, measured with the low-energy sub-detector DeepCore of the IceCube neutrino telescope. AARTSEN 19c adopts looser event selection criteria to prioritize the efficiency of selecting neutrino events, different from tighter event selection criteria which closely follow the criteria used by AARTSEN 18A to measure the ν_μ disappearance.

¹⁵ ACERO 19 is based on a sample size of 12.33×10^{20} protons on target. The fit combines both antineutrino and neutrino data to extract the oscillation parameters. The results favor the normal mass ordering by 1.9σ and θ_{23} values in octant II by 1.6σ . Superseded by ACERO 22.

¹⁶ ALBERT 19 measured the oscillation parameters of atmospheric neutrinos with the ANTARES deep sea neutrino telescope using the data taken from 2007 to 2016 (2830 days of total live time). Supersedes ADRIAN-MARTINEZ 12.

¹⁷ AARTSEN 18A uses three years (April 2012 - May 2015) of neutrino data from full sky with reconstructed energies between 5.6 and 56 GeV, measured with the low-energy sub-detector DeepCore of the IceCube neutrino telescope. AARTSEN 18A also reports the best fit values for the inverted mass ordering as $\Delta m_{32}^2 = -2.32 \times 10^{-3} \text{ eV}^2$ and $\sin^2(\theta_{23}) = 0.51$. Uncertainties for the inverted mass ordering fits were not provided. Supersedes AARTSEN 15A.

¹⁸ ABE 18B uses 328 kton-years of Super-Kamiokande I-IV atmospheric neutrino data to obtain this result. The fit is performed over the four parameters, Δm_{32}^2 , $\sin^2\theta_{23}$, $\sin^2\theta_{13}$, and δ , while the solar parameters are fixed to $\Delta m_{21}^2 = (7.53 \pm 0.18) \times 10^{-5} \text{ eV}^2$ and $\sin^2\theta_{12} = 0.304 \pm 0.014$.

Lepton Particle Listings

Neutrino Mixing

- ¹⁹ ABE 18c data prefers normal ordering with a posterior probability of 87%. Supersedes ABE 17f.
- ²⁰ ABE 18g reports $\Delta m_{13}^2 = (2.432 \pm 0.070) \times 10^{-3} \text{ eV}^2$ for inverted mass ordering. We convert to Δm_{32}^2 using PDG 18 value of $\Delta m_{21}^2 = (7.53 \pm 0.18) \times 10^{-5} \text{ eV}^2$.
- ²¹ ACERO 18 performs a joint fit to the data for ν_μ disappearance and ν_e appearance. The overall best fit favors normal mass ordering and θ_{23} in octant II. No 1σ confidence intervals are presented for the inverted mass ordering scenarios. Superseded by ACERO 19.
- ²² The error for octant I is taken from the result for octant II.
- ²³ ADEY 18a reports results from analysis of 1958 days of data taking with the Daya-Bay experiment, with $3.9 \times 10^6 \bar{\nu}_e$ candidates. The fit to the data gives $\Delta m_{ee}^2 = (2.522 \pm 0.068) \times 10^{-3} \text{ eV}^2$. Solar oscillation parameters are fixed in the analysis using the global averages, $\sin^2(\theta_{12}) = 0.307 \pm 0.013$, $\Delta m_{21}^2 = (7.53 \pm 0.18) \times 10^{-5} \text{ eV}^2$, from PDG 18. Supersedes AN 17a.
- ²⁴ AGAFONOVA 18 assumes maximal θ_{23} mixing.
- ²⁵ SEO 18 reports result of the RENO experiment from a rate and shape analysis of 500 days of data. A simultaneous fit to θ_{13} and Δm_{ee}^2 yields $\Delta m_{ee}^2 = (2.62 \pm 0.21 \pm 0.12) \times 10^{-3} \text{ eV}^2$. We convert the results to Δm_{32}^2 using the PDG 18 values of $\sin^2 \theta_{12}$ and Δm_{21}^2 . SEO 18 is a detailed description of the results published in CHOI 16, which it supersedes. Superseded by BAK 18.
- ²⁶ ABE 17f confidence intervals are obtained using a frequentist analysis including θ_{13} constraint from reactor experiments. Bayesian intervals based on Markov Chain Monte Carlo method are also provided by the authors. Superseded by ABE 18g.
- ²⁷ Superseded by ACERO 18.
- ²⁸ AN 17a report results from combined rate and spectral shape analysis of 1230 days of data taken with the Daya Bay reactor experiment. The data set contains more than 2.5×10^6 inverse beta-decay events with neutron capture on Gd. The fit to the data gives $\Delta_{ee}^2 = (2.50 \pm 0.06 \pm 0.06) \times 10^{-3} \text{ eV}^2$. Superseded by ADEY 18a.
- ²⁹ ABE 16d reports oscillation results using $\bar{\nu}_\mu$ disappearance in an off-axis beam.
- ³⁰ Superseded by ADAMSON 17a.
- ³¹ CHOI 16 reports result of the RENO experiment from a rate and shape analysis of 500 days of data. A simultaneous fit to θ_{13} and Δm_{ee}^2 yields $\Delta m_{ee}^2 = (2.62 \pm 0.21 \pm 0.12) \times 10^{-3} \text{ eV}^2$. We convert the results to Δm_{32}^2 using PDG 18 values of $\sin^2(\theta_{12})$ and Δm_{21}^2 .
- ³² AARTSEN 15a obtains this result by a three-neutrino oscillation analysis using 10–100 GeV muon neutrino sample from a total of 953 days of measurements with the low-energy subdetector DeepCore of the IceCube neutrino telescope. Superseded by AARTSEN 18a.
- ³³ AGAFONOVA 15a result is based on 5 $\nu_\mu \rightarrow \nu_\tau$ appearance candidates with an expected background of 0.25 ± 0.05 events. The best fit is for $\Delta m_{32}^2 = 3.3 \times 10^{-3} \text{ eV}^2$.
- ³⁴ AN 15 uses all eight identical detectors, with four placed near the reactor cores and the remaining four at the far hall to determine prompt energy spectra. The results correspond to the exposure of $6.9 \times 10^5 \text{ GW}_{th}\text{-ton-days}$. They derive $\Delta m_{ee}^2 = (2.42 \pm 0.11) \times 10^{-3} \text{ eV}^2$. Assuming the normal (inverted) ordering, the fitted $\Delta m_{32}^2 = (2.37 \pm 0.11) \times 10^{-3} ((2.47 \pm 0.11) \times 10^{-3}) \text{ eV}^2$. Superseded by AN 17a.
- ³⁵ ABE 14 results are based on ν_μ disappearance using three-neutrino oscillation fit. The confidence intervals are derived from one dimensional profiled likelihoods. In ABE 14 the inverted mass ordering result is reported as $\Delta m_{13}^2 = (2.48 \pm 0.10) \times 10^{-3} \text{ eV}^2$ which we converted to Δm_{32}^2 by adding PDG 14 value of $\Delta m_{21}^2 = (7.53 \pm 0.18) \times 10^{-5} \text{ eV}^2$. Superseded by ABE 17c.
- ³⁶ ADAMSON 14 uses a complete set of accelerator and atmospheric data. The analysis combines the analysis combines the ν_μ disappearance and ν_e appearance data using three-neutrino oscillation fit. The fit results are obtained for normal and inverted mass ordering assumptions.
- ³⁷ AN 14 uses six identical detectors, with three placed near the reactor cores (flux-weighted baselines of 512 and 561 m) and the remaining three at the far hall (at the flux averaged distance of 1579 m from all six reactor cores) to determine prompt energy spectra and derive $\Delta m_{ee}^2 = (2.59 \pm 0.19) \times 10^{-3} \text{ eV}^2$. Assuming the normal (inverted) ordering, the fitted $\Delta m_{32}^2 = (2.54 \pm 0.19) \times 10^{-3} ((2.64 \pm 0.19) \times 10^{-3}) \text{ eV}^2$. Superseded by AN 15.
- ³⁸ FORERO 14 performs a global fit to Δm_{31}^2 using solar, reactor, long-baseline accelerator, and atmospheric neutrino data.
- ³⁹ GONZALEZ-GARCIA 14 result comes from a frequentist global fit. The corresponding Bayesian global fit to the same data results are reported in BERGSTROM 15 as $(2.460 \pm 0.046) \times 10^{-3} \text{ eV}^2$ for normal and $(2.445 \pm 0.047) \times 10^{-3} \text{ eV}^2$ for inverted mass ordering.
- ⁴⁰ The value for normal mass ordering is actually a measurement of Δm_{31}^2 which differs from Δm_{32}^2 by a much smaller value of Δm_{21}^2 .
- ⁴¹ AARTSEN 13b obtained this result by a two-neutrino oscillation analysis using 20–100 GeV muon neutrino sample from a total of 318.9 days of live-time measurement with the low-energy subdetector DeepCore of the IceCube neutrino telescope.
- ⁴² Based on the observation of 58 ν_μ events with $205 \pm 17(\text{syst})$ expected in the absence of neutrino oscillations. Superseded by ABE 14.
- ⁴³ ADAMSON 13b obtained this result from ν_μ and $\bar{\nu}_\mu$ disappearance using ν_μ (10.71×10^{20} POT) and $\bar{\nu}_\mu$ (3.36×10^{20} POT) beams, and atmospheric (37.88 kton-years) data from MINOS. The fit assumed two-flavor neutrino hypothesis and identical ν_μ and $\bar{\nu}_\mu$ oscillation parameters.
- ⁴⁴ ABE 12a obtained this result by a two-neutrino oscillation analysis. The best-fit point is $\Delta m_{32}^2 = 2.65 \times 10^{-3} \text{ eV}^2$.
- ⁴⁵ ADAMSON 12 is a two-neutrino oscillation analysis using antineutrinos.
- ⁴⁶ ADAMSON 12b obtained this result by a two-neutrino oscillation analysis of the L/E distribution using 37.9 kton-yr atmospheric neutrino data with the MINOS far detector.
- ⁴⁷ The 90% single-parameter confidence interval at the best fit point is $\Delta m^2 = 0.0019 \pm 0.0004 \text{ eV}^2$.
- ⁴⁸ The data are separated into pure samples of ν_s and $\bar{\nu}_s$, and separate oscillation parameters for ν_s and $\bar{\nu}_s$ are fit to the data. The best fit point is $(\Delta m^2, \sin^2 2\theta) = (0.0022 \text{ eV}^2, 0.99)$ and $(\Delta \bar{m}^2, \sin^2 2\bar{\theta}) = (0.0016 \text{ eV}^2, 1.00)$. The quoted result is taken from the 90% C.L. contour in the $(\Delta m^2, \sin^2 2\theta)$ plane obtained by minimizing the four parameter log-likelihood function with respect to the other oscillation parameters.
- ⁴⁹ ADRIAN-MARTINEZ 12 measured the oscillation parameters of atmospheric neutrinos with the ANTARES deep sea neutrino telescope using the data taken from 2007 to 2010 (863 days of total live time). Superseded by ALBERT 19.
- ⁵⁰ ABE 11c obtained this result by a two-neutrino oscillation analysis with separate mixing parameters between neutrinos and antineutrinos, using the Super-Kamiokande-I+II+III atmospheric neutrino data. The corresponding 90% CL neutrino oscillation parameter range obtained from this analysis is $\Delta m^2 = 1.7\text{--}3.0 \times 10^{-3} \text{ eV}^2$.
- ⁵¹ ADAMSON 11b obtained this result by a two-neutrino oscillation analysis of antineutrinos in an antineutrino enhanced beam with 1.71×10^{20} protons on target. This result is consistent with the neutrino measurements of ADAMSON 11 at 2% C.L.
- ⁵² ADAMSON 11c obtains this result based on a study of antineutrinos in a neutrino beam and assumes maximal mixing in the two-flavor approximation.
- ⁵³ WENDELL 10 obtained this result by a three-neutrino oscillation analysis with one mass scale dominance ($\Delta m_{21}^2 = 0$) using the Super-Kamiokande-I+II+III atmospheric neutrino data, and updates the HOSAKA 06a result.
- ⁵⁴ ADAMSON 06 obtained this result by a two-neutrino oscillation analysis of the L/E distribution using 4.54 kton yr atmospheric neutrino data with the MINOS far detector.
- ⁵⁵ The best fit in the physical region is for $\Delta m^2 = 2.8 \times 10^{-3} \text{ eV}^2$.
- ⁵⁶ Supersedes ALIU 05.
- ⁵⁷ MICHAEL 06 best fit is $2.74 \times 10^{-3} \text{ eV}^2$. See also ADAMSON 08.
- ⁵⁸ ALLISON 05 result is based on an atmospheric neutrino observation with an exposure of 5.9 kton yr. From a two-flavor oscillation analysis the best-fit point is $\Delta m^2 = 0.0017 \text{ eV}^2$ and $\sin^2 2\theta = 0.97$.
- ⁵⁹ ASHIE 05 obtained this result by a two-neutrino oscillation analysis using 92 kton yr atmospheric neutrino data from the complete Super-Kamiokande I running period. The best fit is for $\Delta m^2 = 2.1 \times 10^{-3} \text{ eV}^2$.
- ⁶⁰ AMBROSIO 04 obtained this result, without using the absolute normalization of the neutrino flux, by combining the angular distribution of upward through-going muon tracks with $E_\mu > 1 \text{ GeV}$, N_{low} and N_{high} , and the numbers of InDown + UpStop and InUp events. Here, N_{low} and N_{high} are the number of events with reconstructed neutrino energies $< 30 \text{ GeV}$ and $> 130 \text{ GeV}$, respectively. InDown and InUp represent events with downward and upward-going tracks starting inside the detector due to neutrino interactions, while UpStop represents entering upward-going tracks which stop in the detector. The best fit is for $\Delta m^2 = 2.3 \times 10^{-3} \text{ eV}^2$.
- ⁶¹ ASHIE 04 obtained this result from the L(flight length)/E(estimated neutrino energy) distribution of ν_μ disappearance probability, using the Super-Kamiokande-I 1489 live-day atmospheric neutrino data. The best fit is for $\Delta m^2 = 2.4 \times 10^{-3} \text{ eV}^2$.
- ⁶² There are several islands of allowed region from this K2K analysis, extending to high values of Δm^2 . We only include the one that overlaps atmospheric neutrino analyses. The best fit is for $\Delta m^2 = 2.8 \times 10^{-3} \text{ eV}^2$.
- ⁶³ AMBROSIO 03 obtained this result on the basis of the ratio $R = N_{low}/N_{high}$, where N_{low} and N_{high} are the number of upward through-going muon events with reconstructed neutrino energy $< 30 \text{ GeV}$ and $> 130 \text{ GeV}$, respectively. The data came from the full detector run started in 1994. The method of FELDMAN 98 is used to obtain the limits. The best fit is for $\Delta m^2 = 2.5 \times 10^{-3} \text{ eV}^2$.
- ⁶⁴ AMBROSIO 03 obtained this result by using the ratio R and the angular distribution of the upward through-going muons. R is given in the previous note and the angular distribution is reported in AMBROSIO 01. The method of FELDMAN 98 is used to obtain the limits. The best fit is for $\Delta m^2 = 2.5 \times 10^{-3} \text{ eV}^2$.
- ⁶⁵ SANCHEZ 03 is based on an exposure of 5.9 kton yr. The result is obtained using a likelihood analysis of the neutrino L/E distribution for a selection μ flavor sample while the e -flavor sample provides flux normalization. The method of FELDMAN 98 is used to obtain the allowed region. The best fit is for $\Delta m^2 = 5.2 \times 10^{-3} \text{ eV}^2$.
- ⁶⁶ AMBROSIO 01 result is based on the angular distribution of upward through-going muon tracks with $E_\mu > 1 \text{ GeV}$. The data came from three different detector configurations, but the statistics is largely dominated by the full detector run, from May 1994 to December 2000. The total live time, normalized to the full detector configuration is 6.17 years. The best fit is obtained outside the physical region. The method of FELDMAN 98 is used to obtain the limits.
- ⁶⁷ AMBROSIO 01 result is based on the angular distribution and normalization of upward through-going muon tracks with $E_\mu > 1 \text{ GeV}$. See the previous footnote.
- ⁶⁸ FUKUDA 99c obtained this result from a total of 537 live days of upward through-going muon data in Super-Kamiokande between April 1996 to January 1998. With a threshold of $E_\mu > 1.6 \text{ GeV}$, the observed flux is $(1.74 \pm 0.07 \pm 0.02) \times 10^{-13} \text{ cm}^{-2}\text{s}^{-1}\text{sr}^{-1}$. The best fit is for $\Delta m^2 = 5.9 \times 10^{-3} \text{ eV}^2$.
- ⁶⁹ FUKUDA 99d obtained this result from a simultaneous fitting to zenith angle distributions of upward-stopping and through-going muons. The flux of upward-stopping muons of minimum energy of 1.6 GeV measured between April 1996 and January 1998 is $(0.39 \pm 0.04 \pm 0.02) \times 10^{-13} \text{ cm}^{-2}\text{s}^{-1}\text{sr}^{-1}$. This is compared to the expected flux of $(0.73 \pm 0.16 (\text{theoretical error})) \times 10^{-13} \text{ cm}^{-2}\text{s}^{-1}\text{sr}^{-1}$. The best fit is for $\Delta m^2 = 3.9 \times 10^{-3} \text{ eV}^2$.
- ⁷⁰ FUKUDA 99d obtained this result from the zenith dependence of the upward-stopping/through-going flux ratio. The best fit is for $\Delta m^2 = 3.1 \times 10^{-3} \text{ eV}^2$.

See key on page 1171

Lepton Particle Listings

Neutrino Mixing

⁷¹ FUKUDA 98c obtained this result by an analysis of 33.0 kton yr atmospheric neutrino data. The best fit is for $\Delta m^2 = 2.2 \times 10^{-3} \text{ eV}^2$.

⁷² HATAKEYAMA 98 obtained this result from a total of 2456 live days of upward-going muon data in Kamiokande between December 1985 and May 1995. With a threshold of $E_\mu > 1.6 \text{ GeV}$, the observed flux of upward through-going muons is $(1.94 \pm 0.10^{+0.07}_{-0.06}) \times 10^{-13} \text{ cm}^{-2} \text{ s}^{-1} \text{ sr}^{-1}$. This is compared to the expected flux of $(2.46 \pm 0.54 \text{ (theoretical error)}) \times 10^{-13} \text{ cm}^{-2} \text{ s}^{-1} \text{ sr}^{-1}$. The best fit is for $\Delta m^2 = 2.2 \times 10^{-3} \text{ eV}^2$.

⁷³ HATAKEYAMA 98 obtained this result from a combined analysis of Kamiokande contained events (FUKUDA 94) and upward going muon events. The best fit is for $\Delta m^2 = 13 \times 10^{-3} \text{ eV}^2$.

⁷⁴ FUKUDA 94 obtained the result by a combined analysis of sub- and multi-GeV atmospheric neutrino events in Kamiokande. The best fit is for $\Delta m^2 = 16 \times 10^{-3} \text{ eV}^2$.

$\sin^2(\theta_{13})$

At present time direct measurements of $\sin^2(\theta_{13})$ are derived from the reactor $\bar{\nu}_e$ disappearance at distances corresponding to the Δm_{32}^2 value, i.e. $L \sim 1 \text{ km}$. Alternatively, limits can also be obtained from the analysis of the solar neutrino data and accelerator-based $\nu_\mu \rightarrow \nu_e$ experiments.

If an experiment reports $\sin^2(2\theta_{13})$ we convert the value to $\sin^2(\theta_{13})$.

VALUE (units 10^{-2})	CL%	DOCUMENT ID	TECN	COMMENT
2.19 ± 0.07	OUR AVERAGE	Error includes scale factor of 1.2.		
2.80 +0.28 -0.65		1 ABE	23F T2K	Normal mass ordering
2.170 ± 0.063		2 AN	23 DAYA	DayaBay, Ling Ao/Ao II reactors
2.70 ± 0.37		3 DE-KERRET	20 DCHZ	Chooz reactors
2.22 ± 0.21 ± 0.37		4 SHIN	20 RENO	Yonggwang reactors
2.29 ± 0.18		5 BAK	18 RENO	Yonggwang reactors
1.81 ± 0.29		6 AN	16A DAYA	DayaBay, Ling Ao/Ao II reactors
• • • We do not use the following data for averages, fits, limits, etc. • • •				
3.10 +0.30 -0.69		1 ABE	23F T2K	Inverted mass ordering
2.41 ± 0.45		7 ABRAHAO	21 DCHZ	Chooz reactors
2.200 +0.069 -0.062		8 SALAS	21 FIT	Normal mass ordering, global fit
2.225 +0.064 -0.070		8 SALAS	21 FIT	Inverted mass ordering, global fit
2.219 +0.062 -0.063		9 ESTEBAN	20A FIT	Normal mass ordering, global fit
2.238 +0.063 -0.062		9 ESTEBAN	20A FIT	Inverted mass ordering, global fit
< 3.9	68	AGAFONOVA	19 OPER	
1.8 +2.9 -1.3		10 ABE	18B SKAM	3ν osc: normal mass ordering, θ ₁₃ free
0.8 +1.7 -0.7		10 ABE	18B SKAM	3ν osc: inverted mass ordering, θ ₁₃ free
2.188 ± 0.076		11 ADEY	18A DAYA	DayaBay, LingAo/Ao II reactors
<12	90	12 AGAFONOVA	18A OPER	OPERA: ν _e appearance
2.160 +0.083 -0.069		DE-SALAS	18 FIT	Normal mass ordering, global fit
2.220 +0.074 -0.076		DE-SALAS	18 FIT	Inverted mass ordering, global fit
2.09 ± 0.23 ± 0.16		13 SEO	18 RENO	Yonggwang reactors
2.7 ± 0.7		14 ABE	17F T2K	Normal mass ordering, T2K only
2.149 ± 0.071 ± 0.050		15 AN	17A DAYA	DayaBay, LingAo/Ao II reactors
2.25 +0.87 -0.86		16 ABE	16B DCHZ	Chooz reactors
2.09 ± 0.23 ± 0.16		17 CHOI	16 RENO	Yonggwang reactors
2.15 ± 0.13		18 AN	15 DAYA	DayaBay, Ling Ao/Ao II reactors
2.6 +1.2 -1.1		19 ABE	14A DCHZ	Chooz reactors
3.0 +1.3 -1.0		20 ABE	14C T2K	Inverted mass ordering
3.6 +1.0 -0.9		20 ABE	14C T2K	Normal mass ordering
2.3 +0.9 -0.8		21 ABE	14H DCHZ	Chooz reactors
2.3 ± 0.2		22 AN	14 DAYA	DayaBay, Ling Ao/Ao II reactors
2.12 ± 0.47		23 AN	14B DAYA	DayaBay, Ling Ao/Ao II reactors
2.34 ± 0.20		24 FORERO	14 FIT	Normal mass ordering
2.40 ± 0.19		24 FORERO	14 FIT	Inverted mass ordering
2.18 ± 0.10		25 GONZALEZ...	14 FIT	Normal mass ordering; global fit
2.19 +0.11 -0.10		25 GONZALEZ...	14 FIT	Inverted mass ordering; global fit
2.5 ± 0.9 ± 0.9		26 ABE	13C DCHZ	Chooz reactors
2.3 +1.3 -1.0		27 ABE	13E T2K	Normal mass ordering
2.8 +1.6 -1.2		27 ABE	13E T2K	Inverted mass ordering

1.6 +1.3 -0.9		28 ADAMSON	13A MINS	Normal mass ordering
3.0 +1.8 -1.6		28 ADAMSON	13A MINS	Inverted mass ordering
<13	90	AGAFONOVA	13 OPER	OPERA: 3ν
< 3.6	95	29 AHARMIM	13 FIT	global solar: 3ν
2.3 ± 0.3 ± 0.1		30 AN	13 DAYA	DayaBay, Ling Ao/Ao II reactors
2.2 ± 1.1 ± 0.8		31 ABE	12 DCHZ	Chooz reactors
2.8 ± 0.8 ± 0.7		32 ABE	12B DCHZ	Chooz reactors
2.9 ± 0.3 ± 0.5		33 AHN	12 RENO	Yonggwang reactors
2.4 ± 0.4 ± 0.1		34 AN	12 DAYA	DayaBay, Ling Ao/Ao II reactors
2.5 +1.8 -1.6		35 ABE	11 FIT	KamLAND + global solar
< 6.1	95	36 ABE	11 FIT	Global solar
1.3 to 5.6	68	37 ABE	11A T2K	Normal mass ordering
1.5 to 5.6	68	38 ABE	11A T2K	Inverted mass ordering
0.3 to 2.3	68	39 ADAMSON	11D MINS	Normal mass ordering
0.8 to 3.9	68	40 ADAMSON	11D MINS	Inverted mass ordering
8 ± 3		41 FOGLI	11 FIT	Global neutrino data
7.8 ± 6.2		42 GANDO	11 FIT	KamLAND + solar: 3ν
12.4 ± 13.3		43 GANDO	11 FIT	KamLAND: 3ν
3 +9 -7	90	44 ADAMSON	10A MINS	Normal mass ordering
6 +14 -6	90	45 ADAMSON	10A MINS	Inverted mass ordering
8 +8 -7		46,47 AHARMIM	10 FIT	KamLAND + global solar: 3ν
< 30	95	46,48 AHARMIM	10 FIT	global solar: 3ν
< 15	90	49 WENDELL	10 SKAM	3ν osc.; normal m ordering
< 33	90	49 WENDELL	10 SKAM	3ν osc.; inverted m ordering
11 +11 -8		50 ADAMSON	09 MINS	Normal mass ordering
18 +15 -11		51 ADAMSON	09 MINS	Inverted mass ordering
6 ± 4		52 FOGLI	08 FIT	Global neutrino data
8 ± 7		53 FOGLI	08 FIT	Solar + KamLAND data
5 ± 5		54 FOGLI	08 FIT	Atmospheric + LBL + CHOOZ
< 36	90	55 YAMAMOTO	06 K2K	Accelerator experiment
< 48	90	56 AHN	04 K2K	Accelerator experiment
< 36	90	57 BOEHM	01	Palo Verde react.
< 45	90	58 BOEHM	00	Palo Verde react.
< 15	90	59 APOLLONIO	99 CHOZ	Reactor Experiment

¹ ABE 23F results are based on data collected between 2010 and 2020 in (anti)neutrino mode and include a neutrino beam exposure of 1.97×10^{21} (1.63×10^{21}) protons on target.

² AN 23 reports results derived from the complete data set collected by the Daya-Bay experiment, corresponding to 3158 days of operation, resulting in $5.55 \times 10^9 \bar{\nu}_e$ candidate events. Solar oscillation parameters are fixed in the analysis to $\sin^2(\theta_{12}) = 0.307 \pm 0.013$, $\Delta m_{21}^2 = (7.53 \pm 0.18) \times 10^{-5} \text{ eV}^2$ from PDG 20. Supersedes ADEY 18A.

³ DE-KERRET 20 uses 481 days of data from single detector operation and also 384 days of data with both near and far detectors operating. A rate and shape analysis is performed on combined neutron captures on H and Gd. Supersedes ABE 16B.

⁴ SHIN 20 uses the RENO detector and 1500 live days of data. The near (far) detector observed 567,690 (90,747) $\bar{\nu}_e$ candidate events with a delayed neutron capture on hydrogen. The extracted value of $\sin^2\theta_{13}$ is consistent with the previous analysis with neutron capture on Gd in BAK 18.

⁵ BAK 18 reports results of the RENO experiment using about 2200 live-days of data taken with detectors placed at 410.6 and 1445.7 m from reactors of the Hanbit Nuclear Power Plant. Supersedes SEO 18.

⁶ AN 16A uses data from the eight antineutrino detectors (404 days) and six antineutrino detectors (217 days) runs to determine the mixing parameter $\sin^2(2\theta_{13})$ using the neutron capture on H only. Supersedes AN 14B.

⁷ ABRAHAO 21 uses 865 days of data collected in both near and far detectors with at least one reactor in operation. The analysis is based on a background model independent approach, so called Reactor Rate Modulation, to determine the mixing angle θ_{13} . Adding the background model reduces the uncertainty to 0.0041. Supersedes ABE 16B.

⁸ SALAS 21 reports results of a global fit to neutrino oscillation data available at the time of the Neutrino 2020 conference.

⁹ ESTEBAN 20A reports results of a global fit to neutrino oscillation data available at the time of the Neutrino2020 conference.

¹⁰ ABE 18b uses 328 kton-years of Super-Kamiokande I-IV atmospheric neutrino data to obtain this result. The fit is performed over the four parameters, Δm_{32}^2 , $\sin^2\theta_{23}$, $\sin^2\theta_{13}$, and δ , while the solar parameters are fixed to $\Delta m_{21}^2 = (7.53 \pm 0.18) \times 10^{-5} \text{ eV}^2$ and $\sin^2\theta_{12} = 0.304 \pm 0.014$.

¹¹ ADEY 18A reports results from analysis of 1958 days of data taking with the Daya-Bay experiment, with $3.9 \times 10^6 \bar{\nu}_e$ candidates. The fit to the data gives $\Delta m_{ee}^2 = (2.522_{-0.070}^{+0.068}) \times 10^{-3} \text{ eV}^2$. Solar oscillation parameters are fixed in the analysis using the global averages, $\sin^2(\theta_{12}) = 0.307_{-0.012}^{+0.013}$, $\Delta m_{21}^2 = (7.53 \pm 0.18) \times 10^{-5} \text{ eV}^2$, from PDG 18. Supersedes AN 17A.

¹² AGAFONOVA 18A reports $\sin^2(2\theta_{13}) < 0.43$ at 90% C.L. The result on the sterile neutrino search in the context of 3+1 model is also reported. A 90% C.L. upper limit on $\sin^2(2\theta_{\mu e}) = 0.021$ for $\Delta m_{41}^2 \geq 0.1 \text{ eV}^2$ is set.

Lepton Particle Listings

Neutrino Mixing

- ¹³ SEO 18 reports results of the RENO experiment using about 500 days of data, performing a rate and shape analysis. Compared to AHN 12, a significant reduction of the systematic uncertainties is reported. A 3% excess of events near 5 MeV of the prompt energy is observed. SEO 18 is a detailed description of the results published in CHOI 16, which it supersedes. Superseded by BAK 18.
- ¹⁴ Using T2K data only. For inverted mass ordering, all values of θ_{13} are ruled out at 68% CL.
- ¹⁵ AN 17A reports results from combined rate and spectral shape analysis of 1230 days of data taken with the Daya Bay reactor experiment. The data set contains more than 2.5×10^6 inverse beta-decay events with neutron capture on Gd. A simultaneous fit to θ_{13} and Δm_{ee}^2 is performed. Superseded by ADEY 18A.
- ¹⁶ ABE 16B uses 455.7 live days of data from a detector 1050 m away from two reactor cores of the Chooz nuclear power station, to determine the mixing parameter $\sin^2(2\theta_{13})$. This analysis uses 7.15 reactor-off days for constraining backgrounds. A rate and shape analysis is performed on combined neutron captures on H and Gd. Supersedes ABE 14H and ABE 13C.
- ¹⁷ CHOI 16 reports results of the RENO experiment using about 500 days of data, performing a rate and shape analysis. Compared to AHN 12, a significant reduction of the systematic uncertainties is reported. A 3% excess of events near 5 MeV of the prompt energy is observed. Supersedes AHN 12.
- ¹⁸ AN 15 uses all eight identical detectors, with four placed near the reactor cores and the remaining four at the far hall to determine the mixing angle θ_{13} using the $\overline{\nu}_e$ observed interaction rates with neutron capture on Gd and energy spectra. The result corresponds to the exposure of 6.9×10^5 GW_{th}-ton-days. Superseded by AN 17A.
- ¹⁹ ABE 14A uses 467.9 live days of one detector, 1050 m away from two reactor cores of the Chooz nuclear power station, to determine the mixing parameter $\sin^2(2\theta_{13})$. The Bugey4 data (DECLAIS 94) is used to constrain the neutrino flux. The data set includes 7.24 reactor-off days. A "rate-modulation" analysis is performed. Supersedes ABE 12B.
- ²⁰ ABE 14C result is for ν_e appearance and assumes $\Delta m_{32}^2 = 2.4 \times 10^{-3}$ eV², $\sin^2(\theta_{23}) = 0.5$, and $\delta = 0$.
- ²¹ ABE 14H uses 467.9 live days of one detector, 1050 m away from two reactor cores of the Chooz nuclear power station, to determine the mixing parameter $\sin^2(2\theta_{13})$. The Bugey4 data (DECLAIS 94) is used to constrain the neutrino flux. The data set includes 7.24 reactor-off days. A rate and shape analysis is performed. Superseded by ABE 16B.
- ²² AN 14 uses six identical detectors, with three placed near the reactor cores (flux-weighted baselines of 512 and 561 m) and the remaining three at the far hall (at the flux averaged distance of 1579 m from all six reactor cores) to determine the mixing angle θ_{13} using the $\overline{\nu}_e$ observed interaction rates with neutron capture on Gd and energy spectra. Supersedes AN 13 and superseded by AN 15.
- ²³ AN 14B uses six identical anti-neutrino detectors with flux-weighted baselines of ~ 500 m and ~ 1.6 km to six power reactors. This rate analysis uses a 217-day data set and neutron capture on protons (not Gd) only. $\Delta m_{31}^2 = 2.32 \times 10^{-3}$ eV² is assumed. Superseded by AN 16A.
- ²⁴ FORERO 14 performs a global fit to neutrino oscillations using solar, reactor, long-baseline accelerator, and atmospheric neutrino data.
- ²⁵ GONZALEZ-GARCIA 14 result comes from a frequentist global fit. The corresponding Bayesian global fit to the same data results are reported in BERGSTROM 15 as $(2.18_{-0.10}^{+0.10}) \times 10^{-2}$ eV² for normal and $(2.19_{-0.10}^{+0.12}) \times 10^{-2}$ eV² for inverted mass ordering.
- ²⁶ ABE 13C uses delayed neutron capture on hydrogen instead of on Gd used previously. The physical volume is thus three times larger. The fit is based on the rate and shape analysis as in ABE 12B. The Bugey4 data (DECLAIS 94) is used to constrain the neutrino flux. Superseded by ABE 16B.
- ²⁷ ABE 13E assumes maximal θ_{23} mixing and CP phase $\delta = 0$.
- ²⁸ ADAMSON 13a results obtained from ν_e appearance, assuming $\delta = 0$, and $\sin^2(2\theta_{23}) = 0.957$.
- ²⁹ AHARMIM 13 obtained this result by a three-neutrino oscillation analysis with the value of Δm_{32}^2 fixed to 2.45×10^{-3} eV², using global solar neutrino data. AHARMIM 13 global solar neutrino data include SNO's all-phases-combined analysis results on the total active ^8B neutrino flux and energy-dependent ν_e survival probability parameters, measurements of Cl (CLEVELAND 98), Ga (ABDURASHITOV 09 which contains combined analysis with GNO (ALTMANN 05 and Ph.D. thesis of F. Kaether)), and ^7Be (BELLINI 11A) rates, and ^8B solar-neutrino recoil electron measurements of SK-I (HOSAKA 06) zenith, SK-II (CRAVENS 08) and SK-III (ABE 11) day/night spectra, and Borexino (BELLINI 10A) spectra. AHARMIM 13 also reported a result combining global solar and KamLAND data, which is $\sin^2(2\theta_{13}) = (9.1_{-3.1}^{+2.9}) \times 10^{-2}$.
- ³⁰ AN 13 uses six identical detectors, with three placed near the reactor cores (flux-weighted baselines of 498 and 555 m) and the remaining three at the far hall (at the flux averaged distance of 1628 m from all six reactor cores) to determine the $\overline{\nu}_e$ interaction rate ratios. Superseded by AN 14.
- ³¹ ABE 12 determines the $\overline{\nu}_e$ interaction rate in a single detector, located 1050 m from the cores of two reactors. A rate and shape analysis is performed. The rate normalization is fixed by the results of the Bugey4 reactor experiment, thus avoiding any dependence on possible very short baseline oscillations. The value of $\Delta m_{31}^2 = 2.4 \times 10^{-3}$ eV² is used in the analysis. Superseded by ABE 12B.
- ³² ABE 12B determines the neutrino mixing angle θ_{13} using a single detector, located 1050 m from the cores of two reactors. This result is based on a spectral shape and rate analysis. The Bugey4 data (DECLAIS 94) is used to constrain the neutrino flux. Superseded by ABE 14A.
- ³³ AHN 12 uses two identical detectors, placed at flux weighted distances of 408.56 m and 1433.99 m from six reactor cores, to determine the mixing angle θ_{13} . This rate-only analysis excludes the no-oscillation hypothesis at 4.9 standard deviations. The value of $\Delta m_{31}^2 = (2.32_{-0.08}^{+0.12}) \times 10^{-3}$ eV² was assumed in the analysis. Superseded by CHOI 16.
- ³⁴ AN 12 uses six identical detectors with three placed near the reactor cores (flux-weighted baselines of 470 m and 576 m) and the remaining three at the far hall (at the flux averaged distance of 1648 m from all six reactor cores) to determine the mixing angle θ_{13} using the $\overline{\nu}_e$ observed interaction rate ratios. This rate-only analysis excludes the no-oscillation hypothesis at 5.2 standard deviations. The value of $\Delta m_{31}^2 = (2.32_{-0.08}^{+0.12}) \times 10^{-3}$ eV² was assumed in the analysis. Superseded by AN 13.
- ³⁵ ABE 11 obtained this result by a three-neutrino oscillation analysis with the value of Δm_{32}^2 fixed to 2.4×10^{-3} eV², using solar neutrino data including Super-Kamiokande, SNO, Borexino (ARPESELLA 08A), Homestake, GALLEX/GNO, SAGE, and KamLAND data. This result implies an upper bound of $\sin^2\theta_{13} < 0.059$ (95% CL) or $\sin^2 2\theta_{13} < 0.22$ (95% CL). The normal neutrino mass ordering and CPT invariance are assumed.
- ³⁶ ABE 11 obtained this result by a three-neutrino oscillation analysis with the value of Δm_{32}^2 fixed to 2.4×10^{-3} eV², using solar neutrino data including Super-Kamiokande, SNO, Borexino (ARPESELLA 08A), Homestake, and GALLEX/GNO data. The normal neutrino mass ordering is assumed.
- ³⁷ The quoted limit is for $\Delta m_{32}^2 = 2.4 \times 10^{-3}$ eV², $\theta_{23} = \pi/2$, $\delta = 0$, and the normal mass ordering. For other values of δ , the 68% region spans from 0.03 to 0.25, and the 90% region from 0.02 to 0.32.
- ³⁸ The quoted limit is for $\Delta m_{32}^2 = 2.4 \times 10^{-3}$ eV², $\theta_{23} = \pi/2$, $\delta = 0$, and the inverted mass ordering. For other values of δ , the 68% region spans from 0.04 to 0.30, and the 90% region from 0.02 to 0.39.
- ³⁹ The quoted limit is for $\Delta m_{32}^2 = 2.32 \times 10^{-3}$ eV², $\theta_{23} = \pi/2$, $\delta = 0$, and the normal mass ordering. For other values of δ , the 68% region spans from 0.02 to 0.12, and the 90% region from 0 to 0.16.
- ⁴⁰ The quoted limit is for $\Delta m_{32}^2 = 2.32 \times 10^{-3}$ eV², $\theta_{23} = \pi/2$, $\delta = 0$, and the inverted mass ordering. For other values of δ , the 68% region spans from 0.02 to 0.16, and the 90% region from 0 to 0.21.
- ⁴¹ FOGLI 11 obtained this result from an analysis using the atmospheric, accelerator long baseline, CHOOZ, solar, and KamLAND data. Recently, MUELLER 11 suggested an average increase of about 3.5% in normalization of the reactor $\overline{\nu}_e$ fluxes, and using these fluxes, the fitted result becomes 0.10 ± 0.03 .
- ⁴² GANDO 11 report $\sin^2\theta_{13} = 0.020 \pm 0.016$. This result was obtained with three-neutrino fit using the KamLAND + solar data.
- ⁴³ GANDO 11 report $\sin^2\theta_{13} = 0.032 \pm 0.037$. This result was obtained with three-neutrino fit using the KamLAND data only.
- ⁴⁴ This result corresponds to the limit of < 0.12 at 90% CL for $\Delta m_{32}^2 = 2.43 \times 10^{-3}$ eV², $\theta_{23} = \pi/2$, and $\delta = 0$. For other values of δ , the 90% CL region spans from 0 to 0.16.
- ⁴⁵ This result corresponds to the limit of < 0.20 at 90% CL for $\Delta m_{32}^2 = 2.43 \times 10^{-3}$ eV², $\theta_{23} = \pi/2$, and $\delta = 0$. For other values of δ , the 90% CL region spans from 0 to 0.21.
- ⁴⁶ AHARMIM 10 global solar neutrino data include SNO's low-energy-threshold analysis survival probability day/night curves, SNO Phase III integral rates (AHARMIM 08), Cl (CLEVELAND 98), SAGE (ABDURASHITOV 09), Gallex/GNO (HAMPEL 99, ALTMANN 05), Borexino (ARPESELLA 08A), SK-I zenith (HOSAKA 06), and SK-II day/night spectra (CRAVENS 08).
- ⁴⁷ AHARMIM 10 obtained this result by a three-neutrino oscillation analysis with the value of Δm_{31}^2 fixed to 2.3×10^{-3} eV², using global solar neutrino data and KamLAND data (ABE 08A). CPT invariance is assumed. This result implies an upper bound of $\sin^2\theta_{13} < 0.057$ (95% CL) or $\sin^2 2\theta_{13} < 0.22$ (95% CL).
- ⁴⁸ AHARMIM 10 obtained this result by a three-neutrino oscillation analysis with the value of Δm_{31}^2 fixed to 2.3×10^{-3} eV², using global solar neutrino data.
- ⁴⁹ WENDELL 10 obtained this result by a three-neutrino oscillation analysis with one mass scale dominance ($\Delta m_{21}^2 = 0$) using the Super-Kamiokande-I+II+III atmospheric neutrino data, and updates the HOSAKA 06A result.
- ⁵⁰ The quoted limit is for $\Delta m_{32}^2 = 2.43 \times 10^{-3}$ eV², $\theta_{23} = \pi/2$, and $\delta = 0$. For other values of δ , the 68% CL region spans from 0.02 to 0.26.
- ⁵¹ The quoted limit is for $\Delta m_{32}^2 = 2.43 \times 10^{-3}$ eV², $\theta_{23} = \pi/2$, and $\delta = 0$. For other values of δ , the 68% CL region spans from 0.04 to 0.34.
- ⁵² FOGLI 08 obtained this result from a global analysis of all neutrino oscillation data, that is, solar + KamLAND + atmospheric + accelerator long baseline + CHOOZ.
- ⁵³ FOGLI 08 obtained this result from an analysis using the solar and KamLAND neutrino oscillation data.
- ⁵⁴ FOGLI 08 obtained this result from an analysis using the atmospheric, accelerator long baseline, and CHOOZ neutrino oscillation data.
- ⁵⁵ YAMAMOTO 06 searched for $\nu_\mu \rightarrow \nu_e$ appearance. Assumes $2 \sin^2(2\theta_{\mu e}) = \sin^2(2\theta_{13})$. The quoted limit is for $\Delta m_{32}^2 = 1.9 \times 10^{-3}$ eV². That value of Δm_{32}^2 is the one- σ low value for AHN 06A. For the AHN 06A best fit value of 2.8×10^{-3} eV², the $\sin^2(2\theta_{13})$ limit is < 0.26 . Supersedes AHN 04.
- ⁵⁶ AHN 04 searched for $\nu_\mu \rightarrow \nu_e$ appearance. Assuming $2 \sin^2(2\theta_{\mu e}) = \sin^2(2\theta_{13})$, a limit on $\sin^2(2\theta_{\mu e})$ is converted to a limit on $\sin^2(2\theta_{13})$. The quoted limit is for $\Delta m_{32}^2 = 1.9 \times 10^{-3}$ eV². That value of Δm_{32}^2 is the one- σ low value for ALIU 05. For the ALIU 05 best fit value of 2.8×10^{-3} eV², the $\sin^2(2\theta_{13})$ limit is < 0.30 .
- ⁵⁷ The quoted limit is for $\Delta m_{32}^2 = 1.9 \times 10^{-3}$ eV². That value of Δm_{32}^2 is the 1- σ low value for ALIU 05. For the ALIU 05 best fit value of 2.8×10^{-3} eV², the $\sin^2 2\theta_{13}$ limit is < 0.19 . In this range, the θ_{13} limit is larger for lower values of Δm_{32}^2 , and smaller for higher values of Δm_{32}^2 .
- ⁵⁸ The quoted limit is for $\Delta m_{32}^2 = 1.9 \times 10^{-3}$ eV². That value of Δm_{32}^2 is the 1- σ low value for ALIU 05. For the ALIU 05 best fit value of 2.8×10^{-3} eV², the $\sin^2 2\theta_{13}$ limit is < 0.23 .
- ⁵⁹ The quoted limit is for $\Delta m_{32}^2 = 2.43 \times 10^{-3}$ eV². That value of Δm_{32}^2 is the central value for ADAMSON 08. For the ADAMSON 08 1- σ low value of 2.30×10^{-3} eV²,

See key on page 1171

Lepton Particle Listings

Neutrino Mixing

the $\sin^2 \theta_{13}$ limit is < 0.16 . See also APOLLONIO 03 for a detailed description of the experiment.

CP violating phase

δ , CP violating phase

Measurements of δ come from atmospheric and accelerator experiments looking at ν_e appearance. We encode values between 0 and 2π , though it is equivalent to use $-\pi$ to π .

VALUE (π rad)	CL%	DOCUMENT ID	TECN	COMMENT
1.19 ± 0.22 OUR AVERAGE		Error includes scale factor of 1.2.		
1.37 ^{+0.31} _{-0.20}		¹ ABE	23F T2K	Normal mass ordering, θ_{13} constrained
0.82 ^{+0.27} _{-0.87}		^{2,3} ACERO	22 NOVA	Normal mass ordering, octant II for θ_{23} , θ_{13} constrained
1.33 ^{+0.45} _{-0.51}		⁴ ABE	18B SKAM	Normal mass ordering, θ_{13} constrained
• • • We do not use the following data for averages, fits, limits, etc. • • •				
1.52 ^{+0.30} _{-0.41}		^{2,5} ACERO	22 NOVA	Inverted mass ordering, octant II for θ_{23} , θ_{13} constrained
1.08 ^{+0.13} _{-0.12}		⁶ SALAS	21 FIT	Normal mass ordering, global fit
1.58 ^{+0.15} _{-0.16}		⁶ SALAS	21 FIT	Inverted mass ordering, global fit
1.40 ^{+0.22} _{-0.18}		⁷ ABE	20F T2K	Normal mass ordering
1.09 ^{+0.15} _{-0.13}		⁸ ESTEBAN	20A FIT	Normal mass ordering, global fit
1.57 ^{+0.14} _{-0.17}		⁸ ESTEBAN	20A FIT	Inverted mass ordering, global fit
0.0 ^{+1.3} _{-0.4}		⁹ ACERO	19 NOVA	Normal mass ordering, octant II for θ_{23}
1.33 ^{+0.46} _{-0.53}		¹⁰ ABE	18B SKAM	3ν osc: normal mass ordering, θ_{13} free
1.22 ^{+0.76} _{-0.67}		¹⁰ ABE	18B SKAM	3ν osc: inverted mass ordering, θ_{13} free
1.33 ^{+0.48} _{-0.53}		⁴ ABE	18B SKAM	3ν osc: inverted mass ordering, θ_{13} constrained
1.40 ± 0.20		¹¹ ABE	18G T2K	Normal mass ordering, θ_{13} constrained
1.54 ^{+0.14} _{-0.12}	95	¹¹ ABE	18G T2K	Inverted mass ordering, θ_{13} constrained
1.21 ^{+0.91} _{-0.30}		¹² ACERO	18 NOVA	Normal mass ordering, octant II for θ_{23}
1.46 ^{+0.56} _{-0.42}		¹² ACERO	18 NOVA	Normal mass order; octant I for θ_{23}
1.32 ^{+0.21} _{-0.15}		DE-SALAS	18 FIT	Normal mass ordering, global fit
1.56 ^{+0.13} _{-0.15}		DE-SALAS	18 FIT	Inverted mass ordering, global fit
1.45 ^{+0.27} _{-0.26}		¹³ ABE	17F T2K	Normal mass ordering
1.54 ^{+0.22} _{-0.23}		¹³ ABE	17F T2K	Inverted mass ordering
1.50 ^{+0.53} _{-0.57}		¹⁴ ADAMSON	17B NOVA	Inverted mass ordering; θ_{23} in octant II
0.74 ^{+0.57} _{-0.93}		¹⁴ ADAMSON	17B NOVA	Normal mass ordering; θ_{23} in octant II
1.48 ^{+0.69} _{-0.58}		¹⁴ ADAMSON	17B NOVA	Normal mass ordering; θ_{23} in octant I
0.0 to 0.1, 0.5 to 2.0	90	^{14,15} ADAMSON	16 NOVA	Inverted mass ordering
0.0 to 2.0	90	¹⁵ ADAMSON	16 NOVA	Normal mass ordering
0 to 0.15, 0.83 to 2	90	ABE	15D T2K	Normal mass ordering
1.09 to 1.92	90	ABE	15D T2K	Inverted mass ordering
0.05 to 1.2	90	¹⁶ ADAMSON	14 MINS	Normal mass ordering
1.34 ^{+0.64} _{-0.38}		FORERO	14 FIT	Normal mass ordering
1.48 ^{+0.34} _{-0.32}		FORERO	14 FIT	Inverted mass ordering
1.70 ^{+0.22} _{-0.39}		¹⁷ GONZALEZ...	14 FIT	Normal mass ordering; global fit
1.41 ^{+0.35} _{-0.34}		¹⁷ GONZALEZ...	14 FIT	Inverted mass ordering; global fit
0 to 1.5 or 1.9 to 2	90	¹⁸ ADAMSON	13A MINS	Normal mass ordering

¹ ABE 23F results are based on data collected between 2010 and 2020 in (anti)neutrino mode and include a neutrino beam exposure of 1.97×10^{21} (1.63×10^{21}) protons on target. For inverted mass ordering, the quoted result is $1.54^{+0.18}_{-0.19}$ π rad. Supersedes ABE 20F.
² ACERO 22 uses data from Jun 29, 2016 to Feb 26, 2019 (12.5×10^{20} POT) and Feb 6, 2014 to Mar 20, 2020 (13.6×10^{20} POT). Results for normal and inverted mass ordering, and θ_{23} octant I and II are presented. Supersedes ACERO 19.
³ For the octant I (lower octant), the 68% CL allowed region is discontinuous, and all delta values are allowed at 90% CL.
⁴ ABE 18B uses 328 kton-years of Super-Kamiokande I-IV atmospheric neutrino data to obtain this result. The fit is performed over the three parameters, Δm_{21}^2 , $\sin^2 \theta_{23}$, and

δ , while the solar parameters and $\sin^2 \theta_{23}$ are fixed to $\Delta m_{21}^2 = (7.53 \pm 0.18) \times 10^{-5}$ eV², $\sin^2 \theta_{12} = 0.304 \pm 0.014$, and $\sin^2 \theta_{13} = 0.0219 \pm 0.0012$.
⁵ The inverted mass ordering is rejected at 1.0 σ . The quoted error bars are based on the local best-fit point.
⁶ SALAS 21 reports results of a global fit to neutrino oscillation data available at the time of the Neutrino 2020 conference.
⁷ ABE 20F results are based on data collected between 2009 and 2018 in (anti)neutrino mode and include a neutrino beam exposure of 1.49×10^{21} (1.64×10^{21}) protons on target. For inverted mass ordering, the quoted result is $1.56^{+0.15}_{-0.17}$ π rad. Supersedes ABE 18G.
⁸ ESTEBAN 20A reports results of a global fit to neutrino oscillation data available at the time of the Neutrino 2020 conference.
⁹ ACERO 19 is based on a sample size of 1.33×10^{20} protons on target with combined antineutrino and neutrino data. Superseded by ACERO 22.
¹⁰ ABE 18B uses 328 kton-years of Super-Kamiokande I-IV atmospheric neutrino data to obtain this result. The fit is performed over the four parameters, Δm_{32}^2 , $\sin^2 \theta_{23}$, $\sin^2 \theta_{13}$, and δ , while the solar parameters are fixed to $\Delta m_{21}^2 = (7.53 \pm 0.18) \times 10^{-5}$ eV² and $\sin^2 \theta_{12} = 0.304 \pm 0.014$.
¹¹ ABE 18G confidence intervals are marginalized over both mass orderings. Normal order preferred with a posterior probability of 87%. The 1-sigma result for normal mass ordering used in the average was provided by the experiment via private communications. Supersedes ABE 17F.
¹² ACERO 18 performs a joint fit to the data for ν_μ disappearance and ν_e appearance. The overall best fit favors normal mass ordering and θ_{23} in octant II. No 1 σ confidence intervals are presented for the inverted mass ordering scenarios. Superseded by ACERO 19.
¹³ ABE 17F confidence intervals are obtained using a frequentist analysis including θ_{13} constraint from reactor experiments. Bayesian intervals based on Markov Chain Monte Carlo method are also provided by the authors. Superseded by ABE 18G.
¹⁴ Errors are projections of 68% C.L. curve of δ_{CP} vs. $\sin^2 \theta_{23}$.
¹⁵ ADAMSON 16 result is based on a data sample with 2.74×10^{20} protons on target. The likelihood-based analysis observed 6 ν_e events with an expected background of 0.99 ± 0.11 events.
¹⁶ ADAMSON 14 result is based on three-flavor formalism and $\theta_{23} > \pi/4$. Likelihood as a function of δ is also shown for the other three combinations of hierarchy and θ_{23} octants; all values of δ are allowed at 90% C.L.
¹⁷ GONZALEZ-GARCIA 14 result comes from a frequentist global fit. The corresponding Bayesian global fit to the same data results are reported in BERGSTROM 15 as 68% CL intervals of 1.24–1.94 for normal and 1.15–1.77 for inverted mass ordering.
¹⁸ ADAMSON 13A result is based on ν_e appearance in MINOS and the calculated $\sin^2(2\theta_{23}) = 0.957$, $\theta_{23} > \pi/4$, and normal mass hierarchy. Likelihood as a function of δ is also shown for the other three combinations of hierarchy and θ_{23} octants; all values of δ are allowed at 90% C.L.

(C) Other neutrino mixing results

The LSND collaboration reported in AGUILAR 01 a signal which is consistent with $\bar{\nu}_\mu \rightarrow \bar{\nu}_e$ oscillations. In a three neutrino framework, this would be a measurement of θ_{12} and Δm_{21}^2 . This does not appear to be consistent with most of the other neutrino data. The following listings include results from $\nu_\mu \rightarrow \nu_e$, $\bar{\nu}_\mu \rightarrow \bar{\nu}_e$ appearance and ν_μ , $\bar{\nu}_\mu$, ν_e , and $\bar{\nu}_e$ disappearance experiments, and searches for CPT violation.

$\Delta(m^2)$ for $\sin^2(2\theta) = 1$ ($\nu_\mu \rightarrow \nu_e$)

VALUE (eV ²)	CL%	DOCUMENT ID	TECN	COMMENT
• • • We do not use the following data for averages, fits, limits, etc. • • •				
0.03 to 0.55	90	¹ AGUILAR-AR...21	MBNE	MiniBooNE $\nu, \bar{\nu}$ combined
0.03 to 0.05	90	² AGUILAR-AR...18c	MBNE	MiniBooNE $\nu, \bar{\nu}$ combined
0.015 to 0.050	90	³ AGUILAR-AR...13A	MBNE	MiniBooNE
<0.34	90	⁴ MAHN	12	MBNE/SciBooNE
<0.034	90	AGUILAR-AR...07	MBNE	MiniBooNE
<0.0008	90	AHN	04	K2K Water Cherenkov
<0.4	90	ASTIER	03	NOMD CERN SPS
<2.4	90	AVVAKUMOV	02	NTEV NUTEV FNAL
		⁵ AGUILAR	01	LSND $\nu_\mu \rightarrow \nu_e$ osc. prob.
0.03 to 0.3	95	⁶ ATHANASSO...98	LSND	$\nu_\mu \rightarrow \nu_e$
<2.3	90	⁷ LOVERRE	96	CHARM/CDHS
<0.9	90	VILAIN	94c	CHM2 CERN SPS
<0.09	90	ANGELINI	86	HLBC BEBC CERN PS

¹ AGUILAR-AREVALO 21 result is based on a total of 18.75×10^{20} POT in neutrino mode, and 11.27×10^{20} POT in anti-neutrino mode. Best fit at 0.043 eV². The allowed region does not extend to large Δm^2 . The quoted value is the entire allowed region of Δm^2 at 90% C.L. for all values of $\sin^2(2\theta)$. Supersedes AGUILAR-AREVALO 18c.
² AGUILAR-AREVALO 18c result is based on $\nu_\mu \rightarrow \nu_e$ appearance of 460.5 ± 99.0 events; The best fit value is $\Delta m^2 = 0.041$ eV². Superseded by AGUILAR-AREVALO 21.
³ AGUILAR-AREVALO 13A result is based on $\nu_\mu \rightarrow \nu_e$ appearance of 162.0 ± 47.8 events; marginally compatible with twoneutrino oscillations. The best fit value is $\Delta m^2 = 3.14$ eV².
⁴ MAHN 12 is a combined spectral fit of MiniBooNE and SciBooNE neutrino data with the range of Δm^2 up to 25 eV². The best limit is 0.04 at 7 eV².

Lepton Particle Listings

Neutrino Mixing

⁵ AGUILAR 01 is the final analysis of the LSND full data set. Search is made for the $\nu_\mu \rightarrow \nu_e$ oscillations using ν_μ from π^+ decay in flight by observing beam-on electron events from $\nu_e C \rightarrow e^- X$. Present analysis results in $8.1 \pm 12.2 \pm 1.7$ excess events in the $60 < E_e < 200$ MeV energy range, corresponding to oscillation probability of $0.10 \pm 0.16 \pm 0.04\%$. This is consistent, though less significant, with the previous result of ATHANASSOPOULOS 98, which it supersedes. The present analysis uses selection criteria developed for the decay at rest region, and is less effective in removing the background above 60 MeV than ATHANASSOPOULOS 98.

⁶ ATHANASSOPOULOS 98 is a search for the $\nu_\mu \rightarrow \nu_e$ oscillations using ν_μ from π^+ decay in flight. The 40 observed beam-on electron events are consistent with $\nu_e C \rightarrow e^- X$; the expected background is 21.9 ± 2.1 . Authors interpret this excess as evidence for an oscillation signal corresponding to oscillations with probability $(0.26 \pm 0.10 \pm 0.05)\%$. Although the significance is only 2.3σ , this measurement is an important and consistent cross check of ATHANASSOPOULOS 96 who reported evidence for $\bar{\nu}_\mu \rightarrow \bar{\nu}_e$ oscillations from μ^+ decay at rest. See also ATHANASSOPOULOS 98b.

⁷ LOVERRE 96 uses the charged-current to neutral-current ratio from the combined CHARM (ALLABY 86) and CDHS (ABRAMOWICZ 86) data from 1986.

$\sin^2(2\theta)$ for "Large" $\Delta(m^2)$ ($\nu_\mu \rightarrow \nu_e$)

VALUE (units 10^{-3})	CL%	DOCUMENT ID	TECN	COMMENT
• • • We do not use the following data for averages, fits, limits, etc. • • •				
6 to 1000	90	1 AGUILAR-AR...21	MBNE	MiniBooNE; $\nu + \bar{\nu}$
< 5	90	2 AGUILAR-AR...18c	MBNE	MiniBooNE; $\nu + \bar{\nu}$
< 7.2	90	AGAFONOVA 13	OPER	$\Delta(m^2) > 0.1$ eV ²
0.8 to 3	90	3 AGUILAR-AR...13a	MBNE	MiniBooNE
< 11	90	4 ANTONELLO 13	ICAR	$\nu_\mu \rightarrow \nu_e$
< 6.8	90	5 ANTONELLO 13a	ICAR	$\nu_\mu \rightarrow \nu_e$
<100	90	6 MAHN 12	MBNE	MiniBooNE/SciBooNE
< 1.8	90	7 AGUILAR-AR...07	MBNE	MiniBooNE
<110	90	8 AHN 04	K2K	Water Cherenkov
< 1.4	90	ASTIER 03	NOMD	CERN SPS
< 1.6	90	AVVAKUMOV 02	NTEV	NUTEV FNAL
		9 AGUILAR 01	LSND	$\nu_\mu \rightarrow \nu_e$ osc. prob.
0.5 to 30	95	10 ATHANASSO...98	LSND	$\nu_\mu \rightarrow \nu_e$
< 3.0	90	11 LOVERRE 96	CHARM/CDHS	
< 9.4	90	VILAIN 94c	CHM2	CERN SPS
< 5.6	90	12 VILAIN 94c	CHM2	CERN SPS

¹ AGUILAR-AREVALO 21 result is based on a total of 18.75×10^{20} POT in neutrino mode, and 11.27×10^{20} POT in anti-neutrino mode. The best fit value is $\sin^2(2\theta) = 0.807$. The allowed region does not extend to large Δm^2 . The quoted value is the entire allowed region of $\sin^2(2\theta)$ at 90% C.L. for all values of Δm^2 . Supersedes AGUILAR-AREVALO 18c.

² AGUILAR-AREVALO 18c result is based on $\nu_\mu \rightarrow \nu_e$ appearance of 460.5 ± 99.0 events; The best fit value is $\sin^2(2\theta) = 0.92$. The quoted limit for the two-neutrino mixing angle θ is valid above $\Delta m^2 = 0.59$ eV². Superseded by AGUILAR-AREVALO 21.

³ AGUILAR-AREVALO 13a result is based on $\nu_\mu \rightarrow \nu_e$ appearance of 162.0 ± 47.8 events; marginally compatible with two neutrino oscillations. The best fit value is $\sin^2(2\theta) = 0.002$.

⁴ ANTONELLO 13 use the ICARUS T600 detector at LNGS and ~ 20 GeV beam of ν_μ from CERN 730 km away to search for an excess of ν_e events. Two events are found with 3.7 ± 0.6 expected from conventional sources. This result excludes some parts of the parameter space expected by LSND. Superseded by ANTONELLO 13a.

⁵ Based on four events with a background of 6.4 ± 0.9 from conventional sources with an average energy of 20 GeV and 730 km from the source of ν_μ .

⁶ MAHN 12 is a combined fit of MiniBooNE and SciBooNE neutrino data.

⁷ The limit is $\sin^2 2\theta < 0.9 \times 10^{-3}$ at $\Delta m^2 = 2$ eV². That value of Δm^2 corresponds to the smallest mixing angle consistent with the reported signal from LSND in AGUILAR 01.

⁸ The limit becomes $\sin^2 2\theta < 0.15$ at $\Delta m^2 = 2.8 \times 10^{-3}$ eV², the best-fit value of the ν_μ disappearance analysis in K2K.

⁹ AGUILAR 01 is the final analysis of the LSND full data set of the search for the $\nu_\mu \rightarrow \nu_e$ oscillations. See footnote in preceding table for further details.

¹⁰ ATHANASSOPOULOS 98 report $(0.26 \pm 0.10 \pm 0.05)\%$ for the oscillation probability; the value of $\sin^2 2\theta$ for large Δm^2 is deduced from this probability. See footnote in preceding table for further details, and see the paper for a plot showing allowed regions. If effect is due to oscillation, it is most likely to be intermediate $\sin^2 2\theta$ and Δm^2 . See also ATHANASSOPOULOS 98b.

¹¹ LOVERRE 96 uses the charged-current to neutral-current ratio from the combined CHARM (ALLABY 86) and CDHS (ABRAMOWICZ 86) data from 1986.

¹² VILAIN 94c limit derived by combining the ν_μ and $\bar{\nu}_\mu$ data assuming CP conservation.

$\Delta(m^2)$ for $\sin^2(2\theta) = 1$ ($\bar{\nu}_\mu \rightarrow \bar{\nu}_e$)

VALUE (eV ²)	CL%	DOCUMENT ID	TECN	COMMENT
• • • We do not use the following data for averages, fits, limits, etc. • • •				
0.023 to 0.060	90	1 AGUILAR-AR...13a	MBNE	MiniBooNE
<0.16	90	2 CHENG 12	MBNE	MiniBooNE/SciBooNE
0.03-0.09	90	3 AGUILAR-AR...10	MBNE	$E_\nu > 475$ MeV
0.03-0.07	90	4 AGUILAR-AR...10	MBNE	$E_\nu > 200$ MeV
<0.06	90	AGUILAR-AR...09b	MBNE	MiniBooNE
<0.055	90	5 ARMBRUSTER02	KAR2	Liquid Sci. calor.
<2.6	90	AVVAKUMOV 02	NTEV	NUTEV FNAL

0.03-0.05		6 AGUILAR 01	LSND	LAMPF
0.05-0.08	90	7 ATHANASSO...96	LSND	LAMPF
0.048-0.090	80	8 ATHANASSO...95		
<0.07	90	9 HILL 95		
<0.9	90	VILAIN 94c	CHM2	CERN SPS
<0.14	90	10 FREEDMAN 93	CNTR	LAMPF

¹ Based on $\bar{\nu}_\mu \rightarrow \bar{\nu}_e$ appearance of 78.4 ± 28.5 events. The best fit values are $\Delta m^2 = 0.043$ eV² and $\sin^2 2\theta = 0.88$.

² CHENG 12 is a combined fit of MiniBooNE and SciBooNE antineutrino data.

³ This value is for a two neutrino oscillation analysis for excess antineutrino events with $E_\nu > 475$ MeV. The best fit is at 0.07. The allowed region is consistent with LSND reported by AGUILAR 01. Supersedes AGUILAR-AREVALO 09b.

⁴ This value is for a two neutrino oscillation analysis for excess antineutrino events with $E_\nu > 200$ MeV with subtraction of the expected 12 events low energy excess seen in the neutrino component of the beam. The best fit value is 0.007 for $\Delta(m^2) = 4.4$ eV².

⁵ ARMBRUSTER 02 is the final analysis of the KARMEN 2 data for 17.7 m distance from the ISIS stopped pion and muon neutrino source. It is a search for $\bar{\nu}_e$, detected by the inverse β -decay reaction on protons and ¹²C. 15 candidate events are observed, and 15.8 ± 0.5 background events are expected, hence no oscillation signal is detected. The results exclude large regions of the parameter area favored by the LSND experiment.

⁶ AGUILAR 01 is the final analysis of the LSND full data set. It is a search for $\bar{\nu}_e$ 30 m from LAMPF beam stop. Neutrinos originate mainly from π^+ decay at rest. $\bar{\nu}_e$ are detected through $\bar{\nu}_e p \rightarrow e^+ n$ ($20 < E_{e^+} < 60$ MeV) in delayed coincidence with $np \rightarrow d\gamma$. Authors observe $87.9 \pm 22.4 \pm 6.0$ total excess events. The observation is attributed to $\bar{\nu}_\mu \rightarrow \bar{\nu}_e$ oscillations with the oscillation probability of $0.264 \pm 0.067 \pm 0.045\%$, consistent with the previously published result. Taking into account all constraints, the most favored allowed region of oscillation parameters is a band of $\Delta(m^2)$ from 0.2-2.0 eV². Supersedes ATHANASSOPOULOS 95, ATHANASSOPOULOS 96, and ATHANASSOPOULOS 98.

⁷ ATHANASSOPOULOS 96 is a search for $\bar{\nu}_e$ 30 m from LAMPF beam stop. Neutrinos originate mainly from π^+ decay at rest. $\bar{\nu}_e$ could come from either $\bar{\nu}_\mu \rightarrow \bar{\nu}_e$ or $\nu_e \rightarrow \bar{\nu}_e$; our entry assumes the first interpretation. They are detected through $\bar{\nu}_e p \rightarrow e^+ n$ (20 MeV $< E_{e^+} < 60$ MeV) in delayed coincidence with $np \rightarrow d\gamma$. Authors observe $51 \pm 20 \pm 8$ total excess events over an estimated background 12.5 ± 2.9 . ATHANASSOPOULOS 96b is a shorter version of this paper.

⁸ ATHANASSOPOULOS 95 error corresponds to the 1.6σ band in the plot. The expected background is 2.7 ± 0.4 events. Corresponds to an oscillation probability of $(0.34 \pm 0.20 \pm 0.16 \pm 0.07)\%$. For a different interpretation, see HILL 95. Replaced by ATHANASSOPOULOS 96.

⁹ HILL 95 is a report by one member of the LSND Collaboration, reporting a different conclusion from the analysis of the data of this experiment (see ATHANASSOPOULOS 95). Contrary to the rest of the LSND Collaboration, Hill finds no evidence for the neutrino oscillation $\bar{\nu}_\mu \rightarrow \bar{\nu}_e$ and obtains only upper limits.

¹⁰ FREEDMAN 93 is a search at LAMPF for $\bar{\nu}_e$ generated from any of the three neutrino types $\nu_\mu, \bar{\nu}_\mu$, and ν_e which come from the beam stop. The $\bar{\nu}_e$'s would be detected by the reaction $\bar{\nu}_e p \rightarrow e^+ n$. FREEDMAN 93 replaces DURKIN 88.

$\sin^2(2\theta)$ for "Large" $\Delta(m^2)$ ($\bar{\nu}_\mu \rightarrow \bar{\nu}_e$)

VALUE (units 10^{-3})	CL%	DOCUMENT ID	TECN	COMMENT
• • • We do not use the following data for averages, fits, limits, etc. • • •				
<640	90	1 ANTONELLO 13a	ICAR	$\bar{\nu}_e$ appearance
<150	90	2 CHENG 12	MBNE	MiniBooNE/SciBooNE
0.4-9.0	99	3 AGUILAR-AR...10	MBNE	$E_\nu > 475$ MeV
0.4-9.0	99	4 AGUILAR-AR...10	MBNE	$E_\nu > 200$ MeV
< 3.3	90	5 AGUILAR-AR...09b	MBNE	MiniBooNE
< 1.7	90	6 ARMBRUSTER02	KAR2	Liquid Sci. calor.
< 1.1	90	AVVAKUMOV 02	NTEV	NUTEV FNAL
5.3±1.3±9.0		7 AGUILAR 01	LSND	LAMPF
6.2±2.4±1.0		8 ATHANASSO...96	LSND	LAMPF
3-12	80	9 ATHANASSO...95		
< 6	90	10 HILL 95		

¹ ANTONELLO 13a obtained the limit by assuming $\bar{\nu}_\mu \rightarrow \bar{\nu}_e$ oscillation from the $\sim 2\%$ of $\bar{\nu}_\mu$ events contamination in the CNGS beam.

² CHENG 12 is a combined fit of MiniBooNE and SciBooNE antineutrino data.

³ This value is for a two neutrino oscillation analysis for excess antineutrino events with $E_\nu > 475$ MeV. At 90% CL there is no solution at high $\Delta(m^2)$. The best fit is at maximal mixing. The allowed region is consistent with LSND reported by AGUILAR 01. Supersedes AGUILAR-AREVALO 09b.

⁴ This value is for a two neutrino oscillation analysis for excess antineutrino events with $E_\nu > 200$ MeV with subtraction of the expected 12 events low energy excess seen in the neutrino component of the beam. At 90% CL there is no solution at high $\Delta(m^2)$. The best fit value is 0.007 for $\Delta(m^2) = 4.4$ eV².

⁵ This result is inconclusive with respect to small amplitude mixing suggested by LSND.

⁶ ARMBRUSTER 02 is the final analysis of the KARMEN 2 data. See footnote in the preceding table for further details, and the paper for the exclusion plot.

⁷ AGUILAR 01 is the final analysis of the LSND full data set. The deduced oscillation probability is $0.264 \pm 0.067 \pm 0.045\%$; the value of $\sin^2 2\theta$ for large $\Delta(m^2)$ is twice this probability (although these values are excluded by other constraints). See footnote in preceding table for further details, and the paper for a plot showing allowed regions. Supersedes ATHANASSOPOULOS 95, ATHANASSOPOULOS 96, and ATHANASSOPOULOS 98.

⁸ATHANASSOPOULOS 96 reports $(0.31 \pm 0.12 \pm 0.05)\%$ for the oscillation probability; the value of $\sin^2 2\theta$ for large $\Delta(m^2)$ should be twice this probability. See footnote in preceding table for further details, and see the paper for a plot showing allowed regions.

⁹ATHANASSOPOULOS 95 error corresponds to the 1.6σ band in the plot. The expected background is 2.7 ± 0.4 events. Corresponds to an oscillation probability of $(0.34 \pm 0.20 \pm 0.07)\%$. For a different interpretation, see HILL 95. Replaced by ATHANASSOPOULOS 96.

¹⁰HILL 95 is a report by one member of the LSND Collaboration, reporting a different conclusion from the analysis of the data of this experiment (see ATHANASSOPOULOS 95). Contrary to the rest of the LSND Collaboration, Hill finds no evidence for the neutrino oscillation $\bar{\nu}_\mu \rightarrow \bar{\nu}_e$ and obtains only upper limits.

Sterile neutrino limits

 $\Delta(m^2)$ for $\sin^2(2\theta) = 1$ ($\nu_\mu \rightarrow \nu_s$)

ν_s means ν_τ or any sterile (noninteracting) ν .

VALUE (10^{-5} eV ²)	CL%	DOCUMENT ID	TECN	COMMENT
-------------------------------------	-----	-------------	------	---------

• • • We do not use the following data for averages, fits, limits, etc. • • •

<3000 (or <550)	90	¹ OYAMA	89	KAMI Water Cherenkov
<4.2 or >54.	90	BIONTA	88	IMB Flux has $\nu_\mu, \bar{\nu}_\mu, \nu_e$, and $\bar{\nu}_e$

¹OYAMA 89 gives a range of limits, depending on assumptions in their analysis. They argue that the region $\Delta(m^2) = (100-1000) \times 10^{-5}$ eV² is not ruled out by any data for large mixing.

Search for ν_μ or $\nu_e \rightarrow \nu_s$

VALUE	CL%	DOCUMENT ID	TECN	COMMENT
-------	-----	-------------	------	---------

• • • We do not use the following data for averages, fits, limits, etc. • • •

<5	$\times 10^{-4}$	95	¹ AKER	23	T β decay
<0.05		95	² ALMAZAN	23	STEREO
<0.02		95	³ AKER	22A	SPEC T β decay
<0.0035		95	⁴ ATIF	22	RENO, NEOS
0.42	$\frac{+0.15}{-0.17}$	68	⁵ BARINOV	22A	BEST
<0.05		95	⁶ ANDRIAMIR...	21	PROSPECT
<0.005		95	⁷ SEREBROV	21	Neutrino-4
<0.008		95	⁸ SKROBOVA	20	DANSS
<0.01		90	⁹ ALEKSEEV	18	DANSS
<0.06		90	¹⁰ ALMAZAN	18	STEREO
<0.1		95	¹¹ ASHENFELT...	18	PROSPECT
<0.4		90	¹² AARTSEN	17B	ICCB IceCube-DeepCore
<8	$\times 10^{-3}$	95	¹³ ABDURASHI...	17	T β decay
<1	$\times 10^{-2}$	90	¹⁴ KO	17	NEOS
<2	$\times 10^{-2}$	90	¹⁵ AARTSEN	16	ICCB IceCube
<4.5	$\times 10^{-4}$	95	¹⁶ ADAMSON	16B	MINOS, DayaBay
<8.6	$\times 10^{-2}$	95	¹⁷ ADAMSON	16C	MINS
<1.1	$\times 10^{-2}$	95	¹⁸ AN	16B	DAYA
			¹⁹ AMBROSIO	01	MCRO matter effects
			²⁰ FUKUDA	00	SKAM neutral currents + matter effects

¹AKER 23 assume a 3+1 neutrino mixing model, use low-rate commissioning data of the KATRIN tritium β decay experiment to place a limit on $\sin^2(\theta_{14})$ for a admixture sterile neutrino mass m_4 of ~ 300 eV.

²ALMAZAN 23 use inverse beta decay data collected by the STEREO experiment, placed 9 to 11 m from the ILL research reactor, to search for $\bar{\nu}_e \rightarrow \bar{\nu}_s$ oscillations. The ILL research reactor uses highly enriched ²³⁵U fuel. No indication of the oscillation to sterile neutrinos is found, the stated limit on $\sin^2(2\theta_{14})$ correspond to $\Delta m_{41}^2 \sim 1$ eV² where the exclusion is maximal. Supersedes ALMAZAN 18.

³AKER 22A uses the first two science runs of the KATRIN tritium β decay neutrino mass experiment to search for an admixture of sterile neutrinos. No evidence is found for a spectral anomaly, indicating such admixture. The resulting limit is on $\sin^2(2\theta_{14})$ for sterile neutrino masses $m_4 < 40$ eV. It is most restrictive at $\Delta m_{41}^2 \sim 400$ eV². A 3+1 model is assumed.

⁴ATIF 22 report results from the combined analysis of the RENO (419 m) and NEOS (24 m) experiments data, collected at the Hanbit Nuclear Power Plant. Results, in terms of $\sin^2(2\theta_{14})$, constrain for $\bar{\nu}_e \rightarrow \bar{\nu}_s$ oscillations. The authors report both excluded and allowed parameter combinations. The exclusion result reported here is based on the Feldman-Cousins method and for $\Delta m_{41}^2 \simeq 0.55$ eV². Part of the allowed area is excluded by the STEREO and PROSPECT experiments.

⁵BARINOV 22A report an event deficit observed using the segmented Baksan Ga neutrino detector, exposed to a 3.4 MCi ⁵¹Cr source. Equal suppression factors are observed for the inner and outer segments. The deficit is interpreted as evidence for oscillations to sterile neutrinos. The result is in terms of $\sin^2(2\theta_{14})$, for a best fit of $\Delta m_{41}^2 = 3.3 \frac{+\infty}{-2.3}$ eV². Some, but not all, of the allowed neutrino parameter space conflicts with other experiments.

⁶ANDRIAMIRADO 21 reports a search for $\bar{\nu}_e \rightarrow \bar{\nu}_s$ oscillations at the HFIR research reactor, at baselines from 6.7 to 9.2 m. The reactor has a ²³⁵U core. 4 tons of ⁶Li-doped liquid scintillator are used in a segmented detector. Oscillations into sterile neutrinos are disfavored. The stated limit for $\sin^2(2\theta_{14})$ is for $\Delta m_{41}^2 \sim 2$ eV² where the sensitivity is maximal.

⁷SEREBROV 21 searches for $\bar{\nu}_e \rightarrow \bar{\nu}_s$ oscillations with a moveable detector with baseline 6–12 m from the SM-3 research reactor with highly enriched ²³⁵U fuel. Analyzing the L/E dependence a χ^2 minimum is found at $\Delta m_{41}^2 = 7.3 \pm 0.13 \pm 1.16$ eV² and $\sin^2(2\theta_{14}) = 0.36 \pm 0.12$. The quoted limit of 0.005 for $\sin^2(2\theta_{14})$ corresponds to $\Delta m_{41}^2 \sim 2$ eV². This is the result from 720 days of reactor ON and 860 days of reactor OFF measurements. The significance of the χ^2 minimum is 2.9 σ . Supersedes SEREBROV 20, SEREBROV 19 and SEREBROV 18A.

⁸SKROBOVA 20 searches for $\bar{\nu}_e - \bar{\nu}_s$ oscillations using the DANSS detector at 10.7, 11.2, and 12.7 m from the 3.1 GW_{th} power reactor. The DANSS detector is highly segmented and moveable; the positions are changed usually 3 times a week. The analysis is based on the ratio of the events at top and bottom position; the middle position is used for checks of consistency. No evidence for sterile neutrinos is found. The quoted limit 0.008, the smallest excluded $\sin^2(2\theta_{14})$, corresponds to $\Delta m_{41}^2 \sim 1.0$ eV². Supersedes ALEKSEEV 18.

⁹ALEKSEEV 18 searches for $\bar{\nu}_e \rightarrow \bar{\nu}_s$ oscillations using the DANSS detector at 10.7, 11.2, and 12.7 m from the 3.1 GW_{th} power reactor. The DANSS detector is highly segmented and moveable; the positions are changed usually 3 times a week. The analysis is based on the ratio of the events at top and bottom position; the middle position is used for checks of consistency. The best fit point is at $\Delta m_{41}^2 = 1.4$ eV² and $\sin^2(2\theta_{14}) = 0.05$ with $\Delta\chi^2 = 13.1$ (statistical errors only) compared to the fit with 3 active neutrinos only. The quoted limit of 0.01 for $\sin^2(2\theta_{14})$ corresponds to $\Delta m_{41}^2 \sim 1.0$ eV². Superseded by SKROBOVA 20.

¹⁰ALMAZAN 18 searches for the $\bar{\nu}_e \rightarrow \bar{\nu}_s$ oscillations with baseline from 9.4 to 11.1 m from the ILL research reactor with highly enriched ²³⁵U fuel. The STEREO detector consists of six separated cells with Gd loaded scintillator, with 15 m water equivalent overburden. The detected rate is 396.3 ± 4.7 $\bar{\nu}_e$ /day with signal to background ratio of about 0.9. The reported results corresponds to 66 days of reactor-on. The analysis uses the relative rates normalized to the cell number 1. No indication of the oscillation to the sterile neutrinos is found, the stated limit on $\sin^2(2\theta_{14})$ correspond to $\Delta m_{41}^2 \sim 3.5$ eV² where the exclusion is maximal. Superseded by ALMAZAN 23.

¹¹ASHENFELTER 18 searches for the $\bar{\nu}_e \rightarrow \bar{\nu}_s$ oscillations at baseline from 6.7 to 9.2 m from the 85 MW research reactor with pure ²³⁵U core. The segmented 4 ton ⁶Li-doped liquid scintillator is operated with about 1 m water equivalent overburden and recorded 25461 \pm 283 IBD events. No indication of oscillations into sterile neutrinos was observed. The stated limit for $\sin^2(2\theta_{14})$ is for $\Delta m_{41}^2 \sim 2$ eV² where the sensitivity is maximal.

¹²AARTSEN 17B uses three years of upward-going atmospheric neutrino data in the energy range of 10–60 GeV to constrain their disappearance into light sterile neutrinos. The reported limit $\sin^2\theta_{24} < 0.11$ at 90% C.L. is for $\Delta m_{41}^2 = 1.0$ eV². We convert the result to $\sin^2 2\theta_{24}$ for the listing. AARTSEN 17B also reports $\cos^2\theta_{24} \cdot \sin^2\theta_{34} < 0.15$ at 90% C.L. for $\Delta m_{41}^2 = 1.0$ eV².

¹³ABDURASHITOV 17 use the Troitsk nu-mass experiment to search for sterile neutrinos with mass 0.1 – 2 keV. We convert the reported limit from $U_{e4}^2 < 0.002$ to $\sin^2 2\theta_{14} < 0.008$ assume $U_{e4} \sim \sin\theta_{14}$. The stated limit corresponds to the smallest U_{e4}^2 . The exclusion curve begins at U_{e4}^2 of 0.02 for $m_4 = 0.1$ keV.

¹⁴KO 17 reports on short baseline reactor oscillation search ($\bar{\nu}_e \rightarrow \bar{\nu}_s$), motivated by the so-called “reactor antineutrino anomaly”. The experiment is conducted at 23.7 m from the core of unit 5 of the Hanbit Nuclear Power Complex in Korea. The reported limit on $\sin^2(2\theta_{41})$ for sterile neutrinos was determined using the reactor antineutrino spectrum determined by the Daya Bay experiment for Δm_{14}^2 around 0.55 eV² where the sensitivity is maximal. A fraction of the parameter space derived from the “reactor antineutrino anomaly” is excluded by this work. Compared to reactor models an event excess is observed at about 5 MeV, in agreement with other experiments.

¹⁵AARTSEN 16 use one year of upward-going atmospheric muon neutrino data in the energy range of 320 GeV to 20 TeV to constrain their disappearance into light sterile neutrinos. Sterile neutrinos are expected to produce distinctive zenith distribution for these energies for $0.01 \leq \Delta m^2 \leq 10$ eV². The stated limit is for $\sin^2 2\theta_{24}$ at Δm^2 around 0.3 eV².

¹⁶ADAMSON 16b combine the results of AN 16B, ADAMSON 16C, and Bugey-3 reactor experiments to constrain ν_μ to ν_e mixing through oscillations into light sterile neutrinos. The stated limit for $\sin^2 2\theta_{\mu e}$ is at $|\Delta m_{41}^2| = 1.2$ eV².

¹⁷ADAMSON 16C use the NuMI beam and exposure of 10.56×10^{20} protons on target to search for the oscillation of ν_μ dominated beam into light sterile neutrinos with detectors at 1.04 and 735 km. The reported limit $\sin^2(\theta_{24}) < 0.022$ at 95% C.L. is for $|\Delta m_{41}^2| = 0.5$ eV². We convert the result to $\sin^2(2\theta_{24})$ for the listing.

¹⁸AN 16B utilize 621 days of data to place limits on the $\bar{\nu}_e$ disappearance into a light sterile neutrino. The stated limit corresponds to the smallest $\sin^2(2\theta_{14})$ at $|\Delta m_{41}^2| \sim 3 \times 10^{-2}$ eV² (obtained from Figure 3 in AN 16B). The exclusion curve begins at $|\Delta m_{41}^2| \sim 1.5 \times 10^{-4}$ eV² and extends to ~ 0.25 eV². The analysis assumes $\sin^2(2\theta_{12}) = 0.846 \pm 0.021$, $\Delta m_{21}^2 = (7.53 \pm 0.18) \times 10^{-5}$ eV², and $|\Delta m_{32}^2| = (2.44 \pm 0.06) \times 10^{-3}$ eV².

¹⁹AMBROSIO 01 tested the pure 2-flavor $\nu_\mu \rightarrow \nu_s$ hypothesis using matter effects which change the shape of the zenith-angle distribution of upward through-going muons. With maximum mixing and Δm^2 around 0.0024 eV², the $\nu_\mu \rightarrow \nu_s$ oscillation is disfavored with 99% confidence level with respect to the $\nu_\mu \rightarrow \nu_\tau$ hypothesis.

²⁰FUKUDA 00 tested the pure 2-flavor $\nu_\mu \rightarrow \nu_s$ hypothesis using three complementary atmospheric-neutrino data samples. With this hypothesis, zenith-angle distributions are expected to show characteristic behavior due to neutral currents and matter effects. In the Δm^2 and $\sin^2 2\theta$ region preferred by the Super-Kamiokande data, the $\nu_\mu \rightarrow \nu_s$ hypothesis is rejected at the 99% confidence level, while the $\nu_\mu \rightarrow \nu_\tau$ hypothesis consistently fits all of the data sample.

FUKUDA	02	PL B539 179	S. Fukuda <i>et al.</i>	(Super-Kamiokande Collab.)
AGUILAR	01	PR D64 112007	A. Aguilar <i>et al.</i>	(LSND Collab.)
AHMAD	01	PRL 87 071301	Q.R. Ahmad <i>et al.</i>	(SNO Collab.)
AMBROSIO	01	PL B517 59	M. Ambrosio <i>et al.</i>	(MACRO Collab.)
BOEHM	01	PR D64 112001	F. Boehm <i>et al.</i>	
FUKUDA	01	PRL 86 5651	S. Fukuda <i>et al.</i>	(Super-Kamiokande Collab.)
AMBROSIO	00	PL B478 5	M. Ambrosio <i>et al.</i>	(MACRO Collab.)
BOEHM	00	PRL 84 3764	F. Boehm <i>et al.</i>	
FUKUDA	00	PRL 85 3939	S. Fukuda <i>et al.</i>	(Super-Kamiokande Collab.)
ALLISON	99	PL B449 137	W.W.M. Allison <i>et al.</i>	(Soudan 2 Collab.)
APOLLONIO	99	PL B466 415	M. Apollonio <i>et al.</i>	(CHOOZ Collab.)
Also		PL B472 434 (errata.)	M. Apollonio <i>et al.</i>	(CHOOZ Collab.)
FUKUDA	99C	PRL 82 2644	Y. Fukuda <i>et al.</i>	(Super-Kamiokande Collab.)
FUKUDA	99D	PRL B467 185	Y. Fukuda <i>et al.</i>	(Super-Kamiokande Collab.)
HAMPEL	99	PL B447 127	W. Hampel <i>et al.</i>	(GALLEX Collab.)
AMBROSIO	98	PL B434 451	M. Ambrosio <i>et al.</i>	(MACRO Collab.)
APOLLONIO	98	PL B420 397	M. Apollonio <i>et al.</i>	(CHOOZ Collab.)
ATHANASSO...	98	PRL 81 1774	C. Athanassopoulos <i>et al.</i>	(LSND Collab.)
ATHANASSO...	98B	PR C58 2489	C. Athanassopoulos <i>et al.</i>	(LSND Collab.)
CLEVELAND	98	APJ 496 505	B.T. Cleveland <i>et al.</i>	(Homestake Collab.)
FELDMAN	98	PR D57 3873	G.J. Feldman, R.D. Cousins	
FUKUDA	98C	PRL 81 1562	Y. Fukuda <i>et al.</i>	(Super-Kamiokande Collab.)
HATAKEYAMA	98	PRL 81 2016	S. Hatakeyama <i>et al.</i>	(Kamiokande Collab.)
CLARK	97	PRL 79 345	R. Clark <i>et al.</i>	(IMB Collab.)
AGLIETTA	96	JETPL 63 791	M. Aglietta <i>et al.</i>	(LSD Collab.)
		Translated from ZETFP 63 753.		
ATHANASSO...	96	PR C54 2685	C. Athanassopoulos <i>et al.</i>	(LSND Collab.)
ATHANASSO...	96B	PRL 77 3082	C. Athanassopoulos <i>et al.</i>	(LSND Collab.)
FUKUDA	96	PRL 77 1683	Y. Fukuda <i>et al.</i>	(Kamiokande Collab.)
FUKUDA	96B	PL B388 397	Y. Fukuda <i>et al.</i>	(Kamiokande Collab.)
GREENWOOD	96	PR D53 6054	Z.D. Greenwood <i>et al.</i>	(UCI, SVR, SUCU)
HAMPEL	96	PL B398 384	W. Hampel <i>et al.</i>	(GALLEX Collab.)
LOVERRE	96	PL B370 156	P.F. Loverre	
ACHKAR	95	NP B434 503	B. Achkar <i>et al.</i>	(SING, SAACL, CPPM, CDEF+)
AHLEN	95	PL B357 481	S.P. Ahlen <i>et al.</i>	(MACRO Collab.)
ATHANASSO...	95	PRL 75 2650	C. Athanassopoulos <i>et al.</i>	(LSND Collab.)
DAUM	95	ZPHY C66 417	K. Daum <i>et al.</i>	(FREJUS Collab.)
HILL	95	PRL 75 2654	J.E. Hill	(PENN)
DECLAIS	94	PL B338 383	Y. Declais <i>et al.</i>	
FUKUDA	94	PL B335 237	Y. Fukuda <i>et al.</i>	(Kamiokande Collab.)
VILAIN	94C	ZPHY C64 539	P. Vilain <i>et al.</i>	(CHARM II Collab.)
FREEDMAN	93	PR D47 811	S.J. Freedman <i>et al.</i>	(LAMPF E645 Collab.)
BECKER-SZ.	92B	PR D46 3720	R.A. Becker-Szendy <i>et al.</i>	(IMB Collab.)
BEIER	92	PL B283 446	E.W. Beier <i>et al.</i>	(KAM2 Collab.)
Also		PTRSL A346 63	R.W. Beier, E.D. Frank	(PENN)
HIRATA	92	PL B280 146	K.S. Hirata <i>et al.</i>	(Kamiokande II Collab.)
CASPER	91	PRL 66 2561	D. Casper <i>et al.</i>	(IMB Collab.)
HIRATA	91	PRL 66 9	K.S. Hirata <i>et al.</i>	(Kamiokande II Collab.)
KUVSHIN...	91	JETPL 54 253	A.A. Kuvshinikov <i>et al.</i>	(KIAE)
BERGER	90B	PL B245 305	C. Berger <i>et al.</i>	(FREJUS Collab.)
HIRATA	90	PRL 65 1297	K.S. Hirata <i>et al.</i>	(Kamiokande II Collab.)
AGLIETTA	89	EPL 8 611	M. Aglietta <i>et al.</i>	(FREJUS Collab.)
DAVIS	89	ARNPS 39 467	R. Davis, A.K. Mann, L. Wolfenstein	(BNL, PENN+)
OYAMA	89	PR D39 1481	Y. Oyama <i>et al.</i>	(Kamiokande II Collab.)
BIONTA	88	PR D38 768	R.M. Bionta <i>et al.</i>	(IMB Collab.)
DURKIN	88	PRL 61 1811	L.S. Durkin <i>et al.</i>	(OSU, ANL, CIT+)
ABRAMOWICZ	86	PRL 57 298	H. Abramowicz <i>et al.</i>	(CDHS Collab.)
ALLABY	86	PL B177 446	J.V. Allaby <i>et al.</i>	(CHARM Collab.)
ANGELINI	86	PL B179 307	C. Angelini <i>et al.</i>	(PISA, ATHU, PADO+)
VUILLEUMIER	82	PL 114B 298	J.L. Vuilleumier <i>et al.</i>	(CIT, SIN, MUNI)
BOLIEV	81	SJNP 34 787	M.M. Boliev <i>et al.</i>	(INRM)
		Translated from YAF 34 1418.		
KWON	81	PR D24 1097	H. Kwon <i>et al.</i>	(CIT, ISNG, MUNI)
BOEHM	80	PL 97B 310	F. Boehm <i>et al.</i>	(ILLG, CIT, ISNG, MUNI)
CROUCH	78	PR D18 2239	M.F. Crouch <i>et al.</i>	(CASE, UCI, WITW)

Heavy Neutral Leptons, Searches for

OMITTED FROM SUMMARY TABLE

We define searches for Heavy Neutral Leptons (HNLs) as searches for Dirac or Majorana fermions with sterile neutrino quantum numbers, that are heavy enough to not disrupt the simplest Big Bang Nucleosynthesis bounds and/or unstable on cosmological timescales: Typically HNLs have mass \sim MeV or higher.

Searches for these particles generically set bounds on the mixing between the HNL and the active neutrinos, as parametrized by the extended 3×4 PMNS matrix elements $U_{\ell X}$ (see the "Neutrino mass, mixing and oscillations" review) where $\ell = e, \mu$ or τ , and we denote the HNL as ν_X . While many measurements may be interpreted to place bounds on various combinations of these matrix elements, we quote below limits only for those cases in which one matrix element is assumed to be much larger than the other two, i.e. $|U_{\ell X}| \gg |U_{\ell' X}|$ for $\ell' \neq \ell$.

Experimental searches make use of various different strategies, including e.g. resonance searches in missing mass decay distributions or specific final states, searches for lepton number violating decays, and trilepton signatures. The resulting bounds on $U_{\ell X}$ are typically dependent on the HNL mass. The quoted limits below are either the best limit near an experimental kinematic threshold, or a characteristic value in the mass range of the experimental sensitivity.

Limits on heavy neutral lepton mixing parameters

Limits on $|U_{eX}|^2$

Quoted limits are either the best limit near the kinematic threshold of the experiment, or a characteristic value in the mass range of the experimental sensitivity

VALUE	CL%	DOCUMENT ID	TECN	COMMENT
$< 5 \times 10^{-7}$	95	¹ AAD	23AO ATLS	$m_{\nu_X} \sim 3\text{--}15$ GeV, pp at 13 TeV

$< 3 \times 10^{-4}$	90	² AGNES	23A DS50	$m_{\nu_X} \sim 7\text{--}35$ keV
$< 3 \times 10^{-8}$	90	³ BAROUKI	22 RVUE	Near $m_{D_s} - m_e$ kin. thres.
$< 1 \times 10^{-6}$	95	⁴ TUMASYAN	22AD CMS	$m_{\nu_X} \sim 8\text{--}14$ GeV, pp at 13 TeV
$< 2 \times 10^{-4}$	95	⁵ FRIEDRICH	21	Near $m_{7\text{Be}} - m_{7\text{Li}}$ kin. thres.
$< 1 \times 10^{-9}$	90	⁶ CORTINA-GIL	20 NA62	$m_{\nu_X} \sim 150\text{--}400$ MeV
$< 2 \times 10^{-5}$	95	⁷ AAD	19F ATLS	$m_{\nu_X} \sim 15\text{--}40$ GeV
$< 1 \times 10^{-9}$	90	⁸ ABE	19B T2K	Near $m_K - m_\pi$ kin. thres.
$< 1 \times 10^{-4}$	90	⁹ ABLIKIM	19AL BES3	$m_{\nu_X} \sim 0.3\text{--}0.7$ GeV
$< 2 \times 10^{-7}$	90	¹⁰ BRYMAN	19 RVUE	$m_{\nu_X} \sim 55$ MeV
$< 1 \times 10^{-8}$	90	¹¹ AGUILAR-AR...	18A PIEN	$m_{\nu_X} \sim 60\text{--}120$ MeV
$< 3 \times 10^{-7}$	90	¹² CORTINA-GIL	18 NA62	$m_{\nu_X} \sim 200\text{--}400$ MeV
$< 1 \times 10^{-6}$	90	¹³ PARK	16 BELL	$m_{\nu_X} \sim 1.4$ GeV
$< 3 \times 10^{-5}$	90	¹⁴ LIVENTSEV	13 BELL	Near $m_{\nu_X} \sim 2\text{--}2.5$ GeV
$< 3 \times 10^{-5}$	95	¹⁵ ABREU	97I DLPH	$m_{\nu_X} \sim 6\text{--}50$ GeV
$< 2 \times 10^{-5}$	95	¹⁶ ABREU	97I DLPH	Near $m_{\nu_X} \sim 3.5$ GeV
$< 1 \times 10^{-5}$	90	¹⁷ BARANOV	93	Near $m_{\pi} - m_e$ kin. thres.
$< 2 \times 10^{-7}$	90	¹⁷ BARANOV	93	Near $m_K - m_e$ kin. thres.
$< 1 \times 10^{-7}$	90	^{18,19} BERNARDI	88 CNTR	Near $m_{\pi} - m_e$ kin. thres.
$< 2 \times 10^{-9}$	90	^{19,20} BERNARDI	88 CNTR	Near $m_K - m_e$ kin. thres.
$< 1 \times 10^{-7}$	90	²¹ DORENBOS...	86 CHR M	Near $m_D - m_e$ kin. thres.
$< 1 \times 10^{-7}$	90	²² COOPER...	85 BEBC	Near $m_D - m_e$ kin. thres.

- AAD 23AO search for $W \rightarrow \nu_X e$, for both Majorana and Dirac HNL scenarios. Also consider scenarios involving multiflavor mixing, with correspondingly weaker limits.
- Search for ionization signals in an LArTPC. Assumes the candidate particle is 100% of dark matter.
- Reanalysis of BEBC results (cf. COOPER-SARKAR 85) to update searches for $D_s^\pm \rightarrow \nu_X e^\pm$ using a corrected formula for the HNL decay probabilities, additional production channels, and an improved fit for the charm meson distributions. Assumes a Majorana HNL.
- TUMASYAN 22AD search for $W \rightarrow e \nu_X, \nu_X \rightarrow e \mu \nu_\mu$ and set limits for Dirac and Majorana Heavy Neutral Leptons. The data correspond to an integrated luminosity of 138 fb $^{-1}$.
- Search in electron capture decay ${}^7\text{Be} \rightarrow {}^7\text{Li} \nu_X$. Kinematic threshold is ~ 850 keV.
- Search for $K^+ \rightarrow e^+ \nu_X$. Assumes lifetime of $\nu_X > 50$ ns.
- Limit from prompt lepton number violating trilepton search.
- $K^+ \rightarrow e^+ \nu_X$, with ν_X decay through U_{eX} . ABE 19B also considers bounds on $|U_{\ell X} U_{\ell' X}|$ for combinations of lepton flavors in the ν_X decay final state.
- Searches for a Majorana Heavy Neutral Lepton producing a $\pi^- e^+$ resonance in the same sign dilepton decay $D \rightarrow K \pi^- e^+ e^+$.
- BRYMAN 19 sets best limits $|U_{eX}|^2 < 1 \times 10^{-4} - 2 \times 10^{-7}$ in the mass range $m_{\nu_X} \sim 2\text{--}55$ MeV, respectively, using the precision branching ratio measurement in AGUILAR-AREVALO 15. See also BRYMAN 19A.
- Search for $\pi^+ \rightarrow e^+ \nu_X$.
- Search for $K^+ \rightarrow e^+ \nu_X$.
- PARK 16 quotes an approximate limit $B(B^+ \rightarrow e^+ \nu_X) < 3 \times 10^{-6}$ in the mass range $m_{\nu_X} \sim 0.2\text{--}1.4$ GeV.
- Search for $B^+ \rightarrow e^+ \nu_X$.
- Search for prompt ν_X decay signatures.
- Search for displaced ν_X decay signatures.
- Searches for K or $\pi \rightarrow e^+ \nu_X, \nu_X \rightarrow e^+ e^- \nu_e$ using a beam dump experiment at the 70 GeV Serpukhov proton synchrotron. BARANOV 93 also considers limits for $|U_{eX} U_{\mu X}|$ from K or $\pi \rightarrow \mu^+ \nu_X, \nu_X \rightarrow e^+ e^- \nu_e$.
- $\pi^+ \rightarrow e^+ \nu_X$, with ν_X decay through U_{eX} .
- BERNARDI 88 also considers bounds on $|U_{eX} U_{\mu X}|$.
- $K^+ \rightarrow e^+ \nu_X$, with ν_X decay through U_{eX} .
- $D^+ \rightarrow e^+ \nu_X$, with $\nu_X \rightarrow e^- \ell^+ \nu_\ell$.
- $D^+ \rightarrow e^+ \nu_X$, with $\nu_X \rightarrow e^- \ell^+ \nu_\ell$ or $\nu_X \rightarrow e^- \pi^+$.

Limits on $|U_{\mu X}|^2$

Quoted limits are either the best limit near the kinematic threshold of the experiment, or a characteristic value in the mass range of the experimental sensitivity

VALUE	CL%	DOCUMENT ID	TECN	COMMENT
$< 5 \times 10^{-7}$	95	¹ AAD	23AO ATLS	$m_{\nu_X} \sim 3\text{--}15$ GeV, pp at 13 TeV
< 0.1	95	² AAD	23CE ATLS	Near $m_{\nu_X} \sim 0.1\text{--}2$ TeV
< 0.1	95	³ TUMASYAN	23AC CMS	Near $m_{\nu_X} \sim 0.1\text{--}3$ TeV
$< 5 \times 10^{-9}$	90	⁴ ABRATENKO	22A MBNE	Near $m_K - m_\mu$ kin. thres.
$< 3 \times 10^{-7}$	95	⁵ TUMASYAN	22AD CMS	$m_{\nu_X} \sim 8\text{--}14$ GeV, pp at 13 TeV
$< 1 \times 10^{-3}$	95	⁶ AAJ	21AA LHCB	$m_{\nu_X} \sim 5\text{--}50$ GeV, pp at 7, 8 TeV
$< 2 \times 10^{-4}$	95	⁷ AAJ	21AA LHCB	$m_{\nu_X} \sim 5\text{--}50$ GeV, pp at 7, 8 TeV
$< 5 \times 10^{-9}$	90	^{8,9} CORTINA-GIL	21 NA62	Near $m_K - m_\mu$ kin. thres.

Lepton Particle Listings

Heavy Neutral Leptons, Searches for

$<2 \times 10^{-2}$	90	10	PRIM	20	BELL	$m_{\nu_X} \sim 1$ GeV
$<2 \times 10^{-5}$	95	11	AAD	19F	ATLS	$m_{\nu_X} \sim 10\text{--}50$ GeV
$<2 \times 10^{-6}$	95	12	AAD	19F	ATLS	$m_{\nu_X} \sim 10$ GeV
$<1 \times 10^{-9}$	90	13	ABE	19B	T2K	Near $m_K - m_\mu$ kin. thres.
$<5 \times 10^{-6}$	90	14,15	AGUILAR-AR...	19B	PIEN	$m_{\nu_X} \sim 16\text{--}30$ MeV
$<1 \times 10^{-5}$	90	15	AGUILAR-AR...	19B	PIEN	Near $m_{\pi^- - m_\mu}$ kin. thres.
$<3 \times 10^{-7}$	90	8	CORTINA-GIL	18	NA62	$m_{\nu_X} \sim 250\text{--}350$ MeV
$<3 \times 10^{-6}$	90	8	LAZZERONI	17A	NA62	Near $m_K - m_\mu$ kin. thres.
$<5 \times 10^{-2}$	90	16	PARK	16	BELL	$m_{\nu_X} \sim 1.4$ GeV
$<1 \times 10^{-8}$	90	8	ARTAMONOV	15A	B949	$m_{\nu_X} \sim 200\text{--}300$ MeV
$<3 \times 10^{-5}$	90	17	LIVENTSEV	13	BELL	Near $m_{\nu_X} \sim 2\text{--}2.5$ GeV
$<2.0 \times 10^{-8}$	95	18	DAUM	00	KARM	$m_{\nu_X} = 33.905$ MeV
$<8 \times 10^{-8}$	90	19	VAITAITIS	99	CCFR	Near $m_K - m_\mu$ kin. thres.
$<6 \times 10^{-8}$	90	20	VAITAITIS	99	CCFR	Near $m_{D_s} - m_\mu$ kin. thres.
$<3 \times 10^{-5}$	95	21	ABREU	97I	DLPH	$m_{\nu_X} \sim 6\text{--}50$ GeV
$<2 \times 10^{-5}$	95	22	ABREU	97I	DLPH	Near $m_{\nu_X} \sim 3.5$ GeV
$<3 \times 10^{-5}$	90	23	VILAIN	95C	CHM2	Near $m_K - m_\mu$ kin. thres.
$<3 \times 10^{-8}$	90	24,25	BERNARDI	88	CNTR	Near $m_{\mu^+ - m_\pi}$ kin. thres.
$<2 \times 10^{-9}$	90	25,26	BERNARDI	88	CNTR	Near $m_K - m_\mu$ kin. thres.
$<1 \times 10^{-7}$	90	27	DORENBOS...	86	CHRM	Near $m_D - m_\mu$ kin. thres.
$<1 \times 10^{-7}$	90	28	COOPER...	85	BEBC	Near $m_D - m_\mu$ kin. thres.

• • • We do not use the following data for averages, fits, limits, etc. • • •

$<1 \times 10^{-7}$ 90 29 ABRATENKO 20 MBNE Superseded by ABRATENKO 22A

1 AAD 23AO search for $W \rightarrow \nu_X \mu$, for both Majorana and Dirac HNL scenarios. Also consider scenarios involving multiflavor mixing, with correspondingly weaker limits.

2 AAD 23CE search for Majorana HNLs via vector boson fusion $W^\pm W^\pm \rightarrow \mu^\pm \mu^\pm$. Limits set in a m_{ν_X} mass range from 50 GeV up to 20 TeV, using the Phenomenological Type-I Seesaw model as a benchmark scenario.

3 TUMASYAN 23AC search for Majorana HNLs via vector boson fusion $W^\pm W^\pm \rightarrow \mu^\pm \mu^\pm$. Limits set in a m_{ν_X} mass range from 50 GeV up to 25 TeV.

4 ABRATENKO 22A search for $K^+ \rightarrow \mu^+ \nu_X$, with $\nu_X \rightarrow \mu^\mp \pi^\pm$, in the mass range $m_{\nu_X} \sim 246\text{--}385$ MeV. Also considers limits from $\nu_X \rightarrow \mu^- \pi^+$ only, for the case of a Dirac HNL.

5 TUMASYAN 22AD search for $W \rightarrow \mu \nu_X$, $\nu_X \rightarrow \mu e \nu_e$ and set limits for Dirac and Majorana Heavy Neutral Leptons. The data correspond to an integrated luminosity of 138 fb^{-1} .

6 Limit from prompt lepton number conserving $W \rightarrow \mu \mu j$ search.

7 Limit from prompt lepton number violating $W \rightarrow \mu \mu j$ search.

8 Search for $K^+ \rightarrow \mu^+ \nu_X$.

9 Assumes a lifetime exceeding 50 ns, and searches over m_{ν_X} range 200–384 MeV.

10 Search for $B^+ \rightarrow \mu^+ \nu_X$ in the mass range $m_{\nu_X} \sim 0\text{--}1.5$ GeV.

11 Limit from prompt lepton number violating trilepton search.

12 Limit from displaced lepton violating or conserving trilepton searches.

13 $K^+ \rightarrow \mu^+ \nu_X$, with ν_X decay through $U_{\mu X}$. ABE 19B also considers bounds on $|U_{\ell X} U_{\ell' X}|$ for combinations of lepton flavors in the ν_X decay final state.

14 Limit requires muon kinetic energy > 1.2 MeV.

15 Search for $\pi^+ \rightarrow \mu^+ \nu_X$.

16 PARK 16 quotes an approximate limit $B(B^+ \rightarrow \mu^+ \nu_X) < 3 \times 10^{-6}$ in the mass range $m_{\nu_X} \sim 0.2\text{--}1.4$ GeV.

17 Search for $B^+ \rightarrow \mu^+ \nu_X$.

18 DAUM 00 quotes a branching ratio bound $B(\pi^+ \rightarrow \mu^+ \nu_X) < 6.0 \times 10^{-10}$ at 95% CL.

19 $K^+ \rightarrow \mu^+ \nu_X$, with $\nu_X \rightarrow \mu X$.

20 $D_s \rightarrow \mu^+ \nu_X$, with $\nu_X \rightarrow \mu X$.

21 Search for prompt ν_X decay signatures.

22 Search for displaced ν_X decay signatures.

23 Search for Heavy Neutral Leptons produced by neutral current muon neutrino interactions, with $\nu_X \rightarrow \mu^+ \mu^- \nu_\mu$.

24 $K^+ \rightarrow \mu^+ \nu_X$, with ν_X decay through $U_{\mu X}$ and $m_{\nu_X} < m_\mu + m_\pi$.

25 BERNARDI 88 also considers bounds on $|U_{eX} U_{\mu X}|$.

26 $K^+ \rightarrow \mu^+ \nu_X$, with $\nu_X \rightarrow \mu^- \pi^+$.

27 $D^+ \rightarrow \mu^+ \nu_X$, with $\nu_X \rightarrow \mu^- \ell^+ \nu_\ell$.

28 $D^+ \rightarrow \mu^+ \nu_X$, with $\nu_X \rightarrow \mu^- \ell^+ \nu_\ell$ or $\nu_X \rightarrow \mu^- \pi^+$.

29 $K^+ \rightarrow \mu^+ \nu_X$, with $\nu_X \rightarrow \mu^- \pi^+$, in the mass range $m_{\nu_X} \sim 260\text{--}385$ MeV. ABRATENKO 20 also considers $\nu_X \rightarrow \mu^+ \pi^-$ for the case of a Majorana HNL.

Limits on $|U_{\tau X}|^2$

Quoted limits are either the best limit near the kinematic threshold of the experiment, or a characteristic value in the mass range of the experimental sensitivity

VALUE	CL%	DOCUMENT ID	TECN	COMMENT
$<1 \times 10^{-5}$	95	1 LEES	23A	BABR Near $m_\tau - 3m_\pi$ kin. thres.
$<2 \times 10^{-6}$	90	2 BAROUKI	22	RVUE Near $m_\tau - m_\nu$ kin. thres.
$<3 \times 10^{-4}$	90	3 ACCIARRI	21	ARNT Near $m_{\nu_X} \lesssim 970$ MeV
$<3 \times 10^{-6}$	90	4 BOIARSKA	21	RVUE Near $m_{\nu_X} \sim 0.8\text{--}1.6$ GeV
$<2 \times 10^{-4}$	90	5 ORLOFF	02	CHRM Near $m_D - m_\tau$ kin. thres.
$<1 \times 10^{-4}$	90	6 ORLOFF	02	CHRM $m_{\nu_X} \sim 200\text{--}250$ MeV
$<3 \times 10^{-5}$	95	7 ABREU	97I	DLPH $m_{\nu_X} \sim 6\text{--}50$ GeV
$<2 \times 10^{-5}$	95	8 ABREU	97I	DLPH Near $m_{\nu_X} \sim 3.5$ GeV

• • • We do not use the following data for averages, fits, limits, etc. • • •

9 LIVENTSEV 23 BELL Near $m_{\nu_X} \sim 0.8\text{--}1.2$ GeV

10 TUMASYAN 22H CMS $p\bar{p}$ at 13 TeV

1 Search for $\tau^\pm \rightarrow \pi^\pm \pi^+ \pi^- \nu_X$.

2 Reanalysis of BEBC results (cf. COOPER-SARKAR 85) to include searches for $D_s^\pm \rightarrow \nu_\tau \tau^\pm$, $\tau^\pm \rightarrow \nu_X \pi^\pm$, $\nu_X \rho^\pm$, or $\nu_X \nu_\tau \ell^\pm$ via $U_{\tau X}$. Assumes a Majorana HNL.

3 Search for $\nu_X \rightarrow \mu^+ \mu^- \nu$.

4 Reanalysis of CHARM results (cf. ORLOFF 02) to include searches for $\nu_X \rightarrow \nu \ell^+ \ell^-$ decays, and including the production of HNLs from τ decays.

5 $D_s \rightarrow \tau^+ \nu_X$, with ν_X decay via $U_{\tau X}$.

6 $D_s \rightarrow \nu_\tau \tau^+$, $\tau^+ \rightarrow \nu_X X$, with ν_X decay via $U_{\tau X}$.

7 Search for prompt ν_X decay signatures.

8 Search for displaced ν_X decay signatures. Kinematical suppression of $\nu_X \rightarrow \tau X$ at lower masses leads to rapid loosening of the $|U_{\tau X}|$ bound compared to that for $|U_{eX}|$ and $|U_{\mu X}|$.

9 Search for $\tau \rightarrow \pi \nu_X$, $\nu_X \rightarrow \pi e$ or $\pi \mu$ in the range 0.2–1.6 GeV. LIVENTSEV 23 reports results for the sum $\sum_{\ell=e,\mu,\tau} |U_{\ell X}|^2$ in a model-dependent context, but which may be roughly reinterpreted as a limit $|U_{eX} U_{\tau X}|^2 + |U_{\mu X} U_{\tau X}|^2 \lesssim 5 \times 10^{-9}$ in either Majorana or Dirac HNL scenarios.

10 TUMASYAN 22H sets limits on an approximately mass-degenerate vector-like lepton SU(2) doublet coupling to the τ . Some of the reported signal region distributions might be used to set limits for heavy neutral leptons coupled to the τ . The data correspond to an integrated luminosity of 138 fb^{-1} .

REFERENCES FOR Heavy Neutral Leptons, Searches for

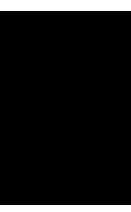
AAD	23AO	PRL 131 061803	G. Aad et al.	(ATLAS Collab.)
AAD	23CE	EPJ C83 824	G. Aad et al.	(ATLAS Collab.)
AGNES	23A	PRL 130 101002	P. Agnes et al.	(DarkSide-50 Collab.)
LEES	23A	PR D107 052009	J.P. Lees et al.	(BABAR Collab.)
LIVENTSEV	23	PRL 131 211802	D. Liventsev et al.	(BELLE Collab.)
TUMASYAN	23AC	PRL 131 011803	A. Tumasyan et al.	(CMS Collab.)
ABRATENKO	22A	PR D106 092006	P. Abratenko et al.	(MicroBooNE Collab.)
BAROUKI	22	SCP 13 118	R. Barouki, G. Marocco, S. Sarkar	(OXF)
TUMASYAN	22AD	JHEP 2207 081	A. Tumasyan et al.	(CMS Collab.)
TUMASYAN	22H	PR D105 112007	A. Tumasyan et al.	(CMS Collab.)
AJJ	21AA	EPJ C81 248	R. Ajij et al.	(LHCb Collab.)
ACCIARRI	21	PRL 127 121801	R. Acciarri et al.	(ArgoNeUT Collab.)
BOIARSKA	21	PR D104 095019	I. Boiarska et al.	(BOHR, LEID)
CORTINA-GIL	21	PL B816 136259	E. Cortina Gil et al.	(NA62 Collab.)
FRIEDRICH	21	PRL 126 021803	S. Friedrich et al.	(BeEST Collab.)
ABRATENKO	20	PR D101 052001	P. Abratenko et al.	(MiniBooNE Collab.)
CORTINA-GIL	16	PR D94 012003	E. Cortina Gil et al.	(NA62 Collab.)
PRIM	20	PR D101 032007	M.T. Prim et al.	(BELLE Collab.)
AAD	19F	JHEP 1910 265	G. Aad et al.	(ATLAS Collab.)
ABE	19B	PR D100 052006	K. Abe et al.	(T2K Collab.)
ABLIKIM	19AL	PR D99 112002	M. Ablikim et al.	(BESIII Collab.)
AGUILAR-AR...	19B	PL B798 134980	A. Aguilar-Arevalo et al.	(PIENU Collab.)
BRYMAN	19	PR D100 053006	D.A. Bryman, R. Shrock	(BRCO, TRIU, STON)
BRYMAN	19A	PR D100 073011	D.A. Bryman, R. Shrock	(BRCO, TRIU, STON)
AGUILAR-AR...	18A	PR D97 072012	A. Aguilar-Arevalo et al.	(PIENU Collab.)
CORTINA-GIL	18	PL B778 137	E. Cortina Gil et al.	(NA62 Collab.)
LAZZERONI	17A	PL B772 712	C. Lazzeroni et al.	(NA62 Collab.)
PARK	16	PR D94 012003	C.-S. Park et al.	(BELLE Collab.)
AGUILAR-AR...	15	PRL 115 071801	A. Aguilar-Arevalo et al.	(PIENU Collab.)
ARTAMONOV	15A	PR D91 052001	A.V. Artamonov et al.	(E949 Collab.)
LIVENTSEV	13	PR D87 071102	D. Liventsev et al.	(BELLE Collab.)
Also	PR D95 099903 (err.)	D. Liventsev et al.	(BELLE Collab.)	
ORLOFF	02	PL B550 8	J. Orloff et al.	(CHARM Collab.)
DAUM	00	PRL 85 1815	M. Daum et al.	(KARMEN Collab.)
VAITAITIS	99	PRL 83 4943	A. Vaitaitis et al.	(CCFR Collab.)
ABREU	97I	ZPHY C74 57	P. Abreu et al.	(DELPHI Collab.)
Also	ZPHY C75 580 (err.)	P. Abreu et al.	(DELPHI Collab.)	
VILAIN	95C	PL B351 387	P. Vilain et al.	(CHARM II Collab.)
Also	PL B343 453	P. Vilain et al.	(CHARM II Collab.)	
BARANOV	93	PL B302 336	S.A. Baranov et al.	(JINR, SERP, BUDA)
BERNARDI	88	PL B203 332	G. Bernardi et al.	(PARIN, CERN, INFN+)
DORENBOS...	86	PL B166 473	J. Dorenbosch et al.	(CHARM Collab.)
COOPER...	85	PL B160B 207	A.M. Cooper-Sarkar et al.	(CERN, LOIC+)

QUARKS

<i>u</i>	1371
<i>d</i>	1371
<i>s</i>	1371
<i>c</i>	1375
<i>b</i>	1377
<i>t</i>	1379
<i>b'</i> (Fourth Generation) Quark	1398
<i>t'</i> (Fourth Generation) Quark	1401
Free Quark Searches	1403

Related Reviews in Volume 1

60. Quark masses (rev.)	834
61. Top quark (rev.)	844





See key on page 1171

Quark Particle Listings

Quarks, *u*, *d*, *s*, Light Quarks (*u*, *d*, *s*)

QUARKS

See the related review(s):

Quark Masses

u $I(J^P) = \frac{1}{2}(\frac{1}{2}^+)$

Mass $m = 2.16 \pm 0.07$ MeV Charge = $\frac{2}{3} e$ $I_z = +\frac{1}{2}$

$m_u/m_d = 0.462 \pm 0.020$

d $I(J^P) = \frac{1}{2}(\frac{1}{2}^+)$

Mass $m = 4.70 \pm 0.07$ MeV Charge = $-\frac{1}{3} e$ $I_z = -\frac{1}{2}$

$m_s/m_d = 17-22$

$\bar{m} = (m_u + m_d)/2 = 3.49 \pm 0.07$ MeV

s $I(J^P) = 0(\frac{1}{2}^+)$

Mass $m = 93.5 \pm 0.8$ MeV Charge = $-\frac{1}{3} e$ Strangeness = -1

$(m_s - (m_u + m_d)/2)/(m_d - m_u) = 27.33^{+0.18}_{-0.14}$

Light Quarks (*u*, *d*, *s*)

OMITTED FROM SUMMARY TABLE
See the related review(s):

Quark Masses

u-QUARK MASS

The *u*-, *d*-, and *s*-quark masses are estimates of so-called "current-quark masses," in a mass-independent subtraction scheme such as \overline{MS} . The ratios m_u/m_d and m_s/m_d are extracted from pion and kaon masses using chiral symmetry. The estimates of *d* and *u* masses are not without controversy and remain under active investigation. Within the literature there are even suggestions that the *u* quark could be essentially massless. The *s*-quark mass is estimated from SU(3) splittings in hadron masses.

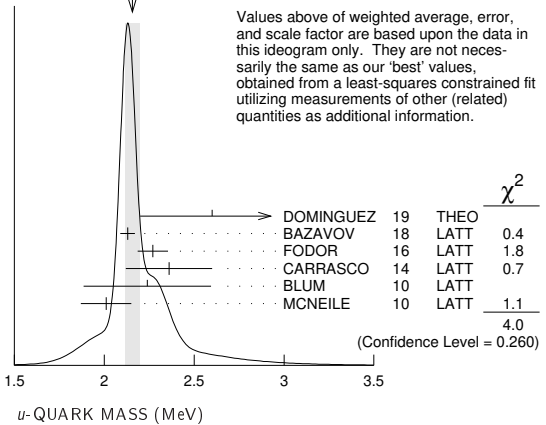
We have normalized the \overline{MS} masses at a renormalization scale of $\mu = 2$ GeV. Results quoted in the literature at $\mu = 1$ GeV have been rescaled by dividing by 1.35. The values of "Our Evaluation" were determined in part via Figures 2 and 3 in the "Quark masses" review.

\overline{MS} MASS (MeV)	CL%	DOCUMENT ID	TECN
2.16 ± 0.07 (CL = 90%) OUR EVALUATION		See the ideogram below.	
2.6 ± 0.4		1 DOMINGUEZ 19	THEO
2.130 ± 0.041		2 BAZAVOV 18	LATT
2.27 ± 0.06 ± 0.06		3 FODOR 16	LATT
2.36 ± 0.24		4 CARRASCO 14	LATT
2.24 ± 0.10 ± 0.34		5 BLUM 10	LATT
2.01 ± 0.14		6 MCNEILE 10	LATT
••• We do not use the following data for averages, fits, limits, etc. •••			
2.57 ± 0.26 ± 0.07		7 AOKI 12	LATT
2.15 ± 0.03 ± 0.10		8 DURR 11	LATT
1.9 ± 0.2		9 BAZAVOV 10	LATT
2.01 ± 0.14		6 DAVIES 10	LATT
2.9 ± 0.2		10 DOMINGUEZ 09	THEO
2.9 ± 0.8		11 DEANDREA 08	THEO
3.02 ± 0.33		12 BLUM 07	LATT
2.7 ± 0.4		13 JAMIN 06	THEO
1.9 ± 0.2		14 MASON 06	LATT
2.8 ± 0.2		15 NARISON 06	THEO
1.7 ± 0.3		16 AUBIN 04A	LATT

- DOMINGUEZ 19 determine the quark mass from a QCD finite energy sum rule for the divergence of the axial current.
- BAZAVOV 18 determine the quark masses using a lattice computation with staggered fermions and four active quark flavors.
- FODOR 16 is a lattice simulation with $n_f = 2 + 1$ dynamical flavors and includes partially quenched QED effects.
- CARRASCO 14 is a lattice QCD computation of light quark masses using $2 + 1 + 1$ dynamical quarks, with $m_u = m_d \neq m_s \neq m_c$. The *u* and *d* quark masses are obtained separately by using the *K* meson mass splittings and lattice results for the electromagnetic contributions.
- BLUM 10 determines light quark masses using a QCD plus QED lattice computation of the electromagnetic mass splittings of the low-lying hadrons. The lattice simulations use $2+1$ dynamical quark flavors.
- DAVIES 10 and MCNEILE 10 determine $\bar{m}_c(\mu)/\bar{m}_s(\mu) = 11.85 \pm 0.16$ using a lattice computation with $n_f = 2 + 1$ dynamical fermions of the pseudoscalar meson masses.

- Mass m_u is obtained from this using the value of m_c from ALLISON 08 or MCNEILE 10 and the BAZAVOV 10 values for the light quark mass ratios, m_s/\bar{m} and m_u/m_d .
- AOKI 12 is a lattice computation using $1 + 1 + 1$ dynamical quark flavors.
 - DURR 11 determine quark mass from a lattice computation of the meson spectrum using $n_f = 2 + 1$ dynamical flavors. The lattice simulations were done at the physical quark mass, so that extrapolation in the quark mass was not needed. The individual m_u , m_d values are obtained using the lattice determination of the average mass m_{ud} and of the ratio m_s/m_{ud} and the value of $Q = (m_s^2 - m_{ud}^2) / (m_d^2 - m_u^2)$ as determined from $\eta \rightarrow 3\pi$ decays.
 - BAZAVOV 10 is a lattice computation using $2+1$ dynamical quark flavors.
 - DOMINGUEZ 09 use QCD finite energy sum rules for the two-point function of the divergence of the axial vector current computed to order α_s^4 .
 - DEANDREA 08 determine $m_u - m_d$ from $\eta \rightarrow 3\pi^0$, and combine with the PDG 06 lattice average value of $m_u + m_d = 7.6 \pm 1.6$ to determine m_u and m_d .
 - BLUM 07 determine quark masses from the pseudoscalar meson masses using a QED plus QCD lattice computation with two dynamical quark flavors.
 - JAMIN 06 determine $m_u(2 \text{ GeV})$ by combining the value of m_s obtained from the spectral function for the scalar *K* π form factor with other determinations of the quark mass ratios.
 - MASON 06 extract light quark masses from a lattice simulation using staggered fermions with an improved action, and three dynamical light quark flavors with degenerate *u* and *d* quarks. Perturbative corrections were included at NNLO order. The quark masses m_u and m_d were determined from their $(m_u + m_d)/2$ measurement and AUBIN 04A m_u/m_d value.
 - NARISON 06 uses sum rules for $e^+ e^- \rightarrow$ hadrons to order α_s^3 to determine m_s combined with other determinations of the quark mass ratios.
 - AUBIN 04A employ a partially quenched lattice calculation of the pseudoscalar meson masses.

WEIGHTED AVERAGE
2.16±0.04 (Error scaled by 1.2)



d-QUARK MASS

See the comment for the *u* quark above.

We have normalized the \overline{MS} masses at a renormalization scale of $\mu = 2$ GeV. Results quoted in the literature at $\mu = 1$ GeV have been rescaled by dividing by 1.35. The values of "Our Evaluation" were determined in part via Figures 2 and 3 in the "Quark masses" review.

\overline{MS} MASS (MeV)	CL%	DOCUMENT ID	TECN
4.70 ± 0.07 (CL = 90%) OUR EVALUATION		See the ideogram below.	
5.3 ± 0.4		1 DOMINGUEZ 19	THEO
4.675 ± 0.056		2 BAZAVOV 18	LATT
4.67 ± 0.06 ± 0.06		3 FODOR 16	LATT
5.03 ± 0.26		4 CARRASCO 14	LATT
4.65 ± 0.15 ± 0.32		5 BLUM 10	LATT
4.77 ± 0.15		6 MCNEILE 10	LATT
••• We do not use the following data for averages, fits, limits, etc. •••			
3.68 ± 0.29 ± 0.10		7 AOKI 12	LATT
4.79 ± 0.07 ± 0.12		8 DURR 11	LATT
4.6 ± 0.3		9 BAZAVOV 10	LATT
4.79 ± 0.16		6 DAVIES 10	LATT
5.3 ± 0.4		10 DOMINGUEZ 09	THEO
4.7 ± 0.8		11 DEANDREA 08	THEO
5.49 ± 0.39		12 BLUM 07	LATT
4.8 ± 0.5		13 JAMIN 06	THEO
4.4 ± 0.3		14 MASON 06	LATT
5.1 ± 0.4		15 NARISON 06	THEO
3.9 ± 0.5		16 AUBIN 04A	LATT

- DOMINGUEZ 19 determine the quark mass from a QCD finite energy sum rule for the divergence of the axial current.
- BAZAVOV 18 determine the quark masses using a lattice computation with staggered fermions and four active quark flavors.
- FODOR 16 is a lattice simulation with $n_f = 2 + 1$ dynamical flavors and includes partially quenched QED effects.

Quark Particle Listings

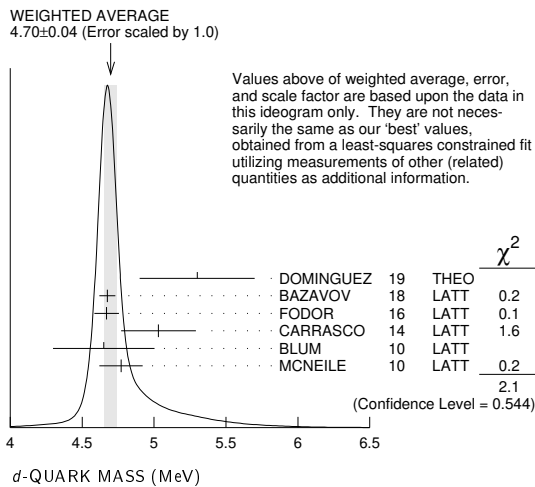
Light Quarks (*u, d, s*)

- ⁴ CARRASCO 14 is a lattice QCD computation of light quark masses using 2 + 1 + 1 dynamical quarks, with $m_u = m_d \neq m_s \neq m_c$. The *u* and *d* quark masses are obtained separately by using the *K* meson mass splittings and lattice results for the electromagnetic contributions.
- ⁵ BLUM 10 determines light quark masses using a QCD plus QED lattice computation of the electromagnetic mass splittings of the low-lying hadrons. The lattice simulations use 2+1 dynamical quark flavors.
- ⁶ DAVIES 10 and MCNEILE 10 determine $\overline{m}_c(\mu)/\overline{m}_s(\mu) = 11.85 \pm 0.16$ using a lattice computation with $n_f = 2 + 1$ dynamical fermions of the pseudoscalar meson masses. Mass m_d is obtained from this using the value of m_c from ALLISON 08 or MCNEILE 10 and the BAZAVOV 10 values for the light quark mass ratios, m_s/\overline{m} and m_u/m_d .
- ⁷ AOKI 12 is a lattice computation using 1 + 1 + 1 dynamical quark flavors.
- ⁸ DURR 11 determine quark mass from a lattice computation of the meson spectrum using $n_f = 2 + 1$ dynamical flavors. The lattice simulations were done at the physical quark mass, so that extrapolation in the quark mass was not needed. The individual m_u, m_d values are obtained using the lattice determination of the average mass m_{ud} and of the ratio m_s/m_{ud} and the value of $Q = (m_s^2 - m_{ud}^2) / (m_d^2 - m_u^2)$ as determined from $\eta \rightarrow 3\pi$ decays.
- ⁹ BAZAVOV 10 is a lattice computation using 2+1 dynamical quark flavors.
- ¹⁰ DOMINGUEZ 09 use QCD finite energy sum rules for the two-point function of the divergence of the axial vector current computed to order α_s^4 .
- ¹¹ DEANDREA 08 determine $m_u - m_d$ from $\eta \rightarrow 3\pi^0$, and combine with the PDG 06 lattice average value of $m_u + m_d = 7.6 \pm 1.6$ to determine m_u and m_d .
- ¹² BLUM 07 determine quark masses from the pseudoscalar meson masses using a QED plus QCD lattice computation with two dynamical quark flavors.
- ¹³ JAMIN 06 determine $m_d(2 \text{ GeV})$ by combining the value of m_s obtained from the spectral function for the scalar *K* π form factor with other determinations of the quark mass ratios.
- ¹⁴ MASON 06 extract light quark masses from a lattice simulation using staggered fermions with an improved action, and three dynamical light quark flavors with degenerate *u* and *d* quarks. Perturbative corrections were included at NNLO order. The quark masses m_u and m_d were determined from their $(m_u + m_d)/2$ measurement and AUBIN 04A m_u/m_d value.
- ¹⁵ NARISON 06 uses sum rules for $e^+e^- \rightarrow$ hadrons to order α_s^3 to determine m_s combined with other determinations of the quark mass ratios.
- ¹⁶ AUBIN 04A perform three flavor dynamical lattice calculation of pseudoscalar meson masses, with continuum estimate of electromagnetic effects in the kaon masses, and one-loop perturbative renormalization constant.

• • • We do not use the following data for averages, fits, limits, etc. • • •

3.59 ± 0.21	¹⁰ AOKI	11A	LATT
3.40 ± 0.07	⁹ DAVIES	10	LATT
4.1 ± 0.2	¹¹ DOMINGUEZ	09	THEO
3.72 ± 0.41	¹² ALLTON	08	LATT
3.85 ± 0.12 ± 0.4	¹³ BLOSSIER	08	LATT
≥ 4.85 ± 0.20	¹⁴ DOMINGUEZ..08B		THEO
3.55 +0.65 -0.28	¹⁵ ISHIKAWA	08	LATT
4.026 ± 0.048	¹⁶ NAKAMURA	08	LATT
4.25 ± 0.35	¹⁷ BLUM	07	LATT
4.08 ± 0.25 ± 0.42	¹⁸ GOCKELER	06	LATT
4.7 ± 0.2 ± 0.3	¹⁹ GOCKELER	06A	LATT
3.2 ± 0.3	²⁰ MASON	06	LATT
3.95 ± 0.3	²¹ NARISON	06	THEO
2.8 ± 0.3	²² AUBIN	04	LATT
4.29 ± 0.14 ± 0.65	²³ AOKI	03	LATT
3.223 ± 0.3	²⁴ AOKI	03B	LATT
4.4 ± 0.1 ± 0.4	²⁵ BECIREVIC	03	LATT
4.1 ± 0.3 ± 1.0	²⁶ CHIU	03	LATT

- ¹ ALEXANDROU 21 determines the quark mass using a lattice calculation of the meson and baryon masses with a twisted mass fermion action. The simulations are carried out using 2+1+1 dynamical quarks with $m_u = m_d \neq m_s \neq m_c$, including gauge ensembles close to the physical pion point.
- ² BRUNO 20 determines the light quark mass using a lattice calculation with $n_f = 2+1$ flavors of Wilson fermions. The scale has been set from t_π and t_K . The tuning was done using the masses of the lightest (π) and strange (*K*) pseudoscalar mesons.
- ³ DOMINGUEZ 19 determine the quark mass from a QCD finite energy sum rule for the divergence of the axial current.
- ⁴ YUAN 17 determine \overline{m} using QCD sum rules in the isospin $I=0$ scalar channel. At the end of the "Numerical Results" section of YUAN 17 the authors discuss the significance of their larger value of the light quark mass compared to previous determinations.
- ⁵ CARRASCO 14 is a lattice QCD computation of light quark masses using 2 + 1 + 1 dynamical quarks, with $m_u = m_d \neq m_s \neq m_c$. The *u* and *d* quark masses are obtained separately by using the *K* meson mass splittings and lattice results for the electromagnetic contributions.
- ⁶ ARTHUR 13 is a lattice computation using 2+1 dynamical domain wall fermions. Masses at $\mu = 3 \text{ GeV}$ have been converted to $\mu = 2 \text{ GeV}$ using conversion factors given in their paper.
- ⁷ DURR 11 determine quark mass from a lattice computation of the meson spectrum using $n_f = 2 + 1$ dynamical flavors. The lattice simulations were done at the physical quark mass, so that extrapolation in the quark mass was not needed.
- ⁸ BLOSSIER 10 determines quark masses from a computation of the hadron spectrum using $n_f=2$ dynamical twisted-mass Wilson fermions.
- ⁹ DAVIES 10 and MCNEILE 10 determine $\overline{m}_c(\mu)/\overline{m}_s(\mu) = 11.85 \pm 0.16$ using a lattice computation with $n_f = 2 + 1$ dynamical fermions of the pseudoscalar meson masses. Mass m_d is obtained from this using the value of m_c from ALLISON 08 or MCNEILE 10 and the BAZAVOV 10 values for the light quark mass ratio, m_s/\overline{m} .
- ¹⁰ AOKI 11A determine quark masses from a lattice computation of the hadron spectrum using $n_f = 2 + 1$ dynamical flavors of domain wall fermions.
- ¹¹ DOMINGUEZ 09 use QCD finite energy sum rules for the two-point function of the divergence of the axial vector current computed to order α_s^4 .
- ¹² ALLTON 08 use a lattice computation of the $\pi, K, \text{ and } \Omega$ masses with 2+1 dynamical flavors of domain wall quarks, and non-perturbative renormalization.
- ¹³ BLOSSIER 08 use a lattice computation of pseudoscalar meson masses and decay constants with 2 dynamical flavors and non-perturbative renormalization.
- ¹⁴ DOMINGUEZ-CLARIMON 08B obtain an inequality from sum rules for the scalar two-point correlator.
- ¹⁵ ISHIKAWA 08 use a lattice computation of the light meson spectrum with 2+1 dynamical flavors of $\mathcal{O}(a)$ improved Wilson quarks, and one-loop perturbative renormalization.
- ¹⁶ NAKAMURA 08 do a lattice computation using quenched domain wall fermions and non-perturbative renormalization.
- ¹⁷ BLUM 07 determine quark masses from the pseudoscalar meson masses using a QED plus QCD lattice computation with two dynamical quark flavors.
- ¹⁸ GOCKELER 06 use an unquenched lattice computation of the axial Ward Identity with $n_f = 2$ dynamical light quark flavors, and non-perturbative renormalization, to obtain $\overline{m}(2 \text{ GeV}) = 4.08 \pm 0.25 \pm 0.19 \pm 0.23 \text{ MeV}$, where the first error is statistical, the second and third are systematic due to the fit range and force scale uncertainties, respectively. We have combined the systematic errors linearly.
- ¹⁹ GOCKELER 06A use an unquenched lattice computation of the pseudoscalar meson masses with $n_f = 2$ dynamical light quark flavors, and non-perturbative renormalization.
- ²⁰ MASON 06 extract light quark masses from a lattice simulation using staggered fermions with an improved action, and three dynamical light quark flavors with degenerate *u* and *d* quarks. Perturbative corrections were included at NNLO order.
- ²¹ NARISON 06 uses sum rules for $e^+e^- \rightarrow$ hadrons to order α_s^3 to determine m_s combined with other determinations of the quark mass ratios.
- ²² AUBIN 04 perform three flavor dynamical lattice calculation of pseudoscalar meson masses, with one-loop perturbative renormalization constant.
- ²³ AOKI 03 uses quenched lattice simulation of the meson and baryon masses with degenerate light quarks. The extrapolations are done using quenched chiral perturbation theory.
- ²⁴ The errors given in AOKI 03b were $+0.046$
 -0.069 . We changed them to ± 0.3 for calculating the overall best values. AOKI 03b uses lattice simulation of the meson and baryon masses with two dynamical light quarks. Simulations are performed using the $\mathcal{O}(a)$ improved Wilson action.
- ²⁵ BECIREVIC 03 perform quenched lattice computation using the vector and axial Ward identities. Uses $\mathcal{O}(a)$ improved Wilson action and nonperturbative renormalization.
- ²⁶ CHIU 03 determines quark masses from the pion and kaon masses using a lattice simulation with a chiral fermion action in quenched approximation.



$$\overline{m} = (m_u + m_d)/2$$

See the comments for the *u* quark above.

We have normalized the \overline{m}_S masses at a renormalization scale of $\mu = 2 \text{ GeV}$. Results quoted in the literature at $\mu = 1 \text{ GeV}$ have been rescaled by dividing by 1.35. The values of "Our Evaluation" were determined in part via Figures 2 and 3 in the "Quark masses" review.

\overline{m}_S MASS (MeV)	CL%	DOCUMENT ID	TECN
3.49 ± 0.07 (CL = 90%) OUR EVALUATION		See the ideogram below.	
3.636 ± 0.066 +0.060 -0.057		¹ ALEXANDROU 21	LATT
3.54 ± 0.12 ± 0.09		² BRUNO 20	LATT
3.9 ± 0.3		³ DOMINGUEZ 19	THEO
4.7 ± 0.8 -0.7		⁴ YUAN 17	THEO
3.70 ± 0.17		⁵ CARRASCO 14	LATT
3.45 ± 0.12		⁶ ARTHUR 13	LATT
3.469 ± 0.047 ± 0.048		⁷ DURR 11	LATT
3.6 ± 0.2		⁸ BLOSSIER 10	LATT
3.39 ± 0.06		⁹ MCNEILE 10	LATT

See key on page 1171

Quark Particle Listings

Light Quarks (*u, d, s*)

s-QUARK MASS

See the comment for the *u* quark above.

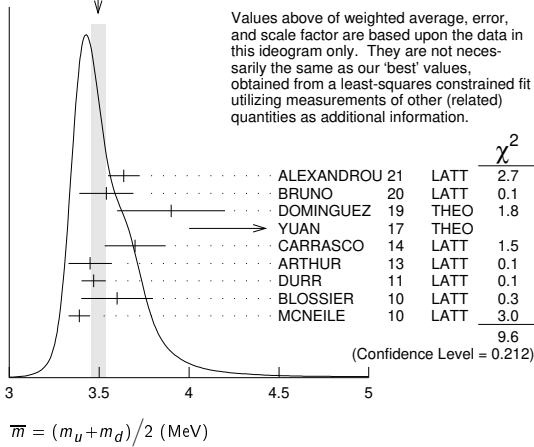
We have normalized the \overline{MS} masses at a renormalization scale of $\mu = 2$ GeV. Results quoted in the literature at $\mu = 1$ GeV have been rescaled by dividing by 1.35.

\overline{MS} MASS (MeV) CL% DOCUMENT ID TECN
93.5 ± 0.8 (CL = 90%) OUR EVALUATION See the ideogram below.

\overline{MS} MASS (MeV)	CL%	DOCUMENT ID	TECN
98.7 ± 2.4 +4.0 -3.2		1 ALEXANDROU 21	LATT
95.7 ± 2.5 ± 2.4		2 BRUNO 20	LATT
92.47 ± 0.69		3 BAZAVOV 18	LATT
93.85 ± 0.75		4 LYTTLE 18	LATT
87.6 ± 6.0		5 ANANTHANA 16	THEO
99.6 ± 4.3		6 CARRASCO 14	LATT
94.4 ± 2.3		7 ARTHUR 13	LATT
94 ± 9		8 BODENSTEIN 13	THEO
95.5 ± 1.1 ± 1.5		9 DURR 11	LATT
93.6 ± 0.8		10 CHAKRABORTY 15	LATT
102 ± 3 ± 1		11 FRITZSCH 12	LATT
96.2 ± 2.7		12 AOKI 11A	LATT
95 ± 6		13 BLOSSIER 10	LATT
97.6 ± 2.9 ± 5.5		14 BLUM 10	LATT
92.4 ± 1.5		15 DAVIES 10	LATT
92.2 ± 1.3		15 MCNEILE 10	LATT
107.3 ± 11.7		16 ALLTON 08	LATT
105 ± 3 ± 9		17 BLOSSIER 08	LATT
102 ± 8		18 DOMINGUEZ 08A	THEO
90.1 +17.2 -6.1		19 SHIKAWA 08	LATT
105.6 ± 1.2		20 NAKAMURA 08	LATT
119.5 ± 9.3		21 BLUM 07	LATT
105 ± 6 ± 7		22 CHETYRKIN 06	THEO
111 ± 6 ± 10		23 GOKELER 06	LATT
119 ± 5 ± 8		24 GOKELER 06A	LATT
92 ± 9		25 JAMIN 06	THEO
87 ± 6		26 MASON 06	LATT
104 ± 15		27 NARISON 06	THEO
≥ 71 ± 4, ≤ 151 ± 14		28 NARISON 06	THEO
96 ± 5 +16 -3 -18		29 BAIKOV 05	THEO
81 ± 22		30 GAMIZ 05	THEO
125 ± 28		31 GORBUNOV 05	THEO
93 ± 32		32 NARISON 05	THEO
76 ± 8		33 AUBIN 04	LATT
116 ± 6 ± 0.65		34 AOKI 03	LATT
84.5 +12 -1.7		35 AOKI 03B	LATT
106 ± 2 ± 8		36 BECIREVIC 03	LATT
92 ± 9 ± 16		37 CHIU 03	LATT
117 ± 17		38 GAMIZ 03	THEO
103 ± 17		39 GAMIZ 03	THEO

- 1 ALEXANDROU 21 determines the quark mass using a lattice calculation of the meson and baryon masses with a twisted mass fermion action. The simulations are carried out using 2+1+1 dynamical quarks with $m_u = m_d \neq m_s \neq m_c$, including gauge ensembles close to the physical pion point.
- 2 BRUNO 20 determines the light quark mass using a lattice calculation with $n_f = 2+1$ flavors of Wilson fermions. The scale has been set from f_π and f_K . The tuning was done using the masses of the lightest (π) and strange (K) pseudoscalar mesons.
- 3 BAZAVOV 18 determine the quark masses using a lattice computation with staggered fermions and four active quark flavors.
- 4 LYTTLE 18 combined with CHAKRABORTY 2015 determine $\overline{m}_s(3 \text{ GeV}) = 84.78 \pm 0.65$ MeV from a lattice simulation with $n_f = 2+1+1$ flavors. They also determine the quoted value $\overline{m}_s(2 \text{ GeV})$ for $n_f = 4$ dynamical flavors.
- 5 ANANTHANA 16 determine $\overline{m}_s(2 \text{ GeV}) = 106.70 \pm 9.36$ MeV and 74.47 ± 7.77 MeV from fits to ALEPH and OPAL τ decay data, respectively. We have used the weighted average of the two.
- 6 CARRASCO 14 is a lattice QCD computation of light quark masses using 2+1+1 dynamical quarks, with $m_u = m_d \neq m_s \neq m_c$. The *u* and *d* quark masses are obtained separately by using the *K* meson mass splittings and lattice results for the electromagnetic contributions.
- 7 ARTHUR 13 is a lattice computation using 2+1 dynamical domain wall fermions. Masses at $\mu = 3$ GeV have been converted to $\mu = 2$ GeV using conversion factors given in their paper.
- 8 BODENSTEIN 13 determines m_s from QCD finite energy sum rules, and the perturbative computation of the pseudoscalar correlator to five-loop order.
- 9 DURR 11 determine quark mass from a lattice computation of the meson spectrum using $n_f = 2+1$ dynamical flavors. The lattice simulations were done at the physical quark mass, so that extrapolation in the quark mass was not needed.
- 10 CHAKRABORTY 15 is a lattice QCD computation that determines m_c and m_c/m_s using pseudoscalar meson masses tuned on gluon field configurations with 2+1+1 dynamical flavors of HISQ quarks with *u/d* masses down to the physical value.
- 11 FRITZSCH 12 determine m_s using a lattice computation with $n_f = 2$ dynamical flavors.
- 12 AOKI 11A determine quark masses from a lattice computation of the hadron spectrum using $n_f = 2+1$ dynamical flavors of domain wall fermions.
- 13 BLOSSIER 10 determines quark masses from a computation of the hadron spectrum using $n_f=2$ dynamical twisted-mass Wilson fermions.

WEIGHTED AVERAGE
3.49±0.04 (Error scaled by 1.2)



Values above of weighted average, error, and scale factor are based upon the data in this ideogram only. They are not necessarily the same as our 'best' values, obtained from a least-squares constrained fit utilizing measurements of other (related) quantities as additional information.

DOCUMENT ID	TECN	χ^2
ALEXANDROU 21	LATT	2.7
BRUNO 20	LATT	0.1
DOMINGUEZ 19	THEO	1.8
YUAN 17	THEO	
CARRASCO 14	LATT	1.5
ARTHUR 13	LATT	0.1
DURR 11	LATT	0.1
BLOSSIER 10	LATT	0.3
MCNEILE 10	LATT	3.0
		9.6

(Confidence Level = 0.212)

$\overline{m} = (m_u + m_d)/2$ (MeV)

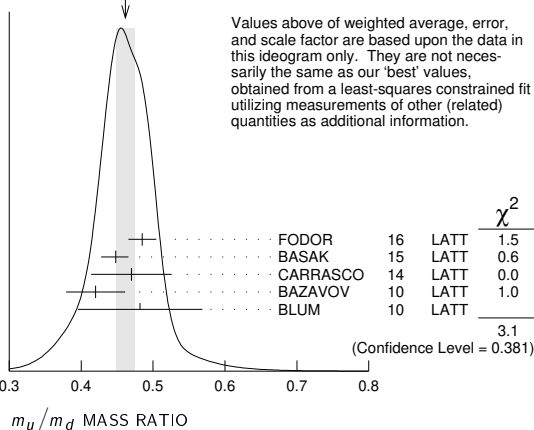
m_u/m_d MASS RATIO

VALUE CL% DOCUMENT ID TECN COMMENT
0.462 ± 0.020 (CL = 90%) OUR EVALUATION See the ideogram below.

0.485 ± 0.011 ± 0.016		1 FODOR 16	LATT
0.4482 +0.0173 -0.0206		2 BASAK 15	LATT
0.470 ± 0.056		3 CARRASCO 14	LATT
0.42 ± 0.01 ± 0.04		4 BAZAVOV 10	LATT
0.4818 ± 0.0096 ± 0.0860		5 BLUM 10	LATT
• • • We do not use the following data for averages, fits, limits, etc. • • •			
0.698 ± 0.051		6 AOKI 12	LATT
0.550 ± 0.031		7 BLUM 07	LATT
0.43 ± 0.08		8 AUBIN 04A	LATT
0.410 ± 0.036		9 NELSON 03	LATT
0.553 ± 0.043		10 LEUTWYLER 96	THEO Compilation

- 1 FODOR 16 is a lattice simulation with $n_f = 2+1$ dynamical flavors and includes partially quenched QED effects.
- 2 BASAK 15 is a lattice computation using 2+1 dynamical quark flavors.
- 3 CARRASCO 14 is a lattice QCD computation of light quark masses using 2+1+1 dynamical quarks, with $m_u = m_d \neq m_s \neq m_c$. The *u* and *d* quark masses are obtained separately by using the *K* meson mass splittings and lattice results for the electromagnetic contributions.
- 4 BAZAVOV 10 is a lattice computation using 2+1 dynamical quark flavors.
- 5 BLUM 10 is a lattice computation using 2+1 dynamical quark flavors.
- 6 AOKI 12 is a lattice computation using 1+1+1 dynamical quark flavors.
- 7 BLUM 07 determine quark masses from the pseudoscalar meson masses using a QED plus QCD lattice computation with two dynamical quark flavors.
- 8 AUBIN 04A perform three flavor dynamical lattice calculation of pseudoscalar meson masses, with continuum estimate of electromagnetic effects in the kaon masses.
- 9 NELSON 03 computes coefficients in the order p^4 chiral Lagrangian using a lattice calculation with three dynamical flavors. The ratio m_u/m_d is obtained by combining this with the chiral perturbation theory computation of the meson masses to order p^4 .
- 10 LEUTWYLER 96 uses a combined fit to $\eta \rightarrow 3\pi$ and $\psi' \rightarrow J/\psi(\pi, \eta)$ decay rates, and the electromagnetic mass differences of the π and *K*.

WEIGHTED AVERAGE
0.462±0.013 (Error scaled by 1.0)



Values above of weighted average, error, and scale factor are based upon the data in this ideogram only. They are not necessarily the same as our 'best' values, obtained from a least-squares constrained fit utilizing measurements of other (related) quantities as additional information.

DOCUMENT ID	TECN	χ^2
FODOR 16	LATT	1.5
BASAK 15	LATT	0.6
CARRASCO 14	LATT	0.0
BAZAVOV 10	LATT	1.0
BLUM 10	LATT	
		3.1

(Confidence Level = 0.381)

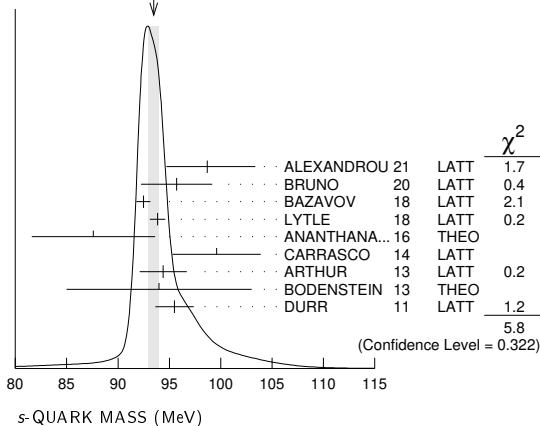
m_u/m_d MASS RATIO

Quark Particle Listings

Light Quarks (*u, d, s*)

- ¹⁴BLUM 10 determines light quark masses using a QCD plus QED lattice computation of the electromagnetic mass splittings of the low-lying hadrons. The lattice simulations use 2+1 dynamical quark flavors.
- ¹⁵DAVIES 10 and MCNEILE 10 determine $\overline{m}_C(\mu)/\overline{m}_S(\mu) = 11.85 \pm 0.16$ using a lattice computation with $n_f = 2 + 1$ dynamical fermions of the pseudoscalar meson masses. Mass m_S is obtained from this using the value of m_C from ALLISON 08 or MCNEILE 10.
- ¹⁶ALLTON 08 use a lattice computation of the π , K , and Ω masses with 2+1 dynamical flavors of domain wall quarks, and non-perturbative renormalization.
- ¹⁷BLOSSIER 08 use a lattice computation of pseudoscalar meson masses and decay constants with 2 dynamical flavors and non-perturbative renormalization.
- ¹⁸DOMINGUEZ 08A make determination from QCD finite energy sum rules for the pseudoscalar two-point function computed to order α_s^4 .
- ¹⁹ISHIKAWA 08 use a lattice computation of the light meson spectrum with 2+1 dynamical flavors of $\mathcal{O}(a)$ improved Wilson quarks, and one-loop perturbative renormalization.
- ²⁰NAKAMURA 08 do a lattice computation using quenched domain wall fermions and non-perturbative renormalization.
- ²¹BLUM 07 determine quark masses from the pseudoscalar meson masses using a QED plus QCD lattice computation with two dynamical quark flavors.
- ²²CHETYRKIN 06 use QCD sum rules in the pseudoscalar channel to order α_s^4 .
- ²³GOCKELER 06 use an unquenched lattice computation of the axial Ward Identity with $n_f = 2$ dynamical light quark flavors, and non-perturbative renormalization, to obtain $\overline{m}_S(2 \text{ GeV}) = 111 \pm 6 \pm 4 \pm 6 \text{ MeV}$, where the first error is statistical, the second and third are systematic due to the fit range and force scale uncertainties, respectively. We have combined the systematic errors linearly.
- ²⁴GOCKELER 06A use an unquenched lattice computation of the pseudoscalar meson masses with $n_f = 2$ dynamical light quark flavors, and non-perturbative renormalization.
- ²⁵JAMIN 06 determine $\overline{m}_S(2 \text{ GeV})$ from the spectral function for the scalar $K\pi$ form factor.
- ²⁶MASON 06 extract light quark masses from a lattice simulation using staggered fermions with an improved action, and three dynamical light quark flavors with degenerate u and d quarks. Perturbative corrections were included at NNLO order.
- ²⁷NARISON 06 uses sum rules for $e^+e^- \rightarrow$ hadrons to order α_s^3 .
- ²⁸NARISON 06 obtains the quoted range from positivity of the spectral functions.
- ²⁹BAIKOV 05 determines $\overline{m}_S(M_\tau) = 100^{+5}_{-3} +^{17}_{-19}$ from sum rules using the strange spectral function in τ decay. The computations were done to order α_s^3 , with an estimate of the α_s^4 terms. We have converted the result to $\mu = 2 \text{ GeV}$.
- ³⁰GAMIZ 05 determines $\overline{m}_S(2 \text{ GeV})$ from sum rules using the strange spectral function in τ decay. The computations were done to order α_s^2 , with an estimate of the α_s^3 terms.
- ³¹GORBUNOV 05 use hadronic tau decays to N3LO, including power corrections.
- ³²NARISON 05 determines $\overline{m}_S(2 \text{ GeV})$ from sum rules using the strange spectral function in τ decay. The computations were done to order α_s^3 .
- ³³AUBIN 04 perform three flavor dynamical lattice calculation of pseudoscalar meson masses, with one-loop perturbative renormalization constant.
- ³⁴AOKI 03 uses quenched lattice simulation of the meson and baryon masses with degenerate light quarks. The extrapolations are done using quenched chiral perturbation theory. Determines $m_s = 113.8 \pm 2.3 \pm^{5.8}_{-2.9}$ using K mass as input and $m_s = 142.3 \pm 5.8 \pm^{22}_{-0}$ using ϕ mass as input. We have performed a weighted average of these values.
- ³⁵AOKI 03B uses lattice simulation of the meson and baryon masses with two dynamical light quarks. Simulations are performed using the $\mathcal{O}(a)$ improved Wilson action.
- ³⁶BEČIREVIĆ 03 perform quenched lattice computation using the vector and axial Ward identities. Uses $\mathcal{O}(a)$ improved Wilson action and nonperturbative renormalization. They also quote $\overline{m}/m_s = 24.3 \pm 0.2 \pm 0.6$.
- ³⁷CHIU 03 determines quark masses from the pion and kaon masses using a lattice simulation with a chiral fermion action in quenched approximation.
- ³⁸GAMIZ 03 determines m_s from SU(3) breaking in the τ hadronic width. The value of V_{us} is chosen to satisfy CKM unitarity.
- ³⁹GAMIZ 03 determines m_s from SU(3) breaking in the τ hadronic width. The value of V_{us} is taken from the PDG.

WEIGHTED AVERAGE
93.5±0.5 (Error scaled by 1.1)



OTHER LIGHT QUARK MASS RATIOS

m_s/m_d MASS RATIO

VALUE	DOCUMENT ID	TECN	COMMENT
17-22 OUR EVALUATION			
20.0	1 GAO 97	97	THEO
18.9±0.8	2 LEUTWYLER 96	96	THEO Compilation
21	3 DONOGHUE 92	92	THEO
18	4 GERARD 90	90	THEO
18 to 23	5 LEUTWYLER 90B	90B	THEO

- ¹GAO 97 uses electromagnetic mass splittings of light mesons.
- ²LEUTWYLER 96 uses a combined fit to $\eta \rightarrow 3\pi$ and $\psi' \rightarrow J/\psi(\pi,\eta)$ decay rates, and the electromagnetic mass differences of the π and K .
- ³DONOGHUE 92 result is from a combined analysis of meson masses, $\eta \rightarrow 3\pi$ using second-order chiral perturbation theory including nonanalytic terms, and $(\psi(2S) \rightarrow J/\psi(1S)\pi)/(\psi(2S) \rightarrow J/\psi(1S)\eta)$.
- ⁴GERARD 90 uses large N and η - η' mixing.
- ⁵LEUTWYLER 90B determines quark mass ratios using second-order chiral perturbation theory for the meson and baryon masses, including nonanalytic corrections. Also uses Weinberg sum rules to determine L_7 .

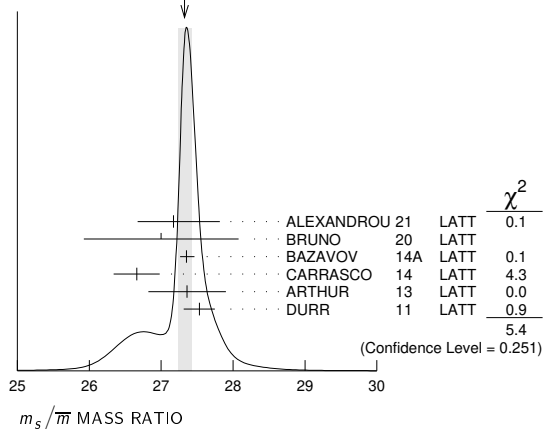
m_s/\overline{m} MASS RATIO

VALUE	CL%	DOCUMENT ID	TECN
27.33±0.18	90%	OUR EVALUATION	See the ideogram below.
-0.14			

27.17±0.32 ^{+0.56} _{-0.38}	1	ALEXANDROU 21	LATT
27.0 ±1.0 ±0.4	2	BRUNO 20	LATT
27.35±0.05 ^{+0.10} _{-0.07}	3	BAZAVOV 14A	LATT
26.66±0.32	4	CARRASCO 14	LATT
27.36±0.54	5	ARTHUR 13	LATT
27.53±0.20±0.08	6	DURR 11	LATT
••• We do not use the following data for averages, fits, limits, etc. •••			
26.8 ±1.4	7	AOKI 11A	LATT
27.3 ±0.9	8	BLOSSIER 10	LATT
28.8 ±1.65	9	ALLTON 08	LATT
27.3 ±0.3 ±1.2	10	BLOSSIER 08	LATT
23.5 ±1.5	11	OLLER 07A	THEO
27.4 ±0.4	12	AUBIN 04	LATT

- ¹ALEXANDROU 21 determines the quark mass using a lattice calculation of the meson and baryon masses with a twisted mass fermion action. The simulations are carried out using 2+1+1 dynamical quarks with $m_u = m_d \neq m_s \neq m_c$, including gauge ensembles close to the physical pion point.
- ²BRUNO 20 determines the light quark mass using a lattice calculation with $n_f = 2+1$ flavors of Wilson fermions. The scale has been set from f_π and f_K . The tuning was done using the masses of the lightest (π) and strange (K) pseudoscalar mesons.
- ³BAZAVOV 14A is a lattice computation using 4 dynamical flavors of HISQ fermions.
- ⁴CARRASCO 14 is a lattice QCD computation of light quark masses using 2+1+1 dynamical quarks, with $m_u = m_d \neq m_s \neq m_c$. The u and d quark masses are obtained separately by using the K meson mass splittings and lattice results for the electromagnetic contributions.
- ⁵ARTHUR 13 is a lattice computation using 2+1 dynamical domain wall fermions.
- ⁶DURR 11 determine quark mass from a lattice computation of the meson spectrum using $n_f = 2 + 1$ dynamical flavors. The lattice simulations were done at the physical quark mass, so that extrapolation in the quark mass was not needed.
- ⁷AOKI 11A determine quark masses from a lattice computation of the hadron spectrum using $n_f = 2 + 1$ dynamical flavors of domain wall fermions.
- ⁸BLOSSIER 10 determines quark masses from a computation of the hadron spectrum using $n_f = 2$ dynamical twisted-mass Wilson fermions.
- ⁹ALLTON 08 use a lattice computation of the π , K , and Ω masses with 2+1 dynamical flavors of domain wall quarks, and non-perturbative renormalization.
- ¹⁰BLOSSIER 08 use a lattice computation of pseudoscalar meson masses and decay constants with 2 dynamical flavors and non-perturbative renormalization.
- ¹¹OLLER 07A use unitarized chiral perturbation theory to order p^4 .
- ¹²Three flavor dynamical lattice calculation of pseudoscalar meson masses.

WEIGHTED AVERAGE
27.33±0.11-0.09 (Error scaled by 1.2)



See key on page 1171

Quark Particle Listings

Light Quarks (*u, d, s, c*)

Q MASS RATIO

$$Q \equiv \sqrt{(m_s^2 - \bar{m}^2)/(m_d^2 - m_u^2)}; \quad \bar{m} \equiv (m_u + m_d)/2$$

VALUE DOCUMENT ID TECN

- • • We do not use the following data for averages, fits, limits, etc. • • •
 - 22.1 ± 0.7 1 COLANGELO 18 THEO
 - 22.0 ± 0.7 2 COLANGELO 17 THEO
 - 21.6 ± 1.1 3 GUO 17 THEO
 - 23.4 ± 0.4 ± 0.5 4 FODOR 16 LATT
 - 21.4 ± 0.4 5 GUO 15F THEO
 - 22.8 ± 0.4 6 MARTEMYA... 05 THEO
 - 22.7 ± 0.8 7 ANISOVICH 96 THEO
- 1 COLANGELO 18 obtain *Q* from a dispersive analysis of $\eta \rightarrow 3\pi$ decay.
 - 2 COLANGELO 17 obtain *Q* from a dispersive analysis of KLOE collaboration data on $\eta \rightarrow \pi^+ \pi^- \pi^0$ decays and chiral perturbation theory input.
 - 3 GUO 17 determine *Q* from a dispersive model fit to KLOE and WASA-at-COSY data on $\eta \rightarrow \pi^+ \pi^- \pi^0$ decay and matching to chiral perturbation theory.
 - 4 FODOR 16 is a lattice simulation with $n_f = 2 + 1$ dynamical flavors and includes partially quenched QED effects.
 - 5 GUO 15F determine *Q* from a Khuri-Treiman analysis of $\eta \rightarrow 3\pi$ decays.
 - 6 MARTEMYANOV 05 determine *Q* from $\eta \rightarrow 3\pi$ decay.
 - 7 ANISOVICH 96 find *Q* from $\eta \rightarrow \pi^+ \pi^- \pi^0$ decay using dispersion relations and chiral perturbation theory.

0.38 ± 0.03. The value 1.2730 ± 0.0046 GeV for the \bar{m}_c mass corresponds to 1.67 ± 0.07 GeV for the pole mass (see the "Note on Quark Masses").

\bar{m}_c MASS (GeV) CL% DOCUMENT ID TECN
1.2730 ± 0.0046 (CL = 90%) OUR EVALUATION See the ideogram below.

\bar{m}_c MASS (GeV)	CL%	DOCUMENT ID	TECN
1.316 ± 0.022 +0.019 -0.010		1 ALEXANDROU 21	LATT
1.296 ± 0.019		2 HEITGER 21	LATT
1.2723 ± 0.0078		3 HATTON 20	LATT
1.266 ± 0.006		4 NARISON 20	THEO
1.290 +0.077 -0.053		5 ABRAMOWICZ18	HERA
1.273 ± 0.010		6 BAZAVOV 18	LATT
1.2737 ± 0.0077		7 LYTLE 18	LATT
1.223 ± 0.033		8 PESET 18	THEO
1.279 ± 0.008		9 CHETYRKIN 17	THEO
1.272 ± 0.008		10 ERLER 17	THEO
1.246 ± 0.023		11 KIYO 16	THEO
1.288 ± 0.020		12 DEHNADI 15	THEO
1.348 ± 0.046		13 CARRASCO 14	LATT
1.24 ± 0.03 +0.03 -0.07		14 ALEKHIN 13	THEO
1.159 ± 0.075		15 SAMOYLOV 13	NOMD
1.278 ± 0.009		16 BODENSTEIN 11	THEO
1.28 +0.07 -0.06		17 LASCHKA 11	THEO
1.196 ± 0.059 ± 0.050		18 AUBERT 10A	BABR
1.25 ± 0.04		19 SJGNER 09	THEO

• • • We do not use the following data for averages, fits, limits, etc. • • •

1.263 ± 0.014		20 NARISON 18A	THEO
1.264 ± 0.006		21 NARISON 18B	THEO
1.335 ± 0.043 +0.040 -0.011		22 BERTONE 16	THEO
1.2715 ± 0.0095		23 CHAKRABOR...15	LATT
1.26 ± 0.05 ± 0.04		24 ABRAMOWICZ13C	COMB
1.282 ± 0.011 ± 0.022		25 DEHNADI 13	THEO
1.286 ± 0.066		26 NARISON 13	THEO
1.36 ± 0.04 ± 0.10		27 ALEKHIN 12	THEO
1.261 ± 0.016		28 NARISON 12A	THEO
1.01 ± 0.09 ± 0.03		29 ALEKHIN 11	THEO
1.28 ± 0.04		30 BLOSSIER 10	LATT
1.299 ± 0.026		31 BODENSTEIN 10	THEO
1.273 ± 0.006		32 MCNEILE 10	LATT
1.261 ± 0.018		33 NARISON 10	THEO
1.279 ± 0.013		34 CHETYRKIN 09	THEO
1.268 ± 0.009		35 ALLISON 08	LATT
1.286 ± 0.013		36 KUHN 07	THEO
1.295 ± 0.015		37 BOUGHEZAL 06	THEO
1.24 ± 0.09		38 BUCHMUEL... 06	THEO
1.224 ± 0.017 ± 0.054		39 HOANG 06	THEO
1.33 ± 0.10		40 AUBERT 04X	THEO
1.29 ± 0.07		41 HOANG 04	THEO
1.319 ± 0.028		42 DEDIVITIIS 03	LATT
1.19 ± 0.11		43 EIDEMULLER 03	THEO
1.289 ± 0.043		44 ERLER 03	THEO
1.26 ± 0.02		45 ZYABLYUK 03	THEO

- 1 ALEXANDROU 21 determines the quark mass using a lattice calculation of the meson and baryon masses with a twisted mass fermion action. We have converted $\bar{m}_c(3 \text{ GeV}) = 1.036 \pm 0.017 \pm 0.015 - 0.008$ to $\bar{m}_c(\bar{m}_c)$. The simulations are carried out using 2+1+1 dynamical quarks with $m_u = m_d \neq m_s \neq m_c$, including gauge ensembles close to the physical pion point.
- 2 HEITGER 21 determines the charm quark mass using a $n_f = 2+1$ flavor lattice QCD simulation with non-perturbatively O(a) improved Wilson fermions. They also determine $\bar{m}_c(3 \text{ GeV}) = 1.007 \pm 0.016 \text{ GeV}$.
- 3 HATTON 20 determines the charm quark mass with a lattice QCD + quenched QED simulation using the HISQ action and including $n_f = 2+1+1$ flavors of sea quarks. m_c is tuned from the J/ψ meson mass giving $\bar{m}_c(3 \text{ GeV}) = 0.9841 \pm 0.0051 \text{ GeV}$.
- 4 NARISON 20 determines the quark mass using QCD Laplace sum rules from the B_c mass, combined with previous determinations of the QCD condensates and c and b masses.
- 5 ABRAMOWICZ 18 determine $\bar{m}_c(\bar{m}_c) = 1.290 \pm 0.046 + 0.062 + 0.003$ from the production of c quarks in $e p$ collisions at HERA using combined H1 and ZEUS data. The experimental/fitting errors, and those from modeling and parameterization have been combined in quadrature.
- 6 BAZAVOV 18 determine the quark masses using a lattice computation with staggered fermions and four active quark flavors.
- 7 LYTLE 18 combined with CHAKRABORTY 15 determine $\bar{m}_c(3 \text{ GeV}) = 0.9874(48) \text{ GeV}$ from a lattice simulation with $n_f = 2+1+1$ flavors. They also determine the quoted value $\bar{m}_c(\bar{m}_c)$ for $n_f = 4$ dynamical flavors.
- 8 PESET 18 determine $\bar{m}_c(\bar{m}_c)$ and $\bar{m}_b(\bar{m}_b)$ using an N3LO calculation of the η_c, η_b and B_c masses.
- 9 CHETYRKIN 17 determine $\bar{m}_c(\mu = 3 \text{ GeV}) = 0.993 \pm 0.008 \text{ GeV}$ and $\bar{m}_c(\bar{m}_c)$ from a four-loop sum-rule computation of the cross-section for $e^+ e^- \rightarrow$ hadrons in the charm threshold region.
- 10 ERLER 17 determine $\bar{m}_c(\bar{m}_c) = 1.272 \pm 0.008 \text{ GeV}$ from a three-loop QCD sum-rule computation of the vector current correlator. This result is for fixed $\alpha_s(M_Z) = 0.1182$. Including an α_s uncertainty of ± 0.0016 , the charm mass error increases from 8 to 9 MeV.
- 11 KIYO 16 determine $\bar{m}_c(\bar{m}_c)$ from the $J/\psi(1S)$ mass at order α_s^3 (N3LO).

LIGHT QUARKS (*u, d, s*) REFERENCES

ALEXANDROU 21	PR D104 074515	C. Alexandrou et al.	(ETM Collab.)
BRUNO 20	EPJ C80 169	M. Bruno et al.	(ALPHA Collab.)
DOMINGUEZ 19	JHEP 1902 057	C.A. Dominguez, A. Mes, K. Schilcher	(CAPE, MAINZ)
BAZAVOV 18	PR D98 054517	A. Bazavov et al.	(Fermilab Lattice, MILC, TUMQCD)
COLANGELO 18	EPJ C78 947	G. Colangelo et al.	
LYTLE 18	PR D98 014513	A.T. Lytle et al.	(HPQCD Collab.)
COLANGELO 17	PRL 118 022001	G. Colangelo et al.	(BERN, IND, JLAB)
GUO 17	PL B771 497	P. Guo et al.	
YUAN 17	PR D96 014024	J.-M. Yuan et al.	
ANANTHANA... 16	PR D94 116014	B. Ananthanarayan, D. Das	(BANG, AHMED)
FODOR 16	PRL 117 082001	Z. Fodor et al.	(BMW Collab.)
BASAK 15	JPCS 640 012052	S. Basak et al.	(MILC Collab.)
CHAKRABOR... 15	PR D91 054508	B. Chakraborty et al.	(HPQCD Collab.)
GUO 15F	PR D92 054016	P. Guo et al.	
BAZAVOV 14A	PR D90 074509	A. Bazavov et al.	(Fermi-LAT and MILC Collabs.)
CARRASCO 14	NP B887 19	N. Carrasco et al.	(European Twisted Mass Collab.)
ARTHUR 13	PR D87 094514	R. Arthur et al.	(RBC and UKQCD Collabs.)
BODENSTEIN 13	JHEP 1307 138	S. Bodenstein, C.A. Dominguez, K. Schilcher	
AOKI 12	PR D86 034507	S. Aoki et al.	(PACS-CS Collab.)
FRITZSCH 12	NP B865 397	P. Fritzsche et al.	(ALPHA Collab.)
AOKI 11A	PR D83 074508	Y. Aoki et al.	(RBC-UKQCD Collab.)
DURR 11	PL B701 265	S. Durr et al.	(BMW Collab.)
BAZAVOV 10	RMP 82 1349	A. Bazavov et al.	(MILC Collab.)
BLOSSIER 10	PR D82 114513	B. Blossier et al.	(ETM Collab.)
BLUM 10	PR D82 094508	T. Blum et al.	
DAVIES 10	PRL 104 132003	C.T.H. Davies et al.	(HPQCD Collab.)
MCNEILE 10	PR D82 034512	C. McNeile et al.	(HPQCD Collab.)
DOMINGUEZ 09	PR D79 014009	C.A. Dominguez et al.	
ALLISON 08	PR D78 054513	I. Allison et al.	(HPQCD Collab.)
ALLTON 08	PR D78 114509	C. Allton et al.	(RBC and UKQCD Collabs.)
BLOSSIER 08	JHEP 0804 020	B. Blossier et al.	(ETM Collab.)
DEANDREA 08	PR D78 034032	A. Deandrea, A. Nehme, P. Talavera	
DOMINGUEZ 08A	JHEP 0805 020	C.A. Dominguez et al.	
DOMINGUEZ... 08B	PL B660 49	A. Dominguez-Clarimon, E. de Rafael, J. Taron	
ISHIKAWA 08	PR D78 011502	T. Ishikawa et al.	(CP-PACS and JLQCD Collabs.)
NAKAMURA 08	PR D78 034502	Y. Nakamura et al.	(CP-PACS Collab.)
BLUM 07	PR D76 114508	T. Blum et al.	(RBC Collab.)
OLLER 07A	EPJ A34 371	J.A. Oller, L. Roca	
CHETYRKIN 06	EPJ C46 721	K.G. Chetyrkin, A. Khodjamirian	
GOCKELER 06	PR D73 054508	M. Gockeler et al.	(QCDSF and UKQCD Collabs.)
GOCKELER 06A	PL B639 307	M. Gockeler et al.	(QCDSF and UKQCD Collabs.)
JAMIN 06	PR D74 074009	M. Jamin, J.A. Oller, A. Pich	
MASON 06	PR D73 114501	Q. Mason et al.	
NARISON 06	PR D74 034013	S. Narison	(HPQCD Collab.)
PDG 06	JP G33 1	W.-M. Yao et al.	(PDG Collab.)
BAIKOV 05	PRL 95 012003	P.A. Baikov, K.G. Chetyrkin, J.H. Kuhn	
GAMIZ 05	PRL 94 011803	E. Gamiz et al.	
GORBUNOV 05	PR D71 013002	D.S. Gorbunov, A.A. Pivovarov	
MARTEMYA... 05	PR D71 017501	B.V. Martemyanov, V.S. Sopot	
NARISON 05	PL B626 101	S. Narison	
AUBIN 04	PR D70 031504	C. Aubin et al.	(HPQCD, MILC, UKQCD Collabs.)
AUBIN 04A	PR D70 114501	C. Aubin et al.	(MILC Collab.)
AOKI 03	PR D67 034503	S. Aoki et al.	(CP-PACS Collab.)
AOKI 03B	PR D68 054502	S. Aoki et al.	(CP-PACS Collab.)
BECIREVIC 03	PL B558 69	D. Becirevic, V. Lubitz, C. Tarantino	
CHIU 03	NP B673 217	T.-W. Chiu, T.-H. Hsieh	
GAMIZ 03	JHEP 0301 060	E. Gamiz et al.	
NELSON 03	PRL 90 021601	D. Nelson, G.T. Fleming, G.W. Kilcup	
GAO 97	PR D56 4115	D.-N. Gao, B.A. Li, M.-L. Yan	
ANISOVICH 96	PL B375 335	A.V. Anisovich, H. Leutwyler	
LEUTWYLER 96	PL B378 313	H. Leutwyler	
DONOGHUE 92	PRL 69 3444	J.F. Donoghue, B.R. Holstein, D. Wyler	(MASA+)
GERARD 90	MPL A5 391	J.M. Gerard	(MPIM)
LEUTWYLER 90B	NP B337 108	H. Leutwyler	(BERN)



$$I(J^P) = 0(\frac{1}{2}^+)$$

$$\text{Charge} = \frac{2}{3} e \quad \text{Charm} = +1$$

c-QUARK MASS

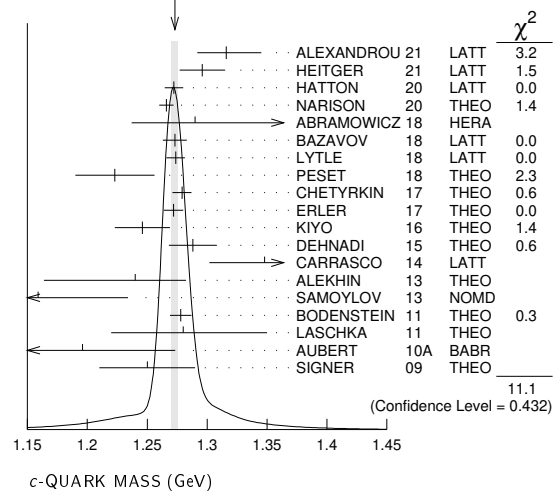
The *c*-quark mass corresponds to the "running" mass $m_c(\mu = m_c)$ in the \bar{m}_c scheme. We have converted masses in other schemes to the \bar{m}_c scheme using two-loop QCD perturbation theory with $\alpha_s(\mu = m_c) =$

Quark Particle Listings

C

- 12 DEHNADI 15 determine $\overline{m}_c(\overline{m}_c)$ using sum rules for $e^+e^- \rightarrow$ hadrons at order α_s^3 (N3LO), and fitting to both experimental data and lattice results.
- 13 CARRASCO 14 is a lattice QCD computation of light quark masses using $2+1+1$ dynamical quarks, with $m_u = m_d \neq m_s \neq m_c$. The u and d quark masses are obtained separately by using the K meson mass splittings and lattice results for the electromagnetic contributions.
- 14 ALEKHIN 13 determines m_c from charm production in deep inelastic scattering at HERA using approximate NNLO QCD.
- 15 SAMOYLOV 13 determines m_c from a study of charm dimuon production in neutrino-iron scattering using the NLO QCD result for the charm quark production cross section.
- 16 BODENSTEIN 11 determine $\overline{m}_c(3 \text{ GeV}) = 0.987 \pm 0.009 \text{ GeV}$ and $\overline{m}_c(\overline{m}_c) = 1.278 \pm 0.009 \text{ GeV}$ using QCD sum rules for the charm quark vector current correlator.
- 17 LASCHKA 11 determine the c mass from the charmonium spectrum. The theoretical computation uses the heavy $Q\overline{Q}$ potential to order $1/m_Q$ obtained by matching the short-distance perturbative result onto lattice QCD result at larger scales.
- 18 AUBERT 10A determine the b - and c -quark masses from a fit to the inclusive decay spectra in semileptonic B decays in the kinetic scheme (and convert it to the \overline{MS} scheme).
- 19 SIGNER 09 determines the c -quark mass using non-relativistic sum rules to analyze the $e^+e^- \rightarrow c\overline{c}$ cross-section near threshold. Also determine the PS mass $m_{PS}(\mu_F = 0.7 \text{ GeV}) = 1.50 \pm 0.04 \text{ GeV}$.
- 20 NARISON 18A determines simultaneously $\overline{m}_c(\overline{m}_c)$ and the 4-dimension gluon condensate using QCD exponential sum rules and their ratios evaluated at the optimal scale $\mu = 2.85 \text{ GeV}$ at N2LO-N3LO of perturbative QCD and including condensates up to dimension 6-8 in the (axial-)vector and (pseudo-)scalar charmonium channels.
- 21 NARISON 18B determines $\overline{m}_c(\overline{m}_c)$ using QCD vector moment sum rules and their ratios at N2LO-N3LO of perturbative QCD and including condensates up to dimension 8.
- 22 BERTONE 16 determine $\overline{m}_c(\overline{m}_c)$ from HERA deep inelastic scattering data using the FONLL scheme. Also determine $\overline{m}_c(\overline{m}_c) = 1.318 \pm 0.054 \pm 0.490 \pm 0.022$ using the fixed flavor number scheme.
- 23 CHAKRABORTY 15 is a lattice QCD computation using $2+1+1$ dynamical flavors. Moments of pseudoscalar current-current correlators are matched to α_s^3 -accurate QCD perturbation theory with the η_c meson mass tuned to experiment.
- 24 ABRAMOWICZ 13c determines m_c from charm production in deep inelastic $e p$ scattering, using the QCD prediction at NLO order. The uncertainties from model and parameterization assumptions, and the value of α_s , of ± 0.03 , ± 0.02 , and ± 0.02 respectively, have been combined in quadrature.
- 25 DEHNADI 13 determines m_c using QCD sum rules for the charmonium spectrum and charm continuum to order α_s^3 (N3LO). The statistical and systematic experimental errors of ± 0.006 and ± 0.009 have been combined in quadrature. The theoretical uncertainties ± 0.019 from truncation of the perturbation series, ± 0.010 from α_s , and ± 0.002 from the gluon condensate have been combined in quadrature.
- 26 NARISON 13 determines m_c using QCD spectral sum rules to order α_s^2 (NNLO) and including condensates up to dimension 6.
- 27 ALEKHIN 12 determines m_c from heavy quark production in deep inelastic scattering at HERA using approximate NNLO QCD.
- 28 NARISON 12A determines m_c using sum rules for the vector current correlator to order α_s^3 , including the effect of gluon condensates up to dimension eight.
- 29 ALEKHIN 11 determines m_c from heavy quark production in deep inelastic scattering using fixed target and HERA data, and approximate NNLO QCD.
- 30 BLOSSIER 10 determines quark masses from a computation of the hadron spectrum using $n_f=2$ dynamical twisted-mass Wilson fermions.
- 31 BODENSTEIN 10 determines $\overline{m}_c(3 \text{ GeV}) = 1.008 \pm 0.026 \text{ GeV}$ using finite energy sum rules for the vector current correlator. The authors have converted this to $\overline{m}_c(\overline{m}_c)$ using $\alpha_s(M_Z) = 0.1189 \pm 0.0020$.
- 32 MCNEILE 10 determines m_c by comparing the order α_s^3 perturbative results for the pseudo-scalar current to lattice simulations with $n_f = 2+1$ sea-quarks by the HPQCD collaboration.
- 33 NARISON 10 determines m_c from ratios of moments of vector current correlators computed to order α_s^3 and including the dimension-six gluon condensate.
- 34 CHETYRKIN 09 determine m_c and m_b from the $e^+e^- \rightarrow Q\overline{Q}$ cross-section and sum rules, using an order α_s^3 computation of the heavy quark vacuum polarization. They also determine $m_c(3 \text{ GeV}) = 0.986 \pm 0.013 \text{ GeV}$.
- 35 ALLISON 08 determine m_c by comparing four-loop perturbative results for the pseudo-scalar current correlator to lattice simulations by the HPQCD collaboration. The result has been updated in MCNEILE 10.
- 36 KUHN 07 determine $\overline{m}_c(\mu = 3 \text{ GeV}) = 0.986 \pm 0.013 \text{ GeV}$ and $\overline{m}_c(\overline{m}_c)$ from a four-loop sum-rule computation of the cross-section for $e^+e^- \rightarrow$ hadrons in the charm threshold region.
- 37 BOUGHEZAL 06 result comes from the first moment of the hadronic production cross-section to order α_s^3 .
- 38 BUCHMUELLER 06 determine m_b and m_c by a global fit to inclusive B decay spectra.
- 39 HOANG 06 determines $\overline{m}_c(\overline{m}_c)$ from a global fit to inclusive B decay data. The B decay distributions were computed to order $\alpha_s^2\beta_0$, and the conversion between different m_c mass schemes to order α_s^3 .
- 40 AUBERT 04x obtain m_c from a fit to the hadron mass and lepton energy distributions in semileptonic B decay. The paper quotes values in the kinetic scheme. The \overline{MS} value has been provided by the BABAR collaboration.
- 41 HOANG 04 determines $\overline{m}_c(\overline{m}_c)$ from moments at order α_s^2 of the charm production cross-section in e^+e^- annihilation.
- 42 DEDIVITIIS 03 use a quenched lattice computation of heavy-heavy and heavy-light meson masses.
- 43 EIDEMULLER 03 determines m_b and m_c using QCD sum rules.
- 44 ERLER 03 determines m_b and m_c using QCD sum rules. Includes recent BES data.
- 45 ZYABLYUK 03 determines m_c by using QCD sum rules in the pseudoscalar channel and comparing with the η_c mass.

WEIGHTED AVERAGE
1.2730±0.0028 (Error scaled by 1.0)



m_c/m_s MASS RATIO

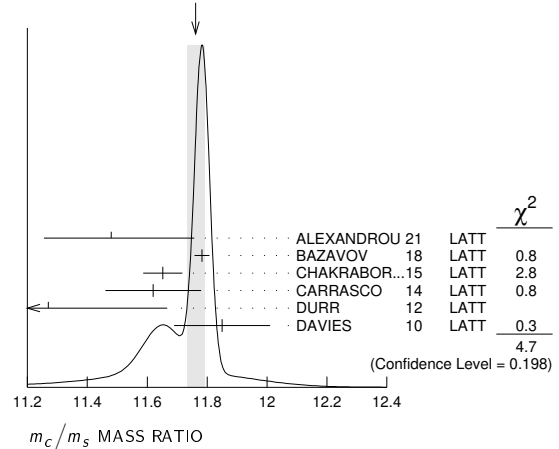
The ratio is that of the \overline{MS} masses at a common scale, for four dynamical quark flavors.

VALUE CL% DOCUMENT ID TECN
11.761±0.047 (CL = 90%) OUR EVALUATION See the ideogram below.

VALUE	CL%	DOCUMENT ID	TECN
11.48 ± 0.12 +0.25 -0.19		1 ALEXANDROU 21	LATT
11.783 ± 0.025		2 BAZAVOV 18	LATT
11.652 ± 0.065		3 CHAKRABOR...15	LATT
11.62 ± 0.16		4 CARRASCO 14	LATT
11.27 ± 0.30 ± 0.26		5 DURR 12	LATT
11.85 ± 0.16		6 DAVIES 10	LATT
11.747 ± 0.019 ± 0.059 -0.043		7 BAZAVOV 14A	LATT
12.0 ± 0.3		8 BLOSSIER 10	LATT

- • • We do not use the following data for averages, fits, limits, etc. • • •
- 1 ALEXANDROU 21 determines the quark mass using a lattice calculation of the meson and baryon masses with a twisted mass fermion action. The simulations are carried out using $2+1+1$ dynamical quarks with $m_u = m_d \neq m_s \neq m_c$, including gauge ensembles close to the physical pion point.
- 2 BAZAVOV 18 determine the quark masses using a lattice computation with staggered fermions and four active quark flavors.
- 3 CHAKRABORTY 15 is a lattice QCD computation on gluon field configurations with $2+1+1$ dynamical flavors of HISQ quarks with u/d masses down to the physical value. m_c and m_s are tuned from pseudoscalar meson masses.
- 4 CARRASCO 14 is a lattice QCD computation of light quark masses using $2+1+1$ dynamical quarks, with $m_u = m_d \neq m_s \neq m_c$. The u and d quark masses are obtained separately by using the K meson mass splittings and lattice results for the electromagnetic contributions.
- 5 DURR 12 determine m_c/m_s using a lattice computation with $n_f = 2$ dynamical fermions. The result is combined with other determinations of m_c to obtain $m_s(2 \text{ GeV}) = 97.0 \pm 2.6 \pm 2.5 \text{ MeV}$.
- 6 DAVIES 10 determine m_c/m_s from meson masses calculated on gluon fields including u , d , and s sea quarks with lattice spacing down to 0.045 fm . The Highly Improved Staggered quark formalism is used for the valence quarks.
- 7 BAZAVOV 14A is a lattice computation using 4 dynamical flavors of HISQ fermions.
- 8 BLOSSIER 10 determine m_c/m_s from a computation of the hadron spectrum using $n_f = 2$ dynamical twisted-mass Wilson fermions.

WEIGHTED AVERAGE
11.761±0.028 (Error scaled by 1.2)



m_b/m_c MASS RATIO

The ratio is that of the \overline{MS} masses at a common scale, for four dynamical quark flavors.

VALUE	DOCUMENT ID	TECN
4.58 ± 0.01 OUR EVALUATION		
4.580 ± 0.007 OUR AVERAGE		
4.586 ± 0.012	¹ HATTON 21	LATT
4.578 ± 0.008	² BAZAVOV 18	LATT
4.528 ± 0.054	³ CHAKRABOR...15	LATT

- HATTON 21 determine $\overline{m}_b(\mu)/\overline{m}_c(\mu) = 4.586 \pm 0.012$ at $\mu = 3$ GeV with a lattice QCD + quenched QED simulation using the HISQ action and including $n_f = 2+1+1$ flavors of sea quarks. The ratio depends weakly on μ because of QED effects.
- BAZAVOV 18 determine the quark masses using a lattice computation with staggered fermions and four active quark flavors for the u, d, s, c quarks and five active flavors for the b quark.
- CHAKRABORTY 15 is a lattice computation using 4 dynamical quark flavors.

$m_b - m_c$ QUARK MASS DIFFERENCE

VALUE (GeV)	DOCUMENT ID	TECN
3.45 ± 0.05 OUR EVALUATION		
• • • We do not use the following data for averages, fits, limits, etc. • • •		
3.472 ± 0.032	¹ AUBERT 10A	BABR
3.42 ± 0.06	² ABDALLAH 06B	DLPH
3.44 ± 0.03	³ AUBERT 04X	BABR
3.41 ± 0.01	³ BAUER 04	THEO

- AUBERT 10A determine the b - and c -quark masses from a fit to the inclusive decay spectra in semileptonic B decays in the kinetic scheme.
- ABDALLAH 06B determine $m_b - m_c$ from moments of the hadron invariant mass and lepton energy spectra in semileptonic inclusive B decays.
- Determine $m_b - m_c$ from a global fit to inclusive B decay spectra.

c-QUARK REFERENCES

ALEXANDROU 21	PR D104 074515	C. Alexandrou et al.	(ETM Collab.)
HATTON 21	PR D103 114508	D. Hatton et al.	(HPQCD Collab.)
HEITGER 21	JHEP 2105 288	J. Heitger, F. Joswig, S. Kuberski	(ALPHA Collab.)
HATTON 20	PR D102 054511	D. Hatton et al.	(HPQCD Collab.)
NARISON 20	PL B802 135221	S. Narison	(MONP)
ABRAMOWICZ 18	EPJ C78 473	H. Abramowicz et al.	(H1 and ZEUS Collabs.)
BAZAVOV 18	PR D98 054517	A. Bazavov et al.	(Fermilab Lattice, MILC, TUMQCD)
LYTLE 18	PR D98 014513	A.T. Lytle et al.	(HPQCD Collab.)
NARISON 18A	IMP A33 1850045	S. Narison	(MONP)
NARISON 18B	PL B704 261	S. Narison	(MONP)
PESET 18	JHEP 1809 167	C. Peset, A. Pineda, J. Segovia	(MONP)
CHETYRKIN 17	PR D96 116007	K.G. Chetyrkin et al.	(BARC, TUM)
ERLER 17	EPJ C77 99	J. Erler, P. Masjuan, H. Spiesberger	
BERTONE 16	JHEP 1608 050	V. Bertone et al.	(xFitter Developers)
KIYO 16	PL B752 122	Y. Kiyo, G. Mishima, Y. Sumino	
CHAKRABOR...15	PR D91 054508	B. Chakraborty et al.	(HPQCD Collab.)
DEHNADI 15	JHEP 1508 155	B. Dehnadi, A.H. Hoang, V. Mateu	
BAZAVOV 14A	PR D90 074509	A. Bazavov et al.	(Fermi-LAT and MILC Collabs.)
CARRASCO 14	NP B887 19	N. Carrasco et al.	(European Twisted Mass Collab.)
ABRAMOWICZ 13C	EPJ C73 2311	H. Abramowicz et al.	(H1 and Zeus Collabs.)
ALEKHIN 13	PL B720 172	S. Alekhin et al.	(SERP, DESY, WUPP+)
DEHNADI 13	JHEP 1309 103	B. Dehnadi et al.	(SHRZ, VIEN, MPIM+)
NARISON 13	PL B718 1321	S. Narison	(MONP)
SAMOYLOV 13	NP B876 339	O. Samoylov et al.	(NOMAD Collab.)
ALEKHIN 12	PL B718 550	S. Alekhin et al.	(SERP, WUPP, DESY+)
DURR 12	PRL 108 122003	S. Durr, G. Koutsou	(WUPP, JULI, CYPR)
NARISON 12A	PL B706 412	S. Narison	(MONP)
ALEKHIN 11	PL B699 345	S. Alekhin, S. Moch	(DESY, SERP)
BODENSTEIN 11	PR D83 074014	S. Bodenstein et al.	
LASCHKA 11	PR D83 094002	A. Laschka, N. Kaiser, W. Weise	
AUBERT 10A	PR D81 032003	B. Aubert et al.	(BABAR Collab.)
BLOSSIER 10	PR D82 114513	B. Blossier et al.	(ETM Collab.)
BODENSTEIN 10	PR D82 114013	S. Bodenstein et al.	
DAVIES 10	PRL 104 132003	C.T.H. Davies et al.	(HPQCD Collab.)
MCNEILE 10	PR D82 034512	C. McNeile et al.	(HPQCD Collab.)
NARISON 10	PL B693 559	S. Narison	(MONP)
Also	PL B705 544 (errata.)	S. Narison	(MONP)
CHETYRKIN 09	PR D80 074010	K.G. Chetyrkin et al.	(KARL, BNL)
SIGNER 09	PL B672 333	A. Signer	(DURR)
ALLISON 08	PR D78 054513	I. Allison et al.	(HPQCD Collab.)
KUHN 07	NP B778 192	J.H. Kuhn, M. Steinhauser, C. Sturm	
ABDALLAH 06B	EPJ C45 35	J. Abdallah et al.	(DELPHI Collab.)
BOUGHEZAL 06	PR D74 074006	R. Boughezal, M. Czakon, T. Schutzmeier	
BUCHMUELL... 06	PR D73 073008	O.L. Buchmueller, H.U. Flacher	(RHBL)
HOANG 06	PL B633 526	A.H. Hoang, A.V. Manohar	
AUBERT 04X	PRL 93 011803	B. Aubert et al.	(BABAR Collab.)
BAUER 04	PR D70 094017	C. Bauer et al.	
HOANG 04	PL B594 127	A.H. Hoang, M. Jamim	
DEDIVITHIS 03	NP B675 309	G.M. de Divitiis et al.	
EIDEMULLER 03	PR D67 113002	M. Eidemuller	
ERLER 03	PL B558 125	J. Erler, M. Luo	
ZYABLYUK 03	JHEP 0301 081	K.N. Zyablyuk	(ITEP)

for the pole mass, using the two-loop conversion formula. A discussion of masses in different schemes can be found in the "Note on Quark Masses."

\overline{MS} MASS (GeV)	CL%	DOCUMENT ID	TECN
4.183 ± 0.007 (CL = 90%) OUR EVALUATION			of \overline{MS} Mass. See the ideogram below.

3.94 +0.46 -0.40	¹ APARISI 22	THEO
4.202 ± 0.021	² HATTON 21	LATT
4.197 ± 0.008	³ NARISON 20	THEO
4.049 +0.138 -0.118	⁴ ABRAMOWICZ18	HERA
4.195 ± 0.014	⁵ BAZAVOV 18	LATT
4.186 ± 0.037	⁶ PESET 18	THEO
4.197 ± 0.022	⁷ KIYO 16	THEO
4.183 ± 0.037	⁸ ALBERTI 15	THEO
4.203 +0.016 -0.034	⁹ BENEKE 15	THEO
4.196 ± 0.023	¹⁰ COLQUHOUN 15	LATT
4.176 ± 0.023	¹¹ DEHNADI 15	THEO
4.21 ± 0.11	¹² BERNARDONI 14	LATT
4.169 ± 0.002 ± 0.008	¹³ PENIN 14	THEO
4.166 ± 0.043	¹⁴ LEE 130	LATT
4.247 ± 0.034	¹⁵ LUCHA 13	THEO
4.171 ± 0.009	¹⁶ BODENSTEIN 12	THEO
4.29 ± 0.14	¹⁷ DIMOPOUL... 12	LATT
4.18 +0.05 -0.04	¹⁸ LASCHKA 11	THEO
4.186 ± 0.044 ± 0.015	¹⁹ AUBERT 10A	BABR
4.163 ± 0.016	²⁰ CHETYRKIN 09	THEO
4.243 ± 0.049	²¹ SCHWANDA 08	BELL

• • • We do not use the following data for averages, fits, limits, etc. • • •

4.184 ± 0.011	²² NARISON 18A	THEO
4.188 ± 0.008	²³ NARISON 18B	THEO
4.07 ± 0.17	²⁴ ABRAMOWICZ14A	ZEUS
4.201 ± 0.043	²⁵ AYALA 14A	THEO
4.236 ± 0.069	²⁶ NARISON 13	THEO
4.213 ± 0.059	²⁷ NARISON 13A	THEO
4.235 ± 0.003 ± 0.055	²⁸ HOANG 12	THEO
4.212 ± 0.032	²⁹ NARISON 12	THEO
4.177 ± 0.011	³⁰ NARISON 12	THEO
4.171 ± 0.014	³¹ NARISON 12A	THEO
4.164 ± 0.023	³² MCNEILE 10	LATT
4.173 ± 0.010	³³ NARISON 10	THEO
5.26 ± 1.2	³⁴ ABDALLAH 08D	DLPH
4.42 ± 0.06 ± 0.08	³⁵ GUAZZINI 08	LATT
4.347 ± 0.048 ± 0.08	³⁶ DELLA-MOR... 07	LATT
4.164 ± 0.025	³⁷ KUHN 07	THEO
4.19 ± 0.40	³⁸ ABDALLAH 06D	DLPH
4.205 ± 0.058	³⁹ BOUGHEZAL 06	THEO
4.20 ± 0.04	⁴⁰ BUCHMUELL... 06	THEO
4.19 ± 0.06	⁴¹ PINEDA 06	THEO
4.4 ± 0.3	⁴² GRAY 05	LATT
4.22 ± 0.06	⁴³ AUBERT 04X	THEO
4.17 ± 0.03	⁴⁴ BAUER 04	THEO
4.22 ± 0.11	⁴⁵ HOANG 04	THEO
4.25 ± 0.11	⁴⁶ MCNEILE 04	LATT
4.22 ± 0.09	⁴⁷ BAUER 03	THEO
4.19 ± 0.05	⁴⁸ BORDES 03	THEO
4.20 ± 0.09	⁴⁹ CORCELLA 03	THEO
4.33 ± 0.10	⁵⁰ DEDIVITHIS 03	LATT
4.24 ± 0.10	⁵¹ EIDEMULLER 03	THEO
4.207 ± 0.03	⁵² ERLER 03	THEO
4.33 ± 0.06 ± 0.10	⁵³ MAHMOOD 03	CLEO
4.190 ± 0.032	⁵⁴ BRAMBILLA 02	THEO
4.346 ± 0.070	⁵⁵ PENIN 02	THEO

- APARISI 22 determine m_b at the Higgs mass, $\overline{m}_b(m_H) = 2.60^{+0.36}_{-0.31}$ GeV from Higgs boson decay rates at the LHC, which is used to obtain $\overline{m}_b(\overline{m}_b)$.
- HATTON 21 determine $\overline{m}_b(3 \text{ GeV}) = 4.513 \pm 0.026$ GeV using a lattice QCD + quenched QED simulation using the HISQ action and including $n_f = 2+1+1$ flavors of sea quarks, by combining their $\overline{m}_b/\overline{m}_c$ and \overline{m}_c determinations.
- NARISON 20 determines the quark mass using QCD Laplace sum rules from the B_c mass, combined with previous determinations of the QCD condensates and c and b masses.
- ABRAMOWICZ 18 determine $\overline{m}_b(\overline{m}_b) = 4.049^{+0.104+0.099+0.001}_{-0.109-0.032-0.031}$ from the production of b quarks in ep collisions at HERA using combined H1 and ZEUS data. The experimental/fitting errors, and those from modeling and parameterization have been combined in quadrature.
- BAZAVOV 18 determine the b mass using a lattice computation with staggered fermions and five active quark flavors.
- PESET 18 determine $\overline{m}_c(\overline{m}_c)$ and $\overline{m}_b(\overline{m}_b)$ using an N3LO calculation of the η_c, η_b and B_c masses.
- KIYO 16 determine $\overline{m}_b(\overline{m}_b)$ from the $\Upsilon(1S)$ mass at order α_s^3 (N3LO).
- ALBERTI 15 determine $\overline{m}_b(\overline{m}_b)$ from fits to inclusive $B \rightarrow X_c e \overline{\nu}$ decay. They also find $m_b^{\text{kin}}(1 \text{ GeV}) = 4.553 \pm 0.020$ GeV.
- BENEKE 15 determine $\overline{m}_b(\overline{m}_b)$ using sum rules for $e^+e^- \rightarrow$ hadrons at order N3LO including finite m_c effects. They find $m_b^{\text{P}}(2 \text{ GeV}) = 4.532^{+0.013}_{-0.035}$ GeV, and $\overline{m}_b(\overline{m}_b) = 4.193^{+0.022}_{-0.035}$ GeV. The value quoted is obtained using the four-loop conversion given in BENEKE 16.



$$J(P) = 0(\frac{1}{2}^+)$$

$$\text{Charge} = -\frac{1}{3} e \quad \text{Bottom} = -1$$

b-QUARK MASS

b -quark mass corresponds to the "running mass" $\overline{m}_b(\mu = \overline{m}_b)$ in the \overline{MS} scheme. We have converted masses in other schemes to the \overline{MS} mass using two-loop QCD perturbation theory with $\alpha_s(\mu = \overline{m}_b) = 0.223 \pm 0.008$. The value $4.18^{+0.04}_{-0.03}$ GeV for the \overline{MS} mass corresponds to 4.78 ± 0.06 GeV

Quark Particle Listings

b

- 10 COLQUHOUN 15 determine $\overline{m}_b(\overline{m}_b)$ from moments of the vector current correlator computed with a lattice simulation using the NRQCD action.
- 11 DEHNADI 15 determine $\overline{m}_b(\overline{m}_b)$ using sum rules for $e^+e^- \rightarrow$ hadrons at order α_s^3 (N3LO), and fitting to both experimental data and lattice results.
- 12 BERNARDONI 14 determine m_b from $n_f = 2$ lattice calculations using heavy quark effective theory non-perturbatively renormalized and matched to QCD at $1/m$ order.
- 13 PENIN 14 determine $\overline{m}_b(\overline{m}_b) = 4.169 \pm 0.008 \pm 0.002 \pm 0.002$ using an estimate of the order α_s^3 b -quark vacuum polarization function in the threshold region, including finite m_c effects. The errors of ± 0.008 from theoretical uncertainties, and ± 0.002 from α_s have been combined in quadrature.
- 14 LEE 13a determine m_b using lattice calculations of the Υ and B_s binding energies in NRQCD, including three light dynamical quark flavors. The quark mass shift in NRQCD is determined to order α_s^2 , with partial α_s^3 contributions.
- 15 LUCHA 13 determines m_b from QCD sum rules for heavy-light currents using the lattice value for Γ_B of 191.5 ± 7.3 GeV.
- 16 BODENSTEIN 12 determine m_b using sum rules for the vector current correlator and the $e^+e^- \rightarrow Q\overline{Q}$ total cross-section.
- 17 DIMOPOULOS 12 determine quark masses from a lattice computation using $n_f = 2$ dynamical flavors of twisted mass fermions.
- 18 LASCHKA 11 determine the b mass from the charmonium spectrum. The theoretical computation uses the heavy $Q\overline{Q}$ potential to order $1/m_Q$ obtained by matching the short-distance perturbative result onto lattice QCD result at larger scales.
- 19 AUBERT 10A determine the b - and c -quark masses from a fit to the inclusive decay spectra in semileptonic B decays in the kinetic scheme (and convert it to the \overline{MS} scheme).
- 20 CHETYRKIN 09 determine m_c and m_b from the $e^+e^- \rightarrow Q\overline{Q}$ cross-section and sum rules, using an order α_s^3 (N3LO) computation of the heavy quark vacuum polarization.
- 21 SCHWANDA 08 measure moments of the inclusive photon spectrum in $B \rightarrow X_s \gamma$ decay to determine m_b^{1S} . We have converted this to \overline{MS} scheme.
- 22 NARISON 18A determines $\overline{m}_b(\overline{m}_b)$ as a function of α_s using QCD exponential sum rules and their ratios evaluated at the optimal scale $\mu = 9.5$ GeV at N2LO-N3LO of perturbative QCD and including condensates up to dimension 6–8 in the (axial-)vector and (pseudo-)scalar bottomonium channels.
- 23 NARISON 18B determines $\overline{m}_b(\overline{m}_b)$ using QCD vector moment sum rules and their ratios at N2LO-N3LO of perturbative QCD and including condensates up to dimension 8.
- 24 ABRAMOWICZ 14A determine $\overline{m}_b(\overline{m}_b) = 4.07 \pm 0.14^{+0.01+0.05+0.08}_{-0.07-0.00-0.05}$ from the production of b quarks in ep collisions at HERA. The errors due to fitting, modeling, PDF parameterization, and theoretical QCD uncertainties due to the values of α_s , m_c , and the renormalization scale μ have been combined in quadrature.
- 25 AYALA 14A determine $\overline{m}_b(\overline{m}_b)$ from the $\Upsilon(1S)$ mass computed to N3LO order in perturbation theory using a renormalon subtracted scheme.
- 26 NARISON 13 determines m_b using QCD spectral sum rules to order α_s^2 (NNLO) and including condensates up to dimension 6.
- 27 NARISON 13A determines m_b using HQET sum rules to order α_s^2 (NNLO) and the B meson mass and decay constant.
- 28 HOANG 12 determine m_b using non-relativistic sum rules for the Υ system at order α_s^2 (NNLO) with renormalization group improvement.
- 29 NARISON 12 determines m_b using exponential sum rules for the vector current correlator to order α_s^2 , including the effect of gluon condensates up to dimension eight.
- 30 Determines m_b to order α_s^3 (N3LO), including the effect of gluon condensates up to dimension eight combining the methods of NARISON 12 and NARISON 12A.
- 31 NARISON 12A determines m_b using sum rules for the vector current correlator to order α_s^3 , including the effect of gluon condensates up to dimension eight.
- 32 MCNEILE 10 determines m_b by comparing order α_s^3 (N3LO) perturbative results for the pseudo-scalar current to lattice simulations with $n_f = 2+1$ sea-quarks by the HPQCD collaboration.
- 33 NARISON 10 determines m_b from ratios of moments of vector current correlators computed to order α_s^2 and including the dimension-six gluon condensate. These values are taken from the erratum to that reference.
- 34 ABDALLAH 08b determine $\overline{m}_b(M_Z) = 3.76 \pm 1.0$ GeV from a leading order study of four-jet rates at LEP.
- 35 GUAZZINI 08 determine $\overline{m}_b(\overline{m}_b)$ from a quenched lattice simulation of heavy meson masses. The ± 0.08 is an estimate of the quenching error.
- 36 DELLA-MORTE 07 determine $\overline{m}_b(\overline{m}_b)$ from a computation of the spin-averaged B meson mass using quenched lattice HQET at order $1/m$. The ± 0.08 is an estimate of the quenching error.
- 37 KUHN 07 determine $\overline{m}_b(\mu = 10 \text{ GeV}) = 3.609 \pm 0.025$ GeV and $\overline{m}_b(\overline{m}_b)$ from a four-loop sum-rule computation of the cross-section for $e^+e^- \rightarrow$ hadrons in the bottom threshold region.
- 38 ABDALLAH 06b determine $m_b(M_Z) = 2.85 \pm 0.32$ GeV from Z -decay three-jet events containing a b -quark.
- 39 BOUGHEZAL 06 \overline{MS} scheme result comes from the first moment of the hadronic production cross-section to order α_s^3 .
- 40 BUCHMUELLER 06 determine m_b and m_c by a global fit to inclusive B decay spectra.
- 41 PINEDA 06 \overline{MS} scheme result comes from a partial NNLL evaluation (complete at order α_s^2 (NNLO)) of sum rules of the bottom production cross-section in e^+e^- annihilation.
- 42 GRAY 05 determines $\overline{m}_b(\overline{m}_b)$ from a lattice computation of the Υ spectrum. The simulations have 2+1 dynamical light flavors. The b quark is implemented using NRQCD.
- 43 AUBERT 04x obtain m_b from a fit to the hadron mass and lepton energy distributions in semileptonic B decay. The paper quotes values in the kinetic scheme. The \overline{MS} value has been provided by the BABAR collaboration.
- 44 BAUER 04 determine m_b , m_c and $m_b - m_c$ by a global fit to inclusive B decay spectra.
- 45 HOANG 04 determines $\overline{m}_b(\overline{m}_b)$ from moments at order α_s^2 of the bottom production cross-section in e^+e^- annihilation.
- 46 MCNEILE 04 use lattice QCD with dynamical light quarks and a static heavy quark to compute the masses of heavy-light mesons.
- 47 BAUER 03 determine the b quark mass by a global fit to B decay observables. The experimental data includes lepton energy and hadron invariant mass moments in semileptonic

$B \rightarrow X_c \ell \nu_\ell$ decay, and the inclusive photon spectrum in $B \rightarrow X_s \gamma$ decay. The theoretical expressions used are of order $1/m^3$, and $\alpha_s^2 \beta_0$.

48 BORDES 03 determines m_b using QCD finite energy sum rules to order α_s^2 .

49 CORCELLA 03 determines \overline{m}_b using sum rules computed to order α_s^2 . Includes charm quark mass effects.

50 DEDIVITIS 03 use a quenched lattice computation of heavy-heavy and heavy-light meson masses.

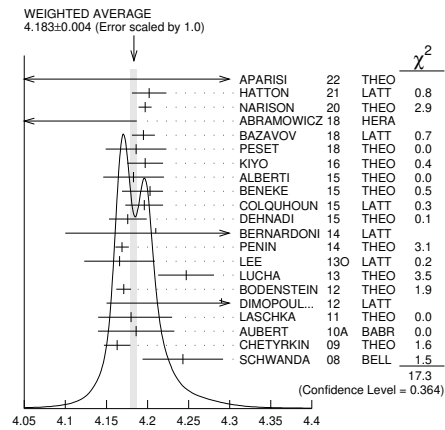
51 EIDEMULLER 03 determines \overline{m}_b and \overline{m}_c using QCD sum rules.

52 ERLER 03 determines \overline{m}_b and \overline{m}_c using QCD sum rules. Includes recent BES data.

53 MAHMOOD 03 determines m_b^{1S} by a fit to the lepton energy moments in $B \rightarrow X_c \ell \nu_\ell$ decay. The theoretical expressions used are of order $1/m^3$ and $\alpha_s^2 \beta_0$. We have converted their result to the \overline{MS} scheme.

54 BRAMBILLA 02 determine $\overline{m}_b(\overline{m}_b)$ from a computation of the $\Upsilon(1S)$ mass to order α_s^4 , including finite m_c corrections.

55 PENIN 02 determines \overline{m}_b from the spectrum of the Υ system.



b -QUARK \overline{MS} MASS (GeV)

m_b/m_s MASS RATIO

VALUE	DOCUMENT ID	TECN
53.88 ± 0.12 OUR AVERAGE		
53.94 ± 0.12	¹ BAZAVOV 18	LATT
52.55 ± 0.55	² CHAKRABORTY 15	LATT

¹ BAZAVOV 18 determine the quark masses using a lattice computation with staggered fermions and four active quark flavors for the u, d, s, c quarks and five active flavors for the b quark.

² CHAKRABORTY 15 determine m_b/m_s from lattice QCD using the HISQ action and including $n_f = 2+1+1$ flavors of sea quarks.

b -QUARK REFERENCES

APARISI 22	PRL 128 122001	J. Aparisi et al.	(VALE, WIEN, PSI+)
HATTON 21	PR D103 114508	D. Hatton et al.	(HPQCD Collab.)
NARISON 20	PL B802 135221	S. Narison	(MONP)
ABRAMOWICZ 18	EPJ C78 473	H. Abramowicz et al.	(HI and ZEUS Collabs.)
BAZAVOV 18	PR D98 054517	A. Bazavov et al.	(Fermilab Lattice, MILC, TUMQCD)
NARISON 18A	IJMP A33 1850045	S. Narison	(MONP)
NARISON 18B	PL B784 261	S. Narison	(MONP)
PESET 18	JHEP 1809 167	C. Peset, A. Pineda, J. Segovia	(BARC, TUM)
BENEKE 16	PoS RADCOR2015 035	M. Beneke et al.	
KIYO 16	PL B752 122	Y. Kiyo, G. Mishima, Y. Sumino	
ALBERTI 15	PRL 114 061802	A. Alberti et al.	
BENEKE 15	NP B891 42	M. Beneke et al.	
CHAKRABORTY 15	PR D91 054508	B. Chakraborty et al.	(HPQCD Collab.)
COLQUHOUN 15	PR D91 074514	B. Colquhoun et al.	(HPQCD Collab.)
DEHNADI 15	JHEP 1508 155	B. Dehnadi, A.H. Hoang, V. Mateu	
ABRAMOWICZ 14A	JHEP 1409 127	H. Abramowicz et al.	(ZEUS Collab.)
AYALA 14A	JHEP 1409 045	C. Ayala, G. Cvetic, A. Pineda	
BERNARDONI 14	PL B730 171	F. Bernardoni et al.	(ALPHA Collab.)
PENIN 14	JHEP 1404 120	A.A. Penin, N. Zerb	
LEE 13a	PR D87 074018	A.J. Lee et al.	(HPQCD Collab.)
LUCHA 13b	PR D88 056011	W. Lucha, D. Melnikov, S. Simula	(VIEN, MOSU+)
NARISON 13A	PL B718 1321	S. Narison	(MONP)
NARISON 13B	PL B721 269	S. Narison	(MONP)
BODENSTEIN 12	PR D85 034003	S. Bodenstein et al.	(CAPE, VALE, MAINZ+)
DIMOPOULOS 12	JHEP 1201 046	P. Dimopoulos et al.	(ETM Collab.)
HOANG 12	JHEP 1210 188	A.H. Hoang, P. Ruiz-Femenia, M. Stahlhofen	(WIEN+)
NARISON 12	PL B707 259	S. Narison	(MONP)
NARISON 12A	PL B706 412	S. Narison	(MONP)
LASCHKA 11	PR D83 094002	A. Laschka, N. Kaiser, W. Weise	
AUBERT 10A	PR D81 032003	B. Aubert et al.	(BABAR Collab.)
MCNEILE 10	PR D82 034512	C. McNeile et al.	(HPQCD Collab.)
NARISON 10	PL B693 559	S. Narison	(MONP)
Also	PL B705 544 (err.)	S. Narison	(MONP)
CHETYRKIN 09	PR D80 074010	K.G. Chetyrkin et al.	(KARL, BNL)
ABDALLAH 08b	EPJ C55 525	J. Abdallah et al.	(DELPHI Collab.)
GUAZZINI 08	JHEP 0801 076	D. Guazzini, R. Sommer, N. Tantalo	(ETM Collab.)
SCHWANDA 08	PR D78 032016	C. Schwanda et al.	
DELLA-MORTE 07	JHEP 0701 007	M. Della Morte et al.	(WIEN+)
KUHN 07	NP B778 192	J.H. Kuhn, M. Steinhauser, C. Sturm	
ABDALLAH 06d	EPJ C46 569	J. Abdallah et al.	(DELPHI Collab.)
BOUGHEZAL 06	PR D74 074006	R. Boughezal, M. Czakon, T. Schutzmeier	
BUCHMUELLER 06	PR D73 073008	O.L. Buchmueller, H.U. Flacher	(RHLL)
PINEDA 06	PR D73 111501	A. Pineda, A. Signer	
GRAY 05	PR D72 094507	A. Gray et al.	(HPQCD and UKQCD Collab.)
AUBERT 04X	PRL 93 011803	B. Aubert et al.	(BABAR Collab.)
BAUER 04	PR D70 094017	C. Bauer et al.	

HOANG	04	PL B594 127	A.H. Hoang, M. Jamin
MCNEILE	04	PL B600 77	C. McNeile, C. Michael, G. Thompson (UKQCD Collab.)
BAUER	03	PR D67 054012	C.W. Bauer <i>et al.</i>
BORDES	03	PL B562 81	J. Bordes, J. Penarrocha, K. Schilcher
CORCELLA	03	PL B554 133	G. Corcella, A.H. Hoang
DEDIVITIS	03	NP B675 309	G.M. de Divitiis <i>et al.</i>
EIDEMULLER	03	PR D67 113002	M. Eidemüller
ERLER	03	PL B558 125	J. Erler, M. Luo
MAHMOOD	03	PR D67 072001	A.H. Mahmood <i>et al.</i> (CLEO Collab.)
BRAMBILLA	02	PR D65 034001	N. Brambilla, Y. Sumino, A. Vairo
PENIN	02	PL B538 335	A. Penin, M. Steinhauser



$$I(J^P) = 0(\frac{1}{2}^+)$$

$$\text{Charge} = \frac{2}{3} e \quad \text{Top} = +1$$

See the related review(s):
Top Quark

t-QUARK MASS

We first list the direct measurements of the top quark mass which employ the event kinematics and then list the measurements which extract a top quark mass from the measured $t\bar{t}$ cross-section using theory calculations. A discussion of the definition of the top quark mass in these measurements can be found in the review "The Top Quark."

For earlier search limits see PDG 96, Physical Review **D54** 1 (1996). We no longer include a compilation of indirect top mass determinations from Standard Model Electroweak fits in the Listings (our last compilation can be found in the Listings of the 2007 partial update). For a discussion of current results see the reviews "The Top Quark" and "Electroweak Model and Constraints on New Physics."

t-Quark Mass (Direct Measurements)

The following measurements extract a t -quark mass from the kinematics of $t\bar{t}$ events. They are sensitive to the top quark mass used in the MC generator that is usually interpreted as the pole mass, but the theoretical uncertainty in this interpretation is hard to quantify. See the review "The Top Quark" and references therein for more information.

OUR AVERAGE of 172.57 ± 0.29 GeV is an average of top mass measurements from LHC and Tevatron Runs. The latest Tevatron average, $174.30 \pm 0.35 \pm 0.54$ GeV, was provided by the Tevatron Electroweak Working Group (TEVEWWG).

VALUE (GeV)	DOCUMENT ID	TECN	COMMENT
172.57 ± 0.29 OUR AVERAGE	Error includes scale factor of 1.5. See the ideogram below.		
174.41 ± 0.39 ± 0.71	1 AAD	23N ATLS	leptonic invariant mass in $\ell + \text{jets}$ channel
171.77 ± 0.37	2 TUMASYAN	23BB CMS	$\ell + \geq 4j$ (2b)
173.06 ± 0.24 ± 0.80	3 TUMASYAN	23Z CMS	boosted top; $\ell + \text{jets}$ channel
172.13 $^{+0.76}_{-0.77}$	4 TUMASYAN	21G CMS	t -channel single top production
172.6 ± 2.5	5 SIRUNYAN	20AR CMS	jet mass from boosted top
172.69 ± 0.25 ± 0.41	6 AABOUD	19AC ATLS	7, 8 TeV ATLAS combination
172.34 ± 0.20 ± 0.70	7 SIRUNYAN	19AP CMS	≥ 6 jets ($\geq 2b$)
172.33 ± 0.14 $^{+0.66}_{-0.72}$	8 SIRUNYAN	19AR CMS	dilepton channel ($e\mu, 2e, 2\mu$)
172.44 ± 0.13 ± 0.47	9 KHACHATRYAN	16AK CMS	7, 8 TeV CMS combination
174.30 ± 0.35 ± 0.54	10 TEVEWWG	16 TEVA	Tevatron combination
• • • We do not use the following data for averages, fits, limits, etc. • • •			
172.08 ± 0.39 ± 0.82	11 AABOUD	19AC ATLS	$\ell + \geq 4j$ (2b)
172.26 ± 0.07 ± 0.61	12 SIRUNYAN	19AP CMS	lepton+jets, all-jets channels
172.25 ± 0.08 ± 0.62	13 SIRUNYAN	18DE CMS	$\ell + \geq 4j$ (2b)
173.72 ± 0.55 ± 1.01	14 AABOUD	17AH ATLS	≥ 5 jets (2b)
174.95 ± 0.40 ± 0.64	15 ABAZOV	17B D0	$\ell + \text{jets}$ and dilepton channels
172.95 ± 0.77 $^{+0.97}_{-0.93}$	16 SIRUNYAN	17L CMS	t -channel single top production
170.8 ± 9.0	17 SIRUNYAN	17N CMS	jet mass in highly-boosted $t\bar{t}$ events
172.22 ± 0.18 $^{+0.89}_{-0.93}$	18 SIRUNYAN	17O CMS	Dilepton channel
172.99 ± 0.41 ± 0.74	19 AABOUD	16T ATLS	dilepton channel
172.84 ± 0.34 ± 0.61	20 AABOUD	16T ATLS	combination of ATLAS
173.32 ± 1.36 ± 0.85	21 ABAZOV	16 D0	$\ell\ell + \cancel{E}_T + \geq 2j$ ($\geq 2b$)
173.93 ± 1.61 ± 0.88	22 ABAZOV	16D D0	$\ell\ell + \cancel{E}_T + \geq 2j$ ($\geq 2b$)
172.35 ± 0.16 ± 0.48	23,24 KHACHATRYAN	16AK CMS	$\ell + \geq 4j$ (2b)
172.32 ± 0.25 ± 0.59	23,24 KHACHATRYAN	16AK CMS	≥ 6 jets (2b)
172.82 ± 0.19 ± 1.22	23,25 KHACHATRYAN	16AK CMS	$(ee/\mu\mu) + \cancel{E}_T + \geq 2b, e\mu + \geq 2b$
173.68 ± 0.20 $^{+1.58}_{-0.97}$	26 KHACHATRYAN	16AL CMS	semi- + di-leptonic channels
173.5 ± 3.0 ± 0.9	27 KHACHATRYAN	16CB CMS	$t \rightarrow (W \rightarrow \ell\nu)(b \rightarrow J/\psi X \rightarrow \mu^+\mu^- X)$
175.1 ± 1.4 ± 1.2	28 AAD	15AW ATLS	small \cancel{E}_T , ≥ 6 jets (2b-tag)
172.99 ± 0.48 ± 0.78	29 AAD	15BF ATLS	$\ell + \text{jets}$ and dilepton
171.5 ± 1.9 ± 2.5	30 AALTONEN	15D CDF	$\ell\ell + \cancel{E}_T + \geq 2j$
175.07 ± 1.19 $^{+1.55}_{-1.58}$	31 AALTONEN	14N CDF	small \cancel{E}_T , 6–8 jets ($\geq 1b$ -tag)
174.98 ± 0.58 ± 0.49	32 ABAZOV	14C D0	$\ell + \cancel{E}_T + 4$ jets ($\geq 1b$ -tag)
173.49 ± 0.69 ± 1.21	33 CHATRCHYAN	14C CMS	≥ 6 jets ($\geq 2b$ -tag)
173.93 ± 1.64 ± 0.87	34 AALTONEN	13H CDF	$\cancel{E}_T + \geq 4$ jets ($\geq 1b$)
173.9 ± 0.9 $^{+1.7}_{-2.1}$	35 CHATRCHYAN	13S CMS	$\ell\ell + \cancel{E}_T + \geq 2b$ -tag (MT2(T))
174.5 ± 0.6 ± 2.3	36 AAD	12I ATLS	$\ell + \cancel{E}_T + \geq 4$ jets ($\geq 1b$), MT

172.85 ± 0.71 ± 0.85	37 AALTONEN	12AI CDF	$\ell + \cancel{E}_T + \geq 4j$ (0,1,2b) template
172.7 ± 9.3 ± 3.7	38 AALTONEN	12AL CDF	$\tau_h + \cancel{E}_T + 4j$ ($\geq 1b$)
173.18 ± 0.56 ± 0.75	39 AALTONEN	12AP TEVA	CDF, D0 combination
172.5 ± 1.4 ± 1.5	40 AALTONEN	12G CDF	6–8 jets with $\geq 1b$
173.7 ± 2.8 ± 1.5	41 ABAZOV	12AB D0	$\ell\ell + \cancel{E}_T + \geq 2j$ (ν WT)
173.9 ± 1.9 ± 1.6	42 ABAZOV	12AB D0	$\ell\ell + \cancel{E}_T + \geq 2j$ (ν WT+MWT)
172.5 ± 0.4 ± 1.5	43 CHATRCHYAN	12BA CMS	$\ell\ell + \cancel{E}_T + \geq 2j$ ($\geq 1b$), MMWT
173.49 ± 0.43 ± 0.98	44 CHATRCHYAN	12BP CMS	$\ell + \cancel{E}_T + \geq 4j$ ($\geq 2b$)
172.4 ± 1.4 ± 1.3	45 AALTONEN	11AC CDF	$\ell + \cancel{E}_T + 4$ jets ($\geq 1b$ -tag)
172.3 ± 2.4 ± 1.0	46 AALTONEN	11AK CDF	Repl. by AALTONEN 13H
172.1 ± 1.1 ± 0.9	47 AALTONEN	11E CDF	$\ell + \text{jets}$ and dilepton
176.9 ± 8.0 ± 2.7	48 AALTONEN	11T CDF	$\ell + \cancel{E}_T + 4$ jets ($\geq 1b$ -tag), $p_T(\ell)$ shape
174.94 ± 0.83 ± 1.24	49 ABAZOV	11P D0	$\ell + \cancel{E}_T + 4$ jets ($\geq 1b$ -tag)
174.0 ± 1.8 ± 2.4	50 ABAZOV	11R D0	dilepton + $\cancel{E}_T + \geq 2$ jets
175.5 ± 4.6 ± 4.6	51 CHATRCHYAN	11F CMS	dilepton + $\cancel{E}_T + \text{jets}$
173.0 ± 0.9 ± 0.9	52 AALTONEN	10AE CDF	$\ell + \cancel{E}_T + 4$ jets ($\geq 1b$ -tag), ME method
169.3 ± 2.7 ± 3.2	53 AALTONEN	10C CDF	dilepton + b -tag (MT2+NVA)
170.7 ± 6.3 ± 2.6	54 AALTONEN	10D CDF	$\ell + \cancel{E}_T + 4$ jets (b -tag)
174.8 ± 2.4 $^{+1.2}_{-1.0}$	55 AALTONEN	10E CDF	≥ 6 jets, vtx b -tag
180.5 ± 12.0 ± 3.6	56 AALTONEN	09AK CDF	$\ell + \cancel{E}_T + \text{jets}$ (soft μ b -tag)
172.7 ± 1.8 ± 1.2	57 AALTONEN	09J CDF	$\ell + \cancel{E}_T + 4$ jets (b -tag)
171.1 ± 3.7 ± 2.1	58 AALTONEN	09K CDF	6 jets, vtx b -tag
171.9 ± 1.7 ± 1.1	59 AALTONEN	09L CDF	$\ell + \text{jets}$, $\ell\ell + \text{jets}$
171.2 ± 2.7 ± 2.9	60 AALTONEN	09O CDF	dilepton
165.5 $^{+3.4}_{-3.3}$ ± 3.1	61 AALTONEN	09X CDF	$\ell\ell + \cancel{E}_T$ ($\nu\phi$ weighting)
174.7 ± 4.4 ± 2.0	62 ABAZOV	09AH D0	dilepton + b -tag (ν WT+MWT)
170.7 $^{+4.2}_{-3.9}$ ± 3.5	63,64 AALTONEN	08C CDF	dilepton, $\sigma_{t\bar{t}}$ constrained
171.5 ± 1.8 ± 1.1	65 ABAZOV	08AH D0	$\ell + \cancel{E}_T + 4$ jets
177.1 ± 4.9 ± 4.7	66,67 AALTONEN	07F CDF	6 jets with $\geq 1b$ vtx
172.3 $^{+10.8}_{-9.6}$ ± 10.8	68 AALTONEN	07B CDF	≥ 4 jets (b -tag)
174.0 ± 2.2 ± 4.8	69 AALTONEN	07D CDF	≥ 6 jets, vtx b -tag
170.8 ± 2.2 ± 1.4	70,71 AALTONEN	07I CDF	lepton + jets (b -tag)
173.7 ± 4.4 $^{+2.1}_{-2.0}$	72 ABAZOV	07F D0	lepton + jets
176.2 ± 9.2 ± 3.9	73 ABAZOV	07W D0	dilepton (MWT)
179.5 ± 7.4 ± 5.6	73 ABAZOV	07W D0	dilepton (ν WT)
164.5 ± 3.9 ± 3.9	71,74 ABULENCIA	07D CDF	dilepton
180.7 $^{+15.5}_{-13.4}$ ± 8.6	75 ABULENCIA	07J CDF	lepton + jets
170.3 $^{+4.1}_{-4.5}$ $^{+1.2}_{-1.8}$	71,76 ABAZOV	06U D0	lepton + jets (b -tag)
173.2 $^{+2.6}_{-2.4}$ ± 3.2	77,78 ABULENCIA	06D CDF	lepton + jets
173.5 $^{+3.7}_{-3.6}$ ± 1.3	64,77 ABULENCIA	06D CDF	lepton + jets
165.2 ± 6.1 ± 3.4	71,79 ABULENCIA	06G CDF	dilepton
170.1 ± 6.0 ± 4.1	64,80 ABULENCIA	06V CDF	dilepton
178.5 ± 13.7 ± 7.7	81,82 ABAZOV	05 D0	6 or more jets
180.1 ± 3.6 ± 3.9	83,84 ABAZOV	04G D0	lepton + jets
176.1 ± 5.1 ± 5.3	85 AFFOLDER	01 CDF	lepton + jets
176.1 ± 6.6	86 AFFOLDER	01 CDF	dilepton, lepton+jets, all-jets
172.1 ± 5.2 ± 4.9	87 ABBOTT	99G D0	di-lepton, lepton+jets
176.0 ± 6.5	88,89 ABE	99B CDF	dilepton, lepton+jets, all-jets
167.4 ± 10.3 ± 4.8	89,90 ABE	99B CDF	dilepton
168.4 ± 12.3 ± 3.6	84 ABBOTT	98D D0	dilepton
173.3 ± 5.6 ± 5.5	84,91 ABBOTT	98F D0	lepton + jets
175.9 ± 4.8 ± 5.3	90,92 ABE	98E CDF	lepton + jets
161 ± 17 ± 10	90 ABE	98F CDF	dilepton
172.1 ± 5.2 ± 4.9	93 BHAT	98B RVUE	dilepton and lepton+jets
173.8 ± 5.0	94 BHAT	98B RVUE	dilepton, lepton+jets, all-jets
173.3 ± 5.6 ± 6.2	84 ABACHI	97E D0	lepton + jets
186 ± 10 ± 5.7	90,95 ABE	97R CDF	6 or more jets
199 $^{+19}_{-21}$ ± 22	ABACHI	95 D0	lepton + jets
176 ± 8 ± 10	ABE	95F CDF	lepton + b -jet
174 ± 10 $^{+13}_{-12}$	ABE	94E CDF	lepton + b -jet

1 AAD 23N based on 36.1 fb^{-1} of pp data at $\sqrt{s} = 13$ TeV. The second error is the sum of systematic (± 0.66) and that from changing parton-shower gluon recoil scheme (± 0.25) uncertainties. The distribution of the invariant mass $m_{\ell\mu}$ (ℓ from W and μ from b -hadron decay) is used, which is less sensitive to jet energy uncertainties and top production modelling.

2 TUMASYAN 23BB based on 36.3 fb^{-1} of pp data at $\sqrt{s} = 13$ TeV. For each event, the mass is reconstructed from a kinematic fit of the decay products to a $t\bar{t}$ hypothesis. A profile likelihood method is applied using up to four observables per event.

3 TUMASYAN 23Z based on 138 fb^{-1} of pp data at $\sqrt{s} = 13$ TeV. The second error is the sum of experimental (± 0.61), model (± 0.47), and theoretical (± 0.23) uncertainties. The products of the hadronic decay of a top quark with $p_T > 400$ GeV, in the $\ell + \text{jets}$ channel of $t\bar{t}$, are reconstructed as a single jet. The top quark mass is determined from the normalized differential cross section measurement in the m_{jet} distribution.

4 TUMASYAN 21G based on 35.9 fb^{-1} of pp data at $\sqrt{s} = 13$ TeV. Events are selected by requiring $1\ell + 2\text{jets}(1b \text{ jet})$ final state.

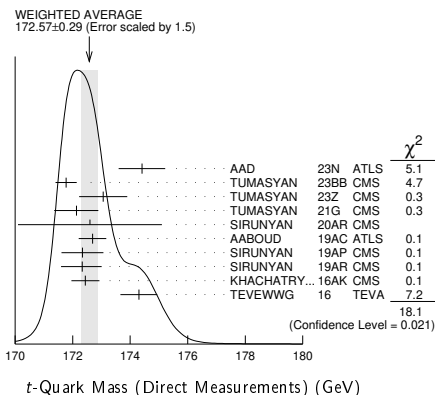
5 SIRUNYAN 20AR based on 35.9 fb^{-1} of pp data at $\sqrt{s} = 13$ TeV. The products of the hadronic decay of a top quark with $p_T > 400$ GeV, in the $\ell + \text{jets}$ channel of $t\bar{t}$ are reconstructed as a single jet. The top quark mass is determined from the normalized differential cross section measurement in the m_{jet} distribution.

Quark Particle Listings

 t

- ⁶ AABOUD 19AC is an ATLAS combination of 7 and 8 TeV top-quark mass determination in the dilepton, lepton + jets, and all jets channels.
- ⁷ SIRUNYAN 19AP based on 35.9 fb⁻¹ of pp data at $\sqrt{s} = 13$ TeV. A kinematical fit is applied to each event assuming the signal event topology. m_t is determined simultaneously with a jet energy scale factor (JSF). The second error represents stat.+JSF. Modeling uncertainties are larger than in the measurements at $\sqrt{s} = 7$ and 8 TeV because of the use of new alternative color reconnection models.
- ⁸ SIRUNYAN 19AR based on 35.9 fb⁻¹ of pp data at $\sqrt{s} = 13$ TeV. Obtained from a simultaneous fit of the cross section and the top quark mass in the POWHEG simulation. The cross section is used also to extract the M_S mass and the strong coupling constant for different PDF sets.
- ⁹ KHACHATRYAN 16AK based on 19.7 fb⁻¹ of pp data at $\sqrt{s} = 8$ TeV. Combination of the three top mass measurements in KHACHATRYAN 16AK and with the CMS results at $\sqrt{s} = 7$ TeV.
- ¹⁰ TEVEWWG 16 is the latest Tevatron average (July 2016) provided by the Tevatron Electroweak Working Group. It takes correlated uncertainties into account and has a χ^2 of 10.8 for 11 degrees of freedom.
- ¹¹ AABOUD 19AC based on 20.2 fb⁻¹ in pp collisions at $\sqrt{s} = 8$ TeV. Uses optimized event selection to suppress less-well-reconstructed events and template fits to determine m_t together with a global jet energy scale factor and a relative b -to-light-jet energy scale factor.
- ¹² SIRUNYAN 19AP based on 35.9 fb⁻¹ of pp data at $\sqrt{s} = 13$ TeV. A combined measurement using the lepton+jets and all-jets channels through a single likelihood function. See SIRUNYAN 18DE.
- ¹³ SIRUNYAN 18DE based on 35.9 fb⁻¹ of pp data at $\sqrt{s} = 13$ TeV. m_t is determined simultaneously with an overall jet energy scale factor constrained by the mass of the hadronically decayed W . Compared to the Run 1 analysis a more advanced treatment of modeling uncertainties are employed, in particular concerning color-reconnection models. Superseded by TUMASYAN 23BB.
- ¹⁴ AABOUD 17AH based on 20.2 fb⁻¹ of pp data at $\sqrt{s} = 8$ TeV. Uses template fits to the ratio of the masses of three-jets (from t candidate) and dijets (from W candidate), to suppress jet energy scale uncertainty. Large QCD background is modelled using a data-driven method.
- ¹⁵ ABAZOV 17B is a combination of measurements of the top quark mass by D0 in the lepton+jets and dilepton channels, using all data collected in Run I (1992–1996) at $\sqrt{s} = 1.8$ TeV and Run II (2001–2011) at $\sqrt{s} = 1.96$ TeV of the Tevatron, corresponding to integrated luminosities of 0.1 fb⁻¹ and 9.7 fb⁻¹, respectively.
- ¹⁶ SIRUNYAN 17L based on 19.7 fb⁻¹ of pp data at $\sqrt{s} = 8$ TeV. m_t is reconstructed from a fit to the invariant mass distribution of $\mu\nu b$, where $p_{T}^{\mu\nu}$ and W mass constraint are used to reconstruct ν momentum. The number of events for various contributions, except for the t -channel single top one, are fixed to the values extracted from simulation. Superseded by TUMASYAN 21G.
- ¹⁷ SIRUNYAN 17N based on 19.7 fb⁻¹ of pp data at $\sqrt{s} = 8$ TeV. The fully hadronic decay of a highly-boosted t is reconstructed in the ℓ +jets channel and unfolded at the particle level. The sensitivity of the peak position of the m_{jet} distribution is used to test quality of the modelling by the simulation.
- ¹⁸ SIRUNYAN 17O based on 19.7 fb⁻¹ of pp data at $\sqrt{s} = 8$ TeV. Analysis is based on the kinematical observables $M(b\ell)$, M_{T2} and $M(b\ell\nu)$. A fit is performed to determine m_t and an overall jet energy scale factor simultaneously.
- ¹⁹ AABOUD 16T based on 20.2 fb⁻¹ of pp data at $\sqrt{s} = 8$ TeV. The analysis is refined using the p_T and invariant mass distributions of ℓ + b -jet system. A combination with measurements from $\sqrt{s} = 7$ TeV data in the dilepton and lepton+jets channels gives $172.84 \pm 0.34 \pm 0.61$ GeV.
- ²⁰ AABOUD 16T is an ATLAS combination of 8 TeV top-quark mass in the dilepton channel with previous measurements from $\sqrt{s} = 7$ TeV data in the dilepton and lepton + jets channels.
- ²¹ ABAZOV 16 based on 9.7 fb⁻¹ of data in $p\bar{p}$ collisions at $\sqrt{s} = 1.96$ TeV. Employs improved fit to minimize statistical errors and improved jet energy calibration, using lepton + jets mode, which reduces error of jet energy scale. Based on previous determination in ABAZOV 12AB with increased integrated luminosity and improved fit and calibrations.
- ²² ABAZOV 16D based on 9.7 fb⁻¹ of data in $p\bar{p}$ collisions at $\sqrt{s} = 1.96$ TeV, using the matrix element technique. Based on previous determination in ABAZOV 11R with increased integrated luminosity. There is a strong correlation with the determination in ABAZOV 16. (See ABAZOV 17B.)
- ²³ KHACHATRYAN 16AK based on 19.7 fb⁻¹ of pp data at $\sqrt{s} = 8$ TeV. Combination of the three top mass measurements in KHACHATRYAN 16AK and with the CMS results at $\sqrt{s} = 7$ TeV gives $172.44 \pm 0.13 \pm 0.47$ GeV.
- ²⁴ The top mass and jet energy scale factor are determined by a fit.
- ²⁵ Uses the analytical matrix weighting technique method.
- ²⁶ KHACHATRYAN 16AL based on 19.7 fb⁻¹ in pp collisions at $\sqrt{s} = 8$ TeV. Determined from the invariant mass distribution of leptons and reconstructed secondary vertices from b decays using only charged particles. The uncertainty is dominated by modeling of b fragmentation and top p_T distribution.
- ²⁷ KHACHATRYAN 16CB based on 666 candidate reconstructed events corresponding to 19.7 fb⁻¹ of pp data at $\sqrt{s} = 8$ TeV. The measurement exploits correlation of m_t with $M(\mu\nu\ell)$ in the same top quark decay, using a high-purity event sample. A study on modeling of b -quark fragmentation is given in Sec.3.3.
- ²⁸ AAD 15AW based on 4.6 fb⁻¹ of pp data at $\sqrt{s} = 7$ TeV. Uses template fits to the ratio of the masses of three-jets (from t candidate) and dijets (from W candidate). Large background from multijet production is modeled with data-driven methods.
- ²⁹ AAD 15BF based on 4.6 fb⁻¹ in pp collisions at $\sqrt{s} = 7$ TeV. Using a three-dimensional template likelihood technique the lepton plus jets ($\geq 1b$ -tagged) channel gives $172.33 \pm 0.75 \pm 1.02$ GeV, while exploiting a one dimensional template method using $m_{\ell b}$ the dilepton channel (1 or 2b-tags) gives $173.79 \pm 0.54 \pm 1.30$ GeV. The results are combined.
- ³⁰ AALTONEN 15D based on 9.1 fb⁻¹ of $p\bar{p}$ data at $\sqrt{s} = 1.96$ TeV. Uses a template technique to fit a distribution of a variable defined by a linear combination of variables sensitive and insensitive to jet energy scale to optimize reduction of systematic errors. b -tagged and non- b -tagged events are separately analyzed and combined.
- ³¹ Based on 9.3 fb⁻¹ of $p\bar{p}$ data at $\sqrt{s} = 1.96$ TeV. Multivariate algorithm is used to discriminate signal from backgrounds, and templates are used to measure m_t .
- ³² Based on 9.7 fb⁻¹ of $p\bar{p}$ data at $\sqrt{s} = 1.96$ TeV. A matrix element method is used to calculate the probability of an event to be signal or background, and the overall jet energy scale is constrained *in situ* by m_W . See ABAZOV 15G for further details.
- ³³ Based on 3.54 fb⁻¹ of pp data at $\sqrt{s} = 7$ TeV. The mass is reconstructed for each event employing a kinematical fit of the jets to a ttbar hypothesis. The combination with the previous CMS measurements in the dilepton and the lepton+jets channels gives $173.54 \pm 0.33 \pm 0.96$ GeV.
- ³⁴ Based on 8.7 fb⁻¹ in $p\bar{p}$ collisions at $\sqrt{s} = 1.96$ TeV. Events with an identified charged lepton or small E_T are rejected from the event sample, so that the measurement is statistically independent from those in the ℓ + jets and all hadronic channels while being sensitive to those events with a τ lepton in the final state.
- ³⁵ Based on 5.0 fb⁻¹ of pp data at $\sqrt{s} = 7$ TeV. CHATRCHYAN 13s studied events with di-lepton + $E_T + \geq 2$ b -jets, and looked for kinematical endpoints of MT2, MT2 $_T$, and subsystem variables.
- ³⁶ AAD 12i based on 1.04 fb⁻¹ of pp data at $\sqrt{s} = 7$ TeV. Uses 2d-template analysis (MT) with m_t and jet energy scale factor (JSF) from m_W mass fit.
- ³⁷ Based on 8.7 fb⁻¹ of data in $p\bar{p}$ collisions at 1.96 TeV. The JES is calibrated by using the dijet mass from the W boson decay.
- ³⁸ Use the ME method based on 2.2 fb⁻¹ of data in $p\bar{p}$ collisions at 1.96 TeV.
- ³⁹ Combination based on up to 5.8 fb⁻¹ of data in $p\bar{p}$ collisions at 1.96 TeV.
- ⁴⁰ Based on 5.8 fb⁻¹ of data in $p\bar{p}$ collisions at 1.96 TeV the quoted value is $m_t = 172.5 \pm 1.4(\text{stat}) \pm 1.0(\text{JES}) \pm 1.1(\text{syst})$ GeV. The measurement is performed with a likelihood fit technique which simultaneously determines m_t and JES (Jet Energy Scale).
- ⁴¹ Based on 4.3 fb⁻¹ of data in p-pbar collisions at 1.96 TeV. The measurement reduces the JES uncertainty by using the single lepton channel study of ABAZOV 11P.
- ⁴² Combination with the result in 1 fb⁻¹ of preceding data reported in ABAZOV 09AH as well as the MWT result of ABAZOV 11R with a statistical correlation of 60%.
- ⁴³ Based on 5.0 fb⁻¹ of pp data at $\sqrt{s} = 7$ TeV. Uses an analytical matrix weighting technique (AMWT) and full kinematic analysis (KIN).
- ⁴⁴ Based on 5.0 fb⁻¹ of pp data at $\sqrt{s} = 7$ TeV. The first error is statistical and JES combined, and the second is systematic. Ideogram method is used to obtain 2D likelihood for the kinematical fit with two parameters m_{top} and JES.
- ⁴⁵ Based on 3.2 fb⁻¹ in $p\bar{p}$ collisions at $\sqrt{s} = 1.96$ TeV. The first error is from statistics and JES combined, and the latter is from the other systematic uncertainties. The result is obtained using an unbinned maximum likelihood method where the top quark mass and the JES are measured simultaneously, with $\Delta_{JES} = 0.3 \pm 0.3(\text{stat})$.
- ⁴⁶ Based on 5.7 fb⁻¹ in $p\bar{p}$ collisions at $\sqrt{s} = 1.96$ TeV. Events with an identified charged lepton or small E_T are rejected from the event sample, so that the measurement is statistically independent from those in the ℓ + jets and all hadronic channels while being sensitive to those events with a τ lepton in the final state. Supersedes AALTONEN 07B.
- ⁴⁷ AALTONEN 11E based on 5.6 fb⁻¹ in $p\bar{p}$ collisions at $\sqrt{s} = 1.96$ TeV. Employs a multi-dimensional template likelihood technique where the lepton plus jets (one or two b -tags) channel gives $172.2 \pm 1.2 \pm 0.9$ GeV while the dilepton channel yields $170.3 \pm 2.0 \pm 3.1$ GeV. The results are combined. OUR EVALUATION includes the measurement in the dilepton channel only.
- ⁴⁸ Uses a likelihood fit of the lepton p_T distribution based on 2.7 fb⁻¹ in $p\bar{p}$ collisions at $\sqrt{s} = 1.96$ TeV.
- ⁴⁹ Based on 3.6 fb⁻¹ in $p\bar{p}$ collisions at $\sqrt{s} = 1.96$ TeV. ABAZOV 11P reports $174.94 \pm 0.83 \pm 0.78 \pm 0.96$ GeV, where the first uncertainty is from statistics, the second from JES, and the last from other systematic uncertainties. We combine the JES and systematic uncertainties. A matrix-element method is used where the JES uncertainty is constrained by the W mass. ABAZOV 11P describes a measurement based on 2.6 fb⁻¹ that is combined with ABAZOV 08AH, which employs an independent 1 fb⁻¹ of data.
- ⁵⁰ Based on a matrix-element method which employs 5.4 fb⁻¹ in $p\bar{p}$ collisions at $\sqrt{s} = 1.96$ TeV. Superseded by ABAZOV 12AB.
- ⁵¹ Based on 36 pb⁻¹ of pp collisions at $\sqrt{s} = 7$ TeV. A Kinematic Method using b -tagging and an analytical Matrix Weighting Technique give consistent results and are combined. Superseded by CHATRCHYAN 12BA.
- ⁵² Based on 5.6 fb⁻¹ in $p\bar{p}$ collisions at $\sqrt{s} = 1.96$ TeV. The likelihood calculated using a matrix element method gives $m_t = 173.0 \pm 0.7(\text{stat}) \pm 0.6(\text{JES}) \pm 0.9(\text{syst})$ GeV, for a total uncertainty of 1.2 GeV.
- ⁵³ Based on 3.4 fb⁻¹ of $p\bar{p}$ collisions at $\sqrt{s} = 1.96$ TeV. The result is obtained by combining the MT2 variable method and the NVA (Neutrino Weighting Algorithm). The MT2 method alone gives $m_t = 168.0^{+4.8}_{-4.0}(\text{stat}) \pm 2.9(\text{syst})$ GeV with smaller systematic error due to small JES uncertainty.
- ⁵⁴ Based on 1.9 fb⁻¹ in $p\bar{p}$ collisions at $\sqrt{s} = 1.96$ TeV. The result is from the measurement using the transverse decay length of b -hadrons and that using the transverse momentum of the W decay muons, which are both insensitive to the JES (jet energy scale) uncertainty. OUR EVALUATION uses only the measurement exploiting the decay length significance which yields $166.9^{+9.5}_{-8.5}(\text{stat}) \pm 2.9(\text{syst})$ GeV. The measurement that uses the lepton transverse momentum is excluded from the average because of a statistical correlation with other samples.
- ⁵⁵ Based on 2.9 fb⁻¹ of $p\bar{p}$ collisions at $\sqrt{s} = 1.96$ TeV. The first error is from statistics and JES uncertainty, and the latter is from the other systematics. Neural-network-based kinematical selection of 6 highest E_T jets with a vtx b -tag is used to distinguish signal from background. Superseded by AALTONEN 12G.
- ⁵⁶ Based on 2 fb⁻¹ of data at $\sqrt{s} = 1.96$ TeV. The top mass is obtained from the measurement of the invariant mass of the lepton (e or μ) from W decays and the soft μ in b -jet. The result is insensitive to jet energy scaling.
- ⁵⁷ Based on 1.9 fb⁻¹ of data at $\sqrt{s} = 1.96$ TeV. The first error is from statistics and jet energy scale uncertainty, and the latter is from the other systematics. Matrix element method with effective propagators.
- ⁵⁸ Based on 943 pb⁻¹ of data at $\sqrt{s} = 1.96$ TeV. The first error is from statistical and jet-energy-scale uncertainties, and the latter is from other systematics. AALTONEN 09k selected 6 jet events with one or more vertex b -tags and used the tree-level matrix element to construct template models of signal and background.
- ⁵⁹ Based on 1.9 fb⁻¹ of data at $\sqrt{s} = 1.96$ TeV. The first error is from statistical and jet-energy-scale (JES) uncertainties, and the second is from other systematics. Events with lepton + jets and those with dilepton + jets were simultaneously fit to constrain m_t and JES. Lepton + jets data only give $m_t = 171.8 \pm 2.2$ GeV, and dilepton data only give $m_t = 171.2^{+5.3}_{-5.1}$ GeV.
- ⁶⁰ Based on 2 fb⁻¹ of data at $\sqrt{s} = 1.96$ TeV. Matrix Element method. Optimal selection criteria for candidate events with two high p_T leptons, high E_T , and two or more jets with and without b -tag are obtained by neural network with neuroevolution technique to minimize the statistical error of m_t .
- ⁶¹ Based on 2.9 fb⁻¹ of data at $\sqrt{s} = 1.96$ TeV. Mass m_t is estimated from the likelihood for the eight-fold kinematical solutions in the plane of the azimuthal angles of the two neutrino momenta.

- ⁶² Based on 1 fb^{-1} of data at $\sqrt{s} = 1.96 \text{ TeV}$. Events with two identified leptons, and those with one lepton plus one isolated track and a b -tag were used to constrain m_t . The result is a combination of the ν WT (ν Weighting Technique) result of $176.2 \pm 4.8 \pm 2.1 \text{ GeV}$ and the MWT (Matrix-element Weighting Technique) result of $173.2 \pm 4.9 \pm 2.0 \text{ GeV}$.
- ⁶³ Reports measurement of $170.7^{+4.2}_{-3.9} \pm 2.6 \pm 2.4 \text{ GeV}$ based on 1.2 fb^{-1} of data at $\sqrt{s} = 1.96 \text{ TeV}$. The last error is due to the theoretical uncertainty on $\sigma_{t\bar{t}}$. Without the cross-section constraint a top mass of $169.7^{+5.2}_{-4.9} \pm 3.1 \text{ GeV}$ is obtained.
- ⁶⁴ Template method.
- ⁶⁵ Result is based on 1 fb^{-1} of data at $\sqrt{s} = 1.96 \text{ TeV}$. The first error is from statistics and jet energy scale uncertainty, and the latter is from the other systematics.
- ⁶⁶ Based on 310 pb^{-1} of data at $\sqrt{s} = 1.96 \text{ TeV}$.
- ⁶⁷ Ideogram method.
- ⁶⁸ Based on 311 pb^{-1} of data at $\sqrt{s} = 1.96 \text{ TeV}$. Events with 4 or more jets with $E_T > 15 \text{ GeV}$, significant missing E_T , and secondary vertex b -tag are used in the fit. About 44% of the signal acceptance is from $\tau\nu + 4$ jets. Events with identified e or μ are vetoed to provide a statistically independent measurement.
- ⁶⁹ Based on 1.02 fb^{-1} of data at $\sqrt{s} = 1.96 \text{ TeV}$. Superseded by AALTONEN 12G.
- ⁷⁰ Based on 955 pb^{-1} of data at $\sqrt{s} = 1.96 \text{ TeV}$. m_t and JES (Jet Energy Scale) are fitted simultaneously, and the first error contains the JES contribution of 1.5 GeV .
- ⁷¹ Matrix element method.
- ⁷² Based on 425 pb^{-1} of data at $\sqrt{s} = 1.96 \text{ TeV}$. The first error is a combination of statistics and JES (Jet Energy Scale) uncertainty, which has been measured simultaneously to give $\text{JES} = 0.989 \pm 0.029(\text{stat})$.
- ⁷³ Based on 370 pb^{-1} of data at $\sqrt{s} = 1.96 \text{ TeV}$. Combined result of MWT (Matrix-element Weighting Technique) and ν WT (ν Weighting Technique) analyses is $178.1 \pm 6.7 \pm 4.8 \text{ GeV}$.
- ⁷⁴ Based on 1.0 fb^{-1} of data at $\sqrt{s} = 1.96 \text{ TeV}$. ABULENCIA 07b improves the matrix element description by including the effects of initial-state radiation.
- ⁷⁵ Based on 695 pb^{-1} of data at $\sqrt{s} = 1.96 \text{ TeV}$. The transverse decay length of the b hadron is used to determine m_t , and the result is free from the JES (jet energy scale) uncertainty.
- ⁷⁶ Based on $\sim 400 \text{ pb}^{-1}$ of data at $\sqrt{s} = 1.96 \text{ TeV}$. The first error includes statistical and systematic jet energy scale uncertainties, the second error is from the other systematics. The result is obtained with the b -tagging information. The result without b -tagging is $169.2^{+5.0+1.5}_{-7.4-1.4} \text{ GeV}$. Superseded by ABAZOV 08AH.
- ⁷⁷ Based on 318 pb^{-1} of data at $\sqrt{s} = 1.96 \text{ TeV}$.
- ⁷⁸ Dynamical likelihood method.
- ⁷⁹ Based on 340 pb^{-1} of data at $\sqrt{s} = 1.96 \text{ TeV}$.
- ⁸⁰ Based on 360 pb^{-1} of data at $\sqrt{s} = 1.96 \text{ TeV}$.
- ⁸¹ Based on $110.2 \pm 5.8 \text{ pb}^{-1}$ at $\sqrt{s} = 1.8 \text{ TeV}$.
- ⁸² Based on the all hadronic decays of $t\bar{t}$ pairs. Single b -quark tagging via the decay chain $b \rightarrow c \rightarrow \mu$ was used to select signal enriched multijet events. The result was obtained by the maximum likelihood method after bias correction.
- ⁸³ Obtained by re-analysis of the lepton + jets candidate events that led to ABBOTT 98f. It is based upon the maximum likelihood method which makes use of the leading order matrix elements.
- ⁸⁴ Based on $125 \pm 7 \text{ pb}^{-1}$ of data at $\sqrt{s} = 1.8 \text{ TeV}$.
- ⁸⁵ Based on $\sim 106 \text{ pb}^{-1}$ of data at $\sqrt{s} = 1.8 \text{ TeV}$.
- ⁸⁶ Obtained by combining the measurements in the lepton + jets [AFFOLDER 01], all-jets [ABE 97r, ABE 99b], and dilepton [ABE 99b] decay topologies.
- ⁸⁷ Obtained by combining the D0 result $m_t(\text{GeV}) = 168.4 \pm 12.3 \pm 3.6$ from 6 di-lepton events (see also ABBOTT 98b) and $m_t(\text{GeV}) = 173.3 \pm 5.6 \pm 5.5$ from lepton+jet events (ABBOTT 98f).
- ⁸⁸ Obtained by combining the CDF results of $m_t(\text{GeV}) = 167.4 \pm 10.3 \pm 4.8$ from 8 dilepton events, $m_t(\text{GeV}) = 175.9 \pm 4.8 \pm 5.3$ from lepton+jet events (ABE 98e), and $m_t(\text{GeV}) = 186.0 \pm 10.0 \pm 5.7$ from all-jet events (ABE 97r). The systematic errors in the latter two measurements are changed in this paper.
- ⁸⁹ See AFFOLDER 01 for details of systematic error re-evaluation.
- ⁹⁰ Based on $109 \pm 7 \text{ pb}^{-1}$ of data at $\sqrt{s} = 1.8 \text{ TeV}$.
- ⁹¹ See ABAZOV 04G.
- ⁹² The updated systematic error is listed. See AFFOLDER 01, appendix C.
- ⁹³ Obtained by combining the D0 results of $m_t(\text{GeV}) = 168.4 \pm 12.3 \pm 3.6$ from 6 dilepton events and $m_t(\text{GeV}) = 173.3 \pm 5.6 \pm 5.5$ from 77 lepton+jet events.
- ⁹⁴ Obtained by combining the D0 results from dilepton and lepton+jet events, and the CDF results (ABE 99b) from dilepton, lepton+jet events, and all-jet events.
- ⁹⁵ Based on the first observation of all hadronic decays of $t\bar{t}$ pairs. Single b -quark tagging with jet-shape variable constraints was used to select signal enriched multi-jet events. The updated systematic error is listed. See AFFOLDER 01, appendix C.

**t-Quark Mass from Cross-Section Measurements**

The top quark \overline{MS} or pole mass can be extracted from a measurement of $\sigma(t\bar{t})$ by using theory calculations. We quote below the \overline{MS} mass. See the review "The Top Quark" and references therein for more information.

VALUE (GeV)	DOCUMENT ID	TECN	COMMENT
162.5^{+2.1}_{-1.5} OUR AVERAGE			
162.9 ± 0.5 ± 1.0 ^{+2.1} _{-1.2}	1 AAD	19G ATLS	$\ell + \cancel{E}_T + \geq 5 j (2b-j)$
160.0 ^{+4.8} _{-4.3}	2 ABAZOV	11s D0	$\sigma(t\bar{t})$ + theory
• • • We do not use the following data for averages, fits, limits, etc. • • •			
	3 ABAZOV	09AG D0	cross sects, theory + exp
	4 ABAZOV	09R D0	cross sects, theory + exp
¹ AAD 19G based on 20.2 fb^{-1} of data in pp collisions at $\sqrt{s} = 8 \text{ TeV}$. Normalized $t\bar{t} + 1$ -jet differential cross section as a function of $t\bar{t}$ invariant mass is measured in the $\ell +$ jets mode. The unfolded parton-level distribution is compared with the NLO QCD prediction. The three errors are from statistics, systematics, and theory.			
² Based on 5.3 fb^{-1} in $p\bar{p}$ collisions at $\sqrt{s} = 1.96 \text{ TeV}$. ABAZOV 11s uses the measured $t\bar{t}$ production cross section of $8.13^{+1.02}_{-0.90} \text{ pb}$ [ABAZOV 11e] in the lepton plus jets channel to obtain the top quark \overline{MS} mass by using an approximate NNLO computation (MOCH 08, LANGENFELD 09). The corresponding top quark pole mass is $167.5^{+5.4}_{-4.9} \text{ GeV}$. A different theory calculation (AHRENS 10, AHRENS 10A) is also used and yields $m_t^{\overline{MS}} = 154.5^{+5.0}_{-4.3} \text{ GeV}$.			
³ Based on 1 fb^{-1} of data at $\sqrt{s} = 1.96 \text{ TeV}$. Uses the $\ell +$ jets, $\ell\ell$, and $\ell\tau +$ jets channels. ABABOV 09AG extract the pole mass of the top quark using two different calculations that yield $169.1^{+5.9}_{-5.2} \text{ GeV}$ (MOCH 08, LANGENFELD 09) and $168.2^{+5.4}_{-5.4} \text{ GeV}$ (KIDONAKIS 08).			
⁴ Based on 1 fb^{-1} of data at $\sqrt{s} = 1.96 \text{ TeV}$. Uses the $\ell\ell$ and $\ell\tau +$ jets channels. ABABOV 09R extract the pole mass of the top quark using two different calculations that yield $173.3^{+9.8}_{-8.6} \text{ GeV}$ (MOCH 08, LANGENFELD 09) and $171.5^{+9.9}_{-8.8} \text{ GeV}$ (CACIARI 08).			

t-Quark Pole Mass from Cross-Section Measurements

VALUE (GeV)	DOCUMENT ID	TECN	COMMENT
172.4 ± 0.7 OUR AVERAGE			
173.4 ^{+1.8} _{-2.0}	1 AAD	23AY LHC	$e^\pm \mu^\mp$ pair; ATLAS+CMS combined
172.93 ± 1.36	2 TUMASYAN	23R CMS	$t\bar{t} + \text{jet}$; $\ell^\pm \ell^\mp$ mode
173.1 ^{+2.0} _{-2.1}	3 AAD	20Q ATLS	$e + \mu + 1$ or 2 b -jets
171.1 ± 0.4 ± 0.9 ^{+0.7} _{-0.3}	4 AAD	19G ATLS	$\ell + \cancel{E}_T + \geq 5 j (2b-j)$
170.6 ± 2.7	5 SIRUNYAN	17w CMS	$\ell + \geq 1 j$
172.8 ± 1.1 ^{+3.3} _{-3.1}	6 ABABOV	16F D0	$\ell\ell, \ell +$ jets channels
173.7 ^{+2.3} _{-2.1}	7 AAD	15BW ATLS	$\ell + \cancel{E}_T + \geq 5 j (2b\text{-tag})$
• • • We do not use the following data for averages, fits, limits, etc. • • •			
170.5 ± 0.8	8 SIRUNYAN	20BV CMS	$t\bar{t}$ normalized multi-differential cross sections
173.2 ± 0.9 ± 0.8 ± 1.2	9 AABOUD	17BC ATLS	$e + \mu + \geq 1 b$ jets
173.8 ^{+1.7} _{-1.8}	10 KHACHATRY...16AW	CMS	$e + \mu + \cancel{E}_T + \geq 0 j$
172.9 ^{+2.5} _{-2.6}	11 AAD	14AY ATLS	pp at $\sqrt{s} = 7, 8 \text{ TeV}$
176.7 ^{+3.0} _{-2.8}	12 CHATRCHYAN14	CMS	pp at $\sqrt{s} = 7 \text{ TeV}$
¹ AAD 23AY based on 5 fb^{-1} and 20 fb^{-1} of pp data at $\sqrt{s} = 7 \text{ TeV}$ and 8 TeV , respectively. The result is obtained from the combined inclusive cross section measurements and the NNLO+NNLL predictions fixing $\alpha_s(m_Z) = 0.118$.			
² TUMASYAN 23R based on 36.3 fb^{-1} of data in pp collisions at $\sqrt{s} = 13 \text{ TeV}$. Normalized $t\bar{t} + 1$ -jet differential cross section as a function of $t\bar{t}$ invariant mass is measured in the dilepton mode. The unfolded parton-level distribution is compared with the NLO QCD prediction. The result depends on the PDF and ABMP16NNLO is used.			
³ AAD 20Q based on 36.1 fb^{-1} of pp data at $\sqrt{s} = 13 \text{ TeV}$. The result is obtained from the inclusive cross section measurement and the NNLO+NNLL prediction.			
⁴ AAD 19G based on 20.2 fb^{-1} of data in pp collisions at $\sqrt{s} = 8 \text{ TeV}$. Normalized $t\bar{t} + 1$ -jet differential cross section as a function of $t\bar{t}$ invariant mass is measured in the $\ell +$ jets mode. The unfolded parton-level distribution is compared with the NLO QCD prediction. The three errors are from statistics, systematics, and theory.			
⁵ SIRUNYAN 17w based on 2.2 fb^{-1} of pp data at $\sqrt{s} = 13 \text{ TeV}$. Events are categorized according to the jet multiplicity and the number of b -tagged jets. The pole mass is obtained from the inclusive cross section measurement and the NNLO prediction.			
⁶ ABABOV 16F based on 9.7 fb^{-1} of data in $p\bar{p}$ collisions at $\sqrt{s} = 1.96 \text{ TeV}$. The result is obtained from the inclusive cross section measurement and the NNLO+NNLL prediction.			
⁷ AAD 15BW based on 4.6 fb^{-1} of pp data at $\sqrt{s} = 7 \text{ TeV}$. Uses normalized differential cross section for $t\bar{t} + 1$ jet as a function of the inverse of the invariant mass of the $t\bar{t} + 1$ jet system. The measured cross section is corrected to the parton level. Then a fit to the data using NLO + parton shower prediction is performed.			
⁸ SIRUNYAN 20BV based on 35.9 fb^{-1} of pp data at $\sqrt{s} = 13 \text{ TeV}$. The error accounts for both experimental and theoretical uncertainties. Events containing two oppositely charged leptons are used. The pole mass is particularly sensitive to the $t\bar{t}$ invariant mass distribution close to the threshold. However, the Coulomb and soft gluon resummation effects are not taken into account, hence, an additional theoretical uncertainty of order $\pm 1 \text{ GeV}$ is assumed.			
⁹ AABOUD 17BC based on 20.2 fb^{-1} of pp data at $\sqrt{s} = 8 \text{ TeV}$. The pole mass is extracted from a fit of NLO predictions to eight single lepton and dilepton differential distributions, while simultaneously constraining uncertainties due to PDFs and QCD scales. The three reported uncertainties come from statistics, experimental systematics, and theoretical sources.			

Quark Particle Listings

t

- ¹⁰ KHACHATRYAN 16AW based on 5.0 fb⁻¹ of pp collisions at 7 TeV and 19.7 fb⁻¹ at 8 TeV. The 7 TeV data include those used in CHATRCHYAN 14. The result is obtained from the inclusive cross sections.
- ¹¹ AAD 14AY used $\sigma(t\bar{t})$ for $e\mu$ events. The result is a combination of the measurements $m_t = 171.4 \pm 2.6$ GeV based on 4.6 fb⁻¹ of data at 7 TeV and $m_t = 174.1 \pm 2.6$ GeV based on 20.3 fb⁻¹ of data at 8 TeV.
- ¹² CHATRCHYAN 14 used $\sigma(t\bar{t})$ from pp collisions at $\sqrt{s} = 7$ TeV measured in CHATRCHYAN 12AX to obtain $m_t(\text{pole})$ for $\alpha_s(m_Z) = 0.1184 \pm 0.0007$. The errors have been corrected in KHACHATRYAN 14K.

 $m_t - m_{\bar{t}}$

Test of CPT conservation. OUR AVERAGE assumes that the systematic uncertainties are uncorrelated.

VALUE (GeV)	DOCUMENT ID	TECN	COMMENT
-0.15 ± 0.20 OUR AVERAGE	Error includes scale factor of 1.1.		
0.83 ^{+1.79} _{-1.35}	¹ TUMASYAN 21G	21G	CMS t-channel single top production
-0.15 ± 0.19 ± 0.09	² CHATRCHYAN17	CMS	$\ell + \cancel{E}_T + \geq 4j$ ($\geq 1b$ j)
0.67 ± 0.61 ± 0.41	³ AAD 14	ATLS	$\ell + \cancel{E}_T + \geq 4j$ (≥ 2 b-tags)
-1.95 ± 1.11 ± 0.59	⁴ AALTONEN 13E	CDF	$\ell + \cancel{E}_T + \geq 4j$ (0,1,2 b-tags)
-0.44 ± 0.46 ± 0.27	⁵ CHATRCHYAN12Y	CMS	$\ell + \cancel{E}_T + \geq 4j$
0.8 ± 1.8 ± 0.5	⁶ ABAZOV 11T	D0	$\ell + \cancel{E}_T + 4$ jets (≥ 1 b-tag)
• • • We do not use the following data for averages, fits, limits, etc. • • •			
-3.0 ± 1.4 ± 1.0	⁷ AALTONEN 11K	CDF	Repl. by AALTONEN 13E
3.8 ± 3.4 ± 1.2	⁸ ABAZOV 09AA	D0	$\ell + \cancel{E}_T + 4$ jets (≥ 1 b-tag)
¹ TUMASYAN 21G based on 35.9 fb ⁻¹ of pp data at $\sqrt{s} = 13$ TeV. Events are selected by requiring $1\ell + 2\text{jets}(1b \text{ jet})$ final state. An average top mass of $172.13^{+0.76}_{-0.77}$ GeV/c ² is obtained.			
² CHATRCHYAN 17 based on 19.6 fb ⁻¹ of pp data at $\sqrt{s} = 8$ TeV and an average top mass of 172.84 ± 0.10 (stat) GeV is obtained.			
³ Based on 4.7 fb ⁻¹ of pp data at $\sqrt{s} = 7$ TeV and an average top mass of 172.5 GeV/c ² .			
⁴ Based on 8.7 fb ⁻¹ of p \bar{p} collisions at $\sqrt{s} = 1.96$ TeV and an average top mass of 172.5 GeV/c ² .			
⁵ Based on 4.96 fb ⁻¹ of pp data at $\sqrt{s} = 7$ TeV. Based on the fitted m_t for ℓ^+ and ℓ^- events using the Ideogram method.			
⁶ Based on a matrix-element method which employs 3.6 fb ⁻¹ in p \bar{p} collisions at $\sqrt{s} = 1.96$ TeV.			
⁷ Based on a template likelihood technique which employs 5.6 fb ⁻¹ in p \bar{p} collisions at $\sqrt{s} = 1.96$ TeV.			
⁸ Based on 1 fb ⁻¹ of data in p \bar{p} collisions at $\sqrt{s} = 1.96$ TeV.			

t-quark DECAY WIDTH

VALUE (GeV)	CL%	DOCUMENT ID	TECN	COMMENT
1.42^{+0.19}_{-0.15} OUR AVERAGE		Error includes scale factor of 1.4.		
1.76 ± 0.33 ^{+0.79} _{-0.68}		¹ AABOUD 18AZ	ATLS	$\ell + \cancel{E}_T + \geq 4j$ (≥ 1 b)
1.36 ± 0.02 ^{+0.14} _{-0.11}		² KHACHATRY...14E	CMS	$\ell\ell + \cancel{E}_T + 2\text{jets}$ (0-2b-tag)
2.00 ^{+0.47} _{-0.43}		³ ABAZOV 12T	D0	$\Gamma(t \rightarrow bW)/B(t \rightarrow bW)$
• • • We do not use the following data for averages, fits, limits, etc. • • •				
< 6.38	95	⁴ AALTONEN 13Z	CDF	$\ell + \cancel{E}_T + \geq 4j$ (≥ 0 b), direct
1.99 ^{+0.69} _{-0.55}		⁵ ABAZOV 11B	D0	Repl. by ABAZOV 12T
> 1.21	95	⁵ ABAZOV 11B	D0	$\Gamma(t \rightarrow Wb)$
< 7.6	95	⁶ AALTONEN 10AC	CDF	$\ell + \text{jets}$, direct
< 13.1	95	⁷ AALTONEN 09M	CDF	$m_t(\text{rec})$ distribution

- ¹ Based on 20.2 fb⁻¹ of pp data at $\sqrt{s} = 8$ TeV. Γ_t is measured using a template fit to the reconstructed invariant mass of the b-jet of the semileptonically decaying top quark and the corresponding lepton, and the angular distance between j_b and j_j in hadronic top decay. Signal templates are generated by reweighting events at parton-level to Breit-Wigner distribution with different Γ_t hypotheses for $m_t = 172.5$ GeV. The result is consistent with the NNLO SM prediction of 1.322 GeV.
- ² Based on 19.7 fb⁻¹ of pp data at $\sqrt{s} = 8$ TeV. The result is obtained by combining the measurement of $R = \Gamma(t \rightarrow Wb)/\Gamma(t \rightarrow Wq (q=b,s,d))$ and a previous CMS measurement of the t-channel single top production cross section of CHATRCHYAN 12BQ, by using the theoretical calculation of $\Gamma(t \rightarrow Wb)$ for $m_t = 172.5$ GeV.
- ³ Based on 5.4 fb⁻¹ of data in p \bar{p} collisions at 1.96 TeV. $\Gamma(t \rightarrow bW)$ is $1.87^{+0.44}_{-0.40}$ GeV is obtained from the observed t-channel single top quark production cross section, whereas $B(t \rightarrow bW) = 0.90 \pm 0.04$ is used assuming $\sum_q B(t \rightarrow qW) = 1$. The result is valid for $m_t = 172.5$ GeV. See the paper for the values for $m_t = 170$ or 175 GeV.
- ⁴ Based on 8.7 fb⁻¹ of data. The two sided 68% CL interval is 1.10 GeV < Γ_t < 4.05 GeV for $m_t = 172.5$ GeV.
- ⁵ Based on 2.3 fb⁻¹ of p \bar{p} collisions at $\sqrt{s} = 1.96$ TeV. ABAZOV 11B extracted Γ_t from the partial width $\Gamma(t \rightarrow Wb) = 1.92^{+0.58}_{-0.51}$ GeV measured using the t-channel single top production cross section, and the branching fraction $\text{br}(t \rightarrow Wb) = 0.962^{+0.068}_{-0.066}(\text{stat})^{+0.064}_{-0.052}(\text{syst})$. The $\Gamma(t \rightarrow Wb)$ measurement gives the 95% CL lowerbound of $\Gamma(t \rightarrow Wb)$ and hence that of Γ_t .
- ⁶ Results are based on 4.3 fb⁻¹ of data in p \bar{p} collisions at $\sqrt{s} = 1.96$ TeV. The top quark mass and the hadronically decaying W boson mass are reconstructed for each candidate events and compared with templates of different top quark width. The two sided 68% CL interval is 0.3 GeV < Γ_t < 4.4 GeV for $m_t = 172.5$ GeV.
- ⁷ Based on 955 pb⁻¹ of p \bar{p} collision data at $\sqrt{s} = 1.96$ TeV. AALTONEN 09M selected $t\bar{t}$ candidate events for the $\ell + \cancel{E}_T + \text{jets}$ channel with one or two b-tags, and examine the decay width dependence of the reconstructed m_t distribution. The result is for $m_t = 175$ GeV, whereas the upper limit is lower for smaller m_t .

t DECAY MODES

Mode	Fraction (Γ_i/Γ)	Confidence level
Γ_1 $Wq (q = b, s, d)$		
Γ_2 Wb		
Γ_3 $e\nu_e b$	(11.10 ± 0.30) %	
Γ_4 $\mu\nu_\mu b$	(11.40 ± 0.20) %	
Γ_5 $\tau\nu_\tau b$	(10.7 ± 0.5) %	
Γ_6 $\ell^+ \bar{q} b$	(66.5 ± 1.4) %	
Γ_7 $\gamma q (q=u,c)$	[a] < 4.5	$\times 10^{-5}$ 95%
Γ_8 $H^+ b, H^+ \rightarrow \tau\nu_\tau$		

 $\Delta T = 1$ weak neutral current (TI) modes

Γ_9 $Zq (q=u,c)$	TI	[b] < 1.2	$\times 10^{-4}$	95%
Γ_{10} Hu	TI	< 1.9	$\times 10^{-4}$	95%
Γ_{11} Hc	TI	< 4.3	$\times 10^{-4}$	95%
Γ_{12} $\ell^+ \bar{q} q' (q=d,s,b; q'=u,c)$	TI	< 1.6	$\times 10^{-3}$	95%

Lepton Family number (LF) violating modes

Γ_{13} $e^\pm \mu^\mp c$	LF	< 8.9	$\times 10^{-7}$
Γ_{14} $e^\pm \mu^\mp u$	LF	< 7	$\times 10^{-8}$

[a] This limit is for $\Gamma(t \rightarrow \gamma q)/\Gamma(t \rightarrow Wb)$.

[b] This limit is for $\Gamma(t \rightarrow Zq)/\Gamma(t \rightarrow Wb)$.

t BRANCHING RATIOS

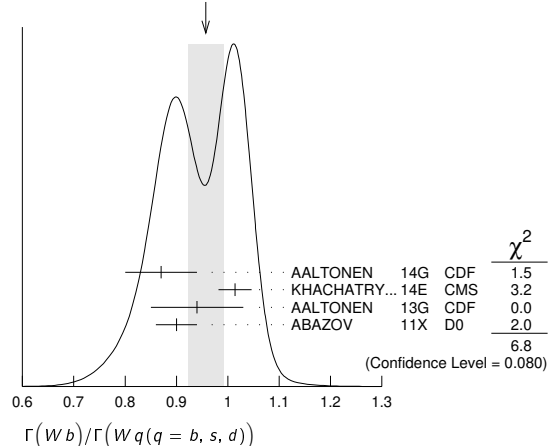
 $\Gamma(Wb)/\Gamma(Wq (q = b, s, d))$

OUR AVERAGE assumes that the systematic uncertainties are uncorrelated.

 Γ_2/Γ_1

VALUE	DOCUMENT ID	TECN	COMMENT
0.957 ± 0.034 OUR AVERAGE	Error includes scale factor of 1.5. See the ideogram below.		
0.87 ± 0.07	¹ AALTONEN 14G	CDF	$\ell\ell + \cancel{E}_T + \geq 2j$ (0,1,2 b-tag)
1.014 ± 0.003 ± 0.032	² KHACHATRY...14E	CMS	$\ell\ell + \cancel{E}_T + 2,3,4j$ (0-2b-tag)
0.94 ± 0.09	³ AALTONEN 13G	CDF	$\ell + \cancel{E}_T + \geq 3\text{jets}$ ($\geq 1b$ -tag)
0.90 ± 0.04	⁴ ABAZOV 11X	D0	
• • • We do not use the following data for averages, fits, limits, etc. • • •			
0.97 ^{+0.09} _{-0.08}	⁵ ABAZOV 08M	D0	$\ell + n$ jets with 0,1,2 b-tag
1.03 ^{+0.19} _{-0.17}	⁶ ABAZOV 06K	D0	
1.12 ^{+0.21} _{-0.19} ± 0.17 -0.13	⁷ ACOSTA 05A	CDF	Repl. by AALTONEN 13G
0.94 ^{+0.26} _{-0.21} ± 0.17 -0.12	⁸ AFFOLDER 01C	CDF	

WEIGHTED AVERAGE
0.957 ± 0.034 (Error scaled by 1.5)



- ¹ Based on 8.7 fb⁻¹ of data. This measurement gives $|V_{tb}| = 0.93 \pm 0.04$ and $|V_{cb}| > 0.85$ (95% CL) in the SM.
- ² Based on 19.7 fb⁻¹ of pp data at $\sqrt{s} = 8$ TeV. The result is obtained by counting the number of b jets per $t\bar{t}$ signal events in the dilepton channel. The $t\bar{t}$ production cross section is measured to be $\sigma(t\bar{t}) = 238 \pm 1 \pm 15$ pb, in good agreement with the SM prediction and the latest CMS measurement of CHATRCHYAN 14F. The measurement gives $R > 0.995$ (95% CL), or $|V_{tb}| > 0.975$ (95% CL) in the SM, requiring $R \leq 1$.
- ³ Based on 8.7 fb⁻¹ of p \bar{p} collisions at $\sqrt{s} = 1.96$ TeV. Measure the fraction of $t \rightarrow Wb$ decays simultaneously with the $t\bar{t}$ cross section. The correlation coefficient between those two measurements is -0.434. Assume unitarity of the 3x3 CKM matrix and set $|V_{tb}| > 0.89$ at 95% CL.
- ⁴ Based on 5.4 fb⁻¹ of data. The error is statistical and systematic combined. The result is a combination of 0.95 ± 0.07 from $\ell + \text{jets}$ channel and 0.86 ± 0.05 from $\ell\ell$ channel. $|V_{tb}| = 0.95 \pm 0.02$ follows from the result by assuming unitarity of the 3x3 CKM matrix.
- ⁵ Result is based on 0.9 fb⁻¹ of data. The 95% CL lower bound $R > 0.79$ gives $|V_{tb}| > 0.89$ (95% CL).

⁶ ABAZOV 06k result is from the analysis of $t\bar{t} \rightarrow \ell\nu + \geq 3$ jets with 230 pb^{-1} of data at $\sqrt{s} = 1.96 \text{ TeV}$. It gives $R > 0.61$ and $|V_{tb}| > 0.78$ at 95% CL. Superseded by ABAZOV 08m.

⁷ ACOSTA 05A result is from the analysis of lepton + jets and di-lepton + jets final states of $t\bar{t}$ candidate events with $\sim 162 \text{ pb}^{-1}$ of data at $\sqrt{s} = 1.96 \text{ TeV}$. The first error is statistical and the second systematic. It gives $R > 0.61$, or $|V_{tb}| > 0.78$ at 95% CL.

⁸ AFFOLDER 01c measures the top-quark decay width ratio $R = \Gamma(Wb)/\Gamma(Wq)$, where q is a d, s , or b quark, by using the number of events with multiple b tags. The first error is statistical and the second systematic. A numerical integration of the likelihood function gives $R > 0.61$ (0.56) at 90% (95%) CL. By assuming three generation unitarity, $|V_{tb}| = 0.97 \pm_{-0.12}^{+0.16}$ or $|V_{tb}| > 0.78$ (0.75) at 90% (95%) CL is obtained. The result is based on 109 pb^{-1} of data at $\sqrt{s} = 1.8 \text{ TeV}$.

$\Gamma(e\nu_e b)/\Gamma_{\text{total}}$		Γ_3/Γ	
VALUE	DOCUMENT ID	TECN	COMMENT
0.111 ± 0.003	¹ AAD	15cc ATLS	$\ell + \text{jets}, \ell\ell + \text{jets}, \ell\tau_h + \text{jets}$

¹ AAD 15cc based on 4.6 fb^{-1} of pp data at $\sqrt{s} = 7 \text{ TeV}$. The original value is given by $13.3 \pm 0.4 \pm 0.5\%$, which includes electrons from the decay of τ leptons. It is assumed that the top branching ratios to leptons and jets add up to one and that only SM processes contribute to the background. The event selection criteria are optimized for the $\ell\tau_h + \text{jets}$ channel. We have converted the original value to eliminate contributions of electrons from τ 's, by using the AAD 15cc measurements of the branching ratios to μ and τ channels, as well as the PDG values of τ branching ratios into e and μ channels.

$\Gamma(\mu\nu_\mu b)/\Gamma_{\text{total}}$		Γ_4/Γ	
VALUE	DOCUMENT ID	TECN	COMMENT
0.114 ± 0.002	¹ AAD	15cc ATLS	$\ell + \text{jets}, \ell\ell + \text{jets}, \ell\tau_h + \text{jets}$

¹ AAD 15cc based on 4.6 fb^{-1} of pp data at $\sqrt{s} = 7 \text{ TeV}$. The original value is given by $13.4 \pm 0.3 \pm 0.5\%$, which includes muons from the decay of τ leptons. It is assumed that the top branching ratios to leptons and jets add up to one and that only SM processes contribute to the background. The event selection criteria are optimized for the $\ell\tau_h + \text{jets}$ channel. We have converted the original value to eliminate contributions of muons from τ 's, by using the AAD 15cc measurements of the branching ratios to μ and τ channels, as well as the PDG values of τ branching ratios into e and τ channels.

$\Gamma(\tau\nu_\tau b)/\Gamma_{\text{total}}$		Γ_5/Γ	
VALUE	DOCUMENT ID	TECN	COMMENT
0.107 ± 0.005 OUR AVERAGE			
$0.1050 \pm 0.0009 \pm 0.0071$	¹ SIRUNYAN	20v CMS	$\ell\tau_h + \geq 3$ jets ($\geq 1b$ -tag)
0.112 ± 0.009	² AAD	15cc ATLS	$\ell + \text{jets}, \ell\ell + \text{jets}, \ell\tau_h + \text{jets}$
0.096 ± 0.028	³ AALTONEN	14A CDF	$\ell + \tau_h + \geq 2$ jets ($\geq 1b$ -tag)

• • • We do not use the following data for averages, fits, limits, etc. • • •

⁴ ABULENCIA 06R CDF $\ell\tau + \text{jets}$

⁵ ABE 97v CDF $\ell\tau + \text{jets}$

¹ SIRUNYAN 20v based on 35.9 fb^{-1} of pp data at $\sqrt{s} = 13 \text{ TeV}$. $t\bar{t}$ events are selected in the $t\bar{t} \rightarrow (\ell\nu_\ell)(\tau\nu_\tau)b\bar{b}$ mode, where τ_h refers to the hadronic decays of τ . The branching ratio is determined with respect to the $t\bar{t}$ inclusive cross section extrapolated from the light dilepton mode. The ratio of the $t\bar{t}$ production cross sections in the $\ell\tau_h$ and $\ell\ell$ channels yields $0.973 \pm 0.009 \pm 0.066$, consistent with lepton universality.

² AAD 15cc based on 4.6 fb^{-1} of pp data at $\sqrt{s} = 7 \text{ TeV}$. The original value is given by $7.0 \pm 0.3 \pm 0.5\%$, which includes only the hadronic decay of τ leptons. It is assumed that the top branching ratios to leptons and jets add up to one and that only SM processes contribute to the background. The event selection criteria are optimized for the $\ell\tau_h + \text{jets}$ channel. We have converted the original value to include leptonic decays of τ 's, by using the AAD 15cc measurements of the branching ratios to e and μ channels, as well as the PDG values of τ branching ratios into e and μ channels.

³ Based on 9 fb^{-1} of data. The measurement is in the channel $t\bar{t} \rightarrow (b\nu)(b\tau\nu)$, where τ decays into hadrons (τ_h), and ℓ (e or μ) include ℓ from τ decays (τ_ℓ). The result is consistent with lepton universality.

⁴ ABULENCIA 06R looked for $t\bar{t} \rightarrow (\ell\nu_\ell)(\tau\nu_\tau)b\bar{b}$ events in 194 pb^{-1} of $p\bar{p}$ collisions at $\sqrt{s} = 1.96 \text{ TeV}$. 2 events are found where 1.00 ± 0.17 signal and 1.29 ± 0.25 background events are expected, giving a 95% CL upper bound for the partial width ratio $\Gamma(t \rightarrow \tau\nu q) / \Gamma_{SM}(t \rightarrow \tau\nu q) < 5.2$.

⁵ ABE 97v searched for $t\bar{t} \rightarrow (\ell\nu_\ell)(\tau\nu_\tau)b\bar{b}$ events in 109 pb^{-1} of $p\bar{p}$ collisions at $\sqrt{s} = 1.8 \text{ TeV}$. They observed 4 candidate events where one expects ~ 1 signal and ~ 2 background events. Three of the four observed events have jets identified as b candidates.

$\Gamma(q\bar{q}b)/\Gamma_{\text{total}}$		Γ_6/Γ	
VALUE	DOCUMENT ID	TECN	COMMENT
0.665 ± 0.004 ± 0.013	¹ AAD	15cc ATLS	$\ell + \text{jets}, \ell\ell + \text{jets}, \ell\tau_h + \text{jets}$

¹ AAD 15cc based on 4.6 fb^{-1} of pp data at $\sqrt{s} = 7 \text{ TeV}$. Branching ratio of top quark into b and jets. It is assumed that the top branching ratios to leptons and jets add up to one and that only SM processes contribute to the background. The event selection criteria are optimized for the $\ell\tau_h + \text{jets}$ channel.

$\Gamma(\gamma q(q=u,c))/\Gamma_{\text{total}}$		Γ_7/Γ	
VALUE	DOCUMENT ID	TECN	COMMENT
< 0.85 × 10⁻⁵	95	¹ AAD	23 ATLS $B(t \rightarrow \gamma u)$, left-handed $t u \gamma$ coupling
< 4.2 × 10⁻⁵	95	¹ AAD	23 ATLS $B(t \rightarrow \gamma c)$, left-handed $t c \gamma$ coupling
< 1.2 × 10⁻⁵	95	¹ AAD	23 ATLS $B(t \rightarrow \gamma u)$, right-handed $t u \gamma$ coupling
< 4.5 × 10⁻⁵	95	¹ AAD	23 ATLS $B(t \rightarrow \gamma c)$, right-handed $t c \gamma$ coupling
< 1.3 × 10 ⁻⁴	95	² KHACHATRYAN...16AS	CMS $B(t \rightarrow \gamma u)$
< 1.7 × 10 ⁻³	95	² KHACHATRYAN...16AS	CMS $B(t \rightarrow \gamma c)$
< 5.9 × 10 ⁻³	95	³ CHEKANOV	03 ZEUS $B(t \rightarrow \gamma u)$

• • • We do not use the following data for averages, fits, limits, etc. • • •

< 2.8 × 10 ⁻⁵	95	⁴ AAD	20B ATLS $B(t \rightarrow \gamma u)$, left-handed $t u \gamma$ coupling, Repl. by AAD 23
< 6.1 × 10 ⁻⁵	95	⁴ AAD	20B ATLS $B(t \rightarrow \gamma u)$, right-handed $t u \gamma$ coupling, Repl. by AAD 23
< 2.2 × 10 ⁻⁴	95	⁴ AAD	20B ATLS $B(t \rightarrow \gamma c)$, left-handed $t c \gamma$ coupling, Repl. by AAD 23
< 1.8 × 10 ⁻⁴	95	⁴ AAD	20B ATLS $B(t \rightarrow \gamma c)$, right-handed $t c \gamma$ coupling, Repl. by AAD 23
< 0.0064	95	⁵ AARON	09A H1 $t \rightarrow \gamma u$
< 0.0465	95	⁶ ABDALLAH	04C DLPH $B(\gamma c \text{ or } \gamma u)$
< 0.0132	95	⁷ AKTAS	04 H1 $B(t \rightarrow \gamma u)$
< 0.041	95	⁸ ACHARD	02 L3 $B(t \rightarrow \gamma c \text{ or } \gamma u)$
< 0.032	95	⁹ ABE	98G CDF $t\bar{t} \rightarrow (Wb)(\gamma c \text{ or } \gamma u)$

¹ AAD 23 based on 139 fb^{-1} of data in pp collisions at $\sqrt{s} = 13 \text{ TeV}$. Anomalous FCNC left-handed and right-handed couplings are searched for through the single top production in association with a photon and in the decay of a top quark in the $t\bar{t}$ production. The SM predictions of the corresponding branching ratios are of the order of 10^{-14} .

² KHACHATRYAN 16AS based on 19.8 fb^{-1} of data in pp collisions at $\sqrt{s} = 8 \text{ TeV}$. FCNC through single top production in association with a photon is searched for in the mode $\mu + \gamma + E_T + \geq 1j$ (0,1b). Bounds on the anomalous FCNC couplings are given by $\kappa_{t u \gamma} < 0.025$ and $\kappa_{t c \gamma} < 0.091$.

³ CHEKANOV 03 looked for single top production via FCNC in the reaction $e^\pm p \rightarrow e^\pm (t \text{ or } \bar{t}) X$ in 130.1 pb^{-1} of data at $\sqrt{s} = 300\text{--}318 \text{ GeV}$. No evidence for top production and its decay into bW was found. The result is obtained for $m_t = 175 \text{ GeV}$ when $B(\gamma c) = B(Zq) = 0$, where q is a u or c quark. Bounds on the effective $t\text{--}u\text{--}\gamma$ and $t\text{--}u\text{--}Z$ couplings are found in their Fig. 4. The conversion to the constraint listed is from private communication, E. Gallo, January 2004.

⁴ AAD 20B based on 81 fb^{-1} of data in pp collisions at $\sqrt{s} = 13 \text{ TeV}$. FCNC through single top production in association with a photon is searched for in the mode $\ell\gamma + E_T + 1j$ (b -tag). Anomalous FCNC left-handed and right-handed couplings are searched for, which result in different kinematical properties of top decay such as the lepton distribution. Limits are set on the $tq\gamma$ couplings in an effective field theory.

⁵ AARON 09A looked for single top production via FCNC in $e^\pm p$ collisions at HERA with 474 pb^{-1} . The upper bound of the cross section gives the bound on the FCNC coupling $\kappa_{t u \gamma} / \Lambda < 1.03 \text{ TeV}^{-1}$, which corresponds to the result for $m_t = 175 \text{ GeV}$.

⁶ ABDALLAH 04c looked for single top production via FCNC in the reaction $e^+e^- \rightarrow \bar{t}c \text{ or } \bar{t}u$ in 541 pb^{-1} of data at $\sqrt{s} = 189\text{--}208 \text{ GeV}$. No deviation from the SM is found, which leads to the bound on $B(t \rightarrow \gamma q)$, where q is a u or a c quark, for $m_t = 175 \text{ GeV}$ when $B(t \rightarrow Zq) = 0$ is assumed. The conversion to the listed bound is from private communication, O. Yushchenko, April 2005. The bounds on the effective $t\text{--}q\text{--}\gamma$ and $t\text{--}q\text{--}Z$ couplings are given in their Fig. 7 and Table 4, for $m_t = 170\text{--}180 \text{ GeV}$, where most conservative bounds are found by choosing the chiral couplings to maximize the negative interference between the virtual γ and Z exchange amplitudes.

⁷ AKTAS 04 looked for single top production via FCNC in e^\pm collisions at HERA with 118.3 pb^{-1} , and found 5 events in the e or μ channels. By assuming that they are due to statistical fluctuation, the upper bound on the $t u \gamma$ coupling $\kappa_{t u \gamma} < 0.27$ (95% CL) is obtained. The conversion to the partial width limit, when $B(\gamma c) = B(Zu) = B(Zc) = 0$, is from private communication, E. Perez, May 2005.

⁸ ACHARD 02i looked for single top production via FCNC in the reaction $e^+e^- \rightarrow \bar{t}c \text{ or } \bar{t}u$ in 634 pb^{-1} of data at $\sqrt{s} = 189\text{--}209 \text{ GeV}$. No deviation from the SM is found, which leads to a bound on the top-quark decay branching fraction $B(\gamma q)$, where q is a u or c quark. The bound assumes $B(Zq) = 0$ and is for $m_t = 175 \text{ GeV}$; bounds for $m_t = 170 \text{ GeV}$ and 180 GeV and $B(Zq) \neq 0$ are given in Fig. 5 and Table 7.

⁹ ABE 98G looked for $t\bar{t}$ events where one t decays into $q\gamma$ while the other decays into bW . The quoted bound is for $\Gamma(\gamma q)/\Gamma(Wb)$.

$\Gamma(H^+ b, H^+ \rightarrow \tau\nu_\tau)/\Gamma_{\text{total}}$		Γ_8/Γ	
VALUE (%)	CL%	DOCUMENT ID	TECN
< 0.25	95	¹ AABOUD	18BWATLS

¹ AABOUD 18BW based on 36.1 fb^{-1} of pp data at $\sqrt{s} = 13 \text{ TeV}$. In the mass range of $m_{H^+} = 90\text{--}160 \text{ GeV}$, assuming the SM cross section for the $t\bar{t}$ production, the upper limit for the branching fraction $B(t \rightarrow bH^+) \times B(H^+ \rightarrow \tau\nu_\tau)$ ranges between 0.25% and 0.031%.

$\Gamma(Z q(q=u,c))/\Gamma_{\text{total}}$		Γ_9/Γ	
VALUE (units 10^{-3})	CL%	DOCUMENT ID	TECN

< 0.062	95	¹ AAD	23AS ATLS $B(t \rightarrow Z u)$, left-handed $t u Z$ coupling
< 0.13	95	¹ AAD	23AS ATLS $B(t \rightarrow Z c)$, left-handed $t c Z$ coupling
< 0.066	95	¹ AAD	23AS ATLS $B(t \rightarrow Z u)$, right-handed $t u Z$ coupling
< 0.12	95	¹ AAD	23AS ATLS $B(t \rightarrow Z c)$, right-handed $t c Z$ coupling
< 0.22	95	² SIRUNYAN	17E CMS $t \rightarrow Z u$
< 0.49	95	² SIRUNYAN	17E CMS $t \rightarrow Z c$
< 0.7	95	³ AAD	16D ATLS $t \rightarrow Z q$ ($q = u, c$)

• • • We do not use the following data for averages, fits, limits, etc. • • •

< 0.17	95	⁴ AABOUD	18AT ATLS $t \rightarrow Z u$
< 0.24	95	⁴ AABOUD	18AT ATLS $t \rightarrow Z c$
< 0.6	95	⁵ CHATRCHYAN14S	CMS $t \rightarrow Z q$ ($q = u, c$)
< 0.5	95	⁶ CHATRCHYAN14S	CMS $t \rightarrow Z q$ ($q = u, c$)
< 2.1	95	⁷ CHATRCHYAN13F	CMS $t \rightarrow Z q$ ($q = u, c$)

Quark Particle Listings

 t

< 7.3	95	⁸ AAD	12BT ATLS	$t\bar{t} \rightarrow \ell^+ \ell^- \ell'^{\pm} + \cancel{E}_T + \text{jets}$
< 32	95	⁹ ABAZOV	11M D0	$t \rightarrow Zq (q = u, c)$
< 83	95	¹⁰ AALTONEN	09AL CDF	$t \rightarrow Zq (q=c)$
< 37	95	¹¹ AALTONEN	08AD CDF	$t \rightarrow Zq (q = u, c)$
< 1.59 × 10 ²	95	¹² ABDALLAH	04C DLPH	$e^+e^- \rightarrow \bar{t}c \text{ or } \bar{t}u$
< 1.37 × 10 ²	95	¹³ ACHARD	02J L3	$e^+e^- \rightarrow \bar{t}c \text{ or } \bar{t}u$
< 1.4 × 10 ²	95	¹⁴ HEISTER	02Q ALEP	$e^+e^- \rightarrow \bar{t}c \text{ or } \bar{t}u$
< 1.37 × 10 ²	95	¹⁵ ABBIENDI	01T OPAL	$e^+e^- \rightarrow \bar{t}c \text{ or } \bar{t}u$
< 1.7 × 10 ²	95	¹⁶ BARATE	00S ALEP	$e^+e^- \rightarrow \bar{t}c \text{ or } \bar{t}u$
< 3.3 × 10 ²	95	¹⁷ ABE	98G CDF	$t\bar{t} \rightarrow (Wb)(Zc \text{ or } Zu)$

¹ AAD 23As based on 139 fb⁻¹ of data in pp collisions at $\sqrt{s} = 13$ TeV. Anomalous FCNC left-handed and right-handed couplings are searched for through the single top production in association with a Z boson and in the decay of a top quark in the $t\bar{t}$ production. Events with $3\ell + \geq 1$ jet(s) (1b-tagged) + \cancel{E}_T are used. The SM predictions of the corresponding branching ratios are of the order of 10⁻¹⁴.

² SIRUNYAN 17E based on 19.7 fb⁻¹ of pp data at $\sqrt{s} = 8$ TeV. The final states $t\bar{t} \rightarrow \ell^+ \ell^- \ell'^{\pm} \nu + \text{jets} (\ell, \ell' = e, \mu)$ are investigated and the cross section $\sigma(pp \rightarrow tZq \rightarrow \ell\nu b\ell^+ \ell^- q) = 10^{+8}_{-7}$ fb is measured, giving no sign of FCNC decays of the top quark.

³ AAD 16D based on 20.3 fb⁻¹ of pp data at $\sqrt{s} = 8$ TeV. The FCNC decay is searched for in $t\bar{t}$ events in the final state $(bW)(qZ)$ when both W and Z decay leptonically, giving 3 charged leptons.

⁴ Based on 36.1 fb⁻¹ of pp data at $\sqrt{s} = 13$ TeV. The final states $t\bar{t} \rightarrow \ell^+ \ell^- \ell'^{\pm} \nu + \text{jets} (\ell, \ell' = e, \mu)$ are investigated and no significant excess over the SM background contributions is observed.

⁵ Based on 19.7 fb⁻¹ of pp data at $\sqrt{s} = 8$ TeV. The flavor changing decay is searched for in $t\bar{t}$ events in the final state $(bW)(qZ)$ when both W and Z decay leptonically, giving 3 charged leptons.

⁶ CHATRCHYAN 14s combined search limit from this and CHATRCHYAN 13F data.

⁷ Based on 5.0 fb⁻¹ of pp data at $\sqrt{s} = 7$ TeV. Search for FCNC decays of the top quark in $t\bar{t} \rightarrow \ell^+ \ell^- \ell'^{\pm} \nu + \text{jets} (\ell, \ell' = e, \mu)$ final states found no excess of signal events.

⁸ Based on 2.1 fb⁻¹ of pp data at $\sqrt{s} = 7$ TeV.

⁹ Based on 4.1 fb⁻¹ of data. ABAZOV 11M searched for FCNC decays of the top quark in $t\bar{t} \rightarrow \ell^+ \ell^- \ell'^{\pm} \nu + \text{jets} (\ell, \ell' = e, \mu)$ final states, and absence of the signal gives the bound.

¹⁰ Based on $p\bar{p}$ data of 1.52 fb⁻¹. AALTONEN 09AL compared $t\bar{t} \rightarrow WbWb \rightarrow \ell\nu bjjb$ and $t\bar{t} \rightarrow ZcWb \rightarrow \ell\ell cjjb$ decay chains, and absence of the latter signal gives the bound. The result is for 100% longitudinally polarized Z boson and the theoretical $t\bar{t}$ production cross section. The results for different Z polarizations and those without the cross section assumption are given in their Table XII.

¹¹ Result is based on 1.9 fb⁻¹ of data at $\sqrt{s} = 1.96$ TeV. $t\bar{t} \rightarrow WbZq$ or $ZqZq$ processes have been looked for in $Z + \geq 4$ jet events with and without b-tag. No signal leads to the bound $B(t \rightarrow Zq) < 0.037 (0.041)$ for $m_t = 175 (170)$ GeV.

¹² ABDALLAH 04C looked for single top production via FCNC in the reaction $e^+e^- \rightarrow \bar{t}c$ or $\bar{t}u$ in 541 pb⁻¹ of data at $\sqrt{s} = 189\text{--}208$ GeV. No deviation from the SM is found, which leads to the bound on $B(t \rightarrow Zq)$, where q is a u or a c quark, for $m_t = 175$ GeV when $B(t \rightarrow \gamma q) = 0$ is assumed. The conversion to the listed bound is from private communication, O. Yushchenko, April 2005. The bounds on the effective t - q - γ and t - q - Z couplings are given in their Fig. 7 and Table 4, for $m_t = 170\text{--}180$ GeV, where most conservative bounds are found by choosing the chiral couplings to maximize the negative interference between the virtual γ and Z exchange amplitudes.

¹³ ACHARD 02J looked for single top production via FCNC in the reaction $e^+e^- \rightarrow \bar{t}c$ or $\bar{t}u$ in 634 pb⁻¹ of data at $\sqrt{s} = 189\text{--}209$ GeV. No deviation from the SM is found, which leads to a bound on the top-quark decay branching fraction $B(Zq)$, where q is a u or c quark. The bound assumes $B(\gamma q) = 0$ and is for $m_t = 175$ GeV; bounds for $m_t = 170$ GeV and 180 GeV and $B(\gamma q) \neq 0$ are given in Fig. 5 and Table 7. Table 6 gives constraints on t - c - e - e four-fermi contact interactions.

¹⁴ HEISTER 02Q looked for single top production via FCNC in the reaction $e^+e^- \rightarrow \bar{t}c$ or $\bar{t}u$ in 214 pb⁻¹ of data at $\sqrt{s} = 204\text{--}209$ GeV. No deviation from the SM is found, which leads to a bound on the branching fraction $B(Zq)$, where q is a u or c quark. The bound assumes $B(\gamma q) = 0$ and is for $m_t = 174$ GeV. Bounds on the effective t - $(c \text{ or } u)$ - γ and t - $(c \text{ or } u)$ - Z couplings are given in their Fig. 2.

¹⁵ ABBIENDI 01T looked for single top production via FCNC in the reaction $e^+e^- \rightarrow \bar{t}c$ or $\bar{t}u$ in 600 pb⁻¹ of data at $\sqrt{s} = 189\text{--}209$ GeV. No deviation from the SM is found, which leads to bounds on the branching fractions $B(Zq)$ and $B(\gamma q)$, where q is a u or c quark. The result is obtained for $m_t = 174$ GeV. The upper bound becomes 9.7% (20.6%) for $m_t = 169 (179)$ GeV. Bounds on the effective t - $(c \text{ or } u)$ - γ and t - $(c \text{ or } u)$ - Z couplings are given in their Fig. 4.

¹⁶ BARATE 00s looked for single top production via FCNC in the reaction $e^+e^- \rightarrow \bar{t}c$ or $\bar{t}u$ in 411 pb⁻¹ of data at c.m. energies between 189 and 202 GeV. No deviation from the SM is found, which leads to a bound on the branching fraction. The bound assumes $B(\gamma q) = 0$. Bounds on the effective t - $(c \text{ or } u)$ - γ and t - $(c \text{ or } u)$ - Z couplings are given in their Fig. 4.

¹⁷ ABE 98G looked for $t\bar{t}$ events where one t decays into three jets and the other decays into qZ with $Z \rightarrow \ell\ell$. The quoted bound is for $\Gamma(Zq)/\Gamma(Wb)$.

$\Gamma(Hu)/\Gamma_{\text{total}}$					Γ_{11}/Γ
VALUE (units 10 ⁻⁴)	CL%	DOCUMENT ID	TECN	COMMENT	
< 1.9	95	¹ TUMASYAN	22A CMS	$t \rightarrow Hu (H \rightarrow \gamma\gamma)$	
•••				••• We do not use the following data for averages, fits, limits, etc. •••	
< 3.8	95	² AAD	23CJ ATLS	$pp \rightarrow tH \text{ or } t \rightarrow Hu (H \rightarrow \gamma\gamma)$	
< 4.0	95	³ AAD	23CJ ATLS	$pp \rightarrow tH \text{ or } t \rightarrow Hu$ (combined with $H \rightarrow \gamma\gamma, H \rightarrow bb, H \rightarrow \tau\tau$)	
< 6.9	95	⁴ AAD	23H ATLS	$pp \rightarrow tH \text{ or } t \rightarrow Hu (H \rightarrow \tau\tau)$	
< 7.9	95	⁵ TUMASYAN	22K CMS	$t \rightarrow Hu (H \rightarrow bb)$	
< 52	95	⁶ AABOUD	19S ATLS	$t \rightarrow Hu (H \rightarrow bb)$	
< 17	95	⁷ AABOUD	19S ATLS	$t \rightarrow Hu (H \rightarrow \tau\tau)$	
< 12	95	⁸ AABOUD	19S ATLS	combination of $t \rightarrow Hu (H \rightarrow WW, ZZ, \tau\tau, \gamma\gamma, b\bar{b})$	

< 19	95	⁹ AABOUD	18X ATLS	$t \rightarrow Hu (H \rightarrow WW, ZZ, \tau\tau)$
< 47	95	¹⁰ SIRUNYAN	18Bc CMS	$t \rightarrow Hu (H \rightarrow bb)$
< 24	95	¹¹ AABOUD	17AV ATLS	$t \rightarrow Hu (H \rightarrow \gamma\gamma)$
< 55	95	¹² KHACHATRYAN..17I	CMS	$t \rightarrow Hu (H \rightarrow WW, ZZ, \tau\tau, \gamma\gamma, b\bar{b})$
< 61	95	¹³ AAD	15C0 ATLS	$t \rightarrow Hu (H \rightarrow bb)$
< 79	95	¹⁴ AAD	14AA ATLS	$t \rightarrow Hq (q=u,c; H \rightarrow \gamma\gamma)$

¹ TUMASYAN 22A based on 137 fb⁻¹ at $\sqrt{s} = 13$ TeV of pp data. The processes considered include both the associated production of a single top quark with a Higgs boson and the decay $t \rightarrow Hu$ in $t\bar{t}$ production using $H \rightarrow \gamma\gamma$.

² AAD 23CJ based on 139 fb⁻¹ at $\sqrt{s} = 13$ TeV of pp data. The processes considered include both the associated production of a single top quark with a Higgs boson and the decay $t \rightarrow Hu$ in $t\bar{t}$ production using $H \rightarrow \gamma\gamma$. Limits on the SMEFT Wilson coefficients are derived.

³ AAD 23CJ based on 139 fb⁻¹ at $\sqrt{s} = 13$ TeV of pp data. The results are combined with searches in the $H \rightarrow \gamma\gamma, H \rightarrow bb$, and $H \rightarrow \tau\tau$ final states. Limits on the SMEFT Wilson coefficients are also derived.

⁴ AAD 23H based on 139 fb⁻¹ at $\sqrt{s} = 13$ TeV of pp data. Uses events with one or two hadronically decaying τ and multiple jets. The limit corresponds to $(3.5^{+1.5}_{-1.0}) \times 10^{-4}$ measurement.

⁵ TUMASYAN 22K based on 137 fb⁻¹ at $\sqrt{s} = 13$ TeV of pp data. Uses events with one isolated lepton and multiple jets (including $\geq 2b$ -jets). Deep neural networks are used for kinematical event reconstruction.

⁶ AABOUD 19s based on 36.1 fb⁻¹ at $\sqrt{s} = 13$ TeV of pp data. Uses events with one isolated lepton and multiple jets (several of them b -tagged with high purity). A multivariate analysis is performed to distinguish the signal from backgrounds.

⁷ AABOUD 19s based on 36.1 fb⁻¹ at $\sqrt{s} = 13$ TeV of pp data. Uses events with one or two hadronically decaying τ and multiple jets. A multivariate analysis is performed to distinguish the signal from backgrounds.

⁸ AABOUD 19s based on 36.1 fb⁻¹ at $\sqrt{s} = 13$ TeV of pp data. The searches using $H \rightarrow bb$ and $H \rightarrow \tau\tau$ are combined with searches in diphoton and multilepton final states. The upper limit on the Yukawa coupling $|Y_{tH}| < 0.066$ (95% CL) is obtained.

⁹ AABOUD 18X based on 36.1 fb⁻¹ at $\sqrt{s} = 13$ TeV of pp data. $\ell\ell$ (same sign) + $\geq 4j$ mode and $\ell\ell\ell + \geq 2j$ mode are targeted and specialized boosted decision trees are used to distinguish signals from backgrounds.

¹⁰ SIRUNYAN 18Bc based on 35.9 fb⁻¹ at $\sqrt{s} = 13$ TeV of pp data. Two channels $pp \rightarrow tH$ and $pp \rightarrow t\bar{t}$ in final states with one isolated lepton and ≥ 3 jets with $\geq 2b$ jets are considered assuming a single tHu FCNC coupling. Reconstructed kinematical variables are fed into a multivariate analysis and no significant deviation is observed from the predicted background.

¹¹ AABOUD 17AV based on 36.1 fb⁻¹ at $\sqrt{s} = 13$ TeV of pp data. Search for $t\bar{t}$ events, where the other top quark decays hadronically or semi-leptonically.

¹² KHACHATRYAN 17I based on 19.7 fb⁻¹ of pp data at $\sqrt{s} = 8$ TeV, using the topologies $t\bar{t} \rightarrow Hq + Wb$, where $q = u, c$.

¹³ AAD 15C0 based on 20.3 fb⁻¹ at $\sqrt{s} = 8$ TeV of pp data. Searches for $t\bar{t}$ events, where the other top quark decays semi-leptonically. Exploits high multiplicity of b -jets and uses a likelihood discriminant. Combining with other ATLAS searches for different Higgs decay modes, $B(t \rightarrow Hc) < 0.46\%$ and $B(t \rightarrow Hu) < 0.45\%$ are obtained.

¹⁴ AAD 14AA based on 4.7 fb⁻¹ at $\sqrt{s} = 7$ TeV and 20.3 fb⁻¹ at $\sqrt{s} = 8$ TeV of pp data. The upper-bound is for the sum of $B(t \rightarrow Hc)$ and $B(t \rightarrow Hu)$. Search for $t\bar{t}$ events, where the other top quark decays hadronically or semi-leptonically. The upper bound constrains the H - t - c Yukawa couplings $\sqrt{|Y_{tL}^H|^2 + |Y_{tR}^H|^2} < 0.17$ (95% CL).

$\Gamma(Hc)/\Gamma_{\text{total}}$					Γ_{11}/Γ
VALUE (units 10 ⁻⁴)	CL%	DOCUMENT ID	TECN	COMMENT	
< 4.3	95	¹ AAD	23CJ ATLS	$pp \rightarrow tH \text{ or } t \rightarrow Hc (H \rightarrow \gamma\gamma)$	
•••				••• We do not use the following data for averages, fits, limits, etc. •••	
< 5.8	95	² AAD	23CJ ATLS	$pp \rightarrow tH \text{ or } t \rightarrow Hc$ (combined with $H \rightarrow \gamma\gamma, H \rightarrow bb, H \rightarrow \tau\tau$)	
< 9.4	95	³ AAD	23H ATLS	$pp \rightarrow tH \text{ or } t \rightarrow Hc (H \rightarrow \tau\tau)$	
< 7.3	95	⁴ TUMASYAN	22A CMS	$t \rightarrow Hc (H \rightarrow \gamma\gamma)$	
< 9.4	95	⁵ TUMASYAN	22K CMS	$t \rightarrow Hc (H \rightarrow bb)$	
< 11	95	⁶ AABOUD	19S ATLS	combination of $t \rightarrow Hc (H \rightarrow WW, ZZ, \tau\tau, \gamma\gamma, b\bar{b})$	
< 42	95	⁷ AABOUD	19S ATLS	$t \rightarrow Hc (H \rightarrow bb)$	
< 19	95	⁸ AABOUD	19S ATLS	$t \rightarrow Hc (H \rightarrow \tau\tau)$	
< 16	95	⁹ AABOUD	18X ATLS	$t \rightarrow Hc (H \rightarrow WW, ZZ, \tau\tau)$	
< 47	95	¹⁰ SIRUNYAN	18Bc CMS	$t \rightarrow Hc (H \rightarrow bb)$	
< 22	95	¹¹ AABOUD	17AV ATLS	$t \rightarrow Hc (H \rightarrow \gamma\gamma)$	
< 40	95	¹² KHACHATRYAN..17I	CMS	$t \rightarrow Hc (H \rightarrow WW, ZZ, \tau\tau, \gamma\gamma, b\bar{b})$	
< 56	95	¹³ AAD	15C0 ATLS	$t \rightarrow Hc (H \rightarrow bb)$	
< 79	95	¹⁴ AAD	14AA ATLS	$t \rightarrow Hq (q=u,c; H \rightarrow \gamma\gamma)$	
< 1.3 × 10 ²	95	¹⁵ CHATRCHYAN14R	CMS	$t \rightarrow Hc (H \rightarrow \geq 2\ell)$	
< 56	95	¹⁶ KHACHATRYAN..14Q	CMS	$t \rightarrow Hc (H \rightarrow \gamma\gamma \text{ or } \text{leptons})$	

¹ AAD 23CJ based on 139 fb⁻¹ at $\sqrt{s} = 13$ TeV of pp data. The processes considered include both the associated production of a single top quark with a Higgs boson and the decay $t \rightarrow Hc$ in $t\bar{t}$ production using $H \rightarrow \gamma\gamma$. Limits on the SMEFT Wilson coefficients are derived.

² AAD 23CJ based on 139 fb⁻¹ at $\sqrt{s} = 13$ TeV of pp data. The results are combined with searches in the $H \rightarrow \gamma\gamma, H \rightarrow bb$, and $H \rightarrow \tau\tau$ final states. Limits on the SMEFT Wilson coefficients are also derived.

³ AAD 23H based on 139 fb⁻¹ at $\sqrt{s} = 13$ TeV of pp data. Uses events with one or two hadronically decaying τ and multiple jets. The limit corresponds to $(4.8^{+2.2}_{-1.4}) \times 10^{-4}$ measurement.

- 4 TUMASYAN 22A based on 137 fb^{-1} at $\sqrt{s} = 13 \text{ TeV}$ of pp data. The processes considered include both the associated production of a single top quark with a Higgs boson and the decay $t \rightarrow Hc$ in $t\bar{t}$ production using $H \rightarrow \gamma\gamma$.
- 5 TUMASYAN 22K based on 137 fb^{-1} at $\sqrt{s} = 13 \text{ TeV}$ of pp data. Uses events with one isolated lepton and multiple jets (including $\geq 2b$ -jets). Deep neural networks are used for kinematical event reconstruction.
- 6 AABOUD 19s based on 36.1 fb^{-1} at $\sqrt{s} = 13 \text{ TeV}$ of pp data. The searches using $H \rightarrow bb$ and $H \rightarrow \tau_h\tau_h$ are combined with searches in diphoton and multilepton final states. The upper limit on the Yukawa coupling $|Y_{tCH}| < 0.064$ (95% CL) is obtained.
- 7 AABOUD 19s based on 36.1 fb^{-1} at $\sqrt{s} = 13 \text{ TeV}$ of pp data. Uses events with one isolated lepton and multiple jets (several of them b -tagged with high purity). A multivariate analysis is performed to distinguish the signal from backgrounds.
- 8 AABOUD 19s based on 36.1 fb^{-1} at $\sqrt{s} = 13 \text{ TeV}$ of pp data. Uses events with one or two hadronically decaying τ and multiple jets. A multivariate analysis is performed to distinguish the signal from backgrounds.
- 9 AABOUD 18x based on 36.1 fb^{-1} at $\sqrt{s} = 13 \text{ TeV}$ of pp data. $\ell\ell$ (same sign) $+ \geq 4j$ mode and $\ell\ell\ell + \geq 2j$ mode are targeted and specialized boosted decision trees are used to distinguish signals from backgrounds.
- 10 SIRUNYAN 18bc based on 35.9 fb^{-1} at $\sqrt{s} = 13 \text{ TeV}$ of pp data. Two channels $pp \rightarrow tH$ and $pp \rightarrow t\bar{t}$ in final states with one isolated lepton and ≥ 3 jets with ≥ 2 b jets are considered assuming a single tHc FCNC coupling. Reconstructed kinematical variables are fed into a multivariate analysis and no significant deviation is observed from the predicted background.
- 11 AABOUD 17AV based on 36.1 fb^{-1} at $\sqrt{s} = 13 \text{ TeV}$ of pp data. Search for $t\bar{t}$ events, where the other top quark decays hadronically or semi-leptonically. The upper bound on the H - t - c Yukawa couplings is 0.090 (95% CL).
- 12 KHACHATRYAN 17i based on 19.7 fb^{-1} of pp data at $\sqrt{s} = 8 \text{ TeV}$, using the topologies $t\bar{t} \rightarrow Hq + Wb$, where $q = u, c$.
- 13 AAD 15CO based on 20.3 fb^{-1} at $\sqrt{s} = 8 \text{ TeV}$ of pp data. Searches for $t\bar{t}$ events, where the other top quark decays semi-leptonically. Exploits high multiplicity of b -jets and uses a likelihood discriminant. Combining with other ATLAS searches for different Higgs decay modes, $B(t \rightarrow Hc) < 0.46\%$ and $B(t \rightarrow Hu) < 0.45\%$ are obtained.
- 14 AAD 14AA based on 4.7 fb^{-1} at $\sqrt{s} = 7 \text{ TeV}$ and 20.3 fb^{-1} at $\sqrt{s} = 8 \text{ TeV}$ of pp data. The upper-bound is for the sum of $B(t \rightarrow Hc)$ and $B(t \rightarrow Hu)$. Search for $t\bar{t}$ events, where the other top quark decays hadronically or semi-leptonically. The upper bound constrains the H - t - c Yukawa couplings $\sqrt{|Y_{tCL}^H|^2 + |Y_{tCR}^H|^2} < 0.17$ (95% CL).
- 15 Based on 19.5 fb^{-1} of pp data at $\sqrt{s} = 8 \text{ TeV}$. Search for final states with 3 or more isolated high E_T charged leptons ($\ell = e, \mu$) bounds the $t \rightarrow Hc$ decay in $t\bar{t}$ events when H decays contain a pair of leptons. The upper bound constrains the H - t - c Yukawa couplings $\sqrt{|Y_{tCL}^H|^2 + |Y_{tCR}^H|^2} < 0.21$ (95% CL).
- 16 KHACHATRYAN 14Q based on 19.5 fb^{-1} at $\sqrt{s} = 8 \text{ TeV}$ of pp data. Search for final states with ≥ 3 isolated charged leptons or with a photon pair accompanied by ≥ 1 lepton(s).

$\Gamma(t^+ \bar{q} q' (q=d,s,b; q'=u,c))/\Gamma_{\text{total}}$ Γ_{12}/Γ

VALUE	CL%	DOCUMENT ID	TECN	COMMENT
$< 1.6 \times 10^{-3}$	95	¹ CHATRCHYAN14O	CMS	$\mu +$ dijets
$< 1.7 \times 10^{-3}$	95	¹ CHATRCHYAN14O	CMS	$e +$ dijets

- ¹ Based on 19.5 fb^{-1} of pp data at $\sqrt{s} = 8 \text{ TeV}$. Baryon number violating decays of the top quark are searched for in $t\bar{t}$ production events where one of the pair decays into hadronic three jets.

$\Gamma(e^{\pm} \mu^{\mp} c)/\Gamma_{\text{total}}$ Γ_{13}/Γ

VALUE	DOCUMENT ID	TECN	COMMENT
$< 8.9 \times 10^{-7}$	¹ TUMASYAN 22Z	CMS	pp at 13 TeV

- ¹ TUMASYAN 22z analysis includes both the production ($c \rightarrow e\mu t$) and decay ($t \rightarrow e\mu c$) modes of the top quark through CFLV interactions. With no significant excess over the standard model expectation, the limits are set at 95% CL on the $B(t \rightarrow e\mu c)$ of 1.31×10^{-6} , 0.89×10^{-6} , 2.59×10^{-6} for vector-, scalar-, and tensor-like CLFV four-fermion effective interactions, respectively.

$\Gamma(e^{\pm} \mu^{\mp} u)/\Gamma_{\text{total}}$ Γ_{14}/Γ

VALUE	DOCUMENT ID	TECN	COMMENT
$< 7 \times 10^{-8}$	¹ TUMASYAN 22z	CMS	pp at 13 TeV

- ¹ TUMASYAN 22z analysis includes both the production ($u \rightarrow e\mu t$) and decay ($t \rightarrow e\mu u$) modes of the top quark through CFLV interactions. With no significant excess over the standard model expectation, the limits are set at 95% CL on the $B(t \rightarrow e\mu u)$ of 0.13×10^{-6} , 0.07×10^{-6} , 0.25×10^{-6} for vector-, scalar-, and tensor-like CLFV four-fermion effective interactions, respectively.

t-quark EW Couplings

W helicity fractions in top decays. F_0 is the fraction of longitudinal and F_{\pm} the fraction of right-handed W bosons. F_{V+A} is the fraction of $V+A$ current in top decays. The effective Lagrangian (cited by ABAZOV 08AI) has terms f_L^V and f_L^A for $V-A$ and $V+A$ couplings, f_2^V and f_2^A for tensor couplings with b_R and b_L respectively.

F_0

VALUE	DOCUMENT ID	TECN	COMMENT
0.693 ± 0.013 OUR AVERAGE			

$0.693 \pm 0.009 \pm 0.011$	¹ AAD	20Y LHC	ATLAS+CMS combined
$0.726 \pm 0.066 \pm 0.067$	² AALTONEN	13D CDF	$F_0 = B(t \rightarrow W_0 b)$
$0.682 \pm 0.030 \pm 0.033$	³ CHATRCHYAN13BH	CMS	$F_0 = B(t \rightarrow W_0 b)$
0.67 ± 0.07	⁴ AAD	12BG ATLAS	$F_0 = B(t \rightarrow W_0 b)$
$0.722 \pm 0.062 \pm 0.052$	⁵ AALTONEN	12Z TEVA	$F_0 = B(t \rightarrow W_0 b)$
$0.669 \pm 0.078 \pm 0.065$	⁶ ABAZOV	11C D0	$F_0 = B(t \rightarrow W_0 b)$
$0.91 \pm 0.37 \pm 0.13$	⁷ AFFOLDER	00B CDF	$F_0 = B(t \rightarrow W_0 b)$

- We do not use the following data for averages, fits, limits, etc. •••

0.70 ± 0.05	⁸ AABOUD	17BB ATLS	$F_0 = 1 - f_1$, Repl by AAD 20Y
$0.681 \pm 0.012 \pm 0.023$	⁹ KHACHATRYAN...16BU	CMS	$F_0 = B(t \rightarrow W_0 b)$, Repl by AAD 20Y
$0.70 \pm 0.07 \pm 0.04$	¹⁰ AALTONEN	10Q CDF	Repl. by AALTONEN 12Z
$0.62 \pm 0.10 \pm 0.05$	¹¹ AALTONEN	09Q CDF	Repl. by AALTONEN 10Q
$0.425 \pm 0.166 \pm 0.102$	¹² ABAZOV	08B D0	Repl. by ABAZOV 11C
$0.85^{+0.15}_{-0.22} \pm 0.06$	¹³ ABULENCIA	07I CDF	$F_0 = B(t \rightarrow W_0 b)$
$0.74^{+0.22}_{-0.34}$	¹⁴ ABULENCIA	06U CDF	$F_0 = B(t \rightarrow W_0 b)$
0.56 ± 0.31	¹⁵ ABAZOV	05G D0	$F_0 = B(t \rightarrow W_0 b)$

- ¹ AAD 20Y based on about 20 fb^{-1} of pp data at $\sqrt{s} = 8 \text{ TeV}$ for each experiment. The first error stands for the sum of the statistical and background uncertainties, and the second error for the remaining systematic uncertainties. The measurements used events with one lepton and different jet multiplicities in the final state. The result is consistent with the NNLO SM prediction of 0.687 ± 0.005 for $m_t = 172.8 \pm 1.3 \text{ GeV}$.
- ² Based on 8.7 fb^{-1} of data in $p\bar{p}$ collisions at $\sqrt{s} = 1.96 \text{ TeV}$ using $t\bar{t}$ events with $\ell + \cancel{E}_T + \geq 4$ jets ($\geq 1 b$), and under the constraint $F_0 + F_{\pm} + F_{\mp} = 1$. The statistical errors of F_0 and F_{\pm} are correlated with correlation coefficient $\rho(F_0, F_{\pm}) = -0.69$.
- ³ Based on 5.0 fb^{-1} of pp data at $\sqrt{s} = 7 \text{ TeV}$. CHATRCHYAN 13BH studied tt events with large \cancel{E}_T and $\ell + \geq 4$ jets using a constrained kinematic fit.
- ⁴ Based on 1.04 fb^{-1} of pp data at $\sqrt{s} = 7 \text{ TeV}$. AAD 12BG studied tt events with large \cancel{E}_T and either $\ell + \geq 4j$ or $\ell\ell + \geq 2j$. The uncertainties are not independent, $\rho(F_0, F_{\pm}) = -0.96$.
- ⁵ Based on 2.7 and 5.1 fb^{-1} of CDF data in $\ell +$ jets and dilepton channels, and 5.4 fb^{-1} of D0 data in $\ell +$ jets and dilepton channels. $F_0 = 0.682 \pm 0.035 \pm 0.046$ if $F_{\pm} = 0.0017(1)$, while $F_{\pm} = -0.015 \pm 0.018 \pm 0.030$ if $F_0 = 0.688(4)$, where the assumed fixed values are the SM prediction for $m_t = 173.3 \pm 1.1 \text{ GeV}$ and $m_W = 80.399 \pm 0.023 \text{ GeV}$.
- ⁶ Results are based on 5.4 fb^{-1} of data in $p\bar{p}$ collisions at 1.96 TeV , including those of ABAZOV 08B. Under the SM constraint of $f_0 = 0.698$ (for $m_t = 173.3 \text{ GeV}$, $m_W = 80.399 \text{ GeV}$), $f_{\pm} = 0.010 \pm 0.022 \pm 0.030$ is obtained.
- ⁷ AFFOLDER 00b studied the angular distribution of leptonic decays of W bosons in $t \rightarrow Wb$ events. The ratio F_0 is the fraction of the helicity zero (longitudinal) W bosons in the decaying top quark rest frame. $B(t \rightarrow W_{\pm} b)$ is the fraction of positive helicity (right-handed) positive charge W bosons in the top quark decays. It is obtained by assuming the Standard Model value of F_0 .
- ⁸ AABOUD 17BB based on 20.2 fb^{-1} of pp data at $\sqrt{s} = 8 \text{ TeV}$. Triple-differential decay rate of top quark in the t -channel single-top production is used to simultaneously determine five generalized Wtb couplings as well as the top polarization. No assumption is made for the other couplings. See this paper for constraints on other couplings not included here. The paper reported f_1 and we converted it to F_0 .
- ⁹ KHACHATRYAN 16BU based on 19.8 fb^{-1} of pp data at $\sqrt{s} = 8 \text{ TeV}$ using $t\bar{t}$ events with $\ell + \cancel{E}_T + \geq 4$ jets ($\geq 2 b$). The errors of F_0 and F_{\pm} are correlated with a correlation coefficient $\rho(F_0, F_{\pm}) = -0.87$. The result is consistent with the NNLO SM prediction of 0.687 ± 0.005 for $m_t = 172.8 \pm 1.3 \text{ GeV}$.
- ¹⁰ Results are based on 2.7 fb^{-1} of data in $p\bar{p}$ collisions at $\sqrt{s} = 1.96 \text{ TeV}$. F_0 result is obtained by assuming $F_{\pm} = 0$, while F_{\pm} result is obtained for $F_0 = 0.70$, the SM value. Model independent fits for the two fractions give $F_0 = 0.88 \pm 0.11 \pm 0.06$ and $F_{\pm} = -0.15 \pm 0.07 \pm 0.06$ with correlation coefficient of -0.59 . The results are for $m_t = 175 \text{ GeV}$.
- ¹¹ Results are based on 1.9 fb^{-1} of data in $p\bar{p}$ collisions at $\sqrt{s} = 1.96 \text{ TeV}$. F_0 result is obtained assuming $F_{\pm} = 0$, while F_{\pm} result is obtained for $F_0 = 0.70$, the SM values. Model independent fits for the two fractions give $F_0 = 0.66 \pm 0.16 \pm 0.05$ and $F_{\pm} = -0.03 \pm 0.06 \pm 0.03$.
- ¹² Based on 1 fb^{-1} at $\sqrt{s} = 1.96 \text{ TeV}$.
- ¹³ Based on 318 pb^{-1} of data at $\sqrt{s} = 1.96 \text{ TeV}$.
- ¹⁴ Based on 200 pb^{-1} of data at $\sqrt{s} = 1.96 \text{ TeV}$. $t \rightarrow Wb \rightarrow \ell\nu b$ ($\ell = e$ or μ). The errors are stat + syst.
- ¹⁵ ABAZOV 05G studied the angular distribution of leptonic decays of W bosons in $t\bar{t}$ candidate events with lepton + jets final states, and obtained the fraction of longitudinally polarized W under the constraint of no right-handed current, $F_{\pm} = 0$. Based on 125 pb^{-1} of data at $\sqrt{s} = 1.8 \text{ TeV}$.

F_{\pm}

VALUE	CL%	DOCUMENT ID	TECN	COMMENT
0.315 ± 0.010 OUR AVERAGE				

$0.315 \pm 0.006 \pm 0.009$	¹ AAD	20Y LHC	ATLAS+CMS combined
$0.310 \pm 0.022 \pm 0.022$	² CHATRCHYAN13BH	CMS	$F_{\pm} = B(t \rightarrow W_{\pm} b)$
0.32 ± 0.04	³ AAD	12BG ATLS	$F_{\pm} = B(t \rightarrow W_{\pm} b)$
$> 0.264 \pm 0.044$	95	⁴ AABOUD	17BB ATLS $F_{\pm} = f_1(1 - f_1^{\pm})$, Repl. by AAD 20Y
$0.323 \pm 0.008 \pm 0.014$		⁵ KHACHATRYAN...16BU	CMS $F_{\pm} = B(t \rightarrow W_{\pm} b)$, Repl. by AAD 20Y

- ¹ AAD 20Y based on about 20 fb^{-1} of pp data at $\sqrt{s} = 8 \text{ TeV}$ for each experiment. The first error stands for the sum of the statistical and background uncertainties, and the second error for the remaining systematic uncertainties. The measurements used events with one lepton and different jet multiplicities in the final state. The result is consistent with the NNLO SM prediction of 0.311 ± 0.005 for $m_t = 172.8 \pm 1.3 \text{ GeV}$.
- ² Based on 5.0 fb^{-1} of pp data at $\sqrt{s} = 7 \text{ TeV}$. CHATRCHYAN 13BH studied tt events with large \cancel{E}_T and $\ell + \geq 4$ jets using a constrained kinematic fit.
- ³ Based on 1.04 fb^{-1} of pp data at $\sqrt{s} = 7 \text{ TeV}$. AAD 12BG studied tt events with large \cancel{E}_T and either $\ell + \geq 4j$ or $\ell\ell + \geq 2j$. The uncertainties are not independent, $\rho(F_0, F_{\pm}) = -0.96$.
- ⁴ AABOUD 17BB based on 20.2 fb^{-1} of pp data at $\sqrt{s} = 8 \text{ TeV}$. Triple-differential decay rate of top quark in the t -channel single-top production is used to simultaneously determine five generalized Wtb couplings as well as the top polarization. No assumption is made for the other couplings. The authors reported $f_1 = 0.30 \pm 0.05$ and $f_1^{\pm} < 0.120$

Quark Particle Listings

t

which we converted to $F_- = f_1(1 - f_1^+)$. See this paper for constraints on other couplings not included here.

⁵ KHACHATRYAN 16BU based on 19.8 fb⁻¹ of pp data at $\sqrt{s} = 8$ TeV using $t\bar{t}$ events with $\ell + \cancel{E}_T + \geq 4$ jets (≥ 2 b). The errors of F_0 and F_- are correlated with a correlation coefficient $\rho(F_0, F_-) = -0.87$. The result is consistent with the NNLO SM prediction of 0.311 ± 0.005 for $m_t = 172.8 \pm 1.3$ GeV.

F_+		CL%	DOCUMENT ID	TECN	COMMENT
-0.005 ± 0.007 OUR AVERAGE					
-0.008 ± 0.005 ± 0.006			1 AAD	20Y LHC	ATLAS+CMS combined
-0.045 ± 0.044 ± 0.058			2 AALTONEN	13D CDF	$F_+ = B(t \rightarrow W_+ b)$
0.008 ± 0.012 ± 0.014			3 CHATRCHYAN	13BH CMS	$F_+ = B(t \rightarrow W_+ b)$
0.01 ± 0.05			4 AAD	12BG ATLS	$F_+ = B(t \rightarrow W_+ b)$
0.023 ± 0.041 ± 0.034			5 ABAZOV	11c D0	$F_+ = B(t \rightarrow W_+ b)$
0.11 ± 0.15			6 AFFOLDER	00B CDF	$F_+ = B(t \rightarrow W_+ b)$
• • • We do not use the following data for averages, fits, limits, etc. • • •					
< 0.036 ± 0.006	95		7 AABOUD	17BB ATLS	$F_+ = f_1 f_1^+$, Repl. by AAD 20Y
-0.004 ± 0.005 ± 0.014			8 KHACHATRY...	16BU CMS	$F_+ = B(t \rightarrow W_+ b)$, Repl. by AAD 20Y
-0.033 ± 0.034 ± 0.031			9 AALTONEN	12Z TEVA	$F_+ = B(t \rightarrow W_+ b)$
-0.01 ± 0.02 ± 0.05			10 AALTONEN	10Q CDF	Repl. by AALTONEN 13D
-0.04 ± 0.04 ± 0.03			11 AALTONEN	09Q CDF	Repl. by AALTONEN 10Q
0.119 ± 0.090 ± 0.053			12 ABAZOV	08B D0	Repl. by ABAZOV 11c
0.056 ± 0.080 ± 0.057			13 ABAZOV	07D D0	$F_+ = B(t \rightarrow W_+ b)$
0.05 \pm 0.11 \pm 0.03			14 ABULENCIA	07I CDF	$F_+ = B(t \rightarrow W_+ b)$
< 0.26	95		14 ABULENCIA	07I CDF	$F_+ = B(t \rightarrow W_+ b)$
< 0.27	95		15 ABULENCIA	06U CDF	$F_+ = B(t \rightarrow W_+ b)$
0.00 ± 0.13 ± 0.07			16 ABAZOV	05L D0	$F_+ = B(t \rightarrow W_+ b)$
< 0.25	95		16 ABAZOV	05L D0	$F_+ = B(t \rightarrow W_+ b)$
< 0.24	95		17 ACOSTA	05D CDF	$F_+ = B(t \rightarrow W_+ b)$

¹ AAD 20Y based on about 20 fb⁻¹ of pp data at $\sqrt{s} = 8$ TeV for each experiment. The first error stands for the sum of the statistical and background uncertainties, and the second error for the remaining systematic uncertainties. The measurements used events with one lepton and different jet multiplicities in the final state. The result is estimated from the measurements of F_0 and F_- assuming unitarity. The value is consistent with the NNLO SM prediction of 0.0017 ± 0.0001 for $m_t = 172.8 \pm 1.3$ GeV.

² Based on 8.7 fb⁻¹ of data in $p\bar{p}$ collisions at $\sqrt{s} = 1.96$ TeV using $t\bar{t}$ events with $\ell + \cancel{E}_T + \geq 4$ jets (≥ 1 b), and under the constraint $F_0 + F_+ + F_- = 1$. The statistical errors of F_0 and F_+ are correlated with correlation coefficient $\rho(F_0, F_+) = -0.69$.

³ Based on 5.0 fb⁻¹ of pp data at $\sqrt{s} = 7$ TeV. CHATRCHYAN 13BH studied tt events with large \cancel{E}_T and $\ell + \geq 4$ jets using a constrained kinematic fit.

⁴ Based on 1.04 fb⁻¹ of pp data at $\sqrt{s} = 7$ TeV. AAD 12BG studied tt events with large \cancel{E}_T and either $\ell + \geq 4$ or $\ell\ell + \geq 2$.

⁵ Results are based on 5.4 fb⁻¹ of data in $p\bar{p}$ collisions at 1.96 TeV, including those of ABAZOV 08B. Under the SM constraint of $f_0 = 0.698$ (for $m_t = 173.3$ GeV, $m_W = 80.399$ GeV), $f_+ = 0.010 \pm 0.022 \pm 0.030$ is obtained.

⁶ AFFOLDER 00B studied the angular distribution of leptonic decays of W bosons in $t \rightarrow Wb$ events. The ratio F_0 is the fraction of the helicity zero (longitudinal) W bosons in the decaying top quark rest frame. $B(t \rightarrow W_+ b)$ is the fraction of positive helicity (right-handed) positive charge W bosons in the top quark decays. It is obtained by assuming the Standard Model value of F_0 .

⁷ AABOUD 17BB based on 20.2 fb⁻¹ of pp data at $\sqrt{s} = 8$ TeV. Triple-differential decay rate of top quark in the t-channel single-top production is used to simultaneously determine five generalized Wtb couplings as well as the top polarization. No assumption is made for the other couplings. The authors reported $f_1 = 0.30 \pm 0.05$ and $f_1^+ < 0.120$ which we converted to $F_+ = f_1 f_1^+$. See this paper for constraints on other couplings not included here.

⁸ KHACHATRYAN 16BU based on 19.8 fb⁻¹ of pp data at $\sqrt{s} = 8$ TeV using $t\bar{t}$ events with $\ell + \cancel{E}_T + \geq 4$ jets (≥ 2 b). The result is consistent with the NNLO SM prediction of 0.0017 ± 0.0001 for $m_t = 172.8 \pm 1.3$ GeV.

⁹ Based on 2.7 and 5.1 fb⁻¹ of CDF data in $\ell +$ jets and dilepton channels, and 5.4 fb⁻¹ of D0 data in $\ell +$ jets and dilepton channels. $F_0 = 0.682 \pm 0.035 \pm 0.046$ if $F_+ = 0.0017(1)$, while $F_+ = -0.015 \pm 0.018 \pm 0.030$ if $F_0 = 0.688(4)$, where the assumed fixed values are the SM prediction for $m_t = 173.3 \pm 1.1$ GeV and $m_W = 80.399 \pm 0.023$ GeV.

¹⁰ Results are based on 2.7 fb⁻¹ of data in $p\bar{p}$ collisions at $\sqrt{s} = 1.96$ TeV. F_0 result is obtained by assuming $F_+ = 0$, while F_+ result is obtained for $F_0 = 0.70$, the SM value. Model independent fits for the two fractions give $F_0 = 0.88 \pm 0.11 \pm 0.06$ and $F_+ = -0.15 \pm 0.07 \pm 0.06$ with correlation coefficient of -0.59 . The results are for $m_t = 175$ GeV.

¹¹ Results are based on 1.9 fb⁻¹ of data in $p\bar{p}$ collisions at $\sqrt{s} = 1.96$ TeV. F_0 result is obtained assuming $F_+ = 0$, while F_+ result is obtained for $F_0 = 0.70$, the SM values. Model independent fits for the two fractions give $F_0 = 0.66 \pm 0.16 \pm 0.05$ and $F_+ = -0.03 \pm 0.06 \pm 0.03$.

¹² Based on 1 fb⁻¹ at $\sqrt{s} = 1.96$ TeV.

¹³ Based on 370 pb⁻¹ of data at $\sqrt{s} = 1.96$ TeV, using the $\ell +$ jets and dilepton decay channels. The result assumes $F_0 = 0.70$, and it gives $F_+ < 0.23$ at 95% CL.

¹⁴ Based on 318 pb⁻¹ of data at $\sqrt{s} = 1.96$ TeV.

¹⁵ Based on 200 pb⁻¹ of data at $\sqrt{s} = 1.96$ TeV. $t \rightarrow Wb \rightarrow \ell\nu b$ ($\ell = e$ or μ). The errors are stat + syst.

¹⁶ ABAZOV 05L studied the angular distribution of leptonic decays of W bosons in $t\bar{t}$ events, where one of the W's from t or \bar{t} decays into e or μ and the other decays hadronically. The fraction of the "+" helicity W boson is obtained by assuming F_0

$= 0.7$, which is the generic prediction for any linear combination of V and A currents. Based on 230 ± 15 pb⁻¹ of data at $\sqrt{s} = 1.96$ TeV.

¹⁷ ACOSTA 05D measures the $m_{\ell b}^2$ distribution in $t\bar{t}$ production events where one or both W's decay leptonically to $\ell = e$ or μ , and finds a bound on the V+A coupling of the $t b W$ vertex. By assuming the SM value of the longitudinal W fraction $F_0 = B(t \rightarrow W_0 b) = 0.70$, the bound on F_+ is obtained. If the results are combined with those of AFFOLDER 00B, the bounds become $F_{V+A} < 0.61$ (95% CL) and $F_+ < 0.18$ (95% CL), respectively. Based on 109 ± 7 pb⁻¹ of data at $\sqrt{s} = 1.8$ TeV (run I).

 F_{V+A}

VALUE	CL%	DOCUMENT ID	TECN	COMMENT
< 0.29	95	1 ABULENCIA	07G CDF	$F_{V+A} = B(t \rightarrow Wb_R)$
• • • We do not use the following data for averages, fits, limits, etc. • • •				
-0.06 ± 0.22 ± 0.12		1 ABULENCIA	07G CDF	$F_{V+A} = B(t \rightarrow Wb_R)$
< 0.80	95	2 ACOSTA	05D CDF	$F_{V+A} = B(t \rightarrow Wb_R)$

¹ Based on 700 pb⁻¹ of data at $\sqrt{s} = 1.96$ TeV.

² ACOSTA 05D measures the $m_{\ell b}^2$ distribution in $t\bar{t}$ production events where one or both W's decay leptonically to $\ell = e$ or μ , and finds a bound on the V+A coupling of the $t b W$ vertex. By assuming the SM value of the longitudinal W fraction $F_0 = B(t \rightarrow W_0 b) = 0.70$, the bound on F_+ is obtained. If the results are combined with those of AFFOLDER 00B, the bounds become $F_{V+A} < 0.61$ (95% CL) and $F_+ < 0.18$ (95% CL), respectively. Based on 109 ± 7 pb⁻¹ of data at $\sqrt{s} = 1.8$ TeV (run I).

 f_1^R

VALUE	CL%	DOCUMENT ID	TECN	COMMENT
• • • We do not use the following data for averages, fits, limits, etc. • • •				
-0.11 < $f_1^R < 0.16$	95	1 AAD	20Y LHC	ATLAS+CMS combined
$ f_1^R/f_1^L < 0.37$	95	2 AABOUD	17BB ATLS	t-channel single top
$ f_1^R < 0.16$	95	3 KHACHATRY...	17G CMS	t-channel single-t prod.
$-0.20 < \text{Re}(V_{tb} f_1^R) < 0.23$	95	4 AAD	12BG ATLS	Constr. on Wtb vtx
$(V_{tb} f_1^R)^2 < 0.93$	95	5 ABAZOV	12E D0	Single-top
$ f_1^R ^2 < 0.30$	95	6 ABAZOV	12I D0	single-t + W helicity
$ f_1^R ^2 < 1.01$	95	7 ABAZOV	09J D0	$ f_1^L = 1, f_1^R = f_1^L = 0$
$ f_1^R ^2 < 2.5$	95	8 ABAZOV	08AI D0	$ f_1^L ^2 = 1.8 \pm 1.0 \pm 1.3$

¹ AAD 20Y based on about 20 fb⁻¹ of pp data at $\sqrt{s} = 8$ TeV for each experiment. The measurements used events with one lepton and different jet multiplicities in the final state. The measurements of F_0 and F_- are used to set the limit. The limit is obtained by assuming the other couplings to have their SM values.

² AABOUD 17BB based on 20.2 fb⁻¹ of pp data at $\sqrt{s} = 8$ TeV. Triple-differential decay rate of top quark is used to simultaneously determine five generalized Wtb couplings as well as the top polarization. No assumption is made for the other couplings. See this paper for constraints on other couplings not included here.

³ KHACHATRYAN 17G based on 5.0 and 19.7 fb⁻¹ of pp data at $\sqrt{s} = 7$ and 8 TeV, respectively. A Bayesian neural network technique is used to discriminate between signal and backgrounds. This is a 95% CL exclusion limit obtained by a three-dimensional fit with simultaneous variation of (f_1^L, f_1^R, f_1^R) .

⁴ Based on 1.04 fb⁻¹ of pp data at $\sqrt{s} = 7$ TeV. AAD 12BG studied tt events with large \cancel{E}_T and either $\ell + \geq 4$ or $\ell\ell + \geq 2$.

⁵ Based on 5.4 fb⁻¹ of data. For each value of the form factor quoted the other two are assumed to have their SM value. Their Fig. 4 shows two-dimensional posterior probability density distributions for the anomalous couplings.

⁶ Based on 5.4 fb⁻¹ of data in $p\bar{p}$ collisions at 1.96 TeV. Results are obtained by combining the limits from the W helicity measurements and those from the single top quark production.

⁷ Based on 1 fb⁻¹ of data at $p\bar{p}$ collisions $\sqrt{s} = 1.96$ TeV. Combined result of the W helicity measurement in $t\bar{t}$ events (ABAZOV 08B) and the search for anomalous tbW couplings in the single top production (ABAZOV 08AI). Constraints when f_1^L and one of the anomalous couplings are simultaneously allowed to vary are given in their Fig. 1 and Table 1.

⁸ Result is based on 0.9 fb⁻¹ of data at $\sqrt{s} = 1.96$ TeV. Single top quark production events are used to measure the Lorentz structure of the tbW coupling. The upper bounds on the non-standard couplings are obtained when only one non-standard coupling is allowed to be present together with the SM one, $f_1^L = V_{tb}^*$.

 f_2^L

VALUE	CL%	DOCUMENT ID	TECN	COMMENT
• • • We do not use the following data for averages, fits, limits, etc. • • •				
-0.08 < $f_2^L < 0.05$	95	1 AAD	20Y LHC	ATLAS+CMS combined
$ f_2^L/f_1^L < 0.29$	95	2 AABOUD	17BB ATLS	t-channel single top
$ f_2^L < 0.057$	95	3 KHACHATRY...	17G CMS	t-channel single-t prod.
$-0.14 < \text{Re}(f_2^L) < 0.11$	95	4 AAD	12BG ATLS	Constr. on Wtb vtx
$(V_{tb} f_2^L)^2 < 0.13$	95	5 ABAZOV	12E D0	Single-top
$ f_2^L ^2 < 0.05$	95	6 ABAZOV	12I D0	single-t + W helicity
$ f_2^L ^2 < 0.28$	95	7 ABAZOV	09J D0	$ f_1^L = 1, f_1^R = f_1^L = 0$
$ f_2^L ^2 < 0.5$	95	8 ABAZOV	08AI D0	$ f_1^L ^2 = 1.4 \pm 0.6 \pm 0.5$

¹ AAD 20Y based on about 20 fb⁻¹ of pp data at $\sqrt{s} = 8$ TeV for each experiment. The measurements used events with one lepton and different jet multiplicities in the final state. The measurements of F_0 and F_- are used to set the limit. The limit is obtained by assuming the other couplings to have their SM values.

² AABOUD 17BB based on 20.2 fb⁻¹ of pp data at $\sqrt{s} = 8$ TeV. Triple-differential decay rate of top quark is used to simultaneously determine five generalized Wtb couplings as well as the top polarization. No assumption is made for the other couplings. See this paper for constraints on other couplings not included here.

³ KHACHATRYAN 17G based on 5.0 and 19.7 fb⁻¹ of pp data at $\sqrt{s} = 7$ and 8 TeV, respectively. A Bayesian neural network technique is used to discriminate between signal and backgrounds. This is a 95% CL exclusion limit obtained by a three-dimensional fit with simultaneous variation of (f_1^L, f_2^L, f_2^R).

⁴ Based on 1.04 fb⁻¹ of pp data at $\sqrt{s} = 7$ TeV. AAD 12B studied tt events with large E_T and either $\ell + \geq 4j$ or $\ell\ell + \geq 2j$.

⁵ Based on 5.4 fb⁻¹ of data. For each value of the form factor quoted the other two are assumed to have their SM value. Their Fig. 4 shows two-dimensional posterior probability density distributions for the anomalous couplings.

⁶ Based on 5.4 fb⁻¹ of data in p \bar{p} collisions at 1.96 TeV. Results are obtained by combining the limits from the W helicity measurements and those from the single top quark production.

⁷ Based on 1 fb⁻¹ of data at p \bar{p} collisions $\sqrt{s} = 1.96$ TeV. Combined result of the W helicity measurement in t \bar{t} events (ABAZOV 08B) and the search for anomalous tbW couplings in the single top production (ABAZOV 08Ai). Constraints when f_1^L and one of the anomalous couplings are simultaneously allowed to vary are given in their Fig. 1 and Table 1.

⁸ Result is based on 0.9 fb⁻¹ of data at $\sqrt{s} = 1.96$ TeV. Single top quark production events are used to measure the Lorentz structure of the tbW coupling. The upper bounds on the non-standard couplings are obtained when only one non-standard coupling is allowed to be present together with the SM one, $f_1^L = V_{tb}^*$.

f_2^R	VALUE	CL%	DOCUMENT ID	TECN	COMMENT
•••	We do not use the following data for averages, fits, limits, etc. •••				
	$-0.04 < f_2^R < 0.02$	95	¹ AAD	20Y LHC	ATLAS+CMS combined
	$-0.12 < \text{Re}(f_2^R/f_1^L) < 0.17$	95	² AABOUD	17BB ATLS	t-channel single top
	$-0.07 < \text{Im}(f_2^R/f_1^L) < 0.06$	95	² AABOUD	17BB ATLS	t-channel single top
	$-0.18 < \text{Im}(f_2^R) < 0.06$	95	³ AABOUD	17I ATLS	t-channel single top
	$-0.049 < f_2^R < 0.048$	95	⁴ KHACHATRYAN..17G	CMS	t-channel single top
	$-0.36 < \text{Re}(f_2^R/f_1^L) < 0.10$	95	⁵ AAD	16AK ATLS	Single-top
	$-0.17 < \text{Im}(f_2^R/f_1^L) < 0.23$	95	⁵ AAD	16AK ATLS	Single-top
	$-0.08 < \text{Re}(f_2^R) < 0.04$	95	⁶ AAD	12BG ATLS	Constr. on Wtb vtx
	$(V_{tb} f_2^R)^2 < 0.06$	95	⁷ ABAZOV	12E D0	Single-top
	$ f_2^R ^2 < 0.12$	95	⁸ ABAZOV	12I D0	single-t + W helicity
	$ f_2^R ^2 < 0.23$	95	⁹ ABAZOV	09J D0	$ f_1^L = 1, f_1^R = f_2^R = 0$
	$ f_2^R ^2 < 0.3$	95	¹⁰ ABAZOV	08Ai D0	$ f_1^L ^2 = 1.4 \pm 0.9$ $ f_1^R ^2 = 1.4 \pm 0.8$

¹ AAD 20Y based on about 20 fb⁻¹ of pp data at $\sqrt{s} = 8$ TeV for each experiment. The measurements used events with one lepton and different jet multiplicities in the final state. The measurements of F_0 and F_- are used to set the limit. The limit is obtained by assuming the other couplings to have their SM values.

² AABOUD 17BB based on 20.2 fb⁻¹ of pp data at $\sqrt{s} = 8$ TeV. Triple-differential decay rate of top quark is used to simultaneously determine five generalized Wtb couplings as well as the top polarization. No assumption is made for the other couplings. See this paper for constraints on other couplings not included here.

³ AABOUD 17I based on 20.2 fb⁻¹ of pp data at $\sqrt{s} = 8$ TeV. A cut-based analysis is used to discriminate between signal and backgrounds. All anomalous couplings other than $\text{Im}(f_2^R)$ are assumed to be zero. See this paper for a number of other asymmetries and measurements that are not included here.

⁴ KHACHATRYAN 17G based on 5.0 and 19.7 fb⁻¹ of pp data at $\sqrt{s} = 7$ and 8 TeV, respectively. A Bayesian neural network technique is used to discriminate between signal and backgrounds. This is a 95% CL exclusion limit obtained by a three-dimensional fit with simultaneous variation of (f_1^L, f_2^L, f_2^R).

⁵ AAD 16AK based on 4.6 fb⁻¹ of pp data at $\sqrt{s} = 7$ TeV. The results are obtained from an analysis of angular distributions of the decay products of single top quarks, assuming $f_1^R = f_2^R = 0$. The fraction of decays containing transversely polarized W is measured to be $F_+ + F_- = 0.37 \pm 0.07$.

⁶ Based on 1.04 fb⁻¹ of pp data at $\sqrt{s} = 7$ TeV. AAD 12B studied tt events with large E_T and either $\ell + \geq 4j$ or $\ell\ell + \geq 2j$.

⁷ Based on 5.4 fb⁻¹ of data. For each value of the form factor quoted the other two are assumed to have their SM value. Their Fig. 4 shows two-dimensional posterior probability density distributions for the anomalous couplings.

⁸ Based on 5.4 fb⁻¹ of data in p \bar{p} collisions at 1.96 TeV. Results are obtained by combining the limits from the W helicity measurements and those from the single top quark production.

⁹ Based on 1 fb⁻¹ of data at p \bar{p} collisions $\sqrt{s} = 1.96$ TeV. Combined result of the W helicity measurement in t \bar{t} events (ABAZOV 08B) and the search for anomalous tbW couplings in the single top production (ABAZOV 08Ai). Constraints when f_1^L and one of the anomalous couplings are simultaneously allowed to vary are given in their Fig. 1 and Table 1.

¹⁰ Result is based on 0.9 fb⁻¹ of data at $\sqrt{s} = 1.96$ TeV. Single top quark production events are used to measure the Lorentz structure of the tbW coupling. The upper bounds on the non-standard couplings are obtained when only one non-standard coupling is allowed to be present together with the SM one, $f_1^L = V_{tb}^*$.

$|f_{LV} V_{tb}|$

Assumed that the top-quark-related CKM matrix elements obey the relation $|V_{td}|, |V_{ts}| \ll |V_{tb}|$ and a form factor f_{LV} is determined for each production mode and centre-of-mass energy.

VALUE	DOCUMENT ID	TECN	COMMENT
0.995 ± 0.021 OUR AVERAGE			
0.988 ± 0.024	¹ SIRUNYAN	20AZ CMS	13 TeV, t-channel single top
1.02 ± 0.04 ± 0.02	² AABOUD	19R LHC	ATLAS + CMS at 7, 8 TeV

¹ SIRUNYAN 20AZ based on 35.9 fb⁻¹ of pp data at $\sqrt{s} = 13$ TeV. Final states enriched in single top quark t-channel events are used. Several theories beyond the standard model are considered, and by releasing all constraints among the involved parameters. Under the standard model assumption of CKM unitarity, the values are found to be $|V_{tb}| > 0.970$ and $|V_{td}|^2 + |V_{ts}|^2 < 0.057$, both at 95% CL.

² The combination of single-top production cross-section measurements in the t-channel, tW, and s-channel production modes from ATLAS and CMS at $\sqrt{s} = 7$ and 8 TeV.

$|f_{LV} \sqrt{|V_{td}|^2 + |V_{ts}|^2}|$

Assumed that the top-quark-related CKM matrix elements obey the relation $|V_{td}|, |V_{ts}| \ll |V_{tb}|$ and a form factor f_{LV} is determined for each production mode and centre-of-mass energy.

VALUE	DOCUMENT ID	TECN	COMMENT
•••	We do not use the following data for averages, fits, limits, etc. •••		
0.24 ± 0.12	¹ SIRUNYAN	20AZ CMS	t-channel single top

¹ We report the square root of SIRUNYAN 20AZ result based on 35.9 fb⁻¹ of pp data at $\sqrt{s} = 13$ TeV measured $|V_{td}|^2 + |V_{ts}|^2 = 0.06 \pm 0.06$ using final states enriched in single top quark t-channel events by releasing all constraints from unitarity of the CKM matrix within the SM. Under the standard model assumption of CKM unitarity, the values are found to be $|V_{tb}| > 0.970$ and $|V_{td}|^2 + |V_{ts}|^2 < 0.057$, both at 95% CL.

Chromo-magnetic dipole moment $\mu_t = g_s \hat{\mu}_t / m_t$

VALUE	CL%	DOCUMENT ID	TECN	COMMENT
•••	We do not use the following data for averages, fits, limits, etc. •••			
$-0.024^{+0.013+0.016}_{-0.009-0.011}$		¹ SIRUNYAN	20AM CMS	$\ell + \text{jets}$
$-0.014 < \hat{\mu}_t < 0.004$	95	² SIRUNYAN	19BX CMS	$\ell\ell + \geq 2j$ ($\geq 1b$)
$-0.053 < \text{Re}(\hat{\mu}_t) < 0.026$	95	³ KHACHATRYAN..16AI	CMS	$\ell\ell + \geq 2j$ ($\geq 1b$)

¹ SIRUNYAN 20AM based on 35.9 fb⁻¹ of pp data at $\sqrt{s} = 13$ TeV. t \bar{t} with low and high boosts are reconstructed through a fit of the kinematic distributions. The $q\bar{q}$ initial subprocess is separated using different dependencies of the distributions on the initial states, and the linearized forward-backward asymmetry is measured to be $A_{FB}^{(1)} = 0.048^{+0.095+0.020}_{-0.087-0.029}$.

² SIRUNYAN 19BX based on 35.9 fb⁻¹ of pp data at $\sqrt{s} = 13$ TeV. A set of parton-level normalized differential cross sections is measured to extract coefficients of the spin-dependent t \bar{t} production density matrix. The coefficients are compared with the NLO MC simulations and with the NLO QCD calculation including EW corrections.

³ KHACHATRYAN 16AI based on 19.5 fb⁻¹ of pp data at $\sqrt{s} = 8$ TeV, using lepton angular distributions as a function of the t \bar{t} -system kinematical variables.

Chromo-electric dipole moment $d_t = g_s \hat{d}_t / m_t$

VALUE	CL%	DOCUMENT ID	TECN	COMMENT
•••	We do not use the following data for averages, fits, limits, etc. •••			
$ \hat{d}_t < 0.015$	95	¹ TUMASYAN	23J CMS	$\ell + \text{jets}$
$-0.014 < \hat{d}_t < 0.027$	95	² TUMASYAN	23U CMS	dilepton channel; $\epsilon(p_t p_{\bar{T}} p_{\ell^+} p_{\ell^-})$
$-0.019 < \hat{d}_t < 0.019$	95	² TUMASYAN	23U CMS	dilepton channel; $\epsilon(p_b p_{\bar{T}} p_{\ell^+} p_{\ell^-})$
$ \hat{d}_t < 0.03$	95	³ SIRUNYAN	20AM CMS	$\ell + \text{jets}$
$-0.020 < \hat{d}_t < 0.012$	95	⁴ SIRUNYAN	19BX CMS	$\ell\ell + \geq 2j$ ($\geq 1b$)
$-0.068 < \text{Im}(\hat{d}_t) < 0.067$	95	⁵ KHACHATRYAN..16AI	CMS	$\ell\ell + \geq 2j$ ($\geq 1b$)

¹ TUMASYAN 23J based on 138 fb⁻¹ of pp data at $\sqrt{s} = 13$ TeV. Four T-odd triple products of momenta of the final-state particles are measured to constrain the dimensionless chromoelectric top quark dipole moment. No evidence of CP-violating effects is found, which is consistent with the SM expectation.

² TUMASYAN 23U based on 35.9 fb⁻¹ of pp data at $\sqrt{s} = 13$ TeV. CP-odd Lorentz pseudo-scalar products $O_1 = \epsilon(p_t p_{\bar{T}} p_{\ell^+} p_{\ell^-})$ and $O_3 = \epsilon(p_b p_{\bar{T}} p_{\ell^+} p_{\ell^-})$ constructed from the momenta of t, \bar{t} , ℓ^+ , ℓ^- and of b, \bar{b} , ℓ^+ , ℓ^- , respectively, are measured and used to constrain the dimensionless chromoelectric top quark dipole moment. No evidence for CP-violating effects is found, which is consistent with the SM expectation.

³ SIRUNYAN 20AM based on 35.9 fb⁻¹ of pp data at $\sqrt{s} = 13$ TeV. t \bar{t} with low and high boosts are reconstructed through a fit of the kinematic distributions. The $q\bar{q}$ initial subprocess is separated using different dependencies of the distributions on the initial states, and the linearized forward-backward asymmetry is measured to be $A_{FB}^{(1)} = 0.048^{+0.095+0.020}_{-0.087-0.029}$.

⁴ SIRUNYAN 19BX based on 35.9 fb⁻¹ of pp data at $\sqrt{s} = 13$ TeV. A set of parton-level normalized differential cross sections is measured to extract coefficients of the spin-dependent t \bar{t} production density matrix and constrain the anomalous chromomagnetic and chromoelectric dipole moments of the top quark. The coefficients are compared with the NLO MC simulations and with the NLO QCD calculation including EW corrections.

⁵ KHACHATRYAN 16AI based on 19.5 fb⁻¹ of pp data at $\sqrt{s} = 8$ TeV, using lepton angular distributions as a function of the t \bar{t} -system kinematical variables.

Spin Correlation in t \bar{t} Production in p \bar{p} Collisions

C is the correlation strength parameter, f is the ratio of events with correlated t and \bar{T} spins (SM prediction: f = 1), and κ is the spin correlation coefficient. See "The Top Quark" review for more information.

VALUE	DOCUMENT ID	TECN	COMMENT
•••	We do not use the following data for averages, fits, limits, etc. •••		
0.89 ± 0.22	¹ ABAZOV	16A D0	f ($\ell\ell + \geq 2j$ jets, $\ell + \geq 4j$ jets)
0.85 ± 0.29	² ABAZOV	12B D0	f ($\ell\ell + \geq 2j$ jets, $\ell + \geq 4j$ jets)
$1.15^{+0.42}_{-0.43}$	³ ABAZOV	12B D0	f ($\ell + \cancel{E}_T + \geq 4j$ jets)
$0.60^{+0.50}_{-0.16}$	⁴ AALTONEN	11AR CDF	κ ($\ell + \cancel{E}_T + \geq 4j$ jets)
$0.74^{+0.40}_{-0.41}$	⁵ ABAZOV	11AE D0	f ($\ell\ell + \cancel{E}_T + \geq 2j$ jets)
0.10 ± 0.45	⁶ ABAZOV	11AF D0	C ($\ell\ell + \cancel{E}_T + \geq 2j$ jets)

¹ ABAZOV 16A based on 9.7 fb⁻¹ of data. A matrix element method is used. It corresponds to evidence of spin correlation at 4.2 σ and is in agreement with the NLO SM prediction $0.80^{+0.01}_{-0.02}$.

² This is a combination of the lepton + jets analysis presented in ABAZOV 12B and the dilepton measurement of ABAZOV 11AE. It provides a 3.1 σ evidence for the t \bar{t} spin correlation.

Quark Particle Listings

t

³ Based on 5.3 fb⁻¹ of data. The error is statistical and systematic combined. A matrix element method is used.

⁴ Based on 4.3 fb⁻¹ of data. The measurement is based on the angular study of the top quark decay products in the helicity basis. The theory prediction is $\kappa \approx 0.40$.

⁵ Based on 5.4 fb⁻¹ of data using a matrix element method. The error is statistical and systematic combined. The no-correlation hypothesis is excluded at the 97.7% CL.

⁶ Based on 5.4 fb⁻¹ of data. The error is statistical and systematic combined. The NLO QCD prediction is $C = 0.78 \pm 0.03$. The neutrino weighting method is used for reconstruction of kinematics.

Spin Correlation in $t\bar{t}$ Production in $p\bar{p}$ Collisions

Spin correlation, f_{SM} , measures the strength of the correlation between the spins of the pair produced $t\bar{t}$. $f_{SM} = 1$ for the SM, while $f_{SM} = 0$ for no spin correlation.

VALUE	DOCUMENT ID	TECN	COMMENT
•••	We do not use the following data for averages, fits, limits, etc. •••		
$0.90 \pm 0.07 \pm 0.09 \pm 0.01$	¹ SIRUNYAN 19BX CMS	C_{kk} in $\ell\ell + \geq 2j (\geq 1b)$	
$1.13 \pm 0.32 \pm 0.32^{+0.10}_{-0.13}$	¹ SIRUNYAN 19BX CMS	C_{rr} in $\ell\ell + \geq 2j (\geq 1b)$	
$1.01 \pm 0.04 \pm 0.05 \pm 0.01$	¹ SIRUNYAN 19BX CMS	C_{nn} in $\ell\ell + \geq 2j (\geq 1b)$	
$0.94 \pm 0.17 \pm 0.26 \pm 0.01$	¹ SIRUNYAN 19BX CMS	$C_{rk} + C_{kr}$ in $\ell\ell + \geq 2j (\geq 1b)$	
$0.98 \pm 0.03 \pm 0.04 \pm 0.01$	¹ SIRUNYAN 19BX CMS	$(C_{kk} + C_{rr} + C_{nn})/3$ in $\ell\ell + \geq 2j (\geq 1b)$	
$0.74 \pm 0.07 \pm 0.19^{+0.06}_{-0.08}$	¹ SIRUNYAN 19BX CMS	$A_{\cos\phi}^{lab}$ in $\ell\ell + \geq 2j (\geq 1b)$	
$1.05 \pm 0.03 \pm 0.08^{+0.09}_{-0.12}$	¹ SIRUNYAN 19BX CMS	$A_{ \Delta\phi(\ell\ell) }$ in $\ell\ell + \geq 2j (\geq 1b)$	
$1.12^{+0.12}_{-0.15}$	² KHACHATRY...16AI CMS	$\ell\ell + \geq 2j (\geq 1b)$	
$0.72 \pm 0.08^{+0.15}_{-0.13}$	³ KHACHATRY...16X CMS	$\mu + 4, 5j$	
$1.20 \pm 0.05 \pm 0.13$	⁴ AAD 15J ATLS	$\Delta\phi(\ell\ell)$ in $\ell\ell + \geq 2j (\geq 1b)$	
$1.19 \pm 0.09 \pm 0.18$	⁵ AAD 14BB ATLS	$\Delta\phi(\ell\ell)$ in $\ell\ell + \geq 2j$ events	
$1.12 \pm 0.11 \pm 0.22$	⁵ AAD 14BB ATLS	$\Delta\phi(\ell j)$ in $\ell + \geq 4j$ events	
$0.87 \pm 0.11 \pm 0.14$	^{5,6} AAD 14BB ATLS	S-ratio in $\ell\ell + \geq 2j$ events	
$0.75 \pm 0.19 \pm 0.23$	^{5,7} AAD 14BB ATLS	$\cos\theta(\ell^+) \cos\theta(\ell^-)$ in $\ell\ell + \geq 2j$ events	
$0.83 \pm 0.14 \pm 0.18$	^{5,8} AAD 14BB ATLS	$\cos\theta(\ell^+) \cos\theta(\ell^-)$ in $\ell\ell + \geq 2j$ events	

¹ SIRUNYAN 19BX based on 35.9 fb⁻¹ of $p\bar{p}$ data at $\sqrt{s} = 13$ TeV. A set of parton-level normalized differential cross sections sensitive to coefficients of the spin-dependent $t\bar{t}$ production density matrix is measured. The distributions and coefficients are compared with the NLO MC simulations and with the NLO QCD calculation including EW corrections. Three errors are from statistics, experimental systematics, and theory.

² KHACHATRYAN 16AI based on 19.5 fb⁻¹ of $p\bar{p}$ data at $\sqrt{s} = 8$ TeV, using lepton angular distributions as a function of the $t\bar{t}$ -system kinematical variables.

³ KHACHATRYAN 16X based on 19.7 fb⁻¹ of $p\bar{p}$ data at $\sqrt{s} = 8$ TeV. Uses a template fit method. Spin correlation strength in the helicity basis is given by $A_{hel} = 0.23 \pm 0.03^{+0.05}_{-0.04}$.

⁴ AAD 15J based on 20.3 fb⁻¹ of $p\bar{p}$ data at $\sqrt{s} = 8$ TeV. Uses a fit including a linear superposition of $\Delta\phi$ distribution from the SM NLO simulation with coefficient f_{SM} and from $t\bar{t}$ simulation without spin correlation with coefficient $(1 - f_{SM})$.

⁵ Based on 4.6 fb⁻¹ of $p\bar{p}$ data at $\sqrt{s} = 7$ TeV. The results are for $m_t = 172.5$ GeV.

⁶ The S-ratio is defined as the SM spin correlation in the like-helicity gluon-gluon collisions normalized to the no spin correlation case; see eq. (6) for the LO expression.

⁷ The polar angle correlation along the helicity axis.

⁸ The polar angle correlation along the direction which maximizes the correlation.

t-quark FCNC Couplings κ^{utg}/Λ and κ^{ctg}/Λ

VALUE (TeV ⁻¹)	CL%	DOCUMENT ID	TECN	COMMENT
•••	We do not use the following data for averages, fits, limits, etc. •••			
<0.0041	95	¹ AAD 22T ATLS	$u\bar{g} \rightarrow t, c\bar{g} \rightarrow t$	
<0.018	95	² KHACHATRY...17G CMS	$ \kappa^{utg} /\Lambda$	
<0.010	95	³ AAD 16AS ATLS	κ^{ctg}/Λ	
<0.023	95	³ AAD 16AS ATLS	κ^{ctg}/Λ	
<0.0069	95	⁴ AAD 12BP ATLS	$t\bar{t}u\bar{g}/\Lambda$ ($t\bar{t}c\bar{g} = 0$)	
<0.016	95	⁴ AAD 12BP ATLS	$t\bar{t}c\bar{g}/\Lambda$ ($t\bar{t}u\bar{g} = 0$)	
<0.013	95	⁵ ABAZOV 10K D0	κ^{utg}/Λ	
<0.057	95	⁵ ABAZOV 10K D0	κ^{ctg}/Λ	
<0.018	95	⁶ AALTONEN 09N CDF	κ^{utg}/Λ ($\kappa^{ctg} = 0$)	
<0.069	95	⁶ AALTONEN 09N CDF	κ^{ctg}/Λ ($\kappa^{utg} = 0$)	
<0.037	95	⁷ ABAZOV 07V D0	κ^{utg}/Λ	
<0.15	95	⁷ ABAZOV 07V D0	κ^{ctg}/Λ	

¹ AAD 22T based on 139 fb⁻¹ of $p\bar{p}$ data at $\sqrt{s} = 13$ TeV. The results are obtained from the 95% CL upper limits on the single top-quark productions $\sigma(q\bar{g} \rightarrow t)\text{B}(t \rightarrow bW)\text{B}(W \rightarrow \ell\nu)$ or $\sigma(c\bar{g} \rightarrow t)\text{B}(t \rightarrow bW)\text{B}(W \rightarrow \ell\nu) < 4.7$ pb. These are interpreted as limits on couplings in an EFT $|C_{uG}^{ut}|/\Lambda^2 < 0.057$ TeV⁻² and $|C_{uG}^{ct}|/\Lambda^2 < 0.14$ TeV⁻². The results also correspond to $\text{B}(t \rightarrow u\bar{g}) < 6.1 \times 10^{-5}$ and $\text{B}(t \rightarrow c\bar{g}) < 3.7 \times 10^{-4}$.

² KHACHATRYAN 17G based on 5.0 and 19.7 fb⁻¹ of $p\bar{p}$ data at $\sqrt{s} = 7$ and 8 TeV, respectively. t -channel single top production is used. The result corresponds to $\text{B}(t \rightarrow u\bar{g}) < 2.0 \times 10^{-5}$ or $\text{B}(t \rightarrow c\bar{g}) < 4.1 \times 10^{-4}$.

³ AAD 16AS based on 20.3 fb⁻¹ of $p\bar{p}$ data at $\sqrt{s} = 8$ TeV. The results are obtained from the 95% CL upper limit on the single top-quark production $\sigma(q\bar{g} \rightarrow t)\text{B}(t \rightarrow bW)\text{B}(W \rightarrow \ell\nu) < 2.9$ pb, $\text{B}(t \rightarrow u\bar{g}) < 4.0 \times 10^{-5}$ and $\text{B}(t \rightarrow c\bar{g}) < 20 \times 10^{-5}$.

⁴ Based on 2.05 fb⁻¹ of $p\bar{p}$ data at $\sqrt{s} = 7$ TeV. The results are obtained from the 95% CL upper limit on the single top-quark production $\sigma(q\bar{g} \rightarrow t)\text{B}(t \rightarrow bW) < 3.9$ pb, for $q=u$ or $q=c$, $\text{B}(t \rightarrow u\bar{g}) < 5.7 \times 10^{-5}$ and $\text{B}(t \rightarrow u\bar{g}) < 2.7 \times 10^{-4}$.

⁵ Based on 2.3 fb⁻¹ of data in $p\bar{p}$ collisions at $\sqrt{s} = 1.96$ TeV. Upper limit of single top quark production cross section 0.20 pb and 0.27 pb via FCNC t - u - g and t - c - g couplings, respectively, lead to the bounds without assuming the absence of the other coupling. $\text{B}(t \rightarrow u + g) < 2.0 \times 10^{-4}$ and $\text{B}(t \rightarrow c + g) < 3.9 \times 10^{-3}$ follow.

⁶ Based on 2.2 fb⁻¹ of data in $p\bar{p}$ collisions at $\sqrt{s} = 1.96$ TeV. Upper limit of single top quark production cross section $\sigma(u(c) + g \rightarrow t) < 1.8$ pb (95% CL) via FCNC t - u - g and t - c - g couplings lead to the bounds. $\text{B}(t \rightarrow u + g) < 3.9 \times 10^{-4}$ and $\text{B}(t \rightarrow c + g) < 5.7 \times 10^{-3}$ follow.

⁷ Result is based on 230 pb⁻¹ of data at $\sqrt{s} = 1.96$ TeV. Absence of single top quark production events via FCNC t - u - g and t - c - g couplings lead to the upper bounds on the dimensioned couplings, κ^{utg}/Λ and κ^{ctg}/Λ , respectively.

t-Quark Yukawa Coupling from $t\bar{t}$ Kinematic Distributions in $p\bar{p}$ Collisions

The ratio of t -quark Yukawa coupling to its standard model predicted value.

VALUE	DOCUMENT ID	TECN	COMMENT
•••	We do not use the following data for averages, fits, limits, etc. •••		
$1.16^{+0.24}_{-0.35}$	¹ SIRUNYAN 20BH CMS	$\ell\ell (\ell=e,\mu) + \text{jets} (\geq 2b_j) + \cancel{E}_T$	
$1.07^{+0.34}_{-0.43}$	² SIRUNYAN 19BY CMS	ℓ -jets, $t\bar{t}$ threshold	
¹ SIRUNYAN 20BH based on 137 fb ⁻¹ of data at $\sqrt{s} = 13$ TeV. Kinematic distributions of $t\bar{t}$ are compared with predictions by different values of the top Yukawa coupling in loop corrections, where the scaling of the SM coupling is used within the κ -framework. The \cancel{E}_T cut applies only to the same-flavor dilepton, not $e\mu$ events.			
² SIRUNYAN 19BY based on 35.8 fb ⁻¹ of data at $\sqrt{s} = 13$ TeV. Experimental sensitivity is enhanced in the low $M_{t\bar{t}}$ region. The distributions of $M_{t\bar{t}}$, $ y_t - y_{\bar{t}} $, and the number of reconstructed jets are compared with predictions by different Yukawa couplings which include NNLO QCD and NLO EW corrections.			

$\sigma(Ht\bar{t})/\sigma(Ht\bar{t})_{SM}$

VALUE	CL%	DOCUMENT ID	TECN	COMMENT
•••	We do not use the following data for averages, fits, limits, etc. •••			
$1.43^{+0.33+0.21}_{-0.31-0.15}$	95	¹ AAD 20Z ATLS	20Z ATLS	$Ht\bar{t}(H \rightarrow \gamma\gamma)$
$1.38^{+0.29+0.21}_{-0.27-0.11}$	95	² SIRUNYAN 20AS CMS	20AS CMS	$Ht\bar{t}(H \rightarrow \gamma\gamma)$
$0.72 \pm 0.24 \pm 0.38$	95	³ SIRUNYAN 19R CMS	19R CMS	$Ht\bar{t}(H \rightarrow b\bar{b}, t\bar{t} \rightarrow \ell\ell + \text{jets or dilepton})$
$0.9 \pm 0.7 \pm 1.3$	95	⁴ SIRUNYAN 18BD CMS	18BD CMS	$Ht\bar{t}(H \rightarrow b\bar{b}, t\bar{t} \rightarrow \text{all jets})$
$1.26^{+0.31}_{-0.26}$	95	⁵ SIRUNYAN 18L CMS	18L CMS	combination of CMS
<6.7	95	⁶ AAD 15 ATLS	15 ATLS	$Ht\bar{t}; H \rightarrow \gamma\gamma$
2.8 ± 1.0	95	⁷ KHACHATRY...14H CMS	14H CMS	$H \rightarrow b\bar{b}, \tau_h\tau_h, \gamma\gamma, WW/ZZ(\text{leptons})$
¹ AAD 20Z based on 139 fb ⁻¹ of $p\bar{p}$ data at 13 TeV. Assuming a CP -even coupling the $t\bar{t}H$ process is observed with a significance of 5.2 σ , and the measured $\sigma_{t\bar{t}H} \cdot B_{\gamma\gamma} = 1.64^{+0.38+0.17}_{-0.36-0.14}$ fb. A CP -mixing angle $ \alpha > 43^\circ$ is excluded at 95% CL.				
² SIRUNYAN 20AS based on 137 fb ⁻¹ of $p\bar{p}$ data at 13 TeV. The $t\bar{t}H$ process is observed with a significance of 6.6 σ , and the measured $\sigma_{t\bar{t}H} \cdot B_{\gamma\gamma} = 1.56^{+0.33+0.09}_{-0.30-0.08}$ fb. The fractional contribution of the CP -odd component is measured to be $f_{CP}^{t\bar{t}H} = 0.00 \pm 0.33$.				
³ SIRUNYAN 19R based on 35.9 fb ⁻¹ of $p\bar{p}$ data at 13 TeV. Multivariate techniques are employed to separate the signal from the dominant $t\bar{t}$ -jets background. The result is for $m_H = 125$ GeV. The measured ratio corresponds to a signal significance of 1.6 σ above the background-only hypothesis.				
⁴ SIRUNYAN 18BD based on 35.9 fb ⁻¹ of $p\bar{p}$ data at 13 TeV. A combined fit of signal and background templates to data is performed in six event categories separated by jet and b -jet multiplicities. An upper limit of 3.8 is obtained for the cross section ratio.				
⁵ SIRUNYAN 18L based on up to 5.1, 19.7, and 35.9 fb ⁻¹ of $p\bar{p}$ data at 7, 8, and 13 TeV, respectively. An excess of events is observed, with a significance of 5.2 standard deviations, over the expectation from the background-only hypothesis. The result is for the Higgs boson mass of 125.09 GeV.				
⁶ Based on 4.5 fb ⁻¹ of data at 7 TeV and 20.3 fb ⁻¹ at 8 TeV. The result is for $m_H = 125.4$ GeV. The measurement constrains the top quark Yukawa coupling strength parameter $\kappa_t = Y_t/Y_t^{SM}$ to be $-1.3 < \kappa_t < 8.0$ (95% CL).				
⁷ Based on 5.1 fb ⁻¹ of $p\bar{p}$ data at 7 TeV and 19.7 fb ⁻¹ at 8 TeV. The results are obtained by assuming the SM decay branching fractions for the Higgs boson of mass 125.6 GeV. The signal strength for individual Higgs decay channels are given in Fig. 13, and the preferred region in the (κ_V, κ_f) space is given in Fig. 14.				

Single t-Quark Production Cross Section in $p\bar{p}$ Collisions at $\sqrt{s} = 1.8$ TeV

Direct probe of the tbW coupling and possible new physics at $\sqrt{s} = 1.8$ TeV.

VALUE (pb)	CL%	DOCUMENT ID	TECN	COMMENT
•••	We do not use the following data for averages, fits, limits, etc. •••			
<24	95	¹ ACOSTA 04H CDF	04H CDF	$p\bar{p} \rightarrow tb + X, tqb + X$
<18	95	² ACOSTA 02 CDF	02 CDF	$p\bar{p} \rightarrow tb + X$
<13	95	³ ACOSTA 02 CDF	02 CDF	$p\bar{p} \rightarrow tqb + X$
¹ ACOSTA 04H bounds single top-quark production from the s -channel W -exchange process, $q'\bar{q} \rightarrow t\bar{b}$, and the t -channel W -exchange process, $q'g \rightarrow qt\bar{b}$. Based on ~ 106 pb ⁻¹ of data.				
² ACOSTA 02 bounds the cross section for single top-quark production via the s -channel W -exchange process, $q'\bar{q} \rightarrow t\bar{b}$. Based on ~ 106 pb ⁻¹ of data.				
³ ACOSTA 02 bounds the cross section for single top-quark production via the t -channel W -exchange process, $q'g \rightarrow qt\bar{b}$. Based on ~ 106 pb ⁻¹ of data.				

Single t-Quark Production Cross Section in pp Collisions at $\sqrt{s} = 1.96$ TeVDirect probes of the tbW coupling and possible new physics at $\sqrt{s} = 1.96$ TeV.

OUR AVERAGE assumes that the systematic uncertainties are uncorrelated.

VALUE (pb)	CL%	DOCUMENT ID	TECN	COMMENT
$3.53^{+1.25}_{-1.16}$		1 AALTONEN	16 CDF	s- + t-channels ($0\ell + \cancel{E}_T + 2, 3j$ ($\geq 1b$ -tag))
$2.25^{+0.29}_{-0.31}$		2 AALTONEN	15H TEVA	t-channel
$3.30^{+0.52}_{-0.40}$		2,3 AALTONEN	15H TEVA	s- + t-channels
$1.12^{+0.61}_{-0.57}$		4 AALTONEN	14K CDF	s-channel ($0\ell + \cancel{E}_T + 2, 3j$ ($\geq 1b$ -tag))
$1.41^{+0.44}_{-0.42}$		5 AALTONEN	14L CDF	s-channel ($\ell + \cancel{E}_T + 2j$ ($\geq 1b$ -tag))
$1.29^{+0.26}_{-0.24}$		6 AALTONEN	14M TEVA	s-channel (CDF + D0)
$3.04^{+0.57}_{-0.53}$		7 AALTONEN	14o CDF	s + t + Wt ($\ell + \cancel{E}_T + 2$ or 3 jets ($\geq 1b$ -tag))
$1.10^{+0.33}_{-0.31}$		8 ABAZOV	13o D0	s-channel
$3.07^{+0.54}_{-0.49}$		8 ABAZOV	13o D0	t-channel
$4.11^{+0.60}_{-0.55}$		8 ABAZOV	13o D0	s- + t-channels
0.98 ± 0.63		9 ABAZOV	11AA D0	s-channel
2.90 ± 0.59		9 ABAZOV	11AA D0	t-channel
$3.43^{+0.73}_{-0.74}$		10 ABAZOV	11AD D0	s- + t-channels
$1.8^{+0.7}_{-0.5}$		11 AALTONEN	10AB CDF	s-channel
0.8 ± 0.4		11 AALTONEN	10AB CDF	t-channel
$4.9^{+2.5}_{-2.2}$		12 AALTONEN	10U CDF	\cancel{E}_T + jets decay
$3.14^{+0.94}_{-0.80}$		13 ABAZOV	10 D0	t-channel
1.05 ± 0.81		13 ABAZOV	10 D0	s-channel
< 7.3	95	14 ABAZOV	10J D0	τ + jets decay
$2.3^{+0.6}_{-0.5}$		15 AALTONEN	09AT CDF	s- + t-channel
3.94 ± 0.88		16 ABAZOV	09Z D0	s- + t-channel
$2.2^{+0.7}_{-0.6}$		17 AALTONEN	08AH CDF	s- + t-channel
4.7 ± 1.3		18 ABAZOV	08i D0	s- + t-channel
4.9 ± 1.4		19 ABAZOV	07H D0	s- + t-channel
< 6.4	95	20 ABAZOV	05P D0	$p\bar{p} \rightarrow tb + X$
< 5.0	95	20 ABAZOV	05P D0	$p\bar{p} \rightarrow tqb + X$
< 10.1	95	21 ACOSTA	05N CDF	$p\bar{p} \rightarrow tqb + X$
< 13.6	95	21 ACOSTA	05N CDF	$p\bar{p} \rightarrow tb + X$
< 17.8	95	21 ACOSTA	05N CDF	$p\bar{p} \rightarrow tb + X, tqb + X$

1 AALTONEN 16 based on 9.5 fb^{-1} of data. This includes, as a part, the result of AALTONEN 14k. Combination of this result with that of AALTONEN 14o gives a s + t cross section of $3.02^{+0.49}_{-0.48} \text{ pb}$ and $|V_{tb}| > 0.84$ (95% CL).

2 AALTONEN 15H based on 9.7 fb^{-1} of data per experiment. The result is for $m_t = 172.5 \text{ GeV}$, and is a combination of the CDF measurements (AALTONEN 16) and the D0 measurements (ABAZOV 13o) on the t-channel single t-quark production cross section. The result is consistent with the NLO+NNLL SM prediction and gives $|V_{tb}| = 1.02^{+0.06}_{-0.05}$ and $|V_{tb}| > 0.92$ (95% CL).

3 AALTONEN 15H is a combined measurement of s-channel single top cross section by CDF + D0. AALTONEN 14M is not included.

4 Based on 9.45 fb^{-1} of data, using neural networks to separate signal from backgrounds. The result is for $m_t = 172.5 \text{ GeV}$. Combination of this result with the CDF measurement in the 1 lepton channel AALTONEN 14L gives $1.36^{+0.37}_{-0.32} \text{ pb}$, consistent with the SM prediction, and is 4.2 sigma away from the background only hypothesis.

5 Based on 9.4 fb^{-1} of data, using neural networks to separate signal from backgrounds. The result is for $m_t = 172.5 \text{ GeV}$. The result is 3.8 sigma away from the background only hypothesis.

6 Based on 9.7 fb^{-1} of data per experiment. The result is for $m_t = 172.5 \text{ GeV}$, and is a combination of the CDF measurements AALTONEN 14L, AALTONEN 14K and the D0 measurement ABAZOV 13o on the s-channel single t-quark production cross section. The result is consistent with the SM prediction of $1.05 \pm 0.06 \text{ pb}$ and the significance of the observation is of 6.3 standard deviations.

7 Based on 7.5 fb^{-1} of data. Neural network is used to discriminate signals (s-, t- and Wt -channel single top production) from backgrounds. The result is consistent with the SM prediction, and gives $|V_{tb}| = 0.95 \pm 0.09(\text{stat} + \text{syst}) \pm 0.05(\text{theory})$ and $|V_{tb}| > 0.78$ (95% CL). The result is for $m_t = 172.5 \text{ GeV}$.

8 Based on 9.7 fb^{-1} of data. Events with $\ell + \cancel{E}_T + 2$ or 3 jets (1 or 2 b-tag) are analysed, assuming $m_t = 172.5 \text{ GeV}$. The combined s- + t-channel cross section gives $|V_{tb}| = 1.12^{+0.09}_{-0.08}$, or $|V_{tb}| > 0.92$ at 95% CL for $r_1^t = 1$ and a flat prior within $0 \leq |V_{tb}|^2 \leq 1$.

9 Based on 5.4 fb^{-1} of data. The result is statistical + systematic combined. The results are for $m_t = 172.5 \text{ GeV}$. Results for other m_t values are given in Table 2 of ABAZOV 11AA.

10 Based on 5.4 fb^{-1} of data and for $m_t = 172.5 \text{ GeV}$. The error is statistical + systematic combined. Results for other m_t values are given in Table III of ABAZOV 11AD. The result is obtained by assuming the SM ratio between tb (s-channel) and tqb (t-channel) productions, and gives $|V_{tb}| = 1.02^{+0.10}_{-0.11}$, or $|V_{tb}| > 0.79$ at 95% CL for a flat prior within $0 < |V_{tb}|^2 < 1$.

11 Based on 3.2 fb^{-1} of data. For combined s- + t-channel result see AALTONEN 09AT.

12 Result is based on 2.1 fb^{-1} of data. Events with large missing E_T and jets with at least one b-jet without identified electron or muon are selected. Result is obtained when observed 2.1σ excess over the background originates from the signal for $m_t = 175 \text{ GeV}$, giving $|V_{tb}| = 1.24^{+0.34}_{-0.29} \pm 0.07(\text{theory})$.

13 Result is based on 2.3 fb^{-1} of data. Events with isolated $\ell + \cancel{E}_T + 2, 3, 4$ jets with one or two b-tags are selected. The analysis assumes $m_t = 170 \text{ GeV}$.

14 Result is based on 4.8 fb^{-1} of data. Events with an isolated reconstructed tau lepton, missing $E_T + 2, 3$ jets with one or two b-tags are selected. When combined with ABAZOV 09Z result for e + μ channels, the s- and t-channels combined cross section is $3.84^{+0.89}_{-0.83} \text{ pb}$.

15 Based on 3.2 fb^{-1} of data. Events with isolated $\ell + \cancel{E}_T$ + jets with at least one b-tag are analyzed and s- and t-channel single top events are selected by using the likelihood function, matrix element, neural-network, boosted decision tree, likelihood function optimized for s-channel process, and neural-networked based analysis of events with \cancel{E}_T that has sensitivity for $W \rightarrow \tau\nu$ decays. The result is for $m_t = 175 \text{ GeV}$, and the mean value decreases by 0.02 pb/GeV for smaller m_t . The signal has 5.0 sigma significance. The result gives $|V_{tb}| = 0.91 \pm 0.11(\text{stat} + \text{syst}) \pm 0.07(\text{theory})$, or $|V_{tb}| > 0.71$ at 95% CL.

16 Based on 2.3 fb^{-1} of data. Events with isolated $\ell + \cancel{E}_T + \geq 2$ jets with 1 or 2 b-tags are analyzed and s- and t-channel single top events are selected by using boosted decision tree, Bayesian neural networks and the matrix element method. The signal has 5.0 sigma significance. The result gives $|V_{tb}| = 1.07 \pm 0.12$, or $|V_{tb}| > 0.78$ at 95% CL. The analysis assumes $m_t = 170 \text{ GeV}$.

17 Result is based on 2.2 fb^{-1} of data. Events with isolated $\ell + \cancel{E}_T + 2, 3$ jets with at least one b-tag are selected, and s- and t-channel single top events are selected by using likelihood, matrix element, and neural network discriminants. The result can be interpreted as $|V_{tb}| = 0.88^{+0.13}_{-0.12}(\text{stat} + \text{syst}) \pm 0.07(\text{theory})$, and $|V_{tb}| > 0.66$ (95% CL) under the $|V_{tb}| < 1$ constraint.

18 Result is based on 0.9 fb^{-1} of data. Events with isolated $\ell + \cancel{E}_T + 2, 3, 4$ jets with one or two b-vertex-tag are selected, and contributions from W + jets, $t\bar{t}$, s- and t-channel single top events are identified by using boosted decision trees, Bayesian neural networks, and matrix element analysis. The result can be interpreted as the measurement of the CKM matrix element $|V_{tb}| = 1.31^{+0.25}_{-0.21}$, or $|V_{tb}| > 0.68$ (95% CL) under the $|V_{tb}| < 1$ constraint.

19 Result is based on 0.9 fb^{-1} of data. This result constrains V_{tb} to $0.68 < |V_{tb}| \leq 1$ at 95% CL.

20 ABAZOV 05P bounds single top-quark production from either the s-channel W -exchange process, $q'\bar{q} \rightarrow t\bar{b}$, or the t-channel W -exchange process, $q'g \rightarrow qt\bar{b}$, based on $\sim 230 \text{ pb}^{-1}$ of data.

21 ACOSTA 05N bounds single top-quark production from the t-channel W -exchange process ($q'g \rightarrow qt\bar{b}$), the s-channel W -exchange process ($q'\bar{q} \rightarrow t\bar{b}$), and from the combined cross section of t- and s-channel. Based on $\sim 162 \text{ pb}^{-1}$ of data.

t-channel Single t Production Cross Section in pp Collisions at $\sqrt{s} = 7$ TeVDirect probe of the tbW coupling and possible new physics at $\sqrt{s} = 7$ TeV.

VALUE (pb)	DOCUMENT ID	TECN	COMMENT
67.5 ± 5.7	1 AABOUD	19R LHC	combination of ATLAS+CMS
$68 \pm 2 \pm 8$	2 AAD	14BI ATLS	$\ell + \cancel{E}_T + 2j$ or $3j$
$83 \pm 4^{+20}_{-19}$	3 AAD	12CH ATLS	t-channel $\ell + \cancel{E}_T + (2,3)j$ (1b)
67.2 ± 6.1	4 CHATRCHYAN12BQ CMS		t-channel $\ell + \cancel{E}_T + \geq 2j$ (1b)
$83.6 \pm 29.8 \pm 3.3$	5 CHATRCHYAN11R CMS		t-channel

1 AABOUD 19R based on 1.17 to 5.1 fb^{-1} of data from ATLAS and CMS at 7 TeV .

2 Based on 4.59 fb^{-1} of data, using neural networks for signal and background separation. $\sigma(tq) = 46 \pm 1 \pm 6 \text{ pb}$ and $\sigma(\bar{t}q) = 23 \pm 1 \pm 3 \text{ pb}$ are separately measured, as well as their ratio $R = \sigma(tq)/\sigma(\bar{t}q) = 2.04 \pm 0.13 \pm 0.12$. The results are for $m_t = 172.5 \text{ GeV}$, and those for other m_t values are given by eq.(4) and Table IV. The measurements give $|V_{tb}| = 1.02 \pm 0.07$ or $|V_{tb}| > 0.88$ (95% CL).

3 Based on 1.04 fb^{-1} of data. The result gives $|V_{tb}| = 1.13^{+0.14}_{-0.13}$ from the ratio $\sigma(\text{exp})/\sigma(\text{th})$, where $\sigma(\text{th})$ is the SM prediction for $|V_{tb}| = 1$. The 95% CL lower bound of $|V_{tb}| > 0.75$ is found if $|V_{tb}| < 1$ is assumed. $\sigma(t) = 59^{+18}_{-16} \text{ pb}$ and $\sigma(\bar{t}) = 33^{+13}_{-12} \text{ pb}$ are found for the separate single t and \bar{t} production cross sections, respectively. The results assume $m_t = 172.5 \text{ GeV}$ for the acceptance.

4 Based on 1.17 fb^{-1} of data for $\ell = \mu, 1.56 \text{ fb}^{-1}$ of data for $\ell = e$ at 7 TeV collected during 2011. The result gives $|V_{tb}| = 1.020 \pm 0.046(\text{meas}) \pm 0.017(\text{th})$. The 95% CL lower bound of $|V_{tb}| > 0.92$ is found if $|V_{tb}| < 1$ is assumed. The results assume $m_t = 172.5 \text{ GeV}$ for the acceptance.

5 Based on 36 pb^{-1} of data. The first error is statistical + systematic combined, the second is luminosity. The result gives $|V_{tb}| = 1.114 \pm 0.22(\text{exp}) \pm 0.02(\text{th})$ from the ratio $\sigma(\text{exp})/\sigma(\text{th})$, where $\sigma(\text{th})$ is the SM prediction for $|V_{tb}| = 1$. The 95% CL lower bound of $|V_{tb}| > 0.62$ (0.68) is found from the 2D (BDT) analysis under the constraint $0 < |V_{tb}|^2 < 1$.

t-channel Single t Production Cross Section in pp Collisions at $\sqrt{s} = 8$ TeV

VALUE (pb)	DOCUMENT ID	TECN	COMMENT
87.7 ± 5.8	1 AABOUD	19R LHC	combination of ATLAS+CMS
$89.6^{+7.1}_{-6.3}$	2 AABOUD	17T ATLS	$\ell + \cancel{E}_T + 2j$ (1b j)
$83.6 \pm 2.3 \pm 7.4$	3 KHACHATRYAN14F CMS		$\ell + \cancel{E}_T + \geq 2j$ (1,2 b, 1 forward j)

1 AABOUD 19R based on 12.2 to 20.3 fb^{-1} of data from ATLAS and CMS at 8 TeV .

2 AABOUD 17T based on 20.2 fb^{-1} of data. A maximum-likelihood fit to neural-network discriminant distributions is used to separate signal and background events. Individual cross sections are measured as $\sigma(tq) = 56.7^{+4.3}_{-3.8} \text{ pb}$ and $\sigma(\bar{t}q) = 32.9^{+3.0}_{-2.7} \text{ pb}$, while their ratio is given by $\sigma(tq)/\sigma(\bar{t}q) = 1.72 \pm 0.09$. A lower limit $|V_{tb}| > 0.92$ (95%

Quark Particle Listings

t

CL) is obtained. Measured total and differential cross sections are described well by the SM.

³Based on 19.7 fb⁻¹ of data. The t and \bar{t} production cross sections are measured separately as $\sigma_{t\text{-}ch.}(t) = 53.8 \pm 1.5 \pm 4.4$ pb and $\sigma_{t\text{-}ch.}(\bar{t}) = 27.6 \pm 1.3 \pm 3.7$ pb, respectively, as well as their ratio $R_{t\text{-}ch} = \sigma_{t\text{-}ch.}(t)/\sigma_{t\text{-}ch.}(\bar{t}) = 1.95 \pm 0.10 \pm 0.19$, in agreement with the SM predictions. Combination with a previous CMS result at $\sqrt{s} = 7$ TeV [CHATRCHYAN 12BQ] gives $|V_{tb}| = 0.998 \pm 0.038 \pm 0.016$. Also obtained is the ratio $R_{8/7} = \sigma_{t\text{-}ch.}(8\text{TeV})/\sigma_{t\text{-}ch.}(7\text{TeV}) = 1.24 \pm 0.08 \pm 0.12$.

s-channel Single t Production Cross Section in pp Collisions at $\sqrt{s} = 8$ TeV

VALUE (pb)	DOCUMENT ID	TECN	COMMENT
4.9 ± 1.4	¹ AABOUD	19R LHC	ATLAS + CMS
4.8 ± 0.8 ^{+1.6} _{-1.3}	² AAD	16U ATLS	$\ell + \cancel{E}_T + 2b$
13.4 ± 7.3	³ KHACHATRYAN	16AZ CMS	$\ell + \cancel{E}_T + 2b$
5.0 ± 4.3	⁴ AAD	15A ATLS	$\ell + \cancel{E}_T + 2b$

- ¹AABOUD 19R based on 12.2 to 20.3 fb⁻¹ of data from ATLAS and CMS at 8 TeV.
²AAD 16U based on 20.3 fb⁻¹ of data, using a maximum-likelihood fit of a matrix element method discriminant. The same data set as in AAD 15A is used. The result corresponds to an observed significance of 3.2 σ .
³KHACHATRYAN 16AZ based on 19.7 fb⁻¹ of data, using a multivariate analysis to separate signal and backgrounds. The same method is applied to 5.1 fb⁻¹ of data at $\sqrt{s} = 7$ TeV, giving 7.1 ± 8.1 pb. Combining both measurements, the observed significance is 2.5 σ . A best fit value of 2.0 ± 0.9 is obtained for the combined ratio of the measured values and SM expectations.
⁴AAD 15A based on 20.3 fb⁻¹ of data, using a multivariate analysis to separate signal and backgrounds. The 95% CL upper bound of the cross section is 14.6 pb. The results are consistent with the SM prediction of 5.61 ± 0.22 pb at approximate NNLO.

t-channel Single t Production Cross Section in pp Collisions at $\sqrt{s} = 13$ TeV

VALUE (pb)	DOCUMENT ID	TECN	COMMENT
130 ± 1 ± 19	¹ SIRUNYAN	20D CMS	$\sigma(tq), \ell + \cancel{E}_T + \geq 2j$
77 ± 1 ± 12	¹ SIRUNYAN	20D CMS	$\sigma(\bar{t}q), \ell + \cancel{E}_T + \geq 2j$
156 ± 5 ± 27 ± 3	² AABOUD	17H ATLS	$\sigma(tq), \ell + \cancel{E}_T + 2j$ (1b, 1 forward j)
91 ± 4 ± 18 ± 2	² AABOUD	17H ATLS	$\sigma(\bar{t}q), \ell + \cancel{E}_T + 2j$ (1b, 1 forward j)
154 ± 8 ± 9 ± 19 ± 4	³ SIRUNYAN	17AA CMS	$\sigma(tq), \mu + \geq 2j$ (1b)
85 ± 10 ± 4 ± 11 ± 2	³ SIRUNYAN	17AA CMS	$\sigma(\bar{t}q), \mu + \geq 2j$ (1b)

- ¹SIRUNYAN 20D based on 35.9 fb⁻¹ of data. Different categories of jet and b jet multiplicity and multivariate discriminators are used to separate signal and background events. The cross section ratio is measured to be $\sigma(tq)/\sigma(\bar{t}q) = 1.68 \pm 0.02 \pm 0.05$. CKM matrix element is obtained as $|f_{LV} V_{tb}| = 0.98 \pm 0.07(\text{exp}) \pm 0.02(\text{theo})$ where f_{LV} is an anomalous form factor. All results are in agreement with the SM.
²AABOUD 17H based on 3.2 fb⁻¹ of data. A maximum-likelihood fit to neural-network discriminant distributions is used to separate signal and background events. The third error is for luminosity. The cross section ratio is measured to be $\sigma(tq)/\sigma(\bar{t}q) = 1.72 \pm 0.09 \pm 0.18$. A lower limit $|V_{tb}| > 0.84$ (95% CL) is obtained. All results are in agreement with the SM.
³SIRUNYAN 17AA based on 2.2 fb⁻¹ of data. A multivariate discriminator is used to separate signal and background events. The four errors are from statistics, experimental systematics, theory, and luminosity. The cross section ratio is measured to be $\sigma(tq)/\sigma(\bar{t}q) = 1.81 \pm 0.18 \pm 0.15$. CKM matrix element is obtained as $|V_{tb}| = 1.05 \pm 0.07(\text{exp}) \pm 0.02(\text{theo})$. All results are in agreement with the SM.

s-channel Single t Production Cross Section in pp Collisions at $\sqrt{s} = 13$ TeV

VALUE (pb)	DOCUMENT ID	TECN	COMMENT
8.2 ± 3.5 _{-2.9}	¹ AAD	23E ATLS	$\ell + \cancel{E}_T + 2b$

- ¹AAD 23E based on 139 fb⁻¹ of data. The signal significance is 3.3 σ over the background-only hypothesis. The result is consistent with the NLO SM prediction of 10.32^{+0.40}_{-0.36} pb.

t \bar{t} Production Cross Section in pp Collisions at $\sqrt{s} = 13$ TeV

VALUE (fb)	DOCUMENT ID	TECN	COMMENT
33 ± 31 ⁺²² ₋₁₇	¹ AAD	22Q ATLS	$H \rightarrow \tau\tau$
670 ± 90 ⁺¹¹⁰ ₋₁₀₀	² AABOUD	18BK ATLS	$H \rightarrow b\bar{b}, WW^*, \tau\tau, \gamma\gamma, Z Z^*$

- ¹AAD 22Q based on 139 fb⁻¹ of data. The measured value includes $B(H \rightarrow \tau\tau)$ and corresponds to the rapidity range $|y_H| < 2.5$. The value is consistent with the SM prediction, where $B(H \rightarrow \tau\tau) = 6.3\%$ for $m_H = 125.09$ GeV.
²AABOUD 18BK based on 79.8 fb⁻¹ of data. The observed significance is 5.8 σ relative to the background-only hypothesis. The measurement is consistent with the NLO SM prediction of 507⁺³⁵₋₅₀ fb. See Table 3 and Fig. 5 for measurements of individual modes. Combined with the measurements at 7 and 8 TeV, the observed significance is 6.3 σ .

Wt Production Cross Section in pp Collisions at $\sqrt{s} = 7$ TeV

VALUE (pb)	DOCUMENT ID	TECN	COMMENT
16.3 ± 4.1	¹ AABOUD	19R LHC	ATLAS + CMS combined
16 ⁺⁵ ₋₄	² CHATRCHYAN	13C CMS	$t + W$ channel, $2\ell + \cancel{E}_T + 1b$

- ¹AABOUD 19R based on 1.17 to 5.1 fb⁻¹ of data from ATLAS and CMS at 7 TeV.
²Based on 4.9 fb⁻¹ of data. The result gives $V_{tb} = 1.01^{+0.16}_{-0.13}(\text{exp}) \pm 0.03(0.04)$. $|V_{tb}| > 0.79$ (95% CL) if $V_{tb} < 1$ is assumed. The results assume $m_t = 172.5$ GeV for the acceptance.

Wt Production Cross Section in pp Collisions at $\sqrt{s} = 8$ TeV

VALUE (pb)	DOCUMENT ID	TECN	COMMENT
26 ± 7	¹ AAD	21AT ATLS	$\ell + \geq 3j$
23.1 ± 3.6	² AABOUD	19R LHC	ATLAS + CMS combined
23.0 ± 1.3 ^{+3.2} _{-3.5} ± 1.1	³ AAD	16B ATLS	$2\ell + \cancel{E}_T + 1b$
23.4 ± 5.4	⁴ CHATRCHYAN	14AC CMS	$t + W$ channel, $2\ell + \cancel{E}_T + 1b$

- ¹AAD 21AT based on 20.2 fb⁻¹ of data. In this single lepton channel, only single neutrino is emitted, so that both W and t can be reconstructed. A neural network is trained to separate signal from background. The measured cross section agrees with the NLO+NNLL SM prediction of 22.4 ± 0.6(scale) ± 1.4(PDF) pb.
²AABOUD 19R based on 12.2 to 20.3 fb⁻¹ of data from ATLAS and CMS at 8 TeV.
³AAD 16B based on 20.3 fb⁻¹ of data. The result gives $|V_{tb}| = 1.01 \pm 0.10$ and $|V_{tb}| > 0.80$ (95% CL) without assuming unitarity of the CKM matrix. The results assume $m_t = 172.5$ GeV for the acceptance.
⁴Based on 12.2 fb⁻¹ of data. Events with two oppositely charged leptons, large \cancel{E}_T and a b -tagged jet are selected, and a multivariate analysis is used to separate the signal from the backgrounds. The result is consistent with the SM prediction of 22.2 ± 0.6(scale) ± 1.4(PDF) pb at approximate NNLO.

Wt Production Cross Section in pp Collisions at $\sqrt{s} = 13$ TeV

VALUE (pb)	DOCUMENT ID	TECN	COMMENT
79.2 ± 0.9 ^{+7.7} _{-8.0} ± 1.2	¹ TUMASYAN	23T CMS	$e^\pm \mu^\mp + \geq 1j(b\text{-tag})$
89 ± 4 ± 12	² TUMASYAN	21E CMS	$1\ell + \text{jets}$
94 ± 10 ⁺²⁸ ₋₂₂ ± 2	³ AABOUD	18H ATLS	$\ell + \ell^- + \geq 1j$
63.1 ± 1.8 ± 6.4 ± 2.1	⁴ SIRUNYAN	18DL CMS	$e^\pm \mu^\mp + \geq 1j(b\text{-tag})$

- ¹TUMASYAN 23T based on 138 fb⁻¹ of data. The result is consistent with the NNLO SM prediction. The differential cross sections are measured as a function of six kinematical variables and are consistent with the NLO SM prediction.
²TUMASYAN 21E based on 36 fb⁻¹ of data. A boosted decision tree is used to separate the signal from the dominant $t\bar{t}$ backgrounds. The result corresponds to an observation with a significance exceeding 5 σ and is consistent with the NNLO QCD prediction of 71.7 ± 1.8(scale) ± 3.4(PDF) pb or with the approximate NNNLO SM prediction of 79.5^{+1.9}_{-1.8}(scale) ± 2.0(PDF) pb.
³AABOUD 18H based on 3.2 fb⁻¹ of data. The last error is from luminosity. A multivariate analysis is used to separate the signal from the backgrounds. The result is consistent with the NLO+NNLL SM prediction of 71.7 ± 1.8(scale) ± 3.4(PDF) pb.
⁴SIRUNYAN 18DL based on 35.9 fb⁻¹ of data. The last error is from luminosity. A multivariate analysis is used to separate the signal from the backgrounds. The result is consistent with the NLO+NNLL SM prediction of 71.7 ± 1.8(scale) ± 3.4(PDF) pb.

Zt Production Cross Section in pp Collisions at $\sqrt{s} = 13$ TeV

VALUE (fb)	DOCUMENT ID	TECN	COMMENT
87.9 ^{+7.5} _{-7.3} ± 7.3 ± 6.0	¹ TUMASYAN	22L CMS	$3\ell + \geq 2j$ ($\geq 1b$)
99 ± 13 ± 7	² AAD	20AB ATLS	$3\ell + 1, 2j + 1b$
111 ± 13 ± 11 ⁻⁹	³ SIRUNYAN	19BF CMS	$3\ell + \geq 2j$ ($\geq 1b$)
600 ± 170 ± 140	⁴ AABOUD	18AE ATLS	$3\ell + 1j + 1b$
123 ± 33 ± 29 ₋₂₃	⁵ SIRUNYAN	18Z CMS	$3\ell + 1j + 1b$

- ¹TUMASYAN 22L based on 138 fb⁻¹ of data at 13 TeV. The result is for a dilepton invariant masses above 30 GeV. It agrees with the NLO SM prediction of 94.2^{+1.9}_{-1.8}(scale) ± 2.5(PDF) fb. The ratio of t and \bar{t} production cross sections is measured as 2.37^{+0.56+0.27}_{-0.42-0.13}. The spin asymmetry is measured to be 0.54 ± 0.16 ± 0.06. Both measurements are in agreement with the SM predictions.
²AAD 20AB based on 139 fb⁻¹ of data at 13 TeV. Neural networks are used to discriminate tZq signal from backgrounds. The result is for the cross section $\sigma(pp \rightarrow tZq \rightarrow \ell^+ \ell^- q)$ for dilepton invariant masses above 30 GeV and is consistent with the NLO SM prediction of 102⁺⁵₋₂ fb.
³SIRUNYAN 19BF based on 77.4 fb⁻¹ of data. Two BDT's are used in the analysis: one to discriminate prompt leptons from non-prompt ones; and one to discriminate tZq signal from backgrounds. The result is for the cross section $\sigma(pp \rightarrow tZq \rightarrow \ell^+ \ell^- q)$ for dilepton invariant masses above 30 GeV and is consistent with the NLO SM prediction of 94.2 ± 3.1 fb.
⁴AABOUD 18AE based on 36.1 fb⁻¹ of data. A multivariate analysis is used to separate the signal from the backgrounds. The result is consistent with the NLO SM prediction of 800 fb with a scale uncertainty of ^{+6.1%}_{-7.4%}.
⁵SIRUNYAN 18Z based on 35.9 fb⁻¹ of data. A multivariate analysis is used to separate the signal from the backgrounds. The result is for the cross section $\sigma(pp \rightarrow tZq \rightarrow Wb\ell^+ \ell^- q)$ and is consistent with the NLO SM prediction of 94.2^{+1.9}_{-1.8}(scale) ± 2.5(PDF) fb. Superseded by SIRUNYAN 19BF.

 γt Production Cross Section in pp Collisions at $\sqrt{s} = 13$ TeV

VALUE (fb)	DOCUMENT ID	TECN	COMMENT
	¹ AAD	23BN ATLS	$\gamma + \ell + \text{jets} + \cancel{E}_T$

- ¹AAD 23BN measured fiducial cross section for $pp \rightarrow t\gamma \rightarrow t\gamma$ at 13 TeV with 139 fb⁻¹ of data. The measured cross section is 688 ± 23⁺⁷⁵₋₇₁ fb, to be compared with the NLO SM prediction of 515 ± 36 fb.

Single t-Quark Production Cross Section in ep Collisions

VALUE (pb)	CL%	DOCUMENT ID	TECN	COMMENT
<0.25	95	1 AARON	09A H1	$e^\pm p \rightarrow e^\pm tX$
<0.55	95	2 AKTAS	04 H1	$e^\pm p \rightarrow e^\pm tX$
<0.225	95	3 CHEKANOV	03 ZEUS	$e^\pm p \rightarrow e^\pm tX$

1 AARON 09A looked for single top production via FCNC in $e^\pm p$ collisions at HERA with 474 pb^{-1} of data at $\sqrt{s} = 301\text{--}319 \text{ GeV}$. The result supersedes that of AKTAS 04.

2 AKTAS 04 looked for single top production via FCNC in e^\pm collisions at HERA with 118.3 pb^{-1} , and found 5 events in the e or μ channels while 1.31 ± 0.22 events are expected from the Standard Model background. No excess was found for the hadronic channel. The observed cross section of $\sigma(ep \rightarrow etX) = 0.29^{+0.15}_{-0.14} \text{ pb}$ at $\sqrt{s} = 319 \text{ GeV}$ gives the quoted upper bound if the observed events are due to statistical fluctuation.

3 CHEKANOV 03 looked in 130.1 pb^{-1} of data at $\sqrt{s} = 301$ and 318 GeV . The limit is for $\sqrt{s} = 318 \text{ GeV}$ and assumes $m_t = 175 \text{ GeV}$.

tT Production Cross Section in pT Collisions at $\sqrt{s} = 1.8 \text{ TeV}$

Only the final combined tT production cross sections obtained from Tevatron Run I by the CDF and D0 experiments are quoted below.

VALUE (pb)	DOCUMENT ID	TECN	COMMENT
$5.69 \pm 1.21 \pm 1.04$	1 ABAZOV	03A D0	Combined Run I data
$6.5^{+1.7}_{-1.4}$	2 AFFOLDER	01A CDF	Combined Run I data

1 Combined result from 110 pb^{-1} of Tevatron Run I data. Assume $m_t = 172.1 \text{ GeV}$.

2 Combined result from 105 pb^{-1} of Tevatron Run I data. Assume $m_t = 175 \text{ GeV}$.

tT Production Cross Section in pT Collisions at $\sqrt{s} = 1.96 \text{ TeV}$

Unless otherwise noted the first quoted error is from statistics, the second from systematic uncertainties, and the third from luminosity. If only two errors are quoted the luminosity is included in the systematic uncertainties.

VALUE (pb)	DOCUMENT ID	TECN	COMMENT
$7.26 \pm 0.13^{+0.57}_{-0.50}$	1 ABAZOV	16F D0	$\ell\ell, \ell + \text{jets}$ channels
8.1 ± 2.1	2 AALTONEN	14A CDF	$\ell + \tau_h + \geq 2\text{jets} (\geq 1b\text{-tag})$
$7.60 \pm 0.20 \pm 0.29 \pm 0.21$	3 AALTONEN	14H TEVA	$\ell\ell, \ell + \text{jets}$, all-jets channels
$8.0 \pm 0.7 \pm 0.6 \pm 0.5$	4 ABAZOV	14K D0	$\ell + \cancel{E}_T + \geq 4 \text{ jets} (\geq 1b\text{-tag})$
7.09 ± 0.84	5 AALTONEN	13AB CDF	$\ell\ell + \cancel{E}_T + \geq 2 \text{ jets}$
7.5 ± 1.0	6 AALTONEN	13G CDF	$\ell + \cancel{E}_T + \geq 3\text{jets} (\geq 1b\text{-tag})$
$8.8 \pm 3.3 \pm 2.2$	7 AALTONEN	12AL CDF	$\tau_h + \cancel{E}_T + 4\text{j} (\geq 1b)$
$8.5 \pm 0.6 \pm 0.7$	8 AALTONEN	11D CDF	$\ell + \cancel{E}_T + \text{jets} (\geq 1b\text{-tag})$
$7.64 \pm 0.57 \pm 0.45$	9 AALTONEN	11W CDF	$\ell + \cancel{E}_T + \text{jets} (\geq 1b\text{-tag})$
$7.99 \pm 0.55 \pm 0.76 \pm 0.46$	10 AALTONEN	11Y CDF	$\cancel{E}_T + \geq 4\text{jets} (0,1,2 b\text{-tag})$
$7.78^{+0.77}_{-0.64}$	11 ABAZOV	11E D0	$\ell + \cancel{E}_T + \geq 2\text{jets}$
$7.56^{+0.63}_{-0.56}$	12 ABAZOV	11Z D0	Combination
$6.27 \pm 0.73 \pm 0.63 \pm 0.39$	13 AALTONEN	10AA CDF	Repl. by AALTONEN 13AB
$7.2 \pm 0.5 \pm 1.0 \pm 0.4$	14 AALTONEN	10E CDF	$\geq 6 \text{ jets}$, vtx b-tag
$7.8 \pm 2.4 \pm 1.6 \pm 0.5$	15 AALTONEN	10V CDF	$\ell + \geq 3 \text{ jets}$, soft-e b-tag
7.70 ± 0.52	16 AALTONEN	10W CDF	$\ell + \cancel{E}_T + \geq 3 \text{ jets} + b\text{-tag}$, norm. to $\sigma(Z \rightarrow \ell\ell)_{TH}$
6.9 ± 2.0	17 ABAZOV	10I D0	$\geq 6 \text{ jets}$ with 2 b-tags
$6.9 \pm 1.2^{+0.8}_{-0.7} \pm 0.4$	18 ABAZOV	10Q D0	$\tau_h + \text{jets}$
$9.6 \pm 1.2^{+0.6}_{-0.5} \pm 0.6$	19 AALTONEN	09AD CDF	$\ell\ell + \cancel{E}_T / \text{vtx } \mu \text{ b-tag}$
$9.1 \pm 1.1^{+1.0}_{-0.9} \pm 0.6$	20 AALTONEN	09H CDF	$\ell + \geq 3 \text{ jets} + \cancel{E}_T / \text{soft } \mu \text{ b-tag}$
$8.18^{+0.98}_{-0.87}$	21 ABAZOV	09AG D0	$\ell + \text{jets}$, $\ell\ell$ and $\ell\tau + \text{jets}$
$7.5 \pm 1.0^{+0.7}_{-0.6} \pm 0.5$	22 ABAZOV	09R D0	$\ell\ell$ and $\ell\tau + \text{jets}$
$8.18^{+0.90}_{-0.84} \pm 0.50$	23 ABAZOV	08M D0	$\ell + n \text{ jets}$ with 0,1,2 b-tag
7.62 ± 0.85	24 ABAZOV	08N D0	$\ell + n \text{ jets} + b\text{-tag}$ or kinematics
$8.5^{+2.7}_{-2.2}$	25 ABULENCIA	08 CDF	$\ell^+ \ell^- (\ell = e, \mu)$
$8.3 \pm 1.0^{+2.0}_{-1.5} \pm 0.5$	26 AALTONEN	07D CDF	$\geq 6 \text{ jets}$, vtx b-tag
$7.4 \pm 1.4 \pm 1.0$	27 ABAZOV	07O D0	$\ell\ell + \text{jets}$, vtx b-tag
$4.5^{+2.0}_{-1.9} \pm 1.4 \pm 0.3$	28 ABAZOV	07P D0	$\geq 6 \text{ jets}$, vtx b-tag
$6.4^{+1.3}_{-1.2} \pm 0.7 \pm 0.4$	29 ABAZOV	07R D0	$\ell + \geq 4 \text{ jets}$
$8.6 \pm 0.9 \pm 0.4$	30 ABAZOV	06X D0	$\ell + \text{jets}$, vtx b-tag
$8.7 \pm 0.9^{+1.1}_{-0.9}$	31 ABULENCIA	06Z CDF	$\ell + \text{jets}$, vtx b-tag
$5.8 \pm 1.2^{+0.9}_{-0.7}$	32 ABULENCIA,A	06C CDF	missing $E_T + \text{jets}$, vtx b-tag
$7.5 \pm 2.1^{+3.3}_{-2.2} \pm 0.5 \pm 0.4$	33 ABULENCIA,A	06E CDF	6–8 jets, b-tag
$8.9 \pm 1.0^{+1.1}_{-1.0}$	34 ABULENCIA,A	06F CDF	$\ell + \geq 3 \text{ jets}$, b-tag
$8.6^{+1.6}_{-1.5} \pm 0.6$	35 ABAZOV	05Q D0	$\ell + n \text{ jets}$
$8.6^{+3.2}_{-2.7} \pm 1.1 \pm 0.6$	36 ABAZOV	05R D0	di-lepton + n jets
$6.7^{+1.4}_{-1.3} \pm 1.6 \pm 0.4$	37 ABAZOV	05X D0	$\ell + \text{jets} / \text{kinematics}$

$5.3 \pm 3.3^{+1.3}_{-1.0}$	38 ACOSTA	05S CDF	$\ell + \text{jets} / \text{soft } \mu \text{ b-tag}$
$6.6 \pm 1.1 \pm 1.5$	39 ACOSTA	05T CDF	$\ell + \text{jets} / \text{kinematics}$
$6.0^{+1.5}_{-1.6} \pm 1.2 \pm 1.3$	40 ACOSTA	05U CDF	$\ell + \text{jets}/\text{kinematics} + \text{vtx } b\text{-tag}$
$5.6^{+1.2}_{-1.1} \pm 0.9 \pm 0.6$	41 ACOSTA	05V CDF	$\ell + n \text{ jets}$
$7.0^{+2.4}_{-2.1} \pm 1.6 \pm 0.4$	42 ACOSTA	04I CDF	di-lepton + jets + missing ET

1 ABAZOV 16F based on 9.7 fb^{-1} of data. The result is for $m_t = 172.5 \text{ GeV}$, and the m_t dependence is shown in Table V and Fig. 9. The result agrees with the NNLO+NNLL SM prediction of $7.35^{+0.23}_{-0.27} \text{ pb}$.

2 Based on 9 fb^{-1} of data. The measurement is in the channel $t\bar{T} \rightarrow (b\ell\nu)(b\tau\nu)$, where τ decays into hadrons (τ_h), and ℓ (e or μ) include ℓ from τ decays (τ_ℓ). The result is for $m_t = 173 \text{ GeV}$.

3 Based on 8.8 fb^{-1} of data. Combination of CDF and D0 measurements given, respectively, by $\sigma(t\bar{T}; \text{CDF}) = 7.63 \pm 0.31 \pm 0.36 \pm 0.16 \text{ pb}$, $\sigma(t\bar{T}; \text{D0}) = 7.56 \pm 0.20 \pm 0.32 \pm 0.46 \text{ pb}$. All the results are for $m_t = 172.5 \text{ GeV}$. The m_t dependence of the mean value is parametrized in eq. (1) and shown in Fig. 2.

4 Based on 9.7 fb^{-1} of data. Differential cross sections with respect to $m_{t\bar{T}}$, $|y(\text{top})|$, $E_T(\text{top})$ are shown in Figs. 9, 10, 11, respectively, and are compared to the predictions of MC models.

5 Based on 8.8 fb^{-1} of $p\bar{p}$ collisions at $\sqrt{s} = 1.96 \text{ TeV}$.

6 Based on 8.7 fb^{-1} of $p\bar{p}$ collisions at $\sqrt{s} = 1.96 \text{ TeV}$. Measure the $t\bar{T}$ cross section simultaneously with the fraction of $t \rightarrow Wb$ decays. The correlation coefficient between those two measurements is -0.434 . Assume unitarity of the 3×3 CKM matrix and set $|V_{tb}| > 0.89$ at 95% CL.

7 Based on 2.2 fb^{-1} of data in $p\bar{p}$ collisions at 1.96 TeV . The result assumes the acceptance for $m_t = 172.5 \text{ GeV}$.

8 Based on 1.12 fb^{-1} and assumes $m_t = 175 \text{ GeV}$, where the cross section changes by $\pm 0.1 \text{ pb}$ for every $\pm 1 \text{ GeV}$ shift in m_t . AALTONEN 11D fits simultaneously the $t\bar{T}$ production cross section and the b-tagging efficiency and find improvements in both measurements.

9 Based on 2.7 fb^{-1} . The first error is from statistics and systematics, the second is from luminosity. The result is for $m_t = 175 \text{ GeV}$. AALTONEN 11W fits simultaneously a jet flavor discriminator between b-, c-, and light-quarks, and find significant reduction in the systematic error.

10 Based on 2.2 fb^{-1} . The result is for $m_t = 172.5 \text{ GeV}$. AALTONEN 11Y selects multi-jet events with large \cancel{E}_T , and vetoes identified electrons and muons.

11 Based on 5.3 fb^{-1} . The error is statistical + systematic + luminosity combined. The result is for $m_t = 172.5 \text{ GeV}$. The results for other m_t values are given in Table XII and eq.(10) of ABAZOV 11E.

12 Combination of a dilepton measurement presented in ABAZOV 11Z (based on 5.4 fb^{-1}), which yields $7.36^{+0.90}_{-0.79}$ (stat+syst) pb, and the lepton + jets measurement of ABAZOV 11E. The result is for $m_t = 172.5 \text{ GeV}$. The results for other m_t values is given by eq.(5) of ABAZOV 11A.

13 Based on 2.8 fb^{-1} . The result is for $m_t = 175 \text{ GeV}$.

14 Based on 2.9 fb^{-1} . Result is obtained from the fraction of signal events in the top quark mass measurement in the all hadronic decay channel.

15 Based on 1.7 fb^{-1} . The result is for $m_t = 175 \text{ GeV}$. AALTONEN 10V uses soft electrons from b-hadron decays to suppress $W + \text{jets}$ background events.

16 Based on 4.6 fb^{-1} . The result is for $m_t = 172.5 \text{ GeV}$. The ratio $\sigma(t\bar{T} \rightarrow \ell + \text{jets}) / \sigma(Z/\gamma^* \rightarrow \ell\ell)$ is measured and then multiplied by the theoretical $Z/\gamma^* \rightarrow \ell\ell$ cross section of $\sigma(Z/\gamma^* \rightarrow \ell\ell) = 251.3 \pm 5.0 \text{ pb}$, which is free from the luminosity error.

17 Based on 1 fb^{-1} . The result is for $m_t = 175 \text{ GeV}$. $7.9 \pm 2.3 \text{ pb}$ is found for $m_t = 170 \text{ GeV}$. ABAZOV 10I uses a likelihood discriminant to separate signal from background, where the background model was created from lower jet-multiplicity data.

18 Based on 1 fb^{-1} . The result is for $m_t = 170 \text{ GeV}$. For $m_t = 175 \text{ GeV}$, the result is $6.3^{+1.2}_{-1.1}(\text{stat}) \pm 0.7(\text{syst}) \pm 0.4(\text{lumi}) \text{ pb}$. Cross section of $t\bar{T}$ production has been measured in the $t\bar{T} \rightarrow \tau_h + \text{jets}$ topology, where τ_h denotes hadronically decaying τ leptons. The result for the cross section times the branching ratio is $\sigma(t\bar{T}) \cdot \text{B}(t\bar{T} \rightarrow \tau_h + \text{jets}) = 0.60^{+0.23}_{-0.22} \pm 0.15 \pm 0.04 \text{ pb}$ for $m_t = 170 \text{ GeV}$.

19 Based on 1.1 fb^{-1} . The result is for $\text{B}(W \rightarrow \ell\nu) = 10.8\%$ and $m_t = 175 \text{ GeV}$; the mean value is 9.8 for $m_t = 172.5 \text{ GeV}$ and 10.1 for $m_t = 170 \text{ GeV}$. AALTONEN 09AD used high p_T e or μ with an isolated track to select $t\bar{T}$ decays into dileptons including $\ell = \tau$. The result is based on the candidate event samples with and without vertex b-tag.

20 Based on 2 fb^{-1} . The result is for $m_t = 175 \text{ GeV}$; the mean value is 3% higher for $m_t = 170 \text{ GeV}$ and 4% lower for $m_t = 180 \text{ GeV}$.

21 Result is based on 1 fb^{-1} of data. The result is for $m_t = 170 \text{ GeV}$, and the mean value decreases with increasing m_t ; see their Fig. 2. The result is obtained after combining $\ell + \text{jets}$, $\ell\ell$, and $\ell\tau$ final states, and the ratios of the extracted cross sections are $R^{\ell\ell/\ell j} = 0.86^{+0.19}_{-0.17}$ and $R^{\ell\tau/\ell\ell - \ell j} = 0.97^{+0.32}_{-0.29}$, consistent with the SM expectation of $R = 1$. This leads to the upper bound of $\text{B}(t \rightarrow bH^+)$ as a function of m_{H^+} . Results are shown in their Fig. 1 for $\text{B}(H^+ \rightarrow \tau\nu) = 1$ and $\text{B}(H^+ \rightarrow c\bar{s}) = 1$ cases. Comparison of the m_t dependence of the extracted cross section and a partial NNLO prediction gives $m_t = 169.1^{+5.9}_{-5.2} \text{ GeV}$.

22 Result is based on 1 fb^{-1} of data. The result is for $m_t = 170 \text{ GeV}$, and the mean value changes by $-0.07 [m_t(\text{GeV}) - 170] \text{ pb}$ near the reference m_t value. Comparison of the m_t dependence of the extracted cross section and a partial NNLO QCD prediction gives $m_t = 171.5^{+9.9}_{-8.8} \text{ GeV}$. The $\ell\tau$ channel alone gives $7.6^{+4.9}_{-4.3} + 3.5^{+1.4}_{-1.4} \text{ pb}$ and the $\ell\ell$ channel gives $7.5^{+1.2}_{-1.1} + 0.7^{+0.7}_{-0.6} \text{ pb}$.

23 Result is based on 0.9 fb^{-1} of data. The first error is from stat + syst, while the latter error is from luminosity. The result is for $m_t = 175 \text{ GeV}$, and the mean value changes by $-0.09 \text{ pb} \cdot [m_t(\text{GeV}) - 175]$.

24 Result is based on 0.9 fb^{-1} of data. The cross section is obtained from the $\ell + \geq 3$ jet event rates with 1 or 2 b-tag, and also from the kinematical likelihood analysis of the $\ell + 3, 4$ jet events. The result is for $m_t = 172.6 \text{ GeV}$, and its m_t dependence shown in Fig. 3 leads to the constraint $m_t = 170 \pm 7 \text{ GeV}$ when compared to the SM prediction.

Quark Particle Listings

t

- ²⁵ Result is based on 360 pb⁻¹ of data. Events with high p_T oppositely charged dileptons $\ell^+ \ell^-$ ($\ell = e, \mu$) are used to obtain cross sections for $t\bar{t}$, W^+W^- , and $Z \rightarrow \tau^+\tau^-$ production processes simultaneously. The other cross sections are given in Table IV.
- ²⁶ Based on 1.02 fb⁻¹ of data. Result is for $m_t = 175$ GeV. Secondary vertex b -tag and neural network selections are used to achieve a signal-to-background ratio of about 1/2.
- ²⁷ Based on 425 pb⁻¹ of data. Result is for $m_t = 175$ GeV. For $m_t = 170.9$ GeV, $7.8 \pm 1.8(\text{stat} + \text{syst})$ pb is obtained.
- ²⁸ Based on 405 ± 25 pb⁻¹ of data. Result is for $m_t = 175$ GeV. The last error is for luminosity. Secondary vertex b -tag and neural network are used to separate the signal events from the background.
- ²⁹ Based on 425 pb⁻¹ of data. Assumes $m_t = 175$ GeV.
- ³⁰ Based on ~ 425 pb⁻¹. Assuming $m_t = 175$ GeV. The first error is combined statistical and systematic, the second one is luminosity.
- ³¹ Based on ~ 318 pb⁻¹. Assuming $m_t = 178$ GeV. The cross section changes by ± 0.08 pb for each \mp GeV change in the assumed m_t . Result is for at least one b -tag. For at least two b -tagged jets, $t\bar{t}$ signal of significance greater than 5σ is found, and the cross section is $10.1^{+1.6+2.0}_{-1.4-1.3}$ pb for $m_t = 178$ GeV.
- ³² Based on ~ 311 pb⁻¹. Assuming $m_t = 178$ GeV. For $m_t = 175$ GeV, the result is $6.0 \pm 1.2^{+0.9}_{-0.7}$. This is the first CDF measurement without lepton identification, and hence it has sensitivity to the $W \rightarrow \tau\nu$ mode.
- ³³ ABULENCIA, A 06E measures the $t\bar{t}$ production cross section in the all hadronic decay mode by selecting events with 6 to 8 jets and at least one b -jet. $S/B = 1/5$ has been achieved. Based on 311 pb⁻¹. Assuming $m_t = 178$ GeV.
- ³⁴ Based on ~ 318 pb⁻¹. Assuming $m_t = 178$ GeV. Result is for at least one b -tag. For at least two b -tagged jets, the cross section is $11.1^{+2.3+2.5}_{-1.9-1.9}$ pb.
- ³⁵ ABAZOV 05Q measures the top-quark pair production cross section with ~ 230 pb⁻¹ of data, based on the analysis of W plus n -jet events where W decays into e or μ plus neutrino, and at least one of the jets is b -jet like. The first error is statistical and systematic, and the second accounts for the luminosity uncertainty. The result assumes $m_t = 175$ GeV; the mean value changes by $(175 - m_t(\text{GeV})) \times 0.06$ pb in the mass range 160 to 190 GeV.
- ³⁶ ABAZOV 05R measures the top-quark pair production cross section with 224–243 pb⁻¹ of data, based on the analysis of events with two charged leptons in the final state. The result assumes $m_t = 175$ GeV; the mean value changes by $(175 - m_t(\text{GeV})) \times 0.08$ pb in the mass range 160 to 190 GeV.
- ³⁷ Based on 230 pb⁻¹. Assuming $m_t = 175$ GeV.
- ³⁸ Based on 194 pb⁻¹. Assuming $m_t = 175$ GeV.
- ³⁹ Based on 194 ± 11 pb⁻¹. Assuming $m_t = 175$ GeV.
- ⁴⁰ Based on 162 ± 10 pb⁻¹. Assuming $m_t = 175$ GeV.
- ⁴¹ ACOSTA 05V measures the top-quark pair production cross section with ~ 162 pb⁻¹ data, based on the analysis of W plus n -jet events where W decays into e or μ plus neutrino, and at least one of the jets is b -jet like. Assumes $m_t = 175$ GeV.
- ⁴² ACOSTA 04I measures the top-quark pair production cross section with 197 ± 12 pb⁻¹ data, based on the analysis of events with two charged leptons in the final state. Assumes $m_t = 175$ GeV.

Ratio of the Production Cross Sections of $t\bar{t}\gamma$ to $t\bar{t}$ at $\sqrt{s} = 1.96$ TeV

VALUE	DOCUMENT ID	TECN	COMMENT
0.024 \pm 0.009	1 AALTONEN 11Z CDF		$E_{T}(\gamma) > 10$ GeV, $ \eta(\gamma) < 1.0$

- • • We do not use the following data for averages, fits, limits, etc. • • •
- ¹ Based on 6.0 fb⁻¹ of data. The error is statistical and systematic combined. Events with lepton + $E_T + \geq 3$ jets ($\geq 1b$) with and without central, high E_T photon are measured. The result is consistent with the SM prediction of 0.024 ± 0.005 . The absolute production cross section is measured to be 0.18 ± 0.08 fb. The statistical significance is 3.0 standard deviations.

$t\bar{t}$ Production Cross Section in pp Collisions at $\sqrt{s} = 7$ TeV

VALUE (pb)	CL%	DOCUMENT ID	TECN	COMMENT
<1.7	95	1 AAD	12BE ATLS	$\ell^+ \ell^+ + E_T + \geq 2j$ + HT

- ¹ Based on 1.04 fb⁻¹ of pp data at $\sqrt{s} = 7$ TeV. The upper bounds are the same for LL, LR and RR chiral components of the two top quarks.

$t\bar{t}$ Production Cross Section in pp Collisions at $\sqrt{s} = 5.02$ TeV

Unless otherwise noted the first quoted error is from statistics, the second from systematic uncertainties, and the third from luminosity. If only two errors are quoted the luminosity is included in the systematic uncertainties.

VALUE (pb)	DOCUMENT ID	TECN	COMMENT
67.5 \pm 0.9 \pm 2.6	1 AAD	23J ATLS	dilepton + single ℓ channels
60.7 \pm 5.0 \pm 2.8 \pm 1.1	2 TUMASYAN 22T CMS		$e + \mu + \geq 2$ jets
63.0 \pm 4.1 \pm 3.0	3 TUMASYAN 22T CMS		combination of $e + \mu + \geq 2$ jets, $\ell +$ jets
69.5 \pm 6.1 \pm 5.6 \pm 1.6	4 SIRUNYAN 18AQ CMS		$\ell +$ jets, $\ell\ell +$ jets

- ¹ AAD 23J based on 257 pb⁻¹ of data from pp collisions. The second error is the sum of systematics (± 2.3), luminosity (± 1.1) and beam energy (± 0.2) uncertainties. The result agrees with the NNLO+NNLL SM prediction of $68.2^{+5.2}_{-5.3}$ pb.
- ² TUMASYAN 22T based on 302 pb⁻¹ of data from pp collisions at $\sqrt{s} = 5.02$ TeV. The errors are from statistics, systematics and luminosity.
- ³ Combination of the measurement by TUMASYAN 22T and the measurement in the $\ell +$ jets channel by SIRUNYAN 18AQ. The errors are from statistics and systematics + luminosity. The result is in agreement with the NNLO+NNLL SM prediction $66.8^{+2.9}_{-3.1}$ pb.
- ⁴ SIRUNYAN 18AQ based on 27.4 pb⁻¹ of data from pp collisions at $\sqrt{s} = 5.02$ TeV. The result is in agreement with the NNLO SM prediction $68.9^{+1.9}_{-2.3}(\text{scale}) \pm 2.3(\text{PDF}) \pm 1.4(\alpha_s)$ pb.

$t\bar{t}$ Production Cross Section in pp Collisions at $\sqrt{s} = 7$ TeV

Unless otherwise noted the first quoted error is from statistics, the second from systematic uncertainties, and the third from luminosity. If only two errors are quoted the luminosity is included in the systematic uncertainties.

VALUE (pb)	DOCUMENT ID	TECN	COMMENT
168.5 \pm 0.7 \pm 6.2 \pm 3.4 -5.9 -3.2	1 AABOUD 23 ATLS		$\ell^+ \ell^+ + \geq 3j$ (0,1,2 b -tagged j)
178.5 \pm 4.7	2 AAD 23AY LHC		$e^\pm \mu^\mp$ pair; ATLAS+CMS combined
161.7 \pm 6.0 \pm 12.0 \pm 3.6	3 KHACHATRYAN...17B CMS		$\ell^+ \ell^+ + \geq 4j$ ($\geq 1b$)
173.6 \pm 2.1 \pm 4.5 \pm 3.8 -4.0 -3.8	4 KHACHATRYAN...16AW CMS		$e + \mu + E_T + \geq 0j$
181.2 \pm 2.8 \pm 10.8 -10.6	5 AAD 15B0 ATLS		$e + \mu + E_T + \geq 0j$
178 \pm 3 \pm 16 \pm 3	6 AAD 15CC ATLS		$\ell +$ jets, $\ell\ell +$ jets, $\ell\tau_h +$ jets
	7 AAIJ 15R LHCB		$\mu + \geq 1j(b\text{-tag})$ forward region
182.9 \pm 3.1 \pm 6.4	8 AAD 14AY ATLS		$e + \mu + 1$ or 2b jets
194 \pm 18 \pm 46	9 AAD 13X ATLS		$\tau_h + E_T + \geq 5j$ ($\geq 2b$)
139 \pm 10 \pm 26	10 CHATRCHYAN 13AY CMS		≥ 6 jets with 2 b -tags
158.1 \pm 2.1 \pm 10.8	11 CHATRCHYAN 13BB CMS		$\ell + E_T +$ jets ($\geq 1b$ -tag)
152 \pm 12 \pm 32	12 CHATRCHYAN 13BE CMS		$\tau_h + E_T + \geq 4$ jets ($\geq 1b$)
177 \pm 20 \pm 14 \pm 7	13 AAD 12B ATLS		Repl. by AAD 12Bf
176 \pm 5 \pm 14 \pm 8 -11	14 AAD 12BF ATLS		$\ell\ell + E_T + \geq 2j$
187 \pm 11 \pm 18 \pm 6 -17	15 AAD 12B0 ATLS		$\ell + E_T + \geq 3j$ with b -tag
186 \pm 13 \pm 20 \pm 7	16 AAD 12CG ATLS		$\ell + \tau_h + E_T + \geq 2j$ ($\geq 1b$)
143 \pm 14 \pm 22 \pm 3	17 CHATRCHYAN 12AC CMS		$\ell + \tau_h + E_T + \geq 2j$ ($\geq 1b$)
161.9 \pm 2.5 \pm 5.1 \pm 3.6 -5.0	18 CHATRCHYAN 12AX CMS		$\ell\ell + E_T + \geq 2b$
145 \pm 31 \pm 42 \pm 7 -27	19 AAD 11A ATLS		$\ell^+ \ell^+ + \geq 4j$, $\ell\ell + E_T + \geq 2j$
173 \pm 39 \pm 7 -32	20 CHATRCHYAN 11AA CMS		$\ell + E_T + \geq 3$ jets
168 \pm 18 \pm 14 \pm 7	21 CHATRCHYAN 11F CMS		$\ell\ell + E_T +$ jets
154 \pm 17 \pm 6	22 CHATRCHYAN 11Z CMS		Combination
194 \pm 72 \pm 24 \pm 21	23 KHACHATRYAN...11A CMS		$\ell\ell + E_T + \geq 2$ jets

- ¹ AABOUD 23 based on 4.6 fb⁻¹ of data. The measurement is performed using a multivariate event classifier based on a binary learning algorithm which differentiates $t\bar{t}$ events from backgrounds in a three-dimensional space. The result is in agreement with the NNLO+NNLL SM prediction of $177^{+5}(\text{scale}) \pm 9(\text{PDF} + \alpha_s)$ pb for $m_t = 172.5$ GeV. Compared to the measured cross section using the dilepton mode of AAD 14AY, significance of discrepancy is between 1.9 σ to 2.1 σ .
- ² AAD 23AY based on 5 fb⁻¹ of data using $m_t = 172.5$ GeV. The ratio of the combined cross section at $\sqrt{s} = 8$ TeV to this one at $\sqrt{s} = 7$ TeV is determined as 1.363 ± 0.032 . The values of the cross sections as well as the ratio are consistent with the NNLO+NNLL SM predictions.
- ³ KHACHATRYAN 17B based on 5.0 fb⁻¹ of data, using a binned likelihood fit of templates to the data. Also the ratio $\sigma(t\bar{t}; 8 \text{ TeV})/\sigma(t\bar{t}; 7 \text{ TeV}) = 1.43 \pm 0.04 \pm 0.07 \pm 0.05$ is reported. The results are in agreement with NNLO SM predictions.
- ⁴ KHACHATRYAN 16AW based on 5.0 fb⁻¹ of data, using a binned likelihood fit to differential distributions of b -tagged and non- b -tagged jets. The result is in good agreement with NNLO SM predictions.
- ⁵ Based on 4.6 fb⁻¹ of data. Uses a template fit to distributions of E_T and jet multiplicities to measure simultaneously $t\bar{t}$, WW , and $Z/\gamma^* \rightarrow \tau\tau$ cross sections, assuming $m_t = 172.5$ GeV.
- ⁶ AAD 15CC based on 4.6 fb⁻¹ of data. The event selection criteria are optimized for the $\ell\tau_h +$ jets channel. Using only this channel $183 \pm 9 \pm 23 \pm 3$ pb is derived for the cross section.
- ⁷ AAIJ 15R, based on 1.0 fb⁻¹ of data, reports $0.239 \pm 0.053 \pm 0.033 \pm 0.024$ pb cross section for the forward fiducial region $p_T(\mu) > 25$ GeV, $2.0 < \eta(\mu) < 4.5$, $50 \text{ GeV} < p_T(b) < 100$ GeV, $2.2 < \eta(b) < 4.2$, $\Delta R(\mu, b) > 0.5$, and $p_T(\mu+b) > 20$ GeV. The three errors are from statistics, systematics, and theory. The result agrees with the SM NLO prediction.
- ⁸ AAD 14AY reports $182.9 \pm 3.1 \pm 4.2 \pm 3.6 \pm 3.3$ pb value based on 4.6 fb⁻¹ of data. The four errors are from statistics, systematic, luminosity, and the 0.66% beam energy uncertainty. We have combined the systematic uncertainties in quadrature. The result is for $m_t = 172.5$ GeV; for other m_t , $\sigma(m_t) = \sigma(172.5 \text{ GeV}) \times [1 - 0.0028 \times (m_t - 172.5 \text{ GeV})]$. The result is consistent with the SM prediction at NNLO.
- ⁹ Based on 1.67 fb⁻¹ of data. The result uses the acceptance for $m_t = 172.5$ GeV.
- ¹⁰ Based on 3.54 fb⁻¹ of data.
- ¹¹ Based on 2.3 fb⁻¹ of data.
- ¹² Based on 3.9 fb⁻¹ of data.
- ¹³ Based on 35 pb⁻¹ of data for an assumed top quark mass of $m_t = 172.5$ GeV.
- ¹⁴ Based on 0.70 fb⁻¹ of data. The 3 errors are from statistics, systematics, and luminosity. The result uses the acceptance for $m_t = 172.5$ GeV.
- ¹⁵ Based on 35 pb⁻¹ of data. The 3 errors are from statistics, systematics, and luminosity. The result uses the acceptance for $m_t = 172.5$ GeV and $173 \pm 17^{+18}_{-16} \pm 6$ pb is found without the b -tag.
- ¹⁶ Based on 2.05 fb⁻¹ of data. The hadronic τ candidates are selected using a BDT technique. The 3 errors are from statistics, systematics, and luminosity. The result uses the acceptance for $m_t = 172.5$ GeV.
- ¹⁷ Based on 2.0 fb⁻¹ and 2.2 fb⁻¹ of data for $\ell = e$ and $\ell = \mu$, respectively. The 3 errors are from statistics, systematics, and luminosity. The result uses the acceptance for $m_t = 172.5$ GeV.
- ¹⁸ Based on 2.3 fb⁻¹ of data. The 3 errors are from statistics, systematics, and luminosity. The result uses the profile likelihood-ratio (PLB) method and an assumed m_t of 172.5 GeV.
- ¹⁹ Based on 2.9 pb⁻¹ of data. The result for single lepton channels is $142 \pm 34^{+50}_{-31}$ pb, while for the dilepton channels is $151 \pm 78 \pm 37$
 $-62 - 24$ pb.

²⁰ Result is based on 36 pb⁻¹ of data. The first uncertainty corresponds to the statistical and systematic uncertainties, and the second corresponds to the luminosity.

²¹ Based on 36 pb⁻¹ of data. The ratio of $t\bar{t}$ and Z/γ^* cross sections is measured as $\sigma(pp \rightarrow t\bar{t})/\sigma(pp \rightarrow Z/\gamma^* \rightarrow e^+e^-/\mu^+\mu^-) = 0.175 \pm 0.018(\text{stat}) \pm 0.015(\text{syst})$ for $60 < m_{\ell\ell} < 120$ GeV, for which they use an NNLO prediction for the denominator cross section of 972 ± 42 pb.

²² Result is based on 36 pb⁻¹ of data. The first error is from statistical and systematic uncertainties, and the second from luminosity. This is a combination of a measurement in the dilepton channel (CHATRCHYAN 11F) and the measurement in the $\ell + \text{jets}$ channel (CHATRCHYAN 11Z) which yields $150 \pm 9 \pm 17 \pm 6$ pb.

²³ Result is based on 3.1 ± 0.3 pb⁻¹ of data.

$t\bar{t}$ Production Cross Section in pp Collisions at $\sqrt{s} = 8$ TeV

Unless otherwise noted the first quoted error is from statistics, the second from systematic uncertainties, and the third from luminosity. If only two errors are quoted the luminosity is included in the systematic uncertainties.

VALUE (pb)	DOCUMENT ID	TECN	COMMENT
------------	-------------	------	---------

• • • We do not use the following data for averages, fits, limits, etc. • • •

$243.3^{+6.0}_{-5.9}$	¹ AAD	23AY LHC	$e^\pm\mu^\mp$ pair; ATLAS+CMS combined
$248.3 \pm 0.7 \pm 13.4 \pm 4.7$	² AABOUD	18BH ATLS	$\ell + \cancel{E}_T + \geq 4j$ ($\geq 1b$)
$239 \pm 4 \pm 28 \pm 5$	³ AABOUD	17Z ATLS	$\tau_h + \cancel{E}_T + \geq 2j$ ($\geq 2b$)
$228.5 \pm 3.8 \pm 13.7 \pm 6.0$	⁴ KHACHATRYAN...17B	CMS	$\ell + \cancel{E}_T + \geq 4j$ ($\geq 1b$)
$242.9 \pm 1.7 \pm 8.6$	⁵ AAD	16BK ATLS	$e + \mu + 1$ or $2b$ jets
$244.9 \pm 1.4^{+6.3}_{-5.5} \pm 6.4$	⁶ KHACHATRYAN...16AW	CMS	$e + \mu + \cancel{E}_T + \geq 0j$
$275.6 \pm 6.1 \pm 37.8 \pm 7.2$	⁷ KHACHATRYAN...16BC	CMS	$\geq 6j$ ($\geq 2b$)
$260 \pm 1 \pm 24 \pm 25$	⁸ AAD	15BP ATLS	$\ell + \cancel{E}_T + \geq 3j$ ($\geq 1b$)
$242.4 \pm 1.7 \pm 10.2$	⁹ AAIJ	15R LHCb	$\mu + \geq 1j$ (b -tag) forward region
$239 \pm 2 \pm 11 \pm 6$	¹⁰ AAD	14AY ATLS	$e + \mu + 1$ or $2b$ jets
$257 \pm 3 \pm 24 \pm 7$	¹¹ CHATRCHYAN14F	CMS	$\ell\ell + \cancel{E}_T + \geq 2j$ (≥ 1 b -tag)
	¹² KHACHATRYAN...14S	CMS	$\ell + \tau_h + \cancel{E}_T + \geq 2j$ ($\geq 1b$)

¹ AAD 23AY based on 20 fb⁻¹ of data using $m_t = 172.5$ GeV. The ratio of this cross section at $\sqrt{s} = 8$ TeV to the combined cross section at $\sqrt{s} = 7$ TeV is determined as 1.363 ± 0.032 . The values of cross sections as well as their ratio are consistent with the NNLO+NNLL SM predictions.

² AABOUD 18BH based on 20.2 fb⁻¹ of data. The result is for $m_t = 172.5$ GeV. To reduce effects of uncertainties in the jet energy scale and b -tagging efficiency, they are included as nuisance parameters in the fit of discriminant distributions, after separating selected events into three regions. Furthermore the W +jets background distribution is modelled using Z +jets event data.

³ AABOUD 17Z based on 20.2 fb⁻¹ of data, using the mode $t\bar{t} \rightarrow \tau\nu q^{\prime}\bar{q}b\bar{b}$ with τ decaying hadronically. Single prong and 3 prong decays of τ are separately analyzed. The result is consistent with the SM. The third quoted uncertainty is due to luminosity.

⁴ KHACHATRYAN 17B based on 19.6 fb⁻¹ of data, using a binned likelihood fit of templates to the data. Also the ratio $\sigma(t\bar{t}; 8\text{TeV})/\sigma(t\bar{t}; 7\text{TeV}) = 1.43 \pm 0.04 \pm 0.07 \pm 0.05$ is reported. The results are in agreement with NNLO SM predictions.

⁵ AAD 16BK is an update of the value from AAD 14AY using the improved luminosity calibration. The value $242.9 \pm 1.7 \pm 5.5 \pm 5.1 \pm 4.2$ pb is reported, where we have combined the systematic uncertainties in quadrature. Also the ratio $\sigma(t\bar{t}; 8\text{TeV})/\sigma(t\bar{t}; 7\text{TeV}) = 1.328 \pm 0.024 \pm 0.015 \pm 0.038 \pm 0.001$ has been updated. The former result is consistent with the SM predictions at NNLO, while the latter result is 2.1 σ below the expectation.

⁶ KHACHATRYAN 16AW based on 19.7 fb⁻¹ of data, using a binned likelihood fit to differential distributions of b -tagged and non- b -tagged jets. The result is in good agreement with NNLO SM predictions.

⁷ KHACHATRYAN 16BC based on 18.4 fb⁻¹ of data. The last uncertainty is due to luminosity. Cuts on kinematical fit probability and $\Delta R(b, b)$ are imposed. The major QCD background is determined from the data. The result is for $m_t = 172.5$ GeV and in agreement with the SM prediction. The top quark p_T spectra, also measured, are significantly softer than theoretical predictions.

⁸ AAD 15BP based on 20.3 fb⁻¹ of data. The result is for $m_t = 172.5$ GeV and in agreement with the SM prediction 253^{+13}_{-15} pb at NNLO+NNLL. Superseded by AABOUD 18BH.

⁹ AAIJ 15R, based on 2.0 fb⁻¹ of data, reports $0.289 \pm 0.043 \pm 0.040 \pm 0.029$ pb cross section for the forward fiducial region $p_T(\mu) > 25$ GeV, $2.0 < \eta(\mu) < 4.5$, $50 \text{ GeV} < p_T(b) < 100$ GeV, $2.2 < \eta(b) < 4.2$, $\Delta R(\mu, b) > 0.5$, and $p_T(\mu+b) > 20$ GeV. The three errors are from statistics, systematics, and theory. The result agrees with the SM NLO prediction.

¹⁰ AAD 14AY reports $242.4 \pm 1.7 \pm 5.5 \pm 7.5 \pm 4.2$ pb value based on 20.3 fb⁻¹ of data. The four errors are from statistics, systematic, luminosity, and the 0.66% beam energy uncertainty. We have combined the systematic uncertainties in quadrature. The result is for $m_t = 172.5$ GeV; for other m_t , $\sigma(m_t) = \sigma(172.5\text{GeV}) \times [1 - 0.0028 \times (m_t - 172.5\text{GeV})]$. Also measured is the ratio $\sigma(t\bar{t}; 8\text{TeV})/\sigma(t\bar{t}; 7\text{TeV}) = 1.326 \pm 0.024 \pm 0.015 \pm 0.049 \pm 0.001$. The results are consistent with the SM predictions at NNLO.

¹¹ Based on 5.3 fb⁻¹ of data. The result is for $m_t = 172.5$ GeV, and a parametrization is given in eq.(6.1) for the mean value at other m_t values. The result is in agreement with the SM prediction $252.9^{+6.4}_{-8.6}$ pb at NNLO.

¹² Based on 19.6 fb⁻¹ of data. The measurement is in the channel $t\bar{t} \rightarrow (b\ell\nu)(b\tau\nu)$, where τ decays into hadrons (τ_h). The result is for $m_t = 172.5$ GeV. For $m_t = 173.3$ GeV, the cross section is lower by 3.1 pb.

$t\bar{t}$ Production Cross Section in pp Collisions at $\sqrt{s} = 13$ TeV

VALUE (pb)	DOCUMENT ID	TECN	COMMENT
------------	-------------	------	---------

• • • We do not use the following data for averages, fits, limits, etc. • • •

$829 \pm 1 \pm 15.4$	¹ AAD	23S ATLS	$e^\pm\mu^\mp + 1$ or 2 b -jets
$791 \pm 1 \pm 21 \pm 14$	² TUMASYAN	21J CMS	$1\ell + \text{jets}$
$830 \pm 0.4 \pm 36 \pm 14$	³ AAD	20AH ATLS	$\ell + \geq 4$ jets ($\geq 1b$ -tag)
$826.4 \pm 3.6 \pm 11.5 \pm 15.8$	⁴ AAD	20Q ATLS	$e\mu + 1$ or 2 b -jets

$781 \pm 7 \pm 62 \pm 20$	⁵ SIRUNYAN	20V CMS	$\ell\tau_h + \geq 3$ jets ($\geq 1b$ -tag)
$803 \pm 2 \pm 25 \pm 20$	⁶ SIRUNYAN	19AR CMS	dilepton channel ($e\mu, 2e, 2\mu$)
	⁷ SIRUNYAN	19P CMS	dilepton channel
$815 \pm 9 \pm 38 \pm 19$	⁸ KHACHATRYAN...17N	CMS	$e\mu + \geq 2j$ ($\geq 1b$ j)
$888 \pm 2 \pm 26 \pm 20$	⁹ SIRUNYAN	17W CMS	$\ell + \geq 1j$
$818 \pm 8 \pm 35$	¹⁰ AABOUD	16R ATLS	$e + \mu + 1$ or $2b$ jets
$746 \pm 58 \pm 53 \pm 36$	¹¹ KHACHATRYAN...16J	CMS	$e + \mu + \geq 2j$

¹ AAD 23S based on 140 fb⁻¹ of data at 13 TeV. The second error is the sum of systematic effects (± 13), luminosity (± 8), and beam energy (± 2) uncertainties. This measurement supersedes that of AAD 20Q. The result is in good agreement with the NNLO+NNLL SM prediction.

² TUMASYAN 21J result is based on 137 fb⁻¹ of data. The last uncertainty is due to the beam luminosity. The result is in agreement with the SM prediction of 832^{+40}_{-46} pb at NNLO+NNLL. Measurements of differential and double-differential cross sections are also presented.

³ AAD 20AH based on 139 fb⁻¹ of data. The last quoted uncertainty is due to the beam luminosity. The result is for $m_t = 172.5$ GeV and in agreement with the SM prediction of $832^{+20}_{-29}(\text{scale}) \pm 35(\text{PDF}+\alpha(s))$ pb at NNLO+NNLL.

⁴ AAD 20Q reports $826.4 \pm 3.6 \pm 11.5 \pm 15.7 \pm 1.9$ pb based on 36.1 fb⁻¹ of data at 13 TeV. The four errors stem from statistics, systematic effects, luminosity, and beam energy, respectively. We have combined luminosity and beam energy uncertainties in quadrature. The result is in agreement with the SM prediction $832^{+20}_{-29}(\text{scale}) \pm 35(\text{PDF}+\alpha(s))$ pb at NNLO+NNLL for $m_t = 172.5$ GeV.

⁵ SIRUNYAN 20V based on 35.9 fb⁻¹ of pp data at $\sqrt{s} = 13$ TeV. The last uncertainty is due to beam luminosity. The $t\bar{t}$ production cross section is measured in the $t\bar{t} \rightarrow (\ell\nu\ell)(\tau_h\nu\tau)bb$ final state, where τ_h refers to the hadronic decays of τ . The result is for $m_t = 172.5$ GeV and in agreement with the SM prediction at NNLO+NNLL.

⁶ SIRUNYAN 19AR based on 35.9 fb⁻¹ of data. Obtained from the visible cross section measured using a template fit to multidifferential distributions categorized according to the b -tagged jet multiplicity. The result is for $m_t = 172.5$ GeV and in agreement with the SM prediction at NNLO+NNLL.

⁷ SIRUNYAN 19P reports differential $t\bar{t}$ cross sections measured using dilepton events at 13 TeV with 35.9 fb⁻¹ and compared to NLO predictions.

⁸ KHACHATRYAN 17N based on 2.2 fb⁻¹ of data. The last quoted uncertainty is due to the beam luminosity. This measurement supersedes that of KHACHATRYAN 16J.

⁹ SIRUNYAN 17W based on 2.2 fb⁻¹ of pp data at $\sqrt{s} = 13$ TeV. Events are categorized according to the jet multiplicity and the number of b -tagged jets. A likelihood fit is performed to the event distributions to compare to the NNLO+NNLL prediction.

¹⁰ AABOUD 16R reported value $818 \pm 8 \pm 27 \pm 19 \pm 12$ pb based on 3.2 fb⁻¹ of data. The four errors are from statistics, systematic, luminosity, and beam energy. We have combined the systematic uncertainties in quadrature. The result is in agreement with the SM prediction $832^{+20}_{-29}(\text{scale}) \pm 35(\text{PDF}+\alpha(s))$ pb at NNLO+NNLL for $m_t = 172.5$ GeV.

¹¹ KHACHATRYAN 16J based on 43 pb⁻¹ of data. The last uncertainty is due to luminosity. The result is for $m_t = 172.5$ GeV and in agreement with the SM prediction $832^{+20}_{-29}(\text{scale}) \pm 35(\text{PDF}+\alpha(s))$ pb at NNLO+NNLL.

$t\bar{t}$ Production Cross Section in pp Collisions at $\sqrt{s} = 13.6$ TeV

VALUE (pb)	DOCUMENT ID	TECN	COMMENT
------------	-------------	------	---------

• • • We do not use the following data for averages, fits, limits, etc. • • •

$850 \pm 3 \pm 27$	¹ AAD	24 ATLS	$e^\pm\mu^\mp + 1$ or 2 b -jets
--------------------	------------------	---------	-------------------------------------

¹ AAD 24 based on 29 fb⁻¹ of data. The last error includes the luminosity uncertainty of ± 20 pb. The result is for $m_t = 172.5$ GeV and in agreement with the SM prediction of $924^{+32}_{-40}(\text{scale}+\text{PDF}+\alpha_s)$ pb. The ratio of the $t\bar{t}$ to the Z production cross section is also measured as $1.145 \pm 0.003 \pm 0.021 \pm 0.002$, which is consistent with the SM prediction of $1.238^{+0.063}_{-0.071}(\text{scale}+\text{PDF}+\alpha_s)$. The uncertainties of luminosity and lepton efficiency largely cancel in the ratio.

$t\bar{t}$ Production Cross Section in Nucleus-Nucleus Collisions

VALUE (μbarn)	DOCUMENT ID	TECN	COMMENT
----------------------------	-------------	------	---------

• • • We do not use the following data for averages, fits, limits, etc. • • •

$2.03^{+0.71}_{-0.64}$	¹ SIRUNYAN	20Bc CMS	Pb-Pb collisions, dilepton + b -jets
$2.54^{+0.84}_{-0.74}$	² SIRUNYAN	20Bc CMS	Pb-Pb collisions, dilepton only

¹ SIRUNYAN 20Bc based on (1.7 ± 0.1) nb⁻¹ of lead-lead collision data at a nucleon-nucleon c.m. energy of 5.02 TeV. It makes use of the final-state dilepton kinematic properties together with requirements on the number of b -jets. The measured value is compatible with QCD predictions.

² SIRUNYAN 20Bc based on (1.7 ± 0.1) nb⁻¹ of lead-lead collision data at a nucleon-nucleon c.m. energy of 5.02 TeV. It makes use of the final-state dilepton kinematic properties alone. The measured value is compatible with QCD predictions.

$t\bar{t}$ $t\bar{t}$ Production Cross Section in pp Collisions at $\sqrt{s} = 8$ TeV

VALUE (fb)	CL%	DOCUMENT ID	TECN	COMMENT
------------	-----	-------------	------	---------

• • • We do not use the following data for averages, fits, limits, etc. • • •

< 23	95	¹ AAD	15AR ATLS	$\ell + \cancel{E}_T + \geq 5j$ ($\geq 2b$)
< 70	95	² AAD	15BY ATLS	$\geq 2\ell + \cancel{E}_T + \geq 2j$ ($\geq 1b$)
< 32	95	³ KHACHATRYAN...14R	CMS	$\ell + \cancel{E}_T + \geq 6j$ ($\geq 2b$)

¹ AAD 15AR based on 20.3 fb⁻¹ of data. A fit to H_T distributions in multi-channels classified by the number of jets and of b -tagged jets is performed.

² AAD 15BY based on 20.3 fb⁻¹ of data. A same-sign lepton pair is required. An excess over the SM prediction reaches 2.5σ for hypotheses involving heavy resonances decaying into $t\bar{t}t\bar{t}$.

³ Based on 19.6 fb⁻¹ of data, using a multivariate analysis to separate signal from backgrounds. About $\sigma(t\bar{t}t\bar{t}) = 1$ fb is expected in the SM.

Quark Particle Listings

t

 $t\bar{t}$ Production Cross Section in pp Collisions at $\sqrt{s} = 13$ TeV

VALUE (fb)	CL%	DOCUMENT ID	TECN	COMMENT
•••				We do not use the following data for averages, fits, limits, etc. •••
$22.5^{+6.6}_{-5.5}$		1 AAD	23bc ATLS	(same-sign 2ℓ) or $\geq 3\ell$
$17.7^{+3.7+2.3}_{-3.5-1.9}$		2 HAYRAPETYAN...23b	CMS	(same-sign 2ℓ), 3ℓ , 4ℓ
36^{+12}_{-11}		3 TUMASYAN	23AQ CMS	$(0,1\ell) + (\ell^\pm\ell^\mp)$ channels
$17 \pm 4 \pm 3$		4 TUMASYAN	23AQ CMS	CMS combined
26^{+17}_{-15}		5 AAD	21bc ATLS	ℓ or $\ell^+\ell^-$ + jets
24^{+7}_{-6}		6 AAD	21bc ATLS	combination of $1\ell/2\ell(\text{OS})$ and $2\ell(\text{SS})/3\ell$
24^{+7}_{-6}		7 AAD	20AR ATLS	(same-sign 2ℓ) or $\geq 3\ell$ + jets
$12.6^{+5.8}_{-5.2}$		8 SIRUNYAN	20c CMS	(same-sign 2ℓ) or 3ℓ + jets
<47	95	9 AABOUD	19AP ATLS	$\ell + \ell^+\ell^-$ channels
<49	95	10 AABOUD	19AP ATLS	combination of ATLAS
13^{+11}_{-9}		11 SIRUNYAN	19CN CMS	combination of CMS
<48	95	12 SIRUNYAN	19CN CMS	ℓ +jets, $\ell^+\ell^-$ +jets channels
<69	95	13 AABOUD	18CE ATLS	$\geq 2\ell(\text{same sign}) + \cancel{E}_T + \geq 1b_j$
$16.9^{+13.8}_{-11.4}$		14 SIRUNYAN	18BU CMS	$t\bar{t}t\bar{t} \rightarrow (\text{same sign } 2\ell \text{ or } \geq 3\ell) + \geq 4j (\geq 2b)$
<94	95	15 SIRUNYAN	17AB CMS	ℓ +jets, $\ell^+\ell^-$ +jets channels
<42	95	16 SIRUNYAN	17s CMS	(same sign 2ℓ) + $\cancel{E}_T + \geq 2j$

1 AAD 23bc result is based on 140 fb^{-1} of data. The result corresponds to observed significance of 6.1σ .

2 HAYRAPETYAN 23b based on 138 fb^{-1} of data. Improvements include the identification of leptons and jets from b hadrons, and from the revised analysis strategy for the signal-background separation by application of machine learning techniques. The result corresponds to the observed significance of 5.6σ and is in agreement with the NLO (QCD+EW) SM prediction of $13.4^{+1.0}_{-1.8} \text{ fb}$ including soft-gluon emission corrections at the next-to-leading logarithmic accuracy.

3 TUMASYAN 23AQ based on up to 138 fb^{-1} of data. The all-hadronic final state is included for the first time.

4 TUMASYAN 23AQ based on up to 138 fb^{-1} of data. It combines earlier CMS results, giving the observed significance of 4.0σ .

5 AAD 21bc result is based on 139 fb^{-1} of data. The events are categorized according to the number of jets and how likely to contain b -hadrons and a multivariate analysis is used to discriminate the signal from backgrounds. The result corresponds to observed significance of 1.9σ .

6 AAD 21bc combines the results of the four-top-quark production cross section measured from the $1\ell/\text{opposite-sign } 2\ell$ channel with that from the same-sign $2\ell/3\ell$ channel (AAD 20AR). The result corresponds to observed significance of 4.7σ and is consistent within 2.0σ with the NLO (QCD+EW) SM prediction of $12.0 \pm 2.4 \text{ fb}$.

7 AAD 20AR based on 139 fb^{-1} of data. Jet multiplicity, jet flavor and event kinematics are used in a multivariate analysis to discriminate the signal from backgrounds. The result corresponds to observed significance of 4.3σ and is consistent within 1.7σ with the NLO (QCD+EW) SM prediction of $12.0 \pm 2.4 \text{ fb}$.

8 SIRUNYAN 20c based on 137 fb^{-1} of data. Both cut-based and multivariate approaches are taken to discriminate the signal from backgrounds. The result is in agreement with the NLO (QCD+EW) SM prediction of $12.0^{+2.2}_{-2.5} \text{ fb}$. The measurement constrains the top quark Yukawa coupling strength parameter to be $|Y_t/Y_t^{\text{SM}}| < 1.7$ (95% CL). It is also used to constrain an oblique parameter of the Higgs boson. Superseded by HAYRAPETYAN 23b.

9 AABOUD 19AP based on 36.1 fb^{-1} of data. The upper limit corresponds to 5.1 times the NLO SM cross section.

10 AABOUD 19AP limit from data combined with AABOUD 18CE. The upper limit corresponds to 5.3 times the NLO SM cross section. Also a limit on the four-top-quark contact interaction of $|C_{4t}|/\Lambda^2 < 1.9 \text{ TeV}^{-2}$ (95% CL) is obtained in an EFT model.

11 SIRUNYAN 19CN based on 35.8 fb^{-1} of data, combined with SIRUNYAN 18BU. The results are also interpreted in the effective field theory framework.

12 SIRUNYAN 19CN based on 35.8 fb^{-1} of data. A multivariate analysis using global event and jet properties is performed to discriminate from $t\bar{t}$ background.

13 AABOUD 18CE based on 36.1 fb^{-1} of proton-proton data taken at $\sqrt{s} = 13 \text{ TeV}$. Events including a same-sign lepton pair are used. The result is consistent with the NLO SM cross section of 9.2 fb .

14 SIRUNYAN 18BU based on 35.9 fb^{-1} of proton-proton data taken at $\sqrt{s} = 13 \text{ TeV}$. Yields from signal regions and control regions defined based on N_{jets} , N_b and N_l are combined in a maximum-likelihood fit. The result is in agreement with the NLO SM prediction $9.2^{+2.9}_{-2.4} \text{ fb}$. The measurement constrains the top quark Yukawa coupling strength parameter to be $|Y_t/Y_t^{\text{SM}}| < 2.1$ (95% CL).

15 SIRUNYAN 17AB based on 2.6 fb^{-1} of data. A multivariate analysis is used to discriminate between $t\bar{t}t\bar{t}$ signal and $t\bar{t}$ background. A combination with a previous search (CMS, KHACHATRYAN 16bJ) in the same-sign dilepton channel gives an upper limit of 69 fb (95% CL), corresponding to $7.4 \times (\text{SM prediction})$.

16 SIRUNYAN 17s based on 35.9 fb^{-1} . The limit is in agreement with the NLO SM prediction $9.2^{+2.9}_{-2.4} \text{ fb}$. Superseded by SIRUNYAN 18BU. The signal events are also used to constrain various new physics models.

 $t\bar{t}W$ Production Cross Section in pp Collisions at $\sqrt{s} = 8 \text{ TeV}$

VALUE (fb)	DOCUMENT ID	TECN	COMMENT
•••			We do not use the following data for averages, fits, limits, etc. •••
$170^{+90}_{-80} \pm 70$	1 KHACHATRY...14N	CMS	$t\bar{t}W \rightarrow \text{same sign dilepton} + \cancel{E}_T + \text{jets}$

1 Based on 19.5 fb^{-1} of data. The result is consistent with the SM prediction of $\sigma(t\bar{t}W) = 206^{+21}_{-23} \text{ fb}$.

 $t\bar{t}W$ Production Cross Section in pp Collisions at $\sqrt{s} = 13 \text{ TeV}$

VALUE (pb)	DOCUMENT ID	TECN	COMMENT
•••			We do not use the following data for averages, fits, limits, etc. •••
$0.868 \pm 0.040 \pm 0.051$	1 TUMASYAN	23AN CMS	2 or 3 $\ell + \cancel{E}_T + \text{jets}$
$0.87 \pm 0.13 \pm 0.14$	2 AABOUD	19AR ATLS	$2,3,4\ell + \cancel{E}_T + \text{jets}$
$0.77^{+0.12+0.13}_{-0.11-0.12}$	3 SIRUNYAN	18Bs CMS	$t\bar{t}W \rightarrow \text{same sign dilepton} + \cancel{E}_T + \text{jets}$
1 TUMASYAN 23AN result is based on 138 fb^{-1} of proton-proton data. The $t\bar{t}W^+$ and $t\bar{t}W^-$ production cross sections, respectively, are measured as $0.553 \pm 0.030 \pm 0.030 \text{ pb}$ and $0.343 \pm 0.026 \pm 0.025 \text{ pb}$. The results are within 2σ deviations from the NLO FxFx SM predictions, $0.592^{+0.155}_{-0.097} \text{ pb}$ ($t\bar{t}W$), $0.384^{+0.053}_{-0.033} \text{ pb}$ ($t\bar{t}W^+$) and $0.198^{+0.026}_{-0.017} \text{ pb}$ ($t\bar{t}W^-$).			
2 AABOUD 19AR result is based on 35.9 fb^{-1} of data. $t\bar{t}W$ and $t\bar{t}Z$ cross sections are simultaneously measured using a combined fit to the events divided into multiple regions. The result is consistent with the SM prediction at NLO $0.60^{+0.08}_{-0.07} \text{ pb}$. It is also used to constrain the Wilson coefficients for dimension-six operators which modify the $t\bar{t}Z$ vertex.			
3 SIRUNYAN 18Bs result is based on 35.9 fb^{-1} of proton-proton data taken at $\sqrt{s} = 13 \text{ TeV}$. The result is consistent with the SM prediction and is used to constrain the Wilson coefficients for dimension-six operators describing new interactions. The result is consistent with the SM prediction at NLO $0.628 \pm 0.082 \text{ pb}$.			

 $t\bar{t}Z$ Production Cross Section in pp Collisions at $\sqrt{s} = 8 \text{ TeV}$

VALUE (fb)	DOCUMENT ID	TECN	COMMENT
•••			We do not use the following data for averages, fits, limits, etc. •••
200^{+80+40}_{-70-30}	1 KHACHATRY...14N	CMS	$t\bar{t}Z \rightarrow 3,4\ell + \cancel{E}_T + \text{jets}$
1 Based on 19.5 fb^{-1} of data. The result is consistent with the SM prediction of $\sigma(t\bar{t}Z) = 197^{+22}_{-25} \text{ fb}$.			

 $t\bar{t}Z$ Production Cross Section in pp Collisions at $\sqrt{s} = 13 \text{ TeV}$

VALUE (pb)	DOCUMENT ID	TECN	COMMENT
•••			We do not use the following data for averages, fits, limits, etc. •••
$0.99 \pm 0.05 \pm 0.08$	1 AAD	21As ATLS	$3,4\ell + \text{jets}$
$0.95 \pm 0.05 \pm 0.06$	2 SIRUNYAN	20Ab CMS	$3,4\ell + \text{jets}$
$0.95 \pm 0.08 \pm 0.10$	3 AABOUD	19AR ATLS	$2,3,4\ell + \cancel{E}_T + \text{jets}$
$0.99^{+0.09+0.12}_{-0.08-0.10}$	4 SIRUNYAN	18Bs CMS	$t\bar{t}Z \rightarrow 3,4\ell + \cancel{E}_T + \text{jets}$
1 AAD 21As based on 139 fb^{-1} of data. The result is consistent with the SM prediction of $0.88^{+0.09}_{-0.10} \text{ pb}$ which includes NLO QCD+EW corrections. Also overall the differential cross sections are in good agreement with the SM predictions.			
2 SIRUNYAN 20Ab based on 77.5 fb^{-1} of data at 13 TeV . The result is consistent with the NLO SM prediction of $0.84 \pm 0.10 \text{ pb}$. Differential cross sections are measured and used to constrain the anomalous couplings and Wilson coefficients for the $t\bar{t}Z$ interaction.			
3 AABOUD 19AR based on 35.9 fb^{-1} of data. $t\bar{t}W$ and $t\bar{t}Z$ cross sections are simultaneously measured using a combined fit to the events divided into multiple regions. The result is consistent with the SM prediction at NLO $0.88^{+0.09}_{-0.11} \text{ pb}$. It is also used to constrain the Wilson coefficients for dimension-six operators which modify the $t\bar{t}Z$ vertex.			
4 Based on 35.9 fb^{-1} of proton-proton data taken at $\sqrt{s} = 13 \text{ TeV}$. The result is consistent with the SM prediction and is used to constrain the Wilson coefficients for dimension-six operators describing new interactions. The result is consistent with the SM prediction at NLO $0.839 \pm 0.101 \text{ pb}$.			

 $t\bar{t}\gamma$ Production Cross Section in pp Collisions at $\sqrt{s} = 13 \text{ TeV}$

VALUE (pb)	DOCUMENT ID	TECN	COMMENT
•••			We do not use the following data for averages, fits, limits, etc. •••
1 TUMASYAN	22W CMS		$1\gamma + \ell^+\ell^- + \geq 1b_j$
2 TUMASYAN	21H CMS		$pp \rightarrow t\bar{t}\gamma$
3 AABOUD	19AD ATLS		$pp \rightarrow t\bar{t}\gamma$
1 TUMASYAN 22W measured fiducial inclusive and differential cross-sections for $pp \rightarrow t\bar{t}\gamma$ at 13 TeV with 138 fb^{-1} of data. The results are in agreement with the SM predictions. The results are used to constrain anomalous couplings of the top quark in the SMEFT framework.			
2 TUMASYAN 21H measured fiducial inclusive and differential cross-sections for $pp \rightarrow t\bar{t}\gamma$ at 13 TeV with 137 fb^{-1} of data. The results are in agreement with the SM predictions. The results are used to constrain anomalous couplings of the top quark in the SMEFT framework.			
3 AABOUD 19AD measured fiducial inclusive and differential cross-sections for $pp \rightarrow t\bar{t}\gamma$ at 13 TeV with 36.1 fb^{-1} of data. The results are in agreement with the theoretical predictions.			

 $f(Q_0)$: $t\bar{t}$ Fraction of Events with a Veto on Additional Central Jet Activity in pp Collisions at $\sqrt{s} = 7 \text{ TeV}$

VALUE (%)	DOCUMENT ID	TECN	COMMENT
•••			We do not use the following data for averages, fits, limits, etc. •••
$80.0 \pm 1.1 \pm 1.6$	1 CHATRCHYAN 14AE	CMS	$Q_0 = 75 \text{ GeV}$ ($ \eta < 2.4$)
$92.0 \pm 0.7 \pm 0.8$	1 CHATRCHYAN 14AE	CMS	$Q_0 = 150 \text{ GeV}$ ($ \eta < 2.4$)
$98.0 \pm 0.3 \pm 0.3$	1 CHATRCHYAN 14AE	CMS	$Q_0 = 300 \text{ GeV}$ ($ \eta < 2.4$)
$56.4 \pm 1.3^{+2.6}_{-2.8}$	2 AAD	12Bl ATLS	$Q_0 = 25 \text{ GeV}$ ($ \eta < 2.1$)
$84.7 \pm 0.9 \pm 1.0$	2 AAD	12Bl ATLS	$Q_0 = 75 \text{ GeV}$ ($ \eta < 2.1$)
$95.2^{+0.5}_{-0.6} \pm 0.4$	2 AAD	12Bl ATLS	$Q_0 = 150 \text{ GeV}$ ($ \eta < 2.1$)

1 CHATRCHYAN 15 based on 5.0 fb^{-1} of data. The $t\bar{t}$ events are selected in the dilepton and lepton + jets decay channels. For other values of Q_0 see Table 5.

2 Based on 2.05 fb^{-1} of data. The $t\bar{t}$ events are selected in the dilepton decay channel with two identified b -jets.

Fraction of $t\bar{t}$ + multi-jet Events in pp Collisions at $\sqrt{s} = 7$ TeV

VALUE	DOCUMENT ID	TECN	COMMENT
0.332±0.090	¹ AAD	15D ATLS	$\ell + \cancel{E}_T + n_j$ ($n=3$ to 8)
0.436±0.098	² CHATRCHYAN14AE	CMS	$t\bar{t}(\ell\ell) + 0$ jet ($E_T > 30$ GeV)
0.232±0.125	² CHATRCHYAN14AE	CMS	$t\bar{t}(\ell\ell) + 1$ jet ($E_T > 30$ GeV)
	² CHATRCHYAN14AE	CMS	$t\bar{t}(\ell\ell) + \geq 2$ jet ($E_T > 30$ GeV)

- ¹ Based on 4.6 fb⁻¹ of data. Fiducial $t\bar{t}$ production cross section is presented as a function of the jet multiplicity for up to eight jets with the jet p_T threshold of 25, 40, 60, and 80 GeV, and as a function of jet p_T up to the 5th jet. MC models can be discriminated by using data for high jet multiplicity and by p_T distributions of the leading and 5th jet.
- ² Based on 5.0 fb⁻¹ of data. Events with two oppositely charged leptons, large \cancel{E}_T and jets with at least 1 b -tag are used to measure the fraction of $t\bar{t}$ plus additional jets. The gap fraction ($n=0$ jet rate) as a function of the jet p_T and that of H_T , the scalar sum of the p_T 's of additional jets, is shown in Fig. 8.

 $t\bar{t}$ Charge Asymmetry (A_C) in pp Collisions at $\sqrt{s} = 7$ TeV

$A_C = (N(\Delta|y| > 0) - N(\Delta|y| < 0)) / (N(\Delta|y| > 0) + N(\Delta|y| < 0))$ where $\Delta|y| = |y_t| - |y_{\bar{t}}|$ is the difference between the absolute values of the top and antitop rapidities and N is the number of events with $\Delta|y|$ positive or negative.

VALUE (%)	DOCUMENT ID	TECN	COMMENT
0.5±0.7±0.6	¹ AABOUD	18AMLHC	ATLAS+CMS combination (lepton + jets)
2.1±2.5±1.7	² AAD	15AJ ATLS	$\ell\ell + \cancel{E}_T + \geq 2j$
0.6±1.0	³ AAD	14I ATLS	$\ell + \cancel{E}_T + \geq 4j$ ($\geq 1b$)
-1.0±1.7±0.8	⁴ CHATRCHYAN14D	CMS	$\ell\ell + \cancel{E}_T + \geq 2j$ ($\geq 1b$)
-1.9±2.8±2.4	⁵ AAD	12BK ATLS	$\ell + \cancel{E}_T + \geq 4j$ ($\geq 1b$)
0.4±1.0±1.1	⁶ CHATRCHYAN12BB	CMS	$\ell + \cancel{E}_T + \geq 4j$ ($\geq 1b$)
-1.3±2.8± ^{2.9} _{-3.1}	⁷ CHATRCHYAN12Bs	CMS	$\ell + \cancel{E}_T + \geq 4j$ ($\geq 1b$)

- ¹ ATLAS and CMS combination based on the data of AAD 14I and CHATRCHYAN 12BB. It takes into account the correlations of the measurements and systematic errors. The result is in agreement with the SM prediction (NLO QCD + NLO EW).
- ² AAD 15AJ based on 4.6 fb⁻¹ of data. After kinematic reconstruction the top quark momenta are corrected for detector resolution and acceptance effects by unfolding, using parton level information of the MC generators. The lepton charge asymmetry is measured as $A_C = 0.024 \pm 0.015 \pm 0.009$. All the measurements are consistent with the SM predictions.
- ³ Based on 4.7 fb⁻¹ of data. The result is consistent with the SM prediction of $A_C = 0.0123 \pm 0.0005$. The asymmetry is 0.011 ± 0.018 if restricted to those events where $\beta_Z(t\bar{t}) > 0.6$, which is also consistent with the SM prediction of $0.020^{+0.006}_{-0.007}$.
- ⁴ Based on 5.0 fb⁻¹ of data. The lepton charge asymmetry is measured as $A_C = 0.009 \pm 0.0010 \pm 0.006$. A_C dependences on $m_{T\bar{T}}$, $|y(t\bar{t})|$, and $p_T(t\bar{t})$ are given in Fig. 5. All measurements are consistent with the SM predictions.
- ⁵ Based on 1.04 fb⁻¹ of data. The result is consistent with $A_C = 0.006 \pm 0.002$ (MC at NLO). No significant dependence of A_C on $m_{t\bar{t}}$ is observed.
- ⁶ Based on 5.0 fb⁻¹ of data at 7 TeV.
- ⁷ Based on 1.09 fb⁻¹ of data. The result is consistent with the SM predictions.

 $t\bar{t}$ Charge Asymmetry (A_C) in pp Collisions at $\sqrt{s} = 8$ TeV

VALUE (%)	DOCUMENT ID	TECN	COMMENT
0.55±0.23±0.25	¹ AABOUD	18AMLHC	ATLAS+CMS combination (lepton + jets)
2.1 ± 1.6	² AAD	16AE ATLS	$\ell\ell + \cancel{E}_T + \geq 2j$
0.9 ± 0.5	³ AAD	16AZ ATLS	$\ell + \cancel{E}_T + \geq 4j$
4.2 ± 3.2	⁴ AAD	16T ATLS	$m_{t\bar{t}} > 0.75$ TeV, $ y_t - y_{\bar{t}} < 2, \ell + \cancel{E}_T + \text{jets}$
1.1 ± 1.1 ± 0.7	⁵ KHACHATRYAN...16AD	CMS	$\ell\ell + \cancel{E}_T + \geq 2j$ ($\geq 1b$)
0.33±0.26±0.33	⁶ KHACHATRYAN...16AH	CMS	$\ell + \cancel{E}_T + \geq 4j$ ($\geq 1b$)
0.10±0.68±0.37	⁷ KHACHATRYAN...16T	CMS	$\ell + \cancel{E}_T + \geq 4j$ ($\geq 1b$)

- ¹ ATLAS and CMS combination based on the data of AAD 16AZ and KHACHATRYAN 16AH. It takes into account the correlations of the measurements and systematic errors. A combination of the differential measurements of the charge asymmetry is also presented. The results are in agreement with the SM prediction (NNLO QCD + NLO EW).
- ² AAD 16AE is based on 20.3 fb⁻¹ of data. After kinematic reconstruction, the top quark momenta are corrected for detector resolution and acceptance effects by unfolding, using parton level information of the MC generators. The lepton charge asymmetry is measured as $A_C = 0.008 \pm 0.006$. All the measurements are consistent with the SM predictions.
- ³ AAD 16AZ based on 20.3 fb⁻¹ of data. All the differential and inclusive measurements are statistically limited and consistent with the SM predictions.
- ⁴ AAD 16T based on 20.3 fb⁻¹ of data. Uses reconstruction techniques for the decay topology of highly boosted top quarks. The observed asymmetry is transformed by unfolding to a parton-level result in the shown fiducial region. The result is consistent with the NLO SM prediction.
- ⁵ KHACHATRYAN 16AD based on 19.5 fb⁻¹ of data. The lepton charge asymmetry is measured as $A_C = 0.003 \pm 0.006 \pm 0.003$. All the measurements are consistent with the SM predictions.
- ⁶ KHACHATRYAN 16AH based on 19.6 fb⁻¹ of data. The same data set as in KHACHATRYAN 16T is used. A template technique is used, which is sensitive to the charge anti-symmetric component of the $t\bar{t}$ rapidity distributions and statistically advantageous. The result is consistent with the SM predictions.
- ⁷ KHACHATRYAN 16T based on 19.7 fb⁻¹ of data. The same data set as in KHACHATRYAN 16AH is used. After kinematic reconstruction the top quark momenta are corrected for detector resolution and acceptance effects by unfolding, using parton level information of the MC generators. All the measurements are consistent with the SM predictions.

 $t\bar{t}$ Charge Asymmetry (A_C) in pp Collisions at $\sqrt{s} = 13$ TeV

VALUE (%)	DOCUMENT ID	TECN	COMMENT
0.68±0.15	¹ AAD	23BA ATLS	single lepton + dilepton channels
0.42 ^{+0.64} _{-0.69}	² TUMASYAN	23BD CMS	$M_{t\bar{t}} > 750$ GeV, single- ℓ channel

- ¹ AAD 23BA is based on 139 fb⁻¹ of data. Inclusive $t\bar{t}$ charge asymmetry is measured to be nonzero with 4.7 σ significance. Also differential $t\bar{t}$ as well as lepton charge asymmetries are measured. All the results are consistent with the SM predictions which include NNLO QCD + NLO EW corrections.
- ² TUMASYAN 23BD is based on 138 fb⁻¹ of data. $t\bar{t}$ charge asymmetry for highly Lorentz-boosted top quarks is measured and is in agreement with the NNLO QCD + NLO EW corrected SM prediction of $0.94^{+0.05}_{-0.07}$ %. The event selection is optimized for highly-boosted top quarks.

 $t\bar{t}W$ leptonic Charge Asymmetry (A_C^ℓ) in pp Collisions at $\sqrt{s} = 13$ TeV

VALUE	DOCUMENT ID	TECN	COMMENT
-0.12±0.14±0.05	¹ AAD	23AA ATLS	$\ell\ell\ell + \geq 1b$

- ¹ AAD 23AA is based on 139 fb⁻¹ of data. The charge-asymmetry in a fiducial volume at particle level is also reported at $-0.11 \pm 0.17 \pm 0.05$ %. All the results are consistent with the SM predictions which include NLO QCD + NLO EW corrections.

 $t\bar{t}\gamma$ Charge Asymmetry (A_C) in pp Collisions at $\sqrt{s} = 13$ TeV

VALUE	DOCUMENT ID	TECN	COMMENT
-0.003±0.029	¹ AAD	23AW ATLS	$\gamma\ell + \geq 4j$ ($\geq 1b$)

- ¹ AAD 23AW is based on 139 fb⁻¹ of data. The measurement is in agreement with the Standard Model expectation.

 t -quark Polarization in $t\bar{t}$ Events in $p\bar{p}$ Collisions at $\sqrt{s} = 1.96$ TeV

VALUE	DOCUMENT ID	TECN	COMMENT
0.070±0.055	¹ ABAZOV	17 D0	$\ell + \cancel{E}_T + \geq 3j$ ($\geq 1b$)
-0.102±0.061	² ABAZOV	17 D0	$\ell + \cancel{E}_T + \geq 3j$ ($\geq 1b$)
0.040±0.035	³ ABAZOV	17 D0	$\ell + \cancel{E}_T + \geq 3j$ ($\geq 1b$)
0.113±0.091±0.019	⁴ ABAZOV	15K D0	A_{FB}^ℓ in $\ell\ell + \cancel{E}_T + \geq 2j$ ($\geq 1b$)

- ¹ ABAZOV 17 based on 9.7 fb⁻¹ of data. The value is top quark polarization times spin analyzing power in the beam basis. Combination with the result of ABAZOV 15K yields 0.081 ± 0.048. This result together with the helicity polarization is shown in a 2-dimensional plot in Fig.4. These results are consistent with the SM prediction.
- ² ABAZOV 17 based on 9.7 fb⁻¹ of data. The value is top quark polarization times spin analyzing power in the helicity basis. The result is consistent with the SM prediction. This result together with the beam polarization is shown in a 2-dimensional plot in Fig.4.
- ³ ABAZOV 17 based on 9.7 fb⁻¹ of data. The value is top quark polarization times spin analyzing power in the transverse basis. The result is consistent with the SM prediction.
- ⁴ ABAZOV 15K based on 9.7 fb⁻¹ of data. The value is top quark polarization times spin analyzing power in the beam basis. The result is consistent with the SM prediction of -0.0019 ± 0.0005 .

 t -quark Polarization in $t\bar{t}$ Events in pp Collisions at $\sqrt{s} = 7$ TeV

The double differential distribution in polar angles, θ_1 (θ_2) of the decay particle of the top (anti-top) decay products, is parametrized as $(1/\sigma)d\sigma/(d\cos\theta_1 d\cos\theta_2) = (1/4) (1 + A_t \cos\theta_1 + A_{\bar{t}} \cos\theta_2 - C \cos\theta_1 \cos\theta_2)$. The charged lepton is used to tag t or \bar{t} . The coefficient A_t and $A_{\bar{t}}$ measure the average helicity of t and \bar{t} , respectively. $A_{CP} = A_t = A_{\bar{t}}$ assumes CP conservation, whereas $A_{CPV} = A_t = -A_{\bar{t}}$ corresponds to maximal CP violation.

VALUE	DOCUMENT ID	TECN	COMMENT
-0.035±0.014±0.037	¹ AAD	13BE ATLS	A_{CP}
0.020±0.016 ^{+0.013} _{-0.017}	¹ AAD	13BE ATLS	A_{CPV}

- ¹ Based on 4.7 fb⁻¹ of data using the final states containing one or two isolated electrons or muons and jets with at least one b -tag.

 t -quark Polarization in $t\bar{t}$ Events in pp Collisions at $\sqrt{s} = 8$ TeV

A_t , $A_{\bar{t}}$, A_{CP} , A_{CPV} , and A_C are defined in header texts in the subsections, just above.

VALUE	DOCUMENT ID	TECN	COMMENT
-0.044±0.038±0.027	¹ AABOUD	17G ATLS	A_t
-0.064±0.040±0.027	¹ AABOUD	17G ATLS	$A_{\bar{t}}$
0.296±0.093±0.037	¹ AABOUD	17G ATLS	A_C
-0.022±0.058	² KHACHATRYAN...16AI	CMS	A_{CP}
0.000±0.016	² KHACHATRYAN...16AI	CMS	A_{CPV}

- ¹ AABOUD 17G based on 20.2 fb⁻¹ of pp data, using events with two leptons and two or more jets with at least one b -tag. Determined from measurements of 15 top quark spin observables. The second error corresponds to a variation of m_t about 172.5 GeV by 0.7 GeV. The values are consistent with the NLO SM predictions.
- ² KHACHATRYAN 16AI based on 19.5 fb⁻¹ of pp data at $\sqrt{s} = 8$ TeV, using events with two leptons and two or more jets with at least one b -tag. Determined from the lepton angular distributions as a function of the $t\bar{t}$ -system kinematical variables.

Quark Particle Listings

t

t-quark Polarization in Single Top Events in pp Collisions at $\sqrt{s} = 8$ TeV

VALUE	CL%	DOCUMENT ID	TECN	COMMENT
• • • We do not use the following data for averages, fits, limits, etc. • • •				
>0.72	95	1 AABOUD 17BB ATLS	$\alpha_\ell P$; t-channel	
$0.97 \pm 0.05 \pm 0.11$		2 AABOUD 17i ATLS	$\alpha_\ell P$; t-channel	
$0.25 \pm 0.08 \pm 0.14$		3 AABOUD 17i ATLS	$(F_+ + F_-)P$; t-channel	
$0.26 \pm 0.03 \pm 0.10$		4 KHACHATRYAN 16Bo CMS	$(\alpha_\mu P)/2$; t-channel	

1 AABOUD 17BB based on 20.2 fb⁻¹ of pp data. Triple-differential decay rate of top quark is used to simultaneously determine five generalized Wtb couplings as well as the top polarization. α_ℓ denotes the spin analyzing power of charged lepton, and the spin axis of the top polarization P is taken along the spectator-quark momentum in the top rest frame. The value is compatible with the SM prediction of about 0.9.

2 AABOUD 17i based on 20.2 fb⁻¹ of pp data. A cut-based analysis is used to discriminate between signal and backgrounds. α_ℓ denotes the spin analyzing power of charged lepton, and the spin axis of the top polarization P is taken along the spectator-quark momentum in the top rest frame. See this paper for a number of other asymmetries and measurements that are not included here.

3 AABOUD 17i based on 20.2 fb⁻¹ of pp data. A cut-based analysis is used to discriminate between signal and backgrounds. F_\pm denotes W helicity fraction, and the spin axis of the top polarization P is taken along the spectator-quark momentum in the top rest frame. See this paper for a number of other asymmetries and measurements that are not included here.

4 KHACHATRYAN 16Bo based on 19.7 fb⁻¹ of data. A high-purity sample with a muon is selected by a multivariate analysis. The value is the top spin asymmetry, given by one half of the spin analyzing power α_μ (=1 at LO of SM) times the top polarization, P , where the spin axis is defined as the direction of the untagged jet in the top rest frame. The value is compatible with the SM prediction of 0.44 with a 2.0 σ deviation.

t-quark Polarization in Single Top Events in pp Collisions at $\sqrt{s} = 13$ TeV

VALUE	DOCUMENT ID	TECN	COMMENT
• • • We do not use the following data for averages, fits, limits, etc. • • •			
0.01 ± 0.18	1 AAD 22Z ATLS	$P_{x'}(t, \text{transverse component})$	
-0.029 ± 0.027	1 AAD 22Z ATLS	$P_{y'}(t, \text{normal component})$	
0.91 ± 0.10	1 AAD 22Z ATLS	$P_{z'}(t, \text{parallel component})$	
-0.02 ± 0.20	1 AAD 22Z ATLS	$P_{x'}(\bar{t}, \text{transverse component})$	
-0.007 ± 0.051	1 AAD 22Z ATLS	$P_{y'}(\bar{t}, \text{normal component})$	
-0.79 ± 0.16	1 AAD 22Z ATLS	$P_{z'}(\bar{t}, \text{parallel component})$	
0.440 ± 0.070	2 SIRUNYAN 20R CMS	$(\alpha_\ell P)/2$; t-channel	

1 AAD 22Z based on 139 fb⁻¹ of data. Three components of t or \bar{t} polarization vector (defined in the t or \bar{t} rest frame) are measured in t-channel single top production using ℓ momentum distribution in the $\ell + \cancel{E}_T + 2j$ (with 1 of them b-jet) channel. The measured values are in agreement with NNLO SM prediction. Constraints on the Wilson coefficients of SMEFT are obtained as $-0.9 < C_{tW} < 1.4$ and $-0.8 < C_{tW} < 0.2$.

2 SIRUNYAN 20R based on 36.1 fb⁻¹ of data. Differential cross sections for t-channel single top production are measured using $1\ell + 2,3\text{-jet}$ mode and found to be in good agreement with SM predictions. The value is the top spin asymmetry, given by 1/2 of the spin analyzing power α_ℓ (=1 at LO of SM) times the top polarization P , where the spin axis is defined as the direction of the spectator quark in the top rest frame at the parton level. It is in good agreement with the NLO SM prediction of 0.436.

gg \rightarrow t \bar{t} Fraction in p \bar{p} Collisions at $\sqrt{s} = 1.96$ TeV

VALUE	CL%	DOCUMENT ID	TECN	COMMENT
• • • We do not use the following data for averages, fits, limits, etc. • • •				
<0.33	68	1 AALTONEN 09F CDF	t \bar{t} correlations	
$0.07 \pm 0.14 \pm 0.07$		2 AALTONEN 08AG CDF	low p_T number of tracks	

1 Based on 955 pb⁻¹. AALTONEN 09F used differences in the t \bar{t} production angular distribution and polarization correlation to discriminate between $gg \rightarrow t\bar{t}$ and $q\bar{q} \rightarrow t\bar{t}$ subprocesses. The combination with the result of AALTONEN 08AG gives $0.07^{+0.15}_{-0.07}$.

2 Result is based on 0.96 fb⁻¹ of data. The contribution of the subprocesses $gg \rightarrow t\bar{t}$ and $q\bar{q} \rightarrow t\bar{t}$ is distinguished by using the difference between quark and gluon initiated jets in the number of small p_T ($0.3 \text{ GeV} < p_T < 3 \text{ GeV}$) charged particles in the central region ($|\eta| < 1.1$).

 A_{FB}^{ℓ} of t \bar{t} in p \bar{p} Collisions at $\sqrt{s} = 1.96$ TeV

A_{FB}^{ℓ} = Forward-backward asymmetry.

VALUE (%)	DOCUMENT ID	TECN	COMMENT
• • • We do not use the following data for averages, fits, limits, etc. • • •			
$12.8 \pm 2.1 \pm 1.4$	1 AALTONEN 18 TEVA	CDF, D0 combination	
$17.5 \pm 5.6 \pm 3.1$	2 ABZOV 15K D0	A_{FB}^{ℓ} in $\ell\ell + \cancel{E}_T + \geq 2j$ ($\geq 1b$)	
7.2 ± 6.0	3 AALTONEN 14F CDF	A_{FB}^{ℓ} in dilepton channel ($\ell\ell + \cancel{E}_T + \geq 2j$)	
7.6 ± 8.2	3 AALTONEN 14F CDF	A_{FB}^{ℓ} in dilepton channel ($\ell\ell + \cancel{E}_T + \geq 2j$)	
$4.2 \pm 2.3^{+1.7}_{-2.0}$	4 ABZOV 14G D0	A_{FB}^{ℓ} ($\ell + \cancel{E}_T + \geq 3j$ ($0,1 \geq 2b$))	
10.6 ± 3.0	5 ABZOV 14H D0	A_{FB}^{ℓ} ($\ell + \cancel{E}_T + \geq 3j$ ($\geq 1b$))	
20.1 ± 6.7	6 AALTONEN 13AD CDF	a_1/a_0 in $\ell + \cancel{E}_T + \geq 4j$ ($\geq 1b$)	
-0.2 ± 3.1	6 AALTONEN 13AD CDF	a_3, a_5, a_7 in $\ell + \cancel{E}_T + \geq 4j$ ($\geq 1b$)	
16.4 ± 4.7	7 AALTONEN 13S CDF	$\ell + \cancel{E}_T + \geq 4$ jets ($\geq 1b\text{-tag}$)	
$9.4^{+3.2}_{-2.9}$	8 AALTONEN 13X CDF	$\ell + \cancel{E}_T + \geq 4$ jets ($\geq 1 b\text{-tag}$)	
11.8 ± 3.2	9 ABZOV 13A D0	$\ell\ell$ & $\ell +$ jets comb.	
-11.6 ± 15.3	10 AALTONEN 11F CDF	$m_{t\bar{t}} < 450 \text{ GeV}$	
47.5 ± 11.4	10 AALTONEN 11F CDF	$m_{t\bar{t}} > 450 \text{ GeV}$	
19.6 ± 6.5	11 ABZOV 11AH D0	$\ell + \cancel{E}_T + \geq 4$ jets ($\geq 1b\text{-tag}$)	
17 ± 8	12 AALTONEN 08AB CDF	p \bar{p} frame	

24 ± 14	12 AALTONEN 08AB CDF	t \bar{t} frame
$12 \pm 8 \pm 1$	13 ABZOV 08L D0	$\ell + \cancel{E}_T + \geq 4$ jets

1 AALTONEN 18 based on 9–10 fb⁻¹ of p \bar{p} data at $\sqrt{s} = 1.96$ TeV. The value is the asymmetry in the number of reconstructed t \bar{t} events with rapidity $y_\ell > y_{\bar{t}}$ and those with $y_\ell < y_{\bar{t}}$. The combined fits to CDF and D0 single lepton and $\ell\ell$ asymmetries give $A_{FB}^{\ell} = 0.073 \pm 0.016 \pm 0.012$ and $A_{FB}^{\ell\ell} = 0.108 \pm 0.043 \pm 0.016$, respectively. The results are consistent with the SM predictions.

2 ABZOV 15K based on 9.7 fb⁻¹ of data. The result is consistent with the SM predictions. By combining with the previous D0 measurement in the $\ell +$ jet channel ABZOV 14H, $A_{FB}^{\ell} = 0.118 \pm 0.025 \pm 0.013$ is obtained.

3 AALTONEN 14F based on 9.1 fb⁻¹ of data. A_{FB}^{ℓ} and $A_{FB}^{\ell\ell}$ denote, respectively, the asymmetries $(N(x>0) - N(x<0))/N_{tot}$ for $x = q\ell\eta_\ell$ (q_ℓ is the charge of ℓ) and $x = \eta_{\ell^+} - \eta_{\ell^-}$. Both results are consistent with the SM predictions. By combining with the previous CDF measurement in the $\ell +$ jet channel AALTONEN 13X, $A_{FB}^{\ell} = 0.098^{+0.028}_{-0.026}$ is obtained. The combined result is about two sigma larger than the SM prediction of $A_{FB}^{\ell} = 0.038 \pm 0.003$.

4 Based on 9.7 fb⁻¹ of p \bar{p} data at $\sqrt{s} = 1.96$ TeV. The asymmetry is corrected for the production level for events with $|y_\ell| < 1.5$. Asymmetry as functions of $E_T(\ell)$ and $|y_\ell|$ are given in Figs. 7 and 8, respectively. Combination with the asymmetry measured in the dilepton channel [ABZOV 13P] gives $A_{FB}^{\ell} = 4.2 \pm 2.0 \pm 1.4\%$, in agreement with the SM prediction of 2.0%.

5 Based on 9.7 fb⁻¹ of data of p \bar{p} data at $\sqrt{s} = 1.96$ TeV. The measured asymmetry is in agreement with the SM predictions of $8.8 \pm 0.9\%$ [BERNREUTHER 12], which includes the EW effects. The dependences of the asymmetry on $|y(t) - y(\bar{t})|$ and $m_{t\bar{t}}$ are shown in Figs. 9 and 10, respectively.

6 Based on 9.4 fb⁻¹ of data. Reported A_{FB}^{ℓ} values come from the determination of a_j coefficients of $d\sigma/d(\cos\theta_\ell) = \sum_i a_i P_i(\cos\theta_\ell)$ measurement. The result of $a_1/a_0 = (40 \pm 12)\%$ seems higher than the NLO SM prediction of $(15^{+7}_{-3})\%$.

7 Based on 9.4 fb⁻¹ of data. The quoted result is the asymmetry at the parton level.

8 Based on 9.4 fb⁻¹ of data. The observed asymmetry is to be compared with the SM prediction of $A_{FB}^{\ell} = 0.038 \pm 0.003$.

9 Based on 5.4 fb⁻¹ of data. ABZOV 13A studied the dilepton channel of the t \bar{t} events and measured the leptonic forward-backward asymmetry to be $A_{FB}^{\ell} = 5.8 \pm 5.1 \pm 1.3\%$, which is consistent with the SM (QCD+EW) prediction of $4.7 \pm 0.1\%$. The result is obtained after combining the measurement ($15.2 \pm 4.0\%$) in the $\ell +$ jets channel ABZOV 11AH. The top quark helicity is measured by using the neutrino weighting method to be consistent with zero in both dilepton and $\ell +$ jets channels.

10 Based on 5.3 fb⁻¹ of data. The error is statistical and systematic combined. Events with lepton + $\cancel{E}_T + \geq 4$ jets ($\geq 1b$) are used. AALTONEN 11F also measures the asymmetry as a function of the rapidity difference $|y_\ell - y_{\bar{t}}|$. The NLO QCD predictions [MCFM] are $(4.0 \pm 0.6)\%$ and $(8.8 \pm 1.3)\%$ for $m_{t\bar{t}} < 450$ and > 450 GeV, respectively.

11 Based on 5.4 fb⁻¹ of data. The error is statistical and systematic combined. The quoted asymmetry is obtained after unfolding to be compared with the MC@NLO prediction of $(5.0 \pm 0.1)\%$. No significant difference between the $m_{t\bar{t}} < 450$ and > 450 GeV data samples is found. A corrected asymmetry based on the lepton from a top quark decay of $(15.2 \pm 4.0)\%$ is measured to be compared to the MC@NLO prediction of $(2.1 \pm 0.1)\%$.

12 Result is based on 1.9 fb⁻¹ of data. The FB asymmetry in the t \bar{t} events has been measured in the $\ell +$ jets mode, where the lepton charge is used as the flavor tag. The asymmetry in the p \bar{p} frame is defined in terms of $\cos(\theta)$ of hadronically decaying t-quark momentum, whereas that in the t \bar{t} frame is defined in terms of the t and \bar{t} rapidity difference. The results are consistent ($\leq 2\sigma$) with the SM predictions.

13 Result is based on 0.9 fb⁻¹ of data. The asymmetry in the number of t \bar{t} events with $y_\ell > y_{\bar{t}}$ and those with $y_\ell < y_{\bar{t}}$ has been measured in the lepton + jets final state. The observed value is consistent with the SM prediction of 0.8% by MC@NLO, and an upper bound on the $Z' \rightarrow t\bar{t}$ contribution for the SM Z-like couplings is given in Fig. 2 for $350 \text{ GeV} < m_{Z'} < 1 \text{ TeV}$.

t-Quark Electric Charge

VALUE	DOCUMENT ID	TECN	COMMENT
$0.64 \pm 0.02 \pm 0.08$	1 AAD 13AY ATLS	$\ell + \cancel{E}_T + \geq 4$ jets ($\geq 1b$)	
• • • We do not use the following data for averages, fits, limits, etc. • • •			
	2 ABZOV 14D D0	$\ell + \cancel{E}_T + \geq 4$ jets ($\geq 2b$)	
	3 AALTONEN 13J CDF	p \bar{p} at 1.96 TeV	
	4 AALTONEN 10S CDF	Repl. by AALTONEN 13J	
	5 ABZOV 07c D0	fraction of $ q =4e/3$ pair	

1 AAD 13AY result is based on 2.05 fb⁻¹ of pp data at $\sqrt{s} = 7$ TeV, the result is obtained by reconstructing t \bar{t} events in the lepton + jets final state, where b-jet charges are tagged by the jet-charge algorithm. This measurement excludes the charge $-4/3$ assignment to the top quark at more than 8 standard deviations.

2 ABZOV 14D result is based on 5.3 fb⁻¹ of p \bar{p} data at $\sqrt{s} = 1.96$ TeV. The electric charge of $b + W$ system in t \bar{t} candidate events is measured from the charges of the leptons from W decay and in b jets. Under the assumption that the $b + W$ system consists of the sum of the top quark and the charge $-4/3$ quark $b'(-4/3)$ of the same mass, the top quark fraction is found to be $f = 0.88 \pm 0.13$ (stat) ± 0.11 (syst), or the upper bound for the $b'(-4/3)$ contamination of $1 - f < 0.46$ (95% CL).

3 AALTONEN 13J excludes the charge $-4/3$ assignment to the top quark at 99% CL, using 5.6 fb⁻¹ of data in p \bar{p} collisions at $\sqrt{s} = 1.96$ TeV. Result is obtained by reconstructing t \bar{t} events in the lepton + jets final state, where b-jet charges are tagged by the jet-charge algorithm.

4 AALTONEN 10S excludes the charge $-4/3$ assignment for the top quark [CHANG 99] at 95% CL, using 2.7 fb⁻¹ of data in p \bar{p} collisions at $\sqrt{s} = 1.96$ TeV. Result is obtained by reconstructing t \bar{t} events in the lepton + jets final state, where b-jet charges are tagged by the SLT (soft lepton tag) algorithm.

5 ABZOV 07c reports an upper limit $\rho < 0.80$ (90% CL) on the fraction ρ of exotic quark pairs $Q\bar{Q}$ with electric charge $|q| = 4e/3$ in t \bar{t} candidate events with high p_T lepton, missing E_T and ≥ 4 jets. The result is obtained by measuring the fraction of

See key on page 1171

Quark Particle Listings

t

events in which the quark pair decays into $W^- + b$ and $W^+ + \bar{b}$, where b and \bar{b} jets are discriminated by using the charge and momenta of tracks within the jet cones. The maximum CL at which the model of CHANG 99 can be excluded is 92%. Based on 370 pb⁻¹ of data at $\sqrt{s} = 1.96$ TeV.

t-Quark REFERENCES

AAD	24	PL B848 138376	G. Aad et al.	(ATLAS Collab.)	KHACHATRYAN...17N	EPJ C77 172	V. Khachatryan et al.	(CMS Collab.)	
AABOUD	23	PR D108 032014	M. Aboud et al.	(ATLAS Collab.)	SIRUNYAN	17AA	PL B772 752	A.M. Sirunyan et al.	(CMS Collab.)
AAD	23	PL B842 137379	G. Aad et al.	(ATLAS Collab.)	SIRUNYAN	17AB	PL B772 336	A.M. Sirunyan et al.	(CMS Collab.)
Also		PL B847 138286 (errata.)	G. Aad et al.	(ATLAS Collab.)	SIRUNYAN	17E	JHEP 1707 003	A.M. Sirunyan et al.	(CMS Collab.)
AAD	23AA	JHEP 2307 033	G. Aad et al.	(ATLAS Collab.)	SIRUNYAN	17L	EPJ C77 354	A.M. Sirunyan et al.	(CMS Collab.)
AAD	23AS	PR D108 032019	G. Aad et al.	(ATLAS Collab.)	SIRUNYAN	17N	EPJ C77 467	A.M. Sirunyan et al.	(CMS Collab.)
AAD	23AW	PL B843 137848	G. Aad et al.	(ATLAS Collab.)	SIRUNYAN	17O	D96 032002	A.M. Sirunyan et al.	(CMS Collab.)
AAD	23AY	JHEP 2307 213	G. Aad et al.	(ATLAS Collab.)	SIRUNYAN	17S	EPJ C77 578	A.M. Sirunyan et al.	(CMS Collab.)
AAD	23BA	JHEP 2308 077	G. Aad et al.	(ATLAS and CMS Collabs.)	SIRUNYAN	17W	JHEP 1709 051	A.M. Sirunyan et al.	(CMS Collab.)
AAD	23BC	EPJ C83 496	G. Aad et al.	(ATLAS Collab.)	AABOUD	16R	PL B761 136	M. Aboud et al.	(ATLAS Collab.)
AAD	23BN	PRL 131 183901	G. Aad et al.	(ATLAS Collab.)	AABOUD	16T	PL B761 350	M. Aboud et al.	(ATLAS Collab.)
AAD	23CJ	JHEP 2312 1195	G. Aad et al.	(ATLAS Collab.)	AAD	16AE	PR D94 032006	G. Aad et al.	(ATLAS Collab.)
AAD	23E	JHEP 2306 191	G. Aad et al.	(ATLAS Collab.)	AAD	16AK	JHEP 1604 023	G. Aad et al.	(ATLAS Collab.)
AAD	23H	JHEP 2306 155	G. Aad et al.	(ATLAS Collab.)	AAD	16AS	EPJ C76 55	G. Aad et al.	(ATLAS Collab.)
AAD	23J	JHEP 2306 138	G. Aad et al.	(ATLAS Collab.)	Also		EPJ C82 70 (errata.)	G. Aad et al.	(ATLAS Collab.)
AAD	23N	JHEP 2306 019	G. Aad et al.	(ATLAS Collab.)	AAD	16AZ	EPJ C76 87	G. Aad et al.	(ATLAS Collab.)
AAD	23S	JHEP 2307 141	G. Aad et al.	(ATLAS Collab.)	AAD	16B	JHEP 1601 064	G. Aad et al.	(ATLAS Collab.)
HAYRAPETYAN...	23B	PL B847 138290	A. Hayrapetyan et al.	(CMS Collab.)	AAD	16BK	EPJ C76 642	G. Aad et al.	(ATLAS Collab.)
TUMASYAN	23AN	JHEP 2307 219	A. Tumasyan et al.	(CMS Collab.)	AAD	16D	EPJ C76 12	G. Aad et al.	(ATLAS Collab.)
TUMASYAN	23AQ	PL B844 138076	A. Tumasyan et al.	(CMS Collab.)	AAD	16E	PL B756 52	G. Aad et al.	(ATLAS Collab.)
TUMASYAN	23BB	EPJ C83 963	A. Tumasyan et al.	(CMS Collab.)	AAD	16F	PL B756 228	G. Aad et al.	(ATLAS Collab.)
TUMASYAN	23BD	PL B846 137703	A. Tumasyan et al.	(CMS Collab.)	AALTONEN	16	PR D93 032011	T. Aaltonen et al.	(CDF Collab.)
TUMASYAN	23J	JHEP 2306 081	A. Tumasyan et al.	(CMS Collab.)	ABAZOV	16	PL B752 18	V.M. Abazov et al.	(DO Collab.)
TUMASYAN	23R	JHEP 2307 077	A. Tumasyan et al.	(CMS Collab.)	ABAZOV	16A	PL B757 199	V.M. Abazov et al.	(DO Collab.)
TUMASYAN	23T	JHEP 2307 044	A. Tumasyan et al.	(CMS Collab.)	ABAZOV	16D	PR D94 032004	V.M. Abazov et al.	(DO Collab.)
TUMASYAN	23U	JHEP 2307 023	A. Tumasyan et al.	(CMS Collab.)	ABAZOV	16F	PR D94 092004	V.M. Abazov et al.	(DO Collab.)
TUMASYAN	23Z	EPJ C83 560	A. Tumasyan et al.	(CMS Collab.)	KHACHATRYAN...	16AD	PL B760 365	V. Khachatryan et al.	(CMS Collab.)
AAD	22Q	JHEP 2208 175	G. Aad et al.	(ATLAS Collab.)	KHACHATRYAN...	16AH	PR D93 034014	V. Khachatryan et al.	(CMS Collab.)
AAD	22T	EPJ C82 334	G. Aad et al.	(ATLAS Collab.)	KHACHATRYAN...	16AI	PR D93 052007	V. Khachatryan et al.	(CMS Collab.)
AAD	22Z	JHEP 2211 040	G. Aad et al.	(ATLAS Collab.)	KHACHATRYAN...	16AJ	PR D93 072004	V. Khachatryan et al.	(CMS Collab.)
TUMASYAN	22A	PRL 129 032001	A. Tumasyan et al.	(CMS Collab.)	KHACHATRYAN...	16AL	PR D93 092000	V. Khachatryan et al.	(CMS Collab.)
TUMASYAN	22K	JHEP 2202 169	A. Tumasyan et al.	(CMS Collab.)	KHACHATRYAN...	16AS	JHEP 1604 035	V. Khachatryan et al.	(CMS Collab.)
TUMASYAN	22L	JHEP 2202 107	A. Tumasyan et al.	(CMS Collab.)	KHACHATRYAN...	16AW	JHEP 1608 029	V. Khachatryan et al.	(CMS Collab.)
TUMASYAN	22T	JHEP 2204 144	A. Tumasyan et al.	(CMS Collab.)	KHACHATRYAN...	16AZ	JHEP 1609 027	V. Khachatryan et al.	(CMS Collab.)
TUMASYAN	22W	JHEP 2205 091	A. Tumasyan et al.	(CMS Collab.)	KHACHATRYAN...	16BC	EPJ C76 128	V. Khachatryan et al.	(CMS Collab.)
TUMASYAN	22Z	JHEP 2206 082	A. Tumasyan et al.	(CMS Collab.)	KHACHATRYAN...	16B	EPJ C76 439	V. Khachatryan et al.	(CMS Collab.)
AAD	21AS	EPJ C81 737	G. Aad et al.	(ATLAS Collab.)	KHACHATRYAN...	16B0	JHEP 1604 073	V. Khachatryan et al.	(CMS Collab.)
AAD	21AT	EPJ C81 720	G. Aad et al.	(ATLAS Collab.)	KHACHATRYAN...	16BU	PL B762 512	V. Khachatryan et al.	(CMS Collab.)
AAD	21BC	JHEP 2111 118	G. Aad et al.	(ATLAS Collab.)	KHACHATRYAN...	16CB	JHEP 1612 123	V. Khachatryan et al.	(CMS Collab.)
TUMASYAN	21E	JHEP 2111 111	A. Tumasyan et al.	(CMS Collab.)	KHACHATRYAN...	16C	PRL 116 052002	V. Khachatryan et al.	(CMS Collab.)
TUMASYAN	21G	JHEP 2112 161	A. Tumasyan et al.	(CMS Collab.)	KHACHATRYAN...	16T	PL B757 154	V. Khachatryan et al.	(CMS Collab.)
TUMASYAN	21H	JHEP 2112 180	A. Tumasyan et al.	(CMS Collab.)	KHACHATRYAN...	16X	PL B758 321	V. Khachatryan et al.	(CMS Collab.)
TUMASYAN	21J	PR D104 092013	A. Tumasyan et al.	(CMS Collab.)	TEVEWVG	16	arXiv:1608.01881	Tevatron Electroweak Working Group	(CMS Collab.)
AAD	20AB	JHEP 2007 124	G. Aad et al.	(ATLAS Collab.)	AAD	15	PL B740 222	G. Aad et al.	(ATLAS Collab.)
AAD	20AD	PL B803 135797	G. Aad et al.	(ATLAS Collab.)	AAD	15A	PL B740 118	G. Aad et al.	(ATLAS Collab.)
AAD	20AR	EPJ C80 1085	G. Aad et al.	(ATLAS Collab.)	AAD	15AJ	JHEP 1505 061	G. Aad et al.	(ATLAS Collab.)
AAD	20B	PL B800 135082	G. Aad et al.	(ATLAS Collab.)	AAD	15AR	JHEP 1508 105	G. Aad et al.	(ATLAS Collab.)
AAD	20Q	EPJ C80 528	G. Aad et al.	(ATLAS Collab.)	AAD	15AW	EPJ C75 158	G. Aad et al.	(ATLAS Collab.)
AAD	20Y	JHEP 2008 051	G. Aad et al.	(ATLAS and CMS Collabs.)	AAD	15BF	EPJ C75 330	G. Aad et al.	(ATLAS Collab.)
AAD	20Z	PRL 125 061802	G. Aad et al.	(ATLAS Collab.)	AAD	15B0	PR D91 052005	G. Aad et al.	(ATLAS Collab.)
SIRUNYAN	20AB	JHEP 2003 056	A.M. Sirunyan et al.	(CMS Collab.)	AAD	15BP	PR D91 12013	G. Aad et al.	(ATLAS Collab.)
SIRUNYAN	20AM	JHEP 2006 146	A.M. Sirunyan et al.	(CMS Collab.)	AAD	15BW	JHEP 1510 121	G. Aad et al.	(ATLAS Collab.)
SIRUNYAN	20AR	PRL 124 202001	A.M. Sirunyan et al.	(CMS Collab.)	AAD	15C	PR D92 072005	G. Aad et al.	(ATLAS Collab.)
SIRUNYAN	20AS	PRL 125 061801	A.M. Sirunyan et al.	(CMS Collab.)	AAD	15CO	JHEP 1512 061	G. Aad et al.	(ATLAS Collab.)
SIRUNYAN	20AZ	PL B808 135609	A.M. Sirunyan et al.	(CMS Collab.)	AAD	15D	JHEP 1501 020	G. Aad et al.	(ATLAS Collab.)
SIRUNYAN	20BC	PRL 125 220011	A.M. Sirunyan et al.	(CMS Collab.)	AAD	15J	PRL 114 142001	G. Aad et al.	(ATLAS Collab.)
SIRUNYAN	20BH	PR D102 092013	A.M. Sirunyan et al.	(CMS Collab.)	AAD	15R	PRL 115 112001	R. Ajij et al.	(LHCb Collab.)
SIRUNYAN	20BY	EPJ C80 658	A.M. Sirunyan et al.	(CMS Collab.)	AALTONEN	15D	PR D92 032003	T. Aaltonen et al.	(CDF Collab.)
SIRUNYAN	20C	EPJ C80 75	A.M. Sirunyan et al.	(CMS Collab.)	AALTONEN	15H	PRL 115 152003	T. Aaltonen et al.	(CDF, DO Collab.)
SIRUNYAN	20D	PL B800 135042	A.M. Sirunyan et al.	(CMS Collab.)	ABAZOV	15G	PR D91 112003	V.M. Abazov et al.	(DO Collab.)
SIRUNYAN	20E	EPJ C80 370	A.M. Sirunyan et al.	(CMS Collab.)	ABAZOV	15K	PR D92 052007	V.M. Abazov et al.	(DO Collab.)
SIRUNYAN	20V	JHEP 2002 191	A.M. Sirunyan et al.	(CMS Collab.)	CHATRCHYAN	15	EPJ C75 216 (errata.)	S. Chatrchyan et al.	(CMS Collab.)
AABOUD	19AC	EPJ C79 290	M. Aboud et al.	(ATLAS Collab.)	AAD	14A	JHEP 1406 008	G. Aad et al.	(ATLAS Collab.)
AABOUD	19AD	EPJ C79 382	M. Aboud et al.	(ATLAS Collab.)	AAD	14AY	EPJ C74 3109	G. Aad et al.	(ATLAS Collab.)
AABOUD	19AP	PR D99 052009	M. Aboud et al.	(ATLAS Collab.)	AAD	14BB	PR D90 112016	G. Aad et al.	(ATLAS Collab.)
AABOUD	19AR	PR D99 072009	M. Aboud et al.	(ATLAS Collab.)	AAD	14B1	PR D90 112006	G. Aad et al.	(ATLAS Collab.)
AABOUD	19B	JHEP 1905 098	M. Aboud et al.	(ATLAS and CMS Collabs.)	AAD	14I	JHEP 1402 107	G. Aad et al.	(ATLAS Collab.)
AABOUD	19S	JHEP 1905 123	M. Aboud et al.	(ATLAS Collab.)	AALTONEN	14A	PR D89 091101	T. Aaltonen et al.	(CDF Collab.)
AAD	19G	JHEP 1911 150	G. Aad et al.	(ATLAS Collab.)	AALTONEN	14F	PRL 113 042001	T. Aaltonen et al.	(CDF Collab.)
SIRUNYAN	19AP	EPJ C79 313	A.M. Sirunyan et al.	(CMS Collab.)	Also		PRL 117 199901 (errata.)	T. Aaltonen et al.	(CDF Collab.)
SIRUNYAN	19AR	EPJ C79 368	A.M. Sirunyan et al.	(CMS Collab.)	AALTONEN	14G	PRL 112 221801	T. Aaltonen et al.	(CDF Collab.)
SIRUNYAN	19BF	PRL 122 132003	A.M. Sirunyan et al.	(CMS Collab.)	AALTONEN	14H	PR D89 072001	T. Aaltonen et al.	(CDF and DO Collab.)
SIRUNYAN	19BX	PR D100 072002	A.M. Sirunyan et al.	(CMS Collab.)	AALTONEN	14K	PRL 112 231805	T. Aaltonen et al.	(CDF Collab.)
SIRUNYAN	19BY	PR D100 072007	A.M. Sirunyan et al.	(CMS Collab.)	AALTONEN	14L	PRL 112 231804	T. Aaltonen et al.	(CDF Collab.)
SIRUNYAN	19CN	JHEP 1911 082	A.M. Sirunyan et al.	(CMS Collab.)	AALTONEN	14M	PRL 112 231803	T. Aaltonen et al.	(CDF and DO Collab.)
SIRUNYAN	19P	JHEP 1902 149	A.M. Sirunyan et al.	(CMS Collab.)	AALTONEN	14N	PR D90 091101	T. Aaltonen et al.	(CDF Collab.)
SIRUNYAN	19R	JHEP 1903 026	A.M. Sirunyan et al.	(CMS Collab.)	AALTONEN	14O	PRL 113 261804	T. Aaltonen et al.	(CDF Collab.)
AABOUD	18AE	PL B780 557	M. Aboud et al.	(ATLAS Collab.)	ABAZOV	14C	PRL 113 032002	V.M. Abazov et al.	(DO Collab.)
AABOUD	18AM	JHEP 1804 033	M. Aboud et al.	(ATLAS and CMS Collabs.)	Also		PR D91 112003	V.M. Abazov et al.	(DO Collab.)
AABOUD	18AT	JHEP 1807 176	M. Aboud et al.	(ATLAS Collab.)	ABAZOV	14D	PR D90 051101	V.M. Abazov et al.	(DO Collab.)
AABOUD	18AZ	EPJ C78 129	M. Aboud et al.	(ATLAS Collab.)	ABAZOV	14E	PR D90 072001	V.M. Abazov et al.	(DO Collab.)
AABOUD	18BH	EPJ C78 487	M. Aboud et al.	(ATLAS Collab.)	ABAZOV	14G	PR D90 072011	V.M. Abazov et al.	(DO Collab.)
AABOUD	18BK	PL B784 173	M. Aboud et al.	(ATLAS Collab.)	ABAZOV	14K	PR D90 092006	V.M. Abazov et al.	(DO Collab.)
AABOUD	18BW	JHEP 1809 139	M. Aboud et al.	(ATLAS Collab.)	CHATRCHYAN	14	PL B728 496	S. Chatrchyan et al.	(CMS Collab.)
AABOUD	18CE	JHEP 1812 039	M. Aboud et al.	(ATLAS Collab.)	CHATRCHYAN	14AC	PRL 112 231802	S. Chatrchyan et al.	(CMS Collab.)
AABOUD	18H	JHEP 1801 063	M. Aboud et al.	(ATLAS Collab.)	CHATRCHYAN	14AE	EPJ C74 3014	S. Chatrchyan et al.	(CMS Collab.)
AABOUD	18X	PR D98 032002	M. Aboud et al.	(ATLAS Collab.)	Also		EPJ C75 216 (errata.)	S. Chatrchyan et al.	(CMS Collab.)
AALTONEN	18R	PRL 120 042001	T. Aaltonen et al.	(CDF and DO Collabs.)	CHATRCHYAN	14C	EPJ C74 2758	S. Chatrchyan et al.	(CMS Collab.)
SIRUNYAN	18AQ	JHEP 1803 115	A.M. Sirunyan et al.	(CMS Collab.)	CHATRCHYAN	14D	JHEP 1404 191	S. Chatrchyan et al.	(CMS Collab.)
SIRUNYAN	18BC	JHEP 1806 102	A.M. Sirunyan et al.	(CMS Collab.)	CHATRCHYAN	14F	JHEP 1402 024	S. Chatrchyan et al.	(CMS Collab.)
SIRUNYAN	18BD	JHEP 1806 101	A.M. Sirunyan et al.	(CMS Collab.)	CHATRCHYAN	14O	PL B731 173	S. Chatrchyan et al.	(CMS Collab.)
SIRUNYAN	18BS	JHEP 1808 011	A.M. Sirunyan et al.	(CMS Collab.)	CHATRCHYAN	14R	PR D90 032006	S. Chatrchyan et al.	(CMS Collab.)
SIRUNYAN	18BU	EPJ C78 140	A.M. Sirunyan et al.	(CMS Collab.)	CHATRCHYAN	14S	PRL 112 171802	S. Chatrchyan et al.	(CMS Collab.)
SIRUNYAN	18DE	EPJ C78 891	A.M. Sirunyan et al.	(CMS Collab.)	KHACHATRYAN...	14E	PL B736 33	V. Khachatryan et al.	(CMS Collab.)
Also		EPJ C82 323 (errata.)	A.M. Sirunyan et al.	(CMS Collab.)	KHACHATRYAN...	14F	JHEP 1406 090	V. Khachatryan et al.	(CMS Collab.)
SIRUNYAN	18DL	JHEP 1810 117	A.M. Sirunyan et al.	(CMS Collab.)	KHACHATRYAN...	14G	JHEP 1409 087	V. Khachatryan et al.	(CMS Collab.)
SIRUNYAN	18L	PRL 120 231801	A.M. Sirunyan et al.	(CMS Collab.)	KHACHATRYAN...	14H	EPJ C74 3060	V. Khachatryan et al.	(CMS Collab.)
SIRUNYAN	18Z	PL B779 358	A.M. Sirunyan et al.	(CMS Collab.)	KHACHATRYAN...	14Q	PR D90 112013	V. Khachatryan et al.	(CMS Collab.)
AABOUD	17AH	JHEP 1709 118	M. Aboud et al.	(ATLAS Collab.)	KHACHATRYAN...	14R	JHEP 1411 154	V. Khachatryan et al.	(CMS Collab.)
AABOUD	17AV	JHEP 1710 129	M. Aboud et al.	(ATLAS Collab.)	KHACHATRYAN...	14S	PL B739 23	V. Khachatryan et al.	(CMS Collab.)
AABOUD	17BB	JHEP 1712 017	M. Aboud et al.	(ATLAS Collab.)	AAD	13AY	JHEP 1311 031	G. Aad et al.	(ATLAS Collab.)
AABOUD	17BC	EPJ C77 804	M. Aboud et al.	(ATLAS Collab.)	AAD	13BE	PRL 111 232002	G. Aad et al.	(ATLAS Collab.)
AABOUD	17G	JHEP 1703 113	M. Aboud et al.	(ATLAS Collab.)	AALTONEN	13X	EPJ C73 2328	G. Aad et al.	(ATLAS Collab.)
AABOUD	17H	JHEP 1704 086	M. Aboud et al.	(ATLAS Collab.)	AALTONEN	13AB	PR D88 091103	T. Aaltonen et al.	(CDF Collab.)
AABOUD	17I	JHEP 1704 124	M. Aboud et al.	(ATLAS Collab.)	AALTONEN	13AD	PRL 111 182002	T. Aaltonen et al.	(CDF Collab.)
AABOUD	17T	EPJ C77 531	M. Aboud et al.	(ATLAS Collab.)	AALTONEN	13D	PR D87 031104	T. Aaltonen et al.	(CDF Collab.)
AABOUD	17Z	PR D95 072003	M. Aboud et al.	(ATLAS Collab.)	AALTONEN	13E	PR D87 052013	T. Aaltonen et al.	(CDF Collab.)
ABAZOV	17	PR D95 011101	V.M. Abazov et al.	(DO Collab.)	AALTONEN	13G	PR D87 111101	T. Aaltonen et al.	(CDF Collab.)
ABAZOV	17B	PR D95 112004	V.M. Abazov et al.	(DO Collab.)	AALTONEN	13H	PR D88 011101	T. Aaltonen et al.	(CDF Collab.)
CHATRCHYAN	17	PL B770 50	S. Chatrchyan et al.	(CMS Collab.)	AALTONEN	13J	PR D88 032003	T. Aaltonen et al.	(CDF Collab.)

Quark Particle Listings

t, b' (Fourth Generation) Quark

CHATRCHYAN	13BH	JHEP 1310 167	S. Chatrchyan et al.	(CMS Collab.)	CACCARI	08	JHEP 0809 127	M. Cacciari et al.	
CHATRCHYAN	13C	PRL 110 022003	S. Chatrchyan et al.	(CMS Collab.)	KIDONAKIS	08	PR D78 074005	N. Kidonakis, R. Vogt	
CHATRCHYAN	13F	PL B718 1252	S. Chatrchyan et al.	(CMS Collab.)	MOCH	08	PR D78 034003	S. Moch, P. Uwer	(BERL, KARLE)
CHATRCHYAN	13S	EPJ C73 2494	S. Chatrchyan et al.	(CMS Collab.)	AALTONEN	07	PRL 98 142001	T. Aaltonen et al.	(CDF Collab.)
AAD	12B	PL B707 459	G. Aad et al.	(ATLAS Collab.)	AALTONEN	07B	PR D75 111103	T. Aaltonen et al.	(CDF Collab.)
AAD	12BE	JHEP 1204 069	G. Aad et al.	(ATLAS Collab.)	AALTONEN	07D	PR D76 072009	T. Aaltonen et al.	(CDF Collab.)
AAD	12BF	JHEP 1205 059	G. Aad et al.	(ATLAS Collab.)	AALTONEN	07I	PRL 99 182002	T. Aaltonen et al.	(CDF Collab.)
AAD	12BG	JHEP 1206 088	G. Aad et al.	(ATLAS Collab.)	ABAZOV	07C	PRL 98 041801	V.M. Abazov et al.	(DO Collab.)
AAD	12BK	EPJ C72 2039	G. Aad et al.	(ATLAS Collab.)	ABAZOV	07D	PR D75 031102	V.M. Abazov et al.	(DO Collab.)
AAD	12BL	EPJ C72 2043	G. Aad et al.	(ATLAS Collab.)	ABAZOV	07F	PR D75 092001	V.M. Abazov et al.	(DO Collab.)
AAD	12BO	PL B711 244	G. Aad et al.	(ATLAS Collab.)	ABAZOV	07H	PRL 98 181802	V.M. Abazov et al.	(DO Collab.)
AAD	12BP	PL B712 351	G. Aad et al.	(ATLAS Collab.)	ABAZOV	07O	PR D76 052006	V.M. Abazov et al.	(DO Collab.)
AAD	12BT	JHEP 1209 139	G. Aad et al.	(ATLAS Collab.)	ABAZOV	07P	PR D76 072007	V.M. Abazov et al.	(DO Collab.)
AAD	12CG	PL B717 89	G. Aad et al.	(ATLAS Collab.)	ABAZOV	07R	PR D76 092007	V.M. Abazov et al.	(DO Collab.)
AAD	12CH	PL B717 330	G. Aad et al.	(ATLAS Collab.)	ABAZOV	07V	PRL 99 191802	V.M. Abazov et al.	(DO Collab.)
AAD	12I	EPJ C72 2046	G. Aad et al.	(ATLAS Collab.)	ABAZOV	07W	PL B655 7	V.M. Abazov et al.	(DO Collab.)
AALTONEN	12AI	PRL 109 152003	T. Aaltonen et al.	(CDF Collab.)	ABULENCIA	07D	PR D75 031105	A. Abulencia et al.	(CDF Collab.)
AALTONEN	12AL	PRL 109 192001	T. Aaltonen et al.	(CDF Collab.)	ABULENCIA	07G	PRL 98 072001	A. Abulencia et al.	(CDF Collab.)
AALTONEN	12AP	PR D86 092003	T. Aaltonen et al.	(CDF, DO Collab.)	ABULENCIA	07J	PR D75 052001	A. Abulencia et al.	(CDF Collab.)
AALTONEN	12G	PL B714 24	T. Aaltonen et al.	(CDF Collab.)	ABULENCIA	07I	PR D75 071102	A. Abulencia et al.	(CDF Collab.)
AALTONEN	12Z	PR D85 071106	T. Aaltonen et al.	(CDF, DO Collab.)	ABAZOV	06K	PL B639 516	V.M. Abazov et al.	(DO Collab.)
ABAZOV	12AB	PR D86 051103	V.M. Abazov et al.	(DO Collab.)	ABAZOV	06U	PR D74 092005	V.M. Abazov et al.	(DO Collab.)
ABAZOV	12B	PR 108 032004	V.M. Abazov et al.	(DO Collab.)	ABAZOV	06X	PR D74 112004	V.M. Abazov et al.	(DO Collab.)
ABAZOV	12E	PL B708 21	V.M. Abazov et al.	(DO Collab.)	ABULENCIA	06D	PRL 96 022004	A. Abulencia et al.	(CDF Collab.)
ABAZOV	12I	PL B713 165	V.M. Abazov et al.	(DO Collab.)	Also	PR D73 032003	A. Abulencia et al.	(CDF Collab.)	
ABAZOV	12T	PR D85 091104	V.M. Abazov et al.	(DO Collab.)	Also	PR D73 092002	A. Abulencia et al.	(CDF Collab.)	
BERNREUTH...	12	PR D86 034026	V. Bernreuther, Z.-G. Si	(AAHC, SHDN)	ABULENCIA	06G	PRL 96 152002	A. Abulencia et al.	(CDF Collab.)
CHATRCHYAN	12AC	PR D85 112007	S. Chatrchyan et al.	(CMS Collab.)	Also	PR D74 032009	A. Abulencia et al.	(CDF Collab.)	
CHATRCHYAN	12AX	JHEP 1211 067	S. Chatrchyan et al.	(CMS Collab.)	ABULENCIA	06R	PL B639 172	A. Abulencia et al.	(CDF Collab.)
CHATRCHYAN	12BA	EPJ C72 2202	S. Chatrchyan et al.	(CMS Collab.)	ABULENCIA	06U	PR D73 111103	A. Abulencia et al.	(CDF Collab.)
CHATRCHYAN	12BB	PL B717 129	S. Chatrchyan et al.	(CMS Collab.)	ABULENCIA	06V	PR D73 112006	A. Abulencia et al.	(CDF Collab.)
CHATRCHYAN	12BF	JHEP 1212 105	S. Chatrchyan et al.	(CMS Collab.)	ABULENCIA	06Z	PRL 97 082004	A. Abulencia et al.	(CDF Collab.)
CHATRCHYAN	12BQ	JHEP 1212 035	S. Chatrchyan et al.	(CMS Collab.)	ABULENCIA,A	06C	PRL 96 202002	A. Abulencia et al.	(CDF Collab.)
CHATRCHYAN	12BS	PL B709 28	S. Chatrchyan et al.	(CMS Collab.)	ABULENCIA,A	06E	PR D74 072005	A. Abulencia et al.	(CDF Collab.)
CHATRCHYAN	12Y	JHEP 1206 109	S. Chatrchyan et al.	(CMS Collab.)	ABULENCIA,A	06F	PR D74 072006	A. Abulencia et al.	(CDF Collab.)
AAD	11A	EPJ C71 1577	G. Aad et al.	(ATLAS Collab.)	ABAZOV	05	PL B606 25	V.M. Abazov et al.	(DO Collab.)
AALTONEN	11AC	PR D84 071105	T. Aaltonen et al.	(CDF Collab.)	ABAZOV	05G	PL B617 1	V.M. Abazov et al.	(DO Collab.)
AALTONEN	11AK	PRL 107 232002	T. Aaltonen et al.	(CDF Collab.)	ABAZOV	05L	PR D72 011104	V.M. Abazov et al.	(DO Collab.)
AALTONEN	11AR	PR D83 031104	T. Aaltonen et al.	(CDF Collab.)	ABAZOV	05P	PL B622 265	V.M. Abazov et al.	(DO Collab.)
AALTONEN	11D	PR D83 071102	T. Aaltonen et al.	(CDF Collab.)	Also	PL B517 282	V.M. Abazov et al.	(DO Collab.)	
AALTONEN	11E	PR D83 111101	T. Aaltonen et al.	(CDF Collab.)	Also	PR D63 031101	B. Abbott et al.	(DO Collab.)	
AALTONEN	11F	PR D83 122003	T. Aaltonen et al.	(CDF Collab.)	Also	PR D75 092007	V.M. Abazov et al.	(DO Collab.)	
AALTONEN	11K	PRL 106 152001	T. Aaltonen et al.	(CDF Collab.)	ABAZOV	05Q	PL B626 35	V.M. Abazov et al.	(DO Collab.)
AALTONEN	11T	PL B698 371	T. Aaltonen et al.	(CDF Collab.)	ABAZOV	05R	PL B628 55	V.M. Abazov et al.	(DO Collab.)
AALTONEN	11W	PR D84 031101	T. Aaltonen et al.	(CDF Collab.)	ABAZOV	05S	PL B626 45	V.M. Abazov et al.	(DO Collab.)
AALTONEN	11Y	PR D84 032003	T. Aaltonen et al.	(CDF Collab.)	ACOSTA	05A	PRL 95 102002	D. Acosta et al.	(CDF Collab.)
AALTONEN	11Z	PR D84 031104	T. Aaltonen et al.	(CDF Collab.)	ACOSTA	05D	PR D71 031101	D. Acosta et al.	(CDF Collab.)
ABAZOV	11A	PL B695 88	V.M. Abazov et al.	(DO Collab.)	ACOSTA	05N	PR D71 012005	D. Acosta et al.	(CDF Collab.)
ABAZOV	11AA	PL B705 313	V.M. Abazov et al.	(DO Collab.)	ACOSTA	05S	PR D72 032002	D. Acosta et al.	(CDF Collab.)
ABAZOV	11AD	PR D84 112001	V.M. Abazov et al.	(DO Collab.)	ACOSTA	05T	PR D72 052003	D. Acosta et al.	(CDF Collab.)
ABAZOV	11AE	PRL 107 032001	V.M. Abazov et al.	(DO Collab.)	ACOSTA	05U	PR D71 072005	D. Acosta et al.	(CDF Collab.)
ABAZOV	11AF	PL B702 16	V.M. Abazov et al.	(DO Collab.)	ACOSTA	05U	PR D71 052003	D. Acosta et al.	(CDF Collab.)
ABAZOV	11AH	PR D84 112005	V.M. Abazov et al.	(DO Collab.)	ABAZOV	04G	NAT 429 638	V.M. Abazov et al.	(DO Collab.)
ABAZOV	11B	PRL 106 022001	V.M. Abazov et al.	(DO Collab.)	ABDALLAH	04C	PL B590 21	J. Abdallah et al.	(DELPHI Collab.)
ABAZOV	11C	PR D83 032009	V.M. Abazov et al.	(DO Collab.)	ACOSTA	04H	PR D69 052003	D. Acosta et al.	(CDF Collab.)
ABAZOV	11E	PR D84 012008	V.M. Abazov et al.	(DO Collab.)	ACOSTA	04I	PRL 93 142001	D. Acosta et al.	(CDF Collab.)
ABAZOV	11M	PL B701 313	V.M. Abazov et al.	(DO Collab.)	AKTAS	04	EPJ C33 9	A. Aktas et al.	(H1 Collab.)
ABAZOV	11P	PR D84 032004	V.M. Abazov et al.	(DO Collab.)	ABAZOV	03A	PR D67 012004	V.M. Abazov et al.	(DO Collab.)
ABAZOV	11R	PRL 107 082004	V.M. Abazov et al.	(DO Collab.)	CHEKANOV	03	PL B559 153	S. Chekanov et al.	(ZEUS Collab.)
ABAZOV	11S	PL B703 422	V.M. Abazov et al.	(DO Collab.)	ACHARD	02J	PL B549 290	P. Achard et al.	(L3 Collab.)
ABAZOV	11T	PR D84 052005	V.M. Abazov et al.	(DO Collab.)	ACOSTA	02	PR D65 091102	D. Acosta et al.	(CDF Collab.)
ABAZOV	11X	PRL 107 121802	V.M. Abazov et al.	(DO Collab.)	HEISTER	02Q	PL B543 173	A. Heister et al.	(ALEPH Collab.)
ABAZOV	11Z	PL B704 403	V.M. Abazov et al.	(DO Collab.)	ABBIENDI	01T	PL B521 181	G. Abbiendi et al.	(OPAL Collab.)
CHATRCHYAN	11AA	EPJ C71 1721	S. Chatrchyan et al.	(CMS Collab.)	AFFOLDER	01	PR D63 032003	T. Affolder et al.	(CDF Collab.)
CHATRCHYAN	11F	JHEP 1107 049	S. Chatrchyan et al.	(CMS Collab.)	CHOLDER	01A	PR D64 032002	T. Cholder et al.	(CDF Collab.)
CHATRCHYAN	11R	PR 107 091802	S. Chatrchyan et al.	(CMS Collab.)	AFFOLDER	01C	PRL 86 3233	T. Affolder et al.	(CDF Collab.)
CHATRCHYAN	11Z	PR D84 092004	S. Chatrchyan et al.	(CMS Collab.)	AFFOLDER	00B	PRL 84 216	T. Affolder et al.	(CDF Collab.)
KHACHATRYAN	11A	PL B695 424	V. Khachatryan et al.	(CMS Collab.)	BARATE	00S	PL B494 33	S. Barate et al.	(ALEPH Collab.)
AALTONEN	10AA	PR D82 052002	T. Aaltonen et al.	(CDF Collab.)	ABBOTT	99G	PR D60 052001	B. Abbott et al.	(DO Collab.)
AALTONEN	10AB	PR D82 112005	T. Aaltonen et al.	(CDF Collab.)	ABE	99B	PRL 82 271	F. Abe et al.	(CDF Collab.)
AALTONEN	10AC	PRL 105 232003	T. Aaltonen et al.	(CDF Collab.)	Also	PRL 82 2808 (errata)	F. Abe et al.	(CDF Collab.)	
AALTONEN	10AE	PRL 105 252001	T. Aaltonen et al.	(CDF Collab.)	CHANG	99	PR D59 091503	D. Chang, W. Chang, E. Ma	
AALTONEN	10C	PR D81 031102	T. Aaltonen et al.	(CDF Collab.)	ABBOTT	88D	PRL 80 2063	B. Abbott et al.	(DO Collab.)
AALTONEN	10D	PR D81 032002	T. Aaltonen et al.	(CDF Collab.)	ABBOTT	98F	PR D58 052001	B. Abbott et al.	(DO Collab.)
AALTONEN	10E	PR D81 052011	T. Aaltonen et al.	(CDF Collab.)	ABE	98E	PRL 80 2767	F. Abe et al.	(CDF Collab.)
AALTONEN	10Q	PRL 105 042002	T. Aaltonen et al.	(CDF Collab.)	ABE	98F	PRL 80 2779	F. Abe et al.	(CDF Collab.)
AALTONEN	10S	PRL 105 101801	T. Aaltonen et al.	(CDF Collab.)	ABE	98G	PRL 80 2525	F. Abe et al.	(CDF Collab.)
AALTONEN	10U	PR D81 072003	T. Aaltonen et al.	(CDF Collab.)	BHAT	98B	JUMP A13 5113	P.C. Bhat, H.B. Prosper, S.S. Snyder	
AALTONEN	10V	PR D81 092002	T. Aaltonen et al.	(CDF Collab.)	ABACHI	97E	PRL 79 1197	S. Abachi et al.	(DO Collab.)
AALTONEN	10W	PRL 105 012001	T. Aaltonen et al.	(CDF Collab.)	ABE	97R	PRL 79 1992	F. Abe et al.	(CDF Collab.)
ABAZOV	10	PL B682 363	V.M. Abazov et al.	(DO Collab.)	ABE	97V	PRL 79 3585	F. Abe et al.	(CDF Collab.)
ABAZOV	10I	PR D82 032002	V.M. Abazov et al.	(DO Collab.)	PDG	96	PR D54 1	R. M. Barnett et al.	(PDG Collab.)
ABAZOV	10J	PL B690 5	V.M. Abazov et al.	(DO Collab.)	ABACHI	95	PRL 74 2632	S. Abachi et al.	(DO Collab.)
ABAZOV	10K	PL B693 81	V.M. Abazov et al.	(DO Collab.)	ABE	95F	PRL 74 2626	F. Abe et al.	(CDF Collab.)
ABAZOV	10Q	PR D82 071102	V.M. Abazov et al.	(DO Collab.)	ABE	94E	PR D50 2966	F. Abe et al.	(CDF Collab.)
AHRENS	10	JHEP 1009 097	V. Ahrens et al.	(MAINZ, HEIDH)	Also	PRL 73 225	F. Abe et al.	(CDF Collab.)	
AHRENS	10A	NPB95, 205-206 48	V. Ahrens et al.	(MAINZ, HEIDH)					
AALTONEN	09AD	PR D79 112007	T. Aaltonen et al.	(CDF Collab.)					
AALTONEN	09AK	PR D80 051104	T. Aaltonen et al.	(CDF Collab.)					
AALTONEN	09AL	PR D80 052001	T. Aaltonen et al.	(CDF Collab.)					
AALTONEN	09AT	PRL 103 092002	T. Aaltonen et al.	(CDF Collab.)					
AALTONEN	09F	PR D79 031101	T. Aaltonen et al.	(CDF Collab.)					
AALTONEN	09H	PR D79 052007	T. Aaltonen et al.	(CDF Collab.)					
AALTONEN	09J	PR D79 072001	T. Aaltonen et al.	(CDF Collab.)					
AALTONEN	09K	PR D79 072010	T. Aaltonen et al.	(CDF Collab.)					
AALTONEN	09L	PR D79 092005	T. Aaltonen et al.	(CDF Collab.)					
AALTONEN	09M	PRL 102 042001	T. Aaltonen et al.	(CDF Collab.)					
AALTONEN	09N	PRL 102 151801	T. Aaltonen et al.	(CDF Collab.)					
AALTONEN	09O	PRL 102 152001	T. Aaltonen et al.	(CDF Collab.)					
AALTONEN	09Q	PL B674 160	T. Aaltonen et al.	(CDF Collab.)					
AALTONEN	09X	PR D79 072005	T. Aaltonen et al.	(CDF Collab.)					
AARON	09A	PL B678 450	F.D. Aaron et al.	(H1 Collab.)					
ABAZOV	09AA	PRL 103 132001	V.M. Abazov et al.	(DO Collab.)					
ABAZOV	09AG	PR D80 071102	V.M. Abazov et al.	(DO Collab.)					
ABAZOV	09AH	PR D80 092006	V.M. Abazov et al.	(DO Collab.)					
ABAZOV	09J	PRL 102 092002	V.M. Abazov et al.	(DO Collab.)					
ABAZOV	09R	PL B679 177	V.M. Abazov et al.	(DO Collab.)					
ABAZOV	09Z	PRL 103 092001	V.M. Abazov et al.	(DO Collab.)					
LANGENFELD	09	PR D80 054009	U. Langenfeld, S. Moch, P. Uwer						
AALTONEN	08AB	PRL 101 202001	T. Aaltonen et al.	(CDF Collab.)	</				

See key on page 1171

Quark Particle Listings

b' (Fourth Generation) Quark

• • • We do not use the following data for averages, fits, limits, etc. • • •

>1460	95	17	AAD	23AG	ATLS	$B(b' \rightarrow Wt) = 1$
>1390	95	3	SIRUNYAN	20Bi	CMS	$B(b' \rightarrow Zb) = 1$
>1130	95	18	SIRUNYAN	19AQ	CMS	$B(b' \rightarrow Zb) = 1$
>1230	95	19	SIRUNYAN	19BW	CMS	$B(b' \rightarrow Wt) = 1$
>1350	95	20	AABOUD	18AW	ATLS	$B(b' \rightarrow Wt) = 1$
> 910	95	21	SIRUNYAN	18BM	CMS	Wt, Zb, hb modes
> 880	95	22	KHACHATRYAN	16AN	CMS	$B(b' \rightarrow Wt) = 1$
<350, 580–635, >700	95	23	AAD	15AR	ATLS	$B(b' \rightarrow Hb) = 1$
> 620	95	24	AAD	15BY	ATLS	Wt, Zb, hb modes
> 730	95	25	AAD	15BY	ATLS	$B(b' \rightarrow Wt) = 1$
> 690	95	26	AAD	15CN	ATLS	$B(b' \rightarrow Wq) = 1$ ($q=u$)
> 755	95	27	AAD	14AZ	ATLS	$B(b' \rightarrow Wt) = 1$
> 675	95	28	CHATRCHYAN	13i	CMS	$B(b' \rightarrow Wt) = 1$
> 480	95	29	AAD	12AT	ATLS	$B(b' \rightarrow Wt) = 1$
> 400	95	30	AAD	12AU	ATLS	$B(b' \rightarrow Zb) = 1$
> 350	95	31	AAD	12bC	ATLS	$B(b' \rightarrow Wq) = 1$ ($q=u,c$)
> 450	95	32	AAD	12bE	ATLS	$B(b' \rightarrow Wt) = 1$
> 685	95	33	CHATRCHYAN	12bH	CMS	$m_{b'} = m_{b''}$
> 611	95	34	CHATRCHYAN	12X	CMS	$B(b' \rightarrow Wt) = 1$
> 372	95	35	AALTONEN	11j	CDF	$b' \rightarrow Wt$
> 361	95	36	CHATRCHYAN	11L	CMS	Repl. by CHA- TRCHYAN 12X
> 338	95	37	AALTONEN	10H	CDF	$b' \rightarrow Wt$
> 380–430	95	38	FLACCO	10	RVUE	$m_{b'} > m_{b''}$
> 268	95	39,40	AALTONEN	07C	CDF	$B(b' \rightarrow Zb) = 1$
> 199	95	41	AFFOLDER	00	CDF	NC: $b' \rightarrow Zb$
> 148	95	42	ABE	98N	CDF	NC: $b' \rightarrow Zb + \text{vertex}$
> 96	95	43	ABACHI	97D	D0	NC: $b' \rightarrow b\gamma$
> 128	95	44	ABACHI	95F	D0	$\ell\ell + \text{jets}, \ell + \text{jets}$
> 75	95	45	MUKHOPAD...	93	RVUE	NC: $b' \rightarrow b\ell\ell$
> 85	95	46	ABE	92	CDF	CC: $\ell\ell$
> 72	95	47	ABE	90B	CDF	CC: $e + \mu$
> 54	95	48	AKESSON	90	UA2	CC: $e + \text{jets} + E_T$
> 43	95	49	ALBAJAR	90B	UA1	CC: $\mu + \text{jets}$
> 34	95	50	ALBAJAR	88	UA1	CC: e or $\mu + \text{jets}$

- AAD 23Ag based on 139 fb⁻¹ of pp data at $\sqrt{s} = 13$ TeV. Pair production of vector-like b' is searched for in the mode $\ell^{\pm}\ell^{\mp} + \geq 2j$ ($\geq 1b$ -tagged) + E_T or with 3ℓ . The data are consistent with the SM background predictions and limits are obtained for different branching ratios.
- TUMASYAN 23v based on 138 fb⁻¹ of pp data at $\sqrt{s} = 13$ TeV. Pair production of vector-like b' is searched for in the single-lepton, same-sign charge dilepton and multi-lepton channels. The data are consistent with the SM background predictions and limits are obtained for different branching ratios.
- SIRUNYAN 20Bi based on 137 fb⁻¹ of pp data at $\sqrt{s} = 13$ TeV. Pair production of vector-like b' is searched for with each b' decaying into Zb or hb . Analysis focuses on final states consisting of jets from six quarks. Mass limits are obtained for a variety of branching ratios of b' decays.
- AABOUD 18Ce based on 36.1 fb⁻¹ of proton-proton data taken at $\sqrt{s} = 13$ TeV. Events including a same-sign lepton pair are used. The limit is for a singlet model, assuming the branching ratios of b' into Zb, Wt and Hb as predicted by the model.
- AABOUD 18cL, AABOUD 18cP based on 36.1 fb⁻¹ of pp data at $\sqrt{s} = 13$ TeV. The limit is for the pair-produced vector-like b' using all-hadronic final state. The analysis is particularly powerful for the $b' \rightarrow hb$ mode. Assuming the pure decay only in this mode sets a limit $m_{b'} > 1010$ GeV.
- AABOUD 18cP based on 36.1 fb⁻¹ of pp data at $\sqrt{s} = 13$ TeV. Pair and single production of vector-like b' are searched for with at least one b' decaying into Zb . In the case of $B(b' \rightarrow Zb) = 1$, the limit is $m_{b'} > 1220$ GeV.
- The limit is for the singlet model, assuming that the branching ratios into Wt, Zb, hb add up to one.
- The limit is for the doublet model, assuming that the branching ratios into Wt, Zb, hb add up to one.
- AABOUD 18cR based on 36.1 fb⁻¹ of pp data at $\sqrt{s} = 13$ TeV. A combination of searches for the pair-produced vector-like b' in various decay channels ($b' \rightarrow Wt, Zb, hb$). Also a model-independent limit is obtained as $m_{b'} > 1.03$ TeV, assuming that the branching ratios into Zb, Wt , and hb add up to one.
- The limit is for the singlet b' .
- The limit is for b' in a weak isospin doublet (t', b') and $|V_{t'b}| \ll |V_{tb}|$. For a b' in a doublet with a charge $-4/3$ vector-like quark, the limit $m_{b'} > 1.14$ TeV is obtained.
- SIRUNYAN 18g based on 19.7 fb⁻¹ of pp data at $\sqrt{s} = 8$ TeV. The limit is for the pair-produced vector-like b' that couple only to light quarks. Upper cross section limits on the single production of a b' and constraints for other decay channels (Zq and Hq) are also given in the paper.
- SIRUNYAN 17AU based on 2.3–2.6 fb⁻¹ of pp data at $\sqrt{s} = 13$ TeV. Limit on pair-produced singlet vector-like b' using one lepton and several jets. The mass bound is given for a b' transforming as a singlet under the electroweak symmetry group, assumed to decay through W, Z or Higgs boson (which decays to jets) and to a third generation quark.
- AAD 15z based on 20.3 fb⁻¹ of pp data at $\sqrt{s} = 8$ TeV. Used events with $\ell + E_T + \geq 6j$ ($\geq 1b$) and at least one pair of jets from weak boson decay, primarily designed to select the signature $b'\bar{b}' \rightarrow WWt\bar{t} \rightarrow JWWWWb\bar{b}$. This is a limit on pair-produced vector-like b' . The lower mass limit is 640 GeV for a vector-like singlet b' .
- Result is based on 1.1 fb⁻¹ of data. No signal is found for the search of long-lived particles which decay into final states with two electrons or photons, and upper bound on the cross section times branching fraction is obtained for $2 < cr < 7000$ mm; see Fig. 3. 95% CL excluded region of b' lifetime and mass is shown in Fig. 4.

- ACOSTA 03 looked for long-lived fourth generation quarks in the data sample of 90 pb⁻¹ of $\sqrt{s} = 1.8$ TeV $p\bar{p}$ collisions by using the muon-like penetration and anomalously high ionization energy loss signature. The corresponding lower mass bound for the charge $(2/3)e$ quark (t') is 220 GeV. The t' bound is higher than the b' bound because t' is more likely to produce charged hadrons than b' . The 95% CL upper bounds for the production cross sections are given in their Fig. 3.
- AAD 23Ag based on 139 fb⁻¹ of pp data at $\sqrt{s} = 13$ TeV. Pair production of vector-like top or b_s is searched for in the mode $1\ell + \geq 4j$ ($\geq 1b$ -tagged) + E_T . The data are consistent with the SM background predictions and limits are obtained for different branching ratios. Masses below 1.59 TeV are excluded assuming a mass-degenerate vector-like doublet (t', b') model.
- SIRUNYAN 19AQ based on 35.9 fb⁻¹ of pp data at $\sqrt{s} = 13$ TeV. Pair production of vector-like b' is searched for with one b' decaying into Zb and the other b' decaying into Wt, Zb, hb . Events with an opposite-sign lepton pair consistent with coming from Z and jets are used. Mass limits are obtained for a variety of branching ratios of b' .
- SIRUNYAN 19BW based on 35.9 fb⁻¹ of pp data at $\sqrt{s} = 13$ TeV. The limit is for the pair-produced vector-like b' using all-hadronic final state. The analysis is made for the Zb, Wt, hb modes and mass limits are obtained for a variety of branching ratios.
- AABOUD 18AW based on 36.1 fb⁻¹ of pp data at $\sqrt{s} = 13$ TeV. The limit is for the pair-produced vector-like b' using lepton-plus-jets final state. The search is also sensitive to the decays into Zb and Hb final states.
- SIRUNYAN 18BM based on 35.9 fb⁻¹ of pp data at $\sqrt{s} = 13$ TeV. The limit is for the pair-produced vector-like b' . Three channels (single lepton, same-charge 2 leptons, or at least 3 leptons) are considered for various branching fraction combinations. Assuming $B(tW) = 1$, the limit is 1240 GeV and for $B(bZ) = 1$ it is 960 GeV.
- KHACHATRYAN 16AN based on 19.7 fb⁻¹ of pp data at $\sqrt{s} = 8$ TeV. Limit on pair-produced vector-like b' using 1, 2, and >2 leptons as well as fully hadronic final states. Other limits depending on the branching fractions to tW, bZ , and bH are given in Table IX.
- AAD 15AR based on 20.3 fb⁻¹ of pp data at $\sqrt{s} = 8$ TeV. Used lepton-plus-jets final state. See Fig. 24 for mass limits in the plane of $B(b' \rightarrow Wt)$ vs. $B(b' \rightarrow Hb)$ from $b'\bar{b}' \rightarrow Hb + X$ searches.
- AAD 15BY based on 20.3 fb⁻¹ of pp data at $\sqrt{s} = 8$ TeV. Limit on pair-produced vector-like b' assuming the branching fractions to W, Z , and h modes of the singlet model. Used events containing $\geq 2\ell + E_T + \geq 2j$ ($\geq 1b$) and including a same-sign lepton pair.
- AAD 15BY based on 20.3 fb⁻¹ of pp data at $\sqrt{s} = 8$ TeV. Limit on pair-produced chiral b' -quark. Used events containing $\geq 2\ell + E_T + \geq 2j$ ($\geq 1b$) and including a same-sign lepton pair.
- AAD 15CN based on 20.3 fb⁻¹ of pp data at $\sqrt{s} = 8$ TeV. Limit on pair-production of chiral b' -quark. Used events with $\ell + E_T + \geq 4j$ (non- b -tagged). Limits on a heavy vector-like quark, which decays into Wq, Zq, hq , are presented in the plane $B(Q \rightarrow Wq)$ vs. $B(Q \rightarrow hq)$ in Fig. 12.
- Based on 20.3 fb⁻¹ of pp data at $\sqrt{s} = 8$ TeV. No significant excess over SM expectation is found in the search for pair production or single production of b' in the events with dilepton from a high $p_T Z$ and additional jets ($\geq 1b$ -tag). If instead of $B(b' \rightarrow Wt) = 1$ an electroweak singlet with $B(b' \rightarrow Wt) \sim 0.45$ is assumed, the limit reduces to 685 GeV.
- Based on 5.0 fb⁻¹ of pp data at $\sqrt{s} = 7$ TeV. CHATRCHYAN 13i looked for events with one isolated electron or muon, large E_T , and at least four jets with large transverse momenta, where one jet is likely to originate from the decay of a bottom quark.
- Based on 1.04 fb⁻¹ of pp data at $\sqrt{s} = 7$ TeV. No signal is found for the search of heavy quark pair production that decay into W and a t quark in the events with a high p_T isolated lepton, large E_T , and at least 6 jets in which one, two or more dijets are from W .
- Based on 2.0 fb⁻¹ of pp data at $\sqrt{s} = 7$ TeV. No $b' \rightarrow Zb$ invariant mass peak is found in the search of heavy quark pair production that decay into Z and a b quark in events with $Z \rightarrow e^+e^-$ and at least one b -jet. The lower mass limit is 358 GeV for a vector-like singlet b' mixing solely with the third SM generation.
- Based on 1.04 fb⁻¹ of pp data at $\sqrt{s} = 7$ TeV. No signal is found for the search of heavy quark pair production that decay into W and a quark in the events with dileptons, large E_T , and ≥ 2 jets.
- Based on 1.04 fb⁻¹ of pp data at $\sqrt{s} = 7$ TeV. AAD 12bE looked for events with two isolated like-sign leptons and at least 2 jets, large E_T and $H_T > 350$ GeV.
- Based on 5 fb⁻¹ of pp data at $\sqrt{s} = 7$ TeV. CHATRCHYAN 12bH searched for QCD and EW production of single and pair of degenerate 4th generation quarks that decay to bW or tW . Absence of signal in events with one lepton, same-sign dileptons or tripletons gives the bound. With a mass difference of 25 GeV/c² between $m_{t'}$ and $m_{b'}$, the corresponding limit shifts by about ± 20 GeV/c².
- Based on 4.9 fb⁻¹ of pp data at $\sqrt{s} = 7$ TeV. CHATRCHYAN 12X looked for events with trileptons or same-sign dileptons and at least one b jet.
- Based on 4.8 fb⁻¹ of data in $p\bar{p}$ collisions at 1.96 TeV. AALTONEN 11j looked for events with $\ell + E_T + \geq 5j$ ($\geq 1b$ or c). No signal is observed and the bound $\sigma(b'\bar{b}') < 30$ fb for $m_{b'} > 375$ GeV is found for $B(b' \rightarrow Wt) = 1$.
- Based on 34 pb⁻¹ of data in pp collisions at 7 TeV. CHATRCHYAN 11L looked for multi-jet events with trileptons or same-sign dileptons. No excess above the SM background excludes $m_{b'}$ between 255 and 361 GeV at 95% CL for $B(b' \rightarrow Wt) = 1$.
- Based on 2.7 fb⁻¹ of data in $p\bar{p}$ collisions at $\sqrt{s} = 1.96$ TeV. AALTONEN 10H looked for pair production of heavy quarks which decay into tW^- or tW^+ , in events with same sign dileptons (e or μ), several jets and large missing E_T . The result is obtained for b' which decays into tW^- . For the charge $5/3$ quark ($T_{5/3}$) which decays into tW^+ , $m_{T_{5/3}} > 365$ GeV (95% CL) is found when it has the charge $-1/3$ partner B of the same mass.
- FLACCO 10 result is obtained from AALTONEN 10H result of $m_{b'} > 338$ GeV, by relaxing the condition $B(b' \rightarrow Wt) = 100\%$ when $m_{b'} > m_{t'}$.
- Result is based on 1.06 fb⁻¹ of data. No excess from the SM Z +jet events is found when Z decays into ee or $\mu\mu$. The $m_{b'}$ bound is found by comparing the resulting upper

Quark Particle Listings

 b' (Fourth Generation) Quark

bound on $\sigma(b'\bar{b}') [1 - (1 - B(b' \rightarrow Zb))^2]$ and the LO estimate of the b' pair production cross section shown in Fig. 38 of the article.

⁴⁰ HUANG 08 reexamined the b' mass lower bound of 268 GeV obtained in AALTONEN 07c that assumes $B(b' \rightarrow Zb) = 1$, which does not hold for $m_{b'} > 255$ GeV. The lower mass bound is given in the plane of $\sin^2(\theta_{tb'})$ and $m_{b'}$.

⁴¹ AFFOLDER 00 looked for b' that decays in to $b+Z$. The signal searched for is bbZ events where one Z decays into e^+e^- or $\mu^+\mu^-$ and the other Z decays hadronically. The bound assumes $B(b' \rightarrow Zb) = 100\%$. Between 100 GeV and 199 GeV, the 95%CL upper bound on $\sigma(b' \rightarrow \bar{b}') \times B^2(b' \rightarrow Zb)$ is also given (see their Fig. 2).

⁴² ABE 98n looked for $Z \rightarrow e^+e^-$ decays with displaced vertices. Quoted limit assumes $B(b' \rightarrow Zb) = 1$ and $c\tau_{b'} = 1$ cm. The limit is lower than m_{Z+m_b} (~ 96 GeV) if $c\tau > 22$ cm or $c\tau < 0.009$ cm. See their Fig. 4.

⁴³ ABACHI 97D searched for b' that decays mainly via FCNC. They obtained 95%CL upper bounds on $B(b'\bar{b}' \rightarrow \gamma + 3 \text{ jets})$ and $B(b'\bar{b}' \rightarrow 2\gamma + 2 \text{ jets})$, which can be interpreted as the lower mass bound $m_{b'} > m_{Z+m_b}$.

⁴⁴ ABACHI 95F bound on the top-quark also applies to b' and t' quarks that decay predominantly into W . See FROGGATT 97.

⁴⁵ MUKHOPADHYAYA 93 analyze CDF dilepton data of ABE 92G in terms of a new quark decaying via flavor-changing neutral current. The above limit assumes $B(b' \rightarrow b\ell^+\ell^-) = 1\%$. For an exotic quark decaying only via virtual Z [$B(b\ell^+\ell^-) = 3\%$], the limit is 85 GeV.

⁴⁶ ABE 92 dilepton analysis limit of >85 GeV at CL=95% also applies to b' quarks, as discussed in ABE 90b.

⁴⁷ ABE 90b exclude the region 28–72 GeV.

⁴⁸ AKESSON 90 searched for events having an electron with $p_T > 12$ GeV, missing momentum > 15 GeV, and a jet with $E_T > 10$ GeV, $|\eta| < 2.2$, and excluded $m_{b'}$ between 30 and 69 GeV.

⁴⁹ For the reduction of the limit due to non-charged-current decay modes, see Fig. 19 of ALBAJAR 90b.

⁵⁰ ALBAJAR 88 study events at $E_{cm} = 546$ and 630 GeV with a muon or isolated electron, accompanied by one or more jets and find agreement with Monte Carlo predictions for the production of charm and bottom, without the need for a new quark. The lower mass limit is obtained by using a conservative estimate for the $b'\bar{b}'$ production cross section and by assuming that it cannot be produced in W decays. The value quoted here is revised using the full $O(\alpha_s^2)$ cross section of ALTARELLI 88.

 $b'(-1/3)$ mass limits from single production in $p\bar{p}$ and pp collisions

VALUE (GeV)	CL%	DOCUMENT ID	TECN	COMMENT
>3000	95	¹ TUMASYAN 220	CMS	$gb \rightarrow b' \rightarrow tW, B(b' \rightarrow tW)=1$
>693	95	² ABAZOV 11F	D0	$qu \rightarrow q'b' \rightarrow q'(Wu)$ $\bar{u}_b b' = 1, B(b' \rightarrow Wu)=1$
>430	95	² ABAZOV 11F	D0	$qd \rightarrow qb' \rightarrow q(Zd)$ $\bar{u}_{db'} = \sqrt{2}, B(b' \rightarrow Zd)=1$
• • • We do not use the following data for averages, fits, limits, etc. • • •				
>2600	95	³ AAD 23CQ	ATLS	$b' \rightarrow bh (h \rightarrow b\bar{b})$
		⁴ SIRUNYAN 21AG	CMS	$gb \rightarrow b' \rightarrow tW, B(b' \rightarrow tW)=1$
		⁵ SIRUNYAN 19AI	CMS	$bZ/tW \rightarrow b' \rightarrow tW$
>1500	95	⁶ AAD 16AH	ATLS	$gb \rightarrow b' \rightarrow tW, B(b' \rightarrow tW)=1$
>1390	95	⁷ KHACHATRY...16i	CMS	$gb \rightarrow b'_L \rightarrow tW, B(b'_L \rightarrow tW)=1$
>1430	95	⁸ KHACHATRY...16i	CMS	$gb \rightarrow b'_R \rightarrow tW, B(b'_R \rightarrow tW)=1$
>1530	95	⁹ KHACHATRY...16i	CMS	$gb \rightarrow b' \rightarrow tW, B(b' \rightarrow tW)=1$

¹ TUMASYAN 220 based on 138 fb^{-1} of data in pp collisions at 13 TeV. No significant excess over SM expectation is found in the search for a left-handed b' assuming 100% decay to tW using a t -tagged jet and a lepton from W . The model assumes that the b' has the excited quark couplings. The bound is from a statistical combination with an earlier analysis by SIRUNYAN 21AG. The 95% CL bounds are also set as 3.0, 3.0, and 3.2 TeV, respectively, for left-handed, right-handed, and vector-like couplings.

² ABAZOV 11F based on 5.4 fb^{-1} of data in $p\bar{p}$ collisions at 1.96 TeV. ABAZOV 11F looked for single production of b' via the W or Z coupling to the first generation up or down quarks, respectively. Model independent cross section limits for the single production processes $p\bar{p} \rightarrow b'q \rightarrow Wuq$, and $p\bar{p} \rightarrow b'q \rightarrow Zdq$ are given in Figs. 3 and 4, respectively, and the mass limits are obtained for the model of ATRE 09 with degenerate bi-doublets of vector-like quarks.

³ AAD 23CQ based on 139 fb^{-1} of data in pp collisions at 13 TeV. No significant excess over SM expectation is found. Limits on mass and production cross section of a vector-like b' are obtained in several theoretical scenarios determined by the couplings between b' and W, Z, h .

⁴ SIRUNYAN 21AG based on 137 fb^{-1} of data in pp collisions at 13 TeV. No significant excess over SM expectation is found in the search for a left-handed b' assuming 100% decay to tW using all hadronic final states, where t and W are tagged as single jets, respectively. The model assumes that the b' has the excited quark couplings. The 95% CL bounds are also set as 2.8 and 3.1 TeV, respectively, for the right-handed and vector-like couplings.

⁵ SIRUNYAN 19AI based on 35.9 fb^{-1} of pp data at $\sqrt{s} = 13$ TeV. Exclusion limits are set on the product of the production cross section and branching fraction for the $b'(-1/3) + b$ and $b'(-1/3) + t$ modes as a function of the vector-like quark mass in Figs. 7 and 8 and in Tab. 2 for relative vector-like quark widths between 1 and 30% for left- and right-handed vector-like quark couplings. No significant deviation from the SM prediction is observed.

⁶ AAD 16AH based on 20.3 fb^{-1} of data in pp collisions at 8 TeV. No significant excess over SM expectation is found in the search for a vector-like b' in the single-lepton and dilepton channels (ℓ or $\ell\ell$) + $1,2,3 j (\geq 1b)$. The model assumes that the b' has the excited quark couplings.

⁷ Based on 19.7 fb^{-1} of data in pp collisions at 8 TeV. Limit on left-handed b' assuming 100% decay to tW and using all-hadronic, lepton + jets, and dilepton final states.

⁸ Based on 19.7 fb^{-1} of data in pp collisions at 8 TeV. Limit on right-handed b' assuming 100% decay to tW and using all-hadronic, lepton + jets, and dilepton final states.

⁹ Based on 19.7 fb^{-1} of data in pp collisions at 8 TeV. Limit on vector-like b' assuming 100% decay to tW and using all-hadronic, lepton+jets, and dilepton final states.

MASS LIMITS for b' (4th Generation) Quark or Hadron in e^+e^- Collisions

Search for hadrons containing a fourth-generation $-1/3$ quark denoted b' .

The last column specifies the assumption for the decay mode (CC denotes the conventional charged-current decay) and the event signature which is looked for.

VALUE (GeV)	CL%	DOCUMENT ID	TECN	COMMENT
>46.0	95	¹ DECAMP 90F	ALEP	any decay
• • • We do not use the following data for averages, fits, limits, etc. • • •				
none 96–103	95	² ABDALLAH 07	DLPH	$b' \rightarrow bZ, cW$
		³ ADRIANI 93G	L3	Quarkonium
>44.7	95	ADRIANI 93M	L3	$\Gamma(Z)$
>45	95	ABREU 91F	DLPH	$\Gamma(Z)$
none 19.4–28.2	95	ABE 90D	VNS	Any decay; event shape
>45.0	95	ABREU 90D	DLPH	$B(CC) = 1$; event shape
>44.5	95	⁴ ABREU 90D	DLPH	$b' \rightarrow cH^-, H^- \rightarrow \bar{c}s, \tau^- \nu$
>40.5	95	⁵ ABREU 90D	DLPH	$\Gamma(Z \rightarrow \text{hadrons})$
>28.3	95	ADACHI 90	TOPZ	$B(\text{FCNC}) = 100\%$; isol. γ or 4 jets
>41.4	95	⁶ AKRAWY 90B	OPAL	Any decay; acoplanarity
>45.2	95	⁶ AKRAWY 90B	OPAL	$B(CC) = 1$; acoplanarity
>46	95	⁷ AKRAWY 90I	OPAL	$b' \rightarrow \gamma + \text{any}$
>27.5	95	⁸ ABE 89E	VNS	$B(CC) = 1$; μ, e
none 11.4–27.3	95	⁹ ABE 89G	VNS	$B(b' \rightarrow b\gamma) > 10\%$; isolated γ
>44.7	95	¹⁰ ABRAMS 89C	MRK2	$B(CC) = 100\%$; isol. track
>42.7	95	¹⁰ ABRAMS 89C	MRK2	$B(bg) = 100\%$; event shape
>42.0	95	¹⁰ ABRAMS 89C	MRK2	Any decay; event shape
>28.4	95	^{11,12} ADACHI 89C	TOPZ	$B(CC) = 1$; μ
>28.8	95	¹³ ENO 89A	AMY	$B(CC) \gtrsim 90\%$; μ, e
>27.2	95	^{13,14} ENO 89A	AMY	any decay; event shape
>29.0	95	¹³ ENO 89A	AMY	$B(b' \rightarrow bg) \gtrsim 85\%$; event shape
>24.4	95	¹⁵ IGARASHI 88A	AMY	μ, e
>23.8	95	¹⁶ SAGAWA 88A	AMY	event shape
>22.7	95	¹⁷ ADEVA 86	MRKJ	μ
>21	95	¹⁸ ALTHOFF 84C	TASS	R , event shape
>19	95	¹⁹ ALTHOFF 84I	TASS	Aplanarity

¹ DECAMP 90F looked for isolated charged particles, for isolated photons, and for four-jet final states. The modes $b' \rightarrow bg$ for $B(b' \rightarrow bg) > 65\%$ or $b' \rightarrow b\gamma$ for $B(b' \rightarrow b\gamma) > 5\%$ are excluded. Charged Higgs decay were not discussed.

² ABDALLAH 07 searched for b' pair production at $E_{cm} = 196\text{--}209$ GeV, with 420 pb^{-1} . No signal leads to the 95% CL upper limits on $B(b' \rightarrow bZ)$ and $B(b' \rightarrow cW)$ for $m_{b'} = 96$ to 103 GeV.

³ ADRIANI 93G search for vector quarkonium states near Z and give limit on quarkonium- Z mixing parameter $\delta m^2 < (10\text{--}30) \text{ GeV}^2$ (95%CL) for the mass 88–94.5 GeV. Using Richardson potential, a $1S(b'\bar{b}')$ state is excluded for the mass range 87.7–94.7 GeV. This range depends on the potential choice.

⁴ ABREU 90D assumed $m_{H^\pm} < m_{b'} - 3$ GeV.

⁵ Superseded by ABREU 91F.

⁶ AKRAWY 90B search was restricted to data near the Z peak at $E_{cm} = 91.26$ GeV at LEP. The excluded region is between 23.6 and 41.4 GeV if no H^\pm decays exist. For charged Higgs decays the excluded regions are between $(m_{H^\pm} + 1.5 \text{ GeV})$ and 45.5 GeV.

⁷ AKRAWY 90I search for isolated photons in hadronic Z decay and derive

$B(Z \rightarrow b'\bar{b}') \cdot B(b' \rightarrow \gamma X) / B(Z \rightarrow \text{hadrons}) < 2.2 \times 10^{-3}$. Mass limit assumes $B(b' \rightarrow \gamma X) > 10\%$.

⁸ ABE 89E search at $E_{cm} = 56\text{--}57$ GeV at TRISTAN for multihadron events with a spherical shape (using thrust and acoplanarity) or containing isolated leptons.

⁹ ABE 89G search was at $E_{cm} = 55\text{--}60.8$ GeV at TRISTAN.

¹⁰ If the photonic decay mode is large ($B(b' \rightarrow b\gamma) > 25\%$), the ABRAMS 89C limit is 45.4 GeV. The limit for Higgs decay ($b' \rightarrow cH^-, H^- \rightarrow \bar{c}s$) is 45.2 GeV.

¹¹ ADACHI 89C search was at $E_{cm} = 56.5\text{--}60.8$ GeV at TRISTAN using multi-hadron events accompanying muons.

¹² ADACHI 89C also gives limits for any mixture of CC and bg decays.

¹³ ENO 89 search at $E_{cm} = 50\text{--}60.8$ at TRISTAN.

¹⁴ ENO 89 considers arbitrary mixture of the charged current, bg , and $b\gamma$ decays.

¹⁵ IGARASHI 88 searches for leptons in low-thrust events and gives $\Delta R(b') < 0.26$ (95% CL) assuming charged current decay, which translates to $m_{b'} > 24.4$ GeV.

¹⁶ SAGAWA 88 set limit $\sigma(\text{top}) < 6.1 \text{ pb}$ at CL=95% for top-flavored hadron production from event shape analyses at $E_{cm} = 52$ GeV. By using the quark parton model cross-section formula near threshold, the above limit leads to lower mass bounds of 23.8 GeV for charge $-1/3$ quarks.

¹⁷ ADEVA 86 give 95%CL upper bound on an excess of the normalized cross section, ΔR , as a function of the minimum c.m. energy (see their figure 3). Production of a pair of $1/3$ charge quarks is excluded up to $E_{cm} = 45.4$ GeV.

¹⁸ ALTHOFF 84C narrow state search sets limit $\Gamma(e^+e^-) / B(\text{hadrons}) < 2.4 \text{ keV}$ CL = 95% and heavy charge $1/3$ quark pair production $m > 21$ GeV, CL = 95%.

¹⁹ ALTHOFF 84I exclude heavy quark pair production for $7 < m < 19$ GeV ($1/3$ charge) using aplanarity distributions (CL = 95%).

b' (Fourth Generation) Quark, t' (Fourth Generation) Quark

REFERENCES FOR Searches for (Fourth Generation) b' Quark

AAD	23AG	EPI C83 719	G. Aad et al.	(ATLAS Collab.)
AAD	23AV	PL B643 138019	G. Aad et al.	(ATLAS Collab.)
AAD	23CQ	JHEP 2311 168	G. Aad et al.	(ATLAS Collab.)
TUMASYAN	23V	JHEP 2307 020	A. Tumasyan et al.	(CMS Collab.)
TUMASYAN	22O	JHEP 2204 048	A. Tumasyan et al.	(CMS Collab.)
SIRUNYAN	21AG	JHEP 2112 106	A.M. Sirunyan et al.	(CMS Collab.)
SIRUNYAN	20BI	PR D102 112004	A.M. Sirunyan et al.	(CMS Collab.)
SIRUNYAN	19AI	EPJ C79 90	A.M. Sirunyan et al.	(CMS Collab.)
SIRUNYAN	19AQ	EPJ C79 364	A.M. Sirunyan et al.	(CMS Collab.)
SIRUNYAN	19BW	PR D100 072001	A.M. Sirunyan et al.	(CMS Collab.)
AABOUD	18AW	JHEP 1808 048	M. Aaboud et al.	(ATLAS Collab.)
AABOUD	18CE	JHEP 1812 039	M. Aaboud et al.	(ATLAS Collab.)
AABOUD	18CL	PR D98 092005	M. Aaboud et al.	(ATLAS Collab.)
AABOUD	18CP	PR D98 112010	M. Aaboud et al.	(ATLAS Collab.)
AABOUD	18CR	PRL 121 211801	M. Aaboud et al.	(ATLAS Collab.)
SIRUNYAN	18BM	JHEP 1808 177	A.M. Sirunyan et al.	(CMS Collab.)
SIRUNYAN	18Q	PR D97 072008	A.M. Sirunyan et al.	(CMS Collab.)
SIRUNYAN	17AU	JHEP 1711 085	A.M. Sirunyan et al.	(CMS Collab.)
AAD	16AH	JHEP 1602 110	G. Aad et al.	(ATLAS Collab.)
KHACHATRYAN...	16AN	PR D93 112009	V. Khachatryan et al.	(CMS Collab.)
KHACHATRYAN...	16I	JHEP 1601 166	V. Khachatryan et al.	(CMS Collab.)
AAD	15AR	JHEP 1508 105	G. Aad et al.	(ATLAS Collab.)
AAD	15BY	JHEP 1510 150	G. Aad et al.	(ATLAS Collab.)
AAD	15CN	PR D92 112007	G. Aad et al.	(ATLAS Collab.)
AAD	15Z	PR D91 112011	G. Aad et al.	(ATLAS Collab.)
AAD	14AZ	JHEP 1411 104	G. Aad et al.	(ATLAS Collab.)
CHATRCHYAN	13I	JHEP 1301 154	S. Chatrchyan et al.	(CMS Collab.)
AAD	12AT	PRL 109 032001	G. Aad et al.	(ATLAS Collab.)
AAD	12AU	PRL 109 071801	G. Aad et al.	(ATLAS Collab.)
AAD	12BC	PR D86 012007	G. Aad et al.	(ATLAS Collab.)
AAD	12BE	JHEP 1204 069	G. Aad et al.	(ATLAS Collab.)
CHATRCHYAN	12BH	PR D86 112003	S. Chatrchyan et al.	(CMS Collab.)
CHATRCHYAN	12X	JHEP 1205 123	S. Chatrchyan et al.	(CMS Collab.)
AALTONEN	11J	PRL 106 141803	T. Aaltonen et al.	(CDF Collab.)
ABAZOV	11F	PRL 106 081801	V.M. Abazov et al.	(D0 Collab.)
CHATRCHYAN	11L	PL B701 204	S. Chatrchyan et al.	(CMS Collab.)
AALTONEN	10H	PRL 104 091801	T. Aaltonen et al.	(CDF Collab.)
FLACCO	10	PRL 105 111801	C.J. Flacco et al.	(UCI, HAIF)
ATRE	09	PR D79 054018	A. Atre et al.	(DO Collab.)
ABAZOV	08X	PRL 101 111802	V.M. Abazov et al.	(DO Collab.)
HUANG	08	PR D77 037302	P.Q. Hung, M. Sher	(UVA, WILL)
AALTONEN	07C	PR D76 072006	T. Aaltonen et al.	(CDF Collab.)
ABDALLAH	07	EPJ C50 507	J. Abdallah et al.	(DELPHI Collab.)
ACOSTA	03	PRL 90 131801	D. Acosta et al.	(CDF Collab.)
AFFOLDER	00	PRL 84 835	A. Affolder et al.	(CDF Collab.)
ABE	98N	PR D58 051102	F. Abe et al.	(CDF Collab.)
ABACHI	97D	PRL 78 3818	S. Abachi et al.	(D0 Collab.)
FROGGATT	97	ZPHY C73 333	C.D. Froggatt, D.J. Smith, H.B. Nielsen	(GLAS+)
ABACHI	95F	PR D52 4877	S. Abachi et al.	(D0 Collab.)
ADRIANI	93G	PL B313 326	O. Adriani et al.	(L3 Collab.)
ADRIANI	93M	PR D51 236 1	O. Adriani et al.	(L3 Collab.)
MUKHOPAD...	93	PR D48 2105	B. Mukhopadhyaya, D.P. Roy	(TATA)
ABE	92	PRL 68 447	F. Abe et al.	(CDF Collab.)
Also		PR D45 3921	F. Abe et al.	(CDF Collab.)
ABE	92G	PR D45 3921	F. Abe et al.	(CDF Collab.)
ABREU	91F	NP B367 511	P. Abreu et al.	(DELPHI Collab.)
ABE	90B	PRL 64 147	F. Abe et al.	(CDF Collab.)
ABE	90D	PL B234 382	K. Abe et al.	(VENUS Collab.)
ABREU	90D	PL B242 536	P. Abreu et al.	(DELPHI Collab.)
ADACHI	90	PL B234 197	I. Adachi et al.	(TOPAZ Collab.)
AKESSON	90	ZPHY C46 179	T. Akesson et al.	(UA2 Collab.)
AKRAWY	90B	PL B236 364	M.Z. Akrawy et al.	(OPAL Collab.)
AKRAWY	90J	PL B246 285	M.Z. Akrawy et al.	(OPAL Collab.)
ALBAJAR	90B	ZPHY C48 1	C. Albajar et al.	(UA1 Collab.)
DECAMP	90F	PL B236 511	D. Decamp et al.	(ALEPH Collab.)
ABE	89E	PR D39 3524	K. Abe et al.	(VENUS Collab.)
ABE	89G	PRL 63 1776	K. Abe et al.	(VENUS Collab.)
ABRAMS	89C	PRL 63 2447	G.S. Abrams et al.	(Mark II Collab.)
ADACHI	89C	PL B229 427	I. Adachi et al.	(TOPAZ Collab.)
ENO	89	PRL 63 1910	S. Eno et al.	(AMY Collab.)
ALBAJAR	88	ZPHY C37 505	C. Albajar et al.	(UA1 Collab.)
ALTARELLI	88	NP B308 724	G. Altarelli et al.	(CERN, ROMA, ETH)
IGARASHI	88	PRL 60 2359	S. Igarashi et al.	(AMY Collab.)
SAGAWA	88	PRL 60 93	H. Sagawa et al.	(AMY Collab.)
ADEVA	86	PR D34 681	B. Adeva et al.	(Mark-J Collab.)
ALTHOFF	84C	PL 138B 441	M. Althoff et al.	(TASSO Collab.)
ALTHOFF	84I	ZPHY C22 307	M. Althoff et al.	(TASSO Collab.)

••• We do not use the following data for averages, fits, limits, etc. •••

>1470	95	20 AAD	23AG ATLS	$B(t' \rightarrow Zt) = 1$
>1280	95	21 SIRUNYAN	19AQ CMS	$B(t' \rightarrow Zt) = 1$
>1370	95	22 SIRUNYAN	19BWCMS	$B(t' \rightarrow ht) = 1$
>1010	95	23 AABOUD	18CL ATLS	$B(t' \rightarrow ht) = 1$
>1160	95	24 AABOUD	17L ATLS	$B(t' \rightarrow Zt) = 1$
> 770	95	25 AAD	15AR ATLS	$B(t' \rightarrow Wb) = 1$
> 590	95	26 AAD	15BY ATLS	Wb, Zt, ht modes
> 745	95	27 KHACHATRYAN...	15AI CMS	$B(t' \rightarrow ht) = 1$
> 700	95	28 CHATRCHYAN14A	CMS	$B(t' \rightarrow Wb) = 1$
> 706	95	28 CHATRCHYAN14A	CMS	$B(t' \rightarrow Zt) = 1$
> 782	95	28 CHATRCHYAN14A	CMS	$B(t' \rightarrow ht) = 1$
> 656	95	29 AAD	13F ATLS	$B(t' \rightarrow Wb) = 1$
> 625	95	30 CHATRCHYAN13I	CMS	$B(t' \rightarrow Zt) = 1$
> 404	95	31 AAD	12AR ATLS	$B(t' \rightarrow Wb) = 1$
> 570	95	32 CHATRCHYAN12BC	CMS	$t'\bar{t}' \rightarrow W^+ b W^- \bar{b}$
> 400	95	33 AALTONEN	11AH CDF	$t' \rightarrow X t (m_X < 70 \text{ GeV})$
> 358	95	34 AALTONEN	11AL CDF	$t' \rightarrow Wb$
> 340	95	34 AALTONEN	11AL CDF	$t' \rightarrow Wq (q=d,s,b)$
> 360	95	35 AALTONEN	11O CDF	$t' \rightarrow X t (m_X < 100 \text{ GeV})$
> 285	95	36 ABAZOV	11Q D0	$t' \rightarrow Wq (q=d,s,b)$
> 256	95	37,38 AALTONEN	08H CDF	$t' \rightarrow Wq$

- AAD 23av based on 139 fb⁻¹ of pp data at $\sqrt{s} = 13$ TeV. Pair production of vector-like t' is searched for in the mode $\ell^\pm \ell'^\mp + \geq 2j$ ($\geq 1b$ -tagged) + \cancel{E}_T or with 3ℓ . The data are consistent with the SM background predictions and limits are obtained for different branching ratios.
- TUMASYAN 23ax based on 138 fb⁻¹ of pp data at $\sqrt{s} = 13$ TeV. A vector-like t' is searched for in the $t + H (H \rightarrow \gamma\gamma)$ decay channel. EW production via a coupling to third-generation quarks of $\kappa_T = 0.25$ is assumed. The branching fractions are assumed to be 50, 25, and 25%, respectively, for bW , tZ , and tH decays.
- TUMASYAN 23v based on 138 fb⁻¹ of pp data at $\sqrt{s} = 13$ TeV. Pair production of vector-like t' is searched for in the single-lepton, same-sign charge dilepton and multi-lepton channels. The data are consistent with the SM background predictions and limits are obtained for different branching ratios. Masses below 1.48 TeV are excluded for all decays to third generation quarks.
- AABOUD 18ce based on 36.1 fb⁻¹ of proton-proton data taken at $\sqrt{s} = 13$ TeV. Events including a same-sign lepton pair are used. The limit is for a singlet model, assuming the branching ratios of t' into Zt , Wb and Ht as predicted by the model.
- AABOUD 18cp based on 36.1 fb⁻¹ of pp data at $\sqrt{s} = 13$ TeV. Pair and single production of vector-like t' are searched for with at least one t' decaying into Zt . In the case of $B(t' \rightarrow Zt) = 1$, the limit is $m_{t'} > 1340$ GeV.
- The limit is for the singlet model, assuming that the branching ratios into Zt , Wb , and Ht add up to one.
- The limit is for the doublet model, assuming that the branching ratios into Zt , Wb , and Ht add up to one.
- AABOUD 18cr based on 36.1 fb⁻¹ of pp data at $\sqrt{s} = 13$ TeV. A combination of searches for the pair-produced vector-like t' in various decay channels ($t' \rightarrow Wb, Zt, ht$). Also a model-independent limit is obtained as $m_{t'} > 1.31$ TeV, assuming that the branching ratios into Zt , Wb and ht add up to one.
- The limit is for the singlet t' .
- The limit is for t' in a weak isospin doublet (t', b') and $|V_{t'b}| \ll |V_{t'c}|$.
- SIRUNYAN 18bm based on 35.9 fb⁻¹ of pp data at $\sqrt{s} = 13$ TeV. The limit is for the pair-produced vector-like t' . Three channels (single lepton, same-charge 2 leptons, or at least 3 leptons) are considered for various branching fraction combinations. Assuming $B(tH) = 1$, the limit is 1270 GeV and for $B(tZ) = 1$ it is 1300 GeV.
- SIRUNYAN 18q based on 19.7 fb⁻¹ of pp data at $\sqrt{s} = 8$ TeV. The limit is for the pair-produced vector-like t' that couple only to light quarks. Constraints for other decay channels (Zq and Hq) are also given in the paper.
- SIRUNYAN 18w based on 35.8 fb⁻¹ of pp data at $\sqrt{s} = 13$ TeV. The limit is for the vector-like t' pair-produced by strong interaction using lepton-plus-jets mode and assuming that $B(t' \rightarrow Wb)$ is 100% product of the production cross section and branching fraction to Wb for any new pair-produced heavy quark decaying to this channel as a narrow resonance.
- SIRUNYAN 17au based on 2.3-2.6 fb⁻¹ of pp data at $\sqrt{s} = 13$ TeV. Limit on pair-produced singlet vector-like t' using one lepton and several jets. The mass bound is given for a t' transforming as a singlet under the electroweak symmetry group, assumed to decay through W, Z or Higgs boson (which decays to jets) and to a third generation quark. For a doublet, the limit is >830 GeV. Other limits are also given in the paper.
- Based on 20.3 fb⁻¹ of pp data at $\sqrt{s} = 8$ TeV. No significant excess over SM expectation is found in the search for pair production or single production of t' in the events with dilepton from a high $P_T Z$ and additional jets ($\geq 1 b$ -tag). If instead of $B(b' \rightarrow Wt) = 1$ an electroweak singlet with $B(b' \rightarrow Wt) \sim 0.45$ is assumed, the limit reduces to 685 GeV.
- Based on 1.04 fb⁻¹ of pp data at $\sqrt{s} = 7$ TeV. No signal is found for the search of heavy quark pair production that decay into W and a quark in the events with dileptons, large \cancel{E}_T , and ≥ 2 jets.
- Based on 1.04 fb⁻¹ of data in pp collisions at 7 TeV. AAD 12c looked for $t'\bar{t}'$ production followed by t' decaying into a top quark and X , an invisible particle, in a final state with an isolated high- P_T lepton, four or more jets, and a large missing transverse energy. No excess over the SM $t\bar{t}$ production gives the upper limit on $t'\bar{t}'$ production cross section as a function of $m_{t'}$ and m_X . The result is obtained for $B(t' \rightarrow Wt) = 1$.
- Based on 5 fb⁻¹ of pp data at $\sqrt{s} = 7$ TeV. CHATRCHYAN 12bh searched for QCD and EW production of single and pair of degenerate 4th generation quarks that decay to Wb or Wt . Absence of signal in events with one lepton, same-sign dileptons or tri-leptons gives the bound. With a mass difference of 25 GeV/c² between $m_{t'}$ and $m_{b'}$, the corresponding limit shifts by about ± 20 GeV/c².

t' (4th Generation) Quark, Searches for

t' (2/3)-quark/hadron mass limits in $p\bar{p}$ and pp collisions

VALUE (GeV)	CL%	DOCUMENT ID	TECN	COMMENT
>1600	95	1 AAD	23AV ATLS	$B(t' \rightarrow Zt) = 1$
> 960	95	2 TUMASYAN	23AX CMS	EW production, $t' \rightarrow Ht$ ($H \rightarrow \gamma\gamma$)
>1500	95	3 TUMASYAN	23V CMS	$B(t' \rightarrow ht) = 1$
> 980	95	4 AABOUD	18CE ATLS	$\geq 2\ell + \cancel{E}_T + \geq 1bj$
>1030	95	5,6 AABOUD	18CP ATLS	2,3 ℓ , singlet model
>1210	95	5,7 AABOUD	18CP ATLS	2,3 ℓ , doublet model
>1310	95	8,9 AABOUD	18CR ATLS	singlet t' . ATLAS combination
>1370	95	8,10 AABOUD	18CR ATLS	t' in a weak isospin doublet (t', b'). ATLAS combination.
>1140	95	11 SIRUNYAN	18BM CMS	Wb, Zt, ht modes
> 845	95	12 SIRUNYAN	18Q CMS	$B(t' \rightarrow Wq) = 1 (q=d,s)$
>1295	95	13 SIRUNYAN	18W CMS	$B(t' \rightarrow Wb) = 1$
> 860	95	14 SIRUNYAN	17AU CMS	
> 735	95	15 AAD	14AZ ATLS	$B(b' \rightarrow Wt) = 1$
> 350	95	16 AAD	12BC ATLS	$B(t' \rightarrow Wq)=1 (q=d,s,b)$
> 420	95	17 AAD	12C ATLS	$t' \rightarrow X t (m_X < 140 \text{ GeV})$
> 685	95	18 CHATRCHYAN12BH	CMS	$m_{b'} = m_{t'}$
> 557	95	19 CHATRCHYAN12P	CMS	$t'\bar{t}' \rightarrow W^+ b W^- \bar{b} \rightarrow b\ell^+ \nu \ell^- \bar{\nu}$

Quark Particle Listings

t' (Fourth Generation) Quark

- ¹⁹Based on 5.0 fb^{-1} of pp data at $\sqrt{s} = 7 \text{ TeV}$. CHATRCHYAN 12P looked for $t'\bar{t}'$ production events with two isolated high p_T leptons, large E_T , and 2 high p_T jets with b -tag. The absence of signal above the SM background gives the limit for $B(t' \rightarrow Wb) = 1$.
- ²⁰AAD 23AG based on 139 fb^{-1} of pp data at $\sqrt{s} = 13 \text{ TeV}$. Pair production of vector-like top or b_s is searched for in the mode $1\ell + \geq 4j$ ($\geq 1b$ -tagged) + E_T . The data are consistent with the SM background predictions and limits are obtained for different branching ratios. Masses below 1.59 TeV are excluded assuming a mass-degenerate vector-like doublet (t', b') model.
- ²¹SIRUNYAN 19AQ based on 35.9 fb^{-1} of pp data at $\sqrt{s} = 13 \text{ TeV}$. Pair production of vector-like t' is searched for with one t' decaying into Zt and the other t' decaying into Wb, Zt, ht . Events with an opposite-sign lepton pair consistent with coming from Z and jets are used. Mass limits are obtained for a variety of branching ratios of t' .
- ²²SIRUNYAN 19BW based on 35.9 fb^{-1} of pp data at $\sqrt{s} = 13 \text{ TeV}$. The limit is for the pair-produced vector-like t' using all-hadronic final state. The analysis is made for the Wb, Zt, ht modes and mass limits are obtained for a variety of branching ratios.
- ²³AABOUD 18CL based on 36.1 fb^{-1} of pp data at $\sqrt{s} = 13 \text{ TeV}$. The limit is for the pair-produced vector-like t' using all-hadronic final state. The analysis is also made for the Wb, Zt, ht modes and mass limits are obtained for a variety of branching ratios.
- ²⁴AABOUD 17L based on 36.1 fb^{-1} of pp data at $\sqrt{s} = 13 \text{ TeV}$. No signal is found in the search for heavy quark pair production that decay into Zt followed by $Z \rightarrow \nu\nu$ in the events with one lepton, large E_T , and ≥ 4 jets. The lower mass limit 0.87 (1.05) TeV is obtained for the singlet (doublet) model with other possible decay modes.
- ²⁵AAD 15AR based on 20.3 fb^{-1} of pp data at $\sqrt{s} = 8 \text{ TeV}$. Used lepton-plus-jets final state. See Fig. 20 for mass limits in the plane of $B(t' \rightarrow Ht)$ vs. $B(t' \rightarrow Wb)$ from a combination of $t'\bar{t}' \rightarrow Wb + X$ and $t'\bar{t}' \rightarrow Ht + X$ searches. Any branching ratio scenario is excluded for mass below 715 GeV .
- ²⁶AAD 15BY based on 20.3 fb^{-1} of pp data at $\sqrt{s} = 8 \text{ TeV}$. Limit on pair-produced vector-like t' assuming the branching fractions to $W, Z,$ and h modes of the singlet model. Used events containing $\geq 2\ell + E_T + \geq 2j$ ($\geq 1b$) and including a same-sign lepton pair.
- ²⁷KHACHATRYAN 15AI based on 19.7 fb^{-1} of pp data at $\sqrt{s} = 8 \text{ TeV}$. The search exploits all-hadronic final states by tagging boosted Higgs boson using jet substructure and b -tagging.
- ²⁸Based on 19.5 fb^{-1} of pp data at $\sqrt{s} = 8 \text{ TeV}$. The t' quark is pair produced and is assumed to decay into three different final states of $bW, tZ,$ and th . The search is carried out using events with at least one isolated lepton.
- ²⁹Based on 4.7 fb^{-1} of pp data at $\sqrt{s} = 7 \text{ TeV}$. No signal is found for the search of heavy quark pair production that decay into W and a b quark in the events with a high p_T isolated lepton, large E_T , and at least 3 jets ($\geq 1b$ -tag). Vector-like quark of charge $2/3$ with $400 < m_{t'} < 550 \text{ GeV}$ and $B(t' \rightarrow Wb) > 0.63$ is excluded at 95% CL.
- ³⁰Based on 5.0 fb^{-1} of pp data at $\sqrt{s} = 7 \text{ TeV}$. CHATRCHYAN 13I looked for events with one isolated electron or muon, large E_T , and at least four jets with large transverse momenta, where one jet is likely to originate from the decay of a bottom quark.
- ³¹Based on 1.04 fb^{-1} of pp data at $\sqrt{s} = 7 \text{ TeV}$. No signal is found in the search for pair produced heavy quarks that decay into W boson and a b quark in the events with a high p_T isolated lepton, large E_T , and at least 3 jets ($\geq 1b$ -tag).
- ³²Based on 5.0 fb^{-1} of pp data at $\sqrt{s} = 7 \text{ TeV}$. CHATRCHYAN 12BC looked for $t'\bar{t}'$ production events with a single isolated high p_T lepton, large E_T and at least 4 high p_T jets with a b -tag. The absence of signal above the SM background gives the limit for $B(t' \rightarrow Wb) = 1$.
- ³³Based on 5.7 fb^{-1} of data in $p\bar{p}$ collisions at 1.96 TeV . AALTONEN 11AH looked for $t'\bar{t}'$ production followed by t' decaying into a top quark and X , an invisible particle, in the all hadronic decay mode of $t\bar{t}$. No excess over the SM $t\bar{t}$ production gives the upper limit on $t'\bar{t}'$ production cross section as a function of $m_{t'}$ and m_X . The result is obtained for $B(t' \rightarrow Xt) = 1$.
- ³⁴Based on 5.6 fb^{-1} of data in $p\bar{p}$ collisions at 1.96 TeV . AALTONEN 11AL looked for $\ell + \geq 4j$ events and set upper limits on $\sigma(t'\bar{t}')$ as functions of $m_{t'}$.
- ³⁵Based on 4.8 fb^{-1} of data in $p\bar{p}$ collisions at 1.96 TeV . AALTONEN 11O looked for $t'\bar{t}'$ production signal when t' decays into a top quark and X , an invisible particle, in $\ell + E_T + \text{jets}$ channel. No excess over the SM $t\bar{t}$ production gives the upper limit on $t'\bar{t}'$ production cross section as a function of $m_{t'}$ and m_X . The result is obtained for $B(t' \rightarrow Xt) = 1$.
- ³⁶Based on 5.3 fb^{-1} of data in $p\bar{p}$ collisions at 1.96 TeV . ABAZOV 11Q looked for $\ell + E_T + \geq 4j$ events and set upper limits on $\sigma(t'\bar{t}')$ as functions of $m_{t'}$.
- ³⁷Searches for pair production of a new heavy top-like quark t' decaying to a W boson and another quark by fitting the observed spectrum of total transverse energy and reconstructed t' mass in the lepton + jets events.
- ³⁸HUANG 08 reexamined the t' mass lower bound of 256 GeV obtained in AALTONEN 08H that assumes $B(b' \rightarrow qZ) = 1$ for $q = u, c$ which does not hold when $m_{b'} < m_{\nu} - m_W$ or the mixing $\sin^2(\theta_{bt'})$ is so tiny that the decay occurs outside of the vertex detector. Fig. 1 gives that lower bound on $m_{t'}$ in the plane of $\sin^2(\theta_{bt'})$ and $m_{b'}$.

$t'(5/3)$ -quark/hadron mass limits in $p\bar{p}$ and pp collisions

VALUE (GeV)	CL%	DOCUMENT ID	TECN	COMMENT
>1460	95	1 AAD	23AG ATLS	$t'(5/3) \rightarrow tW^+$
>1330	95	2 SIRUNYAN	19T CMS	$t'_R(5/3) \rightarrow tW^+$
>1300	95	2 SIRUNYAN	19T CMS	$t'_L(5/3) \rightarrow tW^+$
>1190	95	3 AABOUD	18CE ATLS	$\geq 2\ell + E_T + \geq 1bj$
>1020	95	4 SIRUNYAN	17J CMS	$t'_R(5/3) \rightarrow tW^+$
> 990	95	4 SIRUNYAN	17J CMS	$t'_L(5/3) \rightarrow tW^+$
> 750	95	5 AAD	15BY ATLS	$t'(5/3) \rightarrow tW^+$
> 840	95	6 AAD	15Z ATLS	$t'(5/3) \rightarrow tW^+$
> 800	95	7 CHATRCHYAN	14T CMS	$t'(5/3) \rightarrow tW^+$

• • • We do not use the following data for averages, fits, limits, etc. • • •

- >1350 95 ⁸ AABOUD 18AW ATLS $t'(5/3) \rightarrow tW^+$
- ¹AAD 23AG based on 139 fb^{-1} of pp data at $\sqrt{s} = 13 \text{ TeV}$. Pair production of vector-like top or b' is searched for in the mode $1\ell + \geq 4j$ ($\geq 1b$ -tagged) + E_T . The data are consistent with the SM background predictions and limits are obtained for different branching ratios.
- ²SIRUNYAN 19T based on 35.9 fb^{-1} of pp data at $\sqrt{s} = 13 \text{ TeV}$. Signals are searched in the final states of t' pair production, with same-sign leptons (which come from a t' decay) or a single lepton (which comes from a W out of $4W$ s), along with jets, and no excess over the SM expectation is found.
- ³AABOUD 18CE based on 36.1 fb^{-1} of proton-proton data taken at $\sqrt{s} = 13 \text{ TeV}$. Events including a same-sign lepton pair are used. The limit is for the pair-produced vector-like t' . With single t' production included, assuming $t'tW$ coupling of one, the limit is $m_{t'} > 1.6 \text{ TeV}$.
- ⁴SIRUNYAN 17J based on 2.3 fb^{-1} of pp data at $\sqrt{s} = 13 \text{ TeV}$. Signals are searched in the final states of t' pair production, with same-sign leptons (which come from a t' decay) or a single lepton (which comes from a W out of $4W$ s), along with jets, and no excess over the SM expectation is found.
- ⁵AAD 15BY based on 20.3 fb^{-1} of pp data at $\sqrt{s} = 8 \text{ TeV}$. Limit on $t'(5/3)$ in pair and single production assuming its coupling to Wt is equal to one. Used events containing $\geq 2\ell + E_T + \geq 2j$ ($\geq 1b$) and including a same-sign lepton pair.
- ⁶AAD 15Z based on 20.3 fb^{-1} of pp data at $\sqrt{s} = 8 \text{ TeV}$. Used events with $\ell + E_T + \geq 6j$ ($\geq 1b$) and at least one pair of jets from weak boson decay, sensitive to the final state $b\bar{b}W^+W^-W^+W^-$.
- ⁷CHATRCHYAN 14T based on 19.5 fb^{-1} of pp data at $\sqrt{s} = 8 \text{ TeV}$. Non-observation of anomaly in H_T distribution in the same-sign dilepton events leads to the limit when pair produced $t'(5/3)$ quark decays exclusively into t and W^+ , resulting in the final state with $b\bar{b}W^+W^-W^+W^-$.
- ⁸AABOUD 18AW based on 36.1 fb^{-1} of pp data at $\sqrt{s} = 13 \text{ TeV}$. Limit on $t'(5/3)$ in pair production assuming its coupling to Wt is equal to one. Lepton-plus-jets final state is used, characterized by $\ell + E_T + \text{jets}$ ($\geq 1b$ -tagged).

$t'(2/3)$ mass limits from single production in $p\bar{p}$ and pp collisions

VALUE (GeV)	CL%	DOCUMENT ID	TECN	COMMENT
>950	95	1 AAD	16AV ATLS	$qg \rightarrow q't'b, B(t' \rightarrow Wb)=0.5$
>403	95	2 ABAZOV	11F D0	$qd \rightarrow q't' \rightarrow q'(Wd)$ $\tilde{\kappa}_{d t'}=1, B(t' \rightarrow Wd)=1$
>551	95	2 ABAZOV	11F D0	$qu \rightarrow q't' \rightarrow q(Zu)$ $\tilde{\kappa}_{u t'}=\sqrt{2}, B(t' \rightarrow Zu)=1$
		3 AAD	22G ATLS	$t' \rightarrow Ht$, singlet t'
		4 TUMASYAN	22X CMS	$t' \rightarrow Zt$

• • • We do not use the following data for averages, fits, limits, etc. • • •

- ¹AAD 16AV based on 20.3 fb^{-1} of pp data at $\sqrt{s} = 8 \text{ TeV}$. No significant excess over SM expectation is found in the search for a fully reconstructed vector-like t' in the mode $\ell + E_T + \geq 2j$ ($\geq 1b$). A veto on massive large-radius jets is used to reject the $t\bar{t}$ background.
- ²ABAZOV 11F based on 5.4 fb^{-1} of data in $p\bar{p}$ collisions at 1.96 TeV . It looked for single production of t' via the Z or E coupling to the first generation up or down quarks, respectively. Model independent cross section limits for the single production processes $p\bar{p} \rightarrow t'q \rightarrow (Wd)q$, and $p\bar{p} \rightarrow t'q \rightarrow (Zd)q$ are given in Figs. 3 and 4, respectively, and the mass limits are obtained for the model of ATRE 09 with degenerate bi-doublets of vector-like quarks.
- ³AAD 22G based on 139 fb^{-1} of pp data at $\sqrt{s} = 13 \text{ TeV}$. No significant excess over SM expectation is found in the search for a vector-like t' in the Ht decay channel, where H and t are reconstructed as single jets. The mass range between 1.0 and 2.3 TeV is targeted and 95% CL limits on the production section times the decay branching fraction are set depending on the coupling and mass of t' .
- ⁴TUMASYAN 22X based on 137 fb^{-1} of pp data at $\sqrt{s} = 13 \text{ TeV}$. No significant excess over SM expectation is found in the search for a vector-like t' in the Zt decay channel, where Z decays to neutrinos and t decays hadronically. The 95% CL limits on the production section times the decay branching fraction are set depending on the coupling and mass of t' .

$t'(5/3)$ mass limits from single production in $p\bar{p}$ and pp collisions

VALUE (GeV)	DOCUMENT ID	TECN	COMMENT
	1 SIRUNYAN 19AI CMS	$tW \rightarrow t'(5/3) \rightarrow tW$	

• • • We do not use the following data for averages, fits, limits, etc. • • •

- ¹SIRUNYAN 19AI based on 35.9 fb^{-1} of pp data at $\sqrt{s} = 13 \text{ TeV}$. Exclusion limits are set on the product of the production cross section and branching fraction for the $b'(-1/3) + t$ and $t'(5/3) + t$ modes as a function of the vector-like quark mass in Fig. 8 and Tab. 2 for relative vector-like quark widths between 1 and 30% for left- and right-handed vector-like quark couplings. No significant deviation from the SM prediction is observed.

REFERENCES FOR Searches for (Fourth Generation) t' Quark

AAD	23AG EPJ C83 719	G. Aad et al.	(ATLAS Collab.)
AAD	23AV PL B843 138019	G. Aad et al.	(ATLAS Collab.)
TUMASYAN	23AX JHEP 2309 057	A. Tumasyan et al.	(CMS Collab.)
TUMASYAN	23V JHEP 2307 020	A. Tumasyan et al.	(CMS Collab.)
AAD	22G PR D105 092012	G. Aad et al.	(ATLAS Collab.)
TUMASYAN	22X JHEP 2205 093	A. Tumasyan et al.	(CMS Collab.)
SIRUNYAN	19AI EPJ C79 90	A.M. Sirunyan et al.	(CMS Collab.)
SIRUNYAN	19AQ EPJ C79 364	A.M. Sirunyan et al.	(CMS Collab.)
SIRUNYAN	19BW PR D100 072001	A.M. Sirunyan et al.	(CMS Collab.)
SIRUNYAN	19T JHEP 1903 082	A.M. Sirunyan et al.	(CMS Collab.)
AABOUD	18AW JHEP 1808 048	M. Aaboud et al.	(ATLAS Collab.)

AABOUD	18CE	JHEP 1812 039	M. Aaboud et al.	(ATLAS Collab.)
AABOUD	18CL	PR D98 092005	M. Aaboud et al.	(ATLAS Collab.)
AABOUD	18CP	PR D98 112010	M. Aaboud et al.	(ATLAS Collab.)
AABOUD	18CR	PRL 121 211801	M. Aaboud et al.	(ATLAS Collab.)
SIRUNYAN	18BM	JHEP 1808 177	A.M. Sirunyan et al.	(CMS Collab.)
SIRUNYAN	18Q	PR D97 072008	A.M. Sirunyan et al.	(CMS Collab.)
SIRUNYAN	18W	PL B779 82	A.M. Sirunyan et al.	(CMS Collab.)
AABOUD	17L	JHEP 1708 052	M. Aaboud et al.	(ATLAS Collab.)
SIRUNYAN	17AU	JHEP 1711 085	A.M. Sirunyan et al.	(CMS Collab.)
SIRUNYAN	17J	JHEP 1708 073	A.M. Sirunyan et al.	(CMS Collab.)
AAD	16AV	EPL C76 442	G. Aad et al.	(ATLAS Collab.)
AAD	15AR	JHEP 1508 105	G. Aad et al.	(ATLAS Collab.)
AAD	15BY	JHEP 1510 150	G. Aad et al.	(ATLAS Collab.)
AAD	15Z	PR D91 112011	G. Aad et al.	(ATLAS Collab.)
KHACHATRYAN	15AI	JHEP 1506 080	V. Khachatryan et al.	(CMS Collab.)
AAD	14AZ	JHEP 1411 104	G. Aad et al.	(ATLAS Collab.)
CHATRCHYAN	14A	PL B729 149	S. Chatrchyan et al.	(CMS Collab.)
CHATRCHYAN	14T	PRL 112 171801	S. Chatrchyan et al.	(CMS Collab.)
AAD	13F	PL B718 1284	G. Aad et al.	(ATLAS Collab.)
CHATRCHYAN	13I	JHEP 1301 154	S. Chatrchyan et al.	(CMS Collab.)
AAD	12AR	PRL 108 261802	G. Aad et al.	(ATLAS Collab.)
AAD	12BC	PR D86 012007	G. Aad et al.	(ATLAS Collab.)
AAD	12C	PRL 108 041805	G. Aad et al.	(ATLAS Collab.)
CHATRCHYAN	12BC	PL B718 307	S. Chatrchyan et al.	(CMS Collab.)
CHATRCHYAN	12BH	PR D86 112003	S. Chatrchyan et al.	(CMS Collab.)
CHATRCHYAN	12P	PL B716 103	S. Chatrchyan et al.	(CMS Collab.)
AALTONEN	11AH	PRL 107 191803	T. Aaltonen et al.	(CDF Collab.)
AALTONEN	11AL	PRL 107 261801	T. Aaltonen et al.	(CDF Collab.)
AALTONEN	11O	PRL 106 191801	T. Aaltonen et al.	(CDF Collab.)
ABAZOV	11F	PRL 106 081801	V.M. Abazov et al.	(DO Collab.)
ABAZOV	11Q	PRL 107 082001	V.M. Abazov et al.	(DO Collab.)
ATRE	09	PR D79 054018	A. Atre et al.	(CDF Collab.)
AALTONEN	05H	PRL 100 161803	T. Aaltonen et al.	(CDF Collab.)
HUANG	08	PR D77 037302	P.Q. Hung, M. Sher	(UVA, WILL)

<3.E-37	-1,2	2-5	70	p	0	⁸ ANTIPOV	69B	CNTR
<1.E-35	+1,2	<7	30	p	0	DORFAN	65	CNTR
<2.E-35	-2	<2.5-5	30	p	0	⁹ FRANZINI	65B	CNTR
<5.E-35	+1,2	<2.2	21	p	0	BINGHAM	64	HLBC
<1.E-32	+1,2	<4.0	28	p	0	BLUM	64	HBC
<1.E-35	+1,2	<2.5	31	p	0	⁹ HAGOPIAN	64	HBC
<1.E-34	+1	<2	28	p	0	LEIPUNER	64	CNTR
<1.E-33	+1,2	<2.4	24	p	0	MORRISON	64	HBC

- ¹ CHATRCHYAN 13AR limits assume pair-produced long-lived spin-1/2 particles neutral under $SU(3)_C$ and $SU(2)_L$.
- ² ABE 92I flux limits decrease as the mass increases from 50 to 500 GeV.
- ³ HE 91 limits are for charges of the form $N\pm 1/3$ from 2/3/3 to 38/3.
- ⁴ Hadronic or leptonic quarks.
- ⁵ Cross section cm^2/GeV^2 .
- ⁶ 3×10^{-5} < lifetime $< 1 \times 10^{-3}$ s.
- ⁷ Includes BOTT 72 results.
- ⁸ Assumes isotropic cm production.
- ⁹ Cross section inferred from flux.

Free Quark Searches

FREE QUARK SEARCHES

Quarks are fractionally charged particles, the constituents of hadrons, with charges $1/3 e$ or $2/3 e$. The charge of every known charged system is an integer multiple of $1/3 e$. Quantum Chromodynamics predicts that quarks cannot be observed as freely propagating particles, being confined inside hadrons or deconfined in quark-gluon plasma (QGP). We observe the top quark decaying as still free, because its lifetime is too short to allow its hadronization. Experiments have produced no evidence for free propagating quarks.

Reviews can be found in Refs. 1-5.

References

1. M.L. Perl, E.R. Lee, and D. Lomba, Mod. Phys. Lett. **A19**, 2595 (2004).
2. P.F. Smith, Ann. Rev. Nucl. and Part. Sci. **39**, 73 (1989).
3. L. Lyons, Phys. Reports **129**, 225 (1985).
4. M. Marinelli and G. Morpurgo, Phys. Reports **85**, 161 (1982).
5. L.W. Jones, Rev. Mod. Phys. **49**, 717 (1977).

Quark Production Cross Section — Accelerator Searches

X-SECT (cm^2)	CHG ($e/3$)	MASS (GeV)	ENERGY (GeV)	BEAM	EVTS	DOCUMENT ID	TECN
<1.7-2.3E-39	± 2	100-600	7000	pp	0	¹ CHATRCHYAN13AR	CMS
<14.5.4E-39	± 1	100-600	7000	pp	0	¹ CHATRCHYAN13AR	CMS
<1.3E-36	± 2	45-84	130-172	e^+e^-	0	ABREU	97D DLPH
<2.E-35	+2	250	1800	$p\bar{p}$	0	² ABE	92J CDF
<1.E-35	+4	250	1800	$p\bar{p}$	0	² ABE	92J CDF
<3.8E-28		14.5A	²⁸ Si-Pb		0	³ HE	91 PLAS
<3.2E-28		14.5A	²⁸ Si-Cu		0	³ HE	91 PLAS
<1.E-40	$\pm 1,2$	<10	$p, \nu, \bar{\nu}$		0	BERGSMA	84B CHRMB
<1.E-36	$\pm 1,2$	<9	200 μ		0	AUBERT	83C SPEC
<2.E-10	$\pm 2,4$	1-3	200 p		0	⁴ BUSSIÈRE	80 CNTR
<5.E-38	+1,2	>5	300 p		0	^{5,6} STEVENSON	79 CNTR
<1.E-33	± 1	<20	52 pp		0	BASILE	78 SPEC
<9.E-39	$\pm 1,2$	<6	400 p		0	⁵ ANTREASYAN	77 SPEC
<8.E-35	+1,2	<20	52 pp		0	⁷ FABJAN	75 CNTR
<5.E-38	-1,2	4-9	200 p		0	NASH	74 CNTR
<1.E-32	+2,4	4-24	52 pp		0	ALPER	73 SPEC
<5.E-31	+1,2,4	<12	300 p		0	LEIPUNER	73 CNTR
<6.E-34	$\pm 1,2$	<13	52 pp		0	BOTT	72 CNTR
<1.E-36	-4	4	70 p		0	ANTIPOV	71 CNTR
<1.E-35	$\pm 1,2$	2	28 p		0	⁸ ALLABY	69B CNTR
<4.E-37	-2	<5	70 p		0	⁴ ANTIPOV	69 CNTR

Quark Differential Production Cross Section — Accelerator Searches

X-SECT ($\text{cm}^2\text{sr}^{-1}\text{GeV}^{-1}$)	CHG ($e/3$)	MASS (GeV)	ENERGY (GeV)	BEAM	EVTS	DOCUMENT ID	TECN
<4.E-36	-2,4	1.5-6	70	p	0	BALDIN	76 CNTR
<2.E-33	± 4	5-20	52	pp	0	ALBROW	75 SPEC
<5.E-34	<7	7-15	44	pp	0	JOVANOVA...	75 CNTR
<5.E-35			20	γ	0	¹ GALIK	74 CNTR
<9.E-35	-1,2		200	p	0	NASH	74 CNTR
<4.E-36	-4	2.3-2.7	70	p	0	ANTIPOV	71 CNTR
<3.E-35	$\pm 1,2$	<2.7	27	p	0	ALLABY	69B CNTR
<7.E-38	-1,2	<2.5	70	p	0	ANTIPOV	69B CNTR

¹ Cross section in cm^2/sr /equivalent quanta.

Quark Flux — Accelerator Searches

The definition of FLUX depends on the experiment

- (a) is the ratio of measured free quarks to predicted free quarks if there is no “confinement.”
- (b) is the probability of fractional charge on nuclear fragments. Energy is in GeV/nucleon.
- (c) is the 90%CL upper limit on fractionally-charged particles produced per interaction.
- (d) is quarks per collision.
- (e) is inclusive quark-production cross-section ratio to $\sigma(e^+e^- \rightarrow \mu^+\mu^-)$.
- (f) is quark flux per charged particle.
- (g) is the flux per ν -event.
- (h) is quark yield per π^- yield.
- (i) is 2-body exclusive quark-production cross-section ratio to $\sigma(e^+e^- \rightarrow \mu^+\mu^-)$.

FLUX	CHG ($e/3$)	MASS (GeV)	ENERGY (GeV)	BEAM	EVTS	DOCUMENT ID	TECN
<1.6E-3	b	see note		200	³² S-Pb	0	¹ HUENTRUP 96 PLAS
<6.2E-4	b	see note		10.6	³² S-Pb	0	¹ HUENTRUP 96 PLAS
<0.94E-4	e	± 2	2-30	88-94	e^+e^-	0	AKERS 95R OPAL
<1.7E-4	e	± 2	30-40	88-94	e^+e^-	0	AKERS 95R OPAL
<3.6E-4	e	± 4	5-30	88-94	e^+e^-	0	AKERS 95R OPAL
<1.9E-4	e	± 4	30-45	88-94	e^+e^-	0	AKERS 95R OPAL
<2.E-3	e	+1	5-40	88-94	e^+e^-	0	² BUSKULIC 93C ALEP
<6.E-4	e	+2	5-30	88-94	e^+e^-	0	² BUSKULIC 93C ALEP
<1.2E-3	e	+4	15-40	88-94	e^+e^-	0	² BUSKULIC 93C ALEP
<3.6E-4	i	+4	5.0-10.2	88-94	e^+e^-	0	BUSKULIC 93C ALEP
<3.6E-4	i	+4	16.5-26.0	88-94	e^+e^-	0	BUSKULIC 93C ALEP
<6.9E-4	i	+4	26.0-33.3	88-94	e^+e^-	0	BUSKULIC 93C ALEP
<9.1E-4	i	+4	33.3-38.6	88-94	e^+e^-	0	BUSKULIC 93C ALEP
<1.1E-3	i	+4	38.6-44.9	88-94	e^+e^-	0	BUSKULIC 93C ALEP
<1.6E-4	b	see note	see note			0	³ CECCHINI 93 PLAS
	b	4,5,7,8	2.1A	¹⁶ O	0,20,6		⁴ GHOSH 92 EMUL
<6.4E-5	g	1		$\nu, \bar{\nu}$	1		⁵ BASILE 91 CNTR
<3.7E-5	g	2		$\nu, \bar{\nu}$	1		⁵ BASILE 91 CNTR
<3.9E-5	g	1		$\nu, \bar{\nu}$	1		⁶ BASILE 91 CNTR
<2.8E-5	g	2		$\nu, \bar{\nu}$	1		⁶ BASILE 91 CNTR
<1.9E-4	c		14.5A	²⁸ Si-Pb	0		⁷ HE 91 PLAS
<3.9E-4	c		14.5A	²⁸ Si-Cu	0		⁷ HE 91 PLAS
<1.E-9	c	$\pm 1,2,4$	14.5A	¹⁶ O-Ar	0		MATIS 91 MDRP
<5.1E-10	c	$\pm 1,2,4$	14.5A	¹⁶ O-Hg	0		MATIS 91 MDRP
<8.1E-9	c	$\pm 1,2,4$	14.5A	Si-Hg	0		MATIS 91 MDRP
<1.7E-6	c	$\pm 1,2,4$	60A	¹⁶ O-Hg	0		MATIS 91 MDRP
<3.5E-7	c	$\pm 1,2,4$	200A	¹⁶ O-Hg	0		MATIS 91 MDRP
<1.3E-6	c	$\pm 1,2,4$	200A	S-Hg	0		MATIS 91 MDRP
<5E-2	e	2	19-27	52-60	e^+e^-	0	ADACHI 90C TOPZ
<5E-2	e	4	<24	52-60	e^+e^-	0	ADACHI 90C TOPZ
<1.E-4	e	+2	<3.5	10	e^+e^-	0	BOWCOCK 89B CLEO
<1.E-6	d	$\pm 1,2$	60	¹⁶ O-Hg	0		CALLOWAY 89 MDRP
<3.5E-7	d	$\pm 1,2$	200	¹⁶ O-Hg	0		CALLOWAY 89 MDRP
<1.3E-6	d	$\pm 1,2$	200	S-Hg	0		CALLOWAY 89 MDRP
<1.2E-10	d	± 1	1	800	p-Hg	0	MATIS 89 MDRP

Quark Particle Listings



LIGHT UNFLAVORED MESONS ($S = C = B = 0$)

- π^\pm 1411
- π^0 1414
- η 1416
- $f_0(500)$ aka σ ; was $f_0(600)$, $f_0(400 - 1200)$ 1422
- $\rho(770)$ 1424
- $\omega(782)$ 1430
- $\eta'(958)$ 1435
- $f_0(980)$ 1442
- $a_0(980)$ 1444
- $\phi(1020)$ 1446
- $h_1(1170)$ 1454
- $b_1(1235)$ 1454
- $a_1(1260)$ 1455
- $f_2(1270)$ 1457
- $f_1(1285)$ 1461
- $\eta(1295)$ 1464
- $\pi(1300)$ 1464
- $a_2(1320)$ 1465
- $f_0(1370)$ 1469
- $\pi_1(1400)$ 1471
- $\eta(1405)$ 1472
- $h_1(1415)$ 1475
- $f_1(1420)$ 1475
- $\omega(1420)$ 1477
- $f_2(1430)$ 1478
- $a_0(1450)$ 1478
- $\rho(1450)$ 1479
- $\eta(1475)$ 1483
- $f_0(1500)$ 1484
- $f_1(1510)$ 1486
- $f_2'(1525)$ 1487
- $f_2(1565)$ 1491
- $\rho(1570)$ 1492
- $h_1(1595)$ 1492
- $\pi_1(1600)$ 1493
- $a_1(1640)$ 1494
- $f_2(1640)$ 1495
- $\eta_2(1645)$ 1495
- $\omega(1650)$ 1495
- $\omega_3(1670)$ 1497
- $\pi_2(1670)$ 1497
- $\phi(1680)$ 1499
- $\rho_3(1690)$ 1501
- $\rho(1700)$ 1504
- $a_2(1700)$ 1508
- $a_0(1710)$ 1509
- $f_0(1710)$ 1510
- $X(1750)$ 1512
- $\eta(1760)$ 1512
- $f_0(1770)$ 1513
- $\pi(1800)$ 1514
- $f_2(1810)$ 1515
- $X(1835)$ 1516
- $\phi_3(1850)$ 1517
- $\eta_1(1855)$ 1517
- $\eta_2(1870)$ 1518
- $\pi_2(1880)$ 1518
- $\rho(1900)$ 1519
- $f_2(1910)$ 1519
- $a_0(1950)$ 1520
- $f_2(1950)$ 1520

• Indicates the particle is in the Meson Summary Table

- $a_4(1970)$ 1521
- $\rho_3(1990)$ 1522
- $\pi_2(2005)$ 1523
- $f_2(2010)$ 1523
- $f_0(2020)$ 1523
- $f_4(2050)$ 1524
- $\pi_2(2100)$ 1525
- $f_0(2100)$ 1526
- $f_2(2150)$ 1526
- $\rho(2150)$ 1528
- $\phi(2170)$ 1529
- $f_0(2200)$ 1531
- $f_J(2220)$ 1531
- $\omega(2220)$ 1532
- $\eta(2225)$ 1533
- $\rho_3(2250)$ 1533
- $f_2(2300)$ 1534
- $f_4(2300)$ 1534
- $f_0(2330)$ 1535
- $f_2(2340)$ 1535
- $\rho_5(2350)$ 1536
- $X(2370)$ 1536
- $f_0(2470)$ 1537
- $f_6(2510)$ 1537

STRANGE MESONS ($S = \pm 1, C = B = 0$)

- K^\pm 1538
- K^0 1553
- K_S^0 1554
- K_L^0 1558
- $K_0^*(700)$ aka κ ; was $K_0^*(800)$ 1573
- $K^*(892)$ 1574
- $K_1(1270)$ 1577
- $K_1(1400)$ 1578
- $K^*(1410)$ 1579
- $K_0^*(1430)$ 1580
- $K_2^*(1430)$ 1581
- $K(1460)$ 1583
- $K_2(1580)$ 1584
- $K(1630)$ 1584
- $K_1(1650)$ 1584
- $K^*(1680)$ 1584
- $K_2(1770)$ 1585
- $K_3^*(1780)$ 1586
- $K_2(1820)$ 1587
- $K(1830)$ 1587
- $K_0^*(1950)$ 1588
- $K_2^*(1980)$ 1588
- $K_4^*(2045)$ 1589
- $K_2(2250)$ 1590
- $K_3(2320)$ 1590
- $K_5^*(2380)$ 1590
- $K_4(2500)$ 1590
- $K(3100)$ aka $K_J^*(3100)$ 1591

CHARMED MESONS ($C = \pm 1$)

- D^\pm 1592
- D^0 1610
- $D^*(2007)^0$ 1646
- $D^*(2010)^\pm$ 1647
- $D_0^*(2300)$ was $D_0^*(2400)$ 1648
- $D_1(2420)$ 1649

(Continued on the next page)

- $D_1(2430)^0$ 1650
- $D_2^*(2460)$ 1651
- $D_0(2550)^0$ 1653
- $D_1^*(2600)^0$ was $D(2600)$ 1653
- $D^*(2640)^\pm$ 1654
- $D_2(2740)^0$ was $D(2740)^0$ 1654
- $D_3^*(2750)$ 1654
- $D_1^*(2760)^0$ 1655
- $D(3000)^0$ 1655

CHARMED, STRANGE MESONS ($C = S = \pm 1$)

- D_s^\pm 1657
- $D_s^{*\pm}$ 1673
- $D_{s0}^*(2317)^\pm$ 1674
- $D_{s1}(2460)^\pm$ 1675
- $D_{s1}(2536)^\pm$ 1676
- $D_{s2}^*(2573)$ 1677
- $D_{s0}(2590)^+$ 1678
- $D_{s1}^*(2700)^\pm$ 1678
- $D_{s1}^*(2860)^\pm$ was $D_{sJ}^*(2860)$ 1679
- $D_{s3}^*(2860)^\pm$ 1679
- $D_{sJ}(3040)^\pm$ 1680

BOTTOM MESONS ($B = \pm 1$)

- B^\pm 1682
- B^0 1751
- B^\pm/B^0 ADMIXTURE 1828
- $B^\pm/B^0/B_s^0/b$ -baryon ADMIXTURE 1851
- V_{cb} and V_{ub} CKM Matrix Elements 1859
- B^* 1860
- $B_1(5721)$ 1861
- $B_J^*(5732)$ 1861
- $B_2^*(5747)$ 1862
- $B_J(5840)$ 1862
- $B_J(5970)$ 1863

BOTTOM, STRANGE MESONS ($B = \pm 1, S = \mp 1$)

- B_s^0 1865
- B_s^* 1890
- $B_{s1}(5830)^0$ 1890
- $B_{s2}^*(5840)^0$ 1891
- $B_{sJ}^*(5850)$ 1891
- $B_{sJ}(6063)^0$ 1892
- $B_{sJ}(6114)^0$ 1892

BOTTOM, CHARMED MESONS ($B = C = \pm 1$)

- B_c^+ 1893
- $B_c(2S)^\pm$ 1897

$c\bar{c}$ MESONS

- $\eta_c(1S)$ 1898
- $J/\psi(1S)$ 1907
- $\chi_{c0}(1P)$ 1935
- $\chi_{c1}(1P)$ 1945
- $h_c(1P)$ 1954
- $\chi_{c2}(1P)$ 1956
- $\eta_c(2S)$ 1967
- $\psi(2S)$ 1970
- $\psi(3770)$ 1988
- $\psi_2(3823)$ was $\psi(3823), X(3823)$ 1995
- $\psi_3(3842)$ 1996
- $\chi_{c0}(3860)$ 1996
- $\chi_{c1}(3872)$ aka $X(3872)$ 1996

- $\chi_{c0}(3915)$ was $X(3915)$ 2000
- $\chi_{c2}(3930)$ 2001
- $X(3940)$ 2002
- $T_{c\bar{c}}(4020)$ 2065
- $\psi(4040)$ 2002
- $\chi_{c1}(4140)$ was $X(4140)$ 2005
- $\psi(4160)$ 2005
- $X(4160)$ 2008
- $T_{c\bar{c}}(4250)^+$ 2068
- $\psi(4230)$ aka $Y(4260)$; was $X(4260)$ 2009
- $\chi_{c1}(4274)$ was $X(4274)$ 2014
- $X(4350)$ 2015
- $\psi(4360)$ aka $Y(4360)$; was $X(4360)$ 2015
- $\psi(4415)$ 2017
- $\chi_{c0}(4500)$ was $X(4500)$ 2019
- $X(4630)$ 2019
- $\psi(4660)$ aka $Y(4660)$; was $X(4660)$ 2020
- $\chi_{c1}(4685)$ 2022
- $\chi_{c0}(4700)$ was $X(4700)$ 2022

$b\bar{b}$ MESONS

- $\eta_b(1S)$ 2023
- $\Upsilon(1S)$ 2024
- $\chi_{b0}(1P)$ 2031
- $\chi_{b1}(1P)$ 2033
- $h_b(1P)$ 2035
- $\chi_{b2}(1P)$ 2035
- $\eta_b(2S)$ 2037
- $\Upsilon(2S)$ 2037
- $\Upsilon_2(1D)$ was $\Upsilon(1D)$ 2043
- $\chi_{b0}(2P)$ 2043
- $\chi_{b1}(2P)$ 2045
- $h_b(2P)$ 2047
- $\chi_{b2}(2P)$ 2047
- $\Upsilon(3S)$ 2049
- $\chi_{b1}(3P)$ 2053
- $\chi_{b2}(3P)$ 2053
- $\Upsilon(4S)$ aka $\Upsilon(10580)$ 2054
- $\Upsilon(10753)$ 2056
- $\Upsilon(10860)$ 2056
- $\Upsilon(11020)$ 2060

OTHER MESONS

- $T_{cs0}^*(2870)^0$ was $X_0(2900)$ 2062
- $T_{cs1}^*(2900)^0$ was $X_1(2900)$ 2062
- $T_{cs0}^*(2900)$ 2062
- $T_{c\bar{c}}(3875)^+$ 2062
- $T_{c\bar{c}1}(3900)$ was $Z_c(3900), X(3900)$ 2063
- $T_{c\bar{c}1}(4000)$ was $Z_{cs}(4000)$ 2064
- $T_{c\bar{c}}(4020)$ was $X(4020)$ 2065
- $T_{c\bar{c}}(4050)^+$ was $X(4050)$ 2066
- $T_{c\bar{c}}(4055)^+$ was $X(4055)^\pm$ 2066
- $T_{c\bar{c}}(4100)^+$ was $X(4100)^\pm$ 2067
- $T_{c\bar{c}1}(4200)^+$ was $Z_c(4200), X(4200)^\pm$ 2067
- $T_{c\bar{c}1}(4220)^+$ was $Z_{cs}(4220)^+$ 2067
- $T_{c\bar{c}0}(4240)^+$ was $R_{c0}(4240), X(4240)^\pm$ 2067
- $T_{c\bar{c}}(4250)^+$ was $X(4250)^\pm$ 2068
- $T_{c\bar{c}1}(4430)^+$ was $Z_c(4430), X(4430)^\pm$ 2068
- $T_{b\bar{s}}(5568)^+$ was $X(5568)^\pm$ 2069
- $T_{cc\bar{c}}(6900)^0$ was $X(6900)$ 2069
- $T_{b\bar{b}1}(10610)$ was $Z_b(10610), X(10610)$ 2069
- $T_{b\bar{b}1}(10650)^+$ was $Z_b(10650), X(10650)^\pm$ 2071
- Further States 2072

• Indicates the particle is in the Meson Summary Table

(Continued on next page.)

Notes in the Listings

Charged kaon mass	1538
Dalitz plot parameters for $K \rightarrow 3\pi$ decays	1547
CP -violation in $K_S \rightarrow 3\pi$	1557
Heavy Flavor Averaging Group (rev.)	1681
Charmonium system (rev.)	1898
Branching ratios of $\psi(2S)$ and $\chi_{c0,1,2}$ (rev.)	1934
Bottomonium system (rev.)	2023
Width determination of the Υ states	2023

Related Reviews in Volume 1

62. Form factors for semileptonic kaon ($K_{\ell 3}$), radiative pion ($\pi_{\ell 2\gamma}$) & kaon ($K_{\ell 2\gamma}$) decays (rev.)	871
63. Spectroscopy of light meson resonances (rev.)	874
64. Scalar mesons below 1 GeV (rev.)	888
65. Rare kaon decays (rev.)	896
66. CPT invariance tests in neutral kaon decay (rev.)	902
67. V_{ud} , V_{us} , Cabibbo angle, and CKM unitarity (rev.)	904
68. CP -violation in K_L decays (rev.)	908
69. Review of multibody charm analyses (rev.)	911
70. $D^0-\bar{D}^0$ mixing (rev.)	917
71. D_s^+ branching fractions	927
72. Leptonic decays of charged pseudoscalar mesons (rev.)	929
73. Production and decay of b -flavored hadrons (rev.)	940
74. Polarization in B decays (rev.)	951
75. $B^0-\bar{B}^0$ mixing (rev.)	955
76. Semileptonic B decays, V_{cb} and V_{ub} (rev.)	962
77. CKM angles from B hadrons, determination of (rev.)	980
78. Spectroscopy of mesons containing two heavy quarks (rev.)	985
79. Heavy non- $q\bar{q}$ mesons (rev.)	994



LIGHT UNFLAVORED MESONS
(S = C = B = 0)

For $I = 1$ (π, b, ρ, a): $u\bar{d}, (u\bar{u}-d\bar{d})/\sqrt{2}, d\bar{u}$;
for $I = 0$ ($\eta, \eta', h, h', \omega, \phi, f, f'$): $c_1(u\bar{u} + d\bar{d}) + c_2(s\bar{s})$

π^\pm

$I^G(J^P) = 1^-(0^-)$

We have omitted some results that have been superseded by later experiments. The omitted results may be found in our 1988 edition Physics Letters **B204** 1 (1988).

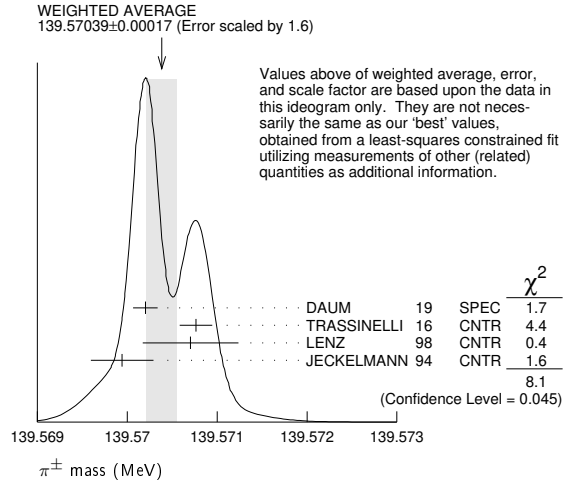
π^\pm MASS

The most accurate charged pion mass measurements are based upon x-ray wavelength measurements for transitions in π^- -mesonic atoms. The observed line is the blend of three components, corresponding to different K-shell occupancies. JECKELMANN 94 revisits the occupancy question, with the conclusion that two sets of occupancy ratios, resulting in two different pion masses (Solutions A and B), are equally probable. We choose the higher Solution B since only this solution is consistent with a positive mass-squared for the muon neutrino, given the precise muon momentum measurements now available (DAUM 91, ASSAMAGAN 94, and ASSAMAGAN 96) for the decay of pions at rest. Earlier mass determinations with π^- -mesonic atoms may have used incorrect K-shell screening corrections.

Measurements with an error of > 0.005 MeV have been omitted from this Listing.

VALUE (MeV)	DOCUMENT ID	TECN	CHG	COMMENT
139.57039 ± 0.00018 OUR FIT	Error includes scale factor of 1.8.			
139.57039 ± 0.00017 OUR AVERAGE	Error includes scale factor of 1.6. See the ideogram below.			
139.57021 ± 0.00014	¹ DAUM 19	SPEC		$\pi^+ \rightarrow \mu^+ \nu_\mu$
139.57077 ± 0.00018	² TRASSINELLI 16	CNTR		X-ray transitions in pionic N2
139.57071 ± 0.00053	³ LENZ 98	CNTR	-	pionic N2-atoms gas target
139.56995 ± 0.00035	⁴ JECKELMANN 94	CNTR	-	π^- atom, Soln. B
• • • We do not use the following data for averages, fits, limits, etc. • • •				
139.57022 ± 0.00014	⁵ ASSAMAGAN 96	SPEC	+	$\pi^+ \rightarrow \mu^+ \nu_\mu$
139.56782 ± 0.00037	⁶ JECKELMANN 94	CNTR	-	π^- atom, Soln. A
139.56996 ± 0.00067	⁷ DAUM 91	SPEC	+	$\pi^+ \rightarrow \mu^+ \nu$
139.56752 ± 0.00037	⁸ JECKELMANN 86b	CNTR	-	Mesonic atoms
139.5704 ± 0.0011	⁷ ABELA 84	SPEC	+	See DAUM 91
139.5664 ± 0.0009	⁹ LU 80	CNTR	-	Mesonic atoms
139.5686 ± 0.0020	⁹ CARTER 76	CNTR	-	Mesonic atoms
139.5660 ± 0.0024	^{9,10} MARUSHEN... 76	CNTR	-	Mesonic atoms

¹ DAUM 19 value is based on their previous (1991+1996) measurements of the μ^+ momentum of 29.79200 ± 0.00011 MeV for π^+ decay at rest. It also uses $m_\mu = 105.6583745 \pm 0.0000024$ MeV, and assumes conservatively $m_{\nu_\mu} = 2.0 \pm 2.0$ MeV. It is the most precise charged pion mass determination.
² TRASSINELLI 16 use the muonic oxygen line for online energy calibration of the pionic line.
³ LENZ 98 result does not suffer K-electron configuration uncertainties as does JECKELMANN 94.
⁴ JECKELMANN 94 Solution B (dominant 2-electron K-shell occupancy), chosen for consistency with positive $m_{\nu_\mu}^2$.
⁵ ASSAMAGAN 96 measures the μ^+ momentum p_μ in $\pi^+ \rightarrow \mu^+ \nu_\mu$ decay at rest to be 29.79200 ± 0.00011 MeV/c. Combined with the μ^+ mass and the assumption $m_{\nu_\mu} = 0$, this gives the π^+ mass above; if $m_{\nu_\mu} > 0$, m_{π^+} given above is a lower limit. Combined instead with m_μ and (assuming CPT) the π^- mass of JECKELMANN 94, p_μ gives an upper limit on m_{ν_μ} (see the ν_μ).
⁶ JECKELMANN 94 Solution A (small 2-electron K-shell occupancy) in combination with either the DAUM 91 or ASSAMAGAN 94 pion decay muon momentum measurement yields a significantly negative $m_{\nu_\mu}^2$. It is accordingly not used in our fits.
⁷ The DAUM 91 value includes the ABELA 84 result. The value is based on a measurement of the μ^+ momentum for π^+ decay at rest, $p_\mu = 29.79179 \pm 0.00053$ MeV, uses $m_\mu = 105.658389 \pm 0.000034$ MeV, and assumes that $m_{\nu_\mu} = 0$. The last assumption means that in fact the value is a lower limit.
⁸ JECKELMANN 86b gives $m_\pi/m_e = 273.12677(71)$. We use $m_e = 0.51099906(15)$ MeV from COHEN 87. The authors note that two solutions for the probability distribution of K-shell occupancy fit equally well, and use other data to choose the lower of the two possible π^\pm masses.
⁹ These values are scaled with a new wavelength-energy conversion factor $V\lambda = 1.23984244(37) \times 10^{-6}$ eV m from COHEN 87. The LU 80 screening correction relies upon a theoretical calculation of inner-shell refilling rates.
¹⁰ This MARUSHENKO 76 value used at the authors' request to use the accepted set of calibration γ energies. Error increased from 0.0017 MeV to include QED calculation error of 0.0017 MeV (12 ppm).



$m_{\pi^+} - m_{\mu^+}$

Measurements with an error > 0.05 MeV have been omitted from this Listing.

VALUE (MeV)	EVTS	DOCUMENT ID	TECN	CHG	COMMENT
• • • We do not use the following data for averages, fits, limits, etc. • • •					
33.91157 ± 0.00067		¹ DAUM 91	SPEC	+	$\pi^+ \rightarrow \mu^+ \nu$
33.9111 ± 0.0011		ABELA 84	SPEC		See DAUM 91
33.925 ± 0.025		BOOTH 70	CNTR	+	Magnetic spect.
33.881 ± 0.035	145	HYMAN 67	HEBC	+	K^- He

¹ The DAUM 91 value assumes that $m_{\nu_\mu} = 0$ and uses our $m_\mu = 105.658389 \pm 0.000034$ MeV.

$(m_{\pi^+} - m_{\pi^-}) / m_{\text{average}}$

A test of CPT invariance.

VALUE (units 10^{-4})	DOCUMENT ID	TECN
2 ± 5	AYRES 71	CNTR

π^\pm MEAN LIFE

Measurements with an error $> 0.02 \times 10^{-8}$ s have been omitted.

VALUE (10^{-8} s)	DOCUMENT ID	TECN	CHG	COMMENT
2.6033 ± 0.0005 OUR AVERAGE	Error includes scale factor of 1.2.			
2.60361 ± 0.0005 2	¹ KOPTEV 95	SPEC	+	Surface μ^+ 's
2.60231 ± 0.0005 0 ± 0.00084	NUMAO 95	SPEC	+	Surface μ^+ 's
2.609 ± 0.008	DUNAITSEV 73	CNTR	+	
2.602 ± 0.004	AYRES 71	CNTR	±	
2.604 ± 0.005	NORDBERG 67	CNTR	+	
2.602 ± 0.004	ECKHAUSE 65	CNTR	+	
• • • We do not use the following data for averages, fits, limits, etc. • • •				
2.640 ± 0.008	² KINSEY 66	CNTR	+	

¹ KOPTEV 95 combines the statistical and systematic errors; the statistical error dominates.
² Systematic errors in the calibration of this experiment are discussed by NORDBERG 67.

$(\tau_{\pi^+} - \tau_{\pi^-}) / \tau_{\text{average}}$

A test of CPT invariance.

VALUE (units 10^{-4})	DOCUMENT ID	TECN
5.5 ± 7.1	AYRES 71	CNTR
• • • We do not use the following data for averages, fits, limits, etc. • • •		
-14 ± 29	PETRUKHIN 68	CNTR
40 ± 70	BARDON 66	CNTR
23 ± 40	¹ LOBKOWICZ 66	CNTR

¹ This is the most conservative value given by LOBKOWICZ 66.

π ELECTRIC POLARIZABILITY α_π

See HOLSTEIN 14 for a general review on hadron polarizability.

VALUE (10^{-4} fm ³)	EVTS	DOCUMENT ID	TECN	COMMENT
2.0 ± 0.6 ± 0.7	63k	¹ ADOLPH 15A	SPEC	$\pi^- \gamma \rightarrow \pi^- \gamma$ Compton scatt.

¹ Value is derived assuming $\alpha_\pi = -\beta_\pi$.

Meson Particle Listings

 π^\pm π^+ DECAY MODES π^- modes are charge conjugates of the modes below.

For decay limits to particles which are not established, see the section on Searches for Axions and Other Very Light Bosons.

Mode	Fraction (Γ_i/Γ)	Confidence level
Γ_1 $\mu^+ \nu_\mu$	[a] (99.98770 ± 0.00004) %	
Γ_2 $\mu^+ \nu_\mu \gamma$	[b] (2.00 ± 0.25) × 10 ⁻⁴	
Γ_3 $e^+ \nu_e$	[a] (1.230 ± 0.004) × 10 ⁻⁴	
Γ_4 $e^+ \nu_e \gamma$	[b] (7.39 ± 0.05) × 10 ⁻⁷	
Γ_5 $e^+ \nu_e \pi^0$	(1.036 ± 0.006) × 10 ⁻⁸	
Γ_6 $e^+ \nu_e e^+ e^-$	(3.2 ± 0.5) × 10 ⁻⁹	
Γ_7 $\mu^+ \nu_\mu \nu \bar{\nu}$	< 9 × 10 ⁻⁶	90%
Γ_8 $e^+ \nu_e \nu \bar{\nu}$	< 1.6 × 10 ⁻⁷	90%

Lepton Family number (LF) or Lepton number (L) violating modes

Γ_9 $\mu^+ \bar{\nu}_e$	L	[c] < 1.5	× 10 ⁻³	90%
Γ_{10} $\mu^+ \nu_e$	LF	[c] < 8.0	× 10 ⁻³	90%
Γ_{11} $\mu^- e^+ e^+ \nu$	LF	< 1.6	× 10 ⁻⁶	90%

[a] Measurements of $\Gamma(e^+ \nu_e)/\Gamma(\mu^+ \nu_\mu)$ always include decays with γ 's, and measurements of $\Gamma(e^+ \nu_e \gamma)$ and $\Gamma(\mu^+ \nu_\mu \gamma)$ never include low-energy γ 's. Therefore, since no clean separation is possible, we consider the modes with γ 's to be subtractions of the modes without them, and let $[\Gamma(e^+ \nu_e) + \Gamma(\mu^+ \nu_\mu)]/\Gamma_{\text{total}} = 100\%$.

[b] See the Particle Listings below for the energy limits used in this measurement; low-energy γ 's are not included.

[c] Derived from an analysis of neutrino-oscillation experiments.

 π^+ BRANCHING RATIOS

$\Gamma(e^+ \nu_e)/\Gamma_{\text{total}}$	Γ_3/Γ
See note [a] in the list of π^+ decay modes just above, and see also the next block of data. See also the note on "Decay Constants of Charged Pseudoscalar Mesons" in the D_s^+ Listings.	

VALUE (units 10 ⁻⁴)	DOCUMENT ID
1.230 ± 0.004 OUR EVALUATION	

$$\frac{\Gamma(e^+ \nu_e) + \Gamma(e^+ \nu_e \gamma)}{\Gamma(\mu^+ \nu_\mu) + \Gamma(\mu^+ \nu_\mu \gamma)} \quad (\Gamma_3 + \Gamma_4)/(\Gamma_1 + \Gamma_2)$$

See note [a] in the list of π^+ decay modes above. See NUMAO 92 for a discussion of $e-\mu$ universality. See also the note on "Decay Constants of Charged Pseudoscalar Mesons" in the D_s^+ Listings.

VALUE (units 10 ⁻⁴)	EVTS	DOCUMENT ID	TECN	CHG	COMMENT
1.2327 ± 0.0023 OUR AVERAGE					
1.2344 ± 0.0023 ± 0.0019	400k	AGUILAR-AR...15	CNTR	+	Stopping π^+
1.2346 ± 0.0035 ± 0.0036	120k	CZAPEK 93	CALO		Stopping π^+
1.2265 ± 0.0034 ± 0.0044	190k	BRITTON 92	CNTR		Stopping π^+
1.218 ± 0.014	32k	BRYMAN 86	CNTR		Stopping π^+
••• We do not use the following data for averages, fits, limits, etc. •••					
1.273 ± 0.028	11k	¹ DICAPUA 64	CNTR		
1.21 ± 0.07		ANDERSON 60	SPEC		
¹ DICAPUA 64 has been updated using the current mean life.					

$\Gamma(\mu^+ \nu_\mu \nu \bar{\nu})/\Gamma_{\text{total}}$	Γ_7/Γ
Note that measurements here do not cover the full kinematic range.	

VALUE (units 10 ⁻⁴)	EVTS	DOCUMENT ID	TECN	CHG	COMMENT
2.0 ± 0.24 ± 0.08		¹ BRESSI 98	CALO	+	Stopping π^+
••• We do not use the following data for averages, fits, limits, etc. •••					
1.24 ± 0.25	26	CASTAGNOLI 58	EMUL		KE $_{\mu} < 3.38$ MeV
¹ BRESSI 98 result is given for $E_\gamma > 1$ MeV only. Result agrees with QED expectation, 2.283×10^{-4} and does not confirm discrepancy of earlier experiment CASTAGNOLI 58.					

$\Gamma(e^+ \nu_e \gamma)/\Gamma_{\text{total}}$	Γ_4/Γ
The very different values reflect the very different kinematic ranges covered (bigger range, bigger value). And none of them covers the whole kinematic range.	

VALUE (units 10 ⁻⁸)	EVTS	DOCUMENT ID	TECN	COMMENT
73.86 ± 0.54	65k	¹ BYCHKOV 09	PIBE	$e^+ \nu_\mu \gamma$ at rest
••• We do not use the following data for averages, fits, limits, etc. •••				
16.1 ± 2.3		² BOLOTOV 90B	SPEC	17 GeV $\pi^- \rightarrow e^- \bar{\nu}_e \gamma$
5.6 ± 0.7	226	³ STETZ 78	SPEC	$P_e > 56$ MeV/c
3.0	143	DEPOMMIER 63B	CNTR	(KE) $_{e^+ \gamma} > 48$ MeV

¹This BYCHKOV 09 value is for $E_\gamma > 10$ MeV and $\Theta_{e^+ \gamma} > 40^\circ$.

²BOLOTOV 90B is for $E_\gamma > 21$ MeV, $E_e > 70 - 0.8 E_\gamma$.

³STETZ 78 is for an $e^- \gamma$ opening angle $> 132^\circ$. Obtains 3.7 when using same cutoffs as DEPOMMIER 63B.

$\Gamma(e^+ \nu_e \pi^0)/\Gamma_{\text{total}}$	Γ_5/Γ				
VALUE (units 10 ⁻⁸)	EVTS	DOCUMENT ID	TECN	CHG	COMMENT
1.036 ± 0.006 OUR AVERAGE					
1.036 ± 0.006	64k	^{1,2} POCANIC 04	PIBE	+	π decay at rest
1.026 ± 0.039	1224	³ MCFARLANE 85	CNTR	+	Decay in flight
1.00 ^{+0.08} _{-0.10}	332	DEPOMMIER 68	CNTR	+	
1.07 ± 0.21	38	⁴ BACASTOW 65	OSPK	+	
1.10 ± 0.26		⁴ BERTRAM 65	OSPK	+	
1.1 ± 0.2	43	⁴ DUNAITSEV 65	CNTR	+	
0.97 ± 0.20	36	⁴ BARTLETT 64	OSPK	+	
••• We do not use the following data for averages, fits, limits, etc. •••					
1.15 ± 0.22	52	⁴ DEPOMMIER 63	CNTR	+	See DEPOMMIER 68

¹ POCANIC 04 normalizes to $e^+ \nu_e$ decays, using the PDG 2004 value $B(\pi^+ \rightarrow e^+ \nu_e) = (1.230 \pm 0.004) \times 10^{-4}$. We add their statistical (0.004×10^{-8}) , systematic (0.004×10^{-8}) and systematic error due to the uncertainty of $B(\pi^+ \rightarrow e^+ \nu_e)$ (0.003×10^{-8}) in quadrature.					
² This result can be used to calculate V_{ud} from pion beta decay: $V_{ud}^{PIBETA} = 0.9728 \pm 0.0030$.					
³ MCFARLANE 85 combines a measured rate $(0.394 \pm 0.015)/s$ with 1982 PDG mean life.					
⁴ DEPOMMIER 68 says the result of DEPOMMIER 63 is at least 10% too large because of a systematic error in the π^0 detection efficiency, and that this may be true of all the previous measurements (also V. Soergel, private communication, 1972).					

$\Gamma(e^+ \nu_e e^+ e^-)/\Gamma(\mu^+ \nu_\mu)$	Γ_6/Γ_1				
VALUE (units 10 ⁻⁹)	CL%	EVTS	DOCUMENT ID	TECN	COMMENT
3.2 ± 0.5 ± 0.2		98	EGLI 89	SPEC	Uses $R_{PAC} = 0.068 \pm 0.004$
••• We do not use the following data for averages, fits, limits, etc. •••					
0.46 ± 0.16 ± 0.07		7	¹ BARANOV 92	SPEC	Stopped π^+
< 4.8		90	KORENCHE... 76B	SPEC	
< 34		90	KORENCHE... 71	OSPK	
¹ This measurement by BARANOV 92 is of the structure-dependent part of the decay. The value depends on values assumed for ratios of form factors.					

$\Gamma(\mu^+ \nu_\mu \nu \bar{\nu})/\Gamma(\mu^+ \nu_\mu)$	Γ_7/Γ_1				
VALUE	CL%	EVTS	DOCUMENT ID	TECN	COMMENT
< 8.6 × 10⁻⁶		90	9.1M	AGUILAR-AR...20A	SPEC fit E_μ spectrum

••• We do not use the following data for averages, fits, limits, etc. •••					
0.46 ± 0.16 ± 0.07		7	¹ BARANOV 92	SPEC	Stopped π^+
< 4.8		90	KORENCHE... 76B	SPEC	
< 34		90	KORENCHE... 71	OSPK	
¹ This measurement by BARANOV 92 is of the structure-dependent part of the decay. The value depends on values assumed for ratios of form factors.					

$\Gamma(e^+ \nu_e \nu \bar{\nu})/\Gamma_{\text{total}}$	Γ_8/Γ				
VALUE	CL%	EVTS	DOCUMENT ID	TECN	COMMENT
< 1.6 × 10⁻⁷		90	1.3M	AGUILAR-AR...20A	SPEC fit E_e spectrum

••• We do not use the following data for averages, fits, limits, etc. •••					
< 5 × 10 ⁻⁶		90		PICCIOTTO 88	SPEC

$\Gamma(\mu^+ \bar{\nu}_e)/\Gamma_{\text{total}}$	Γ_9/Γ
Forbidden by total lepton number conservation. See the note on "Decay Constants of Charged Pseudoscalar Mesons" in the D_s^+ Listings.	

VALUE (units 10 ⁻³)	CL%	DOCUMENT ID	TECN	COMMENT
< 1.5		¹ COOPER 82	HLBC	Wideband ν beam
¹ COOPER 82 limit on $\bar{\nu}_e$ observation is here interpreted as a limit on lepton number violation.				

$\Gamma(\mu^+ \nu_e)/\Gamma_{\text{total}}$	Γ_{10}/Γ
Forbidden by lepton family number conservation.	

VALUE (units 10 ⁻³)	CL%	DOCUMENT ID	TECN	COMMENT
< 8.0		¹ COOPER 82	HLBC	Wideband ν beam
¹ COOPER 82 limit on ν_e observation is here interpreted as a limit on lepton family number violation.				

$\Gamma(\mu^- e^+ e^+ \nu)/\Gamma_{\text{total}}$	Γ_{11}/Γ
Forbidden by lepton family number conservation.	

VALUE (units 10 ⁻⁶)	CL%	DOCUMENT ID	TECN	CHG
< 1.6		90	BARANOV 91B	SPEC +
••• We do not use the following data for averages, fits, limits, etc. •••				
< 7.7		90	KORENCHE... 87	SPEC +

 π^+ — POLARIZATION OF EMITTED μ^+

$\pi^+ \rightarrow \mu^+ \nu$	Tests the Lorentz structure of leptonic charged weak interactions.				
VALUE	CL%	DOCUMENT ID	TECN	CHG	COMMENT
••• We do not use the following data for averages, fits, limits, etc. •••					
< (-0.9959)		90	¹ FETSCHER 84	RVUE +	
-0.99 ± 0.16			² ABELA 83	SPEC -	μ X-rays
¹ FETSCHER 84 uses only the measurement of CARR 83.					
² Sign of measurement reversed in ABELA 83 to compare with μ^+ measurements.					

••• We do not use the following data for averages, fits, limits, etc. •••					
< (-0.9959)		90	¹ FETSCHER 84	RVUE +	
-0.99 ± 0.16			² ABELA 83	SPEC -	μ X-rays
¹ FETSCHER 84 uses only the measurement of CARR 83.					
² Sign of measurement reversed in ABELA 83 to compare with μ^+ measurements.					

See the related review(s):

Form Factors for Semileptonic Kaon ($K_{\ell 3}$), Radiative Pion ($\pi_{\ell 2\gamma}$) and Kaon ($K_{\ell 2\gamma}$) Decays

See key on page 1171

Meson Particle Listings

π^\pm

π^\pm FORM FACTORS

F_V , VECTOR FORM FACTOR

VALUE	EVTS	DOCUMENT ID	TECN	COMMENT
0.0254 ± 0.0017 OUR AVERAGE				
0.0258 ± 0.0017	65k	1 BYCHKOV	09 PIBE	$e^+ \nu \gamma$ at rest
0.014 ± 0.009		2 BOLOTOV	90B SPEC	17 GeV $\pi^- \rightarrow e^- \bar{\nu}_e \gamma$
0.023 $^{+0.015}_{-0.013}$	98	EGLI	89 SPEC	$\pi^+ \rightarrow e^+ \nu_e e^+ e^-$

¹ The BYCHKOV 09 F_A and F_V results are highly (anti-)correlated: $F_A + 1.0286 F_V = 0.03853 \pm 0.00014$.
² BOLOTOV 90b only determines the absolute value.

F_A , AXIAL-VECTOR FORM FACTOR

VALUE	EVTS	DOCUMENT ID	TECN	COMMENT
0.0119 ± 0.0001	65k	1,2 BYCHKOV	09 PIBE	$e^+ \nu \gamma$ at rest
• • • We do not use the following data for averages, fits, limits, etc. • • •				
0.0115 ± 0.0004	41k	1,3 FRLEZ	04 PIBE	$\pi^+ \rightarrow e^+ \nu \gamma$ at rest
0.0106 ± 0.0060		1,4 BOLOTOV	90B SPEC	17 GeV $\pi^- \rightarrow e^- \bar{\nu}_e \gamma$
0.021 $^{+0.011}_{-0.013}$	98	EGLI	89 SPEC	$\pi^+ \rightarrow e^+ \nu_e e^+ e^-$
0.0135 ± 0.0016		1,4 BAY	86 SPEC	$\pi^+ \rightarrow e^+ \nu \gamma$
0.006 ± 0.003		1,4 PHILONEN	86 SPEC	$\pi^+ \rightarrow e^+ \nu \gamma$
0.011 ± 0.003		1,4,5 STETZ	78 SPEC	$\pi^+ \rightarrow e^+ \nu \gamma$

¹ These values come from fixing the vector form factor at the CVC prediction, $F_V = 0.0259 \pm 0.0005$.
² When F_V is released, the BYCHKOV 09 F_A is 0.0117 ± 0.0017 , and F_A and F_V results are highly (anti-)correlated: $F_A + 1.0286 F_V = 0.03853 \pm 0.00014$.
³ The sign of $\gamma = F_A / F_V$ is determined to be positive.
⁴ Only the absolute value of F_A is determined.
⁵ The result of STETZ 78 has a two-fold ambiguity. We take the solution compatible with later determinations.

VECTOR FORM FACTOR SLOPE PARAMETER a

This is a in $F_V(q^2) = F_V(0) (1 + a q^2)$

VALUE	EVTS	DOCUMENT ID	TECN	COMMENT
0.10 ± 0.06	65k	BYCHKOV	09 PIBE	$e^+ \nu \gamma$ at rest

R , SECOND AXIAL-VECTOR FORM FACTOR

VALUE	EVTS	DOCUMENT ID	TECN	COMMENT
0.059 $^{+0.009}_{-0.008}$	98	EGLI	89 SPEC	$\pi^+ \rightarrow e^+ \nu_e e^+ e^-$

π^\pm CHARGE RADIUS

The charge radius of the pion $\sqrt{\langle r_\pi^2 \rangle}$ is defined in relation to the form factor of the pion electromagnetic vertex, called vector form factor VFF, $F_V^{\pi^\pm}$. The VFF is a function of the squared four-momentum transfer t , or of the squared c.m. energy s , depending on the channel in which the photon exchange takes place. In both cases, it is related to the slope of the VFF at zero, namely

$$\langle r_\pi^2 \rangle = 6 \frac{dF_V^{\pi^\pm}(q)}{dq} (q=0) \text{ where } q = t, s$$

The quantity cannot be measured directly. It can be extracted from the cross sections of three processes: pion electroproduction, $eN \rightarrow eN\pi$, and pion electron scattering $e\pi \rightarrow e\pi$, for the t channel, and positron electron annihilation into two charged pions, $e^+e^- \rightarrow \pi^+\pi^-$, for the s channel. We encode all measurements, but we do not use electroproduction data in averaging because the extraction of the pion radius involves, in this case, theoretical uncertainties that cannot be controlled at the needed level of accuracy. In case of analyses based on the same data set, as ANANTHANARAYAN 17 and COLANGELO 19, which cannot be averaged, we combine the results into a common value, with the uncertainty range chosen to cover both analyses. Note that for consistency the form factor needs to be defined in both channels with the vacuum polarisation removed. For details see COLANGELO 19 or Appendix B of ANANTHANARAYAN 16a.

VALUE (fm)	DOCUMENT ID	TECN	COMMENT
0.659 ± 0.004 OUR AVERAGE			
0.656 ± 0.005	1 PDG	19 FIT	
0.65 ± 0.05 ± 0.06	ESCHRICH	01 CNTR	$\pi e \rightarrow \pi e$
0.663 ± 0.006	AMENDOLIA	86 CNTR	$\pi e \rightarrow \pi e$
0.663 ± 0.023	DALLY	82 CNTR	$\pi e \rightarrow \pi e$
• • • We do not use the following data for averages, fits, limits, etc. • • •			
0.640 ± 0.007	2 CUI	21A FIT	Fit existing data
0.655 ± 0.004	3 COLANGELO	19 FIT	Fit existing data
0.657 ± 0.003	4 ANANTHANARA..17	FIT	Fit existing data
0.6603 ± 0.0005 ± 0.0004	5 HANHART	17 FIT	Fit existing data
0.740 ± 0.031	6 LIESENFELD	99 CNTR	$e p \rightarrow e \pi^+ n$
0.661 ± 0.012	7 BIJNENS	98 CNTR	χ PT extraction
0.660 ± 0.024	AMENDOLIA	84 CNTR	$\pi e \rightarrow \pi e$
0.711 ± 0.009 ± 0.016	6 BEBEK	78 CNTR	$e N \rightarrow e \pi N$
0.678 ± 0.004 ± 0.008	8 QUENZER	78 CNTR	$e^+ e^- \rightarrow \pi^+ \pi^-$
0.78 $^{+0.09}_{-0.10}$	ADYLOV	77 CNTR	$\pi e \rightarrow \pi e$

0.74 $^{+0.11}_{-0.13}$	BARDIN	77 CNTR	$e p \rightarrow e \pi^+ n$
0.56 ± 0.04	DALLY	77 CNTR	$\pi e \rightarrow \pi e$

- ¹ This value combines the measurements of ANANTHANARAYAN 17 and COLANGELO 19 which are based on the same data set. The uncertainty range is chosen to cover both results.
- ² CUI 21A perform a fit including spacelike data only. Employ a new mathematical procedure based on interpolation via continued fractions augmented by statistical sampling. Also do not impose the charge conserving normalization condition $F(0) = 1$.
- ³ COLANGELO 19 fit existing F_V data, using an extended Omnes dispersive representation. This analysis is based on the same data set of ANANTHANARAYAN 17. Accordingly, they cannot be averaged. We combine the results into a common value, with the uncertainty range chosen to cover the uncertainty ranges of both analyses.
- ⁴ ANANTHANARAYAN 17 fit existing F_V data, using a mixed phase-modulus dispersive representation. This analysis is based on the same data set of COLANGELO 19. Accordingly, they cannot be averaged. We combine the results into a common value, with the uncertainty range chosen to cover the uncertainty ranges of both analyses.
- ⁵ According to the authors the uncertainty could be underestimated. The value quoted omits the BaBar data AUBERT 09.
- ⁶ The extractions could contain an additional theoretical uncertainty which cannot be sufficiently quantified.
- ⁷ BIJNENS 98 fits existing data.
- ⁸ The extraction is based on a parametrization that does not have correct analytic properties.

π^\pm REFERENCES

We have omitted some papers that have been superseded by later experiments. The omitted papers may be found in our 1988 edition Physics Letters **B204** 1 (1988).

CUI	21A	PL B822 136631	Z.-F. Cui <i>et al.</i>	(NJU, ECT, HZDR)
AGUILAR-AR...	20A	PR D102 012001	A. Aguilar-Arevalo <i>et al.</i>	(PIENU Collab.)
COLANGELO	19	JHEP 1902 006	G. Colangelo, M. Hoferichter, P. Stoffer	(BERN+)
DAUM	19	PL B796 11	M. Daum, R. Frosch, P.-R. Kettle	(PSI)
PDG	19	RPP 2019 at pdg.lbl.gov	M. Tanabashi <i>et al.</i>	(PDG Collab.)
ANANTHANARA..	17	PRL 119 132002	B. Ananthanarayan, I. Caprini, D. Das	
HANHART	17	EPJ C77 98	C. Hanhart <i>et al.</i>	
ANANTHANARA..	16A	PR D93 116007	B. Ananthanarayan <i>et al.</i>	
TRASSINELLI	16	PL B759 533	M. Trassinelli <i>et al.</i>	
ADOLPH	15A	PRL 114 062002	C. Adolph <i>et al.</i>	(COMPASS Collab.)
AGUILAR-AR...	15	PRL 115 071801	A. Aguilar-Arevalo <i>et al.</i>	(PIENU Collab.)
HOLSTEIN	14	ARNPS 64 51	B. Holstein, S. Scherer	(MASA, MAINZ)
AUBERT	09	PR D79 011102	B. Aubert <i>et al.</i>	(BABAR Collab.)
BYCHKOV	09	PRL 103 051802	M. Bychkov <i>et al.</i>	(PSI PIBETA Collab.)
FRLEZ	04	PRL 93 181804	E. Frlez <i>et al.</i>	(PSI PIBETA Collab.)
POCANIC	04	PRL 93 181803	D. Pocanic <i>et al.</i>	(PSI PIBETA Collab.)
ESCHRICH	01	PL B522 233	I. Eschrich <i>et al.</i>	(FNAL SELEX Collab.)
LIESENFELD	99	PL B468 20	A. Liesenfeld <i>et al.</i>	
BIJNENS	98	JHEP 9805 014	J. Bijmens <i>et al.</i>	
BRESSI	98	NP B513 555	G. Bressi <i>et al.</i>	
LENZ	98	PL B416 50	S. Lenz <i>et al.</i>	
ASSAMAGAN	96	PR D53 6065	K.A. Assamagan <i>et al.</i>	(PSI, ZURI, VILL+)
KOPEV	95	JETPL 61 877	V.P. Koptyev <i>et al.</i>	(PNPI)
		Translated from ZETFP 61 865.		
NUMAO	95	PR D52 4855	T. Numao <i>et al.</i>	(TRIU, BROCO)
ASSAMAGAN	94	PL B335 231	K.A. Assamagan <i>et al.</i>	(PSI, ZURI, VILL+)
JECKELMANN	94	PL B335 326	B. Jeckelmann, P.F.A. Goudsmit, H.J. Leisi	(WABRN+)
CZAPEK	93	PRL 70 17	G. Czapek <i>et al.</i>	(BERN, VILL)
BARANOV	92	SJNP 55 1644	V.A. Baranov <i>et al.</i>	(JINR)
		Translated from YAF 55 2940.		
BRITTON	92	PRL 68 3000	D.I. Britton <i>et al.</i>	(TRIU, CARL)
Also		PR D49 28	D.I. Britton <i>et al.</i>	(TRIU, CARL)
NUMAO	92	MPL A7 3357	T. Numao	(TRIU)
BARANOV	91B	SJNP 54 790	V.A. Baranov <i>et al.</i>	(JINR)
		Translated from YAF 54 1298.		
DAUM	91	PL B265 425	M. Daum <i>et al.</i>	(VILL)
BOLOTOV	90B	PL B243 308	V.N. Bolotov <i>et al.</i>	(INRM)
EGLI	89	PL B222 533	S. Egli <i>et al.</i>	(SINDRUM Collab.)
Also		PL B175 97	S. Egli <i>et al.</i>	(AACHS, ETH, SIN, ZURI)
PDG	88	PL B204 1	G.P. Yost <i>et al.</i>	(LBL+)
PICCIOTTO	88	PR D37 1131	C.E. Picciotto <i>et al.</i>	(TRIU, CNCR)
COHEN	87	RMP 59 1121	E.R. Cohen, B.N. Taylor	(RIS, CNB)
KORENCHEN...	87	SJNP 46 192	S.M. Korechenko <i>et al.</i>	(JINR)
		Translated from YAF 46 313.		
AMENDOLIA	86	NP B277 168	S.R. Amendolia <i>et al.</i>	(CERN NA7 Collab.)
BAY	86	PL B174 445	A. Bay <i>et al.</i>	(LAUS, ZURI)
BRYMAN	86	PR D33 1211	D.A. Bryman <i>et al.</i>	(TRIU, CNCR)
Also		PRL 50 7	D.A. Bryman <i>et al.</i>	(TRIU, CNCR)
JECKELMANN	86B	NP A457 709	B. Jeckelmann <i>et al.</i>	(ETH, FRIB)
Also		PRL 56 1444	B. Jeckelmann <i>et al.</i>	(ETH, FRIB)
PHILONEN	86	PRL 57 1402	L.E. Piilonen <i>et al.</i>	(LANL, TEMP, CHIC)
MCFARLANE	85	PR D32 547	W.K. McFarlane <i>et al.</i>	(TEMP, LANL)
ABELA	84	PL 146B 431	R. Abela <i>et al.</i>	(SIN)
Also		PL 74B 126	M. Daum <i>et al.</i>	(SIN)
Also		PR D20 2692	M. Daum <i>et al.</i>	(SIN)
AMENDOLIA	84	PL 146B 116	S.R. Amendolia <i>et al.</i>	(CERN NA7 Collab.)
FETSCHER	84	PL 146B 117	W. Fetscher	(ETH)
ABELA	83	NP A395 413	R. Abela <i>et al.</i>	(BASL, KARLK, KARLE)
CARR	83	PRL 51 627	J. Carr <i>et al.</i>	(LBL, NWES, TRIU)
COOPER	82	PL 112B 97	A.M. Cooper <i>et al.</i>	(RL)
DALLY	82	PRL 48 375	E.B. Dally <i>et al.</i>	
LU	80	PRL 45 1066	D.C. Lu <i>et al.</i>	(YALE, COLU, JHU)
BEBEK	78	PR D17 1693	C.J. Bebek <i>et al.</i>	
QUENZER	78	PL 76B 512	A. Quenzer <i>et al.</i>	(LALO)
STETZ	78	NP B138 285	A.W. Stetz <i>et al.</i>	(LBL, UCLA)
ADYLOV	77	NP B128 461	G.T. Adylov <i>et al.</i>	
BARDIN	77	NP B120 45	G. Bardin <i>et al.</i>	
DALLY	77	PRL 39 1176	E.B. Dally <i>et al.</i>	
CARTER	76	PRL 37 1380	A.L. Carter <i>et al.</i>	(CARL, CNCR, CHIC+)
KORENCHEN...	76B	JETP 44 35	S.M. Korechenko <i>et al.</i>	(JINR)
		Translated from ZETFP 71 69.		
MARUSHEN...	76	JETPL 23 72	V.I. Marushenko <i>et al.</i>	(PNPI)
Also		Translated from ZETFP 23 80.		
Also		Private Comm.	R.E. Shafer	(FNAL)
DUNAITSSEV	73	SJNP 16 292	A. Smirnov	(PNPI)
		Translated from YAF 16 524.	A.F. Dunaitssev <i>et al.</i>	(SERP)
AYRES	71	PR D3 1051	D.S. Ayres <i>et al.</i>	(LRL, UCSB)
Also		PR 157 1288	D.S. Ayres <i>et al.</i>	(LRL)
Also		PRL 21 261	D.S. Ayres <i>et al.</i>	(LRL, UCSB)
Also		Thesis UCRL 18369	D.S. Ayres	(LRL)
Also		PRL 23 1267	A.J. Greenberg <i>et al.</i>	(LRL, UCSB)
KORENCHEN...	71	SJNP 13 189	S.M. Korechenko <i>et al.</i>	(JINR)
		Translated from YAF 13 339.		

Meson Particle Listings

π^\pm, π^0

BOOTH	70	PL 32B 723	P.S.L. Booth <i>et al.</i>	(LIVP)
DEPOMMIER	68	NP B4 189	P. Depommier <i>et al.</i>	(CERN)
PETRUKHIN	68	JINR P1 3862	V.I. Petrukhin <i>et al.</i>	(JINR)
HYMAN	67	PL 25B 376	L.G. Hyman <i>et al.</i>	(ANL, CMU, NWES)
NORDBERG	67	PL 24B 594	M.E. Nordberg, F. Lobkowicz, R.L. Burman	(ROCH)
BARON	66	PRL 16 775	M. Baron <i>et al.</i>	(COLU)
KINSEY	66	PR 144 1132	K.F. Kinsey, F. Lobkowicz, M.E. Nordberg	(ROCH)
LOBKOWICZ	66	PRL 17 548	F. Lobkowicz <i>et al.</i>	(ROCH, BNL)
BACASTOW	65	PR 139 B407	R.B. Bacastow <i>et al.</i>	(LRL, SLAC)
BERTRAM	65	PR 139 B617	W.K. Bertram <i>et al.</i>	(MICH, CMU)
DUNAITSEV	65	JETP 20 58	A.F. Dunaitsev <i>et al.</i>	(JINR)
Translated from ZETF 47 84.				
ECKHAUSE	65	PL 19 348	M. Eckhause <i>et al.</i>	(WILL)
BARTLETT	64	PR 136 B1452	D. Bartlett <i>et al.</i>	(COLU)
DICAPUA	64	PR 133 B1333	M. di Capua <i>et al.</i>	(COLU)
Also Private Comm.				
DEPOMMIER	63	PL 5 61	L. Pondrom	(WIS C)
DEPOMMIER	63B	PL 7 285	P. Depommier <i>et al.</i>	(CERN)
ANDERSON	60	PR 119 2050	H.L. Anderson <i>et al.</i>	(EF1)
CASTAGNOLI	58	PR 112 1779	C. Castagnoli, M. Muchnik	(ROMA)



$$J^{PC} = 1^-(0^+)$$

We have omitted some results that have been superseded by later experiments. The omitted results may be found in our 1988 edition Physics Letters **B204** 1 (1988).

π^0 MASS

The value is calculated from m_{π^\pm} and $(m_{\pi^\pm} - m_{\pi^0})$. See also the notes under the π^\pm Mass Listings.

VALUE (MeV)	DOCUMENT ID
134.9768 ± 0.0005 OUR FIT	Error includes scale factor of 1.1.

$$m_{\pi^\pm} - m_{\pi^0}$$

Measurements with an error > 0.01 MeV have been omitted.

VALUE (MeV)	DOCUMENT ID	TECN	COMMENT
4.5936 ± 0.0005 OUR FIT			
4.5936 ± 0.0005 OUR AVERAGE			
4.59364 ± 0.00048	CRAWFORD 91	CNTR	$\pi^- p \rightarrow \pi^0 n, n$ TOF
4.5930 ± 0.0013	CRAWFORD 86	CNTR	$\pi^- p \rightarrow \pi^0 n, n$ TOF
• • • We do not use the following data for averages, fits, limits, etc. • • •			
4.59366 ± 0.00048	CRAWFORD 88B	CNTR	See CRAWFORD 91
4.6034 ± 0.0052	VASILEVSKY 66	CNTR	
4.6056 ± 0.0055	CZIRR 63	CNTR	

π^0 MEAN LIFE

Most experiments measure the π^0 width which we convert to a lifetime. ATHERTON 85 is the only direct measurement of the π^0 lifetime. The two Primakoff measurements from 1970 have been excluded from our average because they suffered model-related systematics unknown at the time. More information on the π^0 lifetime can be found in BERNSTEIN 13.

VALUE (10^{-17} s)	EVTS	DOCUMENT ID	TECN	COMMENT
8.43 ± 0.13 OUR AVERAGE				Error includes scale factor of 1.2.
8.337 ± 0.056 ± 0.112		¹ LARIN 20	PRMX	Primakoff effect
8.5 ± 1.1		² BYCHKOV 09	PIBE	$\pi^+ \rightarrow e^+ \nu \gamma$ at rest
8.4 ± 0.5 ± 0.5	1182	³ WILLIAMS 88	CBAL	$e^+ e^- \rightarrow e^+ e^- \pi^0$
8.97 ± 0.22 ± 0.17		ATHERTON 85	CNTR	Direct measurement
8.2 ± 0.4		⁴ BROWMAN 74	CNTR	Primakoff effect
• • • We do not use the following data for averages, fits, limits, etc. • • •				
8.32 ± 0.15 ± 0.18		⁵ LARIN 11	PRMX	Primakoff effect
5.6 ± 0.6		BELLETTINI 70	CNTR	Primakoff effect
9 ± 0.68		KRYSHKIN 70	CNTR	Primakoff effect
7.3 ± 1.1		BELLETTINI 65B	CNTR	Primakoff effect

- LARIN 20 reported this lifetime value from a measurement of $\Gamma(\pi^0 \rightarrow \gamma\gamma) = 7.802 \pm 0.052 \pm 0.105$ eV, combining data from PrimEX-II on 12C and 28Si targets with previous PrimEX-I LARIN 11 measurements. This result supersedes LARIN 11.
- BYCHKOV 09 obtains this using the conserved-vector-current relation between the vector form factor F_V and the π^0 lifetime.
- WILLIAMS 88 gives $\Gamma(\gamma\gamma) = 7.7 \pm 0.5 \pm 0.5$ eV. We give here $\tau = \hbar/\Gamma(\text{total})$.
- BROWMAN 74 gives a π^0 width $\Gamma = 8.02 \pm 0.42$ eV. The mean life is \hbar/Γ .
- LARIN 11 reported $\Gamma(\pi^0 \rightarrow \gamma\gamma) = 7.82 \pm 0.14 \pm 0.17$ eV which we converted to mean life $\tau = \hbar/\Gamma(\text{total})$.

π^0 DECAY MODES

For decay limits to particles which are not established, see the appropriate Search sections (A^0 (axion) and Other Light Boson (X^0) Searches, etc.).

Mode	Fraction (Γ_i/Γ)	Scale factor/ Confidence level
Γ_1	2γ	(98.823 ± 0.034) % S=1.5
Γ_2	$e^+ e^- \gamma$	(1.174 ± 0.035) % S=1.5
Γ_3	γ positronium	(1.82 ± 0.29) × 10 ⁻⁹

Γ_4	$e^+ e^+ e^- e^-$	(3.34 ± 0.16) × 10 ⁻⁵	
Γ_5	$e^+ e^-$	(6.46 ± 0.33) × 10 ⁻⁸	
Γ_6	4γ	< 2	× 10 ⁻⁸ CL=90%
Γ_7	invisible	< 4.4	× 10 ⁻⁹ CL=90%
Γ_8	$\nu_e \bar{\nu}_e$	< 1.7	× 10 ⁻⁶ CL=90%
Γ_9	$\nu_\mu \bar{\nu}_\mu$	< 1.6	× 10 ⁻⁶ CL=90%
Γ_{10}	$\nu_\tau \bar{\nu}_\tau$	< 2.1	× 10 ⁻⁶ CL=90%
Γ_{11}	$\gamma \nu \bar{\nu}$	< 1.9	× 10 ⁻⁷ CL=90%

Charge conjugation (C) or Lepton Family number (LF) violating modes

Γ_{12}	3γ	C	< 3.1	× 10 ⁻⁸ CL=90%
Γ_{13}	$\mu^+ e^-$	LF	< 3.8	× 10 ⁻¹⁰ CL=90%
Γ_{14}	$\mu^- e^+$	LF	< 3.2	× 10 ⁻¹⁰ CL=90%
Γ_{15}	$\mu^+ e^- + \mu^- e^+$	LF	< 3.6	× 10 ⁻¹⁰ CL=90%

CONSTRAINED FIT INFORMATION

An overall fit to 2 branching ratios uses 6 measurements and one constraint to determine 3 parameters. The overall fit has a $\chi^2 = 4.6$ for 4 degrees of freedom.

The following *off-diagonal* array elements are the correlation coefficients $\langle \delta x_i \delta x_j \rangle / (\delta x_i \delta x_j)$, in percent, from the fit to the branching fractions, $x_i \equiv \Gamma_i/\Gamma_{\text{total}}$. The fit constrains the x_i whose labels appear in this array to sum to one.

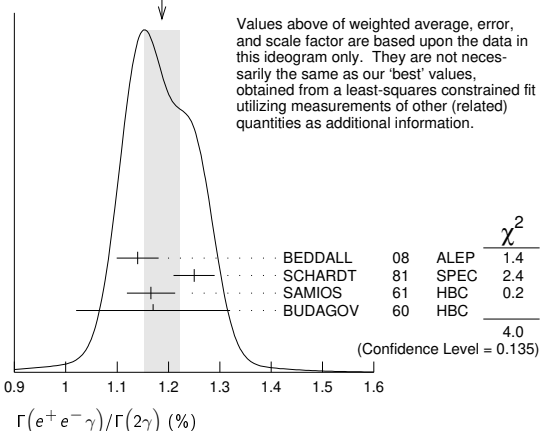
x_2	-100
x_4	0 -1
	x_1 x_2

π^0 BRANCHING RATIOS

$\Gamma(e^+ e^- \gamma)/\Gamma(2\gamma)$	Γ_2/Γ_1			
VALUE (%)	EVTS	DOCUMENT ID	TECN	COMMENT
1.188 ± 0.035 OUR FIT				Error includes scale factor of 1.5.
1.188 ± 0.034 OUR AVERAGE				Error includes scale factor of 1.4. See the ideogram below.
1.140 ± 0.024 ± 0.033	12.5k	¹ BEDDALL 08	ALEP	$e^+ e^- \rightarrow Z \rightarrow \text{hadrons}$
1.25 ± 0.04		SCHARDT 81	SPEC	$\pi^- p \rightarrow n\pi^0$
1.166 ± 0.047	3k	² SAMIOS 61	HBC	$\pi^- p \rightarrow n\pi^0$
1.17 ± 0.15	27	BUDAGOV 60	HBC	
• • • We do not use the following data for averages, fits, limits, etc. • • •				
1.1559 ± 0.0047 ± 0.0106	60k	³ ABOUZAID 19	KTEV	$K_L \rightarrow 3\pi^0$ in flight
1.196		JOSEPH 60	THEO	QED calculation

- BEDDALL 08 value is obtained from ALEPH archived data.
- SAMIOS 61 value uses a Panofsky ratio = 1.62.
- ABOUZAID 19 measured a value of $(0.3920 \pm 0.0016 \pm 0.0036)\%$ from 1999 KTEV data in $K_L \rightarrow 3\pi^0 \rightarrow 5\gamma e^+ e^-$ decays, normalised to $K_L \rightarrow 3\pi^0$, for $m(ee) > 15$ MeV and then extrapolated it to the full $m(ee)$ range using the Mikaelian and Smith predictions for the mass spectrum.

WEIGHTED AVERAGE
1.188 ± 0.034 (Error scaled by 1.4)



$\Gamma(\gamma$ positronium) $/\Gamma(2\gamma)$

VALUE (units 10 ⁻⁹)	EVTS	DOCUMENT ID	TECN	COMMENT
1.84 ± 0.29	277	AFANASYEV 90	CNTR	pC 70 GeV

Γ_3/Γ_1

See key on page 1171

Meson Particle Listings

π^0

$\Gamma(e^+e^-e^-)/\Gamma(2\gamma)$ Γ_4/Γ_1

VALUE (units 10^{-5})	EVTS	DOCUMENT ID	TECN	COMMENT
3.38 ± 0.16 OUR FIT				
3.38 ± 0.16 OUR AVERAGE				
3.46 ± 0.19	30.5k	¹ ABOUZAID 08D	KTEV	$K_L^0 \rightarrow \pi^0 \pi^0 \pi^0_{DD}$
3.18 ± 0.30	146	² SAMIOS 62B	HBC	

¹ This ABOUZAID 08D value includes all radiative final states. The error includes both statistical and systematic errors. The correlation between the Dalitz-pair planes gives a direct measurement of the π^0 parity. The $\pi^0 2\gamma^*$ form factor is measured and limits are placed on a scalar contribution to the decay.
² SAMIOS 62B value uses a Panofsky ratio = 1.62.

$\Gamma(e^+e^-)/\Gamma_{total}$ Γ_5/Γ

Experimental results are listed; branching ratios corrected for radiative effects are given in the footnotes. BERMAN 60 found $B(\pi^0 \rightarrow e^+e^-) \geq 4.69 \times 10^{-8}$ via an exact QED calculation.

VALUE (units 10^{-8})	EVTS	DOCUMENT ID	TECN	CHG	COMMENT
6.44 ± 0.33 OUR AVERAGE					
6.44 ± 0.25 ± 0.22	794	¹ ABOUZAID 07	KTEV		$K_L^0 \rightarrow 3\pi^0$ in flight
6.9 ± 2.3 ± 0.6	21	² DESHPANDE 93	SPEC		$K^+ \rightarrow \pi^+ \pi^0$
7.6 $^{+2.9}_{-2.8}$ ± 0.5	8	³ MCFARLAND 93	SPEC		$K_L^0 \rightarrow 3\pi^0$ in flight

• • • We do not use the following data for averages, fits, limits, etc. • • •
 6.09 ± 0.40 ± 0.24 275 ⁴ ALAVI-HARATI 99c SPEC 0 Repl. by ABOUZAID 07
¹ ABOUZAID 07 result is for $m_{e^+e^-}/m_{\pi^0} > 0.95$. With radiative corrections the result becomes $(7.48 \pm 0.29 \pm 0.25) \times 10^{-8}$.
² The DESHPANDE 93 result with bremsstrahlung radiative corrections is $(8.0 \pm 2.6 \pm 0.6) \times 10^{-8}$.
³ The MCFARLAND 93 result is for $B[\pi^0 \rightarrow e^+e^-, (m_{e^+e^-}/m_{\pi^0})^2 > 0.95]$. With radiative corrections it becomes $(8.8 $^{+4.5}_{-3.2}$ ± 0.6) \times 10^{-8}$.
⁴ ALAVI-HARATI 99c quote result for $B[\pi^0 \rightarrow e^+e^-, (m_{e^+e^-}/m_{\pi^0})^2 > 0.95]$ to minimize radiative contributions from $\pi^0 \rightarrow e^+e^-\gamma$. After radiative corrections they obtain $(7.04 \pm 0.46 \pm 0.28) \times 10^{-8}$.

$\Gamma(e^+e^-)/\Gamma(2\gamma)$ Γ_5/Γ_1

VALUE (units 10^{-7})	CL%	EVTS	DOCUMENT ID	TECN	COMMENT
• • • We do not use the following data for averages, fits, limits, etc. • • •					
<1.3	90		NIEBUHR 89	SPEC	$\pi^- p \rightarrow \pi^0 n$ at rest
<5.3	90		ZEPHAT 87	SPEC	$\pi^- p \rightarrow \pi^0 n$ 0.3 GeV/c
1.7 ± 0.6 ± 0.3		59	FRANK 83	SPEC	$\pi^- p \rightarrow n \pi^0$
1.8 ± 0.6		58	MISCHKE 82	SPEC	See FRANK 83
2.23 $^{+2.40}_{-1.10}$	90	8	FISCHER 78B	SPRK	$K^+ \rightarrow \pi^+ \pi^0$

$\Gamma(4\gamma)/\Gamma_{total}$ Γ_6/Γ

VALUE (units 10^{-8})	CL%	EVTS	DOCUMENT ID	TECN	COMMENT
< 2	90		MCDONOUGH 88	CBOX	$\pi^- p$ at rest
• • • We do not use the following data for averages, fits, limits, etc. • • •					
<160	90		BOLOTOV 86c	CALO	
<440	90	0	AUERBACH 80	CNTR	

$\Gamma(\text{invisible})/\Gamma_{total}$ Γ_7/Γ

The limits apply to all "invisible" channels, including in particular neutrino-antineutrino final states, obtained with laboratory experiments. Astrophysical and cosmological limits exist and are many orders of magnitude lower, but they are model dependent.

VALUE	CL%	DOCUMENT ID	TECN	COMMENT
< 4.4 × 10 ⁻⁹	90	CORTINA-GIL 21c	SPEC	$K^+ \rightarrow \pi^+ \pi^0(\gamma)$
• • • We do not use the following data for averages, fits, limits, etc. • • •				
< 0.27 × 10 ⁻⁶	90	ARTAMONOV 05A	B949	$K^+ \rightarrow \pi^+ \pi^0$
< 0.83 × 10 ⁻⁶	90	ATIYA 91	B787	$K^+ \rightarrow \pi^+ \nu \nu'$
< 24 × 10 ⁻⁶	90	HERCZEG 81	RVUE	$K^+ \rightarrow \pi^+ \nu \nu'$

$\Gamma(\nu_e \bar{\nu}_e)/\Gamma_{total}$ Γ_8/Γ

VALUE (units 10^{-6})	CL%	DOCUMENT ID	TECN	COMMENT
<1.7	90	DORENBOS... 88	CHRM	Beam dump, prompt ν
• • • We do not use the following data for averages, fits, limits, etc. • • •				
<3.1	90	¹ HOFFMAN 88	RVUE	Beam dump, prompt ν
¹ HOFFMAN 88 analyzes data from a 400-GeV BEBC beam-dump experiment.				

$\Gamma(\nu_\mu \bar{\nu}_\mu)/\Gamma_{total}$ Γ_9/Γ

VALUE (units 10^{-6})	CL%	EVTS	DOCUMENT ID	TECN	COMMENT
<1.6	90	8.7	AUERBACH 04	LSND	800 MeV p on Cu
<3.1	90		¹ HOFFMAN 88	RVUE	Beam dump, prompt ν
• • • We do not use the following data for averages, fits, limits, etc. • • •					
<7.8	90		DORENBOS... 88	CHRM	Beam dump, prompt ν
¹ HOFFMAN 88 analyzes data from a 400-GeV BEBC beam-dump experiment.					

$\Gamma(\nu_\tau \bar{\nu}_\tau)/\Gamma_{total}$ Γ_{10}/Γ

VALUE (units 10^{-6})	CL%	DOCUMENT ID	TECN	COMMENT
<2.1	90	¹ HOFFMAN 88	RVUE	Beam dump, prompt ν
• • • We do not use the following data for averages, fits, limits, etc. • • •				
<4.1	90	DORENBOS... 88	CHRM	Beam dump, prompt ν
¹ HOFFMAN 88 analyzes data from a 400-GeV BEBC beam-dump experiment.				

$\Gamma(\gamma\nu\bar{\nu})/\Gamma_{total}$ Γ_{11}/Γ

Standard Model prediction is 6×10^{-18} .

VALUE	CL%	DOCUMENT ID	TECN	COMMENT
<1.9 × 10 ⁻⁷	90	CORTINA-GIL 19	SPEC	$K^+ \rightarrow \pi^+ \gamma \nu \bar{\nu}$
• • • We do not use the following data for averages, fits, limits, etc. • • •				
<6 × 10 ⁻⁴	90	ATIYA 92	CNTR	$K^+ \rightarrow \gamma \nu \bar{\nu} \pi^+$

$\Gamma(3\gamma)/\Gamma_{total}$ Γ_{12}/Γ

Forbidden by C invariance.

VALUE (units 10^{-8})	CL%	EVTS	DOCUMENT ID	TECN	COMMENT
< 3.1	90		MCDONOUGH 88	CBOX	$\pi^- p$ at rest
• • • We do not use the following data for averages, fits, limits, etc. • • •					
< 38	90	0	HIGHLAND 80	CNTR	
<150	90	0	AUERBACH 78	CNTR	
<490	90	0	¹ DUCLOS 65	CNTR	
<490	90		¹ KUTIN 65	CNTR	
¹ These experiments give $B(3\gamma/2\gamma) < 5.0 \times 10^{-6}$.					

$\Gamma(\mu^+e^-)/\Gamma_{total}$ Γ_{13}/Γ

Forbidden by lepton family number conservation.

VALUE (units 10^{-3})	CL%	EVTS	DOCUMENT ID	TECN	COMMENT
< 0.38	90	0	APPEL 00	SPEC	$K^+ \rightarrow \pi^+ \mu^+ e^-$
• • • We do not use the following data for averages, fits, limits, etc. • • •					
<16	90		LEE 90	SPEC	$K^+ \rightarrow \pi^+ \mu^+ e^-$
<78	90		CAMPAGNARI 88	SPEC	See LEE 90

$\Gamma(\mu^-e^+)/\Gamma_{total}$ Γ_{14}/Γ

Forbidden by lepton family number conservation.

VALUE	CL%	DOCUMENT ID	TECN	COMMENT
<3.2 × 10 ⁻¹⁰	90	ALIBERTI 21	NA 62	$K^+ \rightarrow \pi^+ e^+ \mu^-$
• • • We do not use the following data for averages, fits, limits, etc. • • •				
<3.4 × 10 ⁻⁹	90	APPEL 00b	B865	$K^+ \rightarrow \pi^+ e^+ \mu^-$

$[\Gamma(\mu^+e^-) + \Gamma(\mu^-e^+)]/\Gamma_{total}$ Γ_{15}/Γ

Forbidden by lepton family number conservation.

VALUE (units 10^{-3})	CL%	DOCUMENT ID	TECN	COMMENT
< 0.36	90	ABOUZAID 08c	KTEV	$K_L^0 \rightarrow 2\pi^0 \mu^\pm e^\mp$
• • • We do not use the following data for averages, fits, limits, etc. • • •				
< 17.2	90	KROLAK 94	E799	$\ln K_L^0 \rightarrow 3\pi^0$
<140		HERCZEG 84	RVUE	$K^+ \rightarrow \pi^+ \mu e$
< 2 × 10 ⁻⁶		HERCZEG 84	THEO	$\mu^- \rightarrow e^-$ conversion
< 70	90	BRYMAN 82	RVUE	$K^+ \rightarrow \pi^+ \mu e$

π^0 ELECTROMAGNETIC FORM FACTOR

The amplitude for the process $\pi^0 \rightarrow e^+e^-\gamma$ contains a form factor $F(x)$ at the $\pi^0 \gamma \gamma$ vertex, where $x = [m_{e^+e^-}/m_{\pi^0}]^2$. The parameter a in the linear expansion $F(x) = 1 + ax$ is listed below.

All the measurements except that of BEHREND 91 are in the time-like region of momentum transfer.

LINEAR COEFFICIENT OF π^0 ELECTROMAGNETIC FORM FACTOR

VALUE (units 10^{-2})	EVTS	DOCUMENT ID	TECN	COMMENT
3.35 ± 0.31 OUR AVERAGE				
3.68 ± 0.51 ± 0.25	1.1M	LAZZERONI 17	SPEC	$K^\pm \rightarrow \pi^0 \pi^\pm; \pi^0 \rightarrow e^+e^-\gamma$
2.6 ± 2.4 ± 4.8	7.5k	FARZANPAY 92	SPEC	$\pi^- p \rightarrow \pi^0 n$ at rest
2.5 ± 1.4 ± 2.6	54k	MEIJERDREES 92B	SPEC	$\pi^- p \rightarrow \pi^0 n$ at rest
3.26 ± 0.26 ± 0.26	127	¹ BEHREND 91	CELL	$e^+e^- \rightarrow e^+e^- \pi^0$
-11 ± 3 ± 8	32k	FONVIELLE 89	SPEC	Radiation corr.
• • • We do not use the following data for averages, fits, limits, etc. • • •				
12 $^{+5}_{-4}$		² TUPPER 83	THEO	FISCHER 78 data
10 ± 3	31k	³ FISCHER 78	SPEC	Radiation corr.
-1 ± 11	2.2k	DEVONS 69	OSPK	No radiation corr.
-15 ± 10	7.6k	KOBRAK 61	HBC	No radiation corr.
-24 ± 16	3.0k	SAMIOS 61	HBC	No radiation corr.

¹ BEHREND 91 estimates that their systematic error is of the same order of magnitude as their statistical error, and so we have included a systematic error of this magnitude. The value of a is obtained by extrapolation from the region of large space-like momentum transfer assuming vector dominance.
² TUPPER 83 is a theoretical analysis of FISCHER 78 including 2-photon exchange in the corrections.
³ The FISCHER 78 error is statistical only. The result without radiation corrections is $+0.05 \pm 0.03$.

Meson Particle Listings

π^0, η

π^0 REFERENCES

We have omitted some papers that have been superseded by later experiments. The omitted papers may be found in our 1988 edition Physics Letters **B204** 1 (1988).

ALIBERTI 21	PRL 127 131802	R. Aliberti <i>et al.</i>	(NA62 Collab.)
CORTINA-GIL 21C	JHEP 2102 201	E. Cortina Gil <i>et al.</i>	(NA62 Collab.)
LARIN 20	SCI 368 506	I. Larin <i>et al.</i>	(PrimEx II Collab.)
ABOUZAID 19	PR D100 032003	E. Abouzaid <i>et al.</i>	(KTeV Collab.)
CORTINA-GIL 17	JHEP 1905 182	E. Cortina Gil <i>et al.</i>	(NA62 Collab.)
LAZZERONI 17	PL B768 38	C. Lazzeroni <i>et al.</i>	(NA62 Collab.)
BERNSTEIN 13	RMP 85 49	A.M. Bernstein, B. R. Holstein	(AMHT, MIT)
LARIN 11	PRL 106 162303	I. Larin <i>et al.</i>	(PrimEx Collab.)
BYCHKOV 09	PRL 103 051802	M. Bychkov <i>et al.</i>	(PSI PIBETA Collab.)
ABOUZAID 05C	PRL 100 131803	E. Abouzaid <i>et al.</i>	(FNAL KTeV Collab.)
ABOUZAID 08D	PRL 100 182001	E. Abouzaid <i>et al.</i>	(FNAL KTeV Collab.)
BEDDALL 08	EPJ C54 365	A. Beddall, A. Beddall	(UGAZ)
ABOUZAID 07	PR D75 012004	E. Abouzaid <i>et al.</i>	(KTeV Collab.)
ARTAMONOV 05A	PR D72 091102	A.V. Artamonov <i>et al.</i>	(BNL E949 Collab.)
AUERBACH 04	PRL 92 091801	L.B. Auerbach <i>et al.</i>	(LSDN Collab.)
APPEL 00	PRL 85 2450	R. Appel <i>et al.</i>	(BNL 865 Collab.)
Also	Thesis, Yale Univ.	D.R. Bergman	
Also	Thesis, Univ. Zurich	S. Pislak	
APPEL 00B	PRL 85 2977	R. Appel <i>et al.</i>	(BNL 865 Collab.)
ALAVI-HARATI 99C	PRL 83 922	A. Alavi-Harati <i>et al.</i>	(FNAL KTeV Collab.)
KROLAK 94	PL B320 407	P. Krolak <i>et al.</i>	(EFI, UCLA, COLO, ELMT+)
DESHPANDE 93	PRL 71 27	A. Deshpande <i>et al.</i>	(BNL E851 Collab.)
MCFARLAND 93	PRL 71 31	K.S. McFarland <i>et al.</i>	(EFI, UCLA, COLO+)
ATYA 92	PRL 69 733	M.S. Atiya <i>et al.</i>	(BNL, LANL, PRIN+)
FARZANPAY 92	PL B278 413	F. Farzanpay <i>et al.</i>	(ORST, TRIU, BRCO+)
MEIJERDREES 92B	PR D45 1439	P. Meijer Drees <i>et al.</i>	(PSI SINDRUM-I Collab.)
ATYA 91	PRL 66 2189	M.S. Atiya <i>et al.</i>	(BNL, LANL, PRIN+)
BEHREND 91	ZPHY C49 401	H.J. Behrend <i>et al.</i>	(CELLO Collab.)
CRAWFORD 91	PR D43 46	J.F. Crawford <i>et al.</i>	(VILL, UVA)
AFANASYEV 90	PL B236 116	L.G. Afanasyev <i>et al.</i>	(JINR, MOSU, SERP)
Also	SJNP 51 664	L.G. Afanasyev <i>et al.</i>	(JINR)
Translated from YAF 51 1040.			
LEE 90	PRL 64 165	A.M. Lee <i>et al.</i>	(BNL, FNAL, VILL, WASH+)
FONVIELLE 89	PL B233 65	H. Fonvieille <i>et al.</i>	(CLER, LYON, SAACL)
NIEBUHR 89	PR D40 2796	C. Niebuhr <i>et al.</i>	(SINDRUM Collab.)
CAMPAGNARI 88	PRL 61 2062	C. Campagnari <i>et al.</i>	(BNL, FNAL, PSI+)
CRAWFORD 88B	PL B213 391	J.F. Crawford <i>et al.</i>	(PSI, UVA)
DORENBOSCH 88	ZPHY C40 497	J. Dorenbosch <i>et al.</i>	(CHARM Collab.)
HOFMANN 88	PL B208 149	C.M. Hoffman	(LANL)
MCDONOUGH 88	PR D38 2121	J.M. McDonough <i>et al.</i>	(TEMP, LANL, CHIC)
PDG 88	PL B204 1	G.P. Yost <i>et al.</i>	(LBL+)
WILLIAMS 88	PR D38 1365	D.A. Williams <i>et al.</i>	(Crystal Ball Collab.)
ZEPHAT 87	JP G13 1375	A.G. Zephath <i>et al.</i>	(OMICRON Collab.)
BOLOTOV 86C	JETPL 43 520	V.N. Bolotov <i>et al.</i>	(INRM)
Translated from ZETFP 43 405.			
CRAWFORD 86	PRL 56 1043	J.F. Crawford <i>et al.</i>	(SIN, UVA)
ATHERTON 85	PL 158B 81	H.W. Atherton <i>et al.</i>	(CERN, ISU, LUND+)
HERCZEG 84	PR D29 1954	P. Herczeg, C.M. Hoffman	(LANL)
FRANK 83	PR D28 423	J.S. Frank <i>et al.</i>	(LANL, ARZS)
TUPPER 83	PR D28 2905	G.B. Tupper, T.R. Grose, M.A. Samuel	(OKSU)
BRYMAN 82	PR D26 2538	D.A. Bryman	(TRIU)
MISCHKE 82	PRL 48 1153	R.E. Mischke <i>et al.</i>	(LANL, ARZS)
HERCZEG 81	PL 100B 347	P. Herczeg, C.M. Hoffman	(LANL)
SCHARDT 81	PR D23 639	M.A. Schardt <i>et al.</i>	(ARZS, LANL)
AUERBACH 80	PL 90B 317	L.B. Auerbach <i>et al.</i>	(TEMP, LASL)
HIGHLAND 80	PRL 44 628	V.L. Highland <i>et al.</i>	(TEMP, LASL)
AUERBACH 78	PRL 41 275	L.B. Auerbach <i>et al.</i>	(TEMP, LASL)
FISCHER 78	PL 73B 359	J. Fischer <i>et al.</i>	(GEVA, SAACL)
FISCHER 78B	PL 73B 364	J. Fischer <i>et al.</i>	(GEVA, SAACL)
BROWMAN 74	PRL 33 1400	A. Browman <i>et al.</i>	(CORN, BING)
BELLETTINI 70	NC 66A 243	G. Bellettini <i>et al.</i>	(PISA, BONN)
KRYSHKIN 70	JETP 30 1037	V.I. Kryshkin, A.G. Sterligov, Y.P. Usov	(TMSK)
Translated from ZETF 57 1917.			
DEVONS 69	PR 184 1356	S. Devons <i>et al.</i>	(COLU, ROMA)
VASILEVSKIY 66	PL 23 281	I.M. Vasilevskiy <i>et al.</i>	(JINR)
BELLETTINI 65B	NC 40A 1139	G. Bellettini <i>et al.</i>	(PISA, FIRZ)
DUCLOS 65	PL 19 253	J. Duclos <i>et al.</i>	(CERN, HEID)
KUTIN 65	JETPL 2 243	V.M. Kutin, V.I. Petrukhin, Y.D. Prokoshkin	(JINR)
Translated from ZETFP 2 387.			
CZIRR 63	PR 130 341	J.B. Czirr	(LRL)
SAMIOS 62B	PR 126 1844	N.P. Samios <i>et al.</i>	(COLU, BNL)
KOBRACK 61	NC 20 1115	H. Kobrak	(EFI)
SAMIOS 61	PR 121 275	N.P. Samios	(COLU, BNL)
BERMAN 60	NC 18 1192	S. Berman, D. Geffen	(JINR)
BUDAGOV 60	JETP 11 755	Y.A. Budagov <i>et al.</i>	(JINR)
Translated from ZETF 38 1047.			
JOSEPH 60	NC 16 997	D.W. Joseph	(EFI)

η

We have omitted some results that have been superseded by later experiments. The omitted results may be found in our 1988 edition Physics Letters **B204** (1988).

$$I^G(J^{PC}) = 0^+(0^{-+})$$

η MASS

Recent measurements resolve the obvious inconsistency in previous η mass measurements in favor of the higher value first reported by NA48 (LAI 02). We use only precise measurements consistent with this higher mass value for our η mass average.

VALUE (MeV)	EVTS	DOCUMENT ID	TECN	COMMENT
547.862 ± 0.017 OUR AVERAGE				
547.865 ± 0.031 ± 0.062		NIKOLAEV 14	CRYB	$\gamma p \rightarrow p \eta$
547.873 ± 0.005 ± 0.027	1M	GOSLAWSKI 12	SPEC	$d p \rightarrow {}^3\text{He} \eta$
547.874 ± 0.007 ± 0.029		AMBROSINO 07B	KLOE	$e^+ e^- \rightarrow \phi \rightarrow \eta \gamma$
547.785 ± 0.017 ± 0.057	16k	MILLER 07	CLEO	$\psi(2S) \rightarrow J/\psi \eta$
547.843 ± 0.030 ± 0.041	1134	LAI 02	NA48	$\eta \rightarrow 3\pi^0$
••• We do not use the following data for averages, fits, limits, etc. •••				
547.311 ± 0.028 ± 0.032		¹ ABDEL-BARY 05	SPEC	$d p \rightarrow {}^3\text{He} \eta$
547.12 ± 0.06 ± 0.25		KRUSCHE 95D	SPEC	$\gamma p \rightarrow \eta p$, threshold

547.30 ± 0.15	PLOUIN 92	SPEC	$d p \rightarrow {}^3\text{He} \eta$
547.45 ± 0.25	DUANE 74	SPEC	$\pi^- p \rightarrow n$ neutrals
548.2 ± 0.65	FOSTER 65c	HBC	
549.0 ± 0.7	148	FOELSCHKE 64	HBC
548.0 ± 1.0	91	ALFF... 62	HBC
549.0 ± 1.2	53	BASTIEN 62	HBC

¹ ABDEL-BARY 05 disagrees significantly with recent measurements of similar or better precision. See comment in the header.

η WIDTH

This is the partial decay rate $\Gamma(\eta \rightarrow \gamma\gamma)$ divided by the fitted branching fraction for that mode. See the note at the start of the $\Gamma(2\gamma)$ data block, next below.

VALUE (keV) DOCUMENT ID
1.31 ± 0.05 OUR FIT

η DECAY MODES

Mode	Fraction (Γ_i/Γ)	Scale factor/ Confidence level
Neutral modes		
Γ_1 neutral modes	(71.96 ± 0.30) %	S=1.3
Γ_2 2γ	(39.36 ± 0.18) %	S=1.1
Γ_3 $3\pi^0$	(32.57 ± 0.21) %	S=1.2
Γ_4 $\pi^0 2\gamma$	(2.55 ± 0.22) × 10 ⁻⁴	
Γ_5 $2\pi^0 2\gamma$	< 1.2 × 10 ⁻³	CL=90%
Γ_6 4γ	< 2.8 × 10 ⁻⁴	CL=90%
Γ_7 invisible	< 1.0 × 10 ⁻⁴	CL=90%
Charged modes		
Γ_8 charged modes	(28.04 ± 0.30) %	S=1.3
Γ_9 $\pi^+ \pi^- \pi^0$	(23.02 ± 0.25) %	S=1.2
Γ_{10} $\pi^+ \pi^- \gamma$	(4.28 ± 0.07) %	S=1.1
Γ_{11} $e^+ e^- \gamma$	(6.9 ± 0.4) × 10 ⁻³	S=1.2
Γ_{12} $\mu^+ \mu^- \gamma$	(3.1 ± 0.4) × 10 ⁻⁴	
Γ_{13} $e^+ e^-$	< 7 × 10 ⁻⁷	CL=90%
Γ_{14} $\mu^+ \mu^-$	(5.8 ± 0.8) × 10 ⁻⁶	
Γ_{15} $2e^+ 2e^-$	(2.40 ± 0.22) × 10 ⁻⁵	
Γ_{16} $\pi^+ \pi^- e^+ e^- (\gamma)$	(2.68 ± 0.11) × 10 ⁻⁴	
Γ_{17} $e^+ e^- \mu^+ \mu^-$	< 1.6 × 10 ⁻⁴	CL=90%
Γ_{18} $2\mu^+ 2\mu^-$	(5.0 ± 1.3) × 10 ⁻⁹	
Γ_{19} $\mu^+ \mu^- \pi^+ \pi^-$	< 3.6 × 10 ⁻⁴	CL=90%
Γ_{20} $\pi^+ e^- \bar{\nu}_e + c.c.$	< 1.7 × 10 ⁻⁴	CL=90%
Γ_{21} $\pi^+ \pi^- 2\gamma$	< 2.1 × 10 ⁻³	
Γ_{22} $\pi^+ \pi^- \pi^0 \gamma$	< 6 × 10 ⁻⁴	CL=90%
Γ_{23} $\pi^0 \mu^+ \mu^- \gamma$	< 3 × 10 ⁻⁶	CL=90%

Charge conjugation (C), Parity (P), Charge conjugation × Parity (CP), or Lepton Family number (LF) violating modes

Γ_{24} $\pi^0 \gamma$	C	[a] < 9 × 10 ⁻⁵	CL=90%
Γ_{25} $\pi^+ \pi^-$	P, CP	< 4.4 × 10 ⁻⁶	CL=90%
Γ_{26} $2\pi^0$	P, CP	< 3.5 × 10 ⁻⁴	CL=90%
Γ_{27} $2\pi^0 \gamma$	C	< 5 × 10 ⁻⁴	CL=90%
Γ_{28} $3\pi^0 \gamma$	C	< 6 × 10 ⁻⁵	CL=90%
Γ_{29} 3γ	C	< 1.6 × 10 ⁻⁵	CL=90%
Γ_{30} $4\pi^0$	P, CP	< 6.9 × 10 ⁻⁷	CL=90%
Γ_{31} $\pi^0 e^+ e^-$	C	[b] < 8 × 10 ⁻⁶	CL=90%
Γ_{32} $\pi^0 \mu^+ \mu^-$	C	[b] < 5 × 10 ⁻⁶	CL=90%
Γ_{33} $\mu^+ e^- + \mu^- e^+$	LF	< 6 × 10 ⁻⁶	CL=90%

[a] Forbidden by angular momentum conservation.

[b] C parity forbids this to occur as a single-photon process.

CONSTRAINED FIT INFORMATION

An overall fit to 2 decay rate and 22 branching ratios uses 54 measurements and one constraint to determine 9 parameters. The overall fit has a $\chi^2 = 46.2$ for 46 degrees of freedom.

The following *off-diagonal* array elements are the correlation coefficients $\langle \delta x_i \delta x_j \rangle / (\delta x_i \delta x_j)$, in percent, from the fit to the branching fractions, $x_i \equiv \Gamma_i/\Gamma_{\text{total}}$. The fit constrains the x_i whose labels appear in this array to sum to one.

x_3	12																		
x_4	4	0																	
x_9	-69	-76	-3																
x_{10}	-48	-52	-2	53															
x_{11}	-8	-7	0	-4	-3														
x_{12}	-1	-1	0	0	0	0													
x_{16}	0	0	0	0	0	0	0												
Γ	-13	-1	-32	9	6	1	0	0											
		x_2	x_3	x_4	x_9	x_{10}	x_{11}	x_{12}	x_{16}										

Mode	Rate (keV)	Scale factor
Γ_2 2γ	0.515 ± 0.018	
Γ_3 $3\pi^0$	0.426 ± 0.015	
Γ_4 $\pi^0 2\gamma$	(3.34 ± 0.28) × 10 ⁻⁴	
Γ_9 $\pi^+ \pi^- \pi^0$	0.301 ± 0.011	
Γ_{10} $\pi^+ \pi^- \gamma$	0.0559 ± 0.0022	
Γ_{11} $e^+ e^- \gamma$	0.0090 ± 0.0006	1.2
Γ_{12} $\mu^+ \mu^- \gamma$	(4.1 ± 0.5) × 10 ⁻⁴	
Γ_{16} $\pi^+ \pi^- e^+ e^- (\gamma)$	(3.50 ± 0.19) × 10 ⁻⁴	

η DECAY RATES

$\Gamma(2\gamma)$ Γ_2
 See the table immediately above giving the fitted decay rates. Following the advice of NEFKENS 02, we have removed the Primakoff-effect measurement from the average. See also the "Note on the Decay Width ($\eta \rightarrow \gamma\gamma$)," in our 1994 edition, Phys. Rev. D50, 1 August 1994, Part 1, p. 1451, for a discussion of the various measurements.

VALUE (keV)	EVTS	DOCUMENT ID	TECN	COMMENT
0.515 ± 0.018 OUR FIT				
0.516 ± 0.018 OUR AVERAGE				
0.520 ± 0.020 ± 0.013		BABUSCI 13A	KLOE	$e^+ e^- \rightarrow e^+ e^- \eta$
0.51 ± 0.12 ± 0.05	36	BARU 90	MD1	$e^+ e^- \rightarrow e^+ e^- \eta$
0.490 ± 0.010 ± 0.048	2287	ROE 90	ASP	$e^+ e^- \rightarrow e^+ e^- \eta$
0.514 ± 0.017 ± 0.035	1295	WILLIAMS 88	CBAL	$e^+ e^- \rightarrow e^+ e^- \eta$
0.53 ± 0.04 ± 0.04		BARTEL 85E	JADE	$e^+ e^- \rightarrow e^+ e^- \eta$
• • • We do not use the following data for averages, fits, limits, etc. • • •				
0.476 ± 0.062		¹ RODRIGUES 08	CNTR	Reanalysis
0.64 ± 0.14 ± 0.13		AIHARA 86	TPC	$e^+ e^- \rightarrow e^+ e^- \eta$
0.56 ± 0.16	56	WEINSTEIN 83	CBAL	$e^+ e^- \rightarrow e^+ e^- \eta$
0.324 ± 0.046		BROWMAN 74B	CNTR	Primakoff effect
1.00 ± 0.22		² BEMPORAD 67	CNTR	Primakoff effect

¹ RODRIGUES 08 uses a more sophisticated calculation for the inelastic background due to incoherent photoproduction to reanalyze the η photoproduction data on Be and Cu at 9 GeV from BROWMAN 74B. This brings the value of $\Gamma(\eta \rightarrow 2\gamma)$ in line with direct measurements of the width. The error here is only statistical.
² BEMPORAD 67 gives $\Gamma(2\gamma) = 1.21 \pm 0.26$ keV assuming $\Gamma(2\gamma)/\Gamma(\text{total}) = 0.314$. Bemporad private communication gives $\Gamma(2\gamma)^2/\Gamma(\text{total}) = 0.380 \pm 0.083$. We evaluate this using $\Gamma(2\gamma)/\Gamma(\text{total}) = 0.38 \pm 0.01$. Not included in average because the uncertainty resulting from the separation of the coulomb and nuclear amplitudes has apparently been underestimated.

$\Gamma(\pi^0 2\gamma)$ Γ_4

VALUE (eV)	EVTS	DOCUMENT ID	TECN	COMMENT
0.334 ± 0.028 OUR FIT				
0.33 ± 0.03	1200	NEFKENS 14	CRYB	$\gamma p \rightarrow \eta p$

η BRANCHING RATIOS

Neutral modes

$\Gamma(\text{neutral modes})/\Gamma_{\text{total}}$ $\Gamma_1/\Gamma = (\Gamma_2 + \Gamma_3 + \Gamma_4)/\Gamma$

VALUE	EVTS	DOCUMENT ID	TECN	COMMENT
0.7196 ± 0.0030 OUR FIT				Error includes scale factor of 1.3.
0.705 ± 0.008	16k	BASILE 71D	CNTR	MM spectrometer
• • • We do not use the following data for averages, fits, limits, etc. • • •				
0.79 ± 0.08		BUNIATOV 67	OSPK	

$\Gamma(2\gamma)/\Gamma_{\text{total}}$ Γ_2/Γ

VALUE (units 10 ⁻²)	EVTS	DOCUMENT ID	TECN	COMMENT
39.36 ± 0.18 OUR FIT				Error includes scale factor of 1.1.
39.53 ± 0.33 OUR AVERAGE				
39.86 ± 0.04 ± 0.99	2m	¹ ABLIKIM 21AMBES3	$J/\psi \rightarrow \gamma\eta$	
39.49 ± 0.17 ± 0.30	65k	ABEGG 96	SPEC	$p d \rightarrow {}^3\text{He}\eta$
• • • We do not use the following data for averages, fits, limits, etc. • • •				
38.45 ± 0.40 ± 0.36	14k	² LOPEZ 07	CLEO	$\psi(2S) \rightarrow J/\psi\eta$

¹ ABLIKIM 21AM normalize the branching ratio ($\eta \rightarrow \gamma\gamma$) to B($J/\psi \rightarrow \gamma\eta$), which they measured absolutely.
² Not independent of other results listed for LOPEZ 07. Assuming decays of $\eta \rightarrow \gamma\gamma$, $3\pi^0$, $\pi^+ \pi^- \pi^0$, $\pi^+ \pi^- \gamma$, and $e^+ e^- \gamma$ account for all η decays within a contribution of 0.3% to the systematic error.

$\Gamma(2\gamma)/\Gamma(\text{neutral modes})$ $\Gamma_2/\Gamma_1 = \Gamma_2/(\Gamma_2 + \Gamma_3 + \Gamma_4)$

VALUE	EVTS	DOCUMENT ID	TECN	COMMENT
0.5470 ± 0.0018 OUR FIT				
0.548 ± 0.023 OUR AVERAGE				Error includes scale factor of 1.5.
0.535 ± 0.018		BUTTRAM 70	OSPK	
0.59 ± 0.033		BUNIATOV 67	OSPK	
• • • We do not use the following data for averages, fits, limits, etc. • • •				
0.52 ± 0.09	88	ABROSIMOV 80	HLBC	
0.60 ± 0.14	113	KENDALL 74	OSPK	
0.57 ± 0.09		STRUGALSKI 71	HLBC	
0.579 ± 0.052		FELDMAN 67	OSPK	
0.416 ± 0.044		DIGIUGNO 66	CNTR	Error doubled
0.44 ± 0.07		GRUNHAUS 66	OSPK	
0.39 ± 0.06		¹ JONES 66	CNTR	

¹ This result from combining cross sections from two different experiments.

$\Gamma(3\pi^0)/\Gamma_{\text{total}}$ Γ_3/Γ

VALUE (units 10 ⁻²)	EVTS	DOCUMENT ID	TECN	COMMENT
32.57 ± 0.21 OUR FIT				Error includes scale factor of 1.2.
31.96 ± 0.07 ± 0.84	280k	¹ ABLIKIM 21AMBES3	$J/\psi \rightarrow \gamma\eta$	
• • • We do not use the following data for averages, fits, limits, etc. • • •				
34.03 ± 0.56 ± 0.49	1821	² LOPEZ 07	CLEO	$\psi(2S) \rightarrow J/\psi\eta$

¹ ABLIKIM 21AM normalize the branching ratio ($\eta \rightarrow 3\pi^0$) to B($J/\psi \rightarrow \gamma\eta$), which they measured absolutely.
² Not independent of other results listed for LOPEZ 07. Assuming decays of $\eta \rightarrow \gamma\gamma$, $3\pi^0$, $\pi^+ \pi^- \pi^0$, $\pi^+ \pi^- \gamma$, and $e^+ e^- \gamma$ account for all η decays within a contribution of 0.3% to the systematic error.

$\Gamma(3\pi^0)/\Gamma(\text{neutral modes})$ $\Gamma_3/\Gamma_1 = \Gamma_3/(\Gamma_2 + \Gamma_3 + \Gamma_4)$

VALUE	EVTS	DOCUMENT ID	TECN	COMMENT
0.4526 ± 0.0019 OUR FIT				
0.439 ± 0.024				
• • • We do not use the following data for averages, fits, limits, etc. • • •				
0.44 ± 0.08	75	ABROSIMOV 80	HLBC	
0.32 ± 0.09		STRUGALSKI 71	HLBC	
0.41 ± 0.033		BUNIATOV 67	OSPK	Not indep. of $\Gamma(2\gamma)/\Gamma(\text{neutral modes})$
0.177 ± 0.035		FELDMAN 67	OSPK	
0.209 ± 0.054		DIGIUGNO 66	CNTR	Error doubled
0.29 ± 0.10		GRUNHAUS 66	OSPK	

$\Gamma(3\pi^0)/\Gamma(2\gamma)$ Γ_3/Γ_2

VALUE	EVTS	DOCUMENT ID	TECN	COMMENT
0.827 ± 0.006 OUR FIT				
0.829 ± 0.007 OUR AVERAGE				
0.884 ± 0.022 ± 0.019	1821	LOPEZ 07	CLEO	$\psi(2S) \rightarrow J/\psi\eta$
0.817 ± 0.012 ± 0.032	17.4k	¹ AKHMETSHIN 05	CMD2	$e^+ e^- \rightarrow \phi \rightarrow \eta\gamma$
0.826 ± 0.024		ACHASOV 00D	SND	$e^+ e^- \rightarrow \phi \rightarrow \eta\gamma$
0.832 ± 0.005 ± 0.012		KRUSCHE 95D	SPEC	$\gamma p \rightarrow \eta p$, threshold
0.841 ± 0.034		AMSLER 93	CBAR	$\bar{p} p \rightarrow \pi^+ \pi^- \eta$ at rest
0.822 ± 0.009		ALDE 84	GAM2	
• • • We do not use the following data for averages, fits, limits, etc. • • •				
0.796 ± 0.016 ± 0.016		ACHASOV 00	SND	See ACHASOV 00D
0.91 ± 0.14		COX 70B	HB C	
0.75 ± 0.09		DEVONS 70	OSPK	
0.88 ± 0.16		BALTAY 67D	DBC	
1.1 ± 0.2		CENCE 67	OSPK	
1.25 ± 0.39		BACCI 63	CNTR	Inverse BR reported

¹ Uses result from AKHMETSHIN 01B.

$\Gamma(\pi^0 2\gamma)/\Gamma_{\text{total}}$ Γ_4/Γ

VALUE (units 10 ⁻⁴)	CL%	EVTS	DOCUMENT ID	TECN	COMMENT
2.55 ± 0.22 OUR FIT					
2.21 ± 0.24 ± 0.47	≈ 500	¹ PRAKHOV 08	CRYB	$\pi^- p \rightarrow \eta n$ ≈ threshold	
• • • We do not use the following data for averages, fits, limits, etc. • • •					
3.5 ± 0.7 ± 0.6	1.6k	^{2,3} PRAKHOV 05	CRYB	See PRAKHOV 08	
< 8.4	90	7	ACHASOV 01D	SND	$e^+ e^- \rightarrow \phi \rightarrow \eta\gamma$
< 30	90	0	DAVYDOV 81	GAM2	$\pi^- p \rightarrow \eta n$

¹ PRAKHOV 08 is a reanalysis of the data of PRAKHOV 05, using for the first time the invariant-mass spectrum of the two photons.
² Normalized using $\Gamma(\eta \rightarrow 2\gamma)/\Gamma = 0.3943 \pm 0.0026$.
³ This measurement and the independent analysis of the same data by KNECHT 04 both imply a lower value of $\Gamma(\pi^0 2\gamma)$ than the one obtained by ALDE 84 from $\Gamma(\pi^0 2\gamma)/\Gamma(2\gamma)$.

$\Gamma(\pi^0 2\gamma)/\Gamma(2\gamma)$ Γ_4/Γ_2

VALUE (units 10 ⁻³)	EVTS	DOCUMENT ID	TECN	CHG	COMMENT
0.65 ± 0.06 OUR FIT					
1.8 ± 0.4					
• • • We do not use the following data for averages, fits, limits, etc. • • •					
2.5 ± 0.6	70	BINON 82	GAM2		See ALDE 84

Meson Particle Listings

 η $\Gamma(\pi^0 2\gamma)/\Gamma(3\pi^0)$ Γ_4/Γ_3

VALUE (units 10^{-4})	DOCUMENT ID	TECN	COMMENT
7.8 ± 0.7 OUR FIT			
• • • We do not use the following data for averages, fits, limits, etc. • • •			
8.3 ± 2.8 ± 1.4	¹ KNECHT 04	CRYB	$\pi^- \rho \rightarrow n\eta$
	¹ Independent analysis of same data as PRAKHOV 05.		

 $\Gamma(2\pi^0 2\gamma)/\Gamma_{total}$ Γ_5/Γ

VALUE	CL%	DOCUMENT ID	TECN	COMMENT
<1.2 × 10⁻³	90	¹ NEFKENS 05A	CRYB	$\rho(720 \text{ MeV}/c) \pi^- \rightarrow n\eta$
• • • We do not use the following data for averages, fits, limits, etc. • • •				
<4.0 × 10 ⁻³	90	BLIK 07	GAM4	$\pi^- \rho \rightarrow \eta\eta$
	¹ Measurement is done in limited $\gamma\gamma$ energy range.			

 $\Gamma(4\gamma)/\Gamma_{total}$ Γ_6/Γ

VALUE	CL%	DOCUMENT ID	TECN	COMMENT
<2.8 × 10⁻⁴	90	BLIK 07	GAM4	$\pi^- \rho \rightarrow \eta\eta$

 $\Gamma(\text{invisible})/\Gamma(2\gamma)$ Γ_7/Γ_2

VALUE	CL%	DOCUMENT ID	TECN	COMMENT
<2.6 × 10⁻⁴	90	¹ ABLIKIM 13	BES3	$J/\psi \rightarrow \phi\eta$
• • • We do not use the following data for averages, fits, limits, etc. • • •				
<1.65 × 10 ⁻³	90	² ABLIKIM 06q	BES2	$J/\psi \rightarrow \phi\eta$
	¹ Based on 225M J/ψ decays.			
	² Based on 58M J/ψ decays.			

Charged modes

 $\Gamma(\text{charged modes})/\Gamma_{total}$ $\Gamma_8/\Gamma = (\Gamma_9 + \Gamma_{10} + \Gamma_{11} + \Gamma_{12} + \Gamma_{16})/\Gamma$

VALUE	DOCUMENT ID	TECN	COMMENT
0.2804 ± 0.0030 OUR FIT			Error includes scale factor of 1.3.

 $\Gamma(\pi^+ \pi^- \pi^0)/\Gamma_{total}$ Γ_9/Γ

VALUE (units 10^{-2})	EVTS	DOCUMENT ID	TECN	COMMENT
23.02 ± 0.25 OUR FIT				Error includes scale factor of 1.2.
23.04 ± 0.03 ± 0.54	60k	¹ ABLIKIM 21AMBES3		$J/\psi \rightarrow \gamma\eta$
• • • We do not use the following data for averages, fits, limits, etc. • • •				
22.60 ± 0.35 ± 0.29	3915	² LOPEZ 07	CLEO	$\psi(2S) \rightarrow J/\psi\eta$
	¹ ABLIKIM 21AM normalize the branching ratio ($\eta \rightarrow \pi^+ \pi^- \pi^0$) to B($J/\psi \rightarrow \gamma\eta$), which they measured absolutely.			
	² Not independent of other results listed for LOPEZ 07. Assuming decays of $\eta \rightarrow \gamma\gamma$, $3\pi^0$, $\pi^+ \pi^- \pi^0$, $\pi^+ \pi^- \gamma$, and $e^+ e^- \gamma$ account for all η decays within a contribution of 0.3% to the systematic error.			

 $\Gamma(\text{neutral modes})/\Gamma(\pi^+ \pi^- \pi^0)$ $\Gamma_1/\Gamma_9 = (\Gamma_2 + \Gamma_3 + \Gamma_4)/\Gamma_9$

VALUE	EVTS	DOCUMENT ID	TECN	COMMENT
3.13 ± 0.05 OUR FIT				Error includes scale factor of 1.3.
3.26 ± 0.30 OUR AVERAGE				
2.54 ± 1.89	74	KENDALL 74	OSPK	
3.4 ± 1.1	29	AGUILAR...	72B	HBC
2.83 ± 0.80	70	¹ BLOODWO...	72B	HBC
3.6 ± 0.6	244	FLATTE	67B	HBC
2.89 ± 0.56		ALFF...	66	HBC
3.6 ± 0.8	50	KRAEMER	64	DBC
3.8 ± 1.1		PAULI	64	DBC
	¹ Error increased from published value 0.5 by Bloodworth (private communication).			

 $\Gamma(2\gamma)/\Gamma(\pi^+ \pi^- \pi^0)$ Γ_2/Γ_9

VALUE	EVTS	DOCUMENT ID	TECN	COMMENT
1.710 ± 0.025 OUR FIT				Error includes scale factor of 1.2.
1.70 ± 0.04 OUR AVERAGE				
1.704 ± 0.032 ± 0.026	3915	¹ LOPEZ 07	CLEO	$\psi(2S) \rightarrow J/\psi\eta$
1.61 ± 0.14		ABLIKIM 06E	BES2	$e^+ e^- \rightarrow J/\psi \rightarrow \eta\gamma$
1.78 ± 0.10 ± 0.13	1077	AMSLER 95	CBAR	$\bar{p}\rho \rightarrow \pi^+ \pi^- \eta$ at rest
1.72 ± 0.25	401	BAGLIN 69	HLBC	
1.61 ± 0.39		FOSTER 65	HBC	
	¹ LOPEZ 07 reports $\Gamma(\eta \rightarrow \pi^+ \pi^- \pi^0) / \Gamma(\eta \rightarrow 2\gamma) = \Gamma_9/\Gamma_2 = 0.587 \pm 0.011 \pm 0.009$.			

 $\Gamma(3\pi^0)/\Gamma(\pi^+ \pi^- \pi^0)$ Γ_3/Γ_9

VALUE	EVTS	DOCUMENT ID	TECN	COMMENT
1.415 ± 0.023 OUR FIT				Error includes scale factor of 1.2.
1.48 ± 0.05 OUR AVERAGE				
1.46 ± 0.03 ± 0.09		ACHASOV 06A	SND	$e^+ e^- \rightarrow \eta\gamma$
1.52 ± 0.04 ± 0.08	23k	¹ AKHMETSHIN 01B	CMD2	$e^+ e^- \rightarrow \phi \rightarrow \eta\gamma$
1.44 ± 0.09 ± 0.10	1627	AMSLER 95	CBAR	$\bar{p}\rho \rightarrow \pi^+ \pi^- \eta$ at rest
1.50 ^{+0.15} _{-0.29}	199	BAGLIN 69	HLBC	
1.47 ^{+0.20} _{-0.17}		BULLOCK 68	HLBC	
• • • We do not use the following data for averages, fits, limits, etc. • • •				
1.3 ± 0.4		BAGLIN 67B	HLBC	
0.90 ± 0.24		FOSTER 65	HBC	
2.0 ± 1.0		FOELSCH 64	HBC	
0.83 ± 0.32		CRAWFORD 63	HBC	
	¹ AKHMETSHIN 01B uses results from AKHMETSHIN 99F.			

 $\Gamma(\pi^+ \pi^- \pi^0)/[\Gamma(2\gamma) + \Gamma(3\pi^0)]$ $\Gamma_9/(\Gamma_2 + \Gamma_3)$

VALUE	DOCUMENT ID	TECN	COMMENT
0.320 ± 0.005 OUR FIT			Error includes scale factor of 1.2.
0.304 ± 0.012	ACHASOV 00B	SND	$e^+ e^- \rightarrow \phi \rightarrow \eta\gamma$
• • • We do not use the following data for averages, fits, limits, etc. • • •			
0.3141 ± 0.0081 ± 0.0058	ACHASOV 00B	SND	See ACHASOV 00B

 $\Gamma(\pi^+ \pi^- \gamma)/\Gamma_{total}$ Γ_{10}/Γ

VALUE (units 10^{-2})	EVTS	DOCUMENT ID	TECN	COMMENT
4.28 ± 0.07 OUR FIT				Error includes scale factor of 1.1.
4.38 ± 0.02 ± 0.10	200k	¹ ABLIKIM 21AMBES3		$J/\psi \rightarrow \gamma\eta$
• • • We do not use the following data for averages, fits, limits, etc. • • •				
3.96 ± 0.14 ± 0.14	859	² LOPEZ 07	CLEO	$\psi(2S) \rightarrow J/\psi\eta$
	¹ ABLIKIM 21AM normalize the branching ratio ($\eta \rightarrow \pi^+ \pi^- \gamma$) to B($J/\psi \rightarrow \gamma\eta$), which they measured absolutely.			
	² Not independent of other results listed for LOPEZ 07. Assuming decays of $\eta \rightarrow \gamma\gamma$, $3\pi^0$, $\pi^+ \pi^- \pi^0$, $\pi^+ \pi^- \gamma$, and $e^+ e^- \gamma$ account for all η decays within a contribution of 0.3% to the systematic error.			

 $\Gamma(\pi^+ \pi^- \gamma)/\Gamma(\pi^+ \pi^- \pi^0)$ Γ_{10}/Γ_9

VALUE	EVTS	DOCUMENT ID	TECN	COMMENT
0.1858 ± 0.0025 OUR FIT				Error includes scale factor of 1.1.
0.1847 ± 0.0030 OUR AVERAGE				
0.1856 ± 0.0005 ± 0.0028	200k	BABUSCI 13	KLOE	$e^+ e^- \rightarrow \phi \rightarrow \eta\gamma$
0.175 ± 0.007 ± 0.006	859	LOPEZ 07	CLEO	$\psi(2S) \rightarrow J/\psi\eta$
• • • We do not use the following data for averages, fits, limits, etc. • • •				
0.209 ± 0.004	18k	THALER 73	ASPK	
0.201 ± 0.006	7250	GORMLEY 70	ASPK	
0.28 ± 0.04		BALTAY 67B	DBC	
0.25 ± 0.035		LITCHFIELD 67	DBC	
0.30 ± 0.06		CRAWFORD 66	HBC	
0.196 ± 0.041		FOSTER 65c	HBC	

 $\Gamma(e^+ e^- \gamma)/\Gamma_{total}$ Γ_{11}/Γ

VALUE (units 10^{-3})	EVTS	DOCUMENT ID	TECN	COMMENT
6.9 ± 0.4 OUR FIT				Error includes scale factor of 1.2.
6.7 ± 0.5 OUR AVERAGE				Error includes scale factor of 1.2.
6.6 ± 0.4 ± 0.4	1345	BERGHAUSER 11	SPEC	$\gamma p \rightarrow p\eta$
7.8 ± 0.5 ± 0.8	435 ± 31	BERLOWSKI 08	WASA	$p d \rightarrow {}^3\text{He} \eta$
5.15 ± 0.62 ± 0.74	283	ACHASOV 01B	SND	$e^+ e^- \rightarrow \phi \rightarrow \eta\gamma$
7.10 ± 0.64 ± 0.46	323	AKHMETSHIN 01	CMD2	$e^+ e^- \rightarrow \phi \rightarrow \eta\gamma$
• • • We do not use the following data for averages, fits, limits, etc. • • •				
9.4 ± 0.7 ± 0.5	172	¹ LOPEZ 07	CLEO	$\psi(2S) \rightarrow J/\psi\eta$
	¹ Not independent of other results listed for LOPEZ 07. Assuming decays of $\eta \rightarrow \gamma\gamma$, $3\pi^0$, $\pi^+ \pi^- \pi^0$, $\pi^+ \pi^- \gamma$, and $e^+ e^- \gamma$ account for all η decays within a contribution of 0.3% to the systematic error.			

 $\Gamma(e^+ e^- \gamma)/\Gamma(\pi^+ \pi^- \gamma)$ Γ_{11}/Γ_{10}

VALUE	EVTS	DOCUMENT ID	TECN	COMMENT
0.161 ± 0.010 OUR FIT				Error includes scale factor of 1.2.
0.237 ± 0.021 ± 0.015	172	LOPEZ 07	CLEO	$\psi(2S) \rightarrow J/\psi\eta$

 $\Gamma(e^+ e^- \gamma)/\Gamma(\pi^+ \pi^- \pi^0)$ Γ_{11}/Γ_9

VALUE (units 10^{-2})	EVTS	DOCUMENT ID	TECN	COMMENT
2.98 ± 0.19 OUR FIT				Error includes scale factor of 1.3.
2.1 ± 0.5	80	JANE 75B	OSPK	See the erratum

 $\Gamma(\text{neutral modes})/[\Gamma(\pi^+ \pi^- \pi^0) + \Gamma(\pi^+ \pi^- \gamma) + \Gamma(e^+ e^- \gamma)]$ $\Gamma_1/(\Gamma_9 + \Gamma_{10} + \Gamma_{11}) = (\Gamma_2 + \Gamma_3 + \Gamma_4)/(\Gamma_9 + \Gamma_{10} + \Gamma_{11})$

VALUE	EVTS	DOCUMENT ID	TECN	COMMENT
2.57 ± 0.04 OUR FIT				Error includes scale factor of 1.3.
2.64 ± 0.23		BALTAY 67B	DBC	
• • • We do not use the following data for averages, fits, limits, etc. • • •				
4.5 ± 1.0	280	¹ JAMES 66	HBC	
3.20 ± 1.26	53	¹ BASTIEN 62	HBC	
2.5 ± 1.0	10	¹ PICKUP 62	HBC	
	¹ These experiments are not used in the averages as they do not separate clearly $\eta \rightarrow \pi^+ \pi^- \pi^0$ and $\eta \rightarrow \pi^+ \pi^- \gamma$ from each other. The reported values thus probably contain some unknown fraction of $\eta \rightarrow \pi^+ \pi^- \gamma$.			

 $\Gamma(2\gamma)/[\Gamma(\pi^+ \pi^- \pi^0) + \Gamma(\pi^+ \pi^- \gamma) + \Gamma(e^+ e^- \gamma)]$ $\Gamma_2/(\Gamma_9 + \Gamma_{10} + \Gamma_{11})$

VALUE	EVTS	DOCUMENT ID	TECN	COMMENT
1.407 ± 0.020 OUR FIT				Error includes scale factor of 1.2.
1.1 ± 0.4 OUR AVERAGE				
1.51 ± 0.93	75	KENDALL 74	OSPK	
0.99 ± 0.48		CRAWFORD 63	HBC	

 $\Gamma(\mu^+ \mu^- \gamma)/\Gamma_{total}$ Γ_{12}/Γ

VALUE (units 10^{-4})	EVTS	DOCUMENT ID	TECN	COMMENT
3.1 ± 0.4 OUR FIT				
3.1 ± 0.4	600	DZHELADIN 80	SPEC	$\pi^- \rho \rightarrow \eta\eta$
• • • We do not use the following data for averages, fits, limits, etc. • • •				
1.5 ± 0.75	100	BUSHNIN 78	SPEC	See DZHELADIN 80

$\Gamma(e^+e^-)/\Gamma_{\text{total}}$ Γ_{13}/Γ

VALUE	CL%	DOCUMENT ID	TECN	COMMENT
$<7 \times 10^{-7}$	90	ACHASOV	18B	CNTR Inverse reaction $e^+e^- \rightarrow \eta$

• • • We do not use the following data for averages, fits, limits, etc. • • •

$<2.3 \times 10^{-6}$	90	AGAKISHIEV	14	$pp \rightarrow \eta + X$
$<5.6 \times 10^{-6}$	90	¹ AGAKISHIEV	12A	SPEC $pp \rightarrow \eta + X$
$<2.7 \times 10^{-5}$	90	BERLOWSKI	08	WASA $pd \rightarrow {}^3\text{He} \eta$
$<0.77 \times 10^{-4}$	90	BROWDER	97B	CLE2 $e^+e^- \simeq 10.5$ GeV
$<2 \times 10^{-4}$	90	WHITE	96	SPEC $pd \rightarrow \eta {}^3\text{He}$
$<3 \times 10^{-4}$	90	DAVIES	74	RVUE Uses ESTEN 67

¹AGAKISHIEV 12A uses a data sample of 3.5 GeV proton beam collisions on liquid hydrogen target collected by the HADES detector.

 $\Gamma(\mu^+\mu^-)/\Gamma_{\text{total}}$ Γ_{14}/Γ

VALUE (units 10^{-5})	CL%	EVTS	DOCUMENT ID	TECN	COMMENT
5.8 ± 0.8 OUR AVERAGE					

$5.7 \pm 0.7 \pm 0.5$	114	ABEGG	94	SPEC $pd \rightarrow \eta {}^3\text{He}$
6.5 ± 2.1	27	DZHELADIN	80B	SPEC $\pi^- p \rightarrow \eta n$

• • • We do not use the following data for averages, fits, limits, etc. • • •

$5.6^{+0.6}_{-0.7} \pm 0.5$	100	KESSLER	93	SPEC See ABEGG 94
<20	95	0	WEHMANN	68 OSPK

 $\Gamma(\mu^+\mu^-)/\Gamma(2\gamma)$ Γ_{14}/Γ_2

VALUE (units 10^{-5})	DOCUMENT ID	TECN
	HYAMS	69 OSPK

• • • We do not use the following data for averages, fits, limits, etc. • • •

VALUE (units 10^{-5})	CL%	EVTS	DOCUMENT ID	TECN	COMMENT
$2.4 \pm 0.2 \pm 0.1$	362	¹ AMBROSINO	11B	KLOE $e^+e^- \rightarrow \phi \rightarrow \eta \gamma$	

• • • We do not use the following data for averages, fits, limits, etc. • • •

<9.7	90	BERLOWSKI	08	WASA $pd \rightarrow {}^3\text{He} \eta$
<6.9	90	AKHMETSHIN	01	CMD2 $e^+e^- \rightarrow \phi \rightarrow \eta \gamma$

¹This measurement is fully inclusive (includes " $2e^+2e^- \gamma$ " channel).

 $\Gamma(\pi^+\pi^-e^+e^-(\gamma))/\Gamma_{\text{total}}$ Γ_{16}/Γ

VALUE (units 10^{-4})	EVTS	DOCUMENT ID	TECN	COMMENT
2.68 ± 0.11 OUR FIT				

$2.68 \pm 0.09 \pm 0.07$	1555 \pm 52	¹ AMBROSINO	09B	KLOE $e^+e^- \rightarrow \phi \rightarrow \eta \gamma$
--------------------------	---------------	------------------------	-----	--

• • • We do not use the following data for averages, fits, limits, etc. • • •

$4.3^{+2.0}_{-1.6} \pm 0.4$	16	BERLOWSKI	08	WASA $pd \rightarrow {}^3\text{He} \eta$
$4.3 \pm 1.3 \pm 0.4$	16	BARGHOLTZ	07	CNTR See BERLOWSKI 08
$3.7^{+2.5}_{-1.8} \pm 0.3$	4	AKHMETSHIN	01	CMD2 $e^+e^- \rightarrow \phi \rightarrow \eta \gamma$

¹This AMBROSINO 09B value includes radiative events.

 $\Gamma(e^+e^-\mu^+\mu^-)/\Gamma_{\text{total}}$ Γ_{17}/Γ

VALUE	CL%	DOCUMENT ID	TECN	COMMENT
$<1.6 \times 10^{-4}$	90	BERLOWSKI	08	WASA $pd \rightarrow {}^3\text{He} \eta$

 $\Gamma(2\mu^+2\mu^-)/\Gamma(\mu^+\mu^-)$ Γ_{18}/Γ_{14}

VALUE (units 10^{-4})	EVTS	DOCUMENT ID	TECN	COMMENT
$8.6 \pm 1.4 \pm 1.2$	49.6	HAYRAPETY...23A	CMS	pp at 13 TeV

 $\Gamma(\mu^+\mu^-\pi^+\pi^-)/\Gamma_{\text{total}}$ Γ_{19}/Γ

VALUE	CL%	DOCUMENT ID	TECN	COMMENT
$<3.6 \times 10^{-4}$	90	BERLOWSKI	08	WASA $pd \rightarrow {}^3\text{He} \eta$

 $\Gamma(\pi^+e^- \nu_e + c.c.)/\Gamma(\pi^+\pi^-\pi^0)$ Γ_{20}/Γ_9

VALUE	CL%	DOCUMENT ID	TECN	COMMENT
$<7.3 \times 10^{-4}$	90	ABLIKIM	13G	BES3 $J/\psi \rightarrow \phi \eta$

 $\Gamma(\pi^+\pi^-2\gamma)/\Gamma(\pi^+\pi^-\pi^0)$ Γ_{21}/Γ_9

VALUE	CL%	DOCUMENT ID	TECN
$<9 \times 10^{-3}$		PRICE	67 HBC
$<16 \times 10^{-3}$	95	BALTAY	67B DBC

 $\Gamma(\pi^+\pi^-\pi^0\gamma)/\Gamma(\pi^+\pi^-\pi^0)$ Γ_{22}/Γ_9

VALUE	CL%	EVTS	DOCUMENT ID	TECN
$<0.24 \times 10^{-2}$	90	0	THALER	73 ASPK

• • • We do not use the following data for averages, fits, limits, etc. • • •

$<1.7 \times 10^{-2}$	90	ARNOLD	68	HLBC
$<1.6 \times 10^{-2}$	95	BALTAY	67B	DBC
$<7.0 \times 10^{-2}$		FLATTE	67	HBC
$<0.9 \times 10^{-2}$		PRICE	67	HBC

 $\Gamma(\pi^0\mu^+\mu^- \gamma)/\Gamma_{\text{total}}$ Γ_{23}/Γ

VALUE	CL%	DOCUMENT ID	TECN	COMMENT
$<3 \times 10^{-6}$	90	DZHELADIN	81	SPEC $\pi^- p \rightarrow \eta n$

Forbidden modes

 $\Gamma(\pi^0\gamma)/\Gamma_{\text{total}}$ Γ_{24}/Γ

Forbidden by angular momentum conservation.

VALUE	CL%	DOCUMENT ID	TECN	COMMENT
$<9 \times 10^{-5}$	90	NEFKENS	05A	CRYB $p(720 \text{ MeV}/c) \pi^- \rightarrow n \eta$

 $\Gamma(\pi^+\pi^-)/\Gamma_{\text{total}}$ Γ_{25}/Γ

Forbidden by P and CP invariance.

VALUE	CL%	EVTS	DOCUMENT ID	TECN	COMMENT
$<4.4 \times 10^{-6}$	90	83M	¹ BABUSCI	20A	KLOE $e^+e^- \rightarrow \phi \rightarrow \eta \gamma$

• • • We do not use the following data for averages, fits, limits, etc. • • •

$<5.3 \times 10^{-17}$			² ZHEVLAKOV	19	THEO from nEDM limits
$<1.6 \times 10^{-5}$	90	25M	AAIJ	17D	LHCB in $D \rightarrow \pi \pi \pi$ decays
$<3.9 \times 10^{-4}$	90	225M	ABLIKIM	11G	BES3 $e^+e^- \rightarrow J/\psi \rightarrow \eta \gamma$
$<1.3 \times 10^{-5}$	90	16M	AMBROSINO	05A	KLOE $e^+e^- \rightarrow \phi \rightarrow \eta \gamma$
$<3.3 \times 10^{-4}$	90		AKHMETSHIN	99B	CMD2 $e^+e^- \rightarrow \phi \rightarrow \eta \gamma$
$<9 \times 10^{-4}$	90		AKHMETSHIN	97C	CMD2 See AKHMETSHIN 99B
$<15 \times 10^{-4}$		0	THALER	73	ASPK

¹BABUSCI 20A combines new data with the previous AMBROSINO 05A data, and thus supersedes AMBROSINO 05A.

²ZHEVLAKOV 19 derives the value from the experimental limits of nEDM by a calculation using an effective Lagrangian.

 $\Gamma(2\pi^0)/\Gamma_{\text{total}}$ Γ_{26}/Γ

Forbidden by P and CP invariance.

VALUE	CL%	EVTS	DOCUMENT ID	TECN	COMMENT
$<3.5 \times 10^{-4}$	90		BLIK	07	GAM4 $\pi^- p \rightarrow \eta n$

• • • We do not use the following data for averages, fits, limits, etc. • • •

$<2.7 \times 10^{-17}$			¹ ZHEVLAKOV	19	THEO from nEDM limits
$<6.9 \times 10^{-4}$	90	225M	ABLIKIM	11G	BES3 $e^+e^- \rightarrow J/\psi \rightarrow \eta \gamma$
$<4.3 \times 10^{-4}$	90		AKHMETSHIN	99C	CMD2 $e^+e^- \rightarrow \phi \rightarrow \eta \gamma$
$<6 \times 10^{-4}$	90		ACHASOV	98	SND $e^+e^- \rightarrow \phi \rightarrow \eta \gamma$

¹ZHEVLAKOV 19 derives the value from the experimental limits of nEDM by a calculation using an effective Lagrangian.

²ACHASOV 98 observes one event in a $\pm 3\sigma$ region around the η mass, while a Monte Carlo calculation gives 10 ± 5 events. The limit here is the Poisson upper limit for one observed event and no background.

 $\Gamma(2\pi^0\gamma)/\Gamma_{\text{total}}$ Γ_{27}/Γ

Forbidden by C invariance.

VALUE	CL%	DOCUMENT ID	TECN	CHG	COMMENT
$<5 \times 10^{-4}$	90	NEFKENS	05	CRYB	0 $p(720 \text{ MeV}/c) \pi^- \rightarrow n \eta$

• • • We do not use the following data for averages, fits, limits, etc. • • •

$<17 \times 10^{-4}$	90	BLIK	07	GAM4	$\pi^- p \rightarrow \eta n$
----------------------	----	------	----	------	------------------------------

 $\Gamma(3\pi^0)/\Gamma_{\text{total}}$ Γ_{28}/Γ

Forbidden by C invariance.

VALUE	CL%	DOCUMENT ID	TECN	CHG	COMMENT
$<6 \times 10^{-5}$	90	NEFKENS	05	CRYB	0 $p(720 \text{ MeV}/c) \pi^- \rightarrow n \eta$

• • • We do not use the following data for averages, fits, limits, etc. • • •

$<24 \times 10^{-5}$	90	BLIK	07	GAM4	$\pi^- p \rightarrow \eta n$
----------------------	----	------	----	------	------------------------------

 $\Gamma(3\gamma)/\Gamma_{\text{total}}$ Γ_{29}/Γ

Forbidden by C invariance.

VALUE	CL%	DOCUMENT ID	TECN	COMMENT
$<16 \times 10^{-5}$	90	BLIK	07	GAM4 $\pi^- p \rightarrow \eta n$
$<4 \times 10^{-5}$	90	NEFKENS	05A	CRYB $p(720 \text{ MeV}/c) \pi^- \rightarrow n \eta$

• • • We do not use the following data for averages, fits, limits, etc. • • •

$<1.2 \times 10^{-3}$	95	ALDE	84	GAM2 0
-----------------------	----	------	----	--------

 $\Gamma(3\gamma)/\Gamma(2\gamma)$ Γ_{29}/Γ_2

VALUE	CL%	DOCUMENT ID	TECN	CHG
$<1.2 \times 10^{-3}$	95	ALDE	84	GAM2 0

 $\Gamma(3\gamma)/\Gamma(3\pi^0)$ Γ_{29}/Γ_3

VALUE	CL%	DOCUMENT ID	TECN	COMMENT
$<4.9 \times 10^{-5}$	90	ALOISIO	04	KLOE $\phi \rightarrow \eta \gamma$

 $\Gamma(4\pi^0)/\Gamma_{\text{total}}$ Γ_{30}/Γ

Forbidden by P and CP invariance.

VALUE	CL%	DOCUMENT ID	TECN	COMMENT
$<6.9 \times 10^{-7}$	90	PRAKHOV	00	CRYB $\pi^- p \rightarrow n \eta$, 720 MeV/c

• • • We do not use the following data for averages, fits, limits, etc. • • •

$<200 \times 10^{-7}$	90	BLIK	07	GAM4 $\pi^- p \rightarrow \eta n$
-----------------------	----	------	----	-----------------------------------

 $\Gamma(\pi^0e^+e^-)/\Gamma_{\text{total}}$ Γ_{31}/Γ

C parity forbids this to occur as a single-photon process.

VALUE	CL%	DOCUMENT ID	TECN	COMMENT
$<7.5 \times 10^{-6}$	90	ADLARSON	18c	WASA $pd \rightarrow \eta {}^3\text{He}$

• • • We do not use the following data for averages, fits, limits, etc. • • •

$<1.6 \times 10^{-4}$	90	MARTYNOV	76	HLBC
$<8.4 \times 10^{-4}$	90	BAZIN	68	DBC
$<70 \times 10^{-4}$		RITTENBERG	65	HBC

Meson Particle Listings

 η $\Gamma(\pi^0 e^+ e^-)/\Gamma(\pi^+ \pi^- \pi^0)$

C parity forbids this to occur as a single-photon process.

VALUE	CL%	DOCUMENT ID	TECN	COMMENT
$< 3.28 \times 10^{-5}$	90	ADLARSON 18c	WASA	$pd \rightarrow \eta^3\text{He}$
••• We do not use the following data for averages, fits, limits, etc. •••				
$< 1.9 \times 10^{-4}$	90	JANE 75	OSPK	
$< 42 \times 10^{-4}$	90	BAGLIN 67	HLBC	
$< 16 \times 10^{-4}$	90	BILLING 67	HLBC	
$< 77 \times 10^{-4}$		FOSTER 65B	HBC	
$< 110 \times 10^{-4}$		PRICE 65	HBC	

 Γ_{31}/Γ_9 $\Gamma(\pi^0 \mu^+ \mu^-)/\Gamma_{\text{total}}$

C parity forbids this to occur as a single-photon process.

VALUE	CL%	DOCUMENT ID	TECN	COMMENT
$< 5 \times 10^{-6}$	90	DZHELYADIN 81	SPEC	$\pi^- p \rightarrow \eta\eta$
••• We do not use the following data for averages, fits, limits, etc. •••				
$< 500 \times 10^{-6}$		WEHMANN 68	OSPK	

 Γ_{32}/Γ $[\Gamma(\mu^+ e^-) + \Gamma(\mu^- e^+)]/\Gamma_{\text{total}}$

Forbidden by lepton family number conservation.

VALUE	CL%	DOCUMENT ID	TECN	COMMENT
$< 6 \times 10^{-6}$	90	WHITE 96	SPEC	$pd \rightarrow \eta^3\text{He}$

 Γ_{33}/Γ η C-NONCONSERVING DECAY PARAMETERS $\pi^+ \pi^- \pi^0$ LEFT-RIGHT ASYMMETRY PARAMETERMeasurements with an error $> 1.0 \times 10^{-2}$ have been omitted.

VALUE (units 10^{-2})	EVTS	DOCUMENT ID	TECN	COMMENT
$0.09 \pm_{-0.12}^{+0.11}$ OUR AVERAGE				
$+0.09 \pm 0.10 \pm_{-0.14}^{+0.09}$	1.34M	AMBROSINO 08D	KLOE	
0.28 ± 0.26	165k	JANE 74	OSPK	
-0.05 ± 0.22	220k	LAYTER 72	ASPK	
••• We do not use the following data for averages, fits, limits, etc. •••				
1.5 ± 0.5	37k	¹ GORMLEY 68c	ASPK	

¹The GORMLEY 68c asymmetry is probably due to unmeasured ($\mathbf{E} \times \mathbf{B}$) spark chamber effects. New experiments with ($\mathbf{E} \times \mathbf{B}$) controls don't observe an asymmetry. $\pi^+ \pi^- \pi^0$ SEXTANT ASYMMETRY PARAMETERMeasurements with an error $> 2.0 \times 10^{-2}$ have been omitted.

VALUE (units 10^{-2})	EVTS	DOCUMENT ID	TECN	COMMENT
$0.12 \pm_{-0.11}^{+0.10}$ OUR AVERAGE				
$+0.08 \pm 0.10 \pm_{-0.13}^{+0.08}$	1.34M	AMBROSINO 08D	KLOE	
0.20 ± 0.25	165k	JANE 74	OSPK	
0.10 ± 0.22	220k	LAYTER 72	ASPK	
0.5 ± 0.5	37k	GORMLEY 68c	WIRE	

 $\pi^+ \pi^- \pi^0$ QUADRANT ASYMMETRY PARAMETER

VALUE (units 10^{-2})	EVTS	DOCUMENT ID	TECN	COMMENT
-0.09 ± 0.09 OUR AVERAGE				
$-0.05 \pm 0.10 \pm_{-0.05}^{+0.03}$	1.34M	AMBROSINO 08D	KLOE	
-0.30 ± 0.25	165k	JANE 74	OSPK	
-0.07 ± 0.22	220k	LAYTER 72	ASPK	

 $\pi^+ \pi^- \gamma$ LEFT-RIGHT ASYMMETRY PARAMETERMeasurements with an error $> 2.0 \times 10^{-2}$ have been omitted.

VALUE (units 10^{-2})	EVTS	DOCUMENT ID	TECN	COMMENT
0.9 ± 0.4 OUR AVERAGE				
1.2 ± 0.6	35k	JANE 74B	OSPK	
0.5 ± 0.6	36k	THALER 72	ASPK	
1.22 ± 1.56	7257	GORMLEY 70	ASPK	

 $\pi^+ \pi^- \gamma$ PARAMETER β (D -wave)Sensitive to a D -wave contribution: $dN/d\cos\theta = \sin^2\theta (1 + \beta \cos^2\theta)$.

VALUE	EVTS	DOCUMENT ID	TECN	COMMENT
-0.02 ± 0.07 OUR AVERAGE				Error includes scale factor of 1.3.
0.11 ± 0.11	35k	JANE 74B	OSPK	
-0.060 ± 0.065	7250	GORMLEY 70	WIRE	
••• We do not use the following data for averages, fits, limits, etc. •••				
0.12 ± 0.06		¹ THALER 72	ASPK	

¹The authors don't believe this indicates D -wave because the dependence of β on the γ energy is inconsistent with the theoretical prediction. A $\cos^2\theta$ dependence can also come from P - and F -wave interference. η CP-NONCONSERVING DECAY PARAMETER $\pi^+ \pi^- e^+ e^-$ DECAY-PLANE ASYMMETRY PARAMETER A_ϕ In the η rest frame, the total momentum of the $e^+ e^-$ pair is equal and opposite to that of the $\pi^+ \pi^-$ pair. Let \hat{z} be the unit vector along the momentum of the $e^+ e^-$ pair; let \hat{n}_{ee} and $\hat{n}_{\pi\pi}$ be the unit vectors normal to the $e^+ e^-$ and $\pi^+ \pi^-$ planes; and let ϕ be the angle between the two normals. Then

$$\sin\phi \cos\phi = [(\hat{n}_{ee} \times \hat{n}_{\pi\pi}) \cdot \hat{z}] (\hat{n}_{ee} \cdot \hat{n}_{\pi\pi}),$$

and

$$A_\phi \equiv \frac{N_{\sin\phi \cos\phi > 0} - N_{\sin\phi \cos\phi < 0}}{N_{\sin\phi \cos\phi > 0} + N_{\sin\phi \cos\phi < 0}}.$$

VALUE (units 10^{-2})	EVTS	DOCUMENT ID	TECN	COMMENT
$-0.6 \pm 2.5 \pm 1.8$	1555 \pm 52	AMBROSINO 09B	KLOE	$e^+ e^- \rightarrow \phi \rightarrow \eta\gamma$

ENERGY DEPENDENCE OF $\eta \rightarrow 3\pi$ DALITZ PLOTSPARAMETERS FOR $\eta \rightarrow \pi^+ \pi^- \pi^0$ See the "Note on η Decay Parameters," page 1454, in our 1994 edition (Physical Review **D50** 1173 (1994)). The following experiments fit to one or more of the coefficients a, b, c, d, e, f, g for $|\text{matrix element}|^2 = 1 + ay + by^2 + cx + dx^2 + exy + fy^3 + gx^2y$.

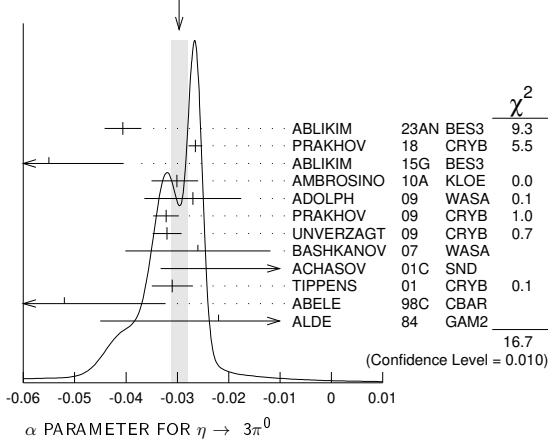
VALUE	EVTS	DOCUMENT ID	TECN	COMMENT
••• We do not use the following data for averages, fits, limits, etc. •••				
631k		¹ ABLIKIM 23AN	BES3	$J/\psi \rightarrow \gamma\eta$
4.7M		² ANASTASI 16A	KLOE	$e^+ e^- \rightarrow \phi \rightarrow \eta\gamma$
79k		ABLIKIM 15G	BES3	$e^+ e^- \rightarrow J/\psi \rightarrow \gamma\eta$
174k		ADLARSON 14A	WASA	$pd \rightarrow \eta^3\text{He}$
1.34M		AMBROSINO 08D	KLOE	
3230		³ ABELE 98D	CBAR	$\bar{p}p \rightarrow \pi^0 \pi^0 \eta$ at rest
1077		⁴ AMSLER 95	CBAR	$\bar{p}p \rightarrow \pi^+ \pi^- \eta$ at rest
81k		LAYTER 73	ASPK	
220k		LAYTER 72	ASPK	
1138		CARPENTER 70	HBC	
349		DANBURG 70	DBC	
7250		GORMLEY 70	WIRE	
526		BAGLIN 69	HLBC	
7170		CNOPS 68	OSPK	
37k		GORMLEY 68c	WIRE	
1300		CLPWY 66	HBC	
705		LARRIBE 66	HBC	

¹ABLIKIM 23AN fit the Dalitz plot density distribution with two parameter sets (a, b, d, f, g), and (a, b, d, f, g).²ANASTASI 16A measure the Dalitz parameters a, b, d, f , and g . This is the first measurement of g .³ABELE 98D obtains $a = -1.22 \pm 0.07$ and $b = 0.22 \pm 0.11$ when c (or d) is fixed at 0.06.⁴AMSLER 95 fits to $(1+ay+by^2)$ and obtains $a = -0.94 \pm 0.15$ and $b = 0.11 \pm 0.27$. α PARAMETER FOR $\eta \rightarrow 3\pi^0$ See the "Note on η Decay Parameters" in our 1994 edition, Phys. Rev. **D50**, 1 August 1994, Part I, p. 1454. The value here is of α in $|\text{matrix element}|^2 = 1 + 2\alpha z$.

VALUE	EVTS	DOCUMENT ID	TECN	COMMENT
-0.0296 ± 0.0016 OUR AVERAGE				Error includes scale factor of 1.7. See the ideogram below.
$-0.0406 \pm 0.0035 \pm 0.0008$	272k	ABLIKIM 23AN	BES3	$J/\psi \rightarrow \gamma\eta$
$-0.0265 \pm 0.0010 \pm 0.0009$	7M	PRAKHOV 18	CRYB	$\gamma p \rightarrow p\eta$
$-0.055 \pm 0.014 \pm 0.004$	33k	ABLIKIM 15G	BES3	$e^+ e^- \rightarrow J/\psi \rightarrow \gamma\eta$
$-0.0301 \pm 0.0035 \pm_{-0.0035}^{+0.0022}$	512k	AMBROSINO 10A	KLOE	$e^+ e^- \rightarrow \phi \rightarrow \eta\gamma$
$-0.027 \pm 0.008 \pm 0.005$	120k	¹ ADOLPH 09	WASA	$pp \rightarrow pp\eta$
$-0.0322 \pm 0.0012 \pm 0.0022$	3M	² PRAKHOV 09	CRYB	$\gamma p \rightarrow p\eta$
$-0.032 \pm 0.002 \pm 0.002$	1.8M	² UNVERZAGT 09	CRYB	$\gamma p \rightarrow p\eta$
$-0.026 \pm 0.010 \pm 0.010$	75k	BASHKANOV 07	WASA	$pp \rightarrow pp\eta$
$-0.010 \pm 0.021 \pm 0.010$	12k	ACHASOV 01c	SND	$e^+ e^- \rightarrow \phi \rightarrow \eta\gamma$
-0.031 ± 0.004	1M	TIPPENS 01	CRYB	$\pi^- p \rightarrow n\eta, 720 \text{ MeV}$
$-0.052 \pm 0.017 \pm 0.010$	98k	ABELE 98c	CBAR	$\bar{p}p \rightarrow 5\pi^0$
-0.022 ± 0.023	50k	ALDE 84	GAM2	
••• We do not use the following data for averages, fits, limits, etc. •••				
$-0.038 \pm 0.003 \pm_{-0.008}^{+0.012}$	1.34M	³ AMBROSINO 08D	KLOE	
-0.32 ± 0.37	192	BAGLIN 70	HLBC	

¹This ADOLPH 09 result is independent of the BASHKANOV 07 result.²The PRAKHOV 09 and UNVERZAGT 09 results are independent.³This AMBROSINO 08D value is an indirect result using $\eta \rightarrow \pi^+ \pi^0 \pi^-$ events and a rescattering matrix that mixes isospin decay amplitudes.

WEIGHTED AVERAGE
-0.0296±0.0016 (Error scaled by 1.7)



PARAMETER Λ IN $\eta \rightarrow \ell^+ \ell^- \gamma$ DECAY

In the pole approximation the electromagnetic transition form factor for a resonance of mass M is given by the expression:
 $|F|^2 = (1 - M_{\ell\ell}^2/\Lambda^2)^{-2}$,
 where for the parameter Λ vector dominance predicts $\Lambda \approx 0.770$ GeV.

VALUE (GeV/c ²)	EVTS	DOCUMENT ID	TECN	COMMENT
0.716 ± 0.011	OUR AVERAGE			
0.712 ± 0.020		1 ADLARSON 17B	A2MM	$\gamma p \rightarrow \eta p$
0.7191 ± 0.0125 ± 0.0093		2 ARNALDI 16	NA60	400 GeV p-A collisions
0.716 ± 0.031 ± 0.009		3 ARNALDI 09	NA60	158A In-In collisions
0.72 ± 0.09	600	DZHELADIN 80	SPEC	$\pi^- p \rightarrow \eta n, \eta \rightarrow \gamma \mu^+ \mu^-$

- ADLARSON 17B reports $\Lambda^{-2}(\eta \rightarrow \gamma e^+ e^-) = 1.97 \pm 0.11$ (GeV/c²)⁻² which we converted to the quoted Λ value and uncertainty (total=statistical plus systematic).
- ARNALDI 16 reports $\Lambda^{-2}(\eta \rightarrow \gamma \mu^+ \mu^-) = 1.934 \pm 0.067 \pm 0.050$ (GeV/c²)⁻² which we converted to the quoted Λ value.
- ARNALDI 09 reports $\Lambda^{-2}(\eta \rightarrow \gamma \mu^+ \mu^-) = 1.95 \pm 0.17 \pm 0.05$ (GeV/c²)⁻² which we converted to the quoted Λ value.

η REFERENCES

ABLIKIM 23AN	PRL D107 092007	M. Ablikim et al.	(BESIII Collab.)
HAYRAPETYAN... 23A	PRL 131 091903	A. Hayrapetyan et al.	(CMS Collab.)
ABLIKIM 21AM	PRL D104 092004	M. Ablikim et al.	(BESIII Collab.)
BABUSCI 20A	JHEP 2010 047	D. Babusci et al.	(KLOE-2 Collab.)
ZHEVLAKOV 19	PR D99 031703	A.S. Zhevlakov et al.	(TMSK, MAINZ, TUBIN+)
ACHASOV 18B	PR D98 052007	M.N. Achasov et al.	(SND Collab.)
ADLARSON 18C	PL B784 378	P. Adlarson et al.	(WASA-at-COSY Collab.)
PRAKHOV 18	PR C97 045203	S. Prakhov et al.	(A2 Collab. at MAMI)
AALU 17D	PL B764 233	R. Aaij et al.	(LHCb Collab.)
ADLARSON 17B	PR C95 035208	P. Adlarson et al.	(A2 Collab. at MAMI)
ANASTASI 16A	JHEP 1605 019	A. Anastasi et al.	(KLOE-2 Collab.)
ARNALDI 16	PL B757 437	R. Arnaldi et al.	(NA60 Collab.)
ABLIKIM 15G	PR D92 012014	M. Ablikim et al.	(BESIII Collab.)
ADLARSON 14A	PR C90 045207	P. Adlarson et al.	(WASA-at-COSY Collab.)
AGAKISHIEV 14	PL B731 265	G. Agakishiev et al.	(HADES Collab.)
NEFKENS 14	PR C90 025206	B.M.K. Nefkens et al.	(A2 Collab. at MAMI)
NIKOLAIEV 14	EPJ A50 58	A. Nikolaev et al.	(MAMI-B, MAINZ, BONN)
ABLIKIM 13G	PR D87 012009	M. Ablikim et al.	(BESIII Collab.)
ABLIKIM 13G	PR D87 032006	M. Ablikim et al.	(BESIII Collab.)
BABUSCI 13	PL B718 910	D. Babusci et al.	(KLOE/KLOE-2 Collab.)
BABUSCI 13A	JHEP 1301 119	D. Babusci et al.	(KLOE-2 Collab.)
AGAKISHIEV 12A	EPJ A48 64	G. Agakishiev et al.	(HADES Collab.)
GOSLAWSKI 12	PR D85 112011	P. Goslawski et al.	(COSY-ANKE Collab.)
ABLIKIM 11G	PR D84 032006	M. Ablikim et al.	(BESIII Collab.)
AMBROSINO 11B	PL B702 324	F. Ambrosino et al.	(KLOE Collab.)
BERGHAUSER 11	PL B701 562	H. Berghauser et al.	(GIES, UCLA, GUTE)
AMBROSINO 10A	PL B694 16	F. Ambrosino et al.	(KLOE Collab.)
ADOLPH 09	PL B677 24	C. Adolph et al.	(WASA-at-COSY Collab.)
AMBROSINO 09B	PL B675 283	F. Ambrosino et al.	(KLOE Collab.)
ARNALDI 09	PL B677 260	R. Arnaldi et al.	(NA60 Collab.)
PRAKHOV 09	PR C79 035204	S. Prakhov et al.	(MAMI-C Crystal Ball Collab.)
UNVERZAGT 09	EPJ A39 169	M. Unverzagt et al.	(MAMI-B Crystal Ball Collab.)
AMBROSINO 08D	JHEP 0805 006	F. Ambrosino et al.	(DAPHNE KLOE Collab.)
BELROWSKI 08	PR D77 032004	M. Belrowski et al.	(CELSIUS/WASA Collab.)
PRAKHOV 08	PR C78 015206	S. Prakhov et al.	(BNL Crystal Ball Collab.)
RODRIGUES 08	PRL 101 012301	T.E. Rodrigues et al.	(USP, FESP, UNESP+)
AMBROSINO 07B	JHEP 0712 073	F. Ambrosino et al.	(KLOE Collab.)
BARGHOLTZ 07	PL B644 299	Chr. Bargholtz et al.	(CELSIUS/WASA Collab.)
BASHKANOV 07	PR C76 048201	M. Bashkanov et al.	(CELSIUS/WASA Collab.)
BLIK 07	PAN 70 693	A.M. Blik et al.	(GAMS Collab.)
LOPEZ 07	PRL 99 122001	A. Lopez et al.	(CLEO Collab.)
MILLER 07	PRL 99 122002	D.H. Miller et al.	(CLEO Collab.)
ABLIKIM 06E	PR D73 052008	M. Ablikim et al.	(BES Collab.)
ABLIKIM 06Q	PRL 97 202002	M. Ablikim et al.	(BES Collab.)
ACHASOV 06A	PR D74 014016	M.N. Achasov et al.	(SND Collab.)
ABDEL-BARY 05	PL B619 281	M. Abdel-Bary et al.	(GEM Collab.)
AKHMETSHIN 05	PL B605 26	R.R. Akhmetshin et al.	(Novosibirsk CMD-2 Collab.)
AMBROSINO 05A	PL B606 276	F. Ambrosino et al.	(KLOE Collab.)
NEFKENS 05	PRL 94 041601	B.M.K. Nefkens et al.	(BNL Crystal Ball Collab.)
NEFKENS 05A	PR C72 035212	B.M.K. Nefkens et al.	(BNL Crystal Ball Collab.)
PRAKHOV 05	PR C72 025201	S. Prakhov et al.	(BNL Crystal Ball Collab.)
ALOISIO 04	PL B591 49	A. Aloisio et al.	(KLOE Collab.)
KNECHT 04	PL B589 14	N. Knecht et al.	(KLOE Collab.)
LAI 02	PL B533 196	A. Lai et al.	(CERN NA48 Collab.)
NEFKENS 02	PS T99 114	B.M.K. Nefkens, J.W. Price	(UCLA)
ACHASOV 01B	PL B504 275	M.N. Achasov et al.	(Novosibirsk SND Collab.)
ACHASOV 01C	JETPL 73 451	M.N. Achasov et al.	(Novosibirsk SND Collab.)

ACHASOV 01D	NP B600 3	M.N. Achasov et al.	(Novosibirsk SND Collab.)
AKHMETSHIN 01	PL B501 191	R.R. Akhmetshin et al.	(Novosibirsk CMD-2 Collab.)
AKHMETSHIN 01B	PL B509 217	R.R. Akhmetshin et al.	(Novosibirsk CMD-2 Collab.)
TIPPENS 01	PRL 87 192001	W.B. Tippens et al.	(BNL Crystal Ball Collab.)
ACHASOV 00	EPJ C12 25	M.N. Achasov et al.	(Novosibirsk SND Collab.)
ACHASOV 00B	JETP 90 17	M.N. Achasov et al.	(Novosibirsk SND Collab.)
ACHASOV 00D	Translated from JETPL 72 282	M.N. Achasov et al.	(Novosibirsk SND Collab.)
PRAKHOV 00	PRL 84 4802	S. Prakhov et al.	(BNL Crystal Ball Collab.)
AKHMETSHIN 99B	PL B462 371	R.R. Akhmetshin et al.	(Novosibirsk CMD-2 Collab.)
AKHMETSHIN 99C	PL B462 380	R.R. Akhmetshin et al.	(Novosibirsk CMD-2 Collab.)
AKHMETSHIN 99F	PL B460 242	R.R. Akhmetshin et al.	(Novosibirsk CMD-2 Collab.)
ABELE 98C	PL B417 193	A. Abele et al.	(Crystal Barrel Collab.)
ABELE 98D	PL B417 197	A. Abele et al.	(Crystal Barrel Collab.)
ACHASOV 98	PL B425 388	M.N. Achasov et al.	(Novosibirsk SND Collab.)
AKHMETSHIN 97C	PL B415 452	R.R. Akhmetshin et al.	(Novosibirsk CMD-2 Collab.)
BROWDER 97B	PR D56 6359	T.E. Browder et al.	(CLEO Collab.)
ABEGG 96	PR D53 11	R. Abegg et al.	(Saturne SPES2 Collab.)
WHITE 96	PR D53 6658	D.B. White et al.	(Saturne SPES2 Collab.)
AMSLER 95	PL B346 203	C. Amisler et al.	(Crystal Barrel Collab.)
KRUSCHE 95D	ZPHY A351 237	B. Krusche et al.	(TAPS + A2 Collab.)
ABEGG 94	PR D50 92	R. Abegg et al.	(Saturne SPES2 Collab.)
PDG 94	PR D50 1173	L. Montanet et al.	(CERN, LBL, BOST+)
AMSLER 93	ZPHY C58 175	C. Amisler et al.	(Crystal Barrel Collab.)
KESLER 93	PRL 70 892	R.S. Kessler et al.	(Saturne SPES2 Collab.)
FLOUIN 92	PL B276 526	F. Flouin et al.	(Saturne SPES4 Collab.)
BARU 90	ZPHY C48 561	S.E. Baru et al.	(MIDI Collab.)
ROE 90	PR D41 17	N.A. Roe et al.	(ASP Collab.)
WILLIAMS 88	PR D38 1365	D.A. Williams et al.	(Crystal Ball Collab.)
AIHARA 86	PR D33 844	H. Aihara et al.	(TPC-2 γ Collab.)
BARTEL 85E	PL 160B 421	W. Bartel et al.	(JADE Collab.)
LANDSBERG 85	PRPL 128 301	L.G. Landsberg	(SERP)
ALDE 84	ZPHY C25 225	D.M. Alde et al.	(SERP, BELG, LAPP)
ALDE 84	SJNP 40 918	D.M. Alde et al.	(SERP, BELG, LAPP)
WEINSTEIN 83	Translated from YAF 40 1447	A.J. Weinstein et al.	(Crystal Ball Collab.)
BINON 82	SJNP 36 391	F.G. Binon et al.	(SERP, BELG, LAPP+)
DAVYDOV 81	NC 71A 497	F.G. Binon et al.	(SERP, BELG, LAPP+)
DAVYDOV 81	LNC 32 45	V.A. Davydov et al.	(SERP, BELG, LAPP+)
DAVYDOV 81	SJNP 33 825	V.A. Davydov et al.	(SERP, BELG, LAPP+)
DZHELADIN 81	PL 10B 239	R.I. Dzheyladin et al.	(SERP)
DZHELADIN 81	SJNP 33 822	R.I. Dzheyladin et al.	(SERP)
ABROSIMOV 80	SJNP 31 195	A.T. Abrosimov et al.	(JINR)
DZHELADIN 80	PL 94B 548	R.I. Dzheyladin et al.	(SERP)
DZHELADIN 80	SJNP 32 516	R.I. Dzheyladin et al.	(SERP)
DZHELADIN 80B	PL 97B 471	R.I. Dzheyladin et al.	(SERP)
DZHELADIN 80B	SJNP 32 518	R.I. Dzheyladin et al.	(SERP)
BUSHNIN 78	PL 79B 147	Y.B. Bushnin et al.	(SERP)
BUSHNIN 78	SJNP 28 775	Y.B. Bushnin et al.	(SERP)
MARTYNOV 76	SJNP 23 48	A.S. Martynov et al.	(JINR)
JANE 75	PL 59B 99	M.R. Jane et al.	(RHEL, LOWC)
JANE 75B	PL 59B 103	M.R. Jane et al.	(RHEL, LOWC)
JANE 75B	PL 73B 503	M.R. Jane et al.	(RHEL, LOWC)
BROWMAN 74B	PRL 32 1067	A. Browman et al.	(CORN, BING)
DAVIES 74	NC 24A 324	J.D. Davies, J.G. Guy, R.K.P. Zia	(BIRM, RHEL+)
DUANE 74	PL 32 425	A. Duane et al.	(LOIC, SHIP)
JANE 74	PL 48B 260	M.R. Jane et al.	(RHEL, LOWC, SUSS)
JANE 74B	PL 48B 265	M.R. Jane et al.	(RHEL, LOWC, SUSS)
KENDALL 74	NC 21A 387	B.N. Kendall et al.	(BROW, BARI, MIT)
LAYTER 73	PR D7 2565	J.G. Layter et al.	(COLU)
THALER 73	PR D7 2569	J.J. Thaler et al.	(COLU)
AGUILAR... 72B	NP D6 29	M. Aguilar-Benitez et al.	(BNL)
BLOODWORTH 72B	NP B39 525	I.J. Bloodworth et al.	(TNTO)
LAYTER 72	PRL 29 316	J.G. Layter et al.	(COLU)
THALER 72	PRL 29 313	J.J. Thaler et al.	(COLU)
BASILE 71D	NC 3A 796	M. Basile et al.	(CERN, BGNA, STRB)
STRUGALSKI 71	NP B27 429	Z.S. Strugalski et al.	(CERN, MFM)
BAGLIN 70	NP B22 66	C. Baglin et al.	(EPOL, MADR, STRB)
BUTTRAM 70	PRL 25 1358	M.T. Buttram, M.N. Kreisler, R.E. Mischke	(PRIN)
CARPENTER 70	PR D1 1303	D.W. Carpenter et al.	(DUKE)
COX 70B	PRL 24 534	B. Cox, L. Fortney, J.P. Goslon	(DUKE)
DANBURG 70	PR D2 2564	J.S. Danburg et al.	(COLU, SYRA)
DEVONS 70	PR D1 1936	S. Devons et al.	(COLU, BNL)
GORMLEY 70	PR D2 501	M. Gormley et al.	(COLU)
BAGLIN 69	PL 29B 445	C. Baglin et al.	(EPOL, UCB, MADR, STRB)
HYAMS 69	NP B22 66	B.D. Hyams et al.	(CERN, MFM)
ARNOLD 68	PL 27B 466	R.G. Arnold et al.	(STRB, MADR, EPOL)
BAZIN 68	PRL 20 895	M.J. Bazin et al.	(PRIN, LOIC)
BULLOCK 68	PL 27B 402	F.W. Bullock et al.	(COLU, BNL)
CNOPS 68	PRL 21 1609	A.M. Cnops et al.	(BNL, ORNL, UCN+)
GORMLEY 68C	PRL 21 402	M. Gormley et al.	(COLU, BNL)
WEHMANN 68	PRL 20 748	A.W. Wehmann et al.	(HARV, CASE, SLA+)
BAGLIN 67B	BAPS 12 567	C. Baglin et al.	(EPOL, UCB)
BALTAJ 67B	PRL 19 1498	C. Baltay et al.	(COLU, STON)
BALTAJ 67D	PRL 19 1495	C. Baltay et al.	(COLU, BRAN)
BEMPORAD 67	PL 25B 300	C. Bemporad et al.	(PIA, BONN)
BILLING 67	PL 25B 435	K.D. Billing et al.	(LOUC, XAF)
BUNIATOV 67	PL 25B 560	S.A. Buniatov et al.	(CERN, ORNL)
CENCE 67	PRL 19 1393	R.J. Cence et al.	(HAWA, LRF)
ESTEN 67	PL 24B 115	M.J. Esten et al.	(LOUC, OXF)
FELDMAN 67	PRL 18 868	M. Feldman et al.	(PENN)
FLATTE 67	PRL 18 976	S.M. Flatte	(LOUC, OXF)
FLATTE 67B	PL 163 1441	S.M. Flatte, C.G. Wohl	(RHEL, SACL)
LITCHFIELD 67	PL 24B 486	P.J. Litchfield et al.	(RHEL, SACL)
PRICE 67	PRL 18 1207	L.R. Price, F.S. Crawford	(LRL)
ALFF... 66	PR 145 1072	C. Alff-Steinberger et al.	(COLU, RUTG)
CLPWV 66	PR 149 104	C. Baltay	(SCUC, LRL, PURD, WISC, YALE)
CRAWFORD 66	PRL 16 333	F.S. Crawford, L.R. Price	(LRL)
DIGUIGNO 66	PRL 16 767	G. di Guigno et al.	(NAPL, TRST, FRAS)
GRUNHAUS 66	Thesis	J. Grunhaus	(COLU)
JAMES 66	PR 142 896	F.E. James, H.L. Kraybill	(YALE, BNL)
JONES 66	PL 23 597	W.G. Jones et al.	(LOIC, RHEL)
LARRIBE 66	PL 23 600	A. Larribe et al.	(SACL, RHEL)
FOSTER 65	PR 138 B652	M. Foster et al.	(WIS, PURD)
FOSTER 65B	Athens Conf.	M. Foster, M. Good, M. Meier	(WIS, C)
FOSTER 65C	Thesis	M. Foster	(WIS, C)
PRICE 65	PRL 15 123	L.R. Price, F.S. Crawford	(LRL)
RITTENBERG 65	PRL 15 556	A. Rittenberg, G.R. Kalbfleisch	(LRL, BNL)
FOELSCH 64	PR 134 B1138	H.W.J. Foelsche, H.L. Kraybill	(YALE)

Meson Particle Listings

 $\eta, f_0(500)$

KRAEMER	64	PR 136 B496	R.W. Kraemer et al.	(JHU, NWES, WOOD)
PAULI	64	PL 13 351	E. Pauli, A. Muller	(SACL)
BACCI	63	PRL 11 37	C. Bacci et al.	(ROMA, FRAS)
CRAWFORD	63	PRL 10 546	F.S.Jr. Crawford, L.J. Lloyd, E.C. Fowler	(LRL+)
Also		PRL 16 907	F.S. Crawford, L.J. Lloyd, E.C. Fowler	(LRL+)
ALFF-...	62	PRL 9 322	C. Alff-Steinberger et al.	(COLU, RUTG)
BASTIEN	62	PRL 8 114	P.L. Bastien et al.	(LRL)
PICKUP	62	PRL 8 329	E. Pickup, D.K. Robinson, E.O. Salant	(CNRC+)

 $f_0(500)$

$$I^G(J^{PC}) = 0^+(0^{++})$$

also known as σ ; was $f_0(600)$, $f_0(400-1200)$

See the related review(s):

Scalar Mesons below 1 GeV

 $f_0(500)$ T-MATRIX POLE \sqrt{s}

Note that $\Gamma = -2 \text{Im}(\sqrt{s})$.

VALUE (MeV)	DOCUMENT ID	TECN	COMMENT
(400-550) - $i(200-350)$ OUR ESTIMATE	(see Fig. 64.3 in the review)		
$(458 \pm 7 \pm 4) - i(245 \pm 6 \pm 7)$	¹ DANILKIN	21	RVUE Compilation
$(410 \pm 20) - i(240 \pm 15)$	SARANTSEV	21	RVUE $J/\psi(1S) \rightarrow \gamma(\pi\pi, K\bar{K}, \eta\eta, \omega\phi)$
$(512 \pm 15) - i(188 \pm 12)$	² ABLIKIM	17	BES3 $J/\psi \rightarrow \gamma 3\pi$
$(440 \pm 10) - i(238 \pm 10)$	³ ALBALADEJO	12	RVUE Compilation
$(445 \pm 25) - i(278 \pm 22)$	^{4,5} GARCIA-MAR..	11	RVUE Compilation
$(457 \pm 14) - i(279 \pm 11)$	^{4,6} GARCIA-MAR..	11	RVUE Compilation
$(442 \pm 5) - i(274 \pm 6)$	⁷ MOUSSALLAM	11	RVUE Compilation
$(452 \pm 13) - i(259 \pm 16)$	⁸ MENNESSIER	10	RVUE Compilation
$(448 \pm 43) - i(266 \pm 43)$	⁹ MENNESSIER	10	RVUE Compilation
$(455 \pm 6 \pm 31) - i(278 \pm 6 \pm 34)$	¹⁰ CAPRINI	08	RVUE Compilation
$(463 \pm 6 \pm 31) - i(259 \pm 6 \pm 33)$	¹¹ CAPRINI	08	RVUE Compilation
$(552 \pm 84) - i(232 \pm 81)$	¹² ABLIKIM	07A	BES2 $\psi(2S) \rightarrow \pi^+\pi^- J/\psi$
$(466 \pm 18) - i(223 \pm 28)$	¹³ BONVICINI	07	CLEO $D^+ \rightarrow \pi^-\pi^+\pi^+$
$(472 \pm 30) - i(271 \pm 30)$	¹⁴ BUGG	07A	RVUE Compilation
$(484 \pm 17) - i(255 \pm 10)$	GARCIA-MAR..	07	RVUE Compilation
$(430) - i(325)$	¹⁵ ANISOVICH	06	RVUE Compilation
$(441 \pm 16) - i(272 \pm 9)$	¹⁶ CAPRINI	06	RVUE $\pi\pi \rightarrow \pi\pi$
$(470 \pm 50) - i(285 \pm 25)$	¹⁷ ZHOU	05	RVUE
$(541 \pm 39) - i(252 \pm 42)$	¹⁸ ABLIKIM	04A	BES2 $J/\psi \rightarrow \omega\pi^+\pi^-$
$(528 \pm 32) - i(207 \pm 23)$	¹⁹ GALLEGOS	04	RVUE Compilation
$(533 \pm 25) - i(249 \pm 25)$	²⁰ BUGG	03	RVUE
$517 - i240$	BLACK	01	RVUE $\pi\pi \rightarrow \pi\pi$
$(470 \pm 30) - i(295 \pm 20)$	¹⁶ COLANGELO	01	RVUE $\pi\pi \rightarrow \pi\pi$
$(535 \pm 14) - i(155 \pm 76)$	²¹ ISHIDA	01	$\Upsilon(3S) \rightarrow \Upsilon\pi\pi$
$610 \pm 14 - i(310 \pm 13)$	²² SUROVTSEV	01	RVUE $\pi\pi \rightarrow \pi\pi, K\bar{K}$
$(540 \pm 29) - i(193 \pm 40)$	ISHIDA	00B	$p\bar{p} \rightarrow \pi^0\pi^0\pi^0$
$445 - i235$	HANNAH	99	RVUE π scalar form factor
$(523 \pm 12) - i(259 \pm 7)$	⁹⁹ KAMINSKI	99	RVUE $\pi\pi \rightarrow \pi\pi, K\bar{K}, \sigma\sigma$
$442 - i 227$	OLLER	99	RVUE $\pi\pi \rightarrow \pi\pi, K\bar{K}$
$469 - i203$	OLLER	99B	RVUE $\pi\pi \rightarrow \pi\pi, K\bar{K}$
$445 - i221$	OLLER	99C	RVUE $\pi\pi \rightarrow \pi\pi, K\bar{K}, \eta\eta$
$420 - i 212$	LOCHER	98	RVUE $\pi\pi \rightarrow \pi\pi, K\bar{K}$
$440 - i245$	²³ DOBADO	97	RVUE Compilation
$(602 \pm 26) - i(196 \pm 27)$	²⁴ ISHIDA	97	$\pi\pi \rightarrow \pi\pi$
$(537 \pm 20) - i(250 \pm 17)$	²⁵ KAMINSKI	97B	RVUE $\pi\pi \rightarrow \pi\pi, K\bar{K}, 4\pi$
$470 - i250$	^{26,27} TORNQVIST	96	RVUE $\pi\pi \rightarrow \pi\pi, K\bar{K}, K\pi, \eta\pi$
$387 - i305$	^{27,28} JANSSEN	95	RVUE $\pi\pi \rightarrow \pi\pi, K\bar{K}$
$420 - i370$	²⁹ ACHASOV	94	RVUE $\pi\pi \rightarrow \pi\pi$
$(506 \pm 10) - i(247 \pm 3)$	KAMINSKI	94	RVUE $\pi\pi \rightarrow \pi\pi, K\bar{K}$
$370 - i356$	³⁰ ZOU	94B	RVUE $\pi\pi \rightarrow \pi\pi, K\bar{K}$
$408 - i342$	^{27,30} ZOU	93	RVUE $\pi\pi \rightarrow \pi\pi, K\bar{K}$
$470 - i208$	³¹ VANBEVEREN	86	RVUE $\pi\pi \rightarrow \pi\pi, K\bar{K}, \eta\eta, \dots$
$(750 \pm 50) - i(450 \pm 50)$	³² ESTABROOKS	79	RVUE $\pi\pi \rightarrow \pi\pi, K\bar{K}$
$(660 \pm 100) - i(320 \pm 70)$	PROTOPOP...	73	HBC $\pi\pi \rightarrow \pi\pi, K\bar{K}$
$650 - i370$	³³ BASDEVANT	72	RVUE $\pi\pi \rightarrow \pi\pi$

¹ Data driven analysis using partial-wave dispersion relations.

² S-matrix pole; 8595 events.

³ Applying the chiral unitary approach at NLO to the K_{e4} data of BATLEY 10 and $\pi N \rightarrow \pi\pi N$ data of HYAMS 73, GRAYER 74, and PROTOPOPESCU 73.

⁴ Uses the K_{e4} data of BATLEY 10c and the $\pi N \rightarrow \pi\pi N$ data of HYAMS 73, GRAYER 74, and PROTOPOPESCU 73.

⁵ Analytic continuation using Roy equations.

⁶ Analytic continuation using GKPY equations.

⁷ Using Roy equations.

⁸ Average of three variants of the analytic K-matrix model. Uses the K_{e4} data of BATLEY 08a and the $\pi N \rightarrow \pi\pi N$ data of HYAMS 73 and GRAYER 74.

⁹ Average of the analyses of three data sets in the K-matrix model. Uses the data of BATLEY 08a, HYAMS 73, and GRAYER 74, partially of COHEN 80 or ETKIN 82b.

¹⁰ From the K_{e4} data of BATLEY 08a and $\pi N \rightarrow \pi\pi N$ data of HYAMS 73.

¹¹ From the K_{e4} data of BATLEY 08a and $\pi N \rightarrow \pi\pi N$ data of PROTOPOPESCU 73, GRAYER 74, and ESTABROOKS 74.

¹² From a mean of three different $f_0(500)$ parametrizations. Uses 40k events.

¹³ From an isobar model using 2.6k events.

¹⁴ Reanalysis of ABLIKIM 04a, PISLAK 01, and HYAMS 73 data.

¹⁵ Using the N/D method.

¹⁶ From the solution of the Roy equation (ROY 71) for the isoscalar S-wave and using a phase-shift analysis of HYAMS 73 and PROTOPOPESCU 73 data.

¹⁷ Reanalysis of the data from PROTOPOPESCU 73, ESTABROOKS 74, GRAYER 74, ROSSELET 77, PISLAK 03, and AKHMETSHIN 04.

¹⁸ From a mean of six different analyses and $f_0(500)$ parameterizations.

¹⁹ Using data on $\psi(2S) \rightarrow J/\psi\pi\pi$ from BAI 00e and on $\Upsilon(nS) \rightarrow \Upsilon(mS)\pi\pi$ from BUTLER 94b and ALEXANDER 98.

²⁰ From a combined analysis of HYAMS 73, AUGUSTIN 89, AITALA 01b, and PISLAK 01.

²¹ A similar analysis (KOMADA 01) finds $(580 \pm 79) - i(190 \pm 107)$ MeV.

²² Coupled channel reanalysis of BATON 70, BENSINGER 71, BAILLON 72, HYAMS 73, HYAMS 75, ROSSELET 77, COHEN 80, and ETKIN 82b using the uniformizing variable.

²³ Using the inverse amplitude method and data of ESTABROOKS 73, GRAYER 74, and PROTOPOPESCU 73.

²⁴ Reanalysis of data from HYAMS 73, GRAYER 74, SRINIVASAN 75, and ROSSELET 77 using the interfering amplitude method.

²⁵ Average and spread of 4 variants ("up" and "down") of KAMINSKI 97B 3-channel model.

²⁶ Uses data from BEIER 72b, OCHS 73, HYAMS 73, GRAYER 74, ROSSELET 77, CASON 83, ASTON 88, and ARMSTRONG 91b. Coupled channel analysis with flavor symmetry and all light two-pseudoscalars systems.

²⁷ Demonstrates explicitly that $f_0(500)$ and $f_0(1370)$ are two different poles.

²⁸ Analysis of data from FALVARD 88.

²⁹ Analysis of data from OCHS 73, ESTABROOKS 75, ROSSELET 77, and MUKHIN 80.

³⁰ Analysis of data from OCHS 73, GRAYER 74, and ROSSELET 77.

³¹ Coupled-channel analysis using data from PROTOPOPESCU 73, HYAMS 73, HYAMS 75, GRAYER 74, ESTABROOKS 74, ESTABROOKS 75, FROGGATT 77, CORDEN 79, BISWAS 81.

³² Analysis of data from APEL 72c, GRAYER 74, CASON 76, PAWLICKI 77. Includes spread and errors of 4 solutions.

³³ Analysis of data from BATON 70, BENSINGER 71, COLTON 71, BAILLON 72, PROTOPOPESCU 73, and WALKER 67.

 $f_0(500)$ BREIT-WIGNER MASS

VALUE (MeV)	DOCUMENT ID	TECN	COMMENT
400 to 800 OUR ESTIMATE			
513 ± 32	³⁴ MURAMATSU	02	CLEO $e^+e^- \approx 10$ GeV
$478 \pm 24 \pm 17$	AITALA	01B E791	$D^+ \rightarrow \pi^-\pi^+\pi^+$
$563 \pm 58 \pm 29$	³⁵ ISHIDA	01	$\Upsilon(3S) \rightarrow \Upsilon\pi\pi$
555	³⁶ ASNER	00	CLE2 $\tau^- \rightarrow \pi^-\pi^0\pi^0\nu_\tau$
540 ± 36	ISHIDA	00B	$p\bar{p} \rightarrow \pi^0\pi^0\pi^0$
750 ± 4	ALEKSEEV	99	SPEC $1.78 \pi^-\rho_{\text{polar}} \rightarrow \pi^-\pi^+n$
744 ± 5	ALEKSEEV	98	SPEC $1.78 \pi^-\rho_{\text{polar}} \rightarrow \pi^-\pi^+n$
759 ± 5	³⁷ TROYAN	98	$5.2 n\rho \rightarrow n\rho\pi^+\pi^-$
780 ± 30	ALDE	97	GAM2 $450 p\bar{p} \rightarrow p\rho\pi^0\pi^0$
585 ± 20	³⁸ ISHIDA	97	$\pi\pi \rightarrow \pi\pi$
761 ± 12	³⁹ SVEC	96	RVUE $6-17 \pi N_{\text{polar}} \rightarrow \pi^+\pi^-N$
~ 860	^{40,41} TORNQVIST	96	RVUE $\pi\pi \rightarrow \pi\pi, K\bar{K}, K\pi, \eta\pi$
1165 ± 50	^{42,43} ANISOVICH	95	RVUE $\pi^-p \rightarrow \pi^0\pi^0n, \bar{p}p \rightarrow \pi^0\pi^0\pi^0, \pi^0\pi^0\eta, \pi^0\eta\eta$
414 ± 20	³⁹ AUGUSTIN	89	DM2

³⁴ Statistical uncertainty only.

³⁵ A similar analysis (KOMADA 01) finds 526 ± 48 MeV.

³⁶ From the best fit of the Dalitz plot.

³⁷ 6σ effect, no PWA.

³⁸ Reanalysis of data from HYAMS 73, GRAYER 74, SRINIVASAN 75, and ROSSELET 77 using the interfering amplitude method.

³⁹ Breit-Wigner fit to S-wave intensity measured in $\pi N \rightarrow \pi^-\pi^+N$ on polarized targets. The fit does not include $f_0(980)$.

⁴⁰ Uses data from ASTON 88, OCHS 73, HYAMS 73, ARMSTRONG 91b, GRAYER 74, CASON 83, ROSSELET 77, and BEIER 72b. Coupled channel analysis with flavor symmetry and all light two-pseudoscalars systems.

⁴¹ Also observed by ASNER 00 in $\tau^- \rightarrow \pi^-\pi^0\pi^0\nu_\tau$ decays.

⁴² Uses $\pi^0\pi^0$ data from ANISOVICH 94, AMSLER 94D, and ALDE 95b, $\pi^+\pi^-$ data from OCHS 73, GRAYER 74 and ROSSELET 77, and $\eta\eta$ data from ANISOVICH 94.

⁴³ The pole is on Sheet III. Demonstrates explicitly that $f_0(500)$ and $f_0(1370)$ are two different poles.

 $f_0(500)$ BREIT-WIGNER WIDTH

VALUE (MeV)	DOCUMENT ID	TECN	COMMENT
100 to 800 OUR ESTIMATE			
335 ± 67	⁴⁴ MURAMATSU	02	CLEO $e^+e^- \approx 10$ GeV
$324 \pm 42 \pm 21$	AITALA	01B E791	$D^+ \rightarrow \pi^-\pi^+\pi^+$
$372 \pm 229 \pm 95$	⁴⁵ ISHIDA	01	$\Upsilon(3S) \rightarrow \Upsilon\pi\pi$
540	⁴⁶ ASNER	00	CLE2 $\tau^- \rightarrow \pi^-\pi^0\pi^0\nu_\tau$
372 ± 80	ISHIDA	00B	$p\bar{p} \rightarrow \pi^0\pi^0\pi^0$
119 ± 13	ALEKSEEV	99	SPEC $1.78 \pi^-\rho_{\text{polar}} \rightarrow \pi^-\pi^+n$
77 ± 22	ALEKSEEV	98	SPEC $1.78 \pi^-\rho_{\text{polar}} \rightarrow \pi^-\pi^+n$

⁴⁴ We do not use the following data for averages, fits, limits, etc. ●●●

⁴⁵ We do not use the following data for averages, fits, limits, etc. ●●●

See key on page 1171

Meson Particle Listings

f_0(500)

Table listing experimental data for f_0(500) decay modes, including columns for value, document ID, technique, and comment. Includes entries like 35 ± 12, 47 TROYAN, 98, 5.2 np → npπ+π-.

Table listing experimental data for f_0(500) decay modes, including columns for value, document ID, technique, and comment. Includes entries like DAI 14A, PR D90 036004, L.-Y. Dai, M.R. Pennington.

f_0(500) DECAY MODES

Table showing decay modes and their fractions. Columns: Mode, Fraction (Γ_i/Γ). Includes ππ and γγ.

f_0(500) PARTIAL WIDTHS

Table header for partial widths with columns: Γ(γγ), VALUE (keV), DOCUMENT ID, TECN, COMMENT, Γ_2.

Main table of partial widths for f_0(500) decay modes, listing values, document IDs, techniques, and comments. Includes entries like 1.37 ± 13, DANILKIN, 21, RVUE, Compilation.

f_0(500) REFERENCES

Table of references for f_0(500) decay modes, listing author names and document IDs.

Table of references for f_0(500) decay modes, listing author names and document IDs. Includes entries like DAI 14A, ALBALADEJO 12, GARCIA-MAR... 11A.

Meson Particle Listings

 $\rho(770)$ $\rho(770)$

$$I^G(J^{PC}) = 1^+(1^{--})$$

 $\rho(770)$ T-MATRIX POLE \sqrt{s}

Note that $\Gamma = -2 \operatorname{Im}(\sqrt{s})$.

VALUE (MeV)	DOCUMENT ID	TECN	COMMENT
(761-765) - i (71-74) OUR ESTIMATE			
$(763.7^{+1.7}_{-1.5}) - i (73.2^{+1.0}_{-1.1})$	1 GARCIA-MAR..11	RVUE	Compilation
$(754 \pm 18) - i (74 \pm 10)$	2 PELAEZ 04A	RVUE	$\pi\pi \rightarrow \pi\pi$
$(762.4 \pm 1.8) - i (72.6 \pm 1.4)$	COLANGELO 01	RVUE	$\pi\pi \rightarrow \pi\pi$

¹ Reanalysis of the K_{e4} data of BATLEY 10c and the $\pi N \rightarrow \pi\pi N$ data of HYAMS 73, GRAYER 74, and PROTOPOESCU 73 using GPKY equations.

² Reanalysis of data from PROTOPOESCU 73, ESTABROOKS 74, GRAYER 74, and COHEN 80 in the unitarized ChPT model.

 $\rho(770)$ MASS

We no longer list S-wave Breit-Wigner fits, or data with high combinatorial background.

NEUTRAL ONLY, e^+e^-

VALUE (MeV)	EVTS	DOCUMENT ID	TECN	COMMENT
775.26 ± 0.23 OUR AVERAGE				
775.3 ± 0.5 ± 0.6		1 ACHASOV 21	SND	$e^+e^- \rightarrow \pi^+\pi^-$
775.02 ± 0.35		2 LEES 12G	BABR	$e^+e^- \rightarrow \pi^+\pi^-\gamma$
775.97 ± 0.46 ± 0.70	900k	3 AKHMETSHIN 07		$e^+e^- \rightarrow \pi^+\pi^-$
774.6 ± 0.4 ± 0.5	800k	4.5 ACHASOV 06	SND	$e^+e^- \rightarrow \pi^+\pi^-$
775.65 ± 0.64 ± 0.50	114k	6.7 AKHMETSHIN 04	CMD2	$e^+e^- \rightarrow \pi^+\pi^-$
775.9 ± 0.5 ± 0.5	1.98M	8 ALOISIO 03	KLOE	$1.02 e^+e^- \rightarrow \pi^+\pi^-\pi^0$
775.8 ± 0.9 ± 2.0	500k	8 ACHASOV 02	SND	$1.02 e^+e^- \rightarrow \pi^+\pi^-\pi^0$
775.9 ± 1.1		9 BARKOV 85	OLYA	$e^+e^- \rightarrow \pi^+\pi^-$
••• We do not use the following data for averages, fits, limits, etc. •••				
763.49 ± 0.53		10 BARTOS 17	RVUE	$e^+e^- \rightarrow \pi^+\pi^-$
758.23 ± 0.46		11 BARTOS 17A	RVUE	$e^+e^- \rightarrow \pi^+\pi^-$
775.8 ± 0.5 ± 0.3	1.98M	12 ALOISIO 03	KLOE	$1.02 e^+e^- \rightarrow \pi^+\pi^-\pi^0$
775.9 ± 0.6 ± 0.5	1.98M	13 ALOISIO 03	KLOE	$1.02 e^+e^- \rightarrow \pi^+\pi^-\pi^0$
775.0 ± 0.6 ± 1.1	500k	14 ACHASOV 02	SND	$1.02 e^+e^- \rightarrow \pi^+\pi^-\pi^0$
775.1 ± 0.7 ± 5.3		15 BENAYOUN 98	RVUE	$e^+e^- \rightarrow \pi^+\pi^-, \mu^+\mu^-$
770.5 ± 1.9 ± 5.1		16 GARDNER 98	RVUE	$0.28-0.92 e^+e^- \rightarrow \pi^+\pi^-$
764.1 ± 0.7		17 O'CONNELL 97	RVUE	$e^+e^- \rightarrow \pi^+\pi^-$
757.5 ± 1.5		18 BERNICHA 94	RVUE	$e^+e^- \rightarrow \pi^+\pi^-$
768 ± 1		19 GESHKEN... 89	RVUE	$e^+e^- \rightarrow \pi^+\pi^-$

¹ From a fit of the cross section in the energy range $0.525 < \sqrt{s} < 0.883$ GeV parameterized by the sum of the Breit-Wigner amplitudes for the $\rho(770)$, ω and $\rho(1450)$ resonances.

² Using the GOUNARIS 68 parametrization with the complex phase of the ρ - ω interference and leaving the masses and widths of the $\rho(1450)$, $\rho(1700)$, and $\rho(2150)$ resonances as free parameters of the fit.

³ A combined fit of AKHMETSHIN 07, AULCHENKO 06, and AULCHENKO 05.

⁴ Supersedes ACHASOV 05A.

⁵ A fit of the SND data from 400 to 1000 MeV using parameters of the $\rho(1450)$ and $\rho(1700)$ from a fit of the data of BARKOV 85, BISELLO 89 and ANDERSON 00A.

⁶ Using the GOUNARIS 68 parametrization with the complex phase of the ρ - ω interference.

⁷ Update of AKHMETSHIN 02.

⁸ Assuming $m_{\rho^+} = m_{\rho^-}$, $\Gamma_{\rho^+} = \Gamma_{\rho^-}$.

⁹ From the GOUNARIS 68 parametrization of the pion form factor.

¹⁰ Applies the Unitary & Analytic Model of the pion electromagnetic form factor of DUBNICKA 10 to analyze the data of LEES 12G and ABLIKIM 16c.

¹¹ Applies the Unitary & Analytic Model of the pion electromagnetic form factor of DUBNICKA 10 to analyze the data of ACHASOV 06, AKHMETSHIN 07, AUBERT 09As, and AMBROSINO 11A.

¹² Assuming $m_{\rho^+} = m_{\rho^-} = m_{\rho^0}$, $\Gamma_{\rho^+} = \Gamma_{\rho^-} = \Gamma_{\rho^0}$.

¹³ Without limitations on masses and widths.

¹⁴ Assuming $m_{\rho^0} = m_{\rho^\pm}$, $g_{\rho^0\pi\pi} = g_{\rho^\pm\pi\pi}$.

¹⁵ Using the data of BARKOV 85 in the hidden local symmetry model.

¹⁶ From the fit to $e^+e^- \rightarrow \pi^+\pi^-$ data from the compilations of HEYN 81 and BARKOV 85, including the GOUNARIS 68 parametrization of the pion form factor.

¹⁷ A fit of BARKOV 85 data assuming the direct $\omega\pi\pi$ coupling.

¹⁸ Applying the S-matrix formalism to the BARKOV 85 data.

¹⁹ Includes BARKOV 85 data. Model-dependent width definition.

CHARGED ONLY, τ DECAYS and e^+e^-

VALUE (MeV)	EVTS	DOCUMENT ID	TECN	CHG	COMMENT
775.11 ± 0.34 OUR AVERAGE					
774.6 ± 0.2 ± 0.5	5.4M	1,2 FUJIKAWA 08	BELL	±	$\tau^- \rightarrow \pi^- \pi^0 \nu_\tau$
775.5 ± 0.7		2,3 SCHAEEL 05c	ALEP		$\tau^- \rightarrow \pi^- \pi^0 \nu_\tau$
775.5 ± 0.5 ± 0.4	1.98M	4 ALOISIO 03	KLOE		$1.02 e^+e^- \rightarrow \pi^+\pi^-\pi^0$
775.1 ± 1.1 ± 0.5	87k	5,6 ANDERSON 00A	CLE2		$\tau^- \rightarrow \pi^- \pi^0 \nu_\tau$

••• We do not use the following data for averages, fits, limits, etc. •••

761.60 ± 0.95		7 BARTOS 17A	RVUE		$\tau^- \rightarrow \pi^- \pi^0 \nu_\tau$
774.8 ± 0.6 ± 0.4	1.98M	8 ALOISIO 03	KLOE	-	$1.02 e^+e^- \rightarrow \pi^+\pi^-\pi^0$
776.3 ± 0.6 ± 0.7	1.98M	8 ALOISIO 03	KLOE	+	$1.02 e^+e^- \rightarrow \pi^+\pi^-\pi^0$
773.9 ± 2.0	± 0.3 -1.0	9 SANZ-CILLERO03	RVUE		$\tau^- \rightarrow \pi^- \pi^0 \nu_\tau$
774.5 ± 0.7 ± 1.5	500k	4 ACHASOV 02	SND	±	$1.02 e^+e^- \rightarrow \pi^+\pi^-\pi^0$
775.1 ± 0.5		10 PICH 01	RVUE		$\tau^- \rightarrow \pi^- \pi^0 \nu_\tau$

¹ $|F_\pi(0)|^2$ fixed to 1.

² From the GOUNARIS 68 parametrization of the pion form factor.

³ The error combines statistical and systematic uncertainties. Supersedes BARATE 97M.

⁴ Assuming $m_{\rho^+} = m_{\rho^-}$, $\Gamma_{\rho^+} = \Gamma_{\rho^-}$.

⁵ $\rho(1700)$ mass and width fixed at 1700 MeV and 235 MeV respectively.

⁶ From the GOUNARIS 68 parametrization of the pion form factor. The second error is a model error taking into account different parametrizations of the pion form factor.

⁷ Applies the Unitary & Analytic Model of the pion electromagnetic form factor of DUBNICKA 10 to analyze the data of FUJIKAWA 08.

⁸ Without limitations on masses and widths.

⁹ Using the data of BARATE 97M and the effective chiral Lagrangian.

¹⁰ From a fit of the model-independent parameterization of the pion form factor to the data of BARATE 97M.

MIXED CHARGES, OTHER REACTIONS

VALUE (MeV)	EVTS	DOCUMENT ID	TECN	CHG	COMMENT
763.0 ± 0.3 ± 1.2					
600k		1 ABELE 99E	CBAR	0 ± 0	$0.0 \bar{p}p \rightarrow \pi^+\pi^-\pi^0$

¹ Assuming the equality of ρ^+ and ρ^- masses and widths.

CHARGED ONLY, HADROPRODUCED

VALUE (MeV)	EVTS	DOCUMENT ID	TECN	CHG	COMMENT
766.5 ± 1.1 OUR AVERAGE					
763.7 ± 3.2		ABELE 97	CBAR		$\bar{p}n \rightarrow \pi^- \pi^0 \pi^0$
768 ± 9		AGUILAR... 91	EHS		400 pp
767 ± 3	2935	1 CAPRARO 87	SPEC	-	200 π^- Cu $\rightarrow \pi^- \pi^0$ Cu
761 ± 5	967	1 CAPRARO 87	SPEC	-	200 π^- Pb $\rightarrow \pi^- \pi^0$ Pb
771 ± 4		HUSTON 86	SPEC	+	202 $\pi^+A \rightarrow \pi^+\pi^0A$
766 ± 7	6500	2 BYERLY 73	OSP	-	5 π^-p
766.8 ± 1.5	9650	3 PISUT 68	RVUE	-	1.7-3.2 π^-p , $t < 10$
767 ± 6	900	1 EISNER 67	HBC	-	4.2 π^-p , $t < 10$

¹ Mass errors enlarged by us to Γ/\sqrt{N} ; see the note with the $K^*(892)$ mass.

² Phase shift analysis. Systematic errors added corresponding to spread of different fits.

³ From fit of 3-parameter relativistic P-wave Breit-Wigner to total mass distribution. Includes BATON 68, MILLER 67B, ALFF-STEINBERGER 66, HAGOPIAN 66, HAGOPIAN 66B, JACOBS 66B, JAMES 66, WEST 66, BLIEDEN 65 and CARMONY 64.

NEUTRAL ONLY, PHOTOPRODUCED

VALUE (MeV)	EVTS	DOCUMENT ID	TECN	COMMENT
769.2 ± 0.9 OUR AVERAGE				
770.8 ± 1.3	± 2.3 -2.4	900k	ANDREEV 20	H1 $ep \rightarrow e\pi^+\pi^-p$
771 ± 2	± 2 -1	63.5k	1 ABRAMOWICZ12	ZEUS $ep \rightarrow e\pi^+\pi^-p$
770 ± 2	± 1	79k	2 BREITWEG 98B	ZEUS 50-100 γp
767.6 ± 2.7			BARTALUCCI 78	CNTR $\gamma p \rightarrow e^+e^-p$
775 ± 5			GLADDING 73	CNTR 2.9-4.7 γp
767 ± 4	1930		BALLAM 72	HBC 2.8 γp
770 ± 4	2430		BALLAM 72	HBC 4.7 γp
765 ± 10			ALVENSLEB... 70	CNTR γA , $t < 0.01$
767.7 ± 1.9	140k		BIGGS 70	CNTR $< 4.1 \gamma C \rightarrow \pi^+\pi^-C$
765 ± 5	4000		ASBURY 67B	CNTR $\gamma + Pb$

••• We do not use the following data for averages, fits, limits, etc. •••

771 ± 2 79k ³ BREITWEG 98B ZEUS 50-100 γp

¹ Using the KUHN 90 parametrization of the pion form factor, neglecting ρ - ω interference.

² From the parametrization according to SOEDING 66.

³ From the parametrization according to ROSS 66.

NEUTRAL ONLY, OTHER REACTIONS

VALUE (MeV)	EVTS	DOCUMENT ID	TECN	COMMENT
769.0 ± 0.9 OUR AVERAGE				
765 ± 6		BERTIN 97c	OBLX	0.0 $\bar{p}p \rightarrow \pi^+\pi^-\pi^0$
773 ± 1.6		WEIDENAUER 93	ASTE	$\bar{p}p \rightarrow \pi^+\pi^-\omega$
762.6 ± 2.6		AGUILAR... 91	EHS	400 pp
770 ± 2		1 HEYN 81	RVUE	Pion form factor
768 ± 4		2,3 BOHACIK 80	RVUE	
769 ± 3		4 WICKLUND 78	ASPK	3,4,6 $\pi^\pm N$
768 ± 1	76k	DEUTSCH... 76	HBC	16 π^+p
767 ± 4	4100	ENGLER 74	DBC	6 $\pi^+n \rightarrow \pi^+\pi^-p$
775 ± 4	32k	2 PROTOPOP... 73	HBC	7.1 π^+p , $t < 0.4$
764 ± 3	6.8k	5 RATCLIFF 72	ASPK	15 π^-p , $t < 0.3$
774 ± 3	1.7k	REYNOLDS 69	HBC	2.26 π^-p
769.2 ± 1.5	13.3k	6 PISUT 68	RVUE	1.7-3.2 π^-p , $t < 10$

See key on page 1171

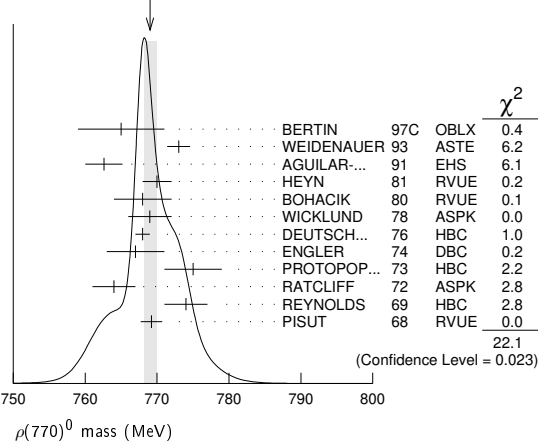
Meson Particle Listings

ρ(770)

Table of experimental data for ρ(770) mass, including columns for value, error, EVTS, DOCUMENT ID, TECN, and COMMENT. Includes entries from BES3, RVUE, CBAR, E665, MIRA, ASPK, LANG, ESTABROOKS, JACOBS, and HYAMS.

- Footnotes 1-15 providing details on data selection, fit methods (Breit-Wigner, relativistic Breit-Wigner), and systematic error treatments.

WEIGHTED AVERAGE 769.0±0.9 (Error scaled by 1.4)

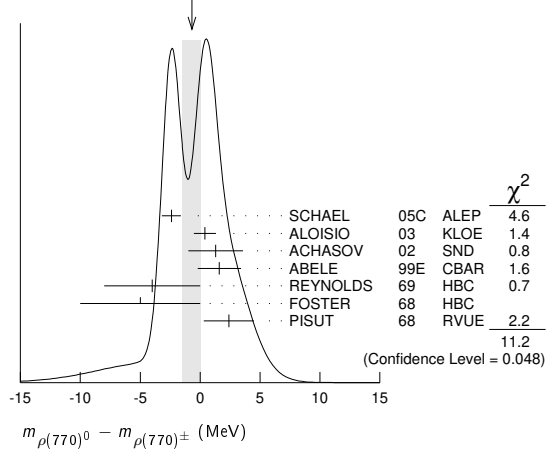


m_ρ(770)0 - m_ρ(770)±

Table of mass differences between ρ(770)0 and ρ(770)±, including columns for VALUE (MeV), EVTS, DOCUMENT ID, TECN, CHG, and COMMENT. Includes entries from SCHAEEL, ALOISIO, ACHASOV, ABELE, REYNOLDS, FOSTER, PISUT, and BARTOS.

- Footnotes 1-5 providing details on data selection, fit methods, and systematic error treatments for the mass difference data.

WEIGHTED AVERAGE -0.7±0.8 (Error scaled by 1.5)



m_ρ(770)+ - m_ρ(770)-

Table of mass differences between ρ(770)+ and ρ(770)-, including columns for VALUE (MeV), EVTS, DOCUMENT ID, TECN, and COMMENT. Includes entry from ALOISIO.

ρ(770) RANGE PARAMETER

The range parameter R enters an energy-dependent correction to the width, of the form (1 + q_r^2 R^2) / (1 + q^2 R^2), where q is the momentum of one of the pions in the ππ rest system. At resonance, q = q_r.

Table of ρ(770) range parameter values, including columns for VALUE (GeV^-1), DOCUMENT ID, TECN, CHG, and COMMENT. Includes entry from CHABAUD.

ρ(770) WIDTH

We no longer list S-wave Breit-Wigner fits, or data with high combinatorial background.

NEUTRAL ONLY, e+e-

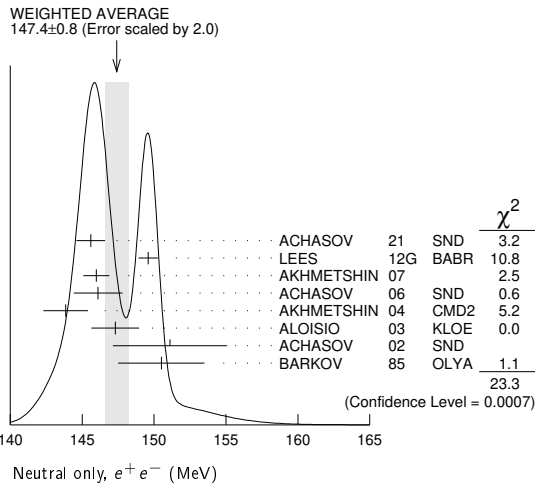
Table of ρ(770) width values for neutral decays, including columns for VALUE (MeV), EVTS, DOCUMENT ID, TECN, and COMMENT. Includes entries from ACHASOV, LEES, AKHMETSHIN, ALOISIO, BARKOV, BARTOS, and GARDNER.

- Footnotes 1-6 providing details on data selection, fit methods, and systematic error treatments for the width data.

Meson Particle Listings

$\rho(770)$

- ⁷ From a fit in the energy range 0.61 to 0.96 GeV. Update of AKHMETSHIN 02.
- ⁸ Assuming $m_{\rho^+} = m_{\rho^-}$, $\Gamma_{\rho^+} = \Gamma_{\rho^-}$.
- ⁹ From the GOUNARIS 68 parametrization of the pion form factor.
- ¹⁰ Applies the Unitary & Analytic Model of the pion electromagnetic form factor of DUBNICKA 10 to analyze the data of LEES 12G and ABLIKIM 16c.
- ¹¹ Applies the Unitary & Analytic Model of the pion electromagnetic form factor of DUBNICKA 10 to analyze the data of ACHASOV 06, AKHMETSHIN 07, AUBERT 09As, and AMBROSINO 11A.
- ¹² Assuming $m_{\rho^+} = m_{\rho^-} = m_{\rho^0}$, $\Gamma_{\rho^+} = \Gamma_{\rho^-} = \Gamma_{\rho^0}$.
- ¹³ Without limitations on masses and widths.
- ¹⁴ Assuming $m_{\rho^0} = m_{\rho^{\pm}}$, $g_{\rho^0\pi\pi} = g_{\rho^{\pm}\pi\pi}$.
- ¹⁵ Using the data of BARKOV 85 in the hidden local symmetry model.
- ¹⁶ From the fit to $e^+e^- \rightarrow \pi^+\pi^-$ data from the compilations of HEYN 81 and BARKOV 85, including the GOUNARIS 68 parametrization of the pion form factor.
- ¹⁷ A fit of BARKOV 85 data assuming the direct $\omega\pi\pi$ coupling.
- ¹⁸ Applying the S-matrix formalism to the BARKOV 85 data.
- ¹⁹ Includes BARKOV 85 data. Model-dependent width definition.



CHARGED ONLY, τ DECAYS and e^+e^-

VALUE (MeV)	EVTS	DOCUMENT ID	TECN	CHG	COMMENT
149.1 ± 0.8	OUR FIT				
149.1 ± 0.8	OUR AVERAGE				
148.1 ± 0.4 ± 1.7	5.4M	^{1,2} FUJIKAWA	08	BELL ±	$\tau^- \rightarrow \pi^- \pi^0 \nu_\tau$
149.0 ± 1.2		^{2,3} SCHAELE	05C	ALEP	$\tau^- \rightarrow \pi^- \pi^0 \nu_\tau$
149.9 ± 2.3 ± 2.0	500k	⁴ ACHASOV	02	SND ±	$1.02 e^+ e^- \rightarrow \pi^+ \pi^- \pi^0$
150.4 ± 1.4 ± 1.4	87k	^{5,6} ANDERSON	00A	CLE2	$\tau^- \rightarrow \pi^- \pi^0 \nu_\tau$
••• We do not use the following data for averages, fits, limits, etc. •••					
139.90 ± 0.46		⁷ BARTOS	17A	RVUE	$\tau^- \rightarrow \pi^- \pi^0 \nu_\tau$
143.7 ± 1.3 ± 1.2	1.98M	⁴ ALOISIO	03	KLOE ±	$1.02 e^+ e^- \rightarrow \pi^+ \pi^- \pi^0$
142.9 ± 1.3 ± 1.4	1.98M	⁸ ALOISIO	03	KLOE -	$1.02 e^+ e^- \rightarrow \pi^+ \pi^- \pi^0$
144.7 ± 1.4 ± 1.2	1.98M	⁸ ALOISIO	03	KLOE +	$1.02 e^+ e^- \rightarrow \pi^+ \pi^- \pi^0$
150.2 ± 2.0 ± 0.7	-1.6	⁹ SANZ-CILLERO03	RVUE		$\tau^- \rightarrow \pi^- \pi^0 \nu_\tau$
150.9 ± 2.2 ± 2.0	500k	¹⁰ ACHASOV	02	SND	$1.02 e^+ e^- \rightarrow \pi^+ \pi^- \pi^0$

- ¹ $|F_\pi(0)|^2$ fixed to 1.
- ² From the GOUNARIS 68 parametrization of the pion form factor.
- ³ The error combines statistical and systematic uncertainties. Supersedes BARATE 97M.
- ⁴ Assuming $m_{\rho^+} = m_{\rho^-}$, $\Gamma_{\rho^+} = \Gamma_{\rho^-}$.
- ⁵ $\rho(1700)$ mass and width fixed at 1700 MeV and 235 MeV respectively.
- ⁶ From the GOUNARIS 68 parametrization of the pion form factor. The second error is a model error taking into account different parametrizations of the pion form factor.
- ⁷ Applies the Unitary & Analytic Model of the pion electromagnetic form factor of DUBNICKA 10 to analyze the data of FUJIKAWA 08.
- ⁸ Without limitations on masses and widths.
- ⁹ Using the data of BARATE 97M and the effective chiral Lagrangian.
- ¹⁰ Assuming $m_{\rho^0} = m_{\rho^{\pm}}$, $g_{\rho^0\pi\pi} = g_{\rho^{\pm}\pi\pi}$.

MIXED CHARGES, OTHER REACTIONS

VALUE (MeV)	EVTS	DOCUMENT ID	TECN	CHG	COMMENT
149.5 ± 1.3	600k	¹ ABELE	99E	CBAR 0±	$0.0 \bar{p}p \rightarrow \pi^+ \pi^- \pi^0$

¹ Assuming the equality of ρ^+ and ρ^- masses and widths.

CHARGED ONLY, HADROPRODUCED

VALUE (MeV)	EVTS	DOCUMENT ID	TECN	CHG	COMMENT
150.2 ± 2.4	OUR FIT				
150.2 ± 2.4	OUR AVERAGE				
152.8 ± 4.3		ABELE	97	CBAR	$\bar{p}n \rightarrow \pi^- \pi^0 \pi^0$
155 ± 11	2.9k	¹ CAPRARO	87	SPEC -	$200 \pi^- \text{Cu} \rightarrow \pi^- \pi^0 \text{Cu}$

154 ± 20	967	¹ CAPRARO	87	SPEC -	$200 \pi^- \text{Pb} \rightarrow \pi^- \pi^0 \text{Pb}$
150 ± 5		HUSTON	86	SPEC +	$202 \pi^+ \text{A} \rightarrow \pi^+ \pi^0 \text{A}$
146 ± 12	6.5k	² BYERLY	73	OSP K -	$5 \pi^- p$
148.2 ± 4.1	9.6k	³ PISUT	68	RVUE -	$1.7-3.2 \pi^- p, t < 10$
146 ± 13	900	EISNER	67	HBC -	$4.2 \pi^- p, t < 10$
••• We do not use the following data for averages, fits, limits, etc. •••					
137.0 ± 0.4		⁴ ABLIKIM	17	BES3	$J/\psi \rightarrow \gamma 3\pi$

¹ Width errors enlarged by us to $4\Gamma/\sqrt{N}$; see the note with the $K^*(892)$ mass.
² Phase shift analysis. Systematic errors added corresponding to spread of different fits.
³ From fit of 3-parameter relativistic P -wave Breit-Wigner to total mass distribution. Includes BATON 68, MILLER 67b, ALFF-STEINBERGER 66, HAGOPIAN 66, HAGOPIAN 66b, JACOBS 66b, JAMES 66, WEST 66, BLIEDEN 65 and CARMONY 64.
⁴ S-matrix pole at a fixed ρ meson mass of 775.49 MeV.

NEUTRAL ONLY, PHOTOPRODUCED

VALUE (MeV)	EVTS	DOCUMENT ID	TECN	COMMENT	
151.5 ± 1.9	OUR AVERAGE				
151.3 ± 2.2 ± 1.6	900k	ANDREEV	20	H1	$e p \rightarrow e \pi^+ \pi^- p$
155 ± 5 ± 2	63.5k	¹ ABRAMOWICZ12	ZEUS	$e p \rightarrow e \pi^+ \pi^- p$	
146 ± 3 ± 13	79k	² BREITWEG	98B	ZEUS	$50-100 \gamma p$
150.9 ± 3.0		BARTALUCCI	78	CNTR	$\gamma p \rightarrow e^+ e^- p$
••• We do not use the following data for averages, fits, limits, etc. •••					
138 ± 3	79k	³ BREITWEG	98B	ZEUS	$50-100 \gamma p$
147 ± 11		GLADDING	73	CNTR	$2.9-4.7 \gamma p$
155 ± 12	2430	BALLAM	72	HBC	$4.7 \gamma p$
145 ± 13	1930	BALLAM	72	HBC	$2.8 \gamma p$
140 ± 5		ALVENSLEB...	70	CNTR	$\gamma A, t < 0.01$
146.1 ± 2.9	140k	BIGGS	70	CNTR	$< 4.1 \gamma C \rightarrow \pi^+ \pi^- C$
160 ± 10		LANZEROTTI	68	CNTR	γp
130 ± 5	4000	ASBURY	67B	CNTR	$\gamma + \text{Pb}$

¹ Using the KUHN 90 parametrization of the pion form factor, neglecting $\rho-\omega$ interference.
² From the parametrization according to SOEDING 66.
³ From the parametrization according to ROSS 66.

NEUTRAL ONLY, OTHER REACTIONS

VALUE (MeV)	EVTS	DOCUMENT ID	TECN	COMMENT	
150.9 ± 1.7	OUR AVERAGE	Error includes scale factor of 1.1.			
122 ± 20		BERTIN	97C	OBLX	$0.0 \bar{p}p \rightarrow \pi^+ \pi^- \pi^0$
145.7 ± 5.3		WEIDENAUER	93	ASTE	$\bar{p}p \rightarrow \pi^+ \pi^- \omega$
144.9 ± 3.7		DUBNICKA	89	RVUE	π form factor
148 ± 6		^{1,2} BOHACIK	80	RVUE	
152 ± 9		³ WICKLUND	78	ASP K	$3,4,6 \pi^\pm p N$
154 ± 2	76k	DEUTSCH...	76	HBC	$16 \pi^+ p$
157 ± 8	6.8k	⁴ RATCLIFF	72	ASP K	$15 \pi^- p, t < 0.3$
143 ± 8	1.7k	REYNOLDS	69	HBC	$2.26 \pi^- p$
••• We do not use the following data for averages, fits, limits, etc. •••					
150.85 ± 0.55 ± 0.67	970k	⁵ ABLIKIM	18C	BES3	$\eta'(958) \rightarrow \gamma \pi^+ \pi^-$
150.18 ± 0.55 ± 0.65	970k	⁶ ABLIKIM	18C	BES3	$\eta'(958) \rightarrow \gamma \pi^+ \pi^-$
147.0 ± 2.5	600k	⁷ ABELE	99E	CBAR	$0.0 \bar{p}p \rightarrow \pi^+ \pi^- \pi^0$
146 ± 3	4.9k	⁸ ADAMS	97	E665	$470 \mu p \rightarrow \mu X B$
160.0 ± 4.1	-4.0	⁹ CHABAUD	83	ASP K	$17 \pi^- p$ polarized
155 ± 1		¹⁰ HEYN	81	RVUE	π form factor
148.0 ± 1.3		^{1,2} LANG	79	RVUE	
146 ± 14	4.1k	ENGLER	74	DBC	$6 \pi^+ n \rightarrow \pi^+ \pi^- p$
143 ± 13		² ESTABROOKS	74	RVUE	$17 \pi^- p \rightarrow \pi^+ \pi^- n$
160 ± 10	32k	¹ PROTOPOP...	73	HBC	$7.1 \pi^+ p, t < 0.4$
145 ± 12	2.2k	^{3,11} HYAMS	68	OSP K	$11.2 \pi^- p$
163 ± 15	13.3k	¹² PISUT	68	RVUE	$1.7-3.2 \pi^- p, t < 10$

- ¹ From pole extrapolation.
- ² From phase shift analysis of GRAYER 74 data.
- ³ Width errors enlarged by us to $4\Gamma/\sqrt{N}$; see the note with the $K^*(892)$ mass.
- ⁴ Published values contain misprints. Corrected by private communication RATCLIFF 74.
- ⁵ From a fit to $\pi^+ \pi^-$ mass using $\rho(770)$ (parametrized with the Gounaris-Sakurai approach), $\omega(782)$, and box anomaly components.
- ⁶ From a fit to $\pi^+ \pi^-$ mass using $\rho(770)$ (parametrized with the Gounaris-Sakurai approach), $\omega(782)$, and $\rho(1450)$ components.
- ⁷ Using relativistic Breit-Wigner and taking into account $\rho-\omega$ interference.
- ⁸ Systematic errors not evaluated.
- ⁹ From fit of 3-parameter relativistic Breit-Wigner to helicity-zero part of P -wave intensity. CHABAUD 83 includes data of GRAYER 74.
- ¹⁰ HEYN 81 includes all spacelike and timelike F_π values until 1978.
- ¹¹ Of HYAMS 68 six parametrizations this is theoretically soundest. MR
- ¹² Includes MALAMUD 69, ARMENISE 68, BACON 67, HUWE 67, MILLER 67b, ALFF-STEINBERGER 66, HAGOPIAN 66, HAGOPIAN 66b, JACOBS 66b, JAMES 66, WEST 66, GOLDBABER 64, ABOLINS 63.

$\Gamma_{\rho(770)^0} - \Gamma_{\rho(770)^\pm}$

VALUE (MeV)	EVTS	DOCUMENT ID	TECN	COMMENT	
0.3 ± 1.3	OUR AVERAGE	Error includes scale factor of 1.4.			
-0.2 ± 1.0		¹ SCHAELE	05C	ALEP	$\tau^- \rightarrow \pi^- \pi^0 \nu_\tau$
3.6 ± 1.8 ± 1.7	1.98M	² ALOISIO	03	KLOE	$1.02 e^+ e^- \rightarrow \pi^+ \pi^- \pi^0$

See key on page 1171

Meson Particle Listings

$\rho(770)$

••• We do not use the following data for averages, fits, limits, etc. •••
 4.66 ± 0.85 ³BARTOS 17A RVUE $e^+e^- \rightarrow \pi^+\pi^-, \tau^- \rightarrow \pi^-\pi^0\nu_\tau$

¹ From the combined fit of the τ^- data from ANDERSON 00A and SCHAEEL 05C and e^+e^- data from the compilation of BARKOV 85, AKHMETSHIN 04, and ALOISIO 05. Supersedes BARATE 97M.
² Assuming $m_{\rho^+} = m_{\rho^-}, \Gamma_{\rho^+} = \Gamma_{\rho^-}$.
³ Applies the Unitary & Analytic Model of the pion electromagnetic form factor of DUBNICKA 10 to analyze the data of ACHASOV 06, AKHMETSHIN 07, AUBERT 09AS, AMBROSINO 11A, and FUJIKAWA 08.

VALUE	EVTS	DOCUMENT ID	TECN	COMMENT
1.8 ± 2.0 ± 0.5	1.98M	¹ ALOISIO 03	KLOE	1.02 $e^+e^- \rightarrow \pi^+\pi^-\pi^0$

¹ Without limitations on masses and widths.

$\rho(770)$ DECAY MODES

Mode	Fraction (Γ_i/Γ)	Scale factor/ Confidence level
$\Gamma_1 \pi\pi$	~ 100	%
$\rho(770)^\pm$ decays		
$\Gamma_2 \pi^\pm\pi^0$	~ 100	%
$\Gamma_3 \pi^\pm\gamma$	(4.5 ± 0.5) × 10 ⁻⁴	S=2.2
$\Gamma_4 \pi^\pm\eta$	< 6	× 10 ⁻³ CL=84%
$\Gamma_5 \pi^\pm\pi^+\pi^-\pi^0$	< 2.0	× 10 ⁻³ CL=84%
$\rho(770)^0$ decays		
$\Gamma_6 \pi^+\pi^-$	~ 100	%
$\Gamma_7 \pi^+\pi^-\gamma$	(9.9 ± 1.6) × 10 ⁻³	
$\Gamma_8 \pi^0\gamma$	(4.7 ± 0.8) × 10 ⁻⁴	S=1.7
$\Gamma_9 \eta\gamma$	(3.00 ± 0.21) × 10 ⁻⁴	
$\Gamma_{10} \pi^0\pi^0\gamma$	(4.5 ± 0.8) × 10 ⁻⁵	
$\Gamma_{11} \mu^+\mu^-$	[a] (4.55 ± 0.28) × 10 ⁻⁵	
$\Gamma_{12} e^+e^-$	[a] (4.72 ± 0.05) × 10 ⁻⁵	
$\Gamma_{13} \pi^+\pi^-\pi^0$	(1.01 ^{+0.54} _{-0.36} ± 0.34) × 10 ⁻⁴	
$\Gamma_{14} \pi^+\pi^-\pi^+\pi^-$	(1.8 ± 0.9) × 10 ⁻⁵	
$\Gamma_{15} \pi^+\pi^-\pi^0\pi^0$	(1.6 ± 0.8) × 10 ⁻⁵	
$\Gamma_{16} \pi^0e^+e^-$	< 1.2	× 10 ⁻⁵ CL=90%
$\Gamma_{17} \eta e^+e^-$		

[a] The $\omega\rho$ interference is then due to $\omega\rho$ mixing only, and is expected to be small. If $e\mu$ universality holds, $\Gamma(\rho^0 \rightarrow \mu^+\mu^-) = \Gamma(\rho^0 \rightarrow e^+e^-) \times 0.99785$.

CONSTRAINED FIT INFORMATION

An overall fit to the total width and a partial width uses 10 measurements and one constraint to determine 3 parameters. The overall fit has a $\chi^2 = 10.7$ for 8 degrees of freedom.

The following *off-diagonal* array elements are the correlation coefficients $\langle \delta p_i \delta p_j \rangle / (\delta p_i \delta p_j)$, in percent, from the fit to parameters p_i , including the branching fractions, $x_i \equiv \Gamma_i/\Gamma_{\text{total}}$. The fit constrains the x_i whose labels appear in this array to sum to one.

x_3	-100	
Γ	15	-15
	x_2	x_3

Mode	Rate (MeV)	Scale factor
$\Gamma_2 \pi^\pm\pi^0$	150.2 ± 2.4	
$\Gamma_3 \pi^\pm\gamma$	0.068 ± 0.007	2.3

CONSTRAINED FIT INFORMATION

An overall fit to the total width, a partial width, and 7 branching ratios uses 21 measurements and one constraint to determine 9 parameters. The overall fit has a $\chi^2 = 9.5$ for 13 degrees of freedom.

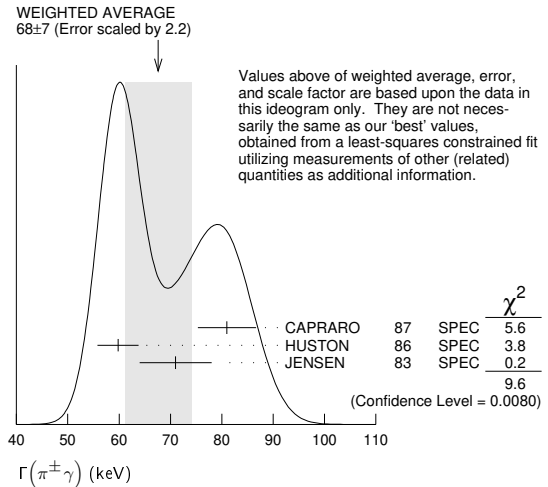
The following *off-diagonal* array elements are the correlation coefficients $\langle \delta p_i \delta p_j \rangle / (\delta p_i \delta p_j)$, in percent, from the fit to parameters p_i , including the branching fractions, $x_i \equiv \Gamma_i/\Gamma_{\text{total}}$. The fit constrains the x_i whose labels appear in this array to sum to one.

x_7	-100							
x_8	-5	0						
x_9	-1	0	1					
x_{10}	-1	0	0	0				
x_{11}	2	-3	0	0	0			
x_{12}	0	0	-6	-9	0	0		
x_{14}	-1	0	0	0	0	0	0	
Γ	0	0	3	5	0	0	-54	
	x_6	x_7	x_8	x_9	x_{10}	x_{11}	x_{12}	x_{14}

Mode	Rate (MeV)	Scale factor
$\Gamma_6 \pi^+\pi^-$	147.5 ± 0.9	
$\Gamma_7 \pi^+\pi^-\gamma$	1.48 ± 0.24	
$\Gamma_8 \pi^0\gamma$	0.070 ± 0.012	1.7
$\Gamma_9 \eta\gamma$	0.0447 ± 0.0032	
$\Gamma_{10} \pi^0\pi^0\gamma$	0.0066 ± 0.0012	
$\Gamma_{11} \mu^+\mu^-$	[a] 0.0068 ± 0.0004	
$\Gamma_{12} e^+e^-$	[a] 0.00704 ± 0.00006	
$\Gamma_{14} \pi^+\pi^-\pi^+\pi^-$	0.0027 ± 0.0014	

$\rho(770)$ PARTIAL WIDTHS

VALUE (keV)	DOCUMENT ID	TECN	CHG	COMMENT
68 ± 7 OUR FIT				Error includes scale factor of 2.3.
68 ± 7 OUR AVERAGE				Error includes scale factor of 2.2. See the ideogram below.
81 ± 4 ± 4	CAPRARO 87	SPEC	-	200 $\pi^-A \rightarrow \pi^-\pi^0A$
59.8 ± 4.0	HUSTON 86	SPEC	+	202 $\pi^+A \rightarrow \pi^+\pi^0A$
71 ± 7	JENSEN 83	SPEC	-	156-260 $\pi^-A \rightarrow \pi^-\pi^0A$



VALUE (keV)	EVTS	DOCUMENT ID	TECN	COMMENT
77 ± 17 ± 11	36500	¹ ACHASOV 03	SND	0.60-0.97 $e^+e^- \rightarrow \pi^0\gamma$
121 ± 31		DOLINSKY 89	ND	$e^+e^- \rightarrow \pi^0\gamma$

••• We do not use the following data for averages, fits, limits, etc. •••
¹ Using $\Gamma_{\text{total}} = 147.9 \pm 1.3$ MeV and $B(\rho \rightarrow \pi^0\gamma)$ from ACHASOV 03.

VALUE (keV)	DOCUMENT ID	TECN	COMMENT
62 ± 17	¹ DOLINSKY 89	ND	$e^+e^- \rightarrow \eta\gamma$

¹ Solution corresponding to constructive $\omega\rho$ interference.

VALUE (keV)	EVTS	DOCUMENT ID	TECN	COMMENT
7.04 ± 0.06 OUR FIT				
7.04 ± 0.06 OUR AVERAGE				

7.048 ± 0.057 ± 0.050	900k	¹ AKHMETSHIN 07		$e^+e^- \rightarrow \pi^+\pi^-$
7.06 ± 0.11 ± 0.05	114k	^{2,3} AKHMETSHIN 04	CMD2	$e^+e^- \rightarrow \pi^+\pi^-$
6.77 ± 0.10 ± 0.30		BARKOV 85	OLYA	$e^+e^- \rightarrow \pi^+\pi^-$
••• We do not use the following data for averages, fits, limits, etc. •••				
7.12 ± 0.02 ± 0.11	800k	⁴ ACHASOV 06	SND	$e^+e^- \rightarrow \pi^+\pi^-$
6.3 ± 0.1		⁵ BENAYOUN 98	RVUE	$e^+e^- \rightarrow \pi^+\pi^-, \mu^+\mu^-$

Meson Particle Listings

$\rho(770)$

- ¹ A combined fit of AKHMETSHIN 07, AULCHENKO 06, and AULCHENKO 05.
- ² Using the GOUNARIS 68 parametrization with the complex phase of the ρ - ω interference.
- ³ From a fit in the energy range 0.61 to 0.96 GeV. Update of AKHMETSHIN 02.
- ⁴ Supersedes ACHASOV 05A.
- ⁵ Using the data of BARKOV 85 in the hidden local symmetry model.

$\Gamma(\pi^+\pi^-\pi^+\pi^-)$ Γ_{14}				
VALUE (keV)	EVTS	DOCUMENT ID	TECN	COMMENT
••• We do not use the following data for averages, fits, limits, etc. •••				
$2.8 \pm 1.4 \pm 0.5$	153	AKHMETSHIN 00	CMD2	$0.6-0.97 e^+e^- \rightarrow \pi^+\pi^-\pi^+\pi^-$

$\rho(770) \Gamma(e^+e^-)\Gamma(i)/\Gamma^2(\text{total})$

$\Gamma(e^+e^-)/\Gamma_{\text{total}} \times \Gamma(\pi^+\pi^-)/\Gamma_{\text{total}}$ $\Gamma_{12}/\Gamma \times \Gamma_6/\Gamma$				
VALUE (units 10^{-5})	EVTS	DOCUMENT ID	TECN	COMMENT
4.89 ± 0.04 OUR AVERAGE				
$4.889 \pm 0.015 \pm 0.039$		¹ ACHASOV 21	SND	$e^+e^- \rightarrow \pi^+\pi^-$
$4.876 \pm 0.023 \pm 0.064$	800k	^{2,3} ACHASOV 06	SND	$e^+e^- \rightarrow \pi^+\pi^-$
••• We do not use the following data for averages, fits, limits, etc. •••				
4.72 ± 0.02		⁴ BENAYOUN 10	RVUE	$0.4-1.05 e^+e^-$

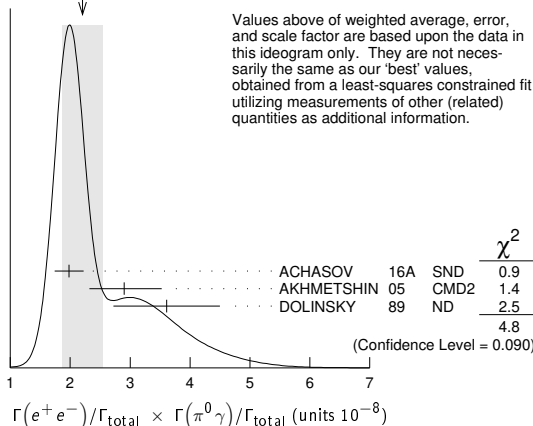
- ¹ From a fit of the cross section in the energy range $0.525 < \sqrt{s} < 0.883$ GeV parameterized by the sum of the Breit-Wigner amplitudes for the $\rho(770)$, ω and $\rho(1450)$ resonances.
- ² Supersedes ACHASOV 05A.
- ³ A fit of the SND data from 400 to 1000 MeV using parameters of the $\rho(1450)$ and $\rho(1700)$ from a fit of the data of BARKOV 85, BISELLO 89 and ANDERSON 00A.
- ⁴ A simultaneous fit of $e^+e^- \rightarrow \pi^+\pi^-$, $\pi^+\pi^-\pi^0$, $\pi^0\gamma$, $\eta\gamma$ data.

$\Gamma(e^+e^-)/\Gamma_{\text{total}} \times \Gamma(\eta\gamma)/\Gamma_{\text{total}}$ $\Gamma_{12}/\Gamma \times \Gamma_9/\Gamma$				
VALUE (units 10^{-8})	EVTS	DOCUMENT ID	TECN	COMMENT
1.42 ± 0.10 OUR FIT				
1.45 ± 0.12 OUR AVERAGE				
$1.32 \pm 0.14 \pm 0.08$	33k	¹ ACHASOV 07B	SND	$0.6-1.38 e^+e^- \rightarrow \eta\gamma$
$1.50 \pm 0.65 \pm 0.09$	17.4k	² AKHMETSHIN 05	CMD2	$0.60-1.38 e^+e^- \rightarrow \eta\gamma$
$1.61 \pm 0.20 \pm 0.11$	23k	^{3,4} AKHMETSHIN 01B	CMD2	$e^+e^- \rightarrow \eta\gamma$
1.85 ± 0.49		⁵ DOLINSKY 89	ND	$e^+e^- \rightarrow \eta\gamma$
••• We do not use the following data for averages, fits, limits, etc. •••				
1.05 ± 0.02		⁶ BENAYOUN 10	RVUE	$0.4-1.05 e^+e^-$

- ¹ From a combined fit of $\sigma(e^+e^- \rightarrow \eta\gamma)$ with $\eta \rightarrow 3\pi^0$ and $\eta \rightarrow \pi^+\pi^-\pi^0$, and fixing $B(\eta \rightarrow 3\pi^0) / B(\eta \rightarrow \pi^+\pi^-\pi^0) = 1.44 \pm 0.04$. Recalculated by us from the cross section at the peak. Supersedes ACHASOV 00D and ACHASOV 06A.
- ² From the $\eta \rightarrow 2\gamma$ decay and using $B(\eta \rightarrow \gamma\gamma) = 39.43 \pm 0.26\%$.
- ³ From the $\eta \rightarrow 3\pi^0$ decay and using $B(\eta \rightarrow 3\pi^0) = (32.24 \pm 0.29) \times 10^{-2}$.
- ⁴ The combined fit from 600 to 1380 MeV taking into account $\rho(770)$, $\omega(782)$, $\phi(1020)$, and $\rho(1450)$ (mass and width fixed at 1450 MeV and 310 MeV respectively).
- ⁵ Recalculated by us from the cross section in the peak.
- ⁶ A simultaneous fit of $e^+e^- \rightarrow \pi^+\pi^-$, $\pi^+\pi^-\pi^0$, $\pi^0\gamma$, $\eta\gamma$ data.

$\Gamma(e^+e^-)/\Gamma_{\text{total}} \times \Gamma(\pi^0\gamma)/\Gamma_{\text{total}}$ $\Gamma_{12}/\Gamma \times \Gamma_8/\Gamma$				
VALUE (units 10^{-8})	EVTS	DOCUMENT ID	TECN	COMMENT
2.2 ± 0.4 OUR FIT Error includes scale factor of 1.7.				
2.21 ± 0.34 OUR AVERAGE Error includes scale factor of 1.6. See the ideogram below.				
$1.98 \pm 0.22 \pm 0.10$		¹ ACHASOV 16A	SND	$0.60-1.38 e^+e^- \rightarrow \pi^0\gamma$
$2.90 \pm 0.60 \pm 0.18$	18k	AKHMETSHIN 05	CMD2	$0.60-1.38 e^+e^- \rightarrow \pi^0\gamma$
$3.61 \pm 0.74 \pm 0.49$	10k	² DOLINSKY 89	ND	$e^+e^- \rightarrow \pi^0\gamma$
••• We do not use the following data for averages, fits, limits, etc. •••				
1.875 ± 0.026		³ BENAYOUN 10	RVUE	$0.4-1.05 e^+e^-$
$2.37 \pm 0.53 \pm 0.33$	36k	⁴ ACHASOV 03	SND	$0.60-0.97 e^+e^- \rightarrow \pi^0\gamma$

WEIGHTED AVERAGE
2.21±0.34 (Error scaled by 1.6)



- ¹ From the VMD model with the $\rho(770)$, $\omega(782)$, $\phi(1020)$ resonances, and an additional resonance describing the total contribution of the $\rho(1450)$ and $\omega(1420)$ states. Supersedes ACHASOV 03.

- ² Recalculated by us from the cross section in the peak.
- ³ A simultaneous fit of $e^+e^- \rightarrow \pi^+\pi^-$, $\pi^+\pi^-\pi^0$, $\pi^0\gamma$, $\eta\gamma$ data.
- ⁴ Using $\sigma_{\phi \rightarrow \pi^0\gamma}$ from ACHASOV 00 and $m_\rho = 775.97$ MeV in the model with the energy-independent phase of ρ - ω interference equal to $(-10.2 \pm 7.0)^\circ$.

$\Gamma(e^+e^-)/\Gamma_{\text{total}} \times \Gamma(\pi^+\pi^-\pi^0)/\Gamma_{\text{total}}$ $\Gamma_{12}/\Gamma \times \Gamma_{13}/\Gamma$				
VALUE (units 10^{-9})	EVTS	DOCUMENT ID	TECN	COMMENT
••• We do not use the following data for averages, fits, limits, etc. •••				
0.903 ± 0.076		¹ BENAYOUN 10	RVUE	$0.4-1.05 e^+e^-$
$4.58 \pm 2.46 \pm 1.56$	1.2M	² ACHASOV 03D	RVUE	$0.44-2.00 e^+e^- \rightarrow \pi^+\pi^-\pi^0$

- ¹ A simultaneous fit of $e^+e^- \rightarrow \pi^+\pi^-$, $\pi^+\pi^-\pi^0$, $\pi^0\gamma$, $\eta\gamma$ data.
- ² Statistical significance is less than 3σ .

$\rho(770)$ BRANCHING RATIOS

$\Gamma(\pi^\pm\eta)/\Gamma(\pi\pi)$ Γ_4/Γ_1				
VALUE (units 10^{-4})	CL%	DOCUMENT ID	TECN	CHG COMMENT
••• We do not use the following data for averages, fits, limits, etc. •••				
<60	84	FERBEL 66	HBC	$\pm \pi^\pm p$ above 2.5

$\Gamma(\pi^\pm\pi^+\pi^-\pi^0)/\Gamma(\pi\pi)$ Γ_5/Γ_1				
VALUE (units 10^{-4})	CL%	DOCUMENT ID	TECN	CHG COMMENT
••• We do not use the following data for averages, fits, limits, etc. •••				
<20	84	FERBEL 66	HBC	$\pm \pi^\pm p$ above 2.5
35 ± 40		JAMES 66	HBC	$+ 2.1 \pi^+ p$

$\Gamma(\pi^+\pi^-\gamma)/\Gamma_{\text{total}}$ Γ_7/Γ				
VALUE	CL%	DOCUMENT ID	TECN	COMMENT
0.0099 ± 0.0016 OUR FIT				
••• We do not use the following data for averages, fits, limits, etc. •••				
0.0111 ± 0.0014		¹ DOLINSKY 91	ND	$e^+e^- \rightarrow \pi^+\pi^-\gamma$
<0.005	90	² VASSERMAN 88	ND	$e^+e^- \rightarrow \pi^+\pi^-\gamma$
		³ VASSERMAN 88	ND	$e^+e^- \rightarrow \pi^+\pi^-\gamma$

- ¹ Bremsstrahlung from a decay pion and for photon energy above 50 MeV.
- ² Superseded by DOLINSKY 91.
- ³ Structure radiation due to quark rearrangement in the decay.

$\Gamma(\pi^0\gamma)/\Gamma_{\text{total}}$ Γ_8/Γ				
VALUE (units 10^{-4})	EVTS	DOCUMENT ID	TECN	COMMENT
••• We do not use the following data for averages, fits, limits, etc. •••				
4.20 ± 0.52		¹ ACHASOV 16A	SND	$0.60-1.38 e^+e^- \rightarrow \pi^0\gamma$
$6.21 \pm 1.28 \pm 0.39$	18k	^{2,3} AKHMETSHIN 05	CMD2	$0.60-1.38 e^+e^- \rightarrow \pi^0\gamma$
$5.22 \pm 1.17 \pm 0.75$	36k	^{3,4} ACHASOV 03	SND	$0.60-0.97 e^+e^- \rightarrow \pi^0\gamma$
6.8 ± 1.7		⁵ BENAYOUN 96	RVUE	$0.54-1.04 e^+e^- \rightarrow \pi^0\gamma$
7.9 ± 2.0		³ DOLINSKY 89	ND	$e^+e^- \rightarrow \pi^0\gamma$

- ¹ Using $B(\rho \rightarrow e^+e^-)$ from PDG 15. Supersedes ACHASOV 03.
- ² Using $B(\rho \rightarrow e^+e^-) = (4.67 \pm 0.09) \times 10^{-5}$.
- ³ Not independent of the corresponding $\Gamma(e^+e^-) \times \Gamma(\pi^0\gamma)/\Gamma_{\text{total}}^2$.
- ⁴ Using $B(\rho \rightarrow e^+e^-) = (4.54 \pm 0.10) \times 10^{-5}$.
- ⁵ Reanalysis of DRUZHININ 84, DOLINSKY 89, and DOLINSKY 91 taking into account a triangle anomaly contribution.

$\Gamma(\eta\gamma)/\Gamma_{\text{total}}$ Γ_9/Γ				
VALUE (units 10^{-4})	EVTS	DOCUMENT ID	TECN	CHG COMMENT
3.00 ± 0.21 OUR FIT				
2.90 ± 0.32 OUR AVERAGE				
$2.79 \pm 0.34 \pm 0.03$	33k	¹ ACHASOV 07B	SND	$0.6-1.38 e^+e^- \rightarrow \eta\gamma$
3.6 ± 0.9		² ANDREWS 77	CNTR 0	$6.7-10 \gamma\text{Cu}$
••• We do not use the following data for averages, fits, limits, etc. •••				
$3.21 \pm 1.39 \pm 0.20$	17.4k	^{3,4} AKHMETSHIN 05	CMD2	$0.60-1.38 e^+e^- \rightarrow \eta\gamma$
$3.39 \pm 0.42 \pm 0.23$		^{2,5,6} AKHMETSHIN 01B	CMD2	$e^+e^- \rightarrow \eta\gamma$
$1.9 \pm 0.6 \pm 0.8$		⁷ BENAYOUN 96	RVUE	$0.54-1.04 e^+e^- \rightarrow \eta\gamma$
4.0 ± 1.1		^{2,4} DOLINSKY 89	ND	$e^+e^- \rightarrow \eta\gamma$

- ¹ ACHASOV 07B reports $[\Gamma(\rho(770) \rightarrow \eta\gamma)/\Gamma_{\text{total}}] \times [B(\rho(770) \rightarrow e^+e^-)] = (1.32 \pm 0.14 \pm 0.08) \times 10^{-8}$ which we divide by our best value $B(\rho(770) \rightarrow e^+e^-) = (4.72 \pm 0.05) \times 10^{-5}$. Our first error is their experiment's error and our second error is the systematic error from using our best value. Supersedes ACHASOV 00D and ACHASOV 06A.
- ² Solution corresponding to constructive ω - ρ interference.
- ³ Using $B(\rho \rightarrow e^+e^-) = (4.67 \pm 0.09) \times 10^{-5}$ and $B(\eta \rightarrow \gamma\gamma) = 39.43 \pm 0.26\%$.
- ⁴ Not independent of the corresponding $\Gamma(e^+e^-) \times \Gamma(\eta\gamma)/\Gamma_{\text{total}}^2$.
- ⁵ The combined fit from 600 to 1380 MeV taking into account $\rho(770)$, $\omega(782)$, $\phi(1020)$, and $\rho(1450)$ (mass and width fixed at 1450 MeV and 310 MeV respectively).
- ⁶ Using $B(\rho \rightarrow e^+e^-) = (4.75 \pm 0.10) \times 10^{-5}$ from AKHMETSHIN 02 and $B(\eta \rightarrow 3\pi^0) = (32.24 \pm 0.29) \times 10^{-2}$.
- ⁷ Reanalysis of DRUZHININ 84, DOLINSKY 89, and DOLINSKY 91 taking into account a triangle anomaly contribution. Constructive ρ - ω interference solution.

See key on page 1171

Meson Particle Listings

ρ(770)

Table with 5 columns: Γ(π⁰π⁰γ)/Γtotal, VALUE (units 10⁻⁵), EVTS, DOCUMENT ID, TECN, COMMENT, Γ10/Γ

4.5 ± 0.9 OUR AVERAGE

Table with 5 columns: VALUE (units 10⁻⁵), EVTS, DOCUMENT ID, TECN, COMMENT, Γ10/Γ

1 This branching ratio includes the conventional VMD mechanism ρ → ωπ⁰, ω → π⁰γ, and the new decay mode ρ → f₀(500)γ, f₀(500) → π⁰π⁰ with a branching ratio (2.0 ± 1.1 ± 0.3) × 10⁻⁵ differing from zero by 2.0 standard deviations.

2 This branching ratio includes the conventional VMD mechanism ρ → ωπ⁰, ω → π⁰γ and the new decay mode ρ → f₀(500)γ, f₀(500) → π⁰π⁰ with a branching ratio (1.9 ± 0.9 ± 0.8 ± 0.4) × 10⁻⁵ differing from zero by 2.4 standard deviations. Supersedes ACHASOV 00G.

3 Superseded by ACHASOV 02F.

Table with 4 columns: Γ(μ⁺μ⁻)/Γ(π⁺π⁻), VALUE (units 10⁻⁵), DOCUMENT ID, TECN, COMMENT, Γ11/Γ6

Table with 5 columns: VALUE (units 10⁻⁵), DOCUMENT ID, TECN, COMMENT, Γ11/Γ6

- 1 Possibly large ρ-ω interference leads us to increase the minus error.
2 Result contains 11 ± 11% correction using SU(3) for central value. The error on the correction takes account of possible ρ-ω interference and the upper limit agrees with the upper limit of ω → μ⁺μ⁻ from this experiment.
3 But he even enlarges his error to take residual ω contamination into account. Since his value is high, seems the other experiments also can't have too many ω's. But maybe Hyams has additional μ's from ρ → ππ, decaying π's.
4 HYAMS 67's mass resolution is 20 MeV. The ω region was excluded.

Table with 4 columns: Γ(e⁺e⁻)/Γ(ππ), VALUE (units 10⁻⁴), DOCUMENT ID, TECN, COMMENT, Γ12/Γ1

- 1 The ρ' contribution is not taken into account.
2 Barkov excludes Auslender and Benakass for large statistical and systematic errors.

Table with 5 columns: Γ(π⁺π⁻π⁰)/Γtotal, VALUE (units 10⁻⁴), CL%, EVTS, DOCUMENT ID, TECN, COMMENT, Γ13/Γ

- 1 From the cross section for e⁺e⁻ → π⁺π⁻π⁰ with contributions from ρ(770), ω(782), φ(1020), ω(1420), and ω(1650). Statistical evidence is more than 6 σ.
2 Statistical significance is less than 3σ.

Table with 5 columns: Γ(π⁺π⁻π⁰)/Γ(ππ), VALUE, CL%, DOCUMENT ID, TECN, CHG, COMMENT, Γ13/Γ1

- 1 Model dependent, assumes l = 1, 2, or 3 for the 3π system.

Table with 5 columns: Γ(π⁺π⁻π⁺π⁻)/Γtotal, VALUE (units 10⁻⁵), CL%, EVTS, DOCUMENT ID, TECN, COMMENT, Γ14/Γ

- 1 Model dependent, assumes l = 1, 2, or 3 for the 3π system.

Table with 5 columns: Γ(π⁺π⁻π⁺π⁻)/Γ(ππ), VALUE (units 10⁻⁴), CL%, DOCUMENT ID, TECN, CHG, COMMENT, Γ14/Γ1

- 1 Model dependent, assumes l = 1, 2, or 3 for the 3π system.

Table with 5 columns: Γ(π⁺π⁻π⁰π⁰)/Γtotal, VALUE (units 10⁻⁵), CL%, DOCUMENT ID, TECN, COMMENT, Γ15/Γ

- 1 Assuming no interference between the ρ and ω contributions.

Table with 5 columns: Γ(π⁰e⁺e⁻)/Γtotal, VALUE (units 10⁻⁵), CL%, DOCUMENT ID, TECN, COMMENT, Γ16/Γ

- 1 Assuming no interference between the ρ and ω contributions.

Table with 5 columns: Γ(ηe⁺e⁻)/Γtotal, VALUE (units 10⁻⁵), CL%, DOCUMENT ID, TECN, COMMENT, Γ17/Γ

ρ(770) REFERENCES

ACHASOV 21 JHEP 2101 113 M.N. Achasov et al. (SND Collab.)
LEES 21B PR D104 112003 J.P. Lees et al. (BABAR Collab.)
ANDREEV 20 EPJ C80 1189 V. Andreev et al. (H1 Collab.)
ABLIKIM 19C PRL 120 242003 M. Ablikim et al. (BESIII Collab.)
ABLIKIM 17 PRL 118 012001 M. Ablikim et al. (BESIII Collab.)
BARTOS 17 PR D96 113004 E. Bartos et al.
BARTOS 17A JUMP A32 1750154 E. Bartos et al.
ABLIKIM 16C PL B753 629 M. Ablikim et al. (BESIII Collab.)
ACHASOV 16A PR D93 092001 M.N. Achasov et al. (SND Collab.)
PDG 15 RPP 2015 at pdg.lbl.gov (PDG Collab.)
ABRAMOWICZ 12 EPJ C72 1869 H. Abramowicz et al. (ZEUS Collab.)
LEES 12A PR D86 032013 J.P. Lees et al. (BABAR Collab.)
AMBROSINO 11G PL B700 102 F. Ambrosino et al. (KLOE Collab.)
GARCIA-MAR... 11 PRL 107 072001 R. Garcia-Martin et al. (MADR, CRAC)
BATLEY 10C EPJ C70 635 J.R. Batley et al. (CERN NA48/2 Collab.)
BENAYOUN 10 EPJ C65 211 M. Benayoun et al.
DUBNICKA 10 APS 60 1 S. Dubnicka, A.Z. Dubnickova
ACHASOV 09A JETP 109 379 M.N. Achasov et al. (SND Collab.)
AUBERT 09AS PRL 103 231801 B. Aubert et al. (BABAR Collab.)
ACHASOV 08 JETP 107 61 M.N. Achasov et al. (SND Collab.)
FUJIKAWA 08 PR D78 072006 M. Fujikawa et al. (BELLE Collab.)
ACHASOV 07B PR D76 077101 M.N. Achasov et al. (SND Collab.)
AKHMETSHIN 07 PL B648 28 R.R. Akhmetshin et al. (Novosibirsk CMD-2 Collab.)
ACHASOV 06 JETP 103 380 M.N. Achasov et al. (Novosibirsk SND Collab.)
ACHASOV 06A PR D74 014016 M.N. Achasov et al. (SND Collab.)
AULCHENKO 06 JETPL 84 413 V.M. Aulchenko et al. (Novosibirsk CMD-2 Collab.)
ACHASOV 05A JETP 101 1053 M.N. Achasov et al. (Novosibirsk SND Collab.)
AKHMETSHIN 05 PL B605 26 R.R. Akhmetshin et al. (Novosibirsk CMD-2 Collab.)
AKHMETSHIN 05A PL B613 29 R.R. Akhmetshin et al. (Novosibirsk CMD-2 Collab.)
ALOISIO 05 PL B606 12 A. Aloisio et al. (KLOE Collab.)
AULCHENKO 05 JETPL 82 743 V.M. Aulchenko et al. (Novosibirsk CMD-2 Collab.)
SCHAEF 05C PRPL 421 191 S. Schaefer et al. (ALEPH Collab.)
AKHMETSHIN 04 PL B578 285 R.R. Akhmetshin et al. (Novosibirsk CMD-2 Collab.)
AKHMETSHIN 04B PL B580 119 R.R. Akhmetshin et al. (Novosibirsk CMD-2 Collab.)
PELAEZ 04A MPL A19 2879 J.R. Pelaez (MADU)
ACHASOV 03 PL B559 171 M.N. Achasov et al. (Novosibirsk SND Collab.)
ACHASOV 03D PR D68 052006 M.N. Achasov et al. (Novosibirsk SND Collab.)
ALOISIO 03 PL B561 55 A. Aloisio et al. (KLOE Collab.)
SANZ-CILLERO 03 EPJ C27 587 J.J. Sanz-Cillero, A. Pich
ACHASOV 02 PR D65 032002 M.N. Achasov et al. (Novosibirsk SND Collab.)
ACHASOV 02F PL B537 201 M.N. Achasov et al. (Novosibirsk SND Collab.)
AKHMETSHIN 02 PL B527 161 R.R. Akhmetshin et al. (Novosibirsk CMD-2 Collab.)
AKHMETSHIN 01B PL B509 217 R.R. Akhmetshin et al. (Novosibirsk CMD-2 Collab.)
COLANGELO 01 NP B603 125 G. Colangelo, J. Gasser, H. Leutwyler
PICH 01 PR D63 093005 A. Pich, J. Portelles
ACHASOV 00 EPJ C12 25 M.N. Achasov et al. (Novosibirsk SND Collab.)
ACHASOV 00D JETPL 72 282 M.N. Achasov et al. (Novosibirsk SND Collab.)
ACHASOV 00G JETPL 71 355 M.N. Achasov et al. (Novosibirsk SND Collab.)
AKHMETSHIN 00 PL B475 190 R.R. Akhmetshin et al. (Novosibirsk CMD-2 Collab.)
ANDERSON 00A PR D61 112002 S. Anderson et al. (CLEO Collab.)
ABELE 99E PL B469 270 A. Abele et al. (Crystal Barrel Collab.)
BENAYOUN 98 EPJ C2 269 M. Benayoun et al. (IPNP, NOVO, ADL+)
BREITWEG 98B EPJ C2 247 J. Breitweg et al. (ZEUS Collab.)
GARDNER 98 PR D57 2716 S. Gardner, H.B. O'Connell
Also PR D62 019903 (err.) S. Gardner, H.B. O'Connell
ABELE 97 PL B391 191 A. Abele et al. (Crystal Barrel Collab.)
ADAMS 97 ZPHY C74 237 M.R. Adams et al. (E665 Collab.)
BARATE 97M ZPHY C76 15 R. Barate et al. (ALEPH Collab.)
BERTIN 97C PL B408 476 A. Bertin et al. (OBELIX Collab.)
BOGOLYUB... 97 PAN 60 46 M.Y. Bogolyubsky et al. (MOSU, SERP)
O'CONNELL 97 NP A623 559 H.B. O'Connell et al. (ADLD)
BENAYOUN 96 ZPHY C72 221 M. Benayoun et al. (IPNP, NOVO)
BERNICHIA 94 PR D50 4454 A. Bernichia, G. Lopez Castro, J. Pestieau (LOUV+)
WEIDENAUER 93 ZPHY C59 387 P. Weidenauser et al. (ASTERIX Collab.)
AGUILAR... 91 ZPHY C50 405 M. Aguilar-Benitez et al. (LEBC-EHS Collab.)
DOLINSKY 91 PRPL 202 99 S.I. Dolinsky et al. (NOVO)
KUHJ 90 ZPHY C48 445 J.H. Kuhn et al. (MFM)
ANTIPOV 89 ZPHY C42 185 Y.M. Antipov et al. (SERP, JINR, BGM+)
BISELLO 89 PL B220 321 D. Bisello et al. (DM2 Collab.)
DOLINSKY 89 ZPHY C42 511 S.I. Dolinsky et al. (NOVO)
DUBNICKA 89 JP G15 1349 S. Dubnicka et al. (JINR, SLOV)
GESHKEN... 89 ZPHY C45 351 B.V. Geshkenbein (ITEP)
KURDADZE 88 JETPL 47 512 L.M. Kurdadze et al. (NOVO)
VASSERMAN 88 SJNP 47 1035 I.B. Vasserman et al. (NOVO)
VASSERMAN 88B SJNP 48 480 I.B. Vasserman et al. (NOVO)
Translated from YAF 47 432.
Translated from YAF 47 1638.
Translated from YAF 48 753.

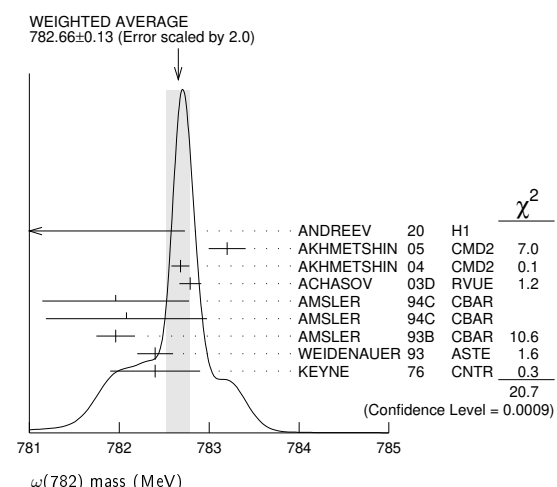
Meson Particle Listings

$\rho(770)$, $\omega(782)$

NAME	CD	REF	STATUS	EXPERIMENT	MODE
AULCHENKO	87C	IFP 87-90	Preprint	V.M. Aulchenko et al.	(NOVO)
CAPRARO	87	NP B288 659		L. Capraro et al.	(CLER, FRAS, MILA+)
BRAMON	86	PL B173 97		A. Bramon, J. Casulleras	(BARC)
HUSTON	86	PR D33 3199		J. Huston et al.	(ROCH, FNAL, MINN)
KURDADZE	86	JETPL 43 643		L.M. Kurdadze et al.	(NOVO)
		Translated from ZETFP 43 497			
BARKOV	85	NP B256 365		L.M. Barkov et al.	(NOVO)
DRUZHININ	84	PL 144B 136		V.P. Druzhinin et al.	(NOVO)
CHABAUD	83	NP B223 1		V. Chabaud et al.	(CERN, CRAC, MPIM)
JENSEN	83	PR D27 26		T. Jensen et al.	(ROCH, FNAL, MINN)
HEYN	81	ZPHY C7 169		M.F. Heyn, C.B. Lang	(GRAZ)
BOHACIK	80	PR D21 1342		J. Bohacik, H. Kuhnelt	(SLOW, WIEN)
COHEN	80	PR D22 2595		D. Cohen et al.	(ANL)
LANG	79	PR D19 956		C.B. Lang, A. Mas-Parada	(ANL)
BARTALUCCI	78	NC 44A 587		S. Bartalucci et al.	(DESY, FRAS)
WICKLUND	78	PR D17 1197		A.B. Wicklund et al.	(ANL)
ANDREWS	77	PRL 38 198		D.E. Andrews et al.	(ROCH)
DEUTSCH...	76	NP B103 426		M. Deuschmann et al.	(AACH3, BERL, BONN+)
ENGLER	74	PR D10 2070		A. Engler et al.	(CMU, CASE)
ESTABROOKS	74	NP B79 301		P.C. Estabrooks, A.D. Martin	(DURH)
GRAYER	74	NP B75 189		G. Grayer et al.	(CERN, MPIM)
RATCLIFF	74	Private Comm.			
BYERLY	73	PR D7 637		W.L. Byerly et al.	(MICH)
GLADDING	73	PR D8 3721		G.E. Gladding et al.	(HARV)
HYAMS	73	NP B64 134		B.D. Hyams et al.	(CERN, MPIM)
PROTOPO...	73	PR D7 1279		S.D. Protopopescu et al.	(LBL)
BALLAM	72	PR D5 545		J. Ballam et al.	(SLAC, LBL, TUFTS)
BENAKSAS	72	PL 39B 289		D. Benaksas et al.	(ORSAY)
JACOBS	72	PR D6 1291		L.D. Jacobs	(SACL)
RATCLIFF	72	PR 38B 345		B.W. Ratcliff et al.	(SLAC)
ABRAMS	71	PR D4 653		G.S. Abrams et al.	(LBL)
ALVENSLEB...	70	PRL 24 786		H. Alvensleben et al.	(DESY)
BIGGS	70	PRL 24 1197		P.J. Biggs et al.	(DARE)
ERBE	69	PR 188 2060		R. Erbe et al.	(German Bubble Chamber Collab.)
MALAMUD	69	Argonne Conf. 93		E.I. Malamud, P.E. Schlein	(UCLA)
REYNOLDS	69	PR 184 1424		B.G. Reynolds et al.	(FSU)
ROTHWELL	69	PRL 23 1521		P.L. Rothwell et al.	(NEAS)
WEHMANN	69	PR 178 2095		A.A. Wehmann et al.	(HARV, CASE, SLAC+)
ARMENISE	68	NC 54A 999		N. Armenise et al.	(BARI, BGNA, FIRZ+)
BATON	68	PR 176 1574		J.P. Baton, G. Laurens	(SACL)
CHUNG	68	PR 165 1491		S.U. Chung et al.	(LRL)
FOSTER	68	NP B6 107		M. Foster et al.	(CERN, CDEF)
GOUNARIS	68	PRL 21 244		G.J. Gounaris, J.J. Sakurai	
HUSON	68	PL 28B 208		R. Huson et al.	(ORSAY, MILA, UCLA)
HYAMS	68	NP B7 1		B.D. Hyams et al.	(CERN, MPIM)
LANZEROTTI	68	PR 166 1365		L.J. Lanzerotti et al.	(HARV)
PISUT	68	NP B6 325		J. Pisut, M. Roos	(CERN)
ASBURY	67B	PRL 19 865		J.G. Asbury et al.	(DESY, COLU)
BACON	67	PR 157 1263		T.C. Bacon et al.	(BNL)
EISNER	67	PR 164 1699		R.L. Eisner et al.	(PURD)
HUWE	67	PL 24B 252		D.O. Huwe et al.	(COLU)
HYAMS	67	PL 24B 534		B.D. Hyams et al.	(CERN, MPIM)
MILLER	67B	PR 153 1423		D.H. Miller et al.	(PURD)
ALFF...	66	PR 145 1072		C. Alff-Steinberger et al.	(COLU, RUTG)
FERBEL	66	PL 21 111		T. Ferbel	(ROCH)
HAGOPIAN	66	PR 145 1128		V. Hagopian et al.	(PENN, SACL)
HAGOPIAN	66B	PR 152 1183		V. Hagopian, Y.L. Pan	(PENN, LRL)
JACOBS	66B	UCRL 16877		L.D. Jacobs	(LRL)
JAMES	66	PR 142 896		F.E. James, H.L. Kraybill	(YALE, BNL)
ROSS	66	PR 149 1172		M. Ross, L. Stodolsky	
SOEDING	66	PL B19 702		P. Soeding	(WIS C)
WEST	66	PR 149 1089		E. West et al.	(WIS C)
BLIEDEN	65	PL 19 444		H.R. Blieden et al.	(CERN MMS Collab.)
CARMONY	64	PRL 12 254		D.D. Carmony et al.	(UCB)
GOLDBERGER	64	PRL 12 336		G. Goldhaber et al.	(LRL, UCBC)
ABOLINS	63	PRL 11 381		M.A. Abolins et al.	(UCSD)

VALUE	EVTS	DOCUMENT ID	TECN	COMMENT
781.0 ± 0.6	510	BIZZARRI 71	HBC	0.0 $\rho\bar{p} \rightarrow K_1 K_1 \omega$
783.7 ± 1.0	3583	12 COYNE 71	HBC	3.7 $\pi^+ p \rightarrow \rho \pi^+ \pi^+ \pi^- \pi^0$
784.1 ± 1.2	750	ABRAMOVI... 70	HBC	3.9 $\pi^- p$
783.2 ± 1.6	13 BIGGS 70B	CNTR	<4.1 $\gamma C \rightarrow \pi^+ \pi^- C$	
782.4 ± 0.5	2400	BIZZARRI 69	HBC	0.0 $\bar{p} p$

- Update of AKHMETSHIN 00c.
- From the combined fit of ANTONELLI 92, ACHASOV 01e, ACHASOV 02e, and ACHASOV 03d data on the $\pi^+ \pi^- \pi^0$ and ANTONELLI 92 on the $\omega \pi^+ \pi^-$ final states. Supersedes ACHASOV 99e and ACHASOV 02e.
- From the $\eta \rightarrow \gamma\gamma$ decay.
- From the $\eta \rightarrow 3\pi^0$ decay.
- Observed by threshold-crossing technique. Mass resolution = 4.8 MeV FWHM.
- The values were extracted from a dispersively improved Breit-Wigner parameterization and do not include vacuum polarization. Inclusion of vacuum polarization gives 782.736 ± 0.024 MeV.
- The ω mass was extracted from a dispersively improved Breit-Wigner parameterization, the ω width fixed at 8.49 ± 0.08 MeV. The value does not include vacuum polarization which would shift the mass to 781.81 ± 0.09 ± 0.03 MeV. The mixing parameter is assumed real valued.
- The values were extracted from a dispersively improved Breit-Wigner parameterization and do not include vacuum polarization.
- From the $\rho - \omega$ interference in the $\pi^+ \pi^-$ mass spectrum using the Breit-Wigner for the ω and leaving its mass and width as free parameters of the fit.
- Systematic uncertainties underestimated.
- Systematic uncertainties not estimated.
- From best-resolution sample of COYNE 71.
- From $\omega - \rho$ interference in the $\pi^+ \pi^-$ mass spectrum assuming ω width 12.6 MeV.



$\omega(782)$

$$J^{PC} = 0^-(1^{--})$$

$\omega(782)$ MASS

VALUE (MeV)	EVTS	DOCUMENT ID	TECN	COMMENT
782.66 ± 0.13 OUR AVERAGE				Error includes scale factor of 2.0. See the ideogram below.
777.9 ± 2.2	+4.3 -2.2	900k	ANDREEV 20	H1 $e p \rightarrow e^+ \pi^+ \pi^- p$
783.20 ± 0.13 ± 0.16	18680	AKHMETSHIN 05	CMD2	0.60-1.38 $e^+ e^- \rightarrow \pi^0 \gamma$
782.68 ± 0.09 ± 0.04	11200	1 AKHMETSHIN 04	CMD2	$e^+ e^- \rightarrow \pi^+ \pi^- \pi^0$
782.79 ± 0.08 ± 0.09	1.2M	2 ACHASOV 03D	RVUE	0.44-2.00 $e^+ e^- \rightarrow \pi^+ \pi^- \pi^0$
781.96 ± 0.17 ± 0.80	11k	3 AMSLER 94C	CBAR	0.0 $\bar{p} p \rightarrow \omega \eta \pi^0$
782.08 ± 0.36 ± 0.82	3463	4 AMSLER 94C	CBAR	0.0 $\bar{p} p \rightarrow \omega \eta \pi^0$
781.96 ± 0.13 ± 0.17	15k	AMSLER 93B	CBAR	0.0 $\bar{p} p \rightarrow \omega \eta \pi^0$
782.4 ± 0.2	270k	WEIDENAUER 93	ASTE	$\bar{p} p \rightarrow 2\pi^+ 2\pi^- \pi^0$
782.4 ± 0.5	7000	5 KEYNE 76	CNTR	$\pi^- p \rightarrow \omega n$
782.58 ± 0.03 ± 0.01		6 HOID 20	RVUE	$e^+ e^- \rightarrow \pi^0 \gamma$
781.68 ± 0.09 ± 0.03		7 COLANGELO 19	RVUE	$e^+ e^- \rightarrow \pi^+ \pi^-$
782.63 ± 0.03 ± 0.01		8 HOFERICHT... 19	RVUE	$e^+ e^- \rightarrow \pi^+ \pi^- \pi^0$
781.91 ± 0.24		9 LEES 12G	BABR	$e^+ e^- \rightarrow \pi^+ \pi^- \gamma$
782.7 ± 0.1 ± 1.5	19500	10 WURZINGER 95	SPEC	1.33 $p d \rightarrow {}^3\text{He} \omega$
781.78 ± 0.10		11 BARKOV 87	CMD	$e^+ e^- \rightarrow \pi^+ \pi^- \pi^0$
782.2 ± 0.4	1488	KURDADZE 83B	OLYA	$e^+ e^- \rightarrow \pi^+ \pi^- \pi^0$
783.3 ± 0.4	433	CORDIER 80	DM1	$e^+ e^- \rightarrow \pi^+ \pi^- \pi^0$
782.5 ± 0.8	33260	ROOS 80	RVUE	0.0-3.6 $\bar{p} p$
782.6 ± 0.8	3000	BENKHEIRI 79	OMEG	9-12 $\pi^{\pm} p$
781.8 ± 0.6	1430	COOPER 78B	HBC	0.7-0.8 $\bar{p} p \rightarrow 5\pi$
782.7 ± 0.9	535	VANAPEL... 78	HBC	7.2 $\bar{p} p \rightarrow \bar{p} p \omega$
783.5 ± 0.8	2100	GESSAROLI 77	HBC	11 $\pi^- p \rightarrow \omega n$
782.5 ± 0.8	418	AGUILAR... 72B	HBC	3.9, 4.6 $K^- p$
783.4 ± 1.0	248	BIZZARRI 71	HBC	0.0 $\rho\bar{p} \rightarrow K^+ K^- \omega$

$\omega(782)$ WIDTH

VALUE (MeV)	EVTS	DOCUMENT ID	TECN	COMMENT
8.68 ± 0.13 OUR AVERAGE				
8.68 ± 0.23 ± 0.10	11200	1 AKHMETSHIN 04	CMD2	$e^+ e^- \rightarrow \pi^+ \pi^- \pi^0$
8.68 ± 0.04 ± 0.15	1.2M	2 ACHASOV 03D	RVUE	0.44-2.00 $e^+ e^- \rightarrow \pi^+ \pi^- \pi^0$
8.65 ± 0.06 ± 0.01		3 HOID 20	RVUE	$e^+ e^- \rightarrow \pi^0 \gamma$
8.71 ± 0.04 ± 0.04		4 HOFERICHT... 19	RVUE	$e^+ e^- \rightarrow \pi^+ \pi^- \pi^0$
8.13 ± 0.45		5 LEES 12G	BABR	$e^+ e^- \rightarrow \pi^+ \pi^- \gamma$
8.2 ± 0.3	19500	6 WURZINGER 95	SPEC	1.33 $p d \rightarrow {}^3\text{He} \omega$
8.4 ± 0.1		7 AULCHENKO 87	ND	$e^+ e^- \rightarrow \pi^+ \pi^- \pi^0$
8.30 ± 0.40		8 BARKOV 87	CMD	$e^+ e^- \rightarrow \pi^+ \pi^- \pi^0$
9.8 ± 0.9	1488	9 KURDADZE 83B	OLYA	$e^+ e^- \rightarrow \pi^+ \pi^- \pi^0$
9.0 ± 0.8	433	10 CORDIER 80	DM1	$e^+ e^- \rightarrow \pi^+ \pi^- \pi^0$
12 ± 2	1430	11 COOPER 78B	HBC	0.7-0.8 $\bar{p} p \rightarrow 5\pi$
9.4 ± 2.5	2100	12 GESSAROLI 77	HBC	11 $\pi^- p \rightarrow \omega n$
10.22 ± 0.43	20000	13 KEYNE 76	CNTR	$\pi^- p \rightarrow \omega n$
13.3 ± 0.2	418	14 AGUILAR... 72B	HBC	3.9, 4.6 $K^- p$
9.1 ± 0.8	451	15 BENAKSAS 72B	OSPK	$e^+ e^- \rightarrow \pi^+ \pi^- \pi^0$
10.5 ± 1.5		16 BORENSTEIN 72	HBC	2.18 $K^- p$
7.70 ± 0.9 ± 1.15	940	17 BROWN 72	MMS	2.5 $\pi^- p \rightarrow n \text{MM}$
10.3 ± 0.4	510	18 BIZZARRI 71	HBC	0.0 $\rho\bar{p} \rightarrow K_1 K_1 \omega$
12.8 ± 3.0	248	19 BIZZARRI 71	HBC	0.0 $\rho\bar{p} \rightarrow K^+ K^- \omega$
9.5 ± 1.0	3583	20 COYNE 71	HBC	3.7 $\pi^+ p \rightarrow \rho \pi^+ \pi^+ \pi^- \pi^0$

- • • We do not use the following data for averages, fits, limits, etc. • • •
- Update of AKHMETSHIN 00c.
- From the combined fit of ANTONELLI 92, ACHASOV 01e, ACHASOV 02e, and ACHASOV 03d data on the $\pi^+ \pi^- \pi^0$ and ANTONELLI 92 on the $\omega \pi^+ \pi^-$ final states. Supersedes ACHASOV 99e and ACHASOV 02e.
- The values were extracted from a dispersively improved Breit-Wigner parameterization and do not include vacuum polarization. Inclusion of vacuum polarization gives 8.63 ± 0.05 MeV.

- ⁴ The values were extracted from a dispersively improved Breit-Wigner parameterization and do not include vacuum polarization.
- ⁵ From the $\rho-\omega$ interference in the $\pi^+\pi^-$ mass spectrum using the Breit-Wigner for the ω and leaving its mass and width as free parameters of the fit.
- ⁶ Systematic uncertainties underestimated.
- ⁷ Relativistic Breit-Wigner includes radiative corrections. Systematic uncertainties not estimated.
- ⁸ Systematic uncertainties not estimated.
- ⁹ Observed by threshold-crossing technique. Mass resolution = 4.8 MeV FWHM.

$\omega(782)$ DECAY MODES

Mode	Fraction (Γ_i/Γ)	Scale factor/ Confidence level
Γ_1 $\pi^+\pi^-\pi^0$	(89.2 ± 0.7) %	
Γ_2 $\pi^0\gamma$	(8.35 ± 0.27) %	S=2.2
Γ_3 $\pi^+\pi^-$	(1.53 ± 0.12) %	S=1.2
Γ_4 neutrals (excluding $\pi^0\gamma$)	(7 ⁺⁸ / ₋₄) × 10 ⁻³	S=1.1
Γ_5 $\eta\gamma$	(4.5 ± 0.4) × 10 ⁻⁴	S=1.1
Γ_6 $\pi^0e^+e^-$	(7.7 ± 0.6) × 10 ⁻⁴	
Γ_7 $\pi^0\mu^+\mu^-$	(1.34 ± 0.18) × 10 ⁻⁴	S=1.5
Γ_8 ηe^+e^-		
Γ_9 e^+e^-	(7.38 ± 0.22) × 10 ⁻⁵	S=1.9
Γ_{10} $\pi^+\pi^-\pi^0\pi^0$	< 2 × 10 ⁻⁴	CL=90%
Γ_{11} $\pi^+\pi^-\gamma$	< 3.6 × 10 ⁻³	CL=95%
Γ_{12} $\pi^+\pi^-\pi^+\pi^-$	< 1 × 10 ⁻³	CL=90%
Γ_{13} $\pi^0\pi^0\gamma$	(6.7 ± 1.1) × 10 ⁻⁵	
Γ_{14} $\eta\pi^0\gamma$	< 3.3 × 10 ⁻⁵	CL=90%
Γ_{15} $\mu^+\mu^-$	(7.4 ± 1.8) × 10 ⁻⁵	
Γ_{16} 3γ	< 1.9 × 10 ⁻⁴	CL=95%

Charge conjugation (C) violating modes			
Γ_{17} $\eta\pi^0$	C	< 2.1 × 10 ⁻⁴	CL=90%
Γ_{18} $2\pi^0$	C	< 2.2 × 10 ⁻⁴	CL=90%
Γ_{19} $3\pi^0$	C	< 2.3 × 10 ⁻⁴	CL=90%
Γ_{20} invisible		< 7 × 10 ⁻⁵	CL=90%

CONSTRAINED FIT INFORMATION

An overall fit to 15 branching ratios uses 48 measurements and one constraint to determine 10 parameters. The overall fit has a $\chi^2 = 48.0$ for 39 degrees of freedom.

The following *off-diagonal* array elements are the correlation coefficients $\langle \delta x_i \delta x_j \rangle / (\delta x_i \delta x_j)$, in percent, from the fit to the branching fractions, $x_i \equiv \Gamma_i/\Gamma_{total}$. The fit constrains the x_i whose labels appear in this array to sum to one.

x_2	23									
x_3	-18	-4								
x_4	-92	-55	1							
x_5	7	23	-1	-15						
x_6	-1	0	0	0	0					
x_7	0	0	0	0	0	0				
x_9	-24	-73	4	47	-31	0	0			
x_{13}	1	4	0	-2	1	0	0	-3		
x_{15}	0	0	0	0	0	0	0	0	0	
	x_1	x_2	x_3	x_4	x_5	x_6	x_7	x_9	x_{13}	x_{15}

$\omega(782)$ PARTIAL WIDTHS

$\Gamma(\pi^0\gamma)$					Γ_2
VALUE (keV)	EVTS	DOCUMENT ID	TECN	COMMENT	
• • • We do not use the following data for averages, fits, limits, etc. • • •					
880 ± 5.0	7815	¹ ACHASOV	13	SND	1.05-2.00 $e^+e^- \rightarrow \pi^0\pi^0\gamma$
788 ± 12 ± 27	36500	² ACHASOV	03	SND	0.60-0.97 $e^+e^- \rightarrow \pi^0\gamma$
764 ± 5.1	10625	DOLINSKY	89	ND	$e^+e^- \rightarrow \pi^0\gamma$

- ¹ Systematic uncertainty not estimated.
- ² Using $\Gamma_\omega = 8.44 \pm 0.09$ MeV and $B(\omega \rightarrow \pi^0\gamma)$ from ACHASOV 03.

$\Gamma(\eta\gamma)$					Γ_5
VALUE (keV)		DOCUMENT ID	TECN	COMMENT	
• • • We do not use the following data for averages, fits, limits, etc. • • •					
6.1 ± 2.5		¹ DOLINSKY	89	ND	$e^+e^- \rightarrow \eta\gamma$

¹ Using $\Gamma_\omega = 8.4 \pm 0.1$ MeV and $B(\omega \rightarrow \eta\gamma)$ from DOLINSKY 89.

$\Gamma(e^+e^-)$

VALUE (keV)	EVTS	DOCUMENT ID	TECN	COMMENT	Γ_9
6.60 ± 0.02 OUR EVALUATION					
• • • We do not use the following data for averages, fits, limits, etc. • • •					
0.591 ± 0.015	11200	^{1,2} AKHMETSHIN 04	CMD2	$e^+e^- \rightarrow \pi^+\pi^-\pi^0$	
0.653 ± 0.003 ± 0.021	1.2M	³ ACHASOV	03D	RVUE	0.44-2.00 $e^+e^- \rightarrow \pi^+\pi^-\pi^0$
0.600 ± 0.031	10625	DOLINSKY	89	ND	$e^+e^- \rightarrow \pi^0\gamma$

¹ Using $B(\omega \rightarrow \pi^+\pi^-\pi^0) = 0.891 \pm 0.007$ and $\Gamma_{total} = 8.44 \pm 0.09$ MeV.
² Update of AKHMETSHIN 00c.
³ Using ACHASOV 03, ACHASOV 03D and $B(\omega \rightarrow \pi^+\pi^-) = (1.70 \pm 0.28)\%$.

$\omega(782) \Gamma(i)\Gamma(e^+e^-)/\Gamma(total)$

$\Gamma(\pi^+\pi^-\pi^0) \times \Gamma(e^+e^-)/\Gamma_{total}$					$\Gamma_1\Gamma_9/\Gamma$
VALUE (eV)	EVTS	DOCUMENT ID	TECN	COMMENT	
569.8 ± 3.1 ± 8.2					
• • • We do not use the following data for averages, fits, limits, etc. • • •					
		¹ LEES	21B	BABR	10.5 $e^+e^- \rightarrow \pi^+\pi^-\pi^0\gamma$

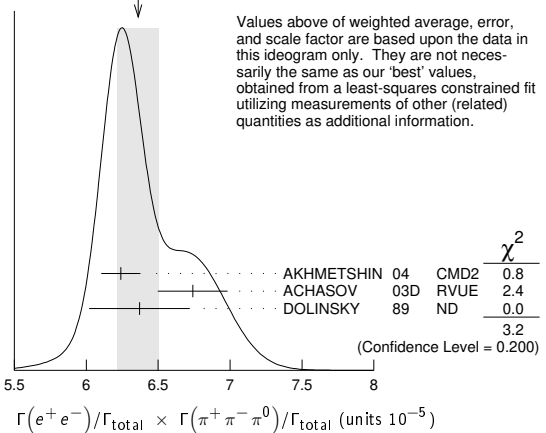
¹ From the cross section for $e^+e^- \rightarrow \pi^+\pi^-\pi^0$ with contributions from $\rho(770)$, $\omega(782)$, $\phi(1020)$, $\omega(1420)$, and $\omega(1650)$.

$\omega(782) \Gamma(e^+e^-)\Gamma(i)/\Gamma^2(total)$

$\Gamma(e^+e^-)/\Gamma_{total} \times \Gamma(\pi^+\pi^-\pi^0)/\Gamma_{total}$					$\Gamma_9/\Gamma \times \Gamma_1/\Gamma$
VALUE (units 10 ⁻⁵)	EVTS	DOCUMENT ID	TECN	COMMENT	
6.59 ± 0.19 OUR FIT					
Error includes scale factor of 2.1.					
6.36 ± 0.14 OUR AVERAGE					
Error includes scale factor of 1.3. See the ideogram below.					
6.24 ± 0.11 ± 0.08	11.2k	¹ AKHMETSHIN 04	CMD2	$e^+e^- \rightarrow \pi^+\pi^-\pi^0$	
6.74 ± 0.04 ± 0.24	1.2M	^{2,3} ACHASOV	03D	RVUE	0.44-2.00 $e^+e^- \rightarrow \pi^+\pi^-\pi^0$
6.37 ± 0.35		² DOLINSKY	89	ND	$e^+e^- \rightarrow \pi^+\pi^-\pi^0$
• • • We do not use the following data for averages, fits, limits, etc. • • •					
6.20 ± 0.13		⁴ BENAYOUN	10	RVUE	0.4-1.05 e^+e^-
6.70 ± 0.06 ± 0.27		⁵ AUBERT,B	04N	BABR	10.6 $e^+e^- \rightarrow \pi^+\pi^-\pi^0\gamma$
6.45 ± 0.24		⁶ BARKOV	87	CMD	$e^+e^- \rightarrow \pi^+\pi^-\pi^0$
5.79 ± 0.42	1488	⁷ KURDADZE	83B	OLYA	$e^+e^- \rightarrow \pi^+\pi^-\pi^0$
5.89 ± 0.54	433	⁶ CORDIER	80	DM1	$e^+e^- \rightarrow \pi^+\pi^-\pi^0$
7.54 ± 0.84	451	⁶ BENAJSAS	72B	OSP K	$e^+e^- \rightarrow \pi^+\pi^-\pi^0$

- ¹ Update of AKHMETSHIN 00c.
- ² Recalculated by us from the cross section in the peak.
- ³ From the combined fit of ANTONELLI 92, ACHASOV 01e, ACHASOV 02e, and ACHASOV 03d data on the $\pi^+\pi^-\pi^0$ and ANTONELLI 92 on the $\omega\pi^+\pi^-$ final states. Supersedes ACHASOV 99e and ACHASOV 02e.
- ⁴ A simultaneous fit of $e^+e^- \rightarrow \pi^+\pi^-$, $\pi^+\pi^-\pi^0$, $\pi^0\gamma$, $\eta\gamma$ data.
- ⁵ Superseded by LEES 21B.
- ⁶ Recalculated by us from the cross section in the peak. Systematic uncertainties underestimated.
- ⁷ Recalculated by us from the cross section in the peak. Systematic uncertainties not estimated.

WEIGHTED AVERAGE
6.36 ± 0.14 (Error scaled by 1.3)



$\Gamma(e^+e^-)/\Gamma_{total} \times \Gamma(\pi^0\gamma)/\Gamma_{total}$

$\Gamma(e^+e^-)/\Gamma_{total} \times \Gamma(\pi^0\gamma)/\Gamma_{total}$					$\Gamma_9/\Gamma \times \Gamma_2/\Gamma$
VALUE (units 10 ⁻⁶)	EVTS	DOCUMENT ID	TECN	COMMENT	
6.16 ± 0.14 OUR FIT					
Error includes scale factor of 1.8.					
6.34 ± 0.10 OUR AVERAGE					
6.336 ± 0.056 ± 0.089		¹ ACHASOV	16A	SND	0.60-1.38 $e^+e^- \rightarrow \pi^0\gamma$
6.47 ± 0.14 ± 0.39	18k	AKHMETSHIN 05	CMD2	0.60-1.38 $e^+e^- \rightarrow \pi^0\gamma$	
6.34 ± 0.21 ± 0.21	10k	² DOLINSKY	89	ND	$e^+e^- \rightarrow \pi^0\gamma$

Meson Particle Listings

$\omega(782)$

••• We do not use the following data for averages, fits, limits, etc. •••
 6.80 ± 0.13 ³ BENAYOUN 10 RVUE 0.4-1.05 e^+e^-
 6.50 ± 0.11 ± 0.20 36k ⁴ ACHASOV 03 SND 0.60-0.97 $e^+e^- \rightarrow \pi^0\gamma$

¹ From the VMD model with the interfering $\rho(770)$, $\omega(782)$, $\phi(1020)$, and an additional resonance describing the total contribution of the $\rho(1450)$ and $\omega(1420)$ states. Supersedes ACHASOV 03.
² Recalculated by us from the cross section in the peak.
³ A simultaneous fit of $e^+e^- \rightarrow \pi^+\pi^-$, $\pi^+\pi^-\pi^0$, $\pi^0\gamma$, $\eta\gamma$ data.
⁴ Using $\sigma(\phi \rightarrow \pi^0\gamma)$ from ACHASOV 00 and $m_\omega = 782.57$ MeV in the model with the energy-independent phase of ρ - ω interference equal to $(-10.2 \pm 7.0)^\circ$.

$\Gamma(e^+e^-)/\Gamma_{total} \times \Gamma(\pi^+\pi^-)/\Gamma_{total}$ $\Gamma_9/\Gamma \times \Gamma_3/\Gamma$

VALUE (units 10^{-6})	EVTS	DOCUMENT ID	TECN	COMMENT
1.28 ± 0.05 OUR AVERAGE				
1.318 ± 0.051 ± 0.021		¹ ACHASOV 21	SND	$e^+e^- \rightarrow \pi^+\pi^-$
1.225 ± 0.058 ± 0.041	800k	² ACHASOV 06	SND	$e^+e^- \rightarrow \pi^+\pi^-$

••• We do not use the following data for averages, fits, limits, etc. •••
 1.166 ± 0.036 ³ BENAYOUN 13 RVUE 0.4-1.05 e^+e^-
 1.05 ± 0.08 ⁴ DAVIER 13 RVUE $e^+e^- \rightarrow \pi^+\pi^-(\gamma)$
¹ From a fit of the cross section in the energy range $0.525 < \sqrt{s} < 0.883$ GeV parameterized by the sum of the Breit-Wigner amplitudes for the $\rho(770)$, ω and $\rho(1450)$ resonances. The measured phase of the $\rho(770)$ - ω interference is $(110.7 \pm 1.5 \pm 1.0)^\circ$.
² Supersedes ACHASOV 05A.
³ A simultaneous fit to $e^+e^- \rightarrow \pi^+\pi^-$, $\pi^+\pi^-\pi^0$, $\pi^0\gamma$, $\eta\gamma$, $K\bar{K}$, and $\tau^- \rightarrow \pi^-\pi^0\nu_\tau$ data. Supersedes BENAYOUN 10.
⁴ From $e^+e^- \rightarrow \pi^+\pi^-(\gamma)$ data of LEES 12G.

$\Gamma(e^+e^-)/\Gamma_{total} \times \Gamma(\eta\gamma)/\Gamma_{total}$ $\Gamma_9/\Gamma \times \Gamma_5/\Gamma$

VALUE (units 10^{-8})	EVTS	DOCUMENT ID	TECN	COMMENT
3.32 ± 0.28 OUR FIT				Error includes scale factor of 1.1.
3.18 ± 0.28 OUR AVERAGE				
3.10 ± 0.31 ± 0.11	33k	¹ ACHASOV 07B	SND	$0.6-1.38 e^+e^- \rightarrow \eta\gamma$
3.17 ^{+1.85} _{-1.31} ± 0.21	17.4k	² AKHMETSHIN 05	CMD2	$0.60-1.38 e^+e^- \rightarrow \eta\gamma$
3.41 ± 0.52 ± 0.21	23k	^{3,4} AKHMETSHIN 01B	CMD2	$e^+e^- \rightarrow \eta\gamma$

••• We do not use the following data for averages, fits, limits, etc. •••
 4.50 ± 0.10 ⁵ BENAYOUN 10 RVUE 0.4-1.05 e^+e^-
¹ From a combined fit of $\sigma(e^+e^- \rightarrow \eta\gamma)$ with $\eta \rightarrow 3\pi^0$ and $\eta \rightarrow \pi^+\pi^-\pi^0$, and fixing $B(\eta \rightarrow 3\pi^0) / B(\eta \rightarrow \pi^+\pi^-\pi^0) = 1.44 \pm 0.04$. Recalculated by us from the cross section at the peak. Supersedes ACHASOV 00D and ACHASOV 06A.
² From the $\eta \rightarrow 2\gamma$ decay and using $B(\eta \rightarrow \gamma\gamma) = 39.43 \pm 0.26\%$.
³ From the $\eta \rightarrow 3\pi^0$ decay and using $B(\eta \rightarrow 3\pi^0) = (32.24 \pm 0.29) \times 10^{-2}$.
⁴ The combined fit from 600 to 1380 MeV taking into account $\rho(770)$, $\omega(782)$, $\phi(1020)$, and $\rho(1450)$ (mass and width fixed at 1450 MeV and 310 MeV respectively).
⁵ A simultaneous fit of $e^+e^- \rightarrow \pi^+\pi^-$, $\pi^+\pi^-\pi^0$, $\pi^0\gamma$, $\eta\gamma$ data.

$\Gamma(e^+e^-)/\Gamma_{total} \times \Gamma(\mu^+\mu^-)/\Gamma_{total}$ $\Gamma_9/\Gamma \times \Gamma_{15}/\Gamma$

VALUE (units 10^{-9})	EVTS	DOCUMENT ID	TECN	COMMENT
4.3 ± 1.8 ± 2.2	4.5 M	¹ ANASTASI 17	KLOE	$e^+e^- \rightarrow \mu^+\mu^-\gamma$

¹ From a fit of the real part of the vacuum polarization by a sum of the leptonic and hadronic contributions, where the hadronic contribution is parameterized as a sum of Breit-Wigner resonances $\omega(782)$, $\phi(1020)$ and using a GOUNARIS 68 parametrization for the $\rho(770)$, and a non-resonant term.

$\omega(782)$ BRANCHING RATIOS

$\Gamma(\pi^+\pi^-\pi^0)/\Gamma_{total}$ Γ_1/Γ
 NIECKNIG 12 describes final-state interactions between the three pions in a dispersive framework using data on the $\pi\pi$ P-wave scattering phase shift.

VALUE	EVTS	DOCUMENT ID	TECN	COMMENT
••• We do not use the following data for averages, fits, limits, etc. •••				
0.9024 ± 0.0019		¹ AMBROSINO 08G	KLOE	$1.0-1.03 e^+e^- \rightarrow \pi^+\pi^-\pi^0, 2\pi^0\gamma$
0.8965 ± 0.0016 ± 0.0048	1.2M	^{2,3} ACHASOV 03D	RVUE	$0.44-2.00 e^+e^- \rightarrow \pi^+\pi^-\pi^0, \pi^+\pi^-\pi^0$
0.880 ± 0.020 ± 0.032	11200	^{3,4} AKHMETSHIN 00C	CMD2	$e^+e^- \rightarrow \pi^+\pi^-\pi^0$
0.8942 ± 0.0062		³ DOLINSKY 89	ND	$e^+e^- \rightarrow \pi^+\pi^-\pi^0$

¹ Not independent of $\Gamma(\pi^0\gamma) / \Gamma(\pi^+\pi^-\pi^0)$ from AMBROSINO 08G.
² Using ACHASOV 03, ACHASOV 03D and $B(\omega \rightarrow \pi^+\pi^-) = (1.70 \pm 0.28)\%$.
³ Not independent of the corresponding $\Gamma(e^+e^-) \times \Gamma(\pi^+\pi^-\pi^0)/\Gamma_{total}^2$.
⁴ Using $\Gamma(e^+e^-) = 0.60 \pm 0.02$ keV.

$\Gamma(\pi^0\gamma)/\Gamma_{total}$ Γ_2/Γ

VALUE (units 10^{-2})	EVTS	DOCUMENT ID	TECN	COMMENT
••• We do not use the following data for averages, fits, limits, etc. •••				
8.88 ± 0.18		¹ ACHASOV 16A	SND	$0.60-1.38 e^+e^- \rightarrow \pi^0\gamma$
8.09 ± 0.14		² AMBROSINO 08G	KLOE	$e^+e^- \rightarrow \pi^+\pi^-\pi^0, 2\pi^0\gamma$
9.06 ± 0.20 ± 0.57	18k	^{3,4} AKHMETSHIN 05	CMD2	$0.60-1.38 e^+e^- \rightarrow \pi^0\gamma$
9.34 ± 0.15 ± 0.31	36k	⁴ ACHASOV 03	SND	$0.60-0.97 e^+e^- \rightarrow \pi^0\gamma$
8.65 ± 0.16 ± 0.42	1.2M	^{5,6} ACHASOV 03D	RVUE	$0.44-2.00 e^+e^- \rightarrow \pi^+\pi^-\pi^0, \pi^+\pi^-\pi^0$
8.39 ± 0.24	9k	⁷ BENAYOUN 96	RVUE	$e^+e^- \rightarrow \pi^0\gamma$
8.88 ± 0.62	10k	⁴ DOLINSKY 89	ND	$e^+e^- \rightarrow \pi^0\gamma$

¹ Using $B(\omega \rightarrow e^+e^-)$ from PDG 15. Supersedes ACHASOV 03.
² Not independent of $\Gamma(\pi^0\gamma) / \Gamma(\pi^+\pi^-\pi^0)$ from AMBROSINO 08G.

³ Using $B(\omega \rightarrow e^+e^-) = (7.14 \pm 0.13) \times 10^{-5}$.
⁴ Not independent of the corresponding $\Gamma(e^+e^-) \times \Gamma(\pi^0\gamma)/\Gamma_{total}^2$.
⁵ Using ACHASOV 03, ACHASOV 03D and $B(\omega \rightarrow \pi^+\pi^-) = (1.70 \pm 0.28)\%$.
⁶ Not independent of the corresponding $\Gamma(e^+e^-) \times \Gamma(\pi^+\pi^-\pi^0)/\Gamma_{total}^2$.
⁷ Reanalysis of DRUZHININ 84, DOLINSKY 89, DOLINSKY 91 taking into account the triangle anomaly contributions.

$\Gamma(\pi^0\gamma)/\Gamma(\pi^+\pi^-\pi^0)$ Γ_2/Γ_1

VALUE (units 10^{-2})	DOCUMENT ID	TECN	COMMENT
9.35 ± 0.30 OUR FIT			Error includes scale factor of 2.4.
9.05 ± 0.27 OUR AVERAGE			Error includes scale factor of 1.8.
8.97 ± 0.16	AMBROSINO 08G	KLOE	$e^+e^- \rightarrow \pi^+\pi^-\pi^0, 2\pi^0\gamma$
9.94 ± 0.36 ± 0.38	¹ AULCHENKO 00A	SND	$e^+e^- \rightarrow \pi^+\pi^-\pi^0, 2\pi^0\gamma$
8.4 ± 1.3	KEYNE 76	CNTR	$\pi^-p \rightarrow \omega n$
10.9 ± 2.5	BENAKSAS 72C	OSPK	$e^+e^- \rightarrow \pi^0\gamma$
8.1 ± 2.0	BALDIN 71	HLBC	$2.9 \pi^+\pi^-$
13 ± 4	JACQUET 69B	HLBC	$2.05 \pi^+\pi^- \rightarrow \pi^+\pi^0$

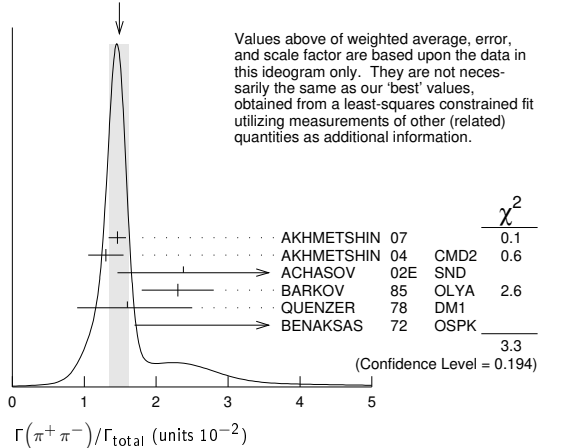
••• We do not use the following data for averages, fits, limits, etc. •••
 9.7 ± 0.2 ± 0.5 ^{2,3} ACHASOV 03D RVUE $0.44-2.00 e^+e^- \rightarrow \pi^+\pi^-\pi^0$
 9.9 ± 0.7 ² DOLINSKY 89 ND $e^+e^- \rightarrow \pi^0\gamma$
¹ From $\sigma_0^{\omega\pi^0 \rightarrow \pi^0\pi^0\gamma}(m_\phi)/\sigma_0^{\omega\pi^0 \rightarrow \pi^+\pi^-\pi^0}(m_\phi)$ with a phase-space correction factor of 1/1.023.
² Not independent of the corresponding $\Gamma(e^+e^-) \times \Gamma(\pi^0\gamma)/\Gamma_{total}^2$.
³ Using ACHASOV 03. Based on 1.2M events.

$\Gamma(\pi^+\pi^-)/\Gamma_{total}$ Γ_3/Γ
 See also $\Gamma(\pi^+\pi^-)/\Gamma(\pi^+\pi^-\pi^0)$.

VALUE (units 10^{-2})	EVTS	DOCUMENT ID	TECN	COMMENT
1.53 ± 0.12 OUR FIT				Error includes scale factor of 1.2.
1.49 ± 0.13 OUR AVERAGE				Error includes scale factor of 1.3. See the ideogram below.
1.46 ± 0.12 ± 0.02	900k	¹ AKHMETSHIN 07		$e^+e^- \rightarrow \pi^+\pi^-$
1.30 ± 0.24 ± 0.05	11.2k	² AKHMETSHIN 04	CMD2	$e^+e^- \rightarrow \pi^+\pi^-$
2.38 ^{+1.77} _{-0.90} ± 0.18	5.4k	³ ACHASOV 02E	SND	$1.1-1.38 e^+e^- \rightarrow \pi^+\pi^-\pi^0$
2.3 ± 0.5		BARKOV 85	OLYA	$e^+e^- \rightarrow \pi^+\pi^-$
1.6 ^{+0.9} _{-0.7}		QUENZER 78	DM1	$e^+e^- \rightarrow \pi^+\pi^-$
3.6 ± 1.9		BENAKSAS 72	OSPK	$e^+e^- \rightarrow \pi^+\pi^-$

••• We do not use the following data for averages, fits, limits, etc. •••
 1.29 ± 0.22 ± 0.03 970k ^{4,5} ABLIKIM 18c BES3 $\eta'(958) \rightarrow \gamma\pi^+\pi^-$
 1.28 ± 0.22 ± 0.03 970k ^{6,7} ABLIKIM 18c BES3 $\eta'(958) \rightarrow \gamma\pi^+\pi^-$
 1.52 ± 0.08 ⁸ HANHART 18 RVUE $e^+e^- \rightarrow \pi^+\pi^-$
 1.75 ± 0.11 4.5M ⁹ ACHASOV 05A SND $e^+e^- \rightarrow \pi^+\pi^-$
 2.01 ± 0.29 ¹⁰ BENAYOUN 03 RVUE $e^+e^- \rightarrow \pi^+\pi^-$
 1.9 ± 0.3 ¹¹ GARDNER 99 RVUE $e^+e^- \rightarrow \pi^+\pi^-$
 2.3 ± 0.4 ¹² BENAYOUN 98 RVUE $e^+e^- \rightarrow \pi^+\pi^-, \mu^+\mu^-$
 1.0 ± 0.11 ¹³ WICKLUND 78 ASPK $3,4,6 \pi^\pm N$
 1.22 ± 0.30 ¹³ ALVENSLEB... 71C CNTR Photoproduction
 1.3^{+1.2}_{-0.9} ¹⁴ MOFFEIT 71 HBC $2.8,4,7 \gamma p$
 0.80^{+0.28}_{-0.20} ¹⁴ BIGGS 70B CNTR $4.2\gamma C \rightarrow \pi^+\pi^-C$

WEIGHTED AVERAGE
 1.49 ± 0.13 (Error scaled by 1.3)



¹ A combined fit of AKHMETSHIN 07, AULCHENKO 06, and AULCHENKO 05.
² Update of AKHMETSHIN 02.
³ From the $m_{\pi^+\pi^-}$ spectrum taking into account the interference of the $\rho\pi$ and $\omega\pi$ amplitudes.
⁴ From a fit to $\pi^+\pi^-$ mass using $\rho(770)$ (parametrized with the Gounaris-Sakurai approach), $\omega(782)$, and box anomaly components.
⁵ ABLIKIM 18c reports $[\Gamma(\omega(782) \rightarrow \pi^+\pi^-)/\Gamma_{total}] \times [B(\eta'(958) \rightarrow \omega\gamma)] = (3.25 \pm 0.21 \pm 0.52) \times 10^{-4}$ which we divide by our best value $B(\eta'(958) \rightarrow \omega\gamma) = (2.52 \pm$

0.07) $\times 10^{-2}$. Our first error is their experiment's error and our second error is the systematic error from using our best value.

⁶From a fit to $\pi^+\pi^-$ mass using $\rho(770)$ (parametrized with the Gounaris-Sakurai approach), $\omega(782)$, and $\rho(1450)$ components.

⁷ABLIKIM 18c reports $[\Gamma(\omega(782) \rightarrow \pi^+\pi^-)/\Gamma_{\text{total}}] \times [B(\eta'(958) \rightarrow \omega\gamma)] = (3.22 \pm 0.21 \pm 0.52) \times 10^{-4}$ which we divide by our best value $B(\eta'(958) \rightarrow \omega\gamma) = (2.52 \pm 0.07) \times 10^{-2}$. Our first error is their experiment's error and our second error is the systematic error from using our best value.

⁸Dispersive analysis. Value extracted from average of data from AUBERT 09AS, AKHMETSHIN 07, ACHASOV 06, AMBROSINO 11A, BABUSCI 13D, ABLIKIM 16b normalised by PDG 16 evaluation for $\Gamma(\omega \rightarrow e^+e^-)$.

⁹Using $\Gamma(\omega \rightarrow e^+e^-)$ from the 2004 Edition of this Review (PDG 04).

¹⁰Using the data of AKHMETSHIN 02 in the hidden local symmetry model.

¹¹Using the data of BARKOV 85.

¹²Using the data of BARKOV 85 in the hidden local symmetry model.

¹³From a model-dependent analysis assuming complete coherence.

¹⁴Re-evaluated under $\Gamma(\pi^+\pi^-)/\Gamma(\pi^+\pi^-\pi^0)$ by BEHREND 71 using more accurate $\omega \rightarrow \rho$ photoproduction cross-section ratio.

$\Gamma(\pi^+\pi^-)/\Gamma(\pi^+\pi^-\pi^0)$ Γ_3/Γ_1

See also $\Gamma(\pi^+\pi^-)/\Gamma_{\text{total}}$.

0.0172 ± 0.0014 OUR FIT Error includes scale factor of 1.2.

0.026 ± 0.005 OUR AVERAGE

VALUE	EVTS	DOCUMENT ID	TECN	COMMENT
0.021 \pm 0.028 -0.009	1,2	RATCLIFF	72	ASPK 15 $\pi^-p \rightarrow n2\pi$
0.028 \pm 0.006	1	BEHREND	71	ASPK Photoproduction
0.022 \pm 0.009 -0.01	3	ROOS	70	RVUE

¹The fitted width of these data is 160 MeV in agreement with present average, thus the ω contribution is overestimated. Assuming ρ width 145 MeV.

²Significant interference effect observed. NB of $\omega \rightarrow 3\pi$ comes from an extrapolation.

³ROOS 70 combines ABRAMOVICH 70 and BIZZARRI 70.

$\Gamma(\pi^+\pi^-)/\Gamma(\pi^0\gamma)$ Γ_3/Γ_2

0.20 ± 0.04

VALUE	EVTS	DOCUMENT ID	TECN	COMMENT
1.98M	1	ALOISIO	03	KLOE 1.02 $e^+e^- \rightarrow \pi^+\pi^-\pi^0$

¹Using the data of ALOISIO 02b.

$\Gamma(\text{neutrals})/\Gamma_{\text{total}}$ $(\Gamma_2+\Gamma_4)/\Gamma$

0.091 ± 0.006 OUR FIT

0.081 ± 0.011 OUR AVERAGE

VALUE	EVTS	DOCUMENT ID	TECN	COMMENT
0.075 \pm 0.025		BIZZARRI	71	HBC 0.0 $p\bar{p}$
0.079 \pm 0.019		DEINET	69B	OSPK 1.5 π^-p
0.084 \pm 0.015		BOLLINI	68C	CNTR 2.1 π^-p
••• We do not use the following data for averages, fits, limits, etc. •••				
0.073 \pm 0.018	42	BASILE	72B	CNTR 1.67 π^-p

$\Gamma(\text{neutrals})/\Gamma(\pi^+\pi^-\pi^0)$ $(\Gamma_2+\Gamma_4)/\Gamma_1$

0.102 ± 0.008 OUR FIT

0.103 ± 0.011 OUR AVERAGE

VALUE	EVTS	DOCUMENT ID	TECN	COMMENT
0.15 \pm 0.04	46	AGUILAR...	72B	HBC 3.9,4.6 K^-p
0.10 \pm 0.03	19	BARASH	67B	HBC 0.0 $\bar{p}p$
0.134 \pm 0.026	850	DIGIUGNO	66B	CNTR 1.4 π^-p
0.097 \pm 0.016	348	FLATTE	66	HBC 1.4 - 1.7 $K^-p \rightarrow \Lambda MM$
0.06 \pm 0.05 -0.02		JAMES	66	HBC 2.1 π^+p
0.08 \pm 0.03	35	KRAEMER	64	DBC 1.2 π^+d
••• We do not use the following data for averages, fits, limits, etc. •••				
0.11 \pm 0.02	20	BUSCHBECK	63	HBC 1.5 K^-p

$\Gamma(\pi^0\gamma)/\Gamma(\text{neutrals})$ $\Gamma_2/(\Gamma_2+\Gamma_4)$

0.78 ± 0.07

VALUE	CL%	DOCUMENT ID	TECN	COMMENT
0.78 \pm 0.07		1 DAKIN	72	OSPK 1.4 $\pi^-p \rightarrow nMM$
>0.81	90	DEINET	69B	OSPK

¹Error statistical only. Authors obtain good fit also assuming $\pi^0\gamma$ as the only neutral decay.

$\Gamma(\text{neutrals})/\Gamma(\text{charged particles})$ $(\Gamma_2+\Gamma_4)/(\Gamma_1+\Gamma_3)$

0.100 ± 0.008 OUR FIT

0.124 ± 0.021

VALUE	DOCUMENT ID	TECN	COMMENT
FELDMAN	67C	OSPK	1.2 π^-p

$\Gamma(\eta\gamma)/\Gamma_{\text{total}}$ Γ_5/Γ

4.5 ± 0.4 OUR FIT Error includes scale factor of 1.1.

6.3 ± 1.3 OUR AVERAGE Error includes scale factor of 1.2.

VALUE	EVTS	DOCUMENT ID	TECN	COMMENT
6.6 \pm 1.7		1 ABELE	97E	CBAR 0.0 $\bar{p}p \rightarrow 5\gamma$
8.3 \pm 2.1		ALDE	93	GAM2 38 $\pi^-p \rightarrow \omega n$
3.0 \pm 2.5 -1.8		2 ANDREWS	77	CNTR 6.7-10 γCu

••• We do not use the following data for averages, fits, limits, etc. •••

4.2 \pm 0.4 \pm 0.1	33k	3 ACHASOV	07B	SND 0.6-1.38 $e^+e^- \rightarrow \eta\gamma$
4.44 \pm 2.59 -1.83 \pm 0.28	17.4k	4,5 AKHMETSHIN	05	CMD2 0.60-1.38 $e^+e^- \rightarrow \eta\gamma$
5.10 \pm 0.72 \pm 0.34	23k	6 AKHMETSHIN	01B	CMD2 $e^+e^- \rightarrow \eta\gamma$
0.7 \pm 0.5		7 CASE	00	CBAR 0.0 $p\bar{p} \rightarrow \eta\eta\gamma$
6.56 \pm 2.41 -2.55	3525	2,8 BENAYOUN	96	RVUE $e^+e^- \rightarrow \eta\gamma$
7.3 \pm 2.9		2,4 DOLINSKY	89	ND $e^+e^- \rightarrow \eta\gamma$

¹No flat $\eta\eta\gamma$ background assumed.

²Solution corresponding to constructive $\omega\rho$ interference.

³ACHASOV 07B reports $[\Gamma(\omega(782) \rightarrow \eta\gamma)/\Gamma_{\text{total}}] \times [B(\omega(782) \rightarrow e^+e^-)] = (3.10 \pm 0.31 \pm 0.11) \times 10^{-8}$ which we divide by our best value $B(\omega(782) \rightarrow e^+e^-) = (7.38 \pm 0.22) \times 10^{-5}$. Our first error is their experiment's error and our second error is the systematic error from using our best value. Supersedes ACHASOV 00D and ACHASOV 06A.

⁴Not independent of the corresponding $\Gamma(e^+e^-) \times \Gamma(\eta\gamma)/\Gamma_{\text{total}}^2$.

⁵Using $B(\omega \rightarrow e^+e^-) = (7.14 \pm 0.13) \times 10^{-5}$ and $B(\eta \rightarrow \gamma\gamma) = 39.43 \pm 0.26\%$.

⁶Using $B(\omega \rightarrow e^+e^-) = (7.07 \pm 0.19) \times 10^{-5}$ and using $B(\eta \rightarrow 3\pi^0) = (32.24 \pm 0.29) \times 10^{-2}$. Solution corresponding to constructive $\omega\rho$ interference. The combined fit from 600 to 1380 MeV taking into account $\rho(770)$, $\omega(782)$, $\phi(1020)$, and $\rho(1450)$ (mass and width fixed at 1450 MeV and 310 MeV respectively). Not independent of the corresponding $\Gamma(e^+e^-) \times \Gamma(\eta\gamma)/\Gamma_{\text{total}}^2$.

⁷Depending on the degree of coherence with the flat $\eta\eta\gamma$ background and using $B(\omega \rightarrow \pi^0\gamma) = (8.5 \pm 0.5) \times 10^{-2}$.

⁸Reanalysis of DRUZHININ 84, DOLINSKY 89, DOLINSKY 91 taking into account the triangle anomaly contributions.

$\Gamma(\eta\gamma)/\Gamma(\pi^0\gamma)$ Γ_5/Γ_2

0.0098 ± 0.0024

VALUE	DOCUMENT ID	TECN	COMMENT	
0.0082 \pm 0.0033	1	ALDE	93	GAM2 38 $\pi^-p \rightarrow \omega n$
0.010 \pm 0.045	2	DOLINSKY	89	ND $e^+e^- \rightarrow \eta\gamma$
		APEL	72B	OSPK 4-8 $\pi^-p \rightarrow n3\gamma$

¹Model independent determination.

²Solution corresponding to constructive $\omega\rho$ interference.

$\Gamma(\pi^0 e^+ e^-)/\Gamma_{\text{total}}$ Γ_6/Γ

7.7 ± 0.6 OUR FIT

7.7 ± 0.6 OUR AVERAGE

VALUE (units 10^{-4})	EVTS	DOCUMENT ID	TECN	COMMENT
7.61 \pm 0.53 \pm 0.64		ACHASOV	08	SND 0.36-0.97 $e^+e^- \rightarrow \pi^0 e^+ e^-$
8.19 \pm 0.71 \pm 0.62		AKHMETSHIN	05A	CMD2 0.72-0.84 e^+e^-
5.9 \pm 1.9	43	DOLINSKY	88	ND $e^+e^- \rightarrow \pi^0 e^+ e^-$

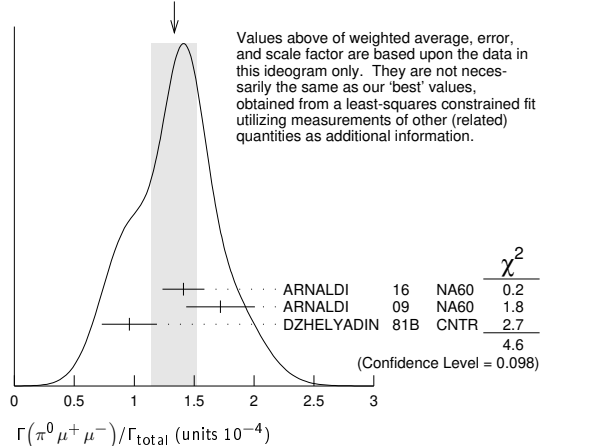
$\Gamma(\pi^0 \mu^+ \mu^-)/\Gamma_{\text{total}}$ Γ_7/Γ

1.34 ± 0.18 OUR FIT Error includes scale factor of 1.5.

1.34 ± 0.19 OUR AVERAGE Error includes scale factor of 1.5. See the ideogram below.

VALUE	EVTS	DOCUMENT ID	TECN	COMMENT
1.41 \pm 0.09 \pm 0.15		ARNALDI	16	NA60 400 GeV (p -A) collisions
1.72 \pm 0.25 \pm 0.14	3k	ARNALDI	09	NA60 158A In-In collisions
0.96 \pm 0.23		DZHELJADIN	81B	CNTR 25-33 $\pi^-p \rightarrow \omega n$

WEIGHTED AVERAGE
1.34 ± 0.19 (Error scaled by 1.5)



$\Gamma(\eta e^+ e^-)/\Gamma_{\text{total}}$ Γ_8/Γ

<1.1

VALUE	DOCUMENT ID	TECN	COMMENT
<1.1	AKHMETSHIN	05A	CMD2 0.72-0.84 e^+e^-

Meson Particle Listings

 $\omega(782)$ $\Gamma(e^+e^-)/\Gamma_{\text{total}}$ Γ_9/Γ

VALUE (units 10^{-4})	EVTS	DOCUMENT ID	TECN	COMMENT
0.738±0.022 OUR FIT	Error includes scale factor of 1.9.			
0.700±0.016	11200	^{1,2} AKHMETSHIN 04	CMD2	$e^+e^- \rightarrow \pi^+\pi^-\pi^0$
0.752±0.004±0.024	1.2M	^{2,3} ACHASOV	03D RVUE	0.44–2.00 $e^+e^- \rightarrow \pi^+\pi^-\pi^0$
0.714±0.036		² DOLINSKY	89 ND	$e^+e^- \rightarrow \pi^+\pi^-\pi^0$
0.72 ± 0.03		² BARKOV	87 CMD	$e^+e^- \rightarrow \pi^+\pi^-\pi^0$
0.64 ± 0.04	1488	² KURDADZE	83B OLYA	$e^+e^- \rightarrow \pi^+\pi^-\pi^0$
0.675±0.069	433	² CORDIER	80 DM1	$e^+e^- \rightarrow \pi^+\pi^-\pi^0$
0.83 ± 0.10	451	² BENAKSAS	72B OSPK	$e^+e^- \rightarrow \pi^+\pi^-\pi^0$
0.77 ± 0.06		⁴ AUGUSTIN	69D OSPK	$e^+e^- \rightarrow \pi^+\pi^-\pi^0$
0.65 ± 0.13	33	⁵ ASTVACAT...	68 OSPK	Assume SU(3)+mixing

¹ Using $B(\omega \rightarrow \pi^+\pi^-\pi^0) = 0.891 \pm 0.007$. Update of AKHMETSHIN 00C.² Not independent of the corresponding $\Gamma(e^+e^-) \times \Gamma(\pi^+\pi^-\pi^0)/\Gamma_{\text{total}}^2$.³ Using ACHASOV 03, ACHASOV 03D and $B(\omega \rightarrow \pi^+\pi^-) = (1.70 \pm 0.28)\%$.⁴ Rescaled by us to correspond to ω width 8.4 MeV. Systematic errors underestimated.⁵ Not resolved from ρ decay. Error statistical only. $\Gamma(\pi^+\pi^-\pi^0\pi^0)/\Gamma_{\text{total}}$ Γ_{10}/Γ

VALUE (units 10^{-4})	CL%	DOCUMENT ID	TECN	COMMENT
< 2	90	ACHASOV	09A SND	$e^+e^- \rightarrow \pi^+\pi^-\pi^0\pi^0$
<200	90	KURDADZE	86 OLYA	$e^+e^- \rightarrow \pi^+\pi^-\pi^0\pi^0$

 $\Gamma(\pi^+\pi^-\gamma)/\Gamma_{\text{total}}$ Γ_{11}/Γ

VALUE	CL%	DOCUMENT ID	TECN	COMMENT
<0.0036	95	WEIDENAUER	90 ASTE	$p\bar{p} \rightarrow \pi^+\pi^-\pi^+\pi^-\gamma$
<0.004	95	BITYUKOV	88B SPEC	$32 \pi^-p \rightarrow \pi^+\pi^-\gamma X$

 $\Gamma(\pi^+\pi^-\gamma)/\Gamma(\pi^+\pi^-\pi^0)$ Γ_{11}/Γ_1

VALUE	CL%	DOCUMENT ID	TECN	COMMENT
<0.066	90	KALBFLEISCH	75 HBC	$2.18 K^-p \rightarrow \Lambda\pi^+\pi^-\gamma$
<0.05	90	FLATTE	66 HBC	$1.2 - 1.7 K^-p \rightarrow \Lambda\pi^+\pi^-\gamma$

 $\Gamma(\pi^+\pi^-\pi^+\pi^-)/\Gamma_{\text{total}}$ Γ_{12}/Γ

VALUE	CL%	DOCUMENT ID	TECN	COMMENT
<1 × 10⁻³	90	KURDADZE	88 OLYA	$e^+e^- \rightarrow \pi^+\pi^-\pi^+\pi^-$

 $\Gamma(\pi^0\pi^0\gamma)/\Gamma_{\text{total}}$ Γ_{13}/Γ

VALUE (units 10^{-5})	EVTS	DOCUMENT ID	TECN	COMMENT
6.7±1.1 OUR FIT				
6.5±1.2 OUR AVERAGE				
6.4 ^{+2.4} _{-2.0} ±0.8	190	¹ AKHMETSHIN 04B	CMD2	0.6–0.97 $e^+e^- \rightarrow \pi^0\pi^0\gamma$
6.6 ^{+1.4} _{-1.3} ±0.6	295	ACHASOV	02F SND	0.36–0.97 $e^+e^- \rightarrow \pi^0\pi^0\gamma$
11.0 ^{+2.1} _{-1.9} ±1.4	190	² AKHMETSHIN 04B	CMD2	0.6–0.97 $e^+e^- \rightarrow \pi^0\pi^0\gamma$
7.8±2.7±2.0	63	^{1,3} ACHASOV	00G SND	$e^+e^- \rightarrow \pi^0\pi^0\gamma$
12.7±2.3±2.5	63	^{2,3} ACHASOV	00G SND	$e^+e^- \rightarrow \pi^0\pi^0\gamma$

¹ In the model assuming the $\rho \rightarrow \pi^0\pi^0\gamma$ decay via the $\omega\pi$ and $f_0(500)\gamma$ mechanisms.² In the model assuming the $\rho \rightarrow \pi^0\pi^0\gamma$ decay via the $\omega\pi$ mechanism only.³ Superseded by ACHASOV 02F. $\Gamma(\pi^0\pi^0\gamma)/\Gamma(\pi^+\pi^-\pi^0)$ Γ_{13}/Γ_1

VALUE	CL%	DOCUMENT ID	TECN	COMMENT
<0.00045	90	DOLINSKY	89 ND	$e^+e^- \rightarrow \pi^0\pi^0\gamma$
<0.08	95	JACQUET	69B HLBC	2.05 $\pi^+p \rightarrow \pi^+\rho\omega$

 $\Gamma(\pi^0\pi^0\gamma)/\Gamma(\pi^0\gamma)$ Γ_{13}/Γ_2

VALUE (units 10^{-4})	CL%	EVTS	DOCUMENT ID	TECN	COMMENT
8.0±1.3 OUR FIT					
8.5±2.9	40 ± 14		ALDE	94B GAM2	$38\pi^-p \rightarrow \pi^0\pi^0\gamma n$
< 50	90		DOLINSKY	89 ND	$e^+e^- \rightarrow \pi^0\pi^0\gamma$
<1800	95		KEYNE	76 CNTR	$\pi^-p \rightarrow \omega n$
<1500	90		BENAKSAS	72C OSPK	e^+e^-
<1400			BALDIN	71 HLBC	2.9 π^+p
<1000	90		BARMIN	64 HLBC	1.3–2.8 π^-p

 $\Gamma(\pi^0\pi^0\gamma)/\Gamma(\text{neutrals})$ $\Gamma_{13}/(\Gamma_2+\Gamma_4)$

VALUE	CL%	DOCUMENT ID	TECN	COMMENT
0.22±0.07		¹ DAKIN	72 OSPK	1.4 $\pi^-p \rightarrow nMM$
<0.19	90	DEINET	69B OSPK	

¹ See $\Gamma(\pi^0\gamma)/\Gamma(\text{neutrals})$. $\Gamma(\eta\pi^0\gamma)/\Gamma_{\text{total}}$ Γ_{14}/Γ

VALUE (units 10^{-5})	CL%	DOCUMENT ID	TECN	COMMENT
<3.3	90	AKHMETSHIN 04B	CMD2	0.6–0.97 $e^+e^- \rightarrow \eta\pi^0\gamma$

 $\Gamma(\mu^+\mu^-)/\Gamma_{\text{total}}$ Γ_{15}/Γ

VALUE (units 10^{-5})	EVTS	DOCUMENT ID	TECN	COMMENT
7.4±1.8 OUR FIT				
7.4±1.8 OUR AVERAGE				
6.6±1.4±1.7	4.5M	¹ ANASTASI	17 KLOE	$e^+e^- \rightarrow \mu^+\mu^-\gamma$
9.0±2.9±1.1	18	HEISTER	02c ALEP	$Z \rightarrow \mu^+\mu^- + X$

¹ Assuming lepton universality in the decay $\omega \rightarrow \ell^+\ell^-$ and correcting for different phase space between electron and muon final states. $\Gamma(\mu^+\mu^-)/\Gamma(\pi^+\pi^-\pi^0)$ Γ_{15}/Γ_1

VALUE (units 10^{-3})	CL%	DOCUMENT ID	TECN	COMMENT
<0.2	90	WILSON	69 OSPK	$12 \pi^-C \rightarrow Fe$
<1.7	74	FLATTE	66 HBC	1.2 – 1.7 $K^-p \rightarrow \Lambda\mu^+\mu^-$
<1.2		BARBARO...	65 HBC	2.7 K^-p

 $\Gamma(\pi^0\mu^+\mu^-)/\Gamma(\mu^+\mu^-)$ Γ_7/Γ_{15}

VALUE	EVTS	DOCUMENT ID	TECN	COMMENT
1.2±0.6	30	¹ DZHELYADIN	79 CNTR	25–33 π^-p

¹ Superseded by DZHELYADIN 81B result above. $\Gamma(3\gamma)/\Gamma_{\text{total}}$ Γ_{16}/Γ

VALUE (units 10^{-4})	CL%	DOCUMENT ID	TECN	COMMENT
<1.9	95	¹ ABELE	97E CBAR	0.0 $\bar{p}p \rightarrow 5\gamma$
<2	90	¹ PROKOSHKIN	95 GAM2	38 $\pi^-p \rightarrow 3\gamma n$

¹ From direct 3γ decay search. $\Gamma(\eta\pi^0)/\Gamma_{\text{total}}$ Γ_{17}/Γ

VALUE	CL%	DOCUMENT ID	TECN	COMMENT
Violates C conservation.				
<0.001	90	ALDE	94B GAM2	$38\pi^-p \rightarrow \eta\pi^0 n$

 $[\Gamma(\eta\pi^0) + \Gamma(\eta\pi^0)]/\Gamma(\pi^+\pi^-\pi^0)$ $(\Gamma_5+\Gamma_{17})/\Gamma_1$

VALUE	CL%	DOCUMENT ID	TECN	COMMENT
<0.016	90	¹ FLATTE	66 HBC	1.2 – 1.7 $K^-p \rightarrow \Lambda\pi^+\pi^-\pi^0$
<0.045	95	JACQUET	69B HLBC	2.05 $\pi^+p \rightarrow \pi^+\rho\omega$

¹ Restated by us using $B(\eta \rightarrow \text{charged modes}) = 29.2\%$. $\Gamma(\eta\pi^0)/\Gamma(\pi^0\gamma)$ Γ_{17}/Γ_2

VALUE (units 10^{-3})	CL%	DOCUMENT ID	TECN	COMMENT
<2.6	90	¹ STAROSTIN	09 CRYM	$\gamma p \rightarrow \eta\pi^0 p$
¹ STAROSTIN 09 reports $[\Gamma(\omega(782) \rightarrow \eta\pi^0)/\Gamma(\omega(782) \rightarrow \pi^0\gamma)] \times [B(\eta \rightarrow 2\gamma)] < 1.01 \times 10^{-3}$ which we divide by our best value $B(\eta \rightarrow 2\gamma) = 39.36 \times 10^{-2}$.				

 $\Gamma(2\pi^0)/\Gamma(\pi^0\gamma)$ Γ_{18}/Γ_2

VALUE (units 10^{-3})	CL%	DOCUMENT ID	TECN	COMMENT
<2.59	90	STAROSTIN	09 CRYM	$\gamma p \rightarrow 2\pi^0 p$

 $\Gamma(3\pi^0)/\Gamma_{\text{total}}$ Γ_{19}/Γ

VALUE	CL%	DOCUMENT ID	TECN	COMMENT
Violates C conservation.				
<3 × 10 ⁻⁴	90	PROKOSHKIN	95 GAM2	38 $\pi^-p \rightarrow 3\pi^0 n$

 $\Gamma(3\pi^0)/\Gamma(\pi^0\gamma)$ Γ_{19}/Γ_2

VALUE (units 10^{-3})	CL%	DOCUMENT ID	TECN	COMMENT
<2.72	90	STAROSTIN	09 CRYM	$\gamma p \rightarrow 3\pi^0 p$

 $\Gamma(3\pi^0)/\Gamma(\pi^+\pi^-\pi^0)$ Γ_{19}/Γ_1

VALUE	CL%	DOCUMENT ID	COMMENT
Violates C conservation.			
<0.009	90	BARBERIS	01 450 $p p \rightarrow p_f 3\pi^0 p_s$

 $\Gamma(\text{invisible})/\Gamma(\pi^+\pi^-\pi^0)$ Γ_{20}/Γ_1

VALUE	CL%	DOCUMENT ID	TECN	COMMENT
<8.1 × 10⁻⁵	90	ABLIKIM	18s BES3	$J/\psi \rightarrow \omega\eta \rightarrow \omega\pi^+\pi^-\pi^0$

See key on page 1171

Meson Particle Listings

$\omega(782), \eta'(958)$

PARAMETER Λ IN $\omega \rightarrow \pi^0 e^+ e^-$ DECAY

In the pole approximation the electromagnetic transition form factor for a resonance of mass M is given by the expression:
 $|F|^2 = (1 - M^2/\Lambda^2)^{-2}$,

where for the parameter Λ vector dominance predicts $\Lambda = M_p \approx 0.770$ GeV. The ARNALDI 09 measurement is in obvious conflict with this expectation. Note that for $\eta \rightarrow \gamma \mu^+ \mu^-$ decay ARNALDI 09 and DZHELJADIN 80 obtain the value of Λ consistent with vector dominance.

PARAMETER Λ IN $\omega \rightarrow \pi^0 \mu^+ \mu^-$ DECAY

VALUE (GeV)	EVTS	DOCUMENT ID	TECN	COMMENT
0.670 ± 0.006 OUR AVERAGE				
0.6707 ± 0.0039 ± 0.0056		¹ ARNALDI 16	NA60	400 GeV (p -A) collisions
0.668 ± 0.009 ± 0.003	3k	² ARNALDI 09	NA60	158A In-In collisions
•••				••• We do not use the following data for averages, fits, limits, etc. •••
0.65 ± 0.03		DZHELJADIN 81B	CNTR	25-33 $\pi^- p \rightarrow \omega n$

¹ARNALDI 16 reports $\Lambda^{-2}(\omega) = 2.223 \pm 0.026 \pm 0.037$ GeV⁻² which we converted to the quoted Λ value.
²ARNALDI 09 reports $\Lambda^{-2}(\omega) = 2.24 \pm 0.06 \pm 0.02$ GeV⁻² which we converted to the quoted Λ value.

PARAMETER Λ IN $\omega \rightarrow \pi^0 e^+ e^-$ DECAY

VALUE (GeV)	EVTS	DOCUMENT ID	TECN	COMMENT
0.709 ± 0.037	1.1k	¹ ADLARSON 17B	A2MM	$\gamma p \rightarrow \omega p$
		¹ ADLARSON 17B		reports $\Lambda^{-2}(\omega\pi^0) = 1.99 \pm 0.21$ GeV ⁻² that we converted to the quoted Λ value.

ENERGY DEPENDENCE OF $\omega \rightarrow \pi^+ \pi^- \pi^0$ DALITZ PLOT

The following experiments fit to one or more of the coefficients α, β, γ for $|matrix element|^2 \propto P(1 + 2\alpha Z + 2\beta Z^2/2 \sin(3\phi) + 2\gamma Z^2 + O(Z^3/2))$ where P is the P -wave phase-space factor and Z, ϕ are kinematical variables as defined in ADLARSON 17.

VALUE	EVTS	DOCUMENT ID	TECN	COMMENT
0.133 ± 0.008 OUR AVERAGE				
0.1321 ± 0.0067 ± 0.0046	260k	¹ ABLIKIM 18AD	BES3	$J/\psi \rightarrow \omega \eta$
0.147 ± 0.036	44k	ADLARSON 17	WASA	α in $p d \rightarrow {}^3\text{He} \omega$, $pp \rightarrow pp \omega$
				¹ Keeping a term linear in Z only. A fit with the terms proportional to Z and Z ^{3/2} gives $\alpha = 0.133 \pm 0.041$ and $\beta = 0.037 \pm 0.054$.

$\omega(782)$ REFERENCES

ACHASOV 21	JHEP 2101 113	M.N. Achasov et al.	(SND Collab.)
LEES 21B	PR D104 112003	J.P. Lees et al.	(BABAR Collab.)
ANDREEV 20	EPJ C80 1189	V. Andreev et al.	(HI Collab.)
HOID 20	EPJ C80 988	B.-L. Hoid, M. Hoferichter, B. Kubis	(BONN, BERN)
COLANGELO 19	JHEP 1902 006	G. Colangelo, M. Hoferichter, P. Stoffer	(BERN+)
HOEFERICHT... 19	JHEP 1908 137	M. Hoferichter, B.-L. Hoid, B. Kubis	(WASH, BONN)
ABLIKIM 18CD	PR D98 112007	M. Ablikim et al.	(BESIII Collab.)
ABLIKIM 18D	PRL 120 242003	M. Ablikim et al.	(BESIII Collab.)
ABLIKIM 18S	PR D98 032001	M. Ablikim et al.	(BESIII Collab.)
HANHART 18	EPJ C78 450	C. Hanhart et al.	
ADLARSON 17	PL B770 418	P. Adlarson et al.	(WASA-at-COSY Collab.)
ADLARSON 17B	PR C95 035208	P. Adlarson et al.	(A2 Collab. at MAMI)
ANASTASI 17	PL B767 485	A. Anastasi et al.	(KLOE-2 Collab.)
ABLIKIM 16B	PL B753 103	M. Ablikim et al.	(BESIII Collab.)
ACHASOV 16A	PR D93 092001	M.N. Achasov et al.	(SND Collab.)
ARNALDI 16	PL B757 437	R. Arnaldi et al.	(NA60 Collab.)
PDG 16	CP C40 100001	C. Patrignani et al.	(PDG Collab.)
PDG 15	RPP 2015 at pdg.lbl.gov		(PDG Collab.)
ACHASOV 13	PR D88 054013	M.N. Achasov et al.	(SND Collab.)
BABUSI 13D	PL B720 336	D. Babusci et al.	(CATA, CALB, BARI)
BENAYOUN 13	EPJ C73 2453	M. Benayoun, P. David, L. DelBuono (PARIN, BERLIN+)	
DAVIER 13	EPJ C73 2597	M. Davier et al.	
LEES 12G	PR D86 032013	J.P. Lees et al.	(BABAR Collab.)
NIECKNIG 12	EPJ C72 2014	F. Niecknig, B. Kubis, S.P. Schneider	(BONN)
AMBROSINO 11A	PL B700 102	F. Ambrosino et al.	(KLOE Collab.)
BENAYOUN 10	EPJ C65 211	M. Benayoun et al.	
ACHASOV 09A	JETP 109 379	M.N. Achasov et al.	(SND Collab.)
	Translated from ZETF 136 442.		
ARNALDI 09	PL B677 260	R. Arnaldi et al.	(NA60 Collab.)
AUBERT 09AS	PRL 103 231801	B. Aubert et al.	(BABAR Collab.)
STAROSTIN 09	PR C79 065201	A. Starostin et al.	(Crystal Ball Collab. at MAMI)
ACHASOV 08	JETP 107 61	M.N. Achasov et al.	(SND Collab.)
	Translated from ZETF 134 80.		
AMBROSINO 08G	PL B669 223	F. Ambrosino et al.	(KLOE Collab.)
ACHASOV 07B	PR D76 077101	M.N. Achasov et al.	(SND Collab.)
AKHMETSHIN 07	PL B648 28	R.R. Akhmetshin et al.	(Novosibirsk CMD-2 Collab.)
ACHASOV 06	JETP 103 380	M.N. Achasov et al.	(Novosibirsk SND Collab.)
	Translated from ZETF 130 437.		
ACHASOV 06A	PR D74 014016	M.N. Achasov et al.	(SND Collab.)
AULCHENKO 06	JETPL 84 413	V.M. Aulchenko et al.	(Novosibirsk CMD-2 Collab.)
	Translated from ZETF 84 491.		
ACHASOV 05A	JETP 101 1053	M.N. Achasov et al.	(Novosibirsk SND Collab.)
	Translated from ZETF 128 1201.		
AKHMETSHIN 05	PL B605 26	R.R. Akhmetshin et al.	(Novosibirsk CMD-2 Collab.)
AKHMETSHIN 05A	PL B613 29	R.R. Akhmetshin et al.	(Novosibirsk CMD-2 Collab.)
AULCHENKO 05	JETPL 82 743	V.M. Aulchenko et al.	(Novosibirsk CMD-2 Collab.)
	Translated from ZETF 82 841.		
AKHMETSHIN 04	PL B578 285	R.R. Akhmetshin et al.	(Novosibirsk CMD-2 Collab.)
AKHMETSHIN 04B	PL B580 119	R.R. Akhmetshin et al.	(Novosibirsk CMD-2 Collab.)
AUBERT, B 04N	PR D70 072004	B. Aubert et al.	(BABAR Collab.)
PDG 04	PL B592 1	S. Eidelman et al.	(PDG Collab.)
ACHASOV 03	PL B559 171	M.N. Achasov et al.	(Novosibirsk SND Collab.)
ACHASOV 03D	PR D68 052006	M.N. Achasov et al.	(Novosibirsk SND Collab.)
ALOISIO 03	PL B561 55	A. Aloisio et al.	(KLOE Collab.)
BENAYOUN 03	EPJ C29 397	M. Benayoun et al.	
ACHASOV 02E	PR D66 032001	M.N. Achasov et al.	(Novosibirsk SND Collab.)
ACHASOV 02F	PL B537 201	M.N. Achasov et al.	(Novosibirsk SND Collab.)
AKHMETSHIN 02	PL B527 161	R.R. Akhmetshin et al.	(Novosibirsk CMD-2 Collab.)
ALOISIO 02D	PL B537 21	A. Aloisio et al.	(KLOE Collab.)
HEISTER 02C	PL B528 19	A. Heister et al.	(ALEPH Collab.)

ACHASOV 01E	PR D63 072002	M.N. Achasov et al.	(Novosibirsk SND Collab.)
AKHMETSHIN 01B	PL B509 217	R.R. Akhmetshin et al.	(Novosibirsk CMD-2 Collab.)
BARBERIS 01	PL B507 14	D. Barberis et al.	
ACHASOV 00	EPJ C12 25	M.N. Achasov et al.	(Novosibirsk SND Collab.)
ACHASOV 00D	JETPL 72 282	M.N. Achasov et al.	(Novosibirsk SND Collab.)
	Translated from ZETF 72 411.		
ACHASOV 00G	JETPL 71 355	M.N. Achasov et al.	(Novosibirsk SND Collab.)
	Translated from ZETF 71 519.		
AKHMETSHIN 00A	PL B476 33	R.R. Akhmetshin et al.	(Novosibirsk CMD-2 Collab.)
AULCHENKO 00C	JETP 90 927	V.M. Aulchenko et al.	(Novosibirsk SND Collab.)
	Translated from ZETF 117 1067.		
CASE 00	PR D61 032002	T. Case et al.	(Crystal Barrel Collab.)
ACHASOV 99E	PL B462 365	M.N. Achasov et al.	(Novosibirsk SND Collab.)
GARDNER 99	PR D59 076002	S. Gardner, H.B. O'Connell	
BENAYOUN 98	EPJ C2 259	M. Benayoun et al.	(IPNP, NOVO, ADL+)
ABELE 97E	PL B411 361	A. Abele et al.	(Crystal Barrel Collab.)
BENAYOUN 96	ZPHY C72 221	M. Benayoun et al.	(IPNP, NOVO)
PROKOSHKIN 95	PD 40 273	Y.D. Prokoshkin, V.D. Samoilenko	(SERP)
	Translated from DANS 342 610.		
WURZINGER 95	PR C51 443	R. Wurzinger et al.	(BONN, ORSAY, SACL+)
ALDE 94B	PL B340 122	D.M. Alde et al.	(SERP, BELG, LANL, LAPP+)
AMSLER 94C	PL B327 425	C. Amisler et al.	(Crystal Barrel Collab.)
ALDE 93	PAN 56 122 9	D.M. Alde et al.	(SERP, LAPP, LANL, BELG+)
	Translated from YAF 56 137.		
Also			
ZPHY C61 35		D.M. Alde et al.	(SERP, LAPP, LANL, BELG+)
AMSLER 93B	PL B311 362	C. Amisler et al.	(Crystal Barrel Collab.)
WEIDENAUER 93	ZPHY C59 387	P. Weidenauer et al.	(ASTERIX Collab.)
ANTONELLI 92	ZPHY C56 15	A. Antonelli et al.	(DM2 Collab.)
DOLINSKY 91	PRPL 202 99	S.I. Dolinsky et al.	(NOVO)
WEIDENAUER 90	ZPHY C47 353	P. Weidenauer et al.	(ASTERIX Collab.)
DOLINSKY 89	ZPHY C42 511	S.I. Dolinsky et al.	(NOVO)
BITYUKOV 88B	SJNP 47 800	S.I. Bitjukov et al.	(SERP)
	Translated from YAF 47 1258.		
DOLINSKY 88	SJNP 48 277	S.I. Dolinsky et al.	(NOVO)
	Translated from YAF 48 442.		
KURDADZE 88	JETPL 47 512	L.M. Kurdadze et al.	(NOVO)
	Translated from ZETF 47 432.		
AULCHENKO 87	PL B186 432	V.M. Aulchenko et al.	(NOVO)
BARKOV 87	JETPL 46 164	L.M. Barkov et al.	(NOVO)
	Translated from ZETF 46 132.		
KURDADZE 86	JETPL 43 643	L.M. Kurdadze et al.	(NOVO)
	Translated from ZETF 43 497.		
BARKOV 85	NP B256 365	L.M. Barkov et al.	(NOVO)
DRUZHININ 84B	PL 144B 136	V.P. Druzhinin et al.	(NOVO)
KURDADZE 83B	JETPL 36 274	L.M. Kurdadze et al.	(NOVO)
	Translated from ZETF 36 221.		
DZHELJADIN 81B	PL 102B 296	R.I. Dzhelezadin et al.	(SERP)
CORDIER 80	NP B172 13	A. Cordier et al.	(LALO)
DZHELJADIN 80	PL 94B 548	R.I. Dzhelezadin et al.	(SERP)
ROOS 80	LNC 27 321	M. Roos, A. Pellinen	(HELS)
BENKHEIRI 79	NP B150 268	P. Benkheiri et al.	(EPOL, CERN, CDF+)
DZHELJADIN 79	PL 84B 143	R.I. Dzhelezadin et al.	(SERP)
COOPER 78B	NP B146 1	A.M. Cooper et al.	(TATA, CERN, CDF+)
QUENZER 78	PL 76B 512	A. Quenzer et al.	(LALO)
VANAPHEL... 78	NP B133 245	V.M. van Apeldoorn et al.	(ZEEM)
WICKLUND 78	PR D17 1197	A.B. Wicklund et al.	(ANL)
ANDREWS 77	PRL 38 198	D.E. Andrews et al.	(ROCH)
GESSAROLI 77	NP B126 382	R. Gessaroli et al.	(BGNA, FIRZ, GENO+)
KEYNE 76	PR D14 28	J. Keyne et al.	(LOIC, SHMP)
	PR D8 2789	D.M. Binnie et al.	(LOIC, SHMP)
Also			
KALBFLEISCH 75	PR D11 987	G.R. Kalbfleisch, R.C. Strand, J.W. Chapman	(BNL+)
AGUILAR... 72B	PR D6 29	M. Aguilar-Benitez et al.	(BNL)
APEL 72B	PL 41B 234	W.D. Apel et al.	(KARLK, KARLE, PISA)
BASILE 72B	Phil. Conf. 153	M. Basile et al.	(CERN)
BENAKSAS 72	PL 39B 209	D. Benaksas et al.	(ORSAY)
BENAKSAS 72B	PL 42B 507	D. Benaksas et al.	(ORSAY)
BENAKSAS 72C	PL 42B 511	D. Benaksas et al.	(ORSAY)
BORNSTEIN 72	PR D5 1559	S.R. Bornstein et al.	(BNL, MICH)
BROWN 72	PL 42B 117	R.M. Brown et al.	(ILL, ILLC)
DAKIN 72	PR D6 2321	J.T. Dakin et al.	(PRIN)
RATCLIFF 72	PL 38B 345	B.N. Ratcliff et al.	(SLAC)
ALVENSEN... 71C	PRL 27 888	H. Alvensleben et al.	(DESY)
BALDIN 71	SJNP 13 758	A.B. Baldin et al.	(ITEP)
	Translated from YAF 13 1318.		
BEHREND 71	PR 27 61	H.J. Behrend et al.	(ROCH, CERN, FNAL)
BIZZARRI 71	NP B27 140	R. Bizzarri et al.	(CERN, CDF)
COYNE 71	NP B32 333	D.G. Coyne et al.	(LRL)
MOFFETT 71	NP B29 349	K.C. Moffett et al.	(LRL, UCB, SLAC+)
ABRAMOV... 70B	NP B20 209	M. Abramovich et al.	(CERN)
BIGGS 70B	PRL 24 1201	P.J. Biggs et al.	(DARE)
BIZZARRI 70	PRL 25 1385	R. Bizzarri et al.	(ROMA, SYRA)
ROOS 70	DNPL/R7 173	M. Roos	(CERN)
	Proc. Daresbury Study Weekend No. 1.		
AUGUSTIN 69D	PL 28B 513	J.E. Augustin et al.	(ORSAY)
BIZZARRI 69	NP B14 169	R. Bizzarri et al.	(CERN, CDF)
DEINET 69B	PL 30B 426	W. Deinet et al.	(KARL, CERN)
JACQUET 69B	NC 63A 743	F. Jacquet et al.	(EPOL, BERG)
WILSON 69	Private Comm.	R. Wilson	(HARV)
	Also		
PR 178 2095		A.A. Wehmhann et al.	(HARV, CASE, SLAC+)
BOLLINI 68C	NC 56A 531	R.G. Astvatsaturov et al.	(JINR, MOSU)
GOUNARIS 68	PRL 21 244	G.J. Gounaris, J.J. Sakurai	(CERN, BGNA, STRB)
BARASH 67B	PR 156 1339	N. Barash et al.	(COLU)
FELDMAN 67C	PR 159 1219	M. Feldman et al.	(PENN)
DI GIUGNO 66B	NC 44A 1272	G. Di Giugno et al.	(NAPL, FRAS, TRST)
FLATTE 66	PR 146 0500	S.M. Flatte et al.	(LRL)
JAMES 66	PR 142 396	F.E. James, H.L. Kraybill	(YALE, BNL)
BARBARO... 65	PRL 14 279	A. Barbaro-Galteri, R.D. Tripp	(LRL)
BARMIN 64	JETP 18 1289	V.V. Barmin et al.	(ITEP)
	Translated from ZETF 45 1879.		
KRAEMER 64	PR 136 B496	R.W. Kraemer et al.	(JHU, NWES, WOOD)
BUSCHBECK 63	Siena Conf. 1 166	B. Buschbeck et al.	(VIEN, CERN, ANIK)

$\eta'(958)$

$$I^G(J^{PC}) = 0^+(0^{-+})$$

$\eta'(958)$ MASS

VALUE (MeV)	EVTS	DOCUMENT ID	TECN	COMMENT
957.78 ± 0.06 OUR AVERAGE				
957.793 ± 0.054 ± 0.036	3.9k	LIBBY 08	CLEO	$J/\psi \rightarrow \gamma \eta'$
957.9 ± 0.2 ± 0.6	4800	WURZINGER 96	SPEC	$1.68 p d \rightarrow {}^3\text{He} \eta'$
957.46 ± 0.33		DUANE 74	MMS	$\pi^- p \rightarrow n \eta'$
958.2 ± 0.5	1414	DANBURG 73	HBC	$2.2 K^- p \rightarrow \Lambda \eta'$
958 ± 1	400	JACOBS 73	HBC	$2.9 K^- p \rightarrow \Lambda \eta'$
956.1 ± 1.1	3415	¹ BASILE 71	CNTR	$1.6 \pi^- p \rightarrow n \eta'$

Meson Particle Listings

 $\eta'(958)$

••• We do not use the following data for averages, fits, limits, etc. •••

957.5 ± 0.2		BAI	04J	BES2	$J/\psi \rightarrow \gamma\gamma\pi^+\pi^-$
959 ± 1	630	² BELADIDZE	92C	VES	$36\pi^-\text{Be} \rightarrow \pi^-\eta'\eta\text{Be}$
958 ± 1	340	² ARMSTRONG	91B	OMEG	$300\rho\rho \rightarrow \rho\rho\eta\pi^+\pi^-$
958.2 ± 0.4	622	² AUGUSTIN	90	DM2	$J/\psi \rightarrow \gamma\eta\pi^+\pi^-$
957.8 ± 0.2	2420	² AUGUSTIN	90	DM2	$J/\psi \rightarrow \gamma\gamma\pi^+\pi^-$
956.3 ± 1.0	143	² GIDAL	87	MRK2	$e^+e^- \rightarrow e^+e^-\eta\pi^+\pi^-$
957.4 ± 1.4	535	³ BASILE	71	CNTR	$1.6\pi^-\rho \rightarrow n\eta'$
957 ± 1		RITTENBERG	69	HBC	$1.7\text{--}2.7\text{K}^-\rho$

¹ Using all η' decays.

² Systematic uncertainty not estimated.

³ Using η' decays into neutrals. Not independent of the other listed BASILE 71 η' mass measurement.

 $\eta'(958)$ WIDTH

VALUE (MeV)	EVTs	DOCUMENT ID	TECN	CHG	COMMENT
0.188 ± 0.006 OUR FIT					
0.230 ± 0.021 OUR AVERAGE					
0.226 ± 0.017 ± 0.014	2300	CZERWINSKI	10	MMS	$\rho\rho \rightarrow \rho\rho\eta'$
0.40 ± 0.22	4800	WURZINGER	96	SPEC	$1.68\rho d \rightarrow {}^3\text{He}\eta'$
0.28 ± 0.10	1000	BINNIE	79	MMS	0 $\pi^-\rho \rightarrow n\text{MM}$
••• We do not use the following data for averages, fits, limits, etc. •••					
0.20 ± 0.04		BAI	04J	BES2	$J/\psi \rightarrow \gamma\gamma\pi^+\pi^-$

 $\eta'(958)$ DECAY MODES

Mode	Fraction (Γ_i/Γ)	Confidence level
Γ_1 $\pi^+\pi^-\eta$	(42.5 ± 0.5) %	
Γ_2 $\rho^0\gamma$ (including non-resonant $\pi^+\pi^-\gamma$)	(29.5 ± 0.4) %	
Γ_3 $\rho^0\gamma$	(22.4 ± 0.5) %	
Γ_4 $\pi^0\pi^0\eta$	(2.52 ± 0.07) %	
Γ_5 $\omega\gamma$	(2.0 ± 0.4) × 10 ⁻⁴	
Γ_6 ωe^+e^-	(2.307 ± 0.033) %	
Γ_7 $\gamma\gamma$	(2.50 ± 0.17) × 10 ⁻³	
Γ_8 $3\pi^0$	(1.13 ± 0.28) × 10 ⁻⁴	
Γ_9 $\mu^+\mu^-\gamma$	(1.9 ± 0.4) × 10 ⁻⁵	
Γ_{10} $\pi^+\pi^-\mu^+\mu^-$	(3.61 ± 0.17) × 10 ⁻³	
Γ_{11} $\pi^+\pi^-\pi^0$	(3.8 ± 0.5) × 10 ⁻³	
Γ_{12} $(\pi^+\pi^-\pi^0)$ S-wave	(7.4 ± 2.3) × 10 ⁻⁴	
Γ_{13} $\pi^-\pi^+\rho^\pm$	(8.3 ± 0.9) × 10 ⁻⁵	
Γ_{14} $2(\pi^+\pi^-\pi^0)$	(1.8 ± 0.4) × 10 ⁻⁴	
Γ_{15} $\pi^+\pi^-\pi^0$	< 1	95%
Γ_{16} $2(\pi^+\pi^-\pi^0)$ neutrals	< 1.8	× 10 ⁻³ 90%
Γ_{17} $2(\pi^+\pi^-\pi^0)$	< 1	% 95%
Γ_{18} $2(\pi^+\pi^-\pi^0)2\pi^0$	< 3.1	× 10 ⁻⁵ 90%
Γ_{19} $3(\pi^+\pi^-\pi^0)$	< 4	× 10 ⁻⁵ 90%
Γ_{20} $K^\pm\pi^\mp$	(2.42 ± 0.10) × 10 ⁻³	
Γ_{21} $\pi^+\pi^-\pi^+\pi^-$	< 2.1	× 10 ⁻⁴ 90%
Γ_{22} $\pi^+e^-\nu_e + \text{c.c.}$	(4.91 ± 0.27) × 10 ⁻⁴	
Γ_{23} γe^+e^-	(3.20 ± 0.24) × 10 ⁻³	
Γ_{24} $\pi^0\gamma\gamma$	(6.2 ± 0.9) × 10 ⁻⁴	
Γ_{25} $\pi^0\gamma\gamma$ (non resonant)	< 1.33	× 10 ⁻⁴ 90%
Γ_{26} $\eta\gamma\gamma$	< 4.94	× 10 ⁻⁵ 90%
Γ_{27} $4\pi^0$	< 5.6	× 10 ⁻⁹ 90%
Γ_{28} e^+e^-	(4.5 ± 1.1) × 10 ⁻⁶	
Γ_{29} $e^+e^-\pi^+\pi^-$	< 6	× 10 ⁻⁴ 90%
Γ_{30} invisible		

Charge conjugation (C), Parity (P), Lepton family number (LF) violating modes

Γ_{31} $\pi^+\pi^-$	P,CP	< 1.8	× 10 ⁻⁵	90%
Γ_{32} $\pi^0\pi^0$	P,CP	< 4	× 10 ⁻⁴	90%
Γ_{33} $\pi^0 e^+ e^-$	C	[a] < 1.4	× 10 ⁻³	90%
Γ_{34} $\pi^0\rho^0$	C	< 4	%	90%
Γ_{35} $\eta e^+ e^-$	C	[a] < 2.4	× 10 ⁻³	90%
Γ_{36} 3γ	C	< 1.0	× 10 ⁻⁴	90%
Γ_{37} $\mu^+\mu^-\pi^0$	C	[a] < 6.0	× 10 ⁻⁵	90%
Γ_{38} $\mu^+\mu^-\eta$	C	[a] < 1.5	× 10 ⁻⁵	90%
Γ_{39} $e\mu$	LF	< 4.7	× 10 ⁻⁴	90%

[a] C parity forbids this to occur as a single-photon process.

CONSTRAINED FIT INFORMATION

An overall fit to the total width, a partial width, 2 combinations of partial widths obtained from integrated cross section, and 20 branching ratios uses 52 measurements and one constraint to determine 9 parameters. The overall fit has a $\chi^2 = 69.5$ for 44 degrees of freedom.

The following *off-diagonal* array elements are the correlation coefficients $\langle \delta p_i \delta p_j \rangle / (\delta p_i \delta p_j)$, in percent, from the fit to parameters p_i , including the branching fractions, $x_i \equiv \Gamma_i / \Gamma_{\text{total}}$. The fit constrains the x_i whose labels appear in this array to sum to one.

x_2	-25							
x_4	-75	-43						
x_5	-7	-6	-2					
x_7	-11	-7	9	-1				
x_8	-17	-10	19	0	2			
x_{11}	-1	-1	-1	0	0	0		
x_{21}	-8	30	-14	-2	-2	-3	0	
Γ	11	-10	-1	1	-40	0	0	-3
	x_1	x_2	x_4	x_5	x_7	x_8	x_{11}	x_{21}

Mode	Rate (MeV)
Γ_1 $\pi^+\pi^-\eta$	0.0799 ± 0.0029
Γ_2 $\rho^0\gamma$ (including non-resonant $\pi^+\pi^-\gamma$)	0.0554 ± 0.0019
Γ_4 $\pi^0\pi^0\eta$	0.0421 ± 0.0017
Γ_5 $\omega\gamma$	0.00474 ± 0.00020
Γ_7 $\gamma\gamma$	0.00434 ± 0.00013
Γ_8 $3\pi^0$	(4.7 ± 0.4) × 10 ⁻⁴
Γ_{11} $\pi^+\pi^-\pi^0$	(6.8 ± 0.4) × 10 ⁻⁴
Γ_{21} $\pi^+\pi^-\pi^+\pi^-$	(4.54 ± 0.23) × 10 ⁻⁴

 $\eta'(958)$ PARTIAL WIDTHS

$\Gamma(\gamma\gamma)$	VALUE (keV)	EVTs	DOCUMENT ID	TECN	COMMENT	Γ_7
4.34 ± 0.14 OUR FIT						
4.28 ± 0.19 OUR AVERAGE						
4.17 ± 0.10 ± 0.27	2000	¹ ACCIARRI	98Q	L3	$e^+e^- \rightarrow e^+e^-\pi^+\pi^-\gamma$	
4.53 ± 0.29 ± 0.51	266	KARCH	92	CBAL	$e^+e^- \rightarrow e^+e^-\eta\pi^0\pi^0$	
3.61 ± 0.13 ± 0.48		² BEHREND	91	CELL	$e^+e^- \rightarrow e^+e^-\eta'(958)$	
4.6 ± 1.1 ± 0.6	23	BARU	90	MD1	$e^+e^- \rightarrow e^+e^-\pi^+\pi^-\gamma$	
4.57 ± 0.25 ± 0.44		BUTLER	90	MRK2	$e^+e^- \rightarrow e^+e^-\eta'(958)$	
5.08 ± 0.24 ± 0.71	547	³ ROE	90	ASP	$e^+e^- \rightarrow e^+e^-\pi^+\pi^-\gamma$	
3.8 ± 0.7 ± 0.6	34	AIHARA	88c	TPC	$e^+e^- \rightarrow e^+e^-\eta\pi^+\pi^-$	
4.9 ± 0.5 ± 0.5	136	⁴ WILLIAMS	88	CBAL	$e^+e^- \rightarrow e^+e^-\pi^+\pi^-\gamma$	
••• We do not use the following data for averages, fits, limits, etc. •••						
4.7 ± 0.6 ± 0.9	143	⁵ GIDAL	87	MRK2	$e^+e^- \rightarrow e^+e^-\eta\pi^+\pi^-$	
4.0 ± 0.9		⁶ BARTEL	85E	JADE	$e^+e^- \rightarrow e^+e^-\pi^+\pi^-\gamma$	

¹ No non-resonant $\pi^+\pi^-$ contribution found.

² Reevaluated by us using $B(\eta' \rightarrow \rho(770)\gamma) = (30.2 \pm 1.3)\%$.

³ Reevaluated by us using $B(\eta' \rightarrow \gamma\gamma) = (2.11 \pm 0.13)\%$.

⁴ Reevaluated by us using $B(\eta' \rightarrow \gamma\gamma) = (2.11 \pm 0.13)\%$.

⁵ Superseded by BUTLER 90.

⁶ Systematic error not evaluated.

$\Gamma(e^+e^-)$	VALUE (eV)	CL%	DOCUMENT ID	TECN	COMMENT	Γ_{28}
< 1.1 × 10⁻³	90	1,2	ACHASOV	15	SND	0.958 $e^+e^- \rightarrow \pi\pi\eta$
••• We do not use the following data for averages, fits, limits, etc. •••						
< 2.0 × 10 ⁻³	90	2	ACHASOV	15	SND	0.958 $e^+e^- \rightarrow \pi\pi\eta$
< 2.4 × 10 ⁻³	90	2	AKHMETSHIN	15	CMD3	0.958 $e^+e^- \rightarrow \pi^+\pi^-\eta$

¹ Combining data of ACHASOV 15 and AKHMETSHIN 15.

² Using η and η' branching fractions from PDG 14.

 $\eta'(958)$ $\Gamma(i)\Gamma(\gamma\gamma)/\Gamma(\text{total})$

This combination of a partial width with the partial width into $\gamma\gamma$ and with the total width is obtained from the integrated cross section into channel(i) in the $\gamma\gamma$ annihilation.

$\Gamma(\gamma\gamma) \times \Gamma(\rho^0\gamma \text{ (including non-resonant } \pi^+\pi^-\gamma)) / \Gamma_{\text{total}}$	VALUE (keV)	EVTs	DOCUMENT ID	TECN	COMMENT	$\Gamma_7\Gamma_2/\Gamma$
1.28 ± 0.04 OUR FIT						
1.26 ± 0.07 OUR AVERAGE						
1.09 ± 0.04 ± 0.13			BEHREND	91	CELL	$e^+e^- \rightarrow e^+e^-\rho(770)^0\gamma$
1.35 ± 0.09 ± 0.21			AIHARA	87	TPC	$e^+e^- \rightarrow e^+e^-\rho\gamma$

Error includes scale factor of 1.2.

1.13±0.04±0.13	867	ALBRECHT	87B	ARG	$e^+e^- \rightarrow e^+e^-\rho\gamma$
1.53±0.09±0.21		ALTHOFF	84E	TASS	$e^+e^- \rightarrow e^+e^-\rho\gamma$
1.14±0.08±0.11	243	BERGER	84B	PLUT	$e^+e^- \rightarrow e^+e^-\rho\gamma$
1.73±0.34±0.35	95	JENNI	83	MRK2	$e^+e^- \rightarrow e^+e^-\rho\gamma$
1.49±0.13±0.027	213	BARTEL	82B	JADE	$e^+e^- \rightarrow e^+e^-\rho\gamma$
•••					We do not use the following data for averages, fits, limits, etc. •••
1.85±0.31±0.24	43	BEHREND	82C	CELL	$e^+e^- \rightarrow e^+e^-\rho\gamma$

 $\Gamma(\gamma\gamma) \times \Gamma(\pi^0\pi^0\eta)/\Gamma_{\text{total}}$ $\Gamma_7\Gamma_4/\Gamma$

VALUE (keV)	DOCUMENT ID	TECN	COMMENT
0.97±0.04 OUR FIT			Error includes scale factor of 1.1.
0.92±0.06±0.11	¹ KARCH	92	CBAL $e^+e^- \rightarrow e^+e^-\eta\pi^0\pi^0$
•••			We do not use the following data for averages, fits, limits, etc. •••
0.95±0.05±0.08	² KARCH	90	CBAL $e^+e^- \rightarrow e^+e^-\eta\pi^0\pi^0$
1.00±0.08±0.10	^{2,3} ANTREASYAN	87	CBAL $e^+e^- \rightarrow e^+e^-\eta\pi^0\pi^0$
¹ Reevaluated by us using $B(\eta \rightarrow \gamma\gamma) = (39.21 \pm 0.34)\%$. Supersedes ANTREASYAN 87 and KARCH 90.			
² Superseded by KARCH 92.			
³ Using $BR(\eta \rightarrow 2\gamma) = (38.9 \pm 0.5)\%$.			

 $\eta'(958) \Gamma(i)(e^+e^-)/\Gamma(\text{total})$
 $\Gamma(\pi^+\pi^-\eta) \times \Gamma(e^+e^-)/\Gamma_{\text{total}}$ $\Gamma_1\Gamma_{28}/\Gamma$

VALUE (10^{-3} eV)	CL%	DOCUMENT ID	TECN	COMMENT
<1.0	90	¹ AKHMETSHIN	15	CMD3 $0.958 e^+e^- \rightarrow \pi^+\pi^-\eta$
¹ AKHMETSHIN 15 reports $[\Gamma(\eta'(958) \rightarrow \pi^+\pi^-\eta) \times \Gamma(\eta'(958) \rightarrow e^+e^-)]/\Gamma_{\text{total}} \times [B(\eta \rightarrow 2\gamma)] < 4.1 \times 10^{-4}$ eV which we divide by our best value $B(\eta \rightarrow 2\gamma) = 39.36 \times 10^{-2}$.				

 $\eta'(958)$ BRANCHING RATIOS
 $\Gamma(\pi^+\pi^-\eta)/\Gamma_{\text{total}}$ Γ_1/Γ

VALUE (units 10^{-2})	EVTS	DOCUMENT ID	TECN	COMMENT
42.5 ± 0.5 OUR FIT				Error includes scale factor of 1.1.
41.24 ± 0.08 ± 1.24	312k	ABLIKIM	19T	BES $J/\psi \rightarrow \gamma\eta'$
•••				We do not use the following data for averages, fits, limits, etc. •••
42.4 ± 1.1 ± 0.4	1.2k	¹ PEDLAR	09	CLEO $J/\psi \rightarrow \gamma\eta'$
¹ Not independent of other η' branching fractions and ratios in PEDLAR 09.				

 $\Gamma(\pi^+\pi^-\eta(\text{charged decay}))/\Gamma_{\text{total}}$ $0.2804\Gamma_1/\Gamma$

VALUE	EVTS	DOCUMENT ID	TECN	COMMENT
0.1191 ± 0.0015 OUR FIT				Error includes scale factor of 1.1.
•••				We do not use the following data for averages, fits, limits, etc. •••
0.123 ± 0.014	107	RITTENBERG	69	HBC $1.7\text{--}2.7 K^-p$
0.10 ± 0.04	10	LONDON	66	HBC $2.24 K^-p \rightarrow \Lambda 2\pi^+ 2\pi^- \pi^0$
0.07 ± 0.04	7	BADIER	65B	HBC $3 K^-p$

 $\Gamma(\pi^+\pi^-\eta(\text{neutral decay}))/\Gamma_{\text{total}}$ $0.7196\Gamma_1/\Gamma$

VALUE	EVTS	DOCUMENT ID	TECN	COMMENT
0.306 ± 0.004 OUR FIT				Error includes scale factor of 1.1.
•••				We do not use the following data for averages, fits, limits, etc. •••
0.314 ± 0.026	281	RITTENBERG	69	HBC $1.7\text{--}2.7 K^-p$

 $\Gamma(\rho^0\gamma(\text{including non-resonant } \pi^+\pi^-\gamma))/\Gamma_{\text{total}}$ Γ_2/Γ

VALUE (units 10^{-2})	EVTS	DOCUMENT ID	TECN	COMMENT
29.5 ± 0.4 OUR FIT				Error includes scale factor of 1.1.
29.90 ± 0.03 ± 0.55	913k	ABLIKIM	19T	BES $J/\psi \rightarrow \gamma\eta'$
•••				We do not use the following data for averages, fits, limits, etc. •••
28.7 ± 0.7 ± 0.4	0.2k	¹ PEDLAR	09	CLEO $J/\psi \rightarrow \gamma\eta'$
32.9 ± 3.3	298	RITTENBERG	69	HBC $1.7\text{--}2.7 K^-p$
20 ± 10	20	LONDON	66	HBC $2.24 K^-p \rightarrow \Lambda \pi^+ \pi^- \gamma$
34 ± 9	35	BADIER	65B	HBC $3 K^-p$
¹ Not independent of other η' branching fractions and ratios in PEDLAR 09.				

 $\Gamma(\rho^0\gamma)/\Gamma_{\text{total}}$ Γ_3/Γ

VALUE (%)	EVTS	DOCUMENT ID	TECN	COMMENT
•••				We do not use the following data for averages, fits, limits, etc. •••
33.34 ± 0.06 ± 1.60	970k	¹ ABLIKIM	18C	BES3 $\eta'(958) \rightarrow \gamma\pi^+\pi^-$
34.43 ± 0.52 ± 1.97	970k	² ABLIKIM	18C	BES3 $\eta'(958) \rightarrow \gamma\pi^+\pi^-$
¹ From a fit to $\pi^+\pi^-$ mass using $\rho(770)$, $\omega(782)$, and box anomaly components.				
² From a fit to $\pi^+\pi^-$ mass using $\rho(770)$, $\omega(782)$, and $\rho(1450)$ components.				

 $\Gamma(\rho^0\gamma(\text{including non-resonant } \pi^+\pi^-\gamma))/\Gamma(\pi^+\pi^-\eta)$ Γ_2/Γ_1

VALUE	DOCUMENT ID	TECN	COMMENT
0.694 ± 0.014 OUR FIT			Error includes scale factor of 1.1.
0.683 ± 0.020 OUR AVERAGE			
0.677 ± 0.024 ± 0.011	PEDLAR	09	CLE3 $J/\psi \rightarrow \eta'\gamma$
0.69 ± 0.03	ABLIKIM	06E	BES2 $J/\psi \rightarrow \eta'\gamma$

 $\Gamma(\rho^0\gamma(\text{including non-resonant } \pi^+\pi^-\gamma))/\Gamma(\pi^+\pi^-\eta(\text{neutral decay}))$ $\Gamma_2/0.714\Gamma_1$

VALUE	EVTS	DOCUMENT ID	TECN	COMMENT
0.972 ± 0.020 OUR FIT				Error includes scale factor of 1.1.
0.97 ± 0.09 OUR AVERAGE				
0.70 ± 0.22		AMSLER	04B	CBAR $0 \bar{p}p \rightarrow \pi^+\pi^-\eta$
1.07 ± 0.17		BELADIDZE	92c	VES $36 \pi^- \text{Be} \rightarrow \pi^- \eta' \eta \text{Be}$
0.92 ± 0.14	473	DANBURG	73	HBC $2.2 K^-p \rightarrow \Lambda X^0$
1.11 ± 0.18	192	JACOBS	73	HBC $2.9 K^-p \rightarrow \Lambda X^0$

 $\Gamma(\pi^0\pi^0\eta)/\Gamma_{\text{total}}$ Γ_4/Γ

VALUE (units 10^{-2})	EVTS	DOCUMENT ID	TECN	COMMENT
22.4 ± 0.6 OUR FIT				Error includes scale factor of 1.1.
21.36 ± 0.10 ± 0.92	52k	ABLIKIM	19T	BES $J/\psi \rightarrow \gamma\eta'$
•••				We do not use the following data for averages, fits, limits, etc. •••
23.5 ± 1.3 ± 0.4	3.2k	¹ PEDLAR	09	CLEO $J/\psi \rightarrow \gamma\eta'$
¹ Not independent of other η' branching fractions and ratios in PEDLAR 09.				

 $\Gamma(\pi^0\pi^0\eta(3\pi^0 \text{ decay}))/\Gamma_{\text{total}}$ $0.321\Gamma_4/\Gamma$

VALUE	EVTS	DOCUMENT ID	TECN	COMMENT
0.0718 ± 0.0018 OUR FIT				Error includes scale factor of 1.1.
•••				We do not use the following data for averages, fits, limits, etc. •••
0.11 ± 0.06	4	BENSINGER	70	DBC $2.2 \pi^+ d$

 $\Gamma(\pi^0\pi^0\eta)/\Gamma(\pi^+\pi^-\eta)$ Γ_4/Γ_1

VALUE	DOCUMENT ID	TECN	COMMENT
0.527 ± 0.019 OUR FIT			Error includes scale factor of 1.1.
0.555 ± 0.043 ± 0.013	PEDLAR	09	CLE3 $J/\psi \rightarrow \eta'\gamma$

 $\Gamma(\rho^0\gamma(\text{including non-resonant } \pi^+\pi^-\gamma))/\Gamma(\pi\pi\eta)$ $\Gamma_2/(\Gamma_1+\Gamma_4)$

VALUE	DOCUMENT ID	TECN	COMMENT
0.454 ± 0.009 OUR FIT			Error includes scale factor of 1.1.
0.43 ± 0.02 ± 0.02	BARBERIS	98c	OMEG 450 $pp \rightarrow p_f \eta' p_s$
•••			We do not use the following data for averages, fits, limits, etc. •••
0.31 ± 0.15	DAVIS	68	HBC $5.5 K^-p$

 $\Gamma(\omega\gamma)/\Gamma_{\text{total}}$ Γ_5/Γ

VALUE (units 10^{-2})	EVTS	DOCUMENT ID	TECN	COMMENT
2.52 ± 0.07 OUR FIT				
2.50 ± 0.07 OUR AVERAGE				
2.489 ± 0.018 ± 0.074	23k	ABLIKIM	19T	BES $J/\psi \rightarrow \gamma\eta'$
2.55 ± 0.03 ± 0.16	33.2k	¹ ABLIKIM	15AD	BES3 $J/\psi \rightarrow \eta'\gamma$
•••				We do not use the following data for averages, fits, limits, etc. •••
2.34 ± 0.30 ± 0.04	70	² PEDLAR	09	CLEO $J/\psi \rightarrow \gamma\eta'$
¹ Using $B(J/\psi \rightarrow \eta'\gamma) = (5.15 \pm 0.16) \times 10^{-3}$ and $B(\omega \rightarrow \pi^+\pi^-\pi^0) = (89.2 \pm 0.7)\%$.				
² Not independent of other η' branching fractions and ratios in PEDLAR 09.				

 $\Gamma(\omega\gamma)/\Gamma(\pi^+\pi^-\eta)$ Γ_5/Γ_1

VALUE	EVTS	DOCUMENT ID	TECN	COMMENT
0.0593 ± 0.0018 OUR FIT				Error includes scale factor of 1.1.
0.055 ± 0.007 ± 0.001		PEDLAR	09	CLE3 $J/\psi \rightarrow \eta'\gamma$
•••				We do not use the following data for averages, fits, limits, etc. •••
0.068 ± 0.013	68	ZANFINO	77	ASP K $8.4 \pi^- p$

 $\Gamma(\omega\gamma)/\Gamma(\pi^0\pi^0\eta)$ Γ_5/Γ_4

VALUE	DOCUMENT ID	TECN	COMMENT
0.113 ± 0.004 OUR FIT			
0.147 ± 0.016	ALDE	87B	GAM2 $38 \pi^- p \rightarrow n 4\gamma$

 $\Gamma(\omega e^+e^-)/\Gamma(\omega\gamma)$ Γ_6/Γ_5

VALUE (units 10^{-3})	DOCUMENT ID	TECN	COMMENT
•••			We do not use the following data for averages, fits, limits, etc. •••
7.71 ± 1.34 ± 0.54	¹ ABLIKIM	15AD	BES3 $J/\psi \rightarrow \eta'\gamma$
¹ Obtained from other ABLIKIM 15AD measurements with common systematics taken into account.			

 $\Gamma(\omega e^+e^-)/\Gamma_{\text{total}}$ Γ_6/Γ

VALUE (units 10^{-4})	EVTS	DOCUMENT ID	TECN	COMMENT
1.97 ± 0.34 ± 0.17	66	¹ ABLIKIM	15AD	BES3 $J/\psi \rightarrow \eta'\gamma$
¹ Using $B(J/\psi \rightarrow \eta'\gamma) = (5.15 \pm 0.16) \times 10^{-3}$ and $B(\omega \rightarrow \pi^+\pi^-\pi^0) = (89.2 \pm 0.7)\%$.				

 $\Gamma(\rho^0\gamma(\text{including non-resonant } \pi^+\pi^-\gamma))/[\Gamma(\pi^+\pi^-\eta) + \Gamma(\pi^0\pi^0\eta) + \Gamma(\omega\gamma)]$ $\Gamma_2/(\Gamma_1+\Gamma_4+\Gamma_5)$

VALUE	DOCUMENT ID	TECN	COMMENT
0.437 ± 0.008 OUR FIT			Error includes scale factor of 1.1.
•••			We do not use the following data for averages, fits, limits, etc. •••
0.25 ± 0.14	DAUBER	64	HBC $1.95 K^-p$

Meson Particle Listings

 $\eta'(958)$

$$[\Gamma(\pi^0\pi^0\eta(\text{charged decay})) + \Gamma(\omega(\text{charged decay})\gamma)]/\Gamma_{\text{total}} \quad (0.286\Gamma_4 + 0.89\Gamma_5)/\Gamma$$

VALUE	EVTS	DOCUMENT ID	TECN	COMMENT
0.0864 ± 0.0017 OUR FIT				Error includes scale factor of 1.1.
• • • We do not use the following data for averages, fits, limits, etc. • • •				
0.045 ± 0.029	42	RITTENBERG 69	HBC	1.7–2.7 K^-p

$$\Gamma(\pi^+\pi^-\text{neutrals})/\Gamma_{\text{total}} \quad (0.714\Gamma_1 + 0.286\Gamma_4 + 0.89\Gamma_5)/\Gamma$$

VALUE	EVTS	DOCUMENT ID	TECN	COMMENT
0.3897 ± 0.0028 OUR FIT				Error includes scale factor of 1.1.
• • • We do not use the following data for averages, fits, limits, etc. • • •				
0.4 ± 0.1	39	LONDON 66	HBC	2.24 $K^-p \rightarrow \Lambda\pi^+\pi^-\text{neutrals}$
0.35 ± 0.06	33	BADIER 65B	HBC	3 K^-p

$$\Gamma(\gamma\gamma)/\Gamma_{\text{total}} \quad \Gamma_7/\Gamma$$

VALUE (units 10^{-2})	EVTS	DOCUMENT ID	TECN	COMMENT
2.307 ± 0.035 OUR FIT				Error includes scale factor of 1.1.
2.31 ± 0.06 OUR AVERAGE				Error includes scale factor of 1.8.
2.331 ± 0.012 ± 0.035	71k	ABLIKIM 19T	BES	$J/\psi \rightarrow \gamma\eta'$
1.99 +0.31 -0.27 ± 0.07	114	1 WICHT 08	BELL	$B^\pm \rightarrow K^\pm\gamma\gamma$
2.00 ± 0.18		2 STANTON 80	SPEC	8.45 $\pi^-p \rightarrow n\pi^+\pi^-2\gamma$
• • • We do not use the following data for averages, fits, limits, etc. • • •				
2.25 ± 0.16 ± 0.03	0.3k	3 PEDLAR 09	CLEO	$J/\psi \rightarrow \gamma\eta'$
1.8 ± 0.2	6000	4 APEL 79	NICE	15–40 $\pi^-p \rightarrow n2\gamma$
2.5 ± 0.7		DUANE 74	MMS	$\pi^-p \rightarrow nMM$
1.71 ± 0.33	68	DALPIAZ 72	CNTR	1.6 $\pi^-p \rightarrow nX^0$
2.0 +0.8 -0.6	31	HARVEY 71	OSPK	3.65 $\pi^-p \rightarrow nX^0$

¹WICHT 08 reports $[\Gamma(\eta'(958) \rightarrow \gamma\gamma)/\Gamma_{\text{total}}] \times [B(B^+ \rightarrow \eta'K^+)] = (1.40^{+0.16+0.15}_{-0.15-0.12}) \times 10^{-6}$ which we divide by our best value $B(B^+ \rightarrow \eta'K^+) = (7.04 \pm 0.25) \times 10^{-5}$. Our first error is their experiment's error and our second error is the systematic error from using our best value.

²Includes APEL 79 result.

³Not independent of other η' branching fractions and ratios in PEDLAR 09.

⁴Data is included in STANTON 80 evaluation.

$$\Gamma(\gamma\gamma)/\Gamma(\pi^+\pi^-\eta) \quad \Gamma_7/\Gamma_1$$

VALUE	DOCUMENT ID	TECN	COMMENT
0.0543 ± 0.0012 OUR FIT			Error includes scale factor of 1.1.
0.053 ± 0.004 ± 0.001	PEDLAR 09	CLE3	$J/\psi \rightarrow \eta'\gamma$

$$\Gamma(\gamma\gamma)/\Gamma(\rho^0\gamma(\text{including non-resonant } \pi^+\pi^-\gamma)) \quad \Gamma_7/\Gamma_2$$

VALUE	DOCUMENT ID	TECN	COMMENT
0.0783 ± 0.0016 OUR FIT			Error includes scale factor of 1.1.
0.080 ± 0.008	ABLIKIM 06E	BES2	$J/\psi \rightarrow \eta'\gamma$

$$\Gamma(\gamma\gamma)/\Gamma(\pi^0\pi^0\eta) \quad \Gamma_7/\Gamma_4$$

VALUE	DOCUMENT ID	TECN	COMMENT
0.1031 ± 0.0028 OUR FIT			Error includes scale factor of 1.9.
0.105 ± 0.010 OUR AVERAGE			
0.091 ± 0.009	AMSLER 93	CBAR	0.0 $\bar{p}p$
0.112 ± 0.002 ± 0.006	ALDE 87B	GAM2	38 $\pi^-p \rightarrow n2\gamma$

$$\Gamma(\gamma\gamma)/\Gamma(\pi^0\pi^0\eta(\text{neutral decay})) \quad \Gamma_7/0.714\Gamma_4$$

VALUE	EVTS	DOCUMENT ID	TECN	COMMENT
0.144 ± 0.004 OUR FIT				• • • We do not use the following data for averages, fits, limits, etc. • • •
0.188 ± 0.058	16	APEL 72	OSPK	3.8 $\pi^-p \rightarrow nX^0$

$$\Gamma(\text{neutrals})/\Gamma_{\text{total}} \quad (0.714\Gamma_4 + 0.09\Gamma_5 + \Gamma_7)/\Gamma$$

VALUE	EVTS	DOCUMENT ID	TECN	COMMENT
0.185 ± 0.004 OUR FIT				Error includes scale factor of 1.1.
• • • We do not use the following data for averages, fits, limits, etc. • • •				
0.185 ± 0.022	535	BASILE 71	CNTR	1.6 $\pi^-p \rightarrow nX^0$
0.189 ± 0.026	123	RITTENBERG 69	HBC	1.7–2.7 K^-p

$$\Gamma(3\pi^0)/\Gamma_{\text{total}} \quad \Gamma_8/\Gamma$$

VALUE (units 10^{-3})	EVTS	DOCUMENT ID	TECN	COMMENT
2.50 ± 0.17 OUR FIT				
3.57 ± 0.26 OUR AVERAGE				
3.522 ± 0.082 ± 0.254	2015	ABLIKIM 17	BES3	$J/\psi \rightarrow \gamma(3\pi^0)$
4.79 ± 0.59 ± 1.14	183	1 ABLIKIM 15P	BES3	$J/\psi \rightarrow K^+K^-3\pi$
• • • We do not use the following data for averages, fits, limits, etc. • • •				
3.56 ± 0.22 ± 0.34	309	2 ABLIKIM 12E	BES3	$J/\psi \rightarrow \gamma(3\pi^0)$

¹We have added all systematic uncertainties in quadrature to a single value.

²Superseded by ABLIKIM 17.

$$\Gamma(3\pi^0)/\Gamma(\pi^0\pi^0\eta) \quad \Gamma_8/\Gamma_4$$

VALUE (units 10^{-4})	EVTS	DOCUMENT ID	TECN	COMMENT
112 ± 8 OUR FIT				
78 ± 10 OUR AVERAGE				
86 ± 19	235	BLIK 08	GAMS	32 $\pi^-p \rightarrow \eta'n$
74 ± 15		ALDE 87B	GAM2	38 $\pi^-p \rightarrow n6\gamma$
75 ± 18		BINON 84	GAM2	30–40 $\pi^-p \rightarrow n6\gamma$

$$\Gamma(\mu^+\mu^-\gamma)/\Gamma(\gamma\gamma) \quad \Gamma_9/\Gamma_7$$

VALUE (units 10^{-3})	EVTS	DOCUMENT ID	TECN	COMMENT
4.9 ± 1.2	33	VIKTOROV 80	CNTR	25,33 $\pi^-p \rightarrow 2\mu\gamma$

$$\Gamma(\pi^+\pi^-\mu^+\mu^-)/\Gamma_{\text{total}} \quad \Gamma_{10}/\Gamma$$

VALUE (units 10^{-5})	CL%	EVTS	DOCUMENT ID	TECN	COMMENT
1.94 ± 0.37 ± 0.02		53	1 ABLIKIM 21I	BES3	$J/\psi \rightarrow \gamma\eta'(958)$
• • • We do not use the following data for averages, fits, limits, etc. • • •					
< 2.9	90		2 ABLIKIM 13O	BES3	$J/\psi \rightarrow \gamma\eta'$
< 24	90		3 NAIK 09	CLEO	$J/\psi \rightarrow \gamma\eta'$

¹ABLIKIM 21I reports $(1.97 \pm 0.33 \pm 0.19) \times 10^{-5}$ from a measurement of $[\Gamma(\eta'(958) \rightarrow \pi^+\pi^-\mu^+\mu^-)/\Gamma_{\text{total}}] \times [B(J/\psi(1S) \rightarrow \gamma\eta'(958))]$ assuming $B(J/\psi(1S) \rightarrow \gamma\eta'(958)) = (5.21 \pm 0.17) \times 10^{-3}$, which we rescale to our best value $B(J/\psi(1S) \rightarrow \gamma\eta'(958)) = (5.28 \pm 0.06) \times 10^{-3}$. Our first error is their experiment's error and our second error is the systematic error from using our best value.

²Using $\Gamma_2/\Gamma = (29.3 \pm 0.6)\%$ from PDG 12.

³Not independent of measured value of Γ_{10}/Γ_1 from NAIK 09.

$$\Gamma(\pi^+\pi^-\mu^+\mu^-)/\Gamma(\pi^+\pi^-\eta) \quad \Gamma_{10}/\Gamma_1$$

VALUE (units 10^{-3})	CL%	DOCUMENT ID	TECN	COMMENT
< 0.5	90	1 NAIK 09	CLEO	$J/\psi \rightarrow \gamma\eta'$
• • • We do not use the following data for averages, fits, limits, etc. • • •				
< 2.9	90			

¹NAIK 09 reports $[\Gamma(\eta'(958) \rightarrow \pi^+\pi^-\mu^+\mu^-)/\Gamma(\eta'(958) \rightarrow \pi^+\pi^-\eta)] / [B(\eta \rightarrow 2\gamma)] < 1.3 \times 10^{-3}$ which we multiply by our best value $B(\eta \rightarrow 2\gamma) = 39.36 \times 10^{-2}$.

$$\Gamma(\pi^+\pi^-\mu^+\mu^-)/\Gamma(\rho^0\gamma(\text{including non-resonant } \pi^+\pi^-\gamma)) \quad \Gamma_{10}/\Gamma_2$$

VALUE (units 10^{-4})	CL%	DOCUMENT ID	TECN	COMMENT
< 1.0	90	ABLIKIM 13O	BES3	$J/\psi \rightarrow \gamma\eta'$

$$\Gamma(\pi^+\pi^-\pi^0)/\Gamma_{\text{total}} \quad \Gamma_{11}/\Gamma$$

VALUE (units 10^{-3})	EVTS	DOCUMENT ID	TECN	COMMENT
3.61 ± 0.18 OUR FIT				
3.61 ± 0.18 OUR AVERAGE				
3.591 ± 0.054 ± 0.174	6067	ABLIKIM 17	BES3	$J/\psi \rightarrow \gamma(\pi^+\pi^-\pi^0)$
4.28 ± 0.49 ± 1.11	78	1 ABLIKIM 15P	BES3	$J/\psi \rightarrow K^+K^-3\pi$
3.7 +1.1 -0.9 ± 0.4		2 NAIK 09	CLEO	$J/\psi \rightarrow \gamma\eta'$

• • • We do not use the following data for averages, fits, limits, etc. • • •

3.83 ± 0.15 ± 0.39 1014 ³ABLIKIM 12E BES3 $J/\psi \rightarrow \gamma(\pi^+\pi^-\pi^0)$

¹We have added all systematic uncertainties in quadrature to a single value.

²Not independent of measured value of Γ_{11}/Γ_1 from NAIK 09.

³Superseded by ABLIKIM 17.

$$\Gamma(\pi^+\pi^-\pi^0)/\Gamma(\pi^+\pi^-\eta) \quad \Gamma_{11}/\Gamma_1$$

VALUE (units 10^{-3})	EVTS	DOCUMENT ID	TECN	COMMENT
8.5 ± 0.4 OUR FIT				Error includes scale factor of 1.1.
8.27 ± 2.49 -2.12 ± 0.04	20	1 NAIK 09	CLEO	$J/\psi \rightarrow \gamma\eta'$

¹NAIK 09 reports $[\Gamma(\eta'(958) \rightarrow \pi^+\pi^-\pi^0)/\Gamma(\eta'(958) \rightarrow \pi^+\pi^-\eta)] / [B(\eta \rightarrow 2\gamma)] = (21^{+6}_{-5} \pm 2) \times 10^{-3}$ which we multiply by our best value $B(\eta \rightarrow 2\gamma) = (39.36 \pm 0.18) \times 10^{-2}$. Our first error is their experiment's error and our second error is the systematic error from using our best value.

$$\Gamma((\pi^+\pi^-\pi^0)\text{ S-wave})/\Gamma_{\text{total}} \quad \Gamma_{12}/\Gamma$$

VALUE (units 10^{-4})	EVTS	DOCUMENT ID	TECN	COMMENT
37.63 ± 0.77 ± 5.00	6580	1 ABLIKIM 17	BES3	$J/\psi \rightarrow \gamma(\pi^+\pi^-\pi^0)$

¹We have added all systematic uncertainties in quadrature.

$$\Gamma(\pi^\mp\rho^\pm)/\Gamma_{\text{total}} \quad \Gamma_{13}/\Gamma$$

VALUE (units 10^{-4})	EVTS	DOCUMENT ID	TECN	COMMENT
7.44 ± 0.60 ± 2.23	1231	1 ABLIKIM 17	BES3	$J/\psi \rightarrow \gamma(\pi^\mp\rho^\pm)$

¹We have added all systematic uncertainties in quadrature.

$$\Gamma(2(\pi^+\pi^-))/\Gamma_{\text{total}} \quad \Gamma_{14}/\Gamma$$

VALUE (units 10^{-5})	CL%	EVTS	DOCUMENT ID	TECN	COMMENT
8.3 ± 0.9 ± 0.1		199	1 ABLIKIM 14M	BES3	$J/\psi \rightarrow \gamma\eta'$
• • • We do not use the following data for averages, fits, limits, etc. • • •					
< 24	90		2 NAIK 09	CLEO	$J/\psi \rightarrow \gamma\eta'$
< 1000	90		RITTENBERG 69	HBC	1.7–2.7 K^-p

¹ABLIKIM 14M reports $[\Gamma(\eta'(958) \rightarrow 2(\pi^+\pi^-))/\Gamma_{\text{total}}] \times [B(J/\psi(1S) \rightarrow \gamma\eta'(958))]$ = $(4.40 \pm 0.35 \pm 0.30) \times 10^{-7}$ which we divide by our best value $B(J/\psi(1S) \rightarrow \gamma\eta'(958)) = (5.28 \pm 0.06) \times 10^{-3}$. Our first error is their experiment's error and our second error is the systematic error from using our best value.

²Not independent of measured value of Γ_{14}/Γ_1 from NAIK 09.

$$\Gamma(2(\pi^+\pi^-))/\Gamma(\pi^+\pi^-\eta) \quad \Gamma_{14}/\Gamma_1$$

VALUE (units 10^{-3})	CL%	DOCUMENT ID	TECN	COMMENT
< 0.6	90	1 NAIK 09	CLEO	$J/\psi \rightarrow \gamma\eta'$
• • • We do not use the following data for averages, fits, limits, etc. • • •				
< 1.4 × 10 ⁻³				

¹NAIK 09 reports $[\Gamma(\eta'(958) \rightarrow 2(\pi^+\pi^-))/\Gamma(\eta'(958) \rightarrow \pi^+\pi^-\eta)] / [B(\eta \rightarrow 2\gamma)] < 1.4 \times 10^{-3}$ which we multiply by our best value $B(\eta \rightarrow 2\gamma) = 39.36 \times 10^{-2}$.

$\Gamma(\pi^+\pi^-2\pi^0)/\Gamma_{\text{total}}$ Γ_{15}/Γ

VALUE (units 10^{-4})	CL%	EVTS	DOCUMENT ID	TECN	COMMENT
$1.78 \pm 0.38 \pm 0.02$		84	¹ ABLIKIM	14M BES3	$J/\psi \rightarrow \gamma\eta'$

• • • We do not use the following data for averages, fits, limits, etc. • • •

<27		90	² NAIK	09 CLEO	$J/\psi \rightarrow \gamma\eta'$
-----	--	----	-------------------	---------	----------------------------------

¹ ABLIKIM 14M reports $[\Gamma(\eta'(958) \rightarrow \pi^+\pi^-2\pi^0)/\Gamma_{\text{total}}] \times [B(J/\psi(1S) \rightarrow \gamma\eta'(958))] = (9.38 \pm 1.79 \pm 0.89) \times 10^{-7}$ which we divide by our best value $B(J/\psi(1S) \rightarrow \gamma\eta'(958)) = (5.28 \pm 0.06) \times 10^{-3}$. Our first error is their experiment's error and our second error is the systematic error from using our best value.

² Not independent of measured value of Γ_{15}/Γ_1 from NAIK 09.

 $\Gamma(\pi^+\pi^-2\pi^0)/\Gamma(\pi^+\pi^-\eta)$ Γ_{15}/Γ_1

VALUE (units 10^{-3})	CL%	DOCUMENT ID	TECN	COMMENT
<6		90	¹ NAIK	09 CLEO $J/\psi \rightarrow \gamma\eta'$

¹ NAIK 09 reports $[\Gamma(\eta'(958) \rightarrow \pi^+\pi^-2\pi^0)/\Gamma(\eta'(958) \rightarrow \pi^+\pi^-\eta)] / [B(\eta \rightarrow 2\gamma)] < 15 \times 10^{-3}$ which we multiply by our best value $B(\eta \rightarrow 2\gamma) = 39.36 \times 10^{-2}$.

 $\Gamma(2(\pi^+\pi^- \text{ neutrals})/\Gamma_{\text{total}}$ Γ_{16}/Γ

VALUE	CL%	DOCUMENT ID	TECN	COMMENT
<0.01		95	DANBURG	73 HBC $2.2 K^-p \rightarrow \Lambda X^0$

• • • We do not use the following data for averages, fits, limits, etc. • • •

<0.01		90	RITTENBERG	69 HBC $1.7-2.7 K^-p$
-------	--	----	------------	-----------------------

 $\Gamma(2(\pi^+\pi^-)\pi^0)/\Gamma_{\text{total}}$ Γ_{17}/Γ

VALUE	CL%	DOCUMENT ID	TECN	COMMENT
<0.002		90	¹ NAIK	09 CLEO $J/\psi \rightarrow \gamma\eta'$

• • • We do not use the following data for averages, fits, limits, etc. • • •

<0.01		90	RITTENBERG	69 HBC $1.7-2.7 K^-p$
-------	--	----	------------	-----------------------

¹ Not independent of measured value of Γ_{17}/Γ_1 from NAIK 09.

 $\Gamma(2(\pi^+\pi^-)\pi^0)/\Gamma(\pi^+\pi^-\eta)$ Γ_{17}/Γ_1

VALUE (units 10^{-3})	CL%	DOCUMENT ID	TECN	COMMENT
<4		90	¹ NAIK	09 CLEO $J/\psi \rightarrow \gamma\eta'$

¹ NAIK 09 reports $[\Gamma(\eta'(958) \rightarrow 2(\pi^+\pi^-)\pi^0)/\Gamma(\eta'(958) \rightarrow \pi^+\pi^-\eta)] / [B(\eta \rightarrow 2\gamma)] < 11 \times 10^{-3}$ which we multiply by our best value $B(\eta \rightarrow 2\gamma) = 39.36 \times 10^{-2}$.

 $\Gamma(2(\pi^+\pi^-)2\pi^0)/\Gamma_{\text{total}}$ Γ_{18}/Γ

VALUE	CL%	DOCUMENT ID	TECN	COMMENT
<0.01		95	KALBFLEISCH	64B HBC $K^-p \rightarrow \Lambda 2(\pi^+\pi^-)+MM$

• • • We do not use the following data for averages, fits, limits, etc. • • •

<0.01		90	LONDON	66 HBC Compilation
-------	--	----	--------	--------------------

 $\Gamma(3(\pi^+\pi^-))/\Gamma_{\text{total}}$ Γ_{19}/Γ

VALUE (units 10^{-5})	CL%	DOCUMENT ID	TECN	COMMENT
< 3.1		90	¹ ABLIKIM	13U BES3 $J/\psi \rightarrow \gamma 3(\pi^+\pi^-)$

• • • We do not use the following data for averages, fits, limits, etc. • • •

< 53		90	² NAIK	09 CLEO $J/\psi \rightarrow \gamma\eta'$
------	--	----	-------------------	--

<500		95	KALBFLEISCH	64B HBC $K^-p \rightarrow \Lambda 2(\pi^+\pi^-)$
------	--	----	-------------	--

¹ Using $B(J/\psi \rightarrow \gamma\eta'(958)) = (5.16 \pm 0.15) \times 10^{-3}$.

² Not independent of measured value of Γ_{19}/Γ_1 from NAIK 09.

 $\Gamma(3(\pi^+\pi^-))/\Gamma(\pi^+\pi^-\eta)$ Γ_{19}/Γ_1

VALUE (units 10^{-3})	CL%	DOCUMENT ID	TECN	COMMENT
<1.2		90	¹ NAIK	09 CLEO $J/\psi \rightarrow \gamma\eta'$

¹ NAIK 09 reports $[\Gamma(\eta'(958) \rightarrow 3(\pi^+\pi^-))/\Gamma(\eta'(958) \rightarrow \pi^+\pi^-\eta)] / [B(\eta \rightarrow 2\gamma)] < 3.0 \times 10^{-3}$ which we multiply by our best value $B(\eta \rightarrow 2\gamma) = 39.36 \times 10^{-2}$.

 $\Gamma(K^\pm\pi^\mp)/\Gamma(\rho^0\gamma(\text{including non-resonant } \pi^+\pi^-\gamma))$ Γ_{20}/Γ_2

VALUE	CL%	DOCUMENT ID	TECN	COMMENT
<1.3 $\times 10^{-4}$		90	ABLIKIM	16M BES3 $e^+e^- \rightarrow J/\psi \rightarrow \text{hadrons}$

 $\Gamma(\pi^+\pi^-e^+e^-)/\Gamma_{\text{total}}$ Γ_{21}/Γ

VALUE (units 10^{-3})	CL%	EVTS	DOCUMENT ID	TECN	COMMENT
2.42 ± 0.10 OUR FIT					

• • • We do not use the following data for averages, fits, limits, etc. • • •

$2.11 \pm 0.12 \pm 0.14$		429	¹ ABLIKIM	13U BES3	$J/\psi \rightarrow \gamma\eta'$
--------------------------	--	-----	----------------------	----------	----------------------------------

$2.5 \pm 1.2 \pm 0.5$			² NAIK	09 CLEO	$J/\psi \rightarrow \gamma\eta'$
-----------------------	--	--	-------------------	---------	----------------------------------

<6		90	RITTENBERG	65 HBC	$2.7 K^-p$
----	--	----	------------	--------	------------

¹ Using $\Gamma_2/\Gamma = (29.3 \pm 0.6)\%$ from PDG 12.

² Not independent of measured value of Γ_{21}/Γ_1 from NAIK 09.

 $\Gamma(\pi^+\pi^-e^+e^-)/\Gamma(\pi^+\pi^-\eta)$ Γ_{21}/Γ_1

VALUE (units 10^{-3})	EVTS	DOCUMENT ID	TECN	COMMENT
5.69 ± 0.25 OUR FIT				

5.51 ± 3.00 ± 0.03

8		¹ NAIK	09 CLEO	$J/\psi \rightarrow \gamma\eta'$
---	--	-------------------	---------	----------------------------------

¹ NAIK 09 reports $[\Gamma(\eta'(958) \rightarrow \pi^+\pi^-e^+e^-)/\Gamma(\eta'(958) \rightarrow \pi^+\pi^-\eta)] / [B(\eta \rightarrow 2\gamma)] = (14 \pm 7 \pm 3) \times 10^{-3}$ which we multiply by our best value $B(\eta \rightarrow 2\gamma) = (39.36 \pm 0.18) \times 10^{-2}$. Our first error is their experiment's error and our second error is the systematic error from using our best value.

 $\Gamma(\pi^+\pi^-e^+e^-)/\Gamma(\rho^0\gamma(\text{including non-resonant } \pi^+\pi^-\gamma))$ Γ_{21}/Γ_2

VALUE (units 10^{-3})	EVTS	DOCUMENT ID	TECN	COMMENT
8.20 ± 0.31 OUR FIT				

8.20 $\pm 0.16 \pm 0.27$

2584		ABLIKIM	21U BES3	$J/\psi \rightarrow \gamma\eta'$
------	--	---------	----------	----------------------------------

• • • We do not use the following data for averages, fits, limits, etc. • • •

$7.2 \pm 0.4 \pm 0.5$		429	¹ ABLIKIM	13U BES3	$J/\psi \rightarrow \gamma\eta'$
-----------------------	--	-----	----------------------	----------	----------------------------------

¹ Superseded by ABLIKIM 21U.

 $\Gamma(\pi^+e^-\nu_e + \text{c.c.})/\Gamma(\pi^+\pi^-\eta)$ Γ_{22}/Γ_1

VALUE (units 10^{-4})	CL%	DOCUMENT ID	TECN	COMMENT
<5.0		90	ABLIKIM	13G BES3 $J/\psi \rightarrow \phi\eta'$

 $\Gamma(\gamma e^+e^-)/\Gamma_{\text{total}}$ Γ_{23}/Γ

VALUE (units 10^{-3})	CL%	DOCUMENT ID	TECN	COMMENT
<0.9		90	BRIERE	00 CLEO $10.6 e^+e^-$

• • • We do not use the following data for averages, fits, limits, etc. • • •

 $\Gamma(\gamma e^+e^-)/\Gamma(\gamma\gamma)$ Γ_{23}/Γ_7

VALUE (units 10^{-2})	EVTS	DOCUMENT ID	TECN	COMMENT
2.13 $\pm 0.09 \pm 0.07$		864	ABLIKIM	15U BES3 $J/\psi \rightarrow \gamma e^+e^-$

• • • We do not use the following data for averages, fits, limits, etc. • • •

 $\Gamma(\pi^0\gamma\gamma)/\Gamma_{\text{total}}$ Γ_{24}/Γ

VALUE (units 10^{-3})	EVTS	DOCUMENT ID	TECN	COMMENT
3.20 $\pm 0.07 \pm 0.23$		3.4k	ABLIKIM	17T BES3 $J/\psi \rightarrow \gamma\eta'$

• • • We do not use the following data for averages, fits, limits, etc. • • •

 $\Gamma(\pi^0\gamma\gamma)/\Gamma(\pi^0\pi^0\eta)$ Γ_{24}/Γ_4

VALUE (units 10^{-4})	CL%	DOCUMENT ID	TECN	COMMENT
<37		90	ALDE	87B GAM2 $38 \pi^-p \rightarrow n4\gamma$

• • • We do not use the following data for averages, fits, limits, etc. • • •

 $\Gamma(\pi^0\gamma\gamma(\text{non resonant}))/\Gamma_{\text{total}}$ Γ_{25}/Γ

VALUE (units 10^{-4})	EVTS	DOCUMENT ID	TECN	COMMENT
6.16 $\pm 0.64 \pm 0.67$		655	ABLIKIM	17T BES3 $J/\psi \rightarrow \gamma\eta'$

• • • We do not use the following data for averages, fits, limits, etc. • • •

 $\Gamma(\eta\gamma\gamma)/\Gamma_{\text{total}}$ Γ_{26}/Γ

VALUE	CL%	DOCUMENT ID	TECN	COMMENT
<1.33 $\times 10^{-4}$		90	ABLIKIM	19AW BES3 $J/\psi \rightarrow \gamma\eta' \rightarrow \gamma\gamma\gamma 2\gamma$

• • • We do not use the following data for averages, fits, limits, etc. • • •

 $\Gamma(4\pi^0)/\Gamma_{\text{total}}$ Γ_{27}/Γ

VALUE	CL%	DOCUMENT ID	TECN	COMMENT
<4.94 $\times 10^{-5}$		90	ABLIKIM	20E BES3 $J/\psi \rightarrow \eta'\gamma$

• • • We do not use the following data for averages, fits, limits, etc. • • •

<3.2 $\times 10^{-4}$		90	DONSKOV	14 GAM4 $32.5 \pi^-p \rightarrow \eta'n$
-----------------------	--	----	---------	--

 $\Gamma(4\pi^0)/\Gamma(\pi^0\pi^0\eta)$ Γ_{27}/Γ_4

VALUE (units 10^{-4})	CL%	DOCUMENT ID	TECN	COMMENT
<23		90	ALDE	87B GAM2 $38 \pi^-p \rightarrow n8\gamma$

• • • We do not use the following data for averages, fits, limits, etc. • • •

 $\Gamma(e^+e^-)/\Gamma_{\text{total}}$ Γ_{28}/Γ

VALUE	CL%	DOCUMENT ID	TECN	COMMENT
< 5.6 $\times 10^{-9}$		90	¹ ACHASOV	15 SND $0.958 e^+e^- \rightarrow \pi\pi\eta$

• • • We do not use the following data for averages, fits, limits, etc. • • •

<12 $\times 10^{-9}$		90	² AKHMETSHIN	15 CMD3 $0.958 e^+e^- \rightarrow \pi^+\pi^-\eta$
----------------------	--	----	-------------------------	---

<2.1 $\times 10^{-7}$		90	VORBYEV	88 ND $e^+e^- \rightarrow \pi^+\pi^-\eta$
-----------------------	--	----	---------	---

¹ Combining data of ACHASOV 15 and AKHMETSHIN 15 and using $\Gamma(\eta') = 0.198 \pm 0.009$ MeV.

² Using $\Gamma_{\eta'(958)} = 198 \pm 9$ keV, $B(\eta'(958) \rightarrow \pi^+\pi^-\eta) = (42.9 \pm 0.7)\%$, and $B(\eta \rightarrow \gamma\gamma) = (39.41 \pm 0.20)\%$.

 $\Gamma(e^+e^-e^+e^-)/\Gamma_{\text{total}}$ Γ_{29}/Γ

VALUE (units 10^{-6})	EVTS	DOCUMENT ID	TECN	COMMENT
4.5 $\pm 1.1 \pm 0.1$		30	¹ ABLIKIM	22E BES3 $J/\psi \rightarrow \gamma\eta'$

¹ ABLIKIM 22E reports $(4.5 \pm 1.0 \pm 0.5) \times 10^{-6}$ from a measurement of $[\Gamma(\eta'(958) \rightarrow e^+e^-e^+e^-)/\Gamma_{\text{total}}] \times [B(J/\psi(1S) \rightarrow \gamma\eta'(958))]$ assuming $B(J/\psi(1S) \rightarrow \gamma\eta'(958)) = (5.25 \pm 0.07) \times 10^{-3}$, which we rescale to our best value $B(J/\psi(1S) \rightarrow \gamma\eta'(958)) = (5.28 \pm 0.06) \times 10^{-3}$. Our first error is their experiment's error and our second error is the systematic error from using our best value.

• • • We do not use the following data for averages, fits, limits, etc. • • •

 $\Gamma(\text{invisible})/\Gamma_{\text{total}}$ Γ_{30}/Γ

VALUE (units 10^{-4})	CL%	DOCUMENT ID	TECN	COMMENT
<9.5		90	¹ NAIK	09 CLEO $J/\psi \rightarrow \gamma\eta'$

• • • We do not use the following data for averages, fits, limits, etc. • • •

¹ Not independent of measured value of Γ_{30}/Γ_1 from NAIK 09.

 $\Gamma(\text{invisible})/\Gamma(\pi^+\pi^-\eta)$ Γ_{30}/Γ_1

VALUE (units 10^{-3})	CL%	DOCUMENT ID	TECN	COMMENT
<2.1		90	¹ NAIK	09 CLEO $J/\psi \rightarrow \gamma\eta'$

• • • We do not use the following data for averages, fits, limits, etc. • • •

¹ NAIK 09 reports $[\Gamma(\eta'(958) \rightarrow \text{invisible})/\Gamma(\eta'(958) \rightarrow \pi^+\pi^-\eta)] / [B(\eta \rightarrow 2\gamma)] < 5.4 \times 10^{-3}$ which we multiply by our best value $B(\eta \rightarrow 2\gamma) = 39.36 \times 10^{-2}$.

Meson Particle Listings

 $\eta'(958)$ $\Gamma(\text{invisible})/\Gamma(\gamma\gamma)$ Γ_{30}/Γ_7

VALUE (units 10^{-4})	CL%	DOCUMENT ID	TECN	COMMENT
<2.4	90	ABLIKIM 13	BES3	$J/\psi \rightarrow \phi\eta'$
••• We do not use the following data for averages, fits, limits, etc. •••				
<6.69	90	ABLIKIM 06Q	BES	$J/\psi \rightarrow \phi\eta'$

 $\Gamma(\pi^+\pi^-)/\Gamma_{\text{total}}$ Γ_{31}/Γ

VALUE (units 10^{-4})	CL%	DOCUMENT ID	TECN	COMMENT
< 0.18	90	¹ AAIJ 17D	LHCB	$D_s^+ \rightarrow \pi^+\pi^-\pi^+$
••• We do not use the following data for averages, fits, limits, etc. •••				
< 0.5	90	² ABLIKIM 11G	BES3	$J/\psi \rightarrow \gamma\pi^+\pi^-$
< 29	90	³ MORI 07A	BELL	$\gamma\gamma \rightarrow \pi^+\pi^-$
< 3.3	90	⁴ MORI 07A	BELL	$\gamma\gamma \rightarrow \pi^+\pi^-$
<800	95	DANBURG 73	HBC	$2.2 K^-p \rightarrow \Lambda X^0$
<200	90	RITTENBERG 69	HBC	$1.7\text{--}2.7 K^-p$

¹ Using branching fractions of D_s^+ decays from PDG 15.

² ABLIKIM 11G reports $[\Gamma(\eta'(958) \rightarrow \pi^+\pi^-)/\Gamma_{\text{total}}] \times [B(J/\psi(1S) \rightarrow \gamma\eta'(958))] < 2.84 \times 10^{-7}$ which we divide by our best value $B(J/\psi(1S) \rightarrow \gamma\eta'(958)) = 5.28 \times 10^{-3}$.

³ Taking into account interference with the $\gamma\gamma \rightarrow \pi^+\pi^-$ continuum.

⁴ Without interference with the $\gamma\gamma \rightarrow \pi^+\pi^-$ continuum.

 $\Gamma(\pi^0\pi^0)/\Gamma_{\text{total}}$ Γ_{32}/Γ

VALUE (units 10^{-4})	CL%	DOCUMENT ID	TECN	COMMENT
< 4×10^{-4}	90	¹ ABLIKIM 11G	BES3	$J/\psi \rightarrow \gamma\pi^0\pi^0$
¹ ABLIKIM 11G reports $[\Gamma(\eta'(958) \rightarrow \pi^+\pi^-)/\Gamma_{\text{total}}] \times [B(J/\psi(1S) \rightarrow \gamma\eta'(958))] < 2.84 \times 10^{-7}$ which we divide by our best value $B(J/\psi(1S) \rightarrow \gamma\eta'(958)) = 5.28 \times 10^{-3}$.				

 $\Gamma(\pi^0\pi^0)/\Gamma(\pi^0\pi^0\eta)$ Γ_{32}/Γ_4

VALUE (units 10^{-4})	CL%	DOCUMENT ID	TECN	COMMENT
<45	90	ALDE 87B	GAM2	$38 \pi^-p \rightarrow n4\gamma$

 $\Gamma(\pi^0 e^+ e^-)/\Gamma_{\text{total}}$ Γ_{33}/Γ

VALUE (units 10^{-3})	CL%	DOCUMENT ID	TECN	COMMENT
< 1.4	90	BRIERE 00	CLEO	$10.6 e^+ e^-$
••• We do not use the following data for averages, fits, limits, etc. •••				
<13	90	RITTENBERG 65	HBC	$2.7 K^-p$

 $\Gamma(\pi^0\rho^0)/\Gamma_{\text{total}}$ Γ_{34}/Γ

VALUE	CL%	DOCUMENT ID	TECN	COMMENT
<0.04	90	RITTENBERG 65	HBC	$2.7 K^-p$

 $\Gamma(\eta e^+ e^-)/\Gamma_{\text{total}}$ Γ_{35}/Γ

VALUE (units 10^{-3})	CL%	DOCUMENT ID	TECN	COMMENT
< 2.4	90	BRIERE 00	CLEO	$10.6 e^+ e^-$
••• We do not use the following data for averages, fits, limits, etc. •••				
<11	90	RITTENBERG 65	HBC	$2.7 K^-p$

 $\Gamma(3\gamma)/\Gamma(\pi^0\pi^0\eta)$ Γ_{36}/Γ_4

VALUE (units 10^{-4})	CL%	DOCUMENT ID	TECN	COMMENT
<4.6	90	ALDE 87B	GAM2	$38 \pi^-p \rightarrow n3\gamma$

 $\Gamma(\mu^+\mu^-\pi^0)/\Gamma_{\text{total}}$ Γ_{37}/Γ

VALUE (units 10^{-5})	CL%	DOCUMENT ID	TECN	COMMENT
<6.0	90	DZHELYADIN 81	CNTR	$30 \pi^-p \rightarrow \eta' n$

 $\Gamma(\mu^+\mu^-\eta)/\Gamma_{\text{total}}$ Γ_{38}/Γ

VALUE (units 10^{-5})	CL%	DOCUMENT ID	TECN	COMMENT
<1.5	90	DZHELYADIN 81	CNTR	$30 \pi^-p \rightarrow \eta' n$

 $\Gamma(e\mu)/\Gamma_{\text{total}}$ Γ_{39}/Γ

VALUE (units 10^{-4})	CL%	DOCUMENT ID	TECN	COMMENT
<4.7	90	BRIERE 00	CLEO	$10.6 e^+ e^-$

 $\eta'(958) \rightarrow \eta\pi\pi$ DECAY PARAMETERS

$$|\text{MATRIX ELEMENT}|^2 = |1 + \alpha Y|^2 + C X + D X^2$$

X and Y are Dalitz variables; α is complex and C , and D are real-valued. Parameters C and D are not necessarily equal to c and d , respectively, in the generalized parameterization following this one. May be different for $\eta'(958) \rightarrow \eta\pi^+\pi^-$ and $\eta'(958) \rightarrow \eta\pi^0\pi^0$ decays. Because of different initial assumptions and strong correlations of the parameters we do not average the parameters in the section below.

 $Re(\alpha)$ decay parameter

VALUE	EVTS	DOCUMENT ID	TECN	COMMENT
-0.034 ± 0.002 ± 0.002	351k	ABLIKIM 18	BES3	$\eta' \rightarrow \eta\pi^+\pi^-$
-0.054 ± 0.004 ± 0.001	56k	ABLIKIM 18	BES3	$\eta' \rightarrow \eta\pi^0\pi^0$

-0.033 ± 0.005 ± 0.003	44k	¹ ABLIKIM 11	BES3	$J/\psi \rightarrow \gamma\eta\pi^+\pi^-$
-0.072 ± 0.012 ± 0.006	7k	² AMELIN 05A	VES	$28 \pi^-A \rightarrow \eta\pi^+\pi^-\pi^-A^*$
-0.021 ± 0.018 ± 0.017	6.7k	³ BRIERE 00	CLEO	$10.6 e^+ e^- \rightarrow \eta\pi^+\pi^-X$
-0.058 ± 0.013 ± 0.003	5.4k	⁴ ALDE 86	GAM2	$38 \pi^-p \rightarrow n\eta\pi^0\pi^0$
-0.08 ± 0.03		^{4,5} KALBFLEISCH 74	RVUE	$\eta' \rightarrow \eta\pi^+\pi^-$

¹ See ABLIKIM 11 for the full correlation matrix.

² Superseded by DOROFEEV 07, which found this parameterization unacceptable. See below.

³ Assuming $\text{Im}(\alpha) = 0$, $C = 0$, and $D = 0$.

⁴ Assuming $C = 0$.

⁵ From the data of DAUBER 64, RITTENBERG 69, AGUILAR-BENITEZ 72B, JACOBS 73, and DANBURG 73.

 $Im(\alpha)$ decay parameter

VALUE	EVTS	DOCUMENT ID	TECN	COMMENT
0.000 ± 0.019 ± 0.001	351k	ABLIKIM 18	BES3	$\eta' \rightarrow \eta\pi^+\pi^-$
0.000 ± 0.038 ± 0.002	56k	ABLIKIM 18	BES3	$\eta' \rightarrow \eta\pi^0\pi^0$
0.000 ± 0.049 ± 0.001	44k	¹ ABLIKIM 11	BES3	$J/\psi \rightarrow \gamma\eta\pi^+\pi^-$
0.0 ± 0.1 ± 0.0	7k	² AMELIN 05A	VES	$28 \pi^-A \rightarrow \eta\pi^+\pi^-\pi^-A^*$
-0.00 ± 0.13 ± 0.00	5.4k	³ ALDE 86	GAM2	$38 \pi^-p \rightarrow n\eta\pi^0\pi^0$
0.0 ± 0.3		^{3,4} KALBFLEISCH 74	RVUE	$\eta' \rightarrow \eta\pi^+\pi^-$

¹ See ABLIKIM 11 for the full correlation matrix.

² Superseded by DOROFEEV 07, which found this parameterization unacceptable. See below.

³ Assuming $C = 0$.

⁴ From the data of DAUBER 64, RITTENBERG 69, AGUILAR-BENITEZ 72B, JACOBS 73, and DANBURG 73.

 C decay parameter

VALUE	EVTS	DOCUMENT ID	TECN	COMMENT
0.0027 ± 0.0024 ± 0.0015	351k	ABLIKIM 18	BES3	$\eta' \rightarrow \eta\pi^+\pi^-$
0.018 ± 0.009 ± 0.003	44k	¹ ABLIKIM 11	BES3	$J/\psi \rightarrow \gamma\eta\pi^+\pi^-$
0.020 ± 0.018 ± 0.004	7k	² AMELIN 05A	VES	$28 \pi^-A \rightarrow \eta\pi^+\pi^-\pi^-A^*$

¹ See ABLIKIM 11 for the full correlation matrix.

² Superseded by DOROFEEV 07, which found this parameterization unacceptable. See below.

 D decay parameter

VALUE	EVTS	DOCUMENT ID	TECN	COMMENT
-0.053 ± 0.004 ± 0.004	351k	ABLIKIM 18	BES3	$\eta' \rightarrow \eta\pi^+\pi^-$
-0.061 ± 0.009 ± 0.005	56k	ABLIKIM 18	BES3	$\eta' \rightarrow \eta\pi^0\pi^0$
-0.059 ± 0.012 ± 0.004	44k	¹ ABLIKIM 11	BES3	$J/\psi \rightarrow \gamma\eta\pi^+\pi^-$
-0.066 ± 0.030 ± 0.015	7k	² AMELIN 05A	VES	$28 \pi^-A \rightarrow \eta\pi^+\pi^-\pi^-A^*$
0.00 ± 0.03 ± 0.00	5.4k	³ ALDE 86	GAM2	$38 \pi^-p \rightarrow n\eta\pi^0\pi^0$
0		^{3,4} KALBFLEISCH 74	RVUE	$\eta' \rightarrow \eta\pi^+\pi^-$

¹ See ABLIKIM 11 for the full correlation matrix.

² Superseded by DOROFEEV 07, which found this parameterization unacceptable. See below.

³ Assuming $C = 0$.

⁴ From the data of DAUBER 64, RITTENBERG 69, AGUILAR-BENITEZ 72B, JACOBS 73, and DANBURG 73.

 $\eta'(958) \rightarrow \eta\pi\pi$ DECAY PARAMETERS

$$|\text{MATRIX ELEMENT}|^2 \propto 1 + a Y + b Y^2 + c X + d X^2$$

X and Y are Dalitz variables and a , b , c , and d are real-valued parameters. May be different for $\eta'(958) \rightarrow \eta\pi^+\pi^-$ and $\eta'(958) \rightarrow \eta\pi^0\pi^0$ decays. We do not average measurements in the section below because parameter values from each experiment are strongly correlated.

 a decay parameter

VALUE	EVTS	DOCUMENT ID	TECN	COMMENT
-0.077 ± 0.003 ± 0.001		¹ ABLIKIM 23AH	BES3	$\eta' \rightarrow \eta\pi^0\pi^0$
-0.056 ± 0.004 ± 0.002	351k	ABLIKIM 18	BES3	$\eta' \rightarrow \eta\pi^+\pi^-$
-0.087 ± 0.009 ± 0.006	56k	ABLIKIM 18	BES3	$\eta' \rightarrow \eta\pi^0\pi^0$
-0.074 ± 0.008 ± 0.006	124k	ADLARSON 18A	A2MM	$\eta' \rightarrow \eta\pi^0\pi^0$
-0.072 ± 0.007 ± 0.008		² GONZALEZ-S. 18A	RVUE	$\eta' \rightarrow \eta\pi^0\pi^0$
-0.047 ± 0.011 ± 0.003	44k	³ ABLIKIM 11	BES3	$J/\psi \rightarrow \gamma\eta\pi^+\pi^-$
-0.066 ± 0.016 ± 0.003	15k	⁴ BLIK 09	GAM4	$32.5 \pi^-p \rightarrow \eta' n$
-0.127 ± 0.016 ± 0.008	20k	⁵ DOROFEEV 07	VES	$27 \pi^-p \rightarrow \eta' n$, $\pi^-A \rightarrow \eta' \pi^-A^*$

¹ Fit IV, ignoring noncup terms. Supersedes ABLIKIM 18.

² Theoretical analysis of ADLARSON 18A using resonance chiral perturbation theory to one loop.

³ See ABLIKIM 11 for the full correlation matrix.

⁴ From $\eta' \rightarrow \eta\pi^0\pi^0$ decay.

⁵ From $\eta' \rightarrow \eta\pi^+\pi^-$ decay.

b decay parameter

VALUE	EVTS	DOCUMENT ID	TECN	COMMENT
• • • We do not use the following data for averages, fits, limits, etc. • • •				
$-0.066 \pm 0.006 \pm 0.001$		¹ ABLIKIM 23AH BES3	$\eta' \rightarrow \eta\pi^0\pi^0$	
$-0.049 \pm 0.006 \pm 0.006$	351k	ABLIKIM 18 BES3	$\eta' \rightarrow \eta\pi^+\pi^-$	
$-0.073 \pm 0.014 \pm 0.005$	56k	ABLIKIM 18 BES3	$\eta' \rightarrow \eta\pi^0\pi^0$	
$-0.063 \pm 0.014 \pm 0.005$	124k	ADLARSON 18A A2MM	$\eta' \rightarrow \eta\pi^0\pi^0$	
$-0.052 \pm 0.001 \pm 0.002$		² GONZALEZ-S...18A RVUE	$\eta' \rightarrow \eta\pi^0\pi^0$	
$-0.069 \pm 0.019 \pm 0.009$	44k	³ ABLIKIM 11 BES3	$J/\psi \rightarrow \gamma\eta\pi^+\pi^-$	
$-0.063 \pm 0.028 \pm 0.004$	15k	⁴ BLIK 09 GAM4	$32.5 \pi^- \rho \rightarrow \eta' n$	
$-0.106 \pm 0.028 \pm 0.014$	20k	⁵ DOROFEEV 07 VES	$27 \pi^- \rho \rightarrow \eta' n$, $\pi^- A \rightarrow \eta' \pi^- A^*$	

- ¹ Fit IV, ignoring noncusp terms. Supersedes ABLIKIM 18.
- ² Theoretical analysis of ADLARSON 18A using resonance chiral perturbation theory to one loop.
- ³ See ABLIKIM 11 for the full correlation matrix.
- ⁴ From $\eta' \rightarrow \eta\pi^0\pi^0$ decay.
- ⁵ From $\eta' \rightarrow \eta\pi^+\pi^-$ decay.

c decay parameter

VALUE	EVTS	DOCUMENT ID	TECN	COMMENT
• • • We do not use the following data for averages, fits, limits, etc. • • •				
$0.0027 \pm 0.0024 \pm 0.0018$	351k	ABLIKIM 18 BES3	$\eta' \rightarrow \eta\pi^+\pi^-$	
$0.019 \pm 0.011 \pm 0.003$	44k	¹ ABLIKIM 11 BES3	$J/\psi \rightarrow \gamma\eta\pi^+\pi^-$	
$-0.107 \pm 0.096 \pm 0.003$	15k	² BLIK 09 GAM4	$32.5 \pi^- \rho \rightarrow \eta' n$	
$0.015 \pm 0.011 \pm 0.014$	20k	³ DOROFEEV 07 VES	$27 \pi^- \rho \rightarrow \eta' n$, $\pi^- A \rightarrow \eta' \pi^- A^*$	

- ¹ See ABLIKIM 11 for the full correlation matrix.
- ² From $\eta' \rightarrow \eta\pi^0\pi^0$ decay.
- ³ From $\eta' \rightarrow \eta\pi^+\pi^-$ decay.

d decay parameter

VALUE	EVTS	DOCUMENT ID	TECN	COMMENT
• • • We do not use the following data for averages, fits, limits, etc. • • •				
$-0.068 \pm 0.004 \pm 0.001$		¹ ABLIKIM 23AH BES3	$\eta' \rightarrow \eta\pi^0\pi^0$	
$-0.063 \pm 0.004 \pm 0.003$	351k	ABLIKIM 18 BES3	$\eta' \rightarrow \eta\pi^+\pi^-$	
$-0.074 \pm 0.009 \pm 0.004$	56k	ABLIKIM 18 BES3	$\eta' \rightarrow \eta\pi^0\pi^0$	
$-0.050 \pm 0.009 \pm 0.005$	124k	ADLARSON 18A A2MM	$\eta' \rightarrow \eta\pi^0\pi^0$	
$-0.051 \pm 0.008 \pm 0.006$		² GONZALEZ-S...18A RVUE	$\eta' \rightarrow \eta\pi^0\pi^0$	
$-0.073 \pm 0.012 \pm 0.003$	44k	³ ABLIKIM 11 BES3	$J/\psi \rightarrow \gamma\eta\pi^+\pi^-$	
$0.018 \pm 0.078 \pm 0.006$	15k	⁴ BLIK 09 GAM4	$32.5 \pi^- \rho \rightarrow \eta' n$	
$-0.082 \pm 0.017 \pm 0.008$	20k	⁵ DOROFEEV 07 VES	$27 \pi^- \rho \rightarrow \eta' n$, $\pi^- A \rightarrow \eta' \pi^- A^*$	

- ¹ Fit IV, ignoring noncusp terms. Supersedes ABLIKIM 18.
- ² Theoretical analysis of ADLARSON 18A using resonance chiral perturbation theory to one loop.
- ³ See ABLIKIM 11 for the full correlation matrix.
- ⁴ From $\eta' \rightarrow \eta\pi^0\pi^0$ decay. If $c \equiv 0$ from Bose-Einstein symmetry, $d = -0.067 \pm 0.020 \pm 0.003$.
- ⁵ From $\eta' \rightarrow \eta\pi^+\pi^-$ decay.

$\eta'(958)$ β PARAMETER
 $|\text{MATRIX ELEMENT}|^2 = (1 + 2\beta Z)$

See the "Note on η Decay Parameters" in our 1994 edition Physical Review D50 1173 (1994), p. 1454.

β decay parameter

VALUE	EVTS	DOCUMENT ID	TECN	COMMENT
-0.61 ± 0.08	OUR AVERAGE	Error includes scale factor of 1.2.		
$-0.640 \pm 0.046 \pm 0.047$	1.8k	ABLIKIM 15G BES3	$J/\psi \rightarrow \gamma(\pi^0\pi^0\pi^0)$	
-0.59 ± 0.18	235	BLIK 08 GAMS	$32 \pi^- \rho \rightarrow \eta' n$	
-0.1 ± 0.3		ALDE 87B GAM2	$38 \pi^- \rho \rightarrow n3\pi^0$	

$\eta'(958)$ C-NONCONSERVING DECAY PARAMETER

See the note on η decay parameters in the Stable Particle Particle Listings for definition of this parameter.

DECAY ASYMMETRY PARAMETER FOR $\pi^+\pi^-\gamma$

VALUE	EVTS	DOCUMENT ID	TECN	COMMENT
-0.03 ± 0.04	OUR AVERAGE			
-0.019 ± 0.056		AIHARA 87 TPC	$2\gamma \rightarrow \pi^+\pi^-\gamma$	
-0.069 ± 0.078	295	GRIGORIAN 75 STRC	$2.1 \pi^- \rho$	
0.00 ± 0.10	103	KALBFLEISCH 75 HBC	$2.18 K^- \rho \rightarrow A\pi^+\pi^-\gamma$	
• • • We do not use the following data for averages, fits, limits, etc. • • •				
0.07 ± 0.08	152	RITTENBERG 65 HBC	$2.1-2.7 K^- \rho$	

$\eta'(958) \rightarrow \gamma\ell^+\ell^-$ TRANSITION FORM FACTOR SLOPE

Related to the effective virtual meson mass A , via slope $\approx A^{-2}$. See e.g. LANDSBERG 85, eq. (3.8), for a detailed definition.

VALUE (GeV ⁻²)	EVTS	DOCUMENT ID	TECN	COMMENT
1.62 ± 0.17	OUR AVERAGE			
$1.60 \pm 0.17 \pm 0.08$	864	¹ ABLIKIM 15G BES3	$J/\psi \rightarrow \gamma e^+ e^-$	
1.7 ± 0.4	33	VIKTOROV 80	$25,33 \pi^- \rho \rightarrow 2\mu\gamma$	

- ¹ In the single-pole Ansatz where slope = $1/(A^2 + \gamma^2)$ with A, γ being a Breit-Wigner mass, width for the effective contributing vector meson.

$\eta'(958)$ REFERENCES

ABLIKIM 23AH	PRL 130 081901	M. Ablikim <i>et al.</i>	(BESIII Collab.)
ABLIKIM 22E	PR D105 112010	M. Ablikim <i>et al.</i>	(BESIII Collab.)
ABLIKIM 21J	PR D103 072006	M. Ablikim <i>et al.</i>	(BESIII Collab.)
ABLIKIM 21I	PR D103 092005	M. Ablikim <i>et al.</i>	(BESIII Collab.)
ABLIKIM 20E	PR D101 032001	M. Ablikim <i>et al.</i>	(BESIII Collab.)
ABLIKIM 19AW	PR D100 052015	M. Ablikim <i>et al.</i>	(BESIII Collab.)
ABLIKIM 19T	PRL 122 142002	M. Ablikim <i>et al.</i>	(BESIII Collab.)
ABLIKIM 18	PR D97 012003	M. Ablikim <i>et al.</i>	(BESIII Collab.)
ABLIKIM 18C	PRL 120 242003	M. Ablikim <i>et al.</i>	(BESIII Collab.)
ADLARSON 18A	PR D98 012001	P. Adlarson <i>et al.</i>	(A2 Collab. at MAMI)
GONZALEZ-S...18A	EPJ C78 758	S. Gonzalez-Solis, E. Passemar	(BEJ, IND+)
AAJ	PL B764 233	R. Aaj <i>et al.</i>	(LHCb Collab.)
ABLIKIM 17	PRL 118 012001	M. Ablikim <i>et al.</i>	(BESIII Collab.)
ABLIKIM 17T	PR D96 012005	M. Ablikim <i>et al.</i>	(BESIII Collab.)
ABLIKIM 16M	PR D93 072008	M. Ablikim <i>et al.</i>	(BESIII Collab.)
ABLIKIM 15AD	PR D92 051101	M. Ablikim <i>et al.</i>	(BESIII Collab.)
ABLIKIM 15G	PR D92 012014	M. Ablikim <i>et al.</i>	(BESIII Collab.)
ABLIKIM 15O	PR D92 012001	M. Ablikim <i>et al.</i>	(BESIII Collab.)
ABLIKIM 15P	PR D92 012007	M. Ablikim <i>et al.</i>	(BESIII Collab.)
ACHASOV 15	PR D91 092010	M.N. Achasov <i>et al.</i>	(SND Collab.)
AKHMETSHIN 15	PL B740 273	R.R. Akhmetshin <i>et al.</i>	(CMD-3 Collab.)
PDG 15	RPP 2015 at pdg.lbl.gov		(PDG Collab.)
ABLIKIM 14M	PRL 112 251801	M. Ablikim <i>et al.</i>	(BESIII Collab.)
DONSKOV 14	MPL A29 1450213	S. Donskov <i>et al.</i>	(GAMS-4 π Collab.)
PDG 14	CP C38 070001	K. Olive <i>et al.</i>	(PDG Collab.)
ABLIKIM 13	PR D87 012009	M. Ablikim <i>et al.</i>	(BESIII Collab.)
ABLIKIM 13G	PR D87 032006	M. Ablikim <i>et al.</i>	(BESIII Collab.)
ABLIKIM 13O	PR D87 092011	M. Ablikim <i>et al.</i>	(BESIII Collab.)
ABLIKIM 13U	PR D88 091502	M. Ablikim <i>et al.</i>	(BESIII Collab.)
ABLIKIM 12E	PRL 108 182001	M. Ablikim <i>et al.</i>	(BESIII Collab.)
PDG 12	PR D86 010001	J. Berlinger <i>et al.</i>	(PDG Collab.)
ABLIKIM 11	PR D83 012003	M. Ablikim <i>et al.</i>	(BESIII Collab.)
ABLIKIM 11G	PR D84 032006	M. Ablikim <i>et al.</i>	(BESIII Collab.)
CZERWINSKI 10	PRL 105 122001	E. Czerwinski <i>et al.</i>	(COSY-11 Collab.)
BLIK 09	PAN 72 231	A.M. Blik <i>et al.</i>	(IHEP (Protvino))
Translated from YAF 72 258.			
NAIK 09	PRL 102 061801	P. Naik <i>et al.</i>	(CLEO Collab.)
PEDLAR 09	PR D79 111101	T.K. Pedlar <i>et al.</i>	(CLEO Collab.)
BLIK 08	PAN 71 2124	A. Blik <i>et al.</i>	(GAMS-4 π Collab.)
Translated from YAF 71 2161.			
LIBBY 08	PRL 101 182002	J. Libby <i>et al.</i>	(CLEO Collab.)
WICHT 08	PL B662 323	J. Wicht <i>et al.</i>	(BELLE Collab.)
DOROFEEV 07	PL B651 22	V. Dorofeev <i>et al.</i>	(VES Collab.)
MORI 07A	JPSJ 76 074102	T. Mori <i>et al.</i>	(BELLE Collab.)
ABLIKIM 06Q	PR D73 052008	M. Ablikim <i>et al.</i>	(BES Collab.)
ABLIKIM 06P	PRL 97 202002	M. Ablikim <i>et al.</i>	(BES Collab.)
AMELIN 05A	PAN 68 372	D.V. Amelin <i>et al.</i>	(VES Collab.)
Translated from YAF 68 401.			
AMSLER 04B	EPJ C33 23	C. Amisler <i>et al.</i>	(Crystal Barrel Collab.)
BAI 04J	PL B594 47	J.Z. Bai <i>et al.</i>	(BES Collab.)
BRIERE 00	PRL 84 26	R. Briere <i>et al.</i>	(CLEO Collab.)
ACCIARRI 98C	PL B418 399	M. Acciari <i>et al.</i>	(L3 Collab.)
BARBERIS 98C	PL B440 225	D. Barberis <i>et al.</i>	(WA 102 Collab.)
WURZINGER 96	PL B374 283	R. Wurzinger <i>et al.</i>	(BONN, ORSAY, SACL+)
PDG 94	PR D50 1173	L. Montanet <i>et al.</i>	(CERN, LBL, BOST+)
AMSLER 93	ZPHY C58 175	C. Amisler <i>et al.</i>	(Crystal Barrel Collab.)
BELADIDZE 92C	SJNP 55 1535	G.M. Beladidze, S.I. Bityukov, G.V. Borisov	(SERP+)
Translated from YAF 55 2748.			
KARCH 92	ZPHY C54 33	K. Karch <i>et al.</i>	(Crystal Ball Collab.)
ARMSTRONG 91B	ZPHY C52 389	T.A. Armstrong <i>et al.</i>	(ATHU, BARI, BIRM+)
BEHREND 91	ZPHY C49 401	H.J. Behrend <i>et al.</i>	(CELLO Collab.)
AUGUSTIN 90	PR D42 10	J.E. Augustin <i>et al.</i>	(DM2 Collab.)
BARU 90	ZPHY C48 681	S.E. Baru <i>et al.</i>	(MD-1 Collab.)
BUTLER 90	PR D42 1368	F. Butler <i>et al.</i>	(Mark II Collab.)
KARCH 90	PL B249 353	K. Karch <i>et al.</i>	(Crystal Ball Collab.)
ROE 90	PR D41 17	N.A. Roe <i>et al.</i>	(ASP Collab.)
AIHARA 88C	PR D38 1	H. Aihara <i>et al.</i>	(TPC-2 γ Collab.)
VOROBYEV 88	SJNP 48 273	P.V. Vorobiev <i>et al.</i>	(NOVO)
Translated from YAF 48 436.			
WILLIAMS 88	PR D38 1365	D.A. Williams <i>et al.</i>	(Crystal Ball Collab.)
AIHARA 87	PR D35 2650	H. Aihara <i>et al.</i>	(TPC-2 γ Collab.)
ALBRECHT 87B	PL B199 457	H. Albrecht <i>et al.</i>	(ARGUS Collab.)
ALDE 87B	ZPHY C36 603	D.M. Alde <i>et al.</i>	(LANL, BELG, SERP, LAPP)
ANTREASIAN 87	PR D36 2633	D. Antreasian <i>et al.</i>	(Crystal Ball Collab.)
GIDAL 87	PRL 59 2012	G. Gidal <i>et al.</i>	(LBL, SLAC, HARV)
ALDE 86	PL B177 115	D.M. Alde <i>et al.</i>	(SERP, BELG, LANL, LAPP)
BARTEL 85E	PL 160B 421	W. Bartel <i>et al.</i>	(JADE Collab.)
LANDSBERG 85	PRPL 128 301	L.G. Landsberg	(SERP)
ALTHOFF 84E	PL 147B 487	M. Althoff <i>et al.</i>	(TASSO Collab.)
BERGER 84B	PL 142B 125	C. Berger	(PLUTO Collab.)
BINON 84	PL 140B 264	F.G. Binon <i>et al.</i>	(SERP, BELG, LAPP+)
JENNI 83	PR D27 1031	P. Jenni <i>et al.</i>	(SLAC, LBL)
BARTEL 82B	PL 113B 190	W. Bartel <i>et al.</i>	(JADE Collab.)
BEHREND 82C	PL 114B 378	H.J. Behrend <i>et al.</i>	(CELLO Collab.)
Also	PL 125B 518 (errata.)	H.J. Behrend <i>et al.</i>	(CELLO Collab.)
DZHELJADIN 81	PL 105B 239	R.I. Dzheyladin <i>et al.</i>	(SERP)
STANTON 80	PL B92 353	N.R. Stanton <i>et al.</i>	(OSU, CARL, MCGIL+)
VIKTOROV 80	SJNP 32 520	V.A. Viktorov <i>et al.</i>	(SERP)
Translated from YAF 32 1005.			
APEL 79	PL 83B 131	W.D. Apel, K.H. Augenstein, E. Bertolucci	(KARLK+)
BINNIE 79	PL 83B 141	D.M. Binnie <i>et al.</i>	(LOIC)
ZANFINO 77	PRL 38 930	C. Zanfino <i>et al.</i>	(CARL, MCGI, OHIO+)
GRIGORIAN 75	NP B91 232	A. Grigorian <i>et al.</i>	(+)
KALBFLEISCH 75	PR D11 187	G.R. Kalbfleisch, R.C. Strand, J.W. Chapman	(BNL+)
DUANE 74	PRL 32 425	A. Duane <i>et al.</i>	(LOIC, SHMP)
KALBFLEISCH 74	PR D10 916	G.R. Kalbfleisch	(BNL)
DANBURG 73	PR D8 3744	J.S. Danburg <i>et al.</i>	(BNL, MICH JP)
JACOBS 73	PR D8 18	S.M. Jacobs <i>et al.</i>	(BRAN, UMD, SYRA+ JP)
AGUILAR... 72B	PR D6 29	M. Aguilar-Benitez <i>et al.</i>	(BNL)
APEL 72	PL 40B 680	W.D. Apel <i>et al.</i>	(KARLK, KARLE, PISA)
DALPIAZ 72	PL 42B 377	P.F. Dalpiaz <i>et al.</i>	(CERN)
BASILE 71	NC 3A 371	M. Basile <i>et al.</i>	(CERN, BGNA, STRB)
HARVEY 71	PRL 27 885	E.H. Harvey <i>et al.</i>	(MINN, MICH)
BENSINGER 70	PL 33B 505	J.R. Bensinger <i>et al.</i>	(WISC)
RITTENBERG 69	Thesis UCRL 18863	A. Rittenberg	(LRL I)
DAVIS 68	PL 27B 532	R. Davis <i>et al.</i>	(NWES, ANL)
LONDON 66	PR 143 1034	G.V. London <i>et al.</i>	(BNL, SYRA IJP)
BADIER 65B	PL 37 337	J. Badier <i>et al.</i>	(EPOL, SAACL AMST)
RITTENBERG 65	PRL 15 556	A. Rittenberg, G.R. Kalbfleisch	(LRL, BNL)
DAUBER 64	PRL 13 449	P.M. Dauber <i>et al.</i>	(UCLA) JP
KALBFLEISCH 64B	PRL 13 349	G.R. Kalbfleisch, O.I. Dahl, A. Rittenberg	(LRL) JP

Meson Particle Listings

$f_0(980)$

$f_0(980)$

$$I^G(J^{PC}) = 0^+(0^{++})$$

See the related review(s):
 Scalar Mesons below 1 GeV

$f_0(980)$ T-MATRIX POLE \sqrt{s}

Note that $\Gamma = -2 \text{Im}(\sqrt{s})$.

VALUE (MeV)	DOCUMENT ID	TECN	COMMENT
(980-1010) - i (20-35) OUR ESTIMATE (see Fig. 64.4 in the review)			
$(993 \pm 2^{+2}_{-1}) - i(21 \pm 3^{+2}_{-4})$	1 DANILKIN 21	RVUE	Compilation
$(1014 \pm 8) - i(35 \pm 5)$	SARANTSEV 21	RVUE	$J/\psi(1S) \rightarrow \gamma(\pi\pi, K\bar{K}, \eta\eta, \omega\phi)$
$(992.8 \pm 1.3) - i(30.7 \pm 2.3)$	2 ALBRECHT 20	RVUE	$0.9 \bar{p}p \rightarrow \pi^0 \pi^0 \eta, \pi^0 \eta\eta, \pi^0 K^+ K^-$
$(1003^{+5}_{-27}) - i(21^{+10}_{-8})$	3 GARCIA-MAR..11	RVUE	Compilation
$(996 \pm 7) - i(25^{+10}_{-6})$	4 GARCIA-MAR..11	RVUE	Compilation
$(996^{+4}_{-14}) - i(24^{+11}_{-3})$	5 MOUSSALLAM11	RVUE	Compilation
$(981 \pm 43) - i(18 \pm 11)$	6 MENNESSIER 10	RVUE	Compilation
$(1030^{+30}_{-10}) - i(35^{+10}_{-16})$	7 ANISOVICH 09	RVUE	$0.0 \bar{p}p, \pi N$
$(973^{+39}_{-127}) - i(11^{+189}_{-11})$	8 PELAEZ 04A	RVUE	$\pi\pi \rightarrow \pi\pi$

- Data driven analysis using partial-wave dispersion relations.
- 5 poles, 5 channels, including scattering data from HYAMS 75 ($\pi\pi$), LONGACRE 86 ($K\bar{K}$), BINON 83 ($\eta\eta$), and BINON 84c ($\eta\eta'$). Based on 18.5k events. Second solution 977.8 ± 1.7 MeV.
- Reanalysis of the K_{e4} data of BATLEY 10c and the $\pi N \rightarrow \pi\pi N$ data of HYAMS 73, GRAYER 74, and PROTOPOESCU 73 using Roy equations.
- Reanalysis of the K_{e4} data of BATLEY 10c and the $\pi N \rightarrow \pi\pi N$ data of HYAMS 73, GRAYER 74, and PROTOPOESCU 73 using GKPY equations.
- Uses Roy equations.
- Average of the analyses of three data sets in the K-matrix model. Uses the data of BATLEY 08a, HYAMS 73, and GRAYER 74, partially of COHEN 80 or ETKIN 82b.
- On sheet II in a 2-pole solution. The other pole is found on sheet III at $(850 - i 100)$ MeV.
- Reanalysis of data from PROTOPOESCU 73, ESTABROOKS 74, GRAYER 74, and COHEN 80 in the unitarized ChPT model.

$f_0(980)$ MASS

VALUE (MeV)	EVTS	DOCUMENT ID	TECN	COMMENT
990 ± 20 OUR ESTIMATE				
• • • We do not use the following data for averages, fits, limits, etc. • • •				
$992.0^{+8.5}_{-7.5} \pm 8.6$		1 AAIJ 19H	LHCB	$pp \rightarrow D^{\pm} X$
989.4 ± 1.3	424	ABLIKIM 15P	BES3	$J/\psi \rightarrow K^+ K^- 3\pi$
989.9 ± 0.4	706	ABLIKIM 12E	BES3	$J/\psi \rightarrow \gamma 3\pi$
$977^{+11}_{-9} \pm 1$	44	2 ECKLUND 09	CLEO	$4.17 e^+ e^- \rightarrow D_s^- D_s^{*+} + c.c.$
$982.2 \pm 1.0^{+8.1}_{-8.0}$		3 UEHARA 08A	BELL	$10.6 e^+ e^- \rightarrow e^+ e^- \pi^0 \pi^0$
$976.8 \pm 0.3^{+10.1}_{-0.6}$	64k	4 AMBROSINO 07	KLOE	$1.02 e^+ e^- \rightarrow \pi^0 \pi^0 \gamma$
$984.7 \pm 0.4^{+2.4}_{-3.7}$	64k	5 AMBROSINO 07	KLOE	$1.02 e^+ e^- \rightarrow \pi^0 \pi^0 \gamma$
973 ± 3	262 ± 30	6 AUBERT 07AK	BABR	$10.6 e^+ e^- \rightarrow \phi \pi^+ \pi^- \gamma$
970 ± 7	54 ± 9	6 AUBERT 07AK	BABR	$10.6 e^+ e^- \rightarrow \phi \pi^0 \pi^0 \gamma$
953 ± 20	2.6k	7 BONVICINI 07	CLEO	$D^+ \rightarrow \pi^- \pi^+ \pi^+$
$985.6^{+1.2+1.1}_{-1.5-1.6}$		8 MORI 07	BELL	$10.6 e^+ e^- \rightarrow e^+ e^- \pi^+ \pi^-$
$983.0 \pm 0.6^{+4.0}_{-3.0}$		9 AMBROSINO 06B	KLOE	$1.02 e^+ e^- \rightarrow \pi^+ \pi^- \gamma$
$977.3 \pm 0.9^{+3.7}_{-4.3}$		10 AMBROSINO 06B	KLOE	$1.02 e^+ e^- \rightarrow \pi^+ \pi^- \gamma$
950 ± 9	4286	11 GARMASH 06	BELL	$B^+ \rightarrow K^+ \pi^+ \pi^-$
965 ± 10		12 ABLIKIM 05	BES2	$J/\psi \rightarrow \phi \pi^+ \pi^-, \phi K^+ K^-$
1031 ± 8		13 ANISOVICH 03	RVUE	
1037 ± 31		TIKHOMIROV 03	SPEC	$40.0 \bar{p} \bar{c} \rightarrow K_S^0 K_S^0 K^0 X$
973 ± 1	2438	14 ALOISIO 02A	KLOE	$e^+ e^- \rightarrow \pi^0 \pi^0 \gamma$
$977 \pm 3 \pm 2$	848	15 AITALA 01D	E791	$D^+ \rightarrow \pi^- \pi^+ \pi^+$
969.8 ± 4.5	419	16 ACHASOV 00H	SND	$e^+ e^- \rightarrow \pi^0 \pi^0 \gamma$
985^{+16}_{-12}	419	17,18 ACHASOV 00H	SND	$e^+ e^- \rightarrow \pi^0 \pi^0 \gamma$
$976 \pm 5 \pm 6$		19 AKHMETSHIN 99B	CMD2	$e^+ e^- \rightarrow \pi^+ \pi^- \gamma$
$977 \pm 3 \pm 6$	268	19 AKHMETSHIN 99C	CMD2	$e^+ e^- \rightarrow \pi^0 \pi^0 \gamma$
$975 \pm 4 \pm 6$		20 AKHMETSHIN 99C	CMD2	$e^+ e^- \rightarrow \pi^0 \pi^0 \gamma$
$975 \pm 4 \pm 6$		21 AKHMETSHIN 99C	CMD2	$e^+ e^- \rightarrow \pi^+ \pi^- \gamma, \pi^0 \pi^0 \gamma$
985 ± 10		BARBERIS 99	OMEG	$450 pp \rightarrow \rho_S \rho_F K^+ K^-$
982 ± 3		BARBERIS 99B	OMEG	$450 pp \rightarrow \rho_S \rho_F \pi^+ \pi^-$

982 ± 3	BARBERIS 99C	OMEG	$450 pp \rightarrow \rho_S \rho_F \pi^0 \pi^0$
$987 \pm 6 \pm 6$	22 BARBERIS 99D	OMEG	$450 pp \rightarrow K^+ K^-, \pi^+ \pi^-$
989 ± 15	BELLAZZINI 99	GAM4	$450 pp \rightarrow \rho \rho \pi^0 \pi^0$
991 ± 3	23 KAMINSKI 99	RVUE	$\pi\pi \rightarrow \pi\pi, K\bar{K}, \sigma\sigma$
~ 980	23 OLLER 99	RVUE	$\pi\pi \rightarrow \pi\pi, K\bar{K}$
~ 993.5	OLLER 99B	RVUE	$\pi\pi \rightarrow \pi\pi, K\bar{K}$
~ 987	23 OLLER 99C	RVUE	$\pi\pi \rightarrow \pi\pi, K\bar{K}, \eta\eta$
957 ± 6	24 ACKERSTAFF 98Q	OPAL	$Z \rightarrow f_0 X$
960 ± 10	ALDE 98	GAM4	
1015 ± 15	23 ANISOVICH 98B	RVUE	Compilation
1008	29 LOCHER 98	RVUE	$\pi\pi \rightarrow \pi\pi, K\bar{K}$
955 ± 10	24 ALDE 97	GAM2	$450 pp \rightarrow \rho \rho \pi^0 \pi^0$
994 ± 9	26 BERTIN 97C	OBLX	$0.0 \bar{p}p \rightarrow \pi^+ \pi^- \pi^0$
$993.2 \pm 6.5 \pm 6.9$	27 ISHIDA 96	RVUE	$\pi\pi \rightarrow \pi\pi, K\bar{K}$
1006	TORNQVIST 96	RVUE	$\pi\pi \rightarrow \pi\pi, K\bar{K}, K\pi, \eta\pi$
997 ± 5	3k	28 ALDE 95B	GAM2 $38 \pi^- p \rightarrow \pi^0 \pi^0 n$
960 ± 10	10k	29 ALDE 95B	GAM2 $38 \pi^- p \rightarrow \pi^0 \pi^0 n$
994 ± 5	AMSLER 95B	CBAR	$0.0 \bar{p}p \rightarrow 3\pi^0$
~ 996	30 AMSLER 95D	CBAR	$0.0 \bar{p}p \rightarrow \pi^0 \pi^0 \pi^0, \pi^0 \eta\eta, \pi^0 \pi^0 \eta$
987 ± 6	31 ANISOVICH 95	RVUE	
1015	JANSEN 95	RVUE	$\pi\pi \rightarrow \pi\pi, K\bar{K}$
983	32 BUGG 94	RVUE	$\bar{p}p \rightarrow \eta 2\pi^0$
973 ± 2	33 KAMINSKI 94	RVUE	$\pi\pi \rightarrow \pi\pi, K\bar{K}$
988	34 ZOU 94B	RVUE	
988 ± 10	35 MORGAN 93	RVUE	$\pi\pi(K\bar{K}) \rightarrow \pi\pi(K\bar{K}), J/\psi \rightarrow \phi \pi\pi(K\bar{K}), D_s \rightarrow \pi(\pi\pi)$
971.1 ± 4.0	24 AGUILAR... 91	EHS	$400 pp$
979 ± 4	36 ARMSTRONG 91	OMEG	$300 pp \rightarrow \rho \rho \pi\pi, \rho \rho K\bar{K}$
956 ± 12	BREAKSTONE 90	SFM	$pp \rightarrow \rho \rho \pi^+ \pi^-$
959.4 ± 6.5	24 AUGUSTIN 89	DM2	$J/\psi \rightarrow \omega \pi^+ \pi^-$
978 ± 9	24 ABACHI 86B	HRS	$e^+ e^- \rightarrow \pi^+ \pi^- X$
$985.0^{+9.0}_{-39.0}$	ETKIN 82B	MPS	$23 \pi^- p \rightarrow n 2K_S^0$
974 ± 4	36 GIDAL 81	MRK2	$J/\psi \rightarrow \pi^+ \pi^- X$
975	37 ACHASOV 80	RVUE	
986 ± 10	36 AGUILAR... 78	HBC	$0.7 \bar{p}p \rightarrow K_S^0 K_S^0$
969 ± 5	36 LEEPER 77	ASPK	$2-2.4 \pi^- p \rightarrow \pi^+ \pi^- n, K^+ K^- n$
987 ± 7	36 BINNIE 73	CNTR	$\pi^- p \rightarrow nMM$
1012 ± 6	38 GRAYER 73	ASPK	$17 \pi^- p \rightarrow \pi^+ \pi^- n$
1007 ± 20	38 HYAMS 73	ASPK	$17 \pi^- p \rightarrow \pi^+ \pi^- n$
997 ± 6	38 PROTOPOP... 73	HBC	$7 \pi^+ p \rightarrow \pi^+ \pi^+ \pi^-$

- From the $D^{\pm} \rightarrow K^{\pm} K^+ K^-$ Dalitz plot fit with the Triple-M amplitude in the multi-meson model of AOUE 18.
- Using a relativistic Breit-Wigner function and taking into account the finite D_s mass.
- Breit-Wigner mass. Using finite width corrections according to FLATTE 76 and ACHASOV 05, and the ratio $g_{f_0} K \bar{K} / g_{f_0} \pi\pi = 0$.
- In the kaon-loop fit.
- In the no-structure fit.
- Systematic errors not estimated.
- FLATTE 76 parameterization. $g_{f_0} \pi\pi = 329 \pm 96$ MeV/c² assuming $g_{f_0} K \bar{K} / g_{f_0} \pi\pi = 2$.
- Breit-Wigner mass. Using finite width corrections according to FLATTE 76 and ACHASOV 05, and the ratio $g_{f_0} K \bar{K} / g_{f_0} \pi\pi = 4.21 \pm 0.25 \pm 0.21$ from ABLIKIM 05.
- In the kaon-loop fit following formalism of ACHASOV 89.
- In the no-structure fit assuming a direct coupling of ϕ to $f_0 \gamma$.
- FLATTE 76 parameterization. Supersedes GARMASH 05.
- FLATTE 76 parameterization. $g_{f_0} K \bar{K} / g_{f_0} \pi\pi = 4.21 \pm 0.25 \pm 0.21$.
- K-matrix pole from combined analysis of $\pi^- p \rightarrow \pi^0 \pi^0 n, \pi^- p \rightarrow K \bar{K} n, \pi^+ \pi^- \rightarrow \pi^+ \pi^-, \bar{p}p \rightarrow \pi^0 \pi^0 \pi^0, \pi^0 \eta\eta, \pi^0 \pi^0 \eta, \pi^+ \pi^- \pi^0, K^+ K^- \pi^0, K_S^0 K_S^0 \pi^0, K^+ K_S^0 \pi^-$ at rest, $\bar{p}n \rightarrow \pi^- \pi^- \pi^+, K_S^0 K^- \pi^0, K_S^0 K_S^0 \pi^-$ at rest.
- From the negative interference with the $f_0(500)$ meson of AITALA 01B using the ACHASOV 89 parameterization for the $f_0(980)$, a Breit-Wigner for the $f_0(500)$, and ACHASOV 01F for the $\rho\pi$ contribution.
- Coupled-channel Breit-Wigner, couplings $g_{\pi} = 0.09 \pm 0.01 \pm 0.01, g_{K} = 0.02 \pm 0.04 \pm 0.03$.
- Supersedes ACHASOV 98i. Using the model of ACHASOV 89.
- Supersedes ACHASOV 98i.
- In the "narrow resonance" approximation.
- Assuming $\Gamma(f_0) = 40$ MeV.
- From a narrow pole fit taking into account $f_0(980)$ and $f_0(1200)$ intermediate mechanisms.
- From the combined fit of the photon spectra in the reactions $e^+ e^- \rightarrow \pi^+ \pi^- \gamma, \pi^0 \pi^0 \gamma$.
- Supersedes BARBERIS 99 and BARBERIS 99B
- T-matrix pole.
- From invariant mass fit.
- On sheet II in a 2 pole solution. The other pole is found on sheet III at $(1039-93i)$ MeV.
- On sheet II in a 2 pole solution. The other pole is found on sheet III at $(963-29i)$ MeV.
- Reanalysis of data from HYAMS 73, GRAYER 74, SRINIVASAN 75, and ROSSELET 77 using the interfering amplitude method.
- At high $|t|$.
- At low $|t|$.

See key on page 1171

Meson Particle Listings

$f_0(980)$

- 30 On sheet II in a 4-pole solution, the other poles are found on sheet III at (953–55i) MeV and on sheet IV at (938–35i) MeV.
- 31 Combined fit of ALDE 95B, ANISOVICH 94, AMSLER 94D.
- 32 On sheet II in a 2 pole solution. The other pole is found on sheet III at (996–103i) MeV.
- 33 From sheet II pole position.
- 34 On sheet II in a 2 pole solution. The other pole is found on sheet III at (797–185i) MeV and can be interpreted as a shadow pole.
- 35 On sheet II in a 2 pole solution. The other pole is found on sheet III at (978–28i) MeV.
- 36 From coupled channel analysis.
- 37 Coupled channel analysis with finite width corrections.
- 38 Included in AGUILAR-BENITEZ 78 fit.

- 30 ± 8
- 48 ± 14
- 32 ± 10
- 30 ± 10
- 54 ± 16
- 27 LEEPER 77 ASPK 2–2.4 $\pi^- p \rightarrow \pi^+ \pi^- n, K^+ K^- n$
- 27 BINNIE 73 CNTR $\pi^- p \rightarrow nMM$
- 30 GRAYER 73 ASPK 17 $\pi^- p \rightarrow \pi^+ \pi^- n$
- 30 HYAMS 73 ASPK 17 $\pi^- p \rightarrow \pi^+ \pi^- n$
- 30 PROTOPOP... 73 HBC 7 $\pi^+ p \rightarrow \pi^+ p \pi^+ \pi^-$

- 1 Using a relativistic Breit-Wigner function and taking into account the finite D_S mass.
- 2 Breit-Wigner $\pi\pi$ width. Using finite width corrections according to FLATTE 76 and ACHASOV 05, and the ratio $g_{f_0} K K / g_{f_0} \pi\pi = 0$.
- 3 Systematic errors not estimated.
- 4 Breit-Wigner $\pi\pi$ width. Using finite width corrections according to FLATTE 76 and ACHASOV 05, and the ratio $g_{f_0} K K / g_{f_0} \pi\pi = 4.21 \pm 0.25 \pm 0.21$ from ABLIKIM 05.
- 5 Breit-Wigner, solution 1, PWA ambiguous.
- 6 K-matrix pole from combined analysis of $\pi^- p \rightarrow \pi^0 \pi^0 n, \pi^- p \rightarrow K \bar{K} n, \pi^+ \pi^- \rightarrow \pi^+ \pi^-, \bar{p} p \rightarrow \pi^0 \pi^0 \pi^0, \pi^0 \eta, \pi^0 \pi^0 \eta, \pi^+ \pi^- \pi^0, K^+ K^- \pi^0, K_S^0 K_S^0 \pi^0, K^+ K_S^0 \pi^-$ at rest, $\bar{p} n \rightarrow \pi^- \pi^+ \pi^+, K_S^0 K^- \pi^0, K_S^0 K_S^0 \pi^-$ at rest.
- 7 Using the data of AKHMETSHIN 99C, ACHASOV 00H, and ALOISIO 02D.
- 8 Breit-Wigner width.
- 9 Supersedes ACHASOV 98i. Using the model of ACHASOV 89.
- 10 Supersedes ACHASOV 98i.
- 11 In the “narrow resonance” approximation.
- 12 From the combined fit of the photon spectra in the reactions $e^+ e^- \rightarrow \pi^+ \pi^- \gamma, \pi^0 \pi^0 \gamma$.
- 13 Supersedes BARBERIS 99 and BARBERIS 99B
- 14 T-matrix pole.
- 15 On sheet II in a 2 pole solution. The other pole is found on sheet III at (1039–93i) MeV.
- 16 From invariant mass fit.
- 17 On sheet II in a 2 pole solution. The other pole is found on sheet III at (963–29i) MeV.
- 18 Reanalysis of data from HYAMS 73, GRAYER 74, SRINIVASAN 75, and ROSSELET 77 using the interfering amplitude method.
- 19 At high $|t|$.
- 20 At low $|t|$.
- 21 On sheet II in a 4-pole solution, the other poles are found on sheet III at (953–55i) MeV and on sheet IV at (938–35i) MeV.
- 22 Combined fit of ALDE 95B, ANISOVICH 94,
- 23 On sheet II in a 2 pole solution. The other pole is found on sheet III at (996–103i) MeV.
- 24 From sheet II pole position.
- 25 On sheet II in a 2 pole solution. The other pole is found on sheet III at (797–185i) MeV and can be interpreted as a shadow pole.
- 26 On sheet II in a 2 pole solution. The other pole is found on sheet III at (978–28i) MeV.
- 27 From coupled channel analysis.
- 28 Coupled channel analysis with finite width corrections.
- 29 From coupled channel fit to the HYAMS 73 and PROTOPODESCU 73 data. With a simultaneous fit to the $\pi\pi$ phase-shifts, inelasticity and to the $K_S^0 K_S^0$ invariant mass.
- 30 Included in AGUILAR-BENITEZ 78 fit.

$f_0(980)$ WIDTH

Width determination very model dependent. Peak width in $\pi\pi$ is about 50 MeV, but decay width can be much larger.

VALUE (MeV)	EVTs	DOCUMENT ID	TECN	COMMENT
10 to 100 OUR ESTIMATE				
• • • We do not use the following data for averages, fits, limits, etc. • • •				
15.3 ± 4.7	424	ABLIKIM	15P BES3	$J/\psi \rightarrow K^+ K^- 3\pi$
9.5 ± 1.1	706	ABLIKIM	12E BES3	$J/\psi \rightarrow \gamma 3\pi$
91 +30 / -22 ± 3	44	1 ECKLUND	09 CLEO	4.17 $e^+ e^- \rightarrow D_S^- D_S^{*+} + c.c.$
66.9 ± 2.2 +17.6 / -12.5		2 UEHARA	08A BELL	10.6 $e^+ e^- \rightarrow \pi^0 \pi^0$
65 ± 13	262 ± 30	3 AUBERT	07AK BABR	10.6 $e^+ e^- \rightarrow \phi \pi^+ \pi^- \gamma$
81 ± 21	54 ± 9	3 AUBERT	07AK BABR	10.6 $e^+ e^- \rightarrow \phi \pi^0 \pi^0 \gamma$
51.3 +20.8 +13.2 / -17.7 -3.8		4 MORI	07 BELL	10.6 $e^+ e^- \rightarrow e^+ e^- \pi^+ \pi^-$
61 ± 9 +14 / -8	2584	5 GARMASH	05 BELL	$B^+ \rightarrow K^+ \pi^+ \pi^-$
64 ± 16		6 ANISOVICH	03 RVUE	
121 ± 23		TIKHOMIROV	03 SPEC	40.0 $\pi^- C \rightarrow K_S^0 K_S^0 K_L^0 X$
~ 70		7 BRAMON	02 RVUE	1.02 $e^+ e^- \rightarrow \pi^0 \pi^0 \gamma$
44 ± 2 ± 2	848	8 AITALA	01A E791	$D^+ \rightarrow \pi^- \pi^+ \pi^+$
201 ± 28	419	9 ACHASOV	00H SND	$e^+ e^- \rightarrow \pi^0 \pi^0 \gamma$
122 ± 13	419	10,11 ACHASOV	00H SND	$e^+ e^- \rightarrow \pi^0 \pi^0 \gamma$
56 ± 20		12 AKHMETSHIN	99C CMD2	$e^+ e^- \rightarrow \pi^0 \pi^0 \gamma$
65 ± 20		BARBERIS	99 OMEG	450 $pp \rightarrow \rho_S \rho_F K^+ K^-$
80 ± 10		BARBERIS	99B OMEG	450 $pp \rightarrow \rho_S \rho_F \pi^+ \pi^-$
80 ± 10		BARBERIS	99C OMEG	450 $pp \rightarrow \rho_S \rho_F \pi^0 \pi^0$
48 ± 12 ± 8		13 BARBERIS	99D OMEG	450 $pp \rightarrow K^+ K^-, \pi^+ \pi^-$
65 ± 25		BELLAZZINI	99 GAM4	450 $pp \rightarrow \rho \rho \pi^0 \pi^0$
71 ± 14		14 KAMINSKI	99 RVUE	$\pi\pi \rightarrow \pi\pi, K \bar{K}, \sigma\sigma$
~ 28		14 OLLER	99 RVUE	$\pi\pi \rightarrow \pi\pi, K \bar{K}$
~ 25		OLLER	99B RVUE	$\pi\pi \rightarrow \pi\pi, K \bar{K}$
~ 14		14 OLLER	99C RVUE	$\pi\pi \rightarrow \pi\pi, K \bar{K}, \eta\eta$
70 ± 20		ALDE	98 GAM4	
86 ± 16		14 ANISOVICH	98B RVUE	Compilation
54		15 LOCHER	98 RVUE	$\pi\pi \rightarrow \pi\pi, K \bar{K}$
69 ± 15		16 ALDE	97 GAM2	450 $pp \rightarrow \rho \rho \pi^0 \pi^0$
38 ± 20		17 BERTIN	97C OBLX	0.0 $\bar{p} p \rightarrow \pi^+ \pi^- \pi^0$
~ 100		18 SHIDA	96 RVUE	$\pi\pi \rightarrow \pi\pi, K \bar{K}$
34		TORNQVIST	96 RVUE	$\pi\pi \rightarrow \pi\pi, K \bar{K}, K\pi, \eta\pi$
48 ± 10	3k	19 ALDE	95B GAM2	38 $\pi^- p \rightarrow \pi^0 \pi^0 n$
95 ± 20	10k	20 ALDE	95B GAM2	38 $\pi^- p \rightarrow \pi^0 \pi^0 n$
26 ± 10		AMSLER	95B CBAR	0.0 $\bar{p} p \rightarrow 3\pi^0$
~ 112		21 AMSLER	95D CBAR	0.0 $\bar{p} p \rightarrow \pi^0 \pi^0 \pi^0, \pi^0 \eta\eta, \pi^0 \pi^0 \eta$
80 ± 12		22 ANISOVICH	95 RVUE	$\pi\pi \rightarrow \pi\pi, K \bar{K}$
30		JANSEN	95 RVUE	$\pi\pi \rightarrow \pi\pi, K \bar{K}$
74		23 BUGG	94 RVUE	$\bar{p} p \rightarrow \eta 2\pi^0$
29 ± 2		24 KAMINSKI	94 RVUE	$\pi\pi \rightarrow \pi\pi, K \bar{K}$
46		25 ZOU	94B RVUE	
48 ± 12		26 MORGAN	93 RVUE	$\pi\pi(K \bar{K}) \rightarrow \pi\pi(K \bar{K}), J/\psi \rightarrow \phi \pi(K \bar{K}), D_S \rightarrow \pi(\pi\pi)$
37.4 ± 10.6		16 AGUILAR-...	91 EHS	400 pp
72 ± 8		27 ARMSTRONG	91 OMEG	300 $pp \rightarrow \rho \rho \pi\pi, \rho \rho K \bar{K}$
110 ± 30		BREAKSTONE	90 SFM	$pp \rightarrow \rho \rho \pi^+ \pi^-$
29 ± 13		16 ABACHI	86B HRS	$e^+ e^- \rightarrow \pi^+ \pi^- X$
120 ± 281 ± 20		ETKIN	82B MPS	23 $\pi^- p \rightarrow n 2K_S^0$
28 ± 10		27 GIDAL	81 MRK2	$J/\psi \rightarrow \pi^+ \pi^- X$
70 to 300		28 ACHASOV	80 RVUE	
100 ± 80		29 AGUILAR-...	78 HBC	0.7 $\bar{p} p \rightarrow K_S^0 K_S^0$

$f_0(980)$ DECAY MODES

Mode	Fraction (Γ_i/Γ)
Γ_1 $\pi\pi$	seen
Γ_2 $K \bar{K}$	seen
Γ_3 $\gamma\gamma$	seen
Γ_4 $e^+ e^-$	

$f_0(980)$ PARTIAL WIDTHS

$\Gamma(\gamma\gamma)$	VALUE (keV)	DOCUMENT ID	TECN	COMMENT	Γ_3	
	0.29 +0.11 / -0.06 OUR AVERAGE					
	0.286 ± 0.017 +0.211 / -0.070	1 UEHARA	08A BELL	10.6 $e^+ e^- \rightarrow e^+ e^- \pi^0 \pi^0$		
	0.205 ± 0.095 +0.147 / -0.083 -0.117	2 MORI	07 BELL	10.6 $e^+ e^- \rightarrow e^+ e^- \pi^+ \pi^-$		
	0.42 ± 0.06 ± 0.18	3 OEST	90 JADE	$e^+ e^- \rightarrow e^+ e^- \pi^0 \pi^0$		
	• • • We do not use the following data for averages, fits, limits, etc. • • •					
	0.32 ± 0.05	4 DAI	14A RVUE	Compilation		
	0.16 ± 0.01	5 MENNESSIER 11	RVUE			
	0.29 ± 0.21 +0.02 / -0.07	6 MOUSSALLAM11	RVUE	Compilation		
	0.42	7,8 PENNINGTON 08	RVUE	Compilation		
	0.10	8,9 PENNINGTON 08	RVUE	Compilation		
	0.28 +0.09 / -0.13	10 BOGLIONE	99 RVUE	$\gamma\gamma \rightarrow \pi^+ \pi^-, \pi^0 \pi^0$		
	0.29 ± 0.07 ± 0.12	11,12 BOYER	90 MRK2	$e^+ e^- \rightarrow e^+ e^- \pi^+ \pi^-$		
	0.31 ± 0.14 ± 0.09	11,12 MARSISKE	90 CBAL	$e^+ e^- \rightarrow e^+ e^- \pi^0 \pi^0$		
	0.63 ± 0.14	13 MORGAN	90 RVUE	$\gamma\gamma \rightarrow \pi^+ \pi^-, \pi^0 \pi^0$		
	1 Using finite width corrections according to FLATTE 76 and ACHASOV 05, and the ratio $g_{f_0} K K / g_{f_0} \pi\pi = 0$.					
	2 Using finite width corrections according to FLATTE 76 and ACHASOV 05, and the ratio $g_{f_0} K K / g_{f_0} \pi\pi = 4.21 \pm 0.25 \pm 0.21$ from ABLIKIM 05.					
	3 OEST 90 quote systematic errors +0.08 / -0.18. We use ±0.18. Observed 60 events.					
	4 Using dispersive analysis with phases from GARCIA-MARTIN 11A and BUETTIGER 04 as input.					

Meson Particle Listings

$f_0(980)$, $a_0(980)$

- ⁵ Uses an analytic K-matrix model. Compilation.
- ⁶ Using dispersion integral with phase input from Roy equations and data from MARSISKE 90, BOYER 90, BEHREND 92, UEHARA 08A, and MORI 07.
- ⁷ Solution A (preferred solution based on χ^2 -analysis).
- ⁸ Dispersion theory based amplitude analysis of BOYER 90, MARSISKE 90, BEHREND 92, and MORI 07.
- ⁹ Solution B (worse than solution A; still acceptable when systematic uncertainties are included).
- ¹⁰ Supersedes MORGAN 90.
- ¹¹ From analysis allowing arbitrary background unconstrained by unitarity.
- ¹² Data included in MORGAN 90, BOGLIONE 99 analyses.
- ¹³ From amplitude analysis of BOYER 90 and MARSISKE 90, data corresponds to resonance parameters $m = 989$ MeV, $\Gamma = 61$ MeV.

$\Gamma(e^+e^-)$		Γ_4			
VALUE (eV)	CL%	DOCUMENT ID	TECN	COMMENT	
<8.4	90	VOROBYEV	88 ND	$e^+e^- \rightarrow \pi^0\pi^0$	

$f_0(980)$ BRANCHING RATIOS

$\Gamma(\pi\pi)/[\Gamma(\pi\pi) + \Gamma(K\bar{K})]$		$\Gamma_1/\Gamma_1 + \Gamma_2$			
VALUE	EVTS	DOCUMENT ID	TECN	COMMENT	

- • • We do not use the following data for averages, fits, limits, etc. • • •
- 0.52 ± 0.12 9.9k 1 AUBERT 06o BABR $B^{\pm} \rightarrow K^{\pm}\pi^{\pm}\pi^{\mp}$
- 0.75 $^{+0.11}_{-0.13}$ 2 ABLIKIM 05q BES2 $\chi_{c0} \rightarrow 2\pi^+2\pi^-$,
 $\pi^+\pi^-K^+K^-$
- 0.84 ± 0.02 3 ANISOVICH 02D SPEC Combined fit
- ~0.68 OLLER 99B RVUE $\pi\pi \rightarrow \pi\pi, K\bar{K}$
- 0.67 ± 0.09 4 LOVERRE 80 HBC $4\pi^-p \rightarrow n2K_S^0$
- 0.81 $^{+0.09}_{-0.04}$ 4 CASON 78 STRC $7\pi^-p \rightarrow n2K_S^0$
- 0.78 ± 0.03 4 WETZEL 76 OSPK $8.9\pi^-p \rightarrow n2K_S^0$

- ¹ Recalculated by us using $\Gamma(K^+K^-)/\Gamma(\pi^+\pi^-) = 0.69 \pm 0.32$ from AUBERT 06o and isospin relations.
- ² Using data from ABLIKIM 04g.
- ³ From a combined K-matrix analysis of Crystal Barrel ($p\bar{p} \rightarrow \pi^0\pi^0\pi^0, \pi^0\eta\eta, \pi^0\pi^0\eta$), GAMS ($\pi\rho \rightarrow \pi^0\pi^0, \eta\eta, \eta\eta'$), and BNL ($\pi\rho \rightarrow K\bar{K}n$) data.
- ⁴ Measure $\pi\pi$ elasticity assuming two resonances coupled to the $\pi\pi$ and $K\bar{K}$ channels only.

$f_0(980)$ REFERENCES

DANILKIN 21 PR D103 114023	I. Danilkin, O. Deineka, M. Vanderhaeghen (MAINZ)
SARANTSEV 21 PL B816 136227	A.V. Sarantsev et al. (BONN, PNPI)
ALBRECHT 20 EPJ C80 453	M. Albrecht et al. (Crystal Barrel Collab.)
AALI 19H JHEP 1904 063	R. Aaij et al. (LHCb Collab.)
AOUDE 18 PR D98 056021	R. Aoude et al.
ABLIKIM 15P PR D92 012007	M. Ablikim et al. (BESIII Collab.)
DAI 14A PR D90 036004	L.-Y. Dai, M.R. Pennington (CEBAF)
ABLIKIM 12E PRL 108 182001	M. Ablikim et al. (BESIII Collab.)
GARCIA-MAR... 11 PRL 107 072001	R. Garcia-Martin et al. (MADR, CRAC)
GARCIA-MAR... 11A PR D83 074004	R. Garcia-Martin et al. (MADR, CRAC)
MENNESSIER 11 PL B696 40	G. Mennessier, S. Narison, X.-G. Wang
MOUSSALLAM 11 EPJ C71 1814	M. Moussallam
BATLEY 10C EPJ C70 635	J.R. Batley et al. (CERN NA48/2 Collab.)
MENNESSIER 10 PL B688 59	G. Mennessier, S. Narison, X.-G. Wang
ANISOVICH 09 IJMP A24 2481	V.V. Anisovich, A.V. Sarantsev (PNPI)
ECKLUND 09 PR D80 052009	K.M. Ecklund et al. (CLEO Collab.)
BATLEY 08A EPJ C54 411	J.R. Batley et al. (CERN NA48/2 Collab.)
PENNINGTON 08 EPJ C56 1	M.R. Pennington et al.
UEHARA 08A PR D78 052004	S. Uehara et al. (BELLE Collab.)
AMBROSINO 07 EPJ C49 473	F. Ambrosino et al. (KLOE Collab.)
AUBERT 07AK PR D76 012008	B. Aubert et al. (BABAR Collab.)
BONVICINI 07 PR D76 012001	G. Bonvicini et al. (CLEO Collab.)
MORI 07 PR D75 051101	T. Mori et al. (BELLE Collab.)
AMBROSINO 06B PL B634 148	F. Ambrosino et al. (KLOE Collab.)
AUBERT 06O PR D74 032003	B. Aubert et al. (BABAR Collab.)
GARMASH 06 PR 96 251803	A. Garmash et al. (BELLE Collab.)
ABLIKIM 05 PL B607 243	M. Ablikim et al. (BES Collab.)
ABLIKIM 05Q PR D72 092002	M. Ablikim et al. (BES Collab.)
ACHASOV 05 PR D72 013006	N.N. Achasov, G.N. Shestakov
GARMASH 05 PR D71 092003	A. Garmash et al. (BELLE Collab.)
ABLIKIM 04G PR D70 092002	M. Ablikim et al. (BES Collab.)
BUETTIGER 04 EPJ C33 409	P. Buettiger, S. Descotes-Genon, B. Moussallam
PELAEZ 04A MPL A19 2879	J.R. Pelaez (MADU)
ANISOVICH 03 EPJ A16 229	V.V. Anisovich et al.
TIKHOMIROV 03 PAN 66 828	G.D. Tikhomirov et al.
ALOISIO 02D Translated from YAF 66 850.	A. Aloisio et al. (KLOE Collab.)
ANISOVICH 02D PAN 65 1545	V.V. Anisovich et al.
BRAMON 02 EPJ C26 253	A. Bramon et al.
ACHASOV 01F PR D63 094007	N.N. Achasov, V.V. Gubin (Novosibirsk SND Collab.)
AITALA 01A PRL 86 765	E.M. Aitala et al. (FNAL E791 Collab.)
AITALA 01B PRL 86 770	E.M. Aitala et al. (FNAL E791 Collab.)
ACHASOV 00H PL B485 349	N.N. Achasov et al. (Novosibirsk SND Collab.)
AKHMETSHTIN 99B PL B492 371	R.R. Akhmetshin et al. (Novosibirsk CMD-2 Collab.)
AKHMETSHTIN 99C PL B462 380	R.R. Akhmetshin et al. (Novosibirsk CMD-2 Collab.)
BARBERIS 99 PL B453 305	D. Barberis et al. (Omega Expt.)
BARBERIS 99B PL B453 316	D. Barberis et al. (Omega Expt.)
BARBERIS 99C PL B453 325	D. Barberis et al. (Omega Expt.)
BARBERIS 99D PL B462 462	D. Barberis et al. (Omega Expt.)
BELLAZZINI 99 PL B467 296	R. Bellazzini et al.
BOGLIONE 99 EPJ C9 11	M. Boglione, M.R. Pennington
KAMINSKI 99 EPJ C9 141	R. Kaminski, L. Lesniak, B. Loiseau (CRAC, PARIN)
OLLER 99 PR D60 099906 (errata.)	J.A. Oller et al.
OLLER 99C NP A652 407 (errata.)	J.A. Oller, E. Oset
ACHASOV 96 PL B407 442	M.N. Achasov et al.
ACKERSTAFF 95Q EPJ C4 19	K. Ackerstaff et al. (OPAL Collab.)
ALDE 98 EPJ A3 361	D. Alde et al. (GAM4 Collab.)
Also PAN 62 405	D. Alde et al. (GAM4 Collab.)
ANISOVICH 98B SPU 41 419	V.V. Anisovich et al.
Translated from UFN 168 481.	

LOCHER 98 EPJ C4 317	M.P. Locher et al. (PSI)
ALDE 97 PL B397 350	D.M. Alde et al. (GAMS Collab.)
BERTIN 97C PL B408 476	A. Bertin et al. (OBELIX Collab.)
ISHIDA 96 PTP 95 745	S. Ishida et al. (TOKY, MIYA, KEK)
TORNQVIST 96 PRL 76 1575	N.A. Tornqvist, M. Roos (HELS)
ALDE 95B ZPHY C66 375	D.M. Alde et al. (GAMS Collab.)
AMSLER 95B PL B342 433	C. Amisler et al. (Crystal Barrel Collab.)
AMSLER 95D PL B355 425	C. Amisler et al. (Crystal Barrel Collab.)
ANISOVICH 95 PL B355 363	V.V. Anisovich et al. (PNPI, SERP)
JANSSSEN 95 PR D52 2690	G. Janssen et al. (STON, ADL, JULI)
AMSLER 94D PL B333 277	C. Amisler et al. (Crystal Barrel Collab.)
ANISOVICH 94 PL B323 233	V.V. Anisovich et al. (Crystal Barrel Collab.)
BUGG 94 PR D50 4412	D.V. Bugg et al. (LOQM)
KAMINSKI 94 PR D50 3145	R. Kaminski, L. Lesniak, J.P. Maillet (CRAC+)
ZOU 94B PR D50 591	B.S. Zou, D.V. Bugg (LOQM)
MORGAN 93 PR D48 1185	D. Morgan, M.R. Pennington (RAL, DURH)
BEHREND 92 ZPHY C56 381	H.J. Behrend (CELLO Collab.)
AGUILAR... 91 ZPHY C50 405	M. Aguilar-Benitez et al. (LEBC-EHS Collab.)
ARMSTRONG 91 ZPHY C51 351	T.A. Armstrong et al. (ATHU, BARI, BIRM+)
BOYER 90 PR D42 1350	J. Boyer et al. (Mark II Collab.)
BREAKSTONE 90 ZPHY C48 569	A.M. Breakstone et al. (ISU, BGN, CERN+)
MARSISKE 90 PR D41 3324	H. Marsiske et al. (Crystal Ball Collab.)
MORGAN 90 ZPHY C48 623	D. Morgan, M.R. Pennington (RAL, DURH)
OEST 90 ZPHY C47 343	T. Oest et al. (JADE Collab.)
ACHASOV 89 NP B315 465	N.N. Achasov, V.N. Ivanchenko
AUGUSTIN 89 NP B320 1	J.E. Augustin, G. Cosme (DM2 Collab.)
VOROBYEV 88 SJNP 48 273	P.V. Vorobyev et al. (NOVO)
Translated from YAF 48 436.	
ABACHI 06B PRL 57 1930	S. Abachi et al. (PURD, ANL, IND, MICH+)
LONGACRE 86 PL B177 223	R.S. Longacre et al. (BNL, BRAN, CUNY+)
BINON 84C NC 80A 363	F.G. Binon et al. (BELG, LAPP, SERP+)
BINON 83 NC 78A 313	F.G. Binon et al. (BELG, LAPP, SERP+)
ETKIN 82B PR D25 1786	A. Etkin et al. (BNL, CUNY, TUFTS, VAND)
GIDAL 81 PL 107B 153	G. Gidal et al. (SLAC, LBL)
ACHASOV 80 SJNP 32 566	N.N. Achasov, S.A. Devyanin, G.N. Shestakov (NOVM)
Translated from YAF 32 1098.	
COHEN 80 PR D22 2595	D. Cohen et al. (ANL) IJP
LOVERRE 80 ZPHY C6 187	P.F. Loverre et al. (CERN, CDEF, MADR+ IJP)
AGUILAR... 78 NP B140 73	M. Aguilar-Benitez et al. (MADR, BOMB+)
CASON 78 PRL 41 271	M.M. Cason et al. (NDAM, ANL)
LEEPER 77 PR D16 2054	R.J. Leeper et al. (ISU)
ROSSELET 77 PR D15 574	L. Rosselet et al. (GEVA, SACL)
FLATTE 76 PL 63B 224	S.M. Flatte (CERN)
WETZEL 76 NP B115 208	W. Wetzel et al. (ETH, CERN, LOIC)
HYAMS 75 NP B100 205	B.D. Hyams et al. (CERN, MPIM)
SRINIVASAN 75 PR D12 681	V. Srinivasan et al. (NDAM, ANL)
ESTABROOKS 74 NP B79 301	P.G. Estabrooks, A.D. Martin (DURH)
GRAYEY 74 NP B75 189	G. Grayey et al. (CERN, MPIM)
BINNIE 73 PRL 31 1534	D.M. Binnie et al. (LOIC, SHMP)
GRAYEY 73 Tallahassee	G. Grayey et al. (CERN, MPIM)
HYAMS 73 NP B64 134	B.D. Hyams et al. (CERN, MPIM)
PROTOPOP... 73 PR D7 1279	S.D. Protopopescu et al. (LBL)

$a_0(980)$

$$I^G(J^{PC}) = 1^-(0^{++})$$

See the related review(s):
Scalar Mesons below 1 GeV

$a_0(980)$ T-MATRIX POLE \sqrt{s}

Note that $\Gamma = -2 \text{Im}(\sqrt{s})$.

VALUE (MeV)	DOCUMENT ID	TECN	COMMENT
(970-1020) - i (30-70) OUR ESTIMATE	(see Fig. 64.2 in the review)		
(1002.4 ± 1.4 ± 6.6) - i (63.5 ± 2.9)	1 ALBRECHT 20 CBAR	0.9 $\bar{p}p \rightarrow \pi^0\pi^0\eta$, $\pi^0\eta\eta, \pi^0K^+K^-$	
(1000.7 ± 12.9) - i (0.7)	2 LU 20 RVUE	$\gamma\gamma \rightarrow \pi^0\eta, K_S^0 K_S^0$	
- i (36.6 ± 12.7) - 2.6			
(989 ± 5) - i (40 ± 5)	3 BUGG 08A RVUE	$\bar{p}p$ annihilation data	
(1117 $^{+24}_{-320}$) - i (12 $^{+43}_{-12}$)	4 PELAEZ 04A RVUE	$\pi\pi \rightarrow \pi\pi, \pi K \rightarrow \pi K$	
(982 ± 3) - i (46 ± 4)	5 ABELE 98 CBAR	0.0 $\bar{p}p \rightarrow K_L^0 K^{\pm}\pi^{\mp}$	

- ¹ Pole mass on sheet closest to the physical axis - the more remote pole is extracted at (1004.1 ± 1.5 ± 6.5) - i (48.6 ± 1.2 ± 3.4) MeV.
- ² T-matrix pole on sheet II.
- ³ T-matrix pole on sheet II. Parameterizes couplings to $\bar{K}K, \pi\eta$, and $\pi\eta'$. Uses AMSLER 94D and ABELE 98.
- ⁴ Reanalysis of data from LINGLIN 73, ESTABROOKS 78, and ASTON 88 in the unitarized ChPT model.
- ⁵ T-matrix pole on sheet II; the pole on sheet III is at (1006 - i 49) MeV.

$a_0(980)$ MASS

VALUE (MeV)	DOCUMENT ID
980 ± 20 OUR ESTIMATE	Mass determination very model dependent

$\eta\pi$ FINAL STATE ONLY

VALUE (MeV)	EVTS	DOCUMENT ID	TECN	CHG	COMMENT
• • • We do not use the following data for averages, fits, limits, etc. • • •					
982.5 ± 1.6 ± 1.1	16.9k	1 AMBROSINO 09F KLOE	09F		1.02 $e^+e^- \rightarrow \eta\pi^0\gamma$
986 ± 4		ANISOVICH 09F RVUE	09F		0.0 $\bar{p}p, \pi\pi$
982.3 $^{+0.6}_{-0.7}$ + 3.1		2 UEHARA 09A BELL	09A		$\gamma\gamma \rightarrow \pi^0\eta$
985 ± 4 ± 6	318	ACHARD 02B L3	02B	L3	183-209 $e^+e^- \rightarrow e^+e^-\eta\pi^+\pi^-$
995 ± 10 - 12	36	3 ACHASOV 00F SND	00F	SND	$e^+e^- \rightarrow \eta\pi^0\gamma$
994 ± 33 - 8	36	4 ACHASOV 00F SND	00F	SND	$e^+e^- \rightarrow \eta\pi^0\gamma$
975 ± 7		BARBERIS 00H	00H		450 $pp \rightarrow \rho f \eta \pi^0 p_S$

988 ± 8	BARBERIS	00H	450 $pp \rightarrow \Delta_F^{++} \eta \pi^- p_S$
~ 1055	⁵ OLLER	99 RVUE	$\eta \pi, K\bar{K}$
~ 1009.2	⁵ OLLER	99B RVUE	$\pi \pi \rightarrow \pi \pi, K\bar{K}$
993.1 ± 2.1	⁶ TEIGE	99 B852	18.3 $\pi^- p \rightarrow \eta \pi^+ \pi^- n$
988 ± 6	⁵ ANISOVICH	98B RVUE	Compilation
987	TORNQVIST	96 RVUE	$\pi \pi \rightarrow \pi \pi, K\bar{K}, K\pi,$ $\eta \pi$
991	JANSSEN	95 RVUE	$\eta \pi \rightarrow \eta \pi, K\bar{K}, K\pi,$ $\eta \pi$
984.45 ± 1.23 ± 0.34	AMSLER	94c CBAR	0.0 $\bar{p} p \rightarrow \omega \eta \pi^0$
982 ± 2	⁷ AMSLER	92 CBAR	0.0 $\bar{p} p \rightarrow \eta \eta \pi^0$
984 ± 4	1040 ⁷ ARMSTRONG	91B OMEG ±	300 $pp \rightarrow pp \eta \pi^+ \pi^-$
976 ± 6	ATKINSON	84E OMEG ±	25-55 $\gamma p \rightarrow \eta \pi n$
986 ± 3	500 ⁸ EVANGELIS...	81 OMEG ±	12 $\pi^- p \rightarrow \eta \pi^+ \pi^- p$
990 ± 7	145 ⁸ GURTU	79 HBC ±	4.2 $K^- p \rightarrow \Lambda \eta 2\pi$
980 ± 11	47 CONFORTO	78 OSPK -	4.5 $\pi^- p \rightarrow p X^-$
978 ± 16	50 CORDEN	78 OMEG ±	12-15 $\pi^- p \rightarrow n \eta 2\pi$
977 ± 7	GRASSLER	77 HBC -	16 $\pi^+ p \rightarrow p \eta 3\pi$
989 ± 4	70 WELLS	75 HBC -	3.1-6 $K^- p \rightarrow \Lambda \eta 2\pi$
972 ± 10	150 DEFOIX	72 HBC ±	0.7 $\bar{p} p \rightarrow 7\pi$
970 ± 15	20 BARNES	69c HBC -	4-5 $K^- p \rightarrow \Lambda \eta 2\pi$
980 ± 10	CAMPBELL	69 DBC	2.7 $\pi^+ d$
980 ± 10	15 MILLER	69B HBC -	4.5 $K^- N \rightarrow \eta \pi \Lambda$
980 ± 10	30 AMMAR	68 HBC ±	5.5 $K^- p \rightarrow \Lambda \eta 2\pi$

95 ± 14	1040 ⁴ ARMSTRONG	91B OMEG ±	300 $pp \rightarrow pp \eta \pi^+ \pi^-$
62 ± 15	500 ⁵ EVANGELIS...	81 OMEG ±	12 $\pi^- p \rightarrow \eta \pi^+ \pi^- p$
60 ± 20	145 ⁵ GURTU	79 HBC ±	4.2 $K^- p \rightarrow \Lambda \eta 2\pi$
60 +50 -30	47 CONFORTO	78 OSPK -	4.5 $\pi^- p \rightarrow p X^-$
86.0 +60.0 -50.0	50 CORDEN	78 OMEG ±	12-15 $\pi^- p \rightarrow n \eta 2\pi$
44 ± 22	GRASSLER	77 HBC -	16 $\pi^+ p \rightarrow p \eta 3\pi$
80 to 300	⁶ FLATTE	76 RVUE -	4.2 $K^- p \rightarrow \Lambda \eta 2\pi$
16.0 +25.0 -16.0	70 ⁷ WELLS	75 HBC -	3.1-6 $K^- p \rightarrow \Lambda \eta 2\pi$
30 ± 5	150 ⁸ DEFOIX	72 HBC ±	0.7 $\bar{p} p \rightarrow 7\pi$
40 ± 15	CAMPBELL	69 DBC	2.7 $\pi^+ d$
60 ± 30	15 MILLER	69B HBC -	4.5 $K^- N \rightarrow \eta \pi \Lambda$
80 ± 30	30 AMMAR	68 HBC ±	5.5 $K^- p \rightarrow \Lambda \eta 2\pi$

- ¹ From a fit with the S-wave amplitude including two interfering Breit-Wigners plus a background term.
- ² T-matrix pole.
- ³ The $\eta \pi$ width.
- ⁴ From a single Breit-Wigner fit.
- ⁵ From $f_1(1285)$ decay.
- ⁶ Using a two-channel resonance parametrization of GAY 76B data.
- ⁷ Weak evidence only for $a_0(980)^+$ production.
- ⁸ This number has very little meaning. Error is much too small. Vlada

$K\bar{K}$ ONLY

VALUE (MeV)	EVTS	DOCUMENT ID	TECN	CHG	COMMENT
-------------	------	-------------	------	-----	---------

- • • We do not use the following data for averages, fits, limits, etc. • • •
- ~ 48 ¹OLLER 99c RVUE $\pi \pi \rightarrow \pi \pi, K\bar{K}$
- ~ 25 ²ASTIER 67 HBC ±
- 57 ± 13 ³ROSENFELD 65 RVUE ±
- ¹ T-matrix pole.
- ² ASTIER 67 includes data of BARLOW 67, CONFORTO 67, ARMENTEROS 65.
- ³ Plus systematic errors.

- ¹ Using the model of ACHASOV 89 and ACHASOV 03B.
- ² From a fit with the S-wave amplitude including two interfering Breit-Wigners plus a background term.
- ³ Using the model of ACHASOV 89. Supersedes ACHASOV 98B.
- ⁴ Using the model of JAFFE 77. Supersedes ACHASOV 98B.
- ⁵ T-matrix pole.
- ⁶ Breit-Wigner fit, average between a_0^{\pm} and a_0^0 . The fit favors a slightly heavier a_0^{\pm} .
- ⁷ From a single Breit-Wigner fit.
- ⁸ From $f_1(1285)$ decay.

$K\bar{K}$ ONLY

VALUE (MeV)	EVTS	DOCUMENT ID	TECN	COMMENT
-------------	------	-------------	------	---------

- • • We do not use the following data for averages, fits, limits, etc. • • •
- 947.7⁺_{-5.0} ± 6.6 ¹AAIJ 19H LHCb $pp \rightarrow D^{\pm} X$
- 925 ± 5 ± 8 190k ²AAIJ 16N LHCb $D^0 \rightarrow K_S^0 K^{\pm} \pi^{\mp}$
- ~ 1053 ³OLLER 99c RVUE $\pi \pi \rightarrow \pi \pi, K\bar{K}$
- 975 ± 15 BERTIN 98B OBLX 0.0 $\bar{p} p \rightarrow K^{\pm} K_S^0 \pi^{\mp}$
- 970 ± 10 316 DEBILLY 80 HBC 1.2-2 $\bar{p} p \rightarrow f_1(1285) \omega$
- 1016 ± 10 100 ⁴ASTIER 67 HBC 0.0 $\bar{p} p$
- 1003.3 ± 7.0 143 ^{5,6}ROSENFELD 65 RVUE

- ¹ From the $D^{\pm} \rightarrow K^{\pm} K^+ K^-$ Dalitz plot fit with the Triple-M amplitude in the multi-meson model of AOUDE 18.
- ² Using a two-channel resonance parametrization with couplings fixed to ABELE 98.
- ³ T-matrix pole.
- ⁴ ASTIER 67 includes data of BARLOW 67, CONFORTO 67, ARMENTEROS 65.
- ⁵ Note on J^P . Main argument for 0^+ is small Q value. Isotropy of decay distribution in $\bar{p} p$ at rest proves nothing. See discussion by Rosenfeld (Oxford) and Butterworth (Heidelberg).
- ⁶ Plus systematic errors.

$a_0(980)$ WIDTH

VALUE (MeV)	EVTS	DOCUMENT ID	TECN	CHG	COMMENT
-------------	------	-------------	------	-----	---------

- 50 to 100 OUR ESTIMATE** Width determination very model dependent. Peak width in $\eta \pi$ is about 60 MeV, but decay width can be much larger.
- • • We do not use the following data for averages, fits, limits, etc. • • •
- 75.6 ± 1.6 +17.4 -10.0 ¹UEHARA 09A BELL $\gamma \gamma \rightarrow \pi^0 \eta$
- 50 ± 13 ± 4 318 ACHARD 02B L3 183-209 $e^+ e^- \rightarrow e^+ e^- \eta \pi^+ \pi^-$
- 72 ± 16 BARBERIS 00H 450 $pp \rightarrow p_f \eta \pi^0 p_S$
- 61 ± 19 BARBERIS 00H 450 $pp \rightarrow \Delta_F^{++} \eta \pi^- p_S$
- ~ 42 ²OLLER 99 RVUE $\eta \pi, K\bar{K}$
- ~ 112 ²OLLER 99B RVUE $\pi \pi \rightarrow \eta \pi, K\bar{K}$
- 71 ± 7 ⁶TEIGE 99 B852 18.3 $\pi^- p \rightarrow \eta \pi^+ \pi^- n$
- 92 ± 20 ²ANISOVICH 98B RVUE Compilation
- 65 ± 10 ³BERTIN 98B OBLX ± 0.0 $\bar{p} p \rightarrow K^{\pm} K_S^0 \pi^{\mp}$
- ~ 100 TORNQVIST 96 RVUE $\pi \pi \rightarrow \pi \pi, K\bar{K}, K\pi,$
 $\eta \pi$
- 202 JANSSEN 95 RVUE $\eta \pi \rightarrow \eta \pi, K\bar{K}, K\pi,$
 $\eta \pi$
- 54.12 ± 0.34 ± 0.12 AMSLER 94c CBAR 0.0 $\bar{p} p \rightarrow \omega \eta \pi^0$
- 54 ± 10 ⁴AMSLER 92 CBAR 0.0 $\bar{p} p \rightarrow \eta \eta \pi^0$

$a_0(980)$ DECAY MODES

Mode	Fraction (Γ_i/Γ)
------	--------------------------------

- | | | |
|------------|-----------------|----------|
| Γ_1 | $\eta \pi$ | seen |
| Γ_2 | $K\bar{K}$ | seen |
| Γ_3 | $\eta' \pi$ | seen |
| Γ_4 | $\rho \pi$ | not seen |
| Γ_5 | $\gamma \gamma$ | seen |
| Γ_6 | $e^+ e^-$ | |

$a_0(980)$ PARTIAL WIDTHS

$\Gamma(\gamma \gamma)$	VALUE (keV)	DOCUMENT ID	TECN	Γ_5
-------------------------	-------------	-------------	------	------------

- • • We do not use the following data for averages, fits, limits, etc. • • •
- 0.30 ± 0.10 ¹AMSLER 98 RVUE
- ¹ Using $\Gamma_{\gamma \gamma} B(a_0(980) \rightarrow \eta \pi) = 0.24 \pm 0.08$ keV.

$a_0(980)$ $\Gamma(\eta \pi)/\Gamma(\text{total})$

$\Gamma(\eta \pi) \times \Gamma(\gamma \gamma)/\Gamma_{\text{total}}$	VALUE (keV)	EVTS	DOCUMENT ID	TECN	COMMENT	$\Gamma_1 \Gamma_5/\Gamma$
---	-------------	------	-------------	------	---------	----------------------------

- 0.21 +0.08 -0.04 OUR AVERAGE**
- 0.128 +0.003 +0.502 -0.002 -0.043 ¹UEHARA 09A BELL $\gamma \gamma \rightarrow \pi^0 \eta$
- 0.28 ± 0.04 ± 0.10 44 OEST 90 JADE $e^+ e^- \rightarrow e^+ e^- \pi^0 \eta$
- 0.19 ± 0.07 +0.10 -0.07 ANTREASYN 86 CBAL $e^+ e^- \rightarrow e^+ e^- \pi^0 \eta$
- ¹ From a fit with the S-wave amplitude including two interfering Breit-Wigners plus a background term.

$\Gamma(\eta \pi) \times \Gamma(e^+ e^-)/\Gamma_{\text{total}}$	VALUE (eV)	CL%	DOCUMENT ID	TECN	COMMENT	$\Gamma_1 \Gamma_6/\Gamma$
---	------------	-----	-------------	------	---------	----------------------------

- <1.5 90 VOROBYEV 88 ND $e^+ e^- \rightarrow \pi^0 \eta$

$a_0(980)$ BRANCHING RATIOS

$\Gamma(K\bar{K})/\Gamma(\eta \pi)$	VALUE	DOCUMENT ID	TECN	CHG	COMMENT	Γ_2/Γ_1
-------------------------------------	-------	-------------	------	-----	---------	---------------------

- 0.172 ± 0.019 OUR AVERAGE**
- 0.137 ± 0.036 ± 0.042 ¹ABLIKIM 22AH BES3 $D_s^+ \rightarrow K_S^0 K^+ \pi^0$
- 0.23 ± 0.05 ²ABELE 98 CBAR 0.0 $\bar{p} p \rightarrow K_L^0 K^{\pm} \pi^{\mp}$
- 0.166 ± 0.01 ± 0.02 ³BARBERIS 98c OMEG 450 $pp \rightarrow p_f f_1(1285) p_S$

Meson Particle Listings

$a_0(980), \phi(1020)$

••• We do not use the following data for averages, fits, limits, etc. •••

$0.138 \pm 0.001 \pm 0.035$	⁴ ALBRECHT	20	CBAR	$0.9 \bar{p}p \rightarrow \pi^0 \pi^0 \eta,$ $\pi^0 \eta \eta, \pi^0 K^+ K^-$
1.20 ± 0.15	⁵ ANISOVICH	09	RVUE	$0.0 \bar{p}p, \pi N$
$1.05 \pm 0.07 \pm 0.05$	⁶ BUGG	08A	RVUE	$\bar{p}p \rightarrow \pi^0 \pi^0 \eta$
0.57 ± 0.16	⁷ BARGIOTTI	03	OBLX	$\bar{p}p$
~ 0.60	OLLER	99B	RVUE	$\pi\pi \rightarrow \eta\pi, K\bar{K}$
0.7 ± 0.3	³ CORDEN	78	OMEG	$12-15 \pi^- p \rightarrow n\eta 2\pi$
0.25 ± 0.08	³ DEFOIX	72	HBC	$\pm 0.7 \bar{p} \rightarrow 7\pi$

- Using $D^+ \rightarrow a_0(980)^+ \pi^0$ from ABLIKIM 19Bc.
- Using $\pi^0 \pi^0 \eta$ from AMSLER 94D.
- From the decay of $f_1(1285)$.
- Residues from T-matrix pole with 2 poles, 2 channels. Solution on adjacent sheet $0.149 \pm 0.001 \pm 0.039$.
- This is a ratio of couplings.
- A ratio of couplings, using AMSLER 94D and ABELE 98. Supersedes BUGG 94.
- Coupled channel analysis of $\pi^+ \pi^- \pi^0, K^+ K^- \pi^0$, and $K^\pm K_S^0 \pi^\mp$.

$\Gamma(\eta'/\pi)/\Gamma_{total}$		Γ_3/Γ			
VALUE	EVTS	DOCUMENT ID	TECN	CHG	COMMENT
seen	116k	¹ CHEN	20A	BELL	$D^0 \rightarrow K^- \pi^+ \eta$

- From an amplitude analysis of the $D^0 \rightarrow K^- \pi^+ \eta$ decay in a three-channel Flatte model with a 10.1σ significance. Earlier observed by ABLIKIM 17K in the $\chi_{c1} \rightarrow \eta \pi^+ \pi^-$ decay with a 8.9σ significance.

$\Gamma(\rho\pi)/\Gamma(\eta\pi)$		Γ_4/Γ_1			
VALUE	CL%	DOCUMENT ID	TECN	CHG	COMMENT
<0.25	70	¹ AMMAR	70	HBC	$\pm 4.1, 5.5 K^- p \rightarrow \Lambda \eta 2\pi$

••• We do not use the following data for averages, fits, limits, etc. •••

- Not clear if they really observed the $a_0(980)$ 3 standard deviations.

$a_0(980)$ REFERENCES

ABLIKIM	22AH	PRL 129 182001	M. Ablikim et al.	(BESIII Collab.)
ALBRECHT	20	EPJ C80 453	M. Albrecht et al.	(Crystal Barrel Collab.)
CHEN	20A	PR D102 012002	Y.Q. Chen et al.	(BELLE Collab.)
LU	20	EPJ C80 436	J. Lu, B. Moussallam	
AAIJ	19H	JHEP 1904 063	R. Aaij et al.	(LHCb Collab.)
ABLIKIM	19BE	PRL 123 112001	M. Ablikim et al.	(BESIII Collab.)
AOUDE	18	PR D98 056021	R.T. Aoude et al.	
ABLIKIM	17K	PR D95 032002	M. Ablikim et al.	(BESIII Collab.)
AAIJ	16N	PR D93 052018	R. Aaij et al.	(LHCb Collab.)
AMBROSINO	09F	PL B681 5	F. Ambrosino et al.	(KLOE Collab.)
ANISOVICH	09	UJMP A24 2481	V.V. Anisovich, A.V. Sarantsev	(PHPI)
UEHARA	09A	PR D80 032001	S. Uehara et al.	(BELLE Collab.)
BUGG	08A	PR D78 074023	J.V. Bugg	(LOQM)
PELAEZ	04A	MPL A19 2879	D.R. Pelaez	(MADU)
ACHASOV	03B	PR D68 014006	N.N. Achasov, A.V. Kiselev	
BARGIOTTI	03	EPJ C26 371	M. Bargiotti et al.	(OBELIX Collab.)
ACHARD	02B	PL B526 269	P. Achard et al.	(L3 Collab.)
ACHASOV	00F	PL B479 53	M.N. Achasov et al.	(Novosibirsk SND Collab.)
BARBERIS	00H	PL B488 225	D. Barberis et al.	(WA 102 Collab.)
OLLER	99	PR D60 099006 (err.)	J.A. Oller et al.	
OLLER	99B	NP A552 407 (err.)	J.A. Oller, E. Oset	
OLLER	99C	PR D60 074023	J.A. Oller, E. Oset	
TEIGE	99	PR D59 012001	S. Teige et al.	(BNL E852 Collab.)
ABELE	98	PR D57 3860	A. Abele et al.	(Crystal Barrel Collab.)
ACHASOV	98B	PL B438 441	M.N. Achasov et al.	(Novosibirsk SND Collab.)
AMSLER	98	RMP 70 1293	C. Amisler	
ANISOVICH	98B	SPU 41 419	V.V. Anisovich et al.	
BARBERIS	98C	PL B440 225	D. Barberis et al.	(WA 102 Collab.)
BERTIN	98B	PL B434 180	A. Bertin et al.	(OBELIX Collab.)
TORNQVIST	96	PR L76 3575	M.A. Tornqvist, M. Roos	(HELS)
JANSEN	95	PR D52 2690	G. Jansen et al.	(STON, ADLD, JULI)
AMSLER	94C	PL B327 425	C. Amisler et al.	(Crystal Barrel Collab.)
AMSLER	94D	PL B333 277	C. Amisler et al.	(Crystal Barrel Collab.)
BUGG	94	PR D50 4412	D.V. Bugg et al.	(LOQM)
AMSLER	92	PL B291 347	C. Amisler et al.	(Crystal Barrel Collab.)
ARMSTRONG	91B	ZPHY C52 389	T.A. Armstrong et al.	(ATHU, BARI, BIRM+)
OEST	90	ZPHY C47 343	T. Oest et al.	(JADE Collab.)
ACHASOV	89	NP B315 465	N.N. Achasov, V.N. Ivanchenko	
ASTON	88	NP B296 493	D. Aston et al.	(SLAC, NAGO, CINC, INUS)
VOROBYEV	88	SJNP 48 273	F.V. Vorobyev et al.	(NOVO)
ANTREASYAN	86	PR D33 1847	D. Antreasyan et al.	(Crystal Ball Collab.)
ATKINSON	84E	PL L38B 459	M. Atkinson et al.	(BONN, CERN, GLAS+)
EVANGELIS...	81	NP B178 197	C. Evangelista et al.	(BARI, BONN, CERN+)
DEBILLY	80	NP B176 1	L. de Billy et al.	(CURIN, LAUS, NEUC+)
GURTU	79	NP B151 181	A. Gurtu et al.	(CERN, ZEEM, NIJM, OXF)
CONFORTO	78	LNC 23 419	B. Conforto et al.	(RHEL, TINTO, CHIC+)
CORDEN	78	NP B144 253	M.J. Corden et al.	(BIRM, RHEL, TELA+)
ESTABROOKS	78	NP B133 490	P.G. Estabrooks et al.	(MCGI, CARL, DURH+)
GRASSLER	77	NP B121 189	H. Grassler et al.	(AACH3, BERL, BONIV+)
JAFFE	77	PR D15 267 281	R. Jaffe	(MIT)
FLATTE	76	PL B3B 224	S.M. Flatte	(CERN)
GAY	76B	PL B3B 220	J.B. Gay et al.	(CERN, AMST, NUMJ JP)
WELLS	75	NP B101 333	J. Wells et al.	(OXF)
LINGLIN	73	NP B55 408	D. Linglin	(CERN)
DEFOIX	72	NP B44 125	C. Defoix et al.	(CDEF, CERN)
AMMAR	70	PR D2 430	R. Ammar et al.	(KANS, NWES, ANL, WIS C)
BARNES	69C	PRL 23 610	V.E. Barnes et al.	(BNL, SYRA)
CAMPBELL	69	PRL 22 1204	J.H. Campbell et al.	(PURD)
MILLER	69B	PL 29B 255	D.H. Miller et al.	(PURD)
Also		PR L80 2011	W.L. Yen et al.	(PURD)
AMMAR	68	PRL 21 1832	R. Ammar et al.	(NWES, ANL)
ASTIER	67	PL 25B 294	A. Astier et al.	(CDEF, CERN, IRAD)
Includes data of	BARLOW	67, CONFORTO	67, and ARMENTEROS	65.
BARLOW	67	NC 50A 701	J. Barlow et al.	(CERN, CDEF, IRAD, LIVP)
CONFORTO	67	NP B3 469	G. Conforto et al.	(CERN, CDEF, IPNP+)
ARMENTEROS	65	PL 17 344	R. Armenteros et al.	(CERN, CDEF)
ROSENFELD	65	Oxford Conf. 58	A.H. Rosenfeld	(LRL)

$\phi(1020)$

$$I^G(J^{PC}) = 0^-(1^{--})$$

$\phi(1020)$ MASS

VALUE (MeV)	EVTS	DOCUMENT ID	TECN	COMMENT
1019.461 ± 0.016 OUR AVERAGE				
1019.463 ± 0.061	2.3M	¹ KOZYREV	18	CMD3 $e^+ e^- \rightarrow K^+ K^-$, $K_S^0 K_L^0$
$1019.462 \pm 0.042 \pm 0.056$	28k	² LEES	14H	BABR $e^+ e^- \rightarrow K_S^0 K_L^0 \gamma$
$1019.51 \pm 0.02 \pm 0.05$		³ LEES	13Q	BABR $e^+ e^- \rightarrow K^+ K^- \gamma$
$1019.30 \pm 0.02 \pm 0.10$	105k	AKHMETSHIN	06	CMD2 $0.98-1.06 e^+ e^- \rightarrow \pi^+ \pi^- \pi^0$
$1019.52 \pm 0.05 \pm 0.05$	17.4k	AKHMETSHIN	05	CMD2 $0.60-1.38 e^+ e^- \rightarrow \eta \gamma$
$1019.483 \pm 0.011 \pm 0.025$	272k	⁴ AKHMETSHIN	04	CMD2 $e^+ e^- \rightarrow K_L^0 K_S^0$
1019.42 ± 0.05	1900k	⁵ ACHASOV	01E	SND $e^+ e^- \rightarrow K^+ K^-$, $K_S^0 K_L^0, \pi^+ \pi^- \pi^0$
$1019.40 \pm 0.04 \pm 0.05$	23k	AKHMETSHIN	01B	CMD2 $e^+ e^- \rightarrow \eta \gamma$
1019.36 ± 0.12		⁶ ACHASOV	00B	SND $e^+ e^- \rightarrow \eta \gamma$
$1019.38 \pm 0.07 \pm 0.08$	2200	⁷ AKHMETSHIN	99F	CMD2 $e^+ e^- \rightarrow \pi^+ \pi^- \geq 2\gamma$
$1019.51 \pm 0.07 \pm 0.10$	11169	AKHMETSHIN	98	CMD2 $e^+ e^- \rightarrow \pi^+ \pi^- \pi^0$
1019.5 ± 0.4		BARBERIS	98	OMEG $450 pp \rightarrow pp 2K^+ 2K^-$
1019.42 ± 0.06	55600	AKHMETSHIN	95	CMD2 $e^+ e^- \rightarrow$ hadrons
1019.7 ± 0.3	2012	DAVENPORT	86	MPSF $400 pA \rightarrow 4 KX$
$1019.7 \pm 0.1 \pm 0.1$	5079	ALBRECHT	85D	ARG $10 e^+ e^- \rightarrow K^+ K^- X$
1019.3 ± 0.1	1500	ARENTON	82	AEMS 11.8 polar. $pp \rightarrow KK$
1019.67 ± 0.17	25080	⁸ PELLINEN	82	RVUE
1019.52 ± 0.13	3681	BUKIN	78C	OLYA $e^+ e^- \rightarrow$ hadrons

••• We do not use the following data for averages, fits, limits, etc. •••

$1018.4 \pm 0.5 \pm 0.1$		⁹ ALBRECHT	20	CBAR $0.9 \bar{p}p \rightarrow K^+ K^- \pi^0$
$1019.21 \pm 0.04 \pm 0.03$		¹⁰ HOID	20	RVUE $e^+ e^- \rightarrow \pi^0 \gamma$
$1019.54 \pm 0.10 \pm 0.51$		¹¹ AAIJ	19H	LHCB $pp \rightarrow D^\pm X$
$1019.20 \pm 0.02 \pm 0.01$		¹² HOFERICHT...	19	RVUE $e^+ e^- \rightarrow \pi^+ \pi^- \pi^0$
1019.469 ± 0.061	1.7M	KOZYREV	18	CMD3 $e^+ e^- \rightarrow K^+ K^-$
1019.457 ± 0.061	610k	KOZYREV	16	CMD3 $e^+ e^- \rightarrow K_S^0 K_L^0$
1019.48 ± 0.01		LEES	13F	BABR $D^+ \rightarrow K^+ K^- \pi^+$
$1019.441 \pm 0.008 \pm 0.080$	542k	AKHMETSHIN	08	CMD2 $1.02 e^+ e^- \rightarrow K^+ K^-$
1019.63 ± 0.07	12540	AUBERT,B	05J	BABR $D^0 \rightarrow \bar{K}^0 K^+ K^-$
1019.8 ± 0.7		ARMSTRONG	86	OMEG $85 \pi^+ / pp \rightarrow \pi^+ / p 4Kp$
1020.1 ± 0.11	5526	ATKINSON	86	OMEG $20-70 \gamma p$
1019.7 ± 1.0		BEBEK	86	CLEO $e^+ e^- \rightarrow \gamma(4S)$
1019.411 ± 0.008	642k	¹⁵ DIJKSTRA	86	SPEC $100-200 \pi^\pm, \bar{p}, p, K^\pm$, on Be
1020.9 ± 0.2		¹⁴ FRAME	86	OMEG $13 K^+ p \rightarrow \phi K^+ p$
1021.0 ± 0.2		¹⁴ ARMSTRONG	83B	OMEG $18.5 K^- p \rightarrow K^- K^+ \Lambda$
1020.0 ± 0.5		¹⁴ ARMSTRONG	83B	OMEG $18.5 K^- p \rightarrow K^- K^+ \Lambda$
1019.7 ± 0.3		¹⁴ BARATE	83	GOLI $190 \pi^- Be \rightarrow 2\mu X$
$1019.8 \pm 0.2 \pm 0.5$	766	IVANOV	81	OLYA $1-1.4 e^+ e^- \rightarrow K^+ K^-$
1019.4 ± 0.5	337	COOPER	78B	HBC $0.7-0.8 \bar{p}p \rightarrow K_S^0 K_L^0 \pi^+ \pi^-$
1020 ± 1	383	¹⁴ BALDI	77	CNTR $10 \pi^- p \rightarrow \pi^- \phi p$
1018.9 ± 0.6	800	COHEN	77	ASPK $6 \pi^\pm N \rightarrow K^+ K^- N$
1019.7 ± 0.5	454	KALBFLEISCH	76	HBC $2.18 K^- p \rightarrow \Lambda K\bar{K}$
1019.4 ± 0.8	984	BESCH	74	CNTR $2 \gamma p \rightarrow p K^+ K^-$
1020.3 ± 0.4	100	BALLAM	73	HBC $2.8-9.3 \gamma p$
1019.4 ± 0.7		BINNIE	73B	CNTR $\pi^- p \rightarrow \phi n$
1019.6 ± 0.5	120	¹⁶ AGUILAR...	72B	HBC $3.9, 4.6 K^- p \rightarrow \Lambda K^+ K^-$
1019.9 ± 0.5	100	¹⁶ AGUILAR...	72B	HBC $3.9, 4.6 K^- p \rightarrow K^- p K^+ K^-$
1020.4 ± 0.5	131	COLLEY	72	HBC $10 K^+ p \rightarrow K^+ \phi p$
1019.9 ± 0.3	410	STOTTLE...	71	HBC $2.9 K^- p \rightarrow \Sigma / \Lambda K\bar{K}$

- Average of KOZYREV 16 and KOZYREV 18 values taking into account the correlated uncertainties. Supersedes individual KOZYREV 16 and KOZYREV 18 results.
- Using a vector meson dominance model with contribution from $\phi(1020)$ and higher mass excitations of $\rho(770), \omega(782)$, and $\phi(1020)$.
- Using a phenomenological model based on KUHN 90 with a sum of Breit-Wigner resonances for $\rho(770), \omega(782), \phi(1020)$ and their higher mass excitations.
- Update of AKHMETSHIN 99b
- From the combined fit assuming that the total $\phi(1020)$ production cross section is saturated by those of $K^+ K^-, K_S^0 K_L^0, \pi^+ \pi^- \pi^0$, and $\eta \gamma$ decays modes and using ACHASOV 00b for the $\eta \gamma$ decay mode.
- Using a total width of 4.43 ± 0.05 MeV. Systematic uncertainty included.
- Using a total width of 4.43 ± 0.05 MeV.

Meson Particle Listings

$\phi(1020)$

$\Gamma(e^+e^-)$ Γ_8

VALUE (keV)	DOCUMENT ID	TECN	COMMENT
1.27 ± 0.04 OUR EVALUATION			
1.251 ± 0.021 OUR AVERAGE			Error includes scale factor of 1.1.
1.235 ± 0.006 ± 0.022	¹ AKHMETSHIN 11	CMD2	1.02 e ⁺ e ⁻ → ϕ
1.32 ± 0.05 ± 0.03	² AMBROSINO 05	KLOE	1.02 e ⁺ e ⁻ → e ⁺ e ⁻
1.28 ± 0.05	AKHMETSHIN 95	CMD2	1.02 e ⁺ e ⁻ → ϕ

¹ Combined analysis of the CMD-2 data on $\phi \rightarrow K^+K^-, K_S^0 K_L^0, \pi^+\pi^-\pi^0, \eta\gamma$ assuming that the sum of their branching fractions is 0.99741 ± 0.00007 .
² From forward-backward asymmetry and using $\Gamma_{\text{total}} = 4.26 \pm 0.05$ MeV from the 2004 edition of this Review.

$(\Gamma(e^+e^-) \times \Gamma(\mu^+\mu^-))^{1/2}$ $(\Gamma_8\Gamma_9)^{1/2}$

VALUE (keV)	DOCUMENT ID	TECN	COMMENT
1.320 ± 0.018 ± 0.017	AMBROSINO 05	KLOE	1.02 e ⁺ e ⁻ → $\mu^+\mu^-$

$\phi(1020) \Gamma(i)\Gamma(e^+e^-)/\Gamma(\text{total})$

$\Gamma(K^+K^-) \times \Gamma(e^+e^-)/\Gamma_{\text{total}}$ $\Gamma_1\Gamma_8/\Gamma$

VALUE (keV)	EVTS	DOCUMENT ID	TECN	COMMENT
0.6340 ± 0.0070 ± 0.0039		¹ LEES	13Q	BABR e ⁺ e ⁻ → K ⁺ K ⁻ γ
• • • We do not use the following data for averages, fits, limits, etc. • • •				
0.669 ± 0.001 ± 0.023	1.7M	KOZYREV	18	CMD3 e ⁺ e ⁻ → K ⁺ K ⁻

¹ Using a phenomenological model based on KUHN 90 with a sum of Breit-Wigner resonances for $\rho(770), \omega(782), \phi(1020)$ and their higher mass excitations. The first error combines statistical and systematic uncertainties. The second one is due to the parametrization of the charged kaon form factor and mass calibration.

$\Gamma(K_S^0 K_L^0) \times \Gamma(e^+e^-)/\Gamma_{\text{total}}$ $\Gamma_2\Gamma_8/\Gamma$

VALUE (keV)	EVTS	DOCUMENT ID	TECN	COMMENT
0.4200 ± 0.0033 ± 0.0123	28k	¹ LEES	14H	BABR e ⁺ e ⁻ → K _S ⁰ K _L ⁰ γ

¹ Using a vector meson dominance model with contribution from $\phi(1020)$ and higher mass excitations of $\rho(770), \omega(782)$, and $\phi(1020)$.

$[\Gamma(\rho\pi) + \Gamma(\pi^+\pi^-\pi^0)] \times \Gamma(e^+e^-)/\Gamma_{\text{total}}$ $\Gamma_3\Gamma_8/\Gamma$

VALUE (eV)	DOCUMENT ID	TECN	COMMENT
184.1 ± 2.1 ± 8.0	¹ LEES	21B	BABR 10.5 e ⁺ e ⁻ → $\pi^+\pi^-\pi^0\gamma$

¹ From the cross section for e⁺e⁻ → $\pi^+\pi^-\pi^0$ with contributions from $\rho(770), \omega(782), \phi(1020), \omega(1420)$, and $\omega(1650)$.

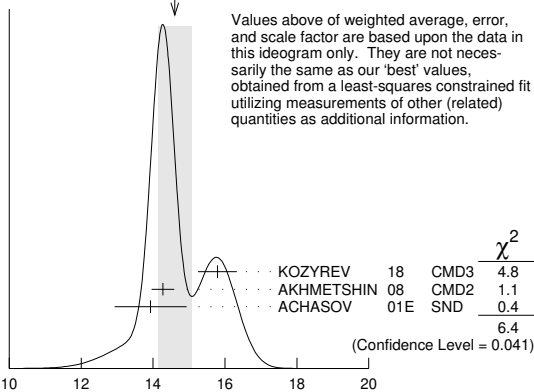
$\phi(1020) \Gamma(i)\Gamma(e^+e^-)/\Gamma^2(\text{total})$

$\Gamma(K^+K^-)/\Gamma_{\text{total}} \times \Gamma(e^+e^-)/\Gamma_{\text{total}}$ $\Gamma_1/\Gamma \times \Gamma_8/\Gamma$

VALUE (units 10 ⁻⁹)	EVTS	DOCUMENT ID	TECN	COMMENT
14.64 ± 0.27 OUR FIT				Error includes scale factor of 1.4.
14.6 ± 0.5 OUR AVERAGE				Error includes scale factor of 1.8. See the ideogram below.
15.789 ± 0.541	1.7M	KOZYREV	18	CMD3 e ⁺ e ⁻ → K ⁺ K ⁻
14.27 ± 0.05 ± 0.31	542k	AKHMETSHIN 08	CMD2	1.02 e ⁺ e ⁻ → K ⁺ K ⁻
13.93 ± 0.14 ± 0.99	1000k	¹ ACHASOV	01E	SND e ⁺ e ⁻ → K ⁺ K ⁻ , K _S ⁰ K _L ⁰ , $\pi^+\pi^-\pi^0$

¹ From the combined fit assuming that the total $\phi(1020)$ production cross section is saturated by those of K⁺K⁻, K_S⁰K_L⁰, $\pi^+\pi^-\pi^0$, and $\eta\gamma$ decays modes and using ACHASOV 00b for the $\eta\gamma$ decay mode.

WEIGHTED AVERAGE
14.6±0.5 (Error scaled by 1.8)



$\Gamma(K^+K^-)/\Gamma_{\text{total}} \times \Gamma(e^+e^-)/\Gamma_{\text{total}}$ (units 10⁻⁵)

$\Gamma(K_L^0 K_S^0)/\Gamma_{\text{total}} \times \Gamma(e^+e^-)/\Gamma_{\text{total}}$ $\Gamma_2/\Gamma \times \Gamma_8/\Gamma$

VALUE (units 10 ⁻⁹)	EVTS	DOCUMENT ID	TECN	COMMENT
10.11 ± 0.12 OUR FIT				
10.07 ± 0.13 OUR AVERAGE				
10.078 ± 0.223	610k	¹ KOZYREV	16	CMD3 e ⁺ e ⁻ → K _S ⁰ K _L ⁰
10.01 ± 0.04 ± 0.17	272k	² AKHMETSHIN 04	CMD2	e ⁺ e ⁻ → K _L ⁰ K _S ⁰
10.27 ± 0.07 ± 0.34	500k	³ ACHASOV	01E	SND e ⁺ e ⁻ → K ⁺ K ⁻ , K _S ⁰ K _L ⁰ , $\pi^+\pi^-\pi^0$

¹ KOZYREV 16 also reports $\Gamma(e^+e^-) B(\phi \rightarrow K_S^0 K_L^0) = (0.428 \pm 0.001 \pm 0.009)$ keV.
² Update of AKHMETSHIN 99d
³ From the combined fit assuming that the total $\phi(1020)$ production cross section is saturated by those of K⁺K⁻, K_S⁰K_L⁰, $\pi^+\pi^-\pi^0$, and $\eta\gamma$ decays modes and using ACHASOV 00b for the $\eta\gamma$ decay mode.

$[\Gamma(\rho\pi) + \Gamma(\pi^+\pi^-\pi^0)]/\Gamma_{\text{total}} \times \Gamma(e^+e^-)/\Gamma_{\text{total}}$ $\Gamma_3/\Gamma \times \Gamma_8/\Gamma$

VALUE (units 10 ⁻⁵)	EVTS	DOCUMENT ID	TECN	COMMENT
4.58 ± 0.11 OUR FIT				Error includes scale factor of 1.1.
4.51 ± 0.14 OUR AVERAGE				

4.51 ± 0.16 ± 0.11	105k	AKHMETSHIN 06	CMD2	0.98-1.06 e ⁺ e ⁻ → $\pi^+\pi^-\pi^0$
4.665 ± 0.042 ± 0.261	400k	¹ ACHASOV	01E	SND e ⁺ e ⁻ → K ⁺ K ⁻ , K _S ⁰ K _L ⁰ , $\pi^+\pi^-\pi^0$
4.35 ± 0.27 ± 0.08	11169	² AKHMETSHIN 98	CMD2	e ⁺ e ⁻ → $\pi^+\pi^-\pi^0$
• • • We do not use the following data for averages, fits, limits, etc. • • •				
4.38 ± 0.12		BENAYOUN 10	RVUE	0.4-1.05 e ⁺ e ⁻
4.30 ± 0.08 ± 0.21		³ AUBERT,B	04N	BABR 10.6 e ⁺ e ⁻ → $\pi^+\pi^-\pi^0\gamma$

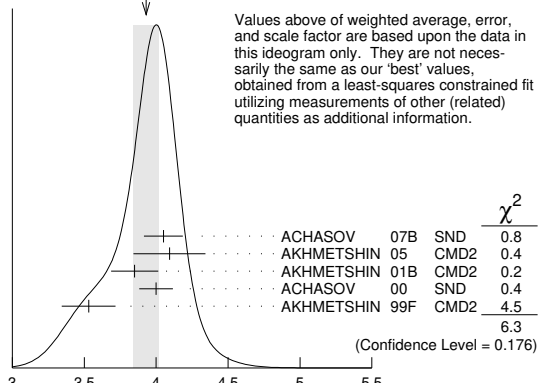
¹ From the combined fit assuming that the total $\phi(1020)$ production cross section is saturated by those of K⁺K⁻, K_S⁰K_L⁰, $\pi^+\pi^-\pi^0$, and $\eta\gamma$ decays modes and using ACHASOV 00b for the $\eta\gamma$ decay mode.
² Recalculated by us from the cross section in the peak.
³ Superseded by LEES 21B.

$\Gamma(\eta\gamma)/\Gamma_{\text{total}} \times \Gamma(e^+e^-)/\Gamma_{\text{total}}$ $\Gamma_5/\Gamma \times \Gamma_8/\Gamma$

VALUE (units 10 ⁻⁶)	EVTS	DOCUMENT ID	TECN	COMMENT
3.88 ± 0.07 OUR FIT				Error includes scale factor of 1.2.
3.93 ± 0.09 OUR AVERAGE				Error includes scale factor of 1.3. See the ideogram below.
4.050 ± 0.067 ± 0.118	33k	¹ ACHASOV	07B	SND 0.6-1.38 e ⁺ e ⁻ → $\eta\gamma$
4.093 ^{+0.040} _{-0.043} ± 0.247	17.4k	² AKHMETSHIN 05	CMD2	0.60-1.38 e ⁺ e ⁻ → $\eta\gamma$
3.850 ± 0.041 ± 0.159	23k	^{3,4} AKHMETSHIN 01B	CMD2	e ⁺ e ⁻ → $\eta\gamma$
4.00 ± 0.04 ± 0.11		⁵ ACHASOV 00	SND	e ⁺ e ⁻ → $\eta\gamma$
3.53 ± 0.08 ± 0.17	2200	^{6,7} AKHMETSHIN 99F	CMD2	e ⁺ e ⁻ → $\eta\gamma$
• • • We do not use the following data for averages, fits, limits, etc. • • •				
4.19 ± 0.06		⁸ BENAYOUN 10	RVUE	0.4-1.05 e ⁺ e ⁻

¹ From a combined fit of $\sigma(e^+e^- \rightarrow \eta\gamma)$ with $\eta \rightarrow 3\pi^0$ and $\eta \rightarrow \pi^+\pi^-\pi^0$, and fixing $B(\eta \rightarrow 3\pi^0) / B(\eta \rightarrow \pi^+\pi^-\pi^0) = 1.44 \pm 0.04$. Recalculated by us from the cross section at the peak. Supersedes ACHASOV 00D and ACHASOV 06A.
² From the $\eta \rightarrow 2\gamma$ decay and using $B(\eta \rightarrow \gamma\gamma) = 39.43 \pm 0.26\%$.
³ From the $\eta \rightarrow 3\pi^0$ decay and using $B(\eta \rightarrow 3\pi^0) = (32.24 \pm 0.29) \times 10^{-2}$.
⁴ The combined fit from 600 to 1380 MeV taking into account $\rho(770), \omega(782), \phi(1020)$, and $\rho(1450)$ (mass and width fixed at 1450 MeV and 310 MeV respectively).
⁵ From the $\eta \rightarrow 2\gamma$ decay and using $B(\eta \rightarrow 2\gamma) = (39.21 \pm 0.34) \times 10^{-2}$.
⁶ Recalculated by the authors from the cross section in the peak.
⁷ From the $\eta \rightarrow \pi^+\pi^-\pi^0$ decay and using $B(\eta \rightarrow \pi^+\pi^-\pi^0) = (23.1 \pm 0.5) \times 10^{-2}$.
⁸ A simultaneous fit of e⁺e⁻ → $\pi^+\pi^-$, $\pi^+\pi^-\pi^0$, $\pi^0\gamma$, $\eta\gamma$ data.

WEIGHTED AVERAGE
3.93±0.09 (Error scaled by 1.3)



$\Gamma(\eta\gamma)/\Gamma_{\text{total}} \times \Gamma(e^+e^-)/\Gamma_{\text{total}}$

$\Gamma_5/\Gamma \times \Gamma_8/\Gamma$

See key on page 1171

Meson Particle Listings

$\phi(1020)$

$\Gamma(\pi^0\gamma)/\Gamma_{total} \times \Gamma(e^+e^-)/\Gamma_{total}$ $\Gamma_6/\Gamma \times \Gamma_8/\Gamma$

VALUE (units 10^{-7})	EVTS	DOCUMENT ID	TECN	COMMENT
3.94 ± 0.16 OUR FIT				
3.95 ± 0.17 OUR AVERAGE				
4.04 ± 0.09 ± 0.19		¹ ACHASOV 16A	SND	0.60-1.38 $e^+e^- \rightarrow \pi^0\gamma$
3.75 ± 0.11 ± 0.29	18k	AKHMETSHIN 05	CMD2	0.60-1.38 $e^+e^- \rightarrow \pi^0\gamma$
• • • We do not use the following data for averages, fits, limits, etc. • • •				
4.29 ± 0.11		² BENAYOUN 10	RVUE	0.4-1.05 e^+e^-
3.67 ± 0.10 $^{+0.27}_{-0.25}$		³ ACHASOV 00	SND	$e^+e^- \rightarrow \pi^0\gamma$

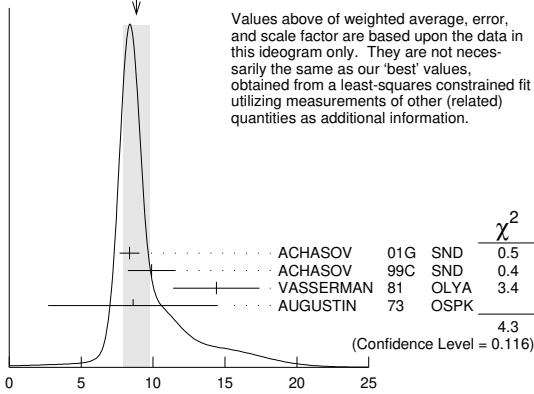
¹ From the VMD model with the interfering $\rho(770)$, $\omega(782)$, $\phi(1020)$ resonances, and an additional resonance describing the total contribution of the $\rho(1450)$ and $\omega(1420)$ states. Supersedes ACHASOV 00.
² A simultaneous fit of $e^+e^- \rightarrow \pi^+\pi^-$, $\pi^+\pi^-\pi^0$, $\pi^0\gamma$, $\eta\gamma$ data.
³ From the $\pi^0 \rightarrow 2\gamma$ decay and using $B(\pi^0 \rightarrow 2\gamma) = (98.798 \pm 0.032) \times 10^{-2}$.

$\Gamma(\mu^+\mu^-)/\Gamma_{total} \times \Gamma(e^+e^-)/\Gamma_{total}$ $\Gamma_9/\Gamma \times \Gamma_8/\Gamma$

VALUE (units 10^{-8})	DOCUMENT ID	TECN	COMMENT
8.5 ± 0.6 OUR FIT	Error includes scale factor of 1.2.		
8.8 ± 0.9 OUR AVERAGE	Error includes scale factor of 1.5. See the ideogram below.		
8.36 ± 0.59 ± 0.37	ACHASOV 01G	SND	$e^+e^- \rightarrow \mu^+\mu^-$
9.9 ± 1.4 ± 0.9	¹ ACHASOV 99c	SND	$e^+e^- \rightarrow \mu^+\mu^-$
14.4 ± 3.0	² VASSERMAN 81	OLYA	$e^+e^- \rightarrow \mu^+\mu^-$
8.6 ± 5.9	² AUGUSTIN 73	OSPK	$e^+e^- \rightarrow \mu^+\mu^-$

¹ Recalculated by the authors from the cross section in the peak.
² Recalculated by us from the cross section in the peak.

WEIGHTED AVERAGE
8.8 ± 0.9 (Error scaled by 1.5)



$\Gamma(\pi^+\pi^-)/\Gamma_{total} \times \Gamma(e^+e^-)/\Gamma_{total}$ $\Gamma_{11}/\Gamma \times \Gamma_8/\Gamma$

VALUE (units 10^{-8})	DOCUMENT ID	TECN	COMMENT
2.2 ± 0.4 OUR FIT			
2.2 ± 0.4 OUR AVERAGE			
2.1 ± 0.3 ± 0.3	¹ ACHASOV 00c	SND	$e^+e^- \rightarrow \pi^+\pi^-$
1.95 $^{+1.15}_{-0.87}$	² GOLUBEV 86	ND	$e^+e^- \rightarrow \pi^+\pi^-$
6.01 $^{+3.19}_{-2.51}$	² VASSERMAN 81	OLYA	$e^+e^- \rightarrow \pi^+\pi^-$
• • • We do not use the following data for averages, fits, limits, etc. • • •			
3.31 ± 0.99	³ BENAYOUN 13	RVUE	0.4-1.05 e^+e^-

¹ Recalculated by the authors from the cross section in the peak.
² Recalculated by us from the cross section in the peak.
³ A simultaneous fit to $e^+e^- \rightarrow \pi^+\pi^-$, $\pi^+\pi^-\pi^0$, $\pi^0\gamma$, $\eta\gamma$, $K\bar{K}$, and $\tau^- \rightarrow \pi^-\pi^0\nu_\tau$ data.

$\Gamma(\omega\pi^0)/\Gamma_{total} \times \Gamma(e^+e^-)/\Gamma_{total}$ $\Gamma_{12}/\Gamma \times \Gamma_8/\Gamma$

VALUE (units 10^{-8})	DOCUMENT ID	TECN	COMMENT
1.40 ± 0.15 OUR FIT			
1.37 ± 0.17 ± 0.01	^{1,2} AMBROSINO 08G	KLOE	$e^+e^- \rightarrow \pi^+\pi^-2\pi^0, 2\pi^0\gamma$

¹ Recalculated by the authors from the cross section at the peak.
² AMBROSINO 08G reports $[\Gamma(\phi(1020) \rightarrow \omega\pi^0)/\Gamma_{total} \times \Gamma(\phi(1020) \rightarrow e^+e^-)/\Gamma_{total}] \times [B(\omega(782) \rightarrow \pi^+\pi^-\pi^0)] = (1.22 \pm 0.13 \pm 0.08) \times 10^{-8}$ which we divide by our best value $B(\omega(782) \rightarrow \pi^+\pi^-\pi^0) = (89.2 \pm 0.7) \times 10^{-2}$. Our first error is their experiment's error and our second error is the systematic error from using our best value.

$\Gamma(\pi^0\pi^0\gamma)/\Gamma_{total} \times \Gamma(e^+e^-)/\Gamma_{total}$ $\Gamma_{17}/\Gamma \times \Gamma_8/\Gamma$

VALUE (units 10^{-8})	DOCUMENT ID	TECN	COMMENT
3.34 ± 0.17 OUR FIT			
3.33 $^{+0.04}_{-0.09} \pm 0.19$	¹ AMBROSINO 07	KLOE	$e^+e^- \rightarrow \pi^0\pi^0\gamma$

¹ Calculated by the authors from the cross section at the peak.

$\Gamma(\pi^+\pi^-\pi^+\pi^-)/\Gamma_{total} \times \Gamma(e^+e^-)/\Gamma_{total}$ $\Gamma_{18}/\Gamma \times \Gamma_8/\Gamma$

VALUE (units 10^{-9})	EVTS	DOCUMENT ID	TECN	COMMENT
1.2 $^{+0.8}_{-0.7}$ OUR FIT				
1.17 ± 0.52 ± 0.64	3285	¹ AKHMETSHIN 00E	CMD2	$e^+e^- \rightarrow \pi^+\pi^-\pi^+\pi^-$
• • • We do not use the following data for averages, fits, limits, etc. • • •				
4.29 ± 0.11		² BENAYOUN 10	RVUE	0.4-1.05 e^+e^-

¹ Recalculated by the authors from the cross section in the peak.

$\phi(1020)$ BRANCHING RATIOS

$\Gamma(K^+K^-)/\Gamma_{total}$ Γ_1/Γ

VALUE	EVTS	DOCUMENT ID	TECN	COMMENT
0.491 ± 0.005 OUR FIT				Error includes scale factor of 1.3.
0.493 ± 0.010 OUR AVERAGE				
0.492 ± 0.012	2913	AKHMETSHIN 95	CMD2	$e^+e^- \rightarrow K^+K^-$
0.44 ± 0.05	321	KALBFLEISCH 76	HBC	$2.18 K^-p \rightarrow \Lambda K^+K^-$
0.49 ± 0.06	270	DEGROOT 74	HBC	$4.2 K^-p \rightarrow \Lambda\phi$
0.540 ± 0.034	565	BALAKIN 71	OSPK	$e^+e^- \rightarrow K^+K^-$
0.48 ± 0.04	252	LINDSEY 66	HBC	$2.1-2.7 K^-p \rightarrow \Lambda K^+K^-$
• • • We do not use the following data for averages, fits, limits, etc. • • •				
0.493 ± 0.003 ± 0.007		¹ AKHMETSHIN 11	CMD2	$1.02 e^+e^- \rightarrow K^+K^-$
0.476 ± 0.017	100k	² ACHASOV 01E	SND	$e^+e^- \rightarrow K^+K^-, K_S^0 K_L^0, \pi^+\pi^-\pi^0$

¹ Combined analysis of the CMD-2 data on $\phi \rightarrow K^+K^-, K_S^0 K_L^0, \pi^+\pi^-\pi^0, \eta\gamma$ assuming that the sum of their branching fractions is 0.99741 ± 0.00007 .
² Using $B(\phi \rightarrow e^+e^-) = (2.93 \pm 0.14) \times 10^{-4}$.

$\Gamma(K_L^0 K_S^0)/\Gamma_{total}$ Γ_2/Γ

VALUE	EVTS	DOCUMENT ID	TECN	COMMENT
0.339 ± 0.004 OUR FIT				Error includes scale factor of 1.2.
0.331 ± 0.009 OUR AVERAGE				
0.335 ± 0.010	40644	AKHMETSHIN 95	CMD2	$e^+e^- \rightarrow K_L^0 K_S^0$
0.326 ± 0.035		DOLINSKY 91	ND	$e^+e^- \rightarrow K_L^0 K_S^0$
0.310 ± 0.024		DRUZHININ 84	ND	$e^+e^- \rightarrow K_L^0 K_S^0$
• • • We do not use the following data for averages, fits, limits, etc. • • •				
0.336 ± 0.002 ± 0.006		¹ AKHMETSHIN 11	CMD2	$1.02 e^+e^- \rightarrow K_S^0 K_L^0$
0.351 ± 0.013	500k	² ACHASOV 01E	SND	$e^+e^- \rightarrow K^+K^-, K_S^0 K_L^0, \pi^+\pi^-\pi^0$
0.27 ± 0.03	133	KALBFLEISCH 76	HBC	$2.18 K^-p \rightarrow \Lambda K_L^0 K_S^0$
0.257 ± 0.030	95	³ BALAKIN 71	OSPK	$e^+e^- \rightarrow K_L^0 K_S^0$
0.40 ± 0.04	167	LINDSEY 66	HBC	$2.1-2.7 K^-p \rightarrow \Lambda K_L^0 K_S^0$

¹ Combined analysis of the CMD-2 data on $\phi \rightarrow K^+K^-, K_S^0 K_L^0, \pi^+\pi^-\pi^0, \eta\gamma$ assuming that the sum of their branching fractions is 0.99741 ± 0.00007 .
² Using $B(\phi \rightarrow e^+e^-) = (2.93 \pm 0.14) \times 10^{-4}$.
³ Balakin error increased by Paul.

$\Gamma(K_L^0 K_S^0)/\Gamma(K^+K^-)$ Γ_2/Γ_1

VALUE	EVTS	DOCUMENT ID	TECN	COMMENT
0.690 ± 0.014 OUR FIT				Error includes scale factor of 1.3.
0.740 ± 0.031 OUR AVERAGE				
0.70 ± 0.06	2732	BUKIN 78c	OLYA	$e^+e^- \rightarrow K_L^0 K_S^0$
0.82 ± 0.08		LOSTY 78	HBC	$4.2 K^-p \rightarrow \phi$ hyperon
0.71 ± 0.05		LAVEN 77	HBC	$10 K^-p \rightarrow K^+K^- \Lambda$
0.71 ± 0.08		LYONS 77	HBC	$3-4 K^-p \rightarrow \Lambda\phi$
0.89 ± 0.10	144	AGUILAR-...	72B	HBC $3.9, 4.6 K^-p$
• • • We do not use the following data for averages, fits, limits, etc. • • •				
0.638 ± 0.022	2.3M	¹ KOZYREV 18	CMD3	$e^+e^- \rightarrow K_L^0 K_S^0, K^+K^-$
0.68 ± 0.03		² AKHMETSHIN 95	CMD2	$e^+e^- \rightarrow K_L^0 K_S^0, K^+K^-$

¹ The prediction taking into account phase-space difference, radiative corrections, isospin breaking, and the Sommerfeld-Gamow-Sakharov factor gives 0.630.
² Theoretical analysis of BRAMON 00 taking into account phase-space difference, electromagnetic radiative corrections, as well as isospin breaking, predicts 0.62. FLOREZ-BAEZ 08 predicts 0.63 considering also structure-dependent radiative corrections. FISCHBACH 02 calculates additional corrections caused by the close threshold and predicts 0.68. See also BENAYOUN 01 and DUBYNSKIY 07. BENAYOUN 12 obtains 0.71 ± 0.01 in the HLS model.

$\Gamma(K_L^0 K_S^0)/\Gamma(K\bar{K})$ $\Gamma_2/(\Gamma_1 + \Gamma_2)$

VALUE	EVTS	DOCUMENT ID	TECN	COMMENT
0.408 ± 0.005 OUR FIT				Error includes scale factor of 1.3.
0.45 ± 0.04 OUR AVERAGE				
0.44 ± 0.07		¹ LONDON 66	HBC	$2.24 K^-p \rightarrow \Lambda K\bar{K}$
0.48 ± 0.07	52	BADIER 65B	HBC	$3 K^-p$
0.40 ± 0.10	34	SCHLEIN 63	HBC	$1.95 K^-p \rightarrow \Lambda K\bar{K}$

¹ This is probably not affected by their controversial background subtraction; the value is from their numbers of $K_1 K_2$ vs K^+K^- events.

$[\Gamma(\rho\pi) + \Gamma(\pi^+\pi^-\pi^0)]/\Gamma_{total}$ Γ_3/Γ

VALUE	EVTS	DOCUMENT ID	TECN	COMMENT
0.154 ± 0.004 OUR FIT				Error includes scale factor of 1.2.
0.151 ± 0.009 OUR AVERAGE				Error includes scale factor of 1.7.
0.161 ± 0.008	11761	AKHMETSHIN 95	CMD2	$e^+e^- \rightarrow \pi^+\pi^-\pi^0$
0.143 ± 0.007		DOLINSKY 91	ND	$e^+e^- \rightarrow \pi^+\pi^-\pi^0$

Meson Particle Listings

 $\phi(1020)$

• • • We do not use the following data for averages, fits, limits, etc. • • •

$0.155 \pm 0.002 \pm 0.005$		¹ AKHMETSHIN 11	CMD2	$1.02 e^+ e^- \rightarrow \pi^+ \pi^- \pi^0$
0.159 ± 0.008	400k	² ACHASOV	01E SND	$e^+ e^- \rightarrow K^+ K^-, K_S^0 K_L^0, \pi^+ \pi^- \pi^0$
$0.145 \pm 0.009 \pm 0.003$	11169	³ AKHMETSHIN 98	CMD2	$e^+ e^- \rightarrow \pi^+ \pi^- \pi^0$
0.139 ± 0.007		⁴ PARROUR	76B OSPK	$e^+ e^-$

¹ Combined analysis of the CMD-2 data on $\phi \rightarrow K^+ K^-, K_S^0 K_L^0, \pi^+ \pi^- \pi^0, \eta\gamma$ assuming that the sum of their branching fractions is 0.99741 ± 0.00007 .

² Using $B(\phi \rightarrow e^+ e^-) = (2.93 \pm 0.14) \times 10^{-4}$.

³ Using $B(\phi \rightarrow e^+ e^-) = (2.99 \pm 0.08) \times 10^{-4}$.

⁴ Using $\Gamma(\phi) = 4.1$ MeV. If interference between the $\rho\pi$ and 3π modes is neglected, the fraction of the $\rho\pi$ is more than 80% at the 90% confidence level.

$$\frac{\Gamma(\rho\pi) + \Gamma(\pi^+ \pi^- \pi^0)}{\Gamma(K^+ K^-)} \quad \Gamma_3/\Gamma_1$$

VALUE	EVTS	DOCUMENT ID	TECN	COMMENT
0.313 ± 0.010 OUR FIT				Error includes scale factor of 1.2.
0.28 ± 0.09	34	AGUILAR-...	72B HBC	$3.9, 4.6 K^- \rho$

$$\frac{\Gamma(\rho\pi) + \Gamma(\pi^+ \pi^- \pi^0)}{\Gamma(K\bar{K})} \quad \Gamma_3/(\Gamma_1 + \Gamma_2)$$

VALUE	DOCUMENT ID	TECN	COMMENT
0.185 ± 0.005 OUR FIT			Error includes scale factor of 1.2.
0.24 ± 0.04 OUR AVERAGE			
0.237 ± 0.039	CERRADA	77B HBC	$4.2 K^- \rho \rightarrow \Lambda 3\pi$
0.30 ± 0.15	LONDON	66 HBC	$2.24 K^- \rho \rightarrow \Lambda \pi^+ \pi^- \pi^0$

$$\frac{\Gamma(\rho\pi) + \Gamma(\pi^+ \pi^- \pi^0)}{\Gamma(K_S^0 K_L^0)} \quad \Gamma_3/\Gamma_2$$

VALUE	EVTS	DOCUMENT ID	TECN	COMMENT
0.453 ± 0.012 OUR FIT				Error includes scale factor of 1.1.
0.51 ± 0.05 OUR AVERAGE				
0.56 ± 0.07	3681	BUKIN	78c OLYA	$e^+ e^- \rightarrow K_L^0 K_S^0, \pi^+ \pi^- \pi^0$
0.47 ± 0.06	516	COSME	74 OSPK	$e^+ e^- \rightarrow \pi^+ \pi^- \pi^0$

$$\Gamma(\pi^+ \pi^- \pi^0)/\Gamma_{\text{total}} \quad \Gamma_4/\Gamma$$

VALUE	CL%	EVTS	DOCUMENT ID	TECN	COMMENT
≈ 0.0087		1.98M	^{1,2} ALOISIO	03 KLOE	$1.02 e^+ e^- \rightarrow \pi^+ \pi^- \pi^0$
< 0.0006	90		³ ACHASOV	02 SND	$1.02 e^+ e^- \rightarrow \pi^+ \pi^- \pi^0$
< 0.23	90		³ CORDIER	80 DM1	$e^+ e^- \rightarrow \pi^+ \pi^- \pi^0$
< 0.20	90		³ PARROUR	76B OSPK	$e^+ e^- \rightarrow \pi^+ \pi^- \pi^0$

¹ From a fit without limitations on charged and neutral ρ masses and widths.

² Adding the direct and $\omega\pi$ contributions and considering the interference between the $\rho\pi$ and $\pi^+ \pi^- \pi^0$.

³ Neglecting the interference between the $\rho\pi$ and $\pi^+ \pi^- \pi^0$.

$$\Gamma(\eta\gamma)/\Gamma_{\text{total}} \quad \Gamma_5/\Gamma$$

VALUE (units 10^{-2})	EVTS	DOCUMENT ID	TECN	COMMENT
1.301 ± 0.024 OUR FIT				Error includes scale factor of 1.2.
1.26 ± 0.04 OUR AVERAGE				
$1.246 \pm 0.025 \pm 0.057$	10k	¹ ACHASOV	98F SND	$e^+ e^- \rightarrow 7\gamma$
1.18 ± 0.11	279	² AKHMETSHIN 95	CMD2	$e^+ e^- \rightarrow \pi^+ \pi^- 3\gamma$
1.30 ± 0.06		³ DRUZHININ 84	ND	$e^+ e^- \rightarrow 3\gamma$
1.4 ± 0.2		⁴ DRUZHININ 84	ND	$e^+ e^- \rightarrow 6\gamma$
0.88 ± 0.20	290	KURDADZE	83c OLYA	$e^+ e^- \rightarrow 3\gamma$
1.35 ± 0.29		ANDREWS	77 CNTR	$6.7-10 \gamma \text{Cu}$
1.5 ± 0.4	54	³ COSME	76 OSPK	$e^+ e^-$

• • • We do not use the following data for averages, fits, limits, etc. • • •

$1.38 \pm 0.02 \pm 0.02$		⁵ AKHMETSHIN 11	CMD2	$1.02 e^+ e^- \rightarrow \eta\gamma$
$1.36 \pm 0.05 \pm 0.01$	33k	⁶ ACHASOV	07B SND	$0.6-1.38 e^+ e^- \rightarrow \eta\gamma$
$1.373 \pm 0.014 \pm 0.085$	17.4k	^{7,8} AKHMETSHIN 05	CMD2	$0.60-1.38 e^+ e^- \rightarrow \eta\gamma$
$1.287 \pm 0.013 \pm 0.063$		^{9,10} AKHMETSHIN 01B	CMD2	$e^+ e^- \rightarrow \eta\gamma$
$1.338 \pm 0.012 \pm 0.052$		¹¹ ACHASOV	00 SND	$e^+ e^- \rightarrow \eta\gamma$
$1.18 \pm 0.03 \pm 0.06$	2200	¹² AKHMETSHIN 99F	CMD2	$e^+ e^- \rightarrow \eta\gamma$
1.21 ± 0.07		¹³ BENAYOUN	96 RVUE	$0.54-1.04 e^+ e^- \rightarrow \eta\gamma$

¹ Using $B(\phi \rightarrow e^+ e^-) = (2.99 \pm 0.08) \times 10^{-4}$ and $B(\eta \rightarrow 3\pi^0) = (32.2 \pm 0.4) \times 10^{-2}$.

² From $\pi^+ \pi^- \pi^0$ decay mode of η .

³ From 2γ decay mode of η .

⁴ From $3\pi^0$ decay mode of η .

⁵ Combined analysis of the CMD-2 data on $\phi \rightarrow K^+ K^-, K_S^0 K_L^0, \pi^+ \pi^- \pi^0, \eta\gamma$ assuming that the sum of their branching fractions is 0.99741 ± 0.00007 .

⁶ ACHASOV 07b reports $[\Gamma(\phi(1020) \rightarrow \eta\gamma)/\Gamma_{\text{total}}] \times [B(\phi(1020) \rightarrow e^+ e^-)] = (4.050 \pm 0.067 \pm 0.118) \times 10^{-6}$ which we divide by our best value $B(\phi(1020) \rightarrow e^+ e^-) = (2.979 \pm 0.033) \times 10^{-4}$. Our first error is their experiment's error and our second error is the systematic error from using our best value. Supersedes ACHASOV 00b and ACHASOV 06a.

⁷ Using $B(\phi \rightarrow e^+ e^-) = (2.98 \pm 0.04) \times 10^{-4}$ and $B(\eta \rightarrow \gamma\gamma) = 39.43 \pm 0.26\%$.

⁸ Not independent of the corresponding $\Gamma(e^+ e^-) \times \Gamma(\eta\gamma)/\Gamma_{\text{total}}^2$.

⁹ Using $B(\phi \rightarrow e^+ e^-) = (2.99 \pm 0.08) \times 10^{-4}$ and $B(\eta \rightarrow 3\pi^0) = (32.24 \pm 0.29) \times 10^{-2}$.

¹⁰ The combined fit from 600 to 1380 MeV taking into account $\rho(770), \omega(782), \phi(1020)$, and $\rho(1450)$ (mass and width fixed at 1450 MeV and 310 MeV respectively).

¹¹ From the $\eta \rightarrow 2\gamma$ decay and using $B(\phi \rightarrow e^+ e^-) = (2.99 \pm 0.08) \times 10^{-4}$.

¹² From $\pi^+ \pi^- \pi^0$ decay mode of η and using $B(\phi \rightarrow e^+ e^-) = (2.99 \pm 0.08) \times 10^{-4}$.

¹³ Reanalysis of DRUZHININ 84, DOLINSKY 89, and DOLINSKY 91 taking into account a triangle anomaly contribution.

$$\Gamma(\pi^0 \gamma)/\Gamma_{\text{total}} \quad \Gamma_6/\Gamma$$

VALUE (units 10^{-3})	EVTS	DOCUMENT ID	TECN	COMMENT
1.32 ± 0.05 OUR FIT				
1.31 ± 0.13 OUR AVERAGE				
1.30 ± 0.13		DRUZHININ	84 ND	$e^+ e^- \rightarrow 3\gamma$
1.4 ± 0.5	32	COSME	76 OSPK	$e^+ e^-$
1.367 ± 0.072		¹ ACHASOV	16A SND	$0.60-1.38 e^+ e^- \rightarrow \pi^0 \gamma$
$1.258 \pm 0.037 \pm 0.077$	18k	^{2,3} AKHMETSHIN 05	CMD2	$0.60-1.38 e^+ e^- \rightarrow \pi^0 \gamma$
$1.226 \pm 0.036 \pm 0.096$		⁴ ACHASOV	00 SND	$e^+ e^- \rightarrow \pi^0 \gamma$
1.26 ± 0.17		⁵ BENAYOUN	96 RVUE	$0.54-1.04 e^+ e^- \rightarrow \pi^0 \gamma$

• • • We do not use the following data for averages, fits, limits, etc. • • •

¹ Using $B(\phi \rightarrow e^+ e^-)$ from PDG 15. Supersedes ACHASOV 00.

² Using $B(\phi \rightarrow e^+ e^-) = (2.98 \pm 0.04) \times 10^{-4}$.

³ Not independent of the corresponding $\Gamma(e^+ e^-) \times \Gamma(\pi^0 \gamma)/\Gamma_{\text{total}}^2$.

⁴ From the $\pi^0 \rightarrow 2\gamma$ decay and using $B(\phi \rightarrow e^+ e^-) = (2.99 \pm 0.08) \times 10^{-4}$.

⁵ Reanalysis of DRUZHININ 84, DOLINSKY 89, and DOLINSKY 91 taking into account a triangle anomaly contribution.

$$\Gamma(\eta\gamma)/\Gamma(\pi^0 \gamma) \quad \Gamma_5/\Gamma_6$$

VALUE	DOCUMENT ID	TECN	COMMENT
$10.9 \pm 0.3 \pm 0.7$			Error includes scale factor of 1.2.
	ACHASOV	00 SND	$e^+ e^- \rightarrow \eta\gamma, \pi^0 \gamma$

$$\Gamma(e^+ e^-)/\Gamma_{\text{total}} \quad \Gamma_8/\Gamma$$

VALUE (units 10^{-4})	EVTS	DOCUMENT ID	TECN	COMMENT
2.979 ± 0.033 OUR FIT				Error includes scale factor of 1.2.
2.98 ± 0.07 OUR AVERAGE				Error includes scale factor of 1.1.
2.93 ± 0.14	1900k	¹ ACHASOV	01E SND	$e^+ e^- \rightarrow K^+ K^-, K_S^0 K_L^0, \pi^+ \pi^- \pi^0$
2.88 ± 0.09	55600	AKHMETSHIN	95 CMD2	$e^+ e^- \rightarrow \text{hadrons}$
3.00 ± 0.21	3681	BUKIN	78c OLYA	$e^+ e^- \rightarrow \text{hadrons}$
3.10 ± 0.14		² PARROUR	76 OSPK	$e^+ e^-$
3.3 ± 0.3		COSME	74 OSPK	$e^+ e^- \rightarrow \text{hadrons}$
2.81 ± 0.25	681	BALAKIN	71 OSPK	$e^+ e^- \rightarrow \text{hadrons}$
3.50 ± 0.27		CHATELUS	71 OSPK	$e^+ e^-$

¹ From the combined fit assuming that the total $\phi(1020)$ production cross section is saturated by those of $K^+ K^-, K_S^0 K_L^0, \pi^+ \pi^- \pi^0$, and $\eta\gamma$ decays modes and using ACHASOV 00b for the $\eta\gamma$ decay mode.

² Using total width 4.2 MeV. They detect 3π mode and observe significant interference with ω tail. This is accounted for in the result quoted above.

$$\Gamma(\mu^+ \mu^-)/\Gamma_{\text{total}} \quad \Gamma_9/\Gamma$$

VALUE (units 10^{-4})	DOCUMENT ID	TECN	COMMENT
2.85 ± 0.22 OUR FIT			Error includes scale factor of 1.2.
2.5 ± 0.4 OUR AVERAGE			
2.69 ± 0.46	¹ HAYES	71 CNTR	$8.3, 9.8 \gamma \text{C} \rightarrow \mu^+ \mu^- \text{X}$
2.17 ± 0.60	¹ EARLES	70 CNTR	$6.0 \gamma \text{C} \rightarrow \mu^+ \mu^- \text{X}$
$2.87 \pm 0.20 \pm 0.14$	² ACHASOV	01g SND	$e^+ e^- \rightarrow \mu^+ \mu^-$
$3.30 \pm 0.45 \pm 0.32$	³ ACHASOV	99c SND	$e^+ e^- \rightarrow \mu^+ \mu^-$
4.83 ± 1.02	⁴ VASSERMAN	81 OLYA	$e^+ e^- \rightarrow \mu^+ \mu^-$
2.87 ± 1.98	⁴ AUGUSTIN	73 OSPK	$e^+ e^- \rightarrow \mu^+ \mu^-$

¹ Neglecting interference between resonance and continuum.

² Using $B(\phi \rightarrow e^+ e^-) = (2.91 \pm 0.07) \times 10^{-4}$.

³ Using $B(\phi \rightarrow e^+ e^-) = (2.99 \pm 0.08) \times 10^{-4}$.

⁴ Recalculated by us using $B(\phi \rightarrow e^+ e^-) = (2.99 \pm 0.08) \times 10^{-4}$.

$$\Gamma(\eta e^+ e^-)/\Gamma_{\text{total}} \quad \Gamma_{10}/\Gamma$$

VALUE (units 10^{-4})	EVTS	DOCUMENT ID	TECN	COMMENT
1.08 ± 0.007 OUR AVERAGE				
$1.075 \pm 0.007 \pm 0.038$	30k	¹ BABUSCI	15 KLOE	$1.02 e^+ e^- \rightarrow \eta e^+ e^-$
$1.19 \pm 0.19 \pm 0.12$	213	² ACHASOV	01B SND	$e^+ e^- \rightarrow \eta e^+ e^-$
$1.14 \pm 0.10 \pm 0.06$	355	³ AKHMETSHIN 01	CMD2	$e^+ e^- \rightarrow \eta e^+ e^-$
$1.13 \pm 0.14 \pm 0.07$	183	⁴ AKHMETSHIN 01	CMD2	$e^+ e^- \rightarrow \eta e^+ e^-$
$1.21 \pm 0.14 \pm 0.09$	130	⁵ AKHMETSHIN 01	CMD2	$e^+ e^- \rightarrow \eta e^+ e^-$
$1.04 \pm 0.20 \pm 0.08$	42	⁶ AKHMETSHIN 01	CMD2	$e^+ e^- \rightarrow \eta e^+ e^-$
1.3 ± 0.8	7	GOLUBEV	85 ND	$e^+ e^- \rightarrow \eta e^+ e^-$

¹ Using $B(\eta \rightarrow 3\pi^0) = (32.57 \pm 0.23)\%$ from PDG 12.

² Using $B(\eta \rightarrow \gamma\gamma) = (39.25 \pm 0.32)\%$, $B(\phi \rightarrow \eta\gamma) = (1.26 \pm 0.06)\%$, and $B(\phi \rightarrow e^+ e^-) = (3.00 \pm 0.06) \times 10^{-4}$.

³ The average of the branching ratios separately obtained from the $\eta \rightarrow \gamma\gamma, 3\pi^0, \pi^+ \pi^- \pi^0$ decays.

⁴ From $\eta \rightarrow \gamma\gamma$ decays and using $B(\eta \rightarrow \gamma\gamma) = (39.33 \pm 0.25) \times 10^{-2}$, $B(\eta \rightarrow \pi^+ \pi^- \gamma) = (4.75 \pm 11) \times 10^{-2}$, and $B(\phi \rightarrow \eta\gamma) = (1.297 \pm 0.033) \times 10^{-2}$.

⁵ From $\eta \rightarrow 3\pi^0$ decays and using $B(\pi^0 \rightarrow \gamma\gamma) = (98.798 \pm 0.033) \times 10^{-2}$, $B(\eta \rightarrow 3\pi^0) = (32.24 \pm 0.29) \times 10^{-2}$, $B(\eta \rightarrow \pi^+ \pi^- \gamma) = (4.75 \pm 0.11) \times 10^{-2}$, and $B(\phi \rightarrow \eta\gamma) = (1.297 \pm 0.033) \times 10^{-2}$.

⁶ From $\eta \rightarrow \pi^+ \pi^- \pi^0$ decays and using $B(\pi^0 \rightarrow \gamma\gamma) = (98.798 \pm 0.033) \times 10^{-2}$, $B(\pi^0 \rightarrow e^+ e^- \gamma) = (1.198 \pm 0.032) \times 10^{-2}$, $B(\eta \rightarrow \pi^+ \pi^- \pi^0) = (23.0 \pm 0.4) \times 10^{-2}$, $B(\phi \rightarrow \pi^+ \pi^- \pi^0) = (15.5 \pm 0.6) \times 10^{-2}$, and $B(\phi \rightarrow \eta\gamma) = (1.297 \pm 0.033) \times 10^{-2}$.

See key on page 1171

Meson Particle Listings

 $\phi(1020)$ $\Gamma(\pi^+\pi^-)/\Gamma_{\text{total}}$ Γ_{11}/Γ

VALUE (units 10^{-4})	CL%	DOCUMENT ID	TECN	COMMENT
0.71 ± 0.11 ± 0.09		1 ACHASOV	00c SND	$e^+e^- \rightarrow \pi^+\pi^-$
0.65 ^{+0.38} _{-0.29}		1 GOLUBEV	86 ND	$e^+e^- \rightarrow \pi^+\pi^-$
2.01 ^{+1.07} _{-0.84}		1 VASSERMAN	81 OLYA	$e^+e^- \rightarrow \pi^+\pi^-$
<6.6	95	BUKIN	78B OLYA	$e^+e^- \rightarrow \pi^+\pi^-$
<2.7	95	ALVENSLEB...	72 CNTR	6.7 γ C \rightarrow $C\pi^+\pi^-$

¹ Using $B(\phi \rightarrow e^+e^-) = (2.99 \pm 0.08) \times 10^{-4}$.

 $\Gamma(\omega\pi^0)/\Gamma_{\text{total}}$ Γ_{12}/Γ

VALUE (units 10^{-5})	DOCUMENT ID	TECN	COMMENT
4.7 ± 0.5 OUR FIT			
5.2 ^{+1.3} _{-1.1}	1,2 AULCHENKO	00A SND	$e^+e^- \rightarrow \pi^+\pi^-\pi^0\pi^0$
4.4 ± 0.6	3 AMBROSINO	08G KLOE	$e^+e^- \rightarrow \pi^+\pi^-\pi^0\pi^0$
~5.4	4 ACHASOV	00E SND	$e^+e^- \rightarrow \pi^0\pi^0\gamma$
5.5 ^{+1.6} _{-1.4} ± 0.3	2,5 AULCHENKO	00A SND	$e^+e^- \rightarrow \pi^+\pi^-\pi^0\pi^0$
4.8 ^{+1.9} _{-1.7} ± 0.8	4 ACHASOV	99 SND	$e^+e^- \rightarrow \pi^+\pi^-\pi^0\pi^0$

¹ Using the 1996 and 1998 data.

² (2.3 ± 0.3)% correction for other decay modes of the $\omega(782)$ applied.

³ Not independent of the corresponding $\Gamma(\omega\pi^0) \times \Gamma(e^+e^-) / \Gamma^2(\text{total})$.

⁴ Using the 1996 data.

⁵ Using the 1998 data.

 $\Gamma(\omega\gamma)/\Gamma_{\text{total}}$ Γ_{13}/Γ

VALUE	CL%	DOCUMENT ID	TECN	COMMENT
<0.05	84	LINDSEY	66 HBC	2.1-2.7 $K^-p \rightarrow \Lambda\pi^+\pi^-$ neutrals

 $\Gamma(\rho\gamma)/\Gamma_{\text{total}}$ Γ_{14}/Γ

VALUE (units 10^{-4})	CL%	DOCUMENT ID	TECN	COMMENT
< 0.12	90	1 AKHMETSHIN	99B CMD2	$e^+e^- \rightarrow \pi^+\pi^-\gamma$
< 7	90	AKHMETSHIN	97C CMD2	$e^+e^- \rightarrow \pi^+\pi^-\gamma$
<200	84	LINDSEY	66 HBC	2.1-2.7 $K^-p \rightarrow \Lambda\pi^+\pi^-$ neutrals

¹ Supersedes AKHMETSHIN 97C.

 $\Gamma(\pi^+\pi^-\gamma)/\Gamma_{\text{total}}$ Γ_{15}/Γ

VALUE (units 10^{-4})	CL%	EVTS	DOCUMENT ID	TECN	COMMENT
0.41 ± 0.12 ± 0.04		30175	1 AKHMETSHIN	99B CMD2	$e^+e^- \rightarrow \pi^+\pi^-\gamma$
< 0.3	90		2 AKHMETSHIN	97C CMD2	$e^+e^- \rightarrow \pi^+\pi^-\gamma$
<600	90		KALBFLEISCH	75 HBC	2.18 $K^-p \rightarrow \Lambda\pi^+\pi^-$ neutrals
< 70	90		COSME	74 OSPK	$e^+e^- \rightarrow \pi^+\pi^-\gamma$
<400	90		LINDSEY	65 HBC	2.1-2.7 $K^-p \rightarrow \Lambda\pi^+\pi^-$ neutrals

¹ For $E_\gamma > 20$ MeV and assuming that $B(\phi(1020) \rightarrow f_0(980)\gamma)$ is negligible. Supersedes AKHMETSHIN 97C.

² For $E_\gamma > 20$ MeV and assuming that $B(\phi(1020) \rightarrow f_0(980)\gamma)$ is negligible.

 $\Gamma(f_0(980)\gamma)/\Gamma_{\text{total}}$ Γ_{16}/Γ

VALUE (units 10^{-4})	CL%	EVTS	DOCUMENT ID	TECN	COMMENT
3.22 ± 0.19 OUR FIT					Error includes scale factor of 1.1.
3.21 ± 0.19 OUR AVERAGE					
3.21 ^{+0.03} _{-0.09} ± 0.18			1 AMBROSINO	07 KLOE	$e^+e^- \rightarrow \pi^0\pi^0\gamma$
2.90 ± 0.21 ± 1.54			2 AKHMETSHIN	99C CMD2	$e^+e^- \rightarrow \pi^+\pi^-\gamma$
4.47 ± 0.21	2438		3 ALOISIO	02D KLOE	$e^+e^- \rightarrow \pi^0\pi^0\gamma$
3.5 ± 0.3 ^{+1.3} _{-0.5}	419	4,5	ACHASOV	00H SND	$e^+e^- \rightarrow \pi^0\pi^0\gamma$
1.93 ± 0.46 ± 0.50	27188		6 AKHMETSHIN	99B CMD2	$e^+e^- \rightarrow \pi^+\pi^-\gamma$
3.05 ± 0.25 ± 0.72	268		7 AKHMETSHIN	99C CMD2	$e^+e^- \rightarrow \pi^0\pi^0\gamma$
1.5 ± 0.5	268		8 AKHMETSHIN	99C CMD2	$e^+e^- \rightarrow \pi^0\pi^0\gamma$
3.42 ± 0.30 ± 0.36	164		4 ACHASOV	98I SND	$e^+e^- \rightarrow 5\gamma$
< 1	90		9 AKHMETSHIN	97C CMD2	$e^+e^- \rightarrow \pi^+\pi^-\gamma$
< 7	90		10 AKHMETSHIN	97C CMD2	$e^+e^- \rightarrow \pi^+\pi^-\gamma$
< 20	90		DRUZHININ	87 ND	$e^+e^- \rightarrow \pi^0\pi^0\gamma$

¹ Obtained by the authors taking into account the $\pi^+\pi^-$ decay mode. Includes a component due to $\pi\pi$ production via the $f_0(500)$ meson. Supersedes ALOISIO 02D.

² From the combined fit of the photon spectra in the reactions $e^+e^- \rightarrow \pi^+\pi^-\gamma$, $\pi^0\pi^0\gamma$.

³ From the negative interference with the $f_0(500)$ meson of AITALA 01B using the ACHASOV 89 parameterization for the $f_0(980)$, a Breit-Wigner for the $f_0(500)$, and ACHASOV 01F for the $\rho\pi$ contribution. Superseded by AMBROSINO 07.

⁴ Assuming that the $\pi^0\pi^0\gamma$ final state is completely determined by the $f_0\gamma$ mechanism, neglecting the decay $B(\phi \rightarrow K\bar{K}\gamma)$ and using $B(f_0 \rightarrow \pi^+\pi^-) = 2B(f_0 \rightarrow \pi^0\pi^0)$.

⁵ Using the value $B(\phi \rightarrow \eta\gamma) = (1.338 \pm 0.053) \times 10^{-2}$.

⁶ For $E_\gamma > 20$ MeV. Supersedes AKHMETSHIN 97C.

⁷ Neglecting other intermediate mechanisms ($\rho\pi, \sigma\gamma$).

⁸ A narrow pole fit taking into account $f_0(980)$ and $f_0(1200)$ intermediate mechanisms.

⁹ For destructive interference with the Bremsstrahlung process

¹⁰ For constructive interference with the Bremsstrahlung process

 $\Gamma(f_0(980)\gamma)/\Gamma(\eta\gamma)$ Γ_{16}/Γ_5

VALUE (units 10^{-2})	EVTS	DOCUMENT ID	TECN	COMMENT
2.48 ± 0.15 OUR FIT				Error includes scale factor of 1.1.
2.6 ± 0.2 ^{+0.8} _{-0.3}	419	1 ACHASOV	00H SND	$e^+e^- \rightarrow \pi^0\pi^0\gamma$

¹ Assuming that the $\pi^0\pi^0\gamma$ final state is completely determined by the $f_0\gamma$ mechanism, neglecting the decay $B(\phi \rightarrow K\bar{K}\gamma)$ and using $B(f_0 \rightarrow \pi^+\pi^-) = 2B(f_0 \rightarrow \pi^0\pi^0)$.

 $\Gamma(\pi^0\pi^0\gamma)/\Gamma_{\text{total}}$ Γ_{17}/Γ

VALUE (units 10^{-4})	CL%	EVTS	DOCUMENT ID	TECN	COMMENT
1.07 ± 0.06 OUR AVERAGE					
1.07 ± 0.01 ± 0.06			1 AMBROSINO	07 KLOE	$e^+e^- \rightarrow \pi^0\pi^0\gamma$
-0.03 -0.06			AKHMETSHIN	99C CMD2	$e^+e^- \rightarrow \pi^0\pi^0\gamma$
1.08 ± 0.17 ± 0.09	268		ACHASOV	00H SND	$e^+e^- \rightarrow \pi^0\pi^0\gamma$
< 1.09 ± 0.03 ± 0.05	2438		ALOISIO	02D KLOE	$e^+e^- \rightarrow \pi^0\pi^0\gamma$
1.158 ± 0.093 ± 0.052	419	2,3	ACHASOV	00H SND	$e^+e^- \rightarrow \pi^0\pi^0\gamma$
< 10	90		DRUZHININ	87 ND	$e^+e^- \rightarrow 5\gamma$

¹ Supersedes ALOISIO 02D.

² Using the value $B(\phi \rightarrow \eta\gamma) = (1.338 \pm 0.053) \times 10^{-2}$.

³ Supersedes ACHASOV 98I. Excluding $\omega\pi^0$.

 $\Gamma(\pi^0\pi^0\gamma)/\Gamma(\eta\gamma)$ Γ_{17}/Γ_5

VALUE (units 10^{-2})	EVTS	DOCUMENT ID	TECN	COMMENT
0.86 ± 0.04 OUR FIT				
0.865 ± 0.070 ± 0.017	419	1 ACHASOV	00H SND	$e^+e^- \rightarrow \pi^0\pi^0\gamma$
0.90 ± 0.08 ± 0.07	164	ACHASOV	98I SND	$e^+e^- \rightarrow 5\gamma$

¹ Supersedes ACHASOV 98I. Excluding $\omega\pi^0$.

 $\Gamma(\pi^+\pi^-\pi^+\pi^-)/\Gamma_{\text{total}}$ Γ_{18}/Γ

VALUE (units 10^{-6})	CL%	EVTS	DOCUMENT ID	TECN	COMMENT
6.5 ± 2.7 ± 1.6		6.8k	1 AKHMETSHIN	17 CMD3	$e^+e^- \rightarrow \pi^+\pi^-\pi^+\pi^-$
3.93 ± 1.74 ± 2.14	3.3k		AKHMETSHIN	00E CMD2	$e^+e^- \rightarrow \pi^+\pi^-\pi^+\pi^-$
< 870	90		CORDIER	79 WIRE	$e^+e^- \rightarrow \pi^+\pi^-\pi^+\pi^-$

¹ Using the cross section at the ϕ meson peak $\sigma(\phi) = 4172 \pm 42$ nb, the nonresonant cross section $\sigma(0) = 1.263 \pm 0.027$ nb and $\text{Re}(Z) = 0.146 \pm 0.030$, $\text{Im}(Z) = -0.002 \pm 0.024$ for the complex amplitude of the $\phi \rightarrow \pi^+\pi^-\pi^+\pi^-$ transition.

 $\Gamma(\pi^+\pi^-\pi^-\pi^0)/\Gamma_{\text{total}}$ Γ_{19}/Γ

VALUE (units 10^{-6})	CL%	DOCUMENT ID	TECN	COMMENT
< 4.6	90	AKHMETSHIN	00E CMD2	$e^+e^- \rightarrow \pi^+\pi^-\pi^-\pi^0$
<150	95	BARKOV	88 CMD	$e^+e^- \rightarrow \pi^+\pi^-\pi^-\pi^0$

 $\Gamma(\pi^0e^+e^-)/\Gamma_{\text{total}}$ Γ_{20}/Γ

VALUE (units 10^{-5})	CL%	EVTS	DOCUMENT ID	TECN	COMMENT
1.33 ± 0.07 OUR AVERAGE					
1.35 ± 0.05 ± 0.05		9.5k	1 ANASTASI	16B KLOE	$e^+e^- \rightarrow \pi^0e^+e^-$
1.01 ± 0.28 ± 0.29	52		2 ACHASOV	02D SND	$e^+e^- \rightarrow \pi^0e^+e^-$
1.22 ± 0.34 ± 0.21	46		3 AKHMETSHIN	01C CMD2	$e^+e^- \rightarrow \pi^0e^+e^-$
< 12	90		DOLINSKY	88 ND	$e^+e^- \rightarrow \pi^0e^+e^-$

¹ Using $B(\pi^0 \rightarrow \gamma\gamma)$ from the 2014 Edition of this Review (PDG 14).

² Using various branching ratios from the 2000 Edition of this Review (PDG 00).

³ Using $B(\pi^0 \rightarrow \gamma\gamma) = 0.98798 \pm 0.00032$, $B(\phi \rightarrow \eta\gamma) = (1.297 \pm 0.033) \times 10^{-2}$, and $B(\eta \rightarrow \pi^+\pi^-\gamma) = (4.75 \pm 0.11) \times 10^{-2}$.

 $\Gamma(\pi^0\eta\gamma)/\Gamma_{\text{total}}$ Γ_{21}/Γ

VALUE (units 10^{-3})	CL%	EVTS	DOCUMENT ID	TECN	COMMENT
7.27 ± 0.30 OUR AVERAGE					Error includes scale factor of 1.5. See the ideogram below.
7.06 ± 0.22	16.9k		1 AMBROSINO	09F KLOE	1.02 $e^+e^- \rightarrow \eta\pi^0\gamma$
8.51 ± 0.51 ± 0.57	607		2 ALOISIO	02C KLOE	$e^+e^- \rightarrow \eta\pi^0\gamma$
7.96 ± 0.60 ± 0.40	197		3 ALOISIO	02C KLOE	$e^+e^- \rightarrow \eta\pi^0\gamma$
8.8 ± 1.4 ± 0.9	36		4 ACHASOV	00F SND	$e^+e^- \rightarrow \eta\pi^0\gamma$
9.0 ± 2.4 ± 1.0	80		AKHMETSHIN	99C CMD2	$e^+e^- \rightarrow \eta\pi^0\gamma$
7.01 ± 0.10 ± 0.20	13.3k		2,5 AMBROSINO	09F KLOE	1.02 $e^+e^- \rightarrow \eta\pi^0\gamma$
7.12 ± 0.13 ± 0.22	3.6k		3,6 AMBROSINO	09F KLOE	1.02 $e^+e^- \rightarrow \eta\pi^0\gamma$
8.3 ± 2.3 ± 1.2	20		ACHASOV	98B SND	$e^+e^- \rightarrow 5\gamma$
< 250	90		DOLINSKY	91 ND	$e^+e^- \rightarrow \pi^0\eta\gamma$

¹ Combined results of $\eta \rightarrow \gamma\gamma$ and $\eta \rightarrow \pi^+\pi^-\pi^0$ decay modes measurements.

Meson Particle Listings

 $\phi(1020)$

² From the decay mode $\eta \rightarrow \gamma\gamma$.

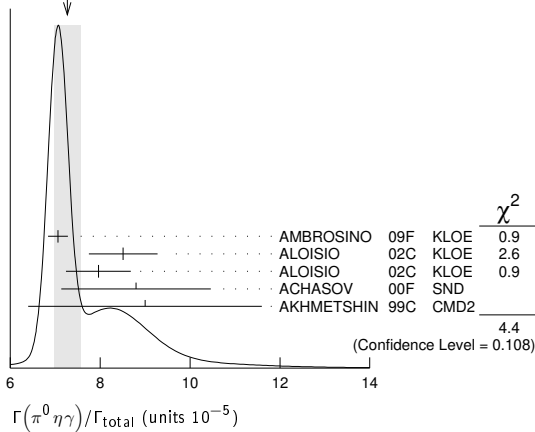
³ From the decay mode $\eta \rightarrow \pi^+\pi^-\pi^0$.

⁴ Supersedes ACHASOV 98B.

⁵ Using $B(\phi \rightarrow \eta\gamma) = (1.304 \pm 0.025)\%$, $B(\eta \rightarrow 3\pi^0) = (32.56 \pm 0.23)\%$, and $B(\eta \rightarrow \gamma\gamma) = (39.31 \pm 0.20)\%$.

⁶ Using $B(\phi \rightarrow \eta\gamma) = (1.304 \pm 0.025)\%$, $B(\eta \rightarrow 3\pi^0) = (32.56 \pm 0.23)\%$, and $B(\eta \rightarrow \pi^+\pi^-\pi^0) = (22.73 \pm 0.28)\%$.

WEIGHTED AVERAGE
7.27±0.30 (Error scaled by 1.5)



$\Gamma(a_0(980)\gamma)/\Gamma_{total}$ Γ₂₂/Γ

VALUE (units 10 ⁻⁵)	CL%	EVTS	DOCUMENT ID	TECN	COMMENT
7.6±0.6 OUR FIT					
7.6±0.6 OUR AVERAGE					
7.4±0.7			1 ALOISIO 02c	KLOE	$e^+e^- \rightarrow \eta\pi^0\gamma$
8.8±1.7	36		2 ACHASOV 00F	SND	$e^+e^- \rightarrow \eta\pi^0\gamma$
••• We do not use the following data for averages, fits, limits, etc. •••					
11 ± 2			3 GOKALP 02	RVUE	$e^+e^- \rightarrow \eta\pi^0\gamma$
<500	90		DOLINSKY 91	ND	$e^+e^- \rightarrow \pi^0\eta\gamma$

¹ Using $M_{a_0(980)} = 984.8$ MeV and assuming $a_0(980)\gamma$ dominance.

² Assuming $a_0(980)\gamma$ dominance in the $\eta\pi^0\gamma$ final state.

³ Using data of ACHASOV 00F.

$\Gamma(f_0(980)\gamma)/\Gamma(a_0(980)\gamma)$ Γ₁₆/Γ₂₂

VALUE	DOCUMENT ID	TECN	COMMENT
6.1±0.6	1 ALOISIO 02c	KLOE	$e^+e^- \rightarrow \eta\pi^0\gamma$

¹ Using results of ALOISIO 02d and assuming that $f_0(980)$ decays into $\pi\pi$ only and $a_0(980)$ into $\eta\pi$ only.

$\Gamma(K^0\bar{K}^0\gamma)/\Gamma_{total}$ Γ₂₃/Γ

VALUE	CL%	DOCUMENT ID	TECN	COMMENT
<1.9 × 10⁻⁸	90	AMBROSINO 09c	KLOE	$e^+e^- \rightarrow K_S^0\bar{K}_S^0\gamma$

$\Gamma(\eta'(958)\gamma)/\Gamma_{total}$ Γ₂₄/Γ

VALUE (units 10 ⁻⁵)	CL%	EVTS	DOCUMENT ID	TECN	COMMENT
6.21±0.20 OUR FIT					
6.21±0.29 OUR AVERAGE					
6.21±0.27±0.11		3407	1 AMBROSINO 07A	KLOE	$1.02 e^+e^- \rightarrow \pi^+\pi^-\pi^0\gamma$

6.7 $\pm^{+2.8}_{-2.4}$ ± 0.8 12 ² AULCHENKO 03B SND $e^+e^- \rightarrow \eta'\gamma$

••• We do not use the following data for averages, fits, limits, etc. •••

6.7 $\pm^{+5.0}_{-4.2}$ ± 1.5 7 AULCHENKO 03B SND $e^+e^- \rightarrow 7\gamma$

6.10±0.61±0.43 120 ³ ALOISIO 02E KLOE $1.02 e^+e^- \rightarrow \pi^+\pi^-\pi^0\gamma$

8.2 $\pm^{+2.1}_{-1.9}$ ± 1.1 21 ⁴ AKHMETSHIN 00B CMD2 $e^+e^- \rightarrow \pi^+\pi^-\pi^0\gamma$

4.9 $\pm^{+2.2}_{-1.8}$ ± 0.6 9 ⁵ AKHMETSHIN 00F CMD2 $e^+e^- \rightarrow \pi^+\pi^-\pi^0\gamma$

6.4 ± 1.6 30 ⁶ AKHMETSHIN 00F CMD2 $e^+e^- \rightarrow \eta'(958)\gamma$

6.7 $\pm^{+3.4}_{-2.9}$ ± 1.0 5 ⁷ AULCHENKO 99 SND $e^+e^- \rightarrow \pi^+\pi^-\pi^0\gamma$

<11 90 AULCHENKO 98 SND $e^+e^- \rightarrow 7\gamma$

6.4 ± 1.6 30 ⁶ AKHMETSHIN 00F CMD2 $e^+e^- \rightarrow \eta'(958)\gamma$

6.7 $\pm^{+3.4}_{-2.9}$ ± 1.0 5 ⁷ AULCHENKO 99 SND $e^+e^- \rightarrow \pi^+\pi^-\pi^0\gamma$

<11 90 AULCHENKO 98 SND $e^+e^- \rightarrow 7\gamma$

6.4 ± 1.6 30 ⁶ AKHMETSHIN 00F CMD2 $e^+e^- \rightarrow \eta'(958)\gamma$

6.7 $\pm^{+3.4}_{-2.9}$ ± 1.0 5 ⁷ AULCHENKO 99 SND $e^+e^- \rightarrow \pi^+\pi^-\pi^0\gamma$

<41 90 DRUZHININ 87 ND $e^+e^- \rightarrow \eta\eta\pi^+\pi^-$

¹ AMBROSINO 07A reports $[\Gamma(\phi(1020) \rightarrow \eta'(958)\gamma)/\Gamma_{total}] / [B(\phi(1020) \rightarrow \eta\gamma)] = (4.77 \pm 0.09 \pm 0.19) \times 10^{-3}$ which we multiply by our best value $B(\phi(1020) \rightarrow \eta\gamma) = (1.301 \pm 0.024) \times 10^{-2}$. Our first error is their experiment's error and our second error is the systematic error from using our best value.

² Averaging AULCHENKO 03B with AULCHENKO 99.

³ Using $B(\phi \rightarrow \eta\gamma) = (1.297 \pm 0.033)\%$.

⁴ Using the value $B(\phi \rightarrow \eta\gamma) = (1.26 \pm 0.06) \times 10^{-2}$.

⁵ Using $B(\phi \rightarrow K_L^0\bar{K}_S^0) = (33.8 \pm 0.6)\%$.

⁶ Averaging AKHMETSHIN 00B with AKHMETSHIN 00F.

⁷ Using the value $B(\eta' \rightarrow \eta\pi^+\pi^-) = (43.7 \pm 1.5) \times 10^{-2}$ and $B(\eta \rightarrow \gamma\gamma) = (39.25 \pm 0.31) \times 10^{-2}$.

$\Gamma(\eta'(958)\gamma)/\Gamma(K_L^0\bar{K}_S^0)$ Γ₂₄/Γ₂

VALUE (units 10 ⁻⁴)	CL%	EVTS	DOCUMENT ID	TECN	COMMENT
1.83±0.06 OUR FIT					
1.46 $\pm^{+0.64}_{-0.54}$ ± 0.18		9	1 AKHMETSHIN 00F	CMD2	$e^+e^- \rightarrow \pi^+\pi^-\pi^+\pi^- \geq 2\gamma$

¹ Using various branching ratios of K_S^0 , K_L^0 , η , η' from the 2000 edition (The European Physical Journal **C15** 1 (2000)) of this Review.

$\Gamma(\eta'(958)\gamma)/\Gamma(\eta\gamma)$ Γ₂₄/Γ₅

VALUE (units 10 ⁻³)	CL%	EVTS	DOCUMENT ID	TECN	COMMENT
4.77±0.15 OUR FIT					
4.78±0.20 OUR AVERAGE					

4.77±0.09±0.19 3407 AMBROSINO 07A KLOE $1.02 e^+e^- \rightarrow \pi^+\pi^-\pi^0\gamma$

4.70±0.47±0.31 120 ¹ ALOISIO 02E KLOE $1.02 e^+e^- \rightarrow \pi^+\pi^-\pi^0\gamma$

6.5 $\pm^{+1.7}_{-1.5}$ ± 0.8 21 AKHMETSHIN 00B CMD2 $e^+e^- \rightarrow \pi^+\pi^-\pi^0\gamma$

••• We do not use the following data for averages, fits, limits, etc. •••

9.5 $\pm^{+5.2}_{-4.0}$ ± 1.4 6 ² AKHMETSHIN 97B CMD2 $e^+e^- \rightarrow \pi^+\pi^-\pi^0\gamma$

¹ From the decay mode $\eta' \rightarrow \eta\pi^+\pi^-$, $\eta \rightarrow \gamma\gamma$.

² Superseded by AKHMETSHIN 00B.

$\Gamma(\eta\pi^0\pi^0)/\Gamma_{total}$ Γ₂₅/Γ

VALUE (units 10 ⁻⁵)	CL%	DOCUMENT ID	TECN	COMMENT
<2	90	AULCHENKO 98	SND	$e^+e^- \rightarrow 7\gamma$

$\Gamma(\mu^+\mu^-)/\Gamma_{total}$ Γ₂₆/Γ

VALUE (units 10 ⁻⁵)	CL%	EVTS	DOCUMENT ID	TECN	COMMENT
1.43±0.45 ± 0.14		27188	1 AKHMETSHIN 99B	CMD2	$e^+e^- \rightarrow \mu^+\mu^-\gamma$

••• We do not use the following data for averages, fits, limits, etc. •••

2.3 ± 1.0 824 ± 33 ² AKHMETSHIN 97C CMD2 $e^+e^- \rightarrow \mu^+\mu^-\gamma$

¹ For $E_\gamma > 20$ MeV. Supersedes AKHMETSHIN 97C.

² For $E_\gamma > 20$ MeV.

$\Gamma(\rho\gamma)/\Gamma_{total}$ Γ₂₇/Γ

VALUE (units 10 ⁻⁴)	CL%	DOCUMENT ID	TECN	COMMENT
<1.2	90	AULCHENKO 08	CMD2	$\phi \rightarrow \pi^+\pi^-\pi^0\gamma$

••• We do not use the following data for averages, fits, limits, etc. •••

<5 90 AKHMETSHIN 98 CMD2 $e^+e^- \rightarrow \pi^+\pi^-\pi^0\gamma$

$\Gamma(\eta\pi^+\pi^-)/\Gamma_{total}$ Γ₂₈/Γ

VALUE (units 10 ⁻⁵)	CL%	DOCUMENT ID	TECN	COMMENT
< 1.8	90	AKHMETSHIN 00E	CMD2	$e^+e^- \rightarrow \pi^+\pi^-\pi^+\pi^- \pi^0$

••• We do not use the following data for averages, fits, limits, etc. •••

< 6.1 90 AULCHENKO 08 CMD2 $\phi \rightarrow \eta\pi^+\pi^-$

<30 90 AKHMETSHIN 98 CMD2 $e^+e^- \rightarrow \pi^+\pi^-\pi^0\gamma$

$\Gamma(\eta\mu^+\mu^-)/\Gamma_{total}$ Γ₂₉/Γ

VALUE (units 10 ⁻⁶)	CL%	DOCUMENT ID	TECN	COMMENT
<9.4	90	AKHMETSHIN 01	CMD2	$e^+e^- \rightarrow \eta e^+e^-$

$\Gamma(\eta U \rightarrow \eta e^+e^-)/\Gamma_{total}$ Γ₃₀/Γ

VALUE	CL%	DOCUMENT ID	TECN	COMMENT
<1 × 10⁻⁶	90	1 BABUSCI 13B	KLOE	$1.02 e^+e^- \rightarrow \eta e^+e^-$

¹ For a narrow vector U with mass between 5 and 470 MeV, from the combined analysis of $\eta \rightarrow \pi^+\pi^-\pi^0$ and $\eta \rightarrow \pi^0\pi^0\pi^0$ from ARCHILLI 12. Measured 90% CL limits as a function of m_U range from 2.2×10^{-8} to 10^{-6} .

$\Gamma(\text{invisible})/\Gamma(K^+K^-)$ Γ₃₁/Γ₁

VALUE	CL%	DOCUMENT ID	TECN	COMMENT
<3.4 × 10⁻⁴	90	ABLIKIM 18s	BES3	$J/\psi \rightarrow \phi \eta \rightarrow \phi\pi^+\pi^-\pi^0$

Lepton Family number (LF) violating modes

$\Gamma(e^\pm\mu^\mp)/\Gamma_{total}$ Γ₃₂/Γ

VALUE	CL%	DOCUMENT ID	TECN	COMMENT
<2 × 10⁻⁶	90	ACHASOV 10A	SND	$e^+e^- \rightarrow e^\pm\mu^\mp$

$\pi^+\pi^-\pi^0 / \rho\pi$ AMPLITUDE RATIO a_1 IN DECAY OF $\phi \rightarrow \pi^+\pi^-\pi^0$

NIECKNIG 12 describes final-state interactions between the three pions in a dispersive framework using data on the $\pi\pi$ P-wave scattering phase shift.

Table with columns: VALUE (units 10^-2), CL% EVTS, DOCUMENT ID, TECN, COMMENT. Row 1: 9.1±1.2 OUR AVERAGE. Row 2: 10.1±4.1±1.7 80k 1 AKHMETSHIN 06 CMD2 1.017-1.021 e+e- -> pi+pi-pi0.

••• We do not use the following data for averages, fits, limits, etc. •••
-6 < a1 < 6 500k 3 ACHASOV 02 SND e+e- -> pi+pi-pi0
-16 < a1 < 11 90 9.8k 1,4 AKHMETSHIN 98 CMD2 e+e- -> pi+pi-gamma

- 1 Dalitz plot analysis taking into account interference between the contact and rho pi amplitudes.
2 From a fit without limitations on charged and neutral rho masses and widths.
3 Recalculated by us to match the notations of AKHMETSHIN 98.
4 Assuming zero phase for the contact term.

PARAMETER beta IN phi -> Pe+e- DECAYS

In the one-pole approximation the electromagnetic transition form factor for phi -> Pe+e- (P = pi, eta) is given as a function of the e+e- invariant mass squared, q^2, by the expression:

|F(q^2)|^2 = (1 - q^2/Lambda^2)^-2,

where vector meson dominance predicts parameter Lambda approx 0.770 GeV (Lambda^-2 approx 1.687 GeV^-2). The slope of this form factor, beta = dF/dq^2(q^2=0), equals Lambda^-2 in this approximation.

The measurements below obtain beta in the one-pole approximation.

PARAMETER beta IN phi -> pi0 e+e- DECAY

Table with columns: VALUE (GeV^-2), EVTS, DOCUMENT ID, TECN, COMMENT. Row 1: 2.02±0.11 9.5k 1 ANASTASI 16b KLOE 1.02 e+e- -> pi0 e+e-

1 The error combines statistical and systematic uncertainties.

PARAMETER beta IN phi -> eta e+e- DECAY

Table with columns: VALUE (GeV^-2), EVTS, DOCUMENT ID, TECN, COMMENT. Row 1: 1.29±0.13 OUR AVERAGE. Row 2: 1.28±0.10+0.09-0.08 30k BABUSCI 15 KLOE 1.02 e+e- -> eta e+e-. Row 3: 3.8 ± 1.8 213 1 ACHASOV 01b SND 1.02 e+e- -> eta e+e-

1 The uncertainty is statistical only. The systematic one is negligible, in comparison.

phi(1020) REFERENCES

LEES 21B PR D104 112003 J.P. Lees et al. (BABAR Collab.)
ALBRECHT 20 EPJ C90 453 M. Albrecht et al. (Crystal Barrel Collab.)
HOID 20 EPJ C90 988 B.-L. Hoid, M. Hoferichter, B. Kubis (BONN, BERN)
AAU 19H JHEP 1904 063 R. Aaij et al. (LHCb Collab.)
HOEFERICH... 19 JHEP 1908 137 M. Hoferichter, B.-L. Hoid, B. Kubis (WASH, BONN)
ALBIKIM 18S PR D98 032001 M. Ablikim et al. (BESIII Collab.)
AOUDE 18 PR D98 056021 R.T. Aoude et al. (CMD-3 Collab.)
KOZYREV 18 PL B779 64 E.A. Kozyrev et al. (CMD-3 Collab.)
AKHMETSHIN 17 PL B768 345 R.R. Akhmetshin et al. (CMD-3 Collab.)
ACHASOV 16A PR D93 092001 M.N. Achasov et al. (SND Collab.)
ANASTASI 16B PL B757 362 A. Anastasi et al. (KLOE-2 Collab.)
KOZYREV 16 PL B760 314 E.A. Kozyrev et al. (CMD-3 Collab.)
BABUSCI 15 PL B742 1 R.D. Babusci et al. (KLOE-2 Collab.)
PDG 15 RPP 2015 at pdg.lbl.gov (PDG Collab.)
LEES 14H PR D89 092002 J.P. Lees et al. (BABAR Collab.)
PDG 14 CP C38 070001 K. Olive et al. (PDG Collab.)
BABUSCI 13B PL B720 111 D. Babusci et al. (KLOE-2 Collab.)
BENAYOUN 13 EPJ C73 2453 M. Benayoun, P. David, L. DelBuono (PARIN, BERLIN+)
LEES 13F PR D87 052010 J.P. Lees et al. (BABAR Collab.)
LEES 13Q PR D88 032013 J.P. Lees et al. (BABAR Collab.)
ARCHILLI 12 PL B706 251 F. Archilli et al. (KLOE-2 Collab.)
BENAYOUN 12 EPJ C72 1848 M. Benayoun et al.
NIECKNIG 12 EPJ C72 2014 F. Niecknig, B. Kubis, S.P. Schneider (BONN)
PDG 12 PR D86 010001 J. Berlinger et al. (PDG Collab.)
AKHMETSHIN 11 PL B695 412 R.R. Akhmetshin et al. (CMD-2 Collab.)
ACHASOV 10A PR D81 057102 M.N. Achasov et al. (Novosibirsk SND Collab.)
BENAYOUN 10 EPJ C65 211 M. Benayoun et al.
AMBROSINO 09C PL B679 10 F. Ambrosino et al. (KLOE Collab.)
AMBROSINO 09F PL B681 5 F. Ambrosino et al. (KLOE Collab.)
AKHMETSHIN 08 PL B669 217 R.R. Akhmetshin et al. (CMD-2 Collab.)
AMBROSINO 08G PL B669 223 F. Ambrosino et al. (KLOE Collab.)
AULCHENKO 08 JETPL 88 85 V.M. Aulchenko et al. (CMD-2 Collab.)
FLOREZ-BAEZ 08 PR D78 077301 F.V. Florez-Baez, G. Lopez Castro
ACHASOV 07B PR D76 077101 M.N. Achasov et al. (SND Collab.)
AMBROSINO 07 EPJ C49 473 F. Ambrosino et al. (KLOE Collab.)
AMBROSINO 07A PL B648 267 F. Ambrosino et al. (KLOE Collab.)
DUBYNSKIY 07 PR D75 113001 S. Dubynskiy et al.
ACHASOV 06A PR D74 014016 M.N. Achasov et al. (SND Collab.)
AKHMETSHIN 06 PL B642 203 R.R. Akhmetshin et al. (CMD-2 Collab.)
AKHMETSHIN 05 PL B605 26 R.R. Akhmetshin et al. (Novosibirsk CMD-2 Collab.)
AMBROSINO 05 PL B608 199 F. Ambrosino et al. (KLOE Collab.)
AUBERT B 05J PR D72 052008 B. Aubert et al. (BABAR Collab.)
AKHMETSHIN 04 PL B578 285 R.R. Akhmetshin et al. (Novosibirsk CMD-2 Collab.)
AUBERT B 04N PR D70 072004 B. Aubert et al. (BABAR Collab.)
ALOISIO 03 PL B561 55 A. Aloisio et al. (KLOE Collab.)
AULCHENKO 03B JETP 97 24 V.M. Aulchenko et al. (Novosibirsk SND Collab.)
ACHASOV 02 PR D65 032002 M.N. Achasov et al. (Novosibirsk SND Collab.)
ACHASOV 02D JETPL 75 449 M.N. Achasov et al. (Novosibirsk SND Collab.)
Translated from ZETFP 75 539.

ALOISIO 02C PL B536 209 A. Aloisio et al. (KLOE Collab.)
ALOISIO 02D PL B537 21 A. Aloisio et al. (KLOE Collab.)
ALOISIO 02E PL B541 45 A. Aloisio et al. (KLOE Collab.)
FISCHBACH 02 PL B526 355 E. Fischbach, A.W. Overhauser, B. Woodahl
GOKALP 02 JP G28 2783 A. Gokalp et al.
ACHASOV 01B PL B504 275 M.N. Achasov et al. (Novosibirsk SND Collab.)
ACHASOV 01E PR D63 072002 M.N. Achasov et al. (Novosibirsk SND Collab.)
ACHASOV 01F PR D63 094007 M.N. Achasov, V.V. Gubin (Novosibirsk SND Collab.)
ACHASOV 01G PRL 86 1639 M.N. Achasov et al. (Novosibirsk SND Collab.)
AITALA 01B PRL 86 770 E.M. Aitala et al. (FNAL E791 Collab.)
AKHMETSHIN 01 PL B501 191 R.R. Akhmetshin et al. (Novosibirsk CMD-2 Collab.)
AKHMETSHIN 01B PL B509 217 R.R. Akhmetshin et al. (Novosibirsk CMD-2 Collab.)
AKHMETSHIN 01C PL B503 237 R.R. Akhmetshin et al. (Novosibirsk CMD-2 Collab.)
BENAYOUN 01 EPJ C22 503 M. Benayoun, H.B. O'Connell (Novosibirsk SND Collab.)
ACHASOV 00 EPJ C12 25 M.N. Achasov et al. (Novosibirsk SND Collab.)
ACHASOV 00B JETP 90 17 M.N. Achasov et al. (Novosibirsk SND Collab.)
Translated from ZETFP 117 22.
ACHASOV 00C PL B474 188 M.N. Achasov et al. (Novosibirsk SND Collab.)
ACHASOV 00D JETPL 72 282 M.N. Achasov et al. (Novosibirsk SND Collab.)
Translated from ZETFP 72 411.
ACHASOV 00E NP B569 158 M.N. Achasov et al. (Novosibirsk SND Collab.)
ACHASOV 00F PL B479 53 M.N. Achasov et al. (Novosibirsk SND Collab.)
ACHASOV 00H PL B485 349 M.N. Achasov et al. (Novosibirsk SND Collab.)
AKHMETSHIN 00B PL B473 337 R.R. Akhmetshin et al. (Novosibirsk CMD-2 Collab.)
AKHMETSHIN 00E PL B491 81 R.R. Akhmetshin et al. (Novosibirsk CMD-2 Collab.)
AKHMETSHIN 00F PL B494 26 R.R. Akhmetshin et al. (Novosibirsk CMD-2 Collab.)
AULCHENKO 00A JETP 90 927 V.M. Aulchenko et al. (Novosibirsk SND Collab.)
Translated from ZETFP 117 1067.
BRAMON 00 PL B486 406 A. Bramon et al.
PDG 00 EPJ C15 1 D.E. Groom et al. (PDG Collab.)
ACHASOV 99 PL B449 122 M.N. Achasov et al.
ACHASOV 99C PL B456 304 M.N. Achasov et al.
AKHMETSHIN 99B PL B462 371 R.R. Akhmetshin et al. (Novosibirsk CMD-2 Collab.)
AKHMETSHIN 99C PL B462 380 R.R. Akhmetshin et al. (Novosibirsk CMD-2 Collab.)
AKHMETSHIN 99D PL B466 385 R.R. Akhmetshin et al. (Novosibirsk CMD-2 Collab.)
Also PL B508 217 (errata.) R.R. Akhmetshin et al. (Novosibirsk CMD-2 Collab.)
AKHMETSHIN 99F PL B460 242 R.R. Akhmetshin et al. (Novosibirsk CMD-2 Collab.)
AULCHENKO 99 JETPL 69 937 V.M. Aulchenko et al.
Translated from ZETFP 69 87.
ACHASOV 98B PL B438 441 M.N. Achasov et al. (Novosibirsk SND Collab.)
ACHASOV 98F JETPL 68 573 M.N. Achasov et al. (Novosibirsk SND Collab.)
ACHASOV 98I PL B440 442 M.N. Achasov et al.
AKHMETSHIN 98 PL B434 426 R.R. Akhmetshin et al. (CMD-2 Collab.)
AULCHENKO 98 PL B436 199 V.M. Aulchenko et al. (Novosibirsk SND Collab.)
BARBERIS 98 PL B432 436 D. Barberis et al. (Omega Expt.)
AKHMETSHIN 97B PL B415 445 R.R. Akhmetshin et al. (NOVO, BOST, PITT+)
AKHMETSHIN 97C PL B415 452 R.R. Akhmetshin et al. (Novosibirsk CMD-2 Collab.)
BENAYOUN 96 ZPHY C72 221 M. Benayoun et al. (IFNP Collab.)
AKHMETSHIN 95 PL B364 199 R.R. Akhmetshin et al. (Novosibirsk CMD-2 Collab.)
DOLINSKY 91 PRPL 202 99 S.I. Dolinsky et al. (NOVO)
KUHN 90 ZPHY C48 445 J.H. Kuhn et al. (MPIM)
ACHASOV 89 NP B315 465 M.N. Achasov, V.N. Ivanchenko
DOLINSKY 89 ZPHY C42 511 S.I. Dolinsky et al. (NOVO)
BARKOV 88 SJNP 47 248 L.M. Barkov et al. (NOVO)
Translated from YAF 47 393.
DOLINSKY 88 SJNP 48 277 S.I. Dolinsky et al. (NOVO)
Translated from YAF 48 442.
DRUZHININ 87 ZPHY C37 1 V.P. Druzhinin et al. (NOVO)
ARMSTRONG 86 PL 166B 245 T.A. Armstrong et al. (ATHU, BARI, BIRM+)
ATKINSON 86 ZPHY C30 521 M. Atkinson et al. (BONN, CERN, GLAS+)
BEBEK 86 PRL 56 1893 C. Bebek et al. (CLEO Collab.)
DAVENPORT 86 PR D33 2519 T.F. Davenport (TUFTS, ARIZ, FSU, NDAM+)
DIJKSTRA 86 ZPHY C31 375 H. Dijkstra et al. (ANIK, BRIS, CERN+)
FRAME 86 NP B276 667 D. Frame et al. (GLAS)
GOLUBEV 86 SJNP 44 409 V.B. Golubev et al. (NOVO)
Translated from YAF 44 633.
ALBRECHT 85D PL 153B 343 H. Albrecht et al. (ARGUS Collab.)
GOLUBEV 85 SJNP 41 756 V.B. Golubev et al. (NOVO)
Translated from YAF 41 1183.
DROZHININ 84 PL 144B 136 V.P. Druzhinin et al. (NOVO)
ARMSTRONG 83B NP B224 193 T.A. Armstrong et al. (BARI, BIRM, CERN+)
BARATE 83 PL 121B 449 R. Barate et al. (SACL, LOIC, SHMF, IND)
KURDADZE 83C JETPL 38 366 L.M. Kurdadze et al. (NOVO)
Translated from ZETFP 38 306.
ARENTOU 82 PR D25 2241 M.W. Arenton et al. (ANL, ILL)
PELLINEN 82 PS 25 599 A. Pellinen, M. Roos (HELS)
DAUM 81 PL 100B 439 C. Daum et al. (AMST, BRIS, CERN, CRAC+)
IVANOV 81 PL 107B 297 P.M. Ivanov et al. (NOVO)
Also Private Comm. S.I. Eidelman (NOVO)
VASSERMAN 81 PL 99B 62 I.B. Vasserman et al. (NOVO)
Also SJNP 35 240 L.M. Kurdadze et al.
Translated from YAF 35 352.
CORDIER 80 NP B172 13 A. Cordier et al. (LALO)
CORDIER 79 PL 81B 389 A. Cordier et al. (LALO)
BUKIN 78B SJNP 27 521 A.D. Bukin et al. (NOVO)
Translated from YAF 27 985.
BUKIN 78C SJNP 27 516 A.D. Bukin et al. (NOVO)
Translated from YAF 27 976.
COOPER 78B NP B146 1 A.M. Cooper et al. (TATA, CERN, CDF+)
LOSTY 78 NP B133 38 M.J. Losty et al. (CERN, AMST, NIJM+)
AKERLOF 77 PRL 39 861 C.W. Akerlof et al. (FNAL, MICH, PURD)
ANDREWS 77 PRL 38 198 D.E. Andrews et al. (ROCH)
BALDI 77 PL 68B 381 R. Baldi et al. (GEVA)
CERRADA 77B NP B126 241 M. Cerrada et al. (AMST, CERN, NIJM+)
COHEN 77 PRL 38 269 D. Cohen et al. (ANL)
LAVEN 77 NP B127 43 H. Laven et al. (AACH3, BERL, CERN, LOIC+)
LYONS 77 NP B125 207 L. Lyons, A.M. Cooper, A.G. Clark (OXF)
COSME 76 PL 63B 352 G. Cosme et al. (ORSAY)
KALBFLEISCH 76 PR D13 32 G.R. Kalbfleisch, R.C. Strand, J.W. Chapman (BNL+)
PARROUR 76 PL 63B 357 G. Parrou et al. (ORSAY)
PARROUR 76B PL 63B 362 G. Parrou et al. (ORSAY)
KALBFLEISCH 75 PR D11 987 G.R. Kalbfleisch, R.C. Strand, J.W. Chapman (BNL+)
AYRES 74 PRL 32 1463 D.S. Ayres et al. (ANL)
BESCH 74 NP B70 257 H.J. Besch et al. (BONN)
COSME 74 PL 48B 155 G. Cosme et al. (ORSAY)
COSME 74B PL 48B 159 G. Cosme et al. (ORSAY)
DEGROOT 74 NP B74 77 A.J. de Groot et al. (AMST, NIJM)
AUGUSTIN 73 PRL 30 462 J.E. Augustin et al. (ORSAY)
BALLAM 73 PR D7 3150 J. Ballam et al. (SLAC, LBL)
BINNIE 73B PR D5 2789 B. Binnie et al. (LOIC, SHMF)
AGUILAR-BENITEZ 72B PR D6 29 M. Aguilar-Benitez et al. (BNL)
ALVENSLEB... 72 PRL 28 66 H. Alvensleben et al. (MIT, DESY)
BORENSTEIN 72 PR D5 1559 S.R. Borenstein et al. (BNL, MICH)
COLLEY 72 NP B50 1 D.C. Colley et al. (BIRM, GLAS)
BALAKIN 71 PL 34B 328 V.E. Balakin et al. (NOVO)
CHATELUS 71 Thesis LAL 1247 Y. Chatelus (STRB)
Also PL 32B 416 J.C. Bizot et al. (ORSAY)
HAYES 71 PR D4 899 S. Hayes et al. (CORN)
STOTTLE... 71 Thesis ORO 2504 170 A.R. Stottleymer (UMD)
BIZOT 70 PL 32B 416 J.C. Bizot et al. (ORSAY)
Also Liverpool Sym. 69 J.P. Perez-Jorba (ORSAY)
EARLES 70 PRL 25 1312 D.R. Earles et al. (NEAS)
LINDSEY 66 PR 147 913 J.S. Lindsey, G. Smith (LRL)

Meson Particle Listings

 $\phi(1020)$, $h_1(1170)$, $b_1(1235)$

LONDON	66	PR 143 1034	G.W. London et al.	(BNL, SYRA) IGJPC
BADIER	65B	PL 17 337	J. Badier et al.	(EPOL, SACL, AMST)
LINDSEY	65	PRL 15 221	J.S. Lindsey, G.A. Smith	(LRL)
LINDSEY	65	d data included in LINDSEY 66.		
SCHLEIN	63	PRL 10 368	P.E. Schlein et al.	(UCLA) IGJP

 $h_1(1170)$

$$J^{PC} = 0^-(1^{+-})$$

 $h_1(1170)$ MASS

VALUE (MeV)	DOCUMENT ID	TECN	CHG	COMMENT
1166 ± 5 ± 3	1 ANDO	92	SPEC	8 $\pi^- p \rightarrow \pi^+ \pi^- \pi^0 n$
• • • We do not use the following data for averages, fits, limits, etc. • • •				
1168 ± 4	ANDO	92	SPEC	8 $\pi^- p \rightarrow \pi^+ \pi^- \pi^0 n$
1190 ± 6	2 DANKOWY...	81	SPEC	0 8 $\pi p \rightarrow 3\pi n$
1 Average and spread of values using 2 variants of the model of BOWLER 75.				
2 Uses the model of BOWLER 75.				

 $h_1(1170)$ WIDTH

VALUE (MeV)	DOCUMENT ID	TECN	CHG	COMMENT
375 ± 6 ± 34	3 ANDO	92	SPEC	8 $\pi^- p \rightarrow \pi^+ \pi^- \pi^0 n$
• • • We do not use the following data for averages, fits, limits, etc. • • •				
345 ± 6	ANDO	92	SPEC	8 $\pi^- p \rightarrow \pi^+ \pi^- \pi^0 n$
320 ± 5	4 DANKOWY...	81	SPEC	0 8 $\pi p \rightarrow 3\pi n$
3 Average and spread of values using 2 variants of the model of BOWLER 75.				
4 Uses the model of BOWLER 75.				

 $h_1(1170)$ DECAY MODES

Mode	Fraction (Γ_i/Γ)
Γ_1 $\rho\pi$	seen

 $h_1(1170)$ BRANCHING RATIOS

$\Gamma(\rho\pi)/\Gamma_{\text{total}}$	VALUE	DOCUMENT ID	TECN	COMMENT	Γ_1/Γ
• • • We do not use the following data for averages, fits, limits, etc. • • •					
seen		ANDO	92	SPEC 8 $\pi^- p \rightarrow \pi^+ \pi^- \pi^0 n$	
seen		ATKINSON	84	OMEG 20-70 $\gamma p \rightarrow \pi^+ \pi^- \pi^0 p$	
seen		DANKOWY...	81	SPEC 8 $\pi p \rightarrow 3\pi n$	

 $h_1(1170)$ REFERENCES

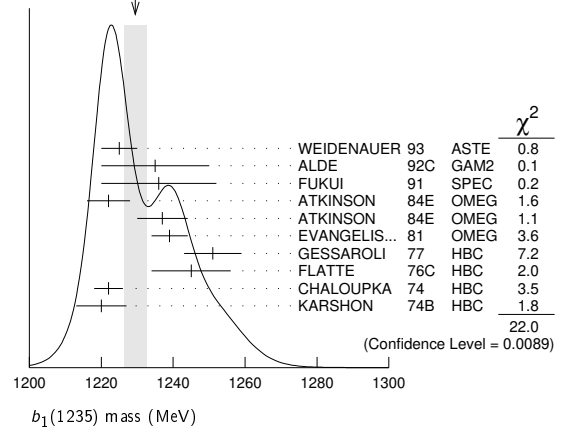
ANDO	92	PL B291 496	A. Ando et al.	(KEK, KYOT, NIRS, SAGA+)
ATKINSON	84	NP B231 15	M. Atkinson et al.	(BONN, CERN, GLAS+)
DANKOWY...	81	PRL 46 580	J.A. Dankowycz et al.	(TNTO, BNL, CARL+)
BOWLER	75	NP B97 227	M.G. Bowler et al.	(OXFTP, DARE)

 $b_1(1235)$

$$J^{PC} = 1^+(1^{+-})$$

 $b_1(1235)$ MASS

VALUE (MeV)	EVTS	DOCUMENT ID	TECN	CHG	COMMENT
1229.5 ± 3.2 OUR AVERAGE					Error includes scale factor of 1.6. See the ideogram below.
1225 ± 5		WEIDENAUER	93	ASTE	$\bar{p}p \rightarrow 2\pi^+ 2\pi^- \pi^0$
1235 ± 15		ALDE	92C	GAM2	38,100 $\pi^- p \rightarrow \omega \pi^0 n$
1236 ± 16		FUKUI	91	SPEC	8.95 $\pi^- p \rightarrow \omega \pi^0 n$
1222 ± 6		ATKINSON	84E	OMEG ±	25-55 $\gamma p \rightarrow \omega \pi X$
1237 ± 7		ATKINSON	84E	OMEG 0	25-55 $\gamma p \rightarrow \omega \pi X$
1239 ± 5		EVANGELIS...	81	OMEG -	12 $\pi^- p \rightarrow \omega \pi p$
1251 ± 8	450	GESSAROLI	77	HBC -	11 $\pi^- p \rightarrow \pi^- \omega p$
1245 ± 11	890	FLATTE	76C	HBC -	4.2 $K^- p \rightarrow \pi^- \omega \Sigma^+$
1222 ± 4	1400	CHALOUPKA	74	HBC -	3.9 $\pi^- p$
1220 ± 7	600	KARSHON	74B	HBC +	4.9 $\pi^+ p$
• • • We do not use the following data for averages, fits, limits, etc. • • •					
1190 ± 10		AUGUSTIN	89	DM2 ±	$e^+ e^- \rightarrow 5\pi$
1213 ± 5		ATKINSON	84C	OMEG 0	20-70 γp
1271 ± 11		COLLICK	84	SPEC +	200 $\pi^+ Z \rightarrow Z \pi \omega$

WEIGHTED AVERAGE
1229.5 ± 3.2 (Error scaled by 1.6) **$b_1(1235)$ WIDTH**

VALUE (MeV)	EVTS	DOCUMENT ID	TECN	CHG	COMMENT
142 ± 9 OUR AVERAGE					Error includes scale factor of 1.2.
113 ± 12		WEIDENAUER	93	ASTE	$\bar{p}p \rightarrow 2\pi^+ 2\pi^- \pi^0$
160 ± 30		ALDE	92C	GAM2	38,100 $\pi^- p \rightarrow \omega \pi^0 n$
151 ± 31		FUKUI	91	SPEC	8.95 $\pi^- p \rightarrow \omega \pi^0 n$
170 ± 15		EVANGELIS...	81	OMEG -	12 $\pi^- p \rightarrow \omega \pi p$
170 ± 5	225	BALTAY	78B	HBC +	15 $\pi^+ p \rightarrow \rho \pi$
155 ± 32	450	GESSAROLI	77	HBC -	11 $\pi^- p \rightarrow \pi^- \omega p$
182 ± 45	890	FLATTE	76C	HBC -	4.2 $K^- p \rightarrow \pi^- \omega \Sigma^+$
135 ± 20	1400	CHALOUPKA	74	HBC -	3.9 $\pi^- p$
156 ± 22	600	KARSHON	74B	HBC +	4.9 $\pi^+ p$
• • • We do not use the following data for averages, fits, limits, etc. • • •					
210 ± 19		AUGUSTIN	89	DM2 ±	$e^+ e^- \rightarrow 5\pi$
231 ± 14		ATKINSON	84C	OMEG 0	20-70 γp
232 ± 29		COLLICK	84	SPEC +	200 $\pi^+ Z \rightarrow Z \pi \omega$

 $b_1(1235)$ DECAY MODES

Mode	Fraction (Γ_i/Γ)	Confidence level
Γ_1 $\omega\pi$	seen	
[D/S amplitude ratio = 0.277 ± 0.027]		
Γ_2 $\pi^\pm \gamma$	(1.6 ± 0.4) × 10 ⁻³	
Γ_3 $\eta\rho$	seen	
Γ_4 $\pi^+ \pi^+ \pi^- \pi^0$	< 50	% 84%
Γ_5 $K^*(892)^\pm K^\mp$	seen	
Γ_6 $(K\bar{K})^\pm \pi^0$	< 8	% 90%
Γ_7 $K_S^0 K_L^0 \pi^\pm$	< 6	% 90%
Γ_8 $K_S^0 K_S^0 \pi^\pm$	< 2	% 90%
Γ_9 $\phi\pi$	< 1.5	% 84%

 $b_1(1235)$ PARTIAL WIDTHS

$\Gamma(\pi^\pm \gamma)$	VALUE (keV)	DOCUMENT ID	TECN	CHG	COMMENT	Γ_2
	230 ± 60	COLLICK	84	SPEC	+ 200 $\pi^+ Z \rightarrow Z \pi \omega$	

 **$b_1(1235)$ D-wave/S-wave AMPLITUDE RATIO
IN DECAY OF $b_1(1235) \rightarrow \omega\pi$**

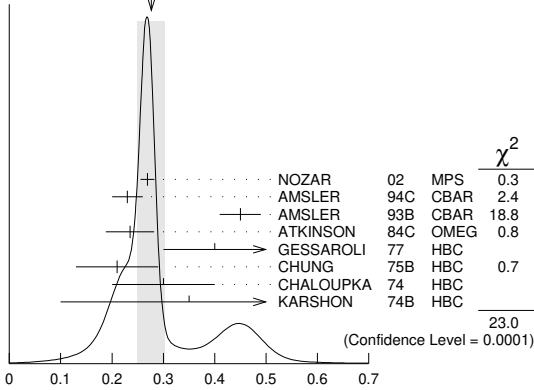
VALUE	EVTS	DOCUMENT ID	TECN	CHG	COMMENT
0.277 ± 0.027 OUR AVERAGE					Error includes scale factor of 2.4. See the ideogram below.
0.269 ± 0.009 ± 0.010		NOZAR	02	MPS -	18 $\pi^- p \rightarrow \omega \pi^- p$
0.23 ± 0.03		AMSLER	94C	CBAR	0.0 $\bar{p}p \rightarrow \omega \eta \pi^0$
0.45 ± 0.04		AMSLER	93B	CBAR	0.0 $\bar{p}p \rightarrow \omega \pi^0 \pi^0$
0.235 ± 0.047		ATKINSON	84C	OMEG	20-70 γp
0.4 + 0.1 - 0.1		GESSAROLI	77	HBC -	11 $\pi^- p \rightarrow \pi^- \omega p$
0.21 ± 0.08		CHUNG	75B	HBC +	7.1 $\pi^+ p$
0.3 ± 0.1		CHALOUPKA	74	HBC -	3.9-7.5 $\pi^- p$
0.35 ± 0.25	600	KARSHON	74B	HBC +	4.9 $\pi^+ p$

See key on page 1171

Meson Particle Listings

$b_1(1235)$, $a_1(1260)$

WEIGHTED AVERAGE
0.277±0.027 (Error scaled by 2.4)



$b_1(1235)$ D-wave/S-wave amplitude ratio in decay of $b_1(1235) \rightarrow \omega\pi$

$b_1(1235)$ D-wave/S-wave AMPLITUDE PHASE DIFFERENCE IN DECAY OF $b_1(1235) \rightarrow \omega\pi$

VALUE (°)	DOCUMENT ID	TECN	CHG	COMMENT
10.5±2.4±3.9	NOZAR	02	MPS	- 18 $\pi^- p \rightarrow \omega\pi^- p$

$b_1(1235)$ BRANCHING RATIOS

$\Gamma(\eta\rho)/\Gamma(\omega\pi)$	DOCUMENT ID	TECN	CHG	COMMENT	Γ_3/Γ_1
<0.10	ATKINSON	84D	OMEG	20-70 γp	

$\Gamma(\pi^+\pi^-\pi^0)/\Gamma(\omega\pi)$	DOCUMENT ID	TECN	CHG	COMMENT	Γ_4/Γ_1
<0.5	ABOLINS	63	HBC	+ 3.5 $\pi^+ p$	

$\Gamma(K^*(892)^\pm K^\mp)/\Gamma_{total}$	DOCUMENT ID	TECN	CHG	COMMENT	Γ_5/Γ
seen	1 ABLIKIM	10E	BES2	$J/\psi \rightarrow K^\pm K_S^0 \pi^\mp \pi^0$	

¹ From a fit including ten additional resonances and energy-independent Breit-Wigner width.

$\Gamma((K\bar{K})^\pm \pi^0)/\Gamma(\omega\pi)$	VALUE	CL%	DOCUMENT ID	TECN	CHG	COMMENT	Γ_6/Γ_1
<0.08	90		BALTAY	67	HBC	± 0.0 $\bar{p}p$	

$\Gamma(K_S^0 K_L^0 \pi^\pm)/\Gamma(\omega\pi)$	VALUE	CL%	DOCUMENT ID	TECN	CHG	COMMENT	Γ_7/Γ_1
<0.06	90		BALTAY	67	HBC	± 0.0 $\bar{p}p$	

$\Gamma(K_S^0 K_L^0 \pi^\pm)/\Gamma(\omega\pi)$	VALUE	CL%	DOCUMENT ID	TECN	CHG	COMMENT	Γ_8/Γ_1
<0.02	90		BALTAY	67	HBC	± 0.0 $\bar{p}p$	

$\Gamma(\phi\pi)/\Gamma(\omega\pi)$	VALUE	CL%	DOCUMENT ID	TECN	CHG	COMMENT	Γ_9/Γ_1
<0.004	95		VIKTOROV	96	SPEC	0 32.5 $\pi^- p \rightarrow K^+ K^- \pi^0 n$	

••• We do not use the following data for averages, fits, limits, etc. •••
 <0.04 95 BIZZARRI 69 HBC ± 0.0 $\bar{p}p$
 <0.015 DAHL 67 HBC 1.6-4.2 $\pi^- p$

$b_1(1235)$ REFERENCES

ABLIKIM	10E	PL B693 88	M. Ablikim et al.	(BES II Collab.)
NOZAR	02	PL B541 35	M. Nozar et al.	
VIKTOROV	96	PAN 59 1184	V.A. Viktorov et al.	(SERP)
Translated from YAF 59 1239.				
AMSLER	94C	PL B327 425	C. Amisler et al.	(Crystal Barrel Collab.)
AMSLER	93B	PL B311 362	C. Amisler et al.	(Crystal Barrel Collab.)
WEIDENAUER	93	ZPHY C59 387	P. Weidenauer et al.	(ASTERIX Collab.)
ALDE	92C	ZPHY C54 553	D.M. Alde et al.	(BELG, SERP, KEK, KYOT+)
FUKUI	91	PL B257 241	S. Fukui et al.	(SUGI, NAGO, KEK, KYOT+)
AUGUSTIN	89	NP B320 1	J.E. Augustin, G. Cosme	(DM2 Collab.)
ATKINSON	84C	NP B243 1	M. Atkinson et al.	(BONN, CERN, GLAS+)
ATKINSON	84D	NP B242 269	M. Atkinson et al.	(BONN, CERN, GLAS+)
ATKINSON	84E	PL B328 459	M. Atkinson et al.	(BONN, CERN, GLAS+)
COLLICK	84	PRL 53 2374	B. Collick et al.	(MINN, ROCH, FNAL)
EVANGELIS...	81	NP B178 197	C. Evangelista et al.	(BARI, BONN, CERN+)
BALTAY	78B	PR D17 62	C. Baltay et al.	(COLU, BING)
GESSAROLI	77	NP B126 382	R. Gessaroli et al.	(BGNA, FIRZ, GENO+)
FLATTE	76C	PL 64B 225	S.M. Flatte et al.	(CERN, AMST, NIJM+)
CHUNG	75B	PR D11 2426	S.U. Chung et al.	(BNL, LBL, UCSC)
CHALOUKPA	74	PL 51B 407	V. Chaloupka et al.	(CERN) JP
KARSHON	74B	PR D10 3608	U. Karshon et al.	(REHO) JP
BIZZARRI	69	NP B14 169	R. Bizzarri et al.	(CERN, CDEF)
BALTAY	67	PRL 18 93	C. Baltay et al.	(COLU)
DAHL	67	PR 163 1377	O.I. Dahl et al.	(LRL)
ABOLINS	63	PRL 11 381	M.A. Abolins et al.	(UCSD)

$a_1(1260)$

$I^G(JPC) = 1^-(1^{++})$

See also our review under the $a_1(1260)$ in PDG 06, Journal of Physics **G33** 1 (2006).

$a_1(1260)$ T-MATRIX POLE \sqrt{s}

Note that $\Gamma = -2 \text{Im}(\sqrt{s})$.

VALUE (MeV)	DOCUMENT ID	TECN	COMMENT
(1209⁺¹³-10) - i(288⁺⁴⁵-12)	OUR ESTIMATE		
(1209 ± 4 - ⁺¹² ₋₉) - i(288 ± 6 - ⁺⁴⁵ ₋₁₀)	MIKHASENKO 18	RVUE	$\tau^- \rightarrow \pi^- \pi^+ \pi^- \nu_\tau$

$a_1(1260)$ MASS

VALUE (MeV)	EVTS	DOCUMENT ID	TECN	COMMENT
1230 ± 40	OUR ESTIMATE			
1299 ± 12	46M	1 AGHASYAN	18B	COMP 190 $\pi^- p \rightarrow \pi^- \pi^+ \pi^- p$

••• We do not use the following data for averages, fits, limits, etc. •••

1195.05 ± 1.05 ± 6.33	894k	AAIJ	18A	LHCB	$D^0 \rightarrow K^\mp \pi^\pm \pi^\pm \pi^\mp$
1225 ± 9 ± 20	7k	2 DARGENT	17	RVUE	$D^0 \rightarrow \pi^- \pi^+ \pi^- \pi^+$
1255 ± 6 ± ⁺⁷ ₋₁₇	420k	3 ALEKSEEV	10	COMP	190 $\pi^- p b \rightarrow \pi^- \pi^+ \pi^- p b'$
1243 ± 12 ± 20		4 AUBERT	07AU	BABR	10.6 $e^+ e^- \rightarrow \rho^0 \pi^+ \pi^- \gamma$
1230-1270	6360	5 LINK	07A	FOCS	$D^0 \rightarrow \pi^- \pi^+ \pi^- \pi^+$
1203 ± 3		6 GOMEZ-DUM.	04	RVUE	$\tau^+ \rightarrow \pi^+ \pi^+ \pi^- \nu_\tau$
1330 ± 24	90k	SALVINI	04	OBLX	$\bar{p}p \rightarrow 2\pi^+ 2\pi^-$
1331 ± 10 ± 3	37k	7 ASNER	00	CLE2	10.6 $e^+ e^- \rightarrow \tau^+ \tau^-$, $\tau^- \rightarrow \pi^- \pi^0 \pi^0 \nu_\tau$
1255 ± 7 ± 6	5904	8 ABREU	98G	DLPH	$e^+ e^-$
1207 ± 5 ± 8	5904	9 ABREU	98G	DLPH	$e^+ e^-$
1196 ± 4 ± 5	5904	10,11 ABREU	98G	DLPH	$e^+ e^-$
1240 ± 10		BARBERIS	98B		450 $pp \rightarrow p_f \pi^+ \pi^- \pi^0 p_S$
1262 ± 9 ± 7		8,12 ACKERSTAFF	97R	OPAL	$E_{cm}^{e^+e^-} = 88-94$, $\tau \rightarrow 3\pi\nu$
1210 ± 7 ± 2		9,12 ACKERSTAFF	97R	OPAL	$E_{cm}^{e^+e^-} = 88-94$, $\tau \rightarrow 3\pi\nu$
1211 ± 7 ± ⁺⁵⁰ ₋₀		9 ALBRECHT	93C	ARG	$\tau^+ \rightarrow \pi^+ \pi^+ \pi^- \nu$
1121 ± 8		13 ANDO	92	SPEC	8 $\pi^- p \rightarrow \pi^+ \pi^- \pi^0 n$
1242 ± 37		14 IVANOV	91	RVUE	$\tau \rightarrow \pi^+ \pi^+ \pi^- \nu$
1260 ± 14		15 IVANOV	91	RVUE	$\tau \rightarrow \pi^+ \pi^+ \pi^- \nu$
1250 ± 9		16 IVANOV	91	RVUE	$\tau \rightarrow \pi^+ \pi^+ \pi^- \nu$
1208 ± 15		ARMSTRONG	90	OMEG	300.0 $pp \rightarrow p p \pi^+ \pi^- \pi^0$
1220 ± 15		17 ISGUR	89	RVUE	$\tau^+ \rightarrow \pi^+ \pi^+ \pi^- \nu$
1260 ± 25		18 BOWLER	88	RVUE	
1166 ± 18 ± 11		BAND	87	MAC	$\tau^+ \rightarrow \pi^+ \pi^+ \pi^- \nu$
1164 ± 41 ± 23		BAND	87	MAC	$\tau^+ \rightarrow \pi^+ \pi^0 \pi^0 \nu$
1250 ± 40		17 TORNQVIST	87	RVUE	
1046 ± 11		ALBRECHT	86B	ARG	$\tau^+ \rightarrow \pi^+ \pi^+ \pi^- \nu$
1056 ± 20 ± 15		RUCKSTUHL	86	DLCO	$\tau^+ \rightarrow \pi^+ \pi^+ \pi^- \nu$
1194 ± 14 ± 10		SCHMIDKE	86	MRK2	$\tau^+ \rightarrow \pi^+ \pi^+ \pi^- \nu$
1255 ± 23		BELLINI	85	SPEC	40 $\pi^- A \rightarrow \pi^- \pi^+ \pi^- A$
1240 ± 80		19 DANKOWY...	81	SPEC	8.45 $\pi^- p \rightarrow n 3\pi$
1280 ± 30		19 DAUM	81B	CNTR	63,94 $\pi^- p \rightarrow p 3\pi$
1041 ± 13		20 GAVILLET	77	HBC	4.2 $K^- p \rightarrow \Sigma 3\pi$

- Statistical error negligible.
- Reanalysis of CLEO data using Breit-Wigner parameterization.
- Superseded by AGHASYAN 2018B.
- The $\rho^\pm \pi^\mp$ state can be also due to the $\pi(1300)$.
- Using the Breit-Wigner parameterization; strong correlation between mass and width.
- Using the data of BARATE 98R.
- From a fit to the 3π mass spectrum including the $K\bar{K}^*(892)$ threshold.
- Uses the model of KUHN 90.
- Uses the model of ISGUR 89.
- Includes the effect of a possible a_1' state.
- Uses the model of FEINDT 90.
- Supersedes AKERS 95P.
- Average and spread of values using 2 variants of the model of BOWLER 75.
- Reanalysis of RUCKSTUHL 86.
- Reanalysis of SCHMIDKE 86.
- Reanalysis of ALBRECHT 86B.
- From a combined reanalysis of ALBRECHT 86B, SCHMIDKE 86, and RUCKSTUHL 86.
- From a combined reanalysis of ALBRECHT 86B and DAUM 81B.
- Uses the model of BOWLER 75.
- Produced in K^- backward scattering.

$a_1(1260)$ WIDTH

VALUE (MeV)	EVTS	DOCUMENT ID	TECN	COMMENT
250 ± 600	OUR ESTIMATE			
380 ± 80	46M	1 AGHASYAN	18B	COMP 190 $\pi^- p \rightarrow \pi^- \pi^+ \pi^- p$

Meson Particle Listings

$a_1(1260)$

• • • We do not use the following data for averages, fits, limits, etc. • • •

422.01 ± 2.10 ± 12.72	894k	AAIJ	18AI	LHCB	$D^0 \rightarrow K^\mp \pi^\pm \pi^\pm \pi^\mp$
430 ± 24 ± 31		2 DARGENT	17	RVUE	$D^0 \rightarrow \pi^- \pi^+ \pi^- \pi^+$
367 ± 9 ± 28/25	420k	3 ALEKSEEV	10	COMP	$190 \pi^- Pb \rightarrow \pi^- \pi^- \pi^+ Pb'$
410 ± 31 ± 30		4 AUBERT	07AU	BABR	$10.6 e^+ e^- \rightarrow \rho^0 \pi^\pm \pi^\mp \gamma$
520-680	6360	5 LINK	07A	FOCS	$D^0 \rightarrow \pi^- \pi^+ \pi^- \pi^+$
480 ± 20		6 GOMEZ-DUM.	04	RVUE	$\tau^+ \rightarrow \pi^+ \pi^+ \pi^- \nu_\tau$
580 ± 41	90k	SALVINI	04	OBLX	$\bar{p} p \rightarrow 2\pi^+ 2\pi^-$
460 ± 85	205	7 DRUTSKOY	02	BELL	$B \rightarrow D^{(*)} K^- K^{*0}$
814 ± 36 ± 13	37k	8 ASNER	00	CLE2	$10.6 e^+ e^- \rightarrow \tau^+ \tau^- \pi^0 \nu_\tau$
450 ± 50	22k	9 AKHMETSHIN	99E	CMD2	$1.05-1.38 e^+ e^- \rightarrow \pi^+ \pi^- \pi^0 \pi^0$
570 ± 10		10 BONDAR	99	RVUE	$e^+ e^- \rightarrow 4\pi, \tau \rightarrow 3\pi \nu_\tau$
587 ± 27 ± 21	5904	11 ABREU	98G	DLPH	$e^+ e^-$
478 ± 3 ± 15	5904	12 ABREU	98G	DLPH	$e^+ e^-$
425 ± 14 ± 8	5904	13,14 ABREU	98G	DLPH	$e^+ e^-$
400 ± 35		BARBERIS	98B		$450 pp \rightarrow p_f \pi^+ \pi^- \pi^0 p_s$
621 ± 32 ± 58		11,15 ACKERSTAFF	97R	OPAL	$E_{cm}^{ee} = 88-94, \tau \rightarrow 3\pi \nu$
457 ± 15 ± 17		12,15 ACKERSTAFF	97R	OPAL	$E_{cm}^{ee} = 88-94, \tau \rightarrow 3\pi \nu$
446 ± 21 ± 140/0		12 ALBRECHT	93C	ARG	$\tau^+ \rightarrow \pi^+ \pi^+ \pi^- \nu$
239 ± 11		ANDO	92	SPEC	$8 \pi^- \rho \rightarrow \pi^+ \pi^- \pi^0 n$
266 ± 13 ± 4		16 ANDO	92	SPEC	$8 \pi^- \rho \rightarrow \pi^+ \pi^- \pi^0 n$
465 ± 228/143		17 IVANOV	91	RVUE	$\tau \rightarrow \pi^+ \pi^+ \pi^- \nu$
298 ± 40/34		18 IVANOV	91	RVUE	$\tau \rightarrow \pi^+ \pi^+ \pi^- \nu$
488 ± 32		19 IVANOV	91	RVUE	$\tau \rightarrow \pi^+ \pi^+ \pi^- \nu$
430 ± 50		ARMSTRONG	90	OMEG	$300.0 pp \rightarrow \rho \rho \pi^+ \pi^- \pi^0$
420 ± 40		20 ISGUR	89	RVUE	$\tau^+ \rightarrow \pi^+ \pi^+ \pi^- \nu$
396 ± 43		21 BOWLER	88	RVUE	
405 ± 75 ± 25		BAND	87	MAC	$\tau^+ \rightarrow \pi^+ \pi^+ \pi^- \nu$
419 ± 108 ± 57		BAND	87	MAC	$\tau^+ \rightarrow \pi^+ \pi^0 \pi^0 \nu$
521 ± 27		ALBRECHT	86B	ARG	$\tau^+ \rightarrow \pi^+ \pi^+ \pi^- \nu$
476 ± 132/120 ± 54		RUCKSTUHL	86	DLCO	$\tau^+ \rightarrow \pi^+ \pi^+ \pi^- \nu$
462 ± 56 ± 30		SCHMIDKE	86	MRK2	$\tau^+ \rightarrow \pi^+ \pi^+ \pi^- \nu$
292 ± 40		BELLINI	85	SPEC	$40 \pi^- A \rightarrow \pi^- \pi^+ \pi^- A$
380 ± 100		22 DANKOWY...	81	SPEC	$8.45 \pi^- \rho \rightarrow n 3\pi$
300 ± 50		22 DAUM	81B	CNTR	$63.94 \pi^- \rho \rightarrow p 3\pi$
230 ± 50		23 GAVILLET	77	HBC	$4.2 K^- \rho \rightarrow \Sigma 3\pi$

1 Statistical error negligible.
 2 Reanalysis of CLEO data using Breit-Wigner parameterization.
 3 Superseded by AGHASYAN 2018B.
 4 The $\rho^\pm \pi^\mp$ state can be also due to the $\pi(1300)$.
 5 Using the Breit-Wigner parameterization; strong correlation between mass and width.
 6 Using the data of BARATE 98R.
 7 From a fit of the $K^- K^{*0}$ distribution assuming $m_{a_1} = 1230$ MeV and purely resonant production of the $K^- K^{*0}$ system.
 8 From a fit to the 3π mass spectrum including the $K \bar{K}^*(892)$ threshold.
 9 Using the $a_1(1260)$ mass of 1230 MeV.
 10 From AKHMETSHIN 99E and ASNER 00 data using the $a_1(1260)$ mass of 1230 MeV.
 11 Uses the model of KUHN 90.
 12 Uses the model of ISGUR 89.
 13 Includes the effect of a possible a_1' state.
 14 Uses the model of FEINDT 90.
 15 Supersedes AKERS 95P.
 16 Average and spread of values using 2 variants of the model of BOWLER 75.
 17 Reanalysis of RUCKSTUHL 86.
 18 Reanalysis of SCHMIDKE 86.
 19 Reanalysis of ALBRECHT 86B.
 20 From a combined reanalysis of ALBRECHT 86B, SCHMIDKE 86, and RUCKSTUHL 86.
 21 From a combined reanalysis of ALBRECHT 86B and DAUM 81B.
 22 Uses the model of BOWLER 75.
 23 Produced in K^- backward scattering.

$a_1(1260)$ DECAY MODES

Mode	Fraction (Γ_i/Γ)
Γ_1 3π	seen
Γ_2 $(\rho\pi)S$ -wave, $\rho \rightarrow \pi\pi$	seen
Γ_3 $(\rho\pi)D$ -wave, $\rho \rightarrow \pi\pi$	seen
Γ_4 $(\rho(1450)\pi)S$ -wave, $\rho \rightarrow \pi\pi$	seen
Γ_5 $(\rho(1450)\pi)D$ -wave, $\rho \rightarrow \pi\pi$	seen
Γ_6 $f_0(500)\pi, f_0 \rightarrow \pi\pi$	seen

Γ_7 $f_0(980)\pi, f_0 \rightarrow \pi\pi$	seen
Γ_8 $f_0(1370)\pi, f_0 \rightarrow \pi\pi$	seen
Γ_9 $f_2(1270)\pi, f_2 \rightarrow \pi\pi$	seen
Γ_{10} $\pi^+ \pi^- \pi^0$	seen
Γ_{11} $\pi^0 \pi^0 \pi^0$	not seen
Γ_{12} $K K \pi$	seen
Γ_{13} $K^*(892) K$	seen
Γ_{14} $\pi \gamma$	seen

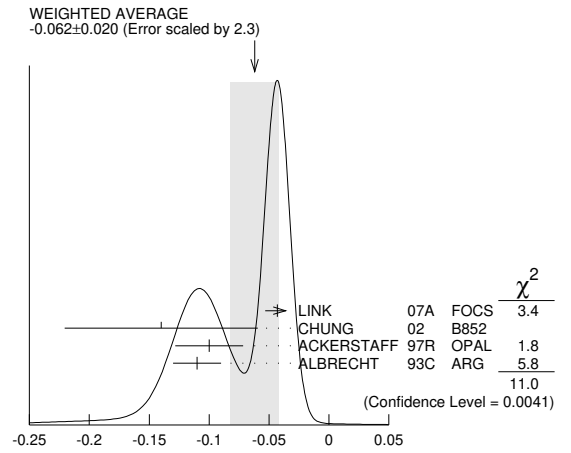
$a_1(1260)$ PARTIAL WIDTHS

$\Gamma(\pi\gamma)$	VALUE (keV)	DOCUMENT ID	TECN	COMMENT
	640 ± 246	ZIELINSKI	84c	SPEC 200 $\pi^+ Z \rightarrow Z 3\pi$

D-wave/S-wave AMPLITUDE RATIO IN DECAY OF $a_1(1260) \rightarrow \rho\pi$

VALUE	DOCUMENT ID	TECN	COMMENT
-0.062 ± 0.020 OUR AVERAGE	Error includes scale factor of 2.3. See the ideogram below.		
-0.043 ± 0.009 ± 0.005	LINK	07A	FOCS $D^0 \rightarrow \pi^- \pi^+ \pi^- \pi^+$
-0.14 ± 0.04 ± 0.07	1 CHUNG	02	B852 $18.3 \pi^- \rho \rightarrow \pi^+ \pi^- \pi^- \rho$
-0.10 ± 0.02 ± 0.02	2,3 ACKERSTAFF	97R	OPAL $E_{cm}^{ee} = 88-94, \tau \rightarrow 3\pi \nu$
-0.11 ± 0.02	2 ALBRECHT	93c	ARG $\tau^+ \rightarrow \pi^+ \pi^+ \pi^- \nu$

1 Deck-type background not subtracted.
 2 Uses the model of ISGUR 89.
 3 Supersedes AKERS 95P.



D-wave/S-wave AMPLITUDE RATIO IN DECAY OF $a_1(1260) \rightarrow \rho\pi$

$a_1(1260)$ BRANCHING RATIOS

$\Gamma((\rho\pi)S\text{-wave}, \rho \rightarrow \pi\pi)/\Gamma_{\text{total}}$	Γ_2/Γ			
VALUE (units 10^{-2})	EVTS	DOCUMENT ID	TECN	COMMENT
• • • We do not use the following data for averages, fits, limits, etc. • • •				
60.19	37k	1 ASNER	00	CLE2 $10.6 e^+ e^- \rightarrow \tau^+ \tau^-, \tau^- \rightarrow \pi^- \pi^0 \pi^0 \nu_\tau$
1 From a fit to the Dalitz plot.				
$\Gamma((\rho\pi)D\text{-wave}, \rho \rightarrow \pi\pi)/\Gamma_{\text{total}}$	Γ_3/Γ			
VALUE (units 10^{-2})	EVTS	DOCUMENT ID	TECN	COMMENT
• • • We do not use the following data for averages, fits, limits, etc. • • •				
1.30 ± 0.60 ± 0.22	37k	1 ASNER	00	CLE2 $10.6 e^+ e^- \rightarrow \tau^+ \tau^-, \tau^- \rightarrow \pi^- \pi^0 \pi^0 \nu_\tau$
1 From a fit to the Dalitz plot.				
$\Gamma((\rho(1450)\pi)S\text{-wave}, \rho \rightarrow \pi\pi)/\Gamma_{\text{total}}$	Γ_4/Γ			
VALUE (units 10^{-2})	EVTS	DOCUMENT ID	TECN	COMMENT
• • • We do not use the following data for averages, fits, limits, etc. • • •				
0.56 ± 0.84 ± 0.32	37k	1,2 ASNER	00	CLE2 $10.6 e^+ e^- \rightarrow \tau^+ \tau^-, \tau^- \rightarrow \pi^- \pi^0 \pi^0 \nu_\tau$
1 From a fit to the Dalitz plot. 2 Assuming for $\rho(1450)$ mass and width of 1370 and 386 MeV respectively.				
$\Gamma((\rho(1450)\pi)D\text{-wave}, \rho \rightarrow \pi\pi)/\Gamma_{\text{total}}$	Γ_5/Γ			
VALUE (units 10^{-2})	EVTS	DOCUMENT ID	TECN	COMMENT
• • • We do not use the following data for averages, fits, limits, etc. • • •				
2.04 ± 1.20 ± 0.28	37k	1,2 ASNER	00	CLE2 $10.6 e^+ e^- \rightarrow \tau^+ \tau^-, \tau^- \rightarrow \pi^- \pi^0 \pi^0 \nu_\tau$
1 From a fit to the Dalitz plot. 2 Assuming for $\rho(1450)$ mass and width of 1370 and 386 MeV respectively.				

See key on page 1171

Meson Particle Listings

a₁(1260), f₂(1270)

Γ(f₀(500)π, f₀ → ππ)/Γ_{total} Γ₆/Γ

Table with columns: VALUE (units 10^-2), EVTS, DOCUMENT ID, TECN, COMMENT. Includes data for CHUNG 02 B852 and ASNER 00 CLE2.

1 From a fit to the Dalitz plot. 2 Assuming for f0(500) (σ) mass and width of 860 and 880 MeV respectively.

Γ(f0(500)π, f0 → ππ)/[Γ((ρπ)S-wave, ρ → ππ) + Γ((ρπ)S-wave, ρ → ππ)] Γ6/(Γ2+Γ2)

Table with columns: VALUE, EVTS, DOCUMENT ID, TECN, COMMENT. Includes data for SALVINI 04 OBLX and AKHMETSHIN 99E CMD2.

1 Uses multichannel Aitchison-Bowler model (BOWLER 75). Uses data from GAVILET 77, DAUM 80, and DANKOWYCH 81.

Γ(f0(980)π, f0 → ππ)/Γ_{total} Γ7/Γ

Table with columns: VALUE, EVTS, DOCUMENT ID, TECN, COMMENT. Includes data for ALEXEEV 21 COMP and ASNER 00 CLE2.

1 The a1(1260)π- → f0(980)π- decay mode via the Triangle Singularity mechanism from MIKHASENKO 15 and ACET1 16 explains the a1(1420)- signal observed by ADOLPH 15c.

Γ(f0(1370)π, f0 → ππ)/Γ_{total} Γ8/Γ

Table with columns: VALUE (units 10^-2), EVTS, DOCUMENT ID, TECN, COMMENT. Includes data for ASNER 00 CLE2.

1 From a fit to the Dalitz plot. 2 Assuming for f0(1370) mass and width of 1186 and 350 MeV respectively.

Γ(f2(1270)π, f2 → ππ)/Γ_{total} Γ9/Γ

Table with columns: VALUE (units 10^-2), EVTS, DOCUMENT ID, TECN, COMMENT. Includes data for ASNER 00 CLE2.

1 From a fit to the Dalitz plot. 2 Assuming for f2(1270) mass and width of 1275 and 185 MeV respectively.

Γ(π+π-π0)/Γ_{total} Γ10/Γ

Table with columns: VALUE, EVTS, DOCUMENT ID, COMMENT. Includes data for BARBERIS 98B.

Γ(π0π0π0)/Γ(π+π-π0) Γ11/Γ10

Table with columns: VALUE, CL%, DOCUMENT ID, COMMENT. Includes data for BARBERIS 01.

1 Inconsistent with observations of σπ, f0(1370)π, and f2(1270)π decay modes.

Γ(K*(892)K)/Γ_{total} Γ13/Γ

Table with columns: VALUE (units 10^-2), EVTS, DOCUMENT ID, TECN, COMMENT. Includes data for COAN 04, DRUTSKOY 02, ASNER 00, and BARATE 99R.

1 Using structure functions from KUHN 92 and DECKER 93a and B(τ- → K-π- K+ντ) = (0.155 ± 0.006 ± 0.009) from BRIERE 03. 2 From a comparison to ALAM 94 assuming purely resonant production of the K- K*0 system. 3 From a fit to the 3π mass spectrum including the K K*(892) threshold. 4 Assuming a1(1260) dominance and taking B(τ → a1(1260)ντ) from BUSKULIC 96.

a1(1260) REFERENCES

Table of references for a1(1260) with columns: AUTHOR, YEAR, DOCUMENT ID, TECN, COMMENT.

Table of references for f2(1270) with columns: AUTHOR, YEAR, DOCUMENT ID, TECN, COMMENT.

f2(1270)

I^{G(JPC)} = 0+(2+ +)

f2(1270) T-MATRIX POLE √S

Note that Γ = -2 Im(√s).

Table of T-matrix poles for f2(1270) with columns: VALUE (MeV), DOCUMENT ID, TECN, COMMENT.

f2(1270) MASS

Table of masses for f2(1270) with columns: VALUE (MeV), EVTS, DOCUMENT ID, TECN, COMMENT.

Meson Particle Listings

$f_2(1270)$

1275 ± 10		AKER	91	CBAR	0.0 $\bar{p}p \rightarrow 3\pi^0$
1220 ± 10		BREAKSTONE	90	SFM	$pp \rightarrow pp\pi^+\pi^-$
1288 ± 12		ABACHI	86B	HRS	$e^+e^- \rightarrow \pi^+\pi^-X$
1284 ± 30	3k	BINON	83	GAM2	$38\pi^-p \rightarrow n2\eta$
1280 ± 20	3k	APEL	82	CNTR	$25\pi^-p \rightarrow n2\pi^0$
1284 ± 10	16000	DEUTSCH...	76	HBC	$16\pi^+p$
1258 ± 10	600	TAKAHASHI	72	HBC	$8\pi^-p \rightarrow n2\pi$
1275 ± 13		ARMENISE	70	HBC	$9\pi^+n \rightarrow p\pi^+\pi^-$
1261 ± 5	1960	³ ARMENISE	68	DBC	$5.1\pi^+n \rightarrow p\pi^+MM^-$
1270 ± 10	360	³ ARMENISE	68	DBC	$5.1\pi^+n \rightarrow p\pi^0MM$
1268 ± 6		¹³ JOHNSON	68	HBC	$3.7-4.2\pi^-p$

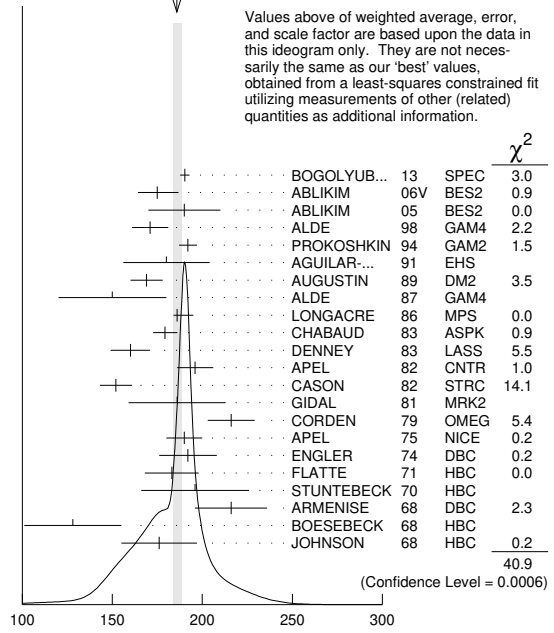
- Averaged over six nuclear targets, no statistically significant dependence on target nucleus observed.
- Breit-Wigner mass.
- Mass errors enlarged by us to Γ/\sqrt{N} ; see the note with the $K^*(892)$ mass.
- From a partial-wave analysis of data using a K-matrix formalism with 5 poles.
- From an energy-independent partial-wave analysis.
- From an amplitude analysis of the reaction $\pi^+\pi^- \rightarrow 2\pi^0$.
- From an amplitude analysis of $\pi^+\pi^- \rightarrow \pi^+\pi^-$ scattering data.
- Fit of the tensor partial waves from BES3 in the multipole basis.
- Using CLEO-c data but not authored by the CLEO Collaboration.
- From a fit to a Breit-Wigner line shape with fixed $\Gamma = 185$ MeV.
- From analysis of L3 data at 91 and 183-209 GeV.
- Systematic uncertainties not estimated.
- JOHNSON 68 includes BONDAR 63, LEE 64, DERADO 65, EISNER 67.

$f_2(1270)$ WIDTH

VALUE (MeV)	EVTS	DOCUMENT ID	TECN	COMMENT
186.6^{+2.8}_{-2.2}		OUR FIT		Error includes scale factor of 1.5.
185.8^{+2.8}_{-2.1}		OUR AVERAGE		Error includes scale factor of 1.6. See the ideogram below.
190.3 ± 1.9 ± 1.8		¹ BOGOLYUB... 13	SPEC	$7\pi^+(K^+,p)A \rightarrow n\gamma + X$
175 ⁺⁶ ₋₄ ± 10		² ABLIKIM 06v	BES2	$e^+e^- \rightarrow J/\psi \rightarrow \gamma\pi^+\pi^-$
190 ± 20		ABLIKIM 05	BES2	$J/\psi \rightarrow \phi\pi^+\pi^-$
171 ± 10		ALDE 98	GAM4	$100\pi^-p \rightarrow \pi^0\pi^0n$
192 ± 5	200k	PROKOSHKIN 94	GAM2	$38\pi^-p \rightarrow \pi^0\pi^0n$
180 ± 24		AGUILAR... 91	EHS	$400pp$
169 ± 9	5730	³ AUGUSTIN 89	DM2	$e^+e^- \rightarrow 5\pi$
150 ± 30	400	³ ALDE 87	GAM4	$100\pi^-p \rightarrow 4\pi^0n$
186 ⁺⁹ ₋₂		⁴ LONGACRE 86	MPS	$22\pi^-p \rightarrow n2K_S^0$
179.2 ^{+6.9} _{-6.6}		⁵ CHABAUD 83	ASPK	$17\pi^-p$ polarized
160 ± 11		DENNEY 83	LASS	$10\pi^+N$
196 ± 10	3k	APEL 82	CNTR	$25\pi^-p \rightarrow n2\pi^0$
152 ± 9		⁶ CASON 82	STRC	$8\pi^+p \rightarrow \Delta^{++}\pi^0\pi^0$
186 ± 27	11600	GIDAL 81	MRK2	J/ψ decay
216 ± 13		⁷ CORDEN 79	OMEG	$12-15\pi^-p \rightarrow n2\pi$
190 ± 10	10k	APEL 75	NICE	$40\pi^-p \rightarrow n2\pi^0$
192 ± 16	4600	ENGLER 74	DBC	$6\pi^+n \rightarrow \pi^+\pi^-p$
183 ± 15	5300	FLATTE 71	HBC	$7\pi^+p \rightarrow \Delta^{++}f_2$
196 ± 30		³ STUNTEBECK 70	HBC	$8\pi^-p, 5.4\pi^+d$
216 ± 20	1960	³ ARMENISE 68	DBC	$5.1\pi^+n \rightarrow p\pi^+MM^-$
128 ± 27		³ BOESEBECK 68	HBC	$8\pi^+p$
176 ± 21		^{3,8} JOHNSON 68	HBC	$3.7-4.2\pi^-p$
•••		We do not use the following data for averages, fits, limits, etc. •••		
168 ± 7		⁹ KLEMPF 22	RVUE	$J/\psi(1S) \rightarrow \gamma\pi^0\pi^0, \gamma K_S^0 K_S^0$
183 ± 2		CARVER 21	CLAS	$\gamma p \rightarrow \pi^0\pi^0 p$
195 ± 15	870	¹⁰ SCHEGELSKY 06A	RVUE	$\gamma\gamma \rightarrow K_S^0 K_S^0$
121 ± 26		TIKHOMIROV 03	SPEC	$40.0\pi^-C \rightarrow K_S^0 K_S^0 K_L^0 X$
187 ± 20		¹¹ ALDE 97	GAM2	$45.0pp \rightarrow pp\pi^0\pi^0$
184 ± 10		¹¹ GRYGOREV 96	SPEC	$40\pi^-N \rightarrow K_S^0 K_S^0 X$
200 ± 10		AKER 91	CBAR	$0.0\bar{p}p \rightarrow 3\pi^0$
240 ± 40	3k	BINON 83	GAM2	$38\pi^-p \rightarrow n2\eta$
187 ± 30	650	³ ANTIPOV 77	CIBS	$25\pi^-p \rightarrow p3\pi$
225 ± 38	16000	DEUTSCH... 76	HBC	$16\pi^+p$
166 ± 28	600	³ TAKAHASHI 72	HBC	$8\pi^-p \rightarrow n2\pi$
173 ± 5.3		³ ARMENISE 70	HBC	$9\pi^+n \rightarrow p\pi^+\pi^-$

- Averaged over six nuclear targets, no statistically significant dependence on target nucleus observed.
- Breit-Wigner width
- Width errors enlarged by us to $4\Gamma/\sqrt{N}$; see the note with the $K^*(892)$ mass.
- From a partial-wave analysis of data using a K-matrix formalism with 5 poles.
- From an energy-independent partial-wave analysis.
- From an amplitude analysis of the reaction $\pi^+\pi^- \rightarrow 2\pi^0$.
- From an amplitude analysis of $\pi^+\pi^- \rightarrow \pi^+\pi^-$ scattering data.
- JOHNSON 68 includes BONDAR 63, LEE 64, DERADO 65, EISNER 67.
- Fit of the tensor partial waves from BES3 in the multipole basis.
- From analysis of L3 data at 91 and 183-209 GeV.
- Systematic uncertainties not estimated.

WEIGHTED AVERAGE
185.8±2.8-2.1 (Error scaled by 1.6)



$f_2(1270)$ DECAY MODES

Mode	Fraction (Γ_i/Γ)	Scale factor/ Confidence level
Γ_1 $\pi\pi$	(84.3 ^{+2.8} _{-1.0}) %	S=1.2
Γ_2 $\pi^+\pi^-2\pi^0$	(7.7 ^{+1.2} _{-3.1}) %	S=1.2
Γ_3 $K\bar{K}$	(4.6 ± 0.4) %	S=2.7
Γ_4 $2\pi^+2\pi^-$	(2.8 ± 0.4) %	S=1.2
Γ_5 $\eta\eta$	(4.0 ± 0.8) × 10 ⁻³	S=2.1
Γ_6 $4\pi^0$	(3.0 ± 1.0) × 10 ⁻³	
Γ_7 $\gamma\gamma$	(1.42 ± 0.24) × 10 ⁻⁵	S=1.4
Γ_8 $\eta\eta\pi$	< 8 × 10 ⁻³	CL=95%
Γ_9 $K^0 K^- \pi^+ + c.c.$	< 3.4 × 10 ⁻³	CL=95%
Γ_{10} e^+e^-	< 6 × 10 ⁻¹⁰	CL=90%

CONSTRAINED FIT INFORMATION

An overall fit to the total width, 4 partial widths, a combination of partial widths obtained from integrated cross sections, and 6 branching ratios uses 44 measurements and one constraint to determine 8 parameters. The overall fit has a $\chi^2 = 82.3$ for 37 degrees of freedom.

The following off-diagonal array elements are the correlation coefficients $\langle \delta p_i \delta p_j \rangle / (\delta p_i \delta p_j)$, in percent, from the fit to parameters p_i , including the branching fractions, $x_i \equiv \Gamma_i/\Gamma_{total}$. The fit constrains the x_i whose labels appear in this array to sum to one.

x_2	-91						
x_3	10	-39					
x_4	10	-38	1				
x_5	1	-6	0	0			
x_6	0	-7	0	0	0		
x_7	4	1	-15	0	0	0	
Γ	-72	66	-10	-7	-1	0	-6
	x_1	x_2	x_3	x_4	x_5	x_6	x_7

Mode	Rate (MeV)	Scale factor
Γ_1 $\pi\pi$	157.2 ^{+5.0} _{-1.0}	
Γ_2 $\pi^+\pi^-2\pi^0$	14.3 ^{+2.3} _{-6.0}	1.3
Γ_3 $K\bar{K}$	8.5 ± 0.8	2.8
Γ_4 $2\pi^+2\pi^-$	5.2 ± 0.7	1.2

Γ_5	$\eta\eta$	0.75	± 0.14	2.1
Γ_6	$4\pi^0$	0.56	± 0.19	
Γ_7	$\gamma\gamma$	0.0026	± 0.0005	1.4

 $f_2(1270)$ PARTIAL WIDTHS

$\Gamma(\pi\pi)$					Γ_1
VALUE (MeV)	EVTS	DOCUMENT ID	TECN	COMMENT	

157.2 \pm 5.0 OUR FIT
-1.0

157.0 \pm 6.0 1 LONGACRE 86 MPS $22\pi^-p \rightarrow n2K_S^0$
-1.0

• • • We do not use the following data for averages, fits, limits, etc. • • •

152 ± 8 870 2 SCHEGELSKY 06A RVUE $\gamma\gamma \rightarrow K_S^0 K_S^0$

1 From a partial-wave analysis of data using a K-matrix formalism with 5 poles.

2 From analysis of L3 data at 91 and 183–209 GeV and using SU(3) relations.

$\Gamma(K\bar{K})$					Γ_3
VALUE (MeV)	EVTS	DOCUMENT ID	TECN	COMMENT	

8.5 \pm 0.8 OUR FIT Error includes scale factor of 2.8.

9.0 \pm 0.7 1 LONGACRE 86 MPS $22\pi^-p \rightarrow n2K_S^0$
-0.3

• • • We do not use the following data for averages, fits, limits, etc. • • •

7.5 ± 2.0 870 2 SCHEGELSKY 06A RVUE $\gamma\gamma \rightarrow K_S^0 K_S^0$

1 From a partial-wave analysis of data using a K-matrix formalism with 5 poles.

2 From analysis of L3 data at 91 and 183–209 GeV and using SU(3) relations.

$\Gamma(\eta\eta)$					Γ_5
VALUE (MeV)	EVTS	DOCUMENT ID	TECN	COMMENT	

0.75 \pm 0.14 OUR FIT Error includes scale factor of 2.1.

1.0 ± 0.1 1 LONGACRE 86 MPS $22\pi^-p \rightarrow n2K_S^0$

• • • We do not use the following data for averages, fits, limits, etc. • • •

1.8 ± 0.4 870 2 SCHEGELSKY 06A RVUE $\gamma\gamma \rightarrow K_S^0 K_S^0$

1 From a partial-wave analysis of data using a K-matrix formalism with 5 poles.

2 From analysis of L3 data at 91 and 183–209 GeV and using SU(3) relations.

$\Gamma(\gamma\gamma)$					Γ_7
VALUE (keV)	EVTS	DOCUMENT ID	TECN	COMMENT	

The value of this width depends on the theoretical model used. Unitary approaches with scalars typically (with exception of PENNINGTON 08) give values clustering around 2.6 keV; without an S-wave contribution, values are systematically higher (typically around 3 keV).

2.6 ± 0.5 OUR FIT Error includes scale factor of 1.4.

2.93 \pm 0.40 1 DAI 14A RVUE Compilation

• • • We do not use the following data for averages, fits, limits, etc. • • •

3.14 ± 0.20 2,3 PENNINGTON 08 RVUE Compilation

3.82 ± 0.30 3,4 PENNINGTON 08 RVUE Compilation

2.55 ± 0.15 870 5 SCHEGELSKY 06A RVUE $\gamma\gamma \rightarrow K_S^0 K_S^0$

2.84 ± 0.35 BOGLIONE 99 RVUE $\gamma\gamma \rightarrow \pi^+\pi^-, \pi^0\pi^0$

2.93 $\pm 0.23 \pm 0.32$ 6 YABUKI 95 VNS

2.58 $\pm 0.13 \pm 0.36$ 7 BEHREND 92 CELL $e^+e^- \rightarrow e^+e^-\pi^+\pi^-$

3.10 $\pm 0.35 \pm 0.35$ 8 BLINOV 92 MD1 $e^+e^- \rightarrow e^+e^-\pi^+\pi^-$

2.27 $\pm 0.47 \pm 0.11$ ADACHI 90D TOPZ $e^+e^- \rightarrow e^+e^-\pi^+\pi^-$

3.15 $\pm 0.04 \pm 0.39$ BOYER 90 MRK2 $e^+e^- \rightarrow e^+e^-\pi^+\pi^-$

3.19 $\pm 0.16 \pm 0.29$ MARSISKE 90 CBAL $e^+e^- \rightarrow e^+e^-\pi^0\pi^0$

2.35 ± 0.65 9 MORGAN 90 RVUE $\gamma\gamma \rightarrow \pi^+\pi^-, \pi^0\pi^0$

3.19 $\pm 0.09 \pm 0.22$ 2177 OEST 90 JADE $e^+e^- \rightarrow e^+e^-\pi^0\pi^0$

3.2 $\pm 0.1 \pm 0.4$ 10 AIHARA 86B TPC $e^+e^- \rightarrow e^+e^-\pi^+\pi^-$

2.5 $\pm 0.1 \pm 0.5$ BEHREND 84B CELL $e^+e^- \rightarrow e^+e^-\pi^+\pi^-$

2.85 $\pm 0.25 \pm 0.5$ 11 BERGER 84 PLUT $e^+e^- \rightarrow e^+e^-2\pi$

2.70 $\pm 0.05 \pm 0.20$ COURAU 84 DLCO $e^+e^- \rightarrow e^+e^-\pi^+\pi^-$

2.52 $\pm 0.13 \pm 0.38$ 12 SMITH 84C MRK2 $e^+e^- \rightarrow e^+e^-\pi^+\pi^-$

2.7 $\pm 0.2 \pm 0.6$ EDWARDS 82F CBAL $e^+e^- \rightarrow e^+e^-2\pi^0$

2.9 $\pm 0.6 \pm 0.6$ 13 EDWARDS 82F CBAL $e^+e^- \rightarrow e^+e^-2\pi^0$

3.2 $\pm 0.2 \pm 0.6$ BRANDELIK 81B TASS $e^+e^- \rightarrow e^+e^-\pi^+\pi^-$

3.6 $\pm 0.3 \pm 0.5$ ROUSSARIE 81 MRK2 $e^+e^- \rightarrow e^+e^-\pi^+\pi^-$

2.3 ± 0.8 14 BERGER 80B PLUT e^+e^-

1 Based on a K-matrix analysis of BELLE data from MORI 07, UEHARA 08A, UEHARA 09 and UEHARA 13. The width is derived for the pole on the third sheet which is closest to the physical axis. Supersedes PENNINGTON 08.

2 Solution A (preferred solution based on χ^2 -analysis).

3 Dispersion theory based amplitude analysis of BOYER 90, MARSISKE 90, BEHREND 92, and MORI 07.

4 Solution B (worse than solution A; still acceptable when systematic uncertainties are included).

5 From analysis of L3 data at 91 and 183–209 GeV and using SU(3) relations.

6 With a narrow scalar state around 1220 MeV.

7 Using a unitarized model with a 300–500 keV wide scalar at 1100 MeV.

8 Using the unitarized model of LYTH 85.

9 Error includes spread of different solutions. Data of MARK2 and CRYSTAL BALL used in the analysis. Authors report strong correlations with $\gamma\gamma$ width of $f_0(1370)$: $\Gamma(f_2) + 1/4 \Gamma(f_0) = 3.6 \pm 0.3$ keV.

¹⁰ Radiative corrections modify the partial widths; for instance the COURAU 84 value becomes 2.66 ± 0.21 in the calculation of LANDRO 86.

¹¹ Using the MENNESSIER 83 model.

¹² Superseded by BOYER 90.

¹³ If helicity = 2 assumption is not made.

¹⁴ Using mass, width and $B(f_2(1270) \rightarrow 2\pi)$ from PDG 78.

$\Gamma(e^+e^-)$					Γ_{10}
VALUE (eV)	CL%	DOCUMENT ID	TECN	COMMENT	

<0.11 90 ACHASOV 00K SND $e^+e^- \rightarrow \pi^0\pi^0$

• • • We do not use the following data for averages, fits, limits, etc. • • •

<1.7 90 VOROBYEV 88 ND $e^+e^- \rightarrow \pi^0\pi^0$

 $f_2(1270)$ $\Gamma(i)\Gamma(\gamma\gamma)/\Gamma(\text{total})$

$\Gamma(K\bar{K}) \times \Gamma(\gamma\gamma)/\Gamma_{\text{total}}$				Γ_3/Γ_7
VALUE (keV)	DOCUMENT ID	TECN	COMMENT	

0.121 \pm 0.020 OUR FIT Error includes scale factor of 1.3.

0.091 \pm 0.007 \pm 0.027 1 ALBRECHT 90G ARG $e^+e^- \rightarrow e^+e^-K^+K^-$

• • • We do not use the following data for averages, fits, limits, etc. • • •

0.104 $\pm 0.007 \pm 0.072$ 2 ALBRECHT 90G ARG $e^+e^- \rightarrow e^+e^-K^+K^-$

1 Using an incoherent background.

2 Using a coherent background.

$\Gamma(\eta\eta) \times \Gamma(\gamma\gamma)/\Gamma_{\text{total}}$				Γ_5/Γ_7
VALUE (eV)	DOCUMENT ID	TECN	COMMENT	

11.5 \pm 1.8 \pm 4.5 1 UEHARA 10A BELL 10.6 $e^+e^- \rightarrow e^+e^-\eta\eta$
-2.0 \pm 3.7

¹ Including interference with the $f_2'(1525)$ (parameters fixed to the values from the 2008 edition of this review, PDG 08) and $f_0(\Upsilon)$.

Helicity-0/Helicity-2 RATIO IN $\gamma\gamma \rightarrow f_2(1270) \rightarrow \pi\pi$

VALUE (units 10^{-2})	DOCUMENT ID	TECN	COMMENT
--------------------------	-------------	------	---------

3.7 \pm 0.3 \pm 15.9 UEHARA 08A BELL 10.6 $e^+e^- \rightarrow e^+e^-\pi^0\pi^0$
-2.9

• • • We do not use the following data for averages, fits, limits, etc. • • •

9.5 ± 1.8 1 DAI 14A RVUE Compilation

13 2,3 PENNINGTON 08 RVUE Compilation

26 3,4 PENNINGTON 08 RVUE Compilation

¹ Based on a K-matrix analysis of BELLE data from MORI 07, UEHARA 08A, UEHARA 09 and UEHARA 13. The width is derived for the pole on the third sheet which is closest to the physical axis.

² Solution A (preferred solution based on χ^2 -analysis).

³ Dispersion theory based amplitude analysis of BOYER 90, MARSISKE 90, BEHREND 92, and MORI 07.

⁴ Solution B (worse than solution A; still acceptable when systematic uncertainties are included).

 $f_2(1270)$ BRANCHING RATIOS

$\Gamma(\pi\pi)/\Gamma_{\text{total}}$					Γ_1/Γ
VALUE	EVTS	DOCUMENT ID	TECN	COMMENT	

0.843 \pm 0.028 OUR FIT Error includes scale factor of 1.2.
-0.010

0.837 \pm 0.020 OUR AVERAGE

0.849 ± 0.025 CHABAUD 83 ASPK 17 π^-p polarized

0.85 ± 0.05 250 BEAUPRE 71 HBC 8 $\pi^+p \rightarrow \Delta^{++}f_2$

0.8 ± 0.04 600 OH 70 HBC 1.26 $\pi^-p \rightarrow \pi^+\pi^-n$

• • • We do not use the following data for averages, fits, limits, etc. • • •

0.856 $\pm 0.001 \pm 0.05$ 1 ALBRECHT 20 RVUE 0.9 $\bar{p}p \rightarrow \pi^0\pi^0, \pi^0\eta\eta, \pi^0K^+K^-$

¹ Residue from T-matrix pole, 4 poles, 4 channels, including scattering data from HYAMS 75 ($\pi\pi$), LONGACRE 86 ($K\bar{K}$), BINON 83 ($\eta\eta$).

$\Gamma(\pi^+\pi^-2\pi^0)/\Gamma(\pi\pi)$				Γ_2/Γ_1
VALUE	EVTS	DOCUMENT ID	TECN	

Should be twice $\Gamma(2\pi^+2\pi^-)/\Gamma(\pi\pi)$ if decay is $\rho\rho$. (See ASCOLI 68D.)

0.091 \pm 0.015 OUR FIT Error includes scale factor of 1.2.
-0.040

0.15 ± 0.06 600 EISENBERG 74 HBC 4.9 $\pi^+p \rightarrow \Delta^{++}f_2$

• • • We do not use the following data for averages, fits, limits, etc. • • •

0.07 EMMS 75D DBC 4 $\pi^+n \rightarrow p f_2$

$\Gamma(K\bar{K})/\Gamma_{\text{total}}$				Γ_3/Γ
VALUE	DOCUMENT ID	TECN	COMMENT	

• • • We do not use the following data for averages, fits, limits, etc. • • •

0.033 $\pm 0.001 \pm 0.005$ 1 ALBRECHT 20 RVUE 0.9 $\bar{p}p \rightarrow \pi^0\pi^0, \pi^0\eta\eta, \pi^0K^+K^-$

¹ Residue from T-matrix pole, 4 poles, 4 channels, including scattering data from HYAMS 75 ($\pi\pi$), LONGACRE 86 ($K\bar{K}$), BINON 83 ($\eta\eta$).

Meson Particle Listings

 $f_2(1270)$ $\Gamma(K\bar{K})/\Gamma(\pi\pi)$

We average only experiments which either take into account $f_2(1270)$ - $a_2(1320)$ interference explicitly or demonstrate that $a_2(1320)$ production is negligible.

VALUE	EVTS	DOCUMENT ID	TECN	COMMENT
0.054 ± 0.005 -0.006				OUR FIT Error includes scale factor of 2.7.

 0.041 ± 0.004
 -0.005 **OUR AVERAGE**

VALUE	EVTS	DOCUMENT ID	TECN	COMMENT
0.045 ± 0.01		¹ BARGIOTTI 03	OBLX	$\bar{p}p$
0.037 ± 0.008 -0.021		ETKIN 82b	MPS	$23 \pi^- p \rightarrow n 2K_S^0$
0.045 ± 0.009		CHABAUD 81	ASPK	$17 \pi^- p$ polarized
0.039 ± 0.008		LOVERRE 80	HBC	$4 \pi^- p \rightarrow K \bar{K} N$
0.052 ± 0.025		ABLIKIM 04e	BES2	$J/\psi \rightarrow \omega K^+ K^-$
0.036 ± 0.005		² COSTA 80	OMEG	$1-2.2 \pi^- p \rightarrow K^+ K^- n$
0.030 ± 0.005		³ MARTIN 79	RVUE	
0.027 ± 0.009		⁴ POLYCHRO... 79	STRC	$7 \pi^- p \rightarrow n 2K_S^0$
0.025 ± 0.015		EMMS 75d	DBC	$4 \pi^+ n \rightarrow p f_2$
0.031 ± 0.012	20	ADERHOLZ 69	HBC	$8 \pi^+ p \rightarrow K^+ K^- \pi^+ p$

¹ Coupled channel analysis of $\pi^+ \pi^- \pi^0$, $K^+ K^- \pi^0$, and $K^\pm K_S^0 \pi^\mp$.

² Re-evaluated by CHABAUD 83.

³ Includes PAWLICKI 77 data.

⁴ Takes into account the $f_2(1270)$ - $f_2'(1525)$ interference.

 $\Gamma(2\pi^+ 2\pi^-)/\Gamma(\pi\pi)$

VALUE	EVTS	DOCUMENT ID	TECN	COMMENT
0.033 ± 0.005				OUR FIT Error includes scale factor of 1.2.
0.033 ± 0.004				OUR AVERAGE Error includes scale factor of 1.1.

VALUE	EVTS	DOCUMENT ID	TECN	COMMENT
0.024 ± 0.006	160	EMMS 75d	DBC	$4 \pi^+ n \rightarrow p f_2$
0.051 ± 0.025	70	EISENBERG 74	HBC	$4.9 \pi^+ p \rightarrow \Delta^{++} f_2$
0.043 ± 0.007 -0.011	285	¹ LOUIE 74	HBC	$3.9 \pi^- p \rightarrow n f_2$
0.037 ± 0.007	154	ANDERSON 73	DBC	$6 \pi^+ n \rightarrow p f_2$
0.047 ± 0.013		OH 70	HBC	$1.26 \pi^- p \rightarrow \pi^+ \pi^- n$

¹ LOUIE 74 was quoted as 0.065 in PDG 74. Factor 2/3 to go from $\pi^+ \pi^- \rightarrow \pi \pi$ forgotten. Mike L.

 $\Gamma(\eta)/\Gamma_{total}$

VALUE (units 10^{-3})	DOCUMENT ID	TECN	COMMENT
4.0 ± 0.8			OUR FIT Error includes scale factor of 2.1.
2.9 ± 0.5			OUR AVERAGE

VALUE	DOCUMENT ID	TECN	COMMENT
2.7 ± 0.7	BINON 05	GAMS	$33 \pi^- p \rightarrow \eta \eta n$
2.8 ± 0.7	ALDE 86d	GAM4	$100 \pi^- p \rightarrow 2 \eta n$
5.2 ± 1.7	BINON 83	GAM2	$38 \pi^- p \rightarrow 2 \eta n$
$4.0 \pm 1.0 \pm 2.0$	¹ ALBRECHT 20	RVUE	$0.9 \bar{p}p \rightarrow \pi^0 \pi^0 \eta$, $\pi^0 \eta \eta$, $\pi^0 K^+ K^-$

¹ Residue from T-matrix pole, 4 poles, 4 channels, including scattering data from HYAMS 75 ($\pi\pi$), LONGACRE 86 ($K\bar{K}$), BINON 83 ($\eta\eta$).

 $\Gamma(\eta\eta)/\Gamma(\pi\pi)$

VALUE	CL%	DOCUMENT ID	TECN	COMMENT
0.003 ± 0.001		BARBERIS 00e		$450 p p \rightarrow p_f \eta \eta p_s$

VALUE	CL%	DOCUMENT ID	TECN	COMMENT
<0.05	95	EDWARDS 82f	CBAL	$e^+ e^- \rightarrow e^+ e^- 2\eta$
<0.016	95	EMMS 75d	DBC	$4 \pi^+ n \rightarrow p f_2$
<0.09	95	EISENBERG 74	HBC	$4.9 \pi^+ p \rightarrow \Delta^{++} f_2$

 $\Gamma(4\pi^0)/\Gamma_{total}$

VALUE	EVTS	DOCUMENT ID	TECN	COMMENT
0.0030 ± 0.0010				OUR FIT
0.003 ± 0.001	400 \pm 50	ALDE 87	GAM4	$100 \pi^- p \rightarrow 4\pi^0 n$

 $\Gamma(\gamma\gamma)/\Gamma_{total}$

VALUE (units 10^{-5})	DOCUMENT ID	TECN	COMMENT
$1.57 \pm 0.01 \pm 1.39$ -0.14	UEHARA 08a	BELL	$10.6 e^+ e^- \rightarrow e^+ e^- \pi^0 \pi^0$

 $\Gamma(\eta\pi\pi)/\Gamma(\pi\pi)$

VALUE	CL%	DOCUMENT ID	TECN	COMMENT
<0.010	95	EMMS 75d	DBC	$4 \pi^+ n \rightarrow p f_2$

 $\Gamma(K^0 K^- \pi^+ + c.c.)/\Gamma(\pi\pi)$

VALUE	CL%	DOCUMENT ID	TECN	COMMENT
<0.004	95	EMMS 75d	DBC	$4 \pi^+ n \rightarrow p f_2$

 $\Gamma(e^+ e^-)/\Gamma_{total}$

VALUE (units 10^{-10})	CL%	DOCUMENT ID	TECN	COMMENT
<6	90	ACHASOV 00k	SND	$e^+ e^- \rightarrow \pi^0 \pi^0$

 $f_2(1270)$ REFERENCES

KLEMP T 22	PL B830 137171	E. Klempt <i>et al.</i>	(BONN)
RODAS 22	EPJ C82 80	A. Rodas <i>et al.</i>	(JPAC Collab.)
CARVER 21	PRL 126 082002	M. Carver <i>et al.</i>	(CLAS Collab.)
ALBRECHT 20	EPJ C80 453	M. Albrecht <i>et al.</i>	(Crystal Barrel Collab.)
DOBBS 15	PR D91 052006	S. Dobbs <i>et al.</i>	(NWES)
DAI 14A	PR D90 036004	L.-Y. Dai, M.R. Pennington	(CEBAF)
BOGOLYUB... 13	PAN 76 1324	M.Yu. Bogolyubsky <i>et al.</i>	(HYPERON-M Collab.)
UEHARA 13	PTEP 2013 123C01	S. Uehara <i>et al.</i>	(BELLE Collab.)
UEHARA 10A	PR D82 114031	S. Uehara <i>et al.</i>	(BELLE Collab.)
ANISOVICH 09	IJMP A24 2481	V.V. Anisovitch, A.V. Sarantsev	
UEHARA 09	PR D79 052009	S. Uehara <i>et al.</i>	(BELLE Collab.)
PDG 08	PL B667 1	C. Amsler <i>et al.</i>	(PDG Collab.)
PENNINGTON 08	EPJ C56 1	M.R. Pennington <i>et al.</i>	
UEHARA 08A	PR D78 052004	S. Uehara <i>et al.</i>	(BELLE Collab.)
MORI 07	PR D75 051101	T. Mori <i>et al.</i>	(BELLE Collab.)
ABLIKIM 06A	PL B642 441	M. Ablikim <i>et al.</i>	(BES Collab.)
SCHEGELSKY 06V	EPJ A27 207	V.A. Schegelsky <i>et al.</i>	
ABLIKIM 05	PL B607 243	M. Ablikim <i>et al.</i>	(BES Collab.)
BINON 05	PAN 68 960	F. Binon <i>et al.</i>	
ABLIKIM 04E	Translated from YAF 66 98	M. Ablikim <i>et al.</i>	(BES Collab.)
BARGIOTTI 03	EPJ C26 371	M. Bargiotti <i>et al.</i>	(OBELIX Collab.)
TIKHOMIROV 03	PAN 66 828	G.D. Tikhomirov <i>et al.</i>	
ACHASOV 00K	PL B492 8	M.N. Achasov <i>et al.</i>	(Novosibirsk SND Collab.)
BARBERIS 00E	PL B479 59	D. Barberis <i>et al.</i>	(WA 102 Collab.)
BOGLIONE 99	EPJ C9 11	M. Boglione, M.R. Pennington	
ALDE 98	PAN 62 405	D. Alde <i>et al.</i>	(GAM4 Collab.)
Also	Translated from YAF 62 446	D. Alde <i>et al.</i>	(GAMS Collab.)
ALDE 97	PL B397 350	D.M. Alde <i>et al.</i>	(GAMS Collab.)
BERTIN 97C	PL B408 476	A. Bertin <i>et al.</i>	(OBELIX Collab.)
GRYGOREV 96	PAN 59 2105	V.K. Grigoriev, O.N. Baloshin, B.P. Barkov	(ITEP)
YABUKI 95	JPS J4 435	F. Yabuki <i>et al.</i>	(VENUS Collab.)
PROKOSHNIK 94	PD 33 420	N.D. Prokoshkin, A.A. Kondashov	(SERP)
BEHREND 92	ZPHY C56 381	H.J. Behrend	(CELLO Collab.)
BLINOV 92	ZPHY C53 33	A.E. Blinov <i>et al.</i>	(NOVO)
AGUILAR... 91	ZPHY C50 405	M. Aguilar-Benitez <i>et al.</i>	(LEBC-EHS Collab.)
AKER 91	PL B260 249	E. Aker <i>et al.</i>	(Crystal Barrel Collab.)
ADACHI 90D	PL B234 185	I. Adachi <i>et al.</i>	(TOPAZ Collab.)
ALBRECHT 90G	ZPHY C48 183	H. Albrecht <i>et al.</i>	(ARGUS Collab.)
BOYER 90	PR D42 1350	J. Boyer <i>et al.</i>	(Mark II Collab.)
BREAKSTONE 90	ZPH C48 569	A.M. Breakstone <i>et al.</i>	(ISU, BGM, CERN+)
MARISKE 90	PR D41 3324	H. Mariske <i>et al.</i>	(Crystal Ball Collab.)
MORGAN 90	ZPHY C48 623	D. Morgan, M.R. Pennington	(RAL, DURH)
OEST 90	ZPHY C47 343	T. Oest <i>et al.</i>	(JADE Collab.)
AUGUSTIN 89	NP B320 1	J.E. Augustin, G. Cosme	(DM2 Collab.)
VOROBYEV 88	SJNP 48 273	P.V. Vorobyev <i>et al.</i>	(NOVO)
Also	Translated from YAF 48 436	P.V. Vorobyev <i>et al.</i>	
ALDE 87	PL B198 286	D.M. Alde <i>et al.</i>	(LANL, BRUX, SERP, LAPP)
AUGUSTIN 87	ZPHY C36 369	J.E. Augustin <i>et al.</i>	(LALO, CLER, FRAS+)
ABACHI 86B	PRL 57 1930	S. Abachi <i>et al.</i>	(PURD, ANL, IND, MICH+)
AIHARA 86B	PRL 57 404	H. Aihara <i>et al.</i>	(T-PC-2+ Collab.)
ALDE 86D	NP B269 485	D.M. Alde <i>et al.</i>	(BELG, LAPP, SERP, CERN+)
LANDRO 86	PL B172 445	M. Landro, K.J. Mork, H.A. Olsen	(UTRO)
LONGACRE 86	PL B177 223	R.S. Longacre <i>et al.</i>	(BNL, BRAN, CUNY+)
LYTH 85	JP G11 459	D.H. Lyth	
BEHREND 84B	ZPHY C23 223	H.J. Behrend <i>et al.</i>	(CELLO Collab.)
BERGER 84	ZPHY C26 199	C. Berger <i>et al.</i>	(PLUTO Collab.)
COURAU 84	PL 147B 227	A. Courau <i>et al.</i>	(CIT, SLAC)
SMITH 84C	PR D30 851	J.R. Smith <i>et al.</i>	(SLAC, LBL, HARV)
BINON 84B	NC 78A 313	F.G. Binon <i>et al.</i>	(BELG, LAPP, SERP+)
Also	SJNP 38 561	F.G. Binon <i>et al.</i>	(BELG, LAPP, SERP+)
Also	Translated from YAF 38 924	F.G. Binon <i>et al.</i>	
CHABAUD 83	NP B223 1	V. Chabaud <i>et al.</i>	(CERN, CRAC, MPIM)
DENNEY 83	PR D28 2726	D.L. Denney <i>et al.</i>	(IOWA, MICH)
MENNESSIER 83	ZPHY C16 241	G. Mennessier	(MONP)
APEL 82	NP B201 197	W.D. Apel <i>et al.</i>	(KARLK, KARLE, PISA, SERP+)
CASON 82	PRL 48 1316	N.M. Cason <i>et al.</i>	(NDAM, ANL)
EDWARDS 82F	PL 110B 82	C. Edwards <i>et al.</i>	(CIT, HARV, PRIN+)
ETKIN 82B	PR D25 1786	A. Etkin <i>et al.</i>	(BNL, CUNY, TUFTS, VAND)
BRANDELIC 81B	ZPHY C10 117	R. Brandelik <i>et al.</i>	(TASSO Collab.)
CHABAUD 81	APP B12 575	V. Chabaud <i>et al.</i>	(CERN, CRAC, MPIM)
GIDAL 81	PL 107B 153	G. Gidal <i>et al.</i>	(SLAC, LBL)
ROUSSARIE 81	PL 105B 304	A. Roussarie <i>et al.</i>	(SLAC, LBL)
BERGER 80B	PL 94B 254	C. Berger <i>et al.</i>	(PLUTO Collab.)
COSTA 80	NP B175 402	G. Costa <i>et al.</i>	(BARI, BONN, CERN, GLAS+)
LOVERRE 80	ZPHY C6 187	P.F. Loverre <i>et al.</i>	(CERN, CDEF, MADR+)
CORDEN 79	NP B157 250	M.J. Corden <i>et al.</i>	(BIRM, RHEL, TELA+)
MARTIN 79	NP B158 520	A.D. Martin, E.N. Ozmutlu	(DURH)
POLYCHRO... 79	PR D19 1317	V.A. Polychronakos <i>et al.</i>	(NDAM, ANL)
PDG 78	PL 75B 1	C. Bricman <i>et al.</i>	(SERP, GEVA)
ANTIPOV 77	NP B119 456	Y.M. Antipov <i>et al.</i>	(ANL)
PAWLICKI 77	PR D15 3196	A.J. Pawlicki <i>et al.</i>	(AACH3, BERL, BONN+)
DEUTSCH... 76	NP B103 426	M. Deuschmann <i>et al.</i>	(KARLK, KARLE, PISA, SERP+)
APEL 75D	PL 57B 398	W.D. Apel <i>et al.</i>	(BIRM, DURH, RHEL)
EMMS 75D	NP B96 155	M.J. Emms <i>et al.</i>	(CERN, MPIM)
HYAMS 75	NP B100 205	B.D. Hyams <i>et al.</i>	(REHO)
EISENBERG 74	PL 52B 239	Y. Eisenberg <i>et al.</i>	(CMU, CASE)
ENGLER 74	PR D10 2070	A. Engler <i>et al.</i>	(SACL, CERN)
LOUIE 74	PL 48B 385	J. Louie <i>et al.</i>	
PDG 73	PL 50B 1	V. Chaloupka <i>et al.</i>	(CMU, CASE)
ANDERSON 73	PRL 31 562	J.C. Anderson <i>et al.</i>	(TOHOK, PENN, NDAM+)
TAKAHASHI 72	PR D6 1266	K. Takahashi <i>et al.</i>	(AACH, BERL, CERN)
BEAUPRE 71	NP B39 77	J.V. Beaupre <i>et al.</i>	(LBL)
FLATTE 71	PL 34B 551	S.M. Flatte <i>et al.</i>	(BARI, BGM, FIRZ)
ARMENISE 70	LNC 4 199	N. Armenise <i>et al.</i>	(WISC, TINTO) JP
OH 70	PR D1 2494	B.Y. Oh <i>et al.</i>	(NDAM)
STUNTEBECK 70	PL 32B 391	P.H. Stuntebeck <i>et al.</i>	(AACH3, BERL, CERN+)
ADERHOLZ 69	NP B11 259	M. Aderholz <i>et al.</i>	(BARI, BGM, FIRZ+)
ARMENISE 68D	NC 54A 999	N. Armenise <i>et al.</i>	(ILL)
ASCOLI 68D	PRL 21 1712	G. Ascoli <i>et al.</i>	(AACH, BERL, CERN)
BOESEBECK 68	NP B4 501	K. Boesebeck <i>et al.</i>	(NDAM, PURD, SLAC)
JOHNSON 68	PR 176 1651	P.B. Johnson <i>et al.</i>	(PURD)
EISNER 67	PR 164 1699	R.L. Eisner <i>et al.</i>	(NDAM)
DERADO 65	PRL 14 372	I. Derado <i>et al.</i>	(MICH)
LEE 64	PR 12 342	Y.Y. Lee <i>et al.</i>	(MICH)
BONDAR 63	PL 5 153	L. Bondar <i>et al.</i>	(AACH, BIRM, BONN, DESY+)

$f_1(1285)$

$$I^G(J^{PC}) = 0^+(1^{++})$$

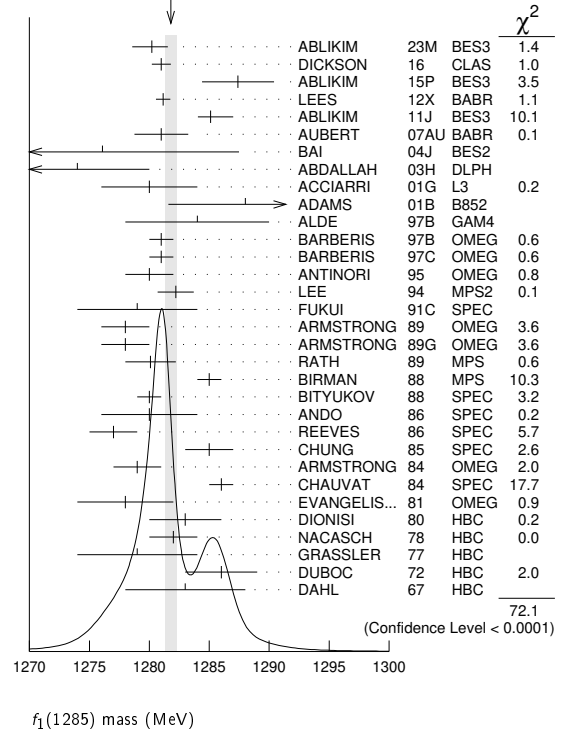
$f_1(1285)$ MASS

VALUE (MeV)	EVTS	DOCUMENT ID	TECN	COMMENT
1281.8 ± 0.5	OUR AVERAGE	Error includes scale factor of 1.7. See the ideogram below.		
1280.2 ± 0.6	126K	ABLIKIM 23M	BES3	$J/\psi \rightarrow \gamma K_S^0 K_S^0 \pi^0$
1281.0 ± 0.8		DICKSON 16	CLAS	$2.55 \gamma p \rightarrow \eta \pi^+ \pi^- p$
1287.4 ± 3.0	87	ABLIKIM 15P	BES3	$J/\psi \rightarrow K^+ K^- 3\pi$
1281.16 ± 0.39 ± 0.45		1 LEES 12X	BABR	$\tau^- \rightarrow \pi^- f_1(1285) \nu_\tau$
1285.1 ± 1.0		2 ABLIKIM 11J	BES3	$J/\psi \rightarrow \omega(\eta \pi^+ \pi^-)$
1281 ± 2 ± 1		AUBERT 07AU	BABR	$10.6 e^+ e^- \rightarrow f_1(1285) \pi^+ \pi^- \gamma$
1276.1 ± 8.1 ± 8.0	203	BAI 04J	BES2	$J/\psi \rightarrow \gamma \gamma \pi^+ \pi^-$
1274 ± 6	237	ABDALLAH 03H	DLPH	$91.2 e^+ e^- \rightarrow K_S^0 K_S^\pm \pi^\mp + X$
1280 ± 4		ACCIARRI 01G	L3	
1288 ± 4 ± 5	20k	ADAMS 01B	B852	$18 \text{ GeV } \pi^- p \rightarrow K^+ K^- \pi^0 n$
1284 ± 6	1400	ALDE 97B	GAM4	$100 \pi^- p \rightarrow \eta \pi^0 \pi^0 n$
1281 ± 1		BARBERIS 97B	OMEG	$450 pp \rightarrow pp 2(\pi^+ \pi^-)$
1281 ± 1		BARBERIS 97C	OMEG	$450 pp \rightarrow pp 2(\pi^+ \pi^-)$
1280 ± 2		3 ANTINORI 95	OMEG	$300,450 pp \rightarrow pp 2(\pi^+ \pi^-)$
1282.2 ± 1.5		LEE 94	MPS2	$18 \pi^- p \rightarrow K^+ \bar{K}^0 2\pi^- p$
1279 ± 5		FUKUI 91C	SPEC	$8.95 \pi^- p \rightarrow \eta \pi^+ \pi^- n$
1278 ± 2	140	ARMSTRONG 89	OMEG	$300 pp \rightarrow K \bar{K} \pi p p$
1278 ± 2		ARMSTRONG 89G	OMEG	$85 \pi^+ p \rightarrow 4\pi p p$
1280.1 ± 2.1	60	RATH 89	MPS	$21.4 \pi^- p \rightarrow K_S^0 K_S^0 \pi^0 n$
1285 ± 1	4750	4 BIRMAN 88	MPS	$8 \pi^- p \rightarrow K^+ \bar{K}^0 \pi^- n$
1280 ± 1	504	BITYUKOV 88	SPEC	$32.5 \pi^- p \rightarrow K^+ K^- \pi^0 n$
1280 ± 4		ANDO 86	SPEC	$8 \pi^- p \rightarrow \eta \pi^+ \pi^- n$
1277 ± 2	420	REEVES 86	SPEC	$6.6 p \bar{p} \rightarrow K K \pi X$
1285 ± 2		CHUNG 85	SPEC	$8 \pi^- p \rightarrow N K \bar{K} \pi$
1279 ± 2	604	ARMSTRONG 84	OMEG	$85 \pi^+ p \rightarrow K \bar{K} \pi p p$
1286 ± 1		CHAUVAT 84	SPEC	$31.5 pp \rightarrow K \bar{K} \pi p p$
1278 ± 4		EVANGELIS... 81	OMEG	$12 \pi^- p \rightarrow \eta \pi^+ \pi^- \pi^- p$
1283 ± 3	103	DIONISI 80	HBC	$4 \pi^- p \rightarrow K \bar{K} \pi n$
1282 ± 2	320	NACASCH 78	HBC	$0.7, 0.76 \bar{p} p \rightarrow K \bar{K} 3\pi$
1279 ± 5	210	GRASSLER 77	HBC	$16 \pi^\mp p$
1286 ± 3	180	DUBOC 72	HBC	$1.2 \bar{p} p \rightarrow 2K 4\pi$
1283 ± 5		DAHL 67	HBC	$1.6-4, 2 \pi^- p$
1289.3 ± 2.8	234	ABLIKIM 19BA	BES3	$e^+ e^- \rightarrow \psi(2S)$
1284.2 ± 2.2	5	AAIJ 14Y	LHCB	$B^0(s) \rightarrow J/\psi 2(\pi^+ \pi^-)$
1281.9 ± 0.5	5	SOSA 99	SPEC	$pp \rightarrow p_{\text{slow}} (K_S^0 K^+ \pi^-) p_{\text{fast}}$
1282.8 ± 0.6	5	SOSA 99	SPEC	$pp \rightarrow p_{\text{slow}} (K_S^0 K^- \pi^+) p_{\text{fast}}$
1270 ± 10		AMELIN 95	VES	$37 \pi^- N \rightarrow \pi^- \pi^+ \pi^- \gamma N$
1280 ± 2		ABATZIS 94	OMEG	$450 pp \rightarrow pp 2(\pi^+ \pi^-)$
1282 ± 4		ARMSTRONG 93C	E760	$\bar{p} p \rightarrow \pi^0 \eta \eta \rightarrow 6\gamma$
1270 ± 6 ± 10		ARMSTRONG 92C	OMEG	$300 pp \rightarrow pp \pi^+ \pi^- \gamma$
1281 ± 1		ARMSTRONG 89E	OMEG	$300 pp \rightarrow pp 2(\pi^+ \pi^-)$
1279 ± 6 ± 10	16	BECKER 87	MRK3	$e^+ e^- \rightarrow \phi K \bar{K} \pi$
1286 ± 9		GIDAL 87	MRK2	$e^+ e^- \rightarrow e^+ e^- \eta \pi^+ \pi^-$
1287 ± 5	353	BITYUKOV 84B	SPEC	$32 \pi^- p \rightarrow K^+ K^- \pi^0 n$
~1279		6 TORNQVIST 82B	RVUE	
1275 ± 6	31	BROMBERG 80	SPEC	$100 \pi^- p \rightarrow K \bar{K} \pi X$
1288 ± 9	200	GURTU 79	HBC	$4.2 K^- p \rightarrow n \eta 2\pi$
~1275.0	46	7 STANTON 79	CNTR	$8.5 \pi^- p \rightarrow n 2\gamma 2\pi$
1271 ± 10	34	CORDEN 78	OMEG	$12-15 \pi^- p \rightarrow K^+ K^- \pi n$
1295 ± 12	85	CORDEN 78	OMEG	$12-15 \pi^- p \rightarrow n 5\pi$
1292 ± 10	150	DEFOIX 72	HBC	$0.7 \bar{p} p \rightarrow 7\pi$
1280 ± 3	500	8 THUN 72	MMS	$13.4 \pi^- p$
1303 ± 8		BARDADIN... 71	HBC	$8 \pi^+ p \rightarrow p 6\pi$
1283 ± 6		BOESEBECK 71	HBC	$16.0 \pi p \rightarrow p 5\pi$
1270 ± 10		CAMPBELL 69	DBC	$2.7 \pi^+ d$
1285 ± 7		LORSTAD 69	HBC	$0.7 \bar{p} p, 4,5\text{-body}$
1290 ± 7		D'ANDLAU 68	HBC	$1.2 \bar{p} p, 5-6 \text{ body}$

¹ Using the $2\pi^+ 2\pi^-$ and $\pi^+ \pi^- \eta$ modes of $f_1(1285)$ decay.

- ² The selected process is $J/\psi \rightarrow \omega a_0(980) \pi$.
- ³ Supersedes ABATZIS 94, ARMSTRONG 89E.
- ⁴ From partial wave analysis of $K^+ \bar{K}^0 \pi^-$ system.
- ⁵ No systematic error given.
- ⁶ From a unitarized quark-model calculation.
- ⁷ From phase shift analysis of $\eta \pi^+ \pi^-$ system.
- ⁸ Seen in the missing mass spectrum.

WEIGHTED AVERAGE
1281.8±0.5 (Error scaled by 1.7)



$f_1(1285)$ WIDTH

Only experiments giving width error less than 20 MeV are kept for averaging.

VALUE (MeV)	EVTS	DOCUMENT ID	TECN	COMMENT
23.0 ± 1.1	OUR AVERAGE	Error includes scale factor of 1.6. See the ideogram below.		
28.2 ± 1.1 ± 5.5	126K	ABLIKIM 23M	BES3	$J/\psi \rightarrow \gamma K_S^0 K_S^0 \pi^0$
18.4 ± 1.4		DICKSON 16	CLAS	$2.55 \gamma p \rightarrow \eta \pi^+ \pi^- p$
18.3 ± 6.3	87	ABLIKIM 15P	BES3	$J/\psi \rightarrow K^+ K^- 3\pi$
22.0 ± 3.1 ± 2.0		1 ABLIKIM 11J	BES3	$J/\psi \rightarrow \omega(\eta \pi^+ \pi^-)$
35 ± 6 ± 4		AUBERT 07AU	BABR	$10.6 e^+ e^- \rightarrow f_1(1285) \pi^+ \pi^- \gamma$
40.0 ± 8.6 ± 9.3	203	BAI 04J	BES2	$J/\psi \rightarrow \gamma \gamma \pi^+ \pi^-$
29 ± 12	237	ABDALLAH 03H	DLPH	$91.2 e^+ e^- \rightarrow K_S^0 K_S^\pm \pi^\mp + X$
45 ± 9 ± 7	20k	ADAMS 01B	B852	$18 \text{ GeV } \pi^- p \rightarrow K^+ K^- \pi^0 n$
55 ± 18	1400	ALDE 97B	GAM4	$100 \pi^- p \rightarrow \eta \pi^0 \pi^0 n$
24 ± 3		BARBERIS 97B	OMEG	$450 pp \rightarrow pp 2(\pi^+ \pi^-)$
20 ± 2		BARBERIS 97C	OMEG	$450 pp \rightarrow pp 2(\pi^+ \pi^-)$
36 ± 5		2 ANTINORI 95	OMEG	$300,450 pp \rightarrow pp 2(\pi^+ \pi^-)$
29.0 ± 4.1		LEE 94	MPS2	$18 \pi^- p \rightarrow K^+ \bar{K}^0 2\pi^- p$
25 ± 4	140	ARMSTRONG 89	OMEG	$300 pp \rightarrow K \bar{K} \pi p p$
22 ± 2	4750	3 BIRMAN 88	MPS	$8 \pi^- p \rightarrow K^+ \bar{K}^0 \pi^- n$
25 ± 4	504	BITYUKOV 88	SPEC	$32.5 \pi^- p \rightarrow K^+ K^- \pi^0 n$
19 ± 5		ANDO 86	SPEC	$8 \pi^- p \rightarrow \eta \pi^+ \pi^- n$
32 ± 8	420	REEVES 86	SPEC	$6.6 p \bar{p} \rightarrow K K \pi X$
22 ± 2		CHUNG 85	SPEC	$8 \pi^- p \rightarrow N K \bar{K} \pi$
32 ± 3	604	ARMSTRONG 84	OMEG	$85 \pi^+ p \rightarrow K \bar{K} \pi p p$
24 ± 3		CHAUVAT 84	SPEC	$31.5 pp \rightarrow K \bar{K} \pi p p$
29 ± 10	103	DIONISI 80	HBC	$4 \pi^- p \rightarrow K \bar{K} \pi n$
28.3 ± 6.7	320	NACASCH 78	HBC	$0.7, 0.76 \bar{p} p \rightarrow K \bar{K} 3\pi$

Meson Particle Listings

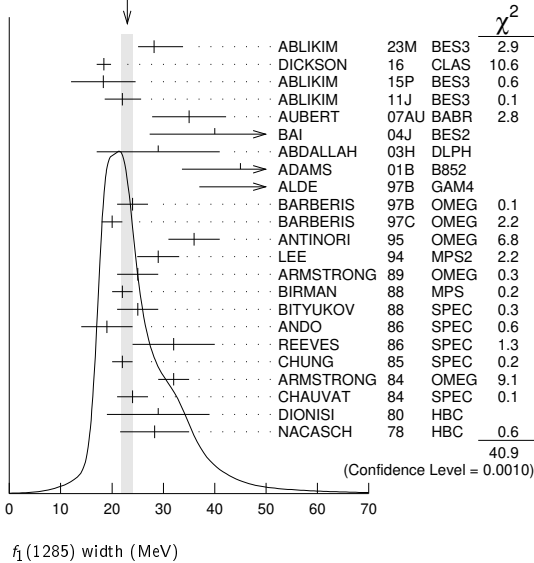
$f_1(1285)$

• • • We do not use the following data for averages, fits, limits, etc. • • •

17.1 ± 3.4	234	ABLIKIM	19BA BES3	$e^+e^- \rightarrow \psi(2S)$
32.4 ± 5.8	4	AAIJ	14Y LHCB	$\bar{B}_{(s)}^0 \rightarrow J/\psi 2(\pi^+\pi^-)$
18.2 ± 1.2	4	SOSA	99 SPEC	$\rho\rho \rightarrow \rho_{slow} (K_S^0 K^+\pi^-)$
19.4 ± 1.5	4	SOSA	99 SPEC	$\rho\rho \rightarrow \rho_{slow} (K_S^0 K^-\pi^+)$
40 ± 5		ABATZIS	94 OMEG	$450 \rho\rho \rightarrow \rho\rho 2(\pi^+\pi^-)$
31 ± 5		ARMSTRONG	89E OMEG	$300 \rho\rho \rightarrow \rho\rho 2(\pi^+\pi^-)$
41 ± 12		ARMSTRONG	89G OMEG	$85 \pi^+\rho \rightarrow 4\pi\pi\rho, \rho\rho \rightarrow 4\pi\rho\rho$
17.9 ± 10.9	60	RATH	89 MPS	$21.4 \pi^-\rho \rightarrow K_S^0 K_S^0 \pi^0 n$
14 $^{+20}_{-14}$ ± 10	16	BECKER	87 MRK3	$e^+e^- \rightarrow \phi K \bar{K} \pi$
26 ± 12		EVANGELIS...	81 OMEG	$12 \pi^-\rho \rightarrow \eta\pi^+\pi^-\pi^-\rho$
25 ± 15	200	GURTU	79 HBC	$4.2 K^-\rho \rightarrow n\eta 2\pi$
~ 10	5	STANTON	79 CNTR	$8.5 \pi^-\rho \rightarrow n 2\gamma 2\pi$
24 ± 18	210	GRASSLER	77 HBC	$16 \pi^+\pi^-\rho$
28 ± 5	150	DEFOIX	72 HBC	$0.7 \bar{p}\rho \rightarrow 7\pi$
46 ± 9	180	DUBOC	72 HBC	$1.2 \bar{p}\rho \rightarrow 2K 4\pi$
37 ± 5	500	THUN	72 MMS	$13.4 \pi^-\rho$
10 ± 10		BOESEBECK	71 HBC	$16.0 \pi\rho \rightarrow p 5\pi$
30 ± 15		CAMPBELL	69 DBC	$2.7 \pi^+ d$
60 ± 15		LORSTAD	69 HBC	$0.7 \bar{p}\rho, 4,5\text{-body}$
35 ± 10		DAHL	67 HBC	$1.6\text{-}4.2 \pi^-\rho$

1 The selected process is $J/\psi \rightarrow \omega a_0(980)\pi$.
 2 Supersedes ABATZIS 94, ARMSTRONG 89E.
 3 From partial wave analysis of $K^+K^0\pi^-$ system.
 4 No systematic error given.
 5 From phase shift analysis of $\eta\pi^+\pi^-$ system.
 6 Resolution is not unfolded.
 7 Seen in the missing mass spectrum.

WEIGHTED AVERAGE
 23.0 ± 1.1 (Error scaled by 1.6)



$f_1(1285)$ DECAY MODES

Mode	Fraction (Γ_i/Γ)	Scale factor/ Confidence level
Γ_1 4π	(32.7 ± 1.8) %	S=1.2
Γ_2 $\pi^0\pi^0\pi^+\pi^-$	(21.8 ± 1.2) %	S=1.2
Γ_3 $2\pi^+2\pi^-$	(10.9 ± 0.6) %	S=1.2
Γ_4 $\rho^0\pi^+\pi^-$	(10.9 ± 0.6) %	S=1.2
Γ_5 $\rho^0\rho^0$	seen	
Γ_6 $4\pi^0$	< 7 × 10 ⁻⁴	CL=90%
Γ_7 $\eta\pi^+\pi^-$	(35 ± 15) %	
Γ_8 $\eta\pi\pi$	(52.2 ± 1.9) %	S=1.2
Γ_9 $a_0(980)\pi$ [ignoring $a_0(980) \rightarrow K\bar{K}$]	(38 ± 4) %	
Γ_{10} $\eta\pi\pi$ [excluding $a_0(980)\pi$]	(14 ± 4) %	
Γ_{11} $K\bar{K}\pi$	(9.0 ± 0.4) %	S=1.1
Γ_{12} $K\bar{K}^*(892)$	not seen	
Γ_{13} $\pi^+\pi^-\pi^0$	(3.0 ± 0.9) × 10 ⁻³	

Γ_{14} $\rho^\pm\pi^\mp$	< 3.1 × 10 ⁻³	CL=95%
Γ_{15} $\gamma\rho^0$	(6.1 ± 1.0) %	S=1.7
Γ_{16} $\phi\gamma$	(7.4 ± 2.6) × 10 ⁻⁴	
Γ_{17} e^+e^-	< 9.4 × 10 ⁻⁹	CL=90%
Γ_{18} $\gamma\gamma^*$		
Γ_{19} $\gamma\gamma$		

CONSTRAINED FIT INFORMATION

An overall fit to 6 branching ratios uses 18 measurements and one constraint to determine 5 parameters. The overall fit has a $\chi^2 = 24.0$ for 14 degrees of freedom.

The following off-diagonal array elements are the correlation coefficients $\langle \delta x_i \delta x_j \rangle / (\delta x_i \delta x_j)$, in percent, from the fit to the branching fractions, $x_i \equiv \Gamma_i/\Gamma_{total}$. The fit constrains the x_i whose labels appear in this array to sum to one.

x_9	-29			
x_{10}	-12	-89		
x_{11}	22	-9	-4	
x_{15}	-24	-8	-3	-27
	x_1	x_9	x_{10}	x_{11}

$f_1(1285)$ $\Gamma(i)/\Gamma(\text{total})$

$\Gamma(\eta\pi\pi) \times \Gamma(\gamma\gamma)/\Gamma_{total}$	$\Gamma_8\Gamma_{19}/\Gamma = (\Gamma_9+\Gamma_{10})\Gamma_{19}/\Gamma$			
VALUE (keV)	CL%	DOCUMENT ID	TECN	COMMENT
<0.62	95	GIDAL	87	MRK2 $e^+e^- \rightarrow e^+e^-\eta\pi^+\pi^-$

$\Gamma(\eta\pi\pi) \times \Gamma(\gamma\gamma^*)/\Gamma_{total}$	$\Gamma_8\Gamma_{18}/\Gamma = (\Gamma_9+\Gamma_{10})\Gamma_{18}/\Gamma$			
VALUE (keV)	EVTs	DOCUMENT ID	TECN	COMMENT
1.4 ± 0.4 OUR AVERAGE				Error includes scale factor of 1.4.
1.18 ± 0.25 ± 0.20	26	1,2 AIHARA	88B	TPC $e^+e^- \rightarrow e^+e^-\eta\pi^+\pi^-$
2.30 ± 0.61 ± 0.42		1,3 GIDAL	87	MRK2 $e^+e^- \rightarrow e^+e^-\eta\pi^+\pi^-$

• • • We do not use the following data for averages, fits, limits, etc. • • •

1.8 ± 0.3 ± 0.3	420	4 ACHARD	02B L3	183-209 $e^+e^- \rightarrow e^+e^-\eta\pi^+\pi^-$
-----------------	-----	----------	--------	---

1 Assuming a ρ -pole form factor.
 2 Published value multiplied by $\eta\pi\pi$ branching ratio 0.49.
 3 Published value divided by 2 and multiplied by the $\eta\pi\pi$ branching ratio 0.49.
 4 Published value multiplied by the $\eta\pi\pi$ branching ratio 0.52.

$f_1(1285)$ BRANCHING RATIOS

$\Gamma(K\bar{K}\pi)/\Gamma(4\pi)$	Γ_{11}/Γ_1		
VALUE	DOCUMENT ID	TECN	COMMENT
0.274 ± 0.017 OUR FIT			Error includes scale factor of 1.4.
0.271 ± 0.016 OUR AVERAGE			Error includes scale factor of 1.2.
0.265 ± 0.014	1	BARBERIS 97C	OMEG 450 $\rho\rho \rightarrow \rho\rho K_S^0 K^\pm\pi^\mp$
0.28 ± 0.05	2	ARMSTRONG 89E	OMEG 300 $\rho\rho \rightarrow \rho\rho f_1(1285)$
0.37 ± 0.03 ± 0.05	3	ARMSTRONG 89G	OMEG 85 $\pi\rho \rightarrow 4\pi X$

1 Using $2(\pi^+\pi^-)$ data from BARBERIS 97B.
 2 Assuming $\rho\pi\pi$ and $a_0(980)\pi$ intermediate states.
 3 4π consistent with being entirely $\rho\pi\pi$.

$\Gamma(\pi^0\pi^0\pi^+\pi^-)/\Gamma_{total}$	$\Gamma_2/\Gamma = \frac{2}{3}\Gamma_1/\Gamma$
VALUE	DOCUMENT ID
0.218 ± 0.012 OUR FIT	
	Error includes scale factor of 1.2.

$\Gamma(2\pi^+2\pi^-)/\Gamma_{total}$	$\Gamma_3/\Gamma = \frac{1}{3}\Gamma_1/\Gamma$
VALUE	DOCUMENT ID
0.109 ± 0.006 OUR FIT	
	Error includes scale factor of 1.2.

$\Gamma(\rho^0\pi^+\pi^-)/\Gamma_{total}$	$\Gamma_4/\Gamma = \frac{1}{3}\Gamma_1/\Gamma$
VALUE	DOCUMENT ID
0.109 ± 0.006 OUR FIT	
	Error includes scale factor of 1.2.

$\Gamma(\rho^0\pi^+\pi^-)/\Gamma(2\pi^+2\pi^-)$	Γ_4/Γ_3		
VALUE	DOCUMENT ID	TECN	COMMENT
1.0 ± 0.4	GRASSLER 77	HBC	16 GeV $\pi^\pm p$

• • • We do not use the following data for averages, fits, limits, etc. • • •

$\Gamma(\rho^0\rho^0)/\Gamma_{total}$	Γ_5/Γ	
VALUE	DOCUMENT ID	COMMENT
seen	BARBERIS 00C	450 $\rho\rho \rightarrow p_f 4\pi p_s$

$\Gamma(4\pi^0)/\Gamma_{total}$	Γ_6/Γ			
VALUE (units 10 ⁻⁴)	CL%	DOCUMENT ID	TECN	COMMENT
<7	90	ALDE 87	GAM4	100 $\pi^-\rho \rightarrow 4\pi^0 n$

$\Gamma(\pi^+\pi^-\pi^0)/\Gamma(\eta\pi^+\pi^-)$		Γ_{13}/Γ_7	
VALUE (%)	EVTS	DOCUMENT ID	TECN COMMENT
0.86±0.16±0.20	2.3k	¹ DOROFEEV 11	VES $\pi^-N \rightarrow \pi^- f_1(1285)N$

¹ Value obtained selecting the region corresponding to $f_0(980)$ in the $\pi^+\pi^-$ mass spectrum.

$\Gamma(\eta\pi\pi)/\Gamma_{total}$		$\Gamma_8/\Gamma = (\Gamma_9+\Gamma_{10})/\Gamma$	
VALUE	DOCUMENT ID	TECN	COMMENT
0.522±0.019 OUR FIT			Error includes scale factor of 1.2.

$\Gamma(4\pi)/\Gamma(\eta\pi\pi)$		$\Gamma_1/\Gamma_8 = \Gamma_1/(\Gamma_9+\Gamma_{10})$	
VALUE	DOCUMENT ID	TECN	COMMENT
0.63±0.06 OUR FIT			Error includes scale factor of 1.2.
0.41±0.14 OUR AVERAGE			
0.37±0.11±0.11	BOLTON 92	MRK3	$J/\psi \rightarrow \gamma f_1(1285)$
0.64±0.40	GURTU 79	HBC	4.2 K^-p
•••			We do not use the following data for averages, fits, limits, etc. •••
0.93±0.30	¹ GRASSLER 77	HBC	16 $\pi^\mp p$

¹ Assuming $\rho\pi\pi$ and $a_0(980)\pi$ intermediate states.

$\Gamma(2\pi^+2\pi^-)/\Gamma(\eta\pi\pi)$		Γ_3/Γ_8	
VALUE	DOCUMENT ID	TECN	COMMENT
0.28±0.02±0.02	¹ LEES 12x	BABR	$\tau^- \rightarrow \pi^- f_1(1285)\nu_\tau$

¹ Assuming $B(f_1(1285) \rightarrow \pi\pi\eta) = 3/2 B(f_1(1285) \rightarrow \pi^+\pi^-\eta)$.

$\Gamma(a_0(980)\pi [\text{ignoring } a_0(980) \rightarrow K\bar{K}])/ \Gamma(\eta\pi\pi)$		$\Gamma_9/\Gamma_8 = \Gamma_9/(\Gamma_9+\Gamma_{10})$	
VALUE	CL%	DOCUMENT ID	TECN COMMENT
0.72±0.08 OUR FIT			
0.72±0.07 OUR AVERAGE			
0.74±0.02±0.09		DICKSON 16	CLAS $\gamma p \rightarrow f_1(1285)p$
0.72±0.15		GURTU 79	HBC 4.2 K^-p
0.6 ^{+0.3} _{-0.2}		CORDEN 78	OMEG 12-15 π^-p

$\Gamma(K\bar{K}\pi)/\Gamma(\eta\pi\pi)$		$\Gamma_{11}/\Gamma_8 = \Gamma_{11}/(\Gamma_9+\Gamma_{10})$	
VALUE	CL%	DOCUMENT ID	TECN COMMENT
0.72±0.08 OUR FIT			
0.72±0.07 OUR AVERAGE			
0.74±0.02±0.09		DICKSON 16	CLAS $\gamma p \rightarrow f_1(1285)p$
0.72±0.15		GURTU 79	HBC 4.2 K^-p
0.6 ^{+0.3} _{-0.2}		CORDEN 78	OMEG 12-15 π^-p
•••			We do not use the following data for averages, fits, limits, etc. •••
>0.69	95	ACHARD 02B	L3 183-209 $e^+e^- \rightarrow e^+e^-\eta\pi^+\pi^-$
0.28±0.07		ALDE 97B	GAM4 100 $\pi^-p \rightarrow \eta\pi^0\pi^0n$
1.0 ±0.3		GRASSLER 77	HBC 16 $\pi^\mp p$

¹ CORDEN 78 assumes low-mass $\eta\pi\pi$ region is dominantly 1^{++} . See BARBERIS 98c and MANAK 00a for discussion.

² $K\bar{K}$ system characterized by the $l = 1$ threshold enhancement. (See under $a_0(980)$).

$\Gamma(K\bar{K}^*(892))/\Gamma_{total}$		Γ_{12}/Γ	
VALUE	DOCUMENT ID	TECN	COMMENT
not seen	NACASCH 78	HBC	0.7, 0.76 $\bar{p}p \rightarrow K\bar{K}^*3\pi$

••• We do not use the following data for averages, fits, limits, etc. •••

¹ ACHARD 07 L3 183-209 $e^+e^- \rightarrow e^+e^-K_S^0K^\pm\pi^\mp$

¹ A clear signal of 19.8 ± 4.4 events observed at high Q^2 .

$\Gamma(\pi^+\pi^-\pi^0)/\Gamma_{total}$		Γ_{13}/Γ	
VALUE (%)	EVTS	DOCUMENT ID	TECN COMMENT
0.30±0.055±0.074	2.3k	¹ DOROFEEV 11	VES $\pi^-N \rightarrow \pi^- f_1(1285)N$

¹ Value obtained selecting the region corresponding to $f_0(980)$ in the $\pi^+\pi^-$ mass spectrum. The systematic error includes the uncertainty on the partial width $f_1 \rightarrow \eta\pi\pi$ obtained from PDG 10 data.

$\Gamma(\pi^\pm\pi^\mp)/\Gamma_{total}$		Γ_{14}/Γ	
VALUE (%)	CL%	DOCUMENT ID	TECN COMMENT
<0.31	95	DOROFEEV 11	VES $\pi^-N \rightarrow \pi^- f_1(1285)N$

$\Gamma(\gamma\rho^0)/\Gamma_{total}$		Γ_{15}/Γ	
VALUE (units 10^{-2})	CL%	DOCUMENT ID	TECN COMMENT
6.1±1.0 OUR FIT			Error includes scale factor of 1.7.

••• We do not use the following data for averages, fits, limits, etc. •••

2.8±0.7±0.6

<5

95

¹ AMELIN 95 VES 37 $\pi^-N \rightarrow \pi^-\pi^+\pi^-\gamma N$

¹ Not an independent measurement.

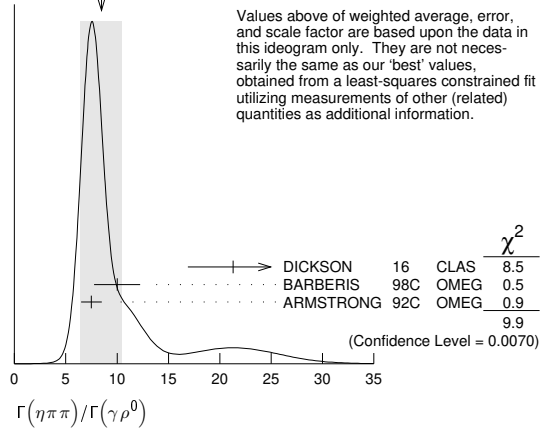
$\Gamma(\gamma\rho^0)/\Gamma(2\pi^+2\pi^-)$		$\Gamma_{15}/\Gamma_3 = \Gamma_{15}/\frac{1}{3}\Gamma_1$	
VALUE	DOCUMENT ID	TECN	COMMENT
0.55±0.10 OUR FIT			Error includes scale factor of 1.5.
0.45±0.18			
	¹ COFFMAN 90	MRK3	$J/\psi \rightarrow \gamma\gamma\pi^+\pi^-$

¹ Using $B(J/\psi \rightarrow \gamma f_1(1285) \rightarrow \gamma\gamma\rho^0) = 0.25 \times 10^{-4}$ and $B(J/\psi \rightarrow \gamma f_1(1285) \rightarrow \gamma 2\pi^+2\pi^-) = 0.55 \times 10^{-4}$ given by MIR 88.

$\Gamma(\eta\pi\pi)/\Gamma(\gamma\rho^0)$		$\Gamma_8/\Gamma_{15} = (\Gamma_9+\Gamma_{10})/\Gamma_{15}$	
VALUE	DOCUMENT ID	TECN	COMMENT
8.6±1.6 OUR FIT			Error includes scale factor of 1.9.
8.5±2.0 OUR AVERAGE			Error includes scale factor of 2.2. See the ideogram below.
21.3±4.4	DICKSON 16	CLAS	$\gamma p \rightarrow f_1(1285)p$
10.0±1.0±2.0	BARBERIS 98c	OMEG	450 $\rho\rho \rightarrow \rho f_1(1285)\rho_S$
7.5±1.0	¹ ARMSTRONG 92c	OMEG	300 $\rho\rho \rightarrow \rho\rho\pi^+\pi^-\gamma, \rho\rho\eta\pi^+\pi^-$

¹ Published value multiplied by 1.5.

WEIGHTED AVERAGE
8.5±2.0 (Error scaled by 2.2)



Values above of weighted average, error, and scale factor are based upon the data in this ideogram only. They are not necessarily the same as our 'best' values, obtained from a least-squares constrained fit utilizing measurements of other (related) quantities as additional information.

$\Gamma(\gamma\rho^0)/\Gamma(K\bar{K}\pi)$		Γ_{15}/Γ_{11}	
VALUE	CL%	DOCUMENT ID	TECN COMMENT
>0.035	90	¹ COFFMAN 90	MRK3 $J/\psi \rightarrow \gamma\gamma\pi^+\pi^-$

••• We do not use the following data for averages, fits, limits, etc. •••

¹ Using $B(J/\psi \rightarrow \gamma f_1(1285) \rightarrow \gamma\gamma\rho^0) = 0.25 \times 10^{-4}$ and $B(J/\psi \rightarrow \gamma f_1(1285) \rightarrow \gamma K\bar{K}\pi) < 0.72 \times 10^{-3}$.

$\Gamma(\phi\gamma)/\Gamma(K\bar{K}\pi)$		Γ_{16}/Γ_{11}		
VALUE (units 10^{-2})	CL%	EVTS	DOCUMENT ID	TECN COMMENT
0.82±0.21±0.20		19	BITYUKOV 88	SPEC 32.5 $\pi^-p \rightarrow K^+K^-\pi^0n$

••• We do not use the following data for averages, fits, limits, etc. •••

<0.50

95

BARBERIS 98c OMEG 450 $\rho\rho \rightarrow \rho f_1(1285)\rho_S$

<0.93

95

A MELIN 95 VES 37 $\pi^-N \rightarrow \pi^-\pi^+\pi^-\gamma N$

$\Gamma(e^+e^-)/\Gamma_{total}$		Γ_{17}/Γ	
VALUE	CL%	DOCUMENT ID	TECN COMMENT
<9.4 × 10⁻⁹	90	¹ ACHASOV 20	SND $e^+e^- \rightarrow \eta\pi^0\pi^0$

¹ ACHASOV 20 reports two candidate events corresponding to a significance of 2.5 σ and the branching fraction of $(5.1^{+3.7}_{-2.7}) \times 10^{-9}$.

$f_1(1285)$ REFERENCES

ABLIKIM 23M	JHEP 2303 121	M. Ablikim et al.	(BESIII Collab.)
ACHASOV 20	PL B800 135074	M.N. Achasov et al.	(SND Collab.)
ABLIKIM 19BA	PR D100 092003	M. Ablikim et al.	(BESIII Collab.)
DICKSON 16	PR C93 065202	R. Dickson et al.	(JLab CLAS Collab.)
ABLIKIM 15P	PR D92 012007	M. Ablikim et al.	(BESIII Collab.)
AAJ 14Y	PRL 112 091802	R. Aaij et al.	(LHCb Collab.)
LEES 12X	PR D86 092010	J.P. Lees et al.	(BABAR Collab.)
ABLIKIM 11J	PRL 107 182001	M. Ablikim et al.	(BESIII Collab.)
DOROFEEV 11	EPJ A47 68	V. Dorofeev et al.	(SERP, MIP) (PDG Collab.)
PDG 10	JP G37 075021	K. Nakamura et al.	(PDG Collab.)
ACHARD 07	JHEP 0703 018	P. Achard et al.	(L3 Collab.)
AUBERT 07AU	PR D76 092005	B. Aubert et al.	(BABAR Collab.)
BAI 04J	PL B594 47	J.Z. Bai et al.	(BES Collab.)
ABDALLAH 03H	PL B569 129	J. Abdallah et al.	(DELPHI Collab.)
ACHARD 02B	PL B526 269	P. Achard et al.	(L3 Collab.)
ACCIARRI 01G	PL B501 1	M. Acciarri et al.	(L3 Collab.)
ADAMS 01B	PL B516 264	G.S. Adams et al.	(BNL E852 Collab.)
BARBERIS 00C	PL B471 440	D. Barberis et al.	(WA 102 Collab.)
MANAK 00A	PR D62 012003	J.J. Manak et al.	(BNL E852 Collab.)
SOSA 99	PRL 83 913	M. Sosa et al.	(BESIII Collab.)
BARBERIS 98B	PL B440 225	D. Barberis et al.	(WA 102 Collab.)
ALDE 97B	PAN 60 366	D. Alde et al.	(GAMS Collab.)
	Translated from YAF 60 458.		
BARBERIS 97C	PL B413 217	D. Barberis et al.	(WA 102 Collab.)
BARBERIS 97C	PL B413 225	D. Barberis et al.	(WA 102 Collab.)
AMELIN 95	ZPHY C66 71	D.V. Amelin et al.	(VES Collab.)
ANTINORI 95	PL B353 589	F. Antinori et al.	(ATHU, BARI, BIRM+)
ABATZIS 94	PL B324 509	S. Abatzis et al.	(ATHU, BARI, BIRM+)
LEE 94	PL B323 227	J.H. Lee et al.	(BNL, IND, KYUN, MASD+)
ARMSTRONG 93C	PL B307 394	T.A. Armstrong et al.	(FNAL, FERR, GENO+)
ARMSTRONG 92C	ZPHY C54 371	T.A. Armstrong et al.	(ATHU, BARI, BIRM+)
BOLTON 92	PL B278 495	T. Bolton et al.	(ATHU, BARI, BIRM+)
BITYUKOV 91B	SJNP 54 318	S.I. Bityukov et al.	(Mark III Collab.)
	Translated from YAF 54 529.		(SERP)

Meson Particle Listings

$f_1(1285), \eta(1295), \pi(1300)$

FUKUI	91C	PL B267 293	S. Fukui et al.	(SUGI, NAGO, KEK, KYOT+)
COFFMAN	90	PR D41 1410	D.M. Coffman et al.	(Mark III Collab.)
ARMSTRONG	89	PL B221 216	T.A. Armstrong et al.	(CERN, CDEF, BIRM+)
ARMSTRONG	89E	PL B228 536	T.A. Armstrong, M. Benayoun	(ATHU, BARI, BIRM+)
ARMSTRONG	89G	ZPHY C43 55	T.A. Armstrong et al.	(CERN, BIRM, BARI+)
RATH	89	PR D40 693	M.G. Rath et al.	(NDAM, BRAN, BNL, CUNY+)
AIHARA	88B	PL B209 107	H. Aihara et al.	(TPC-2 γ Collab.)
BIRMAN	88	PRL 61 1557	A. Birman et al.	(BNL, FSU, IND, MASD) JP
BITYUKOV	88	PL B203 327	S.I. Bityukov et al.	(SERP)
MIR	88	Photon-Photon 88, 126	R. Mir	(Mark III Collab.)
Conference				
ALDE	87	PL B198 286	D.M. Alde et al.	(LANL, BRUX, SERP, LAPP)
BECKER	87	PRL 59 186	J.J. Becker et al.	(Mark III Collab.)
GIDAL	87	PRL 59 2012	G. Gidal et al.	(LBL, SLAC, HARV)
ANDO	86	PRL 57 1296	A. Ando et al.	(KEK, KYOT, NIRS, SAGA+) IJP
REEVES	86	PR D34 1960	D.F. Reeves et al.	(FLOR, BNL, IND+) JP
CHUNG	85	PRL 55 779	S.U. Chung et al.	(BNL, FLOR, IND+) JP
ARMSTRONG	84	PL 146B 273	T.A. Armstrong et al.	(ATHU, BARI, BIRM+) JP
BITYUKOV	84B	PL 144B 133	S.I. Bityukov et al.	(SERP)
CHAUVAT	84	PL 143B 382	P. Chauvat et al.	(CERN, CLER, UCL+)
TORNQVIST	82B	NP B303 268	N.A. Tornqvist	(HELS)
EVANGELIS...	81	NP B178 197	C. Evangelista et al.	(BARI, BONN, CERN+)
BROMBERG	80	PR D22 1513	C.M. Bromberg et al.	(CIT, FNAL, ILLC+)
DIONISI	80	NP B169 1	C. Dionisi et al.	(CERN, MADR, CDEF+)
GURTU	79	NP B151 181	A. Gurtu et al.	(CERN, ZEEM, NIJM, OXF)
STANTON	79	PRL 42 346	N.R. Stanton et al.	(OSU, CARL, MCGI+) JP
CORDEN	78	NP B144 253	M.J. Corden et al.	(BIRM, RHEL, TEL+)
NACASCH	78	NP B135 203	R. Nacasch et al.	(PARIS, MADR, CERN)
GRASSLER	77	NP B121 189	H. Grassler et al.	(AACH3, BERL, BONN+)
DEFOIX	72	NP B44 125	C. Defoix et al.	(CDEF, CERN)
DUBOC	72	NP B46 429	J. Duboc et al.	(PARIS, LIVP)
THUN	72	PRL 28 1733	R. Thun et al.	(STON, NEAS)
BARDADIN...	71	PR D4 2711	M. Bardadin-Otinowska et al.	(WARSA)
BOESEBECK	71	PL 34B 659	K. Boesebeck (AACH, BERL, BONN, CERN, CRAC+)	(PURD)
CAMPBELL	69	PRL 22 1204	J.H. Campbell et al.	(CDEF, CERN) JP
LORSTAD	69	NP B14 63	B. Lorstad et al.	(CDEF, CERN) IJP
D'ANDLAU	68	NP B5 693	C. d'Andlau et al.	(CDEF, CERN, IRAD+) IJP
DAHL	67	PR 163 1377	O.I. Dahl et al.	(LRL) IJP

$\eta(1295)$

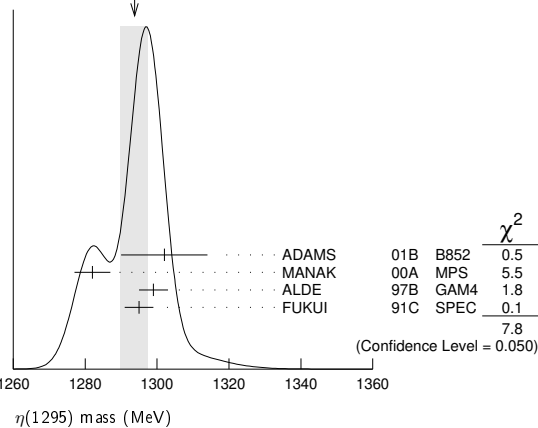
$$I^G(J^{PC}) = 0^+(0^{-+})$$

See the review on "Spectroscopy of Light Meson Resonances."

$\eta(1295)$ MASS

VALUE (MeV)	EVTS	DOCUMENT ID	TECN	COMMENT
1294 ± 4 OUR AVERAGE		Error includes scale factor of 1.6. See the ideogram below.		
1302 ± 9 ± 8	20k	ADAMS	01B B852	18 GeV $\pi^- p \rightarrow K^+ K^- \pi^0 n$
1282 ± 5	9082	MANAK	00A MPS	18 $\pi^- p \rightarrow \eta \pi^+ \pi^- n$
1299 ± 4	2100	ALDE	97B GAM4	100 $\pi^- p \rightarrow \eta \pi^0 \pi^0 n$
1295 ± 4		FUKUI	91C SPEC	8.95 $\pi^- p \rightarrow \eta \pi^+ \pi^- n$
• • • We do not use the following data for averages, fits, limits, etc. • • •				
1264 ± 8		¹ AUGUSTIN	90 DM2	$J/\psi \rightarrow \gamma \eta \pi^+ \pi^-$
~ 1275		STANTON	79 CNTR	8.4 $\pi^- p \rightarrow n \eta 2\pi$

WEIGHTED AVERAGE
1294 ± 4 (Error scaled by 1.6)



¹ PWA analysis of AUGUSTIN 92 assigns 0^{-+} quantum numbers to this state rather than 1^{++} as before.

$\eta(1295)$ WIDTH

VALUE (MeV)	EVTS	DOCUMENT ID	TECN	COMMENT
55 ± 5 OUR AVERAGE				
57 ± 23 ± 21	20k	ADAMS	01B B852	18 GeV $\pi^- p \rightarrow K^+ K^- \pi^0 n$
66 ± 13	9082	MANAK	00A MPS	18 $\pi^- p \rightarrow \eta \pi^+ \pi^- n$
53 ± 6		FUKUI	91C SPEC	8.95 $\pi^- p \rightarrow \eta \pi^+ \pi^- n$
• • • We do not use the following data for averages, fits, limits, etc. • • •				
< 40	2100	ALDE	97B GAM4	100 $\pi^- p \rightarrow \eta \pi^0 \pi^0 n$
44 ± 20		¹ AUGUSTIN	90 DM2	$J/\psi \rightarrow \gamma \eta \pi^+ \pi^-$
~ 70		STANTON	79 CNTR	8.4 $\pi^- p \rightarrow n \eta 2\pi$

¹ PWA analysis of AUGUSTIN 92 assigns 0^{-+} quantum numbers to this state rather than 1^{++} as before.

$\eta(1295)$ DECAY MODES

Mode	Fraction (Γ_i/Γ)
Γ_1 $\eta \pi^+ \pi^-$	seen
Γ_2 $a_0(980) \pi$	seen
Γ_3 $\gamma \gamma$	
Γ_4 $\eta \pi^0 \pi^0$	seen
Γ_5 $\eta(\pi\pi) S$ -wave	seen
Γ_6 $\sigma \eta$	seen
Γ_7 $K \bar{K} \pi$	seen

$\eta(1295) \Gamma(i)/\Gamma(\text{total})$

$\Gamma(\eta \pi^+ \pi^-) \times \Gamma(\gamma \gamma)/\Gamma_{\text{total}}$	$\Gamma_1 \Gamma_3/\Gamma$			
VALUE (keV)	CL%	DOCUMENT ID	TECN	COMMENT
< 0.066	95	ACCIARRI	01G L3	183-202 $e^+ e^- \rightarrow e^+ e^- \eta \pi^+ \pi^-$

• • • We do not use the following data for averages, fits, limits, etc. • • •

< 0.6	90	AIHARA	88C TPC	$e^+ e^- \rightarrow e^+ e^- \eta \pi^+ \pi^-$
< 0.3		ANTREASNYAN	87 CBAL	$e^+ e^- \rightarrow e^+ e^- \eta \pi \pi$

$\Gamma(K \bar{K} \pi) \times \Gamma(\gamma \gamma)/\Gamma_{\text{total}}$

VALUE (keV)	CL%	DOCUMENT ID	TECN	COMMENT
< 0.014	90	^{1,2} AHOHE	05 CLE2	10.6 $e^+ e^- \rightarrow e^+ e^- K_S^0 K^\pm \pi^\mp$

¹ Using $\eta(1295)$ mass and width 1294 MeV and 55 MeV, respectively.

² Assuming three-body phase-space decay to $K_S^0 K^\pm \pi^\mp$.

$\eta(1295)$ BRANCHING RATIOS

$\Gamma(a_0(980) \pi)/\Gamma_{\text{total}}$	Γ_2/Γ		
VALUE	DOCUMENT ID	TECN	COMMENT
• • • We do not use the following data for averages, fits, limits, etc. • • •			
not seen	BERTIN	97 OBLX	0.0 $\bar{p} p \rightarrow K^\pm (K^0) \pi^\mp \pi^+ \pi^-$
seen	BIRMAN	88 MPS	8 $\pi^- p \rightarrow K^+ \bar{K}^0 \pi^- n$
large	ANDO	86 SPEC	8 $\pi^- p \rightarrow \eta \pi^+ \pi^- n$
large	STANTON	79 CNTR	8.4 $\pi^- p \rightarrow n \eta 2\pi$

$\Gamma(a_0(980) \pi)/\Gamma(\eta \pi^0 \pi^0)$	Γ_2/Γ_4		
VALUE	DOCUMENT ID	TECN	COMMENT
0.65 ± 0.10		¹ ALDE	97B GAM4 100 $\pi^- p \rightarrow \eta \pi^0 \pi^0 n$

¹ Assuming that $a_0(980)$ decays only to $\eta \pi$.

$\Gamma(\eta(\pi\pi) S\text{-wave})/\Gamma(\eta \pi^0 \pi^0)$	Γ_5/Γ_4		
VALUE	DOCUMENT ID	TECN	COMMENT
0.35 ± 0.10		ALDE	97B GAM4 100 $\pi^- p \rightarrow \eta \pi^0 \pi^0 n$

$\Gamma(a_0(980) \pi)/\Gamma(\sigma \eta)$	Γ_2/Γ_6			
VALUE	EVTS	DOCUMENT ID	TECN	COMMENT
0.48 ± 0.22	9082	MANAK	00A MPS	18 $\pi^- p \rightarrow \eta \pi^+ \pi^- n$

$\eta(1295)$ REFERENCES

AHOHE	05	PR D71 072001	R. Ahohe et al.	(CLEO Collab.)
ACCIARRI	01G	PL B501 1	M. Acciarri et al.	(L3 Collab.)
ADAMS	01B	PL B516 264	G.S. Adams et al.	(BNL E852 Collab.)
MANAK	00A	PR D62 012003	J.J. Manak et al.	(BNL E852 Collab.)
ALDE	97B	PAN 60 386	D. Alde et al.	(GAMS Collab.)
Translated from YAF 60 458.				
BERTIN	97	PL B400 226	A. Bertin et al.	(OBELIX Collab.)
AUGUSTIN	92	PR D46 1951	J.E. Augustin, G. Cosme	(DM2 Collab.)
FUKUI	91C	PL B267 293	S. Fukui et al.	(SUGI, NAGO, KEK, KYOT+)
AUGUSTIN	90	PR D42 10	J.E. Augustin et al.	(DM2 Collab.)
AIHARA	88C	PR D38 1	H. Aihara et al.	(TPC-2 γ Collab.)
BIRMAN	88	PRL 61 1557	A. Birman et al.	(BNL, FSU, IND, MASD) JP
ANTREASNYAN	87	PR D36 2633	D. Antreasnyan et al.	(Crystal Ball Collab.)
ANDO	86	PRL 57 1296	A. Ando et al.	(KEK, KYOT, NIRS, SAGA+) IJP
STANTON	79	PRL 42 346	N.R. Stanton et al.	(OSU, CARL, MCGI+) JP

$\pi(1300)$

$$I^G(J^{PC}) = 1^-(0^{-+})$$

$\pi(1300)$ MASS

VALUE (MeV)	EVTS	DOCUMENT ID	TECN	COMMENT
1300 ± 10 OUR ESTIMATE				
1128 ± 26 ± 70		DARGENT	17 RVUE	$D^0 \rightarrow \pi^- \pi^+ \pi^- \pi^+$
1345 ± 8 ± 10	18k	¹ SCHEGELSKY	06 RVUE	$\gamma \gamma \rightarrow \pi^+ \pi^- \pi^0$

• • • We do not use the following data for averages, fits, limits, etc. • • •

See key on page 1171

Meson Particle Listings

$\pi(1300)$, $a_2(1320)$

1200 ± 40	90k	SALVINI	04	OBLX	$\bar{p}p \rightarrow 2\pi^+ 2\pi^-$
1343 ± 15 ± 24		CHUNG	02	B852	$18.3 \pi^- p \rightarrow \pi^+ \pi^- \pi^- p$
1375 ± 40		ABELE	01	CBAR	$0.0 \bar{p}d \rightarrow \pi^- 4\pi^0 p$
1275 ± 15		BERTIN	97D	OBLX	$0.05 \bar{p}p \rightarrow 2\pi^+ 2\pi^-$
~ 1114		ABELE	96	CBAR	$0.0 \bar{p}p \rightarrow 5\pi^0$
1190 ± 30		ZIELINSKI	84	SPEC	$200 \pi^+ Z \rightarrow Z 3\pi$
1240 ± 30		BELLINI	82	SPEC	$40 \pi^- A \rightarrow A 3\pi$
1273 ± 50		² AARON	81	RVUE	
1342 ± 20		BONESINI	81	OMEG	$12 \pi^- p \rightarrow p 3\pi$
~ 1400		DAUM	81B	SPEC	$63,94 \pi^- p$

¹ From analysis of L3 data at 183–209 GeV.
² Uses multichannel Aitchison-Bowler model (BOWLER 75). Uses data from DAUM 80 and DANKOWYCH 81.

$\pi(1300)$ WIDTH

VALUE (MeV)	EVTS	DOCUMENT ID	TECN	COMMENT
200 to 600 OUR ESTIMATE				
• • • We do not use the following data for averages, fits, limits, etc. • • •				
314 ± 39 ± 66		DARGENT	17	RVUE $D^0 \rightarrow \pi^- \pi^+ \pi^- \pi^+$
260 ± 20 ± 30	18k	³ SCHEGELSKY	06	RVUE $\gamma\gamma \rightarrow \pi^+ \pi^- \pi^0$
470 ± 120	90k	SALVINI	04	OBLX $\bar{p}p \rightarrow 2\pi^+ 2\pi^-$
449 ± 39 ± 47		CHUNG	02	B852 $18.3 \pi^- p \rightarrow \pi^+ \pi^- \pi^- p$
268 ± 50		ABELE	01	CBAR $0.0 \bar{p}d \rightarrow \pi^- 4\pi^0 p$
218 ± 100		BERTIN	97D	OBLX $0.05 \bar{p}p \rightarrow 2\pi^+ 2\pi^-$
~ 340		ABELE	96	CBAR $0.0 \bar{p}p \rightarrow 5\pi^0$
440 ± 80		ZIELINSKI	84	SPEC $200 \pi^+ Z \rightarrow Z 3\pi$
360 ± 120		BELLINI	82	SPEC $40 \pi^- A \rightarrow A 3\pi$
580 ± 100		⁴ AARON	81	RVUE
220 ± 70		BONESINI	81	OMEG $12 \pi^- p \rightarrow p 3\pi$
~ 600		DAUM	81B	SPEC $63,94 \pi^- p$

³ From analysis of L3 data at 183–209 GeV.
⁴ Uses multichannel Aitchison-Bowler model (BOWLER 75). Uses data from DAUM 80 and DANKOWYCH 81.

$\pi(1300)$ DECAY MODES

Mode	Fraction (Γ_i/Γ)
Γ_1 $\rho\pi$	seen
Γ_2 $\pi(\pi\pi)S$ -wave	seen
Γ_3 $\gamma\gamma$	

$\pi(1300)$ $\Gamma(i)\Gamma(\gamma\gamma)/\Gamma(\text{total})$

$\Gamma(\rho\pi) \times \Gamma(\gamma\gamma)/\Gamma_{\text{total}}$	$\Gamma_1\Gamma_3/\Gamma$			
VALUE (keV)	CL%	DOCUMENT ID	TECN	COMMENT
<0.085	90	ACCIARRI	97T	L3 $e^+e^- \rightarrow e^+e^-\pi^+\pi^-\pi^0$
• • • We do not use the following data for averages, fits, limits, etc. • • •				
<0.8	95	⁵ SCHEGELSKY	06	RVUE $\gamma\gamma \rightarrow \pi^+\pi^-\pi^0$
<0.54	90	ALBRECHT	97B	ARG $e^+e^- \rightarrow e^+e^-\pi^+\pi^-\pi^0$

⁵ From analysis of L3 data at 183–209 GeV.

$\pi(1300)$ BRANCHING RATIOS

$\Gamma(\pi(\pi\pi)S\text{-wave})/\Gamma(\rho\pi)$	Γ_2/Γ_1				
VALUE	CL%	EVTS	DOCUMENT ID	TECN	COMMENT
• • • We do not use the following data for averages, fits, limits, etc. • • •					
2.2 ± 0.4	90k	SALVINI	04	OBLX	$\bar{p}p \rightarrow 2\pi^+ 2\pi^-$
seen		CHUNG	02	B852	$18.3 \pi^- p \rightarrow \pi^+ 2\pi^- p$
<0.15	90	ABELE	01	CBAR	$0.0 \bar{p}d \rightarrow \pi^- 4\pi^0 p$
2.12		⁶ AARON	81	RVUE	

⁶ Uses multichannel Aitchison-Bowler model (BOWLER 75). Uses data from DAUM 80 and DANKOWYCH 81.

$\pi(1300)$ REFERENCES

DARGENT	17	JHEP 1705 143	P. d'Argent et al.	(HEID, BRIS)
SCHEGELSKY	06	EPJ A27 199	V.A. Schegelsky et al.	
SALVINI	04	EPJ C35 21	P. Salvini et al.	(OBELIX Collab.)
CHUNG	02	PR D65 072001	S.U. Chung et al.	(BNL E852 Collab.)
ABELE	01	EPJ C19 667	A. Abele et al.	(Crystal Barrel Collab.)
ACCIARRI	97T	PL B413 147	M. Acciari et al.	(L3 Collab.)
ALBRECHT	97B	ZPHY C74 469	H. Albrecht et al.	(ARGUS Collab.)
BERTIN	97D	PL B414 220	A. Bertin et al.	(OBELIX Collab.)
ABELE	96	PL B380 453	A. Abele et al.	(Crystal Barrel Collab.)
ZIELINSKI	84	PR D30 1855	M. Zielinski et al.	(ROCH, MINN, FNAL)
BELLINI	82	PRL 48 1697	G. Bellini et al.	(MILA, BGNM, JINR)
AARON	81	PR D24 1207	R.A. Aaron, R.S. Longacre	(NEAS, BNL)
BONESINI	81	PL 103B 75	M. Bonesini et al.	(MILA, LIPV, DARE+)
DANKOWYCH...	81	PRL 46 580	J.A. Dankowycz et al.	(TNTO, BNL, CARL+)
DAUM	81B	NP B182 269	C. Daum et al.	(AMST, CERN, CRAC, MPIM+)
DAUM	80	PL 89B 281	C. Daum et al.	(AMST, CERN, CRAC, MPIM+)
BOWLER	75	NP B97 227	M.G. Bowler et al.	(OXFT, DARE)

$a_2(1320)$

$$I^G(J^{PC}) = 1^-(2^{++})$$

$a_2(1320)$ T-MATRIX POLE \sqrt{s}

Note that $\Gamma = -2 \text{Im}(\sqrt{s})$.

VALUE (MeV)	DOCUMENT ID	TECN	COMMENT
(1305–1321)–i(52–58) OUR ESTIMATE			
$(1318.7 \pm 1.9 \pm 1.3) - i(53.8 \pm 2.3 + 1.7 - 0.9)$	¹ KOPF	21	RVUE $0.9 \rho\bar{p} \rightarrow \pi^0 \pi^0 \eta$, $\pi^0 \eta \eta$, $\pi^0 K^+ K^-$ and 191 $\pi^- p \rightarrow \pi^- \pi^- \pi^+ p$
$(1312.5 \pm 0.7 \pm 2.6) - i(53.5 \pm 0.6 \pm 1.9)$	² ALBRECHT	20	RVUE $0.9 \bar{p}p \rightarrow \pi^0 \pi^0 \eta$, $\pi^0 \eta \eta$, $\pi^0 K^+ K^-$
$(1306.0 \pm 0.8 \pm 1.3) - i(57.2 \pm 0.8 \pm 0.0)$	³ RODAS	19	RVUE $91 \pi^- p \rightarrow \eta^{(\prime)} \pi^- p$
$(1309 \pm 4) - i(55 \pm 2)$	⁴ ANISOVICH	09	RVUE $\bar{p}p$, πN

¹ Extraction based on a combined fit of Crystal Barrel and $\pi\pi$ scattering data (ALBRECHT 20), and COMPASS data (ADOLPH 15), using a coupled-channel model of $\eta\pi$, $\eta'\pi$ and $K\bar{K}$ systems.

² T-matrix pole with 2 poles, 2 channels ($\pi^0\eta$ and $K\bar{K}$).

³ Coupled-channel analysis of both the $\eta\pi$ and $\eta'\pi$ systems using ADOLPH 15 data. Superseded JACKURA 18. Performed by JPAC.

⁴ Amplitude did not include dispersive corrections. From analysis of $\eta\pi$ mode.

$a_2(1320)$ MASS

VALUE (MeV)	DOCUMENT ID
1318.2 ± 0.6 OUR AVERAGE	Includes data from the 4 datablocks that follow this one. Error includes scale factor of 1.2.

3 π MODE

VALUE (MeV)	EVTS	DOCUMENT ID	TECN	CHG	COMMENT
The data in this block is included in the average printed for a previous datablock.					

1318.6 ± 1.3 OUR AVERAGE Error includes scale factor of 1.4. See the ideogram below.

1314.5 ± 4.0 / 3.3	46M	¹ AGHASYAN	18B	COMP	190 $\pi^- p \rightarrow \pi^- \pi^+ \pi^- p$
1326 ± 2 ± 2		CHUNG	02	B852	18.3 $\pi^- p \rightarrow \pi^+ \pi^- \pi^- p$
1317 ± 3		BARBERIS	98B		450 $\rho\rho \rightarrow p_f \pi^+ \pi^- \pi^0 p_s$
1323 ± 4 ± 3		ACCIARRI	97T	L3	$e^+e^- \rightarrow e^+e^-\pi^+\pi^-\pi^0$
1320 ± 7		ALBRECHT	97B	ARG	$e^+e^- \rightarrow e^+e^-\pi^+\pi^-\pi^0$
1311.3 ± 1.6 ± 3.0	72.4k	AMELIN	96	VES	36 $\pi^- p \rightarrow \pi^+ \pi^0 \pi^0 n$
1310 ± 5		ARMSTRONG	90	OMEG 0	300.0 $\rho\rho \rightarrow p\rho\pi^+\pi^-\pi^0$
1323.8 ± 2.3	4022	AUGUSTIN	89	DM2 ±	$J/\psi \rightarrow \rho^\pm a_2^\mp$
1320.6 ± 3.1	3562	AUGUSTIN	89	DM2 0	$J/\psi \rightarrow \rho^0 a_2^0$
1317 ± 2	25k	² DAUM	80c	SPEC	63,94 $\pi^- p \rightarrow 3\pi\rho$
1320 ± 10	1097	² BALTAY	78B	HBC +0	15 $\pi^+ p \rightarrow p 4\pi$
1306 ± 8		FERRERSORIA	78	OMEG	9 $\pi^- p \rightarrow p 3\pi$
1318 ± 7	1.6k	² EMMS	75	DBC 0	4 $\pi^+ n \rightarrow p(3\pi)^0$
1315 ± 5		² ANTIPOV	73c	CNTR	25,40 $\pi^- p \rightarrow p\eta\pi^-$
1306 ± 9	1580	CHALOUKKA	73	HBC	3.9 $\pi^- p$

• • • We do not use the following data for averages, fits, limits, etc. • • •

1321 ± 1 + 0 / -7	420k	³ ALEKSEEV	10	COMP	190 $\pi^- Pb \rightarrow \pi^- \pi^+ \pi^+ p b'$
1300 ± 2 ± 4	18k	⁴ SCHEGELSKY	06	RVUE 0	$\gamma\gamma \rightarrow \pi^+ \pi^+ \pi^- \pi^0$
1305 ± 14		CONDO	93	SHF	$\gamma p \rightarrow n\pi^+ \pi^+ \pi^-$
1310 ± 2		² EVANGELIS...	81	OMEG	12 $\pi^- p \rightarrow 3\pi\rho$
1343 ± 11	490	BALTAY	78B	HBC 0	15 $\pi^+ p \rightarrow \Delta 3\pi$
1309 ± 5	5k	BINNIE	71	MMS	$\pi^- p$ near a_2 thresh-old
1299 ± 6	28k	BOWEN	71	MMS	5 $\pi^- p$
1300 ± 6	24k	BOWEN	71	MMS	5 $\pi^+ p$
1309 ± 4	17k	BOWEN	71	MMS	7 $\pi^- p$
1306 ± 4	941	ALSTON...	70	HBC	7.0 $\pi^+ p \rightarrow 3\pi\rho$

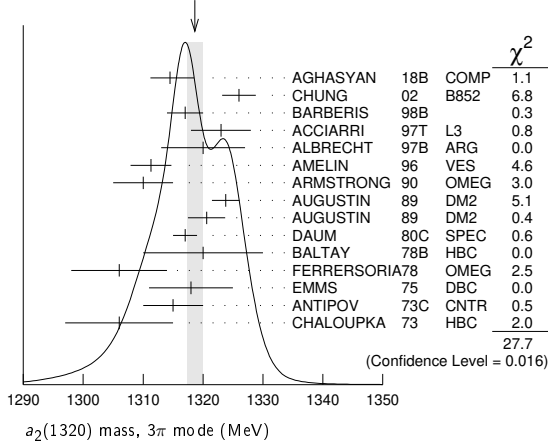
¹ Statistical error negligible.

² From a fit to $J^P = 2^+ \rho\pi$ partial wave.

³ Superseded by AGHASYAN 2018B.

⁴ From analysis of L3 data at 183–209 GeV.

Meson Particle Listings

 $a_2(1320)$ WEIGHTED AVERAGE
1318.6±1.3 (Error scaled by 1.4) $K\bar{K}$ MODE

VALUE (MeV)	EVTs	DOCUMENT ID	TECN	CHG	COMMENT
1318.1± 0.7 OUR AVERAGE					
1319 ± 5	4700	^{1,2} CLELAND	82B	SPEC +	50 $\pi^+ p \rightarrow K_S^0 K^+ p$
1324 ± 6	5200	^{1,2} CLELAND	82B	SPEC -	50 $\pi^- p \rightarrow K_S^0 K^- p$
1320 ± 2	4000	CHABAUD	80	SPEC -	17 $\pi^- A \rightarrow K_S^0 K^- A$
1312 ± 4	11000	CHABAUD	78	SPEC -	9.8 $\pi^- p \rightarrow K^- K_S^0 p$
1316 ± 2	4730	CHABAUD	78	SPEC -	18.8 $\pi^- p \rightarrow K^- K_S^0 p$
1318 ± 1		^{1,3} MARTIN	78D	SPEC -	10 $\pi^- p \rightarrow K_S^0 K^- p$
1320 ± 2	2724	MARGULIE	76	SPEC -	23 $\pi^- p \rightarrow K^- K_S^0 p$
1313 ± 4	730	FOLEY	72	CNTR -	20.3 $\pi^- p \rightarrow K^- K_S^0 p$
1319 ± 3	1500	³ GRAYR	71	ASPK -	17.2 $\pi^- p \rightarrow K^- K_S^0 p$
••• We do not use the following data for averages, fits, limits, etc. •••					
1304 ± 10	870	⁴ SCHEGELSKY	06A	RVUE 0	$\gamma\gamma \rightarrow K_S^0 K_S^0$
1330 ± 11	1000	^{1,2} CLELAND	82B	SPEC +	30 $\pi^+ p \rightarrow K_S^0 K^+ p$
1324 ± 5	350	HYAMS	78	ASPK +	12.7 $\pi^+ p \rightarrow K^+ K_S^0 p$

The data in this block is included in the average printed for a previous datablock.

 $K\bar{K}$ MODE

1 From a fit to $J^P = 2^+$ partial wave.
 2 Number of events evaluated by us.
 3 Systematic error in mass scale subtracted.
 4 From analysis of L3 data at 91 and 183–209 GeV.

1 From a fit to $J^P = 2^+$ partial wave.
 2 From a fit to $J^P = 2^+ \rho\pi$ partial wave.
 3 Width errors enlarged by us to $4\Gamma/\sqrt{N}$; see the note with the $K^*(892)$ mass.
 4 Superseded by AGHASYAN 2018B.
 5 From analysis of L3 data at 183–209 GeV.

 $\eta\pi$ MODE

VALUE (MeV)	EVTs	DOCUMENT ID	TECN	CHG	COMMENT
1317.7± 1.4 OUR AVERAGE					
1308 ± 9		BARBERIS	00H		450 $pp \rightarrow p_f \eta \pi^0 p_S$
1316 ± 9		BARBERIS	00H		450 $pp \rightarrow \Delta_f^{++} \eta \pi^- p_S$
1317 ± 1 ± 2		THOMPSON	97	MPS	18 $\pi^- p \rightarrow \eta \pi^- p$
1315 ± 5 ± 2		¹ AMSLER	94D	CBAR	0.0 $\bar{p}p \rightarrow \pi^0 \pi^0 \eta$
1325.1 ± 5.1		AOYAGI	93	BKEI	$\pi^- p \rightarrow \eta \pi^- p$
1317.7 ± 1.4 ± 2.0		BELADIDZE	93	VES	37 $\pi^- N \rightarrow \eta \pi^- N$
1323 ± 8	1000	² KEY	73	OSPK -	6 $\pi^- p \rightarrow p \pi^- \eta$
••• We do not use the following data for averages, fits, limits, etc. •••					
1307 ± 1 ± 6		³ JACKURA	18	RVUE	$\pi^- p \rightarrow \eta \pi^- p$
1315 ± 12		⁴ ADOLPH	15	COMP	191 $\pi^- p \rightarrow \eta^{(f)} \pi^- p$
1324 ± 5		ARMSTRONG	93C	E760 0	$\bar{p}p \rightarrow \pi^0 \eta \rightarrow 6\gamma$
1336.2 ± 1.7	2561	DELFOSSSE	81	SPEC +	$\pi^\pm p \rightarrow p \pi^\pm \eta$
1330.7 ± 2.4	1653	DELFOSSSE	81	SPEC -	$\pi^\pm p \rightarrow p \pi^\pm \eta$
1324 ± 8	6200	^{2,5} CONFORTO	73	OSPK -	6 $\pi^- p \rightarrow p \pi^- \eta$

The data in this block is included in the average printed for a previous datablock.

 $\eta\pi$ MODE

1 The systematic error of 2 MeV corresponds to the spread of solutions.
 2 Error includes 5 MeV systematic mass-scale error.
 3 Superseded by RODAS 19.
 4 ADOLPH 15 value is derived from a Breit-Wigner fit with mass-dependent width taking the $\eta\pi$ and $\rho\pi$ channels into account.
 5 Missing mass with enriched MMS = $\eta\pi^-$, $\eta = 2\gamma$.

1 From a fit to $J^P = 2^+$ partial wave.
 2 Number of events evaluated by us.
 3 Width errors enlarged by us to $4\Gamma/\sqrt{N}$; see the note with the $K^*(892)$ mass.
 4 From analysis of L3 data at 91 and 183–209 GeV.

 $\eta'\pi$ MODE

VALUE (MeV)	DOCUMENT ID	TECN	COMMENT
1322 ± 7 OUR AVERAGE			
1318 ± 8 $^{+3}_{-5}$	IVANOV	01	B852 18 $\pi^- p \rightarrow \eta' \pi^- p$
1327.0 ± 10.7	BELADIDZE	93	VES 37 $\pi^- N \rightarrow \eta' \pi^- N$

The data in this block is included in the average printed for a previous datablock.

 $\eta'\pi$ MODE

1 The systematic error of 2 MeV corresponds to the spread of solutions.
 2 Error includes 5 MeV systematic mass-scale error.
 3 Superseded by RODAS 19.
 4 ADOLPH 15 value is derived from a Breit-Wigner fit with mass-dependent width taking the $\eta\pi$ and $\rho\pi$ channels into account.
 5 Missing mass with enriched MMS = $\eta\pi^-$, $\eta = 2\gamma$.

1 From a fit to $J^P = 2^+$ partial wave.
 2 Number of events evaluated by us.
 3 Width errors enlarged by us to $4\Gamma/\sqrt{N}$; see the note with the $K^*(892)$ mass.
 4 From analysis of L3 data at 91 and 183–209 GeV.

1 From a fit to $J^P = 2^+$ partial wave.
 2 Number of events evaluated by us.
 3 Width errors enlarged by us to $4\Gamma/\sqrt{N}$; see the note with the $K^*(892)$ mass.
 4 From analysis of L3 data at 91 and 183–209 GeV.

 3π MODE

VALUE (MeV)	EVTs	DOCUMENT ID	TECN	CHG	COMMENT
105.0± 1.7 OUR AVERAGE					
106.6 ± 3.4 $^{+3.4}_{-7.0}$	46M	¹ AGHASYAN	18B	COMP	190 $\pi^- p \rightarrow \pi^- \pi^+ \pi^- p$
108 ± 3 ± 15		CHUNG	02	B852	18.3 $\pi^- p \rightarrow \pi^+ \pi^- \pi^- p$
120 ± 10		BARBERIS	98B		450 $pp \rightarrow p_f \pi^+ \pi^- \pi^0 p_S$
105 ± 10 ± 11		ACCIARRI	97T	L3	$e^+ e^- \rightarrow e^+ e^- \pi^+ \pi^- \pi^0$
120 ± 10		ALBRECHT	97B	ARG	$e^+ e^- \rightarrow e^+ e^- \pi^+ \pi^- \pi^0$
103.0 ± 6.0 ± 3.3 72.4k		AMELIN	96	VES	36 $\pi^- p \rightarrow \pi^+ \pi^- \pi^0 n$
120 ± 10		ARMSTRONG	90	OMEG 0	300.0 $pp \rightarrow p_f \pi^+ \pi^- \pi^0$
107.0 ± 9.7	4022	AUGUSTIN	89	DM2 ±	$J/\psi \rightarrow \rho^\pm a_2^\mp$
118.5 ± 12.5	3562	AUGUSTIN	89	DM2 0	$J/\psi \rightarrow \rho^0 a_2^0$
97 ± 5		² EVANGELIS...	81	OMEG -	12 $\pi^- p \rightarrow 3\pi p$
96 ± 9	25k	² DAUM	80C	SPEC -	63,94 $\pi^- p \rightarrow 3\pi p$
110 ± 15	1097	² BALTAY	78B	HBC +0	15 $\pi^+ p \rightarrow p 4\pi$
112 ± 18	1.6k	² EMMS	75	DBC 0	4 $\pi^+ n \rightarrow p(3\pi)^0$
122 ± 14	1.2k	^{2,3} WAGNER	75	HBC 0	7 $\pi^+ p \rightarrow \Delta^{++}(3\pi)^0$
115 ± 15		² ANTIPOV	73C	CNTR -	25,40 $\pi^- p \rightarrow \rho \eta \pi^-$
99 ± 15	1580	CHALOUPKA	73	HBC -	3.9 $\pi^- p$
105 ± 5	28k	BOWEN	71	MMS -	5 $\pi^- p$
99 ± 5	24k	BOWEN	71	MMS +	5 $\pi^+ p$
103 ± 5	17k	BOWEN	71	MMS -	7 $\pi^- p$
••• We do not use the following data for averages, fits, limits, etc. •••					
110 ± 2 $^{+2}_{-15}$	420k	⁴ ALEKSEEV	10	COMP	190 $\pi^- p \rightarrow \pi^- \pi^+ \pi^- p$
117 ± 6 ± 20	18k	⁵ SCHEGELSKY	06	RVUE 0	$\gamma\gamma \rightarrow \pi^+ \pi^- \pi^0$
120 ± 40		CONDO	93	SHF	$\gamma p \rightarrow n \pi^+ \pi^+ \pi^-$
115 ± 14	490	BALTAY	78B	HBC 0	15 $\pi^+ p \rightarrow \Delta 3\pi$
72 ± 16	5k	BINNIE	71	MMS -	$\pi^- p$ near a_2 threshold
79 ± 12	941	ALSTON...	70	HBC +	7.0 $\pi^+ p \rightarrow 3\pi p$

The data in this block is included in the average printed for a previous datablock.

 3π MODE

1 Statistical error negligible.
 2 From a fit to $J^P = 2^+ \rho\pi$ partial wave.
 3 Width errors enlarged by us to $4\Gamma/\sqrt{N}$; see the note with the $K^*(892)$ mass.
 4 Superseded by AGHASYAN 2018B.
 5 From analysis of L3 data at 183–209 GeV.

1 From a fit to $J^P = 2^+$ partial wave.
 2 Number of events evaluated by us.
 3 Width errors enlarged by us to $4\Gamma/\sqrt{N}$; see the note with the $K^*(892)$ mass.
 4 From analysis of L3 data at 91 and 183–209 GeV.

 $K\bar{K}$ MODE

VALUE (MeV)	EVTs	DOCUMENT ID	TECN	CHG	COMMENT
109.8± 2.4 OUR AVERAGE					
112 ± 20	4700	^{1,2} CLELAND	82B	SPEC +	50 $\pi^+ p \rightarrow K_S^0 K^+ p$
120 ± 25	5200	^{1,2} CLELAND	82B	SPEC -	50 $\pi^- p \rightarrow K_S^0 K^- p$
106 ± 4	4000	CHABAUD	80	SPEC -	17 $\pi^- A \rightarrow K_S^0 K^- A$
126 ± 11	11000	CHABAUD	78	SPEC -	9.8 $\pi^- p \rightarrow K^- K_S^0 p$
101 ± 8	4730	CHABAUD	78	SPEC -	18.8 $\pi^- p \rightarrow K^- K_S^0 p$
113 ± 4		^{1,3} MARTIN	78D	SPEC -	10 $\pi^- p \rightarrow K_S^0 K^- p$
105 ± 8	2724	³ MARGULIE	76	SPEC -	23 $\pi^- p \rightarrow K^- K_S^0 p$
113 ± 19	730	FOLEY	72	CNTR -	20.3 $\pi^- p \rightarrow K^- K_S^0 p$
123 ± 13	1500	³ GRAYR	71	ASPK -	17.2 $\pi^- p \rightarrow K^- K_S^0 p$
••• We do not use the following data for averages, fits, limits, etc. •••					
120 ± 15	870	⁴ SCHEGELSKY	06A	RVUE 0	$\gamma\gamma \rightarrow K_S^0 K_S^0$
121 ± 51	1000	^{1,2} CLELAND	82B	SPEC +	30 $\pi^+ p \rightarrow K_S^0 K^+ p$
110 ± 18	350	HYAMS	78	ASPK +	12.7 $\pi^+ p \rightarrow K^+ K_S^0 p$

The data in this block is included in the average printed for a previous datablock.

 3π MODE

1 From a fit to $J^P = 2^+$ partial wave.
 2 Number of events evaluated by us.
 3 Width errors enlarged by us to $4\Gamma/\sqrt{N}$; see the note with the $K^*(892)$ mass.
 4 From analysis of L3 data at 91 and 183–209 GeV.

1 From a fit to $J^P = 2^+$ partial wave.
 2 Number of events evaluated by us.
 3 Width errors enlarged by us to $4\Gamma/\sqrt{N}$; see the note with the $K^*(892)$ mass.
 4 From analysis of L3 data at 91 and 183–209 GeV.

 $\eta\pi$ MODE

VALUE (MeV)	EVTs	DOCUMENT ID	TECN	CHG	COMMENT
111.1± 2.4 OUR AVERAGE					
115 ± 20		BARBERIS	00H		450 $pp \rightarrow p_f \eta \pi^0 p_S$
112 ± 14		BARBERIS	00H		450 $pp \rightarrow \Delta_f^{++} \eta \pi^- p_S$
112 ± 3 ± 2		¹ AMSLER	94D	CBAR	0.0 $\bar{p}p \rightarrow \pi^0 \pi^0 \eta$
103 ± 6 ± 3		BELADIDZE	93	VES	37 $\pi^- N \rightarrow \eta \pi^- N$
112.2 ± 5.7	2561	DELFOSSSE	81	SPEC +	$\pi^\pm p \rightarrow p \pi^\pm \eta$
116.6 ± 7.7	1653	DELFOSSSE	81	SPEC -	$\pi^\pm p \rightarrow p \pi^\pm \eta$
108 ± 9	1000	KEY	73	OSPK -	6 $\pi^- p \rightarrow p \pi^- \eta$

The data in this block is included in the average printed for a previous datablock.

 $\eta\pi$ MODE

1 From a fit to $J^P = 2^+$ partial wave.
 2 Number of events evaluated by us.
 3 Width errors enlarged by us to $4\Gamma/\sqrt{N}$; see the note with the $K^*(892)$ mass.
 4 From analysis of L3 data at 91 and 183–209 GeV.

1 From a fit to $J^P = 2^+$ partial wave.
 2 Number of events evaluated by us.
 3 Width errors enlarged by us to $4\Gamma/\sqrt{N}$; see the note with the $K^*(892)$ mass.
 4 From analysis of L3 data at 91 and 183–209 GeV.

1 From a fit to $J^P = 2^+$ partial wave.
 2 Number of events evaluated by us.
 3 Width errors enlarged by us to $4\Gamma/\sqrt{N}$; see the note with the $K^*(892)$ mass.
 4 From analysis of L3 data at 91 and 183–209 GeV.

See key on page 1171

Meson Particle Listings

$a_2(1320)$

••• We do not use the following data for averages, fits, limits, etc. •••

112 ± 1 ± 8	² JACKURA	18	RVUE	$\pi^- \rho \rightarrow \eta \pi^- \rho$
119 ± 14	³ ADOLPH	15	COMP	$191 \pi^- \rho \rightarrow \eta^{(\prime)} \pi^- \rho$
127 ± 2 ± 2	⁴ THOMPSON	97	MPS	$18 \pi^- \rho \rightarrow \eta \pi^- \rho$
118 ± 10	ARMSTRONG	93c	E760	0 $\bar{p} p \rightarrow \pi^0 \eta \eta \rightarrow 6 \gamma$
104 ± 9	⁵ CONFORTO	73	OSPK	- $6 \pi^- \rho \rightarrow \rho \text{MM}^-$

- ¹ The systematic error of 2 MeV corresponds to the spread of solutions.
- ² Superseded by RODAS 19.
- ³ ADOLPH 15 value is derived from a Breit-Wigner fit with mass-dependent width taking the $\eta \pi$ and $\rho \pi$ channels into account.
- ⁴ Resolution is not unfolded.
- ⁵ Missing mass with enriched MMS = $\eta \pi^-$, $\eta = 2 \gamma$.

$\eta' \pi$ MODE

VALUE (MeV)	DOCUMENT ID	TECN	COMMENT
119 ± 25 OUR AVERAGE			
140 ± 35 ± 20	IVANOV	01	B852 $18 \pi^- \rho \rightarrow \eta' \pi^- \rho$
106 ± 32	BELADIDZE	93	VES $37 \pi^- N \rightarrow \eta' \pi^- N$

$a_2(1320)$ DECAY MODES

Mode	Fraction (Γ_i/Γ)	Scale factor/ Confidence level
Γ_1 3π	(70.1 ± 2.7) %	S=1.2
Γ_2 $\rho(770)\pi$		
Γ_3 $f_2(1270)\pi$		
Γ_4 $\rho(1450)\pi$		
Γ_5 $\eta \pi$	(14.5 ± 1.2) %	
Γ_6 $\omega \pi \pi$	(10.6 ± 3.2) %	S=1.3
Γ_7 $K\bar{K}$	(4.9 ± 0.8) %	
Γ_8 $\eta'(958)\pi$	(5.5 ± 0.9) × 10 ⁻³	
Γ_9 $\pi^\pm \gamma$	(2.91 ± 0.27) × 10 ⁻³	
Γ_{10} $\gamma \gamma$	(9.4 ± 0.7) × 10 ⁻⁶	
Γ_{11} $e^+ e^-$	< 5 × 10 ⁻⁹	CL=90%

CONSTRAINED FIT INFORMATION

An overall fit to 5 branching ratios uses 18 measurements and one constraint to determine 4 parameters. The overall fit has a $\chi^2 = 9.3$ for 15 degrees of freedom.

The following off-diagonal array elements are the correlation coefficients $\langle \delta x_i \delta x_j \rangle / (\delta x_i \delta x_j)$, in percent, from the fit to the branching fractions, $x_i \equiv \Gamma_i/\Gamma_{\text{total}}$. The fit constrains the x_i whose labels appear in this array to sum to one.

x_5	10		
x_6	-89	-46	
x_7	-1	-2	-24
	x_1	x_5	x_6

$a_2(1320)$ PARTIAL WIDTHS

$\Gamma(\eta \pi)$ Γ_5

VALUE (MeV)	EVTS	DOCUMENT ID	TECN	CHG	COMMENT
••• We do not use the following data for averages, fits, limits, etc. •••					
18.5 ± 3.0	870	¹ SCHEGELSKY	06A	RVUE	0 $\gamma \gamma \rightarrow K_S^0 K_S^0$
¹ From analysis of L3 data at 91 and 183–209 GeV, using $\Gamma(a_2(1320) \rightarrow \gamma \gamma) = 0.91 \text{ keV}$ and SU(3) relations.					

$\Gamma(K\bar{K})$ Γ_7

VALUE (MeV)	EVTS	DOCUMENT ID	TECN	CHG	COMMENT
••• We do not use the following data for averages, fits, limits, etc. •••					
7.0 ^{+2.0} _{-1.5}	870	¹ SCHEGELSKY	06A	RVUE	0 $\gamma \gamma \rightarrow K_S^0 K_S^0$
¹ From analysis of L3 data at 91 and 183–209 GeV, using $\Gamma(a_2(1320) \rightarrow \gamma \gamma) = 0.91 \text{ keV}$ and SU(3) relations.					

$\Gamma(\pi^\pm \gamma)$ Γ_9

VALUE (keV)	EVTS	DOCUMENT ID	TECN	CHG	COMMENT
311 ± 25 OUR AVERAGE					
358 ± 6 ± 42		¹ ADOLPH	14	COMP	- $190 \pi^- \text{Pb} \rightarrow \pi^+ \pi^- \pi^- \text{Pb} / 600 \pi^- A \rightarrow \pi^+ \pi^- \pi^- A$
284 ± 25 ± 25	7.1k	MOLCHANOV	01	SELX	$200 \pi^+ A$
295 ± 60		CIHANGIR	82	SPEC	+ $200 \pi^+ A$
••• We do not use the following data for averages, fits, limits, etc. •••					
461 ± 110		² MAY	77	SPEC	± 9.7 γA
¹ Primakoff reaction using $a_2(1320) \rightarrow 3\pi$ branching ratio of 70.1%.					
² Assuming one-pion exchange.					

$\Gamma(\gamma \gamma)$ Γ_{10}

VALUE (keV)	EVTS	DOCUMENT ID	TECN	CHG	COMMENT
1.00 ± 0.06 OUR AVERAGE					
0.98 ± 0.05 ± 0.09		ACCIARRI	97T	L3	$e^+ e^- \rightarrow e^+ e^- \pi^+ \pi^- \pi^0$
0.96 ± 0.03 ± 0.13		ALBRECHT	97B	ARG	$e^+ e^- \rightarrow e^+ e^- \pi^+ \pi^- \pi^0$
1.26 ± 0.26 ± 0.18	36	BARU	90	MD1	$e^+ e^- \rightarrow e^+ e^- \pi^+ \pi^- \pi^0$
1.00 ± 0.07 ± 0.15	415	BEHREND	90c	CELL	0 $e^+ e^- \rightarrow e^+ e^- \pi^+ \pi^- \pi^0$
1.03 ± 0.13 ± 0.21		BUTLER	90	MRK2	$e^+ e^- \rightarrow e^+ e^- \pi^+ \pi^- \pi^0$
1.01 ± 0.14 ± 0.22	85	OEST	90	JADE	$e^+ e^- \rightarrow e^+ e^- \pi^0 \eta$
0.90 ± 0.27 ± 0.15	56	¹ ALTHOFF	86	TASS	0 $e^+ e^- \rightarrow e^+ e^- 3\pi$
1.14 ± 0.20 ± 0.26		² ANTREASIAN	86	CBAL	0 $e^+ e^- \rightarrow e^+ e^- \pi^0 \eta$
1.06 ± 0.18 ± 0.19		BERGER	84c	PLUT	0 $e^+ e^- \rightarrow e^+ e^- 3\pi$
••• We do not use the following data for averages, fits, limits, etc. •••					
0.81 ± 0.19 ^{+0.42} _{-0.11}	35	¹ BEHREND	82c	CELL	0 $e^+ e^- \rightarrow e^+ e^- 3\pi$
0.77 ± 0.18 ± 0.27	22	² EDWARDS	82F	CBAL	0 $e^+ e^- \rightarrow e^+ e^- \pi^0 \eta$
¹ From $\rho \pi$ decay mode.					
² From $\eta \pi^0$ decay mode.					

$\Gamma(e^+ e^-)$ Γ_{11}

VALUE (eV)	CL%	DOCUMENT ID	TECN	COMMENT
< 0.56	90	ACHASOV	00k	SND $e^+ e^- \rightarrow \pi^0 \pi^0$
••• We do not use the following data for averages, fits, limits, etc. •••				
< 25	90	VOROBYEV	88	ND $e^+ e^- \rightarrow \pi^0 \eta$

$a_2(1320)$ $\Gamma(i)\Gamma(\gamma \gamma)/\Gamma(\text{total})$

$\Gamma(3\pi) \times \Gamma(\gamma \gamma)/\Gamma_{\text{total}}$ $\Gamma_1 \Gamma_{10}/\Gamma$

VALUE (keV)	EVTS	DOCUMENT ID	TECN	COMMENT
••• We do not use the following data for averages, fits, limits, etc. •••				
0.65 ± 0.02 ± 0.02	18k	¹ SCHEGELSKY	06	RVUE $\gamma \gamma \rightarrow \pi^+ \pi^- \pi^0$
¹ From analysis of L3 data at 183–209 GeV.				

$\Gamma(\eta \pi) \times \Gamma(\gamma \gamma)/\Gamma_{\text{total}}$ $\Gamma_5 \Gamma_{10}/\Gamma$

VALUE (keV)	DOCUMENT ID	TECN	COMMENT
••• We do not use the following data for averages, fits, limits, etc. •••			
0.145 ^{+0.097} _{-0.034}	¹ UEHARA	09A	BELL $e^+ e^- \rightarrow e^+ e^- \eta \pi^0$
¹ From the D_2 -wave. The fraction of the D_0 -wave is 3.4 ^{+2.3} _{-1.1} %.			

$\Gamma(K\bar{K}) \times \Gamma(\gamma \gamma)/\Gamma_{\text{total}}$ $\Gamma_7 \Gamma_{10}/\Gamma$

VALUE (keV)	DOCUMENT ID	TECN	COMMENT
0.126 ± 0.007 ± 0.028	¹ ALBRECHT	90g	ARG $e^+ e^- \rightarrow e^+ e^- K^+ K^-$
••• We do not use the following data for averages, fits, limits, etc. •••			
0.081 ± 0.006 ± 0.027	² ALBRECHT	90g	ARG $e^+ e^- \rightarrow e^+ e^- K^+ K^-$
¹ Using an incoherent background.			
² Using a coherent background.			

$a_2(1320)$ BRANCHING RATIOS

$[\Gamma(f_2(1270)\pi) + \Gamma(\rho(1450)\pi)]/\Gamma(\rho(770)\pi)$ $(\Gamma_3 + \Gamma_4)/\Gamma_2$

VALUE	CL%	DOCUMENT ID	TECN	CHG	COMMENT
< 0.12	90	ABRAMOVI...	70B	HBC	- 3.93 $\pi^- \rho$

$\Gamma(\rho(770)\pi)/\Gamma(f_2(1270)\pi)$ Γ_2/Γ_3

VALUE	EVTS	DOCUMENT ID	TECN	COMMENT	
16.5^{+1.2}_{-2.4}	46M	¹ AGHASIAN	18B	COMP	$190 \pi^- \rho \rightarrow \pi^- \pi^+ \pi^- \rho$
¹ Statistical error negligible.					

$\Gamma(\eta \pi)/\Gamma(3\pi)$ Γ_5/Γ_1

VALUE	EVTS	DOCUMENT ID	TECN	CHG	COMMENT
0.207 ± 0.018 OUR FIT					
0.213 ± 0.020 OUR AVERAGE					
0.18 ± 0.05		FORINO	76	HBC	11 $\pi^- \rho$
0.22 ± 0.05	52	ANTIPOV	73	CNTR	- 40 $\pi^- \rho$
0.211 ± 0.044	149	CHALOUKKA	73	HBC	- 3.9 $\pi^- \rho$
0.246 ± 0.042	167	ALSTON-...	71	HBC	+ 7.0 $\pi^+ \rho$
0.25 ± 0.09	15	BOECKMANN	70	HBC	+ 5.0 $\pi^+ \rho$
0.23 ± 0.08	22	ASCOLI	68	HBC	- 5 $\pi^- \rho$
0.12 ± 0.08		CHUNG	68	HBC	- 3.2 $\pi^- \rho$
0.22 ± 0.09		CONTE	67	HBC	- 11.0 $\pi^- \rho$

$\Gamma(\omega \pi \pi)/\Gamma(3\pi)$ Γ_6/Γ_1

VALUE	EVTS	DOCUMENT ID	TECN	CHG	COMMENT
0.15 ± 0.05 OUR FIT					Error includes scale factor of 1.3.
0.15 ± 0.05 OUR AVERAGE					Error includes scale factor of 1.3. See the ideogram below.
0.28 ± 0.09	60	DIAZ	74	DBC	0 6 $\pi^+ \rho$
0.18 ± 0.08		¹ KARSHON	74	HBC	Avg. of above two
0.10 ± 0.05	279	² CHALOUKKA	73	HBC	- 3.9 $\pi^- \rho$

Meson Particle Listings

$a_2(1320)$

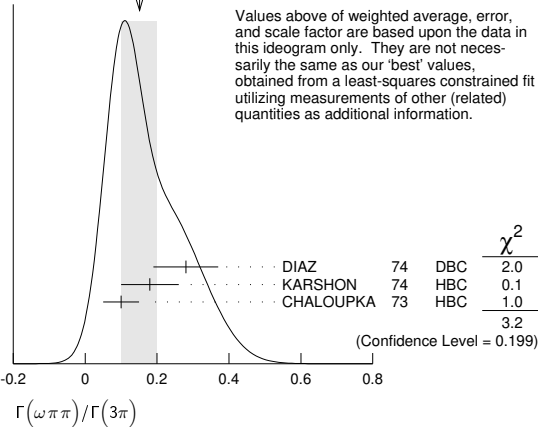
• • • We do not use the following data for averages, fits, limits, etc. • • •

VALUE	EVTS	DOCUMENT ID	TECN	CHG	COMMENT
0.29 ± 0.08	140	¹ KARSHON 74	HBC	0	$4.9 \pi^+ p$
0.10 ± 0.04	60	¹ KARSHON 74	HBC	+	$4.9 \pi^+ p$
0.19 ± 0.08		DEFOIX 73	HBC	0	$0.7 \bar{p} p$

¹ KARSHON 74 suggest an additional $l = 0$ state strongly coupled to $\omega \pi \pi$ which could explain discrepancies in branching ratios and masses. We use a central value and a systematic spread.

² Decays to $b_1(1040) \pi$, $b_1 \rightarrow \omega \pi$. Error increased to account for possible systematic errors of complicated analysis.

WEIGHTED AVERAGE
 0.15 ± 0.05 (Error scaled by 1.3)



$\Gamma(K\bar{K})/\Gamma(3\pi)$ Γ_7/Γ_1

VALUE	EVTS	DOCUMENT ID	TECN	CHG	COMMENT
0.070 ± 0.012 OUR FIT		CHABAUD 78	RVUE		
0.078 ± 0.017					

• • • We do not use the following data for averages, fits, limits, etc. • • •

0.011 ± 0.003		¹ BERTIN 98B	OBLX		$0.0 \bar{p} p \rightarrow \pi^0 \pi^0 \eta, \pi^0 \eta \eta, \pi^0 K^+ K^-$ and $191 \pi^- p \rightarrow \pi^- \pi^- \pi^+ p$
0.056 ± 0.014	50	² CHALOUPKA 73	HBC	-	$3.9 \pi^- p$
0.097 ± 0.018	113	² ALSTON... 71	HBC	+	$7.0 \pi^+ p$
0.06 ± 0.03		² ABRAMOVI... 70B	HBC	-	$3.93 \pi^- p$
0.054 ± 0.022		² CHUNG 68	HBC	-	$3.2 \pi^- p$

¹ Using 4π data from BERTIN 97D.
² Included in CHABAUD 78 review.

$\Gamma(K\bar{K})/\Gamma(\eta\pi)$ Γ_7/Γ_5

VALUE	DOCUMENT ID	TECN	CHG	COMMENT
0.31 ± 0.22	¹ KOPF 21	RVUE		$0.9 \bar{p} p \rightarrow \pi^0 \pi^0 \eta, \pi^0 \eta \eta, \pi^0 K^+ K^-$ and $191 \pi^- p \rightarrow \pi^- \pi^- \pi^+ p$
$0.352 \pm 0.011 \pm 0.175$	² ALBRECHT 20	RVUE		$0.9 \bar{p} p \rightarrow \pi^0 \pi^0 \eta, \pi^0 \eta \eta, \pi^0 K^+ K^-$
0.08 ± 0.02	³ BERTIN 98B	OBLX		$0.0 \bar{p} p \rightarrow K^\pm K_S^\mp \pi^\mp$

¹ From T-matrix pole based on combined fit of Crystal Barrel and $\pi\pi$ scattering data (ALBRECHT 20), and COMPASS data (ADOLPH 15), using a coupled-channel model of $\eta\pi, \eta'\pi$ and $K\bar{K}$ systems.
² Residues from T-matrix pole with 2 poles, 2 channels ($\pi^0 \eta$ and $K\bar{K}$).
³ Using $\eta\pi\pi$ data from AMSLER 94D.

$\Gamma(\eta\pi)/[\Gamma(3\pi) + \Gamma(\eta\pi) + \Gamma(K\bar{K})]$ $\Gamma_5/(\Gamma_1 + \Gamma_5 + \Gamma_7)$

VALUE	EVTS	DOCUMENT ID	TECN	CHG	COMMENT
0.162 ± 0.012 OUR FIT					
0.140 ± 0.028 OUR AVERAGE					
0.13 ± 0.04		ESPIGAT 72	HBC	\pm	$0.0 \bar{p} p$
0.15 ± 0.04	34	BARNHAM 71	HBC	+	$3.7 \pi^+ p$

$\Gamma(K\bar{K})/[\Gamma(3\pi) + \Gamma(\eta\pi) + \Gamma(K\bar{K})]$ $\Gamma_7/(\Gamma_1 + \Gamma_5 + \Gamma_7)$

VALUE	EVTS	DOCUMENT ID	TECN	CHG	COMMENT
0.054 ± 0.009 OUR FIT					
0.048 ± 0.012 OUR AVERAGE					
0.05 ± 0.02		TOET 73	HBC	+	$5 \pi^+ p$
0.09 ± 0.04		TOET 73	HBC	0	$5 \pi^+ p$
0.03 ± 0.02	8	¹ DAMERI 72	HBC	-	$11 \pi^- p$
0.06 ± 0.03	17	BARNHAM 71	HBC	+	$3.7 \pi^+ p$
0.020 ± 0.004		² ESPIGAT 72	HBC	\pm	$0.0 \bar{p} p$

¹ Montanet agrees. Vlada.
² Not averaged because of discrepancy between masses from $K\bar{K}$ and $\rho\pi$ models.

$\Gamma(\eta'(958)\pi)/\Gamma_{total}$ Γ_8/Γ

VALUE	CL%	DOCUMENT ID	TECN	CHG	COMMENT
-------	-----	-------------	------	-----	---------

• • • We do not use the following data for averages, fits, limits, etc. • • •

< 0.006	95	ALDE 92B	GAM2		$38,100 \pi^- p \rightarrow \eta'/\pi^0 n$
< 0.02	97	BARNHAM 71	HBC	+	$3.7 \pi^+ p$
0.004 ± 0.004		¹ BOESEBECK 68	HBC	+	$8 \pi^+ p$

¹ No longer valid since $\Gamma(K\bar{K})/\Gamma(3\pi)$ value has changed (MORRISON 71).

$\Gamma(\eta'(958)\pi)/\Gamma(3\pi)$ Γ_8/Γ_1

VALUE	CL%	DOCUMENT ID	TECN	CHG	COMMENT
-------	-----	-------------	------	-----	---------

• • • We do not use the following data for averages, fits, limits, etc. • • •

< 0.011	90	EISENSTEIN 73	HBC	-	$5 \pi^- p$
< 0.04		ALSTON... 71	HBC	+	$7.0 \pi^+ p$
0.04	$+0.03$ -0.04	BOECKMANN 70	HBC	0	$5.0 \pi^+ p$

$\Gamma(\eta'(958)\pi)/\Gamma(\eta\pi)$ Γ_8/Γ_5

VALUE	DOCUMENT ID	TECN	COMMENT
-------	-------------	------	---------

0.038 ± 0.005 OUR AVERAGE

0.05 ± 0.02	ADOLPH 15	COMP	$191 \pi^- p \rightarrow \eta^{(\prime)} \pi^- p$
0.032 ± 0.009	ABELE 97c	CBAR	$0.0 \bar{p} p \rightarrow \pi^0 \pi^0 \eta'$
$0.047 \pm 0.010 \pm 0.004$	¹ BELADIDZE 93	VES	$37 \pi^- N \rightarrow a_2^- N$
$0.034 \pm 0.008 \pm 0.005$	BELADIDZE 92	VES	$36 \pi^- C \rightarrow a_2^- C$

• • • We do not use the following data for averages, fits, limits, etc. • • •

0.046 ± 0.015	$+0.07$ -0.006	² KOPF 21	RVUE	$0.9 \bar{p} p \rightarrow \pi^0 \pi^0 \eta, \pi^0 \eta \eta, \pi^0 K^+ K^-$ and $191 \pi^- p \rightarrow \pi^- \pi^- \pi^+ p$
-------------------	---------------------	----------------------	------	--

¹ Using $B(\eta' \rightarrow \pi^+ \pi^- \eta) = 0.441$, $B(\eta \rightarrow \gamma\gamma) = 0.389$ and $B(\eta \rightarrow \pi^+ \pi^- \pi^0) = 0.236$.
² From T-matrix pole based on combined fit of Crystal Barrel and $\pi\pi$ scattering data (ALBRECHT 20), and COMPASS data (ADOLPH 15), using a coupled-channel model of $\eta\pi, \eta'\pi$ and $K\bar{K}$ systems.

$\Gamma(\pi^\pm\gamma)/\Gamma_{total}$ Γ_9/Γ

VALUE	DOCUMENT ID	TECN	COMMENT
-------	-------------	------	---------

• • • We do not use the following data for averages, fits, limits, etc. • • •

0.005	$+0.005$ -0.003	¹ EISENBERG 72	HBC	$4.3, 5.25, 7.5 \gamma p$
---------	----------------------	---------------------------	-----	---------------------------

¹ Pion-exchange model used in this estimation.

$\Gamma(e^+e^-)/\Gamma_{total}$ Γ_{11}/Γ

VALUE (units 10^{-3})	CL%	DOCUMENT ID	TECN	COMMENT
--------------------------	-----	-------------	------	---------

• • • We do not use the following data for averages, fits, limits, etc. • • •

< 6	90	ACHASOV 00k	SND	$e^+e^- \rightarrow \pi^0 \pi^0$
-------	----	-------------	-----	----------------------------------

$a_2(1320)$ REFERENCES

KOPF 21	EPJ C81 1056	B. Kopf et al.	(BOCH)
ALBRECHT 20	EPJ C80 453	M. Albrecht et al.	(Crystal Barrel Collab.)
RODAS 19	PRL 122 042002	A. Rodas et al.	(JPAC Collab.)
AGHASYAN 18B	PR D98 092003	M. Aghasyan et al.	(COMPASS Collab.)
JACKURA 18	PL B779 464	A. Jackura et al.	(JPAC and COMPASS Collab.)
ADOLPH 15	PL B740 303	M. Adolph et al.	(COMPASS Collab.)
ADOLPH 14	EPJ A50 79	C. Adolph et al.	(COMPASS Collab.)
ALEKSEEV 10	PRL 104 241803	M.G. Alekseev et al.	(COMPASS Collab.)
ANISOVICH 09	IJMP A21 2481	V.V. Anisovich, A.V. Sarantsev	(PHPI)
UEHARA 09A	PR D80 032001	S. Uehara et al.	(BELLE Collab.)
SCHEGELSKY 06	EPJ A27 199	V.A. Schegelsky et al.	
SCHEGELSKY 06A	EPJ A27 207	V.A. Schegelsky et al.	
CHUNG 02	PR D65 072001	S.U. Chung et al.	(BNL E852 Collab.)
IVANOV 01	PRL 86 3977	E.I. Ivanov et al.	(BNL E852 Collab.)
MOLCHANOV 01	PL B521 171	V.V. Molchanov et al.	(FNAL SELEX Collab.)
ACHASOV 00K	PL B492 8	M.N. Achasov et al.	(Novosibirsk SND Collab.)
BARBERIS 00H	PL B488 225	D. Barberis et al.	(WA 102 Collab.)
BARBERIS 98B	PL B422 399	D. Barberis et al.	(WA 102 Collab.)
BERTIN 98B	PL B434 180	A. Bertin et al.	(OBELIX Collab.)
ABELE 97C	PL B404 179	A. Abele et al.	(Crystal Barrel Collab.)
ACCIARRI 97T	PL B413 147	M. Acciari et al.	(L3 Collab.)
ALBRECHT 97B	ZPHY C74 469	H. Albrecht et al.	(ARGUS Collab.)
THOMPSON 97	PRL 79 1630	D.R. Thompson et al.	(BNL E852 Collab.)
AMELIN 96	ZPHY C70 71	D.V. Amelin et al.	(SERP, TBLI)
AMSLER 94D	PL B333 277	C. Amisler et al.	(Crystal Barrel Collab.)
AOYAGI 93C	PL B314 246	H. Aoyagi et al.	(BKEI Collab.)
ARMSTRONG 93C	PL B307 394	T.A. Armstrong et al.	(FNAL, FERR, GENO+)
BELADIDZE 93	PL B313 276	G.M. Beladidze et al.	(VES Collab.)
CONDO 93	PR D48 3045	G.T. Condo et al.	(SLAC Hybrid Collab.)
ALDE 92B	ZPHY C54 549	D.M. Alde et al.	(SERP, BELG, LANL, LAPP+)
BELADIDZE 92	ZPHY C54 235	G.M. Beladidze et al.	(VES Collab.)
ALBRECHT 90G	ZPHY C48 183	H. Albrecht et al.	(ARGUS Collab.)
ARMSTRONG 90	ZPHY C48 213	T.A. Armstrong, M. Benayoun, W. Beusch	(WA75 Collab.)
BARU 90	ZPHY C48 581	S.E. Baru et al.	(MD-1 Collab.)
BEHREND 90C	ZPHY C46 583	H.J. Behrend et al.	(CELLO Collab.)
BUTLER 90	PR D42 1368	F. Butler et al.	(Mark II Collab.)
OEST 90	ZPHY C47 343	T. Oest et al.	(JADE Collab.)
AUGUSTIN 89	NP B320 1	J.E. Augustin, G. Cosme	(DM2 Collab.)
VOROBYEV 88	SJNP 48 273	P.V. Vorobyev et al.	(NOVO)
ALTHOFF 86	ZPHY C31 537	M. Althoff et al.	(TASSO Collab.)
ANTREAS-YAN 86	PR D33 1847	D. Antreasyan et al.	(Crystal Ball Collab.)
BERGER 84C	PL 149B 427	C. Berger et al.	(PLUTO Collab.)
BEHREND 82C	PL 114B 378	H.J. Behrend et al.	(CELLO Collab.)
Also	PL 125B 518 (errata.)	H.J. Behrend et al.	(CELLO Collab.)
CHANGIR 82	PL 117B 123	S. Cihangir et al.	(FNAL, MINN, ROCH)
CLELAND 82B	NP B208 228	W.E. Cleland et al.	(DURH, GEVA, LAUS+)
EDWARDS 82F	PL 110B 82	C. Edwards et al.	(CIT, HARV, PRIN+)

See key on page 1171

Meson Particle Listings

$a_2(1320)$, $f_0(1370)$

DELFOSSÉ	81	NP B183 349	A. Delfosse et al.	(GEVA, LAUS)
EVAN GELIS...	81	NP B178 197	C. Evangelista et al.	(BARI, BONN, CERN+)
CHABAUD	80	NP B175 189	V. Chabaud et al.	(CERN, MPIM, AMST)
DAUM	80C	PL 89B 276	C. Daum et al.	(AMST, CERN, CRAC, MPIM+)
BALTAY	78B	PR D17 62	C. Baltay et al.	(COLU, BING)
CHABAUD	78	NP B145 349	V. Chabaud et al.	(CERN, MPIM)
FERRERSORIA	78	PL 74B 287	A. Ferrer Soria et al.	(ORSAY, CERN, CDEF+)
HYAMS	78	NP B146 303	B.D. Hyams et al.	(CERN, MPIM, ATEN)
MARTIN	78D	PL 74B 417	A.D. Martin et al.	(DURH, GEVA) JP
MAY	77	PR D16 1903	E.N. May et al.	(ROCH, CORN)
FORINO	76	NC 35A 465	A. Forino et al.	(BGNA, FIRZ, GENO, MILA+)
MARGULIE	76	PR D14 667	M. Margulies et al.	(BNL, CUNY)
EMMS	75	PL 58B 117	M.J. Emms et al.	(BIRM, DURH, RHEL) JP
WAGNER	75	PL 58B 201	F. Wagner, M. Tabak, D.M. Chew	(LBL) JP
DIAZ	74	PRL 32 260	J. Diaz et al.	(CASE, CMU)
KARSHON	74	PRL 32 852	U. Karshon et al.	(REHO)
ANTIPOV	73	NP B63 175	Y.M. Antipov et al.	(CERN, SERP) JP
ANTIPOV	73C	NP B63 153	Y.M. Antipov et al.	(CERN, SERP) JP
CHALOUKPA	73	PL 44B 211	V. Chaloupka et al.	(CERN)
CONFORTO	73	PL 45B 154	G. Conforto et al.	(EFI, FNAL, TNT0+)
DEFOIX	73	PL 43B 141	C. Defoix et al.	(DURH, GEVA)
EISENSTEIN	73	PR D7 278	L. Eisenstein et al.	(CDEF)
KEY	73	PRL 30 503	A.W. Key et al.	(ILL)
TOET	73	NP B63 248	D.Z. Toet et al.	(TNT0, EFI, FNAL, WSIC)
DAMERI	72	NC 9A 1	M. Dameri et al.	(NUM, BONN, DURH, TORI)
EISENBERG	72	PR D5 15	Y. Eisenberg et al.	(GENO, MILA, SAEL)
ESPIGAT	72	NP B36 93	P. Espigat et al.	(REHO, SLAC, TELA)
FOLEY	72	PR D6 747	K.J. Foley et al.	(CERN, CDEF)
ALSTON-...	71	PL 34B 156	M. Alston-Garnjost et al.	(BNL, CUNY)
BARNHAM	71	PRL 26 1494	K.W.J. Barnham et al.	(LRL)
BINNIE	71	PL 36B 257	D.M. Binmie et al.	(LBL)
BOWEN	71	PRL 26 1663	D.R. Bowen et al.	(LOIC, SHMP)
GRAVER	71	PL 34B 333	G. Grayer et al.	(NEAS, STON)
ABRAMOVI...	70B	NP B23 466	M. Abramovich et al.	(CERN, MPIM)
ALSTON-...	70	PL 33B 607	M. Alston-Garnjost et al.	(CERN) JP
BOECKMANN	70	NP B16 221	K. Boeckmann et al.	(LRL)
ASCOLI	68	PRL 20 1321	G. Ascoli et al.	(BONN, DURH, NIJM+)
BOESEBECK	68	NP B4 501	K. Boesebeck et al.	(ILL) JP
CHUNG	68	PR 165 1491	S.U. Chung et al.	(AACH, BERL, CERN)
CONTE	67	NC 51A 175	F. Conte et al.	(LRL)
			(GENO, HAMB, MILA, SAEL)	

$f_0(1370)$

$$J^G(J^{PC}) = 0^+(0^{++})$$

See the review on "Spectroscopy of Light Meson Resonances" and a note on "Non- $q\bar{q}$ Candidates" in PDG 06, Journal of Physics **G33** 1 (2006).

$f_0(1370)$ T-MATRIX POLE \sqrt{s}

Note that $\Gamma = -2 \text{Im}(\sqrt{s})$.

VALUE (MeV)	DOCUMENT ID	TECN	COMMENT
(1250-1440) $-i$ (60-300) OUR ESTIMATE			
$(1245 \pm 40) - i(300^{+30}_{-70})$	1 PELAEZ	23	RVUE Compilation
$(1380 \pm 60) - i(220^{+80}_{-70})$	2 PELAEZ	23	RVUE Compilation
$(1370 \pm 40) - i(195 \pm 20)$	SARANTSEV	21	RVUE $J/\psi(1S) \rightarrow \gamma(\pi\pi, K\bar{K}, \eta\eta, \omega\phi)$
$(1280.6 \pm 1.6 \pm 47.4) - i(205.2 \pm 1.7 \pm 20.7)$	3 ALBRECHT	20	RVUE $0.9 \bar{p}p \rightarrow \pi^0\pi^0\eta, \pi^0\eta, \pi^0 K^+K^-$
$(1290 \pm 50) - i(170^{+20}_{-40})$	4 ANISOVICH	09	RVUE $0.0 \bar{p}p, \pi N$
$(1373 \pm 15) - i(137 \pm 10)$	5 BARGIOTTI	03	OBLX $\bar{p}p$
$(1302 \pm 17) - i(166 \pm 18)$	6 BARBERIS	00C	450 $pp \rightarrow p_f 4\pi p_S$
$(1312 \pm 25 \pm 10) - i(109 \pm 22 \pm 15)$	BARBERIS	99D	OMEG $450 pp \rightarrow K^+K^-, \pi^+\pi^-$
$(1406 \pm 19) - i(80 \pm 6)$	7 KAMINSKI	99	RVUE $\pi\pi \rightarrow \pi\pi, K\bar{K}, \sigma\sigma$
$(1300 \pm 20) - i(120 \pm 20)$	ANISOVICH	98B	RVUE Compilation
$(1290 \pm 15) - i(145 \pm 15)$	BARBERIS	97B	OMEG $450 pp \rightarrow pp 2(\pi^+\pi^-)$
$(1548 \pm 40) - i(560 \pm 40)$	BERTIN	97C	OBLX $0.0 \bar{p}p \rightarrow \pi^+\pi^-\pi^0$
$(1380 \pm 40) - i(180 \pm 25)$	ABELE	96B	CBAR $0.0 \bar{p}p \rightarrow \pi^0 K_L^0 K_L^0$
$(1300 \pm 15) - i(115 \pm 8)$	BUGG	96	RVUE
$(1330 \pm 50) - i(150 \pm 40)$	8 AMSLER	95B	CBAR $\bar{p}p \rightarrow 3\pi^0$
$(1360 \pm 35) - i(150-300)$	8 AMSLER	95C	CBAR $\bar{p}p \rightarrow \pi^0\eta\eta$
$(1390 \pm 30) - i(190 \pm 40)$	9 AMSLER	95D	CBAR $\bar{p}p \rightarrow 3\pi^0, \pi^0\eta\eta, \pi^0\pi^0\eta$
$1346 - i249$	10,11 JANSSEN	95	RVUE $\pi\pi \rightarrow \pi\pi, K\bar{K}$
$1214 - i168$	11,12 TORNQVIST	95	RVUE $\pi\pi \rightarrow \pi\pi, K\bar{K}, K\pi, \eta\pi$
$1364 - i139$	AMSLER	94D	CBAR $\bar{p}p \rightarrow \pi^0\pi^0\eta$
$(1365^{+20}_{-55}) - i(134 \pm 35)$	ANISOVICH	94	CBAR $\bar{p}p \rightarrow 3\pi^0, \pi^0\eta\eta$
$(1340 \pm 40) - i(127^{+30}_{-20})$	13 BUGG	94	RVUE $\bar{p}p \rightarrow 3\pi^0, \eta\eta\pi^0, \eta\pi^0\pi^0$
$(1430 \pm 5) - i(73 \pm 13)$	14 KAMINSKI	94	RVUE $\pi\pi \rightarrow \pi\pi, K\bar{K}$
$1420 - i220$	15 AU	87	RVUE $\pi\pi \rightarrow \pi\pi, K\bar{K}$

1 From forward dispersion relation applied to $\pi\pi$ scattering data.
 2 From partial-wave dispersion relation applied to $\pi\pi \rightarrow \bar{K}K$ data.
 3 T-matrix pole, 5 poles, 5 channels, including scattering data from HYAMS 75 ($\pi\pi$), LONGACRE 86 ($K\bar{K}$), BINON 83 ($\eta\eta$), and BINON 84C ($\eta\eta'$).
 4 Another pole is found at $(1510 \pm 130) - i(800^{+100}_{-150})$ MeV.
 5 Coupled channel analysis of $\pi^+\pi^-\pi^0, K^+K^-\pi^0$, and $K^\pm K_S^0 \pi^\mp$.
 6 Average between $\pi^+\pi^-\pi^0$ and $2(\pi^+\pi^-)$.
 7 T-matrix pole on sheet ---.
 8 Supersedes ANISOVICH 94.
 9 Coupled-channel analysis of $\bar{p}p \rightarrow 3\pi^0, \pi^0\eta\eta$, and $\pi^0\pi^0\eta$ on sheet IV. Demonstrates explicitly that $f_0(500)$ and $f_0(1370)$ are two different poles.

10 Analysis of data from FALVARD 88.
 11 The pole is on Sheet III. Demonstrates explicitly that $f_0(500)$ and $f_0(1370)$ are two different poles.
 12 Uses data from BEIER 72B, OCHS 73, HYAMS 73, GRAYER 74, ROSSELET 77, CASON 83, ASTON 88, and ARMSTRONG 91B. Coupled channel analysis with flavor symmetry and all light two-pseudoscalars systems.
 13 Reanalysis of ANISOVICH 94 data.
 14 T-matrix pole on sheet III.
 15 Analysis of data from OCHS 73, GRAYER 74, BECKER 79, and CASON 83.

$f_0(1370)$ BREIT-WIGNER MASS

VALUE (MeV)	DOCUMENT ID			
1200 to 1500 OUR ESTIMATE				
$\pi\pi$ MODE				
VALUE (MeV)	EVTS	DOCUMENT ID	TECN	COMMENT
••• We do not use the following data for averages, fits, limits, etc. •••				
1400 ± 40		1 AUBERT	09L	BABR $B^\pm \rightarrow \pi^\pm \pi^\pm \pi^\mp$
1470^{+6+72}_{-7-255}		2 UEHARA	08A	BELL $10.6 e^+e^- \rightarrow e^+e^-\pi^0\pi^0$
1259 ± 55	2.6k	BONVICINI	07	CLEO $D^+ \rightarrow \pi^-\pi^+\pi^+$
$1309 \pm 1 \pm 15$		3 BUGG	07A	RVUE $0.0 p\bar{p} \rightarrow 3\pi^0$
1449 ± 13	4.3k	4 GARMASH	06	BELL $B^+ \rightarrow K^+\pi^+\pi^-$
1350 ± 50		ABLIKIM	05	BES2 $J/\psi \rightarrow \phi\pi^+\pi^-$
$1265 \pm 30^{+20}_{-35}$		ABLIKIM	05Q	BES2 $\psi(2S) \rightarrow \gamma\pi^+\pi^-K^+K^-$
$1434 \pm 18 \pm 9$	848	AITALA	01A	E791 $D_s^+ \rightarrow \pi^-\pi^+\pi^+$
1308 ± 10		BARBERIS	99B	OMEG $450 pp \rightarrow p_S p_f \pi^+\pi^-$
1315 ± 50		BELLAZZINI	99	GAM4 $450 pp \rightarrow p p \pi^0\pi^0$
1315 ± 30		ALDE	98	GAM4 $100 \pi^-\pi^+ \rightarrow \pi^0\pi^0\eta$
1280 ± 55		BERTIN	98	OBLX $0.05-0.405 \bar{p}p \rightarrow \pi^+\pi^+\pi^-$
1186		5,6 TORNQVIST	95	RVUE $\pi\pi \rightarrow \pi\pi, K\bar{K}, K\pi, \eta\pi$
1472 ± 12		ARMSTRONG	91	OMEG $300 pp \rightarrow p p \pi\pi, p p K\bar{K}$
1275 ± 20		BREAKSTONE	90	SFM $62 pp \rightarrow p p \pi^+\pi^-$
1420 ± 20		AKESSON	86	SPEC $63 pp \rightarrow p p \pi^+\pi^-$
1256		FROGGATT	77	RVUE $\pi^+\pi^-\pi^0$ channel

1 Breit-Wigner mass.
 2 Breit-Wigner mass. May also be the $f_0(1500)$.
 3 Reanalysis of ABELE 96c data.
 4 Also observed by GARMASH 07 in $B^0 \rightarrow K_S^0 \pi^+\pi^-$ decays. Supersedes GARMASH 05.
 5 Uses data from BEIER 72B, OCHS 73, HYAMS 73, GRAYER 74, ROSSELET 77, CASON 83, ASTON 88, and ARMSTRONG 91B. Coupled channel analysis with flavor symmetry and all light two-pseudoscalars systems.
 6 Also observed by ASNER 00 in $\tau^- \rightarrow \pi^-\pi^0\pi^0\nu_\tau$ decays

$K\bar{K}$ MODE

VALUE (MeV)	EVTS	DOCUMENT ID	TECN	COMMENT
••• We do not use the following data for averages, fits, limits, etc. •••				
$1422 \pm 15 \pm 28$		1 AAJ	19H	LHCb $pp \rightarrow D^\pm X$
$1360 \pm 31 \pm 28$	430	2,3 DOBBS	15	$J/\psi \rightarrow \gamma K^+K^-$
$1350 \pm 48 \pm 15$	168	2,3 DOBBS	15	$\psi(2S) \rightarrow \gamma K^+K^-$
1440 ± 6		VLADIMIRSK...	06	SPEC $40 \pi^-\pi^+ \rightarrow K_S^0 K_L^0 \eta$
1391 ± 10		TIKHOMIROV	03	SPEC $40.0 \pi^-C \rightarrow K_S^0 K_L^0 K_L^0 X$
1440 ± 50		BOLONKIN	88	SPEC $40 \pi^-\pi^+ \rightarrow K_S^0 K_L^0 \eta$
1463 ± 9		ETKIN	82B	MPS $23 \pi^-\pi^+ \rightarrow n 2K_S^0$
1425 ± 15		WICKLUND	80	SPEC $6 \pi N \rightarrow K^+K^-N$
~ 1300		POLYCHRO...	79	STRC $7 \pi^-\pi^+ \rightarrow n 2K_S^0$

1 From the $D^\pm \rightarrow K^\pm K^+K^-$ Dalitz plot fit with the isobar model A.
 2 Using CLEO-c data but not authored by the CLEO Collaboration.
 3 From a fit to a Breit-Wigner line shape with fixed $\Gamma = 346$ MeV.

4π MODE $2(\pi\pi)_S + \rho\rho$

VALUE (MeV)	EVTS	DOCUMENT ID	TECN	COMMENT
••• We do not use the following data for averages, fits, limits, etc. •••				
1395 ± 40		ABELE	01	CBAR $0.0 \bar{p}d \rightarrow \pi^-\pi^0 p$
1374 ± 38		AMSLER	94	CBAR $0.0 \bar{p}p \rightarrow \pi^+\pi^-\pi^0$
1345 ± 12		ADAMO	93	OBLX $\bar{p}p \rightarrow 3\pi^+\pi^-$
1386 ± 30		GASPERO	93	DBC $0.0 \bar{p}n \rightarrow 2\pi^+3\pi^-$
~ 1410	5751	1 BETTINI	66	DBC $0.0 \bar{p}n \rightarrow 2\pi^+3\pi^-$
1 $\rho\rho$ dominant.				

$\eta\eta$ MODE

VALUE (MeV)	DOCUMENT ID	TECN	COMMENT
••• We do not use the following data for averages, fits, limits, etc. •••			
$1262^{+51+82}_{-78-103}$	1 UEHARA	10A	BELL $10.6 e^+e^- \rightarrow e^+e^-\eta\eta$
1430	AMSLER	92	CBAR $0.0 \bar{p}p \rightarrow \pi^0\eta\eta$
1220 ± 40	ALDE	86D	GAM4 $100 \pi^-\pi^+ \rightarrow n 2\eta$

1 Breit-Wigner mass. May also be the $f_0(1500)$.

Meson Particle Listings

 $f_0(1370)$

COUPLED CHANNEL MODE

VALUE (MeV)	DOCUMENT ID	TECN	COMMENT
-------------	-------------	------	---------

• • • We do not use the following data for averages, fits, limits, etc. • • •

$1330.2^{+5.9}_{-6.5} \pm 5.1$	¹ AAIJ	19H	LHCB $pp \rightarrow D^\pm X$
1306 ± 20	² ANISOVICH	03	RVUE

¹ From the $D^\pm \rightarrow K^\pm K^+ K^-$ Dalitz plot fit with the Triple-M amplitude in the multi-meson model of AOUDE 18.
² K-matrix pole from combined analysis of $\pi^- p \rightarrow \pi^0 \pi^0 n$, $\pi^- p \rightarrow K \bar{K} n$, $\pi^+ \pi^- \rightarrow \pi^+ \pi^-$, $\bar{p} p \rightarrow \pi^0 \pi^0 \pi^0$, $\pi^0 \eta \eta$, $\pi^0 \pi^0 \eta$, $\pi^+ \pi^- \pi^0$, $K^+ K^- \pi^0$, $K_S^0 K_S^0 \pi^0$, $K^+ K_S^0 \pi^-$ at rest, $\bar{p} n \rightarrow \pi^- \pi^- \pi^+$, $K_S^0 K^- \pi^0$, $K_S^0 K_S^0 \pi^-$ at rest.

 $f_0(1370)$ BREIT-WIGNER WIDTH

VALUE (MeV)	DOCUMENT ID
-------------	-------------

200 to 500 OUR ESTIMATE

 $\pi\pi$ MODE

VALUE (MeV)	EVTs	DOCUMENT ID	TECN	COMMENT
-------------	------	-------------	------	---------

• • • We do not use the following data for averages, fits, limits, etc. • • •

300 ± 80		¹ AUBERT	09L	BABR $B^\pm \rightarrow \pi^\pm \pi^\pm \pi^\mp$
$90^{+2}_{-1} \pm 50_{-22}$		² UEHARA	08A	BELL $10.6 e^+ e^- \rightarrow e^+ e^- \pi^0 \pi^0$
298 ± 21	2.6k	BONVICINI	07	CLEO $D^+ \rightarrow \pi^- \pi^+ \pi^+$
126 ± 25	4286	³ GARMASH	06	BELL $B^+ \rightarrow K^+ \pi^+ \pi^-$
265 ± 40		ABLIKIM	05	BES2 $J/\psi \rightarrow \phi \pi^+ \pi^-$
$350 \pm 100^{+105}_{-60}$		ABLIKIM	05Q	BES2 $\psi(2S) \rightarrow \gamma \pi^+ \pi^- K^+ K^-$
$173 \pm 32 \pm 6$	848	AITALA	01A	E791 $D_S^+ \rightarrow \pi^- \pi^+ \pi^+$
222 ± 20		BARBERIS	99B	OMEG $450 pp \rightarrow p_S p_f \pi^+ \pi^-$
255 ± 60		BELLAZZINI	99	GAM4 $450 pp \rightarrow p p \pi^0 \pi^0$
190 ± 50		ALDE	98	GAM4 $100 \pi^- p \rightarrow \pi^0 \pi^0 n$
323 ± 13		BERTIN	98	OBLX $0.05-0.405 \bar{p} p \rightarrow \pi^+ \pi^+ \pi^-$
350		^{4,5} TORNQVIST	95	RVUE $\pi\pi \rightarrow \pi\pi$, $K\bar{K}$, $K\pi$, $\eta\pi$
195 ± 33		ARMSTRONG	91	OMEG $300 pp \rightarrow p p \pi\pi$, $p p K\bar{K}$
285 ± 60		BREAKSTONE	90	SFM $62 pp \rightarrow p p \pi^+ \pi^-$
460 ± 50		AKESSON	86	SPEC $63 pp \rightarrow p p \pi^+ \pi^-$
~ 400		⁶ FROGGATT	77	RVUE $\pi^+ \pi^-$ channel

¹ The systematic errors are not reported.

² Breit-Wigner width. May also be the $f_0(1500)$.

³ Also observed by GARMASH 07 in $B^0 \rightarrow K_S^0 \pi^+ \pi^-$ decays. Supersedes GARMASH 05.

⁴ Uses data from BEIER 72b, OCHS 73, HYAMS 73, GRAYER 74, ROSSELET 77, CA-SON 83, ASTON 88, and ARMSTRONG 91b. Coupled channel analysis with flavor symmetry and all light two-pseudoscalars systems.

⁵ Also observed by ASNER 00 in $\tau^- \rightarrow \pi^- \pi^0 \nu_\tau$ decays

⁶ Width defined as distance between 45 and 135° phase shift.

 $K\bar{K}$ MODE

VALUE (MeV)	DOCUMENT ID	TECN	COMMENT
-------------	-------------	------	---------

• • • We do not use the following data for averages, fits, limits, etc. • • •

$324 \pm 38 \pm 42$		¹ AAIJ	19H	LHCB $pp \rightarrow D^\pm X$
121 ± 15		VLADIMIRSK...06	SPEC	$40 \pi^- p \rightarrow K_S^0 K_S^0 n$
55 ± 26		TIKHOMIROV 03	SPEC	$40.0 \pi^- C \rightarrow K_S^0 K_S^0 K_L^0 X$
250 ± 80		BOLONKIN 88	SPEC	$40 \pi^- p \rightarrow K_S^0 K_S^0 n$
118^{+138}_{-16}		ETKIN 82b	MPS	$23 \pi^- p \rightarrow n 2K_S^0$
160 ± 30		WICKLUND 80	SPEC	$6 \pi N \rightarrow K^+ K^- N$
~ 150		POLYCHRO... 79	STRC	$7 \pi^- p \rightarrow n 2K_S^0$

¹ From the $D^\pm \rightarrow K^\pm K^+ K^-$ Dalitz plot fit with the isobar model A.

 4π MODE $2(\pi\pi)_S + \rho\rho$

VALUE (MeV)	EVTs	DOCUMENT ID	TECN	COMMENT
-------------	------	-------------	------	---------

• • • We do not use the following data for averages, fits, limits, etc. • • •

275 ± 55		ABELE	01	CBAR $0.0 \bar{p} d \rightarrow \pi^- 4\pi^0 p$
375 ± 61		AMSLER	94	CBAR $0.0 \bar{p} p \rightarrow \pi^+ \pi^- 3\pi^0$
398 ± 26		ADAMO	93	OBLX $\bar{p} p \rightarrow 3\pi^+ 2\pi^-$
310 ± 50		GASPERO	93	DBC $0.0 \bar{p} n \rightarrow 2\pi^+ 3\pi^-$
~ 90	5751	¹ BETTINI	66	DBC $0.0 \bar{p} n \rightarrow 2\pi^+ 3\pi^-$

¹ $\rho\rho$ dominant.

 $\eta\eta$ MODE

VALUE (MeV)	DOCUMENT ID	TECN	COMMENT
-------------	-------------	------	---------

• • • We do not use the following data for averages, fits, limits, etc. • • •

$484^{+246}_{-170} \pm 246_{-263}$		¹ UEHARA	10A	BELL $10.6 e^+ e^- \rightarrow e^+ e^- \eta \eta$
250		AMSLER	92	CBAR $0.0 \bar{p} p \rightarrow \pi^0 \eta \eta$
320 ± 40		ALDE	86D	GAM4 $100 \pi^- p \rightarrow n 2\eta$

¹ Breit-Wigner width. May also be the $f_0(1500)$.

COUPLED CHANNEL MODE

VALUE (MeV)	DOCUMENT ID	TECN
-------------	-------------	------

• • • We do not use the following data for averages, fits, limits, etc. • • •

147^{+30}_{-50}	¹ ANISOVICH	03	RVUE
-------------------	------------------------	----	------

¹ K-matrix pole from combined analysis of $\pi^- p \rightarrow \pi^0 \pi^0 n$, $\pi^- p \rightarrow K \bar{K} n$, $\pi^+ \pi^- \rightarrow \pi^+ \pi^-$, $\bar{p} p \rightarrow \pi^0 \pi^0 \pi^0$, $\pi^0 \eta \eta$, $\pi^0 \pi^0 \eta$, $\pi^+ \pi^- \pi^0$, $K^+ K^- \pi^0$, $K_S^0 K_S^0 \pi^0$, $K^+ K_S^0 \pi^-$ at rest, $\bar{p} n \rightarrow \pi^- \pi^- \pi^+$, $K_S^0 K^- \pi^0$, $K_S^0 K_S^0 \pi^-$ at rest.

 $f_0(1370)$ DECAY MODES

Mode	Fraction (Γ_i/Γ)
Γ_1 $\pi\pi$	seen
Γ_2 4π	seen
Γ_3 $4\pi^0$	seen
Γ_4 $2\pi^+ 2\pi^-$	seen
Γ_5 $\pi^+ \pi^- 2\pi^0$	seen
Γ_6 $\rho\rho$	seen
Γ_7 $2(\pi\pi)_S$ -wave	seen
Γ_8 $\pi(1300)\pi$	seen
Γ_9 $a_1(1260)\pi$	seen
Γ_{10} $\eta\eta$	seen
Γ_{11} $K\bar{K}$	seen
Γ_{12} $K\bar{K} n\pi$	not seen
Γ_{13} 6π	not seen
Γ_{14} $\omega\omega$	not seen
Γ_{15} $\gamma\gamma$	seen
Γ_{16} $e^+ e^-$	not seen

 $f_0(1370)$ PARTIAL WIDTHS

$\Gamma(\gamma\gamma)$ Γ_{15}
 See $\gamma\gamma$ widths under $f_0(500)$ and MORGAN 90.

$\Gamma(e^+ e^-)$ Γ_{16}

VALUE (eV)	CL%	DOCUMENT ID	TECN	COMMENT
<20	90	VOROBYEV	88	ND $e^+ e^- \rightarrow \pi^0 \pi^0$

 $f_0(1370)$ $\Gamma(i)\Gamma(\gamma\gamma)/\Gamma(\text{total})$

$\Gamma(\eta\eta) \times \Gamma(\gamma\gamma)/\Gamma_{\text{total}}$ $\Gamma_{10}\Gamma_{15}/\Gamma$

VALUE (eV)	DOCUMENT ID	TECN	COMMENT
------------	-------------	------	---------

• • • We do not use the following data for averages, fits, limits, etc. • • •

$121^{+133}_{-53} \pm 169_{-106}$	¹ UEHARA	10A	BELL $10.6 e^+ e^- \rightarrow e^+ e^- \eta \eta$
-----------------------------------	---------------------	-----	---

¹ Including interference with the $f_2'(1525)$ (parameters fixed to the values from the 2008 edition of this review, PDG 08) and $f_2(1270)$. May also be the $f_0(1500)$.

 $f_0(1370)$ BRANCHING RATIOS

$\Gamma(\pi\pi)/\Gamma_{\text{total}}$ Γ_1/Γ

VALUE	CL%	DOCUMENT ID	TECN	COMMENT
-------	-----	-------------	------	---------

• • • We do not use the following data for averages, fits, limits, etc. • • •

<0.10	95	OCHS	13	RVUE
0.26 ± 0.09		BUGG	96	RVUE
<0.15		¹ AMSLER	94	CBAR $\bar{p} p \rightarrow \pi^+ \pi^- 3\pi^0$
<0.06		GASPERO	93	DBC $0.0 \bar{p} n \rightarrow \text{hadrons}$

¹ Using AMSLER 95B ($3\pi^0$).

$\Gamma(4\pi)/\Gamma_{\text{total}}$ $\Gamma_2/\Gamma = (\Gamma_3 + \Gamma_4 + \Gamma_5)/\Gamma$

VALUE	DOCUMENT ID	TECN	COMMENT
-------	-------------	------	---------

• • • We do not use the following data for averages, fits, limits, etc. • • •

>0.72	GASPERO	93	DBC $0.0 \bar{p} n \rightarrow \text{hadrons}$
-------	---------	----	--

$\Gamma(4\pi^0)/\Gamma(4\pi)$ Γ_3/Γ_2

VALUE	DOCUMENT ID	TECN	COMMENT
-------	-------------	------	---------

• • • We do not use the following data for averages, fits, limits, etc. • • •

seen	ABELE	96	CBAR $0.0 \bar{p} p \rightarrow 5\pi^0$
0.068 ± 0.005	¹ GASPERO	93	DBC $0.0 \bar{p} n \rightarrow \text{hadrons}$

¹ Model-dependent evaluation.

$\Gamma(2\pi^+ 2\pi^-)/\Gamma(4\pi)$ $\Gamma_4/\Gamma_2 = \Gamma_4/(\Gamma_3 + \Gamma_4 + \Gamma_5)$

VALUE	DOCUMENT ID	TECN	COMMENT
-------	-------------	------	---------

• • • We do not use the following data for averages, fits, limits, etc. • • •

0.420 ± 0.014	¹ GASPERO	93	DBC $0.0 \bar{p} n \rightarrow 2\pi^+ 3\pi^-$
-------------------	----------------------	----	---

¹ Model-dependent evaluation.

See key on page 1171

Meson Particle Listings

$f_0(1370), \pi_1(1400)$

$\Gamma(\pi^+\pi^-\pi^0)/\Gamma(4\pi)$ $\Gamma_5/\Gamma_2 = \Gamma_5/(\Gamma_3+\Gamma_4+\Gamma_5)$

VALUE	DOCUMENT ID	TECN	COMMENT
0.512±0.019	¹ GASPERO 93	DBC	0.0 $\bar{p}n \rightarrow$ hadrons

• • • We do not use the following data for averages, fits, limits, etc. • • •

¹ Model-dependent evaluation.

$\Gamma(\rho\rho)/\Gamma(4\pi)$ Γ_6/Γ_2

VALUE	DOCUMENT ID	TECN	COMMENT
0.26±0.07	ABELE 01B	CBAR	0.0 $\bar{p}d \rightarrow 5\pi p$

• • • We do not use the following data for averages, fits, limits, etc. • • •

$\Gamma(2(\pi\pi)s\text{-wave})/\Gamma(\pi\pi)$ Γ_7/Γ_1

VALUE	DOCUMENT ID	TECN	COMMENT
5.6±2.6	¹ ABELE 01	CBAR	0.0 $\bar{p}d \rightarrow \pi^- 4\pi^0 p$

• • • We do not use the following data for averages, fits, limits, etc. • • •

¹ From the combined data of ABELE 96 and ABELE 96c.

$\Gamma(2(\pi\pi)s\text{-wave})/\Gamma(4\pi)$ Γ_7/Γ_2

VALUE	DOCUMENT ID	TECN	COMMENT
0.51±0.09	ABELE 01B	CBAR	0.0 $\bar{p}d \rightarrow 5\pi p$

• • • We do not use the following data for averages, fits, limits, etc. • • •

$\Gamma(\rho\rho)/\Gamma(2(\pi\pi)s\text{-wave})$ Γ_6/Γ_7

VALUE	DOCUMENT ID	TECN	COMMENT
large	BARBERIS 00c		450 $pp \rightarrow p_f 4\pi p_s$
1.6 ± 0.2	AMSLER 94	CBAR	$\bar{p}p \rightarrow \pi^+ \pi^- 3\pi^0$
~0.65	GASPERO 93	DBC	0.0 $\bar{p}n \rightarrow$ hadrons

• • • We do not use the following data for averages, fits, limits, etc. • • •

$\Gamma(\pi(1300)\pi)/\Gamma(4\pi)$ Γ_8/Γ_2

VALUE	DOCUMENT ID	TECN	COMMENT
0.17±0.06	ABELE 01B	CBAR	0.0 $\bar{p}d \rightarrow 5\pi p$

• • • We do not use the following data for averages, fits, limits, etc. • • •

$\Gamma(a_1(1260)\pi)/\Gamma(4\pi)$ Γ_9/Γ_2

VALUE	DOCUMENT ID	TECN	COMMENT
0.06±0.02	ABELE 01B	CBAR	0.0 $\bar{p}d \rightarrow 5\pi p$

• • • We do not use the following data for averages, fits, limits, etc. • • •

$\Gamma(\eta\eta)/\Gamma(4\pi)$ $\Gamma_{10}/\Gamma_2 = \Gamma_{10}/(\Gamma_3+\Gamma_4+\Gamma_5)$

VALUE	DOCUMENT ID	TECN	COMMENT
(28 ± 11) × 10 ⁻³	¹ ANISOVICH 02D	SPEC	Combined fit
(4.7 ± 2.0) × 10 ⁻³	BARBERIS 00E		450 $pp \rightarrow p_f \eta p_s$

• • • We do not use the following data for averages, fits, limits, etc. • • •

¹ From a combined K-matrix analysis of Crystal Barrel (0. $p\bar{p} \rightarrow \pi^0 \pi^0 \pi^0, \pi^0 \eta, \pi^0 \pi^0 \eta$), GAMS ($\pi p \rightarrow \pi^0 \pi^0 n, \eta \eta n, \eta \eta' n$), and BNL ($\pi p \rightarrow K \bar{K} n$) data.

$\Gamma(K\bar{K})/\Gamma_{\text{total}}$ Γ_{11}/Γ

VALUE	DOCUMENT ID	TECN	COMMENT
0.35±0.13	BUGG 96	RVUE	

• • • We do not use the following data for averages, fits, limits, etc. • • •

$\Gamma(K\bar{K})/\Gamma(\pi\pi)$ Γ_{11}/Γ_1

VALUE	DOCUMENT ID	TECN	COMMENT
0.08±0.08	ABLIKIM 05	BES2	$J/\psi \rightarrow \phi \pi^+ \pi^-, \phi K^+ K^-$
0.91±0.20	¹ BARGIOTTI 03	OBLX	$\bar{p}p$
0.12±0.06	² ANISOVICH 02D	SPEC	Combined fit
0.46±0.15±0.11	BARBERIS 99D	OMEG	450 $pp \rightarrow K^+ K^-, \pi^+ \pi^-$

• • • We do not use the following data for averages, fits, limits, etc. • • •

¹ Coupled channel analysis of $\pi^+ \pi^- \pi^0, K^+ K^- \pi^0$, and $K^\pm K_S^0 \pi^\mp$.

² From a combined K-matrix analysis of Crystal Barrel (0. $p\bar{p} \rightarrow \pi^0 \pi^0 \pi^0, \pi^0 \eta, \pi^0 \pi^0 \eta$), GAMS ($\pi p \rightarrow \pi^0 \pi^0 n, \eta \eta n, \eta \eta' n$), and BNL ($\pi p \rightarrow K \bar{K} n$) data.

$\Gamma(K\bar{K}n\pi)/\Gamma_{\text{total}}$ Γ_{12}/Γ

VALUE	DOCUMENT ID	TECN	COMMENT
<0.03	GASPERO 93	DBC	0.0 $\bar{p}n \rightarrow$ hadrons

• • • We do not use the following data for averages, fits, limits, etc. • • •

$\Gamma(6\pi)/\Gamma_{\text{total}}$ Γ_{13}/Γ

VALUE	DOCUMENT ID	TECN	COMMENT
<0.22	GASPERO 93	DBC	0.0 $\bar{p}n \rightarrow$ hadrons

• • • We do not use the following data for averages, fits, limits, etc. • • •

$\Gamma(\omega\omega)/\Gamma_{\text{total}}$ Γ_{14}/Γ

VALUE	DOCUMENT ID	TECN	COMMENT
<0.13	GASPERO 93	DBC	0.0 $\bar{p}n \rightarrow$ hadrons

• • • We do not use the following data for averages, fits, limits, etc. • • •

$f_0(1370)$ REFERENCES

PELAEZ 23	PRL 130 051902	J.R. Pelaez, A. Rodas, J. Ruiz de Elvira (MADU+)
SARANTSEV 21	PL B816 136227	A.V. Sarantsev et al. (BONN, PNPI)
ALBRECHT 20	EPJ C80 453	M. Albrecht et al. (Crystal Barrel Collab.)
AAIJ 19H	JHEP 1904 063	R. Aaij et al. (LHCb Collab.)
AOUDE 18	PR D98 056021	R.T. Aoude et al.
DOBBS 15	PR D91 052006	S. Dobbs et al. (NWES)
OCHS 13	JP 640 043001	W. Ochs
UEHARA 10A	PR D82 114031	S. Uehara et al. (BELLE Collab.)
ANISOVICH 09L	IJMP A24 2481	V.V. Anisovich, A.V. Sarantsev (PNPI)
AUBERT 09L	PR D79 072006	B. Aubert et al. (BABAR Collab.)
PDG 08	PL B667 1	C. Amisler et al. (PDG Collab.)
UEHARA 08A	PR D78 052004	S. Uehara et al. (BELLE Collab.)
BONVICINI 07	PR D76 012001	G. Bonvicini et al. (CLEO Collab.)
BUGG 07A	JP G34 151	D.V. Bugg et al.
GARMASH 07	PR D75 012006	A. Garmash et al. (BELLE Collab.)
GARMASH 06	PRL 96 251803	A. Garmash et al. (BELLE Collab.)
PDG 06	JP G33 1	W.-M. Yao et al. (PDG Collab.)
VLADIMIRSK... 06	PAN 69 493	V.V. Vladimirov et al. (ITEP, Moscow)
ABLIKIM 05Q	PL B607 243	M. Ablikim et al. (BES Collab.)
ABLIKIM 05Q	PR D72 092002	M. Ablikim et al. (BES Collab.)
GARMASH 05	PR D71 092003	A. Garmash et al. (BELLE Collab.)
ANISOVICH 03	EPJ A16 229	V.V. Anisovich et al.
BARGIOTTI 03	EPJ C26 371	M. Bargiotti et al. (OBELIX Collab.)
TIKHOMIROV 03	PAN 66 828	G.D. Tikhomirov et al.
ANISOVICH 02D	Translated from YAF 66 860.	V.V. Anisovich et al.
ABELE 01	EPJ C19 667	A. Abele et al. (Crystal Barrel Collab.)
ABELE 01B	EPJ C21 261	A. Abele et al. (Crystal Barrel Collab.)
AITALA 01A	PRL 86 765	E.M. Aitala et al. (FNAL E791 Collab.)
ASNER 00	PR D61 012002	D.M. Asner et al. (CLEO Collab.)
BARBERIS 00C	PL B471 440	D. Barberis et al. (WA 102 Collab.)
BARBERIS 00E	PL B479 59	D. Barberis et al. (WA 102 Collab.)
BARBERIS 99B	PL B453 316	D. Barberis et al. (Omega Expt.)
BARBERIS 99D	PL B462 462	D. Barberis et al. (Omega Expt.)
BELLAZZINI 99	PL B467 296	R. Bellazzini et al.
KAMINSKI 99	EPJ C9 141	R. Kaminski, L. Lesniak, B. Loiseau (CRAC, PARIN)
ALDE 98	EPJ A3 361	D. Alde et al. (GAM4 Collab.)
Also	PAN 62 405	D. Alde et al. (GAMS Collab.)
ANISOVICH 98B	SFU 41 419	V.V. Anisovich et al.
BERTIN 98	PR D57 55	A. Bertin et al. (OBELIX Collab.)
BARBERIS 97B	PL B413 217	D. Barberis et al. (WA 102 Collab.)
BERTIN 97C	PL B408 476	A. Bertin et al. (OBELIX Collab.)
ABELE 96B	PL B380 453	A. Abele et al. (Crystal Barrel Collab.)
ABELE 96B	PL B385 425	A. Abele et al. (Crystal Barrel Collab.)
ABELE 96C	NP A609 562	A. Abele et al. (Crystal Barrel Collab.)
BUGG 96	NP B471 59	D.V. Bugg, A.V. Sarantsev, B.S. Zou (LOQM, PNPI)
AMSLER 95B	PL B342 433	C. Amisler et al. (Crystal Barrel Collab.)
AMSLER 95C	PL B353 571	C. Amisler et al. (Crystal Barrel Collab.)
AMSLER 95D	PL B355 425	C. Amisler et al. (Crystal Barrel Collab.)
JANSSSEN 95	PR D52 2690	G. Janssen et al. (STON, ADL, IULI)
TORNGVIST 95	ZPHY C68 647	N.A. Torngvist (HELS)
AMSLER 94D	PL B322 431	C. Amisler et al. (Crystal Barrel Collab.)
AMSLER 94D	PL B333 277	C. Amisler et al. (Crystal Barrel Collab.)
ANISOVICH 94	PL B323 233	V.V. Anisovich et al. (Crystal Barrel Collab.)
BUGG 94	PR D50 4412	D.V. Bugg et al. (LOQM)
KAMINSKI 94	PR D50 3145	R. Kaminski, L. Lesniak, J.P. Maillet (CRAC+)
ADAMO 93	NP A558 13C	A. Adamo et al. (OBELIX Collab.)
GASPERO 93	NP A562 407	M. Gaspero (ROMA1) JPC
AMSLER 92	PL B291 347	C. Amisler et al. (Crystal Barrel Collab.)
ARMSTRONG 91B	ZPHY C51 351	T.A. Armstrong et al. (ATHU, BARI, BIRH+)
ARMSTRONG 91B	ZPHY C52 389	T.A. Armstrong et al. (ATHU, BARI, BIRH+)
BREAKSTONE 90	ZPHY C48 569	A.M. Breakstone et al. (ISU, BGM, CERN+)
MORGAN 90	ZPHY C48 623	D. Morgan, M.R. Pennington (RAL, DURH)
ASTON 88	NP B296 493	D. Aston et al. (SLAC, MAGO, CINC, INUS)
BOLONKIN 88	NP B309 426	B.V. Bolonkin et al. (ITEP, SERP)
FALVARD 88	PR D38 2706	A. Falvard et al. (CLER, FRAS, LAL O+)
VOROBYEV 88	SJNP 48 273	P.V. Vorobyev et al. (NOVO)
AU 87	PR D35 1633	K.L. Au, D. Morgan, M.R. Pennington (DURH, RAL)
AKESSON 86	NP B264 154	T. Akesson et al. (Axial Field Spec. Collab.)
ALDE 86D	NP B269 485	D.M. Alde et al. (BELG, LAPP, SERP, CERN+)
LONGACRE 86	PL B177 223	R.S. Longacre et al. (BNL, BRAN, CUNY+)
BINON 84C	NC 80A 363	F.G. Binon et al. (BELG, LAPP, SERP+)
BINON 83	NC 78A 313	F.G. Binon et al. (BELG, LAPP, SERP+)
CASON 83	PR D28 1586	N.M. Cason et al. (NDAM, ANL)
ETKIN 82B	PR D25 1786	A. Etkin et al. (BNL, CUNY, TUFTS, VAND)
WICKLUND 80	PRL 45 1469	A.B. Wicklund et al. (ANL)
BECKER 79	NP B151 46	H. Becker et al. (MPIM, CERN, ZEEM, CRAC)
POLYCHRO... 79	PR D19 1317	V.A. Polychronakos et al. (NDAM, ANL)
FROGGATT 77	NP B129 89	C.D. Froggatt, J.L. Petersen (GLAS, NORD)
ROSSELET 77	PR D15 574	L. Rosselet et al. (GEVA, SAACL)
HYAMS 75	NP B100 205	B.D. Hyams et al. (CERN, MPIM)
GRAYEY 74	NP B75 189	G. Grayey et al. (CERN, MPIM)
HYAMS 73	NP B64 134	B.D. Hyams et al. (CERN, MPIM)
OCHS 73	Thesis	W. Ochs (MPIM, MUNI)
BEIER 72B	PRL 29 511	E.W. Beier et al. (PENN)
BETTINI 66	NC 42A 695	A. Bettini et al. (PADO, PISA)

$\pi_1(1400)$

$$I^G(J^{PC}) = 1^-(1^-+)$$

OMITTED FROM SUMMARY TABLE

Coupled channel analyses favor the existence of only one broad 1^-+ isovector state consistent with $\pi_1(1600)$ in the 1400–1600 MeV region. See also $\pi_1(1600)$.

Meson Particle Listings

$\eta(1405)$

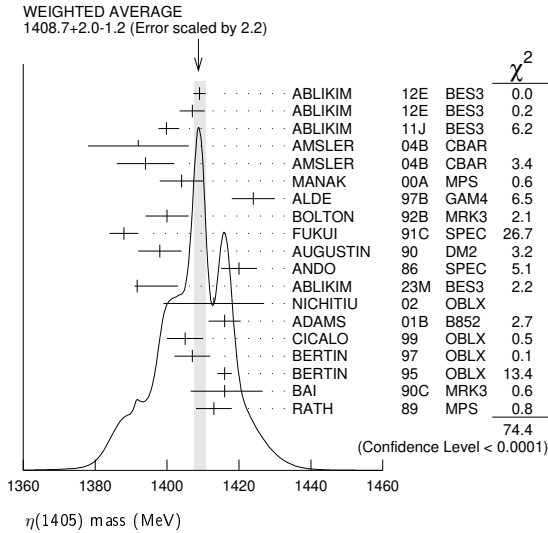
$\eta(1405)$

$$J^G(J^{PC}) = 0^+(0^{-+})$$

See also the $\eta(1475)$.

$\eta(1405)$ MASS

VALUE (MeV) DOCUMENT ID
1408.7 \pm 2.0 OUR AVERAGE Includes data from the 2 datablocks that follow this one.
 Error includes scale factor of 2.2. See the ideogram below.



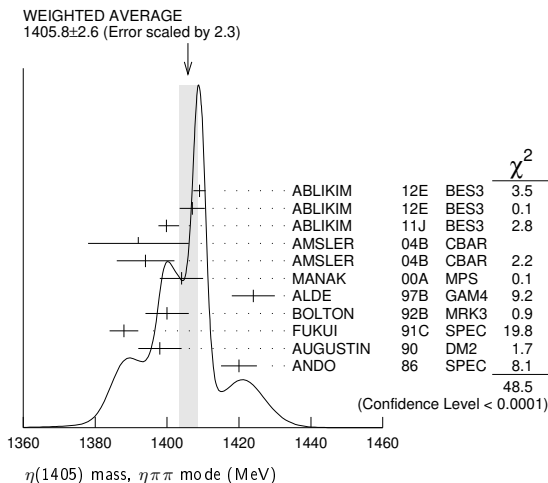
$\eta\pi\pi$ MODE

VALUE (MeV) EVTS DOCUMENT ID TECN COMMENT
 The data in this block is included in the average printed for a previous datablock.

1405.8 \pm 2.6 OUR AVERAGE Error includes scale factor of 2.3. See the ideogram below.

1409.0 \pm 1.7	743	ABLIKIM	12E BES3	$J/\psi \rightarrow \gamma(\pi^+\pi^-\pi^0)$
1407.0 \pm 3.5	198	ABLIKIM	12E BES3	$J/\psi \rightarrow \gamma(\pi^0\pi^0\pi^0)$
1399.8 \pm 2.2 \pm 2.8		1 ABLIKIM	11J BES3	$J/\psi \rightarrow \omega(\eta\pi^+\pi^-)$
1392 \pm 14	900 \pm 375	AMSLER	04B CBAR	$0\bar{p}p \rightarrow \pi^+\pi^-\pi^+\pi^- \eta$
1394 \pm 8	6.6 \pm 2.0k	AMSLER	04B CBAR	$0\bar{p}p \rightarrow \pi^+\pi^-\pi^0\pi^0 \eta$
1404 \pm 6	9082	MANAK	00A MPS	$18\pi^-\pi^- \rightarrow \eta\pi^+\pi^- n$
1424 \pm 6	2200	ALDE	97B GAM4	$100\pi^-\pi^- \rightarrow \eta\pi^0\pi^0 n$
1400 \pm 6		2 BOLTON	92B MRK3	$J/\psi \rightarrow \gamma\eta\pi^+\pi^-$
1388 \pm 4		FUKUI	91C SPEC	$8.95\pi^-\pi^- \rightarrow \eta\pi^+\pi^- n$
1398 \pm 6	261	3 AUGUSTIN	90 DM2	$J/\psi \rightarrow \gamma\eta\pi^+\pi^-$
1420 \pm 5		ANDO	86 SPEC	$8\pi^-\pi^- \rightarrow \eta\pi^+\pi^- n$
1404.0 \pm 11.0	195	ABLIKIM	19B/BES3	$e^+e^- \rightarrow \psi(2S)$
1385 \pm 7		BAI	99 BES	$J/\psi \rightarrow \gamma\eta\pi^+\pi^-$
1409 \pm 3		4 AMSLER	95F CBAR	$0\bar{p}p \rightarrow \pi^+\pi^-\pi^0\pi^0 \eta$

- 1 The selected process is $J/\psi \rightarrow \omega a_0(980)\pi$.
- 2 From fit to the $a_0(980)\pi 0^{-+}$ partial wave.
- 3 Best fit with a single Breit Wigner.
- 4 Superseded by AMSLER 04B.



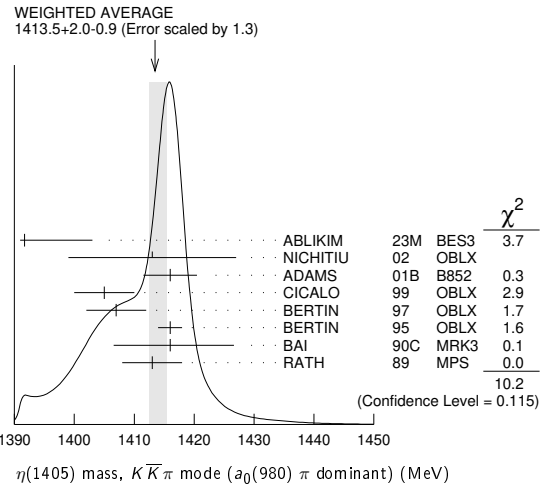
$K\bar{K}\pi$ MODE ($a_0(980)\pi$ or direct $K\bar{K}\pi$)

VALUE (MeV) EVTS DOCUMENT ID TECN COMMENT
 The data in this block is included in the average printed for a previous datablock.

1413.5 \pm 0.9 OUR AVERAGE Error includes scale factor of 1.3. See the ideogram below.

1391.7 \pm 0.7 \pm 11.3	126k	1 ABLIKIM	23M BES3	$J/\psi \rightarrow \gamma K_S^0 K_S^0 \pi^0$
1413 \pm 14	3651	2 NICHITIU	02 OBLX	$0\bar{p}p \rightarrow K^+ K^- \pi^+ \pi^- \pi^0$
1416 \pm 4 \pm 2	20k	ADAMS	01B B852	$18\text{ GeV } \pi^-\pi^- \rightarrow K^+ K^- \pi^0 n$
1405 \pm 5		3 CICALO	99 OBLX	$0\bar{p}p \rightarrow K^\pm K_S^0 \pi^\mp \pi^\pm \pi^-$
1407 \pm 5		3 BERTIN	97 OBLX	$0\bar{p}p \rightarrow K^\pm(K^0) \pi^\mp \pi^\pm \pi^-$
1416 \pm 2		3 BERTIN	95 OBLX	$0\bar{p}p \rightarrow K\bar{K}\pi\pi$
1416 \pm 8 \pm 7	700	4 BAI	90C MRK3	$J/\psi \rightarrow \gamma K_S^0 K^\pm \pi^\mp$
1413 \pm 5		4 RATH	89 MPS	$21.4\pi^-\pi^- \rightarrow n K_S^0 K_S^0 \pi^0$
1459 \pm 5		5 AUGUSTIN	92 DM2	$J/\psi \rightarrow \gamma K\bar{K}\pi$

- 1 ABLIKIM 23M reports for this state a significance from the fit much higher than 35 σ .
- 2 Decaying dominantly directly to $K^+ K^- \pi^0$.
- 3 Decaying into $(K\bar{K})S\pi$, $(K\pi)S\bar{K}$, and $a_0(980)\pi$.
- 4 From fit to the $a_0(980)\pi 0^{-+}$ partial wave. Cannot rule out a $a_0(980)\pi 1^{++}$ partial wave.
- 5 Excluded from averaging because averaging would be meaningless.



$\pi\pi\gamma$ MODE

VALUE (MeV) EVTS DOCUMENT ID TECN COMMENT
1403 \pm 17 OUR AVERAGE Error includes scale factor of 1.8.

1390 \pm 12	235 \pm 91	AMSLER	04B CBAR	$0\bar{p}p \rightarrow \pi^+\pi^-\pi^+\pi^- \eta$
1424 \pm 10 \pm 11	547	BAI	04J BES2	$J/\psi \rightarrow \gamma\gamma\pi^+\pi^-$
1401 \pm 18		1,2 AUGUSTIN	90 DM2	$J/\psi \rightarrow \pi^+\pi^-\gamma\gamma$
1432 \pm 8		2 COFFMAN	90 MRK3	$J/\psi \rightarrow \pi^+\pi^-\gamma\gamma$

- 1 Best fit with a single Breit Wigner.
- 2 This peak in the $\gamma\rho$ channel may not be related to the $\eta(1405)$.

4 π MODE

VALUE (MeV) EVTS DOCUMENT ID TECN COMMENT
 We do not use the following data for averages, fits, limits, etc.

1420 \pm 20		BUGG	95 MRK3	$J/\psi \rightarrow \gamma\pi^+\pi^-\pi^+\pi^-$
1489 \pm 12	3270	1 BISELLO	89B DM2	$J/\psi \rightarrow 4\pi\gamma$

1 Estimated by us from various fits.

$K\bar{K}\pi$ MODE (unresolved)

VALUE (MeV) EVTS DOCUMENT ID TECN COMMENT
 We do not use the following data for averages, fits, limits, etc.

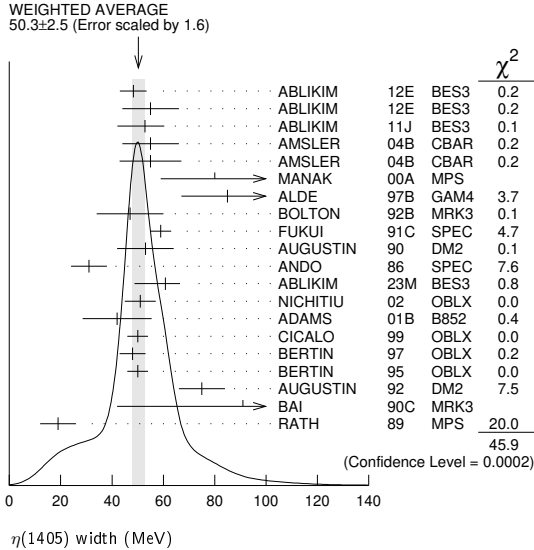
1452.7 \pm 3.3	191	1,2 ABLIKIM	13M BES3	$\psi(2S) \rightarrow \omega K K \pi$
1437.6 \pm 3.2	249 \pm 35	1,2 ABLIKIM	08E BES2	$J/\psi \rightarrow \omega K_S^0 K^+ \pi^- + c.c.$
1445.9 \pm 5.7	62 \pm 18	1,2 ABLIKIM	08E BES2	$J/\psi \rightarrow \omega K^+ K^- \pi^0$
1442 \pm 10	410	1 BAI	98C BES	$J/\psi \rightarrow \gamma K^+ K^- \pi^0$
1445 \pm 8	693	1 AUGUSTIN	90 DM2	$J/\psi \rightarrow \gamma K_S^0 K^\pm \pi^\mp$
1433 \pm 8	296	1 AUGUSTIN	90 DM2	$J/\psi \rightarrow \gamma K^+ K^- \pi^0$
1413 \pm 8	500	1 DUCH	89 ASTE	$\bar{p}p \rightarrow \pi^+\pi^-\pi^\pm \pi^\mp K^0$
1453 \pm 7	170	1 RATH	89 MPS	$21.4\pi^-\pi^- \rightarrow K_S^0 K_S^0 \pi^0 n$
1419 \pm 1	8800	1 BIRMAN	88 MPS	$8\pi^-\pi^- \rightarrow K^+ \bar{K}^0 \pi^- n$
1424 \pm 3	620	1 REEVES	86 SPEC	$6.6\bar{p}p \rightarrow K\bar{K}\pi X$
1421 \pm 2		1 CHUNG	85 SPEC	$8\pi^-\pi^- \rightarrow K\bar{K}\pi n$
1440 \pm 20	174	1 EDWARDS	82E CBAL	$J/\psi \rightarrow \gamma K^+ K^- \pi^0$

1440	+10 -15	1	SCHARRE	80	MRK2	$J/\psi \rightarrow \gamma K_S^0 K^\pm \pi^\mp$
1425	± 7	1,3	BAILLON	67	HBC	$0 \bar{p} p \rightarrow K \bar{K} \pi \pi$

- These experiments identify only one pseudoscalar in the 1400-1500 range. Data could also refer to $\eta(1475)$.
- Systematic uncertainty not evaluated.
- From best fit of 0^-+ partial wave, 50% $K^*(892)K$, 50% $a_0(980)\pi$.

$\eta(1405)$ WIDTH

50.3 ± 2.5 OUR AVERAGE Includes data from the 2 datablocks that follow this one. Error includes scale factor of 1.6. See the ideogram below.

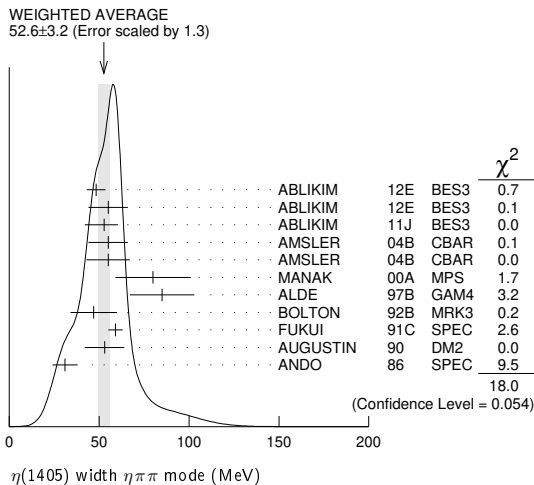


$\eta\pi\pi$ MODE

The data in this block is included in the average printed for a previous datablock.

52.6 ± 3.2 OUR AVERAGE Error includes scale factor of 1.3. See the ideogram below.

48.3 ± 5.2	743	ABLIKIM	12E	BES3	$J/\psi \rightarrow \gamma(\pi^+\pi^-\pi^0)$	
55.0 ± 11.0	198	ABLIKIM	12E	BES3	$J/\psi \rightarrow \gamma(\pi^0\pi^0\pi^0)$	
52.8 ± 7.6 ^{+0.1} _{-7.6}		1	ABLIKIM	11J	BES3	$J/\psi \rightarrow \omega(\eta\pi^+\pi^-)$
55 ± 11	900	AMSLER	04B	CBAR	$0 \bar{p} p \rightarrow \pi^+\pi^-\pi^+\pi^-\eta$	
55 ± 12	6.6k	AMSLER	04B	CBAR	$0 \bar{p} p \rightarrow \pi^+\pi^-\pi^0\pi^0\gamma$	
80 ± 21	9.0k	MANAK	00A	MPS	$18 \pi^- p \rightarrow \eta\pi^+\pi^-n$	
85 ± 18	2.2k	ALDE	97B	GAM4	$100 \pi^- p \rightarrow \eta\pi^0\pi^0n$	
47 ± 13		2	BOLTON	92B	MRK3	$J/\psi \rightarrow \gamma\eta\pi^+\pi^-$
59 ± 4			FUKUI	91C	SPEC	$8.95 \pi^- p \rightarrow \eta\pi^+\pi^-n$
53 ± 11		3	AUGUSTIN	90	DM2	$J/\psi \rightarrow \gamma\eta\pi^+\pi^-$
31 ± 7			ANDO	86	SPEC	$8 \pi^- p \rightarrow \eta\pi^+\pi^-n$
••• We do not use the following data for averages, fits, limits, etc. •••						
79.0 ± 16.0	195	ABLIKIM	19BA	BES3	$e^+e^- \rightarrow \psi(2S)$	
86 ± 10		4	AMSLER	95F	CBAR	$0 \bar{p} p \rightarrow \pi^+\pi^-\pi^0\pi^0\eta$



¹ The selected process is $J/\psi \rightarrow \omega a_0(980)\pi$.

- From fit to the $a_0(980)\pi 0^-+$ partial wave.
- From $\eta\pi^+\pi^-$ mass distribution - mainly $a_0(980)\pi$ - no spin-parity determination available.
- Superseded by AMSLER 04B.

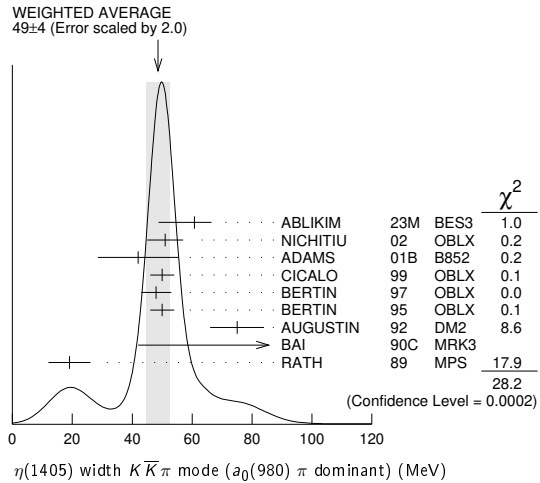
$K\bar{K}\pi$ MODE ($a_0(980)\pi$ or direct $K\bar{K}\pi$)

The data in this block is included in the average printed for a previous datablock.

49 ± 4 OUR AVERAGE Error includes scale factor of 2.0. See the ideogram below.

60.8 ± 1.2 ^{+5.5} _{-12.0}	126K	ABLIKIM	23M	BES3	$J/\psi \rightarrow \gamma K_S^0 K^\pm \pi^0$		
51 ± 6	3651	1	NICHITIU	02	OBLX	$0 \bar{p} p \rightarrow K^+ K^- \pi^+ \pi^- \pi^0$	
42 ± 10 ± 9	20k		ADAMS	01B	B852	$18 \text{ GeV } \pi^- p \rightarrow K^+ K^- \pi^0 n$	
50 ± 4			CICALO	99	OBLX	$0 \bar{p} p \rightarrow K^\pm K_S^0 \pi^\mp \pi^+ \pi^-$	
48 ± 5		2	BERTIN	97	OBLX	$0.0 \bar{p} p \rightarrow K^\pm (K^0) \pi^\mp \pi^+ \pi^-$	
75 ± 4		2	BERTIN	95	OBLX	$0 \bar{p} p \rightarrow K \bar{K} \pi \pi$	
50 ± 9			AUGUSTIN	92	DM2	$J/\psi \rightarrow \gamma K \bar{K} \pi$	
91 ± 6 ⁺⁷ ₋₃₁	⁺¹⁵ ₋₃₈		3	BAI	90C	MRK3	$J/\psi \rightarrow \gamma K_S^0 K^\pm \pi^\mp$
19 ± 7			3	RATH	89	MPS	$21.4 \pi^- p \rightarrow n K_S^0 K^\pm \pi^0$

- Decaying dominantly directly to $K^+ K^- \pi^0$.
- Decaying into $(K\bar{K})_S \pi$, $(K\pi)_S \bar{K}$, and $a_0(980)\pi$.
- From fit to the $a_0(980)\pi 0^-+$ partial wave, but $a_0(980)\pi 1^++$ cannot be excluded.



$\pi\pi\gamma$ MODE

The data in this block is included in the average printed for a previous datablock.

89 ± 17 OUR AVERAGE Error includes scale factor of 1.7.

64 ± 18	235 ± 91	AMSLER	04B	CBAR	$0 \bar{p} p \rightarrow \pi^+\pi^-\pi^+\pi^-\pi^-\gamma$	
101.0 ± 8.8 ± 8.8	547	BAI	04J	BES2	$J/\psi \rightarrow \gamma\gamma\pi^+\pi^-$	
••• We do not use the following data for averages, fits, limits, etc. •••						
174 ± 44			AUGUSTIN	90	DM2	$J/\psi \rightarrow \pi^+\pi^-\pi^-\gamma$
90 ± 26		1	COFFMAN	90	MRK3	$J/\psi \rightarrow \pi^+\pi^-2\gamma$

- This peak in the $\gamma\rho$ channel may not be related to the $\eta(1405)$.

4 π MODE

The data in this block is included in the average printed for a previous datablock.

160 ± 30			BUGG	95	MRK3	$J/\psi \rightarrow \gamma\pi^+\pi^-\pi^+\pi^-$
144 ± 13	3270	1	BISELLO	89B	DM2	$J/\psi \rightarrow 4\pi\gamma$

- Estimated by us from various fits.

$K\bar{K}\pi$ MODE (unresolved)

The data in this block is included in the average printed for a previous datablock.

••• We do not use the following data for averages, fits, limits, etc. •••						
45.9 ± 8.2	191	1,2	ABLIKIM	13M	BES3	$\psi(2S) \rightarrow \omega K K \pi$
48.9 ± 9.0	249 ± 35	1,2	ABLIKIM	08E	BES2	$J/\psi \rightarrow \omega K_S^0 K^+ \pi^- + c.c.$
34.2 ± 18.5	62 ± 18	1,2	ABLIKIM	08E	BES2	$J/\psi \rightarrow \omega K^+ K^- \pi^0$
93 ± 14	296	1	AUGUSTIN	90	DM2	$J/\psi \rightarrow \gamma K^+ K^- \pi^0$
105 ± 10	693	1	AUGUSTIN	90	DM2	$J/\psi \rightarrow \gamma K_S^0 K^\pm \pi^\mp$
62 ± 16	500	1	DUCH	89	ASTE	$\bar{p} p \rightarrow K \bar{K} \pi \pi$
100 ± 11	170	1	RATH	89	MPS	$21.4 \pi^- p \rightarrow K_S^0 K_S^0 \pi^0 n$
66 ± 2	8800	1	BIRMAN	88	MPS	$8 \pi^- p \rightarrow K^+ \bar{K}^0 \pi^- n$
60 ± 10	620	1	REEVES	86	SPEC	$6.6 p \bar{p} \rightarrow K K \pi X$
60 ± 10		1	CHUNG	85	SPEC	$8 \pi^- p \rightarrow K \bar{K} \pi n$
55 ± 20	174	1	EDWARDS	82E	CBAL	$J/\psi \rightarrow \gamma K^+ K^- \pi^0$
50 ± 30		1	SCHARRE	80	MRK2	$J/\psi \rightarrow \gamma K_S^0 K^\pm \pi^\mp$
80 ± 10	800	1,3	BAILLON	67	HBC	$0.0 \bar{p} p \rightarrow K \bar{K} \pi \pi$

- These experiments identify only one pseudoscalar in the 1400-1500 range. Data could also refer to $\eta(1475)$.
- Systematic uncertainty not evaluated.
- From best fit to 0^-+ partial wave, 50% $K^*(892)K$, 50% $a_0(980)\pi$.

Meson Particle Listings

 $\eta(1405)$ $\eta(1405)$ DECAY MODES

Mode	Fraction (Γ_i/Γ)	Confidence level
Γ_1 $K\bar{K}\pi$	seen	
Γ_2 $\eta\pi\pi$	seen	
Γ_3 $a_0(980)\pi$	seen	
Γ_4 $\eta(\pi\pi)$ s-wave	seen	
Γ_5 $f_0(980)\pi^0 \rightarrow \pi^+\pi^-\pi^0$	not seen	
Γ_6 $f_0(980)\eta$	seen	
Γ_7 4π	seen	
Γ_8 $\rho\rho$	<58 %	99.85%
Γ_9 $\gamma\gamma$		
Γ_{10} $\rho^0\gamma$	seen	
Γ_{11} $\phi\gamma$		
Γ_{12} $K^*(892)K$	seen	

 $\eta(1405)$ $\Gamma(\eta)\Gamma(\gamma\gamma)/\Gamma(\text{total})$

VALUE (keV)	CL%	DOCUMENT ID	TECN	COMMENT	$\Gamma_1\Gamma_9/\Gamma$
-------------	-----	-------------	------	---------	---------------------------

••• We do not use the following data for averages, fits, limits, etc. •••

<0.035	90	1,2 AHOHE	05	CLE2	10.6 $e^+e^- \rightarrow e^+e^- K_S^0 K^\pm \pi^\mp$
--------	----	-----------	----	------	--

¹ Using $\eta(1405)$ mass and width 1410 MeV and 51 MeV, respectively.

² Assuming three-body phase-space decay to $K_S^0 K^\pm \pi^\mp$.

VALUE (keV)	CL%	DOCUMENT ID	TECN	COMMENT	$\Gamma_2\Gamma_9/\Gamma$
-------------	-----	-------------	------	---------	---------------------------

<0.095	95	ACCIARRI	01G	L3	183-202 $e^+e^- \rightarrow e^+e^-\eta\pi^+\pi^-$
--------	----	----------	-----	----	---

VALUE (keV)	CL%	DOCUMENT ID	TECN	COMMENT	$\Gamma_{10}\Gamma_9/\Gamma$
-------------	-----	-------------	------	---------	------------------------------

••• We do not use the following data for averages, fits, limits, etc. •••

<1.5	95	ALTHOFF	84E	TASS	$e^+e^- \rightarrow e^+e^-\pi^+\pi^-\gamma$
------	----	---------	-----	------	---

 $\eta(1405)$ BRANCHING RATIOS

VALUE	CL%	DOCUMENT ID	TECN	COMMENT	Γ_2/Γ_1
-------	-----	-------------	------	---------	---------------------

••• We do not use the following data for averages, fits, limits, etc. •••

~0.15		1 BERTIN	95	OBLX	$0\bar{p}p \rightarrow K\bar{K}\pi\pi\pi$
-------	--	----------	----	------	---

<0.5	90	EDWARDS	83B	CBAL	$J/\psi \rightarrow \eta\pi\pi\gamma$
------	----	---------	-----	------	---------------------------------------

<1.1	90	SCHARRE	80	MRK2	$J/\psi \rightarrow \eta\pi\pi\gamma$
------	----	---------	----	------	---------------------------------------

<1.5	95	FOSTER	68B	HBC	$0.0\bar{p}p$
------	----	--------	-----	-----	---------------

¹ Using the data of BAILLON 67 on $\bar{p}p \rightarrow K\bar{K}\pi$.

VALUE	DOCUMENT ID	TECN	COMMENT	Γ_{10}/Γ_2
-------	-------------	------	---------	------------------------

0.111 ± 0.064	AMSLER	04B	CBAR	0 $\bar{p}p$
---------------	--------	-----	------	--------------

VALUE	EVTS	DOCUMENT ID	TECN	COMMENT	Γ_3/Γ_1
-------	------	-------------	------	---------	---------------------

••• We do not use the following data for averages, fits, limits, etc. •••

~0.15		1 BERTIN	95	OBLX	$0\bar{p}p \rightarrow K\bar{K}\pi\pi\pi$
-------	--	----------	----	------	---

~0.8	500	1 DUCH	89	ASTE	$\bar{p}p \rightarrow \pi^+\pi^-\pi^0 K^\pm \pi^\mp K^0$
------	-----	--------	----	------	--

~0.75		1 REEVES	86	SPEC	$6.6\bar{p}p \rightarrow K\bar{K}\pi X$
-------	--	----------	----	------	---

¹ Assuming that the $a_0(980)$ decays only into $K\bar{K}$.

VALUE	EVTS	DOCUMENT ID	TECN	COMMENT	Γ_3/Γ_2
-------	------	-------------	------	---------	---------------------

••• We do not use the following data for averages, fits, limits, etc. •••

0.29 ± 0.10		1 ABELE	98E	CBAR	$0\bar{p}p \rightarrow \eta\pi^0\pi^0\pi^0$
-------------	--	---------	-----	------	---

0.19 ± 0.04		1 ALDE	97B	GAM4	$100\pi^-\pi^0 \rightarrow \eta\pi^0\pi^0\eta$
-------------	--	--------	-----	------	--

0.56 ± 0.04 ± 0.03		1 AMSLER	95F	CBAR	$0\bar{p}p \rightarrow \pi^+\pi^-\pi^0\pi^0\eta$
--------------------	--	----------	-----	------	--

¹ Assuming that the $a_0(980)$ decays only into $\eta\pi$.

VALUE	EVTS	DOCUMENT ID	TECN	COMMENT	Γ_3/Γ_4
-------	------	-------------	------	---------	---------------------

••• We do not use the following data for averages, fits, limits, etc. •••

0.91 ± 0.12		1 ANISOVICH	01	SPEC	$0.0\bar{p}p \rightarrow \eta\pi^+\pi^-\pi^+\pi^-$
-------------	--	-------------	----	------	--

0.15 ± 0.04	9082	1 MANAK	00A	MPS	$18\pi^-\pi^0 \rightarrow \eta\pi^+\pi^-\eta$
-------------	------	---------	-----	-----	---

0.70 ± 0.12 ± 0.20		2 BAI	99	BES	$J/\psi \rightarrow \gamma\eta\pi^+\pi^-$
--------------------	--	-------	----	-----	---

¹ Statistical error only.

² Assuming that the $a_0(980)$ decays only into $\eta\pi$.

VALUE	DOCUMENT ID	TECN	COMMENT	Γ_{10}/Γ_1
-------	-------------	------	---------	------------------------

0.0152 ± 0.0038	1 COFFMAN	90	MRK3	$J/\psi \rightarrow \gamma\gamma\pi^+\pi^-$
-----------------	-----------	----	------	---

¹ Using $B(J/\psi \rightarrow \gamma\eta(1405) \rightarrow \gamma K\bar{K}\pi) = 4.2 \times 10^{-3}$ and $B(J/\psi \rightarrow \gamma\eta(1405) \rightarrow \gamma\gamma\pi^0) = 6.4 \times 10^{-5}$.

 $\Gamma(\gamma\gamma)/\Gamma(K\bar{K}\pi)$ Γ_9/Γ_1

VALUE	CL%	DOCUMENT ID	TECN	COMMENT
-------	-----	-------------	------	---------

<1.78 × 10 ⁻³	90	1 ABLIKIM	180	BES3	$\psi(2S) \rightarrow \pi^+\pi^-\gamma\gamma\gamma$
--------------------------	----	-----------	-----	------	---

¹ Using results from BAI 00d.

 $\Gamma(\eta(\pi\pi)$ s-wave)/ $\Gamma(\eta\pi\pi)$ Γ_4/Γ_2

VALUE	EVTS	DOCUMENT ID	TECN	COMMENT
-------	------	-------------	------	---------

••• We do not use the following data for averages, fits, limits, etc. •••

0.81 ± 0.04	2200	ALDE	97B	GAM4	$100\pi^-\pi^0 \rightarrow \eta\pi^0\pi^0\eta$
-------------	------	------	-----	------	--

 $\Gamma(f_0(980)\eta)/\Gamma(\eta\pi\pi)$ Γ_6/Γ_2

VALUE	DOCUMENT ID	TECN	COMMENT
-------	-------------	------	---------

••• We do not use the following data for averages, fits, limits, etc. •••

0.32 ± 0.07	1 ANISOVICH	00	SPEC	$0.9-1.2\bar{p}p \rightarrow \eta 3\pi^0$
-------------	-------------	----	------	---

¹ Using preliminary Crystal Barrel data.

 $\Gamma(f_0(980)\pi^0 \rightarrow \pi^+\pi^-\pi^0)/\Gamma_{\text{total}}$ Γ_5/Γ

VALUE	DOCUMENT ID	TECN	COMMENT
-------	-------------	------	---------

not seen

	1 ABLIKIM	17AJ	BES3	$\psi(2S) \rightarrow \gamma\pi^+\pi^-\pi^0$
--	-----------	------	------	--

¹ ABLIKIM 17AJ reports $B(\psi(2S) \rightarrow \gamma\eta(1405) \rightarrow \gamma f_0(980)\pi^0 \rightarrow \gamma\pi^+\pi^-\pi^0) < 5.0 \times 10^{-7}$.

 $\Gamma(\rho\rho)/\Gamma_{\text{total}}$ Γ_8/Γ

VALUE	CL%	DOCUMENT ID	TECN	COMMENT
-------	-----	-------------	------	---------

<0.58	99.85	1,2 AMSLER	04B	CBAR	0 $\bar{p}p$
-------	-------	------------	-----	------	--------------

¹ Assuming that the $\eta(1405)$ decays are saturated by the $\pi\pi\eta$, $K\bar{K}\pi$ and $\rho\rho$ modes.

² Using the data of BAILLON 67 on $\bar{p}p \rightarrow K\bar{K}\pi$.

 $\Gamma(K^*(892)K)/\Gamma(a_0(980)\pi)$ Γ_{12}/Γ_3

VALUE	DOCUMENT ID	TECN	COMMENT
-------	-------------	------	---------

••• We do not use the following data for averages, fits, limits, etc. •••

0.084 ± 0.024	1 ADAMS	01B	B852	$18\text{ GeV } \pi^-\pi^0 \rightarrow K^+K^-\pi^0\eta$
---------------	---------	-----	------	---

¹ Statistical error only.

 $\Gamma(\phi\gamma)/\Gamma(\rho^0\gamma)$ Γ_{11}/Γ_{10}

VALUE	CL%	DOCUMENT ID	TECN	COMMENT
-------	-----	-------------	------	---------

••• We do not use the following data for averages, fits, limits, etc. •••

0.09 ± 0.03		1 ABLIKIM	181	BES3	$J/\psi \rightarrow \gamma\gamma\phi(1020)$
-------------	--	-----------	-----	------	---

0.13 ± 0.04		2 ABLIKIM	181	BES3	$J/\psi \rightarrow \gamma\gamma\phi(1020)$
-------------	--	-----------	-----	------	---

<0.77	95	3 BAI	04J	BES2	$J/\psi \rightarrow \gamma\gamma K^+K^-$
-------	----	-------	-----	------	--

¹ Constructive interference between $X(1835)$ and $\eta(1405)/\eta(1475)$ decays to $\gamma\phi$ is assumed. Also see $\eta(1475)$. ABLIKIM 181 reports the inverse as 11.10 ± 3.5 .

² Destructive interference between $X(1835)$ and $\eta(1405)/\eta(1475)$ decays to $\gamma\phi$ is assumed. Also see $\eta(1475)$. ABLIKIM 181 reports the inverse as 7.53 ± 2.49 .

³ Calculated by us from $B(J/\psi \rightarrow \eta(1405)\gamma \rightarrow \phi\gamma\gamma) < 0.82 \times 10^{-4}$ and $B(J/\psi \rightarrow \eta(1405)\gamma \rightarrow \rho^0\gamma\gamma) = (1.07 \pm 0.17 \pm 0.11) \times 10^{-4}$.

 $\eta(1405)$ REFERENCES

ABLIKIM	23M	JHEP	2303	121	M. Ablikim et al.	(BESIII Collab.)
ABLIKIM	198A	PR	D100	092003	M. Ablikim et al.	(BESIII Collab.)
ABLIKIM	181	PR	D97	051101	M. Ablikim et al.	(BESIII Collab.)
ABLIKIM	180	PR	D97	072014	M. Ablikim et al.	(BESIII Collab.)
ABLIKIM	17AJ	PR	D96	112008	M. Ablikim et al.	(BESIII Collab.)
ABLIKIM	13M	PR	D87	092006	M. Ablikim et al.	(BESIII Collab.)
ABLIKIM	11E	PRL	108	182001	M. Ablikim et al.	(BESIII Collab.)
ABLIKIM	12J	PRL	107	182001	M. Ablikim et al.	(BESIII Collab.)
ABLIKIM	08E	PR	D77	032005	M. Ablikim et al.	(BES Collab.)
AHOHE	05	PR	D71	072001	R. Ahohe et al.	(CLEO Collab.)
AMSLER	04B	EPJ	C33	23	C. Amstler et al.	(Crystal Barrel Collab.)
BAI	04J	PL	B594	47	J.Z. Bai et al.	(BES Collab.)
NICHITIU	02	PL	B545	261	F. Nichitiu et al.	(OBELIX Collab.)
ACCIARRI	01G	PL	B501	1	M. Acciarri et al.	(L3 Collab.)
ADAMS	01B	PL	B516	264	G.S. Adams et al.	(BNL E852 Collab.)
ANISOVICH	01	NP	A690	567	A.V. Anisovich et al.	
ANISOVICH	00	PL	B472	168	A.V. Anisovich et al.	
BAI	00D	PL	B476	25	J.Z. Bai et al.	(BES Collab.)
MANAK	00A	PR	D62	012003	J.J. Manak et al.	(BNL E852 Collab.)
BAI	99	PL	B446	356	J.Z. Bai et al.	(BES Collab.)
CICALO	99	PL	B462	453	C. Cicalo et al.	(OBELIX Collab.)
ABELE	98E	NP	B514	45	A. Abele et al.	(Crystal Barrel Collab.)
BAI	98C	PL	B440	217	J.Z. Bai et al.	(BES Collab.)
ALDE	97B	PAN	60	386	D. Alde et al.	(GAMS Collab.)
					Translated from YAF 60 458.	
BERTIN	97	PL	B400	226	B. Bertin et al.	(OBELIX Collab.)
AMSLER	95F	PL	B358	389	C. Amstler et al.	(Crystal Barrel Collab.)
BERTIN	95	PL	B361	187	A. Bertin et al.	(OBELIX Collab.)
BUGG	95	PL	B353	378	D.V. Bugg et al.	(LOQM, PNPI, WASH)
AUGUSTIN	92	PR	D46	1951	J.E. Augustin, G. Cosme	(DM2 Collab.)
BOLTON	92B	PRL	69	1328	T. Bolton et al.	(Mark III Collab.)
FUKUI	91C	PL	B267	293	S. Fukui et al.	(SUGI, NAGO, KEK, KYOT+)
AUGUSTIN	90	PR	D42	10	J.E. Augustin et al.	(DM2 Collab.)
BAI	90C	PRL	65	2507	Z. Bai et al.	(Mark III Collab.)
COFFMAN	90	PR	D41	1410	D.M. Coffman et al.	(Mark III Collab.)
BISELLO	89B	PR	D39	701	G. Bisello et al.	(DM2 Collab.)
DUCH	89	ZPHY	C45	223	K.D. Duch et al.	(ASTERIX Collab.) JP
RATH	89	PR	D40	693	M.G. Rath et al.	(NDAM, BRAN, BNL, CUNY+)
BIRMAN	88	PRL	61	1557	A. Birman et al.	(BNL, FSU, IND, MASD) JP
ANDO	86	PRL	57	1296	A. Ando et al.	(KEK, KYOT, NIRS, SAGA+) JP
REEVES	86	PR	D34	1960	D.F. Reeves et al.	(FLOR, BNL, IND+) JP
CHUNG	85	PRL	55	779	S.U. Chung et al.	(BNL, FLOR, IND+) JP
ALTHOFF	84E	PL	I47B	487	M. Althoff et al.	(TASSO Collab.)
EDWARDS	83B	PRL	51	859	C. Edwards et al.	(CIT, HARV, PRIN+)
EDWARDS	82E	PRL	49	253	C. Edwards et al.	(CIT, HARV, PRIN+)
					Also	
SCHARRE	80	PL	97B	329	D.L. Scharre et al.	(SLAC, LBL)
FOSTER	68B	NP	B8	174	M. Foster et al.	(CERN, CDEF)
BAILLON	67	NC	50A	393	P.H. Baillon et al.	(CERN, CDEF, IRAD)

See key on page 1171

Meson Particle Listings

$h_1(1415), f_1(1420)$

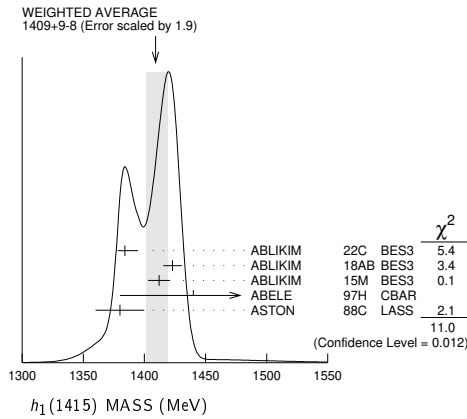
$h_1(1415)$

$$I^G(J^{PC}) = 0^-(1^{+-})$$

$h_1(1415)$ MASS

VALUE (MeV)	EVTS	DOCUMENT ID	TECN	COMMENT
1409⁺⁹₋₈	OUR AVERAGE	Error includes scale factor of 1.9. See the ideogram below.		
1384 ± 6 ⁺⁹ ₋₀		1 ABLIKIM	22C BES3	$J/\psi \rightarrow \gamma \eta' \eta' \rightarrow 4/5 \gamma 2(\pi^+ \pi^-)$
1423 ± 2.1 ± 7.3	2.2k	2 ABLIKIM	18AB BES3	$J/\psi \rightarrow \eta' h_1 \rightarrow \eta' K^* \bar{K}$
1412 ± 4 ± 8		2 ABLIKIM	15M BES3	$\psi(2S) \rightarrow \gamma \chi_{c1,2} \rightarrow \gamma \phi(h_1 \rightarrow K^* \bar{K})$
1440 ± 60		ABELE	97H CBAR	$\bar{p} p \rightarrow K_L^0 K_S^0 \pi^0 \pi^0$
1380 ± 20		ASTON	88C LASS	$11 K^- p \rightarrow K_S^0 K^\pm \pi^\mp \Lambda$

¹ From a partial wave analysis of the systems (γX), with $X \rightarrow \eta' \eta'$, and ($\eta' X$), with $X \rightarrow \gamma \eta'$ in the decay $J/\psi \rightarrow \gamma \eta' \eta'$. The intermediate resonance X is parametrized by a constant-width, relativistic Breit-Wigner.
² Final states $K^+ K^- \pi^0$ and $K_S^0 K^\pm \pi^\mp$.



$h_1(1415)$ WIDTH

VALUE (MeV)	EVTS	DOCUMENT ID	TECN	COMMENT
78 ± 11	OUR AVERAGE			
66 ± 10 ⁺¹² ₋₁₀		1 ABLIKIM	22C BES3	$J/\psi \rightarrow \gamma \eta' \eta' \rightarrow 4/5 \gamma 2(\pi^+ \pi^-)$
90.3 ± 9.8 ± 17.5	2.2k	2 ABLIKIM	18AB BES3	$J/\psi \rightarrow \eta' h_1 \rightarrow \eta' K^* \bar{K}$
84 ± 12 ± 40		2 ABLIKIM	15M BES3	$\psi(2S) \rightarrow \gamma \chi_{c1,2} \rightarrow \gamma \phi(h_1 \rightarrow K^* \bar{K})$
170 ± 80		ABELE	97H CBAR	$\bar{p} p \rightarrow K_L^0 K_S^0 \pi^0 \pi^0$
80 ± 30		ASTON	88C LASS	$11 K^- p \rightarrow K_S^0 K^\pm \pi^\mp \Lambda$

¹ From a partial wave analysis of the systems (γX), with $X \rightarrow \eta' \eta'$, and ($\eta' X$), with $X \rightarrow \gamma \eta'$ in the decay $J/\psi \rightarrow \gamma \eta' \eta'$. The intermediate resonance X is parametrized by a constant-width, relativistic Breit-Wigner.
² Final states $K^+ K^- \pi^0$ and $K_S^0 K^\pm \pi^\mp$.

$h_1(1415)$ DECAY MODES

Mode
$\Gamma_1 K \bar{K}^*(892) + c.c.$

$h_1(1415)$ REFERENCES

ABLIKIM 22C PR D105 072002	M. Ablikim et al. (BESIII Collab.)
ABLIKIM 18AB PR D98 072005	M. Ablikim et al. (BESIII Collab.)
ABLIKIM 15M PR D91 112008	M. Ablikim et al. (BESIII Collab.)
ABELE 97H PL B415 280	A. Abele et al. (Crystal Barrel Collab.)
ASTON 88C PL B201 573	D. Aston et al. (SLAC, NAGO, CINC, INUS)

$f_1(1420)$

$$I^G(J^{PC}) = 0^+(1^{++})$$

See the review on "Spectroscopy of Light Meson Resonances."

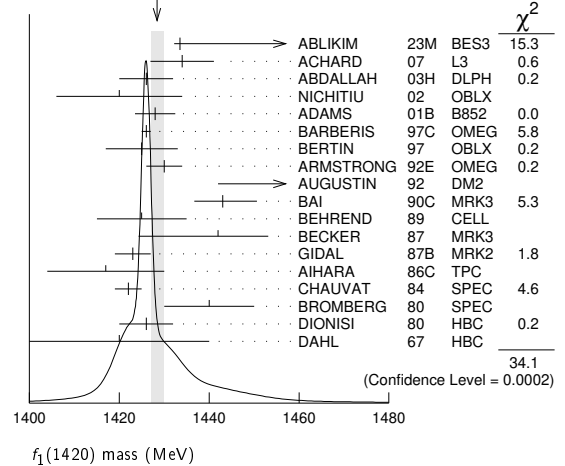
$f_1(1420)$ MASS

VALUE (MeV)	EVTS	DOCUMENT ID	TECN	COMMENT
1428.4^{+1.5}_{-1.3}	OUR AVERAGE	Error includes scale factor of 1.8. See the ideogram below.		
1433.5 ± 1.1 ± 27.9	126K	ABLIKIM	23M BES3	$J/\psi \rightarrow \gamma K_S^0 K_S^0 \pi^0$
1434 ± 5 ± 5	133	1 ACHARD	07 L3	$183-209 e^+ e^- \rightarrow e^+ e^- K_S^0 K^\pm \pi^\mp$

1426 ± 6	711	ABDALLAH	03H DLPH	$91.2 e^+ e^- \rightarrow K_S^0 K^\pm \pi^\mp + X$
1420 ± 14	3651	NICHITIU	02 OBLX	$0 \bar{p} p \rightarrow K^+ K^- \pi^+ \pi^- \pi^0$
1428 ± 4 ± 2	20k	ADAMS	01B B852	$18 \text{ GeV } \pi^- p \rightarrow K^+ K^- \pi^0 n$
1426 ± 1		BARBERIS	97C OMEG	$450 \bar{p} p \rightarrow \bar{p} p K_S^0 K^\pm \pi^\mp$
1425 ± 8		BERTIN	97 OBLX	$0.0 \bar{p} p \rightarrow K^\pm (K^0) \pi^\mp \pi^+ \pi^-$
1430 ± 4		2 ARMSTRONG	92E OMEG	$85,300 \pi^+ p, \bar{p} p \rightarrow \pi^+ p, \bar{p} p (K \bar{K} \pi)$
1462 ± 20		3 AUGUSTIN	92 DM2	$J/\psi \rightarrow \gamma K \bar{K} \pi$
1443 ± 7 ± 3	1100	BAI	90C MRK3	$J/\psi \rightarrow \gamma K_S^0 K^\pm \pi^\mp$
1425 ± 10	17	BEHREND	89 CELL	$\gamma \gamma \rightarrow K_S^0 K^\pm \pi^\mp$
1442 ± 5 ± 10	111	BECKER	87 MRK3	$e^+ e^-, \omega K \bar{K} \pi$
1423 ± 4		GIDAL	87B MRK2	$e^+ e^- \rightarrow e^+ e^- K \bar{K} \pi$
1417 ± 13	13	AIHARA	86C TPC	$e^+ e^- \rightarrow e^+ e^- K \bar{K} \pi$
1422 ± 3		CHAUVAT	84 SPEC	$\text{ISR } 31.5 \text{ pp} \rightarrow e^+ e^- K \bar{K} \pi$
1440 ± 10		4 BROMBERG	80 SPEC	$100 \pi^- p \rightarrow K \bar{K} \pi X$
1426 ± 6	221	DIONISI	80 HBC	$4 \pi^- p \rightarrow K \bar{K} \pi n$
1420 ± 20		DAHL	67 HBC	$1.6-4.2 \pi^- p$
1430.8 ± 0.9		5 SOSA	99 SPEC	$\bar{p} p \rightarrow p_{\text{slow}} (K_S^0 K^\pm \pi^\mp) p_{\text{fast}}$
1433.4 ± 0.8		5 SOSA	99 SPEC	$\bar{p} p \rightarrow p_{\text{slow}} (K_S^0 K^\pm \pi^\mp) p_{\text{fast}}$
1435 ± 9		PROKOSHKIN	97B GAM4	$100 \pi^- p \rightarrow \eta \pi^0 \pi^0 n$
1429 ± 3	389	ARMSTRONG	89 OMEG	$300 \bar{p} p \rightarrow K \bar{K} \pi p p$
1425 ± 2	1520	ARMSTRONG	84 OMEG	$85 \pi^+ p, \bar{p} p \rightarrow (\pi^+, p) (K \bar{K} \pi) p$
~ 1420		BITYUKOV	84 SPEC	$32 K^- p \rightarrow K^+ K^- \pi^0 \gamma$

• • • We do not use the following data for averages, fits, limits, etc. • • •
¹ From a fit with a width fixed at 55 MeV.
² This result supersedes ARMSTRONG 84, ARMSTRONG 89.
³ From fit to the $K^*(892) K 1^{++}$ partial wave.
⁴ Mass error increased to account for $a_0(980)$ mass cut uncertainties.
⁵ No systematic error given.

WEIGHTED AVERAGE
1428.4+1.5-1.3 (Error scaled by 1.8)



$f_1(1420)$ WIDTH

VALUE (MeV)	EVTS	DOCUMENT ID	TECN	COMMENT
56.7 ± 3.3	OUR AVERAGE	Error includes scale factor of 1.3. See the ideogram below.		
95.9 ± 2.3 ± 13.6	126K	ABLIKIM	23M BES3	$J/\psi \rightarrow \gamma K_S^0 K_S^0 \pi^0$
51 ± 14	711	ABDALLAH	03H DLPH	$91.2 e^+ e^- \rightarrow K_S^0 K^\pm \pi^\mp + X$
61 ± 8	3651	NICHITIU	02 OBLX	$0 \bar{p} p \rightarrow K^+ K^- \pi^+ \pi^- \pi^0$
38 ± 9 ± 6	20k	ADAMS	01B B852	$18 \text{ GeV } \pi^- p \rightarrow K^+ K^- \pi^0 n$
58 ± 4		BARBERIS	97C OMEG	$450 \bar{p} p \rightarrow \bar{p} p K_S^0 K^\pm \pi^\mp$
45 ± 10		BERTIN	97 OBLX	$0.0 \bar{p} p \rightarrow K^\pm (K^0) \pi^\mp \pi^+ \pi^-$
58 ± 10		6 ARMSTRONG	92E OMEG	$85,300 \pi^+ p, \bar{p} p \rightarrow \pi^+ p, \bar{p} p (K \bar{K} \pi)$

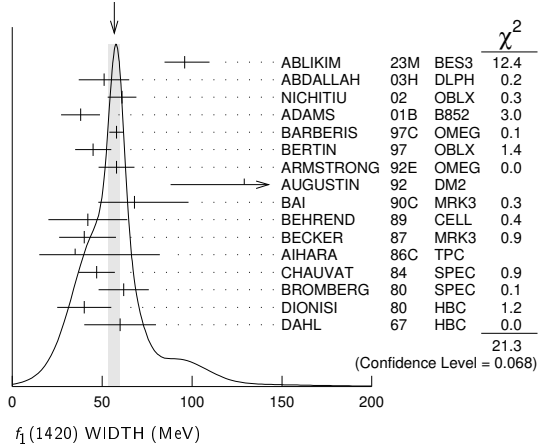
Meson Particle Listings

$f_1(1420)$

Value	CL%	Document ID	TECN	Comment
129 ± 41		7 AUGUSTIN 92 DM2		$J/\psi \rightarrow \gamma K \bar{K} \pi$
68 $^{+29}_{-18} \pm 8$	1100	BAI 90C MRK3		$J/\psi \rightarrow \gamma K_S^0 K^\pm \pi^\mp$
42 ± 22	17	BEHREND 89 CELL		$\gamma \gamma \rightarrow K_S^0 K^\pm \pi^\mp$
40 $^{+17}_{-13} \pm 5$	111	BECKER 87 MRK3		$e^+ e^- \rightarrow \omega K \bar{K} \pi$
35 $^{+47}_{-20}$	13	AIHARA 86C TPC		$e^+ e^- \rightarrow e^+ e^- K \bar{K} \pi$
47 ± 10		CHAUVAT 84 SPEC		ISR 31.5 pp
62 ± 14		BROMBERG 80 SPEC		100 $\pi^- p \rightarrow K \bar{K} \pi X$
40 ± 15	221	DIONISI 80 HBC		4 $\pi^- p \rightarrow K \bar{K} \pi n$
60 ± 20		DAHL 67 HBC		1.6-4.2 $\pi^- p$
68.7 ± 2.9		8 SOSA 99 SPEC		$pp \rightarrow p_{\text{slow}} (K_S^0 K^+ \pi^-) p_{\text{fast}}$
58.8 ± 3.3		8 SOSA 99 SPEC		$pp \rightarrow p_{\text{slow}} (K_S^0 K^- \pi^+) p_{\text{fast}}$
90 ± 25		PROKOSHKIN 97B GAM4		100 $\pi^- p \rightarrow \eta \pi^0 \pi^0 n$
58 ± 8	389	ARMSTRONG 89 OMEG		300 $pp \rightarrow K \bar{K} \pi pp$
62 ± 5	1520	ARMSTRONG 84 OMEG		85 $\pi^+ p, pp \rightarrow (\pi^+, \rho)(K \bar{K} \pi) p$
~ 50		BITYUKOV 84 SPEC		32 $K^- p \rightarrow K^+ K^- \pi^0 \gamma$

6 This result supersedes ARMSTRONG 84, ARMSTRONG 89.
 7 From fit to the $K^*(892) K 1^{++}$ partial wave.
 8 No systematic error given.

WEIGHTED AVERAGE
 56.7±3.3 (Error scaled by 1.3)



$f_1(1420)$ DECAY MODES

Mode	Fraction (Γ_i/Γ)
Γ_1 $K \bar{K} \pi$	seen
Γ_2 $K \bar{K}^*(892) + c.c.$	seen
Γ_3 $\eta \pi \pi$	possibly seen
Γ_4 $a_0(980) \pi$	
Γ_5 $\pi \pi \rho$	
Γ_6 4π	
Γ_7 $\rho^0 \gamma$	
Γ_8 $\phi \gamma$	seen

$f_1(1420) \Gamma(i)\Gamma(\gamma\gamma)/\Gamma(\text{total})$

Value (keV)	CL%	EVTS	Document ID	TECN	Comment
1.9 ± 0.4			OUR AVERAGE		
3.2 ± 0.6 ± 0.7	133	9,10	ACHARD 07 L3		183-209 $e^+ e^- \rightarrow e^+ e^- K_S^0 K^\pm \pi^\mp$
3.0 ± 0.9 ± 0.7		11,12	BEHREND 89 CELL		$e^+ e^- \rightarrow e^+ e^- K_S^0 \pi^\mp$
2.3 $^{+1.0}_{-0.9} \pm 0.8$			HILL 89 JADE		$e^+ e^- \rightarrow e^+ e^- K^\pm K_S^0 \pi^\mp$
1.3 ± 0.5 ± 0.3			AIHARA 88B TPC		$e^+ e^- \rightarrow e^+ e^- K^\pm K_S^0 \pi^\mp$
1.6 ± 0.7 ± 0.3		11,13	GIDAL 87B MRK2		$e^+ e^- \rightarrow e^+ e^- K \bar{K} \pi$
< 8.0	95		JENNI 83 MRK2		$e^+ e^- \rightarrow e^+ e^- K \bar{K} \pi$

9 From a fit with a width fixed at 55 MeV.
 10 The form factor parameter from the fit is 926 ± 78 MeV.
 11 Assume a ρ -pole form factor.
 12 A ϕ -pole form factor gives considerably smaller widths.
 13 Published value divided by 2.

$f_1(1420)$ BRANCHING RATIOS

Value	CL%	Document ID	TECN	Comment
$\Gamma(K \bar{K}^*(892) + c.c.)/\Gamma(K \bar{K} \pi) \Gamma_2/\Gamma_1$				
0.76 ± 0.06		BROMBERG 80 SPEC		100 $\pi^- p \rightarrow K \bar{K} \pi X$
0.86 ± 0.12		DIONISI 80 HBC		4 $\pi^- p \rightarrow K \bar{K} \pi n$

Value	CL%	Document ID	TECN	Comment
$\Gamma(\pi \pi \rho)/\Gamma(K \bar{K} \pi) \Gamma_5/\Gamma_1$				
< 0.3	95	CORDEN 78 OMEG		12-15 $\pi^- p$
< 2.0		DAHL 67 HBC		1.6-4.2 $\pi^- p$

Value	CL%	Document ID	TECN	Comment
$\Gamma(\eta \pi \pi)/\Gamma(K \bar{K} \pi) \Gamma_3/\Gamma_1$				
< 0.1	95	ARMSTRONG 91B OMEG		300 $pp \rightarrow pp \eta \pi^+ \pi^-$
1.35 ± 0.75		KOPKE 89 MRK3		$J/\psi \rightarrow \omega \eta \pi \pi (K \bar{K} \pi)$
< 0.6	90	GIDAL 87 MRK2		$e^+ e^- \rightarrow e^+ e^- \eta \pi^+ \pi^-$
< 0.5	95	CORDEN 78 OMEG		12-15 $\pi^- p$
1.5 ± 0.8		DEFOIX 72 HBC		0.7 $\bar{p} p$

Value	CL%	Document ID	TECN	Comment
$\Gamma(a_0(980) \pi)/\Gamma(\eta \pi \pi) \Gamma_4/\Gamma_3$				
> 0.1	90	PROKOSHKIN 97B GAM4		100 $\pi^- p \rightarrow \eta \pi^0 \pi^0 n$
not seen in either mode		ANDO 86 SPEC		8 $\pi^- p$
not seen in either mode		CORDEN 78 OMEG		12-15 $\pi^- p$
0.4 ± 0.2		DEFOIX 72 HBC		0.7 $\bar{p} p \rightarrow 7\pi$

Value	CL%	Document ID	TECN	Comment
$\Gamma(4\pi)/\Gamma(K \bar{K}^*(892) + c.c.) \Gamma_6/\Gamma_2$				
< 0.90	95	DIONISI 80 HBC		4 $\pi^- p$

Value	CL%	Document ID	TECN	Comment
$\Gamma(K \bar{K} \pi)/[\Gamma(K \bar{K}^*(892) + c.c.) + \Gamma(a_0(980) \pi)] \Gamma_1/(\Gamma_2 + \Gamma_4)$				
0.65 ± 0.27		14 DIONISI 80 HBC		4 $\pi^- p$

14 Calculated using $\Gamma(K \bar{K}^*)/\Gamma(\eta \pi) = 0.24 \pm 0.07$ for $a_0(980)$ fractions.

Value	CL%	Document ID	TECN	Comment
$\Gamma(a_0(980) \pi)/\Gamma(K \bar{K}^*(892) + c.c.) \Gamma_4/\Gamma_2$				
0.44 ± 0.19		ABLIKIM 21U BES3		$D_s^+ \rightarrow f_1(1420) \pi^+$
0.04 ± 0.01 ± 0.01		BARBERIS 98C OMEG		450 $pp \rightarrow p_f f_1(1420) p_s$
< 0.04	68	ARMSTRONG 84 OMEG		85 $\pi^+ p$

Value	CL%	Document ID	TECN	Comment
$\Gamma(4\pi)/\Gamma(K \bar{K} \pi) \Gamma_6/\Gamma_1$				
< 0.62	95	ARMSTRONG 89G OMEG		85 $\pi p \rightarrow 4\pi X$

Value	CL%	Document ID	TECN	Comment
$\Gamma(\rho^0 \gamma)/\Gamma_{\text{total}} \Gamma_7/\Gamma$				
< 0.08	95	15 ARMSTRONG 92C SPEC		300 $pp \rightarrow pp \pi^+ \pi^- \gamma$

15 Using the data on the $\bar{K} K \pi$ mode from ARMSTRONG 89.

Value	CL%	Document ID	TECN	Comment
$\Gamma(\rho^0 \gamma)/\Gamma(K \bar{K} \pi) \Gamma_7/\Gamma_1$				
< 0.02	95	BARBERIS 98C OMEG		450 $pp \rightarrow p_f f_1(1420) p_s$

Value	CL%	Document ID	TECN	Comment
$\Gamma(\phi \gamma)/\Gamma(K \bar{K} \pi) \Gamma_8/\Gamma_1$				
0.003 ± 0.001 ± 0.001		BARBERIS 98C OMEG		450 $pp \rightarrow p_f f_1(1420) p_s$

$f_1(1420)$ REFERENCES

ABLIKIM 23M	JHEP 2303 121	M. Ablikim et al.	(BESIII Collab.)
ABLIKIM 21U	PR D104 032011	M. Ablikim et al.	(BESIII Collab.)
ACHARD 07	JHEP 0703 018	P. Achard et al.	(L3 Collab.)
ABDALLAH 03H	PL B569 129	J. Abdallah et al.	(DELPHI Collab.)
NICHITIU 02	PL B545 261	F. Nichitiu et al.	(OBELIX Collab.)
ADAMS 01B	PL B516 264	G.S. Adams et al.	(BNL E852 Collab.)
SOSA 99	PRL 83 913	M. Sosa et al.	
BARBERIS 98C	PL B440 225	D. Barberis et al.	(WA 102 Collab.)
BARBERIS 97C	PL B413 225	D. Barberis et al.	(WA 102 Collab.)
BERTIN 97	PL B400 226	A. Bertin et al.	(OBELIX Collab.)
PROKOSHKIN 97B	PD 42 298	Yu. D. Prokoshkin, S.A. Sadovskiy	
	Translated from	DANS 354 751	
ARMSTRONG 92C	ZPHY C54 371	T.A. Armstrong et al.	(ATHU, BARI, BIRM+)JPC
ARMSTRONG 92E	ZPHY C56 29	T.A. Armstrong et al.	(ATHU, BARI, BIRM+)JPC

AUGUSTIN	92	PR D46 1951	J.E. Augustin, G. Cosme	(DM2 Collab.)
ARMSTRONG	91B	ZPHY C52 389	T.A. Armstrong et al.	(ATHU, BARI, BIRM+)
BAI	90C	PRL 65 2507	Z. Bai et al.	(Mark III Collab.)
ARMSTRONG	89	PL B221 216	T.A. Armstrong et al.	(CERN, CDEF, BIRM+) JPC
ARMSTRONG	89G	ZPHY C43 55	T.A. Armstrong et al.	(CERN, BIRM, BARI+)
BEHREND	89	ZPHY C42 367	H.J. Behrend et al.	(CELLO Collab.)
HILL	89	ZPHY C42 355	P. Hill et al.	(JADE Collab.) JP
KOPKE	89	PRPL 174 67	L. Kopke et al.	(CERN)
AIHARA	88B	PL B209 107	H. Aihara et al.	(TPC-2 γ Collab.)
BECKER	87	PRL 59 186	J.J. Becker et al.	(Mark III Collab.) JP
GIDAL	87	PRL 59 2012	G. Gidal et al.	(LBL, SLAC, HARV)
GIDAL	87B	PRL 59 2016	G. Gidal et al.	(LBL, SLAC, HARV)
AIHARA	86C	PRL 57 2500	H. Aihara et al.	(TPC-2 γ Collab.) JP
ANDO	86	PRL 57 1296	A. Ando et al.	(KEK, KYOT, NIRS, SAGA+)
ARMSTRONG	84	PL 146B 273	T.A. Armstrong et al.	(ATHU, BARI, BIRM+) JP
BITYUKOV	84	SJNP 39 735	S. Bityukov et al.	(SERP)
		Translated from YAF 39 1165.		
CHAUVAT	84	PL 148B 382	P. Chauvat et al.	(CERN, CLER, UCLA+)
JENNI	83	PR D27 1031	P. Jenni et al.	(SLAC, LBL)
BROMBERG	80	PR D22 1513	C.M. Bromberg et al.	(CIT, FNAL, ILLC+)
DIONISI	80	NP B169 1	C. Dionisi et al.	(CERN, MADR, CDEF+) JUP
CORDEN	78	NP B144 253	M.J. Corden et al.	(BIRM, RHEL, TELA+)
DEFOIX	72	NP B44 125	C. Defoix et al.	(CDEF, CERN)
DAHL	67	PR 163 1377	O.I. Dahl et al.	(LRL) JUP
Also		PRL 14 1074	D.H. Miller et al.	(LRL, UCB)

- 240 ± 70 ⁸ CLEGG 94 RVUE
 174 ± 59 315 ⁹ ANTONELLI 92 DM2 1.34–2.4e⁺e⁻ → ρπ
- From a fit with contributions from ω(1420), ω(1650), and φ(1680). The mass of ω(1420) is fixed to the PDG 18 value of 1420 MeV.
 - From a fit of the interfering ω(1420) and ω(1650) with a relative phase of π and other parameters floating.
 - From a fit with contributions from ω(782), φ(1020), ω(1420), and ω(1650). See ACHASOV 20A for a further analysis of the π⁺π⁻π⁰ data.
 - From a fit of a VMD model with two effective resonances with masses of 1450 MeV and 1700 MeV to describe the excited vector states ω(1420), ρ(1450), ω(1650), and ρ(1700). Systematic errors not evaluated.
 - From the combined fit of ANTONELLI 92, ACHASOV 01E, ACHASOV 02E, and ACHASOV 03D data on the π⁺π⁻π⁰ and ANTONELLI 92 on the ωπ⁺π⁻ final states. Supersedes ACHASOV 99E and ACHASOV 02E.
 - Using results of CORDIER 81 and preliminary data of DOLINSKY 91 and ANTONELLI 92.
 - Using the data of AKHMETSHIN 00D and ANTONELLI 92. The ρπ dominance for the energy dependence of the ω(1420) and ω(1650) width assumed.
 - From a fit to two Breit-Wigner functions interfering between them and with the ω, φ tails with fixed (+, -, +) phases.
 - From a fit to two Breit-Wigner functions interfering between them and with the ω, φ tails with fixed (+, -, +) phases.

ω(1420)

$$I^G(J^{PC}) = 0^-(1^{--})$$

See also the ω(1650) particle listing.

ω(1420) MASS

VALUE (MeV)	EVTS	DOCUMENT ID	TECN	COMMENT
-------------	------	-------------	------	---------

1410 ± 60 OUR ESTIMATE

- • • We do not use the following data for averages, fits, limits, etc. • • •

1418 ± 30 ± 10	824	¹ AKHMETSHIN 17A	CMD3	1.4–2.0 e ⁺ e ⁻ → ωη
1470 ± 50	13.1k	² AULCHENKO 15A	SND	1.05–1.80 e ⁺ e ⁻ → π ⁺ π ⁻ π ⁰
1382 ± 23 ± 70		AUBERT	07AU BABR	10.6 e ⁺ e ⁻ → ωπ ⁺ π ⁻ γ
1350 ± 20 ± 20		AUBERT,B	04N BABR	10.6 e ⁺ e ⁻ → π ⁺ π ⁻ π ⁰ γ
1400 ± 50 ± 130	1.2M	³ ACHASOV 03D	RVUE	0.44–2.00 e ⁺ e ⁻ → π ⁺ π ⁻ π ⁰
1450 ± 10		⁴ HENNER 02	RVUE	1.2–2.0 e ⁺ e ⁻ → ρπ, ωππ
1373 ± 70	177	⁵ AKHMETSHIN 00D	CMD2	1.2–1.38 e ⁺ e ⁻ → ωπ ⁺ π ⁻
1370 ± 25	5095	ANISOVICH 00H	SPEC	0.0 ρπ̄ → ωπ ⁰ π ⁰
1400 ⁺¹⁰⁰ ₋₂₀₀		⁶ ACHASOV 98H	RVUE	e ⁺ e ⁻ → π ⁺ π ⁻ π ⁰
~ 1400		⁷ ACHASOV 98H	RVUE	e ⁺ e ⁻ → ωπ ⁺ π ⁻
~ 1460		⁸ ACHASOV 98H	RVUE	e ⁺ e ⁻ → K ⁺ K ⁻
1440 ± 70		⁹ CLEGG 94	RVUE	
1419 ± 31	315	¹⁰ ANTONELLI 92	DM2	1.34–2.4e ⁺ e ⁻ → ρπ

- From a fit of the interfering ω(1420) and ω(1650) with a relative phase of π and other parameters floating.
- From a fit with contributions from ω(782), φ(1020), ω(1420), and ω(1650). See ACHASOV 20A for a further analysis of the π⁺π⁻π⁰ data.
- From the combined fit of ANTONELLI 92, ACHASOV 01E, ACHASOV 02E, and ACHASOV 03D data on the π⁺π⁻π⁰ and ANTONELLI 92 on the ωπ⁺π⁻ final states. Supersedes ACHASOV 99E and ACHASOV 02E.
- Using results of CORDIER 81 and preliminary data of DOLINSKY 91 and ANTONELLI 92.
- Using the data of AKHMETSHIN 00D and ANTONELLI 92. The ρπ dominance for the energy dependence of the ω(1420) and ω(1650) width assumed.
- Using data from BARKOV 87, DOLINSKY 91, and ANTONELLI 92.
- Using the data from ANTONELLI 92.
- Using the data from IVANOV 81 and BISELLO 88B.
- From a fit to two Breit-Wigner functions and using the data of DOLINSKY 91 and ANTONELLI 92.
- From a fit to two Breit-Wigner functions interfering between them and with the ω, φ tails with fixed (+, -, +) phases.

ω(1420) WIDTH

VALUE (MeV)	EVTS	DOCUMENT ID	TECN	COMMENT
-------------	------	-------------	------	---------

290 ± 190 OUR ESTIMATE

- • • We do not use the following data for averages, fits, limits, etc. • • •

440 ± 125	267	¹ ACHASOV 20B	SND	e ⁺ e ⁻ → ωη → ηπ ⁰ γ
104 ± 35 ± 10	824	² AKHMETSHIN 17A	CMD3	1.4–2.0 e ⁺ e ⁻ → ωη
880 ± 170	13.1k	³ AULCHENKO 15A	SND	1.05–1.80 e ⁺ e ⁻ → π ⁺ π ⁻ π ⁰
480 ± 180		⁴ ACHASOV 10D	SND	1.075–2.0 e ⁺ e ⁻ → π ⁰ γ
130 ± 50 ± 100		AUBERT	07AU BABR	10.6 e ⁺ e ⁻ → ωπ ⁺ π ⁻ γ
450 ± 70 ± 70		AUBERT,B	04N BABR	10.6 e ⁺ e ⁻ → π ⁺ π ⁻ π ⁰ γ
870 ⁺⁵⁰⁰ ₋₃₀₀ ± 450	1.2M	⁵ ACHASOV 03D	RVUE	0.44–2.00 e ⁺ e ⁻ → π ⁺ π ⁻ π ⁰
199 ± 15		⁶ HENNER 02	RVUE	1.2–2.0 e ⁺ e ⁻ → ρπ, ωππ
188 ± 45	177	⁷ AKHMETSHIN 00D	CMD2	1.2–1.38 e ⁺ e ⁻ → ωπ ⁺ π ⁻
360 ⁺¹⁰⁰ ₋₆₀	5095	ANISOVICH 00H	SPEC	0.0 ρπ̄ → ωπ ⁰ π ⁰

ω(1420) DECAY MODES

Mode	Fraction (Γ _i /Γ)
Γ ₁ ρπ	seen
Γ ₂ ωππ	seen
Γ ₃ ωη	
Γ ₄ b ₁ (1235)π	seen
Γ ₅ e ⁺ e ⁻	seen
Γ ₆ π ⁰ γ	

ω(1420) Γ(i)Γ(e⁺e⁻)/Γ²(total)

VALUE (units 10 ⁻⁶)	EVTS	DOCUMENT ID	TECN	COMMENT
---------------------------------	------	-------------	------	---------

- • • We do not use the following data for averages, fits, limits, etc. • • •

0.73 ± 0.08	13.1k	¹ AULCHENKO 15A	SND	1.05–1.80 e ⁺ e ⁻ → π ⁺ π ⁻ π ⁰
0.82 ± 0.05 ± 0.06		AUBERT,B	04N BABR	10.6 e ⁺ e ⁻ → π ⁺ π ⁻ π ⁰ γ
0.65 ± 0.13 ± 0.21	1.2M	^{2,3} ACHASOV 03D	RVUE	0.44–2.00 e ⁺ e ⁻ → π ⁺ π ⁻ π ⁰
0.625 ± 0.160		^{4,5} CLEGG 94	RVUE	
0.466 ± 0.178		^{6,7} ANTONELLI 92	DM2	1.34–2.4e ⁺ e ⁻ → ρπ

- From a fit with contributions from ω(782), φ(1020), ω(1420), and ω(1650). See ACHASOV 20A for a further analysis of the π⁺π⁻π⁰ data.
- Calculated by us from the cross section at the peak.
- From the combined fit of ANTONELLI 92, ACHASOV 01E, ACHASOV 02E, and ACHASOV 03D data on the π⁺π⁻π⁰ and ANTONELLI 92 on the ωπ⁺π⁻ final states. Supersedes ACHASOV 99E and ACHASOV 02E.
- From a fit to two Breit-Wigner functions and using the data of DOLINSKY 91 and ANTONELLI 92.
- From the partial and leptonic width given by the authors.
- From a fit to two Breit-Wigner functions interfering between them and with the ω, φ tails with fixed (+, -, +) phases.
- From the product of the leptonic width and partial branching ratio given by the authors.

Γ(ωππ)/Γ_{total} × Γ(e⁺e⁻)/Γ_{total} Γ₂/Γ × Γ₅/Γ

VALUE (units 10 ⁻⁸)	DOCUMENT ID	TECN	COMMENT
---------------------------------	-------------	------	---------

- • • We do not use the following data for averages, fits, limits, etc. • • •

19.7 ± 5.7	AUBERT	07AU BABR	10.6 e ⁺ e ⁻ → ωπ ⁺ π ⁻ γ
1.9 ± 1.9	¹ AKHMETSHIN 00D	CMD2	1.2–2.4 e ⁺ e ⁻ → ωπ ⁺ π ⁻

- Using the data of AKHMETSHIN 00D and ANTONELLI 92. The ρπ dominance for the energy dependence of the ω(1420) and ω(1650) width assumed.

Γ(ωη)/Γ_{total} × Γ(e⁺e⁻)/Γ_{total} Γ₃/Γ × Γ₅/Γ

VALUE (units 10 ⁻⁸)	EVTS	DOCUMENT ID	TECN	COMMENT
---------------------------------	------	-------------	------	---------

- • • We do not use the following data for averages, fits, limits, etc. • • •

2.5 ± 0.6	267	¹ ACHASOV 20B	SND	e ⁺ e ⁻ → ωη → ηπ ⁰ γ
2.1 ^{+1.0} _{-0.8}		ACHASOV 19	SND	e ⁺ e ⁻ → π ⁺ π ⁻ π ⁰ η
5.0 ± 2.6 ± 0.3	824	² AKHMETSHIN 17A	CMD3	1.4–2.0 e ⁺ e ⁻ → ωη
1.6 ^{+0.9} _{-0.7}	898	³ ACHASOV 16B	SND	1.34–2.00 e ⁺ e ⁻ → ωη

- From a fit with contributions from ω(1420), ω(1650), and φ(1680). The mass of ω(1420) is fixed to the PDG 18 value of 1420 MeV. Fixing also the width of ω(1420) to the PDG 18 value of 220 MeV results in (3.0 ± 1.6) × 10⁻⁸ measurement.
- From a fit of the interfering ω(1420) and ω(1650) with a relative phase of π and other parameters floating. From an alternative fit Γ(ω(1420) → ωη)/Γ_{total} × Γ(ω(1420) → e⁺e⁻) = 5.3 ± 1.6 eV.
- From a fit with contributions from ω(1420), ω(1650), and φ(1680). The mass and the width of ω(1420) are fixed to the 2014 edition (PDG 14) of this review.

Meson Particle Listings

$\omega(1420)$, $f_2(1430)$, $a_0(1450)$

$\Gamma(\pi^0\gamma)/\Gamma_{\text{total}} \times \Gamma(e^+e^-)/\Gamma_{\text{total}}$	$\Gamma_6/\Gamma \times \Gamma_5/\Gamma$
VALUE (units 10^{-8})	DOCUMENT ID TECN COMMENT

0.23±0.14	¹ ACHASOV 10D SND 1.075-2.0 $e^+e^- \rightarrow \pi^0\gamma$
2.03 ^{+0.70} _{-0.75}	² AKHMETSHIN 05 CMD2 0.60-1.38 $e^+e^- \rightarrow \pi^0\gamma$

¹ From a fit of a VMD model with two effective resonances with masses of 1450 MeV and 1700 MeV to describe the excited vector states $\omega(1420)$, $\rho(1450)$, $\omega(1650)$, and $\rho(1700)$. Systematic errors not evaluated.
² Using 1420 MeV and 220 MeV for the $\omega(1420)$ mass and width.

$\omega(1420)$ BRANCHING RATIOS

$\Gamma(\omega\pi\pi)/\Gamma_{\text{total}}$	Γ_2/Γ
VALUE	DOCUMENT ID TECN COMMENT

0.301±0.029	¹ HENNER 02 RVUE 1.2-2.0 $e^+e^- \rightarrow \rho\pi, \omega\pi\pi$ possibly seen
	AKHMETSHIN 00D CMD2 $e^+e^- \rightarrow \omega\pi^+\pi^-$

$\Gamma(\omega\pi\pi)/\Gamma(b_1(1235)\pi)$	Γ_2/Γ_4
VALUE	EVTS DOCUMENT ID TECN COMMENT

0.60±0.16	5095 ANISOVICH 00H SPEC 0.0 $\rho\bar{\rho} \rightarrow \omega\pi^0\pi^0\pi^0$
-----------	--

$\Gamma(\rho\pi)/\Gamma_{\text{total}}$	Γ_1/Γ
VALUE	DOCUMENT ID TECN COMMENT

seen	ACHASOV 20A SND 1.15-2.00 $e^+e^- \rightarrow \pi^+\pi^-\pi^0$
0.699±0.029	¹ HENNER 02 RVUE 1.2-2.0 $e^+e^- \rightarrow \rho\pi, \omega\pi\pi$

$\Gamma(e^+e^-)/\Gamma_{\text{total}}$	Γ_5/Γ
VALUE (units 10^{-7})	EVTS DOCUMENT ID TECN COMMENT

~ 6.6	1.2M ^{2,3} ACHASOV 03D RVUE 0.44-2.00 $e^+e^- \rightarrow \pi^+\pi^-\pi^0$
23 ± 1	¹ HENNER 02 RVUE 1.2-2.0 $e^+e^- \rightarrow \rho\pi, \omega\pi\pi$

¹ Assuming that the $\omega(1420)$ decays into $\rho\pi$ and $\omega\pi\pi$.
² Calculated by us from the cross section at the peak.
³ Assuming that the $\omega(1420)$ decays into $\rho\pi$ only.

$\omega(1420)$ REFERENCES

ACHASOV 20A EPJ C80 993	M.N. Achasov et al.	(SND Collab.)
ACHASOV 20B EPJ C80 1008	M.N. Achasov et al.	(SND Collab.)
ACHASOV 19 PR D99 112004	M.N. Achasov et al.	(SND Collab.)
PDG 18 PR D98 030001	M. Tanabashi et al.	(PDG Collab.)
AKHMETSHIN 17A PL B773 150	R.R. Akhmetshin et al.	(CMD-3 Collab.)
ACHASOV 16B PR D94 092002	M.N. Achasov et al.	(SND Collab.)
AULCHENKO 15A JETP 121 27	V.M. Aulchenko et al.	(SND Collab.)
	Translated from ZETF 148 34.	
PDG 14 CP C38 070001	K. Olive et al.	(PDG Collab.)
ACHASOV 10D PR D98 112001	M.N. Achasov et al.	(SND Collab.)
AUBERT 07AU PR D76 092005	B. Aubert et al.	(BABAR Collab.)
AKHMETSHIN 05 PL B605 26	R.R. Akhmetshin et al.	(Novosibirsk CMD-2 Collab.)
AUBERT,B 04N PR D70 072004	B. Aubert et al.	(BABAR Collab.)
ACHASOV 03D PR D68 052006	M.N. Achasov et al.	(Novosibirsk SND Collab.)
ACHASOV 02E PR D66 032001	M.N. Achasov et al.	(Novosibirsk SND Collab.)
HENNER 02 EPJ C26 3	V.K. Henner et al.	(Novosibirsk SND Collab.)
ACHASOV 01E PR D63 072002	M.N. Achasov et al.	(Novosibirsk SND Collab.)
AKHMETSHIN 00D PL B489 125	R.R. Akhmetshin et al.	(Novosibirsk CMD-2 Collab.)
ANISOVICH 00H PL B485 341	A.V. Anisovich et al.	(Novosibirsk SND Collab.)
ACHASOV 99E PL B462 365	M.N. Achasov et al.	(Novosibirsk SND Collab.)
ACHASOV 98H PR D57 4334	N.N. Achasov, A.A. Kozhevnikov	(Novosibirsk SND Collab.)
CLEGG 94 ZPHY C62 455	A.B. Clegg, A. Donnachie	(LANC, MCHS)
ANTONELLI 92 ZPHY C56 15	A. Antonelli et al.	(DMC2 Collab.)
DOLINSKY 91 PRPL 202 99	S.I. Dolinsky et al.	(NOVO)
BISELLO 88B ZPHY C39 13	D. Bisello et al.	(PADO, CLER, FRAS+)
BARKOV 87 JETPL 46 164	L.M. Barkov et al.	(NOVO)
	Translated from ZETFP 46 132.	
CORDIER 81 PL 106B 155	A. Cordier et al.	(ORSAY)
IVANOV 81 PL 107B 297	P.M. Ivanov et al.	(NOVO)

$f_2(1430)$

$$I^G(J^{PC}) = 0^+(2^{++})$$

OMITTED FROM SUMMARY TABLE

This entry lists nearby peaks observed in the D wave of the $K\bar{K}$ and $\pi^+\pi^-$ systems. Needs confirmation.

$f_2(1430)$ MASS

VALUE (MeV)	DOCUMENT ID	TECN	COMMENT
-------------	-------------	------	---------

~ 1430 OUR ESTIMATE			
1440±11±3	LEES 21A BABR $\gamma\gamma \rightarrow \eta_c(1S) \rightarrow \eta'\pi^+\pi^-$		
1453 ± 4	¹ VLADIMIRSK..01 SPEC $40\pi^-p \rightarrow K_S^0 K_S^0 n$		
1421 ± 5	AUGUSTIN 87 DM2 $J/\psi \rightarrow \gamma\pi^+\pi^-$		
1480±50	AKESSON 86 SPEC $pp \rightarrow pp\pi^+\pi^-$		
1436 ⁺²⁶ ₋₁₆	DAUM 84 CNTR $17-18\pi^-p \rightarrow K^+K^-n$		

••• We do not use the following data for averages, fits, limits, etc. •••

1412± 3	DAUM 84 CNTR $63\pi^-p \rightarrow K_S^0 K_S^0 n, K^+K^-n$
1439 ⁺⁵ ₋₆	² BEUSCH 67 OSPK $5,7,12\pi^-p \rightarrow K_S^0 K_S^0 n$

¹ $J^{PC} = 0^{++}$ or 2^{++} .
² Not seen by WETZEL 76.

$f_2(1430)$ WIDTH

VALUE (MeV)	DOCUMENT ID	TECN	COMMENT
-------------	-------------	------	---------

46±15±5	LEES 21A BABR $\gamma\gamma \rightarrow \eta_c(1S) \rightarrow \eta'\pi^+\pi^-$
13± 5	³ VLADIMIRSK..01 SPEC $40\pi^-p \rightarrow K_S^0 K_S^0 n$
30± 9	AUGUSTIN 87 DM2 $J/\psi \rightarrow \gamma\pi^+\pi^-$
150±50	AKESSON 86 SPEC $pp \rightarrow pp\pi^+\pi^-$
81 ⁺⁵⁶ ₋₂₉	DAUM 84 CNTR $17-18\pi^-p \rightarrow K^+K^-n$
14± 6	DAUM 84 CNTR $63\pi^-p \rightarrow K_S^0 K_S^0 n, K^+K^-n$
43 ⁺¹⁷ ₋₁₈	⁴ BEUSCH 67 OSPK $5,7,12\pi^-p \rightarrow K_S^0 K_S^0 n$

³ $J^{PC} = 0^{++}$ or 2^{++} .
⁴ Not seen by WETZEL 76.

$f_2(1430)$ DECAY MODES

Mode
Γ_1 $K\bar{K}$
Γ_2 $\pi\pi$

$f_2(1430)$ REFERENCES

LEES 21A PR D104 072002	J.P. Lees et al.	(BABAR Collab.)
VLADIMIRSK..01 PAN 64 1895	V.V. Vladimirov et al.	
	Translated from YAF 64 1979.	
AUGUSTIN 87 ZPHY C36 369	J.E. Augustin et al.	(LALO, CLER, FRAS+)
AKESSON 86 NP B264 154	T. Akesson et al.	(Axial Field Spec. Collab.)
DAUM 84 ZPHY C23 339	C. Daum et al.	(AMST, CERN, CRAC, MPIM+)
WETZEL 76 NP B115 208	W. Wetzel et al.	(ETH, CERN, LOIC)
BEUSCH 67 PL 25B 357	W. Beusch et al.	(ETH, CERN)

$a_0(1450)$

$$I^G(J^{PC}) = 1^-(0^{++})$$

See the review on "Spectroscopy of Light Meson Resonances."

$a_0(1450)$ T-MATRIX POLE \sqrt{s}

Note that $\Gamma = -2 \text{Im}(\sqrt{s})$.

VALUE (MeV)	DOCUMENT ID	TECN	COMMENT
-------------	-------------	------	---------

(1290-1500) - i (30-140) OUR ESTIMATE			
(1302.1 ± 1.1 ± 3.9) - i	¹ ALBRECHT 20 RVUE 0.9 $\bar{p}p \rightarrow \pi^0\pi^0\eta,$		
(56.2 ± 0.7 ± 1.7)	$\pi^0\eta\eta, \pi^0 K^+K^-$		
(1515 ± 30) - i (115 ± 18)	ANISOVICH 09 RVUE 0.0 $\bar{p}p, \pi N$		
(1432 ± 13 ± 25) - i (98 ± 5 ± 5)	² BUGG 08A RVUE $\bar{p}p$		
(1441 ⁺⁴⁰ ₋₁₅) - i (55 ± 7)	³ BAKER 03 SPEC $\bar{p}p \rightarrow \omega\pi^+\pi^-\pi^0$		
(1303 ± 16) - i (46 ± 8)	⁴ BARGIOTTI 03 OBLX $\bar{p}p$		
(1296 ± 10) - i (41 ± 11)	AMSLER 02 CBAR 0.9 $\bar{p}p \rightarrow \pi^0\pi^0\eta$		
(1565 ± 30) - i (146 ± 20)	ANISOVICH 98B RVUE Compilation		
(1470 ± 25) - i (132 ± 15)	⁵ AMSLER 95D CBAR 0.0 $\bar{p}p \rightarrow \pi^0\pi^0\pi^0,$		
	$\pi^0\eta\eta, \pi^0\pi^0\eta$		

¹ T-matrix pole, 2 poles, 2 channels ($\pi\eta, K\bar{K}$).
² Using data from AMSLER 94D, ABELE 98, and BAKER 03. Supersedes BUGG 94.
³ From the pole position of a fitted Breit-Wigner amplitude.
⁴ Coupled channel analysis of $\pi^+\pi^-\pi^0, K^+K^-\pi^0$, and $K^\pm K_S^0 \pi^\mp$.
⁵ Coupled-channel analysis of AMSLER 95B, AMSLER 95C, and AMSLER 94D.

$a_0(1450)$ MASS

VALUE (MeV)	EVTS	DOCUMENT ID	TECN	COMMENT
-------------	------	-------------	------	---------

1439 ± 34	OUR AVERAGE	Error includes scale factor of 1.8.		
1480 ± 30	ABELE 98 CBAR 0.0 $\bar{p}p \rightarrow K_L^0 K^\pm \pi^\mp$			
1410 ± 25	ETKIN 82C MPS $23\pi^-p \rightarrow n2K_S^0$			
1458 ± 14 ± 15	190k	¹ AAIJ 16N LHCB $D^0 \rightarrow K_S^0 K^\pm \pi^\mp$		
1316.8 ^{+0.7} _{-1.0} ± 24.7 _{-4.6}		² UEHARA 09A BELL $\gamma\gamma \rightarrow \pi^0\eta$		
1477 ± 10	80k	³ UMAN 06 E835 $5.2\bar{p}p \rightarrow \eta\eta\pi^0$		
1290 ± 10		⁴ BERTIN 98B OBLX 0.0 $\bar{p}p \rightarrow K^\pm K_S^0 \pi^\mp$		
1450 ± 40		AMSLER 94D CBAR 0.0 $\bar{p}p \rightarrow \pi^0\pi^0\eta$		
~ 1300		MARTIN 78 SPEC 10 $K^\pm p \rightarrow K_S^0 \pi p$		
1255 ± 5		⁵ CASON 76		

••• We do not use the following data for averages, fits, limits, etc. •••

¹ Using a model with Gaussian constraints to the PDG averaged values.
² May be a different state.
³ Statistical error only.

See key on page 1171

Meson Particle Listings

$a_0(1450), \rho(1450)$

⁴ Not confirmed by BUGG 08A.
⁵ Isospin 0 not excluded.

$a_0(1450)$ WIDTH

VALUE (MeV)	EVTS	DOCUMENT ID	TECN	COMMENT
258 ± 14	OUR AVERAGE			
265 ± 15		ABELE 98	CBAR	$0.0 \bar{p}p \rightarrow K_L^0 K^\pm \pi^\mp$
230 ± 30		ETKIN 82c	MPS	$23 \pi^- p \rightarrow n 2 K_S^0$
• • • We do not use the following data for averages, fits, limits, etc. • • •				
282 ± 12 ± 13	190k	¹ AAIJ 16N	LHCB	$D^0 \rightarrow K_S^0 K^\pm \pi^\mp$
65.0 ⁺ _{-5.4} 2.1 ⁺ _{-32.6}		² UEHARA 09A	BELL	$\gamma\gamma \rightarrow \pi^0 \eta$
267 ± 11	80k	³ UMAN 06	E835	$5.2 \bar{p}p \rightarrow \eta\eta\pi^0$
80 ± 5		⁴ BERTIN 98B	OBLX	$0.0 \bar{p}p \rightarrow K^\pm K_S \pi^\mp$
270 ± 40		AMSLER 94D	CBAR	$0.0 \bar{p}p \rightarrow \pi^0 \pi^0 \eta$
~ 250		MARTIN 78	SPEC	$10 K^\pm p \rightarrow K_S^0 \pi p$
79 ± 10		⁵ CASON 76		

¹ Using a model with Gaussian constraints to the PDG averaged values .
² May be a different state.
³ Statistical error only.
⁴ Not confirmed by BUGG 08A.
⁵ Isospin 0 not excluded.

$a_0(1450)$ DECAY MODES

Branching fractions are given relative to the one **DEFINED AS 1**.

Mode	Fraction (Γ_i/Γ)
$\Gamma_1 \pi\eta$	0.093 ± 0.020
$\Gamma_2 \pi\eta'(958)$	0.033 ± 0.017
$\Gamma_3 K\bar{K}$	0.082 ± 0.028
$\Gamma_4 \omega\pi\pi$	DEFINED AS 1
$\Gamma_5 a_0(980)\pi\pi$	seen
$\Gamma_6 \gamma\gamma$	seen

$a_0(1450)$ $\Gamma(i)\Gamma(\gamma\gamma)/\Gamma(\text{total})$

$\Gamma(\pi\eta) \times \Gamma(\gamma\gamma)/\Gamma(\text{total})$	$\Gamma_1\Gamma_6/\Gamma$		
VALUE (eV)	DOCUMENT ID	TECN	COMMENT
• • • We do not use the following data for averages, fits, limits, etc. • • •			
432 ± 6 ± 1073 256	¹ UEHARA 09A	BELL	$\gamma\gamma \rightarrow \pi^0 \eta$
¹ May be a different state.			

$a_0(1450)$ BRANCHING RATIOS

$\Gamma(\pi\eta'(958))/\Gamma(\pi\eta)$	Γ_2/Γ_1		
VALUE	DOCUMENT ID	TECN	COMMENT
0.35 ± 0.16	¹ ABELE 98	CBAR	$0.0 \bar{p}p \rightarrow K_L^0 K^\pm \pi^\mp$
• • • We do not use the following data for averages, fits, limits, etc. • • •			
0.43 ± 0.19	ABELE 97c	CBAR	$0.0 \bar{p}p \rightarrow \pi^0 \pi^0 \eta'$
¹ Using $\pi^0 \eta$ from AMSLER 94D.			

$\Gamma(K\bar{K})/\Gamma(\pi\eta)$	Γ_3/Γ_1		
VALUE	DOCUMENT ID	TECN	COMMENT
0.88 ± 0.23	¹ ABELE 98	CBAR	$0.0 \bar{p}p \rightarrow K_L^0 K^\pm \pi^\mp$
• • • We do not use the following data for averages, fits, limits, etc. • • •			
1.887 ± 0.041 ± 0.97	² ALBRECHT 20	RVUE	$0.9 \bar{p}p \rightarrow \pi^0 \pi^0 \eta, \pi^0 \eta\eta, \pi^0 K^+ K^-$
¹ Using $\pi^0 \eta$ from AMSLER 94D. ² Residues from T-matrix pole, 2 poles, 2 channels ($\pi\eta, K\bar{K}$).			

$\Gamma(\omega\pi\pi)/\Gamma(\pi\eta)$	Γ_4/Γ_1			
VALUE	EVTS	DOCUMENT ID	TECN	COMMENT
10.7 ± 2.3	35280	¹ BAKER 03	SPEC	$\bar{p}p \rightarrow \omega\pi^+\pi^-\pi^0$
¹ Using results on $\bar{p}p \rightarrow a_0(1450)\pi^0, a_0(1450) \rightarrow \eta\pi^0$ from ABELE 96c and assuming the $\omega\rho$ mechanism for the $\omega\pi\pi$ state.				

$\Gamma(a_0(980)\pi\pi)/\Gamma(\text{total})$	Γ_5/Γ		
VALUE	DOCUMENT ID	TECN	COMMENT
seen	BUGG 08A	RVUE	$\bar{p}p$

$\Gamma(a_0(980)\pi\pi)/\Gamma(\pi\eta)$	Γ_5/Γ_1			
VALUE	DOCUMENT ID	TECN	CHG	COMMENT
• • • We do not use the following data for averages, fits, limits, etc. • • •				
≤ 4.3	ANISOVICH 01	RVUE	0	$\bar{p}p \rightarrow \eta 2\pi^+ 2\pi^-$

$\Gamma(\gamma\gamma)/\Gamma(\text{total})$

VALUE	DOCUMENT ID	TECN	COMMENT
seen	¹ UEHARA 09A	BELL	$\gamma\gamma \rightarrow \pi^0 \eta$
¹ May be a different state.			

$a_0(1450)$ REFERENCES

ALBRECHT 20	EPJ C80 453	M. Albrecht <i>et al.</i>	(Crystal Barrel Collab.)
AAIJ 16N	PR D93 052018	R. Aaij <i>et al.</i>	(LHCb Collab.)
ANISOVICH 09	IJMP A24 2481	V.V. Anisovich, A.V. Sarantsev	(PnPI)
UEHARA 09A	PR D80 032001	S. Uehara <i>et al.</i>	(BELLE Collab.)
BUGG 08A	PR D78 074023	D.V. Bugg	(LOQM)
UMAN 06	PR D73 052009	I. Uman <i>et al.</i>	(FNAL E835)
BAKER 03	PL B563 140	C.A. Baker <i>et al.</i>	
BARGIOTTI 03	EPJ C26 371	M. Bargiotti <i>et al.</i>	(OBELIX Collab.)
AMSLER 02	EPJ C23 29	C. Amisler <i>et al.</i>	(Crystal Barrel Collab.)
ANISOVICH 01	NP A690 567	A.V. Anisovich <i>et al.</i>	
ABELE 98	PR D57 3860	A. Abele <i>et al.</i>	(Crystal Barrel Collab.)
ANISOVICH 98B	SPU 41 419	V.V. Anisovich <i>et al.</i>	
BERTIN 98B	Translated from UFN 168 481.	A. Bertin <i>et al.</i>	(OBELIX Collab.)
ABELE 97C	PL B404 179	A. Abele <i>et al.</i>	(Crystal Barrel Collab.)
ABELE 96C	NP A609 562	A. Abele <i>et al.</i>	(Crystal Barrel Collab.)
AMSLER 95B	PL B342 433	C. Amisler <i>et al.</i>	(Crystal Barrel Collab.)
AMSLER 95C	PL B353 571	C. Amisler <i>et al.</i>	(Crystal Barrel Collab.)
AMSLER 95D	PL B355 425	C. Amisler <i>et al.</i>	(Crystal Barrel Collab.)
AMSLER 94D	PL B333 277	C. Amisler <i>et al.</i>	(Crystal Barrel Collab.) IGJPC
BUGG 94	PR D50 4412	D.V. Bugg <i>et al.</i>	(LOQM)
ETKIN 82C	PR D25 2446	A. Etkin <i>et al.</i>	(BNL, CUNY, TUFTS, VAND)
MARTIN 78	NP B134 392	A.D. Martin <i>et al.</i>	(DURH, GEVA)
CASON 76	PRL 36 1465	N.M. Cason <i>et al.</i>	(NDAM, ANL)

$\rho(1450)$

$$I^G(J^{PC}) = 1^+(1^{--})$$

$\rho(1450)$ MASS

$\rho(1450)$ MASS

VALUE (MeV) DOCUMENT ID
1465 ± 25 OUR ESTIMATE This is only an educated guess; the error given is larger than the error on the average of the published values.

$\eta\pi^0$ MODE

VALUE (MeV)	EVTS	DOCUMENT ID	TECN	COMMENT
• • • We do not use the following data for averages, fits, limits, etc. • • •				
1506 ± 11	13.4k	¹ GRIBANOV 20	CMD3	$1.1-2.0 e^+ e^- \rightarrow \eta\pi^+ \pi^-$
1500 ± 10	7.4k	² ACHASOV 18	SND	$1.22-2.00 e^+ e^- \rightarrow \eta\pi^+ \pi^-$
1497 ± 14		³ AKHMETSIN 01B	CMD2	$e^+ e^- \rightarrow \eta\gamma$
1421 ± 15		⁴ AKHMETSIN 00D	CMD2	$e^+ e^- \rightarrow \eta\pi^+ \pi^-$
1470 ± 20		ANTONELLI 88	DM2	$e^+ e^- \rightarrow \eta\pi^+ \pi^-$
1446 ± 10		FUKUI 88	SPEC	$8.95 \pi^- p \rightarrow \eta\pi^+ \pi^- n$

¹ Mass and width of the $\rho(770)$ fixed at 775 and 149 MeV, respectively; solution 2 of model 2, $\eta \rightarrow \gamma\gamma$ decays used.
² From the combined fit of AULCHENKO 15 and ACHASOV 18 in the model with the interfering $\rho(1450), \rho(1700)$ and $\rho(2150)$ with the parameters of the $\rho(1450)$ and $\rho(1700)$ floating and the mass and width of the $\rho(2150)$ fixed at 2155 MeV and 320 MeV, respectively. The phases of the resonances are $\pi, 0$ and π , respectively.
³ Using the data of AKHMETSIN 01B on $e^+ e^- \rightarrow \eta\gamma$, AKHMETSIN 00D and ANTONELLI 88 on $e^+ e^- \rightarrow \eta\pi^+ \pi^-$.
⁴ Using the data of ANTONELLI 88, DOLINSKY 91, and AKHMETSIN 00D. The energy-independent width of the $\rho(1450)$ and $\rho(1700)$ mesons assumed.

$\omega\pi$ MODE

VALUE (MeV)	EVTS	DOCUMENT ID	TECN	COMMENT
• • • We do not use the following data for averages, fits, limits, etc. • • •				
1510 ± 7	10.2k	¹ ACHASOV 16D	SND	$1.05-2.00 e^+ e^- \rightarrow \pi^0 \pi^0 \gamma$
1544 ± 22 ± 11 46	821	² MATVIENKO 15	BELL	$\bar{B}^0 \rightarrow D^{*+} \omega \pi^-$
1491 ± 19	7815	³ ACHASOV 13	SND	$1.05-2.00 e^+ e^- \rightarrow \pi^0 \pi^0 \gamma$
1582 ± 17 ± 25	2382	⁴ AKHMETSIN 03B	CMD2	$e^+ e^- \rightarrow \pi^0 \pi^0 \gamma$
1349 ± 25 ± 10 5	341	⁵ ALEXANDER 01B	CLE2	$B \rightarrow D^*(*) \omega \pi^-$
1523 ± 10		⁶ EDWARDS 00A	CLE2	$\tau^- \rightarrow \omega \pi^- \nu_\tau$
1463 ± 25		⁷ CLEGG 94	RVUE	
1250		⁸ ASTON 80C	OMEG	$20-70 \gamma p \rightarrow \omega \pi^0 p$
1290 ± 40		⁸ BARBER 80C	SPEC	$3-5 \gamma p \rightarrow \omega \pi^0 p$

¹ From a phenomenological model based on vector meson dominance with interfering $\rho(770), \rho(1450)$, and $\rho(1700)$. The $\rho(1700)$ mass and width are fixed at 1720 MeV and 250 MeV, respectively. Systematic uncertainties not estimated. Supersedes ACHASOV 13.
² Using Breit-Wigner parameterization of the $\rho(1450)$ and assuming equal probabilities of the $\rho(1450) \rightarrow \pi\pi$ and $\rho(1450) \rightarrow \omega\pi$ decays.
³ From a phenomenological model based on vector meson dominance with the interfering $\rho(1450)$ and $\rho(1700)$ and their widths fixed at 400 and 250 MeV, respectively. Systematic uncertainty not estimated.
⁴ Using the data of AKHMETSIN 03B and BISELLO 91B assuming the $\omega\pi^0$ and $\pi^+\pi^-$ mass dependence of the total width. $\rho(1700)$ mass and width fixed at 1700 MeV and 240 MeV, respectively.
⁵ Using Breit-Wigner parameterization of the $\rho(1450)$ and assuming the $\omega\pi^-$ mass dependence of the total width.
⁶ Mass-independent width parameterization. $\rho(1700)$ mass and width fixed at 1700 MeV and 235 MeV respectively.
⁷ Using data from BISELLO 91B, DOLINSKY 86 and ALBRECHT 87L.
⁸ Not separated from $b_1(1235)$, not pure $J^P = 1^-$ effect.

Meson Particle Listings

 $\rho(1450)$ **4 π MODE**

VALUE (MeV)	DOCUMENT ID	TECN	COMMENT
1435 \pm 40	ABELE 01B	CBAR	0.0 $\bar{p}n \rightarrow 2\pi^- 2\pi^0 \pi^+$
1350 \pm 50	ACHASOV 97	RVUE	$e^+ e^- \rightarrow 2(\pi^+ \pi^-)$
1449 \pm 4	¹ ARMSTRONG 89E	OMEG	300 $p\bar{p} \rightarrow \rho p 2(\pi^+ \pi^-)$

¹ Not clear whether this observation has $l=1$ or 0.

 $\pi\pi$ MODE

VALUE (MeV)	EVTS	DOCUMENT ID	TECN	COMMENT
1326.35 \pm 3.46		¹ BARTOS 17	RVUE	$e^+ e^- \rightarrow \pi^+ \pi^-$
1342.31 \pm 46.62		² BARTOS 17A	RVUE	$e^+ e^- \rightarrow \pi^0 \pi^-$
1373.83 \pm 11.37		³ BARTOS 17A	RVUE	$\tau^- \rightarrow \pi^- \pi^0 \nu_\tau$
1429 \pm 41	20k	⁴ LEES 17c	BABR	$J/\psi \rightarrow \pi^+ \pi^- \pi^0$
1350 \pm 20	$\frac{+20}{-30}$ 63.5k	⁵ ABRAMOWICZ12	ZEUS	$e p \rightarrow e \pi^+ \pi^- p$
1493 \pm 15		⁶ LEES 12g	BABR	$e^+ e^- \rightarrow \pi^+ \pi^- \gamma$
1446 \pm 7	± 28 5.4M	^{7,8} FUJIKAWA 08	BELL	$\tau^- \rightarrow \pi^- \pi^0 \nu_\tau$
1328 \pm 15		⁹ SCHAEEL 05c	ALEP	$\tau^- \rightarrow \pi^- \pi^0 \nu_\tau$
1406 \pm 15	87k	^{7,10} ANDERSON 00A	CLE2	$\tau^- \rightarrow \pi^- \pi^0 \nu_\tau$
\sim 1368		¹¹ ABELE 99c	CBAR	0.0 $\bar{p}d \rightarrow \pi^+ \pi^- \pi^- p$
1348 \pm 33		BERTIN 98	OBLX	0.05–0.405 $\bar{p}p \rightarrow \pi^+ \pi^- \pi^0$
1411 \pm 14		¹² ABELE 97	CBAR	$\bar{p}n \rightarrow \pi^- \pi^0 \pi^0$
1370 $\frac{+90}{-70}$		ACHASOV 97	RVUE	$e^+ e^- \rightarrow \pi^+ \pi^-$
1359 \pm 40		¹⁰ BERTIN 97c	OBLX	0.0 $\bar{p}p \rightarrow \pi^+ \pi^- \pi^0$
1282 \pm 37		BERTIN 97d	OBLX	0.05 $\bar{p}p \rightarrow 2\pi^+ 2\pi^-$
1424 \pm 25		BISELLO 89	DM2	$e^+ e^- \rightarrow \pi^+ \pi^-$
1265.5 \pm 75.3		DUBNICKA 89	RVUE	$e^+ e^- \rightarrow \pi^+ \pi^-$
1292 \pm 17		¹³ KURDADZE 83	OLYA	0.64–1.4 $e^+ e^- \rightarrow \pi^+ \pi^-$

¹ Applies the Unitary & Analytic Model of the pion electromagnetic form factor of DUBNICKA 10 to analyze the data of LEES 12g and ABLIKIM 16c.

² Applies the Unitary & Analytic Model of the pion electromagnetic form factor of DUBNICKA 10 to analyze the data of ACHASOV 06, AKHMETSHIN 07, AUBERT 09As, and AMBROSINO 11A.

³ Applies the Unitary & Analytic Model of the pion electromagnetic form factor of DUBNICKA 10 to analyze the data of FUJIKAWA 08.

⁴ From a Dalitz plot analysis in an isobar model with $\rho(1450)$ and $\rho(1700)$ masses and widths floating.

⁵ Using the KUHN 90 parametrization of the pion form factor, neglecting ρ - ω interference.

⁶ Using the GOUNARIS 68 parametrization of the pion form factor leaving the masses and widths of the $\rho(1450)$, $\rho(1700)$, and $\rho(2150)$ resonances as free parameters of the fit.

⁷ From the GOUNARIS 68 parametrization of the pion form factor.

⁸ $|F_\pi(0)|^2$ fixed to 1.

⁹ From the combined fit of the τ^- data from ANDERSON 00A and SCHAEEL 05c and $e^+ e^-$ data from the compilation of BARKOV 85, AKHMETSHIN 04, and ALOISIO 05. $\rho(1700)$ mass and width fixed at 1713 MeV and 235 MeV, respectively. Supersedes BARATE 97M.

¹⁰ $\rho(1700)$ mass and width fixed at 1700 MeV and 235 MeV, respectively.

¹¹ $\rho(1700)$ mass and width fixed at 1780 MeV and 275 MeV respectively.

¹² T-matrix pole.

¹³ Using for $\rho(1700)$ mass and width 1600 \pm 20 and 300 \pm 10 MeV respectively.

 $K\bar{K}$ MODE

VALUE (MeV)	EVTS	DOCUMENT ID	TECN	CHG	COMMENT
1208 \pm 8 \pm 9	190k	¹ AAIJ 16N	LHCB		$D^0 \rightarrow K_S^0 K^+ \pi^-$
1422.8 \pm 6.5	27k	² ABELE 99D	CBAR	\pm	0.0 $\bar{p}p \rightarrow K^+ K^- \pi^0$

¹ Using the GOUNARIS 68 parametrization with fixed width.

² K-matrix pole. Isospin not determined, could be $\omega(1420)$.

 $K\bar{K}^*(892) + c.c.$ MODE

VALUE (MeV)	DOCUMENT ID	TECN	COMMENT
1505 \pm 19 \pm 7	AUBERT 08s	BABR	10.6 $e^+ e^- \rightarrow K\bar{K}^*(892)\gamma$

 $m_{\rho(1450)^0} - m_{\rho(1450)^\pm}$

VALUE (MeV)	DOCUMENT ID	TECN	COMMENT
-31.53 ± 47.99	¹ BARTOS 17A	RVUE	$e^+ e^- \rightarrow \pi^+ \pi^-$, $\tau^- \rightarrow \pi^- \pi^0 \nu_\tau$

¹ Applies the Unitary & Analytic Model of the pion electromagnetic form factor of DUBNICKA 10 to analyze the data of ACHASOV 06, AKHMETSHIN 07, AUBERT 09As, AMBROSINO 11A, and FUJIKAWA 08.

 $\rho(1450)$ WIDTH **$\rho(1450)$ WIDTH**

VALUE (MeV)	DOCUMENT ID	TECN	COMMENT
400 \pm 60 OUR ESTIMATE	This is only an educated guess; the error given is larger than the error on the average of the published values.		

• • • We do not use the following data for averages, fits, limits, etc. • • •

480 \pm 180 ¹ACHASOV 10D SND 1.075–2.0 $e^+ e^- \rightarrow \pi^0 \gamma$

¹ From a fit of a VMD model with two effective resonances with masses of 1450 MeV and 1700 MeV to describe the excited vector states $\omega(1420)$, $\rho(1450)$, $\omega(1650)$, and $\rho(1700)$. Systematic errors not evaluated.

 $\eta\rho^0$ MODE

VALUE (MeV)	EVTS	DOCUMENT ID	TECN	COMMENT
321 \pm 27	13.4k	¹ GRIBANOV 20	CMD3	1.1–2.0 $e^+ e^- \rightarrow \eta\pi^+ \pi^-$
280 \pm 20	7.4k	² ACHASOV 18	SND	1.22–2.00 $e^+ e^- \rightarrow \eta\pi^+ \pi^-$
226 \pm 44		³ AKHMETSHIN 01B	CMD2	$e^+ e^- \rightarrow \eta\gamma$
211 \pm 31		⁴ AKHMETSHIN 00D	CMD2	$e^+ e^- \rightarrow \eta\pi^+ \pi^-$
230 \pm 30		ANTONELLI 88	DM2	$e^+ e^- \rightarrow \eta\pi^+ \pi^-$
60 \pm 15		FUKUI 88	SPEC	8.95 $\pi^- p \rightarrow \eta\pi^+ \pi^- n$

¹ Mass and width of the $\rho(770)$ fixed at 775 and 149 MeV, respectively; solution 2 of model 2, $\eta \rightarrow \gamma\gamma$ decays used.

² From the combined fit of AULCHENKO 15 and ACHASOV 18 in the model with the interfering $\rho(1450)$, $\rho(1700)$ and $\rho(2150)$ with the parameters of the $\rho(1450)$ and $\rho(1700)$ floating and the mass and width of the $\rho(2150)$ fixed at 2155 MeV and 320 MeV, respectively. The phases of the resonances are π , 0 and π , respectively.

³ Using the data of AKHMETSHIN 01B on $e^+ e^- \rightarrow \eta\gamma$, AKHMETSHIN 00D and ANTONELLI 88 on $e^+ e^- \rightarrow \eta\pi^+ \pi^-$.

⁴ Using the data of ANTONELLI 88, DOLINSKY 91, and AKHMETSHIN 00D. The energy-independent width of the $\rho(1450)$ and $\rho(1700)$ mesons assumed.

 $\omega\pi$ MODE

VALUE (MeV)	EVTS	DOCUMENT ID	TECN	COMMENT
440 \pm 40	10.2k	¹ ACHASOV 16D	SND	1.05–2.00 $e^+ e^- \rightarrow \pi^0 \pi^0 \gamma$
303 \pm $\frac{31+69}{52-7}$	821	² MATVIENKO 15	BELL	$\bar{B}^0 \rightarrow D^* \omega \pi^-$
429 \pm 42 \pm 10	2382	³ AKHMETSHIN 03B	CMD2	$e^+ e^- \rightarrow \pi^0 \pi^0 \gamma$
547 \pm $86 \frac{+46}{-45}$	341	⁴ ALEXANDER 01B	CLE2	$B \rightarrow D^{(*)} \omega \pi^-$
400 \pm 35		⁵ EDWARDS 00A	CLE2	$\tau^- \rightarrow \omega \pi^- \nu_\tau$
311 \pm 62		⁶ CLEGG 94	RVUE	
300		⁷ ASTON 80c	OMEG	20–70 $\gamma p \rightarrow \omega \pi^0 p$
320 \pm 100		⁷ BARBER 80c	SPEC	3–5 $\gamma p \rightarrow \omega \pi^0 p$

¹ From a phenomenological model based on vector meson dominance with interfering $\rho(770)$, $\rho(1450)$, and $\rho(1700)$. The $\rho(1700)$ mass and width are fixed at 1720 MeV and 250 MeV, respectively. Systematic uncertainties not estimated. Supersedes ACHASOV 13.

² Using Breit-Wigner parameterization of the $\rho(1450)$ and assuming equal probabilities of the $\rho(1450) \rightarrow \pi\pi$ and $\rho(1450) \rightarrow \omega\pi$ decays.

³ Using the data of AKHMETSHIN 03B and BISELLO 91B assuming the $\omega\pi^0$ and $\pi^+ \pi^-$ mass dependence of the total width. $\rho(1700)$ mass and width fixed at 1700 MeV and 240 MeV, respectively.

⁴ Using Breit-Wigner parameterization of the $\rho(1450)$ and assuming the $\omega\pi^-$ mass dependence for the total width.

⁵ Mass-independent width parameterization. $\rho(1700)$ mass and width fixed at 1700 MeV and 235 MeV respectively.

⁶ Using data from BISELLO 91B, DOLINSKY 86 and ALBRECHT 87L.

⁷ Not separated from $b_1(1235)$, not pure $J^P = 1^-$ effect.

4 π MODE

VALUE (MeV)	DOCUMENT ID	TECN	COMMENT
325 \pm 100	ABELE 01B	CBAR	0.0 $\bar{p}n \rightarrow 2\pi^- 2\pi^0 \pi^+$

 $\pi\pi$ MODE

VALUE (MeV)	EVTS	DOCUMENT ID	TECN	COMMENT
324.13 \pm 12.01		¹ BARTOS 17	RVUE	$e^+ e^- \rightarrow \pi^+ \pi^-$
492.17 \pm 138.38		² BARTOS 17A	RVUE	$e^+ e^- \rightarrow \pi^+ \pi^-$
340.87 \pm 23.84		³ BARTOS 17A	RVUE	$\tau^- \rightarrow \pi^- \pi^0 \nu_\tau$
576 \pm 29	20k	⁴ LEES 17C	BABR	$J/\psi \rightarrow \pi^+ \pi^- \pi^0$
460 \pm 30	$\frac{+40}{-45}$ 63.5k	⁵ ABRAMOWICZ12	ZEUS	$e p \rightarrow e \pi^+ \pi^- p$
427 \pm 31		⁶ LEES 12G	BABR	$e^+ e^- \rightarrow \pi^+ \pi^- \gamma$
434 \pm 16	± 60 5.4M	^{7,8} FUJIKAWA 08	BELL	$\tau^- \rightarrow \pi^- \pi^0 \nu_\tau$
468 \pm 41		⁹ SCHAEEL 05c	ALEP	$\tau^- \rightarrow \pi^- \pi^0 \nu_\tau$
455 \pm 41	87k	^{7,10} ANDERSON 00A	CLE2	$\tau^- \rightarrow \pi^- \pi^0 \nu_\tau$
\sim 374		¹¹ ABELE 99c	CBAR	0.0 $\bar{p}d \rightarrow \pi^+ \pi^- \pi^- p$
275 \pm 10		BERTIN 98	OBLX	0.05–0.405 $\bar{p}p \rightarrow \pi^+ \pi^- \pi^0$
343 \pm 20		¹² ABELE 97	CBAR	$\bar{p}n \rightarrow \pi^- \pi^0 \pi^0$
310 \pm 40		¹⁰ BERTIN 97c	OBLX	0.0 $\bar{p}p \rightarrow \pi^+ \pi^- \pi^0$
236 \pm 36		BERTIN 97D	OBLX	0.05 $\bar{p}p \rightarrow 2\pi^+ 2\pi^-$
269 \pm 31		BISELLO 89	DM2	$e^+ e^- \rightarrow \pi^+ \pi^-$
391 \pm 70		DUBNICKA 89	RVUE	$e^+ e^- \rightarrow \pi^+ \pi^-$
218 \pm 46		¹³ KURDADZE 83	OLYA	0.64–1.4 $e^+ e^- \rightarrow \pi^+ \pi^-$

¹ Applies the Unitary & Analytic Model of the pion electromagnetic form factor of DUBNICKA 10 to analyze the data of LEES 12g and ABLIKIM 16c.

$\rho(1450)$

- ²Applies the Unitary & Analytic Model of the pion electromagnetic form factor of DUBNICKA 10 to analyze the data of ACHASOV 06, AKHMETSHIN 07, AUBERT 09AS, and AMBROSINO 11A.
- ³Applies the Unitary & Analytic Model of the pion electromagnetic form factor of DUBNICKA 10 to analyze the data of FUJIKAWA 08.
- ⁴From a Dalitz plot analysis in an isobar model with $\rho(1450)$ and $\rho(1700)$ masses and widths floating.
- ⁵Using the KUHN 90 parametrization of the pion form factor, neglecting ρ - ω interference.
- ⁶Using the GOUNARIS 68 parametrization of the pion form factor leaving the masses and widths of the $\rho(1450)$, $\rho(1700)$, and $\rho(2150)$ resonances as free parameters of the fit.
- ⁷From the GOUNARIS 68 parametrization of the pion form factor.
- ⁸ $|F_\pi(0)|^2$ fixed to 1.
- ⁹From the combined fit of the τ^- data from ANDERSON 00A and SCHAEEL 05c and e^+e^- data from the compilation of BARKOV 85, AKHMETSHIN 04, and ALOISIO 05. $\rho(1700)$ mass and width fixed at 1713 MeV and 235 MeV, respectively. Supersedes BARATE 97M.
- ¹⁰ $\rho(1700)$ mass and width fixed at 1700 MeV and 235 MeV, respectively.
- ¹¹ $\rho(1700)$ mass and width fixed at 1780 MeV and 275 MeV respectively.
- ¹²T-matrix pole.
- ¹³Using for $\rho(1700)$ mass and width 1600 ± 20 and 300 ± 10 MeV respectively.

$K\bar{K}$ MODE

VALUE (MeV)	EVTS	DOCUMENT ID	TECN	CHG	COMMENT
• • • We do not use the following data for averages, fits, limits, etc. • • •					
410 ± 19 ± 35	190k	¹ AAIJ	16N	LHCB	$D^0 \rightarrow K_S^0 K^+ \pi^-$
146.5 ± 10.5	27k	² ABELE	99D	CBAR ±	$0.0 \bar{p} p \rightarrow K^+ K^- \pi^0$

- ¹Using the GOUNARIS 68 parameterization with fixed mass.
- ²K-matrix pole. Isospin not determined, could be $\omega(1420)$.

$K\bar{K}^*(892) + c.c.$ MODE

VALUE (MeV)	DOCUMENT ID	TECN	COMMENT
• • • We do not use the following data for averages, fits, limits, etc. • • •			
418 ± 25 ± 4	AUBERT 08s	BABR	$10.6 e^+ e^- \rightarrow K\bar{K}^*(892)\gamma$

$\Gamma_{\rho(1450)^0} - \Gamma_{\rho(1450)^\pm}$

VALUE (MeV)	DOCUMENT ID	TECN	COMMENT
• • • We do not use the following data for averages, fits, limits, etc. • • •			
151.30 ± 140.42	¹ BARTOS	17A	RVUE $e^+ e^- \rightarrow \pi^+ \pi^-, \tau^- \rightarrow \pi^- \pi^0 \nu_\tau$

- ¹Applies the Unitary & Analytic Model of the pion electromagnetic form factor of DUBNICKA 10 to analyze the data of ACHASOV 06, AKHMETSHIN 07, AUBERT 09AS, AMBROSINO 11A, and FUJIKAWA 08.

$\rho(1450)$ DECAY MODES

Mode	Fraction (Γ_i/Γ)
Γ_1 $\pi\pi$	seen
Γ_2 $\pi^+\pi^-$	seen
Γ_3 4π	seen
Γ_4 $\omega\pi$	
Γ_5 $a_1(1260)\pi$	
Γ_6 $h_1(1170)\pi$	
Γ_7 $\pi(1300)\pi$	
Γ_8 $\rho\rho$	
Γ_9 $\rho(\pi\pi)$ s-wave	
Γ_{10} e^+e^-	seen
Γ_{11} $\eta\rho$	seen
Γ_{12} $a_2(1320)\pi$	not seen
Γ_{13} $K\bar{K}$	seen
Γ_{14} K^+K^-	seen
Γ_{15} $K\bar{K}^*(892) + c.c.$	possibly seen
Γ_{16} $\pi^0\gamma$	seen
Γ_{17} $\eta\gamma$	seen
Γ_{18} $f_0(500)\gamma$	not seen
Γ_{19} $f_0(980)\gamma$	not seen
Γ_{20} $f_0(1370)\gamma$	not seen
Γ_{21} $f_2(1270)\gamma$	not seen

$\rho(1450) \Gamma(i)\Gamma(e^+e^-)/\Gamma(\text{total})$

$\Gamma(\pi\pi) \times \Gamma(e^+e^-)/\Gamma(\text{total})$	DOCUMENT ID	TECN	COMMENT	$\Gamma_1\Gamma_{10}/\Gamma$
• • • We do not use the following data for averages, fits, limits, etc. • • •				
0.12	¹ DIEKMAN	88	RVUE $e^+e^- \rightarrow \pi^+\pi^-$	
0.027 + 0.015 - 0.010	² KURDADZE	83	OLYA $0.64-1.4 e^+e^- \rightarrow \pi^+\pi^-$	

- ¹Using total width = 235 MeV.
- ²Using for $\rho(1700)$ mass and width 1600 ± 20 and 300 ± 10 MeV respectively.

$\Gamma(\eta\rho) \times \Gamma(e^+e^-)/\Gamma(\text{total})$

VALUE (eV)	EVTS	DOCUMENT ID	TECN	COMMENT	$\Gamma_{11}\Gamma_{10}/\Gamma$
• • • We do not use the following data for averages, fits, limits, etc. • • •					
335 ± 27 ± 20	13.4k	¹ GRIBANOV	20	CMD3 $1.1-2.0 e^+e^- \rightarrow \eta\pi^+\pi^-$	
210 ± 24 ± 10		² LEES	18	BABR $e^+e^- \rightarrow \eta\pi^+\pi^-$	
74 ± 20		³ AKHMETSHIN 00D	CMD2	$e^+e^- \rightarrow \eta\pi^+\pi^-$	
91 ± 19		ANTONELLI 88	DM2	$e^+e^- \rightarrow \eta\pi^+\pi^-$	

- ¹Mass and width of the $\rho(770)$ fixed at 775 and 149 MeV, respectively; solution 2 of model 2, $\eta \rightarrow \gamma\gamma$ decays used.
- ²Includes non-resonant contribution. The selected fit model includes three ρ excited states. Model uncertainty is 20%.
- ³Using the data of ANTONELLI 88, DOLINSKY 91, and AKHMETSHIN 00D. The energy-independent width of the $\rho(1450)$ and $\rho(1700)$ mesons assumed.

$\Gamma(K\bar{K}^*(892) + c.c.) \times \Gamma(e^+e^-)/\Gamma(\text{total})$

VALUE (eV)	DOCUMENT ID	TECN	COMMENT	$\Gamma_{15}\Gamma_{10}/\Gamma$
• • • We do not use the following data for averages, fits, limits, etc. • • •				
127 ± 15 ± 6	AUBERT 08s	BABR	$10.6 e^+e^- \rightarrow K\bar{K}^*(892)\gamma$	

$\Gamma(\eta\gamma) \times \Gamma(e^+e^-)/\Gamma(\text{total})$

VALUE (eV)	DOCUMENT ID	TECN	COMMENT	$\Gamma_{17}\Gamma_{10}/\Gamma$
• • • We do not use the following data for averages, fits, limits, etc. • • •				
<16.4	¹ AKHMETSHIN 05	CMD2	$0.60-1.38 e^+e^- \rightarrow \eta\gamma$	
2.2 ± 0.5 ± 0.3	² AKHMETSHIN 01B	CMD2	$e^+e^- \rightarrow \eta\gamma$	

- ¹From 2γ decay mode of η using 1465 MeV and 310 MeV for the $\rho(1450)$ mass and width. Recalculated by us.
- ²Using the data of AKHMETSHIN 01B on $e^+e^- \rightarrow \eta\gamma$, AKHMETSHIN 00D and ANTONELLI 88 on $e^+e^- \rightarrow \eta\pi^+\pi^-$. Recalculated by us using width of 226 MeV.

$\rho(1450) \Gamma(i)/\Gamma(\text{total}) \times \Gamma(e^+e^-)/\Gamma(\text{total})$

$\Gamma(\omega\pi)/\Gamma(\text{total}) \times \Gamma(e^+e^-)/\Gamma(\text{total})$

VALUE (units 10^{-6})	EVTS	DOCUMENT ID	TECN	COMMENT	$\Gamma_4/\Gamma \times \Gamma_{10}/\Gamma$
• • • We do not use the following data for averages, fits, limits, etc. • • •					
2.1 ± 0.4	10.2k	¹ ACHASOV	16D	SND $1.05-2.00 e^+e^- \rightarrow \pi^0\pi^0\gamma$	
5.3 ± 0.4	7815	² ACHASOV	13	SND $1.05-2.00 e^+e^- \rightarrow \pi^0\pi^0\gamma$	

- ¹From a phenomenological model based on vector meson dominance with interfering $\rho(770)$, $\rho(1450)$, and $\rho(1700)$. The $\rho(1700)$ mass and width are fixed at 1720 MeV and 250 MeV, respectively. Systematic uncertainties not estimated. Supersedes ACHASOV 13.
- ²From a phenomenological model based on vector meson dominance with the interfering $\rho(1450)$ and $\rho(1700)$ and their widths fixed at 400 and 250 MeV, respectively. Systematic uncertainty not estimated.

$\Gamma(\eta\rho)/\Gamma(\text{total}) \times \Gamma(e^+e^-)/\Gamma(\text{total})$

VALUE (units 10^{-7})	EVTS	DOCUMENT ID	TECN	COMMENT	$\Gamma_{11}/\Gamma \times \Gamma_{10}/\Gamma$
• • • We do not use the following data for averages, fits, limits, etc. • • •					
7.3 ± 0.3	7.4k	¹ ACHASOV	18	SND $1.22-2.00 e^+e^- \rightarrow \eta\pi^+\pi^-$	
4.3 + 1.1 - 0.9 ± 0.2	4.9k	² AULCHENKO	15	SND $1.22-2.00 e^+e^- \rightarrow \eta\pi^+\pi^-$	

- ¹From the combined fit of AULCHENKO 15 and ACHASOV 18 in the model with the interfering $\rho(1450)$, $\rho(1700)$ and $\rho(2150)$ with the parameters of the $\rho(1450)$ and $\rho(1700)$ floating and the mass and width of the $\rho(2150)$ fixed at 2155 MeV and 320 MeV, respectively. The phases of the resonances are π , 0 and π , respectively.
- ²From a fit to the $e^+e^- \rightarrow \eta\pi^+\pi^-$ cross section with vector meson dominance model including $\rho(770)$, $\rho(1450)$, and $\rho(1700)$ decaying exclusively via $\eta\rho(770)$. Masses and widths of vector states are fixed to PDG 14. Coupling constants are assumed to be real.

$\Gamma(\pi^0\gamma)/\Gamma(\text{total}) \times \Gamma(e^+e^-)/\Gamma(\text{total})$

VALUE (units 10^{-9})	DOCUMENT ID	TECN	COMMENT	$\Gamma_{16}/\Gamma \times \Gamma_{10}/\Gamma$
• • • We do not use the following data for averages, fits, limits, etc. • • •				
2.3 ± 1.4	¹ ACHASOV	10D	SND $1.075-2.0 e^+e^- \rightarrow \pi^0\gamma$	

- ¹From a fit of a VMD model with two effective resonances with masses of 1450 MeV and 1700 MeV to describe the excited vector states $\omega(1420)$, $\rho(1450)$, $\omega(1650)$, and $\rho(1700)$. Systematic errors not evaluated.

$\Gamma(f_0(500)\gamma)/\Gamma(\text{total}) \times \Gamma(e^+e^-)/\Gamma(\text{total})$

VALUE (units 10^{-9})	CL%	DOCUMENT ID	TECN	COMMENT	$\Gamma_{19}/\Gamma \times \Gamma_{10}/\Gamma$
<4.0	90	ACHASOV	11	SND $e^+e^- \rightarrow \pi^0\pi^0\gamma$	

$\Gamma(f_0(980)\gamma)/\Gamma(\text{total}) \times \Gamma(e^+e^-)/\Gamma(\text{total})$

VALUE (units 10^{-9})	CL%	DOCUMENT ID	TECN	COMMENT	$\Gamma_{19}/\Gamma \times \Gamma_{10}/\Gamma$
<2.6	90	ACHASOV	11	SND $e^+e^- \rightarrow \pi^0\pi^0\gamma$	

$\Gamma(f_0(1370)\gamma)/\Gamma(\text{total}) \times \Gamma(e^+e^-)/\Gamma(\text{total})$

VALUE (units 10^{-9})	CL%	DOCUMENT ID	TECN	COMMENT	$\Gamma_{20}/\Gamma \times \Gamma_{10}/\Gamma$
<3.5	90	ACHASOV	11	SND $e^+e^- \rightarrow \pi^0\pi^0\gamma$	

Meson Particle Listings

 $\rho(1450)$

$\Gamma(\rho(1270)\gamma)/\Gamma_{\text{total}} \times \Gamma(e^+e^-)/\Gamma_{\text{total}}$		$\Gamma_{21}/\Gamma \times \Gamma_{10}/\Gamma$	
VALUE (units 10^{-3})	CL%	DOCUMENT ID	TECN COMMENT
<0.8	90	¹ ACHASOV	11 SND $e^+e^- \rightarrow \pi^0\pi^0\gamma$
¹ Using Breit-Wigner parametrization of the $\rho(1450)$ with mass and width of 1465 MeV and 400 MeV, respectively.			

 $\rho(1450)$ BRANCHING RATIOS

$\Gamma(\pi\pi)/\Gamma(4\pi)$		Γ_1/Γ_3	
VALUE	DOCUMENT ID	TECN	COMMENT
••• We do not use the following data for averages, fits, limits, etc. •••			
0.37 ± 0.10	^{1,2} ABELE	01B	CBAR $0.0 \bar{p}n \rightarrow 5\pi$
¹ $\omega\pi$ not included.			
² Using ABELE 97.			

$\Gamma(K^+K^-)/\Gamma(\pi^+\pi^-)$		Γ_{14}/Γ_2	
VALUE (%)	EVTS	DOCUMENT ID	TECN COMMENT
$30.7 \pm 8.4 \pm 8.2$	20k	¹ LEES	17C BABR $J/\psi \rightarrow h^+h^-\pi^0$
¹ From Dalitz plot analyses in isobar models.			

$\Gamma(\omega\pi)/\Gamma_{\text{total}}$		Γ_4/Γ	
VALUE	EVTS	DOCUMENT ID	TECN COMMENT
••• We do not use the following data for averages, fits, limits, etc. •••			
seen	821	¹ MATVIENKO	15 BELL $\bar{B}^0 \rightarrow D^{*+}\omega\pi^-$
seen	1.6k	ACHASOV	12 SND $e^+e^- \rightarrow \pi^0\pi^0\gamma$
~ 0.21		CLEGG	94 RVUE
¹ Using Breit-Wigner parametrization of the $\rho(1450)$ and assuming equal probabilities of the $\rho(1450) \rightarrow \pi\pi$ and $\rho(1450) \rightarrow \omega\pi$ decays.			

$\Gamma(\pi\pi)/\Gamma(\omega\pi)$		Γ_1/Γ_4	
VALUE	DOCUMENT ID	TECN	COMMENT
••• We do not use the following data for averages, fits, limits, etc. •••			
~ 0.32		CLEGG	94 RVUE

$\Gamma(\omega\pi)/\Gamma(4\pi)$		Γ_4/Γ_3	
VALUE	DOCUMENT ID	TECN	COMMENT
••• We do not use the following data for averages, fits, limits, etc. •••			
<0.14		CLEGG	88 RVUE

$\Gamma(a_1(1260)\pi)/\Gamma(4\pi)$		Γ_5/Γ_3	
VALUE	DOCUMENT ID	TECN	COMMENT
••• We do not use the following data for averages, fits, limits, etc. •••			
0.27 ± 0.08		¹ ABELE	01B CBAR $0.0 \bar{p}n \rightarrow 5\pi$
¹ $\omega\pi$ not included.			

$\Gamma(h_1(1170)\pi)/\Gamma(4\pi)$		Γ_6/Γ_3	
VALUE	DOCUMENT ID	TECN	COMMENT
••• We do not use the following data for averages, fits, limits, etc. •••			
0.08 ± 0.04		¹ ABELE	01B CBAR $0.0 \bar{p}n \rightarrow 5\pi$
¹ $\omega\pi$ not included.			

$\Gamma(\pi(1300)\pi)/\Gamma(4\pi)$		Γ_7/Γ_3	
VALUE	DOCUMENT ID	TECN	COMMENT
••• We do not use the following data for averages, fits, limits, etc. •••			
0.37 ± 0.13		¹ ABELE	01B CBAR $0.0 \bar{p}n \rightarrow 5\pi$
¹ $\omega\pi$ not included.			

$\Gamma(\rho\rho)/\Gamma(4\pi)$		Γ_8/Γ_3	
VALUE	DOCUMENT ID	TECN	COMMENT
••• We do not use the following data for averages, fits, limits, etc. •••			
0.11 ± 0.05		¹ ABELE	01B CBAR $0.0 \bar{p}n \rightarrow 5\pi$
¹ $\omega\pi$ not included.			

$\Gamma(\rho(\pi\pi)s\text{-wave})/\Gamma(4\pi)$		Γ_9/Γ_3	
VALUE	DOCUMENT ID	TECN	COMMENT
••• We do not use the following data for averages, fits, limits, etc. •••			
0.17 ± 0.09		¹ ABELE	01B CBAR $0.0 \bar{p}n \rightarrow 5\pi$
¹ $\omega\pi$ not included.			

$\Gamma(\eta\rho)/\Gamma_{\text{total}}$		Γ_{11}/Γ	
VALUE	EVTS	DOCUMENT ID	TECN COMMENT
seen	35	¹ ACHASOV	14 SND $1.15\text{--}2.00 e^+e^- \rightarrow \eta\gamma$
••• We do not use the following data for averages, fits, limits, etc. •••			
<0.04		DONNACHIE	87B RVUE

¹From a phenomenological model based on vector meson dominance with $\rho(1450)$ and $\phi(1680)$ masses and widths from the PDG 12.

$\Gamma(\eta\rho)/\Gamma(\omega\pi)$		Γ_{11}/Γ_4	
VALUE	DOCUMENT ID	TECN	COMMENT
••• We do not use the following data for averages, fits, limits, etc. •••			
0.081 ± 0.020		^{1,2} AULCHENKO	15 SND $1.22\text{--}2.00 e^+e^- \rightarrow \eta\pi^+\pi^-$
~ 0.24		³ DONNACHIE	91 RVUE
>2		FUKUI	91 SPEC $8.95 \pi^-\rho \rightarrow \omega\pi^0n$

¹From a fit to the $e^+e^- \rightarrow \eta\pi^+\pi^-$ cross section with vector meson dominance model including $\rho(770)$, $\rho(1450)$, and $\rho(1700)$ decaying exclusively via $\eta\rho(770)$. Masses and widths of vector states are fixed to PDG 14. Coupling constants are assumed to be real.
²Reports the inverse of the quoted value as 12.3 ± 3.1 .
³Using data from BISELLO 91B, DOLINSKY 86 and ALBRECHT 87L.

$\Gamma(\pi\pi)/\Gamma(\eta\rho)$		Γ_1/Γ_{11}	
VALUE	DOCUMENT ID	TECN	COMMENT
••• We do not use the following data for averages, fits, limits, etc. •••			
1.3 ± 0.4		¹ AULCHENKO	15 SND $1.22\text{--}2.00 e^+e^- \rightarrow \eta\pi^+\pi^-$
¹ From a fit to the $e^+e^- \rightarrow \eta\pi^+\pi^-$ cross section with vector meson dominance model including $\rho(770)$, $\rho(1450)$, and $\rho(1700)$ decaying exclusively via $\eta\rho(770)$. Masses and widths of vector states are fixed to PDG 14. Coupling constants are assumed to be real.			

$\Gamma(a_2(1320)\pi)/\Gamma_{\text{total}}$		Γ_{12}/Γ	
VALUE	DOCUMENT ID	TECN	COMMENT
••• We do not use the following data for averages, fits, limits, etc. •••			
not seen		AMELIN	00 VES $37 \pi^-\rho \rightarrow \eta\pi^+\pi^-n$

$\Gamma(K\bar{K})/\Gamma(\omega\pi)$		Γ_{13}/Γ_4	
VALUE	DOCUMENT ID	TECN	COMMENT
••• We do not use the following data for averages, fits, limits, etc. •••			
<0.08		¹ DONNACHIE	91 RVUE
¹ Using data from BISELLO 91B, DOLINSKY 86 and ALBRECHT 87L.			

$\Gamma(K\bar{K}^*(892) + \text{c.c.})/\Gamma_{\text{total}}$		Γ_{15}/Γ	
VALUE	DOCUMENT ID	TECN	COMMENT
••• We do not use the following data for averages, fits, limits, etc. •••			
possibly seen		COAN	04 CLEO $\tau^- \rightarrow K^-\pi^-\pi^+\nu_\tau$

$\Gamma(\eta\gamma)/\Gamma_{\text{total}}$		Γ_{17}/Γ	
VALUE	EVTS	DOCUMENT ID	TECN COMMENT
seen	35	¹ ACHASOV	14 SND $1.15\text{--}2.00 e^+e^- \rightarrow \eta\gamma$
¹ From a phenomenological model based on vector meson dominance with $\rho(1450)$ and $\phi(1680)$ masses and widths from the PDG 12.			

 $\rho(1450)$ REFERENCES

GRIBANOV	20	JHEP 2001 112	S.S. Gribanov <i>et al.</i>	(CMD-3 Collab.)
ACHASOV	18	PR D97 012008	M.N. Achasov <i>et al.</i>	(SND Collab.)
LEES	18	PR D97 052007	J.P. Lees <i>et al.</i>	(BABAR Collab.)
BARTOS	17	PR D96 113004	E. Bartos <i>et al.</i>	
BARTOS	17A	IJMP A32 1750154	E. Bartos <i>et al.</i>	
LEES	17C	PR D95 072007	J.P. Lees <i>et al.</i>	(BABAR Collab.)
AAIJ	16N	PR D93 052018	R. Aaij <i>et al.</i>	(LHCb Collab.)
ABLIKIM	16C	PL B753 629	M. Ablikim <i>et al.</i>	(BESIII Collab.)
ACHASOV	16D	PR D94 112001	M.N. Achasov <i>et al.</i>	(SND Collab.)
AULCHENKO	15	PR D91 052013	V.M. Aulchenko <i>et al.</i>	(SND Collab.)
MATVIENKO	15	PR D92 012013	D. Matvienko <i>et al.</i>	(BELLE Collab.)
ACHASOV	14	PR D90 032002	M.N. Achasov <i>et al.</i>	(SND Collab.)
PDG	14	CP C38 070001	K. Olive <i>et al.</i>	(PDG Collab.)
ACHASOV	13	PR D88 054013	M.N. Achasov <i>et al.</i>	(SND Collab.)
ABRAMOWICZ	12	EPJ C72 1869	H. Abramowicz <i>et al.</i>	(ZEUS Collab.)
ACHASOV	12	JETPL 94 734	M.N. Achasov <i>et al.</i>	
		Translated from ZETFP 94 796.		
LEES	12G	PR D86 032013	J.P. Lees <i>et al.</i>	(BABAR Collab.)
PDG	12	PR D86 010001	J. Beringer <i>et al.</i>	(PDG Collab.)
ACHASOV	11	JETP 113 75	M.N. Achasov <i>et al.</i>	(SND Collab.)
		Translated from ZETF 140 87.		
AMBROSINO	11A	PL B700 102	F. Ambrosino <i>et al.</i>	(KLOE Collab.)
ACHASOV	10D	PR D98 112001	M.N. Achasov <i>et al.</i>	(SND Collab.)
DUBNICKA	10	APS 60 1	S. Dubnicka, A.Z. Dubnickova	
AUBERT	09AS	PRL 103 231801	B. Aubert <i>et al.</i>	(BABAR Collab.)
AUBERT	08S	PR D77 092002	B. Aubert <i>et al.</i>	(BABAR Collab.)
FUJIKAWA	08	PR D78 072006	M. Fujikawa <i>et al.</i>	(BELLE Collab.)
AKHMETSHIN	07	PL B648 28	R.R. Akhmetshin <i>et al.</i>	(Novosibirsk CMD-2 Collab.)
ACHASOV	06	JETP 103 380	M.N. Achasov <i>et al.</i>	(Novosibirsk SND Collab.)
		Translated from ZETF 130 437.		
AKHMETSHIN	05	PL B605 26	R.R. Akhmetshin <i>et al.</i>	(Novosibirsk CMD-2 Collab.)
ALOISIO	05	PL B606 12	A. Aloisio <i>et al.</i>	(KLOE Collab.)
SCHAEEL	05C	PRPL 421 191	S. Schaeel <i>et al.</i>	(ALEPH Collab.)
AKHMETSHIN	04	PL B578 285	R.R. Akhmetshin <i>et al.</i>	(Novosibirsk CMD-2 Collab.)
COAN	04	PRL 92 232001	T.E. Coan <i>et al.</i>	(CLEO Collab.)
AKHMETSHIN	03B	PL B562 173	R.R. Akhmetshin <i>et al.</i>	(Novosibirsk CMD-2 Collab.)
ABELE	01B	EPJ C21 261	A. Abele <i>et al.</i>	(Crystal Barrel Collab.)
AKHMETSHIN	01B	PL B509 217	R.R. Akhmetshin <i>et al.</i>	(Novosibirsk CMD-2 Collab.)
ALEXANDER	01B	PR D64 092001	J.P. Alexander <i>et al.</i>	(CLEO Collab.)
AKHMETSHIN	00D	PL B489 125	R.R. Akhmetshin <i>et al.</i>	(Novosibirsk CMD-2 Collab.)
AMELIN	00	NP A668 83	D. Amelin <i>et al.</i>	(VES Collab.)
ANDERSON	00A	PR D61 112002	S. Anderson <i>et al.</i>	(CLEO Collab.)
EDWARDS	00A	PR D61 072003	K.W. Edwards <i>et al.</i>	(CLEO Collab.)
ABELE	99C	PL B450 275	A. Abele <i>et al.</i>	(Crystal Barrel Collab.)
ABELE	99D	PL B468 178	A. Abele <i>et al.</i>	(Crystal Barrel Collab.)
BERTIN	98	PR D57 55	A. Bertin <i>et al.</i>	(OBELIX Collab.)
ABELE	97	PL B391 191	A. Abele <i>et al.</i>	(Crystal Barrel Collab.)
ACHASOV	97	PR D95 2663	M.N. Achasov <i>et al.</i>	(NOVM)
BARATE	97M	ZPHY C76 15	R. Barate <i>et al.</i>	(ALEPH Collab.)
BERTIN	97C	PL B408 476	A. Bertin <i>et al.</i>	(OBELIX Collab.)
BERTIN	97D	PL B414 220	A. Bertin <i>et al.</i>	(OBELIX Collab.)
CLEGG	94	ZPHY C62 455	A.B. Clegg, A. Donnachie	(LANC, MCHS)

See key on page 1171

Meson Particle Listings

$\rho(1450), \eta(1475)$

BISELLO 91B	NPBPS B21 111	D. Bisello	(DM2 Collab.)
DOLINSKY 91	PRPL 202 99	S.I. Dolinsky et al.	(NOVO)
DONNACHIE 91	ZPHY C51 689	A. Donnachie, A.B. Clegg	(MCHS, LANC)
FUKUI 91	PL B257 241	S. Fukui et al.	(SUGI, NAGO, KEK, KYOT+)
KUHN 90	ZPHY C48 445	J.H. Kuhn et al.	(MPIM)
ARMSTRONG 89E	PL B228 536	T.A. Armstrong, M. Benayoun	(ATHU, BARI, BIRM+)
BISELLO 89	PL B220 321	D. Bisello et al.	(DM2 Collab.)
DUBNICKA 89	JP G15 1349	S. Dubnicka et al.	(JINR, SLOV)
ANTONELLI 88	PL B212 133	A. Antonelli et al.	(DM2 Collab.)
CLEGG 88	ZPHY C40 313	A.B. Clegg, A. Donnachie	(MCHS, LANC)
DIKMAN 88	PRPL 159 99	B. Diekmann	(BONN)
FUKUI 88	PL B202 441	S. Fukui et al.	(SUGI, NAGO, KEK, KYOT+)
ALBRECHT 87L	PL B185 223	H. Albrecht et al.	(ARGUS Collab.)
DONNACHIE 87B	ZPHY C34 257	A. Donnachie, A.B. Clegg	(MCHS, LANC)
DOLINSKY 86	PL B174 453	S.I. Dolinsky et al.	(NOVO)
BARKOV 85	NP B256 365	L.M. Barkov et al.	(NOVO)
KURDADZE 83	JETPL 37 733	L.M. Kurdadze et al.	(NOVO)
Translated from ZETFP 37 613.			
ASTON 80C	PL 92B 211	D. Aston	(BONN, CERN, EPOL, GLAS, LANC+)
BARBER 80C	ZPHY C4 169	D.P. Barber et al.	(DARE, LANC, SHEF)
GOUNARIS 68	PRL 21 244	G.J. Gounaris, J.J. Sakurai	

105 ±15	BERTIN 97	OBLX	0.0 $\bar{p}p \rightarrow K^\pm(K^0)\pi^\mp\pi^+\pi^-$
105 ±15	BERTIN 95	OBLX	0 $\bar{p}p \rightarrow K\bar{K}\pi\pi\pi$
54 $^{+37}_{-21}$ $^{+13}_{-24}$	BAI 90C	MRK3	$J/\psi \rightarrow \gamma K_S^0 K^\pm\pi^\mp$
51 ±13	RATH 89	MPS	$21.4 \pi^- p \rightarrow n K_S^0 K_S^0 \pi^0$

••• We do not use the following data for averages, fits, limits, etc. •••

118 ±22 ±17	¹ ABLIKIM 18i	BES3	$J/\psi \rightarrow \gamma\gamma\phi(1020)$
45 $^{+14}_{-13}$ $^{+21}_{-28}$	² ABLIKIM 15T	BES3	$J/\psi \rightarrow \gamma K_S^0 K_S^0 \eta$
63 ±18	AUGUSTIN 92	DM2	$J/\psi \rightarrow \gamma K\bar{K}\pi$

¹ From a fit to $\gamma\phi$ invariant mass. Angular analysis consistent with $J^{PC} = 0^{-+}$. Other J^{PC} not excluded.
² Could also be the $\eta(1405)$.

$\eta(1475)$

$$J^{PC} = 0^+(0^{-+})$$

See the $\eta(1405)$ and the related review on "Spectroscopy of Light Meson Resonances."

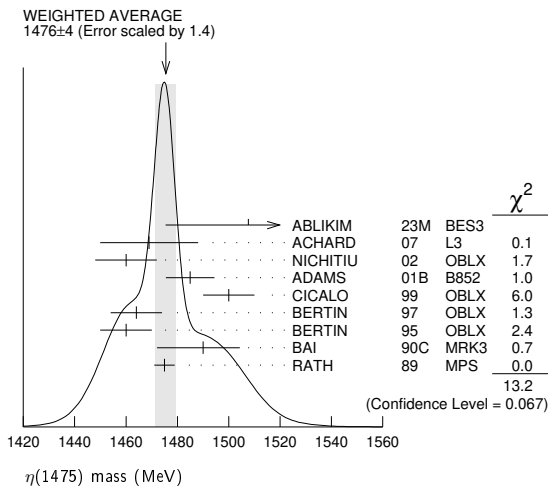
$\eta(1475)$ MASS

VALUE (MeV)	EVTS	DOCUMENT ID	TECN	COMMENT
1476 ± 4 OUR AVERAGE		Error includes scale factor of 1.4. See the ideogram below.		
1507.6 ± 1.6 $^{+15.5}_{-32.2}$	126K	¹ ABLIKIM 23M	BES3	$J/\psi \rightarrow \gamma K_S^0 K_S^0 \pi^0$
1469 ± 14 ± 13	74	ACHARD 07	L3	183-209 $e^+e^- \rightarrow e^+e^- K_S^0 K^\pm\pi^\mp$
1460 ± 12	3651	NICHITIU 02	OBLX	0 $\bar{p}p \rightarrow K^+K^-\pi^+\pi^-\pi^0$
1485 ± 8 ± 5	20k	ADAMS 01B	B852	18 GeV $\pi^- p \rightarrow K^+K^-\pi^0 n$
1500 ± 10		CICALO 99	OBLX	0 $\bar{p}p \rightarrow K^\pm K_S^0 \pi^\mp\pi^+\pi^-$
1464 ± 10		BERTIN 97	OBLX	0 $\bar{p}p \rightarrow K^\pm(K^0)\pi^\mp\pi^+\pi^-$
1460 ± 10		BERTIN 95	OBLX	0 $\bar{p}p \rightarrow K\bar{K}\pi\pi\pi$
1490 $^{+14}_{-8}$ $^{+3}_{-16}$	1100	BAI 90C	MRK3	$J/\psi \rightarrow \gamma K_S^0 K^\pm\pi^\mp$
1475 ± 4		RATH 89	MPS	$21.4 \pi^- p \rightarrow n K_S^0 K_S^0 \pi^0$

••• We do not use the following data for averages, fits, limits, etc. •••

1477 ± 7 ± 13	² ABLIKIM 18i	BES3	$J/\psi \rightarrow \gamma\gamma\phi(1020)$
1565 ± 8 $^{+0}_{-63}$	³ ABLIKIM 15T	BES3	$J/\psi \rightarrow \gamma K_S^0 K_S^0 \eta$
1421 ± 14	AUGUSTIN 92	DM2	$J/\psi \rightarrow \gamma K\bar{K}\pi$

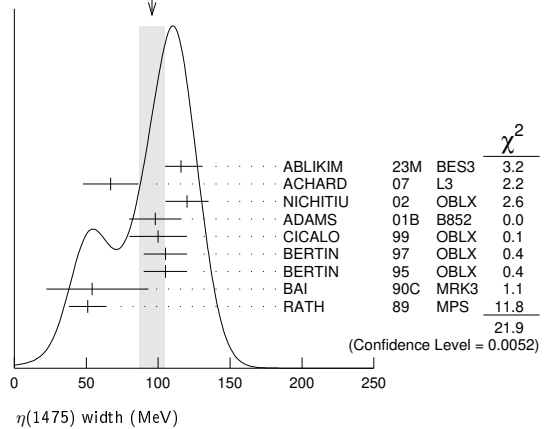
¹ ABLIKIM 23M reports for this state a significance from the fit much higher than 35 σ .
² From a fit to $\gamma\phi$ invariant mass. Angular analysis consistent with $J^{PC} = 0^{-+}$. Other J^{PC} not excluded.
³ Could also be the $\eta(1405)$.



$\eta(1475)$ WIDTH

VALUE (MeV)	EVTS	DOCUMENT ID	TECN	COMMENT
96 ± 9 OUR AVERAGE		Error includes scale factor of 1.7. See the ideogram below.		
115.8 ± 2.4 $^{+14.8}_{-10.9}$	126K	ABLIKIM 23M	BES3	$J/\psi \rightarrow \gamma K_S^0 K_S^0 \pi^0$
67 ± 18 ± 7	74	ACHARD 07	L3	183-209 $e^+e^- \rightarrow e^+e^- K_S^0 K^\pm\pi^\mp$
120 ± 15	3651	NICHITIU 02	OBLX	0 $\bar{p}p \rightarrow K^+K^-\pi^+\pi^-\pi^0$
98 ± 18 ± 3	20k	ADAMS 01B	B852	18 GeV $\pi^- p \rightarrow K^+K^-\pi^0 n$
100 ± 20		CICALO 99	OBLX	0 $\bar{p}p \rightarrow K^\pm K_S^0 \pi^\mp\pi^+\pi^-$

WEIGHTED AVERAGE
96±9 (Error scaled by 1.7)



$\eta(1475)$ DECAY MODES

Mode	Fraction (Γ_i/Γ)
Γ_1 $K\bar{K}\pi$	seen
Γ_2 $K\bar{K}^*(892) + c.c.$	seen
Γ_3 $a_0(980)\pi$	seen
Γ_4 $\gamma\gamma$	seen
Γ_5 $K_S^0 K_S^0 \eta$	possibly seen
Γ_6 $\gamma\phi(1020)$	possibly seen

$\eta(1475)$ $\Gamma(i)/\Gamma(\gamma\gamma)/\Gamma(\text{total})$

VALUE (keV)	CL%	EVTS	DOCUMENT ID	TECN	COMMENT	$\Gamma_1\Gamma_4/\Gamma$
0.23 ± 0.05 ± 0.05		74	¹ ACHARD 07	L3	183-209 $e^+e^- \rightarrow e^+e^- K_S^0 K^\pm\pi^\mp$	
< 0.089	90	2,3	AHOHE 05	CLE2	10.6 $e^+e^- \rightarrow e^+e^- K_S^0 K^\pm\pi^\mp$	

••• We do not use the following data for averages, fits, limits, etc. •••
¹ Supersedes ACCIARRI 01g. Using $B(K_S^0 \rightarrow \pi^+\pi^-) = 0.6895$.
² Using $\eta(1475)$ mass of 1481 MeV and width of 48 MeV. The upper limit increases to 0.140 keV if the world average value, 87 MeV, of the width is used.
³ Assuming three-body phase-space decay to $K_S^0 K^\pm\pi^\mp$.

$\eta(1475)$ BRANCHING RATIOS

$\Gamma(K\bar{K}^*(892) + c.c.)/\Gamma(K\bar{K}\pi)$	Γ_2/Γ_1		
VALUE	DOCUMENT ID	TECN	COMMENT
0.50 ± 0.10	¹ BAILLON 67	HBC	0.0 $\bar{p}p \rightarrow K\bar{K}\pi\pi\pi$

¹ Data could also refer to $\eta(1405)$.

$\Gamma(K\bar{K}^*(892) + c.c.)/[\Gamma(K\bar{K}^*(892) + c.c.) + \Gamma(a_0(980)\pi)]$	$\Gamma_2/(\Gamma_2 + \Gamma_3)$			
VALUE	CL%	DOCUMENT ID	TECN	COMMENT
< 0.25	90	EDWARDS 82E	CBAL	$J/\psi \rightarrow K^+K^-\pi^0\gamma$

••• We do not use the following data for averages, fits, limits, etc. •••

$\Gamma(\gamma\gamma)/\Gamma(K\bar{K}\pi)$	Γ_4/Γ_1			
VALUE	CL%	DOCUMENT ID	TECN	COMMENT
< 1.27 × 10⁻³	90	¹ ABLIKIM 180	BES3	$\psi(2S) \rightarrow \pi^+\pi^-\gamma\gamma\gamma$

¹ Using results from BAI 00d.

Meson Particle Listings

$\eta(1475)$, $f_0(1500)$

$\Gamma(\gamma\phi(1020))/\Gamma_{total}$	Γ_6/Γ		
VALUE	DOCUMENT ID	TECN	COMMENT
possibly seen	1 ABLIKIM	18i	BES3 $J/\psi \rightarrow \gamma\gamma\phi(1020)$
1 Seen as a peak in $\gamma\phi$ invariant mass. Angular analysis consistent with $J^{PC} = 0^{-+}$. Other J^{PC} not excluded. Also see $\eta(1405)$.			

$\eta(1475)$ REFERENCES

ABLIKIM 23M	JHEP 2303 121	M. Ablikim et al.	(BESIII Collab.)
ABLIKIM 18i	PR D97 05101	M. Ablikim et al.	(BESIII Collab.)
ABLIKIM 18O	PR D97 072014	M. Ablikim et al.	(BESIII Collab.)
ABLIKIM 15T	PRL 115 091803	M. Ablikim et al.	(BESIII Collab.)
ACHARD 07	JHEP 0703 018	P. Achard et al.	(L3 Collab.)
AHOHE 05	PR D71 072001	R. Ahohe et al.	(CLEO Collab.)
NICHTIU 02	PL B545 261	F. Nichtiu et al.	(OBELIX Collab.)
ACCIARRI 01G	PL B501 1	M. Acciari et al.	(L3 Collab.)
ADAMS 01B	PL B516 264	G.S. Adams et al.	(BNL E852 Collab.)
BAI 00D	PL B476 25	J.Z. Bai et al.	(BES Collab.)
CICALO 99	PL B462 453	C. Cicalo et al.	(OBELIX Collab.)
BERTIN 97	PL B400 226	A. Bertin et al.	(OBELIX Collab.)
BERTIN 95	PL B361 187	A. Bertin et al.	(OBELIX Collab.)
AUGUSTIN 92	PR D46 1951	J.E. Augustin, G. Cosme	(DM2 Collab.)
BAI 90C	PRL 65 2507	Z. Bai et al.	(Mark III Collab.)
RATH 89	PR D40 693	M.G. Rath et al.	(NDAM, BRAN, BNL, CUNY+)
EDWARDS 82E	PRL 49 259	C. Edwards et al.	(CIT, HARV, PRIN+)
BAILLON 67	NC 50A 393	P.H. Baillon et al.	(CERN, CDF, IRAD)

$f_0(1500)$

$$J^G(J^{PC}) = 0^+(0^{++})$$

See the review on "Spectroscopy of Light Meson Resonances."

$f_0(1500)$ T-MATRIX POLE \sqrt{s}

Note that $\Gamma = -2\text{Im}(\sqrt{s})$.

VALUE (MeV)	DOCUMENT ID	TECN	COMMENT
(1430-1530) - i (40-90) OUR ESTIMATE			
(1450 ± 10) - i (53 ± 8)	1 RODAS	22	RVUE $J/\psi(1S) \rightarrow \gamma(\pi\pi, K\bar{K})$
(1483 ± 15) - i (58 ± 6)	SARANTSEV	21	RVUE $J/\psi(1S) \rightarrow \gamma(\pi\pi, K\bar{K}, \eta\eta, \omega\phi)$
(1496 ± 1.2 ^{+4.4} _{-26.4}) - i (40.4 ± 0.3 ^{+10.0} _{-2.5})	2 ALBRECHT	20	RVUE $0.9 \bar{p}p \rightarrow \pi^0 \pi^0 \eta, \pi^0 \eta \eta, \pi^0 K^+ K^-$
(1465 ± 18) - i (50 ± 9)	3 ROPERTZ	18	RVUE $\bar{B}_s^0 \rightarrow J/\psi(\pi^+ \pi^- / K^+ K^-)$
(1486 ± 10) - i (57 ± 5)	ANISOVICH	09	RVUE $0.0 \bar{p}p, \pi N$
(1489 ⁺⁸ ₋₄) - i (51 ± 5)	4 ANISOVICH	03	RVUE
(1515 ± 12) - i (55 ± 12)	BARBERIS	00A	$450 pp \rightarrow p_f(\eta\eta', \eta'\eta')\rho_S$
(1511 ± 9) - i (51 ± 9)	5 BARBERIS	00C	$450 pp \rightarrow p_f 4\pi\rho_S$
(1510 ± 8) - i (55 ± 8)	BARBERIS	00E	$450 pp \rightarrow p_f \eta\eta\rho_S$
(1502 ± 12 ± 10) - i (49 ± 9 ± 8)	6 BARBERIS	99D	OMEG $450 pp \rightarrow K^+ K^-, \pi^+ \pi^-$
(1447 ± 27) - i (54 ± 23)	7 KAMINSKI	99	RVUE $\pi\pi \rightarrow \pi\pi, K\bar{K}, \sigma\sigma$
(1499 ± 8) - i (65 ± 10)	ANISOVICH	98B	RVUE Compilation.
(1510 ± 20) - i (60 ± 18)	BARBERIS	97B	OMEG $450 pp \rightarrow pp2(\pi^+ \pi^-)$
(1449 ± 20) - i (57 ± 15)	BERTIN	97C	OBLX $0.0 \bar{p}p \rightarrow \pi^+ \pi^- K_L^0 K_L^0$
(1515 ± 20) - i (53 ± 8)	ABELE	96B	CBAR $0.0 \bar{p}p \rightarrow \pi^0 K_L^0 K_L^0$
(1500 ± 8) - i (66 ± 8)	ABELE	96C	RVUE Compilation.
(1500 ± 10) - i (77 ± 15)	8 AMSLER	95D	CBAR $0.0 \bar{p}p \rightarrow \pi^0 \pi^0 \pi^0, \pi^0 \eta \eta, \pi^0 \pi^0 \eta$
(1520 ± 25) - i (74 ⁺¹⁰ ₋₁₃)	9 ANISOVICH	94	CBAR $0.0 \bar{p}p \rightarrow 3\pi^0, \pi^0 \eta \eta$
(1505 ± 20) - i (75 ± 10)	10 BUGG	94	RVUE $\bar{p}p \rightarrow 3\pi^0, \eta \eta \pi^0, \eta \pi^0 \pi^0$

1 T-matrix pole from coupled channel K-matrix fit to data on $J/\psi \rightarrow \gamma\pi^0\pi^0$ (ABLIKIM 15AE) and $J/\psi \rightarrow \gamma K_S^0 K_S^0$ (ABLIKIM 18AA).
 2 T-matrix pole, 5 poles, 5 channels, including scattering data from HYAMS 75 ($\pi\pi$), LONGACRE 86 ($K\bar{K}$), BINON 83 ($\eta\eta$), and BINON 84c ($\eta\eta'$).
 3 T-matrix pole of 3 channel unitary model fit to data from AAIJ 14BR and AAIJ 17V extracted using Pade approximants.
 4 Pole position from combined analysis of $\pi^- p \rightarrow \pi^0 \pi^0 n, \pi^- p \rightarrow K\bar{K}n, \pi^+ \pi^- \rightarrow \pi^+ \pi^-, \bar{p}p \rightarrow \pi^0 \pi^0 \pi^0, \pi^0 \eta \eta, \pi^0 \pi^0 \eta, \pi^+ \pi^- \pi^0, K^+ K^- \pi^0, K_S^0 K_S^0 \pi^0, K^+ K_S^0 \pi^-$ at rest, $\bar{p}n \rightarrow \pi^- \pi^- \pi^+, K_S^0 K^- \pi^0, K_S^0 K_S^0 \pi^-$ at rest.
 5 Average between $\pi^+ \pi^- 2\pi^0$ and $2(\pi^+ \pi^-)$.
 6 Supersedes BARBERIS 99 and BARBERIS 99B.
 7 T-matrix pole on sheet --+.
 8 Coupled-channel analysis of AMSLER 95B, AMSLER 95C, and AMSLER 94D.
 9 From a simultaneous analysis of the annihilations $\bar{p}p \rightarrow 3\pi^0, \pi^0 \eta \eta$.
 10 Reanalysis of ANISOVICH 94 data.

$f_0(1500)$ MASS

VALUE (MeV)	EVTS	DOCUMENT ID	TECN	COMMENT
1522 ± 25		1 BERTIN	98	OBLX $0.05-0.405 \bar{p}p \rightarrow \pi^+ \pi^+ \pi^-$

••• We do not use the following data for averages, fits, limits, etc. •••

1492.5 ± 3.6 ^{+2.4} _{-20.5}		2 ABLIKIM	22G	BES3 $J/\psi \rightarrow \gamma\pi^+ \pi^- \eta'$
1447 ± 16 ± 13	163	3,4 DOBBS	15	$J/\psi \rightarrow \gamma\pi^+ \pi^-$
1442 ± 9 ± 4	261	3,4 DOBBS	15	$\psi(2S) \rightarrow \gamma\pi^+ \pi^-$
1460.9 ± 2.9		5 AAIJ	14BR	LHCB $\bar{B}_s^0 \rightarrow J/\psi\pi^+ \pi^-$
1468 ⁺¹⁴ ₋₁₅ ± 23 ⁺²³ ₋₇₄	5.5k	6 ABLIKIM	13N	BES3 $e^+ e^- \rightarrow J/\psi \rightarrow \gamma\eta\eta$
1470 ± 60	5.68	7 KLEMPPT	08	E791 $D_s^+ \rightarrow \pi^- \pi^+ \pi^+$
1470 ± 7 ± 72 ⁺⁷² ₋₂₅₅		8 UEHARA	08A	BELL $10.6 e^+ e^- \rightarrow e^+ e^- \pi^0 \pi^0$
1466 ± 6 ± 20		9 ABLIKIM	06V	BES2 $e^+ e^- \rightarrow J/\psi \rightarrow \gamma\pi^+ \pi^-$
1495 ± 4		AMSLER	06G	CBAR $0.9 \bar{p}p \rightarrow K^+ K^- \pi^0$
1539 ± 20	9.9k	AUBERT	06G	BABR $B^+ \rightarrow K^+ K^+ K^-$
1473 ± 5	80k	9,10 UMAN	06G	E835 $5.2 \bar{p}p \rightarrow \eta\eta\pi^0$
1478 ± 6		VLADIMIRSK...	06G	SPEC $40 \pi^- p \rightarrow K_S^0 K_S^0 n$
1493 ± 7		BINON	05	GAMS $33 \pi^- p \rightarrow \eta\eta n$
1524 ± 14	1400	11 GARMASH	05	BELL $B^+ \rightarrow K^+ K^+ K^-$
1490 ± 30		9 ABELE	01	CBAR $0.0 \bar{p}d \rightarrow \pi^- 4\pi^0 p$
1497 ± 10		9 BARBERIS	99B	OMEG $450 pp \rightarrow \rho_S \rho_f K^+ K^-$
1502 ± 10		9 BARBERIS	99B	OMEG $450 pp \rightarrow \rho_S \rho_f \pi^+ \pi^-$
1530 ± 45		9 BELLAZZINI	99	GAM4 $450 pp \rightarrow \rho\rho\pi^0\pi^0$
1505 ± 18		9 FRENCH	99	$300 pp \rightarrow \rho_f(K^+ K^-)\rho_S$
1580 ± 80		9 ALDE	98	GAM4 $100 \pi^- p \rightarrow \pi^0 \pi^0 n$
~ 1520		REYES	98	SPEC $800 pp \rightarrow \rho_S \rho_f K_S^0 K_S^0$
~ 1475		FRABETTI	97D	E687 $D_s^\pm \rightarrow \pi^\mp \pi^\pm \pi^\pm$
~ 1505		ABELE	96	CBAR $0.0 \bar{p}p \rightarrow 5\pi^0$
1460 ± 20	120	9 AMELIN	96B	VES $37 \pi^- A \rightarrow \eta\eta\pi^- A$
1500 ± 8		BUGG	96	RVUE
1500 ± 15		12 AMSLER	95B	CBAR $0.0 \bar{p}p \rightarrow 3\pi^0$
1505 ± 15		13 AMSLER	95C	CBAR $0.0 \bar{p}p \rightarrow \eta\eta\pi^0$
1445 ± 5		14 ANTINORI	95	OMEG $300,450 pp \rightarrow pp2(\pi^+ \pi^-)$
1497 ± 30		9 ANTINORI	95	OMEG $300,450 pp \rightarrow pp\pi^+ \pi^-$
~ 1505		BUGG	95	MRK3 $J/\psi \rightarrow \gamma\pi^+ \pi^- \pi^+ \pi^-$
1446 ± 5		9 ABATZIS	94	OMEG $450 pp \rightarrow pp2(\pi^+ \pi^-)$
1545 ± 25		9 AMSLER	94E	CBAR $0.0 \bar{p}p \rightarrow \pi^0 \eta\eta'$
1560 ± 25		9 AMSLER	92C	CBAR $0.0 \bar{p}p \rightarrow \pi^0 \eta\eta$
1550 ± 45 ± 30		9 BELADIDZE	92C	VES $36 \pi^- Be \rightarrow \pi^- \eta' \eta Be$
1449 ± 4		9 ARMSTRONG	89E	OMEG $300 pp \rightarrow pp2(\pi^+ \pi^-)$
1610 ± 20		9 ALDE	88	GAM4 $300 \pi^- N \rightarrow \pi^- N 2\eta$
~ 1525		ASTON	88D	LASS $11 K^- p \rightarrow K_S^0 K_S^0 \Lambda$
1570 ± 20	600	9 ALDE	87	GAM4 $100 \pi^- p \rightarrow 4\pi^0 n$
1575 ± 45		15 ALDE	86D	GAM4 $100 \pi^- p \rightarrow 2\eta n$
1568 ± 33		9 BINON	84C	GAM2 $38 \pi^- p \rightarrow \eta\eta' n$
1592 ± 25		9 BINON	83	GAM2 $38 \pi^- p \rightarrow 2\eta n$
1525 ± 5		9 GRAY	83	DBC $0.0 \bar{p}N \rightarrow 3\pi$

1 Breit-Wigner mass.
 2 The $\pi^+ \pi^-$ mass spectrum is described by a coherent sum of two Breit-Wigner resonances, $f_0(1500)$ and a new $X(1540)$ with mass $1540.2 \pm 7.0^{+36.3}_{-6.1}$ MeV and width $157 \pm 19^{+11}_{-77}$ MeV.
 3 Using CLEO-c data but not authored by the CLEO Collaboration.
 4 From a fit to a Breit-Wigner line shape with fixed $\Gamma = 109$ MeV.
 5 Solution I, statistical error only.
 6 From partial wave analysis including all possible combinations of $0^{++}, 2^{++}$, and 4^{++} resonances.
 7 Reanalysis of AITALA 01A data. This state could also be $f_0(1370)$.
 8 Breit-Wigner mass. May also be the $f_0(1370)$.
 9 Breit-Wigner mass.
 10 Statistical error only.
 11 Breit-Wigner, solution I, PWA ambiguous.
 12 T-matrix pole, supersedes ANISOVICH 94.
 13 T-matrix pole, supersedes ANISOVICH 94 and AMSLER 92.
 14 Supersedes ABATZIS 94, ARMSTRONG 89E. Breit-Wigner mass.
 15 From central value and spread of two solutions. Breit-Wigner mass.

$f_0(1500)$ WIDTH

VALUE (MeV)	EVTS	DOCUMENT ID	TECN	COMMENT
108 ± 33		1 BERTIN	98	OBLX $0.05-0.405 \bar{p}p \rightarrow \pi^+ \pi^+ \pi^-$
107 ± 9 ⁺²¹ ₋₇		2 ABLIKIM	22G	BES3 $J/\psi \rightarrow \gamma\pi^+ \pi^- \eta'$
124 ± 7		3 AAIJ	14BR	LHCB $\bar{B}_s^0 \rightarrow J/\psi\pi^+ \pi^-$
136 ± 41 ± 28 ⁺⁴¹ ₋₁₀₀	5.5k	4 ABLIKIM	13N	BES3 $e^+ e^- \rightarrow J/\psi \rightarrow \gamma\eta\eta$
90 ± 2 ± 50 ⁺² ₋₁ ± 22		5 UEHARA	08A	BELL $10.6 e^+ e^- \rightarrow e^+ e^- \pi^0 \pi^0$
108 ± 14 ⁺¹¹ ₋₁₁ ± 25		6 ABLIKIM	06V	BES2 $e^+ e^- \rightarrow J/\psi \rightarrow \gamma\pi^+ \pi^-$

••• We do not use the following data for averages, fits, limits, etc. •••

121 ± 8		AMSLER	06	CBAR	0.9 $\bar{p}p \rightarrow K^+ K^- \pi^0$
257 ± 33	9.9k	AUBERT	06	BABR	$B^+ \rightarrow K^+ K^+ K^-$
108 ± 9	80k	UMAN	06	E835	5.2 $\bar{p}p \rightarrow \eta \eta \pi^0$
119 ± 10		VLADIMIRSK...	06	SPEC	40 $\pi^- p \rightarrow K_S^0 K_S^0 n$
90 ± 15		BINON	05	GAMS	33 $\pi^- p \rightarrow \eta \eta n$
136 ± 23	1400	GARMASH	05	BELL	$B^+ \rightarrow K^+ K^+ K^-$
140 ± 40		ABELE	01	CBAR	0.0 $\bar{p}d \rightarrow \pi^- 4\pi^0 p$
104 ± 25		BARBERIS	99	OMEG	450 $pp \rightarrow p_S p_f K^+ K^-$
131 ± 15		BARBERIS	99B	OMEG	450 $pp \rightarrow p_S p_f \pi^+ \pi^-$
160 ± 50		BELLAZZINI	99	GAM4	450 $pp \rightarrow p p \pi^0 \pi^0$
100 ± 33		FRENCH	99		300 $pp \rightarrow p_f(K^+ K^-) p_S \pi^0 n$
280 ± 100		ALDE	98	GAM4	100 $\pi^- p \rightarrow \pi^0 \pi^0 n$
~ 100		FRABETTI	97D	E687	$D_s^\pm \rightarrow \pi^\mp \pi^\pm \pi^\pm$
~ 169		ABELE	96	CBAR	0.0 $\bar{p}p \rightarrow 5\pi^0$
100 ± 30	120	AMELIN	96B	VES	37 $\pi^- A \rightarrow \eta \eta \pi^- A$
132 ± 15		BUGG	96	RVUE	
120 ± 25		AMSLER	95B	CBAR	0.0 $\bar{p}p \rightarrow 3\pi^0$
120 ± 30		AMSLER	95C	CBAR	0.0 $\bar{p}p \rightarrow \eta \eta \pi^0$
65 ± 10		ANTINORI	95	OMEG	300,450 $pp \rightarrow p p 2(\pi^+ \pi^-)$
199 ± 30		ANTINORI	95	OMEG	300,450 $pp \rightarrow p p \pi^+ \pi^-$
56 ± 12		ABATZIS	94	OMEG	450 $pp \rightarrow p p 2(\pi^+ \pi^-)$
100 ± 40		AMSLER	94E	CBAR	0.0 $\bar{p}p \rightarrow \pi^0 \eta \eta'$
245 ± 50		AMSLER	92	CBAR	0.0 $\bar{p}p \rightarrow \pi^0 \eta \eta$
153 ± 67 ± 50		BELADIDZE	92C	VES	36 $\pi^- Be \rightarrow \pi^- \eta' \eta Be$
78 ± 18		ARMSTRONG	89E	OMEG	300 $pp \rightarrow p p 2(\pi^+ \pi^-)$
170 ± 40		ALDE	88	GAM4	300 $\pi^- N \rightarrow \pi^- N 2\eta$
150 ± 20	600	ALDE	87	GAM4	100 $\pi^- p \rightarrow 4\pi^0 n$
265 ± 65		ALDE	86D	GAM4	100 $\pi^- p \rightarrow 2\eta n$
260 ± 60		BINON	84C	GAM2	38 $\pi^- p \rightarrow \eta \eta' n$
210 ± 40		BINON	83	GAM2	38 $\pi^- p \rightarrow 2\eta n$
101 ± 13		GRAY	83	DBC	0.0 $\bar{p}N \rightarrow 3\pi$

1 Breit-Wigner width.
 2 The $\pi^+ \pi^-$ mass spectrum is described by a coherent sum of two Breit-Wigner resonances, $f_0(1500)$ and a new $X(1540)$ with mass $1540.2 \pm 7.0_{-6.1}^{+36.3}$ MeV and width $157 \pm 19_{-77}^{+11}$ MeV.
 3 Solution 1, statistical error only.
 4 From partial wave analysis including all possible combinations of 0^{++} , 2^{++} , and 4^{++} resonances.
 5 Breit-Wigner width. May also be the $f_0(1370)$.
 6 Breit-Wigner width.
 7 Statistical error only.
 8 Breit-Wigner, solution 1, PWA ambiguous.
 9 T-matrix pole, supersedes ANISOVICH 94.
 10 T-matrix pole, supersedes ANISOVICH 94 and AMSLER 92.
 11 Supersedes ABATZIS 94, ARMSTRONG 89E. Breit-Wigner mass.
 12 From central value and spread of two solutions. Breit-Wigner mass.

$f_0(1500)$ DECAY MODES

Mode	Fraction (Γ_i/Γ)	Scale factor
Γ_1 $\pi \pi$	(34.5 ± 2.2) %	1.2
Γ_2 $\pi^+ \pi^-$	seen	
Γ_3 $2\pi^0$	seen	
Γ_4 4π	(48.9 ± 3.3) %	1.2
Γ_5 $4\pi^0$	seen	
Γ_6 $2\pi^+ 2\pi^-$	seen	
Γ_7 $2(\pi\pi)_{S\text{-wave}}$	seen	
Γ_8 $\rho\rho$	seen	
Γ_9 $\pi(1300)\pi$	seen	
Γ_{10} $a_1(1260)\pi$	seen	
Γ_{11} $\eta\eta$	(6.0 ± 0.9) %	1.1
Γ_{12} $\eta\eta'(958)$	(2.2 ± 0.8) %	1.4
Γ_{13} $K\bar{K}$	(8.5 ± 1.0) %	1.1
Γ_{14} $\gamma\gamma$	not seen	

CONSTRAINED FIT INFORMATION

An overall fit to 6 branching ratios uses 10 measurements and one constraint to determine 5 parameters. The overall fit has a $\chi^2 = 5.6$ for 6 degrees of freedom.

The following *off-diagonal* array elements are the correlation coefficients $\langle \delta x_i \delta x_j \rangle / (\delta x_i \delta x_j)$, in percent, from the fit to the branching fractions, $x_i \equiv \Gamma_i/\Gamma_{\text{total}}$. The fit constrains the x_i whose labels appear in this array to sum to one.

x_4	-88		
x_{11}	27	-56	
x_{12}	3	-32	26
x_{13}	43	-64	20
			2
	x_1	x_4	x_{11} x_{12}

$f_0(1500)$ $\Gamma(i)\Gamma(\gamma\gamma)/\Gamma(\text{total})$

$\Gamma(\pi\pi) \times \Gamma(\gamma\gamma)/\Gamma_{\text{total}}$	$\Gamma_1/\Gamma_4/\Gamma$			
VALUE (eV)	CL%	DOCUMENT ID	TECN	COMMENT
• • • We do not use the following data for averages, fits, limits, etc. • • •				
$33_{-6}^{+12} + 1809_{-21}$		1 UEHARA	08A BELL	10.6 $e^+ e^- \rightarrow e^+ e^- \pi^0 \pi^0$
not seen		ACCIARRI	01H L3	$\gamma\gamma \rightarrow K_S^0 K_S^0, E_{\text{cm}}^{\text{ee}} = 91, 183-209 \text{ GeV}$
<460	95	BARATE	00E ALEP	$\gamma\gamma \rightarrow \pi^+ \pi^-$
		1 May also be the $f_0(1370)$. Multiplied by us by 3 to obtain the $\pi\pi$ value.		

$f_0(1500)$ BRANCHING RATIOS

$\Gamma(\pi\pi)/\Gamma_{\text{total}}$	Γ_1/Γ		
VALUE	DOCUMENT ID	TECN	COMMENT
• • • We do not use the following data for averages, fits, limits, etc. • • •			
0.454 ± 0.104	BUGG	96	RVUE
$\Gamma(\pi^+ \pi^-)/\Gamma_{\text{total}}$	Γ_2/Γ		
VALUE	DOCUMENT ID	TECN	COMMENT
seen	BERTIN	98	OBLX 0.05-0.405 $\bar{p}p \rightarrow \pi^+ \pi^+ \pi^-$
• • • We do not use the following data for averages, fits, limits, etc. • • •			
possibly seen	FRABETTI	97D	E687 $D_s^\pm \rightarrow \pi^\mp \pi^\pm \pi^\pm$

$\Gamma(4\pi)/\Gamma(\pi\pi)$	Γ_4/Γ_1		
VALUE	DOCUMENT ID	TECN	COMMENT
• • • We do not use the following data for averages, fits, limits, etc. • • •			
1.42 ± 0.18 OUR FIT	Error includes scale factor of 1.2.		
1.42 ± 0.18 OUR AVERAGE	Error includes scale factor of 1.2.		
1.37 ± 0.16	BARBERIS	00D	450 $pp \rightarrow p_f 4\pi p_S$
2.1 ± 0.6	1 AMSLER	98	RVUE
• • • We do not use the following data for averages, fits, limits, etc. • • •			
2.1 ± 0.2	2 ANISOVICH	02D	SPEC Combined fit
3.4 ± 0.8	1 ABELE	96	CBAR 0.0 $\bar{p}p \rightarrow 5\pi^0$
	1 Excluding $\rho\rho$ contribution to 4π .		
	2 From a combined K-matrix analysis of Crystal Barrel (0. $\rho\bar{p} \rightarrow \pi^0 \pi^0 \pi^0, \pi^0 \eta \eta, \pi^0 \pi^0 \eta$), GAMS ($\pi p \rightarrow \pi^0 \pi^0 n, \eta \eta n, \eta \eta' n$), and BNL ($\pi p \rightarrow K\bar{K}n$) data.		

$\Gamma(2(\pi\pi)_{S\text{-wave}})/\Gamma(\pi\pi)$	Γ_7/Γ_1		
VALUE	DOCUMENT ID	TECN	COMMENT
• • • We do not use the following data for averages, fits, limits, etc. • • •			
0.42 ± 0.26	1 ABELE	01	CBAR 0.0 $\bar{p}d \rightarrow \pi^- 4\pi^0 p$
	1 From the combined data of ABELE 96 and ABELE 96c.		

$\Gamma(2(\pi\pi)_{S\text{-wave}})/\Gamma(4\pi)$	Γ_7/Γ_4		
VALUE	DOCUMENT ID	TECN	COMMENT
• • • We do not use the following data for averages, fits, limits, etc. • • •			
0.26 ± 0.07	ABELE	01B	CBAR 0.0 $\bar{p}d \rightarrow 5\pi p$

$\Gamma(\rho\rho)/\Gamma(4\pi)$	Γ_8/Γ_4		
VALUE	DOCUMENT ID	TECN	COMMENT
• • • We do not use the following data for averages, fits, limits, etc. • • •			
0.13 ± 0.08	ABELE	01B	CBAR 0.0 $\bar{p}d \rightarrow 5\pi p$

$\Gamma(\rho\rho)/\Gamma(2(\pi\pi)_{S\text{-wave}})$	Γ_8/Γ_7	
VALUE	DOCUMENT ID	COMMENT
• • • We do not use the following data for averages, fits, limits, etc. • • •		
2.87 ± 0.34 OUR AVERAGE	Error includes scale factor of 1.1.	
3.3 ± 0.5	BARBERIS	00C 450 $pp \rightarrow p_f \pi^+ \pi^- 2\pi^0 p_S$
2.6 ± 0.4	BARBERIS	00C 450 $pp \rightarrow p_f 2(\pi^+ \pi^-) p_S$

$\Gamma(\pi(1300)\pi)/\Gamma(4\pi)$	Γ_9/Γ_4		
VALUE	DOCUMENT ID	TECN	COMMENT
• • • We do not use the following data for averages, fits, limits, etc. • • •			
0.50 ± 0.25	ABELE	01B	CBAR 0.0 $\bar{p}d \rightarrow 5\pi p$

$\Gamma(a_1(1260)\pi)/\Gamma(4\pi)$	Γ_{10}/Γ_4		
VALUE	DOCUMENT ID	TECN	COMMENT
• • • We do not use the following data for averages, fits, limits, etc. • • •			
0.12 ± 0.05	ABELE	01B	CBAR 0.0 $\bar{p}d \rightarrow 5\pi p$

$\Gamma(\eta\eta)/\Gamma_{\text{total}}$	Γ_{11}/Γ		
VALUE	DOCUMENT ID	TECN	COMMENT
• • • We do not use the following data for averages, fits, limits, etc. • • •			
large	ALDE	88	GAM4 300 $\pi^- N \rightarrow \eta \eta \pi^- N$
large	BINON	83	GAM2 38 $\pi^- p \rightarrow 2\eta n$

Meson Particle Listings

$f_0(1500)$, $f_1(1510)$

$\Gamma(\eta\eta)/\Gamma(\pi\pi)$ Γ_{11}/Γ_1

VALUE	DOCUMENT ID	TECN	COMMENT
0.173 ± 0.024 OUR FIT	Error includes scale factor of 1.1.		
0.175 ± 0.027 OUR AVERAGE			
0.18 ± 0.03	BARBERIS	00E	450 $p\bar{p} \rightarrow p_f \eta \eta \bar{p}$
0.157 ± 0.060	¹ AMSLER	95D CBAR	0.0 $\bar{p}p \rightarrow \pi^0 \pi^0 \pi^0, \pi^0 \eta \eta, \pi^0 \pi^0 \eta$
• • • We do not use the following data for averages, fits, limits, etc. • • •			
0.080 ± 0.033	AMSLER	02 CBAR	0.9 $\bar{p}p \rightarrow \pi^0 \eta \eta, \pi^0 \pi^0 \pi^0$
0.11 ± 0.03	² ANISOVICH	02D SPEC	Combined fit
0.078 ± 0.013	³ ABELE	96C RVUE	Compilation
0.230 ± 0.097	⁴ AMSLER	95C CBAR	0.0 $\bar{p}p \rightarrow \eta \eta \pi^0$
¹ Coupled-channel analysis of AMSLER 95B, AMSLER 95C, and AMSLER 94D.			
² From a combined K-matrix analysis of Crystal Barrel (0. $\bar{p}p \rightarrow \pi^0 \pi^0 \pi^0, \pi^0 \eta \eta, \pi^0 \pi^0 \eta$), GAMS ($\pi p \rightarrow \pi^0 \pi^0 n, \eta \eta n, \eta \eta' n$), and BNL ($\pi p \rightarrow K \bar{K} n$) data.			
³ 2π width determined to be 60 ± 12 MeV.			
⁴ Using AMSLER 95B ($3\pi^0$).			

$\Gamma(4\pi^0)/\Gamma(\eta\eta)$ Γ_5/Γ_{11}

VALUE	DOCUMENT ID	TECN	COMMENT
• • • We do not use the following data for averages, fits, limits, etc. • • •			
0.8 ± 0.3	ALDE	87 GAM4	100 $\pi^- p \rightarrow 4\pi^0 n$

$\Gamma(\eta\eta'(958))/\Gamma(\pi\pi)$ Γ_{12}/Γ_1

VALUE (units 10^{-2})	DOCUMENT ID	TECN	COMMENT
6.4 ± 2.2 OUR FIT	Error includes scale factor of 1.4.		
9.5 ± 2.6	BARBERIS	00A	450 $p\bar{p} \rightarrow p_f \eta \eta \bar{p}$
• • • We do not use the following data for averages, fits, limits, etc. • • •			
16.6 ^{+4.2} _{-4.0}	¹ ABLIKIM	22As BES3	$J/\psi(1S) \rightarrow \gamma \eta \eta'$
0.5 ± 0.3	² ANISOVICH	02D SPEC	Combined fit
¹ From a Breit-Wigner fit involving 9 resonances and a resonating exotic $\eta(1855) \rightarrow \eta \eta'/P$ -wave.			
² From a combined K-matrix analysis of Crystal Barrel (0. $\bar{p}p \rightarrow \pi^0 \pi^0 \pi^0, \pi^0 \eta \eta, \pi^0 \pi^0 \eta$), GAMS ($\pi p \rightarrow \pi^0 \pi^0 n, \eta \eta n, \eta \eta' n$), and BNL ($\pi p \rightarrow K \bar{K} n$) data.			

$\Gamma(\eta\eta'(958))/\Gamma(\eta\eta)$ Γ_{12}/Γ_{11}

VALUE	DOCUMENT ID	TECN	COMMENT
0.37 ± 0.13 OUR FIT	Error includes scale factor of 1.5.		
0.29 ± 0.10	¹ AMSLER	95C CBAR	0.0 $\bar{p}p \rightarrow \eta \eta \pi^0$
• • • We do not use the following data for averages, fits, limits, etc. • • •			
0.05 ± 0.03	² ANISOVICH	02D SPEC	Combined fit
0.84 ± 0.23	ABELE	96C RVUE	Compilation
2.7 ± 0.8	BINON	84C GAM2	38 $\pi^- p \rightarrow \eta \eta' n$
¹ Using AMSLER 94E ($\eta \eta' \pi^0$).			
² From a combined K-matrix analysis of Crystal Barrel (0. $\bar{p}p \rightarrow \pi^0 \pi^0 \pi^0, \pi^0 \eta \eta, \pi^0 \pi^0 \eta$), GAMS ($\pi p \rightarrow \pi^0 \pi^0 n, \eta \eta n, \eta \eta' n$), and BNL ($\pi p \rightarrow K \bar{K} n$) data.			

$\Gamma(K\bar{K})/\Gamma_{total}$ Γ_{13}/Γ

VALUE	DOCUMENT ID	TECN	COMMENT
• • • We do not use the following data for averages, fits, limits, etc. • • •			
0.044 ± 0.021	BUGG	96 RVUE	

$\Gamma(K\bar{K})/\Gamma(\pi\pi)$ Γ_{13}/Γ_1

VALUE	DOCUMENT ID	TECN	COMMENT
0.246 ± 0.025 OUR FIT			
0.236 ± 0.026 OUR AVERAGE			
0.25 ± 0.03	¹ BARGIOTTI	03 OBLX	$\bar{p}p$
0.19 ± 0.07	² ABELE	98 CBAR	0.0 $\bar{p}p \rightarrow K_S^0 K_{S\pm}^{\pm} \pi^{\mp}$
0.20 ± 0.08	³ ABELE	96B CBAR	0.0 $\bar{p}p \rightarrow \pi^0 K_S^0 K_L^0$
• • • We do not use the following data for averages, fits, limits, etc. • • •			
0.16 ± 0.05	⁴ ANISOVICH	02D SPEC	Combined fit
0.33 ± 0.03 ± 0.07	BARBERIS	99D OMEG	450 $p\bar{p} \rightarrow K^+ K^-, \pi^+ \pi^-$
¹ Coupled channel analysis of $\pi^+ \pi^- \pi^0, K^+ K^- \pi^0$, and $K^{\pm} K_S^0 \pi^{\mp}$.			
² Using $\pi^0 \pi^0$ from AMSLER 95B.			
³ Using AMSLER 95B ($3\pi^0$), AMSLER 94C ($2\pi^0 \eta$) and SU(3).			
⁴ From a combined K-matrix analysis of Crystal Barrel (0. $\bar{p}p \rightarrow \pi^0 \pi^0 \pi^0, \pi^0 \eta \eta, \pi^0 \pi^0 \eta$), GAMS ($\pi p \rightarrow \pi^0 \pi^0 n, \eta \eta n, \eta \eta' n$), and BNL ($\pi p \rightarrow K \bar{K} n$) data.			

$\Gamma(K\bar{K})/\Gamma(\eta\eta)$ Γ_{13}/Γ_{11}

VALUE	CL%	DOCUMENT ID	TECN	COMMENT
1.43 ± 0.24 OUR FIT	Error includes scale factor of 1.1.			
1.85 ± 0.41				
• • • We do not use the following data for averages, fits, limits, etc. • • •				
1.5 ± 0.6		¹ ANISOVICH	02D SPEC	Combined fit
<0.4	90	² PROKOSHKIN	91	GAM4 300 $\pi^- p \rightarrow \pi^- \rho \eta \eta$
<0.6		³ BINON	83	GAM2 38 $\pi^- p \rightarrow 2\eta n$
¹ From a combined K-matrix analysis of Crystal Barrel (0. $\bar{p}p \rightarrow \pi^0 \pi^0 \pi^0, \pi^0 \eta \eta, \pi^0 \pi^0 \eta$), GAMS ($\pi p \rightarrow \pi^0 \pi^0 n, \eta \eta n, \eta \eta' n$), and BNL ($\pi p \rightarrow K \bar{K} n$) data.				
² Combining results of GAM4 with those of WA76 on $K \bar{K}$ central production.				
³ Using ETKIN 82B and COHEN 80.				

$f_0(1500)$ REFERENCES

ABLIKIM	22AS	PR D106 072012	M. Ablikim et al.	(BESIII Collab.)
Also		PR D107 079001 (err.)	M. Ablikim et al.	(BESIII Collab.)
ABLIKIM	22G	PRL 129 042001	M. Ablikim et al.	(BESIII Collab.)
RODAS	22	EPJ C82 80	A. Rodas et al.	(JPAC Collab.)
SARANTSEV	21	PL B816 136227	A.V. Sarantsev et al.	(BONN, PNPI)
ALBRECHT	20	EPJ C80 453	M. Albrecht et al.	(Crystal Barrel Collab.)
ABLIKIM	18AA	PR D98 072003	M. Ablikim et al.	(BESIII Collab.)
ROPERTZ	18	EPJ C78 1000	S. Ropertz, C. Hanhart, B. Kubis	(BONN, JULI)
AAJ	17V	JHEP 1708 037	R. Aaij et al.	(LHCb Collab.)
ABLIKIM	15AE	PR D92 052003	M. Ablikim et al.	(BESIII Collab.)
DOBBS	15	PR D91 052006	S. Dobbs et al.	(NWES)
AAJ	14BR	PR D89 092006	R. Aaij et al.	(LHCb Collab.)
ABLIKIM	13N	PR D87 092009	M. Ablikim et al.	(BESIII Collab.)
ANISOVICH	09	IJMP A24 2481	V.V. Anisovich, A.V. Sarantsev	(PNPI)
KLEMP	08	EPJ C85 39	E. Klemp, M. Matveev, A.V. Sarantsev	(BONN+)
UEHARA	08A	PR D78 052004	S. Uehara et al.	(BELLE Collab.)
ABLIKIM	06V	PL B642 441	M. Ablikim et al.	(BES Collab.)
ABLIKIM	06	PL B639 165	C. Amisler et al.	(Crystal Barrel Collab.)
AUBERT	06O	PR D74 032003	B. Aubert et al.	(BABAR Collab.)
UMAN	06	PR D73 052009	I. Uman et al.	(FNAL E835)
VLADIMIRSK...	06	PAN 69 493	V.V. Vladimirov et al.	(ITEP, Moscow)
BINON	05	Translated from YAF 69 515.	F. Binon et al.	
		PAN 68 960	F. Binon et al.	
GARMASH	05	PR D71 092003	A. Garmash et al.	(BELLE Collab.)
ANISOVICH	03	EPJ A16 229	V.V. Anisovich et al.	
BARGIOTTI	03	EPJ C26 371	M. Bargiotti et al.	(OBELIX Collab.)
AMSLER	02D	EPJ C23 29	C. Amisler et al.	(Crystal Barrel Collab.)
ANISOVICH	02D	PAN 65 1545	V.V. Anisovich et al.	
		Translated from YAF 65 1583		
ABELE	01	EPJ C19 667	A. Abele et al.	(Crystal Barrel Collab.)
ABELE	01B	EPJ C21 261	A. Abele et al.	(Crystal Barrel Collab.)
ACCIARRI	01H	PL B501 173	M. Acciarri et al.	(L3 Collab.)
AITALA	01A	PRL 86 765	E.M. Aitala et al.	(FNAL E791 Collab.)
BARATE	00E	PL B472 189	R. Barate et al.	(ALEPH Collab.)
BARBERIS	00A	PL B471 429	D. Barberis et al.	(WA 102 Collab.)
BARBERIS	00C	PL B471 440	D. Barberis et al.	(WA 102 Collab.)
BARBERIS	00D	PL B474 423	D. Barberis et al.	(WA 102 Collab.)
BARBERIS	00E	PL B479 59	D. Barberis et al.	(WA 102 Collab.)
BARBERIS	99B	PL B453 305	D. Barberis et al.	(Omega Expt.)
BARBERIS	99B	PL B453 316	D. Barberis et al.	(Omega Expt.)
BARBERIS	99D	PL B462 462	D. Barberis et al.	(Omega Expt.)
BELLAZZINI	99	PL B467 296	R. Bellazzini et al.	
FRENCH	99	PL B460 213	B. French et al.	(WA76 Collab.)
KAMINSKI	99	EPJ C9 141	R. Kaminski, L. Lesniak, B. Loiseau	(CRAC, PARIN)
ABELE	98	PR D57 3860	A. Abele et al.	(Crystal Barrel Collab.)
ALDE	98	EPJ A3 361	D. Alde et al.	(GAM4 Collab.)
Also		PAN 62 405	D. Alde et al.	(GAMS Collab.)
AMSLER	98	RMP 70 1293	C. Amisler	
ANISOVICH	98B	SFU 41 419	V.V. Anisovich et al.	
		Translated from UFN 168 481.		
BERTIN	98	PR D57 55	A. Bertin et al.	(OBELIX Collab.)
REYES	98	PRL 81 4079	M.A. Reyes et al.	
BARBERIS	97B	PL B413 217	D. Barberis et al.	(WA 102 Collab.)
BERTIN	97C	PL B408 476	A. Bertin et al.	(OBELIX Collab.)
FRABETTI	97D	PL B407 79	P.L. Frabetti et al.	(FNAL E687 Collab.)
ABELE	96	PL B380 453	A. Abele et al.	(Crystal Barrel Collab.)
ABELE	96B	PL B365 425	A. Abele et al.	(Crystal Barrel Collab.)
ABELE	96C	NP A009 552	A. Abele et al.	(Crystal Barrel Collab.)
AMELIN	96B	PAN 59 976	D.V. Amelin et al.	(SERP, TBLI)
		Translated from YAF 59 1021.		
BUGG	96	NP B471 59	D.V. Bugg, A.V. Sarantsev, B.S. Zou	(LOQM, PNPI)
AMSLER	95B	PL B342 433	C. Amisler et al.	(Crystal Barrel Collab.)
AMSLER	95C	PL B353 571	C. Amisler et al.	(Crystal Barrel Collab.)
AMSLER	95D	PL B355 425	C. Amisler et al.	(Crystal Barrel Collab.)
ANTINORI	95	PL B353 589	F. Antinori et al.	(ATHU, BARI, BIRM+)
BUGG	95	PL B353 378	D.V. Bugg et al.	(LOQM, PNPI, WASH)
ABATZIS	94	PL B324 509	S. Abatzis et al.	(ATHU, BARI, BIRM+)
AMSLER	94C	PL B327 425	C. Amisler et al.	(Crystal Barrel Collab.)
AMSLER	94D	PL B333 277	C. Amisler et al.	(Crystal Barrel Collab.)
AMSLER	94E	PL B340 259	C. Amisler et al.	(Crystal Barrel Collab.)
ANISOVICH	94	PL B323 233	V.V. Anisovich et al.	(Crystal Barrel Collab.)
BUGG	94	PR D50 4412	D.V. Bugg et al.	(LOQM)
AMSLER	92C	PL B291 347	C. Amisler et al.	(Crystal Barrel Collab.)
BELADIDZE	92C	SJNP 55 1535	G.M. Beladidze, S.I. Bityukov, G.V. Borisov	(SERP+)
		Translated from YAF 55 2748.		
PROKOSHKIN	91	SPD 36 155	Y.D. Prokoshkin	(GAM2 and GAM4 Collab.)
		Translated from DANS 316 900.		
ARMSTRONG	89E	PL B228 536	T.A. Armstrong, M. Benayoun	(ATHU, BARI, BIRM+)
ALDE	88	PL B201 160	D.M. Alde et al.	(SERP, BELG, LANL, LAPP+)
ASTON	88D	NP B301 525	D. Aston et al.	(SLAC, NAGO, CIN, INUS)
ALDE	87	PL B198 286	D.M. Alde et al.	(LANL, BRUX, SERP, LAPP)
ALDE	86D	NP B269 485	D.M. Alde et al.	(BELG, LAPP, SERP, CERN+)
LONGACRE	86	PL B177 223	R.S. Longacre et al.	(BNL, BRAN, CUNY+)
BINON	84C	NC 80A 363	F.G. Binon et al.	(BELG, LAPP, SERP+)
BINON	83	NC 76A 313	F.G. Binon et al.	(BELG, LAPP, SERP+)
Also		SJNP 38 561	F.G. Binon et al.	(BELG, LAPP, SERP+)
		Translated from YAF 38 934.		
GRAY	83	PR D27 307	L. Gray et al.	(SYRA)
ETKIN	82B	PR D25 1786	A. Etkin et al.	(BNL, CUNY, TUFTS, VAND)
COHEN	80	PR D22 2595	D. Cohen et al.	(BNL)
HYAMS	75	NP B100 205	B.D. Hyams et al.	(CERN, MPIM)

$f_1(1510)$

$$I^G(JPC) = 0^+(1^{++})$$

OMITTED FROM SUMMARY TABLE

See the review on "Spectroscopy of Light Meson Resonances."

$f_1(1510)$ MASS

VALUE (MeV)	EVTS	DOCUMENT ID	TECN	COMMENT
1518 ± 5 OUR AVERAGE	Error includes scale factor of 1.7. See the ideogram below.			
1530 ± 10		ASTON	88C LASS	11 $K^- p \rightarrow K_S^0 K_{S\pm}^{\pm} \pi^{\mp} \Lambda$
1512 ± 4	600	¹ BIRMAN	88	MP5 8 $\pi^- p \rightarrow K^+ \bar{K}^0 \pi^- n$
1526 ± 6	271	GAVILLET	82	FBC 4.2 $K^- p \rightarrow \Lambda K K \pi$
• • • We do not use the following data for averages, fits, limits, etc. • • •				
~ 1525		² BAUER	93B	$\gamma \gamma^* \rightarrow \pi^+ \pi^- \pi^0 \pi^0$

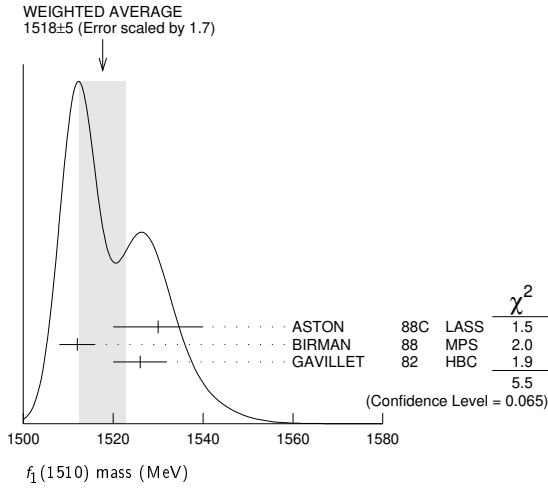
¹ From partial wave analysis of $K^+ \bar{K}^0 \pi^-$ state.

See key on page 1171

Meson Particle Listings

$f_1(1510), f_2'(1525)$

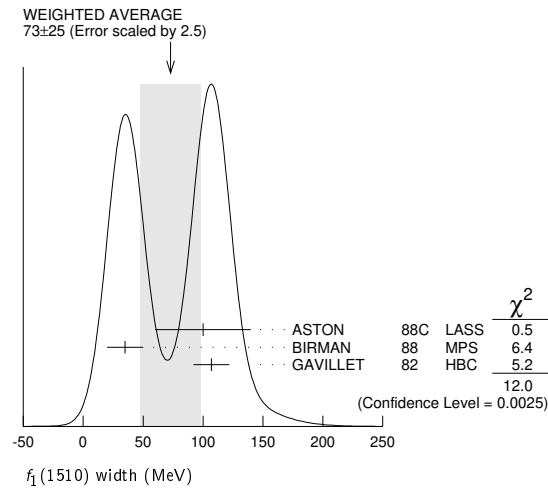
² Not seen by AIHARA 88c in the $K_S^0 K^\pm \pi^\mp$ final state.



$f_1(1510)$ WIDTH

VALUE (MeV)	EVTS	DOCUMENT ID	TECN	COMMENT
73 ± 25 OUR AVERAGE				Error includes scale factor of 2.5. See the ideogram below.
100 ± 40		ASTON 88c	LASS	11 $K^- p \rightarrow K_S^0 K^\pm \pi^\mp \Lambda$
35 ± 15	600	³ BIRMAN 88	MPS	8 $\pi^- p \rightarrow K^+ \bar{K}^0 \pi^- n$
107 ± 15	271	GAVILLET 82	HBC	4.2 $K^- p \rightarrow \Lambda K K \pi$

³ From partial wave analysis of $K^+ \bar{K}^0 \pi^-$ state.



$f_1(1510)$ DECAY MODES

Mode	Fraction (Γ_i/Γ)
Γ_1 $K \bar{K}^*(892) + c.c.$	seen
Γ_2 $\pi^+ \pi^- \eta'$	seen

$f_1(1510)$ BRANCHING RATIOS

$\Gamma(\pi^+ \pi^- \eta')/\Gamma_{total}$	Γ_2/Γ
seen	230
	ABLIKIM 11c BES3
	J/ $\psi \rightarrow \gamma \pi^+ \pi^- \eta'$

$f_1(1510)$ REFERENCES

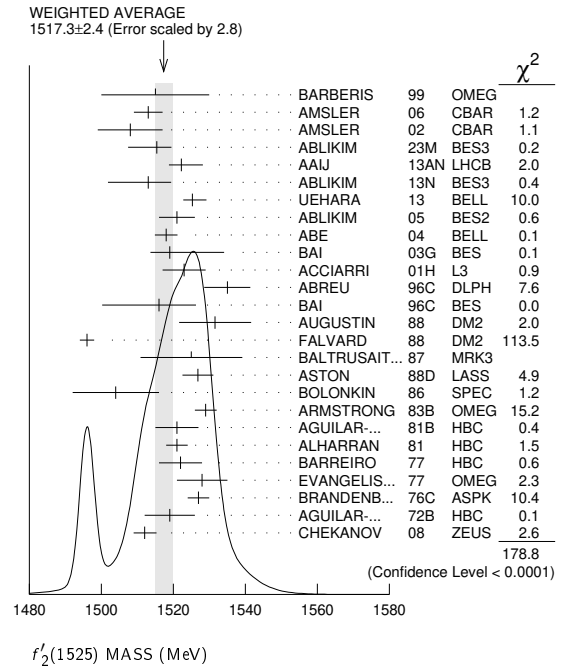
ABLIKIM 11c	PRL 106 072002	M. Ablikim et al.	(BESIII Collab.)
BAUER 93b	PR D48 3976	D.A. Bauer et al.	(SLAC)
AIHARA 88c	PR D38 1	H. Aihara et al.	(TPC-2 γ Collab.)
ASTON 88c	PL B201 573	D. Aston et al.	(SLAC, NAGO, CINC, INUS) JP
BIRMAN 88	PRL 61 1557	A. Birman et al.	(BNL, FSU, IND, MASD) JP
GAVILLET 82	ZPHY C16 119	P. Gavillet et al.	(CERN, CDEF, PADO+)

$f_2'(1525)$

$I^G(JPC) = 0^+(2^{++})$

$f_2'(1525)$ MASS

VALUE (MeV) DOCUMENT ID
1517.3 ± 2.4 OUR AVERAGE Includes data from the 6 datablocks that follow this one. Error includes scale factor of 2.8. See the ideogram below.



PRODUCED BY PION BEAM

VALUE (MeV) EVTS DOCUMENT ID TECN COMMENT
 The data in this block is included in the average printed for a previous datablock.

1521 ± 13		TIKHOMIROV 03	SPEC	40.0 $\pi^- C \rightarrow K_S^0 K_S^0 K_L^0 X$
1547 ± 10	2	¹ LONGACRE 86	MPS	22 $\pi^- p \rightarrow K_S^0 K_S^0 n$
1496 ± 9	8	² CHABAUD 81	ASPK	6 $\pi^- p \rightarrow K^+ K^- n$
1497 ± 9	8	CHABAUD 81	ASPK	18.4 $\pi^- p \rightarrow K^+ K^- n$
1492 ± 29		GORLICH 80	ASPK	17 $\pi^- p$ polarized $\rightarrow K^+ K^- n$
1502 ± 25		³ CORDEN 79	OMEG	12-15 $\pi^- p \rightarrow \pi^+ \pi^- n$
1480	14	CRENNELL 66	HBC	6.0 $\pi^- p \rightarrow K_S^0 K_S^0 n$

¹ From a partial-wave analysis of data using a K-matrix formalism with 5 poles.
² CHABAUD 81 is a reanalysis of PAWLICKI 77 data.
³ From an amplitude analysis where the $f_2'(1525)$ width and elasticity are in complete disagreement with the values obtained from $K \bar{K}$ channel, making the solution dubious.

PRODUCED BY K^\pm BEAM

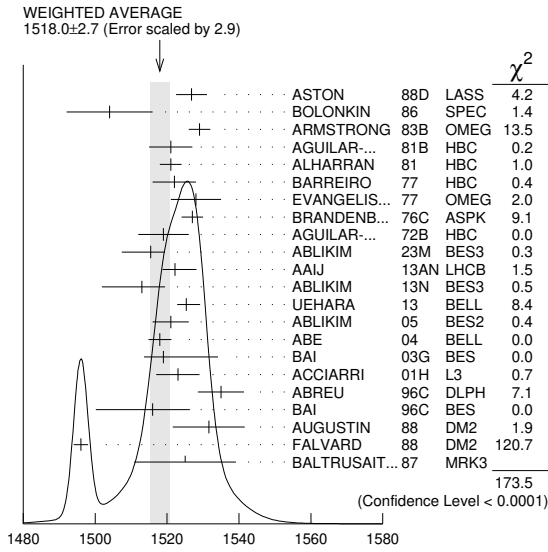
VALUE (MeV) EVTS DOCUMENT ID TECN COMMENT
 The data in this block is included in the average printed for a previous datablock.

VALUE (MeV)	EVTS	DOCUMENT ID	TECN	COMMENT
1518.0 ± 2.7 OUR AVERAGE				Includes data from the datablock that follows this one. Error includes scale factor of 2.9. See the ideogram below.
1526.8 ± 4.3		ASTON 88D	LASS	11 $K^- p \rightarrow K_S^0 K_S^0 \Lambda$
1504 ± 12		BOLONKIN 86	SPEC	40 $K^- p \rightarrow K_S^0 K_S^0 Y$
1529 ± 3		ARMSTRONG 83B	OMEG	18.5 $K^- p \rightarrow K^- K^+ \Lambda$
1521 ± 6	650	AGUILAR... 81B	HBC	4.2 $K^- p \rightarrow \Lambda K^+ K^-$
1521 ± 3	572	ALHARRAN 81	HBC	8.25 $K^- p \rightarrow \Lambda K \bar{K}$
1522 ± 6	123	BARREIRO 77	HBC	4.15 $K^- p \rightarrow \Lambda K_S^0 K_S^0$
1528 ± 7	166	EVANGELIS... 77	OMEG	10 $K^- p \rightarrow K^+ K^- (\Lambda, \Sigma)$
1527 ± 3	120	BRANDENB... 76C	ASPK	13 $K^- p \rightarrow K^+ K^- (\Lambda, \Sigma)$
1519 ± 7	100	AGUILAR... 72B	HBC	3.9, 4.6 $K^- p \rightarrow K \bar{K} (\Lambda, \Sigma)$

••• We do not use the following data for averages, fits, limits, etc. •••
 1514 ± 8 61 BINON 07 GAMS 32.5 $K^- p \rightarrow \eta \eta (\Lambda/\Sigma^0)$
 1513 ± 10 ¹ BARKOV 99 SPEC 40 $K^- p \rightarrow K_S^0 K_S^0 Y$
¹ Systematic errors not estimated.

Meson Particle Listings

$f_2'(1525)$



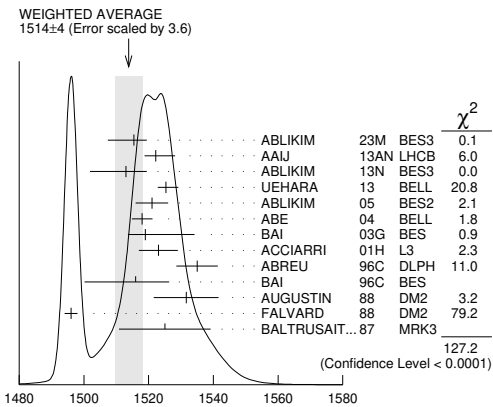
PRODUCED BY K^\pm BEAM (MeV)

PRODUCED IN e^+e^- ANNIHILATION AND PARTICLE DECAYS

VALUE (MeV) EVTS DOCUMENT ID TECN COMMENT
The data in this block is included in the average printed for a previous datablock.

1514 ± 4 OUR AVERAGE Error includes scale factor of 3.6. See the ideogram below.

1515.4 ± 2.5 ± 3.2	126K	ABLIKIM	23M	BES3	$J/\psi \rightarrow \gamma K_S^0 K_S^0 \pi^0$
1522.2 ± 2.8 ± 5.3		AAIJ	13AN	LHCB	$\bar{B}_s^0 \rightarrow J/\psi K^+ K^-$
1513 ± 5 ± 4	5.5k	1 ABLIKIM	13N	BES3	$e^+e^- \rightarrow J/\psi \rightarrow \gamma \eta \eta$
1525.3 ± 1.2 ± 3.7		UEHARA	13	BELL	$\gamma \gamma \rightarrow K_S^0 K_S^0$
1521 ± 5		ABLIKIM	05	BES2	$J/\psi \rightarrow \phi K^+ K^-$
1518 ± 1 ± 3		ABE	04	BELL	10.6 $e^+e^- \rightarrow e^+e^- K^+ K^-$
1519 ± 2 ± 15		BAI	03G	BES	$J/\psi \rightarrow \gamma K \bar{K}$
1523 ± 6	331	2 ACCIARRI	01H	L3	91, 183-209 $e^+e^- \rightarrow e^+e^- K_S^0 K_S^0$
1535 ± 5 ± 4		ABREU	96C	DLPH	$Z^0 \rightarrow K^+ K^- + X$
1516 ± 5 ± 9		BAI	96C	BES	$J/\psi \rightarrow \gamma K^+ K^-$
1531.6 ± 10.0		AUGUSTIN	88	DM2	$J/\psi \rightarrow \gamma K^+ K^-$
1496 ± 2		3 FALVARD	88	DM2	$J/\psi \rightarrow \phi K^+ K^-$
1525 ± 10 ± 10		BALTRUSAIT...87	MRK3		$J/\psi \rightarrow \gamma K^+ K^-$
• • • We do not use the following data for averages, fits, limits, etc. • • •					
1518 ± 3		4 KLEMPPT	22	RVUE	$J/\psi(1S) \rightarrow \gamma \pi^0 \pi^0$, $\gamma K_S^0 K_S^0$
1503 ± 11		5 RODAS	22	RVUE	$J/\psi(1S) \rightarrow \gamma (\pi \pi, K \bar{K})$
1532 ± 3 ± 6	644	6,7 DOBBS	15		$J/\psi \rightarrow \gamma K^+ K^-$
1557 ± 9 ± 3	113	6,7 DOBBS	15		$\psi(2S) \rightarrow \gamma K^+ K^-$
1526 ± 7	29	8 LEES	14H	BABR	$e^+e^- \rightarrow K_S^0 K_S^0 K^+ K^- \gamma$
1523 ± 5	870	9 SCHEGELSKY	06A	RVUE	$\gamma \gamma \rightarrow K_S^0 K_S^0$
1515 ± 5		10 FALVARD	88	DM2	$J/\psi \rightarrow \phi K^+ K^-$



$f_2'(1525)$ mass, e^+e^- annihilation and particle decays (MeV)

¹ From partial wave analysis including all possible combinations of 0^{++} , 2^{++} , and 4^{++} resonances.

- ² Supersedes ACCIARRI 95J.
- ³ From an analysis including interference with $f_0(1710)$.
- ⁴ Fit of the tensor partial waves from BES3 in the multipole basis.
- ⁵ T-matrix pole from coupled channel K-matrix fit to data on $J/\psi \rightarrow \gamma \pi^0 \pi^0$ (ABLIKIM 15AE) and $J/\psi \rightarrow \gamma K_S^0 K_S^0$ (ABLIKIM 18AA).
- ⁶ Using CLEO-c data but not authored by the CLEO Collaboration.
- ⁷ From a fit to a Breit-Wigner line shape with fixed $\Gamma = 73$ MeV.
- ⁸ From a fit to a Breit-Wigner line shape plus a second-order polynomial function. Systematic errors not evaluated.
- ⁹ From analysis of L3 data at 91 and 183-209 GeV.
- ¹⁰ From an analysis ignoring interference with $f_0(1710)$.

PRODUCED IN $\bar{p}p$ ANNIHILATION

VALUE (MeV) DOCUMENT ID TECN COMMENT
The data in this block is included in the average printed for a previous datablock.

1512 ± 4 OUR AVERAGE

1513 ± 4	AMSLER	06	CBAR	0.9	$\bar{p}p \rightarrow K^+ K^- \pi^0$
1508 ± 9	1 AMSLER	02	CBAR	0.9	$\bar{p}p \rightarrow \pi^0 \eta \eta, \pi^0 \pi^0 \pi^0$
• • • We do not use the following data for averages, fits, limits, etc. • • •					
1495.0 ± 1.1 ± 8.1	2 ALBRECHT	20	RVUE	0.9	$\bar{p}p \rightarrow \pi^0 \pi^0 \eta, \pi^0 \eta \eta, \pi^0 K^+ K^-$
1530 ± 12	3 ANISOVICH	09	RVUE	0.0	$\bar{p}p, \pi N$
1	T-matrix pole.				
2	T-matrix pole, 4 poles, 4 channels, including scattering data from HYAMS 75 ($\pi \pi$), LONGACRE 86 ($K \bar{K}$), BINON 83 ($\eta \eta$).				
3	4-poles, 5-channel K matrix fit.				

CENTRAL PRODUCTION

VALUE (MeV) DOCUMENT ID TECN COMMENT
The data in this block is included in the average printed for a previous datablock.

1515 ± 15 BARBERIS 99 OMEG 450 $pp \rightarrow p_S p_f K^+ K^-$

PRODUCED IN $e p$ COLLISIONS

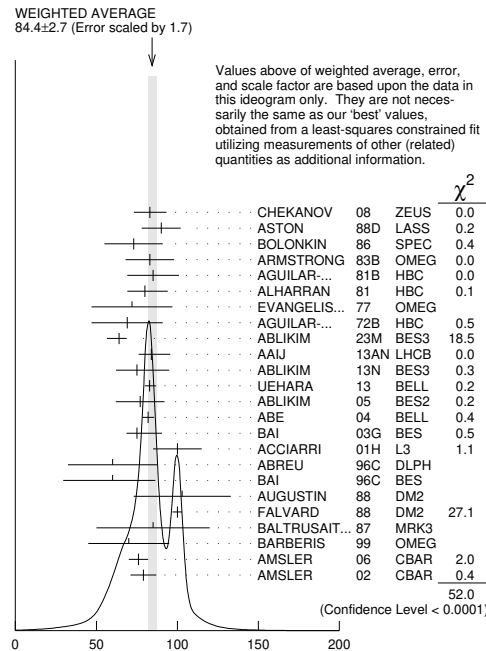
VALUE (MeV) EVTS DOCUMENT ID TECN COMMENT
The data in this block is included in the average printed for a previous datablock.

1512 ± 3 ± 1.4	1 CHEKANOV	08	ZEUS	$e p \rightarrow K_S^0 K_S^0 X$	
• • • We do not use the following data for averages, fits, limits, etc. • • •					
1537 ± 9	84	2 CHEKANOV	04	ZEUS	$e p \rightarrow K_S^0 K_S^0 X$
1	In the SU(3) based model with a specific interference pattern of the $f_2(1270)$, $a_2^0(1320)$, and $f_2'(1525)$ mesons incoherently added to the $f_0(1710)$ and non-resonant background.				
2	Systematic errors not estimated.				

$f_2'(1525)$ WIDTH

VALUE (MeV) DOCUMENT ID

72 ± 7 OUR FIT
84.4 ± 2.7 OUR AVERAGE Includes data from the 6 datablocks that follow this one. Error includes scale factor of 1.7. See the ideogram below.



$f_2'(1525)$ WIDTH (MeV)

See key on page 1171

Meson Particle Listings

$f'_2(1525)$

PRODUCED BY PION BEAM

VALUE (MeV)	DOCUMENT ID	TECN	COMMENT
-------------	-------------	------	---------

The data in this block is included in the average printed for a previous datablock.

102 ± 4.2	TIKHOMIROV 03	SPEC	40.0 $\pi^- C \rightarrow K_S^0 K_S^0 K_L^0 X$
108 ⁺⁵ ₋₂	¹ LONGACRE 86	MPS	22 $\pi^- p \rightarrow K_S^0 K_S^0 n$
69 ⁺²² ₋₁₆	² CHABAUD 81	ASPK	6 $\pi^- p \rightarrow K^+ K^- n$
137 ⁺²³ ₋₂₁	CHABAUD 81	ASPK	18.4 $\pi^- p \rightarrow K^+ K^- n$
150 ⁺⁸³ ₋₅₀	GORLICH 80	ASPK	17 $\pi^- p$ polarized $\rightarrow K^+ K^- n$
165 ± 4.2	³ CORDEN 79	OMEG	12-15 $\pi^- p \rightarrow \pi^+ \pi^- n$
92 ⁺³⁹ ₋₂₂	⁴ POLYCHRO... 79	STRC	7 $\pi^- p \rightarrow n K_S^0 K_S^0$

- From a partial-wave analysis of data using a K-matrix formalism with 5 poles.
- CHABAUD 81 is a reanalysis of PAWLICKI 77 data.
- From an amplitude analysis where the $f'_2(1525)$ width and elasticity are in complete disagreement with the values obtained from $K\bar{K}$ channel, making the solution dubious.
- From a fit to the D with $f_2(1270)$ - $f'_2(1525)$ interference. Mass fixed at 1516 MeV.

PRODUCED BY K^\pm BEAM

VALUE (MeV)	EVTS	DOCUMENT ID	TECN	COMMENT
-------------	------	-------------	------	---------

The data in this block is included in the average printed for a previous datablock.

82 ± 6 OUR AVERAGE				
90 ± 12	ASTON 88D	LASS	11 $K^- p \rightarrow K_S^0 K_S^0 \Lambda$	
73 ± 18	BOLONKIN 86	SPEC	40 $K^- p \rightarrow K_S^0 K_S^0 Y$	
83 ± 15	ARMSTRONG 83B	OMEG	18.5 $K^- p \rightarrow K^- K^+ \Lambda$	
85 ± 16	650 AGUILAR...	81B	HBC 4.2 $K^- p \rightarrow \Lambda K^+ K^-$	
80 ⁺¹⁴ ₋₁₁	572 ALHARRAN...	81B	HBC 8.25 $K^- p \rightarrow \Lambda K\bar{K}$	
72 ± 25	166 EVANGELIS...	77	OMEG 10 $K^- p \rightarrow K^+ K^- (\Lambda, \Sigma)$	
69 ± 22	100 AGUILAR...	72B	HBC 3.9, 4.6 $K^- p \rightarrow K\bar{K} (\Lambda, \Sigma)$	
92 ⁺²⁵ ₋₁₆	61 BINON 07	GAMS	32.5 $K^- p \rightarrow \eta \eta (\Lambda/\Sigma^0)$	
75 ± 20	¹ BARKOV 99	SPEC	40 $K^- p \rightarrow K_S^0 K_S^0 \gamma$	
62 ⁺¹⁹ ₋₁₄	123 BARREIRO 77	HBC	4.15 $K^- p \rightarrow \Lambda K_S^0 K_S^0$	
61 ± 8	120 BRANDENB...	76C	ASPK 13 $K^- p \rightarrow K^+ K^- (\Lambda, \Sigma)$	

- Systematic errors not estimated.

PRODUCED IN $e^+ e^-$ ANNIHILATION AND PARTICLE DECAYS

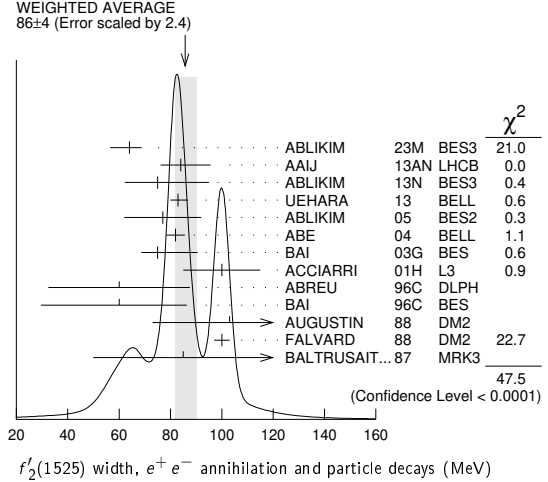
VALUE (MeV)	EVTS	DOCUMENT ID	TECN	COMMENT
-------------	------	-------------	------	---------

The data in this block is included in the average printed for a previous datablock.

86 ± 4 OUR AVERAGE				Error includes scale factor of 2.4. See the ideogram below.
64.0 ± 4.3 ^{+2.0} _{-6.1}	126K	ABLIKIM	23M BES3	$J/\psi \rightarrow \gamma K_S^0 K_S^0 \pi^0$
84 ± 6 ⁺¹⁰ ₋₅		AAIJ	13AN LHCB	$B_S^0 \rightarrow J/\psi K^+ K^-$
75 ⁺¹² ₋₁₀ ⁺¹⁶ ₋₈	5.5k	¹ ABLIKIM	13N BES3	$e^+ e^- \rightarrow J/\psi \rightarrow \gamma \eta \eta$
82.9 ^{+2.1} _{-2.2} ^{+3.3} _{-2.0}		UEHARA	13 BELL	$\gamma \gamma \rightarrow K_S^0 K_S^0$
77 ± 15		ABLIKIM	05 BES2	$J/\psi \rightarrow \phi K^+ K^-$
82 ± 2 ± 3		ABE	04 BELL	10.6 $e^+ e^- \rightarrow e^+ e^- K^+ K^-$
75 ± 4 ⁺¹⁵ ₋₅		BAI	03G BES	$J/\psi \rightarrow \gamma K\bar{K}$
100 ± 15	331	² ACCIARRI	01H L3	91, 183-209 $e^+ e^- \rightarrow e^+ e^- K_S^0 K_S^0$
60 ± 20 ± 19		ABREU	96C DLPH	$Z^0 \rightarrow K^+ K^- + X$
60 ± 23 ⁺¹³ ₋₂₀		BAI	96C BES	$J/\psi \rightarrow \gamma K^+ K^-$
103 ± 30		AUGUSTIN	88 DM2	$J/\psi \rightarrow \gamma K^+ K^-$
100 ± 3		³ FALVARD	88 DM2	$J/\psi \rightarrow \phi K^+ K^-$
85 ± 35		³ BALTRUSAIT...87	MRK3	$J/\psi \rightarrow \gamma K^+ K^-$
78 ± 6		⁴ KLEMPPT	22 RVUE	$J/\psi(1S) \rightarrow \gamma \pi^0 \pi^0$, $\gamma K_S^0 K_S^0$
84 ± 15		⁵ RODAS	22 RVUE	$J/\psi(1S) \rightarrow \gamma (\pi \pi, K\bar{K})$
37 ± 12	29	⁶ LEES	14H BABR	$e^+ e^- \rightarrow K_S^0 K_S^0 K^+ K^- \gamma$
104 ± 10	870	⁷ SCHEGELSKY	06A RVUE	$\gamma \gamma \rightarrow K_S^0 K_S^0$
62 ± 10		⁸ FALVARD	88 DM2	$J/\psi \rightarrow \phi K^+ K^-$

- From partial wave analysis including all possible combinations of 0^{++} , 2^{++} , and 4^{++} resonances.
- Supersedes ACCIARRI 95J.
- From an analysis including interference with $f_0(1710)$.
- Fit of the tensor partial waves from BES3 in the multipole basis.
- T-matrix pole from coupled channel K-matrix fit to data on $J/\psi \rightarrow \gamma \pi^0 \pi^0$ (ABLIKIM 15AE) and $J/\psi \rightarrow \gamma K_S^0 K_S^0$ (ABLIKIM 18AA).
- From a fit to a Breit-Wigner line shape plus a second-order polynomial function. Systematic errors not evaluated.
- From analysis of L3 data at 91 and 183-209 GeV.

⁸ From an analysis ignoring interference with $f_0(1710)$.



PRODUCED IN $\bar{p}p$ ANNIHILATION

VALUE (MeV)	DOCUMENT ID	TECN	COMMENT
-------------	-------------	------	---------

The data in this block is included in the average printed for a previous datablock.

77 ± 5 OUR AVERAGE

76 ± 6	AMSLER 06	CBAR	0.9 $\bar{p}p \rightarrow K^+ K^- \pi^0$
79 ± 8	¹ AMSLER 02	CBAR	0.9 $\bar{p}p \rightarrow \pi^0 \eta \eta, \pi^0 \pi^0 \pi^0$
104.8 ± 0.9 ± 9.8	² ALBRECHT 20	RVUE	0.9 $\bar{p}p \rightarrow \pi^0 \pi^0 \eta, \pi^0 \eta \eta, \pi^0 K^+ K^-$
128 ± 20	³ ANISOVICH 09	RVUE	0.0 $\bar{p}p, \pi N$

- T-matrix pole.
- T-matrix pole, 4 poles, 4 channels, including scattering data from HYAMS 75 ($\pi \pi$), LONGACRE 86 ($K\bar{K}$), BINON 83 ($\eta \eta$).
- K-matrix, 4-poles, 5-channel fit.

CENTRAL PRODUCTION

VALUE (MeV)	DOCUMENT ID	TECN	COMMENT
-------------	-------------	------	---------

The data in this block is included in the average printed for a previous datablock.

70 ± 25	BARBERIS 99	OMEG	450 $p\bar{p} \rightarrow p_S p_f K^+ K^-$
----------------	-------------	------	--

PRODUCED IN $e p$ COLLISIONS

VALUE (MeV)	EVTS	DOCUMENT ID	TECN	COMMENT
-------------	------	-------------	------	---------

The data in this block is included in the average printed for a previous datablock.

83 ± 9⁺⁵₋₄	¹ CHEKANOV 08	ZEUS	$e p \rightarrow K_S^0 K_S^0 X$
---	--------------------------	------	---------------------------------

- We do not use the following data for averages, fits, limits, etc.
 - 84 ² CHEKANOV 04 ZEUS $e p \rightarrow K_S^0 K_S^0 X$

- In the SU(3) based model with a specific interference pattern of the $f_2(1270)$, $a_2^0(1320)$, and $f'_2(1525)$ mesons incoherently added to the $f_0(1710)$ and non-resonant background.
- Systematic errors not estimated.

$f'_2(1525)$ DECAY MODES

Mode	Fraction (Γ_i/Γ)
Γ_1 $K\bar{K}$	(88.8 ± 2.2) %
Γ_2 $\eta \eta$	(10.3 ± 2.2) %
Γ_3 $\pi \pi$	(8.2 ± 1.5) × 10 ⁻³
Γ_4 $K\bar{K}^*(892) + c.c.$	
Γ_5 $\pi K\bar{K}$	
Γ_6 $\pi \pi \eta$	
Γ_7 $\pi^+ \pi^+ \pi^- \pi^-$	
Γ_8 $\gamma \gamma$	(1.12 ± 0.15) × 10 ⁻⁶

CONSTRAINED FIT INFORMATION

An overall fit to 2 partial widths, a combination of partial widths obtained from integrated cross sections, and 3 branching ratios uses 16 measurements and one constraint to determine 5 parameters. The overall fit has a $\chi^2 = 14.2$ for 12 degrees of freedom.

The following *off-diagonal* array elements are the correlation coefficients $\langle \delta x_i \delta x_j \rangle / (\delta x_i \delta x_j)$, in percent, from the fit to the branching fractions, $x_i \equiv \Gamma_i / \Gamma_{\text{total}}$. The fit constrains the x_i whose labels appear in this array to sum to one.

Meson Particle Listings

 $f_2'(1525)$

x_2	-100			
x_3	-5	-1		
x_8	0	0	1	
Γ	-28	28	-1	-62
	x_1	x_2	x_3	x_8

Mode	Rate (MeV)
Γ_1 $K\bar{K}$	64 $^{+6}_{-5}$
Γ_2 $\eta\eta$	7.4 ± 1.9
Γ_3 $\pi\pi$	0.59 ± 0.12
Γ_8 $\gamma\gamma$	(8.1 ± 0.9) $\times 10^{-5}$

 $f_2'(1525)$ PARTIAL WIDTHS

$\Gamma(K\bar{K})$	Γ_1		
VALUE (MeV)	DOCUMENT ID	TECN	COMMENT

64 $^{+6}_{-5}$ OUR FIT63 $^{+6}_{-5}$ 1 LONGACRE 86 MPS 22 $\pi^- p \rightarrow K_S^0 K_S^0 n$

1 From a partial-wave analysis of data using a K-matrix formalism with 5 poles.

$\Gamma(\eta\eta)$	Γ_2			
VALUE (MeV)	EVTS	DOCUMENT ID	TECN	COMMENT

7.4 ± 1.9 OUR FIT

• • • We do not use the following data for averages, fits, limits, etc. • • •

5.0 ± 0.8 870 1 SCHEGELSKY 06A RVUE $\gamma\gamma \rightarrow K_S^0 K_S^0$ 24 $^{+3}_{-1}$ 2 LONGACRE 86 MPS 22 $\pi^- p \rightarrow K_S^0 K_S^0 n$ 1 From analysis of L3 data at 91 and 183–209 GeV, using $\Gamma(f_2'(1525) \rightarrow K\bar{K}) = 68$ MeV and SU(3) relations.

2 From a partial-wave analysis of data using a K-matrix formalism with 5 poles.

$\Gamma(\pi\pi)$	Γ_3			
VALUE (MeV)	EVTS	DOCUMENT ID	TECN	COMMENT

0.59 ± 0.12 OUR FIT1.4 $^{+1.0}_{-0.5}$ 1 LONGACRE 86 MPS 22 $\pi^- p \rightarrow K_S^0 K_S^0 n$

• • • We do not use the following data for averages, fits, limits, etc. • • •

0.2 $^{+1.0}_{-0.2}$ 870 2 SCHEGELSKY 06A RVUE $\gamma\gamma \rightarrow K_S^0 K_S^0$

1 From a partial-wave analysis of data using a K-matrix formalism with 5 poles.

2 From analysis of L3 data at 91 and 183–209 GeV, using $\Gamma(f_2'(1525) \rightarrow K\bar{K}) = 68$ MeV and SU(3) relations.

$\Gamma(\gamma\gamma)$	Γ_8			
VALUE (keV)	EVTS	DOCUMENT ID	TECN	COMMENT

0.081 ± 0.009 OUR FIT

• • • We do not use the following data for averages, fits, limits, etc. • • •

0.13 ± 0.03 870 1 SCHEGELSKY 06A RVUE $\gamma\gamma \rightarrow K_S^0 K_S^0$ 1 From analysis of L3 data at 91 and 183–209 GeV, using $\Gamma(f_2'(1525) \rightarrow K\bar{K}) = 68$ MeV and SU(3) relations.

$\Gamma(K\bar{K})/\Gamma_{total}$	Γ_1/Γ		
VALUE	DOCUMENT ID	TECN	COMMENT

• • • We do not use the following data for averages, fits, limits, etc. • • •

0.746 ± 0.002 $^{+0.166}_{-0.162}$ 1 ALBRECHT 20 RVUE 0.9 $\bar{p}p \rightarrow \pi^0 \pi^0 \eta, \pi^0 \eta\eta, \pi^0 K^+ K^-$ 1 Residue from T-matrix pole, 4 poles, 4 channels, including scattering data from HYAMS 75 ($\pi\pi$), LONGACRE 86 ($K\bar{K}$), BINON 83 ($\eta\eta$). $f_2'(1525)$ $\Gamma(i)\Gamma(\gamma\gamma)/\Gamma_{total}$

$\Gamma(K\bar{K}) \times \Gamma(\gamma\gamma)/\Gamma_{total}$	$\Gamma_1\Gamma_8/\Gamma$			
VALUE (keV)	EVTS	DOCUMENT ID	TECN	COMMENT

0.072 ± 0.007 OUR FIT0.072 ± 0.007 OUR AVERAGE0.048 $^{+0.067}_{-0.008}$ $^{+0.108}_{-0.012}$ UEHARA 13 BELL $\gamma\gamma \rightarrow K_S^0 K_S^0$ 0.0564 ± 0.0048 ± 0.0116 ABE 04 BELL 10.6 $e^+e^- \rightarrow e^+e^- K^+ K^-$ 0.076 ± 0.006 ± 0.011 331 1 ACCIARRI 01H L3 $e^+e^- \rightarrow e^+e^- K_S^0 K_S^0$ 0.067 ± 0.008 ± 0.015 2 ALBRECHT 90G ARG $e^+e^- \rightarrow e^+e^- K^+ K^-$ 0.11 $^{+0.03}_{-0.02}$ ± 0.02 BEHREND 89c CELL $e^+e^- \rightarrow e^+e^- K_S^0 K_S^0$ 0.10 $^{+0.04}_{-0.03}$ $^{+0.03}_{-0.02}$ BERGER 88 PLUT $e^+e^- \rightarrow e^+e^- K_S^0 K_S^0$ 0.12 ± 0.07 ± 0.04 2 AIHARA 86b TPC $e^+e^- \rightarrow e^+e^- K^+ K^-$ 0.11 ± 0.02 ± 0.04 2 ALTHOFF 83 TASS $e^+e^- \rightarrow e^+e^- K\bar{K}$

• • • We do not use the following data for averages, fits, limits, etc. • • •

0.0314 ± 0.0050 ± 0.0077 3 ALBRECHT 90c ARG $e^+e^- \rightarrow e^+e^- K^+ K^-$

1 Supersedes ACCIARRI 95J. From analysis of L3 data at 91 and 183–209 GeV,

2 Using an incoherent background.

3 Using a coherent background.

 $f_2'(1525)$ BRANCHING RATIOS

$\Gamma(\eta\eta)/\Gamma_{total}$	Γ_2/Γ		
VALUE	DOCUMENT ID	TECN	COMMENT

• • • We do not use the following data for averages, fits, limits, etc. • • •

0.059 ± 0.003 ± 0.026 1 ALBRECHT 20 RVUE 0.9 $\bar{p}p \rightarrow \pi^0 \pi^0 \eta, \pi^0 \eta\eta, \pi^0 K^+ K^-$ seen UEHARA 10A BELL 10.6 $e^+e^- \rightarrow e^+e^- \eta\eta$ 0.10 ± 0.03 2 PROKOSHKIN 91 GAM4 300 $\pi^- p \rightarrow \pi^- p \eta\eta$ 1 Residue from T-matrix pole, 4 poles, 4 channels, including scattering data from HYAMS 75 ($\pi\pi$), LONGACRE 86 ($K\bar{K}$), BINON 83 ($\eta\eta$).2 Combining results of GAM4 with those of WA76 on $K\bar{K}$ central production and results of CBAL, MRK3 and DM2 on $J/\psi \rightarrow \gamma\eta\eta$.

$\Gamma(\eta\eta)/\Gamma(K\bar{K})$	Γ_2/Γ_1				
VALUE	CL%	EVTS	DOCUMENT ID	TECN	COMMENT

0.116 ± 0.028 OUR FIT0.115 ± 0.028 OUR AVERAGE0.119 ± 0.015 ± 0.036 61 1 BINON 07 GAMS 32.5 $K^- p \rightarrow \eta\eta(\Lambda/\Sigma^0)$ 2 PROKOSHKIN 91 GAM4 300 $\pi^- p \rightarrow \pi^- p \eta\eta$

• • • We do not use the following data for averages, fits, limits, etc. • • •

< 0.14 90 BARBERIS 00e 450 $pp \rightarrow p_f \eta\eta p_S$ < 0.50 67 BARNES HBC 4.6, 5.0 $K^- p$ 1 Using the compilation of the cross sections for $f_2'(1525)$ production in $K^- p$ collisions from ASTON 88D.2 Combining results of GAM4 with those of WA76 on $K\bar{K}$ central production and results of CBAL, MRK3 and DM2 on $J/\psi \rightarrow \gamma\eta\eta$.

$\Gamma(\pi\pi)/\Gamma_{total}$	Γ_3/Γ			
VALUE (units 10^{-2})	CL%	DOCUMENT ID	TECN	COMMENT

0.82 ± 0.16 OUR FIT0.75 ± 0.16 OUR AVERAGE0.7 ± 0.2 COSTA 80 OMEG 10 $\pi^- p \rightarrow K^+ K^- n$ 2.7 $^{+7.1}_{-1.3}$ 1 GORLICH 80 ASPK 17, 18 $\pi^- p$ 0.75 ± 0.25 1,2 MARTIN 79 RVUE

• • • We do not use the following data for averages, fits, limits, etc. • • •

3.4 ± 1.5 ± 1.0 3 ALBRECHT 20 RVUE 0.9 $\bar{p}p \rightarrow \pi^0 \pi^0 \eta, \pi^0 \eta\eta, \pi^0 K^+ K^-$ < 6 95 AGUILAR... 81B HBC 4.2 $K^- p \rightarrow \Lambda K^+ K^-$ 19 ± 3 CORDEN 79 OMEG 12–15 $\pi^- p \rightarrow \pi^+ \pi^- n$ < 4.5 95 BARREIRO 77 HBC 4.15 $K^- p \rightarrow \Lambda K_S^0 K_S^0$ 1.2 ± 0.4 1 PAWLICKI 77 SPEC 6 $\pi N \rightarrow K^+ K^- N$ < 6.3 90 BRANDENB... 76c ASPK 13 $K^- p \rightarrow K^+ K^- (\Lambda, \Sigma)$ < 0.86 1 BEUSCH 75B OSPK 8.9 $\pi^- p \rightarrow K^0 \bar{K}^0 n$ 1 Assuming that the $f_2'(1525)$ is produced by an one-pion exchange production mechanism.2 MARTIN 79 uses the PAWLICKI 77 data with different input value of the $f_2'(1525) \rightarrow K\bar{K}$ branching ratio.3 Residue from T-matrix pole, 4 poles, 4 channels, including scattering data from HYAMS 75 ($\pi\pi$), LONGACRE 86 ($K\bar{K}$), BINON 83 ($\eta\eta$).

$\Gamma(\pi\pi)/\Gamma(K\bar{K})$	Γ_3/Γ_1		
VALUE	DOCUMENT ID	TECN	COMMENT

0.0092 ± 0.0018 OUR FIT0.075 ± 0.035 AUGUSTIN 87 DM2 $J/\psi \rightarrow \gamma\pi^+ \pi^-$

$[\Gamma(K\bar{K}^*(892) + c.c.) + \Gamma(\pi K\bar{K})]/\Gamma(K\bar{K})$	$(\Gamma_4 + \Gamma_5)/\Gamma_1$			
VALUE	CL%	DOCUMENT ID	TECN	COMMENT

• • • We do not use the following data for averages, fits, limits, etc. • • •

< 0.35 95 AGUILAR... 72B HBC 3.9, 4.6 $K^- p$

< 0.4 67 AMMAR 67 HBC

$\Gamma(\pi\pi\eta)/\Gamma(K\bar{K})$	Γ_6/Γ_1			
VALUE	CL%	DOCUMENT ID	TECN	COMMENT

• • • We do not use the following data for averages, fits, limits, etc. • • •

< 0.41 95 AGUILAR... 72B HBC 3.9, 4.6 $K^- p$

< 0.3 67 AMMAR 67 HBC

$\Gamma(\pi^+ \pi^+ \pi^- \pi^-)/\Gamma(K\bar{K})$	Γ_7/Γ_1			
VALUE	CL%	DOCUMENT ID	TECN	COMMENT

• • • We do not use the following data for averages, fits, limits, etc. • • •

< 0.32 95 AGUILAR... 72B HBC 3.9, 4.6 $K^- p$ $f_2'(1525)$ REFERENCES

ABLIKIM	23M	JHEP 2303 121	M. Ablikim et al.	(BESIII Collab.)
KLEMPIT	22	PL B830 137171	E. Klempit et al.	(BONN)
RODAS	22	EJP C82 80	A. Rodas et al.	(JPAC Collab.)
ALBRECHT	20	EJP C80 453	M. Albrecht et al.	(Crystal Barrel Collab.)
ABLIKIM	18AA	PR D98 072003	M. Ablikim et al.	(BESIII Collab.)
ABLIKIM	15AE	PR D92 052003	M. Ablikim et al.	(BESIII Collab.)
DOBBS	15	PR D91 052006	S. Dobbs et al.	(NWES)
LEES	14H	PR D89 092002	J.P. Lees et al.	(BABAR Collab.)
AAIJ	13AN	PR D87 072004	R. Aaij et al.	(LHCb Collab.)
ABLIKIM	13N	PR D87 092009	M. Ablikim et al.	(BESIII Collab.)
UEHARA	13	PTEP 2013 123C01	S. Uehara et al.	(BELLE Collab.)

See key on page 1171

Meson Particle Listings

$f'_2(1525), f_2(1565)$

UEHARA	10A	PR D82 114031	S. Uehara et al.	(BELLE Collab.)
ANISOVICH	09	JUMP A24 2481	V.V. Anisovich, A.V. Sarantsev	(PNPI)
CHEKANOV	08	PRL 101 112003	S. Chekanov et al.	(ZEUS Collab.)
BINON	07	PAN 70 1713	F. Binon et al.	(GAMS Collab.)
Translated from YAF 70 1758.				
AMSLER	06	PL B639 165	C. Amisler et al.	(Crystal Barrel Collab.)
SCHEGELSKY	08A	EPJ A27 207	V.A. Schegelsky et al.	(BES Collab.)
ABLIKIM	05	PL B607 243	M. Ablikim et al.	(BES Collab.)
ABE	04	EPJ C32 323	K. Abe et al.	(BELLE Collab.)
CHEKANOV	04	PL B578 33	S. Chekanov et al.	(ZEUS Collab.)
BAI	03G	PR D68 052003	J.Z. Bai et al.	(BES Collab.)
TIKHOMIROV	03	PAN 66 828	G.D. Tikhomirov et al.	(BES Collab.)
Translated from YAF 66 860.				
AMSLER	02	EPJ C23 29	C. Amisler et al.	(Crystal Barrel Collab.)
ACCIARRI	01H	PL B501 173	M. Acciari et al.	(L3 Collab.)
BARBERIS	00E	PL B479 59	D. Barberis et al.	(WA 102 Collab.)
BARBERIS	99	PL B453 305	D. Barberis et al.	(Omeg a Expt.)
BARKOV	99	JETPL 70 248	B.P. Barkov et al.	
Translated from ZETFP 70 242.				
ABREU	96C	PL B379 309	P. Abreu et al.	(DELPHI Collab.)
BAI	96C	PRL 77 3959	J.Z. Bai et al.	(BES Collab.)
ACCIARRI	95J	PL B363 118	M. Acciari et al.	(L3 Collab.)
PROKOSHKIN	91	SPD 36 155	Y.D. Prokoshkin	(GAM2 and GAM4 Collab.)
Translated from DANS 316 900.				
ALBRECHT	90G	ZPHY C48 183	H. Albrecht et al.	(ARGUS Collab.)
BEHREND	89C	ZPHY C43 91	H.J. Behrend et al.	(CELLO Collab.)
ASTON	88D	NP B301 525	D. Aston et al.	(SLAC, NAGO, CINC, INUS)
AUGUSTIN	88	PRL 60 2238	J.E. Augustin et al.	(DM2 Collab.)
BERGER	88	ZPHY C37 329	C. Berger et al.	(PLUTO Collab.)
FALVARD	88	PR D38 2706	A. Falvard et al.	(CLER, FRAS, LALO+)
AUGUSTIN	87	ZPHY C36 369	J.E. Augustin et al.	(LALO, CLER, FRAS+)
BALTRUSAITIS	87	PR D35 2077	R.M. Baltrusaitis et al.	(Mark III Collab.)
AIHARA	86B	PRL 57 404	H. Aihara et al.	(TPC-2γ Collab.)
BOLONKIN	86	SJNP 43 776	B.V. Bolonkin et al.	(ITEP) JP
Translated from YAF 43 1211.				
LONGACRE	86	PL B177 223	R.S. Longacre et al.	(BNL, BRAN, CUNY+)
ALTHOFF	83	PL 121B 216	M. Althoff et al.	(TASSO Collab.)
ARMSTRONG	83B	NP B224 193	T.A. Armstrong et al.	(BARI, BIRM, CERN+)
BINON	83	NC 78A 313	F.G. Binon et al.	(BELG, LAPP, SERP+)
AGUILAR...	81B	ZPHY C8 313	M. Aguilar-Benitez et al.	(CERN, CDEF+)
ALHARRAN	81	NP B191 26	S. Al-Harran et al.	(BIRM, CERN, GLAS+)
CHABAUD	81	APP B12 575	V. Chabaud et al.	(CERN, CRAC, MPIM)
COSTA	80	NP B175 402	G. Costa et al.	(BARI, BONN, CERN, GLAS+)
GORLICH	99	NP B174 16	L. Gorlich et al.	(CRAC, MPIM, CERN+)
CORDEN	79	NP B157 250	M.J. Corden et al.	(BIRM, RHEL, TEL+)
MARTIN	79	NP B158 520	A.D. Martin, E.N. Ozmutlu	(DURH)
POLYCHRO...	79	PR D19 1317	V.A. Polychronakos et al.	(NDAM, ANL)
BARREIRO	77	NP B121 237	F. Barreiro et al.	(CERN, AMST, NIJ+)
EVANGELIS...	77	NP B127 384	C. Evangelista et al.	(BARI, BONN, CERN+)
PAWLICKI	77	PR D15 3196	A.J. Pawlicki et al.	(ANL) IJP
BRANDENB...	76C	NP B104 413	G.W. Brandenburg et al.	(SLAC)
BEUSCH	75B	PL 60B 101	W. Beusch et al.	(CERN, ETH)
HYAMS	75	NP B100 205	B.D. Hyams et al.	(CERN, MPIM)
AGUILAR...	72B	PR D6 29	M. Aguilar-Benitez et al.	(BNL)
AMMAR	67	PRL 19 1071	R. Ammar et al.	(NWES, ANL) JP
BARNES	67	PRL 19 964	V.E. Barnes et al.	(BNL, SYR) IJP
CRENNELL	66	PRL 16 1025	D.J. Crennell et al.	(BNL) I

- Breit-Wigner mass.
- From a simultaneous analysis of the annihilations $\bar{p}p \rightarrow 3\pi^0, \pi^0 \eta \eta$ including AKER 91 data.
- J^P not determined, could be partly $f_0(1500)$.
- J^P not determined.
- Superseded by AMSLER 95B.

$f_2(1565)$ WIDTH

VALUE (MeV)	DOCUMENT ID	TECN	COMMENT
132± 23 OUR AVERAGE	Error includes scale factor of 1.1.		
119± 24	¹ BERTIN 98	OBLX	0.05-0.405 $\bar{p}p \rightarrow \pi^+ \pi^+ \pi^-$
170± 40	¹ MAY 90	ASTE	0.0 $\bar{p}p \rightarrow \pi^+ \pi^- \pi^0$
• • • We do not use the following data for averages, fits, limits, etc. • • •			
140± 11	^{1,2} AMELIN 06	VES	36 $\pi^- p \rightarrow \omega \omega n$
130± 20± 40	¹ AMELIN 00	VES	37 $\pi^- p \rightarrow \eta \pi^+ \pi^- n$
263± 101	BALOSHIN 95	SPEC	40 $\pi^- C \rightarrow K_S^0 K_S^0 X$
166± 80 - 20	³ ANISOVICH 94	CBAR	0.0 $\bar{p}p \rightarrow 3\pi^0, \eta \eta \pi^0$
130± 10	⁴ ADAMO 93	OBLX	$\bar{p}p \rightarrow \pi^+ \pi^+ \pi^-$
148± 27	⁵ ARMSTRONG 93C	E760	$\bar{p}p \rightarrow \pi^0 \eta \eta \rightarrow 6\gamma$
103± 15	⁵ ARMSTRONG 93D	E760	$\bar{p}p \rightarrow 3\pi^0 \rightarrow 6\gamma$
111± 10	⁵ ARMSTRONG 93D	E760	$\bar{p}p \rightarrow \eta \pi^0 \pi^0 \rightarrow 6\gamma$
~ 206	⁶ WEIDENAUER 93	ASTE	0.0 $\bar{p}N \rightarrow 3\pi^- 2\pi^+$
132± 37	⁵ ADAMO 92	OBLX	$\bar{p}p \rightarrow \pi^+ \pi^+ \pi^-$
120± 10	⁷ AKER 91	CBAR	0.0 $\bar{p}p \rightarrow 3\pi^0$
116± 9	BRIDGES 86c	DBC	0.0 $\bar{p}N \rightarrow 3\pi^- 2\pi^+$

- Breit-Wigner width.
- Supersedes the $\omega \omega$ state of BELADIDZE 92b earlier assigned to the $f_2(1640)$.
- From a simultaneous analysis of the annihilations $\bar{p}p \rightarrow 3\pi^0, \pi^0 \eta \eta$ including AKER 91 data.
- Supersedes ADAMO 92.
- J^P not determined, could be partly $f_0(1500)$.
- J^P not determined.
- Superseded by AMSLER 95B.

$f_2(1565)$ DECAY MODES

Mode	Fraction (Γ_i/Γ)
Γ_1 $\pi \pi$	seen
Γ_2 $\pi^+ \pi^-$	seen
Γ_3 $\pi^0 \pi^0$	seen
Γ_4 $\rho^0 \rho^0$	seen
Γ_5 $2\pi^+ 2\pi^-$	seen
Γ_6 $\eta \eta$	seen
Γ_7 $\omega \omega$	seen
Γ_8 $K \bar{K}$	seen
Γ_9 $\gamma \gamma$	seen

$f_2(1565)$ PARTIAL WIDTHS

$\Gamma(\eta \eta)$	$\Gamma(K \bar{K})$	$\Gamma(\gamma \gamma)$
1.2± 0.3	2.0± 1.0	0.70± 0.14
• • • We do not use the following data for averages, fits, limits, etc. • • •		
870	870	870
¹ SCHEGELSKY 06A RVUE $\gamma \gamma \rightarrow K_S^0 K_S^0$		
¹ From analysis of L3 data at 91 and 183-209 GeV, using $f_2(1565)$ mass of 1570 MeV, width of 160 MeV, $\Gamma(\pi \pi) = 25$ MeV, and SU(3) relations.		
• • • We do not use the following data for averages, fits, limits, etc. • • •		
¹ SCHEGELSKY 06A RVUE $\gamma \gamma \rightarrow K_S^0 K_S^0$		
¹ From analysis of L3 data at 91 and 183-209 GeV, using $f_2(1565)$ mass of 1570 MeV, width of 160 MeV, $\Gamma(\pi \pi) = 25$ MeV, and SU(3) relations.		
• • • We do not use the following data for averages, fits, limits, etc. • • •		
¹ SCHEGELSKY 06A RVUE $\gamma \gamma \rightarrow K_S^0 K_S^0$		
¹ From analysis of L3 data at 91 and 183-209 GeV, using $f_2(1565)$ mass of 1570 MeV, width of 160 MeV, $\Gamma(\pi \pi) = 25$ MeV, and SU(3) relations.		

$f_2(1565)$ BRANCHING RATIOS

$\Gamma(\pi \pi)/\Gamma_{total}$	Γ_1/Γ
0.05-0.405	0.05-0.405
• • • We do not use the following data for averages, fits, limits, etc. • • •	
0.05-0.405	0.05-0.405
¹ SCHEGELSKY 06A RVUE $\bar{p}p \rightarrow \pi^+ \pi^+ \pi^-$	
¹ From analysis of L3 data at 91 and 183-209 GeV, using $f_2(1565)$ mass of 1570 MeV, width of 160 MeV, $\Gamma(\pi \pi) = 25$ MeV, and SU(3) relations.	

$f_2(1565)$

$$I^G(J^{PC}) = 0^+(2^{++})$$

Seen mostly in antinucleon-nucleon annihilation. See the review on "Spectroscopy of Light Meson Resonances."

$f_2(1565)$ T-MATRIX POLE \sqrt{s}

Note that $\Gamma = -2 \text{Im}(\sqrt{s})$.

VALUE (MeV)	DOCUMENT ID	TECN	COMMENT
(1495-1560) - i (40-110) OUR ESTIMATE			
(1560 ± 15) - i (140 ± 20)	¹ ANISOVICH 09	RVUE	0.0 $\bar{p}p, \pi N$
(1552 ± 13) - i (57 ± 12)	AMSLER 02	CBAR	0.9 $\bar{p}p \rightarrow \pi^0 \eta \eta, \pi^0 \pi^0 \pi^0$
(1507 ± 15) - i (65 ± 10)	BERTIN 97C	OBLX	0.0 $\bar{p}p \rightarrow \pi^+ \pi^- \pi^0$
(1534 ± 20) - i (90 ± 30)	² ABELE 96C	RVUE	Compilation
(~ 1552) - i (~ 71)	³ AMSLER 95D	CBAR	0.0 $\bar{p}p \rightarrow \pi^0 \pi^0 \pi^0, \pi^0 \eta \eta, \pi^0 \pi^0 \eta$

- On sheet II in a two-pole solution.
- T-matrix pole, large coupling to $\rho\rho$ and $\omega\omega$, could be $f_2(1640)$.
- Coupled-channel analysis of AMSLER 95B, AMSLER 95C, and AMSLER 94D.

$f_2(1565)$ MASS

VALUE (MeV)	DOCUMENT ID	TECN	COMMENT
1571 ± 13 OUR AVERAGE			
1575 ± 18	¹ BERTIN 98	OBLX	0.05-0.405 $\bar{p}p \rightarrow \pi^+ \pi^+ \pi^-$
1565 ± 20	¹ MAY 90	ASTE	0.0 $\bar{p}p \rightarrow \pi^+ \pi^- \pi^0$
• • • We do not use the following data for averages, fits, limits, etc. • • •			
1590 ± 10	AMELIN 06	VES	36 $\pi^- p \rightarrow \omega \omega n$
1550 ± 10 ± 20	AMELIN 00	VES	37 $\pi^- p \rightarrow \eta \pi^+ \pi^- n$
1598 ± 11 ± 9	BAKER 99B	SPEC	0 $\bar{p}p \rightarrow \omega \omega \pi^0$
1598 ± 72	BALOSHIN 95	SPEC	40 $\pi^- C \rightarrow K_S^0 K_S^0 X$
1566± 80 - 50	² ANISOVICH 94	CBAR	0.0 $\bar{p}p \rightarrow 3\pi^0, \eta \eta \pi^0$
1502 ± 9	ADAMO 93	OBLX	$\bar{p}p \rightarrow \pi^+ \pi^+ \pi^-$
1488 ± 10	³ ARMSTRONG 93C	E760	$\bar{p}p \rightarrow \pi^0 \eta \eta \rightarrow 6\gamma$
1508 ± 10	³ ARMSTRONG 93D	E760	$\bar{p}p \rightarrow 3\pi^0 \rightarrow 6\gamma$
1525 ± 10	³ ARMSTRONG 93D	E760	$\bar{p}p \rightarrow \eta \pi^0 \pi^0 \rightarrow 6\gamma$
~ 1504	⁴ WEIDENAUER 93	ASTE	0.0 $\bar{p}N \rightarrow 3\pi^- 2\pi^+$
1540 ± 15	³ ADAMO 92	OBLX	$\bar{p}p \rightarrow \pi^+ \pi^+ \pi^-$
1515 ± 10	⁵ AKER 91	CBAR	0.0 $\bar{p}p \rightarrow 3\pi^0$
1477 ± 5	BRIDGES 86c	DBC	0.0 $\bar{p}N \rightarrow 3\pi^- 2\pi^+$

Meson Particle Listings

$f_2(1565)$, $\rho(1570)$, $h_1(1595)$

$\Gamma(\pi^+ \pi^-)/\Gamma_{total}$ Γ_2/Γ

VALUE	DOCUMENT ID	TECN	COMMENT
• • • We do not use the following data for averages, fits, limits, etc. • • •			
seen	BERTIN 98	OBLX	0.05–0.405 $\bar{p}p \rightarrow \pi^+ \pi^+ \pi^-$
not seen	¹ ANISOVICH 94B	RVUE	$\bar{p}p \rightarrow \pi^+ \pi^+ \pi^-$
seen	MAY 89	ASTE	$\bar{p}p \rightarrow \pi^+ \pi^+ \pi^-$

¹ ANISOVICH 94B is from a reanalysis of MAY 90.

$\Gamma(\pi^0 \pi^0)/\Gamma_{total}$ Γ_3/Γ

VALUE	DOCUMENT ID	TECN	COMMENT
seen	AMSLER 95B	CBAR	0.0 $\bar{p}p \rightarrow 3\pi^0$

$\Gamma(\pi^+ \pi^-)/\Gamma(\rho^0 \rho^0)$ Γ_2/Γ_4

VALUE	DOCUMENT ID	TECN	COMMENT
• • • We do not use the following data for averages, fits, limits, etc. • • •			
0.042 ± 0.013	BRIDGES 86B	DBC	$\bar{p}N \rightarrow 3\pi^- 2\pi^+$

$\Gamma(\eta\eta)/\Gamma(\pi^0 \pi^0)$ Γ_6/Γ_3

VALUE	DOCUMENT ID	TECN	COMMENT
• • • We do not use the following data for averages, fits, limits, etc. • • •			
0.024 ± 0.005 ± 0.012	¹ ARMSTRONG 93C	E760	$\bar{p}p \rightarrow \pi^0 \eta \eta \rightarrow 6\gamma$

¹ J^P not determined, could be partly $f_0(1500)$.

$\Gamma(\omega\omega)/\Gamma_{total}$ Γ_7/Γ

VALUE	DOCUMENT ID	TECN	COMMENT
• • • We do not use the following data for averages, fits, limits, etc. • • •			
seen	BAKER 99B	SPEC	0 $\bar{p}p \rightarrow \omega\pi^0$

$f_2(1565)$ REFERENCES

ANISOVICH 09	JMP A24 2481	V.V. Anisovich, A.V. Sarantsev	(PNPI)
AMELIN 06	PAN 69 690	D.V. Amelin et al.	(VES Collab.)
Translated from YAF 69 715.			
SCHEGELSKY 06A	EPJ A27 207	V.A. Schegelsky et al.	
AMSLER 02	EPJ C23 29	C. Amstler et al.	(Crystal Barrel Collab.)
AMELIN 00	NP A668 83	D. Amelin et al.	(VES Collab.)
BAKER 99B	PL B467 147	C.A. Baker et al.	
BERTIN 98	PR D57 55	A. Bertin et al.	(OBELIX Collab.)
BERTIN 97C	PL B408 476	A. Bertin et al.	(OBELIX Collab.)
ABELE 96C	NP A609 562	A. Abele et al.	(Crystal Barrel Collab.)
AMSLER 95B	PL B342 433	C. Amstler et al.	(Crystal Barrel Collab.)
AMSLER 95C	PL B353 571	C. Amstler et al.	(Crystal Barrel Collab.)
AMSLER 95D	PL B355 425	C. Amstler et al.	(Crystal Barrel Collab.)
BALOSHIN 95	PAN 58 46	O.N. Baloshin et al.	(ITEP)
Translated from YAF 58 50.			
AMSLER 94D	PL B333 277	C. Amstler et al.	(Crystal Barrel Collab.)
ANISOVICH 94	PL B323 233	V.V. Anisovich et al.	(Crystal Barrel Collab.)
ANISOVICH 94B	PR D50 1972	V.V. Anisovich et al.	(LOQM)
ADAMO 93	NP A558 13C	A. Adamo et al.	(OBELIX Collab.)
ARMSTRONG 93C	PL B307 394	T.A. Armstrong et al.	(FNAL FERR, GENO+)
ARMSTRONG 93D	PL B307 399	T.A. Armstrong et al.	(FNAL FERR, GENO+)
WEIDENAUER 93	ZPHY C59 387	P. Weidenauer et al.	(ASTERIX Collab.)
ADAMO 92	PL B287 368	A. Adamo et al.	(OBELIX Collab.)
BELADIDZE 92B	ZPHY C54 367	G.M. Beladidze et al.	(VES Collab.)
AKER 91	PL B260 249	E. Aker et al.	(Crystal Barrel Collab.)
MAY 90	ZPHY C46 203	B. May et al.	(ASTERIX Collab.)
MAY 89	PL B225 450	B. May et al.	(ASTERIX Collab.)
BRIDGES 86B	PRL 56 215	D.L. Bridges et al.	(SYRA, CASE)
BRIDGES 86C	PRL 57 1534	D.L. Bridges et al.	(SYRA)

$\rho(1570)$ $I^G(J^{PC}) = 1^+(1^{--})$

OMITTED FROM SUMMARY TABLE
 May be an OZI-violating decay mode of $\rho(1700)$. See the review on "Spectroscopy of Light Meson Resonances."

$\rho(1570)$ MASS

VALUE (MeV)	EVTS	DOCUMENT ID	TECN	COMMENT
1570 ± 36 ± 62	54	¹ AUBERT 08s	BABR	10.6 $e^+ e^- \rightarrow \phi\pi^0 \gamma$
• • • We do not use the following data for averages, fits, limits, etc. • • •				
1614 ± 2		² ACHASOV 23A	SND	$e^+ e^- \rightarrow \omega\pi^0$
1585 ± 15		³ ACHASOV 20c	SND	1.3–2.0 $e^+ e^- \rightarrow K^+ K^- \pi^0$
1480 ± 40		⁴ BITYUKOV 87	SPEC	32.5 $\pi^- p \rightarrow \phi\pi^0 n$

¹ From the fit with two resonances.
² From a vector dominance fit to the Born cross section between 1.05 and 2.0 GeV with $\rho(770)$, $\rho(1570)$, $\rho(1700)$, $\rho(2150)$. The fit also uses SND data from the VEPP-2M collider below 1.02 GeV and from LEES 17H and ABLIKIM 21A above 1.5 GeV.
³ From a fit using a two resonance model in which the mass and width of the other resonance are fixed at the $\rho(1700)$ values from PDG 20.
⁴ Systematic errors not estimated.

$\rho(1570)$ WIDTH

VALUE (MeV)	EVTS	DOCUMENT ID	TECN	COMMENT
144 ± 75 ± 43	54	¹ AUBERT 08s	BABR	10.6 $e^+ e^- \rightarrow \phi\pi^0 \gamma$

• • • We do not use the following data for averages, fits, limits, etc. • • •

492 ± 4	² ACHASOV 23A	SND	$e^+ e^- \rightarrow \omega\pi^0$
75 ± 30	³ ACHASOV 20c	SND	1.3–2.0 $e^+ e^- \rightarrow K^+ K^- \pi^0$
130 ± 60	⁴ BITYUKOV 87	SPEC	32.5 $\pi^- p \rightarrow \phi\pi^0 n$

¹ From the fit with two resonances.
² From a vector dominance fit to the Born cross section between 1.05 and 2.0 GeV with $\rho(770)$, $\rho(1570)$, $\rho(1700)$, $\rho(2150)$. The fit also uses SND data from the VEPP-2M collider below 1.02 GeV and from LEES 17H and ABLIKIM 21A above 1.5 GeV.
³ From a fit using a two resonance model in which the mass and width of the other resonance are fixed at the $\rho(1700)$ values from PDG 20.
⁴ Systematic errors not estimated.

$\rho(1570)$ DECAY MODES

Mode	Fraction (Γ_i/Γ)
Γ_1 $e^+ e^-$	seen
Γ_2 $\phi\pi$	not seen
Γ_3 $\omega\pi$	

$\rho(1570)$ $\Gamma(i)\Gamma(e^+ e^-)/\Gamma(total)$

$\Gamma(\phi\pi) \times \Gamma(e^+ e^-)/\Gamma_{total}$ $\Gamma_2\Gamma_1/\Gamma$

VALUE (eV)	CL%	EVTS	DOCUMENT ID	TECN	COMMENT
3.5 ± 0.9 ± 0.3		54	¹ AUBERT 08s	BABR	10.6 $e^+ e^- \rightarrow \phi\pi^0 \gamma$
• • • We do not use the following data for averages, fits, limits, etc. • • •					
<70		90	² AULCHENKO 87B	ND	$e^+ e^- \rightarrow K_S^0 K_L^0 \pi^0$

¹ From the fit with two resonances.
² Using mass and width of BITYUKOV 87.

$\rho(1570)$ BRANCHING RATIOS

$\Gamma(\phi\pi)/\Gamma_{total}$ Γ_2/Γ

VALUE	DOCUMENT ID	TECN	COMMENT
not seen	ABELE 97H	CBAR	$\bar{p}p \rightarrow K_L^0 K_S^0 \pi^0 \pi^0$
• • • We do not use the following data for averages, fits, limits, etc. • • •			
<0.01	¹ DONNACHIE 91	RVUE	

¹ Using data from BISELLO 91B, DOLINSKY 86, and ALBRECHT 87L.

$\Gamma(\omega\pi)/\Gamma(\omega\pi)$ Γ_2/Γ_3

VALUE	CL%	DOCUMENT ID	TECN	COMMENT
• • • We do not use the following data for averages, fits, limits, etc. • • •				
>0.5		95	BITYUKOV 87	SPEC 32.5 $\pi^- p \rightarrow \phi\pi^0 n$

$\rho(1570)$ REFERENCES

ACHASOV 23A	PR D108 092012	M.N. Achasov et al.	(SND Collab.)
ABLIKIM 21A	PL B813 136059	M. Ablikim et al.	(BESIII Collab.)
ACHASOV 20C	EPJ C80 1139	M.N. Achasov et al.	(SND Collab.)
PDG 20	PTEP 2020 083C01	P.A. Zyla et al.	(PDG Collab.)
LEES 17H	PR D96 092009	J.P. Lees et al.	(BABAR Collab.)
AUBERT 08s	PR D77 092002	B. Aubert et al.	(BABAR Collab.)
ABELE 97H	PL B415 280	A. Abele et al.	(Crystal Barrel Collab.)
BISELLO 91B	NPBPS B21 111	D. Bisello	(DM2 Collab.)
DONNACHIE 91	ZPHY C51 689	A. Donnachie, A.B. Clegg	(MCHS, LANC)
ALBRECHT 87L	PL B185 223	H. Albrecht et al.	(ARGUS Collab.)
AULCHENKO 87B	JETPL 45 145	V.M. Aulchenko et al.	(NOVO)
Translated from ZETFP 45 118.			
BITYUKOV 87	PL B188 383	S.I. Bitiyukov et al.	(SERP)
DOLINSKY 86	PL B174 453	S.I. Dolinsky et al.	(NOVO)

$h_1(1595)$ $I^G(J^{PC}) = 0^-(1^{+-})$

OMITTED FROM SUMMARY TABLE
 Seen in a partial-wave analysis of the $\omega\eta$ system produced in the reaction $\pi^- p \rightarrow \omega\eta n$ at 18 GeV/c.

$h_1(1595)$ MASS

VALUE (MeV)	DOCUMENT ID	TECN	COMMENT
1594 ± 15 ± 10 ± 60	EUGENIO 01	SPEC	18 $\pi^- p \rightarrow \omega\eta n$

$h_1(1595)$ WIDTH

VALUE (MeV)	DOCUMENT ID	TECN	COMMENT
384 ± 60 ± 70 ± 100	EUGENIO 01	SPEC	18 $\pi^- p \rightarrow \omega\eta n$

$h_1(1595)$ DECAY MODES

Mode	Fraction (Γ_i/Γ)
Γ_1 $\omega\eta$	seen

$h_1(1595)$ REFERENCES

EUGENIO 01	PL B497 190	P. Eugenio et al.
------------	-------------	-------------------

$\pi_1(1600)$

$\pi_1(1600)$

$I^G(J^{PC}) = 1^-(1^-+)$

Coupled channel analyses favor the existence of only one broad 1^-+ isovector state consistent with $\pi_1(1600)$ in the 1400–1600 MeV region. Accordingly, the $\pi_1(1400)$ entries of the previous Reviews have been moved into this section. See the review on "Spectroscopy of Light Meson Resonances."

$\pi_1(1600)$ T-Matrix Pole \sqrt{s}

Note that $\Gamma = -2 \text{Im}(\sqrt{s})$.

VALUE (MeV)	DOCUMENT ID	TECN	COMMENT
(1480–1680) – i (150–300) OUR ESTIMATE			
$(1623 \pm 47^{+24}_{-75}) - i(228 \pm 44^{+72}_{-88})$	¹ KOPF	21	RVUE $0.9 \rho\bar{p} \rightarrow \pi^0 \pi^0 \eta$, $\pi^0 \eta \eta$, $\pi^0 K^+ K^-$ and 191 $\pi^- \rho \rightarrow \pi^- \pi^- \pi^+ \rho$
$(1564 \pm 24 \pm 86) - i(246 \pm 27 \pm 51)$	² RODAS	19	RVUE 191 $\pi^- \rho \rightarrow \eta^{(\prime)} \pi^- \rho$

• • • We do not use the following data for averages, fits, limits, etc. • • •

$(1405 \pm 4^{+15}_{-18}) - i(314 \pm 14^{+18}_{-69})$	³ ALBRECHT	20	RVUE $\bar{p} \rho \rightarrow \pi^0 \pi^0 \eta$
--	-----------------------	----	--

¹ From T-matrix pole based on combined fit of Crystal Barrel and $\pi\pi$ scattering data (ALBRECHT 20), and COMPASS data (ADOLPH 15), using a coupled-channel model of $\eta\pi$, $\eta'\pi$ and $K\bar{K}$ systems.
² The coupled-channel analysis of both the $\eta\pi$ and $\eta'\pi$ systems using ADOLPH 15 data.
³ Superseded by KOPF 21.

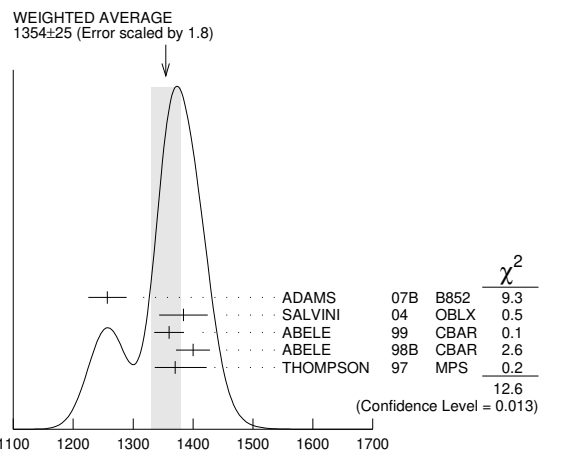
$\pi_1(1600)$ MASS ($\eta\pi$ mode)

Not seen by PROKOSHKIN 95B, BUGG 94, APEL 81, BOUTEMEUR 90, and AGHASYAN 18B.

VALUE (MeV)	EVTS	DOCUMENT ID	TECN	CHG	COMMENT
1354 ± 25 OUR AVERAGE		Error includes scale factor of 1.8. See the ideogram below.			
$1257 \pm 20 \pm 25$	23.5k	ADAMS	07B	B852	$18 \pi^- \rho \rightarrow \eta \pi^0 n$
$1384 \pm 20 \pm 35$	90k	SALVINI	04	OBLX	$\bar{p} \rho \rightarrow 2\pi^+ 2\pi^-$
1360 ± 25		ABELE	99	CBAR	$0.0 \bar{p} \rho \rightarrow \pi^0 \pi^0 \eta$
$1400 \pm 20 \pm 20$		ABELE	98B	CBAR	$0.0 \bar{p} n \rightarrow \pi^- \pi^0 \eta$
$1370 \pm 16 \pm 50_{-30}$		¹ THOMPSON	97	MPS	$18 \pi^- \rho \rightarrow \eta \pi^- \rho$
1323.1 ± 4.6		² AOYAGI	93	BKEI	$\pi^- \rho \rightarrow \eta \pi^- \rho$
1406 ± 20		³ ALDE	88B	GAM4 0	$100 \pi^- \rho \rightarrow \eta \pi^0 n$

• • • We do not use the following data for averages, fits, limits, etc. • • •

¹ Natural parity exchange, questioned by DZIERBA 03.
² Unnatural parity exchange.
³ Seen in the P_0 -wave intensity of the $\eta\pi^0$ system, unnatural parity exchange.



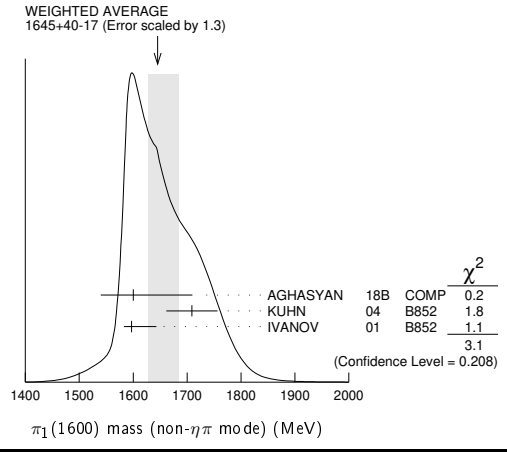
$\pi_1(1600)$ MASS (non- $\eta\pi$ mode)

VALUE (MeV)	EVTS	DOCUMENT ID	TECN	COMMENT
1645 ± 49 OUR AVERAGE		Error includes scale factor of 1.3. See the ideogram below.		
1600^{+110}_{-60}	46M	¹ AGHASYAN	18B	COMP $190 \pi^- \rho \rightarrow \pi^- \pi^+ \pi^- \rho$
$1709 \pm 24 \pm 41$	69k	² KUHN	04	B852 $18 \pi^- \rho \rightarrow \eta \pi^+ \pi^- \pi^- \rho$
$1597 \pm 10^{+45}_{-10}$		² IVANOV	01	B852 $18 \pi^- \rho \rightarrow \eta' \pi^- \rho$

• • • We do not use the following data for averages, fits, limits, etc. • • •

$1660 \pm 10^{+0}_{-64}$	420k	³ ALEKSEEV	10	COMP $190 \pi^- \rho \rightarrow \pi^- \pi^+ \pi^- \rho$
$1664 \pm 8 \pm 10$	145k	⁴ LU	05	B852 $18 \pi^- \rho \rightarrow \omega \pi^- \pi^0 \rho$
$1593 \pm 8^{+29}_{-47}$		^{2,5} ADAMS	98B	B852 $18.3 \pi^- \rho \rightarrow \pi^+ \pi^- \pi^- \rho$

¹ Statistical error negligible. See also the review ALEXEEV 22.
² Natural parity exchange.
³ Superseded by AGHASYAN 2018B.
⁴ May be a different state: natural and unnatural parity exchanges.
⁵ Superseded by DZIERBA 06 excluding this state in a more refined PWA analysis, with 2.6 M events of $\pi^- \rho \rightarrow \pi^- \pi^- \pi^+ \rho$ and 3 M events of $\pi^- \rho \rightarrow \pi^- \pi^0 \pi^0 \rho$ of E852 data.



$\pi_1(1600)$ WIDTH ($\eta\pi$ mode)

Not seen by PROKOSHKIN 95B, BUGG 94, APEL 81, BOUTEMEUR 90, and AGHASYAN 18B.

VALUE (MeV)	EVTS	DOCUMENT ID	TECN	CHG	COMMENT
330 ± 35 OUR AVERAGE		Error includes scale factor of 1.8. See the ideogram below.			
$354 \pm 64 \pm 58$	23.5k	ADAMS	07B	B852	$18 \pi^- \rho \rightarrow \eta \pi^0 n$
$378 \pm 50 \pm 50$	90k	SALVINI	04	OBLX	$\bar{p} \rho \rightarrow 2\pi^+ 2\pi^-$
220 ± 90		ABELE	99	CBAR	$0.0 \bar{p} \rho \rightarrow \pi^0 \pi^0 \eta$
$310 \pm 50 \pm 50_{-30}$		ABELE	98B	CBAR	$0.0 \bar{p} n \rightarrow \pi^- \pi^0 \eta$
$385 \pm 40 \pm 65_{-105}$		¹ THOMPSON	97	MPS	$18 \pi^- \rho \rightarrow \eta \pi^- \rho$

• • • We do not use the following data for averages, fits, limits, etc. • • •

143.2 ± 12.5		² AOYAGI	93	BKEI	$\pi^- \rho \rightarrow \eta \pi^- \rho$
180 ± 20		³ ALDE	88B	GAM4 0	$100 \pi^- \rho \rightarrow \eta \pi^0 n$

¹ Resolution is not unfolded, natural parity exchange, questioned by DZIERBA 03.
² Unnatural parity exchange.
³ Seen in the P_0 -wave intensity of the $\eta\pi^0$ system, unnatural parity exchange.

$\pi_1(1600)$ WIDTH (non- $\eta\pi$ mode)

VALUE (MeV)	EVTS	DOCUMENT ID	TECN	COMMENT
370 ± 50 OUR AVERAGE		Error includes scale factor of 1.3. See the ideogram below.		
580^{+100}_{-230}	46M	¹ AGHASYAN	18B	COMP $190 \pi^- \rho \rightarrow \pi^- \pi^+ \pi^- \rho$
$403 \pm 80 \pm 115$	69k	² KUHN	04	B852 $18 \pi^- \rho \rightarrow \eta \pi^+ \pi^- \pi^- \rho$
$340 \pm 40 \pm 50$		² IVANOV	01	B852 $18 \pi^- \rho \rightarrow \eta' \pi^- \rho$

• • • We do not use the following data for averages, fits, limits, etc. • • •

$269 \pm 21 \pm 42_{-64}$	420k	³ ALEKSEEV	10	COMP $190 \pi^- \rho \rightarrow \pi^- \pi^+ \pi^- \rho$
$185 \pm 25 \pm 28$	145k	⁴ LU	05	B852 $18 \pi^- \rho \rightarrow \omega \pi^- \pi^0 \rho$
$168 \pm 20 \pm 150_{-12}$		^{2,5} ADAMS	98B	B852 $18.3 \pi^- \rho \rightarrow \pi^+ \pi^- \pi^- \rho$

¹ Statistical error negligible. See also the review ALEXEEV 22.
² Natural parity exchange.
³ Superseded by AGHASYAN 2018B.
⁴ May be a different state: natural and unnatural parity exchanges.
⁵ Superseded by DZIERBA 06 excluding this state in a more refined PWA analysis, with 2.6 M events of $\pi^- \rho \rightarrow \pi^- \pi^- \pi^+ \rho$ and 3 M events of $\pi^- \rho \rightarrow \pi^- \pi^0 \pi^0 \rho$ of E852 data.

$\pi_1(1600)$ DECAY MODES

Mode	Fraction (Γ_i/Γ)
Γ_1 $\pi \pi \pi$	seen
Γ_2 $\rho^0 \pi^-$	seen
Γ_3 $f_2(1270) \pi^-$	not seen

Meson Particle Listings

$\pi_1(1600), a_1(1640)$

Γ_4	$b_1(1235)\pi$	seen
Γ_5	$\eta'(958)\pi^-$	seen
Γ_6	$\eta\pi$	seen
Γ_7	$f_1(1285)\pi$	seen

$\pi_1(1600)$ BRANCHING RATIOS

$\Gamma(\rho^0\pi^-)/\Gamma_{total}$	DOCUMENT ID	TECN	COMMENT	Γ_2/Γ
--------------------------------------	-------------	------	---------	-------------------

seen ALEKSEEV 10 COMP 190 $\pi^- Pb \rightarrow \pi^- \pi^- \pi^+ Pb'$
 ••• We do not use the following data for averages, fits, limits, etc. •••
 not seen NOZAR 09 CLAS $\gamma p \rightarrow 2\pi^+ \pi^- n$
 not seen 1 DZIERBA 06 B852 18 $\pi^- p$

¹ From the PWA analysis of 2.6 M $\pi^- p \rightarrow \pi^- \pi^- \pi^+ p$ and 3 M events of $\pi^- p \rightarrow \pi^- \pi^0 \pi^0 p$ of E852 data. Supersedes ADAMS 98B.

$\Gamma(f_2(1270)\pi^-)/\Gamma_{total}$	DOCUMENT ID	TECN	COMMENT	Γ_3/Γ
---	-------------	------	---------	-------------------

not seen 1 DZIERBA 06 B852 18 $\pi^- p$
¹ From the PWA analysis of 2.6 M $\pi^- p \rightarrow \pi^- \pi^- \pi^+ p$ and 3 M events of $\pi^- p \rightarrow \pi^- \pi^0 \pi^0 p$ of E852 data. Supersedes CHUNG 02.

$\Gamma(b_1(1235)\pi)/\Gamma_{total}$	EVTS	DOCUMENT ID	TECN	COMMENT	Γ_4/Γ
---------------------------------------	------	-------------	------	---------	-------------------

seen 35280 1 BAKER 03 SPEC $\bar{p}p \rightarrow \omega\pi^+\pi^-\pi^0$
 ••• We do not use the following data for averages, fits, limits, etc. •••
 seen 145k LU 05 B852 18 $\pi^- p \rightarrow \omega\pi^-\pi^0 p$
¹ $B((b_1\pi)_{D-wave})/B((b_1\pi)_{S-wave}) = 0.3 \pm 0.1$.

$\Gamma(\eta'(958)\pi^-)/\Gamma_{total}$	DOCUMENT ID	TECN	COMMENT	Γ_5/Γ
--	-------------	------	---------	-------------------

seen IVANOV 01 B852 18 $\pi^- p \rightarrow \eta'\pi^-\pi^0 p$

$\Gamma(\eta'(958)\pi^-)/\Gamma(\eta\pi)$	DOCUMENT ID	TECN	COMMENT	Γ_5/Γ_6
---	-------------	------	---------	---------------------

••• We do not use the following data for averages, fits, limits, etc. •••
 $5.54 \pm 1.1^{+1.8}_{-0.27}$ 1 KOPF 21 RVUE 0.9 $\bar{p}p \rightarrow \pi^0\pi^0\eta, \pi^0\eta\eta,$
 $\pi^0 K^+ K^-$ and 191 $\pi^- p \rightarrow \pi^- \pi^- \pi^+ p$

¹ From T-matrix pole based on combined fit of Crystal Barrel and $\pi\pi$ scattering data (ALBRECHT 20), and COMPASS data (ADOLPH 15), using a coupled-channel model of $\eta\pi, \eta'\pi$ and $K\bar{K}$ systems.

$\Gamma(f_1(1285)\pi)/\Gamma(\eta'(958)\pi^-)$	EVTS	DOCUMENT ID	TECN	COMMENT	Γ_7/Γ_5
--	------	-------------	------	---------	---------------------

3.80 ± 0.78 69k 1 KUHN 04 B852 18 $\pi^- p \rightarrow \eta\pi^+\pi^-\pi^- p$
¹ Using $\eta'(958)$ π data from IVANOV 01.

$\pi_1(1600)$ REFERENCES

ALEXEEV 22 PR D105 012005 G.D. Alexeev et al. (COMPASS Collab.)	
KOPF 21 EPJ C81 1056 B. Kopf et al. (BOCH)	
ALBRECHT 20 EPJ C80 453 M. Albrecht et al. (Crystal Barrel Collab.)	
RODAS 19 PRL 122 042002 A. Rodas et al. (JPAC Collab.)	
AGHASYAN 18B PR D98 052003 M. Aghasyan et al. (COMPASS Collab.)	
ADOLPH 15 PRL B740 303 M. Adolph et al. (COMPASS Collab.)	
ALEKSEEV 10 PRL 104 241803 M.G. Alekseev et al. (COMPASS Collab.)	
NOZAR 09 PRL 102 102002 M. Nozar et al. (JLab CLAS Collab.)	
ADAMS 07B PL B657 27 G.S. Adams et al. (BNL E852 Collab.)	
DZIERBA 06 PR D73 072001 A.R. Dzierba et al. (BNL E852 Collab.)	
LU 05 PRL 94 032002 M. Lu et al. (BNL E852 Collab.)	
KUHN 04 PL B595 109 J. Kuhn et al. (BNL E852 Collab.)	
SALVINI 04 EPJ C35 21 P. Salvini et al. (OBELIX Collab.)	
BAKER 03 PL B563 140 C.A. Baker et al. (BNL E852 Collab.)	
DZIERBA 03 PR D67 094015 A.R. Dzierba et al. (BNL E852 Collab.)	
CHUNG 02 PR D65 072001 S.U. Chung et al. (BNL E852 Collab.)	
IVANOV 01 PRL 86 3977 E.I. Ivanov et al. (BNL E852 Collab.)	
ABELE 99 PL B446 349 A. Abele et al. (Crystal Barrel Collab.)	
ABELE 98B PL B423 175 A. Abele et al. (Crystal Barrel Collab.)	
ADAMS 98B PRL 81 5760 G.S. Adams et al. (BNL E852 Collab.)	
THOMPSON 97 PRL 79 1630 D.R. Thompson et al. (BNL E852 Collab.)	
PROKOSHKIN 95B PAN 58 606 Y.D. Prokoshkin, S.A. Sadovsky (SERP)	
Translated from YAF 58 662.	
BUGG 94 PR D50 4412 D.V. Bugg et al. (LOQM)	
AOYAGI 93 PL B314 246 H. Aoyagi et al. (BKEI Collab.)	
BOUTEMEUR 90 Hadron 89 Conf. p 119 M. Boutemeur, M. Poulet (SERP, BELG., LANL+)	
ALDE 85B PL B205 397 D.M. Alde et al. (SERP, BELG., LANL, LAPP)	
APEL 81 NP B193 269 W.D. Apel et al. (SERP, CERN)	

$a_1(1640)$

$$I^G(J^{PC}) = 1^-(1^{++})$$

Possibly seen in the study of the hadronic structure in decay $\tau \rightarrow 3\pi\nu_\tau$ (ABREU 98G and ASNER 00).

$a_1(1640)$ MASS

VALUE (MeV)	EVTS	DOCUMENT ID	TECN	COMMENT
-------------	------	-------------	------	---------

1655 ± 16 OUR AVERAGE Error includes scale factor of 1.2.

1700 ± 35 -130	46M	1 AGHASYAN	18B COMP	$190 \pi^- p \rightarrow \pi^- \pi^+ \pi^- p$
$1691 \pm 18 \pm 30$		DARGENT	17 RVUE	$D^0 \rightarrow \pi^- \pi^+ \pi^- \pi^+$

1630 ± 20	35k	2 BAKER	03 SPEC	$\bar{p}p \rightarrow \omega\pi^+\pi^-\pi^0$
$1714 \pm 9 \pm 36$		CHUNG	02 B852	$18.3 \pi^- p \rightarrow \pi^+\pi^-\pi^- p$
$1640 \pm 12 \pm 30$		BAKER	99 SPEC	$1.94 \bar{p}p \rightarrow 4\pi^0$

••• We do not use the following data for averages, fits, limits, etc. •••

1670 ± 90		BELLINI	85 SPEC	$40 \pi^- A \rightarrow \pi^- \pi^+ \pi^- A$
---------------	--	---------	---------	--

¹ Statistical error negligible.
² Using the $a_1(1260)$ mass and width results of BOWLER 88.

$a_1(1640)$ WIDTH

VALUE (MeV)	EVTS	DOCUMENT ID	TECN	COMMENT
-------------	------	-------------	------	---------

250 ± 40 OUR AVERAGE Error includes scale factor of 1.8. See the ideogram below.

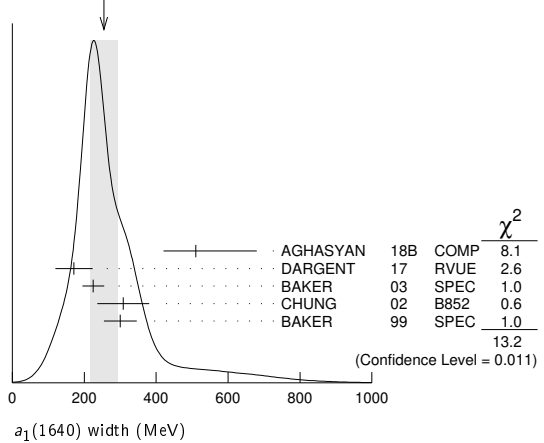
510^{+170}_{-90}	46M	1 AGHASYAN	18B COMP	$190 \pi^- p \rightarrow \pi^- \pi^+ \pi^- p$
$171 \pm 33 \pm 40$		DARGENT	17 RVUE	$D^0 \rightarrow \pi^- \pi^+ \pi^- \pi^+$
225 ± 30	35k	2 BAKER	03 SPEC	$\bar{p}p \rightarrow \omega\pi^+\pi^-\pi^0$
$308 \pm 37 \pm 62$		CHUNG	02 B852	$18.3 \pi^- p \rightarrow \pi^+\pi^-\pi^- p$
$300 \pm 22 \pm 40$		BAKER	99 SPEC	$1.94 \bar{p}p \rightarrow 4\pi^0$

••• We do not use the following data for averages, fits, limits, etc. •••

300 ± 100		BELLINI	85 SPEC	$40 \pi^- A \rightarrow \pi^- \pi^+ \pi^- A$
---------------	--	---------	---------	--

¹ Statistical error negligible.
² Using the $a_1(1260)$ mass and width results of BOWLER 88.

WEIGHTED AVERAGE
 250 ± 40 (Error scaled by 1.8)



$a_1(1640)$ DECAY MODES

Mode	Fraction (Γ_i/Γ)
------	--------------------------------

Γ_1	$\pi\pi\pi$	seen
Γ_2	$f_2(1270)\pi$	seen
Γ_3	$\sigma\pi$	seen
Γ_4	$\rho\pi S$ -wave	seen
Γ_5	$\rho\pi D$ -wave	seen
Γ_6	$\omega\pi\pi$	seen
Γ_7	$f_1(1285)\pi$	seen
Γ_8	$a_1(1260)\eta$	not seen

$a_1(1640)$ BRANCHING RATIOS

$\Gamma(f_2(1270)\pi)/\Gamma(\sigma\pi)$	DOCUMENT ID	TECN	COMMENT	Γ_2/Γ_3
--	-------------	------	---------	---------------------

0.24 ± 0.07 BAKER 99 SPEC 1.94 $\bar{p}p \rightarrow 4\pi^0$

$\Gamma(\rho\pi D$ -wave)/ Γ_{total}	DOCUMENT ID	TECN	COMMENT	Γ_5/Γ
---	-------------	------	---------	-------------------

••• We do not use the following data for averages, fits, limits, etc. •••
 seen CHUNG 02 B852 18.3 $\pi^- p \rightarrow \pi^+\pi^-\pi^- p$
 seen AMELIN 95B VES 36 $\pi^- A \rightarrow \pi^+\pi^-\pi^- A$

$\Gamma(\omega\pi\pi)/\Gamma_{total}$	EVTS	DOCUMENT ID	TECN	COMMENT	Γ_6/Γ
---------------------------------------	------	-------------	------	---------	-------------------

••• We do not use the following data for averages, fits, limits, etc. •••
 seen 35280 1 BAKER 03 SPEC $\bar{p}p \rightarrow \omega\pi^+\pi^-\pi^0$
¹ Assuming the $\omega\rho$ mechanism for the $\omega\pi\pi$ state.

$\Gamma(f_1(1285)\pi)/\Gamma_{total}$	DOCUMENT ID	TECN	COMMENT	Γ_7/Γ
---------------------------------------	-------------	------	---------	-------------------

••• We do not use the following data for averages, fits, limits, etc. •••
 not seen KUHN 04 B852 18 $\pi^- p \rightarrow \eta\pi^+\pi^-\pi^- p$
 seen LEE 94 MPS2 18 $\pi^- p \rightarrow K^+ \bar{K}^0 \pi^- \pi^- p$

See key on page 1171

Meson Particle Listings

$a_1(1640)$, $f_2(1640)$, $\eta_2(1645)$, $\omega(1650)$

$\Gamma(a_1(1260)\eta)/\Gamma_{total}$	DOCUMENT ID	TECN	COMMENT	Γ_8/Γ
not seen	KUHN	04	B852	$18 \pi^- p \rightarrow \eta \pi^+ \pi^- \pi^- p$

$a_1(1640)$ REFERENCES

AGHASYAN	18B	PR D98 092003	M. Aghasyan et al.	(COMPASS Collab.)
DARGENT	17	JHEP 1705 143	P. d'Argent et al.	(HEID, BRIS)
KUHN	04	PL B595 109	J. Kuhn et al.	(BNL E852 Collab.)
BAKER	03	PL B563 140	C.A. Baker et al.	
CHUNG	02	PR D65 072001	S.U. Chung et al.	(BNL E852 Collab.)
ASNER	00	PR D61 012002	D.M. Asner et al.	(CLEO Collab.)
BAKER	99	PL B449 114	C.A. Baker et al.	
ABREU	98G	PL B426 411	P. Abreu et al.	(DELPHI Collab.)
AMELIN	95B	PL B356 595	D.V. Amelin et al.	(SERP, TBIL)
LEE	94	PL B323 227	J.H. Lee et al.	(BNL, IND, KYUN, MASD+)
BOWLER	88	PL B209 99	M.G. Bowler	(OXF)
BELLINI	85	SJNP 41 781	D. Bellini et al.	
Translated from YAF 41 1223.				

$f_2(1640)$

$$I^G(JPC) = 0^+(2^{++})$$

OMITTED FROM SUMMARY TABLE

$f_2(1640)$ MASS

VALUE (MeV)	DOCUMENT ID	TECN	COMMENT
1639 ± 6 OUR AVERAGE	Error includes scale factor of 1.2.		
1620 ± 16	BUGG	95	MRK3 $J/\psi \rightarrow \gamma \pi^+ \pi^- \pi^+ \pi^-$
1647 ± 7	ADAMO	92	OBLX $\bar{\pi} p \rightarrow 3\pi^+ 2\pi^-$
1635 ± 7	ALDE	90	GAM2 $38 \pi^- p \rightarrow \omega \omega n$
• • • We do not use the following data for averages, fits, limits, etc. • • •			
1640 ± 5	AMSLER	06	CBAR $0.9 \bar{p} p \rightarrow K^+ K^- \pi^0$
1659 ± 6	VLADIMIRSK...	06	SPEC $40 \pi^- p \rightarrow K_S^0 K_S^0 n$
1643 ± 7	ALDE	89B	GAM2 $38 \pi^- p \rightarrow \omega \omega n$
¹ Superseded by ALDE 90.			

$f_2(1640)$ WIDTH

VALUE (MeV)	CL%	DOCUMENT ID	TECN	COMMENT
100^{+60}_{-40} OUR AVERAGE	Error includes scale factor of 2.9.			
140^{+60}_{-20}		BUGG	95	MRK3 $J/\psi \rightarrow \gamma \pi^+ \pi^- \pi^+ \pi^-$
58 ± 20		ADAMO	92	OBLX $\bar{\pi} p \rightarrow 3\pi^+ 2\pi^-$
• • • We do not use the following data for averages, fits, limits, etc. • • •				
44 ± 9		AMSLER	06	CBAR $0.9 \bar{p} p \rightarrow K^+ K^- \pi^0$
152 ± 18		VLADIMIRSK...	06	SPEC $40 \pi^- p \rightarrow K_S^0 K_S^0 n$
< 70	90	ALDE	90	GAM2 $38 \pi^- p \rightarrow \omega \omega n$

$f_2(1640)$ DECAY MODES

Mode	Fraction (Γ_i/Γ)
Γ_1 $\omega \omega$	seen
Γ_2 4π	seen
Γ_3 $K\bar{K}$	seen

$f_2(1640)$ BRANCHING RATIOS

$\Gamma(K\bar{K})/\Gamma_{total}$	DOCUMENT ID	TECN	COMMENT	Γ_3/Γ
seen	AMSLER	06	CBAR $0.9 \bar{p} p \rightarrow K^+ K^- \pi^0$	

$f_2(1640)$ REFERENCES

AMSLER	06	PL B639 165	C. Amstler et al.	(Crystal Barrel Collab.)
VLADIMIRSK...	06	PAN 69 493	V.V. Vladimirov et al.	(ITEP, Moscow)
Translated from YAF 69 515.				
BUGG	95	PL B353 378	D.V. Bugg et al.	(LOQM, PNPI, WASH)JP
ADAMO	92	PL B287 368	A. Adamo et al.	(OBELIX Collab.)
ALDE	90	PL B241 600	D.M. Alde et al.	(SERP, BELG, LANL, LAPP+)
ALDE	89B	PL B216 451	D.M. Alde et al.	(SERP, BELG, LANL, LAPP+)IGJPC

$\eta_2(1645)$

$$I^G(JPC) = 0^+(2^{-+})$$

$\eta_2(1645)$ MASS

VALUE (MeV)	DOCUMENT ID	TECN	CHG	COMMENT
1617 ± 5 OUR AVERAGE				
1613 ± 8	BARBERIS	00B		$450 pp \rightarrow p_f \eta \pi^+ \pi^- p_S$
1617 ± 8	BARBERIS	00C		$450 pp \rightarrow p_f 4\pi p_S$
1620 ± 20	BARBERIS	97B	OMEG	$450 pp \rightarrow pp 2(\pi^+ \pi^-)$
$1645 \pm 14 \pm 15$	ADOMEIT	96	CBAR 0	$1.94 \bar{p} p \rightarrow \eta 3\pi^0$
• • • We do not use the following data for averages, fits, limits, etc. • • •				
$1645 \pm 6 \pm 20$	ANISOVICH	00E	SPEC	$0.9-1.94 \bar{p} p \rightarrow \eta 3\pi^0$

$\eta_2(1645)$ WIDTH

VALUE (MeV)	DOCUMENT ID	TECN	CHG	COMMENT
181 ± 11 OUR AVERAGE				
185 ± 17	BARBERIS	00B		$450 pp \rightarrow p_f \eta \pi^+ \pi^- p_S$
177 ± 18	BARBERIS	00C		$450 pp \rightarrow p_f 4\pi p_S$
180 ± 25	BARBERIS	97B	OMEG	$450 pp \rightarrow pp 2(\pi^+ \pi^-)$
$180^{+40}_{-21} \pm 25$	ADOMEIT	96	CBAR 0	$1.94 \bar{p} p \rightarrow \eta 3\pi^0$
• • • We do not use the following data for averages, fits, limits, etc. • • •				
200 ± 25	ANISOVICH	00E	SPEC	$0.9-1.94 \bar{p} p \rightarrow \eta 3\pi^0$

$\eta_2(1645)$ DECAY MODES

Mode	Fraction (Γ_i/Γ)
Γ_1 $a_2(1320)\pi$	seen
Γ_2 $K\bar{K}\pi$	seen
Γ_3 $K^*\bar{K}$	seen
Γ_4 $\eta \pi^+ \pi^-$	seen
Γ_5 $a_0(980)\pi$	seen
Γ_6 $f_2(1270)\eta$	not seen

$\eta_2(1645)$ BRANCHING RATIOS

$\Gamma(K\bar{K}\pi)/\Gamma(a_2(1320)\pi)$	DOCUMENT ID	TECN	COMMENT	Γ_2/Γ_1
0.07 ± 0.03	BARBERIS	97C	OMEG $450 pp \rightarrow pp K\bar{K}\pi$	
¹ Using $2(\pi^+ \pi^-)$ data from BARBERIS 97B.				
$\Gamma(a_2(1320)\pi)/\Gamma(a_0(980)\pi)$	DOCUMENT ID	TECN	COMMENT	Γ_1/Γ_5
13.1 ± 2.3 OUR AVERAGE				
13.5 ± 4.6	ANISOVICH	11	SPEC	$0.9-1.94 p\bar{p}$
13.0 ± 2.7	BARBERIS	00B		$450 pp \rightarrow p_f \eta \pi^+ \pi^- p_S$
² Reanalysis of ADOMEIT 96 and ANISOVICH 00E.				

$\Gamma(f_2(1270)\eta)/\Gamma_{total}$	DOCUMENT ID	COMMENT	Γ_6/Γ
not seen	BARBERIS	00B $450 pp \rightarrow p_f \eta \pi^+ \pi^- p_S$	

$\eta_2(1645)$ REFERENCES

ANISOVICH	11	EPJ C71 1511	A.V. Anisovich et al.	(LOQM, RAL, PNPI)
ANISOVICH	00E	PL B477 19	A.V. Anisovich et al.	
BARBERIS	00B	PL B471 435	D. Barberis et al.	(WA 102 Collab.)
BARBERIS	00C	PL B471 440	D. Barberis et al.	(WA 102 Collab.)
BARBERIS	97B	PL B413 217	D. Barberis et al.	(WA 102 Collab.)
BARBERIS	97C	PL B413 225	D. Barberis et al.	(WA 102 Collab.)
ADOMEIT	96	ZPHY C71 227	J. Adomeit et al.	(Crystal Barrel Collab.)

$\omega(1650)$

$$I^G(JPC) = 0^-(1^{-+})$$

See also the $\omega(1420)$ particle listing.

$\omega(1650)$ MASS

VALUE (MeV)	EVS	DOCUMENT ID	TECN	COMMENT
1670 ± 30 OUR ESTIMATE				
• • • We do not use the following data for averages, fits, limits, etc. • • •				
1660.0 ± 8.4		LICHARD	23	RVUE $e^+ e^- \rightarrow \omega \eta$
1698 ± 10	267	ACHASOV	20B	SND $e^+ e^- \rightarrow \omega \eta \rightarrow \eta \pi^0 \gamma$
$1651 \pm 3^{+16}_{-6}$	183k	ABLIKIM	19AQ	BES $J/\psi \rightarrow K^+ K^- \pi^0$
1673^{+6}_{-7}		ACHASOV	19	SND $e^+ e^- \rightarrow \pi^+ \pi^- \pi^0 \eta$
$1671 \pm 6 \pm 10$	824	AKHMETSHIN	17A	CMD3 $1.4-2.0 e^+ e^- \rightarrow \omega \eta$
1660 ± 10	898	ACHASOV	16B	SND $1.34-2.00 e^+ e^- \rightarrow \omega \eta$
1680 ± 10	13.1k	AULCHENKO	15A	SND $1.05-1.80 e^+ e^- \rightarrow \pi^+ \pi^- \pi^0$
$1667 \pm 13 \pm 6$		AUBERT	07AU	BABR $10.6 e^+ e^- \rightarrow \omega \pi^+ \pi^- \gamma$
1645 ± 8	13	AUBERT	06D	BABR $10.6 e^+ e^- \rightarrow \omega \eta \gamma$
$1660 \pm 10 \pm 2$		AUBERT,B	04N	BABR $10.6 e^+ e^- \rightarrow \pi^+ \pi^- \pi^0 \gamma$
$1770 \pm 50 \pm 60$	1.2M	ACHASOV	03D	RVUE $0.44-2.00 e^+ e^- \rightarrow \pi^+ \pi^- \pi^0$
1619 ± 5		HENNER	02	RVUE $1.2-2.0 e^+ e^- \rightarrow \rho \pi, \omega \pi \pi$
1700 ± 20		EUGENIO	01	SPEC $18 \pi^- p \rightarrow \omega \eta n$
1705 ± 26	612	AKHMETSHIN	00D	CMD2 $e^+ e^- \rightarrow \omega \pi^+ \pi^-$
1820^{+190}_{-150}		ACHASOV	98H	RVUE $e^+ e^- \rightarrow \pi^+ \pi^- \pi^0$

Meson Particle Listings

 $\omega(1650)$

1840	$^{+100}_{-70}$	11	ACHASOV	98H	RVUE	$e^+e^- \rightarrow \omega\pi^+\pi^-$	
1780	$^{+170}_{-300}$	12	ACHASOV	98H	RVUE	$e^+e^- \rightarrow K^+K^-$	
~2100		13	ACHASOV	98H	RVUE	$e^+e^- \rightarrow K_S^0 K^{\pm}\pi^{\mp}$	
1606	± 9	14	CLEGG	94	RVUE		
1662	± 13	750	15	ANTONELLI	92	DM2	$1.34-2.4e^+e^- \rightarrow \rho\pi, \omega\pi\pi$
1670	± 20		ATKINSON	83B	OMEG	$20-70 \gamma\rho \rightarrow 3\pi X$	
1657	± 13		CORDIER	81	DM1	$e^+e^- \rightarrow \omega 2\pi$	
1679	± 34	21	ESPOSITO	80	FRAM	$e^+e^- \rightarrow 3\pi$	
1652	± 17		COSME	79	OSPK	$e^+e^- \rightarrow 3\pi$	

- From a VDM fit to AKHMETSHIN 17A $\omega\eta$ data with two additional resonances of low statistical evidences.
- From a fit with contributions from $\omega(1420)$, $\omega(1650)$, and $\phi(1680)$. The mass of $\omega(1420)$ is fixed to the PDG 18 value of 1420 MeV. Fixing also the width of $\omega(1420)$ to the PDG 18 value of 220 MeV results in 1694 ± 9 MeV measurement.
- Could also be $\rho(1700)$. Branching ratio $J/\psi \rightarrow X\pi^0 \rightarrow K^+K^-\pi^0 = (5.3 \pm 0.3^{+0.6}_{-0.5}) \times 10^{-5}$.
- From a fit of the interfering $\omega(1420)$ and $\omega(1650)$ with a relative phase of π and other parameters floating.
- From a fit with contributions from $\omega(1420)$, $\omega(1650)$, and $\phi(1680)$.
- From a fit with contributions from $\omega(782)$, $\phi(1020)$, $\omega(1420)$, and $\omega(1650)$. See ACHASOV 20A for a further analysis of the $\pi^+\pi^-\pi^0$ data.
- From the combined fit of ANTONELLI 92, ACHASOV 01E, ACHASOV 02E, and ACHASOV 03D data on the $\pi^+\pi^-\pi^0$ and ANTONELLI 92 on the $\omega\pi^+\pi^-$ final states. Supersedes ACHASOV 99E and ACHASOV 02E.
- Using results of CORDIER 81 and preliminary data of DOLINSKY 91 and ANTONELLI 92.
- Using the data of AKHMETSHIN 00D and ANTONELLI 92. The $\rho\pi$ dominance for the energy dependence of the $\omega(1420)$ and $\omega(1650)$ width assumed.
- Using data from BARKOV 87, DOLINSKY 91, and ANTONELLI 92.
- Using the data from ANTONELLI 92.
- Using the data from IVANOV 81 and BISELLO 88B.
- Using the data from BISELLO 91c.
- From a fit to two Breit-Wigner functions and using the data of DOLINSKY 91 and ANTONELLI 92.
- From the combined fit of the $\rho\pi$ and $\omega\pi\pi$ final states.

 $\omega(1650)$ WIDTH

VALUE (MeV)	EVTS	DOCUMENT ID	TECN	COMMENT		
315 ± 35 OUR ESTIMATE						
••• We do not use the following data for averages, fits, limits, etc. •••						
106 ± 15		1	LICHARD	23	RVUE	$e^+e^- \rightarrow \omega\eta$
110 ± 16	267	2	ACHASOV	20B	SND	$e^+e^- \rightarrow \omega\eta \rightarrow \eta\pi^0\gamma$
194 ± 8 $^{+15}_{-7}$	183k	3	ABLIKIM	19A	BES	$J/\psi \rightarrow K^+K^-\pi^0$
95 ± 11			ACHASOV	19	SND	$e^+e^- \rightarrow \pi^+\pi^-\pi^0\eta$
113 ± 9 ± 10	824	4	AKHMETSHIN 17A	CMD3		$1.4-2.0 e^+e^- \rightarrow \omega\eta$
110 ± 20	898	5	ACHASOV	16B	SND	$1.34-2.00 e^+e^- \rightarrow \omega\eta$
310 ± 30	13.1k	6	AULCHENKO	15A	SND	$1.05-1.80 e^+e^- \rightarrow \pi^+\pi^-\pi^0$
222 ± 25 ± 20			AUBERT	07AU	BABR	$10.6 e^+e^- \rightarrow \omega\pi^+\pi^-\gamma$
114 ± 14	13		AUBERT	06D	BABR	$10.6 e^+e^- \rightarrow \omega\eta\gamma$
230 ± 30 ± 20			AUBERT,B	04N	BABR	$10.6 e^+e^- \rightarrow \pi^+\pi^-\pi^0\gamma$
490 $^{+200}_{-150}$ ± 130	1.2M	7	ACHASOV	03D	RVUE	$0.44-2.00 e^+e^- \rightarrow \pi^+\pi^-\pi^0$
250 ± 14		8	HENNER	02	RVUE	$1.2-2.0 e^+e^- \rightarrow \rho\pi, \omega\pi\pi$
250 ± 50			EUGENIO	01	SPEC	$18 \pi^-p \rightarrow \omega\eta\eta$
370 ± 25	612	9	AKHMETSHIN 00D	CMD2		$e^+e^- \rightarrow \omega\pi^+\pi^-$
113 ± 20		10	CLEGG	94	RVUE	
280 ± 24	750	11	ANTONELLI	92	DM2	$1.34-2.4e^+e^- \rightarrow \rho\pi, \omega\pi\pi$
160 ± 20			ATKINSON	83B	OMEG	$20-70 \gamma\rho \rightarrow 3\pi X$
136 ± 46			CORDIER	81	DM1	$e^+e^- \rightarrow \omega 2\pi$
99 ± 49	21		ESPOSITO	80	FRAM	$e^+e^- \rightarrow 3\pi$
42 ± 17			COSME	79	OSPK	$e^+e^- \rightarrow 3\pi$

- From a VDM fit to AKHMETSHIN 17A $\omega\eta$ data with two additional resonances of low statistical evidences.
- From a fit with contributions from $\omega(1420)$, $\omega(1650)$, and $\phi(1680)$. The mass of $\omega(1420)$ is fixed to the PDG 18 value of 1420 MeV. Fixing also the width of $\omega(1420)$ to the PDG 18 value of 220 MeV results in 94 ± 13 MeV measurement.
- Could also be $\rho(1700)$. Branching ratio $J/\psi \rightarrow X\pi^0 \rightarrow K^+K^-\pi^0 = (5.3 \pm 0.3^{+0.6}_{-0.5}) \times 10^{-5}$.
- From a fit of the interfering $\omega(1420)$ and $\omega(1650)$ with a relative phase of π and other parameters floating.
- From a fit with contributions from $\omega(1420)$, $\omega(1650)$, and $\phi(1680)$.
- From a fit with contributions from $\omega(782)$, $\phi(1020)$, $\omega(1420)$, and $\omega(1650)$. See ACHASOV 20A for a further analysis of the $\pi^+\pi^-\pi^0$ data.
- From the combined fit of ANTONELLI 92, ACHASOV 01E, ACHASOV 02E, and ACHASOV 03D data on the $\pi^+\pi^-\pi^0$ and ANTONELLI 92 on the $\omega\pi^+\pi^-$ final states. Supersedes ACHASOV 99E and ACHASOV 02E.
- Using results of CORDIER 81 and preliminary data of DOLINSKY 91 and ANTONELLI 92.
- Using the data of AKHMETSHIN 00D and ANTONELLI 92. The $\rho\pi$ dominance for the energy dependence of the $\omega(1420)$ and $\omega(1650)$ width assumed.
- From a fit to two Breit-Wigner functions and using the data of DOLINSKY 91 and ANTONELLI 92.
- From the combined fit of the $\rho\pi$ and $\omega\pi\pi$ final states.

 $\omega(1650)$ DECAY MODES

Mode	Fraction (Γ_i/Γ)
Γ_1 $\rho\pi$	seen
Γ_2 $\rho(1450)\pi$	seen
Γ_3 $\omega\pi\pi$	seen
Γ_4 $\omega\eta$	seen
Γ_5 e^+e^-	seen
Γ_6 $\pi^0\gamma$	not seen

 $\omega(1650)$ $\Gamma(i)\Gamma(e^+e^-)/\Gamma^2(\text{total})$

$\Gamma(\rho\pi)/\Gamma_{\text{total}} \times \Gamma(e^+e^-)/\Gamma_{\text{total}}$	$\Gamma_1/\Gamma \times \Gamma_5/\Gamma$					
VALUE (units 10^{-6})	EVTS	DOCUMENT ID	TECN	COMMENT		
••• We do not use the following data for averages, fits, limits, etc. •••						
1.56 ± 0.23	13.1k	1	AULCHENKO	15A	SND	$1.05-1.80 e^+e^- \rightarrow \pi^+\pi^-\pi^0$
1.3 ± 0.1 ± 0.1			AUBERT,B	04N	BABR	$10.6 e^+e^- \rightarrow \pi^+\pi^-\pi^0\gamma$
1.2 $^{+0.4}_{-0.1}$ ± 0.8	1.2M	2,3	ACHASOV	03D	RVUE	$0.44-2.00 e^+e^- \rightarrow \pi^+\pi^-\pi^0$
0.921 ± 0.230		4,5	CLEGG	94	RVUE	
0.479 ± 0.050	750	6,7	ANTONELLI	92	DM2	$1.34-2.4e^+e^- \rightarrow \rho\pi, \omega\pi\pi$

- From a fit with contributions from $\omega(782)$, $\phi(1020)$, $\omega(1420)$, and $\omega(1650)$. See ACHASOV 20A for a further analysis of the $\pi^+\pi^-\pi^0$ data.
- Calculated by us from the cross section at the peak.
- From the combined fit of ANTONELLI 92, ACHASOV 01E, ACHASOV 02E, and ACHASOV 03D data on the $\pi^+\pi^-\pi^0$ and ANTONELLI 92 on the $\omega\pi^+\pi^-$ final states. Supersedes ACHASOV 99E and ACHASOV 02E.
- From a fit to two Breit-Wigner functions and using the data of DOLINSKY 91 and ANTONELLI 92.
- From the partial and leptonic width given by the authors.
- From the combined fit of the $\rho\pi$ and $\omega\pi\pi$ final states.
- From the product of the leptonic width and partial branching ratio given by the authors.

 $\Gamma(\omega\pi\pi)/\Gamma_{\text{total}} \times \Gamma(e^+e^-)/\Gamma_{\text{total}}$ $\Gamma_3/\Gamma \times \Gamma_5/\Gamma$

VALUE (units 10^{-7})	EVTS	DOCUMENT ID	TECN	COMMENT		
••• We do not use the following data for averages, fits, limits, etc. •••						
7.0 ± 0.5			AUBERT	07AU	BABR	$10.6 e^+e^- \rightarrow \omega\pi^+\pi^-\gamma$
4.1 ± 0.9 ± 1.3	1.2M	1,2	ACHASOV	03D	RVUE	$0.44-2.00 e^+e^- \rightarrow \pi^+\pi^-\pi^0$
5.40 ± 0.95		3	AKHMETSHIN 00D	CMD2		$1.2-1.38 e^+e^- \rightarrow \omega\pi^+\pi^-$
3.18 ± 0.80		4,5	CLEGG	94	RVUE	
6.07 ± 0.61	750	6,7	ANTONELLI	92	DM2	$1.34-2.4 e^+e^- \rightarrow \rho\pi, \omega\pi\pi$

- Calculated by us from the cross section at the peak.
- From the combined fit of ANTONELLI 92, ACHASOV 01E, ACHASOV 02E, and ACHASOV 03D data on the $\pi^+\pi^-\pi^0$ and ANTONELLI 92 on the $\omega\pi^+\pi^-$ final states. Supersedes ACHASOV 99E and ACHASOV 02E.
- Using the data of AKHMETSHIN 00D and ANTONELLI 92. The $\rho\pi$ dominance for the energy dependence of the $\omega(1420)$ and $\omega(1650)$ width assumed.
- From a fit to two Breit-Wigner functions and using the data of DOLINSKY 91 and ANTONELLI 92.
- From the partial and leptonic width given by the authors.
- From the combined fit of the $\rho\pi$ and $\omega\pi\pi$ final states.
- From the product of the leptonic width and partial branching ratio given by the authors.

 $\Gamma(\omega\eta)/\Gamma_{\text{total}} \times \Gamma(e^+e^-)/\Gamma_{\text{total}}$ $\Gamma_4/\Gamma \times \Gamma_5/\Gamma$

VALUE (units 10^{-7})	EVTS	DOCUMENT ID	TECN	COMMENT		
••• We do not use the following data for averages, fits, limits, etc. •••						
6.4 ± 0.9	267	1	ACHASOV	20B	SND	$e^+e^- \rightarrow \omega\eta \rightarrow \eta\pi^0\gamma$
5.62 $^{+0.45}_{-0.42}$			ACHASOV	19	SND	$e^+e^- \rightarrow \pi^+\pi^-\pi^0\eta$
4.5 ± 0.3 ± 0.3	824	2	AKHMETSHIN 17A	CMD3		$1.4-2.0 e^+e^- \rightarrow \omega\eta$
4.4 ± 0.5	898	3	ACHASOV	16B	SND	$1.34-2.00 e^+e^- \rightarrow \omega\eta$
5.7 ± 0.6	13		AUBERT	06D	BABR	$10.6 e^+e^- \rightarrow \omega\eta\gamma$
< 60 at 90% CL		4	AKHMETSHIN 03B	CMD2		$e^+e^- \rightarrow \eta\pi^0\gamma$

- From a fit with contributions from $\omega(1420)$, $\omega(1650)$, and $\phi(1680)$. The mass of $\omega(1420)$ is fixed to the PDG 18 value of 1420 MeV. Fixing also the width of $\omega(1420)$ to the PDG 18 value of 220 MeV results in $(5.4 \pm 0.6) \times 10^{-7}$ measurement.
- From a fit of the interfering $\omega(1420)$ and $\omega(1650)$ with a relative phase of π and other parameters floating. From an alternative fit $\Gamma(\omega(1650) \rightarrow \omega\eta)/\Gamma_{\text{total}} \times \Gamma(\omega(1650) \rightarrow e^+e^-) = 51 \pm 3$ eV.
- From a fit with contributions from $\omega(1420)$, $\omega(1650)$, and $\phi(1680)$.
- $\omega(1650)$ mass and width fixed at 1700 MeV and 250 MeV, respectively.

 $\omega(1650)$ BRANCHING RATIOS

$\Gamma(\rho\pi)/\Gamma_{\text{total}}$	Γ_1/Γ					
VALUE	EVTS	DOCUMENT ID	TECN	COMMENT		
••• We do not use the following data for averages, fits, limits, etc. •••						
~0.65	1.2M	1	ACHASOV	03D	RVUE	$0.44-2.00 e^+e^- \rightarrow \pi^+\pi^-\pi^0$
0.380 ± 0.014		2	HENNER	02	RVUE	$1.2-2.0 e^+e^- \rightarrow \rho\pi, \omega\pi\pi$

- From the combined fit of ANTONELLI 92, ACHASOV 01E, ACHASOV 02E, and ACHASOV 03D data on the $\pi^+\pi^-\pi^0$ and ANTONELLI 92 on the $\omega\pi^+\pi^-$ final states. Supersedes ACHASOV 99E and ACHASOV 02E.
- Assuming that the $\omega(1650)$ decays into $\rho\pi$ and $\omega\pi\pi$ only.

See key on page 1171

Meson Particle Listings

$\omega(1650), \omega_3(1670), \pi_2(1670)$

$\Gamma(\rho(1450)\pi)/\Gamma_{total}$				Γ_2/Γ
VALUE	DOCUMENT ID	TECN	COMMENT	
seen	ACHASOV	20A	SND	1.15-2.00 $e^+e^- \rightarrow \pi^+\pi^-\pi^0$

$\Gamma(\omega\pi\pi)/\Gamma_{total}$				Γ_3/Γ
VALUE	EVTS	DOCUMENT ID	TECN	COMMENT

• • • We do not use the following data for averages, fits, limits, etc. • • •

~ 0.35 1.2M 1 ACHASOV 03D RVUE 0.44-2.00 $e^+e^- \rightarrow \pi^+\pi^-\pi^0$

0.620±0.014 2 HENNER 02 RVUE 1.2-2.0 $e^+e^- \rightarrow \rho\pi, \omega\pi\pi$

1 From the combined fit of ANTONELLI 92, ACHASOV 01E, ACHASOV 02E, and ACHASOV 03D data on the $\pi^+\pi^-\pi^0$ and ANTONELLI 92 on the $\omega\pi^+\pi^-$ final states. Supersedes ACHASOV 99E and ACHASOV 02E.

2 Assuming that the $\omega(1650)$ decays into $\rho\pi$ and $\omega\pi\pi$ only.

$\Gamma(e^+e^-)/\Gamma_{total}$				Γ_5/Γ
VALUE (units 10^{-7})	EVTS	DOCUMENT ID	TECN	COMMENT

• • • We do not use the following data for averages, fits, limits, etc. • • •

~ 18 1.2M 1,2 ACHASOV 03D RVUE 0.44-2.00 $e^+e^- \rightarrow \pi^+\pi^-\pi^0$

32±1 2 HENNER 02 RVUE 1.2-2.0 $e^+e^- \rightarrow \rho\pi, \omega\pi\pi$

1 Calculated by us from the cross section at the peak.

2 Assuming that the $\omega(1650)$ decays into $\rho\pi$ and $\omega\pi\pi$ only.

$\Gamma(\pi^0\gamma)/\Gamma_{total}$				Γ_6/Γ
VALUE	DOCUMENT ID	TECN	COMMENT	

not seen 1 ACHASOV 10D SND 1.075-2.0 $e^+e^- \rightarrow \pi^0\gamma$

1 From a fit of a VMD model with two effective resonances with masses of 1450 MeV and 1700 MeV to describe the excited vector states $\omega(1420), \rho(1450), \omega(1650)$, and $\rho(1700)$. The width of the highest mass effective resonance is fixed at 315 MeV.

$\omega(1650)$ REFERENCES

LICHARD	23	PR D108 092005	P. Lichard	(OPAV, CTUP)
ACHASOV	20A	EPJ C80 993	M.N. Achasov et al.	(SND Collab.)
ACHASOV	20B	EPJ C80 1008	M.N. Achasov et al.	(SND Collab.)
ABLIKIM	19Aq	PR D100 032004	M. Ablikim et al.	(BESIII Collab.)
ACHASOV	19	PR D99 112004	M.N. Achasov et al.	(SND Collab.)
PDG	18	PR D98 030001	M. Tanabashi et al.	(PDG Collab.)
AKHMETSHPIN	17A	PL B773 150	R.R. Akhmetshin et al.	(CMD-3 Collab.)
ACHASOV	16B	PR D94 092002	M.N. Achasov et al.	(SND Collab.)
AULCHENKO	15A	JETP 121 27	V.M. Aulchenko et al.	(SND Collab.)
Translated from ZETF 148 34.				
ACHASOV	10D	PR D98 112001	M.N. Achasov et al.	(SND Collab.)
AUBERT	07AU	PR D76 092005	B. Aubert et al.	(BABAR Collab.)
AUBERT	06D	PR D73 052003	B. Aubert et al.	(BABAR Collab.)
AUBERT.B	04N	PR D70 072004	B. Aubert et al.	(BABAR Collab.)
ACHASOV	03D	PR D68 052006	M.N. Achasov et al.	(Novosibirsk SND Collab.)
AKHMETSHPIN	03B	PL B562 173	R.R. Akhmetshin et al.	(Novosibirsk CMD-2 Collab.)
ACHASOV	02E	PR D66 032001	M.N. Achasov et al.	(Novosibirsk SND Collab.)
HENNER	02	EPJ C26 3	V.K. Henner et al.	(NOVO)
ACHASOV	01E	PR D63 072002	M.N. Achasov et al.	(Novosibirsk SND Collab.)
EUGENIO	01	PL B497 190	P. Eugenio et al.	(NOVO)
AKHMETSHPIN	00D	PL B489 125	R.R. Akhmetshin et al.	(Novosibirsk CMD-2 Collab.)
ACHASOV	99E	PL B462 365	M.N. Achasov et al.	(Novosibirsk SND Collab.)
ACHASOV	98B	PR D57 4334	N.N. Achasov, A.A. Kozhevnikov	(NOVO)
CLEGG	94	ZPHY C62 455	A.B. Clegg, A. Donnachie	(LANC, MCHS)
ANTONELLI	92	ZPHY C56 15	A. Antonelli et al.	(DM2 Collab.)
BISELLO	91C	ZPHY C52 227	D. Bisello et al.	(NOVO)
DOLINSKY	91	PRPL 202 99	S.I. Dolinsky et al.	(NOVO)
BISELLO	88B	ZPHY C39 13	D. Bisello et al.	(PADO, CLER, FRAS+)
BARKOV	87	JETPL 46 164	L.M. Barkov et al.	(NOVO)
Translated from ZETFP 46 132.				
ATKINSON	83B	PL 127B 132	M. Atkinson et al.	(BONN, CERN, GLAS+)
CORDIER	81	PL 106B 155	A. Cordier et al.	(ORSAY)
IVANOV	81	PL 107B 297	P.M. Ivanov et al.	(NOVO)
ESPOSITO	80	LNC 28 195	B. Esposito et al.	(FRAS, NAPL, PADO+)
COSME	79	NP B152 215	G. Cosme et al.	(IPN)

$\omega_3(1670)$

$$I^G(J^{PC}) = 0^-(3^{--})$$

$\omega_3(1670)$ MASS

VALUE (MeV)	EVTS	DOCUMENT ID	TECN	COMMENT
1667 ± 4 OUR AVERAGE				
1665.3 ± 5.2 ± 4.5	23400	AMELIN	96	VES 36 $\pi^-p \rightarrow \pi^+\pi^-\pi^0n$
1685 ± 20	60	BAUBILLIER	79	HBC 8.2 K^-p backward
1673 ± 12	430	1,2 BALTAY	78E	HBC 15 $\pi^+p \rightarrow \Delta 3\pi$
1650 ± 12		CORDEN	78B	OMEG 8-12 $\pi^-p \rightarrow N 3\pi$
1669 ± 11	600	2 WAGNER	75	HBC 7 $\pi^+p \rightarrow \Delta^{++} 3\pi$
1678 ± 14	500	DIAZ	74	DBC 6 $\pi^+n \rightarrow p 3\pi^0$
1660 ± 13	200	DIAZ	74	DBC 6 $\pi^+n \rightarrow p\omega\pi^0\pi^0$
1679 ± 17	200	MATTHEWS	71D	DBC 7.0 $\pi^+n \rightarrow p 3\pi^0$
1670 ± 20	110	KENYON	69	DBC 8 $\pi^+n \rightarrow p 3\pi^0$
• • • We do not use the following data for averages, fits, limits, etc. • • •				
~ 1700	110	1 CERRADA	77B	HBC 4.2 $K^-p \rightarrow \Lambda 3\pi$
1695 ± 20		BARNES	69B	HBC 4.6 $K^-p \rightarrow \omega 2\pi X$
1636 ± 20		ARMENISE	68B	DBC 5.1 $\pi^+n \rightarrow p 3\pi^0$
1 Phase rotation seen for $J^P = 3^- \rho\pi$ wave.				
2 From a fit to $I(J^P) = 0(3^-) \rho\pi$ partial wave.				

$\omega_3(1670)$ WIDTH

VALUE (MeV)	EVTS	DOCUMENT ID	TECN	COMMENT
168 ± 10 OUR AVERAGE				
149 ± 19 ± 7	23400	AMELIN	96	VES 36 $\pi^-p \rightarrow \pi^+\pi^-\pi^0n$
160 ± 80	60	3 BAUBILLIER	79	HBC 8.2 K^-p backward
173 ± 16	430	4,5 BALTAY	78E	HBC 15 $\pi^+p \rightarrow \Delta 3\pi$
253 ± 39		CORDEN	78B	OMEG 8-12 $\pi^-p \rightarrow N 3\pi$
173 ± 28	600	3,5 WAGNER	75	HBC 7 $\pi^+p \rightarrow \Delta^{++} 3\pi$
167 ± 40	500	DIAZ	74	DBC 6 $\pi^+n \rightarrow p 3\pi^0$
122 ± 39	200	DIAZ	74	DBC 6 $\pi^+n \rightarrow p\omega\pi^0\pi^0$
155 ± 40	200	3 MATTHEWS	71D	DBC 7.0 $\pi^+n \rightarrow p 3\pi^0$
• • • We do not use the following data for averages, fits, limits, etc. • • •				
90 ± 20		BARNES	69B	HBC 4.6 $K^-p \rightarrow \omega 2\pi$
100 ± 40		KENYON	69	DBC 8 $\pi^+n \rightarrow p 3\pi^0$
112 ± 60		ARMENISE	68B	DBC 5.1 $\pi^+n \rightarrow p 3\pi^0$
3 Width errors enlarged by us to $4\Gamma/\sqrt{N}$; see the note with the $K^*(892)$ mass.				
4 Phase rotation seen for $J^P = 3^- \rho\pi$ wave.				
5 From a fit to $I(J^P) = 0(3^-) \rho\pi$ partial wave.				

$\omega_3(1670)$ DECAY MODES

Mode	Fraction (Γ_i/Γ)
Γ_1 $\rho\pi$	seen
Γ_2 $\omega\pi\pi$	seen
Γ_3 $b_1(1235)\pi$	possibly seen

$\omega_3(1670)$ BRANCHING RATIOS

$\Gamma(\omega\pi\pi)/\Gamma(\rho\pi)$				Γ_2/Γ_1
VALUE	EVTS	DOCUMENT ID	TECN	COMMENT

• • • We do not use the following data for averages, fits, limits, etc. • • •

0.71 ± 0.27 100 DIAZ 74 DBC 6 $\pi^+n \rightarrow p 5\pi^0$

$\Gamma(b_1(1235)\pi)/\Gamma(\rho\pi)$				Γ_3/Γ_1
VALUE	DOCUMENT ID	TECN	COMMENT	

possibly seen DIAZ 74 DBC 6 $\pi^+n \rightarrow p 5\pi^0$

$\Gamma(b_1(1235)\pi)/\Gamma(\omega\pi\pi)$				Γ_3/Γ_2
VALUE	CL%	DOCUMENT ID	TECN	COMMENT

• • • We do not use the following data for averages, fits, limits, etc. • • •

> 0.75 68 BAUBILLIER 79 HBC 8.2 K^-p backward

$\omega_3(1670)$ REFERENCES

AMELIN	96	ZPHY C70 71	D.V. Amelin et al.	(SERP, TBIL)
BAUBILLIER	79	PL 89B 331	M. Baubillier et al.	(BIRM, CERN, GLAS+)
BALTAY	78E	PL 40 87	C. Baltay, C.V. Cautis, M. Kalelkar	(COLU) JP
CORDEN	78B	NP B138 235	M.J. Cordén et al.	(BIRM, RHEL, TELU+)
CERRADA	77B	NP B126 241	M. Cerrada et al.	(AMST, CERN, NIJM+ JP)
WAGNER	75	PL 58B 201	F. Wagner, M. Tabak, D.M. Chew	(CASE, CMU)
DIAZ	74	PR L 32 260	J. Diaz et al.	(TINTO, WISC)
MATTHEWS	71D	PR D3 2561	J.A.J. Matthews et al.	(BNL)
BARNES	69B	PR L 23 142	V.E. Barnes et al.	(BNL, UCND, ORNL)
KENYON	69	PR L 23 146	I.R. Kenyon et al.	(BNL, UCND, ORNL)
ARMENISE	68B	PL 26B 336	N. Armenise et al.	(BARI, BGNA, FIRZ+)

$\pi_2(1670)$

$$I^G(J^{PC}) = 1^-(2^{+-})$$

$\pi_2(1670)$ MASS

VALUE (MeV)	EVTS	DOCUMENT ID	TECN	CHG	COMMENT
1670.6 ± 2.9 ± 1.2 OUR AVERAGE					Error includes scale factor of 1.3. See the ideogram below.
1642 ± 12 ± 1	46M	1 AGHASYAN	18B	COMP	190 $\pi^-p \rightarrow \pi^-\pi^+\pi^-\rho$
1749 ± 10 ± 100	145k	LU	05	B852	18 $\pi^-p \rightarrow \omega\pi^-\pi^0\rho$
1676 ± 3 ± 8		2 CHUNG	02	B852	18.3 $\pi^-p \rightarrow \pi^+\pi^-\pi^-\rho$
1685 ± 10 ± 30		BARBERIS	01		450 $pp \rightarrow p f 3\pi^0 p_S$
1687 ± 9 ± 15		AMELIN	99	VES	37 $\pi^-A \rightarrow \omega\pi^-\pi^0 A^*$
1669 ± 4		BARBERIS	98B		450 $pp \rightarrow p f \rho p \rho_S$
1670 ± 4		BARBERIS	98B		450 $pp \rightarrow p f f_2(1270) \pi p_S$
1690 ± 14		3 BERDNIKOV	94	VES	37 $\pi^-A \rightarrow K^+K^-\pi^-A$
1710 ± 20	700	ANTIPOV	87	SIGM	50 $\pi^-Cu \rightarrow \mu^+\mu^-\pi^-Cu$
1676 ± 6		3 EVANGELIS...	81	OMEG	12 $\pi^-p \rightarrow 3\pi\rho$
1657 ± 14		3,4 DAUM	80D	SPEC	63-94 $\pi\rho \rightarrow 3\pi X$
1662 ± 10	2000	3 BALTAY	77	HBC	+ 15 $\pi^+p \rightarrow p 3\pi$

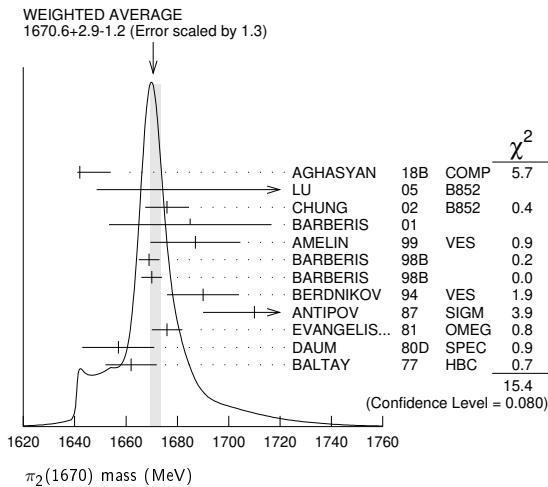
Meson Particle Listings

$\pi_2(1670)$

••• We do not use the following data for averages, fits, limits, etc. •••

1658 ± 3 ± 24 ₈	420k	5	ALEKSEEV	10	COMP	190 $\pi^- Pb \rightarrow \pi^- \pi^+ \pi^+ Pb'$
1730 ± 20		6	AMELIN	95B	VES	36 $\pi^- A \rightarrow \pi^+ \pi^- \pi^- A$
1742 ± 31 ± 49			ANTREASYAN	90	CBAL	$e^+ e^- \rightarrow \pi^0 \pi^0 \pi^0$
1624 ± 21		2	BELLINI	85	SPEC	40 $\pi^- A \rightarrow \pi^- \pi^+ \pi^- A$
1622 ± 35		7	BELLINI	85	SPEC	40 $\pi^- A \rightarrow \pi^- \pi^+ \pi^- A$
1693 ± 28		8	BELLINI	85	SPEC	40 $\pi^- A \rightarrow \pi^- \pi^+ \pi^- A$
1710 ± 20		9	DAUM	81B	SPEC	63,94 $\pi^- p$
1660 ± 10		3	ASCOLI	73	HBC	5-25 $\pi^- p \rightarrow p \pi_2$

- 1 Statistical error negligible.
- 2 From $f_2(1270) \pi$ decay.
- 3 From a fit to $J^P = 2^- S$ -wave $f_2(1270) \pi$ partial wave.
- 4 Clear phase rotation seen in $2^- S, 2^- P, 2^- D$ waves. We quote central value and spread of single-resonance fits to three channels.
- 5 Superseded by AGHASYAN 2018B.
- 6 J^{PC} ambiguous.
- 7 From $\rho \pi$ decay.
- 8 From $\sigma \pi$ decay.
- 9 From a two-resonance fit to four $2^- 0^+$ waves. This should not be averaged with all the single resonance fits.



$\pi_2(1670)$ WIDTH

VALUE (MeV)	EVTS	DOCUMENT ID	TECN	CHG	COMMENT
258⁺⁸₋₉	OUR AVERAGE	Error includes scale factor of 1.2.			
311 ⁺¹² ₋₂₃	46M	10	AGHASYAN	18B	COMP
408 ± 60 ± 250	145k		LU	05	B852
254 ± 3 ± 31		11	CHUNG	02	B852
265 ± 30 ± 40			BARBERIS	01	
168 ± 43 ± 53			AMELIN	99	VES
268 ± 15			BARBERIS	98B	
256 ± 15			BARBERIS	98B	
190 ± 50		12	BERDNIKOV	94	VES
170 ± 80	700		ANTIPOV	87	SIGM
260 ± 20		12	EVANGELIS...	81	OMEG
219 ± 20		12,13	DAUM	80D	SPEC
285 ± 60	2000	12	BALTAY	77	HBC
••• We do not use the following data for averages, fits, limits, etc. •••					
271 ± 9 ⁺²² ₋₂₄	420k	14	ALEKSEEV	10	COMP
310 ± 20		15	AMELIN	95B	VES
236 ± 49 ± 36			ANTREASYAN	90	CBAL
304 ± 22		11	BELLINI	85	SPEC
404 ± 108		16	BELLINI	85	SPEC
330 ± 90		17	BELLINI	85	SPEC
312 ± 50		18	DAUM	81B	SPEC
270 ± 60		12	ASCOLI	73	HBC

- 10 Statistical error negligible.
- 11 From $f_2(1270) \pi$ decay.
- 12 From a fit to $J^P = 2^- f_2(1270) \pi$ partial wave.
- 13 Clear phase rotation seen in $2^- S, 2^- P, 2^- D$ waves. We quote central value and spread of single-resonance fits to three channels.
- 14 Superseded by AGHASYAN 2018B.
- 15 J^{PC} ambiguous.
- 16 From $\rho \pi$ decay.
- 17 From $\sigma \pi$ decay.
- 18 From a two-resonance fit to four $2^- 0^+$ waves. This should not be averaged with all the single resonance fits.

$\pi_2(1670)$ DECAY MODES

Mode	Fraction (Γ_i/Γ)	Confidence level
Γ_1 3π	(95.8 ± 1.4) %	
Γ_2 $\pi^+ \pi^- \pi^0$		
Γ_3 $\pi^0 \pi^0 \pi^0$		
Γ_4 $f_2(1270) \pi$	(56.3 ± 3.2) %	
Γ_5 $\rho \pi$	(31 ± 4) %	
Γ_6 $\sigma \pi$	(10 ± 4) %	
Γ_7 $\pi(\pi\pi)_S$ -wave	(8.7 ± 3.4) %	
Γ_8 $\pi^+ \pi^+ \pi^-$	(53 ± 4) %	
Γ_9 $K \bar{K}^*(892) + c.c.$	(4.2 ± 1.4) %	
Γ_{10} $\omega \rho$	(2.7 ± 1.1) %	
Γ_{11} $\pi^\pm \gamma$	(7.0 ± 1.2) × 10 ⁻⁴	
Γ_{12} $\gamma \gamma$	< 2.8 × 10 ⁻⁷	90%
Γ_{13} $\eta \pi$	< 5 %	
Γ_{14} $\pi^\pm 2\pi^+ 2\pi^-$	< 5 %	
Γ_{15} $\rho(1450) \pi$	< 3.6 × 10 ⁻³	97.7%
Γ_{16} $b_1(1235) \pi$	< 1.9 × 10 ⁻³	97.7%
Γ_{17} $f_1(1285) \pi$	possibly seen	
Γ_{18} $a_2(1320) \pi$	not seen	

CONSTRAINED FIT INFORMATION

An overall fit to 4 branching ratios uses 6 measurements and one constraint to determine 4 parameters. The overall fit has a $\chi^2 = 1.9$ for 3 degrees of freedom.

The following *off-diagonal* array elements are the correlation coefficients $\langle \delta x_i \delta x_j \rangle / (\delta x_i \delta x_j)$, in percent, from the fit to the branching fractions, $x_i \equiv \Gamma_i/\Gamma_{total}$. The fit constrains the x_i whose labels appear in this array to sum to one.

x_5	-53		
x_7	-29	-59	
x_9	-8	-21	-9
	x_4	x_5	x_7

$\pi_2(1670)$ PARTIAL WIDTHS

$\Gamma(\pi^\pm)$	DOCUMENT ID	TECN	CHG	COMMENT	Γ_{11}		
VALUE (keV)							
181 ± 11 ± 27	19	ADOLPH	14	COMP	-	190 $\pi^- Pb \rightarrow \pi^+ \pi^- \pi^- Pb'$	
••• We do not use the following data for averages, fits, limits, etc. •••							
<0.072	90	20	ACCIARRI	97T	L3	$e^+ e^- \rightarrow e^+ e^- \pi^+ \pi^- \pi^0$	
<0.19	90	20	ALBRECHT	97B	ARG	$e^+ e^- \rightarrow e^+ e^- \pi^+ \pi^- \pi^0$	
1.41 ± 0.23 ± 0.28			ANTREASYAN	90	CBAL	0	
0.8 ± 0.3 ± 0.12			21	BEHREND	90C	CELL	0
1.3 ± 0.3 ± 0.2			22	BEHREND	90C	CELL	0
20	Decaying into $f_2(1270) \pi$ and $\rho \pi$.						
21	Constructive interference between $f_2(1270) \pi, \rho \pi$ and background.						
22	Incoherent Ansatz.						

$\pi_2(1670)$ $\Gamma(i)\Gamma(\gamma\gamma)/\Gamma(total)$

$\Gamma(\pi^+ \pi^- \pi^0) \times \Gamma(\gamma\gamma)/\Gamma_{total}$	DOCUMENT ID	TECN	COMMENT	Γ_{12}/Γ		
VALUE (keV)						
<0.1	95	23	SCHEGELSKY	06	RVUE	$\gamma \gamma \rightarrow \pi^+ \pi^- \pi^0$
••• We do not use the following data for averages, fits, limits, etc. •••						
23	From analysis of L3 data at 183-209 GeV.					

See key on page 1171

Meson Particle Listings

$\pi_2(1670), \phi(1680)$

$\pi_2(1670)$ BRANCHING RATIOS

$\Gamma(3\pi)/\Gamma_{\text{total}}$		$\Gamma_1/\Gamma = (\Gamma_4 + \Gamma_5 + \Gamma_7)/\Gamma$
VALUE	DOCUMENT ID	
0.958 ± 0.014 OUR FIT		

$\Gamma(\pi^0 \pi^0 \pi^0)/\Gamma(\pi^+ \pi^- \pi^0)$		Γ_3/Γ_2
VALUE	DOCUMENT ID	COMMENT
0.29 ± 0.03 ± 0.05	BARBERIS 01	450 $pp \rightarrow \rho_f \pi^0 \rho_S$

$\Gamma(\rho\pi)/0.565\Gamma(f_2(1270)\pi)$		$\Gamma_5/0.565\Gamma_4$	
(With $f_2(1270) \rightarrow \pi^+ \pi^-$)			
VALUE	DOCUMENT ID	TECN	COMMENT
0.97 ± 0.09 OUR AVERAGE			Error includes scale factor of 1.9.
0.76 ± 0.07 ± 0.10	CHUNG 02	B852	18.3 $\pi^- p \rightarrow \pi^+ \pi^- \pi^- p$
1.01 ± 0.05	BARBERIS 98B		450 $pp \rightarrow \rho_f \pi^+ \pi^- \pi^0 \rho_S$

$\Gamma(\sigma\pi)/\Gamma(f_2(1270)\pi)$		Γ_6/Γ_4	
VALUE	DOCUMENT ID	TECN	COMMENT
0.17 ± 0.02 ± 0.07	CHUNG 02	B852	18.3 $\pi^- p \rightarrow \pi^+ \pi^- \pi^- p$
0.22 ± 0.10	24,25 BAKER 99	SPEC	1.94 $\bar{p} p \rightarrow 4\pi^0$

$\frac{1}{2}\Gamma(\rho\pi)/\Gamma(\pi^\pm \pi^+ \pi^-)$		$\frac{1}{2}\Gamma_5/\Gamma_8 = \frac{1}{2}\Gamma_5/(0.565\Gamma_4 + \frac{1}{2}\Gamma_5 + 0.624\Gamma_7)$		
VALUE	DOCUMENT ID	TECN	CHG	COMMENT
0.29 ± 0.04 OUR FIT				
0.29 ± 0.05	26 DAUM	81B	SPEC	63,94 $\pi^- p$

$0.565\Gamma(f_2(1270)\pi)/\Gamma(\pi^\pm \pi^+ \pi^-)$		$0.565\Gamma_4/\Gamma_8 = 0.565\Gamma_4/(0.565\Gamma_4 + \frac{1}{2}\Gamma_5 + 0.624\Gamma_7)$		
(With $f_2(1270) \rightarrow \pi^+ \pi^-$)				
VALUE	DOCUMENT ID	TECN	CHG	COMMENT
0.604 ± 0.035 OUR FIT				
0.60 ± 0.05 OUR AVERAGE				Error includes scale factor of 1.3.
0.61 ± 0.04	26 DAUM	81B	SPEC	63,94 $\pi^- p$
0.76 +0.24 -0.34	ARMENISE 69	DBC	+	5.1 $\pi^+ d \rightarrow d 3\pi$
0.35 ± 0.20	BALTAY 68	HBC	+	7-8.5 $\pi^+ p$

$0.624\Gamma(\pi(\pi\pi)_{S\text{-wave}})/\Gamma(\pi^\pm \pi^+ \pi^-)$		$0.624\Gamma_7/\Gamma_8 = 0.624\Gamma_7/(0.565\Gamma_4 + \frac{1}{2}\Gamma_5 + 0.624\Gamma_7)$		
(With $(\pi\pi)_{S\text{-wave}} \rightarrow \pi^+ \pi^-$)				
VALUE	DOCUMENT ID	TECN	COMMENT	
0.10 ± 0.04 OUR FIT				
0.10 ± 0.05	26 DAUM	81B	SPEC	63,94 $\pi^- p$

$\Gamma(K\bar{K}^*(892) + c.c.)/\Gamma(f_2(1270)\pi)$		Γ_9/Γ_4		
VALUE	DOCUMENT ID	TECN	CHG	COMMENT
0.075 ± 0.025 OUR FIT				
0.075 ± 0.025	27 ARMSTRONG 82B	OMEG	-	16 $\pi^- p \rightarrow K^+ K^- \pi^- p$

$\Gamma(\omega\rho)/\Gamma_{\text{total}}$		Γ_{10}/Γ		
VALUE	DOCUMENT ID	TECN	COMMENT	
0.027 ± 0.004 ± 0.010	28 AMELIN	99	VES	37 $\pi^- A \rightarrow \omega \pi^- \pi^0 A^*$

$\Gamma(\eta\pi)/\Gamma(\pi^\pm \pi^+ \pi^-)$		$\Gamma_{13}/\Gamma_8 = \Gamma_{13}/(0.565\Gamma_4 + \frac{1}{2}\Gamma_5 + 0.624\Gamma_7)$		
(All η decays.)				
VALUE	DOCUMENT ID	TECN	CHG	COMMENT
<0.09	BALTAY 68	HBC	+	7-8.5 $\pi^+ p$

$\Gamma(\pi^\pm 2\pi^+ 2\pi^-)/\Gamma(\pi^\pm \pi^+ \pi^-)$		$\Gamma_{14}/\Gamma_8 = \Gamma_{14}/(0.565\Gamma_4 + \frac{1}{2}\Gamma_5 + 0.624\Gamma_7)$		
VALUE	DOCUMENT ID	TECN	CHG	COMMENT
<0.10	CRENNELL 70	HBC	-	6 $\pi^- p \rightarrow f_2 \pi^- N$

$\Gamma(\rho(1450)\pi)/\Gamma_{\text{total}}$		Γ_{15}/Γ		
VALUE	CL%	DOCUMENT ID	TECN	COMMENT
<0.0036	97.7	AMELIN 99	VES	37 $\pi^- A \rightarrow \omega \pi^- \pi^0 A^*$

$\Gamma(b_1(1235)\pi)/\Gamma_{\text{total}}$		Γ_{16}/Γ		
VALUE	CL%	DOCUMENT ID	TECN	COMMENT
<0.0019	97.7	AMELIN 99	VES	37 $\pi^- A \rightarrow \omega \pi^- \pi^0 A^*$

$\Gamma(f_1(1285)\pi)/\Gamma_{\text{total}}$		Γ_{17}/Γ			
VALUE	EVTS	DOCUMENT ID	TECN	COMMENT	
possibly seen	69k	KUHN	04	B852	18 $\pi^- p \rightarrow \eta \pi^+ \pi^- \pi^- p$

$\Gamma(a_2(1320)\pi)/\Gamma_{\text{total}}$		Γ_{18}/Γ			
VALUE	EVTS	DOCUMENT ID	TECN	COMMENT	
not seen	69k	KUHN	04	B852	18 $\pi^- p \rightarrow \eta \pi^+ \pi^- \pi^- p$

D-wave/S-wave RATIO FOR $\pi_2(1670) \rightarrow f_2(1270)\pi$			
VALUE	DOCUMENT ID	TECN	COMMENT
-0.18 ± 0.06	24 BAKER 99	SPEC	1.94 $\bar{p} p \rightarrow 4\pi^0$

F-wave/P-wave RATIO FOR $\pi_2(1670) \rightarrow \rho\pi$			
VALUE	DOCUMENT ID	TECN	COMMENT
-0.72 ± 0.07 ± 0.14	CHUNG 02	B852	18.3 $\pi^- p \rightarrow \pi^+ \pi^- \pi^- p$

$\pi_2(1670)$ REFERENCES

AGHASYAN 18B	PR D98 092003	M. Aghasyan et al.	(COMPASS Collab.)
ADOLPH 14	EPJ A50 79	C. Adolph et al.	(COMPASS Collab.)
ALEKSEEV 10	PRL 104 241803	M.G. Alekseev et al.	(COMPASS Collab.)
SCHEGELSKY 06	EPJ A27 199	V.A. Schegelsky et al.	
LU 05	PRL 94 032002	M. Lu et al.	(BNL E852 Collab.)
KUHN 04	PL B595 109	J. Kuhn et al.	(BNL E852 Collab.)
CHUNG 02	PR D65 072001	S.U. Chung et al.	(BNL E852 Collab.)
BARBERIS 01	PL B507 14	D. Barberis et al.	
AMELIN 99	PAN 62 445	D.V. Amelin et al.	(VES Collab.)
BAKER 99	PL B449 114	C.A. Baker et al.	
BARBERIS 98B	PL B422 399	D. Barberis et al.	(WA 102 Collab.)
ACCIARRI 97T	PL B413 147	M. Acciarri et al.	(L3 Collab.)
ALBRECHT 97B	ZPHY C74 469	H. Albrecht et al.	(ARGUS Collab.)
AMELIN 95B	PL B356 595	D.V. Amelin et al.	(SERP, TBL)
BERDNIKOV 94	PL B337 219	E.B. Berdnikov et al.	(SERP, TBL)
ANTREASYAN 90	ZPHY C48 561	D. Antreasyan et al.	(Crystal Ball Collab.)
BEHREND 80C	ZPHY C46 583	H.J. Behrend et al.	(CELLO Collab.)
ANTIPOV 97	EPL 4 403	Y.M. Antipov et al.	(SERP, JINR, INRM+)
BELLINI 85	SJNP 41 781	D. Bellini et al.	
ARMSTRONG 82B	NP B202 1	T.A. Armstrong, B. Baccari	(AACH3, BARI, BONN+)
DAUM 81B	NP B182 269	C. Daum et al.	(AMST, CERN, CRAC, MPIM+)
EVANGELIS... 81	NP B178 197	C. Evangelista et al.	(BARI, BONN, CERN+)
DAUM 80D	PL B98 285	C. Daum et al.	
BALTAY 77	PRL 39 591	C. Baltay, C.V. Curtis, M. Katelkar	(AMST, CERN, CRAC, MPIM+) JP (COLU) JP
ASCOLI 73	PR D7 669	G. Ascoli	(ILL, TNTO, GENO, HAMB, MILA+) JP
CRENNELL 70	PRL 24 781	D.J. Crennell et al.	(BNL)
ARMENISE 69	LNC 2 501	N. Armenise et al.	(BARI, BGN, FIRZ)
BALTAY 68	PRL 20 887	C. Baltay et al.	(COLU, ROCH, RUTG, YALE) JP
BARTSCH 68	NP B7 345	J. Bartsch et al.	(AACH, BERL, CERN) JP

$\phi(1680)$	$I^G(J^{PC}) = 0^-(1^-)$
--------------------------------	--------------------------

$\phi(1680)$ MASS

e^+e^- PRODUCTION				
VALUE (MeV)	EVTS	DOCUMENT ID	TECN	COMMENT
1680 ± 20 OUR ESTIMATE				

• • • We do not use the following data for averages, fits, limits, etc. • • •

1656.8 ± 4.9	1	LICHARD 23	RVUE	$e^+e^- \rightarrow \Upsilon(nS) \rightarrow \phi\eta\gamma$
1683 ± 7 ± 9	2	ZHU 23	BELL	$e^+e^- \rightarrow \Upsilon(nS) \rightarrow \phi\eta\gamma$
1678 +5 -3 ± 7	3	ZHU 23A	RVUE	$e^+e^- \rightarrow \eta\phi$
1673 ± 5	4	ABLIKIM 22L	BES3	2.0-3.08 $e^+e^- \rightarrow K^+ K^- \pi^0$
1680 +12 -13 ± 21	5	ABLIKIM 20F	BES3	$\psi(2S) \rightarrow K^+ K^- \eta$
1662 ± 20	6	ACHASOV 20C	SND	1.3-2.0 $e^+e^- \rightarrow K^+ K^- \pi^0$
1641 +24 -18		ACHASOV 19	SND	$e^+e^- \rightarrow \pi^+ \pi^- \pi^0 \eta$
1667 ± 5 ± 11	7	IVANOV 19A	CMD3	1.59-2.007 $e^+e^- \rightarrow K^+ K^- \eta$
1700 ± 23	8	ACHASOV 18A	SND	1.3-2.0 $e^+e^- \rightarrow K_S^0 K_L^0 \pi^0$
1674 ± 12 ± 6	9	LEES 14H	BABR	$e^+e^- \rightarrow K_S^0 K_L^0 \gamma$
1733 ± 10 ± 10	10	LEES 12F	BABR	10.6 $e^+e^- \rightarrow \phi\pi^+ \pi^- \gamma$
1689 ± 7 ± 10	11	SHEN 09	BELL	10.6 $e^+e^- \rightarrow K^+ K^- \pi^+ \pi^- \gamma$
1709 ± 20 ± 43	12	AUBERT 08s	BABR	10.6 $e^+e^- \rightarrow \text{hadrons}$
1623 ± 20	13	AKHMETSHIN 03	CMD2	1.05-1.38 $e^+e^- \rightarrow K_L^0 K_S^0$
~ 1500	14	ACHASOV 98H	RVUE	$e^+e^- \rightarrow \pi^+ \pi^- \pi^0, \omega \pi^+ \pi^-, K^+ K^-$

Meson Particle Listings

 $\phi(1680)$

~1900	15	ACHASOV	98H	RVUE	$e^+e^- \rightarrow K_S^0 K^\pm \pi^\mp$
1700 \pm 20	16	CLEGG	94	RVUE	$e^+e^- \rightarrow K^+K^-, K_S^0 K \pi$
1657 \pm 27	367	BISELLO	91C	DM2	$e^+e^- \rightarrow K_S^0 K^\pm \pi^\mp$
1655 \pm 17	17	BISELLO	88B	DM2	$e^+e^- \rightarrow K^+K^-$
1680 \pm 10	18	BUON	82	DM1	$e^+e^- \rightarrow$ hadrons
1677 \pm 12	19	MANE	82	DM1	$e^+e^- \rightarrow K_S^0 K \pi$

- From a VDM fit to ZHU 23 $\eta\phi\gamma$ data with two resonances, $\phi(1680)$, $\phi(2170)$, and a third resonance with mass 1850.7 ± 5.3 MeV and width 25 ± 35 MeV of 1.7 σ statistical evidence.
- From a fit using a vector meson dominance model with contributions from $\phi(1680)$, $\phi(2170)$ and non resonant contribution.
- From the analysis of the combined measurements of $\sigma(e^+e^- \rightarrow \eta\phi)$ from BaBar, Belle, BESIII, CMD3.
- From a partial wave amplitude analysis at $\sqrt{s} = 2.125$ GeV which includes all the possible intermediate states that match J^{PC} conservation in the subsequent two-body decay. The intermediate states are parameterized with the relativistic Breit-Wigner functions. Statistical error only.
- Seen in $\psi(2S)$ decay with branching ratio $\psi(2S) \rightarrow X\eta \rightarrow K^+K^-\eta = (12.0 \pm 1.3^{+6.5}_{-6.9}) \times 10^{-6}$.
- From a fit using a vector meson dominance model with contribution from $\rho(770)$, $\omega(782)$, $\phi(1020)$, $\omega(1420)$, $\rho(1450)$.
- From a fit with coherent interference of the $\phi(1680)$ with a non-resonant contribution.
- Assuming the $K\bar{K}^*(892) + c.c.$ dynamics. Systematic uncertainties not estimated.
- Using a vector meson dominance model with contribution from $\phi(1020)$, $\phi(1680)$, and higher mass excitations of $\rho(770)$ and $\omega(782)$.
- Using events with $\pi\pi$ invariant mass less than 0.85 GeV.
- From a fit with two incoherent Breit-Wigners.
- From the simultaneous fit to the $K\bar{K}^*(892) + c.c.$ and $\phi\eta$ data from AUBERT 08s using the results of AUBERT 07AK.
- From the combined fit of AKHMETSHIN 03 and MANE 81 also including ρ, ω , and ϕ . Neither isospin nor flavor structure known.
- Using data from IVANOV 81, BARKOV 87, BISELLO 88B, DOLINSKY 91, and AN-TONELLI 92.
- Using the data from BISELLO 91C.
- Using BISELLO 88B and MANE 82 data.
- From global fit including ρ, ω, ϕ and $\rho(1700)$ assume mass 1570 MeV and width 510 MeV for ρ radial excitation.
- From global fit of ρ, ω, ϕ and their radial excitations to channels $\omega\pi^+\pi^-, K^+K^-, K_S^0 K_L^0, K_S^0 K^\pm \pi^\mp$. Assume mass 1570 MeV and width 510 MeV for ρ radial excitations, mass 1570 and width 500 MeV for ω radial excitation.
- Fit to one channel only, neglecting interference with $\omega, \rho(1700)$.

 $p\bar{p}$ ANNIHILATION

VALUE (MeV)	DOCUMENT ID	TECN	COMMENT
••• We do not use the following data for averages, fits, limits, etc. •••			
1700 \pm 8	1 AMSLER	06	CBAR 0.9 $\bar{p}p \rightarrow K^+K^-\pi^0$
1 Could also be $\rho(1700)$.			

 $\phi(1680)$ WIDTH e^+e^- PRODUCTION

VALUE (MeV)	EVTS	DOCUMENT ID	TECN	COMMENT
150 \pm 50	OUR ESTIMATE	This is only an educated guess; the error given is larger than the error on the average of the published values.		
••• We do not use the following data for averages, fits, limits, etc. •••				
150.8 \pm 7.0		1 LICHARD	23	RVUE $e^+e^- \rightarrow \Upsilon(nS) \rightarrow \phi\eta\gamma$
149 \pm 12 \pm 13		2 ZHU	23	BELL $e^+e^- \rightarrow \Upsilon(nS) \rightarrow \phi\eta\gamma$
156 \pm 5 \pm 9		3 ZHU	23A	RVUE $e^+e^- \rightarrow \eta\phi$
172 \pm 8		4 ABLIKIM	22L	BES3 $2.0-3.08 e^+e^- \rightarrow K^+K^-\pi^0$
185 $^{+30}_{-26} \pm 25_{-47}$	1.8k	5 ABLIKIM	20F	BES3 $\psi(2S) \rightarrow K^+K^-\eta$
159 \pm 32		6 ACHASOV	20C	SND $1.3-2.0 e^+e^- \rightarrow K^+K^-\pi^0$
103 $^{+26}_{-24}$		ACHASOV	19	SND $e^+e^- \rightarrow \pi^+\pi^-\pi^0\eta$
176 \pm 23 \pm 38	3k	7 IVANOV	19A	CMD3 $1.59-2.007 e^+e^- \rightarrow K^+K^-\eta$
300 \pm 50	2k	8 ACHASOV	18A	SND $1.3-2.0 e^+e^- \rightarrow K_S^0 K_L^0 \pi^0$
165 \pm 38 \pm 70	6.2k	9 LEES	14H	BABR $e^+e^- \rightarrow K_S^0 K_L^0 \gamma$
300 \pm 15 \pm 37		10 LEES	12F	BABR $10.6 e^+e^- \rightarrow \phi\pi^+\pi^-\gamma$
211 \pm 14 \pm 19	4.8k	11 SHEN	09	BELL $10.6 e^+e^- \rightarrow K^+K^-\pi^+\pi^-\gamma$
322 \pm 77 \pm 160		12 AUBERT	08s	BABR $10.6 e^+e^- \rightarrow$ hadrons
139 \pm 60	948	13 AKHMETSHIN	03	CMD2 $1.05-1.38 e^+e^- \rightarrow K_L^0 K_S^0$
300 \pm 60		14 CLEGG	94	RVUE $e^+e^- \rightarrow K^+K^-, K_S^0 K \pi$
146 \pm 55	367	BISELLO	91C	DM2 $e^+e^- \rightarrow K_S^0 K^\pm \pi^\mp$
207 \pm 45		15 BISELLO	88B	DM2 $e^+e^- \rightarrow K^+K^-$
185 \pm 22		16 BUON	82	DM1 $e^+e^- \rightarrow$ hadrons
102 \pm 36		17 MANE	82	DM1 $e^+e^- \rightarrow K_S^0 K \pi$

- From a VDM fit to ZHU 23 $\eta\phi\gamma$ data with two resonances, $\phi(1680)$, $\phi(2170)$, and a third resonance with mass 1850.7 ± 5.3 MeV and width 25 ± 35 MeV of 1.7 σ statistical evidence.
- From a fit using a vector meson dominance model with contributions from $\phi(1680)$, $\phi(2170)$ and non resonant contribution.
- From the analysis of the combined measurements of $\sigma(e^+e^- \rightarrow \eta\phi)$ from BaBar, Belle, BESIII, CMD3.

- From a partial wave amplitude analysis at $\sqrt{s} = 2.125$ GeV which includes all the possible intermediate states that match J^{PC} conservation in the subsequent two-body decay. The intermediate states are parameterized with the relativistic Breit-Wigner functions. Statistical error only.
- Seen in $\psi(2S)$ decay with branching ratio $\psi(2S) \rightarrow X\eta \rightarrow K^+K^-\eta = (12.0 \pm 1.3^{+6.5}_{-6.9}) \times 10^{-6}$.
- From a fit using a vector meson dominance model with contribution from $\rho(770)$, $\omega(782)$, $\phi(1020)$, $\omega(1420)$, $\rho(1450)$.
- From a fit with coherent interference of the $\phi(1680)$ with a non-resonant contribution.
- Assuming the $K\bar{K}^*(892) + c.c.$ dynamics. Systematic uncertainties not estimated.
- Using a vector meson dominance model with contribution from $\phi(1020)$, $\phi(1680)$, and higher mass excitations of $\rho(770)$ and $\omega(782)$.
- Using events with $\pi\pi$ invariant mass less than 0.85 GeV.
- From a fit with two incoherent Breit-Wigners.
- From the simultaneous fit to the $K\bar{K}^*(892) + c.c.$ and $\phi\eta$ data from AUBERT 08s using the results of AUBERT 07AK.
- From the combined fit of AKHMETSHIN 03 and MANE 81 also including ρ, ω , and ϕ . Neither isospin nor flavor structure known.
- Using BISELLO 88B and MANE 82 data.
- From global fit including ρ, ω, ϕ and $\rho(1700)$.
- From global fit of ρ, ω, ϕ and their radial excitations to channels $\omega\pi^+\pi^-, K^+K^-, K_S^0 K_L^0, K_S^0 K^\pm \pi^\mp$. Assume mass 1570 MeV and width 510 MeV for ρ radial excitations, mass 1570 and width 500 MeV for ω radial excitation.
- Fit to one channel only, neglecting interference with $\omega, \rho(1700)$.

 $p\bar{p}$ ANNIHILATION

VALUE (MeV)	DOCUMENT ID	TECN	COMMENT
••• We do not use the following data for averages, fits, limits, etc. •••			
143 \pm 24	1 AMSLER	06	CBAR 0.9 $\bar{p}p \rightarrow K^+K^-\pi^0$
1 Could also be $\rho(1700)$.			

 $\phi(1680)$ DECAY MODES

Mode	Fraction (Γ_i/Γ)
Γ_1 $K\bar{K}^*(892) + c.c.$	seen
Γ_2 $K_S^0 K \pi$	seen
Γ_3 $K\bar{K}$	seen
Γ_4 $K_L^0 K_S^0$	
Γ_5 e^+e^-	seen
Γ_6 $\omega\pi\pi$	not seen
Γ_7 $\phi\pi\pi$	
Γ_8 $K^+K^-\pi^+\pi^-$	seen
Γ_9 $\eta\phi$	seen
Γ_{10} $\eta\gamma$	seen
Γ_{11} $K^+K^-\pi^0$	
Γ_{12} $f_2'(1525)\gamma$	not seen

 $\phi(1680)$ $\Gamma(i)\Gamma(e^+e^-)/\Gamma(\text{total})$

This combination of a partial width with the partial width into e^+e^- and with the total width is obtained from the integrated cross section into channel (i) in e^+e^- annihilation. We list only data that have not been used to determine the partial width $\Gamma(i)$ or the branching ratio $\Gamma(i)/\text{total}$.

 $\Gamma(K_L^0 K_S^0) \times \Gamma(e^+e^-)/\Gamma_{\text{total}}$ $\Gamma_4\Gamma_5/\Gamma$

VALUE (eV)	EVTS	DOCUMENT ID	TECN	COMMENT
••• We do not use the following data for averages, fits, limits, etc. •••				
14.3 \pm 2.4 \pm 6.2	6.2k	1 LEES	14H	BABR $e^+e^- \rightarrow K_S^0 K_L^0 \gamma$
1 Using a vector meson dominance model with contribution from $\phi(1020)$, $\phi(1680)$, and higher mass excitations of $\rho(770)$ and $\omega(782)$.				

 $\Gamma(\phi\pi\pi) \times \Gamma(e^+e^-)/\Gamma_{\text{total}}$ $\Gamma_7\Gamma_5/\Gamma$

VALUE (10^{-2} keV)	DOCUMENT ID	TECN	COMMENT
••• We do not use the following data for averages, fits, limits, etc. •••			
4.2 \pm 0.2 \pm 0.3	LEES	12F	BABR 10.6 $e^+e^- \rightarrow \phi\pi^+\pi^-\gamma$

 $\Gamma(\eta\phi) \times \Gamma(e^+e^-)/\Gamma_{\text{total}}$ $\Gamma_9\Gamma_5/\Gamma$

VALUE (eV)	EVTS	DOCUMENT ID	TECN	COMMENT
••• We do not use the following data for averages, fits, limits, etc. •••				
122 \pm 6 \pm 13		1 ZHU	23	BELL $e^+e^- \rightarrow \Upsilon(nS) \rightarrow \phi\eta\gamma$
65 $^{+5}_{-4} \pm 13$ to 215 $^{+8}_{-5} \pm 11$		2 ZHU	23A	RVUE $e^+e^- \rightarrow \eta\phi$
94 \pm 13 \pm 15	3k	3 IVANOV	19A	CMD3 $1.59-2.007 e^+e^- \rightarrow K^+K^-\eta$

- From a solution of the fit using a vector meson dominance model with contributions from $\phi(1680)$, $\phi(2170)$ and non resonant contribution. Other solutions with equal fit quality give $(219 \pm 15 \pm 18)$ eV, $(163 \pm 11 \pm 13)$ eV and $(203 \pm 12 \pm 18)$ eV.
- From the analysis of the combined measurements of $\sigma(e^+e^- \rightarrow \eta\phi)$ from BaBar, Belle, BESIII, CMD3. Four solutions are found, with equal fit quality: $(79 \pm 4 \pm 16)$ eV, $(127 \pm 5 \pm 12)$ eV, $(65^{+5}_{-4} \pm 13)$ eV, $(215^{+8}_{-5} \pm 11)$ eV.
- From a fit with coherent interference of the $\phi(1680)$ with a non-resonant contribution.

See key on page 1171

Meson Particle Listings

 $\phi(1680), \rho_3(1690)$ $\phi(1680) \Gamma(i)\Gamma(e^+e^-)/\Gamma^2(\text{total})$

This combination of a branching ratio into channel (*i*) and branching ratio into e^+e^- is directly measured and obtained from the cross section at the peak. We list only data that have not been used to determine the branching ratio into (*i*) or e^+e^- .

$\Gamma(K_L^0 K_S^0)/\Gamma_{\text{total}} \times \Gamma(e^+e^-)/\Gamma_{\text{total}} \quad \Gamma_4/\Gamma \times \Gamma_5/\Gamma$

VALUE (units 10^{-6})	EVTS	DOCUMENT ID	TECN	COMMENT
0.131 ± 0.059	948	¹ AKHMETSHIN 03	CMD2	1.05–1.38 $e^+e^- \rightarrow K_L^0 K_S^0$

• • • We do not use the following data for averages, fits, limits, etc. • • •

¹ From the combined fit of AKHMETSHIN 03 and MANE 81 also including ρ, ω , and ϕ . Neither isospin nor flavor structure known. Recalculated by us.

$\Gamma(K\bar{K}^*(892) + \text{c.c.})/\Gamma_{\text{total}} \times \Gamma(e^+e^-)/\Gamma_{\text{total}} \quad \Gamma_1/\Gamma \times \Gamma_5/\Gamma$

VALUE (units 10^{-6})	EVTS	DOCUMENT ID	TECN	COMMENT
1.15 ± 0.16 ± 0.01		¹ AUBERT 08s	BABR	10.6 $e^+e^- \rightarrow K\bar{K}^*(892)\gamma + \text{c.c.}$
3.29 ± 1.57	367	² BISELLO 91c	DM2	1.35–2.40 $e^+e^- \rightarrow K_S^0 K^\pm \pi^\mp$

• • • We do not use the following data for averages, fits, limits, etc. • • •

¹ From the simultaneous fit to the $K\bar{K}^*(892) + \text{c.c.}$ and $\phi\eta$ data from AUBERT 08s using the results of AUBERT 07AK.

² Recalculated by us with the published value of $B(K\bar{K}^*(892) + \text{c.c.}) \times \Gamma(e^+e^-)$.

$\Gamma(\phi\pi\pi)/\Gamma_{\text{total}} \times \Gamma(e^+e^-)/\Gamma_{\text{total}} \quad \Gamma_7/\Gamma \times \Gamma_5/\Gamma$

VALUE (units 10^{-7})	EVTS	DOCUMENT ID	TECN	COMMENT
1.86 ± 0.14 ± 0.21	4.8k	¹ SHEN 09	BELL	10.6 $e^+e^- \rightarrow K^+ K^- \pi^+ \pi^- \gamma$

• • • We do not use the following data for averages, fits, limits, etc. • • •

¹ Multiplied by 3/2 to take into account the $\phi\pi^0\pi^0$ mode. Using $B(\phi \rightarrow K^+ K^-) = (49.2 \pm 0.6)\%$.

$\Gamma(\eta\phi)/\Gamma_{\text{total}} \times \Gamma(e^+e^-)/\Gamma_{\text{total}} \quad \Gamma_9/\Gamma \times \Gamma_5/\Gamma$

VALUE (units 10^{-7})	EVTS	DOCUMENT ID	TECN	COMMENT
5.64 $^{+1.74}_{-1.80}$		ACHASOV 19	SND	$e^+e^- \rightarrow \pi^+ \pi^- \pi^0 \eta$
5.3 ± 0.6 ± 0.9	3k	¹ IVANOV 19A	CMD3	1.59–2.007 $e^+e^- \rightarrow K^+ K^- \eta$
4.3 ± 1.0 ± 0.9		² AUBERT 08s	BABR	10.6 $e^+e^- \rightarrow \phi\eta\gamma$

• • • We do not use the following data for averages, fits, limits, etc. • • •

¹ From a fit with coherent interference of the $\phi(1680)$ with a non-resonant contribution.

² From the simultaneous fit to the $K\bar{K}^*(892) + \text{c.c.}$ and $\phi\eta$ data from AUBERT 08s using the results of AUBERT 07AK.

 $\phi(1680)$ BRANCHING RATIOS

$\Gamma(K\bar{K}^*(892) + \text{c.c.})/\Gamma(K_S^0 K\pi) \quad \Gamma_1/\Gamma_2$

VALUE	DOCUMENT ID	TECN	COMMENT
dominant	MANE 82	DM1	$e^+e^- \rightarrow K_S^0 K^\pm \pi^\mp$

$\Gamma(K\bar{K})/\Gamma(K\bar{K}^*(892) + \text{c.c.}) \quad \Gamma_3/\Gamma_1$

VALUE	DOCUMENT ID	TECN	COMMENT
0.07 ± 0.01	BUON 82	DM1	e^+e^-

• • • We do not use the following data for averages, fits, limits, etc. • • •

$\Gamma(\omega\pi\pi)/\Gamma(K\bar{K}^*(892) + \text{c.c.}) \quad \Gamma_6/\Gamma_1$

VALUE	DOCUMENT ID	TECN	COMMENT
<0.10	BUON 82	DM1	e^+e^-

$\Gamma(\eta\phi)/\Gamma_{\text{total}} \quad \Gamma_9/\Gamma$

VALUE	EVTS	DOCUMENT ID	TECN	COMMENT
seen	35	¹ ACHASOV 14	SND	1.15–2.00 $e^+e^- \rightarrow \eta\gamma$

¹ From a phenomenological model based on vector meson dominance with $\rho(1450)$ and $\phi(1680)$ masses and widths from the PDG 12.

$\Gamma(\eta\phi)/\Gamma(K\bar{K}^*(892) + \text{c.c.}) \quad \Gamma_9/\Gamma_1$

VALUE	DOCUMENT ID	TECN	COMMENT
≈ 0.37	¹ AUBERT 08s	BABR	10.6 $e^+e^- \rightarrow \text{hadrons}$

• • • We do not use the following data for averages, fits, limits, etc. • • •

¹ From the fit including data from AUBERT 07AK.

$\Gamma(\eta\gamma)/\Gamma_{\text{total}} \quad \Gamma_{10}/\Gamma$

VALUE	EVTS	DOCUMENT ID	TECN	COMMENT
seen	35	¹ ACHASOV 14	SND	1.15–2.00 $e^+e^- \rightarrow \eta\gamma$

¹ From a phenomenological model based on vector meson dominance with $\rho(1450)$ and $\phi(1680)$ masses and widths from the PDG 12.

$\Gamma(f_2'(1525)\gamma)/\Gamma_{\text{total}} \quad \Gamma_{12}/\Gamma$

VALUE	DOCUMENT ID	TECN	COMMENT
not seen	¹ ACHASOV 22	SND	1.17–2.00 $e^+e^- \rightarrow \eta\eta\gamma$

¹ The 90% CL upper limit on the Born cross sections $\sigma(e^+e^- \rightarrow \phi(1680) \rightarrow f_2'(1525)\gamma \rightarrow \eta\eta\gamma)$ and $\sigma(e^+e^- \rightarrow \rho(1700) \rightarrow f_0(1500)\gamma \rightarrow \eta\eta\gamma)$ is 10.6 pb.

 $\phi(1680)$ REFERENCES

LICHARD 23	PR D108 092005	P. Lichard	(OPAV, CTUP)
ZHU 23	PR D107 012006	W. Zhu et al.	(BELLE Collab.)
ZHU 23A	CP C47 113003	W. Zhu, X. Wang	(RVUE)
ABLIKIM 22L	JHEP 2207 045	M. Ablikim et al.	(BESIII Collab.)
ACHASOV 22	EPJ C82 168	M.N. Achasov et al.	(SND Collab.)
ABLIKIM 20F	PR D101 032008	M. Ablikim et al.	(BESIII Collab.)
ACHASOV 20C	EPJ C80 1139	M.N. Achasov et al.	(SND Collab.)
ACHASOV 19	PR D99 112004	M.N. Achasov et al.	(SND Collab.)
IVANOV 19A	PL B798 134946	V.L. Ivanov et al.	(CMD-3 Collab.)
ACHASOV 18A	PR D97 032011	M.N. Achasov et al.	(SND Collab.)
ACHASOV 14A	PR D90 032002	M.N. Achasov et al.	(SND Collab.)
LEES 14H	PR D89 092002	J.P. Lees et al.	(BABAR Collab.)
LEES 12F	PR D86 012008	J.P. Lees et al.	(BABAR Collab.)
PDG 12	PR D86 010001	J. Beringer et al.	(PDG Collab.)
SHEN 09	PR D80 031101	C.P. Shen et al.	(BELLE Collab.)
AUBERT 08S	PR D77 092002	B. Aubert et al.	(BABAR Collab.)
AUBERT 07AK	PR D76 012008	B. Aubert et al.	(BABAR Collab.)
AMSLER 06	PL B639 165	C. Amisler et al.	(Crystal Barrel Collab.)
AKHMETSHIN 03	PL B551 27	R.R. Akhmetshin et al.	(Novosibirsk CMD-2 Collab.)
	PAN 65 1222	E.V. Anashkin, V.M. Aulchenko, R.R. Akhmetshin	
	Translated from YAF 65 1255.		
ACHASOV 98H	PR D57 4334	M.N. Achasov, A.A. Kozhevnikov	(LANC, MCHS)
CLEGG 94	ZPHY C62 455	A.B. Clegg, A. Donnachie	(DM2 Collab.)
ANTONELLI 92	ZPHY C56 15	A. Antonelli et al.	(DM2 Collab.)
BISELLO 91C	ZPHY C52 227	D. Bisello et al.	(DM2 Collab.)
DOLINSKY 91	PRPL 202 99	S.I. Dolinsky et al.	(NOVO)
BISELLO 88B	ZPHY C39 13	D. Bisello et al.	(PADO, CLER, FRAS+)
BARKOV 87	JETPL 46 164	L.M. Barkov et al.	(NOVO)
	Translated from ZETFP 46 132.		
BUON 82	PL 1138 221	J. Buon et al.	(LALO, MONP)
MANE 82	PL 112B 178	F. Mane et al.	(LALO)
IVANOV 81	PL 107B 297	P.M. Ivanov et al.	(NOVO)
MANE 81	PL 99B 261	F. Mane et al.	(ORSAY)

 $\rho_3(1690)$

$$I^G(J^{PC}) = 1^+(3^{--})$$

 $\rho_3(1690)$ MASS

VALUE (MeV) DOCUMENT ID
1688.8 ± 2.1 OUR AVERAGE Includes data from the 5 datablocks that follow this one.

2π MODE

VALUE (MeV)	EVTS	DOCUMENT ID	TECN	CHG	COMMENT
The data in this block is included in the average printed for a previous datablock.					

1686 ± 4 OUR AVERAGE

1677 ± 14		EVANGELIS...	81	OMEG	–	12 $\pi^- p \rightarrow 2\pi p$
1679 ± 11	476	BALTAY 78B	HBC	0	15 $\pi^+ p \rightarrow \pi^+ \pi^- n$	
1678 ± 12	175	¹ ANTIPOV 77	CIBS	0	25 $\pi^- p \rightarrow p3\pi$	
1690 ± 7	600	¹ ENGLER 74	DBC	0	6 $\pi^+ n \rightarrow \pi^+ \pi^- p$	
1693 ± 8		² GRAYER 74	ASPK	0	17 $\pi^- p \rightarrow \pi^+ \pi^- n$	
1678 ± 12		MATTHEWS 71c	DBC	0	7 $\pi^+ n$	
• • • We do not use the following data for averages, fits, limits, etc. • • •						
1734 ± 10		³ CORDEN 79	OMEG	–	12–15 $\pi^- p \rightarrow n2\pi$	
1692 ± 12		^{2,4} ESTABROOKS 75	RVUE	0	17 $\pi^- p \rightarrow \pi^+ \pi^- n$	
1737 ± 23		ARMENISE 70	DBC	0	9 $\pi^+ n$	
1650 ± 35	122	BARTSCH 70B	HBC	+	8 $\pi^+ p \rightarrow N2\pi$	
1687 ± 21		STUNTEBECK 70	HDBC	0	8 $\pi^- p, 5.4 \pi^+ d$	
1683 ± 13		ARMENISE 68	DBC	0	5.1 $\pi^+ d$	
1670 ± 30		GOLDBERG 65	HBC	0	6 $\pi^+ d, 8 \pi^- p$	

¹ Mass errors enlarged by us to Γ/\sqrt{N} ; see the note with the $K^*(892)$ mass.

² Uses same data as HYAMS 75.

³ From a phase shift solution containing a $f_2'(1525)$ width two times larger than the $K\bar{K}$ result.

⁴ From phase-shift analysis. Error takes account of spread of different phase-shift solutions.

 $K\bar{K}$ AND $K\bar{K}\pi$ MODES

VALUE (MeV)	EVTS	DOCUMENT ID	TECN	CHG	COMMENT
The data in this block is included in the average printed for a previous datablock.					

1696 ± 4 OUR AVERAGE

1699 ± 5		ALPER 80	CNTR	0	62 $\pi^- p \rightarrow K^+ K^- n$
1698 ± 12	6k	^{5,6} MARTIN 78D	SPEC	0	10 $\pi p \rightarrow K_S^0 K^- p$
1692 ± 6		BLUM 75	ASPK	0	18.4 $\pi^- p \rightarrow nK^+ K^-$
1690 ± 16		ADERHOLZ 69	HBC	+	8 $\pi^+ p \rightarrow K\bar{K}\pi$
• • • We do not use the following data for averages, fits, limits, etc. • • •					
1694 ± 8		⁷ COSTA 80	OMEG	–	10 $\pi^- p \rightarrow K^+ K^- n$

⁵ From a fit to $J^P = 3^-$ partial wave.

⁶ Systematic error on mass scale subtracted.

⁷ They cannot distinguish between $\rho_3(1690)$ and $\omega_3(1670)$.

(4π)± MODE

VALUE (MeV)	EVTS	DOCUMENT ID	TECN	CHG	COMMENT
The data in this block is included in the average printed for a previous datablock.					

1686 ± 5 OUR AVERAGE Error includes scale factor of 1.1.

1694 ± 6		⁸ EVANGELIS...	81	OMEG	–	12 $\pi^- p \rightarrow p4\pi$
1665 ± 15	177	BALTAY 78B	HBC	+	15 $\pi^+ p \rightarrow p4\pi$	
1670 ± 10		THOMPSON 74	HBC	+	13 $\pi^+ p$	
1687 ± 20		CASON 73	HBC	–	8,18.5 $\pi^- p$	
1685 ± 14		⁹ CASON 73	HBC	–	8,18.5 $\pi^- p$	
1680 ± 40	144	BARTSCH 70B	HBC	+	8 $\pi^+ p \rightarrow N4\pi$	
1689 ± 20	102	⁹ BARTSCH 70B	HBC	+	8 $\pi^+ p \rightarrow N2\rho$	
1705 ± 21		CASO 70	HBC	–	11.2 $\pi^- p \rightarrow n\rho2\pi$	

Meson Particle Listings

$\rho_3(1690)$

••• We do not use the following data for averages, fits, limits, etc. •••

1718 ± 10	10	EVANGELIS...	81	OMEG	-	12 $\pi^- p \rightarrow p 4\pi$
1673 ± 9	11	EVANGELIS...	81	OMEG	-	12 $\pi^- p \rightarrow p 4\pi$
1733 ± 9	66	9 KLIGER	74	HBC	-	4.5 $\pi^- p \rightarrow p 4\pi$
1630 ± 15		HOLMES	72	HBC	+	10-12 $K^+ p$
1720 ± 15		BALTAY	68	HBC	+	7, 8.5 $\pi^+ p$

⁸ From $\rho^- \rho^0$ mode, not independent of the other two EVANGELISTA 81 entries.
⁹ From $\rho^\pm \rho^0$ mode.
¹⁰ From $a_2(1320)^- \pi^0$ mode, not independent of the other two EVANGELISTA 81 entries.
¹¹ From $a_2(1320)^0 \pi^-$ mode, not independent of the other two EVANGELISTA 81 entries.

$\omega\pi$ MODE

VALUE (MeV)	DOCUMENT ID	TECN	CHG	COMMENT
-------------	-------------	------	-----	---------

The data in this block is included in the average printed for a previous datablock.

1681 ± 7 OUR AVERAGE

1670 ± 25	12	ALDE	95	GAM2	-	38 $\pi^- p \rightarrow \omega\pi^0 n$
1690 ± 15		EVANGELIS...	81	OMEG	-	12 $\pi^- p \rightarrow \omega\pi p$
1666 ± 14		GESSAROLI	77	HBC	+	11 $\pi^- p \rightarrow \omega\pi p$
1686 ± 9		THOMPSON	74	HBC	+	13 $\pi^+ p$

••• We do not use the following data for averages, fits, limits, etc. •••

1654 ± 24		BARNHAM	70	HBC	+	10 $K^+ p \rightarrow \omega\pi X$
-----------	--	---------	----	-----	---	------------------------------------

¹² Supersedes ALDE 92c.

$\eta\pi^+\pi^-$ MODE

(For difficulties with MMS experiments, see the $a_2(1320)$ mini-review in the 1973 edition.)

VALUE (MeV)	DOCUMENT ID	TECN	CHG	COMMENT
-------------	-------------	------	-----	---------

The data in this block is included in the average printed for a previous datablock.

1682 ± 12 OUR AVERAGE

1685 ± 10 ± 20		AMELIN	00	VES	-	37 $\pi^- p \rightarrow \eta\pi^+\pi^- n$
1680 ± 15		FUKUI	88	SPEC	0	8.95 $\pi^- p \rightarrow \eta\pi^+\pi^- n$

••• We do not use the following data for averages, fits, limits, etc. •••

1700 ± 47	13	ANDERSON	69	MMS	-	16 $\pi^- p$ backward
1632 ± 15	13,14	FOCACCI	66	MMS	-	7-12 $\pi^- p \rightarrow pMM$
1700 ± 15	13,14	FOCACCI	66	MMS	-	7-12 $\pi^- p \rightarrow pMM$
1748 ± 15	13,14	FOCACCI	66	MMS	-	7-12 $\pi^- p \rightarrow pMM$

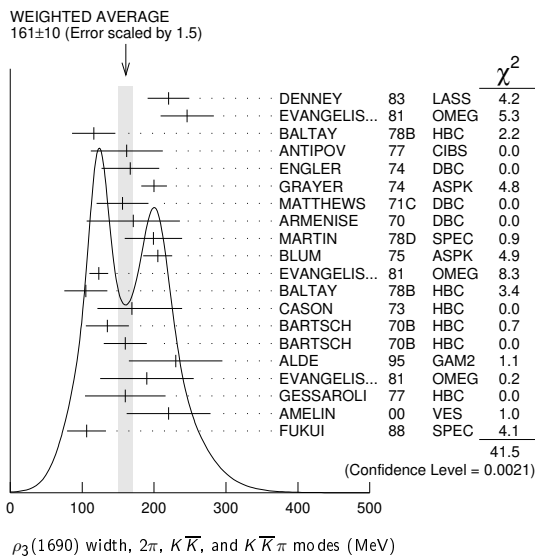
¹³ Seen in 2.5-3 GeV/c $\bar{p}p$. $2\pi^+2\pi^-$, with 0, 1, 2 $\pi^+\pi^-$ pairs in ρ band not seen by OREN 74 (2.3 GeV/c $\bar{p}p$) with more statistics. (Jan. 1976)

¹⁴ Not seen by BOWEN 72.

$\rho_3(1690)$ WIDTH

2 π , $K\bar{K}$, AND $K\bar{K}\pi$ MODES

161 ± 10 OUR AVERAGE Includes data from the 5 datablocks that follow this one. Error includes scale factor of 1.5. See the ideogram below.



2 π MODE

The data in this block is included in the average printed for a previous datablock.

186 ± 14 OUR AVERAGE Error includes scale factor of 1.3. See the ideogram below.

220 ± 29		DENNEY	83	LASS	-	10 $\pi^+ N$
246 ± 37		EVANGELIS...	81	OMEG	-	12 $\pi^- p \rightarrow 2\pi p$

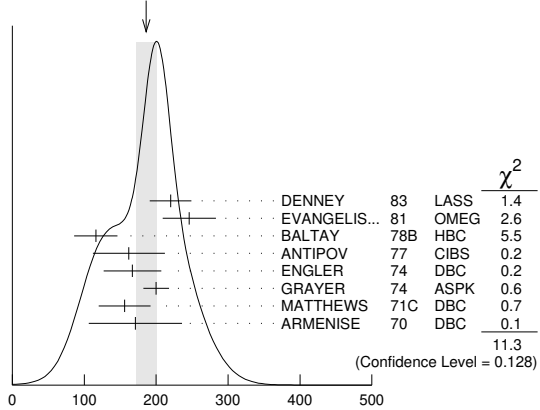
116 ± 30	476	BALTAY	78B	HBC	0	15 $\pi^+ p \rightarrow \pi^+\pi^- n$
162 ± 50	175	15 ANTIPOV	77	CIBS	0	25 $\pi^- p \rightarrow p 3\pi$
167 ± 40	600	ENGLER	74	DBC	0	6 $\pi^+ n \rightarrow \pi^+\pi^- p$
200 ± 18		16 GRAY	74	ASPK	0	17 $\pi^- p \rightarrow \pi^+\pi^- n$
156 ± 36		MATTHEWS	71C	DBC	0	7 $\pi^+ N$
171 ± 65		ARMENISE	70	DBC	0	9 $\pi^+ d$

••• We do not use the following data for averages, fits, limits, etc. •••

322 ± 35	17	CORDEN	79	OMEG	-	12-15 $\pi^- p \rightarrow n 2\pi$
240 ± 30	16,18	ESTABROOKS	75	RVUE	-	17 $\pi^- p \rightarrow \pi^+\pi^- n$
180 ± 30	122	BARTSCH	70B	HBC	+	8 $\pi^+ p \rightarrow N 2\pi$
267 ± 72		STUNTEBECK	70	HDBC	0	8 $\pi^- p, 5.4 \pi^+ d$
188 ± 49		ARMENISE	68	DBC	0	5.1 $\pi^+ d$
180 ± 40		GOLDBERG	65	HBC	0	6 $\pi^+ d, 8 \pi^- p$

¹⁵ Width errors enlarged by us to $4\Gamma/\sqrt{N}$; see the note with the $K^*(892)$ mass.
¹⁶ Uses same data as HYAMS 75 and BECKER 79.
¹⁷ From a phase shift solution containing a $f'_2(1525)$ width two times larger than the $K\bar{K}$ result.
¹⁸ From phase-shift analysis. Error takes account of spread of different phase-shift solutions.

WEIGHTED AVERAGE
186 ± 14 (Error scaled by 1.3)



$\rho_3(1690)$ width, 2 π mode (MeV)

$K\bar{K}$ AND $K\bar{K}\pi$ MODES

The data in this block is included in the average printed for a previous datablock.

204 ± 18 OUR AVERAGE

199 ± 40	6000	19 MARTIN	78D	SPEC	-	10 $\pi p \rightarrow K_S^0 K^- p$
205 ± 20		BLUM	75	ASPK	0	18.4 $\pi^- p \rightarrow n K^+ K^-$

••• We do not use the following data for averages, fits, limits, etc. •••

219 ± 4		ALPER	80	CNTR	0	62 $\pi^- p \rightarrow K^+ K^- n$
186 ± 11	20	COSTA	80	OMEG	-	10 $\pi^- p \rightarrow K^+ K^- n$
112 ± 60		ADERHOLZ	69	HBC	+	8 $\pi^+ p \rightarrow K\bar{K}\pi$

¹⁹ From a fit to $J^P = 3^-$ partial wave.
²⁰ They cannot distinguish between $\rho_3(1690)$ and $\omega_3(1670)$.

(4 π) $^\pm$ MODE

The data in this block is included in the average printed for a previous datablock.

129 ± 10 OUR AVERAGE

123 ± 13	21	EVANGELIS...	81	OMEG	-	12 $\pi^- p \rightarrow p 4\pi$
105 ± 30	177	BALTAY	78B	HBC	+	15 $\pi^+ p \rightarrow p 4\pi$
169 ± 70		CASON	73	HBC	-	8,18.5 $\pi^- p$
135 ± 30	144	BARTSCH	70B	HBC	+	8 $\pi^+ p \rightarrow N 4\pi$
160 ± 30	102	BARTSCH	70B	HBC	+	8 $\pi^+ p \rightarrow N 2\pi$

••• We do not use the following data for averages, fits, limits, etc. •••

230 ± 28	22	EVANGELIS...	81	OMEG	-	12 $\pi^- p \rightarrow p 4\pi$
184 ± 33	23	EVANGELIS...	81	OMEG	-	12 $\pi^- p \rightarrow p 4\pi$
150	66	24 KLIGER	74	HBC	-	4.5 $\pi^- p \rightarrow p 4\pi$
106 ± 25		THOMPSON	74	HBC	+	13 $\pi^+ p$
125 ± 83	24	CASON	73	HBC	-	8,18.5 $\pi^- p$
130 ± 30		HOLMES	72	HBC	+	10-12 $K^+ p$
180 ± 30	90	24 BARTSCH	70B	HBC	+	8 $\pi^+ p \rightarrow N a_2 \pi$
100 ± 35		BALTAY	68	HBC	+	7, 8.5 $\pi^+ p$

²¹ From $\rho^- \rho^0$ mode, not independent of the other two EVANGELISTA 81 entries.
²² From $a_2(1320)^- \pi^0$ mode, not independent of the other two EVANGELISTA 81 entries.
²³ From $a_2(1320)^0 \pi^-$ mode, not independent of the other two EVANGELISTA 81 entries.
²⁴ From $\rho^\pm \rho^0$ mode.

See key on page 1171

Meson Particle Listings

$\rho_3(1690)$

$\omega\pi$ MODE

VALUE (MeV)	DOCUMENT ID	TECN	CHG	COMMENT
-------------	-------------	------	-----	---------

The data in this block is included in the average printed for a previous datablock.

190±40 OUR AVERAGE

230±65	25 ALDE	95	GAM2	38 $\pi^- p \rightarrow \omega\pi^0 n$
190±65	EVANGELIS...	81	OMEG	12 $\pi^- p \rightarrow \omega\pi\rho$
160±56	GESSAROLI	77	HBC	11 $\pi^- p \rightarrow \omega\pi\rho$
89±25	THOMPSON	74	HBC	+ 13 $\pi^+ p$
130 ⁺⁷³ ₋₄₃	BARNHAM	70	HBC	+ 10 $K^+ p \rightarrow \omega\pi X$

²⁵ Supersedes ALDE 92c.

$\eta\pi^+\pi^-$ MODE

(For difficulties with MMS experiments, see the $a_2(1320)$ mini-review in the 1973 edition.)

VALUE (MeV)	DOCUMENT ID	TECN	CHG	COMMENT
-------------	-------------	------	-----	---------

The data in this block is included in the average printed for a previous datablock.

130±40 OUR AVERAGE

VALUE	DOCUMENT ID	TECN	CHG	COMMENT
220±30±50	AMELIN	00	VES	37 $\pi^- p \rightarrow \eta\pi^+\pi^- n$
106±27	FUKUI	88	SPEC	0 8.95 $\pi^- p \rightarrow \eta\pi^+\pi^- n$
< 21	26,27 ANDERSON	69	MMS	- 16 $\pi^- p$ backward
< 30	26,27 FOCACCI	66	MMS	- 7-12 $\pi^- p \rightarrow \rho MM$
< 38	26,27 FOCACCI	66	MMS	- 7-12 $\pi^- p \rightarrow \rho MM$

²⁶ Seen in 2.5-3 GeV/c $\bar{p}p$. $2\pi^+2\pi^-$, with 0, 1, 2 $\pi^+\pi^-$ pairs in ρ^0 band not seen by OREN 74 (2.3 GeV/c $\bar{p}p$) with more statistics. (Jan. 1979)
²⁷ Not seen by BOWEN 72.

$\rho_3(1690)$ DECAY MODES

Mode	Fraction (Γ_i/Γ)	Scale factor
Γ_1 4π	(71.1 ± 1.9) %	
Γ_2 $\pi^\pm\pi^+\pi^-\pi^0$	(67 ± 22) %	
Γ_3 $\omega\pi$	(16 ± 6) %	
Γ_4 $\pi\pi$	(23.6 ± 1.3) %	
Γ_5 $K\bar{K}\pi$	(3.8 ± 1.2) %	
Γ_6 $K\bar{K}$	(1.58 ± 0.26) %	1.2
Γ_7 $\eta\pi^+\pi^-$	seen	
Γ_8 $\rho(770)\eta$	seen	
Γ_9 $\pi\pi\rho$	seen	
Γ_{10} $a_2(1320)\pi$	seen	
Γ_{11} $\rho\rho$	seen	
Γ_{12} $\phi\pi$		
Γ_{13} $\eta\pi$		
Γ_{14} $\pi^\pm 2\pi^+ 2\pi^- \pi^0$		

CONSTRAINED FIT INFORMATION

An overall fit to 5 branching ratios uses 10 measurements and one constraint to determine 4 parameters. The overall fit has a $\chi^2 = 14.7$ for 7 degrees of freedom.

The following off-diagonal array elements are the correlation coefficients $\langle \delta x_i \delta x_j \rangle / (\delta x_i \delta x_j)$, in percent, from the fit to the branching fractions, $x_i \equiv \Gamma_i / \Gamma_{\text{total}}$. The fit constrains the x_i whose labels appear in this array to sum to one.

x_4	-77		
x_5	-74	17	
x_6	-15	2	0
	x_1	x_4	x_5

$\rho_3(1690)$ BRANCHING RATIOS

$\Gamma(\pi\pi)/\Gamma_{\text{total}}$	DOCUMENT ID	TECN	CHG	COMMENT	Γ_4/Γ
0.236±0.013 OUR FIT					
0.243±0.013 OUR AVERAGE					
0.259 ^{+0.018} _{-0.019}	BECKER	79	ASPK	0 17 $\pi^- p$ polarized	
0.23 ± 0.02	CORDEN	79	OMEG	12-15 $\pi^- p \rightarrow n2\pi$	
0.22 ± 0.04	28 MATTHEWS	71c	HDHC	0 7 $\pi^+ n \rightarrow \pi^- p$	
0.245 ± 0.006	29 ESTABROOKS	75	RVUE	17 $\pi^- p \rightarrow \pi^+\pi^- n$	

²⁸ One-pion-exchange model used in this estimation.

²⁹ From phase-shift analysis of HYAMS 75 data.

$\Gamma(\pi\pi)/\Gamma(\pi^\pm\pi^+\pi^-\pi^0)$

VALUE	DOCUMENT ID	TECN	CHG	COMMENT	Γ_4/Γ_2
0.35 ± 0.11	CASON	73	HBC	- 8,18.5 $\pi^- p$	
< 0.2	HOLMES	72	HBC	+ 10-12 $K^+ p$	
< 0.12	BALLAM	71B	HBC	- 16 $\pi^- p$	

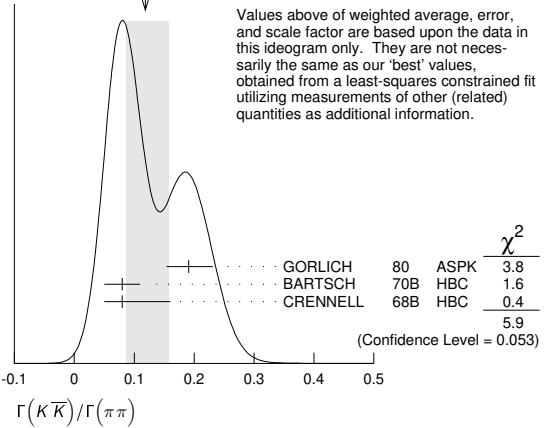
$\Gamma(\pi\pi)/\Gamma(4\pi)$

VALUE	DOCUMENT ID	TECN	CHG	COMMENT	Γ_4/Γ_1
0.332 ± 0.026 OUR FIT				Error includes scale factor of 1.1.	
0.30 ± 0.10	BALTAY	78B	HBC	0 15 $\pi^+ p \rightarrow \rho 4\pi$	

$\Gamma(K\bar{K})/\Gamma(\pi\pi)$

VALUE	DOCUMENT ID	TECN	CHG	COMMENT	Γ_6/Γ_4
0.067 ± 0.011 OUR FIT				Error includes scale factor of 1.2.	
0.118 ± 0.040 -0.032 OUR AVERAGE				Error includes scale factor of 1.7. See the ideogram below.	
0.191 ± 0.040 -0.037	GORLICH	80	ASPK	0 17,18 $\pi^- p$ polarized	
0.08 ± 0.03	BARTSCH	70B	HBC	+ 8 $\pi^+ p$	
0.08 ± 0.08 -0.03	CRENNELL	68B	HBC	6.0 $\pi^- p$	

WEIGHTED AVERAGE
 0.118±0.040-0.032 (Error scaled by 1.7)



$\Gamma(K\bar{K}\pi)/\Gamma(\pi\pi)$

VALUE	DOCUMENT ID	TECN	CHG	COMMENT	Γ_5/Γ_4
0.16 ± 0.05 OUR FIT					
0.16 ± 0.05	30 BARTSCH	70B	HBC	+ 8 $\pi^+ p$	

³⁰ Increased by us to correspond to $B(\rho_3(1690) \rightarrow \pi\pi) = 0.24$.

$[\Gamma(\pi\pi\rho) + \Gamma(a_2(1320)\pi) + \Gamma(\rho\rho)]/\Gamma(\pi^\pm\pi^+\pi^-\pi^0)$

VALUE	DOCUMENT ID	TECN	CHG	COMMENT	$(\Gamma_9 + \Gamma_{10} + \Gamma_{11})/\Gamma_2$
0.94 ± 0.09 OUR AVERAGE					
0.96 ± 0.21	BALTAY	78B	HBC	+ 15 $\pi^+ p \rightarrow \rho 4\pi$	
0.88 ± 0.15	BALLAM	71B	HBC	- 16 $\pi^- p$	
1 ± 0.15	BARTSCH	70B	HBC	+ 8 $\pi^+ p$	
consistent with 1	CASO	68	HBC	- 11 $\pi^- p$	

$\Gamma(\rho\rho)/\Gamma(\pi^\pm\pi^+\pi^-\pi^0)$

VALUE	EVTS	DOCUMENT ID	TECN	CHG	COMMENT	Γ_{11}/Γ_2
0.12 ± 0.11		BALTAY	78B	HBC	+ 15 $\pi^+ p \rightarrow \rho 4\pi$	
0.56	66	KLIGER	74	HBC	- 4.5 $\pi^- p \rightarrow \rho 4\pi$	
0.13 ± 0.09		31 THOMPSON	74	HBC	+ 13 $\pi^+ p$	
0.7 ± 0.15		BARTSCH	70B	HBC	+ 8 $\pi^+ p$	

³¹ $\rho\rho$ and $a_2(1320)\pi$ modes are indistinguishable.

$\Gamma(\rho\rho)/[\Gamma(\pi\pi\rho) + \Gamma(a_2(1320)\pi) + \Gamma(\rho\rho)]$

VALUE	DOCUMENT ID	TECN	CHG	COMMENT	$\Gamma_{11}/(\Gamma_9 + \Gamma_{10} + \Gamma_{11})$
0.48 ± 0.16	CASO	68	HBC	- 11 $\pi^- p$	

$\Gamma(a_2(1320)\pi)/\Gamma(\pi^\pm\pi^+\pi^-\pi^0)$

VALUE	DOCUMENT ID	TECN	CHG	COMMENT	Γ_{10}/Γ_2
0.66 ± 0.08	BALTAY	78B	HBC	+ 15 $\pi^+ p \rightarrow \rho 4\pi$	
0.36 ± 0.14	32 THOMPSON	74	HBC	+ 13 $\pi^+ p$	
not seen	CASON	73	HBC	- 8,18.5 $\pi^- p$	
0.6 ± 0.15	BARTSCH	70B	HBC	+ 8 $\pi^+ p$	
0.6	BALTAY	68	HBC	+ 7,8.5 $\pi^+ p$	

³² $\rho\rho$ and $a_2(1320)\pi$ modes are indistinguishable.

Meson Particle Listings

 $\rho_3(1690)$, $\rho(1700)$ $\Gamma(\omega\pi)/\Gamma(\pi^+\pi^+\pi^-\pi^0)$ Γ_3/Γ_2

VALUE	CL%	DOCUMENT ID	TECN	CHG	COMMENT
0.23±0.05 OUR AVERAGE		Error includes scale factor of 1.2.			
0.33±0.07		THOMPSON 74	HBC	+	13 π^+p
0.12±0.07		BALLAM 71B	HBC	-	16 π^-p
0.25±0.10		BALTAY 68	HBC	+	7,8.5 π^+p
0.25±0.10		JOHNSTON 68	HBC	-	7.0 π^-p
•••		We do not use the following data for averages, fits, limits, etc. •••			
<0.11	95	BALTAY 78B	HBC	+	15 $\pi^+p \rightarrow p4\pi$
<0.09		KLIGER 74	HBC	-	4.5 $\pi^-p \rightarrow p4\pi$

 $\Gamma(\phi\pi)/\Gamma(\pi^+\pi^+\pi^-\pi^0)$ Γ_{12}/Γ_2

VALUE	DOCUMENT ID	TECN	CHG	COMMENT
•••	We do not use the following data for averages, fits, limits, etc. •••			
<0.11	BALTAY 68	HBC	+	7,8.5 π^+p

 $\Gamma(\pi^+2\pi^+2\pi^-\pi^0)/\Gamma(\pi^+\pi^+\pi^-\pi^0)$ Γ_{14}/Γ_2

VALUE	DOCUMENT ID	TECN	CHG	COMMENT
•••	We do not use the following data for averages, fits, limits, etc. •••			
<0.15	BALTAY 68	HBC	+	7,8.5 π^+p

 $\Gamma(\eta\pi)/\Gamma(\pi^+\pi^+\pi^-\pi^0)$ Γ_{13}/Γ_2

VALUE	DOCUMENT ID	TECN	CHG	COMMENT
•••	We do not use the following data for averages, fits, limits, etc. •••			
<0.02	THOMPSON 74	HBC	+	13 π^+p

 $\Gamma(K\bar{K})/\Gamma_{total}$ Γ_6/Γ

VALUE	DOCUMENT ID	TECN	CHG	COMMENT
0.0158±0.0026 OUR FIT	Error includes scale factor of 1.2.			
0.0130±0.0024 OUR AVERAGE				
0.013 ±0.003	COSTA 80	OMEG 0		10 $\pi^-p \rightarrow K^+K^-n$
0.013 ±0.004	33 MARTIN 78B	SPEC -		10 $\pi p \rightarrow K_S^0 K^-p$
33	From $(\Gamma_4\Gamma_6)^{1/2} = 0.056 \pm 0.034$ assuming $B(\rho_3(1690) \rightarrow \pi\pi) = 0.24$.			

 $\Gamma(\omega\pi)/[\Gamma(\omega\pi) + \Gamma(\rho\rho)]$ $\Gamma_3/(\Gamma_3 + \Gamma_{11})$

VALUE	DOCUMENT ID	TECN	CHG	COMMENT
•••	We do not use the following data for averages, fits, limits, etc. •••			
0.22±0.08	CASON 73	HBC	-	8,18.5 π^-p

 $\Gamma(\eta\pi^+\pi^-)/\Gamma_{total}$ Γ_7/Γ

VALUE	DOCUMENT ID	TECN	COMMENT
seen	FUKUI 88	SPEC	8.95 $\pi^-p \rightarrow \eta\pi^+\pi^-n$

 $\Gamma(a_2(1320)\pi)/\Gamma(\rho(770)\eta)$ Γ_{10}/Γ_8

VALUE	DOCUMENT ID	TECN	COMMENT
5.5±2.0	AMELIN 00	VES	37 $\pi^-p \rightarrow \eta\pi^+\pi^-n$

 $\rho_3(1690)$ REFERENCES

AMELIN 00	NP A668 83	D. Amelin et al.	(VES Collab.)
ALDE 95	ZPHY C66 379	D.M. Alde et al.	(GAMS Collab.) JP
ALDE 92C	ZPHY C54 553	D.M. Alde et al.	(BELG, SERP, KEK, LANL+)
FUKUI 88	PL B202 441	S. Fukui et al.	(SUGI, NAGO, KEK, KYOT+)
DENNEY 83	PR D28 2726	D.L. Denney et al.	(IOWA, MICH)
EVANGELIS... 81	NP B178 197	C. Evangelista et al.	(BARI, BONN, CERN+)
ALPER 80	PL 94B 422	B. Alper et al.	(AMST, CERN, CRAC, MPIM+)
COSTA 80	NP B175 402	G. Costa et al.	(BARI, BONN, CERN, GLAS+)
GÖRDLICH 80	NP B174 16	L. Görlich et al.	(CRAC, MPIM, CERN+)
BECKER 79	NP B151 46	H. Becker et al.	(MPIM, CERN, ZEEM, CRAC)
CORDEN 79	NP B157 250	M.J. Corden et al.	(BIRM, RHEL, TEA+)
BALTAY 78B	PR D17 62	C. Baltay et al.	(COLU, BIRG)
MARTIN 78B	NP B140 158	A.D. Martin et al.	(DURH, GEVA)
MARTIN 78D	PL 74B 417	A.D. Martin et al.	(DURH, GEVA)
ANTIPOV 77	NP B119 45	Y.M. Antipov et al.	(SERP, GEVA)
GESSAROLI 77	NP B126 382	R. Gessaroli et al.	(BGNA, FIRZ, GENO+)
BLUM 75	PL 57B 403	W. Blum et al.	(CERN, MPIM) JP
ESTABROOKS 75	NP B95 322	P.G. Estabrooks, A.D. Martin	(DURH)
HYAMS 75	NP B100 205	B.D. Hyams et al.	(CERN, MPIM)
ENGLER 74	PR D10 2070	A. Engler et al.	(CMU, CASE)
GRAYER 74	NP B75 189	G. Grayer et al.	(CERN, MPIM)
KLIGER 74	SJNP 19 428	G.K. Kliger et al.	(ITEP)
OREN 74	NP B71 189	Y. Oren et al.	(ANL, OXF)
THOMPSON 74	NP B69 220	G. Thompson et al.	(PURD)
CASON 73	PR D7 1971	N.M. Cason et al.	(NDAM)
BOWEN 72	PRL 29 890	D.R. Bowen et al.	(NEAS, STON)
HOLMES 72	PR D6 3336	R. Holmes et al.	(ROCH)
BALLAM 71B	PR D3 2606	J. Ballam et al.	(SLAC)
MATTHEWS 71C	NP B33 1	J.A.J. Matthews et al.	(TNTO, WISC) JP
ARMENISE 70	LNC 4 199	N. Armenise et al.	(BARI, BGNA, FIRZ)
BARNHAM 70	PRL 24 1083	K.W.J. Barnham et al.	(BIRM)
BARTSCH 70B	NP B22 109	J. Bartsch et al.	(AACH, BERL, CERN)
CASO 70	LNC 3 707	C. Caso et al.	(GENO, HAMB, MILA, SAEL)
STUNTEBECK 70	PL 32B 391	P.H. Stuntebeck et al.	(NDAM)
ADERHOLZ 69	NP B11 259	M. Aderholz et al.	(AACH3, BERL, CERN+)
ANDERSON 69	PRL 22 1390	E.W. Anderson et al.	(BNL, CMU)
ARMENISE 68	NC 54A 999	N. Armenise et al.	(BARI, BGNA, FIRZ+)
BALTAY 68	PRL 20 887	C. Baltay et al.	(COLU, ROCH, RUTG, YALE)
CASO 68	NC 54A 983	C. Caso et al.	(GENO, HAMB, MILA, SAEL)
CRENNELL 68B	PL 28B 136	D.J. Crennell et al.	(BNL)
JOHNSTON 68	PRL 20 1414	T.F. Johnston et al.	(TNTO, WISC) JP
FOCACCI 66	PRL 17 890	M.N. Focacci et al.	(CERN)
GOLDBERG 65	PL 17 354	M. Goldberg et al.	(CERN, EPOL, ORSAY+)

 $\rho(1700)$

$$I^G(J^{PC}) = 1^+(1^-)$$

See the review on "Spectroscopy of Light Meson Resonances."

 $\rho(1700)$ MASS $\eta\rho^0$ AND $\pi^+\pi^-$ MODES

VALUE (MeV)	DOCUMENT ID
1720±20 OUR ESTIMATE	

 $\eta\rho^0$ MODE

VALUE (MeV)	EVTs	DOCUMENT ID	TECN	COMMENT
The data in this block is included in the average printed for a previous datablock.				

••• We do not use the following data for averages, fits, limits, etc. •••

1834±12	13.4k	¹ GRIBANOV 20	CMD3	1.1-2.0 $e^+e^- \rightarrow \eta\pi^+\pi^-$
1840±10	7.4k	² ACHASOV 18	SND	1.22-2.00 $e^+e^- \rightarrow \eta\pi^+\pi^-$
1740±20		ANTONELLI 88	DM2	$e^+e^- \rightarrow \eta\pi^+\pi^-$
171±15		³ FUKUI 88	SPEC	8.95 $\pi^-p \rightarrow \eta\pi^+\pi^-n$

¹ Mass and width of the $\rho(770)$ fixed at 775 and 149 MeV, respectively; solution 2 of model 2, $\eta \rightarrow \gamma\gamma$ decays used.² From the combined fit of AULCHENKO 15 and ACHASOV 18 in the model with the interfering $\rho(1450)$, $\rho(1700)$ and $\rho(2150)$ with the parameters of the $\rho(1450)$ and $\rho(1700)$ floating and the mass and width of the $\rho(2150)$ fixed at 2155 MeV and 320 MeV, respectively. The phases of the resonances are π , 0 and π , respectively.³ Assuming $\rho^+ f_0(1370)$ decay mode interferes with $a_1(1260)^+\pi$ background. From a two Breit-Wigner fit. $\pi\pi$ MODE

VALUE (MeV)	EVTs	DOCUMENT ID	TECN	COMMENT
The data in this block is included in the average printed for a previous datablock.				

••• We do not use the following data for averages, fits, limits, etc. •••

1770.54 ± 5.49		¹ BARTOS 17	RVUE	$e^+e^- \rightarrow \pi^+\pi^-$
1718.50 ± 65.44		² BARTOS 17A	RVUE	$e^+e^- \rightarrow \pi^+\pi^-$
1766.80 ± 52.36		³ BARTOS 17A	RVUE	$\tau^- \rightarrow \pi^-\pi^0\nu_\tau$
1644 ± 36	20k	⁴ LEES 17c	BABR	$J/\psi \rightarrow \pi^+\pi^-\pi^0$
1780 ± 20	+15 -20	63.5k	⁵ ABRAMOWICZ12	ZEUS $ep \rightarrow e\pi^+\pi^-p$
1861 ± 17		⁶ LEES 12G	BABR	$e^+e^- \rightarrow \pi^+\pi^-\gamma$
1728 ± 17	±89	5.4M	^{7,8} FUJIKAWA 08	BELL $\tau^- \rightarrow \pi^-\pi^0\nu_\tau$
1780 +37 -29		⁹ ABELE 97	CBAR	$\bar{p}n \rightarrow \pi^-\pi^0\pi^0$
1719 ± 15		⁹ BERTIN 97C	OBLX	0.0 $\bar{p}p \rightarrow \pi^+\pi^-\pi^0$
1730 ± 30		CLEGG 94	RVUE	$e^+e^- \rightarrow \pi^+\pi^-$
1768 ± 21		BISELLO 89	DM2	$e^+e^- \rightarrow \pi^+\pi^-$
1745.7 ± 91.9		DUBNICKA 89	RVUE	$e^+e^- \rightarrow \pi^+\pi^-$
1546 ± 26		GESHKEN... 89	RVUE	
1650		¹⁰ ERKAL 85	RVUE	20-70 $\gamma p \rightarrow \gamma p$
1550 ± 70		ABE 84B	HYBR	20 $\gamma p \rightarrow \pi^+\pi^-p$
1590 ± 20		¹¹ ASTON 80	OMEG	20-70 $\gamma p \rightarrow p2\pi$
1600 ± 10		¹² ATIYA 79B	SPEC	50 $\gamma C \rightarrow C2\pi$
1598 +24 -22		BECKER 79	ASPK	17 π^-p polarized
1659 ± 25		¹⁰ LANG 79	RVUE	
1575		¹⁰ MARTIN 78C	RVUE	17 $\pi^-p \rightarrow \pi^+\pi^-n$
1610 ± 30		¹⁰ FROGGATT 77	RVUE	17 $\pi^-p \rightarrow \pi^+\pi^-n$
1590 ± 20		¹³ HYAMS 73	ASPK	17 $\pi^-p \rightarrow \pi^+\pi^-n$

¹ Applies the Unitary & Analytic Model of the pion electromagnetic form factor of DUBNICKA 10 to analyze the data of LEES 12G and ABLIKIM 16C.² Applies the Unitary & Analytic Model of the pion electromagnetic form factor of DUBNICKA 10 to analyze the data of ACHASOV 06, AKHMETSHIN 07, AUBERT 09as, and AMBROSINO 11A.³ Applies the Unitary & Analytic Model of the pion electromagnetic form factor of DUBNICKA 10 to analyze the data of FUJIKAWA 08.⁴ From a Dalitz plot analysis in an isobar model with $\rho(1450)$ and $\rho(1700)$ masses and widths floating.⁵ Using the KUHN 90 parametrization of the pion form factor, neglecting ρ - ω interference.⁶ Using the GOUNARIS 68 parametrization of the pion form factor leaving the masses and widths of the $\rho(1450)$, $\rho(1700)$, and $\rho(2150)$ resonances as free parameters of the fit.⁷ $|F_\pi(0)|^2$ fixed to 1.⁸ From the GOUNARIS 68 parametrization of the pion form factor.⁹ T-matrix pole.¹⁰ From phase shift analysis of HYAMS 73 data.¹¹ Simple relativistic Breit-Wigner fit with constant width.¹² An additional 40 MeV uncertainty in both the mass and width is present due to the choice of the background shape.¹³ Included in BECKER 79 analysis. $\pi\omega$ MODE

VALUE (MeV)	EVTs	DOCUMENT ID	TECN	COMMENT
•••	We do not use the following data for averages, fits, limits, etc. •••			

1723 ± 2 ¹ACHASOV 23A SND $e^+e^- \rightarrow \omega\pi^0$ 1708 ± 41 ²ACHASOV 13 SND 1.05-2.00 $e^+e^- \rightarrow \pi^0\pi^0\gamma$ 1550 to 1620 ³ACHASOV 00i SND $e^+e^- \rightarrow \pi^0\pi^0\gamma$

$\rho(1700)$

1580 to 1710	⁴ ACHASOV	00i	SND	$e^+e^- \rightarrow \pi^0\pi^0\gamma$
1710±90	ACHASOV	97	RVUE	$e^+e^- \rightarrow \omega\pi^0$

- From a vector dominance fit to the Born cross section between 1.05 and 2.0 GeV with $\rho(770)$, $\rho(1570)$, $\rho(1700)$, $\rho(2150)$. The fit also uses SND data from the VEPP-2M collider below 1.02 GeV and from LEES 17H and ABLIKIM 21A above 1.5 GeV.
- From a phenomenological model based on vector meson dominance with the interfering $\rho(1450)$ and $\rho(1700)$ and their widths fixed at 400 and 250 MeV, respectively. Systematic uncertainty not estimated.
- Taking into account both $\rho(1450)$ and $\rho(1700)$ contributions. Using the data of ACHASOV 00i on $e^+e^- \rightarrow \omega\pi^0$ and of EDWARDS 00A on $\tau^- \rightarrow \omega\pi^-\nu_\tau$. $\rho(1450)$ mass and width fixed at 1400 MeV and 500 MeV respectively.
- Taking into account the $\rho(1700)$ contribution only. Using the data of ACHASOV 00i on $e^+e^- \rightarrow \omega\pi^0$ and of EDWARDS 00A on $\tau^- \rightarrow \omega\pi^-\nu_\tau$.

$K\bar{K}$ MODE

VALUE (MeV)	EVTS	DOCUMENT ID	TECN	CHG	COMMENT
••• We do not use the following data for averages, fits, limits, etc. •••					
1688.7 ± 3.1 ^{+141.1} _{1.3}		¹ ALBRECHT	20	RVUE	0.9 $\bar{p}p \rightarrow K^+K^-\pi^0$
1541 ± 12 ± 33	190k	² AAIJ	16N	LHCB	$D^0 \rightarrow K_S^0 K^\pm\pi^\mp$
1740.8 ± 22.2	27k	³ ABELE	99D	CBAR ±	0.0 $\bar{p}p \rightarrow K^+K^-\pi^0$
1582 ± 36	1600	CLELAND	82B	SPEC ±	5.0 $\pi p \rightarrow K_S^0 K^\pm p$

- T-matrix pole, 2 poles, 3 channels, including $\pi\pi$ scattering data from HYAMS 75.
- Using the GOUNARIS 68 parameterization with a fixed width. Value is average using different $K\pi$ S-wave parameterizations in fit.
- K-matrix pole. Isospin not determined, could be $\omega(1650)$ or $\phi(1680)$.

$2(\pi^+\pi^-)$ MODE

VALUE (MeV)	EVTS	DOCUMENT ID	TECN	COMMENT
••• We do not use the following data for averages, fits, limits, etc. •••				
1851 ⁺²⁷ ₋₂₄		ACHASOV	97	RVUE $e^+e^- \rightarrow 2(\pi^+\pi^-)$
1570 ± 20		¹ CORDIER	82	DM1 $e^+e^- \rightarrow 2(\pi^+\pi^-)$
1520 ± 30		² ASTON	81E	OMEG 20-70 $\gamma p \rightarrow p4\pi$
1654 ± 25		³ DIBIANCA	81	DBC $\pi^+d \rightarrow pp2(\pi^+\pi^-)$
1666 ± 39		¹ BACCI	80	FRAG $e^+e^- \rightarrow 2(\pi^+\pi^-)$
1780	34	KILLIAN	80	SPEC 11 $e^-p \rightarrow 2(\pi^+\pi^-)$
1500		⁴ ATIYA	79B	SPEC 50 $\gamma C \rightarrow C4\pi^\pm$
1570 ± 60	65	⁵ ALEXANDER	75	HBC 7.5 $\gamma p \rightarrow p4\pi$
1550 ± 60		² CONVERSI	74	OSPK $e^+e^- \rightarrow 2(\pi^+\pi^-)$
1550 ± 50	160	SCHACHT	74	STRC 5.5-9 $\gamma p \rightarrow p4\pi$
1450 ± 100	340	SCHACHT	74	STRC 9-18 $\gamma p \rightarrow p4\pi$
1430 ± 50	400	BINGHAM	72B	HBC 9.3 $\gamma p \rightarrow p4\pi$

- Simple relativistic Breit-Wigner fit with model dependent width.
- Simple relativistic Breit-Wigner fit with constant width.
- One peak fit result.
- Parameters roughly estimated, not from a fit.
- Skew mass distribution compensated by Ross-Stodolsky factor.

$\pi^+\pi^-\pi^0$ MODE

VALUE (MeV)	DOCUMENT ID	TECN	COMMENT
••• We do not use the following data for averages, fits, limits, etc. •••			
1660 ± 30	ATKINSON	85B	OMEG 20-70 γp

$3(\pi^+\pi^-)$ AND $2(\pi^+\pi^-\pi^0)$ MODES

VALUE (MeV)	DOCUMENT ID	TECN	COMMENT
••• We do not use the following data for averages, fits, limits, etc. •••			
1730 ± 34	¹ FRABETTI	04	E687 $\gamma p \rightarrow 3\pi^+3\pi^-p$
1783 ± 15	CLEGG	90	RVUE $e^+e^- \rightarrow 3(\pi^+\pi^-)2(\pi^+\pi^-\pi^0)$

- From a fit with two resonances with the JACOB 72 continuum.

$$m_{\rho(1700)^0} - m_{\rho(1700)^\pm}$$

VALUE (MeV)	DOCUMENT ID	TECN	COMMENT
••• We do not use the following data for averages, fits, limits, etc. •••			
-48.30 ± 83.81	¹ BARTOS	17A	RVUE $e^+e^- \rightarrow \pi^+\pi^-$, $\tau^- \rightarrow \pi^-\pi^0\nu_\tau$

- Applies the Unitary & Analytic Model of the pion electromagnetic form factor of DUBNICKA 10 to analyze the data of ACHASOV 06, AKHMETSHIN 07, AUBERT 09As, AMBROSINO 11A, and FUJIKAWA 08.

$\rho(1700)$ WIDTH

$\eta\rho^0$ AND $\pi^+\pi^-$ MODES

VALUE (MeV)	DOCUMENT ID
250 ± 100 OUR ESTIMATE	

$\eta\rho^0$ MODE

VALUE (MeV)	EVTS	DOCUMENT ID	TECN	COMMENT
The data in this block is included in the average printed for a previous datablock.				

- We do not use the following data for averages, fits, limits, etc. •••
- 47 ± 19 13.4k ¹ GRIBANOV 20 CMD3 1.1-2.0 $e^+e^- \rightarrow \eta\pi^+\pi^-$
- 132 ± 40 7.4k ² ACHASOV 18 SND 1.22-2.00 $e^+e^- \rightarrow \eta\pi^+\pi^-$

150 ± 30	ANTONELLI	88	DM2	$e^+e^- \rightarrow \eta\pi^+\pi^-$
282 ± 44	³ FUKUI	88	SPEC	8.95 $\pi^-\pi^- \rightarrow \eta\pi^+\pi^-n$

- Mass and width of the $\rho(770)$ fixed at 775 and 149 MeV, respectively; solution 2 of model 2, $\eta \rightarrow \gamma\gamma$ decays used.
- From the combined fit of AULCHENKO 15 and ACHASOV 18 in the model with the interfering $\rho(1450)$, $\rho(1700)$ and $\rho(2150)$ with the parameters of the $\rho(1450)$ and $\rho(1700)$ floating and the mass and width of the $\rho(2150)$ fixed at 2155 MeV and 320 MeV, respectively. The phases of the resonances are π , 0 and π , respectively.
- Assuming $\rho^+\rho^0(1370)$ decay mode interferes with $a_1(1260)^+\pi$ background. From a two Breit-Wigner fit.

$\pi\pi$ MODE

VALUE (MeV)	EVTS	DOCUMENT ID	TECN	COMMENT
The data in this block is included in the average printed for a previous datablock.				

••• We do not use the following data for averages, fits, limits, etc. •••				
268.98 ± 11.40		¹ BARTOS	17	RVUE $e^+e^- \rightarrow \pi^+\pi^-$
489.58 ± 16.95		² BARTOS	17A	RVUE $e^+e^- \rightarrow \pi^+\pi^-$
414.71 ± 119.48		³ BARTOS	17A	RVUE $\tau^- \rightarrow \pi^-\pi^0\nu_\tau$
109 ± 19	20k	⁴ LEES	17C	BABR $J/\psi \rightarrow \pi^+\pi^-\pi^0$
310 ± 30	⁺²⁵ ₋₃₅ 63.5k	⁵ ABRAMOWICZ12	ZEUS	$ep \rightarrow e\pi^+\pi^-p$
316 ± 26		⁶ LEES	12G	BABR $e^+e^- \rightarrow \pi^+\pi^-\gamma$
164 ± 21	⁺⁸⁹ ₋₂₆ 5.4M	^{7,8} FUJIKAWA	08	BELL $\tau^- \rightarrow \pi^-\pi^0\nu_\tau$
275 ± 45		⁹ ABELE	97	CBAR $\bar{p}n \rightarrow \pi^-\pi^0\pi^0$
310 ± 40		⁹ BERTIN	97C	OBLX 0.0 $\bar{p}p \rightarrow \pi^+\pi^-\pi^0$
400 ± 100		CLEGG	94	RVUE $e^+e^- \rightarrow \pi^+\pi^-$
224 ± 22		BISELLO	89	DM2 $e^+e^- \rightarrow \pi^+\pi^-$
242.5 ± 163.0		DUBNICKA	89	RVUE $e^+e^- \rightarrow \pi^+\pi^-$
620 ± 60		GESHKEN...	89	RVUE
<315		¹⁰ ERKAL	85	RVUE 20-70 $\gamma p \rightarrow \gamma\pi$
280 ± 30		ABE	84B	HYBR 20 $\gamma p \rightarrow \pi^+\pi^-p$
230 ± 80		¹¹ ASTON	80	OMEG 20-70 $\gamma p \rightarrow p2\pi$
283 ± 14		¹² ATIYA	79B	SPEC 50 $\gamma C \rightarrow C2\pi$
175 ± 98		BECKER	79	ASPK 17 π^-p polarized
232 ± 34		¹⁰ LANG	79	RVUE
340		¹⁰ MARTIN	78C	RVUE 17 $\pi^-p \rightarrow \pi^+\pi^-n$
300 ± 100		¹⁰ FROGGATT	77	RVUE 17 $\pi^-p \rightarrow \pi^+\pi^-n$
180 ± 50		¹³ HYAMS	73	ASPK 17 $\pi^-p \rightarrow \pi^+\pi^-n$

- Applies the Unitary & Analytic Model of the pion electromagnetic form factor of DUBNICKA 10 to analyze the data of LEES 12G and ABLIKIM 16c.
- Applies the Unitary & Analytic Model of the pion electromagnetic form factor of DUBNICKA 10 to analyze the data of ACHASOV 06, AKHMETSHIN 07, AUBERT 09As, and AMBROSINO 11A.
- Applies the Unitary & Analytic Model of the pion electromagnetic form factor of DUBNICKA 10 to analyze the data of FUJIKAWA 08.
- From a Dalitz plot analysis in an isobar model with $\rho(1450)$ and $\rho(1700)$ masses and widths floating.
- Using the KUHN 90 parameterization of the pion form factor, neglecting $\rho-\omega$ interference.
- Using the GOUNARIS 68 parameterization of the pion form factor leaving the masses and widths of the $\rho(1450)$, $\rho(1700)$, and $\rho(2150)$ resonances as free parameters of the fit.
- $|F_\pi(0)|^2$ fixed to 1.
- From the GOUNARIS 68 parameterization of the pion form factor.
- T-matrix pole.
- From phase shift analysis of HYAMS 73 data.
- Simple relativistic Breit-Wigner fit with constant width.
- An additional 40 MeV uncertainty in both the mass and width is present due to the choice of the background shape.
- Included in BECKER 79 analysis.

$K\bar{K}$ MODE

VALUE (MeV)	EVTS	DOCUMENT ID	TECN	CHG	COMMENT
••• We do not use the following data for averages, fits, limits, etc. •••					
150.9 ± 2.5 ⁺⁶⁰ _{-10.6}		¹ ALBRECHT	20	RVUE	0.9 $\bar{p}p \rightarrow K^+K^-\pi^0$
187.2 ± 26.7	27k	² ABELE	99D	CBAR ±	0.0 $\bar{p}p \rightarrow K^+K^-\pi^0$
265 ± 120	1600	CLELAND	82B	SPEC ±	5.0 $\pi p \rightarrow K_S^0 K^\pm p$

- T-matrix pole, 2 poles, 3 channels, including $\pi\pi$ scattering data from HYAMS 75.
- K-matrix pole. Isospin not determined, could be $\omega(1650)$ or $\phi(1680)$.

$2(\pi^+\pi^-)$ MODE

VALUE (MeV)	EVTS	DOCUMENT ID	TECN	COMMENT
••• We do not use the following data for averages, fits, limits, etc. •••				
510 ± 40		¹ CORDIER	82	DM1 $e^+e^- \rightarrow 2(\pi^+\pi^-)$
400 ± 50		² ASTON	81E	OMEG 20-70 $\gamma p \rightarrow p4\pi$
400 ± 146		³ DIBIANCA	81	DBC $\pi^+d \rightarrow pp2(\pi^+\pi^-)$
700 ± 160		¹ BACCI	80	FRAG $e^+e^- \rightarrow 2(\pi^+\pi^-)$
100	34	KILLIAN	80	SPEC 11 $e^-p \rightarrow 2(\pi^+\pi^-)$
600		⁴ ATIYA	79B	SPEC 50 $\gamma C \rightarrow C4\pi^\pm$
340 ± 160	65	⁵ ALEXANDER	75	HBC 7.5 $\gamma p \rightarrow p4\pi$
360 ± 100		² CONVERSI	74	OSPK $e^+e^- \rightarrow 2(\pi^+\pi^-)$
400 ± 120	160	SCHACHT	74	STRC 5.5-9 $\gamma p \rightarrow p4\pi$
850 ± 200	340	SCHACHT	74	STRC 9-18 $\gamma p \rightarrow p4\pi$
650 ± 100	400	BINGHAM	72B	HBC 9.3 $\gamma p \rightarrow p4\pi$

- Simple relativistic Breit-Wigner fit with model-dependent width.
- Simple relativistic Breit-Wigner fit with constant width.
- One peak fit result.
- Parameters roughly estimated, not from a fit.
- Skew mass distribution compensated by Ross-Stodolsky factor.
- Width errors enlarged by us to $4\Gamma/\sqrt{N}$; see the note with the $K^*(892)$ mass.

Meson Particle Listings

$\rho(1700)$

$\pi^+\pi^-\pi^0\pi^0$ MODE

VALUE (MeV)	DOCUMENT ID	TECN	COMMENT
300 ± 50	ATKINSON	85B	OMEG 20-70 $\gamma\rho$

$\omega\pi^0$ MODE

VALUE (MeV)	DOCUMENT ID	TECN	COMMENT
371 ± 3	1 ACHASOV	23A	SND $e^+e^- \rightarrow \omega\pi^0$
350 to 580	2 ACHASOV	00i	SND $e^+e^- \rightarrow \pi^0\pi^0\gamma$
490 to 1040	3 ACHASOV	00i	SND $e^+e^- \rightarrow \pi^0\pi^0\gamma$

¹ From a vector dominance fit to the Born cross section between 1.05 and 2.0 GeV with $\rho(770)$, $\rho(1570)$, $\rho(1700)$, $\rho(2150)$. The fit also uses SND data from the VEPP-2M collider below 1.02 GeV and from LEES 17H and ABLIKIM 21A above 1.5 GeV.

² Taking into account both $\rho(1450)$ and $\rho(1700)$ contributions. Using the data of ACHASOV 00i on $e^+e^- \rightarrow \omega\pi^0$ and of EDWARDS 00A on $\tau^- \rightarrow \omega\pi^-\nu_\tau$. $\rho(1450)$ mass and width fixed at 1400 MeV and 500 MeV respectively.

³ Taking into account the $\rho(1700)$ contribution only. Using the data of ACHASOV 00i on $e^+e^- \rightarrow \omega\pi^0$ and of EDWARDS 00A on $\tau^- \rightarrow \omega\pi^-\nu_\tau$.

$3(\pi^+\pi^-)$ AND $2(\pi^+\pi^-\pi^0)$ MODES

VALUE (MeV)	DOCUMENT ID	TECN	COMMENT
315 ± 100	1 FRABETTI	04	E687 $\gamma\rho \rightarrow 3\pi^+3\pi^-\rho$
285 ± 20	CLEGG	90	RVUE $e^+e^- \rightarrow 3(\pi^+\pi^-)2(\pi^+\pi^-\pi^0)$

¹ From a fit with two resonances with the JACOB 72 continuum.

$$\Gamma_{\rho(1700)^0} - \Gamma_{\rho(1700)^\pm}$$

VALUE (MeV)	DOCUMENT ID	TECN	COMMENT
74.87 ± 120.67	1 BARTOS	17A	RVUE $e^+e^- \rightarrow \pi^+\pi^-\pi^-\pi^0 \rightarrow \pi^-\pi^0\nu_\tau$

¹ Applies the Unitary & Analytic Model of the pion electromagnetic form factor of DUBNICKA 10 to analyze the data of ACHASOV 06, AKHMETSHIN 07, AUBERT 09AS, AMBROSINO 11A, and FUJIKAWA 08.

$\rho(1700)$ DECAY MODES

Mode	Fraction (Γ_i/Γ)
Γ_1 4π	
Γ_2 $2(\pi^+\pi^-)$	seen
Γ_3 $\rho\pi\pi$	seen
Γ_4 $\rho^0\pi^+\pi^-$	seen
Γ_5 $\rho^0\pi^0\pi^0$	
Γ_6 $\rho^\pm\pi^\mp\pi^0$	seen
Γ_7 $a_1(1260)\pi$	seen
Γ_8 $h_1(1170)\pi$	seen
Γ_9 $\pi(1300)\pi$	seen
Γ_{10} $\rho\rho$	seen
Γ_{11} $\pi^+\pi^-$	seen
Γ_{12} $\pi\pi$	seen
Γ_{13} $K\bar{K}^*(892) + c.c.$	seen
Γ_{14} $\eta\rho$	seen
Γ_{15} $a_2(1320)\pi$	not seen
Γ_{16} $K\bar{K}$	seen
Γ_{17} e^+e^-	seen
Γ_{18} $\pi^0\omega$	seen
Γ_{19} $\pi^0\gamma$	not seen
Γ_{20} $f_0(1500)\gamma$	not seen

$\rho(1700)$ $\Gamma(i)\Gamma(e^+e^-)/\Gamma(\text{total})$

This combination of a partial width with the partial width into e^+e^- and with the total width is obtained from the cross-section into channel i into e^+e^- annihilation.

VALUE (keV)	DOCUMENT ID	TECN	COMMENT	$\Gamma_2\Gamma_{17}/\Gamma$
2.6 ± 0.2	DEL COURT	81B	DM1 $e^+e^- \rightarrow 2(\pi^+\pi^-)$	
2.83 ± 0.42	BACCI	80	FRAG $e^+e^- \rightarrow 2(\pi^+\pi^-)$	

VALUE (keV)	DOCUMENT ID	TECN	COMMENT	$\Gamma_{11}\Gamma_{17}/\Gamma$
0.13	1 DIEKMAN	88	RVUE $e^+e^- \rightarrow \pi^+\pi^-$	
0.029 + 0.016 - 0.012	KURDADZE	83	OLYA 0.64-1.4 $e^+e^- \rightarrow \pi^+\pi^-$	

¹ Using total width = 220 MeV.

VALUE (keV)	DOCUMENT ID	TECN	COMMENT	$\Gamma_{13}\Gamma_{17}/\Gamma$
0.305 ± 0.071	1 BIZOT	80	DM1 e^+e^-	

¹ Model dependent.

VALUE (eV)	EVTS	DOCUMENT ID	TECN	COMMENT	$\Gamma_{14}\Gamma_{17}/\Gamma$
1.35 ± 0.53 ± 0.08	13.4k	1 GRIBANOV	20	CMD3 1.1-2.0 $e^+e^- \rightarrow \eta\pi^+\pi^-$	
84 ± 26 ± 4		2 LEES	18	BABR $e^+e^- \rightarrow \eta\pi^+\pi^-$	
7 ± 3		ANTONELLI	88	DM2 $e^+e^- \rightarrow \eta\pi^+\pi^-$	

¹ Mass and width of the $\rho(770)$ fixed at 775 and 149 MeV, respectively; solution 2 of model 2, $\eta \rightarrow \gamma\gamma$ decays used.

² Includes non-resonant contribution. The selected fit model includes three ρ excited states. Model uncertainty is 80%.

VALUE (keV)	DOCUMENT ID	TECN	COMMENT	$\Gamma_{16}\Gamma_{17}/\Gamma$
0.035 ± 0.029	1 BIZOT	80	DM1 e^+e^-	

¹ Model dependent.

VALUE (keV)	DOCUMENT ID	TECN	COMMENT	$\Gamma_3\Gamma_{17}/\Gamma$
3.510 ± 0.090	1 BIZOT	80	DM1 e^+e^-	

¹ Model dependent.

$\rho(1700)$ $\Gamma(i)/\Gamma(\text{total}) \times \Gamma(e^+e^-)/\Gamma(\text{total})$

VALUE (units 10^{-6})	EVTS	DOCUMENT ID	TECN	COMMENT	$\Gamma_{18}/\Gamma \times \Gamma_{17}/\Gamma$
0.09 ± 0.05	10.2k	1 ACHASOV	16D	SND 1.05-2.00 $e^+e^- \rightarrow \pi^0\pi^0\gamma$	
1.7 ± 0.4	7815	2 ACHASOV	13	SND 1.05-2.00 $e^+e^- \rightarrow \pi^0\pi^0\gamma$	

¹ From a phenomenological model based on vector meson dominance with interfering $\rho(700)$, $\rho(1450)$, and $\rho(1700)$. The $\rho(1700)$ mass and width are fixed at 1720 MeV and 250 MeV, respectively. Systematic uncertainty not estimated. Supersedes ACHASOV 13.

² From a phenomenological model based on vector meson dominance with the interfering $\rho(1450)$ and $\rho(1700)$ and their widths fixed at 400 and 250 MeV, respectively. Systematic uncertainty not estimated.

VALUE (units 10^{-8})	EVTS	DOCUMENT ID	TECN	COMMENT	$\Gamma_{14}/\Gamma \times \Gamma_{17}/\Gamma$
8.3 + 3.8 - 3.1	7.4k	1 ACHASOV	18	SND 1.22-2.00 $e^+e^- \rightarrow \eta\pi^+\pi^-$	

¹ From the combined fit of AULCHENKO 15 and ACHASOV 18 in the model with the interfering $\rho(1450)$, $\rho(1700)$ and $\rho(2150)$ with the parameters of the $\rho(1450)$ and $\rho(1700)$ floating and the mass and width of the $\rho(2150)$ fixed at 2155 MeV and 320 MeV, respectively. The phases of the resonances are π , 0 and π , respectively.

$\rho(1700)$ BRANCHING RATIOS

VALUE	DOCUMENT ID	TECN	COMMENT	Γ_3/Γ_1
0.28 ± 0.06	1 ABELE	01B	CBAR 0.0 $\bar{p}n \rightarrow 5\pi$	

¹ $\omega\pi$ not included.

VALUE	EVTS	DOCUMENT ID	TECN	COMMENT	Γ_4/Γ_2
~ 1.0		DEL COURT	81B	DM1 $e^+e^- \rightarrow 2(\pi^+\pi^-)$	
0.7 ± 0.1	500	SCHACHT	74	STRC 5.5-18 $\gamma\rho \rightarrow p4\pi$	
0.80		1 BINGHAM	72B	HBC 9.3 $\gamma\rho \rightarrow p4\pi$	

¹ The $\pi\pi$ system is in S-wave.

VALUE	DOCUMENT ID	TECN	CHG	COMMENT	Γ_5/Γ_6
< 0.10	ATKINSON	85B	OMEG	20-70 $\gamma\rho$	
< 0.15	ATKINSON	82	OMEG 0	20-70 $\gamma\rho \rightarrow p4\pi$	

VALUE	DOCUMENT ID	TECN	COMMENT	Γ_7/Γ_1
0.16 ± 0.05	1 ABELE	01B	CBAR 0.0 $\bar{p}n \rightarrow 5\pi$	

¹ $\omega\pi$ not included.

$\Gamma(h_1(1170)\pi)/\Gamma(4\pi)$ Γ_8/Γ_1

VALUE	DOCUMENT ID	TECN	COMMENT
0.17±0.06	¹ ABELE	01B	CBAR 0.0 $\bar{p}n \rightarrow 5\pi$
¹ $\omega\pi$ not included.			

$\Gamma(\pi(1300)\pi)/\Gamma(4\pi)$ Γ_9/Γ_1

VALUE	DOCUMENT ID	TECN	COMMENT
0.30±0.10	¹ ABELE	01B	CBAR 0.0 $\bar{p}n \rightarrow 5\pi$
¹ $\omega\pi$ not included.			

$\Gamma(\rho\rho)/\Gamma(4\pi)$ Γ_{10}/Γ_1

VALUE	DOCUMENT ID	TECN	COMMENT
0.09±0.03	¹ ABELE	01B	CBAR 0.0 $\bar{p}n \rightarrow 5\pi$
¹ $\omega\pi$ not included.			

$\Gamma(\pi^+\pi^-)/\Gamma_{total}$ Γ_{11}/Γ

VALUE	DOCUMENT ID	TECN	COMMENT
0.108±0.017 ^{+0.162} _{-0.004}	¹ ALBRECHT	20	RVUE 0.9 $\bar{p}p \rightarrow K^+K^-\pi^0$
0.287 ^{+0.043} _{-0.042}	BECKER	79	ASPK 17 π^-p polarized
0.15 to 0.30	² MARTIN	78C	RVUE 17 $\pi^-p \rightarrow \pi^+\pi^-n$
<0.20	³ COSTA...	77B	RVUE $e^+e^- \rightarrow 2\pi, 4\pi$
0.30 ± 0.05	⁴ FROGGATT	77	RVUE 17 $\pi^-p \rightarrow \pi^+\pi^-n$
<0.15	⁴ EISENBERG	73	HBC 5 $\pi^+p \rightarrow \Delta^{++}2\pi$
0.25 ± 0.05	⁵ HYAMS	73	ASPK 17 $\pi^-p \rightarrow \pi^+\pi^-n$

¹ Residue from T-matrix pole, 2 poles, 3 channels, Chew-Mandelstam functions and simplified analytic continuation for the 4π channel. Includes scattering data from HYAMS 75 and model-independent calculation of GARCIA-MARTIN 11A.
² From phase shift analysis of HYAMS 73 data.
³ Estimate using unitarity, time reversal invariance, Breit-Wigner.
⁴ Estimated using one-pion-exchange model.
⁵ Included in BECKER 79 analysis.

$\Gamma(K\bar{K})/\Gamma_{total}$ Γ_{16}/Γ

VALUE	DOCUMENT ID	TECN	COMMENT
0.007±0.006 ^{+0.041} _{-0.002}	¹ ALBRECHT	20	RVUE 0.9 $\bar{p}p \rightarrow K^+K^-\pi^0$

¹ Residue from T-matrix pole, 2 poles, 3 channels, Chew-Mandelstam functions and simplified analytic continuation for the 4π channel. Includes scattering data from HYAMS 75 and model-independent calculation of GARCIA-MARTIN 11A.

$\Gamma(\pi^+\pi^-)/\Gamma(2(\pi^+\pi^-))$ Γ_{11}/Γ_2

VALUE	DOCUMENT ID	TECN	COMMENT
0.13±0.05	ASTON	80	OMEG 20-70 $\gamma p \rightarrow p2\pi$
<0.14	¹ DAVIER	73	STRC 6-18 $\gamma p \rightarrow p4\pi$
<0.2	² BINGHAM	72B	HBC 9.3 $\gamma p \rightarrow p2\pi$

¹ Upper limit is estimate.
² 2σ upper limit.

$\Gamma(\pi\pi)/\Gamma(4\pi)$ Γ_{12}/Γ_1

VALUE	DOCUMENT ID	TECN	COMMENT
0.16±0.04	^{1,2} ABELE	01B	CBAR 0.0 $\bar{p}n \rightarrow 5\pi$

¹ Using ABELE 97.
² $\omega\pi$ not included.

$\Gamma(K\bar{K}^*(892) + c.c.)/\Gamma_{total}$ Γ_{13}/Γ

VALUE	DOCUMENT ID	TECN	COMMENT
possibly seen	COAN	04	CLEO $\tau^- \rightarrow K^-\pi^-\pi^+\nu_\tau$

$\Gamma(K\bar{K}^*(892) + c.c.)/\Gamma(2(\pi^+\pi^-))$ Γ_{13}/Γ_2

VALUE	DOCUMENT ID	TECN	COMMENT
0.15±0.03	¹ DELCOURT	81B	DM1 $e^+e^- \rightarrow \bar{K}K\pi$

¹ Assuming $\rho(1700)$ and ω radial excitations to be degenerate in mass.

$\Gamma(\eta\rho)/\Gamma_{total}$ Γ_{14}/Γ

VALUE	CL%	DOCUMENT ID	TECN	COMMENT
possibly seen		AKHMETSHIN 00D	CMD2	$e^+e^- \rightarrow \eta\pi^+\pi^-$
<0.04		DONNACHIE 87B	RVUE	
<0.02	58	ATKINSON 86B	OMEG 20-70	γp

$\Gamma(\eta\rho)/\Gamma(2(\pi^+\pi^-))$ Γ_{14}/Γ_2

VALUE	DOCUMENT ID	TECN	COMMENT
0.123±0.027	DELCOURT	82	DM1 $e^+e^- \rightarrow \pi^+\pi^-MM$
~ 0.21	ASTON	80	OMEG 20-70 γp

$\Gamma(\pi^+\pi^- \text{ neutrals})/\Gamma(2(\pi^+\pi^-))$ $(\Gamma_5+\Gamma_6+0.714\Gamma_{14})/\Gamma_2$

VALUE	DOCUMENT ID	TECN	COMMENT
2.6±0.4	¹ BALLAM	74	HBC 9.3 γp

¹ Upper limit. Background not subtracted.

$\Gamma(a_2(1320)\pi)/\Gamma_{total}$ Γ_{15}/Γ

VALUE	DOCUMENT ID	TECN	COMMENT
not seen	AMELIN	00	VES 37 $\pi^-p \rightarrow \eta\pi^+\pi^-n$

$\Gamma(K\bar{K})/\Gamma(2(\pi^+\pi^-))$ Γ_{16}/Γ_2

VALUE	CL%	DOCUMENT ID	TECN	CHG	COMMENT
0.015±0.010		¹ DELCOURT	81B	DM1	$e^+e^- \rightarrow \bar{K}K$
<0.04	95	BINGHAM	72B	HBC	0 9.3 γp

¹ Assuming $\rho(1700)$ and ω radial excitations to be degenerate in mass.

$\Gamma(K\bar{K})/\Gamma(K\bar{K}^*(892) + c.c.)$ Γ_{16}/Γ_{13}

VALUE	DOCUMENT ID	TECN	COMMENT
0.052±0.026	BUON	82	DM1 $e^+e^- \rightarrow$ hadrons

$\Gamma(\pi^0\omega)/\Gamma_{total}$ Γ_{18}/Γ

VALUE	EVTS	DOCUMENT ID	TECN	COMMENT
not seen		MATVIENKO 15	BELL	$\bar{B}^0 \rightarrow D^{*+}\omega\pi^-$
seen	1.6k	ACHASOV 12	SND	$e^+e^- \rightarrow \pi^0\pi^0\gamma$
not seen	2382	AKHMETSHIN 03B	CMD2	$e^+e^- \rightarrow \pi^0\pi^0\gamma$
seen		ACHASOV 97	RVUE	$e^+e^- \rightarrow \omega\pi^0$

$\Gamma(\pi^0\gamma)/\Gamma_{total}$ Γ_{19}/Γ

VALUE	DOCUMENT ID	TECN	COMMENT
not seen	¹ ACHASOV	10D	SND 1.075-2.0 $e^+e^- \rightarrow \pi^0\gamma$

¹ From a fit of a VMD model with two effective resonances with masses of 1450 MeV and 1700 MeV to describe the excited vector states $\omega(1420)$, $\rho(1450)$, $\omega(1650)$, and $\rho(1700)$. The width of the highest mass effective resonance is fixed at 315 MeV.

$\Gamma(f_0(1500)\gamma)/\Gamma_{total}$ Γ_{20}/Γ

VALUE	DOCUMENT ID	TECN	COMMENT
not seen	¹ ACHASOV	22	SND 1.17-2.00 $e^+e^- \rightarrow \eta\eta\gamma$

¹ The 90% CL upper limit on the Born cross sections $\sigma(e^+e^- \rightarrow \phi(1680) \rightarrow f_2'(1525)\gamma \rightarrow \eta\eta\gamma)$ and $\sigma(e^+e^- \rightarrow \rho(1700) \rightarrow f_0(1500)\gamma \rightarrow \eta\eta\gamma)$ is 10.6 pb.

$\rho(1700)$ REFERENCES

ACHASOV	23A	PR D108 092012	M.N. Achasov et al.	(SND Collab.)
ACHASOV	22A	EPJ C82 168	M.N. Achasov et al.	(SND Collab.)
ABLIKIM	21A	PL B813 136059	M. Ablikim et al.	(BESIII Collab.)
ALBRECHT	20	EPJ C60 453	M. Albrecht et al.	(Crystal Barrel Collab.)
GRIBANOV	20	JHEP 2001 112	S.S. Gribanov et al.	(CMD-3 Collab.)
ACHASOV	18	PR D97 012008	M.N. Achasov et al.	(SND Collab.)
LEES	18	PR D97 052007	J.P. Lees et al.	(BABAR Collab.)
BARTOS	17	PR D96 113004	E. Bartos et al.	
BARTOS	17A	IJMP A32 1750154	E. Bartos et al.	
LEES	17C	PR D96 072007	J.P. Lees et al.	(BABAR Collab.)
LEES	17H	PR D96 092009	J.P. Lees et al.	(BABAR Collab.)
AAIJ	16N	PR D93 052018	R. Aaij et al.	(LHCb Collab.)
ABLIKIM	16D	PL B753 629	M. Ablikim et al.	(BESIII Collab.)
ACHASOV	16C	PR D94 112001	M.N. Achasov et al.	(SND Collab.)
AULCHENKO	15	PR D91 052013	V.M. Aulchenko et al.	(SND Collab.)
MATVIENKO	15	PR D92 012013	D. Matvienko et al.	(BELLE Collab.)
ACHASOV	13	PR D88 054013	M.N. Achasov et al.	(SND Collab.)
ABRAMOWICZ	12	EPJ C72 1869	H. Abramowicz et al.	(ZEUS Collab.)
ACHASOV	12	JETPL 94 734	M.N. Achasov et al.	
		Translated from ZETFP 94 796.		
LEES	12G	PR D86 032013	J.P. Lees et al.	(BABAR Collab.)
AMBROSINO	11A	PL B700 102	F. Ambrosino et al.	(KLOE Collab.)
GARCIA-MAR...	11A	PR D83 074004	R. Garcia-Martin et al.	(MADR, CRAC)
ACHASOV	10D	PR D98 112001	M.N. Achasov et al.	(SND Collab.)
DUBNICKA	10	APS 60 1	S. Dubnicka, A.Z. Dubnickova	
AUBERT	09AS	PRL 103 231801	B. Aubert et al.	(BABAR Collab.)
FUJIKAWA	08	PR D78 072006	M. Fujikawa et al.	(BELLE Collab.)
AKHMETSHIN	07	PL B468 28	R.R. Akhmetshin et al.	(Novosibirsk CMD-2 Collab.)
ACHASOV	06	JETP 103 380	M.N. Achasov et al.	(Novosibirsk SND Collab.)
		Translated from ZETF 130 437.		
COAN	04	PRL 92 232001	T.E. Coan et al.	(CLEO Collab.)
FRABETTI	04	PL B578 290	P.L. Frabetti et al.	(FNAL E687 Collab.)
AKHMETSHIN	03B	PL B562 173	R.R. Akhmetshin et al.	(Novosibirsk CMD-2 Collab.)
ABELE	01B	EPJ C21 261	A. Abele et al.	(Crystal Barrel Collab.)
ACHASOV	00I	PL B486 29	M.N. Achasov et al.	(Novosibirsk SND Collab.)
AKHMETSHIN	00D	PL B489 125	R.R. Akhmetshin et al.	(Novosibirsk CMD-2 Collab.)
AMELIN	00	NP A668 83	D. Amelin et al.	(VES Collab.)
EDWARDS	00A	PR D61 072003	K.W. Edwards et al.	(CLEO Collab.)
ABELE	99D	PL B468 178	A. Abele et al.	(Crystal Barrel Collab.)
ABELE	97	PL B391 191	A. Abele et al.	(Crystal Barrel Collab.)
ACHASOV	97	PR D55 2663	M.N. Achasov et al.	(NOVM)
BERTIN	97C	PL B408 476	A. Bertin et al.	(OBELIX Collab.)
CLEGG	94	ZPHY C62 455	A.B. Clegg, A. Donnachie	(LANC, MCHS)
CLEGG	90	ZPHY C45 677	A.B. Clegg, A. Donnachie	(LANC, MCHS)

Meson Particle Listings

$\rho(1700)$, $a_2(1700)$

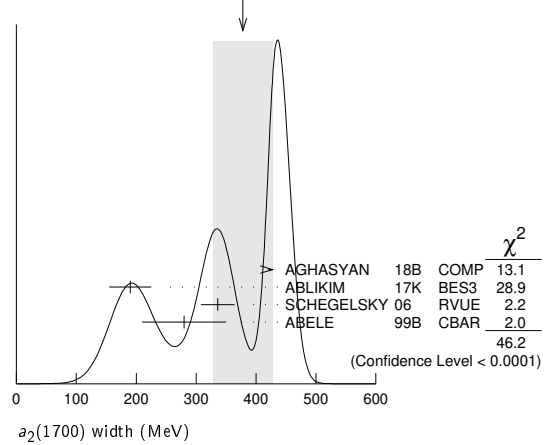
NAME	NO.	EXPERIMENT	EXPERIMENT	EXPERIMENT	EXPERIMENT
KUHN	90	ZPHY C48 445	J.H. Kuhn et al.	(MPIM)	
BISELLO	89	PL B220 321	D. Bisello et al.	(DM2 Collab.)	
DUBNICKA	89	JP G15 1349	S. Dubnicka et al.	(JINR, SLOV)	
GESHKEN...	89	ZPHY C45 351	B.V. Geshkenbein	(ITEP)	
ANTONELLI	88	PL B212 133	A. Antonelli et al.	(DM2 Collab.)	
DIEKMANN	88	PRPL 159 99	B. Diekmann	(BONN)	
FUKUI	88	PL B202 441	S. Fukui et al.	(SUGI, NAGO, KEK, KYOT+)	
DOMNACHIE	87B	ZPHY C34 257	A. Donnachie, A.B. Clegg	(MCHS, LANC)	
ATKINSON	86B	ZPHY C30 531	M. Atkinson et al.	(BONN, CERN, GLAS+)	
ATKINSON	85B	ZPHY C26 499	M. Atkinson et al.	(BONN, CERN, GLAS+)	
ERKAL	85	ZPHY C29 485	C. Erkal, M.G. Olsson	(WISC)	
ABE	84B	PRL 53 751	K. Abe et al.	(SLAC HFP Collab.)	
KURDADZE	83	JETPL 37 733	L.M. Kurdadze et al.	(NOVO)	
Translated from ZETFP 37 613.					
ATKINSON	82	PL 108B 55	M. Atkinson et al.	(BONN, CERN, GLAS+)	
BUON	82	PL 118B 221	J. Buon et al.	(LALO, MONP)	
CLELAND	82B	NP B208 228	W.E. Cleland et al.	(DURH, GEVA, LAUS+)	
CORDIER	82	PL 109B 129	A. Cordier et al.	(LALO)	
DELCOURT	82	PL 113B 93	B. Delcourt et al.	(LALO)	
ASTON	81E	NP B189 15	D. Aston	(BONN, CERN, EPOL, GLAS, LANCA)	
DELCOURT	81B	Bonn Conf. 205	B. Delcourt	(ORSAY)	
Also			A. Cordier et al.	(LALO)	
DIBIANCA	81	PR D23 595	F.A. di Bianca et al.	(CASE, CMU)	
ASTON	80	PL 92B 215	D. Aston	(BONN, CERN, EPOL, GLAS, LANCA)	
BACCI	80	PL 95B 139	C. Bacci et al.	(ROMA, FRAS)	
BIZOT	80	Madison Conf. 546	J.C. Bizot et al.	(LALO, MONP)	
KILLIAN	80	PR D21 3005	T.J. Killian et al.	(CORN)	
ATIYA	79B	PRL 43 1691	M.S. Atiya et al.	(COLU, ILL, FNAL)	
BECKER	79	NP B151 46	H. Becker et al.	(MPIM, CERN, ZEEM, CRAC)	
LANG	79	PR D19 956	C.B. Lang, A. Mas-Parreda	(GRAZ)	
MARTIN	78C	ANP 114 1	A.D. Martin, M.R. Pennington	(CERN)	
COSTA...	77B	PL 71B 345	B. Costa de Beauregard, B. Pire, T.N. Truong	(EPOL)	
FROGGATT	77	NP B129 89	C.D. Froggatt, J.L. Petersen	(GLAS, NORD)	
ALEXANDER	75	PL 57B 487	G. Alexander et al.	(TELA)	
HYAMS	75	NP B100 205	B.D. Hyams et al.	(CERN, MPIM)	
BALLAM	74	NP B76 375	J. Ballam et al.	(SLAC, LBL, MPIM)	
CONVERSI	74	PL 52B 493	M. Conversi et al.	(ROMA, FRAS)	
SCHACHT	74	NP B81 205	P. Schacht et al.	(MPIM)	
DAVIER	73	NP B58 31	M. Davier et al.	(SLAC)	
EISENBERG	73	PL 43B 149	Y. Eisenberg et al.	(REH)	
HYAMS	73	NP B64 134	B.D. Hyams et al.	(CERN, MPIM)	
BINGHAM	72B	PL 41B 635	H.H. Bingham et al.	(CERN, MPIM)	
JACOB	72	PR D5 1847	M. Jacob, R. Slansky	(LBL, UCB, SLAC)IGJP	
GOUNARIS	68	PRL 21 244	G.J. Gounaris, J.J. Sakurai		

$a_2(1700)$ WIDTH

VALUE (MeV)	EVTs	DOCUMENT ID	TECN	COMMENT
380⁺⁶⁰₋₅₀ OUR AVERAGE		Error includes scale factor of 3.9. See the ideogram below.		
436 ⁺²⁰ ₋₁₆	46M	1,2 AGHASYAN	18B	COMP 190 $\pi^- p \rightarrow \pi^- \pi^+ \pi^- p$
190 ± 18 ± 30		2 ABLIKIM	17K	BES3 $\psi(2S) \rightarrow \gamma \eta \pi^+ \pi^-$
336 ± 20 ± 20	18k	3 SCHEGELSKY	06	RVUE $\gamma \gamma \rightarrow \pi^+ \pi^- \pi^0$
280 ± 70		2 ABELE	99B	CBAR 1.94 $\bar{p} p \rightarrow \pi^0 \eta \eta$
• • • We do not use the following data for averages, fits, limits, etc. • • •				
280 ± 10 ± 70		4 JACKURA	18	RVUE $\pi^- p \rightarrow \eta \pi^- p$
270 ± 50		ANISOVICH	09	RVUE 0.0 $\bar{p} p, \pi N$
417 ± 19	80k	5 UMAN	06	E835 5.2 $\bar{p} p \rightarrow \eta \eta \pi^0$
279 ± 49 ± 66	145k	LU	05	B852 18 $\pi^- p \rightarrow \omega \pi^- \pi^0 p$
151 ± 22 ± 24		ABE	04	BELL 10.6 $e^+ e^- \rightarrow \pi^+ \pi^- \pi^0$
187 ± 60	221	6 ACCIARRI	01H	L3 $\gamma \gamma \rightarrow K_S^0 K_S^0, E_{cm}^{ee} = 91, 183-209$ GeV
150 ± 110 ± 34		ACCIARRI	97T	L3 $\gamma \gamma \rightarrow \pi^+ \pi^- \pi^0$

- 1 Statistical error negligible.
- 2 Breit-Wigner width.
- 3 From analysis of L3 data at 183–209 GeV.
- 4 Superseded by RODAS 19.
- 5 Statistical error only.
- 6 Spin 2 dominant, isospin not determined, could also be $I=1$.

WEIGHTED AVERAGE
380+60-50 (Error scaled by 3.9)



$a_2(1700)$

$$I^G(J^{PC}) = 1^-(2^{++})$$

$a_2(1700)$ T-MATRIX POLE \sqrt{s}

Note that $\Gamma = -2 \text{Im}(\sqrt{s})$.

VALUE (MeV)	DOCUMENT ID	TECN	COMMENT
(1630-1780) - i (60-250) OUR ESTIMATE			
(1686 ± 22 ⁺¹⁹ ₋₁₇) - i (211 ± 38 ⁺³² ₋₂₉)	1 KOPF	21	RVUE 0.9 $\bar{p} p \rightarrow \pi^0 \pi^0 \eta, \pi^0 \eta \eta, \pi^0 K^+ K^-$ and 191 $\pi^- p \rightarrow \pi^- \pi^- \pi^+ p$
(1638.9 ± 2.3 ^{+57.4} _{-0.1}) - i (112.0 ± 1.3 ^{+0.9} _{-24.2})	2 ALBRECHT	20	RVUE 0.9 $\bar{p} p \rightarrow \pi^0 \pi^0 \eta, \pi^0 \eta \eta, \pi^0 K^+ K^-$
(1722 ± 15 ± 67) - i (124 ± 9 ± 32)	3 RODAS	19	RVUE 191 $\pi^- p \rightarrow \eta' \pi^- p$
(1698 ± 44) - i (133 ± 28)	AMSLER	02	CBAR 0.9 $\bar{p} p \rightarrow \pi^0 \eta \eta$

- 1 Based on combined fit of Crystal Barrel and $\pi\pi$ scattering data (ALBRECHT 20), and COMPASS data (ADOLPH 15), using a coupled-channel model of $\eta\pi, \eta'\pi$ and $K\bar{K}$ systems.
- 2 Based on 2 poles, 2 channels ($\pi\eta, K\bar{K}$).
- 3 The coupled-channel analysis of both the $\eta\pi$ and $\eta'\pi$ systems using ADOLPH 15 data.

$a_2(1700)$ MASS

VALUE (MeV)	EVTs	DOCUMENT ID	TECN	COMMENT
1706 ± 14 OUR AVERAGE		Error includes scale factor of 1.2.		
1681 ⁺²² ₋₃₅	46M	1,2 AGHASYAN	18B	COMP 190 $\pi^- p \rightarrow \pi^- \pi^+ \pi^- p$
1726 ± 12 ± 25		2 ABLIKIM	17K	BES3 $\psi(2S) \rightarrow \gamma \eta \pi^+ \pi^-$
1722 ± 9 ± 15	18k	3 SCHEGELSKY	06	RVUE $\gamma \gamma \rightarrow \pi^+ \pi^- \pi^0$
1660 ± 40		2 ABELE	99B	CBAR 1.94 $\bar{p} p \rightarrow \pi^0 \eta \eta$
• • • We do not use the following data for averages, fits, limits, etc. • • •				
1720 ± 10 ± 60		4 JACKURA	18	RVUE $\pi^- p \rightarrow \eta \pi^- p$
1675 ± 25		ANISOVICH	09	RVUE 0.0 $\bar{p} p, \pi N$
1702 ± 7	80k	5 UMAN	06	E835 5.2 $\bar{p} p \rightarrow \eta \eta \pi^0$
1721 ± 13 ± 44	145k	LU	05	B852 18 $\pi^- p \rightarrow \omega \pi^- \pi^0 p$
1737 ± 5 ± 7		ABE	04	BELL 10.6 $e^+ e^- \rightarrow \pi^+ \pi^- \pi^0$
1767 ± 14	221	6 ACCIARRI	01H	L3 $\gamma \gamma \rightarrow K_S^0 K_S^0, E_{cm}^{ee} = 91, 183-209$ GeV
~ 1775		7 GRYGOREV	99	SPEC 40 $\pi^- p \rightarrow K_S^0 K_S^0 n$
1752 ± 21 ± 4		ACCIARRI	97T	L3 $\gamma \gamma \rightarrow \pi^+ \pi^- \pi^0$

- 1 Statistical error negligible.
- 2 Breit-Wigner mass.
- 3 From analysis of L3 data at 183–209 GeV.
- 4 Superseded by RODAS 19.
- 5 Statistical error only.
- 6 Spin 2 dominant, isospin not determined, could also be $I=1$.
- 7 Possibly two $J^P = 2^+$ resonances with isospins 0 and 1.

$a_2(1700)$ DECAY MODES

Mode	Fraction (Γ_i/Γ)
Γ_1 $\eta\pi$	(2.5 ± 0.6) %
Γ_2 $\eta'\pi$	seen
Γ_3 $\gamma\gamma$	(7.9 ± 1.7) × 10 ⁻⁷
Γ_4 $\rho\pi$	seen
Γ_5 $f_2(1270)\pi$	seen
Γ_6 $K\bar{K}$	(1.3 ± 0.8) %
Γ_7 $\omega\pi^- \pi^0$	seen
Γ_8 $\omega\rho$	seen

$a_2(1700)$ PARTIAL WIDTHS

$\Gamma(\eta\pi)$	VALUE (MeV)	EVTs	DOCUMENT ID	TECN	COMMENT	Γ_1
9.5 ± 2.0		870	1 SCHEGELSKY 06A	RVUE	$\gamma \gamma \rightarrow K_S^0 K_S^0$	
1 From analysis of L3 data at 91 and 183–209 GeV, using $a_2(1700)$ mass of 1730 MeV and width of 340 MeV, and SU(3) relations.						
$\Gamma(\gamma\gamma)$	VALUE (MeV)	EVTs	DOCUMENT ID	TECN	COMMENT	Γ_3
0.30 ± 0.05		870	1 SCHEGELSKY 06A	RVUE	$\gamma \gamma \rightarrow K_S^0 K_S^0$	
1 From analysis of L3 data at 91 and 183–209 GeV, using $a_2(1700)$ mass of 1730 MeV and width of 340 MeV, and SU(3) relations.						
$\Gamma(K\bar{K})$	VALUE (MeV)	EVTs	DOCUMENT ID	TECN	COMMENT	Γ_6
5.0 ± 3.0		870	1 SCHEGELSKY 06A	RVUE	$\gamma \gamma \rightarrow K_S^0 K_S^0$	
1 From analysis of L3 data at 91 and 183–209 GeV, using $a_2(1700)$ mass of 1730 MeV and width of 340 MeV, and SU(3) relations.						

$a_2(1700) \Gamma(i)\Gamma(\gamma\gamma)/\Gamma(\text{total})$

$$\frac{[\Gamma(\rho\pi) + \Gamma(f_2(1270)\pi)] \times \Gamma(\gamma\gamma)/\Gamma_{\text{total}}}{\Gamma_4 + \Gamma_5} \Gamma_3/\Gamma$$

VALUE (keV)	EVTS	DOCUMENT ID	TECN	COMMENT
$0.29 \pm 0.04 \pm 0.02$		ACCIARRI 97T L3		$\gamma\gamma \rightarrow \pi^+\pi^-\pi^0$
$0.37^{+0.12}_{-0.08} \pm 0.10$	18k	¹ SCHEGELSKY 06	RVUE	$\gamma\gamma \rightarrow \pi^+\pi^-\pi^0$

¹ From analysis of L3 data at 183–209 GeV.

$$\Gamma(K\bar{K}) \times \Gamma(\gamma\gamma)/\Gamma_{\text{total}} \quad \Gamma_6/\Gamma$$

VALUE (eV)	DOCUMENT ID	TECN	COMMENT
$20.6 \pm 4.2 \pm 4.6$	¹ ABE 04 BELL		$10.6 e^+e^- \rightarrow e^+e^-K^+K^-$
$49 \pm 11 \pm 13$	² ACCIARRI 01H L3		$\gamma\gamma \rightarrow K_S^0 K_S^0, E_{\text{cm}}^{\text{eff}} = 91, 183\text{--}209 \text{ GeV}$

¹ Assuming spin 2.

² Spin 2 dominant, isospin not determined, could also be $I=1$.

$a_2(1700)$ BRANCHING RATIOS

$$\Gamma(\rho\pi)/\Gamma(f_2(1270)\pi) \quad \Gamma_4/\Gamma_5$$

VALUE	EVTS	DOCUMENT ID	TECN	COMMENT
$3.4 \pm 0.4 \pm 0.1$	18k	¹ SCHEGELSKY 06	RVUE	$\gamma\gamma \rightarrow \pi^+\pi^-\pi^0$

¹ From analysis of L3 data at 183–209 GeV.

$$\Gamma(K\bar{K})/\Gamma(\eta\pi) \quad \Gamma_6/\Gamma_1$$

VALUE	DOCUMENT ID	TECN	COMMENT
$0.029 \pm 0.04^{+0.011}_{-0.012}$	¹ KOPF 21 RVUE		$0.9 p\bar{p} \rightarrow \pi^0\pi^0\eta, \pi^0\eta\eta, \pi^0K^+K^- \text{ and } 191 \pi^-\rho \rightarrow \pi^-\pi^-\pi^+\rho$
$4.134 \pm 0.106^{+4.909}_{-2.988}$	² ALBRECHT 20 RVUE		$0.9 p\bar{p} \rightarrow \pi^0\pi^0\eta, \pi^0\eta\eta, \pi^0K^+K^-$

¹ From T-matrix pole based on combined fit of Crystal Barrel and $\pi\pi$ scattering data (ALBRECHT 20), and COMPASS data (ADOLPH 15), using a coupled-channel model of $\eta\pi, \eta'\pi$ and $K\bar{K}$ systems.

² Residues from T-matrix pole, 2 poles, 2 channels ($\pi\eta, K\bar{K}$).

$$\Gamma(\eta'\pi)/\Gamma(\eta\pi) \quad \Gamma_2/\Gamma_1$$

VALUE	DOCUMENT ID	TECN	COMMENT
$0.035 \pm 0.044^{+0.069}_{-0.012}$	¹ KOPF 21 RVUE		$0.9 p\bar{p} \rightarrow \pi^0\pi^0\eta, \pi^0\eta\eta, \pi^0K^+K^- \text{ and } 191 \pi^-\rho \rightarrow \pi^-\pi^-\pi^+\rho$

¹ From T-matrix pole based on combined fit of Crystal Barrel and $\pi\pi$ scattering data (ALBRECHT 20), and COMPASS data (ADOLPH 15), using a coupled-channel model of $\eta\pi, \eta'\pi$ and $K\bar{K}$ systems.

$a_2(1700)$ REFERENCES

KOPF 21 EPJ C81 1056	B. Kopf et al. (BOCH)
ALBRECHT 20 EPJ C80 453	M. Albrecht et al. (Crystal Barrel Collab.)
RODAS 19 PRL 122 042002	A. Rodas et al. (JPAC Collab.)
AGHASYAN 18B PR D98 092003	M. Aghasyan et al. (COMPASS Collab.)
JACKURA 18 PL B779 464	A. Jackura et al. (JPAC and COMPASS Collab.)
ABLIKIM 17K PR D95 032002	M. Ablikim et al. (BESIII Collab.)
ADOLPH 15 PL B740 303	M. Adolph et al. (COMPASS Collab.)
ANISOVICH 09 JUMP A24 2481	V.V. Anisovich, A.V. Sarantsev (PNPI)
SCHEGELSKY 06 EPJ A27 199	V.A. Schegelsky et al.
SCHEGELSKY 06A EPJ A27 207	V.A. Schegelsky et al.
UMAN 06 PR D73 052009	I. Uman et al. (FNAL E835)
LU 05 PRL 94 032002	M. Lu et al. (BNL E852 Collab.)
ABE 04 EPJ C32 323	K. Abe et al. (BELLE Collab.)
AMSLER 02 EPJ C23 29	C. Amisler et al. (Crystal Barrel Collab.)
ACCIARRI 01H PL B501 173	M. Acciari et al. (L3 Collab.)
ABELE 99B EPJ C8 67	A. Abele et al. (Crystal Barrel Collab.)
GRYGOREV 99 PAN 62 470	V.K. Grygorev et al.
ACCIARRI 97T PL B413 147	M. Acciari et al. (L3 Collab.)

$a_0(1710)$

$$I^G(J^{PC}) = 1^-(0^{++})$$

OMITTED FROM SUMMARY TABLE

Evidence for this state is also inferred from the interference of the K^+K^- and $K_S^0K_S^0$ decays of the $f_0(1710)$ in $D_s^+ \rightarrow f_0(1710)\pi^+$, leading to a relative branching ratio an order of magnitude larger than expected from isospin symmetry (ABLIKIM 22F). See also the review on "Spectroscopy of Light Meson Resonances."

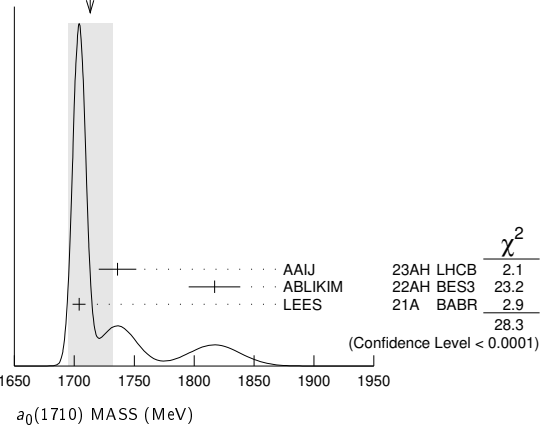
$a_0(1710)$ MASS

VALUE (MeV)	DOCUMENT ID	TECN	COMMENT
1713 ± 19 OUR AVERAGE	Error includes scale factor of 3.8. See the ideogram below.		
$1736 \pm 10 \pm 12$	¹ AAIJ 23AH LHCB		$B^+ \rightarrow K^+(K_S^0 K\pi)$
$1817 \pm 8 \pm 20$	² ABLIKIM 22AH BES3		$D_s^+ \rightarrow K_S^0 K^+\pi^0$
$1704 \pm 5 \pm 2$	LEES 21A BABR		$\eta_C(1S) \rightarrow \pi^+\pi^-\eta$

¹ From Dalitz plot analyses of $\eta_C(1S, 2S) \rightarrow K_S^0 K^+\pi^- + c.c.$

² Observed to decay into $K_S^0 K^+$ in a Breit-Wigner amplitude analysis involving D_s^+ decays into $\bar{K}^*(892)^0 K^+, \bar{K}^*(892)^+ K_S^0, \bar{K}^*(1410)^0 K^+, a_0(980)^+\pi^0,$ and $a_0(1817)^+\pi^0$.

WEIGHTED AVERAGE
1713±19 (Error scaled by 3.8)



$a_0(1710)$ WIDTH

VALUE (MeV)	DOCUMENT ID	TECN	COMMENT
107 ± 15 OUR AVERAGE			
$134 \pm 17 \pm 61$	¹ AAIJ 23AH LHCB		$B^+ \rightarrow K^+(K_S^0 K\pi)$
$97 \pm 22 \pm 15$	² ABLIKIM 22AH BES3		$D_s^+ \rightarrow K_S^0 K^+\pi^0$
$110 \pm 15 \pm 11$	LEES 21A BABR		$\eta_C(1S) \rightarrow \pi^+\pi^-\eta$

¹ From Dalitz plot analyses of $\eta_C(1S, 2S) \rightarrow K_S^0 K^+\pi^- + c.c.$

² Observed to decay into $K_S^0 K^+$ in a Breit-Wigner amplitude analysis involving D_s^+ decays into $\bar{K}^*(892)^0 K^+, \bar{K}^*(892)^+ K_S^0, \bar{K}^*(1410)^0 K^+, a_0(980)^+\pi^0,$ and $a_0(1817)^+\pi^0$.

$a_0(1710)$ DECAY MODES

Mode	Fraction (Γ_i/Γ)
$\Gamma_1 \pi\eta$	seen
$\Gamma_2 K^+K^-$	seen
$\Gamma_3 K_S^0 K_S^0$	seen
$\Gamma_4 K_S^0 K^+$	seen

$$\Gamma(\pi\eta)/\Gamma_{\text{total}} \quad \Gamma_1/\Gamma$$

VALUE	DOCUMENT ID	TECN	COMMENT
seen	LEES 21A BABR		$\eta_C(1S) \rightarrow \pi^+\pi^-\eta$

$$\Gamma(K^+K^-)/\Gamma(K_S^0 K_S^0) \quad \Gamma_2/\Gamma_3$$

VALUE	DOCUMENT ID	TECN	COMMENT
0.32 ± 0.12	¹ ABLIKIM 22F BES3		$D_s^+ \rightarrow K_S^0 K_S^0 \pi^+$

¹ Using $D_s^+ \rightarrow K^+K^-\pi^+$ from ABLIKIM 21AE. The apparent violation of isospin symmetry may be due to a destructive interference with the $f_0(1710)$ in the K^+K^- channel, and a constructive interference in the $K_S^0 K_S^0$ channel.

$$\Gamma(K_S^0 K^+)/\Gamma_{\text{total}} \quad \Gamma_4/\Gamma$$

VALUE	DOCUMENT ID	TECN	COMMENT
seen	ABLIKIM 22AH BES3		$D_s^+ \rightarrow K_S^0 K^+\pi^0$

$a_0(1710)$ REFERENCES

AAIJ 23AH PR D108 032010	R. Aaij et al. (LHCb Collab.)
ABLIKIM 22AH PRL 129 182001	M. Ablikim et al. (BESIII Collab.)
ABLIKIM 22F PR D105 L051103	M. Ablikim et al. (BESIII Collab.)
ABLIKIM 21AE PR D104 012016	M. Ablikim et al. (BESIII Collab.)
LEES 21A PR D104 072002	J.P. Lees et al. (BABAR Collab.)

Meson Particle Listings

$f_0(1710)$

$f_0(1710)$

$$I^G(J^{PC}) = 0^+(0^{++})$$

See the review on "Spectroscopy of Light Meson Resonances."

$f_0(1710)$ T-MATRIX POLE \sqrt{s}

Note that $\Gamma = -2 \text{Im}(\sqrt{s})$.

VALUE (MeV)	DOCUMENT ID	TECN	COMMENT
(1680-1820) - i (50-180) OUR ESTIMATE			
$(1769 \pm 8) - i (78 \pm 6)$	¹ RODAS	22	RVUE $J/\psi(1S) \rightarrow \gamma(\pi\pi, K\bar{K})$
$(1700 \pm 18) - i (127 \pm 12)$	SARANTSEV	21	RVUE $J/\psi(1S) \rightarrow \gamma(\pi\pi, K\bar{K}, \eta\eta, \omega\phi)$
$(1803 \pm 3.5 \pm 45.5 \pm 10.4) - i (145 \pm 2.5 \pm 16.3 \pm 9.6)$	² ALBRECHT	20	RVUE $0.9 \bar{p}p \rightarrow \pi^0 \pi^0 \eta, \pi^0 \eta\eta, \pi^0 K^+ K^-$
$(1732 \pm 15) - i (160 \pm 25 \pm 10)$	³ ANISOVICH	03	RVUE $\pi\pi, K\bar{K}, \eta\eta, \eta\eta', \pi\pi\pi\pi$
$(1698 \pm 18) - i (60 \pm 13)$	BARBERIS	00E	OMEG 450 $p\bar{p} \rightarrow p_f \eta\eta p_S$
$(1770 \pm 12) - i (110 \pm 20)$	⁴ ANISOVICH	99B	SPEC 0.6-1.2 $p\bar{p} \rightarrow \eta\eta\pi^0$
$(1727 \pm 12 \pm 11) - i (63 \pm 8 \pm 9)$	BARBERIS	99D	OMEG 450 $p\bar{p} \rightarrow K^+ K^-, \pi^+ \pi^-$
$(1750 \pm 30) - i (125 \pm 70)$	ANISOVICH	98B	RVUE Compilation

- T-matrix pole from coupled channel K-matrix fit to data on $J/\psi \rightarrow \gamma\pi^0\pi^0$ (ABLIKIM 15AE) and $J/\psi \rightarrow \gamma K_S^0 K_S^0$ (ABLIKIM 18AA).
- T-matrix pole, 5 poles, 5 channels, including scattering data from HYAMS 75 ($\pi\pi$), LONGACRE 86 ($K\bar{K}$), BINON 83 ($\eta\eta$), and BINON 84C ($\eta\eta'$).
- Solution I.
- Not seen by AMSLER 02.

$f_0(1710)$ Breit-Wigner MASS

VALUE (MeV)	EVTS	DOCUMENT ID	TECN	COMMENT
1733 \pm 9 OUR AVERAGE Error includes scale factor of 1.5. See the ideogram below.				
$1757 \pm 24 \pm 9$		LEES	21A	BABR $\eta_C(1S) \rightarrow \eta' K^+ K^-$
$1759 \pm 6 \pm 14 \pm 25$	5.5k	¹ ABLIKIM	13N	BES3 $e^+ e^- \rightarrow J/\psi \rightarrow \gamma\eta\eta$
$1750 \pm 6 \pm 29 \pm 7 \pm 18$		² UEHARA	13	BELL $\gamma\gamma \rightarrow K_S^0 K_S^0$
$1701 \pm 5 \pm 9 \pm 2$	4k	³ CHEKANOV	08	ZEUS $e p \rightarrow K_S^0 K_S^0 X$
$1765 \pm 4 \pm 13$		ABLIKIM	06V	BES2 $e^+ e^- \rightarrow J/\psi \rightarrow \gamma\pi^+ \pi^-$
1738 ± 30		ABLIKIM	04E	BES2 $J/\psi \rightarrow \omega K^+ K^-$
$1740 \pm 4 \pm 10 \pm 25$		BAI	03G	BES $J/\psi \rightarrow \gamma K\bar{K}$
$1740 \pm 30 \pm 25$		BAI	00A	BES $J/\psi \rightarrow \gamma(\pi^+ \pi^- \pi^+ \pi^-)$
1710 ± 25		⁴ FRENCH	99	300 $p\bar{p} \rightarrow p_f(K^+ K^-) p_S$

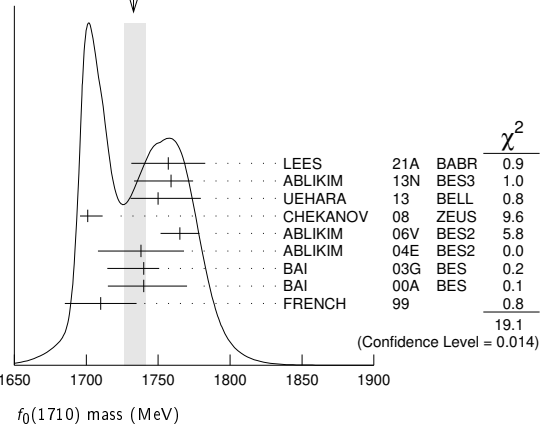
• • • We do not use the following data for averages, fits, limits, etc. • • •

$1744 \pm 7 \pm 5$	381	^{5,6} DOBBS	15	$J/\psi \rightarrow \gamma\pi^+ \pi^-$
$1705 \pm 11 \pm 5$	237	^{5,6} DOBBS	15	$\psi(2S) \rightarrow \gamma\pi^+ \pi^-$
$1706 \pm 4 \pm 5$	1.0k	^{5,6} DOBBS	15	$J/\psi \rightarrow \gamma K^+ K^-$
$1690 \pm 8 \pm 3$	349	^{5,6} DOBBS	15	$\psi(2S) \rightarrow \gamma K^+ K^-$
1750 ± 13		AMSLER	06	CBAR $1.64 \bar{p}p \rightarrow K^+ K^- \pi^0$
1747 ± 5	80k	⁷ UMAN	06	E835 $5.2 \bar{p}p \rightarrow \eta\eta\pi^0$
1776 ± 15		VLADIMIRSK..06	SPEC	40 $\pi^- p \rightarrow K_S^0 K_S^0 n$
1670 ± 20		BINON	05	GAMS $33 \pi^- p \rightarrow \eta\eta n$
1682 ± 16		TIKHOMIROV	03	SPEC $40.0 \pi^- C \rightarrow K_S^0 K_S^0 K_L^0 X$
1670 ± 26	3.6k	⁸ NICHITIU	02	OBLX $0 \bar{p}p \rightarrow K^+ K^- \pi^+ \pi^- \pi^0$
1730 ± 15		BARBERIS	99	OMEG 450 $p\bar{p} \rightarrow p_S p_f K^+ K^-$
1750 ± 20		BARBERIS	99B	OMEG 450 $p\bar{p} \rightarrow p_S p_f \pi^+ \pi^-$
1720 ± 39		BAI	98H	BES $J/\psi \rightarrow \gamma\pi^0 \pi^0$
1775 ± 1.5	57	⁹ BARKOV	98	$\pi^- p \rightarrow K_S^0 K_S^0 n$
1690 ± 11		¹⁰ ABREU	96C	DLPH $Z^0 \rightarrow K^+ K^- X$
$1696 \pm 5 \pm 9 \pm 34$		¹¹ BAI	96C	BES $J/\psi \rightarrow \gamma K^+ K^-$
$1781 \pm 8 \pm 10 \pm 31$		BAI	96C	BES $J/\psi \rightarrow \gamma K^+ K^-$
1768 ± 14		BALOSHIN	95	SPEC $40 \pi^- C \rightarrow K_S^0 K_S^0 X$
1750 ± 15		¹² BUGG	95	MRK3 $J/\psi \rightarrow \gamma\pi^+ \pi^- \pi^+ \pi^-$
1620 ± 16		¹¹ BUGG	95	MRK3 $J/\psi \rightarrow \gamma\pi^+ \pi^- \pi^+ \pi^-$
1748 ± 10		¹³ ARMSTRONG	93C	E760 $\bar{p}p \rightarrow \pi^0 \eta\eta \rightarrow 6\gamma$
~ 1750		BREAKSTONE	93	SFM $p\bar{p} \rightarrow p\bar{p}\pi^+ \pi^- \pi^+ \pi^-$
1744 ± 15		¹⁴ ALDE	92D	GAM2 $38 \pi^- p \rightarrow \eta\eta n$
1713 ± 10		¹⁵ ARMSTRONG	89D	OMEG 300 $p\bar{p} \rightarrow p\bar{p} K^+ K^-$
1706 ± 10		¹⁵ ARMSTRONG	89D	OMEG 300 $p\bar{p} \rightarrow p\bar{p} K_S^0 K_S^0$
1707 ± 10		¹³ AUGUSTIN	88	DM2 $J/\psi \rightarrow \gamma K^+ K^-, K_S^0 K_S^0$
1700 ± 15		¹¹ BOLONKIN	88	SPEC $40 \pi^- p \rightarrow K_S^0 K_S^0 n$
1720 ± 60		BOLONKIN	88	SPEC $40 \pi^- p \rightarrow K_S^0 K_S^0 n$
1638 ± 10		¹⁶ FALVARD	88	DM2 $J/\psi \rightarrow \phi K^+ K^-, K_S^0 K_S^0$
1690 ± 4		¹⁷ FALVARD	88	DM2 $J/\psi \rightarrow \phi K^+ K^-, K_S^0 K_S^0$

1698 ± 15	¹³ AUGUSTIN	87	DM2 $J/\psi \rightarrow \gamma\pi^+ \pi^-$
$1720 \pm 10 \pm 10$	¹¹ BALTRUSAIT..87	MRK3	$J/\psi \rightarrow \gamma K^+ K^-$
1755 ± 8	¹⁸ ALDE	86c	GAM2 $38 \pi^- p \rightarrow n 2\eta$
$1730 \pm 2 \pm 10$	¹⁹ LONGACRE	86	RVUE $22 \pi^- p \rightarrow n 2 K_S^0$
1742 ± 15	¹³ WILLIAMS	84	MPSF $200 \pi^- N \rightarrow 2 K_S^0 X$
1670 ± 50	BLOOM	83	CBAL $J/\psi \rightarrow \gamma 2\eta$
1650 ± 50	BURKE	82	MRK2 $J/\psi \rightarrow \gamma 2\rho$
1640 ± 50	^{20,21} EDWARDS	82D	CBAL $J/\psi \rightarrow \gamma 2\eta$
$1730 \pm 10 \pm 20$	²² ETKIN	82c	MPS $23 \pi^- p \rightarrow n 2 K_S^0$

- From partial wave analysis including all possible combinations of $0^{++}, 2^{++}$, and 4^{++} resonances.
- Spin 0 favored over spin 2.
- In the SU(3) based model with a specific interference pattern of the $f_2(1270), a_2^0(1320)$, and $f_2'(1525)$ mesons incoherently added to the $f_0(1710)$ and non-resonant background.
- $J^P = 0^+$, supersedes ARMSTRONG 89D.
- Using CLEO-c data but not authored by the CLEO Collaboration.
- From a fit to a Breit-Wigner line shape with fixed $\Gamma = 135$ MeV.
- Systematic errors not estimated.
- Decaying to $f_0(1370)\pi\pi$.
- No J^{PC} determination.
- No J^{PC} determination, width not determined.
- $J^P = 2^+$.
- From a fit to the 0^+ partial wave.
- No J^{PC} determination.
- ALDE 92D combines all the GAMS-2000 data.
- $J^P = 2^+$, superseded by FRENCH 99.
- From an analysis ignoring interference with $f_2'(1525)$.
- From an analysis including interference with $f_2'(1525)$.
- Superseded by ALDE 92D.
- Uses MRK3 data. From a partial-wave analysis of data using a K-matrix formalism with 5 poles, but assuming spin 2. Fit with constrained inelasticity.
- $J^P = 2^+$ preferred.
- From fit neglecting nearby $f_2'(1525)$. Replaced by BLOOM 83.
- Superseded by LONGACRE 86.

WEIGHTED AVERAGE
1733+8-7 (Error scaled by 1.5)



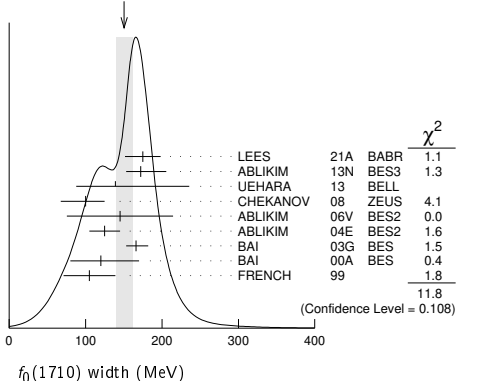
$f_0(1710)$ Breit-Wigner WIDTH

VALUE (MeV)	EVTS	DOCUMENT ID	TECN	COMMENT
150 \pm 12 OUR AVERAGE Error includes scale factor of 1.3. See the ideogram below.				
$175 \pm 23 \pm 4$		LEES	21A	BABR $\eta_C(1S) \rightarrow \eta' K^+ K^-$
$172 \pm 10 \pm 32 \pm 16$	5.5k	¹ ABLIKIM	13N	BES3 $e^+ e^- \rightarrow J/\psi \rightarrow \gamma\eta\eta$
$139 \pm 11 \pm 96 \pm 12 \pm 50$		² UEHARA	13	BELL $\gamma\gamma \rightarrow K_S^0 K_S^0$
$100 \pm 24 \pm 7 \pm 22$	4k	³ CHEKANOV	08	ZEUS $e p \rightarrow K_S^0 K_S^0 X$
$145 \pm 8 \pm 69$		ABLIKIM	06V	BES2 $e^+ e^- \rightarrow J/\psi \rightarrow \gamma\pi^+ \pi^-$
125 ± 20		ABLIKIM	04E	BES2 $J/\psi \rightarrow \omega K^+ K^-$
$166 \pm 5 \pm 15 \pm 10$		BAI	03G	BES $J/\psi \rightarrow \gamma K\bar{K}$
$120 \pm 50 \pm 40$		BAI	00A	BES $J/\psi \rightarrow \gamma(\pi^+ \pi^- \pi^+ \pi^-)$
105 ± 34		⁴ FRENCH	99	300 $p\bar{p} \rightarrow p_f(K^+ K^-) p_S$
• • • We do not use the following data for averages, fits, limits, etc. • • •				
$148 \pm 40 \pm 30$		AMSLER	06	CBAR $1.64 \bar{p}p \rightarrow K^+ K^- \pi^0$
188 ± 13	80k	⁵ UMAN	06	E835 $5.2 \bar{p}p \rightarrow \eta\eta\pi^0$
250 ± 30		VLADIMIRSK..06	SPEC	40 $\pi^- p \rightarrow K_S^0 K_S^0 n$

260 ± 50		BINON	05	GAMS	33	$\pi^- p \rightarrow \eta \eta n$
102 ± 26		TIKHOMIROV	03	SPEC	40.0	$K_S^0 K_S^0 K_S^0 X$
267 ± 44	3651	6 NICHITIU	02	OBLX	0	$\bar{p} p \rightarrow K^+ K^- \pi^+ \pi^- \pi^0$
100 ± 25		BARBERIS	99	OMEG	450	$pp \rightarrow p_S p_f K^+ K^-$
160 ± 30		BARBERIS	99B	OMEG	450	$pp \rightarrow p_S p_f \pi^+ \pi^-$
30 ± 7	57	7 BARKOV	98			$\pi^- p \rightarrow K_S^0 K_S^0 n$
103 ± 18	$^{+30}_{-11}$	8 BAI	96C	BES		$J/\psi \rightarrow \gamma K^+ K^-$
85 ± 24	$^{+22}_{-19}$	BAI	96C	BES		$J/\psi \rightarrow \gamma K^+ K^-$
56 ± 19		BALOSHIN	95	SPEC	40	$\pi^- C \rightarrow K_S^0 K_S^0 X$
160 ± 40		9 BUGG	95	MRK3		$J/\psi \rightarrow \gamma \pi^+ \pi^- \pi^+ \pi^-$
160 ± 60	$^{+20}_{-20}$	8 BUGG	95	MRK3		$J/\psi \rightarrow \gamma \pi^+ \pi^- \pi^+ \pi^-$
264 ± 25		10 ARMSTRONG	93C	E760		$\bar{p} p \rightarrow \pi^0 \eta \eta \rightarrow 6\gamma$
200 to 300		BREAKSTONE	93	SFM		$pp \rightarrow pp \pi^+ \pi^- \pi^+ \pi^-$
< 80 90% CL		11 ALDE	92D	GAM2	38	$\pi^- p \rightarrow \eta \eta n^*$
181 ± 30		12 ARMSTRONG	89D	OMEG	300	$pp \rightarrow pp K^+ K^-$
104 ± 30		12 ARMSTRONG	89D	OMEG	300	$pp \rightarrow pp K_S^0 K_S^0$
166.4 ± 33.2		10 AUGUSTIN	88	DM2		$J/\psi \rightarrow \gamma K^+ K^-, K_S^0 K_S^0$
30 ± 20		8 BOLONKIN	88	SPEC	40	$\pi^- p \rightarrow K_S^0 K_S^0 n$
350 ± 150		BOLONKIN	88	SPEC	40	$\pi^- p \rightarrow K_S^0 K_S^0 n$
148 ± 17		13 FALVARD	88	DM2		$J/\psi \rightarrow \phi K^+ K^-, K_S^0 K_S^0$
184 ± 6		14 FALVARD	88	DM2		$J/\psi \rightarrow \phi K^+ K^-, K_S^0 K_S^0$
136 ± 28		10 AUGUSTIN	87	DM2		$J/\psi \rightarrow \gamma \pi^+ \pi^-$
130 ± 20		8 BALTRUSAITIS	87	MRK3		$J/\psi \rightarrow \gamma K^+ K^-$
122 ± 74	$^{+15}_{-15}$	15 LONGACRE	86	RVUE	22	$\pi^- p \rightarrow n 2K_S^0$
57 ± 38		16 WILLIAMS	84	MPSF	200	$\pi^- N \rightarrow 2K_S^0 X$
160 ± 80		BLOOM	83	CBAL		$J/\psi \rightarrow \gamma 2\eta$
200 ± 100		BURKE	82	MRK2		$J/\psi \rightarrow \gamma 2\rho$
220 ± 100	$^{+70}_{-70}$	17,18 EDWARDS	82D	CBAL		$J/\psi \rightarrow \gamma 2\eta$
200 ± 156	$^{+9}_{-9}$	19 ETKIN	82B	MPS	23	$\pi^- p \rightarrow n 2K_S^0$

- From partial wave analysis including all possible combinations of $0^{++}, 2^{++},$ and 4^{++} resonances.
- Spin 0 favored over spin 2.
- In the SU(3) based model with a specific interference pattern of the $f_2(1270), a_2^0(1320),$ and $f_2'(1525)$ mesons incoherently added to the $f_0(1710)$ and non-resonant background.
- $J^P = 0^+,$ supersedes ARMSTRONG 89D.
- Systematic errors not estimated.
- Decaying to $f_0(1370) \pi \pi.$
- No J^{PC} determination.
- $J^P = 2^+.$
- From a fit to the 0^+ partial wave.
- No J^{PC} determination.
- ALDE 92D combines all the GAMS-2000 data.
- $J^P = 2^+, (0^+ \text{ excluded}).$
- From an analysis ignoring interference with $f_2'(1525).$
- From an analysis including interference with $f_2'(1525).$
- Uses MRK3 data. From a partial-wave analysis of data using a K-matrix formalism with 5 poles, but assuming spin 2. Fit with constrained inelasticity.
- No J^{PC} determination.
- $J^P = 2^+$ preferred.
- From fit neglecting nearby $f_2'(1525).$ Replaced by BLOOM 83.
- From an amplitude analysis of the $K_S^0 K_S^0$ system, superseded by LONGACRE 86.

WEIGHTED AVERAGE
150+12-10 (Error scaled by 1.3)



$f_0(1710)$ DECAY MODES

Mode	Fraction (Γ_i/Γ)
Γ_1 $K\bar{K}$	seen
Γ_2 $\eta\eta$	seen

Γ_3 $\eta\eta'$	not seen
Γ_4 $\pi\pi$	seen
Γ_5 $\gamma\gamma$	seen
Γ_6 $\omega\omega$	seen

$f_0(1710) \Gamma(i)\Gamma(\gamma\gamma)/\Gamma(\text{total})$

$\Gamma(K\bar{K}) \times \Gamma(\gamma\gamma)/\Gamma_{\text{total}}$	VALUE (eV)	CL%	DOCUMENT ID	TECN	COMMENT	$\Gamma_1\Gamma_5/\Gamma$
	$12^{+3}_{-2} + 227$		UEHARA	13	BELL	$\gamma\gamma \rightarrow K_S^0 K_S^0$

• • • We do not use the following data for averages, fits, limits, etc. • • •

VALUE (eV)	CL%	DOCUMENT ID	TECN	COMMENT
<480	95	ALBRECHT	90G	ARG $\gamma\gamma \rightarrow K^+ K^-$
<110	95	1 BEHREND	89C	CELL $\gamma\gamma \rightarrow K_S^0 K_S^0$
<280	95	1 ALTHOFF	85B	TASS $\gamma\gamma \rightarrow K\bar{K}\pi$

1 Assuming helicity 2.

$\Gamma(\pi\pi) \times \Gamma(\gamma\gamma)/\Gamma_{\text{total}}$

VALUE (keV)	CL%	DOCUMENT ID	TECN	COMMENT	$\Gamma_4\Gamma_5/\Gamma$
<0.82	95	1 BARATE	00E	ALEP $\gamma\gamma \rightarrow \pi^+ \pi^-$	

1 Assuming spin 0.

$f_0(1710)$ BRANCHING RATIOS

$\Gamma(K\bar{K})/\Gamma_{\text{total}}$

VALUE	EVTS	DOCUMENT ID	TECN	COMMENT	Γ_1/Γ
seen	1004	1 DOBBS	15	$J/\psi \rightarrow \gamma K^+ K^-$	
seen	349	1 DOBBS	15	$\psi(2S) \rightarrow \gamma K^+ K^-$	
0.36 ± 0.12		ALBALADEJO	08	RVUE	
0.38 ± 0.09		2 LONGACRE	86	MPS $22 \pi^- p \rightarrow n 2K_S^0$	

- Using CLEO-c data but not authored by the CLEO Collaboration.
- From a partial-wave analysis of data using a K-matrix formalism with 5 poles, but assuming spin 2. Fit with constrained inelasticity.

$\Gamma(\eta\eta)/\Gamma_{\text{total}}$

VALUE	DOCUMENT ID	TECN	COMMENT	Γ_2/Γ
0.22 ± 0.12	ALBALADEJO 08	RVUE		
0.18 ± 0.03	1 LONGACRE 86	RVUE		

- From a partial-wave analysis of data using a K-matrix formalism with 5 poles, but assuming spin 2. Fit with constrained inelasticity.

$\Gamma(\eta\eta)/\Gamma(K\bar{K})$

VALUE	CL%	DOCUMENT ID	TECN	COMMENT	Γ_2/Γ_1
0.48 ± 0.15		BARBERIS	00E	$450 pp \rightarrow p_f \eta \eta p_S$	
$0.46^{+0.70}_{-0.38}$		1 ANISOVICH	02D	SPEC Combined fit	
<0.02	90	2 PROKOSHIN	91	GA24 $300 \pi^- p \rightarrow \pi^- \rho \eta \eta$	

- From a combined K-matrix analysis of Crystal Barrel ($0. p\bar{p} \rightarrow \pi^0 \pi^0 \pi^0, \pi^0 \eta \eta, \pi^0 \pi^0 \eta$), GAMS ($\pi p \rightarrow \pi^0 \pi^0 n, \eta \eta n, \eta \eta' n$), and BNL ($\pi p \rightarrow K\bar{K}n$) data.
- Combining results of GAM4 with those of ARMSTRONG 89D.

$\Gamma(\pi\pi)/\Gamma_{\text{total}}$

VALUE	EVTS	DOCUMENT ID	TECN	COMMENT	Γ_4/Γ
seen	381	1 DOBBS	15	$J/\psi \rightarrow \gamma \pi^+ \pi^-$	
seen	237	1 DOBBS	15	$\psi(2S) \rightarrow \gamma \pi^+ \pi^-$	
not seen		AMSLER	02	CBAR $0.9 \bar{p} p \rightarrow \pi^0 \eta \eta, \pi^0 \pi^0 \pi^0$	
$0.039^{+0.002}_{-0.024}$		2 LONGACRE	86	RVUE	

- Using CLEO-c data but not authored by the CLEO Collaboration.
- From a partial-wave analysis of data using a K-matrix formalism with 5 poles, but assuming spin 2. Fit with constrained inelasticity.

$\Gamma(\pi\pi)/\Gamma(K\bar{K})$

VALUE	CL%	DOCUMENT ID	TECN	COMMENT	Γ_4/Γ_1
0.23 ± 0.05	OUR AVERAGE	Error includes scale factor of 1.2.			
$0.64 \pm 0.27 \pm 0.18$		LEES	18A	BABR $\Upsilon(1S) \rightarrow \gamma \pi^+ \pi^-, \gamma K^+ K^-$	
$0.41^{+0.11}_{-0.17}$		ABLIKIM	06V	BES2 $e^+ e^- \rightarrow J/\psi \rightarrow \gamma \pi^+ \pi^-$	
$0.2 \pm 0.024 \pm 0.036$		BARBERIS	99D	OMEG $450 pp \rightarrow K^+ K^-, \pi^+ \pi^-$	
0.39 ± 0.14		ARMSTRONG	91	OMEG $300 pp \rightarrow pp \pi \pi, pp K\bar{K}$	

• • • We do not use the following data for averages, fits, limits, etc. • • •

VALUE	CL%	DOCUMENT ID	TECN	COMMENT	Γ_4/Γ_1
0.32 ± 0.14		ALBALADEJO	08	RVUE	
< 0.11	95	1 ABLIKIM	04E	BES2 $J/\psi \rightarrow \omega K^+ K^-$	
$5.8^{+9.1}_{-5.5}$		2 ANISOVICH	02D	SPEC Combined fit	

- Using data from ABLIKIM 04A.
- From a combined K-matrix analysis of Crystal Barrel ($0. p\bar{p} \rightarrow \pi^0 \pi^0 \pi^0, \pi^0 \eta \eta, \pi^0 \pi^0 \eta$), GAMS ($\pi p \rightarrow \pi^0 \pi^0 n, \eta \eta n, \eta \eta' n$), and BNL ($\pi p \rightarrow K\bar{K}n$) data.

Meson Particle Listings

 $f_0(1710)$, $X(1750)$, $\eta(1760)$ $\Gamma(\eta\eta)/\Gamma(\pi\pi)$

VALUE	CL%	DOCUMENT ID	TECN	COMMENT
$<2.87 \times 10^{-3}$	90	¹ ABLIKIM	22As BES3	$J/\psi(1S) \rightarrow \gamma\eta\eta'$

¹ From a Breit-Wigner fit involving 9 resonances and a resonating exotic $\eta_1(1855) \rightarrow \eta\eta'/P$ -wave.

 $\Gamma(\omega\omega)/\Gamma_{\text{total}}$

VALUE	EVTs	DOCUMENT ID	TECN	COMMENT
seen	180	ABLIKIM	06H BES	$J/\psi \rightarrow \gamma\omega\omega$

 Γ_3/Γ_4 Γ_6/Γ $f_0(1710)$ REFERENCES

ABLIKIM	22As	PR D106 072012	M. Ablikim et al.	(BESIII Collab.)
Also		PR D107 079901 (err.)	M. Ablikim et al.	(BESIII Collab.)
RODAS	22	EPJ C82 80	A. Rodas et al.	(JPAC Collab.)
LEES	21A	PR D104 072002	J.P. Lees et al.	(BABAR Collab.)
SARANTSEV	21	PL B816 136227	A.V. Sarantsev et al.	(BONN, PNPI)
ALBRECHT	20	EPJ C80 453	M. Albrecht et al.	(Crystal Barrel Collab.)
ABLIKIM	18AA	PR D98 072003	M. Ablikim et al.	(BESIII Collab.)
LEES	18A	PR D97 112006	J.P. Lees et al.	(BABAR Collab.)
ABLIKIM	15AE	PR D92 052003	M. Ablikim et al.	(BESIII Collab.)
DOBBS	15	PR D91 052006	S. Dobbs et al.	(NWES)
ABLIKIM	13N	PR D87 092009	M. Ablikim et al.	(BESIII Collab.)
UEHARA	13	PTEP 2013 123C01	S. Uehara et al.	(BELLE Collab.)
ALBALADEJO	08	PRL 101 252002	M. Albaladejo, J.A. Oller	
CHEKANOV	08	PRL 101 112003	S. Chekanov et al.	(ZEUS Collab.)
ABLIKIM	06H	PR D73 112007	M. Ablikim et al.	(BES Collab.)
ABLIKIM	06V	PL B642 441	M. Ablikim et al.	(BES Collab.)
AMSLER	06	PL B639 165	C. Amisler et al.	(Crystal Barrel Collab.)
UMAN	06	PR D73 052009	I. Uman et al.	(FNAL E935)
VLADIMIRSK...	06	PAN 69 493	V.V. Vladimirov et al.	(ITEP, Moscow)
Translated from	YAF 69 515.			
BINON	05	PAN 68 960	F. Binon et al.	
Translated from	YAF 68 938.			
ABLIKIM	04A	PL B598 149	M. Ablikim et al.	(BES Collab.)
ABLIKIM	04E	PL B603 138	M. Ablikim et al.	(BES Collab.)
ANISOVICH	03	EPJ A16 229	V.V. Anisovich et al.	
BAI	03G	PR D68 052003	J.Z. Bai et al.	(BES Collab.)
TIKHOMIROV	03	PAN 66 828	G.D. Tikhomirov et al.	
Translated from	YAF 66 860.			
AMSLER	02	EPJ C23 29	C. Amisler et al.	(Crystal Barrel Collab.)
ANISOVICH	02D	PAN 65 1545	V.V. Anisovich et al.	
Translated from	YAF 65 1583.			
NICHTIU	02	PL B545 261	F. Nichtiu et al.	(OBELIX Collab.)
BAI	00A	PL B472 207	J.Z. Bai et al.	(BES Collab.)
BARATE	00E	PL B472 189	R. Barate et al.	(ALEPH Collab.)
BARBERIS	00E	PL B479 59	D. Barberis et al.	(WA 102 Collab.)
ANISOVICH	99B	PL B449 154	A.V. Anisovich et al.	
BARBERIS	99	PL B453 305	D. Barberis et al.	(Omega Expt.)
BARBERIS	99B	PL B453 316	D. Barberis et al.	(Omega Expt.)
BARBERIS	99D	PL B462 462	D. Barberis et al.	(Omega Expt.)
FRENCH	99	PL B460 213	B. French et al.	(WA76 Collab.)
ANISOVICH	98B	SPU 41 419	V.V. Anisovich et al.	
Translated from	UFN 168 481.			
BAI	98H	PRL 81 1179	J.Z. Bai et al.	(BES Collab.)
BARKOV	98	JETPL 68 764	B.P. Barkov et al.	
ABREU	96C	PL B379 309	P. Abreu et al.	(DELPHI Collab.)
BAI	96C	PRL 77 3959	J.Z. Bai et al.	(BES Collab.)
BALOSHIN	95	PAN 58 46	O.N. Baloshin et al.	(ITEP)
Translated from	YAF 58 50.			
BUGG	95	PL B353 378	D.V. Bugg et al.	(LOQM, PNPI, WASH)
ARMSTRONG	93C	PL B307 394	T.A. Armstrong et al.	(FNAL, FERR, GENO+)
BREAKSTONE	93	ZPHY C58 251	A.M. Breakstone et al.	(IOWA, CERN, DORT+)
ALDE	92D	PL B284 457	D.M. Alde et al.	(GAM2 Collab.)
Also		SJNP 54 451	D.M. Alde et al.	(GAM2 Collab.)
Translated from	YAF 54 745.			
ARMSTRONG	91	ZPHY C51 351	T.A. Armstrong et al.	(ATHU, BARI, BIRM+)
PROKOSHKIN	91	SPD 36 155	Y.D. Prokoshkin	(GAM2 and GAM4 Collab.)
Translated from	DANS 316 900.			
ALBRECHT	90G	ZPHY C48 183	H. Albrecht et al.	(ARGUS Collab.)
ARMSTRONG	89D	PL B227 186	T.A. Armstrong, M. Benayoun	(ATHU, BARI, BIRM+)
BEHREND	89C	ZPHY C43 91	H.J. Behrend et al.	(CELLO Collab.)
AUGUSTIN	88	PRL 60 2238	J.E. Augustin et al.	(DM2 Collab.)
BOLONKIN	88	NP B309 426	B.V. Bolonkin et al.	(ITEP, SERP)
FALVARD	88	PR D38 2706	A. Falvard et al.	(CLER, FRAS, LALO+)
AUGUSTIN	87	ZPHY C36 369	J.E. Augustin et al.	(LALO, CLER, FRAS+)
BALTRUSAITIS..	87	PR D35 2077	R.M. Baltrusaitis et al.	(Mark III Collab.)
ALDE	86C	PL B182 105	D.M. Alde et al.	(SERP, BELG, LANL, LAPP)
LONGACRE	86	PL B177 223	R.S. Longacre et al.	(BNL, BRAN, CUNY+)
ALTHOFF	85B	ZPHY C29 189	J. Althoff et al.	(TASSO Collab.)
BINON	84C	NC 80A 363	F.G. Binon et al.	(BELG, LAPP, SERP+)
WILLIAMS	84	PR D30 877	E.G.H. Williams et al.	(VAND, NDAM, TUFTS+)
BINON	83	NC 78A 313	F.G. Binon et al.	(BELG, LAPP, SERP+)
BLOOM	83	ARNS 33 143	E.D. Bloom, C. Peck	(SLAC, CIT)
BURKE	82	PRL 49 632	D.L. Burke et al.	(LBL, SLAC)
EDWARDS	82D	PRL 48 458	C. Edwards et al.	(CIT, HARV, PRIN+)
ETKIN	82B	PR D25 1786	A. Etkin et al.	(BNL, CUNY, TUFTS, VAND)
ETKIN	82C	PR D25 2446	A. Etkin et al.	(BNL, CUNY, TUFTS, VAND)
HYAMS	75	NP B100 205	B.D. Hyams et al.	(CERN, MPIM)

 $X(1750)$

$$J^{PC} = ?^{-}(1^{-}-)$$

OMITTED FROM SUMMARY TABLE

The $X(1750)$ was separated from the $\phi(1680)$ in the 2022 listings due to its incompatible mass and incompatible pattern of $\bar{K}K$ and $\bar{K}^*(892)K$ branching fractions.

 $X(1750)$ MASS

VALUE (MeV)	EVTs	DOCUMENT ID	TECN	COMMENT
1753.8 ± 2.7 OUR AVERAGE				
1784 ± 12	± 0	ABLIKIM	20F BES3	$\psi(2S) \rightarrow K^+K^-\eta$
$1753.5 \pm 1.5 \pm 2.3$		LINK	02K FOCUS	20-160 $\gamma p \rightarrow K^+K^-\rho$
••• We do not use the following data for averages, fits, limits, etc. •••				
1726 ± 22		BUSENITZ	89 TPS	$\gamma p \rightarrow K^+K^-\chi$
1760 ± 20		ATKINSON	85C OMEG	20-70 $\gamma p \rightarrow K\bar{K}\chi$
1690 ± 10		ASTON	81F OMEG	25-70 $\gamma p \rightarrow K^+K^-\chi$

 $X(1750)$ WIDTH

VALUE (MeV)	EVTs	DOCUMENT ID	TECN	COMMENT
120 ± 10 OUR AVERAGE				
$106 \begin{smallmatrix} +22 \\ -19 \end{smallmatrix} \begin{smallmatrix} +8 \\ -36 \end{smallmatrix}$		ABLIKIM	20F BES3	$\psi(2S) \rightarrow K^+K^-\eta$
$122.2 \pm 6.2 \pm 8.0$		LINK	02K FOCUS	20-160 $\gamma p \rightarrow K^+K^-\rho$
••• We do not use the following data for averages, fits, limits, etc. •••				
121 ± 47		BUSENITZ	89 TPS	$\gamma p \rightarrow K^+K^-\chi$
80 ± 40		ATKINSON	85C OMEG	20-70 $\gamma p \rightarrow K\bar{K}\chi$
100 ± 40		ASTON	81F OMEG	25-70 $\gamma p \rightarrow K^+K^-\chi$

 $X(1750)$ DECAY MODES

Mode	Fraction (Γ_i/Γ)
Γ_1 K^+K^-	seen
Γ_2 $\bar{K}^*(892)^0 K_S^0$	not seen
Γ_3 $K^*(892)^\pm K^\mp$	not seen
Γ_4 $\eta\phi$	not seen

 $\Gamma(\bar{K}^*(892)^0 K_S^0)/\Gamma(K^+K^-)$

VALUE	CL%	DOCUMENT ID	TECN	COMMENT
<0.065	90	LINK	02K FOCUS	$\gamma p \rightarrow K^+K^-\rho$

 $\Gamma(K^*(892)^\pm K^\mp)/\Gamma(K^+K^-)$

VALUE	CL%	DOCUMENT ID	TECN	COMMENT
<0.183	90	LINK	02K FOCUS	$\gamma p \rightarrow K^+K^-\rho$

 $\Gamma(\eta\phi)/\Gamma_{\text{total}}$

VALUE	DOCUMENT ID	TECN	COMMENT
not seen	¹ ZHU	23A RVUE	$e^+e^- \rightarrow \eta\phi$

¹ Reported with a 2σ significance in the fit and an upper limit of $\Gamma(e^+e^-)B(X(1750) \rightarrow \eta\phi)$ in the range 136-322 eV.

 $X(1750)$ REFERENCES

ZHU	23A	CP C47 113003	W. Zhu, X. Wang	(RVUE)
ABLIKIM	20F	PR D101 032008	M. Ablikim et al.	(BESIII Collab.)
LINK	02K	PL B545 50	J.M. Link et al.	(FNAL FOCUS Collab.)
BUSENITZ	89	PR D40 1	J.K. Busewitz et al.	(ILL, FNAL)
ATKINSON	85C	ZPHY C27 233	M. Atkinson et al.	(BONN, CERN, GLAS+)
ASTON	81F	PL 104B 231	D. Aston	(BONN, CERN, EPOL, GLAS, LANC+)

 $\eta(1760)$

$$J^{PC} = 0^+(0^-+)$$

OMITTED FROM SUMMARY TABLE

Seen by DM2 in the $\rho\rho$ system (BISELLO 89B). Structure in this region has been reported before in the same system (BALTRUSAITIS 86B) and in the $\omega\omega$ system (BALTRUSAITIS 85C, BISELLO 87).

 $\eta(1760)$ MASS

VALUE (MeV)	EVTs	DOCUMENT ID	TECN	COMMENT
1751 ± 15 OUR AVERAGE				
$1768 \begin{smallmatrix} +24 \\ -25 \end{smallmatrix} \pm 10$	465	¹ ZHANG	12A BELL	$e^+e^- \rightarrow e^+e^-\eta'\pi^+\pi^-$
$1744 \pm 10 \pm 15$	1045	² ABLIKIM	06H BES	$J/\psi \rightarrow \gamma\omega\omega$
••• We do not use the following data for averages, fits, limits, etc. •••				
$1703 \begin{smallmatrix} +12 \\ -11 \end{smallmatrix} \pm 2$		³ ZHANG	12A BELL	$e^+e^- \rightarrow e^+e^-\eta'\pi^+\pi^-$
1760 ± 11	320	⁴ BISELLO	89B DM2	$J/\psi \rightarrow 4\pi\gamma$

¹ From a single-resonance fit.

² From a partial wave analysis including $\eta(1760)$, $f_0(1710)$, $f_2(1640)$, and $f_2(1910)$.

³ From a two-resonance fit.

⁴ Estimated by us from various fits. Systematic uncertainties not estimated.

 $\eta(1760)$ WIDTH

VALUE (MeV)	EVTs	DOCUMENT ID	TECN	COMMENT
240 ± 30 OUR AVERAGE				
$224 \begin{smallmatrix} +62 \\ -56 \end{smallmatrix} \pm 25$	465	⁵ ZHANG	12A BELL	$e^+e^- \rightarrow e^+e^-\eta'\pi^+\pi^-$
$244 \begin{smallmatrix} +24 \\ -21 \end{smallmatrix} \pm 25$	1045	⁶ ABLIKIM	06H BES	$J/\psi \rightarrow \gamma\omega\omega$
••• We do not use the following data for averages, fits, limits, etc. •••				
$42 \begin{smallmatrix} +36 \\ -22 \end{smallmatrix} \pm 15$		⁷ ZHANG	12A BELL	$e^+e^- \rightarrow e^+e^-\eta'\pi^+\pi^-$
60 ± 16	320	⁸ BISELLO	89B DM2	$J/\psi \rightarrow 4\pi\gamma$
••• We do not use the following data for averages, fits, limits, etc. •••				
⁵ From a single-resonance fit.				
⁶ From a partial wave analysis including $\eta(1760)$, $f_0(1710)$, $f_2(1640)$, and $f_2(1910)$.				
⁷ From a two-resonance fit.				
⁸ Estimated by us from various fits. Systematic uncertainties not estimated.				

See key on page 1171

Meson Particle Listings

$\eta(1760), f_0(1770)$

$\eta(1760)$ DECAY MODES

Mode	Fraction (Γ_i/Γ)
Γ_1 4π	
Γ_2 $2\pi^+2\pi^-$	seen
Γ_3 $\pi^+\pi^-2\pi^0$	seen
Γ_4 $\rho^0\rho^0$	seen
Γ_5 $\rho^+\rho^-$	seen
Γ_6 $\omega\omega$	seen
Γ_7 $\eta'\pi^+\pi^-$	seen
Γ_8 $\gamma\gamma$	seen

$\eta(1760)$ $\Gamma(i)\Gamma(\gamma\gamma)/\Gamma(\text{total})$

$\Gamma(\eta'\pi^+\pi^-) \times \Gamma(\gamma\gamma)/\Gamma_{\text{total}}$	VALUE (eV)	EVTS	DOCUMENT ID	TECN	COMMENT	$\Gamma_7\Gamma_8/\Gamma$
seen	$28.2^{+7.9}_{-7.5} \pm 3.7$	465	⁹ ZHANG	12A BELL	$e^+e^- \rightarrow e^+e^-\eta'/\pi^+\pi^-$	

••• We do not use the following data for averages, fits, limits, etc. •••

seen	$3.0^{+2.0}_{-1.2} \pm 0.8$	52	¹⁰ ZHANG	12A BELL	$e^+e^- \rightarrow e^+e^-\eta'/\pi^+\pi^-$	
seen	$18^{+13}_{-10} \pm 5$	315	¹¹ ZHANG	12A BELL	$e^+e^- \rightarrow e^+e^-\eta'/\pi^+\pi^-$	

⁹ From a single-resonance fit.

¹⁰ From a two-resonance fit. For constructive interference with the X(1835).

¹¹ From a two-resonance fit. For destructive interference with the X(1835).

$\eta(1760)$ BRANCHING RATIOS

$\Gamma(2\pi^+2\pi^-)/\Gamma_{\text{total}}$	VALUE	DOCUMENT ID	TECN	COMMENT	Γ_2/Γ
seen		BISELLO	89B DM2	$J/\psi \rightarrow \gamma 2\pi^+2\pi^-$	

$\Gamma(\pi^+\pi^-2\pi^0)/\Gamma_{\text{total}}$	VALUE	DOCUMENT ID	TECN	COMMENT	Γ_3/Γ
seen		BISELLO	89B DM2	$J/\psi \rightarrow \gamma \pi^+\pi^-2\pi^0$	

$\Gamma(\rho^0\rho^0)/\Gamma_{\text{total}}$	VALUE	DOCUMENT ID	TECN	COMMENT	Γ_4/Γ
seen		BISELLO	89B DM2	$J/\psi \rightarrow \gamma \rho^0\rho^0$	
seen		BALTRUSAIT...86	MRK3	$J/\psi \rightarrow \gamma \rho^0\rho^0$	

$\Gamma(\rho^+\rho^-)/\Gamma_{\text{total}}$	VALUE	DOCUMENT ID	TECN	COMMENT	Γ_5/Γ
seen		BISELLO	89B DM2	$J/\psi \rightarrow \gamma \rho^+\rho^-$	
seen		BALTRUSAIT...86	MRK3	$J/\psi \rightarrow \gamma \rho^+\rho^-$	

$\Gamma(\omega\omega)/\Gamma_{\text{total}}$	VALUE	DOCUMENT ID	TECN	COMMENT	Γ_6/Γ
seen		BISELLO	87 DM2	$J/\psi \rightarrow \omega\omega$	
seen		BALTRUSAIT...85C	MRK3	$J/\psi \rightarrow \gamma\omega\omega$	

$\Gamma(\gamma\gamma)/\Gamma(\omega\omega)$	VALUE	CL%	DOCUMENT ID	TECN	COMMENT	Γ_8/Γ_6
seen	$<2.48 \times 10^{-3}$	90	¹² ABLIKIM	180 BES3	$\psi(2S) \rightarrow \pi^+\pi^-\gamma\gamma\gamma$	

¹² Using results from ABLIKIM 06H.

$\eta(1760)$ REFERENCES

ABLIKIM 180	PR D97 072014	M. Ablikim et al.	(BESIII Collab.)
ZHANG 12A	PR D86 052002	C.C. Zhang et al.	(BELLE Collab.)
ABLIKIM 06H	PR D73 112007	M. Ablikim et al.	(BES Collab.)
BISELLO 89B	PR D39 701	G. Busetto et al.	(DM2 Collab.)
BISELLO 87	PL B192 239	D. Bisello et al.	(PADO, CLER, FRAS-)
BALTRUSAIT...86	PR D33 629	R.M. Baltrusaitis et al.	(Mark III Collab.)
BALTRUSAIT...86B	PR D33 1222	R.M. Baltrusaitis et al.	(Mark III Collab.)
BALTRUSAIT...85C	PRL 55 1723	R.M. Baltrusaitis et al.	(CIT, UCSC-)

$f_0(1770)$

$$I^G(J^{PC}) = 0^+(0^{++})$$

OMITTED FROM SUMMARY TABLE

See the review on "Spectroscopy of Light Meson Resonances."

$f_0(1770)$ Breit-Wigner MASS

VALUE (MeV)	EVTS	DOCUMENT ID	TECN	COMMENT
1784^{+16}_{-14} OUR AVERAGE		Error includes scale factor of 1.1.		
1814 ± 31	7.2k	¹ KHOLODENK..21	VES	$29\pi^-p \rightarrow n\omega\phi$
1795 ± 7^{+23}_{-20}		ABLIKIM	13J BES3	$J/\psi \rightarrow \gamma\omega\phi$
1760 ± 15^{+15}_{-10}		ABLIKIM	05Q BES2	$\psi(2S) \rightarrow \gamma\pi^+\pi^-K^+K^-$

••• We do not use the following data for averages, fits, limits, etc. •••

1765 ± 15		SARANTSEV	21 RVUE	$J/\psi \rightarrow \gamma(\pi\pi, K\bar{K}, \eta\eta, \omega\phi)$
1814 ± 18	2,3	AAIJ	14BR LHCB	$\bar{B}_s^0 \rightarrow J/\psi\pi^+\pi^-$
1812 ± 19^{+26}_{-18}	4	ABLIKIM	06J BES2	$J/\psi \rightarrow \gamma\omega\phi$
1790 ± 40^{+40}_{-30}		ABLIKIM	05 BES2	$J/\psi \rightarrow \phi\pi^+\pi^-$

¹ From partial wave analysis of $\omega\phi$ invariant mass including 0^{++} , 2^{++} , and 0^{-+} resonances.

² Second solution: 1800 ± 22 MeV. The fit favors $f_0(1770)$ to $f_0(1710)$.

³ Statistical error only.

⁴ Not seen by LIU 09 in $B^\pm \rightarrow K^\pm\omega\phi$.

$f_0(1770)$ Breit-Wigner WIDTH

VALUE (MeV)	EVTS	DOCUMENT ID	TECN	COMMENT
161 ± 21 OUR AVERAGE		Error includes scale factor of 1.4. See the ideogram below.		
182 ± 19	7.2k	¹ KHOLODENK..21	VES	$29\pi^-p \rightarrow n\omega\phi$
95 ± 10^{+78}_{-82}		ABLIKIM	13J BES3	$J/\psi \rightarrow \gamma\omega\phi$
125 ± 25^{+10}_{-15}		ABLIKIM	05Q BES2	$\psi(2S) \rightarrow \gamma\pi^+\pi^-K^+K^-$

••• We do not use the following data for averages, fits, limits, etc. •••

180 ± 20		SARANTSEV	21 RVUE	$J/\psi \rightarrow \gamma(\pi\pi, K\bar{K}, \eta\eta, \omega\phi)$
328 ± 34	2,3	AAIJ	14BR LHCB	$\bar{B}_s^0 \rightarrow J/\psi\pi^+\pi^-$
105 ± 20 ± 28	4	ABLIKIM	06J BES2	$J/\psi \rightarrow \gamma\omega\phi$
270 ± 60^{+60}_{-30}	5	ABLIKIM	05 BES2	$J/\psi \rightarrow \phi\pi^+\pi^-$

¹ From partial wave analysis of $\omega\phi$ invariant mass including 0^{++} , 2^{++} , and 0^{-+} resonances.

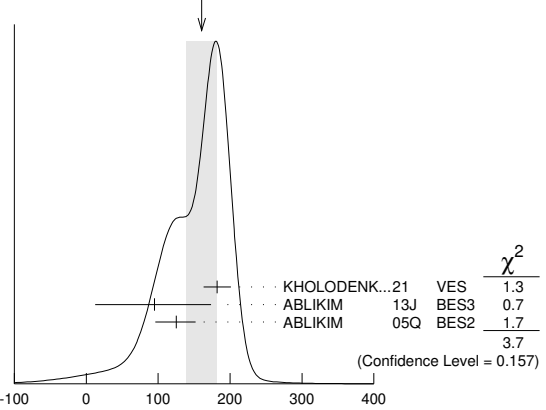
² Second solution: 263 ± 30 MeV. The fit favors $f_0(1770)$ to $f_0(1710)$.

³ Statistical error only.

⁴ Not seen by LIU 09 in $B^\pm \rightarrow K^\pm\omega\phi$.

⁵ $f_0(1710)$ width fixed to PDG value.

WEIGHTED AVERAGE
161 ± 21 (Error scaled by 1.4)



$f_0(1770)$ DECAY MODES

Mode	Fraction (Γ_i/Γ)
Γ_1 $\pi\pi$	seen
Γ_2 $K\bar{K}$	seen
Γ_3 $\eta\eta$	seen
Γ_4 $\omega\phi$	seen

$\Gamma(\pi\pi)/\Gamma_{\text{total}}$	VALUE	DOCUMENT ID	TECN	COMMENT	Γ_1/Γ
seen		SARANTSEV	21 RVUE	$J/\psi \rightarrow \gamma(\pi\pi, K\bar{K}, \eta\eta, \omega\phi)$	
seen		AAIJ	14BR LHCB	$\bar{B}_s^0 \rightarrow J/\psi\pi^+\pi^-$	
seen		ABLIKIM	05 BES2	$J/\psi \rightarrow \phi\pi^+\pi^-$	

$\Gamma(K\bar{K})/\Gamma_{\text{total}}$	VALUE	DOCUMENT ID	TECN	COMMENT	Γ_2/Γ
seen		SARANTSEV	21 RVUE	$J/\psi \rightarrow \gamma(\pi\pi, K\bar{K}, \eta\eta, \omega\phi)$	

$\Gamma(\eta\eta)/\Gamma_{\text{total}}$	VALUE	DOCUMENT ID	TECN	COMMENT	Γ_3/Γ
seen		SARANTSEV	21 RVUE	$J/\psi \rightarrow \gamma(\pi\pi, K\bar{K}, \eta\eta, \omega\phi)$	

Meson Particle Listings

$f_0(1770), \pi(1800)$

$\Gamma(\omega\phi)/\Gamma_{total}$					Γ_4/Γ
VALUE	EVTs	DOCUMENT ID	TECN	COMMENT	
seen	7.2k	KHOLODENK..21	VES	29 $\pi^- p \rightarrow n\omega\phi$	
seen		SARANTSEV 21	RVUE	$J/\psi \rightarrow \gamma(\pi\pi, K\bar{K}, \eta\eta, \omega\phi)$	

$f_0(1770)$ REFERENCES

KHOLODENK..21	PAN 83 1602	M.S. Kholodenko	(VES Collab.)
SARANTSEV 21	PL B816 136227	A.V. Sarantsev et al.	(BONN, PNPI)
AALU 14BR	PR D89 092006	R. Aaij et al.	(LHCb Collab.)
ABLIKIM 13J	PR D87 032008	M. Ablikim et al.	(BESIII Collab.)
LIU 09	PR D79 071102	C. Liu et al.	(BELLE Collab.)
ABLIKIM 06J	PRL 96 162002	M. Ablikim et al.	(BES Collab.)
ABLIKIM 05	PL B607 243	M. Ablikim et al.	(BES Collab.)
ABLIKIM 05Q	PR D72 092002	M. Ablikim et al.	(BES Collab.)

210±30±30	1.2k	AMELIN	96B VES	-	37 $\pi^- A \rightarrow \eta\eta\pi^- A$
190±15±15		12 AMELIN	95B VES	-	36 $\pi^- A \rightarrow \pi^+\pi^-\pi^- A$
210±70		13 BERDNIKOV	94 VES	-	37 $\pi^- A \rightarrow K^+K^-\pi^- A$
225±35±20		BELADIDZE	92C VES	-	36 $\pi^- Be \rightarrow \pi^-\eta'\eta Be$
205±18±32	426	BITYUKOV	91 VES	-	36 $\pi^- C \rightarrow \pi^-\eta\eta C$
310±50	1.1k	BELLINI	82 SPEC	-	40 $\pi^- A \rightarrow 3\pi A$

••• We do not use the following data for averages, fits, limits, etc. •••

208±22±21	420k	14 ALEKSEEV	10 COMP		190 $\pi^- Pb \rightarrow \pi^-\pi^-\pi^+ Pb'$
259±19±6		AMELIN	99 VES		37 $\pi^- A \rightarrow \omega\pi^-\pi^0 A^*$

⁸ Statistical error negligible.

⁹ From a single-pole fit.

¹⁰ In the $f_0(980)\pi$ wave.

¹¹ In the $f_0(500)\pi$ wave.

¹² From a fit to $J^{PC} = 0^- + f_0(980)\pi, f_0(1370)\pi$ waves.

¹³ From a fit to $J^{PC} = 0^- + K_0^*(1430)K^-$ and $f_0(980)\pi^-$ waves.

¹⁴ Superseded by AGHASYAN 2018B.

$\pi(1800)$

$$J^G(J^{PC}) = 1^-(0^- +)$$

See the review on "Spectroscopy of Light Meson Resonances."

$\pi(1800)$ MASS

VALUE (MeV)	EVTs	DOCUMENT ID	TECN	CHG	COMMENT
1810⁺⁹₋₁₁ OUR AVERAGE		Error includes scale factor of 2.2. See the ideogram below.			
1804 ⁺⁶ ₋₉	46M	1 AGHASYAN	18B	COMP	190 $\pi^- p \rightarrow \pi^-\pi^+\pi^- p$
1876±18±16	4k	2 EUGENIO	08	B852	- 18 $\pi^- p \rightarrow \eta\eta\pi^- p$
1774±18±20		3 CHUNG	02	B852	18.3 $\pi^- p \rightarrow \pi^+\pi^-\pi^- p$
1863±9±10		4 CHUNG	02	B852	18.3 $\pi^- p \rightarrow \pi^+\pi^-\pi^- p$
1840±10±10	1.2k	AMELIN	96B	VES	- 37 $\pi^- A \rightarrow \eta\eta\pi^- A$
1775±7±10		5 AMELIN	95B	VES	- 36 $\pi^- A \rightarrow \pi^+\pi^-\pi^- A$
1790±14		6 BERDNIKOV	94	VES	- 37 $\pi^- A \rightarrow K^+K^-\pi^- A$
1873±33±20		BELADIDZE	92C	VES	- 36 $\pi^- Be \rightarrow \pi^-\eta'\eta Be$
1814±10±23	426	BITYUKOV	91	VES	- 36 $\pi^- C \rightarrow \pi^-\eta\eta C$
1770±30	1.1k	BELLINI	82	SPEC	- 40 $\pi^- A \rightarrow 3\pi A$
••• We do not use the following data for averages, fits, limits, etc. •••					
1785±9±12	420k	7 ALEKSEEV	10	COMP	190 $\pi^- Pb \rightarrow \pi^-\pi^-\pi^+ Pb'$
1737±5±15		AMELIN	99	VES	37 $\pi^- A \rightarrow \omega\pi^-\pi^0 A^*$

¹ Statistical error negligible.

² From a single-pole fit.

³ In the $f_0(980)\pi$ wave.

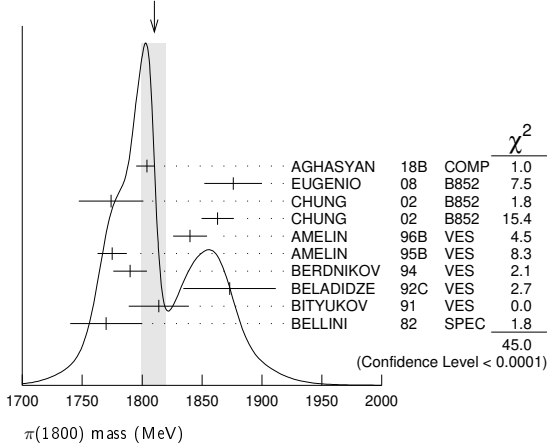
⁴ In the $f_0(500)\pi$ wave.

⁵ From a fit to $J^{PC} = 0^- + f_0(980)\pi, f_0(1370)\pi$ waves.

⁶ From a fit to $J^{PC} = 0^- + K_0^*(1430)K^-$ and $f_0(980)\pi^-$ waves.

⁷ Superseded by AGHASYAN 2018B.

WEIGHTED AVERAGE
1810+9-11 (Error scaled by 2.2)



$\pi(1800)$ WIDTH

VALUE (MeV)	EVTs	DOCUMENT ID	TECN	CHG	COMMENT
215⁺⁸₋₁₁ OUR AVERAGE					
220 ⁺⁸ ₋₁₁	46M	8 AGHASYAN	18B	COMP	190 $\pi^- p \rightarrow \pi^-\pi^+\pi^- p$
221±26±38	4k	9 EUGENIO	08	B852	- 18 $\pi^- p \rightarrow \eta\eta\pi^- p$
223±48±50		10 CHUNG	02	B852	18.3 $\pi^- p \rightarrow \pi^+\pi^-\pi^- p$
191±21±20		11 CHUNG	02	B852	18.3 $\pi^- p \rightarrow \pi^+\pi^-\pi^- p$

$\pi(1800)$ DECAY MODES

Mode	Fraction (Γ_i/Γ)
Γ_1 $\pi^+\pi^-\pi^-$	seen
Γ_2 $f_0(500)\pi^-$	seen
Γ_3 $f_0(980)\pi^-$	seen
Γ_4 $f_0(1370)\pi^-$	seen
Γ_5 $f_0(1500)\pi^-$	not seen
Γ_6 $\rho\pi^-$	not seen
Γ_7 $\eta\eta\pi^-$	seen
Γ_8 $a_0(980)\eta$	seen
Γ_9 $a_2(1320)\eta$	not seen
Γ_{10} $f_2(1270)\pi$	not seen
Γ_{11} $f_0(1370)\pi^-$	not seen
Γ_{12} $f_0(1500)\pi^-$	seen
Γ_{13} $\eta\eta'(958)\pi^-$	seen
Γ_{14} $K_0^*(1430)K^-$	seen
Γ_{15} $K^*(892)K^-$	not seen

$\pi(1800)$ BRANCHING RATIOS

$\Gamma(f_0(980)\pi^-)/\Gamma(f_0(500)\pi^-)$					Γ_3/Γ_2
VALUE	DOCUMENT ID	TECN	CHG	COMMENT	
0.44±0.08±0.38	15 CHUNG	02	B852	18.3 $\pi^- p \rightarrow \pi^+\pi^-\pi^- p$	

$\Gamma(f_0(980)\pi^-)/\Gamma(f_0(1370)\pi^-)$					Γ_3/Γ_4
VALUE	DOCUMENT ID	TECN	CHG	COMMENT	
••• We do not use the following data for averages, fits, limits, etc. •••					
1.7±1.3	16 AMELIN	95B	VES	-	36 $\pi^- A \rightarrow \pi^+\pi^-\pi^- A$

$\Gamma(f_0(1370)\pi^-)/\Gamma_{total}$					Γ_4/Γ
VALUE	DOCUMENT ID	TECN	CHG	COMMENT	
seen	BELLINI	82	SPEC	-	40 $\pi^- A \rightarrow 3\pi A$

$\Gamma(f_0(1500)\pi^-)/\Gamma_{total}$					Γ_5/Γ
VALUE	DOCUMENT ID	TECN	CHG	COMMENT	
not seen	CHUNG	02	B852	18.3 $\pi^- p \rightarrow \pi^+\pi^-\pi^- p$	

$\Gamma(\rho\pi^-)/\Gamma_{total}$					Γ_6/Γ
VALUE	DOCUMENT ID	TECN	CHG	COMMENT	
not seen	BELLINI	82	SPEC	-	40 $\pi^- A \rightarrow 3\pi A$

$\Gamma(\pi\pi^-)/\Gamma(f_0(980)\pi^-)$					Γ_6/Γ_3
VALUE	CL%	DOCUMENT ID	TECN	CHG	COMMENT
••• We do not use the following data for averages, fits, limits, etc. •••					
<0.25		CHUNG	02	B852	18.3 $\pi^- p \rightarrow \pi^+\pi^-\pi^- p$
<0.14	90	AMELIN	95B	VES	- 36 $\pi^- A \rightarrow \pi^+\pi^-\pi^- A$

$\Gamma(\eta\eta\pi^-)/\Gamma(\pi^+\pi^-\pi^-)$					Γ_7/Γ_1
VALUE	EVTs	DOCUMENT ID	TECN	CHG	COMMENT
••• We do not use the following data for averages, fits, limits, etc. •••					
0.5±0.1	1200	16 AMELIN	96B	VES	- 37 $\pi^- A \rightarrow \eta\eta\pi^- A$

$\Gamma(a_2(1320)\eta)/\Gamma_{total}$					Γ_9/Γ
VALUE	DOCUMENT ID	TECN	CHG	COMMENT	
not seen	EUGENIO	08	B852	18 $\pi^- p \rightarrow \eta\eta\pi^- p$	

$\Gamma(f_2(1270)\pi)/\Gamma_{total}$					Γ_{10}/Γ
VALUE	DOCUMENT ID	TECN	CHG	COMMENT	
not seen	EUGENIO	08	B852	18 $\pi^- p \rightarrow \eta\eta\pi^- p$	

See key on page 1171

Meson Particle Listings

$\pi(1800)$, $f_2(1810)$

$\Gamma(f_0(1370)\pi^-)/\Gamma_{total}$				Γ_{11}/Γ
VALUE	DOCUMENT ID	TECN	COMMENT	
not seen	EUGENIO	08	B852	$18 \pi^- \rho \rightarrow \eta \eta \pi^- \rho$

$\Gamma(f_0(1500)\pi^-)/\Gamma(a_0(980)\eta)$					Γ_{12}/Γ_8	
VALUE	EVTS	DOCUMENT ID	TECN	CHG	COMMENT	
• • • We do not use the following data for averages, fits, limits, etc. • • •						
0.48 ± 0.17	4k	16,17	EUGENIO	08	B852	$18 \pi^- \rho \rightarrow \eta \eta \pi^- \rho$
$0.030^{+0.014}_{-0.011}$		16	ANISOVICH	01B	SPEC	$0.6-1.94 \rho \bar{p} \rightarrow \eta \eta \pi^0 \pi^0$
0.08 ± 0.03	1200	16,18	AMELIN	96B	VES	$37 \pi^- A \rightarrow \eta \eta \pi^- A$

$\Gamma(\eta\eta'(958)\pi^-)/\Gamma(\eta\eta\pi^-)$					Γ_{13}/Γ_7	
VALUE	EVTS	DOCUMENT ID	TECN	CHG	COMMENT	
• • • We do not use the following data for averages, fits, limits, etc. • • •						
0.29 ± 0.07		16	BELADIDZE	92C	VES	$36 \pi^- Be \rightarrow \pi^- \eta' \eta Be$
0.3 ± 0.1	426 ± 57	16	BITYUKOV	91	VES	$36 \pi^- C \rightarrow \pi^- \eta \eta C$

$\Gamma(K^*_0(1430)K^-)/\Gamma_{total}$					Γ_{14}/Γ
VALUE	DOCUMENT ID	TECN	CHG	COMMENT	
seen	BERDNIKOV	94	VES	-	$37 \pi^- A \rightarrow K^+ K^- \pi^- A$

$\Gamma(K^*(892)K^-)/\Gamma_{total}$					Γ_{15}/Γ
VALUE	DOCUMENT ID	TECN	CHG	COMMENT	
not seen	BERDNIKOV	94	VES	-	$37 \pi^- A \rightarrow K^+ K^- \pi^- A$
15 Assuming that $f_0(980)$ decays only to $\pi\pi$.					
16 Systematic errors not estimated.					
17 From a single-pole fit.					
18 Assuming that $f_0(1500)$ decays only to $\eta\eta$ and $a_0(980)$ decays only to $\eta\pi$.					

$\pi(1800)$ REFERENCES

AGHASYAN	18B	PR D98 092003	M. Aghasyan et al.	(COMPASS Collab.)
ALEKSEEV	10	PRL 104 241803	M.G. Alekseev et al.	(COMPASS Collab.)
EUGENIO	08	PL B660 466	P. Eugenio et al.	(BNL E852 Collab.)
CHUNG	02	PR D65 072001	S.U. Chung et al.	(BNL E852 Collab.)
ANISOVICH	01B	PL B500 222	A.V. Anisovich et al.	
AMELIN	99	PAN 62 445	D.V. Amelin et al.	(VES Collab.)
AMELIN	96B	Translated from YAF 62 487.	D.V. Amelin et al.	(SERP, TBIL)IGJPC
AMELIN	95B	PAN 59 976	D.V. Amelin et al.	(SERP, TBIL)
BERDNIKOV	94	PL B337 219	E.B. Berdnikov et al.	(SERP, TBIL)
BELADIDZE	92C	SJNP 55 1535	G.M. Beladidze, S.I. Bityukov, G.V. Borisov	(SERP+)
BITYUKOV	91	Translated from YAF 55 2748.	S.I. Bityukov et al.	(SERP, TBIL)
BELLINI	82	PL B268 137	G. Bellini et al.	(MILA, BGNA, JINR)

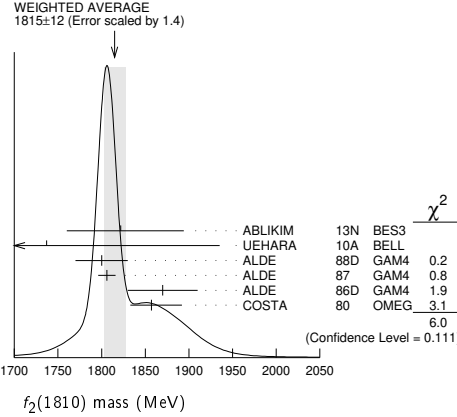
$f_2(1810)$ $I^G(J^{PC}) = 0^+(2^{++})$

OMITTED FROM SUMMARY TABLE
Needs confirmation.

$f_2(1810)$ MASS

VALUE (MeV)	EVTS	DOCUMENT ID	TECN	COMMENT
1815 ± 12	OUR AVERAGE	Error includes scale factor of 1.4. See the ideogram below.		
1822^{+29}_{-24}	$^{+66}_{-57}$	5.5k	1	ABLIKIM 13N BES3 $e^+e^- \rightarrow J/\psi \rightarrow \gamma \eta \eta$
1737 ± 9	$^{+198}_{-65}$		2	UEHARA 10A BELL $10.6 e^+e^- \rightarrow e^+e^- \eta \eta$
1800 ± 30	40	ALDE	88D	GAM4 $300 \pi^- \rho \rightarrow \pi^- \rho 4\pi^0$
1806 ± 10	1600	ALDE	87	GAM4 $100 \pi^- \rho \rightarrow 4\pi^0 n$
1870 ± 40		3	ALDE	86D GAM4 $100 \pi^- \rho \rightarrow \eta \eta n$
1857^{+35}_{-24}		4	COSTA	80 OMEG $10 \pi^- \rho \rightarrow K^+ K^- n$
• • • We do not use the following data for averages, fits, limits, etc. • • •				
$1845.0 \pm 2.2^{+1.6}_{-7.2}$		5	ALBRECHT	20 RVUE $0.9 \bar{p} p \rightarrow \pi^0 \pi^0 \eta, \pi^0 \eta \eta, \pi^0 K^+ K^-$
1858^{+18}_{-71}		6	LONGACRE	86 RVUE Compilation
1799 ± 15		7	CASON	82 STRC $8 \pi^+ \rho \rightarrow \Delta^{++} \pi^0 \pi^0$

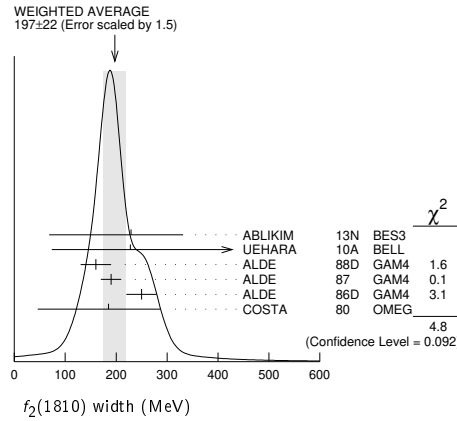
1 From partial wave analysis including all possible combinations of 0^{++} , 2^{++} , and 4^{++} resonances.
 2 Breit-Wigner mass. Could also be the $f_2(1910)$.
 3 Seen in only one solution.
 4 Error increased by spread of two solutions. Included in LONGACRE 86 global analysis.
 5 T-matrix pole, 4 poles, 4 channels, including scattering data from HYAMS 75 ($\pi\pi$), LONGACRE 86 ($K\bar{K}$), BINON 83 ($\eta\eta$).
 6 From a partial-wave analysis of data using a K-matrix formalism with 5 poles. Includes compilation of several other experiments.
 7 From an amplitude analysis of the reaction $\pi^+\pi^- \rightarrow 2\pi^0$. The resonance in the $2\pi^0$ final state is not confirmed by PROKOSHKIN 97.



$f_2(1810)$ WIDTH

VALUE (MeV)	EVTS	DOCUMENT ID	TECN	COMMENT
197 ± 22	OUR AVERAGE	Error includes scale factor of 1.5. See the ideogram below.		
229^{+52}_{-42}	$^{+88}_{-155}$	5.5k	1	ABLIKIM 13N BES3 $e^+e^- \rightarrow J/\psi \rightarrow \gamma \eta \eta$
228^{+21}_{-20}	$^{+234}_{-153}$		2	UEHARA 10A BELL $10.6 e^+e^- \rightarrow e^+e^- \eta \eta$
160 ± 30	40	ALDE	88D	GAM4 $300 \pi^- \rho \rightarrow \pi^- \rho 4\pi^0$
190 ± 20	1600	ALDE	87	GAM4 $100 \pi^- \rho \rightarrow 4\pi^0 n$
250 ± 30		3	ALDE	86D GAM4 $100 \pi^- \rho \rightarrow \eta \eta n$
185^{+102}_{-139}		4	COSTA	80 OMEG $10 \pi^- \rho \rightarrow K^+ K^- n$
• • • We do not use the following data for averages, fits, limits, etc. • • •				
$260.9 \pm 3.9^{+199.9}_{-38.2}$		5	ALBRECHT	20 RVUE $0.9 \bar{p} p \rightarrow \pi^0 \pi^0 \eta, \pi^0 \eta \eta, \pi^0 K^+ K^-$
388^{+15}_{-21}		6	LONGACRE	86 RVUE Compilation
280^{+42}_{-35}		7	CASON	82 STRC $8 \pi^+ \rho \rightarrow \Delta^{++} \pi^0 \pi^0$

1 From partial wave analysis including all possible combinations of 0^{++} , 2^{++} , and 4^{++} resonances.
 2 Breit-Wigner width. Could also be the $f_2(1910)$.
 3 Seen in only one solution.
 4 Error increased by spread of two solutions. Included in LONGACRE 86 global analysis.
 5 T-matrix pole, 4 poles, 4 channels, including scattering data from HYAMS 75 ($\pi\pi$), LONGACRE 86 ($K\bar{K}$), BINON 83 ($\eta\eta$).
 6 From a partial-wave analysis of data using a K-matrix formalism with 5 poles. Includes compilation of several other experiments.
 7 From an amplitude analysis of the reaction $\pi^+\pi^- \rightarrow 2\pi^0$. The resonance in the $2\pi^0$ final state is not confirmed by PROKOSHKIN 97.



$f_2(1810)$ DECAY MODES

Mode	Fraction (Γ_i/Γ)
Γ_1 $\pi\pi$	seen
Γ_2 $\eta\eta$	seen
Γ_3 $4\pi^0$	seen
Γ_4 K^+K^-	seen
Γ_5 $\gamma\gamma$	seen

Meson Particle Listings

 $f_2(1810)$, $X(1835)$ $f_2(1810) \Gamma(i)\Gamma(\gamma\gamma)/\Gamma(\text{total})$

$\Gamma(\eta\eta) \times \Gamma(\gamma\gamma)/\Gamma_{\text{total}}$	DOCUMENT ID	TECN	COMMENT	$\Gamma_2/\Gamma_5/\Gamma$
$5.2^{+0.9}_{-0.8} + 37.3_{-4.5}$	1 UEHARA	10A	BELL	10.6 $e^+e^- \rightarrow e^+e^-\eta\eta$

¹Including interference with the $f_2'(1525)$ (parameters fixed to the values from the 2008 edition of this review, PDG 08) and $f_2(1270)$. May also be the $f_0(1500)$.

 $f_2(1810)$ BRANCHING RATIOS

$\Gamma(\pi\pi)/\Gamma_{\text{total}}$	DOCUMENT ID	TECN	COMMENT	Γ_1/Γ
--	-------------	------	---------	-------------------

not seen	AMSLER	02	CBAR	$0.9 \bar{p}p \rightarrow \pi^0\eta\eta, \pi^0\pi^0\pi^0$
not seen	PROKOSHKIN	97	GAM2	$38 \pi^-\rho \rightarrow \pi^0\pi^0n$
$0.21^{+0.02}_{-0.03}$	1 LONGACRE	86	RVUE	Compilation
0.44 ± 0.03	2 CASON	82	STRC	$8 \pi^+\rho \rightarrow \Delta^{++}\pi^0\pi^0$

¹From a partial-wave analysis of data using a K-matrix formalism with 5 poles. Includes compilation of several other experiments.

²Included in LONGACRE 86 global analysis.

$\Gamma(\eta\eta)/\Gamma_{\text{total}}$	DOCUMENT ID	TECN	COMMENT	Γ_2/Γ
--	-------------	------	---------	-------------------

seen	ABLIKIM	13N	BES3	PWA of $J/\psi \rightarrow \gamma\eta\eta$
$0.008^{+0.028}_{-0.003}$	1 LONGACRE	86	RVUE	Compilation

¹From a partial-wave analysis of data using a K-matrix formalism with 5 poles. Includes compilation of several other experiments.

$\Gamma(\pi\pi)/\Gamma(4\pi^0)$	DOCUMENT ID	TECN	COMMENT	Γ_1/Γ_3
---------------------------------	-------------	------	---------	---------------------

<0.75	ALDE	87	GAM4	$100 \pi^-\rho \rightarrow 4\pi^0n$
-------	------	----	------	-------------------------------------

$\Gamma(4\pi^0)/\Gamma(\eta\eta)$	DOCUMENT ID	TECN	COMMENT	Γ_3/Γ_2
-----------------------------------	-------------	------	---------	---------------------

0.8 ± 0.3	ALDE	87	GAM4	$100 \pi^-\rho \rightarrow 4\pi^0n$
---------------	------	----	------	-------------------------------------

$\Gamma(K^+K^-)/\Gamma_{\text{total}}$	DOCUMENT ID	TECN	COMMENT	Γ_4/Γ
--	-------------	------	---------	-------------------

$0.003^{+0.019}_{-0.002}$	1 LONGACRE	86	RVUE	Compilation
seen	COSTA	80	OMEG	$10 \pi^-\rho \rightarrow K^+K^-n$

¹From a partial-wave analysis of data using a K-matrix formalism with 5 poles. Includes compilation of several other experiments.

 $f_2(1810)$ REFERENCES

ALBRECHT	20	EPJ C80 453	M. Albrecht et al.	(Crystal Barrel Collab.)
ABLIKIM	13N	PR D87 092009	M. Ablikim et al.	(BESIII Collab.)
UEHARA	10A	PR D82 114031	S. Uehara et al.	(BELLE Collab.)
PDG	08	PL B667 1	C. Amstler et al.	(PDG Collab.)
AMSLER	02	EPJ C23 29	C. Amstler et al.	(Crystal Barrel Collab.)
PROKOSHKIN	97	PD 42 117	Y.D. Prokoshkin et al.	(SERP)
ALDE	88D	Translated from DANS 353 323.	D.M. Alde et al.	(SERP, BELG, LANL, LAPP+)
		SJNP 47 819	D.M. Alde et al.	(SERP, BELG, LANL, LAPP+)
		Translated from YAF 47 1273.	D.M. Alde et al.	(LANL, BRUX, SERP, LAPP)
ALDE	87	PL B198 286	D.M. Alde et al.	(BELG, LAPP, SERP, CERN+)
ALDE	86D	NP B269 485	D.M. Alde et al.	(BNL, BRAN, CUNY+)
LONGACRE	86	PL B177 223	R.S. Longacre et al.	(BELG, LAPP, SERP+)
BINON	83	NC 78A 313	F.G. Binon et al.	(NDAM, ANL)
CASON	82	PRL 48 1316	N.M. Cason et al.	(BARI, BONN, CERN, GLAS+)
COSTA	80	NP B175 402	G. Costa et al.	(CERN, MPIM)
HYAMS	75	NP B100 205	B.D. Hyams et al.	(CERN, MPIM)

 $X(1835)$

$$I^G(J^{PC}) = 0^+(0^-+)$$

OMITTED FROM SUMMARY TABLE

Could be a superposition of two states, one with small width appearing as threshold enhancement in $p\bar{p}$, the other one with a larger width. For the former ABLIKIM 12D determine $J^{PC} = 0^-+$.

 $X(1835)$ MASS

VALUE (MeV)	EVTS	DOCUMENT ID	TECN	COMMENT
$1826.5^{+13.0}_{-3.4}$	OUR AVERAGE			
$1825.3 \pm 2.4^{+17.3}_{-2.4}$		1 ABLIKIM	16J	BES3 $J/\psi \rightarrow \gamma\pi^+\pi^-\eta'$
$1844 \pm 9^{+16}_{-25}$		2 ABLIKIM	15T	BES3 $J/\psi \rightarrow \gamma K_S^0 K_S^0 \eta$

• • • We do not use the following data for averages, fits, limits, etc. • • •

$1839 \pm 26 \pm 26$		3 ABLIKIM	18I	BES3 $J/\psi \rightarrow \gamma\gamma\phi(1020)$
$1909.5 \pm 15.9^{+9.4}_{-27.5}$		4 ABLIKIM	16J	BES3 $J/\psi \rightarrow \gamma\pi^+\pi^-\eta'$
$1842.2 \pm 4.2^{+7.1}_{-2.6}$	0.6k	ABLIKIM	13U	BES3 $J/\psi \rightarrow \gamma 3(\pi^+\pi^-)$
$1832^{+19}_{-5} \pm 26$		5 ABLIKIM	12D	BES3 $J/\psi \rightarrow \gamma\rho\bar{p}$
$1836.5 \pm 3.0^{+5.6}_{-2.1}$	4265	6 ABLIKIM	11C	BES3 $J/\psi \rightarrow \gamma\pi^+\pi^-\eta'$
$1877.3 \pm 6.3^{+3.4}_{-7.4}$		7 ABLIKIM	11J	BES3 $J/\psi \rightarrow \omega(\eta\pi^+\pi^-)$
$1837^{+10}_{-12} \pm 7$	231	8,9 ALEXANDER	10	CLEO $J/\psi \rightarrow \gamma\rho\bar{p}$
$1833.7 \pm 6.1 \pm 2.7$	264	ABLIKIM	05R	BES2 $J/\psi \rightarrow \gamma\pi^+\pi^-\eta'$
1831 ± 7		9,10 ABLIKIM	05R	BES2 $J/\psi \rightarrow \gamma\rho\bar{p}$
$1859^{+3}_{-10} \pm 25$		9 BAI	03F	BES2 $J/\psi \rightarrow \gamma\rho\bar{p}$

¹From a fit of the measured $\pi^+\pi^-\eta'$ lineshape that accounts for the abrupt distortion observed at the $p\bar{p}$ threshold through interference with a second previously unseen narrow resonance near 1870 MeV. The fit uses Breit-Wigner functions for the signal shapes and includes known backgrounds and contributors.

²Decay dominated by $f_0(980)\eta$ hence $I^G(J^{PC}) = 0^+(0^-+)$.

³From a fit to $\gamma\phi$ invariant mass. Angular analysis consistent with $J^{PC} = 0^-+$. Other J^{PC} not excluded.

⁴Pole mass from a fit of the measured $\pi^+\pi^-\eta'$ lineshape to a Flatte formula that accounts for the abrupt distortion observed at the $p\bar{p}$ threshold; the fit also includes known backgrounds and contributors, as well as an *ad hoc* Breit-Wigner function ($M \approx 1919$ MeV; $\Gamma \approx 51$ MeV) that is required for a good fit.

⁵From the fit including final state interaction effects in isospin 0 S-wave according to SIBIRTEV 05A. Supersedes ABLIKIM 10G.

⁶From a fit of the $\pi^+\pi^-\eta'$ mass distribution to a combination of $\gamma f_1(1510)$, $\gamma X(1835)$, and two states $\gamma X(2120)$ and $\gamma X(2370)$, for $M(\pi^+\pi^-\eta') < 2.8$ GeV, and accounting for backgrounds from non- η' events and $J/\psi \rightarrow \pi^0\pi^+\pi^-\eta'$.

⁷The selected process is $J/\psi \rightarrow \omega a_0(980)\pi$. This state may be due also to $\eta_2(1870)$ or to a combination of $X(1835)$ and $\eta_2(1870)$.

⁸From a fit of the $p\bar{p}$ mass distribution to a combination of $\gamma X(1835)$, γR with $M(R) = 2100$ MeV and $\Gamma(R) = 160$ MeV, and $\gamma\rho\bar{p}$ phase space, for $M(p\bar{p}) < 2.85$ GeV.

⁹Evidence for a threshold enhancement in the $p\bar{p}$ mass spectrum was also reported by ABE 02K, AUBERT, B 05L, and WANG 05A in $B^+ \rightarrow p\bar{p}K^+$, WANG 05A in $B^0 \rightarrow p\bar{p}K_S^0$, ABE 02W in $\bar{B}^0 \rightarrow p\bar{p}D^0$, DEL-AMO-SANCHEZ 12 in $B \rightarrow D(D^*)\rho\bar{p}(\pi)$, and WEI 08 in $B^+ \rightarrow p\bar{p}\pi^+$ decays. Not seen by ATHAR 06 in $\Upsilon(1S) \rightarrow p\bar{p}\gamma$.

¹⁰From the fit including final state interaction effects in isospin 0 S-wave according to SIBIRTEV 05A. Systematic errors not estimated.

 $X(1835)$ WIDTH

VALUE (MeV)	CL%_EVTS	DOCUMENT ID	TECN	COMMENT
-------------	----------	-------------	------	---------

242^{+14}_{-15} OUR AVERAGE

$245.2 \pm 13.1^{+4.6}_{-9.6}$		1 ABLIKIM	16J	BES3 $J/\psi \rightarrow \gamma\pi^+\pi^-\eta'$
$192^{+20}_{-17} \pm 62_{-43}$		2 ABLIKIM	15T	BES3 $J/\psi \rightarrow \gamma K_S^0 K_S^0 \eta$

• • • We do not use the following data for averages, fits, limits, etc. • • •

$175 \pm 57 \pm 25$		3 ABLIKIM	18I	BES3 $J/\psi \rightarrow \gamma\gamma\phi(1020)$
$273.5 \pm 21.4^{+6.1}_{-64.0}$		4 ABLIKIM	16J	BES3 $J/\psi \rightarrow \gamma\pi^+\pi^-\eta'$
$83 \pm 14 \pm 11$	0.6k	ABLIKIM	13U	BES3 $J/\psi \rightarrow \gamma 3(\pi^+\pi^-)$
< 76	90	5 ABLIKIM	12D	BES3 $J/\psi \rightarrow \gamma\rho\bar{p}$
$190 \pm 9^{+38}_{-36}$	4265	6 ABLIKIM	11C	BES3 $J/\psi \rightarrow \gamma\pi^+\pi^-\eta'$
$57 \pm 12^{+19}_{-4}$		7 ABLIKIM	11J	BES3 $J/\psi \rightarrow \omega(\eta\pi^+\pi^-)$
0^{+44}_{-0}	231	8,9 ALEXANDER	10	CLEO $J/\psi \rightarrow \gamma\rho\bar{p}$
$67.7 \pm 20.3 \pm 7.7$	264	ABLIKIM	05R	BES2 $J/\psi \rightarrow \gamma\pi^+\pi^-\eta'$
< 153	90	9,10 ABLIKIM	05R	BES2 $J/\psi \rightarrow \gamma\rho\bar{p}$
< 30		9 BAI	03F	BES2 $J/\psi \rightarrow \gamma\rho\bar{p}$

¹From a fit of the measured $\pi^+\pi^-\eta'$ lineshape that accounts for the abrupt distortion observed at the $p\bar{p}$ threshold through interference with a second previously unseen narrow resonance near 1870 MeV. The fit uses Breit-Wigner functions for the signal shapes and includes known backgrounds and contributors.

²Decay dominated by $f_0(980)\eta$ hence $I^G(J^{PC}) = 0^+(0^-+)$.

³From a fit to $\gamma\phi$ invariant mass. Angular analysis consistent with $J^{PC} = 0^-+$. Other J^{PC} not excluded.

⁴Pole width from a fit of the measured $\pi^+\pi^-\eta'$ lineshape to a Flatte formula that accounts for the abrupt distortion observed at the $p\bar{p}$ threshold; the fit also includes known backgrounds and contributors, as well as an *ad hoc* Breit-Wigner function ($M \approx 1919$ MeV; $\Gamma \approx 51$ MeV) that is required for a good fit.

⁵From the fit including final state interaction effects in isospin 0 S-wave according to SIBIRTEV 05A. Supersedes ABLIKIM 10G.

⁶From a fit of the $\pi^+\pi^-\eta'$ mass distribution to a combination of $\gamma f_1(1510)$, $\gamma X(1835)$, and two states $\gamma X(2120)$ and $\gamma X(2370)$, for $M(\pi^+\pi^-\eta') < 2.8$ GeV, and accounting for backgrounds from non- η' events and $J/\psi \rightarrow \pi^0\pi^+\pi^-\eta'$.

⁷The selected process is $J/\psi \rightarrow \omega a_0(980)\pi$. This state may be due also to $\eta_2(1870)$ or to a combination of $X(1835)$ and $\eta_2(1870)$.

⁸From a fit of the $p\bar{p}$ mass distribution to a combination of $\gamma X(1835)$, γR with $M(R) = 2100$ MeV and $\Gamma(R) = 160$ MeV, and $\gamma\rho\bar{p}$ phase space, for $M(p\bar{p}) < 2.85$ GeV.

⁹Evidence for a threshold enhancement in the $p\bar{p}$ mass spectrum was also reported by ABE 02K, AUBERT, B 05L, and WANG 05A in $B^+ \rightarrow p\bar{p}K^+$, WANG 05A in $B^0 \rightarrow$

See key on page 1171

Meson Particle Listings

X(1835), $\phi_3(1850)$, $\eta_1(1855)$

$\rho\bar{p}K_S^0$, ABE 02w in $\bar{B}^0 \rightarrow \rho\bar{p}D^0$, DEL-AMO-SANCHEZ 12 in $B \rightarrow D(D^*)\rho\bar{p}(\pi)$, and WEI 08 in $B^+ \rightarrow \rho\bar{p}\pi^+$ decays. Not seen by ATHAR 06 in $\Upsilon(1S) \rightarrow \rho\bar{p}\gamma$.
¹⁰ From the fit including final state interaction effects in isospin 0 S-wave according to SIBIRTSEV 05A. Systematic errors not estimated.

X(1835) DECAY MODES

Mode	Fraction (Γ_i/Γ)
Γ_1 $\rho\bar{p}$	seen
Γ_2 $\eta'\pi^+\pi^-$	seen
Γ_3 $\gamma\gamma$	not seen
Γ_4 $K_S^0 K_S^0 \eta$	seen
Γ_5 $\gamma\phi(1020)$	possibly seen
Γ_6 $3(\pi^+\pi^-)$	seen

X(1835) $\Gamma(i)\Gamma(\gamma\gamma)/\Gamma(\text{total})$

$\Gamma(\eta'\pi^+\pi^-) \times \Gamma(\gamma\gamma)/\Gamma(\text{total})$	$\Gamma_2\Gamma_3/\Gamma$			
VALUE (eV)	CL%	DOCUMENT ID	TECN	COMMENT

••• We do not use the following data for averages, fits, limits, etc. •••
 <35.6 90 1 ZHANG 12A BELL $e^+e^- \rightarrow e^+e^-\eta'\pi^+\pi^-$
 <83 90 2 ZHANG 12A BELL $e^+e^- \rightarrow e^+e^-\eta'\pi^+\pi^-$
¹ From a two-resonance fit and constructive interference of the $\eta(1760)$ and X(1835), a significance of 2.8 σ .
² From a two-resonance fit and destructive interference of the $\eta(1760)$ and X(1835), a significance of 2.8 σ .

X(1835) BRANCHING RATIOS

$\Gamma(\rho\bar{p})/\Gamma(\eta'\pi^+\pi^-)$	Γ_1/Γ_2		
VALUE	DOCUMENT ID	TECN	COMMENT

••• We do not use the following data for averages, fits, limits, etc. •••
 0.333 ABLIKIM 05R BES2 $J/\psi \rightarrow \gamma\pi^+\pi^-\eta'$

$\Gamma(\eta'\pi^+\pi^-)/\Gamma(K_S^0 K_S^0 \eta)$	Γ_2/Γ_4		
VALUE	DOCUMENT ID	TECN	COMMENT

••• We do not use the following data for averages, fits, limits, etc. •••
 6.7 ± 1.8 1 ABLIKIM 15T BES3 $J/\psi \rightarrow \gamma K_S^0 K_S^0 \eta$
¹ Using results from ABLIKIM 05R.

$\Gamma(\eta'\pi^+\pi^-)/\Gamma(\text{total})$	Γ_2/Γ		
VALUE	DOCUMENT ID	TECN	COMMENT

seen 1 ABLIKIM 16J BES3 $J/\psi \rightarrow \gamma\pi^+\pi^-\eta'$
¹ ABLIKIM 16J quotes $B(J/\psi \rightarrow \gamma X(1835)) \times B(X(1835) \rightarrow \pi^+\pi^-\eta') = (3.93 \pm 0.38^{+0.31}_{-0.84}) \times 10^{-4}$ from a fit of the measured $\pi^+\pi^-\eta'$ lineshape that accounts for the abrupt distortion observed at the $\rho\bar{p}$ threshold with a Flatté formula in addition to known backgrounds and contributors, as well as an *ad hoc* Breit-Wigner ($M \approx 1919$ MeV; $\Gamma \approx 51$ MeV) that is required for a good fit. Another explanation for the distortion provided by ABLIKIM 16J is that a second resonance near 1870 MeV interferes with the X(1835); fits to this possibility yield product branching fraction values compatible with that shown within the respective systematic uncertainties.

$\Gamma(\gamma\phi(1020))/\Gamma(\text{total})$	Γ_5/Γ		
VALUE	DOCUMENT ID	TECN	COMMENT

possibly seen 1 ABLIKIM 18I BES3 $J/\psi \rightarrow \gamma\gamma\phi(1020)$
¹ Seen as a peak in $\gamma\phi$ invariant mass. Angular analysis consistent with $J^{PC} = 0^-+$. Other J^{PC} not excluded.

$\Gamma(\gamma\gamma)/\Gamma(\eta'\pi^+\pi^-)$	Γ_3/Γ_2			
VALUE	CL%	DOCUMENT ID	TECN	COMMENT

<9.80 × 10⁻³ 90 1 ABLIKIM 18O BES3 $\psi(2S) \rightarrow \pi^+\pi^-\gamma\gamma\gamma$
¹ Using results from ABLIKIM 16J.

$\Gamma(3(\pi^+\pi^-))/\Gamma(\text{total})$	Γ_6/Γ			
VALUE	EVTS	DOCUMENT ID	TECN	COMMENT

seen 0.6k ABLIKIM 13U BES3 $J/\psi \rightarrow \gamma 3(\pi^+\pi^-)$

X(1835) REFERENCES

ABLIKIM 18I PR D97 051101	M. Ablikim et al.	(BESIII Collab.)
ABLIKIM 18O PR D97 072014	M. Ablikim et al.	(BESIII Collab.)
ABLIKIM 16J PRL 117 042002	M. Ablikim et al.	(BESIII Collab.)
ABLIKIM 15T PRL 115 091803	M. Ablikim et al.	(BESIII Collab.)
ABLIKIM 13U PR D88 091502	M. Ablikim et al.	(BESIII Collab.)
ABLIKIM 12D PRL 108 112003	M. Ablikim et al.	(BESIII Collab.) JPC
DEL-AMO-SA... 12 PR D85 092017	P. del Amo Sanchez et al.	(BABAR Collab.)
ZHANG 12A PR D86 052002	C.C. Zhang et al.	(BELLE Collab.)
ABLIKIM 11C PRL 106 072002	M. Ablikim et al.	(BESIII Collab.)
ABLIKIM 11J PRL 107 182001	M. Ablikim et al.	(BESIII Collab.)
ABLIKIM 10G CP C34 421	M. Ablikim et al.	(BESIII Collab.)
ALEXANDER 10 PR D82 092002	J.P. Alexander et al.	(CLEO Collab.)
WEI 08 PL B659 80	J.-T. Wei et al.	(BELLE Collab.)
ATHAR 06 PR D73 032001	S.B. Athar et al.	(CLEO Collab.)
ABLIKIM 05R PRL 95 262001	M. Ablikim et al.	(BES Collab.)
AUBERT.B 05L PR D72 051101	B. Aubert et al.	(BABAR Collab.)
SIBIRTSEV 05A PR D71 054010	A. Sibirtsev, J. Haidenbauer	
WANG 05A PL B617 141	M.-Z. Wang et al.	(BELLE Collab.)
BAI 03F PRL 91 022001	J.Z. Bai et al.	(BES II Collab.)
ABE 02K PRL 88 181803	K. Abe et al.	(BELLE Collab.)
ABE 02W PRL 89 151802	K. Abe et al.	(BELLE Collab.)

$\phi_3(1850)$

$$I^G(J^{PC}) = 0^-(3^{--})$$

$\phi_3(1850)$ MASS

VALUE (MeV)	EVTS	DOCUMENT ID	TECN	COMMENT
-------------	------	-------------	------	---------

1854 ± 7 OUR AVERAGE
 1855 ± 10 ASTON 88E LASS 11 $K^-p \rightarrow K^-K^+\Lambda$, $K_S^0 K^\pm \pi^\mp \Lambda$
 1870⁺³⁰₋₂₀ 430 ARMSTRONG 82 OMEG 18.5 $K^-p \rightarrow K^-K^+\Lambda$
 1850 ± 10 123 ALHARRAN 81B HBC 8.25 $K^-p \rightarrow K\bar{K}\Lambda$

$\phi_3(1850)$ WIDTH

VALUE (MeV)	EVTS	DOCUMENT ID	TECN	COMMENT
-------------	------	-------------	------	---------

87⁺²³₋₂₃ OUR AVERAGE Error includes scale factor of 1.2.
 64 ± 31 ASTON 88E LASS 11 $K^-p \rightarrow K^-K^+\Lambda$, $K_S^0 K^\pm \pi^\mp \Lambda$
 160⁺⁹⁰₋₅₀ 430 ARMSTRONG 82 OMEG 18.5 $K^-p \rightarrow K^-K^+\Lambda$
 80⁺⁴⁰₋₃₀ 123 ALHARRAN 81B HBC 8.25 $K^-p \rightarrow K\bar{K}\Lambda$

$\phi_3(1850)$ DECAY MODES

Mode	Fraction (Γ_i/Γ)
Γ_1 $K\bar{K}$	seen
Γ_2 $K\bar{K}^*(892) + \text{c.c.}$	seen

$\phi_3(1850)$ BRANCHING RATIOS

$\Gamma(K\bar{K}^*(892) + \text{c.c.})/\Gamma(K\bar{K})$	Γ_2/Γ_1		
VALUE	DOCUMENT ID	TECN	COMMENT

0.55^{+0.85}_{-0.45} ASTON 88E LASS 11 $K^-p \rightarrow K^-K^+\Lambda$, $K_S^0 K^\pm \pi^\mp \Lambda$
 ••• We do not use the following data for averages, fits, limits, etc. •••
 0.8 ± 0.4 ALHARRAN 81B HBC 8.25 $K^-p \rightarrow K\bar{K}\pi\Lambda$

$\phi_3(1850)$ REFERENCES

ASTON 88E PL B208 324	D. Aston et al.	(SLAC, NAGO, CIN, INUS)IGJPC
ARMSTRONG 82 PL 110B 77	T.A. Armstrong et al.	(BARI, BIRM, CERN+)JP
ALHARRAN 81B PL 101B 357	S. Al-Harran et al.	(BIRM, CERN, GLAS+)

$\eta_1(1855)$

$$I^G(J^{PC}) = 0^+(1^{-+})$$

OMITTED FROM SUMMARY TABLE

Meson with exotic (non- $q\bar{q}$) quantum numbers. A state decaying into $\eta\eta'$ with possible quantum numbers 1^{-+} was reported earlier in this mass region BARBERIS 00A in high energy central pp production and by ALDE 91B in π^-p interactions, see the $f_2(1910)$, and the review on "Spectroscopy of Light Meson Resonances."

$\eta_1(1855)$ MASS

VALUE (MeV)	DOCUMENT ID	TECN	COMMENT
-------------	-------------	------	---------

1855 ± 9⁺⁶₋₁ 1 ABLIKIM 22A BES3 $J/\psi(1S) \rightarrow \gamma\eta\eta'$
¹ From a Breit-Wigner fit involving 9 resonances and the resonating exotic $\eta_1(1855) \rightarrow \eta\eta'$ P-wave. For analysis details see ABLIKIM 22As.

$\eta_1(1855)$ WIDTH

VALUE (MeV)	DOCUMENT ID	TECN	COMMENT
-------------	-------------	------	---------

188 ± 18⁺³₋₈ 1 ABLIKIM 22A BES3 $J/\psi(1S) \rightarrow \gamma\eta\eta'$
¹ From a Breit-Wigner fit involving 9 resonances and the resonating exotic $\eta_1(1855) \rightarrow \eta\eta'$ P-wave. For analysis details see ABLIKIM 22As.

$\eta_1(1855)$ DECAY MODES

Mode	Fraction (Γ_i/Γ)
Γ_1 $\eta\eta'$	seen

Meson Particle Listings

 $\eta_1(1855)$, $\eta_2(1870)$, $\pi_2(1880)$ $\Gamma(\eta\eta')/\Gamma_{\text{total}}$

VALUE	DOCUMENT ID	TECN	COMMENT	Γ_1/Γ
seen	ABLIKIM	22A	BES3 $J/\psi \rightarrow \gamma\eta\eta'$	
seen	BARBERIS	00A	450 $pp \rightarrow p_f\eta\eta'\rho_S$	
seen	ALDE	91B	GAM2 $38\pi^-p \rightarrow \eta\eta'n$	

 $\eta_1(1855)$ REFERENCES

ABLIKIM	22A	PRL 129 192002	M. Alikim <i>et al.</i>	(BESIII Collab.)
Also		PR D106 072012	M. Alikim <i>et al.</i>	(BESIII Collab.)
ABLIKIM	22AS	PR D106 072012	M. Alikim <i>et al.</i>	(BESIII Collab.)
Also		PR D107 079901 (errata)	M. Alikim <i>et al.</i>	(BESIII Collab.)
BARBERIS	00A	PL B471 429	D. Barberis <i>et al.</i>	(WA 102 Collab.)
ALDE	91B	SJNP 54 455	D.M. Alde <i>et al.</i>	(SERP, BELG, LANL, LAPP+)
		Translated from YAF 54 751.		

 $\eta_2(1870)$

$$J^{PC} = 0^+(2^-)$$

 $\eta_2(1870)$ MASS

VALUE (MeV)	EVTs	DOCUMENT ID	TECN	COMMENT
1842 ± 8 OUR AVERAGE				
1835 ± 12		BARBERIS	00B	450 $pp \rightarrow p_f\eta\pi^+\pi^-\rho_S$
1844 ± 13		BARBERIS	00C	450 $pp \rightarrow p_f4\pi\rho_S$
1840 ± 25		BARBERIS	97B	OMEG 450 $pp \rightarrow pp2(\pi^+\pi^-)$
1875 ± 20 ± 35		ADOMEIT	96	CBAR 1.94 $\bar{p}p \rightarrow \eta3\pi^0$
1881 ± 32 ± 40	26	KARCH	92	CBAL $e^+e^- \rightarrow e^+e^-\eta\pi^0\pi^0$
• • • We do not use the following data for averages, fits, limits, etc. • • •				
1860 ± 5 ± 15		ANISOVICH	00E	SPEC 0.9-1.94 $\bar{p}p \rightarrow \eta3\pi^0$
1840 ± 15		BAI	99	BES $J/\psi \rightarrow \gamma\eta\pi^+\pi^-$

 $\eta_2(1870)$ WIDTH

VALUE (MeV)	EVTs	DOCUMENT ID	TECN	COMMENT
225 ± 14 OUR AVERAGE				
235 ± 22		BARBERIS	00B	450 $pp \rightarrow p_f\eta\pi^+\pi^-\rho_S$
228 ± 23		BARBERIS	00C	450 $pp \rightarrow p_f4\pi\rho_S$
200 ± 40		BARBERIS	97B	OMEG 450 $pp \rightarrow pp2(\pi^+\pi^-)$
200 ± 25 ± 45		ADOMEIT	96	CBAR 1.94 $\bar{p}p \rightarrow \eta3\pi^0$
221 ± 92 ± 44	26	KARCH	92	CBAL $e^+e^- \rightarrow e^+e^-\eta\pi^0\pi^0$
• • • We do not use the following data for averages, fits, limits, etc. • • •				
250 ± 25 ± 50		ANISOVICH	00E	SPEC 0.9-1.94 $\bar{p}p \rightarrow \eta3\pi^0$
170 ± 40		BAI	99	BES $J/\psi \rightarrow \gamma\eta\pi^+\pi^-$

 $\eta_2(1870)$ DECAY MODES

Mode	Fraction (Γ_i/Γ)
Γ_1 $\eta\pi\pi$	seen
Γ_2 $a_2(1320)\pi$	seen
Γ_3 $f_2(1270)\eta$	seen
Γ_4 $a_0(980)\pi$	seen
Γ_5 $\gamma\gamma$	seen

 $\eta_2(1870)$ BRANCHING RATIOS

$\Gamma(a_2(1320)\pi)/\Gamma(f_2(1270)\eta)$	Γ_2/Γ_3
1.7 ± 0.4 OUR AVERAGE	
1.60 ± 0.40	¹ ANISOVICH 11 SPEC 0.9-1.94 $p\bar{p}$
20.4 ± 6.6	BARBERIS 00B 450 $pp \rightarrow p_f\eta\pi^+\pi^-\rho_S$
4.1 ± 2.3	ADOMEIT 96 CBAR 1.94 $\bar{p}p \rightarrow \eta3\pi^0$
¹ Reanalysis of ADOMEIT 96 and ANISOVICH 00E.	

$\Gamma(a_2(1320)\pi)/\Gamma(a_0(980)\pi)$	Γ_2/Γ_4
32.6 ± 12.6	
	BARBERIS 00B 450 $pp \rightarrow p_f\eta\pi^+\pi^-\rho_S$

$\Gamma(a_0(980)\pi)/\Gamma(f_2(1270)\eta)$	Γ_4/Γ_3
0.48 ± 0.45	
	¹ ANISOVICH 11 SPEC 0.9-1.94 $p\bar{p}$
¹ Reanalysis of ADOMEIT 96 and ANISOVICH 00E.	

$\Gamma(\gamma\gamma)/\Gamma_{\text{total}}$	Γ_5/Γ
seen	KARCH 92 CBAL $e^+e^- \rightarrow e^+e^-\eta\pi^0\pi^0$

 $\eta_2(1870)$ REFERENCES

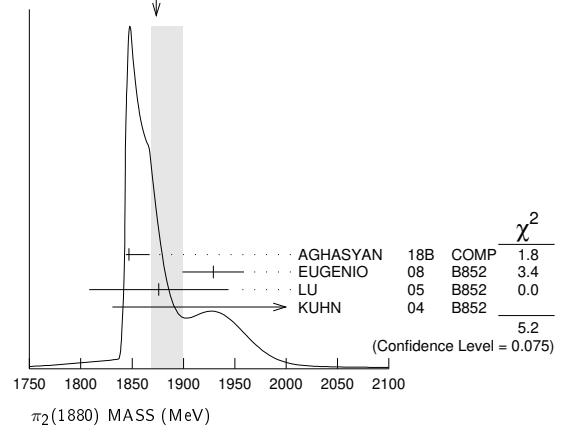
ANISOVICH	11	EPJ C71 1511	A.V. Anisovich <i>et al.</i>	(LOQM, RAL, PNPI)
ANISOVICH	00E	PL B477 19	A.V. Anisovich <i>et al.</i>	
BARBERIS	00B	PL B471 435	D. Barberis <i>et al.</i>	(WA 102 Collab.)
BARBERIS	00C	PL B471 440	D. Barberis <i>et al.</i>	(WA 102 Collab.)
BAI	99	PL B446 356	J.Z. Bai <i>et al.</i>	(BES Collab.)
BARBERIS	97B	PL B413 217	D. Barberis <i>et al.</i>	(WA 102 Collab.)
ADOMEIT	96	ZPHY C71 227	J. Adomeit <i>et al.</i>	(Crystal Barrel Collab.)
KARCH	92	ZPHY C54 33	K. Karch <i>et al.</i>	(Crystal Ball Collab.)

 $\pi_2(1880)$

$$J^{PC} = 1^-(2^-)$$

 $\pi_2(1880)$ MASS

VALUE (MeV)	EVTs	DOCUMENT ID	TECN	CHG	COMMENT
1874 ± 26 ± 5 OUR AVERAGE					Error includes scale factor of 1.6. See the ideogram below.
1847 ± 20	3	46M	¹ AGHASYAN	18B	COMP 190 $\pi^-p \rightarrow \pi^-\pi^+\pi^-p$
1929 ± 24 ± 18	4k	EUGENIO	08	B852	- 18 $\pi^-p \rightarrow \eta\eta\pi^-p$
1876 ± 11 ± 67	145k	LU	05	B852	- 18 $\pi^-p \rightarrow \omega\pi^-\pi^0p$
2003 ± 88 ± 148	69k	KUHN	04	B852	- 18 $\pi^-p \rightarrow \eta\pi^+\pi^-\pi^-p$
• • • We do not use the following data for averages, fits, limits, etc. • • •					
1880 ± 20		ANISOVICH	01B	SPEC	0 0.6-1.94 $\bar{p}p \rightarrow \eta\eta\pi^0\pi^0$
¹ Statistical error negligible.					

WEIGHTED AVERAGE
1874+26-5 (Error scaled by 1.6) $\pi_2(1880)$ WIDTH

VALUE (MeV)	EVTs	DOCUMENT ID	TECN	CHG	COMMENT
237 ± 33 ± 30 OUR AVERAGE					Error includes scale factor of 1.2.
246 ± 28	46M	² AGHASYAN	18B	COMP	190 $\pi^-p \rightarrow \pi^-\pi^+\pi^-p$
323 ± 87 ± 43	4k	EUGENIO	08	B852	- 18 $\pi^-p \rightarrow \eta\eta\pi^-p$
146 ± 17 ± 62	145k	LU	05	B852	- 18 $\pi^-p \rightarrow \omega\pi^-\pi^0p$
306 ± 132 ± 121	69k	KUHN	04	B852	- 18 $\pi^-p \rightarrow \eta\pi^+\pi^-\pi^-p$
• • • We do not use the following data for averages, fits, limits, etc. • • •					
255 ± 45		ANISOVICH	01B	SPEC	0 0.6-1.94 $\bar{p}p \rightarrow \eta\eta\pi^0\pi^0$
² Statistical error negligible.					

 $\pi_2(1880)$ DECAY MODES

Mode	Fraction (Γ_i/Γ)
Γ_1 $\eta\eta\pi^-$	seen
Γ_2 $a_0(980)\eta$	seen
Γ_3 $a_2(1320)\eta$	seen
Γ_4 $f_0(1500)\pi$	seen
Γ_5 $f_1(1285)\pi$	seen
Γ_6 $\omega\pi^-\pi^0$	seen

$\Gamma(a_2(1320)\eta)/\Gamma(f_1(1285)\pi)$	Γ_3/Γ_5
• • • We do not use the following data for averages, fits, limits, etc. • • •	
22.7 ± 7.3	69k KUHN 04 B852 - 18 $\pi^-p \rightarrow \eta\pi^+\pi^-\pi^-p$

$\Gamma(f_0(1500)\pi)/\Gamma(a_0(980)\eta)$	Γ_4/Γ_2
• • • We do not use the following data for averages, fits, limits, etc. • • •	
0.28 ± 0.20	³ ANISOVICH 01B SPEC 0 0.6-1.94 $\bar{p}p \rightarrow \eta\eta\pi^0\pi^0$
0.15 ± 0.15	
³ Systematic errors not estimated.	

 $\pi_2(1880)$ REFERENCES

AGHASYAN	18B	PR D98 092003	M. Aghasyan <i>et al.</i>	(COMPASS Collab.)
EUGENIO	08	PL B660 466	P. Eugenio <i>et al.</i>	(BNL E852 Collab.)
LU	05	PRL 94 032002	M. Lu <i>et al.</i>	(BNL E852 Collab.)
KUHN	04	PL B595 109	J. Kuhn <i>et al.</i>	(BNL E852 Collab.)
ANISOVICH	01B	PL B500 222	A.V. Anisovich <i>et al.</i>	

See key on page 1171

Meson Particle Listings

$\rho(1900)$, $f_2(1910)$

$\rho(1900)$

$I^G(J^{PC}) = 1^+(1^-)$

OMITTED FROM SUMMARY TABLE
See the review on "Spectroscopy of Light Meson Resonances."

$\rho(1900)$ MASS

VALUE (MeV)	EVTs	DOCUMENT ID	TECN	COMMENT
1880 ± 10		¹ ABLIKIM 22L BES3		2.0-3.08 $e^+e^- \rightarrow K^+K^-\pi^0$
1909 ± 17 ± 25	54	² AUBERT 08s BABR		10.6 $e^+e^- \rightarrow \phi\pi^0\gamma$
1880 ± 30		AUBERT 06D BABR		10.6 $e^+e^- \rightarrow 3\pi^+3\pi^-\gamma$
1860 ± 20		AUBERT 06D BABR		10.6 $e^+e^- \rightarrow 2(\pi^+\pi^-\pi^0)\gamma$
1910 ± 10		^{3,4} FRABETTI 04 E687		$\gamma p \rightarrow 3\pi^+3\pi^-p$
1870 ± 10		ANTONELLI 96 SPEC		$e^+e^- \rightarrow$ hadrons

- ¹ From a partial wave amplitude analysis at $\sqrt{s} = 2.125$ GeV which includes all the possible intermediate states that match J^{PC} conservation in the subsequent two-body decay. The intermediate states are parameterized with the relativistic Breit-Wigner functions. Statistical error only.
- ² From the fit with two resonances.
- ³ From a fit with two resonances with the JACOB 72 continuum.
- ⁴ Supersedes FRABETTI 01.

$\rho(1900)$ WIDTH

VALUE (MeV)	EVTs	DOCUMENT ID	TECN	COMMENT
69 ± 15		¹ ABLIKIM 22L BES3		2.0-3.08 $e^+e^- \rightarrow K^+K^-\pi^0$
48 ± 17 ± 2	54	² AUBERT 08s BABR		10.6 $e^+e^- \rightarrow \phi\pi^0\gamma$
130 ± 30		AUBERT 06D BABR		10.6 $e^+e^- \rightarrow 3\pi^+3\pi^-\gamma$
160 ± 20		AUBERT 06D BABR		10.6 $e^+e^- \rightarrow 2(\pi^+\pi^-\pi^0)\gamma$
37 ± 13		^{3,4} FRABETTI 04 E687		$\gamma p \rightarrow 3\pi^+3\pi^-p$
10 ± 5		ANTONELLI 96 SPEC		$e^+e^- \rightarrow$ hadrons

- ¹ From a partial wave amplitude analysis at $\sqrt{s} = 2.125$ GeV which includes all the possible intermediate states that match J^{PC} conservation in the subsequent two-body decay. The intermediate states are parameterized with the relativistic Breit-Wigner functions. Statistical error only.
- ² From the fit with two resonances.
- ³ From a fit with two resonances with the JACOB 72 continuum.
- ⁴ Supersedes FRABETTI 01.

$\rho(1900)$ $\Gamma(\phi)/\Gamma(e^+e^-)/\Gamma^2(\text{total})$

VALUE (units 10^{-8})	EVTs	DOCUMENT ID	TECN	COMMENT
4.2 ± 1.2 ± 0.8	54	¹ AUBERT 08s BABR		10.6 $e^+e^- \rightarrow \phi\pi^0\gamma$

- ¹ From the fit with two resonances.

$\rho(1900)$ DECAY MODES

Mode	Fraction (Γ_i/Γ)
Γ_1 6π	seen
Γ_2 $3\pi^+3\pi^-$	seen
Γ_3 $2\pi^+2\pi^-2\pi^0$	
Γ_4 $\phi\pi$	seen
Γ_5 hadrons	seen
Γ_6 e^+e^-	seen
Γ_7 $\bar{N}N$	not seen

$\rho(1900)$ BRANCHING RATIOS

$\Gamma(6\pi)/\Gamma_{\text{total}}$	VALUE	EVTs	DOCUMENT ID	TECN	COMMENT
seen	8k		AKHMETSHIN 13	CMD3	$e^+e^- \rightarrow 3\pi^+3\pi^-$
not seen			AGNELLO 02	OBLX	$\bar{n}p \rightarrow 3\pi^+2\pi^-\pi^0$
seen			FRABETTI 01	E687	$\gamma p \rightarrow 3\pi^+3\pi^-p$
seen			ANTONELLI 96	SPEC	$e^+e^- \rightarrow$ hadrons

$\rho(1900)$ REFERENCES

ABLIKIM 22L	JHEP 2207 045	M. Ablikim et al.	(BESIII Collab.)
AKHMETSHIN 13	PL B723 82	R.R. Akhmetshin et al.	(CMD-3 Collab.)
AUBERT 08s	PR D77 092002	B. Aubert et al.	(BABAR Collab.)
AUBERT 06D	PR D73 052003	B. Aubert et al.	(BABAR Collab.)
FRABETTI 04	PL B576 290	P.L. Frabetti et al.	(FNAL E687 Collab.)
AGNELLO 02	PL B527 39	M. Agnello et al.	(OBLX Collab.)
FRABETTI 01	PL B514 240	P.L. Frabetti et al.	(FNAL E687 Collab.)
ANTONELLI 96	PL B365 427	A. Antonelli et al.	(FENICE Collab.)
JACOB 72	PR D5 1847	M. Jacob, R. Slansky	

$f_2(1910)$

$I^G(J^{PC}) = 0^+(2^{++})$

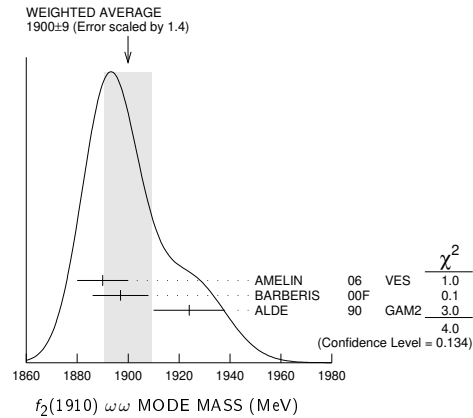
OMITTED FROM SUMMARY TABLE
We list here three different peaks with close masses and widths seen in the mass distributions of $\omega\omega$, $\eta\eta'$, and K^+K^- final states. ALDE 91B argues that they are of different nature.

$f_2(1910)$ MASS

$f_2(1910)$ $\omega\omega$ MODE

VALUE (MeV)	DOCUMENT ID	TECN	COMMENT
1900 ± 9 OUR AVERAGE	Error includes scale factor of 1.4. See the ideogram below.		
1890 ± 10	¹ AMELIN 06 VES		36 $\pi^-p \rightarrow \omega\omega n$
1897 ± 11	BARBERIS 00F		450 $pp \rightarrow p_f\omega\omega p_S$
1924 ± 14	ALDE 90 GAM2		38 $\pi^-p \rightarrow \omega\omega n$

- ¹ Supersedes BELADIDZE 92b.



$f_2(1910)$ $\eta\eta'$ MODE

VALUE (MeV)	DOCUMENT ID	TECN	COMMENT
1934 ± 16	¹ BARBERIS 00A		450 $pp \rightarrow p_f\eta\eta' p_S$
1934 ± 20	² ANISOVICH 00I SPEC		
1911 ± 10	ALDE 91B GAM2		38 $\pi^-p \rightarrow \eta\eta' n$

- ¹ Also compatible with $J^{PC} = 1^-$.
- ² Combined fit with $\eta\eta$, $\pi\pi$, and $\eta\pi\pi$.

$f_2(1910)$ K^+K^- MODE

VALUE (MeV)	DOCUMENT ID	TECN	COMMENT
1941 ± 18	¹ AMSLER 06 CBAR		1.64 $\bar{p}p \rightarrow K^+K^-\pi^0$

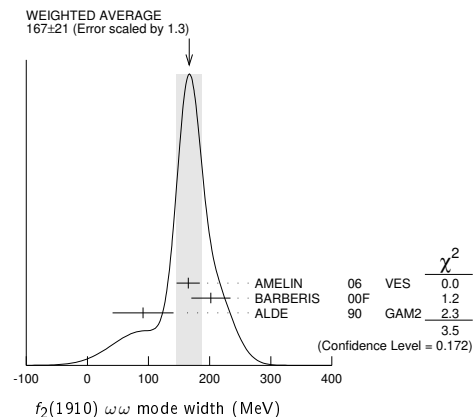
- ¹ Tentative, could be $f_2(1950)$.

$f_2(1910)$ WIDTH

$f_2(1910)$ $\omega\omega$ MODE

VALUE (MeV)	DOCUMENT ID	TECN	COMMENT
167 ± 21 OUR AVERAGE	Error includes scale factor of 1.3. See the ideogram below.		
165 ± 19	¹ AMELIN 06 VES		36 $\pi^-p \rightarrow \omega\omega n$
202 ± 32	BARBERIS 00F		450 $pp \rightarrow p_f\omega\omega p_S$
91 ± 50	ALDE 90 GAM2		38 $\pi^-p \rightarrow \omega\omega n$

- ¹ Supersedes BELADIDZE 92b.



Meson Particle Listings

 $f_2(1910)$, $a_0(1950)$, $f_2(1950)$ $f_2(1910) \eta\eta'$ MODE

VALUE (MeV)	DOCUMENT ID	TECN	COMMENT
141 ± 41	¹ BARBERIS 00A	00A	450 $p\bar{p} \rightarrow p_f \eta \eta' \rho_S$
••• We do not use the following data for averages, fits, limits, etc. •••			
271 ± 25	² ANISOVICH 00J	SPEC	
90 ± 35	ALDE 91B	GAM2	38 $\pi^- p \rightarrow \eta \eta' n$

- ¹ Also compatible with $J^{PC}=1^-+$.
² Combined fit with $\eta\eta$, $\pi\pi$, and $\eta\pi\pi$.

 $f_2(1910) K^+ K^-$ MODE

VALUE (MeV)	DOCUMENT ID	TECN	COMMENT
120 ± 40	AMSLER 06	CBAR	1.64 $\bar{p}p \rightarrow K^+ K^- \pi^0$

- We do not use the following data for averages, fits, limits, etc. •••

 $f_2(1910)$ DECAY MODES

Mode	Fraction (Γ_i/Γ)
Γ_1 $\pi^0 \pi^0$	
Γ_2 $K^+ K^-$	seen
Γ_3 $K_S^0 K_S^0$	
Γ_4 $\eta\eta$	seen
Γ_5 $\omega\omega$	seen
Γ_6 $\eta\eta'$	seen
Γ_7 $\eta'\eta'$	
Γ_8 $\rho\rho$	seen
Γ_9 $a_2(1320)\pi$	seen
Γ_{10} $f_2(1270)\eta$	seen

 $f_2(1910)$ BRANCHING RATIOS

$\Gamma(K^+ K^-)/\Gamma_{\text{total}}$	VALUE	DOCUMENT ID	TECN	COMMENT	Γ_2/Γ_6
seen	1.64	AMSLER 06	CBAR	$\bar{p}p \rightarrow K^+ K^- \pi^0$	

- ¹ Tentative, could be $f_2(1950)$.

$\Gamma(\pi^0 \pi^0)/\Gamma(\eta\eta')$	VALUE	DOCUMENT ID	TECN	COMMENT	Γ_1/Γ_6
••• We do not use the following data for averages, fits, limits, etc. •••					
<0.1		ALDE 89	GAM2	38 $\pi^- p \rightarrow \eta \eta' n$	

$\Gamma(K_S^0 K_S^0)/\Gamma(\eta\eta')$	VALUE	CL%	DOCUMENT ID	TECN	COMMENT	Γ_3/Γ_6
••• We do not use the following data for averages, fits, limits, etc. •••						
<0.066	90		BALOSHIN 86	SPEC	40 $\pi p \rightarrow K_S^0 K_S^0 n$	

$\Gamma(\eta\eta)/\Gamma(\eta\eta')$	VALUE	CL%	DOCUMENT ID	TECN	COMMENT	Γ_4/Γ_6
••• We do not use the following data for averages, fits, limits, etc. •••						
<0.05	90		ALDE 91B	GAM2	38 $\pi^- p \rightarrow \eta \eta' n$	

$\Gamma(\omega\omega)/\Gamma(\eta\eta')$	VALUE	DOCUMENT ID	COMMENT	Γ_5/Γ_6
••• We do not use the following data for averages, fits, limits, etc. •••				
2.6 ± 0.6		BARBERIS 00F	450 $p\bar{p} \rightarrow p_f \omega \omega p_S$	

$\Gamma(\eta'\eta')/\Gamma_{\text{total}}$	VALUE	DOCUMENT ID	TECN	COMMENT	Γ_7/Γ
••• We do not use the following data for averages, fits, limits, etc. •••					
probably not seen		BARBERIS 00A		450 $p\bar{p} \rightarrow p_f \eta' \eta' \rho_S$	
possibly seen		BELADIDZE 92D	VES	37 $\pi^- p \rightarrow \eta' \eta' n$	

$\Gamma(\rho\rho)/\Gamma(\omega\omega)$	VALUE	DOCUMENT ID	COMMENT	Γ_8/Γ_5
••• We do not use the following data for averages, fits, limits, etc. •••				
2.6 ± 0.4		BARBERIS 00F	450 $p\bar{p} \rightarrow p_f \omega \omega p_S$	

$\Gamma(f_2(1270)\eta)/\Gamma(a_2(1320)\pi)$	VALUE	DOCUMENT ID	TECN	COMMENT	Γ_{10}/Γ_9
0.09 ± 0.05		¹ ANISOVICH 11	SPEC	0.9–1.94 $p\bar{p}$	

- ¹ Reanalysis of ADOEIT 96 and ANISOVICH 00E.

 $f_2(1910)$ REFERENCES

ANISOVICH 11	EPI C71 1511	A.V. Anisovich et al.	(LOQM, RAL, PNPI)
AMELIN 06	PAN 69 690	D.V. Amelin et al.	(VES Collab.)
	Translated from YAF 69 715.		

AMSLER 06	PL B639 165	C. Amshler et al.	(Crystal Barrel Collab.)
ANISOVICH 00E	PL B477 19	A.V. Anisovich et al.	
ANISOVICH 00J	PL B491 47	A.V. Anisovich et al.	(RAL, LOQM, PNPI+)
BARBERIS 00A	PL B471 429	D. Barberis et al.	(WA 102 Collab.)
BARBERIS 00F	PL B484 198	D. Barberis et al.	(WA 102 Collab.)
ADOMEIT 96	ZPHY C71 227	J. Adomeit et al.	(Crystal Barrel Collab.)
BELADIDZE 92B	ZPHY C54 367	G.M. Beladidze et al.	(VES Collab.)
BELADIDZE 92D	ZPHY C57 13	G.M. Beladidze et al.	(VES Collab.)
ALDE 91B	SJNP 54 455	D.M. Alde et al.	(SERP, BELG, LANL, LAPP+)
	Translated from YAF 54 751.		
	PL B276 375	D.M. Alde et al.	(BELG, SERP, KEK, LANL+)
ALDE 90	PL B241 600	D.M. Alde et al.	(SERP, BELG, LANL, LAPP+)
ALDE 89	PL B216 447	D.M. Alde et al.	(SERP, BELG, LANL, LAPP)
	SJNP 48 1035	D.M. Alde et al.	(BELG, SERP, LANL, LAPP)
	Translated from YAF 48 1724.		
BALOSHIN 86	SJNP 43 959	O.N. Baloshin et al.	(ITEP)
	Translated from YAF 43 1467.		

 $a_0(1950)$

$$I^G(J^{PC}) = 1^-(0^{++})$$

OMITTED FROM SUMMARY TABLE

Needs confirmation. Seen in $\gamma\gamma \rightarrow \eta_c(1S) \rightarrow K\bar{K}\pi$ by LEES 16A with significance 2.5 σ in $K_S^0 K^\pm \pi^\mp$ and 4.2 σ in $K^+ K^- \pi^0$.

 $a_0(1950)$ MASS

VALUE (MeV)	EVTS	DOCUMENT ID	TECN	COMMENT
1931 ± 14 ± 22	12k	^{1,2} LEES	16A	BABR $\gamma\gamma \rightarrow \eta_c(1S) \rightarrow K\bar{K}\pi$
••• We do not use the following data for averages, fits, limits, etc. •••				
1949 ± 32 ± 76	8k	¹ LEES	16A	BABR $\gamma\gamma \rightarrow \eta_c(1S) \rightarrow K_S^0 K^\pm \pi^\mp$
1927 ± 15 ± 23	4k	¹ LEES	16A	BABR $\gamma\gamma \rightarrow \eta_c(1S) \rightarrow K^+ K^- \pi^0$

- ¹ From a model-independent partial wave analysis fit to a relativistic Breit-Wigner function with a floating width.

- ² Weighted average of the $K_S^0 K^\pm$ and $K^+ K^-$ decay modes.

 $a_0(1950)$ WIDTH

VALUE (MeV)	EVTS	DOCUMENT ID	TECN	COMMENT
271 ± 22 ± 29	12k	^{1,2} LEES	16A	BABR $\gamma\gamma \rightarrow \eta_c(1S) \rightarrow K\bar{K}\pi$
••• We do not use the following data for averages, fits, limits, etc. •••				
265 ± 36 ± 110	8k	¹ LEES	16A	BABR $\gamma\gamma \rightarrow \eta_c(1S) \rightarrow K_S^0 K^\pm \pi^\mp$
274 ± 28 ± 30	4k	¹ LEES	16A	BABR $\gamma\gamma \rightarrow \eta_c(1S) \rightarrow K^+ K^- \pi^0$

- ¹ From a model-independent partial wave analysis fit to a relativistic Breit-Wigner function with a floating mass.

- ² Weighted average of the $K_S^0 K^\pm$ and $K^+ K^-$ decay modes.

 $a_0(1950)$ DECAY MODES

Mode	Fraction (Γ_i/Γ)
Γ_1 $K\bar{K}$	seen

 $a_0(1950)$ BRANCHING RATIOS

$\Gamma(K\bar{K})/\Gamma_{\text{total}}$	VALUE	EVTS	DOCUMENT ID	TECN	COMMENT	Γ_1/Γ
seen	12k	¹ LEES	16A	BABR	$\gamma\gamma \rightarrow \eta_c(1S) \rightarrow K\bar{K}\pi$	

- ¹ From a model-independent partial wave analysis.

 $a_0(1950)$ REFERENCES

LEES 16A	PR D93 012005	J.P. Lees et al.	(BABAR Collab.)
----------	---------------	------------------	-----------------

 $f_2(1950)$

$$I^G(J^{PC}) = 0^+(2^{++})$$

 $f_2(1950)$ T-MATRIX POLE \sqrt{S}

Note that $\Gamma = -2 \text{Im}(\sqrt{s})$.

VALUE (MeV)	DOCUMENT ID	TECN	COMMENT
(1830–2020) — i (110–220) OUR ESTIMATE			
(1955 ± 75) — i (175 ± 57)	¹ RODAS 22	RVUE	$J/\psi(1S) \rightarrow \gamma(\pi\pi, K\bar{K})$
(1978.2 ± 1.8 ± 28.4) — i (16.9 ± 7.8)	² ALBRECHT 20	RVUE	0.9 $\bar{p}p \rightarrow \pi^0 \pi^0 \eta, \pi^0 \eta\eta, \pi^0 K^+ K^-$
(118.8 ± 0.8 ± 20.8)			
(1867 ± 46) — i (193 ± 29)	AMSLER 02	CBAR	0.9 $\bar{p}p \rightarrow \pi^0 \eta\eta, \pi^0 \pi^0 \pi^0$

- ¹ T-matrix pole from coupled channel K-matrix fit to data on $J/\psi \rightarrow \gamma \pi^0 \pi^0$ (ABLIIKIM 15AE) and $J/\psi \rightarrow \gamma K_S^0 K_S^0$ (ABLIIKIM 18AA).

- ² T-matrix pole, 4 poles, 4 channels, including scattering data from HYAMS 75 ($\pi\pi$), LONGACRE 86 ($K\bar{K}$), BINON 83 ($\eta\eta$).

See key on page 1171

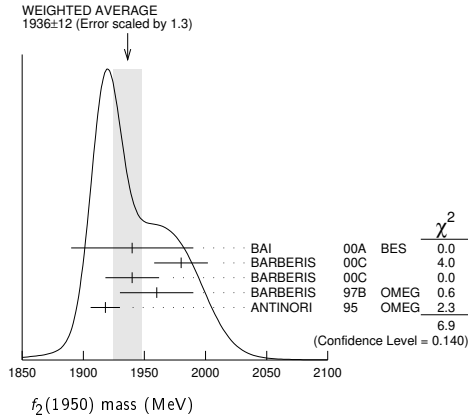
Meson Particle Listings

$f_2(1950)$, $a_4(1970)$

$f_2(1950)$ MASS

VALUE (MeV)	DOCUMENT ID	TECN	COMMENT
1936±12 OUR AVERAGE	Error includes scale factor of 1.3. See the ideogram below.		
1940±50	BAI	00A	BES $J/\psi \rightarrow \gamma(\pi^+\pi^-\pi^+\pi^-)$
1980±22	1 BARBERIS	00c	450 $pp \rightarrow pp4\pi$
1940±22	2 BARBERIS	00c	450 $pp \rightarrow pp2\pi^0$
1960±30	BARBERIS	97B	OMEG 450 $pp \rightarrow pp2(\pi^+\pi^-)$
1918±12	ANTINORI	95	OMEG 300,450 $pp \rightarrow pp2(\pi^+\pi^-)$
• • • We do not use the following data for averages, fits, limits, etc. • • •			
2038 ⁺¹³⁺¹² ₋₁₁₋₇₃	3 UEHARA	09	BELL 10.6 $e^+e^- \rightarrow e^+e^-\pi^0\pi^0$
1930±25	4 BINON	05	GAMS 33 $\pi^-p \rightarrow \eta\eta n$
1980±2±14	ABE	04	BELL 10.6 $e^+e^- \rightarrow e^+e^-K^+K^-$
2010±25	ANISOVICH	00j	SPEC
1980±50	ANISOVICH	99B	SPEC 1.35-1.94 $p\bar{p} \rightarrow \eta\eta\pi^0$
~1990	5 OAKDEN	94	RVUE 0.36-1.55 $p\bar{p} \rightarrow \pi\pi$
1950±15	6 ASTON	91	LASS 11 $K^-p \rightarrow \Lambda K\bar{K}\pi\pi$

- 1 Decaying into $\pi^+\pi^-2\pi^0$.
- 2 Decaying into $2(\pi^+\pi^-)$.
- 3 Taking into account $f_4(2050)$.
- 4 First solution, PWA is ambiguous.
- 5 From solution B of amplitude analysis of data on $p\bar{p} \rightarrow \pi\pi$. See however KLOET 96 who fit $\pi^+\pi^-$ only and find waves only up to $J = 3$ to be important but not significantly resonant.
- 6 Cannot determine spin to be 2.



$f_2(1950)$ WIDTH

VALUE (MeV)	DOCUMENT ID	TECN	COMMENT
464±24 OUR AVERAGE	Error includes scale factor of 1.3. See the ideogram below.		
380 ⁺¹²⁰ ₋₉₀	BAI	00A	BES $J/\psi \rightarrow \gamma(\pi^+\pi^-\pi^+\pi^-)$
520±50	1 BARBERIS	00c	450 $pp \rightarrow pp4\pi$
485±55	2 BARBERIS	00c	450 $pp \rightarrow pp4\pi$
460±40	BARBERIS	97B	OMEG 450 $pp \rightarrow pp2(\pi^+\pi^-)$
390±60	ANTINORI	95	OMEG 300,450 $pp \rightarrow pp2(\pi^+\pi^-)$
• • • We do not use the following data for averages, fits, limits, etc. • • •			
441 ⁺²⁷⁺²⁸ ₋₂₅₋₁₉₂	3 UEHARA	09	BELL 10.6 $e^+e^- \rightarrow e^+e^-\pi^0\pi^0$
450±50	4 BINON	05	GAMS 33 $\pi^-p \rightarrow \eta\eta n$
297±12±6	ABE	04	BELL 10.6 $e^+e^- \rightarrow e^+e^-K^+K^-$
495±35	ANISOVICH	00j	SPEC
500±100	ANISOVICH	99B	SPEC 1.35-1.94 $p\bar{p} \rightarrow \eta\eta\pi^0$
~100	5 OAKDEN	94	RVUE 0.36-1.55 $p\bar{p} \rightarrow \pi\pi$
250±50	6 ASTON	91	LASS 11 $K^-p \rightarrow \Lambda K\bar{K}\pi\pi$

- 1 Decaying into $\pi^+\pi^-2\pi^0$.
- 2 Decaying into $2(\pi^+\pi^-)$.
- 3 Taking into account $f_4(2050)$.
- 4 First solution, PWA is ambiguous.
- 5 From solution B of amplitude analysis of data on $p\bar{p} \rightarrow \pi\pi$. See however KLOET 96 who fit $\pi^+\pi^-$ only and find waves only up to $J = 3$ to be important but not significantly resonant.
- 6 Cannot determine spin to be 2.

$f_2(1950)$ DECAY MODES

Mode	Fraction (Γ_i/Γ)
Γ_1 $K^*(892)\bar{K}^*(892)$	seen
Γ_2 $\pi\pi$	seen
Γ_3 $\pi^+\pi^-$	seen
Γ_4 $\pi^0\pi^0$	seen
Γ_5 4π	seen

Γ_6 $\pi^+\pi^-\pi^+\pi^-$	
Γ_7 $a_2(1320)\pi$	
Γ_8 $\eta\eta$	seen
Γ_9 $K\bar{K}$	seen
Γ_{10} $\gamma\gamma$	seen
Γ_{11} $\rho\bar{\rho}$	seen

$f_2(1950)$ $\Gamma(i)\Gamma(\gamma\gamma)/\Gamma(\text{total})$

VALUE (eV)	DOCUMENT ID	TECN	COMMENT	$\Gamma_9/\Gamma_{10}/\Gamma$
------------	-------------	------	---------	-------------------------------

- • • We do not use the following data for averages, fits, limits, etc. • • •
| 122±4±26 | 1 ABE | 04 | BELL 10.6 $e^+e^- \rightarrow e^+e^-K^+K^-$ | |
- 1 Assuming spin 2.

VALUE	DOCUMENT ID	TECN	COMMENT	$\Gamma_2/\Gamma_{10}/\Gamma$
-------	-------------	------	---------	-------------------------------

- • • We do not use the following data for averages, fits, limits, etc. • • •
| 162⁺⁶⁹⁺¹¹³⁷₋₄₂₋₂₀₄ | 1 UEHARA | 09 | BELL 10.6 $e^+e^- \rightarrow e^+e^-\pi^0\pi^0$ | |
- 1 Taking into account $f_4(2050)$.

$f_2(1950)$ BRANCHING RATIOS

$\Gamma(K^*(892)\bar{K}^*(892))/\Gamma_{\text{total}}$	DOCUMENT ID	TECN	CHG	COMMENT	Γ_1/Γ
--	-------------	------	-----	---------	-------------------

VALUE	DOCUMENT ID	TECN	COMMENT	Γ_7/Γ
-------	-------------	------	---------	-------------------

- • • We do not use the following data for averages, fits, limits, etc. • • •
| not seen | BARBERIS | 00B | 450 $pp \rightarrow p_f\eta\pi^+\pi^-p_s$ | |
| not seen | BARBERIS | 00c | 450 $pp \rightarrow p_f4\pi p_s$ | |
| possibly seen | BARBERIS | 97B | OMEG 450 $pp \rightarrow pp2(\pi^+\pi^-)$ | |

$\Gamma(\eta\eta)/\Gamma(4\pi)$	CL%	DOCUMENT ID	COMMENT	Γ_8/Γ_5
---------------------------------	-----	-------------	---------	---------------------

- • • We do not use the following data for averages, fits, limits, etc. • • •
| <5.0 × 10⁻³ | 90 | BARBERIS | 00E 450 $pp \rightarrow p_f\eta\eta p_s$ | |

$\Gamma(\eta\eta)/\Gamma(\pi^+\pi^-)$	DOCUMENT ID	TECN	COMMENT	Γ_8/Γ_3
---------------------------------------	-------------	------	---------	---------------------

0.14±0.05	AMSLER	02	CBAR 0.9 $p\bar{p} \rightarrow \pi^0\eta\eta, \pi^0\pi^0\pi^0$	
-----------	--------	----	--	--

$\Gamma(\rho\bar{\rho})/\Gamma_{\text{total}}$	EVTS	DOCUMENT ID	TECN	COMMENT	Γ_{11}/Γ
--	------	-------------	------	---------	----------------------

seen	111	ALEXANDER	10	CLEO $\psi(2S) \rightarrow \gamma\rho\bar{\rho}$	
------	-----	-----------	----	--	--

$f_2(1950)$ REFERENCES

RODAS	22	EPJ C82 80	A. Rodas et al.	(JPAC Collab.)
ALBRECHT	20	EPJ C80 453	M. Albrecht et al.	(Crystal Barrel Collab.)
ABLIKIM	18AA	PR D98 072003	M. Ablikim et al.	(BESIII Collab.)
ABLIKIM	15AE	PR D92 052003	M. Ablikim et al.	(BESIII Collab.)
ALEXANDER	10	PR D82 092002	J.P. Alexander et al.	(CLEO Collab.)
UEHARA	09	PR D79 052009	S. Uehara et al.	(BELLE Collab.)
BINON	05	PAN 68 960	F. Binon et al.	
Translated from YAF 68 998.				
ABE	04	EPJ C32 323	K. Abe et al.	(BELLE Collab.)
AMSLER	02	EPJ C23 29	C. Amisler et al.	(Crystal Barrel Collab.)
ANISOVICH	00j	PL B491 47	A.V. Anisovich et al.	(RAL, LOQM, FNPI)
BAI	00A	PL B472 207	J.Z. Bai et al.	(BES Collab.)
BARBERIS	00B	PL B471 435	D. Barberis et al.	(WA 102 Collab.)
BARBERIS	00C	PL B471 440	D. Barberis et al.	(WA 102 Collab.)
BARBERIS	00E	PL B479 59	D. Barberis et al.	(WA 102 Collab.)
ANISOVICH	99B	PL B449 154	A.V. Anisovich et al.	
BARBERIS	97B	PL B413 217	D. Barberis et al.	(WA 102 Collab.)
KLOET	96	PR D53 6120	W.M. Kloet, F. Myhrer	(RUTG, NORD)
ANTINORI	95	PL B353 589	F. Antinori et al.	(ATHU, BARI, BIRM+JP)
OAKDEN	94	NP A574 731	M.N. Oakden, M.R. Pennington	(DURH)
ASTON	91	NPBPS B21 5	D. Aston et al.	(LASS Collab.)
LONGACRE	86	PL B177 223	R.S. Longacre et al.	(BNL, BRAN, CUNY+)
BINON	83	NC 78A 313	F.G. Binon et al.	(BELG, LAPP, SERP+)
HYAMS	75	NP B100 205	B.D. Hyams et al.	(CERN, MFM)

$a_4(1970)$

$I^G(J^{PC}) = 1^-(4^{++})$

$a_4(1970)$ MASS

VALUE (MeV)	EVTS	DOCUMENT ID	TECN	CHG	COMMENT
-------------	------	-------------	------	-----	---------

- 1935⁺¹¹₋₁₃
 - 46M
 - 1 AGHASYAN
 - 18B
 - COMP
 - 190 $\pi^-p \rightarrow \pi^-\pi^+\pi^-p$
- 1900⁺⁸⁰₋₂₀
 - ADOLPH
 - 15
 - COMP
 - 191 $\pi^-p \rightarrow \eta^{(\prime)}\pi^-p$
- 1985±10±13
 - 145k
 - LU
 - 05
 - B852
 - 18 $\pi^-p \rightarrow \omega\pi^-\pi^0p$
- 1996±25±43
 - CHUNG
 - 02
 - B852
 - 18.3 $\pi^-p \rightarrow 3\pi p$
- 2000±40⁺⁶⁰₋₂₀
 - IVANOV
 - 01
 - B852
 - 18 $\pi^-p \rightarrow \eta'\pi^-p$
- 2010±20
 - 2 ALDE
 - 96
 - GAM2 0
 - 38 $\pi^-p \rightarrow \eta\pi^0 n$
- 2040±30
 - 3 CLELAND
 - 82B
 - SPEC ±
 - 50 $\pi p \rightarrow K_S^0 K^\pm p$

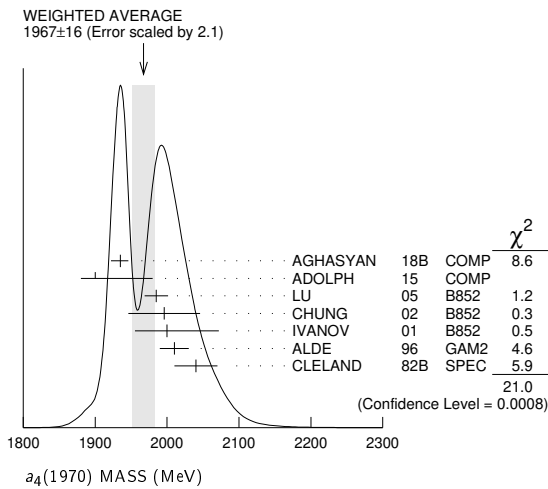
Meson Particle Listings

$a_4(1970), \rho_3(1990)$

••• We do not use the following data for averages, fits, limits, etc. •••

1885 ± 13 ⁺⁵⁰ ₋₂	420k	4	ALEKSEEV	10	COMP	190 $\pi^- Pb \rightarrow \pi^- \pi^+ \pi^+ Pb'$
2004 ± 6	80k	5	UMAN	06	E835	5.2 $\bar{p}p \rightarrow \eta \eta \pi^0$
2005 ⁺²⁵ ₋₄₅		6	ANISOVICH	01F	SPEC	2.0 $\bar{p}p \rightarrow 3\pi^0, \pi^0 \eta, \pi^0 \eta'$
1944 ± 8 ± 50		7	AMELIN	99	VES	37 $\pi^- A \rightarrow \omega \pi^- \pi^0 A^*$
1903 ± 10		8	BALDI	78	SPEC	10 $\pi^- p \rightarrow \rho K_S^0 K^-$
2030 ± 50		9	CORDEN	78c	OMEG 0	15 $\pi^- p \rightarrow 3\pi n$

- 1 Statistical error negligible.
- 2 From a simultaneous fit to the G_\perp and G_0 wave intensities.
- 3 From an amplitude analysis.
- 4 Superseded by AGHASYAN 2018B.
- 5 Statistical error only.
- 6 From the combined analysis of ANISOVICH 99c, ANISOVICH 99e, and ANISOVICH 01f.
- 7 May be a different state.
- 8 From a fit to the Y_8^0 moment. Limited by phase space.
- 9 $J^P = 4^+$ is favored, though $J^P = 2^+$ cannot be excluded.



$a_4(1970)$ WIDTH

VALUE (MeV)	EVTS	DOCUMENT ID	TECN	CHG	COMMENT
324⁺¹⁵₋₁₈ OUR AVERAGE					
333 ⁺¹⁶ ₋₂₁	46M	¹ AGHASYAN	18b	COMP	190 $\pi^- p \rightarrow \pi^- \pi^+ \pi^- p$
300 ⁺⁸⁰ ₋₁₀₀		ADOLPH	15	COMP	191 $\pi^- p \rightarrow \eta^{(\prime)} \pi^- p$
231 ± 30 ± 46	145k	LU	05	B852	18 $\pi^- p \rightarrow \omega \pi^- \pi^0 p$
298 ± 81 ± 85		CHUNG	02	B852	18.3 $\pi^- p \rightarrow 3\pi p$
350 ± 100 ⁺⁷⁰ ₋₅₀		IVANOV	01	B852	18 $\pi^- p \rightarrow \eta' \pi^- p$
370 ± 80		² ALDE	96	GAM2 0	38 $\pi^- p \rightarrow \eta \pi^0 n$
380 ± 150		³ CLELAND	82b	SPEC ±	50 $\pi p \rightarrow K_S^0 K^\pm p$

••• We do not use the following data for averages, fits, limits, etc. •••

294 ± 25 ⁺⁴⁶ ₋₁₉	420k	4	ALEKSEEV	10	COMP	190 $\pi^- Pb \rightarrow \pi^- \pi^+ \pi^+ Pb'$
401 ± 16	80k	5	UMAN	06	E835	5.2 $\bar{p}p \rightarrow \eta \eta \pi^0$
180 ± 30		6	ANISOVICH	01F	SPEC	2.0 $\bar{p}p \rightarrow 3\pi^0, \pi^0 \eta, \pi^0 \eta'$
324 ± 26 ± 75		7	AMELIN	99	VES	37 $\pi^- A \rightarrow \omega \pi^- \pi^0 A^*$
166 ± 43		8	BALDI	78	SPEC	10 $\pi^- p \rightarrow \rho K_S^0 K^-$
510 ± 200		9	CORDEN	78c	OMEG 0	15 $\pi^- p \rightarrow 3\pi n$

- 1 Statistical error negligible.
- 2 From a simultaneous fit to the G_\perp and G_0 wave intensities.
- 3 From an amplitude analysis.
- 4 Superseded by AGHASYAN 2018B.
- 5 Statistical error only.
- 6 From the combined analysis of ANISOVICH 99c, ANISOVICH 99e, and ANISOVICH 01f.
- 7 May be a different state.
- 8 From a fit to the Y_8^0 moment. Limited by phase space.
- 9 $J^P = 4^+$ is favored, though $J^P = 2^+$ cannot be excluded.

$a_4(1970)$ DECAY MODES

Mode	Fraction (Γ_i/Γ)
Γ_1 $K\bar{K}$	seen
Γ_2 $\pi^+ \pi^- \pi^0$	seen
Γ_3 $\rho \pi$	seen

Γ_4 $f_2(1270) \pi$	seen
Γ_5 $\omega \pi^- \pi^0$	seen
Γ_6 $\omega \rho$	seen
Γ_7 $\eta \pi$	seen
Γ_8 $\eta'(958) \pi$	seen

$a_4(1970)$ BRANCHING RATIOS

$\Gamma(K\bar{K})/\Gamma_{total}$	VALUE	DOCUMENT ID	TECN	CHG	COMMENT	Γ_1/Γ
seen		BALDI	78	SPEC	±	10 $\pi^- p \rightarrow K_S^0 K^- p$

$\Gamma(\pi^+ \pi^- \pi^0)/\Gamma_{total}$	VALUE	DOCUMENT ID	TECN	CHG	COMMENT	Γ_2/Γ
seen		CORDEN	78c	OMEG 0		15 $\pi^- p \rightarrow 3\pi n$

$\Gamma(\rho \pi)/\Gamma(f_2(1270) \pi)$	VALUE	EVTS	DOCUMENT ID	TECN	COMMENT	Γ_3/Γ_4
--	-------	------	-------------	------	---------	---------------------

1.7^{+0.9}_{-0.8} OUR AVERAGE Error includes scale factor of 3.7.

2.9 ^{+0.6} _{-0.4}	46M	¹ AGHASYAN	18b	COMP	190 $\pi^- p \rightarrow \pi^- \pi^+ \pi^- p$
1.1 ± 0.2 ± 0.2		CHUNG	02	B852	18.3 $\pi^- p \rightarrow 3\pi p$

¹ Statistical error negligible.

$\Gamma(\eta \pi)/\Gamma_{total}$	VALUE	DOCUMENT ID	TECN	CHG	COMMENT	Γ_7/Γ
seen		ALDE	96	GAM2 0	38 $\pi^- p \rightarrow \eta \pi^0 n$	

$\Gamma(\eta'(958) \pi)/\Gamma(\eta \pi)$	VALUE	DOCUMENT ID	TECN	COMMENT	Γ_8/Γ_7
0.23 ± 0.07		ADOLPH	15	COMP	191 $\pi^- p \rightarrow \eta^{(\prime)} \pi^- p$

$\Gamma(\omega \rho)/\Gamma_{total}$	VALUE	EVTS	DOCUMENT ID	TECN	COMMENT	Γ_6/Γ
seen	145k		LU	05	B852	18 $\pi^- p \rightarrow \omega \pi^- \pi^0 p$

$a_4(1970)$ REFERENCES

AGHASYAN 18B	PR D98 092003	M. Aghasyan et al.	(COMPASS Collab.)
ADOLPH 15	PL B740 303	M. Adolph et al.	(COMPASS Collab.)
ALEKSEEV 10	PRL 104 241803	M.G. Alekseev et al.	(COMPASS Collab.)
UMAN 06	PR D73 052009	I. Uman et al.	(FNAL E835)
LU 05	PRL 94 032002	M. Lu et al.	(BNL E852 Collab.)
CHUNG 02	PR D65 072001	S.U. Chung et al.	(BNL E852 Collab.)
ANISOVICH 01F	PL B517 261	A.V. Anisovich et al.	
IVANOV 01	PRL 86 3377	E.I. Ivanov et al.	(BNL E852 Collab.)
AMELIN 99	PAN 62 445	D.V. Amelin et al.	(VES Collab.)
ANISOVICH 99C	PL B452 173	A.V. Anisovich et al.	
ANISOVICH 99E	PL B452 187	A.V. Anisovich et al.	
ALDE 96	PAN 59 982	S.V. Donskov et al.	(GAMS Collab.) IJGPC
CLELAND 82B	NP B208 228	W.E. Cleland et al.	(DURH, GEVA, LAUS+)
BALDI 78	PL 74B 413	R. Baldi et al.	(GEVA) JP
CORDEN 78c	NP B136 77	M.J. Corden et al.	(BIRM, RHEL, TELA+) JP

$\rho_3(1990)$

$$I^G(J^{PC}) = 1^+(3^{--})$$

OMITTED FROM SUMMARY TABLE

$\rho_3(1990)$ MASS

VALUE (MeV)	DOCUMENT ID	TECN	COMMENT
••• We do not use the following data for averages, fits, limits, etc. •••			
1982 ± 14	¹ ANISOVICH	02	SPEC 0.6-1.9 $\rho \bar{p} \rightarrow \omega \pi^0, \omega \eta \pi^0, \pi^+ \pi^-$
~ 2007	HASAN	94	RVUE $\bar{p} p \rightarrow \pi \pi$

¹ From the combined analysis of ANISOVICH 00j, ANISOVICH 01d, ANISOVICH 01e, and ANISOVICH 02.

$\rho_3(1990)$ WIDTH

VALUE (MeV)	DOCUMENT ID	TECN	COMMENT
••• We do not use the following data for averages, fits, limits, etc. •••			
188 ± 24	² ANISOVICH	02	SPEC 0.6-1.9 $\rho \bar{p} \rightarrow \omega \pi^0, \omega \eta \pi^0, \pi^+ \pi^-$
~ 287	HASAN	94	RVUE $\bar{p} p \rightarrow \pi \pi$

² From the combined analysis of ANISOVICH 00j, ANISOVICH 01d, ANISOVICH 01e, and ANISOVICH 02.

$\rho_3(1990)$ REFERENCES

ANISOVICH 02	PL B542 8	A.V. Anisovich et al.	
ANISOVICH 01D	PL B508 6	A.V. Anisovich et al.	
ANISOVICH 01E	PL B513 281	A.V. Anisovich et al.	
ANISOVICH 00J	PL B491 47	A.V. Anisovich et al.	(RAL, LOQM, PNPI+)
HASAN 94	PL B334 215	A. Hasan, D.V. Bugg	(LOQM)

See key on page 1171

Meson Particle Listings

$\pi_2(2005)$, $f_2(2100)$, $f_0(2020)$

$\pi_2(2005)$

$$J^{PC} = 1^-(2^-+)$$

OMITTED FROM SUMMARY TABLE

$\pi_2(2005)$ MASS

VALUE (MeV)	EVTs	DOCUMENT ID	TECN	COMMENT
1963⁺¹⁷₋₂₇ OUR AVERAGE				
1962 ⁺¹⁷ ₋₂₉	46M	¹ AGHASYAN	18B	COMP 190 $\pi^- p \rightarrow \pi^- \pi^+ \pi^- p$
1974 ⁺¹⁴ ₋₈₃	145k	LU	05	B852 18 $\pi^- p \rightarrow \omega \pi^- \pi^0 p$
• • • We do not use the following data for averages, fits, limits, etc. • • •				
2005 ⁺¹⁵		ANISOVICH	01F	SPEC 2.0 $\bar{p} p \rightarrow 3\pi^0, \pi^0 \eta, \pi^0 \eta'$
¹ Statistical uncertainty negligible.				

$\pi_2(2005)$ WIDTH

VALUE (MeV)	EVTs	DOCUMENT ID	TECN	COMMENT
370⁺¹⁶₋₉₀ OUR AVERAGE				
371 ⁺¹⁶ ₋₁₂₀	46M	¹ AGHASYAN	18B	COMP 190 $\pi^- p \rightarrow \pi^- \pi^+ \pi^- p$
341 ⁺⁶¹ ₋₁₃₉	145k	LU	05	B852 18 $\pi^- p \rightarrow \omega \pi^- \pi^0 p$
• • • We do not use the following data for averages, fits, limits, etc. • • •				
200 ⁺⁴⁰		ANISOVICH	01F	SPEC 2.0 $\bar{p} p \rightarrow 3\pi^0, \pi^0 \eta, \pi^0 \eta'$
¹ Statistical uncertainty negligible.				

$\pi_2(2005)$ DECAY MODES

Mode	Fraction (Γ_i/Γ)
Γ_1 $\pi^- \pi^+ \pi^-$	seen
Γ_2 $\omega \pi^0 \pi^-$	seen

$\pi_2(2005)$ BRANCHING RATIOS

$\Gamma(\pi^- \pi^+ \pi^-)/\Gamma_{total}$	Γ_1/Γ		
VALUE	DOCUMENT ID	TECN	COMMENT
seen	AGHASYAN	18B	COMP 190 $\pi^- p \rightarrow \pi^- \pi^+ \pi^- p$
$\Gamma(\omega \pi^0 \pi^-)/\Gamma_{total}$	Γ_2/Γ		
VALUE	DOCUMENT ID	TECN	COMMENT
seen	LU	05	B852 18 $\pi^- p \rightarrow \omega \pi^- \pi^0 p$

$\pi_2(2005)$ REFERENCES

AGHASYAN	18B	PR D98 092003	M. Aghasyan et al.	(COMPASS Collab.)
LU	05	PRL 94 032002	M. Lu et al.	(BNL E852 Collab.)
ANISOVICH	01F	PL B517 261	A.V. Anisovich et al.	

$f_2(2100)$

$$J^{PC} = 0^+(2^{++})$$

$f_2(2100)$ MASS

VALUE (MeV)	DOCUMENT ID	TECN	COMMENT
2011⁺⁶²₋₇₆ OUR AVERAGE			
2062 ⁺⁶ ₋₁₀	² ABLIKIM	22As	BES3 $J/\psi(1S) \rightarrow \gamma \eta \eta'$
2005 ⁺¹²	VLADIMIRSK..06	SPEC	40 $\pi^- p \rightarrow K_S^0 K_S^0 n$
1980 ⁺²⁰	³ BOLONKIN	88	SPEC 40 $\pi^- p \rightarrow K_S^0 K_S^0 n$
2050 ⁺⁹⁰ ₋₅₀	ETKIN	85	MPS 22 $\pi^- p \rightarrow 2\phi n$
2120 ⁺²⁰ ₋₁₂₀	LINDENBAUM	84	RVUE
2160 ⁺⁵⁰	ETKIN	82	MPS 22 $\pi^- p \rightarrow 2\phi n$
¹ Includes data of ETKIN 85. The percentage of the resonance going into $\phi\phi$, $2^+ + S_2$, D_2 , and D_0 is $98\pm\frac{1}{3}$, $0\pm\frac{1}{0}$, and $2\pm\frac{2}{1}$, respectively.			
² From a Breit-Wigner fit involving 9 resonances and a resonating exotic $\eta_1(1855) \rightarrow \eta \eta'$ P-wave.			
³ Statistically very weak, only 1.4 s.d.			

$f_2(2100)$ WIDTH

VALUE (MeV)	DOCUMENT ID	TECN	COMMENT
202⁺⁶⁷₋₆₂	⁴ ETKIN	88	MPS 22 $\pi^- p \rightarrow \phi\phi n$

• • • We do not use the following data for averages, fits, limits, etc. • • •

165 ⁺¹⁷ ₋₅	⁵ ABLIKIM	22As	BES3 $J/\psi(1S) \rightarrow \gamma \eta \eta'$
209 ⁺³²	VLADIMIRSK..06	SPEC	40 $\pi^- p \rightarrow K_S^0 K_S^0 n$
145 ⁺⁵⁰	⁶ BOLONKIN	88	SPEC 40 $\pi^- p \rightarrow K_S^0 K_S^0 n$
200 ⁺¹⁶⁰ ₋₅₀	ETKIN	85	MPS 22 $\pi^- p \rightarrow 2\phi n$
300 ⁺¹⁵⁰ ₋₅₀	LINDENBAUM	84	RVUE
310 ⁺⁷⁰	ETKIN	82	MPS 22 $\pi^- p \rightarrow 2\phi n$

⁴ Includes data of ETKIN 85.

⁵ From a Breit-Wigner fit involving 9 resonances and a resonating exotic $\eta_1(1855) \rightarrow \eta \eta'$ P-wave.

⁶ Statistically very weak, only 1.4 s.d.

$f_2(2100)$ DECAY MODES

Mode	Fraction (Γ_i/Γ)
Γ_1 $\phi\phi$	seen
Γ_2 $K\bar{K}$	seen

$f_2(2100)$ BRANCHING RATIOS

$\Gamma(K\bar{K})/\Gamma_{total}$	Γ_2/Γ		
VALUE	DOCUMENT ID	TECN	COMMENT
seen	VLADIMIRSK..06	SPEC	40 $\pi^- p \rightarrow K_S^0 K_S^0 n$

$f_2(2100)$ REFERENCES

ABLIKIM	22As	PR D106 072012	M. Ablikim et al.	(BESIII Collab.)
Also		PR D107 079901 (errata.)	M. Ablikim et al.	(BESIII Collab.)
VLADIMIRSK..06		PAN 69 493	V.V. Vladimirov et al.	(ITEP, Moscow)
Translated from		YAF 69 515		
BOLONKIN	88	NP B309 426	B.V. Bolonkin et al.	(ITEP, SERP)
ETKIN	88	PL B201 568	A. Etkin et al.	(BNL, CUNY)
ETKIN	85	PL 165B 217	A. Etkin et al.	(BNL, CUNY)
LINDENBAUM	84	CNPP 13 285	S.J. Lindenbaum	(CUNY)
ETKIN	82	PRL 49 1620	A. Etkin et al.	(BNL, CUNY)
Also		Brighton Conf. 351	S.J. Lindenbaum	(BNL, CUNY)

$f_0(2020)$

$$J^{PC} = 0^+(0^{++})$$

Needs confirmation.

$f_0(2020)$ T-MATRIX POLE \sqrt{s}

Note that $\Gamma = -2 \text{Im}(\sqrt{s})$.

VALUE (MeV)	DOCUMENT ID	TECN	COMMENT
(1870–2080) – i (120–240) OUR ESTIMATE			
(2038 ⁺⁴⁸ – i (156 ⁺⁴¹))	¹ RODAS	22	RVUE $J/\psi(1S) \rightarrow \gamma(\pi\pi, K\bar{K})$
(1925 ⁺²⁵ – i (160 ⁺¹⁸))	SARANTSEV	21	RVUE $J/\psi(1S) \rightarrow \gamma(\pi\pi, K\bar{K}, \eta\eta, \omega\phi)$
(1910 ⁺⁵⁰ – i (199 ⁺⁴⁰))	² ROPERTZ	18	RVUE $\bar{B}_s^0 \rightarrow J/\psi(\pi^+ \pi^- / K^+ K^-)$
(1992 ⁺¹⁶ – i (221 ⁺³⁰))	³ BARBERIS	00c	450 $pp \rightarrow p_f 4\pi p_S$
(2020 ⁺³⁵ – i (205 ⁺²⁵))	BARBERIS	97B	OMEG 450 $pp \rightarrow pp 2(\pi^+ \pi^-)$
¹ T-matrix pole from coupled channel K-matrix fit to data on $J/\psi \rightarrow \gamma \pi^0 \pi^0$ (ABLIKIM 15AE) and $J/\psi \rightarrow \gamma K_S^0 K_S^0$ (ABLIKIM 18AA).			
² T-matrix pole of a 3 channel unitary model fit to data from AAIJ 14BR and AAIJ 17V extracted using Pade approximants.			
³ Average between $\pi^+ \pi^- 2\pi^0$ and $2(\pi^+ \pi^-)$.			

$f_0(2020)$ MASS

VALUE (MeV)	EVTs	DOCUMENT ID	TECN	COMMENT
1982⁺³₋₅₀				
1982 ⁺³ ₋₅₀	¹ ABLIKIM	22c	BES3 $J/\psi \rightarrow \gamma \eta' \eta' \rightarrow 4/5 \gamma 2(\pi^+ \pi^-)$	
• • • We do not use the following data for averages, fits, limits, etc. • • •				
2010 ⁺⁶ ₋₄	² ABLIKIM	22As	BES3 $J/\psi(1S) \rightarrow \gamma \eta \eta'$	
2037 ⁺⁸	³ UMAN	06	E835 5.2 $\bar{p} p \rightarrow \eta \eta \pi^0$	
2040 ⁺³⁸	ANISOVICH	00I	SPEC	
2010 ⁺⁶⁰	ALDE	98	GAM4 100 $\pi^- p \rightarrow \pi^0 \pi^0 n$	

¹ From a partial wave analysis of the systems (γX) , with $X \rightarrow \eta' \eta'$, and $(\eta' X)$, with $X \rightarrow \gamma \eta'$ in the decay $J/\psi \rightarrow \gamma \eta' \eta'$. The intermediate resonance X is parametrized by a constant-width, relativistic Breit-Wigner.

² From a Breit-Wigner fit involving 9 resonances and a resonating exotic $\eta_1(1855) \rightarrow \eta \eta'$ P-wave.

³ Statistical error only.

$f_0(2020)$ WIDTH

VALUE (MeV)	EVTs	DOCUMENT ID	TECN	COMMENT
436⁺⁴₋₄₉				
436 ⁺⁴ ₋₄₉	¹ ABLIKIM	22c	BES3 $J/\psi \rightarrow \gamma \eta' \eta' \rightarrow 4/5 \gamma 2(\pi^+ \pi^-)$	

Meson Particle Listings

$f_0(2020)$, $f_4(2050)$

• • • We do not use the following data for averages, fits, limits, etc. • • •

203 ± 9 ⁺¹³ ₋₁₁	2	ABLIKIM	22As	BES3	$J/\psi(1S) \rightarrow \gamma\eta\eta'$
296 ± 17	80k	3	UMAN	06	E835 $5.2 \bar{p}p \rightarrow \eta\eta\pi^0$
405 ± 40			ANISOVICH	00J	SPEC
240 ± 100			ALDE	98	GAM4 $100 \pi^- p \rightarrow \pi^0 \pi^0 n$

¹ From a partial wave analysis of the systems (γX), with $X \rightarrow \eta'\eta'$, and ($\eta' X$), with $X \rightarrow \gamma\eta'$ in the decay $J/\psi \rightarrow \gamma\eta'\eta'$. The intermediate resonance X is parametrized by a constant-width, relativistic Breit-Wigner.

² From a Breit-Wigner fit involving 9 resonances and a resonating exotic $\eta_1(1855) \rightarrow \eta\eta'$ P-wave.

³ Statistical error only.

$f_0(2020)$ DECAY MODES

Mode	Fraction (Γ_i/Γ)
Γ_1 $\rho\pi\pi$	seen
Γ_2 $\pi^0\pi^0$	seen
Γ_3 $\rho\rho$	seen
Γ_4 $\omega\omega$	seen
Γ_5 $\eta\eta$	seen
Γ_6 $\eta'\eta'$	seen

$f_0(2020)$ BRANCHING RATIOS

$\Gamma(\rho\rho)/\Gamma(\omega\omega)$	DOCUMENT ID	COMMENT	Γ_3/Γ_4
~ 3	BARBERIS	00F $450 \bar{p}p \rightarrow \rho_f \omega \rho_S$	

• • • We do not use the following data for averages, fits, limits, etc. • • •

$\Gamma(\eta\eta)/\Gamma_{total}$	DOCUMENT ID	TECN	COMMENT	Γ_5/Γ
seen	UMAN	06	E835 $5.2 \bar{p}p \rightarrow \eta\eta\pi^0$	

$\Gamma(\eta'\eta')/\Gamma_{total}$	DOCUMENT ID	TECN	COMMENT	Γ_6/Γ
seen	¹ ABLIKIM	22c	BES3 $J/\psi \rightarrow \gamma\eta'\eta' \rightarrow 4/5\gamma 2(\pi^+\pi^-)$	

¹ From a partial wave analysis of the systems (γX), with $X \rightarrow \eta'\eta'$, and ($\eta' X$), with $X \rightarrow \gamma\eta'$ in the decay $J/\psi \rightarrow \gamma\eta'\eta'$. The intermediate resonance X is parametrized by a constant-width, relativistic Breit-Wigner.

$f_0(2020)$ REFERENCES

ABLIKIM	22As	PR D106 072012	M. Ablikim et al.	(BESIII Collab.)
Also		PR D107 079901 (errata)	M. Ablikim et al.	(BESIII Collab.)
ABLIKIM	22C	PR D105 072002	M. Ablikim et al.	(BESIII Collab.)
RODAS	22	EPJ C82 80	A. Rodas et al.	(JPAK Collab.)
SARANTSEV	21	PL B816 136227	A.V. Sarantsev et al.	(BONN, PNPI)
ABLIKIM	18AA	PR D98 072003	M. Ablikim et al.	(BESIII Collab.)
ROPERTZ	18	EPJ C78 1000	S. Ropertz, C. Hanhart, B. Kubis	(BONN, JULI)
AAIJ	17V	JHEP 1708 037	R. Aaij et al.	(LHCb Collab.)
ABLIKIM	15AE	PR D92 052003	M. Ablikim et al.	(BESIII Collab.)
AAIJ	14BR	PR D89 092006	R. Aaij et al.	(LHCb Collab.)
UMAN	06	PR D73 052009	I. Uman et al.	(FNAL E835)
ANISOVICH	00J	PL B491 47	A.V. Anisovich et al.	(RAL, LOQM, PNPI+)
BARBERIS	00C	PL B471 440	D. Barberis et al.	(WA 102 Collab.)
BARBERIS	00F	PL B484 198	D. Barberis et al.	(WA 102 Collab.)
ALDE	98	EPJ A3 361	D. Alde et al.	(GAM4 Collab.)
Also		PAN 62 405	D. Alde et al.	(GAM4 Collab.)
Translated from		YAF 62 446		
BARBERIS	97B	PL B413 217	D. Barberis et al.	(WA 102 Collab.)

$f_4(2050)$

$$I^G(J^{PC}) = 0^+(4^{++})$$

$f_4(2050)$ MASS

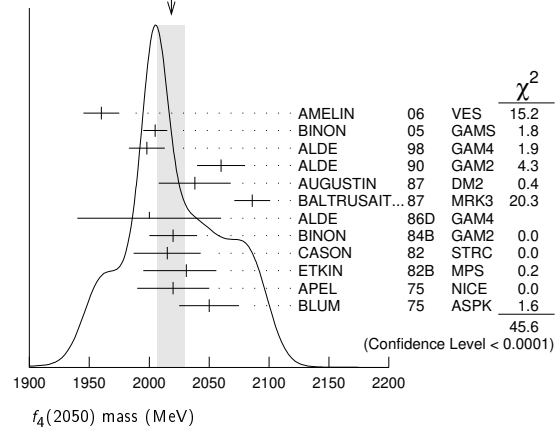
VALUE (MeV)	EVTS	DOCUMENT ID	TECN	COMMENT
2018 ± 11	OUR AVERAGE	Error includes scale factor of 2.1. See the ideogram below.		
1960 ± 15		AMELIN	06	VES $36 \pi^- p \rightarrow \omega\omega n$
2005 ± 10		¹ BINON	05	GAMS $33 \pi^- p \rightarrow \eta\eta n$
1998 ± 15		ALDE	98	GAM4 $100 \pi^- p \rightarrow \pi^0 \pi^0 n$
2060 ± 20		ALDE	90	GAM2 $38 \pi^- p \rightarrow \omega\omega n$
2038 ± 30		AUGUSTIN	87	DM2 $J/\psi \rightarrow \gamma\pi^+\pi^-$
2086 ± 15		BALTRUSAIT..	87	MRK3 $J/\psi \rightarrow \gamma\pi^+\pi^-$
2000 ± 60		ALDE	86D	GAM4 $100 \pi^- p \rightarrow n2\eta$
2020 ± 20	40k	² BINON	84B	GAM2 $38 \pi^- p \rightarrow n2\pi^0$
2015 ± 28		³ CASON	82	STRC $8 \pi^+ p \rightarrow \Delta^{++} \pi^0 \pi^0$
2031 ⁺²⁵ ₋₃₆		ETKIN	82B	MPS $23 \pi^- p \rightarrow n2K^0_S$
2020 ± 30	700	APEL	75	NICE $40 \pi^- p \rightarrow n2\pi^0$
2050 ± 25		BLUM	75	ASPK $18.4 \pi^- p \rightarrow nK^+ K^-$

• • • We do not use the following data for averages, fits, limits, etc. • • •

1966 ± 25	4	ANISOVICH	09	RVUE	0.0 $\bar{p}p, \pi N$
1885 ⁺¹⁴⁺²¹⁸ ₋₁₃₋₂₅	5	UEHARA	09	BELL	10.6 $e^+e^- \rightarrow e^+e^-\pi^0\pi^0$
2018 ± 6		ANISOVICH	00J	SPEC	2.0 $\bar{p}p \rightarrow \eta\pi^0\pi^0, \pi^0\pi^0,$ $\eta\eta, \eta\eta', \pi\pi$
~ 2000	6	MARTIN	98	RVUE	$N\bar{N} \rightarrow \pi\pi$
~ 2010	7	MARTIN	97	RVUE	$N\bar{N} \rightarrow \pi\pi$
~ 2040	8	OAKDEN	94	RVUE	0.36-1.55 $\bar{p}p \rightarrow \pi\pi$
~ 1990	9	OAKDEN	94	RVUE	0.36-1.55 $\bar{p}p \rightarrow \pi\pi$
1978 ± 5	10	ALPER	80	CNTR	62 $\pi^- p \rightarrow K^+ K^- n$
2040 ± 10	10	ROZANSKA	80	SPRK	18 $\pi^- p \rightarrow \rho\bar{p}n$
1935 ± 13	10	CORDEN	79	OMEG	12-15 $\pi^- p \rightarrow n2\pi$
1988 ± 7		EVANGELIS..	79B	OMEG	10 $\pi^- p \rightarrow K^+ K^- n$
1922 ± 14	11	ANTIPOV	77	CIBS	25 $\pi^- p \rightarrow \rho3\pi$

- From the first PWA solution.
- From a partial-wave analysis of the data.
- From an amplitude analysis of the reaction $\pi^+\pi^- \rightarrow 2\pi^0$.
- K matrix pole.
- Taking into account the $f_2(1950)$. Helicity-2 production favored.
- Energy-dependent analysis.
- Single energy analysis.
- From solution A of amplitude analysis of data on $\bar{p}p \rightarrow \pi\pi$. See however KLOET 96 who fit $\pi^+\pi^-$ only and find waves only up to $J = 3$ to be important but not significantly resonant.
- From solution B of amplitude analysis of data on $\bar{p}p \rightarrow \pi\pi$. See however KLOET 96 who fit $\pi^+\pi^-$ only and find waves only up to $J = 3$ to be important but not significantly resonant.
- $I(J^{PC}) = 0(4^+)$ from amplitude analysis assuming one-pion exchange.
- Width errors enlarged by us to $4\Gamma/\sqrt{N}$; see the note with the $K^*(892)$ mass.

WEIGHTED AVERAGE
2018 ± 11 (Error scaled by 2.1)



$f_4(2050)$ WIDTH

VALUE (MeV)	EVTS	DOCUMENT ID	TECN	COMMENT
237 ± 18	OUR AVERAGE	Error includes scale factor of 1.9. See the ideogram below.		
290 ± 20		AMELIN	06	VES $36 \pi^- p \rightarrow \omega\omega n$
340 ± 80		¹² BINON	05	GAMS $33 \pi^- p \rightarrow \eta\eta n$
395 ± 40		ALDE	98	GAM4 $100 \pi^- p \rightarrow \pi^0 \pi^0 n$
170 ± 60		ALDE	90	GAM2 $38 \pi^- p \rightarrow \omega\omega n$
304 ± 60		AUGUSTIN	87	DM2 $J/\psi \rightarrow \gamma\pi^+\pi^-$
210 ± 63		BALTRUSAIT..	87	MRK3 $J/\psi \rightarrow \gamma\pi^+\pi^-$
400 ± 100		ALDE	86D	GAM4 $100 \pi^- p \rightarrow n2\eta$
240 ± 40	40k	¹³ BINON	84B	GAM2 $38 \pi^- p \rightarrow n2\pi^0$
190 ± 14		DENNEY	83	LASS $10 \pi^+ n/\pi^+ p$
186 ⁺¹⁰³ ₋₅₈		¹⁴ CASON	82	STRC $8 \pi^+ p \rightarrow \Delta^{++} \pi^0 \pi^0$
305 ⁺³⁶ ₋₁₁₉		ETKIN	82B	MPS $23 \pi^- p \rightarrow n2K^0_S$
180 ± 60	700	APEL	75	NICE $40 \pi^- p \rightarrow n2\pi^0$
225 ⁺¹²⁰ ₋₇₀		BLUM	75	ASPK $18.4 \pi^- p \rightarrow nK^+ K^-$

• • • We do not use the following data for averages, fits, limits, etc. • • •

260 ± 40	15	ANISOVICH	09	RVUE	0.0 $\bar{p}p, \pi N$
453 ± 20 ⁺³¹ ₋₁₂₉	16	UEHARA	09	BELL	10.6 $e^+e^- \rightarrow e^+e^-\pi^0\pi^0$
182 ± 7		ANISOVICH	00J	SPEC	2.0 $\bar{p}p \rightarrow \eta\pi^0\pi^0, \pi^0\pi^0,$ $\eta\eta, \eta\eta', \pi\pi$
~ 170	17	MARTIN	98	RVUE	$N\bar{N} \rightarrow \pi\pi$
~ 200	18	MARTIN	97	RVUE	$N\bar{N} \rightarrow \pi\pi$
~ 60	19	OAKDEN	94	RVUE	0.36-1.55 $\bar{p}p \rightarrow \pi\pi$

See key on page 1171

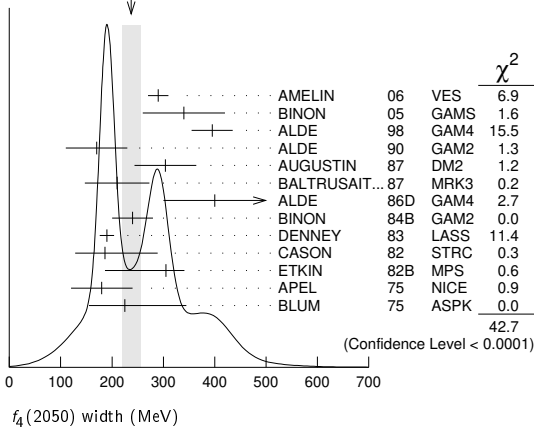
Meson Particle Listings

$f_4(2050), \pi_2(2100)$

~ 80	20 OAKDEN	94 RVUE	0.36-1.55	$\bar{p}p \rightarrow \pi\pi$
243 ± 16	21 ALPER	80 CNTR	62	$\pi^- p \rightarrow K^+ K^- n$
140 ± 15	21 ROZANSKA	80 SPRK	18	$\pi^- p \rightarrow p \bar{p} n$
263 ± 57	21 CORDEN	79 OMEG	12-15	$\pi^- p \rightarrow n 2\pi$
100 ± 28	EVANGELIS...	79B OMEG	10	$\pi^- p \rightarrow K^+ K^- n$
107 ± 56	22 ANTIPOV	77 CIBS	25	$\pi^- p \rightarrow p 3\pi$

- 12 From the first PWA solution.
 13 From a partial-wave analysis of the data.
 14 From an amplitude analysis of the reaction $\pi^+ \pi^- \rightarrow 2\pi^0$.
 15 K matrix pole.
 16 Taking into account the $f_2(1950)$. Helicity-2 production favored.
 17 Energy-dependent analysis.
 18 Single energy analysis.
 19 From solution A of amplitude analysis of data on $\bar{p}p \rightarrow \pi\pi$. See however KLOET 96 who fit $\pi^+ \pi^-$ only and find waves only up to $J = 3$ to be important but not significantly resonant.
 20 From solution B of amplitude analysis of data on $\bar{p}p \rightarrow \pi\pi$. See however KLOET 96 who fit $\pi^+ \pi^-$ only and find waves only up to $J = 3$ to be important but not significantly resonant.
 21 $J(J^P) = 0(4^+)$ from amplitude analysis assuming one-pion exchange.
 22 Width errors enlarged by us to $4\Gamma/\sqrt{N}$; see the note with the $K^*(892)$ mass.

WEIGHTED AVERAGE
237±18 (Error scaled by 1.9)



$f_4(2050)$ DECAY MODES

Mode	Fraction (Γ_i/Γ)
Γ_1 $\omega\omega$	seen
Γ_2 $\pi\pi$	(17.0 ± 1.5) %
Γ_3 $K\bar{K}$	(6.8 ^{+3.4} _{-1.8}) × 10 ⁻³
Γ_4 $\eta\eta$	(2.1 ± 0.8) × 10 ⁻³
Γ_5 $4\pi^0$	< 1.2 %
Γ_6 $\gamma\gamma$	seen
Γ_7 $a_2(1320)\pi$	seen

$f_4(2050)$ $\Gamma(i)\Gamma(\gamma\gamma)/\Gamma(\text{total})$

VALUE (keV)	CL%	DOCUMENT ID	TECN	COMMENT	$\Gamma_3\Gamma_6/\Gamma$
-------------	-----	-------------	------	---------	---------------------------

• • • We do not use the following data for averages, fits, limits, etc. • • •
 <0.29 95 ALTHOFF 85B TASS $\gamma\gamma \rightarrow K\bar{K}\pi$

VALUE (eV)	CL%	EVTS	DOCUMENT ID	TECN	COMMENT	$\Gamma_2\Gamma_6/\Gamma$
------------	-----	------	-------------	------	---------	---------------------------

• • • We do not use the following data for averages, fits, limits, etc. • • •
 23.1^{+3.6+70.5}_{-3.3-15.6} 23 UEHARA 09 BELL 10.6 $e^+e^- \rightarrow e^+e^-\pi^0\pi^0$
 <1100 95 13 ± 4 OEST 90 JADE $e^+e^- \rightarrow e^+e^-\pi^0\pi^0$

23 Taking into account the $f_2(1950)$. Helicity-2 production favored.

$f_4(2050)$ BRANCHING RATIOS

$\Gamma(\omega\omega)/\Gamma_{\text{total}}$	VALUE	DOCUMENT ID	TECN	COMMENT	Γ_1/Γ
--	-------	-------------	------	---------	-------------------

seen AMELIN 06 VES 36 $\pi^- p \rightarrow \omega\omega n$
 • • • We do not use the following data for averages, fits, limits, etc. • • •
 not seen BARBERIS 00F 450 $pp \rightarrow p f \omega p \pi_S$

$\Gamma(\omega\omega)/\Gamma(\pi\pi)$	VALUE	DOCUMENT ID	TECN	COMMENT	Γ_1/Γ_2
---------------------------------------	-------	-------------	------	---------	---------------------

1.5 ± 0.3 ALDE 90 GAM2 38 $\pi^- p \rightarrow \omega\omega n$

$\Gamma(\pi\pi)/\Gamma_{\text{total}}$	VALUE	DOCUMENT ID	TECN	COMMENT	Γ_2/Γ
--	-------	-------------	------	---------	-------------------

0.170 ± 0.015 OUR AVERAGE
 0.18 ± 0.03 24 BINON 83C GAM2 38 $\pi^- p \rightarrow n 4\gamma$
 0.16 ± 0.03 24 CASON 82 STRC 8 $\pi^+ p \rightarrow \Delta^{++} \pi^0 \pi^0$
 0.17 ± 0.02 24 CORDEN 79 OMEG 12-15 $\pi^- p \rightarrow n 2\pi$
 24 Assuming one pion exchange.

$\Gamma(K\bar{K})/\Gamma(\pi\pi)$	VALUE	DOCUMENT ID	TECN	COMMENT	Γ_3/Γ_2
-----------------------------------	-------	-------------	------	---------	---------------------

0.04^{+0.02}_{-0.01} ETKIN 82B MPS 23 $\pi^- p \rightarrow n 2K_S^0$

$\Gamma(\eta\eta)/\Gamma_{\text{total}}$	VALUE (units 10 ⁻³)	DOCUMENT ID	TECN	COMMENT	Γ_4/Γ
--	---------------------------------	-------------	------	---------	-------------------

2.1 ± 0.8 ALDE 86D GAM4 100 $\pi^- p \rightarrow n 4\gamma$

$\Gamma(4\pi^0)/\Gamma_{\text{total}}$	VALUE	DOCUMENT ID	TECN	COMMENT	Γ_5/Γ
--	-------	-------------	------	---------	-------------------

<0.012 ALDE 87 GAM4 100 $\pi^- p \rightarrow 4\pi^0 n$

$\Gamma(a_2(1320)\pi)/\Gamma_{\text{total}}$	VALUE	DOCUMENT ID	TECN	COMMENT	Γ_7/Γ
--	-------	-------------	------	---------	-------------------

seen AMELIN 00 VES 37 $\pi^- p \rightarrow \eta\pi^+\pi^- n$

$f_4(2050)$ REFERENCES

ANISOVICH 09	IJMP A24 2481	V.V. Anisovich, A.V. Sarantsev	(PNPI)
UEHARA 09	PR D79 052009	S. Uehara et al.	(BELLE Collab.)
AMELIN 06	PAN 69 590	D.V. Amelin et al.	(VES Collab.)
Translated from YAF 69 715.			
BINON 05	PAN 68 960	F. Binon et al.	
Translated from YAF 68 998.			
AMELIN 00J	NP A668 83	D. Amelin et al.	(VES Collab.)
ANISOVICH 00J	PL B491 47	A.V. Anisovich et al.	(RAL, LOQM, PNPI+)
BARBERIS 00F	PL B484 198	D. Barberis et al.	(WA 102 Collab.)
ALDE 90	EPL A3 361	D. Alde et al.	(GAM4 Collab.)
Also translated from YAF 62 446.			
MARTIN 98	PR C57 3492	B.R. Martin et al.	
MARTIN 97	PR C56 1114	B.R. Martin, G.C. Oades	(LOUC, AARH)
KLOET 96	PR D53 6120	W.M. Kloet, F. Myhrer	(RUTG, NORD)
OAKDEN 94	NP A574 731	M.N. Oakden, M.R. Pennington	(DURH)
ALDE 90	PL B241 600	D.M. Alde et al.	(SERP, BELG, LANL, LAPP+)
OEST 90	ZPHY C47 343	T. Oest et al.	(JADE Collab.)
ALDE 87	PL B198 286	D.M. Alde et al.	(LANL, BRUX, SERP, LAPP)
AUGUSTIN 87	ZPHY C36 369	J.E. Augustin et al.	(LANL, CLER, FRAS+)
BALTRUSAITIS... 87	PR D35 2077	R.M. Baltrusaitis et al.	(Mark III Collab.)
ALDE 86D	NP B269 485	D.M. Alde et al.	(BELG, LAPP, SERP, CERN+)
ALTHOFF 85B	ZPHY C29 189	M. Althoff et al.	(TASSO Collab.)
BINON 84B	LNC 39 41	F.G. Binon et al.	(SERP, BELG, LAPP)
BINON 83C	SJNP 38 723	F.G. Binon et al.	(SERP, BRUX+)
Translated from YAF 38 1199.			
DENNEY 83	PR D28 2726	D.L. Denney et al.	(IOWA, MICH)
CASON 82	PRL 48 1316	N.M. Cason et al.	(NDAM, ANL)
ETKIN 82B	PR D25 1786	A. Etkin et al.	(BNL, CUNY, TUFTS, VAND)
ALPER 80	PL 94B 422	B. Alper et al.	(AMST, CERN, CRAC, MPIM+)
ROZANSKA 80	NP B162 505	M. Rozanska et al.	(MPIM, CERN)
CORDEN 79	NP B157 250	M.J. Corden et al.	(BIRM, RHEL, TEA+JP)
EVANGELIS... 79B	NP B154 381	C. Evangelista et al.	(BARI, BONN, CERN+)
ANTIPOV 77	NP B119 45	Y.M. Antipov et al.	(SERP, GEVA)
APEL 75	PL 57B 398	W.D. Apel et al.	(KARLK, KARLE, PISA, SERP+JP)
BLUM 75	PL 57B 403	W. Blum et al.	(CERN, MPIM)JP

$\pi_2(2100)$

$$I^G(J^{PC}) = 1^-(2^-+)$$

OMITTED FROM SUMMARY TABLE
 Needs confirmation.

$\pi_2(2100)$ MASS

VALUE (MeV)	DOCUMENT ID	TECN	COMMENT
-------------	-------------	------	---------

2090 ± 29 OUR AVERAGE
 2090 ± 30 1 AMELIN 95B VES 36 $\pi^- A \rightarrow \pi^+ \pi^- \pi^- A$
 2100 ± 150 2 DAUM 81B CNTR 63,94 $\pi^- p \rightarrow 3\pi X$
 1 From a fit to $J^{PC} = 2^-+ f_2(1270)\pi, (\pi\pi)_S\pi$ waves.
 2 From a two-resonance fit to four 2^-0^+ waves.

$\pi_2(2100)$ WIDTH

VALUE (MeV)	DOCUMENT ID	TECN	COMMENT
-------------	-------------	------	---------

620 ± 50 OUR AVERAGE Error includes scale factor of 1.2.
 520 ± 100 3 AMELIN 95B VES 36 $\pi^- A \rightarrow \pi^+ \pi^- \pi^- A$
 651 ± 50 4 DAUM 81B CNTR 63,94 $\pi^- p \rightarrow 3\pi X$
 3 From a fit to $J^{PC} = 2^-+ f_2(1270)\pi, (\pi\pi)_S\pi$ waves.
 4 From a two-resonance fit to four 2^-0^+ waves.

Meson Particle Listings

 $\pi_2(2100)$, $f_0(2100)$, $f_2(2150)$ $\pi_2(2100)$ DECAY MODES

Mode	Fraction (Γ_i/Γ)
Γ_1 3π	seen
Γ_2 $\rho\pi$	seen
Γ_3 $f_2(1270)\pi$	seen
Γ_4 $(\pi\pi)_S\pi$	seen

 $\pi_2(2100)$ BRANCHING RATIOS

$\Gamma(\rho\pi)/\Gamma(3\pi)$	Γ_2/Γ_1		
VALUE	DOCUMENT ID	TECN	COMMENT
0.19 ± 0.05	⁵ DAUM	81B	CNTR 63,94 $\pi^- \rho$
$\Gamma(f_2(1270)\pi)/\Gamma(3\pi)$	Γ_3/Γ_1		
VALUE	DOCUMENT ID	TECN	COMMENT
0.36 ± 0.09	⁵ DAUM	81B	CNTR 63,94 $\pi^- \rho$
$\Gamma((\pi\pi)_S\pi)/\Gamma(3\pi)$	Γ_4/Γ_1		
VALUE	DOCUMENT ID	TECN	COMMENT
0.45 ± 0.07	⁵ DAUM	81B	CNTR 63,94 $\pi^- \rho$
D-wave/S-wave RATIO FOR $\pi_2(2100) \rightarrow f_2(1270)\pi$			
VALUE	DOCUMENT ID	TECN	COMMENT
0.39 ± 0.23	⁵ DAUM	81B	CNTR 63,94 $\pi^- \rho$

⁵ From a two-resonance fit to four 2^-0^+ waves.

 $\pi_2(2100)$ REFERENCES

AMELIN	95B	PL B356 595	D.V. Amelin <i>et al.</i>	(SERP; TBIL)
DAUM	81B	NP B182 269	C. Daum <i>et al.</i>	(AMST, CERN, CRAC, MPIM+)

 $f_0(2100)$

$$I^G(J^{PC}) = 0^+(0^{++})$$

OMITTED FROM SUMMARY TABLE
Needs confirmation.

 $f_0(2100)$ MASS

VALUE (MeV)	EVTS	DOCUMENT ID	TECN	COMMENT
2095^{+17}_{-19} OUR AVERAGE				
$2116 \pm 27 \pm 17$		LEES	21A	BABR $\gamma\gamma \rightarrow \eta_c(1S) \rightarrow \eta' \pi^+ \pi^-$
$2081 \pm 13^{+24}_{-36}$	5.5k	¹ ABLIKIM	13N	BES3 $e^+e^- \rightarrow J/\psi \rightarrow \gamma \eta \eta$
2090 ± 30		BAI	00A	BES $J/\psi \rightarrow \gamma(\pi^+ \pi^- \pi^+ \pi^-)$
• • • We do not use the following data for averages, fits, limits, etc. • • •				
2075 ± 20		SARANTSEV	21	RVUE $J/\psi(1S) \rightarrow \gamma(\pi\pi, K\bar{K}, \eta\eta, \omega\phi)$
$2090 \pm 10 \pm 6$	529	^{2,3} DOBBS	15	$J/\psi \rightarrow \gamma \pi^+ \pi^-$
$2099 \pm 17 \pm 8$	283	^{2,3} DOBBS	15	$\psi(2S) \rightarrow \gamma \pi^+ \pi^-$
2105 ± 8	80k	⁴ UMAN	06	E835 $5.2 \bar{p}p \rightarrow \eta \eta \pi^0$
2102 ± 13		⁵ ANISOVICH	00J	SPEC $2.0 \bar{p}p \rightarrow \eta \pi^0 \pi^0, \pi^0 \pi^0, \eta \eta, \eta \eta', \pi^+ \pi^-$
2105 ± 10		ANISOVICH	99K	SPEC $0.6-1.94 \bar{p}p \rightarrow \eta \eta, \eta \eta'$
~ 2104		BUGG	95	$J/\psi \rightarrow \gamma \pi^+ \pi^- \pi^+ \pi^-$
~ 2122		HASAN	94	RVUE $\bar{p}p \rightarrow \pi \pi$

¹ From partial wave analysis including all possible combinations of 0^{++} , 2^{++} , and 4^{++} resonances.
² Using CLEO-c data but not authored by the CLEO Collaboration.
³ From a fit to a Breit-Wigner line shape with fixed $\Gamma = 209$ MeV.
⁴ Statistical error only.
⁵ Includes the data of ANISOVICH 00B indicating to exotic decay pattern.

 $f_0(2100)$ WIDTH

VALUE (MeV)	EVTS	DOCUMENT ID	TECN	COMMENT
287^{+32}_{-24} OUR AVERAGE				
$289 \pm 34 \pm 15$		LEES	21A	BABR $\gamma\gamma \rightarrow \eta_c(1S) \rightarrow \eta' \pi^+ \pi^-$
273^{+27+70}_{-24-23}	5.5k	¹ ABLIKIM	13N	BES3 $e^+e^- \rightarrow J/\psi \rightarrow \gamma \eta \eta$
330 ± 100		BAI	00A	BES $J/\psi \rightarrow \gamma(\pi^+ \pi^- \pi^+ \pi^-)$
• • • We do not use the following data for averages, fits, limits, etc. • • •				
260 ± 25		SARANTSEV	21	RVUE $J/\psi(1S) \rightarrow \gamma(\pi\pi, K\bar{K}, \eta\eta, \omega\phi)$
236 ± 14	80k	² UMAN	06	E835 $5.2 \bar{p}p \rightarrow \eta \eta \pi^0$
211 ± 29		³ ANISOVICH	00J	SPEC $2.0 \bar{p}p \rightarrow \eta \pi^0 \pi^0, \pi^0 \pi^0, \eta \eta, \eta \eta', \pi^+ \pi^-$
200 ± 25		ANISOVICH	99K	SPEC $0.6-1.94 \bar{p}p \rightarrow \eta \eta, \eta \eta'$
~ 203		BUGG	95	$J/\psi \rightarrow \gamma \pi^+ \pi^- \pi^+ \pi^-$
~ 273		HASAN	94	RVUE $\bar{p}p \rightarrow \pi \pi$

¹ From partial wave analysis including all possible combinations of 0^{++} , 2^{++} , and 4^{++} resonances.
² Statistical error only.
³ Includes the data of ANISOVICH 00B indicating to exotic decay pattern.

 $f_0(2100)$ REFERENCES

LEES	21A	PR D104 072002	J.P. Lees <i>et al.</i>	(BABAR Collab.)
SARANTSEV	21	PL B616 136227	A.V. Sarantsev <i>et al.</i>	(BONN, FNPI)
DOBBS	15	PR D91 052006	S. Dobbs <i>et al.</i>	(NWES)
ABLIKIM	13N	PR D87 092009	M. Ablikim <i>et al.</i>	(BESIII Collab.)
UMAN	06	PR D73 052009	I. Uman <i>et al.</i>	(FNAL E835)
ANISOVICH	00B	NP A662 319	A.V. Anisovich <i>et al.</i>	
ANISOVICH	00J	PL B491 47	A.V. Anisovich <i>et al.</i>	(RAL, LOQM, PNPI+)
BAI	00A	PL B472 207	J.Z. Bai <i>et al.</i>	(BES Collab.)
ANISOVICH	99K	PL B468 309	A.V. Anisovich <i>et al.</i>	
BUGG	95	PL B353 378	D.V. Bugg <i>et al.</i>	(LOQM, PNPI, WASH)
HASAN	94	PL B334 215	A. Hasan, D.V. Bugg	(LOQM)

 $f_2(2150)$

$$I^G(J^{PC}) = 0^+(2^{++})$$

OMITTED FROM SUMMARY TABLE
This entry was previously called T_0 .

 $f_2(2150)$ MASS $f_2(2150)$ MASS, COMBINED MODES (MeV)

VALUE (MeV)	EVTS	DOCUMENT ID	TECN	COMMENT
2157 ± 12 OUR AVERAGE				Includes data from the datablock that follows this one.
• • • We do not use the following data for averages, fits, limits, etc. • • •				
2170 ± 6	80k	¹ UMAN	06	E835 $5.2 \bar{p}p \rightarrow \eta \eta \pi^0$

¹ Statistical error only.

 $\eta \eta$ MODE

VALUE (MeV)	DOCUMENT ID	TECN	COMMENT
The data in this block is included in the average printed for a previous datablock.			

 2157 ± 12 OUR AVERAGE

2151 ± 16	BARBERIS	00E	450 $pp \rightarrow p_f \eta \eta p_S$
2175 ± 20	PROKOSHKIN	95D	GAM4 $300 \pi^- N \rightarrow \pi^- N 2\eta, 450 pp \rightarrow pp 2\eta$
2130 ± 35	SINGOVSKI	94	GAM4 $450 pp \rightarrow pp 2\eta$
• • • We do not use the following data for averages, fits, limits, etc. • • •			
2140 ± 30	² ABELE	99B	CBAR $1.94 \bar{p}p \rightarrow \pi^0 \eta \eta$
2104 ± 20	³ ARMSTRONG	93C	E760 $\bar{p}p \rightarrow \pi^0 \eta \eta \rightarrow 6\gamma$

² Spin not determined.
³ No J^{PC} determination.

 $\eta \pi \pi$ MODE

VALUE (MeV)	DOCUMENT ID	TECN	CHG	COMMENT
• • • We do not use the following data for averages, fits, limits, etc. • • •				
$2135 \pm 20 \pm 45$	⁴ ADOMEIT	96	CBAR	0 $1.94 \bar{p}p \rightarrow \eta 3\pi^0$

⁴ ANISOVICH 00E recommends to withdraw ADOMEIT 96 that assumed a single $J^P = 2^+$ resonance.

 $\bar{p}p \rightarrow \pi \pi$

VALUE (MeV)	DOCUMENT ID	TECN	COMMENT
• • • We do not use the following data for averages, fits, limits, etc. • • •			
~ 2090	⁵ OAKDEN	94	RVUE $0.36-1.55 \bar{p}p \rightarrow \pi \pi$
~ 2120	⁶ OAKDEN	94	RVUE $0.36-1.55 \bar{p}p \rightarrow \pi \pi$
~ 2170	⁷ MARTIN	80B	RVUE
~ 2150	⁷ MARTIN	80C	RVUE
~ 2150	⁸ DULUDE	78B	OSPK $1-2 \bar{p}p \rightarrow \pi^0 \pi^0$

⁵ OAKDEN 94 makes an amplitude analysis of LEAR data on $\bar{p}p \rightarrow \pi \pi$ using a method based on Barrelet zeros. This is solution A. The amplitude analysis of HASAN 94 includes earlier data as well, and assume that the data can be parametrized in terms of towers of nearly degenerate resonances on the leading Regge trajectory. See also KLOET 96 and MARTIN 97 who make related analyses.
⁶ From solution B of amplitude analysis of data on $\bar{p}p \rightarrow \pi \pi$.
⁷ $I(J^P) = 0(2^+)$ from simultaneous analysis of $p\bar{p} \rightarrow \pi^- \pi^+ \pi^0$ and $\pi^0 \pi^0$.
⁸ $I^G(J^P) = 0^+(2^+)$ from partial-wave amplitude analysis.

S-CHANNEL $\bar{p}p, \bar{N}N$ or $K\bar{K}$

VALUE (MeV)	DOCUMENT ID	TECN	CHG	COMMENT
• • • We do not use the following data for averages, fits, limits, etc. • • •				
2139^{+8}_{-9}	⁹ EVANGELIS...	97	SPEC	$0.6-2.4 \bar{p}p \rightarrow K_S^0 K_S^0$
~ 2190	⁹ CUTTS	78B	CNTR	$0.97-3 \bar{p}p \rightarrow \bar{N}N$
2155 ± 15	^{9,10} COUPLAND	77	CNTR	0 $0.7-2.4 \bar{p}p \rightarrow \bar{p}p$
2193 ± 2	^{9,11} ALSPECTOR	73	CNTR	$\bar{p}p$ S channel

⁹ Isospins 0 and 1 not separated.
¹⁰ From a fit to the total elastic cross section.
¹¹ Referred to as T or T region by ALSPECTOR 73.

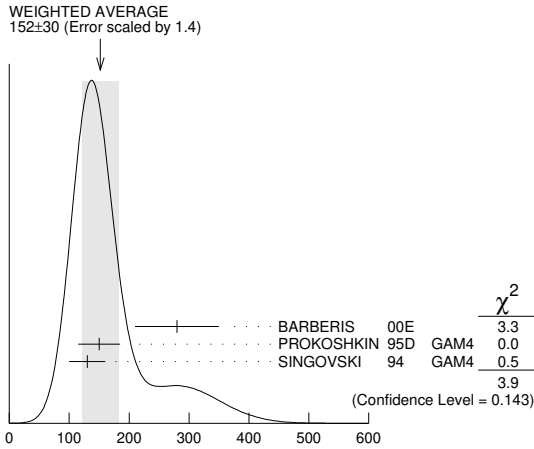
 $K\bar{K}$ MODE

VALUE (MeV)	DOCUMENT ID	TECN	COMMENT
• • • We do not use the following data for averages, fits, limits, etc. • • •			
2200 ± 13	VLADIMIRSK..	06	SPEC $40 \pi^- p \rightarrow K_S^0 K_S^0 n$
2150 ± 20	ABLIKIM	04E	BES2 $J/\psi \rightarrow \omega K^+ K^-$
2130 ± 35	BARBERIS	99	OMEG $450 pp \rightarrow p_S p_f K^+ K^-$

$f_2(2150)$ WIDTH

$f_2(2150)$ WIDTH, COMBINED MODES (MeV)

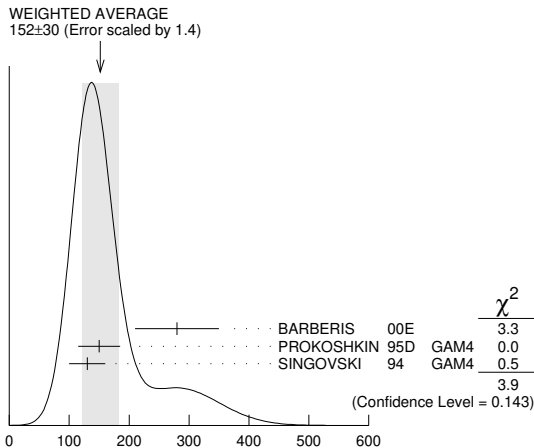
VALUE (MeV)	EVTS	DOCUMENT ID	TECN	COMMENT
152±30 OUR AVERAGE				Includes data from the datablock that follows this one. Error includes scale factor of 1.4. See the ideogram below.
• • •				We do not use the following data for averages, fits, limits, etc. • • •
182±11	80k	12 UMAN	06 E835	5.2 $\bar{p}p \rightarrow \eta\eta\pi^0$
12 Statistical error only.				



$f_2(2150)$ width, combined modes (MeV)

$\eta\eta$ MODE

VALUE (MeV)	DOCUMENT ID	TECN	COMMENT
The data in this block is included in the average printed for a previous datablock.			
152±30 OUR AVERAGE			Error includes scale factor of 1.4. See the ideogram below.
280±70	BARBERIS 00E		450 $pp \rightarrow p_f \eta \eta p_s$
150±35	PROKOSHKIN 95D	GAM4	300 $\pi^- N \rightarrow \pi^- N 2\eta$, 450 $pp \rightarrow pp 2\eta$
130±30	SINGOVSKI 94	GAM4	450 $pp \rightarrow pp 2\eta$
• • •			We do not use the following data for averages, fits, limits, etc. • • •
310±50	13 ABELE 99B	CBAR	1.94 $\bar{p}p \rightarrow \pi^0 \eta \eta$
203±10	14 ARMSTRONG 93C	E760	$\bar{p}p \rightarrow \pi^0 \eta \eta \rightarrow 6\gamma$
13 Spin not determined. 14 No J^PC determination.			



$f_2(2150)$ width, $\eta\eta$ mode (MeV)

$\eta\pi\pi$ MODE

VALUE (MeV)	DOCUMENT ID	TECN	CHG	COMMENT
• • •				We do not use the following data for averages, fits, limits, etc. • • •
250±25±45	15 ADOMEIT 96	CBAR	0	1.94 $\bar{p}p \rightarrow \eta 3\pi^0$
15 ANISOVICH 00E recommends to withdraw ADOMEIT 96 that assumed a single $J^P = 2^+$ resonance.				

$\bar{p}p \rightarrow \pi\pi$

VALUE (MeV)	DOCUMENT ID	TECN	COMMENT
250 OUR ESTIMATE			
• • •			We do not use the following data for averages, fits, limits, etc. • • •
~ 70	16 OAKDEN 94	RVUE	0.36-1.55 $\bar{p}p \rightarrow \pi\pi$
~ 250	17 MARTIN 80B	RVUE	
~ 250	17 MARTIN 80C	RVUE	
~ 250	18 DULUDE 78B	OSPK	1-2 $\bar{p}p \rightarrow \pi^0 \pi^0$
16 See however KLOET 96 who fit $\pi^+ \pi^-$ only and find waves only up to $J = 3$ to be important but not significantly resonant.			
17 $I(J^P) = 0(2^+)$ from simultaneous analysis of $\bar{p}p \rightarrow \pi^- \pi^+$ and $\pi^0 \pi^0$.			
18 $I^G(J^P) = 0^+(2^+)$ from partial-wave amplitude analysis.			

S-CHANNEL $\bar{p}p, \bar{N}N$ or $\bar{K}K$

VALUE (MeV)	DOCUMENT ID	TECN	CHG	COMMENT
• • •				We do not use the following data for averages, fits, limits, etc. • • •
56 ⁺³¹ ₋₁₆	19 EVANGELIS... 97	SPEC		0.6-2.4 $\bar{p}p \rightarrow K_S^0 K_S^0$
135±75	20,21 COUPLAND 77	CNTR	0	0.7-2.4 $\bar{p}p \rightarrow \bar{p}p$
98±8	21 ALSPECTOR 73	CNTR		$\bar{p}p$ S channel
19 Isospin 0 and 2 not separated.				
20 From a fit to the total elastic cross section.				
21 Isospins 0 and 1 not separated.				

$K\bar{K}$ MODE

VALUE (MeV)	DOCUMENT ID	TECN	COMMENT
• • •			We do not use the following data for averages, fits, limits, etc. • • •
91±62	VLADIMIRSK...06	SPEC	40 $\pi^- p \rightarrow K_S^0 K_S^0 n$
150±30	ABLIKIM 04E	BES2	$J/\psi \rightarrow \omega K^+ K^-$
270±50	BARBERIS 99	OMEG	450 $pp \rightarrow p_s p_f K^+ K^-$

$f_2(2150)$ DECAY MODES

Mode	Fraction (Γ_i/Γ)
Γ_1	$\pi\pi$
Γ_2	$\eta\eta$
Γ_3	$K\bar{K}$
Γ_4	$f_2(1270)\eta$
Γ_5	$a_2(1320)\pi$
Γ_6	$p\bar{p}$

$f_2(2150)$ BRANCHING RATIOS

VALUE	CL%	DOCUMENT ID	TECN	COMMENT	Γ_3/Γ_2
1.28±0.23		BARBERIS 00E		450 $pp \rightarrow p_f \eta \eta p_s$	
• • •				We do not use the following data for averages, fits, limits, etc. • • •	
<0.1	95	22 PROKOSHKIN 95D	GAM4	300 $\pi^- N \rightarrow \pi^- N 2\eta$, 450 $pp \rightarrow pp 2\eta$	
22 Using data from ARMSTRONG 89D.					
VALUE	CL%	DOCUMENT ID	TECN	COMMENT	Γ_1/Γ_2
<0.33	95	23 PROKOSHKIN 95D	GAM4	300 $\pi^- N \rightarrow \pi^- N 2\eta$, 450 $pp \rightarrow pp 2\eta$	
23 Derived from a $\pi^0 \pi^0 / \eta\eta$ limit.					
VALUE	DOCUMENT ID	TECN	COMMENT	Γ_4/Γ_5	
0.79±0.11	24 ADOMEIT 96	CBAR	1.94 $\bar{p}p \rightarrow \eta 3\pi^0$		
24 Using $B(a_2(1320) \rightarrow \eta\pi) = 0.145$					
VALUE	EVTS	DOCUMENT ID	TECN	COMMENT	Γ_6/Γ
seen	73	ALEXANDER 10	CLEO	$\psi(2S) \rightarrow \gamma p \bar{p}$	

$f_2(2150)$ REFERENCES

ALEXANDER 10	PR D82 092002	J.P. Alexander et al.	(CLEO Collab.)
UMAN 06	PR D73 052009	I. Uman et al.	(FNAL E835)
VLADIMIRSK...06	PAN 69 493	N.V. Vladimirov et al.	(ITEP, Moscow)
Translated from YAF 69 515.			
ABLIKIM 04E	PL B603 138	M. Ablikim et al.	(BES Collab.)
ANISOVICH 00E	PL B477 19	A.V. Anisovich et al.	
BARBERIS 00E	PL B479 59	D. Barberis et al.	(WA 102 Collab.)
ABELE 99B	EPJ C8 67	A. Abele et al.	(Crystal Barrel Collab.)
BARBERIS 99	PL B453 305	D. Barberis et al.	(Omega Expt.)
EVANGELIS... 97	PR D56 3803	C. Evangelista et al.	(LEAR Collab.)
MARTIN 97	PR C56 1114	B.R. Martin, G.C. Oades	(LOUC, AARRH)
ADOMEIT 96	ZPHY C71 227	J. Adomeit et al.	(Crystal Barrel Collab.)
KLOET 96	PR D53 6120	W.M. Kloet, F. Myhrer	(RUTG, NORD)
PROKOSHKIN 95D	PD 40 495	Y.D. Prokoshkin	(SERP)IGJPC
Translated from DANS 344 469.			

Meson Particle Listings

 $f_2(2150), \rho(2150)$

HASAN	94	PL B334 215	A. Hasan, D.V. Bugg	(LOQM)
OKADEN	94	NP A574 731	M.N. Oakden, M.R. Pennington	(DURH)
SINGOVSKI	94	NC A107 1911	A.V. Singovsky	(SERP)
ARMSTRONG	93C	PL B307 394	T.A. Armstrong <i>et al.</i>	(FNAL, FERR, GENO+)
ARMSTRONG	89D	PL B227 186	T.A. Armstrong, M. Benayoun	(ATHU, BARI, BIRM+)
MARTIN	80B	NP B176 355	B.R. Martin, D. Morgan	(LOUC, RHEL) JP
MARTIN	80C	NP B169 216	A.D. Martin, M.R. Pennington	(DURH) JP
CUTTS	78B	PR D17 16	D. Cutts <i>et al.</i>	(STON, WIS C)
DULUDE	78B	PL 79B 335	R.S. Dulude <i>et al.</i>	(BROW, MIT, BARI) JP
COUPLAND	77	PL 71B 460	M. Coupland <i>et al.</i>	(LOQM, RHEL)
ALSPECTOR	73	PRL 30 511	J. Alspector <i>et al.</i>	(RUTG, UPNJ)

 $\rho(2150)$

$$I^G(J^{PC}) = 1^+(1^{--})$$

OMITTED FROM SUMMARY TABLE

This entry was previously called $T_1(2190)$. See the review on "Spectroscopy of Light Meson Resonances." $\rho(2150)$ MASS e^+e^- PRODUCED

VALUE (MeV)	EVTS	DOCUMENT ID	TECN	COMMENT
••• We do not use the following data for averages, fits, limits, etc. •••				
2044 ± 31 ± 4		¹ ABLIKIM	23BQ BES3	$e^+e^- \rightarrow a_2(1320)^+ \pi^- +$ c.c. $\rightarrow \eta \pi^+ \pi^-$
2095 ± 4		² ACHASOV	23A SND	$e^+e^- \rightarrow \omega \pi^0$
2034 ± 13 ± 9		³ ABLIKIM	21A BES3	$e^+e^- \rightarrow \omega \pi^0$
2111 ± 43 ± 25		⁴ ABLIKIM	21X BES3	$e^+e^- \rightarrow \eta' \pi^+ \pi^-$
2255 +17 +50 -18 -41	1.8k	⁵ ABLIKIM	20F BES3	$\psi(2S) \rightarrow K^+ K^- \eta$
2201 ± 19		⁶ LEES	20 BABR	$e^+e^- \rightarrow K^+ K^- \gamma$
2227 ± 9 ± 9		⁷ LEES	20 RVUE	$e^+e^- \rightarrow K^+ K^-$
2039 ± 8 +36 -18		⁸ ABLIKIM	19AQ BES	$J/\psi \rightarrow K^+ K^- \pi^0$
2239.2 ± 7.1 ± 11.3		⁹ ABLIKIM	19L BES3	$e^+e^- \rightarrow K^+ K^-$
2254 ± 22		¹⁰ LEES	12G BABR	$e^+e^- \rightarrow \pi^+ \pi^- \gamma$
2150 ± 40 ± 50		AUBERT	07AU BABR	$10.6 e^+e^- \rightarrow$ $f_1(1285) \pi^+ \pi^- \gamma$
1990 ± 80		AUBERT	07AU BABR	$10.6 e^+e^- \rightarrow \eta' \pi^+ \pi^- \gamma$
2153 ± 37		BIAGINI	91 RVUE	$e^+e^- \rightarrow \pi^+ \pi^-, K^+ K^-$
2110 ± 50		¹¹ CLEGG	90 RVUE	$e^+e^- \rightarrow 3(\pi^+ \pi^-),$ $2(\pi^+ \pi^- \pi^0)$

¹ From a fit to the cross section between 2.00 and 3.08 GeV with a coherent sum of a Breit-Wigner resonance and a non-resonant contribution. Could be another state.² From a vector dominance fit to the Born cross section between 1.05 and 2.0 GeV with $\rho(770), \rho(1570), \rho(1700), \rho(2150)$. The fit also uses SND data from the VEPP-2M collider below 1.02 GeV and from LEES 17H and ABLIKIM 21A above 1.5 GeV.³ From a fit to the cross section between 2.00 and 3.08 GeV with a coherent sum of Breit-Wigner amplitudes, including contributions from $\rho(770), \rho(1450)$ and $\rho(1700)$. Could be another state.⁴ From a Breit-Wigner fit to the Born cross section, including an s -dependent continuum amplitude.⁵ Seen in $\psi(2S)$ decay with branching ratio $\psi(2S) \rightarrow X \eta \rightarrow K^+ K^- \eta = (21.7 \pm 1.9 + 7.7 - 8.3) \times 10^{-6}$.⁶ From the fit to the BABAR data of LEES 13Q assuming a coherent sum of a single Breit-Wigner resonance and a nonresonant contribution. The resonance significance is 3.5σ .⁷ From the fit to the BABAR data of LEES 13Q and BESIII data of ABLIKIM 19L assuming a coherent sum of a single Breit-Wigner resonance and a nonresonant contribution.⁸ Could also be another state. Seen in J/ψ decay with branching ratio $J/\psi \rightarrow X \pi^0 \rightarrow K^+ K^- \pi^0 = (6.7 \pm 1.1 + 2.2 - 1.8) \times 10^{-6}$.⁹ The observed structure can be due to both the $\phi(2170)$ and $\rho(2150)$.¹⁰ Using the GOUNARIS 68 parametrization of the pion form factor leaving the masses and widths of the $\rho(1450), \rho(1700)$, and $\rho(2150)$ resonances as free parameters of the fit.¹¹ Includes ATKINSON 85. $\bar{p}p \rightarrow \pi\pi$

VALUE (MeV)	DOCUMENT ID	TECN	COMMENT
••• We do not use the following data for averages, fits, limits, etc. •••			
~ 2191	HASAN	94 RVUE	$\bar{p}p \rightarrow \pi\pi$
~ 2070	¹ OAKDEN	94 RVUE	$0.36-1.55 \bar{p}p \rightarrow \pi\pi$
~ 2170	² MARTIN	80B RVUE	
~ 2100	² MARTIN	80C RVUE	

¹ See however KLOET 96 who fit $\pi^+ \pi^-$ only and find waves only up to $J = 3$ to be important but not significantly resonant.² $I(J^P) = 1(1^-)$ from simultaneous analysis of $p\bar{p} \rightarrow \pi^- \pi^+$ and $\pi^0 \pi^0$.S-CHANNEL $\bar{N}N$

VALUE (MeV)	DOCUMENT ID	TECN	COMMENT
••• We do not use the following data for averages, fits, limits, etc. •••			
2110 ± 35	¹ ANISOVICH	02 SPEC	$0.6-1.9 p\bar{p} \rightarrow \omega \pi^0, \omega \eta \pi^0, \pi^+ \pi^-$
~ 2190	² CUTTS	78B CNTR	$0.97-3 \bar{p}p \rightarrow \bar{N}N$
2155 ± 15	^{2,3} COUPLAND	77 CNTR	$0.7-2.4 \bar{p}p \rightarrow \bar{p}p$
2193 ± 2	^{2,4} ALSPECTOR	73 CNTR	$\bar{p}p$ S channel
2190 ± 10	⁵ ABRAMS	70 CNTR	S channel $\bar{p}N$

¹ From the combined analysis of ANISOVICH 00J, ANISOVICH 01D, ANISOVICH 01E, and ANISOVICH 02.² Isospins 0 and 1 not separated.³ From a fit to the total elastic cross section.⁴ Referred to as T or T' region by ALSPECTOR 73.⁵ Seen as bump in $l = 1$ state. See also COOPER 68. PEASLEE 75 confirm $\bar{p}p$ results of ABRAMS 70, no narrow structure. $\pi^- p \rightarrow \omega \pi^0 n$

VALUE (MeV)	DOCUMENT ID	TECN	COMMENT
••• We do not use the following data for averages, fits, limits, etc. •••			
2140 ± 30	ALDE	95 GAM2	$38 \pi^- p \rightarrow \omega \pi^0 n$
2170 ± 30	ALDE	92C GAM4	$100 \pi^- p \rightarrow \omega \pi^0 n$

 $\rho(2150)$ WIDTH e^+e^- PRODUCED

VALUE (MeV)	EVTS	DOCUMENT ID	TECN	COMMENT
••• We do not use the following data for averages, fits, limits, etc. •••				
163 ± 69 ± 24		¹ ABLIKIM	23BQ BES3	$e^+e^- \rightarrow a_2(1320)^+ \pi^- +$ c.c. $\rightarrow \eta \pi^+ \pi^-$
270 ± 3		² ACHASOV	23A SND	$e^+e^- \rightarrow \omega \pi^0$
234 ± 30 ± 25		³ ABLIKIM	21A BES3	$e^+e^- \rightarrow \omega \pi^0$
135 ± 34 ± 30		⁴ ABLIKIM	21X BES3	$e^+e^- \rightarrow \eta' \pi^+ \pi^-$
460 ± 54 +160 -48 -90	1.8k	⁵ ABLIKIM	20F BES3	$\psi(2S) \rightarrow K^+ K^- \eta$
70 ± 38		⁶ LEES	20 BABR	$e^+e^- \rightarrow K^+ K^- \gamma$
127 ± 14 ± 4		⁷ LEES	20 RVUE	$e^+e^- \rightarrow K^+ K^-$
196 ± 23 +25 -27		⁸ ABLIKIM	19AQ BES	$J/\psi \rightarrow K^+ K^- \pi^0$
139.8 ± 12.3 ± 20.6		⁹ ABLIKIM	19L BES3	$e^+e^- \rightarrow K^+ K^-$
109 ± 76		¹⁰ LEES	12G BABR	$e^+e^- \rightarrow \pi^+ \pi^- \gamma$
350 ± 40 ± 50		AUBERT	07AU BABR	$10.6 e^+e^- \rightarrow$ $f_1(1285) \pi^+ \pi^- \gamma$
310 ± 140		AUBERT	07AU BABR	$10.6 e^+e^- \rightarrow \eta' \pi^+ \pi^- \gamma$
389 ± 79		BIAGINI	91 RVUE	$e^+e^- \rightarrow \pi^+ \pi^-, K^+ K^-$
410 ± 100		¹¹ CLEGG	90 RVUE	$e^+e^- \rightarrow 3(\pi^+ \pi^-),$ $2(\pi^+ \pi^- \pi^0)$

¹ From a fit to the cross section between 2.00 and 3.08 GeV with a coherent sum of a Breit-Wigner resonance and a non-resonant contribution. Could be another state.² From a vector dominance fit to the Born cross section between 1.05 and 2.0 GeV with $\rho(770), \rho(1570), \rho(1700), \rho(2150)$. The fit also uses SND data from the VEPP-2M collider below 1.02 GeV and from LEES 17H and ABLIKIM 21A above 1.5 GeV.³ From a fit to the cross section between 2.00 and 3.08 GeV with a coherent sum of Breit-Wigner amplitudes, including contributions from $\rho(770), \rho(1450)$ and $\rho(1700)$. Could be another state.⁴ From a Breit-Wigner fit to the Born cross section, including an s -dependent continuum amplitude.⁵ Seen in $\psi(2S)$ decay with branching ratio $\psi(2S) \rightarrow X \eta \rightarrow K^+ K^- \eta = (21.7 \pm 1.9 + 7.7 - 8.3) \times 10^{-6}$.⁶ From the fit to the BABAR data of LEES 13Q assuming a coherent sum of a single Breit-Wigner resonance and a nonresonant contribution. The resonance significance is 3.5σ .⁷ From the fit to the BABAR data of LEES 13Q and BESIII data of ABLIKIM 19L assuming a coherent sum of a single Breit-Wigner resonance and a nonresonant contribution.⁸ Could also be another state. Seen in J/ψ decay with branching ratio $J/\psi \rightarrow X \pi^0 \rightarrow K^+ K^- \pi^0 = (6.7 \pm 1.1 + 2.2 - 1.8) \times 10^{-6}$.⁹ The observed structure can be due to both the $\phi(2170)$ and $\rho(2150)$.¹⁰ Using the GOUNARIS 68 parametrization of the pion form factor leaving the masses and widths of the $\rho(1450), \rho(1700)$, and $\rho(2150)$ resonances as free parameters of the fit.¹¹ Includes ATKINSON 85. $\bar{p}p \rightarrow \pi\pi$

VALUE (MeV)	DOCUMENT ID	TECN	COMMENT
••• We do not use the following data for averages, fits, limits, etc. •••			
~ 296	HASAN	94 RVUE	$\bar{p}p \rightarrow \pi\pi$
~ 40	¹ OAKDEN	94 RVUE	$0.36-1.55 \bar{p}p \rightarrow \pi\pi$
~ 250	² MARTIN	80B RVUE	
~ 200	² MARTIN	80C RVUE	

¹ See however KLOET 96 who fit $\pi^+ \pi^-$ only and find waves only up to $J = 3$ to be important but not significantly resonant.² $I(J^P) = 1(1^-)$ from simultaneous analysis of $p\bar{p} \rightarrow \pi^- \pi^+$ and $\pi^0 \pi^0$.S-CHANNEL $\bar{N}N$

VALUE (MeV)	DOCUMENT ID	TECN	COMMENT
••• We do not use the following data for averages, fits, limits, etc. •••			
230 ± 50	¹ ANISOVICH	02 SPEC	$0.6-1.9 p\bar{p} \rightarrow \omega \pi^0, \omega \eta \pi^0, \pi^+ \pi^-$
135 ± 75	^{2,3} COUPLAND	77 CNTR	$0.7-2.4 \bar{p}p \rightarrow \bar{p}p$
98 ± 8	³ ALSPECTOR	73 CNTR	$\bar{p}p$ S channel
~ 85	⁴ ABRAMS	70 CNTR	S channel $\bar{p}N$

¹ From the combined analysis of ANISOVICH 00J, ANISOVICH 01D, ANISOVICH 01E, and ANISOVICH 02.² From a fit to the total elastic cross section.³ Isospins 0 and 1 not separated.⁴ Seen as bump in $l = 1$ state. See also COOPER 68. PEASLEE 75 confirm $\bar{p}p$ results of ABRAMS 70, no narrow structure. $\pi^- p \rightarrow \omega \pi^0 n$

VALUE (MeV)	DOCUMENT ID	TECN	COMMENT
••• We do not use the following data for averages, fits, limits, etc. •••			
320 ± 70	ALDE	95 GAM2	$38 \pi^- p \rightarrow \omega \pi^0 n$
~ 300	ALDE	92C GAM4	$100 \pi^- p \rightarrow \omega \pi^0 n$

See key on page 1171

Meson Particle Listings

$\rho(2150), \phi(2170)$

$\rho(2150)$ DECAY MODES

Mode	Fraction (Γ_i/Γ)
Γ_1 e^+e^-	
Γ_2 $\pi^+\pi^-$	seen
Γ_3 K^+K^-	seen
Γ_4 $3(\pi^+\pi^-)$	seen
Γ_5 $2(\pi^+\pi^-\pi^0)$	seen
Γ_6 $\eta'\pi^+\pi^-$	seen
Γ_7 $f_1(1285)\pi^+\pi^-$	seen
Γ_8 $\omega\pi^0$	seen
Γ_9 $\omega\pi^0\eta$	seen
Γ_{10} $a_2(1320)\pi$	
Γ_{11} $\rho\bar{\rho}$	

$\rho(2150)$ $\Gamma(\eta'\pi^+\pi^-)/\Gamma(\text{total})$

VALUE (eV)	DOCUMENT ID	TECN	COMMENT	$\Gamma_6\Gamma_1/\Gamma$
------------	-------------	------	---------	---------------------------

••• We do not use the following data for averages, fits, limits, etc. •••
 $23.3 \pm 5.3 \pm 3.3$ ¹ ABLIKIM 21X BES3 $e^+e^- \rightarrow \eta'\pi^+\pi^-$
¹ From a Breit-Wigner fit to the Born cross section interfering constructively with the continuum. For destructive interference the value is $0.64 \pm 0.49 \pm 0.42$ eV.

VALUE (eV)	DOCUMENT ID	TECN	COMMENT	$\Gamma_8\Gamma_1/\Gamma$
------------	-------------	------	---------	---------------------------

••• We do not use the following data for averages, fits, limits, etc. •••
 $34 \pm 11 \pm 16$ ABLIKIM 21A BES3 $e^+e^- \rightarrow \omega\pi^0$

VALUE (eV)	DOCUMENT ID	TECN	COMMENT	$\Gamma_{10}\Gamma_1/\Gamma$
------------	-------------	------	---------	------------------------------

••• We do not use the following data for averages, fits, limits, etc. •••
 $34.6 \pm 17.1 \pm 6.0$ ¹ ABLIKIM 23BQ BES3 $e^+e^- \rightarrow a_2(1320)^+\pi^- + c.c. \rightarrow \eta\pi^+\pi^-$

¹ From a solution of the fit to the cross section between 2.00 and 3.08 GeV using a coherent sum of a single Breit-Wigner resonance and a non-resonant contribution. $B(a_2(1320) \rightarrow \eta\pi) \times B(\eta \rightarrow \gamma\gamma)$ fixed to 0.057. Another solution with equal fit quality gives $137.1 \pm 73.3 \pm 2.1$ eV.

$\rho(2150)$ $\Gamma(f_1(1285)\pi^+\pi^-)/\Gamma^2(\text{total})$

VALUE (units 10^{-7})	DOCUMENT ID	TECN	COMMENT	$\Gamma_7/\Gamma \times \Gamma_1/\Gamma$
--------------------------	-------------	------	---------	--

$3.1 \pm 0.6 \pm 0.5$ ¹ AUBERT 07AU BABR $10.6 e^+e^- \rightarrow f_1(1285)\pi^+\pi^-\gamma$
¹ Calculated by us from the reported value of cross section at the peak.

VALUE (units 10^{-8})	DOCUMENT ID	TECN	COMMENT	$\Gamma_6/\Gamma \times \Gamma_1/\Gamma$
--------------------------	-------------	------	---------	--

••• We do not use the following data for averages, fits, limits, etc. •••
 4.9 ± 1.9 ¹ AUBERT 07AU BABR $10.6 e^+e^- \rightarrow \eta'\pi^+\pi^-\gamma$
¹ Calculated by us from the reported value of cross section at the peak.

$\rho(2150)$ REFERENCES

ABLIKIM	23BQ	PR D108 L111101	M. Ablikim et al.	(BESIII Collab.)
ACHASOV	23A	PR D108 092012	M.N. Achasov et al.	(SND Collab.)
ABLIKIM	21A	PL B813 136059	M. Ablikim et al.	(BESIII Collab.)
ABLIKIM	21X	PR D103 072007	M. Ablikim et al.	(BESIII Collab.)
ABLIKIM	20F	PR D101 032008	M. Ablikim et al.	(BESIII Collab.)
LEES	20	PR D101 012011	J.P. Lees et al.	(BESIII Collab.)
ABLIKIM	19AQ	PR D100 032004	M. Ablikim et al.	(BESIII Collab.)
ABLIKIM	19L	PR D99 032001	M. Ablikim et al.	(BESIII Collab.)
LEES	17H	PR D96 092009	J.P. Lees et al.	(BABAR Collab.)
LEES	13Q	PR D88 032013	J.P. Lees et al.	(BABAR Collab.)
LEES	12G	PR D86 032013	J.P. Lees et al.	(BABAR Collab.)
AUBERT	07AU	PR D76 092005	B. Aubert et al.	(BABAR Collab.)
ANISOVICH	02	PL B542 8	A.V. Anisovich et al.	
ANISOVICH	01D	PL B508 6	A.V. Anisovich et al.	
ANISOVICH	01E	PL B513 281	A.V. Anisovich et al.	
ANISOVICH	00J	PL B491 47	A.V. Anisovich et al.	(RAL, LOQM, PNPI+)
KLOET	96	PR D53 6130	W.M. Kloet, F. Myhrer	(RUTG, NORD)
ALDE	95	ZPHY C66 379	D.M. Alde et al.	(GAMS Collab.) JP
HASAN	94	PL B334 215	A. Hasan, D.V. Bugg	(LOQM)
OAKDEN	94	NP A574 731	M.N. Oakden, M.R. Pennington	(DURH)
ALDE	92C	ZPHY C54 553	D.M. Alde et al.	(BELG, SERP, KEK, LANL+)
BIAGINI	91	NC 104A 363	F. Biagini et al.	(FRAS, PRAG)
CLEGG	90	ZPHY C45 677	A.B. Clegg, A. Donnachie	(LANC, MCHS)
ATKINSON	85	ZPHY C29 333	M. Atkinson et al.	(BONN, CER, GLAS+)
MARTIN	80B	NP B176 355	B.R. Martin, D. Morgan	(LOUCL, RHEL) JP
MARTIN	80C	NP B169 216	A.D. Martin, M.R. Pennington	(DURH) JP
CUTTS	78B	PR D17 16	D. Cutts et al.	(STON, WISC)
COUPLAND	77	PL 71B 460	M. Coupland et al.	(LOQM, RHEL)
PEASLEE	75	PL 57B 189	D.C. Peaslee et al.	(CANB, BARI, BROW+)
ALSPECTOR	73	PRL 30 511	J. Alspector et al.	(RUTG, UPJN)
ABRAMS	70	PR D1 1917	R.J. Abrams et al.	(BNL)
COOPER	68	PRL 20 1059	W.A. Cooper et al.	(ANL)
GOUNARIS	68	PRL 21 244	G.J. Gounaris, J.J. Sakurai	

$\phi(2170)$

$$J^G(J^{PC}) = 0^-(1^{--})$$

See the review on "Spectroscopy of Light Meson Resonances."

$\phi(2170)$ MASS

VALUE (MeV)	EVTS	DOCUMENT ID	TECN	COMMENT
2164 ± 6	OUR AVERAGE			
2178 ± 20 ± 5		¹ ABLIKIM 23AX BES3		$e^+e^- \rightarrow \phi\pi^+\pi^-$
2190 ± 19 ± 37		² ABLIKIM 22L BES3		$2.0-3.08 e^+e^- \rightarrow K^+K^-\pi^0$
2176 ± 24 ± 3		³ ABLIKIM 21A BES3		$e^+e^- \rightarrow \omega\eta$
2163.5 ± 6.2 ± 3.0		⁴ ABLIKIM 21T BES3		$e^+e^- \rightarrow \phi\eta$
2177.5 ± 4.8 ± 19.5		⁵ ABLIKIM 20M BES3		$e^+e^- \rightarrow \eta'\phi$
2126.5 ± 16.8 ± 12.4		⁶ ABLIKIM 20S BES3		$e^+e^- \rightarrow K^+K^-\pi^0\pi^0$
•••				We do not use the following data for averages, fits, limits, etc. •••
2215.7 ± 8.3		⁷ LICHARD 23 RVUE		$e^+e^- \rightarrow \Upsilon(nS) \rightarrow \phi\eta\gamma$
2169 ± 5 ± 6		⁸ ZHU 23A RVUE		$e^+e^- \rightarrow \eta\phi$
2273.7 ± 5.7 ± 19.3		⁹ ABLIKIM 21AP BES3		$e^+e^- \rightarrow K_S^0 K_L^0$
2135 ± 8 ± 9	95	ABLIKIM 19I BES3		$e^+e^- \rightarrow \eta\phi f_0(980)$
2239.2 ± 7.1 ± 11.3		¹⁰ ABLIKIM 19L BES3		$e^+e^- \rightarrow K^+K^-$
2200 ± 6 ± 5	471	ABLIKIM 15H BES3		$J/\psi \rightarrow \eta\phi\pi^+\pi^-$
2180 ± 8 ± 8	11,12	LEES 12F BABR		$10.6 e^+e^- \rightarrow \phi\pi^+\pi^-\gamma$
2079 ± 13 ± 79-28	4.8k	¹³ SHEN 09 BELL		$10.6 e^+e^- \rightarrow K^+K^-\pi^+\pi^-\gamma$
2186 ± 10 ± 6	52	ABLIKIM 08F BES		$J/\psi \rightarrow \eta\phi f_0(980)$
2125 ± 22 ± 10	483	AUBERT 08S BABR		$10.6 e^+e^- \rightarrow \phi\eta\gamma$
2192 ± 14	116	¹⁴ AUBERT 07AK BABR		$10.6 e^+e^- \rightarrow K^+K^-\pi^+\pi^-\gamma$
2169 ± 20	149	¹⁴ AUBERT 07AK BABR		$10.6 e^+e^- \rightarrow K^+K^-\pi^0\pi^0\gamma$
2175 ± 10 ± 15	201	^{12,15} AUBERT_BE 06D BABR		$10.6 e^+e^- \rightarrow K^+K^-\pi\pi\gamma$

- From a fit to the e^+e^- cross section between 2.00 and 3.08 GeV with a sum of Breit-Wigner amplitude and a non-resonant contribution.
- By a simultaneous fit of the $K_S^0(1430)+K^-$ and $K^*(892)+K^-$ intermediate channels in a partial-wave analysis, assuming the same structure, modelled with a coherent sum of a nonresonant component and a resonant component by a Breit-Wigner function.
- From a fit to the cross section between 2.00 and 3.08 GeV with a coherent sum of Breit-Wigner amplitudes, including contributions from $\omega(1420)$ and $\omega(1650)/\phi(1680)$.
- From a fit to the cross section below 3.5 GeV measured by BaBar and BESIII with a coherent sum of two modified Breit-Wigner amplitudes ($\phi(1680)$ and $\phi(2170)$) and a nonresonant term.
- From a fit using a coherent sum of a phase-space modified Breit-Wigner function and a phase-space term.
- By a simultaneous fit of the intermediate channels in a partial-wave analysis, assuming the same structure, modelled with a coherent sum of a nonresonant component and a resonant component by a Breit-Wigner function.
- From a VDM fit to ZHU 23 $\eta\phi\gamma$ data with two resonances, $\phi(1680)$, $\phi(2170)$, and a third resonance with mass 1850.7 ± 5.3 MeV and width 25 ± 35 MeV of 1.7 σ statistical evidence.
- From the analysis of the combined measurements of $\sigma(e^+e^- \rightarrow \eta\phi)$ from BaBar, Belle, BESIII, CMD3. The statistical significance for $\phi(2170)$ is 7.2 σ .
- From a fit to the cross section between 2.00 and 3.08 GeV with a sum of Breit-Wigner amplitude and a nonresonant contribution. The observed structure can be also due to $\rho(2150)$.
- The observed structure can be due to both the $\phi(2170)$ and $\rho(2150)$.
- Fit includes interference with the $\phi(1680)$.
- From the $\phi f_0(980)$ component.
- From a fit with two incoherent Breit-Wigners.
- From the $K^+K^-\pi^0$ component.
- Superseded by LEES 12F.

$\phi(2170)$ WIDTH

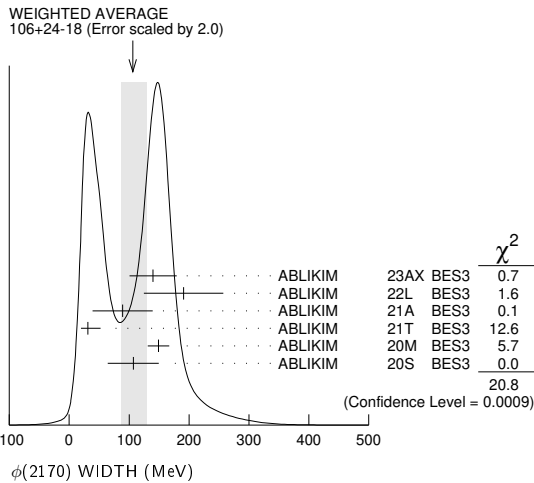
VALUE (MeV)	EVTS	DOCUMENT ID	TECN	COMMENT
106 +24-18	OUR AVERAGE			Error includes scale factor of 2.0. See the ideogram below.
140 ± 36 ± 16		¹ ABLIKIM 23AX BES3		$e^+e^- \rightarrow \phi\pi^+\pi^-$
191 ± 28 ± 60		² ABLIKIM 22L BES3		$2.0-3.08 e^+e^- \rightarrow K^+K^-\pi^0$
89 ± 50 ± 5		³ ABLIKIM 21A BES3		$e^+e^- \rightarrow \omega\eta$
31.1 +21.1-11.6 ± 1.1		⁴ ABLIKIM 21T BES3		$e^+e^- \rightarrow \phi\eta$
149.0 ± 15.6 ± 8.9		⁵ ABLIKIM 20S BES3		$e^+e^- \rightarrow \eta'\phi$
106.9 ± 32.1 ± 28.1		⁶ ABLIKIM 20M BES3		$e^+e^- \rightarrow K^+K^-\pi^0\pi^0$
•••				We do not use the following data for averages, fits, limits, etc. •••
35 ± 23		⁷ LICHARD 23 RVUE		$e^+e^- \rightarrow \Upsilon(nS) \rightarrow \phi\eta\gamma$
96 +17-14 ± 9		⁸ ZHU 23A RVUE		$e^+e^- \rightarrow \eta\phi$
86 ± 44 ± 51		⁹ ABLIKIM 21AP BES3		$e^+e^- \rightarrow K_S^0 K_L^0$
104 ± 24 ± 12	95	ABLIKIM 19I BES3		$e^+e^- \rightarrow \eta\phi f_0(980)$
139.8 ± 12.3 ± 20.6		¹⁰ ABLIKIM 19L BES3		$e^+e^- \rightarrow K^+K^-$
104 ± 15 ± 15	471	ABLIKIM 15H BES3		$J/\psi \rightarrow \eta\phi\pi^+\pi^-$
77 ± 15 ± 10	11,12	LEES 12F BABR		$10.6 e^+e^- \rightarrow \phi\pi^+\pi^-\gamma$

Meson Particle Listings

$\phi(2170)$

192	± 23	$^{+25}_{-61}$	4.8k	13	SHEN	09	BELL	$10.6 e^+ e^- \rightarrow K^+ K^- \pi^+ \pi^- \gamma$
65	± 23	± 17	52		ABLIKIM	08F	BES	$J/\psi \rightarrow \eta \phi f_0(980)$
61	± 50	± 13	483		AUBERT	08S	BABR	$10.6 e^+ e^- \rightarrow \phi \eta \gamma$
71	± 21		116	14	AUBERT	07AK	BABR	$10.6 e^+ e^- \rightarrow K^+ K^- \pi^+ \pi^- \gamma$
102	± 27		149	14	AUBERT	07AK	BABR	$10.6 e^+ e^- \rightarrow K^+ K^- \pi^0 \pi^0 \gamma$
58	± 16	± 20	201	12,15	AUBERT, BE	06D	BABR	$10.6 e^+ e^- \rightarrow K^+ K^- \pi \pi \gamma$

- 1 From a fit to the $e^+ e^-$ cross section between 2.00 and 3.08 GeV with a sum of Breit-Wigner amplitude and a non-resonant contribution.
- 2 By a simultaneous fit of the $K_S^0(1430) + K^-$ and $K^*(892) + K^-$ intermediate channels in a partial-wave analysis, assuming the same structure, modelled with a coherent sum of a nonresonant component and a resonant component by a Breit-Wigner function.
- 3 From a fit to the cross section between 2.00 and 3.08 GeV with a coherent sum of Breit-Wigner amplitudes, including contributions from $\omega(1420)$ and $\omega(1650)/\phi(1680)$.
- 4 From a fit to the cross section below 3.5 GeV measured by BaBar and BESIII with a coherent sum of two modified Breit-Wigner amplitudes ($\phi(1680)$ and $\phi(2170)$) and a nonresonant term.
- 5 From a fit using a coherent sum of a phase-space modified Breit-Wigner function and a phase-space term.
- 6 By a simultaneous fit of the intermediate channels in a partial-wave analysis, assuming the same structure, modelled with a coherent sum of a nonresonant component and a resonant component by a Breit-Wigner function.
- 7 From a VDM fit to ZHU 23 $\eta \phi \gamma$ data with two resonances, $\phi(1680)$, $\phi(2170)$, and a third resonance with mass 1850.7 ± 5.3 MeV and width 25 ± 35 MeV of 1.7 σ statistical evidence.
- 8 From the analysis of the combined measurements of $\sigma(e^+ e^- \rightarrow \eta \phi)$ from BaBar, Belle, BESIII, CMD3. The statistical significance for $\phi(2170)$ is 7.2 σ .
- 9 From a fit to the cross section between 2.00 and 3.08 GeV with a sum of Breit-Wigner amplitude and a nonresonant contribution. The observed structure can be also due to $\rho(2150)$.
- 10 The observed structure can be due to both the $\phi(2170)$ and $\rho(2150)$.
- 11 Fit includes interference with the $\phi(1680)$.
- 12 From the $\phi f_0(980)$ component.
- 13 From a fit with two incoherent Breit-Wigners.
- 14 From the $K^+ K^- f_0(980)$ component.
- 15 Superseded by LEES 12F.



$\phi(2170)$ DECAY MODES

Mode	Fraction (Γ_i/Γ)
$\Gamma_1 e^+ e^-$	seen
$\Gamma_2 \phi \eta$	seen
$\Gamma_3 \omega \eta$	seen
$\Gamma_4 \phi \eta'$	seen
$\Gamma_5 \phi \pi \pi$	seen
$\Gamma_6 \phi f_0(980)$	seen
$\Gamma_7 K_S^0 K_L^0$	
$\Gamma_8 K^+ K^- \pi^+ \pi^-$	
$\Gamma_9 K^+ K^- f_0(980) \rightarrow K^+ K^- \pi^+ \pi^-$	seen
$\Gamma_{10} K^+ K^- \pi^0 \pi^0$	
$\Gamma_{11} K^+ K^- f_0(980) \rightarrow K^+ K^- \pi^0 \pi^0$	seen
$\Gamma_{12} K^{*0} K^{\pm} \pi^{\mp}$	not seen
$\Gamma_{13} K^*(892)^0 \bar{K}^*(892)^0$	not seen
$\Gamma_{14} K^*(892)^+ K^*(892)^-$	
$\Gamma_{15} K^*(892)^+ K^- + c.c.$	
$\Gamma_{16} K(1460)^+ K^- + c.c.$	
$\Gamma_{17} K_1(1270)^+ K^- + c.c.$	
$\Gamma_{18} K_1(1400)^+ K^- + c.c.$	
$\Gamma_{19} K_2^*(1430)^+ K^- + c.c.$	

$\phi(2170) \Gamma(i)\Gamma(e^+ e^-)/\Gamma(\text{total})$

$\Gamma(\phi \eta) \times \Gamma(e^+ e^-)/\Gamma_{\text{total}}$	$\Gamma_2 \Gamma_1/\Gamma$	
VALUE (eV)	CL% EVTS DOCUMENT ID TECN COMMENT	
0.17	90	1 ZHU 23 BELL $e^+ e^- \rightarrow \gamma(nS) \rightarrow \phi \eta \gamma$
$0.36^{+0.05}_{-0.03} \pm 0.07$		2 ZHU 23A RVUE $e^+ e^- \rightarrow \eta \phi$
$0.24^{+0.12}_{-0.07}$		3 ABLIKIM 21T BES3 $e^+ e^- \rightarrow \phi \eta$
$1.7 \pm 0.7 \pm 1.3$	483	AUBERT 08S BABR $10.6 e^+ e^- \rightarrow \phi \eta \gamma$

- 1 From a solution of the fit using a vector meson dominance model with contributions from $\phi(1680)$, $\phi(2170)$ and non resonant contribution with mass and width of $\phi(2170)$ fixed at 2163.5 MeV and 31.1 MeV respectively. Four solutions are found with equal fit quality giving 0.17 eV (solution I and II) and 18.6 eV (III and IV) at 90% CL.
- 2 From the analysis of the combined measurements of $\sigma(e^+ e^- \rightarrow \eta \phi)$ from BaBar, Belle, BESIII, CMD3. The statistical significance for $\phi(2170)$ is 7.2 σ . Four solutions are found, with equal fit quality: $(0.56^{+0.03}_{-0.02} \pm 0.07)$ eV, $(0.36^{+0.05}_{-0.03} \pm 0.07)$ eV, $(38 \pm 1 \pm 5)$ eV, $(41 \pm 2 \pm 6)$ eV.
- 3 From a solution of the fit to the cross section below 3.5 GeV measured by BaBar and BESIII with a coherent sum of two modified Breit-Wigner amplitudes ($\phi(1680)$ and $\phi(2170)$) and a nonresonant term. The other solution gives $10.11^{+3.87}_{-3.13}$ eV.

$\Gamma(\omega \eta) \times \Gamma(e^+ e^-)/\Gamma_{\text{total}}$	$\Gamma_3 \Gamma_1/\Gamma$
VALUE (eV)	DOCUMENT ID TECN COMMENT
$0.43 \pm 0.15 \pm 0.04$	1 ABLIKIM 21A BES3 $e^+ e^- \rightarrow \omega \eta$

- 1 For constructive interference with $\omega(1420)$ and $\omega(1650)/\phi(1680)$. For destructive interference: $1.25 \pm 0.48 \pm 0.18$ eV.

$\Gamma(\phi \eta') \times \Gamma(e^+ e^-)/\Gamma_{\text{total}}$	$\Gamma_4 \Gamma_1/\Gamma$
VALUE (eV)	DOCUMENT ID TECN COMMENT
$7.1 \pm 0.7 \pm 0.7$	1 ABLIKIM 20M BES3 $e^+ e^- \rightarrow \eta' \phi$

- 1 From a fit using a coherent sum of a phase-space modified Breit-Wigner function and a phase-space term.

$\Gamma(\phi f_0(980)) \times \Gamma(e^+ e^-)/\Gamma_{\text{total}}$	$\Gamma_6 \Gamma_1/\Gamma$
VALUE (eV)	EVTS DOCUMENT ID TECN COMMENT

- 2.3 $\pm 0.3 \pm 0.3$ 1,2 LEES 12F BABR $10.6 e^+ e^- \rightarrow \phi \pi^+ \pi^- \gamma$
- 2.5 $\pm 0.8 \pm 0.4$ 201 2,3 AUBERT, BE 06D BABR $10.6 e^+ e^- \rightarrow K^+ K^- \pi \pi \gamma$
- 1 From a fit with constructive interference with the $\phi(1680)$. In a fit with destructive interference, the value is larger by a factor of 12.
- 2 For $f_0(980) \rightarrow \pi \pi$.
- 3 Superseded by LEES 12F.

$\Gamma(K_S^0 K_L^0) \times \Gamma(e^+ e^-)/\Gamma_{\text{total}}$	$\Gamma_7 \Gamma_1/\Gamma$
VALUE (eV)	DOCUMENT ID TECN COMMENT

- 0.9 $\pm 0.6 \pm 0.7$ 1 ABLIKIM 21AP BES3 $e^+ e^- \rightarrow K_S^0 K_L^0$
- 1 From a fit to the cross section between 2.00 and 3.08 GeV with a sum of Breit-Wigner amplitude and a nonresonant contribution. The observed structure can be also due to $\rho(2150)$.

$\Gamma(K^*(892)^+ K^*(892)^-) \times \Gamma(e^+ e^-)/\Gamma_{\text{total}}$	$\Gamma_{14} \Gamma_1/\Gamma$
VALUE (eV)	CL% DOCUMENT ID TECN COMMENT

- <1.9 90 1 ABLIKIM 20S BES3 $e^+ e^- \rightarrow K^+ K^- \pi^0 \pi^0$
- 1 By a simultaneous fit of the intermediate channels in a partial-wave analysis, assuming the same structure, modelled with a coherent sum of a nonresonant component and a resonant component by a Breit-Wigner function.

$\Gamma(K^*(892)^+ K^- + c.c.) \times \Gamma(e^+ e^-)/\Gamma_{\text{total}}$	$\Gamma_{15} \Gamma_1/\Gamma$
VALUE (eV)	DOCUMENT ID TECN COMMENT

- 1.0 ± 0.3 1 ABLIKIM 22L BES3 $2.0\text{-}3.08 e^+ e^- \rightarrow K^+ K^- \pi^0$
- 1 From a solution of a simultaneous fit of the $K_2^*(1430) + K^-$ and $K^*(892) + K^-$ intermediate channels in a partial-wave analysis, assuming the same structure, modelled with a coherent sum of a nonresonant component and a resonant component by a Breit-Wigner function. The other solution gives 7.1 ± 0.9 eV. Significance 3.7 σ .

$\Gamma(K(1460)^+ K^- + c.c.) \times \Gamma(e^+ e^-)/\Gamma_{\text{total}}$	$\Gamma_{16} \Gamma_1/\Gamma$
VALUE (eV)	DOCUMENT ID TECN COMMENT

- 3.0 ± 3.8 1 ABLIKIM 20S BES3 $e^+ e^- \rightarrow K^+ K^- \pi^0 \pi^0$
- 1 By a simultaneous fit of the intermediate channels in a partial-wave analysis, assuming the same structure, modelled with a coherent sum of a nonresonant component and a resonant component by a Breit-Wigner function.

$\Gamma(K_1(1270)^+ K^- + c.c.) \times \Gamma(e^+ e^-)/\Gamma_{\text{total}}$	$\Gamma_{17} \Gamma_1/\Gamma$
VALUE (eV)	CL% DOCUMENT ID TECN COMMENT

- <12.5 90 1 ABLIKIM 20S BES3 $e^+ e^- \rightarrow K^+ K^- \pi^0 \pi^0$
- 1 By a simultaneous fit of the intermediate channels in a partial-wave analysis, assuming the same structure, modelled with a coherent sum of a nonresonant component and a resonant component by a Breit-Wigner function. A second solution of the fit with equal fit quality gives an upper limit value of 297.6 eV.

See key on page 1171

Meson Particle Listings

$\phi(2170)$, $f_0(2200)$, $f_J(2220)$

$\Gamma(K_1(1400)^+ K^- + c.c.) \times \Gamma(e^+ e^-) / \Gamma_{\text{total}}$ $\Gamma_{18} \Gamma_1 / \Gamma$

VALUE (eV)	DOCUMENT ID	TECN	COMMENT
4.7 ± 3.3	¹ ABLIKIM 20s BES3		$e^+ e^- \rightarrow K^+ K^- \pi^0 \pi^0$

¹ By a simultaneous fit of the intermediate channels in a partial-wave analysis, assuming the same structure, modelled with a coherent sum of a nonresonant component and a resonant component by a Breit-Wigner function. A second solution of the fit with equal fit quality gives a value of 98.8 ± 7.8 eV.

$\Gamma(K_2^*(1430)^+ K^- + c.c.) \times \Gamma(e^+ e^-) / \Gamma_{\text{total}}$ $\Gamma_{19} \Gamma_1 / \Gamma$

VALUE (eV)	DOCUMENT ID	TECN	COMMENT
12.6 ± 2.4	¹ ABLIKIM 22L BES3		$2.0\text{--}3.08 e^+ e^- \rightarrow K^+ K^- \pi^-$

¹ From a solution of a simultaneous fit of the $K_2^*(1430)^+ K^-$ and $K^*(892)^+ K^-$ intermediate channels in a partial-wave analysis, assuming the same structure, modelled with a coherent sum of a nonresonant component and a resonant component by a Breit-Wigner function. The other solution gives 161.1 ± 20.6 eV.

$\phi(2170) \Gamma(i) \Gamma(e^+ e^-) / \Gamma^2(\text{total})$

$\Gamma(\phi \pi \pi) / \Gamma_{\text{total}} \times \Gamma(e^+ e^-) / \Gamma_{\text{total}}$ $\Gamma_5 / \Gamma \times \Gamma_1 / \Gamma$

VALUE (units 10^{-7})	EVTS	DOCUMENT ID	TECN	COMMENT
1.65 ± 0.15 ± 0.18	4.8k	¹ SHEN 09 BELL		$10.6 e^+ e^- \rightarrow K^+ K^- \pi^+ \pi^- \gamma$

¹ Multiplied by 3/2 to take into account the $\phi \pi^0 \pi^0$ mode. Using $B(\phi \rightarrow K^+ K^-) = (49.2 \pm 0.6)\%$.

$\phi(2170)$ BRANCHING RATIOS

$\Gamma(\phi \pi \pi) / \Gamma_{\text{total}}$ Γ_5 / Γ

VALUE	DOCUMENT ID	TECN	COMMENT
seen	¹ ABLIKIM 23AX BES3		$e^+ e^- \rightarrow \phi \pi^+ \pi^-$

¹ From a fit to the $e^+ e^-$ cross section between 2.00 and 3.08 GeV with a sum of Breit-Wigner amplitude and a non-resonant contribution.

$\Gamma(K^+ K^- f_0(980) \rightarrow K^+ K^- \pi^+ \pi^-) / \Gamma_{\text{total}}$ Γ_9 / Γ

VALUE	DOCUMENT ID	TECN	COMMENT
seen	AUBERT 07AK BABR		$10.6 e^+ e^- \rightarrow K^+ K^- \pi^+ \pi^- \gamma$

$\Gamma(K^+ K^- f_0(980) \rightarrow K^+ K^- \pi^0 \pi^0) / \Gamma_{\text{total}}$ Γ_{11} / Γ

VALUE	DOCUMENT ID	TECN	COMMENT
seen	AUBERT 07AK BABR		$10.6 e^+ e^- \rightarrow K^+ K^- \pi^0 \pi^0 \gamma$

$\Gamma(K^*0 K^\pm \pi^\mp) / \Gamma_{\text{total}}$ Γ_{12} / Γ

VALUE	DOCUMENT ID	TECN	COMMENT
not seen	AUBERT 07AK BABR		$10.6 \text{ GeV } e^+ e^-$

$\Gamma(K^*(892)^0 \bar{K}^*(892)^0) / \Gamma_{\text{total}}$ Γ_{13} / Γ

VALUE	DOCUMENT ID	TECN	COMMENT
not seen	ABLIKIM 10C BES2		$J/\psi \rightarrow \eta K^+ \pi^- K^- \pi^+$

$\phi(2170)$ REFERENCES

ABLIKIM 23AX	PR D108 032011	M. Ablikim et al.	(BESIII Collab.)
LICHARD 23	PR D108 092005	P. Lichard	(OPAV, CTUP)
ZHU 23	PR D107 012006	W. Zhu et al.	(BELLE Collab.)
ZHU 23A	CP C47 113003	W. Zhu, X. Wang	(RVUE)
ABLIKIM 22L	JHEP 2207 045	M. Ablikim et al.	(BESIII Collab.)
ABLIKIM 21A	PL B813 136059	M. Ablikim et al.	(BESIII Collab.)
ABLIKIM 21AP	PR D104 092014	M. Ablikim et al.	(BESIII Collab.)
ABLIKIM 21T	PR D104 032007	M. Ablikim et al.	(BESIII Collab.)
ABLIKIM 20M	PR D102 012008	M. Ablikim et al.	(BESIII Collab.)
ABLIKIM 20S	PRL 124 112001	M. Ablikim et al.	(BESIII Collab.)
ABLIKIM 19I	PR D99 012014	M. Ablikim et al.	(BESIII Collab.)
ABLIKIM 19L	PR D99 032001	M. Ablikim et al.	(BESIII Collab.)
ABLIKIM 15H	PR D91 052017	M. Ablikim et al.	(BESIII Collab.)
LEES 12F	PR D86 012008	J.P. Lees et al.	(BABAR Collab.)
ABLIKIM 10C	PL B685 27	M. Ablikim et al.	(BES II Collab.)
SHEN 09	PR D80 031101	C.P. Shen et al.	(BELLE Collab.)
ABLIKIM 08F	PRL 100 102003	M. Ablikim et al.	(BES Collab.)
AUBERT 08S	PR D77 092002	B. Aubert et al.	(BABAR Collab.)
AUBERT 07AK	PR D76 012008	B. Aubert et al.	(BABAR Collab.)
AUBERT_BE 06D	PR D74 091103	B. Aubert et al.	(BABAR Collab.)

$f_0(2200)$

$$I^G(J^{PC}) = 0^+(0^{++})$$

OMITTED FROM SUMMARY TABLE
 Seen in $K_S^0 K_S^0$ (AUGUSTIN 88), $K^+ K^-$ (ABLIKIM 05Q) and $\eta \eta$ (BINON 05) system. Not seen in $\Upsilon(1S)$ radiative decays (BARU 89).

$f_0(2200)$ MASS

VALUE (MeV)	EVTS	DOCUMENT ID	TECN	COMMENT
2187 ± 14 OUR AVERAGE				
2170 ± 20 ⁺¹⁰ ₋₁₅		ABLIKIM 05Q BES2		$\psi(2S) \rightarrow \gamma \pi^+ \pi^- K^+ K^-$
2197 ± 17		¹ AUGUSTIN 88 DM2		$J/\psi \rightarrow \gamma K_S^0 K_S^0$

• • • We do not use the following data for averages, fits, limits, etc. • • •

2200 ± 25		SARANTSEV 21	RVUE	$J/\psi(1S) \rightarrow \gamma(\pi \pi, K \bar{K}, \eta \eta, \omega \phi)$
2206 ± 12 ± 8	381	^{2,3} DOBBS	15	$J/\psi \rightarrow \gamma K^+ K^-$
2188 ± 17 ± 16	203	^{2,3} DOBBS	15	$\psi(2S) \rightarrow \gamma K^+ K^-$
2210 ± 50		⁴ BINON	05	GAMS $33 \pi^- p \rightarrow \eta \eta n$
~ 2122		HASAN 94	RVUE	$\bar{p} p \rightarrow \pi \pi$
~ 2321		HASAN 94	RVUE	$\bar{p} p \rightarrow \pi \pi$

¹ Cannot determine spin to be 0.
² Using CLEO-c data but not authored by the CLEO Collaboration.
³ From a fit to a Breit-Wigner line shape with fixed $\Gamma = 238$ MeV.
⁴ First solution, PWA is ambiguous.

$f_0(2200)$ WIDTH

VALUE (MeV)	DOCUMENT ID	TECN	COMMENT
210 ± 40 OUR AVERAGE			
220 ± 60 ⁺⁴⁰ ₋₄₅		ABLIKIM 05Q BES2	$\psi(2S) \rightarrow \gamma \pi^+ \pi^- K^+ K^-$
201 ± 51		⁵ AUGUSTIN 88 DM2	$J/\psi \rightarrow \gamma K_S^0 K_S^0$

• • • We do not use the following data for averages, fits, limits, etc. • • •

150 ± 30		SARANTSEV 21	RVUE	$J/\psi(1S) \rightarrow \gamma(\pi \pi, K \bar{K}, \eta \eta, \omega \phi)$
380 ± 90		⁶ BINON 05	GAMS	$33 \pi^- p \rightarrow \eta \eta n$
~ 273		HASAN 94	RVUE	$\bar{p} p \rightarrow \pi \pi$
~ 223		HASAN 94	RVUE	$\bar{p} p \rightarrow \pi \pi$

⁵ Cannot determine spin to be 0.
⁶ First solution, PWA is ambiguous.

$f_0(2200)$ REFERENCES

SARANTSEV 21	PL B816 136227	A.V. Sarantsev et al.	(BONN, PNPI)
DOBBS 15	PR D91 052006	S. Dobbs et al.	(NWES)
ABLIKIM 05Q	PR D72 092002	M. Ablikim et al.	(BES Collab.)
BINON 05	PAN 68 960	F. Binon et al.	
	Translated from YAF 68 998.		
HASAN 94	PL B334 215	A. Hasan, D.V. Bugg	(LOQM)
BARU 89	ZPHY C42 505	S.E. Baru et al.	(NOVO)
AUGUSTIN 88	PRL 60 2238	J.E. Augustin et al.	(DM2 Collab.)

$f_J(2220)$

$$I^G(J^{PC}) = 0^+(2^{++} \text{ or } 4^{++})$$

OMITTED FROM SUMMARY TABLE
 See our mini-review in the 2004 edition of this Review, PDG 04.

$f_J(2220)$ MASS

VALUE (MeV)	EVTS	DOCUMENT ID	TECN	COMMENT
2231.1 ± 3.5 OUR AVERAGE				
2235 ± 4 ± 6	74	BAI 96B	BES	$e^+ e^- \rightarrow J/\psi \rightarrow \gamma \pi^+ \pi^-$
2230 ± 6 ⁺⁷ ₋₇ ± 16	46	BAI 96B	BES	$e^+ e^- \rightarrow J/\psi \rightarrow \gamma K^+ K^-$
2232 ± 8 ⁺⁷ ₋₇ ± 15	23	BAI 96B	BES	$e^+ e^- \rightarrow J/\psi \rightarrow \gamma K_S^0 K_S^0$
2235 ± 4 ± 5	32	BAI 96B	BES	$e^+ e^- \rightarrow J/\psi \rightarrow \gamma \rho \bar{\rho}$
2209 ± 17 ⁺¹⁵ ₋₁₅ ± 10		ASTON 88F	LASS	$11 K^- p \rightarrow K^+ K^- \Lambda$
2230 ± 20		BOLONKIN 88	SPEC	$40 \pi^- p \rightarrow K_S^0 K_S^0 n$
2220 ± 10	41	¹ ALDE 86B	GA24	$38\text{--}100 \pi p \rightarrow n \eta \eta'$
2230 ± 6 ± 14	93	BALTRUSAIT..86D	MRK3	$e^+ e^- \rightarrow \gamma K^+ K^-$
2232 ± 7 ± 7	23	BALTRUSAIT..86D	MRK3	$e^+ e^- \rightarrow \gamma K_S^0 K_S^0$

• • • We do not use the following data for averages, fits, limits, etc. • • •

2223.9 ± 2.5		² VLADIMIRSK..08	SPEC	$40 \pi^- p \rightarrow K_S^0 K_S^0 n + m \pi^0$
2246 ± 36		BAI 98H	BES	$J/\psi \rightarrow \gamma \pi^0 \pi^0$

¹ ALDE 86B uses data from both the GAMS-2000 and GAMS-4000 detectors.
² $J^{PC} = 2^{++}$. Systematic uncertainties not evaluated.

$f_J(2220)$ WIDTH

VALUE (MeV)	CL%	EVTS	DOCUMENT ID	TECN	COMMENT
23 ± 8 OUR AVERAGE					
19 ± 13 ⁺¹¹ ₋₁₁ ± 12		74	BAI 96B	BES	$e^+ e^- \rightarrow J/\psi \rightarrow \gamma \pi^+ \pi^-$
20 ± 20 ⁺¹⁵ ₋₁₅ ± 17		46	BAI 96B	BES	$e^+ e^- \rightarrow J/\psi \rightarrow \gamma K^+ K^-$
20 ± 25 ⁺¹⁶ ₋₁₆ ± 14		23	BAI 96B	BES	$e^+ e^- \rightarrow J/\psi \rightarrow \gamma K_S^0 K_S^0$
15 ± 12 ⁺⁹ ₋₉ ± 9		32	BAI 96B	BES	$e^+ e^- \rightarrow J/\psi \rightarrow \gamma \rho \bar{\rho}$
60 ± 107 ⁺⁵⁷ ₋₅₇			ASTON 88F	LASS	$11 K^- p \rightarrow K^+ K^- \Lambda$
80 ± 30			BOLONKIN 88	SPEC	$40 \pi^- p \rightarrow K_S^0 K_S^0 n$

Meson Particle Listings

 $f_J(2220), \omega(2220)$

$26^{+20}_{-16} \pm 17$	93	BALTRUSAIT...86D	MRK3	$e^+e^- \rightarrow \gamma K^+ K^-$
$18^{+23}_{-15} \pm 10$	23	BALTRUSAIT...86D	MRK3	$e^+e^- \rightarrow \gamma K_S^0 K_S^0$
8.6 ± 2.5		¹ VLADIMIRSK...08	SPEC	$40 \pi^- p \rightarrow K_S^0 K_S^0 n$ $+ m \pi^0$
< 80	90	ALDE	87c	GAM2 $38 \pi^- p \rightarrow \eta' \eta n$
¹ $J^{PC} = 2^+ +$. Systematic uncertainties not evaluated				

 $f_J(2220)$ DECAY MODES

Mode	Fraction (Γ_i/Γ)
Γ_1 $\pi\pi$	not seen
Γ_2 $\pi^+\pi^-$	not seen
Γ_3 $K\bar{K}$	not seen
Γ_4 $\rho\bar{\rho}$	not seen
Γ_5 $\gamma\gamma$	not seen
Γ_6 $\eta\eta'(958)$	seen
Γ_7 $\phi\phi$	not seen
Γ_8 $\eta\eta$	not seen

 $f_J(2220)$ $\Gamma(i)\Gamma(\gamma\gamma)/\Gamma(\text{total})$

$\Gamma(K\bar{K}) \times \Gamma(\gamma\gamma)/\Gamma_{\text{total}}$	CL%	DOCUMENT ID	TECN	COMMENT	Γ_3/Γ_7
< 1.4	95	¹ ACCIARRI	01H	L3 $\gamma\gamma \rightarrow K_S^0 K_S^0, E_{\text{cm}}^{\text{res}} = 91, 183-209 \text{ GeV}$	
< 5.6	95	¹ GODANG	97	CLE2 $\gamma\gamma \rightarrow K_S^0 K_S^0$	
< 86	95	¹ ALBRECHT	90G	ARG $\gamma\gamma \rightarrow K^+ K^-$	
< 1000	95	² ALTHOFF	85B	TASS $\gamma\gamma, K\bar{K}\pi$	

$\Gamma(\pi\pi) \times \Gamma(\gamma\gamma)/\Gamma_{\text{total}}$	CL%	DOCUMENT ID	TECN	COMMENT	Γ_1/Γ_5
< 2.5	95	ALAM	98C	CLE2 $\gamma\gamma \rightarrow \pi^+\pi^-$	
¹ Assuming $J^P = 2^+$.					
² True for $J^P = 0^+$ and $J^P = 2^+$.					

 $f_J(2220)$ $\Gamma(i)\Gamma(\rho\bar{\rho})/\Gamma^2(\text{total})$

$\Gamma(\rho\bar{\rho})/\Gamma_{\text{total}} \times \Gamma(\pi\pi)/\Gamma_{\text{total}}$	CL%	DOCUMENT ID	TECN	COMMENT	$\Gamma_4/\Gamma \times \Gamma_1/\Gamma$
< 18	95	¹ AMSLER	01	CBAR $1.4-1.5 \rho\bar{\rho} \rightarrow \pi^0 \pi^0$	
$< (11-42)$	99	² HASAN	96	SPEC $1.35-1.55 \rho\bar{\rho} \rightarrow \pi^+\pi^-$	

$\Gamma(\rho\bar{\rho})/\Gamma_{\text{total}} \times \Gamma(\phi\phi)/\Gamma_{\text{total}}$	CL%	DOCUMENT ID	TECN	COMMENT	$\Gamma_4/\Gamma \times \Gamma_7/\Gamma$
< 6	95	³ EVANGELIS...	98	SPEC $1.1-2.0 \rho\bar{\rho} \rightarrow \phi\phi$	

$\Gamma(\rho\bar{\rho})/\Gamma_{\text{total}} \times \Gamma(\eta\eta)/\Gamma_{\text{total}}$	CL%	DOCUMENT ID	TECN	COMMENT	$\Gamma_4/\Gamma \times \Gamma_8/\Gamma$
< 4	95	¹ AMSLER	01	CBAR $1.4-1.5 \rho\bar{\rho} \rightarrow \eta\eta$	

- ¹ For $J^P = 2^+$ in the mass range 2222-2240 MeV and the total width between 10 and 20 MeV.
² For $J^P = 2^+$ and $J^P = 4^+$ in the mass range 2220-2245 MeV and the total width of 15 MeV.
³ For $J^P = 2^+$, the mass of 2235 MeV and the total width of 15 MeV.

 $f_J(2220)$ BRANCHING RATIOS

$\Gamma(\pi\pi)/\Gamma_{\text{total}}$	DOCUMENT ID	COMMENT	Γ_1/Γ
not seen	¹ DOBBS	15 $J/\psi \rightarrow \gamma\pi\pi$	
not seen	¹ DOBBS	15 $\psi(2S) \rightarrow \gamma\pi\pi$	
¹ Using CLEO-c data but not authored by the CLEO Collaboration.			

$\Gamma(K\bar{K})/\Gamma_{\text{total}}$	DOCUMENT ID	COMMENT	Γ_3/Γ
not seen	¹ DOBBS	15 $J/\psi \rightarrow \gamma K\bar{K}$	
not seen	¹ DOBBS	15 $\psi(2S) \rightarrow \gamma K\bar{K}$	
¹ Using CLEO-c data but not authored by the CLEO Collaboration.			

$\Gamma(\pi\pi)/\Gamma(K\bar{K})$	DOCUMENT ID	TECN	COMMENT	Γ_1/Γ_3
1.0 ± 0.5	BAI	96B	BES $e^+e^- \rightarrow J/\psi \rightarrow \gamma 2\pi, K\bar{K}$	

 $\Gamma(\rho\bar{\rho})/\Gamma_{\text{total}}$ Γ_4/Γ

VALUE (units 10^{-4})	CL%	DOCUMENT ID	TECN	COMMENT
not seen		¹ AUBERT	07AV	BABR $B \rightarrow \rho\bar{\rho} K^{(*)}$
not seen		WANG	05A	BELL $B^+ \rightarrow \bar{p} p K^+$
< 3.0	95	² EVANGELIS...	97	SPEC $1.96-2.40 \bar{p} p \rightarrow K_S^0 K_S^0$
< 1.1	99.7	³ BARNES	93	SPEC $1.3-1.57 \bar{p} p \rightarrow K_S^0 K_S^0$
< 2.6	99.7	³ BARDIN	87	CNTR $1.3-1.5 \bar{p} p \rightarrow K^+ K^-$
< 3.6	99.7	³ SCULLI	87	CNTR $1.29-1.55 \bar{p} p \rightarrow K^+ K^-$
¹ Assuming $\Gamma < 30 \text{ MeV}$.				
² Assuming $\Gamma \sim 20 \text{ MeV}$, $J^P = 2^+$ and $B(f_J(2220) \rightarrow K\bar{K}) = 100\%$.				
³ Assuming $\Gamma = 30-35 \text{ MeV}$, $J^P = 2^+$ and $B(f_J(2220) \rightarrow K\bar{K}) = 100\%$.				

 $\Gamma(\rho\bar{\rho})/\Gamma(K\bar{K})$ Γ_4/Γ_3

VALUE	DOCUMENT ID	TECN	COMMENT
0.17 ± 0.09	BAI	96B	BES $e^+e^- \rightarrow J/\psi \rightarrow \gamma\rho\bar{\rho}, K\bar{K}$

 $f_J(2220)$ REFERENCES

DOBBS	15	PR D91 052006	S. Dobbs et al.	(NWES)
VLADIMIRSK...	08	PAN 71 2129	V.V. Vladimirov et al.	(ITEP)
Translated from YAF 71 2166.				
AUBERT	07AV	PR D76 092004	B. Aubert et al.	(BABAR Collab.)
WANG	05A	PL B617 141	M.-Z. Wang et al.	(BELLE Collab.)
PDG	04	PL B592 1	S. Eidelman et al.	(PDG Collab.)
ACCIARRI	01H	PL B501 173	M. Acciarri et al.	(L3 Collab.)
AMSLER	01	PL B520 175	C. Amisler et al.	(Crystal Barrel Collab.)
ALAM	98C	PRL 81 3328	M.S. Alam et al.	(CLEO Collab.)
BAI	98B	PRL 81 1179	J.Z. Bai et al.	(BES Collab.)
EVANGELIS...	98	PR D57 6370	C. Evangelista et al.	(JETSET Collab.)
EVANGELIS...	97	PR D56 3803	C. Evangelista et al.	(LEAR Collab.)
GODANG	97	PRL 79 3829	R. Godang et al.	(CLEO Collab.)
BAI	96B	PRL 76 3502	J.Z. Bai et al.	(BES Collab.)
HASAN	96	PL B388 376	A. Hasan, D.V. Bugg	(BRUN, LOQM)
BARNES	93	PL B309 469	P.D. Barnes et al.	(PS185 Collab.)
ALBRECHT	90G	ZPHY C48 183	H. Albrecht et al.	(ARGUS Collab.)
ASTON	88F	PL B215 199	D. Aston et al.	(SLAC, NAGO, CIN, INUS) JP
BOLONKIN	88	NP B309 426	B.V. Bolonkin et al.	(ITEP, SERP)
ALDE	87C	SJNP 45 255	D. Alde et al.	
Translated from YAF 45 405.				
BARDIN	87	PL B195 292	G. Bardini et al.	(SACL, FERR, CERN, PADO+)
SCULLI	87	PRL 58 1715	J. Sculli et al.	(NYU, BNL)
ALDE	86B	PL B177 120	D.M. Alde et al.	(SERP, BELG, LANL, LAPP)
BALTRUSAIT...	86D	PRL 56 107	R.M. Baltusaitis	(CIT, UCSC, ILL, SLA+)
ALTHOFF	85B	ZPHY C29 189	M. Althoff et al.	(TASSO Collab.)

OTHER RELATED PAPERS

DEL-AMO-SA...	100	PRL 105 172001	P. del Amo Sanchez et al.	(BABAR Collab.)
---------------	-----	----------------	---------------------------	-----------------

 $\omega(2220)$

$$I^G(J^{PC}) = 0^-(1^-)$$

OMITTED FROM SUMMARY TABLE

 $\omega(2220)$ MASS

VALUE (MeV)	DOCUMENT ID	TECN	COMMENT
$2232 \pm 19 \pm 27$	¹ ABLIKIM	23G	BES3 $2.0-3.1 e^+e^- \rightarrow \omega\pi\pi$
$2250 \pm 25 \pm 27$	² ABLIKIM	23G	BES3 $2.0-3.1 e^+e^- \rightarrow \omega\pi^+\pi^-$
$2222 \pm 7 \pm 2$	³ ABLIKIM	22I	BES3 $2.0-3.8 e^+e^- \rightarrow \omega\pi^0\pi^0$
2205 ± 30	⁴ ANISOVICH	02B	SPEC $0.6-1.9 \rho\bar{\rho} \rightarrow \omega\eta, \omega\pi^0\pi^0$
¹ From a fit to $\omega\pi^+\pi^-$ and $\omega\pi^0\pi^0$ with a Breit-Wigner resonance interfering with the continuum. Supersedes ABLIKIM 22I.			
² From a fit to $\omega\pi^+\pi^-$ with a Breit-Wigner resonance interfering with the continuum.			
³ From the fit to the cross section by the coherent sum of resonant component parametrized by a modified Breit-Wigner amplitude and a phase-space contribution for the continuum.			
⁴ From the combined analysis of ANISOVICH 00D, ANISOVICH 01C, and ANISOVICH 02B.			

 $\omega(2220)$ WIDTH

VALUE (MeV)	DOCUMENT ID	TECN	COMMENT
$93 \pm 53 \pm 20$	⁵ ABLIKIM	23G	BES3 $2.0-3.1 e^+e^- \rightarrow \omega\pi\pi$
$125 \pm 43 \pm 15$	⁶ ABLIKIM	23G	BES3 $2.0-3.1 e^+e^- \rightarrow \omega\pi^+\pi^-$
$59 \pm 30 \pm 6$	⁷ ABLIKIM	22I	BES3 $2.0-3.8 e^+e^- \rightarrow \omega\pi^0\pi^0$
350 ± 90	⁸ ANISOVICH	02B	SPEC $0.6-1.9 \rho\bar{\rho} \rightarrow \omega\eta, \omega\pi^0\pi^0$
⁵ From a fit to $\omega\pi^+\pi^-$ and $\omega\pi^0\pi^0$ with a Breit-Wigner resonance interfering with the continuum. Supersedes ABLIKIM 22I.			
⁶ From a fit to $\omega\pi^+\pi^-$ with a Breit-Wigner resonance interfering with the continuum.			
⁷ From the fit to the cross section by the coherent sum of resonant component parametrized by a modified Breit-Wigner amplitude and a phase-space contribution for the continuum.			
⁸ From the combined analysis of ANISOVICH 00D, ANISOVICH 01C, and ANISOVICH 02B.			

See key on page 1171

Meson Particle Listings

$\omega(2220), \eta(2225), \rho_3(2250)$

$\omega(2220)$ DECAY MODES

Mode	Fraction (Γ_i/Γ)
$\Gamma_1 \quad \omega \pi \pi$	seen
$\Gamma_2 \quad \omega \pi^+ \pi^-$	seen
$\Gamma_3 \quad \omega \pi^0 \pi^0$	seen
$\Gamma_4 \quad e^+ e^-$	seen

$\omega(2220) \Gamma(i)\Gamma(e^+e^-)/\Gamma(\text{total})$

$\Gamma(\omega \pi^0 \pi^0) \times \Gamma(e^+e^-)/\Gamma_{\text{total}}$	$\Gamma_3 \Gamma_4 / \Gamma$		
VALUE (eV)	DOCUMENT ID	TECN	COMMENT

••• We do not use the following data for averages, fits, limits, etc. •••
 $0.3 \pm 0.1 \pm 0.1$ ⁹ ABLIKIM 22i BES3 2.0-3.8 $e^+e^- \rightarrow \omega \pi^0 \pi^0$
⁹ Superseded by ABLIKIM 23G.

$\Gamma(\omega \pi^+ \pi^-) \times \Gamma(e^+e^-)/\Gamma_{\text{total}}$	$\Gamma_2 \Gamma_4 / \Gamma$		
VALUE (eV)	DOCUMENT ID	TECN	COMMENT

••• We do not use the following data for averages, fits, limits, etc. •••
 $0.9 \pm 0.4 \pm 0.4$ ¹⁰ ABLIKIM 23G BES3 2.0-3.1 $e^+e^- \rightarrow \omega \pi^+ \pi^-$
¹⁰ From a fit to $\omega \pi^+ \pi^-$ with a Breit-Wigner resonance interfering with the continuum. Solution with constructive interference: $52.9 \pm 17.0 \pm 13.1$ eV.

$\Gamma(\omega \pi \pi) \times \Gamma(e^+e^-)/\Gamma_{\text{total}}$	$\Gamma_1 \Gamma_4 / \Gamma$		
VALUE (eV)	DOCUMENT ID	TECN	COMMENT

$0.9 \pm 0.5 \pm 0.2$ ¹¹ ABLIKIM 23G BES3 2.0-3.1 $e^+e^- \rightarrow \omega \pi \pi$
¹¹ From a fit to $\omega \pi^+ \pi^-$ and $\omega \pi^0 \pi^0$ with a Breit-Wigner resonance interfering with the continuum. Solution with constructive interference: $61.1 \pm 32.1 \pm 15.4$ eV. Supersedes ABLIKIM 22i.

$\omega(2220)$ REFERENCES

ABLIKIM 23G	JHEP 2301 111	M. Ablikim et al.	(BESIII Collab.)
Also	JHEP 2303 093 (errat.)	M. Ablikim, et. al.	(BESIII Collab.)
ABLIKIM 22i	PR D105 032005	M. Ablikim et al.	(BESIII Collab.)
ANISOVICH 02B	PL B542 19	A.V. Anisovich et al.	
ANISOVICH 01C	PL B507 23	A.V. Anisovich et al.	
ANISOVICH 00D	PL B476 15	A.V. Anisovich et al.	

$\eta(2225)$

$$J^{PC} = 0^+(0^-+)$$

OMITTED FROM SUMMARY TABLE

Seen in $J/\psi \rightarrow \gamma \phi \phi$. Possibly seen in $B \rightarrow \phi \phi K$ by LEES 11A.

$\eta(2225)$ MASS

VALUE (MeV)	EVTS	DOCUMENT ID	TECN	COMMENT
-------------	------	-------------	------	---------

2221^{+13}_{-10} OUR AVERAGE

$2216^{+4}_{-5} \pm 21_{-11}$		¹ ABLIKIM 16N BES3		$J/\psi \rightarrow \gamma K^+ K^- K^+ K^-$
$2240^{+30}_{-20} \pm 30_{-20}$	196 ± 19	ABLIKIM 08i BES		$J/\psi \rightarrow \gamma K^+ K^- K_S^0 K_L^0$
$2230 \pm 25 \pm 15$		BAI 90B MRK3		$J/\psi \rightarrow \gamma K^+ K^- K^+ K^-$
$2214 \pm 20 \pm 13$		BAI 90B MRK3		$J/\psi \rightarrow \gamma K^+ K^- K_S^0 K_L^0$

••• We do not use the following data for averages, fits, limits, etc. •••
 ~ 2220 BISELLO 86B DM2 $J/\psi \rightarrow \gamma K^+ K^- K^+ K^-$
¹ From a partial wave analysis of $J/\psi \rightarrow \gamma \phi \phi$ that also finds significant signals for $\eta(2100), 0^-+$ phase space, $f_0(2100), f_2(2010), f_2(2300), f_2(2340)$, and a previously unseen 0^-+ state $X(2500)$ ($M = 2470^{+15}_{-19} \pm 101_{-23}$ MeV, $\Gamma = 230^{+64}_{-35} \pm 56_{-33}$ MeV).

$\eta(2225)$ WIDTH

VALUE (MeV)	EVTS	DOCUMENT ID	TECN	COMMENT
-------------	------	-------------	------	---------

185^{+40}_{-20} OUR AVERAGE

$185^{+12}_{-14} \pm 43_{-17}$		¹ ABLIKIM 16N BES3		$J/\psi \rightarrow \gamma K^+ K^- K^+ K^-$
$190 \pm 30^{+60}_{-40}$	196 ± 19	ABLIKIM 08i BES		$J/\psi \rightarrow \gamma K^+ K^- K_S^0 K_L^0$
$150^{+300}_{-60} \pm 60$		BAI 90B MRK3		$J/\psi \rightarrow \gamma K^+ K^- K^+ K^-$

••• We do not use the following data for averages, fits, limits, etc. •••
 ~ 80 BISELLO 86B DM2 $J/\psi \rightarrow \gamma K^+ K^- K^+ K^-$
¹ From a partial wave analysis of $J/\psi \rightarrow \gamma \phi \phi$ that also finds significant signals for $\eta(2100), 0^-+$ phase space, $f_0(2100), f_2(2010), f_2(2300), f_2(2340)$, and a previously unseen 0^-+ state $X(2500)$ ($M = 2470^{+15}_{-19} \pm 101_{-23}$ MeV, $\Gamma = 230^{+64}_{-35} \pm 56_{-33}$ MeV).

$\eta(2225)$ REFERENCES

ABLIKIM 16N	PR D93 112011	M. Ablikim	(BESIII Collab.)
LEES 11A	PR D94 012001	J.P. Lees et al.	(BABAR Collab.)
ABLIKIM 08i	PL B662 330	M. Ablikim et al.	(BES Collab.)
BAI 90B	PRL 65 1309	Z. Bai et al.	(Mark III Collab.)
BISELLO 86B	PL B179 294	D. Bisello et al.	(DM2 Collab.)

$\rho_3(2250)$

$$J^{PC} = 1^+(3^-)$$

OMITTED FROM SUMMARY TABLE

Contains results mostly from formation experiments. For further production experiments see the Further States entry. See also $\rho(2150), f_2(2150), f_4(2300), \rho_5(2350)$.

$\rho_3(2250)$ MASS

$\bar{p}p \rightarrow \pi\pi$ or $K\bar{K}$

VALUE (MeV)	EVTS	DOCUMENT ID	TECN	CHG	COMMENT
-------------	------	-------------	------	-----	---------

••• We do not use the following data for averages, fits, limits, etc. •••
 $2248^{+17}_{-5} \pm 59_{-1.3} \times 1.8k$ ¹ ABLIKIM 20F BES3 $\psi(2S) \rightarrow K^+ K^- \eta$
 ~ 2232 HASAN 94 RVUE $\bar{p}p \rightarrow \pi\pi$
 ~ 2090 ² OAKDEN 94 RVUE $0.36-1.55 \bar{p}p \rightarrow \pi\pi$
 ~ 2250 ³ MARTIN 80B RVUE
 ~ 2300 ³ MARTIN 80C RVUE
 ~ 2140 ⁴ CARTER 78B CNTR 0 $0.7-2.4 \bar{p}p \rightarrow K^- K^+$
 ~ 2150 ⁵ CARTER 77 CNTR 0 $0.7-2.4 \bar{p}p \rightarrow \pi\pi$

¹ Seen in $\psi(2S)$ decay with branching ratio $\psi(2S) \rightarrow X\eta \rightarrow K^+ K^- \eta = (1.9 \pm 0.4^{+0.5}_{-1.3}) \times 10^{-6}$.
² See however KLOET 96 who fit $\pi^+ \pi^-$ only and find waves only up to $J = 3$ to be important but not significantly resonant.
³ $I(J^P) = 1(3^-)$ from simultaneous analysis of $p\bar{p} \rightarrow \pi^- \pi^+$ and $\pi^0 \pi^0$.
⁴ $l = 0, 1, J^P = 3^-$ from Barrelet-zero analysis.
⁵ $I(J^P) = 1(3^-)$ from amplitude analysis.

S-CHANNEL $\bar{N}N$

VALUE (MeV)	DOCUMENT ID	TECN	CHG	COMMENT
-------------	-------------	------	-----	---------

••• We do not use the following data for averages, fits, limits, etc. •••
 2260 ± 20 ⁶ ANISOVICH 02 SPEC $0.6-1.9 \bar{p}\bar{p} \rightarrow \omega \pi^0, \omega \eta \pi^0, \pi^+ \pi^-$
 ~ 2190 ⁷ CUTTS 78B CNTR $0.97-3 \bar{p}p \rightarrow \bar{N}N$
 2155 ± 15 ^{7,8} COUPLAND 77 CNTR 0 $0.7-2.4 \bar{p}p \rightarrow \bar{p}p$
 2193 ± 2 ^{7,9} ALSPECTOR 73 CNTR $\bar{p}p$ S channel
 2190 ± 10 ¹⁰ ABRAMS 70 CNTR S channel $\bar{p}N$
⁶ From the combined analysis of ANISOVICH 00j, ANISOVICH 01d, ANISOVICH 01E, and ANISOVICH 02.
⁷ Isospins 0 and 1 not separated.
⁸ From a fit to the total elastic cross section.
⁹ Referred to as T or T region by ALSPECTOR 73.
¹⁰ Seen as bump in $l = 1$ state. See also COOPER 68. PEASLEE 75 confirm $\bar{p}p$ results of ABRAMS 70, no narrow structure.

Other processes

VALUE (MeV)	DOCUMENT ID	TECN	COMMENT
-------------	-------------	------	---------

••• We do not use the following data for averages, fits, limits, etc. •••
 $2290 \pm 20 \pm 30$ AMELIN 00 VES $37 \pi^- p \rightarrow \eta \pi^+ \pi^- n$

$\rho_3(2250)$ WIDTH

$\bar{p}p \rightarrow \pi\pi$ or $K\bar{K}$

VALUE (MeV)	EVTS	DOCUMENT ID	TECN	CHG	COMMENT
-------------	------	-------------	------	-----	---------

••• We do not use the following data for averages, fits, limits, etc. •••
 $185^{+31}_{-26} \pm 17_{-103} \times 1.8k$ ¹¹ ABLIKIM 20F BES3 $\psi(2S) \rightarrow K^+ K^- \eta$
 ~ 220 HASAN 94 RVUE $\bar{p}p \rightarrow \pi\pi$
 ~ 60 ¹² OAKDEN 94 RVUE $0.36-1.55 \bar{p}p \rightarrow \pi\pi$
 ~ 250 ¹³ MARTIN 80B RVUE
 ~ 200 ¹³ MARTIN 80C RVUE
 ~ 150 ¹⁴ CARTER 78B CNTR 0 $0.7-2.4 \bar{p}p \rightarrow K^- K^+$
 ~ 200 ¹⁵ CARTER 77 CNTR 0 $0.7-2.4 \bar{p}p \rightarrow \pi\pi$

¹¹ Seen in $\psi(2S)$ decay with branching ratio $\psi(2S) \rightarrow X\eta \rightarrow K^+ K^- \eta = (1.9 \pm 0.4^{+0.5}_{-1.3}) \times 10^{-6}$.
¹² See however KLOET 96 who fit $\pi^+ \pi^-$ only and find waves only up to $J = 3$ to be important but not significantly resonant.
¹³ $I(J^P) = 1(3^-)$ from simultaneous analysis of $p\bar{p} \rightarrow \pi^- \pi^+$ and $\pi^0 \pi^0$.
¹⁴ $l = 0, 1, J^P = 3^-$ from Barrelet-zero analysis.
¹⁵ $I(J^P) = 1(3^-)$ from amplitude analysis.

S-CHANNEL $\bar{N}N$

VALUE (MeV)	DOCUMENT ID	TECN	CHG	COMMENT
-------------	-------------	------	-----	---------

••• We do not use the following data for averages, fits, limits, etc. •••
 160 ± 25 ¹⁶ ANISOVICH 02 SPEC $0.6-1.9 \bar{p}\bar{p} \rightarrow \omega \pi^0, \omega \eta \pi^0, \pi^+ \pi^-$
 135 ± 75 ^{17,18} COUPLAND 77 CNTR 0 $0.7-2.4 \bar{p}p \rightarrow \bar{p}p$
 98 ± 8 ¹⁸ ALSPECTOR 73 CNTR $\bar{p}p$ S channel
 ~ 85 ¹⁹ ABRAMS 70 CNTR S channel $\bar{p}N$
¹⁶ From the combined analysis of ANISOVICH 00j, ANISOVICH 01d, ANISOVICH 01E, and ANISOVICH 02.
¹⁷ From a fit to the total elastic cross section.
¹⁸ Isospins 0 and 1 not separated.
¹⁹ Seen as bump in $l = 1$ state. See also COOPER 68. PEASLEE 75 confirm $\bar{p}p$ results of ABRAMS 70, no narrow structure.

Meson Particle Listings

$\rho_3(2250)$, $f_2(2300)$, $f_4(2300)$

Other processes

VALUE (MeV)	DOCUMENT ID	TECN	COMMENT
• • • We do not use the following data for averages, fits, limits, etc. • • •			
230 ± 50 ± 80	AMELIN	00	VES 37 $\pi^- p \rightarrow \eta \pi^+ \pi^- n$

$\rho_3(2250)$ REFERENCES

ABLIKIM	20F	PR D101 032008	M. Ablikim et al.	(BESIII Collab.)
ANISOVICH	02	PL B542 8	A.V. Anisovich et al.	
ANISOVICH	01D	PL B508 6	A.V. Anisovich et al.	
ANISOVICH	01E	PL B513 281	A.V. Anisovich et al.	
AMELIN	00	NP A668 83	D. Amelin et al.	(VES Collab.)
ANISOVICH	00J	PL B491 47	A.V. Anisovich et al.	(RAL, LOQM, PNPI+)
KLOET	96	PR D53 6120	W.M. Kloet, F. Myhrer	(RUTG, RHELD)
HASAN	94	PL B334 215	A. Hasan, D.V. Bugg	(LOQM)
OAKDEN	94	NP A574 731	M.N. Oakden, M.R. Pennington	(DURH)
MARTIN	80B	NP B176 355	B.R. Martin, D. Morgan	(LOUC, RHELD)JP
MARTIN	80C	NP B169 216	A.D. Martin, M.R. Pennington	(DURH)JP
CARTER	78B	NP B141 467	A.A. Carter	(LOQM)
CUTTS	78B	PR D17 16	D. Cutts et al.	(STON, WIS C)
CARTER	77	PL 67B 117	A.A. Carter et al.	(LOQM, RHELD)JP
COUPLAND	77	PL 71B 460	M. Coupland et al.	(LOQM, RHELD)
PEASLEE	75	PL 57B 189	D.C. Peaslee et al.	(CANB, BARI, BROW+)
ALSPECTOR	73	PRL 30 511	J. Alspector et al.	(RUTG, UPNJ)
ABRAMS	70	PR D1 1917	R.J. Abrams et al.	(BNL)
COOPER	68	PRL 20 1059	W.A. Cooper et al.	(ANL)

$f_2(2300)$

$$I^G(J^{PC}) = 0^+(2^{++})$$

$f_2(2300)$ MASS

VALUE (MeV)	DOCUMENT ID	TECN	COMMENT
2297 ± 28	¹ ETKIN	88	MPS 22 $\pi^- p \rightarrow \phi \phi n$
• • • We do not use the following data for averages, fits, limits, etc. • • •			
2262 ± 4 ± 28	² ABLIKIM	21A1	BES3 3.51-4.60 $e^+ e^- \rightarrow \phi \Lambda \bar{\Lambda}$
2243 ± $\begin{matrix} 7+ \\ -6-29 \end{matrix}$	³ UEHARA	13	BELL $\gamma\gamma \rightarrow K_S^0 K_S^0$
2270 ± 12	VLADIMIRSK...06	SPEC	40 $\pi^- p \rightarrow K_S^0 K_S^0 n$
2327 ± 9 ± 6	ABE	04	BELL 10.6 $e^+ e^- \rightarrow e^+ e^- K^+ K^-$
2231 ± 10	BOOTH	86	OMEG 85 $\pi^- Be \rightarrow 2\phi Be$
2220 ± $\begin{matrix} 90 \\ -20 \end{matrix}$	LINDENBAUM	84	RVUE
2320 ± 40	ETKIN	82	MPS 22 $\pi^- p \rightarrow 2\phi n$

- ¹ Includes data of ETKIN 85. The percentage of the resonance going into $\phi\phi$ 2^{++} , S_2 , D_2 , and D_0 is 6^{+15}_{-5} , 25^{+18}_{-14} , and 69^{+16}_{-27} , respectively.
- ² Threshold enhancement in $\Lambda\bar{\Lambda}$, preferred J^{PC} are 2^{++} , 2^{-+} , or 1^{++} . Could be another state.
- ³ Spin 2 preferred, tentatively assigned to $f_2(2300)$.

$f_2(2300)$ WIDTH

VALUE (MeV)	DOCUMENT ID	TECN	COMMENT
149 ± 41	¹ ETKIN	88	MPS 22 $\pi^- p \rightarrow \phi \phi n$
• • • We do not use the following data for averages, fits, limits, etc. • • •			
72 ± 5 ± 43	² ABLIKIM	21A1	BES3 3.51-4.60 $e^+ e^- \rightarrow \phi \Lambda \bar{\Lambda}$
145 ± $\begin{matrix} 12+ \\ -27 \end{matrix}$	³ UEHARA	13	BELL $\gamma\gamma \rightarrow K_S^0 K_S^0$
90 ± 29	VLADIMIRSK...06	SPEC	40 $\pi^- p \rightarrow K_S^0 K_S^0 n$
275 ± 36 ± 20	ABE	04	BELL 10.6 $e^+ e^- \rightarrow e^+ e^- K^+ K^-$
133 ± 50	BOOTH	86	OMEG 85 $\pi^- Be \rightarrow 2\phi Be$
200 ± 50	LINDENBAUM	84	RVUE
220 ± 70	ETKIN	82	MPS 22 $\pi^- p \rightarrow 2\phi n$

- ¹ Includes data of ETKIN 85.
- ² Threshold enhancement in $\Lambda\bar{\Lambda}$, preferred J^{PC} are 2^{++} , 2^{-+} , or 1^{++} . Could be another state.
- ³ Spin 2 preferred, tentatively assigned to $f_2(2300)$.

$f_2(2300)$ DECAY MODES

Mode	Fraction (Γ_i/Γ)
Γ_1 $\phi\phi$	seen
Γ_2 $K\bar{K}$	seen
Γ_3 $\gamma\gamma$	seen
Γ_4 $\Lambda\bar{\Lambda}$	seen

$f_2(2300)$ $\Gamma(i)\Gamma(\gamma\gamma)/\Gamma(\text{total})$

$\Gamma(K\bar{K}) \times \Gamma(\gamma\gamma)/\Gamma(\text{total})$	DOCUMENT ID	TECN	COMMENT	$\Gamma_2\Gamma_3/\Gamma$
• • • We do not use the following data for averages, fits, limits, etc. • • •				
$3.2^{+0.5+1.3}_{-0.4-2.2}$	UEHARA	13	BELL $\gamma\gamma \rightarrow K_S^0 K_S^0$	
44 ± 6 ± 12	¹ ABE	04	BELL 10.6 $e^+ e^- \rightarrow e^+ e^- K^+ K^-$	

¹ Assuming spin 2.

$f_2(2340)$ BRANCHING RATIOS

$\Gamma(\phi\phi)/\Gamma(\text{total})$	DOCUMENT ID	TECN	COMMENT	Γ_1/Γ
VALUE				
seen	BOOTH	86	OMEG 85 $\pi^- Be \rightarrow 2\phi Be$	
seen	ETKIN	82	MPS 22 $\pi^- p \rightarrow 2\phi n$	

$\Gamma(K\bar{K})/\Gamma(\text{total})$	DOCUMENT ID	TECN	COMMENT	Γ_2/Γ
VALUE				
seen	VLADIMIRSK...06	SPEC	40 $\pi^- p \rightarrow K_S^0 K_S^0 n$	
seen	ABE	04	BELL 10.6 $e^+ e^- \rightarrow e^+ e^- K^+ K^-$	

$\Gamma(\gamma\gamma)/\Gamma(\text{total})$	DOCUMENT ID	TECN	COMMENT	Γ_3/Γ
VALUE				
seen	UEHARA	13	BELL $\gamma\gamma \rightarrow K_S^0 K_S^0$	

$\Gamma(\Lambda\bar{\Lambda})/\Gamma(\text{total})$	DOCUMENT ID	TECN	COMMENT	Γ_4/Γ
VALUE				
seen	¹ ABLIKIM	21A1	BES3 3.51-4.60 $e^+ e^- \rightarrow \phi \Lambda \bar{\Lambda}$	

¹ Threshold enhancement in $\Lambda\bar{\Lambda}$, preferred J^{PC} are 2^{++} , 2^{-+} , or 1^{++} . Could be another state.

$f_2(2300)$ REFERENCES

ABLIKIM	21A1	PR D104 052006	M. Ablikim et al.	(BESIII Collab.)
UEHARA	13	PTEP 2013 123C01	S. Uehara et al.	(BELLE Collab.)
VLADIMIRSK...06	06	PAN 69 493	V.V. Vladimirov et al.	(ITEP, Moscow)
		Translated from YAF 69 515.		
ABE	04	EPJ C32 323	K. Abe et al.	(BELLE Collab.)
ETKIN	88	PL B201 568	A. Etkin et al.	(BNL, CUNY)
BOOTH	86	NP B273 677	P.S.L. Booth et al.	(LIVP, GLAS, CERN)
ETKIN	85	PL 165B 217	A. Etkin et al.	(BNL, CUNY)
LINDENBAUM	84	CNPP 13 285	S.J. Lindenbaum	(CUNY)
ETKIN	82	PRL 49 1620	A. Etkin et al.	(BNL, CUNY)

$f_4(2300)$

$$I^G(J^{PC}) = 0^+(4^{++})$$

OMITTED FROM SUMMARY TABLE

This entry was previously called $U_0(2350)$. Contains results mostly from formation experiments. For further production experiments see the Further States entry. See also $\rho(2150)$, $f_2(2150)$, $\rho_3(2250)$, $\rho_5(2350)$.

$f_4(2300)$ MASS

$\bar{p}p \rightarrow \pi\pi$ or $\bar{K}K$	DOCUMENT ID	TECN	COMMENT
VALUE (MeV)			
• • • We do not use the following data for averages, fits, limits, etc. • • •			
~ 2314	HASAN	94	RVUE $\bar{p}p \rightarrow \pi\pi$
~ 2300	¹ MARTIN	80B	RVUE
~ 2300	¹ MARTIN	80C	RVUE
~ 2340	² CARTER	78B	CNTR 0.7-2.4 $\bar{p}p \rightarrow K^- K^+$
~ 2330	DULUDE	78B	OSPK 1-2 $\bar{p}p \rightarrow \pi^0 \pi^0$
~ 2310	³ CARTER	77	CNTR 0.7-2.4 $\bar{p}p \rightarrow \pi\pi$

- ¹ $I(J^P) = 0(4^+)$ from simultaneous analysis of $\bar{p}p \rightarrow \pi^- \pi^+$ and $\pi^0 \pi^0$.
- ² $I(J^P) = 0(4^+)$ from Barrelet-zero analysis.
- ³ $I(J^P) = 0(4^+)$ from amplitude analysis.

S-CHANNEL $\bar{p}p$ or $\bar{N}N$

VALUE (MeV)	DOCUMENT ID	TECN	COMMENT
• • • We do not use the following data for averages, fits, limits, etc. • • •			
2283 ± 17	⁴ ANISOVICH	00J	SPEC
~ 2380	⁵ CUTTS	78B	CNTR 0.97-3 $\bar{p}p \rightarrow \bar{N}N$
2345 ± 15	^{5,6} COUPLAND	77	CNTR 0.7-2.4 $\bar{p}p \rightarrow \bar{p}p$
2359 ± 2	^{5,7} ALSPECTOR	73	CNTR $\bar{p}p$ S channel
2375 ± 10	ABRAMS	70	CNTR S channel $\bar{N}N$

- ⁴ From the combined analysis of ANISOVICH 99c and ANISOVICH 99f on $\bar{p}p \rightarrow \eta \pi^0 \pi^0$, $\pi^0 \pi^0$, $\eta\eta$, $\eta\eta'$, $\pi^+ \pi^-$.
- ⁵ Isospins 0 and 1 not separated.
- ⁶ From a fit to the total elastic cross section.
- ⁷ Referred to as U or U region by ALSPECTOR 73.

$\pi^- p \rightarrow \eta \pi \pi n$

VALUE (MeV)	DOCUMENT ID	TECN	COMMENT
• • • We do not use the following data for averages, fits, limits, etc. • • •			
2330 ± 20 ± 40	AMELIN	00	VES 37 $\pi^- p \rightarrow \eta \pi^+ \pi^- n$

$\rho\rho$ CENTRAL PRODUCTION

VALUE (MeV)	DOCUMENT ID	COMMENT
2320 ± 60 OUR ESTIMATE		
• • • We do not use the following data for averages, fits, limits, etc. • • •		
2332 ± 15	BARBERIS	00F 450 $\rho\rho \rightarrow \rho_f \omega \rho_s$

See key on page 1171

Meson Particle Listings

$f_4(2300)$, $f_0(2330)$, $f_2(2340)$

$f_4(2300)$ WIDTH

$\bar{p}p \rightarrow \pi\pi$ or $\bar{K}K$

VALUE (MeV)	DOCUMENT ID	TECN	COMMENT
•••	We do not use the following data for averages, fits, limits, etc. •••		
~ 278	HASAN 94	RVUE	$\bar{p}p \rightarrow \pi\pi$
~ 200	⁸ MARTIN 80C	RVUE	
~ 150	⁹ CARTER 78B	CNTR	0.7-2.4 $\bar{p}p \rightarrow K^-K^+$
~ 210	¹⁰ CARTER 77	CNTR	0.7-2.4 $\bar{p}p \rightarrow \pi\pi$
⁸ $I(J^P) = 0(4^+)$ from simultaneous analysis of $p\bar{p} \rightarrow \pi^-\pi^+$ and $\pi^0\pi^0$.			
⁹ $I(J^P) = 0(4^+)$ from Barrelet-zero analysis.			
¹⁰ $I(J^P) = 0(4^+)$ from amplitude analysis.			

S-CHANNEL $\bar{p}p$ or $\bar{N}N$

VALUE (MeV)	DOCUMENT ID	TECN	COMMENT
•••	We do not use the following data for averages, fits, limits, etc. •••		
310 ± 25	¹¹ ANISOVICH 00J	SPEC	
135 ⁺¹⁵⁰ - 65	^{12,13} COUPLAND 77	CNTR	0.7-2.4 $\bar{p}p \rightarrow \bar{p}p$
165 ⁺¹⁸ - 8	¹³ ALSPECTOR 73	CNTR	$\bar{p}p$ S channel
~ 190	ABRAMS 70	CNTR	S channel $\bar{N}N$
¹¹ From the combined analysis of ANISOVICH 99C and ANISOVICH 99F on $\bar{p}p \rightarrow \eta\pi^0\pi^0$, $\pi^0\pi^0$, $\eta\eta$, $\eta\eta'$, $\pi^+\pi^-$.			
¹² From a fit to the total elastic cross section.			
¹³ Isospins 0 and 1 not separated.			

$\pi^-\rho \rightarrow \eta\pi\pi$

VALUE (MeV)	DOCUMENT ID	TECN	COMMENT
•••	We do not use the following data for averages, fits, limits, etc. •••		
235 ± 50 ± 40	AMELIN 00	VES	37 $\pi^-\rho \rightarrow \eta\pi^+\pi^-n$

pp CENTRAL PRODUCTION

VALUE (MeV)	DOCUMENT ID	COMMENT
250 ± 80 OUR ESTIMATE		
•••	We do not use the following data for averages, fits, limits, etc. •••	
260 ± 57	BARBERIS 00F	450 $pp \rightarrow p_f\omega p_S$

$f_4(2300)$ DECAY MODES

Mode	Fraction (Γ_i/Γ)
Γ_1 $\rho\rho$	seen
Γ_2 $\omega\omega$	seen
Γ_3 $\eta\pi\pi$	seen
Γ_4 $\pi\pi$	seen
Γ_5 $K\bar{K}$	seen
Γ_6 $N\bar{N}$	seen

$f_4(2300)$ BRANCHING RATIOS

$\Gamma(\rho\rho)/\Gamma(\omega\omega)$	Γ_1/Γ_2	
•••	We do not use the following data for averages, fits, limits, etc. •••	
2.8 ± 0.5	BARBERIS 00F	450 $pp \rightarrow p_f\omega p_S$

$f_4(2300)$ REFERENCES

AMELIN 00 NP A668 83	D. Amelin et al.	(VES Collab.)
ANISOVICH 00J PL B491 47	A.V. Anisovich et al.	(RAL, LOQM, PNPI+)
BARBERIS 00F PL B484 198	D. Barberis et al.	(WA 102 Collab.)
ANISOVICH 99C PL B452 173	A.V. Anisovich et al.	
ANISOVICH 99F NP A651 253	A.V. Anisovich et al.	
HASAN 94 PL B334 215	A. Hasan, D.V. Bugg	(LOQM)
MARTIN 80B NP B176 355	B.R. Martin, D. Morgan	(LOUC, RHEL)JP
MARTIN 80C NP B169 216	A.D. Martin, M.R. Pennington	(DURH)JP
CARTER 78B NP B141 467	A.A. Carter	(LOQM)
CUTTS 78B PR D17 16	D. Cutts et al.	(STON, WIS C)
DULUDE 78B PL 79B 335	R.S. Dulude et al.	(BROW, MIT, BARI)JP
CARTER 77 PL 67B 117	A.A. Carter et al.	(LOQM, RHEL)JP
COUPLAND 77 PL 71B 460	M. Coupland et al.	(LOQM, RHEL)
ALSPECTOR 73 PRL 30 511	J. Alspector et al.	(RUTG, UPNJ)
ABRAMS 70 PR D1 1917	R.J. Abrams et al.	(BNL)

$f_0(2330)$

$$I^G(J^{PC}) = 0^+(0^{++})$$

OMITTED FROM SUMMARY TABLE

$f_0(2330)$ MASS

VALUE (MeV)	DOCUMENT ID	TECN	COMMENT
•••	We do not use the following data for averages, fits, limits, etc. •••		
2312 ± 7 ⁺⁷ - 3	¹ ABLIKIM 22As BES3		$J/\psi(1S) \rightarrow \gamma\eta\eta'$
2312 ± 2 ⁺¹⁰ - 0	² ABLIKIM 22c BES3		$J/\psi \rightarrow \gamma\eta'\eta' \rightarrow 4/5\gamma 2(\pi^+\pi^-)$
2419 ± 64	³ RODAS 22 RVUE		$J/\psi(1S) \rightarrow \gamma(\pi\pi, K\bar{K})$

2340 ± 20	SARANTSEV 21 RVUE		$J/\psi(1S) \rightarrow \gamma(\pi\pi, K\bar{K}, \eta\eta, \omega\phi)$
2314 ± 25	⁴ BUGG 04A RVUE		
2337 ± 14	ANISOVICH 00J SPEC		2.0 $\bar{p}p \rightarrow \pi\pi, \eta\eta$
~ 2321	HASAN 94 RVUE		$\bar{p}p \rightarrow \pi\pi$

- From a Breit-Wigner fit involving 9 resonances and a resonating exotic $\eta_1(1855) \rightarrow \eta\eta'$ P-wave.
- From a partial wave analysis of the systems (γX), with $X \rightarrow \eta'\eta'$, and ($\eta'X$), with $X \rightarrow \gamma\eta'$ in the decay $J/\psi \rightarrow \gamma\eta'\eta'$. The intermediate resonance X is parametrized by a constant-width, relativistic Breit-Wigner.
- T-matrix pole from coupled channel K-matrix fit to data on $J/\psi \rightarrow \gamma\pi^0\pi^0$ (ABLIKIM 15AE) and $J/\psi \rightarrow \gamma K_S^0 K_S^0$ (ABLIKIM 18AA).
- Partial wave analysis of the data on $p\bar{p} \rightarrow \bar{\Lambda}\Lambda$ from BARNES 00.

$f_0(2330)$ WIDTH

VALUE (MeV)	DOCUMENT ID	TECN	COMMENT
•••	We do not use the following data for averages, fits, limits, etc. •••		
65 ± 10 ⁺³ - 12	¹ ABLIKIM 22As BES3		$J/\psi(1S) \rightarrow \gamma\eta\eta'$
134 ± 5 ⁺³⁰ - 9	² ABLIKIM 22c BES3		$J/\psi \rightarrow \gamma\eta'\eta' \rightarrow 4/5\gamma 2(\pi^+\pi^-)$
274 ± 94	³ RODAS 22 RVUE		$J/\psi(1S) \rightarrow \gamma(\pi\pi, K\bar{K})$
165 ± 25	SARANTSEV 21 RVUE		$J/\psi(1S) \rightarrow \gamma(\pi\pi, K\bar{K}, \eta\eta, \omega\phi)$
144 ± 20	⁴ BUGG 04A RVUE		
217 ± 33	ANISOVICH 00J SPEC		2.0 $\bar{p}p \rightarrow \pi\pi, \eta\eta$
~ 223	HASAN 94 RVUE		$\bar{p}p \rightarrow \pi\pi$

- From a Breit-Wigner fit involving 9 resonances and a resonating exotic $\eta_1(1855) \rightarrow \eta\eta'$ P-wave.
- From a partial wave analysis of the systems (γX), with $X \rightarrow \eta'\eta'$, and ($\eta'X$), with $X \rightarrow \gamma\eta'$ in the decay $J/\psi \rightarrow \gamma\eta'\eta'$. The intermediate resonance X is parametrized by a constant-width, relativistic Breit-Wigner.
- T-matrix pole from coupled channel K-matrix fit to data on $J/\psi \rightarrow \gamma\pi^0\pi^0$ (ABLIKIM 15AE) and $J/\psi \rightarrow \gamma K_S^0 K_S^0$ (ABLIKIM 18AA).
- Partial wave analysis of the data on $p\bar{p} \rightarrow \bar{\Lambda}\Lambda$ from BARNES 00.

$f_0(2330)$ REFERENCES

ABLIKIM 22As PR D106 072012	M. Ablikim et al.	(BESIII Collab.)
Also PR D107 079901 (errata)	M. Ablikim et al.	(BESIII Collab.)
ABLIKIM 22C PR D105 072002	M. Ablikim et al.	(BESIII Collab.)
RODAS 22 EPJ C82 80	A. Rodas et al.	(JPAC Collab.)
SARANTSEV 21 PL B816 136227	A.V. Sarantsev et al.	(BONN, PNPI)
ABLIKIM 18AA PR D98 072003	M. Ablikim et al.	(BESIII Collab.)
ABLIKIM 15AE PR D92 052003	M. Ablikim et al.	(BESIII Collab.)
BUGG 04A EPJ C36 161	D.V. Bugg	
ANISOVICH 00J PL B491 47	A.V. Anisovich et al.	(RAL, LOQM, PNPI+)
BARNES 00 PR C62 055203	P.D. Barnes et al.	
HASAN 94 PL B334 215	A. Hasan, D.V. Bugg	(LOQM)

$f_2(2340)$

$$I^G(J^{PC}) = 0^+(2^{++})$$

$f_2(2340)$ MASS

VALUE (MeV)	EVTS	DOCUMENT ID	TECN	COMMENT
2346 ⁺²¹ - 10 OUR AVERAGE				
2346 ± 8 ⁺²² - 6		¹ ABLIKIM 22c BES3		$J/\psi \rightarrow \gamma\eta'\eta' \rightarrow 4/5\gamma 2(\pi^+\pi^-)$
2362 ⁺³¹ - 30 ⁺¹⁴⁰ - 63	5.5k	² ABLIKIM 13N BES3		$e^+e^- \rightarrow J/\psi \rightarrow \gamma\eta\eta$
2339 ± 55		³ ETKIN 88 MPS		22 $\pi^-\rho \rightarrow \phi\phi n$
•••	We do not use the following data for averages, fits, limits, etc. •••			
2350 ± 7	80k	⁴ UMAN 06 E835		5.2 $\bar{p}p \rightarrow \eta\eta\pi^0$
2392 ± 10		BOOTH 86 OMEG		85 $\pi^-\text{Be} \rightarrow 2\phi\text{Be}$
2360 ± 20		LINDENBAUM 84 RVUE		

- From a partial wave analysis of the systems (γX), with $X \rightarrow \eta'\eta'$, and ($\eta'X$), with $X \rightarrow \gamma\eta'$ in the decay $J/\psi \rightarrow \gamma\eta'\eta'$. The intermediate resonance X is parametrized by a constant-width, relativistic Breit-Wigner.
- From partial wave analysis including all possible combinations of 0^{++} , 2^{++} , and 4^{++} resonances.
- Includes data of ETKIN 85. The percentage of the resonance going into $\phi\phi 2^{++} S_2$, D_2 , and D_0 is 37 ± 19, 4 ⁺¹² - 4, and 59 ⁺²¹ - 19, respectively.
- Statistical error only.

$f_2(2340)$ WIDTH

VALUE (MeV)	EVTS	DOCUMENT ID	TECN	COMMENT
331 ⁺²⁷ - 18 OUR AVERAGE				
332 ± 14 ⁺²⁶ - 12		¹ ABLIKIM 22c BES3		$J/\psi \rightarrow \gamma\eta'\eta' \rightarrow 4/5\gamma 2(\pi^+\pi^-)$
334 ⁺⁶² - 54 ⁺¹⁶⁵ - 100	5.5k	² ABLIKIM 13N BES3		$e^+e^- \rightarrow J/\psi \rightarrow \gamma\eta\eta$
319 ⁺⁸¹ - 69		³ ETKIN 88 MPS		22 $\pi^-\rho \rightarrow \phi\phi n$

Meson Particle Listings

$f_2(2340)$, $\rho_5(2350)$, $X(2370)$

••• We do not use the following data for averages, fits, limits, etc. •••

218 ± 16	80k	4 UMAN	06	E835	5.2	$\bar{p}p \rightarrow \eta\eta\pi^0$
198 ± 50		BOOTH	86	OMEG	85	$\pi^- \text{Be} \rightarrow 2\phi\text{Be}$
150 ⁺¹⁵⁰ ₋₅₀		LINDENBAUM	84	RVUE		

- From a partial wave analysis of the systems (γX), with $X \rightarrow \eta'\eta'$, and ($\eta' X$), with $X \rightarrow \gamma\eta'$ in the decay $J/\psi \rightarrow \gamma\eta'\eta'$. The intermediate resonance X is parametrized by a constant-width, relativistic Breit-Wigner.
- From partial wave analysis including all possible combinations of 0^{++} , 2^{++} , and 4^{++} resonances.
- Includes data of ETKIN 85.
- Statistical error only.

$f_2(2340)$ DECAY MODES

Mode	Fraction (Γ_i/Γ)
Γ_1 $\phi\phi$	seen
Γ_2 $\eta\eta$	seen
Γ_3 $\eta'\eta'$	seen

$f_2(2340)$ BRANCHING RATIOS

$\Gamma(\eta\eta)/\Gamma_{\text{total}}$	Γ_2/Γ			
VALUE	DOCUMENT ID	TECN	CHG	COMMENT
seen	UMAN	06	E835	5.2 $\bar{p}p \rightarrow \eta\eta\pi^0$

$\Gamma(\eta'\eta')/\Gamma_{\text{total}}$	Γ_3/Γ			
VALUE	DOCUMENT ID	TECN	CHG	COMMENT
seen	¹ ABLIKIM	22c	BES3	$J/\psi \rightarrow \gamma\eta'\eta' \rightarrow 4/5\gamma 2(\pi^+\pi^-)$

- From a partial wave analysis of the systems (γX), with $X \rightarrow \eta'\eta'$, and ($\eta' X$), with $X \rightarrow \gamma\eta'$ in the decay $J/\psi \rightarrow \gamma\eta'\eta'$. The intermediate resonance X is parametrized by a constant-width, relativistic Breit-Wigner.

$f_2(2340)$ REFERENCES

ABLIKIM	22c	PR D105 072002	M. Ablikim et al.	(BESIII Collab.)
ABLIKIM	13n	PR D87 092009	M. Ablikim et al.	(BESIII Collab.)
UMAN	06	PR D73 052009	I. Uman et al.	(FNAL E835)
ETKIN	85	PL B201 959	A. Etkin et al.	(BNL, CUNY)
BOOTH	86	NP B373 677	P.S.L. Booth et al.	(LIVP, GLAS, CERN)
ETKIN	85	PL 165B 217	A. Etkin et al.	(BNL CUNY)
LINDENBAUM	84	CNPP 13 285	S.J. Lindenbaum	(CUNY)

$\rho_5(2350)$

$$I^G(J^{PC}) = 1^+(5^{--})$$

OMITTED FROM SUMMARY TABLE
 This entry was previously called $U_1(2400)$. See also $\rho(2150)$, $f_2(2150)$, $\rho_3(2250)$, $f_4(2300)$.

$\rho_5(2350)$ MASS

$\pi^- p \rightarrow \omega\pi^0 n$	VALUE (MeV)	DOCUMENT ID	TECN	CHG	COMMENT
2330 ± 35		ALDE	95	GAM2	38 $\pi^- p \rightarrow \omega\pi^0 n$

$\bar{p}p \rightarrow \pi\pi$ or $\bar{K}K$

VALUE (MeV)	DOCUMENT ID	TECN	CHG	COMMENT
••• We do not use the following data for averages, fits, limits, etc. •••				
~ 2303	HASAN	94	RVUE	$\bar{p}p \rightarrow \pi\pi$
~ 2300	¹ MARTIN	80B	RVUE	
~ 2250	¹ MARTIN	80C	RVUE	
~ 2500	² CARTER	78B	CNTR 0	0.7-2.4 $\bar{p}p \rightarrow K^- K^+$
~ 2480	³ CARTER	77	CNTR 0	0.7-2.4 $\bar{p}p \rightarrow \pi\pi$

S-CHANNEL $\bar{N}N$

VALUE (MeV)	DOCUMENT ID	TECN	CHG	COMMENT
••• We do not use the following data for averages, fits, limits, etc. •••				
2300 ± 45	⁴ ANISOVICH	02	SPEC	0.6-1.9 $p\bar{p} \rightarrow \omega\pi^0$, $\omega\eta\pi^0, \pi^+\pi^-$
2295 ± 30	ANISOVICH	00J	SPEC	
~ 2380	⁵ CUTTS	78B	CNTR	0.97-3 $\bar{p}p \rightarrow \bar{N}N$
2345 ± 15	^{5,6} COUPLAND	77	CNTR 0	0.7-2.4 $\bar{p}p \rightarrow \bar{p}p$
2359 ± 2	^{5,7} ALSPECTOR	73	CNTR	$\bar{p}p$ S channel
2350 ± 10	⁸ ABRAMS	70	CNTR	S channel $\bar{N}N$
2360 ± 25	⁹ OH	70B	HDBC -0	$\bar{p}(p,n), K^* K 2\pi$

$\pi^- p \rightarrow K^+ K^- n$

VALUE (MeV)	DOCUMENT ID	TECN	CHG	COMMENT
••• We do not use the following data for averages, fits, limits, etc. •••				
2307 ± 6	ALPER	80	CNTR 0	62 $\pi^- p \rightarrow K^+ K^- n$
¹ $I(J^P) = 1(5^-)$				from simultaneous analysis of $p\bar{p} \rightarrow \pi^- \pi^+$ and $\pi^0 \pi^0$.

² $I = 0(1); J^P = 5^-$ from Barrelet-zero analysis.

³ $I(J^P) = 1(5^-)$ from amplitude analysis.

⁴ From the combined analysis of ANISOVICH 00J, ANISOVICH 01D, ANISOVICH 01E, and ANISOVICH 02.

⁵ Isospins 0 and 1 not separated.

⁶ From a fit to the total elastic cross section.

⁷ Referred to as U or U region by ALSPECTOR 73.

⁸ For $I = 1 \bar{N}N$.

⁹ No evidence for this bump seen in the $\bar{p}p$ data of CHAPMAN 71B. Narrow state not confirmed by OH 73 with more data.

$\rho_5(2350)$ WIDTH

$\pi^- p \rightarrow \omega\pi^0 n$

VALUE (MeV)	DOCUMENT ID	TECN	CHG	COMMENT
400 ± 100	ALDE	95	GAM2	38 $\pi^- p \rightarrow \omega\pi^0 n$

$\bar{p}p \rightarrow \pi\pi$ or $\bar{K}K$

VALUE (MeV)	DOCUMENT ID	TECN	CHG	COMMENT
••• We do not use the following data for averages, fits, limits, etc. •••				
~ 169	HASAN	94	RVUE	$\bar{p}p \rightarrow \pi\pi$
~ 250	¹⁰ MARTIN	80B	RVUE	
~ 300	¹⁰ MARTIN	80C	RVUE	
~ 150	¹¹ CARTER	78B	CNTR 0	0.7-2.4 $\bar{p}p \rightarrow K^- K^+$
~ 210	¹² CARTER	77	CNTR 0	0.7-2.4 $\bar{p}p \rightarrow \pi\pi$

S-CHANNEL $\bar{N}N$

VALUE (MeV)	DOCUMENT ID	TECN	CHG	COMMENT
••• We do not use the following data for averages, fits, limits, etc. •••				
260 ± 75	¹³ ANISOVICH	02	SPEC	0.6-1.9 $p\bar{p} \rightarrow \omega\pi^0$, $\omega\eta\pi^0, \pi^+\pi^-$
235 ± ⁶⁵ ₄₀	ANISOVICH	00J	SPEC	
135 ± ¹⁵⁰ ₆₅	^{14,15} COUPLAND	77	CNTR 0	0.7-2.4 $\bar{p}p \rightarrow \bar{p}p$
165 ± ¹⁸ ₈	¹⁵ ALSPECTOR	73	CNTR	$\bar{p}p$ S channel
< 60	¹⁶ OH	70B	HDBC -0	$\bar{p}(p,n), K^* K 2\pi$
~ 140	ABRAMS	67C	CNTR	S channel $\bar{p}N$

$\pi^- p \rightarrow K^+ K^- n$

VALUE (MeV)	DOCUMENT ID	TECN	CHG	COMMENT
••• We do not use the following data for averages, fits, limits, etc. •••				
245 ± 20	ALPER	80	CNTR 0	62 $\pi^- p \rightarrow K^+ K^- n$
¹⁰ $I(J^P) = 1(5^-)$				from simultaneous analysis of $p\bar{p} \rightarrow \pi^- \pi^+$ and $\pi^0 \pi^0$.
¹¹ $I = 0(1); J^P = 5^-$				from Barrelet-zero analysis.
¹² $I(J^P) = 1(5^-)$				from amplitude analysis.
¹³ From the combined analysis of ANISOVICH 00J, ANISOVICH 01D, ANISOVICH 01E, and ANISOVICH 02.				
¹⁴ From a fit to the total elastic cross section.				
¹⁵ Isospins 0 and 1 not separated.				
¹⁶ No evidence for this bump seen in the $\bar{p}p$ data of CHAPMAN 71B. Narrow state not confirmed by OH 73 with more data.				

$\rho_5(2350)$ REFERENCES

ANISOVICH	02	PL B542 8	A.V. Anisovich et al.	
ANISOVICH	01D	PL B508 6	A.V. Anisovich et al.	
ANISOVICH	01E	PL B513 281	A.V. Anisovich et al.	
ANISOVICH	00J	PL B491 47	A.V. Anisovich et al.	(RAL, LOQM, PNP1+)
ALDE	95	ZPHY C66 379	D.M. Alde et al.	(GAMS Collab.)JP
HASAN	94	PL B334 215	A. Hasan, D.V. Bugg	(LOQM)
ALPER	80	PL 94B 422	B. Alper et al.	(AMST, CERN, CRAC, MPIM+)
MARTIN	80B	NP B176 355	B.R. Martin, D. Morgan	(LOUC, RHEL)JP
MARTIN	80C	NP B169 216	A.D. Martin, M.R. Pennington	(DURH)JP
CARTER	78B	NP B141 467	A.A. Carter	(LOQM)
CUTTS	78B	PR D17 16	D. Cutts et al.	(STON, WIS C)
CARTER	77	PL 67B 117	A.A. Carter et al.	(LOQM, RHEL)JP
COUPLAND	77	PL 71B 460	M. Coupland et al.	(LOQM, RHEL)
ALSPECTOR	73	PRL 30 511	J. Alspector et al.	(RUTG, UPNI)
OH	73	NP B51 57	B.Y. Oh et al.	(MSU)
CHAPMAN	71B	PR D4 1275	J.W. Chapman et al.	(MICH)
ABRAMS	70	PR D1 1917	R.J. Abrams et al.	(BNL)
OH	70B	PRL 24 1257	B.Y. Oh et al.	(MSU)
ABRAMS	67C	PRL 18 1209	R.J. Abrams et al.	(BNL)

$X(2370)$

$$I^G(J^{PC}) = ?(???)$$

OMITTED FROM SUMMARY TABLE

$X(2370)$ MASS

VALUE (MeV)	EVTS	DOCUMENT ID	TECN	COMMENT
2341.6 ± 6.5 ± 5.7		¹ ABLIKIM	20q	BES3 $J/\psi \rightarrow \gamma K \bar{K} \eta'$
2376.3 ± 8.7 ^{+3.2} _{-4.3}	565	ABLIKIM	11c	BES3 $J/\psi \rightarrow \gamma\pi^+\pi^-\eta'$

- The state observed by ABLIKIM 11c at 2120 MeV is not observed with 90% CL upper limit of 1.49×10^{-5} for $J/\psi \rightarrow \gamma X(2120) \rightarrow \gamma K^+ K^- \eta'$ and 6.38×10^{-6} for $K_S^0 K_S^0 \eta'$.

See key on page 1171

Meson Particle Listings
X(2370), $f_0(2470)$, $f_6(2510)$

X(2370) WIDTH

VALUE (MeV)	DOCUMENT ID	TECN	COMMENT
114^{+12}_{-10} OUR AVERAGE			
$117 \pm 10 \pm 8$	¹ ABLIKIM	20Q BES3	$J/\psi \rightarrow \gamma K \bar{K} \eta'$
$83 \pm 17^{+44}_{-6}$	ABLIKIM	11c BES3	$J/\psi \rightarrow \gamma \pi^+ \pi^- \eta'$

¹ The state observed by ABLIKIM 11c at 2120 MeV is not observed with 90% CL upper limit of 1.49×10^{-5} for $J/\psi \rightarrow \gamma X(2120) \rightarrow \gamma K^+ K^- \eta'$ and 6.38×10^{-6} for $K_S^0 K_S^0 \eta'$.

X(2370) DECAY MODES

Mode	Fraction (Γ_i/Γ)
Γ_1 $K^+ K^- \eta'$	seen
Γ_2 $K_S^0 K_S^0 \eta'$	seen
Γ_3 $\pi^+ \pi^- \eta'$	seen
Γ_4 $\eta \eta \eta'$	not seen

X(2370) BRANCHING RATIOS

$\Gamma(K^+ K^- \eta')/\Gamma_{\text{total}}$	DOCUMENT ID	TECN	COMMENT	Γ_1/Γ
seen	ABLIKIM	20Q BES3	$J/\psi \rightarrow \gamma K^+ K^- \eta'$	
$\Gamma(K_S^0 K_S^0 \eta')/\Gamma_{\text{total}}$	DOCUMENT ID	TECN	COMMENT	Γ_2/Γ
seen	ABLIKIM	20Q BES3	$J/\psi \rightarrow \gamma K_S^0 K_S^0 \eta'$	
$\Gamma(\pi^+ \pi^- \eta')/\Gamma_{\text{total}}$	DOCUMENT ID	TECN	COMMENT	Γ_3/Γ
seen	ABLIKIM	11c BES3	$J/\psi \rightarrow \gamma \pi^+ \pi^- \eta'$	
$\Gamma(\eta \eta \eta')/\Gamma_{\text{total}}$	DOCUMENT ID	TECN	COMMENT	Γ_4/Γ
not seen	¹ ABLIKIM	21c BES3	$J/\psi(1S) \rightarrow \gamma \eta \eta \eta'$	

¹ ABLIKIM 21c measured $B(J/\psi(1S) \rightarrow \gamma X(2370) \rightarrow \gamma \eta \eta \eta') < 9.2 \times 10^{-6}$.

X(2370) REFERENCES

ABLIKIM	21c	PR D103 012009	M. Ablikim et al.	(BESIII Collab.)
ABLIKIM	20Q	EPJ C80 746	M. Ablikim et al.	(BESIII Collab.)
ABLIKIM	11c	PRL 106 072002	M. Ablikim et al.	(BESIII Collab.)

 $f_0(2470)$

$$J^G(J^{PC}) = 0^+(0^{++})$$

OMITTED FROM SUMMARY TABLE

Seen by ABLIKIM 22c with a significance of 5.2σ in a partial-wave analysis of the systems (γX) , $X \rightarrow \eta' \eta'$ and $(\eta' X)$, $X \rightarrow \gamma \eta'$ in the decay $J/\psi \rightarrow \gamma \eta' \eta'$.

 $f_0(2470)$ MASS

VALUE (MeV)	DOCUMENT ID	TECN	COMMENT
$2470 \pm 4^{+4}_{-6}$	¹ ABLIKIM	22c BES3	$J/\psi \rightarrow \gamma \eta' \eta' \rightarrow 4/5 \gamma 2(\pi^+ \pi^-)$

¹ From a partial wave analysis of the systems (γX) , with $X \rightarrow \eta' \eta'$, and $(\eta' X)$, with $X \rightarrow \gamma \eta'$ in the decay $J/\psi \rightarrow \gamma \eta' \eta'$. The intermediate resonance X is parametrized by a constant-width, relativistic Breit-Wigner.

 $f_0(2470)$ WIDTH

VALUE (MeV)	DOCUMENT ID	TECN	COMMENT
$75 \pm 9^{+11}_{-8}$	¹ ABLIKIM	22c BES3	$J/\psi \rightarrow \gamma \eta' \eta' \rightarrow 4/5 \gamma 2(\pi^+ \pi^-)$

¹ From a partial wave analysis of the systems (γX) , with $X \rightarrow \eta' \eta'$, and $(\eta' X)$, with $X \rightarrow \gamma \eta'$ in the decay $J/\psi \rightarrow \gamma \eta' \eta'$. The intermediate resonance X is parametrized by a constant-width, relativistic Breit-Wigner.

 $f_0(2470)$ DECAY MODES

Mode	Fraction (Γ_i/Γ)
Γ_1 $\eta' \eta'$	seen

$\Gamma(\eta' \eta')/\Gamma_{\text{total}}$	DOCUMENT ID	TECN	COMMENT	Γ_1/Γ
seen	¹ ABLIKIM	22c BES3	$J/\psi \rightarrow \gamma \eta' \eta' \rightarrow 4/5 \gamma 2(\pi^+ \pi^-)$	

¹ From a partial wave analysis of the systems (γX) , with $X \rightarrow \eta' \eta'$, and $(\eta' X)$, with $X \rightarrow \gamma \eta'$ in the decay $J/\psi \rightarrow \gamma \eta' \eta'$. The intermediate resonance X is parametrized by a constant-width, relativistic Breit-Wigner.

 $f_0(2470)$ REFERENCES

ABLIKIM	22c	PR D105 072002	M. Ablikim et al.	(BESIII Collab.)
---------	-----	----------------	-------------------	------------------

 $f_6(2510)$

$$J^G(J^{PC}) = 0^+(6^{++})$$

OMITTED FROM SUMMARY TABLE

Needs confirmation.

 $f_6(2510)$ MASS

VALUE (MeV)	DOCUMENT ID	TECN	COMMENT
2470 ± 50 OUR AVERAGE			Error includes scale factor of 2.1.
2420 ± 30	ALDE	98 GAM4	$100 \pi^- p \rightarrow \pi^0 \pi^0 n$
2510 ± 30	BINON	84B GAM2	$38 \pi^- p \rightarrow n 2\pi^0$
2485 ± 40	¹ ANISOVICH	00J SPEC	$1.92\text{--}2.41 p\bar{p}$

¹ From the combined analysis of ANISOVICH 99c, ANISOVICH 99f, ANISOVICH 99j, ANISOVICH 99k, and ANISOVICH 00b.

 $f_6(2510)$ WIDTH

VALUE (MeV)	DOCUMENT ID	TECN	COMMENT
260 ± 40 OUR AVERAGE			
270 ± 60	ALDE	98 GAM4	$100 \pi^- p \rightarrow \pi^0 \pi^0 n$
240 ± 60	BINON	84B GAM2	$38 \pi^- p \rightarrow n 2\pi^0$
410 ± 90	² ANISOVICH	00J SPEC	$1.92\text{--}2.41 p\bar{p}$

² From the combined analysis of ANISOVICH 99c, ANISOVICH 99f, ANISOVICH 99j, ANISOVICH 99k, and ANISOVICH 00b.

 $f_6(2510)$ DECAY MODES

Mode	Fraction (Γ_i/Γ)
Γ_1 $\pi \pi$	$(6.0 \pm 1.0) \%$

 $f_6(2510)$ BRANCHING RATIOS

$\Gamma(\pi \pi)/\Gamma_{\text{total}}$	DOCUMENT ID	TECN	COMMENT	Γ_1/Γ
0.06 ± 0.01	³ BINON	83c GAM2	$38 \pi^- p \rightarrow n 4\gamma$	

³ Assuming one pion exchange and using data of BOLOTOV 74.

 $f_6(2510)$ REFERENCES

ANISOVICH	00B	NP A662 319	A.V. Anisovich et al.	
ANISOVICH	00J	PL B491 47	A.V. Anisovich et al.	(RAL, LOQM, PNPI+)
ANISOVICH	99C	PL B452 173	A.V. Anisovich et al.	
ANISOVICH	99F	NP A651 253	A.V. Anisovich et al.	
ANISOVICH	99J	PL B471 271	A.V. Anisovich et al.	
ANISOVICH	99K	PL B468 309	A.V. Anisovich et al.	
ALDE	98	EPJ A3 361	D. Alde et al.	(GAM4 Collab.)
Also		PAN 62 405	D. Alde et al.	(GAMS Collab.)
		Translated from YAF 62 446.		
BINON	84B	LINC 39 41	F.G. Binon et al.	(SERP, BELG, LAPP) JP
BINON	83C	SJNP 38 723	F.G. Binon et al.	(SERP, BRUX+)
		Translated from YAF 38 1199.		
BOLOTOV	74	PL 52B 489	V.N. Bolotov et al.	(SERP)

Meson Particle Listings

 K^\pm

STRANGE MESONS
($S = \pm 1, C = B = 0$)

$K^+ = u\bar{s}, K^0 = d\bar{s}, \bar{K}^0 = \bar{d}s, K^- = \bar{u}s,$ similarly for K^{*s}

 K^\pm

$$I(J^P) = \frac{1}{2}(0^-)$$

CHARGED KAON MASS

Revised 1994 by T.G. Trippe (LBNL).

The average of the six charged kaon mass measurements which we use in the Particle Listings is

$$m_{K^\pm} = 493.677 \pm 0.013 \text{ MeV } (S = 2.4), \quad (1)$$

where the error has been increased by the scale factor S . The large scale factor indicates a serious disagreement between different input data. The average before scaling the error is

$$m_{K^\pm} = 493.677 \pm 0.005 \text{ MeV},$$

$$\chi^2 = 22.9 \text{ for } 5 \text{ D.F.}, \text{ Prob.} = 0.04\%, \quad (2)$$

where the high χ^2 and correspondingly low χ^2 probability further quantify the disagreement.

The main disagreement is between the two most recent and precise results,

$$m_{K^\pm} = 493.696 \pm 0.007 \text{ MeV} \quad \text{DENISOV 91}$$

$$m_{K^\pm} = 493.636 \pm 0.011 \text{ MeV } (S = 1.5) \quad \text{GALL 88}$$

$$\text{Average} = 493.679 \pm 0.006 \text{ MeV}$$

$$\chi^2 = 21.2 \text{ for } 1 \text{ D.F.}, \text{ Prob.} = 0.0004\%, \quad (3)$$

both of which are measurements of x-ray energies from kaonic atoms. Comparing the average in Eq. (3) with the overall average in Eq. (2), it is clear that DENISOV 91 [1] and GALL 88 [2] dominate the overall average, and that their disagreement is responsible for most of the high χ^2 .

The GALL 88 measurement was made using four different kaonic atom transitions, $K^- \text{Pb } (9 \rightarrow 8)$, $K^- \text{Pb } (11 \rightarrow 10)$, $K^- \text{W } (9 \rightarrow 8)$, and $K^- \text{W } (11 \rightarrow 10)$. The m_{K^\pm} values they obtain from each of these transitions is shown in the Particle Listings and in Fig. 1. Their $K^- \text{Pb } (9 \rightarrow 8)$ m_{K^\pm} is below and somewhat inconsistent with their other three transitions. The average of their four measurements is

$$m_{K^\pm} = 493.636 \pm 0.007,$$

$$\chi^2 = 7.0 \text{ for } 3 \text{ D.F.}, \text{ Prob.} = 7.2\%. \quad (4)$$

This is a low but acceptable χ^2 probability so, to be conservative, GALL 88 scaled up the error on their average by $S=1.5$ to obtain their published error ± 0.011 shown in Eq. (3) above and used in the Particle Listings average.

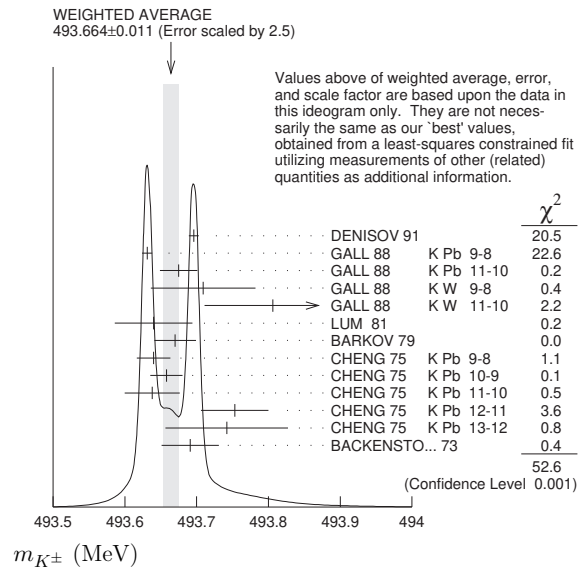


Figure 1: Ideogram of m_{K^\pm} mass measurements. GALL 88 and CHENG 75 measurements are shown separately for each transition they measured.

The ideogram in Fig. 1 shows that the DENISOV 91 measurement and the GALL 88 $K^- \text{Pb } (9 \rightarrow 8)$ measurement yield two well-separated peaks. One might suspect the GALL 88 $K^- \text{Pb } (9 \rightarrow 8)$ measurement since it is responsible both for the internal inconsistency in the GALL 88 measurements and the disagreement with DENISOV 91.

To see if the disagreement could result from a systematic problem with the $K^- \text{Pb } (9 \rightarrow 8)$ transition, we have separated the CHENG 75 [3] data, which also used $K^- \text{Pb}$, into its separate transitions. Figure 1 shows that the CHENG 75 and GALL 88 $K^- \text{Pb } (9 \rightarrow 8)$ values are consistent, suggesting the possibility of a common effect such as contaminant nuclear γ rays near the $K^- \text{Pb } (9 \rightarrow 8)$ transition energy, although the CHENG 75 errors are too large to make a strong conclusion. The average of all 13 measurements has a χ^2 of 52.6 as shown in Fig. 1 and the first line of Table 1, yielding an unacceptable χ^2 probability of 0.00005%. The second line of Table 1 excludes both the GALL 88 and CHENG 75 measurements of the $K^- \text{Pb } (9 \rightarrow 8)$ transition and yields a χ^2 probability of 43%. The third [fourth] line of Table 1 excludes only the GALL 88 $K^- \text{Pb } (9 \rightarrow 8)$ [DENISOV 91] measurement and yields a χ^2 probability of 20% [8.6%]. Table 1 shows that removing both measurements of the $K^- \text{Pb } (9 \rightarrow 8)$ transition produces the most consistent set of data, but that excluding only the GALL 88 $K^- \text{Pb } (9 \rightarrow 8)$ transition or DENISOV 91 also produces acceptable probabilities.

Table 1: m_{K^\pm} averages for some combinations of Fig. 1 data.

m_{K^\pm} (MeV)	χ^2	D.F.	Prob. (%)	Measurements used
493.664 ± 0.004	52.6	12	0.00005	all 13 measurements
493.690 ± 0.006	10.1	10	43	no K^- Pb(9→8)
493.687 ± 0.006	14.6	11	20	no GALL 88 K^- Pb(9→8)
493.642 ± 0.006	17.8	11	8.6	no DENISOV 91

Yu.M. Ivanov, representing DENISOV 91, has estimated corrections needed for the older experiments because of improved ^{192}Ir and ^{198}Au calibration γ -ray energies. He estimates that CHENG 75 and BACKENSTOSS 73 [4] m_{K^\pm} values could be raised by about 15 keV and 22 keV, respectively. With these estimated corrections, Table 1 becomes Table 2. The last line of Table 2 shows that if such corrections are assumed, then GALL 88 K^- Pb (9 → 8) is inconsistent with the rest of the data even when DENISOV 91 is excluded. Yu.M. Ivanov warns that these are rough estimates. Accordingly, we do not use Table 2 to reject the GALL 88 K^- Pb (9 → 8) transition, but we note that a future reanalysis of the CHENG 75 data could be useful because it might provide supporting evidence for such a rejection.

Table 2: m_{K^\pm} averages for some combinations of Fig. 1 data after raising CHENG 75 and BACKENSTOSS 73 values by 0.015 and 0.022 MeV respectively.

m_{K^\pm} (MeV)	χ^2	D.F.	Prob. (%)	Measurements used
493.666 ± 0.004	53.9	12	0.00003	all 13 measurements
493.693 ± 0.006	9.0	10	53	no K^- Pb(9→8)
493.690 ± 0.006	11.5	11	40	no GALL 88 K^- Pb(9→8)
493.645 ± 0.006	23.0	11	1.8	no DENISOV 91

The GALL 88 measurement uses a Ge semiconductor spectrometer which has a resolution of about 1 keV, so they run the risk of some contaminant nuclear γ rays. Studies of γ rays following stopped π^- and Σ^- absorption in nuclei (unpublished) do not show any evidence for contaminants according to GALL 88 spokesperson, B.L. Roberts. The DENISOV 91 measurement uses a crystal diffraction spectrometer with a resolution of 6.3 eV for radiation at 22.1 keV to measure the 4f-3d transition in K^- ^{12}C . The high resolution and the light nucleus reduce the probability for overlap by contaminant γ rays, compared with the measurement of GALL 88. The DENISOV 91 measurement is supported by their high-precision measurement of the 4d-2p transition energy in π^- ^{12}C , which is good agreement with the calculated energy.

While we suspect that the GALL 88 K^- Pb (9 → 8) measurements could be the problem, we are unable to find clear grounds for rejecting it. Therefore, we retain their measurement in the average and accept the large scale factor until further information can be obtained from new measurements and/or from reanalysis of GALL 88 and CHENG 75 data.

We thank B.L. Roberts (Boston Univ.) and Yu.M. Ivanov (Petersburg Nuclear Physics Inst.) for their extensive help in understanding this problem.

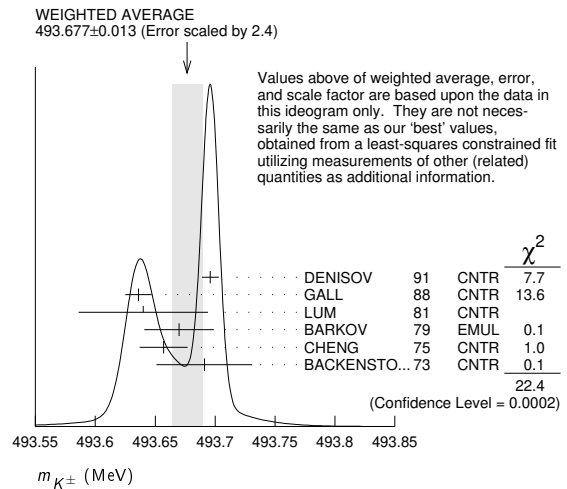
References

1. A.S. Denisov, *et al.* [DENISOV 91], Sov. Phys. JETP Lett. **54**, 558 (1991).
2. K.P. Gall, *et al.* [GALL 88], Phys. Rev. Lett. **60**, 186 (1988).
3. S.C. Cheng, *et al.* [CHENG 75], Nucl. Phys. **A254**, 381 (1975).
4. G. Backenstoss, *et al.* [BACKENSTOSS 73], Phys. Lett. **43B**, 431 (1973).

K^\pm MASS

VALUE (MeV)	DOCUMENT ID	TECN	CHG	COMMENT
493.677 ± 0.015 OUR FIT	Error includes scale factor of 2.8.			
493.677 ± 0.013 OUR AVERAGE	Error includes scale factor of 2.4. See the ideogram below.			
493.696 ± 0.007	¹ DENISOV	91	CNTR	— Kaonic atoms
493.636 ± 0.011	² GALL	88	CNTR	— Kaonic atoms
493.640 ± 0.054	LUM	81	CNTR	— Kaonic atoms
493.670 ± 0.029	BARKOV	79	EMUL	± $e^+ e^- \rightarrow K^+ K^-$
493.657 ± 0.020	² CHENG	75	CNTR	— Kaonic atoms
493.691 ± 0.040	BACKENSTO...73	CNTR	—	Kaonic atoms
● ● ● We do not use the following data for averages, fits, limits, etc. ● ● ●				
493.631 ± 0.007	GALL	88	CNTR	— K^- Pb (9 → 8)
493.675 ± 0.026	GALL	88	CNTR	— K^- Pb (11 → 10)
493.709 ± 0.073	GALL	88	CNTR	— K^- W (9 → 8)
493.806 ± 0.095	GALL	88	CNTR	— K^- W (11 → 10)
$493.640 \pm 0.022 \pm 0.008$	³ CHENG	75	CNTR	— K^- Pb (9 → 8)
$493.658 \pm 0.019 \pm 0.012$	³ CHENG	75	CNTR	— K^- Pb (10 → 9)
$493.638 \pm 0.035 \pm 0.016$	³ CHENG	75	CNTR	— K^- Pb (11 → 10)
$493.753 \pm 0.042 \pm 0.021$	³ CHENG	75	CNTR	— K^- Pb (12 → 11)
$493.742 \pm 0.081 \pm 0.027$	³ CHENG	75	CNTR	— K^- Pb (13 → 12)

¹ Error increased from 0.0059 based on the error analysis in IVANOV 92.
² This value is the authors' combination of all of the separate transitions listed for this paper.
³ The CHENG 75 values for separate transitions were calculated from their Table 7 transition energies. The first error includes a 20% systematic error in the noncircular contaminant shift. The second error is due to a ± 5 eV uncertainty in the theoretical transition energies.



$m_{K^+} - m_{K^-}$

Test of CPT.

VALUE (MeV)	EVTS	DOCUMENT ID	TECN	CHG
-0.032 ± 0.090	1.5 M	¹ FORD	72	ASPK ±

¹ FORD 72 uses $m_{\pi^+} - m_{\pi^-} = +28 \pm 70$ keV.

Meson Particle Listings

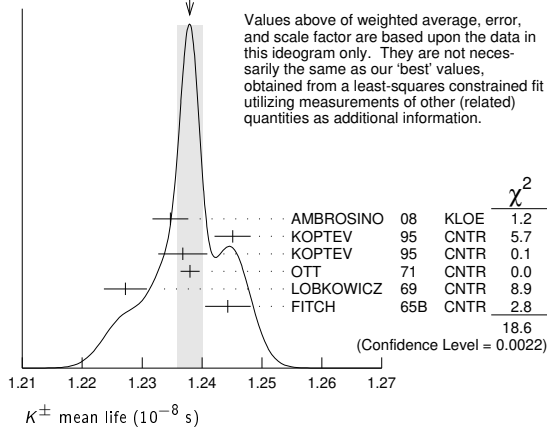
K^\pm

K^\pm MEAN LIFE

VALUE (10^{-8} s)	EVTS	DOCUMENT ID	TECN	CHG	COMMENT
1.2380 ± 0.0020 OUR FIT		Error includes scale factor of 1.8.			
1.2379 ± 0.0021 OUR AVERAGE		Error includes scale factor of 1.9. See the ideogram below.			
1.2347 ± 0.0030	15M	¹ AMBROSINO	08	KLOE ±	$\phi \rightarrow K^+ K^-$
1.2451 ± 0.0030	250k	KOPTEV	95	CNTR	K at rest, U target
1.2368 ± 0.0041	150k	KOPTEV	95	CNTR	K at rest, Cu target
1.2380 ± 0.0016	3M	OTT	71	CNTR +	K at rest
1.2272 ± 0.0036		LOBKOWICZ	69	CNTR +	K in flight
1.2443 ± 0.0038		FITCH	65B	CNTR +	K at rest
• • • We do not use the following data for averages, fits, limits, etc. • • •					
1.2415 ± 0.0024	400k	² KOPTEV	95	CNTR	K at rest
1.221 ± 0.011		FORD	67	CNTR ±	
1.231 ± 0.011		BOYARSKI	62	CNTR +	

¹ Result obtained by averaging the decay length and decay time analyses taking correlations into account.
² KOPTEV 95 report this weighted average of their U-target and Cu-target results, where they have weighted by $1/\sigma$ rather than $1/\sigma^2$.

WEIGHTED AVERAGE
 1.2379 ± 0.0021 (Error scaled by 1.9)



$$(\tau_{K^+} - \tau_{K^-}) / \tau_{\text{average}}$$

This quantity is a measure of *CPT* invariance in weak interactions.

VALUE (%)	DOCUMENT ID	TECN
0.10 ± 0.09 OUR AVERAGE	Error includes scale factor of 1.2.	
-0.4 ± 0.4	AMBROSINO	08
0.090 ± 0.078	LOBKOWICZ	69
0.47 ± 0.30	FORD	67

See the related review(s):

Rare Kaon Decays

K^+ DECAY MODES

K^- modes are charge conjugates of the modes below.

Mode	Fraction (Γ_i/Γ)	Scale factor/ Confidence level
Leptonic and semileptonic modes		
Γ_1 $e^+ \nu_e$	(1.582 ± 0.007) × 10 ⁻⁵	
Γ_2 $\mu^+ \nu_\mu$	(63.56 ± 0.11) %	S=1.2
Γ_3 $\pi^0 e^+ \nu_e$	(5.07 ± 0.04) %	S=2.1
Called K_{e3}^+ .		
Γ_4 $\pi^0 \mu^+ \nu_\mu$	(3.352 ± 0.034) %	S=1.9
Called $K_{\mu 3}^+$.		
Γ_5 $\pi^0 \pi^0 e^+ \nu_e$	(2.55 ± 0.04) × 10 ⁻⁵	S=1.1
Γ_6 $\pi^+ \pi^- e^+ \nu_e$	(4.247 ± 0.024) × 10 ⁻⁵	
Γ_7 $\pi^+ \pi^- \mu^+ \nu_\mu$	(1.4 ± 0.9) × 10 ⁻⁵	
Γ_8 $\pi^0 \pi^0 \pi^0 e^+ \nu_e$	< 3.5 × 10 ⁻⁶	CL=90%
Hadronic modes		
Γ_9 $\pi^+ \pi^0$	(20.67 ± 0.08) %	S=1.2
Γ_{10} $\pi^+ \pi^0 \pi^0$	(1.760 ± 0.023) %	S=1.1
Γ_{11} $\pi^+ \pi^+ \pi^-$	(5.583 ± 0.024) %	

Leptonic and semileptonic modes with photons

Γ_{12} $\mu^+ \nu_\mu \gamma$	[a,b] (6.2 ± 0.8) × 10 ⁻³	
Γ_{13} $\mu^+ \nu_\mu \gamma (SD^+)$	[c,d] (1.33 ± 0.22) × 10 ⁻⁵	
Γ_{14} $\mu^+ \nu_\mu \gamma (SD^+ INT)$	[c,d] < 2.7 × 10 ⁻⁵	CL=90%
Γ_{15} $\mu^+ \nu_\mu \gamma (SD^- + SD^- INT)$	[c,d] < 2.6 × 10 ⁻⁴	CL=90%
Γ_{16} $e^+ \nu_e \gamma$	(1.03 ± 0.14) × 10 ⁻⁵	
Γ_{17} $\pi^0 e^+ \nu_e \gamma$	[a,b] (2.698 ± 0.033) × 10 ⁻⁴	
Γ_{18} $\pi^0 e^+ \nu_e \gamma (SD)$	[c,d] < 5.3 × 10 ⁻⁵	CL=90%
Γ_{19} $\pi^0 \mu^+ \nu_\mu \gamma$	[a,b] (1.25 ± 0.25) × 10 ⁻⁵	
Γ_{20} $\pi^0 \pi^0 e^+ \nu_e \gamma$	< 5 × 10 ⁻⁶	CL=90%

Hadronic modes with photons or $\ell\bar{\ell}$ pairs

Γ_{21} $\pi^+ \pi^0 \gamma (INT)$	(- 4.2 ± 0.9) × 10 ⁻⁶	
Γ_{22} $\pi^+ \pi^0 \gamma (DE)$	[a,e] (6.0 ± 0.4) × 10 ⁻⁶	
Γ_{23} $\pi^+ \pi^0 e^+ e^-$	(4.24 ± 0.14) × 10 ⁻⁶	
Γ_{24} $\pi^+ \pi^0 \pi^0 \gamma$	[a,b] (7.6 ± 3.0) × 10 ⁻⁶	
Γ_{25} $\pi^+ \pi^+ \pi^- \gamma$	[a,b] (7.1 ± 0.5) × 10 ⁻⁶	
Γ_{26} $\pi^+ \gamma \gamma$	[a] (1.01 ± 0.06) × 10 ⁻⁶	
Γ_{27} $\pi^+ 3\gamma$	[a] < 1.0 × 10 ⁻⁴	CL=90%
Γ_{28} $\pi^+ e^+ e^- \gamma$	(1.19 ± 0.13) × 10 ⁻⁸	

Leptonic modes with $\ell\bar{\ell}$ pairs

Γ_{29} $e^+ \nu_e \nu\bar{\nu}$	< 6 × 10 ⁻⁵	CL=90%
Γ_{30} $\mu^+ \nu_\mu \nu\bar{\nu}$	< 1.0 × 10 ⁻⁶	CL=90%
Γ_{31} $e^+ \nu_e e^+ e^-$	(2.48 ± 0.20) × 10 ⁻⁸	
Γ_{32} $\mu^+ \nu_\mu e^+ e^-$	(7.06 ± 0.31) × 10 ⁻⁸	
Γ_{33} $e^+ \nu_e \mu^+ \mu^-$	(1.7 ± 0.5) × 10 ⁻⁸	
Γ_{34} $\mu^+ \nu_\mu \mu^+ \mu^-$	< 4.1 × 10 ⁻⁷	CL=90%

Lepton family number (*LF*), Lepton number (*L*), $\Delta S = \Delta Q$ (*SQ*) violating modes, or $\Delta S = 1$ weak neutral current (*S1*) modes

Γ_{35} $\pi^+ \pi^+ e^- \bar{\nu}_e$	<i>SQ</i> < 1.3 × 10 ⁻⁸	CL=90%
Γ_{36} $\pi^+ \pi^+ \mu^- \bar{\nu}_\mu$	<i>SQ</i> < 3.0 × 10 ⁻⁶	CL=95%
Γ_{37} $\pi^+ e^+ e^-$	<i>S1</i> (3.00 ± 0.09) × 10 ⁻⁷	
Γ_{38} $\pi^+ \mu^+ \mu^-$	<i>S1</i> (9.17 ± 0.14) × 10 ⁻⁸	S=1.8
Γ_{39} $\pi^+ e^+ e^- e^+ e^-$	< 1.4 × 10 ⁻⁸	CL=90%
Γ_{40} $\pi^+ \nu\bar{\nu}$	<i>S1</i> (1.14 ± 0.40 / -0.33) × 10 ⁻¹⁰	
Γ_{41} $\pi^+ \pi^0 \nu\bar{\nu}$	<i>S1</i> < 4.3 × 10 ⁻⁵	CL=90%
Γ_{42} $\mu^- \nu e^+ e^+$	<i>LF</i> < 8.1 × 10 ⁻¹¹	CL=90%
Γ_{43} $\mu^+ \nu_e$	<i>LF</i> [f] < 4 × 10 ⁻³	CL=90%
Γ_{44} $\pi^+ \mu^+ e^-$	<i>LF</i> < 1.3 × 10 ⁻¹¹	CL=90%
Γ_{45} $\pi^- \mu^- e^+$	<i>LF</i> < 6.6 × 10 ⁻¹¹	CL=90%
Γ_{46} $\pi^- \mu^+ e^+$	<i>L</i> < 4.2 × 10 ⁻¹¹	CL=90%
Γ_{47} $\pi^- e^+ e^+$	<i>L</i> < 5.3 × 10 ⁻¹¹	CL=90%
Γ_{48} $\pi^- \mu^+ \mu^+$	<i>L</i> < 4.2 × 10 ⁻¹¹	CL=90%
Γ_{49} $\pi^- \pi^0 e^+ e^+$	<i>L</i> < 8.5 × 10 ⁻¹⁰	CL=90%
Γ_{50} $\mu^+ \bar{\nu}_e$	<i>L</i> [f] < 3.3 × 10 ⁻³	CL=90%
Γ_{51} $\pi^0 e^+ \bar{\nu}_e$	<i>L</i> < 3 × 10 ⁻³	CL=90%
Γ_{52} $\pi^+ \gamma$	[g] < 2.3 × 10 ⁻⁹	CL=90%

- [a] See the Particle Listings below for the energy limits used in this measurement.
- [b] Most of this radiative mode, the low-momentum γ part, is also included in the parent mode listed without γ 's.
- [c] Structure-dependent part.
- [d] See the review on "Form Factors for Radiative Pion and Kaon Decays" for definitions and details.
- [e] Direct-emission branching fraction.
- [f] Derived from an analysis of neutrino-oscillation experiments.
- [g] Violates angular-momentum conservation.

CONSTRAINED FIT INFORMATION

An overall fit to the mean life, a decay rate, and 15 branching ratios uses 35 measurements and one constraint to determine 8 parameters. The overall fit has a $\chi^2 = 53.4$ for 28 degrees of freedom.

The following *off-diagonal* array elements are the correlation coefficients $\langle \delta p_i \delta p_j \rangle / (\delta p_i \delta p_j)$, in percent, from the fit to parameters p_i , including the branching fractions, $x_i \equiv \Gamma_i / \Gamma_{\text{total}}$. The fit constrains the x_i whose labels appear in this array to sum to one.

x_3	-66						
x_4	-64	89					
x_5	-12	-5	-5				
x_9	-67	0	-1	-6			
x_{10}	-13	-6	-5	91	-6		
x_{11}	-14	-6	-6	2	-7	2	
Γ	3	1	1	0	2	0	-24
	x_2	x_3	x_4	x_5	x_9	x_{10}	x_{11}

Mode	Rate (10^8 s^{-1})	Scale factor
$\Gamma_2 \mu^+ \nu_\mu$	0.5134 ± 0.0012	1.5
$\Gamma_3 \pi^0 e^+ \nu_e$ Called K_{e3}^+ .	0.0410 ± 0.0004	2.1
$\Gamma_4 \pi^0 \mu^+ \nu_\mu$ Called $K_{\mu 3}^+$.	0.02707 ± 0.00028	1.9
$\Gamma_5 \pi^0 \pi^0 e^+ \nu_e$	$(2.059 \pm 0.029) \times 10^{-5}$	1.1
$\Gamma_9 \pi^+ \pi^0$	0.1670 ± 0.0007	1.3
$\Gamma_{10} \pi^+ \pi^0 \pi^0$	0.01421 ± 0.00018	1.1
$\Gamma_{11} \pi^+ \pi^+ \pi^-$	0.04510 ± 0.00019	

K^\pm DECAY RATES

$\Gamma(\mu^+ \nu_\mu) \quad \Gamma_2$

VALUE (10^6 s^{-1})	DOCUMENT ID	TECN	CHG
51.34 ± 0.12 OUR FIT	Error includes scale factor of 1.5.		
• • • We do not use the following data for averages, fits, limits, etc. • • •			
51.2 ± 0.8	FORD	67	CNTR ±

$\Gamma(\pi^+ \pi^+ \pi^-) \quad \Gamma_{11}$

VALUE (10^6 s^{-1})	EVTS	DOCUMENT ID	TECN	CHG
4.510 ± 0.019 OUR FIT				
4.511 ± 0.024		¹ FORD	70	ASPK
• • • We do not use the following data for averages, fits, limits, etc. • • •				
4.529 ± 0.032	3.2M	¹ FORD	70	ASPK
4.496 ± 0.030		¹ FORD	67	CNTR ±
¹ First FORD 70 value is second FORD 70 combined with FORD 67.				

K^+ BRANCHING RATIOS

Leptonic and semileptonic modes

$\Gamma(e^+ \nu_e)/\Gamma(\mu^+ \nu_\mu) \quad \Gamma_1/\Gamma_2$

See the note on "Decay Constants of Charged Pseudoscalar Mesons" in the D_S^\pm Listings.

VALUE (units 10^{-5})	EVTS	DOCUMENT ID	TECN	CHG
2.488 ± 0.009 OUR AVERAGE				
$2.488 \pm 0.007 \pm 0.007$	150k	¹ LAZZERONI	13	NA62 ±
$2.493 \pm 0.025 \pm 0.019$	13.8k	² AMBROSINO	09E	KLOE ±
• • • We do not use the following data for averages, fits, limits, etc. • • •				
$2.487 \pm 0.011 \pm 0.007$	60k	³ LAZZERONI	11	NA62 +
2.51 ± 0.15	404	HEINTZE	76	SPEC +
2.37 ± 0.17	534	HEARD	75B	SPEC +
2.42 ± 0.42	112	CLARK	72	OSPK +

¹ LAZZERONI 13 uses full data sample collected from 2007 to 2008. This ratio is defined to be fully inclusive, including internal-bremsstrahlung.

² The ratio is defined to include internal-bremsstrahlung, ignoring direct-emission contributions. AMBROSINO 09E determined the ratio from the measurement of $\Gamma(K \rightarrow e\nu(\gamma))$, $E_\gamma < 10 \text{ MeV}$ / $\Gamma(K \rightarrow \mu\nu(\gamma))$. 89.8% of $K \rightarrow e\nu(\gamma)$ events had $E_\gamma < 10 \text{ MeV}$.

³ This ratio is defined to be fully inclusive, including internal-bremsstrahlung.

$\Gamma(\mu^+ \nu_\mu)/\Gamma_{\text{total}} \quad \Gamma_2/\Gamma$

See the note on "Decay Constants of Charged Pseudoscalar Mesons" in the D_S^\pm Listings.

VALUE (units 10^{-2})	EVTS	DOCUMENT ID	TECN	CHG	COMMENT
63.56 ± 0.11 OUR FIT					Error includes scale factor of 1.2.
63.60 ± 0.16 OUR AVERAGE					
$63.66 \pm 0.09 \pm 0.15$	865k	¹ AMBROSINO	06A	KLOE	+
63.24 ± 0.44	62k	CHIANG	72	OSPK	+ 1.84 GeV/c K^+

¹ Fully inclusive. Used tagged kaons from ϕ decays.

$\Gamma(\pi^0 e^+ \nu_e)/\Gamma_{\text{total}} \quad \Gamma_3/\Gamma$

VALUE (units 10^{-2})	EVTS	DOCUMENT ID	TECN	CHG	COMMENT
5.07 ± 0.04 OUR FIT					Error includes scale factor of 2.1.
4.94 ± 0.05 OUR AVERAGE					
$4.965 \pm 0.038 \pm 0.037$		¹ AMBROSINO	08A	KLOE	±
4.86 ± 0.10	3516	CHIANG	72	OSPK	+ 1.84 GeV/c K^+
• • • We do not use the following data for averages, fits, limits, etc. • • •					
4.7 ± 0.3	429	SHAKLEE	64	HLBC	+
5.0 ± 0.5		ROE	61	HLBC	+

¹ Depends on K^+ lifetime τ . AMBROSINO 08A uses PDG 06 value of $\tau = (1.2385 \pm 0.0024) \times 10^{-8} \text{ sec}$. The correlation between K_{e3}^+ and $K_{\mu 3}^+$ branching fraction measurements is 62.7%.

$\Gamma(\pi^0 e^+ \nu_e)/\Gamma(\mu^+ \nu_\mu) \quad \Gamma_3/\Gamma_2$

VALUE	EVTS	DOCUMENT ID	TECN	CHG
0.0798 ± 0.0008 OUR FIT				Error includes scale factor of 1.9.
• • • We do not use the following data for averages, fits, limits, etc. • • •				
0.069 ± 0.006	350	ZELLER	69	ASPK +
0.0775 ± 0.0033	960	BOTTERILL	68c	ASPK +
0.069 ± 0.006	561	GARLAND	68	OSPK +
0.0791 ± 0.0054	295	¹ AUERBACH	67	OSPK +

¹ AUERBACH 67 changed from 0.0797 ± 0.0054 . See comment with ratio $\Gamma(\pi^0 \mu^+ \nu_\mu)/\Gamma(\mu^+ \nu_\mu)$. The value 0.0785 ± 0.0025 given in AUERBACH 67 is an average of AUERBACH 67 $\Gamma(\pi^0 e^+ \nu_e)/\Gamma(\mu^+ \nu_\mu)$ and CESTER 66 $\Gamma(\pi^0 e^+ \nu_e)/[\Gamma(\mu^+ \nu_\mu) + \Gamma(\pi^+ \pi^0)]$.

$\Gamma(\pi^0 e^+ \nu_e)/[\Gamma(\mu^+ \nu_\mu) + \Gamma(\pi^+ \pi^0)] \quad \Gamma_3/(\Gamma_2 + \Gamma_9)$

VALUE (units 10^{-2})	EVTS	DOCUMENT ID	TECN	CHG
6.02 ± 0.06 OUR FIT				Error includes scale factor of 2.1.
6.02 ± 0.15 OUR AVERAGE				
6.16 ± 0.22	5110	ESCHSTRUTH	68	OSPK +
5.89 ± 0.21	1679	CESTER	66	OSPK +
• • • We do not use the following data for averages, fits, limits, etc. • • •				
5.92 ± 0.65		¹ WEISSENBERG	76	SPEC +

¹ Value calculated from WEISSENBERG 76 ($\pi^0 e\nu$), ($\mu\nu$), and ($\pi\pi^0$) values to eliminate dependence on our 1974 ($\pi 2\pi^0$) and ($\pi\pi^+ \pi^-$) fractions.

$\Gamma(\pi^0 e^+ \nu_e)/[\Gamma(\pi^0 \mu^+ \nu_\mu) + \Gamma(\pi^+ \pi^0) + \Gamma(\pi^+ \pi^0 \pi^0)] \quad \Gamma_3/(\Gamma_4 + \Gamma_9 + \Gamma_{10})$

VALUE	EVTS	DOCUMENT ID	TECN	CHG
0.1967 ± 0.0016 OUR FIT				Error includes scale factor of 2.5.
$0.1962 \pm 0.0008 \pm 0.0035$	71k	SHER	03	B865 +

$\Gamma(\pi^0 e^+ \nu_e)/\Gamma(\pi^+ \pi^0) \quad \Gamma_3/\Gamma_9$

VALUE	EVTS	DOCUMENT ID	TECN	CHG	COMMENT
0.2454 ± 0.0023 OUR FIT					Error includes scale factor of 2.6.
0.2467 ± 0.0011 OUR AVERAGE					Error includes scale factor of 1.1.
$0.2423 \pm 0.0015 \pm 0.0037$	31k	UVAROV	14	ISTR	- ISTR+
$0.2470 \pm 0.0009 \pm 0.0004$	87k	BATLEY	07A	NA48	±
• • • We do not use the following data for averages, fits, limits, etc. • • •					
0.221 ± 0.012	786	¹ LUCAS	73B	HBC	- Dalitz pairs only

¹ LUCAS 73B gives $N(K_{e3}) = 786 \pm 3.1\%$, $N(2\pi) = 3564 \pm 3.1\%$. We use these values to obtain quoted result.

$\Gamma(\pi^0 e^+ \nu_e)/\Gamma(\pi^+ \pi^+ \pi^-) \quad \Gamma_3/\Gamma_{11}$

VALUE	EVTS	DOCUMENT ID	TECN	CHG
0.908 ± 0.009 OUR FIT				Error includes scale factor of 1.6.
• • • We do not use the following data for averages, fits, limits, etc. • • •				
0.867 ± 0.027	2768	BARMIN	87	XEBC +
0.856 ± 0.040	2827	BRAUN	75	HLBC +
0.850 ± 0.019	4385	¹ HAIDT	71	HLBC +
0.846 ± 0.021	4385	¹ EICHTEN	68	HLBC +
0.94 ± 0.09	854	BELLOTTI	67B	HLBC
0.90 ± 0.06	230	BORREANI	64	HBC +

¹ HAIDT 71 is a reanalysis of EICHTEN 68. Not included in average because of large discrepancy in $\Gamma(\pi^0 \mu^+ \nu)/\Gamma(\pi^0 e^+ \nu)$ with more precise results.

$\Gamma(\pi^0 \mu^+ \nu_\mu)/\Gamma_{\text{total}} \quad \Gamma_4/\Gamma$

VALUE (units 10^{-2})	EVTS	DOCUMENT ID	TECN	CHG	COMMENT
3.352 ± 0.034 OUR FIT					Error includes scale factor of 1.9.
3.24 ± 0.04 OUR AVERAGE					
$3.233 \pm 0.029 \pm 0.026$		¹ AMBROSINO	08A	KLOE	±
3.33 ± 0.16	2345	CHIANG	72	OSPK	+ 1.84 GeV/c K^+
• • • We do not use the following data for averages, fits, limits, etc. • • •					
2.8 ± 0.4		² TAYLOR	59	EMUL	+

¹ Depends on K^+ lifetime τ . AMBROSINO 08A uses PDG 06 value of $\tau = (1.2385 \pm 0.0024) \times 10^{-8} \text{ sec}$. The correlation between K_{e3}^+ and $K_{\mu 3}^+$ branching fraction measurements is 62.7%.

² Earlier experiments not averaged.

$\Gamma(\pi^0 \mu^+ \nu_\mu)/\Gamma(\mu^+ \nu_\mu) \quad \Gamma_4/\Gamma_2$

VALUE	EVTS	DOCUMENT ID	TECN	CHG
0.0527 ± 0.0006 OUR FIT				Error includes scale factor of 1.8.
• • • We do not use the following data for averages, fits, limits, etc. • • •				
0.054 ± 0.009	240	ZELLER	69	ASPK +
0.0480 ± 0.0037	424	¹ GARLAND	68	OSPK +
0.0486 ± 0.0040	307	² AUERBACH	67	OSPK +

¹ GARLAND 68 changed from 0.055 ± 0.004 in agreement with μ -spectrum calculation of GAILLARD 70 appendix B. L.G.Pondrom, (private communication 73).

² AUERBACH 67 changed from 0.0602 ± 0.0046 by erratum which brings the μ -spectrum calculation into agreement with GAILLARD 70 appendix B.

Meson Particle Listings

 K^\pm $\Gamma(\pi^0 \mu^+ \nu_\mu) / \Gamma(\pi^0 e^+ \nu_e)$ Γ_4 / Γ_3

VALUE	EVTS	DOCUMENT ID	TECN	CHG	COMMENT
0.6608 ± 0.0031 OUR FIT					Error includes scale factor of 1.2.
0.6618 ± 0.0027 OUR AVERAGE					
0.663 ± 0.003 ± 0.001	77k	BATLEY	07A	NA48	±
0.671 ± 0.007 ± 0.008	24k	HORIE	01	SPEC	
0.670 ± 0.014		¹ HEINTZE	77	SPEC	+
0.667 ± 0.017	5601	BOTTERILL	68B	ASPK	+
0.6511 ± 0.0064		² AMBROSINO	08A	KLOE	±
0.608 ± 0.014	1585	³ BRAUN	75	HLBC	+
0.705 ± 0.063	554	⁴ LUCAS	73B	HBC	- Dalitz pairs only
0.698 ± 0.025	3480	⁵ CHIANG	72	OSPK	+ 1.84 GeV/c K^\pm
0.596 ± 0.025		⁶ HAIDT	71	HLBC	+
0.604 ± 0.022	1398	⁶ EICHTEN	68	HLBC	
0.703 ± 0.056	1509	CALLAHAN	66B	HLBC	

- ¹ HEINTZE 77 value from fit to λ_0 . Assumes μ -e universality.
² Not used in the fit. This result enters the fit via correlation of K_{e3}^+ and $K_{\mu 3}^+$ branching fraction measurements of AMBROSINO 08A.
³ BRAUN 75 value is from form factor fit. Assumes μ -e universality.
⁴ LUCAS 73B gives $N(K_{\mu 3}) = 554 \pm 7.6\%$, $N(K_{e3}) = 786 \pm 3.1\%$. We divide.
⁵ CHIANG 72 $\Gamma(\pi^0 \mu^+ \nu_\mu) / \Gamma(\pi^0 e^+ \nu_e)$ is statistically independent of CHIANG 72 $\Gamma(\pi^0 \mu^+ \nu_\mu) / \Gamma_{\text{total}}$ and $\Gamma(\pi^0 e^+ \nu_e) / \Gamma_{\text{total}}$.
⁶ HAIDT 71 is a reanalysis of EICHTEN 68. Not included in average because of large discrepancy with more precise results.

 $[\Gamma(\pi^0 \mu^+ \nu_\mu) + \Gamma(\pi^+ \pi^0)] / \Gamma_{\text{total}}$ $(\Gamma_4 + \Gamma_9) / \Gamma$

We combine these two modes for experiments measuring them in xenon bubble chamber because of difficulties of separating them there.

VALUE (units 10^{-2})	EVTS	DOCUMENT ID	TECN	CHG
24.02 ± 0.08 OUR FIT				Error includes scale factor of 1.2.
25.4 ± 0.9	886	SHAKLEE	64	HLBC +
23.4 ± 1.1		ROE	61	HLBC +

 $\Gamma(\pi^0 \mu^+ \nu_\mu) / \Gamma(\pi^+ \pi^0)$ Γ_4 / Γ_9

VALUE	EVTS	DOCUMENT ID	TECN	CHG
0.1637 ± 0.0006 ± 0.0003	77k	BATLEY	07A	NA48 ±

 $\Gamma(\pi^0 \mu^+ \nu_\mu) / \Gamma(\pi^+ \pi^+ \pi^-)$ Γ_4 / Γ_{11}

VALUE	EVTS	DOCUMENT ID	TECN	CHG	COMMENT
0.600 ± 0.007 OUR FIT					Error includes scale factor of 1.6.
0.503 ± 0.019	1505	¹ HAIDT	71	HLBC	+
0.510 ± 0.017	1505	¹ EICHTEN	68	HLBC	+
0.63 ± 0.07	2845	² BISI	65B	BC	+ HBC+HLBC

- ¹ HAIDT 71 is a reanalysis of EICHTEN 68. Not included in average because of large discrepancy in $\Gamma(\pi^0 \mu^+ \nu) / \Gamma(\pi^0 e^+ \nu)$ with more precise results.
² Error enlarged for background problems. See GAILLARD 70.

 $\Gamma(\pi^0 \pi^0 e^+ \nu_e) / \Gamma_{\text{total}}$ Γ_5 / Γ

VALUE (units 10^{-5})	EVTS	DOCUMENT ID	TECN	CHG
2.55 ± 0.04 OUR FIT				Error includes scale factor of 1.1.
2.54 ± 0.89	10	BARMIN	88B	HLBC +

 $\Gamma(\pi^0 \pi^0 e^+ \nu_e) / \Gamma(\pi^+ \pi^0 \pi^0)$ Γ_5 / Γ_{10}

VALUE (units 10^{-3})	EVTS	DOCUMENT ID	TECN	CHG
1.449 ± 0.008 OUR FIT				
1.449 ± 0.006 ± 0.006	65.2k	¹ BATLEY	14A	NA48 ±

- ¹ Data collected in 2003–2004. This leads to the scalar form factor $(1 + \delta_{PM}) f_5 = 6.079 \pm 0.012 \pm 0.027 \pm 0.046$ where the last error is due to the normalizing decay mode uncertainty.

 $\Gamma(\pi^0 \pi^0 e^+ \nu_e) / \Gamma(\pi^0 e^+ \nu_e)$ Γ_5 / Γ_3

VALUE (units 10^{-4})	EVTS	DOCUMENT ID	TECN	CHG
5.03 ± 0.09 OUR FIT				Error includes scale factor of 1.2.
4.1 +1.0 -0.7 OUR AVERAGE				
4.2 +1.0 -0.9	25	BOLOTOV	86B	CALO -
3.8 +5.0 -1.2	2	LJUNG	73	HLBC +

 $\Gamma(\pi^+ \pi^- e^+ \nu_e) / \Gamma(\pi^+ \pi^+ \pi^-)$ Γ_6 / Γ_{11}

VALUE (units 10^{-4})	EVTS	DOCUMENT ID	TECN	CHG
7.606 ± 0.029 OUR AVERAGE				
7.615 ± 0.008 ± 0.028	1.1M	¹ BATLEY	12	NA48 ±
7.35 ± 0.01 ± 0.19	388k	² PISLAK	01	B865
7.21 ± 0.32	30k	ROSSELET	77	SPEC +

• • • We do not use the following data for averages, fits, limits, etc. • • •

7.36 ± 0.68	500	BOURQUIN	71	ASPK
7.0 ± 0.9	106	SCHWEIN...	71	HLBC +
5.83 ± 0.63	269	ELY	69	HLBC +

- ¹ BATLEY 12 uses data collected in 2003–2004. The result is inclusive of $K^\pm \rightarrow \pi^+ \pi^- e^\pm \nu \gamma$ decays. Using PDG 12 value for $\Gamma(\pi^+ \pi^- \pi^+) / \Gamma = (5.59 \pm 0.04) \times 10^{-2}$.
 BATLEY 12 obtains $B(\pi^+ \pi^- e \nu) = (4.257 \pm 0.004 \pm 0.035) \times 10^{-5}$ where the syst. error is dominated by the error on the normalization mode.
² PISLAK 01 reports $\Gamma(\pi^+ \pi^- e^+ \nu_e) / \Gamma_{\text{total}} = (4.109 \pm 0.008 \pm 0.110) \times 10^{-5}$ using the PDG 00 value $\Gamma(\pi^+ \pi^+ \pi^-) / \Gamma_{\text{total}} = (5.59 \pm 0.05) \times 10^{-2}$. We divide by the PDG value and unfold its error from the systematic error. PISLAK 03 and PISLAK 10A give additional details on the branching ratio measurement and give improved errors on the S-wave π - π scattering length: $a_0^0 = 0.235 \pm 0.013$ and $a_0^2 = -0.0410 \pm 0.0027$.

 $\Gamma(\pi^+ \pi^- \mu^+ \nu_\mu) / \Gamma_{\text{total}}$ Γ_7 / Γ

VALUE (units 10^{-5})	EVTS	DOCUMENT ID	TECN	CHG
0.77 +0.54 -0.50	1	CLINE	65	FBC +

 $\Gamma(\pi^+ \pi^- \mu^+ \nu_\mu) / \Gamma(\pi^+ \pi^+ \pi^-)$ Γ_7 / Γ_{11}

VALUE (units 10^{-4})	EVTS	DOCUMENT ID	TECN	CHG
2.57 ± 1.55	7	BISI	67	DBC +
~ 2.5	1	GREINER	64	EMUL +

 $\Gamma(\pi^0 \pi^0 \pi^0 e^+ \nu_e) / \Gamma_{\text{total}}$ Γ_8 / Γ

VALUE (units 10^{-6})	CL%	EVTS	DOCUMENT ID	TECN	CHG
<3.5	90	0	BOLOTOV	88	SPEC -
<9	90	0	BARMIN	92	XEBC +

Hadronic modes

 $\Gamma(\pi^+ \pi^0) / \Gamma_{\text{total}}$ Γ_9 / Γ

VALUE (units 10^{-2})	EVTS	DOCUMENT ID	TECN	CHG	COMMENT
20.67 ± 0.08 OUR FIT					Error includes scale factor of 1.2.
20.70 ± 0.16 OUR AVERAGE					Error includes scale factor of 1.8.
20.65 ± 0.05 ± 0.08	1.4M	¹ AMBROSINO	08E	KLOE	+ $\phi \rightarrow K^+ K^-$
21.18 ± 0.28	16k	CHIANG	72	OSPK	+ 1.84 GeV/c K^\pm
21.0 ± 0.6		CALLAHAN	65	HLBC	See Γ_9 / Γ_{11}

- ¹ Fully inclusive of final-state radiation. The branching ratio is evaluated using K^+ lifetime, $\tau = 12.385$ ns.

 $\Gamma(\pi^+ \pi^0) / \Gamma(\mu^+ \nu_\mu)$ Γ_9 / Γ_2

VALUE	EVTS	DOCUMENT ID	TECN	CHG	COMMENT
0.3252 ± 0.0016 OUR FIT					Error includes scale factor of 1.2.
0.3325 ± 0.0032 OUR AVERAGE					
0.3329 ± 0.0047 ± 0.0010	45k	USHER	92	SPEC	+ $p\bar{p}$ at rest
0.3355 ± 0.0057		¹ WEISSENBE...	76	SPEC	+
0.3277 ± 0.0065	4517	² AUERBACH	67	OSPK	+
0.328 ± 0.005	25k	¹ WEISSENBE...	74	STRC	+
0.305 ± 0.018	1600	ZELLER	69	ASPK	+

- ¹ WEISSENBERG 76 revises WEISSENBERG 74.
² AUERBACH 67 changed from 0.3253 ± 0.0065. See comment with ratio $\Gamma(\pi^0 \mu^+ \nu_\mu) / \Gamma(\mu^+ \nu_\mu)$.

 $\Gamma(\pi^+ \pi^0) / \Gamma(\pi^+ \pi^+ \pi^-)$ Γ_9 / Γ_{11}

VALUE	EVTS	DOCUMENT ID	TECN	CHG
3.702 ± 0.022 OUR FIT				Error includes scale factor of 1.1.
3.96 ± 0.15	1045	CALLAHAN	66	FBC +

 $\Gamma(\pi^+ \pi^0 \pi^0) / \Gamma_{\text{total}}$ Γ_{10} / Γ

VALUE (units 10^{-2})	EVTS	DOCUMENT ID	TECN	CHG	COMMENT
1.760 ± 0.023 OUR FIT					Error includes scale factor of 1.1.
1.775 ± 0.028 OUR AVERAGE					Error includes scale factor of 1.2.
1.763 ± 0.013 ± 0.022		ALOISIO	04A	KLOE	±
1.84 ± 0.06	1307	CHIANG	72	OSPK	+ 1.84 GeV/c K^\pm
1.53 ± 0.11	198	¹ PANDOULAS	70	EMUL	+
1.8 ± 0.2	108	SHAKLEE	64	HLBC	+
1.7 ± 0.2		ROE	61	HLBC	+
1.5 ± 0.2		² TAYLOR	59	EMUL	+

- ¹ Includes events of TAYLOR 59.
² Earlier experiments not averaged.

$\Gamma(\pi^+\pi^0\pi^0)/\Gamma(\pi^+\pi^0)$		Γ_{10}/Γ_9	
VALUE	EVTS	DOCUMENT ID	TECN CHG COMMENT
0.0851 ± 0.0012 OUR FIT			Error includes scale factor of 1.1.
•••			We do not use the following data for averages, fits, limits, etc. •••
0.081 ± 0.005	574	¹ LUCAS	73B HBC — Dalitz pairs only
		¹ LUCAS 73B	gives $N(\pi^2\pi^0) = 574 \pm 5.9\%$, $N(2\pi) = 3564 \pm 3.1\%$. We quote $0.5N(\pi^2\pi^0)/N(2\pi)$ where 0.5 is because only Dalitz pair π^0 's were used.

$\Gamma(\pi^+\pi^0\pi^0)/\Gamma(\pi^+\pi^+\pi^-)$		Γ_{10}/Γ_{11}	
VALUE	EVTS	DOCUMENT ID	TECN CHG COMMENT
0.315 ± 0.004 OUR FIT			Error includes scale factor of 1.1.
0.303 ± 0.009	2027	BISI	65 BC + HBC+HLBC
•••			We do not use the following data for averages, fits, limits, etc. •••
0.393 ± 0.099	17	YOUNG	65 EMUL +

$\Gamma(\pi^+\pi^+\pi^-)/\Gamma_{total}$		Γ_{11}/Γ	
VALUE (units 10^{-2})	EVTS	DOCUMENT ID	TECN CHG COMMENT
5.583 ± 0.024 OUR FIT			
5.565 ± 0.031 ± 0.025	68k	¹ BABUSCI	14B KLOE +
•••			We do not use the following data for averages, fits, limits, etc. •••
5.56 ± 0.20	2330	² CHIANG	72 OSPK + 1.84 GeV/c K^+
5.34 ± 0.21	693	³ PANDOULAS	70 EMUL +
5.71 ± 0.15		DEMARCO	65 HBC
6.0 ± 0.4	44	YOUNG	65 EMUL +
5.54 ± 0.12	2332	CALLAHAN	64 HLBC +
5.1 ± 0.2	540	SHAKLEE	64 HLBC +
5.7 ± 0.3		ROE	61 HLBC +

- ¹Inclusive of final-state radiation. Result obtained from averaging two branching ratios: one from a sample with $K^- \rightarrow \mu\nu(\gamma)$ tagging and another with $K^- \rightarrow \pi^-\pi^0(\gamma)$ tagging.
- ²Value is not independent of CHIANG 72 $\Gamma(\mu^+\nu_\mu)/\Gamma_{total}$, $\Gamma(\pi^+\pi^0)/\Gamma_{total}$, $\Gamma(\pi^+\pi^0\pi^0)/\Gamma_{total}$, $\Gamma(\pi^0\mu^+\nu_\mu)/\Gamma_{total}$, and $\Gamma(\pi^0e^+\nu_e)/\Gamma_{total}$.
- ³Includes events of TAYLOR 59.

Leptonic and semileptonic modes with photons

$\Gamma(\mu^+\nu_\mu\gamma)/\Gamma_{total}$		Γ_{12}/Γ	
VALUE (units 10^{-3})	EVTS	DOCUMENT ID	TECN CHG COMMENT
6.2 ± 0.8 OUR AVERAGE			
6.6 ± 1.5		^{1,2} DEMIDOV	90 XEBC $P(\mu) < 231.5$ MeV/c
6.0 ± 0.9		BARMIN	88 HLBC + $P(\mu) < 231.5$ MeV/c
•••			We do not use the following data for averages, fits, limits, etc. •••
3.5 ± 0.8		^{2,3} DEMIDOV	90 XEBC $E(\gamma) > 20$ MeV
3.2 ± 0.5	57	⁴ BARMIN	88 HLBC + $E(\gamma) > 20$ MeV
5.4 ± 0.3		⁵ AKIBA	85 SPEC $P(\mu) < 231.5$ MeV/c

- ¹ $P(\mu)$ cut given in DEMIDOV 90 paper, 235.1 MeV/c, is a misprint according to authors (private communication).
- ²DEMIDOV 90 quotes only inner bremsstrahlung (IB) part.
- ³Not independent of above DEMIDOV 90 value. Cuts differ.
- ⁴Not independent of above BARMIN 88 value. Cuts differ.
- ⁵Assumes μ - e universality and uses constraints from $K \rightarrow e\nu\gamma$.

$\Gamma(\mu^+\nu_\mu\gamma(SD^+))/\Gamma_{total}$		Γ_{13}/Γ	
VALUE (units 10^{-5})	CL% EVTS	DOCUMENT ID	TECN
1.33 ± 0.12 ± 0.18	2588	¹ ADLER	00B B787
•••			We do not use the following data for averages, fits, limits, etc. •••
<3.0	90	AKIBA	85 SPEC

- ¹ADLER 00B obtains the branching ratio by extrapolating the measurement in the kinematic region $E_\mu > 137$ MeV, $E_\gamma > 90$ MeV to the full SD^+ phase-space. Also reports $|F_V + F_A| = 0.165 \pm 0.007 \pm 0.011$ and $-0.04 < F_V - F_A < 0.24$ at 90% CL.

$\Gamma(\mu^+\nu_\mu\gamma(SD^+INT))/\Gamma_{total}$		Γ_{14}/Γ	
VALUE (units 10^{-5})	CL% EVTS	DOCUMENT ID	TECN
<2.7	90	AKIBA	85 SPEC

- Interference term between internal Bremsstrahlung and SD^+ term. See the "Note on $\pi^\pm \rightarrow \ell^\pm\nu\gamma$ and $K^\pm \rightarrow \ell^\pm\nu\gamma$ Form Factors" in the π^\pm section of the Particle Data Listings above.

$\Gamma(\mu^+\nu_\mu\gamma(SD^- + SD^-INT))/\Gamma_{total}$		Γ_{15}/Γ	
VALUE (units 10^{-4})	CL% EVTS	DOCUMENT ID	TECN
<2.6	90	¹ AKIBA	85 SPEC

- ¹Assumes μ - e universality and uses constraints from $K \rightarrow e\nu\gamma$.

$\Gamma(e^+\nu_e\gamma)/\Gamma(\mu^+\nu_\mu)$		Γ_{16}/Γ_2	
VALUE (units 10^{-5})	EVTS	DOCUMENT ID	TECN CHG COMMENT
1.62 ± 0.22 OUR AVERAGE			Error includes scale factor of 3.9.
1.98 ± 0.11	95	¹ KOBAYASHI	23 E36 E_γ in 10–250 MeV, $p_e > 200$ MeV/c
1.483 ± 0.066 ± 0.013	1.4k	² AMBROSINO	09E KLOE ± E_γ in 10–250 MeV, $p_e > 200$ MeV/c
•••			We do not use the following data for averages, fits, limits, etc. •••
1.85 ± 0.11 ± 0.07	574	^{3,4} ITO	22 E36 + E_γ in 10–250 MeV, $p_e > 200$ MeV/c

- ¹KOBAYASHI 23 observed 95 ± 10 $K_{e2\gamma}^{SD^+}$ events and derived $B(K_{e2\gamma}^{SD^+})/B(K_{e2\gamma}) = 1.25 \pm 0.14 \pm 0.08$. The authors obtained the R_γ value $(1.98 \pm 0.11) \times 10^{-5}$ by averaging KOBAYASHI 23 with ITO 22 after updating the ITO 22 result to include internal bremsstrahlung process in the acceptance calculation.
- ²AMBROSINO 09E measured the differential width $dR_\gamma/dE_\gamma = (1/\Gamma(K \rightarrow \mu\nu)) (d\Gamma(K \rightarrow e\nu\gamma)/dE_\gamma)$. Result obtained by integrating the differential width over E_γ from 10 to 250 MeV.
- ³ITO 22 result derived from $B(K_{e2\gamma}^{SD^+})/B(K_{e2\gamma}) = 1.12 \pm 0.07 \pm 0.04$.
- ⁴superseded by KOBAYASHI 2023

$\Gamma(\pi^0e^+\nu_e\gamma)/\Gamma(\pi^0e^+\nu_e)$		Γ_{17}/Γ_3	
VALUE (units 10^{-3})	EVTS	DOCUMENT ID	TECN CHG COMMENT
5.32 ± 0.05 OUR AVERAGE			
5.33 ± 0.03 ± 0.04	130k	¹ CORTINA-GIL	23D NA62 + $E_\gamma > 10$ MeV, $0.6 < \cos(\theta_{e\gamma}) < 0.9$
5.32 ± 0.10 ± 0.12	7248	² POLYARUSH	21 OKA + $E_\gamma > 10$ MeV, $0.6 < \cos(\theta_{e\gamma}) < 0.9$
4.7 ± 0.2 ± 0.3	1456	³ AKIMENKO	07 ISTR — $E_\gamma > 10$ MeV, $0.6 < \cos(\theta_{e\gamma}) < 0.9$
4.6 ± 0.8	82	⁴ BARMIN	91 XEBC $E_\gamma > 10$ MeV, $0.6 < \cos(\theta_{e\gamma}) < 0.9$
5.6 ± 0.4	192	⁵ BOLOTOV	86B CALO — $E_\gamma > 10$ MeV
•••			We do not use the following data for averages, fits, limits, etc. •••
18.1 ± 0.3 ± 0.7	4476	³ AKIMENKO	07 ISTR — $E_\gamma > 10$ MeV, $\theta_{e\gamma} > 10^\circ$
6.3 ± 0.2 ± 0.3		³ AKIMENKO	07 ISTR — $E_\gamma > 30$ MeV, $\theta_{e\gamma} > 20^\circ$
15.1 ± 2.5	82	⁴ BARMIN	91 XEBC $E_\gamma > 10$ MeV, $\cos(\theta_{e\gamma}) < 0.98$
4.8 ± 2.0	16	⁶ LJUNG	73 HLBC + $E_\gamma > 30$ MeV
2.2 $^{+1.5}_{-1.0}$		⁶ LJUNG	73 HLBC + $E_\gamma > 30$ MeV
7.6 ± 2.8	13	⁷ ROMANO	71 HLBC $E_\gamma > 10$ MeV
5.3 ± 2.2		⁷ ROMANO	71 HLBC + $E_\gamma > 30$ MeV
12 ± 8		BELLOTTI	67 HLBC $E_\gamma > 30$ MeV

- ¹CORTINA-GIL 23D provides values for three kinematic regions. For averaging, we use value with $E_\gamma > 10$ MeV and $0.6 < \cos(\theta_{e\gamma}) < 0.9$.
- ²POLYARUSH 21 provides values for three kinematic regions. For averaging, we use value with $E_\gamma > 10$ MeV and $0.6 < \cos(\theta_{e\gamma}) < 0.9$.
- ³AKIMENKO 07 provides values for three kinematic regions. For averaging, we use value with $E_\gamma > 10$ MeV and $0.6 < \cos(\theta_{e\gamma}) < 0.9$.
- ⁴BARMIN 91 quotes branching ratio $\Gamma(K \rightarrow e\pi^0\nu\gamma)/\Gamma_{all}$. The measured normalization is $[\Gamma(K \rightarrow e\pi^0\nu) + \Gamma(K \rightarrow \pi^+\pi^+\pi^-)]$. For comparison with other experiments we used $\Gamma(K \rightarrow e\pi^0\nu)/\Gamma_{all} = 0.0482$ to calculate the values quoted here.
- ⁵ $\cos(\theta_{e\gamma})$ between 0.6 and 0.9.
- ⁶First LJUNG 73 value is for $\cos(\theta_{e\gamma}) < 0.9$, second value is for $\cos(\theta_{e\gamma})$ between 0.6 and 0.9 for comparison with ROMANO 71.
- ⁷Both ROMANO 71 values are for $\cos(\theta_{e\gamma})$ between 0.6 and 0.9. Second value is for comparison with second LJUNG 73 value. We use lowest E_γ cut for Summary Table value. See ROMANO 71 for E_γ dependence.

$\Gamma(\pi^0e^+\nu_e\gamma(SD))/\Gamma_{total}$		Γ_{18}/Γ	
VALUE (units 10^{-5})	CL% EVTS	DOCUMENT ID	TECN CHG COMMENT
<5.3	90	BOLOTOV	86B CALO —

$\Gamma(\pi^0\mu^+\nu_\mu\gamma)/\Gamma_{total}$		Γ_{19}/Γ	
VALUE (units 10^{-5})	CL% EVTS	DOCUMENT ID	TECN CHG COMMENT
1.25 ± 0.25 OUR AVERAGE			
1.10 ± 0.32 ± 0.05	23	¹ ADLER	10 B787 $30 < E_\gamma < 60$ MeV
1.46 ± 0.22 ± 0.32	153	² TCHIKILEV	07 ISTR — $30 < E_\gamma < 60$ MeV
•••			We do not use the following data for averages, fits, limits, etc. •••
2.4 ± 0.5 ± 0.6	125	SHIMIZU	06 K470 + $E_\gamma > 30$ MeV; $\theta_{\mu\gamma} > 20^\circ$
<6.1	90	0	LJUNG 73 HLBC + $E(\gamma) > 30$ MeV
¹ Value obtained from $B(K^+ \rightarrow \pi^0\mu^+\nu_\mu\gamma) = (2.51 \pm 0.74 \pm 0.12) \times 10^{-5}$ obtained in the kinematic region $E_\gamma > 20$ MeV, and then theoretical $K_{\mu 3\gamma}$ spectrum has been used. Also $B(K^+ \rightarrow \pi^0\mu^+\nu_\mu\gamma) = (1.58 \pm 0.46 \pm 0.08) \times 10^{-5}$, for $E_\gamma > 30$ MeV and $\theta_{\mu\gamma} > 20^\circ$, was determined.			
² Obtained from measuring $B(K_{\mu 3\gamma})/B(K_{\mu 3})$ and using PDG 02 value $B(K_{\mu 3}) = 3.27\%$. $B(K_{\mu 3\gamma}) = (8.82 \pm 0.94 \pm 0.86) \times 10^{-5}$ is obtained for 5 MeV $< E_\gamma < 30$ MeV.			

Meson Particle Listings

K^\pm

$\Gamma(\pi^0 \pi^0 e^+ \nu_e \gamma)/\Gamma_{\text{total}}$			Γ_{20}/Γ			
VALUE (units 10^{-6})	CL%	EVTS	DOCUMENT ID	TECN	CHG	COMMENT
<5	90	0	BARMIN	92	XEBC	+ $E_\gamma > 10$ MeV

Hadronic modes with photons

$\Gamma(\pi^+ \pi^0 \gamma(\text{INT}))/\Gamma_{\text{total}}$			Γ_{21}/Γ		
The $K^+ \rightarrow \pi^+ \pi^0 \gamma$ differential decay rate can be described in terms of T_{π^+} , the charged pion kinetic energy, and $W^2 = (P_{K^+} \cdot P_\gamma)(P_{\pi^+} \cdot P_\gamma) / (m_K m_{\pi^+})^2$; then we can write $d^2\Gamma(K^+ \rightarrow \pi^+ \pi^0 \gamma) / (dT_{\pi^+} dW^2) = d^2\Gamma(K^+ \rightarrow \pi^+ \pi^0 \gamma)_{IB} / (dT_{\pi^+} dW^2) [1 + 2 \cos(\pm\phi + \delta_1^+ - \delta_0^+) m_\pi^2 m_K^2 W^2 X_E + m_\pi^4 m_K^4 (X_E^2 + X_M^2) W^4]$. The IB differential and total branching ratios are expressed in terms of the non-radiative experimental width $\Gamma(K^+ \rightarrow \pi^+ \pi^0)$ by Low's theorem. Using PDG 10 $B(K^+ \rightarrow \pi^+ \pi^0) = 0.2066 \pm 0.0008$, one obtains respectively $B(K^+ \rightarrow \pi^+ \pi^0 \gamma)_{IB}$ ($55 < T_{\pi^+} < 90$ MeV) $= 2.55 \times 10^{-4}$ and $B(K^+ \rightarrow \pi^+ \pi^0 \gamma)_{IB}$ ($0 < T_{\pi^+} < 80$ MeV) $= 1.80 \times 10^{-4}$. Fitting respectively the piece proportional to W^2 and the piece proportional to W^4 , the interference contribution (INT), proportional to X_E , and the direct contribution (DE) proportional to $X_E^2 + X_M^2$ are extracted.					

VALUE (units 10^{-6})	EVTS	DOCUMENT ID	TECN	CHG	COMMENT
$-4.24 \pm 0.63 \pm 0.70$	600k	¹ BATLEY	10A	NA48	\pm T_{π^+} 0-80 MeV

¹ The cut on the photon energy implies $W^2 > 0.2$. BATLEY 10A obtains the INT and DE fractional branchings with respect to IB from a simultaneous kinematical fit of INT and DE and then we use the PDG 10 value for $B(K^+ \rightarrow \pi^+ \pi^0) = 20.66 \pm 0.08$ to determine the IB. The INT and DE correlation coefficients -0.83 . Assuming a constant electric amplitude, X_E , this INT value implies $X_E = -24 \pm 6 \text{ GeV}^{-4}$.

$\Gamma(\pi^+ \pi^0 \gamma(\text{DE}))/\Gamma_{\text{total}}$			Γ_{22}/Γ		
Direct emission (DE) part of $\Gamma(\pi^+ \pi^0 \gamma)/\Gamma_{\text{total}}$, assuming that interference (INT) component is zero.					

VALUE (units 10^{-6})	EVTS	DOCUMENT ID	TECN	CHG	COMMENT
$5.99 \pm 0.27 \pm 0.25$	600k	¹ BATLEY	10A	NA48	\pm T_{π^+} 0-80 MeV

• • • We do not use the following data for averages, fits, limits, etc. • • •

$3.8 \pm 0.8 \pm 0.7$	10k	ALIEV	06	K470	+ T_{π^+} 55-90 MeV
$3.7 \pm 3.9 \pm 1.0$	930	UVAROV	06	ISTR	- T_{π^+} 55-90 MeV
$3.2 \pm 1.3 \pm 1.0$	4k	ALIEV	03	K470	+ T_{π^+} 55-90 MeV
$6.1 \pm 2.5 \pm 1.9$	4k	ALIEV	03	K470	+ T_{π^+} full range
$4.7 \pm 0.8 \pm 0.3$	20k	² ADLER	00c	B787	+ T_{π^+} 55-90 MeV
20.5 ± 4.6	$+3.9$ -2.3	BOLOTOV	87	WIRE	- T_{π^+} 55-90 MeV
$15.6 \pm 3.5 \pm 5.0$		ABRAMS	72	ASPK	\pm T_{π^+} 55-90 MeV

¹ The cut on the photon energy implies $W^2 > 0.2$. BATLEY 10A obtains the INT and DE fractional branchings with respect to IB from a simultaneous kinematical fit of INT and DE and then we use the PDG 10 value for $B(K^+ \rightarrow \pi^+ \pi^0) = 20.66 \pm 0.08$ to determine the IB. The INT and DE correlation coefficients -0.93 . Assuming constant electric and magnetic amplitudes, X_E and X_M , these INT and DE values imply $X_E = -24 \pm 6 \text{ GeV}^{-4}$ and $X_M = -254 \pm 9 \text{ GeV}^{-4}$.

² ADLER 00c measures the INT component to be $(-0.4 \pm 1.6)\%$ of the inner bremsstrahlung (IB) component.

$\Gamma(\pi^+ \pi^0 e^+ e^-)/\Gamma_{\text{total}}$			Γ_{23}/Γ		
VALUE (units 10^{-6})	EVTS	DOCUMENT ID	TECN	CHG	COMMENT
4.24 ± 0.14	4.9k	¹ BATLEY	19	NA48	

¹ BATLEY 19 result is obtained from an exposure of 1.7×10^{11} charged kaon decays recorded in 2003-2004. The study of the kinematic space shows evidence for a structure dependent contribution consistent with predictions from chiral perturbation theory.

$\Gamma(\pi^+ \pi^0 \pi^0 \gamma)/\Gamma(\pi^+ \pi^0 \pi^0)$			Γ_{24}/Γ_{10}		
VALUE (units 10^{-4})	DOCUMENT ID	TECN	CHG	COMMENT	
4.3 ± 3.2 -1.7	BOLOTOV	85	SPEC	-	$E(\gamma) > 10$ MeV

$\Gamma(\pi^+ \pi^+ \pi^- \gamma)/\Gamma_{\text{total}}$			Γ_{25}/Γ		
VALUE (units 10^{-4})	EVTS	DOCUMENT ID	TECN	CHG	COMMENT
0.071 ± 0.005	OUR AVERAGE				
0.071 ± 0.005	450	SHAPKIN	19	OKA	+ $E(\gamma) > 30$ MeV
1.10 ± 0.48	7	BARMIN	89	XEBC	$E(\gamma) > 5$ MeV
1.0 ± 0.4		STAMER	65	EMUL	+ $E(\gamma) > 11$ MeV

$\Gamma(\pi^+ \gamma \gamma)/\Gamma_{\text{total}}$			Γ_{26}/Γ			
VALUE (units 10^{-7})	CL%	EVTS	DOCUMENT ID	TECN	CHG	COMMENT
10.1 ± 0.6	OUR AVERAGE					
$10.03 \pm 0.51 \pm 0.24$	215	¹ LAZZERONI	14	NA62	\pm	
$11 \pm 3 \pm 1$	31	² KITCHING	97	B787	+	
• • • We do not use the following data for averages, fits, limits, etc. • • •						
$9.10 \pm 0.72 \pm 0.22$	149	³ BATLEY	14	NA48	\pm	
< 0.083	90	⁴ ARTAMONOV	05	B949	+ $P_\pi > 213$ MeV/c	
< 10	90	ATIYA	90b	B787	+ T_π 117-127 MeV	
< 84	90	ASANO	82	CNTR	+ T_π 117-127 MeV	
-420 ± 520	0	ABRAMS	77	SPEC	+ $T_\pi < 92$ MeV	
< 350	90	LJUNG	73	HLBC	+ 6-102, 114-127 MeV	

< 500	90	0	KLEMS	71	OSPK	+ $T_\pi < 117$ MeV
-100 ± 600			CHEN	68	OSPK	+ T_π 60-90 MeV

¹ LAZZERONI 14 combines NA62 and NA48/2 results. The result for the full kinematic range is extrapolated from the model-independent branching fraction $(9.65 \pm 0.61 \pm 0.14) \times 10^{-7}$ for $(m_{\gamma\gamma}/m_K)^2 > 0.2$. The measured ChPT parameter $\tilde{c} = 1.86 \pm 0.25$.

² KITCHING 97 is extrapolated from their model-independent branching fraction $(6.0 \pm 1.5 \pm 0.7) \times 10^{-7}$ for $100 \text{ MeV} < P_{\pi^+} < 180 \text{ MeV}/c$ using Chiral Perturbation Theory.

³ BATLEY 14 uses data collected in 2003 and 2004. Branching ratio is obtained by determining the parameter $\tilde{c} = 1.41 \pm 0.38 \pm 0.11$ and integrating the $\mathcal{O}(p^6)$ chiral spectrum. A model independent value for the branching ratio is also obtained $(8.77 \pm 0.87 \pm 0.17) \times 10^{-7}$ for kinematic range $(m_{\gamma\gamma}/m_K)^2 > 0.2$.

⁴ ARTAMONOV 05 limit assumes ChPT with $\tilde{c} = 1.8$ with unitarity corrections. With $\tilde{c} = 1.6$ and no unitarity corrections they obtain $< 2.3 \times 10^{-8}$ at 90% CL. This partial branching ratio is predicted to be 6.10×10^{-9} and 0.49×10^{-9} for the cases with and without unitarity correction.

$\Gamma(\pi^+ 3\gamma)/\Gamma_{\text{total}}$			Γ_{27}/Γ		
Values given here assume a phase space pion energy spectrum.					

VALUE (units 10^{-4})	CL%	DOCUMENT ID	TECN	CHG	COMMENT
<1.0	90	ASANO	82	CNTR	+ $T(\pi)$ 117-127 MeV

• • • We do not use the following data for averages, fits, limits, etc. • • •

<3.0	90	KLEMS	71	OSPK	+ $T(\pi) > 117$ MeV
------	----	-------	----	------	----------------------

$\Gamma(\pi^+ e^+ e^- \gamma)/\Gamma_{\text{total}}$			Γ_{28}/Γ		
VALUE (units 10^{-8})	EVTS	DOCUMENT ID	TECN	CHG	COMMENT
$1.19 \pm 0.12 \pm 0.04$	113	¹ BATLEY	08	NA48	$m_{ee\gamma} > 260$ MeV

¹ BATLEY 08 also reports the Chiral Perturbation Theory parameter $\tilde{c} = 0.9 \pm 0.45$ obtained using the shape of the $e^+ e^- \gamma$ invariant mass spectrum. By extrapolating the theoretical amplitude to $m_{ee\gamma} < 260$ MeV, it obtains the inclusive $B(K^+ \rightarrow \pi^+ e^+ e^- \gamma) = (1.29 \pm 0.13 \pm 0.03) \times 10^{-8}$, where the first error is the combined statistical and systematic errors and the second error is from the uncertainty in \tilde{c} .

Leptonic modes with $\ell\bar{\ell}$ pairs

$\Gamma(e^+ \nu_e \nu \bar{\nu})/\Gamma(e^+ \nu_e)$			Γ_{29}/Γ_1			
VALUE	CL%	EVTS	DOCUMENT ID	TECN	CHG	COMMENT
<3.8	90	0	HEINTZE	79	SPEC	+

$\Gamma(\mu^+ \nu_\mu \nu \bar{\nu})/\Gamma_{\text{total}}$			Γ_{30}/Γ		
VALUE	CL%	DOCUMENT ID	TECN	CHG	COMMENT
<1.0 × 10 ⁻⁶	90	¹ CORTINA-GIL	21	NA62	+

• • • We do not use the following data for averages, fits, limits, etc. • • •

<2.4 × 10 ⁻⁶	90	² ARTAMONOV	16	B949	+
<6.0 × 10 ⁻⁶	90	³ PANG	73	CNTR	+

¹ CORTINA-GIL 21 assumes Standard Model μ spectrum. The search is performed in the reconstructed missing mass interval $m_{\text{miss}} > 316 \text{ MeV}/c^2$.

² ARTAMONOV 16 assumes Standard model μ spectrum. The search is performed in the muon momentum region between 130 and 175 MeV/c.

³ PANG 73 assumes μ spectrum from ν - ν interaction of BARDIN 70.

$\Gamma(e^+ \nu_e e^+ e^-)/\Gamma_{\text{total}}$			Γ_{31}/Γ		
VALUE (units 10^{-8})	EVTS	DOCUMENT ID	TECN	CHG	COMMENT
$2.48 \pm 0.14 \pm 0.14$	410	POBLAGUEV	02	B865	+ $m_{ee} > 150$ MeV

• • • We do not use the following data for averages, fits, limits, etc. • • •

20 ± 20	4	DIAMANT-...	76	SPEC	+ $m_{e^+e^-} > 140$ MeV
-------------	---	-------------	----	------	--------------------------

$\Gamma(\mu^+ \nu_\mu e^+ e^-)/\Gamma_{\text{total}}$			Γ_{32}/Γ		
VALUE (units 10^{-8})	EVTS	DOCUMENT ID	TECN	CHG	COMMENT
$7.06 \pm 0.16 \pm 0.26$	2.7k	POBLAGUEV	02	B865	+ $m_{ee} > 145$ MeV

• • • We do not use the following data for averages, fits, limits, etc. • • •

100 ± 30	14	DIAMANT-...	76	SPEC	+ $m_{e^+e^-} > 140$ MeV
--------------	----	-------------	----	------	--------------------------

$\Gamma(e^+ \nu_e \mu^+ \mu^-)/\Gamma_{\text{total}}$			Γ_{33}/Γ		
VALUE (units 10^{-8})	CL%	DOCUMENT ID	TECN	CHG	COMMENT
1.72 ± 0.45		MA	06	B865	

• • • We do not use the following data for averages, fits, limits, etc. • • •

<50	90	ADLER	98	B787	
-----	----	-------	----	------	--

$\Gamma(\mu^+ \nu_\mu \mu^+ \mu^-)/\Gamma_{\text{total}}$			Γ_{34}/Γ		
VALUE (units 10^{-7})	CL%	DOCUMENT ID	TECN	CHG	COMMENT
<4.1	90	ATIYA	89	B787	+

Lepton Family number (LF), Lepton number (L), $\Delta S = \Delta Q$ (SQ) violating modes, or $\Delta S = 1$ weak neutral current (S1) modes

$\Gamma(\pi^+ \pi^+ e^- \nu_e)/\Gamma_{\text{total}}$			Γ_{35}/Γ		
Test of $\Delta S = \Delta Q$ rule.					

• • • We do not use the following data for averages, fits, limits, etc. • • •

VALUE (units 10^{-7})	CL%	EVTS	DOCUMENT ID	TECN	CHG	COMMENT
< 9.0	95	0	SCHWEINB...	71	HLBC	+
< 6.9	95	0	ELY	69	HLBC	+
<20.	95	0	BIRGE	65	FBC	+

$\Gamma(\pi^+ \pi^+ e^- \bar{\nu}_e) / \Gamma(\pi^+ \pi^- e^+ \nu_e)$

Test of $\Delta S = \Delta Q$ rule.

VALUE (units 10^{-4})	CL%	EVTs	DOCUMENT ID	TECN
< 3	90	3	¹ BLOCH 76	SPEC

••• We do not use the following data for averages, fits, limits, etc. •••

<130.	95	0	BOURQUIN 71	ASPK
-------	----	---	-------------	------

¹BLOCH 76 quotes 3.6×10^{-4} at CL = 95%, we convert.

Γ_{35} / Γ_6

••• We do not use the following data for averages, fits, limits, etc. •••

$0.48^{+0.72}_{-0.48}$			³ CORTINA-GIL 20c	NA62 +
< 11	90	1	⁴ CORTINA-GIL 19b	NA62 + decay-in-flight
$7.89^{+9.26}_{-5.10}$			⁵ ARTAMONOV 08	B949 + $140 < P_\pi < 199$ MeV
< 22	90	1	⁶ ADLER 04	B787 + $211 < P_\pi < 229$ MeV
< 27	90		ADLER 04	B787 + Scalar
< 18	90		ADLER 04	B787 + Tensor
$1.47^{+1.30}_{-0.89}$			⁷ ANISIMOVSK..04	B949 + $211 < P_\pi < 229$ MeV
$1.57^{+1.75}_{-0.82}$			ADLER 02	B787 + $P_\pi > 211$ MeV/c
< 42	90	1	ADLER 02c	B787 + $140 < P_\pi < 195$ MeV
< 47	90		ADLER 02c	B787 + Scalar
< 25	90		ADLER 02c	B787 + Tensor
$1.5^{+3.4}_{-1.2}$			ADLER 00	B787 In ADLER 02
$4.2^{+9.7}_{-3.5}$			ADLER 97	B787
< 24	90		ADLER 96	B787
< 75	90		ATIYA 93	B787 + $T(\pi)$ 115–127 MeV
< 52	90		ATIYA 93	B787 +
< 170	90	0	ATIYA 93b	B787 + $T(\pi)$ 60–100 MeV
< 340	90		ATIYA 90	B787 +
<1400	90		ASANO 81b	CNTR + $T(\pi)$ 116–127 MeV

$\Gamma(\pi^+ \pi^+ \mu^- \bar{\nu}_\mu) / \Gamma_{total}$

Test of $\Delta S = \Delta Q$ rule.

VALUE (units 10^{-6})	CL%	EVTs	DOCUMENT ID	TECN	CHG
<3.0	95	0	BIRGE 65	FBC	+

Γ_{36} / Γ

$\Gamma(\pi^+ e^+ e^-) / \Gamma_{total}$

Test for $\Delta S = 1$ weak neutral current. Allowed by combined first-order weak and electromagnetic interactions.

VALUE (units 10^{-7})	EVTs	DOCUMENT ID	TECN	CHG
3.00 ± 0.09 OUR AVERAGE				

$3.11 \pm 0.04 \pm 0.12$	7253	¹ BATLEY 09	NA48	±
$2.94 \pm 0.05 \pm 0.14$	10300	² APPEL 99	SPEC	±
$2.75 \pm 0.23 \pm 0.13$	500	³ ALLIEGRO 92	SPEC	+
2.7 ± 0.5	41	⁴ BLOCH 75	SPEC	+

Γ_{37} / Γ

¹ Value extrapolated from a measurement in the region $z = (m_{e\bar{e}}/m_K)^2 > 0.08$. BATLEY 09 also evaluated the shape of the form factor using four different theoretical models.

² APPEL 99 establishes vector nature of this decay and determines form factor $f(z) = f_0(1 + \delta z)$, $Z = M_{e\bar{e}}^2/m_K^2$, $\delta = 2.14 \pm 0.13 \pm 0.15$. Also reports constraints on scalar and tensor interactions: $|f_S| < 6.6 \times 10^{-5}$, $|f_T| < 3.7 \times 10^{-4}$ at 90% C.L.

³ ALLIEGRO 92 assumes a vector interaction with a form factor given by $\lambda = 0.105 \pm 0.035 \pm 0.015$ and a correlation coefficient of -0.82 .

⁴ BLOCH 75 assumes a vector interaction.

$\Gamma(\pi^+ \mu^+ \mu^-) / \Gamma_{total}$

Test for $\Delta S = 1$ weak neutral current. Allowed by higher-order electroweak interactions.

VALUE (units 10^{-8})	CL%	EVTs	DOCUMENT ID	TECN	CHG	COMMENT
9.17 ± 0.14 OUR AVERAGE						Error includes scale factor of 1.8.
$9.15 \pm 0.06 \pm 0.05$	28k	¹ CORTINA-GIL 22a	NA62			2017–18 data
$9.62 \pm 0.21 \pm 0.13$	3120	² BATLEY 11a	NA48	±		2003–04 data
$9.8 \pm 1.0 \pm 0.5$	110	³ PARK 02	HYCP	±		
$9.22 \pm 0.60 \pm 0.49$	402	⁴ MA 00	B865	+		
$5.0 \pm 0.4 \pm 0.9$	207	⁵ ADLER 97c	B787	+		

••• We do not use the following data for averages, fits, limits, etc. •••

$9.7 \pm 1.2 \pm 0.4$	65	PARK 02	HYCP	+
$10.0 \pm 1.9 \pm 0.7$	35	PARK 02	HYCP	–
<23	90	ATIYA 89	B787	+

¹ CORTINA-GIL 22a also studies the form factor $f(z)$ dependence of the decay, described via single photon exchange: assuming a linear form factor including $\pi\pi$ rescattering, $W_{\pi\pi^+}$, as in DAMBROSIO 98a, finding $f(z) = G_F m_K^2 (a_+ + b_+ z) + W_{\pi\pi}(z)$, $a_+ = -0.575 \pm 0.013$, $b_+ = -0.722 \pm 0.043$.

² BATLEY 11a also studies the form factor $f(z)$ dependence of the decay, described via single photon exchange: i) assuming a linear form factor, $f(z) = f_0(1 + \delta z)$, $z = (M_{\mu\mu}/m_K)^2$, finding $f_0 = 0.470 \pm 0.040$ and $\delta = 3.11 \pm 0.57$ and ii) assuming a linear form factor including $\pi\pi$ rescattering, $W_{\pi\pi}$, as in DAMBROSIO 98a, finding $f(z) = G_F m_K^2 (a_+ + b_+ z) + W_{\pi\pi}(z)$, $a_+ = -0.575 \pm 0.039$, $b_+ = -0.813 \pm 0.145$.

³ PARK 02 “±” result comes from combining $K^+ \rightarrow \pi^+ \mu^+ \mu^-$ and $K^- \rightarrow \pi^- \mu^+ \mu^-$, assuming CP is conserved.

⁴ MA 00 establishes vector nature of this decay and determines form factor $f(z) = f_0(1 + \delta z)$, $z = (M_{\mu\mu}/m_K)^2$, $\delta = 2.45^{+1.30}_{-0.95}$.

⁵ ADLER 97c gives systematic error 0.7×10^{-8} and theoretical uncertainty 0.6×10^{-8} , which we combine in quadrature to obtain our second error.

$\Gamma(\pi^+ e^+ e^- e^+ e^-) / \Gamma_{total}$

VALUE	CL%	DOCUMENT ID	TECN	CHG
< 1.4×10^{-8}	90	¹ CORTINA-GIL 23b	NA62	+

Γ_{39} / Γ

¹ Quoted limit is obtained using data collected from 2017 to 2018. CORTINA-GIL 23b also reports upper limits at 90% C.L. at the level of 10^{-9} for the branching ratios of two prompt decay chains involving pair-production of hidden-sector mediators: $K^+ \rightarrow \pi^+ a a$, $a \rightarrow e^+ e^-$ and $K^+ \rightarrow \pi^+ S$, $S \rightarrow X X$, $X \rightarrow e^+ e^-$.

$\Gamma(\pi^+ \nu \bar{\nu}) / \Gamma_{total}$

Test for $\Delta S = 1$ weak neutral current. Allowed by higher-order electroweak interactions. Branching ratio values are extrapolated from the momentum or energy regions shown in the comments assuming Standard Model phase space except for those labeled “Scalar” or “Tensor” to indicate the assumed non-Standard-Model interaction.

VALUE (units 10^{-10})	CL%	EVTs	DOCUMENT ID	TECN	CHG	COMMENT
1.14 ± 0.40 OUR AVERAGE						
$1.06^{+0.41}_{-0.35}$	20	¹ CORTINA-GIL 21b	NA62	+		
$1.73^{+1.15}_{-1.05}$	7	² ARTAMONOV 08	B949	+		$140 < P_\pi < 199$ MeV, $211 \lesseqgtr P_\pi < 229$ MeV

$\Gamma(\pi^+ \pi^0 \nu \bar{\nu}) / \Gamma_{total}$

Test for $\Delta S = 1$ weak neutral current. Allowed by higher-order electroweak interactions.

VALUE (units 10^{-5})	CL%	DOCUMENT ID	TECN
<4.3	90	¹ ADLER 01	SPEC

¹ Search region defined by $90 \text{ MeV}/c < P_{\pi^+} < 188 \text{ MeV}/c$ and $135 \text{ MeV} < E_{\pi^0} < 180 \text{ MeV}$.

$\Gamma(\mu^- \nu e^+ e^+) / \Gamma_{total}$

VALUE	CL%	DOCUMENT ID	TECN
< 8.1×10^{-11}	90	¹ CORTINA-GIL 23	NA62

¹ Performed using the dataset collected by the NA62 experiment at CERN from 2016 to 2018.

$\Gamma(\mu^- \nu e^+ e^+) / \Gamma(\pi^+ \pi^- e^+ \nu_e)$

Test of lepton family number conservation.

VALUE (units 10^{-3})	CL%	EVTs	DOCUMENT ID	TECN	CHG
<0.5	90	0	¹ DIAMANT-...	76	SPEC +

¹ DIAMANT-BERGER 76 quotes this result times our 1975 $\pi^+ \pi^- e \nu$ BR ratio.

$\Gamma(\mu^+ \nu_e) / \Gamma_{total}$

Forbidden by lepton family number conservation.

VALUE	CL%	EVTs	DOCUMENT ID	TECN	COMMENT
<0.004	90	0	¹ LYONS 81	HLBC	200 GeV K^+ narrow band ν beam

••• We do not use the following data for averages, fits, limits, etc. •••

<0.012	90	¹ COOPER 82	HLBC	Wideband ν beam
--------	----	------------------------	------	---------------------

¹ COOPER 82 and LYONS 81 limits on ν_e observation are here interpreted as limits on lepton family number violation in the absence of mixing.

Meson Particle Listings

 K^\pm $\Gamma(\pi^+ \mu^+ e^-)/\Gamma_{\text{total}}$

Test of lepton family number conservation.

VALUE (units 10^{-10})	CL%	DOCUMENT ID	TECN	CHG
<0.13	90	¹ SHER 05	RVUE	+
<0.21	90	SHER 05	B865	+
<0.39	90	APPEL 00	B865	+
<2.1	90	LEE 90	SPEC	+

¹ This result combines SHER 05 1998 data, APPEL 00 1996 data, and data from BERGMAN 97 and PISLAK 97 theses, all from BNL-E865, with LEE 90 BNL-E777 data.

 Γ_{44}/Γ $\Gamma(\pi^+ \mu^- e^+)/\Gamma_{\text{total}}$

Test of lepton family number conservation.

VALUE	CL%	DOCUMENT ID	TECN	CHG
< 6.6×10^{-11}	90	ALIBERTI 21	NA62	+
< 5.2×10^{-10}	90	APPEL 00B	B865	+
< 70×10^{-10}	90	¹ DIAMANT-...	76 SPEC	+

¹ Measurement actually applies to the sum of the $\pi^+ \mu^- e^+$ and $\pi^- \mu^+ e^+$ modes.

 Γ_{45}/Γ $\Gamma(\pi^- \mu^+ e^+)/\Gamma_{\text{total}}$

Test of total lepton number conservation.

VALUE	CL%	DOCUMENT ID	TECN	CHG
< 4.2×10^{-11}	90	ALIBERTI 21	NA62	+
< 5.0×10^{-10}	90	APPEL 00B	B865	+
< 70×10^{-10}	90	¹ DIAMANT-...	76 SPEC	+

¹ Measurement actually applies to the sum of the $\pi^+ \mu^- e^+$ and $\pi^- \mu^+ e^+$ modes.

 Γ_{46}/Γ $\Gamma(\pi^- e^+ e^+)/\Gamma_{\text{total}}$

Test of total lepton number conservation.

VALUE	CL%	DOCUMENT ID	TECN	CHG	COMMENT
< 5.3×10^{-11}	90	¹ CORTINA-GIL 22	NA62	+	decay-in-flight
< 2.2×10^{-10}	90	² CORTINA-GIL 19A	NA62	+	decay-in-flight
< 6.4×10^{-10}	90	APPEL 00B	B865	+	
< 9.2×10^{-9}	90	DIAMANT-...	76 SPEC	+	
< 1.5×10^{-5}	90	CHANG 68	HBC	-	

¹ CORTINA-GIL 22 uses the complete dataset collected by the NA62 experiment at CERN from 2016 to 2018. Supersedes CORTINA-GIL 19A.

² CORTINA-GIL 19A results are obtained with 2017 data. Superseded by CORTINA-GIL 22

 Γ_{47}/Γ $\Gamma(\pi^- \mu^+ \mu^+)/\Gamma_{\text{total}}$

Forbidden by total lepton number conservation.

VALUE	CL%	DOCUMENT ID	TECN	CHG	COMMENT
< 4.2×10^{-11}	90	¹ CORTINA-GIL 19A	NA62	+	decay-in-flight
< 8.6×10^{-11}	90	² BATLEY 17	NA48	±	
< 1.1×10^{-9}	90	BATLEY 11A	NA48	±	
< 3.0×10^{-9}	90	APPEL 00B	B865	+	
< 1.5×10^{-4}	90	³ LITTENBERG 92	HBC		

¹ CORTINA-GIL 19A results are obtained with 2017 data.

² BATLEY 17 result is based on data taken in 2003 to 2004. Limits for two-body resonance X in $K^\pm \rightarrow \pi \mu \mu$ decays are also reported.

³ LITTENBERG 92 is from retroactive data analysis of CHANG 68 bubble chamber data.

 Γ_{48}/Γ $\Gamma(\pi^- \pi^0 e^+ e^+)/\Gamma_{\text{total}}$

Test of total lepton number conservation.

VALUE	CL%	DOCUMENT ID	TECN	CHG	COMMENT
< 8.5×10^{-10}	90	¹ CORTINA-GIL 22	NA62	+	decay-in-flight

¹ CORTINA-GIL 22 uses the complete dataset collected by the NA62 experiment at CERN from 2016 to 2018.

 Γ_{49}/Γ $\Gamma(\mu^+ \bar{\nu}_e)/\Gamma_{\text{total}}$

Forbidden by total lepton number conservation.

VALUE (units 10^{-3})	CL%	DOCUMENT ID	TECN	COMMENT
<3.3	90	¹ COOPER 82	HLBC	Wideband ν beam

¹ COOPER 82 limit on $\bar{\nu}_e$ observation is here interpreted as a limit on lepton number violation in the absence of mixing.

 Γ_{50}/Γ $\Gamma(\pi^0 e^+ \bar{\nu}_e)/\Gamma_{\text{total}}$

Forbidden by total lepton number conservation.

VALUE	CL%	DOCUMENT ID	TECN	COMMENT
<0.003	90	¹ COOPER 82	HLBC	Wideband ν beam

¹ COOPER 82 limit on $\bar{\nu}_e$ observation is here interpreted as a limit on lepton number violation in the absence of mixing.

 Γ_{51}/Γ $\Gamma(\pi^\pm \gamma)/\Gamma_{\text{total}}$

Violates angular momentum conservation and gauge invariance. Current interest in this decay is as a search for non-commutative space-time effects as discussed in ARTAMONOV 05 and for exotic physics such as a vacuum expectation value of a new vector field, non-local Superstring effects, or departures from Lorentz invariance, as discussed in ADLER 02b.

VALUE	CL%	DOCUMENT ID	TECN	CHG
< 2.3×10^{-9}	90	ARTA MONOV 05	B949	+
< 360×10^{-9}	90	ADLER 02B	B787	+
< 1400×10^{-9}	90	ASANO 82	CNTR	+
< 4000×10^{-9}	90	¹ KLEMS 71	OSPK	+

¹ Test of model of Selleri, Nuovo Cimento **60A** 291 (1969).

 Γ_{52}/Γ CPT VIOLATION TESTS IN K^\pm DECAYS

$$\Delta = (\Gamma(K^+) - \Gamma(K^-)) / (\Gamma(K^+) + \Gamma(K^-))$$

 $\Delta(K^\pm \rightarrow \mu^\pm \nu_\mu)$ RATE DIFFERENCE/SUM

VALUE (%)	DOCUMENT ID	TECN
-0.27 ± 0.21	FORD 67	CNTR

 $\Delta(K^\pm \rightarrow \pi^\pm \pi^0)$ RATE DIFFERENCE/SUM

VALUE (%)	DOCUMENT ID	TECN
0.4 ± 0.6	HERZO 69	OSPK

CP VIOLATION TESTS IN K^\pm DECAYS

$$\Delta = (\Gamma(K^+) - \Gamma(K^-)) / (\Gamma(K^+) + \Gamma(K^-))$$

 $\Delta(K^\pm \rightarrow \pi^\pm e^+ e^-)$ RATE DIFFERENCE/SUM

VALUE (units 10^{-2})	DOCUMENT ID	TECN
$-2.2 \pm 1.5 \pm 0.6$	¹ BATLEY 09	NA48

¹ This implies an upper limit of 2.1×10^{-2} at 90% CL.

 $\Delta(K^\pm \rightarrow \pi^\pm \mu^+ \mu^-)$ RATE DIFFERENCE/SUM

VALUE	DOCUMENT ID	TECN
0.010 ± 0.023 OUR AVERAGE		
0.011 ± 0.023	¹ BATLEY 11A	NA48
$-0.02 \pm 0.11 \pm 0.04$	PARK 02	HYCP

¹ This corresponds to the asymmetry upper limit of $< 2.9 \times 10^{-2}$ at 90% CL.

 $\Delta(K^\pm \rightarrow \pi^\pm \pi^0 \gamma)$ RATE DIFFERENCE/SUM

VALUE (units 10^{-3})	EVTS	DOCUMENT ID	TECN	CHG	COMMENT
0.0 ± 1.2 OUR AVERAGE					
$0.0 \pm 1.0 \pm 0.6$	1M	¹ BATLEY 10A	NA48		
4 ± 29	2461	SMITH 76	WIRE	±	E_π 55–90 MeV
5 ± 20	4000	ABRAMS 73B	ASPK	±	E_π 51–100 MeV

¹ This value implies the upper bound for this asymmetry 1.5×10^{-3} at 90% CL.

 $\Delta(K^\pm \rightarrow \pi^\pm \pi^+ \pi^-)$ RATE DIFFERENCE/SUM

VALUE (%)	EVTS	DOCUMENT ID	TECN	CHG
0.04 ± 0.06		¹ FORD 70	ASPK	
-0.01 ± 0.08		² SMITH 73	ASPK	±
0.05 ± 0.07	3.2M	¹ FORD 70	ASPK	
-0.25 ± 0.45		FLETCHER 67	OSPK	
-0.02 ± 0.11		¹ FORD 67	CNTR	

¹ First FORD 70 value is second FORD 70 combined with FORD 67.

² SMITH 73 value of $K^\pm \rightarrow \pi^\pm \pi^+ \pi^-$ rate difference is derived from SMITH 73 value of $K^\pm \rightarrow \pi^\pm 2\pi^0$ rate difference.

 $\Delta(K^\pm \rightarrow \pi^\pm \pi^0 \pi^0)$ RATE DIFFERENCE/SUM

VALUE (%)	EVTS	DOCUMENT ID	TECN	CHG
-0.02 ± 0.28 OUR AVERAGE				
0.04 ± 0.29		SMITH 73	ASPK	±
-0.6 ± 0.9	1802	HERZO 69	OSPK	

T VIOLATION TESTS IN K^+ AND K^- DECAYS P_T in $K^+ \rightarrow \pi^0 \mu^+ \nu_\mu$

T-violating muon polarization. Sensitive to new sources of CP violation beyond the Standard Model.

VALUE (units 10^{-3})	EVTS	DOCUMENT ID	TECN	CHG
$-1.7 \pm 2.3 \pm 1.1$		¹ ABE 04F	K246	+
$-4.2 \pm 4.9 \pm 0.9$	3.9M	ABE 99S	K246	+

¹ Includes three sets of data: 96-97 (ABE 99S), 98, and 99-00 totaling about three times the ABE 99S data sample. Corresponds to $P_T < 5.0 \times 10^{-3}$ at 90% CL.

P_T in $K^+ \rightarrow \mu^+ \nu_\mu \gamma$

T-violating muon polarization. Sensitive to new sources of CP violation beyond the Standard Model.

VALUE (units 10^{-2})	EVTS	DOCUMENT ID	TECN	CHG
$-0.64 \pm 1.85 \pm 0.10$	114k	¹ ANISIMOVSK...03	K246	+

¹ Muons stopped and polarization measured from decay to positrons.

 $\text{Im}(\xi)$ in $K^+ \rightarrow \pi^0 \mu^+ \nu_\mu$ DECAY (from transverse μ pol.)

Test of T reversal invariance.

VALUE	EVTS	DOCUMENT ID	TECN	CHG	COMMENT
-0.006 ± 0.008 OUR AVERAGE					
$-0.0053 \pm 0.0071 \pm 0.0036$		¹ ABE	04F K246	+	
-0.016 ± 0.025	20M	CAMPBELL	81 CNTR	+	Pol.

••• We do not use the following data for averages, fits, limits, etc. •••

$-0.013 \pm 0.016 \pm 0.003$	3.9M	ABE	99s CNTR	+	$p_T K^+$ at rest
------------------------------	------	-----	----------	---	-------------------

¹ Includes three sets of data: 96-97 (ABE 99s), 98, and 99-00 totaling about three times the ABE 99s data sample. Corresponds to $\text{Im}(\xi) < 0.016$ at 90% CL.

DALITZ PLOT PARAMETERS FOR $K \rightarrow 3\pi$ DECAYS

Revised 1999 by T.G. Trippe (LBNL).

The Dalitz plot distribution for $K^\pm \rightarrow \pi^\pm \pi^\pm \pi^\mp$, $K^\pm \rightarrow \pi^0 \pi^0 \pi^\pm$, and $K_L^0 \rightarrow \pi^+ \pi^- \pi^0$ can be parameterized by a series expansion such as that introduced by Weinberg [1]. We use the form

$$\begin{aligned} |M|^2 &\propto 1 + g \frac{(s_3 - s_0)}{m_{\pi^+}^2} + h \left[\frac{s_3 - s_0}{m_{\pi^+}^2} \right]^2 \\ &+ j \frac{(s_2 - s_1)}{m_{\pi^+}^2} + k \left[\frac{s_2 - s_1}{m_{\pi^+}^2} \right]^2 \\ &+ f \frac{(s_2 - s_1)(s_3 - s_0)}{m_{\pi^+}^2 m_{\pi^+}^2} + \dots, \end{aligned} \quad (1)$$

where $m_{\pi^+}^2$ has been introduced to make the coefficients g , h , j , and k dimensionless, and

$$s_i = (P_K - P_i)^2 = (m_K - m_i)^2 - 2m_K T_i, \quad i = 1, 2, 3,$$

$$s_0 = \frac{1}{3} \sum_i s_i = \frac{1}{3} (m_K^2 + m_1^2 + m_2^2 + m_3^2).$$

Here the P_i are four-vectors, m_i and T_i are the mass and kinetic energy of the i^{th} pion, and the index 3 is used for the odd pion.

The coefficient g is a measure of the slope in the variable s_3 (or T_3) of the Dalitz plot, while h and k measure the quadratic dependence on s_3 and $(s_2 - s_1)$, respectively. The coefficient j is related to the asymmetry of the plot and must be zero if CP invariance holds. Note also that if CP is good, g , h , and k must be the same for $K^+ \rightarrow \pi^+ \pi^+ \pi^-$ as for $K^- \rightarrow \pi^- \pi^- \pi^+$.

Since different experiments use different forms for $|M|^2$, in order to compare the experiments we have converted to g , h , j , and k whatever coefficients have been measured. Where such conversions have been done, the measured coefficient a_y , a_t , a_u , or a_v is given in the comment at the right. For definitions of these coefficients, details of this conversion, and discussion of the data, see the April 1982 version of this note [2].

References

1. S. Weinberg, Phys. Rev. Lett. **4**, 87 (1960).
2. Particle Data Group, Phys. Lett. **111B**, 69 (1982).

ENERGY DEPENDENCE OF K^\pm DALITZ PLOT

$$|\text{matrix element}|^2 = 1 + gu + hu^2 + kv^2$$

where $u = (s_3 - s_0) / m_\pi^2$ and $v = (s_2 - s_1) / m_\pi^2$

LINEAR COEFFICIENT g FOR $K^\pm \rightarrow \pi^\pm \pi^+ \pi^-$

Some experiments use Dalitz variables x and y . In the comments we give a_y = coefficient of y term. See note above on "Dalitz Plot Parameters for $K \rightarrow 3\pi$ Decays." For discussion of the conversion of a_y to g , see the earlier version of the same note in the Review published in Physics Letters **111B** 70 (1982).

VALUE	EVTS	DOCUMENT ID	TECN	CHG	COMMENT
-0.21134 ± 0.00017	471M	¹ BATLEY	07B NA48	\pm	
••• We do not use the following data for averages, fits, limits, etc. •••					
-0.2221 ± 0.0065	225k	DEVAUX	77 SPEC	+	$a_y = .2814 \pm .0082$
-0.199 ± 0.008	81k	² LUCAS	73 HBC	-	$a_y = 0.252 \pm 0.011$
-0.2157 ± 0.0028	750k	FORD	72 ASPK	+	$a_y = .2734 \pm .0035$
-0.2186 ± 0.0028	750k	FORD	72 ASPK	-	$a_y = .2770 \pm .0035$
-0.200 ± 0.009	39819	³ HOFFMASTER	72 HLBC	+	
-0.196 ± 0.012	17898	⁴ GRAUMAN	70 HLBC	+	$a_y = 0.228 \pm 0.030$
-0.193 ± 0.010	50919	MAST	69 HBC	-	$a_y = 0.244 \pm 0.013$
-0.218 ± 0.016	9994	⁵ BUTLER	68 HBC	+	$a_y = 0.277 \pm 0.020$
-0.190 ± 0.023	5778	^{5,6} MOSCOSO	68 HBC	-	$a_y = 0.242 \pm 0.029$
-0.22 ± 0.024	5428	^{5,6} ZINCHENKO	67 HBC	+	$a_y = 0.28 \pm 0.03$
-0.220 ± 0.035	1347	⁷ FERRO-LUZZI	61 HBC	-	$a_y = 0.28 \pm 0.045$

¹ Final state strong interaction and radiative corrections not included in the fit.

² Quadratic dependence is required by K_L^0 experiments.

³ HOFFMASTER 72 includes GRAUMAN 70 data.

⁴ Emulsion data added — all events included by HOFFMASTER 72.

⁵ Experiments with large errors not included in average.

⁶ Also includes DBC events.

⁷ No radiative corrections included.

QUADRATIC COEFFICIENT h FOR $K^\pm \rightarrow \pi^\pm \pi^+ \pi^-$

VALUE (units 10^{-2})	EVTS	DOCUMENT ID	TECN	CHG
1.848 ± 0.040	471M	¹ BATLEY	07B NA48	\pm

••• We do not use the following data for averages, fits, limits, etc. •••

-0.06 ± 1.43	225k	DEVAUX	77 SPEC	+
1.87 ± 0.62	750k	FORD	72 ASPK	+
1.25 ± 0.62	750k	FORD	72 ASPK	-
-0.9 ± 1.4	39819	HOFFMASTER	72 HLBC	+
-0.1 ± 1.2	50919	MAST	69 HBC	-

¹ Final state strong interaction and radiative corrections not included in the fit.

QUADRATIC COEFFICIENT k FOR $K^\pm \rightarrow \pi^\pm \pi^+ \pi^-$

VALUE (units 10^{-3})	EVTS	DOCUMENT ID	TECN	CHG
-4.63 ± 0.14	471M	¹ BATLEY	07B NA48	\pm

••• We do not use the following data for averages, fits, limits, etc. •••

-20.5 ± 3.9	225k	DEVAUX	77 SPEC	+
-7.5 ± 1.9	750k	FORD	72 ASPK	+
-8.3 ± 1.9	750k	FORD	72 ASPK	-
-10.5 ± 4.5	39819	HOFFMASTER	72 HLBC	+
-14 ± 12	50919	MAST	69 HBC	-

¹ Final state strong interaction and radiative corrections not included in the fit.

 $(g_+ - g_-) / (g_+ + g_-)$ FOR $K^\pm \rightarrow \pi^\pm \pi^+ \pi^-$

This is a CP violating asymmetry between linear coefficients g_\pm for $K^+ \rightarrow \pi^+ \pi^+ \pi^-$ decay and g_- for $K^- \rightarrow \pi^- \pi^+ \pi^-$ decay.

VALUE (units 10^{-4})	EVTS	DOCUMENT ID	TECN
$-1.5 \pm 1.5 \pm 1.6$	3.1G	¹ BATLEY	07E NA48

••• We do not use the following data for averages, fits, limits, etc. •••

$1.7 \pm 2.1 \pm 2.0$	1.7G	² BATLEY	06 NA48
-70.0 ± 53	3.2M	FORD	70 ASPK

¹ BATLEY 07E includes data from BATLEY 06. Uses quadratic parametrization and value $g_+ + g_- = 2g$ from BATLEY 07B. This measurement neglects any possible charge asymmetries in higher order slope parameters h or k .

² This measurement neglects any possible charge asymmetries in higher order slope parameters h or k .

LINEAR COEFFICIENT g FOR $K^\pm \rightarrow \pi^\pm \pi^0 \pi^0$

Unless otherwise stated, all experiments include terms quadratic in $(s_3 - s_0) / m_\pi^2$. See note above on "Dalitz Plot Parameters for $K \rightarrow 3\pi$ Decays."

See BATUSOV 98 for a discussion of the discrepancy between their result and others, especially BOLOTOV 86. At this time we have no way to resolve the discrepancy so we depend on the large scale factor as a warning.

VALUE	EVTS	DOCUMENT ID	TECN	CHG	COMMENT
0.626 ± 0.007 OUR AVERAGE					
$0.6259 \pm 0.0043 \pm 0.0093$	493k	AKOPDZHAN..05B	TNF	\pm	
$0.627 \pm 0.004 \pm 0.010$	252k	^{1,2} AJINENKO	03B ISTR	-	

Meson Particle Listings

 K^\pm

• • • We do not use the following data for averages, fits, limits, etc. • • •

0.736 ± 0.014 ± 0.012	33k	BATUSOV	98	SPEC	+
0.582 ± 0.021	43k	BOLOTOV	86	CALO	-
0.670 ± 0.054	3263	BRAUN	76B	HLBC	+
0.630 ± 0.038	5635	SHEAFF	75	HLBC	+
0.510 ± 0.060	27k	SMITH	75	WIRE	+
0.67 ± 0.06	1365	AUBERT	72	HLBC	+
0.544 ± 0.048	4048	DAVISON	69	HLBC	+

¹ Measured using in-flight decays of the 25 GeV negative secondary beam.

² They form new world averages $g_- = (0.617 \pm 0.018)$ and $g_+ = (0.684 \pm 0.033)$ which give $\Delta g_{\pi^0} = 0.051 \pm 0.028$.

QUADRATIC COEFFICIENT h FOR $K^\pm \rightarrow \pi^\pm \pi^0 \pi^0$

VALUE	EVTS	DOCUMENT ID	TECN	CHG	COMMENT
0.052 ± 0.008 OUR AVERAGE					
0.0551 ± 0.0044 ± 0.0086	493k	AKOPDZHAN.05B	TNF	±	
0.046 ± 0.004 ± 0.012	252k	¹ AJINENKO	03B	ISTR	-

• • • We do not use the following data for averages, fits, limits, etc. • • •

0.128 ± 0.015 ± 0.024	33k	BATUSOV	98	SPEC	+
0.037 ± 0.024	43k	BOLOTOV	86	CALO	-
0.152 ± 0.082	3263	BRAUN	76B	HLBC	+
0.041 ± 0.030	5635	SHEAFF	75	HLBC	+
0.009 ± 0.040	27k	SMITH	75	WIRE	+
-0.01 ± 0.08	1365	AUBERT	72	HLBC	+
0.026 ± 0.050	4048	DAVISON	69	HLBC	+

¹ Measured using in-flight decays of the 25 GeV negative secondary beam.

QUADRATIC COEFFICIENT k FOR $K^\pm \rightarrow \pi^\pm \pi^0 \pi^0$

VALUE	EVTS	DOCUMENT ID	TECN	CHG	
0.0054 ± 0.0035 OUR AVERAGE					
0.0082 ± 0.0011 ± 0.0014	493k	AKOPDZHAN.05B	TNF	±	
0.001 ± 0.001 ± 0.002	252k	¹ AJINENKO	03B	ISTR	-

• • • We do not use the following data for averages, fits, limits, etc. • • •

0.0197 ± 0.0045 ± 0.0029	33k	BATUSOV	98	SPEC	+
1.8 ± 2.2 ± 1.3	47M	³ BATLEY	06A	NA48	±

¹ Measured using in-flight decays of the 25 GeV negative secondary beam.

 $(g_+ - g_-) / (g_+ + g_-)$ FOR $K^\pm \rightarrow \pi^\pm \pi^0 \pi^0$

A nonzero value for this quantity indicates CP violation.

VALUE (units 10^{-4})	EVTS	DOCUMENT ID	TECN
1.8 ± 1.8 OUR AVERAGE			
1.8 ± 1.7 ± 0.6	91.3M	¹ BATLEY	07E NA48
2 ± 18 ± 5	619k	² AKOPDZHAN.05	TNF

• • • We do not use the following data for averages, fits, limits, etc. • • •

1.8 ± 2.2 ± 1.3	47M	³ BATLEY	06A	NA48	±
-----------------	-----	---------------------	-----	------	---

¹ BATLEY 07E includes data from BATLEY 06A. Uses quadratic parametrization and PDG 06 value $g = 0.626 \pm 0.007$ to obtain $g_+ - g_- = (2.2 \pm 2.1 \pm 0.7) \times 10^{-4}$. Neglects any possible charge asymmetries in higher order slope parameters h or k .

² Asymmetry obtained assuming that $g_+ + g_- = 2 \times 0.652$ (PDG 02) and that asymmetries in h and k are zero.

³ Linear and quadratic slopes from PDG 04 are used. Any possible charge asymmetries in higher order slope parameters h or k are neglected.

ALTERNATIVE PARAMETRIZATIONS OF $K^\pm \rightarrow \pi^\pm \pi^0 \pi^0$ DALITZ PLOT

The following functional form for the matrix element suggested by $\pi\pi$ rescattering in $K^+ \rightarrow \pi^+ \pi^+ \pi^- \pi^0 \rightarrow \pi^+ \pi^0 \pi^0$ is used for this fit (CABIBBO 04A, CABIBBO 05): Matrix element = $M_0 + M_1$ where $M_0 = 1 + (1/2)g_0 u + (1/2)h' u^2 + (1/2)k_0 v^2$ with $u = (s_3 - s_0)/(m_{\pi^+})^2$, $v = (s_2 - s_1)/(m_{\pi^+})^2$ and where M_1 takes into account the non-analytic piece due to $\pi\pi$ rescattering amplitudes a_0 and a_2 ; The parameters g_0 and h' are related to the parameters g and h of the matrix element squared given in the previous section by the approximations $g_0 \sim g^{PDG}$ and $h' \sim h^{PDG} - (g/2)^2$ and $k_0 \sim k^{PDG}$.

In addition, we also consider the effective field theory framework of COLANGELO 06A and BISSEGGGER 09 to extract g_{BB} and h'_{BB} .

LINEAR COEFFICIENT g_0 FOR $K^\pm \rightarrow \pi^\pm \pi^0 \pi^0$

VALUE	EVTS	DOCUMENT ID	TECN	CHG
0.6525 ± 0.0009 ± 0.0033	60M	¹ BATLEY	09A	NA48 ±
0.645 ± 0.004 ± 0.009	23M	² BATLEY	06B	NA48 ±

¹ This fit is obtained with the CABIBBO 05 matrix element in the $2\pi^0$ invariant mass squared range $0.074094 < m_{2\pi^0}^2 < 0.104244$ GeV². Electromagnetic corrections and CHPT constraints for $\pi\pi$ phase shifts (a_0 and a_2) have been used. Also measured ($a_0 - a_2$) $m_{\pi^+} = 0.2646 \pm 0.0021 \pm 0.0023$, where k_0 was kept fixed in the fit at -0.0099 .

² Superseded by BATLEY 09A. This fit is obtained with the CABIBBO 05 matrix element in the $2\pi^0$ invariant mass squared range 0.074 GeV² $< m_{2\pi^0}^2 < 0.097$ GeV², assuming $k = 0$ (no term proportional to $(s_2 - s_1)^2$) and excluding the kinematic region around the cusp ($m_{2\pi^0}^2 = (2m_{\pi^+})^2 \pm 0.000525$ GeV²). Also $\pi\pi$ phase shifts a_0 and a_2 are measured: ($a_0 - a_2$) $m_{\pi^+} = 0.268 \pm 0.010 \pm 0.004 \pm 0.013$ (external) and $a_2 m_{\pi^+} = -0.041 \pm 0.022 \pm 0.014$.

QUADRATIC COEFFICIENT h' FOR $K^\pm \rightarrow \pi^\pm \pi^0 \pi^0$

VALUE	EVTS	DOCUMENT ID	TECN	CHG
-0.0433 ± 0.0008 ± 0.0026	60M	¹ BATLEY	09A	NA48 ±
-0.047 ± 0.012 ± 0.011	23M	² BATLEY	06B	NA48 ±

• • • We do not use the following data for averages, fits, limits, etc. • • •

¹ This fit is obtained with the CABIBBO 05 matrix element in the $2\pi^0$ invariant mass squared range $0.074094 < m_{2\pi^0}^2 < 0.104244$ GeV². Electromagnetic corrections and CHPT constraints for $\pi\pi$ phase shifts (a_0 and a_2) have been used. Also measured ($a_0 - a_2$) $m_{\pi^+} = 0.2646 \pm 0.0021 \pm 0.0023$, where k_0 was kept fixed in the fit at -0.0099 .

² Superseded by BATLEY 09A. This fit is obtained with the CABIBBO 05 matrix element in the $2\pi^0$ invariant mass squared range 0.074 GeV² $< m_{2\pi^0}^2 < 0.097$ GeV², assuming $k = 0$ (no term proportional to $(s_2 - s_1)^2$) and excluding the kinematic region around the cusp ($m_{2\pi^0}^2 = (2m_{\pi^+})^2 \pm 0.000525$ GeV²). Also $\pi\pi$ phase shifts a_0 and a_2 are measured: ($a_0 - a_2$) $m_{\pi^+} = 0.268 \pm 0.010 \pm 0.004 \pm 0.013$ (external) and $a_2 m_{\pi^+} = -0.041 \pm 0.022 \pm 0.014$.

QUADRATIC COEFFICIENT k_0 FOR $K^\pm \rightarrow \pi^\pm \pi^0 \pi^0$

VALUE	EVTS	DOCUMENT ID	TECN	CHG
0.0095 ± 0.00017 ± 0.00048	60M	¹ BATLEY	09A	NA48 ±

¹ Assumed $a_2 m_{\pi^+} = -0.0044$ in the fit.

LINEAR COEFFICIENT g_{BB} FOR $K^\pm \rightarrow \pi^\pm \pi^0 \pi^0$

VALUE	EVTS	DOCUMENT ID	TECN	CHG
0.6219 ± 0.0009 ± 0.0033	60M	¹ BATLEY	09A	NA48 ±

¹ This fit is obtained using parametrizations of COLANGELO 06A and BISSEGGGER 09 in the $2\pi^0$ invariant mass squared range $0.074094 < m_{2\pi^0}^2 < 0.104244$ GeV². Electromagnetic corrections and CHPT constraints for $\pi\pi$ phase shifts (a_0 and a_2) have been used. Also measured ($a_0 - a_2$) $m_{\pi^+} = 0.2633 \pm 0.0024 \pm 0.0024$, where k_0 was kept fixed in the fit at 0.0085.

QUADRATIC COEFFICIENT h'_{BB} FOR $K^\pm \rightarrow \pi^\pm \pi^0 \pi^0$

VALUE	EVTS	DOCUMENT ID	TECN	CHG
-0.0520 ± 0.0009 ± 0.0026	60M	¹ BATLEY	09A	NA48 ±

¹ This fit is obtained using parametrizations of COLANGELO 06A and BISSEGGGER 09 in the $2\pi^0$ invariant mass squared range $0.074094 < m_{2\pi^0}^2 < 0.104244$ GeV². Electromagnetic corrections and CHPT constraints for $\pi\pi$ phase shifts (a_0 and a_2) have been used. Also measured ($a_0 - a_2$) $m_{\pi^+} = 0.2633 \pm 0.0024 \pm 0.0024$, where k_0 was kept fixed in the fit at 0.0085.

 $K_{\pi^0}^\pm$ FORM FACTORS

In the form factor comments, the following symbols are used.

f_+ and f_- are form factors for the vector matrix element.

f_S and f_T refer to the scalar and tensor term.

$f_0 = f_+ + f_- t / (m_{K^\pm}^2 - m_{\pi^0}^2)$.

t = momentum transfer to the π .

λ_+ and λ_0 are the linear expansion coefficients of f_+ and f_0 :

$f_+(t) = f_+(0) (1 + \lambda_+ t / m_{\pi^+}^2)$

For quadratic expansion

$f_+(t) = f_+(0) (1 + \lambda'_+ t / m_{\pi^+}^2 + \frac{\lambda''_+}{2} t^2 / m_{\pi^+}^4)$

as used by KTeV. If there is a non-vanishing quadratic term, then λ_+ represents an average slope, which is then different from λ'_+ .

NA48/2 and OKA quadratic expansion coefficients are converted with $\lambda'_+ PDG = \lambda'_+ NA48/2$ and $\lambda''_+ PDG = 2 \lambda''_+ NA48/2$

$\lambda'_+ PDG = (\frac{m_{\pi^+}}{m_{\pi^0}})^2 \lambda'_+ OKA$ and

$\lambda''_+ PDG = 2 (\frac{m_{\pi^+}}{m_{\pi^0}})^4 \lambda''_+ OKA$

OKA linear expansion coefficients are converted with $\lambda_+ PDG = (\frac{m_{\pi^+}}{m_{\pi^0}})^2 \lambda_+ OKA$ and $\lambda_0 PDG = (\frac{m_{\pi^+}}{m_{\pi^0}})^2 \lambda_0 OKA$

The pole parametrization is

$f_+(t) = f_+(0) (\frac{M_V^2}{M_V^2 - t})$

$f_0(t) = f_0(0) (\frac{M_S^2}{M_S^2 - t})$

where M_V and M_S are the vector and scalar pole masses.

The following abbreviations are used:

DP = Dalitz plot analysis.

PI = π spectrum analysis.

MU = μ spectrum analysis.

POL = μ polarization analysis.

BR = $K_{\mu^3}^\pm / K_{e^3}^\pm$ branching ratio analysis.

E = positron or electron spectrum analysis.

RC = radiative corrections.

For previous λ'_+ and λ''_+ parametrizations used by NA48 (e.g. LA1 07A) and ISTRA (e.g. YUSHCHENKO 04B) see PDG 18.

λ_+ (LINEAR ENERGY DEPENDENCE OF f_+ IN K_{e3}^\pm DECAY)

These results are for a linear expansion only. See the next section for fits including a quadratic term. For radiative correction of the K_{e3}^\pm Dalitz plot, see GINSBERG 67, BECHERRAWY 70, CIRIGLIANO 02, CIRIGLIANO 04, and ANDRE 07. Results labeled OUR FIT are discussed in the review “ K_{e3}^\pm and $K_{\mu 3}^0$ Form Factors” above. For earlier, lower statistics results, see the 2004 edition of this review, Physics Letters **B592** 1 (2004).

VALUE (units 10^{-2})	EVTS	DOCUMENT ID	TECN	CHG	COMMENT
2.959 ± 0.025 OUR FIT	Assuming μ -e universality				
2.956 ± 0.025 OUR AVERAGE					
2.95 ± 0.022 ± 0.018	5.25M	YUSHCHENKO 18	OCA	+	
3.044 ± 0.083 ± 0.074	1.1M	AKOPDZANOV 09	TNF	±	
2.966 ± 0.050 ± 0.034	919k	¹ YUSHCHENKO 04B	ISTR	- DP	
2.78 ± 0.26 ± 0.30	41k	SHIMIZU 00	SPEC	+ DP	
2.84 ± 0.27 ± 0.20	32k	² AKIMENKO 91	SPEC	PI, no RC	
2.9 ± 0.4	62k	³ BOLOTOV 88	SPEC	PI, no RC	
• • • We do not use the following data for averages, fits, limits, etc. • • •					
3.06 ± 0.09 ± 0.06	550k	^{1,4} AJINENKO 03C	ISTR	- DP	
2.93 ± 0.15 ± 0.2	130k	⁴ AJINENKO 02	SPEC	DP	

¹ Rescaled to agree with our conventions as noted above.

² AKIMENKO 91 state that radiative corrections would raise λ_+ by 0.0013.

³ BOLOTOV 88 state radiative corrections of GINSBERG 67 would raise λ_+ by 0.002.

⁴ Superseded by YUSHCHENKO 04B.

 λ_+ (LINEAR ENERGY DEPENDENCE OF f_+ IN $K_{\mu 3}^\pm$ DECAY)

Results labeled OUR FIT are discussed in the review “ K_{e3}^\pm and $K_{\mu 3}^0$ Form Factors” above. For earlier, lower statistics results, see the 2004 edition of this review, Physics Letters **B592** 1 (2004).

VALUE (units 10^{-2})	EVTS	DOCUMENT ID	TECN	CHG	COMMENT
2.959 ± 0.025 OUR FIT	Assuming μ -e universality				
3.09 ± 0.25 OUR FIT	Error includes scale factor of 1.5. Not assuming μ -e universality				
2.96 ± 0.14 ± 0.10	540k	¹ YUSHCHENKO04	ISTR	- DP	
• • • We do not use the following data for averages, fits, limits, etc. • • •					
3.21 ± 0.45	112k	² AJINENKO 03	ISTR	- DP	
¹ Rescaled to agree with our conventions as noted above.					
² Superseded by YUSHCHENKO 04.					

 λ_0 (LINEAR ENERGY DEPENDENCE OF f_0 IN $K_{\mu 3}^\pm$ DECAY)

Results labeled OUR FIT are discussed in the review “ K_{e3}^\pm and $K_{\mu 3}^0$ Form Factors” above. For earlier, lower statistics results, see the 2004 edition of this review, Physics Letters **B592** 1 (2004).

VALUE (units 10^{-2})	$d\lambda_0/d\lambda_+$	EVTS	DOCUMENT ID	TECN	CHG	COMMENT
1.76 ± 0.25 OUR FIT	Error includes scale factor of 2.7. Assuming μ -e universality					
1.73 ± 0.27 OUR FIT	Error includes scale factor of 2.6. Not assuming μ -e universality					
1.420 ± 0.114 ± 0.107		2.3M	¹ BATLEY 18	NA48	±	
1.96 ± 0.12 ± 0.06	-0.348	540k	² YUSHCHENKO04	ISTR	- DP	
• • • We do not use the following data for averages, fits, limits, etc. • • •						
2.09 ± 0.45	-0.46	112k	³ AJINENKO 03	ISTR	- DP	
1.9 ± 0.64		24k	⁴ HORIE 01	SPEC	+ BR	
1.9 ± 1.0	+0.03	55k	⁵ HEINTZE 77	SPEC	+ BR	

¹ Data collected in 2004 by NA48/2. Obtained from a fit with a quadratic vector form factor. Correlation coefficient with linear slope is 0.511, with quadratic slope is -0.513. $\chi^2/NDF = 409.9/381$. BATLEY 18 also performed a combined K_{e3}^\pm and $K_{\mu 3}^\pm$ fit assuming μ -e universality and obtained $(14.47 \pm 0.63 \pm 1.17) \times 10^{-3}$.

² Rescaled to agree with our conventions as noted above.

³ Superseded by YUSHCHENKO 04.

⁴ HORIE 01 assumes μ -e universality in K_{e3}^\pm decay and uses SHIMIZU 00 value $\lambda = 0.0278 \pm 0.0040$ from K_{e3}^\pm decay.

⁵ HEINTZE 77 uses $\lambda_+ = 0.029 \pm 0.003$. $d\lambda_0/d\lambda_+$ estimated by us.

 λ_+^* (LINEAR K_{e3}^\pm FORM FACTOR FROM QUADRATIC FIT)

VALUE (units 10^{-2})	EVTS	DOCUMENT ID	TECN	CHG	COMMENT
2.59 ± 0.04 OUR AVERAGE					
2.426 ± 0.078 ± 0.130	4.4M	¹ BATLEY 18	NA48	±	
2.611 ± 0.035 ± 0.028	5.25M	YUSHCHENKO18	OCA	+	
2.485 ± 0.163 ± 0.034	919k	^{2,3} YUSHCHENKO04B	ISTR	- DP	
• • • We do not use the following data for averages, fits, limits, etc. • • •					
3.07 ± 0.21	550k	^{2,4} AJINENKO 03C	ISTR	- DP	

¹ Data collected in 2004 by NA48/2. Correlation coefficient with quadratic slope is -0.929. $\chi^2/NDF = 569.1/687$. BATLEY 18 also performed a combined K_{e3}^\pm and $K_{\mu 3}^\pm$ fit assuming μ -e universality and obtained $(24.24 \pm 0.75 \pm 1.3) \times 10^{-3}$.

² Rescaled to agree with our conventions as noted above.

³ YUSHCHENKO 04B λ_+^* and λ_+^{**} are strongly correlated with coefficient $\rho(\lambda_+^*, \lambda_+^{**}) = -0.95$.

⁴ Superseded by YUSHCHENKO 04B.

 λ_+^{**} (QUADRATIC K_{e3}^\pm FORM FACTOR)

VALUE (units 10^{-2})	EVTS	DOCUMENT ID	TECN	CHG	COMMENT
0.186 ± 0.021 OUR AVERAGE					
0.164 ± 0.030 ± 0.039	4.4M	¹ BATLEY 18	NA48	±	
0.191 ± 0.019 ± 0.014	5.25M	YUSHCHENKO18	OCA	+	
0.192 ± 0.062 ± 0.071	919k	^{2,3} YUSHCHENKO04B	ISTR	- DP	

• • • We do not use the following data for averages, fits, limits, etc. • • •

-0.5 ± 0.7 ± 1.5 550k ^{2,4}AJINENKO 03C ISTR - DP

¹ Data collected in 2004 by NA48/2. Correlation coefficient with quadratic slope is -0.929. $\chi^2/NDF = 569.1/687$. BATLEY 18 also performed a combined K_{e3}^\pm and $K_{\mu 3}^\pm$ fit assuming μ -e universality and obtained $(1.67 \pm 0.29 \pm 0.41) \times 10^{-3}$.

² Rescaled to agree with our conventions as noted above.

³ YUSHCHENKO 04B λ_+^* and λ_+^{**} are strongly correlated with coefficient $\rho(\lambda_+^*, \lambda_+^{**}) = -0.95$.

⁴ Superseded by YUSHCHENKO 04B.

 λ_+^* (LINEAR $K_{\mu 3}^\pm$ FORM FACTOR FROM QUADRATIC FIT)

VALUE (units 10^{-3})	EVTS	DOCUMENT ID	TECN	CHG
24.27 ± 2.88 ± 2.89	2.3M	¹ BATLEY 18	NA48	±

¹ Data collected in 2004 by NA48/2. Correlation coefficient with quadratic slope is -0.974, with scalar slope is 0.511. $\chi^2/NDF = 409.9/381$. BATLEY 18 also performed a combined K_{e3}^\pm and $K_{\mu 3}^\pm$ fit assuming μ -e universality and obtained $(24.24 \pm 0.75 \pm 1.3) \times 10^{-3}$.

 λ_+^{**} (QUADRATIC $K_{\mu 3}^\pm$ FORM FACTOR)

VALUE (units 10^{-3})	EVTS	DOCUMENT ID	TECN	CHG
1.83 ± 1.05 ± 1.09	2.3M	¹ BATLEY 18	NA48	±

¹ Data collected in 2004 by NA48/2. Correlation coefficient with linear slope is -0.974, with scalar slope is 0.513. $\chi^2/NDF = 409.9/381$. BATLEY 18 also performed a combined K_{e3}^\pm and $K_{\mu 3}^\pm$ fit assuming μ -e universality and obtained $(1.67 \pm 0.29 \pm 0.41) \times 10^{-3}$.

 M_V (VECTOR POLE MASS FOR K_{e3}^\pm DECAY)

See the review on K_{e3}^\pm and $K_{\mu 3}^0$ Form Factors for details.

VALUE (MeV)	EVTS	DOCUMENT ID	TECN	CHG
890.3 ± 2.8 OUR AVERAGE				
885.2 ± 3.3 ± 7.2	4.4M	¹ BATLEY 18	NA48	±
891 ± 3	5.25M	² YUSHCHENKO18	OCA	+

¹ Data collected in 2004 by NA48/2. $\chi^2/NDF = 568.9/688$. BATLEY 18 also performed a combined K_{e3}^\pm and $K_{\mu 3}^\pm$ fit assuming μ -e universality and obtained $884.4 \pm 3.1 \pm 6.7$ MeV.

² Assumed no scalar or tensor contributions to the form factor.

 M_V (VECTOR POLE MASS FOR $K_{\mu 3}^\pm$ DECAY)

VALUE (MeV)	EVTS	DOCUMENT ID	TECN	CHG
878.4 ± 8.8 ± 8.3	2.3M	¹ BATLEY 18	NA48	±

¹ Data collected in 2004 by NA48/2. $\chi^2/NDF = 409.9/382$. BATLEY 18 also performed a combined K_{e3}^\pm and $K_{\mu 3}^\pm$ fit assuming μ -e universality and obtained $884.4 \pm 3.1 \pm 6.7$ MeV.

 M_S (SCALAR POLE MASS FOR $K_{\mu 3}^\pm$ DECAY)

VALUE (MeV)	EVTS	DOCUMENT ID	TECN	CHG
1214.8 ± 23.5 ± 49.2	2.3M	¹ BATLEY 18	NA48	±

¹ Data collected in 2004 by NA48/2. $\chi^2/NDF = 409.9/382$. BATLEY 18 also performed a combined K_{e3}^\pm and $K_{\mu 3}^\pm$ fit assuming μ -e universality and obtained $1208.3 \pm 21.2 \pm 47.5$ MeV.

 A_+ (DISPERSIVE VECTOR FORM FACTOR IN K_{e3}^\pm DECAY)

See the review on K_{e3}^\pm and $K_{\mu 3}^0$ Form Factors for details.

VALUE (units 10^{-2})	EVTS	DOCUMENT ID	TECN	CHG
2.460 ± 0.017 OUR AVERAGE				
2.494 ± 0.021 ± 0.064	4.4M	¹ BATLEY 18	NA48	±
2.458 ± 0.018	5.25M	² YUSHCHENKO18	OCA	+

¹ Data collected in 2004 by NA48/2. $\chi^2/NDF = 569.0/688$. BATLEY 18 also performed a combined K_{e3}^\pm and $K_{\mu 3}^\pm$ fit assuming μ -e universality and obtained $(24.99 \pm 0.20 \pm 0.62) \times 10^{-3}$.

² Assumed no scalar or tensor contributions to the form factor.

 A_+ (DISPERSIVE VECTOR FORM FACTOR IN $K_{\mu 3}^\pm$ DECAY)

VALUE (units 10^{-3})	EVTS	DOCUMENT ID	TECN	CHG
25.36 ± 0.58 ± 0.72	2.3M	¹ BATLEY 18	NA48	±

¹ Data collected in 2004 by NA48/2. $\chi^2/NDF = 410.3/382$. BATLEY 18 also performed a combined K_{e3}^\pm and $K_{\mu 3}^\pm$ fit assuming μ -e universality and obtained $(24.99 \pm 0.20 \pm 0.62) \times 10^{-3}$.

 $\ln(C)$ (DISPERSIVE SCALAR FORM FACTOR IN $K_{\mu 3}^\pm$ decays)

VALUE (units 10^{-3})	EVTS	DOCUMENT ID	TECN	CHG
182.17 ± 6.31 ± 14.45	2.3M	¹ BATLEY 18	NA48	±

¹ Data collected in 2004 by NA48/2. Combined fit with dispersive vector form factor $A_+ = 25.36 \pm 0.58 \pm 0.72$. Correlation coefficient is 0.104. $\chi^2/NDF = 410.3/382$. BATLEY 18 also performed a combined K_{e3}^\pm and $K_{\mu 3}^\pm$ fit assuming μ -e universality and obtained $(183.65 \pm 5.92 \pm 14.25) \times 10^{-3}$.

Meson Particle Listings

 K^\pm $|f_S/f_+|$ FOR K_{e3}^\pm DECAYRatio of scalar to f_+ couplings.

VALUE (units 10^{-2})	CL%	EVTS	DOCUMENT ID	TECN	CHG	COMMENT	
-0.08 ± 0.34						OUR AVERAGE	
0.01 ± 0.38		5.25M	YUSHCHENKO18	OKA	+	$\lambda'_+, \lambda''_+, f_S$ fit	
$-0.37 \pm 0.66 \pm 0.41$		919k	YUSHCHENKO04B	ISTR	-	$\lambda'_+, \lambda''_+, f_S$ fit	
$0.2 \pm 2.6 \pm 1.4$		41k	SHIMIZU	00	SPEC	λ_+, f_S, f_T fit	
••• We do not use the following data for averages, fits, limits, etc. •••							
0.2 ± 2.0		550k	1 AJINENKO	03c	ISTR	λ_+, f_S, f_T fit	
-1.9 ± 1.6		130k	1 AJINENKO	02	SPEC	λ_+, f_S fit	
$7.0 \pm 1.6 \pm 1.6$		32k	AKIMENKO	91	SPEC	$\lambda_+, f_S, f_T, \phi$ fit	
0 ± 10		2827	2 BRAUN	75	HLBC	+	
< 13		90	4017	CHIANG	72	OSPK	+
14 ± 3		2707	2 STEINER	71	HLBC	$\lambda_+, f_S, f_T, \phi$ fit	
< 23		90	BOTTERILL	68c	ASP		
< 18		90	BELLOTTI	67b	HLBC		
< 30		95	KALMUS	67	HLBC	+	

¹ Superseded by YUSHCHENKO 04b.² Statistical errors only. $|f_T/f_+|$ FOR K_{e3}^\pm DECAYRatio of tensor to f_+ couplings.

VALUE (units 10^{-2})	EVTS	DOCUMENT ID	TECN	CHG	COMMENT
-1.2 ± 1.3					OUR AVERAGE
-1.24 ± 1.6	5.25M	YUSHCHENKO18	OKA	+	$\lambda'_+, \lambda''_+, f_T$ fit
$-1.2 \pm 2.1 \pm 1.1$	919k	YUSHCHENKO04B	ISTR	-	$\lambda'_+, \lambda''_+, f_T$ fit
$1 \pm 14 \pm 9$	41k	SHIMIZU	00	SPEC	λ_+, f_S, f_T fit
••• We do not use the following data for averages, fits, limits, etc. •••					
$2.1 \pm 6.4 \pm 2.6$	550k	1 AJINENKO	03c	ISTR	λ_+, f_S, f_T fit
-4.5 ± 6.0	130k	1 AJINENKO	02	SPEC	λ_+, f_T fit
$53 \pm 9 \pm 10$	32k	AKIMENKO	91	SPEC	$\lambda_+, f_S, f_T, \phi$ fit

¹ Superseded by YUSHCHENKO 04b. f_S/f_+ FOR $K_{\mu 3}^\pm$ DECAYRatio of scalar to f_+ couplings.

VALUE (units 10^{-2})	EVTS	DOCUMENT ID	TECN	CHG	COMMENT
$0.17 \pm 0.14 \pm 0.54$	540k	1 YUSHCHENKO04	ISTR	-	DP
••• We do not use the following data for averages, fits, limits, etc. •••					
$0.4 \pm 0.5 \pm 0.5$	112k	2 AJINENKO	03	ISTR	DP

¹ The second error is the theoretical error from the uncertainty in the chiral perturbation theory prediction for λ_0 , ± 0.0053 , combined in quadrature with the systematic error ± 0.0009 .² The second error is the theoretical error from the uncertainty in the chiral perturbation theory prediction for λ_0 . Superseded by YUSHCHENKO 04. f_T/f_+ FOR $K_{\mu 3}^\pm$ DECAYRatio of tensor to f_+ couplings.

VALUE (units 10^{-2})	EVTS	DOCUMENT ID	TECN	CHG	COMMENT
$-0.07 \pm 0.71 \pm 0.20$	540k	YUSHCHENKO04	ISTR	-	DP
••• We do not use the following data for averages, fits, limits, etc. •••					
$-2.1 \pm 2.8 \pm 1.4$	112k	1 AJINENKO	03	ISTR	DP
2 ± 12	1585	BRAUN	75	HLBC	

¹ The second error is the theoretical error from the uncertainty in the chiral perturbation theory prediction for λ_0 . Superseded by YUSHCHENKO 04. K_{e4}^\pm FORM FACTORSBased on the parametrizations of AMOROS 99, the K_{e4}^\pm form factors can be expressed as

$$F_S = f_S + f'_S q^2 + f''_S q^4 + f'_e S_e / 4m_\pi^2$$

$$F_P = f_P$$

$$G_P = g_P + g'_P q^2$$

$$H_P = h_P$$

where $q^2 = (S_\pi / 4m_\pi^2) - 1$, S_π is the invariant mass squared of the dipion, and S_e is the invariant mass squared of the dilepton. f_S FOR $K^\pm \rightarrow \pi^+ \pi^- e^\pm \nu$ DECAY

VALUE	EVTS	DOCUMENT ID	TECN	CHG
5.712 ± 0.032				
$5.705 \pm 0.003 \pm 0.035$	1.1M	1 BATLEY	12	NA48 ±
$5.75 \pm 0.02 \pm 0.08$	400k	2 PISLAK	03	B865 ±

¹ BATLEY 12 uses data collected in 2003–2004. The result is obtained from a measurement of $\Gamma(\pi^+ \pi^- e \nu) / \Gamma(\pi^+ \pi^- \pi^+)$ and assumed PDG 12 value of $\Gamma(\pi^+ \pi^- \pi^+) / \Gamma = (5.59 \pm 0.04) \times 10^{-2}$.² Radiative corrections included. Using Roy equations and not including isospin breaking, PISLAK 03 obtains the following $\pi\pi$ scattering lengths $a_0^0 = 0.228 \pm 0.012 \pm 0.004 \pm 0.012$ (theor.) and $a_0^2 = -0.0365 \pm 0.0023 \pm 0.0008 \pm 0.0031$ (theor.). f'_S/f_S FOR $K^\pm \rightarrow \pi^+ \pi^- e^\pm \nu$ DECAY

VALUE (units 10^{-2})	EVTS	DOCUMENT ID	TECN	CHG
$15.2 \pm 0.7 \pm 0.5$	1.13M	1 BATLEY	10c	NA48 ±

••• We do not use the following data for averages, fits, limits, etc. •••

$17.2 \pm 0.9 \pm 0.6$	670k	2 BATLEY	08A	NA48 ±
------------------------	------	----------	-----	--------

¹ Radiative corrections included. Using Roy equations and including isospin breaking, BATLEY 10c obtains the following scattering lengths $a_0^0 = 0.2220 \pm 0.0128 \pm 0.0050 \pm 0.0037$ (theor.), $a_0^2 = -0.0432 \pm 0.0086 \pm 0.0034 \pm 0.0028$ (theor.). The correlation with $f''_S/f_S = -0.954$ and with $f'_e/f_S = 0.080$. Supersedes BATLEY 08A.² Radiative corrections included. Using Roy equations and not including isospin breaking, BATLEY 08A obtains the following $\pi\pi$ scattering length $a_0^0 = 0.233 \pm 0.016 \pm 0.007$, $a_0^2 = -0.0471 \pm 0.011 \pm 0.004$. f''_S/f_S FOR $K^\pm \rightarrow \pi^+ \pi^- e^\pm \nu$ DECAY

VALUE (units 10^{-2})	EVTS	DOCUMENT ID	TECN	CHG
$-7.3 \pm 0.7 \pm 0.6$	1.13M	1 BATLEY	10c	NA48 ±

••• We do not use the following data for averages, fits, limits, etc. •••

$-9.0 \pm 0.9 \pm 0.7$	670k	2 BATLEY	08A	NA48 ±
------------------------	------	----------	-----	--------

¹ Radiative corrections included. Using Roy equations and including isospin breaking, BATLEY 10c obtains the following scattering lengths $a_0^0 = 0.2220 \pm 0.0128 \pm 0.0050 \pm 0.0037$ (theor.), $a_0^2 = -0.0432 \pm 0.0086 \pm 0.0034 \pm 0.0028$ (theor.). The correlation with $f'_S/f_S = -0.954$ and with $f'_e/f_S = 0.019$. Supersedes BATLEY 08A.² Radiative corrections included. Using Roy equations and not including isospin breaking, BATLEY 08A obtains the following $\pi\pi$ scattering length $a_0^0 = 0.233 \pm 0.016 \pm 0.007$, $a_0^2 = -0.0471 \pm 0.011 \pm 0.004$. f'_e/f_S FOR $K^\pm \rightarrow \pi^+ \pi^- e^\pm \nu$ DECAY

VALUE (units 10^{-2})	EVTS	DOCUMENT ID	TECN	CHG
$6.8 \pm 0.6 \pm 0.7$	1.13M	1 BATLEY	10c	NA48 ±

••• We do not use the following data for averages, fits, limits, etc. •••

$8.1 \pm 0.8 \pm 0.9$	670k	2 BATLEY	08A	NA48 ±
-----------------------	------	----------	-----	--------

¹ Radiative corrections included. Using Roy equations and including isospin breaking, BATLEY 10c obtains the following scattering lengths $a_0^0 = 0.2220 \pm 0.0128 \pm 0.0050 \pm 0.0037$ (theor.), $a_0^2 = -0.0432 \pm 0.0086 \pm 0.0034 \pm 0.0028$ (theor.). The correlation with $f'_S/f_S = 0.080$ and with $f''_S/f_S = 0.019$. Supersedes BATLEY 08A.² Radiative corrections included. Using Roy equations and not including isospin breaking, BATLEY 08A obtains the following $\pi\pi$ scattering length $a_0^0 = 0.233 \pm 0.016 \pm 0.007$, $a_0^2 = -0.0471 \pm 0.011 \pm 0.004$. f_P/f_S FOR $K^\pm \rightarrow \pi^+ \pi^- e^\pm \nu$ DECAY

VALUE (units 10^{-2})	EVTS	DOCUMENT ID	TECN	CHG
$-4.8 \pm 0.3 \pm 0.4$	1.13M	1 BATLEY	10c	NA48 ±

••• We do not use the following data for averages, fits, limits, etc. •••

$-4.8 \pm 0.4 \pm 0.4$	670k	2 BATLEY	08A	NA48 ±
------------------------	------	----------	-----	--------

¹ Radiative corrections included. Using Roy equations and including isospin breaking, BATLEY 10c obtains the following scattering lengths $a_0^0 = 0.2220 \pm 0.0128 \pm 0.0050 \pm 0.0037$ (theor.), $a_0^2 = -0.0432 \pm 0.0086 \pm 0.0034 \pm 0.0028$ (theor.). Supersedes BATLEY 08A.² Radiative corrections included. Using Roy equations and not including isospin breaking, BATLEY 08A obtains the following $\pi\pi$ scattering length $a_0^0 = 0.233 \pm 0.016 \pm 0.007$, $a_0^2 = -0.0471 \pm 0.011 \pm 0.004$. g_P/f_S FOR $K^\pm \rightarrow \pi^+ \pi^- e^\pm \nu$ DECAY

VALUE (units 10^{-2})	EVTS	DOCUMENT ID	TECN	CHG
$86.8 \pm 1.0 \pm 1.0$	1.13M	1 BATLEY	10c	NA48 ±

••• We do not use the following data for averages, fits, limits, etc. •••

$87.3 \pm 1.3 \pm 1.2$	670k	2 BATLEY	08A	NA48 ±
$80.9 \pm 0.9 \pm 1.2$	400k	3 PISLAK	03	B865 ±

¹ Radiative corrections included. Using Roy equations and including isospin breaking, BATLEY 10c obtains the following scattering lengths $a_0^0 = 0.2220 \pm 0.0128 \pm 0.0050 \pm 0.0037$ (theor.), $a_0^2 = -0.0432 \pm 0.0086 \pm 0.0034 \pm 0.0028$ (theor.). Supersedes BATLEY 08A. The correlation with $g'_P/f_S = -0.914$. Supersedes BATLEY 08A.² Radiative corrections included. Using Roy equations and not including isospin breaking, BATLEY 08A obtains the following $\pi\pi$ scattering length $a_0^0 = 0.233 \pm 0.016 \pm 0.007$, $a_0^2 = -0.0471 \pm 0.011 \pm 0.004$.³ Radiative corrections included. Using Roy equations PISLAK 03 obtains the following scattering lengths $a_0^0 = 0.203 \pm 0.033 \pm 0.004$, $a_0^2 = -0.055 \pm 0.023 \pm 0.003$. g'_P/f_S FOR $K^\pm \rightarrow \pi^+ \pi^- e^\pm \nu$ DECAY

VALUE (units 10^{-2})	EVTS	DOCUMENT ID	TECN	CHG
$8.9 \pm 1.7 \pm 1.3$	1.13M	1 BATLEY	10c	NA48 ±

• • • We do not use the following data for averages, fits, limits, etc. • • •

8.1±2.2±1.5	670k	² BATLEY	08A	NA48	±
12.0±1.9±0.7	400k	³ PISLAK	03	B865	±

¹ Radiative corrections included. Using Roy equations and including isospin breaking, BATLEY 10c obtains the following scattering lengths $a_0^0 = 0.2220 \pm 0.0128 \pm 0.0050 \pm 0.0037$ (theor.), $a_0^2 = -0.0432 \pm 0.0086 \pm 0.0034 \pm 0.0028$ (theor.). The correlation with $g_p/f_s = -0.914$. Supersedes BATLEY 08A.

² Radiative corrections included. Using Roy equations and not including isospin breaking, BATLEY 08A obtains the following $\pi\pi$ scattering length $a_0^0 = 0.233 \pm 0.016 \pm 0.007$, $a_0^2 = -0.0471 \pm 0.011 \pm 0.004$.

³ Radiative corrections included. Using Roy equations PISLAK 03 obtains the following scattering lengths $a_0^0 = 0.203 \pm 0.033 \pm 0.004$, $a_0^2 = -0.055 \pm 0.023 \pm 0.003$.

h_p/f_s FOR $K^\pm \rightarrow \pi^+ \pi^- e^\pm \nu$ DECAY

VALUE (units 10^{-2})	EVTS	DOCUMENT ID	TECN	CHG
--------------------------	------	-------------	------	-----

• • • We do not use the following data for averages, fits, limits, etc. • • •

-39.8±1.5±0.8	1.13M	¹ BATLEY	10C	NA48	±
-41.1±1.9±0.8	670k	² BATLEY	08A	NA48	±
-51.3±3.3±3.5	400k	³ PISLAK	03	B865	±

¹ Radiative corrections included. Using Roy equations and including isospin breaking, BATLEY 10c obtains the following scattering lengths $a_0^0 = 0.2220 \pm 0.0128 \pm 0.0050 \pm 0.0037$ (theor.), $a_0^2 = -0.0432 \pm 0.0086 \pm 0.0034 \pm 0.0028$ (theor.). Supersedes BATLEY 08A.

² Radiative corrections included. Using Roy equations and not including isospin breaking, BATLEY 08A obtains the following $\pi\pi$ scattering length $a_0^0 = 0.233 \pm 0.016 \pm 0.007$, $a_0^2 = -0.0471 \pm 0.011 \pm 0.004$.

³ Radiative corrections included. Using Roy equations PISLAK 03 obtains the following scattering lengths $a_0^0 = 0.203 \pm 0.033 \pm 0.004$, $a_0^2 = -0.055 \pm 0.023 \pm 0.003$.

DECAY FORM FACTOR FOR $K^\pm \rightarrow \pi^0 \pi^0 e^\pm \nu$

Given in BOLOTOV 86b, BARMIN 88b, and SHIMIZU 04.

$K^\pm \rightarrow \ell^\pm \nu \gamma$ FORM FACTORS

For definitions of the axial-vector F_A and vector F_V form factor, see the "Note on $\pi^\pm \rightarrow \ell^\pm \nu \gamma$ and $K^\pm \rightarrow \ell^\pm \nu \gamma$ Form Factors" in the π^\pm section. In the kaon literature, often different definitions $a_K = F_A/m_K$ and $v_K = F_V/m_K$ are used.

$F_A + F_V$, SUM OF AXIAL-VECTOR AND VECTOR FORM FACTOR FOR $K \rightarrow e\nu e\gamma$

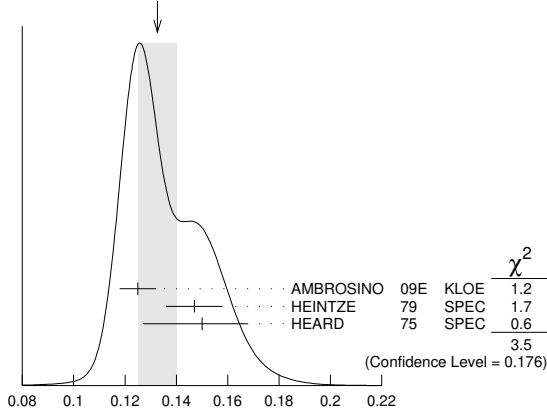
VALUE	EVTS	DOCUMENT ID	TECN	COMMENT
0.133±0.008 OUR AVERAGE				Error includes scale factor of 1.3. See the ideogram below.
0.125±0.007±0.001	1.4k	¹ AMBROSINO	09E	KLOE E_γ in 10–250 MeV, $p_e > 200$ MeV/c
0.147±0.011	51	² HEINTZE	79	SPEC
0.150±0.018 -0.023	56	³ HEARD	75	SPEC

¹ AMBROSINO 09E measures the absolute value $|F_A + F_V|$ which is parametrized as $|F_A + F_V| = F_V (1 + \lambda(1-x)) + F_A$, $x = 2E_\gamma/m_K$. ($F_A + F_V$) and λ are fit parameters. The fitted value of $\lambda = 0.38 \pm 0.20 \pm 0.02$ with a correlation of -0.93 between ($F_A + F_V$) and λ .

² HEINTZE 79 quotes absolute value of $|F_A + F_V| \sin\theta_C$. We use $\sin\theta_C = V_{us} = 0.2205$.

³ HEARD 75 quotes absolute value of $|F_A + F_V| \sin\theta_C$. We use $\sin\theta_C = V_{us} = 0.2205$.

WEIGHTED AVERAGE
0.133±0.008 (Error scaled by 1.3)



$F_A + F_V$, SUM OF AXIAL-VECTOR AND VECTOR FORM FACTOR FOR $K \rightarrow e\nu e\gamma$

$F_A + F_V$, SUM OF AXIAL-VECTOR AND VECTOR FORM FACTOR FOR $K \rightarrow \mu\nu\mu\gamma$

VALUE	CL%	EVTS	DOCUMENT ID	TECN	CHG
0.165±0.007±0.011		2588	¹ ADLER	00B	B787 +

• • • We do not use the following data for averages, fits, limits, etc. • • •

-1.2 to 1.1	90	DEMIDOV	90	XEBC
< 0.23	90	¹ AKIBA	85	SPEC

¹ Quotes absolute value. Sign not determined.

$F_A - F_V$, DIFFERENCE OF AXIAL-VECTOR AND VECTOR FORM FACTOR FOR $K \rightarrow e\nu e\gamma$

VALUE	CL%	DOCUMENT ID	TECN	
<0.49	90	¹ HEINTZE	79	SPEC

¹ HEINTZE 79 quotes $|F_A - F_V| < \sqrt{11} |F_A + F_V|$.

$F_A - F_V$, DIFFERENCE OF AXIAL-VECTOR AND VECTOR FORM FACTOR FOR $K \rightarrow \mu\nu\mu\gamma$

VALUE	CL%	EVTS	DOCUMENT ID	TECN	CHG
-0.153±0.033 OUR AVERAGE					Error includes scale factor of 1.1.
-0.134±0.021±0.027	95k	KRAVTSOV	19	OKA	+
-0.21±0.06	22k	DUK	11	ISTR	-

• • • We do not use the following data for averages, fits, limits, etc. • • •

-0.24 to 0.04	90	2588	ADLER	00B	B787 +
-2.2 to 0.6	90	DEMIDOV	90	XEBC	
-2.5 to 0.3	90	AKIBA	85	SPEC	

K^\pm CHARGE RADIUS

VALUE (fm)	DOCUMENT ID	COMMENT
0.560±0.031 OUR AVERAGE		
0.580±0.040	AMENDOLIA 86B	$Ke \rightarrow Ke$
0.530±0.050	DALLY 80	$Ke \rightarrow Ke$
0.620±0.037	BLATNK 79	VMD + dispersion relations

• • • We do not use the following data for averages, fits, limits, etc. • • •

K^+ LONGITUDINAL POLARIZATION OF EMITTED μ^+

VALUE	CL%	DOCUMENT ID	TECN	CHG	COMMENT
<-0.990	90	¹ AOKI	94	SPEC	+
<-0.990	90	IMAZATO	92	SPEC	+ Repl. by AOKI 94
-0.970±0.047		² YAMANAKA	86	SPEC	+
-1.0 ±0.1		² CUTTS	69	SPRK	+
-0.96 ±0.12		² COOMBES	57	CNTR	+

¹ AOKI 94 measures $\xi P_\mu = -0.9996 \pm 0.0030 \pm 0.0048$. The above limit is obtained by summing the statistical and systematic errors in quadrature, normalizing to the physically significant region ($|\xi P_\mu| < 1$) and assuming that $\xi=1$, its maximum value.

² Assumes $\xi=1$.

FORWARD-BACKWARD ASYMMETRY IN K^\pm DECAYS

$$A_{FB}(K^\pm_{\pi\mu\mu}) = \frac{\Gamma(\cos(\theta_{K\mu}) > 0) - \Gamma(\cos(\theta_{K\mu}) < 0)}{\Gamma(\cos(\theta_{K\mu}) > 0) + \Gamma(\cos(\theta_{K\mu}) < 0)}$$

VALUE	CL%	DOCUMENT ID	TECN	COMMENT
<0.9 × 10⁻²	90	¹ CORTINA-GIL	22A	NA62 2017–18 data
<2.3 × 10 ⁻²	90	² BATLEY	11A	NA48

¹ CORTINA-GIL 22A measured the asymmetry $A_{FB} = (0.0 \pm 0.7) \times 10^{-2}$. The quoted 90% C.L. was obtained via private communication and also presented at the Moriond 2023 conference. The authors will publish this limit in an addendum to the publication.

² BATLEY 11A gives a corresponding value of the asymmetry $A_{FB} = (-2.4 \pm 1.8) \times 10^{-2}$.

K^\pm REFERENCES

CORTINA-GIL 23	PL B838	137679	E. Cortina Gil et al.	(NA62 Collab.)
CORTINA-GIL 23B	PL B846	138193	E. Cortina-Gil et al.	(NA62 Collab.)
CORTINA-GIL 23D	JHEP	2309 040	E. Cortina Gil et al.	(NA62 Collab.)
KOBAYASHI 23	PL B843	138020	A. Kobayashi et al.	(J-PARC E36 Collab.)
CORTINA-GIL 22	PL B830	137172	E. Cortina Gil et al.	(NA62 Collab.)
CORTINA-GIL 22A	JHEP	2211 011	E. Cortina Gil et al.	(NA62 Collab.)
ITO 22	PL B826	136913	H. Ito et al.	(J-PARC E36 Collab.)
ALIBERTI 21	PRL	127 131802	R. Aliberti et al.	(NA62 Collab.)
CORTINA-GIL 21	PL B816	136259	E. Cortina Gil et al.	(NA62 Collab.)
CORTINA-GIL 21B	JHEP	2106 093	E. Cortina Gil et al.	(NA62 Collab.)
POLYARUSH 21	EPJ	C81 161	A.Yu. Polyarush et al.	(OKA Collab.)
CORTINA-GIL 20C	JHEP	2011 042	E. Cortina Gil et al.	(NA62 Collab.)
BATLEY 19	PL B788	552	J.R. Batley et al.	(NA48/2 Collab.)
CORTINA-GIL 19A	PL B797	134794	E. Cortina Gil et al.	(NA62 Collab.)
CORTINA-GIL 19B	PL B791	156	E. Cortina Gil et al.	(NA62 Collab.)
KRAVTSOV 19	EPJ	C79 635	V.I. Kravtsov et al.	(OKA Collab.)
SHAPKIN 19	EPJ	C79 296	M.M. Shapkin et al.	(OKA Collab.)
BATLEY 18	JHEP	1810 150	J.R. Batley et al.	(NA48/2 Collab.)
PDG 18	PR	D98 030001	M. Tanabashi et al.	(PDG Collab.)
YUSHCHENKO 18	JETPL	107 139	O.P. Yushchenko et al.	(OKA Collab.)
BATLEY 17	PL B769	67	J.R. Batley et al.	(NA48/2 Collab.)
ARTAMONOV 16	PR	D94 032012	A.V. Artamonov et al.	(BNL E949 Collab.)
BABUSCI 14B	PL B738	128	D. Babusci et al.	(KLOE and KLOE-2 Collab.)
BATLEY 14	PL B730	141	J.R. Batley et al.	(CERN NA48/2 Collab.)
BATLEY 14A	JHEP	1408 159	J.R. Batley et al.	(CERN NA48/2 Collab.)
LAZZERONI 14	PL B732	65	C. Lazzeroni et al.	(CERN NA62 Collab.)
UVAROV 14	PAN	77 725	V.A. Uvarov et al.	(ISTRA+ Collab.)

Translated from YAF 77 765.

Meson Particle Listings

 K^{\pm}

LAZZERONI	13	PL B719 326	C. Lazzeroni et al.	(CERN NA62 Collab.)	AKIMENKO	91	PL B259 225	S.A. Akimenko et al.	(SERP, JINR, TBIL+)
BATLEY	12	PL B715 105	J.R. Batley et al.	(CERN NA48/2 Collab.)	BARMIN	91	SJNP 53 606	V.V. Barmin et al.	(ITEP)
PDG	12	PR D86 010001	J. Berlinger et al.	(PDG)			Translated from YAF 53 981.		
BATLEY	11A	PL B697 107	J.R. Batley et al.	(CERN NA48/2 Collab.)	DENISOV	91	JETPL 54 558	A.S. Denisov et al.	(PNPI)
DUK	11	PL B695 59	V.A. Duk et al.	(ISTRA+ Collab.)			Translated from ZETFP 54 557.		
LAZZERONI	11	PL B698 105	C. Lazzeroni et al.	(CERN NA62 Collab.)	ATYA	90	PRL 64 21	M.S. Atiya et al.	(BNL E787 Collab.)
ADLER	10	PR D81 092001	S. Adler et al.	(BNL E787 Collab.)	ATYA	90B	PRL 65 1188	M.S. Atiya et al.	(BNL E787 Collab.)
BATLEY	10A	EPJ C68 75	J.R. Batley et al.	(CERN NA48/2 Collab.)	DEMIDOV	90	SJNP 52 1006	V.S. Demidov et al.	(ITEP)
BATLEY	10C	EPJ C70 835	J.R. Batley et al.	(CERN NA48/2 Collab.)			Translated from YAF 52 1595.		
PDG	10	JP G37 075021	K. Nakamura et al.	(PDG Collab.)	LEE	90	PRL 64 165	A.M. Lee et al.	(BNL, FNAL, VILL, WASH+)
PISLAK	10A	PRL 105 019901E	S. Pislak et al.	(BNL E865 Collab.)	ATYA	89	PRL 63 2177	M.S. Atiya et al.	(BNL E787 Collab.)
AKOPDZHANOV	09	PAN 71 2074	G.A. Akopdzhanov et al.	(IHEP)	BARMIN	89	SJNP 50 421	V.V. Barmin et al.	(ITEP)
		Translated from YAF 71 2108.			BARMIN	88	SJNP 47 643	V.V. Barmin et al.	(ITEP)
AMBROSINO	09E	EPJ C64 627	F. Ambrosino et al.	(KLOE Collab.)	BARMIN	88B	SJNP 48 1032	V.V. Barmin et al.	(ITEP)
Also		EPJ C65 703 (errata.)	F. Ambrosino et al.	(KLOE Collab.)			Translated from YAF 48 1011.		
BATLEY	09	PL B677 246	J.R. Batley et al.	(CERN NA48/2 Collab.)	BOLOTOV	88	JETPL 47 7	V.M. Bolotov et al.	(ASCI)
BATLEY	09A	EPJ C64 589	J.R. Batley et al.	(CERN NA48/2 Collab.)			Translated from ZETFP 47 8.		
BISSEGGER	09	NP B006 178	M. Bissegger et al.	(KLOE Collab.)	GALL	88	PRL 60 186	K.P. Gall et al.	(BOST, MIT, WILL, CIT+)
AMBROSINO	08	JHEP 0801 073	F. Ambrosino et al.	(KLOE Collab.)	BARMIN	87	SJNP 45 62	V.V. Barmin et al.	(ITEP)
AMBROSINO	08A	JHEP 0802 098	F. Ambrosino et al.	(KLOE Collab.)	BOLOTOV	87	SJNP 45 1023	V.N. Bolotov et al.	(INRM)
AMBROSINO	08E	PL B666 305	F. Ambrosino et al.	(KLOE Collab.)			Translated from YAF 45 1652.		
ARTAMONOV	08	PRL 101 191802	A.V. Artamonov et al.	(BNL E949 Collab.)	AMENDOLIA	86B	PL B78 435	S.R. Amendolia et al.	(CERN NA7 Collab.)
Also		PR D79 092004	A.V. Artamonov et al.	(BNL E949 Collab.)	BOLOTOV	86	SJNP 44 73	V.N. Bolotov et al.	(INRM)
BATLEY	08	PL B659 493	J.R. Batley et al.	(CERN NA48/2 Collab.)	BOLOTOV	86B	SJNP 44 68	V.N. Bolotov et al.	(INRM)
BATLEY	08A	EPJ C54 411	J.R. Batley et al.	(CERN NA48/2 Collab.)			Translated from YAF 44 117.		
AKIMENKO	07	PAN 70 702	S.A. Akimenko et al.	(ISTRA+ Collab.)			Translated from YAF 44 108.		
		Translated from YAF 70 734.			YAMANAKA	86	PR D34 85	T. Yamanaka et al.	(KEK, TOKY)
ANDRE	07	ANP 322 2518	T. Andre	(EFI)	Also		PRL 52 329	R.S. Hayano et al.	(TOKY, KEK)
BATLEY	07A	EPJ C50 329	J.R. Batley et al.	(CERN NA48/2 Collab.)	AKIBA	85	PL 52 2911	Y. Akiba et al.	(TOKY, TINT, TSUK, KEK)
Also		EPJ C52 1021 (errata.)	J.R. Batley et al.	(CERN NA48/2 Collab.)	BOLOTOV	85	JETPL 42 481	V.M. Bolotov et al.	(INRM)
BATLEY	07B	PL B649 349	J.R. Batley et al.	(CERN NA48/2 Collab.)			Translated from ZETFP 42 390.		
BATLEY	07E	EPJ C52 875	J.R. Batley et al.	(CERN NA48/2 Collab.)	ASANO	82	PL 113B 195	Y. Asano et al.	(KEK, TOKY, INUS, OSAK)
LAI	07A	PL B647 341	A. Lai et al.	(CERN NA48 Collab.)	COOPER	82	PL 112B 97	A.M. Cooper et al.	(RL)
TCHIKILEV	07	PAN 70 29	O.G. Tchikilev et al.	(ISTRA+ Collab.)	PDG	82B	PL 111B 70	M. Roos et al.	(HELS, CIT, CERN)
ALIEV	06	EPJ C46 61	M.A. Aliev et al.	(KEK E470 Collab.)	ASANO	81B	PL 107B 159	Y. Asano et al.	(KEK, TOKY, INUS, OSAK)
AMBROSINO	06A	PL B632 76	F. Ambrosino et al.	(KLOE Collab.)	CAMPBELL	81	PRL 47 1032	M.K. Campbell et al.	(YALE, BNL)
BATLEY	06	PL B634 474	J.R. Batley et al.	(CERN NA48/2 Collab.)	Also		PR D27 1056	S.R. Blatt et al.	(YALE, BNL)
BATLEY	06A	PL B638 22	J.R. Batley et al.	(CERN NA48/2 Collab.)	LUM	81	PR D33 2522	K. Lum et al.	(LBL, NBS+)
Also		PL B640 297 (errata.)	J.R. Batley et al.	(CERN NA48/2 Collab.)	LYONS	81	ZPHY C10 215	L. Lyons, C. Albajar, G. Myatt	(OXF)
BATLEY	06B	PL B633 173	J.R. Batley et al.	(CERN NA48/2 Collab.)	DALLY	80	PRL 45 232	E.B. Dally et al.	(UCLA+)
COLANGELO	06A	PL B638 187	G. Colangelo et al.	(CERN NA48/2 Collab.)	BARKOV	79	NP B148 53	L.M. Barkov et al.	(NOVO, KIAE)
MA	06	PR D73 037101	H. Ma et al.	(BNL E865 Collab.)	BLATNIK	79	LNC 24 39	S. Blatnik, J. Stahov, C.B. Lang	(TUZL, GRAZ)
PDG	06	JP G33 1	W.-M. Yao et al.	(PDG Collab.)	HEINTZE	79	NP B149 365	J. Heintze et al.	(HEIDP, CERN)
SHIMIZU	06	PL B633 190	S. Shimizu et al.	(KEK E470 Collab.)	ABRAMS	77	PR D15 22	R.J. Abrams et al.	(BNL)
UVAROV	06	PAN 69 26	V.A. Uvarov et al.	(ISTRA+ Collab.)	DEVAUX	77	NP B126 11	B. Devaux et al.	(SACL, GEVA)
AKOPDZHANOV	05	EPJ C40 343	G.A. Akopdzhanov et al.	(IHEP)	HEINTZE	77	PL 70B 482	J. Heintze et al.	(HEIDP, CERN)
Also		PAN 68 948	G.A. Akopdzhanov et al.	(IHEP)	ROSSELET	77	PR D15 574	L. Rosselet et al.	(GEVA, SACL)
		Translated from YAF 68 966.			BLOCH	76	PL 60B 333	P. Bloch et al.	(GEVA, SACL)
AKOPDZHANOV	05B	JETPL 82 675	G.A. Akopdzhanov et al.	(IHEP)	BRAUN	76B	LNC 17 521	H.M. Braun et al.	(AACH3, BARI, BELG+)
		Translated from ZETFP 82 771.			DIAMANT-...	76	PL 62B 485	A.M. Diamant-Berger et al.	(SACL, GEVA)
ARTAMONOV	05	PL B623 192	A.V. Artamonov et al.	(BNL E949 Collab.)	HEINTZE	76	PL 60B 302	J. Heintze et al.	(HEIDP)
CABIBBO	05	JHEP 0503 021	N. Cabibbo, G. Isidori	(CERN, ROMAI, FRAS)	SMITH	76	NP B109 173	K.M. Smith et al.	(GLAS, LIVP, OXF+)
SHER	05	PR D72 012005	A. Sher et al.	(BNL E865 Collab.)	WEISSENB...	76	NP B115 55	A.O. Weissenberg et al.	(ITEP, LEBD)
ABE	04F	PRL 93 131601	M. Abe et al.	(KEK E246 Collab.)	BLOCH	75	PL 56B 201	P. Bloch et al.	(SACL, GEVA)
Also		PR D73 072005	M. Abe et al.	(KEK E246 Collab.)	BRAUN	75	NP B89 210	H.M. Braun et al.	(AACH3, BARI, BRUX+)
ADLER	04	PR D70 037102	S. Adler et al.	(KEK E246 Collab.)	CHENG	75	NP A254 381	S.C. Cheng et al.	(COLU, YALE)
ALOISIO	04A	PL B597 139	A. Aloisio et al.	(KLOE Collab.)	HEARD	75	PL 55B 324	K.S. Heard et al.	(CERN, HEIDH)
ANISIMOVSKY	04	PRL 93 031801	V.V. Anisimovskiy et al.	(BNL E949 Collab.)	HEARD	75B	PL 55B 327	K.S. Heard et al.	(CERN, HEIDH)
Also		PR D77 052003	S. Adler et al.	(BNL E949 Collab.)	SHEAFF	75	PR D12 2570	M. Sheaff	(WISC)
CABIBBO	04A	PRL 93 121801	N. Cabibbo	(CERN, ROMAI)	SMITH	75	NP B31 45	K.M. Smith et al.	(GLAS, LIVP, OXF+)
CIRIGLIANO	04	EPJ C35 53	V. Cirigliano, H. Neufeld, H. Pichl	(CIT, VALE+)	WEISSENB...	75	PL 48B 474	A.O. Weissenberg et al.	(ITEP, LEBD)
PDG	04	PL B592 1	S. Eidelman et al.	(PDG Collab.)	ABRAMS	73B	PRL 30 500	R.J. Abrams et al.	(BNL)
SHIMIZU	04	PR D70 037101	S. Shimizu et al.	(KEK E470 Collab.)	BACKENSTO...	73	PL 43B 431	G. Backenstoss et al.	(CERN, KARLK, KARLE+)
YUSHCHENKO	04B	PL B581 31	O.P. Yushchenko et al.	(INRM, INRM)	LUJUNG	73	PR D8 1307	D. Ljung, D. Cline	(WISC)
YUSHCHENKO	04B	PL B589 111	O.P. Yushchenko et al.	(INRM)	Also		PRL 28 523	D. Ljung	(WISC)
AJINENKO	03	PAN 66 105	I.V. Ajinenko et al.	(IHEP, INRM)	Also		PRL 28 1287	D. Cline, D. Ljung	(WISC)
		Translated from YAF 66 107.			Also		PRL 23 326	U. Camerini et al.	(WISC)
AJINENKO	03B	PL B567 159	I.V. Ajinenko et al.	(IHEP, INRM)	LUCAS	73	PR D8 719	P.W. Lucas, H.D. Taft, W.J. Willis	(YALE)
AJINENKO	03C	PL B574 14	I.V. Ajinenko et al.	(IHEP, INRM)	LUCAS	73B	PR D8 727	P.W. Lucas, H.D. Taft, W.J. Willis	(YALE)
ALIEV	03	PL B554 7	M.A. Aliev et al.	(KEK E470 Collab.)	PANG	73	PR D8 1989	C.Y. Pang et al.	(EFI, ARIZ, LBL)
ANISIMOVSKY	03	PL B562 166	V.V. Anisimovskiy et al.	(BNL E865 Collab.)	Also		PL 40B 8	G.D. Cabib et al.	(EFI, LBL)
PISLAK	03	PR D67 072004	S. Pislak et al.	(BNL E865 Collab.)	SMITH	73	NP B60 411	K.M. Smith et al.	(GLAS, LIVP, OXF+)
Also		PR D81 119903E	S. Pislak et al.	(BNL E865 Collab.)	ABRAMS	72	PRL 29 1118	R.J. Abrams et al.	(BNL)
SHER	03	PRL 91 261802	A. Sher et al.	(BNL E865 Collab.)	AUBERT	72	NC 12A 509	B. Aubert et al.	(ORSAY, BRUX, EPOL)
ADLER	02	PR 88 041803	S. Adler et al.	(BNL E787 Collab.)	CHIANG	72	PR D6 1254	I.H. Chiang et al.	(ROCH, WISC)
ADLER	02B	PR D65 052009	S. Adler et al.	(BNL E787 Collab.)	CLARK	72	PRL 29 1274	A.R. Clark et al.	(LBL)
ADLER	02C	PL B537 211	S. Adler et al.	(BNL E787 Collab.)	FORD	72	PL 38B 335	W.T. Ford et al.	(PRIN)
AJINENKO	02	PAN 65 2064	I.V. Ajinenko et al.	(IHEP, INRM)	HOFFMASTER	72	NP B36 1	S. Hoffmaster et al.	(STEV, SETO, LEHI)
		Translated from YAF 65 2125.			BOURQUIN	71	PL 36B 615	M.H. Bourquin et al.	(GEVA, SACL)
CIRIGLIANO	02	EPJ C23 121	V. Cirigliano et al.	(VIEN, VALE, MARS)	HAIDT	71	PR D3 10	D. Haidt et al.	(AACH, BARI, CERN, EPOL, NIJH+)
PARK	02	PRL 88 111801	H.K. Park et al.	(FNAL HyperCP Collab.)			PL 29B 619	D. Haidt et al.	(AACH, BARI, CERN, EPOL+)
PDG	02	PR D66 010001	K. Hagiwara et al.	(PDG Collab.)	KLEMS	71	PR D4 66	J.H. Klems, R.H. Hildebrand, R. Stiening	(CHC+)
POBLAGUEV	02	PRL 89 061803	A.A. Poblaguev et al.	(BNL 865 Collab.)	Also		PRL 24 1086	J.H. Klems, R.H. Hildebrand, R. Stiening	(LRL+)
ADLER	01	PR D63 032004	S. Adler et al.	(BNL E787 Collab.)	Also		PRL 25 473	J.H. Klems, R.H. Hildebrand, R. Stiening	(LRL+)
HORIE	01	PL B513 311	K. Horie et al.	(KEK E426 Collab.)	OTT	71	PR D3 52	R.J. Ott, T.W. Pritchard	(LOQM)
PISLAK	01	PRL 87 221801	S. Pislak et al.	(BNL E865 Collab.)	ROMANO	71	PL 36B 525	F. Romano et al.	(BARI, CERN, ORSAY)
Also		PR D67 072004	S. Pislak et al.	(BNL E865 Collab.)	SCHWEINB...	71	PL 36B 246	W. Schweinberger	(AACH, BELG, CERN, NIJH+)
Also		PRL 105 019901E	S. Pislak et al.	(BNL E865 Collab.)	STEINER	71	PL 36B 521	H.J. Steiner	(AACH, BARI, CERN, EPOL, ORSAY+)
ADLER	00	PRL 84 3748	S. Adler et al.	(BNL E787 Collab.)	BARDIN	70	PL 32B 121	D.Y. Bardin, S.N. Bilenky, B.M. Pontecorvo	(JINR)
ADLER	00B	PRL 85 2256	S. Adler et al.	(BNL E787 Collab.)	BECHERRAWY	70	PR D1 1452	T. Becherrawy	(ROCH)
ADLER	00C	PRL 85 4856	S. Adler et al.	(BNL E787 Collab.)	FORD	70	PRL 25 1370	W.T. Ford et al.	(PRIN)
APPEL	00	PRL 85 2450	R. Appel et al.	(BNL 865 Collab.)	GAILLARD	70	CERN 70-14	J.M. Gaillard, L.M. Chounet	(CERN, ORSAY)
Also		Thesis, Yale Univ.	D.R. Bergman		GRAUMAN	70	PR D1 1277	J.J. Grauman et al.	(STEV, SETO, LEHI)
Also		Thesis, Univ. Zurich	S. Pislak		Also		PR 23 737	J.J. Grauman et al.	(STEV, SETO, LEHI)
APPEL	00B	PRL 85 2877	R. Appel et al.	(BNL 865 Collab.)	PANDOULAS	70	PR D2 1205	D. Pandoulas et al.	(STEV, SETO)
MA	00	PRL 84 2580	H. Ma et al.	(BNL 865 Collab.)	CUTTS	69	PR 184 1380	D. Cutts et al.	(LRL, MIT)
PDG	00	EPJ C51 1	D.E. Groom et al.	(PDG Collab.)	Also		PRL 20 955	D. Cutts et al.	(LRL, MIT)
SHIMIZU	00	PL B495 33	S. Shimizu et al.	(KEK E246 Collab.)	DAVISON	69	PR 180 1333	D.C. Davison et al.	(UCR)
ABE	99S	PRL 83 4253	M. Abe et al.	(KEK E246 Collab.)	ELY	69	PR 180 1319	R.P.J. Ely et al.	(LOUC, WISC, LRL)
AMOROS	99	JP G25 1607	G. Amoros, J. Bijmiers	(LUND, HELS)	HERZO	69	PR 186 1403	D. Herzo et al.	(ILL)
APPEL	99	PRL 83 4482	R. Appel et al.	(BNL 865 Collab.)	LOBKOWICZ	69	PR 185 1676	F. Lobkowicz et al.	(ROCH, BNL)
ADLER	98	PR D58 012003	S. Adler et al.	(BNL E787 Collab.)	Also		PRL 17 548	F. Lobkowicz et al.	(ROCH, BNL)
BATUSOV	98	NP B516 3	V.Y. Batusov et al.		MAST	69	PR 183 1200	T.S. Mast et al.	(LRL)
DAMBROSIO	98A	JHEP 9808 004	G. D'Ambrosio et al.		SELLER	69	NC 60A 291	F. Seller	(LRL)
ADLER	97	PRL 79 2204	S. Adler et al.	(BNL E787 Collab.)	ZELLER	69	PR 182 1420	H. Zeller et al.	(UCLA, LRL)
ADLER	97C	PRL 79 4756	S. Adler et al.	(BN					

See key on page 1171

Meson Particle Listings

K^\pm, K^0

NAME	REF	YEAR	STATUS	AUTHOR	INSTITUTION
BISI	67	PL 25B 572		V. Bisi et al.	(TORI)
FLETCHER	67	PRL 19 98		C.R. Fletcher et al.	(ILL)
FORD	67	PRL 18 1214		W.T. Ford et al.	(PRIN)
GINSBERG	67	PR 162 1570		E.S. Ginsberg	(MASB)
KALMUS	67	PR 159 1187		G.E. Kalmus, A. Kernan	(LRL)
ZINCHENKO	67	Thesis Rutgers		A.I. Zinchenko	(RUTG)
CALLAHAN	66	NC 44A 90		A.C. Callahan	(WISC)
CALLAHAN	66B	PR 150 1153		A.C. Callahan et al.	(WISC, LRL, UCRL)
CESTER	66	PL 21 343		R. Cester et al.	(PPA)
See footnote 1 in AUERBACH 67.					
Also PR 155 1505					
BIRGE	65	PR 139 B1600		L.B. Auerbach et al.	(PENN, PRIN)
BISI	65	NC 35 768		R.W. Birge et al.	(LRL, WISC)
BISI	65B	PR 139 B1068		V. Bisi et al.	(TORI)
CALLAHAN	65	PRL 15 129		A. Callahan, D. Cline	(WISC)
CLINE	65	PL 15 293		D. Cline, W.F. Fry	(WISC)
DEMARCO	65	PR 140 B1430		A. de Marco, C. Grosso, G. Rinaudo	(TORI, CERN)
FITCH	65B	PR 140 B1088		V.L. Fitch, C.A. Quarles, H.C. Wilkins	(PRIN+)
STAMER	65	PR 138 B440		P. Stamer et al.	(STEVE)
YOUNG	65	Thesis UCRL 16362		P.S. Young	(LRL)
Also PR 156 1464					
BORREANI	64	PL 12 123		G. Borreani, W.Z. Osborne, W.H. Barkas	(LRL)
CALLAHAN	64	PR 136 B1463		G. Borreani, G. Rinaudo, A.E. Werbrouck	(TORI)
GREINER	64	PRL 13 284		A. Callahan, R. March, R. Stark	(WISC)
SHAKLEE	64	PR 136 B1423		D.E. Greiner, W.Z. Osborne, W.H. Barkas	(LRL)
BOYARSKI	62	PR 128 2398		F.S. Shaklee et al.	(MICH)
FERRU-LUZZI	61	NC 22 1087		A.M. Boyarski et al.	(MIT)
ROE	61	PRL 7 346		M. Ferro-Luzzi et al.	(LRL)
TAYLOR	59	PR 114 359		B.P. Roe et al.	(MICH, LRL)
COOMBES	57	PR 108 1348		S. Taylor et al.	(COLU)
C.A. Coombes et al. (LBL)					

OTHER RELATED PAPERS

NAME	REF	YEAR	STATUS	AUTHOR	INSTITUTION
LITTENBERG	93	ARNPS 43 729		L.S. Littenberg, G. Valencia	(BNL, FNAL)
Rare and Radiative Kaon Decays					
RITCHIE	93	RMP 65 1149		J.L. Ritchie, S.G. Wojcicki	
BATTISTON	92	PRPL 214 293		R. Battiston et al.	(PGIA, CERN, TRSTT)
Status and Perspectives of K Decay Physics					
BRYMAN	89	IJMP A4 79		D.A. Bryman	(TRIU)
Rare Kaon Decays					
CHOUNET	72	PRPL 4C 199		L.M. Chounet, J.M. Gaillard, M.K. Gaillard	(ORSAY+)
FEARING	70	PR D2 542		H.W. Fearing, E. Fischbach, J. Smith	(STON, BOHR)
HAIDT	69B	PL 29B 696		D. Haidt et al.	(AACH, BARI, CERN, EPOL+)
CRONIN	68B	Vienna Conf. 241		J.W. Cronin	(PRIN)
Rapporteur talk.					
WILLIS	67	Heidelberg Conf. 273		W.J. Willis	(YALE)
Rapporteur talk.					
CABIBBO	66	Berkeley Conf. 33		N. Cabibbo	(CERN)
ADAIR	64	PL 12 67		R.K. Adair, L.B. Leipuner	(YALE, BNL)
CABIBBO	64	PL 9 352		N. Cabibbo, A. Maksymowicz	(CERN)
Also PL 11 360					
Also PL 14 72					
BIRGE	63	PRL 11 35		R.W. Birge et al.	(LRL, WISC, BARI)
BLOCK	62B	CERN Conf. 371		M.M. Block, L. Lendinara, L. Monari	(NWES, BGNA)
BRENE	61	NP 22 553		N. Brene, L. Egardt, B. Qvist	(NORD)



$$I(J^P) = \frac{1}{2}(0^-)$$

K^0 MASS

VALUE (MeV)	EVTS	DOCUMENT ID	TECN	COMMENT
497.611 ± 0.013 OUR FIT				Error includes scale factor of 1.2.
497.611 ± 0.013 OUR AVERAGE				Error includes scale factor of 1.2.
497.607 ± 0.007 ± 0.015	261k	¹ TOMARADZE 14		$\psi(2S) \rightarrow K_S^0 X$
497.583 ± 0.005 ± 0.020	35k	AMBROSINO 07B	KLOE	$e^+e^- \rightarrow K_L^0 K_S^0$
497.625 ± 0.001 ± 0.031	655k	LAI 02	NA48	K_L^0 beam
497.661 ± 0.033	3713	BARKOV 87B	CMD	$e^+e^- \rightarrow K_L^0 K_S^0$
497.742 ± 0.085	780	BARKOV 85B	CMD	$e^+e^- \rightarrow K_L^0 K_S^0$
• • • We do not use the following data for averages, fits, limits, etc. • • •				
497.44 ± 0.50		FITCH 67	OSPK	
498.9 ± 0.5	4500	BALTAY 66	HBC	K^0 from $\bar{p}p$
497.44 ± 0.33	2223	KIM 65B	HBC	K^0 from $\bar{p}p$
498.1 ± 0.4		CHRISTENS... 64	OSPK	

¹ Obtained by analyzing CLEO-c data but not authored by the CLEO Collaboration.

$m_{K^0} - m_{K^\pm}$

VALUE (MeV)	EVTS	DOCUMENT ID	TECN	CHG	COMMENT
3.934 ± 0.020 OUR FIT					Error includes scale factor of 1.6.
• • • We do not use the following data for averages, fits, limits, etc. • • •					
3.95 ± 0.21	417	HILL 68B	DBC	+	$K^+d \rightarrow K^0 pp$
3.90 ± 0.25	9	BURNSTEIN 65	HBC	-	
3.71 ± 0.35	7	KIM 65B	HBC	-	$K^-p \rightarrow n\bar{K}^0$
5.4 ± 1.1		CRAWFORD 59	HBC	+	
3.9 ± 0.6		ROSENFELD 59	HBC	-	

K^0 MEAN SQUARE CHARGE RADIUS

VALUE (fm ²)	EVTS	DOCUMENT ID	TECN	COMMENT
-0.077 ± 0.010 OUR AVERAGE				
-0.077 ± 0.007 ± 0.011	5037	ABOUZAID 06	KTEV	$K_L^0 \rightarrow \pi^+ \pi^- e^+ e^-$
-0.090 ± 0.021		LAI 03C	NA48	$K_L^0 \rightarrow \pi^+ \pi^- e^+ e^-$
-0.054 ± 0.026		MOLZON 78		K_S regen. by electrons
• • • We do not use the following data for averages, fits, limits, etc. • • •				
-0.087 ± 0.046		BLATNIK 79		VMD + dispersion relations
-0.050 ± 0.130		FOETH 69B		K_S regen. by electrons

T-VIOLATION PARAMETER IN K^0 - \bar{K}^0 MIXING

The asymmetry $A_T = \frac{\Gamma(\bar{K}^0 \rightarrow K^0) - \Gamma(K^0 \rightarrow \bar{K}^0)}{\Gamma(\bar{K}^0 \rightarrow K^0) + \Gamma(K^0 \rightarrow \bar{K}^0)}$ must vanish if T invariance holds.

ASYMMETRY A_T IN K^0 - \bar{K}^0 MIXING

VALUE (units 10 ⁻³)	EVTS	DOCUMENT ID	TECN
6.6 ± 1.3 ± 1.0	640k	¹ ANGELOPO... 98E	CPLR

¹ ANGELOPOULOS 98E measures the asymmetry $A_T = [\Gamma(\bar{K}^0_{t=0} \rightarrow e^+ \pi^- \nu_{t=\tau}) - \Gamma(K^0_{t=0} \rightarrow e^- \pi^+ \bar{\nu}_{t=\tau})] / [\Gamma(\bar{K}^0_{t=0} \rightarrow e^+ \pi^- \nu_{t=\tau}) + \Gamma(K^0_{t=0} \rightarrow e^- \pi^+ \bar{\nu}_{t=\tau})]$ as a function of the neutral-kaon eigentime τ . The initial strangeness of the neutral kaon is tagged by the charge of the accompanying charged kaon in the reactions $p\bar{p} \rightarrow K^- \pi^+ K^0$ and $p\bar{p} \rightarrow K^+ \pi^- \bar{K}^0$. The strangeness at the time of the decay is tagged by the lepton charge. The reported result is the average value of A_T over the interval $1\tau_S < \tau < 20\tau_S$. From this value of A_T ANGELOPOULOS 01B, assuming CPT invariance in the $e\nu$ decay amplitude, determine the T -violating $\Delta S = \Delta S$ conserving parameter (for its definition, see Review below) $4\text{Re}(\epsilon) = (6.2 \pm 1.4 \pm 1.0) \times 10^{-3}$.

See the related review(s):

[CPT Invariance Tests in Neutral Kaon Decay](#)

CP-VIOLATION PARAMETERS

Re(ϵ)	VALUE (units 10 ⁻³)	DOCUMENT ID	TECN
1.596 ± 0.013		¹ AMBROSINO 06H	KLOE
• • • We do not use the following data for averages, fits, limits, etc. • • •			
1.664 ± 0.010		² LAI 05A	NA48

¹ AMBROSINO 06H uses Bell-Steinberger relations with the following measurements: $B(K_L^0 \rightarrow \pi^+ \pi^-)$ in AMBROSINO 06F, $B(K_S^0 \rightarrow \pi^0 \pi^0 \pi^0)$ in AMBROSINO 05B, the K_S^0 -semileptonic charge asymmetry in AMBROSINO 06E, and K^0 -semileptonic results in ANGELOPOULOS 98F.

² LAI 05A values are obtained through unitarity (Bell-Steinberger relations), improving determination of η_{000} and combining other data from PDG 04 and APOSTOLAKIS 99B.

CPT-VIOLATION PARAMETERS

In K^0 - \bar{K}^0 mixing, if CP -violating interactions include a T conserving part then

$$|K_S\rangle = [|K_1\rangle + (\epsilon + \delta)|K_2\rangle] / \sqrt{1 + |\epsilon + \delta|^2}$$

$$|K_L\rangle = [|K_2\rangle + (\epsilon - \delta)|K_1\rangle] / \sqrt{1 + |\epsilon - \delta|^2}$$

where

$$|K_1\rangle = [|K^0\rangle + |\bar{K}^0\rangle] / \sqrt{2}$$

$$|K_2\rangle = [|K^0\rangle - |\bar{K}^0\rangle] / \sqrt{2}$$

and

$$|\bar{K}^0\rangle = CP|K^0\rangle.$$

The parameter δ specifies the CP -violating part.

Estimates of δ are given below assuming the validity of the $\Delta S = \Delta Q$ rule. See also THOMSON 95 for a test of CP -symmetry conservation in K^0 decays using the Bell-Steinberger relation.

REAL PART OF δ

A nonzero value violates CPT invariance.

VALUE (units 10 ⁻⁴)	EVTS	DOCUMENT ID	TECN	COMMENT
2.51 ± 2.25		¹ ABOUZAID 11	KTEV	
• • • We do not use the following data for averages, fits, limits, etc. • • •				
2.3 ± 2.7		² AMBROSINO 06H	KLOE	
2.4 ± 2.8		³ APOSTOLA... 99B	RVUE	
2.9 ± 2.6 ± 0.6	1.3M	⁴ ANGELOPO... 98F	CPLR	
180 ± 200	6481	⁵ DEMIDOV 95		$K_{\ell 3}$ reanalysis

¹ ABOUZAID 11 uses Bell-Steinberger relations.

² AMBROSINO 06H uses Bell-Steinberger relations with the following measurements: $B(K_L^0 \rightarrow \pi^+ \pi^-)$ in AMBROSINO 06F, $B(K_S^0 \rightarrow \pi^0 \pi^0 \pi^0)$ in AMBROSINO 05B, the K_S^0 -semileptonic charge asymmetry in AMBROSINO 06E, and K^0 -semileptonic results in ANGELOPOULOS 98F.

³ APOSTOLAKIS 99B assumes only unitarity and combines CPLEAR and other results.

⁴ ANGELOPOULOS 98F use $\Delta S = \Delta Q$. If $\Delta S = \Delta Q$ is not assumed, they find $\text{Re}(\delta) = (3.0 \pm 3.3 \pm 0.6) \times 10^{-4}$.

⁵ DEMIDOV 95 reanalyzes data from HART 73 and NIEBERGALL 74.

IMAGINARY PART OF δ

A nonzero value violates CPT invariance.

VALUE (units 10 ⁻⁵)	EVTS	DOCUMENT ID	TECN	COMMENT
-1.5 ± 1.6		¹ ABOUZAID 11	KTEV	
• • • We do not use the following data for averages, fits, limits, etc. • • •				
0.4 ± 2.1		² AMBROSINO 06H	KLOE	
-0.2 ± 2.0		³ LAI 05A	NA48	
2.4 ± 5.0		⁴ APOSTOLA... 99B	RVUE	
-90 ± 290 ± 100	1.3M	⁵ ANGELOPO... 98F	CPLR	
2100 ± 3700	6481	⁶ DEMIDOV 95		$K_{\ell 3}$ reanalysis

¹ ABOUZAID 11 uses Bell-Steinberger relations.

Meson Particle Listings

K^0, K_S^0

- ²AMBROSINO 06H uses Bell-Steinberger relations with the following measurements: $B(K_L^0 \rightarrow \pi^+ \pi^-)$ in AMBROSINO 06F, $B(K_S^0 \rightarrow \pi^0 \pi^0 \pi^0)$ in AMBROSINO 05B, the K_S^0 -semileptonic charge asymmetry in AMBROSINO 06E, and K^0 -semileptonic results in ANGELOPOULOS 98F.
³LAI 05A values are obtained through unitarity (Bell-Steinberger relations), improving determination of η_{000} and combining other data from PDG 04 and APOSTOLAKIS 99B.
⁴APOSTOLAKIS 99B assumes only unitarity and combines CPLEAR and other results.
⁵If $\Delta S = \Delta Q$ is not assumed, ANGELOPOULOS 98F finds $\text{Im}\delta = (-15 \pm 23 \pm 3) \times 10^{-3}$.
⁶DEMIDOV 95 reanalyzes data from HART 73 and NIEBERGALL 74.

Re(y)

A non-zero value would violate CPT invariance in $\Delta S = \Delta Q$ amplitude. $\text{Re}(y)$ is the following combination of K_{e3} decay amplitudes:

$$\text{Re}(y) = \text{Re} \left(\frac{A(K^0 \rightarrow e^+ \pi^+ \bar{\nu}_e) - A(K^0 \rightarrow e^+ \pi^- \nu_e)}{A(K^0 \rightarrow e^- \pi^+ \bar{\nu}_e) + A(K^0 \rightarrow e^- \pi^- \nu_e)} \right)$$

VALUE (units 10^{-3})	EVTS	DOCUMENT ID	TECN
0.4 ± 2.5	13k	¹ AMBROSINO 06E	KLOE

• • • We do not use the following data for averages, fits, limits, etc. • • •

0.3 ± 3.1		² APOSTOLA... 99B	CPLR
---------------	--	------------------------------	------

- ¹They use the PDG 04 for the K_L^0 semileptonic charge asymmetry and PDG 04 (CP reviewed, CPT NOT ASSUMED) for $\text{Re}(\epsilon)$.
²Constrained by Bell-Steinberger (or unitarity) relation.

Re(x₋)

A non-zero value would violate CPT invariance in decay amplitudes with $\Delta S \neq \Delta Q$. x_{\pm} , used here to define $\text{Re}(x_{\pm})$, and x_{\pm} , used below in the $\Delta S = \Delta Q$ section are the following combinations of K_{e3} decay amplitudes:

$$x_{\pm} = \frac{1}{2} \left(\frac{A(K^0 \rightarrow \pi^- e^+ \nu_e)}{A(K^0 \rightarrow \pi^- e^- \bar{\nu}_e)} \pm \frac{A(K^0 \rightarrow \pi^+ e^- \bar{\nu}_e)}{A(K^0 \rightarrow \pi^+ e^+ \nu_e)} \right)$$

VALUE (units 10^{-3})	EVTS	DOCUMENT ID	TECN	COMMENT
-2.9 ± 2.0		¹ AMBROSINO 06H	KLOE	

• • • We do not use the following data for averages, fits, limits, etc. • • •

-0.8 ± 2.5	13k	² AMBROSINO 06E	KLOE	
-0.5 ± 3.0		³ APOSTOLA... 99B	CPLR	Strangeness tagged
$2 \pm 13 \pm 3$	650k	ANGELOPO... 98F	CPLR	Strangeness tagged

- ¹AMBROSINO 06H uses Bell-Steinberger relations with the following measurements: $B(K_L^0 \rightarrow \pi^+ \pi^-)$ in AMBROSINO 06F, $B(K_S^0 \rightarrow \pi^0 \pi^0 \pi^0)$ in AMBROSINO 05B, the K_S^0 -semileptonic charge asymmetry in AMBROSINO 06E, and K^0 -semileptonic results in ANGELOPOULOS 98F.
²Uses PDG 04 for the K_L^0 semileptonic charge asymmetry and $\text{Re}(\delta)$ from CPLEAR, ANGELOPOULOS 98F.
³Constrained by Bell-Steinberger (or unitarity) relation.

$$\left| m_{K^0} - m_{\bar{K}^0} \right| / m_{\text{average}}$$

A test of CPT invariance. "Our Evaluation" is described in the "Tests of Conservation Laws" section. It assumes CPT invariance in the decay and neglects some contributions from decay channels other than $\pi\pi$.

VALUE	CL%	DOCUMENT ID	TECN
$< 6 \times 10^{-19}$	90	PDG 12	

• • • We do not use the following data for averages, fits, limits, etc. • • •

$(-3 \pm 4) \times 10^{-18}$		¹ ANGELOPO... 99B	RVUE
------------------------------	--	------------------------------	------

- ¹ANGELOPOULOS 99B assumes only unitarity and combines CPLEAR and other results.

$$(\Gamma_{K^0} - \Gamma_{\bar{K}^0}) / m_{\text{average}}$$

A test of CPT invariance.

VALUE	DOCUMENT ID	TECN
$(7.8 \pm 8.4) \times 10^{-18}$	¹ ANGELOPO... 99B	RVUE

- ¹ANGELOPOULOS 99B assumes only unitarity and combines CPLEAR with other results. Correlated with $(m_{K^0} - m_{\bar{K}^0}) / m_{\text{average}}$ with a correlation coefficient of -0.95 .

TESTS OF $\Delta S = \Delta Q$ RULE

Re(x₊)

A non-zero value would violate the $\Delta S = \Delta Q$ rule in CPT conserving transitions. x_{\pm} is defined above in the $\text{Re}(x_{\pm})$ section.

VALUE (units 10^{-3})	EVTS	DOCUMENT ID	TECN
-0.9 ± 3.0 OUR AVERAGE			
-2 ± 10		¹ BATLEY 07D	NA48
-0.5 ± 3.6	13k	² AMBROSINO 06E	KLOE
-1.8 ± 6.1		³ ANGELOPO... 98D	CPLR

- ¹Result obtained from the measurement $\Gamma(K_S^0 \rightarrow \pi e \nu) / \Gamma(K_L^0 \rightarrow \pi e \nu) = 0.993 \pm 0.34$, neglecting possible CPT non-invariance and using PDG 06 values of $B(K_L^0 \rightarrow \pi e \nu) = 0.4053 \pm 0.0015$, $\tau_L = (5.114 \pm 0.021) \times 10^{-8}$ s and $\tau_S = (0.8958 \pm 0.0005) \times 10^{-10}$ s.
² $\text{Re}(x_{\pm})$ can be shown to be equal to the following combination of rates:

$$\text{Re}(x_{\pm}) = \frac{1}{2} \frac{\Gamma(K_S^0 \rightarrow \pi e \nu) - \Gamma(K_L^0 \rightarrow \pi e \nu)}{\Gamma(K_S^0 \rightarrow \pi e \nu) + \Gamma(K_L^0 \rightarrow \pi e \nu)}$$

which is valid up to first order in terms violating CPT and/or the $\Delta S = \Delta Q$ rule.

- ³Obtained neglecting CPT violating amplitudes.

K^0 REFERENCES

TOMARADZE 14	PR D89 031501	A. Tomaradze et al.	(NWES, WAYN)
PDG 12	PR D86 010001	J. Beringer et al.	(PDG Collab.)
ABOUZAID 11	PR D83 092001	E. Abouzaid et al.	(FNAL KTeV Collab.)
AMBROSINO 07B	JHEP 0712 073	F. Ambrosino et al.	(KLOE Collab.)
BATLEY 07D	PL B653 145	J.R. Batley et al.	(CERN NA48 Collab.)
ABOUZAID 06	PRL 96 101801	E. Abouzaid et al.	(KTeV Collab.)
AMBROSINO 06E	PL B636 173	F. Ambrosino et al.	(KLOE Collab.)
AMBROSINO 06F	PL B638 140	F. Ambrosino et al.	(KLOE Collab.)
AMBROSINO 06H	JHEP 0612 011	F. Ambrosino et al.	(KLOE Collab.)
PDG 06	JP 633 1	W.-M. Yao et al.	(PDG Collab.)
AMBROSINO 05B	PL B619 61	F. Ambrosino et al.	(KLOE Collab.)
LAI 05A	PL B610 165	A. Lai et al.	(CERN NA48 Collab.)
PDG 04	PL B592 1	S. Eidelman et al.	(PDG Collab.)
LAI 03C	EPJ C30 33	A. Lai et al.	(CERN NA48 Collab.)
LAI 02	PL B533 196	A. Lai et al.	(CERN NA48 Collab.)
ANGELOPO... 01B	EPJ C22 55	A. Angelopoulos et al.	(CPLEAR Collab.)
ANGELOPO... 99B	PL B471 332	A. Angelopoulos et al.	(CPLEAR Collab.)
APOSTOLA... 99B	PL B456 297	A. Apostolakis et al.	(CPLEAR Collab.)
ANGELOPO... 98D	PL B444 38	A. Angelopoulos et al.	(CPLEAR Collab.)
Also	EPJ C22 55	A. Angelopoulos et al.	(CPLEAR Collab.)
ANGELOPO... 98E	PL B444 43	A. Angelopoulos et al.	(CPLEAR Collab.)
ANGELOPO... 98F	PL B444 52	A. Angelopoulos et al.	(CPLEAR Collab.)
Also	EPJ C22 55	A. Angelopoulos et al.	(CPLEAR Collab.)
DEMIDOV 95	PAN 58 968	V. Demidov, K. Gusev, E. Shabalina	(ITEP)
From YAF 58	1041.		
THOMSON 95	PR D51 1412	G.B. Thomson, Y. Zou	(RUTG)
BARKOV 87B	SJNP 46 630	L.M. Barkov et al.	(NOVO)
	Translated from YAF 46	1088.	
BARKOV 85B	JETPL 42 138	L.M. Barkov et al.	(NOVO)
	Translated from ZETFP 42	113.	
BLATNIK 79	LNC 24 39	S. Blatnik, J. Stahov, C.B. Lang	(TUZL, GRAZ)
MOLZON 78	PRL 41 1213	W.R. Molzon et al.	(EFI+)
NIEBERGALL 74	PL 49B 103	F. Niebergall et al.	(CERN, ORSAY, VIEN)
HART 73	NP B66 317	J.C. Hart et al.	(CAVE, RHEL)
FOETH 69B	PL 30B 276	H. Foeth et al.	(AACH, CERN, TORI)
HILL 68B	PR 168 1534	D.G. Hill et al.	(BNL, CMU)
FITCH 67	PR 164 1711	V.L. Fitch et al.	(PRIN)
BALTAY 66	PR 142 332	C. Baltay et al.	(YALE, BNL)
BURNSTEIN 65	PR 138 B895	R.A. Burnstein, H.A. Rubin	(UMD)
KIM 65B	PR 140 B1334	J.K. Kim, L. Kirsch, D. Miller	(COLU)
CHRISTENS... 64	PRL 13 138	J.H. Christenson et al.	(PRIN)
CRAWFORD 59	PRL 2 112	F.S. Crawford et al.	(LRL)
ROSENFELD 59	PRL 2 110	A.H. Rosenfeld, F.T. Solmitz, R.D. Tripp	(LRL)



$$I(J^P) = \frac{1}{2}(0^-)$$

K_S^0 MEAN LIFE

For earlier measurements, beginning with BOLDT 58b, see our 1986 edition, Physics Letters **170B** 130 (1986).

OUR FIT is described in the note on "CP violation in K_L^0 decays" in the K^0 Particle Listings. The result labeled "OUR FIT Assuming CP^T " ["OUR FIT Not assuming CP^T "] includes all measurements except those with the comment "Not assuming CP^T " ["Assuming CP^T "]. Measurements with neither comment do not assume CPT and enter both fits.

VALUE (10^{-10} s)	EVTS	DOCUMENT ID	TECN	COMMENT
0.8954 ± 0.0004 OUR FIT				Error includes scale factor of 1.1. Assuming CP^T
0.89564 ± 0.00033 OUR FIT				Not assuming CP^T
0.89589 ± 0.00070		^{1,2} ABOUZAID 11	KTEV	Not assuming CP^T
0.89623 ± 0.00047		^{1,3} ABOUZAID 11	KTEV	Assuming CP^T
$0.89562 \pm 0.00029 \pm 0.00043$	20M	⁴ AMBROSINO 11	KLOE	Not assuming CP^T
$0.89598 \pm 0.00048 \pm 0.00051$	16M	LAI 02C	NA48	
0.8971 ± 0.0021		BERTANZA 97	NA31	
$0.8941 \pm 0.0014 \pm 0.0009$		SCHWINGEN... 95	E773	Assuming CP^T
0.8929 ± 0.0016		GIBBONS 93	E731	Assuming CP^T

• • • We do not use the following data for averages, fits, limits, etc. • • •

0.8965 ± 0.0007		⁵ ALAVI-HARATI 03	KTEV	Assuming CP^T
0.8958 ± 0.0013		⁶ ALAVI-HARATI 03	KTEV	Not assuming CP^T
0.8920 ± 0.0044	214k	GROSSMAN 87	SPEC	
0.905 ± 0.007		⁷ ARONSON 82B	SPEC	
0.881 ± 0.009	26k	ARONSON 76	SPEC	
$0.8926 \pm 0.0032 \pm 0.0002$		⁸ CARITHERS 75	SPEC	
0.8937 ± 0.0048	6M	GEWENGER 74B	ASPK	
0.8958 ± 0.0045	50k	⁹ SK JEGGEST... 72	HBC	
0.856 ± 0.008	19994	¹⁰ DONALD 68B	HBC	
0.872 ± 0.009	20000	^{9,10} HILL 68	DBC	

- ¹The two ABOUZAID 11 values use the same full KTeV dataset from 1996, 1997, and 1999. The first enters the "assuming CP^T " fit and the second enters the "not assuming CP^T " fit.
²ABOUZAID 11 fit has Δm , τ_S , ϕ_e , $\text{Re}(e'/\epsilon)$, and $\text{Im}(e'/\epsilon)$ as free parameters. See $\text{Im}(e'/\epsilon)$ in the " K_L^0 CP violation" section for correlation information.
³ABOUZAID 11 fit has Δm and τ_S free but constrains ϕ_{\pm} to the Superweak value, i.e. assumes CP^T . This τ_S value is correlated with their $\Delta m = m_{K_L^0} - m_{K_S^0}$ measurement in the K_L^0 listings. The correlation coefficient $\rho(\tau_S, \Delta m) = -0.670$.
⁴Fit to the proper time distribution.
⁵This ALAVI-HARATI 03 fit has Δm and τ_S free but constrains ϕ_{\pm} to the Superweak value, i.e. assumes CP^T . This τ_S value is correlated with their $\Delta m = m_{K_L^0} - m_{K_S^0}$ measurement in the K_L^0 listings. The correlation coefficient $\rho(\tau_S, \Delta m) = -0.396$. Superseded by ABOUZAID 11.
⁶This ALAVI-HARATI 03 fit has Δm , ϕ_{\pm} , and τ_{K_S} free. See ϕ_{\pm} in the " K_L CP violation" section for correlation information. Superseded by ABOUZAID 11.

⁷ARONSON 82 find that K_S^0 mean life may depend on the kaon energy.
⁸CARTHERS 75 measures the Δm dependence of the total decay rate (inverse mean life) to be $\Gamma(K_S^0) = [(1.122 \pm 0.004) + 0.16(\Delta m - 0.5348)/\Delta m]10^{10}/s$, or, in terms of mean life, CARTHERS 75 measures $\tau_S = (0.8913 \pm 0.0032) - 0.238[\Delta m - 0.5348](10^{-10} s)$. We have adjusted the measurement to use our best values of $(\Delta m = 0.5293 \pm 0.0009)(10^{10} \hbar s^{-1})$. Our first error is their experiment's error and our second error is the systematic error from using our best values.
⁹HILL 68 has been changed by the authors from the published value (0.865 ± 0.009) because of a correction in the shift due to η_{+-} . SKJEGGESTAD 72 and HILL 68 give detailed discussions of systematics encountered in this type of experiment.
¹⁰Pre-1971 experiments are excluded from the average because of disagreement with later more precise experiments.

K_S^0 DECAY MODES

Mode	Fraction (Γ_i/Γ)	Scale factor/ Confidence level
Hadronic modes		
Γ_1 $\pi^0\pi^0$	$(30.69 \pm 0.05) \%$	
Γ_2 $\pi^+\pi^-$	$(69.20 \pm 0.05) \%$	
Γ_3 $\pi^+\pi^-\pi^0$	$(3.5^{+1.1}_{-0.9}) \times 10^{-7}$	
Modes with photons or $\ell\bar{\ell}$ pairs		
Γ_4 $\pi^+\pi^-\gamma$	[a,b] $(1.79 \pm 0.05) \times 10^{-3}$	
Γ_5 $\pi^+\pi^-e^+e^-$	$(4.79 \pm 0.15) \times 10^{-5}$	
Γ_6 $\pi^0\gamma\gamma$	[a] $(4.9 \pm 1.8) \times 10^{-8}$	
Γ_7 $\gamma\gamma$	$(2.63 \pm 0.17) \times 10^{-6}$	S=3.1
Γ_8 $\mu^+\mu^-\mu^+\mu^-$	$< 5.1 \times 10^{-12}$	CL=90%
Semileptonic modes		
Γ_9 $\pi^\pm e^\mp \nu_e$	[c] $(7.14 \pm 0.06) \times 10^{-4}$	
Γ_{10} $\pi^\pm \mu^\mp \nu_\mu$	[c,d] $(4.56 \pm 0.20) \times 10^{-4}$	
CP violating (CP) and $\Delta S = 1$ weak neutral current (S1) modes		
Γ_{11} $3\pi^0$	CP $< 2.6 \times 10^{-8}$	CL=90%
Γ_{12} $\mu^+\mu^-$	S1 $< 2.1 \times 10^{-10}$	CL=90%
Γ_{13} e^+e^-	S1 $< 9 \times 10^{-9}$	CL=90%
Γ_{14} $\pi^0 e^+ e^-$	S1 [a] $(3.0^{+1.5}_{-1.2}) \times 10^{-9}$	
Γ_{15} $\pi^0 \mu^+ \mu^-$	S1 $(2.9^{+1.5}_{-1.2}) \times 10^{-9}$	

[a] See the Particle Listings below for the energy limits used in this measurement.
 [b] Most of this radiative mode, the low-momentum γ part, is also included in the parent mode listed without γ 's.
 [c] The value is for the sum of the charge states or particle/antiparticle states indicated.
 [d] Not a measurement. Calculated as $0.666 \cdot B(\pi^\pm e^\mp \nu_e)$.

CONSTRAINED FIT INFORMATION

An overall fit to 4 branching ratios uses 5 measurements and one constraint to determine 4 parameters. The overall fit has a $\chi^2 = 0.6$ for 2 degrees of freedom.

The following *off-diagonal* array elements are the correlation coefficients $\langle \delta x_i \delta x_j \rangle / (\delta x_i \delta x_j)$, in percent, from the fit to the branching fractions, $x_i \equiv \Gamma_i/\Gamma_{total}$. The fit constrains the x_i whose labels appear in this array to sum to one.

x_2	-100		
x_9	-9	8	
x_{10}	-1	-3	0
	x_1	x_2	x_9

K_S^0 DECAY RATES

$\Gamma(\pi^\pm e^\mp \nu_e)$	Γ_9			
VALUE ($10^6 s^{-1}$)	EVTS	DOCUMENT ID	TECN	COMMENT
● ● ● We do not use the following data for averages, fits, limits, etc. ● ● ●				
8.1 ± 1.6	75	¹ AKHMETSHIN 99	CMD2	Tagged K_S^0 using $\phi \rightarrow K_L^0 K_S^0$
7.50 ± 0.08		² PDG	98	
seen		BURGUN	72	HBC $K^+p \rightarrow K^0 p \pi^+$
9.3 ± 2.5		AUBERT	65	HLBC $\Delta S = \Delta Q$, CP cons. not assumed
¹ AKHMETSHIN 99 is from a measured branching ratio $B(K_S^0 \rightarrow \pi e \nu_e) = (7.2 \pm 1.4) \times 10^{-4}$ and $\tau_{K_S^0} = (0.8934 \pm 0.0008) \times 10^{-10} s$. Not independent of measured branching ratio.				
² PDG 98 from K_L^0 measurements, assuming that $\Delta S = \Delta Q$ in K^0 decay so that $\Gamma(K_S^0 \rightarrow \pi^\pm e^\mp \nu_e) = \Gamma(K_L^0 \rightarrow \pi^\pm e^\mp \nu_e)$.				

$\Gamma(\pi^\pm \mu^\mp \nu_\mu)$	Γ_{10}
VALUE ($10^6 s^{-1}$)	DOCUMENT ID
● ● ● We do not use the following data for averages, fits, limits, etc. ● ● ●	
5.25 ± 0.07	¹ PDG 98
¹ PDG 98 from K_L^0 measurements, assuming that $\Delta S = \Delta Q$ in K^0 decay so that $\Gamma(K_S^0 \rightarrow \pi^\pm \mu^\mp \nu_\mu) = \Gamma(K_L^0 \rightarrow \pi^\pm \mu^\mp \nu_\mu)$.	

K_S^0 BRANCHING RATIOS

Hadronic modes				
$\Gamma(\pi^0\pi^0)/\Gamma_{total}$	Γ_1/Γ			
VALUE	EVTS	DOCUMENT ID	TECN	
0.3069 ± 0.0005 OUR FIT				
● ● ● We do not use the following data for averages, fits, limits, etc. ● ● ●				
0.335 ± 0.014	1066	BROWN	63 HLBC	
0.288 ± 0.021	198	CHRETIEN	63 HLBC	
0.30 ± 0.035		BROWN	61 HLBC	
$\Gamma(\pi^+\pi^-)/\Gamma_{total}$	Γ_2/Γ			
VALUE	EVTS	DOCUMENT ID	TECN	COMMENT
0.6920 ± 0.0005 OUR FIT				
● ● ● We do not use the following data for averages, fits, limits, etc. ● ● ●				
0.670 ± 0.010	3447	DOYLE	69 HBC	$\pi^-p \rightarrow \Lambda K^0$
$\Gamma(\pi^+\pi^-)/\Gamma(\pi^0\pi^0)$	Γ_2/Γ_1			
VALUE	EVTS	DOCUMENT ID	TECN	COMMENT
2.255 ± 0.005 OUR FIT				
2.2549 ± 0.0054				
● ● ● We do not use the following data for averages, fits, limits, etc. ● ● ●				
$2.2555 \pm 0.0012 \pm 0.0054$		¹ AMBROSINO	06c	KLOE
$2.236 \pm 0.003 \pm 0.015$	766k	² ALOISIO	02b	KLOE
2.11 ± 0.09	1315	EVERHART	76	WIRE $\pi^-p \rightarrow \Lambda K^0$
2.169 ± 0.094	16k	COWELL	74	OSPK $\pi^-p \rightarrow \Lambda K^0$
2.16 ± 0.08	4799	HILL	73	DBC $K^+d \rightarrow K^0 p p$
2.22 ± 0.10	3068	³ ALITTI	72	HBC $K^+p \rightarrow \pi^+ p K^0$
2.22 ± 0.08	6380	MORSE	72b	DBC $K^+n \rightarrow K^0 p$
2.10 ± 0.11	701	⁴ NAGY	72	HLBC $K^+n \rightarrow K^0 p$
2.22 ± 0.095	6150	⁵ BALTAY	71	HBC $Kp \rightarrow K^0$ neutrals
2.282 ± 0.043	7944	⁶ MOFFETT	70	OSPK $K^+n \rightarrow K^0 p$
2.12 ± 0.17	267	⁴ BOZOKI	69	HLBC
2.285 ± 0.055	3016	⁶ GOBBI	69	OSPK $K^+n \rightarrow K^0 p$
2.10 ± 0.06	3700	MORFIN	69	HLBC $K^+n \rightarrow K^0 p$

¹ This result combines AMBROSINO 06c KLOE 2001-02 data with ALOISIO 02b KLOE 2000 data. $K_S^0 \rightarrow \pi^+\pi^-$ fully inclusive.
² Includes radiative decays $\pi^+\pi^-\gamma$.
³ The directly measured quantity is $K_S^0 \rightarrow \pi^+\pi^-/all K^0 = 0.345 \pm 0.005$.
⁴ NAGY 72 is a final result which includes BOZOKI 69.
⁵ The directly measured quantity is $K_S^0 \rightarrow \pi^+\pi^-/all \bar{K}^0 = 0.345 \pm 0.005$.
⁶ MOFFETT 70 is a final result which includes GOBBI 69.

$\Gamma(\pi^+\pi^-\pi^0)/\Gamma_{total}$	Γ_3/Γ			
VALUE (units 10^{-7})	EVTS	DOCUMENT ID	TECN	COMMENT
3.5 ± 1.1 OUR AVERAGE				
$4.7^{+2.2+1.7}_{-1.7-1.5}$		¹ BATLEY	05	NA48
$2.5^{+1.3+0.5}_{-1.0-0.6}$	500k	² ADLER	97b	CPLR
$4.8^{+2.2}_{-1.6} \pm 1.1$		³ ZOU	96	E621
● ● ● We do not use the following data for averages, fits, limits, etc. ● ● ●				
$4.1^{+2.5+0.5}_{-1.9-0.6}$		⁴ ADLER	96E	CPLR Sup. by ADLER 97b
$3.9^{+5.4+0.9}_{-1.8-0.7}$		⁵ THOMSON	94	E621 Sup. by ZOU 96

¹ BATLEY 05 is obtained by measuring the interference parameters in $K_S, K_L \rightarrow \pi^+\pi^-\pi^0$: $Re(\lambda) = 0.038 \pm 0.008 \pm 0.006$ and $Im(\lambda) = -0.013 \pm 0.005 \pm 0.004$; the correlation coeff. between $Re(\lambda)$ and $Im(\lambda)$ is 0.66 (statistical only).
² ADLER 97b find the CP-conserving parameters $Re(\lambda) = (28 \pm 7 \pm 3) \times 10^{-3}$, $Im(\lambda) = (-10 \pm 8 \pm 2) \times 10^{-3}$. They estimate $B(K_S^0 \rightarrow \pi^+\pi^-\pi^0)$ from $Re(\lambda)$ and the K_L^0 decay parameters. See also ANGELOPOULOS 98c.
³ ZOU 96 is from the the measured quantities $|\rho_{+-0}| = 0.039^{+0.009}_{-0.006} \pm 0.005$ and $\phi_p = (-9 \pm 18)^\circ$.
⁴ ADLER 96E is from the measured quantities $Re(\lambda) = 0.036 \pm 0.010^{+0.002}_{-0.003}$ and $Im(\lambda)$ consistent with zero. Note that the quantity λ is the same as ρ_{+-0} used in other footnotes.
⁵ THOMSON 94 calculates this branching ratio from their measurements $|\rho_{+-0}| = 0.035^{+0.019}_{-0.011} \pm 0.004$ and $\phi_p = (-59 \pm 48)^\circ$ where $|\rho_{+-0}| e^{i\phi_p} = A(K_S^0 \rightarrow \pi^+\pi^-\pi^0, l=2)/A(K_L^0 \rightarrow \pi^+\pi^-\pi^0)$.

Meson Particle Listings

 K_S^0 Modes with photons or $\ell\bar{\ell}$ pairs $\Gamma(\pi^+\pi^-\gamma)/\Gamma(\pi^+\pi^-)$ Γ_4/Γ_2

VALUE (units 10^{-3})	EVTS	DOCUMENT ID	TECN	COMMENT
2.59 ± 0.08 OUR AVERAGE				
2.56 ± 0.09	1286	RAMBERG	93 E731	$p_\gamma > 50$ MeV/c
2.68 ± 0.15		¹ TAUREG	76 SPEC	$p_\gamma > 50$ MeV/c
7.10 ± 0.22	3723	RAMBERG	93 E731	$p_\gamma > 20$ MeV/c
3.0 ± 0.6	29	² BOBISUT	74 HLBC	$p_\gamma > 40$ MeV/c
2.8 ± 0.6		³ BURGUN	73 HBC	$p_\gamma > 50$ MeV/c

- • • We do not use the following data for averages, fits, limits, etc. • • •
- ¹TAUREG 76 find direct emission contribution < 0.06 , CL = 90%.
- ²BOBISUT 74 not included in average because p_γ cut differs. Estimates direct emission contribution to be 0.5 or less, CL = 95%.
- ³BURGUN 73 estimates that direct emission contribution is 0.3 ± 0.6 .

 $\Gamma(\pi^+\pi^-e^+e^-)/\Gamma_{\text{total}}$ Γ_5/Γ

VALUE (units 10^{-5})	EVTS	DOCUMENT ID	TECN	COMMENT
4.79 ± 0.15 OUR AVERAGE				
4.83 ± 0.11 ± 0.14	23k	¹ BATLEY	11 NA48	2002 data
4.69 ± 0.30	676	² LAI	03c NA48	1998+1999 data
4.71 ± 0.23 ± 0.22	620	^{2,3} LAI	03c NA48	1999 data
4.5 ± 0.7 ± 0.4	56	LAI	00b NA48	1998 data

- • • We do not use the following data for averages, fits, limits, etc. • • •
- ¹BATLEY 11 reports $[\Gamma(K_S^0 \rightarrow \pi^+\pi^-e^+e^-)/\Gamma_{\text{total}}] / [B(K_L^0 \rightarrow \pi^+\pi^-\pi^0)] / [B(\pi^0 \rightarrow e^+e^-\gamma)] = (3.28 \pm 0.06 \pm 0.04) \times 10^{-2}$ which we multiply by our best values $B(K_L^0 \rightarrow \pi^+\pi^-\pi^0) = (12.54 \pm 0.05) \times 10^{-2}$, $B(\pi^0 \rightarrow e^+e^-\gamma) = (1.174 \pm 0.035) \times 10^{-2}$. Our first error is their experiment's error and our second error is the systematic error from using our best values. Also a limit on the absolute value of the interference between bremsstrahlung and E1 transition is given: $< 4 \times 10^{-7}$ at 90% C.L.
- ²Uses normalization $\text{BR}(K_L \rightarrow \pi^+\pi^-\pi^0) \cdot \text{BR}(\pi^0 \rightarrow e^+e^-) = (1.505 \pm 0.047) \times 10^{-3}$ from our 2000 Edition.
- ³Second error is $0.16(\text{syst}) \pm 0.15(\text{norm})$ combined in quadrature.

 $\Gamma(\pi^0\gamma\gamma)/\Gamma_{\text{total}}$ Γ_6/Γ

VALUE (units 10^{-3})	CL%	EVTS	DOCUMENT ID	TECN	COMMENT
4.9 ± 1.6 ± 0.9		17	¹ LAI	04 NA48	$m_{\gamma\gamma}^2/m_K^2 > 0.2$
< 33	90		LAI	03b NA48	$m_{\gamma\gamma}^2/m_K^2 > 0.2$

- • • We do not use the following data for averages, fits, limits, etc. • • •
- ¹Spectrum also measured and found consistent with the one generated by a constant matrix element.

 $\Gamma(\gamma\gamma)/\Gamma_{\text{total}}$ Γ_7/Γ

VALUE (units 10^{-6})	CL%	EVTS	DOCUMENT ID	TECN	COMMENT
2.63 ± 0.17 OUR AVERAGE					Error includes scale factor of 3.1.
2.26 ± 0.12 ± 0.06		711	¹ AMBROSINO	08c KLOE	$\phi \rightarrow K_S^0 K_L^0$
2.713 ± 0.063 ± 0.005		7.5k	² LAI	03 NA48	
2.58 ± 0.36 ± 0.22	149		LAI	00 NA48	
2.2 ± 1.1	16		³ BARR	95b NA31	
2.4 ± 0.9	35		⁴ BARR	95b NA31	
< 13	90		BALATS	89 SPEC	
2.4 ± 1.2	19		BURKHARDT	87 NA31	
< 133	90		BARMIN	86b XEBC	

- • • We do not use the following data for averages, fits, limits, etc. • • •
- ¹AMBROSINO 08c reports $(2.26 \pm 0.12 \pm 0.06) \times 10^{-6}$ from a measurement of $[\Gamma(K_S^0 \rightarrow \gamma\gamma)/\Gamma_{\text{total}}] \times [B(K_S^0 \rightarrow \pi^0\pi^0)]$ assuming $B(K_S^0 \rightarrow \pi^0\pi^0) = (30.69 \pm 0.05) \times 10^{-2}$.
- ²LAI 03 reports $[\Gamma(K_S^0 \rightarrow \gamma\gamma)/\Gamma_{\text{total}}] / [B(K_S^0 \rightarrow \pi^0\pi^0)] = (8.84 \pm 0.18 \pm 0.10) \times 10^{-6}$ which we multiply by our best value $B(K_S^0 \rightarrow \pi^0\pi^0) = (30.69 \pm 0.05) \times 10^{-2}$. Our first error is their experiment's error and our second error is the systematic error from using our best value.
- ³BARR 95b result is calculated using $B(K_L \rightarrow \gamma\gamma) = (5.86 \pm 0.17) \times 10^{-4}$.
- ⁴BARR 95b quotes this as the combined BARR 95b + BURKHARDT 87 result after rescaling BURKHARDT 87 to use same branching ratios and lifetimes as BARR 95b.

 $\Gamma(\mu^+\mu^-\mu^+\mu^-)/\Gamma_{\text{total}}$ Γ_8/Γ

VALUE	CL%	DOCUMENT ID	TECN
< 5.1 × 10⁻¹²	90	¹ AAIJ	23AE LHCB

- ¹AAIJ 23AE uses 5.1 fb⁻¹ of LHCB data recorded from 2016 to 2018.

Semileptonic modes

 $\Gamma(\pi^\pm e^\mp \nu_e)/\Gamma_{\text{total}}$ Γ_9/Γ

VALUE (units 10^{-4})	EVTS	DOCUMENT ID	TECN	COMMENT
7.14 ± 0.06 OUR FIT				
7.04 ± 0.08 OUR AVERAGE				
7.046 ± 0.18 ± 0.16		¹ BATLEY	07d NA48	$K^0(\bar{K}^0)(t) \rightarrow \pi e \nu$
6.91 ± 0.34 ± 0.15	624	² ALOISIO	02 KLOE	Tagged K_S^0 using $\phi \rightarrow K_L^0 K_S^0$

- • • We use the following data for averages but not for fits. • • •

7.05 ± 0.09 13k ³AMBROSINO 06E KLOE Not fitted

- • • We do not use the following data for averages, fits, limits, etc. • • •

7.2 ± 1.4 75 AKHMETSHIN 99 CMD2 Tagged K_S^0 using $\phi \rightarrow K_L^0 K_S^0$

- Reconstructed from $K^0(\bar{K}^0)(t) \rightarrow \pi e \nu$ distributions using PDG values of $B(K_L^0 \rightarrow \pi e \nu) = 0.4053 \pm 0.0015$, $\tau_L = (5.114 \pm 0.021) \times 10^{-8}$ s and $\tau_S = (0.8958 \pm 0.0005) \times 10^{-10}$ s.
- Uses the PDG 00 value for $B(K_S^0 \rightarrow \pi^+\pi^-)$.
- Obtained by imposing $\Sigma_i B(K_S^0 \rightarrow i) = 1$, where i runs over all the four branching ratios $\pi^+\pi^-$, $\pi^0\pi^0$, $\pi e \nu$, and $\pi \mu \nu$. Input value of $B(K_S^0 \rightarrow \pi^+\pi^-) / B(K_S^0 \rightarrow \pi^0\pi^0)$ from AMBROSINO 06c is used. To derive $\Gamma(K_S^0 \rightarrow \pi^+\mu\nu) / \Gamma(K_S^0 \rightarrow \pi^+e\nu)$, lepton universality is assumed, radiative corrections from ANDRE 07 are used, and phase space integrals are taken from KTeV, ALEXOPOULOS 04A. This branching fraction enters our fit via their $\Gamma(\pi^\pm e^\mp \nu_e) / \Gamma(\pi^+\pi^-)$ branching ratio measurement.

 $\Gamma(\pi^\pm \mu^\mp \nu_\mu)/\Gamma_{\text{total}}$ Γ_{10}/Γ

VALUE (units 10^{-4})	EVTS	DOCUMENT ID	TECN	COMMENT
4.56 ± 0.20 OUR FIT				
4.56 ± 0.11 ± 0.17	7223	¹ BABUSCI	20 KLOE	direct measurement

- ¹Value obtained by normalizing to the KLOE measurement $B(K_S^0 \rightarrow \pi^+\pi^-) = (69.196 \pm 0.051)\%$. Also comparison with the PDG 18 based derived value leads to a lepton flavor universality test $|V_{us} f_+(0)|_{K_S^0 \rightarrow \pi\mu\nu}^2 / |V_{us} f_+(0)|_{K_S^0 \rightarrow \pi e\nu}^2 = 0.975 \pm 0.044$.

 $\Gamma(\pi^\pm e^\mp \nu_e)/\Gamma(\pi^+\pi^-)$ Γ_9/Γ_2

VALUE (units 10^{-3})	EVTS	DOCUMENT ID	TECN
1.032 ± 0.008 OUR FIT			
1.0338 ± 0.0054 ± 0.0064		¹ BABUSCI	23 KLOE

- • • We do not use the following data for averages, fits, limits, etc. • • •

1.019 ± 0.011 ± 0.007 13k ²AMBROSINO 06E KLOE

- ¹BABUSCI 23 measured $\Gamma(K_S^0 \rightarrow \pi e \nu)/\Gamma(K_S^0 \rightarrow \pi^+\pi^-) = (1.0421 \pm 0.0066 \pm 0.0075) \times 10^{-3}$ based on data collected from 2004 to 2005. About 50k signal events were reconstructed from the dataset corresponding to an integrated luminosity of 1.63 fb⁻¹. The quoted value is their combination of this result with the previous measurement of AMBROSINO 06E. The correlation coefficient between the two measurements is 12%.
- ²AMBROSINO 06E result is included in BABUSCI 23.

CP violating (CP) and $\Delta S = 1$ weak neutral current (S1) modes $\Gamma(3\pi^0)/\Gamma_{\text{total}}$ Γ_{11}/Γ

VALUE (units 10^{-7})	CL%	EVTS	DOCUMENT ID	TECN	COMMENT
< 0.26	90	590M	¹ BABUSCI	13c KLOE	$\phi \rightarrow K_L^0 K_S^0$

- • • We do not use the following data for averages, fits, limits, etc. • • •

< 1.2	90	37.8M	AMBROSINO	05b KLOE
< 7.4	90	4.9M	² LAI	05A NA48
< 140	90	7M	ACHASOV	99b SND
< 190	90	17300	³ ANGELOPO...	98b CPLR
< 370	90		BARMIN	83 HLBC

- ¹BABUSCI 13c uses 1.7 fb⁻¹ of data of $\phi \rightarrow K_L^0 K_S^0$ decays with K_L^0 interaction in the calorimeter, collected from 2004 to 2005. No candidate events were found in the data with an expected background of $0.04_{-0.03}^{+0.15}$ events. Upper limit is obtained by normalizing to $K_S^0 \rightarrow 2\pi^0$ decays.
- ²LAI 05A value is obtained from their bound on $|\eta_{000}|$ (not assuming CP T) and $B(K_L^0 \rightarrow 3\pi^0) = 0.211 \pm 0.003$, and PDG 04 values for K_L^0 and K_S^0 lifetimes. If CPT is assumed then $B(K_S^0 \rightarrow 3\pi^0)_{CPT} < 2.3 \times 10^{-7}$ at 90% CL
- ³ANGELOPOULOS 98b is from $\text{Im}(\eta_{000}) = -0.05 \pm 0.12 \pm 0.05$, assuming $\text{Re}(\eta_{000}) = \text{Re}(\epsilon) = 1.635 \times 10^{-3}$ and using the value $B(K_L^0 \rightarrow \pi^0\pi^0\pi^0) = 0.2112 \pm 0.0027$.

 $\Gamma(\mu^+\mu^-)/\Gamma_{\text{total}}$ Γ_{12}/Γ

VALUE	CL%	DOCUMENT ID	TECN
< 2.1 × 10⁻¹⁰	90	¹ AAIJ	20AE LHCB

- • • We do not use the following data for averages, fits, limits, etc. • • •

< 8 × 10 ⁻¹⁰	90	² AAIJ	17bQ LHCB
< 9 × 10 ⁻⁹	90	³ AAIJ	13G LHCB
< 3.2 × 10 ⁻⁷	90	GJESDAL	73 ASPK
< 7 × 10 ⁻⁶	90	HYAMS	69b OSPK

- ¹AAIJ 20AE uses 8.6 fb⁻¹ of LHCB data from 2011 to 2012 and 2016 to 2018. The result utilizes the normalization mode branching fraction $B(K_S^0 \rightarrow \pi^+\pi^-) = (69.20 \pm 0.05) \times 10^{-2}$ from PDG 18. Supersedes AAJ 17bQ.
- ²AAIJ 17bQ uses 3.0 fb⁻¹ of pp collisions at $\sqrt{s} = 7$ and 8 TeV. The result utilizes the normalization mode branching fraction $B(K_S^0 \rightarrow \pi^+\pi^-) = (69.20 \pm 0.05) \times 10^{-2}$ from PDG 16. Supersedes AAJ 13G.
- ³AAIJ 13G uses 1.0 fb⁻¹ of pp collisions at $\sqrt{s} = 7$ TeV. They obtained $B(K_S^0 \rightarrow \mu^+\mu^-) < 11 \times 10^{-9}$ at 95% C.L.

See key on page 1171

Meson Particle Listings

 K_S^0 $\Gamma(e^+e^-)/\Gamma_{\text{total}}$ Γ_{13}/Γ Test for $\Delta S = 1$ weak neutral current. Allowed by first-order weak interaction combined with electromagnetic interaction.

VALUE (units 10^{-7})	CL%	DOCUMENT ID	TECN	COMMENT
< 0.09	90	¹ AMBROSINO 09A	KLOE	$e^+e^- \rightarrow \phi \rightarrow K_S^0 K_L^0$
• • • We do not use the following data for averages, fits, limits, etc. • • •				
< 1.4	90	ANGELOPO...	97 CPLR	
< 28	90	BLICK 94	CNTR	Hyperon facility
<100	90	BARMIN 86	XEBC	

¹AMBROSINO 09A reports $< 0.09 \times 10^{-7}$ from a measurement of $[\Gamma(K_S^0 \rightarrow e^+e^-)/\Gamma_{\text{total}}] / [B(K_S^0 \rightarrow \pi^+\pi^-)]$ assuming $B(K_S^0 \rightarrow \pi^+\pi^-) = (69.20 \pm 0.05) \times 10^{-2}$. $\Gamma(\pi^0 e^+ e^-)/\Gamma_{\text{total}}$ Γ_{14}/Γ Test for $\Delta S = 1$ weak neutral current. Allowed by first-order weak interaction combined with electromagnetic interaction.

VALUE (units 10^{-9})	CL%	EVTS	DOCUMENT ID	TECN	COMMENT
$3.0^{+1.5}_{-1.2} \pm 0.2$		7	¹ BATLEY 03	NA48	$m_{ee} > 0.165$ GeV
• • • We do not use the following data for averages, fits, limits, etc. • • •					
< 140	90		LAI 01	NA48	
< 1100	90	0	BARR 93B	NA31	
<45000	90		GIBBONS 88	E731	

¹BATLEY 03 extrapolate also to the full kinematical region using a constant form factor and a vector matrix element. The resulting branching ratio is $(5.8^{+2.9}_{-2.4}) \times 10^{-9}$. $\Gamma(\pi^0 \mu^+ \mu^-)/\Gamma_{\text{total}}$ Γ_{15}/Γ Test for $\Delta S = 1$ weak neutral current. Allowed by first-order weak interaction combined with electromagnetic interaction.

VALUE (units 10^{-9})	EVTS	DOCUMENT ID	TECN	COMMENT
$2.9^{+1.5}_{-1.2} \pm 0.2$	6	¹ BATLEY 04A	NA48	NA48/1 K_S^0 beam

¹Background estimate is $0.22^{+0.18}_{-0.11}$ events. Branching ratio assumes a vector matrix element and unit form factor. K_S^0 FORM FACTORS

For discussion, see note on K_{f3} form factors in the K^\pm section of the Particle Listings above. Because the semileptonic branching fraction is smaller in K_S^0 than K_L^0 by the ratio of the mean lives, the K_S^0 semileptonic form factor has so far been measured only in the K_{e3} mode using the linear expansion $f_+(t) = f_+(0) (1 + \lambda_+ t / m_\pi^2)$, which gives the vector form factor $f_+(t)$ relative to its value at $t = 0$.

 λ_+ (LINEAR ENERGY DEPENDENCE OF f_+ IN K_{e3}^0 DECAY)

VALUE (units 10^{-2})	EVTS	DOCUMENT ID	TECN
3.39 ± 0.41	15k	AMBROSINO 06E	KLOE

 CP VIOLATION IN $K_S \rightarrow 3\pi$

Written 1996 by T. Nakada (Paul Scherrer Institute) and L. Wolfenstein (Carnegie-Mellon University).

The possible final states for the decay $K^0 \rightarrow \pi^+\pi^-\pi^0$ have isospin $I = 0, 1, 2$, and 3 . The $I = 0$ and $I = 2$ states have $CP = +1$ and K_S can decay into them without violating CP symmetry, but they are expected to be strongly suppressed by centrifugal barrier effects. The $I = 1$ and $I = 3$ states, which have no centrifugal barrier, have $CP = -1$ so that the K_S decay to these requires CP violation.

In order to see CP violation in $K_S \rightarrow \pi^+\pi^-\pi^0$, it is necessary to observe the interference between K_S and K_L decay, which determines the amplitude ratio

$$\eta_{+-0} = \frac{A(K_S \rightarrow \pi^+\pi^-\pi^0)}{A(K_L \rightarrow \pi^+\pi^-\pi^0)}. \quad (1)$$

If η_{+-0} is obtained from an integration over the whole Dalitz plot, there is no contribution from the $I = 0$ and $I = 2$ final states and a nonzero value of η_{+-0} is entirely due to CP violation.

Only $I = 1$ and $I = 3$ states, which are $CP = -1$, are allowed for $K^0 \rightarrow \pi^0\pi^+\pi^0$ decays and the decay of K_S into $3\pi^0$

is an unambiguous sign of CP violation. Similarly to η_{+-0} , η_{000} is defined as

$$\eta_{000} = \frac{A(K_S \rightarrow \pi^0\pi^0\pi^0)}{A(K_L \rightarrow \pi^0\pi^0\pi^0)}. \quad (2)$$

If one assumes that CPT invariance holds and that there are no transitions to $I = 3$ (or to nonsymmetric $I = 1$ states), it can be shown that

$$\begin{aligned} \eta_{+-0} &= \eta_{000} \\ &= \epsilon + i \frac{\text{Im } a_1}{\text{Re } a_1}. \end{aligned} \quad (3)$$

With the Wu-Yang phase convention, a_1 is the weak decay amplitude for K^0 into $I = 1$ final states; ϵ is determined from CP violation in $K_L \rightarrow 2\pi$ decays. The real parts of η_{+-0} and η_{000} are equal to $\text{Re}(\epsilon)$. Since currently-known upper limits on $|\eta_{+-0}|$ and $|\eta_{000}|$ are much larger than $|\epsilon|$, they can be interpreted as upper limits on $\text{Im}(\eta_{+-0})$ and $\text{Im}(\eta_{000})$ and so as limits on the CP -violating phase of the decay amplitude a_1 .

 CP -VIOLATION PARAMETERS IN K_S^0 DECAY

$A_S = [\Gamma(K_S^0 \rightarrow \pi^- e^+ \nu_e) - \Gamma(K_S^0 \rightarrow \pi^+ e^- \bar{\nu}_e)] / \text{SUM}$
Such asymmetry violates CP . If CP is assumed then $A_S = 2 \text{Re}(\epsilon)$.

VALUE (units 10^{-3})	EVTS	DOCUMENT ID	TECN
$-3.8 \pm 5.0 \pm 2.6$	83k	¹ ANASTASI 18A	KLOE
• • • We do not use the following data for averages, fits, limits, etc. • • •			
$1.5 \pm 9.6 \pm 2.9$	13k	AMBROSINO 06E	KLOE

¹ANASTASI 18A result is a combination of the new measurement and AMBROSINO 06E. The new ANASTASI 18A measurement using data collected from 2004–2005, which corresponds to an integrated luminosity of 1.63 fb^{-1} is $A_S = (-4.9 \pm 5.7 \pm 2.6) \times 10^{-3}$.PARAMETERS FOR $K_S^0 \rightarrow 3\pi$ DECAY

$\text{Im}(\eta_{+-0})^2 = \Gamma(K_S^0 \rightarrow \pi^+\pi^-\pi^0, CP\text{-violating}) / \Gamma(K_L^0 \rightarrow \pi^+\pi^-\pi^0)$
 CP assumed valid (i.e. $\text{Re}(\eta_{+-0}) \simeq 0$).

VALUE	CL%	EVTS	DOCUMENT ID	TECN
<0.23	90	601	¹ BARMIN 85	HLBC
<0.12	90	384	METCALF 72	ASPK

¹BARMIN 85 find $\text{Re}(\eta_{+-0}) = (0.05 \pm 0.17)$ and $\text{Im}(\eta_{+-0}) = (0.15 \pm 0.33)$. Includes events of BALDO-CEOLIN 75.

$\text{Im}(\eta_{+-0}) = \text{Im}[A(K_S^0 \rightarrow \pi^+\pi^-\pi^0, CP\text{-violating}) / A(K_L^0 \rightarrow \pi^+\pi^-\pi^0)]$

VALUE	EVTS	DOCUMENT ID	TECN	COMMENT
$-0.002 \pm 0.009^{+0.002}_{-0.001}$	500k	¹ ADLER 97B	CPLR	
• • • We do not use the following data for averages, fits, limits, etc. • • •				
$-0.002 \pm 0.018 \pm 0.003$	137k	² ADLER 96D	CPLR	Sup. by ADLER 97B
$-0.015 \pm 0.017 \pm 0.025$	272k	³ ZOU 94	SPEC	

¹ADLER 97B also find $\text{Re}(\eta_{+-0}) = -0.002 \pm 0.007^{+0.004}_{-0.001}$. See also ANGELOPOULOS 98c.²The ADLER 96D fit also yields $\text{Re}(\eta_{+-0}) = 0.006 \pm 0.013 \pm 0.001$ with a correlation $+0.66$ between real and imaginary parts. Their results correspond to $|\eta_{+-0}| < 0.037$ with 90% CL.³ZOU 94 use theoretical constraint $\text{Re}(\eta_{+-0}) = \text{Re}(\epsilon) = 0.0016$. Without this constraint they find $\text{Im}(\eta_{+-0}) = 0.019 \pm 0.061$ and $\text{Re}(\eta_{+-0}) = 0.019 \pm 0.027$.

$\text{Im}(\eta_{000})^2 = \Gamma(K_S^0 \rightarrow 3\pi^0) / \Gamma(K_L^0 \rightarrow 3\pi^0)$

 CP assumed valid (i.e. $\text{Re}(\eta_{000}) \simeq 0$). This limit determines branching ratio $\Gamma(3\pi^0)/\Gamma_{\text{total}}$ above.

VALUE	CL%	EVTS	DOCUMENT ID	TECN	COMMENT
• • • We do not use the following data for averages, fits, limits, etc. • • •					
<0.1	90	632	¹ BARMIN 83	HLBC	
<0.28	90		² GJESDAL 74B	SPEC	Indirect meas.

¹BARMIN 83 find $\text{Re}(\eta_{000}) = (-0.08 \pm 0.18)$ and $\text{Im}(\eta_{000}) = (-0.05 \pm 0.27)$. Assuming CP invariance they obtain the limit quoted above.²GJESDAL 74B uses $K_{2\pi}$, $K_{\mu 3}$, and K_{e3} decay results, unitarity, and CP . Calculates $|\langle \eta_{000} \rangle| = 0.26 \pm 0.20$. We convert to upper limit.

Meson Particle Listings

K_S^0, K_L^0

$\text{Im}(\eta_{000}) = \text{Im}(A(K_S^0 \rightarrow \pi^0 \pi^0 \pi^0)/A(K_L^0 \rightarrow \pi^0 \pi^0 \pi^0))$
 $K_S^0 \rightarrow \pi^0 \pi^0 \pi^0$ violates CP conservation, in contrast to $K_S^0 \rightarrow \pi^+ \pi^- \pi^0$ which has a CP-conserving part.

VALUE	EVTs	DOCUMENT ID	TECN	COMMENT
-0.001 ± 0.016 OUR AVERAGE				
0.000 ± 0.009 ± 0.013	4.9M	¹ LAI 05A	NA48	Assumes CPT
-0.05 ± 0.12 ± 0.05	17300	² ANGELOPO... 98B	CPLR	Assumes CPT

¹ LAI 05A assumes $\text{Re}(\eta_{000}) = \text{Re}(\epsilon) = 1.66 \times 10^{-3}$. The equivalent limit is $|\eta_{000}|_{CPT} < 0.025$ at 90% CL Without assuming CPT invariance, they obtain $\text{Re}(\eta_{000}) = -0.002 \pm 0.011 \pm 0.015$ and $\text{Im}(\eta_{000}) = -0.003 \pm 0.013 \pm 0.017$ with a statistical correlation coefficient of 0.77 and an overall correlation coefficient of 0.57 between imaginary and real part. The equivalent limit is $|\eta_{000}| < 0.045$ at 90% CL

² ANGELOPOULOS 98B assumes $\text{Re}(\eta_{000}) = \text{Re}(\epsilon) = 1.635 \times 10^{-3}$. Without assuming CPT invariance, they obtain $\text{Re}(\eta_{000}) = 0.18 \pm 0.14 \pm 0.06$ and $\text{Im}(\eta_{000}) = 0.15 \pm 0.20 \pm 0.03$.

$|\eta_{000}| = |A(K_S^0 \rightarrow 3\pi^0)/A(K_L^0 \rightarrow 3\pi^0)|$
 A non-zero value violates CP invariance.

VALUE	CL%	EVTs	DOCUMENT ID	TECN	COMMENT
<0.0088	90	590M	BABUSCI	13C	KLOE
••• We do not use the following data for averages, fits, limits, etc. •••					
<0.018	90	37.8M	AMBROSINO	05B	KLOE
<0.045	90	4.9M	LAI	05A	NA48

DECAY-PLANE ASYMMETRY IN $\pi^+ \pi^- e^+ e^-$ DECAYS

This is the CP-violating asymmetry

$$A = \frac{N_{\sin\phi\cos\phi>0.0} - N_{\sin\phi\cos\phi<0.0}}{N_{\sin\phi\cos\phi>0.0} + N_{\sin\phi\cos\phi<0.0}}$$

where ϕ is the angle between the $e^+ e^-$ and $\pi^+ \pi^-$ planes in the K_S^0 rest frame.

CP asymmetry A in $K_S^0 \rightarrow \pi^+ \pi^- e^+ e^-$

VALUE (%)	DOCUMENT ID	TECN	COMMENT
-0.4 ± 0.8 OUR AVERAGE			
-0.4 ± 0.8	¹ BATLEY 11	NA48	2002 data
-1.1 ± 4.1	LAI 03C	NA48	1998+1999 data
••• We do not use the following data for averages, fits, limits, etc. •••			
0.5 ± 4.0 ± 1.6	LAI 03C	NA48	1999 data

¹ The result is used to set the limit $A < 1.5\%$ at 90% C.L.

K_S^0 REFERENCES

AJAI 23AE PR D108 L031102	R. Ajai et al. (LHCb Collab.)
BABUSCI 23 JHEP 2302 098	D. Babusci et al. (KLOE-2 Collab.)
AJAI 20AE PRL 125 231801	R. Ajai et al. (LHCb Collab.)
BABUSCI 20 PL B804 135378	D. Babusci et al. (KLOE-2 Collab.)
ANASTASI 18A JHEP 1809 021	A. Anastasi et al. (KLOE-2 Collab.)
PDG 18 PR D98 030001	M. Tanabashi et al. (PDG Collab.)
AJAI 17BQ EPJ C77 678	R. Ajai et al. (PDG Collab.)
PDG 16 CP C40 100001	C. Patrignani et al. (PDG Collab.)
AJAI 13G JHEP 1301 090	R. Ajai et al. (LHCb Collab.)
BABUSCI 13C PL B723 54	D. Babusci et al. (KLOE-2 Collab.)
ABOUZAID 11 PR D83 092001	E. Abouzaid et al. (FNAL KTeV Collab.)
AMBROSINO 11 EPJ C71 1604	F. Ambrosino et al. (KLOE Collab.)
BATLEY 11 PL B694 301	J.R. Batley et al. (CERN NA48/1 Collab.)
AMBROSINO 09A PL B672 203	F. Ambrosino et al. (KLOE Collab.)
AMBROSINO 08C JHEP 0805 051	F. Ambrosino et al. (KLOE Collab.)
ANDRE 07 ANP 322 2518	T. Andre (EFI)
BATLEY 07D PL B653 145	J.R. Batley et al. (CERN NA48 Collab.)
AMBROSINO 06C EPJ C48 767	F. Ambrosino et al. (KLOE Collab.)
AMBROSINO 05B PL B636 173	F. Ambrosino et al. (KLOE Collab.)
AMBROSINO 05B PL B619 61	F. Ambrosino et al. (KLOE Collab.)
BATLEY 05 PL B630 31	J.R. Batley et al. (NA48 Collab.)
LAI 05A PL B610 165	A. Lai et al. (CERN NA48 Collab.)
ALEXOPOU... 04A PR D70 092007	T. Alexopoulos et al. (FNAL KTeV Collab.)
BATLEY 04A PL B599 197	J.R. Batley et al. (NA48 Collab.)
LAI 04 PL B578 276	A. Lai et al. (CERN NA48 Collab.)
PDG 04 PL B592 1	S. Edelman et al. (PDG Collab.)
ALAVI-HARATI 03 PR D67 012005	A. Alavi-Harati et al. (FNAL KTeV Collab.)
Also PR D70 079904 (errata.)	A. Alavi-Harati et al. (FNAL KTeV Collab.)
BATLEY 03 PL B576 43	J.R. Batley et al. (CERN NA48 Collab.)
LAI 03 PL B551 7	A. Lai et al. (CERN NA48 Collab.)
LAI 03B PL B556 105	A. Lai et al. (CERN NA48 Collab.)
LAI 03C EPJ C30 33	A. Lai et al. (CERN NA48 Collab.)
ALOISIO 02 PL B535 37	A. Aloisio et al. (KLOE Collab.)
ALOISIO 02B PL B538 21	A. Aloisio et al. (KLOE Collab.)
LAI 02C PL B537 28	A. Lai et al. (CERN NA48 Collab.)
LAI 01 PL B514 253	A. Lai et al. (CERN NA48 Collab.)
PDG 00 PL B493 29	A. Lai et al. (CERN NA48 Collab.)
LAI 00B PL B496 137	A. Lai et al. (CERN NA48 Collab.)
PDG 00 EPJ C15 1	D.E. Groom et al. (PDG Collab.)
ACHASOV 99D PL B459 674	M.N. Achasov et al. (Novosibirsk CMD-2 Collab.)
AKHMETSHIN 99 PL B456 90	R.R. Akhmetshin et al. (Novosibirsk CMD-2 Collab.)
ANGELOPO... 98B PL B425 391	A. Angelopoulos et al. (CLEAR Collab.)
ANGELOPO... 98C EPJ C5 389	A. Angelopoulos et al. (CLEAR Collab.)
PDG 98 EPJ C3 1	C. Caso et al. (PDG Collab.)
ADLER 97B PL B407 193	R. Adler et al. (CLEAR Collab.)
ANGELOPO... 97 PL B413 232	A. Angelopoulos et al. (CLEAR Collab.)
BERTANZO 97 ZPHY C73 629	L. Bertanza (PISA, CERN, EDIN, MAINZ, ORSAY+)
ADLER 96D PL B370 167	R. Adler et al. (CLEAR Collab.)
ADLER 96E PL B374 313	R. Adler et al. (CLEAR Collab.)
ZOU 96 PL B369 362	Y. Zou et al. (RUTG, MINN, MICH)
BARR 95B PL B351 579	G.D. Barr et al. (CERN, EDIN, MAINZ, LALO+)
SCHWINGEN... 95 PRL 74 4376	B. Schwinger et al. (EFI, CHC+)
BLICK 94 PL B334 234	A.M. Blick et al. (SERP, JINR)
THOMSON 94 PL B337 411	G.B. Thomson et al. (RUTG, MINN, MICH)
ZOU 94 PL B329 519	Y. Zou et al. (RUTG, MINN, MICH)
BARR 93B PL B304 381	G.D. Barr et al. (CERN, EDIN, MAINZ, LALO+)
GIBBONS 93 PRL 70 1199	L.K. Gibbons et al. (FNAL E731 Collab.)
Also PR D55 6625	L.K. Gibbons et al. (FNAL E731 Collab.)
RAMBERG 93 PRL 70 2525	E. Ramberg et al. (FNAL E731 Collab.)
BALATS 89 SJNP 49 828	M.Y. Balats et al. (ITEP)
Translated from YAF 49 1332.	

GIBBONS 88 PRL 61 2661	L.K. Gibbons et al. (FNAL E731 Collab.)
BURKHARDT 87 PL B199 139	H. Burkhardt et al. (CERN, EDIN, MAINZ+)
GROSSMAN 87 PRL 59 18	N. Grossman et al. (MINN, MICH, RUTG)
BARMIN 86 SJNP 44 622	V.V. Barmin et al. (ITEP)
Also Translated from YAF 44 965.	
BARMIN 86B NC 96A 159	V.V. Barmin et al. (ITEP, PADO)
PDG 86B PL 170B 130	M. Aguilar-Benitez et al. (CERN, CIT+)
BARMIN 85 NC 85A 67	V.V. Barmin et al. (ITEP, PADO)
Also SJNP 41 759	V.V. Barmin et al. (ITEP)
Also Translated from YAF 41 1187.	
BARMIN 83 PL 128B 129	V.V. Barmin et al. (ITEP, PADO)
Also SJNP 39 269	V.V. Barmin et al. (ITEP, PADO)
Also Translated from YAF 39 428.	
ARONSON 82B PRL 48 1078	S.H. Aronson et al. (BNL, CHIC, STAN+)
ARONSON 82B PRL 48 1306	S.H. Aronson et al. (BNL, CHIC, PURD)
Also PL 116B 73	E. Fischbach et al. (PURD, BNL, CHIC)
Also PR D28 476	S.H. Aronson et al. (BNL, CHIC, PURD)
Also PR D28 495	S.H. Aronson et al. (BNL, CHIC, PURD)
ARONSON 76 NC 32A 236	S.H. Aronson et al. (WISC, EFI, UCSD+)
EVERHART 76 PR D14 661	G.C. Everhart et al. (PERN)
TAUREG 76 PL 65B 92	H. Taureg et al. (HEIDH, CERN, DORT)
BALDO... 75 NC 25A 688	M. Baldo-Golin et al. (PADO, WISC)
CARITHERS 75 PRL 34 1244	W.C. Carithers et al. (COLU, NYU)
BOBISUT 74 LNC 11 646	F. Bobisut et al. (PADO)
COWELL 74 PR D10 2083	PL. Cowell et al. (STON, COLU)
GEWENIGER 74B PL 48B 487	C. Geweniger et al. (CERN, HEIDH)
GJESDAL 74B PL 52B 119	S. Gjesdal et al. (CERN, HEIDH)
BURGUN 73 PL 46B 481	G. Burgun et al. (SACL, CERN)
GJESDAL 73 PL 44B 217	S. Gjesdal et al. (CERN, HEIDH)
HILL 73 PR D8 1290	D.G. Hill et al. (BNL, CMU)
ALITTI 72 PL 39B 568	J. Alitti, E. Lesquoy, A. Muller (SACL)
BURGUN 72 NP B50 194	G. Burgun et al. (SACL, CERN, OSLO)
METCALF 72 PL 40B 703	M. Metcalf et al. (CERN, IPN, WIEN)
MORSE 72B PRL 28 388	R. Morse et al. (COLO, PRIN, UMD)
NAGY 72 NP B47 94	E. Nagy, F. Tebbs, G. Vestergombi (BUDA)
Also PL 30B 498	G. Bozoki et al. (BUDA)
SKJEGGEST... 72 NP B48 343	O. Skjeggstad et al. (OSLO, CERN, SACL)
BALTAY 71 PRL 27 1678	C. Baltay et al. (COLU)
Also Thesis Nevis 187	W.A. Cooper (COLU)
MOFFETT 70 BAPS 15 512	R. Moffett et al. (ROCH)
BOZOKI 69 PL 30B 498	G. Bozoki et al. (BUDA)
DOYLE 69 Thesis UCLR 18139	J.C. Doyle (LRL)
GOBBI 69 PRL 22 682	B. Gobbi et al. (ROCH)
HYAMS 69B PL 29B 521	B.D. Hyams et al. (CERN, MFM)
MORFIN 69 PRL 23 660	J.G. Morfin, D. Sinclair (MICH)
DONALD 68 PL 27B 58	R.A. Donald et al. (LIVP, CERN, IPN+)
HILL 68 PR 171 1418	D.G. Hill et al. (BNL, CMU)
AUBERT 65 PL 17 59	B. Aubert et al. (EPOL, ORSAY)
BROWN 63 PR 130 769	J.L. Brown et al. (LRL, MICH)
CHRETIEN 63 PR 131 2208	M. Chretien et al. (BRAN, BROW, HARV+)
BROWN 61 NC 19 1155	J.L. Brown et al. (MICH)
BOLDT 58B PRL 1 150	E. Boldt, D.O. Caldwell, Y. Pal (MIT)

OTHER RELATED PAPERS

LITTENBERG 93 ARNPS 43 729	L.S. Littenberg, G. Valencia (BNL, FNAL)
Rare and Radiative Kaon Decays	
BATTISTON 92 PRL 214 293	R. Battiston et al. (PGIA, CERN, TRSTT)
Status and Perspectives of K Decay Physics	
TRILLING 65B UCRL 16473	G.N. Trilling (LRL)
Updated from 1965 Argonne Conference, page 115.	
CRAWFORD 62 CERN Conf. 827	F.S. Crawford (LRL)
FITCH 61 NC 22 1160	V.L. Fitch, P.A. Piroue, R.B. Perkins (PRIN+)
GOOD 61 PR 124 1223	R.H. Good et al. (LRL, WISC)
BIRGE 60 Rochester Conf. 601	R.W. Birge et al. (LRL, WISC)
MULLER 60 PRL 4 418	F. Muller et al. (LRL, BNL)



$$J(P) = \frac{1}{2}(0^-)$$

$$m_{K_L^0} - m_{K_S^0}$$

For earlier measurements, beginning with GOOD 61 and FITCH 61, see our 1986 edition, Physics Letters 170B 132 (1986).

OUR FIT is described in the note on "CP violation in K_L decays" in the K_S^0 Particle Listings. The result labeled "OUR FIT Assuming CPT" ["OUR FIT Not assuming CPT"] includes all measurements except those with the comment "Not assuming CPT" ["Assuming CPT"]. Measurements with neither comment do not assume CPT and enter both fits.

VALUE (10^{10} s^{-1})	DOCUMENT ID	TECN	COMMENT
0.5293 ± 0.0009 OUR FIT	Error includes scale factor of 1.3. Assuming CPT		
0.5289 ± 0.0010 OUR FIT	Not assuming CPT		
0.52797 ± 0.00195	^{1,2} ABOUZAID 11	KTEV	Not assuming CPT
0.52699 ± 0.00123	^{1,3} ABOUZAID 11	KTEV	Assuming CPT
0.5240 ± 0.0044 ± 0.0033	APOSTOLA... 99c	CPLR	$K^0 - \bar{K}^0$ to $\pi^+ \pi^-$
0.5297 ± 0.0030 ± 0.0022	⁴ SCHWINGEN... 95	E773	20-160 GeV K beams
0.5286 ± 0.0028	⁵ GIBBONS 93	E731	Assuming CPT
0.5257 ± 0.0049 ± 0.0021	⁴ GIBBONS 93c	E731	Not assuming CPT
0.5340 ± 0.0025 ± 0.0015	⁶ GEWENIGER 74c	SPEC	Gap method
0.5334 ± 0.0040 ± 0.0015	^{6,7} GJESDAL 74	SPEC	Assuming CPT
••• We do not use the following data for averages, fits, limits, etc. •••			
0.5261 ± 0.0015	⁸ ALAVI-HARATI 03	KTEV	Assuming CPT
0.5288 ± 0.0043	⁹ ALAVI-HARATI 03	KTEV	Not assuming CPT
0.5343 ± 0.0063 ± 0.0025	¹⁰ ANGELOPO... 01	CPLR	
0.5295 ± 0.0020 ± 0.0003	¹¹ ANGELOPO... 98D	CPLR	Assuming CPT
0.5307 ± 0.0013	¹² ADLER 96c	RVUE	
0.5274 ± 0.0029 ± 0.0005	¹¹ ADLER 95	CPLR	Sup. by ANGELOPOU-L0S 98D
0.482 ± 0.014	¹³ ARONSON 82B	SPEC	$E=30-110$ GeV
0.534 ± 0.007	¹⁴ CARNEGIE 71	ASP K	Gap method
0.542 ± 0.006	¹⁴ ARONSON 70	ASP K	Gap method
0.542 ± 0.006	CULLEN 70	CNTR	

¹ The two ABOUZAID 11 values use the same data. The first enters the "assuming CPT" fit and the second enters the "not assuming CPT" fit.

See key on page 1171

Meson Particle Listings

K_L^0

- ²ABOUZAID 11 fit has Δm , τ_S , ϕ_e , $\text{Re}(e'/\epsilon)$, and $\text{Im}(e'/\epsilon)$ as free parameters. See $\text{Im}(e'/\epsilon)$ in the " K_L^0 CP violation" section for correlation information.
- ³ABOUZAID 11 fit has Δm and τ_S free but constrains ϕ_e to the Superweak value, i.e. assumes CP T. See " K_S^0 Mean Life" section for correlation information.
- ⁴Fits Δm and ϕ_{+-} simultaneously. GIBBONS 93c systematic error is from B. Winstein via private communication. 20–160 GeV K beams.
- ⁵GIBBONS 93 value assume $\phi_{+-} = \phi_{00} = \phi_{\text{SW}} = (43.7 \pm 0.2)^\circ$, i.e. assumes CP T. 20–160 GeV K beams.
- ⁶These two experiments have a common systematic error due to the uncertainty in the momentum scale, as pointed out in WAHL 89.
- ⁷GJESDAL 74 uses charge asymmetry in K_{S}^0 decays.
- ⁸ALAVI-HARATI 03 fit Δm and $\tau_{K_{\text{S}}^0}$ simultaneously. ϕ_{+-} is constrained to the Superweak value, i.e. CP T is assumed. See " K_{S}^0 Mean Life" section for correlation information. Superseded by ABOUZAID 11.
- ⁹ALAVI-HARATI 03 fit Δm , ϕ_{+-} , and $\tau_{K_{\text{S}}^0}$ simultaneously. See ϕ_{+-} in the " K_{L}^0 CP violation" section for correlation information. Superseded by ABOUZAID 11.
- ¹⁰ANGELOPOULOS 01 uses strong interactions strangeness tagging at two different times.
- ¹¹Uses K_{e3}^0 and $K_{\mu 3}^0$ strangeness tagging at production and decay. Assumes CP T conservation on $\Delta S = -\Delta Q$ transitions.
- ¹²ADLER 96c is the result of a fit which includes nearly the same data as entered into the "OUR FIT" value above.
- ¹³ARONSON 82 find that Δm may depend on the kaon energy
- ¹⁴ARONSON 70 and CARNEGIE 71 use K_{S}^0 mean life = $(0.862 \pm 0.006) \times 10^{-10}$ s. We have not attempted to adjust these values for the subsequent change in the K_{S}^0 mean life or in η_{+-} .

K_L^0 MEAN LIFE

VALUE (10^{-8} s)	EVTS	DOCUMENT ID	TECN	COMMENT	
5.116 ± 0.021 OUR FIT	Error	includes scale factor of 1.1.			
5.099 ± 0.021 OUR AVERAGE					
5.072 ± 0.011 ± 0.035	13M	1 AMBROSINO 06	KLOE	$\sum_i B_i = 1$	
5.092 ± 0.017 ± 0.025	15M	AMBROSINO 05c	KLOE		
5.154 ± 0.044	0.4M	VOSBURGH 72	CNTR		
• • •		We do not use the following data for averages, fits, limits, etc. • • •			
5.15 ± 0.14		DEVLIN 67	CNTR		
¹ AMBROSINO 06 uses $\phi \rightarrow K_{\text{L}} K_{\text{S}}$ with K_{L} tagged by $K_{\text{S}} \rightarrow \pi^+ \pi^-$. The four major K_{L} BR's are measured, the small remainder ($\pi^+ \pi^-, \pi^0 \pi^0, \gamma \gamma$) is taken from PDG 04. This KLOE K_{L} lifetime is obtained by imposing $\sum_i B_i = 1$. The correlation matrix among the four measured K_{L} BR's and this K_{L} lifetime is					
	K_{e3}	$K_{\mu 3}$	$3\pi^0$	$\pi^+ \pi^- \pi^0$	$\tau_{K_{\text{L}}}$
K_{e3}	1	-0.25	-0.56	-0.07	0.25
$K_{\mu 3}$		1	-0.43	-0.20	0.33
$3\pi^0$			1	-0.39	-0.21
$\pi^+ \pi^- \pi^0$				1	-0.39
$\tau_{K_{\text{L}}}$					1

These correlations are taken into account in our fit. The average of this KLOE mean life measurement and the independent KLOE measurement in AMBROSINO 05c is $(5.084 \pm 0.023) \times 10^{-8}$ s.

K_L^0 DECAY MODES

Mode	Fraction (Γ_i/Γ)	Scale factor/ Confidence level
Semileptonic modes		
Γ_1 $\pi^\pm e^\mp \nu_e$ Called K_{e3}^0 .	[a] (40.55 ± 0.11) %	S=1.7
Γ_2 $\pi^\pm \mu^\mp \nu_\mu$ Called $K_{\mu 3}^0$.	[a] (27.04 ± 0.07) %	S=1.1
Γ_3 ($\pi \mu$ atom) ν	(1.05 ± 0.11) × 10 ⁻⁷	
Γ_4 $\pi^0 \pi^\pm e^\mp \nu$	[a] (5.20 ± 0.11) × 10 ⁻⁵	
Γ_5 $\pi^\pm e^\mp \nu e^+ e^-$	[a] (1.26 ± 0.04) × 10 ⁻⁵	
Hadronic modes, including Charge conjugation × Parity Violating (CPV) modes		
Γ_6 $3\pi^0$	(19.52 ± 0.12) %	S=1.6
Γ_7 $\pi^+ \pi^- \pi^0$	(12.54 ± 0.05) %	
Γ_8 $\pi^+ \pi^-$	CPV [b] (1.967 ± 0.010) × 10 ⁻³	S=1.5
Γ_9 $\pi^0 \pi^0$	CPV (8.64 ± 0.06) × 10 ⁻⁴	S=1.8
Semileptonic modes with photons		
Γ_{10} $\pi^\pm e^\mp \nu_e \gamma$	[a,c,d] (3.79 ± 0.06) × 10 ⁻³	
Γ_{11} $\pi^\pm \mu^\mp \nu_\mu \gamma$	(5.65 ± 0.23) × 10 ⁻⁴	
Hadronic modes with photons or $\ell\bar{\ell}$ pairs		
Γ_{12} $\pi^0 \pi^0 \gamma$	< 2.43 × 10 ⁻⁷	CL=90%
Γ_{13} $\pi^+ \pi^- \gamma$	[c,d] (4.15 ± 0.15) × 10 ⁻⁵	S=2.8
Γ_{14} $\pi^+ \pi^- \pi^- \gamma$ (DE)	(2.84 ± 0.11) × 10 ⁻⁵	S=2.0
Γ_{15} $\pi^0 2\gamma$	[c] (1.273 ± 0.033) × 10 ⁻⁶	
Γ_{16} $\pi^0 \gamma e^+ e^-$	(1.62 ± 0.17) × 10 ⁻⁸	

Other modes with photons or $\ell\bar{\ell}$ pairs

Γ_{17} 2γ	(5.47 ± 0.04) × 10 ⁻⁴	S=1.1
Γ_{18} 3γ	< 7.4 × 10 ⁻⁸	CL=90%
Γ_{19} $e^+ e^- \gamma$	(9.4 ± 0.4) × 10 ⁻⁶	S=2.0
Γ_{20} $\mu^+ \mu^- \gamma$	(3.59 ± 0.11) × 10 ⁻⁷	S=1.3
Γ_{21} $\mu^+ \mu^- \mu^+ \mu^-$	< 2.3 × 10 ⁻⁹	CL=90%
Γ_{22} $e^+ e^- \gamma \gamma$	[c] (5.95 ± 0.33) × 10 ⁻⁷	
Γ_{23} $\mu^+ \mu^- \gamma \gamma$	[c] (1.0 ± _{-0.6} ^{+0.8}) × 10 ⁻⁸	

Charge conjugation × Parity (CP) or Lepton Family number (LF) violating modes, or $\Delta S = 1$ weak neutral current (S1) modes

Γ_{24} $\mu^+ \mu^-$	S1 (6.84 ± 0.11) × 10 ⁻⁹	
Γ_{25} $e^+ e^-$	S1 (9 ± ₋₄ ⁺⁶) × 10 ⁻¹²	
Γ_{26} $\pi^+ \pi^- e^+ e^-$	S1 [c] (3.11 ± 0.19) × 10 ⁻⁷	
Γ_{27} $\pi^0 \pi^0 e^+ e^-$	S1 < 6.6 × 10 ⁻⁹	CL=90%
Γ_{28} $\pi^0 \pi^0 \mu^+ \mu^-$	S1 < 9.2 × 10 ⁻¹¹	CL=90%
Γ_{29} $\mu^+ \mu^- e^+ e^-$	S1 (2.69 ± 0.27) × 10 ⁻⁹	
Γ_{30} $e^+ e^- e^+ e^-$	S1 (3.56 ± 0.21) × 10 ⁻⁸	
Γ_{31} $\pi^0 \mu^+ \mu^-$	CP,S1 [e] < 3.8 × 10 ⁻¹⁰	CL=90%
Γ_{32} $\pi^0 e^+ e^-$	CP,S1 [e] < 2.8 × 10 ⁻¹⁰	CL=90%
Γ_{33} $\pi^0 \nu \bar{\nu}$	CP,S1 [f] < 3.0 × 10 ⁻⁹	CL=90%
Γ_{34} $\pi^0 \pi^0 \nu \bar{\nu}$	S1 < 8.1 × 10 ⁻⁷	CL=90%
Γ_{35} $e^\pm \mu^\mp$	LF [a] < 4.7 × 10 ⁻¹²	CL=90%
Γ_{36} $e^\pm e^\pm \mu^\mp \mu^\mp$	LF [a] < 4.12 × 10 ⁻¹¹	CL=90%
Γ_{37} $\pi^0 \mu^\pm e^\mp$	LF [a] < 7.6 × 10 ⁻¹¹	CL=90%
Γ_{38} $\pi^0 \pi^0 \mu^\pm e^\mp$	LF < 1.7 × 10 ⁻¹⁰	CL=90%

Lorentz invariance violating modes

Γ_{39} $\pi^0 \gamma$	< 1.7 × 10 ⁻⁷	CL=90%
------------------------------	--------------------------	--------

- [a] The value is for the sum of the charge states or particle/antiparticle states indicated.
- [b] This mode includes gammas from inner bremsstrahlung but not the direct emission mode $K_L^0 \rightarrow \pi^+ \pi^- \gamma$ (DE).
- [c] See the Particle Listings below for the energy limits used in this measurement.
- [d] Most of this radiative mode, the low-momentum γ part, is also included in the parent mode listed without γ 's.
- [e] Allowed by higher-order electroweak interactions.
- [f] Violates CP in leading order. Test of direct CP violation since the indirect CP-violating and CP-conserving contributions are expected to be suppressed.

CONSTRAINED FIT INFORMATION

An overall fit to the mean life and 15 branching ratios uses 27 measurements and one constraint to determine 11 parameters. The overall fit has a $\chi^2 = 37.4$ for 17 degrees of freedom.

The following off-diagonal array elements are the correlation coefficients $\langle \delta p_i \delta p_j \rangle / (\delta p_i \delta p_j)$, in percent, from the fit to parameters p_i , including the branching fractions, $x_i \equiv \Gamma_i / \Gamma_{\text{total}}$. The fit constrains the x_i whose labels appear in this array to sum to one.

x_2	-21																		
x_6	-77	-29																	
x_7	-15	-20	-18																
x_8	53	-11	-47	4															
x_9	30	-23	-11	-12	64														
x_{13}	6	-1	-6	0	12	8													
x_{14}	6	-1	-6	0	11	7	93												
x_{17}	-46	-22	64	-14	-21	8	-3	-3											
x_{19}	-5	-2	7	-1	-3	-1	0	0	4										
Γ	-27	-9	24	15	-13	-6	-2	-2	15	2									
	x_1	x_2	x_6	x_7	x_8	x_9	x_{13}	x_{14}	x_{17}	x_{19}									

Mode	Rate (10^8 s^{-1})	Scale factor
Γ_1 $\pi^\pm e^\mp \nu_e$ Called K_{e3}^0 .	[a] 0.07927 ± 0.00034	1.1
Γ_2 $\pi^\pm \mu^\mp \nu_\mu$ Called $K_{\mu 3}^0$.	[a] 0.05286 ± 0.00025	1.1

Meson Particle Listings

 K_L^0

Γ_6	$3\pi^0$	0.03815 ± 0.00030	1.5
Γ_7	$\pi^+\pi^-\pi^0$	0.02451 ± 0.00015	
Γ_8	$\pi^+\pi^-$	[b] $(3.844 \pm 0.023) \times 10^{-4}$	1.2
Γ_9	$\pi^0\pi^0$	$(1.690 \pm 0.013) \times 10^{-4}$	1.4
Γ_{13}	$\pi^+\pi^-\gamma$	[c,d] $(8.11 \pm 0.29) \times 10^{-6}$	2.7
Γ_{14}	$\pi^+\pi^-\gamma(\text{DE})$	$(5.55 \pm 0.21) \times 10^{-6}$	2.0
Γ_{17}	2γ	$(1.069 \pm 0.010) \times 10^{-4}$	1.2
Γ_{19}	$e^+e^-\gamma$	$(1.84 \pm 0.08) \times 10^{-6}$	1.9

 K_L^0 DECAY RATES

$\Gamma(\pi^+\pi^-\pi^0)$ Γ_7				
VALUE (10^6 s^{-1})	EVTS	DOCUMENT ID	TECN	COMMENT
2.451 ± 0.015 OUR FIT				

••• We do not use the following data for averages, fits, limits, etc. •••

2.32 ± 0.13 -0.15	192	BALDO...	75	HLBC	Assumes CP
2.35 ± 0.20	180	¹ JAMES	72	HBC	Assumes CP
2.71 ± 0.28	99	CHO	71	DBC	Assumes CP
2.5 ± 0.3	98	¹ JAMES	71	HBC	Assumes CP
2.12 ± 0.33	50	MEISNER	71	HBC	Assumes CP
2.20 ± 0.35	53	WEBBER	70	HBC	Assumes CP
2.62 ± 0.28 -0.27	136	BEHR	66	HLBC	Assumes CP
3.26 ± 0.77	18	ANDERSON	65	HBC	
1.4 ± 0.4	14	FRANZINI	65	HBC	

¹ JAMES 72 is a final measurement and includes JAMES 71.

$\Gamma(\pi^\pm e^\mp \nu_e)$ Γ_1				
VALUE (10^6 s^{-1})	EVTS	DOCUMENT ID	TECN	COMMENT
7.927 ± 0.034 OUR FIT				Error includes scale factor of 1.1.

••• We do not use the following data for averages, fits, limits, etc. •••

7.81 ± 0.56	620	CHAN	71	HBC	
7.52 ± 0.85 -0.72		AUBERT	65	HLBC	$\Delta S = \Delta Q$, CP assumed

$\Gamma(\pi^\pm e^\mp \nu_e) + \Gamma(\pi^\pm \mu^\mp \nu_\mu)$ $(\Gamma_1 + \Gamma_2)$				
VALUE (10^6 s^{-1})	EVTS	DOCUMENT ID	TECN	COMMENT
13.21 ± 0.05 OUR FIT				

••• We do not use the following data for averages, fits, limits, etc. •••

12.4 ± 0.7	410	¹ BURGUN	72	HBC	$K^+p \rightarrow K^0 p \pi^+$
8.47 ± 1.69	126	¹ MANN	72	HBC	$K^-p \rightarrow n \bar{K}^0$
13.1 ± 1.3	252	¹ WEBBER	71	HBC	$K^-p \rightarrow n \bar{K}^0$
11.6 ± 0.9	393	^{1,2} CHO	70	DBC	$K^+n \rightarrow K^0 p$
10.3 ± 0.8	335	² HILL	67	DBC	$K^+n \rightarrow K^0 p$
9.85 ± 1.15 -1.05	109	¹ FRANZINI	65	HBC	

¹ Assumes $\Delta S = \Delta Q$ rule.

² CHO 70 includes events of HILL 67.

 K_L^0 BRANCHING RATIOS

Semileptonic modes

$\Gamma(\pi^\pm e^\mp \nu_e)/\Gamma_{\text{total}}$ Γ_1/Γ				
VALUE	EVTS	DOCUMENT ID	TECN	COMMENT
0.4055 ± 0.0011 OUR FIT				Error includes scale factor of 1.7.

••• We do not use the following data for averages, fits, limits, etc. •••

0.4007 $\pm 0.0005 \pm 0.0015$	13M	¹ AMBROSINO 06	KLOE	
0.4067 ± 0.0011		² ALEXOPOU... 04	KTEV	

¹ There are correlations between these five KLOE measurements: $B(K_L \rightarrow \pi e \nu)$, $B(K_L \rightarrow \pi \mu \nu)$, $B(K_L \rightarrow 3\pi^0)$, $B(K_L \rightarrow \pi^+\pi^-\pi^0)$, and τ_{K_L} measured in AMBROSINO 06. See the footnote for the τ_{K_L} measurement for the correlation matrix.

² ALEXOPOULOS 04 constrains $\sum_i B_i = 0.9993$ for the six major K_L branching fractions. The correlations among these branching fractions are taken into account in our fit. The correlation matrix is

	K_{e3}	$K_{\mu 3}$	$3\pi^0$	$\pi^+\pi^-\pi^0$	$\pi^+\pi^-$	$\pi^0\pi^0$
K_{e3}	1					
$K_{\mu 3}$	0.15	1				
$3\pi^0$	-0.77	-0.62	1			
$\pi^+\pi^-\pi^0$	0.18	0.08	-0.54	1		
$\pi^+\pi^-$	0.28	0.22	-0.48	0.49	1	
$\pi^0\pi^0$	-0.72	-0.54	0.89	-0.46	-0.39	1

$\Gamma(\pi^\pm \mu^\mp \nu_\mu)/\Gamma_{\text{total}}$ Γ_2/Γ				
VALUE	EVTS	DOCUMENT ID	TECN	COMMENT
0.2704 ± 0.0007 OUR FIT				Error includes scale factor of 1.1.

••• We do not use the following data for averages, fits, limits, etc. •••

0.2698 $\pm 0.0005 \pm 0.0015$	13M	¹ AMBROSINO 06	KLOE	
0.2701 ± 0.0009		² ALEXOPOU... 04	KTEV	

¹ There are correlations between these five KLOE measurements: $B(K_L \rightarrow \pi e \nu)$, $B(K_L \rightarrow \pi \mu \nu)$, $B(K_L \rightarrow 3\pi^0)$, $B(K_L \rightarrow \pi^+\pi^-\pi^0)$, and τ_{K_L} measured in AMBROSINO 06. See the footnote for the τ_{K_L} measurement for the correlation matrix.

² For correlations with other ALEXOPOULOS 04 measurements, see the footnote with their $B(K_L \rightarrow \pi e \nu)$ measurement.

$[\Gamma(\pi^\pm e^\mp \nu_e) + \Gamma(\pi^\pm \mu^\mp \nu_\mu)]/\Gamma_{\text{total}}$ $(\Gamma_1 + \Gamma_2)/\Gamma$

VALUE	DOCUMENT ID
0.6760 ± 0.0012 OUR FIT	Error includes scale factor of 1.6.

$\Gamma(\pi^\pm \mu^\mp \nu_\mu)/\Gamma(\pi^\pm e^\mp \nu_e)$ Γ_2/Γ_1

VALUE	EVTS	DOCUMENT ID	TECN	COMMENT
0.6669 ± 0.0027 OUR FIT				Error includes scale factor of 1.2.

••• We use the following data for averages but not for fits. •••

0.6740 ± 0.0059	13M	¹ AMBROSINO 06	KLOE	Not in fit
0.6640 $\pm 0.0014 \pm 0.0022$	394k	² ALEXOPOU... 04	KTEV	Not in fit

••• We do not use the following data for averages, fits, limits, etc. •••

0.702 ± 0.011	33k	CHO	80	HBC
0.662 ± 0.037	10k	WILLIAMS	74	ASP
0.741 ± 0.044	6700	BRANDENB...	73	HBC
0.662 ± 0.030	1309	EVANS	73	HLBC
0.68 ± 0.08	3548	BASILE	70	OSP
0.71 ± 0.05	770	BUDAGOV	68	HLBC

¹ AMBROSINO 06 enters the fit via their separate measurements of these two modes.

² ALEXOPOULOS 04 enters the fit via their separate measurements of these two modes.

$\Gamma((\pi \text{ atom})\nu)/\Gamma(\pi^\pm \mu^\mp \nu_\mu)$ Γ_3/Γ_2

VALUE (units 10^{-7})	EVTS	DOCUMENT ID	TECN	COMMENT
3.90 ± 0.39	155	¹ ARONSON 86	SPEC	

••• We do not use the following data for averages, fits, limits, etc. •••

seen	18	COOMBES	76	WIRE
------	----	---------	----	------

¹ ARONSON 86 quote theoretical value of $(4.31 \pm 0.08) \times 10^{-7}$.

$\Gamma(\pi^0 \pi^\pm e^\mp \nu)/\Gamma_{\text{total}}$ Γ_4/Γ

VALUE (units 10^{-5})	CL%	EVTS	DOCUMENT ID	TECN	COMMENT
5.20 ± 0.11 OUR AVERAGE					

••• We do not use the following data for averages, fits, limits, etc. •••

5.21 $\pm 0.07 \pm 0.09$	5402	BATLEY	04	NA48
5.16 $\pm 0.20 \pm 0.22$	729	MAKOFF	93	E731

••• We do not use the following data for averages, fits, limits, etc. •••

6.2 ± 2.0	16	CARROLL	80c	SPEC
< 220	90	¹ DONALDSON 74	SPEC	

¹ DONALDSON 74 uses $K_L^0 \rightarrow \pi^+\pi^-\pi^0$ /(all K_L^0) decays = 0.126.

$\Gamma(\pi^\pm e^\mp \nu e^+e^-)/\Gamma(\pi^+\pi^-\pi^0)$ Γ_5/Γ_7

VALUE (units 10^{-5})	EVTS	DOCUMENT ID	TECN	COMMENT
$10.02 \pm 0.17 \pm 0.29$	19k	¹ ABOUZAIID 07c	KTEV	$M_{ee} > 5 \text{ MeV}$, $E_{ee}^* > 30 \text{ MeV}$

¹ E_{ee}^* is the energy of the e^+e^- pair in the kaon rest frame. ABOUZAIID 07c reports $[\Gamma(K_L^0 \rightarrow \pi^\pm e^\mp \nu e^+e^-)/\Gamma(K_L^0 \rightarrow \pi^+\pi^-\pi^0)] / [B(\pi^0 \rightarrow e^+e^-\gamma)] = (8.54 \pm 0.07 \pm 0.13) \times 10^{-3}$ which we multiply by our best value $B(\pi^0 \rightarrow e^+e^-\gamma) = (1.174 \pm 0.035) \times 10^{-2}$. Our first error is their experiment's error and our second error is the systematic error from using our best value.

Hadronic modes,

including Charge conjugation x Parity Violating (CPV) modes

$\Gamma(3\pi^0)/\Gamma_{\text{total}}$ Γ_6/Γ

VALUE	EVTS	DOCUMENT ID	TECN	COMMENT
0.1952 ± 0.0012 OUR FIT				Error includes scale factor of 1.6.

••• We use the following data for averages but not for fits. •••

0.1969 ± 0.0026 OUR AVERAGE Error includes scale factor of 2.0.

••• We do not use the following data for averages, fits, limits, etc. •••

0.1997 $\pm 0.0003 \pm 0.0019$	13M	¹ AMBROSINO 06	KLOE	Not fitted
0.1945 ± 0.0018		¹ ALEXOPOU... 04	KTEV	Not fitted

¹ We exclude these $B(K_L \rightarrow 3\pi^0)$ measurements from our fit because the authors have constrained K_L branching fractions to sum to one. It enters our fit via the other measurements from the experiment and their correlations, along with our constraint that the fitted branching fractions sum to one.

$\Gamma(3\pi^0)/\Gamma(\pi^\pm e^\mp \nu_e)$ Γ_6/Γ_1

VALUE	EVTS	DOCUMENT ID	TECN	COMMENT
0.481 ± 0.004 OUR FIT				Error includes scale factor of 1.8.

••• We use the following data for averages but not for fits. •••

$0.4782 \pm 0.0014 \pm 0.0053$ 209k ¹ ALEXOPOU... 04 KTEV Not in fit

••• We do not use the following data for averages, fits, limits, etc. •••

0.545 $\pm 0.004 \pm 0.009$	38k	KREUTZ	95	NA31
-----------------------------	-----	--------	----	------

¹ This measurement enters the fit via their separate measurements of these two modes.

$\Gamma(3\pi^0)/[\Gamma(\pi^\pm e^\mp \nu_e) + \Gamma(\pi^\pm \mu^\mp \nu_\mu) + \Gamma(\pi^+\pi^-\pi^0)]$ $\Gamma_6/(\Gamma_1 + \Gamma_2 + \Gamma_7)$

VALUE	EVTS	DOCUMENT ID	TECN	COMMENT
0.2436 ± 0.0018 OUR FIT				Error includes scale factor of 1.6.

••• We do not use the following data for averages, fits, limits, etc. •••

0.251 ± 0.014 549 BUDAGOV 68 HLBC ORSAV meas.

0.277 ± 0.021 444 BUDAGOV 68 HLBC Ecole polytec.meas

0.31 ± 0.07 29 KULYUKINA 68 CC

0.24 ± 0.08 24 ANIKINA 64 CC

$\Gamma(3\pi^0)/\Gamma(\pi^+\pi^-\pi^0)$ Γ_6/Γ_7

VALUE	EVTS	DOCUMENT ID	TECN	COMMENT
1.557 ± 0.012 OUR FIT				Error includes scale factor of 1.3.

••• We use the following data for averages but not for fits. •••

1.582 ± 0.027 13M ¹ AMBROSINO 06 KLOE Not in fit

See key on page 1171

Meson Particle Listings

K_L^0

• • • We do not use the following data for averages, fits, limits, etc. • • •

1.611 ± 0.014 ± 0.034	28k	KREUTZ	95	NA31	
1.65 ± 0.07	883	BARMIN	72B	HLBC	Error statistical only
1.80 ± 0.13	1010	BUDAGOV	68	HLBC	
2.0 ± 0.6	188	ALEKSANYAN	64B	FBC	

¹ AMBROSINO 06 enters the fit via their separate measurements of these two modes.

$\Gamma(\pi^+ \pi^- \pi^0)/\Gamma_{total}$ Γ_7/Γ

VALUE	EVTS	DOCUMENT ID	TECN	COMMENT
0.1254 ± 0.0005 OUR FIT				Error includes scale factor of 1.3.
0.1255 ± 0.0006 OUR AVERAGE				
0.1263 ± 0.0004 ± 0.0011	13M	¹ AMBROSINO 06	KLOE	
0.1252 ± 0.0007		² ALEXOPOU... 04	KTEV	

¹ There are correlations between these five KLOE measurements: $B(K_L \rightarrow \pi e \nu)$, $B(K_L \rightarrow \pi \mu \nu)$, $B(K_L \rightarrow 3\pi^0)$, $B(K_L \rightarrow \pi^+ \pi^- \pi^0)$, and τ_{K_L} measured in AMBROSINO 06. See the footnote for the τ_{K_L} measurement for the correlation matrix.

² For correlations with other ALEXOPOULOS 04 measurements, see the footnote with their $B(K_L \rightarrow \pi e \nu)$ measurement.

$\Gamma(\pi^+ \pi^- \pi^0)/\Gamma(\pi^\pm e^\mp \nu_e)$ Γ_7/Γ_1

VALUE	EVTS	DOCUMENT ID	TECN	COMMENT
0.3092 ± 0.0016 OUR FIT				Error includes scale factor of 1.1.
• • • We use the following data for averages but not for fits. • • •				
0.3078 ± 0.0005 ± 0.0017	799k	¹ ALEXOPOU... 04	KTEV	Not in fit
• • • We do not use the following data for averages, fits, limits, etc. • • •				
0.336 ± 0.003 ± 0.007	28k	KREUTZ	95	NA31

¹ This measurement enters the fit via their separate measurements for the two modes.

$\Gamma(\pi^+ \pi^- \pi^0)/[\Gamma(\pi^\pm e^\mp \nu_e) + \Gamma(\pi^\pm \mu^\mp \nu_\mu) + \Gamma(\pi^+ \pi^- \pi^0)]$ $\Gamma_7/(\Gamma_1 + \Gamma_2 + \Gamma_7)$

VALUE	EVTS	DOCUMENT ID	TECN	COMMENT
0.1565 ± 0.0006 OUR FIT				Error includes scale factor of 1.1.
• • • We do not use the following data for averages, fits, limits, etc. • • •				
0.163 ± 0.003	6499	CHO	77	HBC
0.1605 ± 0.0038	1590	ALEXANDER	73B	HBC
0.146 ± 0.004	3200	BRANDENB...	73	HBC
0.159 ± 0.010	558	EVANS	73	HLBC
0.167 ± 0.016	1402	KULYUKINA	68	CC
0.161 ± 0.005		HOPKINS	67	HBC
0.162 ± 0.015	126	HAWKINS	66	HBC
0.159 ± 0.015	326	AUSTBURY	65B	CC
0.178 ± 0.017	566	GUIDONI	65	HBC
0.144 ± 0.004	1729	HOPKINS	65	HBC See HOPKINS 67

$\Gamma(\pi^+ \pi^-)/\Gamma_{total}$ Γ_8/Γ

Violates CP conservation.

VALUE (units 10 ⁻³)	EVTS	DOCUMENT ID	TECN	COMMENT
1.967 ± 0.010 OUR FIT				Error includes scale factor of 1.5.
1.975 ± 0.012		¹ ALEXOPOU... 04	KTEV	

¹ For correlations with other ALEXOPOULOS 04 measurements, see the footnote with their $B(K_L \rightarrow \pi e \nu)$ measurement.

$\Gamma(\pi^+ \pi^-)/\Gamma(\pi^\pm e^\mp \nu_e)$ Γ_8/Γ_1

VALUE (units 10 ⁻³)	EVTS	DOCUMENT ID	TECN	COMMENT
4.849 ± 0.020 OUR FIT				Error includes scale factor of 1.1.
4.840 ± 0.020 OUR AVERAGE				
4.826 ± 0.022 ± 0.016	47k	¹ LAI	07	NA48
• • • We use the following data for averages but not for fits. • • •				
4.856 ± 0.017 ± 0.023	84k	² ALEXOPOU... 04	KTEV	Not in fit

¹ The LAI 07 central value of 4.835×10^{-3} has been reduced by 0.19% to 4.826×10^{-3} to subtract the contribution from the direct emission mode $K_L^0 \rightarrow \pi^+ \pi^- \gamma$ (DE).

² This measurement enters the fit via their separate measurements for the two modes.

$[\Gamma(\pi^+ \pi^-) + \Gamma(\pi^+ \pi^- \gamma \text{ (DE)})]/\Gamma(\pi^\pm \mu^\mp \nu_\mu)$ $(\Gamma_8 + \Gamma_{14})/\Gamma_2$

VALUE (units 10 ⁻³)	EVTS	DOCUMENT ID	TECN	COMMENT
7.38 ± 0.04 OUR FIT				Error includes scale factor of 1.4.
7.275 ± 0.042 ± 0.054	45k	¹ AMBROSINO 06F	KLOE	

¹ Fully inclusive. Taking $B(K_L^0 \rightarrow \pi \mu \nu)$ from KLOE, AMBROSINO 06, $B(K_L^0 \rightarrow \pi^+ \pi^- + \pi^+ \pi^- \gamma \text{ (DE)}) = (1.963 \pm 0.012 \pm 0.017) \times 10^{-3}$ is obtained.

$\Gamma(\pi^+ \pi^-)/[\Gamma(\pi^\pm e^\mp \nu_e) + \Gamma(\pi^\pm \mu^\mp \nu_\mu)]$ $\Gamma_8/(\Gamma_1 + \Gamma_2)$

Violates CP conservation.

VALUE (units 10 ⁻³)	EVTS	DOCUMENT ID	TECN	COMMENT
2.909 ± 0.013 OUR FIT				Error includes scale factor of 1.3.
• • • We do not use the following data for averages, fits, limits, etc. • • •				
3.13 ± 0.14	1687	COUPAL	85	SPEC $\eta_{+-} = 2.28 \pm 0.06$
3.04 ± 0.14	2703	DEVOE	77	SPEC $\eta_{+-} = 2.25 \pm 0.05$
2.51 ± 0.23	309	¹ DEBOUARD	67	OSPK $\eta_{+-} = 2.00 \pm 0.09$
2.35 ± 0.19	525	¹ FITCH	67	OSPK $\eta_{+-} = 1.94 \pm 0.08$

¹ Old experiments excluded from fit. See subsection on η_{+-} in section on "PARAMETERS FOR $K_L^0 \rightarrow 2\pi$ DECAY" below for average η_{+-} of these experiments and for note on discrepancy.

$\Gamma(\pi^\pm e^\mp \nu_e)/\Gamma(2 \text{ tracks})$ $\Gamma_1/(\Gamma_1 + \Gamma_2 + 0.03508\Gamma_6 + \Gamma_7 + \Gamma_8)$

$\Gamma(2 \text{ tracks}) = \Gamma(\pi^\pm e^\mp \nu_e) + \Gamma(\pi^\pm \mu^\mp \nu_\mu) + 0.03508 \Gamma(3\pi^0) + \Gamma(\pi^+ \pi^- \pi^0) + \Gamma(\pi^+ \pi^-)$ where 0.03508 is the fraction of $3\pi^0$ events with one Dalitz decay ($\pi^0 \rightarrow \gamma e^+ e^-$).

VALUE	EVTS	DOCUMENT ID	TECN	COMMENT
0.5006 ± 0.0009 OUR FIT				Error includes scale factor of 1.3.
0.4978 ± 0.0035	6.8M	LAI	04B	NA48

$\Gamma(\pi^+ \pi^-)/[\Gamma(\pi^\pm e^\mp \nu_e) + \Gamma(\pi^\pm \mu^\mp \nu_\mu) + \Gamma(\pi^+ \pi^- \pi^0)]$ $\Gamma_8/(\Gamma_1 + \Gamma_2 + \Gamma_7)$

Violates CP conservation.

VALUE (units 10 ⁻³)	EVTS	DOCUMENT ID	TECN	COMMENT
2.454 ± 0.011 OUR FIT				Error includes scale factor of 1.3.
• • • We do not use the following data for averages, fits, limits, etc. • • •				
2.60 ± 0.07	4200	¹ MESSNER	73	ASPK $\eta_{+-} = 2.23 \pm 0.05$

¹ From same data as $\Gamma(\pi^+ \pi^-)/\Gamma(\pi^+ \pi^- \pi^0)$ MESSNER 73, but with different normalization.

$\Gamma(\pi^+ \pi^-)/\Gamma(\pi^+ \pi^- \pi^0)$ Γ_8/Γ_7

Violates CP conservation.

VALUE (units 10 ⁻²)	EVTS	DOCUMENT ID	TECN	COMMENT
1.568 ± 0.010 OUR FIT				Error includes scale factor of 1.3.
• • • We do not use the following data for averages, fits, limits, etc. • • •				
1.64 ± 0.04	4200	MESSNER	73	ASPK $\eta_{+-} = 2.23$

$\Gamma(\pi^0 \pi^0)/\Gamma_{total}$ Γ_9/Γ

Violates CP conservation.

VALUE (units 10 ⁻³)	EVTS	DOCUMENT ID	TECN	COMMENT
0.864 ± 0.006 OUR FIT				Error includes scale factor of 1.8.
0.865 ± 0.012		¹ ALEXOPOU... 04	KTEV	

¹ For correlations with other ALEXOPOULOS 04 measurements, see the footnote with their $B(K_L \rightarrow \pi e \nu)$ measurement.

$\Gamma(\pi^0 \pi^0)/\Gamma(\pi^+ \pi^-)$ Γ_9/Γ_8

Violates CP conservation.

VALUE	EVTS	DOCUMENT ID	TECN	COMMENT
0.4395 ± 0.0023 OUR FIT				Error includes scale factor of 2.0.
0.4390 ± 0.0012		ETAFIT	16	

$\Gamma(\pi^0 \pi^0)/\Gamma(3\pi^0)$ Γ_9/Γ_6

Violates CP conservation.

VALUE (units 10 ⁻²)	EVTS	DOCUMENT ID	TECN	COMMENT
0.443 ± 0.004 OUR FIT				Error includes scale factor of 2.1.
• • • We use the following data for averages but not for fits. • • •				
0.4446 ± 0.0016 ± 0.0019	100k	¹ ALEXOPOU... 04	KTEV	Not in fit

• • • We do not use the following data for averages, fits, limits, etc. • • •

0.37 ± 0.08	29	BARMIN	70	HLBC $\eta_{00} = 2.02 \pm 0.23$
0.32 ± 0.15	30	BUDAGOV	70	HLBC $\eta_{00} = 1.9 \pm 0.5$
0.46 ± 0.11	57	BANNER	69	OSPK $\eta_{00} = 2.2 \pm 0.3$

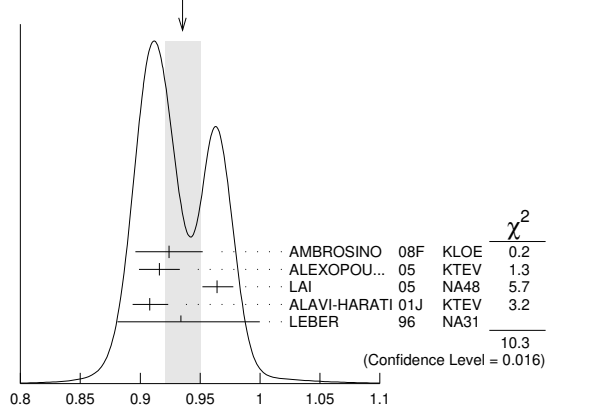
¹ This measurement enters the fit via their separate measurements for the two modes.

———— Semileptonic modes with photons ————

$\Gamma(\pi^\pm e^\mp \nu_e \gamma)/\Gamma(\pi^\pm e^\mp \nu_e)$ Γ_{10}/Γ_1

VALUE (units 10 ⁻²)	EVTS	DOCUMENT ID	TECN	COMMENT
0.935 ± 0.015 OUR AVERAGE				Error includes scale factor of 1.9. See the ideogram below.
0.924 ± 0.023 ± 0.016	9k	¹ AMBROSINO 08F	KLOE	$E_\gamma^* > 30 \text{ MeV}$, $\theta_{e\gamma}^* > 20^\circ$
0.916 ± 0.017	4309	² ALEXOPOU... 05	KTEV	$E_\gamma^* > 30 \text{ MeV}$, $\theta_{e\gamma}^* > 20^\circ$
0.964 ± 0.008 ± 0.011	19k	LAI	05	NA48 $E_\gamma^* > 30 \text{ MeV}$, $\theta_{e\gamma}^* > 20^\circ$
0.908 ± 0.008 ± 0.013	15k	ALAVI-HARATI 01J	KTEV	$E_\gamma^* \geq 30 \text{ MeV}$, $\theta_{e\gamma}^* \geq 20^\circ$
0.934 ± 0.036 ± 0.055	1384	LEBER	96	NA31 $E_\gamma^* \geq 30 \text{ MeV}$, $\theta_{e\gamma}^* \geq 20^\circ$

WEIGHTED AVERAGE
0.935 ± 0.015 (Error scaled by 1.9)



¹ Direct emission contribution measured $\langle X \rangle = -2.3 \pm 1.3 \pm 1.4$.

Meson Particle Listings

K_L^0

² Also measured cut $E_\gamma^* > 10$ MeV, $\theta_{e\gamma}^* > 0^\circ$ 14221 evts: $\Gamma(\pi^\pm e^\mp \nu_e \gamma) / \Gamma(\pi^\pm e^\mp \nu_e) = (4.942 \pm 0.062)\%$.

$\Gamma(\pi^\pm \mu^\mp \nu_\mu \gamma) / \Gamma(\pi^\pm \mu^\mp \nu_\mu)$ Γ_{11}/Γ_2

VALUE (units 10^{-3})	CL%	EVTS	DOCUMENT ID	TECN	COMMENT
2.09 ± 0.08 OUR AVERAGE					
2.09 ± 0.09			¹ ALEXOPOU... 05	KTEV	$E_\gamma^* > 30$ MeV
2.08 ± 0.17 ^{+0.16} _{-0.21}		252	BENDER 98	NA48	$E_\gamma^* \geq 30$ MeV

¹ Also measured cut $E_\gamma^* > 10$ MeV, 1385 evts: $\Gamma(\pi^\pm \mu^\mp \nu_\mu \gamma) / \Gamma(\pi^\pm \mu^\mp \nu_\mu) = (0.530 \pm 0.014 \pm 0.012)\%$.

Hadronic modes with photons or $\ell\bar{\ell}$ pairs

$\Gamma(\pi^0 \pi^0 \gamma) / \Gamma_{total}$ Γ_{12}/Γ

VALUE (units 10^{-6})	CL%	DOCUMENT ID	TECN	COMMENT
< 0.243	90	ABOUZAID 08b	KTEV	$K_L^0 \rightarrow \pi^0 \pi_D^0 \gamma, \pi_D^0 \rightarrow e e \gamma$
••• We do not use the following data for averages, fits, limits, etc. •••				
< 5.6	90	BARR 94	NA31	
< 230	90	ROBERTS 94	E799	

$\Gamma(\pi^+ \pi^- \gamma) / \Gamma(\pi^+ \pi^- \pi^0)$ Γ_{13}/Γ_7

For earlier limits see our 1992 edition Physical Review **D45** S1 (1992).

VALUE (units 10^{-4})	EVTS	DOCUMENT ID	TECN	COMMENT
••• We do not use the following data for averages, fits, limits, etc. •••				
1.23 ± 0.13	516	^{1,2} CARROLL 80b	SPEC	$E_\gamma^* > 20$ MeV
2.33 ± 0.23	546	^{1,3} CARROLL 80b	SPEC	
3.56 ± 0.26	1062	^{1,4} CARROLL 80b	SPEC	$E_\gamma^* > 20$ MeV

¹ CARROLL 80b quotes $B(\pi^+ \pi^- \gamma)$ using normalization $B(\pi^+ \pi^- \pi^0) = 0.1239$. We divide by this value to obtain their measured $\Gamma(\pi^+ \pi^- \gamma) / \Gamma(\pi^+ \pi^- \pi^0)$.
² Internal Bremsstrahlung component only.
³ Direct γ emission component only.
⁴ Both IB and DE components.

$\Gamma(\pi^+ \pi^- \gamma) / \Gamma(\pi^+ \pi^-)$ Γ_{13}/Γ_8

VALUE (units 10^{-2})	EVTS	DOCUMENT ID	TECN	COMMENT
2.11 ± 0.08 OUR FIT				Error includes scale factor of 2.9.
2.11 ± 0.08 OUR AVERAGE				Error includes scale factor of 2.9.
2.08 ± 0.02 ± 0.02	8669	¹ ALAVI-HARATI 01b	KTEV	$E_\gamma^* > 20$ MeV
2.30 ± 0.07	3136	RAMBERG 93	E731	$E_\gamma^* > 20$ MeV

¹ ALAVI-HARATI 01b includes both Direct Emission (DE) and Inner Bremsstrahlung (IB) processes.

$\Gamma(\pi^+ \pi^- \gamma (DE)) / \Gamma(\pi^+ \pi^-)$ Γ_{14}/Γ_{13}

These values assume that $\Gamma(K_L^0 \rightarrow \pi^+ \pi^- \gamma) = \Gamma(K_L^0 \rightarrow \pi^+ \pi^- \gamma (DE)) + \Gamma(K_L^0 \rightarrow \pi^+ \pi^- \gamma (IB))$, the sum of widths for the direct emission (DE) and inner bremsstrahlung (IB) processes, with no IB-DE interference. DE assumes a form factor as described in RAMBERG 93.

VALUE	EVTS	DOCUMENT ID	TECN	COMMENT
0.684 ± 0.009 OUR FIT				
0.684 ± 0.009 OUR AVERAGE				
0.689 ± 0.021	111k	ABOUZAID 06a	KTEV	$E_\gamma^* > 20$ MeV
0.683 ± 0.011	8669	ALAVI-HARATI 01b	KTEV	$E_\gamma^* > 20$ MeV
0.685 ± 0.041	3136	RAMBERG 93	E731	$E_\gamma^* > 20$ MeV

$\Gamma(\pi^0 2\gamma) / \Gamma_{total}$ Γ_{15}/Γ

VALUE (units 10^{-6})	CL%	EVTS	DOCUMENT ID	TECN	COMMENT
1.273 ± 0.033 OUR AVERAGE					
1.28 ± 0.06 ± 0.01	1.4k		¹ ABOUZAID 08	KTEV	
1.27 ± 0.04 ± 0.01	2.5k		² LAI 02b	NA48	
••• We do not use the following data for averages, fits, limits, etc. •••					
1.68 ± 0.07 ± 0.08		884	³ ALAVI-HARATI 99b	KTEV	
1.7 ± 0.2 ± 0.2		63	⁴ BARR 92	NA31	
1.86 ± 0.60 ± 0.60		60	PAPADIMITR...91	E731	$m_{\gamma\gamma} > 280$ MeV
< 5.1		90	PAPADIMITR...91	E731	$m_{\gamma\gamma} < 264$ MeV
2.1 ± 0.6		14	⁵ BARR 90c	NA31	$m_{\gamma\gamma} > 280$ MeV

¹ ABOUZAID 08 reports $(1.29 \pm 0.03 \pm 0.05) \times 10^{-6}$ from a measurement of $[\Gamma(K_L^0 \rightarrow \pi^0 2\gamma) / \Gamma_{total}] / [B(K_L^0 \rightarrow \pi^0 \pi^0)]$ assuming $B(K_L^0 \rightarrow \pi^0 \pi^0) = (8.69 \pm 0.04) \times 10^{-4}$, which we rescale to our best value $B(K_L^0 \rightarrow \pi^0 \pi^0) = (8.64 \pm 0.06) \times 10^{-4}$. Our first error is their experiment's error and our second error is the systematic error from using our best value.
² LAI 02b reports $[\Gamma(K_L^0 \rightarrow \pi^0 2\gamma) / \Gamma_{total}] / [B(K_L^0 \rightarrow \pi^0 \pi^0)] = (1.467 \pm 0.032 \pm 0.032) \times 10^{-3}$ which we multiply by our best value $B(K_L^0 \rightarrow \pi^0 \pi^0) = (8.64 \pm 0.06) \times 10^{-4}$. Our first error is their experiment's error and our second error is the systematic error from using our best value. They also find that $B(\pi^0 2\gamma, m_{\gamma\gamma} < 110$ MeV) $< 0.6 \times 10^{-8}$ (90% CL).
³ ALAVI-HARATI 99b finds that $\Gamma(\pi^0 2\gamma, m_{\gamma\gamma} < 240$ MeV) / $\Gamma(\pi^0 2\gamma) = (17.3 \pm 1.3 \pm 1.5)\%$. Superseded by ABOUZAID 08.
⁴ BARR 92 find that $\Gamma(\pi^0 2\gamma, m_{\gamma\gamma} < 240$ MeV) / $\Gamma(\pi^0 2\gamma) < 0.09$ (90% CL).
⁵ BARR 90c superseded by BARR 92.

$\Gamma(\pi^0 \gamma e^+ e^-) / \Gamma_{total}$ Γ_{16}/Γ

VALUE (units 10^{-8})	CL%	EVTS	DOCUMENT ID	TECN
1.62 ± 0.14 ± 0.09		125	¹ ABOUZAID 07d	KTEV
••• We do not use the following data for averages, fits, limits, etc. •••				
2.34 ± 0.35 ± 0.13		44	ALAVI-HARATI 01e	KTEV
< 71		90	MURAKAMI 99	SPEC

¹ ABOUZAID 07d includes 1997 (ALAVI-HARATI 01e) and 1999 data. It measures the ratio of $B(K_L^0 \rightarrow \pi^0 \gamma e^+ e^-) / B(K_L^0 \rightarrow \pi^0 \pi_D^0)$, where π_D^0 is the Dalitz decaying π^0 , and uses PDG 06 values $B(K_L^0 \rightarrow \pi^0 \pi^0) = (8.69 \pm 0.04) \times 10^{-4}$, and $B(\pi_D^0 \rightarrow e^+ e^- \gamma) = (1.198 \pm 0.032) \times 10^{-2}$. Supersedes ALAVI-HARATI 01e result.

Other modes with photons or $\ell\bar{\ell}$ pairs

$\Gamma(2\gamma) / \Gamma_{total}$ Γ_{17}/Γ

VALUE (units 10^{-4})	EVTS	DOCUMENT ID	TECN	COMMENT
5.47 ± 0.04 OUR FIT				Error includes scale factor of 1.1.
••• We do not use the following data for averages, fits, limits, etc. •••				
4.54 ± 0.84		¹ BANNER 72b	OSPK	
4.5 ± 1.0	23	ENSTROM 71	OSPK	K_L^0 1.5-9 GeV/c
5.0 ± 1.0		² REPELLIN 71	OSPK	
5.5 ± 1.1	90	KUNZ 68	OSPK	Norm.to 3 $\pi(C+N)$

¹ This value uses $(\eta_{00}/\eta_{+-})^2 = 1.05 \pm 0.14$. In general, $\Gamma(2\gamma) / \Gamma_{total} = [(4.32 \pm 0.55) \times 10^{-4}] [(\eta_{00}/\eta_{+-})^2]$.
² Assumes regeneration amplitude in copper at 2 GeV is 22 mb. To evaluate for a given regeneration amplitude and error, multiply by (regeneration amplitude/22mb)².

$\Gamma(2\gamma) / \Gamma(3\pi^0)$ Γ_{17}/Γ_6

VALUE (units 10^{-3})	EVTS	DOCUMENT ID	TECN	COMMENT
2.802 ± 0.017 OUR FIT				
2.802 ± 0.018 OUR AVERAGE				
2.79 ± 0.02 ± 0.02	27k	ADINOLFI 03	KLOE	
2.81 ± 0.01 ± 0.02		LAI 03	NA48	
••• We do not use the following data for averages, fits, limits, etc. •••				
2.13 ± 0.43	28	BARMIN 71	HLBC	
2.24 ± 0.28	115	BANNER 69	OSPK	
2.5 ± 0.7	16	ARNOLD 68b	HLBC	Vacuum decay

$\Gamma(2\gamma) / \Gamma(\pi^0 \pi^0)$ Γ_{17}/Γ_9

VALUE	EVTS	DOCUMENT ID	TECN
0.633 ± 0.006 OUR FIT			Error includes scale factor of 1.4.
0.632 ± 0.004 ± 0.008	110k	BURKHARDT 87	NA31

$\Gamma(3\gamma) / \Gamma_{total}$ Γ_{18}/Γ

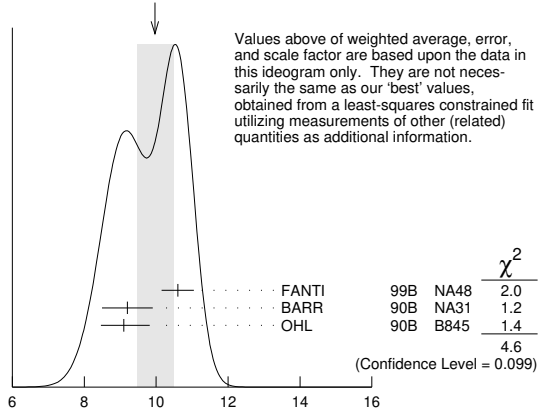
VALUE	CL%	DOCUMENT ID	TECN
< 7.4 × 10⁻⁸	90	¹ TUNG 11	K391
••• We do not use the following data for averages, fits, limits, etc. •••			
< 2.4 × 10 ⁻⁷	90	² BARR 95c	NA31

¹ TUNG 11 reports the result assuming parity violating interaction and using 2005 data (Run-II and III). Assuming parity conserving or phase space interaction, the 90% upper limits obtained are 7.5×10^{-8} and 8.6×10^{-8} , respectively.
² Assumes a phase-space decay distribution.

$\Gamma(e^+ e^- \gamma) / \Gamma_{total}$ Γ_{19}/Γ

VALUE (units 10^{-6})	EVTS	DOCUMENT ID	TECN
9.4 ± 0.4 OUR FIT			Error includes scale factor of 2.0.
10.0 ± 0.5 OUR AVERAGE			Error includes scale factor of 1.5. See the ideogram below.
10.6 ± 0.2 ± 0.4	6864	¹ FANTI 99b	NA48
9.2 ± 0.5 ± 0.5	1053	BARR 90b	NA31
9.1 ± 0.4 ^{+0.6} _{-0.5}	919	OHL 90b	B845

WEIGHTED AVERAGE
10.0 ± 0.5 (Error scaled by 1.5)



¹ For FANTI 99b, the ± 0.4 systematic error includes for uncertainties in the calculation, primarily uncertainties in the $\pi^0 \rightarrow e^+ e^- \gamma$ and $K_L^0 \rightarrow \pi^0 \pi^0$ branching ratios, evaluated using our 1999 Web edition values.

$\Gamma(e^+e^- \gamma)/\Gamma(3\pi^0)$ Γ_{19}/Γ_6

VALUE (units 10^{-5})	EVTS	DOCUMENT ID	TECN
4.82 ± 0.21 OUR FIT			Error includes scale factor of 2.0.
4.63 ± 0.04 ± 0.13	83k	¹ ABOUZAID	07B KTEV

¹ABOUZAID 07B reports $[\Gamma(K_L^0 \rightarrow e^+e^-\gamma)/\Gamma(K_L^0 \rightarrow 3\pi^0)] / [3\Gamma(\pi^0 \rightarrow 2\gamma)/\Gamma_{\text{total}} \times \Gamma(\pi^0 \rightarrow e^+e^-\gamma)/\Gamma_{\text{total}}] = (1.3302 \pm 0.0046 \pm 0.0103) \times 10^{-3}$ which we multiply by our best value $3\Gamma(\pi^0 \rightarrow 2\gamma)/\Gamma_{\text{total}} \times \Gamma(\pi^0 \rightarrow e^+e^-\gamma)/\Gamma_{\text{total}} = 0.0348 \pm 0.0010$. Our first error is their experiment's error and our second error is the systematic error from using our best value.

$\Gamma(\mu^+ \mu^- \gamma)/\Gamma_{\text{total}}$ Γ_{20}/Γ

VALUE (units 10^{-7})	EVTS	DOCUMENT ID	TECN
3.59 ± 0.11 OUR AVERAGE			Error includes scale factor of 1.3.
3.62 ± 0.04 ± 0.08	9100	ALAVI-HARATI01G	KTEV
3.4 ± 0.6 ± 0.4	45	FANTI	97 NA48
3.23 ± 0.23 ± 0.19	197	SPENCER	95 E799

$\Gamma(\mu^+ \mu^- \mu^+ \mu^-)/\Gamma_{\text{total}}$ Γ_{21}/Γ

VALUE	CL%	DOCUMENT ID	TECN
< 2.3 × 10⁻⁹	90	¹ AALIJ	23AE LHCB

¹AALIJ 23AE uses 5.1 fb⁻¹ of LHCb data recorded from 2016 to 2018.

$\Gamma(e^+e^- \gamma \gamma)/\Gamma_{\text{total}}$ Γ_{22}/Γ

VALUE (units 10^{-7})	EVTS	DOCUMENT ID	TECN	COMMENT
5.95 ± 0.33 OUR AVERAGE				
5.84 ± 0.15 ± 0.32	1543	ALAVI-HARATI01F	KTEV	$E_\gamma^* > 5$ MeV
8.0 ± 1.5 ^{+1.4} / _{-1.2}	40	SETZU	98 NA31	$E_\gamma^* > 5$ MeV
6.5 ± 1.2 ± 0.6	58	NAKAYA	94 E799	$E_\gamma^* > 5$ MeV
6.6 ± 3.2		MORSE	92 B845	$E_\gamma^* > 5$ MeV

$\Gamma(\mu^+ \mu^- \gamma \gamma)/\Gamma_{\text{total}}$ Γ_{23}/Γ

VALUE (units 10^{-9})	EVTS	DOCUMENT ID	TECN	COMMENT
10.4 ^{+7.5}/_{-5.9} ± 0.7	4	ALAVI-HARATI00E	KTEV	$m_{\gamma\gamma} \geq 1$ MeV/c ²

Charge conjugation × Parity (CP) or Lepton Family number (LF) violating modes, or $\Delta S = 1$ weak neutral current (S1) modes

$\Gamma(\mu^+ \mu^-)/\Gamma(\pi^+ \pi^-)$ Γ_{24}/Γ_8

Test for $\Delta S = 1$ weak neutral current. Allowed by higher-order electroweak interaction.

VALUE (units 10^{-6})	EVTS	DOCUMENT ID	TECN	COMMENT
3.48 ± 0.05 OUR AVERAGE				
3.474 ± 0.057	6210	AMBROSE	00 B871	
3.87 ± 0.30	179	¹ AKAGI	95 SPEC	
3.38 ± 0.17	707	HEINSON	95 B791	

••• We do not use the following data for averages, fits, limits, etc. •••

3.9 ± 0.3 ± 0.1	178	² AKAGI	91B SPEC	ln AKAGI 95
3.45 ± 0.18 ± 0.13	368	³ HEINSON	91 SPEC	ln HEINSON 95
4.1 ± 0.5	54	INAGAKI	89 SPEC	ln AKAGI 91B
2.8 ± 0.3 ± 0.2	87	MATHIAZIAH...	89B SPEC	ln HEINSON 91

¹AKAGI 95 gives this number multiplied by the PDG 1992 average for $\Gamma(K_L^0 \rightarrow \pi^+ \pi^-)/\Gamma_{\text{total}}$.
²AKAGI 91B give this number multiplied by the 1990 PDG average for $\Gamma(K_L^0 \rightarrow \pi^+ \pi^-)/\Gamma_{\text{total}}$.
³HEINSON 91 give $\Gamma(K_L^0 \rightarrow \mu\mu)/\Gamma_{\text{total}}$. We divide out the $\Gamma(K_L^0 \rightarrow \pi^+ \pi^-)/\Gamma_{\text{total}}$ PDG average which they used.

$\Gamma(e^+e^-)/\Gamma_{\text{total}}$ Γ_{25}/Γ

Test for $\Delta S = 1$ weak neutral current. Allowed by higher-order electroweak interaction.

VALUE (units 10^{-10})	CL%	EVTS	DOCUMENT ID	TECN
0.087 ^{+0.057}/_{-0.041}		4	AMBROSE	98 B871

••• We do not use the following data for averages, fits, limits, etc. •••

< 1.6	90	1	AKAGI	95 SPEC
< 0.41	90	0	¹ ARISAKA	93B B791

¹ARISAKA 93B includes all events with < 6 MeV radiated energy.

$\Gamma(\pi^+ \pi^- e^+ e^-)/\Gamma_{\text{total}}$ Γ_{26}/Γ

Test for $\Delta S = 1$ weak neutral current. Allowed by higher-order electroweak interaction.

VALUE (units 10^{-7})	CL%	EVTS	DOCUMENT ID	TECN	COMMENT
3.11 ± 0.19 OUR AVERAGE					
3.08 ± 0.09 ± 0.18	1125	¹ LAI	03c NA48		
3.2 ± 0.6 ± 0.4	37	ADAMS	98 KTEV		
4.4 ± 1.3 ± 0.5	13	TAKEUCHI	98 SPEC		

••• We do not use the following data for averages, fits, limits, etc. •••

< 4.6	90		NOMURA	97 SPEC	$m_{ee} > 4$ MeV
-------	----	--	--------	---------	------------------

¹LAI 03c second error is 0.15(syst) ± 0.10(norm) combined in quadrature. The normalization uses $BR(K_L \rightarrow \pi^+ \pi^- \pi^0) * BR(\pi^0 \rightarrow e^+ e^-) = (1.505 \pm 0.047) \times 10^{-3}$ from our 2000 Edition.

$\Gamma(\pi^0 \pi^0 e^+ e^-)/\Gamma_{\text{total}}$ Γ_{27}/Γ

Test for $\Delta S = 1$ weak neutral current. Allowed by higher-order electroweak interaction.

VALUE (units 10^{-9})	CL%	EVTS	DOCUMENT ID	TECN
< 6.6	90	1	ALAVI-HARATI02C	E799

$\Gamma(\pi^0 \pi^0 \mu^+ \mu^-)/\Gamma_{\text{total}}$ Γ_{28}/Γ

Test for $\Delta S = 1$ weak neutral current. Allowed by higher-order electroweak interaction.

VALUE	CL%	DOCUMENT ID	TECN
< 9.2 × 10⁻¹¹	90	¹ ABOUZAID	11A E799

¹ABOUZAID 11A also reports $B(K_L^0 \rightarrow \pi^0 \pi^0 X^0 \rightarrow \pi^0 \pi^0 \mu^+ \mu^-) < 1.0 \times 10^{-10}$ at 90% C.L., where the X^0 is a possible new neutral boson that was reported by PARK 05 with a mass of 214.3 ± 0.5 MeV/c².

$\Gamma(\mu^+ \mu^- e^+ e^-)/\Gamma_{\text{total}}$ Γ_{29}/Γ

Test for $\Delta S = 1$ weak neutral current. Allowed by higher-order electroweak interaction.

VALUE (units 10^{-9})	CL%	EVTS	DOCUMENT ID	TECN	COMMENT
2.69 ± 0.27 OUR AVERAGE					
2.69 ± 0.24 ± 0.12		131	¹ ALAVI-HARATI03B	KTEV	
2.9 ^{+6.7} / _{-2.4}		1	GU	96 E799	

••• We do not use the following data for averages, fits, limits, etc. •••

2.62 ± 0.40 ± 0.17		43	ALAVI-HARATI01H	KTEV	Sup. by ALAVI-HARATI 03B
--------------------	--	----	-----------------	------	--------------------------

< 4900 90 BALATS 83 SPEC
¹ALAVI-HARATI 03B also measures the linear slope $\alpha = -1.59 \pm 0.37$.

$\Gamma(e^+e^- e^+e^-)/\Gamma_{\text{total}}$ Γ_{30}/Γ

Test for $\Delta S = 1$ weak neutral current. Allowed by higher-order electroweak interaction.

VALUE (units 10^{-8})	EVTS	DOCUMENT ID	TECN	COMMENT
3.56 ± 0.21 OUR AVERAGE				
3.30 ± 0.24 ± 0.25	200	¹ LAI	05B NA48	
3.72 ± 0.18 ± 0.23	441	ALAVI-HARATI01D	KTEV	
3.96 ± 0.78 ± 0.32	27	GU	94 E799	
3.07 ± 1.25 ± 0.26	6	VAGINS	93 B845	

••• We do not use the following data for averages, fits, limits, etc. •••

6 ± 2 ± 1	18	² AKAGI	95 SPEC	$m_{ee} > 470$ MeV
7 ± 3 ± 2	6	² AKAGI	95 SPEC	$m_{ee} > 470$ MeV
10.4 ± 3.7 ± 1.1	8	³ BARR	95 NA31	
6 ± 2 ± 1	18	AKAGI	93 CNTR	Sup. by AKAGI 95
4 ± 3	2	BARR	91 NA31	Sup. by BARR 95

¹LAI 05B uses 1998 and 1999 data. Data are normalized to the observed events of $K_L^0 \rightarrow \pi^+ \pi^- \pi^0$ (π^0 into Dalitz pair) and PDG 04 values are used for $B(K_L^0 \rightarrow \pi^+ \pi^- \pi^0)$ and $B(\pi^0 \rightarrow e^+ e^- \gamma)$. The systematic error includes a normalization error of ± 0.10.
²Values are for the total branching fraction, acceptance-corrected for the m_{ee} cuts shown.
³Distribution of angles between two e^+e^- pair planes favors $CP = -1$ for K_L^0 .

$\Gamma(\pi^0 \mu^+ \mu^-)/\Gamma_{\text{total}}$ Γ_{31}/Γ

Violates CP in leading order. Test for $\Delta S = 1$ weak neutral current. Allowed by higher-order electroweak interaction.

VALUE (units 10^{-9})	CL%	EVTS	DOCUMENT ID	TECN
< 0.38	90		ALAVI-HARATI00D	KTEV

••• We do not use the following data for averages, fits, limits, etc. •••

< 5.1	90	0	HARRIS	93 E799
-------	----	---	--------	---------

$\Gamma(\pi^0 e^+ e^-)/\Gamma_{\text{total}}$ Γ_{32}/Γ

Violates CP in leading order. Direct and indirect CP-violating contributions are expected to be comparable and to dominate the CP-conserving part. LAI 02B result suggests that CP-violation effects dominate. Test for $\Delta S = 1$ weak neutral current. Allowed by higher-order electroweak interaction.

VALUE (units 10^{-10})	CL%	EVTS	DOCUMENT ID	TECN	COMMENT
< 2.8	90		¹ ALAVI-HARATI04A	KTEV	combined result

••• We do not use the following data for averages, fits, limits, etc. •••

< 3.5	90		ALAVI-HARATI04A	KTEV	
0.0047 ^{+0.0022} / _{-0.0018}			² LAI	02B NA48	CP-conserving part
< 5.1	90	2	ALAVI-HARATI01	KTEV	
< 0.01 to 0.02			ALAVI-HARATI99B	KTEV	CP-conserving part
< 43	90	0	HARRIS	93B E799	
< 75	90	0	BARKER	90 E731	
< 55	90	0	OHL	90 B845	
< 400	90		BARR	88 NA31	
< 3200	90		JASTRZEM...	88 SPEC	

¹Combined result of ALAVI-HARATI 04A 1999-2000 data set and ALAVI-HARATI 01 1997 data set.
²LAI 02B uses the absence of a signal in $K_L^0 \rightarrow \pi^0 \gamma \gamma$ with $m(\gamma\gamma) < m(\pi^0)$ and their a_V value to predict this value.

$\Gamma(\pi^0 \nu \bar{\nu})/\Gamma_{\text{total}}$ Γ_{33}/Γ

Violates CP in leading order. Test of direct CP violation since the indirect CP-violating and CP-conserving contributions are expected to be suppressed. Test of $\Delta S = 1$ weak neutral current.

VALUE (units 10^{-8})	CL%	DOCUMENT ID	TECN
< 0.49	90	¹ AHN	21 KOTO
< 0.30	90	² AHN	19 KOTO

Meson Particle Listings

K_L^0

• • • We do not use the following data for averages, fits, limits, etc. • • •

< 5.1	90	³ AHN	17	KOTO
< 2.6	90	⁴ AHN	10	K391
< 6.7	90	⁵ AHN	08	K391
< 21	90	⁶ AHN	06	K391
< 59	90	ALAVI-HARATI	00	KTEV

¹AHN 21 result is based on data collected in 2016, 2017 and 2018, which corresponds to 3.05×10^{19} protons on target. A single event sensitivity of $(7.20 \pm 0.05 \pm 0.66) \times 10^{-10}$ was achieved with 3 candidate events observed and total 1.22 ± 0.26 background events.

²AHN 19 result is based on data collected in 2015, which corresponds to 2.2×10^{19} protons on target. A single event sensitivity of $(1.30 \pm 0.01 \pm 0.14) \times 10^{-9}$ was achieved with no candidate events observed. An upper limit of $< 2.4 \times 10^{-9}$ at the 90% C.L. for the $K_L^0 \rightarrow \pi^0 X^0$ decay was also set, where X^0 is an invisible particle with a mass of 135 MeV/c².

³AHN 17 result is based on the first 100 hours of physics running in 2013. One candidate event was observed with an expected background of 0.34 ± 0.16 events. An upper limit of $< 3.7 \times 10^{-8}$ at the 90% C.L. for the $K_L^0 \rightarrow \pi^0 X^0$ decay was also set, where X^0 is an invisible particle with a mass of 135 MeV/c².

⁴Obtained combining Run-2 (AHN 08) and Run-3 data.

⁵Value obtained using data from February to April 2005.

⁶Value obtained analyzing 10% of data of RUN 1 (performed in 2004).

$\Gamma(\pi^0 \pi^0 \nu \bar{\nu})/\Gamma_{\text{total}}$ Γ₃₄/Γ

VALUE	CL%	DOCUMENT ID	TECN
< 8.1 × 10⁻⁷	90	¹ OGATA	11 K391

• • • We do not use the following data for averages, fits, limits, etc. • • •

< 4.7 × 10 ⁻⁵	90	² NIX	07 K391
--------------------------	----	------------------	---------

¹Using 2005 Run-1 data. OGATA 11 also sets a limit on the $K_L^0 \rightarrow \pi^0 \pi^0 X \rightarrow$ invisible particles process: the limit on the branching fraction varied from 7.0×10^{-7} to 4.0×10^{-5} for the mass of X ranging from 50 to 200 MeV/c².

²Observed 1 event with expected background of 0.43 ± 0.35 events. NIX 07 also measured $B(K_L^0 \rightarrow \pi^0 \pi^0 P) < 1.2 \times 10^{-6}$ at 90% CL, where P is the pseudoscalar particle and $m_P < 100$ MeV.

$\Gamma(e^\pm \mu^\mp)/\Gamma_{\text{total}}$ Γ₃₅/Γ

Test of lepton family number conservation.

VALUE (units 10 ⁻¹¹)	CL%	EVTS	DOCUMENT ID	TECN
< 0.47	90	0	AMBROSE	98B B871

• • • We do not use the following data for averages, fits, limits, etc. • • •

< 9.4	90	0	AKAGI	95 SPEC
< 3.9	90	0	ARISAKA	93 B791
< 3.3	90	0	¹ ARISAKA	93 B791

¹This is the combined result of ARISAKA 93 and MATHIAZHAGAN 89.

$\Gamma(e^\pm e^\pm \mu^\mp \mu^\mp)/\Gamma_{\text{total}}$ Γ₃₆/Γ

Test of lepton family number conservation.

VALUE (units 10 ⁻¹¹)	CL%	EVTS	DOCUMENT ID	TECN	COMMENT
< 4.12	90	0	ALAVI-HARATI	03B	KTEV

• • • We do not use the following data for averages, fits, limits, etc. • • •

< 12.3	90	0	¹ ALAVI-HARATI	01H	KTEV	Sup. by ALAVI-HARATI 03B
< 61.0	90	0	¹ GU	96	E799	

¹Assuming uniform phase space distribution.

$\Gamma(\pi^0 \mu^\pm e^\mp)/\Gamma_{\text{total}}$ Γ₃₇/Γ

Test of lepton family number conservation.

VALUE (units 10 ⁻¹⁰)	CL%	DOCUMENT ID	TECN
< 0.76	90	ABOUZAID	08c KTEV

• • • We do not use the following data for averages, fits, limits, etc. • • •

< 62	90	ARISAKA	98 E799
------	----	---------	---------

$\Gamma(\pi^0 \pi^0 \mu^\pm e^\mp)/\Gamma_{\text{total}}$ Γ₃₈/Γ

Test of lepton family number conservation.

VALUE (units 10 ⁻¹⁰)	CL%	DOCUMENT ID	TECN
< 1.7	90	ABOUZAID	08c KTEV

Lorentz invariance violating modes

$\Gamma(\pi^0 \gamma)/\Gamma_{\text{total}}$ Γ₃₉/Γ

VALUE	CL%	DOCUMENT ID	TECN
< 1.7 × 10⁻⁷	90	¹ SHIMIZU	20 KOTO

¹SHIMIZU 20 uses data collected from 2016 to 2018 at the J-PARC KOTO experiment. The single event sensitivity is $(7.1 \pm 0.3 \pm 1.6) \times 10^{-8}$. No candidate event was observed.

See the related review(s):

V_{ud}, V_{us} the Cabibbo Angle, and CKM Unitarity

ENERGY DEPENDENCE OF K_L^0 DALITZ PLOT

For discussion, see note on Dalitz plot parameters in the K^\pm section of the Particle Listings above. For definitions of $a_V, a_T, a_U,$ and $a_Y,$ see the earlier version of the same note in the 1982 edition of this Review published in Physics Letters **111B** 70 (1982).

$$|\text{matrix element}|^2 = 1 + gu + hu^2 + jv + kv^2 + iuv$$

$$\text{where } u = (s_3 - s_0) / m_\pi^2 \text{ and } v = (s_2 - s_1) / m_\pi^2$$

LINEAR COEFFICIENT g FOR $K_L^0 \rightarrow \pi^+ \pi^- \pi^0$

VALUE	EVTS	DOCUMENT ID	TECN	COMMENT
0.678 ± 0.008 OUR AVERAGE				Error includes scale factor of 1.5. See the ideogram below.

0.6823 ± 0.0044 ± 0.0044	500k	ANGELOPO...	98c	CPLR
0.681 ± 0.024	6499	CHO	77	HBC
0.620 ± 0.023	4709	PEACH	77	HBC
0.677 ± 0.010	509k	MESSNER	74	ASPK $a_Y = -0.917 \pm 0.013$

• • • We do not use the following data for averages, fits, limits, etc. • • •

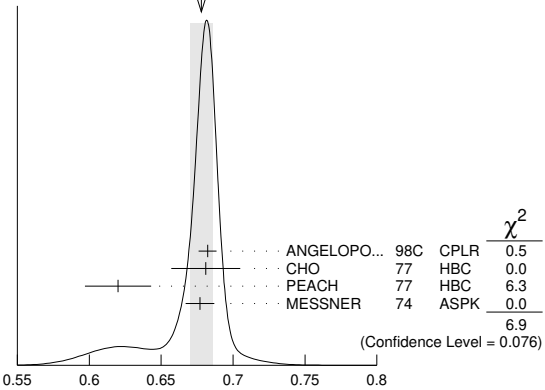
0.69 ± 0.07	192	¹ BALDO...	75	HLBC
0.590 ± 0.022	56k	¹ BUCHANAN	75	SPEC $a_U = -0.277 \pm 0.010$
0.619 ± 0.027	20k	^{1,2} BISI	74	ASPK $a_T = -0.282 \pm 0.011$
0.612 ± 0.032		¹ ALEXANDER	73B	HBC
0.73 ± 0.04	3200	¹ BRANDEN...	73	HBC
0.608 ± 0.043	1486	¹ KRENZ	72	HLBC $a_T = -0.277 \pm 0.018$
0.650 ± 0.012	29k	¹ ALBROW	70	ASPK $a_Y = -0.858 \pm 0.015$
0.593 ± 0.022	36k	^{1,3} BUCHANAN	70	SPEC $a_U = -0.278 \pm 0.010$
0.664 ± 0.056	4400	¹ SMITH	70	OSPK $a_T = -0.306 \pm 0.024$
0.400 ± 0.045	2446	¹ BASILE	68B	OSPK $a_T = -0.188 \pm 0.020$
0.649 ± 0.044	1350	¹ HOPKINS	67	HBC $a_T = -0.294 \pm 0.018$
0.428 ± 0.055	1198	¹ NEFKENS	67	OSPK $a_U = -0.204 \pm 0.025$

¹Quadratic dependence required by some experiments. (See sections on "QUADRATIC COEFFICIENT h " and "QUADRATIC COEFFICIENT k " below.) Correlations prevent us from averaging results of fits not including $g, h,$ and k terms.

²BISI 74 value comes from quadratic fit with quad. term consistent with zero. g error is thus larger than if linear fit were used.

³BUCHANAN 70 result revised by BUCHANAN 75 to include radiative correlations and to use more reliable K_L^0 momentum spectrum of second experiment (had same beam).

WEIGHTED AVERAGE
0.678±0.008 (Error scaled by 1.5)



Linear coeff. g for $K_L^0 \rightarrow \pi^+ \pi^- \pi^0$ matrix element squared

QUADRATIC COEFFICIENT h FOR $K_L^0 \rightarrow \pi^+ \pi^- \pi^0$

See notes in section "LINEAR COEFFICIENT g FOR $K_L^0 \rightarrow \pi^+ \pi^- \pi^0$ [MATRIX ELEMENT]²" above.

VALUE	EVTS	DOCUMENT ID	TECN
0.076 ± 0.006 OUR AVERAGE			

0.061 ± 0.004 ± 0.015	500k	ANGELOPO...	98c CPLR
0.095 ± 0.032	6499	CHO	77 HBC
0.048 ± 0.036	4709	PEACH	77 HBC
0.079 ± 0.007	509k	MESSNER	74 ASPK

• • • We do not use the following data for averages, fits, limits, etc. • • •

-0.011 ± 0.018	29k	¹ ALBROW	70 ASPK
0.043 ± 0.052	4400	¹ SMITH	70 OSPK

¹Quadratic coefficients h and k required by some experiments. (See section on "QUADRATIC COEFFICIENT k " below.) Correlations prevent us from averaging results of fits not including $g, h,$ and k terms.

QUADRATIC COEFFICIENT k FOR $K_L^0 \rightarrow \pi^+ \pi^- \pi^0$

VALUE	EVTS	DOCUMENT ID	TECN
0.0099 ± 0.0015 OUR AVERAGE			

0.0104 ± 0.0017 ± 0.0024	500k	ANGELOPO...	98c CPLR
0.024 ± 0.010	6499	CHO	77 HBC
-0.008 ± 0.012	4709	PEACH	77 HBC
0.0097 ± 0.0018	509k	MESSNER	74 ASPK

LINEAR COEFFICIENT j FOR $K_L^0 \rightarrow \pi^+ \pi^- \pi^0$ (CP-VIOLATING TERM)

Listed in CP-violation section below.

QUADRATIC COEFFICIENT f FOR $K_L^0 \rightarrow \pi^+ \pi^- \pi^0$ (CP-VIOLATING TERM)

Listed in CP-violation section below.

QUADRATIC COEFFICIENT h FOR $K_L^0 \rightarrow \pi^0 \pi^0 \pi^0$

We do not average measurements that do not account for the effect of final state rescattering.

VALUE (units 10^{-3})	EVTS	DOCUMENT ID	TECN
+0.59 ± 0.20 ± 1.16	68M	¹ ABOUZAIID 08A	KTEV

• • • We do not use the following data for averages, fits, limits, etc. • • •

-6.1 ± 0.9 ± 0.5	14.7M	² LAI	01B NA48
-3.3 ± 1.1 ± 0.7	5M	^{2,3} SOMALWAR	92 E731

¹ Result obtained using Cl3pl model of CABIBBO 05 to include $\pi\pi$ rescattering effects. The systematic error includes an external error of 1.06×10^{-3} from the parametrization input of $(a_0 - a_2) m_{\pi^+} = 0.268 \pm 0.017$ from BATLEY 06b.

² LAI 01B and SOMALWAR 92 results do not include $\pi\pi$ final state rescattering effects.

³ SOMALWAR 92 chose m_{π^+} as normalization to make it compatible with the Particle Data Group $K_L^0 \rightarrow \pi^+ \pi^- \pi^0$ definitions.

K_L^0 FORM FACTORS

For discussion, see note on form factors in the K^\pm section of the Particle Listings above.

In the form factor comments, the following symbols are used.

f_+ and f_- are form factors for the vector matrix element.

f_S and f_T refer to the scalar and tensor term.

$$f_0(t) = f_+(t) + f_-(t) / (m_{K^0}^2 - m_{\pi^+}^2).$$

t = momentum transfer to the π .

λ_+ and λ_0 are the linear expansion coefficients of f_+ and f_0 :

$$f_+(t) = f_+(0) (1 + \lambda_+ t / m_{\pi^+}^2)$$

For quadratic expansion

$$f_+(t) = f_+(0) (1 + \lambda'_+ t / m_{\pi^+}^2 + \frac{\lambda''_+}{2} t^2 / m_{\pi^+}^4)$$

as used by KTeV. If there is a non-vanishing quadratic term, then λ_+

represents an average slope, which is then different from λ'_+ .

NA48 (K_{e3}) and ISTRA quadratic expansion coefficients are converted with

$$\lambda'_+ PDG = \lambda'_+ NA48 \text{ and } \lambda''_+ PDG = 2 \lambda'_+ NA48$$

$$\lambda'_+ PDG = (\frac{m_{\pi^+}}{m_{\pi^0}})^2 \lambda'_+ ISTRA \text{ and}$$

$$\lambda''_+ PDG = 2 (\frac{m_{\pi^+}}{m_{\pi^0}})^4 \lambda''_+ ISTRA$$

ISTRA linear expansion coefficients are converted with

$$\lambda_+ PDG = (\frac{m_{\pi^+}}{m_{\pi^0}})^2 \lambda_+ ISTRA \text{ and } \lambda_0 PDG = (\frac{m_{\pi^+}}{m_{\pi^0}})^2 \lambda_0 ISTRA$$

The pole parametrization is

$$f_+(t) = f_+(0) (\frac{M_V^2}{M_V^2 - t})$$

$$f_0(t) = f_0(0) (\frac{M_S^2}{M_S^2 - t})$$

where M_V and M_S are the vector and scalar pole masses.

The dispersive parametrization is

$$f_+(t) = f_+(0) \exp[\frac{t}{m_{\pi^+}^2} (\Lambda_+ + H(t))];$$

$$f_0(t) = f_+(0) \exp[\frac{t}{m_K^2 - m_{\pi^+}^2} (\ln[C] - G(t))],$$

where Λ_+ is the slope parameter and $\ln[C] = \ln[f_0(m_K^2 - m_{\pi^+}^2)]$

is the logarithm of the scalar form factor at the Callan-Treiman point.

$H(t)$ and $G(t)$ are dispersive integrals.

The following abbreviations are used:

DP = Dalitz plot analysis.

PI = π spectrum analysis.

MU = μ spectrum analysis.

POL = μ polarization analysis.

BR = $K_{\mu 3}^0 / K_{e 3}^0$ branching ratio analysis.

E = positron or electron spectrum analysis.

RC = radiative corrections.

λ_+ (LINEAR ENERGY DEPENDENCE OF f_+ IN $K_{e 3}^0$ DECAY)

For radiative correction of $K_{e 3}^0$ DP, see GINSBERG 67, BECHERRAWY 70, CIRIGLIANO 02, CIRIGLIANO 04, and ANDRE 07. Results labeled OUR FIT are discussed in the review " $K_{e 3}^\pm$ and $K_{e 3}^0$ Form Factors" in the K^\pm Listings. For earlier, lower statistics results, see the 2004 edition of this review, Physics Letters **B592** 1 (2004).

VALUE (units 10^{-2})	EVTS	DOCUMENT ID	TECN	COMMENT
2.82 ± 0.04 OUR FIT				Error includes scale factor of 1.1. Assuming μ -e universality
2.85 ± 0.04 OUR AVERAGE				
2.86 ± 0.05 ± 0.04	2M	AMBROSINO 06D	KLOE	
2.832 ± 0.037 ± 0.043	1.9M	ALEXOPOU... 04A	KTEV	PI, no $\mu = e$
2.88 ± 0.04 ± 0.11	5.6M	¹ LAI	04C NA48	DP

• • • We do not use the following data for averages, fits, limits, etc. • • •

2.84 ± 0.07 ± 0.13	5.6M	² LAI	04C NA48	DP
2.45 ± 0.12 ± 0.22	366k	APOSTOLA...	00 CPLR	DP
3.06 ± 0.34	74k	BIRULEV	81 SPEC	DP
3.12 ± 0.25	500k	GJESDAL	76 SPEC	DP
2.70 ± 0.28	25k	BLUMENTHAL75	SPEC	DP

¹ Results from linear fit and assuming only vector and axial couplings.

² Results from linear fit with $|f_S/f_+|$ and $|f_T/f_+|$ free.

λ_+ (LINEAR ENERGY DEPENDENCE OF f_+ IN $K_{\mu 3}^0$ DECAY)

Results labeled OUR FIT are discussed in the review " $K_{e 3}^\pm$ and $K_{e 3}^0$ Form Factors" in the K^\pm Listings. For earlier, lower statistics results, see the 2004 edition of this review, Physics Letters **B592** 1 (2004).

VALUE (units 10^{-2})	EVTS	DOCUMENT ID	TECN	COMMENT
2.82 ± 0.04 OUR FIT				Error includes scale factor of 1.1. Assuming μ -e universality
2.71 ± 0.10 OUR FIT				Error includes scale factor of 1.4. Not assuming μ -e universality
2.67 ± 0.06 ± 0.08	2.3M	¹ LAI	07A NA48	DP
2.745 ± 0.088 ± 0.063	1.5M	ALEXOPOU... 04A	KTEV	DP, no $\mu = e$
2.813 ± 0.051	3.4M	ALEXOPOU... 04A	KTEV	PI, DP, $\mu = e$
3.0 ± 0.3	1.6M	DONALDSON 74B	SPEC	DP

• • • We do not use the following data for averages, fits, limits, etc. • • •

4.27 ± 0.44	150k	BIRULEV	81 SPEC	DP
-------------	------	---------	---------	----

¹ LAI 07A gives a correlation -0.40 between their λ_0 and λ_+ measurements.

λ_0 (LINEAR ENERGY DEPENDENCE OF f_0 IN $K_{\mu 3}^0$ DECAY)

Wherever possible, we have converted the above values of $\xi(0)$ into values of λ_0 using the associated λ_+^μ and $d\xi(0)/d\lambda_+$. Results labeled OUR FIT are discussed in the review " $K_{e 3}^\pm$ and $K_{e 3}^0$ Form Factors" in the K^\pm Listings. For earlier, lower statistics results, see the 2004 edition of this review, Physics Letters **B592** 1 (2004).

VALUE (units 10^{-2})	$d\lambda_0/d\lambda_+$	EVTS	DOCUMENT ID	TECN	COMMENT
1.38 ± 0.18 OUR FIT					Error includes scale factor of 2.2. Assuming μ -e universality
1.42 ± 0.23 OUR FIT					Error includes scale factor of 2.8. Not assuming μ -e universality
1.17 ± 0.07 ± 0.10		2.3M	¹ LAI	07A NA48	DP
1.657 ± 0.125	-0.44	1.5M	² ALEXOPOU...	04A KTEV	DP, no $\mu = e$
1.635 ± 0.121	-0.85	3.4M	³ ALEXOPOU...	04A KTEV	PI, DP, $\mu = e$
+1.9 ± 0.4	-0.47	1.6M	⁴ DONALDSON 74B	SPEC	DP

• • • We do not use the following data for averages, fits, limits, etc. • • •

3.41 ± 0.67	unknown	150k	⁵ BIRULEV	81 SPEC	DP
-------------	---------	------	----------------------	---------	----

¹ LAI 07A gives a correlation -0.40 between their λ_0 and λ_+ measurements.

² ALEXOPOULOS 04A gives a correlation -0.38 between their λ_0 and λ_+ measurements.

³ ALEXOPOULOS 04A gives a correlation -0.36 between their λ_0 and λ_+ measurements.

⁴ DONALDSON 74B $d\lambda_0/d\lambda_+$ obtained from figure 18.

⁵ BIRULEV 81 gives $d\lambda_0/d\lambda_+ = -1.5$, giving an unreasonably narrow error ellipse which dominates all other results. We use $d\lambda_0/d\lambda_+ = 0$.

λ'_+ (LINEAR $K_{e 3}^0$ FORM FACTOR FROM QUADRATIC FIT)

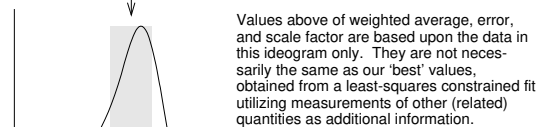
VALUE (units 10^{-2})	EVTS	DOCUMENT ID	TECN	COMMENT
2.40 ± 0.12 OUR FIT				Error includes scale factor of 1.2. Assuming μ -e universality
2.49 ± 0.13 OUR FIT				Error includes scale factor of 1.1. Not assuming μ -e universality
2.48 ± 0.17 OUR AVERAGE				Error includes scale factor of 1.5. See the ideogram below.
2.55 ± 0.15 ± 0.10	2M	¹ AMBROSINO 06D	KLOE	
2.167 ± 0.137 ± 0.143	1.9M	² ALEXOPOU...	04A KTEV	PI, no $\mu = e$
2.80 ± 0.19 ± 0.15	5.6M	³ LAI	04C NA48	DP

¹ We use AMBROSINO 06D result in the fit not assuming μ -e universality. This result enters the fit assuming μ -e universality via AMBROSINO 07C measurement of λ'_+ in $K_{\mu 3}$ decays. AMBROSINO 06D gives a correlation -0.95 between their λ'_+ and λ''_+ .

² ALEXOPOULOS 04A gives a correlation -0.97 between their λ'_+ and λ''_+ .

³ For LAI 04C we calculate a correlation -0.88 between their λ'_+ and λ''_+ .

WEIGHTED AVERAGE
2.48 ± 0.17 (Error scaled by 1.5)



				χ^2
AMBROSINO	06D	KLOE	0.2	
ALEXOPOU...	04A	KTEV	2.4	
LAI	04C	NA48	1.8	
			4.4	
			4.4	

(Confidence Level = 0.111)
 λ'_+ (LINEAR $K_{e 3}^0$ FORM FACTOR FROM QUADRATIC FIT) (units 10^{-2})

Meson Particle Listings

K_L^0

χ''_+ (QUADRATIC K_{e3}^0 FORM FACTOR)

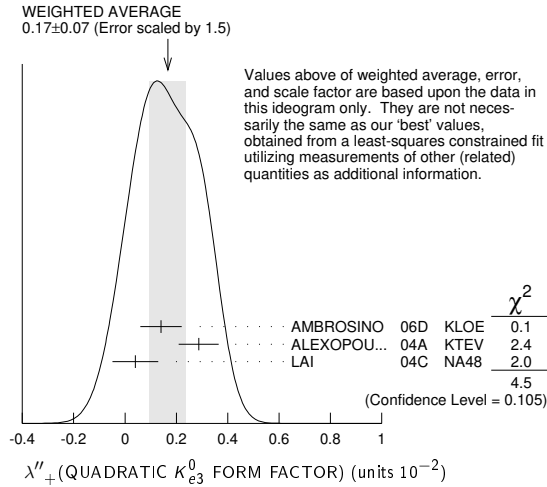
VALUE (units 10^{-2})	EVTS	DOCUMENT ID	TECN	COMMENT
0.20 ± 0.05	OUR FIT	Error includes scale factor of 1.2. Assuming μ -e universality		
0.16 ± 0.05	OUR FIT	Error includes scale factor of 1.1. Not assuming μ -e universality		
0.17 ± 0.07	OUR AVERAGE	Error includes scale factor of 1.5. See the ideogram below.		
0.14 ± 0.07 ± 0.04	2M	¹ AMBROSINO 06D	KLOE	
0.287 ± 0.057 ± 0.053	1.9M	² ALEXOPOU... 04A	KTEV	PI, no $\mu = e$
0.04 ± 0.08 ± 0.04	5.6M	^{3,4} LAI 04C	NA48	DP

¹ We use AMBROSINO 06D result in the fit not assuming μ -e universality. This result enters the fit assuming μ -e universality via AMBROSINO 07C measurement of χ''_+ in $K_{\mu 3}$ decays. AMBROSINO 06D gives a correlation -0.95 between their χ'_+ and χ''_+ .

² ALEXOPOULOS 04A gives a correlation -0.97 between their χ'_+ and χ''_+ .

³ Values doubled to agree with PDG conventions described above.

⁴ LAI 04C gives a correlation -0.88 between their χ'_+ and χ''_+ .



χ'_+ (LINEAR K_{e3}^0 FORM FACTOR FROM QUADRATIC FIT)

VALUE (units 10^{-2})	EVTS	DOCUMENT ID	TECN	COMMENT
2.40 ± 0.12	OUR FIT	Error includes scale factor of 1.2. Assuming μ -e universality		
1.89 ± 0.24	OUR FIT	Not assuming μ -e universality		
2.23 ± 0.98 ± 0.37	1.8M	¹ AMBROSINO 07C	KLOE	no $\mu = e$
2.56 ± 0.15 ± 0.09	3.8M	¹ AMBROSINO 07C	KLOE	$\mu = e$
2.05 ± 0.22 ± 0.24	2.3M	¹ LAI 07A	NA48	DP
1.703 ± 0.319 ± 0.177	1.5M	¹ ALEXOPOU... 04A	KTEV	DP, no $\mu = e$
2.064 ± 0.175	3.4M	¹ ALEXOPOU... 04A	KTEV	PI, DP, $\mu = e$

¹ See section λ_0 below for correlations.

χ''_+ (QUADRATIC $K_{\mu 3}^0$ FORM FACTOR)

VALUE (units 10^{-2})	EVTS	DOCUMENT ID	TECN	COMMENT
0.20 ± 0.05	OUR FIT	Error includes scale factor of 1.2. Assuming μ -e universality		
0.37 ± 0.12	OUR FIT	Error includes scale factor of 1.3. Not assuming μ -e universality		
0.48 ± 0.49 ± 0.16	1.8M	¹ AMBROSINO 07C	KLOE	no $\mu = e$
0.15 ± 0.07 ± 0.04	3.8M	¹ AMBROSINO 07C	KLOE	$\mu = e$
0.26 ± 0.09 ± 0.10	2.3M	¹ LAI 07A	NA48	DP
0.443 ± 0.131 ± 0.072	1.5M	¹ ALEXOPOU... 04A	KTEV	DP, no $\mu = e$
0.320 ± 0.069	3.4M	¹ ALEXOPOU... 04A	KTEV	PI, DP, $\mu = e$

¹ See section λ_0 below for correlations.

λ_0 (LINEAR $f_0 K_{\mu 3}^0$ FORM FACTOR FROM QUADRATIC FIT)

VALUE (units 10^{-2})	EVTS	DOCUMENT ID	TECN	COMMENT
1.16 ± 0.09	OUR FIT	Error includes scale factor of 1.2. Assuming μ -e universality		
1.07 ± 0.14	OUR FIT	Error includes scale factor of 1.3. Not assuming μ -e universality		
0.91 ± 0.59 ± 0.26	1.8M	¹ AMBROSINO 07C	KLOE	no $\mu = e$
1.54 ± 0.18 ± 0.13	3.8M	² AMBROSINO 07C	KLOE	$\mu = e$
0.95 ± 0.11 ± 0.08	2.3M	³ LAI 07A	NA48	DP
1.281 ± 0.136 ± 0.122	1.5M	⁴ ALEXOPOU... 04A	KTEV	DP, no $\mu = e$
1.372 ± 0.131	3.4M	⁵ ALEXOPOU... 04A	KTEV	PI, DP, $\mu = e$

¹ AMBROSINO 07C, not assuming μ -e universality, gives a correlation matrix

$$\begin{matrix} \chi'_+ & \chi''_+ \\ \chi''_+ & -0.97 & 1 \\ \lambda_0 & 0.81 & -0.91 & 1 \end{matrix}$$

² AMBROSINO 07C, assuming μ -e universality, gives a correlation matrix

$$\begin{matrix} \chi'_+ & \chi''_+ \\ \chi''_+ & -0.95 & 1 \\ \lambda_0 & 0.29 & -0.38 & 1 \end{matrix}$$

³ LAI 07A gives a correlation matrix

$$\begin{matrix} \chi'_+ & \chi''_+ \\ \chi''_+ & -0.96 & 1 \\ \lambda_0 & 0.63 & -0.73 & 1 \end{matrix}$$

⁴ ALEXOPOULOS 04A, not assuming μ -e universality, gives a correlation matrix

$$\begin{matrix} \chi'_+ & \chi''_+ & \lambda_0 \\ \chi''_+ & -0.96 & 1 \\ \lambda_0 & 0.65 & -0.75 & 1 \end{matrix}$$

⁵ ALEXOPOULOS 04A, assuming μ -e universality, gives a correlation matrix

$$\begin{matrix} \chi'_+ & \chi''_+ & \lambda_0 \\ \chi''_+ & -0.97 & 1 \\ \lambda_0 & 0.34 & -0.44 & 1 \end{matrix}$$

M_V^e (POLE MASS FOR K_{e3}^0 DECAY)

VALUE (MeV)	EVTS	DOCUMENT ID	TECN	COMMENT
878 ± 6	OUR FIT	Error includes scale factor of 1.1. Assuming μ -e universality		
875 ± 5	OUR AVERAGE			
870 ± 6 ± 7	2M	AMBROSINO 06D	KLOE	
881.03 ± 5.12 ± 4.94	1.9M	ALEXOPOU... 04A	KTEV	PI, no $\mu = e$
859 ± 18	5.6M	LAI 04C	NA48	

M_V^μ (POLE MASS FOR $K_{\mu 3}^0$ DECAY)

VALUE (MeV)	EVTS	DOCUMENT ID	TECN	COMMENT
878 ± 6	OUR FIT	Error includes scale factor of 1.1. Assuming μ -e universality		
900 ± 21	OUR FIT	Error includes scale factor of 1.7. Not assuming μ -e universality		
905 ± 9 ± 17	2.3M	¹ LAI 07A	NA48	DP
889.19 ± 12.81 ± 9.92	1.5M	¹ ALEXOPOU... 04A	KTEV	DP, no $\mu = e$
882.32 ± 6.54	3.4M	¹ ALEXOPOU... 04A	KTEV	PI, DP, $\mu = e$

¹ See section M_S^μ below for correlations.

M_S^μ (POLE MASS FOR $K_{\mu 3}^0$ DECAY)

VALUE (MeV)	EVTS	DOCUMENT ID	TECN	COMMENT
1250 ± 90	OUR FIT	Error includes scale factor of 2.6. Assuming μ -e universality		
1220 ± 80	OUR FIT	Error includes scale factor of 2.3. Not assuming μ -e universality		
1400 ± 46 ± 53	2.3M	¹ LAI 07A	NA48	DP
1167.14 ± 28.30 ± 31.04	1.5M	² ALEXOPOU... 04A	KTEV	PI, no $\mu = e$
1173.80 ± 39.47	3.4M	³ ALEXOPOU... 04A	KTEV	PI, DP, $\mu = e$

¹ LAI 07A gives a correlation -0.47 between their M_S^μ and M_V^μ measurements, not assuming μ -e universality.

² ALEXOPOULOS 04A gives a correlation -0.46 between their M_S^μ and M_V^μ and measurements, not assuming μ -e universality.

³ ALEXOPOULOS 04A gives a correlation -0.40 between their M_S^μ and M_V^μ and measurements, assuming μ -e universality.

Λ_+ (DISPERSIVE VECTOR FORM FACTOR FOR $K_{\mu 3}^0$ DECAY)

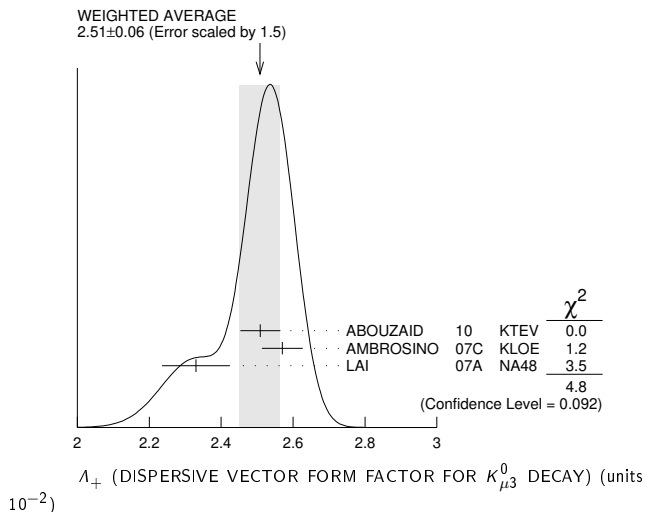
See the review on " K_{e3}^0 and $K_{\mu 3}^0$ Form Factors" for details of the dispersive parametrization.

VALUE (units 10^{-2})	EVTS	DOCUMENT ID	TECN	COMMENT
2.51 ± 0.06	OUR AVERAGE	Error includes scale factor of 1.5. See the ideogram below.		
2.509 ± 0.035 ± 0.043	3.4M	¹ ABOUZAID 10	KTEV	$\mu = e$
2.57 ± 0.04 ± 0.04	3.8M	² AMBROSINO 07C	KLOE	$\mu = e$
2.33 ± 0.05 ± 0.08	2.3M	³ LAI 07A	NA48	DP

¹ Obtained from a sample of 1.9 M K_{e3} and 1.5 M $K_{\mu 3}$. The correlation between Λ_+ and $\ln(C)$ is -0.269 .

² AMBROSINO 07C results include 2M K_{e3} events from AMBROSINO 06D. The correlation between Λ_+ and $\ln(C)$ is -0.26 .

³ LAI 07A gives a correlation -0.44 between their Λ_+ and $\ln(C)$ measurements.



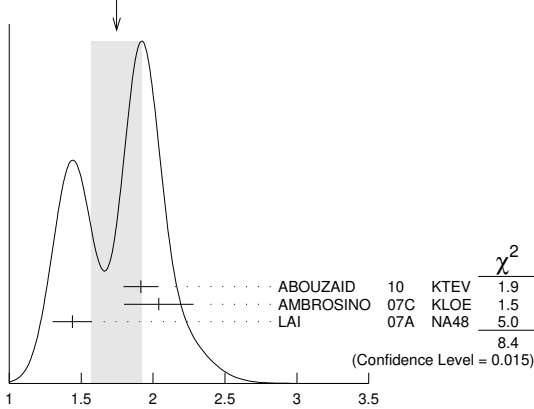
ln(C) (DISPERSIVE SCALAR FORM FACTOR FOR $K_{\mu 3}^0$ DECAY)

See the review on " K_{e3}^{\pm} and $K_{\mu 3}^0$ Form Factors" for details of the dispersive parametrization.

VALUE (units 10^{-1})	EVTS	DOCUMENT ID	TECN	COMMENT
1.75 ± 0.18 OUR AVERAGE				Error includes scale factor of 2.0. See the ideogram below.
1.915 ± 0.078 ± 0.094	3.4M	¹ ABOUZAID	10 KTEV	$\mu = e$
2.04 ± 0.19 ± 0.15	3.8M	² AMBROSINO	07c KLOE	$\mu = e$
1.438 ± 0.080 ± 0.112	2.3M	³ LAI	07A NA48	DP

- ¹ Obtained from a sample of 1.9 M K_{e3} and 1.5 M $K_{\mu 3}$. The correlation between A_+ and $\ln(C)$ is -0.269 .
- ² AMBROSINO 07c results include 2M K_{e3} events from AMBROSINO 06d. We convert (A_+, A_0) to $(A_+, \ln(C))$ parametrization using $\ln(C) = (A_0 \cdot 11.713 + 0.0398) \pm 0.0041$, where the error is due to theory parametrization of the form factor. The correlation between A_+ and $\ln(C)$ is -0.26 .
- ³ LAI 07A gives a correlation -0.44 between their A_+ and $\ln(C)$ measurements.

WEIGHTED AVERAGE
1.75 ± 0.18 (Error scaled by 2.0)



ln(C) (DISPERSIVE SCALAR FORM FACTOR FOR $K_{\mu 3}^0$ DECAY) (units 10^{-1})

$a_1(t_0, Q^2)$ FORM FACTOR PARAMETER

See HILL 06 for a definition of this parameter.

VALUE	EVTS	DOCUMENT ID	TECN
1.023 ± 0.028 ± 0.029	2M	¹ ABOUZAID	06c KTEV

- ¹ $Q^2 = 2 \text{ GeV}^2$, $t_0 = 0.49 (m_K - m_\pi)^2$. Correlation between a_1 and a_2 : $\rho_{12} = -0.064$.

$a_2(t_0, Q^2)$ FORM FACTOR PARAMETER

See HILL 06 for a definition of this parameter.

VALUE	EVTS	DOCUMENT ID	TECN
0.75 ± 1.58 ± 1.47	2M	¹ ABOUZAID	06c KTEV

- ¹ $Q^2 = 2 \text{ GeV}^2$, $t_0 = 0.49 (m_K - m_\pi)^2$. Correlation between a_1 and a_2 : $\rho_{12} = -0.064$.

$|f_S/f_+|$ FOR K_{e3}^0 DECAY

Ratio of scalar to f_+ couplings.

VALUE (units 10^{-2})	CL%	EVTS	DOCUMENT ID	TECN	COMMENT
1.5^{+0.7}_{-1.0} ± 1.2		5.6M	¹ LAI	04c	NA48

- • • We do not use the following data for averages, fits, limits, etc. • • •
- <9.5 95 18k HILL 78 STRC
- <7. 68 48k BIRULEV 76 SPEC See also BIRULEV 81
- <4. 68 25k BLUMENTHAL75 SPEC

- ¹ Results from linear fit with $|f_S/f_+|$ and $|f_T/f_+|$ free.

$|f_T/f_+|$ FOR K_{e3}^0 DECAY

Ratio of tensor to f_+ couplings.

VALUE (units 10^{-2})	CL%	EVTS	DOCUMENT ID	TECN	COMMENT
5⁺³₋₄ ± 3		5.6M	¹ LAI	04c	NA48

- • • We do not use the following data for averages, fits, limits, etc. • • •
- <40. 95 18k HILL 78 STRC
- <34. 68 48k BIRULEV 76 SPEC See also BIRULEV 81
- <23. 68 25k BLUMENTHAL75 SPEC

- ¹ Results from linear fit with $|f_S/f_+|$ and $|f_T/f_+|$ free.

$|f_T/f_+|$ FOR $K_{\mu 3}^0$ DECAY

Ratio of tensor to f_+ couplings.

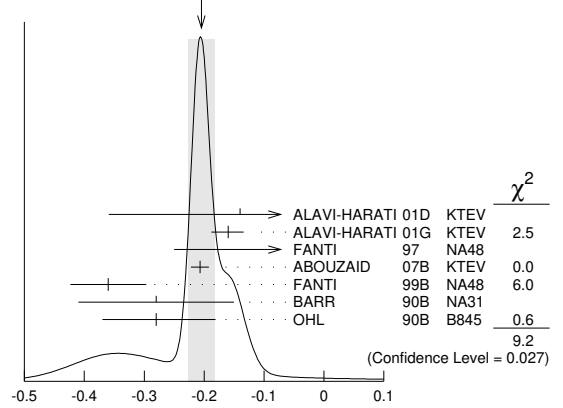
VALUE (units 10^{-2})	DOCUMENT ID	TECN
12 ± 12.	BIRULEV 81	SPEC

α_{K^*} DECAY FORM FACTOR FOR $K_L \rightarrow e^+ e^- \gamma$, $K_L^0 \rightarrow e^+ e^- e^+ e^-$

Average of all α_{K^*} measurements (from each of three datablocks following this one) assuming lepton universality.

VALUE	DOCUMENT ID
-0.205 ± 0.022 OUR AVERAGE	Includes data from the 3 datablocks that follow this one. Error includes scale factor of 1.8. See the ideogram below.

WEIGHTED AVERAGE
-0.205 ± 0.022 (Error scaled by 1.8)



α_{K^*} DECAY FORM FACTOR FOR $K_L \rightarrow e^+ e^- \gamma$, $K_L^0 \rightarrow e^+ e^- e^+ e^-$

α_{K^*} DECAY FORM FACTOR FOR $K_L \rightarrow e^+ e^- \gamma$

α_{K^*} is the constant in the model of BERGSTROM 83 which measures the relative strength of the vector-vector transition $K_L \rightarrow K^* \gamma$ with $K^* \rightarrow \rho, \omega, \phi \rightarrow \gamma^*$ and the pseudoscalar-pseudoscalar transition $K_L \rightarrow \pi, \eta, \eta' \rightarrow \gamma \gamma^*$.

VALUE	EVTS	DOCUMENT ID	TECN
-0.217 ± 0.034 OUR AVERAGE			Error includes scale factor of 2.4.
-0.207 ± 0.012 ± 0.009	83k	¹ ABOUZAID	07B KTEV
-0.36 ± 0.06 ± 0.02	6864	FANTI	99B NA48
-0.28 ± 0.13		BARR	90B NA31
-0.280 ^{+0.099} _{-0.090}		OHL	90B B845

- ¹ ABOUZAID 07b measures $C \cdot \alpha_{K^*} = -0.517 \pm 0.030 \pm 0.022$. We assume $C = 2.5$, as in all other measurements.

α_{K^*} DECAY FORM FACTOR FOR $K_L \rightarrow \mu^+ \mu^- \gamma$

α_{K^*} is the constant in the model of BERGSTROM 83 described in the previous section.

VALUE	EVTS	DOCUMENT ID	TECN
-0.158 ± 0.027 OUR AVERAGE			
-0.160 ^{+0.026} _{-0.028}	9100	ALAVI-HARATI 01G	KTEV
-0.04 ± 0.24		FANTI	97 NA48
-0.21			

$\alpha_{K^*}^{\text{eff}}$ DECAY FORM FACTOR FOR $K_L \rightarrow e^+ e^- e^+ e^-$

$\alpha_{K^*}^{\text{eff}}$ is the parameter describing the relative strength of an intermediate pseudoscalar decay amplitude and a vector meson decay amplitude in the model of BERGSTROM 83. It takes into account both the radiative effects and the form factor. Since there are two $e^+ e^-$ pairs here compared with one in $e^+ e^- \gamma$ decays, a factorized expression is used for the $e^+ e^- e^+ e^-$ decay form factor.

VALUE	EVTS	DOCUMENT ID	TECN
-0.14 ± 0.16 ± 0.15	441	ALAVI-HARATI 01D	KTEV

α_{DIP} DECAY FORM FACTOR FOR $K_L^0 \rightarrow e^+ e^- \gamma$, $K_L^0 \rightarrow e^+ e^- e^+ e^-$

Average of all α_{DIP} measurements (from each of three datablocks following this one) assuming lepton universality.

VALUE	DOCUMENT ID
-1.69 ± 0.08 OUR AVERAGE	Includes data from the 3 datablocks that follow this one. Error includes scale factor of 1.7.

α_{DIP} DECAY FORM FACTOR FOR $K_L^0 \rightarrow e^+ e^- \gamma$

α_{DIP} parameter in $K_L^0 \rightarrow \gamma^* \gamma^*$ form factor by DAMBROSIO 98, motivated by vector meson dominance and a proper short distance behavior.

VALUE	EVTS	DOCUMENT ID	TECN
-1.729 ± 0.043 ± 0.028	83k	ABOUZAID	07B KTEV

α_{DIP} DECAY FORM FACTOR FOR $K_L^0 \rightarrow \mu^+ \mu^- \gamma$

α_{DIP} is a constant in the model of DAMBROSIO 98 described in the previous section.

VALUE	EVTS	DOCUMENT ID	TECN
-1.54 ± 0.10	9100	ALAVI-HARATI 01G	KTEV

Meson Particle Listings

 K_L^0 α_{DIP} DECAY FORM FACTOR FOR $K_L^0 \rightarrow e^+ e^- \mu^+ \mu^-$ α_{DIP} is a constant in the model of DAMBROSIO 98 described in the previous section.

VALUE	EVTS	DOCUMENT ID	TECN
The data in this block is included in the average printed for a previous datablock.			

-1.59 ± 0.37	131	ALAVI-HARATI03B	KTEV
--------------	-----	-----------------	------

 a_1/a_2 FORM FACTOR FOR M1 DIRECT EMISSION AMPLITUDEForm factor = $\hat{g}_{M1} \left[1 + \frac{\alpha_1/\alpha_2}{(M_p^2 - M_K^2) + 2M_K E_\gamma} \right]$ as described in ALAVI-HARATI 00b.

VALUE (GeV ²)	EVTS	DOCUMENT ID	TECN	COMMENT
-0.737 ± 0.014 OUR AVERAGE				
-0.744 ± 0.027 ± 0.032	5241	¹ ABOUZAID	06 KTEV	$\pi^+ \pi^- e^+ e^-$
-0.738 ± 0.007 ± 0.018	111k	² ABOUZAID	06A KTEV	$\pi^+ \pi^+ \gamma$
-0.81 \pm $\frac{+0.07}{-0.13}$ ± 0.02		³ LAI	03C NA48	$\pi^+ \pi^- e^+ e^-$
-0.737 ± 0.026 ± 0.022		⁴ ALAVI-HARATI01B		$\pi^+ \pi^- \gamma$
-0.720 ± 0.028 ± 0.009	1766	⁵ ALAVI-HARATI00B	KTEV	$\pi^+ \pi^- e^+ e^-$
¹ ABOUZAID 06 also measured $ \hat{g}_{M1} = 1.11 \pm 0.14$.				
² ABOUZAID 06A also measured $ \hat{g}_{M1} = 1.198 \pm 0.035 \pm 0.086$.				
³ LAI 03c also measured $\hat{g}_{M1} = 0.99 \pm \frac{+0.28}{-0.27} \pm 0.07$.				
⁴ ALAVI-HARATI 01B fit gives $\chi^2/\text{DOF} = 38.8/27$. Linear and quadratic fits give $\chi^2/\text{DOF} = 43.2/27$ and $37.6/26$ respectively.				
⁵ ALAVI-HARATI 00b also measured $ \hat{g}_{M1} = 1.35 \pm \frac{+0.20}{-0.17} \pm 0.04$.				

 \tilde{f}_S DECAY FORM FACTOR FOR $K_L^0 \rightarrow \pi^\pm \pi^0 e^\mp \nu_e$

VALUE	DOCUMENT ID	TECN
0.049 ± 0.011 OUR AVERAGE Error includes scale factor of 1.7.		
0.052 ± 0.006 ± 0.002	BATLEY 04	NA48
0.010 ± 0.016 ± 0.017	MAKOFF 93	E731

 \tilde{f}_P DECAY FORM FACTOR FOR $K_L^0 \rightarrow \pi^\pm \pi^0 e^\mp \nu_e$

VALUE	DOCUMENT ID	TECN
-0.052 ± 0.012 OUR AVERAGE		
-0.051 ± 0.011 ± 0.005	BATLEY 04	NA48
-0.079 ± 0.049 ± 0.022	MAKOFF 93	E731

 λ_γ DECAY FORM FACTOR FOR $K_L^0 \rightarrow \pi^\pm \pi^0 e^\mp \nu_e$

VALUE	DOCUMENT ID	TECN
0.085 ± 0.020 OUR AVERAGE		
0.087 ± 0.019 ± 0.006	BATLEY 04	NA48
0.014 ± 0.087 ± 0.070	MAKOFF 93	E731

 \tilde{h} DECAY FORM FACTOR FOR $K_L^0 \rightarrow \pi^\pm \pi^0 e^\mp \nu_e$

VALUE	DOCUMENT ID	TECN
-0.30 ± 0.13 OUR AVERAGE		
-0.32 ± 0.12 ± 0.07	BATLEY 04	NA48
-0.07 ± 0.31 ± 0.31	MAKOFF 93	E731

 L_3 CHIRAL PERT. THEO. PARAM. FOR $K_L^0 \rightarrow \pi^\pm \pi^0 e^\mp \nu_e$

VALUE (units 10 ⁻³)	DOCUMENT ID	TECN
-3.96 ± 0.28 OUR AVERAGE Error includes scale factor of 1.6.		
-4.1 ± 0.2	BATLEY 04	NA48
-3.4 ± 0.4	¹ MAKOFF 93	E731

¹ MAKOFF 93 sign has been changed to negative to agree with the sign convention used in BATLEY 04. a_V VECTOR MESON EXCHANGE CONTRIBUTION

VALUE	EVTS	DOCUMENT ID	TECN	COMMENT
-0.43 ± 0.06 OUR AVERAGE Error includes scale factor of 1.5.				
-0.31 ± 0.05 ± 0.07	1.4k	¹ ABOUZAID	08 KTEV	
-0.46 ± 0.03 ± 0.04		LAI	02B NA48	$K_L^0 \rightarrow \pi^0 2\gamma$
-0.67 ± 0.21 ± 0.12		ALAVI-HARATI01E	KTEV	$K_L^0 \rightarrow \pi^0 e^+ e^- \gamma$
• • • We do not use the following data for averages, fits, limits, etc. • • •				
-0.72 ± 0.05 ± 0.06		² ALAVI-HARATI99B	KTEV	$K_L^0 \rightarrow \pi^0 2\gamma$

¹ Using KTeV dataset collected in 1996, 1997, and 1999.² Superseded by ABOUZAID 08.

See the related review(s):

[CP Violation in \$K_L^0\$ Decays](#)CP-VIOLATION PARAMETERS IN K_L^0 DECAYSCHARGE ASYMMETRY IN K_{L3}^0 DECAYSSuch asymmetry violates CP. It is related to $\text{Re}(\epsilon)$. $A_L =$ weighted average of $A_L(\mu)$ and $A_L(e)$ In previous editions and in the literature the symbol used for this asymmetry was δ_L or δ . We use A_L for consistency with B^0 asymmetry notation and with recent K_S^0 notation.

VALUE (%)	EVTS	DOCUMENT ID	TECN	COMMENT
0.332 ± 0.006 OUR AVERAGE Includes data from the 2 datablocks that follow this one.				
0.333 ± 0.050	33M	WILLIAMS 73	ASPK	$K_{\mu 3} + K_{e 3}$

 $A_L(\mu) = [\Gamma(\pi^- \mu^+ \nu_\mu) - \Gamma(\pi^+ \mu^- \bar{\nu}_\mu)]/\text{SUM}$

Only the combined value below is put into the Meson Summary Table.

VALUE (%)	EVTS	DOCUMENT ID	TECN
The data in this block is included in the average printed for a previous datablock.			

0.304 ± 0.025 OUR AVERAGE

0.313 ± 0.029	15M	GEWENIGER 74	ASPK
0.278 ± 0.051	7.7M	PICCONI 72	ASPK

• • • We do not use the following data for averages, fits, limits, etc. • • •

0.60 ± 0.14	4.1M	MCCARTHY 73	CNTR
0.57 ± 0.17	1M	¹ PACIOTTI 69	OSPK
0.403 ± 0.134	1M	¹ DORFAN 67	OSPK

¹ PACIOTTI 69 is a reanalysis of DORFAN 67 and is corrected for $\mu^+ \mu^-$ range difference in MCCARTHY 72. $A_L(e) = [\Gamma(\pi^- e^+ \nu_e) - \Gamma(\pi^+ e^- \bar{\nu}_e)]/\text{SUM}$

Only the combined value below is put into the Meson Summary Table.

VALUE (%)	EVTS	DOCUMENT ID	TECN
The data in this block is included in the average printed for a previous datablock.			

0.334 ± 0.007 OUR AVERAGE

0.3322 ± 0.0058 ± 0.0047	298M	ALAVI-HARATI02	
0.341 ± 0.018	34M	GEWENIGER 74	ASPK
0.318 ± 0.038	40M	FITCH 73	ASPK
0.346 ± 0.033	10M	MARX 70	CNTR

• • • We do not use the following data for averages, fits, limits, etc. • • •

0.36 ± 0.18	600k	ASHFORD 72	ASPK
0.246 ± 0.059	10M	¹ SAAL 69	CNTR
0.224 ± 0.036	10M	¹ BENNETT 67	CNTR

¹ SAAL 69 is a reanalysis of BENNETT 67.PARAMETERS FOR $K_L^0 \rightarrow 2\pi$ DECAY

$$\eta_{+-} = A(K_L^0 \rightarrow \pi^+ \pi^-) / A(K_S^0 \rightarrow \pi^+ \pi^-)$$

$$\eta_{00} = A(K_L^0 \rightarrow \pi^0 \pi^0) / A(K_S^0 \rightarrow \pi^0 \pi^0)$$

The fitted values of $|\eta_{+-}|$ and $|\eta_{00}|$ given below are the results of a fit to $|\eta_{+-}|$, $|\eta_{00}|$, $|\eta_{00}/\eta_{+-}|$, and $\text{Re}(\epsilon'/\epsilon)$. Independent information on $|\eta_{+-}|$ and $|\eta_{00}|$ can be obtained from the fitted values of the $K_L^0 \rightarrow \pi\pi$ and $K_S^0 \rightarrow \pi\pi$ branching ratios and the K_L^0 and K_S^0 lifetimes. This information is included as data in the $|\eta_{+-}|$ and $|\eta_{00}|$ sections with a Document ID "BRFIT." See the note "CP violation in K_L decays" above for details. $|\eta_{00}| = |A(K_L^0 \rightarrow 2\pi^0) / A(K_S^0 \rightarrow 2\pi^0)|$

VALUE (units 10 ⁻³)	DOCUMENT ID	TECN	COMMENT
2.220 ± 0.011 OUR FIT Error includes scale factor of 1.8.			
2.243 ± 0.014	BRFIT	16	

• • • We do not use the following data for averages, fits, limits, etc. • • •

2.47 ± 0.31 ± 0.24	ANGELOPO... 98	CPLR	
2.49 ± 0.40	¹ ADLER 96B	CPLR	Sup. by ANGELOPOULOS 98
2.33 ± 0.18	CHRISTENS... 79	ASPK	
2.71 ± 0.37	² WOLFF 71	OSPK	Cu reg., 4 γ 's
2.95 ± 0.63	² CHOLLET 70	OSPK	Cu reg., 4 γ 's

¹ Error is statistical only.² CHOLLET 70 gives $|\eta_{00}| = (1.23 \pm 0.24) \times (\text{regeneration amplitude, 2 GeV/c Cu})/10000\text{mb}$. WOLFF 71 gives $|\eta_{00}| = (1.13 \pm 0.12) \times (\text{regeneration amplitude, 2 GeV/c Cu})/10000\text{mb}$. We compute both $|\eta_{00}|$ values for (regeneration amplitude, 2 GeV/c Cu) = $24 \pm 2\text{mb}$. This regeneration amplitude results from averaging over FAISSNER 69, extrapolated using optical-model calculations of Bohm et al., Physics Letters **27B** 594 (1968) and the data of BALATS 71. (From H. Faissner, private communication). $|\eta_{+-}| = |A(K_L^0 \rightarrow \pi^+ \pi^-) / A(K_S^0 \rightarrow \pi^+ \pi^-)|$

VALUE (units 10 ⁻³)	EVTS	DOCUMENT ID	TECN	COMMENT
2.232 ± 0.011 OUR FIT Error includes scale factor of 1.8.				
2.226 ± 0.007	BRFIT	16		

• • • We do not use the following data for averages, fits, limits, etc. • • •

2.223 ± 0.012	¹ LAI 07	NA48	
2.219 ± 0.013	² AMBROSINO 06F	KLOE	
2.228 ± 0.010	³ ALEXOPOU... 04	KTEV	
2.286 ± 0.023 ± 0.026	70M	⁴ APOSTOLA... 99c	CPLR K^0 - \bar{K}^0 asymmetry
2.310 ± 0.043 ± 0.031		⁵ ADLER 95B	CPLR K^0 - \bar{K}^0 asymmetry
2.32 ± 0.14 ± 0.03	10 ⁵	ADLER 92B	CPLR K^0 - \bar{K}^0 asymmetry
2.30 ± 0.035		GEWENIGER 74B	ASPK

¹ Value obtained from the NA48 measurements of $\Gamma(K_L^0 \rightarrow \pi^+ \pi^-)/\Gamma(K_L^0 \rightarrow \pi^0 \nu_e)$ and $\tau_{K_S^0}$ and KLOE measurements of $B(K_S^0 \rightarrow \pi^+ \pi^-)$ and $\tau_{K_L^0}$. $\Gamma(K_L^0 \rightarrow \pi^+ \pi^-)$ is defined to include the inner bremsstrahlung component $\Gamma(K_L^0 \rightarrow \pi^+ \pi^- \gamma(\text{IB}))$ but exclude the direct emission component $B(K_S^0 \rightarrow \pi^+ \pi^- (\text{DE}))$. Their $|\eta_{+-}|$ value is not directly used in our fit, but enters the fit via their branching ratio and lifetime measurements.² AMBROSINO 06f uses KLOE branching ratios and τ_L together with τ_S from PDG 04. Their $|\eta_{+-}|$ value is not directly used in our fit, but enters the fit via their branching ratio and lifetime measurements.

- ³ALEXOPOULOS 04 $|\eta_{+-}|$ uses their $K_L^0 \rightarrow \pi\pi$ branching fractions, $\tau_S = (0.8963 \pm 0.0005) \times 10^{-10}$ s from the average of KTeV and NA48 τ_S measurements, and assumes that $\Gamma(K_S^0 \rightarrow \pi\ell\nu_\ell) = \Gamma(K_L^0 \rightarrow \pi\ell\nu_\ell)$ giving $B(K_S^0 \rightarrow \pi\ell\nu_\ell) = 0.118\%$. Their η_{+-} is not directly used in our fit, but enters our fit via their branching ratio measurements.
- ⁴APOSTOLAKIS 99c report $(2.264 \pm 0.023 \pm 0.026 + 9.1[\tau_S - 0.8934]) \times 10^{-3}$. We evaluate for our 2006 best value $\tau_S = (0.8958 \pm 0.0005) \times 10^{-10}$ s.
- ⁵ADLER 95b report $(2.312 \pm 0.043 \pm 0.030 - 1[\Delta m - 0.5274] + 9.1[\tau_S - 0.8926]) \times 10^{-3}$. We evaluate for our 1996 best values $\Delta m = (0.5304 \pm 0.0014) \times 10^{-10}$ $\hbar s^{-1}$ and $\tau_S = (0.8927 \pm 0.0009) \times 10^{-10}$ s. Superseded by APOSTOLAKIS 99c.

$$|\epsilon| = (2|\eta_{+-}| + |\eta_{00}|)/3$$

This expression is a very good approximation, good to about one part in 10^{-4} because of the small measured value of $\phi_{00} - \phi_{+-}$ and small theoretical ambiguities.

VALUE (units 10^{-3})	DOCUMENT ID	TECN	COMMENT
0.9950 ± 0.0007 OUR FIT			Error includes scale factor of 1.6.
0.9930 ± 0.0020 OUR AVERAGE			

$$|\eta_{00}/\eta_{+-}|$$

VALUE	EVTS	DOCUMENT ID	TECN
0.9950 ± 0.0007 OUR FIT			Error includes scale factor of 1.6.
0.9930 ± 0.0020 OUR AVERAGE			
0.9931 ± 0.0020	1,2	BARR 93D NA31	
0.9904 ± 0.0084 ± 0.0036	3	WOODS 88 E731	
• • • We do not use the following data for averages, fits, limits, etc. • • •			
0.9939 ± 0.0013 ± 0.0015	1M	1 BARR 93D NA31	
0.9899 ± 0.0020 ± 0.0025	1	BURKHARDT 88 NA31	

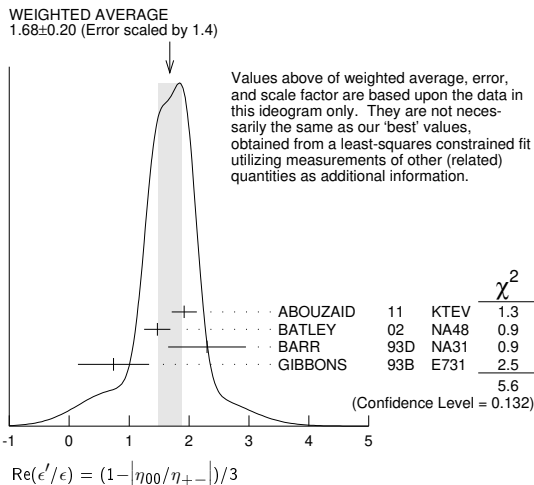
- ¹This is the square root of the ratio R given by BURKHARDT 88 and BARR 93D.
- ²This is the combined results from BARR 93D and BURKHARDT 88, taking into account a common systematic uncertainty of 0.0014.
- ³We calculate $|\eta_{00}/\eta_{+-}| = 1 - 3(\epsilon'/\epsilon)$ from WOODS 88 (ϵ'/ϵ) value.

$$\text{Re}(\epsilon'/\epsilon) = (1 - |\eta_{00}/\eta_{+-}|)/3$$

We have neglected terms of order $\omega \cdot \text{Re}(\epsilon'/\epsilon)$, where $\omega = \text{Re}(A_2)/\text{Re}(A_0) \simeq 1/22$. If included, this correction would lower $\text{Re}(\epsilon'/\epsilon)$ by about 0.04×10^{-3} . See SOZZI 04.

VALUE (units 10^{-3})	DOCUMENT ID	TECN	COMMENT
1.66 ± 0.23 OUR FIT			Error includes scale factor of 1.6.
1.68 ± 0.20 OUR AVERAGE			Error includes scale factor of 1.4. See the ideogram below.
1.92 ± 0.21	1	ABOUZAID 11 KTEV Assuming CPT	
1.47 ± 0.22		BATLEY 02 NA48	
0.74 ± 0.52 ± 0.29		GIBBONS 93B E731	
• • • We use the following data for averages but not for fits. • • •			
2.3 ± 0.65	2,3	BARR 93D NA31	
• • • We do not use the following data for averages, fits, limits, etc. • • •			
2.110 ± 0.343	1,4	ABOUZAID 11 KTEV Not assuming CPT	
2.07 ± 0.28		ALAVI-HARATI 03 KTEV In ABOUZAID 11	
1.53 ± 0.26		LAI 01C NA48 Incl. in BATLEY 02	
2.80 ± 0.30 ± 0.28		ALAVI-HARATI 99D KTEV In ALAVI-HARATI 03	
1.85 ± 0.45 ± 0.58		FANTI 99C NA48 In LAI 01C	
2.0 ± 0.7	5	BARR 93D NA31	
-0.4 ± 1.4 ± 0.6		PATTERSON 90 E731 in GIBBONS 93B	
3.3 ± 1.1	5	BURKHARDT 88 NA31	
3.2 ± 2.8 ± 1.2	2	WOODS 88 E731	

- ¹The two ABOUZAID 11 values use the same data. The fits are performed with and without CPT invariance requirement.
- ²These values are derived from $|\eta_{00}/\eta_{+-}|$ measurements. They enter the average in this section but enter the fit via the $|\eta_{00}/\eta_{+-}|$ only.
- ³This is the combined results from BARR 93D and BURKHARDT 88, taking into account their common systematic uncertainty.
- ⁴We use ABOUZAID 11 $\text{Re}(\epsilon'/\epsilon)$ value with CPT assumption in our fits for $|\eta_{+-}|$, $|\eta_{00}|$, and $\text{Re}(\epsilon'/\epsilon)$.
- ⁵These values are derived from $|\eta_{00}/\eta_{+-}|$ measurements.



ϕ_{+-} , PHASE OF η_{+-}

The dependence of the phase on Δm and τ_S is given for each experiment in the comments below, where Δm is the $K_L^0 - K_S^0$ mass difference in units $10^{10} \hbar s^{-1}$ and τ_S is the K_S mean life in units 10^{-10} s. We also give the regeneration phase ϕ_f in the comments below.

OUR FIT is described in the note on "CP violation in K_L decays" in the K_L^0 Particle Listings. Most experiments in this section are included in both the "Not Assuming CPT" and "Assuming CPT" fits. In the latter fit, they have little direct influence on ϕ_{+-} because their errors are large compared to that assuming CPT, but they influence Δm and τ_S through their dependencies on these parameters, which are given in the footnotes.

VALUE (°)	EVTS	DOCUMENT ID	TECN	COMMENT
43.51 ± 0.05 OUR FIT				Error includes scale factor of 1.2. Assuming CPT
43.4 ± 0.5 OUR FIT				Error includes scale factor of 1.2. Not assuming CPT
42.9 ± 0.6 ± 0.3	70M	1 APOSTOLA... 99C	CPLR	$K^0 - \bar{K}^0$ asymmetry
42.9 ± 0.8 ± 0.2		2,3 SCHWINGEN... 95	E773	$CH_{1,1}$ regenerator
41.4 ± 0.9 ± 0.2		3,4 GIBBONS 93	E731	$B_4 C$ regenerator
44.5 ± 1.6 ± 0.5		5 CAROSI 90	NA31	Vacuum regen.
43.3 ± 1.0 ± 0.5		6 GEWENIGER 74B	ASP K	Vacuum regen.
• • • We do not use the following data for averages, fits, limits, etc. • • •				
43.76 ± 0.64		7 ABOUZAID 11	KTEV	Not assuming CPT
44.12 ± 0.72 ± 1.20		8 ALAVI-HARATI 03	KTEV	Not assuming CPT
42.5 ± 0.4 ± 0.3		9,10 ADLER 96C	RVUE	
43.4 ± 1.1 ± 0.3		11 ADLER 95B	CPLR	$K^0 - \bar{K}^0$ asymmetry
42.3 ± 4.4 ± 1.4	100k	12 ADLER 92B	CPLR	$K^0 - \bar{K}^0$ asymmetry
47.7 ± 2.0 ± 0.9		3,13 KARLSSON 90	E731	
44.3 ± 2.8 ± 0.2		14 CARITHERS 75	SPEC	C regenerator

- ¹APOSTOLAKIS 99c measures $\phi_{+-} = (43.19 \pm 0.53 \pm 0.28) + 300 [\Delta m - 0.5301] (^\circ)$. We have adjusted the measurement to use our best values of $(\Delta m = 0.5293 \pm 0.0009) (10^{10} \hbar s^{-1})$. Our first error is their experiment's error and our second error is the systematic error from using our best values.
- ²SCHWINGENHEUER 95 measures $\phi_{+-} = (43.53 \pm 0.76) + 173 [\Delta m - 0.5282] - 275 [\tau_S - 0.8926] (^\circ)$. We have adjusted the measurement to use our best values of $(\Delta m = 0.5293 \pm 0.0009) (10^{10} \hbar s^{-1})$, $(\tau_S = 0.8954 \pm 0.0004) (10^{-10} s)$. Our first error is their experiment's error and our second error is the systematic error from using our best values.
- ³These experiments measure $\phi_{+-} - \phi_f$ and calculate the regeneration phase from the power law momentum dependence of the regeneration amplitude using analyticity and dispersion relations. SCHWINGENHEUER 95 [GIBBONS 93] includes a systematic error of $0.35^\circ [0.5^\circ]$ for uncertainties in their modeling of the regeneration amplitude.
- ⁴GIBBONS 93 measures $\phi_{+-} = (42.21 \pm 0.9) + 189 [\Delta m - 0.5257] - 460 [\tau_S - 0.8922] (^\circ)$. We have adjusted the measurement to use our best values of $(\Delta m = 0.5293 \pm 0.0009) (10^{10} \hbar s^{-1})$, $(\tau_S = 0.8954 \pm 0.0004) (10^{-10} s)$. Our first error is their experiment's error and our second error is the systematic error from using our best values. This is actually reported in SCHWINGENHEUER 95, footnote 8. GIBBONS 93 reports $\phi_{+-} (42.2 \pm 1.4)^\circ$. They measure $\phi_{+-} - \phi_f$ and calculate the regeneration phase ϕ_f from the power law momentum dependence of the regeneration amplitude using analyticity. An error of 0.6° is included for possible uncertainties in the regeneration phase.
- ⁵CAROSI 90 measures $\phi_{+-} = (46.9 \pm 1.4 \pm 0.7) + 579 [\Delta m - 0.5351] + 303 [\tau_S - 0.8922] (^\circ)$. We have adjusted the measurement to use our best values of $(\Delta m = 0.5293 \pm 0.0009) (10^{10} \hbar s^{-1})$, $(\tau_S = 0.8954 \pm 0.0004) (10^{-10} s)$. Our first error is their experiment's error and our second error is the systematic error from using our best values.
- ⁶GEWENIGER 74B measures $\phi_{+-} = (49.4 \pm 1.0) + 565 [\Delta m - 0.540] (^\circ)$. We have adjusted the measurement to use our best values of $(\Delta m = 0.5293 \pm 0.0009) (10^{10} \hbar s^{-1})$. Our first error is their experiment's error and our second error is the systematic error from using our best values.
- ⁷Not independent of other phase parameters reported in ABOUZAID 11.
- ⁸ALAVI-HARATI 03 ϕ_{+-} is correlated with their $\Delta m = m_{K_L^0} - m_{K_S^0}$ and τ_{K_S} measurements in the K_L^0 and K_S^0 sections respectively. The correlation coefficients are $\rho(\phi_{+-}, \Delta m) = +0.955$, $\rho(\phi_{+-}, \tau_S) = -0.871$, and $\rho(\tau_S, \Delta m) = -0.840$. CPT is not assumed. Uses scintillator Pb regenerator. Superseded by ABOUZAID 11.
- ⁹ADLER 96c measures $\phi_{+-} = (43.82 \pm 0.41) + 339 [\Delta m - 0.5307] - 252 [\tau_S - 0.8922] (^\circ)$. We have adjusted the measurement to use our best values of $(\Delta m = 0.5293 \pm 0.0009) (10^{10} \hbar s^{-1})$, $(\tau_S = 0.8954 \pm 0.0004) (10^{-10} s)$. Our first error is their experiment's error and our second error is the systematic error from using our best values.
- ¹⁰ADLER 96c is the result of a fit which includes nearly the same data as entered into the "OUR FIT" value in the 1996 edition of this Review (Physical Review D54 1 (1996)).
- ¹¹ADLER 95B measures $\phi_{+-} = (42.7 \pm 0.9 \pm 0.6) + 316 [\Delta m - 0.5274] + 30 [\tau_S - 0.8926] (^\circ)$. We have adjusted the measurement to use our best values of $(\Delta m = 0.5293 \pm 0.0009) (10^{10} \hbar s^{-1})$, $(\tau_S = 0.8954 \pm 0.0004) (10^{-10} s)$. Our first error is their experiment's error and our second error is the systematic error from using our best values.
- ¹²ADLER 92B quote separately two systematic errors: ± 0.4 from their experiment and ± 1.0 degrees due to the uncertainty in the value of Δm .
- ¹³KARLSSON 90 systematic error does not include regeneration phase uncertainty.
- ¹⁴CARITHERS 75 measures $\phi_{+-} = (45.5 \pm 2.8) + 224 [\Delta m - 0.5348] (^\circ)$. We have adjusted the measurement to use our best values of $(\Delta m = 0.5293 \pm 0.0009) (10^{10} \hbar s^{-1})$. Our first error is their experiment's error and our second error is the systematic error from using our best values. $\phi_f = -40.9 \pm 2.6^\circ$.

Meson Particle Listings

 K_L^0 ϕ_{00} , PHASE OF η_{00}

See comment in ϕ_{+-} header above for treatment of Δm and τ_S dependence, as well as for the inclusion of data in both the "Assuming CPT " and "Not Assuming CPT " fits.

OUR FIT is described in the note on "CP violation in K_L decays" in the K_L^0 Particle Listings.

VALUE (%)	DOCUMENT ID	TECN	COMMENT
43.52 ± 0.05 OUR FIT			Error includes scale factor of 1.2. Assuming CPT
43.7 ± 0.6 OUR FIT			Error includes scale factor of 1.2. Not assuming CPT
44.5 ± 2.3 ± 0.5	¹ CAROSI	90	NA31
• • •			We do not use the following data for averages, fits, limits, etc. • • •
44.06 ± 0.68	² ABOUZAID	11	KTEV Not assuming CPT
41.7 ± 5.9 ± 0.2	³ ANGELOPO...	98	CPLR
50.8 ± 7.1 ± 1.7	⁴ ADLER	96B	CPLR Sup. by ANGELOPOULOS 98
47.4 ± 1.4 ± 0.9	⁵ KARLSSON	90	E731

¹CAROSI 90 measures $\phi_{00} = (47.1 \pm 2.1 \pm 1.0) + 579 [\Delta m - 0.5351] + 252 [\tau_S - 0.8922]$ (°). We have adjusted the measurement to use our best values of ($\Delta m = 0.5293 \pm 0.0009$) (10^{10} h s^{-1}), ($\tau_S = 0.8954 \pm 0.0004$) (10^{-10} s). Our first error is their experiment's error and our second error is the systematic error from using our best values.

²Not independent of other phase parameters reported in ABOUZAID 11.

³ANGELOPOULOS 98 measures $\phi_{00} = (42.0 \pm 5.6 \pm 1.9) + 240 [\Delta m - 0.5307]$ (°). We have adjusted the measurement to use our best values of ($\Delta m = 0.5293 \pm 0.0009$) (10^{10} h s^{-1}). Our first error is their experiment's error and our second error is the systematic error from using our best values. The τ_S dependence is negligible.

⁴ADLER 96B identified initial neutral kaon individually as being a K^0 or a \bar{K}^0 . The systematic uncertainty is $\pm 1.5^\circ$ combined in quadrature with $\pm 0.8^\circ$ due to Δm .

⁵KARLSSON 90 systematic error does not include regeneration phase uncertainty.

 $\phi_\epsilon = (2\phi_{+-} + \phi_{00})/3$

This expression is a very good approximation, good to about 10^{-3} degrees because of the small measured values of $\phi_{00} - \phi_{+-}$ and $\text{Re } \epsilon'/\epsilon$, and small theoretical ambiguities.

VALUE (%)	DOCUMENT ID	TECN	COMMENT
43.52 ± 0.04 OUR FIT			Error includes scale factor of 1.2. Assuming CPT
43.5 ± 0.5 OUR FIT			Error includes scale factor of 1.3. Not assuming CPT
43.5164 ± 0.0002 ± 0.0509	¹ SUPERWEAK	16	Assuming CPT
43.86 ± 0.63	² ABOUZAID	11	KTEV Not assuming CPT

¹SUPERWEAK 16 is a fake measurement used to impose the CPT or Superweak constraint $\phi_{+-} = \phi_{SW} = \tan^{-1}[2 \frac{\Delta m}{\hbar} (\frac{\tau_S \tau_L}{\tau_S - \tau_L})]$. This "measurement" is linearized using values near the PDG 04 edition values of Δm , τ_S and τ_L , and then adjusted to our current values as described in the following "measurement". SUPERWEAK 16 measures $\phi_\epsilon = (43.50258 \pm 0.00021) + 54.1 [\Delta m - 0.5289] + 32.0 [\tau_S - 0.89564]$ (°). We have adjusted the measurement to use our best values of ($\Delta m = 0.5293 \pm 0.0009$) (10^{10} h s^{-1}), ($\tau_S = 0.8954 \pm 0.0004$) (10^{-10} s). Our first error is their experiment's error and our second error is the systematic error from using our best values.

²ABOUZAID 11 uses the full KTeV dataset collected in 1996, 1997, and 1999. See $\text{Im}(\epsilon'/\epsilon)$ section for correlation information.

 $\text{Im}(\epsilon'/\epsilon) = -(\phi_{00} - \phi_{+-})/3$

For small $|\epsilon'/\epsilon|$, $\text{Im}(\epsilon'/\epsilon)$ is related to the phases of η_{00} and η_{+-} by the above expression.

VALUE (%)	DOCUMENT ID	TECN	COMMENT
-0.002 ± 0.005 OUR FIT			Error includes scale factor of 1.7. Assuming CPT
-0.11 ± 0.11 OUR FIT			Not assuming CPT
-0.0985 ± 0.1157	¹ ABOUZAID	11	KTEV Not assuming CPT

¹ABOUZAID 11 uses the full KTeV dataset collected in 1996, 1997, and 1999. The fit has Δm , τ_S , ϕ_ϵ , $\text{Re}(\epsilon'/\epsilon)$, and $\text{Im}(\epsilon'/\epsilon)$ as free parameters. The reported value of $\text{Im}(\epsilon'/\epsilon) = (-17.20 \pm 20.20) \times 10^{-4}$ rad. The correlation coefficients are $\rho(\phi_\epsilon, \Delta m) = 0.828$, $\rho(\phi_\epsilon, \tau_S) = -0.765$, $\rho(\Delta m, \tau_S) = -0.858$, $\rho(\text{Im}(\epsilon'/\epsilon), \phi_\epsilon) = -0.041$, $\rho(\text{Im}(\epsilon'/\epsilon), \Delta m) = 0.026$, $\rho(\text{Im}(\epsilon'/\epsilon), \tau_S) = -0.010$.

DECAY-PLANE ASYMMETRY IN $\pi^+ \pi^- e^+ e^-$ DECAYS

This is the CP -violating asymmetry

$$A = \frac{N_{\sin\phi\cos\phi>0.0} - N_{\sin\phi\cos\phi<0.0}}{N_{\sin\phi\cos\phi>0.0} + N_{\sin\phi\cos\phi<0.0}}$$

where ϕ is the angle between the $e^+ e^-$ and $\pi^+ \pi^-$ planes in the K_L^0 rest frame.

CP ASYMMETRY A in $K_L^0 \rightarrow \pi^+ \pi^- e^+ e^-$

VALUE (%)	DOCUMENT ID	TECN	COMMENT
13.7 ± 1.5 OUR AVERAGE			
13.6 ± 1.4 ± 1.5	ABOUZAID	06	KTEV
14.2 ± 3.0 ± 1.9	LAI	03C	NA48
13.6 ± 2.5 ± 1.2	ALAVI-HARATI00B		KTEV

PARAMETERS FOR $e^+ e^- e^+ e^-$ DECAYS

These are the CP -violating parameters in the ϕ distribution, where ϕ is the angle between the planes of the two $e^+ e^-$ pairs in the kaon rest frame:

$$\frac{d\Gamma}{d\phi} \propto 1 + \beta_{CP} \cos(2\phi) + \gamma_{CP} \sin(2\phi)$$

where $\beta_{CP} = -0.20$ and $\gamma_{CP} = 0$ values correspond to no CP violation.

 β_{CP} from $K_L^0 \rightarrow e^+ e^- e^+ e^-$

VALUE (%)	DOCUMENT ID	TECN	COMMENT
-0.19 ± 0.07 OUR AVERAGE			
-0.13 ± 0.10 ± 0.03	¹ LAI	05B	NA48
-0.23 ± 0.09 ± 0.02	ALAVI-HARATI01D		KTEV $M_{ee} > 8 \text{ MeV}/c^2$

¹LAI 05B obtains $\beta_{CP} = -0.13 \pm 0.10$ (stat) if $\gamma_{CP} = 0$ is assumed.

 γ_{CP} from $K_L^0 \rightarrow e^+ e^- e^+ e^-$

VALUE	EVTS	DOCUMENT ID	TECN	COMMENT
0.01 ± 0.11 OUR AVERAGE				Error includes scale factor of 1.6.
+0.13 ± 0.10 ± 0.03	200	LAI	05B	NA48
-0.09 ± 0.09 ± 0.02	441	ALAVI-HARATI01D		KTEV $M_{ee} > 8 \text{ MeV}/c^2$

CHARGE ASYMMETRY IN $\pi^+ \pi^- \pi^0$ DECAYS

These are CP -violating charge-asymmetry parameters, defined at beginning of section "LINEAR COEFFICIENT g FOR $K_L^0 \rightarrow \pi^+ \pi^- \pi^0$ " above.

See also note on Dalitz plot parameters in K^\pm section and note on "CP violation in K_L decays" above.

LINEAR COEFFICIENT j FOR $K_L^0 \rightarrow \pi^+ \pi^- \pi^0$

VALUE	EVTS	DOCUMENT ID	TECN
0.0012 ± 0.0008 OUR AVERAGE			
0.0010 ± 0.0024 ± 0.0030	500k	ANGELOPO...	98C CPLR
-0.001 ± 0.011	6499	CHO	77
0.001 ± 0.003	4709	PEACH	77
0.0013 ± 0.0009	3M	SCRIBANO	70
0.0 ± 0.017	4400	SMITH	70 OSPK
0.001 ± 0.004	238k	BLANPIED	68

QUADRATIC COEFFICIENT f FOR $K_L^0 \rightarrow \pi^+ \pi^- \pi^0$

VALUE	EVTS	DOCUMENT ID	TECN
0.0045 ± 0.0024 ± 0.0059	500k	ANGELOPO...	98C CPLR

PARAMETERS for $K_L^0 \rightarrow \pi^+ \pi^- \gamma$ DECAY

$$|\eta_{+-\gamma}| = |A(K_L^0 \rightarrow \pi^+ \pi^- \gamma, CP \text{ violating})/A(K_S^0 \rightarrow \pi^+ \pi^- \gamma)|$$

VALUE (units 10^{-3})	EVTS	DOCUMENT ID	TECN
2.35 ± 0.07 OUR AVERAGE			
2.359 ± 0.062 ± 0.040	9045	MATTHEWS	95 E773
2.15 ± 0.26 ± 0.20	3671	RAMBERG	93B E731

 $\phi_{+-\gamma} = \text{phase of } \eta_{+-\gamma}$

VALUE (°)	EVTS	DOCUMENT ID	TECN
44 ± 4 OUR AVERAGE			
43.8 ± 3.5 ± 1.9	9045	MATTHEWS	95 E773
72 ± 23 ± 17	3671	RAMBERG	93B E731

 $|\epsilon'_{+-\gamma}|/\epsilon$ for $K_L^0 \rightarrow \pi^+ \pi^- \gamma$

VALUE	CL%	EVTS	DOCUMENT ID	TECN
<0.3		90	3671	¹ RAMBERG 93B E731

¹RAMBERG 93B limit on $|\epsilon'_{+-\gamma}|/\epsilon$ assumes that any difference between η_{+-} and $\eta_{+-\gamma}$ is due to direct CP violation.

 $|g_{E1}|$ for $K_L^0 \rightarrow \pi^+ \pi^- \gamma$

This parameter is the amplitude of the direct emission of a CP violating E1 electric dipole photon.

VALUE	CL%	EVTS	DOCUMENT ID	TECN	COMMENT
<0.21		90	111k	ABOUZAID 06A	KTEV $E_\gamma^* > 20 \text{ MeV}$

T VIOLATION TESTS IN K_L^0 DECAYS $\text{Im}(\xi)$ in $K_{\mu 3}^0$ DECAY (from transverse μ pol.)

Test of T reversal invariance.

VALUE	EVTS	DOCUMENT ID	TECN	COMMENT
-0.007 ± 0.026 OUR AVERAGE				
0.009 ± 0.030	12M	MORSE	80	CNTR Polarization
0.35 ± 0.30	207k	¹ CLARK	77	SPEC POL, $t=0$
-0.085 ± 0.064	2.2M	² SANDWEISS	73	CNTR POL, $t=0$
-0.02 ± 0.08		LONGO	69	CNTR POL, $t=3.3$
-0.2 ± 0.6		ABRAMS	68B	OSPK Polarization

• • • We do not use the following data for averages, fits, limits, etc. • • •

0.012 ± 0.026 SCHMIDT 79 CNTR Repl. by MORSE 80

¹CLARK 77 value has additional $\xi(0)$ dependence $+0.21\text{Re}[\xi(0)]$.

²SANDWEISS 73 value corrected from value quoted in their paper due to new value of $\text{Re}(\xi)$. See footnote 4 of SCHMIDT 79.

CPT-INVARIANCE TESTS IN K_L^0 DECAYSPHASE DIFFERENCE $\phi_{00} - \phi_{+-}$

Test of CPT .

OUR FIT is described in the note on "CP violation in K_L decays" in the K_L^0 Particle Listings.

VALUE (%)	DOCUMENT ID	TECN	COMMENT
0.006 ± 0.014 OUR FIT			Error includes scale factor of 1.7. Assuming CPT
0.34 ± 0.32 OUR FIT			Not assuming CPT
0.006 ± 0.008	¹ SUPERWEAK	16	Assuming CPT
-0.30 ± 0.88	² SCHWINGEN...	95	Combined E731, E773

- • • We do not use the following data for averages, fits, limits, etc. • • •
- 0.30 ± 0.35 ³ ABOUZAID 11 KTEV Not assuming CPT
- 0.39 ± 0.22 ± 0.45 ⁴ ALAVI-HARATI 03 KTEV
- 0.62 ± 0.71 ± 0.75 SCHWINGEN... 95 E773
- 1.6 ± 1.2 ⁵ GIBBONS 93 E731
- 0.2 ± 2.6 ± 1.2 ⁶ CAROSI 90 NA31
- 0.3 ± 2.4 ± 1.2 KARLSSON 90 E731

¹ SUPERWEAK 16 is a fake experiment to constrain $\phi_{00} - \phi_{+-}$ to a small value as described in the note "CP violation in K_L decays."

² This SCHWINGENHEUER 95 values is the combined result of SCHWINGENHEUER 95 and GIBBONS 93, accounting for correlated systematic errors.

³ Not independent of other phase parameters reported in ABOUZAID 11.

⁴ ALAVI-HARATI 03 fit $\text{Re}(\epsilon'/\epsilon)$, $\text{Im}(\epsilon'/\epsilon)$, Δm , τ_S , and ϕ_{+-} simultaneously, not assuming CPT. Phase difference is obtained from $\phi_{00} - \phi_{+-} \approx -3\text{Im}(\epsilon'/\epsilon)$ for small $|\epsilon'/\epsilon|$. Superseded by ABOUZAID 11.

⁵ GIBBONS 93 give detailed dependence of systematic error on lifetime (see the section on the K_S^0 mean life) and mass difference (see the section on $m_{K_L^0} - m_{K_S^0}$).

⁶ CAROSI 90 is excluded from the fit because it is not independent of ϕ_{+-} and ϕ_{00} values.

PHASE DIFFERENCE $\phi_{+-} - \phi_{SW}$

Test of CPT. The Superweak phase $\phi_{SW} \equiv \tan^{-1}(2\Delta m/\Delta\Gamma)$ where $\Delta m = m_{K_L^0} - m_{K_S^0}$ and $\Delta\Gamma = \hbar(\tau_L - \tau_S)/(\tau_L\tau_S)$.

VALUE (°)	DOCUMENT ID	TECN	COMMENT
0.61 ± 0.62 ± 1.01	¹ ALAVI-HARATI 03	KTEV	

¹ ALAVI-HARATI 03 fit is the same as their ϕ_{+-} , τ_{K_S} , Δm fit, except that the parameter $\phi_{+-} - \phi_{SW}$ is used in place of ϕ .

$\text{Re}(\frac{2}{3}\eta_{+-} + \frac{1}{3}\eta_{00}) - \frac{A_L}{2}$

Test of CPT

VALUE (units 10 ⁻⁶)	DOCUMENT ID	TECN	COMMENT
-3 ± 35	¹ ALAVI-HARATI 02	E799	Uses A_L from K_{e3} decays

¹ ALAVI-HARATI 02 uses PDG 00 values of η_{+-} and η_{00} .

$\Delta S = \Delta Q$ IN K^0 DECAYS

The relative amount of $\Delta S \neq \Delta Q$ component present is measured by the parameter x , defined as

$$x = A(\bar{K}^0 \rightarrow \pi^- \ell^+ \nu) / A(K^0 \rightarrow \pi^- \ell^+ \nu)$$

We list $\text{Re}\{x\}$ and $\text{Im}\{x\}$ for K_{e3} and $K_{\mu 3}$ combined.

$$x = A(\bar{K}^0 \rightarrow \pi^- \ell^+ \nu) / A(K^0 \rightarrow \pi^- \ell^+ \nu) = A(\Delta S = -\Delta Q) / A(\Delta S = \Delta Q)$$

REAL PART OF x

VALUE	EVTS	DOCUMENT ID	TECN	COMMENT
-0.0018 ± 0.0041 ± 0.0045		ANGELOPO... 98D	CPLR	K_{e3} from K^0

- • • We do not use the following data for averages, fits, limits, etc. • • •

0.10 +0.18 -0.19	79	SMITH	75B WIRE	$\pi^- p \rightarrow K^0 \Lambda$
0.04 ± 0.03	4724	NIEBERGALL	74 ASPK	$K^+ p \rightarrow K^0 p \pi^+$
-0.008 ± 0.044	1757	FACKLER	73 OSPK	K_{e3} from K^0
-0.03 ± 0.07	1367	HART	73 OSPK	K_{e3} from $K^0 \Lambda$
-0.070 ± 0.036	1079	MALLARY	73 OSPK	K_{e3} from $K^0 \Lambda X$
0.03 ± 0.06	410	¹ BURGUN	72 HBC	$K^+ p \rightarrow K^0 p \pi^+$
0.04 +0.10 -0.13	100	² GRAHAM	72 OSPK	$K_{\mu 3}$ from $K^0 \Lambda$
-0.05 ± 0.09	442	² GRAHAM	72 OSPK	$\pi^- p \rightarrow K^0 \Lambda$
0.26 +0.10 -0.14	126	MANN	72 HBC	$K^- p \rightarrow n \bar{K}^0$
-0.13 ± 0.11	342	² MANTSCH	72 OSPK	K_{e3} from $K^0 \Lambda$
0.04 +0.07 -0.08	222	¹ BURGUN	71 HBC	$K^+ p \rightarrow K^0 p \pi^+$
0.25 +0.07 -0.09	252	WEBBER	71 HBC	$K^- p \rightarrow n \bar{K}^0$
0.12 ± 0.09	215	³ CHO	70 DBC	$K^+ d \rightarrow K^0 p p$
-0.020 ± 0.025	69	⁴ BENNETT	CNTR	Charge asym + Cu regen.
0.09 +0.14 -0.16	686	LITTENBERG	69 OSPK	$K^+ n \rightarrow K^0 p$
0.03 ± 0.03	68	⁴ BENNETT	CNTR	
0.09 +0.07 -0.09	121	JAMES	68 HBC	$\bar{p} p$
0.17 +0.16 -0.35	116	FELDMAN	67B OSPK	$\pi^- p \rightarrow K^0 \Lambda$
0.17 ± 0.10	335	³ HILL	67 DBC	$K^+ d \rightarrow K^0 p p$
0.035 +0.11 -0.13	196	AUBERT	65 HLBC	K^+ charge exch.
0.06 +0.18 -0.44	152	⁵ BALDO...	65 HLBC	K^+ charge exch.
-0.08 +0.16 -0.28	109	⁶ FRANZINI	65 HBC	$\bar{p} p$

¹ BURGUN 72 is a final result which includes BURGUN 71.

- ² First GRAHAM 72 value is second GRAHAM 72 value combined with MANTSCH 72.
- ³ CHO 70 is analysis of unambiguous events in new data and HILL 67.
- ⁴ BENNETT 69 is a reanalysis of BENNETT 68.
- ⁵ BALDO-CEOLIN 65 gives x and θ converted by us to $\text{Re}(x)$ and $\text{Im}(x)$.
- ⁶ FRANZINI 65 gives x and θ for $\text{Re}(x)$ and $\text{Im}(x)$. See SCHMIDT 67.

IMAGINARY PART OF x

Assumes $m_{K_L^0} - m_{K_S^0}$ positive. See Listings above.

VALUE	EVTS	DOCUMENT ID	TECN	COMMENT
0.0012 ± 0.0019 ± 0.0009	640k	ANGELOPO... 01B	CPLR	K_{e3} from K^0
• • • We do not use the following data for averages, fits, limits, etc. • • •				
0.0012 ± 0.0019	640k	¹ ANGELOPO... 98E	CPLR	K_{e3} from K^0
-0.10 +0.16 -0.19	79	SMITH	75B WIRE	$\pi^- p \rightarrow K^0 \Lambda$
-0.06 ± 0.05	4724	NIEBERGALL	74 ASPK	$K^+ p \rightarrow K^0 p \pi^+$
-0.017 ± 0.060	1757	FACKLER	73 OSPK	K_{e3} from K^0
0.09 ± 0.07	1367	HART	73 OSPK	K_{e3} from $K^0 \Lambda$
0.107 +0.092 -0.074	1079	MALLARY	73 OSPK	K_{e3} from $K^0 \Lambda X$
0.07 +0.06 -0.07	410	² BURGUN	72 HBC	$K^+ p \rightarrow K^0 p \pi^+$
0.12 +0.17 -0.16	100	³ GRAHAM	72 OSPK	$K_{\mu 3}$ from $K^0 \Lambda$
0.05 ± 0.13	442	³ GRAHAM	72 OSPK	$\pi^- p \rightarrow K^0 \Lambda$
0.21 +0.15 -0.12	126	MANN	72 HBC	$K^- p \rightarrow n \bar{K}^0$
-0.04 ± 0.16	342	³ MANTSCH	72 OSPK	K_{e3} from $K^0 \Lambda$
0.12 +0.08 -0.09	222	² BURGUN	71 HBC	$K^+ p \rightarrow K^0 p \pi^+$
0.0 ± 0.08	252	WEBBER	71 HBC	$K^- p \rightarrow n \bar{K}^0$
-0.08 ± 0.07	215	⁴ CHO	70 DBC	$K^+ d \rightarrow K^0 p p$
-0.11 +0.10 -0.11	686	LITTENBERG	69 OSPK	$K^+ n \rightarrow K^0 p$
+0.22 +0.37 -0.29	121	JAMES	68 HBC	$\bar{p} p$
0.0 ± 0.25	116	FELDMAN	67B OSPK	$\pi^- p \rightarrow K^0 \Lambda$
-0.20 ± 0.10	335	⁴ HILL	67 DBC	$K^+ d \rightarrow K^0 p p$
-0.21 +0.11 -0.15	196	AUBERT	65 HLBC	K^+ charge exch.
-0.44 +0.32 -0.19	152	⁵ BALDO...	65 HLBC	K^+ charge exch.
+0.24 +0.40 -0.30	109	⁶ FRANZINI	65 HBC	$\bar{p} p$

- ¹ Superseded by ANGELOPOULOS 01B.
- ² BURGUN 72 is a final result which includes BURGUN 71.
- ³ First GRAHAM 72 value is second GRAHAM 72 value combined with MANTSCH 72.
- ⁴ Footnote 10 of HILL 67 should read +0.58, not -0.58 (private communication) CHO 70 is analysis of unambiguous events in new data and HILL 67.
- ⁵ BALDO-CEOLIN 65 gives x and θ converted by us to $\text{Re}(x)$ and $\text{Im}(x)$.
- ⁶ FRANZINI 65 gives x and θ for $\text{Re}(x)$ and $\text{Im}(x)$. See SCHMIDT 67.

K_L^0 REFERENCES

AAIJ	23AE	PR D108 L031102	R. Aaij et al.	(LHCb Collab.)
AHN	21	PRL 126 121801	J.K. Ahn et al.	(KOTO Collab.)
SHIMIZU	20	PR D102 051103	N. Shimizu et al.	(KOTO Collab.)
AHN	19	PRL 122 021802	J.K. Ahn et al.	(KOTO Collab.)
AHN	17	PTEP 2017 021C01	J.K. Ahn et al.	(KOTO Collab.)
BRFIT	16	RPP 2016 edition	C.-J. Lin	(PDG Collab.)
ETAFIT	16	RPP 2016 edition	C.-J. Lin	(PDG Collab.)
SUPERWEAK	16	RPP 2016 edition	C.-J. Lin	(PDG Collab.)
ABOUZAID	11	PR D83 092001	E. Abouzaid et al.	(FNAL KTeV Collab.)
ABOUZAID	11A	PRL 107 201803	E. Abouzaid et al.	(KTeV Collab.)
OGATA	11	PR D84 052009	R. Ogata et al.	(KEK E391A Collab.)
TUNG	11	PR D83 031101	Y.C. Tung et al.	(KEK E391A Collab.)
ABOUZAID	10	PR D81 052001	E. Abouzaid et al.	(FNAL KTeV Collab.)
AHN	10	PR D81 072004	J.K. Ahn et al.	(KEK E391A Collab.)
ABOUZAID	08	PR D77 112004	E. Abouzaid et al.	(FNAL KTeV Collab.)
ABOUZAID	08A	PR D78 032009	E. Abouzaid et al.	(FNAL KTeV Collab.)
ABOUZAID	08B	PR D78 032014	E. Abouzaid et al.	(FNAL KTeV Collab.)
ABOUZAID	08C	PRL 100 131803	J.K. Ahn et al.	(FNAL KTeV Collab.)
AHN	08	PRL 100 201802	J.K. Ahn et al.	(KEK E391A Collab.)
AMBROSINO	08F	EPJ C55 539	F. Ambrosino et al.	(KLOE Collab.)
ABOUZAID	07B	PRL 99 051804	E. Abouzaid et al.	(FNAL KTeV Collab.)
ABOUZAID	07C	PRL 99 081803	E. Abouzaid et al.	(FNAL KTeV Collab.)
ABOUZAID	07D	PR D76 052001	E. Abouzaid et al.	(FNAL KTeV Collab.)
AMBROSINO	07C	JHEP 0712 105	F. Ambrosino et al.	(KLOE Collab.)
ANDRE	07	ANP 322 2518	T. Andre	(EFI)
LAI	07	PL B645 26	A. Lai et al.	(CERN NA48 Collab.)
LAI	07A	PL B647 341	A. Lai et al.	(CERN NA48 Collab.)
NIX	07	PR D76 011101	J. Nix et al.	(KEK E391A Collab.)
ABOUZAID	06	PRL 96 101801	E. Abouzaid et al.	(KTeV Collab.)
ABOUZAID	06A	PR D74 032004	E. Abouzaid et al.	(KTeV Collab.)
Also		PR D74 039905 (errat.)	E. Abouzaid et al.	(KTeV Collab.)
ABOUZAID	06C	PR D74 097101	E. Abouzaid et al.	(KTeV Collab.)
AHN	06	PR D74 051105	J.K. Ahn et al.	(KEK E391A Collab.)
Also		PR D74 079901 (errat.)	J.K. Ahn et al.	(KEK E391A Collab.)
AMBROSINO	06	PL B632 43	F. Ambrosino et al.	(KLOE Collab.)
AMBROSINO	06D	PL B636 166	F. Ambrosino et al.	(KLOE Collab.)
AMBROSINO	06F	PL B638 140	F. Ambrosino et al.	(KLOE Collab.)
BATLEY	06B	PL B633 173	J.R. Batley et al.	(CERN NA48/2 Collab.)
HILL	06	PR D74 096006	R.J. Hill	(FNAL)
PDG	06	JP 033 1	W.-M. Yao et al.	(PDG Collab.)
ALEXOPOU... 05	PR D71 012001	T. Alexopoulos et al.	(FNAL KTeV Collab.)	
AMBROSINO 05C	PL B626 15	F. Ambrosino et al.	(KLOE Collab.)	
CABIBBO	05	JHEP 0503 021	N. Cabibbo, G. Isidori	(CERN, ROMA1, FRAS)
LAI	05	PL B605 247	A. Lai et al.	(CERN NA48 Collab.)
LAI	05B	PL B615 31	A. Lai et al.	(CERN NA48 Collab.)
PARK	05	PRL 94 021801	H.K. Park et al.	(FNAL HyperCP Collab.)
ALAVI-HARATI 04A	PRL 93 021805	A. Alavi-Harati et al.	(FNAL KTeV/E799 Collab.)	
ALEXOPOU... 04	PR D70 092006	T. Alexopoulos et al.	(FNAL KTeV Collab.)	
ALEXOPOU... 04A	PR D70 092007	T. Alexopoulos et al.	(FNAL KTeV Collab.)	
BATLEY	04	PL B595 75	J.R. Batley et al.	(CERN NA48 Collab.)
CIRIGLIANO	04	EPJ C35 53	V. Cirigliano, H. Neufeld, H. Pichl	(CIT, VALE+)

Meson Particle Listings

 K_L^0

LAI	04B	PL B602 41	A. Lai et al.	(CERN N448 Collab.)	PDG	86C	PL 170B 132	M. Aguilar-Benitez et al.	(CERN, CIT+)
LAI	04C	PL B604 1	A. Lai et al.	(CERN N448 Collab.)	COUPL	85	PRL 55 566	D.P. Coupl et al.	(CHIC, SLAC)
PDG	04	PL B592 1	S. Edelman et al.	(PDG Collab.)	BALATS	83	SJNP 38 556	M.Y. Balats et al.	(ITEP)
SOZZI	04	EPJ C36 37	M. Sozzi	(PISA)			Translated from YAF 38 927.		
ADINOLFI	03	PL B566 61	M. Adinolfi et al.	(KLOE Collab.)	BERGSTROM	83	PL 131B 229	L. Bergstrom, E. Masso, P. Singer	(CERN)
ALAVI-HARATI	03	PR D67 012005	A. Alavi-Harati et al.	(FNAL KTeV Collab.)	ARONSON	82B	PRL 48 1078	S.H. Aronson et al.	(BNL, CHIC, STAN+)
Also		PR D70 079904 (err.)	A. Alavi-Harati et al.	(FNAL KTeV Collab.)	ARONSON	82B	PRL 48 1306	S.H. Aronson et al.	(BNL, CHIC, PURD)
ALAVI-HARATI	03B	PRL 90 141801	A. Alavi-Harati et al.	(FNAL KTeV Collab.)	Also		PL 116B 73	E. Fischbach et al.	(PURD, BNL, CHIC)
LAI	03	PL B551 33	A. Lai et al.	(CERN N448 Collab.)	Also		PR D28 476	S.H. Aronson et al.	(BNL, CHIC, PURD)
LAI	03C	EPJ C30 33	A. Lai et al.	(CERN N448 Collab.)	Also		PR D28 495	S.H. Aronson et al.	(BNL, CHIC, PURD)
ALAVI-HARATI	02	PRL 88 181601	A. Alavi-Harati et al.	(FNAL KTeV Collab.)	PDG	82B	PL 111B 70	M. Roos et al.	(HELS, CIT, CERN)
ALAVI-HARATI	02C	PRL 89 211801	A. Alavi-Harati et al.	(FNAL KTeV Collab.)	BIRULEV	81	NP B182 1	V.K. Birulev et al.	(JINR)
BATLEY	02	PL B544 97	J.R. Batley et al.	(CERN N448 Collab.)	Also		SJNP 31 622	V.K. Birulev et al.	(JINR)
CIRIGLIANO	02	EPJ C23 121	V. Cirigliano et al.	(VIEN, VALE, MARS)			Translated from YAF 31 1204.		
LAI	02B	PL B536 229	A. Lai et al.	(CERN N448 Collab.)	CARROLL	80B	PRL 44 529	A.S. Carroll et al.	(BNL, ROCH)
ALAVI-HARATI	01	PRL 86 397	A. Alavi-Harati et al.	(FNAL KTeV Collab.)	CARROLL	80C	PL 96B 407	A.S. Carroll et al.	(BNL, ROCH)
ALAVI-HARATI	01B	PRL 86 761	A. Alavi-Harati et al.	(FNAL KTeV Collab.)	CHO	80	PR D22 2688	Y. Cho et al.	(ANL, CMU)
ALAVI-HARATI	01D	PRL 86 5425	A. Alavi-Harati et al.	(FNAL KTeV Collab.)	MORSE	80	PR D21 1750	W.M. Morse et al.	(BNL, YALE)
ALAVI-HARATI	01E	PRL 87 021801	A. Alavi-Harati et al.	(FNAL KTeV Collab.)	CHRISTENS...	79	PRL 43 1209	J.H. Christenson et al.	(NYU)
ALAVI-HARATI	01F	PR D64 012003	A. Alavi-Harati et al.	(FNAL KTeV Collab.)	SCHMIDT	79	PRL 43 556	M.P. Schmidt et al.	(YALE, BNL)
ALAVI-HARATI	01G	PRL 87 071801	A. Alavi-Harati et al.	(FNAL KTeV Collab.)	HILL	78	PL 73B 883	D.G. Hill et al.	(BNL, SLAC, SBER)
ALAVI-HARATI	01H	PRL 87 111802	A. Alavi-Harati et al.	(FNAL KTeV Collab.)	CHO	77	PR D15 587	Y. Cho et al.	(ANL, CMU)
ALAVI-HARATI	01J	PR D64 112004	A. Alavi-Harati et al.	(FNAL KTeV Collab.)	CLARK	77	PR D15 553	A.R. Clark et al.	(LBL)
ANGELOPO...	01	PL B503 49	A. Angelopoulos et al.	(CLEAR Collab.)	Also		Thesis LBL-4275	G. Shen	(LBL)
ANGELOPO...	01B	EPJ C22 55	A. Angelopoulos et al.	(CLEAR Collab.)	DEVOE	77	PR D16 565	R. Devoe et al.	(EFI, ANL)
LAI	01B	PL B515 261	A. Lai et al.	(CERN N448 Collab.)	PEACH	77	NP B127 399	K.J. Peach et al.	(BGNA, EDIN, GLAS+)
LAI	01C	EPJ C22 231	A. Lai et al.	(CERN N448 Collab.)	BIRULEV	76	SJNP 24 178	V.K. Birulev et al.	(JINR)
ALAVI-HARATI	00	PR D61 072006	A. Alavi-Harati et al.	(FNAL KTeV Collab.)			Translated from YAF 24 340.		
ALAVI-HARATI	00B	PRL 84 408	A. Alavi-Harati et al.	(FNAL KTeV Collab.)	COOMBES	76	PRL 37 249	R.W. Coombes et al.	(STAN, NYU)
ALAVI-HARATI	00D	PRL 84 5279	A. Alavi-Harati et al.	(FNAL KTeV Collab.)	GJESDAL	76	NP B109 118	G. Gjesdal et al.	(CERN, HEID)
ALAVI-HARATI	00E	PR D62 112001	A. Alavi-Harati et al.	(FNAL KTeV Collab.)	BALDO...	75	NC 25A 688	M. Baldo-Ceolin et al.	(PADO, WISC)
AMBRROSE	00	PRL 84 1389	D. Ambrose et al.	(BNL E871 Collab.)	BLUMENTHAL	75	PRL 34 164	R.B. Blumenthal et al.	(PENN, CHIC, TEMP)
APOSTOLA...	00	PL B473 186	A. Apostolakis et al.	(CLEAR Collab.)	BUCHANAN	75	PR D11 457	C.D. Buchanan et al.	(UCLA, SLAC, JHU)
PDG	00	EPJ C15 1	D.E. Groom et al.	(PDG Collab.)	CARITHERS	75	PRL 34 1244	W.C.J. Carithers et al.	(COLU, NYU)
ALAVI-HARATI	99B	PRL 83 917	A. Alavi-Harati et al.	(FNAL KTeV Collab.)	SMITH	75B	Thesis UCSD unpub.	J.G. Smith	(UCSD)
ALAVI-HARATI	99D	PRL 83 22	A. Alavi-Harati et al.	(FNAL KTeV Collab.)	BISI	74	PL 90B 504	V. Bisi, M.I. Ferrero	(TORI)
APOSTOLA...	99C	PL B458 545	A. Apostolakis et al.	(CLEAR Collab.)	DONALDSON	74	Thesis SLAC-0184	G. Donaldson	(SLAC)
Also		EPJ C18 41	A. Apostolakis et al.	(CLEAR Collab.)	Also		PR D14 2839	G. Donaldson et al.	(SLAC)
FANTI	99B	PL B458 553	V. Fanti et al.	(CERN N448 Collab.)	DONALDSON	74B	PR D9 2960	G. Donaldson et al.	(SLAC, UCSC)
FANTI	99C	PL B465 335	V. Fanti et al.	(CERN N448 Collab.)	Also		PRL 31 337	G. Donaldson et al.	(SLAC, UCSC)
MURAKAMI	99	PL B463 333	K. Murakami et al.	(KEK E162 Collab.)	GEWENIGER	74	PL 48B 483	C. Geweniger et al.	(CERN, HEID)
ADAMS	98	PRL 80 4123	J. Adams et al.	(FNAL KTeV Collab.)	Also		Thesis CERN Int. 74-4	V. Luth	(CERN)
AMBRROSE	98	PRL 81 4309	D. Ambrose et al.	(BNL E871 Collab.)	GEWENIGER	74B	PL 48B 487	C. Geweniger et al.	(CERN, HEID)
AMBRROSE	98B	PRL 81 5734	D. Ambrose et al.	(BNL E871 Collab.)	Also		PL 52B 119	S. Gjesdal et al.	(CERN, HEID)
ANGELOPO...	98	PL B420 191	A. Angelopoulos et al.	(CLEAR Collab.)	GEWENIGER	74C	PL 52B 108	C. Geweniger et al.	(CERN, HEID)
ANGELOPO...	98C	EPJ C5 389	A. Angelopoulos et al.	(CLEAR Collab.)	GJESDAL	74	PL 52B 113	S. Gjesdal et al.	(CERN, HEID)
ANGELOPO...	98D	PL B444 38	A. Angelopoulos et al.	(CLEAR Collab.)	MESSNER	74	PRL 33 1458	R. Messner et al.	(COLO, SLAC, UCSC)
Also		EPJ C22 55	A. Angelopoulos et al.	(CLEAR Collab.)	NIEBERGALL	74	PL 49B 103	F. Niebergall et al.	(CERN, ORSAY, VIEN)
ANGELOPO...	98E	PL B444 43	A. Angelopoulos et al.	(CLEAR Collab.)	WILLIAMS	74	PR 33 2103	H.H. Williams et al.	(BNL, YALE)
ARISAKA	98	PL B432 230	K. Arisaka et al.	(FNAL E799 Collab.)	ALEXANDER	73B	NP B65 301	G. Alexander et al.	(TELA, HEID)
BENDER	98	PL B418 411	M. Bender et al.	(CERN N448 Collab.)	BRANDENB...	73	PR D8 1978	G.W. Brandenburg et al.	(SLAC)
DAMBROSIO	98	PL B423 385	G. D'Ambrósio, G. Isidori, J. Portoles		EVANS	73	PR D7 36	G.R. Evans et al.	(EDIN, CERN)
SETZU	98	PL B420 205	M. G. Setzu et al.		Also		PRL 23 427	G.R. Evans et al.	(EDIN, CERN)
TAKEUCHI	98	PL B443 409	Y. Takeuchi et al.	(KYOT, KEK, HIRO)	FACKLER	73	PRL 31 847	O. Fackler et al.	(MIT)
FANTI	97	ZPHY C76 653	V. Fanti et al.	(CERN N448 Collab.)	FITCH	73	PRL 31 1524	V.L. Fitch et al.	(PRIN)
NOMURA	97	PL B408 445	T. Nomura et al.	(KYOT, KEK, HIRO)	Also		Thesis COO-3072-13	R.C. Webb	(PRIN)
ADLER	96B	ZPHY C70 211	R. Adler et al.	(CLEAR Collab.)	HART	73	NP B66 317	J.C. Hart et al.	(CAVE, RHEL)
ADLER	96C	PL B369 367	R. Adler et al.	(CLEAR Collab.)	MALLARY	73	PR D7 1953	M.L. Mallary et al.	(CIT)
GU	96	PRL 76 4312	P. Gu et al.	(RUTG, UCLA, EFI, COLO+)	Also		PRL 25 1214	F.J. Sciulli et al.	(CIT)
LEBER	96	PL B369 69	F. Leber et al.	(MAINZ, CERN, EDIN, ORSAY+)	MCCARTHY	73	PR D7 687	R.L. McCarthy et al.	(LBL)
PDG	96	PR D54 1	R. M. Barnett et al.	(PDG Collab.)	Also		PL 42B 291	R.L. McCarthy et al.	(LBL)
ADLER	95	PL B363 237	R. Adler et al.	(CLEAR Collab.)	MESSNER	73	Thesis LBL-550	R.L. McCarthy	(LBL)
ADLER	95B	PL B363 243	R. Adler et al.	(CLEAR Collab.)	SANDWEISS	73	PRL 30 876	R. Messner et al.	(COLO, SLAC, UCSC)
AKAGI	95	PR D51 2061	T. Akagi et al.	(TOHOK, TOKY, KYOT, KEK)	WILLIAMS	73	PRL 31 1521	J. Sandweiss et al.	(YALE, ANL)
BARR	95	ZPHY C65 361	G.D. Barr et al.	(CERN, EDIN, MAINZ, LALO+)	ASHFORD	72	PL 38B 47	H.H. Williams et al.	(BNL, YALE)
BARR	95C	PL B358 399	G.D. Barr et al.	(CERN, EDIN, MAINZ, LALO+)	BANNER	72B	PR 29 237	V.A. Ashford et al.	(CHIC, UCSD)
HEINSON	95	PR D51 985	A.P. Heinson et al.	(BNL E791 Collab.)	BARMIN	72B	SJNP 15 638	M. Banner et al.	(PRIN)
KREUTZ	95	ZPHY C65 67	A. Kreutz et al.	(SIEG, EDIN, MAINZ, ORSAY+)	Also		SJNP 15 638	V.V. Barmin et al.	(ITEP)
MATTHEWS	95	PRL 75 2803	J.N. Matthews et al.	(RUTG, EFI, ELMT+)	BURGUN	72	NP B50 194	G. Burgun et al.	(SACL, CERN, OSLO)
SCHWINGEN...	95	PRL 74 4376	B. Schwingenheuer et al.	(EFI, CHIC+)	GRAHAM	72	NC 9A 166	M.F. Graham et al.	(ILL, NEAS)
SPENCER	95	PRL 74 3323	M.B. Spencer et al.	(UCLA, EFI, COLO+)	JAMES	72	NP B49 1	F. James et al.	(CERN, SACL, OSLO)
BARR	94	PL B328 528	G.D. Barr et al.	(CERN, EDIN, MAINZ, LALO+)	KRENZ	72	LNC 4 213	W. Krenz et al.	(AACH, CERN, EDIN)
GU	94	PRL 72 3000	P. Gu et al.	(RUTG, UCLA, EFI, COLO+)	MANN	72	PR D6 137	W.A. Mann et al.	(MASA, BNL, YALE)
NAKAYA	94	PRL 73 2169	T. Nakaya et al.	(OSAK, UCLA, EFI, COLO+)	MANTSCH	72	NC 9A 160	P.M. Mantsch et al.	(ILL, NEAS)
ROBERTS	94	PR D50 1874	D. Roberts et al.	(UCLA, EFI, COLO+)	MCCARTHY	72	PL 42B 291	R.L. McCarthy et al.	(SLAC)
AKAGI	93	PL B371 2444	T. Akagi et al.	(TOHOK, TOKY, KYOT, KEK)	PICCIONI	72	PRL 29 1412	R. Piccioni et al.	(SLAC)
ARISAKA	93	PRL 70 1049	K. Arisaka et al.	(BNL E791 Collab.)	Also		PR D9 2939	R. Piccioni et al.	(SLAC, UCSC, COLO)
ARISAKA	93B	PRL 71 3910	K. Arisaka et al.	(BNL E791 Collab.)	VOSBURGH	72	PR D6 1834	K.G. Vosburgh et al.	(RUTG, MASA)
BARR	93D	PL B317 233	G.D. Barr et al.	(CERN, EDIN, MAINZ, LALO+)	Also		PR D6 966	K.G. Vosburgh et al.	(RUTG, MASA)
GIBBONS	93	PRL 70 1199	L.K. Gibbons et al.	(FNAL E731 Collab.)	BALATS	71	SJNP 13 53	M.Y. Balats et al.	(ITEP)
Also		PR D55 6625	L.K. Gibbons et al.	(FNAL E731 Collab.)	Also		Translated from YAF 13 93.		
GIBBONS	93B	PRL 70 1203	L.K. Gibbons et al.	(FNAL E731 Collab.)	BARMIN	71	PL 35B 604	V.V. Barmin et al.	(ITEP)
GIBBONS	93C	Thesis RX-1487	L.K. Gibbons	(CHIC)	BURGUN	71	LNC 2 1169	G. Burgun et al.	(SACL, CERN, OSLO)
Also		PR D55 6625	L.K. Gibbons et al.	(FNAL E731 Collab.)	CARNEGIE	71	PR D4 1	R.K. Carnegie et al.	(PRIN)
HARRIS	93	PRL 71 3914	D.A. Harris et al.	(EFI, UCLA, COLO+)	CHAN	71	Thesis LBL-350	J.H.S. Chan	(CERN, BNL, CASE)
HARRIS	93B	PRL 71 3918	D.A. Harris et al.	(EFI, UCLA, COLO+)	CHO	71	PR D3 1557	Y. Cho et al.	(CMU, BNL, LBL)
MAKOFF	93	PRL 70 1571	G. Makoff et al.	(FNAL E731 Collab.)	ENSTROM	71	PR D4 2629	J. Enstrom et al.	(SLAC, STAN)
Also		PR 75 2019 (err.)	G. Makoff et al.	(FNAL E731 Collab.)	Also		Thesis SLAC-0125	J.E. Enstrom	(STAN)
RAMBERG	93	PRL 70 2525	E. Ramberg et al.	(FNAL E731 Collab.)	JAMES	71	PL 35B 215	F. James et al.	(CERN, SACL, OSLO)
RAMBERG	93B	PRL 70 2529	E.J. Ramberg et al.	(FNAL E731 Collab.)	MEISNER	71	PR D3 59	G.W. Meisner et al.	(MASA, BNL, YALE)
VAGINS	93	PRL 71 35	M.R. Vagins et al.	(BNL E845 Collab.)	REPELLIN	71	PL 36B 603	J.P. Repellin et al.	(ORSAY, CERN)
ADLER	92B	PL B286 180	R. Adler et al.	(CLEAR Collab.)	WEBBER	71	PR D3 64	B.R. Webber et al.	(LRL)
Also		SJNP 55 840	R. Adler et al.	(CLEAR Collab.)	Also		PRL 21 498	B.R. Webber et al.	(LRL)
BARR	92	PL B284 440	G.D. Barr et al.	(CERN, EDIN, MAINZ, LALO+)	Also		Thesis UCRL 19226	B.R. Webber	(LRL)
MORSE	92	PR D45 36	W.M. Morse et al.	(BNL, VALE, VASS)	WOLFF	71	PL 36B 517	B. Wolff et al.	(ORSAY, CERN)
PDG	92	PR D45 51	K. Hikasa et al.	(KEK, LBL, BOST+)	ALBROW	70	PL 33B 516	M.G. Albrow et al.	(MCHS, DARE)
SOMALWAR	92	PRL 68 2580	S.V. Somalwar et al.	(FNAL E731 Collab.)	ARONSON	70	PRL 25 1057	S.H. Aronson et al.	(EFI, ILLC, SLAC)
AKAGI	91B	PR 67 2618	T. Akagi et al.	(TOHOK, TOKY, KYOT, KEK)	BARMIN	70	PL 33B 377	V.V. Barmin et al.	(ITEP, JINR)
BARR	91	PL B259 309	G.D. Barr et al.	(CERN, EDIN, MAINZ, LALO+)	BASEL	70	PR D2 787	P. Basel et al.	(SACL)
HEINSON	91	PR D44 1	A.P. Heinson et al.	(UCL, UCLA, LANL+)	BECHERAWY	70	PR D1 1452	T. Becherawy	(ROCH)
PAPADIMITR...	91	PR D44 573	V. Papadimitriou et al.	(FNAL E731 Collab.)	BUCHANAN	70	PL 33B 623	C.D. Buchanan et al.	(SLAC, JHU, UCLA)
BARKER	90	PR D41 3546	A.R. Barker et al.	(FNAL E731 Collab.)	Also		Private Comm.	A.J. Cox	
Also		PRL 61 2661	L.K. Gibbons et al.	(FNAL E731 Collab.)	BUDAGOV	70	PR D2 815	I.A. Budagov et al.	(CERN, ORSAY, EPOL)
BARR	90B	PL B240 283	G.D. Barr et al.	(CERN, EDIN, MAINZ, LALO+)	Also		PL 28B 215	I.A. Budagov et al.	(CERN, ORSAY, EPOL)
BARR	90C	PL B242 523	G.D. Barr et al.	(CERN, EDIN, MAINZ, LALO+)	CHO	70	PR D1 3031	Y. Cho et al.	(CMU, BNL, CASE)
CAROSI	90	PL B237 303	R. Carosi et al.	(CERN, EDIN, MAINZ, LALO+)	Also		PRL 19 668	D.G. Hill et al.	(BNL, CMU)
KARLSSON	90	PRL 64 2976	M. Karlsson et al.	(FNAL E731 Collab.)	CHOLLET	70	PL 31B 658	J.C. Chollet et al.	(CERN)
OHL	90	PRL 64 2755	K.E. Ohi et al.	(BNL E845 Collab.)	CULLEN	70	PL 32B 523	M. Cullen et al.	(AACH, CERN, TORI)
OHL	90B	PRL 65 1407	K.E. Ohi et al.	(BNL E845 Collab.)	MARX	70	PL 32B 219	J. Marx et al.	(COLU, HARV, CERN)
PATTERSON	90	PRL 64 1493	J.R. Patterson et al.	(FNAL E731 Collab.)	Also		Thesis Nevis 179	J. Marx	(COLU)
INAGAKI	89	PR D40 1712	T. Inagaki et al.	(KEK, TOKY, KYOT)	SCRIBANO	70	PL 32B 224	A. Scribano et al.	(PISA, COLU, HARV)
MATHIAZH...	89	PRL 63 2181	C. Mathiazhagan et al.	(UCL, UCLA, LANL+)	SMITH	70	PL 32B 133	R.C. Smith et al.	(UMD, BNL)
MATHIAZH...	89B	PRL 63 2185	C. Mathiazhagan et al.	(UCL, UCLA, LANL+)	WEBBER	70	PR D1 1967	B.R. Webber et al.	(LRL)
WAHL	89	CERN-EP/89-86	H. Wahl	(CERN)	Also		Thesis UCRL 19226	B.R. Webber	(LRL)
BARR	88	PL B214 303	G.D. Barr et al.	(CERN, EDIN, MAINZ, LALO+)	BANNER	69	PR 188 2033	M. Banner et al.	(PRIN)
BURKHARDT	88	PL B206 169	H. Burkhardt et al.	(CERN, EDIN, MAINZ, Z+)	Also		PRL 21 1103	M. Banner et al.	(PRIN)
JASTRZEM...	88	PRL 61 2300	E. Jastrzembski et al.						

See key on page 1171

Meson Particle Listings

$K_L^0, K_0^*(700)$

SAAL	69	Thesis	H.J. Saal	(COLU)
ABRAMS	68B	PR 176 1603	R.G. Abrams <i>et al.</i>	(ILL)
ARNOLD	68B	PL 28B 56	R.G. Arnold <i>et al.</i>	(CERN, ORSAY)
BASILE	68B	PL 28B 58	P. Basile <i>et al.</i>	(SACL)
BENNETT	68	PL 27B 244	S. Bennett <i>et al.</i>	(COLU, CERN)
BLANPIED	68	PRL 21 1650	W.A. Blanpied <i>et al.</i>	(CASE, HARV, MCGI)
BOHM	68B	PL 27B 594	A. Bohm <i>et al.</i>	
BUDAGOV	68	NC 57A 182	I.A. Budagov <i>et al.</i>	(CERN, ORSAY, IPNP)
Also		PL 28B 215	I.A. Budagov <i>et al.</i>	(CERN, ORSAY, EPOL)
JAMES	68	NP B3 365	F. James, H. Briand	(IPNP, CERN)
Also		PRL 21 257	J.A. Holland, M.J. Longo, K.K. Young	(UCLA, MICH)
KULYUKINA	68	JETP 26 20	L.A. Kulyukina <i>et al.</i>	(JINR)
Also		Translated from ZETF 53 29		
KUNZ	68	Thesis PU-68-46	P.F. Kunz	(PRIN)
BENNETT	67	PRL 19 993	S. Bennett <i>et al.</i>	(COLU)
DEBOUARD	67	NC 52A 662	X. de Bouard <i>et al.</i>	(CERN)
Also		PL 15 58	X. de Bouard <i>et al.</i>	(CERN, ORSAY, MPIM)
DEVLIN	67	PRL 18 54	T.J. Devlin <i>et al.</i>	(PRIN, UMD)
Also		PR 169 1045	G.A. Sayer <i>et al.</i>	(UMD, PPA, PRIN)
DORFAN	67	PRL 19 987	D.E. Dorfman <i>et al.</i>	(SLAC, LRL)
FELDMAN	67B	PR 155 1611	L. Feldman <i>et al.</i>	(PRIN)
FITCH	67	PR 164 1711	V.L. Fitch <i>et al.</i>	(PRIN)
GINSBERG	67	PR 162 1570	E.S. Ginsberg	(MASB)
HILL	67	PRL 19 668	D.G. Hill <i>et al.</i>	(BNL, CMU)
HOPKINS	67	PRL 19 185	H.W.K. Hopkins, T.C. Bacon, F.R. Eisler	(BNL)
NEFKENS	67	PR 157 1233	B.M.K. Nefkens <i>et al.</i>	(ILL)
SCHMIDT	67	Thesis Nevis 160	P. Schmidt	(COLU)
BEHR	66	PL 22 540	L. Behr <i>et al.</i>	(EPOL, MILA, PADO, ORSAY)
HAWKINS	66	PL 21 238	C.J.B. Hawkins	(YALE)
Also		PR 156 1444	C.J.B. Hawkins	(YALE)
ANDERSON	65	PRL 14 475	J.A. Anderson <i>et al.</i>	(LRL, WIS-C)
ASTBURY	65B	PL 18 175	P. Astbury <i>et al.</i>	(CERN, ZURI)
AUBERT	65	PL 17 59	B. Aubert <i>et al.</i>	(EPOL, ORSAY)
Also		PL 24B 75	J.P. Lowys <i>et al.</i>	(EPOL, ORSAY)
BALDO...	65	NC 38 684	M. Baldo-Geolin <i>et al.</i>	(PADO)
FRANZINI	65	PR 140 B127	P. Franzini <i>et al.</i>	(COLU, RUTG)
GUIDONI	65	Argonne Conf. 49	P. Guidoni <i>et al.</i>	(BNL, YALE)
HOPKINS	65	Argonne Conf. 67	H.W.K. Hopkins, T.C. Bacon, F. Eisler	(VAND+)
ALEKSANYAN	64B	Dubna Conf. 2 102	A.S. Aleksanyan <i>et al.</i>	(YERE)
Also		JETP 19 1019	A.S. Aleksanyan <i>et al.</i>	(LEBD, MPEI, YERE)
Also		Translated from ZETF 46 1504		
ANIKINA	64	JETP 19 42	M.K. Anikina <i>et al.</i>	(GEOR, JINR)
Also		Translated from ZETF 46 59		
FITCH	61	NC 22 1160	V.L. Fitch, P.A. Piroue, R.B. Perkins	(PRIN+)
GOOD	61	PR 124 1223	R.H. Good <i>et al.</i>	(LRL)

OTHER RELATED PAPERS

HAYAKAWA	93	PR D48 1150	M. Hayakawa, A.J. Sanda	(NAGO)
Also		"Searching for $T, CP, CPT, \Delta S = \Delta Q$ Rule Violations in the Neutral K Meson System: A Guide"		
LITTENBERG	93	ARNPS 43 729	R.L. Littenberg, G. Valencia	(BNL, FNAL)
Also		Rare and Radiative Kaon Decays		
RITCHIE	93	RMP 65 1149	J.L. Ritchie, S.G. Wojcicki	
Also		"Rare K Decays"		
WINSTEIN	93	RMP 65 1113	B. Winstein, L. Wolfenstein	
Also		"The Search for Direct CP Violation"		
BATTISTON	92	PRPL 214 293	R. Battiston <i>et al.</i>	(PGIA, CERN, TRSTT)
Also		Status and Perspectives of K Decay Physics		
DIB	92	PR D46 2265	C.O. Dib, R.D. Peccei	(UCLA)
Also		Tests of CPT conservation in the neutral kaon system.		
KLEINKNECHT	92	CNPP 20 281	K. Kleinknecht	(MAINZ)
Also		New Results on CP Violation in Decays of Neutral K Mesons.		
KLEINKNECHT	90	ZPHY C46 557	K. Kleinknecht	(MAINZ)
PEACH	90	JP G16 131	D.J. Peach	(EDIN)
BRYMAN	89	IJMP A4 79	K.A. Bryman	(TRIU)
Also		"Rare Kaon Decays"		
KLEINKNECHT	76	ARNS 26 1	K. Kleinknecht	(DORT)
GINSBERG	75	PR D8 3887	E.S. Ginsberg, J. Smith	(MIT, STON)
GINSBERG	70	PR D1 229	E.S. Ginsberg	(HAIF)
HEUSSE	70	LNC 3 449	P. Heusse <i>et al.</i>	(ORSAY)
CRONIN	68C	Vienna Conf. 281	J.W. Cronin	(PRIN)
RUBBIA	67	PL 24B 531	C. Rubbia, J. Steinberger	(CERN, COLU)
Also		PL 23 167	C. Rubbia, J. Steinberger	(CERN, COLU)
Also		PL 20 207	C. Alf-Steinberger <i>et al.</i>	(CERN)
Also		PL 21 595	C. Alf-Steinberger <i>et al.</i>	(CERN)
AUERBACH	66	PR 149 1052	L.B. Auerbach <i>et al.</i>	(PENN)
Also		PRL 14 192	L.B. Auerbach <i>et al.</i>	(PENN)
FIRESTONE	66B	PRL 17 116	A. Firestone <i>et al.</i>	(YALE, BNL)
BEHR	65	Argonne Conf. 59	L. Behr <i>et al.</i>	(EPOL, MILA, PADO)
MESTVIRISH...	65	JINR P 2449	A.N. Mestvirishvili <i>et al.</i>	(JINR)
TRILLING	65B	UCRL 16473	G.N. Trilling	(LRL)
Also		Updated from 1965 Argonne Conference, page 115.		
JOVANOV...	63	BNL Conf. 42	J.V. Jovanovich <i>et al.</i>	(BNL, UMD)

$K_0^*(700)$

$$I(J^P) = \frac{1}{2}(0^+)$$

also known as κ ; was $K_0^*(800)$
See the related review(s):
Scalar Mesons below 1 GeV

$K_0^*(700)$ T-Matrix Pole \sqrt{s}

VALUE (MeV)	DOCUMENT ID	TECN	COMMENT
(630-730) - i (260-340) OUR ESTIMATE	(see Fig. 64.1 in the review)		
$(702 \pm 12^{+4}_{-5}) - i (285 \pm 16^{+8}_{-13})$	¹ DANILKIN	21	RVUE Compilation
$(648 \pm 7) - i (280 \pm 16)$	² PELAEZ	20	RVUE $\pi K \rightarrow \pi K$
$(670 \pm 18) - i (295 \pm 28)$	³ PELAEZ	17	RVUE $\pi K \rightarrow \pi K$
$(764 \pm 63^{+71}_{-34}) - i (306 \pm 149^{+143}_{-85})$	⁴ ABLIKIM	11B	BES2 1.3k $J/\psi \rightarrow K_S^0 K_S^0 \pi^+ \pi^-$
$(665 \pm 9) - i (268^{+21}_{-6})$	⁵ GUO	11B	RVUE
$(849 \pm 77^{+18}_{-14}) - i (256 \pm 40^{+46}_{-22})$	⁴ ABLIKIM	10E	BES2 1.4k $J/\psi \rightarrow K^\pm K_S^0 \pi^\mp \pi^0$
$(663 \pm 8 \pm 34) - i (329 \pm 5 \pm 22)$	⁶ BUGG	10	RVUE S-matrix pole
$(706.0 \pm 1.8 \pm 22.8) - i (319.4 \pm 2.2 \pm 20.2)$	⁷ BONVICINI	08A	CLEO 141k $D^+ \rightarrow K^- \pi^+ \pi^+$

$(841 \pm 30^{+81}_{-73}) - i (309 \pm 45^{+48}_{-72})$	⁴ ABLIKIM	06c	BES2 25k $J/\psi \rightarrow \overline{K}^*(892)^0 K^+ \pi^-$
$(750^{+30}_{-55}) - i (342 \pm 60)$	⁸ BUGG	06	RVUE
$(658 \pm 13) - i (279 \pm 12)$	⁹ DESCOTES-G.	06	RVUE $\pi K \rightarrow \pi K$
$(757 \pm 33) - i (279 \pm 41)$	¹⁰ GUO	06	RVUE
$(694 \pm 53) - i (303 \pm 30)$	¹¹ ZHOU	06	RVUE $K\rho \rightarrow K^- \pi^+ n$
$(594 \pm 79) - i (362 \pm 166)$	¹¹ ZHENG	04	RVUE $K^- \rho \rightarrow K^- \pi^+ n$
$(722 \pm 60) - i (386 \pm 50)$	¹¹ BUGG	03	RVUE 11 $K^- \rho \rightarrow K^- \pi^+ n$
$(875 \pm 75) - i (335 \pm 110)$	¹² ISHIDA	97B	RVUE 11 $K^- \rho \rightarrow K^- \pi^+ n$
$727 - i 263$	¹³ VANBEVEREN	86	RVUE

- Data driven analysis using partial-wave dispersion relations.
- Extracted employing πK partial wave analysis from ESTABROOKS 78 and ASTON 88, Roy-Steiner equations and once subtracted forward dispersion relations.
- Reanalysis of ESTABROOKS 78 and ASTON 88 satisfying Forward Dispersion Relations and using sequences of Pade approximants.
- Extracted from Breit-Wigner parameters.
- Fit to scattering phase shifts using UChPT amplitudes with explicit resonances.
- Supersedes BUGG 06. Combined analysis of ASTON 88, ABLIKIM 06c, AITALA 06, and LINK 09 using an s -dependent width with couplings to $K\pi$ and $K\eta'$, and the Adler zero near thresholds.
- From a complex pole included in the fit. Using parameters from the model that fits data best.
- Reanalysis of ASTON 88, AITALA 02, and ABLIKIM 06c using for the κ an s -dependent width with an Adler zero near threshold.
- Using Roy-Steiner equations (ROY 71) consistent with unitarity, analyticity and crossing symmetry constraints.
- From UChPT fitted to MERCER 71, BINGHAM 72 and ESTABROOKS 78. Amplitude shown to be consistent with data of ABLIKIM 06c.
- Reanalysis of ASTON 88 data.
- Reanalysis of ASTON 88 using interfering Breit-Wigner amplitudes. Extracted from Breit-Wigner parameters.
- Unitarized Quark Model.

$K_0^*(700)$ Breit-Wigner Mass

VALUE (MeV)	EVTS	DOCUMENT ID	TECN	COMMENT
845 ± 17 OUR AVERAGE				
$826 \pm 49^{+49}_{-34}$	1.3k	¹ ABLIKIM	11B	BES2 $J/\psi \rightarrow K_S^0 K_S^0 \pi^+ \pi^-$
$810 \pm 68^{+15}_{-24}$	1.4k	² ABLIKIM	10E	BES2 $J/\psi \rightarrow K^\pm K_S^0 \pi^\mp \pi^0$
$856 \pm 17 \pm 13$	54k	LINK	07B	FOCS $D^+ \rightarrow K^- \pi^+ \pi^+$
$878 \pm 23^{+64}_{-55}$	25k	³ ABLIKIM	06c	BES2 $J/\psi \rightarrow \overline{K}^*(892)^0 K^+ \pi^-$
$797 \pm 19 \pm 43$	15k	^{4,5} AITALA	02	E791 $D^+ \rightarrow K^- \pi^+ \pi^+$
888.0 ± 1.9	141k	⁶ BONVICINI	08A	CLEO $D^+ \rightarrow K^- \pi^+ \pi^+$
855 ± 15	0.6k	⁷ CAWLFIELD	06A	CLEO $D^0 \rightarrow K^+ K^- \pi^0$
905^{+65}_{-30}		⁸ ISHIDA	97B	RVUE 11 $K^- \rho \rightarrow K^- \pi^+ n$

- • • We do not use the following data for averages, fits, limits, etc. • • •
- The Breit-Wigner parameters from a fit with seven intermediate resonances. The S -matrix pole position is $(764 \pm 63^{+71}_{-54}) - i (306 \pm 149^{+143}_{-85})$ MeV.
 - From a fit including ten additional resonances and energy-independent Breit-Wigner width.
 - A fit in the $K_0^*(700) + K^*(892) + K^*(1410)$ model with mass and width of the $K_0^*(700)$ from ABLIKIM 06c well describes the left slope of the $K_S^0 \pi^-$ invariant mass spectrum in $\tau^- \rightarrow K_0^* \pi^- \nu_\tau$ decay studied by EPIFANOV 07. Averaged value from different parameterizations.
 - Not seen by KOPP 01 using 7070 events of $D^0 \rightarrow K^- \pi^+ \pi^0$. LINK 02e and LINK 05i show clear evidence for a constant non-resonant scalar amplitude rather than $K_0^*(700)$ in their high statistics analysis of $D^+ \rightarrow K^- \pi^+ \mu^+ \nu_\mu$.
 - AUBERT 07r does not find evidence for the charged $K_0^*(700)$ using 11k events of $D^0 \rightarrow K^- K^+ \pi^0$.
 - Using parameters from the model that fits data best.
 - Breit-Wigner parameters. A significant S -wave can be also modeled as a non-resonant contribution.
 - Reanalysis of ASTON 88 using interfering Breit-Wigner amplitudes.

$K_0^*(700)$ Breit-Wigner Width

VALUE (MeV)	EVTS	DOCUMENT ID	TECN	COMMENT
468 ± 30 OUR AVERAGE				
$449 \pm 156^{+144}_{-81}$	1.3k	¹ ABLIKIM	11B	BES2 $J/\psi \rightarrow K_S^0 K_S^0 \pi^+ \pi^-$
$536 \pm 87^{+106}_{-47}$	1.4k	² ABLIKIM	10E	BES2 $J/\psi \rightarrow K^\pm K_S^0 \pi^\mp \pi^0$
$464 \pm 28 \pm 22$	54k	LINK	07B	FOCS $D^+ \rightarrow K^- \pi^+ \pi^+$
$499 \pm 52^{+55}_{-87}$	25k	³ ABLIKIM	06c	BES2 $J/\psi \rightarrow \overline{K}^*(892)^0 K^+ \pi^-$
$410 \pm 43 \pm 87$	15k	^{4,5} AITALA	02	E791 $D^+ \rightarrow K^- \pi^+ \pi^+$
550.4 ± 11.8	141k	⁶ BONVICINI	08A	CLEO $D^+ \rightarrow K^- \pi^+ \pi^+$
251 ± 48	0.6k	⁷ CAWLFIELD	06A	CLEO $D^0 \rightarrow K^+ K^- \pi^0$
545^{+235}_{-110}		⁸ ISHIDA	97B	RVUE 11 $K^- \rho \rightarrow K^- \pi^+ n$

- The Breit-Wigner parameters from a fit with seven intermediate resonances. The S -matrix pole position is $(764 \pm 63^{+71}_{-54}) - i (306 \pm 149^{+143}_{-85})$ MeV.

Meson Particle Listings

$K_0^*(700)$, $K^*(892)$

- ²From a fit including ten additional resonances and energy-independent Breit-Wigner width.
- ³A fit in the $K_0^*(700) + K^*(892) + K^*(1410)$ model with mass and width of the $K_0^*(700)$ from ABLIKIM 06c well describes the left slope of the $K_S^0 \pi^-$ invariant mass spectrum in $\tau^- \rightarrow K_S^0 \pi^- \nu_\tau$ decay studied by EPIFANOV 07. Averaged value from different parameterizations.
- ⁴Not seen by KOPP 01 using 7070 events of $D^0 \rightarrow K^- \pi^+ \pi^0$. LINK 02e and LINK 05i show clear evidence for a constant non-resonant scalar amplitude rather than $K_0^*(700)$ in their high statistics analysis of $D^+ \rightarrow K^- \pi^+ \mu^+ \nu_\mu$.
- ⁵AUBERT 07t does not find evidence for the charged $K_0^*(700)$ using 11k events of $D^0 \rightarrow K^- K^+ \pi^0$.
- ⁶Using parameters from the model that fits data best.
- ⁷Statistical error only. A fit to the Dalitz plot including the $K_0^*(700)^\pm$, $K^*(892)^\pm$, and ϕ resonances modeled as Breit-Wigners. A significant S-wave can be also modeled as a non-resonant contribution.
- ⁸Reanalysis of ASTON 88 using interfering Breit-Wigner amplitudes.

$K_0^*(700)$ DECAY MODES

Mode	Fraction (Γ_i/Γ)
Γ_1 $K \pi$	100 %

$K_0^*(700)$ REFERENCES

DANILKIN 21	PR D103 114023	I. Danilkin, O. Deineka, M. Vanderhaeghen (MAINZ)
PELAEZ 20	PRL 124 172001	J.R. Pelaez et al.
PELAEZ 17	EPJ C77 91	J.R. Pelaez, A.Rodas, J.R. de Elvira
ABLIKIM 11B	PL B698 183	M. Ablikim et al. (BES II Collab.)
GUO 11B	PR D84 034005	Z.-H. Guo, J.A. Oller
ABLIKIM 10E	PL B693 88	M. Ablikim et al. (BES II Collab.)
BUGG 10	PR D81 014002	D.V. Bugg (LOQM)
LINK 09	PL B681 14	J.M. Link et al. (FNAL FOCUS Collab.)
BONVICINI 08A	PR D78 052001	G. Bonvicini et al. (CLEO Collab.)
AUBERT 07T	PR D76 011102	B. Aubert et al. (BABAR Collab.)
EPIFANOV 07	PL B654 85	D. Epifanov et al. (BELLE Collab.)
LINK 07B	PL B653 1	J.M. Link et al. (FNAL FOCUS Collab.)
ABLIKIM 06C	PL B633 681	M. Ablikim et al. (BES Collab.)
AITALA 06	PR D73 032004	E.M. Aitala et al. (FNAL E791 Collab.)
Also	PR D74 059901 (errata)	E.M. Aitala et al. (FNAL E791 Collab.)
BUGG 06	PL B632 471	D.V. Bugg (LOQM)
CAWLFIELD 06A	PR D74 031108	C. Cawfield et al. (CLEO Collab.)
DESCOTES-G...06	EPJ C48 553	S. Descotes-Genon, B. Moussallam
GUO 06	NP A773 78	F.K. Guo et al.
ZHOU 06	NP A775 212	Z.Y. Zhou, H.Q. Zheng
LINK 05I	PL B621 72	J.M. Link et al. (FNAL FOCUS Collab.)
ZHENG 04	NP A733 235	H.Q. Zheng et al.
BUGG 03	PL B572 1	D.V. Bugg
AITALA 02	PRL 89 121801	E.M. Aitala et al. (FNAL E791 Collab.)
LINK 02E	PL B535 43	J.M. Link et al. (FNAL FOCUS Collab.)
KOPP 01	PR D63 092001	S. Kopp et al. (CLEO Collab.)
ISHIDA 97B	PTP 98 621	S. Ishida et al.
ASTON 88	NP B296 493	D. Aston et al. (SLAC, NAGO, CINC, INUS)
VANBEVEREN 86	ZPHY C30 615	E. van Beveren et al. (NUM, BIEL)
ESTABROOKS 78	NP B133 490	P.G. Estabrooks et al. (MCGI, CARL, DURH+)
BINGHAM 72	NP B41 1	H.H. Bingham et al. (International K^* Collab.)
MERCER 71	NP B32 381	R. Mercer et al. (JHU)
ROY 71	PL 36B 353	S.M. Roy

891.7 ± 0.6	6706	COOPER 78	HBC ±	0.76 $\bar{p}p \rightarrow (K\pi)^\pm X$
891.9 ± 0.7	9000	¹ PALER 75	HBC -	14.3 $K^- p \rightarrow (K\pi)^- X$
892.2 ± 1.5	4404	AGUILAR... 71B	HBC -	3.9,4.6 $K^- p \rightarrow (K\pi)^- p$
891 ± 2	1000	CRENNELL 69D	DBC -	3.9 $K^- N \rightarrow K^0 \pi^- X$
890 ± 3.0	720	BARLOW 67	HBC ±	1.2 $\bar{p}p \rightarrow (K^0 \pi)^\pm K^\mp$
889 ± 3.0	600	BARLOW 67	HBC ±	1.2 $\bar{p}p \rightarrow (K^0 \pi)^\pm K \pi$
891 ± 2.3	620	² DEBAERE 67B	HBC +	3.5 $K^+ p \rightarrow K^0 \pi^+ p$
891.0 ± 1.2	1700	³ WOJCICKI 64	HBC -	1.7 $K^- p \rightarrow \bar{K}^0 \pi^- p$

• • • We do not use the following data for averages, fits, limits, etc. • • •

893.6 ± 0.1 $^{+0.2}_{-0.3}$	183k	ABLIKIM 19A	BES ±	$J/\psi \rightarrow K^+ K^- \pi^0$
895.6 ± 0.8	4k	⁴ LEES 17c	BABR	$J/\psi \rightarrow K_S^0 K^\pm \pi^\mp$
893.2 ± 0.1 ± 1.0	190k	⁵ AAIJ 16N	LHCB	$D^0 \rightarrow K_S^0 K^\pm \pi^\mp$
893.5 ± 1.1	27k	⁶ ABELE 99D	CBAR ±	0.0 $\bar{p}p \rightarrow K^+ K^- \pi^0$
890.4 ± 0.2 ± 0.5	80k	⁷ BIRD 89	LASS -	11 $K^- p \rightarrow \bar{K}^0 \pi^- p$
890.0 ± 2.3	800	^{2,3} CLELAND 82	SPEC +	30 $K^+ p \rightarrow K_S^0 \pi^+ p$
896.0 ± 1.1	3200	^{2,3} CLELAND 82	SPEC +	50 $K^+ p \rightarrow K_S^0 \pi^+ p$
893 ± 1	3600	^{2,3} CLELAND 82	SPEC -	50 $K^+ p \rightarrow K_S^0 \pi^- p$
896.0 ± 1.9	380	DELFOSSSE 81	SPEC +	50 $K^\pm p \rightarrow K^\pm \pi^0 p$
886.0 ± 2.3	187	DELFOSSSE 81	SPEC -	50 $K^\pm p \rightarrow K^\pm \pi^0 p$
894.2 ± 2.0	765	² CLARK 73	HBC -	3.13 $K^- p \rightarrow \bar{K}^0 \pi^- p$
894.3 ± 1.5	1150	^{2,3} CLARK 73	HBC -	3.3 $K^- p \rightarrow \bar{K}^0 \pi^- p$
892.0 ± 2.6	341	² SCHWEING...68	HBC -	5.5 $K^- p \rightarrow \bar{K}^0 \pi^- p$

- ¹Inclusive reaction. Complicated background and phase-space effects.
- ²Mass errors enlarged by us to Γ/\sqrt{N} . See note.
- ³Number of events in peak reevaluated by us.
- ⁴From a Dalitz plot analysis in an isobar model with charged and neutral $K^*(892)$ masses and widths floating.
- ⁵Average of fit results with different parameterizations for the $K \pi$ S-wave.
- ⁶K-matrix pole.
- ⁷From a partial wave amplitude analysis.

CHARGED ONLY, PRODUCED IN τ LEPTON DECAYS

VALUE (MeV)	EVTS	DOCUMENT ID	TECN	COMMENT
895.47 ± 0.20 ± 0.74	53k	¹ EPIFANOV 07	BELL	$\tau^- \rightarrow K_S^0 \pi^- \nu_\tau$
892.0 ± 0.5		² BOITO 10	RVUE	$\tau^- \rightarrow K_S^0 \pi^- \nu_\tau$
892.0 ± 0.9		^{3,4} BOITO 09	RVUE	$\tau^- \rightarrow K_S^0 \pi^- \nu_\tau$
895.3 ± 0.2		^{4,5} JAMIN 08	RVUE	$\tau^- \rightarrow K_S^0 \pi^- \nu_\tau$
896.4 ± 0.9	12k	⁶ BONVICINI 02	CLEO	$\tau^- \rightarrow K^- \pi^0 \nu_\tau$
895 ± 2		⁷ BARATE 99R	ALEP	$\tau^- \rightarrow K^- \pi^0 \nu_\tau$

- • • We do not use the following data for averages, fits, limits, etc. • • •
- ¹From a fit in the $K_0^*(700) + K^*(892) + K^*(1410)$ model.
- ²From the pole position of the $K \pi$ vector form factor using EPIFANOV 07 and constraints from K_{J3} decays in ANTONELLI 10.
- ³From the pole position of the $K \pi$ vector form factor in the complex s-plane and using EPIFANOV 07 data.
- ⁴Systematic uncertainties not estimated.
- ⁵Reanalysis of EPIFANOV 07 using resonance chiral theory.
- ⁶Calculated by us from the shift by 4.7 ± 0.9 MeV (statistical uncertainty only) reported in BONVICINI 02 with respect to the world average value from PDG 00.
- ⁷With mass and width of the $K^*(1410)$ fixed at 1412 MeV and 227 MeV, respectively.

NEUTRAL ONLY

VALUE (MeV)	EVTS	DOCUMENT ID	TECN	COMMENT
895.55 ± 0.20 OUR AVERAGE		Error includes scale factor of 1.7. See the ideogram below.		
894.68 ± 0.25 ± 0.05		¹ ABLIKIM 16F	BES3	$D^+ \rightarrow K^- \pi^+ e^+ \nu_e$
895.4 ± 0.2 ± 0.2	243k	² DEL-AMO-SA...11A	BABR	$D^+ \rightarrow K^- \pi^+ e^+ \nu_e$
895.7 ± 0.2 ± 0.3	141k	³ BONVICINI 08A	CLEO	$D^+ \rightarrow K^- \pi^+ e^+ \nu_e$
895.41 ± 0.32 $^{+0.35}_{-0.43}$	18k	⁴ LINK 05I	FOCS	$D^+ \rightarrow K^- \pi^+ \mu^+ \nu_\mu$
896 ± 2		BARBERIS 98E	OMEG	450 $pp \rightarrow p_f p_S K^* \bar{K}^*$
895.9 ± 0.5 ± 0.2		ASTON 88	LASS	11 $K^- p \rightarrow K^- \pi^+ n$
894.52 ± 0.63	25k	⁵ ATKINSON 86	OMEG	20-70 γp
894.63 ± 0.76	20k	⁵ ATKINSON 86	OMEG	20-70 γp
897 ± 1	28k	EVANGELIS... 80	OMEG	10 $\pi^- p \rightarrow K^+ \pi^- (\Lambda, \Sigma)$
898.4 ± 1.4	1180	AGUILAR... 78B	HBC	0.76 $\bar{p}p \rightarrow K^\mp K_S^0 \pi^\pm$
894.9 ± 1.6		WICKLUND 78	ASPK	3,4,6 $K^\pm N \rightarrow (K\pi)^0 N$
897.6 ± 0.9		BOWLER 77	DBC	5.4 $K^+ d \rightarrow K^+ \pi^- pp$
895.5 ± 1.0	3600	MCCUBBIN 75	HBC	3.6 $K^- p \rightarrow K^- \pi^+ n$
897.1 ± 0.7	22k	⁵ PALER 75	HBC	14.3 $K^- p \rightarrow (K\pi)^0 X$
896.0 ± 0.6	10k	FOX 74	RVUE	2 $K^- p \rightarrow K^- \pi^+ n$
896.0 ± 0.6		FOX 74	RVUE	2 $K^+ n \rightarrow K^+ \pi^- p$
896 ± 2		⁶ MATISON 74	HBC	12 $K^+ p \rightarrow K^+ \pi^- \Delta$
896 ± 1	3186	LEWIS 73	HBC	2.1-2.7 $K^+ p \rightarrow K \pi \pi p$
894.0 ± 1.3		⁶ LINGLIN 73	HBC	2-13 $K^+ p \rightarrow K^+ \pi^- \pi^+ p$
898.4 ± 1.3	1700	⁷ BUCHNER 72	DBC	4.6 $K^+ n \rightarrow K^+ \pi^- p$
897.9 ± 1.1	2934	⁷ AGUILAR... 71B	HBC	3.9,4.6 $K^- p \rightarrow K^- \pi^+ n$
898.0 ± 0.7	5362	⁷ AGUILAR... 71B	HBC	3.9,4.6 $K^- p \rightarrow K^- \pi^+ \pi^- p$
895 ± 1	4300	⁸ HABER 70	DBC	3 $K^- N \rightarrow K^- \pi^+ X$
893.7 ± 2.0	10k	DAVIS 69	HBC	12 $K^+ p \rightarrow K^+ \pi^- \pi^+ p$
894.7 ± 1.4	1040	⁷ DAUBER 67B	HBC	2.0 $K^- p \rightarrow K^- \pi^+ \pi^- p$

$K^*(892)$

$$J(P) = \frac{1}{2}(1^-)$$

$K^*(892)$ T-Matrix Pole \sqrt{s}

VALUE (MeV)	DOCUMENT ID	TECN	COMMENT
(890 ± 14) - i (26 ± 6) OUR ESTIMATE			
(890 ± 2) - i (25.6 ± 1.2)	¹ PELAEZ 20	RVUE	$\pi K \rightarrow \pi K$
(892 ± 1) - i (29 ± 1)	² PELAEZ 17	RVUE	$\pi K \rightarrow \pi K$
(889 ± 13) - i (24 ± 4)	³ PELAEZ 04A	RVUE	$\pi K \rightarrow \pi K$

- ¹Extracted employing πK partial wave analysis from ESTABROOKS 78 and ASTON 88, Roy-Steiner equations and once subtracted forward dispersion relations.
- ²Reanalysis of ESTABROOKS 78 and ASTON 88 satisfying Forward Dispersion Relations and using sequences of Pade approximants.
- ³Reanalysis of data from ESTABROOKS 78 and ASTON 88 in the unitarized ChPT model.

$K^*(892)$ MASS

CHARGED ONLY, HADROPRODUCED

VALUE (MeV)	EVTS	DOCUMENT ID	TECN	CHG	COMMENT
891.67 ± 0.26 OUR AVERAGE					
892.2 ± 0.5 ± 1.7		ALBRECHT 20	CBAR		0.9 $\bar{p}p \rightarrow K^+ K^- \pi^0$
892.6 ± 0.5	5840	BAUBILLIER 84B	HBC -		8.25 $K^- p \rightarrow \bar{K}^0 \pi^- p$
888 ± 3		NAPIER 84	SPEC +		200 $\pi^- p \rightarrow 2K_S^0 X$
891 ± 1		NAPIER 84	SPEC -		200 $\pi^- p \rightarrow 2K_S^0 X$
891.7 ± 2.1	3700	BARTH 83	HBC +		70 $K^+ p \rightarrow K^0 \pi^+ X$
891 ± 1	4100	TOAFF 81	HBC -		6.5 $K^- p \rightarrow \bar{K}^0 \pi^- p$
892.8 ± 1.6		AJINENKO 80	HBC +		32 $K^+ p \rightarrow K^0 \pi^+ X$
890.7 ± 0.9	1800	AGUILAR... 78B	HBC ±		0.76 $\bar{p}p \rightarrow K^\mp K_S^0 \pi^\pm$
886.6 ± 2.4	1225	BALAND 78	HBC ±		12 $\bar{p}p \rightarrow (K\pi)^\pm X$

See key on page 1171

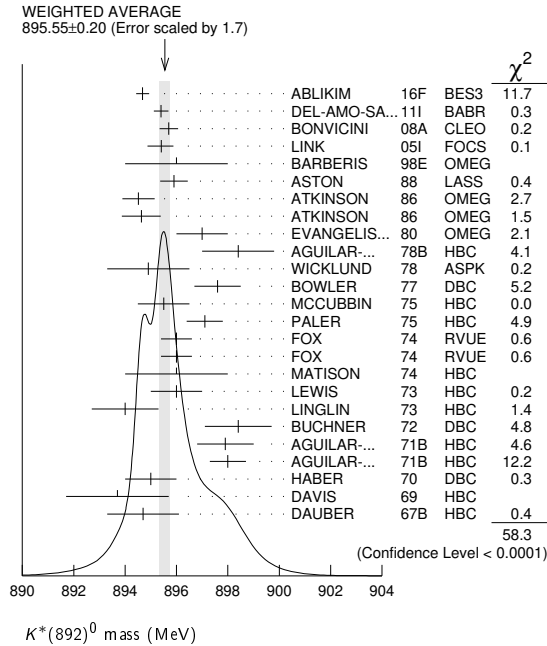
Meson Particle Listings

$K^*(892)$

• • • We do not use the following data for averages, fits, limits, etc. • • •

895.50 ± 0.92 ± 2.6		9 ADUSZKIEW...20A	NA61	158	pp
898.1 ± 1.0	4k	10 LEES	17C	BABR	$J/\psi \rightarrow K_S^0 K^\pm \pi^\mp$
895.53 ± 0.17		LEES	13F	BABR	$D^+ \rightarrow K^+ K^- \pi^+$
894.9 ± 0.5 ± 0.7	14.4k	11 MITCHELL	09A	CLEO	$D_s^+ \rightarrow K^+ K^- \pi^+$
896.2 ± 0.3	20k	12 AUBERT	07AK	BABR	$10.6 e^+ e^- \rightarrow K^{*0} K^\pm \pi^\mp \gamma$
900.7 ± 1.1	5900	BARTH	83	HBC	$70 K^+ p \rightarrow K^+ \pi^- X$

- 1 Taking also into account the $K_S^*(1430)^0$ and $K_2^*(1430)^0$.
- 2 Taking into account the $K^*(892)^0$, S -wave and P -wave ($K^*(1410)^0$).
- 3 From the isobar model with a complex pole for the κ .
- 4 Fit to $K\pi$ mass spectrum includes a non-resonant scalar component.
- 5 Inclusive reaction. Complicated background and phase-space effects.
- 6 From pole extrapolation.
- 7 Mass errors enlarged by us to Γ/\sqrt{N} . See note.
- 8 Number of events in peak reevaluated by us.
- 9 For transverse momenta between 0.6 and 0.8 GeV/c and rapidity $0 < y < 0.5$.
- 10 From a Dalitz plot analysis in an isobar model with charged and neutral $K^*(892)$ masses and widths floating.
- 11 This value comes from a fit with χ^2 of 178/117.
- 12 Systematic uncertainties not estimated.



$K^*(892)$ MASSES AND MASS DIFFERENCES

Unrealistically small errors have been reported by some experiments. We use simple “realistic” tests for the minimum errors on the determination of a mass and width from a sample of N events:

$$\delta_{\min}(m) = \frac{\Gamma}{\sqrt{N}}, \quad \delta_{\min}(\Gamma) = 4 \frac{\Gamma}{\sqrt{N}}. \quad (1)$$

We consistently increase unrealistic errors before averaging. For a detailed discussion, see the 1971 edition of this Note.

$m_{K^*(892)^0} - m_{K^*(892)^\pm}$

VALUE (MeV)	EVTs	DOCUMENT ID	TECN	CHG	COMMENT
6.7 ± 1.2 OUR AVERAGE					
7.7 ± 1.7	2980	AGUILAR...	78B	HBC	±0 0.76 $\bar{p}p \rightarrow K^\mp K_S^0 \pi^\pm$
5.7 ± 1.7	7338	AGUILAR...	71B	HBC	-0 3.9, 4.6 $K^- p$
6.3 ± 4.1	283	1 BARASH	67B	HBC	0.0 $\bar{p}p$

1 Number of events in peak reevaluated by us.

$K^*(892)$ RANGE PARAMETER

All from partial wave amplitude analyses.

VALUE (GeV ⁻¹)	EVTs	DOCUMENT ID	TECN	CHG	COMMENT
2.1 ± 0.5 ± 0.5	243k	1 DEL-AMO-SA..11i	BABR	0	$D^+ \rightarrow K^- \pi^+ e^+ \nu_e$
3.96 ± 0.54 ± 1.31	18k	2 LINK	05I	FOCS	0 $D^+ \rightarrow K^- \pi^+ \mu^+ \nu_\mu$
3.4 ± 0.7		ASTON	88	LASS	0 11 $K^- p \rightarrow K^- \pi^+ n$
12.1 ± 3.2 ± 3.0		BIRD	89	LASS	- 11 $K^- p \rightarrow \bar{K}^0 \pi^- p$

- • • We do not use the following data for averages, fits, limits, etc. • • •
- 1 Taking into account the $K^*(892)^0$, S -wave and P -wave ($K^*(1410)^0$).
- 2 Fit to $K\pi$ mass spectrum includes a non-resonant scalar component.

$K^*(892)$ WIDTH

CHARGED ONLY, HADROPRODUCED

VALUE (MeV)	EVTs	DOCUMENT ID	TECN	CHG	COMMENT
51.4 ± 0.8 OUR FIT					
51.4 ± 0.8 OUR AVERAGE					
54.4 ± 0.9 ± 1.7		ALBRECHT 20	CBAR		0.9 $\bar{p}p \rightarrow K^+ K^- \pi^0$
49 ± 2	5840	BAUBILLIER 84B	HBC	-	8.25 $K^- p \rightarrow \bar{K}^0 \pi^- p$
56 ± 4		NAPIER 84	SPEC	-	200 $\pi^- p \rightarrow 2K_S^0 X$
51 ± 2	4100	TOAFF 81	HBC	-	6.5 $K^- p \rightarrow \bar{K}^0 \pi^- p$
50.5 ± 5.6		AJINENKO 80	HBC	+	32 $K^+ p \rightarrow K^0 \pi^+ X$
45.8 ± 3.6	1800	AGUILAR...	78B	HBC	± 0.76 $\bar{p}p \rightarrow K^\mp K_S^0 \pi^\pm$
52.0 ± 2.5	6706	1 COOPER 78	HBC	±	0.76 $\bar{p}p \rightarrow (K\pi)^\pm X$
52.1 ± 2.2	9000	2 PALER 75	HBC	-	14.3 $K^- p \rightarrow (K\pi)^- X$
46.3 ± 6.7	765	1 CLARK 73	HBC	-	3.13 $K^- p \rightarrow \bar{K}^0 \pi^- p$
48.2 ± 5.7	1150	1,3 CLARK 73	HBC	-	3.3 $K^- p \rightarrow \bar{K}^0 \pi^- p$
54.3 ± 3.3	4404	1 AGUILAR...	71B	HBC	- 3.9, 4.6 $K^- p \rightarrow (K\pi)^- p$
46 ± 5	1700	1,3 WOJCICKI 64	HBC	-	1.7 $K^- p \rightarrow \bar{K}^0 \pi^- p$
• • • We do not use the following data for averages, fits, limits, etc. • • •					
46.7 ± 0.2 ± 0.1	183k	ABLIKIM 19Aq	BES	±	$J/\psi \rightarrow K^+ K^- \pi^0$
43.6 ± 1.3	4k	4 LEES 17C	BABR		$J/\psi \rightarrow K_S^0 K^\pm \pi^\mp$
47.2 ± 0.3 ± 2.3	190k	5 AAIJ 16N	LHCB		$D^0 \rightarrow K_S^0 K^\pm \pi^\mp$
54.8 ± 1.7	27k	6 ABELE 99D	CBAR	±	0.0 $\bar{p}p \rightarrow K^+ K^- \pi^0$
45.2 ± 1 ± 2	80k	7 BIRD 89	LASS	-	11 $K^- p \rightarrow \bar{K}^0 \pi^- p$
42.8 ± 7.1	3700	BARTH 83	HBC	+	70 $K^+ p \rightarrow K^0 \pi^+ X$
64.0 ± 9.2	800	1,3 CLELAND 82	SPEC	+	30 $K^+ p \rightarrow K^0 \pi^+ p$
62.0 ± 4.4	3200	1,3 CLELAND 82	SPEC	+	50 $K^+ p \rightarrow K^0 \pi^+ p$
55 ± 4	3600	1,3 CLELAND 82	SPEC	-	50 $K^+ p \rightarrow K_S^0 \pi^- p$
62.6 ± 3.8	380	DELFOSSSE 81	SPEC	+	50 $K^\pm p \rightarrow K^\pm \pi^0 p$
50.5 ± 3.9	187	DELFOSSSE 81	SPEC	-	50 $K^\pm p \rightarrow K^\pm \pi^0 p$

- 1 Width errors enlarged by us to $4 \times \Gamma/\sqrt{N}$; see note.
- 2 Inclusive reaction. Complicated background and phase-space effects.
- 3 Number of events in peak reevaluated by us.
- 4 From a Dalitz plot analysis in an isobar model with charged and neutral $K^*(892)$ masses and widths floating.
- 5 Average of fit results with different parametrizations for the $K\pi$ S -wave.
- 6 K -matrix pole.
- 7 From a partial wave amplitude analysis.

CHARGED ONLY, PRODUCED IN τ LEPTON DECAYS

VALUE (MeV)	EVTs	DOCUMENT ID	TECN	COMMENT
46.2 ± 0.6 ± 1.2	53k	1 EPIFANOV 07	BELL	$\tau^- \rightarrow K_S^0 \pi^- \nu_\tau$
• • • We do not use the following data for averages, fits, limits, etc. • • •				
46.5 ± 1.1		2 BOITO 10	RVUE	$\tau^- \rightarrow K_S^0 \pi^- \nu_\tau$
46.2 ± 0.4		3,4 BOITO 09	RVUE	$\tau^- \rightarrow K_S^0 \pi^- \nu_\tau$
47.5 ± 0.4		4,5 JAMIN 08	RVUE	$\tau^- \rightarrow K_S^0 \pi^- \nu_\tau$
55 ± 8		6 BARATE 99R	ALEP	$\tau^- \rightarrow K^- \pi^0 \nu_\tau$

- 1 From a fit in the $K_S^*(700) + K^*(892) + K^*(1410)$ model.
- 2 From the pole position of the $K\pi$ vector form factor using EPIFANOV 07 and constraints from K_{J3} decays in ANTONELLI 10.
- 3 From the pole position of the $K\pi$ vector form factor in the complex s -plane and using EPIFANOV 07 data.
- 4 Systematic uncertainties not estimated.
- 5 Reanalysis of EPIFANOV 07 using resonance chiral theory.
- 6 With mass and width of the $K^*(1410)$ fixed at 1412 MeV and 227 MeV, respectively.

NEUTRAL ONLY

VALUE (MeV)	EVTs	DOCUMENT ID	TECN	COMMENT
47.3 ± 0.5 OUR FIT				Error includes scale factor of 2.0.
47.3 ± 0.5 OUR AVERAGE				Error includes scale factor of 2.0. See the ideogram below.
46.53 ± 0.56 ± 0.31		1 ABLIKIM 16F	BES3	$D^+ \rightarrow K^- \pi^+ e^+ \nu_e$
46.5 ± 0.3 ± 0.2	243k	2 DEL-AMO-SA..11i	BABR	$D^+ \rightarrow K^- \pi^+ e^+ \nu_e$
45.3 ± 0.5 ± 0.6	141k	3 BONVICINI 08A	CLEO	$D^+ \rightarrow K^- \pi^+ \pi^+$
47.79 ± 0.86 ± 1.32	18k	4 LINK 05I	FOCS	$D^+ \rightarrow K^- \pi^+ \mu^+ \nu_\mu$

See key on page 1171

Meson Particle Listings

$K^*(892), K_1(1270)$

DEL-AMO-SA... 111	PR D83 072001	P. del Amo Sanchez et al.	(BABAR Collab.)
ANTONELLI 10	EPJ C69 399	M. Antonelli et al.	(FlaviNet Working Group)
BOITO 10	JHEP 1009 031	D.R. Boito, R. Escribano, M. Jamin	(BARC)
BOITO 09	EPJ C59 821	D.R. Boito, R. Escribano, M. Jamin	(CLEO Collab.)
MITCHELL 09A	PR D79 072008	R.E. Mitchell et al.	(CLEO Collab.)
BONVICINI 08A	PR D78 052001	G. Bonvicini et al.	(CLEO Collab.)
JAMIN 08	PL B664 78	M. Jamin, A. Pich, J. Portoles	
AUBERT 07AK	PR D76 012008	B. Aubert et al.	(BABAR Collab.)
EPIFANOV 07	B654 65	D. Epifanov et al.	(BELLE Collab.)
LINK 05I	PL B621 72	J.M. Link et al.	(FNAL FOCUS Collab.)
PELAEZ 04A	MPL A19 2879	J.R. Pelaez	(MADU)
BONVICINI 02	PRL 88 111803	G. Bonvicini et al.	(CLEO Collab.)
PDG 00	EPJ C15 1	D.E. Groom et al.	(PDG Collab.)
ABELE 99D	PL B468 178	A. Abele et al.	(Crystal Barrel Collab.)
BARATE 99R	EPJ C11 599	R. Barate et al.	(ALEPH Collab.)
BARBERIS 98E	PL B436 204	D. Barberis et al.	(Omega Expt.)
BIRD 89	SLAC-332	P.F. Bird	(SLAC)
ASTON 88	NP B296 493	D. Aston et al.	(SLAC, NAGO, CINC, INUS)
ATKINSON 86	ZPHY C30 521	M. Atkinson et al.	(BONN. CERN, GLAS+)
CARLSMITH 86	PRL 56 18	D. Carlsmith et al.	(EFI, SAFL)
BAUBILLIER 84B	ZPHY C26 37	M. Baubillier et al.	(BIRM, CERN, GLAS+)
NAPIER 84	PL 149B 514	A. Napier et al.	(TUFTS, ARIZ, FNAL, FLOR+)
BARTH 83	NP B223 296	M. Barth et al.	(BRUX, CERN, GENO, MONS+)
BERG 83	Thesis UMI 83-21652	D.M. Berg	(ROCH)
CHANDLEE 83	PRL 51 168	C. Chandlee et al.	(ROCH, FNAL, MINN)
CLELAND 82	NP B208 189	W.E. Cleland et al.	(DURH, GEVA, LAUS+)
DELFOSE 81	NP B183 349	A. Delfosse et al.	(GEVA, LAUS)
TOAFF 81	PR D23 1500	S. Toaff et al.	(ANL, KANS)
AJINENKO 80	ZPHY C5 177	I.V. Ajinenko et al.	(SERP, BRUX, MONS+)
EVANGELIS... 80	NP B165 383	C. Evangelista et al.	(BARI, BONN, CERN+)
AGUILAR... 78B	NP B141 101	M. Aguilar-Benitez et al.	(MADR, TATA+)
BALAND 78	NP B140 220	J.F. Baland et al.	(MONS, BELG, CERN+)
COOPER 78	NP B136 365	A.M. Cooper et al.	(TATA, CERN, CDEF+)
ESTABROOKS 78	NP B133 490	P.G. Estabrooks et al.	(MCGI, CARL, DURH+)
Also	PR D17 658	P.G. Estabrooks et al.	(MCGI, CARL, DURH+)
JONGEJANS 78	NP B139 383	B. Jongejans et al.	(ZEEM, CERN, NIJM+)
WICKLUND 78	PR D17 1197	A.B. Wicklund et al.	(ANL)
BOWLER 77	NP B126 31	M.B. Bowler et al.	(OXF)
CARITHERS 75B	PRL 35 349	W.C.J. Carithers et al.	(ROCH, MCGI)
MCCUBBIN 75	NP B86 13	N.A. McCubbin, L. Lyons	(OXF)
PALER 75	NP B96 1	K. Paler et al.	(RHEL, SAFL, EPOL)
FOX 74	NP B80 403	G.C. Fox, M.L. Griss	(CIT)
MATISON 74	PR D9 1872	M.J. Matison et al.	(LBL)
BEMPORAD 73	NP B51 1	C. Bemporad et al.	(CERN, ETH, LOIC)
CLARK 73	NP B54 432	A.G. Clark, L. Lyons, D. Radojicic	(OXF)
LEWIS 73	NP B60 283	P.H. Lewis et al.	(LOWC, LOIC, CDEF)
LINGLIN 73	NP B55 408	D. Linglin	(CERN)
BUCHNER 72	NP B45 333	K. Buchner et al.	(MPIM, CERN, BRUX)
AGUILAR... 71B	PR D4 2583	M. Aguilar-Benitez, R.L. Eisner, J.B. Kinson	(BNL)
HABER 70	NP B17 289	B. Haber et al.	(REHO, SAFL, BGNA, EPOL)
CRENNELL 69D	PRL 22 487	D.J. Crennell et al.	(BNL)
DAVIS 69	PRL 23 1071	P.J. Davis et al.	(LRL)
SCHWEING... 68	PR 166 1317	F. Schweingruber et al.	(ANL, NWES)
BARASH 67B	PR 156 1399	N. Barash et al.	(COLU)
BARLOW 67	NC 50A 701	J. Barlow et al.	(CERN, CDEF, IRAD, LIVP)
DAUBER 67B	NP 153 1403	P.M. Dauber et al.	(UCLA)
DEBAERE 67B	NC 51A 401	W. de Baere et al.	(BRUX, CERN)
WOJCICKI 64	PR 135 B484	S.G. Wojcicki	(LRL)

••• We do not use the following data for averages, fits, limits, etc. •••

~1276	² TORNQVIST 82B	RVUE	
~1300	VERGEEST 79	HBC -	4.2 $K^-p \rightarrow (\bar{K}\pi\pi)^-p$
1289±25	³ CARNEGIE 77	ASPK ±	13 $K^\pm p \rightarrow (K\pi\pi)^\pm p$
~1300	BRANDENB... 76	ASPK ±	13 $K^\pm p \rightarrow (K\pi\pi)^\pm p$
~1270	OTTER 76	HBC -	10,14,16 $K^-p \rightarrow (\bar{K}\pi\pi)^-p$
1260	DAVIS 72	HBC +	12 K^+p
1234±12	FIRESTONE 72B	DBC +	12 K^+d

¹ Well described in the chiral unitary approach of GENG 07 with two poles at 1195 and 1284 MeV and widths of 246 and 146 MeV, respectively.
² From a unitarized quark-model calculation.
³ From a model-dependent fit with Gaussian background to BRANDENBURG 76 data.

PRODUCED BY BEAMS OTHER THAN K MESONS

VALUE (MeV)	EVTS	DOCUMENT ID	TECN	CHG	COMMENT
The data in this block is included in the average printed for a previous datablock.					
1248.1 ± 3.3 ± 1.4		GULER 11	BELL	B ⁺	$J/\psi K^+ \pi^+ \pi^-$
••• We do not use the following data for averages, fits, limits, etc. •••					
1289.81 ± 0.56 ± 1.66	894k	AAIJ 18A1	LHCB	D ⁰	$K^+ \pi^\pm \pi^\pm \pi^\mp$
1279 ± 10	25k	¹ ABLIKIM 06c	BES2	J/ψ	$\bar{K}^*(892)^0 K^+ \pi^-$
1294 ± 10	310	RODEBACK 81	HBC	4 π ⁻ p	$\Lambda K 2\pi$
1300	40	CRENNELL 72	HBC	4.5 π ⁻ p	$\Lambda K 2\pi$
1242 + ⁹ / ₋₁₀		² ASTIER 69	HBC		$\bar{p}p$
1300	45	CRENNELL 67	HBC	6 π ⁻ p	$\Lambda K 2\pi$

¹ Systematic errors not estimated.
² This was called the C meson.

PRODUCED IN τ LEPTON DECAYS

VALUE (MeV)	EVTS	DOCUMENT ID	TECN	CHG	COMMENT
The data in this block is included in the average printed for a previous datablock.					
1254 ± 33 ± 34	7k	ASNER	00B	CLEO ±	$\tau^- \rightarrow K^- \pi^+ \pi^- \nu_\tau$

$K_1(1270)$ WIDTH

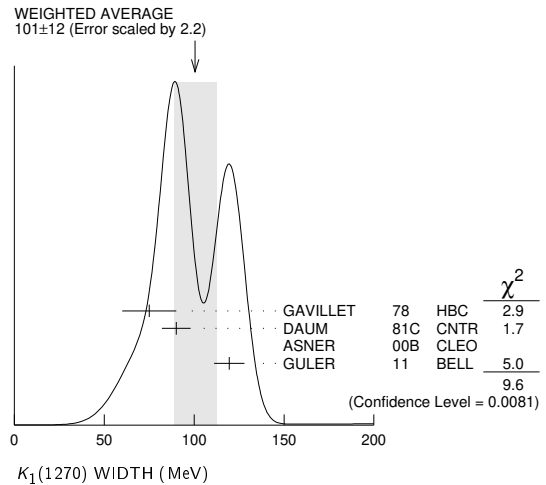
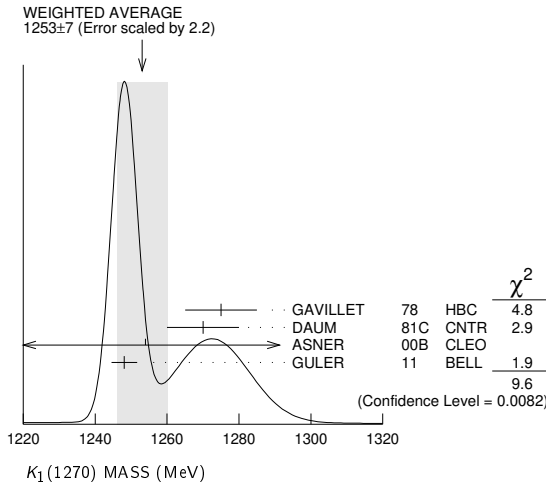
VALUE (MeV) DOCUMENT ID
90 ± 20 OUR ESTIMATE This is only an educated guess; the error given is larger than the error on the average of the published values.
101 ± 12 OUR AVERAGE Includes data from the 4 datablocks that follow this one. Error includes scale factor of 2.2. See the ideogram below.

$K_1(1270)$

$$J(P) = \frac{1}{2}(1^+)$$

$K_1(1270)$ MASS

VALUE (MeV) DOCUMENT ID
1253 ± 7 OUR AVERAGE Includes data from the 4 datablocks that follow this one. Error includes scale factor of 2.2. See the ideogram below.



PRODUCED BY K⁻, BACKWARD SCATTERING, HYPERON EXCHANGE

VALUE (MeV)	EVTS	DOCUMENT ID	TECN	CHG	COMMENT
The data in this block is included in the average printed for a previous datablock.					
75 ± 15	700	GAVILLET 78	HBC	+	4.2 $K^-p \rightarrow \Xi^- K\pi\pi$

PRODUCED BY K BEAMS

VALUE (MeV)	DOCUMENT ID	TECN	CHG	COMMENT
The data in this block is included in the average printed for a previous datablock.				
90 ± 8	¹ DAUM 81c	CNTR -		63 $K^-p \rightarrow K^- 2\pi p$

••• We do not use the following data for averages, fits, limits, etc. •••

~150	VERGEEST 79	HBC -	4.2 $K^-p \rightarrow (\bar{K}\pi\pi)^-p$
~150±71	² CARNEGIE 77	ASPK ±	13 $K^\pm p \rightarrow (K\pi\pi)^\pm p$
~200	BRANDENB... 76	ASPK ±	13 $K^\pm p \rightarrow (K\pi\pi)^\pm p$
120	DAVIS 72	HBC +	12 K^+p
188±21	FIRESTONE 72B	DBC +	12 K^+d

¹ Well described in the chiral unitary approach of GENG 07 with two poles at 1195 and 1284 MeV and widths of 246 and 146 MeV, respectively.
² From a model-dependent fit with Gaussian background to BRANDENBURG 76 data.

PRODUCED BY K⁻, BACKWARD SCATTERING, HYPERON EXCHANGE

VALUE (MeV)	EVTS	DOCUMENT ID	TECN	CHG	COMMENT
The data in this block is included in the average printed for a previous datablock.					
1275 ± 10	700	GAVILLET 78	HBC	+	4.2 $K^-p \rightarrow \Xi^- (K\pi\pi)^+$

PRODUCED BY K BEAMS

VALUE (MeV)	DOCUMENT ID	TECN	CHG	COMMENT
The data in this block is included in the average printed for a previous datablock.				
1270 ± 10	¹ DAUM	81c	CNTR -	63 $K^-p \rightarrow K^- 2\pi p$

Meson Particle Listings

$K_1(1270), K_1(1400)$

PRODUCED BY BEAMS OTHER THAN K MESONS

VALUE (MeV)	EVTS	DOCUMENT ID	TECN	COMMENT
-------------	------	-------------	------	---------

The data in this block is included in the average printed for a previous datablock.

$119.5 \pm 5.2 \pm 6.7$		GULER	11	BELL	$B^+ \rightarrow J/\psi K^+ \pi^+ \pi^-$
• • • We do not use the following data for averages, fits, limits, etc. • • •					
$116.11 \pm 1.65 \pm 2.96$	894k	AAIJ	18A1	LHCB	$D^0 \rightarrow K^+ \pi^+ \pi^- \pi^+$
131	± 21	25k	1	ABLIKIM	06C BES2 $J/\psi \rightarrow \bar{K}^*(892)^0 K^+ \pi^-$
66	± 15	310		RODEBACK	81 HBC $4 \pi^- p \rightarrow \Lambda K 2\pi$
60		40		CRENNELL	72 HBC $4.5 \pi^- p \rightarrow \Lambda K 2\pi$
127	$+7$ -25			ASTIER	69 HBC $\bar{p} p$
60		45		CRENNELL	67 HBC $6 \pi^- p \rightarrow \Lambda K 2\pi$

¹ Systematic errors not estimated.

PRODUCED IN τ LEPTON DECAYS

VALUE (MeV)	EVTS	DOCUMENT ID	TECN	CHG	COMMENT
-------------	------	-------------	------	-----	---------

The data in this block is included in the average printed for a previous datablock.

$260^{+90}_{-70} \pm 80$	7k	ASNER	00B	CLEO	$\tau^- \rightarrow K^- \pi^+ \pi^- \nu_\tau$
--------------------------	----	-------	-----	------	---

$K_1(1270)$ DECAY MODES

Mode	Fraction (Γ_i/Γ)	Scale factor
Γ_1 $K \rho$	(38 \pm 13) %	2.2
Γ_2 $K_0^*(1430) \pi$	(28 \pm 4) %	
Γ_3 $K^*(892) \pi$	(21 \pm 10) %	2.2
Γ_4 $K \omega$	(11.0 \pm 2.0) %	
Γ_5 $K f_0(1370)$	(3.0 \pm 2.0) %	
Γ_6 γK^0	seen	

$K_1(1270)$ PARTIAL WIDTHS

$\Gamma(K \rho)$ Γ_1

VALUE (MeV)	DOCUMENT ID	TECN	CHG	COMMENT
• • • We do not use the following data for averages, fits, limits, etc. • • •				
57 \pm 5	MAZZUCATO	79	HBC	+ 4.2 $K^- p \rightarrow \Xi^- (K \pi \pi)^+$
75 \pm 6	CARNEGIE	77B	ASPK	\pm 13 $K^\pm p \rightarrow (K \pi \pi)^\pm p$

$\Gamma(K_0^*(1430) \pi)$ Γ_2

VALUE (MeV)	DOCUMENT ID	TECN	CHG	COMMENT
• • • We do not use the following data for averages, fits, limits, etc. • • •				
26 \pm 6	CARNEGIE	77B	ASPK	\pm 13 $K^\pm p \rightarrow (K \pi \pi)^\pm p$

$\Gamma(K^*(892) \pi)$ Γ_3

VALUE (MeV)	DOCUMENT ID	TECN	CHG	COMMENT
• • • We do not use the following data for averages, fits, limits, etc. • • •				
14 \pm 11	MAZZUCATO	79	HBC	+ 4.2 $K^- p \rightarrow \Xi^- (K \pi \pi)^+$
2 \pm 2	CARNEGIE	77B	ASPK	\pm 13 $K^\pm p \rightarrow (K \pi \pi)^\pm p$

$\Gamma(K \omega)$ Γ_4

VALUE (MeV)	DOCUMENT ID	TECN	CHG	COMMENT
• • • We do not use the following data for averages, fits, limits, etc. • • •				
4 \pm 4	MAZZUCATO	79	HBC	+ 4.2 $K^- p \rightarrow \Xi^- (K \pi \pi)^+$
24 \pm 3	CARNEGIE	77B	ASPK	\pm 13 $K^\pm p \rightarrow (K \pi \pi)^\pm p$

$\Gamma(K f_0(1370))$ Γ_5

VALUE (MeV)	DOCUMENT ID	TECN	CHG	COMMENT
• • • We do not use the following data for averages, fits, limits, etc. • • •				
22 \pm 5	CARNEGIE	77B	ASPK	\pm 13 $K^\pm p \rightarrow (K \pi \pi)^\pm p$

$\Gamma(\gamma K^0)$ Γ_6

VALUE (keV)	DOCUMENT ID	TECN	COMMENT
73.2 \pm 6.1 \pm 28.3	ALAVI-HARATI02B	KTEV	$K + A \rightarrow K^* + A$

$K_1(1270)$ BRANCHING RATIOS

$\Gamma(K \rho)/\Gamma_{total}$ Γ_1/Γ

VALUE	DOCUMENT ID	TECN	COMMENT
0.38 \pm 0.13 OUR FIT	Error includes scale factor of 2.2.		
0.42 \pm 0.06	1 DAUM	81c CNTR	63 $K^- p \rightarrow K^- 2\pi p$
• • • We do not use the following data for averages, fits, limits, etc. • • •			
0.584 \pm 0.043	2 GULER	11 BELL	$B^+ \rightarrow J/\psi K^+ \pi^+ \pi^-$
dominant	RODEBACK	81 HBC	$4 \pi^- p \rightarrow \Lambda K 2\pi$

$\Gamma(K_0^*(1430) \pi)/\Gamma_{total}$ Γ_2/Γ

VALUE	DOCUMENT ID	TECN	COMMENT
0.28 \pm 0.04	1 DAUM	81c CNTR	63 $K^- p \rightarrow K^- 2\pi p$
• • • We do not use the following data for averages, fits, limits, etc. • • •			
0.0201 \pm 0.0064	2 GULER	11 BELL	$B^+ \rightarrow J/\psi K^+ \pi^+ \pi^-$

$\Gamma(K^*(892) \pi)/\Gamma_{total}$ Γ_3/Γ

VALUE	DOCUMENT ID	TECN	COMMENT
0.21 \pm 0.10 OUR FIT	Error includes scale factor of 2.2.		
0.16 \pm 0.05	1 DAUM	81c CNTR	63 $K^- p \rightarrow K^- 2\pi p$
• • • We do not use the following data for averages, fits, limits, etc. • • •			
0.171 \pm 0.023	2 GULER	11 BELL	$B^+ \rightarrow J/\psi K^+ \pi^+ \pi^-$

$\Gamma(K^*(892) \pi)/\Gamma(K \rho)$ Γ_3/Γ_1

VALUE	DOCUMENT ID	TECN	COMMENT
0.56 \pm 0.29 OUR FIT	Error includes scale factor of 2.2.		
0.99 \pm 0.15 \pm 0.18	ABLIKIM	21U BES3	$D_s^+ \rightarrow \bar{K}_1(1270)^0 K^+$

$\Gamma(K \omega)/\Gamma_{total}$ Γ_4/Γ

VALUE	DOCUMENT ID	TECN	COMMENT
0.11 \pm 0.02	1 DAUM	81c CNTR	63 $K^- p \rightarrow K^- 2\pi p$
• • • We do not use the following data for averages, fits, limits, etc. • • •			
0.225 \pm 0.052	2 GULER	11 BELL	$B^+ \rightarrow J/\psi K^+ \pi^+ \pi^-$

$\Gamma(K \omega)/\Gamma(K \rho)$ Γ_4/Γ_1

VALUE	CL%	DOCUMENT ID	TECN	COMMENT
• • • We do not use the following data for averages, fits, limits, etc. • • •				
<0.30	95	RODEBACK	81 HBC	$4 \pi^- p \rightarrow \Lambda K 2\pi$

$\Gamma(K f_0(1370))/\Gamma_{total}$ Γ_5/Γ

VALUE	DOCUMENT ID	TECN	COMMENT
0.03 \pm 0.02	1 DAUM	81c CNTR	63 $K^- p \rightarrow K^- 2\pi p$

D-wave/S-wave RATIO FOR $K_1(1270) \rightarrow K^*(892) \pi$

VALUE	DOCUMENT ID	TECN	COMMENT
1.0 \pm 0.7	1 DAUM	81c CNTR	63 $K^- p \rightarrow K^- 2\pi p$

¹ Average from low and high t data.

² Assuming that decays are saturated by the $K \rho, K_0^*(1430) \pi, K^*(892) \pi, K \omega$ decay modes and neglecting interference between them. The values $B(\omega \rightarrow \pi^+ \pi^-) = (1.53^{+0.11}_{-0.13})$ and $B(K_0^*(1430) \rightarrow K \pi) = (93 \pm 10)\%$ are used. Systematic uncertainties not estimated.

$K_1(1270)$ REFERENCES

ABLIKIM	21U	PR D104 032011	M. Ablikim et al.	(BESIII Collab.)
AAIJ	18A1	EPJ C78 443	R. Aaij et al.	(LHCb Collab.)
GULER	11	PR D83 032005	H. Guler et al.	(BELLE Collab.)
GENG	07	PR D75 014017	L.S. Geng et al.	
ABLIKIM	06C	PL B633 681	M. Ablikim et al.	(BES Collab.)
ALAVI-HARATI	02B	PRL 89 072001	A. Alavi-Harati et al.	(FNAL KTeV Collab.)
ASNER	00B	PR D62 072006	D.M. Asner et al.	(CLEO Collab.)
TORNQVIST	82B	NP B203 268	N.A. Tornqvist	(HELS)
DAUM	81c	NP B187 1	C. Daum et al.	(AMST, CERN, CRAC, MPIM+)
RODEBACK	81	ZPHY C9 9	S. Rodeback et al.	(CERN, CDEF, MADR+)
MAZZUCATO	79	NP B156 532	M. Mazzucato et al.	(CERN, ZEEM, NIJM+)
VERGEEST	79	NP B158 265	J.S.M. Vergeest et al.	(NUM, AMST, CERN+)
GAVILLET	78	PL 76B 517	P. Gavillet et al.	(AMST, CERN, NIJM+)
CARNEGIE	77B	PL B127 509	R.K. Carnegie et al.	(SLAC)
CARNEGIE	77B	PL 68B 287	R.K. Carnegie et al.	(SLAC)
BRANDENB...	76	PRL 36 703	G.W. Brandenburg et al.	(SLAC) JP
OTTER	76	NP B106 77	G. Otter et al.	(AACH3, BERL, CERN, LOIC+)
CRENNELL	72	PR D6 1220	D.J. Crennell et al.	(BNL)
DAVIS	72	PR D5 2688	P.J. Davis et al.	(LBL)
FIRESTONE	72B	PR D5 505	A. Firestone et al.	(LBL)
ASTIER	69	NP B10 65	A. Astier et al.	(CDEF, CERN, IPNP, LVP, IUP)
CRENNELL	67	PRL 19 44	D.J. Crennell et al.	(BNL)

$K_1(1400)$

$$I(J^P) = \frac{1}{2}(1^+)$$

$K_1(1400)$ MASS

VALUE (MeV)	EVTS	DOCUMENT ID	TECN	CHG	COMMENT
1403 \pm 7 OUR AVERAGE					
1463 \pm 64 \pm 68	7k	ASNER	00B	CLEO	$\tau^- \rightarrow K^- \pi^+ \pi^- \nu_\tau$
1373 \pm 14 \pm 18		1 ASTON	87	LASS	0 11 $K^- p \rightarrow \bar{K}^0 \pi^+ \pi^- n$
1392 \pm 18		BAUBILLIER	82B	HBC	0 8.25 $K^- p \rightarrow K_S^0 \pi^+ \pi^- n$
1410 \pm 25		DAUM	81c	CNTR	- 63 $K^- p \rightarrow K^- 2\pi p$
1415 \pm 15		ETKIN	80	MPS	0 6 $K^- p \rightarrow \bar{K}^0 \pi^+ \pi^- n$
1404 \pm 10		2 CARNEGIE	77	ASPK	\pm 13 $K^\pm p \rightarrow (K \pi \pi)^\pm p$
• • • We do not use the following data for averages, fits, limits, etc. • • •					
1418 \pm 8	25k	3 ABLIKIM	06c	BES2	$J/\psi \rightarrow \bar{K}^*(892)^0 K^+ \pi^-$
\sim 1350		4 TORNQVIST	82B	RVUE	
\sim 1400		VERGEEST	79	HBC	- 4.2 $K^- p \rightarrow (\bar{K} \pi \pi)^- p$
\sim 1400		BRANDENB...	76	ASPK	\pm 13 $K^\pm p \rightarrow (K \pi \pi)^\pm p$
1420		DAVIS	72	HBC	+ 12 $K^+ p$
1368 \pm 18		FIRESTONE	72B	DBC	+ 12 $K^+ d$

¹ From partial-wave analysis of $K^0 \pi^+ \pi^-$ system.

² From a model-dependent fit with Gaussian background to BRANDENBURG 76 data.

³ Systematic errors not estimated.

⁴ From a unitarized quark-model calculation.

See key on page 1171

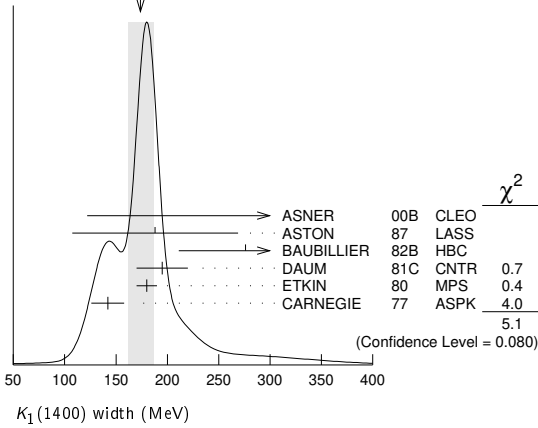
Meson Particle Listings

$K_1(1400)$, $K^*(1410)$

$K_1(1400)$ WIDTH

VALUE (MeV)	EVTS	DOCUMENT ID	TECN	CHG	COMMENT
174 ± 13 OUR AVERAGE		Error includes scale factor of 1.6. See the ideogram below.			
300 ⁺³⁷⁰ ₋₁₁₀ ± 140	7k	ASNER	00B	CLEO	± $\tau^- \rightarrow K^- \pi^+ \pi^- \nu_\tau$
188 ± 54 ± 60		¹ ASTON	87	LASS	0 11 $K^- p \rightarrow \bar{K}^0 \pi^+ \pi^- n$
276 ± 65		BAUBILLIER	82B	HBC	0 8.25 $K^- p \rightarrow K_S^0 \pi^+ \pi^- n$
195 ± 25		DAUM	81C	CNTR	- 63 $K^- p \rightarrow K^- 2\pi p$
180 ± 10		ETKIN	80	MPS	0 6 $K^- p \rightarrow \bar{K}^0 \pi^+ \pi^- n$
142 ± 16		² CARNEGIE	77	ASPK	± 13 $K^\pm p \rightarrow (K\pi\pi)^\pm p$
• • • We do not use the following data for averages, fits, limits, etc. • • •					
152 ± 16	25k	³ ABLIKIM	06c	BES2	$J/\psi \rightarrow \bar{K}^*(892)^0 K^+ \pi^-$
~ 200		VERGEEST	79	HBC	- 4.2 $K^- p \rightarrow (\bar{K}\pi\pi)^- p$
~ 160		BRANDENB...	76	ASPK	± 13 $K^\pm p \rightarrow (K\pi\pi)^\pm p$
80		DAVIS	72	HBC	+ 12 $K^+ p$
241 ± 30		FIRESTONE	72B	DBC	+ 12 $K^+ d$

WEIGHTED AVERAGE
174±13 (Error scaled by 1.6)



$K_1(1400)$ DECAY MODES

Mode	Fraction (Γ_i/Γ)
Γ_1 $K^*(892)\pi$	(94 ± 6 %) %
Γ_2 $K\rho$	(3.0 ± 3.0 %) %
Γ_3 $K f_0(1370)$	(2.0 ± 2.0 %) %
Γ_4 $K\omega$	(1.0 ± 1.0 %) %
Γ_5 $K_S^0(1430)\pi$	not seen
Γ_6 γK^0	seen
Γ_7 $K\phi$	seen

$K_1(1400)$ PARTIAL WIDTHS

$\Gamma(K^*(892)\pi)$	Γ_1
VALUE (MeV)	DOCUMENT ID TECN CHG COMMENT
117 ± 10	CARNEGIE 77 ASPK ± 13 $K^\pm p \rightarrow (K\pi\pi)^\pm p$
$\Gamma(K\rho)$	Γ_2
VALUE (MeV)	DOCUMENT ID TECN CHG COMMENT
2 ± 1	CARNEGIE 77 ASPK ± 13 $K^\pm p \rightarrow (K\pi\pi)^\pm p$
$\Gamma(K\omega)$	Γ_4
VALUE (MeV)	DOCUMENT ID TECN CHG COMMENT
23 ± 12	CARNEGIE 77 ASPK ± 13 $K^\pm p \rightarrow (K\pi\pi)^\pm p$
$\Gamma(\gamma K^0)$	Γ_6
VALUE (keV)	DOCUMENT ID TECN COMMENT
280.8 ± 23.2 ± 40.4	ALAVI-HARATI02B KTEV $K + A \rightarrow K^* + A$

$K_1(1400)$ BRANCHING RATIOS

$\Gamma(K^*(892)\pi)/\Gamma_{total}$	Γ_1/Γ
VALUE	DOCUMENT ID TECN COMMENT
0.94 ± 0.06	¹ DAUM 81c CNTR 63 $K^- p \rightarrow K^- 2\pi p$
¹ Average from low and high t data.	

$\Gamma(K\rho)/\Gamma_{total}$	Γ_2/Γ
VALUE	DOCUMENT ID TECN COMMENT
0.03 ± 0.03	¹ DAUM 81c CNTR 63 $K^- p \rightarrow K^- 2\pi p$
¹ Average from low and high t data.	

$\Gamma(K f_0(1370))/\Gamma_{total}$	Γ_3/Γ
VALUE	DOCUMENT ID TECN COMMENT
0.02 ± 0.02	¹ DAUM 81c CNTR 63 $K^- p \rightarrow K^- 2\pi p$
¹ Average from low and high t data.	

$\Gamma(K\omega)/\Gamma_{total}$	Γ_4/Γ
VALUE	DOCUMENT ID TECN COMMENT
0.01 ± 0.01	¹ DAUM 81c CNTR 63 $K^- p \rightarrow K^- 2\pi p$
¹ Average from low and high t data.	

$\Gamma(K\phi)/\Gamma_{total}$	Γ_7/Γ
VALUE	EVTS DOCUMENT ID TECN COMMENT
seen	24k ¹ AAIJ 21E LHCB $B^+ \rightarrow J/\psi \phi K^+$
¹ From an amplitude analysis of the decay $B^+ \rightarrow J/\psi \phi K^+$ with a significance of 9.2 σ .	

$\Gamma(K_S^0(1430)\pi)/\Gamma_{total}$	Γ_5/Γ
VALUE	DOCUMENT ID TECN COMMENT
not seen	¹ DAUM 81c CNTR 63 $K^- p \rightarrow K^- 2\pi p$
¹ Average from low and high t data.	

D-wave/S-wave RATIO FOR $K_1(1400) \rightarrow K^*(892)\pi$

VALUE	DOCUMENT ID	TECN	COMMENT
0.04 ± 0.01	¹ DAUM 81c CNTR 63	$K^- p \rightarrow K^- 2\pi p$	
¹ Average from low and high t data.			

$K_1(1400)$ REFERENCES

AAIJ 21E PRL 127 082001 R. Aaij et al. (LHCb Collab.)
ABLIKIM 06c PL B633 681 M. Ablikim et al. (BES Collab.)
ALAVI-HARATI 02B PRL 89 072001 A. Alavi-Harati et al. (FNAL KTeV Collab.)
ASNER 00B PR D62 072006 D.M. Asner et al. (CLEO Collab.)
ASTON 87 NP B292 693 D. Aston et al. (SLAC, NAGO, CIN, INUS)
BAUBILLIER 82B NP B202 21 M. Baubillier et al. (BIRM, CERN, GLAS+)
TORNQVIST 82B NP B203 268 N.A. Tornqvist (HELS)
DAUM 81C NP B187 1 C. Daum et al. (AMST, CERN, CRAC, MPIM+J)
ETKIN 80 PR D22 42 A. Etkin et al. (BNL, CUNY)JP
VERGEEST 79 NP B158 265 J.S.M. Vergeest et al. (NUM, AMST, CERN+)
CARNEGIE 77 NP B127 509 R.K. Carnegie et al. (SLAC)
BRANDENB... 76 PRL 36 703 G.W. Brandenburg et al. (SLAC)JP
DAVIS 72 PR D5 2688 P.J. Davis et al. (LBL)
FIRESTONE 72B PR D5 505 A. Firestone et al. (LBL)

$K^*(1410)$

$I(J^P) = \frac{1}{2}(1^-)$

$K^*(1410)$ T-MATRIX POLE \sqrt{s}

Note that $\Gamma = -2 \text{Im}(\sqrt{s})$.

VALUE (MeV)	DOCUMENT ID	TECN	COMMENT
(1368 ± 38) - i(106 ± 48)	OUR ESTIMATE		
(1368 ± 38) - i(106 ± 48)	¹ PELAEZ 17	RVUE	$\pi K \rightarrow \pi K$
¹ Reanalysis of ESTABROOKS 78 and ASTON 88 satisfying Forward Dispersion Relations and using sequences of Pade approximants.			

$K^*(1410)$ MASS

VALUE (MeV)	EVTS	DOCUMENT ID	TECN	CHG	COMMENT
1414 ± 15 OUR AVERAGE	Error includes scale factor of 1.3.				
1380 ± 21 ± 19		ASTON 88	LASS	0	11 $K^- p \rightarrow K^- \pi^+ n$
1420 ± 7 ± 10		ASTON 87	LASS	0	11 $K^- p \rightarrow \bar{K}^0 \pi^+ \pi^- n$
• • • We do not use the following data for averages, fits, limits, etc. • • •					
1437 ± 8 ± 16	190k	¹ AAIJ 16N	LHCB		$D^0 \rightarrow (K_S^0 \pi^\mp) K^\pm$
1426 ± 8 ± 24	190k	² AAIJ 16N	LHCB		$D^0 \rightarrow K_S^0 (K^\pm \pi^\mp)$
1276 ⁺⁷² ₋₇₇		^{3,4} BOITO 09	RVUE		$\tau^- \rightarrow K_S^0 \pi^- \nu_\tau$
1367 ± 54		BIRD 89	LASS	-	11 $K^- p \rightarrow \bar{K}^0 \pi^- p$
1474 ± 25		BAUBILLIER 82B	HBC	0	8.25 $K^- p \rightarrow \bar{K}^0 2\pi n$
1500 ± 30		ETKIN 80	MPS	0	6 $K^- p \rightarrow \bar{K}^0 \pi^+ \pi^- n$
¹ Using a parametrization for the $K\pi$ S-wave similar to ASTON 88 with fixed resonance width.					
² Using a $K\pi$ S-wave parametrization with resonant and non-resonant contributions.					
³ From the pole position of the $K\pi$ vector form factor in the complex s -plane and using EPIFANOV 07 data.					
⁴ Systematic uncertainties not estimated.					

$K^*(1410)$ WIDTH

VALUE (MeV)	EVTS	DOCUMENT ID	TECN	CHG	COMMENT
232 ± 21 OUR AVERAGE	Error includes scale factor of 1.1.				
176 ± 52 ± 22		ASTON 88	LASS	0	11 $K^- p \rightarrow K^- \pi^+ n$
240 ± 18 ± 12		ASTON 87	LASS	0	11 $K^- p \rightarrow \bar{K}^0 \pi^+ \pi^- n$

Meson Particle Listings

$K^*(1410)$, $K_0^*(1430)$

••• We do not use the following data for averages, fits, limits, etc. •••

210 ± 20 ± 60	190k	1 AAIJ	16N LHCB	$D^0 \rightarrow (K_S^0 \pi^\mp) K^\pm$
270 ± 20 ± 40	190k	1 AAIJ	16N LHCB	$D^0 \rightarrow K_S^0(K^\pm \pi^\mp)$
198 ⁺⁶¹ ₋₈₇		2,3 BOITO	09 RVUE	$\tau^- \rightarrow K_S^0 \pi^- \nu_\tau$
114 ± 101		BIRD	89 LASS	$11 K^- p \rightarrow \bar{K}^0 \pi^- p$
275 ± 65		BAUBILLIER	82B HBC	$0.825 K^- p \rightarrow \bar{K}^0 2\pi n$
500 ± 100		ETKIN	80 MPS	$0.6 K^- p \rightarrow \bar{K}^0 \pi^+ \pi^- n$

- Using a $K\pi$ S-wave parametrization with resonant and non-resonant contributions.
- From the pole position of the $K\pi$ vector form factor in the complex s -plane and using EPIFANOV 07 data.
- Systematic uncertainties not estimated.

$K^*(1410)$ DECAY MODES

Mode	Fraction (Γ_i/Γ)	Confidence level
Γ_1 $K^*(892)\pi$	> 40 %	95%
Γ_2 $K\pi$	(6.6 ± 1.3) %	
Γ_3 $K\rho$	< 7 %	95%
Γ_4 γK^0	< 2.3 × 10 ⁻⁴	90%
Γ_5 $K\phi$	seen	

$K^*(1410)$ PARTIAL WIDTHS

$\Gamma(\gamma K^0)$	CL%	DOCUMENT ID	TECN	COMMENT	Γ_4
VALUE (keV)					
<52.9	90	ALAVI-HARATI02B	KTEV	$K + A \rightarrow K^* + A$	

$K^*(1410)$ BRANCHING RATIOS

$\Gamma(K\rho)/\Gamma(K^*(892)\pi)$	CL%	DOCUMENT ID	TECN	CHG	COMMENT	Γ_3/Γ_1
VALUE						
<0.17	95	ASTON	84 LASS	0	$11 K^- p \rightarrow \bar{K}^0 2\pi n$	

$\Gamma(K\pi)/\Gamma(K^*(892)\pi)$	CL%	DOCUMENT ID	TECN	CHG	COMMENT	Γ_2/Γ_1
VALUE						
<0.16	95	ASTON	84 LASS	0	$11 K^- p \rightarrow \bar{K}^0 2\pi n$	

$\Gamma(K\pi)/\Gamma_{total}$	CL%	DOCUMENT ID	TECN	CHG	COMMENT	Γ_2/Γ
VALUE						
0.066 ± 0.010 ± 0.008		ASTON	88 LASS	0	$11 K^- p \rightarrow K^- \pi^+ n$	

$\Gamma(K\phi)/\Gamma_{total}$	EVTS	DOCUMENT ID	TECN	COMMENT	Γ_5/Γ
VALUE					
seen	24k	1 AAIJ	21E LHCB	$B^+ \rightarrow J/\psi \phi K^+$	

- From an amplitude analysis of the decay $B^+ \rightarrow J/\psi \phi K^+$ with a significance of 7.7 σ .

$K^*(1410)$ REFERENCES

AAIJ	21E	PRL 127 082001	R. Aaij et al.	(LHCb Collab.)
PELAEZ	17	EPJ C77 91	J.R. Peláez, A.Rodas, J.R. de Elvira	
AAIJ	16N	PR D93 052018	R. Aaij et al.	(LHCb Collab.)
BOITO	09	EPJ C59 821	D.R. Boito, R. Escribano, M. Jamin	
EPIFANOV	07	PL B654 65	D. Epifanov et al.	(BELLE Collab.)
ALAVI-HARATI 02B		PRL 89 072001	A. Alavi-Harati et al.	(FNAL KTeV Collab.)
BIRD	89	SLAC-332	P.F. Bird	(SLAC)
ASTON	88	NP B296 493	D. Aston et al.	(SLAC, NAGO, CINC, INUS)
ASTON	87	NP B292 693	D. Aston et al.	(SLAC, NAGO, CINC, INUS)
ASTON	84	PL 149B 258	D. Aston et al.	(SLAC, CARL, OTTA JP)
BAUBILLIER	82B	NP B202 21	M. Baubillier et al.	(BIRM, CERN, GLAS-)
ETKIN	80	PR D22 42	A. Etkin et al.	(BNL, CUNY) JP
ESTABROOKS	78	NP B133 490	P.G. Estabrooks et al.	(MCGI, CARL, DURH-)

$K_0^*(1430)$

$$I(J^P) = \frac{1}{2}(0^+)$$

$K_0^*(1430)$ T-MATRIX POLE \sqrt{s}

Note that $\Gamma = -2 \text{Im}(\sqrt{s})$.

VALUE (MeV)	DOCUMENT ID	TECN	COMMENT
(1431 ± 6) - i (110 ± 19) OUR ESTIMATE			
(1431 ± 6) - i (110 ± 19)	1 PELAEZ	17 RVUE	$\pi K \rightarrow \pi K$

- Reanalysis of ESTABROOKS 78 and ASTON 88 satisfying Forward Dispersion Relations and using sequences of Padé approximants.

$K_0^*(1430)$ MASS

VALUE (MeV)	EVTS	DOCUMENT ID	TECN	COMMENT
1425 ± 50 OUR ESTIMATE				

••• We do not use the following data for averages, fits, limits, etc. •••

1493 ± 4 ± 7		1 AAIJ	23AH LHCB	$B^+ \rightarrow K^+(K_S^0 K\pi)$
1449 ± 17 ± 2		2 LEES	21A BABR	$\eta_c(1S) \rightarrow \eta' K^+ K^-$
1438 ± 8 ± 4	5.4k	3 LEES	14E BABR	$\eta_c(1S) \rightarrow K^+ K^- \eta/\pi^0$
1427 ± 4 ± 13		4 BUGG	10 RVUE	S-matrix pole
1466.6 ± 0.7 ± 3.4	141k	5 BONVICINI	08A CLEO	$D^+ \rightarrow K^- \pi^+ \pi^+$
~ 1412		6 LINK	07 FOCS	$D^+ \rightarrow K^- K^+ \pi^+$
1461.0 ± 4.0 ± 2.1	54k	7 LINK	07B FOCS	$D^+ \rightarrow K^- \pi^+ \pi^+$
1406 ± 29		8 BUGG	06 RVUE	
1435 ± 6		9 ZHOU	06 RVUE	$K\rho \rightarrow K^- \pi^+ n$
1455 ± 20 ± 15		ABLIKIM	05Q BES2	$\psi(2S) \rightarrow \gamma \pi^+ \pi^- K^+ K^-$
1456 ± 8		10 ZHENG	04 RVUE	$K^- p \rightarrow K^- \pi^+ n$
~ 1419		11 BUGG	03 RVUE	$11 K^- p \rightarrow K^- \pi^+ n$
~ 1440		12 LI	03 RVUE	$11 K^- p \rightarrow K^- \pi^+ n$
1459 ± 9	15k	13 AITALA	02 E791	$D^+ \rightarrow K^- \pi^+ \pi^+$
~ 1440		14 JAMIN	00 RVUE	$K\rho \rightarrow K\rho$
1436 ± 8		15 BARBERIS	98E OMEG	450 pp \rightarrow $p\bar{f}p_S K^+ K^- \pi^+ \pi^-$
1415 ± 25		11 ANISOVICH	97C RVUE	$11 K^- p \rightarrow K^- \pi^+ n$
~ 1450		16 TORNQVIST	96 RVUE	$\pi\pi \rightarrow \pi\pi, K\bar{K}, K\pi$
1412 ± 6		17 ASTON	88 LASS	$11 K^- p \rightarrow K^- \pi^+ n$
~ 1430		BAUBILLIER	84B HBC	$8.25 K^- p \rightarrow \bar{K}^0 \pi^- p$
~ 1425		18 ESTABROOKS	78 ASPK	$13 K^\pm p \rightarrow K^\pm \pi^\pm(n, \Delta)$
~ 1450.0		MARTIN	78 SPEC	$10 K^\pm p \rightarrow K_S^0 \pi p$

- From Dalitz plot analyses of $\eta_c(1S, 2S) \rightarrow K_S^0 K^+ \pi^- + c.c.$
- Using a $K\pi - K\eta'$ coupled channel Breit-Wigner function.
- Using both $\eta \rightarrow \gamma\gamma$ and $\eta \rightarrow \pi^+ \pi^- \pi^0$. From a likelihood scan in the presence of several interfering scalar-meson resonances with fixed width $\Gamma(K_0^*(1430)) = 210$ MeV.
- S-Matrix pole. Supersedes BUGG 06. Combined analysis of ASTON 88, ABLIKIM 06c, AITALA 06, and LINK 09 using an s-dependent width with couplings to $K\pi$ and $K\eta'$, and the Adler zero near thresholds.
- From the isobar model with a complex pole for the κ .
- From a non-parametric analysis.
- A Breit-Wigner mass and width.
- S-matrix pole. Reanalysis of ASTON 88, AITALA 02, and ABLIKIM 06c including the κ with an s-dependent width and an Adler zero near threshold.
- S-matrix pole. Using ASTON 88 and assuming $K_0^*(700)$, $K_0^*(1950)$.
- Using ASTON 88 and assuming $K_0^*(700)$.
- T-matrix pole. Reanalysis of ASTON 88 data.
- Breit-Wigner fit. Using ASTON 88.
- Assuming a low-mass scalar $K\pi$ resonance, $\kappa(700)$.
- T-matrix pole. Using data from ESTABROOKS 78 and ASTON 88.
- J^P not determined, could be $K_2^*(1430)$.
- T-matrix pole.
- Uses a model for the background, without this background they get a mass 1340 MeV, where the phase shift passes 90°.
- Mass defined by pole position. From elastic $K\pi$ partial-wave analysis.

$K_0^*(1430)$ WIDTH

VALUE (MeV)	EVTS	DOCUMENT ID	TECN	COMMENT
270 ± 80 OUR ESTIMATE				

••• We do not use the following data for averages, fits, limits, etc. •••

215 ± 7 ± 4		1 AAIJ	23AH LHCB	$B^+ \rightarrow K^+(K_S^0 K\pi)$
210 ± 20 ± 12	5.4k	2 LEES	14E BABR	$\eta_c(1S) \rightarrow K^+ K^- \eta/\pi^0$
270 ± 10 ± 40		3 BUGG	10 RVUE	S-matrix pole
174.2 ± 1.9 ± 3.2	141k	4 BONVICINI	08A CLEO	$D^+ \rightarrow K^- \pi^+ \pi^+$
~ 500		5 LINK	07 FOCS	$D^+ \rightarrow K^- K^+ \pi^+$
177.0 ± 8.0 ± 3.4	54k	6 LINK	07B FOCS	$D^+ \rightarrow K^- \pi^+ \pi^+$
350 ± 40		7 BUGG	06 RVUE	
288 ± 22		8 ZHOU	06 RVUE	$K\rho \rightarrow K^- \pi^+ n$
270 ± 45	+30 -35	ABLIKIM	05Q BES2	$\psi(2S) \rightarrow \gamma \pi^+ \pi^- K^+ K^-$
217 ± 31		9 ZHENG	04 RVUE	$K^- p \rightarrow K^- \pi^+ n$
~ 316		10 BUGG	03 RVUE	$11 K^- p \rightarrow K^- \pi^+ n$
~ 350		11 LI	03 RVUE	$11 K^- p \rightarrow K^- \pi^+ n$
175 ± 17	15k	12 AITALA	02 E791	$D^+ \rightarrow K^- \pi^+ \pi^+$
~ 300		13 JAMIN	00 RVUE	$K\rho \rightarrow K\rho$
196 ± 45		14 BARBERIS	98E OMEG	450 pp \rightarrow $p\bar{f}p_S K^+ K^- \pi^+ \pi^-$
330 ± 50		10 ANISOVICH	97C RVUE	$11 K^- p \rightarrow K^- \pi^+ n$
~ 320		15 TORNQVIST	96 RVUE	$\pi\pi \rightarrow \pi\pi, K\bar{K}, K\pi$
294 ± 23		ASTON	88 LASS	$11 K^- p \rightarrow K^- \pi^+ n$
~ 200		BAUBILLIER	84B HBC	$8.25 K^- p \rightarrow \bar{K}^0 \pi^- p$
200 to 300		16 ESTABROOKS	78 ASPK	$13 K^\pm p \rightarrow K^\pm \pi^\pm(n, \Delta)$

- From Dalitz plot analyses of $\eta_c(1S, 2S) \rightarrow K_S^0 K^+ \pi^- + c.c.$
- Using both $\eta \rightarrow \gamma\gamma$ and $\eta \rightarrow \pi^+ \pi^- \pi^0$. From a likelihood scan in the presence of several interfering scalar-meson resonances with fixed mass $M(K_0^*(1430)) = 1435$ MeV.
- S-Matrix pole. Supersedes BUGG 06. Combined analysis of ASTON 88, ABLIKIM 06c, AITALA 06, and LINK 09 using an s-dependent width with couplings to $K\pi$ and $K\eta'$, and the Adler zero near thresholds.
- From the isobar model with a complex pole for the κ .

See key on page 1171

Meson Particle Listings

$K_0^*(1430)$, $K_2^*(1430)$

- ⁵ From a non-parametric analysis.
- ⁶ A Breit-Wigner mass and width.
- ⁷ S-matrix pole. Reanalysis of ASTON 88, AITALA 02, and ABLIKIM 06c including the κ with an s-dependent width and an Adler zero near threshold.
- ⁸ S-matrix pole. Using ASTON 88 and assuming $K_0^*(700)$, $K_0^*(1950)$.
- ⁹ Using ASTON 88 and assuming $K_0^*(700)$.
- ¹⁰ T-matrix pole. Reanalysis of ASTON 88 data.
- ¹¹ Breit-Wigner fit. Using ASTON 88.
- ¹² Assuming a low-mass scalar $K\pi$ resonance, $\kappa(700)$.
- ¹³ T-matrix pole. Using data from ESTABROOKS 78 and ASTON 88.
- ¹⁴ J^P not determined, could be $K_2^*(1430)$.
- ¹⁵ T-matrix pole.
- ¹⁶ From elastic $K\pi$ partial-wave analysis.

$K_0^*(1430)$ DECAY MODES

Mode	Fraction (Γ_i/Γ)
Γ_1 $K\pi$	(93 \pm 10) %
Γ_2 $K\eta$	(8.6 \pm 2.7 / 3.4) %
Γ_3 $K\eta'(958)$	seen

$K_0^*(1430)$ BRANCHING RATIOS

$\Gamma(K\pi)/\Gamma_{total}$	Γ_1/Γ			
VALUE	DOCUMENT ID	TECN	CHG	COMMENT
0.93 \pm 0.04 \pm 0.09	ASTON	88	LASS	0 11 $K^-p \rightarrow K^- \pi^+ n$

$\Gamma(K\eta)/\Gamma(K\pi)$	Γ_2/Γ_1			
VALUE (%)	EVTS	DOCUMENT ID	TECN	COMMENT
9.2 \pm 2.5 \pm 1.0 / 2.5	5.4k	¹ LEES	14E	BABR $\eta_c(1S) \rightarrow K^+ K^- \eta/\pi^0$

¹ Using both $\eta \rightarrow \gamma\gamma$ and $\eta \rightarrow \pi^+ \pi^- \pi^0$. From a Dalitz analysis in the presence of several interfering scalar-meson resonances.

$\Gamma(K\eta'(958))/\Gamma_{total}$	Γ_3/Γ		
VALUE	DOCUMENT ID	TECN	COMMENT
seen	ABLIKIM	14J	BES3 $\psi(2S) \rightarrow \gamma K^+ K^- \eta'(958)$

$\Gamma(K\eta'(958))/\Gamma(K\pi)$	Γ_3/Γ_1		
VALUE	DOCUMENT ID	TECN	COMMENT
0.397 \pm 0.064 \pm 0.054	¹ LEES	21A	BABR $\eta_c(1S) \rightarrow \eta' K^+ K^-$

¹ Using $K\pi$ data from LEES 14E.

$K_0^*(1430)$ REFERENCES

AAJ	23AH	PR D108 032010	R. Aaj <i>et al.</i>	(LHCb Collab.)
LEES	21A	PR D104 072002	J.P. Lees <i>et al.</i>	(BABAR Collab.)
PELAEZ	17	EPJ C71 91	J.R. Pelaez, A.Rodas, J.R. de Elvira	(BESIII Collab.)
ABLIKIM	14J	PR D89 074030	M. Ablikim <i>et al.</i>	(BABAR Collab.)
LEES	14E	PR D89 112004	J.P. Lees <i>et al.</i>	(BABAR Collab.)
BUGG	10	PR D81 014002	D.V. Bugg	(LOQM)
LINK	09	PL B681 14	J.M. Link <i>et al.</i>	(FNAL FOCUS Collab.)
BONVICINI	08A	PR D78 052001	G. Bonvicini <i>et al.</i>	(CLEO Collab.)
LINK	07	PL B648 156	J.M. Link <i>et al.</i>	(FNAL FOCUS Collab.)
LINK	07B	PL B653 1	J.M. Link <i>et al.</i>	(FNAL FOCUS Collab.)
ABLIKIM	06C	PL B633 681	M. Ablikim <i>et al.</i>	(BES Collab.)
AITALA	06	PR D73 032004	E.M. Aitala <i>et al.</i>	(FNAL E791 Collab.)
BUGG	Also	PR D74 059901 (errata.)	E.M. Aitala <i>et al.</i>	(FNAL E791 Collab.)
BUGG	06	PL B632 471	D.V. Bugg	(LOQM)
ZHOU	06	NP A775 212	Z.Y. Zhou, H.Q. Zheng	(BES Collab.)
ABLIKIM	05Q	PR D72 092002	M. Ablikim <i>et al.</i>	(BES Collab.)
ZHENG	04	NP A733 235	H.Q. Zheng <i>et al.</i>	(BES Collab.)
BUGG	03	PL B572 1	D.V. Bugg	(LOQM)
LI	03	PR D67 034025	L. Li, B. Zou, G. Li	(FNAL E791 Collab.)
AITALA	02	PRL 89 121801	E.M. Aitala <i>et al.</i>	(FNAL E791 Collab.)
JAMIN	00	NP B587 331	M. Jamin <i>et al.</i>	(Omega Expt.)
BARBERIS	98E	PL B436 204	D. Barberis <i>et al.</i>	(Omega Expt.)
ANISOVICH	97C	PL B413 137	A.V. Anisovich, A.V. Sarantsev	(HELs)
TORNQVIST	96	PRL 76 1575	N.A. Tornqvist, M. Roos	(HELs)
ASTON	88	NP B296 493	D. Aston <i>et al.</i>	(SLAC, NAGO, CINC, INUS)
BAUBILLIER	84B	ZPHY C26 37	M. Baubillier <i>et al.</i>	(BIRM, CERN, GLAS-)
ESTABROOKS	78	NP B133 490	P.G. Estabrooks <i>et al.</i>	(MCGI, CARL, DURH-)
MARTIN	78	NP B134 392	A.D. Martin <i>et al.</i>	(DURH, GEVA)

$K_2^*(1430)$

$I(J^P) = \frac{1}{2}(2^+)$

We consider that phase-shift analyses provide more reliable determinations of the mass and width.

$K_2^*(1430)$ T-MATRIX POLE \sqrt{s}

Note that $\Gamma = -2 \text{Im}(\sqrt{s})$.

VALUE (MeV)	DOCUMENT ID	TECN	COMMENT
(1424 \pm 4) - i (66 \pm 2) OUR ESTIMATE			
(1424 \pm 4) - i (66 \pm 2)	¹ PELAEZ	17	RVUE $\pi K \rightarrow \pi K$

¹ Reanalysis of ESTABROOKS 78 and ASTON 88 satisfying Forward Dispersion Relations and using sequences of Padé approximants.

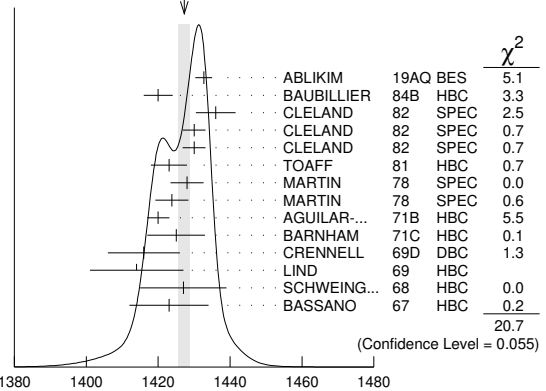
$K_2^*(1430)$ MASS

CHARGED ONLY, WITH FINAL STATE $K\pi$

VALUE (MeV)	EVTS	DOCUMENT ID	TECN	CHG	COMMENT
1427.3 \pm 1.5 OUR AVERAGE					Error includes scale factor of 1.3. See the ideogram below.
1432.7 \pm 0.7 \pm 2.2 / 2.3	183k	ABLIKIM	19AQ	BES	\pm $J/\psi \rightarrow K^+ K^- \pi^0$
1420 \pm 4	1587	BAUBILLIER	84B	HBC	- 8.25 $K^- p \rightarrow \bar{K}^0 \pi^- p$
1436 \pm 5.5	400	^{1,2} CLELAND	82	SPEC	+ 30 $K^+ p \rightarrow K_0^0 \pi^+ p$
1430 \pm 3.2	1500	^{1,2} CLELAND	82	SPEC	+ 50 $K^+ p \rightarrow K_S^0 \pi^+ p$
1430 \pm 3.2	1200	^{1,2} CLELAND	82	SPEC	- 50 $K^+ p \rightarrow K_S^0 \pi^- p$
1423 \pm 5	935	TOAFF	81	HBC	- 6.5 $K^- p \rightarrow \bar{K}^0 \pi^- p$
1428.0 \pm 4.6		³ MARTIN	78	SPEC	+ 10 $K^\pm p \rightarrow K_S^0 \pi p$
1423.8 \pm 4.6		³ MARTIN	78	SPEC	- 10 $K^\pm p \rightarrow K_S^0 \pi p$
1420.0 \pm 3.1	1400	AGUILAR-...	71B	HBC	+ 3.9,4.6 $K^- p$
1425 \pm 8.0	225	^{1,2} BARNHAM	71c	HBC	+ $K^+ p \rightarrow K^0 \pi^+ p$
1416 \pm 10	220	CRENNELL	69D	DBC	- 3.9 $K^- N \rightarrow \bar{K}^0 \pi^- N$
1414 \pm 13.0	60	¹ LIND	69	HBC	+ 9 $K^+ p \rightarrow K^0 \pi^+ p$
1427 \pm 12	63	¹ SCHWEING...	68	HBC	- 5.5 $K^- p \rightarrow \bar{K} \pi N$
1423 \pm 11.0	39	¹ BASSANO	67	HBC	- 4.6-5.0 $K^- p \rightarrow \bar{K}^0 \pi^- p$
1428 \pm 2	4300	⁴ ABLIKIM	22L	BES3	2.0-3.08 $e^+ e^- \rightarrow K^+ K^- \pi^0$
1423.4 \pm 2 \pm 3	24809 \pm 820	⁵ BIRD	89	LASS	- 11 $K^- p \rightarrow \bar{K}^0 \pi^- p$

- • • We do not use the following data for averages, fits, limits, etc. • • •
- ¹ Errors enlarged by us to Γ/\sqrt{N} ; see the note with the $K^*(892)$ mass.
- ² Number of events in peak re-evaluated by us.
- ³ Systematic error added by us.
- ⁴ From a partial wave amplitude analysis at $\sqrt{s} = 2.125$ GeV which includes all the possible intermediate states that match J^{PC} conservation in the subsequent two-body decay. The intermediate states are parameterized with the relativistic Breit-Wigner functions. Statistical error only.
- ⁵ From a partial wave amplitude analysis.

WEIGHTED AVERAGE
1427.3 \pm 1.5 (Error scaled by 1.3)



$K_2^*(1430)$ mass, combined neutral and charged (MeV)

NEUTRAL ONLY

VALUE (MeV)	EVTS	DOCUMENT ID	TECN	COMMENT
1432.4 \pm 1.3 OUR AVERAGE				
1431.2 \pm 1.8 \pm 0.7		¹ ASTON	88	LASS 11 $K^- p \rightarrow K^- \pi^+ n$
1434 \pm 4 \pm 6		¹ ASTON	87	LASS 11 $K^- p \rightarrow \bar{K}^0 \pi^+ \pi^- n$
1433 \pm 6 \pm 10		¹ ASTON	84B	LASS 11 $K^- p \rightarrow \bar{K}^0 2\pi n$
1471 \pm 12		¹ BAUBILLIER	82B	HBC 8.25 $K^- p \rightarrow NK_S^0 \pi$
1428 \pm 3		¹ ASTON	81c	LASS 11 $K^- p \rightarrow K^- \pi^+ n$
1434 \pm 2		¹ ESTABROOKS	78	ASP 13 $K^\pm p \rightarrow pK\pi$
1440 \pm 10		¹ BOWLER	77	DBC 5.5 $K^+ d \rightarrow K\pi pp$
1428.5 \pm 3.9	1786 \pm 127	² AUBERT	07AK	BABR 10.6 $e^+ e^- \rightarrow K^{*0} K_S^\pm \pi^\mp \gamma$
1420 \pm 7	300	HENDRICK	76	DBC 8.25 $K^+ N \rightarrow K^+ \pi N$
1421.6 \pm 4.2	800	MCCUBBIN	75	HBC 3.6 $K^- p \rightarrow K^- \pi^+ n$
1420.1 \pm 4.3		³ LINGLIN	73	HBC 2-13 $K^+ p \rightarrow K^+ \pi^- X$
1419.1 \pm 3.7	1800	AGUILAR-...	71B	HBC 3.9,4.6 $K^- p$
1416 \pm 6	600	CORDS	71	DBC 9 $K^+ n \rightarrow K^+ \pi^- p$
1421.1 \pm 2.6	2200	DAVIS	69	HBC 12 $K^+ p \rightarrow K^+ \pi^- X$

- • • We do not use the following data for averages, fits, limits, etc. • • •
- ¹ From phase shift or partial-wave analysis.
- ² Systematic errors not estimated.
- ³ From pole extrapolation, using world $K^+ p$ data summary tape.

Meson Particle Listings

$K_2^*(1430)$

$K_2^*(1430)$ WIDTH

CHARGED ONLY, WITH FINAL STATE $K\pi$

VALUE (MeV)	EVTS	DOCUMENT ID	TECN	CHG	COMMENT
100.0 ± 2.2 OUR FIT					Error includes scale factor of 1.1.
100.0 ± 2.2 OUR AVERAGE					Error includes scale factor of 1.1.
102.5 ± 1.6 ^{+3.1} / _{-2.8}	183k	ABLIKIM	19AQ	BES	± $J/\psi \rightarrow K^+ K^- \pi^0$
109 ± 22	400	1,2 CLELAND	82	SPEC	+ 30 $K^+ p \rightarrow K_S^0 \pi^+ p$
124 ± 12.8	1500	1,2 CLELAND	82	SPEC	+ 50 $K^+ p \rightarrow K_S^0 \pi^+ p$
113 ± 12.8	1200	1,2 CLELAND	82	SPEC	- 50 $K^+ p \rightarrow K_S^0 \pi^+ p$
85 ± 16	935	TOAFF	81	HBC	- 6.5 $K^- p \rightarrow \bar{K}^0 \pi^- p$
96.5 ± 3.8		MARTIN	78	SPEC	+ 10 $K^\pm p \rightarrow K_S^0 \pi p$
97.7 ± 4.0		MARTIN	78	SPEC	- 10 $K^\pm p \rightarrow K_S^0 \pi p$
94.7 ^{+15.1} / _{-12.5}	1400	AGUILAR-...	71B	HBC	- 3,9,4,6 $K^- p$

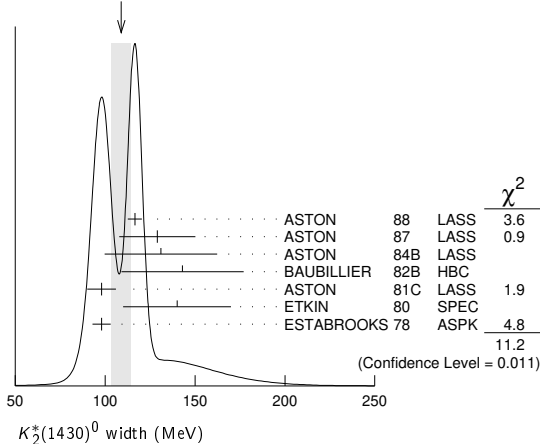
- • • We do not use the following data for averages, fits, limits, etc. • • •
 - 107 ± 4 4300³ ABLIKIM 22L BES3 2.0-3.08 $e^+ e^- \rightarrow K^+ K^- \pi^0$
 - 98 ± 4 ± 4 25k⁴ BIRD 89 LASS - 11 $K^- p \rightarrow \bar{K}^0 \pi^- p$
- ¹ Errors enlarged by us to $4\Gamma/\sqrt{N}$; see the note with the $K^*(892)$ mass.
² Number of events in peak re-evaluated by us.
³ From a partial wave amplitude analysis at $\sqrt{s} = 2.125$ GeV which includes all the possible intermediate states that match J^{PC} conservation in the subsequent two-body decay. The intermediate states are parameterized with the relativistic Breit-Wigner functions. Statistical error only.
⁴ From a partial wave amplitude analysis.

NEUTRAL ONLY

VALUE (MeV)	EVTS	DOCUMENT ID	TECN	COMMENT
109 ± 5 OUR AVERAGE				Error includes scale factor of 1.9. See the ideogram below.
116.5 ± 3.6 ± 1.7		¹ ASTON 88 LASS	11	$K^- p \rightarrow K^- \pi^+ n$
129 ± 15 ± 15		¹ ASTON 87 LASS	11	$K^- p \rightarrow \bar{K}^0 \pi^+ \pi^- n$
131 ± 24 ± 20		¹ ASTON 84B LASS	11	$K^- p \rightarrow \bar{K}^0 2\pi n$
143 ± 34		¹ BAUBILLIER 82B HBC	8.25	$K^- p \rightarrow N K_S^0 \pi\pi$
98 ± 8		¹ ASTON 81c LASS	11	$K^- p \rightarrow K^- \pi^+ n$
140 ± 30		¹ ETKIN 80 SPEC	6	$K^- p \rightarrow \bar{K}^0 \pi^+ \pi^- n$
98 ± 5		¹ ESTABROOKS 78 ASPK	13	$K^\pm p \rightarrow p K \pi$

- • • We do not use the following data for averages, fits, limits, etc. • • •
 - 113.7 ± 9.2 1786 ± 127² AUBERT 07AK BABR 10.6 $e^+ e^- \rightarrow K^* K^\pm \pi^\mp \gamma$
 - 125 ± 29 300³ HENDRICK 76 DBC 8.25 $K^+ N \rightarrow K^+ \pi N$
 - 116 ± 18 800 MCCUBBIN 75 HBC 3.6 $K^- p \rightarrow K^- \pi^+ n$
 - 61 ± 14 4 LINGLIN 73 HBC 2-13 $K^+ p \rightarrow K^+ \pi^+ X$
 - 116.6^{+10.3}/_{-15.5} 1800 AGUILAR-... 71B HBC 3,9,4,6 $K^- p$
 - 144 ± 24.0 600³ CORDS 71 DBC 9 $K^+ n \rightarrow K^+ \pi^- p$
 - 101 ± 10 2200 DAVIS 69 HBC 12 $K^+ p \rightarrow K^+ \pi^- \pi^+ p$
- ¹ From phase shift or partial-wave analysis.
² Systematic errors not estimated.
³ Errors enlarged by us to $4\Gamma/\sqrt{N}$; see the note with the $K^*(892)$ mass.
⁴ From pole extrapolation, using world $K^+ p$ data summary tape.

WEIGHTED AVERAGE
109±5 (Error scaled by 1.9)



$K_2^*(1430)$ DECAY MODES

Mode	Fraction (Γ_i/Γ)	Scale factor/ Confidence level
Γ_1 $K\pi$	(49.9 ± 1.2) %	
Γ_2 $K^*(892)\pi$	(24.7 ± 1.5) %	
Γ_3 $K^*(892)\pi\pi$	(13.4 ± 2.2) %	
Γ_4 $K\rho$	(8.7 ± 0.8) %	S=1.2

Γ_5 $K\omega$	(2.9 ± 0.8) %	
Γ_6 $K^+\gamma$	(2.4 ± 0.5) × 10 ⁻³	S=1.1
Γ_7 $K\eta$	(1.5 ^{+3.4} / _{-1.0}) × 10 ⁻³	S=1.3
Γ_8 $K\omega\pi$	< 7.2 × 10 ⁻⁴	CL=95%
Γ_9 $K^0\gamma$	< 9 × 10 ⁻⁴	CL=90%

CONSTRAINED FIT INFORMATION

An overall fit to the total width, a partial width, and 10 branching ratios uses 32 measurements and one constraint to determine 8 parameters. The overall fit has a $\chi^2 = 21.1$ for 25 degrees of freedom.

The following *off-diagonal* array elements are the correlation coefficients $\langle \delta p_i \delta p_j \rangle / (\delta p_i \delta p_j)$, in percent, from the fit to parameters p_i , including the branching fractions, $x_i \equiv \Gamma_i/\Gamma_{\text{total}}$. The fit constrains the x_i whose labels appear in this array to sum to one.

x_2	-9						
x_3	-40	-73					
x_4	-8	36	-52				
x_5	-11	-3	-26	-7			
x_6	-1	-1	-1	-1	0		
x_7	-4	-7	-5	-5	-2	0	
Γ	0	0	0	0	0	-11	0
	x_1	x_2	x_3	x_4	x_5	x_6	x_7

Mode	Rate (MeV)	Scale factor
Γ_1 $K\pi$	49.9 ± 1.6	
Γ_2 $K^*(892)\pi$	24.7 ± 1.6	
Γ_3 $K^*(892)\pi\pi$	13.5 ± 2.3	
Γ_4 $K\rho$	8.7 ± 0.8	1.2
Γ_5 $K\omega$	2.9 ± 0.8	
Γ_6 $K^+\gamma$	0.24 ± 0.05	1.1
Γ_7 $K\eta$	0.15 ^{+0.34} / _{-0.10}	1.3

$K_2^*(1430)$ PARTIAL WIDTHS

Mode	VALUE (keV)	DOCUMENT ID	TECN	CHG	COMMENT
$\Gamma(K^+\gamma)$	240 ± 50 OUR FIT				Error includes scale factor of 1.1.
Γ_6	240 ± 45	CIHANGIR 82 SPEC	+		200 $K^+ Z \rightarrow Z K^+ \pi^0$, $Z K_S^0 \pi^+$

Mode	VALUE (keV)	CL%	DOCUMENT ID	TECN	CHG	COMMENT
$\Gamma(K^0\gamma)$	< 5.4	90	ALAVI-HARATI02B KTEV			$K^+ A \rightarrow K^+ + A$
Γ_9	< 84	90	CARLSMITH 87 SPEC	0		60-200 $K_L^0 A \rightarrow K_S^0 \pi^0 A$

$K_2^*(1430)$ BRANCHING RATIOS

$\Gamma(K\pi)/\Gamma_{\text{total}}$	VALUE	DOCUMENT ID	TECN	CHG	COMMENT	Γ_1/Γ
0.499 ± 0.012 OUR FIT						
0.488 ± 0.014 OUR AVERAGE						
0.485 ± 0.006 ± 0.020		¹ ASTON 88 LASS	0		11 $K^- p \rightarrow K^- \pi^+ n$	
0.49 ± 0.02		¹ ESTABROOKS 78 ASPK	±		13 $K^\pm p \rightarrow p K \pi$	

¹ From phase shift analysis.

$\Gamma(K^*(892)\pi)/\Gamma(K\pi)$	VALUE	DOCUMENT ID	TECN	CHG	COMMENT	Γ_2/Γ_1
0.496 ± 0.034 OUR FIT						
0.47 ± 0.04 OUR AVERAGE						
0.44 ± 0.09		ASTON 84B LASS	0		11 $K^- p \rightarrow \bar{K}^0 2\pi n$	
0.62 ± 0.19		LAUSCHER 75 HBC	0		10,16 $K^- p \rightarrow K^- \pi^+ n$	
0.54 ± 0.16		DEHM 74 DBC	0		4.6 $K^+ N$	
0.47 ± 0.08		AGUILAR-... 71B HBC			3,9,4,6 $K^- p$	
0.47 ± 0.10		BASSANO 67 HBC	-0		4,6,5,0 $K^- p$	
0.45 ± 0.13		BADIER 65c HBC	-		3 $K^- p$	

$\Gamma(K\omega)/\Gamma(K\pi)$	VALUE	DOCUMENT ID	TECN	CHG	COMMENT	Γ_5/Γ_1
0.059 ± 0.017 OUR FIT						
0.070 ± 0.035 OUR AVERAGE						
0.05 ± 0.04		AGUILAR-... 71B HBC			3,9,4,6 $K^- p$	
0.13 ± 0.07		BASSOMPIE... 69 HBC	0		5 $K^+ p$	

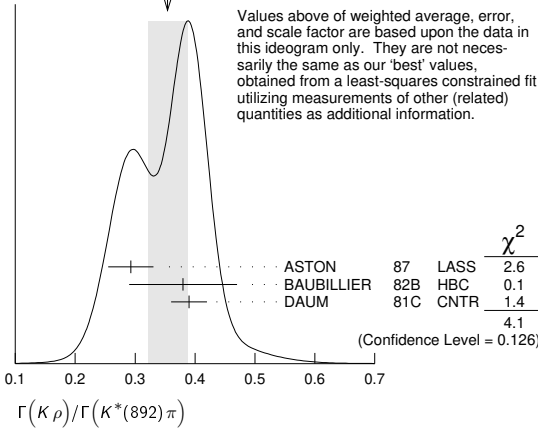
$\Gamma(K\rho)/\Gamma(K\pi)$ Γ_4/Γ_1

VALUE	DOCUMENT ID	TECN	CHG	COMMENT
0.174 ± 0.017 OUR FIT	Error includes scale factor of 1.2.			
0.150 +0.029 -0.017 OUR AVERAGE				
0.18 ± 0.05	ASTON	84B	LASS	0 11 $K^-p \rightarrow \bar{K}^0 2\pi n$
0.02 +0.10 -0.02	DEHM	74	DBC	0 4.6 $K^+ N$
0.16 ± 0.05	AGUILAR...	71B	HBC	3,9,4,6 K^-p
0.14 ± 0.10	BASSANO	67	HBC	-0 4,6,5,0 K^-p
0.14 ± 0.07	BADIER	65c	HBC	- 3 K^-p

$\Gamma(K\rho)/\Gamma(K^*(892)\pi)$ Γ_4/Γ_2

VALUE	DOCUMENT ID	TECN	CHG	COMMENT
0.350 ± 0.031 OUR FIT	Error includes scale factor of 1.4.			
0.354 ± 0.033 OUR AVERAGE	Error includes scale factor of 1.4. See the ideogram below.			
0.293 ± 0.032 ± 0.020	ASTON	87	LASS	0 11 $K^-p \rightarrow \bar{K}^0 \pi^+ \pi^- n$
0.38 ± 0.09	BAUBILLIER	82B	HBC	0 8.25 $K^-p \rightarrow N K_0^0 \pi \pi$
0.39 ± 0.03	DAUM	81c	CNTR	63 $K^-p \rightarrow K^- 2\pi p$

WEIGHTED AVERAGE
0.354 ± 0.033 (Error scaled by 1.4)



$\Gamma(K\omega)/\Gamma(K^*(892)\pi)$ Γ_5/Γ_2

VALUE	DOCUMENT ID	TECN	CHG	COMMENT
0.118 ± 0.034 OUR FIT				
0.10 ± 0.04	FIELD	67	HBC	- 3.8 K^-p

$\Gamma(K\eta)/\Gamma(K^*(892)\pi)$ Γ_7/Γ_2

VALUE	DOCUMENT ID	TECN	CHG	COMMENT
0.006 +0.014 -0.004 OUR FIT	Error includes scale factor of 1.2.			
0.07 ± 0.04	FIELD	67	HBC	- 3.8 K^-p

$\Gamma(K\eta)/\Gamma(K\pi)$ Γ_7/Γ_1

VALUE	CL%	DOCUMENT ID	TECN	CHG	COMMENT
0.0030 +0.0070 -0.0020 OUR FIT	Error includes scale factor of 1.3.				
0 ± 0.0056	¹ ASTON 88B LASS - 11 $K^-p \rightarrow K^- \eta p$				
• • • We do not use the following data for averages, fits, limits, etc. • • •					
<0.04	95	AGUILAR...	71B	HBC	3,9,4,6 K^-p
<0.065		² BASSOMPIE...	69	HBC	5.0 $K^+ p$
<0.02		BISHOP	69	HBC	3.5 $K^+ p$
¹ ASTON 88B quote < 0.0092 at CL=95%. We convert this to a central value and 1 sigma error in order to be able to use it in our constrained fit.					
² Restated by us.					

$\Gamma(K^*(892)\pi\pi)/\Gamma_{total}$ Γ_3/Γ

VALUE	DOCUMENT ID	TECN	CHG	COMMENT
0.134 ± 0.022 OUR FIT				
0.12 ± 0.04	¹ GOLDBERG	76	HBC	- 3 $K^-p \rightarrow \rho \bar{K}^0 \pi \pi \pi$
¹ Assuming $\pi\pi$ system has isospin 1, which is supported by the data.				

$\Gamma(K^*(892)\pi\pi)/\Gamma(K\pi)$ Γ_3/Γ_1

VALUE	DOCUMENT ID	TECN	CHG	COMMENT
0.27 ± 0.05 OUR FIT				
0.21 ± 0.08	^{1,2} JONGEJANS	78	HBC	- 4 $K^-p \rightarrow \rho \bar{K}^0 \pi \pi \pi$
¹ Restated by us.				
² Assuming $\pi\pi$ system has isospin 1, which is supported by the data.				

$\Gamma(K\omega\pi)/\Gamma_{total}$ Γ_8/Γ

VALUE (units 10^{-3})	CL%	EVTS	DOCUMENT ID	TECN	COMMENT
<0.72	95	0	JONGEJANS	78	HBC 4 $K^-p \rightarrow \rho \bar{K}^0 4\pi$

$K_2^*(1430)$ REFERENCES

ABLIKIM 22L	JHEP 2207 045	M. Ablikim <i>et al.</i>	(BESIII Collab.)
ABLIKIM 19AQ	PR D100 032004	M. Ablikim <i>et al.</i>	(BESIII Collab.)
PELAEZ 17	EPJ C77 91	J.R. Pelaez, A.Rodas, J.R. de Elvira	(BESIII Collab.)
AUBERT 07AK	PR D76 012008	B. Aubert <i>et al.</i>	(BABAR Collab.)
ALAVI-HARATI 02B	PRL 89 072001	A. Alavi-Harati <i>et al.</i>	(FNAL KTeV Collab.)
BIRD 89	SLAC-332	P.F. Bird	(SLAC)
ASTON 88	NP B296 493	D. Aston <i>et al.</i>	(SLAC, NAGO, CINC, INUS)
ASTON 88B	PL B201 169	D. Aston <i>et al.</i>	(SLAC, NAGO, CINC, INUS)
ASTON 87	NP B292 693	D. Aston <i>et al.</i>	(SLAC, NAGO, CINC, INUS)
CARLSMITH 87	PR D36 3502	D. Carlsmith <i>et al.</i>	(EFI, SACL)
ASTON 84B	NP B247 261	D. Aston <i>et al.</i>	(SLAC, CARL, OTTA)
BAUBILLIER 84B	ZPHY C26 37	M. Baubillier <i>et al.</i>	(BIRM, CERN, GLAS+)
BAUBILLIER 82B	NP B202 21	M. Baubillier <i>et al.</i>	(BIRM, CERN, GLAS+)
CHANGIR 82	PL 117B 123	S. Changir <i>et al.</i>	(FNAL, MINN, ROCH)
CLELAND 82	NP B208 189	W.E. Cleland <i>et al.</i>	(DURH, GEVA, LAUS+)
ASTON 81C	PL 106B 235	D. Aston <i>et al.</i>	(SLAC, CARL, OTTA) JP
DAUM 81C	NP B187 1	C. Daum <i>et al.</i>	(AMST, CERN, CRAC, MPIM+)
TOAFF 81	PR D23 1500	S. Toaff <i>et al.</i>	(ANL, KANS)
ETKIN 80	NP D22 42	A. Etkin <i>et al.</i>	(BNL, CUNY) JP
ESTABROOKS 78	NP B133 490	P.G. Estabrooks <i>et al.</i>	(MCGI, CARL, DURH+)
Also	PR D17 658	P.G. Estabrooks <i>et al.</i>	(MCGI, CARL, DURH+)
JONGEJANS 78	NP B139 383	B. Jongejans <i>et al.</i>	(ZEEM, CERN, NIJM+)
MARTIN 78	NP B134 392	A.D. Martin <i>et al.</i>	(DURH, GEVA)
BOWLER 77	NP B126 31	M.G. Bowler <i>et al.</i>	(OXF)
GOLDBERG 76	LNC 117 253	J. Goldberg	(HAF)
HENDRICK 76	NP B112 189	K. Hendrickx <i>et al.</i>	(MONS, SACL, PARIS+)
LAUSCHER 75	NP B86 189	P. Lauscher <i>et al.</i>	(ABCLV Collab.) JP
MCCUBBIN 75	NP B86 13	N.A. McCubbin, L. Lyons	(OXF)
DEHM 74	NP B75 47	G. Dehm <i>et al.</i>	(MPIM, BRUX, MONS, CERN)
LINGLIN 73	NP B55 408	D. Linglin	(CERN)
AGUILAR... 71B	PR D4 2583	M. Aguilar-Benitez, R.L. Eisner, J.B. Kinson	(BNL)
BARNHAM 71C	NP B28 171	K.W.J. Barnham <i>et al.</i>	(BIRM, GLAS)
CORDS 71	PR D4 1974	D. Cords <i>et al.</i>	(PURD, UCD, IUPU)
BASSOMPIE... 69	NP B13 189	G. Bassompierre <i>et al.</i>	(CERN, BRUX) JP
BISHOP 69	NP B9 403	J.M. Bishop <i>et al.</i>	(WISC)
CRENNELL 69D	PRL 22 487	D.J. Crennell <i>et al.</i>	(BNL)
DAVIS 69	PRL 23 1071	P.J. Davis <i>et al.</i>	(LRL)
LIND 69	NP B14 1	V.G. Lind <i>et al.</i>	(LRL) JP
SCHWEING... 68	PR 166 1317	F. Schweingruber <i>et al.</i>	(ANL, NWES)
Also	Thesis	F.L. Schweingruber	(NWES, NWES)
BASSANO 67	PRL 19 968	D. Bassano <i>et al.</i>	(BNL, SYRA)
FIELD 67	PL 24B 638	J.H. Field <i>et al.</i>	(UCSD)
BADIER 65C	PL 19 612	J. Badier <i>et al.</i>	(EPOL, SACL, AMST)

$K(1460)$

$I(J^P) = \frac{1}{2}(0^-)$

Observed in $K\pi\pi$ partial-wave analysis.

$K(1460)$ MASS

VALUE (MeV)	EVTS	DOCUMENT ID	TECN	CHG	COMMENT
• • • We do not use the following data for averages, fits, limits, etc. • • •					
1482.40 ± 3.58 ± 15.22	894k	AAIJ	18A	LHCB	$D^0 \rightarrow K^\mp 2\pi^\pm \pi^\mp$
~ 1460	63	DAUM	81c	CNTR	- $K^-p \rightarrow K^- 2\pi p$
~ 1400	13	¹ BRANDENB...	76B	ASPK ±	$K^\pm p \rightarrow K^\mp 2\pi p$
¹ Coupled mainly to $K f_0(1370)$. Decay into $K^*(892)\pi$ seen.					

$K(1460)$ WIDTH

VALUE (MeV)	EVTS	DOCUMENT ID	TECN	CHG	COMMENT
• • • We do not use the following data for averages, fits, limits, etc. • • •					
335.60 ± 6.20 ± 8.65	894k	AAIJ	18A	LHCB	$D^0 \rightarrow K^\mp 2\pi^\pm \pi^\mp$
~ 260	63	DAUM	81c	CNTR	- $K^-p \rightarrow K^- 2\pi p$
~ 250	15	¹ BRANDENB...	76B	ASPK ±	$K^\pm p \rightarrow K^\mp 2\pi p$
¹ Coupled mainly to $K f_0(1370)$. Decay into $K^*(892)\pi$ seen.					

$K(1460)$ DECAY MODES

Mode	Fraction (Γ_i/Γ)
Γ_1 $K^*(892)\pi$	seen
Γ_2 $K\rho$	seen
Γ_3 $K_0^*(1430)\pi$	seen
Γ_4 $K\phi$	seen

$K(1460)$ PARTIAL WIDTHS

$\Gamma(K^*(892)\pi)$ Γ_1			
VALUE (MeV)	DOCUMENT ID	TECN	COMMENT
• • • We do not use the following data for averages, fits, limits, etc. • • •			
~ 109	DAUM	81c	CNTR 63 $K^-p \rightarrow K^- 2\pi p$
$\Gamma(K\rho)$ Γ_2			
VALUE (MeV)	DOCUMENT ID	TECN	COMMENT
• • • We do not use the following data for averages, fits, limits, etc. • • •			
~ 34	DAUM	81c	CNTR 63 $K^-p \rightarrow K^- 2\pi p$
$\Gamma(K_0^*(1430)\pi)$ Γ_3			
VALUE (MeV)	DOCUMENT ID	TECN	COMMENT
• • • We do not use the following data for averages, fits, limits, etc. • • •			
~ 117	DAUM	81c	CNTR 63 $K^-p \rightarrow K^- 2\pi p$

Meson Particle Listings

 $K(1460)$, $K_2(1580)$, $K(1630)$, $K_1(1650)$, $K^*(1680)$ $\Gamma(K\phi)/\Gamma_{\text{total}}$ Γ_4/Γ

VALUE	EVTS	DOCUMENT ID	TECN	CHG	COMMENT
seen	24k	¹ AAIJ	21E	LHCB	$B^+ \rightarrow J/\psi\phi K^+$

¹ From an amplitude analysis of the decay $B^+ \rightarrow J/\psi\phi K^+$ with a significance of 12 σ .

 $K(1460)$ REFERENCES

AAIJ	21E	PRL 127 082001	R. Aaij et al.	(LHCb Collab.)
AAIJ	18AI	EPJ C78 443	R. Aaij et al.	(LHCb Collab.)
DAUM	81C	NP B187 1	C. Daum et al.	(AMST, CERN, CRAC, MPIM+)
BRANDENB...	76B	PRL 36 1239	G.W. Brandenburg et al.	(SLAC)JP

 $K_2(1580)$

$$I(J^P) = \frac{1}{2}(2^-)$$

OMITTED FROM SUMMARY TABLE

Seen in partial-wave analysis of the $K^- \pi^+ \pi^-$ system. Needs confirmation.

 $K_2(1580)$ MASS

VALUE (MeV)	DOCUMENT ID	CHG	COMMENT
••• We do not use the following data for averages, fits, limits, etc. •••			
~ 1580	OTTER	79	10,14,16 $K^- p$

 $K_2(1580)$ WIDTH

VALUE (MeV)	DOCUMENT ID	CHG	COMMENT
••• We do not use the following data for averages, fits, limits, etc. •••			
~ 110	OTTER	79	10,14,16 $K^- p$

 $K_2(1580)$ DECAY MODES

Mode	Fraction (Γ_i/Γ)
Γ_1 $K^*(892)\pi$	seen
Γ_2 $K_2^*(1430)\pi$	possibly seen

 $K_2(1580)$ BRANCHING RATIOS $\Gamma(K^*(892)\pi)/\Gamma_{\text{total}}$ Γ_1/Γ

VALUE	DOCUMENT ID	TECN	CHG	COMMENT
seen	OTTER	79	HBC	10,14,16 $K^- p$

••• We do not use the following data for averages, fits, limits, etc. •••
possibly seen GULER 11 BELL $B^+ \rightarrow J/\psi K^+ \pi^+ \pi^-$

 $\Gamma(K_2^*(1430)\pi)/\Gamma_{\text{total}}$ Γ_2/Γ

VALUE	DOCUMENT ID	TECN	CHG	COMMENT
possibly seen	OTTER	79	HBC	10,14,16 $K^- p$

 $K_2(1580)$ REFERENCES

GULER	11	PR D83 032005	H. Guler et al.	(BELLE Collab.)
OTTER	79	NP B147 1	G. Otter et al.	(AACH3, BERL, CERN, LOIC+)JP

 $K(1630)$

$$I(J^P) = \frac{1}{2}(?^?)$$

OMITTED FROM SUMMARY TABLE

Seen as a narrow peak, compatible with the experimental resolution, in the invariant mass of the $K_S^0 \pi^+ \pi^-$ system produced in $\pi^- p$ interactions at high momentum transfers.

 $K(1630)$ MASS

VALUE (MeV)	EVTS	DOCUMENT ID	TECN	COMMENT
1629 ± 7	~ 75	KARNAUKHOV98	BC	$16.0 \pi^- p \rightarrow (K_S^0 \pi^+ \pi^-) X^+ \pi^- X^0$

 $K(1630)$ WIDTH

VALUE (MeV)	EVTS	DOCUMENT ID	TECN	COMMENT
16 ± 19 16	~ 75	¹ KARNAUKHOV98	BC	$16.0 \pi^- p \rightarrow (K_S^0 \pi^+ \pi^-) X^+ \pi^- X^0$

¹ Compatible with an experimental resolution of 14 ± 1 MeV.

 $K(1630)$ DECAY MODES

Mode
Γ_1 $K_S^0 \pi^+ \pi^-$

 $K(1630)$ REFERENCES

KARNAUKHOV 98	PAN 61 203	V.M. Karnaukhov, C. Coca, V.I. Moroz
		Translated from YAF 61 252.

 $K_1(1650)$

$$I(J^P) = \frac{1}{2}(1^+)$$

This entry contains various peaks in strange meson systems ($K^+ \phi$, $K \pi \pi$) reported in partial-wave analysis in the 1600–1900 mass region.

 $K_1(1650)$ MASS

VALUE (MeV)	EVTS	DOCUMENT ID	TECN	CHG	COMMENT
1650 ± 50		FRAME	86	OMEG +	$13 K^+ p \rightarrow \phi K^+ p$

••• We do not use the following data for averages, fits, limits, etc. •••

1861 ± 10 ⁺¹⁶ ₋₄₆	24k	¹ AAIJ	21E	LHCB	$B^+ \rightarrow J/\psi\phi K^+$
1911 ± 37 ⁺¹²⁴ ₋₄₈	24k	¹ AAIJ	21E	LHCB	$B^+ \rightarrow J/\psi\phi K^+$
1793 ± 59 ⁺¹⁵³ ₋₁₀₁	4289	^{2,3} AAIJ	17C	LHCB	$B^+ \rightarrow J/\psi\phi K^+$
~ 1840		ARMSTRONG 83	OMEG -		$18.5 K^- p \rightarrow 3Kp$
~ 1800		DAUM	81c	CNTR -	$63 K^- p \rightarrow K^- 2\pi p$

¹ One of two K_1 states reported by AAIJ 21E. From an amplitude analysis of the decay $B^+ \rightarrow J/\psi\phi K^+$ with a significance of 4.5 σ .
² From an amplitude analysis of the decay $B^+ \rightarrow J/\psi\phi K^+$ with a significance of 7.6 σ .
³ Superseded by AAIJ 21E.

 $K_1(1650)$ WIDTH

VALUE (MeV)	EVTS	DOCUMENT ID	TECN	CHG	COMMENT
150 ± 50		FRAME	86	OMEG +	$13 K^+ p \rightarrow \phi K^+ p$

••• We do not use the following data for averages, fits, limits, etc. •••

149 ± 41 ⁺²³¹ ₋₂₃	24k	¹ AAIJ	21E	LHCB	$B^+ \rightarrow J/\psi\phi K^+$
276 ± 50 ⁺³¹⁹ ₋₁₅₉	24k	¹ AAIJ	21E	LHCB	$B^+ \rightarrow J/\psi\phi K^+$
365 ± 157 ⁺¹³⁸ ₋₂₁₅	4289	^{2,3} AAIJ	17C	LHCB	$B^+ \rightarrow J/\psi\phi K^+$
~ 250		DAUM	81c	CNTR -	$63 K^- p \rightarrow K^- 2\pi p$

¹ One of two K_1 states reported by AAIJ 21E. From an amplitude analysis of the decay $B^+ \rightarrow J/\psi\phi K^+$ with a significance of 4.5 σ .
² From an amplitude analysis of the decay $B^+ \rightarrow J/\psi\phi K^+$ with a significance of 7.6 σ .
³ Superseded by AAIJ 21E.

 $K_1(1650)$ DECAY MODES

Mode
Γ_1 $K \pi \pi$
Γ_2 $K \phi$

 $K_1(1650)$ REFERENCES

AAIJ	21E	PRL 127 082001	R. Aaij et al.	(LHCb Collab.)
AAIJ	17C	PRL 118 022003	R. Aaij et al.	(LHCb Collab.)
	Also	PR D95 012002	R. Aaij et al.	(LHCb Collab.)
FRAME	86	NP B276 667	D. Frame et al.	(GLAS)
ARMSTRONG	83	NP B221 1	T.A. Armstrong et al.	(BARI, BIRM, CERN+)
DAUM	81C	NP B187 1	C. Daum et al.	(AMST, CERN, CRAC, MPIM+)

 $K^*(1680)$

$$I(J^P) = \frac{1}{2}(1^-)$$

 $K^*(1680)$ MASS

VALUE (MeV)	EVTS	DOCUMENT ID	TECN	CHG	COMMENT
1718 ± 18 OUR AVERAGE					
1722 ± 20 ⁺³³ ₋₁₀₉	4289	¹ AAIJ	17c	LHCB	$B^+ \rightarrow J/\psi\phi K^+$
$1677 \pm 10 \pm 32$		ASTON	88	LASS 0	$11 K^- p \rightarrow K^- \pi^+ n$
$1735 \pm 10 \pm 20$		ASTON	87	LASS 0	$11 K^- p \rightarrow \bar{K}^0 \pi^+ \pi^- n$

••• We do not use the following data for averages, fits, limits, etc. •••

1678 ± 64		BIRD	89	LASS -	$11 K^- p \rightarrow \bar{K}^0 \pi^- p$
1800 ± 70		ETKIN	80	MPS 0	$6 K^- p \rightarrow \bar{K}^0 \pi^+ \pi^- n$
~ 1650		ESTABROOKS 78	ASPK 0		$13 K^\pm p \rightarrow K^\pm \pi^\pm n$

¹ From an amplitude analysis of the decay $B^+ \rightarrow J/\psi\phi K^+$ with a significance of 8.5 σ .

See key on page 1171

Meson Particle Listings

$K^*(1680)$, $K_2(1770)$

 $K^*(1680)$ WIDTH

VALUE (MeV)	EVTS	DOCUMENT ID	TECN	CHG	COMMENT
320 ± 110 OUR AVERAGE Error includes scale factor of 4.2.					
354 ± 75 ⁺¹⁴⁰ ₋₁₈₁	4289	² AAIJ	17c	LHCB	$B^+ \rightarrow J/\psi \phi K^+$
205 ± 16 ± 34		ASTON	88	LASS	0 11 $K^- \rho \rightarrow K^- \pi^+ n$
423 ± 18 ± 30		ASTON	87	LASS	0 11 $K^- \rho \rightarrow \bar{K}^0 \pi^+ \pi^- n$
• • • We do not use the following data for averages, fits, limits, etc. • • •					
454 ± 270		BIRD	89	LASS	- 11 $K^- \rho \rightarrow \bar{K}^0 \pi^- \rho$
170 ± 30		ETKIN	80	MPS	0 6 $K^- \rho \rightarrow \bar{K}^0 \pi^+ \pi^- n$
250 to 300		ESTABROOKS	78	ASPK	0 13 $K^\pm \rho \rightarrow K^\pm \pi^\pm n$

²From an amplitude analysis of the decay $B^+ \rightarrow J/\psi \phi K^+$ with a significance of 8.5 σ .

 $K^*(1680)$ DECAY MODES

Mode	Fraction (Γ_i/Γ)
Γ_1 $K\pi$	(38.7 ± 2.5) %
Γ_2 $K\rho$	(31.4 ^{+5.0} _{-2.1}) %
Γ_3 $K^*(892)\pi$	(29.9 ^{+2.2} _{-5.0}) %
Γ_4 $K\phi$	seen
Γ_5 $K\eta$	(1.4 ^{+1.0} _{-0.8}) %

CONSTRAINED FIT INFORMATION

An overall fit to 4 branching ratios uses 4 measurements and one constraint to determine 3 parameters. The overall fit has a $\chi^2 = 2.9$ for 2 degrees of freedom.

The following *off-diagonal* array elements are the correlation coefficients $\langle \delta x_i \delta x_j \rangle / (\delta x_i \delta x_j)$, in percent, from the fit to the branching fractions, $x_i \equiv \Gamma_i/\Gamma_{\text{total}}$. The fit constrains the x_i whose labels appear in this array to sum to one.

x_2	-36	
x_3	-39	-72
	x_1	x_2

 $K^*(1680)$ BRANCHING RATIOS

$\Gamma(K\pi)/\Gamma_{\text{total}}$	DOCUMENT ID	TECN	CHG	COMMENT	Γ_1/Γ
0.387 ± 0.026 OUR FIT					
0.388 ± 0.014 ± 0.022	ASTON	88	LASS	0 11 $K^- \rho \rightarrow K^- \pi^+ n$	
$\Gamma(K\pi)/\Gamma(K^*(892)\pi)$	DOCUMENT ID	TECN	CHG	COMMENT	Γ_1/Γ_3
1.30^{+0.23}_{-0.14} OUR FIT					
2.8 ± 1.1	ASTON	84	LASS	0 11 $K^- \rho \rightarrow \bar{K}^0 2\pi n$	
$\Gamma(K\rho)/\Gamma(K\pi)$	DOCUMENT ID	TECN	CHG	COMMENT	Γ_2/Γ_1
0.81^{+0.14}_{-0.09} OUR FIT					
1.2 ± 0.4	ASTON	84	LASS	0 11 $K^- \rho \rightarrow \bar{K}^0 2\pi n$	
$\Gamma(K\rho)/\Gamma(K^*(892)\pi)$	DOCUMENT ID	TECN	CHG	COMMENT	Γ_2/Γ_3
1.05^{+0.27}_{-0.11} OUR FIT					
0.97 ± 0.09^{+0.30}_{-0.10}	ASTON	87	LASS	0 11 $K^- \rho \rightarrow \bar{K}^0 \pi^+ \pi^- n$	
$\Gamma(K\phi)/\Gamma_{\text{total}}$	EVTS	DOCUMENT ID	TECN	COMMENT	Γ_4/Γ
seen	24k	³ AAIJ	21E	LHCB $B^+ \rightarrow J/\psi \phi K^+$	
• • • We do not use the following data for averages, fits, limits, etc. • • •					
seen	4289	^{4,5} AAIJ	17c	LHCB $B^+ \rightarrow J/\psi \phi K^+$	

³From an amplitude analysis of the decay $B^+ \rightarrow J/\psi \phi K^+$ with a significance of 4.7 σ .

⁴From an amplitude analysis of the decay $B^+ \rightarrow J/\psi \phi K^+$ with a significance of 8.5 σ .

⁵Superseded by AAJ 21E.

 $\Gamma(K\eta)/\Gamma(K\pi)$

VALUE	EVTS	DOCUMENT ID	TECN	COMMENT	Γ_5/Γ_1
0.037 ± 0.007^{+0.024}_{-0.018}	116k	⁶ CHEN	20A	BELL $D^0 \rightarrow K^- \pi^+ \eta$	
⁶ CHEN 20A quotes the ratio $\Gamma(K^*(1680)^- \rightarrow K^- \eta)/\Gamma(K^*(1680)^- \rightarrow K^- \pi^0) = 0.11 \pm 0.02+0.06-0.04 \pm 0.04$ (BPDG) where the last uncertainty comes from $B(\eta \rightarrow \gamma\gamma) = (39.41 \pm 0.20)\%$. We divide it by 3 taking into account that $\Gamma(K^*(1680)^- \rightarrow K^- \pi^0)/\Gamma(K^*(1680)^- \rightarrow (K\pi)^-) = 1/3$.					

 $\Gamma(K\eta)/\Gamma_{\text{total}}$

VALUE (units 10^{-2})	EVTS	DOCUMENT ID	TECN	COMMENT	Γ_5/Γ
• • • We do not use the following data for averages, fits, limits, etc. • • •					
1.44 ± 0.21 ^{+0.96} _{-0.73}	116k	⁷ CHEN	20A	BELL $D^0 \rightarrow K^- \pi^+ \eta$	
⁷ From an amplitude analysis of the decay $D^0 \rightarrow K^- \pi^+ \eta$ with a significance of 16 σ . Not independent of the CHEN 20A measurement of $\Gamma(K^*(1680) \rightarrow K\eta)/\Gamma(K^*(1680) \rightarrow K\pi)$.					

 $K^*(1680)$ REFERENCES

AAIJ	21E	PRL 127 082001	R. Aaij et al.	(LHCb Collab.)
CHEN	20A	PR D102 012002	Y.Q. Chen et al.	(BELLE Collab.)
AAIJ	17C	PRL 118 022003	R. Aaij et al.	(LHCb Collab.)
Also		PR D95 012002	R. Aaij et al.	(LHCb Collab.)
BIRD	89	SLAC-332	P.F. Bird	(SLAC)
ASTON	88	NP B296 493	D. Aston et al.	(SLAC, NAGO, CIN, INUS)
ASTON	87	NP B292 693	D. Aston et al.	(SLAC, NAGO, CIN, INUS)
ASTON	84	PL 149B 258	D. Aston et al.	(SLAC, CARL, OTTA)JP
ETKIN	80	PR D22 42	A. Etkin et al.	(BNL, CUNY)JP
ESTABROOKS	78	NP B133 490	P.G. Estabrooks et al.	(MCGI, CARL, DURH+)JP

 $K_2(1770)$

$$I(J^P) = \frac{1}{2}(2^-)$$

See our mini-review in the 2004 edition of this Review, PDG 04.

 $K_2(1770)$ MASS

VALUE (MeV)	EVTS	DOCUMENT ID	TECN	CHG	COMMENT
1773 ± 8 OUR AVERAGE					
1777 ± 35 ⁺¹²² ₋₇₇	4289	¹ AAIJ	17c	LHCB	$B^+ \rightarrow J/\psi \phi K^+$
1773 ± 8		² ASTON	93	LASS	11 $K^- \rho \rightarrow K^- \omega p$
• • • We do not use the following data for averages, fits, limits, etc. • • •					
1743 ± 15		TIKHOMIROV	03	SPEC	$40.0 \pi^- C \rightarrow K_S^0 K_S^0 K_L^0 X$
1810 ± 20		FRAME	86	OMEG +	13 $K^+ p \rightarrow \phi K^+ p$
~ 1730		ARMSTRONG	83	OMEG -	18.5 $K^- p \rightarrow 3K p$
~ 1780		³ DAUM	81c	CNTR -	63 $K^- p \rightarrow K^- 2\pi p$
1710 ± 15	60	CHUNG	74	HBC -	7.3 $K^- p \rightarrow K^- \omega p$
1767 ± 6		BLIEDEN	72	MMS -	11-16 $K^- p$
1730 ± 20	306	⁴ FIRESTONE	72B	DBC +	12 $K^+ d$
1765 ± 40		⁵ COLLEY	71	HBC +	10 $K^+ p \rightarrow K_2 \pi N$
1740		DENEGRI	71	DBC -	12.6 $K^- d \rightarrow \bar{K} 2\pi d$
1745 ± 20		AGUILAR...	70c	HBC -	4.6 $K^- p$
1780 ± 15		BARTSCH	70c	HBC -	10.1 $K^- p$
1760 ± 15		LUDLAM	70	HBC -	12.6 $K^- p$

¹From an amplitude analysis of the decay $B^+ \rightarrow J/\psi \phi K^+$ with a significance of 5.0 σ .

²From a partial wave analysis of the $K^- \omega$ system.

³From a partial wave analysis of the $K^- 2\pi$ system.

⁴Produced in conjunction with excited deuteron.

⁵Systematic errors added correspond to spread of different fits.

 $K_2(1770)$ WIDTH

VALUE (MeV)	EVTS	DOCUMENT ID	TECN	CHG	COMMENT
186 ± 14 OUR AVERAGE					
217 ± 116 ⁺²²¹ ₋₁₅₄	4289	⁶ AAIJ	17c	LHCB	$B^+ \rightarrow J/\psi \phi K^+$
186 ± 14		⁷ ASTON	93	LASS	11 $K^- \rho \rightarrow K^- \omega p$
• • • We do not use the following data for averages, fits, limits, etc. • • •					
147 ± 70		TIKHOMIROV	03	SPEC	$40.0 \pi^- C \rightarrow K_S^0 K_S^0 K_L^0 X$
140 ± 40		FRAME	86	OMEG +	13 $K^+ p \rightarrow \phi K^+ p$
~ 220		ARMSTRONG	83	OMEG -	18.5 $K^- p \rightarrow 3K p$
~ 210		⁸ DAUM	81c	CNTR -	63 $K^- p \rightarrow K^- 2\pi p$
110 ± 50	60	CHUNG	74	HBC -	7.3 $K^- p \rightarrow K^- \omega p$
100 ± 26		BLIEDEN	72	MMS -	11-16 $K^- p$
210 ± 30	306	⁹ FIRESTONE	72B	DBC +	12 $K^+ d$
90 ± 70		¹⁰ COLLEY	71	HBC +	10 $K^+ p \rightarrow K_2 \pi N$
130		DENEGRI	71	DBC -	12.6 $K^- d \rightarrow \bar{K} 2\pi d$
100 ± 50		AGUILAR...	70c	HBC -	4.6 $K^- p$
138 ± 40		BARTSCH	70c	HBC -	10.1 $K^- p$
50 ± 40		LUDLAM	70	HBC -	12.6 $K^- p$
- 20					

⁶From an amplitude analysis of the decay $B^+ \rightarrow J/\psi \phi K^+$ with a significance of 5.0 σ .

Meson Particle Listings

$K_2(1770), K_3^*(1780)$

- ⁷ From a partial wave analysis of the $K^- \omega$ system.
- ⁸ From a partial wave analysis of the $K^- 2\pi$ system.
- ⁹ Produced in conjunction with excited deuteron.
- ¹⁰ Systematic errors added correspond to spread of different fits.

$K_2(1770)$ DECAY MODES

Mode	Fraction (Γ_i/Γ)
Γ_1 $K \pi \pi$	
Γ_2 $K_2^*(1430) \pi$	seen
Γ_3 $K^*(892) \pi$	seen
Γ_4 $K f_2(1270)$	seen
Γ_5 $K f_0(980)$	possibly seen
Γ_6 $K \phi$	seen
Γ_7 $K \omega$	seen

$K_2(1770)$ BRANCHING RATIOS

$\Gamma(K_2^*(1430)\pi)/\Gamma(K\pi\pi)$ Γ_2/Γ_1
 $(K_2^*(1430) \rightarrow K\pi)$

VALUE	DOCUMENT ID	TECN	CHG	COMMENT
•••	We do not use the following data for averages, fits, limits, etc. •••			
~ 0.03	DAUM	81c	CNTR	63 $K^- p \rightarrow K^- 2\pi p$
~ 1.0	11 FIRESTONE	72B	DBC +	12 $K^+ d$
< 1.0	COLLEY	71	HBC	10 $K^+ p$
0.2 ± 0.2	AGUILAR...	70c	HBC -	4.6 $K^- p$
< 1.0	BARTSCH	70c	HBC -	10.1 $K^- p$
1.0	BARBARO...	69	HBC +	12.0 $K^+ p$

¹¹ Produced in conjunction with excited deuteron.

$\Gamma(K^*(892)\pi)/\Gamma(K\pi\pi)$ Γ_3/Γ_1

VALUE	DOCUMENT ID	TECN	COMMENT
•••	We do not use the following data for averages, fits, limits, etc. •••		
~ 0.23	DAUM	81c	CNTR 63 $K^- p \rightarrow K^- 2\pi p$

$\Gamma(K f_2(1270))/\Gamma(K\pi\pi)$ Γ_4/Γ_1
 $(f_2(1270) \rightarrow \pi\pi)$

VALUE	DOCUMENT ID	TECN	COMMENT
•••	We do not use the following data for averages, fits, limits, etc. •••		
~ 0.74	DAUM	81c	CNTR 63 $K^- p \rightarrow K^- 2\pi p$

$\Gamma(K f_0(980))/\Gamma_{total}$ Γ_5/Γ

VALUE	DOCUMENT ID	TECN	COMMENT
•••	We do not use the following data for averages, fits, limits, etc. •••		
possibly seen	TIKHOMIROV	03	SPEC 40.0 $\frac{B^- C^-}{K_S^0 K_S^0 K_L^0 X}$

$\Gamma(K\phi)/\Gamma_{total}$ Γ_6/Γ

VALUE	EVTs	DOCUMENT ID	TECN	CHG	COMMENT
seen	24k	12 AAIJ	21E	LHCB	$B^+ \rightarrow J/\psi \phi K^+$
•••	We do not use the following data for averages, fits, limits, etc. •••				
seen	4289	13,14 AAIJ	17c	LHCB	$B^+ \rightarrow J/\psi \phi K^+$

¹² From an amplitude analysis of the decay $B^+ \rightarrow J/\psi \phi K^+$ with a significance of 7.9 σ .

¹³ From an amplitude analysis of the decay $B^+ \rightarrow J/\psi \phi K^+$ with a significance of 5.0 σ .

¹⁴ Superseded by AAIJ 21E.

$\Gamma(K\omega)/\Gamma_{total}$ Γ_7/Γ

VALUE	DOCUMENT ID	TECN	CHG	COMMENT
seen	OTTER	81	HBC	\pm 8.25,10,16 $K^\pm p$
seen	CHUNG	74	HBC	- 7.3 $K^- p \rightarrow K^- \omega p$

$K_2(1770)$ REFERENCES

AAIJ	21E	PRL 127 082001	R. Aaij et al.	(LHCb Collab.)
AAIJ	17C	PRL 118 022003	R. Aaij et al.	(LHCb Collab.)
Also		PR D95 012002	R. Aaij et al.	(LHCb Collab.)
PDG	04	PL B592 1	S. Eidelman et al.	(PDG Collab.)
TIKHOMIROV	03	PAN 66 828	G.D. Tikhomirov et al.	
		Translated from YAF 66 860.		
ASTON	93	PL B308 186	D. Aston et al.	(SLAC, NAGO, CINC, INUS)
FRAME	86	NP B276 667	D. Frame et al.	(GLAS)
ARMSTRONG	83	NP B221 1	T.A. Armstrong et al.	(BARI, BIRM, CERN+)
DAUM	81c	NP B187 1	C. Daum et al.	(AMST, CERN, CRAC, MPIM+)
OTTER	81	NP B181 1	G. Otter	(AACH3, BERL, LOIC, VIEN, BIRM+)
CHUNG	74	PL 51B 413	S.U. Chung et al.	(BNL)
BLIEDEN	72	PL 39B 668	H.R. Blieden et al.	(STON, NEAS)
FIRESTONE	72B	PR D5 505	A. Firestone et al.	(LBL)
COLLEY	71	NP B26 71	D.C. Colley et al.	(BIRM, GLAS)
DENEGRY	71	NP B28 13	D. Denezri et al.	(JHU) JP
AGUILAR...	70c	PRL 25 54	M. Aguilar-Benitez et al.	(BNL)
BARTSCH	70c	PL 33B 186	J. Bartsch et al.	(AACH, BERL, CERN+)
LUDLAM	70	PR D2 1234	T. Ludlam, J. Sandweiss, A.J. Slaughter	(YALE)
BARBARO...	69	PRL 22 1207	A. Barbaro-Galiteri et al.	(LRL)

$K_3^*(1780)$

$$I(J^P) = \frac{1}{2}(3^-)$$

$K_3^*(1780)$ T-MATRIX POLE \sqrt{s}

Note that $\Gamma = -2 \text{Im}(\sqrt{s})$.

VALUE (MeV)	DOCUMENT ID	TECN	COMMENT
(1754 \pm 13) - i (119 \pm 14) OUR EVALUATION			
(1754 \pm 13) - i (119 \pm 14)	¹ PELAEZ	17	RVUE $\pi K \rightarrow \pi K$

¹ Reanalysis of ESTABROOKS 78 and ASTON 88 satisfying Forward Dispersion Relations and using sequences of Pade approximants.

$K_3^*(1780)$ MASS

VALUE (MeV)	EVTs	DOCUMENT ID	TECN	CHG	COMMENT
1779 \pm 8 OUR AVERAGE		Error includes scale factor of 1.2.			
1813 \pm 15 $^{+65}_{-16}$	18k	¹ ABLIKIM	20F	BES3	$\psi(2S) \rightarrow K^+ K^- \eta$
1781 \pm 8 \pm 4		² ASTON	88	LASS	0 11 $K^- p \rightarrow K^- \pi^+ n$
1740 \pm 14 \pm 15		² ASTON	87	LASS	0 11 $K^- p \rightarrow \bar{K}^0 \pi^+ \pi^- n$
1779 \pm 11		³ BALDI	76	SPEC	+ 10 $K^+ p \rightarrow K^0 \pi^+ p$
1776 \pm 26		⁴ BRANDENB...	76D	ASPK	0 13 $K^\pm p \rightarrow K^\pm \pi^\mp N$
•••	We do not use the following data for averages, fits, limits, etc. •••				
1720 \pm 10 \pm 15	6111	⁵ BIRD	89	LASS	- 11 $K^- p \rightarrow \bar{K}^0 \pi^- p$
1749 \pm 10		ASTON	88B	LASS	- 11 $K^- p \rightarrow K^- \eta p$
1780 \pm 9	300	BAUBILLIER	84B	HBC	- 8.25 $K^- p \rightarrow \bar{K}^0 \pi^- p$
1790 \pm 15		BAUBILLIER	82B	HBC	0 8.25 $K^- p \rightarrow K_S^0 \pi^\pm p$
1784 \pm 9	2060	CLELAND	82	SPEC	\pm 50 $K^+ p \rightarrow K_S^0 \pi^\pm p$
1786 \pm 15		⁶ ASTON	81D	LASS	0 11 $K^- p \rightarrow K^- \pi^+ n$
1762 \pm 9	190	TOAFF	81	HBC	- 6.5 $K^- p \rightarrow \bar{K}^0 \pi^- p$
1850 \pm 50		ETKIN	80	MPS	0 6 $K^- p \rightarrow \bar{K}^0 \pi^+ \pi^-$
1812 \pm 28		BEUSCH	78	OMEG	10 $K^- p \rightarrow \bar{K}^0 \pi^+ \pi^- n$
1786 \pm 8		CHUNG	78	MPS	0 6 $K^- p \rightarrow K^- \pi^+ n$

¹ Seen in $\psi(2S)$ decay with branching ratio $\psi(2S) \rightarrow K^\pm X \rightarrow K^+ K^- \eta = (2.0 \pm 0.4 \pm 1.9) \times 10^{-6}$.

² From energy-independent partial-wave analysis.

³ From a fit to Y_2^0 moment. $J^P = 3^-$ found.

⁴ Confirmed by phase shift analysis of ESTABROOKS 78, yields $J^P = 3^-$.

⁵ From a partial wave amplitude analysis.

⁶ From a fit to the Y_0^0 moment.

$K_3^*(1780)$ WIDTH

VALUE (MeV)	EVTs	DOCUMENT ID	TECN	CHG	COMMENT
161 \pm 17 OUR AVERAGE		Error includes scale factor of 1.1.			
191 $^{+43}_{-37}$ \pm 81	1.8k	¹ ABLIKIM	20F	BES3	$\psi(2S) \rightarrow K^+ K^- \eta$
203 \pm 30 \pm 8		² ASTON	88	LASS	0 11 $K^- p \rightarrow K^- \pi^+ n$
171 \pm 42 \pm 20		² ASTON	87	LASS	0 11 $K^- p \rightarrow \bar{K}^0 \pi^+ \pi^- n$
135 \pm 22		³ BALDI	76	SPEC	+ 10 $K^+ p \rightarrow K^0 \pi^+ p$
•••	We do not use the following data for averages, fits, limits, etc. •••				
187 \pm 31 \pm 20	6111	⁴ BIRD	89	LASS	- 11 $K^- p \rightarrow \bar{K}^0 \pi^- p$
193 $^{+51}_{-37}$		ASTON	88B	LASS	- 11 $K^- p \rightarrow K^- \eta p$
99 \pm 30	300	BAUBILLIER	84B	HBC	- 8.25 $K^- p \rightarrow \bar{K}^0 \pi^- p$
~ 130		BAUBILLIER	82B	HBC	0 8.25 $K^- p \rightarrow K_S^0 \pi^\pm p$
191 \pm 24	2060	CLELAND	82	SPEC	\pm 50 $K^+ p \rightarrow K_S^0 \pi^\pm p$
225 \pm 60		⁵ ASTON	81D	LASS	0 11 $K^- p \rightarrow K^- \pi^+ n$
~ 80	190	TOAFF	81	HBC	- 6.5 $K^- p \rightarrow \bar{K}^0 \pi^- p$
240 \pm 50		ETKIN	80	MPS	0 6 $K^- p \rightarrow \bar{K}^0 \pi^+ \pi^-$
181 \pm 44		⁶ BEUSCH	78	OMEG	10 $K^- p \rightarrow \bar{K}^0 \pi^+ \pi^- n$
96 \pm 31		CHUNG	78	MPS	0 6 $K^- p \rightarrow K^- \pi^+ n$
270 \pm 70		⁷ BRANDENB...	76D	ASPK	0 13 $K^\pm p \rightarrow K^\pm \pi^\mp N$

¹ Seen in $\psi(2S)$ decay with branching ratio $\psi(2S) \rightarrow K^\pm X \rightarrow K^+ K^- \eta = (2.0 \pm 0.4 \pm 1.9) \times 10^{-6}$.

² From energy-independent partial-wave analysis.

³ From a fit to Y_2^0 moment. $J^P = 3^-$ found.

⁴ From a partial wave amplitude analysis.

⁵ From a fit to Y_0^0 moment.

⁶ Errors enlarged by us to $4\Gamma/\sqrt{N}$; see the note with the $K^*(892)$ mass.

⁷ ESTABROOKS 78 find that BRANDENBURG 76D data are consistent with 175 MeV width. Not averaged.

See key on page 1171

Meson Particle Listings

$K_3^*(1780)$, $K_2(1820)$, $K(1830)$

 $K_3^*(1780)$ DECAY MODES

Mode	Fraction (Γ_i/Γ)	Confidence level
Γ_1 $K\rho$	(31 ± 9) %	
Γ_2 $K^*(892)\pi$	(20 ± 5) %	
Γ_3 $K\pi$	(18.8 ± 1.0) %	
Γ_4 $K\eta$	(30 ± 13) %	
Γ_5 $K_2^*(1430)\pi$	< 16 %	95%

CONSTRAINED FIT INFORMATION

An overall fit to 3 branching ratios uses 4 measurements and one constraint to determine 4 parameters. The overall fit has a $\chi^2 = 0.0$ for 1 degrees of freedom.

The following *off-diagonal* array elements are the correlation coefficients $\langle \delta x_i \delta x_j \rangle / (\delta x_i \delta x_j)$, in percent, from the fit to the branching fractions, $x_i \equiv \Gamma_i/\Gamma_{\text{total}}$. The fit constrains the x_i whose labels appear in this array to sum to one.

x_2	85		
x_3	18	21	
x_4	-98	-94	-27
	x_1	x_2	x_3

 $K_3^*(1780)$ BRANCHING RATIOS

$\Gamma(K\rho)/\Gamma(K^*(892)\pi)$	VALUE	DOCUMENT ID	TECN	CHG	COMMENT	Γ_1/Γ_2
1.52 ± 0.23 OUR FIT						
1.52 ± 0.21 ± 0.10	ASTON	87	LASS	0	11 $K^-p \rightarrow \bar{K}^0\pi^+\pi^-n$	

$\Gamma(K^*(892)\pi)/\Gamma(K\pi)$	VALUE	DOCUMENT ID	TECN	CHG	COMMENT	Γ_2/Γ_3
1.09 ± 0.26 OUR FIT						
1.09 ± 0.26	ASTON	84B	LASS	0	11 $K^-p \rightarrow \bar{K}^0\pi^+n$	

$\Gamma(K\pi)/\Gamma_{\text{total}}$	VALUE	DOCUMENT ID	TECN	CHG	COMMENT	Γ_3/Γ
0.188 ± 0.010 OUR FIT						
0.188 ± 0.010 OUR AVERAGE						
0.187 ± 0.008 ± 0.008	ASTON	88	LASS	0	11 $K^-p \rightarrow K^-\pi^+n$	
0.19 ± 0.02	ESTABROOKS	78	ASPK	0	13 $K^\pm p \rightarrow K\pi N$	

$\Gamma(K\eta)/\Gamma(K\pi)$	VALUE	DOCUMENT ID	TECN	CHG	COMMENT	Γ_4/Γ_3
1.6 ± 0.7 OUR FIT						
• • • We do not use the following data for averages, fits, limits, etc. • • •						
0.41 ± 0.050	¹ BIRD	89	LASS	-	11 $K^-p \rightarrow \bar{K}^0\pi^-p$	
0.50 ± 0.18	ASTON	88B	LASS	-	11 $K^-p \rightarrow K^-\eta p$	

¹ This result supersedes ASTON 88B.

$\Gamma(K_2^*(1430)\pi)/\Gamma(K^*(892)\pi)$	VALUE	CL%	DOCUMENT ID	TECN	CHG	COMMENT	Γ_5/Γ_2
< 0.78	95		ASTON	87	LASS	0	11 $K^-p \rightarrow \bar{K}^0\pi^+\pi^-n$

 $K_3^*(1780)$ REFERENCES

ABLIKIM	20F	PR D101 032008	M. Ablikim et al.	(BESIII Collab.)
PELAEZ	17	EPJ C77 91	J.R. Pelaez, A.Rodas, J.R. de Elvira	
BIRD	89	SLAC-332	P.F. Bird	(SLAC)
ASTON	88	NP B296 493	D. Aston et al.	(SLAC, NAGO, CINC, INUS)
ASTON	88B	PL B201 169	D. Aston et al.	(SLAC, NAGO, CINC, INUS) JP
ASTON	87	NP B292 693	D. Aston et al.	(SLAC, NAGO, CINC, INUS)
ASTON	84B	NP B247 261	D. Aston et al.	(SLAC, CARL, OTTA)
BAUBILLIER	84B	ZPHY C26 37	M. Baubillier et al.	(BIRM, CERN, GLAS+)
BAUBILLIER	82B	NP B202 21	M. Baubillier et al.	(BIRM, CERN, GLAS+)
CLELAND	82	NP B208 189	W.E. Cleland et al.	(DURH, GEVA, LAUS+)
ASTON	81D	PL 99B 502	D. Aston et al.	(SLAC, CARL, OTTA) JP
TOAFF	81	PR D23 1500	S. Toaff et al.	(ANL, KANS)
ETKIN	80	PR D22 42	A. Etkin et al.	(BNL, CUNY) JP
BEUSCH	78	PL 74B 282	W. Beusch et al.	(CERN, AACH3, ETH) JP
CHUNG	78	PRL 40 355	S.U. Chung et al.	(BNL, BRAN, CUNY+) JP
ESTABROOKS	78	NP B133 490	P.G. Estabrooks et al.	(MCGI, CARL, DURH+) JP
Also		PR D17 658	P.G. Estabrooks et al.	(MCGI, CARL, DURH+)
BALDI	76	PL 63B 344	R. Baldi et al.	(GEVA) JP
BRANDENB...	76D	PL 60B 478	G.W. Brandenburg et al.	(SLAC) JP

 $K_2(1820)$ MASS

VALUE (MeV)	EVTS	DOCUMENT ID	TECN	COMMENT
1819 ± 12 OUR AVERAGE				
1853 ± 27 ⁺¹⁸ ₋₃₅	4289	¹ AAIJ	17c	LHCB $B^+ \rightarrow J/\psi\phi K^+$
1816 ± 13		² ASTON	93	LASS $11K^-p \rightarrow K^-\omega p$
• • • We do not use the following data for averages, fits, limits, etc. • • •				
~ 1840		³ DAUM	81c	CNTR $63K^-p \rightarrow K^-2\pi p$

¹ From an amplitude analysis of the decay $B^+ \rightarrow J/\psi\phi K^+$ with a significance of 3.0 σ .
² From a partial wave analysis of the $K^-\omega$ system.
³ From a partial wave analysis of the $K^-2\pi$ system.

 $K_2(1820)$ WIDTH

VALUE (MeV)	EVTS	DOCUMENT ID	TECN	COMMENT
264 ± 34 OUR AVERAGE				
167 ± 58 ⁺⁸² ₋₇₂	4289	¹ AAIJ	17c	LHCB $B^+ \rightarrow J/\psi\phi K^+$
276 ± 35		² ASTON	93	LASS $11K^-p \rightarrow K^-\omega p$
• • • We do not use the following data for averages, fits, limits, etc. • • •				
~ 230		³ DAUM	81c	CNTR $63K^-p \rightarrow K^-2\pi p$

¹ From an amplitude analysis of the decay $B^+ \rightarrow J/\psi\phi K^+$ with a significance of 3.0 σ .
² From a partial wave analysis of the $K^-\omega$ system.
³ From a partial wave analysis of the $K^-2\pi$ system.

 $K_2(1820)$ DECAY MODES

Mode	Fraction (Γ_i/Γ)
Γ_1 $K\pi\pi$	seen
Γ_2 $K_2^*(1430)\pi$	seen
Γ_3 $K^*(892)\pi$	seen
Γ_4 $Kf_2(1270)$	seen
Γ_5 $K\omega$	seen
Γ_6 $K\phi$	seen

 $K_2(1820)$ BRANCHING RATIOS

$\Gamma(K_2^*(1430)\pi)/\Gamma(K\pi\pi)$	VALUE	DOCUMENT ID	TECN	COMMENT	Γ_2/Γ_1
• • • We do not use the following data for averages, fits, limits, etc. • • •					
~ 0.77	DAUM	81c	CNTR	$63K^-p \rightarrow \bar{K}2\pi p$	

$\Gamma(K^*(892)\pi)/\Gamma(K\pi\pi)$	VALUE	DOCUMENT ID	TECN	COMMENT	Γ_3/Γ_1
• • • We do not use the following data for averages, fits, limits, etc. • • •					
~ 0.05	DAUM	81c	CNTR	$63K^-p \rightarrow \bar{K}2\pi p$	

$\Gamma(Kf_2(1270))/\Gamma(K\pi\pi)$	VALUE	DOCUMENT ID	TECN	COMMENT	Γ_4/Γ_1
• • • We do not use the following data for averages, fits, limits, etc. • • •					
~ 0.18	DAUM	81c	CNTR	$63K^-p \rightarrow \bar{K}2\pi p$	

$\Gamma(K\phi)/\Gamma_{\text{total}}$	VALUE	EVTS	DOCUMENT ID	TECN	COMMENT	Γ_6/Γ
seen		24k	¹ AAIJ	21E	LHCB $B^+ \rightarrow J/\psi\phi K^+$	
• • • We do not use the following data for averages, fits, limits, etc. • • •						
seen		4289	^{2,3} AAIJ	17c	LHCB $B^+ \rightarrow J/\psi\phi K^+$	

¹ From an amplitude analysis of the decay $B^+ \rightarrow J/\psi\phi K^+$ with a significance of 5.8 σ .
² From an amplitude analysis of the decay $B^+ \rightarrow J/\psi\phi K^+$ with a significance of 3.0 σ .
³ Superseded by AAJ 21E.

 $K_2(1820)$ REFERENCES

AAIJ	21E	PRL 127 082001	R. Aaij et al.	(LHCb Collab.)
AAIJ	17C	PRL 118 022003	R. Aaij et al.	(LHCb Collab.)
Also		PR D35 012002	R. Aaij et al.	(LHCb Collab.)
PDG	04	PL B592 1	S. Eidelman et al.	(PDG Collab.)
ASTON	93	PL B308 186	D. Aston et al.	(SLAC, NAGO, CINC, INUS)
DAUM	81C	NP B187 1	C. Daum et al.	(AMST, CERN, CRAC, MPIM+)

 $K_2(1820)$

$$I(J^P) = \frac{1}{2}(2^-)$$

See our mini-review in the 2004 edition of this Review (PDG 04) under $K_2(1770)$.

 $K(1830)$

$$I(J^P) = \frac{1}{2}(0^-)$$

OMITTED FROM SUMMARY TABLE

Seen in partial-wave analysis of $K\phi$ system. Needs confirmation.

Meson Particle Listings

$K(1830)$, $K_0^*(1950)$, $K_2^*(1980)$

$K(1830)$ MASS

VALUE (MeV)	EVTS	DOCUMENT ID	TECN	CHG	COMMENT
$1874 \pm 43^{+59}_{-115}$	4289	1,2 AAIJ	17c	LHCB	$B^+ \rightarrow J/\psi \phi K^+$

~ 1830 ARMSTRONG 83 OMEG - $18.5 K^- p \rightarrow 3Kp$
¹ From an amplitude analysis of the decay $B^+ \rightarrow J/\psi \phi K^+$ with a significance of 3.5σ .
² A subsequent amplitude analysis of $B^+ \rightarrow J/\psi \phi K^+$ by AAIJ 21E did not confirm this measurement.

$K(1830)$ WIDTH

VALUE (MeV)	EVTS	DOCUMENT ID	TECN	CHG	COMMENT
$168 \pm 90^{+280}_{-104}$	4289	3,4 AAIJ	17c	LHCB	$B^+ \rightarrow J/\psi \phi K^+$

~ 250 ARMSTRONG 83 OMEG - $18.5 K^- p \rightarrow 3Kp$
³ From an amplitude analysis of the decay $B^+ \rightarrow J/\psi \phi K^+$ with a significance of 3.5σ .
⁴ A subsequent amplitude analysis of $B^+ \rightarrow J/\psi \phi K^+$ by AAIJ 21E did not confirm this measurement.

$K(1830)$ DECAY MODES

Mode	Fraction (Γ_i/Γ)
$\Gamma_1 K \phi$	$(52 \pm 14) \%$

$K(1830)$ REFERENCES

AAIJ 21E PRL 127 082001 R. Aaij et al. (LHCb Collab.)
AAIJ 17C PRL 118 022003 R. Aaij et al. (LHCb Collab.)
Also PR D95 012002 R. Aaij et al. (LHCb Collab.)
ARMSTRONG 83 NP B221 1 T.A. Armstrong et al. (BARI, BIRM, CERN+)JP

$K_0^*(1950)$

$$I(J^P) = \frac{1}{2}(0^+)$$

Seen in partial-wave analysis of the $K^- \pi^+$ system. Needs confirmation.

$K_0^*(1950)$ MASS

VALUE (MeV)	DOCUMENT ID	TECN	CHG	COMMENT
1957 ± 14 OUR AVERAGE				

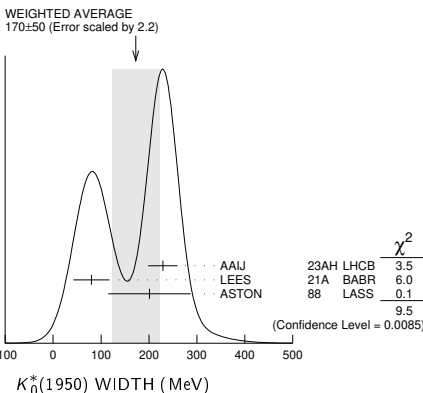
$1980 \pm 14 \pm 19$	¹ AAIJ	23AH	LHCB	$B^+ \rightarrow K^+(K_S^0 K \pi)$
$1942 \pm 22 \pm 21$	LEES	21A	BABR	$\gamma \gamma \rightarrow \eta_c(1S) \rightarrow \eta' K^+ K^-$
$1945 \pm 10 \pm 20$	² ASTON	88	LASS 0	$11 K^- p \rightarrow K^- \pi^+ n$
1917 ± 12	³ ZHOU	06	RVUE	$Kp \rightarrow K^- \pi^+ n$
1820 ± 40	⁴ ANISOVICH	97C	RVUE	$11 K^- p \rightarrow K^- \pi^+ n$

¹ From Dalitz plot analyses of $\eta_c(1S, 2S) \rightarrow K_S^0 K^+ \pi^- + c.c.$
² We take the central value of the two solutions and the larger error given.
³ S-matrix pole. Using ASTON 88 and assuming $K_0^*(700)$, $K_0^*(1430)$.
⁴ T-matrix pole. Reanalysis of ASTON 88 data.

$K_0^*(1950)$ WIDTH

VALUE (MeV)	DOCUMENT ID	TECN	CHG	COMMENT
170 ± 50 OUR AVERAGE				Error includes scale factor of 2.2. See the ideogram below.

$229 \pm 26 \pm 16$	¹ AAIJ	23AH	LHCB	$B^+ \rightarrow K^+(K_S^0 K \pi)$
$80 \pm 32 \pm 20$	LEES	21A	BABR	$\gamma \gamma \rightarrow \eta_c(1S) \rightarrow \eta' K^+ K^-$
$201 \pm 34 \pm 79$	² ASTON	88	LASS 0	$11 K^- p \rightarrow K^- \pi^+ n$
145 ± 38	³ ZHOU	06	RVUE	$Kp \rightarrow K^- \pi^+ n$
250 ± 100	⁴ ANISOVICH	97C	RVUE	$11 K^- p \rightarrow K^- \pi^+ n$



¹ From Dalitz plot analyses of $\eta_c(1S, 2S) \rightarrow K_S^0 K^+ \pi^- + c.c.$

² We take the central value of the two solutions and the larger error given.

³ S-matrix pole. Using ASTON 88 and assuming $K_0^*(700)$, $K_0^*(1430)$.

⁴ T-matrix pole. Reanalysis of ASTON 88 data.

$K_0^*(1950)$ DECAY MODES

Mode	Fraction (Γ_i/Γ)
$\Gamma_1 K^- \pi^+$	$(52 \pm 14) \%$

$K_0^*(1950)$ BRANCHING RATIOS

$\Gamma(K^- \pi^+)/\Gamma_{total}$	Γ_1/Γ
------------------------------------	-------------------

VALUE	DOCUMENT ID	TECN	CHG	COMMENT
$0.52 \pm 0.08 \pm 0.12$	¹ ASTON	88	LASS 0	$11 K^- p \rightarrow K^- \pi^+ n$

² We do not use the following data for averages, fits, limits, etc. ●●●
 ~ 0.60 ² ZHOU 06 RVUE $Kp \rightarrow K^- \pi^+ n$

¹ We take the central value of the two solutions and the larger error given.

² S-matrix pole. Using ASTON 88 and assuming $K_0^*(700)$, $K_0^*(1430)$.

$K_0^*(1950)$ REFERENCES

AAIJ 23AH PR D108 032010 R. Aaij et al. (LHCb Collab.)
LEES 21A PR D104 072002 J.P. Lees et al. (BABAR Collab.)
ZHOU 06 NP A775 212 Z.Y. Zhou, H.Q. Zheng
ANISOVICH 97C PL B413 137 A.V. Anisovich, A.V. Sarantsev
ASTON 88 NP B296 493 D. Aston et al. (SLAC, NAGO, CIN, INUS)

$K_2^*(1980)$

$$I(J^P) = \frac{1}{2}(2^+)$$

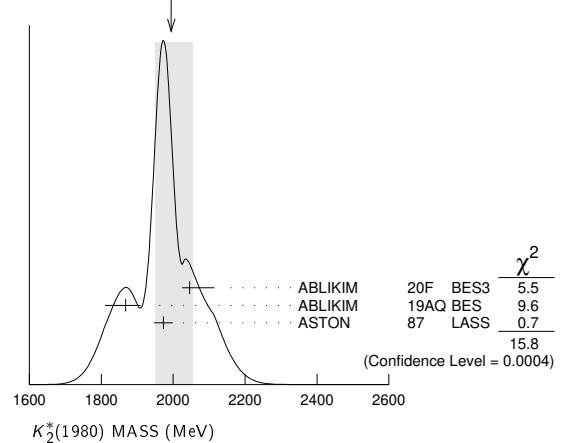
$K_2^*(1980)$ MASS

VALUE (MeV)	EVTS	DOCUMENT ID	TECN	CHG	COMMENT
1990^{+60}_{-50} OUR AVERAGE					Error includes scale factor of 2.8. See the ideogram below.

2046^{+17+67}_{-16-15}	1.8k	¹ ABLIKIM	20F	BES3	$\psi(2S) \rightarrow K^+ K^- \eta$
$1868 \pm 8^{+40}_{-57}$	183k	ABLIKIM	19AQ	BES ±	$J/\psi \rightarrow K^+ K^- \pi^0$
$1973 \pm 8 \pm 25$		ASTON	87	LASS 0	$11 K^- p \rightarrow \bar{K}^0 \pi^+ \pi^- n$
$2073 \pm 94^{+245}_{-240}$	4289	^{2,3} AAIJ	17c	LHCB	$B^+ \rightarrow J/\psi \phi K^+$
2020 ± 20		TIKHOMIROV 03	SPEC		$40.0 \pi^- C \rightarrow K_S^0 K_S^0 K_L^0 X$
1978 ± 40	241	BIRD	89	LASS -	$11 K^- p \rightarrow \bar{K}^0 \pi^- p$

¹ Seen in $\psi(2S)$ decay with branching ratio $\psi(2S) \rightarrow K^\pm X \rightarrow K^+ K^- \eta = (7.0 \pm 0.5^{+3.7}_{-0.6}) \times 10^{-6}$.
² From an amplitude analysis of the decay $B^+ \rightarrow J/\psi \phi K^+$ with a significance of 5.4σ .
³ A reanalysis by AAIJ 21E using a larger data sample did not confirm this measurement, the new result having a significance of only 1.6σ .

WEIGHTED AVERAGE
 1990+60-50 (Error scaled by 2.8)



$K_2^*(1980)$ WIDTH

VALUE (MeV)	EVTS	DOCUMENT ID	TECN	CHG	COMMENT
348^{+38+72}_{-34-44} OUR AVERAGE					Error includes scale factor of 1.3. See the ideogram below.

408^{+38+72}_{-34-44}	1.8k	¹ ABLIKIM	20F	BES3	$\psi(2S) \rightarrow K^+ K^- \eta$
$272 \pm 24^{+50}_{-15}$	183k	ABLIKIM	19AQ	BES ±	$J/\psi \rightarrow K^+ K^- \pi^0$
$373 \pm 33 \pm 60$		ASTON	87	LASS 0	$11 K^- p \rightarrow \bar{K}^0 \pi^+ \pi^- n$

See key on page 1171

Meson Particle Listings

$K_2^*(1980), K_4^*(2045)$

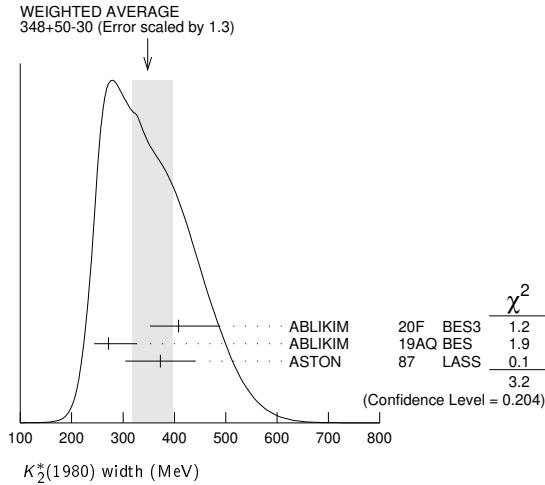
••• We do not use the following data for averages, fits, limits, etc. •••

678 ± 311 ⁺¹¹⁵³ ₋₅₅₉	4289	2,3	AAIJ	17c	LHCB	$B^+ \rightarrow J/\psi \phi K^+$
180 ± 70			TIKHOMIROV	03	SPEC	$40.0 \pi^- C \rightarrow K_S^0 K_S^0 K_L^0 X$
398 ± 47	241		BIRD	89	LASS	$11 K^- p \rightarrow \bar{K}^0 \pi^- p$

¹ Seen in $\psi(2S)$ decay with branching ratio $\psi(2S) \rightarrow K^\pm X \rightarrow K^+ K^- \eta = (7.0 \pm 0.5 \pm 3.7) \times 10^{-6}$.

² From an amplitude analysis of the decay $B^+ \rightarrow J/\psi \phi K^+$ with a significance of 5.4 σ .

³ A reanalysis by AAIJ 21E using a larger data sample did not confirm this measurement, the new result having a significance of only 1.6 σ .



$K_2^*(1980)$ DECAY MODES

Mode	Fraction (Γ_i/Γ)
Γ_1 $K^*(892)\pi$	possibly seen
Γ_2 $K\rho$	possibly seen
Γ_3 $K f_2(1270)$	possibly seen
Γ_4 $K\phi$	seen
Γ_5 $K\eta$	seen

$K_2^*(1980)$ BRANCHING RATIOS

$\Gamma(K^*(892)\pi)/\Gamma_{total}$	Γ_1/Γ
possibly seen	GULER 11 BELL $B^+ \rightarrow J/\psi K^+ \pi^+ \pi^-$

$\Gamma(K\rho)/\Gamma_{total}$	Γ_2/Γ
possibly seen	GULER 11 BELL $B^+ \rightarrow J/\psi K^+ \pi^+ \pi^-$

$\Gamma(K\rho)/\Gamma(K^*(892)\pi)$	Γ_2/Γ_1
$1.49 \pm 0.24 \pm 0.09$	ASTON 87 LASS 0 $11 K^- p \rightarrow \bar{K}^0 \pi^+ \pi^- n$

$\Gamma(K f_2(1270))/\Gamma_{total}$	Γ_3/Γ
possibly seen	TIKHOMIROV 03 SPEC $40.0 \pi^- C \rightarrow K_S^0 K_S^0 K_L^0 X$

$\Gamma(K\phi)/\Gamma_{total}$	Γ_4/Γ
seen	4289 1,2 AAIJ 17c LHCB $B^+ \rightarrow J/\psi \phi K^+$

¹ From an amplitude analysis of the decay $B^+ \rightarrow J/\psi \phi K^+$ with a significance of 5.4 σ .
² A reanalysis by AAIJ 21E using a larger data sample did not confirm this measurement, the new result having a significance of only 1.6 σ .

$\Gamma(K\eta)/\Gamma_{total}$	Γ_5/Γ
seen	1.8k 1 ABLIKIM 20F BES3 $\psi(2S) \rightarrow K^+ K^- \eta$
seen	116k 2 CHEN 20A BELL $D^0 \rightarrow K^- \pi^+ \eta$

¹ Seen decaying to $K\eta$ in an amplitude analysis of $\psi(2S) \rightarrow K^+ K^- \eta$.
² From an amplitude analysis of the decay $D^0 \rightarrow K^- \pi^+ \eta$ with a significance of 17 σ .

$K_2^*(1980)$ REFERENCES

AAIJ	21E	PRL 127 082001	R. Aaij et al.	(LHCb Collab.)
ABLIKIM	20F	PR D101 032008	M. Ablikim et al.	(BESIII Collab.)
CHEN	20A	PR D102 012002	Y.Q. Chen et al.	(BELLE Collab.)
ABLIKIM	19AQ	PR D100 032004	M. Ablikim et al.	(BESIII Collab.)

AAIJ	17C	PRL 118 022003	R. Aaij et al.	(LHCb Collab.)
Also		PR D95 012002	R. Aaij et al.	(LHCb Collab.)
GULER	11	PR D83 032005	H. Guler et al.	(BELLE Collab.)
TIKHOMIROV	03	PAN 66 828	G.D. Tikhomirov et al.	
		Translated from YAF 66 860.		
BIRD	89	SLAC-332	P.F. Bird	(SLAC)
ASTON	87	NP B292 693	D. Aston et al.	(SLAC, NAGO, CIN, INUS)

$K_4^*(2045)$

$J(P) = \frac{1}{2}(4^+)$

$K_4^*(2045)$ MASS

VALUE (MeV)	EVTS	DOCUMENT ID	TECN	CHG	COMMENT
2048 ± 8		OUR AVERAGE			Error includes scale factor of 1.1.
2090 ± 9 ⁺¹¹ ₋₂₉	183k	ABLIKIM	19AQ BES	±	$J/\psi \rightarrow K^+ K^- \pi^0$
2062 ± 14 ± 13		¹ ASTON	86 LASS	0	$11 K^- p \rightarrow K^- \pi^+ n$
2039 ± 10	400	^{2,3} CLELAND	82 SPEC	±	$50 K^+ p \rightarrow K_S^0 \pi^\pm p$
2070 ± 100		⁴ ASTON	81c LASS	0	$11 K^- p \rightarrow K^- \pi^+ n$

••• We do not use the following data for averages, fits, limits, etc. •••

2079 ± 7	431	TORRES	86 MPSF	400 pA	$\rightarrow 4KX$
2088 ± 20	650	BAUBILLIER	82 HBC	-	$8.25 K^- p \rightarrow K_S^0 \pi^- p$
2115 ± 46	488	CARMONY	77 HBC	0	$9 K^+ d \rightarrow K^+ \pi^+ X$

¹ From a fit to all moments.
² From a fit to 8 moments.
³ Number of events evaluated by us.
⁴ From energy-independent partial-wave analysis.

$K_4^*(2045)$ WIDTH

VALUE (MeV)	EVTS	DOCUMENT ID	TECN	CHG	COMMENT
199 ± 27		OUR AVERAGE			
201 ± 19 ⁺⁵⁷ ₋₁₇	183k	ABLIKIM	19AQ BES	±	$J/\psi \rightarrow K^+ K^- \pi^0$
221 ± 48 ± 27		⁵ ASTON	86 LASS	0	$11 K^- p \rightarrow K^- \pi^+ n$
189 ± 35	400	^{6,7} CLELAND	82 SPEC	±	$50 K^+ p \rightarrow K_S^0 \pi^\pm p$

••• We do not use the following data for averages, fits, limits, etc. •••

61 ± 58	431	TORRES	86 MPSF	400 pA	$\rightarrow 4KX$
170 ± 100	650	BAUBILLIER	82 HBC	-	$8.25 K^- p \rightarrow K_S^0 \pi^- p$
240 ± 500		⁸ ASTON	81c LASS	0	$11 K^- p \rightarrow K^- \pi^+ n$
300 ± 200		CARMONY	77 HBC	0	$9 K^+ d \rightarrow K^+ \pi^+ X$

⁵ From a fit to all moments.
⁶ From a fit to 8 moments.
⁷ Number of events evaluated by us.
⁸ From energy-independent partial-wave analysis.

$K_4^*(2045)$ DECAY MODES

Mode	Fraction (Γ_i/Γ)
Γ_1 $K\pi$	(9.9 ± 1.2) %
Γ_2 $K^*(892)\pi\pi$	(9 ± 5) %
Γ_3 $K^*(892)\pi\pi\pi$	(7 ± 5) %
Γ_4 $\rho K\pi$	(5.7 ± 3.2) %
Γ_5 $\omega K\pi$	(5.0 ± 3.0) %
Γ_6 $\phi K\pi$	(2.8 ± 1.4) %
Γ_7 $\phi K^*(892)$	(1.4 ± 0.7) %

$K_4^*(2045)$ BRANCHING RATIOS

$\Gamma(K\pi)/\Gamma_{total}$	Γ_1/Γ
0.099 ± 0.012	ASTON 88 LASS 0 $11 K^- p \rightarrow K^- \pi^+ n$

$\Gamma(K^*(892)\pi\pi)/\Gamma(K\pi)$	Γ_2/Γ_1
0.89 ± 0.53	BAUBILLIER 82 HBC - $8.25 K^- p \rightarrow p K_S^0 3\pi$

$\Gamma(K^*(892)\pi\pi\pi)/\Gamma(K\pi)$	Γ_3/Γ_1
0.75 ± 0.49	BAUBILLIER 82 HBC - $8.25 K^- p \rightarrow p K_S^0 3\pi$

$\Gamma(\rho K\pi)/\Gamma(K\pi)$	Γ_4/Γ_1
0.58 ± 0.32	BAUBILLIER 82 HBC - $8.25 K^- p \rightarrow p K_S^0 3\pi$

$\Gamma(\omega K\pi)/\Gamma(K\pi)$	Γ_5/Γ_1
0.50 ± 0.30	BAUBILLIER 82 HBC - $8.25 K^- p \rightarrow p K_S^0 3\pi$

Meson Particle Listings

 $K_4^*(2045)$, $K_2(2250)$, $K_3(2320)$, $K_5^*(2380)$, $K_4(2500)$

$\Gamma(\phi K \pi)/\Gamma_{\text{total}}$					Γ_6/Γ
VALUE	DOCUMENT ID	TECN	CHG	COMMENT	
0.028 ± 0.014	⁹ TORRES	86	MPSF	400 pA → 4KX	

$\Gamma(\phi K^*(892))/\Gamma_{\text{total}}$					Γ_7/Γ
VALUE	DOCUMENT ID	TECN	CHG	COMMENT	
0.014 ± 0.007	⁹ TORRES	86	MPSF	400 pA → 4KX	

⁹ Error determination is model dependent.

 $K_4^*(2045)$ REFERENCES

ABLIKIM	19AQ	PR	D100	032004	M. Ablikim et al.	(BESIII Collab.)
ASTON	88	NP	B296	493	D. Aston et al.	(SLAC, NAGO, CINC, INUS)
ASTON	86	PL	B180	308	D. Aston et al.	(SLAC, NAGO, CINC, INUS)
TORRES	86	PR	D34	707	S. Torres et al.	(VPI, ARIZ, FNAL, FSU+)
BAUBILLIER	82	PL	118B	447	M. Baubillier et al.	(BIRM, CERN, GLAS+)
CLELAND	82	NP	B208	189	W.E. Cleland et al.	(DURH, GEVA, LAUS+)
ASTON	81C	PL	106B	235	D. Aston et al.	(SLAC, CARL, OTTA) JP
CARMONY	77	PR	D16	1251	D.D. Carmony et al.	(PURD, UCD, IUPU)

 $K_2(2250)$

$$I(J^P) = \frac{1}{2}(2^-)$$

OMITTED FROM SUMMARY TABLE

This entry contains various peaks in strange meson systems reported in the 2150–2260 MeV region, as well as enhancements seen in the antihyperon-nucleon system, either in the mass spectra or in the $J^P = 2^-$ wave.

 $K_2(2250)$ MASS

VALUE (MeV)	EVTS	DOCUMENT ID	TECN	CHG	COMMENT
2247 ± 17 OUR AVERAGE					
2200 ± 40		¹ ARMSTRONG	83c	OMEG	– 18 $K^- p \rightarrow \Lambda \bar{p} X$
2235 ± 50		¹ BAUBILLIER	81	HBC	– 8 $K^- p \rightarrow \Lambda \bar{p} X$
2260 ± 20		¹ CLELAND	81	SPEC	± 50 $K^+ p \rightarrow \Lambda \bar{p} X$
• • • We do not use the following data for averages, fits, limits, etc. • • •					
2280 ± 20		TIKHOMIROV	03	SPEC	40.0 $\pi^- C \rightarrow$ $K_S^0 K_S^0 K_L^0 X$
2147 ± 4	37	CHLIAPNIK...	79	HBC	+ 32 $K^+ p \rightarrow \bar{\Lambda} p X$
2240 ± 20	20	LISSAUER	70	HBC	9 $K^+ p$

¹ $J^P = 2^-$ from moments analysis.

 $K_2(2250)$ WIDTH

VALUE (MeV)	EVTS	DOCUMENT ID	TECN	CHG	COMMENT
180 ± 30 OUR AVERAGE					Error includes scale factor of 1.4.
150 ± 30		² ARMSTRONG	83c	OMEG	– 18 $K^- p \rightarrow \Lambda \bar{p} X$
210 ± 30		² CLELAND	81	SPEC	± 50 $K^+ p \rightarrow \Lambda \bar{p} X$
• • • We do not use the following data for averages, fits, limits, etc. • • •					
180 ± 60		TIKHOMIROV	03	SPEC	40.0 $\pi^- C \rightarrow$ $K_S^0 K_S^0 K_L^0 X$
~ 200		² BAUBILLIER	81	HBC	– 8 $K^- p \rightarrow \Lambda \bar{p} X$
~ 40	37	CHLIAPNIK...	79	HBC	+ 32 $K^+ p \rightarrow \bar{\Lambda} p X$
80 ± 20	20	LISSAUER	70	HBC	9 $K^+ p$

² $J^P = 2^-$ from moments analysis.

 $K_2(2250)$ DECAY MODES

Mode	Fraction (Γ_i/Γ)
Γ_1 $K \pi \pi$	(6.1 ± 1.2) %
Γ_2 $K f_2(1270)$	
Γ_3 $K^*(892) f_0(980)$	
Γ_4 $\rho \bar{\Lambda}$	

 $K_2(2250)$ REFERENCES

TIKHOMIROV	03	PAN	66	828	G.D. Tikhomirov et al.	
		Translated from	YAF	66	860.	
ARMSTRONG	83c	NP	B227	365	T.A. Armstrong et al.	(BARI, BIRM, CERN+)
BAUBILLIER	81	NP	B183	1	M. Baubillier et al.	(BIRM, CERN, GLAS+)
CLELAND	81	NP	B184	1	W.E. Cleland et al.	(PITT, GEVA, LAUS+)
CHLIAPNIK...	79	NP	B158	253	P.V. Chliapnikov et al.	(CERN, BELG, MONS)
LISSAUER	70	NP	B18	491	D. Lissauer et al.	(LBL)

 $K_3(2320)$

$$I(J^P) = \frac{1}{2}(3^+)$$

OMITTED FROM SUMMARY TABLE

Seen in the $J^P = 3^+$ wave of the antihyperon-nucleon system. Needs confirmation.

 $K_3(2320)$ MASS

VALUE (MeV)	DOCUMENT ID	TECN	CHG	COMMENT
2324 ± 24 OUR AVERAGE				
2330 ± 40	¹ ARMSTRONG	83c	OMEG	– 18 $K^- p \rightarrow \Lambda \bar{p} X$
2320 ± 30	¹ CLELAND	81	SPEC	± 50 $K^+ p \rightarrow \Lambda \bar{p} X$

¹ $J^P = 3^+$ from moments analysis.

 $K_3(2320)$ WIDTH

VALUE (MeV)	DOCUMENT ID	TECN	CHG	COMMENT
150 ± 30	² ARMSTRONG	83c	OMEG	– 18 $K^- p \rightarrow \Lambda \bar{p} X$
• • • We do not use the following data for averages, fits, limits, etc. • • •				
~ 250	² CLELAND	81	SPEC	± 50 $K^+ p \rightarrow \Lambda \bar{p} X$

² $J^P = 3^+$ from moments analysis.

 $K_3(2320)$ DECAY MODES

Mode	Fraction (Γ_i/Γ)
Γ_1 $\rho \bar{\Lambda}$	

 $K_3(2320)$ REFERENCES

ARMSTRONG	83c	NP	B227	365	T.A. Armstrong et al.	(BARI, BIRM, CERN+)
CLELAND	81	NP	B184	1	W.E. Cleland et al.	(PITT, GEVA, LAUS+)

 $K_5^*(2380)$

$$I(J^P) = \frac{1}{2}(5^-)$$

OMITTED FROM SUMMARY TABLE

Needs confirmation.

 $K_5^*(2380)$ MASS

VALUE (MeV)	DOCUMENT ID	TECN	CHG	COMMENT
2382 ± 14 ± 19	¹ ASTON	86	LASS	0 11 $K^- p \rightarrow K^- \pi^+ n$

¹ From a fit to all the moments.

 $K_5^*(2380)$ WIDTH

VALUE (MeV)	DOCUMENT ID	TECN	CHG	COMMENT
178 ± 37 ± 32	² ASTON	86	LASS	0 11 $K^- p \rightarrow K^- \pi^+ n$

² From a fit to all the moments.

 $K_5^*(2380)$ DECAY MODES

Mode	Fraction (Γ_i/Γ)
Γ_1 $K \pi$	(6.1 ± 1.2) %

 $K_5^*(2380)$ BRANCHING RATIOS

$\Gamma(K \pi)/\Gamma_{\text{total}}$					Γ_1/Γ
VALUE	DOCUMENT ID	TECN	CHG	COMMENT	
0.061 ± 0.012	ASTON	88	LASS	0 11 $K^- p \rightarrow K^- \pi^+ n$	

 $K_5^*(2380)$ REFERENCES

ASTON	88	NP	B296	493	D. Aston et al.	(SLAC, NAGO, CINC, INUS)
ASTON	86	PL	B180	308	D. Aston et al.	(SLAC, NAGO, CINC, INUS)

 $K_4(2500)$

$$I(J^P) = \frac{1}{2}(4^-)$$

OMITTED FROM SUMMARY TABLE

Needs confirmation.

 $K_4(2500)$ MASS

VALUE (MeV)	DOCUMENT ID	TECN	CHG	COMMENT
2490 ± 20	¹ CLELAND	81	SPEC	± 50 $K^+ p \rightarrow \Lambda \bar{p}$

¹ $J^P = 4^-$ from moments analysis.

 $K_4(2500)$ WIDTH

VALUE (MeV)	DOCUMENT ID	TECN	CHG	COMMENT
• • • We do not use the following data for averages, fits, limits, etc. • • •				
~ 250	² CLELAND	81	SPEC	± 50 $K^+ p \rightarrow \Lambda \bar{p}$

² $J^P = 4^-$ from moments analysis.

See key on page 1171

Meson Particle Listings
 $K_4(2500), K(3100)$

$K_4(2500)$ DECAY MODES

Mode
$\Gamma_1 \quad p\bar{\Lambda}$

$K_4(2500)$ REFERENCES

CLELAND 81 NP B184 1 W.E. Cleland *et al.* (PITT, GEVA, LAUS+)

$K(3100)$

$$I^G(J^{PC}) = ?^?(?^{??})$$

OMITTED FROM SUMMARY TABLE
 also known as $K_J^?(3100)$

Narrow peak observed in several ($\Lambda\bar{p}$ + pions) and ($\bar{\Lambda}p$ + pions) states in Σ^- Be reactions by BOURQUIN 86 and in np and nA reactions by ALEEV 93. Not seen by BOEHNLEIN 91. If due to strong decays, this state has exotic quantum numbers ($B=0, Q=+1, S=-1$ for $\Lambda\bar{p}\pi^+\pi^+$ and $I \geq 3/2$ for $\Lambda\bar{p}\pi^-$). Needs confirmation.

$K(3100)$ MASS

VALUE (MeV)	DOCUMENT ID
≈ 3100 OUR ESTIMATE	

3-BODY DECAYS

VALUE (MeV)	DOCUMENT ID	TECN	COMMENT
3054 ± 11 OUR AVERAGE			
3060 ± 7 ± 20	¹ ALEEV 93 BIS2		$K(3100) \rightarrow \Lambda\bar{p}\pi^+$
3056 ± 7 ± 20	¹ ALEEV 93 BIS2		$K(3100) \rightarrow \bar{\Lambda}p\pi^-$
3055 ± 8 ± 20	¹ ALEEV 93 BIS2		$K(3100) \rightarrow \Lambda\bar{p}\pi^-$
3045 ± 8 ± 20	¹ ALEEV 93 BIS2		$K(3100) \rightarrow \bar{\Lambda}p\pi^+$

4-BODY DECAYS

VALUE (MeV)	DOCUMENT ID	TECN	COMMENT
3059 ± 11 OUR AVERAGE			
3067 ± 6 ± 20	¹ ALEEV 93 BIS2		$K(3100) \rightarrow \Lambda\bar{p}\pi^+\pi^+$
3060 ± 8 ± 20	¹ ALEEV 93 BIS2		$K(3100) \rightarrow \Lambda\bar{p}\pi^+\pi^-$
3055 ± 7 ± 20	¹ ALEEV 93 BIS2		$K(3100) \rightarrow \bar{\Lambda}p\pi^-\pi^-$
3052 ± 8 ± 20	¹ ALEEV 93 BIS2		$K(3100) \rightarrow \bar{\Lambda}p\pi^-\pi^+$

• • • We do not use the following data for averages, fits, limits, etc. • • •

VALUE	DOCUMENT ID	TECN	COMMENT
3105 ± 30	BOURQUIN 86 SPEC		$K(3100) \rightarrow \Lambda\bar{p}\pi^+\pi^+$
3115 ± 30	BOURQUIN 86 SPEC		$K(3100) \rightarrow \Lambda\bar{p}\pi^+\pi^-$

5-BODY DECAYS

VALUE (MeV)	DOCUMENT ID	TECN	COMMENT
• • • We do not use the following data for averages, fits, limits, etc. • • •			
3095 ± 30	BOURQUIN 86 SPEC		$K(3100) \rightarrow \Lambda\bar{p}\pi^+\pi^+\pi^-$
¹ Supersedes ALEEV 90.			

$K(3100)$ WIDTH

3-BODY DECAYS

VALUE (MeV)	DOCUMENT ID	TECN	COMMENT
• • • We do not use the following data for averages, fits, limits, etc. • • •			
42 ± 16	² ALEEV 93 BIS2		$K(3100) \rightarrow \Lambda\bar{p}\pi^+$
36 ± 15	² ALEEV 93 BIS2		$K(3100) \rightarrow \bar{\Lambda}p\pi^-$
50 ± 18	² ALEEV 93 BIS2		$K(3100) \rightarrow \Lambda\bar{p}\pi^-$
30 ± 15	² ALEEV 93 BIS2		$K(3100) \rightarrow \bar{\Lambda}p\pi^+$

4-BODY DECAYS

VALUE (MeV)	CL%	DOCUMENT ID	TECN	COMMENT
• • • We do not use the following data for averages, fits, limits, etc. • • •				
22 ± 8		² ALEEV 93 BIS2		$K(3100) \rightarrow \Lambda\bar{p}\pi^+\pi^+$
28 ± 12		² ALEEV 93 BIS2		$K(3100) \rightarrow \Lambda\bar{p}\pi^+\pi^-$
32 ± 15		² ALEEV 93 BIS2		$K(3100) \rightarrow \bar{\Lambda}p\pi^-\pi^-$
30 ± 15		² ALEEV 93 BIS2		$K(3100) \rightarrow \bar{\Lambda}p\pi^-\pi^+$
<30	90	BOURQUIN 86 SPEC		$K(3100) \rightarrow \Lambda\bar{p}\pi^+\pi^+$
<80	90	BOURQUIN 86 SPEC		$K(3100) \rightarrow \Lambda\bar{p}\pi^+\pi^-$

5-BODY DECAYS

VALUE (MeV)	CL%	DOCUMENT ID	TECN	COMMENT
• • • We do not use the following data for averages, fits, limits, etc. • • •				
<30	90	BOURQUIN 86 SPEC		$K(3100) \rightarrow \Lambda\bar{p}\pi^+\pi^+\pi^-$
² Supersedes ALEEV 90.				

$K(3100)$ DECAY MODES

Mode
$\Gamma_1 \quad K(3100)^0 \rightarrow \Lambda\bar{p}\pi^+$
$\Gamma_2 \quad K(3100)^{--} \rightarrow \Lambda\bar{p}\pi^-$
$\Gamma_3 \quad K(3100)^- \rightarrow \Lambda\bar{p}\pi^+\pi^-$
$\Gamma_4 \quad K(3100)^+ \rightarrow \Lambda\bar{p}\pi^+\pi^+$
$\Gamma_5 \quad K(3100)^0 \rightarrow \Lambda\bar{p}\pi^+\pi^+\pi^-$
$\Gamma_6 \quad K(3100)^0 \rightarrow \Sigma(1385)^+\bar{p}$

$\Gamma(\Sigma(1385)^+\bar{p})/\Gamma(\Lambda\bar{p}\pi^+)$

Γ_6/Γ_1

VALUE	CL%	DOCUMENT ID	TECN	COMMENT
<0.04	90	ALEEV 93 BIS2		$K(3100)^0 \rightarrow \Sigma(1385)^+\bar{p}$

$K(3100)$ REFERENCES

ALEEV 93 PAN 56 1358	A.N. Aleev <i>et al.</i>	(BIS-2 Collab.)
Translated from YAF 56 100.		
BOEHNLEIN 91 NPBPS B21 174	A. Boehnlein <i>et al.</i>	(FLOR, BNL, IND+)
ALEEV 90 ZPHY C47 533	A.N. Aleev <i>et al.</i>	(BIS-2 Collab.)
BOURQUIN 86 PL B172 113	M.H. Bourquin <i>et al.</i>	(GEVA, RAL, HEIDP+)

Meson Particle Listings

 D^\pm

CHARMED MESONS

($C = \pm 1$)

$$D^+ = c\bar{d}, D^0 = c\bar{u}, \bar{D}^0 = \bar{c}u, D^- = \bar{c}d, \text{ similarly for } D^{*s}$$
 D^\pm

$$J(P) = \frac{1}{2}(0^-)$$

 D^\pm MASS

The fit includes $D^\pm, D^0, D_s^\pm, D^{*\pm}, D^{*0}, D_1(2420)^0, D_2^*(2460)^0$, and $D_{s1}(2536)^\pm$ mass and mass difference measurements.

VALUE (MeV)	EVTS	DOCUMENT ID	TECN	COMMENT
1869.66 ± 0.05 OUR FIT				
1869.5 ± 0.4 OUR AVERAGE				
1869.53 ± 0.49 ± 0.20	110 ± 15	ANASHIN	10A	KEDR e^+e^- at $\psi(3770)$
1870.0 ± 0.5 ± 1.0	317	BARLAG	90c	ACCM π^- Cu 230 GeV
1869.4 ± 0.6		¹ TRILLING	81	RVUE e^+e^- 3.77 GeV
••• We do not use the following data for averages, fits, limits, etc. •••				
1875 ± 10	9	ADAMOVIČ	87	EMUL Photoproduction
1860 ± 16	6	ADAMOVIČ	84	EMUL Photoproduction
1863 ± 4		DERRICK	84	HRS e^+e^- 29 GeV
1868.4 ± 0.5		¹ SCHINDLER	81	MRK2 e^+e^- 3.77 GeV
1874 ± 5		GOLDBABER	77	MRK1 D^0, D^+ recoil spectra
1868.3 ± 0.9		¹ PERUZZI	77	LGW e^+e^- 3.77 GeV
1874 ± 11		PICCOLO	77	MRK1 e^+e^- 4.03, 4.41 GeV
1876 ± 15	50	PERUZZI	76	MRK1 $K^\mp\pi^\pm\pi^\pm$

¹PERUZZI 77 and SCHINDLER 81 errors do not include the 0.13% uncertainty in the absolute SPEAR energy calibration. TRILLING 81 uses the high precision $J/\psi(1S)$ and $\psi(2S)$ measurements of ZHOLENTZ 80 to determine this uncertainty and combines the PERUZZI 77 and SCHINDLER 81 results to obtain the value quoted.

 D^\pm MEAN LIFE

Measurements with an error $> 100 \times 10^{-15}$ s have been omitted from the Listings.

VALUE (10^{-15} s)	EVTS	DOCUMENT ID	TECN	COMMENT
1033 ± 5 OUR AVERAGE				
1030.4 ± 4.7 ± 3.1	171k	¹ ABUDINEN	21A	BEL2 e^+e^- at $\Upsilon(4S)$
1039.4 ± 4.3 ± 7.0	110k	LINK	02F	FOCS γ nucleus, ≈ 180 GeV
••• We do not use the following data for averages, fits, limits, etc. •••				
1033.6 ± 22.1 ± 9.9 -12.7	3.7k	BONVICINI	99	CLEO $e^+e^- \approx \Upsilon(4S)$
1048 ± 15 ± 11	9k	FRABETTI	94D	E687 $D^+ \rightarrow K^-\pi^+\pi^+$
1075 ± 40 ± 18	2.4k	FRABETTI	91	E687 γ Be, $D^+ \rightarrow K^-\pi^+\pi^+$
1030 ± 80 ± 60	200	ALVAREZ	90	NA14 $\gamma, D^+ \rightarrow K^-\pi^+\pi^+$
1050 ± 77 -72	317	² BARLAG	90c	ACCM π^- Cu 230 GeV
1050 ± 80 ± 70	363	ALBRECHT	88i	ARG e^+e^- 10 GeV
1090 ± 30 ± 25	2.9k	RAAB	88	E691 Photoproduction

¹ABUDINEN 21A determines the lifetime ratio $\tau(D^+)/\tau(D^0) = 2.510 \pm 0.013 \pm 0.007$.

²BARLAG 90c estimates the systematic error to be negligible.

 D^+ DECAY MODES

Most decay modes (other than the semileptonic modes) that involve a neutral K meson are now given as K_S^0 modes, not as \bar{K}^0 modes. Nearly always it is a K_S^0 that is measured, and interference between Cabibbo-allowed and doubly Cabibbo-suppressed modes can invalidate the assumption that $2\Gamma(K_S^0) = \Gamma(\bar{K}^0)$.

Mode	Fraction (Γ_i/Γ)	Scale factor/ Confidence level
------	--------------------------------	-----------------------------------

Inclusive modes

Γ_1	e^+ semileptonic	(16.07 ± 0.30) %	
Γ_2	μ^+ anything	(17.6 ± 3.2) %	
Γ_3	K^- anything	(25.7 ± 1.4) %	
Γ_4	K_S^0 anything	(33.1 ± 0.4) %	
Γ_5	K^+ anything	(5.9 ± 0.8) %	
Γ_6	$\bar{K}^*(892)^-$ anything	(6 ± 5) %	
Γ_7	$\bar{K}^*(892)^0$ anything	(23 ± 5) %	
Γ_8	$K^*(892)^0$ anything	< 6.6 %	CL=90%
Γ_9	η anything	(6.3 ± 0.7) %	
Γ_{10}	η' anything	(1.04 ± 0.18) %	
Γ_{11}	ϕ anything	(1.12 ± 0.04) %	
Γ_{12}	$\pi^+\pi^+\pi^-$ anything	(15.25 ± 0.20) %	

Leptonic and semileptonic modes

Γ_{13}	$e^+\nu_e$	< 8.8	$\times 10^{-6}$	CL=90%
Γ_{14}	$\gamma e^+\nu_e$	< 3.0	$\times 10^{-5}$	CL=90%
Γ_{15}	$\mu^+\nu_\mu$	(3.74 ± 0.17)	$\times 10^{-4}$	
Γ_{16}	$\tau^+\nu_\tau$	(1.20 ± 0.27)	$\times 10^{-3}$	
Γ_{17}	$\bar{K}^0 e^+\nu_e$	(8.72 ± 0.09) %		
Γ_{18}	$\bar{K}^0 \mu^+\nu_\mu$	(8.76 ± 0.19) %		
Γ_{19}	$K^-\pi^+ e^+\nu_e$	(4.02 ± 0.18) %		S=3.2
Γ_{20}	$\bar{K}^*(892)^0 e^+\nu_e, \bar{K}^*(892)^0 \rightarrow K^-\pi^+$	(3.77 ± 0.17) %		
Γ_{21}	$(K^-\pi^+)_{[0.8-1.0]\text{GeV}} e^+\nu_e$	(3.39 ± 0.09) %		
Γ_{22}	$(K^-\pi^+)_{S\text{-wave}} e^+\nu_e$	(2.28 ± 0.11)	$\times 10^{-3}$	
Γ_{23}	$\bar{K}^*(1410)^0 e^+\nu_e, \bar{K}^*(1410)^0 \rightarrow K^-\pi^+$	< 6	$\times 10^{-3}$	CL=90%
Γ_{24}	$\bar{K}_2^*(1430)^0 e^+\nu_e, \bar{K}_2^*(1430)^0 \rightarrow K^-\pi^+$	< 5	$\times 10^{-4}$	CL=90%
Γ_{25}	$K^-\pi^+ e^+\nu_e$ nonresonant	< 7	$\times 10^{-3}$	CL=90%
Γ_{26}	$\bar{K}^*(892)^0 e^+\nu_e$	(5.40 ± 0.10) %		S=1.1
Γ_{27}	$K^-\pi^+ \mu^+\nu_\mu$	(3.65 ± 0.34) %		
Γ_{28}	$\bar{K}^*(892)^0 \mu^+\nu_\mu, \bar{K}^*(892)^0 \rightarrow K^-\pi^+$	(3.52 ± 0.10) %		
Γ_{29}	$K^-\pi^+ \mu^+\nu_\mu$ nonresonant	(1.9 ± 0.5)	$\times 10^{-3}$	
Γ_{30}	$\bar{K}^*(892)^0 \mu^+\nu_\mu$	(5.27 ± 0.15) %		
Γ_{31}	$K^-\pi^+ \pi^0 \mu^+\nu_\mu$	< 1.5	$\times 10^{-3}$	CL=90%
Γ_{32}	$\bar{K}_1^*(1270)^0 e^+\nu_e, \bar{K}_1^0 \rightarrow K^-\pi^+ \pi^0$	(1.06 ± 0.15)	$\times 10^{-3}$	
Γ_{33}	$\bar{K}_0^*(1430)^0 \mu^+\nu_\mu$	< 2.3	$\times 10^{-4}$	CL=90%
Γ_{34}	$\bar{K}^*(1680)^0 \mu^+\nu_\mu$	< 1.5	$\times 10^{-3}$	CL=90%
Γ_{35}	$\pi^0 e^+\nu_e$	(3.72 ± 0.17)	$\times 10^{-3}$	S=2.0
Γ_{36}	$\pi^0 \mu^+\nu_\mu$	(3.50 ± 0.15)	$\times 10^{-3}$	
Γ_{37}	$\eta e^+\nu_e$	(1.11 ± 0.07)	$\times 10^{-3}$	
Γ_{38}	$\eta \mu^+\nu_\mu$	(1.04 ± 0.11)	$\times 10^{-3}$	
Γ_{39}	$\pi^-\pi^+ e^+\nu_e$	(2.49 ± 0.11)	$\times 10^{-3}$	S=1.2
Γ_{40}	$f_0(500)^0 e^+\nu_e, f_0(500)^0 \rightarrow \pi^+\pi^-$	(6.4 ± 0.6)	$\times 10^{-4}$	
Γ_{41}	$\rho^0 e^+\nu_e$	(1.90 ± 0.10)	$\times 10^{-3}$	S=1.2
Γ_{42}	$\rho^0 \mu^+\nu_\mu$	(2.4 ± 0.4)	$\times 10^{-3}$	
Γ_{43}	$\omega e^+\nu_e$	(1.69 ± 0.11)	$\times 10^{-3}$	
Γ_{44}	$\omega \mu^+\nu_\mu$	(1.77 ± 0.21)	$\times 10^{-3}$	
Γ_{45}	$\eta'(958) e^+\nu_e$	(2.0 ± 0.4)	$\times 10^{-4}$	
Γ_{46}	$a(980)^0 e^+\nu_e, a(980)^0 \rightarrow \eta\pi^0$	(1.7 ± 0.8)	$\times 10^{-4}$	
Γ_{47}	$b_1(1235)^0 e^+\nu_e, b_1^0 \rightarrow \omega\pi^0$	< 1.75	$\times 10^{-4}$	CL=90%
Γ_{48}	$\phi e^+\nu_e$	< 1.3	$\times 10^{-5}$	CL=90%
Γ_{49}	$D^0 e^+\nu_e$	< 1.0	$\times 10^{-4}$	CL=90%

Hadronic modes with a \bar{K} or $\bar{K}K\bar{K}$

Γ_{50}	$K_L^0 \pi^+$	(1.562 ± 0.031) %		S=1.7
Γ_{51}	$K_L^0 \pi^+$	(1.46 ± 0.05) %		
Γ_{52}	$K^- 2\pi^+$	[a] (9.38 ± 0.16) %		S=1.6
Γ_{53}	$(K^-\pi^+)_{S\text{-wave}} \pi^+$	(7.52 ± 0.17) %		
Γ_{54}	$\bar{K}_0^*(700)^0 \pi^+, \bar{K}_0^* \rightarrow K^-\pi^+$	(1.25 ± 0.06) %	[b]	
Γ_{55}	$\bar{K}_0^*(1430)^0 \pi^+, \bar{K}_0^*(1430)^0 \rightarrow K^-\pi^+$	(1.04 ± 0.12) %		
Γ_{56}	$\bar{K}^*(892)^0 \pi^+, \bar{K}^*(892)^0 \rightarrow K^-\pi^+$	not seen		
Γ_{57}	$\bar{K}^*(1410)^0 \pi^+, \bar{K}^{*0} \rightarrow K^-\pi^+$	(2.3 ± 0.7)	$\times 10^{-4}$	[b]
Γ_{58}	$\bar{K}_2^*(1430)^0 \pi^+, \bar{K}_2^*(1430)^0 \rightarrow K^-\pi^+$	(2.2 ± 1.1)	$\times 10^{-4}$	[b]
Γ_{59}	$\bar{K}^*(1680)^0 \pi^+, \bar{K}^*(1680)^0 \rightarrow K^-\pi^+$	(1.45 ± 0.26) %		
Γ_{60}	$K^-(2\pi^+)_{J=2}$	(7.36 ± 0.20) %		[a]
Γ_{61}	$K^- 2\pi^+$ nonresonant	(6.14 ± 0.35) %		
Γ_{62}	$K_S^0 \pi^+ \pi^0$	(1.5 ± 1.2)	$\times 10^{-3}$	
Γ_{63}	$K_S^0 \rho^+$	(2.64 ± 0.32)	$\times 10^{-3}$	
Γ_{64}	$K_S^0 \rho(1450)^+, \rho^+ \rightarrow \pi^+\pi^0$	(2.7 ± 0.9)	$\times 10^{-3}$	
Γ_{65}	$\bar{K}^*(892)^0 \pi^+, \bar{K}^*(892)^0 \rightarrow K_S^0 \pi^0$			
Γ_{66}	$\bar{K}_0^*(1430)^0 \pi^+, \bar{K}_0^{*0} \rightarrow K_S^0 \pi^0$			

Γ_{67}	$\bar{K}_0^*(1680)^0 \pi^+, \bar{K}_0^{*0} \rightarrow K_S^0 \pi^0$	$(10 \pm 7) \times 10^{-4}$	
Γ_{68}	$\bar{\pi}^0 \pi^+, \bar{K}^0 \rightarrow K_S^0 \pi^0$	$(6 \pm 5) \times 10^{-3}$	
Γ_{69}	$K_S^0 \pi^+ \pi^0$ nonresonant	$(3 \pm 4) \times 10^{-3}$	
Γ_{70}	$K_S^0 \pi^+ \pi^0$ nonresonant and $\bar{\pi}^0 \pi^+$	$(1.37 \pm 0.21) \%$	
Γ_{71}	$(K_S^0 \pi^0)_{S\text{-wave}} \pi^+$	$(1.27 \pm 0.27) \%$	
Γ_{72}	$K_S^0 \pi^+ \omega$	$(7.1 \pm 0.5) \times 10^{-3}$	
Γ_{73}	$K_S^0 \pi^+ \eta$	$(1.31 \pm 0.05) \%$	
Γ_{74}	$K_S^0 \pi^+ \eta'(958)$	$(1.90 \pm 0.21) \times 10^{-3}$	
Γ_{75}	$K^- 2\pi^+ \pi^0$	[c] $(6.25 \pm 0.18) \%$	
Γ_{76}	$K_S^0 2\pi^+ \pi^-$	[c] $(3.10 \pm 0.09) \%$	
Γ_{77}	$K_S^0 \pi^+ 2\pi^0$	$(2.89 \pm 0.09) \%$	
Γ_{78}	$K_S^0 a_1(1260)^+, a_1^+ \rightarrow \rho(770)^+ \pi^0$	$(8.7 \pm 1.6) \times 10^{-3}$	
Γ_{79}	$K_S^0 a_1(1260)^+, a_1^+ \rightarrow f_0(500) \pi^+, f_0 \rightarrow \pi^0 \pi^0$	$(1.0 \pm 0.6) \times 10^{-3}$	
Γ_{80}	$\bar{K}_1(1400)^0 \pi^+, \bar{K}_1^0 \rightarrow \bar{K}^*(892)^0 \pi^0, \bar{K}^{*0} \rightarrow K_S^0 \pi^0$	$(2.3 \pm 0.4) \times 10^{-3}$	
Γ_{81}	$\bar{K}^*(892)^0 \rho^+, \bar{K}^{*0} \rightarrow K_S^0 \pi^0$	$(9.7 \pm 0.9) \times 10^{-3}$	
Γ_{82}	$\bar{K}^*(892)^0 \pi^+ \pi^0$ non-resonant, $\bar{K}^{*0} \rightarrow K_S^0 \pi^0$	$(2.6 \pm 0.7) \times 10^{-3}$	
Γ_{83}	$K_S^0 \rho^+ \pi^0$ non-resonant	$(4.8 \pm 0.5) \times 10^{-3}$	
Γ_{84}	$K^- 2\pi^+ \eta$	$(1.35 \pm 0.12) \times 10^{-3}$	
Γ_{85}	$K_S^0 \pi^+ \pi^0 \eta$	$(1.22 \pm 0.25) \times 10^{-3}$	
Γ_{86}	$K^- 3\pi^+ \pi^-$	[a] $(5.7 \pm 0.5) \times 10^{-3}$	
Γ_{87}	$\bar{K}^*(892)^0 2\pi^+ \pi^-, \bar{K}^*(892)^0 \rightarrow K^- \pi^+$	$(1.2 \pm 0.4) \times 10^{-3}$	S=1.1
Γ_{88}	$\bar{K}^*(892)^0 \rho^0 \pi^+, K^*(892)^0 \rightarrow K^- \pi^+$	$(2.3 \pm 0.4) \times 10^{-3}$	
Γ_{89}	$\bar{K}^*(892)^0 a_1(1260)^+$	[d] $(9.3 \pm 1.9) \times 10^{-3}$	
Γ_{90}	$\bar{K}^*(892)^0 2\pi^+ \pi^-$ no- ρ , $\bar{K}^*(892)^0 \rightarrow K^- \pi^+$		
Γ_{91}	$K^- \rho^0 2\pi^+$	$(1.72 \pm 0.28) \times 10^{-3}$	
Γ_{92}	$K^- 3\pi^+ \pi^-$ nonresonant	$(4.0 \pm 2.9) \times 10^{-4}$	
Γ_{93}	$K_S^0 2\pi^+ \pi^- \pi^0$	$(1.53 \pm 0.08) \%$	
Γ_{94}	$K_S^0 \pi^+ 3\pi^0$	$(5.5 \pm 0.5) \times 10^{-3}$	
Γ_{95}	$K^- 2\pi^+ 2\pi^0$	$(4.95 \pm 0.32) \times 10^{-3}$	
Γ_{96}	$K^+ 2K_S^0$	$(2.54 \pm 0.13) \times 10^{-3}$	
Γ_{97}	$K^+ K^- K_S^0 \pi^+$	$(2.4 \pm 0.5) \times 10^{-4}$	

Pionic modes

Γ_{98}	$\pi^+ \pi^0$	$(1.247 \pm 0.033) \times 10^{-3}$	
Γ_{99}	$2\pi^+ \pi^-$	$(3.27 \pm 0.09) \times 10^{-3}$	
Γ_{100}	$\rho^0 \pi^+$	$(8.4 \pm 0.8) \times 10^{-4}$	
Γ_{101}	$\pi^+ (\pi^+ \pi^-)_{S\text{-wave}}$	$(2.01 \pm 0.06) \times 10^{-3}$	
Γ_{102}	$\sigma \pi^+, \sigma \rightarrow \pi^+ \pi^-$	$(1.38 \pm 0.10) \times 10^{-3}$	
Γ_{103}	$f_0(980) \pi^+, f_0 \rightarrow \pi^+ \pi^-$	$(1.57 \pm 0.32) \times 10^{-4}$	
Γ_{104}	$f_0(1370) \pi^+, f_0 \rightarrow \pi^+ \pi^-$	$(8 \pm 4) \times 10^{-5}$	
Γ_{105}	$\omega \pi^+, \omega \rightarrow \pi^+ \pi^-$	$(3.4 \pm 0.5) \times 10^{-6}$	
Γ_{106}	$f_2(1270) \pi^+, f_2 \rightarrow \pi^+ \pi^-$	$(4.58 \pm 0.28) \times 10^{-4}$	
Γ_{107}	$\rho(1450)^0 \pi^+, \rho^0 \rightarrow \pi^+ \pi^-$	$(1.8 \pm 0.5) \times 10^{-4}$	
Γ_{108}	$\rho(1700)^0 \pi^+, \rho^0 \rightarrow \pi^+ \pi^-$	$(1.9 \pm 0.5) \times 10^{-4}$	
Γ_{109}	$f_0(1500) \pi^+, f_0 \rightarrow \pi^+ \pi^-$	$(1.1 \pm 0.4) \times 10^{-4}$	
Γ_{110}	$f_0(1710) \pi^+, f_0 \rightarrow \pi^+ \pi^-$	$< 5 \times 10^{-5}$	CL=95%
Γ_{111}	$f_0(1790) \pi^+, f_0 \rightarrow \pi^+ \pi^-$	$< 7 \times 10^{-5}$	CL=95%
Γ_{112}	$(\pi^+ \pi^+)_{S\text{-wave}} \pi^-$	$< 1.2 \times 10^{-4}$	CL=95%
Γ_{113}	$2\pi^+ \pi^-$ nonresonant	$< 1.1 \times 10^{-4}$	CL=95%
Γ_{114}	$\pi^+ 2\pi^0$	$(4.61 \pm 0.15) \times 10^{-3}$	
Γ_{115}	$2\pi^+ \pi^- \pi^0$	$(1.165 \pm 0.030) \%$	
Γ_{116}	$\pi^+ 3\pi^0$	$(4.17 \pm 0.26) \times 10^{-3}$	
Γ_{117}	$\pi^+ 4\pi^0$	$(1.9 \pm 0.4) \times 10^{-3}$	
Γ_{118}	$2\pi^+ \pi^- 2\pi^0$	$(1.07 \pm 0.05) \%$	
Γ_{119}	$3\pi^+ 2\pi^-$	$(1.66 \pm 0.16) \times 10^{-3}$	S=1.1
Γ_{120}	$2\pi^+ \pi^- 3\pi^0$	$(3.42 \pm 0.35) \times 10^{-3}$	
Γ_{121}	$3\pi^+ 2\pi^- \pi^0$	$(2.34 \pm 0.27) \times 10^{-3}$	
Γ_{122}	$\eta \pi^+$	$(3.77 \pm 0.09) \times 10^{-3}$	
Γ_{123}	$\eta \pi^+ \pi^0$	$(2.05 \pm 0.35) \times 10^{-3}$	S=2.2
Γ_{124}	$\eta 2\pi^+ \pi^-$	$(3.41 \pm 0.20) \times 10^{-3}$	
Γ_{125}	$\eta \pi^+ 2\pi^0$	$(3.20 \pm 0.33) \times 10^{-3}$	
Γ_{126}	$\eta \pi^+ 3\pi^0$	$(2.9 \pm 0.5) \times 10^{-3}$	

Γ_{127}	$\eta 2\pi^+ \pi^- \pi^0$	$(3.88 \pm 0.34) \times 10^{-3}$
Γ_{128}	$\eta \eta \pi^+$	$(2.96 \pm 0.26) \times 10^{-3}$
Γ_{129}	$\omega \pi^+$	$(2.8 \pm 0.6) \times 10^{-4}$
Γ_{130}	$\omega \pi^+ \pi^0$	$(3.9 \pm 0.9) \times 10^{-3}$
Γ_{131}	$\eta'(958) \pi^+$	$(4.97 \pm 0.19) \times 10^{-3}$
Γ_{132}	$\eta'(958) \pi^+ \pi^0$	$(1.6 \pm 0.5) \times 10^{-3}$

Hadronic modes with a $K\bar{K}$ pair

Γ_{133}	$K_S^0 K^+$	$(3.04 \pm 0.09) \times 10^{-3}$	S=2.2
Γ_{134}	$K_S^0 K^+$	$(3.21 \pm 0.16) \times 10^{-3}$	
Γ_{135}	$K_S^0 K^+ \pi^0$	$(5.07 \pm 0.30) \times 10^{-3}$	
Γ_{136}	$K^*(892)^+ K_S^0, K^{*+} \rightarrow K^+ K^- \pi^+$	$(2.89 \pm 0.30) \times 10^{-3}$	
Γ_{137}	$\bar{K}^*(892)^0 K^+, \bar{K}^{*0} \rightarrow K_S^0 \pi^0$	$(5.2 \pm 1.4) \times 10^{-4}$	
Γ_{138}	$K^*(892)^+ K_S^0$		
Γ_{139}	$K_S^0 K^+ \pi^0$	$(5.24 \pm 0.31) \times 10^{-3}$	
Γ_{140}	$K^+ K^- \pi^+$	[a] $(9.68 \pm 0.18) \times 10^{-3}$	
Γ_{141}	$K^+ \bar{K}^*(892)^0, \bar{K}^*(892)^0 \rightarrow K^- \pi^+$	$(2.49 \pm 0.08) \times 10^{-3}$	
Γ_{142}	$K^+ \bar{K}_0^*(1430)^0, \bar{K}_0^*(1430)^0 \rightarrow K^- \pi^+$	$(1.82 \pm 0.35) \times 10^{-3}$	
Γ_{143}	$K^+ \bar{K}_2^*(1430)^0, \bar{K}_2^0 \rightarrow K^- \pi^+$	$(1.6 \pm 1.2) \times 10^{-4}$	
Γ_{144}	$K^+ \bar{K}_0^*(700), \bar{K}_0^0 \rightarrow K^- \pi^+$	$(6.8 \pm 3.5) \times 10^{-4}$	
Γ_{145}	$a_0(1450)^0 \pi^+, a_0^0 \rightarrow K^+ K^-$	$(4.5 \pm 7.0) \times 10^{-4}$	
Γ_{146}	$\phi(1680) \pi^+, \phi \rightarrow K^+ K^-$	$(4.9 \pm 4.0) \times 10^{-5}$	
Γ_{147}	$\phi \pi^+, \phi \rightarrow K^+ K^-$	$(2.69 \pm 0.07) \times 10^{-3}$	
Γ_{148}	$\phi \pi^+$	$(5.70 \pm 0.14) \times 10^{-3}$	
Γ_{149}	$K^+ K^- \pi^+ \pi^0$	$(6.62 \pm 0.32) \times 10^{-3}$	
Γ_{150}	$K_S^0 K_S^0 \pi^+$	$(2.70 \pm 0.13) \times 10^{-3}$	
Γ_{151}	$K_S^0 K_S^0 \pi^+ \pi^0$	$(1.34 \pm 0.21) \times 10^{-3}$	
Γ_{152}	$K_S^0 K^+ \eta$	$(1.8 \pm 0.5) \times 10^{-4}$	
Γ_{153}	$K_S^0 K^0 \pi^+ \pi^-$	$(1.89 \pm 0.13) \times 10^{-3}$	
Γ_{154}	$K_S^0 K^+ \pi^0 \pi^0$	$(5.8 \pm 1.3) \times 10^{-4}$	
Γ_{155}	$K_S^0 K^- 2\pi^+$	$(2.27 \pm 0.13) \times 10^{-3}$	
Γ_{156}	$K^+ K^- 2\pi^+ \pi^-$	$(2.3 \pm 1.2) \times 10^{-4}$	

A few poorly measured branching fractions:

Γ_{157}	$\phi \pi^+ \pi^0$	$(2.3 \pm 1.0) \%$	
Γ_{158}	$\phi \rho^+$	$< 1.5 \%$	CL=90%
Γ_{159}	$K^+ K^- \pi^+ \pi^0$ non- ϕ	$(1.5 \pm 0.7) \%$	

Doubly Cabibbo-suppressed modes

Γ_{160}	$K^+ \pi^0$	$(2.08 \pm 0.21) \times 10^{-4}$	S=1.4
Γ_{161}	$K^+ \eta$	$(1.25 \pm 0.16) \times 10^{-4}$	S=1.1
Γ_{162}	$K^+ \eta'(958)$	$(1.85 \pm 0.20) \times 10^{-4}$	
Γ_{163}	$K^+ 2\pi^0$	$(2.1 \pm 0.4) \times 10^{-4}$	
Γ_{164}	$K^*(892)^+ \pi^0$	$(3.4 \pm 1.4) \times 10^{-4}$	
Γ_{165}	$K^+ \pi^+ \pi^-$	$(4.91 \pm 0.09) \times 10^{-4}$	
Γ_{166}	$K^+ \rho^0$	$(1.9 \pm 0.5) \times 10^{-4}$	
Γ_{167}	$K^+ \eta \pi^0$	$(2.1 \pm 0.5) \times 10^{-4}$	
Γ_{168}	$K^*(892)^+ \eta$	$(4.4 \pm 1.8) \times 10^{-4}$	
Γ_{169}	$K^*(892)^0 \pi^+, K^*(892)^0 \rightarrow K^+ \pi^-$	$(2.3 \pm 0.4) \times 10^{-4}$	
Γ_{170}	$K^+ f_0(980), f_0(980) \rightarrow \pi^+ \pi^-$	$(4.4 \pm 2.6) \times 10^{-5}$	
Γ_{171}	$K_2^*(1430)^0 \pi^+, K_2^*(1430)^0 \rightarrow K^+ \pi^-$	$(3.9 \pm 2.7) \times 10^{-5}$	
Γ_{172}	$K^+ \pi^+ \pi^-$ nonresonant	not seen	
Γ_{173}	$K^+ \pi^+ \pi^- \pi^0$	$(1.21 \pm 0.09) \times 10^{-3}$	
Γ_{174}	$K^+ \pi^+ \pi^- \pi^0$ nonresonant	$(1.10 \pm 0.07) \times 10^{-3}$	
Γ_{175}	$K^+ \omega$	$(5.7 \pm 2.5) \times 10^{-5}$	
Γ_{176}	$2K^+ K^-$	$(6.14 \pm 0.11) \times 10^{-5}$	
Γ_{177}	$\phi(1020)^0 K^+$	$< 2.1 \times 10^{-5}$	CL=90%
Γ_{178}	$K^+ \phi(1020), \phi \rightarrow K^+ K^-$	$(4.4 \pm 0.6) \times 10^{-6}$	
Γ_{179}	$K^+ (K^+ K^-)_{S\text{-wave}}$	$(5.77 \pm 0.12) \times 10^{-5}$	

$\Delta C = 1$ weak neutral current (C1) modes, or Lepton Family number (LF), or Lepton number (L), or Baryon number (B) violating modes

Γ_{180}	$\pi^+ e^+ e^-$	C1 $< 1.1 \times 10^{-6}$	CL=90%
Γ_{181}	$\pi^+ \pi^0 e^+ e^-$	$< 1.4 \times 10^{-5}$	CL=90%

Meson Particle Listings

 D^\pm

Γ ₁₈₂	$\pi^+\phi, \phi \rightarrow e^+e^-$	[e]	$(1.7 \pm_{-0.9}^{+1.4}) \times 10^{-6}$		
Γ ₁₈₃	$\pi^+\mu^+\mu^-$	CI	< 6.7	$\times 10^{-8}$	CL=90%
Γ ₁₈₄	$\pi^+\phi, \phi \rightarrow \mu^+\mu^-$	[e]	$(1.8 \pm 0.8) \times 10^{-6}$		
Γ ₁₈₅	$\rho^+\mu^+\mu^-$	CI	< 5.6	$\times 10^{-4}$	CL=90%
Γ ₁₈₆	$K^+e^+e^-$	[f]	< 8.5	$\times 10^{-7}$	CL=90%
Γ ₁₈₇	$K^+\pi^0e^+e^-$		< 1.5	$\times 10^{-5}$	CL=90%
Γ ₁₈₈	$K^0_S \pi^+e^+e^-$		< 2.6	$\times 10^{-5}$	CL=90%
Γ ₁₈₉	$K^0_S K^+e^+e^-$		< 1.1	$\times 10^{-5}$	CL=90%
Γ ₁₉₀	$K^+\mu^+\mu^-$	[f]	< 5.4	$\times 10^{-8}$	CL=90%
Γ ₁₉₁	$\pi^+e^+\mu^-$	LF	< 2.1	$\times 10^{-7}$	CL=90%
Γ ₁₉₂	$\pi^+e^-\mu^+$	LF	< 2.2	$\times 10^{-7}$	CL=90%
Γ ₁₉₃	$K^+e^+\mu^-$	LF	< 7.5	$\times 10^{-8}$	CL=90%
Γ ₁₉₄	$K^+e^-\mu^+$	LF	< 1.0	$\times 10^{-7}$	CL=90%
Γ ₁₉₅	π^-2e^+	L	< 5.3	$\times 10^{-7}$	CL=90%
Γ ₁₉₆	$\pi^-2\mu^+$	L	< 1.4	$\times 10^{-8}$	CL=90%
Γ ₁₉₇	$\pi^-e^+\mu^+$	L	< 1.3	$\times 10^{-7}$	CL=90%
Γ ₁₉₈	$\rho^-2\mu^+$	L	< 5.6	$\times 10^{-4}$	CL=90%
Γ ₁₉₉	K^-2e^+	L	< 9	$\times 10^{-6}$	CL=90%
Γ ₂₀₀	$K^0_S \pi^-2e^+$		< 3.3	$\times 10^{-6}$	CL=90%
Γ ₂₀₁	$K^- \pi^0 2e^+$		< 8.5	$\times 10^{-6}$	CL=90%
Γ ₂₀₂	$K^-2\mu^+$	L	< 1.0	$\times 10^{-5}$	CL=90%
Γ ₂₀₃	$K^-e^+\mu^+$	L	< 1.9	$\times 10^{-6}$	CL=90%
Γ ₂₀₄	$K^*(892)^-2\mu^+$	L	< 8.5	$\times 10^{-4}$	CL=90%
Γ ₂₀₅	Λe^+	L,B	< 1.1	$\times 10^{-6}$	CL=90%
Γ ₂₀₆	$\bar{\Lambda} e^+$	L,B	< 6.5	$\times 10^{-7}$	CL=90%
Γ ₂₀₇	$\Sigma^0 e^+$	L,B	< 1.7	$\times 10^{-6}$	CL=90%
Γ ₂₀₈	$\bar{\Sigma}^0 e^+$	L,B	< 1.3	$\times 10^{-6}$	CL=90%
Γ ₂₀₉	$\bar{n} e^+$		< 1.43	$\times 10^{-5}$	CL=90%
Γ ₂₁₀	$n e^+$		< 2.91	$\times 10^{-5}$	CL=90%

[a] The branching fraction for this mode may differ from the sum of the submodes that contribute to it, due to interference effects. See the relevant papers.

[b] These subfractions of the $K^-2\pi^+$ mode are uncertain: see the Particle Listings.

[c] See the listings under " $D \rightarrow K\pi\pi\pi$ partial wave analyses" and our 2008 Review (Physics Letters **B667** 1 (2008)) for measurements of submodes of this mode.

[d] The unseen decay modes of the resonances are included.

[e] This is *not* a test for the $\Delta C=1$ weak neutral current, but leads to the $\pi^+\ell^+\ell^-$ final state.

[f] This mode is not a useful test for a $\Delta C=1$ weak neutral current because both quarks must change flavor in this decay.

FIT INFORMATION

An overall fit to 33 branching ratios uses 43 measurements to determine 17 parameters. The overall fit has a $\chi^2 = 64.4$ for 26 degrees of freedom.

The following *off-diagonal* array elements are the correlation coefficients $\langle \delta x_i \delta x_j \rangle / (\delta x_i \delta x_j)$, in percent, from the fit to the branching fractions, $x_i \equiv \Gamma_i / \Gamma_{\text{total}}$.

x_{19}	0									
x_{26}	0	0								
x_{30}	7	1	0							
x_{39}	0	0	0	0						
x_{41}	0	0	0	0	83					
x_{50}	0	5	0	1	0	0				
x_{52}	0	28	0	3	0	0	19			
x_{86}	0	5	0	1	0	0	4	19		
x_{98}	0	6	0	1	0	0	4	22	4	
x_{119}	0	5	0	0	0	0	3	17	75	4
x_{122}	0	4	0	0	0	0	3	14	3	3
x_{131}	0	5	0	1	0	0	4	19	4	4
x_{133}	0	9	0	1	0	0	29	31	6	7
x_{160}	0	1	0	0	0	0	1	5	1	1
x_{161}	0	1	0	0	0	0	2	0	0	0
x_{162}	0	2	0	0	0	0	1	6	1	1

x_{122}	2							
x_{131}	3	3						
x_{133}	5	4	6					
x_{160}	1	1	1	1				
x_{161}	0	14	0	1	0			
x_{162}	1	1	32	2	0	0		

 D^+ BRANCHING RATIOS

Some now-obsolete measurements have been omitted from these Listings.

c-quark decays

 $\Gamma(c \rightarrow e^+ \text{ anything}) / \Gamma(c \rightarrow \text{ anything})$

For the Summary Table, we only use the average of e^+ and μ^+ measurements from $Z^0 \rightarrow c\bar{c}$ decays; see the second data block below.

VALUE	EVTS	DOCUMENT ID	TECN	COMMENT
$0.103 \pm 0.009 \pm_{-0.008}^{+0.009}$	378	¹ ABBENDI	99K OPAL	$Z^0 \rightarrow c\bar{c}$

¹ABBENDI 99K uses the excess of right-sign over wrong-sign leptons opposite reconstructed $D^*(2010)^+ \rightarrow D^0\pi^+$ decays in $Z^0 \rightarrow c\bar{c}$.

 $\Gamma(c \rightarrow \mu^+ \text{ anything}) / \Gamma(c \rightarrow \text{ anything})$

For the Summary Table, we only use the average of e^+ and μ^+ measurements from $Z^0 \rightarrow c\bar{c}$ decays; see the next data block.

VALUE	EVTS	DOCUMENT ID	TECN	COMMENT
0.082 ± 0.005 OUR AVERAGE				
$0.073 \pm 0.008 \pm 0.002$	73	KAYIS-TOPAK.05	CHRS	ν_μ emulsion
$0.095 \pm 0.007 \pm_{-0.014}^{+0.013}$	2829	ASTIER	00D NOMD	$\nu_\mu \text{ Fe} \rightarrow \mu^- \mu^+ X$
$0.090 \pm 0.007 \pm_{-0.006}^{+0.007}$	476	¹ ABBENDI	99K OPAL	$Z^0 \rightarrow c\bar{c}$
$0.086 \pm 0.017 \pm_{-0.007}^{+0.008}$	69	² ALBRECHT	92F ARG	$e^+e^- \approx 10 \text{ GeV}$
$0.078 \pm 0.009 \pm 0.012$		ONG	88 MRK2	$e^+e^- 29 \text{ GeV}$
$0.078 \pm 0.015 \pm 0.02$		BARTEL	87 JADE	$e^+e^- 34.6 \text{ GeV}$
$0.082 \pm 0.012 \pm_{-0.01}^{+0.02}$		ALTHOFF	84G TASS	$e^+e^- 34.5 \text{ GeV}$
• • • We do not use the following data for averages, fits, limits, etc. • • •				
$0.093 \pm 0.009 \pm 0.009$	88	KAYIS-TOPAK.02	CHRS	See KAYIS-TOPAKSU 05
$0.089 \pm 0.018 \pm 0.025$		BARTEL	85J JADE	See BARTEL 87

¹ABBENDI 99K uses the excess of right-sign over wrong-sign leptons opposite reconstructed $D^*(2010)^+ \rightarrow D^0\pi^+$ decays in $Z^0 \rightarrow c\bar{c}$.

²ALBRECHT 92F uses the excess of right-sign over wrong-sign leptons in a sample of events tagged by fully reconstructed $D^*(2010)^+ \rightarrow D^0\pi^+$ decays.

 $\Gamma(c \rightarrow \ell^+ \text{ anything}) / \Gamma(c \rightarrow \text{ anything})$

This is an average (not a sum) of e^+ and μ^+ measurements.

VALUE	EVTS	DOCUMENT ID	TECN	COMMENT
0.096 ± 0.004 OUR AVERAGE				
$0.0958 \pm 0.0042 \pm 0.0028$	1828	¹ ABREU	00o DLPH	$Z^0 \rightarrow c\bar{c}$
$0.095 \pm 0.006 \pm_{-0.006}^{+0.007}$	854	² ABBENDI	99K OPAL	$Z^0 \rightarrow c\bar{c}$

¹ABREU 00o uses leptons opposite fully reconstructed $D^*(2010)^+, D^+, \text{ or } D^0$ mesons.

²ABBENDI 99K uses the excess of right-sign over wrong-sign leptons opposite reconstructed $D^*(2010)^+ \rightarrow D^0\pi^+$ decays in $Z^0 \rightarrow c\bar{c}$.

 $\Gamma(c \rightarrow D^*(2010)^+ \text{ anything}) / \Gamma(c \rightarrow \text{ anything})$

VALUE	EVTS	DOCUMENT ID	TECN	COMMENT
$0.255 \pm 0.015 \pm 0.008$	2371	¹ ABREU	00o DLPH	$Z^0 \rightarrow c\bar{c}$

¹ABREU 00o uses slow pions opposite fully reconstructed $D^*(2010)^+, D^+, \text{ or } D^0$ mesons as a signal of $D^*(2010)^-$ production.

Inclusive modes

 $\Gamma(e^+ \text{ semileptonic}) / \Gamma_{\text{total}}$

The sum of our $\bar{K}^0 e^+ \nu_e, \bar{K}^*(892)^0 e^+ \nu_e, \pi^0 e^+ \nu_e, \eta e^+ \nu_e, \rho^0 e^+ \nu_e,$ and $\omega e^+ \nu_e$ branching fractions is $15.3 \pm 0.3\%$.

VALUE (%)	EVTS	DOCUMENT ID	TECN	COMMENT
$16.13 \pm 0.10 \pm 0.29$	$26.2 \pm 0.2k$	¹ ASNER	10 CLEO	e^+e^- at 3774 MeV
$15.2 \pm 0.9 \pm 0.8$	521 ± 32	ABLICKIM	07G BES2	$e^+e^- \approx \psi(3770)$
$16.13 \pm 0.20 \pm 0.33$	8798 ± 105	² ADAM	06A CLEO	See ASNER 10
$17.0 \pm 1.9 \pm 0.7$	158	BALTRUSAIT...85B	MRK3	$e^+e^- 3.77 \text{ GeV}$

• • • We do not use the following data for averages, fits, limits, etc. • • •

¹Using the D^+ and D^0 lifetimes, ASNER 10 finds that the ratio of the D^+ and D^0 semileptonic widths is $0.985 \pm 0.015 \pm 0.024$.

²Using the D^+ and D^0 lifetimes, ADAM 06A finds that the ratio of the D^+ and D^0 inclusive e^+ widths is $0.985 \pm 0.028 \pm 0.015$, consistent with the isospin-invariance prediction of 1.

Γ(μ+ anything)/Γtotal Γ2/Γ

Table with columns: VALUE (%), EVTS, DOCUMENT ID, TECN, COMMENT. Row 1: 17.6±2.7±1.8, 100±12, 1 ABLIKIM 08L BES2 e+e- ≈ ψ(3772)

1 ABLIKIM 08L finds the ratio of D+ → μ+ X and D0 → μ+ X branching fractions to be 2.59 ± 0.70 ± 0.25, in accord with the ratio of D+ and D0 lifetimes, 2.54 ± 0.02.

Γ(K- anything)/Γtotal Γ3/Γ

Table with columns: VALUE (%), EVTS, DOCUMENT ID, TECN, COMMENT. Row 1: 25.7±1.4 OUR AVERAGE

Table with columns: VALUE (%), EVTS, DOCUMENT ID, TECN, COMMENT. Row 1: 24.7±1.3±1.2, 631±33, ABLIKIM 07G BES2 e+e- ≈ ψ(3770)

Γ(K0 anything)/Γtotal Γ4/Γ

Table with columns: VALUE (%), EVTS, DOCUMENT ID, TECN, COMMENT. Row 1: 33.11±0.13±0.36, 95k, ABLIKIM 23A0 BES3 e+e- at 3.773 GeV

• • • We do not use the following data for averages, fits, limits, etc. • • •

Table with columns: VALUE (%), EVTS, DOCUMENT ID, TECN, COMMENT. Row 1: 30.25±2.75±1.65, 244, 1 ABLIKIM 06U BES2 e+e- at 3773 MeV

1 ABLIKIM 06U reports B(D0 → K0 X or K0 X) = (60.5 ± 5.5 ± 3.3) × 10−2 which we take as twice the branching fraction for D+ → K0 X.

2 COFFMAN 91 reports B(D+ → K0 X or K0 X) = (61.2 ± 6.5 ± 4.3) × 10−2 which we take as twice the branching fraction for D+ → K0 X.

Γ(K+ anything)/Γtotal Γ5/Γ

Table with columns: VALUE (%), EVTS, DOCUMENT ID, TECN, COMMENT. Row 1: 5.9±0.8 OUR AVERAGE

Table with columns: VALUE (%), EVTS, DOCUMENT ID, TECN, COMMENT. Row 1: 6.1±0.9±0.4, 189±27, ABLIKIM 07G BES2 e+e- ≈ ψ(3770)

Γ(K*(892)- anything)/Γtotal Γ6/Γ

Table with columns: VALUE (%), EVTS, DOCUMENT ID, TECN, COMMENT. Row 1: 5.7±5.2±0.7, 7.2±6.5, ABLIKIM 06U BES2 e+e- at 3773 MeV

Γ(K*(892)0 anything)/Γtotal Γ7/Γ

Table with columns: VALUE (%), EVTS, DOCUMENT ID, TECN, COMMENT. Row 1: 23.2±4.5±3.0, 189±36, ABLIKIM 05P BES e+e- ≈ 3773 MeV

Γ(K*(892)0 anything)/Γtotal Γ8/Γ

Table with columns: VALUE (%), CL%, DOCUMENT ID, TECN, COMMENT. Row 1: <6.6, 90, ABLIKIM 05P BES e+e- ≈ 3773 MeV

Γ(η anything)/Γtotal Γ9/Γ

This ratio includes η particles from η' decays.

Table with columns: VALUE (%), EVTS, DOCUMENT ID, TECN, COMMENT. Row 1: 6.3±0.5±0.5, 1972±142, HUANG 06B CLEO e+e- at ψ(3770)

Γ(η' anything)/Γtotal Γ10/Γ

Table with columns: VALUE (%), EVTS, DOCUMENT ID, TECN, COMMENT. Row 1: 1.04±0.16±0.09, 82±13, HUANG 06B CLEO e+e- at ψ(3770)

Γ(φ anything)/Γtotal Γ11/Γ

Table with columns: VALUE (%), EVTS, DOCUMENT ID, TECN, COMMENT. Row 1: 1.12 ± 0.04 OUR AVERAGE

Table with columns: VALUE (%), EVTS, DOCUMENT ID, TECN, COMMENT. Row 1: 1.135±0.034±0.031, 2.7k, ABLIKIM 19AY BES3 e+e- at 3773 MeV

Γ(π+ π+ π- anything)/Γtotal Γ12/Γ

Table with columns: VALUE (%), EVTS, DOCUMENT ID, TECN, COMMENT. Row 1: 15.25±0.09±0.18, 124k, ABLIKIM 23A1 BES3 2.93 fb−1, e+e- at ψ(3770)

Leptonic and semileptonic modes

Γ(e+ νe)/Γtotal Γ13/Γ

Table with columns: VALUE, CL%, DOCUMENT ID, TECN, COMMENT. Row 1: <8.8 × 10−6, 90, EISENSTEIN 08 CLEO e+e- at ψ(3770)

Table with columns: VALUE, CL%, DOCUMENT ID, TECN, COMMENT. Row 1: <2.4 × 10−5, 90, ARTUSO 05A CLEO See EISENSTEIN 08

Γ(γ e+ νe)/Γtotal Γ14/Γ

Table with columns: VALUE, CL%, DOCUMENT ID, TECN, COMMENT. Row 1: <3.0 × 10−5, 90, 1 ABLIKIM 17M BES3 e+e- at 3.773 GeV

1 This ABLIKIM 17M limit is for photons with energies greater than 10 MeV.

Γ(μ+ νμ)/Γtotal Γ15/Γ

See the note on "Decay Constants of Charged Pseudoscalar Mesons" in the D± Listings.

Table with columns: VALUE (units 10−4), EVTS, DOCUMENT ID, TECN, COMMENT. Row 1: 3.74±0.17 OUR AVERAGE

Table with columns: VALUE, EVTS, DOCUMENT ID, TECN, COMMENT. Row 1: 3.71±0.19±0.06, 409±21, 1 ABLIKIM 14F BES3 e+e- at ψ(3770)

Table with columns: VALUE, EVTS, DOCUMENT ID, TECN, COMMENT. Row 1: 3.82±0.32±0.09, 150±12, 2 EISENSTEIN 08 CLEO e+e- at ψ(3770)

• • • We do not use the following data for averages, fits, limits, etc. • • •

Table with columns: VALUE, EVTS, DOCUMENT ID, TECN, COMMENT. Row 1: 12.2 +11.1−5.3 ±1.0, 3, 3 ABLIKIM 05D BES e+e- ≈ 3.773 GeV

Table with columns: VALUE, EVTS, DOCUMENT ID, TECN, COMMENT. Row 1: 4.40±0.66±0.09, 47±7, 4 ARTUSO 05A CLEO See EISENSTEIN 08

Table with columns: VALUE, EVTS, DOCUMENT ID, TECN, COMMENT. Row 1: 3.5 ± 1.4 ± 0.6, 7, 5 BONVICINI 04A CLEO Incl. in ARTUSO 05A

Table with columns: VALUE, EVTS, DOCUMENT ID, TECN, COMMENT. Row 1: 8 +16−5 +5−2, 1, 6 BAI 98B BES e+e- → D*+ D−

1 ABLIKIM 14F obtain |Vcd| · fD+ = (45.75 ± 1.20 ± 0.39) MeV, and using |Vcd| = 0.22520 ± 0.00065 gets fD+ = (203.2 ± 5.3 ± 1.8) MeV.

2 EISENSTEIN 08, using the D+ lifetime and assuming |Vcd| = |Vus|, gets fD+ = (205.8 ± 8.5 ± 2.5) MeV from this measurement.

3 ABLIKIM 05D finds a background-subtracted 2.67 ± 1.74 D+ → μ+ νμ events, and from this obtains fD+ = 371 +129−119 ± 25 MeV.

4 ARTUSO 05A obtains fD+ = 222.6 ± 16.7 +2.8−3.4 MeV from this measurement.

5 BONVICINI 04A finds eight events with an estimated background of one, and from the branching fraction obtains fD+ = 202 ± 41 ± 17 MeV.

6 BAI 98B obtains fD+ = (300 +180+80−150−40) MeV from this measurement.

Γ(τ+ ντ)/Γtotal Γ16/Γ

Table with columns: VALUE (units 10−3), CL%, EVTS, DOCUMENT ID, TECN, COMMENT. Row 1: 1.20±0.24±0.12, 137, 1 ABLIKIM 19BG BES3 e+e- at 3773 MeV

• • • We do not use the following data for averages, fits, limits, etc. • • •

Table with columns: VALUE, EVTS, DOCUMENT ID, TECN, COMMENT. Row 1: <1.2, 90, EISENSTEIN 08 CLEO e+e- at ψ(3770)

Table with columns: VALUE, EVTS, DOCUMENT ID, TECN, COMMENT. Row 1: <2.1, 90, RUBIN 06A CLEO See EISENSTEIN 08

1 ABLIKIM 19BG observe this mode with a significance of 5.1 σ.

Γ(K0 e+ νe)/Γtotal Γ17/Γ

Table with columns: VALUE (%), EVTS, DOCUMENT ID, TECN, COMMENT. Row 1: 8.72 ± 0.09 OUR AVERAGE

Table with columns: VALUE, EVTS, DOCUMENT ID, TECN, COMMENT. Row 1: 8.68 ± 0.14 ± 0.16, 1172, ABLIKIM 21BA BES3 e+e- at 3.773 GeV

Table with columns: VALUE, EVTS, DOCUMENT ID, TECN, COMMENT. Row 1: 8.60 ± 0.06 ± 0.15, 26k, ABLIKIM 17S BES3 Using K0 → π+ π−

Table with columns: VALUE, EVTS, DOCUMENT ID, TECN, COMMENT. Row 1: 8.59 ± 0.14 ± 0.21, 5013, ABLIKIM 16V BES3 Using K0 → 2π0

Table with columns: VALUE, EVTS, DOCUMENT ID, TECN, COMMENT. Row 1: 8.962±0.054±0.206, 40k, 1 ABLIKIM 15AF BES3 from D+ → KL e+ νe

Table with columns: VALUE, EVTS, DOCUMENT ID, TECN, COMMENT. Row 1: 8.83 ± 0.10 ± 0.20, 8.5k, 2 BESSON 09 CLEO from D+ → KS e+ νe

Table with columns: VALUE, EVTS, DOCUMENT ID, TECN, COMMENT. Row 1: 8.95 ± 1.59 ± 0.67, 34, 3 ABLIKIM 05A BES from D+ → KS e+ νe

• • • We do not use the following data for averages, fits, limits, etc. • • •

Table with columns: VALUE, EVTS, DOCUMENT ID, TECN, COMMENT. Row 1: 8.53 ± 0.13 ± 0.23, 4 DOBBS 08 CLEO See BESSON 09

Table with columns: VALUE, EVTS, DOCUMENT ID, TECN, COMMENT. Row 1: 8.71 ± 0.38 ± 0.37, 545, HUANG 05B CLEO See DOBBS 08

1 ABLIKIM 15AF report Γ(D+ → KL e+ νe)/Γtotal = (4.481 ± 0.027 ± 0.103)%. See also the form-factor parameters near the end of this D+ Listing.

2 See the form-factor parameters near the end of this D+ Listing.

3 The ABLIKIM 05A result together with the D0 → K− e+ νe branching fraction of ABLIKIM 04C and Particle Data Group lifetimes gives Γ(D0 → K− e+ νe) / Γ(D+ → K0 e+ νe) = 1.08 ± 0.22 ± 0.07; isospin invariance predicts the ratio is 1.0.

4 DOBBS 08 establishes |Vcd / Vcs · fK(0) / fK(0)| = 0.188 ± 0.008 ± 0.002 from the D+ and D0

decays to K e+ νe and π e+ νe. It also finds Γ(D0 → K− e+ νe) / Γ(D+ → K0 e+ νe) = 1.06 ± 0.02 ± 0.03; isospin invariance predicts the ratio is 1.0.

Γ(K0 μ+ νμ)/Γtotal Γ18/Γ

Table with columns: VALUE (units 10−2), EVTS, DOCUMENT ID, TECN, COMMENT. Row 1: 8.76±0.19 OUR FIT

Table with columns: VALUE, EVTS, DOCUMENT ID, TECN, COMMENT. Row 1: 8.72±0.07±0.18, 21k, ABLIKIM 16G BES3 e+e- at 3773 MeV

Table with columns: VALUE, EVTS, DOCUMENT ID, TECN, COMMENT. Row 1: 10.3 ± 2.3 ± 0.8, 29 ± 6, ABLIKIM 07 BES2 e+e- at 3773 MeV

Γ(K0 μ+ νμ)/Γ(K− 2π+)

Table with columns: VALUE, EVTS, DOCUMENT ID, TECN, COMMENT. Row 1: 0.934±0.025 OUR FIT Error includes scale factor of 1.2.

Table with columns: VALUE, EVTS, DOCUMENT ID, TECN, COMMENT. Row 1: 1.019±0.076±0.065, 555 ± 39, LINK 04E FOCS γ nucleus, Eγ ≈ 180 GeV

Γ(K− π+ e+ νe)/Γtotal Γ19/Γ

Table with columns: VALUE (units 10−2), EVTS, DOCUMENT ID, TECN, COMMENT. Row 1: 4.02±0.18 OUR FIT Error includes scale factor of 3.2.

Table with columns: VALUE, EVTS, DOCUMENT ID, TECN, COMMENT. Row 1: 3.77±0.03±0.08, 18.3k, ABLIKIM 16F BES3 e+e- at ψ(3770)

Table with columns: VALUE, EVTS, DOCUMENT ID, TECN, COMMENT. Row 1: 3.50±0.75±0.27, 29, ABLIKIM 06G BES2 e+e- at 3773 MeV

Table with columns: VALUE, EVTS, DOCUMENT ID, TECN, COMMENT. Row 1: 3.5 +1.2−0.7 ± 0.4, 14, BAI 91 MRK3 e+e- ≈ 3.77 GeV

Γ(K− π+ e+ νe)/Γ(K− 2π+)

Table with columns: VALUE, EVTS, DOCUMENT ID, TECN, COMMENT. Row 1: 0.428 ± 0.018 OUR FIT Error includes scale factor of 3.7.

Table with columns: VALUE, EVTS, DOCUMENT ID, TECN, COMMENT. Row 1: 0.4380±0.0036±0.0042, 70k±363, DEL-AMO-SA..111 BABR e+e- ≈ 10.6 GeV

Γ(K*(892)0 e+ νe, K*(892)0 → K− π+)/Γ(K− π+ e+ νe)

Table with columns: VALUE (%), DOCUMENT ID, TECN, COMMENT. Row 1: 93.93±0.27 OUR AVERAGE

Table with columns: VALUE, EVTS, DOCUMENT ID, TECN, COMMENT. Row 1: 93.93±0.22±0.18, ABLIKIM 16F BES3 e+e- at ψ(3770)

Table with columns: VALUE, EVTS, DOCUMENT ID, TECN, COMMENT. Row 1: 94.11±0.74±0.75, DEL-AMO-SA..111 BABR e+e- ≈ 10.6 GeV

Meson Particle Listings

 D^\pm $\Gamma((K^- \pi^+) [0.8-1.0] \text{GeV } e^+ \nu_e) / \Gamma_{\text{total}}$ Γ_{21} / Γ

VALUE (units 10^{-2})	EVTS	DOCUMENT ID	TECN	COMMENT
3.39 ± 0.03 ± 0.08	16.2k	ABLIKIM	16F BES3	$e^+ e^-$ at $\psi(3770)$

 $\Gamma((K^- \pi^+)_{S\text{-wave}} e^+ \nu_e) / \Gamma_{\text{total}}$ Γ_{22} / Γ

VALUE (units 10^{-3})	DOCUMENT ID	TECN	COMMENT
2.28 ± 0.08 ± 0.08	ABLIKIM 16F BES3		$e^+ e^-$ at $\psi(3770)$

 $\Gamma((K^- \pi^+)_{S\text{-wave}} e^+ \nu_e) / \Gamma(K^- \pi^+ e^+ \nu_e)$ $\Gamma_{22} / \Gamma_{19}$

VALUE (%)	DOCUMENT ID	TECN	COMMENT
5.89 ± 0.17 OUR AVERAGE			
6.05 ± 0.22 ± 0.18	ABLIKIM 16F BES3		$e^+ e^-$ at $\psi(3770)$
5.79 ± 0.16 ± 0.15	DEL-AMO-SA...11i BABR		$e^+ e^- \approx 10.6$ GeV

 $\Gamma(\bar{K}^*(1410)^0 e^+ \nu_e, \bar{K}^*(1410)^0 \rightarrow K^- \pi^+) / \Gamma_{\text{total}}$ Γ_{23} / Γ

VALUE	CL%	DOCUMENT ID	TECN	COMMENT
< 6 × 10⁻³	90	DEL-AMO-SA...11i BABR		$e^+ e^- \approx 10.6$ GeV

 $\Gamma(\bar{K}_2^*(1430)^0 e^+ \nu_e, \bar{K}_2^*(1430)^0 \rightarrow K^- \pi^+) / \Gamma_{\text{total}}$ Γ_{24} / Γ

VALUE	CL%	DOCUMENT ID	TECN	COMMENT
< 5 × 10⁻⁴	90	DEL-AMO-SA...11i BABR		$e^+ e^- \approx 10.6$ GeV

 $\Gamma(K^- \pi^+ e^+ \nu_e \text{ nonresonant}) / \Gamma_{\text{total}}$ Γ_{25} / Γ

VALUE	CL%	DOCUMENT ID	TECN	COMMENT
< 0.007	90	ANJOS 89B E691		Photoproduction

 $\Gamma(\bar{K}^*(892)^0 e^+ \nu_e) / \Gamma_{\text{total}}$ Γ_{26} / Γ

Unseen decay modes of $\bar{K}^*(892)^0$ are included. See the end of the D^+ Listings for measurements of $D^+ \rightarrow \bar{K}^*(892)^0 \ell^+ \nu_\ell$ form-factor ratios.

VALUE (units 10^{-2})	EVTS	DOCUMENT ID	TECN	COMMENT
5.40 ± 0.10 OUR FIT				Error includes scale factor of 1.1.
5.40 ± 0.10 OUR AVERAGE				Error includes scale factor of 1.1.
5.31 ± 0.05 ± 0.12	16.2k	ABLIKIM 16F BES3		$e^+ e^-$ at $\psi(3770)$
5.52 ± 0.07 ± 0.13	≈ 5k	BRIERE 10 CLEO		$e^+ e^-$ at $\psi(3770)$
• • • We do not use the following data for averages, fits, limits, etc. • • •				
5.06 ± 1.21 ± 0.40	28 ± 7	ABLIKIM 06o BES2		$e^+ e^-$ at 3773 MeV
5.56 ± 0.27 ± 0.23	422 ± 21	¹ HUANG 05B CLEO		$e^+ e^-$ at $\psi(3770)$
¹ HUANG 05B finds $\Gamma(D^0 \rightarrow K^{*0} e^+ \nu_e) / \Gamma(D^+ \rightarrow \bar{K}^{*0} e^+ \nu_e) = 0.98 \pm 0.08 \pm 0.04$; isospin invariance predicts the ratio is 1.0.				

 $\Gamma(\bar{K}^*(892)^0 e^+ \nu_e) / \Gamma(K^- 2\pi^+)$ $\Gamma_{26} / \Gamma_{52}$

Unseen decay modes of the $\bar{K}^*(892)^0$ are included. See the end of the D^+ Listings for measurements of $D^+ \rightarrow \bar{K}^*(892)^0 \ell^+ \nu_\ell$ form-factor ratios.

VALUE	EVTS	DOCUMENT ID	TECN	COMMENT
• • • We do not use the following data for averages, fits, limits, etc. • • •				
0.74 ± 0.04 ± 0.05		BRANDENB... 02 CLEO		$e^+ e^- \approx \gamma(4S)$
0.62 ± 0.15 ± 0.09	35	ADAMOVICH 91 OMEG		$\pi^- 340$ GeV
0.55 ± 0.08 ± 0.10	880	ALBRECHT 91 ARG		$e^+ e^- \approx 10.4$ GeV
0.49 ± 0.04 ± 0.05		ANJOS 89B E691		Photoproduction

 $\Gamma(K^- \pi^+ \mu^+ \nu_\mu) / \Gamma(\bar{K}^0 \mu^+ \nu_\mu)$ $\Gamma_{27} / \Gamma_{18}$

VALUE	EVTS	DOCUMENT ID	TECN	COMMENT
0.417 ± 0.030 ± 0.023	555 ± 39	LINK 04E FOCS		γ nucleus, $\bar{E}_\gamma \approx 180$ GeV

 $\Gamma(K^- \pi^+ \mu^+ \nu_\mu \text{ nonresonant}) / \Gamma(K^- \pi^+ \mu^+ \nu_\mu)$ $\Gamma_{29} / \Gamma_{27}$

VALUE	EVTS	DOCUMENT ID	TECN	COMMENT
0.0530 ± 0.0074 ± 0.0099 ± 0.0096	14k	LINK 05i FOCS		γ nucleus, $\bar{E}_\gamma \approx 180$ GeV

 $\Gamma(\bar{K}^*(892)^0 \mu^+ \nu_\mu) / \Gamma_{\text{total}}$ Γ_{30} / Γ

Unseen decay modes of the $\bar{K}^*(892)^0$ are included. See the end of the D^+ Listings for measurements of $D^+ \rightarrow \bar{K}^*(892)^0 \ell^+ \nu_\ell$ form-factor ratios.

VALUE (units 10^{-2})	EVTS	DOCUMENT ID	TECN	COMMENT
5.27 ± 0.15 OUR FIT				Error includes scale factor of 1.1.
5.27 ± 0.15 OUR AVERAGE				Error includes scale factor of 1.1.
5.27 ± 0.07 ± 0.14	≈ 5k	BRIERE 10 CLEO		$e^+ e^-$ at $\psi(3770)$

 $\Gamma(\bar{K}^*(892)^0 \mu^+ \nu_\mu) / \Gamma(\bar{K}^0 \mu^+ \nu_\mu)$ $\Gamma_{30} / \Gamma_{18}$

Unseen decay modes of the $\bar{K}^*(892)^0$ are included. See the end of the D^+ Listings for measurements of $D^+ \rightarrow \bar{K}^*(892)^0 \ell^+ \nu_\ell$ form-factor ratios.

VALUE	EVTS	DOCUMENT ID	TECN	COMMENT
0.602 ± 0.020 OUR FIT				Error includes scale factor of 1.1.
0.594 ± 0.043 ± 0.033	555 ± 39	LINK 04E FOCS		γ nucleus, $\bar{E}_\gamma \approx 180$ GeV

 $\Gamma(\bar{K}^*(892)^0 \mu^+ \nu_\mu) / \Gamma(K^- 2\pi^+)$ $\Gamma_{30} / \Gamma_{52}$

Unseen decay modes of the $\bar{K}^*(892)^0$ are included. See the end of the D^+ Listings for measurements of $D^+ \rightarrow \bar{K}^*(892)^0 \ell^+ \nu_\ell$ form-factor ratios.

VALUE	EVTS	DOCUMENT ID	TECN	COMMENT
0.57 ± 0.06 OUR FIT				Error includes scale factor of 1.2.
0.57 ± 0.06 OUR AVERAGE				Error includes scale factor of 1.2.

VALUE	CL%	DOCUMENT ID	TECN	COMMENT
0.72 ± 0.10 ± 0.05		BRANDENB... 02 CLEO		$e^+ e^- \approx \gamma(4S)$
0.56 ± 0.04 ± 0.06	875	FRABETTI 93E E687		γ Be $\bar{E}_\gamma \approx 200$ GeV
0.46 ± 0.07 ± 0.08	224	KODAMA 92C E653		π^- emulsion 600 GeV
• • • We do not use the following data for averages, fits, limits, etc. • • •				
0.602 ± 0.010 ± 0.021	12k	¹ LINK 02j FOCS		γ nucleus, ≈ 180 GeV
¹ This LINK 02j result includes the effects of an interference of a small S-wave $K^- \pi^+$ amplitude with the dominant \bar{K}^{*0} amplitude. (The interference effect is reported in LINK 02E.) This result is redundant with results of LINK 04E elsewhere in these Listings.				

 $\Gamma(K^- \pi^+ \pi^0 \mu^+ \nu_\mu) / \Gamma(K^- \pi^+ \mu^+ \nu_\mu)$ $\Gamma_{31} / \Gamma_{27}$

VALUE	CL%	DOCUMENT ID	TECN	COMMENT
< 0.042	90	FRABETTI 93E E687		γ Be $\bar{E}_\gamma \approx 200$ GeV

 $\Gamma(\bar{K}_1^*(1270)^0 e^+ \nu_e, \bar{K}_1^*(1270)^0 \rightarrow K^- \pi^+ \pi^0) / \Gamma_{\text{total}}$ Γ_{32} / Γ

VALUE (units 10^{-3})	EVTS	DOCUMENT ID	TECN	COMMENT
1.06 ± 0.12 ± 0.08 ± 0.10	120	¹ ABLIKIM 19BH BES3		$e^+ e^-$ at 3773 MeV
¹ ABLIKIM 19BH quotes $B(D^+ \rightarrow \bar{K}_1^*(1270)^0 e^+ \nu_e) = (2.30 \pm 0.26 \pm 0.18 \pm 0.25) \times 10^{-3}$, where the last uncertainty is due to $B(\bar{K}_1^*(1270)^0 \rightarrow K^- \pi^+ \pi^0) = 0.467 \pm 0.050$.				

 $\Gamma(\bar{K}_0^*(1430)^0 \mu^+ \nu_\mu) / \Gamma(K^- \pi^+ \mu^+ \nu_\mu)$ $\Gamma_{33} / \Gamma_{27}$

VALUE	CL%	DOCUMENT ID	TECN	COMMENT
< 0.0064	90	LINK 05i FOCS		γ A, $\bar{E}_\gamma \approx 180$ GeV

 $\Gamma(\bar{K}^*(1680)^0 \mu^+ \nu_\mu) / \Gamma(K^- \pi^+ \mu^+ \nu_\mu)$ $\Gamma_{34} / \Gamma_{27}$

VALUE	CL%	DOCUMENT ID	TECN	COMMENT
< 0.04	90	LINK 05i FOCS		γ A, $\bar{E}_\gamma \approx 180$ GeV

 $\Gamma(\pi^0 e^+ \nu_e) / \Gamma_{\text{total}}$ Γ_{35} / Γ

VALUE (%)	EVTS	DOCUMENT ID	TECN	COMMENT
0.372 ± 0.017 OUR AVERAGE				Error includes scale factor of 2.0.
0.363 ± 0.008 ± 0.005	3.4k	ABLIKIM 17s BES3		Using $\pi^0 \rightarrow 2\gamma$
0.405 ± 0.016 ± 0.009	838	¹ BESSON 09 CLEO		$e^+ e^-$ at $\psi(3770)$
• • • We do not use the following data for averages, fits, limits, etc. • • •				
0.373 ± 0.022 ± 0.013		² DOBBS 08 CLEO		See BESSON 09
0.44 ± 0.06 ± 0.03	63 ± 9	HUANG 05B CLEO		See DOBBS 08
¹ See the form-factor parameters near the end of this D^+ Listing.				
² DOBBS 08 establishes $ \frac{V_{cs} d}{V_{cs} s} \cdot \frac{f_\pi(0)}{f_{K^*}(0)} = 0.188 \pm 0.008 \pm 0.002$ from the D^+ and D^0 decays to $\bar{K} e^+ \nu_e$ and $\pi e^+ \nu_e$. It finds $\Gamma(D^0 \rightarrow \pi^- e^+ \nu_e) / \Gamma(D^+ \rightarrow \pi^0 e^+ \nu_e) = 2.03 \pm 0.14 \pm 0.08$; isospin invariance predicts the ratio is 2.0.				

 $\Gamma(\pi^0 \mu^+ \nu_\mu) / \Gamma_{\text{total}}$ Γ_{36} / Γ

VALUE (%)	EVTS	DOCUMENT ID	TECN	COMMENT
0.350 ± 0.011 ± 0.010	1.3k	ABLIKIM 18Ae BES3		$e^+ e^-$, 3773 MeV

 $\Gamma(\eta e^+ \nu_e) / \Gamma_{\text{total}}$ Γ_{37} / Γ

VALUE (units 10^{-4})	EVTS	DOCUMENT ID	TECN	COMMENT
11.1 ± 0.7 OUR AVERAGE				
10.74 ± 0.81 ± 0.51	373	ABLIKIM 18R BES3		$e^+ e^-$, 3773 MeV
11.4 ± 0.9 ± 0.4		YELTON 11 CLEO		$e^+ e^-$ at $\psi(3770)$
• • • We do not use the following data for averages, fits, limits, etc. • • •				
13.3 ± 2.0 ± 0.6	46	MITCHELL 09B CLEO		See YELTON 11

 $\Gamma(\eta \mu^+ \nu_\mu) / \Gamma_{\text{total}}$ Γ_{38} / Γ

VALUE (units 10^{-4})	EVTS	DOCUMENT ID	TECN	COMMENT
10.41 ± 1.12 ± 0.05	234	¹ ABLIKIM 20T BES3		$e^+ e^-$, 3773 MeV
¹ ABLIKIM 20T reports $(10.4 \pm 1.0 \pm 0.5) \times 10^{-4}$ from a measurement of $[\Gamma(D^+ \rightarrow \eta \mu^+ \nu_\mu) / \Gamma_{\text{total}}] \times [B(\eta \rightarrow 2\gamma)]$ assuming $B(\eta \rightarrow 2\gamma) = (39.41 \pm 0.20) \times 10^{-2}$, which we rescale to our best value $B(\eta \rightarrow 2\gamma) = (39.36 \pm 0.18) \times 10^{-2}$. Our first error is their experiment's error and our second error is the systematic error from using our best value.				

 $\Gamma(\pi^- \pi^+ e^+ \nu_e) / \Gamma_{\text{total}}$ Γ_{39} / Γ

VALUE (units 10^{-3})	EVTS	DOCUMENT ID	TECN	COMMENT
2.49 ± 0.11 OUR FIT				Error includes scale factor of 1.2.
2.449 ± 0.074 ± 0.073	1.7k	ABLIKIM 19C BES3		$e^+ e^-$ at 3773 MeV

 $\Gamma(\rho(500)^0 e^+ \nu_e, \rho(500)^0 \rightarrow \pi^+ \pi^-) / \Gamma(\pi^- \pi^+ e^+ \nu_e)$ $\Gamma_{40} / \Gamma_{39}$

VALUE (units 10^{-2})	EVTS	DOCUMENT ID	TECN	COMMENT
25.7 ± 1.6 ± 1.1	1.5k	ABLIKIM 19C BES3		$\pi^- \pi^+ e^+ \nu_e$ events

 $\Gamma(\rho^0 e^+ \nu_e) / \Gamma_{\text{total}}$ Γ_{41} / Γ

VALUE (units 10^{-3})	EVTS	DOCUMENT ID	TECN	COMMENT
1.90 ± 0.10 OUR FIT				Error includes scale factor of 1.2.
2.17 ± 0.12 ± 0.12	447 ± 25	¹ DOBBS 13 CLEO		$e^+ e^-$ at $\psi(3770)$

• • • We do not use the following data for averages, fits, limits, etc. • • •

2.1 ± 0.4 ± 0.1 27 ± 6 ²HUANG 05B CLEO See DOBBS 13
¹ DOBBS 13 finds $\Gamma(D^0 \rightarrow \rho^- e^+ \nu_e) / 2 \Gamma(D^+ \rightarrow \rho^0 e^+ \nu_e) = 1.03 \pm 0.09^{+0.08}_{-0.02}$,
 isospin invariance predicts the ratio is 1.0.
² HUANG 05B finds $\Gamma(D^0 \rightarrow \rho^- e^+ \nu_e) / 2 \Gamma(D^+ \rightarrow \rho^0 e^+ \nu_e) = 1.2^{+0.4}_{-0.3} \pm 0.1$;
 isospin invariance predicts the ratio is 1.0.

$\Gamma(\rho^0 e^+ \nu_e) / \Gamma(\pi^- \pi^+ e^+ \nu_e)$ $\Gamma_{41} / \Gamma_{39}$

VALUE (units 10^{-2})	EVTS	DOCUMENT ID	TECN	COMMENT
76.5 ± 2.3 OUR FIT				Error includes scale factor of 1.2.
76.0 ± 1.7 ± 1.1	1.5k	ABLIKIM 19C	BES3	$\pi^- \pi^+ e^+ \nu_e$ events

$\Gamma(\rho^0 e^+ \nu_e) / \Gamma(\bar{K}^*(892)^0 e^+ \nu_e)$ $\Gamma_{41} / \Gamma_{26}$

VALUE	EVTS	DOCUMENT ID	TECN	COMMENT
0.0353 ± 0.0020 OUR FIT				Error includes scale factor of 1.1.
0.045 ± 0.014 ± 0.009	49	¹ AITALA	97 E791	π^- nucleus, 500 GeV

¹ AITALA 97 explicitly subtracts $D^+ \rightarrow \eta' e^+ \nu_e$ and other backgrounds to get this result.

$\Gamma(\rho^0 \mu^+ \nu_\mu) / \Gamma(\bar{K}^*(892)^0 \mu^+ \nu_\mu)$ $\Gamma_{42} / \Gamma_{30}$

VALUE	EVTS	DOCUMENT ID	TECN	COMMENT
0.045 ± 0.007 OUR AVERAGE				Error includes scale factor of 1.1.
0.041 ± 0.006 ± 0.004	320 ± 44	LINK	06B FOCS	γA , $\bar{E}_\gamma \approx 180$ GeV
0.051 ± 0.015 ± 0.009	54	¹ AITALA	97 E791	π^- nucleus, 500 GeV
0.079 ± 0.019 ± 0.013	39	² FRABETTI	97 E687	γBe , $\bar{E}_\gamma \approx 220$ GeV

¹ AITALA 97 explicitly subtracts $D^+ \rightarrow \eta' \mu^+ \nu_\mu$ and other backgrounds to get this result.
² Because the reconstruction efficiency for photons is low, this FRABETTI 97 result also includes any $D^+ \rightarrow \eta' \mu^+ \nu_\mu \rightarrow \gamma \rho^0 \mu^+ \nu_\mu$ events in the numerator.

$\Gamma(\omega e^+ \nu_e) / \Gamma_{total}$ Γ_{43} / Γ

VALUE (units 10^{-3})	EVTS	DOCUMENT ID	TECN	COMMENT
1.69 ± 0.11 OUR AVERAGE				
1.63 ± 0.11 ± 0.08	491 ± 32	ABLIKIM 15W	BES3	292 fb ⁻¹ , 3773 MeV
1.82 ± 0.18 ± 0.07	129 ± 13	DOBBS 13	CLEO	$e^+ e^-$ at $\psi(3770)$

• • • We do not use the following data for averages, fits, limits, etc. • • •

1.6	$^{+0.7}_{-0.6} \pm 0.1$	7.6	$^{+3.3}_{-2.7}$	HUANG 05B	CLEO	See DOBBS 13
-----	--------------------------	-----	------------------	-----------	------	--------------

$\Gamma(\omega e^+ \nu_e) / \Gamma(\pi^- \pi^+ e^+ \nu_e)$ $\Gamma_{43} / \Gamma_{39}$

VALUE (units 10^{-2})	EVTS	DOCUMENT ID	TECN	COMMENT
1.28 ± 0.41 ± 0.15	1.5k	ABLIKIM 19C	BES3	$\pi^- \pi^+ e^+ \nu_e$ events

$\Gamma(\omega \mu^+ \nu_\mu) / \Gamma_{total}$ Γ_{44} / Γ

VALUE (units 10^{-4})	EVTS	DOCUMENT ID	TECN	COMMENT
17.7 ± 2.1 ± 0.1	194	¹ ABLIKIM 20H	BES3	$e^+ e^-$, 3773 MeV

¹ ABLIKIM 20H reports $(17.7 \pm 1.8 \pm 1.1) \times 10^{-4}$ from a measurement of $[\Gamma(D^+ \rightarrow \omega \mu^+ \nu_\mu) / \Gamma_{total}] \times [B(\omega(782) \rightarrow \pi^+ \pi^- \pi^0)]$ assuming $B(\omega(782) \rightarrow \pi^+ \pi^- \pi^0) = (89.3 \pm 0.6) \times 10^{-2}$, which we rescale to our best value $B(\omega(782) \rightarrow \pi^+ \pi^- \pi^0) = (89.2 \pm 0.7) \times 10^{-2}$. Our first error is their experiment's error and our second error is the systematic error from using our best value.

$\Gamma(\eta'(958) e^+ \nu_e) / \Gamma_{total}$ Γ_{45} / Γ

VALUE (units 10^{-4})	CL%	EVTS	DOCUMENT ID	TECN	COMMENT
2.0 ± 0.4 OUR AVERAGE					
1.91 ± 0.51 ± 0.13		32	ABLIKIM 18R	BES3	$e^+ e^-$, 3773 MeV
2.16 ± 0.53 ± 0.07			YELTON 11	CLEO	$e^+ e^-$ at $\psi(3770)$

• • • We do not use the following data for averages, fits, limits, etc. • • •

<3.5		90	MITCHELL 09B	CLEO	See YELTON 11
------	--	----	--------------	------	---------------

$\Gamma(a(980)^0 e^+ \nu_e, a(980)^0 \rightarrow \eta \pi^0) / \Gamma_{total}$ Γ_{46} / Γ

VALUE (units 10^{-4})	EVTS	DOCUMENT ID	TECN	COMMENT
1.66 ± 0.81 ± 0.11	10^{+5}_{-4}	¹ ABLIKIM 18F	BES3	$e^+ e^-$ at 3773 MeV

¹ Signal observed at 2.9 σ C.L.

$\Gamma(b_1(1235)^0 e^+ \nu_e, b_1^0 \rightarrow \omega \pi^0) / \Gamma_{total}$ Γ_{47} / Γ

VALUE	CL%	DOCUMENT ID	TECN	COMMENT
<1.75 × 10⁻⁴	90	ABLIKIM 20AF	BES3	$e^+ e^-$, 3773 MeV

$\Gamma(\phi e^+ \nu_e) / \Gamma_{total}$ Γ_{48} / Γ
 Unseen decay modes of the ϕ are included.

VALUE	CL%	DOCUMENT ID	TECN	COMMENT
<1.3 × 10⁻⁵	90	ABLIKIM 15W	BES3	292 fb ⁻¹ , 3773 MeV

• • • We do not use the following data for averages, fits, limits, etc. • • •

<0.9	$\times 10^{-4}$	90	YELTON 11	CLEO $e^+ e^-$ at $\psi(3770)$
<1.6	$\times 10^{-4}$	90	MITCHELL 09B	CLEO See YELTON 11
<0.0201		90	ABLIKIM 06P	BES2 $e^+ e^-$ at 3773 MeV
<0.0209		90	BAI 91	MRK3 $e^+ e^- \approx 3.77$ GeV

$\Gamma(D^0 e^+ \nu_e) / \Gamma_{total}$ Γ_{49} / Γ

VALUE	CL%	DOCUMENT ID	TECN	COMMENT
<1.0 × 10⁻⁴	90	ABLIKIM 17AD	BES3	$e^+ e^-$ at 3.773 GeV

Hadronic modes with a \bar{K} or $\bar{K}K\bar{K}$

$\Gamma(K_S^0 \pi^+) / \Gamma_{total}$ Γ_{50} / Γ

VALUE (units 10^{-2})	EVTS	DOCUMENT ID	TECN	COMMENT
1.562 ± 0.031 OUR FIT				Error includes scale factor of 1.7.
1.591 ± 0.006 ± 0.030	94k	ABLIKIM 18W	BES3	$e^+ e^-$, 3773 MeV

• • • We do not use the following data for averages, fits, limits, etc. • • •

1.526 ± 0.022 ± 0.038		¹ DOBBS 07	CLEO	See MENDEZ 10
1.55 ± 0.05 ± 0.06	2.2k	¹ HE 05	CLEO	See DOBBS 07
1.6 ± 0.3 ± 0.1	161	ADLER 88c	MRK3	$e^+ e^-$ 3.77 GeV

¹ DOBBS 07 and HE 05 use single- and double-tagged events in an overall fit. DOBBS 07 supersedes HE 05.

$\Gamma(K_S^0 \pi^+) / \Gamma(K^- 2\pi^+)$ $\Gamma_{50} / \Gamma_{52}$

VALUE	EVTS	DOCUMENT ID	TECN	COMMENT
0.167 ± 0.004 OUR FIT				Error includes scale factor of 2.4.
0.162 ± 0.009 OUR AVERAGE				Error includes scale factor of 4.5.
0.171 ± 0.002 ± 0.002		BONVICINI 14	CLEO	All CLEO-c runs
0.1530 ± 0.0023 ± 0.0016	10.6k	LINK 02B	FOCS	γ nucleus, $\bar{E}_\gamma \approx 180$ GeV

• • • We do not use the following data for averages, fits, limits, etc. • • •

0.1682 ± 0.0012 ± 0.0037	30k	MENDEZ 10	CLEO	See BONVICINI 14
0.174 ± 0.012 ± 0.011	473	¹ BISHAI 97	CLEO	$e^+ e^- \approx \gamma(4S)$
0.137 ± 0.015 ± 0.016	264	ANJOS 90c	E691	Photoproduction

¹ See BISHAI 97 for an isospin analysis of $D^+ \rightarrow \bar{K} \pi$ amplitudes.

$\Gamma(K_L^0 \pi^+) / \Gamma_{total}$ Γ_{51} / Γ

VALUE (units 10^{-2})	EVTS	DOCUMENT ID	TECN	COMMENT
1.460 ± 0.040 ± 0.035	2023 ± 54	¹ HE 08	CLEO	$e^+ e^-$ at $\psi(3770)$

¹ The difference of CLEO $D^+ \rightarrow K_S^0 \pi^+$ and $K_L^0 \pi^+$ branching fractions over the sum (DOBBS 07 and HE 08) is $+0.022 \pm 0.016 \pm 0.018$.

$\Gamma(K^- 2\pi^+) / \Gamma_{total}$ Γ_{52} / Γ

VALUE (units 10^{-2})	EVTS	DOCUMENT ID	TECN	COMMENT
9.38 ± 0.16 OUR FIT				Error includes scale factor of 1.6.
9.224 ± 0.059 ± 0.157				
		BONVICINI 14	CLEO	All CLEO-c runs

• • • We do not use the following data for averages, fits, limits, etc. • • •

9.14 ± 0.10 ± 0.17		¹ DOBBS 07	CLEO	See BONVICINI 14
9.5 ± 0.2 ± 0.3	15.1k	¹ HE 05	CLEO	See DOBBS 07
9.3 ± 0.6 ± 0.8	1502	² BALEST 94	CLEO	$e^+ e^- \approx \gamma(4S)$
6.4	$^{+1.5}_{-1.4}$	³ BARLAG 92c	ACCM	π^- Cu 230 GeV
9.1 ± 1.3 ± 0.4	1164	ADLER 88c	MRK3	$e^+ e^-$ 3.77 GeV
9.1 ± 1.9	239	⁴ SCHINDLER 81	MRK2	$e^+ e^-$ 3.771 GeV

¹ DOBBS 07 and HE 05 use single- and double-tagged events in an overall fit. DOBBS 07 supersedes HE 05.
² BALEST 94 measures the ratio of $D^+ \rightarrow K^- \pi^+ \pi^+$ and $D^0 \rightarrow K^- \pi^+$ branching fractions to be $2.35 \pm 0.16 \pm 0.16$ and uses their absolute measurement of the $D^0 \rightarrow K^- \pi^+$ fraction (AKERIB 93).
³ BARLAG 92c computes the branching fraction by topological normalization.
⁴ SCHINDLER 81 (MARK-2) measures $\sigma(e^+ e^- \rightarrow \psi(3770)) \times$ branching fraction to be 0.38 ± 0.05 nb. We use the MARK-3 (ADLER 88c) value of $\sigma = 4.2 \pm 0.6 \pm 0.3$ nb.

See the related review(s):

Review of Multibody Charm Analyses

$\Gamma((K^- \pi^+)_{S\text{-wave}} \pi^+) / \Gamma(K^- 2\pi^+)$ $\Gamma_{53} / \Gamma_{52}$
 This is the "fit fraction" from the Dalitz-plot analysis. The $K^- \pi^+$ S-wave includes a broad scalar κ ($\bar{K}_0^*(700)$), the $\bar{K}_0^*(1430)^0$, and non-resonant background.

VALUE	DOCUMENT ID	TECN	COMMENT
0.801 ± 0.012 OUR AVERAGE			
0.8024 ± 0.0138 ± 0.0043	¹ LINK 09	FOCS	MIPWA fit, 53k evts
0.838 ± 0.038	² BONVICINI 08A	CLEO	QMIPWA fit, 141k evts
0.786 ± 0.014 ± 0.018	AITALA 06	E791	Dalitz fit, 15.1k events

• • • We do not use the following data for averages, fits, limits, etc. • • •

0.8323 ± 0.0150 ± 0.0008	³ LINK 07B	FOCS	See LINK 09
--------------------------	-----------------------	------	-------------

¹ This LINK 09 model-independent partial-wave analysis of the $K^- \pi^+$ S-wave slices the $K^- \pi^+$ mass range into 39 bins.
² The BONVICINI 08A QMIPWA (quasi-model-independent partial-wave analysis) of the $K^- \pi^+$ S-wave amplitude slices the $K^- \pi^+$ mass range into 26 bins but keeps the Breit-Wigner $\bar{K}_0^*(1430)^0$.
³ This LINK 07B fit uses a K matrix. The $K^- \pi^+$ S-wave fit fraction given above breaks down into $(207.3 \pm 25.5 \pm 12.4)\%$ isospin-1/2 and $(40.5 \pm 9.6 \pm 3.2)\%$ isospin-3/2 — with large interference between the two. The isospin-1/2 component includes the κ (or $\bar{K}_0^*(700)^0$) and $\bar{K}_0^*(1430)^0$.

$\Gamma(\bar{K}_0^*(700)^0 \pi^+, \bar{K}_0^*(700)^0 \rightarrow K^- \pi^+) / \Gamma(K^- 2\pi^+)$ $\Gamma_{54} / \Gamma_{52}$
 This is the "fit fraction" from the Dalitz-plot analysis.

VALUE	DOCUMENT ID	TECN	COMMENT
0.478 ± 0.121 ± 0.053	AITALA 02	E791	See AITALA 06

• • • We do not use the following data for averages, fits, limits, etc. • • •

$\Gamma(\bar{K}_0^*(1430)^0 \pi^+, \bar{K}_0^*(1430)^0 \rightarrow K^- \pi^+) / \Gamma(K^- 2\pi^+)$ $\Gamma_{55} / \Gamma_{52}$
 This is the "fit fraction" from the Dalitz-plot analysis.

VALUE	DOCUMENT ID	TECN	COMMENT
0.1330 ± 0.0062	BONVICINI 08A	CLEO	QMIPWA fit, 141k evts

Meson Particle Listings

D^\pm

• • • We do not use the following data for averages, fits, limits, etc. • • •

0.125 ± 0.014 ± 0.005	AITALA	02	E791	See AITALA 06
0.284 ± 0.022 ± 0.059	FRABETTI	94G	E687	Dalitz fit, 8800 evts
0.248 ± 0.019 ± 0.017	ANJOS	93	E691	γ Be 90–260 GeV

$\Gamma(\bar{K}^*(892)^0 \pi^+, \bar{K}^*(892)^0 \rightarrow K^- \pi^+)/\Gamma(K^- 2\pi^+)$ Γ_{56}/Γ_{52}
 This is the “fit fraction” from the Dalitz-plot analysis.

VALUE	DOCUMENT ID	TECN	COMMENT
0.111 ± 0.012 OUR AVERAGE			Error includes scale factor of 3.7.
0.1236 ± 0.0034 ± 0.0034	LINK 09	FOCS	MIPWA fit, 53k evts
0.0988 ± 0.0046	BONVICINI 08A	CLEO	QMIPWA fit, 141k evts
0.119 ± 0.002 ± 0.020	AITALA 06	E791	Dalitz fit, 15.1k events
• • • We do not use the following data for averages, fits, limits, etc. • • •			
0.1361 ± 0.0041 ± 0.0030	¹ LINK 07B	FOCS	See LINK 09
0.123 ± 0.010 ± 0.009	AITALA 02	E791	See AITALA 06
0.137 ± 0.006 ± 0.009	FRABETTI 94G	E687	Dalitz fit, 8800 evts
0.170 ± 0.009 ± 0.034	ANJOS 93	E691	γ Be 90–260 GeV
0.14 ± 0.04 ± 0.04	ALVAREZ 91B	NA14	Photoproduction
0.13 ± 0.01 ± 0.07	ADLER 87	MRK3	e^+e^- 3.77 GeV

¹The statistical error on this LINK 07B value is corrected in LINK 09.

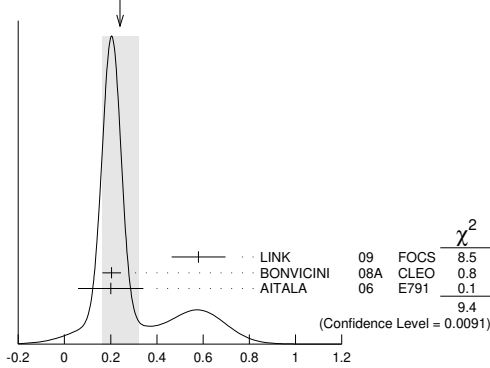
$\Gamma(\bar{K}^*(1410)^0 \pi^+, \bar{K}^*(1410)^0 \rightarrow K^- \pi^+)/\Gamma(K^- 2\pi^+)$ Γ_{57}/Γ_{52}

VALUE (units 10 ⁻³)	DOCUMENT ID	TECN	COMMENT
not seen	LINK 09	FOCS	MIPWA fit, 53k evts
not seen	BONVICINI 08A	CLEO	QMIPWA fit, 141k evts
• • • We do not use the following data for averages, fits, limits, etc. • • •			
4.8 ± 2.1 ± 1.7	LINK 07B	FOCS	See LINK 09

$\Gamma(\bar{K}_2^*(1430)^0 \pi^+, \bar{K}_2^*(1430)^0 \rightarrow K^- \pi^+)/\Gamma(K^- 2\pi^+)$ Γ_{58}/Γ_{52}
 This is the “fit fraction” from the Dalitz-plot analysis.

VALUE (units 10 ⁻²)	DOCUMENT ID	TECN	COMMENT
0.24 ± 0.08 OUR AVERAGE			Error includes scale factor of 2.2. See the ideogram below.
0.58 ± 0.10 ± 0.06	LINK 09	FOCS	MIPWA fit, 53k evts
0.204 ± 0.040	BONVICINI 08A	CLEO	QMIPWA fit, 141k evts
0.2 ± 0.1 ± 0.1	AITALA 06	E791	Dalitz fit, 15.1k events
• • • We do not use the following data for averages, fits, limits, etc. • • •			
0.39 ± 0.09 ± 0.05	LINK 07B	FOCS	See LINK 09
0.5 ± 0.1 ± 0.2	AITALA 02	E791	See AITALA 06

WEIGHTED AVERAGE
0.24±0.08 (Error scaled by 2.2)



$\Gamma(\bar{K}_2^*(1430)^0 \pi^+, \bar{K}_2^*(1430)^0 \rightarrow K^- \pi^+)/\Gamma(K^- 2\pi^+)$ Γ_{58}/Γ_{52}
 (units 10⁻²)

$\Gamma(\bar{K}^*(1680)^0 \pi^+, \bar{K}^*(1680)^0 \rightarrow K^- \pi^+)/\Gamma(K^- 2\pi^+)$ Γ_{59}/Γ_{52}
 This is the “fit fraction” from the Dalitz-plot analysis.

VALUE (units 10 ⁻²)	DOCUMENT ID	TECN	COMMENT
0.23 ± 0.12 OUR AVERAGE			
1.75 ± 0.62 ± 0.54	LINK 09	FOCS	MIPWA fit, 53k evts
0.196 ± 0.118	BONVICINI 08A	CLEO	QMIPWA fit, 141k evts
1.2 ± 0.6 ± 1.2	AITALA 06	E791	Dalitz fit, 15.1k events
• • • We do not use the following data for averages, fits, limits, etc. • • •			
1.90 ± 0.63 ± 0.43	LINK 07B	FOCS	See LINK 09
2.5 ± 0.7 ± 0.3	AITALA 02	E791	See AITALA 06
4.7 ± 0.6 ± 0.7	FRABETTI 94G	E687	Dalitz fit, 8800 evts
3.0 ± 0.4 ± 1.3	ANJOS 93	E691	γ Be 90–260 GeV

$\Gamma(K^- (2\pi^+)_{I=2})/\Gamma(K^- 2\pi^+)$ Γ_{60}/Γ_{52}

VALUE	DOCUMENT ID	TECN	COMMENT
0.155 ± 0.028	BONVICINI 08A	CLEO	QMIPWA fit, 141k evts

$\Gamma(K^- 2\pi^+ \text{ nonresonant})/\Gamma(K^- 2\pi^+)$ Γ_{61}/Γ_{52}
 This is the “fit fraction” from the Dalitz-plot analysis. Later analyses find little need for this decay mode.

VALUE	DOCUMENT ID	TECN	COMMENT
• • • We do not use the following data for averages, fits, limits, etc. • • •			
0.130 ± 0.058 ± 0.044	AITALA 02	E791	See AITALA 06
0.998 ± 0.037 ± 0.072	FRABETTI 94G	E687	Dalitz fit, 8800 evts

0.838 ± 0.088 ± 0.275	ANJOS 93	E691	γ Be 90–260 GeV
0.79 ± 0.07 ± 0.15	ADLER 87	MRK3	e^+e^- 3.77 GeV

$\Gamma(K_S^0 \pi^+ \pi^0)/\Gamma_{\text{total}}$ Γ_{62}/Γ

VALUE (units 10 ⁻²)	EVTS	DOCUMENT ID	TECN	COMMENT
• • • We do not use the following data for averages, fits, limits, etc. • • •				
6.99 ± 0.09 ± 0.25		¹ DOBBS 07	CLEO	See BONVICINI 14
7.2 ± 0.2 ± 0.4	5.1k	¹ HE 05	CLEO	See DOBBS 07
5.1 ± 1.3 ± 0.8	159	ADLER 88c	MRK3	e^+e^- 3.77 GeV

¹ DOBBS 07 and HE 05 use single- and double-tagged events in an overall fit. DOBBS 07 supersedes HE 05.

$\Gamma(K_S^0 \pi^+ \pi^0)/\Gamma(K^- 2\pi^+)$ Γ_{62}/Γ_{52}

VALUE	DOCUMENT ID	TECN	COMMENT
0.785 ± 0.007 ± 0.016	BONVICINI 14	CLEO	All CLEO-c runs

$\Gamma(K_S^0 \rho^+)/\Gamma(K_S^0 \pi^+ \pi^0)$ Γ_{63}/Γ_{62}
 This is the “fit fraction” from the Dalitz-plot analysis.

VALUE (units 10 ⁻²)	DOCUMENT ID	TECN	COMMENT
83.4 ± 2.2 ± 7.1	¹ ABLIKIM 14E	BES3	e^+e^- at $\psi(3770)$

¹ Fit fraction from Dalitz plot analysis of 142k $D^+ \rightarrow K_S^0 \pi^+ \pi^0$ events.

$\Gamma(K_S^0 \rho(1450)^+, \rho^+ \rightarrow \pi^+ \pi^0)/\Gamma(K_S^0 \pi^+ \pi^0)$ Γ_{64}/Γ_{62}
 This is the “fit fraction” from the Dalitz-plot analysis.

VALUE (%)	DOCUMENT ID	TECN	COMMENT
2.1 ± 0.3 ± 1.6	ABLIKIM 14E	BES3	e^+e^- at $\psi(3770)$

$\Gamma(\bar{K}^*(892)^0 \pi^+, \bar{K}^*(892)^0 \rightarrow K_S^0 \pi^0)/\Gamma(K_S^0 \pi^+ \pi^0)$ Γ_{65}/Γ_{62}
 This is the “fit fraction” from the Dalitz-plot analysis.

VALUE (units 10 ⁻²)	DOCUMENT ID	TECN	COMMENT
3.58 ± 0.17 ± 0.39	¹ ABLIKIM 14E	BES3	e^+e^- at $\psi(3770)$

¹ Fit fraction from Dalitz plot analysis of 142k $D^+ \rightarrow K_S^0 \pi^+ \pi^0$ events.

$\Gamma(\bar{K}_0^*(1430)^0 \pi^+, \bar{K}_0^*(1430)^0 \rightarrow K_S^0 \pi^0)/\Gamma(K_S^0 \pi^+ \pi^0)$ Γ_{66}/Γ_{62}
 This is the “fit fraction” from the Dalitz-plot analysis.

VALUE (%)	DOCUMENT ID	TECN	COMMENT
3.7 ± 0.6 ± 1.1	ABLIKIM 14E	BES3	e^+e^- at $\psi(3770)$

$\Gamma(\bar{K}_0^*(1680)^0 \pi^+, \bar{K}_0^*(1680)^0 \rightarrow K_S^0 \pi^0)/\Gamma(K_S^0 \pi^+ \pi^0)$ Γ_{67}/Γ_{62}
 This is the “fit fraction” from the Dalitz-plot analysis.

VALUE (%)	DOCUMENT ID	TECN	COMMENT
1.3 ± 0.2 ± 0.9	ABLIKIM 14E	BES3	e^+e^- at $\psi(3770)$

$\Gamma(\bar{\pi}^0 \pi^+, \bar{\pi}^0 \rightarrow K_S^0 \pi^0)/\Gamma(K_S^0 \pi^+ \pi^0)$ Γ_{68}/Γ_{62}
 This is the “fit fraction” from the Dalitz-plot analysis.

VALUE (%)	DOCUMENT ID	TECN	COMMENT
7.7 ± 1.2 ± 6.5	ABLIKIM 14E	BES3	e^+e^- at $\psi(3770)$

$\Gamma(K_S^0 \pi^+ \pi^0 \text{ nonresonant})/\Gamma(K_S^0 \pi^+ \pi^0)$ Γ_{69}/Γ_{62}
 This is the “fit fraction” from the Dalitz-plot analysis.

VALUE (units 10 ⁻²)	DOCUMENT ID	TECN	COMMENT
4.6 ± 0.7 ± 5.4	¹ ABLIKIM 14E	BES3	e^+e^- at $\psi(3770)$

¹ Fit fraction from Dalitz plot analysis of 142k $D^+ \rightarrow K_S^0 \pi^+ \pi^0$ events.

$\Gamma(K_S^0 \pi^+ \pi^0 \text{ nonresonant and } \bar{\pi}^0 \pi^+)/\Gamma(K_S^0 \pi^+ \pi^0)$ Γ_{70}/Γ_{62}
 This is the “fit fraction” from the Dalitz-plot analysis.

VALUE (%)	DOCUMENT ID	TECN	COMMENT
18.6 ± 1.7 ± 2.3	ABLIKIM 14E	BES3	e^+e^- at $\psi(3770)$

$\Gamma((K_S^0 \pi^0)_{S\text{-wave}} \pi^+)/\Gamma(K_S^0 \pi^+ \pi^0)$ Γ_{71}/Γ_{62}
 The numerator here is the coherent sum of the $\bar{K}_0^*(1430)^0 \pi^+$, $\bar{\pi}^0 \pi^+$, and nonresonant contributions.

VALUE (%)	DOCUMENT ID	TECN	COMMENT
17.3 ± 1.4 ± 3.4	ABLIKIM 14E	BES3	e^+e^- at $\psi(3770)$

$\Gamma(K_S^0 \pi^+ \omega)/\Gamma_{\text{total}}$ Γ_{72}/Γ

VALUE (units 10 ⁻²)	EVTS	DOCUMENT ID	TECN	COMMENT
0.707 ± 0.041 ± 0.029	523	¹ ABLIKIM 22U	BES3	e^+e^- at 3.773 GeV

¹ ABLIKIM 22U determines the ratio $B(D^+ \rightarrow K_S^0 \pi^+ \omega)/B(D^0 \rightarrow K^- \pi^+ \omega) = 0.21 \pm 0.01 \pm 0.01$, in significant tension with statistical isospin model expectation of 0.9.

$\Gamma(K_S^0 \pi^+ \eta)/\Gamma_{\text{total}}$ Γ_{73}/Γ

VALUE (units 10 ⁻³)	EVTS	DOCUMENT ID	TECN	COMMENT
13.09 ± 0.37 ± 0.31	1.3k	ABLIKIM 20V	BES3	e^+e^- , 3773 MeV

$\Gamma(K_S^0 \pi^+ \eta'(958))/\Gamma_{\text{total}}$ Γ_{74}/Γ

VALUE (units 10 ⁻³)	EVTS	DOCUMENT ID	TECN	COMMENT
1.90 ± 0.17 ± 0.13	267	ABLIKIM 18Ac	BES3	e^+e^- , 3773 MeV

$\Gamma(K^- 2\pi^+ \pi^0)/\Gamma_{\text{total}}$ Γ_{75}/Γ

See the listings under " $D \rightarrow K\pi\pi$ partial wave analyses" and our 2008 Review (Physics Letters **B667** 1 (2008)) for measurements of submodes of this mode.

VALUE (units 10^{-2})	EVTS	DOCUMENT ID	TECN	COMMENT
$5.98 \pm 0.08 \pm 0.16$		¹ DOBBS	07 CLEO	See BONVICINI 14
$6.0 \pm 0.2 \pm 0.2$	4.8k	¹ HE	05 CLEO	See DOBBS 07
$5.8 \pm 1.2 \pm 1.2$	142	COFFMAN	92B MRK3	$e^+ e^-$ 3.77 GeV
$6.3 \pm 1.4 \pm 1.2$	175	BALTRUSAIT...86E	MRK3	See COFFMAN 92B

¹ DOBBS 07 and HE 05 use single- and double-tagged events in an overall fit. DOBBS 07 supersedes HE 05.

 $\Gamma(K^- 2\pi^+ \pi^0)/\Gamma(K^- 2\pi^+)$ Γ_{75}/Γ_{52}

VALUE	DOCUMENT ID	TECN	COMMENT
$0.666 \pm 0.006 \pm 0.014$	BONVICINI 14	CLEO	All CLEO-c runs

 $\Gamma(K_S^0 2\pi^+ \pi^-)/\Gamma_{\text{total}}$ Γ_{76}/Γ

See the listings under " $D \rightarrow K\pi\pi$ partial wave analyses" and our 2008 Review (Physics Letters **B667** 1 (2008)) for measurements of submodes of this mode.

VALUE (units 10^{-2})	EVTS	DOCUMENT ID	TECN	COMMENT
$3.122 \pm 0.046 \pm 0.096$		¹ DOBBS	07 CLEO	See BONVICINI 14
$3.2 \pm 0.1 \pm 0.2$	3.2k	¹ HE	05 CLEO	See DOBBS 07
$2.1 \pm 1.0 \pm 0.9$		² BARLAG	92c ACCM	π^- Cu 230 GeV
$3.3 \pm 0.8 \pm 0.2$	168	ADLER	88c MRK3	$e^+ e^-$ 3.77 GeV

¹ DOBBS 07 and HE 05 use single- and double-tagged events in an overall fit. DOBBS 07 supersedes HE 05.

² BARLAG 92c computes the branching fraction by topological normalization.

 $\Gamma(K_S^0 2\pi^+ \pi^-)/\Gamma(K^- 2\pi^+)$ Γ_{76}/Γ_{52}

VALUE	DOCUMENT ID	TECN	COMMENT
$0.331 \pm 0.004 \pm 0.006$	BONVICINI 14	CLEO	All CLEO-c runs

 $\Gamma(K_S^0 \pi^+ 2\pi^0)/\Gamma_{\text{total}}$ Γ_{77}/Γ

VALUE (units 10^{-3})	EVTS	DOCUMENT ID	TECN	COMMENT
$28.88 \pm 0.58 \pm 0.69$	3.7k	ABLIKIM	23BW BES3	$e^+ e^-$ at 3.773 GeV
$29.04 \pm 0.62 \pm 0.87$	3.4k	¹ ABLIKIM	22Y BES3	$e^+ e^-$ at 3.773 GeV

¹ See ABLIKIM 23BW.

 $\Gamma(K_S^0 a_1(1260)^+, a_1^+ \rightarrow \rho(770)^+ \pi^0)/\Gamma(K_S^0 \pi^+ 2\pi^0)$ Γ_{78}/Γ_{77}

VALUE (units 10^{-2})	DOCUMENT ID	TECN	COMMENT
$30.0 \pm 3.6 \pm 4.2$	¹ ABLIKIM	23BW BES3	$D^+ \rightarrow K_S^0 \pi^+ 2\pi^0$

¹ Amplitude analysis of 1.4k $D^+ \rightarrow K_S^0 \pi^+ 2\pi^0$ events.

 $\Gamma(K_S^0 a_1(1260)^+, a_1^+ \rightarrow f_0(500) \pi^+, f_0 \rightarrow \pi^0 \pi^0)/\Gamma(K_S^0 \pi^+ 2\pi^0)$ Γ_{79}/Γ_{77}

VALUE (units 10^{-2})	DOCUMENT ID	TECN	COMMENT
$3.5 \pm 1.1 \pm 1.9$	¹ ABLIKIM	23BW BES3	$D^+ \rightarrow K_S^0 \pi^+ 2\pi^0$

¹ Amplitude analysis of 1.4k $D^+ \rightarrow K_S^0 \pi^+ 2\pi^0$ events.

 $\Gamma(K_1(1400)^0 \pi^+, K_1^0 \rightarrow \bar{K}^*(892)^0 \pi^0, \bar{K}^{*0} \rightarrow K_S^0 \pi^0)/\Gamma(K_S^0 \pi^+ 2\pi^0)$ Γ_{80}/Γ_{77}

VALUE (units 10^{-2})	DOCUMENT ID	TECN	COMMENT
$8.0 \pm 1.2 \pm 0.4$	¹ ABLIKIM	23BW BES3	$D^+ \rightarrow K_S^0 \pi^+ 2\pi^0$

¹ Amplitude analysis of 1.4k $D^+ \rightarrow K_S^0 \pi^+ 2\pi^0$ events.

 $\Gamma(\bar{K}^*(892)^0 \rho^+, \bar{K}^{*0} \rightarrow K_S^0 \pi^0)/\Gamma(K_S^0 \pi^+ 2\pi^0)$ Γ_{81}/Γ_{77}

VALUE (units 10^{-2})	DOCUMENT ID	TECN	COMMENT
$33.6 \pm 2.7 \pm 1.4$	¹ ABLIKIM	23BW BES3	$D^+ \rightarrow K_S^0 \pi^+ 2\pi^0$

¹ Amplitude analysis of 1.4k $D^+ \rightarrow K_S^0 \pi^+ 2\pi^0$ events.

 $\Gamma(\bar{K}^*(892)^0 \pi^+ \pi^0 \text{ non-resonant}, \bar{K}^{*0} \rightarrow K_S^0 \pi^0)/\Gamma(K_S^0 \pi^+ 2\pi^0)$ Γ_{82}/Γ_{77}

VALUE (units 10^{-2})	DOCUMENT ID	TECN	COMMENT
$9.1 \pm 2.0 \pm 1.0$	¹ ABLIKIM	23BW BES3	$D^+ \rightarrow K_S^0 \pi^+ 2\pi^0$

¹ Amplitude analysis of 1.4k $D^+ \rightarrow K_S^0 \pi^+ 2\pi^0$ events.

 $\Gamma(K_S^0 \rho^+ \pi^0 \text{ non-resonant})/\Gamma(K_S^0 \pi^+ 2\pi^0)$ Γ_{83}/Γ_{77}

VALUE (units 10^{-2})	DOCUMENT ID	TECN	COMMENT
$16.5 \pm 1.6 \pm 0.3$	¹ ABLIKIM	23BW BES3	$D^+ \rightarrow K_S^0 \pi^+ 2\pi^0$

¹ Amplitude analysis of 1.4k $D^+ \rightarrow K_S^0 \pi^+ 2\pi^0$ events.

 $\Gamma(K^- 2\pi^+ \eta)/\Gamma_{\text{total}}$ Γ_{84}/Γ

VALUE (units 10^{-3})	EVTS	DOCUMENT ID	TECN	COMMENT
$1.35 \pm 0.11 \pm 0.04$	190	ABLIKIM	20V BES3	$e^+ e^-$, 3773 MeV

 $\Gamma(K_S^0 \pi^+ \pi^0 \eta)/\Gamma_{\text{total}}$ Γ_{85}/Γ

VALUE (units 10^{-3})	EVTS	DOCUMENT ID	TECN	COMMENT
$1.22 \pm 0.24 \pm 0.06$	50	ABLIKIM	20V BES3	$e^+ e^-$, 3773 MeV

 $\Gamma(K^- 3\pi^+ \pi^-)/\Gamma(K^- 2\pi^+)$ Γ_{86}/Γ_{52}

VALUE	EVTS	DOCUMENT ID	TECN	COMMENT
0.061 ± 0.005 OUR FIT				Error includes scale factor of 1.1.
0.062 ± 0.008 OUR AVERAGE				Error includes scale factor of 1.3.
$0.058 \pm 0.002 \pm 0.006$	2923	LINK	03D FOCUS	$\gamma A, \bar{E}_\gamma \approx 180$ GeV
$0.077 \pm 0.008 \pm 0.010$	239	FRABETTI	97c E687	$\gamma \text{Be}, \bar{E}_\gamma \approx 200$ GeV
$0.09 \pm 0.01 \pm 0.01$	113	ANJOS	90D E691	Photoproduction

 $\Gamma(\bar{K}^*(892)^0 2\pi^+ \pi^-, \bar{K}^*(892)^0 \rightarrow K^- \pi^+)/\Gamma(K^- 3\pi^+ \pi^-)$ Γ_{87}/Γ_{86}

VALUE	DOCUMENT ID	TECN	COMMENT
$0.21 \pm 0.04 \pm 0.06$	LINK	03D FOCUS	$\gamma A, \bar{E}_\gamma \approx 180$ GeV

 $\Gamma(\bar{K}^*(892)^0 \rho^0 \pi^+, \bar{K}^*(892)^0 \rightarrow K^- \pi^+)/\Gamma(K^- 2\pi^+)$ Γ_{88}/Γ_{52}

VALUE	DOCUMENT ID	TECN	COMMENT
$0.016 \pm 0.007 \pm 0.004$	FRABETTI 97c	E687	$\gamma \text{Be}, \bar{E}_\gamma \approx 200$ GeV

 $\Gamma(\bar{K}^*(892)^0 \rho^0 \pi^+, \bar{K}^*(892)^0 \rightarrow K^- \pi^+)/\Gamma(K^- 3\pi^+ \pi^-)$ Γ_{88}/Γ_{86}

VALUE	DOCUMENT ID	TECN	COMMENT
$0.40 \pm 0.03 \pm 0.06$	LINK	03D FOCUS	$\gamma A, \bar{E}_\gamma \approx 180$ GeV

 $\Gamma(\bar{K}^*(892)^0 a_1(1260)^+)/\Gamma(K^- 2\pi^+)$ Γ_{89}/Γ_{52}

Unseen decay modes of the $\bar{K}^*(892)^0$ and $a_1(1260)^+$ are included.

VALUE	DOCUMENT ID	TECN	COMMENT
$0.099 \pm 0.008 \pm 0.018$	LINK	03D FOCUS	$\gamma A, \bar{E}_\gamma \approx 180$ GeV

 $\Gamma(\bar{K}^*(892)^0 2\pi^+ \pi^- \text{ no-}\rho, \bar{K}^*(892)^0 \rightarrow K^- \pi^+)/\Gamma(K^- 2\pi^+)$ Γ_{90}/Γ_{52}

VALUE	DOCUMENT ID	TECN	COMMENT
$0.032 \pm 0.010 \pm 0.008$	FRABETTI 97c	E687	$\gamma \text{Be}, \bar{E}_\gamma \approx 200$ GeV

 $\Gamma(K^- \rho^0 2\pi^+)/\Gamma(K^- 2\pi^+)$ Γ_{91}/Γ_{52}

VALUE	DOCUMENT ID	TECN	COMMENT
$0.034 \pm 0.009 \pm 0.005$	FRABETTI 97c	E687	$\gamma \text{Be}, \bar{E}_\gamma \approx 200$ GeV

 $\Gamma(K^- \rho^0 2\pi^+)/\Gamma(K^- 3\pi^+ \pi^-)$ Γ_{91}/Γ_{86}

VALUE	DOCUMENT ID	TECN	COMMENT
$0.30 \pm 0.04 \pm 0.01$	LINK	03D FOCUS	$\gamma A, \bar{E}_\gamma \approx 180$ GeV

 $\Gamma(K^- 3\pi^+ \pi^- \text{ nonresonant})/\Gamma(K^- 3\pi^+ \pi^-)$ Γ_{92}/Γ_{86}

VALUE	CL%	DOCUMENT ID	TECN	COMMENT
$0.07 \pm 0.05 \pm 0.01$		LINK	03D FOCUS	$\gamma A, \bar{E}_\gamma \approx 180$ GeV
< 0.026	90	FRABETTI 97c	E687	$\gamma \text{Be}, \bar{E}_\gamma \approx 200$ GeV

 $\Gamma(K_S^0 2\pi^+ \pi^- \pi^0)/\Gamma_{\text{total}}$ Γ_{93}/Γ

VALUE (units 10^{-3})	EVTS	DOCUMENT ID	TECN	COMMENT
$15.28 \pm 0.57 \pm 0.60$	1k	ABLIKIM	22Y BES3	$e^+ e^-$ at 3.773 GeV

 $\Gamma(K_S^0 \pi^+ 3\pi^0)/\Gamma_{\text{total}}$ Γ_{94}/Γ

VALUE (units 10^{-3})	EVTS	DOCUMENT ID	TECN	COMMENT
$5.54 \pm 0.44 \pm 0.32$	285	ABLIKIM	22Y BES3	$e^+ e^-$ at 3.773 GeV

 $\Gamma(K^- 2\pi^+ 2\pi^0)/\Gamma_{\text{total}}$ Γ_{95}/Γ

VALUE (units 10^{-3})	EVTS	DOCUMENT ID	TECN	COMMENT
$4.95 \pm 0.26 \pm 0.19$	756	ABLIKIM	22Y BES3	$e^+ e^-$ at 3.773 GeV

 $\Gamma(K^+ 2K_S^0)/\Gamma_{\text{total}}$ Γ_{96}/Γ

VALUE (units 10^{-4})	EVTS	DOCUMENT ID	TECN	COMMENT
$25.4 \pm 0.5 \pm 1.2$	3551	ABLIKIM	17A BES3	$e^+ e^- \rightarrow \psi(3770)$

 $\Gamma(K^+ 2K_S^0)/\Gamma(K^- 2\pi^+)$ Γ_{96}/Γ_{52}

VALUE	EVTS	DOCUMENT ID	TECN	COMMENT
$0.035 \pm 0.010 \pm 0.005$	39 ± 9	ALBRECHT	94I ARG	$e^+ e^- \approx 10$ GeV
0.085 ± 0.018	70 ± 12	AMMAR	91 CLEO	$e^+ e^- \approx 10.5$ GeV

 $\Gamma(\phi(1020)^0 K^+)/\Gamma_{\text{total}}$ Γ_{177}/Γ

VALUE	CL%	DOCUMENT ID	TECN	COMMENT
$< 2.1 \times 10^{-5}$	90	ABLIKIM	19B BES3	$e^+ e^-$ at 3773 MeV

Meson Particle Listings

D^\pm

$\Gamma(K^+ K^- K_S^0 \pi^+)/\Gamma(K_S^0 2\pi^+ \pi^-)$

Γ_{97}/Γ_{76}

VALUE (units 10^{-3})	EVTs	DOCUMENT ID	TECN	COMMENT
7.7 ± 1.5 ± 0.9	35 ± 7	LINK	01c FOCS	γ nucleus, $\bar{E}_\gamma \approx 180$ GeV

Piononic modes

$\Gamma(\pi^+ \pi^0)/\Gamma_{total}$

Γ_{98}/Γ

VALUE (units 10^{-3})	EVTs	DOCUMENT ID	TECN	COMMENT
1.247 ± 0.033 OUR FIT				
1.259 ± 0.033 ± 0.023	10k	ABLIKIM	18w BES3	$e^+ e^-$, 3773 MeV

$\Gamma(\pi^+ \pi^0)/\Gamma(K^- 2\pi^+)$

Γ_{98}/Γ_{52}

VALUE (units 10^{-2})	EVTs	DOCUMENT ID	TECN	COMMENT
1.33 ± 0.04 OUR FIT				Error includes scale factor of 1.1.
1.31 ± 0.06 OUR AVERAGE				
1.29 ± 0.04 ± 0.05	2649 ± 76	MENDEZ	10 CLEO	$e^+ e^-$ at 3774 MeV
1.33 ± 0.11 ± 0.09	1229 ± 99	AUBERT,B	06F BABR	$e^+ e^- \approx \Upsilon(4S)$
1.44 ± 0.19 ± 0.10	171 ± 22	ARMS	04 CLEO	$e^+ e^- \approx 10$ GeV
• • • We do not use the following data for averages, fits, limits, etc. • • •				
1.33 ± 0.07 ± 0.06	914 ± 46	RUBIN	06 CLEO	See MENDEZ 10

$\Gamma(2\pi^+ \pi^-)/\Gamma_{total}$

Γ_{99}/Γ

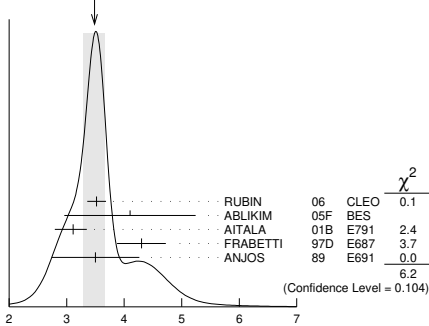
VALUE (units 10^{-4})	EVTs	DOCUMENT ID	TECN	COMMENT
32.7 ± 0.7 ± 0.5	2.6k	ABLIKIM	22B G BES3	$e^+ e^-$ at 3.773 GeV

$\Gamma(2\pi^+ \pi^-)/\Gamma(K^- 2\pi^+)$

Γ_{99}/Γ_{52}

VALUE (units 10^{-2})	EVTs	DOCUMENT ID	TECN	COMMENT
3.48 ± 0.19 OUR AVERAGE				Error includes scale factor of 1.4. See the ideogram below.
3.52 ± 0.11 ± 0.12	3303 ± 95	RUBIN	06 CLEO	$e^+ e^-$ at $\psi(3770)$
4.1 ± 1.1 ± 0.3	85 ± 22	ABLIKIM	05F BES	$e^+ e^- \approx \psi(3770)$
3.11 ± 0.18 ^{+0.16} _{-0.26}	1172	AITALA	01B E791	π^- nucleus, 500 GeV
4.3 ± 0.3 ± 0.3	236	FRABETTI	97D E687	γ Be ≈ 200 GeV
3.5 ± 0.7 ± 0.3	83	ANJOS	89 E691	Photoproduction

WEIGHTED AVERAGE
3.48 ± 0.19 (Error scaled by 1.4)



$\Gamma(\rho^0 \pi^+)/\Gamma(2\pi^+ \pi^-)$

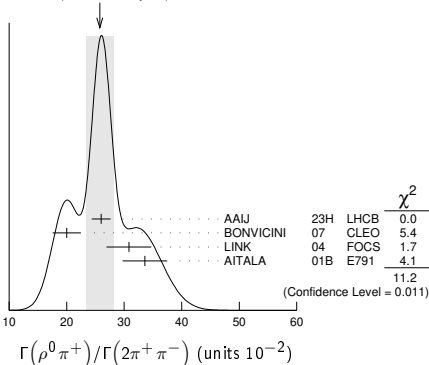
Γ_{100}/Γ_{99}

This is the "fit fraction" from the Dalitz-plot analysis.

VALUE (units 10^{-2})	EVTs	DOCUMENT ID	TECN	COMMENT
25.8 ± 2.4 OUR AVERAGE				Error includes scale factor of 1.9. See the ideogram below.
26 ± 0.3 ± 1.6 ± 0.3	572k	¹ AAIJ	23H LHCB	Dalitz plot fit
20.0 ± 2.3 ± 0.9		BONVICINI	07 CLEO	Dalitz fit, ≈ 2240 evts
30.82 ± 3.14 ± 2.30		LINK	04 FOCS	Dalitz fit, 1527 ± 51 evts
33.6 ± 3.2 ± 2.2		AITALA	01B E791	Dalitz fit, 1172 evts

¹ The last error reflects the uncertainty on the amplitude model.

WEIGHTED AVERAGE
25.8 ± 2.4 (Error scaled by 1.9)



$\Gamma(\pi^+ (\pi^+ \pi^-)_{S\text{-wave}})/\Gamma(2\pi^+ \pi^-)$

Γ_{101}/Γ_{99}

This is the "fit fraction" from the Dalitz-plot analysis. See also the next three data blocks.

VALUE (units 10^{-2})	EVTs	DOCUMENT ID	TECN	COMMENT
61.5 ± 0.9 OUR AVERAGE				
61.8 ± 0.5 ± 0.6 ± 0.5	572k	^{1,2} AAIJ	23H LHCB	Dalitz plot fit
56.00 ± 3.24 ± 2.14		³ LINK	04 FOCS	Dalitz fit, 1527 ± 51 evts

¹ AAIJ 23H parameterise the $\pi^+ \pi^-$ S-wave using one complex number per bin in 50 bins of $\pi^+ \pi^-$ invariant mass.

² The last error reflects the uncertainty on the amplitude model.

³ LINK 04 borrows a K-matrix parametrization from ANISOVICH 03 of the full $\pi-\pi$ S-wave isoscalar scattering amplitude to describe the $\pi^+ \pi^-$ S-wave component of the $\pi^+ \pi^+ \pi^-$ state. The fit fraction given above is a sum over five f_0 mesons, the $f_0(980)$, $f_0(1300)$, $f_0(1200-1600)$, $f_0(1500)$, and $f_0(1750)$. See LINK 04 for details and discussion.

$\Gamma(\sigma \pi^+, \sigma \rightarrow \pi^+ \pi^-)/\Gamma(2\pi^+ \pi^-)$

Γ_{102}/Γ_{99}

This is the "fit fraction" from the Dalitz-plot analysis.

VALUE	DOCUMENT ID	TECN	COMMENT
0.422 ± 0.027 OUR AVERAGE			
0.418 ± 0.014 ± 0.025	BONVICINI 07	CLEO	Dalitz fit, ≈ 2240 evts
0.463 ± 0.090 ± 0.021	AITALA 01B	E791	Dalitz fit, 1172 evts

$\Gamma(f_0(980) \pi^+, f_0 \rightarrow \pi^+ \pi^-)/\Gamma(2\pi^+ \pi^-)$

Γ_{103}/Γ_{99}

This is the "fit fraction" from the Dalitz-plot analysis.

VALUE	DOCUMENT ID	TECN	COMMENT
0.048 ± 0.010 OUR AVERAGE			Error includes scale factor of 1.3.
0.041 ± 0.009 ± 0.003	BONVICINI 07	CLEO	Dalitz fit, ≈ 2240 evts
0.062 ± 0.013 ± 0.004	AITALA 01B	E791	Dalitz fit, 1172 evts

$\Gamma(f_0(1370) \pi^+, f_0 \rightarrow \pi^+ \pi^-)/\Gamma(2\pi^+ \pi^-)$

Γ_{104}/Γ_{99}

This is the "fit fraction" from the Dalitz-plot analysis.

VALUE	DOCUMENT ID	TECN	COMMENT
0.024 ± 0.013 OUR AVERAGE			
0.026 ± 0.018 ± 0.006	BONVICINI 07	CLEO	Dalitz fit, ≈ 2240 evts
0.023 ± 0.015 ± 0.008	AITALA 01B	E791	Dalitz fit, 1172 evts

$\Gamma(\omega \pi^+, \omega \rightarrow \pi^+ \pi^-)/\Gamma(2\pi^+ \pi^-)$

Γ_{105}/Γ_{99}

VALUE (units 10^{-3})	EVTs	DOCUMENT ID	TECN	COMMENT
1.03 ± 0.08 ± 0.14 ± 0.02	572k	¹ AAIJ	23H LHCB	Dalitz plot fit

¹ The last error reflects the uncertainty on the amplitude model.

$\Gamma(f_2(1270) \pi^+, f_2 \rightarrow \pi^+ \pi^-)/\Gamma(2\pi^+ \pi^-)$

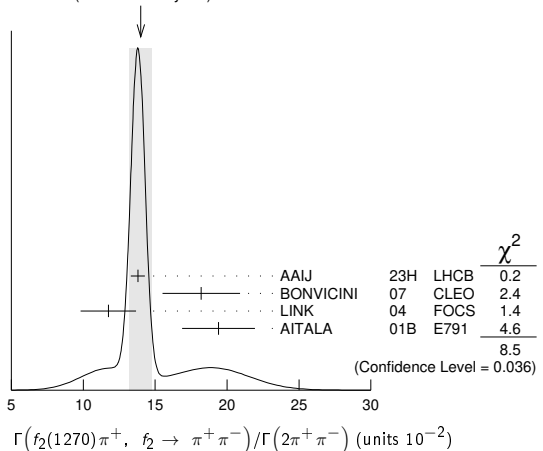
Γ_{106}/Γ_{99}

This is the "fit fraction" from the Dalitz-plot analysis.

VALUE (units 10^{-2})	EVTs	DOCUMENT ID	TECN	COMMENT
14.0 ± 0.8 OUR AVERAGE				Error includes scale factor of 1.7. See the ideogram below.
13.8 ± 0.2 ± 0.4 ± 0.2	572k	¹ AAIJ	23H LHCB	Dalitz plot fit
18.2 ± 2.6 ± 0.7		BONVICINI	07 CLEO	Dalitz fit, ≈ 2240 evts
11.74 ± 1.90 ± 0.29		LINK	04 FOCS	Dalitz fit, 1527 ± 51 evts
19.4 ± 2.5 ± 0.4		AITALA	01B E791	Dalitz fit, 1172 evts

¹ The last error reflects the uncertainty on the amplitude model.

WEIGHTED AVERAGE
14.0 ± 0.8 (Error scaled by 1.7)



$\Gamma(\rho(1450)^0 \pi^+, \rho^0 \rightarrow \pi^+ \pi^-)/\Gamma(2\pi^+ \pi^-)$

Γ_{107}/Γ_{99}

This is the "fit fraction" from the Dalitz-plot analysis.

VALUE (units 10^{-2})	CL%	EVTs	DOCUMENT ID	TECN	COMMENT
5.4 ± 0.4 ± 1.3 ± 0.8		572k	¹ AAIJ	23H LHCB	Dalitz plot fit
<2.4	95		BONVICINI	07 CLEO	Dalitz fit, ≈ 2240 evts
0.7 ± 0.7 ± 0.3			AITALA	01B E791	Dalitz fit, 1172 evts

¹ The last error reflects the uncertainty on the amplitude model.

$\Gamma(\rho(1700)^0 \pi^+, \rho^0 \rightarrow \pi^+ \pi^-)/\Gamma(2\pi^+ \pi^-)$ Γ_{108}/Γ_{99}

VALUE (units 10^{-2})	EVTS	DOCUMENT ID	TECN	COMMENT
$5.7 \pm 0.5 \pm 1.0 \pm 1.0$	572k	¹ AAIJ	23H LHCb	Dalitz plot fit

¹ The last error reflects the uncertainty on the amplitude model.

 $\Gamma(f_0(1500) \pi^+, f_0 \rightarrow \pi^+ \pi^-)/\Gamma(2\pi^+ \pi^-)$ Γ_{109}/Γ_{99}

This is the "fit fraction" from the Dalitz-plot analysis.

VALUE	DOCUMENT ID	TECN	COMMENT
$0.034 \pm 0.010 \pm 0.008$	BONVICINI 07	CLEO	Dalitz fit, ≈ 2240 evts

 $\Gamma(f_0(1710) \pi^+, f_0 \rightarrow \pi^+ \pi^-)/\Gamma(2\pi^+ \pi^-)$ Γ_{110}/Γ_{99}

This is the "fit fraction" from the Dalitz-plot analysis.

VALUE	CL%	DOCUMENT ID	TECN	COMMENT
<0.016	95	BONVICINI 07	CLEO	Dalitz fit, ≈ 2240 evts

 $\Gamma(f_0(1790) \pi^+, f_0 \rightarrow \pi^+ \pi^-)/\Gamma(2\pi^+ \pi^-)$ Γ_{111}/Γ_{99}

This is the "fit fraction" from the Dalitz-plot analysis.

VALUE	CL%	DOCUMENT ID	TECN	COMMENT
<0.02	95	BONVICINI 07	CLEO	Dalitz fit, ≈ 2240 evts

 $\Gamma((\pi^+ \pi^+)_{S\text{-wave}} \pi^-)/\Gamma(2\pi^+ \pi^-)$ Γ_{112}/Γ_{99}

This is the "fit fraction" from the Dalitz-plot analysis.

VALUE	CL%	DOCUMENT ID	TECN	COMMENT
<0.037	95	BONVICINI 07	CLEO	Dalitz fit, ≈ 2240 evts

 $\Gamma(2\pi^+ \pi^- \text{ nonresonant})/\Gamma(2\pi^+ \pi^-)$ Γ_{113}/Γ_{99}

This is the "fit fraction" from the Dalitz-plot analysis.

VALUE	CL%	DOCUMENT ID	TECN	COMMENT
<0.035	95	BONVICINI 07	CLEO	Dalitz fit, ≈ 2240 evts
• • • We do not use the following data for averages, fits, limits, etc. • • •				
$0.078 \pm 0.060 \pm 0.027$		AITALA 01B	E791	Dalitz fit, 1172 evts

 $\Gamma(\pi^+ 2\pi^0)/\Gamma_{\text{total}}$ Γ_{114}/Γ

VALUE (units 10^{-4})	EVTS	DOCUMENT ID	TECN	COMMENT
$46.1 \pm 1.2 \pm 0.9$	2k	ABLIKIM	22B BES3	$e^+ e^-$ at 3.773 GeV

 $\Gamma(\pi^+ 2\pi^0)/\Gamma(K^- 2\pi^+)$ Γ_{114}/Γ_{52}

VALUE (units 10^{-2})	EVTS	DOCUMENT ID	TECN	COMMENT
$5.0 \pm 0.3 \pm 0.3$	1535 ± 89	RUBIN 06	CLEO	$e^+ e^-$ at $\psi(3770)$

 $\Gamma(\pi^+ 3\pi^0)/\Gamma_{\text{total}}$ Γ_{116}/Γ

VALUE (units 10^{-4})	EVTS	DOCUMENT ID	TECN	COMMENT
$41.7 \pm 2.2 \pm 1.3$	570	ABLIKIM	22B BES3	$e^+ e^-$ at 3.773 GeV

 $\Gamma(2\pi^+ \pi^- \pi^0)/\Gamma_{\text{total}}$ Γ_{115}/Γ

VALUE (units 10^{-4})	EVTS	DOCUMENT ID	TECN	COMMENT
$116.5 \pm 2.1 \pm 2.1$	4.6k	ABLIKIM	22B BES3	$e^+ e^-$ at 3.773 GeV

 $\Gamma(2\pi^+ \pi^- \pi^0)/\Gamma(K^- 2\pi^+)$ Γ_{115}/Γ_{52}

VALUE (units 10^{-2})	EVTS	DOCUMENT ID	TECN	COMMENT
$12.4 \pm 0.5 \pm 0.6$	5701 ± 205	RUBIN 06	CLEO	$e^+ e^-$ at $\psi(3770)$

 $\Gamma(\pi^+ 4\pi^0)/\Gamma_{\text{total}}$ Γ_{117}/Γ

VALUE (units 10^{-4})	EVTS	DOCUMENT ID	TECN	COMMENT
$19.5 \pm 3.6 \pm 2.3$	57	ABLIKIM	22B BES3	$e^+ e^-$ at 3.773 GeV

 $\Gamma(2\pi^+ \pi^- 2\pi^0)/\Gamma_{\text{total}}$ Γ_{118}/Γ

VALUE (units 10^{-4})	EVTS	DOCUMENT ID	TECN	COMMENT
$107.4 \pm 4.0 \pm 3.0$	1.2k	ABLIKIM	22B BES3	$e^+ e^-$ at 3.773 GeV

 $\Gamma(3\pi^+ 2\pi^-)/\Gamma_{\text{total}}$ Γ_{119}/Γ

VALUE (units 10^{-4})	EVTS	DOCUMENT ID	TECN	COMMENT
$18.2 \pm 1.1 \pm 1.0$	460	ABLIKIM	22B BES3	$e^+ e^-$ at 3.773 GeV

 $\Gamma(3\pi^+ 2\pi^-)/\Gamma(K^- 2\pi^+)$ Γ_{119}/Γ_{52}

VALUE (units 10^{-2})	EVTS	DOCUMENT ID	TECN	COMMENT
1.77 ± 0.17 OUR FIT				
$1.73 \pm 0.20 \pm 0.17$	732 ± 77	RUBIN 06	CLEO	$e^+ e^-$ at $\psi(3770)$
• • • We do not use the following data for averages, fits, limits, etc. • • •				
$2.3 \pm 0.4 \pm 0.2$	58	FRABETTI 97C	E687	γ Be, $\bar{E}_\gamma \approx 200$ GeV

 $\Gamma(3\pi^+ 2\pi^-)/\Gamma(K^- 3\pi^+ \pi^-)$ Γ_{119}/Γ_{86}

VALUE	EVTS	DOCUMENT ID	TECN	COMMENT
0.289 ± 0.019 OUR FIT				
$0.290 \pm 0.017 \pm 0.011$	835	LINK 03D	FOCS	γ A, $\bar{E}_\gamma \approx 180$ GeV

 $\Gamma(2\pi^+ \pi^- 3\pi^0)/\Gamma_{\text{total}}$ Γ_{120}/Γ

VALUE (units 10^{-4})	EVTS	DOCUMENT ID	TECN	COMMENT
$34.2 \pm 3.1 \pm 1.6$	186	ABLIKIM	22B BES3	$e^+ e^-$ at 3.773 GeV

 $\Gamma(3\pi^+ 2\pi^- \pi^0)/\Gamma_{\text{total}}$ Γ_{121}/Γ

VALUE (units 10^{-4})	EVTS	DOCUMENT ID	TECN	COMMENT
$23.4 \pm 2.2 \pm 1.5$	183	ABLIKIM	22B BES3	$e^+ e^-$ at 3.773 GeV

 $\Gamma(\eta \pi^+)/\Gamma_{\text{total}}$ Γ_{122}/Γ

Unseen decay modes of the η are included.

VALUE (units 10^{-4})	EVTS	DOCUMENT ID	TECN	COMMENT
37.7 ± 0.9 OUR FIT				
$37.90 \pm 0.70 \pm 0.68$	12k	ABLIKIM	18W BES3	$e^+ e^-$, 3773 MeV
• • • We do not use the following data for averages, fits, limits, etc. • • •				
$30.7 \pm 2.2 \pm 1.3$	258	ABLIKIM	16D BES3	$e^+ e^-$ at 3773 MeV
$34.3 \pm 1.4 \pm 1.7$	1033 ± 42	ARTUSO 08	CLEO	See MENDEZ 10

 $\Gamma(\eta \pi^+)/\Gamma(K^- 2\pi^+)$ Γ_{122}/Γ_{52}

Unseen decay modes of the η are included.

VALUE (units 10^{-2})	EVTS	DOCUMENT ID	TECN	COMMENT
4.02 ± 0.11 OUR FIT				Error includes scale factor of 1.1.
$3.87 \pm 0.09 \pm 0.19$	2940 ± 68	MENDEZ 10	CLEO	$e^+ e^-$ at 3774 MeV
• • • We do not use the following data for averages, fits, limits, etc. • • •				
$3.81 \pm 0.26 \pm 0.21$	377 ± 26	RUBIN 06	CLEO	See ARTUSO 08

 $\Gamma(\eta \pi^+ \pi^0)/\Gamma_{\text{total}}$ Γ_{123}/Γ

VALUE (units 10^{-4})	EVTS	DOCUMENT ID	TECN	COMMENT
20.5 ± 3.5 OUR AVERAGE				Error includes scale factor of 2.2.
$22.3 \pm 1.5 \pm 1.0$	381	ABLIKIM	20G BES3	$e^+ e^-$, 3773 MeV
$13.8 \pm 3.1 \pm 1.6$	149 ± 34	ARTUSO 08	CLEO	$e^+ e^-$ at $\psi(3770)$
• • • We do not use the following data for averages, fits, limits, etc. • • •				
$24.7 \pm 9.3 \pm 1.6$	42	ABLIKIM	20AA BES3	$e^+ e^-$, 3773 MeV

 $\Gamma(\eta 2\pi^+ \pi^-)/\Gamma_{\text{total}}$ Γ_{124}/Γ

VALUE (units 10^{-3})	EVTS	DOCUMENT ID	TECN	COMMENT
$3.41 \pm 0.17 \pm 0.10$	515	ABLIKIM	20V BES3	$e^+ e^-$, 3773 MeV

 $\Gamma(\eta \pi^+ 2\pi^0)/\Gamma_{\text{total}}$ Γ_{125}/Γ

VALUE (units 10^{-3})	EVTS	DOCUMENT ID	TECN	COMMENT
$3.20 \pm 0.28 \pm 0.17$	190	ABLIKIM	20V BES3	$e^+ e^-$, 3773 MeV

 $\Gamma(\eta \pi^+ 3\pi^0)/\Gamma_{\text{total}}$ Γ_{126}/Γ

VALUE (units 10^{-4})	EVTS	DOCUMENT ID	TECN	COMMENT
$28.9 \pm 4.0 \pm 2.2$	80	ABLIKIM	22B BES3	$e^+ e^-$ at 3.773 GeV

 $\Gamma(\eta 2\pi^+ \pi^- \pi^0)/\Gamma_{\text{total}}$ Γ_{127}/Γ

VALUE (units 10^{-4})	EVTS	DOCUMENT ID	TECN	COMMENT
$38.8 \pm 3.2 \pm 1.2$	190	ABLIKIM	22B BES3	$e^+ e^-$ at 3.773 GeV

 $\Gamma(\eta \eta \pi^+)/\Gamma_{\text{total}}$ Γ_{128}/Γ

VALUE (units 10^{-4})	EVTS	DOCUMENT ID	TECN	COMMENT
$29.6 \pm 2.4 \pm 1.0$	179	ABLIKIM	20G BES3	$e^+ e^-$, 3773 MeV

 $\Gamma(\omega \pi^+)/\Gamma_{\text{total}}$ Γ_{129}/Γ

Unseen decay modes of the ω are included.

VALUE (units 10^{-4})	CL%	EVTS	DOCUMENT ID	TECN	COMMENT
$2.79 \pm 0.57 \pm 0.16$		79	ABLIKIM	16D BES3	$e^+ e^-$ at 3773 MeV
• • • We do not use the following data for averages, fits, limits, etc. • • •					
<3.4		90	RUBIN 06	CLEO	$e^+ e^-$ at $\psi(3770)$

 $\Gamma(\omega \pi^+ \pi^0)/\Gamma_{\text{total}}$ Γ_{130}/Γ

VALUE (units 10^{-3})	EVTS	DOCUMENT ID	TECN	COMMENT
$3.87 \pm 0.83 \pm 0.25$	233	¹ ABLIKIM	20AA BES3	$e^+ e^-$, 3773 MeV
¹ ABLIKIM 20AA reports a statistical significance of 7.7 σ for this measurement.				

 $\Gamma(\eta'(958) \pi^+)/\Gamma_{\text{total}}$ Γ_{131}/Γ

Unseen decay modes of the $\eta'(958)$ are included.

VALUE (units 10^{-4})	EVTS	DOCUMENT ID	TECN	COMMENT
49.7 ± 1.9 OUR FIT				
$51.2 \pm 1.4 \pm 2.1$	3.1k	ABLIKIM	18W BES3	$e^+ e^-$, 3773 MeV
• • • We do not use the following data for averages, fits, limits, etc. • • •				
$44.2 \pm 2.5 \pm 2.9$	352 ± 20	ARTUSO 08	CLEO	See MENDEZ 10

 $\Gamma(\eta'(958) \pi^+)/\Gamma(K^- 2\pi^+)$ Γ_{131}/Γ_{52}

Unseen decay modes of the $\eta'(958)$ are included.

VALUE (units 10^{-2})	EVTS	DOCUMENT ID	TECN	COMMENT
5.30 ± 0.21 OUR FIT				
$5.12 \pm 0.17 \pm 0.25$	1037 ± 35	MENDEZ 10	CLEO	$e^+ e^-$ at 3774 MeV

 $\Gamma(\eta'(958) \pi^+ \pi^0)/\Gamma_{\text{total}}$ Γ_{132}/Γ

Unseen decay modes of the $\eta'(958)$ are included.

VALUE (units 10^{-4})	EVTS	DOCUMENT ID	TECN	COMMENT
$15.7 \pm 4.3 \pm 2.5$	33 ± 9	ARTUSO 08	CLEO	$e^+ e^-$ at $\psi(3770)$

Meson Particle Listings

D^\pm

Hadronic modes with a $K\bar{K}$ pair

$\Gamma(K_S^0 K^+)/\Gamma_{\text{total}}$					Γ_{133}/Γ
VALUE (units 10^{-3})	EVTS	DOCUMENT ID	TECN	COMMENT	
3.04 ± 0.09 OUR FIT				Error includes scale factor of 2.2.	
3.183 ± 0.029 ± 0.060	18k	ABLIKIM	18w BES3	e^+e^- , 3773 MeV	
• • • We do not use the following data for averages, fits, limits, etc. • • •					
3.02 ± 0.09 ± 0.08	780	ABLIKIM	19M BES3	See ABLIKIM 18w.	
3.14 ± 0.09 ± 0.08	1971 ± 51	BONVICINI	08 CLEO	See MENDEZ 10	

$\Gamma(K_S^0 K^+)/\Gamma(K_S^0 \pi^+)$					Γ_{133}/Γ_{50}
VALUE	EVTS	DOCUMENT ID	TECN	COMMENT	
0.194 ± 0.006 OUR FIT				Error includes scale factor of 2.8.	
0.1901 ± 0.0024 OUR AVERAGE					
0.1899 ± 0.0011 ± 0.0022	101k ± 561	WON	09 BELL	e^+e^- at $\Upsilon(4S)$	
0.1892 ± 0.0155 ± 0.0073	278 ± 21	ARMS	04 CLEO	$e^+e^- \approx 10$ GeV	
0.1996 ± 0.0119 ± 0.0096	949	LINK	02b FOCS	$\gamma A, \bar{E}_\gamma \approx 180$ GeV	
• • • We do not use the following data for averages, fits, limits, etc. • • •					
0.222 ± 0.037 ± 0.013	63 ± 10	ABLIKIM	05F BES	$e^+e^- \approx \psi(3770)$	
0.222 ± 0.041 ± 0.019	70	BISHAI	97 CLEO	See ARMS 04	
0.25 ± 0.04 ± 0.02	129	FRABETTI	95 E687	$\gamma Be, \bar{E}_\gamma \approx 200$ GeV	
0.271 ± 0.065 ± 0.039	69	ANJOS	90c E691	γBe	
0.317 ± 0.086 ± 0.048	31	BALTRUSAIT.	.85E MRK3	e^+e^- 3.77 GeV	
0.25 ± 0.15	6	SCHINDLER	81 MRK2	e^+e^- 3.771 GeV	

$\Gamma(K_S^0 K^+)/\Gamma(K^- 2\pi^+)$					Γ_{133}/Γ_{52}
VALUE (units 10^{-2})	EVTS	DOCUMENT ID	TECN	COMMENT	
3.24 ± 0.09 OUR FIT				Error includes scale factor of 2.3.	
3.35 ± 0.06 ± 0.07	5161 ± 86	MENDEZ	10 CLEO	e^+e^- at 3774 MeV	
• • • We do not use the following data for averages, fits, limits, etc. • • •					
3.02 ± 0.18 ± 0.15	949	¹ LINK	02b FOCS	γ nucleus, $\bar{E}_\gamma \approx 180$ GeV	
¹ This LINK 02b result is redundant with a result in the previous datablock.					

$\Gamma(K_S^0 K^+)/\Gamma_{\text{total}}$					Γ_{134}/Γ
VALUE (units 10^{-3})	EVTS	DOCUMENT ID	TECN	COMMENT	
3.21 ± 0.11 ± 0.11	650	ABLIKIM	19M BES3	e^+e^- at 3773 MeV	

$\Gamma(K_S^0 K^+ \pi^0)/\Gamma_{\text{total}}$					Γ_{135}/Γ
VALUE (units 10^{-3})	EVTS	DOCUMENT ID	TECN	COMMENT	
5.07 ± 0.19 ± 0.23	470	ABLIKIM	19M BES3	e^+e^- at 3773 MeV	

$\Gamma(K^*(892)^+ K_S^0, K^{*+} \rightarrow K^+ \pi^0)/\Gamma(K_S^0 K^+ \pi^0)$					$\Gamma_{136}/\Gamma_{135}$
VALUE	EVTS	DOCUMENT ID	TECN	COMMENT	
0.571 ± 0.026 ± 0.042	692	¹ ABLIKIM	21AD BES3	e^+e^- at 3.773 GeV	
¹ ABLIKIM 21AD value is a fit fraction from an amplitude analysis of $D^+ \rightarrow K^+ K_S^0 \pi^0$ with four components. Reconstructs the $K^*(892)^+$ from its $K^+ \pi^0$ final state.					

$\Gamma(\bar{K}^*(892)^0 K^+, \bar{K}^{*0} \rightarrow K_S^0 \pi^0)/\Gamma(K_S^0 K^+ \pi^0)$					$\Gamma_{137}/\Gamma_{135}$
VALUE	EVTS	DOCUMENT ID	TECN	COMMENT	
1.02 ± 0.015 ± 0.022	692	¹ ABLIKIM	21AD BES3	e^+e^- at 3.773 GeV	
¹ ABLIKIM 21AD value is a fit fraction from an amplitude analysis of $D^+ \rightarrow K^+ K_S^0 \pi^0$ with four components. Reconstructs the $\bar{K}^*(892)^0$ from its $K_S^0 \pi^0$ final state.					

$\Gamma(K^*(892)^+ K_S^0)/\Gamma(K_S^0 \pi^+)$					Γ_{138}/Γ_{50}
VALUE	EVTS	DOCUMENT ID	TECN	COMMENT	
Unseen decay modes of the $K^*(892)^+$ are included.					
• • • We do not use the following data for averages, fits, limits, etc. • • •					
1.1 ± 0.3 ± 0.4	67	FRABETTI	95 E687	$\gamma Be, \bar{E}_\gamma \approx 200$ GeV	

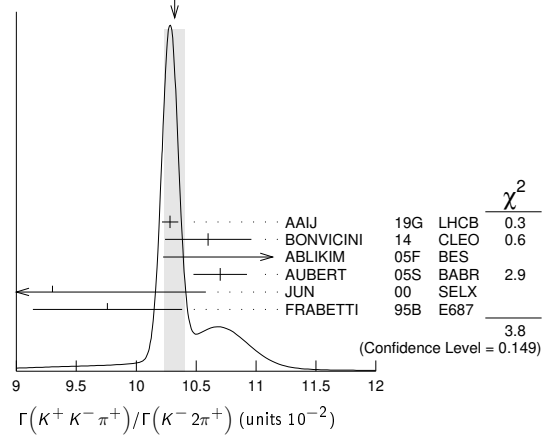
$\Gamma(K_S^0 K^+ \pi^0)/\Gamma_{\text{total}}$					Γ_{139}/Γ
VALUE (units 10^{-3})	EVTS	DOCUMENT ID	TECN	COMMENT	
5.24 ± 0.22 ± 0.22	410	ABLIKIM	19M BES3	e^+e^- at 3773 MeV	

$\Gamma(K^+ K^- \pi^+)/\Gamma_{\text{total}}$					Γ_{140}/Γ
VALUE (units 10^{-2})	EVTS	DOCUMENT ID	TECN	COMMENT	
• • • We do not use the following data for averages, fits, limits, etc. • • •					
0.935 ± 0.017 ± 0.024		¹ DOBBS	07 CLEO	See BONVICINI 14	
0.97 ± 0.04 ± 0.04	1250 ± 40	¹ HE	05 CLEO	See DOBBS 07	
¹ DOBBS 07 and HE 05 use single- and double-tagged events in an overall fit. DOBBS 07 supersedes HE 05.					

$\Gamma(K^+ K^- \pi^+)/\Gamma(K^- 2\pi^+)$					Γ_{140}/Γ_{52}
VALUE (units 10^{-2})	EVTS	DOCUMENT ID	TECN	COMMENT	
10.32 ± 0.09 OUR AVERAGE				Error includes scale factor of 1.4. See the ideogram below.	
10.282 ± 0.002 ± 0.068	23M	AAIJ	19G LHCB	pp at 8 TeV	
10.6 ± 0.2 ± 0.3		BONVICINI	14 CLEO	All CLEO-c runs	
11.7 ± 1.3 ± 0.7	181 ± 20	ABLIKIM	05F BES	$e^+e^- \approx \psi(3770)$	
10.7 ± 0.1 ± 0.2	43k	AUBERT	05S BABR	$e^+e^- \approx \Upsilon(4S)$	

9.3 ± 1.0 $^{+0.8}_{-0.6}$	JUN	00 SELX	Σ^- nucleus, 600 GeV
9.76 ± 0.42 ± 0.46	FRABETTI	95b E687	$\gamma Be, \bar{E}_\gamma \approx 200$ GeV

WEIGHTED AVERAGE
10.32 ± 0.09 (Error scaled by 1.4)



$\Gamma(K^+ \bar{K}^*(892)^0, \bar{K}^*(892)^0 \rightarrow K^- \pi^+)/\Gamma(K^+ K^- \pi^+)$					$\Gamma_{141}/\Gamma_{140}$
VALUE (%)	DOCUMENT ID	TECN	COMMENT		
25.7 ± 0.5 ± 0.4	RUBIN	08 CLEO	Dalitz fit, 19,458 ± 163 evts		
• • • We do not use the following data for averages, fits, limits, etc. • • •					
30.1 ± 2.0 ± 2.5	FRABETTI	95b E687	Dalitz fit, 915 evts		

$\Gamma(K^+ \bar{K}_S^*(1430)^0, \bar{K}_S^*(1430)^0 \rightarrow K^- \pi^+)/\Gamma(K^+ K^- \pi^+)$					$\Gamma_{142}/\Gamma_{140}$
VALUE (%)	DOCUMENT ID	TECN	COMMENT		
18.8 ± 1.2 ± 3.3	RUBIN	08 CLEO	Dalitz fit, 19,458 ± 163 evts		
• • • We do not use the following data for averages, fits, limits, etc. • • •					
37.0 ± 3.5 ± 1.8	FRABETTI	95b E687	Dalitz fit, 915 evts		

$\Gamma(K^+ \bar{K}_2^*(1430)^0, \bar{K}_2^*(1430)^0 \rightarrow K^- \pi^+)/\Gamma(K^+ K^- \pi^+)$					$\Gamma_{143}/\Gamma_{140}$
VALUE (%)	DOCUMENT ID	TECN	COMMENT		
1.7 ± 0.4 ± 1.2	RUBIN	08 CLEO	Dalitz fit, 19,458 ± 163 evts		

$\Gamma(K^+ \bar{K}_0^*(700), \bar{K}_0^*(700) \rightarrow K^- \pi^+)/\Gamma(K^+ K^- \pi^+)$					$\Gamma_{144}/\Gamma_{140}$
VALUE (%)	DOCUMENT ID	TECN	COMMENT		
7.0 ± 0.8 ± 3.5	RUBIN	08 CLEO	Dalitz fit, 19,458 ± 163 evts		

$\Gamma(a_0(1450)^0 \pi^+, a_0^0 \rightarrow K^+ K^-)/\Gamma(K^+ K^- \pi^+)$					$\Gamma_{145}/\Gamma_{140}$
VALUE (%)	DOCUMENT ID	TECN	COMMENT		
4.6 ± 0.6 ± 7.2	RUBIN	08 CLEO	Dalitz fit, 19,458 ± 163 evts		

$\Gamma(\phi(1680) \pi^+, \phi \rightarrow K^+ K^-)/\Gamma(K^+ K^- \pi^+)$					$\Gamma_{146}/\Gamma_{140}$
VALUE (%)	DOCUMENT ID	TECN	COMMENT		
0.51 ± 0.11 ± 0.37	RUBIN	08 CLEO	Dalitz fit, 19,458 ± 163 evts		

$\Gamma(\phi \pi^+, \phi \rightarrow K^+ K^-)/\Gamma(K^+ K^- \pi^+)$					$\Gamma_{147}/\Gamma_{140}$
VALUE (%)	DOCUMENT ID	TECN	COMMENT		
27.8 ± 0.4 ± 0.2	RUBIN	08 CLEO	Dalitz fit, 19,458 ± 163 evts		
• • • We do not use the following data for averages, fits, limits, etc. • • •					
29.2 ± 3.1 ± 3.0	FRABETTI	95b E687	Dalitz fit, 915 evts		

$\Gamma(\phi \pi^+)/\Gamma_{\text{total}}$					Γ_{148}/Γ
VALUE (units 10^{-3})	EVTS	DOCUMENT ID	TECN	COMMENT	
5.70 ± 0.05 ± 0.13	18k	ABLIKIM	19b1 BES3	e^+e^- at 3773 MeV	

$\Gamma(K^+ K^- \pi^+ \pi^0)/\Gamma_{\text{total}}$					Γ_{149}/Γ
VALUE (units 10^{-3})	EVTS	DOCUMENT ID	TECN	COMMENT	
6.62 ± 0.20 ± 0.25	1.3k	ABLIKIM	20ac BES3	e^+e^- at 3.773 GeV	

$\Gamma(K^+ K^- \pi^+ \pi^0)/\Gamma(K^- 2\pi^+ \pi^0)$					Γ_{149}/Γ_{75}
VALUE (units 10^{-2})	EVTS	DOCUMENT ID	TECN	COMMENT	
11.32 ± 0.13 ± 0.26	50k	LI	23G BELL	e^+e^- at/near $\Upsilon(nS)$, $n=1, \dots, 5$	

$\Gamma(K_S^0 K_S^0 \pi^+)/\Gamma_{\text{total}}$		Γ_{150}/Γ	
VALUE (units 10^{-4})	EVTS	DOCUMENT ID	TECN COMMENT
$27.0 \pm 0.5 \pm 1.2$	4897	ABLIKIM	17A BES3 $e^+e^- \rightarrow \psi(3770)$

$\Gamma(K_S^0 K_S^0 \pi^+ \pi^0)/\Gamma_{\text{total}}$		Γ_{151}/Γ	
VALUE (units 10^{-3})	EVTS	DOCUMENT ID	TECN COMMENT
$1.34 \pm 0.20 \pm 0.06$	80	ABLIKIM	20Ac BES3 e^+e^- at 3.773 GeV

$\Gamma(K_S^0 K^+ \eta)/\Gamma_{\text{total}}$		Γ_{152}/Γ	
VALUE (units 10^{-4})	EVTS	DOCUMENT ID	TECN COMMENT
$1.85 \pm 0.52 \pm 0.08$	14	ABLIKIM	20v BES3 e^+e^- , 3773 MeV

$\Gamma(K^+ K_S^0 \pi^+ \pi^-)/\Gamma_{\text{total}}$		Γ_{153}/Γ	
VALUE (units 10^{-3})	EVTS	DOCUMENT ID	TECN COMMENT
$1.89 \pm 0.12 \pm 0.05$	277	ABLIKIM	20Ac BES3 e^+e^- at 3.773 GeV

$\Gamma(K^+ K_S^0 \pi^+ \pi^-)/\Gamma(K_S^0 2\pi^+ \pi^-)$		Γ_{153}/Γ_{76}	
VALUE (units 10^{-2})	EVTS	DOCUMENT ID	TECN COMMENT
$5.62 \pm 0.39 \pm 0.40$	469 ± 32	LINK	01c FOCS γ nucleus, $\bar{E}_\gamma \approx 180$ GeV

$\Gamma(K_S^0 K^+ \pi^0 \pi^0)/\Gamma_{\text{total}}$		Γ_{154}/Γ	
VALUE (units 10^{-4})	EVTS	DOCUMENT ID	TECN COMMENT
$5.8 \pm 1.2 \pm 0.4$	34	ABLIKIM	20Ac BES3 e^+e^- at 3.773 GeV

$\Gamma(K_S^0 K^- 2\pi^+)/\Gamma_{\text{total}}$		Γ_{155}/Γ	
VALUE (units 10^{-3})	EVTS	DOCUMENT ID	TECN COMMENT
$2.27 \pm 0.12 \pm 0.06$	467	ABLIKIM	20Ac BES3 e^+e^- at 3.773 GeV

$\Gamma(K_S^0 K^- 2\pi^+)/\Gamma(K_S^0 2\pi^+ \pi^-)$		Γ_{155}/Γ_{76}	
VALUE (units 10^{-2})	EVTS	DOCUMENT ID	TECN COMMENT
$7.68 \pm 0.41 \pm 0.32$	670 ± 35	LINK	01c FOCS γ nucleus, $\bar{E}_\gamma \approx 180$ GeV

$\Gamma(K^+ K^- 2\pi^+ \pi^-)/\Gamma(K^- 3\pi^+ \pi^-)$		Γ_{156}/Γ_{86}	
VALUE	EVTS	DOCUMENT ID	TECN COMMENT
$0.040 \pm 0.009 \pm 0.019$	38	LINK	03D FOCS $\gamma A, \bar{E}_\gamma \approx 180$ GeV

$\Gamma(\phi \pi^+ \pi^0)/\Gamma_{\text{total}}$		Γ_{157}/Γ	
VALUE	DOCUMENT ID	TECN	COMMENT
0.023 ± 0.010	¹ BARLAG	92c ACCM	π^- Cu 230 GeV
¹ BARLAG 92c computes the branching fraction using topological normalization.			

$\Gamma(\phi \rho^+)/\Gamma(K^- 2\pi^+)$		Γ_{158}/Γ_{52}	
VALUE	CL%	DOCUMENT ID	TECN COMMENT
<0.16	90	DAOUDI	92 CLEO $e^+e^- \approx 10.5$ GeV

$\Gamma(K^+ K^- \pi^+ \pi^0 \text{ non-}\phi)/\Gamma_{\text{total}}$		Γ_{159}/Γ	
VALUE	DOCUMENT ID	TECN	COMMENT
0.015 ± 0.007 -0.006	¹ BARLAG	92c ACCM	π^- Cu 230 GeV
¹ BARLAG 92c computes the branching fraction using topological normalization.			

$\Gamma(K^+ K^- \pi^+ \pi^0 \text{ non-}\phi)/\Gamma(K^- 2\pi^+)$		Γ_{159}/Γ_{52}	
VALUE	CL%	DOCUMENT ID	TECN COMMENT
<0.25	90	ANJOS	89E E691 Photoproduction

———— Doubly Cabibbo-suppressed modes ————

$\Gamma(K^+ \pi^0)/\Gamma_{\text{total}}$		Γ_{160}/Γ	
VALUE (units 10^{-4})	EVTS	DOCUMENT ID	TECN COMMENT
2.08 ± 0.21 OUR FIT	Error includes scale factor of 1.4.		
2.35 ± 0.20 OUR AVERAGE			
$2.32 \pm 0.21 \pm 0.06$	1.8k	ABLIKIM	18w BES3 e^+e^- , 3773 MeV
$2.52 \pm 0.47 \pm 0.26$	189 ± 37	AUBERT,B	06F BABR $e^+e^- \approx \mathcal{T}(4S)$
• • • We do not use the following data for averages, fits, limits, etc. • • •			
$2.28 \pm 0.36 \pm 0.17$	148 ± 23	DYTMAN	06 CLEO See MENDEZ 10

$\Gamma(K^+ \pi^0)/\Gamma(K^- 2\pi^+)$		Γ_{160}/Γ_{52}	
VALUE (units 10^{-3})	EVTS	DOCUMENT ID	TECN COMMENT
2.21 ± 0.23 OUR FIT	Error includes scale factor of 1.5.		
$1.9 \pm 0.2 \pm 0.1$	343 ± 37	MENDEZ	10 CLEO e^+e^- at 3774 MeV

$\Gamma(K^+ \eta)/\Gamma_{\text{total}}$		Γ_{161}/Γ	
VALUE (units 10^{-3})	EVTS	DOCUMENT ID	TECN COMMENT
0.125 ± 0.016 OUR FIT	Error includes scale factor of 1.1.		
$0.151 \pm 0.025 \pm 0.014$	439	ABLIKIM	18w BES3 e^+e^- , 3773 MeV

$\Gamma(K^+ \eta)/\Gamma(\eta \pi^+)$		$\Gamma_{161}/\Gamma_{122}$	
VALUE (%)	EVTS	DOCUMENT ID	TECN COMMENT
3.3 ± 0.4 OUR FIT	Error includes scale factor of 1.1.		
$3.06 \pm 0.43 \pm 0.14$	166 ± 23	WON	11 BELL $e^+e^- \approx \mathcal{T}(4S)$

$\Gamma(K^+ \eta'(958))/\Gamma_{\text{total}}$		Γ_{162}/Γ	
VALUE (units 10^{-3})	EVTS	DOCUMENT ID	TECN COMMENT
0.185 ± 0.020 OUR FIT			
$0.164 \pm 0.051 \pm 0.024$	87	ABLIKIM	18w BES3 e^+e^- , 3773 MeV

$\Gamma(K^+ \eta'(958))/\Gamma(\eta'(958) \pi^+)$		$\Gamma_{162}/\Gamma_{131}$	
VALUE (%)	EVTS	DOCUMENT ID	TECN COMMENT
3.7 ± 0.4 OUR FIT			
$3.77 \pm 0.39 \pm 0.10$	180 ± 19	WON	11 BELL $e^+e^- \approx \mathcal{T}(4S)$

$\Gamma(K^+ 2\pi^0)/\Gamma_{\text{total}}$		Γ_{163}/Γ	
VALUE (units 10^{-4})	EVTS	DOCUMENT ID	TECN COMMENT
$2.1 \pm 0.4 \pm 0.1$	43	ABLIKIM	22Bk BES3 e^+e^- at 3.773 GeV

$\Gamma(K^*(892)^+ \pi^0)/\Gamma_{\text{total}}$		Γ_{164}/Γ	
VALUE (units 10^{-4})	EVTS	DOCUMENT ID	TECN COMMENT
$3.4 \pm 1.3 \pm 0.1$	17	¹ ABLIKIM	22Bk BES3 e^+e^- at 3.773 GeV

¹ ABLIKIM 22Bk report a 2.7 σ significance for the observation of this decay and assign an upper limit for this branching fraction of 5.4×10^{-4} at 90% CL. In their analysis, ABLIKIM 22Bk assume negligible interference between $D^+ \rightarrow K^{*+} \pi^0 \rightarrow K^+ \pi^0 \pi^0$ and the non-resonant decay to the same final state.

$\Gamma(K^+ \pi^+ \pi^-)/\Gamma(K^- 2\pi^+)$		Γ_{165}/Γ_{52}	
VALUE (units 10^{-3})	EVTS	DOCUMENT ID	TECN COMMENT
5.238 ± 0.025 OUR AVERAGE			
$5.231 \pm 0.009 \pm 0.023$	795k	AAIJ	19G LHCB pp at 8 TeV
$5.69 \pm 0.18 \pm 0.14$	2638 ± 84	KO	09 BELL e^+e^- at $\mathcal{T}(4S)$
$6.5 \pm 0.8 \pm 0.4$	189 ± 24	LINK	04F FOCS $\gamma A, \bar{E}_\gamma \approx 180$ GeV
$7.7 \pm 1.7 \pm 0.8$	59 ± 13	AITALA	97c E791 $\pi^- A, 500$ GeV
$7.2 \pm 2.3 \pm 1.7$	21	FRABETTI	95E E687 $\gamma Be, \bar{E}_\gamma = 220$ GeV

$\Gamma(K^+ \rho^0)/\Gamma(K^+ \pi^+ \pi^-)$		$\Gamma_{166}/\Gamma_{165}$	
VALUE	DOCUMENT ID	TECN	COMMENT
0.39 ± 0.09 OUR AVERAGE			
$0.3943 \pm 0.0787 \pm 0.0815$	LINK	04F FOCS	Dalitz fit, 189 evts
$0.37 \pm 0.14 \pm 0.07$	AITALA	97c E791	Dalitz fit, 59 evts

This is the "fit fraction" from the Dalitz-plot analysis.

$\Gamma(K^+ \eta \pi^0)/\Gamma_{\text{total}}$		Γ_{167}/Γ	
VALUE (units 10^{-4})	EVTS	DOCUMENT ID	TECN COMMENT
$2.1 \pm 0.5 \pm 0.1$	19	ABLIKIM	22Bk BES3 e^+e^- at 3.773 GeV

$\Gamma(K^*(892)^+ \eta)/\Gamma_{\text{total}}$		Γ_{168}/Γ	
VALUE (units 10^{-4})	EVTS	DOCUMENT ID	TECN COMMENT
$4.4 \pm 1.8 \pm 0.2$	11	¹ ABLIKIM	22Bk BES3 e^+e^- at 3.773 GeV

¹ ABLIKIM 22Bk report a 3.2 σ significance for the observation of this decay mode. In their analysis, ABLIKIM 22Bk assume negligible interference between $D^+ \rightarrow K^{*+} \eta \rightarrow K^+ \eta \pi^0$ and the non-resonant decay to the same final state.

$\Gamma(K^*(892)^0 \pi^+, K^*(892)^0 \rightarrow K^+ \pi^-)/\Gamma(K^+ \pi^+ \pi^-)$		$\Gamma_{169}/\Gamma_{165}$	
VALUE	DOCUMENT ID	TECN	COMMENT
0.47 ± 0.08 OUR AVERAGE			
$0.5220 \pm 0.0684 \pm 0.0638$	LINK	04F FOCS	Dalitz fit, 189 evts
$0.35 \pm 0.14 \pm 0.01$	AITALA	97c E791	Dalitz fit, 59 evts

This is the "fit fraction" from the Dalitz-plot analysis.

$\Gamma(K^+ f_0(980), f_0(980) \rightarrow \pi^+ \pi^-)/\Gamma(K^+ \pi^+ \pi^-)$		$\Gamma_{170}/\Gamma_{165}$	
VALUE	DOCUMENT ID	TECN	COMMENT
$0.0892 \pm 0.0333 \pm 0.0412$	LINK	04F FOCS	Dalitz fit, 189 evts

This is the "fit fraction" from the Dalitz-plot analysis.

$\Gamma(K_S^2(1430)^0 \pi^+, K_S^2(1430)^0 \rightarrow K^+ \pi^-)/\Gamma(K^+ \pi^+ \pi^-)$		$\Gamma_{171}/\Gamma_{165}$	
VALUE	DOCUMENT ID	TECN	COMMENT
$0.0803 \pm 0.0372 \pm 0.0391$	LINK	04F FOCS	Dalitz fit, 189 evts

This is the "fit fraction" from the Dalitz-plot analysis.

$\Gamma(K^+ \pi^+ \pi^- \text{ nonresonant})/\Gamma(K^+ \pi^+ \pi^-)$		$\Gamma_{172}/\Gamma_{165}$	
VALUE	DOCUMENT ID	TECN	COMMENT
$0.36 \pm 0.14 \pm 0.07$	¹ AITALA	97c E791	Dalitz fit, 59 evts

This is the "fit fraction" from the Dalitz-plot analysis.

• • • We do not use the following data for averages, fits, limits, etc. • • •

¹ LINK 04F, with three times as many events, finds no need for a nonresonant amplitude.

Meson Particle Listings

 D^\pm $\Gamma(K^+\pi^+\pi^-\pi^0)/\Gamma_{\text{total}}$ Γ_{173}/Γ

VALUE (units 10^{-3})	EVTS	DOCUMENT ID	TECN	COMMENT
$1.21 \pm 0.08 \pm 0.03$	350	¹ ABLIKIM	20z BES3	e^+e^- at 3773 MeV

¹ ABLIKIM 20z subtracted the known branching fractions of $D^+ \rightarrow K^+\eta$, $D^+ \rightarrow K^+\phi$, and $D^+ \rightarrow K^+\omega$ to obtain an estimate of the non-resonant component (ignoring interference effects and possible additional resonant contributions) $B(D^+ \rightarrow K^+\pi^+\pi^-\pi^0 \text{ non-resonant}) = (1.13 \pm 0.08 \pm 0.03) \times 10^{-3}$.

 $\Gamma(K^+\pi^+\pi^-\pi^0)/\Gamma(K^-2\pi^+\pi^0)$ Γ_{173}/Γ_{75}

VALUE (units 10^{-2})	EVTS	DOCUMENT ID	TECN	COMMENT
$1.68 \pm 0.11 \pm 0.03$	3.6k	LI	23g BELL	e^+e^- at/near $\mathcal{T}(nS)$, $n=1, \dots, 5$

 $\Gamma(K^+\pi^+\pi^-\pi^0 \text{ nonresonant})/\Gamma_{\text{total}}$ Γ_{174}/Γ

VALUE (units 10^{-3})	EVTS	DOCUMENT ID	TECN	COMMENT
1.10 ± 0.07 OUR AVERAGE				
$1.03 \pm 0.12 \pm 0.06$	112	¹ ABLIKIM	21B BES3	e^+e^- at 3.773 GeV
$1.13 \pm 0.08 \pm 0.03$	350	² ABLIKIM	20z BES3	e^+e^- at 3.773 GeV

¹ ABLIKIM 21B result has subtracted the known branching fractions of $D^+ \rightarrow K^+\eta$, $D^+ \rightarrow K^+\phi$, and $D^+ \rightarrow K^+\omega$ resonances (ignoring interference effects). The result including these components is measured to be $B(D^+ \rightarrow K^+\pi^+\pi^-\pi^0) = (1.11 \pm 0.12) \times 10^{-3}$, where the uncertainty is statistical only.

² ABLIKIM 20z result has subtracted the known branching fractions of $D^+ \rightarrow K^+\eta$, $D^+ \rightarrow K^+\phi$, and $D^+ \rightarrow K^+\omega$, ignoring interference effects. The result including these components is measured to be $(1.21 \pm 0.08 \pm 0.03) \times 10^{-3}$.

 $\Gamma(K^+\omega)/\Gamma_{\text{total}}$ Γ_{175}/Γ

VALUE (units 10^{-5})	EVTS	DOCUMENT ID	TECN	COMMENT
$5.7 \pm 2.3 \pm 0.2$	9	ABLIKIM	20z BES3	e^+e^- , 3773 MeV

 $\Gamma(2K^+K^-)/\Gamma(K^-2\pi^+)$ Γ_{176}/Γ_{52}

VALUE (units 10^{-4})	EVTS	DOCUMENT ID	TECN	COMMENT
6.54 ± 0.05 OUR AVERAGE				
$6.541 \pm 0.025 \pm 0.042$	134k	AAIJ	19g LHCb	pp at 8 TeV
$9.49 \pm 2.17 \pm 0.22$	65	¹ LINK	02i FOCS	γ nucleus, ≈ 180 GeV

¹ LINK 02i finds little evidence for ϕK^+ or $f_0(980) K^+$ submodes.

 $\Gamma(K^+\phi(1020), \phi \rightarrow K^+K^-)/\Gamma(2K^+K^-)$ $\Gamma_{178}/\Gamma_{176}$

VALUE (%)	DOCUMENT ID	TECN	COMMENT
7.1 ± 0.9	¹ AAIJ	19H LHCb	pp at 8 TeV

¹ Fit fraction from a Dalitz plot analysis of $D^+ \rightarrow K^+K^+K^-$ decays. The last uncertainty is due to the amplitude model.

 $\Gamma(K^+(K^+K^-)_{s\text{-wave}})/\Gamma(2K^+K^-)$ $\Gamma_{179}/\Gamma_{176}$

VALUE	DOCUMENT ID	TECN	COMMENT
0.94 ± 0.01	¹ AAIJ	19H LHCb	pp at 8 TeV

¹ Fit fraction from a Dalitz plot analysis of $D^+ \rightarrow K^+K^+K^-$ decays. The last uncertainty is due to the amplitude model.

Rare or forbidden modes

 $\Gamma(\pi^+e^+e^-)/\Gamma_{\text{total}}$ Γ_{180}/Γ

A test for the $\Delta C = 1$ weak neutral current. Allowed by higher-order electroweak interactions.

VALUE	CL%	DOCUMENT ID	TECN	COMMENT
$<1.1 \times 10^{-6}$	90	LEES	11g BABR	$e^+e^- \approx \mathcal{T}(4S)$
$<1.1 \times 10^{-6}$	90	AAIJ	21t LHCb	$1.6 \text{ fb}^{-1} pp$
$<1.6 \times 10^{-6}$	90	¹ RUBIN	10 CLEO	e^+e^- at $\psi(3770)$
$<5.9 \times 10^{-6}$	90	HE	05A CLEO	See RUBIN 10
$<7.4 \times 10^{-6}$	90	HE	05A CLEO	See RUBIN 10
$<5.2 \times 10^{-5}$	90	AITALA	99g E791	$\pi^- N$ 500 GeV
$<1.1 \times 10^{-4}$	90	FRABETTI	97B E687	γ Be, $\bar{E}_\gamma \approx 220$ GeV
$<6.6 \times 10^{-5}$	90	AITALA	96 E791	$\pi^- N$ 500 GeV
$<2.5 \times 10^{-3}$	90	WEIR	90B MRK2	e^+e^- 29 GeV
$<2.6 \times 10^{-3}$	90	HAAS	88 CLEO	e^+e^- 10 GeV

¹ This RUBIN 10 limit is for the e^+e^- mass in the continuum away from the $\phi(1020)$. See the next data block.

 $\Gamma(\pi^+\pi^0e^+e^-)/\Gamma_{\text{total}}$ Γ_{181}/Γ

VALUE	CL%	DOCUMENT ID	TECN	COMMENT
$<1.4 \times 10^{-5}$	90	ABLIKIM	18P BES3	e^+e^- , 3773 MeV

 $\Gamma(\pi^+\phi, \phi \rightarrow e^+e^-)/\Gamma_{\text{total}}$ Γ_{182}/Γ

This is not a test for the $\Delta C = 1$ weak neutral current, but leads to the $\pi^+e^+e^-$ final state.

VALUE	EVTS	DOCUMENT ID	TECN	COMMENT
$(1.7 \pm 1.4 \pm 0.1) \times 10^{-6}$	4	¹ RUBIN	10 CLEO	e^+e^- at $\psi(3770)$

$\bullet \bullet \bullet$ We do not use the following data for averages, fits, limits, etc. $\bullet \bullet \bullet$

$(2.7 \pm 3.6 \pm 0.2) \times 10^{-6}$	2	HE	05A CLEO	See RUBIN 10
--	---	----	----------	--------------

¹ This RUBIN 10 result is consistent with the known $D^+ \rightarrow \phi\pi^+$ and $\phi \rightarrow e^+e^-$ fractions.

 $\Gamma(\pi^+\mu^+\mu^-)/\Gamma_{\text{total}}$ Γ_{183}/Γ

A test for the $\Delta C = 1$ weak neutral current. Allowed by higher-order electroweak interactions.

VALUE	CL%	DOCUMENT ID	TECN	COMMENT
$<6.7 \times 10^{-8}$	90	AAIJ	21t LHCb	$1.6 \text{ fb}^{-1} pp$
$<6.7 \times 10^{-8}$	90	AAIJ	21t LHCb	$1.6 \text{ fb}^{-1} pp$
$<7.3 \times 10^{-8}$	90	AAIJ	13AF LHCb	pp at 7 TeV
$<6.5 \times 10^{-6}$	90	LEES	11g BABR	$e^+e^- \approx \mathcal{T}(4S)$
$<3.9 \times 10^{-6}$	90	¹ ABAZOV	08D D0	$p\bar{p}$, $E_{\text{cm}} = 1.96$ TeV
$<8.8 \times 10^{-6}$	90	LINK	03F FOCS	γA , $\bar{E}_\gamma \approx 180$ GeV
$<1.5 \times 10^{-5}$	90	AITALA	99G E791	$\pi^- N$ 500 GeV
$<8.9 \times 10^{-5}$	90	FRABETTI	97B E687	γ Be, $\bar{E}_\gamma \approx 220$ GeV
$<1.8 \times 10^{-5}$	90	AITALA	96 E791	$\pi^- N$ 500 GeV
$<2.2 \times 10^{-4}$	90	KODAMA	95 E653	π^- emulsion 600 GeV
$<5.9 \times 10^{-3}$	90	WEIR	90B MRK2	e^+e^- 29 GeV
$<2.9 \times 10^{-3}$	90	HAAS	88 CLEO	e^+e^- 10 GeV

¹ This ABAZOV 08D limit is for the $\mu^+\mu^-$ mass in the continuum away from the $\phi(1020)$. See the next data block.

 $\Gamma(\pi^+\phi, \phi \rightarrow \mu^+\mu^-)/\Gamma_{\text{total}}$ Γ_{184}/Γ

This is not a test for the $\Delta C = 1$ weak neutral current, but leads to the $\pi^+\mu^+\mu^-$ final state.

VALUE	DOCUMENT ID	TECN	COMMENT
$(1.8 \pm 0.5 \pm 0.6) \times 10^{-6}$	¹ ABAZOV	08D D0	$p\bar{p}$, $E_{\text{cm}} = 1.96$ TeV

¹ This ABAZOV 08D value is consistent with the known $D^+ \rightarrow \phi\pi^+$ and $\phi \rightarrow \mu^+\mu^-$ fractions.

 $\Gamma(\rho^+\mu^+\mu^-)/\Gamma_{\text{total}}$ Γ_{185}/Γ

A test for the $\Delta C = 1$ weak neutral current. Allowed by higher-order electroweak interactions.

VALUE	CL%	DOCUMENT ID	TECN	COMMENT
$<5.6 \times 10^{-4}$	90	KODAMA	95 E653	π^- emulsion 600 GeV

 $\Gamma(K^+e^+e^-)/\Gamma_{\text{total}}$ Γ_{186}/Γ

Both quarks would have to change flavor for this decay to occur.

VALUE	CL%	DOCUMENT ID	TECN	COMMENT
$<8.5 \times 10^{-7}$	90	AAIJ	21t LHCb	$1.6 \text{ fb}^{-1} pp$
$<8.5 \times 10^{-7}$	90	AAIJ	21t LHCb	$1.6 \text{ fb}^{-1} pp$
$<1.0 \times 10^{-6}$	90	LEES	11g BABR	$e^+e^- \approx \mathcal{T}(4S)$
$<3.0 \times 10^{-6}$	90	RUBIN	10 CLEO	e^+e^- at $\psi(3770)$
$<6.2 \times 10^{-6}$	90	HE	05A CLEO	See RUBIN 10
$<2.0 \times 10^{-4}$	90	AITALA	99G E791	$\pi^- N$ 500 GeV
$<2.0 \times 10^{-4}$	90	FRABETTI	97B E687	γ Be, $\bar{E}_\gamma \approx 220$ GeV
$<4.8 \times 10^{-3}$	90	WEIR	90B MRK2	e^+e^- 29 GeV

 $\Gamma(K^+\pi^0e^+e^-)/\Gamma_{\text{total}}$ Γ_{187}/Γ

VALUE	CL%	DOCUMENT ID	TECN	COMMENT
$<1.5 \times 10^{-5}$	90	ABLIKIM	18P BES3	e^+e^- , 3773 MeV

 $\Gamma(K_S^0\pi^+e^+e^-)/\Gamma_{\text{total}}$ Γ_{188}/Γ

VALUE	CL%	DOCUMENT ID	TECN	COMMENT
$<2.6 \times 10^{-5}$	90	ABLIKIM	18P BES3	e^+e^- , 3773 MeV

 $\Gamma(K_S^0K^+e^+e^-)/\Gamma_{\text{total}}$ Γ_{189}/Γ

VALUE	CL%	DOCUMENT ID	TECN	COMMENT
$<1.1 \times 10^{-5}$	90	ABLIKIM	18P BES3	e^+e^- , 3773 MeV

 $\Gamma(K^+\mu^+\mu^-)/\Gamma_{\text{total}}$ Γ_{190}/Γ

Both quarks would have to change flavor for this decay to occur.

VALUE	CL%	DOCUMENT ID	TECN	COMMENT
$<5.4 \times 10^{-8}$	90	AAIJ	21t LHCb	$1.6 \text{ fb}^{-1} pp$
$<5.4 \times 10^{-8}$	90	AAIJ	21t LHCb	$1.6 \text{ fb}^{-1} pp$
$<4.3 \times 10^{-6}$	90	LEES	11g BABR	$e^+e^- \approx \mathcal{T}(4S)$
$<9.2 \times 10^{-6}$	90	LINK	03F FOCS	γA , $\bar{E}_\gamma \approx 180$ GeV
$<4.4 \times 10^{-5}$	90	AITALA	99G E791	$\pi^- N$ 500 GeV
$<9.7 \times 10^{-5}$	90	FRABETTI	97B E687	γ Be, $\bar{E}_\gamma \approx 220$ GeV
$<3.2 \times 10^{-4}$	90	KODAMA	95 E653	π^- emulsion 600 GeV
$<9.2 \times 10^{-3}$	90	WEIR	90B MRK2	e^+e^- 29 GeV

 $\Gamma(\pi^+e^+\mu^-)/\Gamma_{\text{total}}$ Γ_{191}/Γ

A test of lepton-family-number conservation.

VALUE	CL%	DOCUMENT ID	TECN	COMMENT
$<2.1 \times 10^{-7}$	90	AAIJ	21t LHCb	$1.6 \text{ fb}^{-1} pp$
$<2.1 \times 10^{-7}$	90	AAIJ	21t LHCb	$1.6 \text{ fb}^{-1} pp$
$<2.9 \times 10^{-6}$	90	LEES	11g BABR	$e^+e^- \approx \mathcal{T}(4S)$
$<1.1 \times 10^{-4}$	90	FRABETTI	97B E687	γ Be, $\bar{E}_\gamma \approx 220$ GeV
$<3.3 \times 10^{-3}$	90	WEIR	90B MRK2	e^+e^- 29 GeV

 $\Gamma(\pi^+e^-\mu^+)/\Gamma_{\text{total}}$ Γ_{192}/Γ

A test of lepton-family-number conservation.

VALUE	CL%	DOCUMENT ID	TECN	COMMENT
$<2.2 \times 10^{-7}$	90	AAIJ	21t LHCb	$1.6 \text{ fb}^{-1} pp$
$<2.2 \times 10^{-7}$	90	AAIJ	21t LHCb	$1.6 \text{ fb}^{-1} pp$
$<3.6 \times 10^{-6}$	90	LEES	11g BABR	$e^+e^- \approx \mathcal{T}(4S)$
$<1.3 \times 10^{-4}$	90	FRABETTI	97B E687	γ Be, $\bar{E}_\gamma \approx 220$ GeV
$<3.3 \times 10^{-3}$	90	WEIR	90B MRK2	e^+e^- 29 GeV

Γ(K⁺e⁺μ⁻)/Γ_{total} **Γ₁₉₃/Γ**

A test of lepton-family-number conservation.

VALUE	CL%	DOCUMENT ID	TECN	COMMENT
<7.5 × 10 ⁻⁸	90	AAIJ	21T	LHCB 1.6 fb ⁻¹ pp
••• We do not use the following data for averages, fits, limits, etc. •••				
<1.2 × 10 ⁻⁶	90	LEES	11G	BABR e ⁺ e ⁻ ≈ 7(45)
<1.3 × 10 ⁻⁴	90	FRABETTI	97B	E687 γ Be, E _γ ≈ 220 GeV
<3.4 × 10 ⁻³	90	WEIR	90B	MRK2 e ⁺ e ⁻ 29 GeV

Γ(K⁺e⁻μ⁺)/Γ_{total} **Γ₁₉₄/Γ**

A test of lepton-family-number conservation.

VALUE	CL%	DOCUMENT ID	TECN	COMMENT
<1.0 × 10 ⁻⁷	90	AAIJ	21T	LHCB 1.6 fb ⁻¹ pp
••• We do not use the following data for averages, fits, limits, etc. •••				
<2.8 × 10 ⁻⁶	90	LEES	11G	BABR e ⁺ e ⁻ ≈ 7(45)
<1.2 × 10 ⁻⁴	90	FRABETTI	97B	E687 γ Be, E _γ ≈ 220 GeV
<3.4 × 10 ⁻³	90	WEIR	90B	MRK2 e ⁺ e ⁻ 29 GeV

Γ(π⁻2e⁺)/Γ_{total} **Γ₁₉₅/Γ**

A test of lepton-number conservation.

VALUE	CL%	DOCUMENT ID	TECN	COMMENT
<5.3 × 10 ⁻⁷	90	AAIJ	21T	LHCB 1.6 fb ⁻¹ pp
••• We do not use the following data for averages, fits, limits, etc. •••				
<1.9 × 10 ⁻⁶	90	LEES	11G	BABR e ⁺ e ⁻ ≈ 7(45)
<1.1 × 10 ⁻⁶	90	RUBIN	10	CLEO e ⁺ e ⁻ at ψ(3770)
<3.6 × 10 ⁻⁶	90	HE	05A	CLEO See RUBIN 10
<9.6 × 10 ⁻⁵	90	AITALA	99G	E791 π ⁻ N 500 GeV
<1.1 × 10 ⁻⁴	90	FRABETTI	97B	E687 γ Be, E _γ ≈ 220 GeV
<4.8 × 10 ⁻³	90	WEIR	90B	MRK2 e ⁺ e ⁻ 29 GeV

Γ(π⁻2μ⁺)/Γ_{total} **Γ₁₉₆/Γ**

A test of lepton-number conservation.

VALUE	CL%	DOCUMENT ID	TECN	COMMENT
<1.4 × 10 ⁻⁸	90	AAIJ	21T	LHCB 1.6 fb ⁻¹ pp
••• We do not use the following data for averages, fits, limits, etc. •••				
<2.2 × 10 ⁻⁸	90	AAIJ	13AF	LHCB pp at 7 TeV
<2.0 × 10 ⁻⁶	90	LEES	11G	BABR e ⁺ e ⁻ ≈ 7(45)
<4.8 × 10 ⁻⁶	90	LINK	03F	FOCS γ A, E _γ ≈ 180 GeV
<1.7 × 10 ⁻⁵	90	AITALA	99G	E791 π ⁻ N 500 GeV
<8.7 × 10 ⁻⁵	90	FRABETTI	97B	E687 γ Be, E _γ ≈ 220 GeV
<2.2 × 10 ⁻⁴	90	KODAMA	95	E653 π ⁻ emulsion 600 GeV
<6.8 × 10 ⁻³	90	WEIR	90B	MRK2 e ⁺ e ⁻ 29 GeV

Γ(π⁻e⁺μ⁺)/Γ_{total} **Γ₁₉₇/Γ**

A test of lepton-number conservation.

VALUE	CL%	DOCUMENT ID	TECN	COMMENT
<1.3 × 10 ⁻⁷	90	AAIJ	21T	LHCB 1.6 fb ⁻¹ pp
••• We do not use the following data for averages, fits, limits, etc. •••				
<2.0 × 10 ⁻⁶	90	LEES	11G	BABR e ⁺ e ⁻ ≈ 7(45)
<5.0 × 10 ⁻⁵	90	AITALA	99G	E791 π ⁻ N 500 GeV
<1.1 × 10 ⁻⁴	90	FRABETTI	97B	E687 γ Be, E _γ ≈ 220 GeV
<3.7 × 10 ⁻³	90	WEIR	90B	MRK2 e ⁺ e ⁻ 29 GeV

Γ(ρ⁻2μ⁺)/Γ_{total} **Γ₁₉₈/Γ**

A test of lepton-number conservation.

VALUE	CL%	DOCUMENT ID	TECN	COMMENT
<5.6 × 10 ⁻⁴	90	KODAMA	95	E653 π ⁻ emulsion 600 GeV

Γ(K⁻2e⁺)/Γ_{total} **Γ₁₉₉/Γ**

A test of lepton-number conservation.

VALUE	CL%	DOCUMENT ID	TECN	COMMENT
<0.9 × 10 ⁻⁶	90	LEES	11G	BABR e ⁺ e ⁻ ≈ 7(45)
••• We do not use the following data for averages, fits, limits, etc. •••				
<3.5 × 10 ⁻⁶	90	RUBIN	10	CLEO e ⁺ e ⁻ at ψ(3770)
<4.5 × 10 ⁻⁶	90	HE	05A	CLEO See RUBIN 10
<1.2 × 10 ⁻⁴	90	FRABETTI	97B	E687 γ Be, E _γ ≈ 220 GeV
<9.1 × 10 ⁻³	90	WEIR	90B	MRK2 e ⁺ e ⁻ 29 GeV

Γ(K_S⁰π⁻2e⁺)/Γ_{total} **Γ₂₀₀/Γ**

VALUE	CL%	DOCUMENT ID	TECN	COMMENT
<3.3 × 10 ⁻⁶	90	ABLIKIM	19AL	BES3 e ⁺ e ⁻ at 3773 MeV

Γ(K⁻π⁰2e⁺)/Γ_{total} **Γ₂₀₁/Γ**

VALUE	CL%	DOCUMENT ID	TECN	COMMENT
<8.5 × 10 ⁻⁶	90	ABLIKIM	19AL	BES3 e ⁺ e ⁻ at 3773 MeV

Γ(K⁻2μ⁺)/Γ_{total} **Γ₂₀₂/Γ**

A test of lepton-number conservation.

VALUE	CL%	DOCUMENT ID	TECN	COMMENT
<10 × 10 ⁻⁶	90	LEES	11G	BABR e ⁺ e ⁻ ≈ 7(45)
••• We do not use the following data for averages, fits, limits, etc. •••				
< 1.3 × 10 ⁻⁵	90	LINK	03F	FOCS γ A, E _γ ≈ 180 GeV
< 1.2 × 10 ⁻⁴	90	FRABETTI	97B	E687 γ Be, E _γ ≈ 220 GeV
< 3.2 × 10 ⁻⁴	90	KODAMA	95	E653 π ⁻ emulsion 600 GeV
< 4.3 × 10 ⁻³	90	WEIR	90B	MRK2 e ⁺ e ⁻ 29 GeV

Γ(K⁻e⁺μ⁺)/Γ_{total} **Γ₂₀₃/Γ**

A test of lepton-number conservation.

VALUE	CL%	DOCUMENT ID	TECN	COMMENT
<1.9 × 10 ⁻⁶	90	LEES	11G	BABR e ⁺ e ⁻ ≈ 7(45)
••• We do not use the following data for averages, fits, limits, etc. •••				
<1.3 × 10 ⁻⁴	90	FRABETTI	97B	E687 γ Be, E _γ ≈ 220 GeV
<4.0 × 10 ⁻³	90	WEIR	90B	MRK2 e ⁺ e ⁻ 29 GeV

Γ(K*(892)⁻2μ⁺)/Γ_{total} **Γ₂₀₄/Γ**

A test of lepton-number conservation.

VALUE	CL%	DOCUMENT ID	TECN	COMMENT
<8.5 × 10 ⁻⁴	90	KODAMA	95	E653 π ⁻ emulsion 600 GeV

Γ(Λe⁺)/Γ_{total} **Γ₂₀₅/Γ**

VALUE	CL%	DOCUMENT ID	TECN	COMMENT
<1.1 × 10 ⁻⁶	90	ABLIKIM	20D	BES3 e ⁺ e ⁻ , 3773 MeV

Γ(Λ̄e⁺)/Γ_{total} **Γ₂₀₆/Γ**

VALUE	CL%	DOCUMENT ID	TECN	COMMENT
<6.5 × 10 ⁻⁷	90	ABLIKIM	20D	BES3 e ⁺ e ⁻ , 3773 MeV

Γ(Σ⁰e⁺)/Γ_{total} **Γ₂₀₇/Γ**

VALUE	CL%	DOCUMENT ID	TECN	COMMENT
<1.7 × 10 ⁻⁶	90	ABLIKIM	20D	BES3 e ⁺ e ⁻ , 3773 MeV

Γ(Σ⁰e⁺)/Γ_{total} **Γ₂₀₈/Γ**

VALUE	CL%	DOCUMENT ID	TECN	COMMENT
<1.3 × 10 ⁻⁶	90	ABLIKIM	20D	BES3 e ⁺ e ⁻ , 3773 MeV

Γ(π̄e⁺)/Γ_{total} **Γ₂₀₉/Γ**

VALUE	CL%	DOCUMENT ID	TECN	COMMENT
<1.43 × 10 ⁻⁵	90	ABLIKIM	22BJ	BES3 2.93fb ⁻¹ e ⁺ e ⁻ at 3.773 GeV

Γ(ne⁺)/Γ_{total} **Γ₂₁₀/Γ**

VALUE	CL%	DOCUMENT ID	TECN	COMMENT
<2.91 × 10 ⁻⁵	90	ABLIKIM	22BJ	BES3 2.93fb ⁻¹ e ⁺ e ⁻ at 3.773 GeV

D[±] CP-VIOLATING DECAY-RATE ASYMMETRIES

This is the difference between D⁺ and D⁻ partial widths for the decay to state f, divided by the sum of the widths:
 $A_{CP}(f) = [\Gamma(D^+ \to f) - \Gamma(D^- \to \bar{f})] / [\Gamma(D^+ \to f) + \Gamma(D^- \to \bar{f})]$.

A_{CP}(μ[±]ν) in D⁺ → μ⁺ν_μ, D⁻ → μ⁻ν_μ

VALUE (%)	DOCUMENT ID	TECN	COMMENT
+8 ± 8	EISENSTEIN	08	CLEO e ⁺ e ⁻ at ψ(3770)

A_{CP}(K_L⁰e[±]ν) in D⁺ → K_L⁰e⁺ν_e, D⁻ → K_L⁰e⁻ν_e

VALUE (%)	DOCUMENT ID	TECN	COMMENT
-0.59 ± 0.60 ± 1.48	ABLIKIM	15AF	BES3 e ⁺ e ⁻ 3773 MeV

A_{CP}(K_S⁰π[±]) in D[±] → K_S⁰π[±]

VALUE (%)	EVTS	DOCUMENT ID	TECN	COMMENT
-0.41 ± 0.09 OUR AVERAGE				
-1.1 ± 0.6 ± 0.2		BONVICINI	14	CLEO All CLEO-c runs
-0.363 ± 0.094 ± 0.067	1738k	¹ KO	12A	BELL e ⁺ e ⁻ ≈ 7(nS)
-0.44 ± 0.13 ± 0.10	807k			DEL-AMO-SA...11H BABR e ⁺ e ⁻ ≈ 7(45)
-1.6 ± 1.5 ± 0.9	10.6k	² LINK	02B	FOCS γ nucleus, E _γ ≈ 180 GeV
••• We do not use the following data for averages, fits, limits, etc. •••				
-0.71 ± 0.19 ± 0.20		KO	10	BELL See KO 12A
-1.3 ± 0.7 ± 0.3	30k	MENDEZ	10	CLEO See BONVICINI 14
-0.6 ± 1.0 ± 0.3		DOBBS	07	CLEO See MENDEZ 10

¹ KO 12A finds that after subtracting the contribution due to K⁰ - π⁰ mixing, the CP asymmetry due to the change of charm is (-0.024 ± 0.094 ± 0.067)%, consistent with zero.

² LINK 02B measures N(D⁺ → K_S⁰π⁺)/N(D⁺ → K⁻π⁺π⁺), the ratio of numbers of events observed, and similarly for the D⁻.

A_{CP}(K_L⁰K[±]) in D[±] → K_L⁰K[±]

VALUE (units 10 ⁻²)	EVTS	DOCUMENT ID	TECN	COMMENT
-4.2 ± 3.2 ± 1.2	650	ABLIKIM	19M	BES3 e ⁺ e ⁻ at 3773 MeV

A_{CP}(K[±]2π[±]) in D⁺ → K⁻2π⁺, D⁻ → K⁺2π⁻

VALUE (%)	EVTS	DOCUMENT ID	TECN	COMMENT
-0.18 ± 0.16 OUR AVERAGE				
-0.16 ± 0.15 ± 0.09	2.3M	ABAZOV	14L	D0 p _T , √s = 1.96 TeV
-0.3 ± 0.2 ± 0.4		BONVICINI	14	CLEO All CLEO-c runs
••• We do not use the following data for averages, fits, limits, etc. •••				
-0.1 ± 0.4 ± 0.9	231k	MENDEZ	10	CLEO See BONVICINI 14
-0.5 ± 0.4 ± 0.9		DOBBS	07	CLEO See MENDEZ 10

Meson Particle Listings

 D^\pm $A_{CP}(K^\mp \pi^\pm \pi^\pm \pi^0)$ in $D^+ \rightarrow K^- \pi^+ \pi^+ \pi^0$, $D^- \rightarrow K^+ \pi^- \pi^- \pi^0$

VALUE (%)	DOCUMENT ID	TECN	COMMENT
$-0.3 \pm 0.6 \pm 0.4$	BONVICINI	14	CLEO All CLEO-c runs
••• We do not use the following data for averages, fits, limits, etc. •••			
$1.0 \pm 0.9 \pm 0.9$	DOBBS	07	CLEO See BONVICINI 14

 $A_{CP}(K_S^0 \pi^\pm \pi^0)$ in $D^+ \rightarrow K_S^0 \pi^+ \pi^0$, $D^- \rightarrow K_S^0 \pi^- \pi^0$

VALUE (%)	DOCUMENT ID	TECN	COMMENT
$-0.1 \pm 0.7 \pm 0.2$	BONVICINI	14	CLEO All CLEO-c runs
••• We do not use the following data for averages, fits, limits, etc. •••			
$0.3 \pm 0.9 \pm 0.3$	DOBBS	07	CLEO See BONVICINI 14

 $A_{CP}(K_S^0 \pi^\pm \eta)$ in $D^\pm \rightarrow K_S^0 \pi^\pm \eta$

VALUE (units 10^{-2})	EVTS	DOCUMENT ID	TECN	COMMENT
$-0.9 \pm 2.9 \pm 1.0$	1.3k	ABLIKIM	20v	BES3 $e^+ e^-$, 3773 MeV

 $A_{CP}(K_S^0 \pi^\pm \pi^+ \pi^-)$ in $D^+ \rightarrow K_S^0 \pi^\pm \pi^+ \pi^-$, $D^- \rightarrow K_S^0 \pi^\mp \pi^- \pi^+$

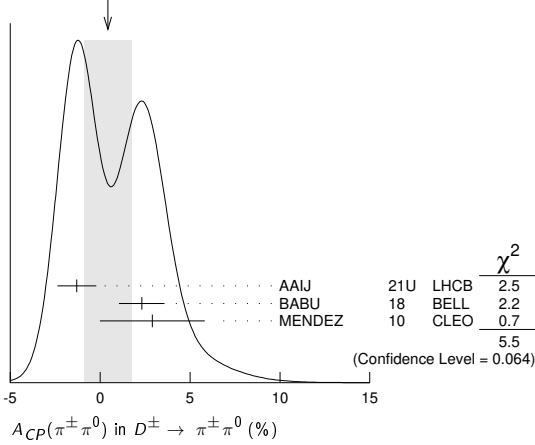
VALUE (%)	DOCUMENT ID	TECN	COMMENT
$0.0 \pm 1.2 \pm 0.3$	BONVICINI	14	CLEO All CLEO-c runs
••• We do not use the following data for averages, fits, limits, etc. •••			
$0.1 \pm 1.1 \pm 0.6$	DOBBS	07	CLEO See BONVICINI 14

 $A_{CP}(K^\pm \pi^+ \pi^- \pi^0)$ in $D^\pm \rightarrow K^\pm \pi^+ \pi^- \pi^0$

VALUE (%)	EVTS	DOCUMENT ID	TECN	COMMENT
$-0.04 \pm 0.06 \pm 0.01$	350	ABLIKIM	20z	BES3 $e^+ e^-$, 3773 MeV

 $A_{CP}(\pi^\pm \pi^0)$ in $D^\pm \rightarrow \pi^\pm \pi^0$

VALUE (%)	EVTS	DOCUMENT ID	TECN	COMMENT
0.4 ± 1.3 OUR AVERAGE	Error includes scale factor of 1.7.			See the ideogram below.
$-1.3 \pm 0.9 \pm 0.6$	28.7k	AAIJ	21u	LHCB pp at 7, 8, 13 TeV
$2.31 \pm 1.24 \pm 0.23$	108k	BABU	18	BELL At/near $\Upsilon(4S)$, $\Upsilon(5S)$
$2.9 \pm 2.9 \pm 0.3$	2.6k	MENDEZ	10	CLEO $e^+ e^-$ at 3774 MeV

WEIGHTED AVERAGE
 0.4 ± 1.3 (Error scaled by 1.7) $A_{CP}(\pi^\pm \eta)$ in $D^\pm \rightarrow \pi^\pm \eta$

VALUE (%)	EVTS	DOCUMENT ID	TECN	COMMENT
0.3 ± 0.5 OUR AVERAGE				
$0.34 \pm 0.66 \pm 0.16 \pm 0.05$	111k	¹ AAIJ	23E	LHCB 6 fb^{-1} , pp at 13 TeV, $\eta \rightarrow \gamma \pi \pi$
$-0.2 \pm 0.8 \pm 0.4$	32.7k	AAIJ	21u	LHCB pp at 13 TeV
$+1.74 \pm 1.13 \pm 0.19$		WON	11	BELL $e^+ e^- \approx \Upsilon(4S)$
$-2.0 \pm 2.3 \pm 0.3$	2.9k	MENDEZ	10	CLEO $e^+ e^-$ at 3774 MeV

¹The last uncertainty is due to the uncertainty on the CP asymmetry of the control channel, $D^+ \rightarrow \phi \pi^+$.

 $A_{CP}(\pi^\pm \pi^0 \eta)$ in $D^\pm \rightarrow \pi^\pm \pi^0 \eta$

VALUE (units 10^{-2})	EVTS	DOCUMENT ID	TECN	COMMENT
$-5.8 \pm 6.6 \pm 1.8$	381	ABLIKIM	20g	BES3 $e^+ e^-$ at 3.773 GeV

 $A_{CP}(\pi^\pm \eta \eta)$ in $D^\pm \rightarrow \pi^\pm \eta \eta$

VALUE (units 10^{-2})	EVTS	DOCUMENT ID	TECN	COMMENT
$8.0 \pm 8.3 \pm 1.9$	179	ABLIKIM	20g	BES3 $e^+ e^-$ at 3.773 GeV

 $A_{CP}(\pi^\pm \eta'(958))$ in $D^\pm \rightarrow \pi^\pm \eta'(958)$

VALUE (%)	EVTS	DOCUMENT ID	TECN	COMMENT
0.41 ± 0.23 OUR AVERAGE	Error includes scale factor of 1.2.			
$0.49 \pm 0.18 \pm 0.06 \pm 0.05$	555k	¹ AAIJ	23E	LHCB 6 fb^{-1} , pp at 13 TeV, $\eta \rightarrow \gamma \pi \pi$
$-0.61 \pm 0.72 \pm 0.54$	63k	AAIJ	17AF	LHCB pp at 7, 8 TeV
$-0.12 \pm 1.12 \pm 0.17$		WON	11	BELL $e^+ e^- \approx \Upsilon(4S)$
$-4.0 \pm 3.4 \pm 0.3$	1.0k	MENDEZ	10	CLEO $e^+ e^-$ at 3774 MeV

¹The last uncertainty is due to the uncertainty on the CP asymmetry of the control channel, $D^+ \rightarrow \phi \pi^+$.

 $A_{CP}(K^0/K^0 K^\pm)$ in $D^+ \rightarrow \bar{K}^0 K^+$, $D^- \rightarrow K^0 K^-$

VALUE (%)	EVTS	DOCUMENT ID	TECN	COMMENT
0.11 ± 0.17 OUR AVERAGE				
$0.03 \pm 0.17 \pm 0.14$	1.0M	¹ AAIJ	14BD	LHCB pp at 7, 8 TeV
$0.08 \pm 0.28 \pm 0.14$	277k	KO	13	BELL $e^+ e^-$ at $\Upsilon(4S)$
$0.46 \pm 0.36 \pm 0.25$	159k	LEES	13E	BABR $e^+ e^-$ at $\Upsilon(4S)$

¹AAIJ 14BD reports its result as $A_{CP}(D^\pm \rightarrow K_S^0 \pi^\pm)$ with CP -violation effects in the $K^0 - \bar{K}^0$ system subtracted. It also measures $A_{CP}(D^\pm \rightarrow \bar{K}^0/K^0 K^\pm) + A_{CP}(D_S^\pm \rightarrow \bar{K}^0/K^0 \pi^\pm) = (0.41 \pm 0.49 \pm 0.26)\%$.

 $A_{CP}(K_S^0 K^\pm)$ in $D^\pm \rightarrow K_S^0 K^\pm$

VALUE (%)	EVTS	DOCUMENT ID	TECN	COMMENT
-0.01 ± 0.07 OUR AVERAGE				
$-0.004 \pm 0.061 \pm 0.045$	6M	AAIJ	19t	LHCB pp at 7, 8, 13 TeV
$-1.8 \pm 2.7 \pm 1.6$	780	ABLIKIM	19M	BES3 $e^+ e^-$ at 3773 MeV
$-0.25 \pm 0.28 \pm 0.14$	277k	KO	13	BELL $e^+ e^-$ at $\Upsilon(nS)$
$0.13 \pm 0.36 \pm 0.25$	159k	LEES	13E	BABR $e^+ e^-$ at $\Upsilon(4S)$
$-0.2 \pm 1.5 \pm 0.9$	5.2k	MENDEZ	10	CLEO $e^+ e^-$ at 3774 MeV
$7.1 \pm 6.1 \pm 1.2$	949	¹ LINK	02B	FOCS γ nucleus, $\bar{E}_\gamma \approx 180$ GeV

••• We do not use the following data for averages, fits, limits, etc. •••

$-0.16 \pm 0.58 \pm 0.25$		KO	10	BELL $e^+ e^- \approx \Upsilon(4S)$
$6.9 \pm 6.0 \pm 1.5$	949	² LINK	02B	FOCS γ nucleus, $\bar{E}_\gamma \approx 180$ GeV

¹LINK 02B measures $N(D^+ \rightarrow K_S^0 K^+)/N(D^+ \rightarrow K_S^0 \pi^+)$, the ratio of numbers of events observed, and similarly for the D^- .

²LINK 02B measures $N(D^+ \rightarrow K_S^0 K^+)/N(D^+ \rightarrow K^- \pi^+ \pi^+)$, the ratio of numbers of events observed, and similarly for the D^- .

 $A_{CP}(K_S^0 K^\pm \pi^0)$ in $D^\pm \rightarrow K_S^0 K^\pm \pi^0$

VALUE (units 10^{-2})	EVTS	DOCUMENT ID	TECN	COMMENT
$1.4 \pm 3.7 \pm 2.4$	470	ABLIKIM	19M	BES3 $e^+ e^-$ at 3773 MeV

 $A_{CP}(K_L^0 K^\pm \pi^0)$ in $D^\pm \rightarrow K_L^0 K^\pm \pi^0$

VALUE (units 10^{-2})	EVTS	DOCUMENT ID	TECN	COMMENT
$-0.6 \pm 4.1 \pm 1.7$	410	ABLIKIM	19M	BES3 $e^+ e^-$ at 3773 MeV

 $A_{CP}(K^+ K^- \pi^\pm)$ in $D^\pm \rightarrow K^+ K^- \pi^\pm$

See also AAJ 11G for a search for CP asymmetry in the $D^\pm \rightarrow K^+ K^- \pi^\pm$ Dalitz plots using 370k decays and four different binning schemes. No evidence for CP asymmetry was found.

VALUE (%)	EVTS	DOCUMENT ID	TECN	COMMENT
0.37 ± 0.29 OUR AVERAGE				
$0.37 \pm 0.30 \pm 0.15$	224k	¹ LEES	13F	BABR $e^+ e^-$ at $\Upsilon(4S)$
$-0.03 \pm 0.84 \pm 0.29$		RUBIN	08	CLEO $e^+ e^-$ at 3774 MeV
$1.4 \pm 1.0 \pm 0.8$	43k	² AUBERT	05s	BABR $e^+ e^-$ at $\Upsilon(4S)$
$0.6 \pm 1.1 \pm 0.5$	14k	³ LINK	00B	FOCS
-1.4 ± 2.9		³ AITALA	97B	E791 $-0.062 < A_{CP} < +0.034$ (90% CL)
-3.1 ± 6.8		³ FRABETTI	94I	E687 $-0.14 < A_{CP} < +0.081$ (90% CL)

••• We do not use the following data for averages, fits, limits, etc. •••

$-0.1 \pm 0.9 \pm 0.4$ ⁴BONVICINI 14 CLEO See RUBIN 08
 $-0.1 \pm 1.5 \pm 0.8$ DOBBS 07 CLEO See BONVICINI 14 and RUBIN 08

¹This is the integrated CP asymmetry. LEES 13F also searches for CP asymmetries in four regions of the Dalitz plots (two of which are listed below); in comparisons of binned D^+ and D^- Dalitz plots; in parametrized fits to those plots, including 2-body submodes; and in comparisons of Legendre-polynomial distributions for the $K^+ K^-$ and $K^- \pi^+$ systems.

²AUBERT 05s measures $N(D^+ \rightarrow K^+ K^- \pi^+)/N(D_S^+ \rightarrow K^+ K^- \pi^+)$, the ratio of the numbers of events observed, and similarly for the D^- .

³FRABETTI 94I, AITALA 98C, and LINK 00B measure $N(D^+ \rightarrow K^- K^+ \pi^+)/N(D^+ \rightarrow K^- \pi^+ \pi^+)$, the ratio of numbers of events observed, and similarly for the D^- .

⁴RUBIN 08 performs a dedicated analysis of this decay mode on the same dataset, with slightly better precision. We therefore take that BONVICINI 14 does not supersede RUBIN 08's A_{CP} result.

 $A_{CP}(K^\pm K^*0)$ in $D^+ \rightarrow K^+ \bar{K}^{*0}$, $D^- \rightarrow K^- K^{*0}$

VALUE (%)	EVTS	DOCUMENT ID	TECN	COMMENT
-0.3 ± 0.4 OUR AVERAGE				
$-0.3 \pm 0.4 \pm 0.2$	73k	¹ LEES	13F	BABR $e^+ e^-$ at $\Upsilon(4S)$
$-0.4 \pm 2.0 \pm 0.6$		RUBIN	08	CLEO Fit-fraction asymmetry
$+0.9 \pm 1.7 \pm 0.7$	11k	² AUBERT	05s	BABR $e^+ e^-$ at $\Upsilon(4S)$
-1.0 ± 5.0		³ AITALA	97B	E791 $-0.092 < A_{CP} < +0.072$ (90% CL)
-12 ± 13		³ FRABETTI	94I	E687 $-0.33 < A_{CP} < +0.094$ (90% CL)

¹This LEES 13F result is for the $K^\mp \pi^\pm$ mass-squared between 0.4 and 1.0 GeV^2 , and does not actually separate out the K^* .

²AUBERT 05s measures $N(D^+ \rightarrow K^+ \bar{K}^{*0})/N(D_S^+ \rightarrow K^+ K^- \pi^+)$, the ratio of the numbers of events observed, and similarly for the D^- .

³FRABETTI 94I and AITALA 97B measure $N(D^+ \rightarrow K^+ \bar{K}^*(892)^0)/N(D^+ \rightarrow K^- \pi^+ \pi^+)$, the ratio of numbers of events observed, and similarly for the D^- .

See key on page 1171

Meson Particle Listings

 D^\pm $A_{CP}(\phi\pi^\pm)$ in $D^\pm \rightarrow \phi\pi^\pm$

VALUE (%)	EVTS	DOCUMENT ID	TECN	COMMENT
0.01 ± 0.09 OUR AVERAGE		Error includes scale factor of 1.8.		
0.003 ± 0.040 ± 0.029	55M	AAIJ	19T	LHCb pp at 7, 8, 13 TeV
-0.3 ± 0.3 ± 0.5	97k	¹ LEES	13F	BABR e^+e^- at $\Upsilon(4S)$
+0.51 ± 0.28 ± 0.05	237k	STARIC	12	BELL Mainly at $\Upsilon(4S)$
-1.8 ± 1.6 $\begin{smallmatrix} +0.2 \\ -0.4 \end{smallmatrix}$		RUBIN	08	CLEO Fit-fraction asymmetry
+0.2 ± 1.5 ± 0.6	10k	² AUBERT	05s	BABR e^+e^- at $\Upsilon(4S)$
-2.8 ± 3.6		³ AITALA	97B	E791 $-0.087 < A_{CP} < +0.031$ (90% CL)
+6.6 ± 8.6		³ FRABETTI	94I	E687 $-0.075 < A_{CP} < +0.21$ (90% CL)

• • • We do not use the following data for averages, fits, limits, etc. • • •

-0.04 ± 0.14 ± 0.14	1.58M	⁴ AAIJ	13W	LHCb pp at 7 TeV
¹ This LEES 13F result is for the K^+K^- mass-squared less than 1.3 GeV ² and the $K^\mp\pi^\pm$ mass-squared above 1.0 GeV ² , and does not actually separate out the ϕ .				
² AUBERT 05s measures $N(D^+ \rightarrow \phi\pi^+)/N(D_S^+ \rightarrow K^+K^-\pi^+)$, the ratio of the numbers of events observed, and similarly for the D^- .				
³ FRABETTI 94I and AITALA 97B measure $N(D^+ \rightarrow \phi\pi^+)/N(D^+ \rightarrow K^-\pi^+\pi^+)$, the ratio of numbers of events observed, and similarly for the D^- .				
⁴ See AAJ 19T.				

 $A_{CP}(K^\pm K_0^*(1430)^0)$ in $D^+ \rightarrow K^+ \bar{K}_0^*(1430)^0$, $D^- \rightarrow K^- K_0^*(1430)^0$

VALUE (%)	DOCUMENT ID	TECN	COMMENT
+8 ± 6 $\begin{smallmatrix} +4 \\ -2 \end{smallmatrix}$	RUBIN	08	CLEO Fit-fraction asymmetry

 $A_{CP}(K^\pm K_2^*(1430)^0)$ in $D^+ \rightarrow K^+ \bar{K}_2^*(1430)^0$, $D^- \rightarrow K^- K_2^*(1430)^0$

VALUE (%)	DOCUMENT ID	TECN	COMMENT
+43 ± 19 $\begin{smallmatrix} +5 \\ -18 \end{smallmatrix}$	RUBIN	08	CLEO Fit-fraction asymmetry

 $A_{CP}(K^\pm K_0^*(700))$ in $D^+ \rightarrow K^+ \bar{K}_0^*(700)$, $D^- \rightarrow K^- K_0^*(700)$

VALUE (%)	DOCUMENT ID	TECN	COMMENT
-12 ± 11 $\begin{smallmatrix} +14 \\ -6 \end{smallmatrix}$	RUBIN	08	CLEO Fit-fraction asymmetry

 $A_{CP}(a_0(1450)^0\pi^\pm)$ in $D^\pm \rightarrow a_0(1450)^0\pi^\pm$

VALUE (%)	DOCUMENT ID	TECN	COMMENT
-19 ± 12 $\begin{smallmatrix} +8 \\ -11 \end{smallmatrix}$	RUBIN	08	CLEO Fit-fraction asymmetry

 $A_{CP}(\phi(1680)\pi^\pm)$ in $D^\pm \rightarrow \phi(1680)\pi^\pm$

VALUE (%)	DOCUMENT ID	TECN	COMMENT
-9 ± 22 ± 14	RUBIN	08	CLEO Fit-fraction asymmetry

 $A_{CP}(\pi^\pm 2\pi^0)$ in $D^\pm \rightarrow \pi^\pm 2\pi^0$

VALUE (%)	EVTS	DOCUMENT ID	TECN	COMMENT
+5.6 ± 2.7 ± 0.5	2k	ABLIKIM	22B G	BES3 e^+e^- at 3.773 GeV

 $A_{CP}(\pi^+\pi^-\pi^\pm)$ in $D^\pm \rightarrow \pi^+\pi^-\pi^\pm$

See also AAJ 14c for a search for CP violation in $D^\pm \rightarrow \pi^+\pi^-\pi^\pm$ Dalitz plots using model-independent binned and unbinned methods. No evidence was found.

VALUE (%)	EVTS	DOCUMENT ID	TECN	COMMENT
0.5 ± 2.0 OUR AVERAGE				
+1.2 ± 2.2 ± 0.6	2.6k	ABLIKIM	22B G	BES3 e^+e^- at 3.773 GeV
-1.7 ± 4.2		¹ AITALA	97B	E791 $-0.086 < A_{CP} < +0.052$ (90% CL)

¹AITALA 97B measure $N(D^+ \rightarrow \pi^+\pi^-\pi^+)/N(D^+ \rightarrow K^-\pi^+\pi^+)$, the ratio of numbers of events observed, and similarly for the D^- .

 $A_{CP}(2\pi^\pm\pi^\mp\pi^0)$ in $D^\pm \rightarrow 2\pi^\pm\pi^\mp\pi^0$

VALUE (%)	EVTS	DOCUMENT ID	TECN	COMMENT
+0.3 ± 1.8 ± 0.8	4.6k	ABLIKIM	22B G	BES3 e^+e^- at 3.773 GeV

 $A_{CP}(2\pi^\pm\pi^\mp 2\pi^0)$ in $D^\pm \rightarrow 2\pi^\pm\pi^\mp 2\pi^0$

VALUE (%)	EVTS	DOCUMENT ID	TECN	COMMENT
-4.2 ± 3.8 ± 1.3	1.2k	ABLIKIM	22B G	BES3 e^+e^- at 3.773 GeV

 $A_{CP}(\pi^+\pi^-\pi^\pm\eta)$ in $D^\pm \rightarrow \pi^+\pi^-\pi^\pm\eta$

VALUE (units 10^{-2})	EVTS	DOCUMENT ID	TECN	COMMENT
2.5 ± 5.0 ± 1.6	510	ABLIKIM	20V	BES3 e^+e^- , 3773 MeV

 $A_{CP}(K_S^0 K^\pm\pi^+\pi^-)$ in $D^\pm \rightarrow K_S^0 K^\pm\pi^+\pi^-$

VALUE (%)	EVTS	DOCUMENT ID	TECN	COMMENT
-4.2 ± 6.4 ± 2.2	523 ± 32	LINK	05E	FOCS γA , $\bar{E}_{\gamma} \approx 180$ GeV

 $A_{CP}(K^\pm\pi^0)$ in $D^\pm \rightarrow K^\pm\pi^0$

VALUE (%)	EVTS	DOCUMENT ID	TECN	COMMENT
-3 ± 5 OUR AVERAGE				
-3.2 ± 4.7 ± 2.1	2.5k	AAIJ	21U	LHCb pp at 7, 8, 13 TeV
-3.5 ± 10.7 ± 0.9	343	MENDEZ	10	CLEO e^+e^- at 3774 MeV

 $A_{CP}(K^\pm\eta)$ in $D^\pm \rightarrow K^\pm\eta$

VALUE (units 10^{-2})	EVTS	DOCUMENT ID	TECN	COMMENT
-6 ± 10 ± 4	880	AAIJ	21U	LHCb pp at 13 TeV

 $D^\pm \chi^2$ TESTS OF CP -VIOLATION (CPV)

We list model-independent searches for local CP violation in phase-space distributions of multi-body decays.

Most of these searches divide phase space (Dalitz plot for 3-body decays, five-dimensional equivalent for 4-body decays) into bins, and perform a χ^2 test comparing normalised yields N_i, \bar{N}_i in CP -conjugate bin pairs i : $\chi^2 = \sum_i (N_i - \alpha \bar{N}_i) / \sigma(N_i - \alpha \bar{N}_i)$. The factor $\alpha = (\sum_i N_i) / (\sum_i \bar{N}_i)$ removes the dependence on phase-space-integrated rate asymmetries. The result is used to obtain the probability (p-value) to obtain the measured χ^2 or larger under the assumption of CP conservation [AUBERT 08A0, BEDIAGA 09]. Alternative methods obtain p-values from other test variables based on unbinned analyses [WILLIAMS 11, AAJ 14C]. Results can be combined using Fisher's method [MOSTELLER 48].

Local CPV in $D^\pm \rightarrow \pi^+\pi^-\pi^\pm$

p-value (%)	EVTS	DOCUMENT ID	TECN	COMMENT
78.1	3.1M	¹ AAIJ	14C	LHCb χ^2

¹AAIJ 14C uses binned and unbinned methods, and finds slightly better sensitivity with the former. We took the first value in the table of results for the binned method.

Local CPV in $D^\pm \rightarrow K^+K^-\pi^\pm$

p-value (%)	EVTS	DOCUMENT ID	TECN	COMMENT
31 OUR EVALUATION				
72	224k	LEES	13F	BABR χ^2
12.7	370k	¹ AAIJ	11G	LHCb χ^2

¹AAIJ 11G publishes results for several binning schemes. We picked the first value in their table of results.

Local CPV in $D^\pm \rightarrow K^+K^-K^\pm$

VALUE (%)	EVTS	DOCUMENT ID	TECN	COMMENT
31.6	1.27M	AAIJ	23L	LHCb χ^2

 CP VIOLATING ASYMMETRIES OF P -ODD (T -ODD) MOMENTS $A_{Tviol}(K_S^0 K^\pm\pi^+\pi^-)$ in $D^\pm \rightarrow K_S^0 K^\pm\pi^+\pi^-$

$C_T \equiv \bar{p}_{K^+} \cdot (\bar{p}_{\pi^+} \times \bar{p}_{\pi^-})$ is a parity-odd correlation of the K^+ , π^+ , and π^- momenta for the D^+ . $\bar{C}_T \equiv \bar{p}_{K^-} \cdot (\bar{p}_{\pi^-} \times \bar{p}_{\pi^+})$ is the corresponding quantity for the D^- . Then

$A_T \equiv [\Gamma(C_T > 0) - \Gamma(C_T < 0)] / [\Gamma(C_T > 0) + \Gamma(C_T < 0)]$, and
 $\bar{A}_T \equiv [\Gamma(-\bar{C}_T > 0) - \Gamma(-\bar{C}_T < 0)] / [\Gamma(-\bar{C}_T > 0) + \Gamma(-\bar{C}_T < 0)]$, and

$A_{Tviol} \equiv \frac{1}{2}(A_T - \bar{A}_T)$. C_T and \bar{C}_T are commonly referred to as T -odd moments, because they are odd under T reversal. However, the T -conjugate process $K_S^0 K^\pm\pi^+\pi^- \rightarrow D^\pm$ is not accessible, while the P -conjugate process is.

VALUE (units 10^{-3})	EVTS	DOCUMENT ID	TECN	COMMENT
-3 ± 8 OUR AVERAGE		Error includes scale factor of 1.1.		
3.4 ± 8.7 ± 3.2	19k	MOON	23	BELL 980 fb ⁻¹ at $\sim \Upsilon(4S)$
-12.0 ± 10.0 ± 4.6	21k	LEES	11E	BABR $e^+e^- \approx \Upsilon(4S)$
• • • We do not use the following data for averages, fits, limits, etc. • • •				
23 ± 62 ± 22	523	LINK	05E	FOCS γA , $\bar{E}_{\gamma} \approx 180$ GeV

 $A_{Tviol}(K^+K^-K_S^0\pi^\pm)$ in $D^\pm \rightarrow K^+K^-K_S^0\pi^\pm$

$C_T \equiv \bar{p}_{K^+} \cdot (\bar{p}_{\pi^+} \times \bar{p}_{K^-})$ is a parity-odd correlation of the K^+ , π^+ , and K^- momenta for the D^+ . $\bar{C}_T \equiv \bar{p}_{K^-} \cdot (\bar{p}_{\pi^-} \times \bar{p}_{K^+})$ is the corresponding quantity for the D^- . Then

$A_T \equiv [\Gamma(C_T > 0) - \Gamma(C_T < 0)] / [\Gamma(C_T > 0) + \Gamma(C_T < 0)]$, and
 $\bar{A}_T \equiv [\Gamma(-\bar{C}_T > 0) - \Gamma(-\bar{C}_T < 0)] / [\Gamma(-\bar{C}_T > 0) + \Gamma(-\bar{C}_T < 0)]$, and

$A_{Tviol} \equiv \frac{1}{2}(A_T - \bar{A}_T)$. C_T and \bar{C}_T are commonly referred to as T -odd moments, because they are odd under T reversal. However, the T -conjugate process $K^+K^-K_S^0\pi^\pm \rightarrow D^\pm$ is not accessible, while the P -conjugate process is.

VALUE (%)	EVTS	DOCUMENT ID	TECN	COMMENT
-3.34 ± 2.66 ± 0.35	1.4k	MOON	23	BELL 980 fb ⁻¹ at $\sim \Upsilon(4S)$

SEMLEPTONIC FORM FACTORS

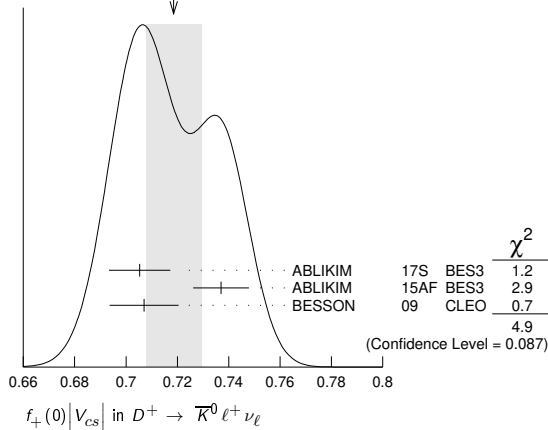
 $f_+(0)|V_{cs}|$ in $D^+ \rightarrow \bar{K}^0\ell^+\nu_\ell$

VALUE	DOCUMENT ID	TECN	COMMENT
0.719 ± 0.011 OUR AVERAGE	Error includes scale factor of 1.6. See the ideogram below.		
0.7053 ± 0.0040 ± 0.0112	ABLIKIM	17s	BES3 $K_S^0 e^+\nu_e$ 2-parameter fit
0.737 ± 0.006 ± 0.009	¹ ABLIKIM	15AF	BES3 $K_L e^+\nu_e$ 3-parameter fit
0.707 ± 0.010 ± 0.009	² BESSION	09	CLEO $K_S e^+\nu_e$ 3-parameter fit

¹ABLIKIM 15AF finds 0.728 ± 0.006 ± 0.011 for a 2-parameter fit.

²BESSION 09 finds 0.716 ± 0.007 ± 0.009 for a 2-parameter fit.

Meson Particle Listings

 D^\pm WEIGHTED AVERAGE
0.719±0.011 (Error scaled by 1.6) $r_1 \equiv a_1/a_0$ in $D^+ \rightarrow \bar{K}^0 \ell^+ \nu_\ell$

VALUE	EVTS	DOCUMENT ID	TECN	COMMENT
-2.13±0.14 OUR AVERAGE				
-2.18±0.14±0.05		ABLIKIM 17s BES3		$K_S^0 e^+ \nu_e$ 2-parameter fit
-2.23±0.42±0.53	40k	1 ABLIKIM 15AF BES3		$K_L e^+ \nu_e$ 3-parameter fit
-1.66±0.44±0.10		2 BESSON 09 CLEO		$K_S e^+ \nu_e$ 3-parameter fit

¹ ABLIKIM 15AF finds $r_1 = -1.91 \pm 0.33 \pm 0.28$ for a 2-parameter fit.
² BESSON 09 finds $r_1 = -2.10 \pm 0.25 \pm 0.08$ for 2-parameter fit.

 $r_2 \equiv a_2/a_0$ in $D^+ \rightarrow \bar{K}^0 \ell^+ \nu_\ell$

VALUE	EVTS	DOCUMENT ID	TECN	COMMENT
-3±12 OUR AVERAGE				Error includes scale factor of 1.5.
+11±9±9	40k	ABLIKIM 15AF BES3		$K_L e^+ \nu_e$ 3-parameter fit
-14±11±1		BESSON 09 CLEO		$K_S e^+ \nu_e$ 3-parameter fit

 $f_+(0)|V_{cd}|$ in $D^+ \rightarrow \pi^0 \ell^+ \nu_\ell$

VALUE	EVTS	DOCUMENT ID	TECN	COMMENT
0.1407±0.0025 OUR AVERAGE				
0.1400±0.0026±0.0007		ABLIKIM 17s BES3		$\pi^0 e^+ \nu_e$ 2-parameter fit
0.146±0.007±0.002		BESSON 09 CLEO		$\pi^0 e^+ \nu_e$ 3-parameter fit

 $r_1 \equiv a_1/a_0$ in $D^+ \rightarrow \pi^0 \ell^+ \nu_\ell$

VALUE	EVTS	DOCUMENT ID	TECN	COMMENT
-2.00±0.13 OUR AVERAGE				
-2.01±0.13±0.02		ABLIKIM 17s BES3		$\pi^0 e^+ \nu_e$ 2-parameter fit
-1.37±0.88±0.24		BESSON 09 CLEO		$\pi^0 e^+ \nu_e$ 3-parameter fit

 $r_2 \equiv a_2/a_0$ in $D^+ \rightarrow \pi^0 \ell^+ \nu_\ell$

VALUE	EVTS	DOCUMENT ID	TECN	COMMENT
-4±5±1		BESSON 09 CLEO		$\pi^0 e^+ \nu_e$ 3-parameter fit

 $f_+(0)|V_{cd}|$ in $D^+ \rightarrow \eta \ell^+ \nu_\ell$ ($\ell = e$ or ν)

VALUE (units 10^{-2})	EVTS	DOCUMENT ID	TECN	COMMENT
8.4±0.4 OUR AVERAGE				
8.7±0.8±0.2	234	ABLIKIM 20T BES3		$\eta \mu^+ \nu_\mu$, z expansion
7.86±0.64±0.21	373	ABLIKIM 18R BES3		$\eta e^+ \nu_e$, z expansion
8.6±0.6±0.1		YELTON 11 CLEO		$\eta e^+ \nu_e$, z expansion

 $r_1 \equiv a_1/a_0$ in $D^+ \rightarrow \eta e^+ \nu_e$

VALUE	EVTS	DOCUMENT ID	TECN	COMMENT
-5.3±2.7 OUR AVERAGE				Error includes scale factor of 1.9.
-7.33±1.69±0.40	373	ABLIKIM 18R BES3		z expansion
-1.83±2.23±0.28		YELTON 11 CLEO		z expansion

 $r_V \equiv V(0)/A_1(0)$ in $D^+ \rightarrow \omega e^+ \nu_e$

VALUE	EVTS	DOCUMENT ID	TECN	COMMENT
1.24±0.09±0.06		ABLIKIM 15W BES3		292 fb ⁻¹ , 3773 MeV

 $r_2 \equiv A_2(0)/A_1(0)$ in $D^+ \rightarrow \omega e^+ \nu_e$

VALUE	EVTS	DOCUMENT ID	TECN	COMMENT
1.06±0.15±0.05		ABLIKIM 15W BES3		292 fb ⁻¹ , 3773 MeV

 $r_V \equiv V(0)/A_1(0)$ in $D^+, D^0 \rightarrow \rho e^+ \nu_e$

VALUE	EVTS	DOCUMENT ID	TECN	COMMENT
1.64±0.10 OUR AVERAGE				Error includes scale factor of 1.2.
1.695±0.083±0.051	2.5k	1 ABLIKIM 19c BES3		$e^+ e^-$ at 3773 MeV
1.48±0.15±0.05		1,2 DOBBS 13 CLEO		$e^+ e^-$ at $\psi(3770)$

¹ Uses both D^+ and D^0 events.
² Using PDG 10 values of V_{cd} and lifetimes, DOBBS 13 gets $A_1(0) = 0.56 \pm 0.01 \pm 0.02$, $A_2(0) = 0.47 \pm 0.06 \pm 0.04$, and $V(0) = 0.84 \pm 0.09 \pm 0.05$.

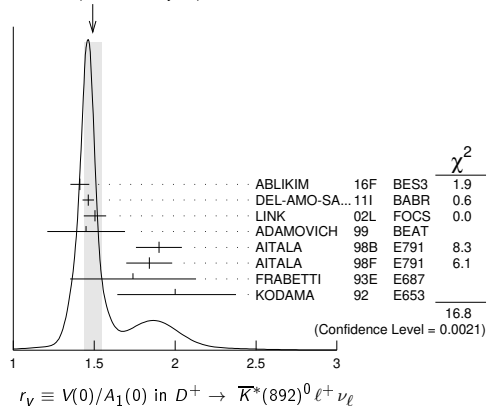
 $r_2 \equiv A_2(0)/A_1(0)$ in $D^+, D^0 \rightarrow \rho e^+ \nu_e$

VALUE	EVTS	DOCUMENT ID	TECN	COMMENT
0.84±0.06 OUR AVERAGE				
0.845±0.056±0.039	2.5k	1 ABLIKIM 19c BES3		$e^+ e^-$ at 3773 MeV
0.83±0.11±0.04		1,2 DOBBS 13 CLEO		$e^+ e^-$ at $\psi(3770)$

¹ Uses both D^+ and D^0 events.² Using PDG 10 values of V_{cd} and lifetimes, DOBBS 13 gets $A_1(0) = 0.56 \pm 0.01 \pm 0.02$, $A_2(0) = 0.47 \pm 0.06 \pm 0.04$, and $V(0) = 0.84 \pm 0.09 \pm 0.05$. $r_V \equiv V(0)/A_1(0)$ in $D^+ \rightarrow \bar{K}^*(892)^0 \ell^+ \nu_\ell$ See also BRIERE 10 for $\bar{K}^* \ell^+ \nu_\ell$ helicity-basis form-factor measurements.

VALUE	EVTS	DOCUMENT ID	TECN	COMMENT
1.49±0.05 OUR AVERAGE				Error includes scale factor of 2.1. See the ideogram below.
1.411±0.058±0.007	16.2k	ABLIKIM 16F BES3		$\bar{K}^*(892)^0 e^+ \nu_e$
1.463±0.017±0.031		1 DEL-AMO-SA...111 BABR		
1.504±0.057±0.039	15k	2 LINK 02L FOCS		$\bar{K}^*(892)^0 \mu^+ \nu_\mu$
1.45±0.23±0.07	763	ADAMOVICH 99 BEAT		$\bar{K}^*(892)^0 \mu^+ \nu_\mu$
1.90±0.11±0.09	3000	3 AITALA 98B E791		$\bar{K}^*(892)^0 e^+ \nu_e$
1.84±0.11±0.09	3034	AITALA 98F E791		$\bar{K}^*(892)^0 \mu^+ \nu_\mu$
1.74±0.27±0.28	874	FRABETTI 93E E687		$\bar{K}^*(892)^0 \mu^+ \nu_\mu$
2.00±0.34±0.32±0.16	305	KODAMA 92 E653		$\bar{K}^*(892)^0 \mu^+ \nu_\mu$

••• We do not use the following data for averages, fits, limits, etc. •••

2.0±0.6±0.3 183 ANJOS 90E E691 $\bar{K}^*(892)^0 e^+ \nu_e$ ¹ DEL-AMO-SANCHEZ 111 finds the pole mass $m_A = (2.63 \pm 0.10 \pm 0.13)$ GeV (m_V is fixed at 2 GeV).² LINK 02L includes the effects of interference with an S-wave background. This much improves the goodness of fit, but does not much shift the values of the form factors.³ This is slightly different from the AITALA 98B value: see ref. [5] in AITALA 98F.WEIGHTED AVERAGE
1.49±0.05 (Error scaled by 2.1) $r_2 \equiv A_2(0)/A_1(0)$ in $D^+ \rightarrow \bar{K}^*(892)^0 \ell^+ \nu_\ell$ See also BRIERE 10 for $\bar{K}^* \ell^+ \nu_\ell$ helicity-basis form-factor measurements.

VALUE	EVTS	DOCUMENT ID	TECN	COMMENT
0.802±0.021 OUR AVERAGE				
0.788±0.042±0.008	16.2k	ABLIKIM 16F BES3		$\bar{K}^*(892)^0 e^+ \nu_e$
0.801±0.020±0.020		1 DEL-AMO-SA...111 BABR		
0.875±0.049±0.064	15k	2 LINK 02L FOCS		$\bar{K}^*(892)^0 \mu^+ \nu_\mu$
1.00±0.15±0.03	763	ADAMOVICH 99 BEAT		$\bar{K}^*(892)^0 \mu^+ \nu_\mu$
0.71±0.08±0.09	3000	AITALA 98B E791		$\bar{K}^*(892)^0 e^+ \nu_e$
0.75±0.08±0.09	3034	AITALA 98F E791		$\bar{K}^*(892)^0 \mu^+ \nu_\mu$
0.78±0.18±0.10	874	FRABETTI 93E E687		$\bar{K}^*(892)^0 \mu^+ \nu_\mu$
0.82±0.22±0.23±0.11	305	KODAMA 92 E653		$\bar{K}^*(892)^0 \mu^+ \nu_\mu$

••• We do not use the following data for averages, fits, limits, etc. •••

0.0±0.5±0.2 183 ANJOS 90E E691 $\bar{K}^*(892)^0 e^+ \nu_e$ ¹ DEL-AMO-SANCHEZ 111 finds the pole mass $m_A = (2.63 \pm 0.10 \pm 0.13)$ GeV (m_V is fixed at 2 GeV).² LINK 02L includes the effects of interference with an S-wave background. This much improves the goodness of fit, but does not much shift the values of the form factors. $r_3 \equiv A_3(0)/A_1(0)$ in $D^+ \rightarrow \bar{K}^*(892)^0 \ell^+ \nu_\ell$ See also BRIERE 10 for $\bar{K}^* \ell^+ \nu_\ell$ helicity-basis form-factor measurements.

VALUE	EVTS	DOCUMENT ID	TECN	COMMENT
0.04±0.33±0.29	3034	AITALA 98F E791		$\bar{K}^*(892)^0 \mu^+ \nu_\mu$

 Γ_L/Γ_T in $D^+ \rightarrow \bar{K}^*(892)^0 \ell^+ \nu_\ell$ See also BRIERE 10 for $\bar{K}^* \ell^+ \nu_\ell$ helicity-basis form-factor measurements.

VALUE	EVTS	DOCUMENT ID	TECN	COMMENT
1.13±0.08 OUR AVERAGE				
1.09±0.10±0.02	763	ADAMOVICH 99 BEAT		$\bar{K}^*(892)^0 \mu^+ \nu_\mu$
1.20±0.13±0.13	874	FRABETTI 93E E687		$\bar{K}^*(892)^0 \mu^+ \nu_\mu$
1.18±0.18±0.08	305	KODAMA 92 E653		$\bar{K}^*(892)^0 \mu^+ \nu_\mu$

Meson Particle Listings

D^\pm, D^0

DAOUDI	92	PR D45 3965	M. Daoudi et al.	(CLEO Collab.)
KODAMA	92	PL B274 246	K. Kodama et al.	(FNAL E653 Collab.)
KODAMA	92C	PL B286 187	K. Kodama et al.	(FNAL E653 Collab.)
ADAMOVIICH	91	PL B268 142	M.I. Adamovich et al.	(WA82 Collab.)
ALBRECHT	91	PL B255 634	H. Albrecht et al.	(ARGUS Collab.)
ALVAREZ	91B	ZPHY C50 11	M.P. Alvarez et al.	(CERN NA14/2 Collab.)
AMMAR	91	PR D44 3383	R. Ammar et al.	(CLEO Collab.)
BAI	91	PRL 66 1011	Z. Bai et al.	(Mark III Collab.)
COFFMAN	91	PL B263 135	D.M. Coffman et al.	(Mark III Collab.)
FRABETTI	91	PL B263 584	P.L. Frabetti et al.	(FNAL E687 Collab.)
ALVAREZ	90	ZPHY C47 539	M.P. Alvarez et al.	(CERN NA14/2 Collab.)
ANJOS	90C	PR D41 2705	J.C. Anjos et al.	(FNAL E691 Collab.)
ANJOS	90D	PR D42 2414	J.C. Anjos et al.	(FNAL E691 Collab.)
ANJOS	90E	PRL 65 2630	J.C. Anjos et al.	(FNAL E691 Collab.)
BARLAG	90C	ZPHY C46 563	S. Barlag et al.	(ACCMOR Collab.)
WEIR	90B	PR D41 1384	A.J. Weir et al.	(Mark II Collab.)
ANJOS	89	PRL 62 125	J.C. Anjos et al.	(FNAL E691 Collab.)
ANJOS	89B	PRL 62 722	J.C. Anjos et al.	(FNAL E691 Collab.)
ANJOS	89E	PL B223 267	J.C. Anjos et al.	(FNAL E691 Collab.)
ADLER	88C	PRL 60 99	J. Adler et al.	(Mark III Collab.)
ALBRECHT	88I	PL B210 267	H. Albrecht et al.	(ARGUS Collab.)
HAAS	88	PRL 60 1614	P. Haas et al.	(CLEO Collab.)
ONG	88	PRL 60 2587	R.A. Ong et al.	(Mark II Collab.)
RAAB	88	PR D37 2391	J.R. Raab et al.	(FNAL E691 Collab.)
ADAMOVIICH	87	EPL 4 887	M.I. Adamovich et al.	(Photon Emulsion Collab.)
ADLER	87	PL B196 107	J. Adler et al.	(Mark III Collab.)
BARTEL	87	ZPHY C33 339	W. Bartel et al.	(JADE Collab.)
BALTUSAITIS	86E	PRL 56 2140	R.M. Baltusaitis et al.	(Mark III Collab.)
BALTUSAITIS	85B	PRL 54 1976	R.M. Baltusaitis et al.	(Mark III Collab.)
BALTUSAITIS	85E	PRL 55 150	R.M. Baltusaitis et al.	(Mark III Collab.)
BARTEL	85J	PL B13B 277	W. Bartel et al.	(JADE Collab.)
ADAMOVIICH	84	PL 140B 119	M.I. Adamovich et al.	(CERN WA58 Collab.)
ALTHOFF	84G	ZPHY C22 219	M. Althoff et al.	(TASSO Collab.)
DERRICK	84	PRL 53 1971	M. Derrick et al.	(HRS Collab.)
SCHINDLER	81	PR D24 78	R.H. Schindler et al.	(Mark II Collab.)
TRILLING	81	PRPL 75 57	G.H. Trilling	(LBL, UCBLJ)
ZHOLENTZ	80	PL 96B 214	A.A. Zholents et al.	(NOVO)
Also		SJNP 34 814	A.A. Zholents et al.	(NOVO)
Translated from YAF 34		1471	A.A. Zholents et al.	(NOVO)
GOLDBERGER	77	PL 99B 503	S. Goldhaber et al.	(Mark I Collab.)
PERUZZI	77	PRL 39 1301	I. Peruzzi et al.	(LWG Collab.)
PICCOLO	77	PL 70B 260	M. Piccolo et al.	(Mark I Collab.)
PERUZZI	76	PRL 37 569	I. Peruzzi et al.	(Mark I Collab.)
MOSTELLER	48	Am.Stat.3 No.5 30	R.A. Fisher, F. Mosteller	

OTHER RELATED PAPERS

RICHMAN	95	RMP 67 893	J.D. Richman, P.R. Burchat	(UCSB, STAN)
ROSNER	95	CNPP 21 369	J. Rosner	(CHIC)



$$I(J^P) = \frac{1}{2}(0^-)$$

D^0 MASS

The fit includes $D^\pm, D^0, D_S^\pm, D^{*\pm}, D^{*0}, D_1(2420)^0, D_2^*(2460)^0$, and $D_{S1}(2536)^\pm$ mass and mass difference measurements.

Given the recent addition of much more precise measurements, we have omitted all those masses published up through 1990. See any Review before 2015 for those earlier results.

VALUE (MeV)	EVTS	DOCUMENT ID	TECN	COMMENT
1864.84 ± 0.05	OUR FIT			
1864.84 ± 0.05	OUR AVERAGE			
1864.845 ± 0.025 ± 0.057	63k	1 TOMARADZE 14	D ⁰ → K ⁻ 2π ⁺ π ⁻	
1864.75 ± 0.15 ± 0.11		AAIJ 13v	LHCB D ⁰ → K ⁺ 2K ⁻ π ⁺	
1864.841 ± 0.048 ± 0.063	4.3k	2 LEES 13s	BABR e ⁺ e ⁻ at $\Upsilon(4S)$	
1865.30 ± 0.33 ± 0.23	0.1k	ANASHIN 10A	KEDR e ⁺ e ⁻ at $\psi(3770)$	
1864.847 ± 0.150 ± 0.095	0.3k	CAWLFIELD 07	CLEO D ⁰ → K _S ⁰ φ	

¹ Obtained by analyzing CLEO-c data but not authored by the CLEO Collaboration. The largest source of error in the TOMARADZE 14 value is from the uncertainties in the K⁻ and K_S⁰ masses. The systematic error given above is the addition in quadrature of ±0.022 ± 0.053 MeV, where the second error is from those mass uncertainties.

² The largest source of error in the LEES 13s value is from the uncertainty of the K⁺ mass. The quoted systematic error is in fact ±0.043 + 3 (m_{K⁺} - 493.677), in MeV.

$m_{D^\pm} - m_{D^0}$

The fit includes $D^\pm, D^0, D_S^\pm, D^{*\pm}, D^{*0}, D_1(2420)^0, D_2^*(2460)^0$, and $D_{S1}(2536)^\pm$ mass and mass difference measurements.

VALUE (MeV)	DOCUMENT ID	TECN	COMMENT
4.822 ± 0.015	OUR FIT		
4.76 ± 0.12 ± 0.07	AAIJ 13v	LHCB	D ⁺ → K ⁺ K ⁻ π ⁺

D^0 MEAN LIFE

Measurements with an error > 10 × 10⁻¹⁵ s have been omitted from the average.

VALUE (10 ⁻¹⁵ s)	EVTS	DOCUMENT ID	TECN	COMMENT
410.3 ± 1.0	OUR AVERAGE			
410.5 ± 1.1 ± 0.8	171k	1 ABUDINEN 21A	BEL2	e ⁺ e ⁻ at $\Upsilon(4S)$
409.6 ± 1.1 ± 1.5	210k	LINK 02F	FOCS	γ nucleus, ≈ 180 GeV
407.9 ± 6.0 ± 4.3	10k	KUSHNIR... 01	SELX	K ⁻ π ⁺ , K ⁻ π ⁺ π ⁺ π ⁻
413 ± 3 ± 4	35k	AITALA 99E	E791	K ⁻ π ⁺
408.5 ± 4.1 ⁺ _{-3.4}	25k	BONVICINI 99	CLE2	e ⁺ e ⁻ ≈ $\Upsilon(4S)$
413 ± 4 ± 3	16k	FRABETTI 94D	E687	K ⁻ π ⁺ , K ⁻ π ⁺ π ⁺ π ⁻

• • • We do not use the following data for averages, fits, limits, etc. • • •

424 ± 11 ± 7	5118	FRABETTI 91	E687	K ⁻ π ⁺ , K ⁻ π ⁺ π ⁺ π ⁻
417 ± 18 ± 15	890	ALVAREZ 90	NA14	K ⁻ π ⁺ , K ⁻ π ⁺ π ⁺ π ⁻
388 ⁺²³ ₋₂₁	641	2 BARLAG 90c	ACCM	π ⁻ Cu 230 GeV
480 ± 40 ± 30	776	ALBRECHT 88I	ARG	e ⁺ e ⁻ 10 GeV
422 ± 8 ± 10	4212	RAAB 88	E691	Photoproduction
420 ± 50	90	BARLAG 87B	ACCM	K ⁻ and π ⁻ 200 GeV

¹ ABUDINEN 21A determines the lifetime ratio $\tau(D^+)/\tau(D^0) = 2.510 \pm 0.013 \pm 0.007$.

² BARLAG 90c estimate systematic error to be negligible.

See the related review(s):

$D^0 - \bar{D}^0$ Mixing

$$|m_{D_1^0} - m_{D_2^0}| = x \Gamma$$

The D_1^0 and D_2^0 are the mass eigenstates of the D^0 meson, as described in the note on " $D^0 - \bar{D}^0$ Mixing," above. The experiments usually present $x \equiv \Delta m/\Gamma$. Then $\Delta m = x \Gamma = x \hbar/\tau$.

VALUE (10 ¹⁰ h s ⁻¹)	CL%	DOCUMENT ID	TECN	COMMENT
0.997 ± 0.116	OUR EVALUATION			(Produced by HFLAV)
0.94 ± 0.11	OUR AVERAGE			
1.05 ± 0.36 ± 0.06		1 AAIJ	23Bc LHCB	pp at 13 TeV, D ⁰ → K _S ⁰ π ⁺ π ⁻
0.97 ^{+0.14} _{-0.13}		2 AAIJ	21AB LHCB	pp at 13 TeV, D ⁰ → K _S ⁰ π ⁺ π ⁻
0.66 ± 0.41 ^{+0.18} _{-0.37}		3 AAIJ	19x LHCB	pp at 7, 8 TeV, D ⁰ → K _S ⁰ π ⁺ π ⁻
		4 AAIJ	18K LHCB	pp at 7, 8, 13 TeV
		5 AAIJ	16V LHCB	pp at 7 TeV
		6 LEES	16D BABR	e ⁺ e ⁻ , 10.6 GeV
		7 KO	14 BELL	e ⁺ e ⁻ → $\Upsilon(nS)$
		8 PENG	14 BELL	e ⁺ e ⁻ → $\Upsilon(nS)$
		9 AALTONEN	13AE CDF	p \bar{p} at 1.96 TeV
0.39 ± 0.56 ± 0.35		10 DEL-AMO-SA...10D	BABR	e ⁺ e ⁻ , 10.6 GeV
		11 AAIJ	17A0 LHCB	Repl. by AAIJ 18K
		12 AAIJ	13CE LHCB	Repl. by AAIJ 17A0
		13 AAIJ	13N LHCB	Repl. by AAIJ 13Ce
6.4 ^{+1.4} _{-1.7} ± 1.0		14 AUBERT	09AN BABR	e ⁺ e ⁻ at 10.58 GeV
		15 LOWREY	09	CLEO e ⁺ e ⁻ at $\psi(3770)$
1.98 ± 0.73 ^{+0.32} _{-0.41}		16 ZHANG	07B BELL	Repl. by PENG 14
< 7	95	17 ZHANG	06 BELL	e ⁺ e ⁻
-11 to +22		16 ASNER	05 CLEO	e ⁺ e ⁻ ≈ 10 GeV
< 11	90	BITENC	05 BELL	
< 30	90	CAWLFIELD	05 CLEO	
< 7	95	17 LI	05A BELL	See ZHANG 06
< 22	95	18 LINK	05H FOCS	γ nucleus
< 23	95	AUBERT	04Q BABR	
< 11	95	17 AUBERT	03Z BABR	e ⁺ e ⁻ , 10.6 GeV
< 7	95	19 GODANG	00 CLE2	e ⁺ e ⁻
< 32	90	20,21 AITALA	98 E791	π ⁻ nucleus, 500 GeV
< 24	90	22 AITALA	96C E791	π ⁻ nucleus, 500 GeV
< 21	90	21,23 ANJOS	88C E691	Photoproduction

• • • We do not use the following data for averages, fits, limits, etc. • • •

- ¹ AAIJ 23Bc analysis of $D^0 \rightarrow K_S^0 \pi^+ \pi^-$ from $B \rightarrow D^0 \mu \nu X$ events allows for CP violation (none seen).
- ² AAIJ 21AB measurement allows for CP violation (none seen).
- ³ AAIJ 19x D^0 come from D^{*+} and $\bar{B} \rightarrow D^0 \mu^- X$ decays (and c.c.). Measurement allows for CP violation (none seen).
- ⁴ The result was established with D^0 from prompt and secondary D^* . Based on 5 fb⁻¹ of data collected at $\sqrt{s} = 7, 8, 13$ TeV. Assumes no CP violation. Reported $x'^2 = (3.9 \pm 2.7) \times 10^{-5}$ and $y' = (5.28 \pm 0.52) \times 10^{-3}$, where $x' = x \cos(\delta) + y \sin(\delta)$, $y' = y$.
- ⁵ Model-independent measurement of the charm mixing parameters in the decay $D^0 \rightarrow K_S^0 \pi^+ \pi^-$ using 1.0 fb⁻¹ of LHCB data at $\sqrt{s} = 7$ TeV.
- ⁶ Time-dependent amplitude analysis of $D^0 \rightarrow \pi^+ \pi^- \pi^0$.
- ⁷ Based on 976 fb⁻¹ of data collected at Y(nS) resonances. Assumes no CP violation. Reported $x'^2 = (0.09 \pm 0.22) \times 10^{-3}$ and $y' = (4.6 \pm 3.4) \times 10^{-3}$, where $x' = x \cos(\delta) + y \sin(\delta)$, $y' = y \cos(\delta) - x \sin(\delta)$ and δ is the strong phase between $D^0 \rightarrow K^+ \pi^-$ and $\bar{D}^0 \rightarrow K^+ \pi^-$.
- ⁸ The time-dependent Dalitz-plot analysis of $D^0 \rightarrow K_S^0 \pi^+ \pi^-$ is employed. Decay-time information and interference on the Dalitz plot are used to distinguish doubly Cabibbo-suppressed decays from mixing and to measure the relative phase between $D^0 \rightarrow K^{*+} \pi^-$ and $\bar{D}^0 \rightarrow K^{*+} \pi^-$. This value allows CP violation and is sensitive to the sign of Δm .
- ⁹ Based on 9.6 fb⁻¹ of data collected at the Tevatron. Assumes no CP violation. Reported $x'^2 = (0.08 \pm 0.18) \times 10^{-3}$ and $y' = (4.3 \pm 4.3) \times 10^{-3}$, where $x' = x \cos(\delta) + y$.

- $\sin(\delta), y' = y \cos(\delta) - x \sin(\delta)$ and δ is the strong phase between the $D^0 \rightarrow K^+ \pi^-$ and $\bar{D}^0 \rightarrow K^+ \pi^-$.
- ¹⁰ DEL-AMO-SANCHEZ 10D uses $540,800 \pm 800 K_S^0 \pi^+ \pi^-$ and $79,900 \pm 300 K_S^0 K^+ K^-$ events in a time-dependent amplitude analysis of the D^0 and \bar{D}^0 Dalitz plots. No evidence was found for CP violation, and the values here assume no such violation.
- ¹¹ The result was established with D^0 from prompt and secondary D^* . Based on 3 fb^{-1} of data collected at $\sqrt{s} = 7, 8 \text{ TeV}$. Assumes no CP violation. Reported $x'^2 = (3.6 \pm 4.3) \times 10^{-5}$ and $y' = (5.23 \pm 0.84) \times 10^{-3}$, where $x' = x \cos(\delta) + y \sin(\delta), y' = y \cos(\delta) - x \sin(\delta)$ and δ is the strong phase between the $D^0 \rightarrow K^+ \pi^-$ and $\bar{D}^0 \rightarrow K^+ \pi^-$.
- ¹² Based on 3 fb^{-1} of data collected at $\sqrt{s} = 7, 8 \text{ TeV}$. Assumes no CP violation. Reported $x'^2 = (5.5 \pm 4.9) \times 10^{-4}$ and $y' = (4.8 \pm 1.0) \times 10^{-3}$, where $x' = x \cos(\delta) + y \sin(\delta), y' = y \cos(\delta) - x \sin(\delta)$ and δ is the strong phase between the $D^0 \rightarrow K^+ \pi^-$ and $\bar{D}^0 \rightarrow K^+ \pi^-$.
- ¹³ Based on 1 fb^{-1} of data collected at $\sqrt{s} = 7 \text{ TeV}$ in 2011. Assumes no CP violation. Reported $x'^2 = (-0.9 \pm 1.3) \times 10^{-4}$ and $y' = (7.2 \pm 2.4) \times 10^{-3}$, where $x' = x \cos(\delta) + y \sin(\delta), y' = y \cos(\delta) - x \sin(\delta)$ and δ is the strong phase between the $D^0 \rightarrow K^+ \pi^-$ and $\bar{D}^0 \rightarrow K^+ \pi^-$.
- ¹⁴ The AUBERT 09AN values are inferred from the branching ratio $\Gamma(D^0 \rightarrow K^+ \pi^- \pi^0)$ via $\bar{D}^0/\Gamma(D^0 \rightarrow K^+ \pi^- \pi^0)$ given near the end of this Listings. Mixing is distinguished from DCS decays using decay-time information. Interference between mixing and DCS is allowed. The phase between $D^0 \rightarrow K^+ \pi^- \pi^0$ and $\bar{D}^0 \rightarrow K^+ \pi^- \pi^0$ is assumed to be small. The width difference here is y'' , which is not the same as y_{CP} in the note on $D^0-\bar{D}^0$ mixing.
- ¹⁵ LOWREY 09 uses quantum correlations in $e^+ e^- \rightarrow D^0 \bar{D}^0$ at the $\psi(3770)$. See below for coherence factors and average relative strong phases for both $D^0 \rightarrow K^- \pi^+ \pi^0$ and $D^0 \rightarrow K^- \pi^- 2\pi^+$. A fit that includes external measurements of charm mixing parameters gets $\Delta m = (2.34 \pm 0.61) \times 10^{10} \text{ h}^{-1}$.
- ¹⁶ The ASNER 05 and ZHANG 07B values are from the time-dependent Dalitz-plot analysis of $D^0 \rightarrow K_S^0 \pi^+ \pi^-$. Decay-time information and interference on the Dalitz plot are used to distinguish doubly Cabibbo-suppressed decays from mixing and to measure the relative phase between $D^0 \rightarrow K^* \pi^-$ and $\bar{D}^0 \rightarrow K^* \pi^-$. This value allows CP violation and is sensitive to the sign of Δm .
- ¹⁷ The AUBERT 03Z, LI 05A, and ZHANG 06 limits are inferred from the $D^0-\bar{D}^0$ mixing ratio $\Gamma(K^+ \pi^- \text{ via } \bar{D}^0)/\Gamma(K^+ \pi^-)$ given near the end of this D^0 Listings. Decay-time information is used to distinguish DCS decays from $D^0-\bar{D}^0$ mixing. The limit allows interference between the DCS and mixing ratios, and also allows CP violation. AUBERT 03Z assumes the strong phase between $D^0 \rightarrow K^+ \pi^-$ and $\bar{D}^0 \rightarrow K^+ \pi^-$ amplitudes is small; if an arbitrary phase is allowed, the limit degrades by 20%. The LI 05A and ZHANG 06 limits are valid for an arbitrary strong phase.
- ¹⁸ This LINK 05H limit is inferred from the $D^0-\bar{D}^0$ mixing ratio $\Gamma(K^+ \pi^- \text{ via } \bar{D}^0)/\Gamma(K^+ \pi^-)$ given near the end of this D^0 Listings. Decay-time information is used to distinguish DCS decays from $D^0-\bar{D}^0$ mixing. The limit allows interference between the DCS and mixing ratios, and also allows CP violation. The strong phase between $D^0 \rightarrow K^+ \pi^-$ and $\bar{D}^0 \rightarrow K^+ \pi^-$ is assumed to be small. If an arbitrary relative strong phase is allowed, the limit degrades by 25%.
- ¹⁹ This GODANG 00 limit is inferred from the $D^0-\bar{D}^0$ mixing ratio $\Gamma(K^+ \pi^- \text{ via } \bar{D}^0)/\Gamma(K^+ \pi^-)$ given near the end of this D^0 Listings. Decay-time information is used to distinguish DCS decays from $D^0-\bar{D}^0$ mixing. The limit allows interference between the DCS and mixing ratios, and also allows CP violation. The strong phase between $D^0 \rightarrow K^+ \pi^-$ and $\bar{D}^0 \rightarrow K^+ \pi^-$ is assumed to be small. If an arbitrary relative strong phase is allowed, the limit degrades by a factor of two.
- ²⁰ AITALA 98 allows interference between the doubly Cabibbo-suppressed and mixing amplitudes, and also allows CP violation in this term, but assumes that $A_D = A_R = 0$. See the note on " $D^0-\bar{D}^0$ Mixing," above.
- ²¹ This limit is inferred from R_M for $f = K^+ \pi^-$ and $f = K^+ \pi^- \pi^+ \pi^-$. See the note on " $D^0-\bar{D}^0$ Mixing," above. Decay-time information is used to distinguish doubly Cabibbo-suppressed decays from $D^0-\bar{D}^0$ mixing.
- ²² This limit is inferred from R_M for $f = K^+ \ell^- \bar{\nu}_\ell$. See the note on " $D^0-\bar{D}^0$ Mixing," above.
- ²³ ANJOS 88C assumes that $y = 0$. See the note on " $D^0-\bar{D}^0$ Mixing," above. Without this assumption, the limit degrades by about a factor of two.

Some early results have been omitted. See our 2006 Review (Journal of Physics G33 1 (2006)).

VALUE (units 10^{-2})	EVTS	DOCUMENT ID	TECN	COMMENT
1.394 ± 0.056 OUR EVALUATION		(Produced by HFLAV)		
1.35 ± 0.08 OUR AVERAGE		Error includes scale factor of 1.5. See the ideogram below.		
2.52 ± 0.62 ± 0.17		1 AAIJ	23BC LHCB	pp at 13 TeV, $D^0 \rightarrow K_S^0 \pi^+ \pi^-$
1.392 ± 0.052 ± 0.026		2 AAIJ	22O LHCB	$y_{CP} = y_{CP}(K\pi)$, pp at 13 TeV
0.92 + 0.30 - 0.28	30.6M	3 AAIJ	21AB LHCB	pp at 13 TeV
1.92 ± 1.82 +1.29 -1.24	91k	4 NAYAK	20 BELL	$D^0 \rightarrow K_S^0 \omega$
1.14 ± 0.26 ± 0.18		5 AAIJ	19 LHCB	pp at 7, 8 TeV
1.48 ± 0.74	2.3M	6 AAIJ	19X LHCB	$D^0 \rightarrow K_S^0 \pi^+ \pi^-$
		7 AAIJ	18K LHCB	pp at 7, 8, 13 TeV
		8 AAIJ	16V LHCB	pp at 7 TeV
0.06 ± 0.92 ± 0.26		9 LEES	16D BABR	$e^+ e^-$, 10.6 GeV
0.4 ± 1.8 ± 1.0		10 STARIC	16 BELL	$e^+ e^- \rightarrow \Upsilon(nS)$
2.22 ± 0.44 ± 0.18		11 ABLIKIM	15D BES3	$e^+ e^- \rightarrow \psi(3770)$
-4.0 ± 2.6 ± 1.4		12 KO	14 BELL	$e^+ e^- \rightarrow \Upsilon(nS)$
0.60 ± 0.30 +0.10 -0.17		13 PENG	14 BELL	$e^+ e^- \rightarrow \Upsilon(nS)$
1.44 ± 0.36 ± 0.24		14 AALTONEN	13AE CDF	$p\bar{p}$ at 1.96 TeV
0.55 ± 0.63 ± 0.41		15 LEES	13 BABR	pp at 7, 8 TeV
1.14 ± 0.40 ± 0.30		16 AAIJ	12K LHCB	pp at 7 TeV
0.22 ± 1.22 ± 1.04		17 DEL-AMO-SA...	10D BABR	$e^+ e^-$, 10.6 GeV
		18 ZUPANC	09 BELL	$e^+ e^- \approx \Upsilon(4S)$
-1.0 ± 2.0 +1.4 -1.6	18k	19 ABE	02I BELL	$e^+ e^- \approx \Upsilon(4S)$
-2.4 ± 5.0 ± 2.8	3393	20 CSORNA	02 CLE2	$e^+ e^- \approx \Upsilon(4S)$
6.84 ± 2.78 ± 1.48	10k	19 LINK	00 FOCUS	γ nucleus
+1.6 ± 5.8 ± 2.1		19 AITALA	99E E791	$K^- \pi^+, K^+ K^-$
••• We do not use the following data for averages, fits, limits, etc. •••				
		21 AAIJ	17AO LHCB	Repl. by AAIJ 18K
		22 AAIJ	13CE LHCB	Repl. by AAIJ 17AO
		23 AAIJ	13N LHCB	Repl. by AAIJ 13CE
2.32 ± 0.44 ± 0.36		24 AUBERT	09AI BABR	See LEES 13
-0.12 ± 1.10 ± 1.28 ± 0.68		25 AUBERT	09AN BABR	$e^+ e^-$ at 10.58 GeV
1.4 + 4.8 - 5.4		26 LOWREY	09 CLEO	$e^+ e^-$ at $\psi(3770)$
1.70 ± 1.52	13k	27 AALTONEN	08E CDF	$p\bar{p}, \sqrt{s} = 1.96 \text{ TeV}$
2.06 ± 0.66 ± 0.38		28 AUBERT	08U BABR	See AUBERT 09AI
1.94 ± 0.88 ± 0.62	4k	27 AUBERT	07W BABR	$e^+ e^- \approx 10.6 \text{ GeV}$
2.62 ± 0.64 ± 0.50	160k	29 STARIC	07 BELL	Repl. by STARIC 16
0.74 ± 0.50 +0.20 -0.31	534k	30 ZHANG	07B BELL	Repl. by PENG 14
-0.7 ± 4.9	4k	27,31 ZHANG	06 BELL	$e^+ e^-$
-3.0 ± 5.0 +1.6 -4.8 -0.8		30 ASNER	05 CLEO	$e^+ e^- \approx 10 \text{ GeV}$
-0.3 ± 5.7		27,31 LI	05A BELL	See ZHANG 06
-5.2 +18.4 -16.8		27,31 LINK	05H FOCUS	γ nucleus
1.6 ± 0.8 +1.0 -0.8	450k	32 AUBERT	03P BABR	See AUBERT 08U
1.6 + 6.2 -12.8		27,31 AUBERT	03Z BABR	$e^+ e^-$, 10.6 GeV
-5.0 + 2.8 -3.2 ± 0.6		27 GODANG	00 CLE2	$e^+ e^-$

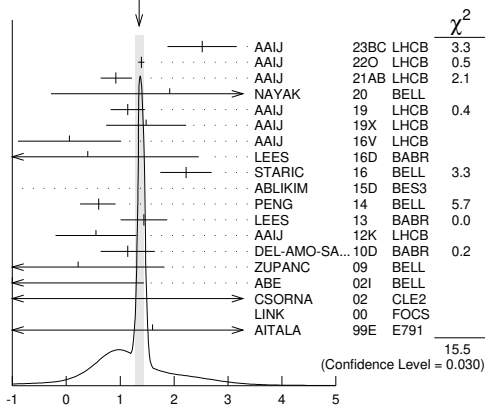
$$(\Gamma_{D_1^0} - \Gamma_{D_2^0})/\Gamma = 2y$$

The D_1^0 and D_2^0 are the mass eigenstates of the D^0 meson, as described in the note on " $D^0-\bar{D}^0$ Mixing," above.

Due to the strong phase difference between $D^0 \rightarrow K^+ \pi^-$ and $\bar{D}^0 \rightarrow K^+ \pi^-$, we exclude from the average those measurements of y' that are inferred from the $D^0-\bar{D}^0$ mixing ratio $\Gamma(K^+ \pi^- \text{ via } \bar{D}^0) / \Gamma(K^+ \pi^-)$ given near the end of this D^0 Listings. OUR AVERAGE assumes CP conservation, though this is disfavored by data.

In the absence of CP violation, the experimental measurement of the observable y_{CP} corresponds to y . In the presence of CP violation, y_{CP} is approximately equal to y up to a CP -violating weak phase cosine, that is very close to unity, and higher order CP -violating effects. Many experiments measure y_{CP} with respect to a reference channel, such that the quoted results below are often $y_{CP} \pm y_{CP}(\text{reference})$. We denote the actual observable and the reference channel below for those experiments with sufficient sensitivity such that $y_{CP}(\text{reference})$ cannot be neglected.

WEIGHTED AVERAGE
1.35±0.08 (Error scaled by 1.5)



$$(\Gamma_1 - \Gamma_2)/\Gamma = 2y$$

¹ AAIJ 23BC analysis of $D^0 \rightarrow K_S^0 \pi^+ \pi^-$ from $B \rightarrow D^0 \mu \nu X$ events allows for CP violation (none seen).

Meson Particle Listings

 D^0

- ² AAIJ 22o is the combination of the measurement in the $D^0 \rightarrow \pi^- \pi^+$ channel and the one in the $D^0 \rightarrow K^- K^+$ channel, that are $(1.314 \pm 0.106 \pm 0.032)\%$ and $(1.416 \pm 0.060 \pm 0.028)\%$ respectively, assuming fully correlated systematics except those related to peaking backgrounds.
- ³ AAIJ 21AB analysis of $D^0 \rightarrow K_S^0 \pi^+ \pi^-$ events allows for CP violation (none seen).
- ⁴ NAYAK 20 reports $(1.92 \pm 1.82 \pm 1.24 \pm 0.34) \times 10^{-2}$ where the last uncertainty is due to possible presence of CP -even decays in the data sample. Extracts $y_{CP} = (\Gamma_{CP+} - \Gamma_{CP-}) / (\Gamma_{CP+} + \Gamma_{CP-})$ in $D^0 \rightarrow K_S^0 \omega$ versus $\bar{D}^0 \rightarrow K_S^0 \omega$, by measuring the decay lifetime of $D^0 \rightarrow K_S^0 \omega$ with $\omega \rightarrow \pi^+ \pi^- \pi^0$ versus $\bar{D}^0 \rightarrow K^- \pi^+$. We list $2y_{CP} = 2y (= \Delta\Gamma/\Gamma)$ in the absence of CP violation.
- ⁵ Based on 3 fb^{-1} of data collected at $\sqrt{s} = 7, 8 \text{ TeV}$. Measures the lifetime difference between $D^0 \rightarrow K^- K^+$ and $D^0 \rightarrow \pi^- \pi^+$ (CP -even) decays and $D^0 \rightarrow K^- \pi^+$ (CP -mixed) decays, or $y_{CP} = (\Gamma_{CP+} - \Gamma_{CP-}) / (\Gamma_{CP+} + \Gamma_{CP-})$. The D^0 mesons are required to originate from semimuonic decays of B mesons. We list $2y_{CP} = \Delta\Gamma/\Gamma$.
- ⁶ AAIJ 19x D^0 come from D^{*+} and $\bar{B} \rightarrow D^0 \mu^- X$ decays (and c.c.) in pp collisions at 7 and 8 TeV. Measurement allows for CP violation (none seen).
- ⁷ The result was established with D^0 from prompt and secondary D^* . Based on 5 fb^{-1} of data collected at $\sqrt{s} = 7, 8, 13 \text{ TeV}$. Assumes no CP violation. Reported $x'^2 = (3.9 \pm 2.7) \times 10^{-5}$ and $y' = (5.28 \pm 0.52) \times 10^{-3}$, where $x' = x \cos(\delta) + y \sin(\delta)$, $y' = y \cos(\delta) - x \sin(\delta)$ and δ is the strong phase between the $D^0 \rightarrow K^+ \pi^-$ and $\bar{D}^0 \rightarrow K^+ \pi^-$.
- ⁸ Model-independent measurement of the charm mixing parameters in the decay $D^0 \rightarrow K_S^0 \pi^+ \pi^-$ using 1.0 fb^{-1} of LHCb data at $\sqrt{s} = 7 \text{ TeV}$.
- ⁹ Time-dependent amplitude analysis of $D^0 \rightarrow \pi^+ \pi^- \pi^0$.
- ¹⁰ An improved measurement of $\bar{D}^0 - D^0$ mixing and a search for CP violation in D^0 decays to CP -even final states $K^+ K^-$ and $\pi^+ \pi^-$ using the final Belle data sample of 976 fb^{-1} .
- ¹¹ ABLIKIM 15D uses quantum correlations in $e^+ e^- \rightarrow D^0 \bar{D}^0$ at the $\psi(3770)$.
- ¹² Based on 976 fb^{-1} of data collected at $Y(\text{nS})$ resonances. Assumes no CP violation. Reported $x'^2 = (0.09 \pm 0.22) \times 10^{-3}$ and $y' = (4.6 \pm 3.4) \times 10^{-3}$, where $x' = x \cos(\delta) + y \sin(\delta)$, $y' = y \cos(\delta) - x \sin(\delta)$ and δ is the strong phase between $D^0 \rightarrow K^+ \pi^-$ and $\bar{D}^0 \rightarrow K^+ \pi^-$.
- ¹³ The time-dependent Dalitz-plot analysis of $D^0 \rightarrow K_S^0 \pi^+ \pi^-$ is employed. Decay-time information and interference on the Dalitz plot are used to distinguish doubly Cabibbo-suppressed decays from mixing and to measure the relative phase between $D^0 \rightarrow K^{*+} \pi^-$ and $\bar{D}^0 \rightarrow K^{*+} \pi^-$. This value allows CP violation and is sensitive to the sign of Δm .
- ¹⁴ Based on 9.6 fb^{-1} of data collected at the Tevatron. Assumes no CP violation. Reported $x'^2 = (0.08 \pm 0.18) \times 10^{-3}$ and $y' = (4.3 \pm 4.3) \times 10^{-3}$, where $x' = x \cos(\delta) + y \sin(\delta)$, $y' = y \cos(\delta) - x \sin(\delta)$ and δ is the strong phase between the $D^0 \rightarrow K^+ \pi^-$ and $\bar{D}^0 \rightarrow K^+ \pi^-$.
- ¹⁵ Obtained $y_{CP} = (0.72 \pm 0.18 \pm 0.12)\%$ based on three effective D^0 lifetimes measured in $K^+ \pi^+$, $K^- K^+$, and $\pi^- \pi^+$. We list $2y_{CP} = \Delta\Gamma/\Gamma$.
- ¹⁶ Compared the lifetimes of D^0 decay to the CP eigenstate $K^+ K^-$ with D^0 decay to $\pi^+ K^-$. The values here assume no CP violation.
- ¹⁷ DEL-AMO-SANCHEZ 10b uses $540,800 \pm 800 K_S^0 \pi^+ \pi^-$ and $79,900 \pm 300 K_S^0 K^+ K^-$ events in a time-dependent amplitude analyses of the D^0 and \bar{D}^0 Dalitz plots. No evidence was found for CP violation, and the values here assume no such violation.
- ¹⁸ ZUPANC 09 uses a method based on measuring the mean decay time of $D^0 \rightarrow K_S^0 K^+ K^-$ events for different $K^+ K^-$ mass intervals.
- ¹⁹ LINK 00, AITALA 99E, and ABE 02i measure the lifetime difference between $D^0 \rightarrow K^- K^+$ (CP -even) decays and $D^0 \rightarrow K^- \pi^+$ (CP -mixed) decays, or $y_{CP} = [(\Gamma_{CP+} - \Gamma_{CP-}) / (\Gamma_{CP+} + \Gamma_{CP-})]$. We list $2y_{CP} = \Delta\Gamma/\Gamma$.
- ²⁰ CSORNA 02 measures the lifetime difference between $D^0 \rightarrow K^- K^+$ and $\pi^- \pi^+$ (CP -even) decays and $D^0 \rightarrow K^- \pi^+$ (CP -mixed) decays, or $y_{CP} = [(\Gamma_{CP+} - \Gamma_{CP-}) / (\Gamma_{CP+} + \Gamma_{CP-})]$. We list $2y_{CP} = \Delta\Gamma/\Gamma$.
- ²¹ The result was established with D^0 from prompt and secondary D^* . Based on 3 fb^{-1} of data collected at $\sqrt{s} = 7, 8 \text{ TeV}$. Assumes no CP violation. Reported $x'^2 = (3.6 \pm 4.3) \times 10^{-5}$ and $y' = (5.23 \pm 0.84) \times 10^{-3}$, where $x' = x \cos(\delta) + y \sin(\delta)$, $y' = y \cos(\delta) - x \sin(\delta)$ and δ is the strong phase between the $D^0 \rightarrow K^+ \pi^-$ and $\bar{D}^0 \rightarrow K^+ \pi^-$.
- ²² Based on 3 fb^{-1} of data collected at $\sqrt{s} = 7, 8 \text{ TeV}$. Assumes no CP violation. Reported $x'^2 = (5.5 \pm 4.9) \times 10^{-4}$ and $y' = (4.8 \pm 1.0) \times 10^{-3}$, where $x' = x \cos(\delta) + y \sin(\delta)$, $y' = y \cos(\delta) - x \sin(\delta)$ and δ is the strong phase between the $D^0 \rightarrow K^+ \pi^-$ and $\bar{D}^0 \rightarrow K^+ \pi^-$.
- ²³ Based on 1 fb^{-1} of data collected at $\sqrt{s} = 7 \text{ TeV}$ in 2011. Assumes no CP violation. Reported $x'^2 = (-0.9 \pm 1.3) \times 10^{-4}$ and $y' = (7.2 \pm 2.4) \times 10^{-3}$, where $x' = x \cos(\delta) + y \sin(\delta)$, $y' = y \cos(\delta) - x \sin(\delta)$ and δ is the strong phase between the $D^0 \rightarrow K^+ \pi^-$ and $\bar{D}^0 \rightarrow K^+ \pi^-$.
- ²⁴ This combines the $y_{CP} = (\tau_{K^+ \pi^+} / \tau_{K^- K^+}) - 1$ using untagged $K^- \pi^+$ and $K^- K^+$ events of AUBERT 09A1 with the disjoint y_{CP} using tagged $K^- \pi^+$, $K^- K^+$, and $\pi^- \pi^+$ events of AUBERT 08U.
- ²⁵ The AUBERT 09AN values are inferred from the branching ratio $\Gamma(D^0 \rightarrow K^+ \pi^- \pi^0) / \Gamma(D^0 \rightarrow K^- \pi^+ \pi^0)$ given near the end of this Listings. Mixing is distinguished from DCS decays using decay-time information. Interference between mixing and DCS is allowed. The phase between $D^0 \rightarrow K^+ \pi^- \pi^0$ and $\bar{D}^0 \rightarrow K^+ \pi^- \pi^0$ is assumed to be small. The width difference here is y'' , which is not the same as y_{CP} in the note on $D^0 - \bar{D}^0$ mixing.
- ²⁶ LOWREY 09 uses quantum correlations in $e^+ e^- \rightarrow D^0 \bar{D}^0$ at the $\psi(3770)$. See below for coherence factors and average relative strong phases for both $D^0 \rightarrow K^- \pi^+ \pi^0$ and $D^0 \rightarrow K^- \pi^- \pi^+$. A fit that includes external measurements of charm mixing parameters gets $2y = (1.62 \pm 0.32) \times 10^{-2}$.
- ²⁷ The GODANG 00, AUBERT 03z, LINK 05H, LI 05A, ZHANG 06, AUBERT 07w, and AALTONEN 08E limits are inferred from the $D^0 - \bar{D}^0$ mixing ratio $\Gamma(K^+ \pi^-) / \Gamma(K^- \pi^+)$ given near the end of this D^0 Listings. Decay-time information is used to distinguish DCS decays from $D^0 - \bar{D}^0$ mixing. The limits allow interference between

the DCS and mixing ratios, and all except AUBERT 07w and AALTONEN 08E also allow CP violation. The phase between $D^0 \rightarrow K^+ \pi^-$ and $\bar{D}^0 \rightarrow K^+ \pi^-$ is assumed to be small. This is a measurement of y' and is not the same as the y_{CP} of our note above on " $D^0 - \bar{D}^0$ Mixing."

- ²⁸ This value combines the results of AUBERT 08U and AUBERT 03P.
- ²⁹ STARIC 07 compares the lifetimes of D^0 decay to the CP eigenstates $K^+ K^-$ and $\pi^+ \pi^-$ with D^0 decay to $K^- \pi^+$.
- ³⁰ The ASNER 05 and ZHANG 07b values are from the time-dependent Dalitz-plot analysis of $D^0 \rightarrow K_S^0 \pi^+ \pi^-$. Decay-time information and interference on the Dalitz plot are used to distinguish doubly Cabibbo-suppressed decays from mixing and to measure the relative phase between $D^0 \rightarrow K^{*+} \pi^-$ and $\bar{D}^0 \rightarrow K^{*+} \pi^-$. This limit allows CP violation.
- ³¹ The ranges of AUBERT 03z, LINK 05H, LI 05A, and ZHANG 06 measurements are for 95% confidence level.
- ³² AUBERT 03P measures $Y \equiv 2\tau^0 / (\tau^+ + \tau^-) - 1$, where τ^0 is the $D^0 \rightarrow K^- \pi^+$ (and $\bar{D}^0 \rightarrow K^+ \pi^-$) lifetime, and τ^+ and τ^- are the D^0 and \bar{D}^0 lifetimes to CP -even states (here $K^- K^+$ and $\pi^- \pi^+$). In the limit of CP conservation, $Y = y \equiv \Delta\Gamma / 2\Gamma$ (we list $2y = \Delta\Gamma/\Gamma$). AUBERT 03P also uses $\tau^+ - \tau^-$ to get $\Delta Y = -0.008 \pm 0.006 \pm 0.002$.

 $|q/p|$

The mass eigenstates D_1^0 and D_2^0 are related to the $C = \pm 1$ states by $|D_{1,2}^0\rangle = p |D^0\rangle + q |\bar{D}^0\rangle$. See the note on " $D^0 - \bar{D}^0$ Mixing" above.

VALUE	EVTS	DOCUMENT ID	TECN	COMMENT
0.995 ± 0.016 OUR EVALUATION				(Produced by HFLAV) see the note on " $D^0 - \bar{D}^0$ Mixing."
0.99 ± 0.05 OUR AVERAGE				
0.996 ± 0.052	30.6M	1 AAIJ	21AB LHCb	pp at 13 TeV
1.05 $^{+0.22}_{-0.17}$	2.3M	2 AAIJ	19x LHCb	pp at 7, 8 TeV
		3 AAIJ	18k LHCb	pp at 7, 8, 13 TeV
0.90 $^{+0.16}_{-0.15}$ $^{+0.08}_{-0.06}$		4 PENG	14 BELL	$e^+ e^- \rightarrow \Upsilon(\text{nS})$
• • • We do not use the following data for averages, fits, limits, etc. • • •				
		5 AAIJ	13CE LHCb	Repl. by AAIJ 18k
0.86 $^{+0.30}_{-0.29}$ $^{+0.10}_{-0.08}$		6 ZHANG	07B BELL	Repl. by PENG 14

- ¹ AAIJ 21AB result comes from analysis of $D^0 \rightarrow K_S^0 \pi^+ \pi^-$ events.
- ² AAIJ 19x measurement comes from analysis of $D^0 \rightarrow K_S^0 \pi^+ \pi^-$ decays. D^0 come from D^{*+} and $\bar{B} \rightarrow D^0 \mu^- X$ decays (and c.c.) in pp collisions at 7 and 8 TeV.
- ³ Based on 5 fb^{-1} of data collected at $\sqrt{s} = 7, 8, 13 \text{ TeV}$. Allowing for CP violation, the direct CP violation in mixing is reported $1.00 < |q/p| < 1.35$ at the 68.3% CL for the $D^0 \rightarrow K^+ \pi^-$ and $\bar{D}^0 \rightarrow K^+ \pi^-$.
- ⁴ The time-dependent Dalitz-plot analysis of $D^0 \rightarrow K_S^0 \pi^+ \pi^-$ is employed. Decay-time information and interference on the Dalitz plot are used to distinguish doubly Cabibbo-suppressed decays from mixing and to measure the relative phase between $D^0 \rightarrow K^{*+} \pi^-$ and $\bar{D}^0 \rightarrow K^{*+} \pi^-$. This value allows CP violation and is sensitive to the sign of Δm .
- ⁵ Based on 3 fb^{-1} of data collected at $\sqrt{s} = 7, 8 \text{ TeV}$. Allowing for CP violation, the direct CP violation in mixing is reported $0.75 < |q/p| < 1.24$ at the 68.3% CL for the $D^0 \rightarrow K^+ \pi^-$ and $\bar{D}^0 \rightarrow K^+ \pi^-$.
- ⁶ The phase of p/q is $(-14 \pm 16 \pm 5)^\circ$. The ZHANG 07b value is from the time-dependent Dalitz-plot analysis of $D^0 \rightarrow K_S^0 \pi^+ \pi^-$. Decay-time information and interference on the Dalitz plot are used to distinguish doubly Cabibbo-suppressed decays from mixing and to measure the relative phase between $D^0 \rightarrow K^{*+} \pi^-$ and $\bar{D}^0 \rightarrow K^{*+} \pi^-$. This value allows CP violation.

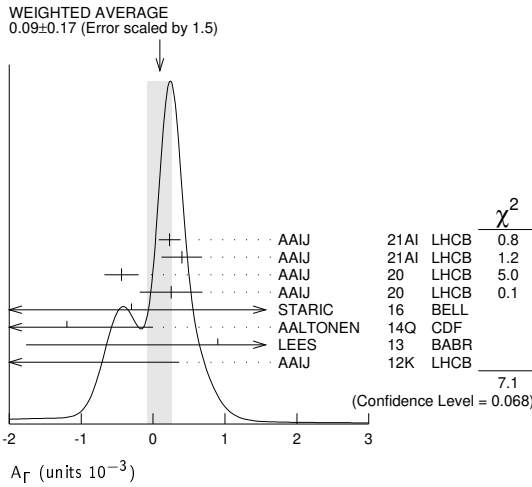
 A_Γ

A_Γ is the decay-rate asymmetry for CP -even final states $A_\Gamma = (\bar{\tau}_+ - \tau_+) / (\bar{\tau}_+ + \tau_+)$. See the note on " $D^0 - \bar{D}^0$ Mixing" above.

VALUE (units 10^{-3})	EVTS	DOCUMENT ID	TECN	COMMENT
0.089 ± 0.113 OUR EVALUATION				
0.09 ± 0.17 OUR AVERAGE				Error includes scale factor of 1.5. See the ideogram below.
0.23 ± 0.15 ± 0.03		1 AAIJ	21AI LHCb	$D^0 \rightarrow K^+ K^-$
0.40 ± 0.28 ± 0.04		1 AAIJ	21AI LHCb	$D^0 \rightarrow \pi^+ \pi^-$
-0.44 ± 0.23 ± 0.06	21M	2 AAIJ	20 LHCb	$D^0 \rightarrow K^+ K^-$
0.25 ± 0.43 ± 0.07	7M	3 AAIJ	20 LHCb	$D^0 \rightarrow \pi^+ \pi^-$
-0.3 ± 2.0 ± 0.7		4 STARIC	16 BELL	$e^+ e^- \rightarrow \Upsilon(\text{nS})$
-1.2 ± 1.2	1.8M	5 AALTONEN	14Q CDF	$p\bar{p}$, $\sqrt{s} = 1.96 \text{ TeV}$
0.9 ± 2.6 ± 0.6	0.7M	LEES	13 BABR	$e^+ e^- \rightarrow \Upsilon(4S)$
-5.9 ± 5.9 ± 2.1		6 AAIJ	12K LHCb	pp at 7 TeV, 2010 data.
• • • We do not use the following data for averages, fits, limits, etc. • • •				
-0.30 ± 0.32 ± 0.10	9.6M	6 AAIJ	17AK LHCb	Repl. by AAIJ 20
0.46 ± 0.58 ± 0.12	3.0M	7 AAIJ	17AK LHCb	Repl. by AAIJ 20
-1.34 ± 0.77 $^{+0.26}_{-0.34}$	2.3M	8 AAIJ	15AA LHCb	Repl. by AAIJ 20
-0.92 ± 1.45 $^{+0.25}_{-0.33}$	0.8M	9 AAIJ	15AA LHCb	Repl. by AAIJ 20
-0.35 ± 0.62 ± 0.12		6 AAIJ	14AL LHCb	Repl. by AAIJ 17AK
0.33 ± 1.06 ± 0.14		7 AAIJ	14AL LHCb	Repl. by AAIJ 17AK
2.6 ± 3.6 ± 0.8		AUBERT	08U BABR	See LEES 13
0.1 ± 3.0 ± 2.5		STARIC	07 BELL	Repl. by STARIC 16
8 ± 6 ± 2		AUBERT	03P BABR	$e^+ e^- \approx \Upsilon(4S)$

- ¹ Requires D^0 to originate from $D^{*+}(2010)^+ \rightarrow D^0 \pi^+$. AAIJ 21AI measures the parameter $\Delta Y_f \approx -A_f^2$ up to 1% corrections from y_{CP}^f .

- ² Measured using $D^0 \rightarrow K^+K^-$ decays, combines measurements with D^0 either from partially reconstructed semileptonic B hadron decays or from $D^{*+} \rightarrow D^0\pi^+$.
- ³ Measured using $D^0 \rightarrow \pi^+\pi^-$ decays, combines measurements with D^0 either from partially reconstructed semileptonic B hadron decays or from $D^{*+} \rightarrow D^0\pi^+$.
- ⁴ An improved measurement of $\overline{D}^0 - D^0$ mixing and a search for CP violation in D^0 decays to CP -even final states K^+K^- and $\pi^+\pi^-$ using the final Belle data sample of 976 fb^{-1} .
- ⁵ Combined result from $D^0 \rightarrow K^+K^-$ and $D^0 \rightarrow \pi^+\pi^-$, with D^0 from $D^{*+} \rightarrow D^0\pi^+$ (and cc).
- ⁶ Measured using $D^{*+} \rightarrow D^0\pi^+$, $D^0 \rightarrow K^+K^-$ decays (and cc).
- ⁷ Measured using $D^{*+} \rightarrow D^0\pi^+$, $D^0 \rightarrow \pi^+\pi^-$ decays (and cc).
- ⁸ Measured using $D^0 \rightarrow K^+K^-$ decays, with D^0 from partially reconstructed semileptonic B hadron decays.
- ⁹ Measured using $D^0 \rightarrow \pi^+\pi^-$ decays, with D^0 from partially reconstructed semileptonic B hadron decays.



$\phi_{K_S^0\pi\pi}$

Parametrizes CP violation in the interference between D^0 mixing and decay. The mass eigenstates D_1^0 and D_2^0 are related to the $C = \pm 1$ states by $|D_{1,2}^0\rangle = p|D^0\rangle + q|\overline{D}^0\rangle$. In the absence of CP violation in the decay, and using the usual phase convention where CP conservation implies q/p is real, $\phi_{K_S^0\pi\pi}$ is identical to the decay-mode-independent parameter $\phi = \arg(q/p)$.

VALUE	EVTS	DOCUMENT ID	TECN	COMMENT
0.02 ± 0.04 -0.05	OUR AVERAGE			
0.056 ± 0.047 -0.051	30.6M	¹ AAIJ	21AB LHCb	pp at 13 TeV
-0.09 ± 0.11 -0.16	2.3M	² AAIJ	19x LHCb	pp at 7, 8 TeV
-0.10 ± 0.19 ± 0.07 -0.09	1.2M	³ PENG	14 BELL	e^+e^- at $\Upsilon(4S, 5S)$

- ¹ AAIJ 21AB result comes from analysis of $D^0 \rightarrow K_S^0\pi^+\pi^-$ events.
- ² AAIJ 19x result comes from analysis of $D^0 \rightarrow K_S^0\pi^+\pi^-$ events. D^0 come from D^{*+} and $\overline{B} \rightarrow D^0\mu^-X$ decays (and c.c.) in pp collisions at 7 and 8 TeV.
- ³ PENG 14 reports $-0.10 \pm 0.19 \pm 0.05 \pm 0.05$ value where the last uncertainty is due to the amplitude model. We have added the systematic uncertainties in quadrature.

$\cos \delta$

δ is the $D^0 \rightarrow K^+\pi^-$ relative strong phase.

VALUE	EVTS	DOCUMENT ID	TECN	COMMENT
0.990 ± 0.025 -0.015	OUR AVERAGE			
0.991 ± 0.021 ± 0.012 0.022 ± 0.015		¹ ABLIKIM	22bMBES3	$e^+e^- \rightarrow D^0\overline{D}^0$, 3.77 GeV
1.02 ± 0.11 ± 0.06		² ABLIKIM	14c BES3	$e^+e^- \rightarrow D^0\overline{D}^0$, 3.77 GeV
0.81 ± 0.22 ± 0.07 -0.18 ± 0.05		³ ASNER	12 CLEO	$e^+e^- \rightarrow D^0\overline{D}^0$, 3.77 GeV
1.03 ± 0.31 ± 0.06 -0.17		⁴ ASNER	08 CLEO	Repl. by ASNER 12

- ¹ Uses quantum correlations in $e^+e^- \rightarrow D^0\overline{D}^0$ at the $\psi(3770)$ to measure the asymmetry of the branching fraction of $D^0 \rightarrow K^-\pi^+$ in CP -odd and CP -even eigenstates to be $(13.2 \pm 1.1 \pm 0.7)\%$ and $(13.0 \pm 1.2 \pm 0.8)\%$ when using the predominantly CP -even tag $D^0 \rightarrow \pi^+\pi^-\pi^0$. A fit that includes external measurements of charm mixing parameters finds the value quoted above.
- ² Uses quantum correlations in $e^+e^- \rightarrow D^0\overline{D}^0$ at the $\psi(3770)$ to measure the asymmetry of the branching fraction of $D^0 \rightarrow K^-\pi^+$ in CP -odd and CP -even eigenstates to be $(12.7 \pm 1.3 \pm 0.7)\%$. A fit that includes external measurements of charm mixing parameters finds the value quoted above.
- ³ Uses quantum correlations in $e^+e^- \rightarrow D^0\overline{D}^0$ at the $\psi(3770)$, where decay rates of CP -tagged $K\pi$ final states depend on the strong phases between the decays of $D^0 \rightarrow K^+\pi^-$ and $\overline{D}^0 \rightarrow K^+\pi^-$. The measurements obtained $\sin(\delta) = -0.01 \pm 0.41 \pm 0.04$ and $|\delta| = (10_{-53}^{+28+13})^\circ$ as well. A fit that includes external measurements of charm

mixing parameters finds $\cos(\delta) = 1.15_{-0.17}^{+0.19+0.00}$, $\sin(\delta) = 0.56_{-0.31}^{+0.32+0.21}$, and $|\delta| = (18_{-17}^{+11})^\circ$.

- ⁴ ASNER 08 uses quantum correlations in $e^+e^- \rightarrow D^0\overline{D}^0$ at the $\psi(3770)$, where decay rates of CP -tagged $K\pi$ final states depend on $\cos \delta$ because of interfering amplitudes. The above measurement implies $|\delta| < 75^\circ$ with a confidence level of 95%. A fit that includes external measurements of charm mixing parameters finds $\cos \delta = 1.10 \pm 0.35 \pm 0.07$. See also the note on " $D^0 - \overline{D}^0$ Mixing" p. 783 in our 2008 Review (PDG 08).

$D^0 \rightarrow K^-\pi^+\pi^0$ COHERENCE FACTOR $R_{K\pi\pi^0}$

See the note on ' $D^0 - \overline{D}^0$ Mixing' for the definition. $R_{K\pi\pi^0}$ can have any value between 0 and 1. A value near 1 indicates the decay is dominated by a few intermediate states with limited interference.

VALUE	EVTS	DOCUMENT ID	TECN	COMMENT
0.792 ± 0.033	OUR AVERAGE			
0.78 ± 0.04	62.4k	¹ ABLIKIM	21AA BES3	$e^+e^- \rightarrow D^0\overline{D}^0$ at $\psi(3770)$
0.82 ± 0.06		^{1,2,3} EVANS	16	$e^+e^- \rightarrow D^0\overline{D}^0$ at $\psi(3770)$
0.82 ± 0.07		^{1,3} LIBBY	14	Repl. by EVANS 16
0.78 ± 0.11 -0.25		⁴ LOWREY	09 CLEO	Repl. by LIBBY 14

- ¹ Uses quantum correlations in $e^+e^- \rightarrow D^0\overline{D}^0$ at the $\psi(3770)$, where the decay rates of CP -tagged $K^-\pi^+\pi^0$ final states depend on $R_{K\pi\pi^0}$ and $\delta^{K\pi\pi^0}$.
- ² A combined fit with a recent LHCb $D^0\overline{D}^0$ mixing results in AAIJ 16F is also reported to be 0.81 ± 0.06 .
- ³ Obtained by analyzing CLEO-c data but not authored by the CLEO Collaboration.
- ⁴ LOWREY 09 uses quantum correlations in $e^+e^- \rightarrow D^0\overline{D}^0$ at the $\psi(3770)$, where the decay rates of CP -tagged $K^-\pi^+\pi^0$ final states depend on $R_{K\pi\pi^0}$ and $\delta^{K\pi\pi^0}$. A fit that includes external measurements of charm mixing parameters gets $R_{K\pi\pi^0} = 0.84 \pm 0.07$.

$D^0 \rightarrow K^-\pi^+\pi^0$ AVERAGE RELATIVE STRONG PHASE $\delta^{K\pi\pi^0}$

The quoted value of δ is based on the same sign CP phase of D^0 and \overline{D}^0 convention.

VALUE ($^\circ$)	EVTS	DOCUMENT ID	TECN	COMMENT
198 ± 10	OUR AVERAGE			
196 ± 14 -15	62.4k	¹ ABLIKIM	21AA BES3	$e^+e^- \rightarrow D^0\overline{D}^0$ at $\psi(3770)$
199 ± 13 -14		^{1,2,3} EVANS	16	$e^+e^- \rightarrow D^0\overline{D}^0$ at $\psi(3770)$
164 ± 20 -14		^{1,3} LIBBY	14	Repl. by EVANS 16
239 ± 32 -28		⁴ LOWREY	09 CLEO	Repl. by LIBBY 14

- ¹ Uses quantum correlations in $e^+e^- \rightarrow D^0\overline{D}^0$ at the $\psi(3770)$, where the decay rates of CP -tagged $K^-\pi^+\pi^0$ final states depend on $R_{K\pi\pi^0}$ and $\delta^{K\pi\pi^0}$.
- ² A combined fit with a recent LHCb $D^0\overline{D}^0$ mixing results in AAIJ 16F is also reported to be 198_{-15}^{+14} degree.
- ³ Obtained by analyzing CLEO-c data but not authored by the CLEO Collaboration.
- ⁴ LOWREY 09 uses quantum correlations in $e^+e^- \rightarrow D^0\overline{D}^0$ at the $\psi(3770)$, where the decay rates of CP -tagged $K^-\pi^+\pi^0$ final states depend on $R_{K\pi\pi^0}$ and $\delta^{K\pi\pi^0}$. A fit that includes external measurements of charm mixing parameters gets $\delta^{K\pi\pi^0} = (227_{-17}^{+14})^\circ$.

$D^0 \rightarrow K^-\pi^-2\pi^+$ COHERENCE FACTOR $R_{K3\pi}$

See the note on ' $D^0 - \overline{D}^0$ Mixing' for the definition. $R_{K3\pi}$ can have any value between 0 and 1. A value near 1 indicates the decay is dominated by a few intermediate states with limited interference.

VALUE	EVTS	DOCUMENT ID	TECN	COMMENT
0.52 ± 0.10 -0.09	OUR AVERAGE			
0.52 ± 0.12 -0.10	8.6k	¹ ABLIKIM	21AA BES3	$e^+e^- \rightarrow D^0\overline{D}^0$ at $\psi(3770)$
0.53 ± 0.18 -0.21		^{1,2,3} EVANS	16	$e^+e^- \rightarrow D^0\overline{D}^0$ at $\psi(3770)$, pp at 7, 8 TeV
0.458 ± 0.010 ± 0.023	0.9M, 3k	⁴ AAIJ	18AI LHCb	amplitude models
0.32 ± 0.20 -0.28		^{1,3} LIBBY	14	Repl. by EVANS 16
0.36 ± 0.24 -0.30		⁵ LOWREY	09 CLEO	Repl. by LIBBY 14

- ¹ Uses quantum correlations in $e^+e^- \rightarrow D^0\overline{D}^0$ at the $\psi(3770)$, where the decay rates of CP -tagged $K^-\pi^-2\pi^+$ final states depend on $R_{K3\pi}$ and $\delta^{K3\pi}$.
- ² A combined fit with a recent LHCb $D^0\overline{D}^0$ mixing results in AAIJ 16F is also reported, to be $0.43_{-0.13}^{+0.17}$.
- ³ Obtained by analyzing CLEO-c data but not authored by the CLEO Collaboration.
- ⁴ Calculated from amplitude models to $D^0 \rightarrow K^-\pi^-2\pi^+$ and $D^0 \rightarrow K^+\pi^+2\pi^-$ and cc. Reports $0.458 \pm 0.010 \pm 0.012 \pm 0.020$ value where the 3rd uncertainty is the model uncertainty. We combined both systematic uncertainties in quadrature. Because of the importance of model independence in the practical use of the coherence factor, we do not include model-derived results in the average.
- ⁵ LOWREY 09 uses quantum correlations in $e^+e^- \rightarrow D^0\overline{D}^0$ at the $\psi(3770)$, where the decay rates of CP -tagged $K^-\pi^-2\pi^+$ final states depend on $R_{K3\pi}$ and $\delta^{K3\pi}$. A fit that includes external measurements of charm mixing parameters gets $R_{K3\pi} = 0.33_{-0.23}^{+0.26}$.

Meson Particle Listings

 D^0 $D^0 \rightarrow K^- \pi^- 2\pi^+$ AVERAGE RELATIVE STRONG PHASE $\delta^{K^*3\pi}$

The quoted value of δ is based on the same sign CP phase of D^0 and \bar{D}^0 convention.

VALUE (°)	EVTS	DOCUMENT ID	TECN	COMMENT
-----------	------	-------------	------	---------

149⁺²⁶₋₁₆ OUR AVERAGE Error includes scale factor of 1.4.

167 ⁺³¹ ₋₁₉	8.6k	¹ ABLIKIM	21AA BES3	$e^+e^- \rightarrow D^0 \bar{D}^0$ at $\psi(3770)$
-----------------------------------	------	----------------------	-----------	--

125 ⁺²² ₋₁₄	1.2,3	EVANS	16	$e^+e^- \rightarrow D^0 \bar{D}^0$ at $\psi(3770)$
-----------------------------------	-------	-------	----	--

• • • We do not use the following data for averages, fits, limits, etc. • • •

255 ⁺²¹ ₋₇₈	1.3	LIBBY	14	Repl. by EVANS 16
-----------------------------------	-----	-------	----	-------------------

118 ⁺⁶² ₋₅₃	4	LOWREY	09	CLEO Repl. by LIBBY 14
-----------------------------------	---	--------	----	------------------------

¹ Uses quantum correlations in $e^+e^- \rightarrow D^0 \bar{D}^0$ at the $\psi(3770)$, where the decay rates of CP -tagged $K^- \pi^- 2\pi^+$ final states depend on $R_{K^*3\pi}$ and $\delta^{K^*3\pi}$.

² A combined fit with a recent LHCb $D^0 \bar{D}^0$ mixing results in AAIJ 16F is also reported to be $(128 \pm 28)^\circ$.

³ Obtained by analyzing CLEO-c data but not authored by the CLEO Collaboration.

⁴ LOWREY 09 uses quantum correlations in $e^+e^- \rightarrow D^0 \bar{D}^0$ at the $\psi(3770)$, where the decay rates of CP -tagged $K^- \pi^- 2\pi^+$ final states depend on $R_{K^*3\pi}$ and $\delta^{K^*3\pi}$.

A fit that includes external measurements of charm mixing parameters gets $\delta^{K^*3\pi} = (114 \pm 26)^\circ$.

 $D^0 \rightarrow K^- \pi^- 2\pi^+$, $R_{K^*3\pi}$ ($y \cos \delta^{K^*3\pi} - x \sin \delta^{K^*3\pi}$)

VALUE (10^{-3}TeV^{-1})	EVTS	DOCUMENT ID	TECN	COMMENT
-------------------------------------	------	-------------	------	---------

-3.0 ± 0.7	42.5k	¹ AAIJ	16F	LHCb $p\bar{p}$ at 7, 8 TeV
-------------------	-------	-------------------	-----	-----------------------------

¹ From a time-dependent analysis of D mixing in $D^0 \rightarrow K^+ \pi^- \pi^+ \pi^-$. This result uses external constraints on $R_{M^j} = 1/2(x^2 + y^2)$. Without such constraints, AAIJ 16F measure $(0.3 \pm 1.8) \times 10^{-3}$, with a large correlation coefficient to R_{M^j} .

 $D^0 \rightarrow K_S^0 K^+ \pi^-$ COHERENCE FACTOR $R_{K_S^0 K^+ \pi^-}$

VALUE	DOCUMENT ID	TECN	COMMENT
-------	-------------	------	---------

0.70 ± 0.08	¹ INSLER	12	CLEO $e^+e^- \rightarrow D^0 \bar{D}^0$ at 3.77 GeV
--------------------	---------------------	----	---

¹ Uses quantum correlations in $e^+e^- \rightarrow D^0 \bar{D}^0$ at the $\psi(3770)$, where the signal side D decays to $K_S^0 K^+ \pi^-$ and the tag-side D decays to $K\pi$, $K\pi\pi\pi$, $K\pi\pi^0$, and 10 additional CP -even, CP -odd, and mixed CP modes involving K_S^0 or K_L^0 .

 $D^0 \rightarrow K_S^0 K^+ \pi^-$ AVERAGE RELATIVE STRONG PHASE $\delta^{K_S^0 K^+ \pi^-}$

The quoted value of δ is based on the same sign CP phase of D^0 and \bar{D}^0 convention.

VALUE (°)	DOCUMENT ID	TECN	COMMENT
-----------	-------------	------	---------

0.1 ± 15.7	¹ INSLER	12	CLEO $e^+e^- \rightarrow D^0 \bar{D}^0$ at 3.77 GeV
-------------------	---------------------	----	---

¹ Uses quantum correlations in $e^+e^- \rightarrow D^0 \bar{D}^0$ at the $\psi(3770)$, where the signal side D decays to $K_S^0 K^+ \pi^-$ and the tag-side D decays to $K\pi$, $K\pi\pi\pi$, $K\pi\pi^0$, and 10 additional CP -even, CP -odd, and mixed CP modes involving K_S^0 or K_L^0 .

 $D^0 \rightarrow K^* K$ COHERENCE FACTOR $R_{K^* K}$

VALUE	DOCUMENT ID	TECN	COMMENT
-------	-------------	------	---------

0.94 ± 0.12	¹ INSLER	12	CLEO $e^+e^- \rightarrow D^0 \bar{D}^0$ at 3.77 GeV
--------------------	---------------------	----	---

¹ Uses quantum correlations in $e^+e^- \rightarrow D^0 \bar{D}^0$ at the $\psi(3770)$, where the signal side D decays to $K_S^0 K^+ \pi^-$ and the tag-side D decays to $K\pi$, $K\pi\pi\pi$, $K\pi\pi^0$, and 10 additional CP -even, CP -odd, and mixed CP modes involving K_S^0 or K_L^0 .

 $D^0 \rightarrow K^* K$ AVERAGE RELATIVE STRONG PHASE $\delta^{K^* K}$

The quoted value of δ is based on the same sign CP phase of D^0 and \bar{D}^0 convention.

VALUE (°)	DOCUMENT ID	TECN	COMMENT
-----------	-------------	------	---------

-16.6 ± 18.4	¹ INSLER	12	CLEO $e^+e^- \rightarrow D^0 \bar{D}^0$ at 3.77 GeV
---------------------	---------------------	----	---

¹ Uses quantum correlations in $e^+e^- \rightarrow D^0 \bar{D}^0$ at the $\psi(3770)$, where the signal side D decays to $K_S^0 K^+ \pi^-$ and the tag-side D decays to $K\pi$, $K\pi\pi\pi$, $K\pi\pi^0$, and 10 additional CP -even, CP -odd, and mixed CP modes involving K_S^0 or K_L^0 .

 D^0 DECAY MODES

Most decay modes (other than the semileptonic modes) that involve a neutral K meson are now given as K_S^0 modes, not as \bar{K}^0 modes. Nearly always it is a K_S^0 that is measured, and interference between Cabibbo-allowed and doubly Cabibbo-suppressed modes can invalidate the assumption that $2\Gamma(K_S^0) = \Gamma(\bar{K}^0)$.

Mode	Fraction (Γ_i/Γ)	Scale factor/ Confidence level
------	--------------------------------	-----------------------------------

Topological modes

Γ_1	0-prongs	[a] (15 ± 6) %
Γ_2	2-prongs	(71 ± 6) %
Γ_3	4-prongs	[b] (14.6 ± 0.5) %
Γ_4	6-prongs	[c] (6.5 ± 1.3) × 10 ⁻⁴

Inclusive modes

Γ_5	e^+ anything	[d] (6.49 ± 0.11) %	
Γ_6	μ^+ anything	(6.8 ± 0.6) %	
Γ_7	K^- anything	(54.7 ± 2.8) %	S=1.3
Γ_8	K_S^0 anything	(20.75 ± 0.23) %	
Γ_9	K^+ anything	(3.4 ± 0.4) %	
Γ_{10}	$K^*(892)^-$ anything	(15 ± 9) %	
Γ_{11}	$\bar{K}^*(892)^0$ anything	(9 ± 4) %	
Γ_{12}	$K^*(892)^+$ anything	< 3.6 %	CL=90%
Γ_{13}	$K^*(892)^0$ anything	(2.8 ± 1.3) %	
Γ_{14}	η anything	(9.5 ± 0.9) %	
Γ_{15}	η' anything	(2.48 ± 0.27) %	
Γ_{16}	ϕ anything	(1.08 ± 0.04) %	
Γ_{17}	$\pi^+ \pi^+ \pi^-$ anything	(17.60 ± 0.25) %	
Γ_{18}	invisibles	< 9.4 × 10 ⁻⁵	CL=90%

Semileptonic modes

Γ_{19}	$K^- \ell^+ \nu_\ell$	(3.549 ± 0.026) %	S=1.2
Γ_{20}	$K^- e^+ \nu_e$	(3.41 ± 0.04) %	
Γ_{21}	$K^- \mu^+ \nu_\mu$	(2.15 ± 0.16) %	
Γ_{22}	$K^*(892)^- e^+ \nu_e$	(1.89 ± 0.24) %	
Γ_{23}	$K^*(892)^- \mu^+ \nu_\mu$	(1.6 ± 1.3) %	
Γ_{24}	$K^- \pi^0 e^+ \nu_e$	(1.44 ± 0.04) %	
Γ_{25}	$\bar{K}^0 \pi^- e^+ \nu_e$	(7.9 ± 1.7) × 10 ⁻⁴	
Γ_{26}	$(\bar{K}^0 \pi^-)_{S\text{-wave}} e^+ \nu_e$	(2.8 ± 1.4) × 10 ⁻⁴	
Γ_{27}	$K^- \pi^+ \pi^- e^+ \nu_e$	(1.01 ± 0.18) × 10 ⁻³	
Γ_{28}	$K_1(1270)^- e^+ \nu_e$	< 1.3 × 10 ⁻³	CL=90%
Γ_{29}	$K^- \pi^+ \pi^- \mu^+ \nu_\mu$	< 1.5 × 10 ⁻³	CL=90%
Γ_{30}	$(\bar{K}^*(892) \pi)^- \mu^+ \nu_\mu$	(2.91 ± 0.04) × 10 ⁻³	
Γ_{31}	$\pi^- e^+ \nu_e$	(2.67 ± 0.12) × 10 ⁻³	S=1.3
Γ_{32}	$\pi^- \mu^+ \nu_\mu$	(1.45 ± 0.07) × 10 ⁻³	
Γ_{33}	$\pi^- \pi^0 e^+ \nu_e$	(1.50 ± 0.12) × 10 ⁻³	S=1.9
Γ_{34}	$\rho^- e^+ \nu_e$	(1.35 ± 0.13) × 10 ⁻³	
Γ_{35}	$\rho^- \mu^+ \nu_\mu$	(1.33 ± 0.34) × 10 ⁻⁴	
Γ_{36}	$a(980)^- e^+ \nu_e, a^- \rightarrow \eta \pi^-$	< 1.12 × 10 ⁻⁴	CL=90%
Γ_{37}	$b_1(1235)^- e^+ \nu_e, b_1^- \rightarrow \omega \pi^-$		

Hadronic modes with one \bar{K}

Γ_{38}	$K^- \pi^+$	(3.947 ± 0.030) %	S=1.2
Γ_{39}	$K_S^0 \pi^0$	(1.240 ± 0.022) %	
Γ_{40}	$K_L^0 \pi^0$	(9.76 ± 0.32) × 10 ⁻³	
Γ_{41}	$K^0 \eta$	(4.34 ± 0.16) × 10 ⁻³	
Γ_{42}	$K^0 \eta'$	(8.12 ± 0.35) × 10 ⁻³	S=1.3
Γ_{43}	$K^0 \omega$	(1.16 ± 0.04) %	
Γ_{44}	$K_S^0 \pi^+ \pi^-$	[e] (2.80 ± 0.18) %	S=1.1
Γ_{45}	$K_S^0 \rho^0$	(6.3 ± 0.6) × 10 ⁻³	
Γ_{46}	$K_S^0 \omega, \omega \rightarrow \pi^+ \pi^-$	(2.0 ± 0.6) × 10 ⁻⁴	
Γ_{47}	$K_S^0 (\pi^+ \pi^-)_{S\text{-wave}}$	(3.3 ± 0.8) × 10 ⁻³	
Γ_{48}	$K_S^0 f_0(980), f_0 \rightarrow \pi^+ \pi^-$	(1.20 ± 0.40) × 10 ⁻³	
Γ_{49}	$K_S^0 f_0(1370), f_0 \rightarrow \pi^+ \pi^-$	(2.8 ± 0.9) × 10 ⁻³	
Γ_{50}	$K_S^0 f_2(1270), f_2 \rightarrow \pi^+ \pi^-$	(9 ± 10) × 10 ⁻⁵	
Γ_{51}	$K^*(892)^- \pi^+, K^{*-} \rightarrow K_S^0 \pi^-$	(1.64 ± 0.14) %	
Γ_{52}	$K_0^*(1430)^- \pi^+, K_0^{*-} \rightarrow K_S^0 \pi^-$	(2.67 ± 0.40) × 10 ⁻³	
Γ_{53}	$K_2^*(1430)^- \pi^+, K_2^{*-} \rightarrow K_S^0 \pi^-$	(3.4 ± 1.9) × 10 ⁻⁴	
Γ_{54}	$K^*(1680)^- \pi^+, K^{*-} \rightarrow K_S^0 \pi^-$	(4.4 ± 3.5) × 10 ⁻⁴	
Γ_{55}	$K^*(892)^+ \pi^-, K^{*+} \rightarrow K_S^0 \pi^+$	[f] (1.13 ± 0.60) × 10 ⁻⁴	
Γ_{56}	$K_0^*(1430)^+ \pi^-, K_0^{*+} \rightarrow K_S^0 \pi^+$	[f] < 1.4 × 10 ⁻⁵	CL=95%
Γ_{57}	$K_2^*(1430)^+ \pi^-, K_2^{*+} \rightarrow K_S^0 \pi^+$	[f] < 3.4 × 10 ⁻⁵	CL=95%

Γ ₅₈	$K_S^0 \pi^+ \pi^-$ nonresonant	(2.5 \pm 6.0 \pm 1.6) $\times 10^{-4}$		Γ ₁₁₃	$K^*(892)^- 2\pi^+ \pi^-$, $K^*(892)^- \rightarrow K_S^0 \pi^-$, no ρ^0	(5 \pm 7) $\times 10^{-4}$	
Γ ₅₉	$K^- \pi^+ \pi^0$	[e] (14.4 \pm 0.6) %	S=2.2	Γ ₁₁₄	$K^*(892)^- \rho^0 \pi^+$, $K^*(892)^- \rightarrow K_S^0 \pi^-$	(1.6 \pm 0.6) $\times 10^{-3}$	
Γ ₆₀	$K^- \rho^+$	(11.2 \pm 0.7) %		Γ ₁₁₅	$K_S^0 2\pi^+ 2\pi^-$ nonresonant	< 1.2	$\times 10^{-3}$ CL=90%
Γ ₆₁	$K^- \rho(1700)^+$, $\rho^+ \rightarrow \pi^+ \pi^0$	(8.2 \pm 1.8) $\times 10^{-3}$		Γ ₁₁₆	$\bar{K}^0 \pi^+ \pi^- 2\pi^0 (\pi^0)$		
Γ ₆₂	$K^*(892)^- \pi^+$, $K^*(892)^- \rightarrow K^- \pi^+$	(2.31 \pm 0.40 \pm 0.20) %		Γ ₁₁₇	$K^- 3\pi^+ 2\pi^-$	(2.2 \pm 0.6) $\times 10^{-4}$	
Γ ₆₃	$\bar{K}^*(892)^0 \pi^0$, $\bar{K}^*(892)^0 \rightarrow K^- \pi^+$	(1.95 \pm 0.25) %		Fractions of some of the following modes with resonances have already appeared above as submodes of particular charged-particle modes. These nine modes below are all corrected for unseen decays of the resonances.			
Γ ₆₄	$K_0^*(1430)^- \pi^+$, $K_0^{*-} \rightarrow K^- \pi^+$	(4.8 \pm 2.2) $\times 10^{-3}$		Γ ₁₁₈	$K_S^0 \eta$	(5.09 \pm 0.13) $\times 10^{-3}$	
Γ ₆₅	$\bar{K}_0^*(1430)^0 \pi^0$, $\bar{K}_0^{*0} \rightarrow K^- \pi^+$	(5.9 \pm 5.0 \pm 1.6) $\times 10^{-3}$		Γ ₁₁₉	$K_S^0 \omega$	(1.11 \pm 0.06) %	
Γ ₆₆	$K^*(1680)^- \pi^+$, $K^{*-} \rightarrow K^- \pi^0$	(1.9 \pm 0.7) $\times 10^{-3}$		Γ ₁₂₀	$K_S^0 \eta'(958)$	(9.49 \pm 0.32) $\times 10^{-3}$	
Γ ₆₇	$K^- \pi^+ \pi^0$ nonresonant	(1.15 \pm 0.60 \pm 0.20) %		Γ ₁₂₁	$\bar{K}^*(892)^0 \pi^+ \pi^- \pi^0$	(1.9 \pm 0.9) %	
Γ ₆₈	$K_S^0 2\pi^0$	(9.1 \pm 1.1) $\times 10^{-3}$	S=2.2	Γ ₁₂₂	$\bar{K}^*(892)^0 \eta$	(1.41 \pm 0.12) %	
Γ ₆₉	$K_L^0 \pi^0 \pi^0$	(1.26 \pm 0.06) %		Γ ₁₂₃	$K^- \pi^+ \eta'(958)$	(6.43 \pm 0.34) $\times 10^{-3}$	
Γ ₇₀	$K_S^0 (2\pi^0)_S$ -wave	(2.6 \pm 0.7) $\times 10^{-3}$		Γ ₁₂₄	$K_S^0 \eta'(958) \pi^0$	(2.52 \pm 0.27) $\times 10^{-3}$	
Γ ₇₁	$\bar{K}^*(892)^0 \pi^0$, $\bar{K}^{*0} \rightarrow K_S^0 \pi^0$	(8.1 \pm 0.7) $\times 10^{-3}$		Γ ₁₂₅	$\bar{K}^*(892)^0 \eta'(958)$	< 1.0	$\times 10^{-3}$ CL=90%
Γ ₇₂	$\bar{K}^*(1430)^0 \pi^0$, $\bar{K}^{*0} \rightarrow K_S^0 \pi^0$	(4 \pm 23) $\times 10^{-5}$		Hadronic modes with three K's			
Γ ₇₃	$\bar{K}^*(1680)^0 \pi^0$, $\bar{K}^{*0} \rightarrow K_S^0 \pi^0$	(1.0 \pm 0.4) $\times 10^{-3}$		Γ ₁₂₆	$K_S^0 K^+ K^-$	(4.42 \pm 0.32) $\times 10^{-3}$	
Γ ₇₄	$K_S^0 f_2(1270)$, $f_2 \rightarrow 2\pi^0$	(2.3 \pm 1.1) $\times 10^{-4}$		Γ ₁₂₇	$K_S^0 a_0(980)^0$, $a_0^0 \rightarrow K^+ K^-$	(2.9 \pm 0.4) $\times 10^{-3}$	
Γ ₇₅	$2K_S^0$, one $K_S^0 \rightarrow 2\pi^0$	(3.2 \pm 1.1) $\times 10^{-4}$		Γ ₁₂₈	$K^- a_0(980)^+$, $a_0^+ \rightarrow K^+ K_S^0$	(5.9 \pm 1.8) $\times 10^{-4}$	
Γ ₇₆	$K_S^0 2\pi^0$ nonresonant			Γ ₁₂₉	$K^+ a_0(980)^-$, $a_0^- \rightarrow K^- K_S^0$	< 1.1	$\times 10^{-4}$ CL=95%
Γ ₇₇	$K_S^0 3\pi^0$	(7.6 \pm 0.4) $\times 10^{-3}$		Γ ₁₃₀	$K_S^0 f_0(980)$, $f_0 \rightarrow K^+ K^-$	< 9	$\times 10^{-5}$ CL=95%
Γ ₇₈	$K^- 2\pi^+ \pi^-$	[e] (8.22 \pm 0.14) %		Γ ₁₃₁	$K_S^0 \phi$, $\phi \rightarrow K^+ K^-$	(2.03 \pm 0.15) $\times 10^{-3}$	
Γ ₇₉	$K^- \pi^+ \rho^0$ total	(6.87 \pm 0.31) %		Γ ₁₃₂	$K_S^0 \phi$	(4.14 \pm 0.23) $\times 10^{-3}$	
Γ ₈₀	$K^- \pi^+ \rho^0$ 3-body	(6.1 \pm 1.6) $\times 10^{-3}$		Γ ₁₃₃	$K_S^0 f_0(1370)$, $f_0 \rightarrow K^+ K^-$	(1.7 \pm 1.1) $\times 10^{-4}$	
Γ ₈₁	$\bar{K}^*(892)^0 \rho^0$, $\bar{K}^{*0} \rightarrow K^- \pi^+$	(1.01 \pm 0.05) %		Γ ₁₃₄	$3K_S^0$	(7.5 \pm 0.7) $\times 10^{-4}$	S=1.4
Γ ₈₂	$\bar{K}^*(892)^0 \rho^0$ transverse, $\bar{K}^{*0} \rightarrow K^- \pi^+$	(1.2 \pm 0.4) %		Γ ₁₃₅	$K^+ 2K^- \pi^+$	(2.25 \pm 0.32) $\times 10^{-4}$	
Γ ₈₃	$K^- a_1(1260)^+$, $a_1^+ \rightarrow \rho^0 \pi^+$	(4.32 \pm 0.32) %		Γ ₁₃₆	$K^+ K^- \bar{K}^*(892)^0$, $\bar{K}^{*0} \rightarrow K^- \pi^+$	(4.5 \pm 1.8) $\times 10^{-5}$	
Γ ₈₄	$K_1(1270)^- \pi^+$, $K_1^- \rightarrow K^- \pi^+$	(3.9 \pm 0.4) $\times 10^{-3}$		Γ ₁₃₇	$K^- \pi^+ \phi$, $\phi \rightarrow K^+ K^-$	(4.0 \pm 1.7) $\times 10^{-5}$	
Γ ₈₅	$\bar{K}^*(892)^0 \pi^+ \pi^-$ total, $\bar{K}^{*0} \rightarrow K^- \pi^+$			Γ ₁₃₈	$\phi \bar{K}^*(892)^0$, $\phi \rightarrow K^+ K^-$, $\bar{K}^{*0} \rightarrow K^- \pi^+$	(1.08 \pm 0.21) $\times 10^{-4}$	
Γ ₈₆	$\bar{K}^*(892)^0 \pi^+ \pi^-$ 3-body, $\bar{K}^{*0} \rightarrow K^- \pi^+$			Γ ₁₃₉	$K^+ 2K^- \pi^+$ nonresonant	(3.4 \pm 1.5) $\times 10^{-5}$	
Γ ₈₇	$K_1(1270)^- \pi^+$, $K_1^- \rightarrow K^- \pi^+$	(6.6 \pm 2.3) $\times 10^{-4}$		Γ ₁₄₀	$2K_S^0 K^\pm \pi^\mp$	(5.9 \pm 1.3) $\times 10^{-4}$	
Γ ₈₈	$K^- 2\pi^+ \pi^-$ nonresonant	(1.81 \pm 0.07) %		Pionic modes			
Γ ₈₉	$K_S^0 \pi^+ \pi^- \pi^0$	[g] (5.2 \pm 0.6) %		Γ ₁₄₁	$\pi^+ \pi^-$	(1.454 \pm 0.024) $\times 10^{-3}$	S=1.4
Γ ₉₀	$K_S^0 \eta$, $\eta \rightarrow \pi^+ \pi^- \pi^0$	(1.17 \pm 0.03) $\times 10^{-3}$		Γ ₁₄₂	$2\pi^0$	(8.26 \pm 0.25) $\times 10^{-4}$	
Γ ₉₁	$K_S^0 \omega$, $\omega \rightarrow \pi^+ \pi^- \pi^0$	(9.9 \pm 0.6) $\times 10^{-3}$		Γ ₁₄₃	$\pi^+ \pi^- \pi^0$	(1.49 \pm 0.07) %	S=2.3
Γ ₉₂	$K^- \pi^+ 2\pi^0$	(8.86 \pm 0.23) %		Γ ₁₄₄	$\rho^+ \pi^-$	(1.01 \pm 0.05) %	
Γ ₉₃	$K^- \pi^+ 3\pi^0$	(9.5 \pm 0.4) $\times 10^{-3}$		Γ ₁₄₅	$\rho^0 \pi^0$	(3.86 \pm 0.24) $\times 10^{-3}$	
Γ ₉₄	$K_S^0 \pi^+ \pi^- 2\pi^0$	(1.27 \pm 0.06) %		Γ ₁₄₆	$\rho^- \pi^+$	(5.15 \pm 0.26) $\times 10^{-3}$	
Γ ₉₅	$K^- 2\pi^+ \pi^- \pi^0$	(4.3 \pm 0.4) %		Γ ₁₄₇	$\rho(1450)^+ \pi^-$, $\rho^+ \rightarrow \pi^+ \pi^0$	(1.6 \pm 2.1) $\times 10^{-5}$	
Γ ₉₆	$\bar{K}^*(892)^0 \pi^+ \pi^- \pi^0$, $\bar{K}^{*0} \rightarrow K^- \pi^+$	(1.3 \pm 0.6) %		Γ ₁₄₈	$\rho(1450)^0 \pi^0$, $\rho^0 \rightarrow \pi^+ \pi^-$	(4.5 \pm 2.0) $\times 10^{-5}$	
Γ ₉₇	$\bar{K}^*(892)^0 \omega$, $\bar{K}^{*0} \rightarrow K^- \pi^+$, $\omega \rightarrow \pi^+ \pi^- \pi^0$	(6.5 \pm 3.0) $\times 10^{-3}$		Γ ₁₄₉	$\rho(1450)^- \pi^+$, $\rho^- \rightarrow \pi^- \pi^0$	(2.7 \pm 0.4) $\times 10^{-4}$	
Γ ₉₈	$K^- \pi^+ \omega$	(3.39 \pm 0.10) %		Γ ₁₅₀	$\rho(1700)^+ \pi^-$, $\rho^+ \rightarrow \pi^+ \pi^0$	(6.1 \pm 1.5) $\times 10^{-4}$	
Γ ₉₉	$\bar{K}^*(892)^0 \omega$	(1.1 \pm 0.5) %		Γ ₁₅₁	$\rho(1700)^0 \pi^0$, $\rho^0 \rightarrow \pi^+ \pi^-$	(7.4 \pm 1.8) $\times 10^{-4}$	
Γ ₁₀₀	$K_S^0 \pi^0 \omega$	(8.5 \pm 0.6) $\times 10^{-3}$		Γ ₁₅₂	$\rho(1700)^- \pi^+$, $\rho^- \rightarrow \pi^- \pi^0$	(4.8 \pm 1.1) $\times 10^{-4}$	
Γ ₁₀₁	$K_S^0 \eta \pi^0$	(1.01 \pm 0.05) %		Γ ₁₅₃	$f_0(980) \pi^0$, $f_0 \rightarrow \pi^+ \pi^-$	(3.7 \pm 0.9) $\times 10^{-5}$	
Γ ₁₀₂	$K_S^0 a_0(980)$, $a_0 \rightarrow \eta \pi^0$	(1.20 \pm 0.28) %		Γ ₁₅₄	$f_0(500) \pi^0$, $f_0 \rightarrow \pi^+ \pi^-$	(1.22 \pm 0.22) $\times 10^{-4}$	
Γ ₁₀₃	$\bar{K}^*(892)^0 \eta$, $\bar{K}^{*0} \rightarrow K_S^0 \pi^0$	(2.9 \pm 0.7) $\times 10^{-3}$		Γ ₁₅₅	$f_0(1370) \pi^0$, $f_0 \rightarrow \pi^+ \pi^-$	(5.5 \pm 2.1) $\times 10^{-5}$	
Γ ₁₀₄	$K^- \pi^+ \eta$	(1.88 \pm 0.05) %	S=1.4	Γ ₁₅₆	$f_0(1500) \pi^0$, $f_0 \rightarrow \pi^+ \pi^-$	(5.8 \pm 1.6) $\times 10^{-5}$	
Γ ₁₀₅	$K^*(892)^0 \eta$, $K^{*0} \rightarrow K^- \pi^+$	(8.9 \pm 0.8 \pm 0.6) $\times 10^{-3}$		Γ ₁₅₇	$f_0(1710) \pi^0$, $f_0 \rightarrow \pi^+ \pi^-$	(4.6 \pm 1.6) $\times 10^{-5}$	
Γ ₁₀₆	$a_0(980)^+ K^-$, $a_0^+ \rightarrow \eta \pi^+$	(7.4 \pm 0.9 \pm 0.7) $\times 10^{-3}$		Γ ₁₅₈	$f_2(1270) \pi^0$, $f_2 \rightarrow \pi^+ \pi^-$	(1.97 \pm 0.21) $\times 10^{-4}$	
Γ ₁₀₇	$K_2^*(1980)^- \pi^+$, $K_2^{*-} \rightarrow K^- \eta$	(2.2 \pm 1.7 \pm 1.9) $\times 10^{-4}$		Γ ₁₅₉	$\pi^+ \pi^- \pi^0$ nonresonant	(1.3 \pm 0.4) $\times 10^{-4}$	
Γ ₁₀₈	$K^- \pi^+ \pi^0 \eta$	(4.49 \pm 0.27) $\times 10^{-3}$		Γ ₁₆₀	$3\pi^0$	(2.0 \pm 0.5) $\times 10^{-4}$	
Γ ₁₀₉	$K_S^0 \pi^+ \pi^- \eta$	(2.80 \pm 0.21) $\times 10^{-3}$		Γ ₁₆₁	$2\pi^+ 2\pi^-$	(7.56 \pm 0.20) $\times 10^{-3}$	
Γ ₁₁₀	$K_S^0 2\pi^0 \eta$	(1.76 \pm 0.26) $\times 10^{-3}$		Γ ₁₆₂	$a_1(1260)^+ \pi^-$, $a_1^+ \rightarrow 2\pi^+ \pi^-$ total	(4.53 \pm 0.31) $\times 10^{-3}$	
Γ ₁₁₁	$K_S^0 2\pi^+ 2\pi^-$	(2.66 \pm 0.30) $\times 10^{-3}$		Γ ₁₆₃	$a_1(1260)^+ \pi^-$, $a_1^+ \rightarrow \rho^0 \pi^+ S$ -wave	(3.13 \pm 0.21) $\times 10^{-3}$	
Γ ₁₁₂	$K_S^0 \rho^0 \pi^+ \pi^-$, no $K^*(892)^-$	(1.1 \pm 0.7) $\times 10^{-3}$		Γ ₁₆₄	$a_1(1260)^+ \pi^-$, $a_1^+ \rightarrow \rho^0 \pi^+ D$ -wave	(1.9 \pm 0.5) $\times 10^{-4}$	
				Γ ₁₆₅	$a_1(1260)^+ \pi^-$, $a_1^+ \rightarrow \sigma \pi^+$	(6.4 \pm 0.7) $\times 10^{-4}$	
				Γ ₁₆₆	$a_1(1260)^- \pi^+$, $a_1^- \rightarrow \rho^0 \pi^- S$ -wave	(2.3 \pm 0.9) $\times 10^{-4}$	
				Γ ₁₆₇	$a_1(1260)^- \pi^+$, $a_1^- \rightarrow \sigma \pi^-$	(6.0 \pm 3.4) $\times 10^{-5}$	

Meson Particle Listings

 D^0

Γ_{168}	$\pi(1300)^+\pi^-, \pi(1300)^+ \rightarrow \sigma\pi^+$	$(5.1 \pm 2.7) \times 10^{-4}$		Γ_{225}	$K^*(892)^0 K_S^0, K^{*0} \rightarrow K^+\pi^-, K^*(892)^- K^+, K^{*-} \rightarrow K_S^0\pi^-$	$(1.12 \pm 0.21) \times 10^{-4}$	
Γ_{169}	$\pi(1300)^-\pi^+, \pi(1300)^- \rightarrow \sigma\pi^-$	$(2.3 \pm 2.2) \times 10^{-4}$		Γ_{226}	$K^*(1410)^0 K_S^0, K^{*0} \rightarrow K^+\pi^+, K^*(1410)^- K^+, K^{*-} \rightarrow K_S^0\pi^-$	$(6.2 \pm 1.1) \times 10^{-4}$	
Γ_{170}	$a_1(1640)^+\pi^-, a_1^+ \rightarrow \rho^0\pi^+ D\text{-wave}$	$(3.2 \pm 1.6) \times 10^{-4}$		Γ_{227}	$(K^+\pi^-)_{S\text{-wave}} K_S^0, (K_S^0\pi^-)_{S\text{-wave}} K^+$	$(5 \pm 8) \times 10^{-5}$	
Γ_{171}	$a_1(1640)^+\pi^-, a_1^+ \rightarrow \sigma\pi^+$	$(1.8 \pm 1.4) \times 10^{-4}$		Γ_{228}	$\rho(1700)^+\pi^-, \rho^+ \rightarrow K_S^0 K^+$	$(2.6 \pm 2.0) \times 10^{-4}$	
Γ_{172}	$\pi_2(1670)^+\pi^-, \pi_2^+ \rightarrow f_2(1270)^0\pi^+, f_2^0 \rightarrow \pi^+\pi^-$	$(2.0 \pm 0.9) \times 10^{-4}$		Γ_{229}	$a_0(980)^+\pi^-, a_0^+ \rightarrow K_S^0 K^+$	$(3.7 \pm 1.9) \times 10^{-4}$	
Γ_{173}	$\pi_2(1670)^+\pi^-, \pi_2^+ \rightarrow \sigma\pi^+$	$(2.6 \pm 1.0) \times 10^{-4}$		Γ_{230}	$a_0(1450)^+\pi^-, a_0^+ \rightarrow K_S^0 K^+$	$(1.4 \pm 0.6) \times 10^{-4}$	
Γ_{174}	$2\rho^0$ total	$(1.85 \pm 0.13) \times 10^{-3}$		Γ_{231}	$\rho(1700)^+\pi^-, \rho^+ \rightarrow K_S^0 K^+$	$(6 \pm 4) \times 10^{-4}$	
Γ_{175}	$2\rho^0$, parallel helicities	$(8.3 \pm 3.2) \times 10^{-5}$		Γ_{232}	$K^+(892)^+ K^-, K^*(892)^+ \rightarrow K^+\pi^0$	$(3.2 \pm 2.5) \times 10^{-5}$	
Γ_{176}	$2\rho^0$, perpendicular helicities	$(4.8 \pm 0.6) \times 10^{-4}$		Γ_{233}	$K^*(892)^- K^+, K^*(892)^- \rightarrow K^-\pi^0$	$(1.1 \pm 0.6) \times 10^{-5}$	
Γ_{177}	$2\rho^0$, longitudinal helicities	$(1.27 \pm 0.10) \times 10^{-3}$		Γ_{234}	$(K^+\pi^0)_{S\text{-wave}} K^-, (K^-\pi^0)_{S\text{-wave}} K^+$	$(3.42 \pm 0.15) \times 10^{-3}$	
Γ_{178}	$2\rho(770)^0, S\text{-wave}$	$(1.8 \pm 1.3) \times 10^{-4}$		Γ_{235}	$f_0(980)\pi^0, f_0 \rightarrow K^+ K^-$	$(1.52 \pm 0.08) \times 10^{-3}$	
Γ_{179}	$2\rho(770)^0, P\text{-wave}$	$(5.3 \pm 1.3) \times 10^{-4}$		Γ_{236}	$\phi\pi^0, \phi \rightarrow K^+ K^-$	$(5.4 \pm 0.4) \times 10^{-4}$	
Γ_{180}	$2\rho(770)^0, D\text{-wave}$	$(6.2 \pm 3.0) \times 10^{-4}$		Γ_{237}	$K^+ K^-\pi^0$ nonresonant	$(6.6 \pm 0.4) \times 10^{-4}$	
Γ_{181}	Resonant $(\pi^+\pi^-)\pi^+\pi^-$ 3-body total	$(1.51 \pm 0.12) \times 10^{-3}$		Γ_{238}	$2K_S^0\pi^0$	$< 1.45 \times 10^{-4}$	CL=90%
Γ_{182}	$\sigma\pi^+\pi^-$	$(6.2 \pm 0.9) \times 10^{-4}$		Γ_{239}	$K^+ K^-\eta$	$(5.9 \pm 1.9) \times 10^{-5}$	
Γ_{183}	$\sigma\rho(770)^0$	$(5.0 \pm 2.5) \times 10^{-4}$		Γ_{240}	$\phi(1020)\eta$	$(1.84 \pm 0.12) \times 10^{-4}$	
Γ_{184}	$f_0(980)\pi^+\pi^-, f_0 \rightarrow \pi^+\pi^-$	$(1.8 \pm 0.5) \times 10^{-4}$		Γ_{241}	$K^+ K^-\eta$ nonresonant	$(9.9 \pm 0.9) \times 10^{-5}$	
Γ_{185}	$f_2(1270)\pi^+\pi^-, f_2 \rightarrow \pi^+\pi^-$	$(3.7 \pm 0.6) \times 10^{-4}$		Γ_{242}	$2K_S^0\eta$	$(1.3 \pm 0.6) \times 10^{-4}$	
Γ_{186}	$2f_2(1270), f_2 \rightarrow \pi^+\pi^-$	$(1.6 \pm 1.8) \times 10^{-4}$		Γ_{243}	$K^+ K^-\pi^0\pi^0$	$(6.9 \pm 0.8) \times 10^{-4}$	
Γ_{187}	$f_0(1370)\sigma, f_0 \rightarrow \pi^+\pi^-$	$(1.6 \pm 0.5) \times 10^{-3}$		Γ_{244}	$K^+ K^-\pi^+\pi^-$	$(2.47 \pm 0.11) \times 10^{-3}$	
Γ_{188}	$\pi^+\pi^-\pi^0$	$(1.002 \pm 0.031) \%$		Γ_{245}	$\phi(\pi^+\pi^-)_{S\text{-wave}}, \phi \rightarrow K^+ K^-$	$(10 \pm 5) \times 10^{-5}$	
Γ_{189}	$4\pi^0$	$(7.6 \pm 1.1) \times 10^{-4}$		Γ_{246}	$(\phi\rho^0)_{S\text{-wave}}, \phi \rightarrow K^+ K^-$	$(6.9 \pm 0.6) \times 10^{-4}$	
Γ_{190}	$\eta\pi^0$	$[h] (6.3 \pm 0.6) \times 10^{-4}$	S=1.1	Γ_{247}	$(\phi\rho^0)_{P\text{-wave}}, \phi \rightarrow K^+ K^-$	$(4.0 \pm 1.9) \times 10^{-5}$	
Γ_{191}	$\omega\pi^0$	$[h] (1.17 \pm 0.35) \times 10^{-4}$		Γ_{248}	$(\phi\rho^0)_{D\text{-wave}}, \phi \rightarrow K^+ K^-$	$(4.2 \pm 1.4) \times 10^{-5}$	
Γ_{192}	$\omega\eta$	$(1.98 \pm 0.18) \times 10^{-3}$	S=1.1	Γ_{249}	$K^*(892)^0 \bar{K}^*(892)^0, K^{*0} \rightarrow K^{\pm}\pi^{\mp}$		
Γ_{193}	$2\pi^+2\pi^-\pi^0$	$(3.46 \pm 0.21) \times 10^{-3}$		Γ_{250}	$K^+ K^-\rho^0$ 3-body		
Γ_{194}	$\pi^+\pi^-\pi^0$	$(1.53 \pm 0.21) \times 10^{-3}$		Γ_{251}	$f_0(980)\pi^+\pi^-, f_0 \rightarrow K^+ K^-$	$(2.24 \pm 0.13) \times 10^{-4}$	
Γ_{195}	$2\pi^+2\pi^-\pi^0$	$(4.8 \pm 0.4) \times 10^{-3}$		Γ_{252}	$(K^*(892)^0 \bar{K}^*(892)^0)_{S\text{-wave}}, K^{*0} \rightarrow K^{\pm}\pi^{\mp}$		
Γ_{196}	$\eta\pi^+\pi^-$	$[h] (1.16 \pm 0.07) \times 10^{-3}$		Γ_{253}	$(K^*(892)^0 \bar{K}^*(892)^0)_{P\text{-wave}}, K^* \rightarrow K^{\pm}\pi^{\mp}$	$(1.20 \pm 0.08) \times 10^{-4}$	
Γ_{197}	$\omega\pi^+\pi^-$	$[h] (1.33 \pm 0.20) \times 10^{-3}$		Γ_{254}	$(K^*(892)^0 \bar{K}^*(892)^0)_{D\text{-wave}}, K^* \rightarrow K^{\pm}\pi^{\mp}$	$(4.7 \pm 0.4) \times 10^{-5}$	
Γ_{198}	$\omega\pi^0\pi^0$	$< 1.10 \times 10^{-3}$	CL=90%	Γ_{255}	$K^*(892)^0 K^{\mp}\pi^{\pm} 3\text{-body}, K^{*0} \rightarrow K^{\pm}\pi^{\mp}$		
Γ_{199}	$\eta 2\pi^0$	$(3.8 \pm 1.3) \times 10^{-4}$		Γ_{256}	$K^*(892)^0 (K^-\pi^+)_{S\text{-wave}} 3\text{-body}, K^{*0} \rightarrow K^+\pi^-$	$(1.4 \pm 0.6) \times 10^{-4}$	
Γ_{200}	$\pi^+\pi^-\pi^0\eta$	$(3.23 \pm 0.22) \times 10^{-3}$		Γ_{257}	$(K^-\pi^+)_{P\text{-wave}}, (K^+\pi^-)_{S\text{-wave}}$		
Γ_{201}	$\eta 3\pi^0$	$(2.36 \pm 0.28) \times 10^{-3}$		Γ_{258}	$K_1(1270)^{\pm} K^{\mp}, K_1^{\pm} \rightarrow K^{\pm}\pi^{\mp}\pi^-$	$(1.4 \pm 0.9) \times 10^{-4}$	
Γ_{202}	$\eta 2\pi^+2\pi^-$	$(6.0 \pm 1.2) \times 10^{-4}$		Γ_{259}	$K_1(1270)^+ K^-, K_1^+ \rightarrow K^+\pi^-\pi^+$	$(1.5 \pm 0.5) \times 10^{-4}$	
Γ_{203}	$3\pi^+3\pi^-$	$(4.3 \pm 1.2) \times 10^{-4}$		Γ_{260}	$K_1(1270)^+ K^-, K_1^+ \rightarrow K^+\pi^-\rho^0 K^+$	$(2.2 \pm 0.6) \times 10^{-4}$	
Γ_{204}	$\eta'(958)\pi^0$	$(9.2 \pm 1.0) \times 10^{-4}$		Γ_{261}	$K_1(1270)^+ K^-, K_1^+ \rightarrow \omega(782) K^+, \omega \rightarrow \pi^+\pi^-$	$(1.5 \pm 1.2) \times 10^{-5}$	
Γ_{205}	$\eta'(958)\pi^+\pi^-$	$(4.5 \pm 1.7) \times 10^{-4}$		Γ_{262}	$K_1(1270)^- K^+, K_1^- \rightarrow \bar{K}^{*0}\pi^-$		
Γ_{206}	2η	$(2.11 \pm 0.19) \times 10^{-3}$	S=2.2	Γ_{263}	$K_1(1270)^- K^+, K_1^- \rightarrow \rho^0 K^-$	$(1.3 \pm 0.4) \times 10^{-4}$	
Γ_{207}	$2\eta\pi^0$	$(7.3 \pm 2.2) \times 10^{-4}$		Γ_{264}	$K_1(1400)^{\pm} K^{\mp}, K_1^{\pm} \rightarrow K^{\pm}\pi^{\mp}\pi^-$		
Γ_{208}	$2\eta\pi^+\pi^-$	$(8.5 \pm 1.4) \times 10^{-4}$		Γ_{265}	$K_1(1400)^+ K^-, K_1^+ \rightarrow K^*(892)^0\pi^+, K^{*0} \rightarrow K^+\pi^-$	$(4.6 \pm 0.4) \times 10^{-4}$	
Γ_{209}	3η	$< 1.3 \times 10^{-4}$	CL=90%	Γ_{266}	$K^*(1410)^+ K^-, K^{*+} \rightarrow K^+\pi^-$		
Γ_{210}	$\eta\eta'(958)$	$(1.01 \pm 0.19) \times 10^{-3}$		Γ_{267}	$K^*(1410)^+ K^-, K^{*+} \rightarrow K_S^0\pi^+$		
Hadronic modes with a $K\bar{K}$ pair				Γ_{268}	$(K^-\pi^+)_{S\text{-wave}} K_S^0, (K_S^0\pi^+)_{S\text{-wave}} K^-$		
Γ_{211}	$K^+ K^-$	$(4.08 \pm 0.06) \times 10^{-3}$	S=1.6	Γ_{269}	$a_0(980)^-\pi^+, a_0^- \rightarrow K_S^0 K^-$		
Γ_{212}	$2K_S^0$	$(1.41 \pm 0.05) \times 10^{-4}$	S=1.1	Γ_{270}	$a_2(1320)^-\pi^+, a_2^- \rightarrow K_S^0 K^-$		
Γ_{213}	$K_S^0 K^-\pi^+$	$(3.3 \pm 0.5) \times 10^{-3}$	S=1.1	Γ_{271}	$\rho(1450)^-\pi^+, \rho^- \rightarrow K_S^0 K^-$	$(4.6 \pm 2.5) \times 10^{-5}$	
Γ_{214}	$\bar{K}^*(892)^0 K_S^0, \bar{K}^{*0} \rightarrow K^-\pi^+, K^*(892)^+ K^-, K^{*+} \rightarrow K_S^0\pi^+$	$(8.2 \pm 1.6) \times 10^{-5}$		Γ_{272}	$K_S^0 K^-\pi^-$	$(2.17 \pm 0.35) \times 10^{-3}$	S=1.1
Γ_{215}	$\bar{K}^*(1410)^0 K_S^0, \bar{K}^{*0} \rightarrow K^-\pi^+, K^*(892)^+ K^-, K^{*+} \rightarrow K_S^0\pi^+$	$(1.89 \pm 0.30) \times 10^{-3}$					
Γ_{216}	$\bar{K}^*(1410)^0 K_S^0, \bar{K}^{*0} \rightarrow K^-\pi^+, K^*(892)^+ K^-, K^{*+} \rightarrow K_S^0\pi^+$	$(1.3 \pm 1.9) \times 10^{-4}$					
Γ_{217}	$\bar{K}^*(1410)^+ K^-, K^{*+} \rightarrow K^-\pi^+, K^*(892)^+ K^-, K^{*+} \rightarrow K_S^0\pi^+$	$(3.2 \pm 1.9) \times 10^{-4}$					
Γ_{218}	$(K^-\pi^+)_{S\text{-wave}} K_S^0$	$(6.0 \pm 2.9) \times 10^{-4}$					
Γ_{219}	$(K_S^0\pi^+)_{S\text{-wave}} K^-$	$(3.9 \pm 1.0) \times 10^{-4}$					
Γ_{220}	$a_0(980)^-\pi^+, a_0^- \rightarrow K_S^0 K^-$	$(1.3 \pm 1.4) \times 10^{-4}$					
Γ_{221}	$a_0(1450)^-\pi^+, a_0^- \rightarrow K_S^0 K^-$	$(2.5 \pm 2.0) \times 10^{-5}$					
Γ_{222}	$a_2(1320)^-\pi^+, a_2^- \rightarrow K_S^0 K^-$	$(5 \pm 5) \times 10^{-6}$					
Γ_{223}	$\rho(1450)^-\pi^+, \rho^- \rightarrow K_S^0 K^-$	$(4.6 \pm 2.5) \times 10^{-5}$					
Γ_{224}	$K_S^0 K^+\pi^-$	$(2.17 \pm 0.35) \times 10^{-3}$	S=1.1				

See key on page 1171

Meson Particle Listings

 D^0

Γ ₂₇₂	$K^*(1410)^- K^+, K^{*-} \rightarrow \bar{K}^{*0} \pi^-$	$(7.0 \pm 1.1) \times 10^{-5}$			
Γ ₂₇₃	$K_1(1680)^+ K^-, K_1^+ \rightarrow K^{*0} \pi^+, K^{*0} \rightarrow K^+ \pi^-$	$(8.9 \pm 3.2) \times 10^{-5}$			
Γ ₂₇₄	$K^+ K^- \pi^+ \pi^-$ non-resonant	$(2.7 \pm 0.6) \times 10^{-4}$			
Γ ₂₇₅	$2K_S^0 \pi^+ \pi^-$	$(5.3 \pm 0.9) \times 10^{-4}$			
Γ ₂₇₆	$K_S^0 K^- \pi^+ \pi^0$	$(1.32 \pm 0.16) \times 10^{-3}$			
Γ ₂₇₇	$K_S^0 K^+ \pi^- \pi^0$	$(6.5 \pm 0.7) \times 10^{-4}$			
Γ ₂₇₈	$K_S^0 K^- 2\pi^+ \pi^-$	< 1.4	$\times 10^{-4}$	CL=90%	
Γ ₂₇₉	$K^+ K^- \pi^+ \pi^- \pi^0$	$(3.1 \pm 2.0) \times 10^{-3}$			
Other $K\bar{K}X$ modes. They include all decay modes of the ϕ , η , and ω .					
Γ ₂₈₀	$\phi \pi^0$	$(1.17 \pm 0.04) \times 10^{-3}$			
Γ ₂₈₁	$\phi \eta$	$(1.8 \pm 0.5) \times 10^{-4}$			
Γ ₂₈₂	$\phi \omega$	$(6.5 \pm 1.0) \times 10^{-4}$			
Radiative modes					
Γ ₂₈₃	$\rho^0 \gamma$	$(1.82 \pm 0.32) \times 10^{-5}$			
Γ ₂₈₄	$\omega \gamma$	< 2.4	$\times 10^{-4}$	CL=90%	
Γ ₂₈₅	$\phi \gamma$	$(2.81 \pm 0.19) \times 10^{-5}$			
Γ ₂₈₆	$\bar{K}^*(892)^0 \gamma$	$(4.1 \pm 0.7) \times 10^{-4}$			
Doubly Cabibbo suppressed (DC) modes or $\Delta C = 2$ forbidden via mixing (C2M) modes					
Γ ₂₈₇	$K^+ \ell^- \bar{\nu}_\ell$ via \bar{D}^0	$[i] < 2.2$	$\times 10^{-5}$	CL=90%	
Γ ₂₈₈	K^+ or $K^*(892)^+$ $e^- \bar{\nu}_e$ via \bar{D}^0	< 6	$\times 10^{-5}$	CL=90%	
Γ ₂₈₉	$K^+ \pi^-$ DC	$(1.50 \pm 0.07) \times 10^{-4}$		S=3.0	
Γ ₂₉₀	$K^+ \pi^-$ via DCS	$(1.363 \pm 0.025) \times 10^{-4}$			
Γ ₂₉₁	$K^+ \pi^-$ via \bar{D}^0	< 1.6	$\times 10^{-5}$	CL=95%	
Γ ₂₉₂	$K_S^0 \pi^+ \pi^-$ in $D^0 \rightarrow \bar{D}^0$	< 1.8	$\times 10^{-4}$	CL=95%	
Γ ₂₉₃	$K^*(892)^+ \pi^-, K^{*+} \rightarrow K_S^0 \pi^+$ DC	$(1.13 \pm_{-0.34}^{0.60}) \times 10^{-4}$			
Γ ₂₉₄	$K_0^*(1430)^+ \pi^-, K_0^{*+} \rightarrow K_S^0 \pi^+$ DC	< 1.4	$\times 10^{-5}$		
Γ ₂₉₅	$K_2^*(1430)^+ \pi^-, K_2^{*+} \rightarrow K_S^0 \pi^+$ DC	< 3.4	$\times 10^{-5}$		
Γ ₂₉₆	$K^+ \pi^- \pi^0$ DC	$(3.06 \pm 0.16) \times 10^{-4}$		S=1.4	
Γ ₂₉₇	$K^+ \pi^- \pi^0$ via \bar{D}^0	$(7.6 \pm_{-0.6}^{0.5}) \times 10^{-4}$			
Γ ₂₉₈	$K^+ \pi^- 2\pi^0$	< 3.6	$\times 10^{-4}$	CL=90%	
Γ ₂₉₉	$K^+ \pi^+ 2\pi^-$ via DCS	$(2.49 \pm 0.07) \times 10^{-4}$			
Γ ₃₀₀	$K^+ \pi^+ 2\pi^-$ DC	$(2.65 \pm 0.06) \times 10^{-4}$			
Γ ₃₀₁	$K^+ \pi^+ 2\pi^-$ via \bar{D}^0	$(7.9 \pm 3.0) \times 10^{-6}$			
Γ ₃₀₂	$K^+ \pi^-$ or $K^+ \pi^+ 2\pi^-$ via \bar{D}^0				
Γ ₃₀₃	μ^- anything via \bar{D}^0	< 4	$\times 10^{-4}$	CL=90%	
$\Delta C = 1$ weak neutral current (C1) modes, Lepton Family number (LF) violating modes, Lepton (L) or Baryon (B) number violating modes					
Γ ₃₀₄	$\gamma \gamma$ C1	< 8.5	$\times 10^{-7}$	CL=90%	
Γ ₃₀₅	$e^+ e^-$ C1	< 7.9	$\times 10^{-8}$	CL=90%	
Γ ₃₀₆	$\mu^+ \mu^-$ C1	< 3.1	$\times 10^{-9}$	CL=90%	
Γ ₃₀₇	$\pi^0 e^+ e^-$ C1	< 4	$\times 10^{-6}$	CL=90%	
Γ ₃₀₈	$\pi^0 \mu^+ \mu^-$ C1	< 1.8	$\times 10^{-4}$	CL=90%	
Γ ₃₀₉	$\pi^0 \nu \bar{\nu}$ C1	< 2.1	$\times 10^{-4}$	CL=90%	
Γ ₃₁₀	$\eta e^+ e^-$ C1	< 3	$\times 10^{-6}$	CL=90%	
Γ ₃₁₁	$\eta \mu^+ \mu^-$ C1	< 5.3	$\times 10^{-4}$	CL=90%	
Γ ₃₁₂	$\pi^+ \pi^- e^+ e^-$ C1	< 7	$\times 10^{-6}$	CL=90%	
Γ ₃₁₃	$\rho^0 e^+ e^-$ C1	< 1.0	$\times 10^{-4}$	CL=90%	
Γ ₃₁₄	$\pi^+ \pi^- \mu^+ \mu^-$ C1	$(9.6 \pm 1.2) \times 10^{-7}$			
Γ ₃₁₅	$\pi^+ \pi^- \mu^+ \mu^-$ (non-res) C1	< 5.5	$\times 10^{-7}$	CL=90%	
Γ ₃₁₆	$\rho^0 \mu^+ \mu^-$ C1	< 2.2	$\times 10^{-5}$	CL=90%	
Γ ₃₁₇	$\omega e^+ e^-$ C1	< 6	$\times 10^{-6}$	CL=90%	
Γ ₃₁₈	$\omega \mu^+ \mu^-$ C1	< 8.3	$\times 10^{-4}$	CL=90%	
Γ ₃₁₉	$K^- K^+ e^+ e^-$ C1	< 1.1	$\times 10^{-5}$	CL=90%	
Γ ₃₂₀	$\phi e^+ e^-$ C1	< 5.2	$\times 10^{-5}$	CL=90%	
Γ ₃₂₁	$K^- K^+ \mu^+ \mu^-$ C1	$(1.54 \pm 0.32) \times 10^{-7}$			
Γ ₃₂₂	$K^- K^+ \mu^+ \mu^-$ (non-res) C1	< 3.3	$\times 10^{-5}$	CL=90%	
Γ ₃₂₃	$\phi \mu^+ \mu^-$ C1	< 3.1	$\times 10^{-5}$	CL=90%	
Γ ₃₂₄	$\bar{K}^0 e^+ e^-$ [j]	< 2.4	$\times 10^{-5}$	CL=90%	
Γ ₃₂₅	$\bar{K}^0 \mu^+ \mu^-$ [j]	< 2.6	$\times 10^{-4}$	CL=90%	
Γ ₃₂₆	$K^- \pi^+ e^+ e^-$				
Γ ₃₂₇	$K^- \pi^+ e^+ e^-, 675 < m_{ee} < 875$ MeV	$(4.0 \pm 0.5) \times 10^{-6}$			
Γ ₃₂₈	$K^- \pi^+ e^+ e^-, 1.005 < m_{ee} < 1.035$ GeV	< 5	$\times 10^{-7}$	CL=90%	
Γ ₃₂₉	$\bar{K}^*(892)^0 e^+ e^-$ [j]	< 4.7	$\times 10^{-5}$	CL=90%	
Γ ₃₃₀	$K^- \pi^+ \mu^+ \mu^-$ C1	< 3.59	$\times 10^{-4}$	CL=90%	
Γ ₃₃₁	$K^- \pi^+ \mu^+ \mu^-, 675 < m_{\mu\mu} < 875$ MeV	$(4.2 \pm 0.4) \times 10^{-6}$			
Γ ₃₃₂	$\bar{K}^*(892)^0 \mu^+ \mu^-$ [j]	< 2.4	$\times 10^{-5}$	CL=90%	
Γ ₃₃₃	$\pi^+ \pi^- \pi^0 \mu^+ \mu^-$ C1	< 8.1	$\times 10^{-4}$	CL=90%	
Γ ₃₃₄	$\mu^\pm e^\mp$ LF	[k] < 1.3	$\times 10^{-8}$	CL=90%	
Γ ₃₃₅	$\pi^0 e^\pm \mu^\mp$ LF	[k] < 8.0	$\times 10^{-7}$	CL=90%	
Γ ₃₃₆	$\eta e^\pm \mu^\mp$ LF	[k] < 2.25	$\times 10^{-6}$	CL=90%	
Γ ₃₃₇	$\pi^+ \pi^- e^\pm \mu^\mp$ LF	[k] < 1.71	$\times 10^{-6}$	CL=90%	
Γ ₃₃₈	$\rho^0 e^\pm \mu^\mp$ LF	[k] < 5.0	$\times 10^{-7}$	CL=90%	
Γ ₃₃₉	$\omega e^\pm \mu^\mp$ LF	[k] < 1.71	$\times 10^{-6}$	CL=90%	
Γ ₃₄₀	$K^- K^+ e^\pm \mu^\mp$ LF	[k] < 1.00	$\times 10^{-6}$	CL=90%	
Γ ₃₄₁	$\phi e^\pm \mu^\mp$ LF	[k] < 5.1	$\times 10^{-7}$	CL=90%	
Γ ₃₄₂	$\bar{K}^0 e^\pm \mu^\mp$ LF	[k] < 1.74	$\times 10^{-6}$	CL=90%	
Γ ₃₄₃	$K^- \pi^+ e^\pm \mu^\mp$ LF	[k] < 1.90	$\times 10^{-6}$	CL=90%	
Γ ₃₄₄	$\bar{K}^*(892)^0 e^\pm \mu^\mp$ LF	[k] < 1.25	$\times 10^{-6}$	CL=90%	
Γ ₃₄₅	$2\pi^- 2e^+$ L	< 9.1	$\times 10^{-7}$	CL=90%	
Γ ₃₄₆	$2\pi^- 2\mu^+$ L	< 15.2	$\times 10^{-6}$	CL=90%	
Γ ₃₄₇	$K^- \pi^- 2e^+$ L	< 5.0	$\times 10^{-7}$	CL=90%	
Γ ₃₄₈	$K^- \pi^- 2\mu^+$ L	< 5.3	$\times 10^{-7}$	CL=90%	
Γ ₃₄₉	$2K^- 2e^+$ L	< 3.4	$\times 10^{-7}$	CL=90%	
Γ ₃₅₀	$2K^- 2\mu^+$ L	< 1.0	$\times 10^{-7}$	CL=90%	
Γ ₃₅₁	$\pi^- \pi^- e^+ \mu^+$ L	< 3.06	$\times 10^{-6}$	CL=90%	
Γ ₃₅₂	$K^- \pi^- e^+ \mu^+$ L	< 2.10	$\times 10^{-6}$	CL=90%	
Γ ₃₅₃	$2K^- e^+ \mu^+$ L	< 5.8	$\times 10^{-7}$	CL=90%	
Γ ₃₅₄	$p e^+$ L,B	< 2.2	$\times 10^{-6}$	CL=90%	
Γ ₃₅₅	$\bar{p} e^+$ L,B	< 1.2	$\times 10^{-6}$	CL=90%	
Γ ₃₅₆	Unaccounted decay modes				
[a] This value is obtained by subtracting the branching fractions for 2-, 4- and 6-prongs from unity.					
[b] This is the sum of our $K^- 2\pi^+ \pi^-$, $K^- 2\pi^+ \pi^- \pi^0$, $\bar{K}^0 2\pi^+ 2\pi^-$, $K^+ 2K^- \pi^+$, $2\pi^+ 2\pi^-$, $2\pi^+ 2\pi^- \pi^0$, $K^+ K^- \pi^+ \pi^-$, and $K^+ K^- \pi^+ \pi^- \pi^0$, branching fractions.					
[c] This is the sum of our $K^- 3\pi^+ 2\pi^-$ and $3\pi^+ 3\pi^-$ branching fractions.					
[d] The branching fractions for the $K^- e^+ \nu_e$, $K^*(892)^- e^+ \nu_e$, $\pi^- e^+ \nu_e$, and $\rho^- e^+ \nu_e$ modes add up to $6.17 \pm 0.17\%$.					
[e] The branching fraction for this mode may differ from the sum of the submodes that contribute to it, due to interference effects. See the relevant papers.					
[f] This is a doubly Cabibbo-suppressed mode.					
[g] Submodes of the $D^0 \rightarrow K_S^0 \pi^+ \pi^- \pi^0$ mode with a K^* and/or ρ were studied by COFFMAN 92B, but with only 140 events. With nothing new for 18 years, we refer to our 2008 edition, Physics Letters B667 1 (2008), for those results.					
[h] This branching fraction includes all the decay modes of the resonance in the final state.					
[i] This limit assumes the average of $B(D^0 \rightarrow K^- e^+ \nu_e)$ and $B(D^0 \rightarrow K^- \mu^+ \nu_\mu)$ for the $B(D^0 \rightarrow K^- \ell^+ \nu_\ell)$ value.					
[j] This mode is not a useful test for a $\Delta C=1$ weak neutral current because both quarks must change flavor in this decay.					
[k] The value is for the sum of the charge states or particle/antiparticle states indicated.					
FIT INFORMATION					
An overall fit to 68 branching ratios uses 134 measurements to determine 33 parameters. The overall fit has a $\chi^2 = 149.3$ for 101 degrees of freedom.					
The following off-diagonal array elements are the correlation coefficients $\langle \delta x_i \delta x_j \rangle / (\delta x_i \delta x_j)$, in percent, from the fit to the branching fractions, $x_i \equiv \Gamma_i / \Gamma_{\text{total}}$.					

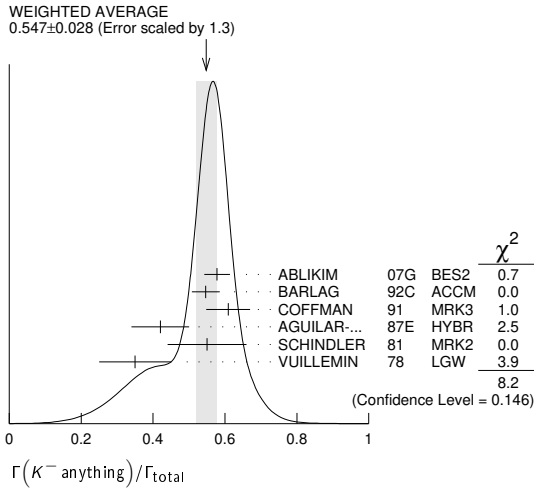
See key on page 1171

Meson Particle Listings

D^0

$\Gamma(\mu^+ \text{ anything})/\Gamma_{\text{total}}$					Γ_6/Γ
VALUE (%)	EVTS	DOCUMENT ID	TECN	COMMENT	
6.8 ± 0.6 OUR FIT					
6.4 ± 0.8 OUR AVERAGE					
6.8 ± 1.5 ± 0.8	79 ± 10	¹ ABLIKIM	08L BES2	$e^+e^- \approx \psi(3772)$	
6.5 ± 1.2 ± 0.3	36	KAYIS-TOPAK.05	CHRS	ν_μ emulsion	
6.0 ± 0.7 ± 1.2	310	ALBRECHT	96C ARG	$e^+e^- \approx 10$ GeV	
¹ ABLIKIM 08L finds the ratio of $D^+ \rightarrow \mu^+ X$ and $D^0 \rightarrow \mu^+ X$ branching fractions to be $2.59 \pm 0.70 \pm 0.25$, in accord with the ratio of D^+ and D^0 lifetimes, 2.54 ± 0.02 .					

$\Gamma(K^- \text{ anything})/\Gamma_{\text{total}}$					Γ_7/Γ
VALUE	EVTS	DOCUMENT ID	TECN	COMMENT	
0.547 ± 0.028 OUR AVERAGE					
Error includes scale factor of 1.3. See the ideogram below.					
0.578 ± 0.016 ± 0.032	2098 ± 59	ABLIKIM	07G BES2	$e^+e^- \approx \psi(3770)$	
0.546 ^{+0.039} _{-0.038}		¹ BARLAG	92C ACCM	π^- Cu 230 GeV	
0.609 ± 0.032 ± 0.052		COFFMAN	91 MRK3	e^+e^- 3.77 GeV	
0.42 ± 0.08		AGUILAR-...	87E HYBR	$\pi p, pp$ 360, 400 GeV	
0.55 ± 0.11	121	SCHINDLER	81 MRK2	e^+e^- 3.771 GeV	
0.35 ± 0.10	19	VUILLEMIN	78 LGW	e^+e^- 3.772 GeV	
¹ BARLAG 92c computes the branching fraction using topological normalization.					



$\Gamma(K_S^0 \text{ anything})/\Gamma_{\text{total}}$					Γ_8/Γ
VALUE (%)	EVTS	DOCUMENT ID	TECN	COMMENT	
20.75 ± 0.12 ± 0.20					
• • • We do not use the following data for averages, fits, limits, etc. • • •					
23.8 ± 2.4 ± 1.5	250	¹ ABLIKIM	06U BES2	e^+e^- at 3773 MeV	
22.8 ± 2.5 ± 1.6		² COFFMAN	91 MRK3	e^+e^- 3.77 GeV	
¹ ABLIKIM 06U reports $B(D^0 \rightarrow K_S^0 X \text{ or } \bar{K}_S^0 X) = 0.476 \pm 0.048 \pm 0.030$ which we take as twice the branching fraction for $D^0 \rightarrow K_S^0 X$.					
² COFFMAN 91 reports $B(D^0 \rightarrow K_S^0 X \text{ or } \bar{K}_S^0 X) = 0.455 \pm 0.050 \pm 0.032$ which we take as twice the branching fraction for $D^0 \rightarrow K_S^0 X$.					

$\Gamma(K^+ \text{ anything})/\Gamma_{\text{total}}$					Γ_9/Γ
VALUE	EVTS	DOCUMENT ID	TECN	COMMENT	
0.034 ± 0.004 OUR AVERAGE					
0.035 ± 0.007 ± 0.003	119 ± 23	ABLIKIM	07G BES2	$e^+e^- \approx \psi(3770)$	
0.034 ^{+0.007} _{-0.005}		¹ BARLAG	92C ACCM	π^- Cu 230 GeV	
0.028 ± 0.009 ± 0.004		COFFMAN	91 MRK3	e^+e^- 3.77 GeV	
0.03 ^{+0.05} _{-0.02}		AGUILAR-...	87E HYBR	$\pi p, pp$ 360, 400 GeV	
0.08 ± 0.03	25	SCHINDLER	81 MRK2	e^+e^- 3.771 GeV	
¹ BARLAG 92c computes the branching fraction using topological normalization.					

$\Gamma(K^*(892)^- \text{ anything})/\Gamma_{\text{total}}$					Γ_{10}/Γ
VALUE	EVTS	DOCUMENT ID	TECN	COMMENT	
0.153 ± 0.083 ± 0.019					
0.153 ± 0.083 ± 0.019	28 ± 15	ABLIKIM	06U BES2	e^+e^- at 3773 MeV	

$\Gamma(\bar{K}^*(892)^0 \text{ anything})/\Gamma_{\text{total}}$					Γ_{11}/Γ
VALUE	EVTS	DOCUMENT ID	TECN	COMMENT	
0.087 ± 0.040 ± 0.012					
0.087 ± 0.040 ± 0.012	96 ± 44	ABLIKIM	05P BES	$e^+e^- \approx 3773$ MeV	

$\Gamma(K^*(892)^+ \text{ anything})/\Gamma_{\text{total}}$					Γ_{12}/Γ
VALUE	CL%	DOCUMENT ID	TECN	COMMENT	
<0.036					
<0.036	90	ABLIKIM	06U BES2	e^+e^- at 3773 MeV	

$\Gamma(K^*(892)^0 \text{ anything})/\Gamma_{\text{total}}$					Γ_{13}/Γ
VALUE	EVTS	DOCUMENT ID	TECN	COMMENT	
0.028 ± 0.012 ± 0.004					
0.028 ± 0.012 ± 0.004	31 ± 12	ABLIKIM	05P BES	$e^+e^- \approx 3773$ MeV	

$\Gamma(\eta \text{ anything})/\Gamma_{\text{total}}$					Γ_{14}/Γ
VALUE (%)	EVTS	DOCUMENT ID	TECN	COMMENT	
This ratio includes η particles from η' decays.					
9.5 ± 0.4 ± 0.8					
9.5 ± 0.4 ± 0.8	4463 ± 197	HUANG	06B CLEO	e^+e^- at $\psi(3770)$	

$\Gamma(\eta' \text{ anything})/\Gamma_{\text{total}}$					Γ_{15}/Γ
VALUE (%)	EVTS	DOCUMENT ID	TECN	COMMENT	
2.48 ± 0.17 ± 0.21					
2.48 ± 0.17 ± 0.21	299 ± 21	HUANG	06B CLEO	e^+e^- at $\psi(3770)$	

$\Gamma(\phi \text{ anything})/\Gamma_{\text{total}}$					Γ_{16}/Γ
VALUE (%)	EVTS	DOCUMENT ID	TECN	COMMENT	
1.08 ± 0.04 OUR AVERAGE					
1.091 ± 0.027 ± 0.035	4.1k	ABLIKIM	19AYBES3	e^+e^- at 3773 MeV	
1.05 ± 0.08 ± 0.07	368 ± 24	HUANG	06B CLEO	e^+e^- at $\psi(3770)$	
• • • We do not use the following data for averages, fits, limits, etc. • • •					
1.71 ^{+0.76} _{-0.71}	± 0.17	9	BAI	00c BES	$e^+e^- \rightarrow D\bar{D}^*, D^*\bar{D}^*$

$\Gamma(\pi^+ \pi^+ \pi^- \text{ anything})/\Gamma_{\text{total}}$					Γ_{17}/Γ
VALUE (%)	EVTS	DOCUMENT ID	TECN	COMMENT	
17.60 ± 0.11 ± 0.22					
17.60 ± 0.11 ± 0.22	95k	ABLIKIM	23A1 BES3	$2.93 \text{ fb}^{-1}, e^+e^-$ at $\psi(3770)$	

$\Gamma(\text{invisibles})/\Gamma_{\text{total}}$					Γ_{18}/Γ
VALUE	CL%	DOCUMENT ID	TECN	COMMENT	
<9.4 × 10⁻⁵					
<9.4 × 10 ⁻⁵	90	LAI	17 BELL	e^+e^- at $\Upsilon(nS), n=4,5$	

Semileptonic modes

$\Gamma(K^- e^+ \nu_e)/\Gamma_{\text{total}}$					Γ_{20}/Γ
VALUE (%)	EVTS	DOCUMENT ID	TECN	COMMENT	
3.549 ± 0.026 OUR FIT					
Error includes scale factor of 1.2.					
3.525 ± 0.023 OUR AVERAGE					
3.567 ± 0.031 ± 0.025	4040	ABLIKIM	21BA BES3	e^+e^- at 3.773 GeV	
3.505 ± 0.014 ± 0.033	71k	¹ ABLIKIM	15X BES3	$2.92 \text{ fb}^{-1}, 3.773$ GeV	
3.50 ± 0.03 ± 0.04	14.1k	¹ BESSON	09 CLEO	e^+e^- at $\psi(3770)$	
3.45 ± 0.10 ± 0.19	1.3k	² WIDHALM	06 BELL	$e^+e^- \approx \Upsilon(4S)$	
3.82 ± 0.40 ± 0.27	104	ABLIKIM	04C BES	e^+e^- , 3.773 GeV	
3.4 ± 0.5 ± 0.4	55	ADLER	89 MRK3	e^+e^- 3.77 GeV	
• • • We do not use the following data for averages, fits, limits, etc. • • •					
3.56 ± 0.03 ± 0.09		³ DOBBS	08 CLEO	See BESSON 09	
3.44 ± 0.10 ± 0.10	1.3k	COAN	05 CLEO	See DOBBS 08	

- See the form-factor parameters near the end of this D^0 Listing.
- The $\pi^- e^+ \nu_e$ and $K^- e^+ \nu_e$ results of WIDHALM 06 give $|\frac{V_{cd}}{V_{cs}} \cdot \frac{f_+^\pi(0)}{f_+^K(0)}|^2 = 0.042 \pm 0.003 \pm 0.003$.
- DOBBS 08 establishes $|\frac{V_{cd}}{V_{cs}} \cdot \frac{f_+^\pi(0)}{f_+^K(0)}| = 0.188 \pm 0.008 \pm 0.002$ from the D^+ and D^0 decays to $\bar{K} e^+ \nu_e$ and $\pi e^+ \nu_e$.

$\Gamma(K^- e^+ \nu_e)/\Gamma(K^- \pi^+)$					Γ_{20}/Γ_{38}
VALUE	EVTS	DOCUMENT ID	TECN	COMMENT	
0.899 ± 0.009 OUR FIT					
Error includes scale factor of 1.3.					
0.930 ± 0.013 OUR AVERAGE					
0.927 ± 0.007 ± 0.012	76k ± 323	¹ AUBERT	07BG BABR	$e^+e^- \approx \Upsilon(4S)$	
0.978 ± 0.027 ± 0.044	2510	² BEAN	93C CLE2	$e^+e^- \approx \Upsilon(4S)$	
0.90 ± 0.06 ± 0.06	584	³ CRAWFORD	91B CLEO	$e^+e^- \approx 10.5$ GeV	
0.91 ± 0.07 ± 0.11	250	⁴ ANJOS	89F E691	Photoproduction	

- The event samples in this AUBERT 07BG result include radiative photons. The $D^0 \rightarrow K^- e^+ \nu_e$ form factor at $q^2 = 0$ is $f_+^K(0) = 0.727 \pm 0.007 \pm 0.005 \pm 0.007$.
- BEAN 93C uses $K^- \mu^+ \nu_\mu$ as well as $K^- e^+ \nu_e$ events and makes a small phase-space adjustment to the number of the μ^+ events to use them as e^+ events. A pole mass of $2.00 \pm 0.12 \pm 0.18$ GeV/ c^2 is obtained from the q^2 dependence of the decay rate.
- CRAWFORD 91B uses $K^- e^+ \nu_e$ and $K^- \mu^+ \nu_\mu$ candidates to measure a pole mass of $2.1_{-0.2}^{+0.4} \pm 0.3$ GeV/ c^2 from the q^2 dependence of the decay rate.
- ANJOS 89F measures a pole mass of $2.1_{-0.2}^{+0.4} \pm 0.2$ GeV/ c^2 from the q^2 dependence of the decay rate.

$\Gamma(K^- \mu^+ \nu_\mu)/\Gamma_{\text{total}}$					Γ_{21}/Γ
VALUE (%)	EVTS	DOCUMENT ID	TECN	COMMENT	
3.41 ± 0.04 OUR FIT					
3.41 ± 0.04 OUR AVERAGE					
3.413 ± 0.019 ± 0.035	47k	ABLIKIM	19B BES3	e^+e^- , 3773 MeV	
3.45 ± 0.10 ± 0.21	1249 ± 43	WIDHALM	06 BELL	$e^+e^- \approx \Upsilon(4S)$	

$\Gamma(K^- \mu^+ \nu_\mu)/\Gamma(\mu^+ \text{ anything})$					Γ_{21}/Γ_6
VALUE	EVTS	DOCUMENT ID	TECN	COMMENT	
0.50 ± 0.04 OUR FIT					
0.472 ± 0.051 ± 0.040					
0.472 ± 0.051 ± 0.040	232	KODAMA	94 E653	π^- emulsion 600 GeV	
• • • We do not use the following data for averages, fits, limits, etc. • • •					
0.32 ± 0.05 ± 0.05	124	KODAMA	91 EMUL	pA 800 GeV	

Meson Particle Listings

 D^0 $\Gamma(K^-\mu^+\nu_\mu)/\Gamma(K^-\pi^+)$ Γ_{21}/Γ_{38}

VALUE	EVTS	DOCUMENT ID	TECN	COMMENT
0.864 ± 0.012 OUR FIT				Error includes scale factor of 1.1.
0.84 ± 0.04 OUR AVERAGE				
0.852 ± 0.034 ± 0.028	1897	¹ FRABETTI 95G	E687	γ Be $\overline{E}_\gamma = 220$ GeV
0.82 ± 0.13 ± 0.13	338	² FRABETTI 93I	E687	γ Be $\overline{E}_\gamma = 221$ GeV
0.79 ± 0.08 ± 0.09	231	³ CRAWFORD 91B	CLEO	$e^+e^- \approx 10.5$ GeV

¹ FRABETTI 95G extracts the ratio of form factors $f_-(0)/f_+(0) = -1.3^{+3.6}_{-3.4} \pm 0.6$, and measures a pole mass of $1.87^{+0.11+0.07}_{-0.08-0.06}$ GeV/ c^2 from the q^2 dependence of the decay rate.

² FRABETTI 93I measures a pole mass of $2.1^{+0.7+0.7}_{-0.3-0.3}$ GeV/ c^2 from the q^2 dependence of the decay rate.

³ CRAWFORD 91B measures a pole mass of $2.00 \pm 0.12 \pm 0.18$ GeV/ c^2 from the q^2 dependence of the decay rate.

 $\Gamma(K^*(892)^-e^+\nu_e)/\Gamma_{\text{total}}$ Γ_{22}/Γ

Both decay modes of the $K^*(892)^-$ are included.

VALUE (%)	EVTS	DOCUMENT ID	TECN	COMMENT
2.15 ± 0.16 OUR FIT				
2.16 ± 0.15 ± 0.08	219 ± 16	¹ COAN 05	CLEO	e^+e^- at $\psi(3770)$

¹ COAN 05 uses both $K^-\pi^0$ and $K_S^0\pi^-$ events.

 $\Gamma(K^*(892)^-e^+\nu_e)/\Gamma(K_S^0\pi^-e^+\nu_e)$ Γ_{22}/Γ_{25}

VALUE (units 10^{-2})	EVTS	DOCUMENT ID	TECN	COMMENT
94.52 ± 0.97 ± 0.62	3.1k	ABLIKIM 19G	BES3	$K_S^0\pi^-e^+\nu_e$ events

 $\Gamma(K^*(892)^-e^+\nu_e)/\Gamma(K_S^0\pi^+\pi^-)$ Γ_{22}/Γ_{44}

Unseen decay modes of the $K^*(892)^-$ are included.

VALUE	EVTS	DOCUMENT ID	TECN	COMMENT
0.77 ± 0.07 OUR FIT				
0.76 ± 0.12 ± 0.06	152	¹ BEAN 93C	CLE2	$e^+e^- \approx \gamma(4S)$

¹ BEAN 93C uses $K^*\mu^+\nu_\mu$ as well as $K^*e^+\nu_e$ events and makes a small phase-space adjustment to the number of the μ^+ events to use them as e^+ events.

 $\Gamma(K^*(892)^-\mu^+\nu_\mu)/\Gamma(K_S^0\pi^+\pi^-)$ Γ_{23}/Γ_{44}

Unseen decay modes of the $K^*(892)^-$ are included.

VALUE	EVTS	DOCUMENT ID	TECN	COMMENT
0.674 ± 0.068 ± 0.026	175 ± 17	¹ LINK 05B	FOCS	γA , $\overline{E}_\gamma \approx 180$ GeV

¹ LINK 05B finds that in $D^0 \rightarrow \overline{K}^0\pi^-\mu^+\nu_\mu$ the $\overline{K}^0\pi^-$ system is 6% in S-wave.

 $\Gamma(K^-\pi^0e^+\nu_e)/\Gamma_{\text{total}}$ Γ_{24}/Γ

VALUE	EVTS	DOCUMENT ID	TECN	COMMENT
0.016 ± 0.013 ± 0.002	4	¹ BAI 91	MRK3	$e^+e^- \approx 3.77$ GeV

¹ BAI 91 finds that a fraction $0.79^{+0.15+0.09}_{-0.17-0.03}$ of combined D^+ and D^0 decays to $\overline{K}\pi e^+\nu_e$ (24 events) are $\overline{K}^*(892)e^+\nu_e$. BAI 91 uses 56 $K^-e^+\nu_e$ events to measure a pole mass of $1.8 \pm 0.3 \pm 0.2$ GeV/ c^2 from the q^2 dependence of the decay rate.

 $\Gamma(\overline{K}^0\pi^-e^+\nu_e)/\Gamma_{\text{total}}$ Γ_{25}/Γ

VALUE (%)	EVTS	DOCUMENT ID	TECN	COMMENT
1.44 ± 0.04 OUR AVERAGE				
1.434 ± 0.029 ± 0.032	3.1k	ABLIKIM 19G	BES3	e^+e^- at 3773 MeV
2.61 ± 1.04 ± 0.28	9 ± 3	ABLIKIM 06O	BES2	e^+e^- at 3773 MeV
2.8 $\pm_{-0.8}^{+1.7}$ ± 0.3	6	¹ BAI 91	MRK3	$e^+e^- \approx 3.77$ GeV

¹ BAI 91 finds that a fraction $0.79^{+0.15+0.09}_{-0.17-0.03}$ of combined D^+ and D^0 decays to $\overline{K}\pi e^+\nu_e$ (24 events) are $\overline{K}^*(892)e^+\nu_e$.

 $\Gamma(\overline{K}^0\pi^-)_{S\text{-wave}}e^+\nu_e)/\Gamma(\overline{K}^0\pi^-e^+\nu_e)$ Γ_{26}/Γ_{25}

VALUE (units 10^{-2})	EVTS	DOCUMENT ID	TECN	COMMENT
5.51 ± 0.97 ± 0.62	3.1k	ABLIKIM 19G	BES3	$K_S^0\pi^-e^+\nu_e$ events

 $\Gamma(K^-\pi^+\pi^-e^+\nu_e)/\Gamma_{\text{total}}$ Γ_{27}/Γ

VALUE (units 10^{-4})	EVTS	DOCUMENT ID	TECN	COMMENT
2.8 $\pm_{-1.1}^{+1.4}$ ± 0.3	8	ARTUSO 07A	CLEO	e^+e^- at $\gamma(3770)$

 $\Gamma(K_1(1270)^-e^+\nu_e)/\Gamma_{\text{total}}$ Γ_{28}/Γ

VALUE (units 10^{-4})	EVTS	DOCUMENT ID	TECN	COMMENT
10.1 ± 1.8 OUR AVERAGE				
10.9 ± 1.3 $\pm_{-1.6}^{+0.9}$ ± 1.2	109	¹ ABLIKIM 21AY	BES3	e^+e^- at 3773 GeV
7.6 $\pm_{-3.0}^{+4.1}$ ± 0.9	8	² ARTUSO 07A	CLEO	e^+e^- at $\gamma(3770)$

¹ Uses $B(K_1(1270)^- \rightarrow K^-\pi^+\pi^-) = (32.9 \pm 3.6)\%$, which is the source of the third uncertainty.

² This ARTUSO 07A result is corrected for all decay modes of the $K_1(1270)^-$.

 $\Gamma(K^-\pi^+\pi^-\mu^+\nu_\mu)/\Gamma(K^-\mu^+\nu_\mu)$ Γ_{29}/Γ_{21}

VALUE	CL%	DOCUMENT ID	TECN	COMMENT
<0.037	90	KODAMA 93B	E653	π^- emulsion 600 GeV

 $\Gamma(\overline{K}^*(892)\pi^-\mu^+\nu_\mu)/\Gamma(K^-\mu^+\nu_\mu)$ Γ_{30}/Γ_{21}

VALUE	CL%	DOCUMENT ID	TECN	COMMENT
<0.043	90	¹ KODAMA 93B	E653	π^- emulsion 600 GeV

¹ KODAMA 93B searched in $K^-\pi^+\pi^-\mu^+\nu_\mu$, but the limit includes other ($\overline{K}^*(892)\pi^-$) charge states.

 $\Gamma(\pi^-e^+\nu_e)/\Gamma_{\text{total}}$ Γ_{31}/Γ

VALUE (%)	EVTS	DOCUMENT ID	TECN	COMMENT
0.291 ± 0.004 OUR FIT				
0.293 ± 0.004 OUR AVERAGE				
0.295 ± 0.004 ± 0.003	6.3k	¹ ABLIKIM 15X	BES3	2.92 fb $^{-1}$, 3.773 GeV
0.288 ± 0.008 ± 0.003	1.3k	¹ BESSON 09	CLEO	e^+e^- at $\psi(3770)$
0.279 ± 0.027 ± 0.016	126	² WIDHALM 06	BELL	$e^+e^- \approx \gamma(4S)$
0.299 ± 0.011 ± 0.009		³ DOBBS 08	CLEO	See BESSON 09
0.262 ± 0.025 ± 0.008	117	COAN 05	CLEO	See DOBBS 08

¹ See the form-factor parameters near the end of this D^0 Listing.

² The $\pi^-e^+\nu_e$ and $K^-e^+\nu_e$ results of WIDHALM 06 give $|\frac{V_{cd}}{V_{cs}} \cdot \frac{f_+^\pi(0)}{f_+^K(0)}|^2 = 0.042 \pm 0.003 \pm 0.003$.

³ DOBBS 08 establishes $|\frac{V_{cd}}{V_{cs}} \cdot \frac{f_+^\pi(0)}{f_+^K(0)}| = 0.188 \pm 0.008 \pm 0.002$ from the D^+ and D^0 decays to $\overline{K}e^+\nu_e$ and $\pi e^+\nu_e$.

 $\Gamma(\pi^-e^+\nu_e)/\Gamma(K^-e^+\nu_e)$ Γ_{31}/Γ_{20}

VALUE	EVTS	DOCUMENT ID	TECN	COMMENT
0.0821 ± 0.0013 OUR FIT				Error includes scale factor of 1.1.
0.085 ± 0.007 OUR AVERAGE				
0.082 ± 0.006 ± 0.005		¹ HUANG 05	CLEO	$e^+e^- \approx \gamma(4S)$
0.101 ± 0.020 ± 0.003	91	² FRABETTI 96B	E687	γ Be, $\overline{E}_\gamma \approx 200$ GeV
0.103 ± 0.039 ± 0.013	87	³ BUTLER 95	CLE2	< 0.156 (90% CL)

¹ HUANG 05 uses both e and μ events, and makes a small correction to the μ events to make them effectively e events. This result gives $|\frac{V_{cd}}{V_{cs}} \cdot \frac{f_+^\pi(0)}{f_+^K(0)}|^2 = 0.038^{+0.006+0.005}_{-0.007-0.003}$.

² FRABETTI 96B uses both e and μ events, and makes a small correction to the μ events to make them effectively e events. This result gives $|\frac{V_{cd}}{V_{cs}} \cdot \frac{f_+^\pi(0)}{f_+^K(0)}|^2 = 0.050 \pm 0.011 \pm 0.002$.

³ BUTLER 95 has 87 ± 33 $\pi^-e^+\nu_e$ events. The result gives $|\frac{V_{cd}}{V_{cs}} \cdot \frac{f_+^\pi(0)}{f_+^K(0)}|^2 = 0.052 \pm 0.020 \pm 0.007$.

 $\Gamma(\pi^-e^+\nu_e)/\Gamma(K^-\pi^+)$ Γ_{31}/Γ_{38}

VALUE (units 10^{-2})	EVTS	DOCUMENT ID	TECN	COMMENT
7.38 ± 0.12 OUR FIT				Error includes scale factor of 1.1.
7.02 ± 0.17 ± 0.23	375k	¹ LEES 15F	BABR	347 fb $^{-1}$, 10.58 GeV

¹ See the form-factor parameters near the end of the D^0 Listing.

 $\Gamma(\pi^-\mu^+\nu_\mu)/\Gamma_{\text{total}}$ Γ_{32}/Γ

VALUE (%)	EVTS	DOCUMENT ID	TECN	COMMENT
0.267 ± 0.012 OUR FIT				Error includes scale factor of 1.3.
0.268 ± 0.012 OUR AVERAGE				Error includes scale factor of 1.2.
0.272 ± 0.008 ± 0.006	2.3k	ABLIKIM 18A	BES3	e^+e^- , 3773 MeV
0.231 ± 0.026 ± 0.019	106 ± 13	WIDHALM 06	BELL	$e^+e^- \approx \gamma(4S)$

 $\Gamma(\pi^-\mu^+\nu_\mu)/\Gamma(K^-\mu^+\nu_\mu)$ Γ_{32}/Γ_{21}

VALUE	EVTS	DOCUMENT ID	TECN	COMMENT
0.0784 ± 0.0035 OUR FIT				Error includes scale factor of 1.2.
0.074 ± 0.008 ± 0.007	288 ± 29	¹ LINK 05	FOCS	γA , $\overline{E}_\gamma \approx 180$ GeV

¹ LINK 05 finds the form-factor ratio $|f_0^\pi(0)/f_0^K(0)|$ to be $0.85 \pm 0.04 \pm 0.04 \pm 0.01$.

 $\Gamma(\pi^-\pi^0e^+\nu_e)/\Gamma_{\text{total}}$ Γ_{33}/Γ

VALUE (units 10^{-3})	EVTS	DOCUMENT ID	TECN	COMMENT
1.445 ± 0.058 ± 0.039	1.1k	¹ ABLIKIM 19C	BES3	e^+e^- at 3773 MeV

¹ Seen 100% via $D^0 \rightarrow \rho(770)^-e^+\nu_e$, and also reported as the branching fraction for $D^0 \rightarrow \rho(770)^-e^+\nu_e$.

 $\Gamma(\rho^-e^+\nu_e)/\Gamma_{\text{total}}$ Γ_{34}/Γ

VALUE (units 10^{-3})	EVTS	DOCUMENT ID	TECN	COMMENT
1.50 ± 0.12 OUR AVERAGE				Error includes scale factor of 1.9.
1.445 ± 0.058 ± 0.039	1.1k	¹ ABLIKIM 19C	BES3	e^+e^- at 3773 MeV
1.77 ± 0.12 ± 0.10	305 ± 21	^{2,3} DOBBS 13	CLEO	e^+e^- at $\psi(3770)$
1.94 ± 0.39 ± 0.13	31 ± 6	COAN 05	CLEO	See DOBBS 13

¹ This result is the same as the one reported for $D^0 \rightarrow \pi^-\pi^0e^+\nu_e$ which ABLIKIM 19C found to proceed 100% via $D^0 \rightarrow \rho(770)^-e^+\nu_e$.

² DOBBS 13 finds $\Gamma(D^0 \rightarrow \rho^-e^+\nu_e) / 2 \Gamma(D^+ \rightarrow \rho^0e^+\nu_e) = 1.03 \pm 0.09^{+0.08}_{-0.02}$; isospin invariance predicts the ratio is 1.0.

³ See the D^+ Listings for $D \rightarrow \rho e^+\nu_e$ form factors.

See key on page 1171

Meson Particle Listings

 D^0

$\Gamma(\rho^-\mu^+\nu_\mu)/\Gamma_{\text{total}}$					Γ_{35}/Γ
VALUE (units 10^{-3})	EVTS	DOCUMENT ID	TECN	COMMENT	
$1.35 \pm 0.09 \pm 0.09$	570	ABLIKIM	21bC BES3	e^+e^- at 3.773 GeV	

$\Gamma(a(980)^- e^+ \nu_e, a^- \rightarrow \eta \pi^-)/\Gamma_{\text{total}}$					Γ_{36}/Γ
VALUE (units 10^{-4})	EVTS	DOCUMENT ID	TECN	COMMENT	
$1.33 \pm 0.33 \pm 0.09$	26	¹ ABLIKIM	18F BES3	e^+e^- at 3773 MeV	

¹ Signal observed at 6.4σ C.L.

$\Gamma(b_1(1235)^- e^+ \nu_e, b_1^- \rightarrow \omega \pi^-)/\Gamma_{\text{total}}$					Γ_{37}/Γ
VALUE	CL%	DOCUMENT ID	TECN	COMMENT	
$<1.12 \times 10^{-4}$	90	ABLIKIM	20Af BES3	e^+e^- , 3773 MeV	

Hadronic modes with a single \bar{K}

$\Gamma(K^- \pi^+)/\Gamma_{\text{total}}$					Γ_{38}/Γ
VALUE (%)	EVTS	DOCUMENT ID	TECN	COMMENT	
3.947 ± 0.030 OUR FIT				Error includes scale factor of 1.2.	
3.909 ± 0.034 OUR AVERAGE					

$3.883 \pm 0.006 \pm 0.051$	0.5M	¹ ABLIKIM	18W BES3	e^+e^- , 3773 MeV	
$3.934 \pm 0.021 \pm 0.061$		BONVICINI	14 CLEO	All CLEO-c runs	
$4.007 \pm 0.037 \pm 0.072$	33.8k	AUBERT	08L BABR	e^+e^- at $\Upsilon(4S)$	
$3.82 \pm 0.07 \pm 0.12$		² ARTUSO	98 CLE2	CLEO average	
$3.90 \pm 0.09 \pm 0.12$	5.4k	³ BARATE	97c ALEP	From Z decays	
$3.41 \pm 0.12 \pm 0.28$	1.2k	³ ALBRECHT	94F ARG	$e^+e^- \approx \Upsilon(4S)$	
$3.62 \pm 0.34 \pm 0.44$		³ DECAMP	91J ALEP	From Z decays	
• • • We do not use the following data for averages, fits, limits, etc. • • •					
$3.891 \pm 0.035 \pm 0.069$		⁴ DOBBS	07 CLEO	See BONVICINI 14	
$3.91 \pm 0.08 \pm 0.09$	10.3k	⁴ HE	05 CLEO	See DOBBS 07	
$3.81 \pm 0.15 \pm 0.16$	1.2k	⁵ ARTUSO	98 CLE2	e^+e^- at $\Upsilon(4S)$	
$3.69 \pm 0.11 \pm 0.16$		⁶ COAN	98 CLE2	See ARTUSO 98	
$4.5 \pm 0.6 \pm 0.4$		⁷ ALBRECHT	94 ARG	$e^+e^- \approx \Upsilon(4S)$	
$3.95 \pm 0.08 \pm 0.17$	4.2k	^{3,8} AKERIB	93 CLE2	See ARTUSO 98	
$4.5 \pm 0.8 \pm 0.5$	56	³ ABACHI	88 HRS	e^+e^- 29 GeV	
$4.2 \pm 0.4 \pm 0.4$	0.9k	ADLER	88c MRK3	e^+e^- 3.77 GeV	
4.1 ± 0.6	0.3k	⁹ SCHINDLER	81 MRK2	e^+e^- 3.771 GeV	
4.3 ± 1.0	130	¹⁰ PERUZZI	77 LGW	e^+e^- 3.77 GeV	

¹ ABLIKIM 18W measured the combined $K^{\pm}\pi^{\pm}$ branching fraction to be 3.898%. We have subtracted off the doubly Cabibbo-suppressed branching fraction $B(D^0 \rightarrow K^+\pi^-) = (1.50 \pm 0.07) \times 10^{-4}$, even though it is less than one-third of the uncertainty of the combined measurement, in order to treat this as a measurement of $B(D^0 \rightarrow K^-\pi^+)$.² This combines the CLEO results of ARTUSO 98, COAN 98, and AKERIB 93.³ ABACHI 88, DECAMP 91J, AKERIB 93, ALBRECHT 94F, and BARATE 97c use $D^*(2010)^+ \rightarrow D^0\pi^+$ decays. The π^+ is both slow and of low p_T with respect to the event thrust axis or nearest jet ($\approx D^{*+}$ direction). The excess number of such π^+ 's over background gives the number of $D^*(2010)^+ \rightarrow D^0\pi^+$ events, and the fraction with $D^0 \rightarrow K^-\pi^+$ gives the $D^0 \rightarrow K^-\pi^+$ branching fraction.⁴ DOBBS 07 and HE 05 use single- and double-tagged events in an overall fit. DOBBS 07 supersedes HE 05.⁵ ARTUSO 98, following ALBRECHT 94, uses D^0 mesons from $\bar{B}^0 \rightarrow D^*(2010)^+ X \ell^- \bar{\nu}_\ell$ decays. Our average uses the CLEO average of this value with the values of COAN 98 and AKERIB 93.⁶ COAN 98 assumes that $\Gamma(B \rightarrow \bar{D} X \ell^+ \nu)/\Gamma(B \rightarrow X \ell^+ \nu) = 1.0 - 3|V_{ub}/V_{cb}|^2 - 0.010 \pm 0.005$, the last term accounting for $\bar{B} \rightarrow D_s^+ K X \ell^- \bar{\nu}$. COAN 98 is included in the CLEO average in ARTUSO 98.⁷ ALBRECHT 94 uses D^0 mesons from $\bar{B}^0 \rightarrow D^{*+} \ell^- \bar{\nu}_\ell$ decays. This is a different set of events than used by ALBRECHT 94F.⁸ This AKERIB 93 value includes radiative corrections; without them, the value is $0.0391 \pm 0.0008 \pm 0.0017$. AKERIB 93 is included in the CLEO average in ARTUSO 98.⁹ SCHINDLER 81 (MARK-2) measures $\sigma(e^+e^- \rightarrow \psi(3770)) \times$ branching fraction to be 0.24 ± 0.02 nb. We use the MARK-3 (ADLER 88c) value of $\sigma = 5.8 \pm 0.5 \pm 0.6$ nb.¹⁰ PERUZZI 77 (MARK-1) measures $\sigma(e^+e^- \rightarrow \psi(3770)) \times$ branching fraction to be 0.25 ± 0.05 nb. We use the MARK-3 (ADLER 88c) value of $\sigma = 5.8 \pm 0.5 \pm 0.6$ nb.

$\Gamma(K_S^0 \pi^0)/\Gamma_{\text{total}}$					Γ_{39}/Γ
VALUE (%)	EVTS	DOCUMENT ID	TECN	COMMENT	
1.239 ± 0.022 OUR FIT					
$1.240 \pm 0.006 \pm 0.027$	67k	ABLIKIM	18W BES3	e^+e^- , 3773 MeV	

• • • We do not use the following data for averages, fits, limits, etc. • • •

$1.240 \pm 0.017 \pm 0.056$	614	HE	08 CLEO	See MENDEZ 10
-----------------------------	-----	----	---------	---------------

$\Gamma(K_S^0 \pi^0)/[\Gamma(K^- \pi^+) + \Gamma(K^+ \pi^-)]$					$\Gamma_{39}/(\Gamma_{38} + \Gamma_{289})$
VALUE (units 10^{-2})	EVTS	DOCUMENT ID	TECN	COMMENT	
31.3 ± 0.6 OUR FIT					
$30.4 \pm 0.3 \pm 0.9$	20k	MENDEZ	10 CLEO	e^+e^- at 3774 MeV	

$\Gamma(K_S^0 \pi^0)/\Gamma(K_S^0 \pi^+ \pi^-)$					Γ_{39}/Γ_{44}
VALUE	EVTS	DOCUMENT ID	TECN	COMMENT	
0.44 ± 0.02 OUR FIT					
$0.44 \pm 0.02 \pm 0.05$	1942 \pm 64	PROCARIO	93B CLE2	e^+e^- 10.36–10.7 GeV	

• • • We do not use the following data for averages, fits, limits, etc. • • •

$0.34 \pm 0.04 \pm 0.02$	92	¹ ALBRECHT	92P ARG	$e^+e^- \approx 10$ GeV
$0.36 \pm 0.04 \pm 0.08$	104	KINOSHITA	91 CLEO	$e^+e^- \sim 10.7$ GeV

¹ This value is calculated from numbers in Table 1 of ALBRECHT 92P.

$\Gamma(K_L^0 \pi^0)/\Gamma_{\text{total}}$					Γ_{40}/Γ
VALUE (%)	EVTS	DOCUMENT ID	TECN	COMMENT	
$0.97 \pm 0.03 \pm 0.02$	2590				
0.976 ± 0.032 OUR AVERAGE					
$0.998 \pm 0.049 \pm 0.048$	1116	¹ HE	08 CLEO	e^+e^- at $\psi(3770)$	

¹ The difference of HE 08 $D^0 \rightarrow K_S^0 \pi^0$ and $K_L^0 \pi^0$ branching fractions over the sum is $0.108 \pm 0.025 \pm 0.024$. This is consistent with U-spin symmetry and the Cabibbo angle.

$\Gamma(K_L^0 \eta)/\Gamma_{\text{total}}$					Γ_{41}/Γ
VALUE (units 10^{-3})	EVTS	DOCUMENT ID	TECN	COMMENT	
4.34 ± 0.16 OUR AVERAGE					
$4.39 \pm 0.24 \pm 0.15$	543	¹ ABLIKIM	22W BES3	e^+e^- at 3.773 GeV	
$4.31 \pm 0.14 \pm 0.13$	2.1k	² ABLIKIM	22W BES3	e^+e^- at 3.773 GeV	

¹ Uses $\eta \rightarrow \pi^+\pi^-\pi^0$ with branching fraction $(23.02 \pm 0.25) \times 10^{-2}$.² Uses $\eta \rightarrow \gamma\gamma$ with branching fraction $(39.36 \pm 0.18) \times 10^{-2}$.

$\Gamma(K_L^0 \eta')/\Gamma_{\text{total}}$					Γ_{42}/Γ
VALUE (units 10^{-3})	EVTS	DOCUMENT ID	TECN	COMMENT	
8.12 ± 0.35 OUR AVERAGE				Error includes scale factor of 1.3.	
$8.57 \pm 0.37 \pm 0.22$	684	¹ ABLIKIM	22W BES3	e^+e^- at 3.773 GeV	
$7.85 \pm 0.24 \pm 0.23$	2k	² ABLIKIM	22W BES3	e^+e^- at 3.773 GeV	

¹ Uses $\eta' \rightarrow \pi^+\pi^-\eta$ with branching fraction 0.425 ± 0.005 .² Uses $\eta' \rightarrow \rho^0\gamma$ with branching fraction 0.295 ± 0.004 .

$\Gamma(K_L^0 \omega)/\Gamma_{\text{total}}$					Γ_{43}/Γ
VALUE (units 10^{-2})	EVTS	DOCUMENT ID	TECN	COMMENT	
$1.164 \pm 0.022 \pm 0.028$	6.1k	ABLIKIM	22W BES3	e^+e^- at 3.773 GeV	
• • • We do not use the following data for averages, fits, limits, etc. • • •					
$1.09 \pm 0.06 \pm 0.03$	1360	ABLIKIM	22BMBES3	e^+e^- at $\psi(3770)$	

$\Gamma(K_S^0 \pi^+ \pi^-)/\Gamma_{\text{total}}$					Γ_{44}/Γ
VALUE (%)	EVTS	DOCUMENT ID	TECN	COMMENT	
• • • We do not use the following data for averages, fits, limits, etc. • • •					
$2.52 \pm 0.20 \pm 0.25$	284 \pm 22	¹ ALBRECHT	94F ARG	$e^+e^- \approx \Upsilon(4S)$	
$3.2 \pm 0.3 \pm 0.5$		ADLER	87 MRK3	e^+e^- 3.77 GeV	
2.6 ± 0.8	32 \pm 8	² SCHINDLER	81 MRK2	e^+e^- 3.771 GeV	
4.0 ± 1.2	28	³ PERUZZI	77 LGW	e^+e^- 3.77 GeV	

¹ See the footnote on the ALBRECHT 94F measurement of $\Gamma(K^- \pi^+)/\Gamma_{\text{total}}$ for the method used.² SCHINDLER 81 (MARK-2) measures $\sigma(e^+e^- \rightarrow \psi(3770)) \times$ branching fraction to be 0.30 ± 0.08 nb. We use the MARK-3 (ADLER 88c) value of $\sigma = 5.8 \pm 0.5 \pm 0.6$ nb.³ PERUZZI 77 (MARK-1) measures $\sigma(e^+e^- \rightarrow \psi(3770)) \times$ branching fraction to be 0.46 ± 0.12 nb. We use the MARK-3 (ADLER 88c) value of $\sigma = 5.8 \pm 0.5 \pm 0.6$ nb.

$\Gamma(K_S^0 \pi^+ \pi^-)/\Gamma(K^- \pi^+)$					Γ_{44}/Γ_{38}
VALUE	EVTS	DOCUMENT ID	TECN	COMMENT	
0.71 ± 0.05 OUR FIT				Error includes scale factor of 1.1.	
$0.81 \pm 0.05 \pm 0.08$	856 \pm 35	FRABETTI	94J E687	γ Be $\bar{E}_{\gamma} = 220$ GeV	
• • • We do not use the following data for averages, fits, limits, etc. • • •					
0.85 ± 0.40	35	AVERY	80 SPEC	$\gamma N \rightarrow D^{*+}$	
1.4 ± 0.5	116	PICCOLO	77 MRK1	e^+e^- 4.03, 4.41 GeV	

$\Gamma(K_S^0 \rho^0)/\Gamma(K_S^0 \pi^+ \pi^-)$					Γ_{45}/Γ_{44}
VALUE	EVTS	DOCUMENT ID	TECN	COMMENT	
0.224 ± 0.017 OUR AVERAGE				Error includes scale factor of 1.7.	
0.210 ± 0.016		¹ AUBERT	08AL BABR	Dalitz fit, ≈ 487 k evts	
$0.264 \pm 0.009 \pm 0.010$		MURAMATSU	02 CLE2	Dalitz fit, 5299 evts	

This is the "fit fraction" from the Dalitz-plot analysis.

• • • We do not use the following data for averages, fits, limits, etc. • • •

$0.267 \pm 0.011 \pm 0.009$		ASNER	04A CLEO	See MURAMATSU 02
$0.350 \pm 0.028 \pm 0.067$		FRABETTI	94G E687	Dalitz fit, 597 evts
$0.227 \pm 0.032 \pm 0.009$		ALBRECHT	93D ARG	Dalitz fit, 440 evts
$0.215 \pm 0.051 \pm 0.037$		ANJOS	93 E691	γ Be 90–260 GeV
$0.20 \pm 0.06 \pm 0.03$		FRABETTI	92B E687	γ Be, $\bar{E}_{\gamma} = 221$ GeV
$0.12 \pm 0.01 \pm 0.07$		ADLER	87 MRK3	e^+e^- 3.77 GeV

¹ The error on this AUBERT 08AL value includes both statistical and systematic uncertainties; the latter dominates.

$\Gamma(K_S^0 \omega, \omega \rightarrow \pi^+ \pi^-)/\Gamma(K_S^0 \pi^+ \pi^-)$					Γ_{46}/Γ_{44}
VALUE	EVTS	DOCUMENT ID	TECN	COMMENT	
0.0073 ± 0.0020 OUR AVERAGE					
0.009 ± 0.010		¹ AUBERT	08AL BABR	Dalitz fit, ≈ 487 k evts	
$0.0072 \pm 0.0018 \pm 0.0010$		MURAMATSU	02 CLE2	Dalitz fit, 5299 evts	

This is the "fit fraction" from the Dalitz-plot analysis.

• • • We do not use the following data for averages, fits, limits, etc. • • •

$0.0081 \pm 0.0019 \pm 0.0018$		ASNER	04A CLEO	See MURAMATSU 02
--------------------------------	--	-------	----------	------------------

¹ The error on this AUBERT 08AL value includes both statistical and systematic uncertainties; the latter dominates.

Meson Particle Listings

 D^0 $\Gamma(K_S^0(\pi^+\pi^-)_{S\text{-wave}})/\Gamma(K_S^0\pi^+\pi^-)$ Γ_{47}/Γ_{44}

This is the "fit fraction" from the Dalitz-plot analysis. The $(\pi^+\pi^-)_{S\text{-wave}}$ includes what in isobar models are the $f_0(980)$ and $f_0(1370)$; see the following two data blocks.

VALUE	DOCUMENT ID	TECN	COMMENT
0.119±0.026	¹ AUBERT	08AL BABR	Dalitz fit, ≈ 487 k evts

¹The error on this AUBERT 08AL value includes both statistical and systematic uncertainties; the latter dominates.

 $\Gamma(K_S^0 f_0(980), f_0 \rightarrow \pi^+\pi^-)/\Gamma(K_S^0\pi^+\pi^-)$ Γ_{48}/Γ_{44}

Fit fraction from the Dalitz plot analyses.

VALUE	DOCUMENT ID	TECN	COMMENT
0.043±0.005^{+0.012}_{-0.006}	MURAMATSU 02	CLE2	Dalitz fit, 5299 evts

• • • We do not use the following data for averages, fits, limits, etc. • • •

0.042±0.005 ^{+0.011} _{-0.005}	ASNER	04A CLEO	See MURAMATSU 02
0.068±0.016±0.018	FRABETTI	94G E687	Dalitz fit, 597 evts
0.046±0.018±0.006	ALBRECHT	93D ARG	Dalitz fit, 440 evts

 $\Gamma(K_S^0 f_0(1370), f_0 \rightarrow \pi^+\pi^-)/\Gamma(K_S^0\pi^+\pi^-)$ Γ_{49}/Γ_{44}

This is the "fit fraction" from the Dalitz-plot analysis.

VALUE	DOCUMENT ID	TECN	COMMENT
0.099±0.011^{+0.028}_{-0.044}	MURAMATSU 02	CLE2	Dalitz fit, 5299 evts

• • • We do not use the following data for averages, fits, limits, etc. • • •

0.098±0.014 ^{+0.026} _{-0.036}	ASNER	04A CLEO	See MURAMATSU 02
0.077±0.022±0.031	FRABETTI	94G E687	Dalitz fit, 597 evts
0.082±0.028±0.013	ALBRECHT	93D ARG	Dalitz fit, 440 evts

 $\Gamma(K_S^0 f_2(1270), f_2 \rightarrow \pi^+\pi^-)/\Gamma(K_S^0\pi^+\pi^-)$ Γ_{50}/Γ_{44}

This is the "fit fraction" from the Dalitz-plot analysis.

VALUE	DOCUMENT ID	TECN	COMMENT
0.0032^{+0.0035}_{-0.0022} OUR AVERAGE			

0.006 ± 0.007	¹ AUBERT	08AL BABR	Dalitz fit, ≈ 487 k evts
0.0027±0.0015 ^{+0.0037} _{-0.0017}	MURAMATSU 02	CLE2	Dalitz fit, 5299 evts

• • • We do not use the following data for averages, fits, limits, etc. • • •

0.0036±0.0022 ^{+0.0032} _{-0.0019}	ASNER	04A CLEO	See MURAMATSU 02
0.037 ± 0.014 ± 0.017	FRABETTI	94G E687	Dalitz fit, 597 evts
0.050 ± 0.021 ± 0.008	ALBRECHT	93D ARG	Dalitz fit, 440 evts

¹The error on this AUBERT 08AL value includes both statistical and systematic uncertainties; the latter dominates.

 $\Gamma(K^*(892)^-\pi^+, K^{*-} \rightarrow K_S^0\pi^-)/\Gamma(K_S^0\pi^+\pi^-)$ Γ_{51}/Γ_{44}

This is the "fit fraction" from the Dalitz-plot analysis.

VALUE	DOCUMENT ID	TECN	COMMENT
0.588^{+0.034}_{-0.050} OUR AVERAGE			Error includes scale factor of 2.0.

0.557±0.028	¹ AUBERT	08AL BABR	Dalitz fit, ≈ 487 k evts
0.657±0.013 ^{+0.018} _{-0.040}	MURAMATSU 02	CLE2	Dalitz fit, 5299 evts

• • • We do not use the following data for averages, fits, limits, etc. • • •

0.663±0.013 ^{+0.024} _{-0.043}	ASNER	04A CLEO	See MURAMATSU 02
0.625±0.036±0.026	FRABETTI	94G E687	Dalitz fit, 597 evts
0.718±0.042±0.030	ALBRECHT	93D ARG	Dalitz fit, 440 evts
0.480±0.097	ANJOS	93 E691	γ Be 90–260 GeV
0.56 ± 0.04 ± 0.05	ADLER	87 MRK3	e^+e^- 3.77 GeV

¹The error on this AUBERT 08AL value includes both statistical and systematic uncertainties; the latter dominates.

 $\Gamma(K_S^0(1430)^-\pi^+, K_0^{*-} \rightarrow K_S^0\pi^-)/\Gamma(K_S^0\pi^+\pi^-)$ Γ_{52}/Γ_{44}

This is the "fit fraction" from the Dalitz-plot analysis.

VALUE	DOCUMENT ID	TECN	COMMENT
0.095^{+0.014}_{-0.010} OUR AVERAGE			

0.102±0.015	¹ AUBERT	08AL BABR	Dalitz fit, ≈ 487 k evts
0.073±0.007 ^{+0.031} _{-0.011}	MURAMATSU 02	CLE2	Dalitz fit, 5299 evts

• • • We do not use the following data for averages, fits, limits, etc. • • •

0.072±0.007 ^{+0.014} _{-0.013}	ASNER	04A CLEO	See MURAMATSU 02
0.109±0.027±0.029	FRABETTI	94G E687	Dalitz fit, 597 evts
0.129±0.034±0.021	ALBRECHT	93D ARG	Dalitz fit, 440 evts

¹The error on this AUBERT 08AL value includes both statistical and systematic uncertainties; the latter dominates.

 $\Gamma(K_S^0(1430)^-\pi^+, K_2^{*-} \rightarrow K_S^0\pi^-)/\Gamma(K_S^0\pi^+\pi^-)$ Γ_{53}/Γ_{44}

This is the "fit fraction" from the Dalitz-plot analysis.

VALUE	DOCUMENT ID	TECN	COMMENT
0.0120^{+0.0070}_{-0.0035} OUR AVERAGE			

0.022 ± 0.016	¹ AUBERT	08AL BABR	Dalitz fit, ≈ 487 k evts
0.011 ± 0.002 ^{+0.007} _{-0.003}	MURAMATSU 02	CLE2	Dalitz fit, 5299 evts

• • • We do not use the following data for averages, fits, limits, etc. • • •

0.011 ± 0.002 ^{+0.005} _{-0.003}	ASNER	04A CLEO	See MURAMATSU 02
---	-------	----------	------------------

¹The error on this AUBERT 08AL value includes both statistical and systematic uncertainties; the latter dominates.

 $\Gamma(K^*(1680)^-\pi^+, K^{*-} \rightarrow K_S^0\pi^-)/\Gamma(K_S^0\pi^+\pi^-)$ Γ_{54}/Γ_{44}

This is the "fit fraction" from the Dalitz-plot analysis.

VALUE	DOCUMENT ID	TECN	COMMENT
0.016±0.013 OUR AVERAGE			

0.007±0.019	¹ AUBERT	08AL BABR	Dalitz fit, ≈ 487 k evts
0.022±0.004 ^{+0.018} _{-0.015}	MURAMATSU 02	CLE2	Dalitz fit, 5299 evts

• • • We do not use the following data for averages, fits, limits, etc. • • •

0.023±0.005 ^{+0.007} _{-0.014}	ASNER	04A CLEO	See MURAMATSU 02
---	-------	----------	------------------

¹The error on this AUBERT 08AL value includes both statistical and systematic uncertainties; the latter dominates.

 $\Gamma(K^*(892)^+\pi^-, K^{*+} \rightarrow K_S^0\pi^+)/\Gamma(K_S^0\pi^+\pi^-)$ Γ_{55}/Γ_{44}

This is a doubly Cabibbo-suppressed mode.

VALUE (units 10^{-3})	DOCUMENT ID	TECN	COMMENT
4.0^{+2.0}_{-1.2} OUR AVERAGE			

4.6±2.3	¹ AUBERT	08AL BABR	Dalitz fit, ≈ 487 k evts
3.4±1.3 ^{+4.1} _{-0.4}	MURAMATSU 02	CLE2	Dalitz fit, 5299 evts

• • • We do not use the following data for averages, fits, limits, etc. • • •

3.4±1.3 ^{+3.6} _{-0.5}	ASNER	04A CLEO	See MURAMATSU 02
---	-------	----------	------------------

¹The error on this AUBERT 08AL value includes both statistical and systematic uncertainties; the latter dominates.

 $\Gamma(K_S^0(1430)^+\pi^-, K_0^{*+} \rightarrow K_S^0\pi^+)/\Gamma(K_S^0\pi^+\pi^-)$ Γ_{56}/Γ_{44}

This is a doubly Cabibbo-suppressed mode.

VALUE	CL%	DOCUMENT ID	TECN	COMMENT
<5 × 10⁻⁴	95	AUBERT	08AL BABR	Dalitz fit, ≈ 487 k evts

 $\Gamma(K_S^0(1430)^+\pi^-, K_2^{*+} \rightarrow K_S^0\pi^+)/\Gamma(K_S^0\pi^+\pi^-)$ Γ_{57}/Γ_{44}

This is a doubly Cabibbo-suppressed mode.

VALUE	CL%	DOCUMENT ID	TECN	COMMENT
<1.2 × 10⁻³	95	AUBERT	08AL BABR	Dalitz fit, ≈ 487 k evts

 $\Gamma(K_S^0\pi^+\pi^- \text{ nonresonant})/\Gamma(K_S^0\pi^+\pi^-)$ Γ_{58}/Γ_{44}

This is the "fit fraction" from the Dalitz-plot analysis. Neither FRABETTI 94G nor ALBRECHT 93D (quoted in many of the earlier submodes of $K_S^0\pi^+\pi^-$) sees evidence for a nonresonant component.

VALUE	DOCUMENT ID	TECN	COMMENT
0.009±0.004^{+0.020}_{-0.004}	MURAMATSU 02	CLE2	Dalitz fit, 5299 evts

• • • We do not use the following data for averages, fits, limits, etc. • • •

0.007±0.007 ^{+0.021} _{-0.006}	ASNER	04A CLEO	See MURAMATSU 02
0.263±0.024±0.041	ANJOS	93 E691	γ Be 90–260 GeV
0.26 ± 0.08 ± 0.05	FRABETTI	92B E687	γ Be, $\bar{E}_\gamma = 221$ GeV
0.33 ± 0.05 ± 0.10	ADLER	87 MRK3	e^+e^- 3.77 GeV

 $\Gamma(K^-\pi^+\pi^0)/\Gamma_{\text{total}}$ Γ_{59}/Γ

VALUE (%)	EVTS	DOCUMENT ID	TECN	COMMENT
14.57±0.12±0.38		¹ DOBBS	07 CLEO	See BONVICINI 14

14.9 ± 0.3 ± 0.5	19k ± 150	¹ HE	05 CLEO	See DOBBS 07
13.3 ± 1.2 ± 1.3	931	ADLER	88c MRK3	e^+e^- 3.77 GeV
11.7 ± 4.3	37	² SCHINDLER	81 MRK2	e^+e^- 3.771 GeV

¹DOBBS 07 and HE 05 use single- and double-tagged events in an overall fit. DOBBS 07 supersedes HE 05.

²SCHINDLER 81 (MARK-2) measures $\sigma(e^+e^- \rightarrow \psi(3770)) \times$ branching fraction to be 0.68 ± 0.23 nb. We use the MARK-3 (ADLER 88c) value of $\sigma = 5.8 \pm 0.5 \pm 0.6$ nb.

 $\Gamma(K^-\pi^+\pi^0)/\Gamma(K^-\pi^+)$ Γ_{59}/Γ_{38}

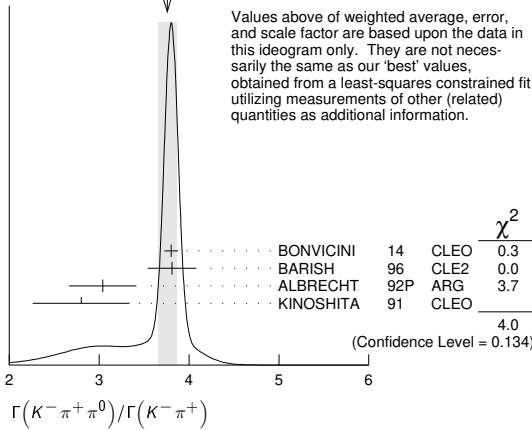
VALUE	EVTS	DOCUMENT ID	TECN	COMMENT
3.65±0.14 OUR FIT				Error includes scale factor of 2.3.

3.76±0.10 OUR AVERAGE				Error includes scale factor of 1.4. See the ideogram below.
------------------------------	--	--	--	---

3.802±0.022±0.073		BONVICINI	14 CLEO	All CLEO-c runs
3.81 ± 0.07 ± 0.26	10k	BARISH	96 CLE2	$e^+e^- \approx \mathcal{T}(4S)$
3.04 ± 0.16 ± 0.34	931	¹ ALBRECHT	92P ARG	$e^+e^- \approx 10$ GeV
2.8 ± 0.14 ± 0.52	1050	KINOSHITA	91 CLEO	$e^+e^- \sim 10.7$ GeV

¹This value is calculated from numbers in Table 1 of ALBRECHT 92P.

WEIGHTED AVERAGE
3.76±0.10 (Error scaled by 1.4)



Values above of weighted average, error, and scale factor are based upon the data in this ideogram only. They are not necessarily the same as our 'best' values, obtained from a least-squares constrained fit utilizing measurements of other (related) quantities as additional information.

$\Gamma(K^-\rho^+\pi^0)/\Gamma(K^-\pi^+\pi^0)$ Γ60/Γ59

This is the "fit fraction" from the Dalitz-plot analysis.

VALUE	DOCUMENT ID	TECN	COMMENT
0.78 ± 0.04 OUR AVERAGE			
0.788 ± 0.019 ± 0.048	KOPP 01	CLE2	Dalitz fit, ≈ 7,000 evts
0.765 ± 0.041 ± 0.054	FRABETTI 94G	E687	Dalitz fit, 530 evts
••• We do not use the following data for averages, fits, limits, etc. •••			
0.647 ± 0.039 ± 0.150	ANJOS 93	E691	γ Be 90–260 GeV
0.81 ± 0.03 ± 0.06	ADLER 87	MRK3	e^+e^- 3.77 GeV

$\Gamma(K^-\rho(1700)^+\pi^0)/\Gamma(K^-\pi^+\pi^0)$ Γ61/Γ59

This is the "fit fraction" from the Dalitz-plot analysis.

VALUE	DOCUMENT ID	TECN	COMMENT
0.057 ± 0.008 ± 0.009	KOPP 01	CLE2	Dalitz fit, ≈ 7,000 evts

$\Gamma(K^*(892)^-\pi^+, K^*(892)^-\pi^0)/\Gamma(K^-\pi^+\pi^0)$ Γ62/Γ59

This is the "fit fraction" from the Dalitz-plot analysis.

VALUE	DOCUMENT ID	TECN	COMMENT
0.160 ± 0.025 OUR AVERAGE -0.013			
0.161 ± 0.007 ± 0.027 -0.011	KOPP 01	CLE2	Dalitz fit, ≈ 7,000 evts
0.148 ± 0.028 ± 0.049	FRABETTI 94G	E687	Dalitz fit, 530 evts
••• We do not use the following data for averages, fits, limits, etc. •••			
0.084 ± 0.011 ± 0.012	ANJOS 93	E691	γ Be 90–260 GeV
0.12 ± 0.02 ± 0.03	ADLER 87	MRK3	e^+e^- 3.77 GeV

$\Gamma(\bar{K}^*(892)^0\pi^0, \bar{K}^*(892)^0\pi^+)/\Gamma(K^-\pi^+\pi^0)$ Γ63/Γ59

This is the "fit fraction" from the Dalitz-plot analysis.

VALUE	DOCUMENT ID	TECN	COMMENT
0.135 ± 0.016 OUR AVERAGE			
0.127 ± 0.009 ± 0.016	KOPP 01	CLE2	Dalitz fit, ≈ 7,000 evts
0.165 ± 0.031 ± 0.015	FRABETTI 94G	E687	Dalitz fit, 530 evts
••• We do not use the following data for averages, fits, limits, etc. •••			
0.142 ± 0.018 ± 0.024	ANJOS 93	E691	γ Be 90–260 GeV
0.13 ± 0.02 ± 0.03	ADLER 87	MRK3	e^+e^- 3.77 GeV

$\Gamma(K_0^{*0}(1430)^-\pi^+, K_0^{*0}(1430)^-\pi^0)/\Gamma(K^-\pi^+\pi^0)$ Γ64/Γ59

This is the "fit fraction" from the Dalitz-plot analysis.

VALUE	DOCUMENT ID	TECN	COMMENT
0.033 ± 0.006 ± 0.014	KOPP 01	CLE2	Dalitz fit, ≈ 7,000 evts

$\Gamma(\bar{K}_0^{*0}(1430)^0\pi^0, \bar{K}_0^{*0}(1430)^0\pi^+)/\Gamma(K^-\pi^+\pi^0)$ Γ65/Γ59

This is the "fit fraction" from the Dalitz-plot analysis.

VALUE	DOCUMENT ID	TECN	COMMENT
0.041 ± 0.006 ± 0.032 -0.009	KOPP 01	CLE2	Dalitz fit, ≈ 7,000 evts

$\Gamma(K^*(1680)^-\pi^+, K^*(1680)^-\pi^0)/\Gamma(K^-\pi^+\pi^0)$ Γ66/Γ59

This is the "fit fraction" from the Dalitz-plot analysis.

VALUE	DOCUMENT ID	TECN	COMMENT
0.013 ± 0.003 ± 0.004	KOPP 01	CLE2	Dalitz fit, ≈ 7,000 evts

$\Gamma(K^-\pi^+\pi^0 \text{ nonresonant})/\Gamma(K^-\pi^+\pi^0)$ Γ67/Γ59

This is the "fit fraction" from the Dalitz-plot analysis.

VALUE	EVTS	DOCUMENT ID	TECN	COMMENT
0.080 ± 0.040 -0.014				OUR AVERAGE
0.075 ± 0.009 ± 0.056 -0.011		KOPP 01	CLE2	Dalitz fit, ≈ 7,000 evts
0.101 ± 0.033 ± 0.040		FRABETTI 94G	E687	Dalitz fit, 530 evts
••• We do not use the following data for averages, fits, limits, etc. •••				
0.036 ± 0.004 ± 0.018		ANJOS 93	E691	γ Be 90–260 GeV
0.09 ± 0.02 ± 0.04		ADLER 87	MRK3	e^+e^- 3.77 GeV
0.51 ± 0.22	21	SUMMERS 84	E691	Photoproduction

$\Gamma(K_S^0 2\pi^0)/\Gamma_{\text{total}}$ Γ68/Γ

VALUE (units 10 ⁻³)	EVTS	DOCUMENT ID	TECN	COMMENT
9.1 ± 1.1 OUR AVERAGE				Error includes scale factor of 2.2.
10.58 ± 0.38 ± 0.73	1259	LOWREY 11	CLEO	$e^+e^- \approx 3.77$ GeV
8.34 ± 0.45 ± 0.42		ASNER 08	CLEO	$e^+e^- \rightarrow D^0\bar{D}^0$, 3.77 GeV

$\Gamma(K_L^0 \pi^0 \pi^0)/\Gamma_{\text{total}}$ Γ69/Γ

VALUE (%)	EVTS	DOCUMENT ID	TECN	COMMENT
1.26 ± 0.05 ± 0.03	1300	ABLIKIM 22BMBES3		e^+e^- at $\psi(3770)$

$\Gamma(K_S^0(2\pi^0)_S\text{-wave})/\Gamma(K_S^0 2\pi^0)$ Γ70/Γ68

This is the "fit fraction" from the Dalitz-plot analysis.

VALUE (units 10 ⁻²)	DOCUMENT ID	TECN	COMMENT
28.9 ± 6.3 ± 3.1	LOWREY 11	CLEO	Dalitz analysis, 1259 evts

$\Gamma(\bar{K}^*(892)^0\pi^0, \bar{K}^{*0} \rightarrow K_S^0\pi^0)/\Gamma(K_S^0 2\pi^0)$ Γ71/Γ39

This is the "fit fraction" from the Dalitz-plot analysis.

VALUE (units 10 ⁻²)	DOCUMENT ID	TECN	COMMENT	
65.6 ± 5.3 ± 2.5	LOWREY 11	CLEO	Dalitz analysis, 1259 evts	
••• We do not use the following data for averages, fits, limits, etc. •••				
55 ⁺¹³ / ₋₁₀ ± 7		PROCARIO 93B	CLE2	Dalitz plot fit, 122 evts

$\Gamma(\bar{K}^*(1430)^0\pi^0, \bar{K}^{*0} \rightarrow K_S^0\pi^0)/\Gamma(K_S^0 2\pi^0)$ Γ72/Γ68

This is the "fit fraction" from the Dalitz-plot analysis.

VALUE (units 10 ⁻²)	DOCUMENT ID	TECN	COMMENT
0.49 ± 0.45 ± 2.51	LOWREY 11	CLEO	Dalitz analysis, 1259 evts

$\Gamma(\bar{K}^*(1680)^0\pi^0, \bar{K}^{*0} \rightarrow K_S^0\pi^0)/\Gamma(K_S^0 2\pi^0)$ Γ73/Γ68

This is the "fit fraction" from the Dalitz-plot analysis.

VALUE (units 10 ⁻²)	DOCUMENT ID	TECN	COMMENT
11.2 ± 2.7 ± 2.5	LOWREY 11	CLEO	Dalitz analysis, 1259 evts

$\Gamma(K_S^0 f_2(1270), f_2 \rightarrow 2\pi^0)/\Gamma(K_S^0 2\pi^0)$ Γ74/Γ68

This is the "fit fraction" from the Dalitz-plot analysis.

VALUE (units 10 ⁻²)	DOCUMENT ID	TECN	COMMENT
2.48 ± 0.91 ± 0.78	LOWREY 11	CLEO	Dalitz analysis, 1259 evts

$\Gamma(2K_0^{*0}, \text{one } K_0^{*0} \rightarrow 2\pi^0)/\Gamma(K_S^0 2\pi^0)$ Γ75/Γ68

This is the "fit fraction" from the Dalitz-plot analysis.

VALUE (units 10 ⁻²)	DOCUMENT ID	TECN	COMMENT
3.46 ± 0.92 ± 0.66	LOWREY 11	CLEO	Dalitz analysis, 1259 evts

$\Gamma(K_S^0 2\pi^0 \text{ nonresonant})/\Gamma(K_S^0 \pi^0)$ Γ76/Γ39

This is the "fit fraction" from the Dalitz-plot analysis.

VALUE	DOCUMENT ID	TECN	COMMENT
••• We do not use the following data for averages, fits, limits, etc. •••			
0.37 ± 0.08 ± 0.04	PROCARIO 93B	CLE2	Dalitz plot fit, 122 evts

$\Gamma(K_S^0 3\pi^0)/\Gamma_{\text{total}}$ Γ77/Γ

VALUE (units 10 ⁻³)	EVTS	DOCUMENT ID	TECN	COMMENT
7.64 ± 0.30 ± 0.29	870	ABLIKIM 22Y	BES3	e^+e^- at 3.773 GeV

$\Gamma(K^- 2\pi^+ \pi^-)/\Gamma_{\text{total}}$ Γ78/Γ

This is the "fit fraction" from the Dalitz-plot analysis.

VALUE (%)	EVTS	DOCUMENT ID	TECN	COMMENT
••• We do not use the following data for averages, fits, limits, etc. •••				
8.30 ± 0.07 ± 0.20		¹ DOBBS 07	CLEO	See BONVICINI 14
8.3 ± 0.2 ± 0.3	15k	¹ HE 05	CLEO	See DOBBS 07
7.9 ± 1.5 ± 0.9		² ALBRECHT 94	ARG	$e^+e^- \approx \Upsilon(4S)$
6.80 ± 0.27 ± 0.57	1.4k	³ ALBRECHT 94F	ARG	$e^+e^- \approx \Upsilon(4S)$
9.1 ± 0.8 ± 0.8	992	ADLER 88c	MRK3	e^+e^- 3.77 GeV
11.7 ± 2.5	185	⁴ SCHINDLER 81	MRK2	e^+e^- 3.771 GeV
6.2 ± 1.9	44	⁵ PERUZZI 77	LGW	e^+e^- 3.77 GeV

¹ DOBBS 07 and HE 05 use single- and double-tagged events in an overall fit. DOBBS 07 supersedes HE 05.
² ALBRECHT 94 uses D^0 mesons from $\bar{B}^0 \rightarrow D^{*+} \ell^- \bar{\nu}_\ell$ decays. This is a different set of events than used by ALBRECHT 94F.
³ See the footnote on the ALBRECHT 94F measurement of $\Gamma(K^-\pi^+)/\Gamma_{\text{total}}$ for the method used.
⁴ SCHINDLER 81 (MARK-2) measures $\sigma(e^+e^- \rightarrow \psi(3770)) \times$ branching fraction to be 0.68 ± 0.11 nb. We use the MARK-3 (ADLER 88c) value of $\sigma = 5.8 \pm 0.5 \pm 0.6$ nb.
⁵ PERUZZI 77 (MARK-1) measures $\sigma(e^+e^- \rightarrow \psi(3770)) \times$ branching fraction to be 0.36 ± 0.10 nb. We use the MARK-3 (ADLER 88c) value of $\sigma = 5.8 \pm 0.5 \pm 0.6$ nb.

$\Gamma(K^- 2\pi^+ \pi^-)/\Gamma(K^-\pi^+)$ Γ78/Γ38

VALUE	EVTS	DOCUMENT ID	TECN	COMMENT
2.083 ± 0.031 OUR FIT				
2.087 ± 0.032 OUR AVERAGE				
2.106 ± 0.013 ± 0.032		BONVICINI 14	CLEO	All CLEO-c runs
1.94 ± 0.07 ± 0.09 -0.11		JUN 00	SELX	Σ^- nucleus, 600 GeV
1.7 ± 0.2 ± 0.2	1745	ANJOS 92c	E691	γ Be 90–260 GeV
1.90 ± 0.25 ± 0.20	337	ALVAREZ 91B	NA14	Photoproduction
2.12 ± 0.16 ± 0.09		BORTOLETTO 88	CLEO	e^+e^- 10.55 GeV
2.17 ± 0.28 ± 0.23		ALBRECHT 85F	ARG	e^+e^- 10 GeV

Meson Particle Listings

 D^0

• • • We do not use the following data for averages, fits, limits, etc. • • •

2.0 ± 0.9	48	BAILEY	86	ACCM	π^- Be fixed target
2.0 ± 1.0	10	BAILEY	83B	SPEC	π^- Be → D^0
2.2 ± 0.8	214	PICCOLO	77	MRK1	e^+e^- 4.03, 4.41 GeV

$\Gamma(K^- \pi^+ \rho^0 \text{ total}) / \Gamma(K^- 2\pi^+ \pi^-)$		$\Gamma_{79} / \Gamma_{78}$			
VALUE (units 10^{-2})	EVTS	DOCUMENT ID	TECN	COMMENT	
83.5 ± 3.5 OUR AVERAGE					
80 ± 3 ± 5		ANJOS	92C	E691	1745 $K^- 2\pi^+ \pi^-$ evts
85.5 ± 3.2 ± 3.0		COFFMAN	92B	MRK3	1281 ± 45 $K^- 2\pi^+ \pi^-$ evts

$\Gamma(K^- \pi^+ \rho^0 \text{ 3-body}) / \Gamma(K^- 2\pi^+ \pi^-)$		$\Gamma_{80} / \Gamma_{78}$			
VALUE (units 10^{-2})	EVTS	DOCUMENT ID	TECN	COMMENT	
7.4 ± 2.0 OUR AVERAGE					
8.4 ± 1.1 ± 2.5	16k	ABLIKIM	17o	BES3	$D^0 \rightarrow K^- 2\pi^+ \pi^-$
5 ± 3 ± 2		ANJOS	92C	E691	1745 $K^- 2\pi^+ \pi^-$ evts
8.4 ± 2.2 ± 4.0		COFFMAN	92B	MRK3	1281 ± 45 $K^- 2\pi^+ \pi^-$ evts

$\Gamma(\bar{K}^*(892)^0 \rho^0, \bar{K}^{*0} \rightarrow K^- \pi^+) / \Gamma(K^- 2\pi^+ \pi^-)$		$\Gamma_{81} / \Gamma_{78}$			
VALUE (units 10^{-2})	EVTS	DOCUMENT ID	TECN	COMMENT	
12.3 ± 0.6 OUR AVERAGE					
12.3 ± 0.4 ± 0.5	16k	ABLIKIM	17o	BES3	$D^0 \rightarrow K^- 2\pi^+ \pi^-$
13 ± 2 ± 2		ANJOS	92C	E691	1745 $K^- 2\pi^+ \pi^-$ evts

$\Gamma(\bar{K}^*(892)^0 \rho^0 \text{ transverse}, \bar{K}^{*0} \rightarrow K^- \pi^+) / \Gamma(K^- 2\pi^+ \pi^-)$		$\Gamma_{82} / \Gamma_{78}$			
VALUE	EVTS	DOCUMENT ID	TECN	COMMENT	
0.142 ± 0.016 ± 0.05	1281	COFFMAN	92B	MRK3	$K^- 2\pi^+ \pi^-$ evts

$\Gamma(K^- a_1(1260)^+, a_1^+ \rightarrow \rho^0 \pi^+) / \Gamma(K^- 2\pi^+ \pi^-)$		$\Gamma_{83} / \Gamma_{78}$			
VALUE (units 10^{-2})	EVTS	DOCUMENT ID	TECN	COMMENT	
53 ± 4 OUR AVERAGE					
54.6 ± 2.8 ± 3.7	16k	ABLIKIM	17o	BES3	$D^0 \rightarrow K^- 2\pi^+ \pi^-$
47 ± 5 ± 10	1745	ANJOS	92C	E691	$K^- 2\pi^+ \pi^-$ evts
49.2 ± 2.4 ± 8.0	1281	COFFMAN	92B	MRK3	$K^- 2\pi^+ \pi^-$ evts

$\Gamma(K_1(1270)^- \pi^+, K_1^- \rightarrow K^- \pi^+ \pi^- \text{ total}) / \Gamma(K^- 2\pi^+ \pi^-)$		$\Gamma_{84} / \Gamma_{78}$			
VALUE (units 10^{-2})	EVTS	DOCUMENT ID	TECN	COMMENT	
4.8 ± 0.4 OUR AVERAGE					
4.6 ± 0.05 ± 0.39 ± 0.24	891k	¹ AAIJ	18A1	LHCB	$D^0 \rightarrow K^- 2\pi^+ \pi^-$
6.6 ± 1.9 ± 0.3	1281	COFFMAN	92B	MRK3	$K^- 2\pi^+ \pi^-$ evts

¹ The 3rd error is due to the uncertainty in the amplitude model composition.

$\Gamma(K_1(1270)^- \pi^+, K_1^- \rightarrow \bar{K}^*(892)^0 \pi^-, \bar{K}^{*0} \rightarrow K^- \pi^+) / \Gamma(K^- 2\pi^+ \pi^-)$		$\Gamma_{87} / \Gamma_{78}$			
VALUE (units 10^{-2})	EVTS	DOCUMENT ID	TECN	COMMENT	
0.8 ± 0.2 ± 0.2	16k	ABLIKIM	17o	BES3	$D^0 \rightarrow K^- 2\pi^+ \pi^-$

$\Gamma(K^- 2\pi^+ \pi^- \text{ nonresonant}) / \Gamma(K^- 2\pi^+ \pi^-)$		$\Gamma_{88} / \Gamma_{78}$			
VALUE (units 10^{-2})	EVTS	DOCUMENT ID	TECN	COMMENT	
22.0 ± 0.8 OUR AVERAGE					
22.04 ± 0.28 ± 2.09 ± 1.51	891k	¹ AAIJ	18A1	LHCB	$D^0 \rightarrow K^- 2\pi^+ \pi^-$
21.9 ± 0.6 ± 0.6	16k	² ABLIKIM	17o	BES3	$D^0 \rightarrow K^- 2\pi^+ \pi^-$
23 ± 2 ± 3	1.7k	ANJOS	92C	E691	$D^0 \rightarrow K^- 2\pi^+ \pi^-$
24.2 ± 2.5 ± 6.0	1.2k	COFFMAN	92B	MRK3	$D^0 \rightarrow K^- 2\pi^+ \pi^-$

¹ The 3rd error is due to the uncertainty in the amplitude model composition.² In addition to the 14 ABLIKIM 17o branching ratios we have listed, the paper gives 15 more ratios for mostly non-resonant modes. Four of the 15 have less than 2-standard-deviation significance. Here are some of the omitted modes, with S, P, V, A, and T for scalar, pseudo-scalar, vector, axial-vector, and tensor spin sub-structures: $\pi^+(K^- \rho^0)_P$, $\pi^+(K^- \rho^0)_V$, $\pi^+(\bar{K}^{*0} \pi^-)_P$, $\pi^+(\bar{K}^{*0} \pi^-)_V$, $\pi^+(\pi^-(K^- \pi^+)_{S\text{-wave}})_A$, $(K^- \pi^+)_V$, $(\pi^+ \pi^-)_S$, $(K^- \pi^+)_T$, $(\pi^+ \pi^-)_S$...

$\Gamma(K_S^0 \pi^+ \pi^- \pi^0) / \Gamma_{\text{total}}$		Γ_{89} / Γ			
VALUE (%)	EVTS	DOCUMENT ID	TECN	COMMENT	
5.2 ± 0.6 OUR FIT					
5.2 ± 1.1 ± 1.2	140	COFFMAN	92B	MRK3	e^+e^- 3.77 GeV

• • • We do not use the following data for averages, fits, limits, etc. • • •

6.7 ± 1.6	¹ BARLAG	92c	ACCM	π^- Cu 230 GeV
-1.7				

¹ BARLAG 92c computes the branching fraction using topological normalization.

$\Gamma(K_S^0 \pi^+ \pi^- \pi^0) / \Gamma(K_S^0 \pi^+ \pi^-)$		$\Gamma_{89} / \Gamma_{44}$			
VALUE	EVTS	DOCUMENT ID	TECN	COMMENT	
1.85 ± 0.20 OUR FIT					
1.86 ± 0.23 OUR AVERAGE					
1.80 ± 0.20 ± 0.21	190	¹ ALBRECHT	92P	ARG	$e^+e^- \approx 10$ GeV
2.8 ± 0.8 ± 0.8	46	ANJOS	92C	E691	γ Be 90-260 GeV
1.85 ± 0.26 ± 0.30	158	KINOSHITA	91	CLEO	$e^+e^- \sim 10.7$ GeV

¹ This value is calculated from numbers in Table 1 of ALBRECHT 92P.

$\Gamma(K^- \pi^+ 2\pi^0) / \Gamma_{\text{total}}$		Γ_{92} / Γ			
VALUE (%)	EVTS	DOCUMENT ID	TECN	COMMENT	
8.86 ± 0.13 ± 0.19	6.1k	ABLIKIM	19Ak	BES3	e^+e^- at 3773 MeV

• • • We do not use the following data for averages, fits, limits, etc. • • •

17.7 ± 2.9	¹ BARLAG	92c	ACCM	π^- Cu 230 GeV
14.9 ± 3.7 ± 3.0	² ADLER	88c	MRK3	e^+e^- 3.77 GeV
20.9 ^{+7.4} _{-4.3} ± 1.2	¹ AGUILAR...	87F	HYBR	$\pi p, pp$ 360, 400 GeV

¹ AGUILAR-BENITEZ 87F and BARLAG 92c compute the branching fraction using topological normalization. They do not distinguish the presence of a third π^0 , and thus are not included in the average.² ADLER 88c uses an absolute normalization method finding this decay channel opposite a detected $\bar{D}^0 \rightarrow K^+ \pi^-$ in pure $D\bar{D}$ events.

$\Gamma(K^- \pi^+ 3\pi^0) / \Gamma_{\text{total}}$		Γ_{93} / Γ			
VALUE (units 10^{-3})	EVTS	DOCUMENT ID	TECN	COMMENT	
9.54 ± 0.30 ± 0.31	1.6k	ABLIKIM	22Y	BES3	e^+e^- at 3.773 GeV

$\Gamma(K_S^0 \pi^+ \pi^- 2\pi^0) / \Gamma_{\text{total}}$		Γ_{94} / Γ			
VALUE (units 10^{-3})	EVTS	DOCUMENT ID	TECN	COMMENT	
12.66 ± 0.45 ± 0.43	1.2k	ABLIKIM	22Y	BES3	e^+e^- at 3.773 GeV

$\Gamma(K^- 2\pi^+ \pi^- \pi^0) / \Gamma(K^- \pi^+)$		$\Gamma_{95} / \Gamma_{38}$			
VALUE	EVTS	DOCUMENT ID	TECN	COMMENT	
1.09 ± 0.10 OUR FIT					
0.98 ± 0.11 ± 0.11	225	¹ ALBRECHT	92P	ARG	$e^+e^- \approx 10$ GeV

¹ This value is calculated from numbers in Table 1 of ALBRECHT 92P.

$\Gamma(K^- 2\pi^+ \pi^- \pi^0) / \Gamma(K^- 2\pi^+ \pi^-)$		$\Gamma_{95} / \Gamma_{78}$			
VALUE	EVTS	DOCUMENT ID	TECN	COMMENT	
0.52 ± 0.05 OUR FIT					
0.56 ± 0.07 OUR AVERAGE					
0.55 ± 0.07 ^{+0.12} _{-0.09}	167	KINOSHITA	91	CLEO	$e^+e^- \sim 10.7$ GeV
0.57 ± 0.06 ± 0.05	180	ANJOS	90D	E691	Photoproduction

$\Gamma(\bar{K}^*(892)^0 \pi^+ \pi^- \pi^0, \bar{K}^{*0} \rightarrow K^- \pi^+) / \Gamma_{\text{total}}$		Γ_{96} / Γ			
VALUE (units 10^{-2})	EVTS	DOCUMENT ID	TECN	COMMENT	
1.3 ± 0.6 OUR EVALUATION					
seen		ALBRECHT	92P	ARG	$e^+e^- \approx 10$ GeV

$\Gamma(\bar{K}^*(892)^0 \omega, \bar{K}^{*0} \rightarrow K^- \pi^+, \omega \rightarrow \pi^+ \pi^- \pi^0) / \Gamma_{\text{total}}$		Γ_{97} / Γ			
VALUE (units 10^{-3})	EVTS	DOCUMENT ID	TECN	COMMENT	
6.5 ± 3.0		¹ ALBRECHT	92P	ARG	$e^+e^- \approx 10$ GeV

¹ This value is calculated from numbers in Table 2 of ALBRECHT 92P.

$\Gamma(K^- \pi^+ \omega) / \Gamma_{\text{total}}$		Γ_{98} / Γ			
VALUE (units 10^{-2})	EVTS	DOCUMENT ID	TECN	COMMENT	
3.392 ± 0.044 ± 0.085	10.1k	¹ ABLIKIM	22U	BES3	e^+e^- at 3.773 GeV

¹ ABLIKIM 22U determines the ratios $B(D^0 \rightarrow K_S^0 \pi^0 \omega) / B(D^0 \rightarrow K^- \pi^+ \omega) = 0.23 \pm 0.01 \pm 0.01$ and $B(D^+ \rightarrow K_S^0 \pi^+ \omega) / B(D^0 \rightarrow K^- \pi^+ \omega) = 0.21 \pm 0.01 \pm 0.01$, in significant tension with statistical isospin model expectations of 0.4 and 0.9 respectively.

$\Gamma(K^- \pi^+ \omega) / \Gamma(K^- \pi^+)$		$\Gamma_{98} / \Gamma_{38}$			
VALUE	EVTS	DOCUMENT ID	TECN	COMMENT	
0.78 ± 0.12 ± 0.10	99	¹ ALBRECHT	92P	ARG	$e^+e^- \approx 10$ GeV

¹ This value is calculated from numbers in Table 1 of ALBRECHT 92P.

$\Gamma(\bar{K}^*(892)^0 \omega) / \Gamma(K^- \pi^+)$		$\Gamma_{99} / \Gamma_{38}$			
VALUE	EVTS	DOCUMENT ID	TECN	COMMENT	
0.28 ± 0.11 ± 0.04	17	¹ ALBRECHT	92P	ARG	$e^+e^- \approx 10$ GeV

¹ This value is calculated from numbers in Table 1 of ALBRECHT 92P.

$\Gamma(K_S^0 \pi^0 \omega) / \Gamma_{\text{total}}$		Γ_{100} / Γ			
VALUE (units 10^{-2})	EVTS	DOCUMENT ID	TECN	COMMENT	
0.848 ± 0.046 ± 0.031	697	¹ ABLIKIM	22U	BES3	e^+e^- at 3.773 GeV

¹ ABLIKIM 22U determines the ratio $B(D^0 \rightarrow K_S^0 \pi^0 \omega) / B(D^0 \rightarrow K^- \pi^+ \omega) = 0.23 \pm 0.01 \pm 0.01$, in significant tension with statistical isospin model expectation of 0.4.

$\Gamma(K_S^0 \eta \pi^0) / \Gamma_{\text{total}}$		Γ_{101} / Γ			
VALUE (units 10^{-3})	EVTS	DOCUMENT ID	TECN	COMMENT	
10.06 ± 0.34 ± 0.30	1.1k	ABLIKIM	20V	BES3	e^+e^- , 3773 MeV

$\Gamma(K_S^0 \eta \pi^0) / \Gamma(K_S^0 \pi^0)$		$\Gamma_{101} / \Gamma_{39}$			
VALUE	EVTS	DOCUMENT ID	TECN	COMMENT	
0.46 ± 0.07 ± 0.06	155 ± 22	¹ RUBIN	04	CLEO	$e^+e^- \approx 10$ GeV

¹ The η here is detected in its $\gamma\gamma$ mode, but other η modes are included in the value given.

See key on page 1171

Meson Particle Listings

 D^0 $\Gamma(K_S^0 a_0(980), a_0 \rightarrow \eta \pi^0) / \Gamma(K_S^0 \eta \pi^0)$ $\Gamma_{102} / \Gamma_{101}$

This is the "fit fraction" from the Dalitz-plot analysis, with interference.

VALUE	DOCUMENT ID	TECN	COMMENT
1.19 ± 0.09 ± 0.26	1 RUBIN	04	CLEO Dalitz fit, 155 evts

¹ In addition to $K_S^0 a_0(980)$ and $\bar{K}^*(892)^0 \eta$ modes, RUBIN 04 finds a fit fraction of $0.246 \pm 0.092 \pm 0.091$ for other, undetermined modes.

 $\Gamma(\bar{K}^*(892)^0 \eta, \bar{K}^{*0} \rightarrow K_S^0 \pi^0) / \Gamma(K_S^0 \eta \pi^0)$ $\Gamma_{103} / \Gamma_{101}$

This is the "fit fraction" from the Dalitz-plot analysis, with interference.

VALUE	DOCUMENT ID	TECN	COMMENT
0.293 ± 0.062 ± 0.035	1 RUBIN	04	CLEO Dalitz fit, 155 evts

¹ See the note on RUBIN 04 in the preceding data block.

 $\Gamma(K^- \pi^+ \eta) / \Gamma_{total}$ Γ_{104} / Γ

Unseen decay modes of the η are included.

VALUE (units 10^{-2})	EVTS	DOCUMENT ID	TECN	COMMENT
1.88 ± 0.05 OUR FIT				Error includes scale factor of 1.4.
1.853 ± 0.025 ± 0.031	6.1k	ABLIKIM	20v	BES3 $e^+ e^-$, 3773 MeV

 $\Gamma(K^- \pi^+ \eta) / \Gamma(K^- \pi^+)$ $\Gamma_{104} / \Gamma_{38}$

Unseen decay modes of the η are included.

VALUE (units 10^{-2})	EVTS	DOCUMENT ID	TECN	COMMENT
50.1 ± 2.0 ± 0.2	116k	1 CHEN	20A	BELL $e^+ e^-$ at $\gamma(4S)$

¹ CHEN 20A reports $0.500 \pm 0.002 \pm 0.020 \pm 0.003$ from a measurement of $[\Gamma(D^0 \rightarrow K^- \pi^+ \eta) / \Gamma(D^0 \rightarrow K^- \pi^+)] \times [B(\eta \rightarrow 2\gamma)]$ assuming $B(\eta \rightarrow 2\gamma) = (39.41 \pm 0.20) \times 10^{-2}$, which we rescale to our best value $B(\eta \rightarrow 2\gamma) = (39.36 \pm 0.18) \times 10^{-2}$. Our first error is their experiment's error and our second error is the systematic error from using our best value. The third reported uncertainty is the uncertainty from $B(\eta \rightarrow 2\gamma)$.

 $\Gamma(K^*(892)^0 \eta, K^{*0} \rightarrow K^- \pi^+) / \Gamma(K^- \pi^+ \eta)$ $\Gamma_{105} / \Gamma_{104}$

Unseen decay modes of the η are included.

VALUE (units 10^{-2})	DOCUMENT ID	TECN	COMMENT
47.61 ± 1.32 ± 0.24 + 3.64 - 0.49 - 2.71	1 CHEN	20A	BELL $e^+ e^-$ at $\gamma(4S)$

¹ The third uncertainty is due to the uncertainty from the Dalitz model.

 $\Gamma(a_0(980)^+ K^-, a_0^+ \rightarrow \eta \pi^+) / \Gamma(K^- \pi^+ \eta)$ $\Gamma_{106} / \Gamma_{104}$

Unseen decay modes of the η are included.

VALUE (units 10^{-2})	DOCUMENT ID	TECN	COMMENT
39.28 ± 1.50 ± 1.58 + 4.38 - 0.51 - 3.30	1 CHEN	20A	BELL $e^+ e^-$ at $\gamma(4S)$

¹ The third uncertainty is due to the uncertainty from the Dalitz model.

 $\Gamma(K_2^-(1980)^- \pi^+, K_2^{*-} \rightarrow K^- \eta) / \Gamma_{total}$ Γ_{107} / Γ

Unseen decay modes of the η are included.

VALUE (units 10^{-4})	DOCUMENT ID	TECN	COMMENT
2.2 + 1.7 - 1.9	CHEN	20A	BELL $e^+ e^-$ at $\gamma(4S)$

 $\Gamma(K^- \pi^+ \pi^0 \eta) / \Gamma_{total}$ Γ_{108} / Γ

Unseen decay modes of the η are included.

VALUE (units 10^{-3})	EVTS	DOCUMENT ID	TECN	COMMENT
4.49 ± 0.22 ± 0.15	580	ABLIKIM	20v	BES3 $e^+ e^-$, 3773 MeV

 $\Gamma(K_S^0 \pi^+ \pi^- \eta) / \Gamma_{total}$ Γ_{109} / Γ

Unseen decay modes of the η are included.

VALUE (units 10^{-3})	EVTS	DOCUMENT ID	TECN	COMMENT
2.80 ± 0.19 ± 0.10	250	ABLIKIM	20v	BES3 $e^+ e^-$, 3773 MeV

 $\Gamma(K_S^0 2\pi^0 \eta) / \Gamma_{total}$ Γ_{110} / Γ

Unseen decay modes of the η are included.

VALUE (units 10^{-3})	EVTS	DOCUMENT ID	TECN	COMMENT
1.76 ± 0.23 ± 0.13	65	ABLIKIM	20v	BES3 $e^+ e^-$, 3773 MeV

 $\Gamma(K_S^0 2\pi^+ 2\pi^-) / \Gamma(K_S^0 \pi^+ \pi^-)$ $\Gamma_{111} / \Gamma_{44}$

Unseen decay modes of the η are included.

VALUE	EVTS	DOCUMENT ID	TECN	COMMENT
0.095 ± 0.005 ± 0.007	1283 ± 57	LINK	04d	FOCS $\gamma A, \bar{E}_\gamma \approx 180$ GeV

• • • We do not use the following data for averages, fits, limits, etc. • • •

0.07 ± 0.02 ± 0.01	11	¹ ALBRECHT	92P	ARG $e^+ e^- \approx 10$ GeV
0.149 ± 0.026	56	AMMAR	91	CLEO $e^+ e^- \approx 10.5$ GeV
0.18 ± 0.07 ± 0.04	6	ANJOS	90D	E691 Photoproduction

¹ This value is calculated from numbers in Table 1 of ALBRECHT 92P.

 $\Gamma(K_S^0 \rho^0 \pi^+ \pi^-, \text{no } K^*(892)^-) / \Gamma(K_S^0 2\pi^+ 2\pi^-)$ $\Gamma_{112} / \Gamma_{111}$

Unseen decay modes of the η are included.

VALUE	DOCUMENT ID	TECN	COMMENT
0.40 ± 0.24 ± 0.07	LINK	04d	FOCS $\gamma A, \bar{E}_\gamma \approx 180$ GeV

 $\Gamma(K^*(892)^- 2\pi^+ \pi^-, K^*(892)^- \rightarrow K_S^0 \pi^-, \text{no } \rho^0) / \Gamma(K_S^0 2\pi^+ 2\pi^-)$ $\Gamma_{113} / \Gamma_{111}$

Unseen decay modes of the η are included.

VALUE	DOCUMENT ID	TECN	COMMENT
0.17 ± 0.28 ± 0.02	LINK	04d	FOCS $\gamma A, \bar{E}_\gamma \approx 180$ GeV

 $\Gamma(K^*(892)^- \rho^0 \pi^+, K^*(892)^- \rightarrow K_S^0 \pi^-) / \Gamma(K_S^0 2\pi^+ 2\pi^-)$ $\Gamma_{114} / \Gamma_{111}$

Unseen decay modes of the η are included.

VALUE	DOCUMENT ID	TECN	COMMENT
0.60 ± 0.21 ± 0.09	LINK	04d	FOCS $\gamma A, \bar{E}_\gamma \approx 180$ GeV

 $\Gamma(K_S^0 2\pi^+ 2\pi^- \text{ nonresonant}) / \Gamma(K_S^0 2\pi^+ 2\pi^-)$ $\Gamma_{115} / \Gamma_{111}$

Unseen decay modes of the η are included.

VALUE	CL%	DOCUMENT ID	TECN	COMMENT
<0.46	90	LINK	04d	FOCS $\gamma A, \bar{E}_\gamma \approx 180$ GeV

 $\Gamma(K^- 3\pi^+ 2\pi^-) / \Gamma(K^- 2\pi^+ \pi^-)$ $\Gamma_{117} / \Gamma_{78}$

Unseen decay modes of the η are included.

VALUE (units 10^{-3})	EVTS	DOCUMENT ID	TECN	COMMENT
2.70 ± 0.58 ± 0.38	48 ± 10	LINK	04B	FOCS $\gamma A, \bar{E}_\gamma \approx 180$ GeV

 $\Gamma(K_S^0 \eta) / \Gamma_{total}$ Γ_{118} / Γ

Unseen decay modes of the η are included.

VALUE (units 10^{-3})	EVTS	DOCUMENT ID	TECN	COMMENT
5.09 ± 0.13 OUR FIT				
5.13 ± 0.07 ± 0.12	9.5k	ABLIKIM	18w	BES3 $e^+ e^-$, 3773 MeV
• • •				We do not use the following data for averages, fits, limits, etc. • • •
4.42 ± 0.15 ± 0.28		ASNER	08	CLEO See MENDEZ 10

 $\Gamma(K_S^0 \eta) / [\Gamma(K^- \pi^+) + \Gamma(K^+ \pi^-)]$ $\Gamma_{118} / (\Gamma_{38} + \Gamma_{289})$

Unseen decay modes of the η are included.

VALUE (units 10^{-2})	EVTS	DOCUMENT ID	TECN	COMMENT
12.83 ± 0.33 OUR FIT				
12.3 ± 0.3 ± 0.17	2864 ± 65	MENDEZ	10	CLEO $e^+ e^-$ at 3774 MeV

 $\Gamma(K_S^0 \eta) / \Gamma(K_S^0 \pi^0)$ $\Gamma_{118} / \Gamma_{39}$

Unseen decay modes of the η are included.

VALUE	EVTS	DOCUMENT ID	TECN	COMMENT
0.32 ± 0.04 ± 0.03	225 ± 30	PROCARIO	93B	CLE2 $\eta \rightarrow \gamma \gamma$

 $\Gamma(K_S^0 \eta) / \Gamma(K_S^0 \pi^+ \pi^-)$ $\Gamma_{118} / \Gamma_{44}$

Unseen decay modes of the η are included.

VALUE	EVTS	DOCUMENT ID	TECN	COMMENT
0.14 ± 0.02 ± 0.02	80 ± 12	PROCARIO	93B	CLE2 $\eta \rightarrow \pi^+ \pi^- \pi^0$

 $\Gamma(K_S^0 \omega) / \Gamma_{total}$ Γ_{119} / Γ

Unseen decay modes of the ω are included.

VALUE (%)	DOCUMENT ID	TECN	COMMENT
1.11 ± 0.06 OUR FIT			
1.12 ± 0.04 ± 0.05	ASNER	08	CLEO $e^+ e^- \rightarrow D^0 \bar{D}^0$, 3.77 GeV

 $\Gamma(K_S^0 \omega) / \Gamma(K^- \pi^+)$ $\Gamma_{119} / \Gamma_{38}$

Unseen decay modes of the ω are included.

VALUE	DOCUMENT ID	TECN	COMMENT
0.50 ± 0.18 ± 0.10	ALBRECHT	89D	ARG $e^+ e^-$ 10 GeV

 $\Gamma(K_S^0 \omega) / \Gamma(K_S^0 \pi^+ \pi^-)$ $\Gamma_{119} / \Gamma_{44}$

Unseen decay modes of the ω are included.

VALUE	EVTS	DOCUMENT ID	TECN	COMMENT
0.396 ± 0.030 OUR FIT				
0.33 ± 0.09 OUR AVERAGE				Error includes scale factor of 1.1.
0.29 ± 0.08 ± 0.05	16	¹ ALBRECHT	92P	ARG $e^+ e^- \approx 10$ GeV
0.54 ± 0.14 ± 0.16	40	KINOSHITA	91	CLEO $e^+ e^- \sim 10.7$ GeV

¹ This value is calculated from numbers in Table 1 of ALBRECHT 92P.

 $\Gamma(K_S^0 \omega) / \Gamma(K_S^0 \pi^+ \pi^- \pi^0)$ $\Gamma_{119} / \Gamma_{89}$

Unseen decay modes of the ω are included.

VALUE	DOCUMENT ID	TECN	COMMENT
0.215 ± 0.026 OUR FIT			
0.220 ± 0.048 ± 0.0116	COFFMAN	92B	MRK3 1281 ± 45 $K^- 2\pi^+ \pi^-$ evts

 $\Gamma(K_S^0 \eta'(958)) / \Gamma_{total}$ Γ_{120} / Γ

Unseen decay modes of the $\eta'(958)$ are included.

VALUE (units 10^{-3})	EVTS	DOCUMENT ID	TECN	COMMENT
9.49 ± 0.32 OUR FIT				
9.49 ± 0.20 ± 0.36	3k	ABLIKIM	18w	BES3 $e^+ e^-$, 3773 MeV

 $\Gamma(K_S^0 \eta'(958)) / [\Gamma(K^- \pi^+) + \Gamma(K^+ \pi^-)]$ $\Gamma_{120} / (\Gamma_{38} + \Gamma_{289})$

Unseen decay modes of the $\eta'(958)$ are included.

VALUE (units 10^{-2})	EVTS	DOCUMENT ID	TECN	COMMENT
24.0 ± 0.8 OUR FIT				
24.3 ± 0.8 ± 1.1	1321 ± 42	MENDEZ	10	CLEO $e^+ e^-$ at 3774 MeV

 $\Gamma(K_S^0 \eta'(958)) / \Gamma(K_S^0 \pi^+ \pi^-)$ $\Gamma_{120} / \Gamma_{44}$

Unseen decay modes of the $\eta'(958)$ are included.

VALUE	EVTS	DOCUMENT ID	TECN	COMMENT
0.339 ± 0.022 OUR FIT				
0.32 ± 0.04 OUR AVERAGE				
0.31 ± 0.02 ± 0.04	594	PROCARIO	93B	CLE2 $\eta' \rightarrow \eta \pi^+ \pi^-, \rho^0 \gamma$
0.37 ± 0.13 ± 0.06	18	¹ ALBRECHT	92P	ARG $e^+ e^- \approx 10$ GeV

¹ This value is calculated from numbers in Table 1 of ALBRECHT 92P.

 $\Gamma(\bar{K}^*(892)^0 \pi^+ \pi^- \pi^0) / \Gamma(K^- 2\pi^+ \pi^- \pi^0)$ $\Gamma_{121} / \Gamma_{95}$

Unseen decay modes of the $\bar{K}^*(892)^0$ are included.

VALUE	DOCUMENT ID	TECN	COMMENT
0.45 ± 0.15 ± 0.15	ANJOS	90D	E691 Photoproduction

Meson Particle Listings

 D^0

$\Gamma(\bar{K}^*(892)^0 \eta) / \Gamma_{\text{total}}$ Γ_{122} / Γ
 VALUE (units 10^{-2}) DOCUMENT ID TECN COMMENT

1.41 ± 0.13 ± 0.01 ¹ CHEN 20A BELL $e^+ e^-$ at $\Upsilon(4S)$

¹ CHEN 20A reports $(1.41 \pm 0.04 \pm 0.12 \pm 0.01) \times 10^{-2}$ from a measurement of $[\Gamma(D^0 \rightarrow \bar{K}^*(892)^0 \eta) / \Gamma_{\text{total}}] \times [B(\eta \rightarrow 2\gamma)]$ assuming $B(\eta \rightarrow 2\gamma) = (39.41 \pm 0.20) \times 10^{-2}$, which we rescale to our best value $B(\eta \rightarrow 2\gamma) = (39.36 \pm 0.18) \times 10^{-2}$. Our first error is their experiment's error and our second error is the systematic error from using our best value. The third reported uncertainty is the uncertainty from $B(\eta \rightarrow 2\gamma)$.

$\Gamma(\bar{K}^*(892)^0 \eta) / \Gamma(K^- \pi^+)$ $\Gamma_{122} / \Gamma_{38}$

Unseen decay modes of the $\bar{K}^*(892)^0$ and η are included.

VALUE EVTS DOCUMENT ID TECN COMMENT

• • • We do not use the following data for averages, fits, limits, etc. • • •

0.58 ± 0.19 ± 0.24 46 KINOSHITA 91 CLEO $e^+ e^- \sim 10.7$ GeV

$\Gamma(\bar{K}^*(892)^0 \eta) / \Gamma(K^- \pi^+ \pi^0)$ $\Gamma_{122} / \Gamma_{59}$

Unseen decay modes of the $\bar{K}^*(892)^0$ and η are included.

VALUE EVTS DOCUMENT ID TECN COMMENT

• • • We do not use the following data for averages, fits, limits, etc. • • •

0.13 ± 0.02 ± 0.03 214 PROCARIO 93B CLE2 $\bar{K}^{*0} \eta \rightarrow K^- \pi^+ / \gamma \gamma$

$\Gamma(K^- \pi^+ \eta'(958)) / \Gamma_{\text{total}}$ Γ_{123} / Γ

VALUE (units 10^{-3}) EVTS DOCUMENT ID TECN COMMENT

6.43 ± 0.15 ± 0.31 2.5k ABLIKIM 18Ac BES3 $e^+ e^-$, 3773 MeV

$\Gamma(K^- \pi^+ \eta'(958)) / \Gamma(K^- 2\pi^+ \pi^-)$ $\Gamma_{123} / \Gamma_{78}$

Unseen decay modes of the $\eta'(958)$ are included.

VALUE EVTS DOCUMENT ID TECN COMMENT

0.093 ± 0.014 ± 0.019 286 PROCARIO 93B CLE2 $\eta' \rightarrow \eta \pi^+ \pi^-, \rho^0 \gamma$

$\Gamma(K_S^0 \eta'(958) \pi^0) / \Gamma_{\text{total}}$ Γ_{124} / Γ

VALUE (units 10^{-3}) EVTS DOCUMENT ID TECN COMMENT

2.52 ± 0.22 ± 0.15 289 ABLIKIM 18Ac BES3 $e^+ e^-$, 3773 MeV

$\Gamma(\bar{K}^*(892)^0 \eta'(958)) / \Gamma(K^- \pi^+ \eta'(958))$ $\Gamma_{125} / \Gamma_{123}$

Unseen decay modes of the $\bar{K}^*(892)^0$ are included.

VALUE CL% DOCUMENT ID TECN COMMENT

<0.15 90 PROCARIO 93B CLE2

Hadronic modes with three K 's

$\Gamma(K_S^0 K^+ K^-) / \Gamma(K_S^0 \pi^+ \pi^-)$ $\Gamma_{126} / \Gamma_{44}$

VALUE EVTS DOCUMENT ID TECN COMMENT

0.158 ± 0.001 ± 0.005 14k ± 116 AUBERT,B 05J BABR $e^+ e^- \approx \Upsilon(4S)$

• • • We do not use the following data for averages, fits, limits, etc. • • •

0.20 ± 0.05 ± 0.04 47 FRABETTI 92B E687 γ Be, $\bar{E}_\gamma \approx 221$ GeV

0.170 ± 0.022 136 AMMAR 91 CLEO $e^+ e^- \approx 10.5$ GeV

0.24 ± 0.08 BEBEK 86 CLEO $e^+ e^-$ near $\Upsilon(4S)$

0.185 ± 0.055 52 ALBRECHT 85B ARG $e^+ e^- 10$ GeV

$\Gamma(K_S^0 a_0(980)^0, a_0^0 \rightarrow K^+ K^-) / \Gamma(K_S^0 K^+ K^-)$ $\Gamma_{127} / \Gamma_{126}$

This is the "fit fraction" from the Dalitz-plot analysis, with interference.

VALUE DOCUMENT ID TECN COMMENT

0.664 ± 0.016 ± 0.070 AUBERT,B 05J BABR Dalitz fit, 12540 ± 112 evts

$\Gamma(K^- a_0(980)^+, a_0^+ \rightarrow K^+ K_S^0) / \Gamma(K_S^0 K^+ K^-)$ $\Gamma_{128} / \Gamma_{126}$

This is the "fit fraction" from the Dalitz-plot analysis, with interference.

VALUE DOCUMENT ID TECN COMMENT

0.134 ± 0.011 ± 0.037 AUBERT,B 05J BABR Dalitz fit, 12540 ± 112 evts

$\Gamma(K^+ a_0(980)^-, a_0^- \rightarrow K^- K_S^0) / \Gamma(K_S^0 K^+ K^-)$ $\Gamma_{129} / \Gamma_{126}$

This is a doubly Cabibbo-suppressed mode.

VALUE CL% DOCUMENT ID TECN COMMENT

<0.025 95 AUBERT,B 05J BABR Dalitz fit, 12540 ± 112 evts

$\Gamma(K_S^0 f_0(980), f_0 \rightarrow K^+ K^-) / \Gamma(K_S^0 K^+ K^-)$ $\Gamma_{130} / \Gamma_{126}$

VALUE CL% DOCUMENT ID TECN COMMENT

<0.021 95 AUBERT,B 05J BABR Dalitz fit, 12540 ± 112 evts

$\Gamma(K_S^0 \phi, \phi \rightarrow K^+ K^-) / \Gamma(K_S^0 K^+ K^-)$ $\Gamma_{131} / \Gamma_{126}$

This is the "fit fraction" from the Dalitz-plot analysis, with interference.

VALUE DOCUMENT ID TECN COMMENT

0.459 ± 0.007 ± 0.007 AUBERT,B 05J BABR Dalitz fit, 12540 ± 112 evts

$\Gamma(K_S^0 \phi) / \Gamma_{\text{total}}$ Γ_{132} / Γ

VALUE (units 10^{-3}) EVTS DOCUMENT ID TECN COMMENT

4.14 ± 0.21 ± 0.10 904 ¹ ABLIKIM 22w BES3 $e^+ e^-$ at 3.773 GeV

¹ ABLIKIM 22w reports $(0.414 \pm 0.021 \pm 0.010) \times 10^{-2}$ from a measurement of $[\Gamma(D^0 \rightarrow K_S^0 \phi) / \Gamma_{\text{total}}] \times [B(\phi(1020) \rightarrow K^+ K^-)]$ assuming $B(\phi(1020) \rightarrow K^+ K^-) = 0.491 \pm 0.005$.

$\Gamma(K_S^0 f_0(1370), f_0 \rightarrow K^+ K^-) / \Gamma(K_S^0 K^+ K^-)$ $\Gamma_{133} / \Gamma_{126}$

This is the "fit fraction" from the Dalitz-plot analysis, with interference.

VALUE DOCUMENT ID TECN COMMENT

0.038 ± 0.007 ± 0.023 ¹ AUBERT,B 05J BABR Dalitz fit, 12540 ± 112 evts

¹ AUBERT,B 05J calls the mode $K_S^0 f_0(1400)$, but insofar as it is seen here at all, it is certainly the same as $f_0(1370)$.

$\Gamma(3K_S^0) / \Gamma_{\text{total}}$ Γ_{134} / Γ

VALUE (units 10^{-4}) EVTS DOCUMENT ID TECN COMMENT

7.5 ± 0.7 OUR FIT Error includes scale factor of 1.4.

7.21 ± 0.33 ± 0.44 597 ABLIKIM 17A BES3 $e^+ e^- \rightarrow \psi(3770)$

$\Gamma(3K_S^0) / \Gamma(K_S^0 \pi^+ \pi^-)$ $\Gamma_{134} / \Gamma_{44}$

VALUE (units 10^{-2}) EVTS DOCUMENT ID TECN COMMENT

2.70 ± 0.26 OUR FIT Error includes scale factor of 1.2.

3.2 ± 0.4 OUR AVERAGE

3.58 ± 0.54 ± 0.52 170 ± 26 LINK 05A FOCS γ Be, $\bar{E}_\gamma \approx 180$ GeV

2.78 ± 0.38 ± 0.48 61 ASNER 96B CLE2 $e^+ e^- \approx \Upsilon(4S)$

7.0 ± 2.4 ± 1.2 10 ± 3 FRABETTI 94J E687 γ Be, $\bar{E}_\gamma \approx 220$ GeV

3.2 ± 1.0 22 AMMAR 91 CLEO $e^+ e^- \approx 10.5$ GeV

3.4 ± 1.4 ± 1.0 5 ALBRECHT 90c ARG $e^+ e^- \approx 10$ GeV

$\Gamma(K^+ 2K^- \pi^+) / \Gamma(K^- 2\pi^+ \pi^-)$ $\Gamma_{135} / \Gamma_{78}$

VALUE EVTS DOCUMENT ID TECN COMMENT

0.0027 ± 0.0004 OUR AVERAGE Error includes scale factor of 1.1.

0.00257 ± 0.00034 ± 0.00024 143 LINK 03G FOCS γ A, $\bar{E}_\gamma \approx 180$ GeV

0.0054 ± 0.0016 ± 0.0008 18 AITALA 01D E791 π^- A, 500 GeV

0.0028 ± 0.0007 ± 0.0001 20 FRABETTI 95c E687 γ Be, $\bar{E}_\gamma \approx 200$ GeV

$\Gamma(K^+ K^- \bar{K}^*(892)^0, \bar{K}^{*0} \rightarrow K^- \pi^+) / \Gamma(K^+ 2K^- \pi^+)$ $\Gamma_{136} / \Gamma_{135}$

VALUE DOCUMENT ID TECN COMMENT

0.20 ± 0.07 ± 0.02 LINK 03G FOCS γ A, $\bar{E}_\gamma \approx 180$ GeV

$\Gamma(K^- \pi^+ \phi, \phi \rightarrow K^+ K^-) / \Gamma(K^+ 2K^- \pi^+)$ $\Gamma_{137} / \Gamma_{135}$

VALUE DOCUMENT ID TECN COMMENT

0.18 ± 0.06 ± 0.04 LINK 03G FOCS γ A, $\bar{E}_\gamma \approx 180$ GeV

$\Gamma(\phi \bar{K}^*(892)^0, \phi \rightarrow K^+ K^-, \bar{K}^{*0} \rightarrow K^- \pi^+) / \Gamma(K^+ 2K^- \pi^+)$ $\Gamma_{138} / \Gamma_{135}$

VALUE DOCUMENT ID TECN COMMENT

0.48 ± 0.06 ± 0.01 LINK 03G FOCS γ A, $\bar{E}_\gamma \approx 180$ GeV

$\Gamma(K^+ 2K^- \pi^+ \text{nonresonant}) / \Gamma(K^+ 2K^- \pi^+)$ $\Gamma_{139} / \Gamma_{135}$

VALUE DOCUMENT ID TECN COMMENT

0.15 ± 0.06 ± 0.02 LINK 03G FOCS γ A, $\bar{E}_\gamma \approx 180$ GeV

$\Gamma(2K_S^0 K^\pm \pi^\mp) / \Gamma(K_S^0 \pi^+ \pi^-)$ $\Gamma_{140} / \Gamma_{44}$

VALUE (units 10^{-2}) EVTS DOCUMENT ID TECN COMMENT

2.12 ± 0.38 ± 0.20 57 ± 10 LINK 05A FOCS γ Be, $\bar{E}_\gamma \approx 180$ GeV

Pionic modes

$\Gamma(\pi^+ \pi^-) / \Gamma_{\text{total}}$ Γ_{141} / Γ

VALUE (units 10^{-3}) EVTS DOCUMENT ID TECN COMMENT

1.454 ± 0.024 OUR FIT Error includes scale factor of 1.4.

1.508 ± 0.018 ± 0.022 21k ABLIKIM 18w BES3 $e^+ e^-$, 3773 MeV

$\Gamma(\pi^+ \pi^-) / \Gamma(K^- \pi^+)$ $\Gamma_{141} / \Gamma_{38}$

VALUE (units 10^{-2}) EVTS DOCUMENT ID TECN COMMENT

3.68 ± 0.06 OUR FIT Error includes scale factor of 1.3.

3.59 ± 0.06 OUR AVERAGE

3.594 ± 0.054 ± 0.040 7334 ± 97 ACOSTA 05c CDF $p\bar{p}$, $\sqrt{s} = 1.96$ TeV

3.53 ± 0.12 ± 0.06 3453 LINK 03 FOCS γ A, $\bar{E}_\gamma \approx 180$ GeV

3.51 ± 0.16 ± 0.17 710 CSORNA 02 CLE2 $e^+ e^- \approx \Upsilon(4S)$

4.0 ± 0.2 ± 0.3 2043 AITALA 98c E791 π^- A, 500 GeV

• • • We do not use the following data for averages, fits, limits, etc. • • •

3.62 ± 0.10 ± 0.08 2085 ± 54 RUBIN 06 CLEO See MENDEZ 10

3.4 ± 0.7 ± 0.1 76 ± 15 ABLIKIM 05F BES $e^+ e^- \approx \psi(3770)$

4.3 ± 0.7 ± 0.3 177 FRABETTI 94c E687 γ Be $\bar{E}_\gamma \approx 220$ GeV

3.48 ± 0.30 ± 0.23 227 SELEN 93 CLE2 $e^+ e^- \approx \Upsilon(4S)$

5.5 ± 0.8 ± 0.5 120 ANJOS 91d E691 Photoproduction

5.0 ± 0.7 ± 0.5 110 ALEXANDER 90 CLEO $e^+ e^- 10.5\text{--}11$ GeV

$\Gamma(\pi^+ \pi^-) / [\Gamma(K^- \pi^+) + \Gamma(K^+ \pi^-)]$ $\Gamma_{141} / (\Gamma_{38} + \Gamma_{289})$

VALUE (units 10^{-2}) EVTS DOCUMENT ID TECN COMMENT

3.67 ± 0.06 OUR FIT Error includes scale factor of 1.3.

3.70 ± 0.06 ± 0.09 6210 ± 93 MENDEZ 10 CLEO $e^+ e^-$ at 3774 MeV

$\Gamma(2\pi^0) / \Gamma_{\text{total}}$ Γ_{142} / Γ

VALUE (units 10^{-4}) EVTS DOCUMENT ID TECN COMMENT

8.26 ± 0.25 OUR FIT

8.29 ± 0.30 OUR AVERAGE

8.24 ± 0.21 ± 0.30 6k ABLIKIM 15F BES3 $e^+ e^-$ at 3.773 GeV

8.4 ± 0.1 ± 0.5 26k LEES 12L BABR $e^+ e^- \approx 10.58$ GeV

$\Gamma(2\pi^0)/\Gamma(K^-\pi^+)$ Γ_{142}/Γ_{38}

VALUE (units 10^{-2})	EVTS	DOCUMENT ID	TECN	COMMENT
• • • We do not use the following data for averages, fits, limits, etc. • • •				
$2.05 \pm 0.13 \pm 0.16$	499 ± 32	RUBIN	06 CLEO	See MENDEZ 10
$2.2 \pm 0.4 \pm 0.4$	40	SELEN	93 CLE2	$e^+e^- \rightarrow \Upsilon(4S)$

$\Gamma(2\pi^0)/[\Gamma(K^-\pi^+) + \Gamma(K^+\pi^-)]$ $\Gamma_{142}/(\Gamma_{38} + \Gamma_{289})$

VALUE (units 10^{-2})	EVTS	DOCUMENT ID	TECN	COMMENT
2.08 ± 0.07 OUR FIT				
$2.06 \pm 0.07 \pm 0.10$	1567 ± 54	MENDEZ	10 CLEO	e^+e^- at 3774 MeV

$\Gamma(\pi^+\pi^-\pi^0)/\Gamma(K^-\pi^+)$ Γ_{143}/Γ_{38}

VALUE (units 10^{-2})	EVTS	DOCUMENT ID	TECN	COMMENT
37.7 ± 1.7 OUR FIT				Error includes scale factor of 2.4.
$34.4 \pm 0.5 \pm 1.2$	11k ± 164	RUBIN	06 CLEO	e^+e^- at $\psi(3770)$

$\Gamma(\pi^+\pi^-\pi^0)/\Gamma(K^-\pi^+\pi^0)$ Γ_{143}/Γ_{59}

VALUE (units 10^{-2})	EVTS	DOCUMENT ID	TECN	COMMENT
10.32 ± 0.25 OUR FIT				Error includes scale factor of 2.3.
10.41 ± 0.23 OUR AVERAGE				Error includes scale factor of 2.0.
$10.12 \pm 0.04 \pm 0.18$	123k ± 490	ARINSTEIN	08 BELL	$e^+e^- \approx \Upsilon(4S)$
$10.59 \pm 0.06 \pm 0.13$	60k ± 343	AUBERT,B	06x BABR	$e^+e^- \approx \Upsilon(4S)$

$\Gamma(\pi^+\pi^-\pi^0)/\Gamma_{total}$ Γ_{143}/Γ

VALUE (units 10^{-4})	EVTS	DOCUMENT ID	TECN	COMMENT
$134.3 \pm 1.3 \pm 1.6$	12.8k	ABLIKIM	22B G BES3	e^+e^- at 3.773 GeV

$\Gamma(\rho^+\pi^-)/\Gamma(\pi^+\pi^-\pi^0)$ $\Gamma_{144}/\Gamma_{143}$

This is the "fit fraction" from the Dalitz-plot analysis, with interference. See GASPERO 08 and BHATTACHARYA 10A for isospin decompositions of the $D^0 \rightarrow \pi^+\pi^-\pi^0$ Dalitz plot, both based on the amplitudes of AUBERT 07Bj. They quantify the conclusion that the final state is dominantly isospin 0.

VALUE (units 10^{-2})	DOCUMENT ID	TECN	COMMENT
68.1 ± 0.6 OUR AVERAGE			
$67.8 \pm 0.0 \pm 0.6$	AUBERT	07Bj BABR	Dalitz fit, 45k events
$76.3 \pm 1.9 \pm 2.5$	CRONIN-HEN..05	CLEO	$e^+e^- \approx 10$ GeV

$\Gamma(\rho^0\pi^0)/\Gamma(\pi^+\pi^-\pi^0)$ $\Gamma_{145}/\Gamma_{143}$

This is the "fit fraction" from the Dalitz-plot analysis, with interference.

VALUE (units 10^{-2})	DOCUMENT ID	TECN	COMMENT
25.9 ± 1.1 OUR AVERAGE			
$26.2 \pm 0.5 \pm 1.1$	AUBERT	07Bj BABR	Dalitz fit, 45k events
$24.4 \pm 2.0 \pm 2.1$	CRONIN-HEN..05	CLEO	$e^+e^- \approx 10$ GeV

$\Gamma(\rho^-\pi^+)/\Gamma(\pi^+\pi^-\pi^0)$ $\Gamma_{146}/\Gamma_{143}$

This is the "fit fraction" from the Dalitz-plot analysis, with interference.

VALUE (units 10^{-2})	DOCUMENT ID	TECN	COMMENT
34.6 ± 0.8 OUR AVERAGE			
$34.6 \pm 0.8 \pm 0.3$	AUBERT	07Bj BABR	Dalitz fit, 45k events
$34.5 \pm 2.4 \pm 1.3$	CRONIN-HEN..05	CLEO	$e^+e^- \approx 10$ GeV

$\Gamma(\rho(1450)^+\pi^-, \rho^+ \rightarrow \pi^+\pi^0)/\Gamma(\pi^+\pi^-\pi^0)$ $\Gamma_{147}/\Gamma_{143}$

This is the "fit fraction" from the Dalitz-plot analysis.

VALUE (units 10^{-2})	DOCUMENT ID	TECN	COMMENT
$0.11 \pm 0.07 \pm 0.12$	AUBERT	07Bj BABR	Dalitz fit, 45k events

$\Gamma(\rho(1450)^0\pi^0, \rho^0 \rightarrow \pi^+\pi^-)/\Gamma(\pi^+\pi^-\pi^0)$ $\Gamma_{148}/\Gamma_{143}$

This is the "fit fraction" from the Dalitz-plot analysis.

VALUE (units 10^{-2})	DOCUMENT ID	TECN	COMMENT
$0.30 \pm 0.11 \pm 0.07$	AUBERT	07Bj BABR	Dalitz fit, 45k events

$\Gamma(\rho(1450)^-\pi^+, \rho^- \rightarrow \pi^-\pi^0)/\Gamma(\pi^+\pi^-\pi^0)$ $\Gamma_{149}/\Gamma_{143}$

This is the "fit fraction" from the Dalitz-plot analysis.

VALUE (units 10^{-2})	DOCUMENT ID	TECN	COMMENT
$1.79 \pm 0.22 \pm 0.12$	AUBERT	07Bj BABR	Dalitz fit, 45k events

$\Gamma(\rho(1700)^+\pi^-, \rho^+ \rightarrow \pi^+\pi^0)/\Gamma(\pi^+\pi^-\pi^0)$ $\Gamma_{150}/\Gamma_{143}$

This is the "fit fraction" from the Dalitz-plot analysis.

VALUE (units 10^{-2})	DOCUMENT ID	TECN	COMMENT
$4.1 \pm 0.7 \pm 0.7$	AUBERT	07Bj BABR	Dalitz fit, 45k events

$\Gamma(\rho(1700)^0\pi^0, \rho^0 \rightarrow \pi^+\pi^-)/\Gamma(\pi^+\pi^-\pi^0)$ $\Gamma_{151}/\Gamma_{143}$

This is the "fit fraction" from the Dalitz-plot analysis.

VALUE (units 10^{-2})	DOCUMENT ID	TECN	COMMENT
$5.0 \pm 0.6 \pm 1.0$	AUBERT	07Bj BABR	Dalitz fit, 45k events

$\Gamma(\rho(1700)^-\pi^+, \rho^- \rightarrow \pi^-\pi^0)/\Gamma(\pi^+\pi^-\pi^0)$ $\Gamma_{152}/\Gamma_{143}$

This is the "fit fraction" from the Dalitz-plot analysis.

VALUE (units 10^{-2})	DOCUMENT ID	TECN	COMMENT
$3.2 \pm 0.4 \pm 0.6$	AUBERT	07Bj BABR	Dalitz fit, 45k events

$\Gamma(f_0(980)\pi^0, f_0 \rightarrow \pi^+\pi^-)/\Gamma(\pi^+\pi^-\pi^0)$ $\Gamma_{153}/\Gamma_{143}$

This is the "fit fraction" from the Dalitz-plot analysis.

VALUE (units 10^{-2})	DOCUMENT ID	TECN	COMMENT
$0.25 \pm 0.04 \pm 0.04$	AUBERT	07Bj BABR	Dalitz fit, 45k events

$\Gamma(f_0(500)\pi^0, f_0 \rightarrow \pi^+\pi^-)/\Gamma(\pi^+\pi^-\pi^0)$ $\Gamma_{154}/\Gamma_{143}$

The $f_0(500)$ is the σ . This is the "fit fraction" from the Dalitz-plot analysis.

VALUE (units 10^{-2})	DOCUMENT ID	TECN	COMMENT
$0.82 \pm 0.10 \pm 0.10$	AUBERT	07Bj BABR	Dalitz fit, 45k events

$\Gamma(f_0(1370)\pi^0, f_0 \rightarrow \pi^+\pi^-)/\Gamma(\pi^+\pi^-\pi^0)$ $\Gamma_{155}/\Gamma_{143}$

This is the "fit fraction" from the Dalitz-plot analysis.

VALUE (units 10^{-2})	DOCUMENT ID	TECN	COMMENT
$0.37 \pm 0.11 \pm 0.09$	AUBERT	07Bj BABR	Dalitz fit, 45k events

$\Gamma(f_0(1500)\pi^0, f_0 \rightarrow \pi^+\pi^-)/\Gamma(\pi^+\pi^-\pi^0)$ $\Gamma_{156}/\Gamma_{143}$

This is the "fit fraction" from the Dalitz-plot analysis.

VALUE (units 10^{-2})	DOCUMENT ID	TECN	COMMENT
$0.39 \pm 0.08 \pm 0.07$	AUBERT	07Bj BABR	Dalitz fit, 45k events

$\Gamma(f_0(1710)\pi^0, f_0 \rightarrow \pi^+\pi^-)/\Gamma(\pi^+\pi^-\pi^0)$ $\Gamma_{157}/\Gamma_{143}$

This is the "fit fraction" from the Dalitz-plot analysis.

VALUE (units 10^{-2})	DOCUMENT ID	TECN	COMMENT
$0.31 \pm 0.07 \pm 0.08$	AUBERT	07Bj BABR	Dalitz fit, 45k events

$\Gamma(f_2(1270)\pi^0, f_2 \rightarrow \pi^+\pi^-)/\Gamma(\pi^+\pi^-\pi^0)$ $\Gamma_{158}/\Gamma_{143}$

This is the "fit fraction" from the Dalitz-plot analysis.

VALUE (units 10^{-2})	DOCUMENT ID	TECN	COMMENT
$1.32 \pm 0.08 \pm 0.10$	AUBERT	07Bj BABR	Dalitz fit, 45k events

$\Gamma(\pi^+\pi^-\pi^0 \text{ nonresonant})/\Gamma(\pi^+\pi^-\pi^0)$ $\Gamma_{159}/\Gamma_{143}$

This is the "fit fraction" from the Dalitz-plot analysis.

VALUE (units 10^{-2})	DOCUMENT ID	TECN	COMMENT
$0.84 \pm 0.21 \pm 0.12$	AUBERT	07Bj BABR	Dalitz fit, 45k events

$\Gamma(3\pi^0)/\Gamma_{total}$ Γ_{160}/Γ

VALUE (units 10^{-4})	CL%	EVTS	DOCUMENT ID	TECN	COMMENT
$2.0 \pm 0.4 \pm 0.3$		60	1 ABLIKIM	18x BES3	e^+e^- , 3773 MeV

• • • We do not use the following data for averages, fits, limits, etc. • • •

<3.5	90		RUBIN	06 CLEO	e^+e^- at $\psi(3770)$
------	----	--	-------	---------	--------------------------

¹ Significance of signal reported by ABLIKIM 18x is 4.8σ .

$\Gamma(4\pi^0)/\Gamma_{total}$ Γ_{189}/Γ

VALUE (units 10^{-4})	EVTS	DOCUMENT ID	TECN	COMMENT
$7.6 \pm 0.9 \pm 0.7$	96	ABLIKIM	22B G BES3	e^+e^- at 3.773 GeV

$\Gamma(2\pi^+2\pi^-)/\Gamma(K^-\pi^+)$ Γ_{161}/Γ_{38}

VALUE (units 10^{-2})	EVTS	DOCUMENT ID	TECN	COMMENT
19.1 ± 0.5 OUR FIT				
$19.1 \pm 0.4 \pm 0.6$	7331 ± 130	RUBIN	06 CLEO	e^+e^- at $\psi(3770)$

$\Gamma(2\pi^+2\pi^-)/\Gamma(K^-2\pi^+\pi^-)$ Γ_{161}/Γ_{78}

VALUE (units 10^{-2})	EVTS	DOCUMENT ID	TECN	COMMENT
9.19 ± 0.22 OUR FIT				
9.20 ± 0.26 OUR AVERAGE				
$9.14 \pm 0.18 \pm 0.22$	6360 ± 115	LINK	07A FOCS	γ Be, $\overline{E}_\gamma \approx 180$ GeV
$7.9 \pm 1.8 \pm 0.5$	162	ABLIKIM	05F BES	$e^+e^- \approx \psi(3770)$
$9.5 \pm 0.7 \pm 0.2$	814	FRABETTI	95C E687	γ Be, $\overline{E}_\gamma \approx 200$ GeV
10.2 ± 1.3	345	AMMAR	91 CLEO	$e^+e^- \approx 10.5$ GeV

• • • We do not use the following data for averages, fits, limits, etc. • • •

$11.5 \pm 2.3 \pm 1.6$	64	ADAMOVICH	92 OMEG	π^- 340 GeV
$10.8 \pm 2.4 \pm 0.8$	79	FRABETTI	92 E687	γ Be
$9.6 \pm 1.8 \pm 0.7$	66	ANJOS	91 E691	γ Be 80–240 GeV

$\Gamma(a_1(1260)^+\pi^-, a_1^+ \rightarrow 2\pi^+\pi^- \text{ total})/\Gamma(2\pi^+2\pi^-)$ $\Gamma_{162}/\Gamma_{161}$

This is the fit fraction from the coherent amplitude analysis.

VALUE (units 10^{-2})	DOCUMENT ID	TECN	COMMENT
$60.0 \pm 3.0 \pm 2.4$	LINK	07A FOCS	4-body fit, $\approx 5.7k$ evts

$\Gamma(a_1(1260)^+\pi^-, a_1^+ \rightarrow \rho^0\pi^+ \text{ S-wave})/\Gamma(2\pi^+2\pi^-)$ $\Gamma_{163}/\Gamma_{161}$

This is the fit fraction from the coherent amplitude analysis.

VALUE (units 10^{-2})	DOCUMENT ID	TECN	COMMENT
41.5 ± 2.5 OUR AVERAGE			
$38.1 \pm 2.3 \pm 3.6$	¹ DARGENT	17	4-body fit, 7.3k 4 π evts
$43.3 \pm 2.5 \pm 1.9$	LINK	07A FOCS	4-body fit, $\approx 5.7k$ evts

¹ Obtained by analyzing CLEO-c data but not authored by the CLEO Collaboration.

$\Gamma(a_1(1260)^+\pi^-, a_1^+ \rightarrow \rho^0\pi^+ \text{ D-wave})/\Gamma(2\pi^+2\pi^-)$ $\Gamma_{164}/\Gamma_{161}$

This is the fit fraction from the coherent amplitude analysis.

VALUE (units 10^{-2})	DOCUMENT ID	TECN	COMMENT
$2.5 \pm 0.5 \pm 0.4$	¹ LINK	07A FOCS	4-body fit, $\approx 5.7k$ evts

¹ DARGENT 17 using 7.3k events find this contribution negligible.

$\Gamma(a_1(1260)^+\pi^-, a_1^+ \rightarrow \sigma\pi^+)/\Gamma(2\pi^+2\pi^-)$ $\Gamma_{165}/\Gamma_{161}$

This is the fit fraction from the coherent amplitude analysis.

VALUE (units 10^{-2})	DOCUMENT ID	TECN	COMMENT
8.4 ± 0.9 OUR AVERAGE			
$10.2 \pm 1.4 \pm 3.3$	¹ DARGENT	17	7.3k 4-body fit, 4 π evts
$8.3 \pm 0.7 \pm 0.6$	LINK	07A FOCS	4-body fit, $\approx 5.7k$ evts

¹ Obtained by analyzing CLEO-c data but not authored by the CLEO Collaboration.

Meson Particle Listings

 D^0 $\Gamma(a_1(1260)^-\pi^+, a_1^- \rightarrow \rho^0\pi^- S\text{-wave})/\Gamma(2\pi^+2\pi^-)$ $\Gamma_{166}/\Gamma_{161}$

This is the fit fraction from a coherent amplitude analysis.

VALUE (units 10^{-2})	EVTS	DOCUMENT ID	TECN	COMMENT
$3.1 \pm 0.6 \pm 1.0$	7.3k	¹ DARGENT 17	FOCS	4-body fit, 4 π evts

¹ Obtained by analyzing CLEO-c data but not authored by the CLEO Collaboration. $\Gamma(a_1(1260)^-\pi^+, a_1^- \rightarrow \sigma\pi^-)/\Gamma(2\pi^+2\pi^-)$ $\Gamma_{167}/\Gamma_{161}$

This is the fit fraction from a coherent amplitude analysis.

VALUE (units 10^{-2})	EVTS	DOCUMENT ID	TECN	COMMENT
$0.8 \pm 0.2 \pm 0.4$	7.3k	¹ DARGENT 17	FOCS	4-body fit, 4 π evts

¹ Obtained by analyzing CLEO-c data but not authored by the CLEO Collaboration. $\Gamma(\pi(1300)^+\pi^-, \pi(1300)^+ \rightarrow \sigma\pi^+)/\Gamma(2\pi^+2\pi^-)$ $\Gamma_{168}/\Gamma_{161}$

This is the fit fraction from a coherent amplitude analysis.

VALUE (units 10^{-2})	EVTS	DOCUMENT ID	TECN	COMMENT
$6.8 \pm 0.9 \pm 3.4$	7.3k	¹ DARGENT 17	FOCS	4-body fit, 4 π evts

¹ Obtained by analyzing CLEO-c data but not authored by the CLEO Collaboration. $\Gamma(\pi(1300)^-\pi^+, \pi(1300)^- \rightarrow \sigma\pi^-)/\Gamma(2\pi^+2\pi^-)$ $\Gamma_{169}/\Gamma_{161}$

This is the fit fraction from a coherent amplitude analysis.

VALUE (units 10^{-2})	EVTS	DOCUMENT ID	TECN	COMMENT
$3.0 \pm 0.6 \pm 2.8$	7.3k	¹ DARGENT 17	FOCS	4-body fit, 4 π evts

¹ Obtained by analyzing CLEO-c data but not authored by the CLEO Collaboration. $\Gamma(a_1(1640)^+\pi^-, a_1^+ \rightarrow \rho^0\pi^+ D\text{-wave})/\Gamma(2\pi^+2\pi^-)$ $\Gamma_{170}/\Gamma_{161}$

This is the fit fraction from a coherent amplitude analysis.

VALUE (units 10^{-2})	EVTS	DOCUMENT ID	TECN	COMMENT
$4.2 \pm 0.6 \pm 2.0$	7.3k	^{1,2} DARGENT 17	FOCS	4-body fit, 4 π evts

¹ Obtained by analyzing CLEO-c data but not authored by the CLEO Collaboration.² 4-body fit, 4 π evts $\Gamma(a_1(1640)^+\pi^-, a_1^+ \rightarrow \sigma\pi^+)/\Gamma(2\pi^+2\pi^-)$ $\Gamma_{171}/\Gamma_{161}$

This is the fit fraction from a coherent amplitude analysis.

VALUE (units 10^{-2})	EVTS	DOCUMENT ID	TECN	COMMENT
$2.4 \pm 0.7 \pm 1.7$	7.3k	¹ DARGENT 17	FOCS	4-body fit, 4 π evts

¹ Obtained by analyzing CLEO-c data but not authored by the CLEO Collaboration. $\Gamma(\pi_2(1670)^+\pi^-, \pi_2^+ \rightarrow f_2(1270)^0\pi^+, f_2^+ \rightarrow \pi^+\pi^-)/\Gamma(2\pi^+2\pi^-)$ $\Gamma_{172}/\Gamma_{161}$

This is the fit fraction from a coherent amplitude analysis.

VALUE (units 10^{-2})	EVTS	DOCUMENT ID	TECN	COMMENT
$2.7 \pm 0.6 \pm 1.1$	7.3k	¹ DARGENT 17	FOCS	4-body fit, 4 π evts

¹ Obtained by analyzing CLEO-c data but not authored by the CLEO Collaboration. $\Gamma(\pi_2(1670)^+\pi^-, \pi_2^+ \rightarrow \sigma\pi^+)/\Gamma(2\pi^+2\pi^-)$ $\Gamma_{173}/\Gamma_{161}$

This is the fit fraction from a coherent amplitude analysis.

VALUE (units 10^{-2})	EVTS	DOCUMENT ID	TECN	COMMENT
$3.5 \pm 0.6 \pm 1.2$	7.3k	¹ DARGENT 17	FOCS	4-body fit, 4 π evts

¹ Obtained by analyzing CLEO-c data but not authored by the CLEO Collaboration. $\Gamma(2\rho^0\text{total})/\Gamma(2\pi^+2\pi^-)$ $\Gamma_{174}/\Gamma_{161}$

This is the fit fraction from the coherent amplitude analysis.

VALUE (units 10^{-2})	DOCUMENT ID	TECN	COMMENT
$24.5 \pm 1.3 \pm 1.0$	LINK 07A	FOCS	4-body fit, $\approx 5.7k$ evts

 $\Gamma(2\rho^0, \text{parallel helicities})/\Gamma(2\pi^+2\pi^-)$ $\Gamma_{175}/\Gamma_{161}$

This is the fit fraction from the coherent amplitude analysis.

VALUE (units 10^{-2})	DOCUMENT ID	TECN	COMMENT
$1.1 \pm 0.3 \pm 0.3$	LINK 07A	FOCS	4-body fit, $\approx 5.7k$ evts

 $\Gamma(2\rho^0, \text{perpendicular helicities})/\Gamma(2\pi^+2\pi^-)$ $\Gamma_{176}/\Gamma_{161}$

This is the fit fraction from the coherent amplitude analysis.

VALUE (units 10^{-2})	DOCUMENT ID	TECN	COMMENT
$6.4 \pm 0.6 \pm 0.5$	LINK 07A	FOCS	4-body fit, $\approx 5.7k$ evts

 $\Gamma(2\rho^0, \text{longitudinal helicities})/\Gamma(2\pi^+2\pi^-)$ $\Gamma_{177}/\Gamma_{161}$

This is the fit fraction from the coherent amplitude analysis.

VALUE (units 10^{-2})	DOCUMENT ID	TECN	COMMENT
$16.8 \pm 1.0 \pm 0.8$	LINK 07A	FOCS	4-body fit, $\approx 5.7k$ evts

 $\Gamma(2\rho(770)^0, S\text{-wave})/\Gamma(2\pi^+2\pi^-)$ $\Gamma_{178}/\Gamma_{161}$

This is the fit fraction from a coherent amplitude analysis.

VALUE (units 10^{-2})	EVTS	DOCUMENT ID	TECN	COMMENT
$2.4 \pm 0.7 \pm 1.5$	7.3k	¹ DARGENT 17	FOCS	4-body fit, 4 π evts

¹ Obtained by analyzing CLEO-c data but not authored by the CLEO Collaboration. $\Gamma(2\rho(770)^0, P\text{-wave})/\Gamma(2\pi^+2\pi^-)$ $\Gamma_{179}/\Gamma_{161}$

This is the fit fraction from a coherent amplitude analysis.

VALUE (units 10^{-2})	EVTS	DOCUMENT ID	TECN	COMMENT
$7.0 \pm 0.5 \pm 1.6$	7.3k	¹ DARGENT 17	FOCS	4-body fit, 4 π evts

¹ Obtained by analyzing CLEO-c data but not authored by the CLEO Collaboration. $\Gamma(2\rho(770)^0, D\text{-wave})/\Gamma(2\pi^+2\pi^-)$ $\Gamma_{180}/\Gamma_{161}$

This is the fit fraction from a coherent amplitude analysis.

VALUE (units 10^{-2})	EVTS	DOCUMENT ID	TECN	COMMENT
$8.2 \pm 1.0 \pm 3.9$	7.3k	¹ DARGENT 17	FOCS	4-body fit, 4 π evts

¹ Obtained by analyzing CLEO-c data but not authored by the CLEO Collaboration. $\Gamma(\text{Resonant } (\pi^+\pi^-)\pi^+\pi^- \text{ 3-body total})/\Gamma(2\pi^+2\pi^-)$ $\Gamma_{181}/\Gamma_{161}$

This is the fit fraction from the coherent amplitude analysis.

VALUE (units 10^{-2})	DOCUMENT ID	TECN	COMMENT
$20.0 \pm 1.2 \pm 1.0$	LINK 07A	FOCS	4-body fit, $\approx 5.7k$ evts

 $\Gamma(\sigma\pi^+\pi^-)/\Gamma(2\pi^+2\pi^-)$ $\Gamma_{182}/\Gamma_{161}$

This is the fit fraction from the coherent amplitude analysis.

VALUE (units 10^{-2})	DOCUMENT ID	TECN	COMMENT
$8.2 \pm 0.9 \pm 0.7$	LINK 07A	FOCS	4-body fit, $\approx 5.7k$ evts

 $\Gamma(\sigma\rho(770)^0)/\Gamma(2\pi^+2\pi^-)$ $\Gamma_{183}/\Gamma_{161}$

This is the fit fraction from a coherent amplitude analysis.

VALUE (units 10^{-2})	EVTS	DOCUMENT ID	TECN	COMMENT
$6.6 \pm 1.0 \pm 3.2$	7.3k	¹ DARGENT 17	FOCS	4-body fit, 4 π evts

¹ Obtained by analyzing CLEO-c data but not authored by the CLEO Collaboration. $\Gamma(f_0(1370)\sigma, f_0 \rightarrow \pi^+\pi^-)/\Gamma(2\pi^+2\pi^-)$ $\Gamma_{187}/\Gamma_{161}$

This is the fit fraction from a coherent amplitude analysis.

VALUE (units 10^{-2})	EVTS	DOCUMENT ID	TECN	COMMENT
$21.2 \pm 1.8 \pm 6.7$	7.3k	¹ DARGENT 17	FOCS	4-body fit, 4 π evts

¹ Obtained by analyzing CLEO-c data but not authored by the CLEO Collaboration. $\Gamma(f_0(980)\pi^+\pi^-, f_0 \rightarrow \pi^+\pi^-)/\Gamma(2\pi^+2\pi^-)$ $\Gamma_{184}/\Gamma_{161}$

This is the fit fraction from the coherent amplitude analysis.

VALUE (units 10^{-2})	DOCUMENT ID	TECN	COMMENT
$2.4 \pm 0.5 \pm 0.4$	LINK 07A	FOCS	4-body fit, $\approx 5.7k$ evts

 $\Gamma(f_2(1270)\pi^+\pi^-, f_2 \rightarrow \pi^+\pi^-)/\Gamma(2\pi^+2\pi^-)$ $\Gamma_{185}/\Gamma_{161}$

This is the fit fraction from the coherent amplitude analysis.

VALUE (units 10^{-2})	DOCUMENT ID	TECN	COMMENT
$4.9 \pm 0.6 \pm 0.5$	LINK 07A	FOCS	4-body fit, $\approx 5.7k$ evts

 $\Gamma(2f_2(1270), f_2 \rightarrow \pi^+\pi^-)/\Gamma(2\pi^+2\pi^-)$ $\Gamma_{186}/\Gamma_{161}$

This is the fit fraction from a coherent amplitude analysis.

VALUE (units 10^{-2})	EVTS	DOCUMENT ID	TECN	COMMENT
$2.1 \pm 0.5 \pm 2.3$	7.3k	¹ DARGENT 17	FOCS	4-body fit, 4 π evts

¹ Obtained by analyzing CLEO-c data but not authored by the CLEO Collaboration. $\Gamma(\pi^+\pi^-2\pi^0)/\Gamma_{\text{total}}$ Γ_{188}/Γ

VALUE (units 10^{-3})	EVTS	DOCUMENT ID	TECN	COMMENT
$10.02 \pm 0.19 \pm 0.24$	3.8k	ABLIKIM 228g	BES3	e^+e^- at 3.773 GeV

 $\Gamma(\pi^+\pi^-2\pi^0)/\Gamma(K^-\pi^+)$ Γ_{188}/Γ_{38}

VALUE (units 10^{-2})	EVTS	DOCUMENT ID	TECN	COMMENT
$25.8 \pm 1.5 \pm 1.8$	2724 \pm 166	RUBIN 06	CLEO	e^+e^- at $\psi(3770)$

 $\Gamma(\eta\pi^0)/\Gamma_{\text{total}}$ Γ_{190}/Γ Unseen decay modes of the η are included.

VALUE (units 10^{-4})	EVTS	DOCUMENT ID	TECN	COMMENT
6.3 ± 0.6 OUR FIT	Error includes scale factor of 1.1.			

$5.8 \pm 0.5 \pm 0.5$	1.7k	ABLIKIM 18L	BES3	e^+e^- , 3773 MeV
• • •	We do not use the following data for averages, fits, limits, etc. • • •			
$6.5 \pm 0.9 \pm 0.4$	75	ABLIKIM 16D	BES3	See ABLIKIM 18L
$6.4 \pm 1.0 \pm 0.4$	156 \pm 24	ARTUSO 08	CLEO	See MENDEZ 10

 $\Gamma(\eta\pi^0)/\Gamma(K^-\pi^+)$ Γ_{190}/Γ_{38} Unseen decay modes of the η are included.

VALUE (units 10^{-2})	EVTS	DOCUMENT ID	TECN	COMMENT
• • •	We do not use the following data for averages, fits, limits, etc. • • •			
$1.47 \pm 0.34 \pm 0.11$	62 \pm 14	RUBIN 06	CLEO	See ARTUSO 08

 $\Gamma(\eta\pi^0)/[\Gamma(K^-\pi^+) + \Gamma(K^+\pi^-)]$ $\Gamma_{190}/(\Gamma_{38} + \Gamma_{289})$ Unseen decay modes of the η are included.

VALUE (units 10^{-2})	EVTS	DOCUMENT ID	TECN	COMMENT
1.60 ± 0.14 OUR FIT	Error includes scale factor of 1.1.			
$1.74 \pm 0.15 \pm 0.11$	481 \pm 40	MENDEZ 10	CLEO	e^+e^- at 3774 MeV

 $\Gamma(\omega\pi^0)/\Gamma_{\text{total}}$ Γ_{191}/Γ Unseen decay modes of the ω are included.

VALUE (units 10^{-4})	EVTS	DOCUMENT ID	TECN	COMMENT
$1.17 \pm 0.34 \pm 0.07$	45	ABLIKIM 16D	BES3	e^+e^- , 3773 MeV

 $\Gamma(2\pi^+2\pi^-\pi^0)/\Gamma_{\text{total}}$ Γ_{193}/Γ

VALUE (units 10^{-4})	EVTS	DOCUMENT ID	TECN	COMMENT
$34.6 \pm 1.5 \pm 1.5$	940	ABLIKIM 228g	BES3	e^+e^- at 3.773 GeV

$\Gamma(2\pi^+2\pi^-\pi^0)/\Gamma(K^-\pi^+)$ Γ_{193}/Γ_{38}

VALUE (units 10 ⁻²)	EVTS	DOCUMENT ID	TECN	COMMENT
10.7±1.2±0.5	1614 ± 171	RUBIN	06 CLEO	e ⁺ e ⁻ at $\psi(3770)$

$\Gamma(\pi^+\pi^-\pi^0)/\Gamma_{total}$ Γ_{194}/Γ

VALUE (units 10 ⁻⁴)	EVTS	DOCUMENT ID	TECN	COMMENT
15.3±1.7±1.3	180	ABLIKIM	22B BES3	e ⁺ e ⁻ at 3.773 GeV

$\Gamma(2\pi^+2\pi^-\pi^0)/\Gamma_{total}$ Γ_{195}/Γ

VALUE (units 10 ⁻⁴)	EVTS	DOCUMENT ID	TECN	COMMENT
47.7±3.1±2.1	350	ABLIKIM	22B BES3	e ⁺ e ⁻ at 3.773 GeV

$\Gamma(\eta\pi^+\pi^-)/\Gamma_{total}$ Γ_{196}/Γ

Unseen decay modes of the η are included.

VALUE (units 10 ⁻⁴)	EVTS	DOCUMENT ID	TECN	COMMENT
11.6±0.7 OUR AVERAGE				
10.6±1.8±0.7	96	ABLIKIM	20AA BES3	e ⁺ e ⁻ , 3773 MeV
12.0±0.7±0.4	450	ABLIKIM	20G BES3	e ⁺ e ⁻ , 3773 MeV
10.9±1.3±0.9	257	ARTUSO	08 CLEO	e ⁺ e ⁻ at $\psi(3770)$

$\Gamma(\eta\pi^+\pi^-)/\Gamma(K^-\pi^+\eta)$ $\Gamma_{196}/\Gamma_{104}$

VALUE (units 10 ⁻²)	EVTS	DOCUMENT ID	TECN	COMMENT
6.49±0.09±0.12	13k	LI	21G BELL	e ⁺ e ⁻ at $\Upsilon(nS)$

$\Gamma(\eta2\pi^0)/\Gamma_{total}$ Γ_{199}/Γ

VALUE (units 10 ⁻⁴)	CL%	EVTS	DOCUMENT ID	TECN	COMMENT
3.8±1.1±0.7		42	¹ ABLIKIM	18x BES3	e ⁺ e ⁻ , 3773 MeV
••• We do not use the following data for averages, fits, limits, etc. •••					
<23.8		90	ABLIKIM	20AA BES3	e ⁺ e ⁻ , 3773 MeV
¹ Significance of signal reported by ABLIKIM 18x is 3.8 σ .					

$\Gamma(\pi^+\pi^-\pi^0\eta)/\Gamma_{total}$ Γ_{200}/Γ

VALUE (units 10 ⁻³)	EVTS	DOCUMENT ID	TECN	COMMENT
3.23±0.17±0.14	510	ABLIKIM	20v BES3	e ⁺ e ⁻ , 3773 MeV

$\Gamma(\eta3\pi^0)/\Gamma_{total}$ Γ_{201}/Γ

VALUE (units 10 ⁻⁴)	EVTS	DOCUMENT ID	TECN	COMMENT
23.6±2.2±1.7	155	ABLIKIM	22B BES3	e ⁺ e ⁻ at 3.773 GeV

$\Gamma(\eta2\pi^+2\pi^-)/\Gamma_{total}$ Γ_{202}/Γ

VALUE (units 10 ⁻⁴)	EVTS	DOCUMENT ID	TECN	COMMENT
6.0±1.0±0.6	49	ABLIKIM	22B BES3	e ⁺ e ⁻ at 3.773 GeV

$\Gamma(\omega\eta)/\Gamma_{total}$ Γ_{192}/Γ

VALUE (units 10 ⁻³)	EVTS	DOCUMENT ID	TECN	COMMENT
1.98±0.18 OUR AVERAGE				Error includes scale factor of 1.1.
2.15±0.17±0.15	2.2k	ABLIKIM	18L BES3	e ⁺ e ⁻ , 3773 MeV
1.78±0.19±0.15	600	¹ SMITH	18	e ⁺ e ⁻ , 3773 MeV
¹ Obtained by analyzing CLEO-c data but not authored by the CLEO Collaboration.				

$\Gamma(\omega\pi^+\pi^-)/\Gamma_{total}$ Γ_{197}/Γ

VALUE (units 10 ⁻³)	EVTS	DOCUMENT ID	TECN	COMMENT
1.33±0.16±0.12	411	ABLIKIM	20AA BES3	e ⁺ e ⁻ , 3773 MeV

$\Gamma(\omega\pi^+\pi^-)/\Gamma(K^-\pi^+)$ Γ_{197}/Γ_{38}

Unseen decay modes of the ω are included.

VALUE (units 10 ⁻²)	EVTS	DOCUMENT ID	TECN	COMMENT
4.1±1.2±0.4	472 ± 132	RUBIN	06 CLEO	e ⁺ e ⁻ at $\psi(3770)$

$\Gamma(\omega\pi^0\pi^0)/\Gamma_{total}$ Γ_{198}/Γ

VALUE	CL%	DOCUMENT ID	TECN	COMMENT
<1.10 × 10 ⁻³		90	ABLIKIM	20AA BES3 e ⁺ e ⁻ , 3773 MeV

$\Gamma(3\pi^+3\pi^-)/\Gamma(K^-2\pi^+\pi^-)$ Γ_{203}/Γ_{78}

VALUE (units 10 ⁻³)	EVTS	DOCUMENT ID	TECN	COMMENT
5.23±0.59±1.35	149 ± 17	LINK	04B FOCS	$\gamma_A, \bar{E}_\gamma \approx 180$ GeV

$\Gamma(3\pi^+3\pi^-)/\Gamma(K^-3\pi^+2\pi^-)$ $\Gamma_{203}/\Gamma_{117}$

VALUE	DOCUMENT ID	TECN	COMMENT
••• We do not use the following data for averages, fits, limits, etc. •••			
1.93±0.47±0.48	¹ LINK	04B FOCS	$\gamma_A, \bar{E}_\gamma \approx 180$ GeV
¹ This LINK 04B result is not independent of other results in these Listings.			

$\Gamma(\eta'(958)\pi^0)/\Gamma_{total}$ Γ_{204}/Γ

Unseen decay modes of the $\eta'(958)$ are included.

VALUE (units 10 ⁻⁴)	EVTS	DOCUMENT ID	TECN	COMMENT
9.2±1.0 OUR FIT				
9.3±1.1±0.9	469 ± 56	ABLIKIM	18L BES3	e ⁺ e ⁻ , 3773 MeV
••• We do not use the following data for averages, fits, limits, etc. •••				
8.1±1.5±0.6	50 ± 9	ARTUSO	08 CLEO	See MENDEZ 10

$\Gamma(\eta'(958)\pi^0)/[\Gamma(K^-\pi^+) + \Gamma(K^+\pi^-)]$ $\Gamma_{204}/(\Gamma_{38}+\Gamma_{289})$

Unseen decay modes of the $\eta'(958)$ are included.

VALUE (units 10 ⁻²)	EVTS	DOCUMENT ID	TECN	COMMENT
2.32±0.25 OUR FIT				
2.3 ± 0.3 ± 0.2	159 ± 19	MENDEZ	10 CLEO	e ⁺ e ⁻ at 3774 MeV

$\Gamma(\eta'(958)\pi^+\pi^-)/\Gamma_{total}$ Γ_{205}/Γ

Unseen decay modes of the $\eta'(958)$ are included.

VALUE (units 10 ⁻⁴)	EVTS	DOCUMENT ID	TECN	COMMENT
4.5±1.6±0.5	21 ± 8	ARTUSO	08 CLEO	e ⁺ e ⁻ at $\psi(3770)$

$\Gamma(2\eta)/\Gamma_{total}$ Γ_{206}/Γ

Unseen decay modes of the η are included.

VALUE (units 10 ⁻⁴)	EVTS	DOCUMENT ID	TECN	COMMENT
21.1±1.9 OUR FIT				Error includes scale factor of 2.2.
22.0±0.7±0.6	3.4k	ABLIKIM	18L BES3	e ⁺ e ⁻ , 3773 MeV
••• We do not use the following data for averages, fits, limits, etc. •••				
16.7±1.4±1.3	255 ± 22	ARTUSO	08 CLEO	See MENDEZ 10

$\Gamma(2\eta)/[\Gamma(K^-\pi^+) + \Gamma(K^+\pi^-)]$ $\Gamma_{206}/(\Gamma_{38}+\Gamma_{289})$

Unseen decay modes of the η are included.

VALUE (units 10 ⁻²)	EVTS	DOCUMENT ID	TECN	COMMENT
5.3±0.5 OUR FIT				Error includes scale factor of 2.2.
4.3±0.3±0.4	430 ± 29	MENDEZ	10 CLEO	e ⁺ e ⁻ at 3774 MeV

$\Gamma(2\eta\pi^0)/\Gamma_{total}$ Γ_{207}/Γ

VALUE (units 10 ⁻⁴)	EVTS	DOCUMENT ID	TECN	COMMENT
7.3±1.6±1.5	27	¹ ABLIKIM	18x BES3	e ⁺ e ⁻ , 3773 MeV
¹ Significance of signal reported by ABLIKIM 18x is 5.5 σ .				

$\Gamma(2\eta\pi^+\pi^-)/\Gamma_{total}$ Γ_{208}/Γ

VALUE (units 10 ⁻⁴)	EVTS	DOCUMENT ID	TECN	COMMENT
8.5±1.3±0.4	43	ABLIKIM	22B BES3	e ⁺ e ⁻ at 3.773 GeV

$\Gamma(3\eta)/\Gamma_{total}$ Γ_{209}/Γ

VALUE	CL%	DOCUMENT ID	TECN	COMMENT
<1.3 × 10 ⁻⁴		90	ABLIKIM	18x BES3 e ⁺ e ⁻ , 3773 MeV

$\Gamma(\eta\eta'(958))/\Gamma_{total}$ Γ_{210}/Γ

Unseen decay modes of the η and $\eta'(958)$ are included.

VALUE (units 10 ⁻⁴)	EVTS	DOCUMENT ID	TECN	COMMENT
10.1±1.9 OUR FIT				
9.4±2.5±1.1	158 ± 41	ABLIKIM	18L BES3	e ⁺ e ⁻ , 3773 MeV
••• We do not use the following data for averages, fits, limits, etc. •••				
12.6±2.5±1.1	46 ± 9	ARTUSO	08 CLEO	See MENDEZ 10

$\Gamma(\eta\eta'(958))/[\Gamma(K^-\pi^+) + \Gamma(K^+\pi^-)]$ $\Gamma_{210}/(\Gamma_{38}+\Gamma_{289})$

Unseen decay modes of the η and $\eta'(958)$ are included.

VALUE (units 10 ⁻²)	EVTS	DOCUMENT ID	TECN	COMMENT
2.5±0.5 OUR FIT				
2.7±0.6±0.3	66 ± 15	MENDEZ	10 CLEO	e ⁺ e ⁻ at 3774 MeV

Hadronic modes with a $K\bar{K}$ pair

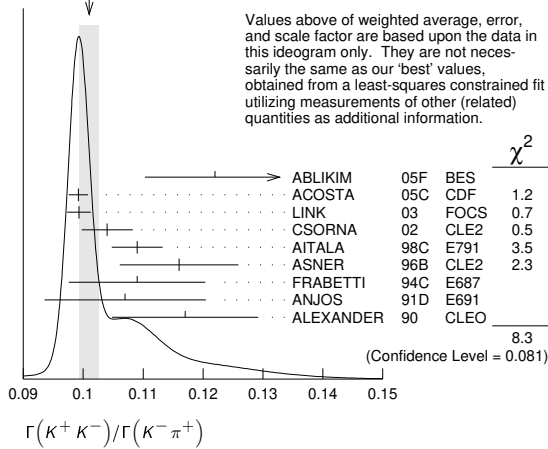
$\Gamma(K^+K^-)/\Gamma_{total}$ Γ_{211}/Γ

VALUE (units 10 ⁻³)	EVTS	DOCUMENT ID	TECN	COMMENT
4.08 ± 0.06 OUR FIT				Error includes scale factor of 1.6.
4.233±0.021±0.064	56k	ABLIKIM	18W BES3	e ⁺ e ⁻ , 3773 MeV
••• We do not use the following data for averages, fits, limits, etc. •••				
4.08 ± 0.08 ± 0.09	4.7k	BONVICINI	08 CLEO	See MENDEZ 10

$\Gamma(K^+K^-)/\Gamma(K^-\pi^+)$ Γ_{211}/Γ_{38}

VALUE	EVTS	DOCUMENT ID	TECN	COMMENT
0.1033±0.0013 OUR FIT				Error includes scale factor of 1.6.
0.1010±0.0016 OUR AVERAGE				Error includes scale factor of 1.4. See the ideogram below.
0.122 ± 0.011 ± 0.004	242 ± 20	ABLIKIM	05F BES	e ⁺ e ⁻ $\approx \psi(3770)$
0.0992±0.0011±0.0012	16k±200	ACOSTA	03C CDF	$p\bar{p}, \sqrt{s}=1.96$ TeV
0.0993±0.0014±0.0014	11k	LINK	05C FOCS	γ nucleus, $\bar{E}_\gamma \approx 180$ GeV
0.1040 ± 0.0033 ± 0.0027	1900	CSORNA	02 CLE2	e ⁺ e ⁻ $\approx \Upsilon(4S)$
0.109 ± 0.003 ± 0.003	3317	AITALA	98C E791	π^- nucleus, 500 GeV
0.116 ± 0.007 ± 0.007	1102	ASNER	96B CLE2	e ⁺ e ⁻ $\approx \Upsilon(4S)$
0.109 ± 0.007 ± 0.009	581	FRABETTI	93C E687	γ Be $\bar{E}_\gamma = 220$ GeV
0.107 ± 0.010 ± 0.009	193	ANJOS	91D E691	Photoproduction
0.117 ± 0.010 ± 0.007	249	ALEXANDER	90 CLEO	e ⁺ e ⁻ 10.5–11 GeV
••• We do not use the following data for averages, fits, limits, etc. •••				
0.107 ± 0.029 ± 0.015	103	ADAMOVICH	92 OMEG	π^- 340 GeV
0.138 ± 0.027 ± 0.010	155	FRABETTI	92 E687	γ Be
0.16 ± 0.05	34	ALVAREZ	91B NA14	Photoproduction
0.10 ± 0.02 ± 0.01	131	ALBRECHT	90C ARG	e ⁺ e ⁻ ≈ 10 GeV
0.122 ± 0.018 ± 0.012	118	BALTRUSAITIS	85E MRK3	e ⁺ e ⁻ 3.77 GeV
0.113 ± 0.030		ABRAMS	79D MRK2	e ⁺ e ⁻ 3.77 GeV

Meson Particle Listings

 D^0 WEIGHTED AVERAGE
0.1010±0.0016 (Error scaled by 1.4) $\Gamma(K^+K^-)/[\Gamma(K^-\pi^+) + \Gamma(K^+\pi^-)]$ $\Gamma_{211}/(\Gamma_{38} + \Gamma_{289})$

VALUE (units 10^{-2})	EVTS	DOCUMENT ID	TECN	COMMENT
10.29±0.13 OUR FIT				Error includes scale factor of 1.6.
10.41±0.11±0.12	13.8k	MENDEZ	10	CLEO e^+e^- at 3774 MeV

 $\Gamma(K^+K^-)/\Gamma(\pi^+\pi^-)$ $\Gamma_{211}/\Gamma_{141}$

The unused results here are redundant with $\Gamma(K^+K^-)/\Gamma(K^-\pi^+)$ and $\Gamma(\pi^+\pi^-)/\Gamma(K^-\pi^+)$ measurements by the same experiments.

VALUE	EVTS	DOCUMENT ID	TECN	COMMENT
• • • We do not use the following data for averages, fits, limits, etc. • • •				
2.760±0.040±0.034	7334	ACOSTA	05c	CDF $p\bar{p}$, $\sqrt{s}=1.96$ TeV
2.81±0.10±0.06		LINK	03	FOCS γ nucleus, $\bar{E}_\gamma \approx 180$ GeV
2.96±0.16±0.15	710	CSORNA	02	CLE2 $e^+e^- \approx \Upsilon(4S)$
2.75±0.15±0.16		AITALA	98c	E791 π^- nucleus, 500 GeV
2.53±0.46±0.19		FRABETTI	94c	E687 γ Be $\bar{E}_\gamma = 220$ GeV
2.23±0.81±0.46		ADAMOVIICH	92	OMEG π^- 340 GeV
1.95±0.34±0.22		ANJOS	91D	E691 Photoproduction
2.5±0.7		ALBRECHT	90c	ARG $e^+e^- \approx 10$ GeV
2.35±0.37±0.28		ALEXANDER	90	CLEO e^+e^- 10.5–11 GeV

 $\Gamma(2K_S^0)/\Gamma_{total}$ Γ_{212}/Γ

VALUE (units 10^{-4})	EVTS	DOCUMENT ID	TECN	COMMENT
1.41±0.05 OUR FIT				Error includes scale factor of 1.1.
1.67±0.11±0.11	576	ABLIKIM	17A	BES3 $e^+e^- \rightarrow \psi(3770)$
• • • We do not use the following data for averages, fits, limits, etc. • • •				
1.46±0.32±0.09	68±15	BONVICINI	08	CLEO See MENDEZ 10

 $\Gamma(2K_S^0)/[\Gamma(K^-\pi^+) + \Gamma(K^+\pi^-)]$ $\Gamma_{212}/(\Gamma_{38} + \Gamma_{289})$

VALUE (units 10^{-2})	EVTS	DOCUMENT ID	TECN	COMMENT
0.357±0.013 OUR FIT				Error includes scale factor of 1.1.
0.41±0.04±0.02	215±23	MENDEZ	10	CLEO e^+e^- at 3774 MeV

 $\Gamma(2K_S^0)/\Gamma(K_S^0\pi^+\pi^-)$ Γ_{212}/Γ_{44}

This is the same as $\Gamma(K^0\bar{K}^0)/\Gamma(\bar{K}^0\pi^+\pi^-)$ because $D^0 \rightarrow K_S^0 K_L^0$ is forbidden by CP conservation.

VALUE (units 10^{-2})	EVTS	DOCUMENT ID	TECN	COMMENT
0.506±0.033 OUR FIT				
1.20±0.22 OUR AVERAGE				
1.44±0.32±0.16	79±17	LINK	05A	FOCS γ Be, $\bar{E}_\gamma \approx 180$ GeV
1.01±0.22±0.16	26	ASNER	96B	CLE2 $e^+e^- \approx \Upsilon(4S)$
3.9±1.3±1.3	20±7	FRABETTI	94J	E687 γ Be $\bar{E}_\gamma = 220$ GeV
• • • We do not use the following data for averages, fits, limits, etc. • • •				
2.1 $^{+1.1}_{-0.8}$ ±0.2	5	ALEXANDER	90	CLEO e^+e^- 10.5–11 GeV

 $\Gamma(2K_S^0)/\Gamma(K_S^0\pi^0)$ Γ_{212}/Γ_{39}

VALUE (units 10^{-2})	EVTS	DOCUMENT ID	TECN	COMMENT
1.14±0.04 OUR FIT				Error includes scale factor of 1.1.
1.101±0.023±0.030	4.8k	DASH	17	BELL At/near $\Upsilon(4S)$, $\Upsilon(5S)$

 $\Gamma(K_S^0K^-\pi^+)/\Gamma(K^-\pi^+)$ Γ_{213}/Γ_{38}

VALUE	DOCUMENT ID	TECN	COMMENT
0.084±0.013 OUR FIT			Error includes scale factor of 1.1.
0.08±0.03	¹ ANJOS	91	E691 γ Be 80–240 GeV

¹The factor 100 at the top of column 2 of Table I of ANJOS 91 should be omitted.

 $\Gamma(\phi\pi^0)/\Gamma_{total}$ Γ_{280}/Γ

VALUE (units 10^{-3})	EVTS	DOCUMENT ID	TECN	COMMENT
1.168±0.028±0.028	3.3k	ABLIKIM	19B1	BES3 e^+e^- at 3773 MeV

 $\Gamma(\phi\eta)/\Gamma_{total}$ Γ_{281}/Γ

VALUE (units 10^{-4})	EVTS	DOCUMENT ID	TECN	COMMENT
1.81±0.46±0.06	102	ABLIKIM	19B1	BES3 e^+e^- at 3773 MeV

 $\Gamma(K_S^0K^-\pi^+)/\Gamma(K_S^0\pi^+\pi^-)$ Γ_{213}/Γ_{44}

VALUE	EVTS	DOCUMENT ID	TECN	COMMENT
0.118±0.017 OUR FIT				Error includes scale factor of 1.1.
0.119±0.021 OUR AVERAGE				Error includes scale factor of 1.3.
0.108±0.019	61	AMMAR	91	CLEO $e^+e^- \approx 10.5$ GeV
0.16±0.03±0.02	39	ALBRECHT	90c	ARG $e^+e^- \approx 10$ GeV

 $\Gamma(\bar{K}^*(892)^0 K_S^0, \bar{K}^{*0} \rightarrow K^-\pi^+)/\Gamma(K_S^0K^-\pi^+)$ $\Gamma_{214}/\Gamma_{213}$

Fit fraction from Dalitz plot analyses. The fraction for the $K_S^0\pi^+$ mass between 792 and 992 MeV is $0.370 \pm 0.003 \pm 0.012$.

VALUE (units 10^{-2})	EVTS	DOCUMENT ID	TECN	COMMENT
2.47±0.15±0.23	113k	¹ AAIJ	16N	LHCB Dalitz plot fit

¹AAIJ 16N gives results for two S-wave parameterisations. We take the values from the model with LASS parametrization, and the difference as a systematic uncertainty.

 $\Gamma(K^*(892)^+K^-, K^{*+} \rightarrow K_S^0\pi^+)/\Gamma(K_S^0K^-\pi^+)$ $\Gamma_{215}/\Gamma_{213}$

Fit fraction from Dalitz plot analyses.

VALUE (units 10^{-2})	EVTS	DOCUMENT ID	TECN	COMMENT
56.9±0.6±1.1	113k	¹ AAIJ	16N	LHCB Dalitz plot fit

¹AAIJ 16N gives results for two S-wave parameterisations. We take the values from the model with LASS parametrization, and the difference as a systematic uncertainty.

 $\Gamma(\bar{K}^*(1410)^0 K_S^0, \bar{K}^{*0} \rightarrow K^-\pi^+)/\Gamma(K_S^0K^-\pi^+)$ $\Gamma_{216}/\Gamma_{213}$

Fit fraction from Dalitz plot analyses.

VALUE (units 10^{-2})	EVTS	DOCUMENT ID	TECN	COMMENT
3.8±0.5±5.6	113k	¹ AAIJ	16N	LHCB Dalitz plot fit

¹AAIJ 16N gives results for two S-wave parameterisations. We take the values from the model with LASS parametrization, and the difference as a uncertainty (which in this case dominates)

 $\Gamma(K^*(1410)^+K^-, K^{*+} \rightarrow K_S^0\pi^+)/\Gamma(K_S^0K^-\pi^+)$ $\Gamma_{217}/\Gamma_{213}$

Fit fraction from Dalitz plot analyses.

VALUE (units 10^{-2})	EVTS	DOCUMENT ID	TECN	COMMENT
9.6±1.1±5.4	113k	¹ AAIJ	16N	LHCB Dalitz plot fit

¹AAIJ 16N gives results for two S-wave parameterisations. We take the values from the model with LASS parametrization, and the difference as a systematic uncertainty (which in this case dominates).

 $\Gamma((K^-\pi^+)_{S\text{-wave}}K_S^0)/\Gamma(K_S^0K^-\pi^+)$ $\Gamma_{218}/\Gamma_{213}$

Fit fraction from Dalitz plot analyses.

VALUE (units 10^{-2})	EVTS	DOCUMENT ID	TECN	COMMENT
18±2±8	113k	¹ AAIJ	16N	LHCB Dalitz plot fit

¹AAIJ 16N gives results for two S-wave parameterisations. We take the values from the model with LASS parametrization, and the difference as a systematic uncertainty (which in this case dominates).

 $\Gamma((K_S^0\pi^+)_{S\text{-wave}}K^-)/\Gamma(K_S^0K^-\pi^+)$ $\Gamma_{219}/\Gamma_{213}$

Fit fraction from Dalitz plot analyses.

VALUE (units 10^{-2})	EVTS	DOCUMENT ID	TECN	COMMENT
11.7±1.0±2.3	113k	¹ AAIJ	16N	LHCB Dalitz plot fit

¹AAIJ 16N gives results for two S-wave parameterisations. We take the values from the model with LASS parametrization, and the difference as a systematic uncertainty.

 $\Gamma(a_0(980)^-\pi^+, a_0^- \rightarrow K_S^0K^-)/\Gamma(K_S^0K^-\pi^+)$ $\Gamma_{220}/\Gamma_{213}$

Fit fraction from Dalitz plot analyses.

VALUE (units 10^{-2})	EVTS	DOCUMENT ID	TECN	COMMENT
4.0±0.7±4.1	113k	¹ AAIJ	16N	LHCB Dalitz plot fit

¹AAIJ 16N gives results for two S-wave parameterisations. We take the values from the model with LASS parametrization, and the difference as a systematic uncertainty (which in this case dominates).

 $\Gamma(a_0(1450)^-\pi^+, a_0^- \rightarrow K_S^0K^-)/\Gamma(K_S^0K^-\pi^+)$ $\Gamma_{221}/\Gamma_{213}$

Fit fraction from Dalitz plot analyses.

VALUE (units 10^{-2})	EVTS	DOCUMENT ID	TECN	COMMENT
0.74±0.15±0.57	113k	¹ AAIJ	16N	LHCB Dalitz plot fit

¹AAIJ 16N gives results for two S-wave parameterisations. We take the values from the model with LASS parametrization, and the difference as a systematic uncertainty (which in this case dominates).

 $\Gamma(a_2(1320)^-\pi^+, a_2^- \rightarrow K_S^0K^-)/\Gamma(K_S^0K^-\pi^+)$ $\Gamma_{222}/\Gamma_{213}$

Fit fraction from Dalitz plot analyses.

VALUE (units 10^{-2})	EVTS	DOCUMENT ID	TECN	COMMENT
0.15±0.06±0.14	113k	¹ AAIJ	16N	LHCB Dalitz plot fit

¹AAIJ 16N gives results for two S-wave parameterisations. We take the values from the model with LASS parametrization, and the difference as a systematic uncertainty.

 $\Gamma(\rho(1450)^-\pi^+, \rho^- \rightarrow K_S^0K^-)/\Gamma(K_S^0K^-\pi^+)$ $\Gamma_{223}/\Gamma_{213}$

Fit fraction from Dalitz plot analyses.

VALUE (units 10^{-2})	EVTS	DOCUMENT ID	TECN	COMMENT
1.4±0.2±0.7	113k	¹ AAIJ	16N	LHCB Dalitz plot fit

¹AAIJ 16N gives results for two S-wave parameterisations. We take the values from the model with LASS parametrization, and the difference as a systematic uncertainty.

$\Gamma(K_S^0 K^+ \pi^-) / \Gamma(K^- \pi^+) \quad \Gamma_{224} / \Gamma_{38}$

VALUE	DOCUMENT ID	TECN	COMMENT
0.05 ± 0.025	¹ ANJOS	91	E691 γ Be 80–240 GeV

¹ The factor 100 at the top of column 2 of Table I of ANJOS 91 should be omitted.

 $\Gamma(K_S^0 K^+ \pi^-) / \Gamma(K_S^0 \pi^+ \pi^-) \quad \Gamma_{224} / \Gamma_{44}$

VALUE	EVTS	DOCUMENT ID	TECN	COMMENT
0.098 ± 0.020	55	AMMAR	91	CLEO $e^+ e^- \approx 10.5$ GeV

 $\Gamma(K_S^0 K^+ \pi^-) / \Gamma(K_S^0 K^- \pi^+) \quad \Gamma_{224} / \Gamma_{213}$

VALUE	EVTS	DOCUMENT ID	TECN	COMMENT
0.654 ± 0.007 OUR FIT				
0.654 ± 0.007 OUR AVERAGE				
0.655 ± 0.004 ± 0.006	76k, 113k	AAIJ	16N	LHCB pp at 7, 8 TeV
0.592 ± 0.044 ± 0.018		INSLER	12	CLEO $e^+ e^- \rightarrow D^0 \bar{D}^0$ at 3.77 GeV

 $\Gamma(K^*(892)^0 K_S^0, K^{*0} \rightarrow K^+ \pi^-) / \Gamma(\bar{K}^{*0}(892)^0 K_S^0, \bar{K}^{*0} \rightarrow K^- \pi^+) \quad \Gamma_{225} / \Gamma_{214}$

VALUE	CL%	DOCUMENT ID	TECN	COMMENT
0.356 ± 0.034 ± 0.007		¹ INSLER	12	CLEO $e^+ e^- \rightarrow D^0 \bar{D}^0$, 3.77 GeV

• • • We do not use the following data for averages, fits, limits, etc. • • •

< 0.010 90 AMMAR 91 CLEO $e^+ e^- \approx 10.5$ GeV

¹ Uses quantum correlations in $e^+ e^- \rightarrow D^0 \bar{D}^0$ at the $\psi(3770)$, where the signal side D decays to $K_S^0 K \pi$ and the tag-side D decays to $K \pi$, $K \pi \pi \pi$, $K \pi \pi^0$, and 10 additional CP -even, CP -odd, and mixed CP modes involving K_S^0 or K_L^0 .

 $\Gamma(K^*(892)^0 K_S^0, K^{*0} \rightarrow K^+ \pi^-) / \Gamma(K_S^0 K^+ \pi^-) \quad \Gamma_{225} / \Gamma_{224}$

VALUE (units 10^{-2})	EVTS	DOCUMENT ID	TECN	COMMENT
5.17 ± 0.21 ± 0.47	76k	¹ AAIJ	16N	LHCB Dalitz plot fit

¹ AAIJ 16N gives results for two S-wave parameterisations. We take the values from the model with LASS parametrization, and the difference as a systematic uncertainty.

 $\Gamma(K^*(892)^- K^+, K^{*-} \rightarrow K_S^0 \pi^-) / \Gamma(K_S^0 K^+ \pi^-) \quad \Gamma_{226} / \Gamma_{224}$

VALUE (units 10^{-2})	EVTS	DOCUMENT ID	TECN	COMMENT
28.8 ± 0.4 ± 1.5	76k	¹ AAIJ	16N	LHCB Dalitz plot fit

¹ AAIJ 16N gives results for two S-wave parameterisations. We take the values from the model with LASS parametrization, and the difference as a systematic uncertainty.

 $\Gamma(K^*(1410)^0 K_S^0, K^{*0} \rightarrow K^+ \pi^-) / \Gamma(K_S^0 K^+ \pi^-) \quad \Gamma_{227} / \Gamma_{224}$

VALUE (units 10^{-2})	EVTS	DOCUMENT ID	TECN	COMMENT
2.2 ± 0.6 ± 3.7	76k	¹ AAIJ	16N	LHCB Dalitz plot fit

¹ AAIJ 16N gives results for two S-wave parameterisations. We take the values from the model with LASS parametrization, and the difference as a systematic uncertainty (which in this case dominates).

 $\Gamma(K^*(1410)^- K^+, K^{*-} \rightarrow K_S^0 \pi^-) / \Gamma(K_S^0 K^+ \pi^-) \quad \Gamma_{228} / \Gamma_{224}$

VALUE (units 10^{-2})	EVTS	DOCUMENT ID	TECN	COMMENT
11.9 ± 1.5 ± 9.1	76k	¹ AAIJ	16N	LHCB Dalitz plot fit

¹ AAIJ 16N gives results for two S-wave parameterisations. We take the values from the model with LASS parametrization, and the difference as a systematic uncertainty (which in this case dominates).

 $\Gamma((K^+ \pi^-)_{S\text{-wave}} K_S^0) / \Gamma(K_S^0 K^+ \pi^-) \quad \Gamma_{229} / \Gamma_{224}$

VALUE (units 10^{-2})	EVTS	DOCUMENT ID	TECN	COMMENT
17 ± 2 ± 8	76k	¹ AAIJ	16N	LHCB Dalitz plot fit

¹ AAIJ 16N gives results for two S-wave parameterisations. We take the values from the model with LASS parametrization, and the difference as a systematic uncertainty.

 $\Gamma((K_S^0 \pi^-)_{S\text{-wave}} K^+) / \Gamma(K_S^0 K^+ \pi^-) \quad \Gamma_{230} / \Gamma_{224}$

VALUE (units 10^{-2})	EVTS	DOCUMENT ID	TECN	COMMENT
6.3 ± 0.9 ± 2.3	76k	¹ AAIJ	16N	LHCB Dalitz plot fit

¹ AAIJ 16N gives results for two S-wave parameterisations. We take the values from the model with LASS parametrization, and the difference as a systematic uncertainty.

 $\Gamma(a_0(980)^+ \pi^-, a_0^+ \rightarrow K_S^0 K^+) / \Gamma(K_S^0 K^+ \pi^-) \quad \Gamma_{231} / \Gamma_{224}$

VALUE (units 10^{-2})	EVTS	DOCUMENT ID	TECN	COMMENT
26 ± 2 ± 18	76k	¹ AAIJ	16N	LHCB Dalitz plot fit

¹ AAIJ 16N gives results for two S-wave parameterisations. We take the values from the model with LASS parametrization, and the difference as a systematic uncertainty (which in this case dominates).

 $\Gamma(a_0(1450)^+ \pi^-, a_0^+ \rightarrow K_S^0 K^+) / \Gamma(K_S^0 K^+ \pi^-) \quad \Gamma_{232} / \Gamma_{224}$

VALUE (units 10^{-2})	EVTS	DOCUMENT ID	TECN	COMMENT
1.5 ± 0.3 ± 1.1	76k	¹ AAIJ	16N	LHCB Dalitz plot fit

¹ AAIJ 16N gives results for two S-wave parameterisations. We take the values from the model with LASS parametrization, and the difference as a systematic uncertainty (which in this case dominates).

 $\Gamma(\rho(1700)^+ \pi^-, \rho^+ \rightarrow K_S^0 K^+) / \Gamma(K_S^0 K^+ \pi^-) \quad \Gamma_{233} / \Gamma_{224}$

VALUE (units 10^{-2})	EVTS	DOCUMENT ID	TECN	COMMENT
0.53 ± 0.11 ± 0.23	76k	¹ AAIJ	16N	LHCB Dalitz plot fit

¹ AAIJ 16N gives results for two S-wave parameterisations. We take the values from the model with LASS parametrization, and the difference as a systematic uncertainty.

 $\Gamma(K^+ K^- \pi^0) / \Gamma(K^- \pi^+ \pi^0) \quad \Gamma_{234} / \Gamma_{59}$

VALUE (units 10^{-2})	EVTS	DOCUMENT ID	TECN	COMMENT
2.37 ± 0.03 ± 0.04	11k ± 122	AUBERT, B	06x	BABR $e^+ e^- \approx \Upsilon(4S)$

• • • We do not use the following data for averages, fits, limits, etc. • • •

0.95 ± 0.26 151 ASNER 96B

 $\Gamma(K^*(892)^+ K^-, K^*(892)^+ \rightarrow K^+ \pi^0) / \Gamma(K^+ K^- \pi^0) \quad \Gamma_{235} / \Gamma_{234}$

VALUE (units 10^{-2})	DOCUMENT ID	TECN	COMMENT
44.4 ± 0.8 ± 0.6	AUBERT	07T	BABR Dalitz fit II, 11k evts

• • • We do not use the following data for averages, fits, limits, etc. • • •

46.1 ± 3.1 ¹ CAWLFIELD 06A CLEO Dalitz fit, 627 ± 30 evts

¹ The error on this CAWLFIELD 06A result is statistical only.

 $\Gamma(K^*(892)^- K^+, K^*(892)^- \rightarrow K^- \pi^0) / \Gamma(K^+ K^- \pi^0) \quad \Gamma_{236} / \Gamma_{234}$

VALUE (units 10^{-2})	DOCUMENT ID	TECN	COMMENT
15.9 ± 0.7 ± 0.6	AUBERT	07T	BABR Dalitz fit II, 11k evts

• • • We do not use the following data for averages, fits, limits, etc. • • •

12.3 ± 2.2 ¹ CAWLFIELD 06A CLEO Dalitz fit, 627 ± 30 evts

¹ The error on this CAWLFIELD 06A result is statistical only.

 $\Gamma((K^+ \pi^0)_{S\text{-wave}} K^-) / \Gamma(K^+ K^- \pi^0) \quad \Gamma_{237} / \Gamma_{234}$

VALUE (units 10^{-2})	DOCUMENT ID	TECN	COMMENT
71.1 ± 3.7 ± 1.9	¹ AUBERT	07T	BABR Dalitz fit II, 11k evts

¹ The only major difference between fits I and II in the AUBERT 07T analysis is in this mode, where the fit-I fraction is (16.3 ± 3.4 ± 2.1)%.

 $\Gamma((K^- \pi^0)_{S\text{-wave}} K^+) / \Gamma(K^+ K^- \pi^0) \quad \Gamma_{238} / \Gamma_{234}$

VALUE (units 10^{-2})	DOCUMENT ID	TECN	COMMENT
3.9 ± 0.9 ± 1.0	AUBERT	07T	BABR Dalitz fit II, 11k evts

 $\Gamma(f_0(980) \pi^0, f_0 \rightarrow K^+ K^-) / \Gamma(K^+ K^- \pi^0) \quad \Gamma_{239} / \Gamma_{234}$

VALUE (units 10^{-2})	DOCUMENT ID	TECN	COMMENT
10.5 ± 1.1 ± 1.2	¹ AUBERT	07T	BABR Dalitz fit II, 11k evts

¹ When AUBERT 07T replace the $f_0(980) \pi^0$ mode with $a_0(980) \pi^0$, the fit fraction is a negligibly different (11.0 ± 1.5 ± 1.2)%.

 $\Gamma(\phi \pi^0, \phi \rightarrow K^+ K^-) / \Gamma(K^+ K^- \pi^0) \quad \Gamma_{240} / \Gamma_{234}$

VALUE (units 10^{-2})	DOCUMENT ID	TECN	COMMENT
19.4 ± 0.6 ± 0.5	AUBERT	07T	BABR Dalitz fit II, 11k evts

• • • We do not use the following data for averages, fits, limits, etc. • • •

14.9 ± 1.6 ¹ CAWLFIELD 06A CLEO Dalitz fit, 627 ± 30 evts

¹ The error on this CAWLFIELD 06A result is statistical only.

 $\Gamma(K^+ K^- \pi^0 \text{ nonresonant}) / \Gamma(K^+ K^- \pi^0) \quad \Gamma_{241} / \Gamma_{234}$

VALUE	DOCUMENT ID	TECN	COMMENT
0.360 ± 0.037	¹ CAWLFIELD	06A	CLEO Dalitz fit, 627 ± 30 evts

¹ The error is statistical only. CAWLFIELD 06A also fits the Dalitz plot replacing this flat nonresonant background with broad S-wave $\kappa^\pm \rightarrow K^\pm \pi^0$ resonances. There is no significant improvement in the fit, and $K^{*\pm} K \pi$ and $\phi \pi^0$ results are not much changed.

 $\Gamma(K_S^0 \pi^0) / \Gamma_{\text{total}} \quad \Gamma_{242} / \Gamma$

VALUE	CL%	DOCUMENT ID	TECN	COMMENT
< 1.45 × 10⁻⁴	90	ABLIKIM	22Y	BES3 $e^+ e^-$ at 3.773 GeV
< 5.9 × 10 ⁻⁴	90	ASNER	96B	CLE2 $e^+ e^- \approx \Upsilon(4S)$

Meson Particle Listings

 D^0 $\Gamma(K^+K^-)/\Gamma_{\text{total}}$ Γ_{243}/Γ

VALUE (units 10^{-4})	EVTS	DOCUMENT ID	TECN	COMMENT
$0.59 \pm 0.18 \pm 0.05$	13	ABLIKIM	20v BES3	e^+e^- , 3773 MeV

 $\Gamma(K^+K^-)/\Gamma(K^-\pi^+\eta)$ $\Gamma_{243}/\Gamma_{104}$

VALUE (units 10^{-3})	EVTS	DOCUMENT ID	TECN	COMMENT
$9.57^{+0.36}_{-0.33} \pm 0.20$	1.4k	LI	21g BELL	e^+e^- at $\mathcal{T}(\text{NS})$

 $\Gamma(\phi(1020)\eta)/\Gamma(K^-\pi^+\eta)$ $\Gamma_{244}/\Gamma_{104}$

VALUE (units 10^{-3})	EVTS	DOCUMENT ID	TECN	COMMENT
$9.8 \pm 0.6 \pm 0.1$	1.4k	¹ LI	21g BELL	e^+e^- at $\mathcal{T}(\text{NS})$

¹LI 21g reports $[\Gamma(D^0 \rightarrow \phi(1020)\eta)/\Gamma(D^0 \rightarrow K^-\pi^+\eta)] \times [B(\phi(1020) \rightarrow K^+K^-)] = (4.82 \pm 0.23 \pm 0.16) \times 10^{-3}$ which we divide by our best value $B(\phi(1020) \rightarrow K^+K^-) = (49.1 \pm 0.5) \times 10^{-2}$. Our first error is their experiment's error and our second error is the systematic error from using our best value.

 $\Gamma(K^+K^-\eta_{\text{nonresonant}})/\Gamma(K^-\pi^+\eta)$ $\Gamma_{245}/\Gamma_{104}$

VALUE (units 10^{-3})	EVTS	DOCUMENT ID	TECN	COMMENT
$5.26^{+0.45}_{-0.38} \pm 0.11$	1.4k	LI	21g BELL	e^+e^- at $\mathcal{T}(\text{NS})$

 $\Gamma(2K_S^0)/\Gamma_{\text{total}}$ Γ_{246}/Γ

VALUE (units 10^{-4})	EVTS	DOCUMENT ID	TECN	COMMENT
$1.33 \pm 0.59 \pm 0.18$	7	ABLIKIM	20v BES3	e^+e^- , 3773 MeV

 $\Gamma(K^+K^-\pi^0\pi^0)/\Gamma_{\text{total}}$ Γ_{247}/Γ

VALUE (units 10^{-4})	EVTS	DOCUMENT ID	TECN	COMMENT
$6.9 \pm 0.7 \pm 0.4$	132	ABLIKIM	20ac BES3	e^+e^- at 3.773 GeV

 $\Gamma(K^+K^-\pi^+\pi^-)/\Gamma(K^-2\pi^+\pi^-)$ Γ_{248}/Γ_{78}

VALUE (units 10^{-2})	EVTS	DOCUMENT ID	TECN	COMMENT
3.00 ± 0.13 OUR AVERAGE				

$2.95 \pm 0.11 \pm 0.08$	2669 \pm 101	¹ LINK	05g FOCS	γBe , $\overline{E}_\gamma \approx 180$ GeV
$3.13 \pm 0.37 \pm 0.36$	136 \pm 15	AITALA	98d E791	π^- nucleus, 500 GeV
$3.5 \pm 0.4 \pm 0.2$	244 \pm 26	FRABETTI	95c E687	γBe , $\overline{E}_\gamma \approx 200$ GeV
$4.4 \pm 1.8 \pm 0.5$	19 \pm 8	ABLIKIM	05f BES	$e^+e^- \approx \psi(3770)$
$4.1 \pm 0.7 \pm 0.5$	114 \pm 20	ALBRECHT	94i ARG	$e^+e^- \approx 10$ GeV
3.14 ± 1.0	89 \pm 29	AMMAR	91 CLEO	$e^+e^- \approx 10.5$ GeV
$2.8^{+0.8}_{-0.7}$		ANJOS	91 E691	γBe 80–240 GeV

¹LINK 05g uses a smaller, cleaner subset of 1279 \pm 48 events for the amplitude analysis that gives the results in the next data blocks.

 $\Gamma(\phi(\pi^+\pi^-)_{S\text{-wave}} \phi \rightarrow K^+K^-)/\Gamma(K^+K^-\pi^+\pi^-)$ $\Gamma_{249}/\Gamma_{248}$

VALUE (units 10^{-2})	EVTS	DOCUMENT ID	TECN	COMMENT
$4.0 \pm 0.6 \pm 2.1$	3k	¹ DARGENT	17	4-body fit, $KK\pi\pi$ events

• • • We do not use the following data for averages, fits, limits, etc. • • •

$10.3 \pm 1.0 \pm 0.8$	3k	² ARTUSO	12 CLEO	4-body fit, $KK\pi\pi$ events
1 ± 1	1.3k	LINK	05g FOCS	4-body fit, $KK\pi\pi$ events

¹Obtained by analyzing CLEO data but not authored by the CLEO Collaboration.
²See DARGENT 17

 $\Gamma((\phi\rho^0)_{S\text{-wave}} \phi \rightarrow K^+K^-)/\Gamma(K^+K^-\pi^+\pi^-)$ $\Gamma_{250}/\Gamma_{248}$

VALUE (units 10^{-2})	EVTS	DOCUMENT ID	TECN	COMMENT
$28.1 \pm 1.3 \pm 1.7$	2.9k	^{1,2} DARGENT	17	4-body fit, $KK\pi\pi$ evts

• • • We do not use the following data for averages, fits, limits, etc. • • •

$38.3 \pm 2.5 \pm 3.8$		^{1,3} ARTUSO	12 CLEO	Fitting 2959 evts.
$29 \pm 2 \pm 1$		LINK	05g FOCS	Fits 1279 \pm 48 evts.

¹ARTUSO 12 and DARGENT 17 use the same dataset, but ARTUSO 12 uses a formulation for the D-wave component that is in fact a mix of S- and D-wave, while DARGENT 17 uses a pure D-wave. This explains the discrepancy in their $\rho\phi$ S- and D-wave components.

²Obtained by analyzing CLEO data but not authored by the CLEO Collaboration.
³See DARGENT 17

 $\Gamma((\phi\rho^0)_{P\text{-wave}} \phi \rightarrow K^+K^-)/\Gamma(K^+K^-\pi^+\pi^-)$ $\Gamma_{251}/\Gamma_{248}$

VALUE (units 10^{-2})	EVTS	DOCUMENT ID	TECN	COMMENT
$1.6 \pm 0.3 \pm 0.7$	2.9k	¹ DARGENT	17	4-body fit, $KK\pi\pi$ evts

¹Obtained by analyzing CLEO data but not authored by the CLEO Collaboration.

 $\Gamma((\phi\rho^0)_{D\text{-wave}} \phi \rightarrow K^+K^-)/\Gamma(K^+K^-\pi^+\pi^-)$ $\Gamma_{252}/\Gamma_{248}$

VALUE (units 10^{-2})	EVTS	DOCUMENT ID	TECN	COMMENT
$1.7 \pm 0.4 \pm 0.4$	2.9k	^{1,2} DARGENT	17	4-body fit, $KK\pi\pi$ evts

• • • We do not use the following data for averages, fits, limits, etc. • • •

$3.4 \pm 0.7 \pm 0.6$ ^{1,3}ARTUSO 12 CLEO Fitting 2959 evts.

¹ARTUSO 12 use a formulation for the D-wave component that is in fact a mix of S- and D-wave, while DARGENT 17 uses a pure D-wave.

²Obtained by analyzing CLEO data but not authored by the CLEO Collaboration.

³See DARGENT 17

 $\Gamma(K^*(892)^0\overline{K}^*(892)^0, K^{*0} \rightarrow K^\pm\pi^\mp)/\Gamma(K^+K^-\pi^+\pi^-)$ $\Gamma_{253}/\Gamma_{248}$

VALUE (units 10^{-2})	DOCUMENT ID	TECN	COMMENT
$3 \pm 2 \pm 1$	LINK	05g FOCS	Fits 1279 \pm 48 evts.

• • • We do not use the following data for averages, fits, limits, etc. • • •

$3 \pm 2 \pm 1$ LINK 05g FOCS Fits 1279 \pm 48 evts.

 $\Gamma(K^+K^-\rho^0\text{3-body})/\Gamma(K^+K^-\pi^+\pi^-)$ $\Gamma_{254}/\Gamma_{248}$

VALUE (units 10^{-2})	DOCUMENT ID	TECN	COMMENT
$3 \pm 2 \pm 1$	LINK	05g FOCS	Fits 1279 \pm 48 evts.

• • • We do not use the following data for averages, fits, limits, etc. • • •

$2 \pm 2 \pm 2$ LINK 05g FOCS Fits 1279 \pm 48 evts.

 $\Gamma(f_0(980)\pi^+\pi^-, f_0 \rightarrow K^+K^-)/\Gamma(K^+K^-\pi^+\pi^-)$ $\Gamma_{255}/\Gamma_{248}$

VALUE (units 10^{-2})	DOCUMENT ID	TECN	COMMENT
$15 \pm 3 \pm 2$	LINK	05g FOCS	Fits 1279 \pm 48 evts.

• • • We do not use the following data for averages, fits, limits, etc. • • •

$15 \pm 3 \pm 2$ LINK 05g FOCS Fits 1279 \pm 48 evts.

 $\Gamma((K^*(892)^0\overline{K}^*(892)^0)_{S\text{-wave}}, K^{*0} \rightarrow K^\pm\pi^\mp)/\Gamma(K^+K^-\pi^+\pi^-)$ $\Gamma_{256}/\Gamma_{248}$

VALUE (units 10^{-2})	EVTS	DOCUMENT ID	TECN	COMMENT
9.06 ± 0.35 OUR AVERAGE				

$9.18 \pm 0.21 \pm 0.28$	163k	AAIJ	19c LHCB	4-body fit, $KK\pi\pi$ evts
$4.5 \pm 0.8 \pm 2.0$	3k	¹ DARGENT	17	4-body fit, $KK\pi\pi$ evts

• • • We do not use the following data for averages, fits, limits, etc. • • •

$6.1 \pm 0.8 \pm 0.9$ 3k ²ARTUSO 12 CLEO 4-body fit, $KK\pi\pi$ evts

¹Obtained by analyzing CLEO data but not authored by the CLEO Collaboration.

²See DARGENT 17

 $\Gamma((K^*(892)^0\overline{K}^*(892)^0)_{P\text{-wave}}, K^* \rightarrow K^\pm\pi^\mp)/\Gamma(K^+K^-\pi^+\pi^-)$ $\Gamma_{257}/\Gamma_{248}$

VALUE (units 10^{-2})	EVTS	DOCUMENT ID	TECN	COMMENT
4.87 ± 0.24 OUR AVERAGE				

$4.90 \pm 0.16 \pm 0.18$	163k	AAIJ	19c LHCB	4-body fit, $KK\pi\pi$ evts
$3.6 \pm 0.7 \pm 1.5$	2.9k	¹ DARGENT	17	4-body fit, $KK\pi\pi$ evts

• • • We do not use the following data for averages, fits, limits, etc. • • •

$6.1 \pm 0.8 \pm 0.9$ 3k ²ARTUSO 12 CLEO 4-body fit, $KK\pi\pi$ evts

¹Obtained by analyzing CLEO data but not authored by the CLEO Collaboration.

²See DARGENT 17

 $\Gamma((K^*(892)^0\overline{K}^*(892)^0)_{D\text{-wave}}, K^* \rightarrow K^\pm\pi^\mp)/\Gamma(K^+K^-\pi^+\pi^-)$ $\Gamma_{258}/\Gamma_{248}$

VALUE (units 10^{-2})	EVTS	DOCUMENT ID	TECN	COMMENT
1.89 ± 0.13 OUR AVERAGE				

$1.85 \pm 0.09 \pm 0.10$	163k	AAIJ	19c LHCB	4-body fit, $KK\pi\pi$ evts
$4.0 \pm 0.6 \pm 0.7$	2.9k	¹ DARGENT	17	4-body fit, $KK\pi\pi$ evts

• • • We do not use the following data for averages, fits, limits, etc. • • •

$4.0 \pm 0.6 \pm 0.7$ 2.9k ¹DARGENT 17 4-body fit, $KK\pi\pi$ evts

¹Obtained by analyzing CLEO data but not authored by the CLEO Collaboration.

 $\Gamma(K^*(892)^0K^\mp\pi^\pm\text{3-body}, K^{*0} \rightarrow K^\pm\pi^\mp)/\Gamma(K^+K^-\pi^+\pi^-)$ $\Gamma_{259}/\Gamma_{248}$

VALUE (units 10^{-2})	DOCUMENT ID	TECN	COMMENT
$11 \pm 2 \pm 1$	LINK	05g FOCS	Fits 1279 \pm 48 evts.

• • • We do not use the following data for averages, fits, limits, etc. • • •

$11 \pm 2 \pm 1$ LINK 05g FOCS Fits 1279 \pm 48 evts.

 $\Gamma(K^*(892)^0(K^-\pi^+)_{S\text{-wave}}\text{3-body}, K^{*0} \rightarrow K^+\pi^-)/\Gamma(K^+K^-\pi^+\pi^-)$ $\Gamma_{260}/\Gamma_{248}$

VALUE (units 10^{-2})	EVTS	DOCUMENT ID	COMMENT
$5.8 \pm 1.2 \pm 2.1$	2.9k	¹ DARGENT	17 4-body fit, $KK\pi\pi$ evts

¹Obtained by analyzing CLEO data but not authored by the CLEO Collaboration.

 $\Gamma((K^-\pi^+)_{P\text{-wave}}, (K^+\pi^-)_{S\text{-wave}})/\Gamma(K^+K^-\pi^+\pi^-)$ $\Gamma_{261}/\Gamma_{248}$

VALUE (units 10^{-2})	DOCUMENT ID	TECN	COMMENT
$10.9 \pm 1.2 \pm 1.7$	¹ ARTUSO	12 CLEO	Fitting 2959 evts.

• • • We do not use the following data for averages, fits, limits, etc. • • •

$10.9 \pm 1.2 \pm 1.7$ ¹ARTUSO 12 CLEO Fitting 2959 evts.

¹See DARGENT 17

 $\Gamma(K_1^+(1270)^\pm K^\mp, K_1^\pm \rightarrow K^\pm\pi^+\pi^-)/\Gamma(K^+K^-\pi^+\pi^-)$ $\Gamma_{262}/\Gamma_{248}$

VALUE (units 10^{-2})	DOCUMENT ID	TECN	COMMENT
$33 \pm 6 \pm 4$	¹ LINK	05g FOCS	Fits 1279 \pm 48 evts.

• • • We do not use the following data for averages, fits, limits, etc. • • •

$33 \pm 6 \pm 4$ ¹LINK 05g FOCS Fits 1279 \pm 48 evts.

¹This LINK 05g value includes $K_1^+(1270)^\pm \rightarrow \rho^0 K^\pm \rightarrow K_6^*(1430)^0 \pi^\pm$, and $K^*(892)^0 \pi^\pm$.

$\Gamma(K_1(1270)^+ K^-, K_1^+ \rightarrow K^{*0} \pi^+)/\Gamma(K^+ K^- \pi^+ \pi^-)$ $\Gamma_{263}/\Gamma_{248}$

VALUE (units 10^{-2})	EVTS	DOCUMENT ID	TECN	COMMENT
5.5 ± 1.4 ± 3.4	3k	¹ DARGENT 17		4-body fit, $K K \pi \pi$ evts
••• We do not use the following data for averages, fits, limits, etc. •••				
7.3 ± 0.8 ± 1.9	3k	² ARTUSO 12	CLEO	4-body fit, $K K \pi \pi$ events

¹ Obtained by analyzing CLEO data but not authored by the CLEO Collaboration.
² See DARGENT 17

 $\Gamma(K_1(1270)^+ K^-, K_1^+ \rightarrow K^*(1430)^0 \pi^+, K^{*0} \rightarrow K^+ \pi^-)/\Gamma(K^+ K^- \pi^+ \pi^-)$ $\Gamma_{264}/\Gamma_{248}$

This is the fit fraction from a coherent amplitude analysis.

VALUE (units 10^{-2})	EVTS	DOCUMENT ID	TECN	COMMENT
6.1 ± 1.2 ± 1.8	2.9k	¹ DARGENT 17		4-body fit, $K K \pi \pi$ evts

¹ Obtained by analyzing CLEO data but not authored by the CLEO Collaboration.

 $\Gamma(K_1(1270)^+ K^-, K_1^+ \rightarrow \rho^0 K^+)/\Gamma(K^+ K^- \pi^+ \pi^-)$ $\Gamma_{265}/\Gamma_{248}$

VALUE (units 10^{-2})	EVTS	DOCUMENT ID	TECN	COMMENT
9.1 ± 1.5 ± 1.9	2.9k	¹ DARGENT 17		4-body fit, $K K \pi \pi$ evts
••• We do not use the following data for averages, fits, limits, etc. •••				
4.7 ± 0.7 ± 0.8		² ARTUSO 12	CLEO	Fitting 2959 evts.

¹ Obtained by analyzing CLEO data but not authored by the CLEO Collaboration.
² See DARGENT 17

 $\Gamma(K_1(1270)^+ K^-, K_1^+ \rightarrow \omega(782) K^+, \omega \rightarrow \pi^+ \pi^-)/\Gamma(K^+ K^- \pi^+ \pi^-)$ $\Gamma_{266}/\Gamma_{248}$

This is the fit fraction from a coherent amplitude analysis.

VALUE (units 10^{-2})	EVTS	DOCUMENT ID	TECN	COMMENT
0.6 ± 0.3 ± 0.4	2.9k	¹ DARGENT 17		4-body fit, $K K \pi \pi$ evts

¹ Obtained by analyzing CLEO data but not authored by the CLEO Collaboration.

 $\Gamma(K_1(1270)^- K^+, K_1^- \rightarrow \bar{K}^{*0} \pi^-)/\Gamma(K^+ K^- \pi^+ \pi^-)$ $\Gamma_{267}/\Gamma_{248}$

VALUE (units 10^{-2})	EVTS	DOCUMENT ID	TECN	COMMENT
0.9 ± 0.3 ± 0.4		¹ ARTUSO 12	CLEO	Fitting 2959 evts.

¹ See DARGENT 17

 $\Gamma(K_1(1270)^- K^+, K_1^- \rightarrow \rho^0 K^-)/\Gamma(K^+ K^- \pi^+ \pi^-)$ $\Gamma_{268}/\Gamma_{248}$

VALUE (units 10^{-2})	EVTS	DOCUMENT ID	TECN	COMMENT
5.4 ± 0.7 ± 1.3	2.9k	¹ DARGENT 17		4-body fit, $K K \pi \pi$ evts
••• We do not use the following data for averages, fits, limits, etc. •••				
6.0 ± 0.8 ± 0.6		² ARTUSO 12	CLEO	Fitting 2959 evts.

¹ Obtained by analyzing CLEO data but not authored by the CLEO Collaboration.
² See DARGENT 17

 $\Gamma(K_1(1400)^\pm K^\mp, K_1^\pm \rightarrow K^\pm \pi^+ \pi^-)/\Gamma(K^+ K^- \pi^+ \pi^-)$ $\Gamma_{269}/\Gamma_{248}$

This is the fraction from a coherent amplitude analysis.

VALUE (units 10^{-2})	DOCUMENT ID	TECN	COMMENT
22 ± 3 ± 4	LINK 05g	FOCS	Fits 1279 ± 48 evts.

 $\Gamma(K_1(1400)^+ K^-, K_1^+ \rightarrow K^*(892)^0 \pi^+, K^{*0} \rightarrow K^+ \pi^-)/\Gamma(K^+ K^- \pi^+ \pi^-)$ $\Gamma_{270}/\Gamma_{248}$

This is the fit fraction from a coherent amplitude analysis.

VALUE (units 10^{-2})	EVTS	DOCUMENT ID	TECN	COMMENT
18.7 ± 1.5 OUR AVERAGE				
19.08 ± 0.60 ± 1.46	163k	AAIJ 19c	LHCB	4-body fit, $K K \pi \pi$ evts
12.4 ± 2.6 ± 6.3	2.9k	¹ DARGENT 17		4-body fit, $K K \pi \pi$ evts

¹ Obtained by analyzing CLEO data but not authored by the CLEO Collaboration.

 $\Gamma(K^*(1410)^+ K^-, K^{*+} \rightarrow K^{*0} \pi^+)/\Gamma(K^+ K^- \pi^+ \pi^-)$ $\Gamma_{271}/\Gamma_{248}$

VALUE (units 10^{-2})	DOCUMENT ID	TECN	COMMENT
4.2 ± 0.7 ± 0.8	^{1,2} ARTUSO 12	CLEO	Fitting 2959 evts.

¹ DARGENT 17 find $K^*(1410)^+ \pi^-$ and $K^*(1680)^+ \pi^-$, which both peak outside the $D^0 \rightarrow K K \pi \pi$ kinematic range, effectively indistinguishable; we list their result under $K^*(1680)^+ \pi^-$.
² See DARGENT 17

 $\Gamma(K^*(1410)^- K^+, K^{*-} \rightarrow \bar{K}^{*0} \pi^-)/\Gamma(K^+ K^- \pi^+ \pi^-)$ $\Gamma_{272}/\Gamma_{248}$

VALUE (units 10^{-2})	EVTS	DOCUMENT ID	TECN	COMMENT
2.82 ± 0.19 ± 0.39	163k	AAIJ 19c	LHCB	4-body fit, $K K \pi \pi$ evts
••• We do not use the following data for averages, fits, limits, etc. •••				
4.7 ± 0.7 ± 0.7	3k	¹ ARTUSO 12	CLEO	4-body fit, $K K \pi \pi$ evts

¹ See DARGENT 17.

 $\Gamma(K_1(1680)^+ K^-, K_1^+ \rightarrow K^{*0} \pi^+, K^{*0} \rightarrow K^+ \pi^-)/\Gamma(K^+ K^- \pi^+ \pi^-)$ $\Gamma_{273}/\Gamma_{248}$

This is the fit fraction from a coherent amplitude analysis.

VALUE (units 10^{-2})	EVTS	DOCUMENT ID	TECN	COMMENT
3.6 ± 0.8 ± 1.0	2.9k	^{1,2} DARGENT 17		4-body fit, $K K \pi \pi$ evts

¹ DARGENT 17 find $K^*(1410)^+ \pi^-$ and $K^*(1680)^+ \pi^-$, which both peak outside the $D^0 \rightarrow K K \pi \pi$ kinematic range, effectively indistinguishable.

² Obtained by analyzing CLEO data but not authored by the CLEO Collaboration.

 $\Gamma(K^+ K^- \pi^+ \pi^- \text{ non-resonant})/\Gamma(K^+ K^- \pi^+ \pi^-)$ $\Gamma_{274}/\Gamma_{248}$

This is the fit fraction from a coherent amplitude analysis.

VALUE (units 10^{-2})	EVTS	DOCUMENT ID	TECN	COMMENT
11.1 ± 1.2 ± 2.2	2.9k	¹ DARGENT 17		4-body fit, $K K \pi \pi$ evts

¹ Obtained by analyzing CLEO data but not authored by the CLEO Collaboration.

 $\Gamma(2K_S^0 \pi^+ \pi^-)/\Gamma_{\text{total}}$ Γ_{275}/Γ

VALUE (units 10^{-4})	EVTS	DOCUMENT ID	TECN	COMMENT
5.3 ± 0.9 ± 0.3	63	ABLIKIM	20Ac	BES3 $e^+ e^-$ at 3.773 GeV

 $\Gamma(2K_S^0 \pi^+ \pi^-)/\Gamma(K_S^0 \pi^+ \pi^-)$ Γ_{275}/Γ_{44}

VALUE (units 10^{-2})	EVTS	DOCUMENT ID	TECN	COMMENT
1.72 ± 0.05 OUR AVERAGE				
1.71 ± 0.03 ± 0.04	6095	SANGAL 23	BELL	$e^+ e^-$ at $\Upsilon(4S, 5S)$, 10.520 GeV
4.16 ± 0.70 ± 0.42	113	LINK 05A	FOCS	γ Be, $\bar{E}_\gamma \approx 180$ GeV
6.2 ± 2.0 ± 1.6	25	ALBRECHT 94i	ARG	$e^+ e^- \approx 10$ GeV

 $\Gamma(K_S^0 K^- \pi^+ \pi^0)/\Gamma_{\text{total}}$ Γ_{276}/Γ

VALUE (units 10^{-3})	EVTS	DOCUMENT ID	TECN	COMMENT
1.32 ± 0.14 ± 0.07	195	ABLIKIM	20Ac	BES3 $e^+ e^-$ at 3.773 GeV

 $\Gamma(K_S^0 K^+ \pi^- \pi^0)/\Gamma_{\text{total}}$ Γ_{277}/Γ

VALUE (units 10^{-4})	EVTS	DOCUMENT ID	TECN	COMMENT
6.5 ± 0.7 ± 0.2	119	ABLIKIM	20Ac	BES3 $e^+ e^-$ at 3.773 GeV

 $\Gamma(K_S^0 K^- 2\pi^+ \pi^-)/\Gamma(K_S^0 2\pi^+ 2\pi^-)$ $\Gamma_{278}/\Gamma_{111}$

VALUE	CL%	DOCUMENT ID	TECN	COMMENT
<0.054	90	LINK 04b	FOCS	γ A, $\bar{E}_\gamma \approx 180$ GeV

 $\Gamma(K^+ K^- \pi^+ \pi^- \pi^0)/\Gamma_{\text{total}}$ Γ_{279}/Γ

VALUE	DOCUMENT ID	TECN	COMMENT
0.0031 ± 0.0020	¹ BARLAG 92c	ACCM	π^- Cu 230 GeV

¹ BARLAG 92c computes the branching fraction using topological normalization.

 $\Gamma(\phi \pi^0)/\Gamma(K^+ K^-)$ $\Gamma_{280}/\Gamma_{211}$

VALUE	EVTS	DOCUMENT ID	TECN	COMMENT
0.194 ± 0.006 ± 0.009	1254	TAJIMA 04	BELL	$e^+ e^-$ at $\Upsilon(4S)$

 $\Gamma(\phi \eta)/\Gamma(K^+ K^-)$ $\Gamma_{281}/\Gamma_{211}$

VALUE (units 10^{-2})	EVTS	DOCUMENT ID	TECN	COMMENT
3.59 ± 1.14 ± 0.18	31	TAJIMA 04	BELL	$e^+ e^-$ at $\Upsilon(4S)$

 $\Gamma(\phi \omega)/\Gamma_{\text{total}}$ Γ_{282}/Γ

VALUE (units 10^{-4})	CL%	EVTS	DOCUMENT ID	TECN	COMMENT
6.48 ± 0.96 ± 0.40		196	¹ ABLIKIM 22	BES3	$e^+ e^-$ at 3.773 GeV

••• We do not use the following data for averages, fits, limits, etc. •••

<21 90 ALBRECHT 94i ARG $e^+ e^- \approx 10$ GeV

¹ ABLIKIM 22 determines the longitudinal polarization fraction of the ϕ and ω , $f_L = 0.00 \pm 0.10 \pm 0.08$, corresponding to $f_L < 0.24$ at 95% CL.

Radiative modes

 $\Gamma(\rho^0 \gamma)/\Gamma(\pi^+ \pi^-)$ $\Gamma_{283}/\Gamma_{141}$

VALUE (units 10^{-2})	EVTS	DOCUMENT ID	TECN	COMMENT
1.25 ± 0.21 ± 0.05	500	NANUT 17	BELL	$e^+ e^-$ at $\Upsilon(nS)$, $n=2,3,4,5$

 $\Gamma(\omega \gamma)/\Gamma_{\text{total}}$ Γ_{284}/Γ

VALUE	CL%	DOCUMENT ID	TECN	COMMENT
<2.4 × 10⁻⁴	90	ASNER 98	CLE2	

 $\Gamma(\phi \gamma)/\Gamma(K^- \pi^+)$ Γ_{285}/Γ_{38}

VALUE (units 10^{-4})	EVTS	DOCUMENT ID	TECN	COMMENT
7.1 ± 0.5 OUR FIT				
7.15 ± 0.78 ± 0.69	243 ± 25	AUBERT	08Az	BABR $e^+ e^- \approx 10.6$ GeV

 $\Gamma(\phi \gamma)/\Gamma(K^+ K^-)$ $\Gamma_{285}/\Gamma_{211}$

VALUE (units 10^{-3})	EVTS	DOCUMENT ID	TECN	COMMENT
6.9 ± 0.5 OUR FIT				
6.88 ± 0.47 ± 0.21	524	NANUT 17	BELL	$e^+ e^-$ at $\Upsilon(nS)$, $n=2,3,4,5$

Meson Particle Listings

D^0

• • • We do not use the following data for averages, fits, limits, etc. • • •

6.31^{+1.70+0.30}_{-1.48-0.36} 28 TAJIMA 04 BELL See NANUT 17

$\Gamma(K^*(892)^0 \gamma) / \Gamma(K^- \pi^+)$ $\Gamma_{286} / \Gamma_{38}$

VALUE (units 10 ⁻³)	EVTS	DOCUMENT ID	TECN	COMMENT
10.5 ± 1.7 OUR AVERAGE				Error includes scale factor of 3.1.
11.9 ± 0.5 ± 0.5	9.1k	NANUT	17 BELL	e ⁺ e ⁻ at $\Upsilon(nS)$, n=2,3,4,5
8.43 ± 0.51 ± 0.70	2.2k	AUBERT	08AZ BABR	e ⁺ e ⁻ ≈ 10.6 GeV

Doubly Cabibbo-suppressed / Mixing modes

$\Gamma(K^+ \ell^- \bar{\nu}_\ell \text{ via } \bar{D}^0) / \Gamma(K^- \ell^+ \nu_\ell)$ $\Gamma_{287} / \Gamma_{19}$

This is a limit on R_M without the complications of possible doubly Cabibbo-suppressed decays that occur when using hadronic modes. For the limits on $|m_1 - m_2|$ and $(\Gamma_1 - \Gamma_2) / \Gamma$ that come from the best mixing limit, see near the beginning of these D^0 Listings.

VALUE	CL%	DOCUMENT ID	TECN	COMMENT
< 6.1 × 10⁻⁴	90	1 BITENC	08 BELL	e ⁺ e ⁻ , 10.58 GeV

• • • We do not use the following data for averages, fits, limits, etc. • • •

< 50 × 10 ⁻⁴	90	2 AITALA	96c E791	π^- nucleus, 500 GeV
-------------------------	----	----------	----------	--------------------------

¹ The BITENC 08 right-sign sample includes about 15% of $D^0 \rightarrow K^- \pi^0 \ell^+ \nu_\ell$ and other decays.

² AITALA 96c uses $D^{*+} \rightarrow D^0 \pi^+$ (and charge conjugate) decays to identify the charm at production and $D^0 \rightarrow K^- \ell^+ \nu_\ell$ (and charge conjugate) decays to identify the charm at decay.

$\Gamma(K^+ \text{ or } K^*(892)^+ e^- \bar{\nu}_e \text{ via } \bar{D}^0) / [\Gamma(K^- e^+ \nu_e) + \Gamma(K^*(892)^- e^+ \nu_e)]$ $\Gamma_{288} / (\Gamma_{20} + \Gamma_{22})$

This is a limit on R_M without the complications of possible doubly Cabibbo-suppressed decays that occur when using hadronic modes. The experiments use $D^{*+} \rightarrow D^0 \pi^+$ (and charge conjugate) decays to identify the charm at production and the charge of the e to identify the charm at decay. These limits do not allow CP violation. For the limits on $|m_1 - m_2|$ and $(\Gamma_1 - \Gamma_2) / \Gamma$ that come from the best mixing limit, see near the beginning of these D^0 Listings.

VALUE	CL%	DOCUMENT ID	TECN	COMMENT
< 0.001	90	BITENC	05 BELL	e ⁺ e ⁻ ≈ 10.6 GeV

• • • We do not use the following data for averages, fits, limits, etc. • • •

-0.0013 < R < +0.0012	90	AUBERT	07AB BABR	e ⁺ e ⁻ ≈ 10.58 GeV
< 0.0078	90	CAWFIELD	05 CLEO	e ⁺ e ⁻ ≈ 10.6 GeV
< 0.0042	90	AUBERT,B	04Q BABR	See AUBERT 07AB

$\Gamma(K^+ \pi^-) / \Gamma(K^- \pi^+)$ $\Gamma_{289} / \Gamma_{38}$

This is R , the time-integrated wrong-sign rate compared to the right-sign rate. See the note on " D^0 - \bar{D}^0 Mixing," near the start of the D^0 Listings.

The experiments here use the charge of the pion in $D^*(2010)^\pm \rightarrow (D^0 \text{ or } \bar{D}^0) \pi^\pm$ decay to tell whether a D^0 or a \bar{D}^0 was born. The $D^0 \rightarrow K^+ \pi^-$ decay can occur directly by doubly Cabibbo-suppressed (DCS) decay, or indirectly by $D^0 \rightarrow \bar{D}^0$ mixing followed by $\bar{D}^0 \rightarrow K^+ \pi^-$ decay. Some of the experiments can use the decay-time information to disentangle the two mechanisms. Here, we list the experimental branching ratio, which if there is no mixing is the DCS ratio. See the next data block for values of the DCS ratio R_D , and the following data block for limits on the mixing ratio R_M . See the section on CP-violating asymmetries near the end of this D^0 Listing for values of A_D , and the note on " D^0 - \bar{D}^0 Mixing" for limits on x' and y'.

Some early limits have been omitted from this Listing; see our 1998 edition (The European Physical Journal **C3** 1 (1998)) and our 2006 edition (Journal of Physics **G33** 1 (2006)).

VALUE (units 10 ⁻³)	EVTS	DOCUMENT ID	TECN	COMMENT
3.79 ± 0.18 OUR FIT				Error includes scale factor of 3.3.

3.79 ± 0.18 OUR AVERAGE Error includes scale factor of 3.3. See the ideogram below.

4.15 ± 0.10	12.7 ± 0.3k	1 AALTONEN	08E CDF	$p\bar{p}$, $\sqrt{s} = 1.96$ TeV
3.53 ± 0.08 ± 0.04	4030 ± 90	2 AUBERT	07W BABR	e ⁺ e ⁻ ≈ 10.6 GeV
3.77 ± 0.08 ± 0.05	4024 ± 88	1 ZHANG	06 BELL	e ⁺ e ⁻

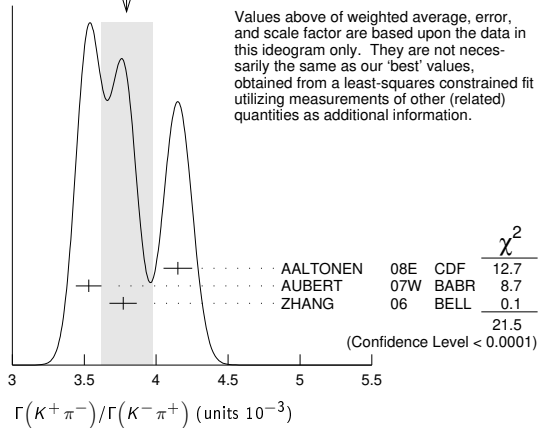
• • • We do not use the following data for averages, fits, limits, etc. • • •

4.05 ± 0.21 ± 0.11	2.0 ± 0.1k	3 ABULENCIA	06x CDF	See AALTONEN 08E
3.81 ± 0.17 ± 0.08	845 ± 40	2 LI	05A BELL	See ZHANG 06

4.29 ^{+0.63} _{-0.61} ± 0.27	234	4 LINK	05H FOCS	γ nucleus
3.57 ± 0.22 ± 0.27		5 AUBERT	03Z BABR	See AUBERT 07w
4.04 ± 0.85 ± 0.25	149	6 LINK	01 FOCS	γ nucleus
3.32 ^{+0.63} _{-0.65} ± 0.40	45	1 GODANG	00 CLE2	e ⁺ e ⁻
6.8 ^{+3.4} _{-3.3} ± 0.7	34	2 AITALA	98 E791	π^- nucl., 500 GeV

- GODANG 00, ZHANG 06, and AALTONEN 08E allow CP violation.
- AITALA 98, LI 05A, and AUBERT 07w assume no CP violation.
- This ABULENCIA 06x result assumes no mixing.
- This LINK 05H result assumes no mixing but allows CP violation. If neither mixing nor CP violation is allowed, $R = (4.29 \pm 0.63 \pm 0.28) \times 10^{-3}$.
- This AUBERT 03z result allows CP violation. If CP violation is not allowed, $R = 0.00359 \pm 0.00020 \pm 0.00027$.
- This LINK 01 result assumes no mixing or CP violation.

WEIGHTED AVERAGE
3.79±0.18 (Error scaled by 3.3)



$\Gamma(K^+ \pi^- \text{ via DCS}) / \Gamma(K^- \pi^+)$ $\Gamma_{290} / \Gamma_{38}$

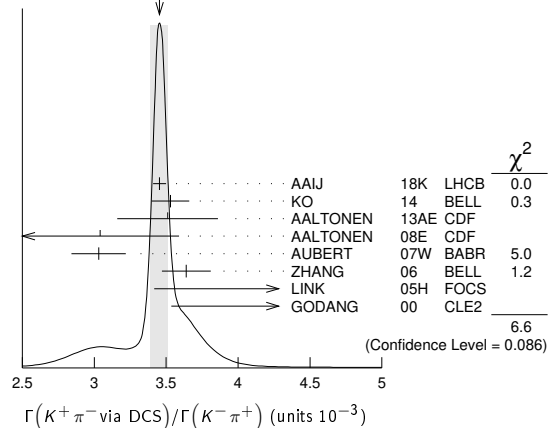
This is R_D , the doubly Cabibbo-suppressed ratio when mixing is allowed.

VALUE (units 10 ⁻³)	EVTS	DOCUMENT ID	TECN	COMMENT
3.45 ± 0.06 OUR AVERAGE				Error includes scale factor of 1.5. See the ideogram below.

3.454 ± 0.040 ± 0.020	722k	1 AAIJ	18K LHCb	$p\bar{p}$ at 7, 8, 13 TeV
3.53 ± 0.13		2 KO	14 BELL	e ⁺ e ⁻ → $\Upsilon(nS)$
3.51 ± 0.35		3 AALTONEN	13AE CDF	$p\bar{p}$ at 1.96 TeV
3.04 ± 0.55	13k	AALTONEN	08E CDF	$p\bar{p}$, $\sqrt{s} = 1.96$ TeV
3.03 ± 0.16 ± 0.10	4.0k	4 AUBERT	07W BABR	e ⁺ e ⁻ ≈ 10.6 GeV
3.64 ± 0.17	4.0k	5 ZHANG	06 BELL	e ⁺ e ⁻
5.17 ^{+1.47} _{-1.58} ± 0.76	234	6 LINK	05H FOCS	γ nucleus
4.8 ± 1.2 ± 0.4	45	7 GODANG	00 CLE2	e ⁺ e ⁻
3.533 ± 0.054	236k	8 AAIJ	17A0 LHCb	See AAIJ 18k
3.568 ± 0.066		9 AAIJ	13CE LHCb	$p\bar{p}$ at 7, 8 TeV
3.52 ± 0.15		10 AAIJ	13N LHCb	Repl. by AAIJ 13CE
2.87 ± 0.37	0.8k	LI	05A BELL	See ZHANG 06

- This AAIJ 18k value is for direct and indirect CP violation allowed. The value is the same if either one or the other is not allowed, but in each case the error then is $(0.028 \pm 0.014) \times 10^{-3}$.
- Based on 976 fb⁻¹ of data collected at $\Upsilon(nS)$ resonances. Assumes no CP violation.
- Based on 9.6 fb⁻¹ of data collected at the Tevatron. Assumes no CP violation.
- Result is the same whether or not CP violation is allowed.
- This ZHANG 06 assumes no CP violation.
- This LINK 05H result allows CP violation. Allowing mixing but not CP violation, $R_D = (3.81^{+1.67}_{-1.63} ± 0.92) \times 10^{-3}$.
- This GODANG 00 result allows CP violation.
- The result was established with D^0 from prompt and secondary D^* assuming no CPV or no direct CPV.
- Based on 3 fb⁻¹ of data collected at $\sqrt{s} = 7, 8$ TeV. Assumes no CP violation.
- Based on 1 fb⁻¹ of data collected at $\sqrt{s} = 7$ TeV in 2011. Assumes no CP violation.

WEIGHTED AVERAGE
3.45±0.06 (Error scaled by 1.5)



See key on page 1171

Meson Particle Listings

D^0

$\Gamma(K^+\pi^- \text{ via } \bar{D}^0)/\Gamma(K^-\pi^+)$ Γ_{291}/Γ_{38}

This is R_M in the note on " $D^0-\bar{D}^0$ Mixing" near the start of the D^0 Listings. The experiments here (1) use the charge of the pion in $D^*(2010)^\pm \rightarrow (D^0 \text{ or } \bar{D}^0)\pi^\pm$ decay to tell whether a D^0 or a \bar{D}^0 was born; and (2) use the decay-time distribution to disentangle doubly Cabibbo-suppressed decay and mixing. For the limits on $|m_1 - m_2|$ and $(\Gamma_1 - \Gamma_2)/\Gamma$ that come from the best mixing limit, see near the beginning of these D^0 Listings.

VALUE	CL%	DOCUMENT ID	TECN	COMMENT
<0.00040	95	¹ ZHANG	06 BELL	e^+e^-
• • • We do not use the following data for averages, fits, limits, etc. • • •				
<0.00046	95	² LI	05A BELL	See ZHANG 06
<0.0063	95	³ LINK	05H FOCS	γ nucleus
<0.0013	95	⁴ AUBERT	03Z BABR	e^+e^- , 10.6 GeV
<0.00041	95	⁵ GODANG	00 CLE2	e^+e^-
<0.0092	95	⁶ BARATE	98W ALEP	e^+e^- at Z^0
<0.005	90	⁷ ANJOS	88c E691	Photoproduction

- This ZHANG 06 result allows CP violation, but the result does not change if CP violation is not allowed.
- This LI 05A result allows CP violation. The limit becomes < 0.00042 (95% CL) if CP violation is not allowed.
- LINK 05H obtains the same result whether or not CP violation is allowed.
- This AUBERT 03Z result allows CP violation and assumes that the strong phase between $D^0 \rightarrow K^+\pi^-$ and $\bar{D}^0 \rightarrow K^+\pi^-$ is small, and limits only $D^0 \rightarrow \bar{D}^0$ transitions via off-shell intermediate states. The limit on transitions via on-shell intermediate states is 0.0016.
- This GODANG 00 result allows CP violation and assumes that the strong phase between $D^0 \rightarrow K^+\pi^-$ and $\bar{D}^0 \rightarrow K^+\pi^-$ is small, and limits only $D^0 \rightarrow \bar{D}^0$ transitions via off-shell intermediate states. The limit on transitions via on-shell intermediate states is 0.0017.
- This BARATE 98W result assumes no interference between the DCS and mixing amplitudes ($\gamma = 0$ in the note on " $D^0-\bar{D}^0$ Mixing" near the start of the D^0 Listings). When interference is allowed, the limit degrades to 0.036 (95%CL).
- This ANJOS 88c result assumes no interference between the DCS and mixing amplitudes ($\gamma = 0$ in the note on " $D^0-\bar{D}^0$ Mixing" near the start of the D^0 Listings). When interference is allowed, the limit degrades to 0.019.

$\Gamma(K_S^0\pi^+\pi^- \text{ in } D^0 \rightarrow \bar{D}^0)/\Gamma(K_S^0\pi^+\pi^-)$ Γ_{292}/Γ_{44}

This is R_M in the note on " $D^0-\bar{D}^0$ Mixing" near the start of the D^0 Listings. The experiments here (1) use the charge of the pion in $D^*(2010)^\pm \rightarrow (D^0 \text{ or } \bar{D}^0)\pi^\pm$ decay to tell whether a D^0 or a \bar{D}^0 was born; and (2) use the decay-time distribution to disentangle doubly Cabibbo-suppressed decay and mixing. For the limits on $|m_1 - m_2|$ and $(\Gamma_1 - \Gamma_2)/\Gamma$ that come from the best mixing limit, see near the beginning of these D^0 Listings.

VALUE	CL%	DOCUMENT ID	TECN	COMMENT
<0.0063	95	¹ ASNER	05 CLEO	$e^+e^- \approx 10$ GeV

- This ASNER 05 limit allows CP violation. If CP violation is not allowed, the limit is 0.0042 at 95% CL.

$\Gamma(K^+\pi^-\pi^0)/\Gamma_{\text{total}}$ Γ_{296}/Γ

VALUE (units 10^{-4})	EVTS	DOCUMENT ID	TECN	COMMENT
3.06 ± 0.16	OUR FIT	Error includes scale factor of 1.4.		
3.13 ± 0.60	± 0.15	46	¹ ABLIKIM	22X BES3 e^+e^- at 3.773 GeV

- Uses the semileptonic tag method of ABLIKIM 21BB.

$\Gamma(K^+\pi^-\pi^0)/\Gamma(K^-\pi^+\pi^0)$ Γ_{296}/Γ_{59}

The experiments here use the charge of the pion in $D^*(2010)^\pm \rightarrow (D^0 \text{ or } \bar{D}^0)\pi^\pm$ decay to tell whether a D^0 or a \bar{D}^0 was born. The $D^0 \rightarrow K^+\pi^-\pi^0$ decay can occur directly by doubly Cabibbo-suppressed (DCS) decay, or indirectly by $D^0 \rightarrow \bar{D}^0$ mixing followed by $\bar{D}^0 \rightarrow K^+\pi^-\pi^0$ decay.

VALUE (units 10^{-3})	EVTS	DOCUMENT ID	TECN	COMMENT
2.12 ± 0.07	OUR FIT			
2.12 ± 0.07	OUR AVERAGE			
2.01 ± 0.11		¹ EVANS	16 CLEO	$e^+e^- \rightarrow D^0\bar{D}^0$ at $\psi(3770)$
$2.14 \pm 0.08 \pm 0.08$	763	² AUBERT,B	06N BABR	$e^+e^- \approx \Upsilon(4S)$
$2.29 \pm 0.15 \pm 0.13$	± 0.09	1.9k	TIAN	05 BELL $e^+e^- \approx \Upsilon(4S)$
4.3 ± 1.1	± 0.7	38	BRANDENB...	01 CLE2 $e^+e^- \approx \Upsilon(4S)$

- A combined fit with a recent LHCb $D^0\bar{D}^0$ mixing results in AAIJ 16F is also reported to be $(2.00 \pm 0.11) \times 10^{-3}$.
- This AUBERT,B 06N result assumes no mixing.

$\Gamma(K^+\pi^-\pi^0 \text{ via } \bar{D}^0)/\Gamma(K^-\pi^+\pi^0)$ Γ_{297}/Γ_{59}

This is R_M in the note on " $D^0-\bar{D}^0$ Mixing" near the start of the D^0 Listings. The experiments here (1) use the charge of the pion in $D^*(2010)^\pm \rightarrow (D^0 \text{ or } \bar{D}^0)\pi^\pm$ decay to tell whether a D^0 or a \bar{D}^0 was born; and (2) use the decay-time distribution to disentangle doubly Cabibbo-suppressed decay and mixing. For the limits on $|m_1 - m_2|$ and $(\Gamma_1 - \Gamma_2)/\Gamma$ that come from the best mixing limit, see near the beginning of these D^0 Listings.

VALUE (units 10^{-3})	CL%	DOCUMENT ID	TECN	COMMENT
5.25 ± 0.25	± 0.31	AUBERT	09AN BABR	e^+e^- at 10.58 GeV

- • • We do not use the following data for averages, fits, limits, etc. • • •

<0.54 95 ¹ AUBERT,B 06N BABR $e^+e^- \approx \Upsilon(4S)$

- This AUBERT,B 06N limit assumes no CP violation. The measured value corresponding to the limit is $(2.3 \pm 1.8 \pm 0.4) \times 10^{-4}$. If CP violation is allowed, this becomes $(1.0 \pm 0.7 \pm 0.3) \times 10^{-4}$.

$\Gamma(K^+\pi^-\pi^0)/\Gamma_{\text{total}}$ Γ_{298}/Γ

VALUE	CL%	DOCUMENT ID	TECN	COMMENT
< 3.6×10^{-4}	90	¹ ABLIKIM	22X BES3	e^+e^- at 3.773 GeV

- Uses the semileptonic tag method of ABLIKIM 21BB.

$\Gamma(K^+\pi^+\pi^-\text{ via DCS})/\Gamma(K^-\pi^+\pi^-)$ Γ_{299}/Γ_{78}

VALUE (units 10^{-3})	EVTS	DOCUMENT ID	TECN	COMMENT
3.03 ± 0.07	OUR AVERAGE			
3.025 ± 0.077	42k,11M	¹ AAIJ	16F LHCb	pp at 7, 8 TeV
3.03 ± 0.13		² EVANS	16 CLEO	$e^+e^- \rightarrow D^0\bar{D}^0$ at $\psi(3770)$

- This result uses external input on the mixing parameters x, y . Without this input, the result is $(3.215 \pm 0.136) \times 10^{-3}$.
- A combined fit with a recent LHCb $D^0\bar{D}^0$ mixing results in AAIJ 16F is also reported to be $(3.01 \pm 0.07) \times 10^{-3}$.

$\Gamma(K^+\pi^+\pi^-)/\Gamma(K^-\pi^+\pi^-)$ Γ_{300}/Γ_{78}

The experiments here use the charge of the pion in $D^*(2010)^\pm \rightarrow (D^0 \text{ or } \bar{D}^0)\pi^\pm$ decay to tell whether a D^0 or a \bar{D}^0 was born. The $D^0 \rightarrow K^+\pi^+\pi^-$ decay can occur directly by doubly Cabibbo-suppressed (DCS) decay, or indirectly by $D^0 \rightarrow \bar{D}^0$ mixing followed by $\bar{D}^0 \rightarrow K^+\pi^+\pi^-$ decay. Some of the experiments can use the decay-time information to disentangle the two mechanisms. Here, we list the experimental branching ratio, which if there is no mixing is the DCS ratio; in the next data block we give the limits on the mixing ratio.

Some early limits have been omitted from this Listing; see our 1998 edition (EPJ C31).

VALUE (units 10^{-3})	CL%	EVTS	DOCUMENT ID	TECN	COMMENT
3.22 ± 0.05	OUR AVERAGE				
3.22 ± 0.05		42k,11M	¹ AAIJ	16F LHCb	pp at 7, 8 TeV
$3.24 \pm 0.08 \pm 0.07$		3.3k	² WHITE	13 BELL	$e^+e^- \approx \Upsilon(4S)$
4.4 ± 1.3	± 0.4	54	² DYTMAN	01 CLE2	$e^+e^- \approx \Upsilon(4S)$
2.5 ± 3.6	± 0.3		³ AITALA	98 E791	π^- nucl., 500 GeV

- • • We do not use the following data for averages, fits, limits, etc. • • •

3.20 ± 0.18	± 0.13	1.7k	² TIAN	05 BELL	See WHITE 13
<18	90		² AMMAR	91 CLEO	$e^+e^- \approx 10.5$ GeV
<18	90		⁴ ANJOS	88c E691	Photoproduction

- AAIJ 16F result comes from time-dependent analysis that uses external input on the mixing parameters x, y . Without this input, the result is $(3.29 \pm 0.08) \times 10^{-3}$.
- AMMAR 91 cannot and DYTMAN 01, TIAN 05 do not distinguish between doubly Cabibbo-suppressed decay and $D^0-\bar{D}^0$ mixing.
- This AITALA 98 result assumes no $D^0-\bar{D}^0$ mixing (R_M in the note on " $D^0-\bar{D}^0$ Mixing"). It becomes $-0.0020 \pm 0.0117 \pm 0.0035$ when mixing is allowed and decay-time information is used to distinguish doubly Cabibbo-suppressed decays from mixing.
- ANJOS 88c uses decay-time information to distinguish doubly Cabibbo-suppressed (DCS) decays from $D^0-\bar{D}^0$ mixing. However, the result assumes no interference between the DCS and mixing amplitudes ($\gamma = 0$ in the note on " $D^0-\bar{D}^0$ Mixing" near the start of the D^0 Listings). When interference is allowed, the limit degrades to 0.033.

$\Gamma(K^+\pi^+\pi^-\text{ via } \bar{D}^0)/\Gamma(K^-\pi^+\pi^-)$ Γ_{301}/Γ_{78}

This is a $D^0-\bar{D}^0$ mixing limit. The experiments here (1) use the charge of the pion in $D^*(2010)^\pm \rightarrow (D^0 \text{ or } \bar{D}^0)\pi^\pm$ decay to tell whether a D^0 or a \bar{D}^0 was born; and (2) use the decay-time distribution to disentangle doubly Cabibbo-suppressed decay and mixing. For the limits on $|m_{D_1^0} - m_{D_2^0}|$ and $(\Gamma_{D_1^0} - \Gamma_{D_2^0})/\Gamma_{D_0}$ that come from the best mixing limit, see near the beginning of these D^0 Listings.

VALUE (units 10^{-5})	CL%	DOCUMENT ID	TECN	COMMENT
9.6 ± 3.6		¹ AAIJ	16F LHCb	pp at 7, 8 TeV

- • • We do not use the following data for averages, fits, limits, etc. • • •

- AAIJ 16F result comes from an unconstrained decay-time dependent fit to the wrong-sign to right-sign decay rates ratio as $(x^2 + y^2)/2$.
- ANJOS 88c uses decay-time information to distinguish doubly Cabibbo-suppressed (DCS) decays from $D^0-\bar{D}^0$ mixing. However, the result assumes no interference between the DCS and mixing amplitudes ($\gamma = 0$ in the note on " $D^0-\bar{D}^0$ Mixing" near the start of the D^0 Listings). When interference is allowed, the limit degrades to 0.007.

Meson Particle Listings

 D^0 $\Gamma(K^+\pi^- \text{ or } K^+\pi^+2\pi^- \text{ via } \bar{D}^0)/\Gamma(K^-\pi^+ \text{ or } K^-2\pi^+\pi^-)$ Γ_{302}/Γ_0

This is a $D^0\text{-}\bar{D}^0$ mixing limit. For the limits on $|m_{D_1^0} - m_{D_2^0}|$ and $(\Gamma_{D_1^0} - \Gamma_{D_2^0})/\Gamma_{D^0}$ that come from the best mixing limit, see near the beginning of these D^0 Listings.

VALUE	CL%	DOCUMENT ID	TECN	COMMENT
•••				We do not use the following data for averages, fits, limits, etc. •••
<0.0085	90	¹ AITALA	98	E791 π^- nucleus, 500 GeV
<0.0037	90	² ANJOS	88c	E691 Photoproduction

¹ AITALA 98 uses decay-time information to distinguish doubly Cabibbo-suppressed decays from $D^0\text{-}\bar{D}^0$ mixing. The fit allows interference between the two amplitudes, and also allows CP violation in this term. The central value obtained is $0.0039^{+0.0036}_{-0.0032} \pm 0.0016$. When interference is disallowed, the result becomes $0.0021 \pm 0.0009 \pm 0.0002$.

² This combines results of ANJOS 88c on $K^+\pi^-$ and $K^+\pi^+\pi^-$ (via \bar{D}^0) reported in the data block above (see footnotes there). It assumes no interference.

 $\Gamma(\mu^- \text{ anything via } \bar{D}^0)/\Gamma(\mu^+ \text{ anything})$ Γ_{303}/Γ_6

This is a $D^0\text{-}\bar{D}^0$ mixing limit. See the somewhat better limits above.

VALUE	CL%	DOCUMENT ID	TECN	COMMENT
<0.0056	90	LOUIS	86	SPEC π^- W 225 GeV
•••				We do not use the following data for averages, fits, limits, etc. •••
<0.012	90	BENVENUTI	85	CNTR μ C, 200 GeV
<0.044	90	BODEK	82	SPEC π^- , pFe $\rightarrow D^0$

Rare or forbidden modes

 $\Gamma(\gamma\gamma)/\Gamma_{\text{total}}$ Γ_{304}/Γ

$D^0 \rightarrow \gamma\gamma$ is a flavor-changing neutral-current decay, forbidden in the Standard Model at the tree level.

VALUE	CL%	DOCUMENT ID	TECN	COMMENT
< 8.5 $\times 10^{-7}$	90	NISAR	16	BELL e^+e^- at $\Upsilon(4S)$, $\Upsilon(5S)$
•••				We do not use the following data for averages, fits, limits, etc. •••
< 3.8 $\times 10^{-6}$	90	ABLIKIM	15F	BES3 e^+e^- at 3.773 GeV
< 2.2 $\times 10^{-6}$	90	LEES	12L	BABR $e^+e^- \approx 10.58$ GeV
< 2.9 $\times 10^{-6}$	90	COAN	03	CLE2 $e^+e^- \approx \Upsilon(4S)$

 $\Gamma(e^+e^-)/\Gamma_{\text{total}}$ Γ_{305}/Γ

A test for the $\Delta C = 1$ weak neutral current. Allowed by first-order weak interaction combined with electromagnetic interaction.

VALUE	CL%	DOCUMENT ID	TECN	COMMENT
<7.9 $\times 10^{-8}$	90	PETRIC	10	BELL $e^+e^- \approx \Upsilon(4S)$
•••				We do not use the following data for averages, fits, limits, etc. •••
<1.7 $\times 10^{-7}$	90	LEES	12Q	BABR $e^+e^- \approx 10.58$ GeV
<1.2 $\times 10^{-6}$	90	AUBERT,B	04Y	BABR $e^+e^- \approx \Upsilon(4S)$
<8.19 $\times 10^{-6}$	90	PRIPSTEIN	00	E789 p nucleus, 800 GeV
<6.2 $\times 10^{-6}$	90	AITALA	99G	E791 π^- N 500 GeV
<1.3 $\times 10^{-5}$	90	FREYBERGER	96	CLE2 $e^+e^- \approx \Upsilon(4S)$
<1.3 $\times 10^{-4}$	90	ADLER	88	MRK3 e^+e^- 3.77 GeV
<1.7 $\times 10^{-4}$	90	ALBRECHT	88G	ARG e^+e^- 10 GeV
<2.2 $\times 10^{-4}$	90	HAAS	88	CLEO e^+e^- 10 GeV

 $\Gamma(\mu^+\mu^-)/\Gamma_{\text{total}}$ Γ_{306}/Γ

A test for the $\Delta C = 1$ weak neutral current. Allowed by first-order weak interaction combined with electromagnetic interaction.

VALUE	CL%	DOCUMENT ID	TECN	COMMENT
<3.1 $\times 10^{-9}$	90	¹ AAIJ	23R	LHCB pp at 7, 8, 13 TeV
•••				We do not use the following data for averages, fits, limits, etc. •••
<6.2 $\times 10^{-9}$	90	² AAIJ	13AI	LHCB pp at 7 TeV
0.6–8.1 $\times 10^{-7}$	90	³ LEES	12Q	BABR $e^+e^- \approx 10.58$ GeV
<2.1 $\times 10^{-7}$	90	AALTONEN	10X	CDF $p\bar{p}$, $\sqrt{s} = 1.96$ TeV
<1.4 $\times 10^{-7}$	90	PETRIC	10	BELL $e^+e^- \approx \Upsilon(4S)$
<2.0 $\times 10^{-6}$	90	ABT	04	HERB pA , 920 GeV
<1.3 $\times 10^{-6}$	90	AUBERT,B	04Y	BABR $e^+e^- \approx \Upsilon(4S)$
<2.5 $\times 10^{-6}$	90	ACOSTA	03F	CDF See AALTONEN 10x
<1.56 $\times 10^{-5}$	90	PRIPSTEIN	00	E789 p nucleus, 800 GeV
<5.2 $\times 10^{-6}$	90	AITALA	99G	E791 π^- N 500 GeV
<4.1 $\times 10^{-6}$	90	ADAMOVICH	97	BEAT π^- Cu, W 350 GeV
<4.2 $\times 10^{-6}$	90	ALEXOPOU...	96	E771 p Si, 800 GeV
<3.4 $\times 10^{-5}$	90	FREYBERGER	96	CLE2 $e^+e^- \approx \Upsilon(4S)$
<7.6 $\times 10^{-6}$	90	ADAMOVICH	95	BEAT See ADAMOVICH 97
<4.4 $\times 10^{-5}$	90	KODAMA	95	E653 π^- emulsion 600 GeV
<3.1 $\times 10^{-5}$	90	⁴ MISHRA	94	E789 -4.1 ± 4.8 events
<7.0 $\times 10^{-5}$	90	ALBRECHT	88G	ARG e^+e^- 10 GeV
<1.1 $\times 10^{-5}$	90	LOUIS	86	SPEC π^- W 225 GeV
<3.4 $\times 10^{-4}$	90	AUBERT	85	EMC Deep inelast. μ^- N

¹ AAIJ 23R reports a 95% CL limit of $< 3.5 \times 10^{-9}$.

² Superseded by AAIJ 23R.

³ LEES 12Q gives a 2-sided range.

⁴ Here MISHRA 94 uses "the statistical approach advocated by the PDG." For an alternate approach, giving a limit of 9×10^{-6} at 90% confidence level, see the paper.

 $\Gamma(\pi^0 e^+ e^-)/\Gamma_{\text{total}}$ Γ_{307}/Γ

A test for the $\Delta C = 1$ weak neutral current. Allowed by higher-order electroweak interactions.

VALUE	CL%	DOCUMENT ID	TECN	COMMENT
<4 $\times 10^{-6}$	90	ABLIKIM	18P	BES3 e^+e^- , 3773 MeV
•••				We do not use the following data for averages, fits, limits, etc. •••
<4.5 $\times 10^{-5}$	90	FREYBERGER	96	CLE2 $e^+e^- \approx \Upsilon(4S)$

 $\Gamma(\pi^0 \mu^+ \mu^-)/\Gamma_{\text{total}}$ Γ_{308}/Γ

A test for the $\Delta C = 1$ weak neutral current. Allowed by higher-order electroweak interactions.

VALUE	CL%	DOCUMENT ID	TECN	COMMENT
<1.8 $\times 10^{-4}$	90	KODAMA	95	E653 π^- emulsion 600 GeV
•••				We do not use the following data for averages, fits, limits, etc. •••
<5.4 $\times 10^{-4}$	90	FREYBERGER	96	CLE2 $e^+e^- \approx \Upsilon(4S)$

 $\Gamma(\pi^0 \nu \bar{\nu})/\Gamma_{\text{total}}$ Γ_{309}/Γ

A test for the $\Delta C = 1$ weak neutral current. Allowed by higher-order electroweak interactions.

VALUE	CL%	DOCUMENT ID	TECN	COMMENT
<2.1 $\times 10^{-4}$	90	¹ ABLIKIM	22V	BES3 e^+e^- at 3773 MeV

¹ ABLIKIM 22V measurement comes from a sample of 10.6×10^6 $D^0\bar{D}^0$ pairs.

 $\Gamma(\eta e^+ e^-)/\Gamma_{\text{total}}$ Γ_{310}/Γ

A test for the $\Delta C = 1$ weak neutral current. Allowed by higher-order electroweak interactions.

VALUE	CL%	DOCUMENT ID	TECN	COMMENT
<3 $\times 10^{-6}$	90	ABLIKIM	18P	BES3 e^+e^- , 3773 MeV
•••				We do not use the following data for averages, fits, limits, etc. •••
<1.1 $\times 10^{-4}$	90	FREYBERGER	96	CLE2 $e^+e^- \approx \Upsilon(4S)$

 $\Gamma(\eta \mu^+ \mu^-)/\Gamma_{\text{total}}$ Γ_{311}/Γ

A test for the $\Delta C = 1$ weak neutral current. Allowed by higher-order electroweak interactions.

VALUE	CL%	DOCUMENT ID	TECN	COMMENT
<5.3 $\times 10^{-4}$	90	FREYBERGER	96	CLE2 $e^+e^- \approx \Upsilon(4S)$

 $\Gamma(\pi^+\pi^-\pi^+e^+e^-)/\Gamma_{\text{total}}$ Γ_{312}/Γ

A test for the $\Delta C = 1$ weak neutral current. Allowed by higher-order electroweak interactions.

VALUE	CL%	DOCUMENT ID	TECN	COMMENT
<7 $\times 10^{-6}$	90	ABLIKIM	18P	BES3 e^+e^- , 3773 MeV
•••				We do not use the following data for averages, fits, limits, etc. •••
<3.73 $\times 10^{-4}$	90	AITALA	01C	E791 π^- nucleus, 500 GeV

 $\Gamma(\rho^0 e^+ e^-)/\Gamma_{\text{total}}$ Γ_{313}/Γ

A test for the $\Delta C = 1$ weak neutral current. Allowed by higher-order electroweak interactions.

VALUE	CL%	DOCUMENT ID	TECN	COMMENT
<1.0 $\times 10^{-4}$	90	¹ FREYBERGER	96	CLE2 $e^+e^- \approx \Upsilon(4S)$
•••				We do not use the following data for averages, fits, limits, etc. •••
<1.24 $\times 10^{-4}$	90	AITALA	01C	E791 π^- nucleus, 500 GeV
<4.5 $\times 10^{-4}$	90	HAAS	88	CLEO e^+e^- 10 GeV

¹ This FREYBERGER 96 limit is obtained using a phase-space model. The limit changes to $< 1.8 \times 10^{-4}$ using a photon pole amplitude model.

 $\Gamma(\pi^+\pi^-\mu^+\mu^-)/\Gamma_{\text{total}}$ Γ_{314}/Γ

A test for the $\Delta C = 1$ weak neutral current. Allowed by higher-order electroweak interactions.

VALUE (units 10^{-7})	EVTS	DOCUMENT ID	TECN	COMMENT
9.64 $\pm 0.48 \pm 1.10$	561	¹ AAIJ	17B	LHCB pp at 8 TeV

¹ The second AAIJ 17B error is the systematic 0.51×10^{-7} and normalization 0.97×10^{-7} mode errors added in quadrature.

 $\Gamma(\pi^+\pi^-\mu^+\mu^- \text{ (non-res)})/\Gamma_{\text{total}}$ Γ_{315}/Γ

A test for the $\Delta C = 1$ weak neutral current. Allowed by higher-order electroweak interactions.

VALUE	CL%	DOCUMENT ID	TECN	COMMENT
<5.5 $\times 10^{-7}$	90	¹ AAIJ	14B	LHCB pp at 7 TeV
•••				We do not use the following data for averages, fits, limits, etc. •••
<3.0 $\times 10^{-5}$	90	AITALA	01C	E791 π^- nucleus, 500 GeV

¹ AAIJ 14B measures this branching-fraction limit relative to the $\pi^+\pi^-\phi, \phi \rightarrow \mu^+\mu^-$ fraction. The above limit excludes the resonant (ϕ, ω, ρ) regions, and then fills those gaps with a phase-space model.

 $\Gamma(\rho^0 \mu^+ \mu^-)/\Gamma_{\text{total}}$ Γ_{316}/Γ

A test for the $\Delta C = 1$ weak neutral current. Allowed by higher-order electroweak interactions.

VALUE	CL%	DOCUMENT ID	TECN	COMMENT
<2.2 $\times 10^{-5}$	90	AITALA	01C	E791 π^- nucleus, 500 GeV
•••				We do not use the following data for averages, fits, limits, etc. •••
<4.9 $\times 10^{-4}$	90	¹ FREYBERGER	96	CLE2 $e^+e^- \approx \Upsilon(4S)$
<2.3 $\times 10^{-4}$	90	KODAMA	95	E653 π^- emulsion 600 GeV
<8.1 $\times 10^{-4}$	90	HAAS	88	CLEO e^+e^- 10 GeV

¹ This FREYBERGER 96 limit is obtained using a phase-space model. The limit changes to $< 4.5 \times 10^{-4}$ using a photon pole amplitude model.

$\Gamma(\omega e^+ e^-)/\Gamma_{\text{total}}$ Γ_{317}/Γ
 A test for the $\Delta C = 1$ weak neutral current. Allowed by higher-order electroweak interactions.

VALUE	CL%	DOCUMENT ID	TECN	COMMENT
$<6 \times 10^{-6}$	90	ABLIKIM 18P BES3		$e^+ e^-$, 3773 MeV
••• We do not use the following data for averages, fits, limits, etc. •••				
$<1.8 \times 10^{-4}$	90	¹ FREYBERGER 96	CLE2	$e^+ e^- \approx \Upsilon(4S)$

¹This FREYBERGER 96 limit is obtained using a phase-space model. The limit changes to $<2.7 \times 10^{-4}$ using a photon pole amplitude model.

$\Gamma(\omega \mu^+ \mu^-)/\Gamma_{\text{total}}$ Γ_{318}/Γ
 A test for the $\Delta C = 1$ weak neutral current. Allowed by higher-order electroweak interactions.

VALUE	CL%	DOCUMENT ID	TECN	COMMENT
$<8.3 \times 10^{-4}$	90	¹ FREYBERGER 96	CLE2	$e^+ e^- \approx \Upsilon(4S)$

¹This FREYBERGER 96 limit is obtained using a phase-space model. The limit changes to $<6.5 \times 10^{-4}$ using a photon pole amplitude model.

$\Gamma(K^- K^+ e^+ e^-)/\Gamma_{\text{total}}$ Γ_{319}/Γ
 A test for the $\Delta C = 1$ weak neutral current. Allowed by higher-order electroweak interactions.

VALUE	CL%	DOCUMENT ID	TECN	COMMENT
$<1.1 \times 10^{-5}$	90	ABLIKIM 18P BES3		$e^+ e^-$, 3773 MeV
••• We do not use the following data for averages, fits, limits, etc. •••				
$<3.15 \times 10^{-4}$	90	AITALA 01c E791		π^- nucleus, 500 GeV

$\Gamma(K^- \pi^+ e^+ e^-, 675 < m_{ee} < 875 \text{ MeV})/\Gamma_{\text{total}}$ Γ_{327}/Γ
 A test for the $\Delta C = 1$ weak neutral current. Allowed by higher-order electroweak interactions.

VALUE (units 10^{-6})	EVTS	DOCUMENT ID	TECN	COMMENT
$4.0 \pm 0.5 \pm 0.2 \pm 0.1$	68	^{1,2} LEES 19A BABR		$e^+ e^-$ near $\Upsilon(4S)$

¹Observation with 9.7 σ significance. The last uncertainty is due to the uncertainty on the branching fraction of the normalization mode, $D^0 \rightarrow K^- \pi^+ \pi^+ \pi^-$. The second uncertainty is other systematic and is dominated by the model parameterization.

²LEES 19A also sets an upper limit for non-resonant regions, where long-distance effects are expected to be small: $<3.1 \times 10^{-6}$ at 90% CL.

$\Gamma(K^- \pi^+ e^+ e^-, 1.005 < m_{ee} < 1.035 \text{ GeV})/\Gamma_{\text{total}}$ Γ_{328}/Γ
 A test for the $\Delta C = 1$ weak neutral current. Allowed by higher-order electroweak interactions.

VALUE	CL%	DOCUMENT ID	TECN	COMMENT
$<5 \times 10^{-7}$	90	¹ LEES 19A BABR		$e^+ e^-$ near $\Upsilon(4S)$

¹LEES 19A also sets an upper limit for non-resonant regions, where long-distance effects are expected to be small: $<3.1 \times 10^{-6}$ at 90% CL.

$\Gamma(\phi e^+ e^-)/\Gamma_{\text{total}}$ Γ_{320}/Γ
 A test for the $\Delta C = 1$ weak neutral current. Allowed by higher-order electroweak interactions.

VALUE	CL%	DOCUMENT ID	TECN	COMMENT
$<5.2 \times 10^{-5}$	90	¹ FREYBERGER 96	CLE2	$e^+ e^- \approx \Upsilon(4S)$
••• We do not use the following data for averages, fits, limits, etc. •••				
$<5.9 \times 10^{-5}$	90	AITALA 01c E791		π^- nucleus, 500 GeV

¹This FREYBERGER 96 limit is obtained using a phase-space model. The limit changes to $<7.6 \times 10^{-5}$ using a photon pole amplitude model.

$\Gamma(K^- K^+ \mu^+ \mu^-)/\Gamma_{\text{total}}$ Γ_{321}/Γ
 A test for the $\Delta C = 1$ weak neutral current. Allowed by higher-order electroweak interactions.

VALUE (units 10^{-7})	EVTS	DOCUMENT ID	TECN	COMMENT
$1.54 \pm 0.27 \pm 0.18$	34	¹ AAIJ 17BG LHCB		pp at 8 TeV

¹The second AAIJ 17BG error is the systematic 0.09×10^{-7} and normalization 0.16×10^{-7} mode errors added in quadrature.

$\Gamma(K^- K^+ \mu^+ \mu^- (\text{non-res}))/\Gamma_{\text{total}}$ Γ_{322}/Γ
 A test for the $\Delta C = 1$ weak neutral current. Allowed by higher-order electroweak interactions.

VALUE	CL%	DOCUMENT ID	TECN	COMMENT
$<3.3 \times 10^{-5}$	90	AITALA 01c E791		π^- nucleus, 500 GeV

$\Gamma(\phi \mu^+ \mu^-)/\Gamma_{\text{total}}$ Γ_{323}/Γ
 A test for the $\Delta C = 1$ weak neutral current. Allowed by higher-order electroweak interactions.

VALUE	CL%	DOCUMENT ID	TECN	COMMENT
$<3.1 \times 10^{-5}$	90	AITALA 01c E791		π^- nucleus, 500 GeV
••• We do not use the following data for averages, fits, limits, etc. •••				
$<4.1 \times 10^{-4}$	90	¹ FREYBERGER 96	CLE2	$e^+ e^- \approx \Upsilon(4S)$

¹This FREYBERGER 96 limit is obtained using a phase-space model. The limit changes to $<2.4 \times 10^{-4}$ using a photon pole amplitude model.

$\Gamma(\bar{K}^0 e^+ e^-)/\Gamma_{\text{total}}$ Γ_{324}/Γ
 Not a useful test for $\Delta C = 1$ weak neutral current because both quarks must change flavor.

VALUE	CL%	DOCUMENT ID	TECN	COMMENT
$<2.4 \times 10^{-5}$	90	¹ ABLIKIM 18P BES3		$e^+ e^-$, 3773 MeV
••• We do not use the following data for averages, fits, limits, etc. •••				
$<1.1 \times 10^{-4}$	90	FREYBERGER 96	CLE2	$e^+ e^- \approx \Upsilon(4S)$
$<1.7 \times 10^{-3}$	90	ADLER 89c MRK3		$e^+ e^-$ 3.77 GeV

¹ABLIKIM 18P report a 90% C.L. limit on $D^0 \rightarrow K_S^0 e^+ e^-$ of 1.2×10^{-5} which is here interpreted in terms of $D^0 \rightarrow \bar{K}^0 e^+ e^-$.

$\Gamma(\bar{K}^0 \mu^+ \mu^-)/\Gamma_{\text{total}}$ Γ_{325}/Γ
 Not a useful test for $\Delta C = 1$ weak neutral current because both quarks must change flavor.

VALUE	CL%	DOCUMENT ID	TECN	COMMENT
$<2.6 \times 10^{-4}$	90	KODAMA 95 E653		π^- emulsion 600 GeV
••• We do not use the following data for averages, fits, limits, etc. •••				
$<6.7 \times 10^{-4}$	90	FREYBERGER 96	CLE2	$e^+ e^- \approx \Upsilon(4S)$

$\Gamma(K^- \pi^+ e^+ e^-)/\Gamma_{\text{total}}$ Γ_{326}/Γ
 A test for the $\Delta C = 1$ weak neutral current. Allowed by higher-order electroweak interactions.

VALUE	CL%	DOCUMENT ID	TECN	COMMENT
••• We do not use the following data for averages, fits, limits, etc. •••				
$<4.1 \times 10^{-5}$	90	ABLIKIM 18P BES3		see LEES 19A
$<3.85 \times 10^{-4}$	90	AITALA 01c E791		π^- nucleus, 500 GeV

$\Gamma(K^*(892)^0 e^+ e^-)/\Gamma_{\text{total}}$ Γ_{329}/Γ
 Not a useful test for $\Delta C = 1$ weak neutral current because both quarks must change flavor.

VALUE	CL%	DOCUMENT ID	TECN	COMMENT
$<4.7 \times 10^{-5}$	90	AITALA 01c E791		π^- nucleus, 500 GeV
••• We do not use the following data for averages, fits, limits, etc. •••				
$<1.4 \times 10^{-4}$	90	¹ FREYBERGER 96	CLE2	$e^+ e^- \approx \Upsilon(4S)$

¹This FREYBERGER 96 limit is obtained using a phase-space model. The limit changes to $<2.0 \times 10^{-4}$ using a photon pole amplitude model.

$\Gamma(K^- \pi^+ \mu^+ \mu^-)/\Gamma_{\text{total}}$ Γ_{330}/Γ
 A test for the $\Delta C = 1$ weak neutral current. Allowed by higher-order electroweak interactions.

VALUE	CL%	DOCUMENT ID	TECN	COMMENT
$<3.59 \times 10^{-4}$	90	AITALA 01c E791		π^- nucleus, 500 GeV

$\Gamma(K^- \pi^+ \mu^+ \mu^-, 675 < m_{\mu\mu} < 875 \text{ MeV})/\Gamma_{\text{total}}$ Γ_{331}/Γ
 A test for the $\Delta C = 1$ weak neutral current. Allowed by higher-order electroweak interactions.

VALUE (units 10^{-6})	EVTS	DOCUMENT ID	TECN	COMMENT
$4.17 \pm 0.12 \pm 0.40$	2.4k	¹ AAIJ 16i LHCB		pp at 8 TeV

¹AAIJ 16i uses $B(D^0 \rightarrow K^- \pi^+ \pi^+ \pi^-) = (8.287 \pm 0.043 \pm 0.200) \times 10^{-2}$ value for the normalization mode.

$\Gamma(\bar{K}^*(892)^0 \mu^+ \mu^-)/\Gamma_{\text{total}}$ Γ_{332}/Γ
 Not a useful test for $\Delta C = 1$ weak neutral current because both quarks must change flavor.

VALUE	CL%	DOCUMENT ID	TECN	COMMENT
$<2.4 \times 10^{-5}$	90	AITALA 01c E791		π^- nucleus, 500 GeV
••• We do not use the following data for averages, fits, limits, etc. •••				
$<1.18 \times 10^{-3}$	90	¹ FREYBERGER 96	CLE2	$e^+ e^- \approx \Upsilon(4S)$

¹This FREYBERGER 96 limit is obtained using a phase-space model. The limit changes to $<1.0 \times 10^{-3}$ using a photon pole amplitude model.

$\Gamma(\pi^+ \pi^- \pi^0 \mu^+ \mu^-)/\Gamma_{\text{total}}$ Γ_{333}/Γ
 A test for the $\Delta C = 1$ weak neutral current. Allowed by higher-order electroweak interactions.

VALUE	CL%	DOCUMENT ID	TECN	COMMENT
$<8.1 \times 10^{-4}$	90	KODAMA 95 E653		π^- emulsion 600 GeV

$\Gamma(\mu^\pm e^\mp)/\Gamma_{\text{total}}$ Γ_{334}/Γ
 A test of lepton family number conservation.

VALUE	CL%	DOCUMENT ID	TECN	COMMENT
$<1.3 \times 10^{-8}$	90	AAIJ 16H LHCB		pp at 7, 8 GeV
••• We do not use the following data for averages, fits, limits, etc. •••				
$<3.3 \times 10^{-7}$	90	LEES 12Q BABR		$e^+ e^- \approx 10.58 \text{ GeV}$
$<2.6 \times 10^{-7}$	90	PETRIC 10 BELL		$e^+ e^- \approx \Upsilon(4S)$
$<8.1 \times 10^{-7}$	90	AUBERT.B 04Y BABR		$e^+ e^- \approx \Upsilon(4S)$
$<1.72 \times 10^{-5}$	90	PRIPSTEIN 00 E789		p nucleus, 800 GeV
$<8.1 \times 10^{-6}$	90	AITALA 99G E791		$\pi^- N$ 500 GeV
$<1.9 \times 10^{-5}$	90	¹ FREYBERGER 96	CLE2	$e^+ e^- \approx \Upsilon(4S)$
$<1.0 \times 10^{-4}$	90	ALBRECHT 88G ARG		$e^+ e^-$ 10 GeV
$<2.7 \times 10^{-4}$	90	HAAS 88 CLEO		$e^+ e^-$ 10 GeV
$<1.2 \times 10^{-4}$	90	BECKER 87C MRK3		$e^+ e^-$ 3.77 GeV
$<9 \times 10^{-4}$	90	PALKA 87 SILI		200 GeV pp
$<21 \times 10^{-4}$	90	² RILES 87 MRK2		$e^+ e^-$ 29 GeV

¹This is the corrected result given in the erratum to FREYBERGER 96.

²RILES 87 assumes $B(D \rightarrow K\pi) = 3.0\%$ and has production model dependency.

$\Gamma(\pi^0 e^\pm \mu^\mp)/\Gamma_{\text{total}}$ Γ_{335}/Γ
 A test of lepton family number conservation. The value is for the sum of the two charge states.

VALUE	CL%	DOCUMENT ID	TECN	COMMENT
$<8.0 \times 10^{-7}$	90	LEES 20A BABR		$e^+ e^-$ at $\Upsilon(4S)$
••• We do not use the following data for averages, fits, limits, etc. •••				
$<8.6 \times 10^{-5}$	90	FREYBERGER 96	CLE2	$e^+ e^- \approx \Upsilon(4S)$

Meson Particle Listings

 D^0

$\Gamma(\eta e^\pm \mu^\mp)/\Gamma_{\text{total}}$ Γ_{336}/Γ
 A test of lepton family number conservation. The value is for the sum of the two charge states.

VALUE	CL%	DOCUMENT ID	TECN	COMMENT
$<22.5 \times 10^{-7}$	90	¹ LEES	20A	BABR e^+e^- at $\Upsilon(4S)$
••• We do not use the following data for averages, fits, limits, etc. •••				
$<1.0 \times 10^{-4}$	90	FREYBERGER 96	CLE2	$e^+e^- \approx \Upsilon(4S)$
¹ LEES 20A quotes separate limits $B(D^0 \rightarrow \eta e^\pm \mu^\mp, \eta \rightarrow \gamma\gamma) < 24.0 \times 10^{-7}$ and $B(D^0 \rightarrow \eta e^\pm \mu^\mp, \eta \rightarrow \pi^+\pi^-\pi^0) < 43.0 \times 10^{-7}$.				

$\Gamma(\pi^+\pi^- e^\pm \mu^\mp)/\Gamma_{\text{total}}$ Γ_{337}/Γ
 A test of lepton family-number conservation.

VALUE	CL%	DOCUMENT ID	TECN	COMMENT
$<1.71 \times 10^{-6}$	90	LEES	20B	BABR e^+e^- at $\Upsilon(4S)$
••• We do not use the following data for averages, fits, limits, etc. •••				
$<1.5 \times 10^{-5}$	90	AITALA	01c	E791 π^- nucleus, 500 GeV

$\Gamma(\rho^0 e^\pm \mu^\mp)/\Gamma_{\text{total}}$ Γ_{338}/Γ
 A test of lepton family number conservation. The value is for the sum of the two charge states.

VALUE	CL%	DOCUMENT ID	TECN	COMMENT
$<5.0 \times 10^{-7}$	90	LEES	20A	BABR e^+e^- at $\Upsilon(4S)$
••• We do not use the following data for averages, fits, limits, etc. •••				
$<6.6 \times 10^{-5}$	90	AITALA	01c	E791 π^- nucleus, 500 GeV
$<4.9 \times 10^{-5}$	90	¹ FREYBERGER 96	CLE2	$e^+e^- \approx \Upsilon(4S)$

¹ This FREYBERGER 96 limit is obtained using a phase-space model. The limit changes to $<5.0 \times 10^{-5}$ using a photon pole amplitude model.

$\Gamma(\omega e^\pm \mu^\mp)/\Gamma_{\text{total}}$ Γ_{339}/Γ
 A test of lepton family number conservation. The value is for the sum of the two charge states.

VALUE	CL%	DOCUMENT ID	TECN	COMMENT
$<17.1 \times 10^{-7}$	90	LEES	20A	BABR e^+e^- at $\Upsilon(4S)$
••• We do not use the following data for averages, fits, limits, etc. •••				
$<1.2 \times 10^{-4}$	90	¹ FREYBERGER 96	CLE2	$e^+e^- \approx \Upsilon(4S)$

¹ This FREYBERGER 96 limit is obtained using a phase-space model. The same limit is obtained using a photon pole amplitude model.

$\Gamma(K^- K^+ e^\pm \mu^\mp)/\Gamma_{\text{total}}$ Γ_{340}/Γ
 A test of lepton family-number conservation.

VALUE	CL%	DOCUMENT ID	TECN	COMMENT
$<1.00 \times 10^{-6}$	90	LEES	20B	BABR e^+e^- at $\Upsilon(4S)$
••• We do not use the following data for averages, fits, limits, etc. •••				
$<1.8 \times 10^{-4}$	90	AITALA	01c	E791 π^- nucleus, 500 GeV

$\Gamma(\phi e^\pm \mu^\mp)/\Gamma_{\text{total}}$ Γ_{341}/Γ
 A test of lepton family number conservation. The value is for the sum of the two charge states.

VALUE	CL%	DOCUMENT ID	TECN	COMMENT
$<5.1 \times 10^{-7}$	90	LEES	20A	BABR e^+e^- at $\Upsilon(4S)$
••• We do not use the following data for averages, fits, limits, etc. •••				
$<4.7 \times 10^{-5}$	90	AITALA	01c	E791 π^- nucleus, 500 GeV
$<3.4 \times 10^{-5}$	90	¹ FREYBERGER 96	CLE2	$e^+e^- \approx \Upsilon(4S)$

¹ This FREYBERGER 96 limit is obtained using a phase-space model. The limit changes to $<3.3 \times 10^{-5}$ using a photon pole amplitude model.

$\Gamma(K^0 e^\pm \mu^\mp)/\Gamma_{\text{total}}$ Γ_{342}/Γ
 A test of lepton family number conservation. The value is for the sum of the two charge states.

VALUE	CL%	DOCUMENT ID	TECN	COMMENT
$<17.4 \times 10^{-7}$	90	¹ LEES	20A	BABR e^+e^- at $\Upsilon(4S)$
••• We do not use the following data for averages, fits, limits, etc. •••				
$<1.0 \times 10^{-4}$	90	FREYBERGER 96	CLE2	$e^+e^- \approx \Upsilon(4S)$
¹ LEES 20A quotes $B(D^0 \rightarrow K_S^0 e^\pm \mu^\mp) < 8.7 \times 10^{-7}$ at 90% CL.				

$\Gamma(K^- \pi^+ e^\pm \mu^\mp)/\Gamma_{\text{total}}$ Γ_{343}/Γ
 A test of lepton family-number conservation.

VALUE	CL%	DOCUMENT ID	TECN	COMMENT
$<1.90 \times 10^{-6}$	90	LEES	20B	BABR e^+e^- at $\Upsilon(4S)$
••• We do not use the following data for averages, fits, limits, etc. •••				
$<5.53 \times 10^{-4}$	90	AITALA	01c	E791 π^- nucleus, 500 GeV

$\Gamma(K^*(892)^0 e^\pm \mu^\mp)/\Gamma_{\text{total}}$ Γ_{344}/Γ
 A test of lepton family number conservation. The value is for the sum of the two charge states.

VALUE	CL%	DOCUMENT ID	TECN	COMMENT
$<12.5 \times 10^{-7}$	90	LEES	20A	BABR e^+e^- at $\Upsilon(4S)$
••• We do not use the following data for averages, fits, limits, etc. •••				
$<8.3 \times 10^{-5}$	90	AITALA	01c	E791 π^- nucleus, 500 GeV
$<1.0 \times 10^{-4}$	90	¹ FREYBERGER 96	CLE2	$e^+e^- \approx \Upsilon(4S)$

¹ This FREYBERGER 96 limit is obtained using a phase-space model. The same limit is obtained using a photon pole amplitude model.

$\Gamma(2\pi^- 2e^+)/\Gamma_{\text{total}}$ Γ_{345}/Γ
 A test of lepton-number conservation.

VALUE	CL%	DOCUMENT ID	TECN	COMMENT
$<9.1 \times 10^{-7}$	90	LEES	20B	BABR e^+e^- at $\Upsilon(4S)$
••• We do not use the following data for averages, fits, limits, etc. •••				
$<1.12 \times 10^{-4}$	90	¹ AITALA	01c	E791 π^- nucleus, 500 GeV
¹ Value includes decay to the charge conjugate state.				

$\Gamma(2\pi^- 2\mu^+)/\Gamma_{\text{total}}$ Γ_{346}/Γ
 A test of lepton-number conservation.

VALUE	CL%	DOCUMENT ID	TECN	COMMENT
$<1.52 \times 10^{-6}$	90	LEES	20B	BABR e^+e^- at $\Upsilon(4S)$
••• We do not use the following data for averages, fits, limits, etc. •••				
$<2.9 \times 10^{-5}$	90	¹ AITALA	01c	E791 π^- nucleus, 500 GeV
¹ Value includes decay to the charge conjugate state.				

$\Gamma(K^- \pi^- 2e^+)/\Gamma_{\text{total}}$ Γ_{347}/Γ
 A test of lepton-number conservation.

VALUE	CL%	DOCUMENT ID	TECN	COMMENT
$<5.0 \times 10^{-7}$	90	LEES	20B	BABR e^+e^- at $\Upsilon(4S)$
••• We do not use the following data for averages, fits, limits, etc. •••				
$<2.8 \times 10^{-6}$	90	ABLIKIM	19AL	BES3 e^+e^- at 3773 MeV
$<2.06 \times 10^{-4}$	90	¹ AITALA	01c	E791 π^- nucleus, 500 GeV
¹ Value includes decay to the charge conjugate state.				

$\Gamma(K^- \pi^- 2\mu^+)/\Gamma_{\text{total}}$ Γ_{348}/Γ
 A test of lepton-number conservation.

VALUE	CL%	DOCUMENT ID	TECN	COMMENT
$<5.3 \times 10^{-7}$	90	LEES	20B	BABR e^+e^- at $\Upsilon(4S)$
••• We do not use the following data for averages, fits, limits, etc. •••				
$<3.9 \times 10^{-4}$	90	¹ AITALA	01c	E791 π^- nucleus, 500 GeV
¹ Value includes decay to the charge conjugate state.				

$\Gamma(2K^- 2e^+)/\Gamma_{\text{total}}$ Γ_{349}/Γ
 A test of lepton-number conservation.

VALUE	CL%	DOCUMENT ID	TECN	COMMENT
$<3.4 \times 10^{-7}$	90	LEES	20B	BABR e^+e^- at $\Upsilon(4S)$
••• We do not use the following data for averages, fits, limits, etc. •••				
$<1.52 \times 10^{-4}$	90	¹ AITALA	01c	E791 π^- nucleus, 500 GeV
¹ Value includes decay to the charge conjugate state.				

$\Gamma(2K^- 2\mu^+)/\Gamma_{\text{total}}$ Γ_{350}/Γ
 A test of lepton-number conservation.

VALUE	CL%	DOCUMENT ID	TECN	COMMENT
$<1.0 \times 10^{-7}$	90	LEES	20B	BABR e^+e^- at $\Upsilon(4S)$
••• We do not use the following data for averages, fits, limits, etc. •••				
$<9.4 \times 10^{-5}$	90	¹ AITALA	01c	E791 π^- nucleus, 500 GeV
¹ Value includes decay to the charge conjugate state.				

$\Gamma(\pi^- \pi^- e^+ \mu^+)/\Gamma_{\text{total}}$ Γ_{351}/Γ
 A test of lepton-number conservation.

VALUE	CL%	DOCUMENT ID	TECN	COMMENT
$<3.06 \times 10^{-6}$	90	LEES	20B	BABR e^+e^- at $\Upsilon(4S)$
••• We do not use the following data for averages, fits, limits, etc. •••				
$<7.9 \times 10^{-5}$	90	¹ AITALA	01c	E791 π^- nucleus, 500 GeV
¹ Value includes decay to the charge conjugate state.				

$\Gamma(K^- \pi^- e^+ \mu^+)/\Gamma_{\text{total}}$ Γ_{352}/Γ
 A test of lepton-number conservation.

VALUE	CL%	DOCUMENT ID	TECN	COMMENT
$<2.10 \times 10^{-6}$	90	LEES	20B	BABR e^+e^- at $\Upsilon(4S)$
••• We do not use the following data for averages, fits, limits, etc. •••				
$<2.18 \times 10^{-4}$	90	¹ AITALA	01c	E791 π^- nucleus, 500 GeV
¹ Value includes decay to the charge conjugate state.				

$\Gamma(2K^- e^+ \mu^+)/\Gamma_{\text{total}}$ Γ_{353}/Γ
 A test of lepton-number conservation.

VALUE	CL%	DOCUMENT ID	TECN	COMMENT
$<5.8 \times 10^{-7}$	90	LEES	20B	BABR e^+e^- at $\Upsilon(4S)$
••• We do not use the following data for averages, fits, limits, etc. •••				
$<5.7 \times 10^{-5}$	90	¹ AITALA	01c	E791 π^- nucleus, 500 GeV
¹ Value includes decay to the charge conjugate state.				

$\Gamma(p e^-)/\Gamma_{\text{total}}$ Γ_{354}/Γ
 A test of baryon- and lepton-number conservation.

VALUE	CL%	DOCUMENT ID	TECN	COMMENT
$<2.2 \times 10^{-6}$	90	ABLIKIM	22T	BES3 e^+e^- at 3.773 GeV
••• We do not use the following data for averages, fits, limits, etc. •••				
$<1.0 \times 10^{-5}$	90	¹ RUBIN	09	CLEO e^+e^- at $\psi(3770)$
¹ This RUBIN 09 limit is for either $D^0 \rightarrow p e^-$ or $\bar{D}^0 \rightarrow \bar{p} e^-$ decay.				

$\Gamma(\bar{p}e^+)/\Gamma_{\text{total}}$

A test of baryon- and lepton-number conservation.

VALUE	CL%	DOCUMENT ID	TECN	COMMENT
$<1.2 \times 10^{-6}$	90	ABLIKIM 22T	BES3	e^+e^- at 3.773 GeV
••• We do not use the following data for averages, fits, limits, etc. •••				
$<1.1 \times 10^{-5}$	90	¹ RUBIN 09	CLEO	e^+e^- at $\psi(3770)$
¹ This RUBIN 09 limit is for either $D^0 \rightarrow \bar{p}e^+$ or $\bar{D}^0 \rightarrow \bar{p}e^+$ decay.				

 Γ_{355}/Γ D^0 CP-VIOLATING DECAY-RATE ASYMMETRIESThis is the difference between D^0 and \bar{D}^0 partial widths for the decay to state f , divided by the sum of the widths:

$$A_{CP}(f) = [\Gamma(D^0 \rightarrow f) - \Gamma(\bar{D}^0 \rightarrow \bar{f})] / [\Gamma(D^0 \rightarrow f) + \Gamma(\bar{D}^0 \rightarrow \bar{f})].$$

 $A_{CP}(K^+K^-)$ in $D^0, \bar{D}^0 \rightarrow K^+K^-$

VALUE (units 10^{-4})	EVTS	DOCUMENT ID	TECN	COMMENT
4 ± 5 OUR AVERAGE				
6.8 ± 5.4 ± 1.6	37M	¹ AAIJ	23Ac	LHCB pp at 13 TeV
4 ± 12 ± 10	4.56M	AAIJ	17M	LHCB pp 7, 8 TeV
-24 ± 22 ± 9	476k	² AALTONEN	12B	CDF $p\bar{p}$, $\sqrt{s}=1.96$ TeV
0 ± 34 ± 13	129k	³ AUBERT	08M	BABR $e^+e^- \approx 10.6$ GeV
-43 ± 30 ± 11	120k	⁴ STARIC	08	BELL $e^+e^- \approx \Upsilon(4S)$
200 ± 120 ± 60		⁵ ACOSTA	05c	CDF $p\bar{p}$, $\sqrt{s}=1.96$ TeV
0 ± 220 ± 80	3023	⁵ CSORNA	02	CLE2 $e^+e^- \approx \Upsilon(4S)$
-10 ± 220 ± 150	3330	⁵ LINK	00B	FOCS
-100 ± 490 ± 120	609	⁵ AITALA	98c	E791 $-0.093 < A_{CP} < +0.073$ (90% CL)

••• We do not use the following data for averages, fits, limits, etc. •••

-6 ± 15 ± 10 1.8M ²AAIJ 14Ak LHCB See AAIJ 17M

¹AAIJ 23Ac result comes from 5.7 fb⁻¹ of data. Also reports the values of the direct CP asymmetries, $a_{CP}^{\pi\pi} = (23.2 \pm 6.1) \times 10^{-4}$ and $a_{CP}^{KK} = (7.7 \pm 5.7) \times 10^{-4}$, with a correlation of 88%, obtained using previous determinations of $A_{CP}(K^+K^-)$, ΔA_{CP} , ΔY , the reconstructed mean decay times of $D^0 \rightarrow \pi\pi$ and $D^0 \rightarrow KK$ in the aforementioned measurements, and the world average of the D^0 lifetime (PDG 22).

²See also "D⁰ CP-violating asymmetry differences" at the end of the CP-violating asymmetries.

³AUBERT 08M uses corrected numbers of events directly, not ratios with $K^{\mp}\pi^{\pm}$ events.

⁴STARIC 08 uses $D^0 \rightarrow K^-\pi^+$ and $\bar{D}^0 \rightarrow K^+\pi^-$ decays to correct for detector-induced asymmetries.

⁵AITALA 98c, LINK 00B, CSORNA 02, and ACOSTA 05c measure $N(D^0 \rightarrow K^+K^-)/N(D^0 \rightarrow K^-\pi^+)$, the ratio of numbers of events observed, and similarly for the \bar{D}^0 .

 $A_{CP}(K_S^0 K_S^0)$ in $D^0, \bar{D}^0 \rightarrow K_S^0 K_S^0$

VALUE (%)	EVTS	DOCUMENT ID	TECN	COMMENT
-1.9 ± 1.1 OUR AVERAGE				Error includes scale factor of 1.1.
-3.1 ± 1.2 ± 0.5	8.1k	¹ AAIJ	21X	LHCB pp at 13 TeV
-0.02 ± 1.53 ± 0.17	5.4k	² DASH	17	BELL At/near $\Upsilon(4S)$, $\Upsilon(5S)$
-2.9 ± 5.2 ± 2.2	630	AAIJ	15At	LHCB pp at 7, 8 TeV
-23 ± 19	65	BONVICINI	01	CLE2 $e^+e^- \approx 10.6$ GeV

••• We do not use the following data for averages, fits, limits, etc. •••

2.3 ± 2.8 ± 0.9 1.7k AAIJ 18Av LHCB see AAIJ 21X

¹AAIJ 21X reports a value of $(-3.1 \pm 1.2 \pm 0.4 \pm 0.2) \times 10^{-2}$ where the third uncertainty is from $A_{CP}(K^+K^-) = 0.04 \pm 0.12 \pm 0.10\%$, as measured by LHCB. We have added the systematic uncertainties in quadrature. Supersedes AAIJ 18Av.

²The systematic uncertainty is dominated by the uncertainty on A_{CP} in the control channel $D^0 \rightarrow K_S^0 \pi^0$.

 $A_{CP}(\pi^+\pi^-)$ in $D^0, \bar{D}^0 \rightarrow \pi^+\pi^-$

VALUE (%)	EVTS	DOCUMENT ID	TECN	COMMENT
0.13 ± 0.14 OUR AVERAGE				
0.07 ± 0.14 ± 0.11		¹ AAIJ	17M	LHCB pp 7, 8 TeV
0.22 ± 0.24 ± 0.11	215k	² AALTONEN	12B	CDF $p\bar{p}$, $\sqrt{s}=1.96$ TeV
-0.24 ± 0.52 ± 0.22	63.7k	³ AUBERT	08M	BABR $e^+e^- \approx 10.6$ GeV
0.43 ± 0.52 ± 0.12	51k	⁴ STARIC	08	BELL $e^+e^- \approx \Upsilon(4S)$
1.0 ± 1.3 ± 0.6		⁵ ACOSTA	05c	CDF $p\bar{p}$, $\sqrt{s}=1.96$ TeV
1.9 ± 3.2 ± 0.8	1136	⁵ CSORNA	02	CLE2 $e^+e^- \approx \Upsilon(4S)$
4.8 ± 3.9 ± 2.5	1177	⁵ LINK	00B	FOCS
-4.9 ± 7.8 ± 3.0	343	⁵ AITALA	98c	E791 $-0.186 < A_{CP} < +0.088$ (90% CL)

••• We do not use the following data for averages, fits, limits, etc. •••

-0.20 ± 0.19 ± 0.10 774k ^{2,6}AAIJ 14Ak LHCB See AAIJ 17M

¹AAIJ 17M value combines $\Delta A_{CP}(\pi\pi, K^+K^-)$ from AAIJ 16d, $A_{CP}(K^+K^-)$ from AAIJ 17M, and $A_{CP}(\pi\pi)$ from AAIJ 14Ak.

²See also "D⁰ CP-violating asymmetry differences" at the end of the CP-violating asymmetries.

³AUBERT 08M uses corrected numbers of events directly, not ratios with $K^{\mp}\pi^{\pm}$ events.

⁴STARIC 08 uses $D^0 \rightarrow K^-\pi^+$ and $\bar{D}^0 \rightarrow K^+\pi^-$ decays to correct for detector-induced asymmetries.

⁵AITALA 98c, LINK 00B, CSORNA 02, and ACOSTA 05c measure $N(D^0 \rightarrow \pi^+\pi^-)/N(D^0 \rightarrow K^-\pi^+)$, the ratio of numbers of events observed, and similarly for the \bar{D}^0 .

⁶AAIJ 14Ak uses $\Delta A_{CP}(\pi\pi, K^+K^-)$ and $A_{CP}(K^+K^-)$ reported in the same paper.

 $A_{CP}(\pi^0\pi^0)$ in $D^0, \bar{D}^0 \rightarrow \pi^0\pi^0$

VALUE (%)	EVTS	DOCUMENT ID	TECN	COMMENT
0.0 ± 0.6 OUR AVERAGE				
-0.03 ± 0.64 ± 0.10	34k	NISAR	14	BELL e^+e^- at/near Υ 's
0.1 ± 4.8	810	BONVICINI	01	CLE2 $e^+e^- \approx 10.6$ GeV

 D^0 CP-EVEN FRACTIONS

The CP-even fraction F_+ , defined for self-conjugate final states, like the coherence factor is useful for measuring the unitary triangle angle γ in $B \rightarrow DK$ decays. A purely CP-even state has $F_+ = 1$, a CP-odd one has $F_+ = 0$. For details, see NAYAK 15.

CP-even fraction in $D^0 \rightarrow K_S^0 \pi^+ \pi^- \pi^0$ decays

VALUE (%)	DOCUMENT ID	TECN	COMMENT
23.6 ± 0.9 OUR AVERAGE			
23.5 ± 1.0 ± 0.2	ABLIKIM 23Av	BES3	e^+e^- at $\psi(3770)$, 2.93 fb ⁻¹
23.8 ± 1.2 ± 1.2	¹ RESMI 18		Uses CLEO-c data
¹ Obtained by analyzing CLEO-c data but not authored by the CLEO Collaboration.			

CP-even fraction in $D^0 \rightarrow \pi^+ \pi^- \pi^0$ decays

VALUE (%)	DOCUMENT ID	TECN	COMMENT
97.3 ± 1.7	MALDE 15		Uses CLEO data
••• We do not use the following data for averages, fits, limits, etc. •••			
96.8 ± 1.7 ± 0.6	NAYAK 15		see MALDE 15

CP-even fraction in $D^0 \rightarrow \pi^+ \pi^- \pi^+ \pi^-$ decays

VALUE (%)	DOCUMENT ID	TECN	COMMENT
74.6 ± 1.6 OUR AVERAGE			Error includes scale factor of 1.2.
73.5 ± 1.5 ± 0.5	¹ ABLIKIM 22Bf	BES3	2.93 fb ⁻¹ in e^+e^- at 3.773 GeV
76.9 ± 2.1 ± 1.0	² HARNEW 18		Uses CLEO-c data
••• We do not use the following data for averages, fits, limits, etc. •••			
72.9 ± 0.9 ± 1.8	^{2,3} DARGENT 17		from amplitude model
73.7 ± 2.8	MALDE 15		CLEO amplitude model independent

¹A combination of three consistent measurements with CP-eigenstate, quasi-CP-eigenstate and CP-mixed tags.

²Obtained by analyzing CLEO-c data but not authored by the CLEO Collaboration.

³MALDE 15 and DARGENT 17 use different CLEO data sets, so in principle their results could be averaged. However, given the importance that model-independence has in the use of this value, we exclude the amplitude model-derived result from the average.

CP-even fraction in $D^0 \rightarrow \pi^+ \pi^- 2\pi^0$ decays

VALUE	EVTS	DOCUMENT ID	TECN	COMMENT
0.682 ± 0.077	236	ABLIKIM 22Bg	BES3	e^+e^- at 3.773 GeV

CP-even fraction in $D^0 \rightarrow 2\pi^+ 2\pi^- \pi^0$ decays

VALUE	EVTS	DOCUMENT ID	TECN	COMMENT
0.438 ± 0.104	73	ABLIKIM 22Bg	BES3	e^+e^- at 3.773 GeV

CP-even fraction in $D^0 \rightarrow \pi^+ \pi^- 3\pi^0$ decays

VALUE	EVTS	DOCUMENT ID	TECN	COMMENT
0.520 +0.338 -0.269	12 ^{+4.9} _{-3.9}	ABLIKIM 22Bg	BES3	e^+e^- at 3.773 GeV

CP-even fraction in $D^0 \rightarrow 2\pi^+ 2\pi^- 2\pi^0$ decays

VALUE	EVTS	DOCUMENT ID	TECN	COMMENT
0.790 +0.269 -0.255	19	ABLIKIM 22Bg	BES3	e^+e^- at 3.773 GeV

CP-even fraction in $D^0 \rightarrow K^+ K^- \pi^0$ decays

VALUE (%)	DOCUMENT ID	TECN	COMMENT
73.2 ± 5.5	MALDE 15		Uses CLEO data
••• We do not use the following data for averages, fits, limits, etc. •••			
73.1 ± 5.8 ± 2.1	NAYAK 15		see MALDE 15

CP-even fraction in $D^0 \rightarrow K^+ K^- \pi^+ \pi^-$ decays

VALUE (%)	DOCUMENT ID	TECN	COMMENT
74.1 ± 3.0 OUR AVERAGE			
73.0 ± 3.7 ± 2.1	¹ ABLIKIM 23Aj	BES3	2.93 fb ⁻¹ , e^+e^- at $\psi(3770)$
75.3 ± 1.8 ± 3.9	² DARGENT 17		from amplitude model

¹A combined measurement of the CP-even fraction using both CP tags and $K_{S,L}^0 \pi^+ \pi^-$ tags. ABLIKIM 23Aj reports CP-even fractions $0.704 \pm 0.042 \pm 0.028$ and $0.798 \pm 0.077 \pm 0.019$ for the former and latter tags, respectively.

²Obtained by analyzing CLEO data but not authored by the CLEO Collaboration.

Meson Particle Listings

 D^0 $A_{CP}(\rho\gamma)$ in $D^0, \bar{D}^0 \rightarrow \rho\gamma$

VALUE (units 10^{-2})	DOCUMENT ID	TECN	COMMENT
$5.6 \pm 15.2 \pm 0.6$	NANUT	17	BELL e^+e^- at $\Upsilon(nS)$, $n=2,3,4,5$

 $A_{CP}(\phi\gamma)$ in $D^0, \bar{D}^0 \rightarrow \phi\gamma$

VALUE (units 10^{-2})	DOCUMENT ID	TECN	COMMENT
$-9.4 \pm 6.6 \pm 0.1$	NANUT	17	BELL e^+e^- at $\Upsilon(nS)$, $n=2,3,4,5$

 $A_{CP}(K^*(892)^0\gamma)$ in $D^0, \bar{D}^0 \rightarrow K^*(892)^0\gamma$

VALUE (units 10^{-2})	DOCUMENT ID	TECN	COMMENT
$-0.3 \pm 2.0 \pm 0.0$	NANUT	17	BELL e^+e^- at $\Upsilon(nS)$, $n=2,3,4,5$

 $A_{CP}(\pi^+\pi^-\pi^0)$ in $D^0, \bar{D}^0 \rightarrow \pi^+\pi^-\pi^0$

VALUE (%)	EVTS	DOCUMENT ID	TECN	COMMENT
0.4 ± 0.4	OUR AVERAGE			
$+0.6 \pm 0.9 \pm 0.4$	12.8k	ABLIKIM	22Bg BES3	e^+e^- at 3.773 GeV
0.43 ± 1.30	123k	ARINSTEIN	08 BELL	$e^+e^- \approx \Upsilon(4S)$
$0.31 \pm 0.41 \pm 0.17$	80k	¹ AUBERT	08a0 BABR	$e^+e^- \approx 10.6$ GeV
$1 \pm \frac{+9}{-7} \pm 5$		CRONIN-HEN..05	CLEO	$e^+e^- \approx 10$ GeV

¹ AUBERT 08a0 report their result using a different sign convention.

 $A_{CP}(\eta\pi^+\pi^-)$ in $D^0, \bar{D}^0 \rightarrow \eta\pi^+\pi^-$

VALUE (units 10^{-2})	EVTS	DOCUMENT ID	TECN	COMMENT
$0.9 \pm 1.2 \pm 0.5$	13k	LI	21g BELL	e^+e^- at $\Upsilon(nS)$
• • • We do not use the following data for averages, fits, limits, etc. • • •				
$9.6 \pm 5.4 \pm 1.8$	450	ABLIKIM	20g BES3	e^+e^- at 3.773 GeV

 $A_{CP}(\rho(770)^+\pi^-)$ in $D^0 \rightarrow \pi^+\pi^-\pi^0$ in $D^0 \rightarrow \rho^+\pi^-, \bar{D}^0 \rightarrow \rho^-\pi^+$

VALUE (%)	DOCUMENT ID	TECN	COMMENT
$+1.2 \pm 0.8 \pm 0.3$	AUBERT	08a0 BABR	Table 1, -Col.5/2×Col.2

 $A_{CP}(\rho(770)^0\pi^0)$ in $D^0, \bar{D}^0 \rightarrow \rho^0\pi^0$

VALUE (%)	DOCUMENT ID	TECN	COMMENT
$-3.1 \pm 2.7 \pm 1.2$	AUBERT	08a0 BABR	Table 1, -Col.5/2×Col.2

 $A_{CP}(\rho(770)^-\pi^+)$ in $D^0 \rightarrow \pi^+\pi^-\pi^0$ in $D^0 \rightarrow \rho^-\pi^+, \bar{D}^0 \rightarrow \rho^+\pi^-$

VALUE (%)	DOCUMENT ID	TECN	COMMENT
$-1.0 \pm 1.6 \pm 0.7$	AUBERT	08a0 BABR	Table 1, -Col.5/2×Col.2

 $A_{CP}(\rho(1450)^+\pi^-)$ in $D^0 \rightarrow \pi^+\pi^-\pi^0$ in $D^0 \rightarrow \rho(1450)^+\pi^-, \bar{D}^0 \rightarrow c.c.$

VALUE (%)	DOCUMENT ID	TECN	COMMENT
$0 \pm 50 \pm 50$	AUBERT	08a0 BABR	Table 1, -Col.5/2×Col.2

 $A_{CP}(\rho(1450)^0\pi^0)$ in $D^0, \bar{D}^0 \rightarrow \rho(1450)^0\pi^0$

VALUE (%)	DOCUMENT ID	TECN	COMMENT
$-17 \pm 33 \pm 17$	AUBERT	08a0 BABR	Table 1, -Col.5/2×Col.2

 $A_{CP}(\rho(1450)^-\pi^+)$ in $D^0 \rightarrow \pi^+\pi^-\pi^0$ in $D^0 \rightarrow \rho(1450)^-\pi^+, \bar{D}^0 \rightarrow c.c.$

VALUE (%)	DOCUMENT ID	TECN	COMMENT
$+6 \pm 8 \pm 3$	AUBERT	08a0 BABR	Table 1, -Col.5/2×Col.2

 $A_{CP}(\rho(1700)^+\pi^-)$ in $D^0 \rightarrow \pi^+\pi^-\pi^0$ in $D^0 \rightarrow \rho(1700)^+\pi^-, \bar{D}^0 \rightarrow c.c.$

VALUE (%)	DOCUMENT ID	TECN	COMMENT
$-5 \pm 13 \pm 5$	AUBERT	08a0 BABR	Table 1, -Col.5/2×Col.2

 $A_{CP}(\rho(1700)^0\pi^0)$ in $D^0, \bar{D}^0 \rightarrow \rho(1700)^0\pi^0$

VALUE (%)	DOCUMENT ID	TECN	COMMENT
$+13 \pm 8 \pm 3$	AUBERT	08a0 BABR	Table 1, -Col.5/2×Col.2

 $A_{CP}(\rho(1700)^-\pi^+)$ in $D^0 \rightarrow \pi^+\pi^-\pi^0$ in $D^0 \rightarrow \rho(1700)^-\pi^+, \bar{D}^0 \rightarrow c.c.$

VALUE (%)	DOCUMENT ID	TECN	COMMENT
$+8 \pm 10 \pm 5$	AUBERT	08a0 BABR	Table 1, -Col.5/2×Col.2

 $A_{CP}(f_0(980)\pi^0)$ in $D^0, \bar{D}^0 \rightarrow f_0(980)\pi^0$

VALUE (%)	DOCUMENT ID	TECN	COMMENT
$0 \pm 25 \pm 25$	AUBERT	08a0 BABR	Table 1, -Col.5/2×Col.2

 $A_{CP}(f_0(1370)\pi^0)$ in $D^0, \bar{D}^0 \rightarrow f_0(1370)\pi^0$

VALUE (%)	DOCUMENT ID	TECN	COMMENT
$+25 \pm 13 \pm 13$	AUBERT	08a0 BABR	Table 1, -Col.5/2×Col.2

 $A_{CP}(f_0(1500)\pi^0)$ in $D^0, \bar{D}^0 \rightarrow f_0(1500)\pi^0$

VALUE (%)	DOCUMENT ID	TECN	COMMENT
$0 \pm 13 \pm 13$	AUBERT	08a0 BABR	Table 1, -Col.5/2×Col.2

 $A_{CP}(f_0(1710)\pi^0)$ in $D^0, \bar{D}^0 \rightarrow f_0(1710)\pi^0$

VALUE (%)	DOCUMENT ID	TECN	COMMENT
$0 \pm 17 \pm 17$	AUBERT	08a0 BABR	Table 1, -Col.5/2×Col.2

 $A_{CP}(f_2(1270)\pi^0)$ in $D^0, \bar{D}^0 \rightarrow f_2(1270)\pi^0$

VALUE (%)	DOCUMENT ID	TECN	COMMENT
$-4 \pm 4 \pm 4$	AUBERT	08a0 BABR	Table 1, -Col.5/2×Col.2

 $A_{CP}(\sigma(400)\pi^0)$ in $D^0, \bar{D}^0 \rightarrow \sigma(400)\pi^0$

VALUE (%)	DOCUMENT ID	TECN	COMMENT
$+6 \pm 6 \pm 6$	AUBERT	08a0 BABR	Table 1, -Col.5/2×Col.2

 $A_{CP}(\text{nonresonant } \pi^+\pi^-\pi^0)$ in $D^0, \bar{D}^0 \rightarrow \text{nonresonant } \pi^+\pi^-\pi^0$

VALUE (%)	DOCUMENT ID	TECN	COMMENT
$-13 \pm 19 \pm 13$	AUBERT	08a0 BABR	Table 1, -Col.5/2×Col.2

 $A_{CP}(\pi^+\pi^-\pi^0)$ in $D^0, \bar{D}^0 \rightarrow \pi^+\pi^-\pi^0$

VALUE (%)	EVTS	DOCUMENT ID	TECN	COMMENT
$-2.5 \pm 1.9 \pm 0.7$	3.8k	ABLIKIM	22Bg BES3	e^+e^- at 3.773 GeV

 $A_{CP}(2\pi^+2\pi^-)$ in $D^0, \bar{D}^0 \rightarrow 2\pi^+2\pi^-$

VALUE (%)	EVTS	DOCUMENT ID	TECN	COMMENT
$0.54 \pm 1.04 \pm 0.51$	7.3k	^{1,2} DARGENT	17	e^+e^- at $\psi(3770)$

¹ Decay rate asymmetry integrated in decay time and across full 4π phase space.

² Obtained by analyzing CLEO-c data but not authored by the CLEO Collaboration.

 $A_{CP}(a_1(1260)^+\pi^-)$ in $D^0 \rightarrow 2\pi^+2\pi^-$ in $D^0 \rightarrow a_1(1260)^+\pi^-, \bar{D}^0 \rightarrow c.c.$

VALUE (%)	EVTS	DOCUMENT ID	COMMENT
$4.7 \pm 2.6 \pm 4.9$	7.3k	¹ DARGENT	17 4-body fit, 4π evts

¹ Obtained by analyzing CLEO-c data but not authored by the CLEO Collaboration.

 $A_{CP}(a_1(1260)^-\pi^+)$ in $D^0 \rightarrow 2\pi^+2\pi^-$ in $D^0 \rightarrow a_1(1260)^-\pi^+, \bar{D}^0 \rightarrow c.c.$

VALUE (%)	EVTS	DOCUMENT ID	COMMENT
$13.7 \pm 13.8 \pm 11.4$	7.3k	¹ DARGENT	17 4-body fit, 4π evts

¹ Obtained by analyzing CLEO-c data but not authored by the CLEO Collaboration.

 $A_{CP}(\pi(1300)^+\pi^-)$ in $D^0 \rightarrow 2\pi^+2\pi^-$ in $D^0 \rightarrow \pi(1300)^+\pi^-, \bar{D}^0 \rightarrow c.c.$

VALUE (%)	EVTS	DOCUMENT ID	COMMENT
$-1.6 \pm 12.9 \pm 6.7$	7.3k	¹ DARGENT	17 4-body fit, 4π evts

¹ Obtained by analyzing CLEO-c data but not authored by the CLEO Collaboration.

 $A_{CP}(\pi(1300)^-\pi^+)$ in $D^0 \rightarrow 2\pi^+2\pi^-$ in $D^0 \rightarrow \pi(1300)^-\pi^+, \bar{D}^0 \rightarrow c.c.$

VALUE (%)	EVTS	DOCUMENT ID	COMMENT
$-5.6 \pm 11.9 \pm 27.7$	7.3k	¹ DARGENT	17 4-body fit, 4π evts

¹ Obtained by analyzing CLEO-c data but not authored by the CLEO Collaboration.

 $A_{CP}(a_1(1640)^+\pi^-)$ in $D^0 \rightarrow 2\pi^+2\pi^-$ in $D^0 \rightarrow a_1(1640)^+\pi^-, \bar{D}^0 \rightarrow c.c.$

VALUE (%)	EVTS	DOCUMENT ID	COMMENT
$8.6 \pm 17.8 \pm 19.3$	7.3k	¹ DARGENT	17 4-body fit, 4π evts

¹ Obtained by analyzing CLEO-c data but not authored by the CLEO Collaboration.

 $A_{CP}(\pi_2(1670)^+\pi^-)$ in $D^0 \rightarrow 2\pi^+2\pi^-$ in $D^0 \rightarrow \pi_2(1670)^+\pi^-, \bar{D}^0 \rightarrow c.c.$

VALUE (%)	EVTS	DOCUMENT ID	COMMENT
$7.3 \pm 15.1 \pm 10.4$	7.3k	¹ DARGENT	17 4-body fit, 4π evts

¹ Obtained by analyzing CLEO-c data but not authored by the CLEO Collaboration.

 $A_{CP}(\sigma f_0(1370))$ in $D^0, \bar{D}^0 \rightarrow \sigma f_0(1370)$

VALUE (%)	EVTS	DOCUMENT ID	COMMENT
$-14.6 \pm 16.5 \pm 9.4$	7.3k	¹ DARGENT	17 4-body fit, 4π evts

¹ Obtained by analyzing CLEO-c data but not authored by the CLEO Collaboration.

 $A_{CP}(\sigma\rho(770)^0)$ in $D^0, \bar{D}^0 \rightarrow \sigma\rho(770)^0$

VALUE (%)	EVTS	DOCUMENT ID	COMMENT
$2.5 \pm 16.8 \pm 20.8$	7.3k	¹ DARGENT	17 4-body fit, 4π evts

¹ Obtained by analyzing CLEO-c data but not authored by the CLEO Collaboration.

 $A_{CP}(2\rho(770)^0)$ in $D^0, \bar{D}^0 \rightarrow 2\rho(770)^0$

VALUE (%)	EVTS	DOCUMENT ID	COMMENT
$-5.6 \pm 5.0 \pm 2.9$	7.3k	¹ DARGENT	17 4-body fit, 4π evts

¹ Obtained by analyzing CLEO-c data but not authored by the CLEO Collaboration.

 $A_{CP}(2f_2(1270))$ in $D^0, \bar{D}^0 \rightarrow 2f_2(1270)$

VALUE (%)	EVTS	DOCUMENT ID	COMMENT
$-28.3 \pm 12.3 \pm 20.9$	7.3k	¹ DARGENT	17 4-body fit, 4π evts

¹ Obtained by analyzing CLEO-c data but not authored by the CLEO Collaboration.

 $A_{CP}(\pi^+\pi^-\pi^0\eta)$ in $D^0, \bar{D}^0 \rightarrow \pi^+\pi^-\pi^0\eta$

VALUE (units 10^{-2})	EVTS	DOCUMENT ID	TECN	COMMENT
$-5.5 \pm 5.2 \pm 2.4$	510	ABLIKIM	20v BES3	e^+e^- , 3773 MeV

 $A_{CP}(K^+K^-\pi^0)$ in $D^0, \bar{D}^0 \rightarrow K^+K^-\pi^0$

VALUE (%)	EVTS	DOCUMENT ID	TECN	COMMENT
$-1.00 \pm 1.67 \pm 0.25$	11 ± 0.11 k	AUBERT	08a0 BABR	$e^+e^- \approx 10.6$ GeV

 $A_{CP}(K^*(892)^+K^-)$ in $D^0 \rightarrow K^+K^-\pi^0$ in $D^0 \rightarrow K^*(892)^+K^-, \bar{D}^0 \rightarrow c.c.$

VALUE (%)	DOCUMENT ID	TECN	COMMENT
$-0.9 \pm 1.2 \pm 0.4$	¹ AUBERT	08a0 BABR	Table 1, -Col.5/2×Col.2

¹ AUBERT 08a0 report their result using a different sign convention.

$A_{CP}(K^*(1410)^+ K^- \rightarrow K^+ K^- \pi^0)$ in $D^0, \bar{D}^0 \rightarrow K^*(1410)^+ K^-, \bar{D}^0 \rightarrow$ c.c.

VALUE (%)	DOCUMENT ID	TECN	COMMENT
$-21 \pm 23 \pm 8$	AUBERT	08A0 BABR	Table 1, -Col.5/2×Col.2

 $A_{CP}((K^+ \pi^0)_{S-wave} K^- \rightarrow K^+ K^- \pi^0)$ in $D^0, \bar{D}^0 \rightarrow (K^+ \pi^0)_S K^-, \bar{D}^0 \rightarrow$ c.c.

VALUE (%)	DOCUMENT ID	TECN	COMMENT
$+7 \pm 15 \pm 3$	AUBERT	08A0 BABR	Table 1, -Col.5/2×Col.2

 $A_{CP}(\phi(1020) \pi^0 \rightarrow K^+ K^- \pi^0)$ in $D^0, \bar{D}^0 \rightarrow \phi(1020) \pi^0$

VALUE (%)	DOCUMENT ID	TECN	COMMENT
$+1.1 \pm 2.1 \pm 0.5$	AUBERT	08A0 BABR	Table 1, -Col.5/2×Col.2

 $A_{CP}(f_0(980) \pi^0 \rightarrow K^+ K^- \pi^0)$ in $D^0, \bar{D}^0 \rightarrow f_0(980) \pi^0$

VALUE (%)	DOCUMENT ID	TECN	COMMENT
$-3 \pm 19 \pm 1$	AUBERT	08A0 BABR	Table 1, -Col.5/2×Col.2

 $A_{CP}(a_0(980) \pi^0 \rightarrow K^+ K^- \pi^0)$ in $D^0, \bar{D}^0 \rightarrow a_0(980) \pi^0$

VALUE (%)	DOCUMENT ID	TECN	COMMENT
$-5 \pm 16 \pm 2$	¹ AUBERT	08A0 BABR	Table 1, -Col.5/2×Col.2

¹This AUBERT 08A0 value is obtained when the $a_0(980)^0$ replaces the $f_0(980)$ in the fit.

 $A_{CP}(f'_2(1525) \pi^0 \rightarrow K^+ K^- \pi^0)$ in $D^0, \bar{D}^0 \rightarrow f'_2(1525) \pi^0$

VALUE (%)	DOCUMENT ID	TECN	COMMENT
$0 \pm 50 \pm 150$	AUBERT	08A0 BABR	Table 1, -Col.5/2×Col.2

 $A_{CP}(K^*(892)^- K^+ \rightarrow K^+ K^- \pi^0)$ in $D^0 \rightarrow K^*(892)^- K^+, \bar{D}^0 \rightarrow$ c.c.

VALUE (%)	DOCUMENT ID	TECN	COMMENT
$-5 \pm 4 \pm 1$	AUBERT	08A0 BABR	Table 1, -Col.5/2×Col.2

 $A_{CP}(K^*(1410)^- K^+ \rightarrow K^+ K^- \pi^0)$ in $D^0 \rightarrow K^*(1410)^- K^+, \bar{D}^0 \rightarrow$ c.c.

VALUE (%)	DOCUMENT ID	TECN	COMMENT
$-17 \pm 28 \pm 7$	AUBERT	08A0 BABR	Table 1, -Col.5/2×Col.2

 $A_{CP}((K^- \pi^0)_{S-wave} K^+ \rightarrow K^+ K^- \pi^0)$ in $D^0 \rightarrow (K^- \pi^0)_S K^+, \bar{D}^0 \rightarrow$ c.c.

VALUE (%)	DOCUMENT ID	TECN	COMMENT
$-7 \pm 40 \pm 8$	AUBERT	08A0 BABR	Table 1, -Col.5/2×Col.2

 $A_{CP}(K^+ K^- \eta)$ in $D^0, \bar{D}^0 \rightarrow K^+ K^- \eta$

VALUE (units 10^{-2})	EVTS	DOCUMENT ID	TECN	COMMENT
$-1.4 \pm 3.3 \pm 1.1$	1.4k	LI	21G BELL	$e^+ e^-$ at $\Upsilon(nS)$

 $A_{CP}(\phi(1020) \eta \rightarrow K^+ K^- \eta)$ in $D^0, \bar{D}^0 \rightarrow \phi(1020) \eta$

VALUE (units 10^{-2})	EVTS	DOCUMENT ID	TECN	COMMENT
$-1.9 \pm 4.4 \pm 0.6$	1.4k	LI	21G BELL	$e^+ e^-$ at $\Upsilon(nS)$

 $A_{CP}(K_S^0 \pi^0)$ in $D^0, \bar{D}^0 \rightarrow K_S^0 \pi^0$

VALUE (%)	EVTS	DOCUMENT ID	TECN	COMMENT
-0.20 ± 0.17 OUR AVERAGE				

$-0.21 \pm 0.16 \pm 0.07$	467k	¹ NISAR	14 BELL	$e^+ e^-$ at near Υ 's
0.1 ± 1.3	9099	BONVICINI	01 CLE2	$e^+ e^- \approx 10.6$ GeV

••• We do not use the following data for averages, fits, limits, etc. •••

$-0.28 \pm 0.19 \pm 0.10$	326k	KO	11 BELL	See NISAR 14
-1.8 ± 3.0		BARTELT	95 CLE2	See BONVICINI 01

¹After subtracting CPV in $K^0 - \bar{K}^0$ mixing, NISAR 14 gets $A_{CP} = (+0.12 \pm 0.16 \pm 0.07)\%$.

 $A_{CP}(K_S^0 \eta)$ in $D^0, \bar{D}^0 \rightarrow K_S^0 \eta$

VALUE (%)	EVTS	DOCUMENT ID	TECN	COMMENT
$+0.54 \pm 0.51 \pm 0.16$	46k	KO	11 BELL	$e^+ e^- \approx \Upsilon(4S)$

 $A_{CP}(K_S^0 \eta')$ in $D^0, \bar{D}^0 \rightarrow K_S^0 \eta'$

VALUE (%)	EVTS	DOCUMENT ID	TECN	COMMENT
$+0.98 \pm 0.67 \pm 0.14$	27k	KO	11 BELL	$e^+ e^- \approx \Upsilon(4S)$

 $A_{CP}(K_S^0 \phi)$ in $D^0, \bar{D}^0 \rightarrow K_S^0 \phi$

VALUE (%)	DOCUMENT ID	TECN	COMMENT
-2.8 ± 9.4	BARTELT	95 CLE2	$-18.2 < A_{CP} < +12.6\%$ (90% CL)

 $A_{CP}(K^\mp \pi^\pm)$ in $D^0 \rightarrow K^- \pi^+, \bar{D}^0 \rightarrow K^+ \pi^-$

VALUE (%)	EVTS	DOCUMENT ID	TECN	COMMENT
0.2 ± 0.5 OUR AVERAGE				

-0.01 ± 0.91		AAIJ	18k LHCB	pp at 7, 8, 13 TeV
$0.3 \pm 0.3 \pm 0.6$		BONVICINI	14 CLEO	All CLEO-c runs

••• We do not use the following data for averages, fits, limits, etc. •••

$+0.5 \pm 0.4 \pm 0.9$	150k	MENDEZ	10 CLEO	See BONVICINI 14
$-0.4 \pm 0.5 \pm 0.9$		DOBBS	07 CLEO	See BONVICINI 14

 $A_{CP}(K^\pm \pi^\mp)$ in $D^0 \rightarrow K^+ \pi^-, \bar{D}^0 \rightarrow K^- \pi^+$

VALUE (%)	EVTS	DOCUMENT ID	TECN	COMMENT
-0.9 ± 1.4 OUR AVERAGE				

-1.7 ± 1.6		^{1,2} AAIJ	17A0 LHCB	pp at 7,8 TeV
$-2.1 \pm 5.2 \pm 1.5$	4.0k	AUBERT	07W BABR	$e^+ e^- \approx 10.6$ GeV
$+2.3 \pm 4.7$	4.0k	³ ZHANG	06 BELL	$e^+ e^-$

$+18 \pm 14 \pm 4$		⁴ LINK	05H FOCS	γ nucleus
$+9.5 \pm 6.1 \pm 8.3$		⁵ AUBERT	03z BABR	$e^+ e^-$, 10.6 GeV
$+2 \pm 19 \pm 20$	± 1	⁶ GODANG	00 CLE2	$e^+ e^-$

••• We do not use the following data for averages, fits, limits, etc. •••

-0.7 ± 1.9		¹ AAIJ	13CE LHCB	Repl. by AAJ 17A0
-8.0 ± 7.7	0.8k	⁷ LI	05A BELL	See ZHANG 06

¹Based on 3 fb⁻¹ of data collected at $\sqrt{s} = 7, 8$ TeV. Allowing for CP violation, the direct CP-violation in mixing is reported for the $D^0 \rightarrow K^+ \pi^-$ and $\bar{D}^0 \rightarrow K^+ \pi^-$.

²The CPV is derived from $A_{CP} = (R_D^+ - R_D^-)/(R_D^+ + R_D^-)$.

³This ZHANG 06 result allows mixing.

⁴This LINK 05H result assumes no mixing. If mixing is allowed, it becomes $0.13_{-0.25}^{+0.33} \pm 0.10$.

⁵This AUBERT 03z limit assumes no mixing. If mixing is allowed, the 95% confidence-level interval is $(-2.8 < A_D < 4.9) \times 10^{-3}$.

⁶This GODANG 00 result assumes no $D^0 - \bar{D}^0$ mixing and becomes $-0.43 < A_{CP} < +0.34$ at 95% CL. If mixing is allowed $A_{CP} = -0.01_{-0.17}^{+0.16} \pm 0.01$.

⁷This LI 05A result allows mixing.

 $A_{CP}(K^- \pi^+) \text{ in } D_{CP(\pm 1)} \rightarrow K^\mp \pi^\pm$

$$A_{CP}(K^- \pi^+) = [B(D_{CP(-)} \rightarrow K^- \pi^+) - B(D_{CP(+)} \rightarrow K^- \pi^+)] / \text{Sum}$$

VALUE (%)	DOCUMENT ID	TECN	COMMENT
13.1 ± 1.0 OUR AVERAGE			

$13.2 \pm 1.1 \pm 0.7$	¹ ABLIKIM	22BMBES3	$e^+ e^-$ at $\psi(3770)$
------------------------	----------------------	----------	---------------------------

$13.0 \pm 1.2 \pm 0.8$	² ABLIKIM	22BMBES3	$D^0 \rightarrow \pi^+ \pi^- \pi^0$ reference
------------------------	----------------------	----------	---

••• We do not use the following data for averages, fits, limits, etc. •••

$12.7 \pm 1.3 \pm 0.7$	³ ABLIKIM	14c BES3	$e^+ e^- \rightarrow D^0 \bar{D}^0$, 3.77 GeV
------------------------	----------------------	----------	--

¹ABLIKIM 22b uses quantum correlations in $e^+ e^- \rightarrow D^0 \bar{D}^0$ at the $\psi(3770)$ to measure the asymmetry of the branching fraction of $D^0 \rightarrow K^- \pi^+$ in CP-odd and CP-even eigenstates. It then extracts the strong-phase difference $\delta_{K\pi}$.

²ABLIKIM 22b uses quantum correlations in $e^+ e^- \rightarrow D^0 \bar{D}^0$ at the $\psi(3770)$ to measure the asymmetry of the branching fraction of $D^0 \rightarrow K^- \pi^+$ in CP-odd and CP-even eigenstates, using the predominantly CP-even decay $D^0 \rightarrow \pi^+ \pi^- \pi^0$ mode as reference. It then extracts the strong-phase difference $\delta_{K\pi}$.

³ABLIKIM 14c uses quantum correlations in $e^+ e^- \rightarrow D^0 \bar{D}^0$ at the $\psi(3770)$ to measure the asymmetry of the branching fraction of $D^0 \rightarrow K^- \pi^+$ in CP-odd and CP-even eigenstates. It then extracts the strong-phase difference $\delta_{K\pi}$. Superseded by ABLIKIM 22b.

 $A_{CP}(K^\mp \pi^\pm \pi^0)$ in $D^0 \rightarrow K^- \pi^+ \pi^0, \bar{D}^0 \rightarrow K^+ \pi^- \pi^0$

VALUE (%)	DOCUMENT ID	TECN	COMMENT
0.1 ± 0.5 OUR AVERAGE			

$0.1 \pm 0.3 \pm 0.4$	BONVICINI	14 CLEO	All CLEO-c runs
-----------------------	-----------	---------	-----------------

-3.1 ± 8.6	¹ KOPP	01 CLE2	$e^+ e^- \approx 10.6$ GeV
----------------	-------------------	---------	----------------------------

••• We do not use the following data for averages, fits, limits, etc. •••

$0.2 \pm 0.4 \pm 0.8$	DOBBS	07 CLEO	See BONVICINI 14
-----------------------	-------	---------	------------------

¹KOPP 01 fits separately the D^0 and \bar{D}^0 Dalitz plots and then calculates the integrated difference of normalized densities divided by the integrated sum.

 $A_{CP}(K^\pm \pi^\mp \pi^0)$ in $D^0 \rightarrow K^+ \pi^- \pi^0, \bar{D}^0 \rightarrow K^- \pi^+ \pi^0$

VALUE (%)	EVTS	DOCUMENT ID	TECN	COMMENT
0 ± 5 OUR AVERAGE				

-0.6 ± 5.3	1978 ± 104	TIAN	05 BELL	$e^+ e^- \approx \Upsilon(4S)$
----------------	----------------	------	---------	--------------------------------

$+9 \pm 25 \pm 22$	38	BRANDENB...	01 CLE2	$e^+ e^- \approx \Upsilon(4S)$
--------------------	----	-------------	---------	--------------------------------

 $A_{CP}(K_S^0 \pi^+ \pi^-)$ in $D^0, \bar{D}^0 \rightarrow K_S^0 \pi^+ \pi^-$

VALUE (%)	EVTS	DOCUMENT ID	TECN	COMMENT
-0.1 ± 0.8 OUR AVERAGE				

$-0.05 \pm 0.57 \pm 0.54$	350k	¹ AALTONEN	12AD CDF	
---------------------------	------	-----------------------	----------	--

$-0.9 \pm 2.1 \pm 1.6 \pm 5.7$	4854	² ASNER	04A CLEO	$e^+ e^- \approx 10$ GeV
--------------------------------	------	--------------------	----------	--------------------------

¹This is the overall result of AALTONEN 12AD. Following are the 15 CP fit-fraction asymmetries from the amplitude analysis of the D^0 and $\bar{D}^0 \rightarrow K_S^0 \pi^+ \pi^-$ Dalitz plots.

²This is the overall result of ASNER 04A; CP-violating limits are also given below for each of the 10 resonant submodes found in an amplitude analysis of the D^0 and $\bar{D}^0 \rightarrow K_S^0 \pi^+ \pi^-$ Dalitz plots.

 $A_{CP}(K^\mp \pi^\pm \eta)$ in $D^0, \bar{D}^0 \rightarrow K^\mp \pi^\pm \eta$

VALUE (units 10^{-2})	EVTS	DOCUMENT ID	TECN	COMMENT
$-1.9 \pm 1.3 \pm 1.0$	6.1k	ABLIKIM	20V BES3	$e^+ e^-$, 3773 MeV

 $A_{CP}(K_S^0 \pi^0 \eta)$ in $D^0, \bar{D}^0 \rightarrow K_S^0 \pi^0 \eta$

VALUE (units 10^{-2})	EVTS	DOCUMENT ID	TECN	COMMENT
$-3.9 \pm 3.2 \pm 0.8$	1.1k	ABLIKIM	20V BES3	$e^+ e^-$, 3773 MeV

 $A_{CP}(K^\mp \pi^\pm \pi^0 \eta)$ in $D^0, \bar{D}^0 \rightarrow K^\mp \pi^\pm \pi^0 \eta$

VALUE (units 10^{-2})	EVTS	DOCUMENT ID	TECN	COMMENT
$-7.9 \pm 4.8 \pm 2.5$	580	ABLIKIM	20V BES3	$e^+ e^-$, 3773 MeV

Meson Particle Listings

 D^0

$A_{CP}(K^*(892)^{\mp}\pi^{\pm} \rightarrow K_S^0\pi^+\pi^-)$ in $D^0 \rightarrow K^{*-}\pi^+, \bar{D}^0 \rightarrow K^{*+}\pi^-$

VALUE (%)	DOCUMENT ID	TECN	COMMENT
$+0.36 \pm 0.33 \pm 0.40$	AALTONEN	12AD CDF	Dalitz fit, $\sim 350k$ evts
••• We do not use the following data for averages, fits, limits, etc. •••			
$+2.5 \pm 1.9 \pm_{-0.8}^{+3.3}$	ASNER	04A CLEO	Dalitz fit, 4854 evts

$A_{CP}(K^*(892)^{\pm}\pi^{\mp} \rightarrow K_S^0\pi^+\pi^-)$ in $D^0 \rightarrow K^{*+}\pi^-, \bar{D}^0 \rightarrow K^{*-}\pi^+$

This is a doubly Cabibbo-suppressed mode.

VALUE (%)	DOCUMENT ID	TECN	COMMENT
$+1.0 \pm 5.7 \pm 2.1$	AALTONEN	12AD CDF	Dalitz fit, $\sim 350k$ evts
••• We do not use the following data for averages, fits, limits, etc. •••			
$-21 \pm 42 \pm 28$	ASNER	04A CLEO	Dalitz fit, 4854 evts

$A_{CP}(K_S^0\rho^0 \rightarrow K_S^0\pi^+\pi^-)$ in $D^0 \rightarrow \bar{K}^0\rho^0, \bar{D}^0 \rightarrow K^0\rho^0$

VALUE (%)	DOCUMENT ID	TECN	COMMENT
$-0.05 \pm 0.50 \pm 0.08$	AALTONEN	12AD CDF	Dalitz fit, $\sim 350k$ evts
••• We do not use the following data for averages, fits, limits, etc. •••			
$+3.1 \pm 3.8 \pm_{-2.2}^{+2.7}$	ASNER	04A CLEO	Dalitz fit, 4854 evts

$A_{CP}(K_S^0\omega \rightarrow K_S^0\pi^+\pi^-)$ in $D^0 \rightarrow \bar{K}^0\omega, \bar{D}^0 \rightarrow K^0\omega$

VALUE (%)	DOCUMENT ID	TECN	COMMENT
$-12.6 \pm 6.0 \pm 2.6$	AALTONEN	12AD CDF	Dalitz fit, $\sim 350k$ evts
••• We do not use the following data for averages, fits, limits, etc. •••			
$-26 \pm 24 \pm_{-4}^{+22}$	ASNER	04A CLEO	Dalitz fit, 4854 evts

$A_{CP}(K_S^0f_0(980) \rightarrow K_S^0\pi^+\pi^-)$ in $D^0 \rightarrow \bar{K}^0f_0(980), \bar{D}^0 \rightarrow K^0f_0(980)$

VALUE (%)	DOCUMENT ID	TECN	COMMENT
$-0.4 \pm 2.2 \pm 1.6$	AALTONEN	12AD CDF	Dalitz fit, $\sim 350k$ evts
••• We do not use the following data for averages, fits, limits, etc. •••			
$-4.7 \pm 11.0 \pm_{-8.8}^{+24.9}$	ASNER	04A CLEO	Dalitz fit, 4854 evts

$A_{CP}(K_S^0f_2(1270) \rightarrow K_S^0\pi^+\pi^-)$ in $D^0 \rightarrow \bar{K}^0f_2(1270), \bar{D}^0 \rightarrow K^0f_2(1270)$

VALUE (%)	DOCUMENT ID	TECN	COMMENT
$-4.0 \pm 3.4 \pm 3.0$	AALTONEN	12AD CDF	Dalitz fit, $\sim 350k$ evts
••• We do not use the following data for averages, fits, limits, etc. •••			
$+34 \pm 51 \pm_{-79}^{+33}$	ASNER	04A CLEO	Dalitz fit, 4854 evts

$A_{CP}(K_S^0f_0(1370) \rightarrow K_S^0\pi^+\pi^-)$ in $D^0 \rightarrow \bar{K}^0f_0(1370), \bar{D}^0 \rightarrow K^0f_0(1370)$

VALUE (%)	DOCUMENT ID	TECN	COMMENT
$-0.5 \pm 4.6 \pm 7.7$	AALTONEN	12AD CDF	Dalitz fit, $\sim 350k$ evts
••• We do not use the following data for averages, fits, limits, etc. •••			
$+18 \pm 10 \pm_{-22}^{+13}$	ASNER	04A CLEO	Dalitz fit, 4854 evts

$A_{CP}(K_S^0\rho^0(1450) \rightarrow K_S^0\pi^+\pi^-)$ in $D^0 \rightarrow \bar{K}^0\rho^0(1450), \bar{D}^0 \rightarrow K^0\rho^0(1450)$

VALUE (%)	DOCUMENT ID	TECN	COMMENT
$-4.1 \pm 5.2 \pm 8.1$	AALTONEN	12AD CDF	Dalitz fit, $\sim 350k$ evts

$A_{CP}(K_S^0f_0(600) \rightarrow K_S^0\pi^+\pi^-)$ in $D^0 \rightarrow \bar{K}^0f_0(600), \bar{D}^0 \rightarrow K^0f_0(600)$

VALUE (%)	DOCUMENT ID	TECN	COMMENT
$-2.7 \pm 2.7 \pm 3.6$	AALTONEN	12AD CDF	Dalitz fit, $\sim 350k$ evts

$A_{CP}(K^*(1410)^{\mp}\pi^{\pm} \rightarrow K^*(1410)^-\pi^+, \bar{D}^0 \rightarrow K^*(1410)^+\pi^-$

VALUE (%)	DOCUMENT ID	TECN	COMMENT
$-2.3 \pm 5.7 \pm 6.4$	AALTONEN	12AD CDF	Dalitz fit, $\sim 350k$ evts

$A_{CP}(K_0^*(1430)^{\mp}\pi^{\pm} \rightarrow K_S^0\pi^+\pi^-)$ in $D^0 \rightarrow K_0^*(1430)^-\pi^+, \bar{D}^0 \rightarrow c.c.$

VALUE (%)	DOCUMENT ID	TECN	COMMENT
$4.0 \pm 2.4 \pm 3.8$	AALTONEN	12AD CDF	Dalitz fit, $\sim 350k$ evts
••• We do not use the following data for averages, fits, limits, etc. •••			
$-0.2 \pm 11.3 \pm_{-5.0}^{+8.8}$	ASNER	04A CLEO	Dalitz fit, 4854 evts

$A_{CP}(K_0^*(1430)^{\pm}\pi^{\mp} \rightarrow K_0^*(1430)^+\pi^-, \bar{D}^0 \rightarrow K_0^*(1430)^-\pi^+$

This is a doubly Cabibbo-suppressed mode.

VALUE (%)	DOCUMENT ID	TECN	COMMENT
$+12 \pm 11 \pm 10$	AALTONEN	12AD CDF	Dalitz fit, $\sim 350k$ evts

$A_{CP}(K_2^*(1430)^{\mp}\pi^{\pm} \rightarrow K_S^0\pi^+\pi^-)$ in $D^0 \rightarrow K_2^*(1430)^-\pi^+, \bar{D}^0 \rightarrow c.c.$

VALUE (%)	DOCUMENT ID	TECN	COMMENT
$+2.9 \pm 4.0 \pm 4.1$	AALTONEN	12AD CDF	Dalitz fit, $\sim 350k$ evts
••• We do not use the following data for averages, fits, limits, etc. •••			
$-7 \pm 25 \pm_{-26}^{+13}$	ASNER	04A CLEO	Dalitz fit, 4854 evts

$A_{CP}(K_2^*(1430)^{\pm}\pi^{\mp} \rightarrow K_2^*(1430)^+\pi^-, \bar{D}^0 \rightarrow K_2^*(1430)^-\pi^+$

This is a doubly Cabibbo-suppressed mode.

VALUE (%)	DOCUMENT ID	TECN	COMMENT
$-10 \pm 14 \pm 29$	AALTONEN	12AD CDF	Dalitz fit, $\sim 350k$ evts

$A_{CP}(K^*(1680)^{\mp}\pi^{\pm} \rightarrow K_S^0\pi^+\pi^-)$ in $D^0 \rightarrow K^*(1680)^-\pi^+, \bar{D}^0 \rightarrow c.c.$

VALUE (%)	DOCUMENT ID	TECN	COMMENT
••• We do not use the following data for averages, fits, limits, etc. •••			
$-36 \pm 19 \pm_{-35}^{+10}$	ASNER	04A CLEO	Dalitz fit, 4854 evts

$A_{CP}(K^-\pi^+\pi^+\pi^-)$ in $D^0 \rightarrow K^-\pi^+\pi^+\pi^-, \bar{D}^0 \rightarrow K^+\pi^-\pi^-\pi^+$

VALUE (%)	DOCUMENT ID	TECN	COMMENT
$0.2 \pm 0.3 \pm 0.4$	BONVICINI	14 CLEO	All CLEO-c runs
••• We do not use the following data for averages, fits, limits, etc. •••			
$+0.7 \pm 0.5 \pm 0.9$	DOBBS	07 CLEO	See BONVICINI 14

$A_{CP}(K^{\pm}\pi^{\mp}\pi^+\pi^-)$ in $D^0 \rightarrow K^+\pi^-\pi^+\pi^-, \bar{D}^0 \rightarrow K^-\pi^+\pi^+\pi^-$

VALUE (%)	EVTS	DOCUMENT ID	TECN	COMMENT
-1.8 ± 4.4	1721 \pm 75	TIAN	05 BELL	$e^+e^- \approx T(4S)$

$A_{CP}(K^+K^-\pi^+\pi^-)$ in $D^0, \bar{D}^0 \rightarrow K^+K^-\pi^+\pi^-$

See also AAIJ 13BR for a search for CP violation in $D^0 \rightarrow K^+K^-\pi^+\pi^-$ in binned phase space. No evidence of CP violation was found.

VALUE (%)	EVTS	DOCUMENT ID	TECN	COMMENT
1.3 ± 1.7	OUR AVERAGE			
$1.84 \pm 1.74 \pm 0.3$	2.9k	¹ DARGENT	17	e^+e^-
$-8.2 \pm 5.6 \pm 4.7$	828 \pm 46	LINK	05e	FOCS $\gamma A, \bar{E}_{\gamma} \approx 180$ GeV

¹ Obtained by analyzing CLEO data but not authored by the CLEO Collaboration.

$A_{CP}(2K_S^0\pi^+\pi^-)$ in $D^0, \bar{D}^0 \rightarrow 2K_S^0\pi^+\pi^-$

VALUE (units 10^{-2})	EVTS	DOCUMENT ID	TECN	COMMENT
$-2.54 \pm 1.44 \pm_{-0.10}^{+0.11}$	6095	¹ SANGAL	23 BELL	e^+e^- at $T(4S,5S), 10,520$ GeV

¹ SANGAL 23 also measures the parity asymmetry A_T in the sign of the triple product of momenta between one K_S^0 (the one with higher momentum) and the two charged pions, and reports the resulting CP asymmetry between the CP conjugate modes $(A_T - \bar{A}_T)/2 = (-1.95 \pm 1.42 \pm_{-0.12}^{+0.14}) \times 10^{-2}$.

$A_{CP}(K_1^*(1270)^+K^- \rightarrow K^+K^-\pi^+\pi^-)$ in $D^0 \rightarrow K_1^*(1270)^+K^-, \bar{D}^0 \rightarrow c.c.$

Including the full $K_1^*(1270)^+$ phase space accessible in this decay chain, with its various resonance contributions.

VALUE (%)	EVTS	DOCUMENT ID	TECN	COMMENT
-2.3 ± 1.7	OUR AVERAGE			
$-2.6 \pm 1.7 \pm 0.2$	163k	AAIJ	19c	LHCB 4-body fit, $KK\pi\pi$ evts
$25.3 \pm 9.7 \pm 12.7$	2.9k	¹ DARGENT	17	4-body fit, $KK\pi\pi$ evts

¹ Obtained by analyzing CLEO data but not authored by the CLEO Collaboration.

$A_{CP}(K_1^*(1270)^+K^- \rightarrow K^*0\pi^+K^-)$ in $D^0 \rightarrow K_1^*(1270)^+K^-, \bar{D}^0 \rightarrow c.c.$

VALUE (%)	DOCUMENT ID	TECN	COMMENT
-0.7 ± 10.4	ARTUSO	12 CLEO	Amplitude fit, 2959 evts.

$A_{CP}(K_1^*(1270)^-K^+ \rightarrow \bar{K}^*0\pi^-K^+)$ in $D^0 \rightarrow K_1^*(1270)^-K^+, \bar{D}^0 \rightarrow c.c.$

VALUE (%)	DOCUMENT ID	TECN	COMMENT
-10.0 ± 31.5	ARTUSO	12 CLEO	Amplitude fit, 2959 evts.

$A_{CP}(K_1^*(1270)^-K^+ \rightarrow K^+K^-\pi^+\pi^-)$ in $D^0 \rightarrow K_1^*(1270)^-K^+, \bar{D}^0 \rightarrow c.c.$

Including the full $K_1^*(1270)^-$ phase space accessible in this decay chain, with its various resonance contributions.

VALUE (%)	EVTS	DOCUMENT ID	TECN	COMMENT
1.7 ± 3.5	OUR AVERAGE			
$3.3 \pm 3.5 \pm 0.5$	163k	AAIJ	19c	LHCB 4-body fit, $KK\pi\pi$ evts
$-50.4 \pm 12.0 \pm 16.1$	2.9k	¹ DARGENT	17	4-body fit, $KK\pi\pi$ evts

¹ Obtained by analyzing CLEO data but not authored by the CLEO Collaboration.

$A_{CP}(K_1^*(1270)^+K^- \rightarrow \rho^0K^+K^-)$ in $D^0 \rightarrow K_1^*(1270)^+K^-, \bar{D}^0 \rightarrow c.c.$

VALUE (%)	DOCUMENT ID	TECN	COMMENT
-6.5 ± 16.9	ARTUSO	12 CLEO	Amplitude fit, 2959 evts.

$A_{CP}(K_1^*(1270)^-K^+ \rightarrow \rho^0K^-K^+)$ in $D^0 \rightarrow K_1^*(1270)^-K^+, \bar{D}^0 \rightarrow c.c.$

VALUE (%)	DOCUMENT ID	TECN	COMMENT
$+9.6 \pm 12.9$	ARTUSO	12 CLEO	Amplitude fit, 2959 evts.

$A_{CP}(K_1(1400)^+K^- \rightarrow K^+K^-\pi^+\pi^-)$ in $D^0 \rightarrow K_1(1400)^+K^-, \bar{D}^0 \rightarrow c.c.$

Including the full $K_1(1400)^+$ phase space accessible in this decay chain, with its various resonance contributions.

VALUE (%)	EVTS	DOCUMENT ID	TECN	COMMENT
-4.4 ± 2.1	OUR AVERAGE			
$-4.5 \pm 2.1 \pm 0.3$	163k	AAIJ	19c	LHCB 4-body fit, $KK\pi\pi$ evts
$9.2 \pm 15.2 \pm 20.3$	2.9k	¹ DARGENT	17	4-body fit, $KK\pi\pi$ evts

¹ Obtained by analyzing CLEO data but not authored by the CLEO Collaboration.

$A_{CP}(K^*(1410)^+K^- \rightarrow K^*0\pi^+K^-)$ in $D^0 \rightarrow K^*(1410)^+K^-, \bar{D}^0 \rightarrow c.c.$

VALUE (%)	DOCUMENT ID	TECN	COMMENT
-20.0 ± 16.8	ARTUSO	12 CLEO	Amplitude fit, 2959 evts.

$A_{CP}(K^*(1410)^- K^+ \rightarrow \bar{K}^{*0} \pi^- K^+)$ in $D^0 \rightarrow K^*(1410)^- K^+, \bar{D}^0 \rightarrow c.c.$

VALUE (%)	EVTS	DOCUMENT ID	TECN	COMMENT
-1.1 ± 13.7		ARTUSO	12	CLEO Amplitude fit, 2959 evts.

$A_{CP}(K^*(1680)^+ K^- \rightarrow K^+ K^- \pi^+ \pi^-)$ in $D^0 \rightarrow K^*(1680)^+ K^-, \bar{D}^0 \rightarrow c.c.$
 Including the full $K^*(1680)^+$ phase space accessible in this decay chain, with its various resonance contributions.

VALUE (%)	EVTS	DOCUMENT ID	TECN	COMMENT
$-17.1 \pm 21.8 \pm 18.5$	2.9k	¹ DARGENT	17	4-body fit, $K K \pi \pi$ evts

¹ Obtained by analyzing CLEO data but not authored by the CLEO Collaboration.

$A_{CP}(K^{*0} \bar{K}^{*0})$ in $D^0, \bar{D}^0 \rightarrow K^{*0} \bar{K}^{*0}$
 Including S, P, D wave

VALUE (%)	EVTS	DOCUMENT ID	TECN	COMMENT
$-4.6 \pm 9.0 \pm 11.3$	2.9k	¹ DARGENT	17	4-body fit, $K K \pi \pi$ evts

¹ Obtained by analyzing CLEO data but not authored by the CLEO Collaboration.

$A_{CP}(K^{*0} \bar{K}^{*0} S\text{-wave})$ in $D^0, \bar{D}^0 \rightarrow K^{*0} \bar{K}^{*0} S\text{-wave}$

VALUE (%)	EVTS	DOCUMENT ID	TECN	COMMENT
-3.9 ± 2.2 OUR AVERAGE				
$-4.3 \pm 2.2 \pm 0.5$	163k	AAIJ	19c	LHCb 4-body fit, $K K \pi \pi$ evts
$+9.5 \pm 13.5$	3k	ARTUSO	12	CLEO 4-body fit, $K K \pi \pi$ evts

$A_{CP}(\phi \rho^0)$ in $D^0, \bar{D}^0 \rightarrow \phi \rho^0$
 Including S, P, D wave

VALUE (%)	EVTS	DOCUMENT ID	TECN	COMMENT
$1.5 \pm 4.6 \pm 8.0$	2.9k	¹ DARGENT	17	4-body fit, $K K \pi \pi$ evts

¹ Obtained by analyzing CLEO data but not authored by the CLEO Collaboration.

$A_{CP}(\phi \rho^0 S\text{-wave})$ in $D^0, \bar{D}^0 \rightarrow \phi \rho^0 S\text{-wave}$

VALUE (%)	DOCUMENT ID	TECN	COMMENT
-2.7 ± 5.3	ARTUSO	12	CLEO Amplitude fit, 2959 evts.

$A_{CP}(\phi \rho^0 D\text{-wave})$ in $D^0, \bar{D}^0 \rightarrow \phi \rho^0 D\text{-wave}$

VALUE (%)	DOCUMENT ID	TECN	COMMENT
-37.1 ± 19.0	ARTUSO	12	CLEO Amplitude fit, 2959 evts.

$A_{CP}(\phi(\pi^+ \pi^-) S\text{-wave})$ in $D^0, \bar{D}^0 \rightarrow \phi(\pi^+ \pi^-) S\text{-wave}$

VALUE (%)	EVTS	DOCUMENT ID	TECN	COMMENT
6 ± 6 OUR AVERAGE				
$5.8 \pm 6.1 \pm 0.8$	163k	AAIJ	19c	LHCb 4-body fit, $K K \pi \pi$ evts
$-4.0 \pm 18.0 \pm 44.6$	3k	¹ DARGENT	17	4-body fit, $K K \pi \pi$ evts

- • • We do not use the following data for averages, fits, limits, etc. • • •

-8.6 ± 10.4	3k	² ARTUSO	12	CLEO 4-body fit, $K K \pi \pi$ evts
-----------------	----	---------------------	----	-------------------------------------

¹ Obtained by analyzing CLEO data but not authored by the CLEO Collaboration.
² See DARGENT 17

$A_{CP}(K^*(892)^0 (K^- \pi^+) S\text{-wave})$ in $D^0, \bar{D}^0 \rightarrow K^*(892)^0 (K^- \pi^+) S\text{-wave}$

VALUE (%)	EVTS	DOCUMENT ID	TECN	COMMENT
$-13.1 \pm 17.9 \pm 31.2$	2.9k	¹ DARGENT	17	4-body fit, $K K \pi \pi$ evts

¹ Obtained by analyzing CLEO data but not authored by the CLEO Collaboration.

$A_{CP}(K^+ K^- \pi^+ \pi^- \text{non-resonant})$ in $D^0, \bar{D}^0 \rightarrow K^+ K^- \pi^+ \pi^- \text{non-resonant}$

VALUE (%)	DOCUMENT ID	COMMENT
$+8.2 \pm 10.9 \pm 17.1$	¹ DARGENT	17 4-body fit, 2.9k $K K \pi \pi$ evts

¹ Obtained by analyzing CLEO data but not authored by the CLEO Collaboration.

$A_{CP}((K^- \pi^+) P\text{-wave} (K^+ \pi^-) S\text{-wave})$ in $D^0 \rightarrow (K^- \pi^+) P\text{-wave} (K^+ \pi^-) S\text{-wave}, \bar{D}^0 \rightarrow c.c.$

VALUE (%)	DOCUMENT ID	TECN	COMMENT
$+2.7 \pm 10.6$	ARTUSO	12	CLEO Amplitude fit, 2959 evts.

$A_{CP}(K^+ K^- \mu^+ \mu^-)$ in $D^0, \bar{D}^0 \rightarrow K^+ K^- \mu^+ \mu^-$

VALUE (%)	EVTS	DOCUMENT ID	TECN	COMMENT
$-2.3 \pm 6.3 \pm 0.6$	318	¹ AAIJ	22L	LHCb pp at 7, 8, 13TeV

- • • We do not use the following data for averages, fits, limits, etc. • • •

$0 \pm 11 \pm 2$	110	AAIJ	18I	LHCb pp at 7, 8, 13TeV
------------------	-----	------	-----	--------------------------

¹ Supersedes AAIJ 18I. This analysis provides the first complete angular analysis of $D^0 \rightarrow K^+ K^- \mu^+ \mu^-$, and measures angular moments for several bins in the dimuon invariant mass. The mass of the dihadron system is required to be less than 1200 MeV.

$A_{CP}(\pi^+ \pi^- \mu^+ \mu^-)$ in $D^0, \bar{D}^0 \rightarrow \pi^+ \pi^- \mu^+ \mu^-$

VALUE (%)	EVTS	DOCUMENT ID	TECN	COMMENT
$2.9 \pm 2.1 \pm 0.4$	3.6k	¹ AAIJ	22L	LHCb pp at 7, 8, 13 TeV

- • • We do not use the following data for averages, fits, limits, etc. • • •

$4.9 \pm 3.8 \pm 0.7$	1.1k	AAIJ	18I	LHCb pp at 7, 8, 13TeV
-----------------------	------	------	-----	--------------------------

¹ Supersedes AAIJ 18I. This analysis provides the first complete angular analysis of $D^0 \rightarrow \pi^+ \pi^- \mu^+ \mu^-$, and measures angular moments for several bins in the dimuon invariant mass. The mass of the dihadron system is required to be less than 1200 MeV.

D^0 CP-VIOLATING ASYMMETRY DIFFERENCES

$\Delta A_{CP} = A_{CP}(K^+ K^-) - A_{CP}(\pi^+ \pi^-)$

CP violation in these modes can come from the decay amplitudes (direct) and/or from mixing or interference of mixing and decay (indirect). The difference ΔA_{CP} is primarily sensitive to the direct component, and only retains a second-order dependence on the indirect component for measurements where the mean decay time of the $K^+ K^-$ and $\pi^+ \pi^-$ samples are not identical. The results below are averaged assuming the indirect component can be neglected.

VALUE (%)	EVTS	DOCUMENT ID	TECN	COMMENT
-0.154 ± 0.029	53M,17M	AAIJ	19D	LHCb Time-integrated
• • • We do not use the following data for averages, fits, limits, etc. • • •				
$-0.10 \pm 0.08 \pm 0.03$	6.5M,2.2M	AAIJ	16D	LHCb See AAIJ 19D
$0.14 \pm 0.16 \pm 0.08$	2.2M,0.8M	AAIJ	14AK	LHCb See AAIJ 19D
$0.49 \pm 0.30 \pm 0.14$	0.56M,0.22M	AAIJ	13AD	LHCb See AAIJ 14AK
$-0.82 \pm 0.21 \pm 0.11$	1.4M,0.4M	AAIJ	12G	LHCb See AAIJ 16D
$-0.46 \pm 0.31 \pm 0.12$		AALTONEN	12B	CDF See AALTONEN 120
$-0.62 \pm 0.21 \pm 0.10$		AALTONEN	120	CDF Time-integrated
$0.24 \pm 0.62 \pm 0.26$		¹ AUBERT	08M	BABR Time-integrated
$-0.86 \pm 0.60 \pm 0.07$	120k	STARIC	08	BELL Time-integrated

¹ Calculated from the AUBERT 08M values of $A_{CP}(K^+ K^-)$ and $A_{CP}(\pi^+ \pi^-)$. The systematic error here combines the systematic errors in quadrature, and therefore somewhat over-estimates it.

D^0 TESTS OF LOCAL CP-VIOLATION (CPV)

We list model-independent searches for local CP violation in phase-space distributions of multi-body decays.

Most of these searches divide phase space (Dalitz plot for 3-body decays, five-dimensional equivalent for 4-body decays) into bins, and perform a χ^2 test comparing normalised yields N_i, \bar{N}_i in CP -conjugate bin pairs i : $\chi^2 = \sum_i (N_i - \alpha \bar{N}_i) / \sigma(N_i - \alpha \bar{N}_i)$. The factor $\alpha = (\sum_j N_j) / (\sum_j \bar{N}_j)$ removes the dependence on phase-space-integrated rate asymmetries. The result is used to obtain the probability (p-value) to obtain the measured χ^2 or larger under the assumption of CP conservation [AUBERT 08AO, BEDIAGA 09]. Alternative methods obtain p-values from other test variables based on unbinned analyses [WILLIAMS 11, AAIJ 14C]. Results can be combined using Fisher's method [MOSTELLER 48].

Local CPV in $D^0, \bar{D}^0 \rightarrow \pi^+ \pi^- \pi^0$

p-value (%)	EVTS	DOCUMENT ID	TECN	COMMENT
10.6 OUR EVALUATION				
62	2.5M	AAIJ	23AW	LHCb unbinned method
2.6	566k	¹ AAIJ	15A	LHCb unbinned method
32.8	82k	AUBERT	08AO	BABR χ^2

¹ Unusually, AAIJ 15A assigns an uncertainty on the p value of $\pm 0.5\%$. This results from limited test statistics.

Local CPV in $D^0, \bar{D}^0 \rightarrow \pi^+ \pi^- \pi^+ \pi^-$

p-value (%)	EVTS	DOCUMENT ID	TECN	COMMENT
0.6 ± 0.2	1.0M	¹ AAIJ	17AE	LHCb unbinned, P-odd
• • • We do not use the following data for averages, fits, limits, etc. • • •				
4.6 ± 0.5	1.0M	^{2,3} AAIJ	17AE	LHCb unbinned, P-even
41	330k	^{2,4} AAIJ	13BR	LHCb χ^2, P -even

¹ This AAIJ 17AE value tests CP Violation in P -odd variables.
² This value tests CP Violation in P -even variables.
³ Not included in average as correlation to P -odd measurement using the same data is unclear.
⁴ See AAIJ 17AE.

Local CPV in $D^0, \bar{D}^0 \rightarrow K_S^0 \pi^+ \pi^-$

p-value (%)	EVTS	DOCUMENT ID	TECN	COMMENT
96	350k	AALTONEN	12AD	CDF χ^2

Local CPV in $D^0, \bar{D}^0 \rightarrow K^+ K^- \pi^0$

p-value (%)	EVTS	DOCUMENT ID	TECN	COMMENT
16.6	11k	AUBERT	08AO	BABR χ^2

Local CPV in $D^0, \bar{D}^0 \rightarrow K^+ K^- \pi^+ \pi^-$

p-value (%)	EVTS	DOCUMENT ID	TECN	COMMENT
9.1	57k	AAIJ	13BR	LHCb χ^2

CP VIOLATING ASYMMETRIES OF P-ODD (T-ODD) MOMENTS

The CP -sensitive P -odd (T -odd) correlation in D^0, \bar{D}^0 decays. The D^0 and \bar{D}^0 are distinguished by the charge of the parent D^* : $D^{*+} \rightarrow D^0 \pi^+$ and $D^{*-} \rightarrow \bar{D}^0 \pi^-$.

$A_{T\text{odd}}(K^+ K^- \pi^+ \pi^-)$ in $D^0, \bar{D}^0 \rightarrow K^+ K^- \pi^+ \pi^-$

$C_T \equiv \bar{p}_{K^+} \cdot (\bar{p}_{\pi^+} \times \bar{p}_{\pi^-})$ is a parity-odd correlation of the K^+ , π^+ , and π^- momenta (evaluated in the D^0 rest frame) for the D^0 . $\bar{C}_T \equiv \bar{p}_{K^-} \cdot (\bar{p}_{\pi^-} \times \bar{p}_{\pi^+})$ is the corresponding quantity for the \bar{D}^0 . Then
 $\frac{A_T}{A} \equiv \frac{[\Gamma(C_T > 0) - \Gamma(C_T < 0)]}{[\Gamma(C_T > 0) + \Gamma(C_T < 0)]}$, and
 $\bar{A}_T \equiv \frac{[\Gamma(-\bar{C}_T > 0) - \Gamma(-\bar{C}_T < 0)]}{[\Gamma(-\bar{C}_T > 0) + \Gamma(-\bar{C}_T < 0)]}$, and

Meson Particle Listings

D^0

$A_{Tviol} \equiv \frac{1}{2}(A_T - \bar{A}_T)$. C_T and \bar{C}_T are commonly referred to as T -odd moments, because they are odd under T reversal. However, the T -conjugate process $K^+ K^- \pi^+ \pi^- \rightarrow D^0$ is not accessible, while the CP -conjugate process is.

VALUE (units 10^{-3})	EVTS	DOCUMENT ID	TECN	COMMENT
2.9 ± 2.2 OUR AVERAGE				
$5.2 \pm 3.7 \pm 0.7$	110k	¹ KIM	19	BELL $e^+ e^-$ at $\Upsilon(1S) - \Upsilon(6S)$
$1.8 \pm 2.9 \pm 0.4$	171k	AAIJ	14BC	LHCB $B \rightarrow D^0 \mu^- X$
$1.0 \pm 5.1 \pm 4.4$	47k	DEL-AMO-SA..10	BABR	$e^+ e^- \approx 10.6$ GeV
$10 \pm 57 \pm 37$	0.8k	LINK	05E	FOCS $\gamma A, \bar{E}_\gamma \approx 180$ GeV

¹ KIM 19 also study CP -violating asymmetries in several other kinematic variables. No evidence for CP violation is found in any of them.

$A_{Tviol}(2K_S^0 \pi^+ \pi^-)$ in $D^0, \bar{D}^0 \rightarrow 2K_S^0 \pi^+ \pi^-$

$C_T \equiv \bar{p}_{K_S^0} \cdot (\bar{p}_{\pi^+} \times \bar{p}_{\pi^-})$ is a parity-odd correlation of the K_S^0 (with higher momentum), π^+ , and π^- momenta (evaluated in the D^0 rest frame) for the D^0 . $\bar{C}_T \equiv \bar{p}_{K_S^0} \cdot (\bar{p}_{\pi^-} \times \bar{p}_{\pi^+})$ is the corresponding quantity for the \bar{D}^0 . Then $A_T \equiv [\Gamma(C_T > 0) - \Gamma(C_T < 0)] / [\Gamma(C_T > 0) + \Gamma(C_T < 0)]$, and $\bar{A}_T \equiv [\Gamma(-\bar{C}_T > 0) - \Gamma(-\bar{C}_T < 0)] / [\Gamma(-\bar{C}_T > 0) + \Gamma(-\bar{C}_T < 0)]$, and $A_{Tviol} \equiv \frac{1}{2}(A_T - \bar{A}_T)$. C_T and \bar{C}_T are commonly referred to as T -odd moments, because they are odd under T reversal. However, the T -conjugate process $K_S^0 K_S^0 \pi^+ \pi^- \rightarrow D^0$ is not accessible, while the CP -conjugate process is.

VALUE (units 10^{-2})	EVTS	DOCUMENT ID	TECN	COMMENT
$-1.95 \pm 1.42^{+0.14}_{-0.12}$	6095	SANGAL	23	BELL $e^+ e^-$ at $\Upsilon(4S, 5S), 10.520$ GeV

$A_{Tviol}(K_S^0 \pi^+ \pi^- \pi^0)$ in $D^0, \bar{D}^0 \rightarrow K_S^0 \pi^+ \pi^- \pi^0$

$C_T \equiv \bar{p}_{K_S^0} \cdot (\bar{p}_{\pi^+} \times \bar{p}_{\pi^-})$ is a parity-odd correlation evaluated in the D^0 rest frame. \bar{C}_T is defined as the CP -conjugate observable with \bar{D}^0 daughter particles. Then $A_T \equiv [\Gamma(C_T > 0) - \Gamma(C_T < 0)] / [\Gamma(C_T > 0) + \Gamma(C_T < 0)]$, and $\bar{A}_T \equiv [\Gamma(-\bar{C}_T > 0) - \Gamma(-\bar{C}_T < 0)] / [\Gamma(-\bar{C}_T > 0) + \Gamma(-\bar{C}_T < 0)]$, and $A_{Tviol} \equiv \frac{1}{2}(A_T - \bar{A}_T)$. C_T and \bar{C}_T are commonly referred to as T -odd moments, because they are odd under T reversal. However, the T -conjugate process $K_S^0 \pi^+ \pi^- \pi^0 \rightarrow D^0$ is not accessible, while the CP -conjugate process is.

VALUE (units 10^{-3})	EVTS	DOCUMENT ID	TECN	COMMENT
$-0.20 \pm 1.38^{+0.23}_{-0.76}$	745k	¹ PRASANTH	17	BELL $e^+ e^-$ at $\Upsilon(nS)$'s

¹ PRASANTH 17 also measures A_{Tviol} in sub-regions of the $D^0 \rightarrow K_S^0 \pi^+ \pi^- \pi^0$ phase-space. No evidence of T violation is found.

D^0 CPT-VIOLATING DECAY-RATE ASYMMETRIES

$A_{CPT}(K^\mp \pi^\pm)$ in $D^0 \rightarrow K^- \pi^+, \bar{D}^0 \rightarrow K^+ \pi^-$

$A_{CPT}(t)$ is defined in terms of the time-dependent decay probabilities $P(D^0 \rightarrow K^- \pi^+)$ and $\bar{P}(\bar{D}^0 \rightarrow K^+ \pi^-)$ by $A_{CPT}(t) = (\bar{P} - P) / (\bar{P} + P)$. For small mixing parameters $x \equiv \Delta m / \Gamma$ and $y \equiv \Delta \Gamma / 2\Gamma$ (as is the case), and times $t, A_{CPT}(t)$ reduces to $[y \operatorname{Re} \xi - x \operatorname{Im} \xi] \Gamma t$, where ξ is the CP -violating parameter.

The following is actually $y \operatorname{Re} \xi - x \operatorname{Im} \xi$.

VALUE	DOCUMENT ID	TECN	COMMENT
$0.0083 \pm 0.0065 \pm 0.0041$	LINK	03B	FOCS γ nucleus, $\bar{E}_\gamma \approx 180$ GeV

$D^0 \rightarrow K^*(892)^- \ell^+ \nu_\ell$ FORM FACTORS

$r_V \equiv V(0)/A_1(0)$ in $D^0 \rightarrow K^*(892)^- \ell^+ \nu_\ell$

VALUE	EVTS	DOCUMENT ID	TECN	COMMENT
1.46 ± 0.07 OUR AVERAGE				
$1.46 \pm 0.07 \pm 0.02$	3k	ABLIKIM	19G	BES3 $K^*(892)^- e^+ \nu_e$
$1.71 \pm 0.68 \pm 0.34$		LINK	05B	FOCS $K^*(892)^- \mu^+ \nu_\mu$

$r_2 \equiv A_2(0)/A_1(0)$ in $D^0 \rightarrow K^*(892)^- \ell^+ \nu_\ell$

VALUE	EVTS	DOCUMENT ID	TECN	COMMENT
0.68 ± 0.06 OUR AVERAGE				
$0.67 \pm 0.06 \pm 0.01$	3k	ABLIKIM	19G	BES3 $K^*(892)^- e^+ \nu_e$
$0.91 \pm 0.37 \pm 0.10$		LINK	05B	FOCS $K^*(892)^- \mu^+ \nu_\mu$

$D^0 \rightarrow K^- / \pi^- \ell^+ \nu_\ell$ FORM FACTORS

$f_+(0)$ in $D^0 \rightarrow K^- \ell^+ \nu_\ell$

VALUE	EVTS	DOCUMENT ID	TECN	COMMENT
0.736 ± 0.004 OUR AVERAGE				
$0.7368 \pm 0.0026 \pm 0.0036$	71k	ABLIKIM	15X	BES3 $\ell=e, 2$ -parameter fit
$0.727 \pm 0.007 \pm 0.009$		AUBERT	07Bg	BABR $\ell=e, 2$ -parameter fit

$f_+(0)|V_{cb}|$ in $D^0 \rightarrow K^- \ell^+ \nu_\ell$

VALUE	EVTS	DOCUMENT ID	TECN	COMMENT
0.7166 ± 0.0030 OUR AVERAGE				
$0.7133 \pm 0.0038 \pm 0.0029$	47k	ABLIKIM	19B	BES3 $\ell=\mu, 2$ -parameter fit
$0.7172 \pm 0.0025 \pm 0.0035$	71k	¹ ABLIKIM	15X	BES3 $\ell=e, 2$ -parameter fit
$0.726 \pm 0.008 \pm 0.004$		BESSION	09	CLEO $\ell=e, 3$ -parameter fit

¹ The 3-parameter fit yields $0.7195 \pm 0.0035 \pm 0.0041$.

$r_1 \equiv a_1/a_0$ in $D^0 \rightarrow K^- \ell^+ \nu_\ell$

VALUE	EVTS	DOCUMENT ID	TECN	COMMENT
-2.40 ± 0.16 OUR AVERAGE				
$-2.33 \pm 0.16 \pm 0.08$	71k	¹ ABLIKIM	15X	BES3 $\ell=e, 3$ -parameter fit
$-2.65 \pm 0.34 \pm 0.08$		BESSION	09	CLEO $\ell=e, 3$ -parameter fit

¹ The 2-parameter fit yields $-2.23 \pm 0.09 \pm 0.06$.

$r_2 \equiv a_2/a_0$ in $D^0 \rightarrow K^- \ell^+ \nu_\ell$

VALUE	EVTS	DOCUMENT ID	TECN	COMMENT
5 ± 4 OUR AVERAGE				
$3.4 \pm 3.9 \pm 2.4$	71k	ABLIKIM	15X	BES3 $\ell=e, 3$ -parameter fit
$13 \pm 9 \pm 1$		BESSION	09	CLEO $\ell=e, 3$ -parameter fit

$f_+(0)$ in $D^0 \rightarrow \pi^- \ell^+ \nu_\ell$

VALUE	EVTS	DOCUMENT ID	TECN	COMMENT
$0.6372 \pm 0.0080 \pm 0.0044$	6.3k	ABLIKIM	15X	BES3 $\ell=e, 2$ -parameter fit

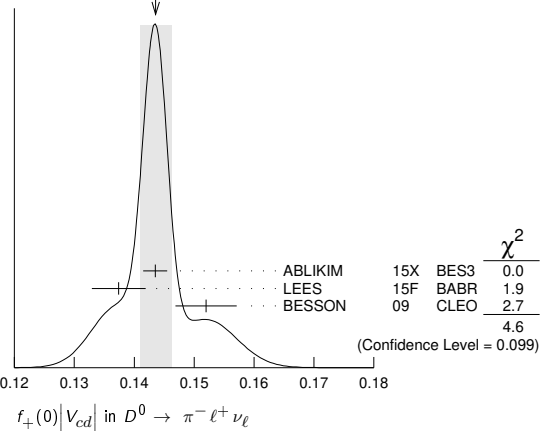
$f_+(0)|V_{cd}|$ in $D^0 \rightarrow \pi^- \ell^+ \nu_\ell$

VALUE	EVTS	DOCUMENT ID	TECN	COMMENT
0.1436 ± 0.0026 OUR AVERAGE				Error includes scale factor of 1.5. See the ideogram below.
$0.1435 \pm 0.0018 \pm 0.0009$	6.3k	¹ ABLIKIM	15X	BES3 $\ell=e, 2$ -parameter fit
$0.1374 \pm 0.0038 \pm 0.0024$	5.3k	² LEES	15F	BABR $\ell=e, 3$ -parameter fit
$0.152 \pm 0.005 \pm 0.001$		BESSION	09	CLEO $\ell=e, 3$ -parameter fit

¹ The 3-parameter fit yields $0.1420 \pm 0.0024 \pm 0.0010$.

² LEES 15F reports a value $0.1374 \pm 0.0038 \pm 0.0022 \pm 0.0009$, where the last uncertainty is due to the uncertainties of the $D^0 \rightarrow K^- \pi^+$ branching fraction.

WEIGHTED AVERAGE
 0.1436 ± 0.0026 (Error scaled by 1.5)

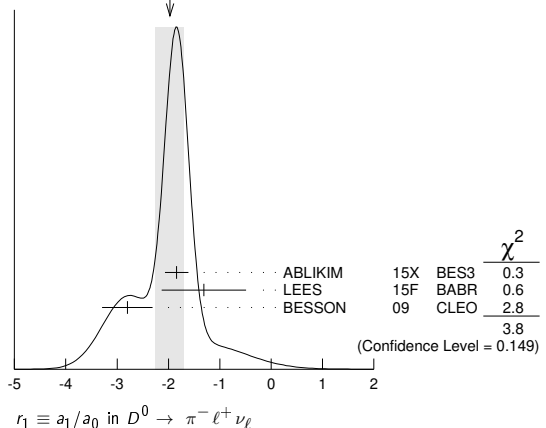


$r_1 \equiv a_1/a_0$ in $D^0 \rightarrow \pi^- \ell^+ \nu_\ell$

VALUE	EVTS	DOCUMENT ID	TECN	COMMENT
-1.97 ± 0.28 OUR AVERAGE				Error includes scale factor of 1.4. See the ideogram below.
$-1.84 \pm 0.22 \pm 0.07$	6.3k	¹ ABLIKIM	15X	BES3 $\ell=e, 3$ -parameter fit
$-1.31 \pm 0.70 \pm 0.43$	5.3k	LEES	15F	BABR $\ell=e, 3$ -parameter fit
$-2.80 \pm 0.49 \pm 0.04$		BESSION	09	CLEO $\ell=e, 3$ -parameter fit

¹ The 2-parameter fit yields $-2.04 \pm 0.08 \pm 0.03$.

WEIGHTED AVERAGE
 -1.97 ± 0.28 (Error scaled by 1.4)



See key on page 1171

Meson Particle Listings

$D^*(2007)^0, D^*(2010)^\pm$

• • • We do not use the following data for averages, fits, limits, etc. • • •
 142.2 ± 2.0 SADROZINSKI 80 CBAL $D^{*0} \rightarrow D^0 \pi^0$
 142.7 ± 1.7 2 GOLDHABER 77 MRK1 $e^+ e^-$
 1 Obtained by analyzing CLEO-c data but not authored by the CLEO Collaboration. This value comes from the average of the results for two decay modes, $D^0 \rightarrow K^- \pi^+$ and $D^0 \rightarrow K^- \pi^+ \pi^- \pi^+$.
 2 From simultaneous fit to $D^*(2010)^+, D^*(2007)^0, D^+$, and D^0 .

$D^*(2007)^0$ WIDTH

VALUE (MeV)	CL%	DOCUMENT ID	TECN	COMMENT
<2.1	90	1 ABACHI	88B	HRS $D^{*0} \rightarrow D^+ \pi^-$

1 Assuming $m_{D^{*0}} = 2007.2 \pm 2.1$ MeV/c².

$D^*(2007)^0$ DECAY MODES

$\bar{D}^*(2007)^0$ modes are charge conjugates of modes below.

Mode	Fraction (Γ_i/Γ)	Confidence level
Γ_1 $D^0 \pi^0$	(64.7 ± 0.9) %	
Γ_2 $D^0 \gamma$	(35.3 ± 0.9) %	
Γ_3 $D^0 e^+ e^-$	(3.91 ± 0.33) × 10 ⁻³	
Γ_4 $\mu^+ \mu^-$	< 2.5 × 10 ⁻⁸	90%
Γ_5 $e^+ e^-$	< 1.7 × 10 ⁻⁶	90%

CONSTRAINED FIT INFORMATION

An overall fit to 2 branching ratios uses 5 measurements and one constraint to determine 2 parameters. The overall fit has a $\chi^2 = 2.5$ for 4 degrees of freedom.

The following off-diagonal array elements are the correlation coefficients $\langle \delta x_i \delta x_j \rangle / (\delta x_i \delta x_j)$, in percent, from the fit to the branching fractions, $x_i \equiv \Gamma_i/\Gamma_{\text{total}}$. The fit constrains the x_i whose labels appear in this array to sum to one.

$$x_2 \begin{vmatrix} -100 \\ x_1 \end{vmatrix}$$

$D^*(2007)^0$ BRANCHING RATIOS

$\Gamma(D^0 \pi^0)/\Gamma_{\text{total}}$	VALUE	EVTS	DOCUMENT ID	TECN	COMMENT	Γ_1/Γ
0.647 ± 0.009 OUR FIT						
0.655 ± 0.008 ± 0.005	3.2k	1	ABLIKIM	15B	BES3	$e^+ e^- \rightarrow$ hadrons
0.635 ± 0.003 ± 0.017	69k	1	AUBERT,BE	05G	BABR	10.6 $e^+ e^- \rightarrow$ hadrons
0.596 ± 0.035 ± 0.028	858	2	ALBRECHT	95F	ARG	$e^+ e^- \rightarrow$ hadrons
0.636 ± 0.023 ± 0.033	1097	2	BUTLER	92	CLE2	$e^+ e^- \rightarrow$ hadrons

1 Derived from the ratio $\Gamma(D^0 \pi^0) / \Gamma(D^0 \gamma)$ assuming that the branching fractions of $D^{*0} \rightarrow D^0 \pi^0$ and $D^{*0} \rightarrow D^0 \gamma$ decays sum to 100%.
 2 The BUTLER 92 and ALBRECHT 95F branching ratios are not independent, they have been constrained by the authors to sum to 100%.

$\Gamma(D^0 \gamma)/\Gamma_{\text{total}}$	VALUE	EVTS	DOCUMENT ID	TECN	COMMENT	Γ_2/Γ
0.353 ± 0.009 OUR FIT						
0.381 ± 0.029 OUR AVERAGE						
0.404 ± 0.035 ± 0.028	456	1	ALBRECHT	95F	ARG	$e^+ e^- \rightarrow$ hadrons
0.364 ± 0.023 ± 0.033	621	1	BUTLER	92	CLE2	$e^+ e^- \rightarrow$ hadrons
0.37 ± 0.08 ± 0.08			ADLER	88D	MRK3	$e^+ e^-$
0.345 ± 0.008 ± 0.005	1.8k	2	ABLIKIM	15B	BES3	$e^+ e^- \rightarrow$ hadrons
0.365 ± 0.003 ± 0.017	68k	2	AUBERT,BE	05G	BABR	10.6 $e^+ e^- \rightarrow$ hadrons
0.47 ± 0.23			LOW	87	HRS	29 GeV $e^+ e^-$
0.53 ± 0.13			BARTEL	85G	JADE	$e^+ e^-$, hadrons
0.47 ± 0.12			COLES	82	MRK2	$e^+ e^-$
0.45 ± 0.15			GOLDHABER	77	MRK1	$e^+ e^-$

1 The BUTLER 92 and ALBRECHT 95F branching ratios are not independent, they have been constrained by the authors to sum to 100%.
 2 Derived from the ratio $\Gamma(D^0 \pi^0) / \Gamma(D^0 \gamma)$ assuming that the branching fractions of $D^{*0} \rightarrow D^0 \pi^0$ and $D^{*0} \rightarrow D^0 \gamma$ decays sum to 100%.

$\Gamma(D^0 \pi^0)/\Gamma(D^0 \gamma)$	VALUE	EVTS	DOCUMENT ID	TECN	COMMENT	Γ_1/Γ_2
1.83 ± 0.07 OUR FIT						
1.85 ± 0.07 OUR AVERAGE						
1.90 ± 0.07 ± 0.05	4.9k		ABLIKIM	15B	BES3	10.6 $e^+ e^- \rightarrow$ hadrons
1.74 ± 0.02 ± 0.13			AUBERT,BE	05G	BABR	10.6 $e^+ e^- \rightarrow$ hadrons
1.789 ± 0.082		1	AAIJ	22N	LHCB	$B^0, B_s^0 \rightarrow \bar{D}^{*0}(K \pi, \pi \pi)$

1 Statistical error only.

$\Gamma(D^0 e^+ e^-)/\Gamma(D^0 \gamma)$	VALUE (units 10 ⁻³)	EVTS	DOCUMENT ID	TECN	COMMENT	Γ_3/Γ_2
11.08 ± 0.76 ± 0.49		421	ABLIKIM	21BD	BES3	4.178 GeV $e^+ e^-$

$\Gamma(\mu^+ \mu^-)/\Gamma_{\text{total}}$	VALUE	CL%	DOCUMENT ID	TECN	COMMENT	Γ_4/Γ
<2.5 × 10⁻⁸		90	1 AAIJ	23D	LHCB	$B^- \rightarrow \pi^- \mu^+ \mu^-$

1 AAIJ 23D reports $< 2.6 \times 10^{-8}$ from a measurement of $[\Gamma(D^*(2007)^0 \rightarrow \mu^+ \mu^-) / \Gamma_{\text{total}}] \times [B(B^+ \rightarrow \bar{D}^*(2007)^0 \pi^+)]$ assuming $B(B^+ \rightarrow \bar{D}^*(2007)^0 \pi^+) = (4.90 \pm 0.17) \times 10^{-3}$, which we rescale to our best value $B(B^+ \rightarrow \bar{D}^*(2007)^0 \pi^+) = 5.17 \times 10^{-3}$. The reported value also assumes $B(B^- \rightarrow J/\psi(1S) K^-) = (10.20 \pm 0.19) \times 10^{-4}$ and $B(J/\psi(1S) \rightarrow \mu^+ \mu^-) = (59.61 \pm 0.33) \times 10^{-3}$ for the normalization mode $B^- \rightarrow J/\psi(1S) K^-$.

$\Gamma(e^+ e^-)/\Gamma_{\text{total}}$	VALUE	CL%	DOCUMENT ID	TECN	COMMENT	Γ_5/Γ
<1.7 × 10⁻⁶		90	SHEMYAKIN	20	CMD3	$e^+ e^- \rightarrow D^0 \pi^0, D^0 \gamma$

$D^*(2007)^0$ REFERENCES

AAIJ 23D EPJ C83 666 R. Aaij et al. (LHCb Collab.)
 ABLIKIM 23AZ PL B846 138245 M. Ablikim et al. (BESIII Collab.) JP
 AAIJ 22N PR D105 072005 R. Aaij et al. (LHCb Collab.)
 ABLIKIM 21BD PR D104 112012 M. Ablikim et al. (BESIII Collab.)
 SHEMYAKIN 20 PAN 83 954 D.N. Shemyakin (CMD-3 Collab.)
 ABLIKIM 15B PR D91 031101 M. Ablikim et al. (BESIII Collab.)
 TOMARADZE 15 PR D91 011102 A. Tomaradze et al. (NWES)
 AUBERT,BE 05G PR D72 091101 B. Aubert et al. (BABAR Collab.)
 ALBRECHT 95F ZPHY C66 63 H. Albrecht et al. (ARGUS Collab.)
 BORTOLETTO 92B PRL 69 2046 D. Bortoletto et al. (CLEO Collab.)
 BUTLER 92 PRL 69 2041 F. Butler et al. (CLEO Collab.)
 ABACHI 88B PL B212 533 S. Abachi et al. (ANL, IND, MICH, PURD+)
 ADLER 88D PL B208 152 J. Adler et al. (Mark III Collab.)
 LOW 87 PL B183 232 E.H. Low et al. (HRS Collab.)
 BARTEL 85G PL B16B 197 W. Bartel et al. (JADE Collab.)
 COLES 82 PR D26 2190 M.W. Coles et al. (LBL, SLAC)
 SADROZINSKI 80 Madison Conf. 681 H.F.W. Sadrozinski et al. (PRIN, CIT+)
 GOLDHABER 77 PL 69B 503 G. Goldhaber et al. (Mark I Collab.)

$D^*(2010)^\pm$

$I(J^P) = \frac{1}{2}(1^-)$

$J^P = 1^-$ established by ABLIKIM 23AZ.

$D^*(2010)^\pm$ MASS

The fit includes $D^\pm, D^0, D_s^\pm, D^{*±}, D^{*0}, D_s^{*±}, D_1(2420)^0, D_2^*(2460)^0$, and $D_{s1}(2536)^\pm$ mass and mass difference measurements.

VALUE (MeV)	EVTS	DOCUMENT ID	TECN	CHG	COMMENT
2010.26 ± 0.05 OUR FIT					
2008 ± 3		1 GOLDHABER 77	MRK1	±	$e^+ e^-$
2008.6 ± 1.0		2 PERUZZI 77	LGW	±	$e^+ e^-$

1 From simultaneous fit to $D^*(2010)^\pm, D^*(2007)^0, D^+$, and D^0 ; not independent of FELDMAN 77B mass difference below.
 2 PERUZZI 77 mass not independent of FELDMAN 77B mass difference below and PERUZZI 77 D^0 mass value.

$m_{D^*(2010)^+ - m_{D^+}}$

The fit includes $D^\pm, D^0, D_s^\pm, D^{*±}, D^{*0}, D_s^{*±}, D_1(2420)^0, D_2^*(2460)^0$, and $D_{s1}(2536)^\pm$ mass and mass difference measurements.

VALUE (MeV)	EVTS	DOCUMENT ID	TECN	COMMENT
140.603 ± 0.015 OUR FIT				
140.602 ± 0.014 OUR AVERAGE				
140.6010 ± 0.0068 ± 0.0129	151k	LEES	17F	BABR $e^+ e^- \rightarrow$ hadrons
140.64 ± 0.08 ± 0.06	620	BORTOLETTO92B	CLE2	$e^+ e^- \rightarrow$ hadrons

$m_{D^*(2010)^+ - m_{D^0}}$

The fit includes $D^\pm, D^0, D_s^\pm, D^{*±}, D^{*0}, D_s^{*±}, D_1(2420)^0, D_2^*(2460)^0$, and $D_{s1}(2536)^\pm$ mass and mass difference measurements.

VALUE (MeV)	EVTS	DOCUMENT ID	TECN	COMMENT
145.4258 ± 0.017 OUR FIT				
145.4258 ± 0.0020 OUR AVERAGE				
145.4259 ± 0.0004 ± 0.0017	312.8k	LEES	13X	BABR $D^{*±} \rightarrow D^0 \pi^\pm \rightarrow (K \pi, K 3\pi) \pi^\pm$
145.412 ± 0.002 ± 0.012		ANASTASSOV 02	CLE2	$D^{*±} \rightarrow D^0 \pi^\pm \rightarrow (K \pi) \pi^\pm$
145.54 ± 0.08	611	1 ADINOLFI 99	BEAT	$D^{*±} \rightarrow D^0 \pi^\pm$
145.45 ± 0.02		1 BREITWEG 99	ZEUS	$D^{*±} \rightarrow D^0 \pi^\pm \rightarrow (K \pi) \pi^\pm$
145.42 ± 0.05		1 BREITWEG 99	ZEUS	$D^{*±} \rightarrow D^0 \pi^\pm \rightarrow (K^- 3\pi) \pi^\pm$
145.5 ± 0.15	103	2 ADLOFF 97B	H1	$D^{*±} \rightarrow D^0 \pi^\pm$

Error includes scale factor of 1.2.

Meson Particle Listings

$D^*(2010)^\pm, D_0^*(2300)$

VALUE	CL%	EVTS	DOCUMENT ID	TECN	COMMENT
145.44 ± 0.08		152	² BREITWEG 97	ZEUS	$D^{*\pm} \rightarrow D^0 \pi^\pm$
145.42 ± 0.11		199	² BREITWEG 97	ZEUS	$D^{*\pm} \rightarrow D^0 \pi^\pm$
145.4 ± 0.2		48	² DERRICK 95	ZEUS	$D^{*\pm} \rightarrow D^0 \pi^\pm$
145.39 ± 0.06 ± 0.03			BARLAG 92B	ACCM	$\pi^- 230 \text{ GeV}$
145.5 ± 0.2		115	² ALEXANDER 91B	OPAL	$D^{*\pm} \rightarrow D^0 \pi^\pm$
145.30 ± 0.06			² DECAMP 91J	ALEP	$D^{*\pm} \rightarrow D^0 \pi^\pm$
145.40 ± 0.05 ± 0.10			ABACHI 88B	HRS	$D^{*\pm} \rightarrow D^0 \pi^\pm$
145.46 ± 0.07 ± 0.03			ALBRECHT 85F	ARG	$D^{*\pm} \rightarrow D^0 \pi^\pm$
145.5 ± 0.3		28	BAILEY 83	SPEC	$D^{*\pm} \rightarrow D^0 \pi^\pm$
145.5 ± 0.3		60	FITCH 81	SPEC	$\pi^- A$
145.3 ± 0.5		30	FELDMAN 77B	MRK1	$D^{*\pm} \rightarrow D^0 \pi^\pm$

••• We do not use the following data for averages, fits, limits, etc. •••
 145.4256 ± 0.0006 ± 0.0017 138.5k LEES 13x BABR $D^{*\pm} \rightarrow D^0 \pi^\pm \rightarrow (K^- \pi^+) \pi^\pm$

$m_{D^*(2010)^+ - m_{D^*(2007)^0}$

VALUE (MeV)	DOCUMENT ID	TECN	COMMENT
2.6 ± 1.8	¹ PERUZZI 77	LGW	$e^+ e^-$

1 Not independent of FELDMAN 77B mass difference above, PERUZZI 77 D^0 mass, and GOLDHABER 77 $D^*(2007)^0$ mass.

$D^*(2010)^\pm$ WIDTH

VALUE (keV)	CL%	EVTS	DOCUMENT ID	TECN	COMMENT
83.4 ± 1.8 OUR AVERAGE					
83.3 ± 1.2 ± 1.4	1.4	312.8k	¹ LEES 13x	BABR	$D^{*\pm} \rightarrow D^0 \pi^\pm \rightarrow (K \pi, K 3\pi) \pi^\pm$
96 ± 4 ± 22			¹ ANASTASSOV 02	CLE2	$D^{*\pm} \rightarrow D^0 \pi^\pm \rightarrow (K \pi) \pi^\pm$
83.4 ± 1.7 ± 1.5	1.5	138.5k	¹ LEES 13x	BABR	$D^{*\pm} \rightarrow D^0 \pi^\pm \rightarrow (K^- \pi^+) \pi^\pm$
83.2 ± 1.5 ± 2.6	2.6	174.3k	¹ LEES 13x	BABR	$D^{*\pm} \rightarrow D^0 \pi^\pm \rightarrow (K^- 2\pi^+ \pi^-) \pi^\pm$
<131	90	110	BARLAG 92B	ACCM	$\pi^- 230 \text{ GeV}$

1 Ignoring the electromagnetic contribution from $D^{*\pm} \rightarrow D^\pm \gamma$.

$D^*(2010)^\pm$ DECAY MODES

$D^*(2010)^-$ modes are charge conjugates of the modes below.

Mode	Fraction (Γ_j/Γ)
$\Gamma_1 D^0 \pi^+$	(67.7 ± 0.5) %
$\Gamma_2 D^+ \pi^0$	(30.7 ± 0.5) %
$\Gamma_3 D^+ \gamma$	(1.6 ± 0.4) %

CONSTRAINED FIT INFORMATION

An overall fit to 3 branching ratios uses 6 measurements and one constraint to determine 3 parameters. The overall fit has a $\chi^2 = 0.3$ for 4 degrees of freedom.

The following *off-diagonal* array elements are the correlation coefficients $\langle \delta x_i \delta x_j \rangle / (\delta x_i \delta x_j)$, in percent, from the fit to the branching fractions, $x_i \equiv \Gamma_i/\Gamma_{\text{total}}$. The fit constrains the x_i whose labels appear in this array to sum to one.

x_2	-62	
x_3	-43	-44
	x_1	x_2

$D^*(2010)^+$ BRANCHING RATIOS

$\Gamma(D^0 \pi^+)/\Gamma_{\text{total}}$	DOCUMENT ID	TECN	COMMENT	Γ_1/Γ
0.677 ± 0.005 OUR FIT				
0.677 ± 0.006 OUR AVERAGE				
0.6759 ± 0.0029 ± 0.0064	^{1,2,3} BARTELT 98	CLE2	$e^+ e^-$	
0.688 ± 0.024 ± 0.013	ALBRECHT 95F	ARG	$e^+ e^- \rightarrow$ hadrons	
0.681 ± 0.010 ± 0.013	¹ BUTLER 92	CLE2	$e^+ e^- \rightarrow$ hadrons	

••• We do not use the following data for averages, fits, limits, etc. •••

0.57 ± 0.04 ± 0.04	ADLER 88D	MRK3	$e^+ e^-$
0.44 ± 0.10	COLES 82	MRK2	$e^+ e^-$
0.6 ± 0.15	³ GOLDHABER 77	MRK1	$e^+ e^-$

1 The branching ratios are not independent, they have been constrained by the authors to sum to 100%.
 2 Systematic error includes theoretical error on the prediction of the ratio of hadronic modes.
 3 Assuming that isospin is conserved in the decay.

$\Gamma(D^+ \pi^0)/\Gamma_{\text{total}}$

VALUE	CL%	EVTS	DOCUMENT ID	TECN	COMMENT
0.3073 ± 0.0013 ± 0.0062					
0.312 ± 0.011 ± 0.008	1.4	1404	^{1,2,3} BARTELT 98	CLE2	$e^+ e^-$
0.308 ± 0.004 ± 0.008	410		¹ BUTLER 92	CLE2	$e^+ e^- \rightarrow$ hadrons
0.26 ± 0.02 ± 0.02			ADLER 88D	MRK3	$e^+ e^-$
0.34 ± 0.07			COLES 82	MRK2	$e^+ e^-$

1 The branching ratios are not independent, they have been constrained by the authors to sum to 100%.
 2 Systematic error includes theoretical error on the prediction of the ratio of hadronic modes.
 3 Assuming that isospin is conserved in the decay.

$\Gamma(D^+ \gamma)/\Gamma_{\text{total}}$

VALUE	CL%	EVTS	DOCUMENT ID	TECN	COMMENT
0.016 ± 0.004 OUR FIT					
0.016 ± 0.005 OUR AVERAGE					
0.0168 ± 0.0042 ± 0.0029			^{1,2} BARTELT 98	CLE2	$e^+ e^-$
0.011 ± 0.014 ± 0.016	12		¹ BUTLER 92	CLE2	$e^+ e^- \rightarrow$ hadrons

••• We do not use the following data for averages, fits, limits, etc. •••

<0.052	90		ALBRECHT 95F	ARG	$e^+ e^- \rightarrow$ hadrons
0.17 ± 0.05 ± 0.05			ADLER 88D	MRK3	$e^+ e^-$
0.22 ± 0.12			³ COLES 82	MRK2	$e^+ e^-$

1 The branching ratios are not independent, they have been constrained by the authors to sum to 100%.
 2 Systematic error includes theoretical error on the prediction of the ratio of hadronic modes.
 3 Not independent of $\Gamma(D^0 \pi^+)/\Gamma_{\text{total}}$ and $\Gamma(D^+ \pi^0)/\Gamma_{\text{total}}$ measurement.

$D^*(2010)^\pm$ REFERENCES

ABLIKIM 23A2	PL B846 138245	M. Ablikim et al.	(BESIII Collab.) JP
LEES 17F	PRL 119 202003	J.P. Lees et al.	(BABAR Collab.)
LEES 13X	PRL 111 111801	J.P. Lees et al.	(BABAR Collab.)
Also	PR D88 052003	J.P. Lees et al.	(BABAR Collab.)
Also	PR D88 079902 (err.)	J.P. Lees et al.	(BABAR Collab.)
ANASTASSOV 02	PR D65 032003	A. Anastassov et al.	(CLEO Collab.)
ADINOLFI 99	NP B547 3	M. Adinolfi et al.	(Beatrice Collab.)
BREITWEG 99	EPL C6 67	J. Breitweg et al.	(ZEUS Collab.)
BARTELT 98	PRL 80 3919	J. Bartelt et al.	(CLEO Collab.)
ADLOFF 97B	ZPHY C72 593	C. Adloff et al.	(H1 Collab.)
BREITWEG 97	PL B401 192	J. Breitweg et al.	(ZEUS Collab.)
BREITWEG 97B	PL B407 402	J. Breitweg et al.	(ZEUS Collab.)
ALBRECHT 95F	ZPHY C66 63	H. Albrecht et al.	(ARGUS Collab.)
DERRICK 95	PL B349 225	M. Derrick et al.	(ZEUS Collab.)
BARLAG 92B	PL B278 480	S. Barlag et al.	(ACCMOR Collab.)
BORTOLETTO 92B	PRL 69 2046	D. Bortoletto et al.	(CLEO Collab.)
BUTLER 92	PRL 69 2041	F. Butler et al.	(CLEO Collab.)
ALEXANDER 91B	PL B262 341	G. Alexander et al.	(OPAL Collab.)
DECAMP 91J	PL B266 218	D. Decamp et al.	(ALEPH Collab.)
ABACHI 88B	PL B212 533	S. Abachi et al.	(ANL, IND, MICH, PURD+)
ADLER 88D	PL B208 152	J. Adler et al.	(Mark III Collab.)
ALBRECHT 85F	PL 150B 235	H. Albrecht et al.	(ARGUS Collab.)
AHLEN 83	PRL 51 1147	S.P. Ahlen et al.	(ANL, IND, LBL+)
BAILEY 83	PL 132B 230	R. Bailey et al.	(AMST, BRIS, CERN, CRAC+)
COLES 82	PR D26 2190	M.W. Coles et al.	(LBL, SLAC)
YELTON 82	PRL 49 430	J.M. Yelton et al.	(SLAC, LBL, UCB+)
FITCH 81	PRL 46 761	V.L. Fitch et al.	(PRIN, SAFL, TORI+)
AVERY 80	PRL 44 1309	P. Avery et al.	(ILL, FNAL, COLU)
BLIETSCHAU 79	PL 86B 108	J. Blietschau et al.	(AACH3, BONN, CERN+)
FELDMAN 77B	PRL 38 1313	G.J. Feldman et al.	(Mark I Collab.)
GOLDHABER 77	PL 69B 503	G. Goldhaber et al.	(Mark I Collab.)
PERUZZI 77	PRL 39 1301	I. Peruzzi et al.	(LGW Collab.)

$D_0^*(2300)$

$I(J^P) = \frac{1}{2}(0^+)$

was $D_0^*(2400)$

There is a strong evidence that recent data on $B \rightarrow D \pi \pi$ (AAIJ 15Y, AAIJ 16AH) and $B \rightarrow D \pi K$ (AAIJ 14BH, AAIJ 15V, AAIJ 15X) call for two poles in the scalar $I = 1/2 \pi D$ amplitude in this mass range. The data are consistent with a lower pole at $(2105^{+6}_{-8}) - i(102^{+10}_{-11})$ MeV and a higher pole at $(2451^{+35}_{-26}) - i(134^{+7}_{-8})$ MeV (DU 18A, DU 19, DU 21). For details see review on "Heavy Non- $q\bar{q}$ Mesons."

$D_0^*(2300)$ MASS

VALUE (MeV)	EVTS	DOCUMENT ID	TECN	CHG	COMMENT
2343 ± 10 OUR AVERAGE					Error includes scale factor of 1.5. See the ideogram below.
2360 ± 15 ± 30		¹ AAIJ 15X	LHCB	+	$B^0 \rightarrow \bar{D}^0 K^+ \pi^-$
2349 ± 6 ± 4		² AAIJ 15Y	LHCB	+	$B^0 \rightarrow \bar{D}^0 \pi^+ \pi^-$
2297 ± 8 ± 20	3.4k	AUBERT 09AB	BABR	0	$B^- \rightarrow D^+ \pi^- \pi^-$
2308 ± 17 ± 32		ABE 04D	BELL	0	$B^- \rightarrow D^+ \pi^- \pi^-$

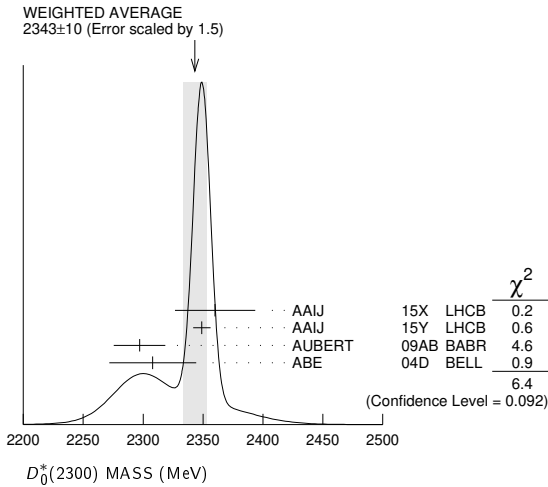
See key on page 1171

Meson Particle Listings

$D_0^*(2300)$, $D_1(2420)$

••• We do not use the following data for averages, fits, limits, etc. •••
 2354 ± 7 ± 11 3 AAIJ 15Y LHCb + $B^0 \rightarrow \bar{D}^0 \pi^+ \pi^-$
 2403 ± 14 ± 35 18.8k 4 LINK 04A FOCS + γA
 2407 ± 21 ± 35 9.8k 4 LINK 04A FOCS 0 γA

¹ From the Dalitz plot analysis including various K^* and D^{**} mesons as well as broad structures in the $K \pi$ S-wave and the $D \pi$ S- and P-waves.
² Modeling the $\pi^+ \pi^-$ S-wave with the Isobar formalism.
³ Modeling the $\pi^+ \pi^-$ S-wave with the K-matrix formalism.
⁴ Possibly the feed-down from another state.



$D_0^*(2300)$ WIDTH

VALUE (MeV)	EVTS	DOCUMENT ID	TECN	CHG	COMMENT
229 ± 16 OUR AVERAGE					
255 ± 26 ± 51		¹ AAIJ	15X	LHCb	+ $B^0 \rightarrow \bar{D}^0 K^+ \pi^-$
217 ± 13 ± 13		² AAIJ	15Y	LHCb	+ $B^0 \rightarrow \bar{D}^0 \pi^+ \pi^-$
273 ± 12 ± 48	3.4k	AUBERT	09AB	BABR	0 $B^- \rightarrow D^+ \pi^- \pi^-$
276 ± 21 ± 63		ABE	04D	BELL	0 $B^- \rightarrow D^+ \pi^- \pi^-$
••• We do not use the following data for averages, fits, limits, etc. •••					
230 ± 15 ± 21		³ AAIJ	15Y	LHCb	+ $B^0 \rightarrow \bar{D}^0 \pi^+ \pi^-$
283 ± 24 ± 34	18.8k	⁴ LINK	04A	FOCS	+ γA
240 ± 55 ± 59	9.8k	⁴ LINK	04A	FOCS	0 γA

¹ From the Dalitz plot analysis including various K^* and D^{**} mesons as well as broad structures in the $K \pi$ S-wave and the $D \pi$ S- and P-waves.
² Modeling the $\pi^+ \pi^-$ S-wave with the Isobar formalism.
³ Modeling the $\pi^+ \pi^-$ S-wave with the K-matrix formalism.
⁴ Possibly the feed-down from another state.

$D_0^*(2300)$ DECAY MODES

Mode	Fraction (Γ_i/Γ)
Γ_1 $D \pi^\pm$	seen

$\Gamma(D \pi^\pm)/\Gamma_{total}$	Γ_1/Γ
seen	AAIJ 15X LHCb + $D^*(2300)^+ \rightarrow D^0 \pi^+$
seen	AAIJ 15Y LHCb + $D^*(2300)^+ \rightarrow D^0 \pi^+$
seen	3.4k AUBERT 09AB BABR 0 $D^*(2300)^0 \rightarrow D^+ \pi^-$
seen	ABE 04D BELL 0 $D^*(2300)^0 \rightarrow D^+ \pi^-$
seen	18.8k LINK 04A FOCS + $D^*(2300)^+ \rightarrow D^0 \pi^+$

$D_0^*(2300)$ REFERENCES

DU	21	PRL 126 192001	M.-L. Du et al.	(LHCb Collab.)
DU	19	PR D99 114002	M.-L. Du, F.-K. Guo, U.-G. Meissner	(LHCb Collab.)
DU	18A	PR D98 094018	M.-L. Du et al.	(LHCb Collab.)
AAIJ	16AH	PR D94 072001	R. Aaij et al.	(LHCb Collab.)
AAIJ	15V	PR D91 092002	R. Aaij et al.	(LHCb Collab.)
Also		PR D93 119901 (err.)	R. Aaij et al.	(LHCb Collab.)
AAIJ	15X	PR D92 012012	R. Aaij et al.	(LHCb Collab.)
AAIJ	15Y	PR D92 032002	R. Aaij et al.	(LHCb Collab.)
AAIJ	14BH	PR D90 072003	R. Aaij et al.	(LHCb Collab.)
AUBERT	09AB	PR D79 112004	B. Aubert et al.	(BABAR Collab.)
ABE	04D	PR D69 112002	K. Abe et al.	(BELLE Collab.)
LINK	04A	PL B586 11	J.M. Link et al.	(FOCUS Collab.)

$D_1(2420)$

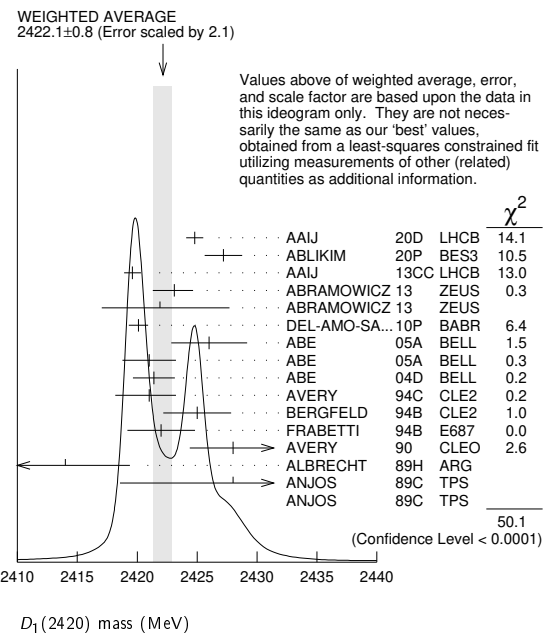
$I(J^P) = \frac{1}{2}(1^+)$

$D_1(2420)$ MASS

The fit includes D^\pm , D^0 , D_s^\pm , D_s^{*0} , D_s^{*+} , $D_1(2420)^0$, $D_2^*(2460)^0$, and $D_{s1}(2536)^\pm$ mass and mass difference measurements.

VALUE (MeV)	EVTS	DOCUMENT ID	TECN	CHG	COMMENT	
2422.1 ± 0.6 OUR FIT Error includes scale factor of 1.7.						
2422.1 ± 0.8 OUR AVERAGE Error includes scale factor of 2.1. See the ideogram below.						
2424.8 ± 0.1 ± 0.7	79k	¹ AAIJ	20D	LHCb	0 $B^- \rightarrow D^{*+} \pi^- \pi^-$	
2427.2 ± 1.0 ± 1.2	4207	ABLIKIM	20P	BES3	+ $e^+ e^- \rightarrow D^+ D^- \pi^+ \pi^-$	
2419.6 ± 0.1 ± 0.7	210k	AAIJ	13cc	LHCb	0 $p p \rightarrow D^{*+} \pi^- X$	
2423.1 ± 1.5 ± 0.4	2.7k	² ABRAMOWICZ13	ZEUS	0	$e^\pm p \rightarrow D^{(*)+} \pi^- X$	
2421.9 ± 4.7 ± 3.4	759	³ ABRAMOWICZ13	ZEUS	+	$e^\pm p \rightarrow D^{(*)0} \pi^+ X$	
2420.1 ± 0.1 ± 0.8	103k	DEL-AMO-SA...	10P	BABR	0 $e^+ e^- \rightarrow D^{*+} \pi^- X$	
2426 ± 3 ± 1	151	ABE	05A	BELL	0 $B^- \rightarrow D^0 \pi^+ \pi^- \pi^-$	
2421 ± 2 ± 1	124	ABE	05A	BELL	+ $\bar{B}^0 \rightarrow D^+ \pi^+ \pi^- \pi^-$	
2421.4 ± 1.5 ± 0.9		⁴ ABE	04D	BELL	0 $B^- \rightarrow D^{*+} \pi^- \pi^-$	
2421 ± 1 ± 2	± 2	286	AVERY	94c	CLE2	0 $e^+ e^- \rightarrow D^{*+} \pi^- X$
2425 ± 2 ± 2	146	BERGFELD	94B	CLE2	+ $e^+ e^- \rightarrow D^{*0} \pi^+ X$	
2422 ± 2 ± 2	51	FRABETTI	94B	E687	0 $\gamma Be \rightarrow D^{*+} \pi^- X$	
2428 ± 3 ± 2	279	AVERY	90	CLEO	0 $e^+ e^- \rightarrow D^{*+} \pi^- X$	
2414 ± 2 ± 5	171	ALBRECHT	89H	ARG	0 $e^+ e^- \rightarrow D^{*+} \pi^- X$	
2428 ± 8 ± 5	171	ANJOS	89c	TPS	0 $\gamma N \rightarrow D^{*+} \pi^- X$	
2443 ± 7 ± 5	190	ANJOS	89c	TPS	+ $\gamma N \rightarrow D^0 \pi^+ X^0$	
••• We do not use the following data for averages, fits, limits, etc. •••						
2420.5 ± 2.1 ± 0.9	3.1k	⁵ CHEKANOV	09	ZEUS	0 $e^\pm p \rightarrow D^{*+} \pi^- X$	
2421.7 ± 0.7 ± 0.6	7.5k	ABULENCIA	06A	CDF	0 1900 $p \bar{p} \rightarrow D^{*+} \pi^- X$	
2425 ± 3	235	⁶ ABREU	98M	DLPH	0 $e^+ e^-$	

¹ From a full four-body amplitude analysis of the $B^- \rightarrow D^{*+} \pi^- \pi^-$ decay.
² From the combined fit of the $M(D^+ \pi^-)$ and $M(D^{*+} \pi^-)$ distributions. and A_{D_2} fixed to the theoretical prediction of -1.
³ From the fit of the $M(D^0 \pi^+)$ distribution. The widths of the D_1^+ and D_2^+ are fixed to 25 MeV and 37 MeV, and A_{D_1} and A_{D_2} are fixed to the theoretical predictions of 3 and -1, respectively.
⁴ Fit includes the contribution from $D_1^*(2430)^0$.
⁵ Calculated using the mass difference $m(D_1^0) - m(D^{*+})_{PDG}$ reported below and $m(D^{*+})_{PDG} = 2010.27 \pm 0.17$ MeV. The 0.17 MeV uncertainty of the PDG mass value should be added to the experimental uncertainty of 0.9 MeV.
⁶ No systematic error given.



Meson Particle Listings

 $D_1(2420), D_1(2430)^0$ $m_{D_1(2420)^0} - m_{D^{*+}}$

The fit includes $D^\pm, D^0, D_s^\pm, D^{*±}, D^{*0}, D_1(2420)^0, D_2^*(2460)^0$, and $D_{s1}(2536)^\pm$ mass and mass difference measurements.

VALUE (MeV)	EVTS	DOCUMENT ID	TECN	COMMENT
411.8±0.6 OUR FIT				Error includes scale factor of 1.7.
411.5±0.8 OUR AVERAGE				
410.2±2.1±0.9	3.1k	CHEKANOV 09	ZEUS	$e^\pm p \rightarrow D^{*+} \pi^- X$
411.7±0.7±0.4	7.5k	ABULENCIA 06A	CDF	1900 $p\bar{p} \rightarrow D^{*+} \pi^- X$

 $m_{D_1(2420)^\pm} - m_{D_1(2420)^0}$

VALUE (MeV)	DOCUMENT ID	TECN	COMMENT
4$^{+2}_{-3}$±3	BERGFELD 94B	CLE2	$e^+ e^- \rightarrow$ hadrons

 $D_1(2420)$ WIDTH

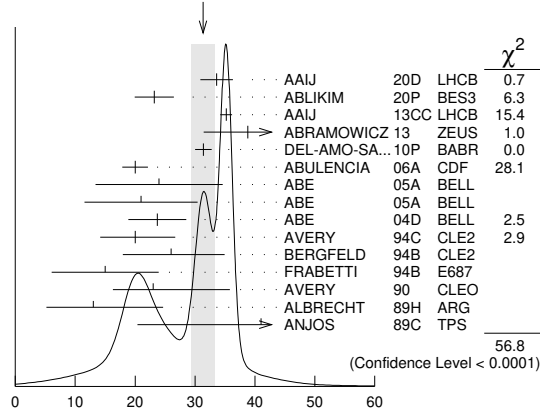
VALUE (MeV)	EVTS	DOCUMENT ID	TECN	CHG	COMMENT
31.3±1.9 OUR AVERAGE					Error includes scale factor of 2.8. See the ideogram below.
33.6±0.3±2.7	79k	¹ AAIJ 20D	LHCB	0	$B^- \rightarrow D^{*+} \pi^- \pi^-$
23.2±2.3±2.3	4207	ABLIKIM 20P	BES3	+	$e^+ e^- \rightarrow D^{*+} D^- \pi^+ \pi^-$
35.2±0.4±0.9	210k	AAIJ 13CC	LHCB	0	$p\bar{p} \rightarrow D^{*+} \pi^- X$
38.8±5.0 $^{+1.9}_{-5.4}$	2.7k	² ABRAMOWICZ13	ZEUS	0	$e^\pm p \rightarrow D^{(*)+} \pi^- X$
31.4±0.5±1.3	103k	DEL-AMO-SA...10P	BABR	0	$e^+ e^- \rightarrow D^{*+} \pi^- X$
20.0±1.7±1.3	7.5k	ABULENCIA 06A	CDF	0	1900 $p\bar{p} \rightarrow D^{*+} \pi^- X$
24 ± 7 ± 8	151	ABE 05A	BELL	0	$B^- \rightarrow D^0 \pi^+ \pi^- \pi^-$
21 ± 5 ± 8	124	ABE 05A	BELL	+	$\bar{B}^0 \rightarrow D^+ \pi^+ \pi^- \pi^-$
23.7±2.7±4.0		³ ABE 04D	BELL	0	$B^- \rightarrow D^{*+} \pi^- \pi^-$
20 $^{+6}_{-5}$ ± 3	286	AVERY 94C	CLE2	0	$e^+ e^- \rightarrow D^{*+} \pi^- X$
26 $^{+8}_{-7}$ ± 4	146	BERGFELD 94B	CLE2	+	$e^+ e^- \rightarrow D^{*0} \pi^+ X$
15 ± 8 ± 4	51	FRABETTI 94B	E687	0	$\gamma Be \rightarrow D^{*+} \pi^- X$
23 $^{+6}_{-8}$ $^{+10}_{-3}$	279	AVERY 90	CLEO	0	$e^+ e^- \rightarrow D^{*+} \pi^- X$
13 ± 6 $^{+10}_{-5}$	171	ALBRECHT 89H	ARG	0	$e^+ e^- \rightarrow D^{*+} \pi^- X$
41 ± 19 ± 8	190	ANJOS 89C	TPS	+	$\gamma N \rightarrow D^0 \pi^+ X^0$
••• We do not use the following data for averages, fits, limits, etc. •••					
53.2±7.2±3.3 $^{+3.3}_{-4.9}$	3.1k	CHEKANOV 09	ZEUS	0	$e^\pm p \rightarrow D^{*+} \pi^- X$
58 ± 14 ± 10	171	ANJOS 89C	TPS	0	$\gamma N \rightarrow D^{*+} \pi^- X$

¹ From a full four-body amplitude analysis of the $B^- \rightarrow D^{*+} \pi^- \pi^-$ decay.

² From the combined fit of the $M(D^+ \pi^-)$ and $M(D^{*+} \pi^-)$ distributions. and A_{D_2} fixed to the theoretical prediction of -1 .

³ Fit includes the contribution from $D_1^*(2430)^0$.

WEIGHTED AVERAGE
31.3±1.9 (Error scaled by 2.8)



$D_1(2420)$ WIDTH (MeV)

 $D_1(2420)$ DECAY MODES

$\bar{D}_1(2420)$ modes are charge conjugates of modes below.

Mode	Fraction (Γ_i/Γ)
Γ_1 $D^*(2007)^0 \pi$	seen
Γ_2 $D \pi^+ \pi^-$	
Γ_3 $D \rho^0$	

Γ_4 $D f_0(500)$
Γ_5 $D_0^*(2300)^0 \pi$
Γ_6 $D^0 \pi$
Γ_7 $D^* \pi^+ \pi^-$

 $D_1(2420)$ BRANCHING RATIOS

$\Gamma(D^*(2007)^0 \pi)/\Gamma_{\text{total}}$	Γ_1/Γ			
VALUE	DOCUMENT ID	TECN	CHG	COMMENT
seen	ACKERSTAFF 97W	OPAL	0	$e^+ e^- \rightarrow D^{*+} \pi^- X$
seen	AVERY 90	CLEO	0	$e^+ e^- \rightarrow D^{*+} \pi^- X$
seen	ALBRECHT 89H	ARG	0	$e^+ e^- \rightarrow D^* \pi^- X$
seen	ANJOS 89C	TPS	0	$\gamma N \rightarrow D^{*+} \pi^- X$
seen	ANJOS 89C	TPS	+	$\gamma N \rightarrow D^0 \pi^+ X^0$

 $\Gamma(D^0 \pi)/\Gamma(D^*(2007)^0 \pi)$

VALUE	CL%	DOCUMENT ID	TECN	CHG	COMMENT
<0.18	90	BERGFELD 94B	CLE2	+	$e^+ e^- \rightarrow$ hadrons
••• We do not use the following data for averages, fits, limits, etc. •••					
<0.24	90	AVERY 90	CLEO	0	$e^+ e^- \rightarrow D^+ \pi^- X$

 $D_1(2420)$ POLARIZATION AMPLITUDE A_{D_1}

A polarization amplitude A_{D_1} is a parameter that depends on the initial polarization of the D_1 and is sensitive to a possible S-wave contribution to its decay. For D_1 decays the helicity angle, θ_h , distribution varies like $1 + A_{D_1} \cos^2 \theta_h$, where θ_h is the angle in the D^* rest frame between the two pions emitted by the $D_1 \rightarrow D^* \pi$ and the $D^* \rightarrow D \pi$.

Unpolarized D_1 decaying purely via D-wave is predicted to give $A_{D_1} = 3$.

VALUE	EVTS	DOCUMENT ID	TECN	CHG	COMMENT
5.73±0.25 OUR AVERAGE					
7.8 $^{+6.7}_{-2.7}$ ± 1.8	2.7k	¹ ABRAMOWICZ13	ZEUS	0	$e^\pm p \rightarrow D^{(*)+} \pi^- X$
5.72±0.25	103k	DEL-AMO-SA...10P	BABR	0	$e^+ e^- \rightarrow D^{*+} \pi^- X$
5.9 $^{+3.0}_{-1.7}$ $^{+2.4}_{-1.0}$		CHEKANOV 09	ZEUS	0	$e^\pm p \rightarrow D^{*+} \pi^- X$
••• We do not use the following data for averages, fits, limits, etc. •••					
3.30±0.48	210k	² AAIJ 13CC	LHCB	0	$p\bar{p} \rightarrow D^{*+} \pi^- X$
3.8 ± 0.6 ± 0.8		³ AUBERT 09Y	BABR	0	$B^+ \rightarrow D_1^0 \ell^+ \nu_\ell$
3.8 ± 0.6 ± 0.8		³ AUBERT 09Y	BABR	+	$B^0 \rightarrow D_1^- \ell^+ \nu_\ell$
2.74 $^{+1.40}_{-0.93}$		⁴ AVERY 94C	CLE2	0	$e^+ e^- \rightarrow D^{*+} \pi^- X$

¹ From the combined fit of the $M(D^+ \pi^-)$ and $M(D^{*+} \pi^-)$ distributions. and A_{D_2} fixed to the theoretical prediction of -1 . A pure D-wave not excluded although some S-wave mixing possible.

² Systematic uncertainty not estimated. Resonance parameters fixed.

³ Assuming $\Gamma(\Upsilon(4S) \rightarrow B^+ B^-) / \Gamma(\Upsilon(4S) \rightarrow B^0 \bar{B}^0) = 1.065 \pm 0.026$ and equal partial widths and helicity angle distributions for charged and neutral D_1 mesons.

⁴ Systematic uncertainties not estimated.

 $D_1(2420)$ REFERENCES

AAIJ 20D	PR D101 032005	R. Aaij et al.	(LHCB Collab.)
ABLIKIM 20P	PL B804 135395	M. Ablikim et al.	(BESIII Collab.)
AAIJ 13CC	JHEP 1309 145	R. Aaij et al.	(LHCB Collab.)
ABRAMOWICZ 13	NP B866 229	H. Abramowicz et al.	(ZEUS Collab.)
DEL-AMO-SA...10P	PR D82 111101	P. del Amo Sanchez et al.	(BABAR Collab.)
AUBERT 09Y	PRL 103 051803	B. Aubert et al.	(BABAR Collab.)
CHEKANOV 09	EPJ C60 25	S. Chekanov et al.	(ZEUS Collab.)
ABULENCIA 06A	PR D73 051104	A. Abulencia et al.	(CDF Collab.)
ABE 05A	PRL 94 221805	K. Abe et al.	(BELLE Collab.)
ABE 04D	PR D69 112002	K. Abe et al.	(BELLE Collab.)
ABREU 98M	PL B426 231	P. Abreu et al.	(DELPHI Collab.)
ACKERSTAFF 97W	ZPHY C76 425	K. Ackerstaff et al.	(OPAL Collab.)
AVERY 94C	PL B331 236	P. Avery et al.	(CLEO Collab.)
BERGFELD 94B	PL B340 194	T. Bergfeld et al.	(CLEO Collab.)
FRABETTI 94B	PRL 72 324	P.L. Frabetti et al.	(FNAL E687 Collab.)
AVERY 90	PR D41 774	P. Avery, D. Basson	(CLEO Collab.)
ALBRECHT 89H	PL B232 398	H. Albrecht et al.	(ARGUS Collab.)
ANJOS 89C	PRL 62 1717	J.C. Anjos et al.	(FNAL E691 Collab.)

 $D_1(2430)^0$

$$J^P = \frac{1}{2}(1^+)$$

$J^P = 1^+$ determined by AAJ 20D.

 $D_1(2430)^0$ MASS

VALUE (MeV)	EVTS	DOCUMENT ID	TECN	COMMENT
2412±9 OUR AVERAGE				
2411 ± 3 ± 9	79k	¹ AAIJ 20D	LHCB	$B^- \rightarrow D^{*+} \pi^- \pi^-$
2427 ± 26 ± 25		ABE 04D	BELL	$B^- \rightarrow D^{*+} \pi^- \pi^-$
••• We do not use the following data for averages, fits, limits, etc. •••				
2477 ± 28		² AUBERT 06L	BABR	$\bar{B}^0 \rightarrow D^{*+} \omega \pi^-$

¹ From a full four-body amplitude analysis of the $B^- \rightarrow D^{*+} \pi^- \pi^-$ decay.

² Systematic errors not estimated.

$D_1(2430)^0, D_2^*(2460)$

$D_1(2430)^0$ WIDTH

VALUE (MeV)	EVTS	DOCUMENT ID	TECN	COMMENT
314 ± 29 OUR AVERAGE				
309 ± 9 ± 28	79k	¹ AAIJ	20D LHCb	$B^- \rightarrow D^{*+} \pi^- \pi^-$
384 $_{-75}^{+107}$ ± 74		ABE	04D BELL	$B^- \rightarrow D^{*+} \pi^- \pi^-$
• • • We do not use the following data for averages, fits, limits, etc. • • •				
266 ± 97		² AUBERT	06L BABR	$\bar{B}^0 \rightarrow D^{*+} \omega \pi^-$

¹ From a full four-body amplitude analysis of the $B^- \rightarrow D^{*+} \pi^- \pi^-$ decay.
² Systematic errors not estimated.

$D_1(2430)^0$ DECAY MODES

Mode	Fraction (Γ_i/Γ)
Γ_1 $D^*(2010)^+ \pi^-$	seen

$D_1(2430)^0$ REFERENCES

AAIJ	20D	PR D101 032005	R. Aaij <i>et al.</i>	(LHCb Collab.) JP
AUBERT	06L	PR D74 012001	B. Aubert <i>et al.</i>	(BABAR Collab.)
ABE	04D	PR D69 112002	K. Abe <i>et al.</i>	(BELLE Collab.)

$D_2^*(2460)$

$I(J^P) = \frac{1}{2}(2^+)$

$D_2^*(2460)$ MASS

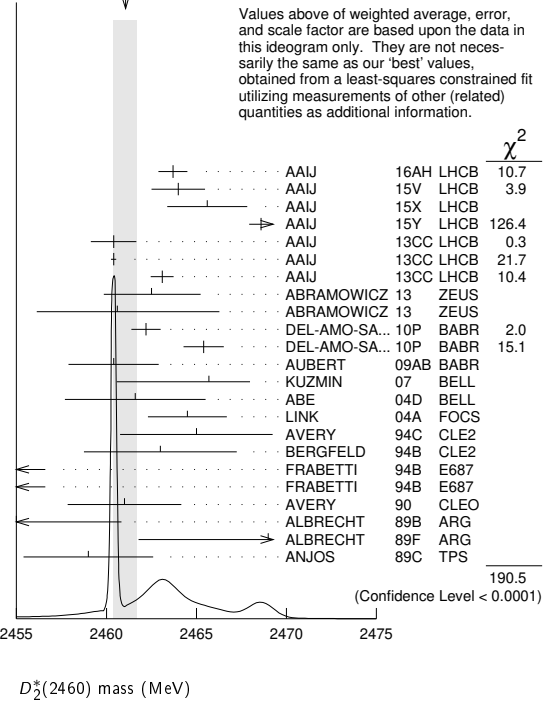
The fit includes $D^\pm, D^0, D_s^\pm, D^{*\pm}, D^{*0}, D_s^{*\pm}, D_1(2420)^0, D_2^*(2460)^0$, and $D_{s1}(2536)^\pm$ mass and mass difference measurements.

VALUE (MeV)	EVTS	DOCUMENT ID	TECN	CHG	COMMENT
2461.1 ± 0.8 OUR FIT					Error includes scale factor of 6.3.
2461.1 ± 0.7 OUR AVERAGE					Error includes scale factor of 5.2. See the ideogram below.
2463.7 ± 0.4 ± 0.7	28k	¹ AAIJ	16AH LHCb	0	$B^- \rightarrow D^+ \pi^- \pi^-$
2464.0 ± 1.4 ± 0.5	2k	² AAIJ	15V LHCb	0	$B^- \rightarrow D^+ K^- \pi^-$
2465.6 ± 1.8 ± 1.3		³ AAIJ	15X LHCb	+	$B^0 \rightarrow \bar{D}^0 K^+ \pi^-$
2468.6 ± 0.6 ± 0.3		⁴ AAIJ	15Y LHCb	+	$B^0 \rightarrow \bar{D}^0 \pi^+ \pi^-$
2460.4 ± 0.4 ± 1.2	82k	AAIJ	13CC LHCb	0	$pp \rightarrow D^{*+} \pi^- X$
2460.4 ± 0.1 ± 0.1	675k	AAIJ	13CC LHCb	0	$pp \rightarrow D^+ \pi^- X$
2463.1 ± 0.2 ± 0.6	342k	AAIJ	13CC LHCb	+	$pp \rightarrow D^0 \pi^+ X$
2462.5 ± 2.4 $_{-1.1}^{+1.3}$	2.3k	⁵ ABRAMOWICZ13	ZEUS	0	$e^\pm p \rightarrow D^*(*) \pi^- X$
2460.6 ± 4.4 $_{-0.8}^{+3.6}$	1371	⁶ ABRAMOWICZ13	ZEUS	+	$e^\pm p \rightarrow D^*(*)^0 \pi^+ X$
2462.2 ± 0.1 ± 0.8	243k	DEL-AMO-SA...10P	BABR	0	$e^+ e^- \rightarrow D^+ \pi^- X$
2465.4 ± 0.2 ± 1.1	111k	⁷ DEL-AMO-SA...10P	BABR	+	$e^+ e^- \rightarrow D^0 \pi^+ X$
2460.4 ± 1.2 ± 2.2	3.4k	AUBERT	09AB BABR	0	$B^- \rightarrow D^+ \pi^- \pi^-$
2465.7 ± 1.8 $_{-4.8}^{+1.4}$	2909	KUZMIN	07 BELL	+	$e^+ e^- \rightarrow$ hadrons
2461.6 ± 2.1 ± 3.3		⁸ ABE	04D BELL	0	$B^- \rightarrow D^+ \pi^- \pi^-$
2464.5 ± 1.1 ± 1.9	5.8k	⁸ LINK	04A FOCS	0	γA
2465 ± 3 ± 3	486	AVERY	94C CLE2	0	$e^+ e^- \rightarrow D^+ \pi^- X$
2463 ± 3 ± 3	310	BERGFELD	94B CLE2	+	$e^+ e^- \rightarrow D^0 \pi^+ X$
2453 ± 3 ± 2	128	FRABETTI	94B E687	0	$\gamma Be \rightarrow D^+ \pi^- X$
2453 ± 3 ± 2	185	FRABETTI	94B E687	+	$\gamma Be \rightarrow D^0 \pi^+ X$
2461 ± 3 ± 1	440	AVERY	90 CLEO	0	$e^+ e^- \rightarrow D^{*+} \pi^- X$
2455 ± 3 ± 5	337	ALBRECHT	89B ARG	0	$e^+ e^- \rightarrow D^+ \pi^- X$
2469 ± 4 ± 6		ALBRECHT	89F ARG	+	$e^+ e^- \rightarrow D^0 \pi^+ X$
2459 ± 3 ± 2	153	ANJOS	89C TPS	0	$\gamma N \rightarrow D^+ \pi^- X$
• • • We do not use the following data for averages, fits, limits, etc. • • •					
2468.1 ± 0.6 ± 0.5		⁹ AAIJ	15Y LHCb	+	$B^0 \rightarrow \bar{D}^0 \pi^+ \pi^-$
2469.1 ± 3.7 $_{-1.3}^{+1.2}$	1.5k	¹⁰ CHEKANOV	09 ZEUS	0	$e^\pm p \rightarrow D^*(*) \pi^- X$
2463.3 ± 0.6 ± 0.8	20k	ABULENCIA	06A CDF	0	1900 $p\bar{p} \rightarrow D^+ \pi^- X$
2467.6 ± 1.5 ± 0.8	3.5k	¹¹ LINK	04A FOCS	+	γA
2461 ± 6 ± 126		¹² ABREU	98M DLPH	0	$e^+ e^-$
2466 ± 7 ± 1		ASRATYAN	95 BEBC	0	53,40 $\nu(\bar{\nu}) \rightarrow pX, dX$

¹ From the amplitude analysis in the model describing the $D^+ \pi^-$ wave together with virtual contributions from the $D^*(2007)^0$ and B^{*0} states, and components corresponding to the $D_2^*(2460)^0, D_1^*(2680)^0, D_3^*(2760)^0$, and $D_2^*(3000)^0$ resonances.
² From the amplitude analysis in the model describing the $D^+ \pi^-$ wave together with virtual contributions from the $D^*(2007)^0$ and B^{*0} states, nonresonant spin-0 and spin-1 components as well as the $D_2^*(2400)^0, D_2^*(2460)^0$ and $D_1^*(2760)^0$ resonances.
³ From the Dalitz plot analysis including various K^* and D^{**} mesons as well as broad structures in the $K\pi$ S-wave and the $D\pi$ S- and P-waves.
⁴ Modeling the $\pi^+ \pi^-$ S-wave with the isobar formalism.
⁵ From the combined fit of the $M(D^+ \pi^-)$ and $M(D^{*+} \pi^-)$ distributions, and A_{D_2} fixed to the theoretical prediction of -1.
⁶ From the fit of the $M(D^0 \pi^+)$ distribution. The widths of the D_1^+ and D_2^{*+} are fixed to 25 MeV and 37 MeV, and A_{D_1} and A_{D_2} are fixed to the theoretical predictions of 3 and -1, respectively.
⁷ At a fixed width of 50.5 MeV.

⁸ Fit includes the contribution from $D_2^*(2400)^0$.
⁹ Modeling the $\pi^+ \pi^-$ S-wave with the K-matrix formalism.
¹⁰ Calculated using the mass difference $m(D_2^{*0}) - m(D^{*+})_{PDG}$ reported below and $m(D^{*+})_{PDG} = 2010.27 \pm 0.17$ MeV. The 0.17 MeV uncertainty of the PDG mass value should be added to the experimental uncertainty of $_{-1.3}^{+1.2}$ MeV.
¹¹ Fit includes the contribution from $D_2^*(2400)^\pm$. Not independent of the corresponding mass difference measurement, $(m_{D_2^*(2460)^\pm}) - (m_{D_2^*(2460)^0})$.
¹² No systematic error given.

WEIGHTED AVERAGE
2461.1 ± 0.7 (Error scaled by 5.2)



$m_{D_2^*(2460)^0} - m_{D^+}$

The fit includes $D^\pm, D^0, D_s^\pm, D^{*\pm}, D^{*0}, D_s^{*\pm}, D_1(2420)^0, D_2^*(2460)^0$, and $D_{s1}(2536)^\pm$ mass and mass difference measurements.

VALUE (MeV)	EVTS	DOCUMENT ID	TECN	COMMENT
591.5 ± 0.8 OUR FIT				Error includes scale factor of 6.0.
593.9 ± 0.6 ± 0.5	20k	ABULENCIA	06A CDF	1900 $p\bar{p} \rightarrow D^+ \pi^- X$

$m_{D_2^*(2460)^0} - m_{D^{*+}}$

The fit includes $D^\pm, D^0, D_s^\pm, D^{*\pm}, D^{*0}, D_s^{*\pm}, D_1(2420)^0, D_2^*(2460)^0$, and $D_{s1}(2536)^\pm$ mass and mass difference measurements.

VALUE (MeV)	EVTS	DOCUMENT ID	TECN	COMMENT
450.9 ± 0.8 OUR FIT				Error includes scale factor of 6.0.
458.8 ± 3.7 $_{-1.3}^{+1.2}$	1.5k	CHEKANOV	09 ZEUS	$e^\pm p \rightarrow D^*(*) \pi^- X$

$m_{D_2^*(2460)^\pm} - m_{D_2^*(2460)^0}$

VALUE (MeV)	DOCUMENT ID	TECN	COMMENT
2.4 ± 1.7 OUR AVERAGE			
3.1 ± 1.9 ± 0.9	LINK	04A FOCS	γA
- 2 ± 4 ± 4	BERGFELD	94B CLE2	$e^+ e^- \rightarrow$ hadrons
0 ± 4	FRABETTI	94B E687	$\gamma Be \rightarrow D\pi X$
14 ± 5 ± 8	ALBRECHT	89F ARG	$e^+ e^- \rightarrow D^0 \pi^+ X$

$D_2^*(2460)$ WIDTH

VALUE (MeV)	EVTS	DOCUMENT ID	TECN	CHG	COMMENT
47.3 ± 0.8 OUR AVERAGE					Error includes scale factor of 1.5. See the ideogram below.
47.0 ± 0.8 ± 1.0	28k	¹ AAIJ	16AH LHCb	0	$B^- \rightarrow D^+ \pi^- \pi^-$
43.8 ± 2.9 ± 1.8	2k	² AAIJ	15V LHCb	0	$B^- \rightarrow D^+ K^- \pi^-$

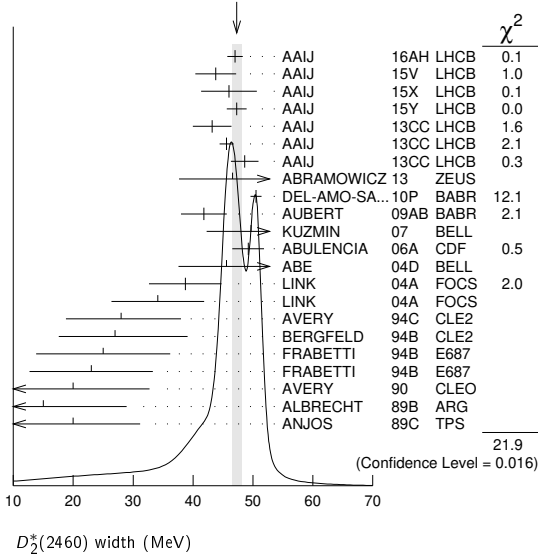
Meson Particle Listings

$D_2^*(2460)$

$46.0 \pm 3.4 \pm 3.2$	³ AAIJ	15X LHC B	+	$B^0 \rightarrow \bar{D}^0 K^+ \pi^-$
$47.3 \pm 1.5 \pm 0.7$	⁴ AAIJ	15Y LHC B	+	$B^0 \rightarrow \bar{D}^0 \pi^+ \pi^-$
$43.2 \pm 1.2 \pm 3.0$	82k AAIJ	13CC LHC B	0	$pp \rightarrow D^{*+} \pi^- X$
$45.6 \pm 0.4 \pm 1.1$	675k AAIJ	13CC LHC B	0	$pp \rightarrow D^+ \pi^- X$
$48.6 \pm 1.3 \pm 1.9$	342k AAIJ	13CC LHC B	+	$pp \rightarrow D^0 \pi^+ X$
$46.6 \pm 8.1 \pm 5.9$ 3.8	⁵ ABRAMOWICZ13	ZEUS	0	$e^+ p \rightarrow D^{(*)+} \pi^- X$
$50.5 \pm 0.6 \pm 0.7$	DEL-AMO-SA...10P	BABR	0	$e^+ e^- \rightarrow D^+ \pi^- X$
$41.8 \pm 2.5 \pm 2.9$	AUBERT	09AB BABR	0	$B^- \rightarrow D^+ \pi^- \pi^-$
$49.7 \pm 3.8 \pm 6.4$	KUZMIN	07 BELL	+	$e^+ e^- \rightarrow \text{hadrons}$
$49.2 \pm 2.3 \pm 1.3$	20k ABULENCIA	06A CDF	0	$1900 p\bar{p} \rightarrow D^+ \pi^- X$
$45.6 \pm 4.4 \pm 6.7$	⁶ ABE	04D BELL	0	$B^- \rightarrow D^+ \pi^- \pi^-$
$38.7 \pm 5.3 \pm 2.9$	⁶ LINK	04A FOCS	0	γA
$34.1 \pm 6.5 \pm 4.2$	⁷ LINK	04A FOCS	+	γA
$28 \pm 8 \pm 6$	486 AVERY	94C CLE2	0	$e^+ e^- \rightarrow D^+ \pi^- X$
$27 \pm 11 \pm 5$	310 BERGFELD	94B CLE2	+	$e^+ e^- \rightarrow D^0 \pi^+ X$
$25 \pm 10 \pm 5$	128 FRABETTI	94B E687	0	$\gamma Be \rightarrow D^+ \pi^- X$
$23 \pm 9 \pm 5$	185 FRABETTI	94B E687	+	$\gamma Be \rightarrow D^0 \pi^+ X$
$20 \pm 9 \pm 9$ -10	440 AVERY	90 CLEO	0	$e^+ e^- \rightarrow D^{*+} \pi^- X$
$15 \pm 13 \pm 5$ -10	337 ALBRECHT	89B ARG	0	$e^+ e^- \rightarrow D^+ \pi^- X$
$20 \pm 10 \pm 5$	153 ANJOS	89c TPS	0	$\gamma N \rightarrow D^+ \pi^- X$

- • • We do not use the following data for averages, fits, limits, etc. • • •
- ¹ From the amplitude analysis in the model describing the $D^+ \pi^-$ wave together with virtual contributions from the $D^*(2007)^0$ and B^{*0} states, and components corresponding to the $D_2^*(2460)^0$, $D_1^*(2680)^0$, $D_3^*(2760)^0$, and $D_2^*(3000)^0$ resonances.
- ² From the amplitude analysis in the model describing the $D^+ \pi^-$ wave together with virtual contributions from the $D^*(2007)^0$ and B^{*0} states, nonresonant spin-0 and spin-1 components as well as the $D_0^*(2400)^0$, $D_2^*(2460)^0$ and $D_1^*(2760)^0$ resonances.
- ³ From the Dalitz plot analysis including various K^* and D^{**} mesons as well as broad structures in the $K \pi S$ -wave and the $D \pi S$ - and P -waves.
- ⁴ Modeling the $\pi^+ \pi^- S$ -wave with the isobar formalism.
- ⁵ From the combined fit of the $M(D^+ \pi^-)$ and $M(D^{*+} \pi^-)$ distributions. and A_{D_2} fixed to the theoretical prediction of -1 .
- ⁶ Fit includes the contribution from $D_3^*(2400)^0$.
- ⁷ Fit includes the contribution from $D_0^*(2400)^0$.
- ⁸ Modeling the $\pi^+ \pi^- S$ -wave with the K-matrix formalism.

WEIGHTED AVERAGE
47.3±0.8 (Error scaled by 1.5)



$D_2^*(2460)$ DECAY MODES

$\bar{D}_2^*(2460)$ modes are charge conjugates of modes below.

Mode	Fraction (Γ_i/Γ)
Γ_1 $D \pi^-$	seen
Γ_2 $D^*(2010) \pi^-$	seen
Γ_3 $D^+ \pi^+ \pi^-$	
Γ_4 $D^* \pi^+ \pi^-$	

$D_2^*(2460)$ BRANCHING RATIOS

$\Gamma(D \pi^-)/\Gamma_{total}$		Γ_1/Γ			
VALUE	EVTS	DOCUMENT ID	TECN	CHG	COMMENT
seen	3.4k	AUBERT	09AB BABR	0	$B^- \rightarrow D^+ \pi^- \pi^-$
seen	337	ALBRECHT	89B ARG	0	$e^+ e^- \rightarrow D^+ \pi^- X$
seen		ALBRECHT	89F ARG	+	$e^+ e^- \rightarrow D^0 \pi^+ X$
seen		ANJOS	89c TPS	0	$\gamma N \rightarrow D^+ \pi^- X$

$\Gamma(D^*(2010) \pi^-)/\Gamma_{total}$		Γ_2/Γ			
VALUE	EVTS	DOCUMENT ID	TECN	CHG	COMMENT
seen		ACKERSTAFF	97W OPAL	0	$e^+ e^- \rightarrow D^{*+} \pi^- X$
seen		AVERY	90 CLEO	0	$e^+ e^- \rightarrow D^{*+} \pi^- X$
seen		ALBRECHT	89H ARG	0	$e^+ e^- \rightarrow D^* \pi^- X$

$\Gamma(D \pi^-)/\Gamma(D^*(2010) \pi^-)$		Γ_1/Γ_2			
VALUE	EVTS	DOCUMENT ID	TECN	CHG	COMMENT
1.52 ± 0.14 OUR AVERAGE					
$1.4 \pm 0.3 \pm 0.3$	2.3k	¹ ABRAMOWICZ13	ZEUS	0	$e^\pm p \rightarrow D^{(*)+} \pi^- X$
$1.1 \pm 0.4 \pm 0.3$ 0.2	1371	² ABRAMOWICZ13	ZEUS	+	$e^\pm p \rightarrow D^{(*)0} \pi^+ X$
$1.47 \pm 0.03 \pm 0.16$	379k	DEL-AMO-SA...10P	BABR	0	$e^+ e^- \rightarrow D^{(*)+} \pi^- X$
$2.8 \pm 0.8 \pm 0.5$ -0.6	1.5k	CHEKANOV	09 ZEUS	0	$e^\pm p \rightarrow D^{(*)+} \pi^- X$
$2.2 \pm 0.7 \pm 0.6$		AVERY	94C CLE2	0	$e^+ e^- \rightarrow D^{*+} \pi^- X$
$1.9 \pm 1.1 \pm 0.3$		BERGFELD	94B CLE2	+	$e^+ e^- \rightarrow \text{hadrons}$
2.3 ± 0.8		AVERY	90 CLEO	0	$e^+ e^-$
$3.0 \pm 1.1 \pm 1.5$		ALBRECHT	89H ARG	0	$e^+ e^- \rightarrow D^* \pi^- X$
• • • We do not use the following data for averages, fits, limits, etc. • • •					
1.9 ± 0.5		ABE	04D BELL	0	$B^- \rightarrow D^{(*)+} \pi^- \pi^-$

- ¹ From the combined fit of the $M(D^+ \pi^-)$ and $M(D^{*+} \pi^-)$ distributions. and A_{D_2} fixed to the theoretical prediction of -1 .
- ² From the fit of the $M(D^0 \pi^+)$ distribution. The widths of the D_1^+ and D_2^+ are fixed to 25 MeV and 37 MeV, and A_{D_1} and A_{D_2} are fixed to the theoretical predictions of 3 and -1 , respectively.

$\Gamma(D \pi^-)/[\Gamma(D \pi^-) + \Gamma(D^*(2010) \pi^-)]$		$\Gamma_1/(\Gamma_1 + \Gamma_2)$			
VALUE	EVTS	DOCUMENT ID	TECN	CHG	COMMENT
$0.62 \pm 0.03 \pm 0.02$	8414	¹ AUBERT	09Y BABR	0	$B^+ \rightarrow D_2^{*0} \ell^+ \nu_\ell$
$0.62 \pm 0.03 \pm 0.02$	3361	¹ AUBERT	09Y BABR	+	$\bar{B}^0 \rightarrow D_2^{*+} \ell^- \nu_\ell$

- • • We do not use the following data for averages, fits, limits, etc. • • •
- ¹ Assuming $\Gamma(\Upsilon(4S) \rightarrow B^+ B^-) / \Gamma(\Upsilon(4S) \rightarrow B^0 \bar{B}^0) = 1.065 \pm 0.026$ and equal partial widths for charged and neutral D_2^* mesons.

$D_2^*(2460)$ POLARIZATION AMPLITUDE A_{D_2}

A polarization amplitude A_{D_2} is a parameter that depends on the initial polarization of the D_2 . For D_2 decays the helicity angle, θ_H , distribution varies like $1 + A_{D_2} \cos^2(\theta_H)$, where θ_H is the angle in the D^* rest frame between the two pions emitted by the $D_2 \rightarrow D^* \pi$ and $D^* \rightarrow D \pi$.

VALUE	EVTS	DOCUMENT ID	TECN	CHG	COMMENT
-1.16 ± 0.35	2.3k	¹ ABRAMOWICZ13	ZEUS	0	$e^\pm p \rightarrow D^{(*)+} \pi^- X$
consistent with -1	243k	DEL-AMO-SA...10P	BABR	0	$e^+ e^- \rightarrow D^+ \pi^- X$
-0.74 ± 0.49 -0.38		² AVERY	94C CLE2	0	$e^+ e^- \rightarrow D^{*+} \pi^- X$

- ¹ From the combined fit of the $M(D^+ \pi^-)$ and $M(D^{*+} \pi^-)$ distributions.
- ² Systematic uncertainties not estimated.

$D_2^*(2460)$ REFERENCES

AAIJ 16AH PR D94 072001	R. Aaij et al.	(LHCb Collab.)
AAIJ 15Y PR D91 092002	R. Aaij et al.	(LHCb Collab.)
Also PR D93 119901 (errata.)	R. Aaij et al.	(LHCb Collab.)
AAIJ 15X PR D92 012012	R. Aaij et al.	(LHCb Collab.)
AAIJ 15Y PR D92 032002	R. Aaij et al.	(LHCb Collab.)
AAIJ 13CC JHEP 1309 145	R. Aaij et al.	(LHCb Collab.)
ABRAMOWICZ 13 NP B866 229	H. Abramowicz et al.	(ZEUS Collab.)
DEL-AMO-SA...10P PR D82 111101	P. del Amo Sanchez et al.	(BABAR Collab.)
AUBERT 09AB PR D79 112004	B. Aubert et al.	(BABAR Collab.)
AUBERT 09Y PRL 103 051803	B. Aubert et al.	(BABAR Collab.)
CHEKANOV 09 EPJ C60 25	S. Chekanov et al.	(ZEUS Collab.)
KUZMIN 07 PR D76 012006	A. Kuzmin et al.	(BELLE Collab.)
ABULENCIA 06A PR D73 051104	A. Abulencia et al.	(CDF Collab.)
ABE 04D PR D69 112002	K. Abe et al.	(BELLE Collab.)
LINK 04A PL B586 11	J.M. Link et al.	(FOCUS Collab.)
ABREU 98M PL B426 231	P. Abreu et al.	(DELPHI Collab.)
ACKERSTAFF 97W ZPHY C76 425	K. Ackerstaff et al.	(OPAL Collab.)
ASRATYAN 95 ZPHY C68 43	A.E. Asratyan et al.	(BIRM, BELG, CERN+)
AVERY 94C PL B331 236	P. Avery et al.	(CLEO Collab.)
BERGFELD 94B PL B340 194	T. Bergfeld et al.	(CLEO Collab.)
FRABETTI 94B PRL 72 324	P.L. Frabetti et al.	(FNAL E687 Collab.)
AVERY 90 PR D41 774	P. Avery, D. Besson	(CLEO Collab.)
ALBRECHT 89B PL B221 422	H. Albrecht et al.	(ARGUS Collab.)
ALBRECHT 89F PL B231 208	H. Albrecht et al.	(ARGUS Collab.)
ALBRECHT 89H PL B232 398	H. Albrecht et al.	(ARGUS Collab.)
ANJOS 89C PRL 62 1717	J.C. Anjos et al.	(FNAL E691 Collab.)

See key on page 1171

Meson Particle Listings

$D_0(2550)^0, D_1^*(2600)^0$

$D_0(2550)^0$

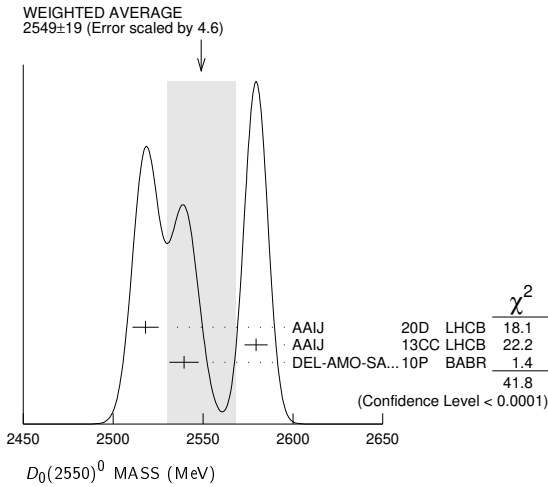
$I(J^P) = \frac{1}{2}(0^-)$

OMITTED FROM SUMMARY TABLE
 $J^P = 0^-$ determined by AAIJ 20D.

$D_0(2550)^0$ MASS

VALUE (MeV)	EVTS	DOCUMENT ID	TECN	COMMENT
2549 ± 19 OUR AVERAGE		Error includes scale factor of 4.6. See the ideogram below.		
2518 ± 2 ± 7	79k	¹ AAIJ	20D LHCB	$B^- \rightarrow D^{*+} \pi^- \pi^-$
2579.5 ± 3.4 ± 5.5	60k	AAIJ	13CC LHCB	$pp \rightarrow D^{*+} \pi^- X$
2539.4 ± 4.5 ± 6.8	34k	DEL-AMO-SA...10P	BABR	$e^+ e^- \rightarrow D^{*+} \pi^- X$

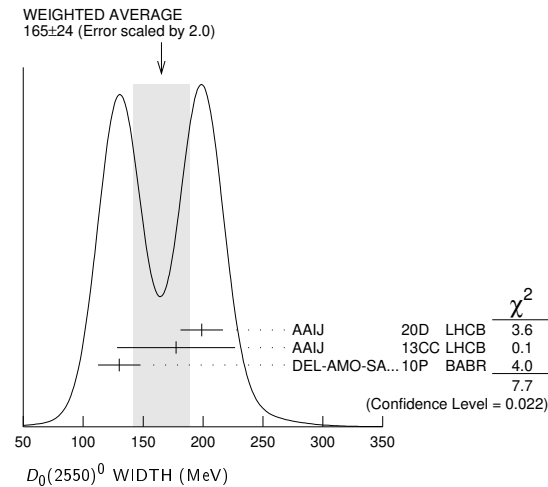
¹ From a full four-body amplitude analysis of the $B^- \rightarrow D^{*+} \pi^- \pi^-$ decay.



$D_0(2550)^0$ WIDTH

VALUE (MeV)	EVTS	DOCUMENT ID	TECN	COMMENT
165 ± 24 OUR AVERAGE		Error includes scale factor of 2.0. See the ideogram below.		
199 ± 5 ± 17	79k	¹ AAIJ	20D LHCB	$B^- \rightarrow D^{*+} \pi^- \pi^-$
177.5 ± 17.8 ± 46.0	60k	AAIJ	13CC LHCB	$pp \rightarrow D^{*+} \pi^- X$
130 ± 12 ± 13	34k	DEL-AMO-SA...10P	BABR	$e^+ e^- \rightarrow D^{*+} \pi^- X$

¹ From a full four-body amplitude analysis of the $B^- \rightarrow D^{*+} \pi^- \pi^-$ decay.



$D_0(2550)^0$ DECAY MODES

Mode	Fraction (Γ_i/Γ)
$\Gamma_1 D^{*+} \pi^-$	seen

$D_0(2550)^0$ POLARIZATION AMPLITUDE A_{D_J}

A polarization amplitude A_{D_J} is a parameter that depends on the initial polarization of the D_J . For D_J decays the helicity angle, θ_H , distribution varies like $1 + A_{D_J} \cos^2(\theta_H)$, where θ_H is the angle in the D_J rest frame between the two pions emitted in the $D_J \rightarrow D^* \pi$ and $D^* \rightarrow D \pi$ decays.

VALUE	EVTS	DOCUMENT ID	TECN	COMMENT
-------	------	-------------	------	---------

• • • We do not use the following data for averages, fits, limits, etc. • • •

4.2 ± 1.3	60k	¹ AAIJ	13CC LHCB	$pp \rightarrow D^{*+} \pi^- X$
-----------	-----	-------------------	-----------	---------------------------------

¹ Systematic uncertainty not estimated.

$D_0(2550)^0$ REFERENCES

AAIJ 20D PR D101 032005	R. Aaij et al.	(LHCb Collab.)JP
AAIJ 13CC JHEP 1309 145	R. Aaij et al.	(LHCb Collab.)
DEL-AMO-SA...10P PR D82 111101	P. del Amo Sanchez et al.	(BABAR Collab.)

$D_1^*(2600)^0$

$I(J^P) = \frac{1}{2}(1^-)$

OMITTED FROM SUMMARY TABLE
was $D_1^*(2600)$

$J^P = 1^-$ determined by AAIJ 20D.

$D_1^*(2600)^0$ MASS

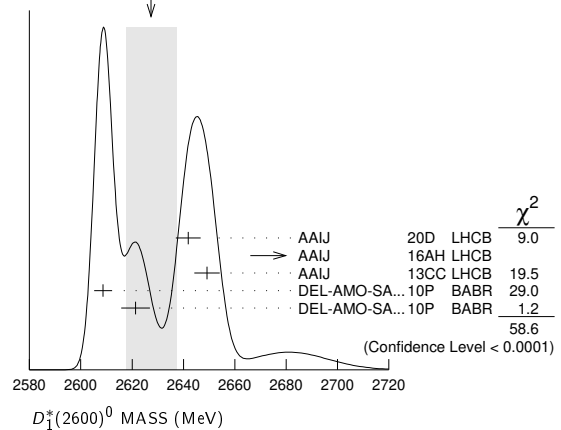
VALUE (MeV)	EVTS	DOCUMENT ID	TECN	CHG	COMMENT
2627 ± 10 OUR AVERAGE		Error includes scale factor of 4.4. See the ideogram below.			
2641.9 ± 1.8 ± 4.5	79k	¹ AAIJ	20D LHCB		$B^- \rightarrow D^{*+} \pi^- \pi^-$
2681.1 ± 5.6 ± 14.0	28k	² AAIJ	16AH LHCB		$B^- \rightarrow D^+ \pi^- \pi^-$
2649.2 ± 3.5 ± 3.5	51k	AAIJ	13CC LHCB		$pp \rightarrow D^{*+} \pi^- X$
2608.7 ± 2.4 ± 2.5	26k	DEL-AMO-SA...10P	BABR	0	$e^+ e^- \rightarrow D^+ \pi^- X$
2621.3 ± 3.7 ± 4.2	13k	³ DEL-AMO-SA...10P	BABR	+	$e^+ e^- \rightarrow D^0 \pi^+ X$

¹ From a full four-body amplitude analysis of the $B^- \rightarrow D^{*+} \pi^- \pi^-$ decay.

² From the amplitude analysis in the model describing the $D^+ \pi^-$ wave together with virtual contributions from the $D^*(2007)^0$ and B^*0 states, and components corresponding to the $D_2^*(2460)^0, D_1^*(2680)^0, D_3^*(2760)^0$, and $D_2^*(3000)^0$ resonances.

³ At a fixed width of 93 MeV.

WEIGHTED AVERAGE
2627 ± 10 (Error scaled by 4.4)



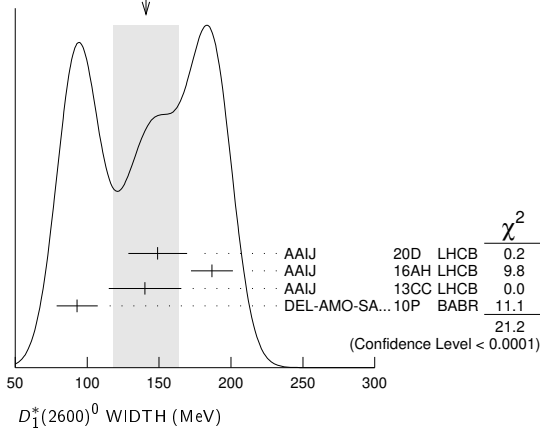
$D_1^*(2600)^0$ WIDTH

VALUE (MeV)	EVTS	DOCUMENT ID	TECN	COMMENT
141 ± 23 OUR AVERAGE		Error includes scale factor of 2.7. See the ideogram below.		
149 ± 4 ± 20	79k	¹ AAIJ	20D LHCB	$B^- \rightarrow D^{*+} \pi^- \pi^-$
186.7 ± 8.5 ± 11.9	28k	² AAIJ	16AH LHCB	$B^- \rightarrow D^+ \pi^- \pi^-$
140.2 ± 17.1 ± 18.6	51k	AAIJ	13CC LHCB	$pp \rightarrow D^{*+} \pi^- X$
93 ± 6 ± 13	26k	DEL-AMO-SA...10P	BABR	$e^+ e^- \rightarrow D^+ \pi^- X$

¹ From a full four-body amplitude analysis of the $B^- \rightarrow D^{*+} \pi^- \pi^-$ decay.

² From the amplitude analysis in the model describing the $D^+ \pi^-$ wave together with virtual contributions from the $D^*(2007)^0$ and B^*0 states, and components corresponding to the $D_2^*(2460)^0, D_1^*(2680)^0, D_3^*(2760)^0$, and $D_2^*(3000)^0$ resonances.

Meson Particle Listings

 $D_1^*(2600)^0$, $D^*(2640)^\pm$, $D_2(2740)^0$, $D_3^*(2750)$ WEIGHTED AVERAGE
141±23 (Error scaled by 2.7) $D_1^*(2600)^0$ DECAY MODES

Mode	Fraction (Γ_i/Γ)
Γ_1 $D\pi$	seen
Γ_2 $D^+\pi^-$	seen
Γ_3 $D^0\pi^\pm$	seen
Γ_4 $D^*\pi$	seen
Γ_5 $D^{*+}\pi^-$	seen

 $D_1^*(2600)^0$ BRANCHING RATIOS

VALUE	EVTS	DOCUMENT ID	TECN	COMMENT	Γ_2/Γ_5
$0.32 \pm 0.02 \pm 0.09$	76k	DEL-AMO-SA...10P	BABR	$e^+e^- \rightarrow D^{*+}\pi^- X$	

 $D_1^*(2600)^0$ REFERENCES

AAIJ	20D	PR D101 032005	R. Aaij et al.	(LHCb Collab.) JP
AAIJ	16AH	PR D94 072001	R. Aaij et al.	(LHCb Collab.)
AAIJ	13CC	JHEP 1309 145	R. Aaij et al.	(LHCb Collab.)
DEL-AMO-SA...10P	PR D82 111101	P. del Amo Sanchez et al.	(BABAR Collab.)	

 $D^*(2640)^\pm$

$I(J^P) = \frac{1}{2}(?^?)$

OMITTED FROM SUMMARY TABLE

Seen in Z decays by ABREU 98M. Not seen by ABBIENDI 01N and CHEKANOV 09. Needs confirmation.

 $D^*(2640)^\pm$ MASS

VALUE (MeV)	EVTS	DOCUMENT ID	TECN	COMMENT
$2637 \pm 2 \pm 6$	66 ± 14	ABREU	98M	DLPH $e^+e^- \rightarrow D^{*+}\pi^+\pi^- X$

 $D^*(2640)^\pm$ WIDTH

VALUE (MeV)	CL%	DOCUMENT ID	TECN	COMMENT
<15	95	ABREU	98M	DLPH $e^+e^- \rightarrow D^{*+}\pi^+\pi^- X$

 $D^*(2640)^+$ DECAY MODES $D^*(2640)^-$ modes are charge conjugates of modes below.

Mode	Fraction (Γ_i/Γ)
Γ_1 $D^*(2010)^+\pi^+\pi^-$	seen

 $D^*(2640)^\pm$ REFERENCES

CHEKANOV	09	EPJ C60 25	S. Chekanov et al.	(ZEUS Collab.)
ABBIENDI	01N	EPJ C20 445	G. Abbiendi et al.	(OPAL Collab.)
ABREU	98M	PL B426 231	P. Abreu et al.	(DELPHI Collab.)

 $D_2(2740)^0$

$I(J^P) = \frac{1}{2}(2^-)$

OMITTED FROM SUMMARY TABLE

was $D(2740)^0$ $J^P = 2^-$ determined by (AAIJ 20D). $D_2(2740)^0$ MASS

VALUE (MeV)	EVTS	DOCUMENT ID	TECN	COMMENT
2747 ± 6 OUR AVERAGE				
2751 ± 3 ± 7	79k	¹ AAIJ	20D	LHCB $B^- \rightarrow D^{*+}\pi^-\pi^-$
2737.0 ± 3.5 ± 11.2	7.7k	AAIJ	13CC	LHCB $pp \rightarrow D^{*+}\pi^- X$

¹ From a full four-body amplitude analysis of the $B^- \rightarrow D^{*+}\pi^-\pi^-$ decay. $D_2(2740)^0$ WIDTH

VALUE (MeV)	EVTS	DOCUMENT ID	TECN	COMMENT
88 ± 19 OUR AVERAGE				
102 ± 6 ± 26	79k	¹ AAIJ	20D	LHCB $B^- \rightarrow D^{*+}\pi^-\pi^-$
73.2 ± 13.4 ± 25.0	7.7k	AAIJ	13CC	LHCB $pp \rightarrow D^{*+}\pi^- X$

¹ From a full four-body amplitude analysis of the $B^- \rightarrow D^{*+}\pi^-\pi^-$ decay. $D_2(2740)^0$ DECAY MODES

Mode	Fraction (Γ_i/Γ)
Γ_1 $D^{*+}\pi^-$	seen

 $D_2(2740)^0$ POLARIZATION AMPLITUDE A_{D_J} A polarization amplitude A_{D_J} is a parameter that depends on the initial polarization of the D_J . For D_J decays the helicity angle, θ_H , distribution varies like $1 + A_{D_J} \cos^2(\theta_H)$, where θ_H is the angle in the D_J rest frame between the two pions emitted in the $D_J \rightarrow D^*\pi$ and $D^* \rightarrow D\pi$ decays.

VALUE	EVTS	DOCUMENT ID	TECN	COMMENT
3.1 ± 2.2	7.7k	¹ AAIJ	13CC	LHCB $pp \rightarrow D^{*+}\pi^- X$

¹ Systematic uncertainty not estimated. $D_2(2740)^0$ REFERENCES

AAIJ	20D	PR D101 032005	R. Aaij et al.	(LHCb Collab.) JP
AAIJ	13CC	JHEP 1309 145	R. Aaij et al.	(LHCb Collab.)

 $D_3^*(2750)$

$I(J^P) = \frac{1}{2}(3^-)$

 J^P determined by AAIJ 15Y from the Dalitz plot analysis of $B^0 \rightarrow \bar{D}^0\pi^+\pi^-$ decays. $D_3^*(2750)$ MASS

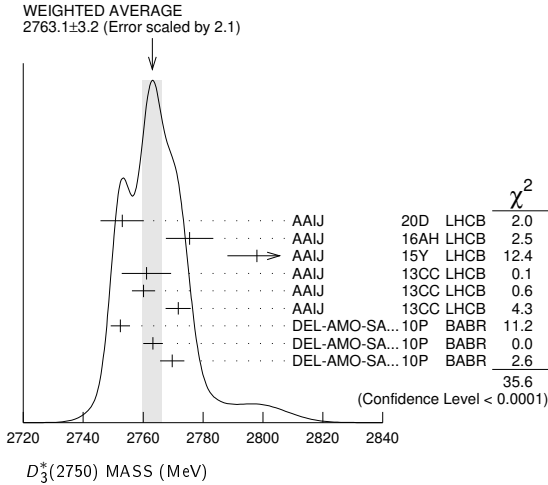
VALUE (MeV)	EVTS	DOCUMENT ID	TECN	CHG	COMMENT
2763.1 ± 3.2 OUR AVERAGE					Error includes scale factor of 2.1. See the ideogram below.
2753 ± 4 ± 6	79k	¹ AAIJ	20D	LHCB	$B^- \rightarrow D^{*+}\pi^-\pi^-$
2775.5 ± 4.5 ± 6.5	28k	² AAIJ	16AH	LHCB	$B^- \rightarrow D^+\pi^-\pi^-$
2798 ± 7 ± 7		³ AAIJ	15Y	LHCB	$B^0 \rightarrow \bar{D}^0\pi^+\pi^-$
2761.1 ± 5.1 ± 6.5	14k	AAIJ	13CC	LHCB	0 $pp \rightarrow D^{*+}\pi^- X$
2760.1 ± 1.1 ± 3.7	56k	AAIJ	13CC	LHCB	0 $pp \rightarrow D^+\pi^- X$
2771.7 ± 1.7 ± 3.8	20k	AAIJ	13CC	LHCB	+ $pp \rightarrow \bar{D}^0\pi^+ X$
2752.4 ± 1.7 ± 2.7	235k	⁴ DEL-AMO-SA...10P	BABR	0	$e^+e^- \rightarrow D^{*+}\pi^- X$
2763.3 ± 2.3 ± 2.3	11.3k	⁴ DEL-AMO-SA...10P	BABR	0	$e^+e^- \rightarrow D^+\pi^- X$
2769.7 ± 3.8 ± 1.5	5.7k	^{4,5} DEL-AMO-SA...10P	BABR	+	$e^+e^- \rightarrow \bar{D}^0\pi^+ X$
2802 ± 11 ± 10		⁶ AAIJ	15Y	LHCB	$B^0 \rightarrow \bar{D}^0\pi^+\pi^-$

¹ From a full four-body amplitude analysis of the $B^- \rightarrow D^{*+}\pi^-\pi^-$ decay.² From the amplitude analysis in the model describing the $D^+\pi^-$ wave together with virtual contributions from the $D^*(2007)^0$ and B^{*0} states, and components corresponding to the $D_2^*(2460)^0$, $D_1^*(2680)^0$, $D_3^*(2760)^0$, and $D_2^*(3000)^0$ resonances.³ Modeling the $\pi^+\pi^-$ S-wave with the Isobar formalism.⁴ The states observed in the $D^*\pi$ and $D\pi$ final states are not necessarily the same.⁵ At a fixed width of 60.9 MeV.⁶ Modeling the $\pi^+\pi^-$ S-wave with the K-matrix formalism.

See key on page 1171

Meson Particle Listings

$D_3^*(2750)$, $D_1^*(2760)^0$, $D(3000)^0$



$D_3^*(2750)$ REFERENCES

AAIJ	20D	PR D101 032005	R. Aaij et al.	(LHCb Collab.)
AAIJ	16AH	PR D94 072001	R. Aaij et al.	(LHCb Collab.)
AAIJ	15Y	PR D92 032002	R. Aaij et al.	(LHCb Collab.) JP
AAIJ	13CC	JHEP 1309 145	R. Aaij et al.	(LHCb Collab.)
DEL-AMO-SA...10P	PR D82	111101	P. del Amo Sanchez et al.	(BABAR Collab.)

$D_1^*(2760)^0$

$I(J^P) = \frac{1}{2}(1^-)$

OMITTED FROM SUMMARY TABLE

J^P determined by AAIJ 15V from the Dalitz plot analysis of $B^- \rightarrow D^+ K^- \pi^-$ decays.

$D_1^*(2760)^0$ MASS

VALUE (MeV)	EVTS	DOCUMENT ID	TECN	COMMENT
2781 ± 18 ± 13	2k	¹ AAIJ	15V LHCB	$B^- \rightarrow D^+ K^- \pi^-$

¹ From the amplitude analysis in the model describing the $D^+ \pi^-$ wave together with virtual contributions from the $D^*(2007)^0$ and B^{*0} states, nonresonant spin-0 and spin-1 components as well as the $D_0^*(2400)^0$, $D_2^*(2460)^0$ and $D_1^*(2760)^0$ resonances.

$D_1^*(2760)^0$ WIDTH

VALUE (MeV)	EVTS	DOCUMENT ID	TECN	COMMENT
177 ± 32 ± 21	2k	¹ AAIJ	15V LHCB	$B^- \rightarrow D^+ K^- \pi^-$

¹ From the amplitude analysis in the model describing the $D^+ \pi^-$ wave together with virtual contributions from the $D^*(2007)^0$ and B^{*0} states, nonresonant spin-0 and spin-1 components as well as the $D_0^*(2400)^0$, $D_2^*(2460)^0$ and $D_1^*(2760)^0$ resonances.

$D_1^*(2760)^0$ DECAY MODES

Mode	Fraction (Γ_i/Γ)
Γ_1 $D^+ \pi^-$	seen

$D_1^*(2760)^0$ BRANCHING RATIOS

$\Gamma(D^+ \pi^-)/\Gamma_{total}$	Γ_1/Γ
seen	¹ AAIJ 15V LHCB $B^- \rightarrow D^+ K^- \pi^-$

¹ From the amplitude analysis in the model describing the $D^+ \pi^-$ wave together with virtual contributions from the $D^*(2007)^0$ and B^{*0} states, nonresonant spin-0 and spin-1 components as well as the $D_0^*(2400)^0$, $D_2^*(2460)^0$ and $D_1^*(2760)^0$ resonances.

$D_1^*(2760)^0$ REFERENCES

AAIJ	15V	PR D91 092002	R. Aaij et al.	(LHCb Collab.) JP
Also		PR D93 119901 (err.)	R. Aaij et al.	(LHCb Collab.)

$D(3000)^0$

$I(J^P) = \frac{1}{2}(2^{??})$

OMITTED FROM SUMMARY TABLE

Both natural- and unnatural-parity components observed depending on the decay mode (AAIJ 13CC).

$D(3000)^0$ MASS

VALUE (MeV)	EVTS	DOCUMENT ID	TECN	COMMENT
3214 ± 29 ± 49	28k	¹ AAIJ	16AH LHCB	$B^- \rightarrow D^+ \pi^- \pi^-$

• • • We do not use the following data for averages, fits, limits, etc. • • •

2971.8 ± 8.7	9.5k	^{2,3} AAIJ	13CC LHCB	$pp \rightarrow D^* \pi^- X$
3008.1 ± 4.0	17.6k	^{2,4} AAIJ	13CC LHCB	$pp \rightarrow D^+ \pi^- X$

¹ From the amplitude analysis in the model describing the $D^+ \pi^-$ wave together with virtual contributions from the $D^*(2007)^0$ and B^{*0} states, and components corresponding to the $D_2^*(2460)^0$, $D_1^*(2680)^0$, $D_3^*(2760)^0$, and $D_2^*(3000)^0$ resonances.

² Systematic uncertainty not estimated.

³ Unnatural parity preferred.

⁴ Natural parity state. A state $D(3000)^+$ is possibly seen in $D^0 \pi^+$ final state.

$D(3000)^0$ WIDTH

VALUE (MeV)	EVTS	DOCUMENT ID	TECN	COMMENT
186 ± 38 ± 72	28k	⁵ AAIJ	16AH LHCB	$B^- \rightarrow D^+ \pi^- \pi^-$

$D_3^*(2750)$ WIDTH

VALUE (MeV)	EVTS	DOCUMENT ID	TECN	CHG	COMMENT
66 ± 5	OUR AVERAGE				
66 ± 10 ± 14	79k	¹ AAIJ	20D LHCB		$B^- \rightarrow D^* \pi^- \pi^-$
95.3 ± 9.6 ± 34.0	28k	² AAIJ	16AH LHCB		$B^- \rightarrow D^+ \pi^- \pi^-$
105 ± 18 ± 24		³ AAIJ	15Y LHCB		$B^0 \rightarrow \bar{D}^0 \pi^+ \pi^-$
74.4 ± 3.4 ± 37.0	14k	AAIJ	13CC LHCB	0	$pp \rightarrow D^* \pi^- X$
74.4 ± 3.4 ± 19.1	56k	AAIJ	13CC LHCB	0	$pp \rightarrow D^+ \pi^- X$
66.7 ± 6.6 ± 10.5	20k	AAIJ	13CC LHCB	+	$pp \rightarrow D^0 \pi^+ X$
71 ± 6 ± 11	23.5k	⁴ DEL-AMO-SA...10P	BABR		$e^+ e^- \rightarrow D^* \pi^- X$
60.9 ± 5.1 ± 3.6	11.3k	⁴ DEL-AMO-SA...10P	BABR		$e^+ e^- \rightarrow D^+ \pi^- X$
154 ± 27 ± 16		⁵ AAIJ	15Y LHCB		$B^0 \rightarrow \bar{D}^0 \pi^+ \pi^-$

- • • We do not use the following data for averages, fits, limits, etc. • • •
- ¹ From a full four-body amplitude analysis of the $B^- \rightarrow D^* \pi^- \pi^-$ decay.
- ² From the amplitude analysis in the model describing the $D^+ \pi^-$ wave together with virtual contributions from the $D^*(2007)^0$ and B^{*0} states, and components corresponding to the $D_2^*(2460)^0$, $D_1^*(2680)^0$, $D_3^*(2760)^0$, and $D_2^*(3000)^0$ resonances.
- ³ Modeling the $\pi^+ \pi^-$ S-wave with the Isobar formalism.
- ⁴ The states observed in the $D^* \pi$ and $D \pi$ final states are not necessarily the same.
- ⁵ Modeling the $\pi^+ \pi^-$ S-wave with the K-matrix formalism.

$D_3^*(2750)$ DECAY MODES

Mode	Fraction (Γ_i/Γ)
Γ_1 $D \pi$	seen
Γ_2 $D^+ \pi^-$	seen
Γ_3 $D^0 \pi^\pm$	seen
Γ_4 $D^* \pi$	seen
Γ_5 $D^* \pi^-$	seen

$D_3^*(2750)$ BRANCHING RATIOS

$\Gamma(D^+ \pi^-)/\Gamma(D^* \pi^-)$	Γ_2/Γ_5
0.42 ± 0.05 ± 0.11	

VALUE	EVTS	DOCUMENT ID	TECN	COMMENT
0.42 ± 0.05 ± 0.11	34.8k	¹ DEL-AMO-SA...10P	BABR	$e^+ e^- \rightarrow D^* \pi^- X$

¹ The states observed in the $D^* \pi$ and $D \pi$ final states are not necessarily the same.

$D_3^*(2750)$ POLARIZATION AMPLITUDE A_D

A polarization amplitude A_D is a parameter that depends on the initial polarization of the $D_3^*(2750)$. For $D_3^*(2750)$ decays the helicity angle, θ_H , distribution varies like $1 + A_D \cos(\theta_H)$, where θ_H is the angle in the D^* rest frame between the two pions emitted by the $D_3^*(2750) \rightarrow D^* \pi$ and $D^* \rightarrow D \pi$.

VALUE	EVTS	DOCUMENT ID	TECN	COMMENT
-0.33 ± 0.28	23.5k	¹ DEL-AMO-SA...10P	BABR	$e^+ e^- \rightarrow D^* \pi^- X$

- • • We do not use the following data for averages, fits, limits, etc. • • •
- ¹ Systematic uncertainties not estimated. The states observed in the $D^* \pi$ and $D \pi$ final states are not necessarily the same.

Meson Particle Listings

 $D(3000)^0$

• • • We do not use the following data for averages, fits, limits, etc. • • •

188.1±44.8 9.5k ^{6,7} AAIJ 13cc LHCb $pp \rightarrow D^{*+} \pi^- X$
 110.5±11.5 17.6k ^{6,8} AAIJ 13cc LHCb $pp \rightarrow D^+ \pi^- X$

⁵ From the amplitude analysis in the model describing the $D^+ \pi^-$ wave together with virtual contributions from the $D^*(2007)^0$ and B^{*0} states, and components corresponding to the $D_2^*(2460)^0$, $D_1^*(2680)^0$, $D_3^*(2760)^0$, and $D_2^*(3000)^0$ resonances.

⁶ Systematic uncertainty not estimated.

⁷ Unnatural parity preferred.

⁸ Natural parity state. A state $D(3000)^+$ is possibly seen in $D^0 \pi^+$ final state.

 $D(3000)^0$ DECAY MODES

Mode	Fraction (Γ_i/Γ)
Γ_1 $D^{*+} \pi^-$	seen

 $D(3000)^0$ POLARIZATION AMPLITUDE A_{D_J}

A polarization amplitude A_{D_J} is a parameter that depends on the initial polarization of the D_J . For D_J decays the helicity angle, θ_H , distribution varies like $1 + A_{D_J} \cos^2(\theta_H)$, where θ_H is the angle in the D_J rest frame between the two pions emitted in the $D_J \rightarrow D^* \pi$ and $D^* \rightarrow D \pi$ decays.

VALUE EVTS DOCUMENT ID TECN COMMENT

• • • We do not use the following data for averages, fits, limits, etc. • • •

1.5±0.9 9.5k ⁹ AAIJ 13cc LHCb $pp \rightarrow D^{*+} \pi^- X$

⁹ Systematic uncertainty not estimated.

 $D(3000)^0$ REFERENCES

AAIJ	16AH PR D94 072001	R. Aaij <i>et al.</i>	(LHCb Collab.)
AAIJ	13CC JHEP 1309 145	R. Aaij <i>et al.</i>	(LHCb Collab.)

CHARMED, STRANGE MESONS
($C = \pm 1, S = \pm 1$)
(including possibly non- $q\bar{q}$ states)

$D_s^+ = c\bar{s}, D_s^- = \bar{c}s,$ similarly for $D_s^{* \pm}$'s

D_s^\pm

$J(P) = 0(0^-)$

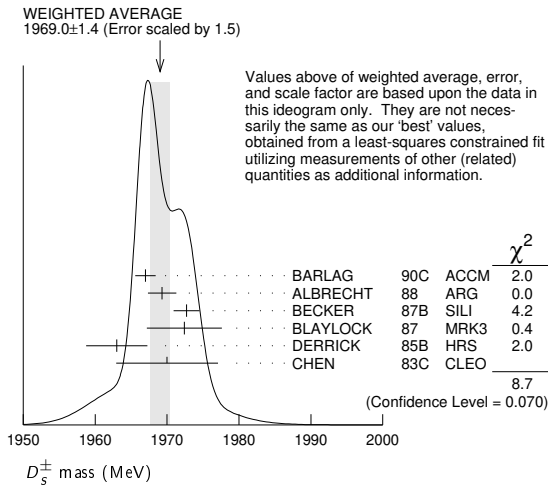
The angular distributions of the decays of the ϕ and $\bar{K}^*(892)^0$ in the $\phi\pi^+$ and $K^+\bar{K}^*(892)^0$ modes strongly indicate that the spin is zero. The parity given is that expected of a $c\bar{s}$ ground state.

D_s^\pm MASS

The fit includes $D^\pm, D^0, D_s^\pm, D^{*\pm}, D^{*0}, D_s^{* \pm}, D_1(2420)^0, D_2^*(2460)^0,$ and $D_{s1}(2536)^\pm$ mass and mass difference measurements. Measurements of the D_s^\pm mass with an error greater than 10 MeV are omitted from the fit and average. A number of early measurements have been omitted altogether.

VALUE (MeV)	EVTS	DOCUMENT ID	TECN	COMMENT
1968.35 ± 0.07 OUR FIT				
1969.0 ± 1.4 OUR AVERAGE				Error includes scale factor of 1.5. See the ideogram below.
1967.0 ± 1.0 ± 1.0	54	BARLAG	90C	ACCM π^- Cu 230 GeV
1969.3 ± 1.4 ± 1.4		ALBRECHT	88	ARG e^+e^- 9.4-10.6 GeV
1972.7 ± 1.5 ± 1.0	21	BECKER	87B	SILI 200 GeV π, K, p
1972.4 ± 3.7 ± 3.7	27	BLAYLOCK	87	MRK3 e^+e^- 4.14 GeV
1963 ± 3 ± 3	30	DERRICK	85B	HRS e^+e^- 29 GeV
1970 ± 5 ± 5	104	CHEN	83c	CLEO e^+e^- 10.5 GeV
••• We do not use the following data for averages, fits, limits, etc. •••				
1968.3 ± 0.7 ± 0.7	290	¹ ANJOS	88	E691 Photoproduction
1980 ± 15	6	USHIDA	86	EMUL ν wideband
1973.6 ± 2.6 ± 3.0	163	ALBRECHT	85D	ARG e^+e^- 10 GeV
1948 ± 28 ± 10	65	AIHARA	84D	TPC e^+e^- 29 GeV
1975 ± 9 ± 10	49	ALTHOFF	84	TASS e^+e^- 14-25 GeV
1975 ± 4	3	BAILEY	84	ACCM hadron ⁺ Be → $\phi\pi^+X$

¹ANJOS 88 enters the fit via $m_{D_s^\pm} - m_{D^\pm}$ (see below).



$m_{D_s^\pm} - m_{D^\pm}$

The fit includes $D^\pm, D^0, D_s^\pm, D^{*\pm}, D^{*0}, D_s^{* \pm}, D_1(2420)^0, D_2^*(2460)^0,$ and $D_{s1}(2536)^\pm$ mass and mass difference measurements.

VALUE (MeV)	EVTS	DOCUMENT ID	TECN	COMMENT
98.69 ± 0.05 OUR FIT				
98.69 ± 0.05 OUR AVERAGE				
98.68 ± 0.03 ± 0.04		AAIJ	13V	LHCB $D_s^+ \rightarrow K^+K^-\pi^+$
99.41 ± 0.38 ± 0.21		ACOSTA	03D	CDF2 $\bar{p}p, \sqrt{s} = 1.96$ TeV
98.4 ± 0.1 ± 0.3	48k	AUBERT	02G	BABR $e^+e^- \approx \gamma(4S)$
99.5 ± 0.6 ± 0.3		BROWN	94	CLE2 $e^+e^- \approx \gamma(4S)$
98.5 ± 1.5	555	CHEN	89	CLEO e^+e^- 10.5 GeV
99.0 ± 0.8	290	ANJOS	88	E691 Photoproduction

D_s^\pm MEAN LIFE

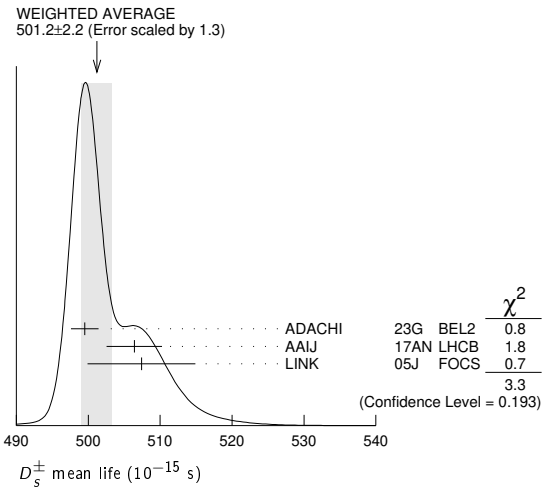
Measurements with an error greater than 100×10^{-15} s or with fewer than 100 events have been omitted from the Listings.

VALUE (10^{-15} s)	EVTS	DOCUMENT ID	TECN	COMMENT
501.2 ± 2.2 OUR AVERAGE				Error includes scale factor of 1.3. See the ideogram below.
499.5 ± 1.7 ± 0.9	116k	ADACHI	23G	BEL2 $D_s^+ \rightarrow \phi\pi^+$
506.4 ± 3.0 ± 1.7 ± 1.7		¹ AAIJ	17AN	LHCB pp at 7, 8 TeV
507.4 ± 5.5 ± 5.1	13.6k	LINK	05J	FOCS $\phi\pi^+$ and $\bar{K}^{*0}K^+$
••• We do not use the following data for averages, fits, limits, etc. •••				
472.5 ± 17.2 ± 6.6	760	IORI	01	SELX 600 GeV Σ^-, π^-, p
518 ± 14 ± 7	1662	AITALA	99	E791 π^- nucleus, 500 GeV
486.3 ± 15.0 ⁺ _{-5.1}	2167	² BONVICINI	99	CLE2 $e^+e^- \approx \gamma(4S)$
475 ± 20 ± 7	900	FRABETTI	93F	E687 γ Be, $\phi\pi^+$
500 ± 60 ± 30	104	FRABETTI	90	E687 γ Be, $\phi\pi^+$
470 ± 40 ± 20	228	RAAB	88	E691 Photoproduction

¹This AAIJ 17AN value is derived from the difference between the D_s^- and D^- widths.

The 3rd uncertainty, $\pm 1.7 \times 10^{-15}$ s, arises from the uncertainty of the D^- width.

²BONVICINI 99 obtains 1.19 ± 0.04 for the ratio of D_s^+ to D^0 lifetimes.



D_s^\pm DECAY MODES

Unless otherwise noted, the branching fractions for modes with a resonance in the final state include all the decay modes of the resonance. D_s^- modes are charge conjugates of the modes below.

Mode	Fraction (Γ_i/Γ)	Scale factor / Confidence level
Inclusive modes		
Γ_1 e^+ semileptonic	[a] (6.33 ± 0.15) %	
Γ_2 π^+ anything	(19.3 ± 1.4) %	
Γ_3 π^- anything	(43.2 ± 0.9) %	
Γ_4 π^0 anything	(123 ± 7) %	
Γ_5 K^- anything	(18.7 ± 0.5) %	
Γ_6 K^+ anything	(28.9 ± 0.7) %	
Γ_7 K_S^0 anything	(19.0 ± 1.1) %	
Γ_8 η anything	[b] (29.9 ± 2.8) %	
Γ_9 ω anything	(6.1 ± 1.4) %	
Γ_{10} η' anything	[c] (10.3 ± 1.4) %	S=1.1
Γ_{11} $f_0(980)$ anything, $f_0 \rightarrow \pi^+\pi^-$	< 1.3	CL=90%
Γ_{12} ϕ anything	(15.7 ± 1.0) %	
Γ_{13} K^+K^- anything	(15.8 ± 0.7) %	
Γ_{14} $K_S^0 K^+$ anything	(5.8 ± 0.5) %	
Γ_{15} $K_S^0 K^-$ anything	(1.9 ± 0.4) %	
Γ_{16} $2K_S^0$ anything	(1.70 ± 0.32) %	
Γ_{17} $2K^+$ anything	< 2.6	$\times 10^{-3}$ CL=90%
Γ_{18} $2K^-$ anything	< 6	$\times 10^{-4}$ CL=90%
Γ_{19} $2\pi^+\pi^-$ anything	(32.8 ± 0.7) %	
Leptonic and semileptonic modes		
Γ_{20} $e^+\nu_e$	< 8.3	$\times 10^{-5}$ CL=90%
Γ_{21} $\mu^+\nu_\mu$	(5.35 ± 0.12) $\times 10^{-3}$	
Γ_{22} $\tau^+\nu_\tau$	(5.36 ± 0.10) %	
Γ_{23} $\gamma e^+\nu_e$	< 1.3	$\times 10^{-4}$ CL=90%
Γ_{24} $K^+K^-e^+\nu_e$	—	

Meson Particle Listings

D_S^\pm

Γ ₂₅	$K_S^0 K_S^0 e^+ \nu_e$	< 3.8	$\times 10^{-4}$	CL=90%
Γ ₂₆	$\phi e^+ \nu_e$	[d] (2.39 ± 0.16) %		S=1.3
Γ ₂₇	$K_1(1270)^0 e^+ \nu_e$	< 4.1	$\times 10^{-4}$	CL=90%
Γ ₂₈	$b_1(1235)^0 e^+ \nu_e, b_1^0 \rightarrow \omega \pi^0$	< 6.4	$\times 10^{-4}$	CL=90%
Γ ₂₉	$\phi \mu^+ \nu_\mu$	(2.24 ± 0.11) %		
Γ ₃₀	$\eta e^+ \nu_e + \eta'(958) e^+ \nu_e$	[d] (3.03 ± 0.24) %		
Γ ₃₁	$\eta e^+ \nu_e$	[d] (2.26 ± 0.06) %		
Γ ₃₂	$\eta'(958) e^+ \nu_e$	[d] (8.0 ± 0.4) $\times 10^{-3}$		
Γ ₃₃	$\eta \mu^+ \nu_\mu$	(2.4 ± 0.5) %		
Γ ₃₄	$\eta'(958) \mu^+ \nu_\mu$	(1.1 ± 0.5) %		
Γ ₃₅	$\omega e^+ \nu_e$	[e] < 2.0	$\times 10^{-3}$	CL=90%
Γ ₃₆	$K^0 e^+ \nu_e$	(3.4 ± 0.4) $\times 10^{-3}$		
Γ ₃₇	$K^*(892)^0 e^+ \nu_e$	[d] (2.15 ± 0.28) $\times 10^{-3}$		S=1.1
Γ ₃₈	$f_0(500) e^+ \nu_e, f_0 \rightarrow \pi^0 \pi^0$	< 7.3	$\times 10^{-4}$	CL=90%
Γ ₃₉	$f_0(980) e^+ \nu_e, f_0 \rightarrow \pi^0 \pi^0$	(7.9 ± 1.5) $\times 10^{-4}$		
Γ ₄₀	$f_0(980) e^+ \nu_e, f_0 \rightarrow \pi^+ \pi^-$			
Γ ₄₁	$f_0(980) \mu^+ \nu_\mu, f_0 \rightarrow K^+ K^-$	< 5.45	$\times 10^{-4}$	CL=90%
Γ ₄₂	$a_0(980)^0 e^+ \nu_e, a_0^0 \rightarrow \pi^0 \eta$	< 1.2	$\times 10^{-4}$	CL=90%
Γ ₄₃	$\pi^0 e^+ \nu_e$	< 6.4	$\times 10^{-5}$	CL=90%

Hadronic modes with a $K\bar{K}$ pair

Γ ₄₄	$K^+ K_S^0$	(1.450 ± 0.035) %		
Γ ₄₅	$K^+ K^0$	(1.49 ± 0.06) %		
Γ ₄₆	$K^+ \bar{K}^0$	(2.95 ± 0.14) %		
Γ ₄₇	$K^+ K^- \pi^+$	[f] (5.37 ± 0.10) %		S=1.1
Γ ₄₈	$\phi \pi^+$	[d,g] (4.5 ± 0.4) %		
Γ ₄₉	$\phi \pi^+, \phi \rightarrow K^+ K^-$	[g] (2.21 ± 0.06) %		
Γ ₅₀	$K^+ \bar{K}^*(892)^0$	(12.7 $\begin{smallmatrix} +4.0 \\ -3.1 \end{smallmatrix}$) %		
Γ ₅₁	$K^+ \bar{K}^*(892)^0, \bar{K}^{*0} \rightarrow K^- \pi^+$	(2.58 ± 0.06) %		
Γ ₅₂	$K^+ \bar{K}^*(892)^0, \bar{K}^{*0} \rightarrow K_S^0 \pi^0$	(4.8 ± 0.5) $\times 10^{-3}$		
Γ ₅₃	$f_0(980) \pi^+, f_0 \rightarrow K^+ K^-$	(1.11 ± 0.19) %		
Γ ₅₄	$f_0(1370) \pi^+, f_0 \rightarrow K^+ K^-$	(7.1 ± 2.9) $\times 10^{-4}$		
Γ ₅₅	$f_0(1710) \pi^+, f_0 \rightarrow K^+ K^-$	(6.7 ± 2.8) $\times 10^{-4}$		
Γ ₅₆	$a_0(980)^+ \pi^0, a_0^+ \rightarrow K^+ K_S^0$	(1.1 ± 0.4) $\times 10^{-3}$		
Γ ₅₇	$a_0(1710)^+ \pi^0, a_0^+ \rightarrow K^+ K_S^0$	(3.5 ± 0.6) $\times 10^{-3}$		
Γ ₅₈	$K^+ \bar{K}_0^*(1430)^0, \bar{K}_0^0 \rightarrow K^- \pi^+$	(1.76 ± 0.25) $\times 10^{-3}$		
Γ ₅₉	$K^+ \bar{K}^*(1410)^0, \bar{K}_0^0 \rightarrow K_S^0 \pi^0$	(8.8 ± 2.8) $\times 10^{-4}$		
Γ ₆₀	$K^+ K_S^0 \pi^0$	(1.47 ± 0.07) %		
Γ ₆₁	$K^*(892)^+ K_S^0, K^{*+} \rightarrow K^+ \pi^0$	(2.04 ± 0.33) $\times 10^{-3}$		
Γ ₆₂	$2K_S^0 \pi^+$	(7.1 ± 0.4) $\times 10^{-3}$		S=1.3
Γ ₆₃	$f_0(980) \pi^+, f_0 \rightarrow K_S^0 K_S^0$	< 1.8	$\times 10^{-4}$	CL=90%
Γ ₆₄	$f_0(1710) \pi^+, f_0 \rightarrow K_S^0 K_S^0$	(3.3 ± 0.4) $\times 10^{-3}$		
Γ ₆₅	$K^*(892)^+ K_S^0, K^{*+} \rightarrow K_S^0 \pi^+$	(3.09 ± 0.33) $\times 10^{-3}$		
Γ ₆₆	$K^0 \bar{K}^0 \pi^+$	—		
Γ ₆₇	$K^*(892)^+ \bar{K}^0$	[d] (5.4 ± 1.2) %		
Γ ₆₈	$K^+ K^- \pi^+ \pi^0$	(5.50 ± 0.24) %		S=1.3
Γ ₆₉	$\phi \rho^+$	[d] (5.59 ± 0.34) %		
Γ ₇₀	$\bar{K}_1(1270)^0 K^+, \bar{K}_1(1270)^0 \rightarrow K^- \rho^+$	(5.7 ± 0.6) $\times 10^{-3}$		
Γ ₇₁	$\bar{K}_1(1270)^0 K^+, \bar{K}_1(1270)^0 \rightarrow K^*(892) \pi$	(1.31 ± 0.25) %		
Γ ₇₂	$\bar{K}_1(1400)^0 K^+, \bar{K}_1(1400)^0 \rightarrow K^*(892) \pi$	(2.0 ± 0.4) %		
Γ ₇₃	$a_0(980)^0 \rho^+, a_0^0 \rightarrow K^+ K^-$	(1.9 ± 0.4) $\times 10^{-3}$		
Γ ₇₄	$f_1(1420)^0 \pi^+, f_1(1420)^0 \rightarrow K^*(892)^\mp K^\pm$	(3.9 ± 0.7) $\times 10^{-3}$		
Γ ₇₅	$f_1(1420)^0 \pi^+, f_1(1420)^0 \rightarrow a_0(980)^0 \pi^0, a_0(980)^0 \rightarrow K^+ K^-$	(4.0 ± 1.4) $\times 10^{-4}$		
Γ ₇₆	$\eta(1475) \pi^+, \eta(1475) \rightarrow a_0(980)^0 \pi^0, a_0(980)^0 \rightarrow K^+ K^-$	(7.0 ± 2.8) $\times 10^{-4}$		
Γ ₇₇	$K_S^0 K^- 2\pi^+$	(1.53 ± 0.08) %		S=1.5
Γ ₇₈	$K^+ K^- K_S^0 \pi^+$	(1.29 ± 0.18) $\times 10^{-4}$		
Γ ₇₉	$K^*(892)^+ \bar{K}^*(892)^0$	[d] (5.64 ± 0.35) %		
Γ ₈₀	$\eta(1475) K_S^0, \eta \rightarrow K^*(892)^0 \pi^+, K^{*0} \rightarrow K^- \pi^+$	(3.4 ± 1.0) $\times 10^{-4}$		

Γ ₈₁	$\eta(1475) \pi^+, \eta \rightarrow \bar{K}^*(892)^+ K^-, \bar{K}^{*+} \rightarrow K_S^0 \pi^+$	(3.4 ± 1.0) $\times 10^{-4}$		
Γ ₈₂	$\eta(1475) \pi^+, \eta \rightarrow a_0(980)^- \pi^+, a_0^- \rightarrow K_S^0 K^-$	(1.7 ± 0.9) $\times 10^{-3}$		
Γ ₈₃	$f_1(1285) \pi^+, f_1 \rightarrow a_0(980)^- \pi^+, a_0^- \rightarrow K_S^0 K^-$	(3.4 ± 0.8) $\times 10^{-4}$		
Γ ₈₄	$K^+ K_S^0 \pi^+ \pi^-$	(9.5 ± 0.8) $\times 10^{-3}$		S=1.1
Γ ₈₅	$K^+ K^- 2\pi^+ \pi^-$	(6.6 ± 0.6) $\times 10^{-3}$		
Γ ₈₆	$\phi 2\pi^+ \pi^-$	[d] (1.21 ± 0.16) %		
Γ ₈₇	$\phi \rho^0 \pi^+, \phi \rightarrow K^+ K^-$	(4.9 ± 0.7) $\times 10^{-3}$		
Γ ₈₈	$\phi a_1(1260)^+, \phi \rightarrow K^+ K^-, a_1^+ \rightarrow \rho^0 \pi^+$	(7.4 ± 1.2) $\times 10^{-3}$		
Γ ₈₉	$\phi 2\pi^+ \pi^-$ non- $\rho, \phi \rightarrow K^+ K^-$	(1.4 ± 0.5) $\times 10^{-3}$		
Γ ₉₀	$K^+ K^- \rho^0 \pi^+ \pi^-$ non- ϕ	< 2.0	$\times 10^{-4}$	CL=90%
Γ ₉₁	$K^+ K^- 2\pi^+ \pi^-$ nonresonant	(1.0 ± 0.4) $\times 10^{-3}$		
Γ ₉₂	$2K_S^0 2\pi^+ \pi^-$	(7.8 ± 3.3) $\times 10^{-4}$		

Hadronic modes without K 's

Γ ₉₃	$\pi^+ \pi^0$	< 1.2	$\times 10^{-4}$	CL=90%
Γ ₉₄	$2\pi^+ \pi^-$	(1.08 ± 0.04) %		
Γ ₉₅	$\rho^0 \pi^+$	(1.12 ± 0.17) $\times 10^{-4}$		
Γ ₉₆	$\pi^+ (\pi^+ \pi^-)_{S\text{-wave}}$	[h] (9.12 ± 0.35) $\times 10^{-3}$		
Γ ₉₇	$f_0(980) \pi^+, f_0 \rightarrow \pi^+ \pi^-$			
Γ ₉₈	$f_0(1370) \pi^+, f_0 \rightarrow \pi^+ \pi^-$			
Γ ₉₉	$f_0(1500) \pi^+, f_0 \rightarrow \pi^+ \pi^-$			
Γ ₁₀₀	$f_2(1270) \pi^+, f_2 \rightarrow \pi^+ \pi^-$	(1.40 ± 0.11) $\times 10^{-3}$		
Γ ₁₀₁	$f_2'(1525)^0 \pi^+, f_2' \rightarrow \pi^+ \pi^-$	(5.7 ± 2.0) $\times 10^{-6}$		
Γ ₁₀₂	$\rho(1450)^0 \pi^+, \rho^0 \rightarrow \pi^+ \pi^-$	(1.8 ± 0.6) $\times 10^{-4}$		
Γ ₁₀₃	$\rho(1700)^0 \pi^+, \rho^0 \rightarrow \pi^+ \pi^-$	(4 ± 4) $\times 10^{-5}$		
Γ ₁₀₄	$\pi^+ 2\pi^0$	(5.2 ± 0.5) $\times 10^{-3}$		S=1.1
Γ ₁₀₅	$f_0(980) \pi^+, f_0 \rightarrow \pi^0 \pi^0$	(2.9 ± 0.6) $\times 10^{-3}$		
Γ ₁₀₆	$f_0(1370) \pi^+, f_0 \rightarrow \pi^0 \pi^0$	(1.3 ± 0.6) $\times 10^{-3}$		
Γ ₁₀₇	$f_2(1270) \pi^+, f_2 \rightarrow \pi^0 \pi^0$	(5.0 ± 3.5) $\times 10^{-4}$		
Γ ₁₀₈	$2\pi^+ \pi^- \pi^0$	—		
Γ ₁₀₉	$\eta \pi^+$	[d] (1.67 ± 0.09) %		S=1.1
Γ ₁₁₀	$\omega \pi^+$	[d] (1.92 ± 0.30) $\times 10^{-3}$		
Γ ₁₁₁	$\omega \pi^+, \omega \rightarrow \pi^+ \pi^-$	(3.9 ± 0.5) $\times 10^{-5}$		
Γ ₁₁₂	$3\pi^+ 2\pi^-$	(7.8 ± 0.8) $\times 10^{-3}$		
Γ ₁₁₃	$2\pi^+ \pi^- 2\pi^0$	—		
Γ ₁₁₄	$\eta \rho^+$	[d] (8.9 ± 0.8) %		
Γ ₁₁₅	$\eta \pi^+ \pi^0$	(9.5 ± 0.5) %		
Γ ₁₁₆	$\eta (\pi^+ \pi^0)_{P\text{-wave}}$	(5.1 ± 3.1) $\times 10^{-3}$		
Γ ₁₁₇	$a_0(980)^+ 0 \pi^0, a_0(980)^+ 0 \rightarrow \eta \pi^+ 0$	(2.2 ± 0.4) %		
Γ ₁₁₈	$\omega \pi^+ \pi^0$	[d] (2.8 ± 0.7) %		
Γ ₁₁₉	$2\pi^+ \pi^- \eta$	(3.12 ± 0.16) %		
Γ ₁₂₀	$a_1(1260)^+ \eta, a_1^+ \rightarrow \rho(770)^0 \pi^+, \rho^0 \rightarrow \pi^+ \pi^-$	(1.73 ± 0.16) %		
Γ ₁₂₁	$a_1(1260)^+ \eta, a_1^+ \rightarrow f_0(500) \pi^+, f_0 \rightarrow \pi^+ \pi^-$	(2.5 ± 0.9) $\times 10^{-3}$		
Γ ₁₂₂	$a_0(980)^+ \rho(770)^0, a_0^+ \rightarrow \eta \pi^+$	(2.1 ± 0.9) $\times 10^{-3}$		
Γ ₁₂₃	$\eta(1405) \pi^+, \eta(1405) \rightarrow a_0(980)^- \pi^+, a_0^- \rightarrow \eta \pi^-$	(2.2 ± 0.7) $\times 10^{-4}$		
Γ ₁₂₄	$\eta(1405) \pi^+, \eta(1405) \rightarrow a_0(980)^+ \pi^-, a_0^+ \rightarrow \eta \pi^+$	(2.2 ± 0.7) $\times 10^{-4}$		
Γ ₁₂₅	$f_1(1420) \pi^+, f_1 \rightarrow a_0(980)^- \pi^+, a_0^- \rightarrow \eta \pi^-$	(5.9 ± 1.8) $\times 10^{-4}$		
Γ ₁₂₆	$f_1(1420) \pi^+, f_1 \rightarrow a_0(980)^+ \pi^-, a_0^+ \rightarrow \eta \pi^+$	(5.3 ± 1.8) $\times 10^{-4}$		
Γ ₁₂₇	$3\pi^+ 2\pi^- \pi^0$	(4.9 ± 3.2) %		
Γ ₁₂₈	$\omega 2\pi^+ \pi^-$	[d] (1.6 ± 0.5) %		
Γ ₁₂₉	$\eta'(958) \pi^+$	[c,d] (3.94 ± 0.25) %		
Γ ₁₃₀	$3\pi^+ 2\pi^- 2\pi^0$	—		
Γ ₁₃₁	$\omega \eta \pi^+$	[d] (5.4 ± 1.3) $\times 10^{-3}$		
Γ ₁₃₂	$\eta'(958) \rho^+$	[c,d] (5.8 ± 1.5) %		
Γ ₁₃₃	$\eta'(958) \pi^+ \pi^0$	(6.08 ± 0.29) %		
Γ ₁₃₄	$\eta'(958) \pi^+ \pi^0$ nonresonant	< 5.1 %		CL=90%

See key on page 1171

Meson Particle Listings

D_s^\pm

Modes with one or three K 's

Γ_{135}	$K^+\pi^0$	(7.4 ± 0.5) × 10 ⁻⁴	
Γ_{136}	$K_S^0\pi^+$	(1.09 ± 0.05) × 10 ⁻³	
Γ_{137}	$K^+\eta$	[d] (1.73 ± 0.08) × 10 ⁻³	
Γ_{138}	$K^+\omega$	[d] (9.9 ± 1.5) × 10 ⁻⁴	
Γ_{139}	$K^+\eta'(958)$	[d] (2.64 ± 0.24) × 10 ⁻³	
Γ_{140}	$K^+\pi^+\pi^-$	(6.20 ± 0.19) × 10 ⁻³	
Γ_{141}	$K^+\rho^0$	(2.17 ± 0.25) × 10 ⁻³	
Γ_{142}	$K^+\rho(1450)^0, \rho^0 \rightarrow \pi^+\pi^-$	(7.2 ± 1.7) × 10 ⁻⁴	
Γ_{143}	$K^+f_0(500), f_0 \rightarrow \pi^+\pi^-$	(4.5 ± 3.0) × 10 ⁻⁴	
Γ_{144}	$K^+f_0(980), f_0 \rightarrow \pi^+\pi^-$	(2.8 ± 1.1) × 10 ⁻⁴	
Γ_{145}	$K^+f_0(1370), f_0 \rightarrow \pi^+\pi^-$	(1.2 ± 0.6) × 10 ⁻³	
Γ_{146}	$K^*(892)^0\pi^+, K^{*0} \rightarrow$ $K^+\pi^-$	(1.67 ± 0.26) × 10 ⁻³	
Γ_{147}	$K^*(1410)^0\pi^+, K^{*0} \rightarrow$ $K^+\pi^-$	(6 ± 4) × 10 ⁻⁴	
Γ_{148}	$K^*(1430)^0\pi^+, K^{*0} \rightarrow$ $K^+\pi^-$	(9.3 ± 3.1) × 10 ⁻⁴	
Γ_{149}	$K^+\pi^+\pi^-$ nonresonant	(9.9 ± 3.2) × 10 ⁻⁴	
Γ_{150}	$K_S^0\pi^+\pi^0$		
Γ_{151}	$K_S^0\pi^+\pi^0$	(5.38 ± 0.32) × 10 ⁻³	
Γ_{152}	$K_S^0\rho(770)^+, \rho^+ \rightarrow \pi^+\pi^0$	(2.7 ± 0.5) × 10 ⁻³	
Γ_{153}	$K_S^0\rho(1450)^+, \rho^+ \rightarrow \pi^+\pi^0$	(1.10 ± 0.34) × 10 ⁻³	
Γ_{154}	$K^*(892)^0\pi^+, K^{*0} \rightarrow K_S^0\pi^0$	(4.5 ± 1.3) × 10 ⁻⁴	
Γ_{155}	$K^*(892)^+\pi^0, K^{*+} \rightarrow$ $K_S^0\pi^+$	(2.5 ± 0.8) × 10 ⁻⁴	
Γ_{156}	$K^*(1410)^0\pi^+, K^{*0} \rightarrow$ $K_S^0\pi^0$	(1.8 ± 0.9) × 10 ⁻⁴	
Γ_{157}	$K_S^0 2\pi^+\pi^-$	(2.8 ± 1.0) × 10 ⁻³	
Γ_{158}	$K^+\pi^+\pi^-\pi^0$	(9.7 ± 0.6) × 10 ⁻³	
Γ_{159}	$K^*(892)^0\rho^+, K^{*0} \rightarrow K^+\pi^-$	(3.9 ± 0.4) × 10 ⁻³	
Γ_{160}	$K^*(892)^+\rho^0, K^{*+} \rightarrow K^+\pi^0$	(4.2 ± 1.2) × 10 ⁻⁴	
Γ_{161}	$K_1(1270)^0\pi^+, K_1^0 \rightarrow K^+\rho^-$	(3.9 ± 1.3) × 10 ⁻⁴	
Γ_{162}	$K_1(1400)^0\pi^+, K_1^0 \rightarrow$ $K^*(890)^+\pi^-, K^{*+} \rightarrow$ $K^+\pi^0$	(5.4 ± 0.9) × 10 ⁻⁴	
Γ_{163}	$K_1(1400)^0\pi^+, K_1^0 \rightarrow$ $K^*(890)^0\pi^0, K^{*0} \rightarrow$ $K^+\pi^-$	(5.9 ± 1.0) × 10 ⁻⁴	
Γ_{164}	$K^+a_1(1260)^0, a_1 \rightarrow \rho^+\pi^-$	(1.8 ± 1.1) × 10 ⁻⁴	
Γ_{165}	$K^+a_1(1260)^0, a_1 \rightarrow \rho^-\pi^+$	(1.8 ± 1.1) × 10 ⁻⁴	
Γ_{166}	$K^+\pi^+\pi^-\pi^0$ nonresonant	(9.2 ± 2.4) × 10 ⁻⁴	
Γ_{167}	$(K^+\pi^0)\rho$ -wave ρ^0	(1.01 ± 0.21) × 10 ⁻³	
Γ_{168}	$K^+\omega\pi^0$	[d] < 8.2 × 10 ⁻³	CL=90%
Γ_{169}	$K^+\omega\pi^+\pi^-$	[d] < 5.4 × 10 ⁻³	CL=90%
Γ_{170}	$K^+\omega\eta$	[d] < 7.9 × 10 ⁻³	CL=90%
Γ_{171}	$2K^+K^-$	(2.15 ± 0.20) × 10 ⁻⁴	
Γ_{172}	$\phi K^+, \phi \rightarrow K^+K^-$	(8.8 ± 2.0) × 10 ⁻⁵	

Doubly Cabibbo-suppressed modes

Γ_{173}	$2K^+\pi^-$	(1.274 ± 0.031) × 10 ⁻⁴	
Γ_{174}	$K^+K^*(892)^0, K^{*0} \rightarrow$ $K^+\pi^-$	(6.0 ± 3.4) × 10 ⁻⁵	

Baryon-antibaryon mode

Γ_{175}	$\rho\bar{\rho}$	(1.22 ± 0.11) × 10 ⁻³	
Γ_{176}	$\rho\bar{\rho}e^+\nu_e$	< 2.0 × 10 ⁻⁴	CL=90%

**$\Delta C = 1$ weak neutral current (CI) modes,
Lepton family number (LF), or
Lepton number (L) violating modes**

Γ_{177}	$\pi^+e^+e^-$	[j] < 5.5 × 10 ⁻⁶	CL=90%
Γ_{178}	$\pi^+\phi, \phi \rightarrow e^+e^-$	[j] (6 $\begin{smallmatrix} +8 \\ -4 \end{smallmatrix}$) × 10 ⁻⁶	
Γ_{179}	$\pi^+\mu^+\mu^-$	[j] < 1.8 × 10 ⁻⁷	CL=90%
Γ_{180}	$K^+e^+e^-$	CI < 3.7 × 10 ⁻⁶	CL=90%
Γ_{181}	$K^+\mu^+\mu^-$	CI < 1.4 × 10 ⁻⁷	CL=90%
Γ_{182}	$K^*(892)^+\mu^+\mu^-$	CI < 1.4 × 10 ⁻³	CL=90%
Γ_{183}	$\pi^+e^+\mu^-$	LF < 1.1 × 10 ⁻⁶	CL=90%
Γ_{184}	$\pi^+e^-\mu^+$	LF < 9.4 × 10 ⁻⁷	CL=90%
Γ_{185}	$K^+e^+\mu^-$	LF < 7.9 × 10 ⁻⁷	CL=90%
Γ_{186}	$K^+e^-\mu^+$	LF < 5.6 × 10 ⁻⁷	CL=90%
Γ_{187}	π^-2e^+	L < 1.4 × 10 ⁻⁶	CL=90%
Γ_{188}	$\pi^-2\mu^+$	L < 8.6 × 10 ⁻⁸	CL=90%
Γ_{189}	$\pi^-e^+\mu^+$	L < 6.3 × 10 ⁻⁷	CL=90%
Γ_{190}	K^-2e^+	L < 7.7 × 10 ⁻⁷	CL=90%

Γ_{191}	$K^-2\mu^+$	L < 2.6 × 10 ⁻⁸	CL=90%
Γ_{192}	$K^-e^+\mu^+$	L < 2.6 × 10 ⁻⁷	CL=90%
Γ_{193}	$K^*(892)^-2\mu^+$	L < 1.4 × 10 ⁻³	CL=90%

[a] This is the purely e^+ semileptonic branching fraction: the e^+ fraction from τ^+ decays has been subtracted off. The sum of our (non- τ) e^+ exclusive fractions — an $e^+\nu_e$ with an η, η', ϕ, K^0 , or K^{*0} — is $5.99 \pm 0.31\%$.

[b] This fraction includes η from η' decays.

[c] The sum of our exclusive η' fractions — $\eta'e^+\nu_e, \eta'\mu^+\nu_\mu, \eta'\pi^+, \eta'\rho^+$, and $\eta'K^+$ — is $11.8 \pm 1.6\%$.

[d] This branching fraction includes all the decay modes of the final-state resonance.

[e] A test for $u\bar{u}$ or $d\bar{d}$ content in the D_s^+ . Neither Cabibbo-favored nor Cabibbo-suppressed decays can contribute, and ω - ϕ mixing is an unlikely explanation for any fraction above about 2×10^{-4} .

[f] The branching fraction for this mode may differ from the sum of the submodes that contribute to it, due to interference effects. See the relevant papers.

[g] We decouple the $D_s^+ \rightarrow \phi\pi^+$ branching fraction obtained from mass projections (and used to get some of the other branching fractions) from the $D_s^+ \rightarrow \phi\pi^+, \phi \rightarrow K^+K^-$ branching fraction obtained from the Dalitz-plot analysis of $D_s^+ \rightarrow K^+K^-\pi^+$. That is, the ratio of these two branching fractions is not exactly the $\phi \rightarrow K^+K^-$ branching fraction 0.491.

[h] This is the average of a model-independent and a K -matrix parametrization of the $\pi^+\pi^-$ S-wave and is a sum over several f_0 mesons.

[i] This mode is not a useful test for a $\Delta C=1$ weak neutral current because both quarks must change flavor in this decay.

[j] This is *not* a test for the $\Delta C=1$ weak neutral current, but leads to the $\pi^+\ell^+\ell^-$ final state.

FIT INFORMATION

An overall fit to 16 branching ratios uses 25 measurements to determine 11 parameters. The overall fit has a $\chi^2 = 12.7$ for 14 degrees of freedom.

The following *off-diagonal* array elements are the correlation coefficients $\langle \delta x_i \delta x_j \rangle / (\delta x_i \delta x_j)$, in percent, from the fit to the branching fractions, $x_i \equiv \Gamma_i / \Gamma_{\text{total}}$.

x_{47}	27									
x_{68}	8	0								
x_{77}	24	4	14							
x_{84}	18	3	12	45						
x_{94}	17	33	1	6	4					
x_{109}	1	15	-8	-15	-12	6				
x_{110}	0	1	0	-1	0	0	4			
x_{138}	0	0	0	0	0	0	0	0		
x_{140}	7	3	4	8	6	2	-4	0	0	
x_{158}	0	0	0	0	0	0	0	26	0	
	x_{44}	x_{47}	x_{68}	x_{77}	x_{84}	x_{94}	x_{109}	x_{110}	x_{138}	x_{140}

See the related review(s):

[D_s[±] Branching Fractions](#)

D_s[±] BRANCHING RATIOS

A number of older, now obsolete results have been omitted. They may be found in earlier editions.

Inclusive modes

$\Gamma(e^+ \text{ semileptonic}) / \Gamma_{\text{total}}$					Γ_1 / Γ
This is the purely e^+ semileptonic branching fraction: the e^+ fraction from τ^+ decays has been subtracted off.					
<u>VALUE (%)</u>	<u>EVTS</u>	<u>DOCUMENT ID</u>	<u>TECN</u>	<u>COMMENT</u>	
6.33 ± 0.15 OUR AVERAGE					
6.30 ± 0.13 ± 0.10	17k	^{1,2} ABLIKIM	21AC BES3	e^+e^- at 4.178–4.230 GeV	
6.52 ± 0.39 ± 0.15	0.5k	³ ASNER	10 CLEO	e^+e^- at 3774 MeV	
¹ ABLIKIM 21AC finds that the ratio of the D_s^+ and D^0 semielectronic widths is $0.790 \pm 0.016 \pm 0.020$.					

Meson Particle Listings

 D_S^\pm

²ABLIKIM 21AC reports a value of $(6.30 \pm 0.13 \pm 0.09 \pm 0.04) \times 10^{-2}$, where the last uncertainty is an external systematic from $B(D_S^+ \rightarrow \tau \nu)$. We have added the systematic uncertainties in quadrature.

³Using the D_S^+ and D^0 lifetimes, ASNER 10 finds that the ratio of the D_S^+ and D^0 semileptonic widths is $0.828 \pm 0.051 \pm 0.025$.

$\Gamma(\pi^+ \text{ anything})/\Gamma_{\text{total}}$		Γ_2/Γ	
Events with two π^+ 's count twice, etc. But π^+ 's from $K_S^0 \rightarrow \pi^+ \pi^-$ are not included.			
VALUE (%)	DOCUMENT ID	TECN	COMMENT
119.3 ± 1.2 ± 0.7	DOBBS	09	CLEO $e^+ e^-$ at 4170 MeV

$\Gamma(\pi^- \text{ anything})/\Gamma_{\text{total}}$		Γ_3/Γ	
Events with two π^- 's count twice, etc. But π^- 's from $K_S^0 \rightarrow \pi^+ \pi^-$ are not included.			
VALUE (%)	DOCUMENT ID	TECN	COMMENT
43.2 ± 0.9 ± 0.3	DOBBS	09	CLEO $e^+ e^-$ at 4170 MeV

$\Gamma(\pi^0 \text{ anything})/\Gamma_{\text{total}}$		Γ_4/Γ	
Events with two π^0 's count twice, etc. But π^0 's from $K_S^0 \rightarrow 2\pi^0$ are not included.			
VALUE (%)	DOCUMENT ID	TECN	COMMENT
123.4 ± 3.8 ± 5.3	DOBBS	09	CLEO $e^+ e^-$ at 4170 MeV

$\Gamma(K^- \text{ anything})/\Gamma_{\text{total}}$		Γ_5/Γ	
VALUE (%)	DOCUMENT ID	TECN	COMMENT
18.7 ± 0.5 ± 0.2	DOBBS	09	CLEO $e^+ e^-$ at 4170 MeV

$\Gamma(K^+ \text{ anything})/\Gamma_{\text{total}}$		Γ_6/Γ	
VALUE (%)	DOCUMENT ID	TECN	COMMENT
28.9 ± 0.6 ± 0.3	DOBBS	09	CLEO $e^+ e^-$ at 4170 MeV

$\Gamma(K_S^0 \text{ anything})/\Gamma_{\text{total}}$		Γ_7/Γ	
VALUE (%)	DOCUMENT ID	TECN	COMMENT
19.0 ± 1.0 ± 0.4	DOBBS	09	CLEO $e^+ e^-$ at 4170 MeV

$\Gamma(\eta \text{ anything})/\Gamma_{\text{total}}$		Γ_8/Γ	
This ratio includes η particles from η' decays.			
VALUE (%)	DOCUMENT ID	TECN	COMMENT
29.9 ± 2.2 ± 1.7	DOBBS	09	CLEO $e^+ e^-$ at 4170 MeV
••• We do not use the following data for averages, fits, limits, etc. •••			
23.5 ± 3.1 ± 2.0	674 ± 91	HUANG	06B CLEO See DOBBS 09

$\Gamma(\omega \text{ anything})/\Gamma_{\text{total}}$		Γ_9/Γ	
VALUE (%)	DOCUMENT ID	TECN	COMMENT
6.1 ± 1.4 ± 0.3	DOBBS	09	CLEO $e^+ e^-$ at 4170 MeV

$\Gamma(\eta' \text{ anything})/\Gamma_{\text{total}}$		Γ_{10}/Γ	
VALUE (%)	DOCUMENT ID	TECN	COMMENT
10.3 ± 1.4 OUR AVERAGE	Error includes scale factor of 1.1.		
8.8 ± 1.8 ± 0.5	68	ABLIKIM	15Z BES3 482 pb ⁻¹ , 4009 MeV
11.7 ± 1.7 ± 0.7		DOBBS	09 CLEO $e^+ e^-$ at 4170 MeV
••• We do not use the following data for averages, fits, limits, etc. •••			
8.7 ± 1.9 ± 0.8	68	HUANG	06B CLEO See DOBBS 09

$\Gamma(f_0(980) \text{ anything, } f_0 \rightarrow \pi^+ \pi^-)/\Gamma_{\text{total}}$		Γ_{11}/Γ	
VALUE (%)	DOCUMENT ID	TECN	COMMENT
<1.3	90	DOBBS	09 CLEO $e^+ e^-$ at 4170 MeV

$\Gamma(\phi \text{ anything})/\Gamma_{\text{total}}$		Γ_{12}/Γ	
VALUE (%)	DOCUMENT ID	TECN	COMMENT
15.7 ± 0.8 ± 0.6	DOBBS	09	CLEO $e^+ e^-$ at 4170 MeV
••• We do not use the following data for averages, fits, limits, etc. •••			
16.1 ± 1.2 ± 1.1	398 ± 27	HUANG	06B CLEO See DOBBS 09

$\Gamma(K^+ K^- \text{ anything})/\Gamma_{\text{total}}$		Γ_{13}/Γ	
VALUE (%)	DOCUMENT ID	TECN	COMMENT
15.8 ± 0.6 ± 0.3	DOBBS	09	CLEO $e^+ e^-$ at 4170 MeV

$\Gamma(K_S^0 K^+ \text{ anything})/\Gamma_{\text{total}}$		Γ_{14}/Γ	
VALUE (%)	DOCUMENT ID	TECN	COMMENT
5.8 ± 0.5 ± 0.1	DOBBS	09	CLEO $e^+ e^-$ at 4170 MeV

$\Gamma(K_S^0 K^- \text{ anything})/\Gamma_{\text{total}}$		Γ_{15}/Γ	
VALUE (%)	DOCUMENT ID	TECN	COMMENT
1.9 ± 0.4 ± 0.1	DOBBS	09	CLEO $e^+ e^-$ at 4170 MeV

$\Gamma(2K_S^0 \text{ anything})/\Gamma_{\text{total}}$		Γ_{16}/Γ	
VALUE (%)	DOCUMENT ID	TECN	COMMENT
1.7 ± 0.3 ± 0.1	DOBBS	09	CLEO $e^+ e^-$ at 4170 MeV

$\Gamma(2K^+ \text{ anything})/\Gamma_{\text{total}}$		Γ_{17}/Γ	
VALUE (%)	DOCUMENT ID	TECN	COMMENT
<0.26	90	DOBBS	09 CLEO $e^+ e^-$ at 4170 MeV

$\Gamma(2K^- \text{ anything})/\Gamma_{\text{total}}$		Γ_{18}/Γ	
VALUE (%)	DOCUMENT ID	TECN	COMMENT
<0.06	90	DOBBS	09 CLEO $e^+ e^-$ at 4170 MeV

$\Gamma(2\pi^+ \pi^- + \text{ anything})/\Gamma_{\text{total}}$		Γ_{19}/Γ	
VALUE (%)	DOCUMENT ID	TECN	COMMENT
32.81 ± 0.35 ± 0.63	25k	¹ ABLIKIM	23AV BES3 $e^+ e^-$ at 4.178 GeV
¹ Charged pions from K_S^0 meson decays are excluded from this measurement			

Leptonic and semileptonic modes

See the related review(s): Leptonic Decays of Charged Pseudoscalar Mesons

$\Gamma(e^+ \nu_e)/\Gamma_{\text{total}}$		Γ_{20}/Γ	
VALUE	DOCUMENT ID	TECN	COMMENT
<0.83 × 10⁻⁴	90	¹ ZUPANC	13 BELL $e^+ e^-$ at $\Upsilon(4S), \Upsilon(5S)$

••• We do not use the following data for averages, fits, limits, etc. •••

<2.3 × 10 ⁻⁴	90	DEL-AMO-SA...10J	BABR $e^+ e^-$, 10.58 GeV
<1.2 × 10 ⁻⁴	90	ALEXANDER	09 CLEO $e^+ e^-$ at 4170 MeV
<1.3 × 10 ⁻⁴	90	PEDLAR	07A CLEO See ALEXANDER 09

¹ZUPANC 13 also gives the limit as $<1.0 \times 10^{-4}$ at 95% CL.

$\Gamma(\mu^+ \nu_\mu)/\Gamma_{\text{total}}$		Γ_{21}/Γ	
See the note on "Decay Constants of Charged Pseudoscalar Mesons."			
VALUE (units 10 ⁻³)	DOCUMENT ID	TECN	COMMENT
5.35 ± 0.12 OUR AVERAGE			
5.294 ± 0.108 ± 0.085	2.5k	ABLIKIM	23BR BES3 $e^+ e^-$ at 4.128–4.226 GeV
5.17 ± 0.75 ± 0.21	69	¹ ABLIKIM	16o BES3 $e^+ e^-$ at 4.009 GeV
5.31 ± 0.28 ± 0.20	490	² ZUPANC	13 BELL $e^+ e^-$ at $\Upsilon(4S), \Upsilon(5S)$
6.02 ± 0.38 ± 0.34	270	³ DEL-AMO-SA...10J	BABR $e^+ e^-$, 10.58 GeV
5.65 ± 0.45 ± 0.17	230	ALEXANDER	09 CLEO $e^+ e^-$ at 4170 MeV
••• We do not use the following data for averages, fits, limits, etc. •••			
5.35 ± 0.13 ± 0.16	2.2k	⁴ ABLIKIM	21BE BES3 $e^+ e^-$, 4.178, 4.226 GeV
5.49 ± 0.16 ± 0.15	1.1k	⁴ ABLIKIM	19E BES3 $e^+ e^-$ at 4178 MeV
6.44 ± 0.76 ± 0.57	170	⁵ WIDHALM	08 BELL See ZUPANC 13
5.94 ± 0.66 ± 0.31	88	⁶ PEDLAR	07A CLEO See ALEXANDER 09
6.8 ± 1.1 ± 1.8	553	⁷ HEISTER	02i ALEP Z decays

¹ABLIKIM 16o also reports that when constrained by the Standard Model ratio of $\Gamma(D^+ \rightarrow \tau^+ \nu_\tau)/\Gamma(D^+ \rightarrow \mu^+ \nu_\mu) = 9.76$, the branching fraction is found to be $(0.495 \pm 0.067 \pm 0.026)\%$. The constrained value is used to obtain the decay constant, $f_{D^+} = (241.0 \pm 16.3 \pm 6.6)$ MeV.

²ZUPANC 13 uses both $\mu^+ \nu$ and $\tau^+ \nu$ events to get $f_{D^+} = (255.5 \pm 4.2 \pm 5.1)$ MeV.

³DEL-AMO-SANCHEZ 10J uses $\mu^+ \nu_\mu$ and $\tau^+ \nu_\tau$ events together to get $f_{D^+} = (258.6 \pm 6.4 \pm 7.5)$ MeV.

⁴Superseded by ABLIKIM 23BR.

⁵WIDHALM 08 gets $f_{D^+} = (275 \pm 16 \pm 12)$ MeV from the branching fraction.

⁶PEDLAR 07A also fits μ^+ and τ^+ events together and gets an effective $\mu^+ \nu_\mu$ branching fraction of $(6.38 \pm 0.59 \pm 0.33) \times 10^{-3}$

⁷This HEISTER 02i result is not actually an independent measurement of the absolute $\mu^+ \nu_\mu$ branching fraction, but is in fact based on our $\phi\pi^+$ branching fraction of $3.6 \pm 0.9\%$, so it cannot be included in our overall fit. HEISTER 02i combines its $D_S^+ \rightarrow \tau^+ \nu_\tau$ and $\mu^+ \nu_\mu$ branching fractions to get $f_{D^+} = (285 \pm 19 \pm 40)$ MeV.

$\Gamma(\mu^+ \nu_\mu)/\Gamma(\phi\pi^+)$		Γ_{21}/Γ_{48}	
See the note on "Decay Constants of Charged Pseudoscalar Mesons" above.			
VALUE	DOCUMENT ID	TECN	COMMENT

••• We do not use the following data for averages, fits, limits, etc. •••

0.143 ± 0.018 ± 0.006	489 ± 55	¹ AUBERT	07v BABR $e^+ e^- \approx \Upsilon(4S)$
0.23 ± 0.06 ± 0.04	18	² ALEXANDROV	00 BEAT π^- nucleus, 350 GeV
0.173 ± 0.023 ± 0.035	182	³ CHADHA	98 CLE2 $e^+ e^- \approx \Upsilon(4S)$
0.245 ± 0.052 ± 0.074	39	⁴ ACOSTA	94 CLE2 See CHADHA 98

¹AUBERT 07v gets $f_{D^+} = (283 \pm 17 \pm 16)$ MeV, using $\Gamma(D_S^+ \rightarrow \phi\pi^+)/\Gamma(\text{total}) = (4.71 \pm 0.46)\%$.

²ALEXANDROV 00 uses $f_D^2/f_{D^+}^2 = 0.82 \pm 0.09$ from a lattice-gauge-theory calculation to get the relative numbers of $D^+ \rightarrow \mu^+ \nu_\mu$ and $D_S^+ \rightarrow \mu^+ \nu_\mu$ events. The present result leads to $f_{D^+} = (323 \pm 44 \pm 36)$ MeV.

³CHADHA 98 obtains $f_{D^+} = (280 \pm 19 \pm 28 \pm 34)$ MeV from this measurement, using $\Gamma(D_S^+ \rightarrow \phi\pi^+)/\Gamma(\text{total}) = 0.036 \pm 0.009$.

⁴ACOSTA 94 obtains $f_{D^+} = (344 \pm 37 \pm 52 \pm 42)$ MeV from this measurement, using $\Gamma(D_S^+ \rightarrow \phi\pi^+)/\Gamma(\text{total}) = 0.037 \pm 0.009$.

$\Gamma(\tau^+ \nu_\tau)/\Gamma_{\text{total}}$		Γ_{22}/Γ	
See the note on "Decay Constants of Charged Pseudoscalar Mesons" above.			
VALUE (%)	DOCUMENT ID	TECN	COMMENT
5.36 ± 0.10 OUR AVERAGE			
5.44 ± 0.17 ± 0.13	2.4k	¹ ABLIKIM	23BP BES3 $e^+ e^-$ at 4.128–4.226 GeV

5.37±0.17±0.15	2.3k	² ABLIKIM	23BX BES3	e^+e^- at 4.128-4.226 GeV
5.29±0.25±0.20	1.7k	³ ABLIKIM	21AF BES3	e^+e^- at 4.178, 4.226 GeV
5.27±0.10±0.12	4.9k	⁴ ABLIKIM	21AZ BES3	e^+e^- at 4.178, 4.226 GeV
3.28±1.83±0.37	33	⁵ ABLIKIM	16o BES3	e^+e^- at 4.009 GeV
5.70±0.21 $^{+0.31}_{-0.30}$	2.2k	⁶ ZUPANC	13 BELL	e^+e^- at $\Upsilon(4S)$, $\Upsilon(5S)$
4.96±0.37±0.57	748	⁷ DEL-AMO-SA...	10J BABR	$e^- \bar{\nu}_e \nu_\tau, \mu^- \bar{\nu}_\mu \nu_\tau$
6.42±0.81±0.18	126	⁸ ALEXANDER	09 CLEO	$\tau^+ \rightarrow \pi^+ \bar{\nu}_\tau$
5.52±0.57±0.21	155	⁸ NAIK	09A CLEO	$\tau^+ \rightarrow \rho^+ \bar{\nu}_\tau$
5.30±0.47±0.22	181	⁸ ONYISI	09 CLEO	$\tau^+ \rightarrow e^+ \nu_e \bar{\nu}_\tau$

••• We do not use the following data for averages, fits, limits, etc. •••

5.21±0.25±0.17	950	⁹ ABLIKIM	21BE BES3	e^+e^- at 4.178, 4.226 GeV
6.17±0.71±0.34	102	¹⁰ ECKLUND	08 CLEO	See ONYISI 09
8.0 ±1.3 ±0.4	47	¹⁰ PEDLAR	07A CLEO	See ALEXANDER 09
5.79±0.77±1.84	881	¹¹ HEISTER	02I ALEP	Z decays
7.0 ±2.1 ±2.0	22	¹² ABBIENDI	01L OPAL	$D_s^{*+} \rightarrow \gamma D_s^+$ from Z^0 's
7.4 ±2.8 ±2.4	16	¹³ ACCIARRI	97F L3	$D_s^{*+} \rightarrow \gamma D_s^+$ from Z^0 's

- 1 ABLIKIM 23BP uses $\tau^+ \rightarrow \pi^+ \bar{\nu}_\tau$ decays.
- 2 ABLIKIM 23BX uses $\tau^+ \rightarrow \mu^+ \nu_\mu \bar{\nu}_\tau$ decays.
- 3 ABLIKIM 21AF uses $\tau^+ \rightarrow \pi^+ \pi^0 \bar{\nu}_\tau$ decays.
- 4 ABLIKIM 21AZ uses $\tau^+ \rightarrow e^+ \nu_e \bar{\nu}_\tau$ decays.
- 5 ABLIKIM 16o also reports that when constrained by the Standard Model ratio of $\Gamma(D_s^+ \rightarrow \tau^+ \nu_\tau)/\Gamma(D_s^+ \rightarrow \mu^+ \nu_\mu) = 9.75$; the branching fraction is found to be $(4.83 \pm 0.65 \pm 0.26)\%$.
- 6 ZUPANC 13 uses both $\mu^+ \nu$ and $\tau^+ \nu$ events to get $f_{D_s} = (255.5 \pm 4.2 \pm 5.1)$ MeV.
- 7 DEL-AMO-SANCHEZ 10j (with a small correction; see LEES 15d) uses $\mu^+ \nu_\mu$ and $\tau^+ \nu_\tau$ events together to get $f_{D_s} = (259.9 \pm 6.6 \pm 7.6)$ MeV.
- 8 ALEXANDER 09, NAIK 09A, and ONYISI 09 use different τ decay modes and are independent. The three papers combined give $f_{D_s} = (259.7 \pm 7.8 \pm 3.4)$ MeV.
- 9 ABLIKIM 21BE uses $\tau^+ \rightarrow \pi^+ \bar{\nu}_\tau$ decays. When constrained by the Standard Model ratio of $\Gamma(D_s^+ \rightarrow \tau^+ \nu_\tau)/\Gamma(D_s^+ \rightarrow \mu^+ \nu_\mu) = 9.75$, the branching fraction is found to be $(5.22 \pm 0.10 \pm 0.14)\%$. Superseded by ABLIKIM 23BP.
- 10 ECKLUND 08 and PEDLAR 07A are independent: ECKLUND 08 uses $\tau^+ \rightarrow e^+ \nu_e \bar{\nu}_\tau$ events, PEDLAR 07A uses $\tau^+ \rightarrow \pi^+ \bar{\nu}_\tau$ events.
- 11 HEISTER 02 combines its $D_s^+ \rightarrow \tau^+ \nu_\tau$ and $\mu^+ \nu_\mu$ branching fractions to get $f_{D_s} = (285 \pm 19 \pm 40)$ MeV.
- 12 This ABBIENDI 01L value gives a decay constant f_{D_s} of $(286 \pm 44 \pm 41)$ MeV.
- 13 The second ACCIARRI 97F error here combines in quadrature systematic (0.016) and normalization (0.018) errors. The branching fraction gives $f_{D_s} = (309 \pm 58 \pm 33 \pm 38)$ MeV.

$\Gamma(\tau^+ \nu_\tau)/\Gamma(\mu^+ \nu_\mu)$		Γ_{22}/Γ_{21}		
VALUE	EVTs	DOCUMENT ID	TECN	COMMENT

- We do not use the following data for averages, fits, limits, etc. •••
- | | | | | |
|-------------------------------|----------|----------------------|---------|---|
| 10.73±0.69 $^{+0.56}_{-0.53}$ | 2.2k/492 | ¹ ZUPANC | 13 BELL | e^+e^- at $\Upsilon(4S)$, $\Upsilon(5S)$ |
| 11.0 ±1.4 ±0.6 | 102 | ² ECKLUND | 08 CLEO | See ONYISI 09 |
- 1 This ZUPANC 13 ratio is not independent of the separate $\tau\nu$ and $\mu\nu$ fractions listed above.
 - 2 This ECKLUND 08 value also uses results from PEDLAR 07A, and it is not independent of other results in these Listings. Combined with earlier CLEO results, the decay constant f_{D_s} is $274 \pm 10 \pm 5$ MeV.

$\Gamma(\gamma e^+ \nu_e)/\Gamma_{total}$		Γ_{23}/Γ		
VALUE	CL%	DOCUMENT ID	TECN	COMMENT

- We do not use the following data for averages, fits, limits, etc. •••
- | | | | | |
|-------------------------|----|---------|-----------|-------------------------|
| <1.3 × 10 ⁻⁴ | 90 | ABLIKIM | 19AD BES3 | for $E_\gamma > 10$ MeV |
|-------------------------|----|---------|-----------|-------------------------|

$\Gamma(K^+ K^- e^+ \nu_e)/\Gamma(K^+ K^- \pi^+)$		Γ_{24}/Γ_{47}		
VALUE	DOCUMENT ID	TECN	COMMENT	

- We do not use the following data for averages, fits, limits, etc. •••
- | | | | |
|-------------------|---------------------|-----------|----------------------------|
| 0.558±0.007±0.016 | ¹ AUBERT | 08AN BABR | e^+e^- at $\Upsilon(4S)$ |
|-------------------|---------------------|-----------|----------------------------|
- 1 This AUBERT 08AN ratio is only for the $K^+ K^-$ mass in the range 1.01-to-1.03 GeV in the numerator and 1.0095-to-1.0295 GeV in the denominator.

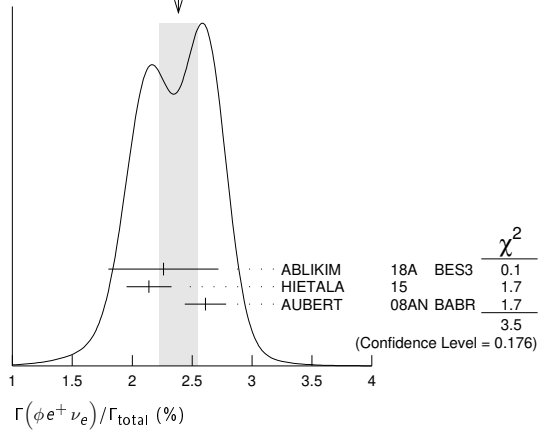
$\Gamma(K_s^0 K_s^0 e^+ \nu_e)/\Gamma_{total}$		Γ_{25}/Γ		
VALUE	CL%	DOCUMENT ID	TECN	COMMENT

- We do not use the following data for averages, fits, limits, etc. •••
- | | | | | |
|-------------------------|----|---------|----------|-----------------------------|
| <3.8 × 10 ⁻⁴ | 90 | ABLIKIM | 22j BES3 | e^+e^- at 4.178-4.226 GeV |
|-------------------------|----|---------|----------|-----------------------------|

$\Gamma(\phi e^+ \nu_e)/\Gamma_{total}$		Γ_{26}/Γ		
VALUE (%)	EVTs	DOCUMENT ID	TECN	COMMENT

- See the end of the D_s^+ Listings for measurements of $D_s^+ \rightarrow \phi e^+ \nu_e$ form factors. Unseen decay modes of the ϕ are included.
- We do not use the following data for averages, fits, limits, etc. •••
- | | | | | |
|----------------|-----|---------|-----------|----------------------------|
| 2.26±0.45±0.09 | 26 | ABLIKIM | 18A BES3 | e^+e^- at 4.009 GeV |
| 2.14±0.17±0.08 | 207 | HIETALA | 15 | Uses CLEO data |
| 2.61±0.03±0.17 | 25k | AUBERT | 08AN BABR | e^+e^- at $\Upsilon(4S)$ |
- We do not use the following data for averages, fits, limits, etc. •••
- | | | | | |
|----------------|-----|---------|---------|----------------|
| 2.36±0.23±0.13 | 106 | ECKLUND | 09 CLEO | See HIETALA 15 |
| 2.29±0.37±0.11 | 45 | YELTON | 09 CLEO | See ECKLUND 09 |

WEIGHTED AVERAGE
2.39±0.16 (Error scaled by 1.3)



$\Gamma(\phi e^+ \nu_e)/\Gamma(\phi \pi^+)$		Γ_{26}/Γ_{48}		
VALUE	EVTs	DOCUMENT ID	TECN	COMMENT

- As noted in the comment column, most of these measurements use $\phi\mu^+\nu_\mu$ events in addition to or instead of $\phi e^+\nu_e$ events.
- We do not use the following data for averages, fits, limits, etc. •••
- | | | | | |
|-------------------------------|-----|-----------|-----------|---|
| 0.540±0.033±0.048 | 793 | LINK | 02J FOCUS | Uses $\phi\mu^+\nu_\mu$ |
| 0.54 ±0.05 ±0.04 | 367 | BUTLER | 94 CLE2 | Uses $\phi e^+\nu_e$ and $\phi\mu^+\nu_\mu$ |
| 0.58 ±0.17 ±0.07 | 97 | FRABETTI | 93G E687 | Uses $\phi\mu^+\nu_\mu$ |
| 0.57 ±0.15 ±0.15 | 104 | ALBRECHT | 91 ARG | Uses $\phi e^+\nu_e$ |
| 0.49 ±0.10 $^{+0.10}_{-0.14}$ | 54 | ALEXANDER | 90B CLEO | Uses $\phi e^+\nu_e$ and $\phi\mu^+\nu_\mu$ |

$\Gamma(\phi\mu^+ \nu_\mu)/\Gamma_{total}$		Γ_{29}/Γ		
VALUE (%)	EVTs	DOCUMENT ID	TECN	COMMENT

- We do not use the following data for averages, fits, limits, etc. •••
- | | | | | |
|----------------|------|---------|-----------|-----------------------------|
| 2.25±0.09±0.07 | 1.7k | ABLIKIM | 23bz BES3 | e^+e^- at 4.128-4.226 GeV |
| 1.94±0.53±0.09 | 22 | ABLIKIM | 18A BES3 | e^+e^- at 4.009 GeV |

$\Gamma(\eta e^+ \nu_e)/\Gamma_{total}$		Γ_{31}/Γ		
VALUE (%)	EVTs	DOCUMENT ID	TECN	COMMENT

- Unseen decay modes of the η are included.
- We do not use the following data for averages, fits, limits, etc. •••
- | | | | | |
|-------------------|------|----------------------|-----------|---------------------------|
| 2.255±0.039±0.051 | 4k | ABLIKIM | 23bo BES3 | e^+e^- at 4128-4226 MeV |
| 2.30 ±0.31 ±0.08 | 63 | ABLIKIM | 16T BES3 | e^+e^- at 4.009 GeV |
| 2.28 ±0.14 ±0.19 | 358 | ¹ HIETALA | 15 | Uses CLEO data |
| 2.323±0.063±0.063 | 1.8k | ² ABLIKIM | 19s BES3 | e^+e^- at 4178 MeV |
| 2.48 ±0.29 ±0.13 | 82 | YELTON | 09 CLEO | See HIETALA 15 |
- 1 Obtained by analyzing CLEO-c data but not authored by the CLEO Collaboration.
 - 2 Superseded by ABLIKIM 23bo

$\Gamma(\eta e^+ \nu_e)/\Gamma(\phi e^+ \nu_e)$		Γ_{31}/Γ_{26}		
VALUE	EVTs	DOCUMENT ID	TECN	COMMENT

- Unseen decay modes of the η and the ϕ are included.
- We do not use the following data for averages, fits, limits, etc. •••
- | | | | | |
|----------------|-----|--------------------------|---------|----------------|
| 1.24±0.12±0.15 | 440 | ¹ BRANDENB... | 95 CLE2 | See HIETALA 15 |
|----------------|-----|--------------------------|---------|----------------|
- 1 BRANDENBURG 95 uses both e^+ and μ^+ events and makes a phase-space adjustment to use the μ^+ events as e^+ events.

$\Gamma(\eta'(958) e^+ \nu_e)/\Gamma_{total}$		Γ_{32}/Γ		
VALUE (%)	EVTs	DOCUMENT ID	TECN	COMMENT

- Unseen decay modes of the $\eta'(958)$ are included.
- We do not use the following data for averages, fits, limits, etc. •••
- | | | | | |
|-------------------|-----|----------------------|-----------|---------------------------|
| 0.810±0.038±0.024 | 675 | ABLIKIM | 23bo BES3 | e^+e^- at 4128-4226 MeV |
| 0.93 ±0.30 ±0.05 | 14 | ABLIKIM | 16T BES3 | e^+e^- at 4.009 MeV |
| 0.68 ±0.15 ±0.06 | 20 | ¹ HIETALA | 15 | Uses CLEO data |
| 0.824±0.073±0.027 | 261 | ² ABLIKIM | 19s BES3 | e^+e^- at 4178 MeV |
| 0.91 ±0.33 ±0.05 | 7.5 | YELTON | 09 CLEO | See HIETALA 15 |
- 1 Obtained by analyzing CLEO-c data but not authored by the CLEO Collaboration.
 - 2 Superseded by ABLIKIM 23bo

$\Gamma(\eta'(958) e^+ \nu_e)/\Gamma(\phi e^+ \nu_e)$		Γ_{32}/Γ_{26}		
VALUE	EVTs	DOCUMENT ID	TECN	COMMENT

- Unseen decay modes of the resonances are included.
- We do not use the following data for averages, fits, limits, etc. •••
- | | | | | |
|----------------|----|--------------------------|---------|----------------|
| 0.43±0.11±0.07 | 29 | ¹ BRANDENB... | 95 CLE2 | See HIETALA 15 |
|----------------|----|--------------------------|---------|----------------|
- 1 BRANDENBURG 95 uses both e^+ and μ^+ events and makes a phase-space adjustment to use the μ^+ events as e^+ events.

Meson Particle Listings

 D_S^\pm

$$\frac{\Gamma(\eta e^+ \nu_e) + \Gamma(\eta(958) e^+ \nu_e)}{\Gamma(\phi e^+ \nu_e)} \quad \Gamma_{30}/\Gamma_{26} = (\Gamma_{31} + \Gamma_{32})/\Gamma_{26}$$

Unseen decay modes of the resonances are included.

VALUE (%)	CL%	DOCUMENT ID	TECN	COMMENT
$1.67 \pm 0.17 \pm 0.17$		1 BRANDENB...	95 CLE2	See HIETALA 15

• • • We do not use the following data for averages, fits, limits, etc. • • •

1 This BRANDENBURG 95 data is redundant with data in previous blocks.

$$\frac{\Gamma(\eta \mu^+ \nu_\mu)}{\Gamma_{\text{total}}} \quad \Gamma_{33}/\Gamma$$

VALUE (%)	EVTS	DOCUMENT ID	TECN	COMMENT
$2.42 \pm 0.46 \pm 0.11$	44	ABLIKIM	18A BES3	$e^+ e^-$ at 4.009 GeV

$$\frac{\Gamma(\eta'(958) \mu^+ \nu_\mu)}{\Gamma_{\text{total}}} \quad \Gamma_{34}/\Gamma$$

VALUE (%)	EVTS	DOCUMENT ID	TECN	COMMENT
$1.06 \pm 0.54 \pm 0.07$	10	ABLIKIM	18A BES3	$e^+ e^-$ at 4.009 GeV

$$\frac{\Gamma(\omega e^+ \nu_e)}{\Gamma_{\text{total}}} \quad \Gamma_{35}/\Gamma$$

A test for $u\bar{u}$ or $d\bar{d}$ content in the D_S^+ . Neither Cabibbo-favored nor Cabibbo-suppressed decays can contribute, and $\omega - \phi$ mixing is an unlikely explanation for any fraction above about 2×10^{-4} .

VALUE (%)	CL%	DOCUMENT ID	TECN	COMMENT
< 0.20	90	MARTIN	11 CLEO	$e^+ e^-$ at 4170 MeV

$$\frac{\Gamma(K^0 e^+ \nu_e)}{\Gamma_{\text{total}}} \quad \Gamma_{36}/\Gamma$$

VALUE (%)	EVTS	DOCUMENT ID	TECN	COMMENT
0.34 ± 0.04	OUR AVERAGE			
$0.325 \pm 0.038 \pm 0.016$	117	1 ABLIKIM	19D BES3	$e^+ e^-$ at 4178 MeV
$0.39 \pm 0.08 \pm 0.03$	42	HIETALA	15	Uses CLEO data

• • • We do not use the following data for averages, fits, limits, etc. • • •

$0.37 \pm 0.10 \pm 0.02$ 14 YELTON 09 CLEO See HIETALA 15

1 K^0 reconstructed via $K^0 \rightarrow K_S^0 \rightarrow \pi^+ \pi^-$ decays.

$$\frac{\Gamma(K_1(1270)^0 e^+ \nu_e)}{\Gamma_{\text{total}}} \quad \Gamma_{27}/\Gamma$$

VALUE (%)	CL%	DOCUMENT ID	TECN	COMMENT
$< 4.1 \times 10^{-4}$	90	1 ABLIKIM	23Bs BES3	$e^+ e^-$ at 4.128-4.226 GeV

1 ABLIKIM 23Bs uses $K_1(1270)^0 \rightarrow K^- \pi^+ \pi^0$ decays.

$$\frac{\Gamma(K^*(892)^0 e^+ \nu_e)}{\Gamma_{\text{total}}} \quad \Gamma_{37}/\Gamma$$
Unseen decay modes of the $K^*(892)^0$ are included.

VALUE (%)	EVTS	DOCUMENT ID	TECN	COMMENT
0.215 ± 0.028	OUR AVERAGE			Error includes scale factor of 1.1.
$0.237 \pm 0.026 \pm 0.020$	155	ABLIKIM	19D BES3	$e^+ e^-$ at 4178 MeV
$0.18 \pm 0.04 \pm 0.01$	32	1 HIETALA	15	$e^+ e^-$ at 4.170 GeV

• • • We do not use the following data for averages, fits, limits, etc. • • •

$0.18 \pm 0.07 \pm 0.01$ 7.5 YELTON 09 CLEO See HIETALA 15

1 Uses CLEO data, but not authored by the CLEO collaboration

$$\frac{\Gamma(f_0(500) e^+ \nu_e, f_0 \rightarrow \pi^0 \pi^0)}{\Gamma_{\text{total}}} \quad \Gamma_{38}/\Gamma$$

VALUE (%)	CL%	DOCUMENT ID	TECN	COMMENT
$< 7.3 \times 10^{-4}$	90	ABLIKIM	22J BES3	$e^+ e^-$ at 4.178-4.226 GeV

$$\frac{\Gamma(f_0(980) e^+ \nu_e, f_0 \rightarrow \pi^0 \pi^0)}{\Gamma_{\text{total}}} \quad \Gamma_{39}/\Gamma$$

VALUE (units 10^{-4})	EVTS	DOCUMENT ID	TECN	COMMENT
$7.9 \pm 1.4 \pm 0.4$	55	1 ABLIKIM	22J BES3	$e^+ e^-$ at 4.178-4.226 GeV

1 Assuming $B(f_0 \rightarrow \pi^0 \pi^0) = 1/3$ via the isospin limit, this result implies $B(D_S^+ \rightarrow f_0(980) e^+ \nu_e) = (2.4 \pm 0.4) \times 10^{-3}$.

$$\frac{\Gamma(f_0(980) e^+ \nu_e, f_0 \rightarrow \pi^+ \pi^-)}{\Gamma_{\text{total}}} \quad \Gamma_{40}/\Gamma$$

VALUE (%)	EVTS	DOCUMENT ID	TECN	COMMENT
$0.13 \pm 0.03 \pm 0.01$	42	1 HIETALA	15	Uses CLEO data
$0.20 \pm 0.03 \pm 0.01$	44	ECKLUND	09 CLEO	See HIETALA 15
$0.13 \pm 0.04 \pm 0.01$	13	YELTON	09 CLEO	See ECKLUND 09

• • • We do not use the following data for averages, fits, limits, etc. • • •

1 HIETALA 15 uses a tighter cut on the reconstructed $\pi^+ \pi^-$ mass (± 60 MeV around the f_0) than ECKLUND 09. It finds that applying the same tight cut to both analyses gives consistent results.

$$\frac{\Gamma(f_0(980) \mu^+ \nu_\mu, f_0 \rightarrow K^+ K^-)}{\Gamma_{\text{total}}} \quad \Gamma_{41}/\Gamma$$

VALUE (%)	CL%	DOCUMENT ID	TECN	COMMENT
$< 5.45 \times 10^{-4}$	90	1 ABLIKIM	23Bz BES3	$e^+ e^-$ at 4.128-4.226 GeV

1 Partial wave analysis of 939 $D_S^+ \rightarrow K^+ K^- \mu^+ \nu_\mu$ events, assuming $K^+ K^-$ S-wave is 100% $f_0(980)$.

$$\frac{\Gamma(a_0(980)^0 e^+ \nu_e, a_0^0 \rightarrow \pi^0 \eta)}{\Gamma_{\text{total}}} \quad \Gamma_{42}/\Gamma$$

VALUE (%)	CL%	DOCUMENT ID	TECN	COMMENT
$< 1.2 \times 10^{-4}$	90	ABLIKIM	21Y BES3	$e^+ e^-$ at 4.178-4.226 GeV

$$\frac{\Gamma(\pi^0 e^+ \nu_e)}{\Gamma_{\text{total}}} \quad \Gamma_{43}/\Gamma$$

VALUE (%)	CL%	DOCUMENT ID	TECN	COMMENT
$< 6.4 \times 10^{-5}$	90	ABLIKIM	22BH BES3	6.32 fb^{-1} of $e^+ e^-$ at 4.178-4.226 GeV

$$\frac{\Gamma(b_1(1235)^0 e^+ \nu_e, b_1^0 \rightarrow \omega \pi^0)}{\Gamma_{\text{total}}} \quad \Gamma_{28}/\Gamma$$

VALUE (%)	CL%	DOCUMENT ID	TECN	COMMENT
$< 6.4 \times 10^{-4}$	90	ABLIKIM	23Bs BES3	$e^+ e^-$ at 4.128-4.226 GeV

Hadronic modes with a $K\bar{K}$ pair
$$\frac{\Gamma(K^+ K_S^0)}{\Gamma_{\text{total}}} \quad \Gamma_{44}/\Gamma$$

VALUE (%)	EVTS	DOCUMENT ID	TECN	COMMENT
1.450 ± 0.035	OUR FIT			
1.46 ± 0.05	OUR AVERAGE			Error includes scale factor of 1.2.
$1.425 \pm 0.038 \pm 0.031$	1.8k	ABLIKIM	19AMBES3	$e^+ e^-$ at 4178 MeV
$1.52 \pm 0.05 \pm 0.03$		ONYISI	13 CLEO	$e^+ e^-$ at 4.17 GeV

• • • We do not use the following data for averages, fits, limits, etc. • • •

$1.49 \pm 0.07 \pm 0.05$ 1 ALEXANDER 08 CLEO See ONYISI 13

1 ALEXANDER 08 uses single- and double-tagged events in an overall fit.

$$\frac{\Gamma(K^+ K_S^0)}{\Gamma(K^+ K^- \pi^+)} \quad \Gamma_{44}/\Gamma_{47}$$

VALUE (units 10^{-2})	EVTS	DOCUMENT ID	TECN	COMMENT
$27.55 \pm 0.18 \pm 0.50$	40k	ABLIKIM	20R BES3	$e^+ e^-$, 4178 ~ 4226 MeV

$$\frac{\Gamma(K^+ K_S^0)}{\Gamma_{\text{total}}} \quad \Gamma_{45}/\Gamma$$

VALUE (%)	EVTS	DOCUMENT ID	TECN	COMMENT
$1.485 \pm 0.039 \pm 0.046$	2.3k	ABLIKIM	19AMBES3	$e^+ e^-$ at 4178 MeV

$$\frac{\Gamma(K^+ \bar{K}^0)}{\Gamma_{\text{total}}} \quad \Gamma_{46}/\Gamma$$

VALUE (%)	EVTS	DOCUMENT ID	TECN	COMMENT
$2.95 \pm 0.11 \pm 0.09$	2.0k	1 ZUPANC	13 BELL	$e^+ e^-$ at $\Upsilon(4S), \Upsilon(5S)$

1 ZUPANC 13 finds the \bar{K}^0 from its missing-mass squared, not from $K_S^0 \rightarrow \pi^+ \pi^-$.

The DCS ($D_S^+ \rightarrow K^+ K^0$) contribution to this fraction is estimated to be an order of magnitude below the statistical uncertainty.

$$\frac{\Gamma(K^+ K^- \pi^+)}{\Gamma_{\text{total}}} \quad \Gamma_{47}/\Gamma$$

VALUE (%)	EVTS	DOCUMENT ID	TECN	COMMENT
5.37 ± 0.10	OUR FIT			Error includes scale factor of 1.1.
5.45 ± 0.11	OUR AVERAGE			Error includes scale factor of 1.1.
$5.47 \pm 0.08 \pm 0.13$	5.1k	ABLIKIM	21AE BES3	$e^+ e^-$ at 4.178 GeV
$5.55 \pm 0.14 \pm 0.13$		ONYISI	13 CLEO	$e^+ e^-$ at 4.17 GeV
$5.06 \pm 0.15 \pm 0.21$	4.1k	ZUPANC	13 BELL	$e^+ e^-$ at $\Upsilon(4S), \Upsilon(5S)$
$5.78 \pm 0.20 \pm 0.30$		DEL-AMO-SA.10j	BABR	$e^+ e^-$, 10.58 GeV

• • • We do not use the following data for averages, fits, limits, etc. • • •

$5.50 \pm 0.23 \pm 0.16$ 1 ALEXANDER 08 CLEO See ONYISI 13

1 ALEXANDER 08 uses single- and double-tagged events in an overall fit.

$$\frac{\Gamma(\phi \pi^+)}{\Gamma_{\text{total}}} \quad \Gamma_{48}/\Gamma$$

The results here are model-independent. For earlier, model-dependent results, see our PDG 06 edition. We decouple the $D_S^+ \rightarrow \phi \pi^+$ branching fraction obtained from mass projections (and used to get some of the other branching fractions) from the $D_S^+ \rightarrow \phi \pi^+, \phi \rightarrow K^+ K^-$ branching fraction obtained from the Dalitz-plot analysis of $D_S^+ \rightarrow K^+ K^- \pi^+$. That is, the ratio of these two branching fractions is not exactly the $\phi \rightarrow K^+ K^-$ branching fraction 0.491.

VALUE (%)	EVTS	DOCUMENT ID	TECN	COMMENT
4.5 ± 0.4	OUR AVERAGE			
$4.62 \pm 0.36 \pm 0.51$		1 AUBERT	06N BABR	$e^+ e^-$ at $\Upsilon(4S)$
$4.81 \pm 0.52 \pm 0.38$	212 ± 19	2 AUBERT	05V BABR	$e^+ e^- \approx \Upsilon(4S)$
$3.59 \pm 0.77 \pm 0.48$		3 ARTUSO	96 CLE2	$e^+ e^-$ at $\Upsilon(4S)$

• • • We do not use the following data for averages, fits, limits, etc. • • •

$3.9 \pm 5.1 \pm 1.8$ 4 BAI 95c BES $e^+ e^-$ 4.03 GeV

1 This AUBERT 06N measurement uses $\bar{B}^0 \rightarrow D_s^{(*)-} D^{(*)+}$ and $B^- \rightarrow D_s^{(*)-} D^{(*)0}$ decays, including some from other papers. However, the result is independent of AUBERT 05V.

2 AUBERT 05V uses the ratio of $B^0 \rightarrow D^{*-} D_S^{*+}$ events seen in two different ways, in both of which the $D^{*-} \rightarrow \bar{D}^0 \pi^-$ decay is fully reconstructed: (1) The $D_S^{*+} \rightarrow D_S^+ \gamma$, $D_S^+ \rightarrow \phi \pi^+$ decay is fully reconstructed. (2) The number of events in the D_S^+ peak in the missing mass spectrum against the $D^{*-} \gamma$ is measured.

3 ARTUSO 96 uses partially reconstructed $\bar{B}^0 \rightarrow D^{*+} D_S^{*-}$ decays to get a model-independent value for $\Gamma(D_S^- \rightarrow \phi \pi^-)/\Gamma(D^0 \rightarrow K^- \pi^+)$ of $0.92 \pm 0.20 \pm 0.11$.

4 BAI 95c uses $e^+ e^- \rightarrow D_S^+ D_S^-$ events in which one or both of the D_S^\pm are observed to obtain the first model-independent measurement of the $D_S^+ \rightarrow \phi \pi^+$ branching fraction, without assumptions about $\sigma(D_S^\pm)$. However, with only two "doubly-tagged" events, the statistical error is very large.

See key on page 1171

Meson Particle Listings

D_s^\pm

$\Gamma(\phi\pi^+, \phi \rightarrow K^+K^-)/\Gamma(K^+K^-\pi^+)$ Γ_{49}/Γ_{47}

This is the "fit fraction" from the Dalitz-plot analysis. We decouple the $D_s^+ \rightarrow \phi\pi^+$ branching fraction obtained from mass projections (and used to get some of the other branching fractions) from the $D_s^+ \rightarrow \phi\pi^+, \phi \rightarrow K^+K^-$ branching fraction obtained from the Dalitz-plot analysis of $D_s^+ \rightarrow K^+K^-\pi^+$. That is, the ratio of these two branching fractions is not exactly the $\phi \rightarrow K^+K^-$ branching fraction 0.491.

VALUE (units 10^{-2})	EVTS	DOCUMENT ID	TECN	COMMENT
41.2±0.7 OUR AVERAGE				
40.5±0.7±0.9	18.6k	ABLIKIM	21AE BES3	e^+e^- at 4.178 GeV
41.4±0.8±0.5		DEL-AMO-SA...11G	BABR	Dalitz fit, 96k evts
42.2±1.6±0.3		MITCHELL	09A CLEO	Dalitz fit, 12k evts
••• We do not use the following data for averages, fits, limits, etc. •••				
39.6±3.3±4.7		FRABETTI	95B E687	Dalitz fit, 701 evts

$\Gamma(K^+\bar{K}^*(892)^0)/\Gamma(K^*(892)^+\bar{K}^0)$ Γ_{50}/Γ_{67}

VALUE	DOCUMENT ID	TECN	COMMENT
2.35$^{+0.42}_{-0.23}$±0.10	ABLIKIM	22AH BES3	Dalitz plot fit to 990 $D_s^\pm \rightarrow K^\pm K_S^0 \pi^0$ evts

$\Gamma(K^+\bar{K}^*(892)^0, \bar{K}^{*0} \rightarrow K^-\pi^+)/\Gamma(K^+K^-\pi^+)$ Γ_{51}/Γ_{47}

This is the "fit fraction" from the Dalitz-plot analysis.

VALUE (units 10^{-2})	EVTS	DOCUMENT ID	TECN	COMMENT
47.9±0.6 OUR AVERAGE				
48.3±0.9±0.6	18.6k	ABLIKIM	21AE BES3	e^+e^- at 4.178 GeV
47.9±0.5±0.5		DEL-AMO-SA...11G	BABR	Dalitz fit, 96k evts
47.4±1.5±0.4		MITCHELL	09A CLEO	Dalitz fit, 12k evts
••• We do not use the following data for averages, fits, limits, etc. •••				
47.8±4.6±4.0		FRABETTI	95B E687	Dalitz fit, 701 evts

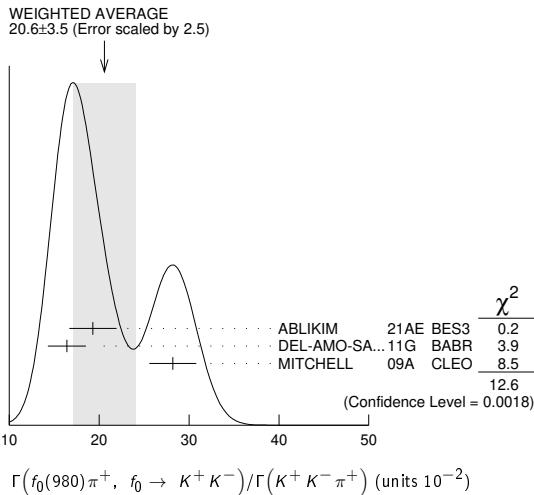
$\Gamma(K^+\bar{K}^*(892)^0, \bar{K}^{*0} \rightarrow K_S^0\pi^0)/\Gamma(K^+K_S^0\pi^0)$ Γ_{52}/Γ_{60}

VALUE (units 10^{-2})	DOCUMENT ID	TECN	COMMENT
32.7±2.2±1.9	ABLIKIM	22AH BES3	Dalitz plot fit, 990 evts

$\Gamma(f_0(980)\pi^+, f_0 \rightarrow K^+K^-)/\Gamma(K^+K^-\pi^+)$ Γ_{53}/Γ_{47}

This is the "fit fraction" from the Dalitz-plot analysis. This is likely a superposition of $D_s^+ \rightarrow f_0(980)\pi$ and $D_s^+ \rightarrow a_0(980)\pi$ which are indistinguishable in such an analysis.

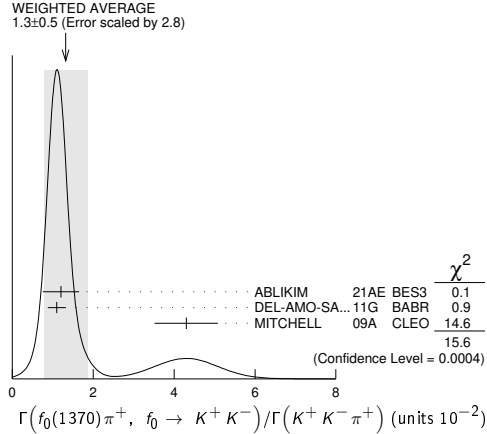
VALUE (units 10^{-2})	EVTS	DOCUMENT ID	TECN	COMMENT
20.6±3.5 OUR AVERAGE				Error includes scale factor of 2.5. See the ideogram below.
19.3±1.7±2.0	18.6k	ABLIKIM	21AE BES3	e^+e^- at 4.178 GeV
16.4±0.7±2.0		DEL-AMO-SA...11G	BABR	Dalitz fit, 96k evts
28.2±1.9±1.8		MITCHELL	09A CLEO	Dalitz fit, 12k evts
••• We do not use the following data for averages, fits, limits, etc. •••				
11.0±3.5±2.6		FRABETTI	95B E687	Dalitz fit, 701 evts



$\Gamma(f_0(1370)\pi^+, f_0 \rightarrow K^+K^-)/\Gamma(K^+K^-\pi^+)$ Γ_{54}/Γ_{47}

This is the "fit fraction" from the Dalitz-plot analysis.

VALUE (units 10^{-2})	EVTS	DOCUMENT ID	TECN	COMMENT
1.3±0.5 OUR AVERAGE				Error includes scale factor of 2.8. See the ideogram below.
1.2±0.4±0.2	18.6k	ABLIKIM	21AE BES3	e^+e^- at 4.178 GeV
1.1±0.1±0.2		DEL-AMO-SA...11G	BABR	Dalitz fit, 96k evts
4.3±0.6±0.5		MITCHELL	09A CLEO	Dalitz fit, 12k evts



$\Gamma(f_0(1710)\pi^+, f_0 \rightarrow K^+K^-)/\Gamma(K^+K^-\pi^+)$ Γ_{55}/Γ_{47}

This is the "fit fraction" from the Dalitz-plot analysis. This is likely a superposition of $D_s^+ \rightarrow f_0(1710)\pi$ and $D_s^+ \rightarrow a_0(1710)\pi$ which are indistinguishable in such an analysis.

VALUE (units 10^{-2})	EVTS	DOCUMENT ID	TECN	COMMENT
1.3±0.5 OUR AVERAGE				Error includes scale factor of 3.8.
1.9±0.4±0.6	18.6k	ABLIKIM	21AE BES3	e^+e^- at 4.178 GeV
1.1±0.1±0.1		DEL-AMO-SA...11G	BABR	Dalitz fit, 96k evts
3.4±0.5±0.3		MITCHELL	09A CLEO	Dalitz fit, 12k evts
••• We do not use the following data for averages, fits, limits, etc. •••				
3.4±2.3±3.5		FRABETTI	95B E687	Dalitz fit, 701 evts

$\Gamma(a_0(980)+\pi^0, a_0^+ \rightarrow K^+K_S^0)/\Gamma(K^+K_S^0\pi^0)$ Γ_{56}/Γ_{60}

VALUE (units 10^{-2})	DOCUMENT ID	TECN	COMMENT
7.7±1.7±1.8	ABLIKIM	22AH BES3	Dalitz plot fit, 990 evts

$\Gamma(a_0(1710)+\pi^0, a_0^+ \rightarrow K^+K_S^0)/\Gamma(K^+K_S^0\pi^0)$ Γ_{57}/Γ_{60}

VALUE (units 10^{-2})	DOCUMENT ID	TECN	COMMENT
23.6±3.4±2.0	¹ ABLIKIM	22AH BES3	Dalitz plot fit, 990 evts

¹ ABLIKIM 22AH observe an a_0 -like state with mass $m_{a_0} = 1.817 \pm 0.008 \pm 0.020$ GeV, and name the intermediate resonance $a_0(1817)$. We interpret this as the $a_0(1710)$ observed by LEES 21A.

$\Gamma(K^+\bar{K}_S^*(1430)^0, \bar{K}_0^{*0} \rightarrow K^-\pi^+)/\Gamma(K^+K^-\pi^+)$ Γ_{58}/Γ_{47}

This is the "fit fraction" from the Dalitz-plot analysis.

VALUE (units 10^{-2})	EVTS	DOCUMENT ID	TECN	COMMENT
3.3±0.5 OUR AVERAGE				
3.0±0.6±0.5	18.6k	ABLIKIM	21AE BES3	e^+e^- at 4.178 GeV
2.4±0.3±1.0		DEL-AMO-SA...11G	BABR	Dalitz fit, 96k evts
3.9±0.5±0.5		MITCHELL	09A CLEO	Dalitz fit, 12k evts
••• We do not use the following data for averages, fits, limits, etc. •••				
9.3±3.2±3.2		FRABETTI	95B E687	Dalitz fit, 701 evts

$\Gamma(K^+\bar{K}^*(1410)^0, \bar{K}_0^{*0} \rightarrow K_S^0\pi^0)/\Gamma(K^+K_S^0\pi^0)$ Γ_{59}/Γ_{60}

VALUE (units 10^{-2})	DOCUMENT ID	TECN	COMMENT
6.0±1.4±1.3	ABLIKIM	22AH BES3	Dalitz plot fit, 990 evts

$\Gamma(K^+K_S^0\pi^0)/\Gamma_{total}$ Γ_{60}/Γ

VALUE (%)	EVTS	DOCUMENT ID	TECN	COMMENT
1.47±0.07 OUR AVERAGE				
1.46±0.06±0.05	990	ABLIKIM	22AH BES3	e^+e^- at 4.178-4.226 GeV
1.52±0.09±0.20		ONYISI	13 CLEO	e^+e^- at 4.17 GeV

$\Gamma(K^*(892)^+K_S^0, K^{*+} \rightarrow K^+\pi^0)/\Gamma(K^+K_S^0\pi^0)$ Γ_{61}/Γ_{60}

VALUE (units 10^{-2})	DOCUMENT ID	TECN	COMMENT
13.9±1.7±1.3	ABLIKIM	22AH BES3	Dalitz plot fit, 990 evts

$\Gamma(2K_S^0\pi^+)/\Gamma_{total}$ Γ_{62}/Γ

VALUE (%)	EVTS	DOCUMENT ID	TECN	COMMENT
0.71±0.04 OUR AVERAGE				Error includes scale factor of 1.3.
0.68±0.04±0.01	370	ABLIKIM	22F BES3	e^+e^- at 4.178-4.226 GeV
0.77±0.05±0.03		ONYISI	13 CLEO	e^+e^- at 4.17 GeV

$\Gamma(f_0(980)\pi^+, f_0 \rightarrow K_S^0K_S^0)/\Gamma_{total}$ Γ_{63}/Γ

This is the "fit fraction" from the Dalitz-plot analysis. This is likely a superposition of $D_s^+ \rightarrow f_0(980)\pi$ and $D_s^+ \rightarrow a_0(980)\pi$ which are indistinguishable in such an analysis.

VALUE	CL%	DOCUMENT ID	TECN	COMMENT
<1.8 × 10⁻⁴	90	¹ ABLIKIM	22F BES3	Dalitz plot fit

¹ Based on isospin considerations, the authors interpret the suppression in the observed rate of this mode compared to $D_s^\pm \rightarrow f_0(980)\pi^+, f_0 \rightarrow K^+K^-$ as likely due to the destructive interference between $a_0(980)$ and $f_0(980)$ in decays to $K_S^0K_S^0$.

Meson Particle Listings

 D_S^\pm $\Gamma(\rho_0(1710)\pi^+, \rho_0 \rightarrow K_S^0 K_S^0)/\Gamma(2K_S^0\pi^+)$ Γ_{64}/Γ_{62}

This is the "fit fraction" from the Dalitz-plot analysis. This is likely a superposition of $D_S^+ \rightarrow \rho_0(1710)\pi$ and $D_S^+ \rightarrow \rho_0(1700)\pi$ which are indistinguishable in such an analysis.

VALUE (units 10^{-2})	DOCUMENT ID	TECN	COMMENT
46.3±4.0±1.2	ABLIKIM	22F	BES3 Dalitz plot fit, 400 evts

 $\Gamma(K^*(892)^+ K_S^0, K^{*+} \rightarrow K_S^0 \pi^+)/\Gamma(2K_S^0 \pi^+)$ Γ_{65}/Γ_{62}

VALUE (units 10^{-2})	DOCUMENT ID	TECN	COMMENT
43.5±3.9±0.5	ABLIKIM	22F	BES3 Dalitz plot fit, 400 evts

 $\Gamma(K^*(892)^+ \bar{K}^0)/\Gamma(\phi\pi^+)$ Γ_{67}/Γ_{48}

Unseen decay modes of the resonances are included.

VALUE	DOCUMENT ID	TECN	COMMENT
1.20±0.21±0.13	CHEN	89	CLEO e^+e^- 10 GeV

 $\Gamma(K^+ K^- \pi^+ \pi^0)/\Gamma_{total}$ Γ_{68}/Γ

VALUE (%)	EVTS	DOCUMENT ID	TECN	COMMENT
5.50±0.24 OUR FIT				Error includes scale factor of 1.3.
5.51±0.28 OUR AVERAGE				Error includes scale factor of 1.5.

5.42±0.10±0.17	3k	¹ ABLIKIM	21U	BES3 e^+e^- at 4.178–4.226 GeV
6.37±0.21±0.56		ONYISI	13	CLEO e^+e^- at 4.17 GeV

• • • We do not use the following data for averages, fits, limits, etc. • • •

5.65±0.29±0.40		² ALEXANDER	08	CLEO See ONYISI 13
		¹ ABLIKIM	21U	uses an amplitude analysis of $D_S^+ \rightarrow K^+ K^- \pi^+ \pi^0$ with 9 components.
		² ALEXANDER	08	uses single- and double-tagged events in an overall fit.

 $\Gamma(\phi\rho^+)/\Gamma_{total}$ Γ_{69}/Γ

VALUE (units 10^{-2})	EVTS	DOCUMENT ID	TECN	COMMENT
5.59±0.15±0.30	3k	¹ ABLIKIM	21U	BES3 e^+e^- at 4.178–4.226 GeV

¹ABLIKIM 21U uses an amplitude analysis of $D_S^+ \rightarrow K^+ K^- \pi^+ \pi^0$ with 9 components.

 $\Gamma(\phi\rho^+)/\Gamma(\phi\pi^+)$ Γ_{69}/Γ_{48}

VALUE	EVTS	DOCUMENT ID	TECN	COMMENT
1.86±0.26±0.29 _{0.40}	253	AVERY	92	CLE2 $e^+e^- \approx 10.5$ GeV

 $\Gamma(\bar{K}_1(1270)^0 K^+, \bar{K}_1(1270)^0 \rightarrow K^- \rho^+)/\Gamma_{total}$ Γ_{70}/Γ

VALUE (units 10^{-2})	EVTS	DOCUMENT ID	TECN	COMMENT
0.57±0.05±0.04	3k	¹ ABLIKIM	21U	BES3 e^+e^- at 4.178–4.226 GeV

¹ABLIKIM 21U uses an amplitude analysis of $D_S^+ \rightarrow K^+ K^- \pi^+ \pi^0$ with 9 components.

 $\Gamma(\bar{K}_1(1270)^0 K^+, \bar{K}_1(1270)^0 \rightarrow K^*(892)\pi)/\Gamma_{total}$ Γ_{71}/Γ

VALUE (units 10^{-2})	EVTS	DOCUMENT ID	TECN	COMMENT
1.31±0.18±0.18	3k	^{1,2} ABLIKIM	21U	BES3 e^+e^- at 4.178–4.226 GeV

¹ABLIKIM 21U uses an amplitude analysis of $D_S^+ \rightarrow K^+ K^- \pi^+ \pi^0$ with 9 components.
² $\bar{K}_1(1270)^0 \rightarrow K^*(892)\pi$ denotes a sum over $\bar{K}(892)^0\pi^0$ and $K(892)^-\pi^+$ final states, which are assumed to have relative branching ratio 1/2, as per isospin.

 $\Gamma(\bar{K}_1(1400)^0 K^+, \bar{K}_1(1400)^0 \rightarrow K^*(892)\pi)/\Gamma_{total}$ Γ_{72}/Γ

VALUE (units 10^{-2})	EVTS	DOCUMENT ID	TECN	COMMENT
1.98±0.27±0.32	3k	¹ ABLIKIM	21U	BES3 e^+e^- at 4.178–4.226 GeV

¹ $\bar{K}_1(1400)^0 \rightarrow K^*(892)\pi$ denotes a sum over $\bar{K}(892)^0\pi^0$ and $K(892)^-\pi^+$ final states, which are assumed to have relative branching ratio 1/2, as per isospin.

 $\Gamma(a_0(980)^0 \rho^+, a_0^0 \rightarrow K^+ K^-)/\Gamma_{total}$ Γ_{73}/Γ

VALUE (units 10^{-2})	EVTS	DOCUMENT ID	TECN	COMMENT
0.19±0.03±0.03	3k	¹ ABLIKIM	21U	BES3 e^+e^- at 4.178–4.226 GeV

¹ABLIKIM 21U uses an amplitude analysis of $D_S^+ \rightarrow K^+ K^- \pi^+ \pi^0$ with 9 components.

 $\Gamma(\bar{K}_1(1420)^0 \pi^+, \bar{K}_1(1420)^0 \rightarrow K^*(892)\bar{K}^\pm)/\Gamma_{total}$ Γ_{74}/Γ

VALUE (units 10^{-2})	EVTS	DOCUMENT ID	TECN	COMMENT
0.39±0.06±0.03	3k	¹ ABLIKIM	21U	BES3 e^+e^- at 4.178–4.226 GeV

¹ABLIKIM 21U uses an amplitude analysis of $D_S^+ \rightarrow K^+ K^- \pi^+ \pi^0$ with 9 components.

 $\Gamma(\bar{K}_1(1420)^0 \pi^+, \bar{K}_1(1420)^0 \rightarrow a_0(980)^0 \pi^0, a_0(980)^0 \rightarrow K^+ K^-)/\Gamma_{total}$ Γ_{75}/Γ

VALUE (units 10^{-2})	EVTS	DOCUMENT ID	TECN	COMMENT
0.04±0.01±0.01	3k	¹ ABLIKIM	21U	BES3 e^+e^- at 4.178–4.226 GeV

¹ABLIKIM 21U uses an amplitude analysis of $D_S^+ \rightarrow K^+ K^- \pi^+ \pi^0$ with 9 components.

 $\Gamma(\eta(1475)\pi^+, \eta(1475) \rightarrow a_0(980)^0 \pi^0, a_0(980)^0 \rightarrow K^+ K^-)/\Gamma_{total}$ Γ_{76}/Γ

VALUE (units 10^{-2})	EVTS	DOCUMENT ID	TECN	COMMENT
0.07±0.02±0.02	3k	¹ ABLIKIM	21U	BES3 e^+e^- at 4.178–4.226 GeV

¹ABLIKIM 21U uses an amplitude analysis of $D_S^+ \rightarrow K^+ K^- \pi^+ \pi^0$ with 9 components.

 $\Gamma(K_S^0 K^- 2\pi^+)/\Gamma_{total}$ Γ_{77}/Γ

VALUE (%)	EVTS	DOCUMENT ID	TECN	COMMENT
1.53±0.08 OUR FIT				Error includes scale factor of 1.5.
1.53±0.11 OUR AVERAGE				Error includes scale factor of 1.8.

1.46±0.05±0.05	1.3k	ABLIKIM	21K	BES3 e^+e^- at 4.178–4.226 GeV
1.69±0.07±0.08		ONYISI	13	CLEO e^+e^- at 4.17 GeV

• • • We do not use the following data for averages, fits, limits, etc. • • •

1.64±0.10±0.07		¹ ALEXANDER	08	CLEO See ONYISI 13
		¹ ALEXANDER	08	uses single- and double-tagged events in an overall fit.

 $\Gamma(K^+ K^- K_S^0 \pi^+)/\Gamma(K^+ K_S^0 \pi^+ \pi^-)$ Γ_{78}/Γ_{84}

VALUE (%)	EVTS	DOCUMENT ID	TECN	COMMENT
1.36±0.15±0.04	645	MOON	23	BELL 980 fb ⁻¹ at $\sim \mathcal{T}(4S)$

 $\Gamma(K^*(892)^+ \bar{K}^*(892)^0)/\Gamma_{total}$ Γ_{79}/Γ

VALUE (units 10^{-2})	EVTS	DOCUMENT ID	TECN	COMMENT
5.64±0.23±0.27	3k	¹ ABLIKIM	21U	BES3 e^+e^- at 4.178–4.226 GeV

¹ABLIKIM 21U uses an amplitude analysis of $D_S^+ \rightarrow K^+ K^- \pi^+ \pi^0$ with 9 components.

 $\Gamma(K^*(892)^+ \bar{K}^*(892)^0)/\Gamma(\phi\pi^+)$ Γ_{79}/Γ_{48}

VALUE	DOCUMENT ID	TECN	COMMENT
1.6±0.4±0.4	ALBRECHT	92B	ARG $e^+e^- \approx 10.4$ GeV

 $\Gamma(K^*(892)^+ \bar{K}^*(892)^0)/\Gamma(K_S^0 K^- 2\pi^+)$ Γ_{79}/Γ_{77}

VALUE (units 10^{-2})	EVTS	DOCUMENT ID	TECN	COMMENT
40.6±2.9±4.9	1.3k	^{1,2} ABLIKIM	21K	BES3 e^+e^- at 4.178–4.226 GeV

¹Predominantly S-wave, with a significant D-wave component.

² $D_S^+ \rightarrow K_S^0 K^- 2\pi^+$ amplitude analysis with 13 components.

 $\Gamma(\eta(1475) K_S^0, \eta \rightarrow K^*(892)^0 \pi^+, K^{*0} \rightarrow K^- \pi^+)/\Gamma(K_S^0 K^- 2\pi^+)$ Γ_{80}/Γ_{77}

VALUE (units 10^{-2})	EVTS	DOCUMENT ID	TECN	COMMENT
2.2±0.6±0.2	1.3k	¹ ABLIKIM	21K	BES3 e^+e^- at 4.178–4.226 GeV

¹ $D_S^+ \rightarrow K_S^0 K^- 2\pi^+$ amplitude analysis with 13 components.

 $\Gamma(\eta(1475)\pi^+, \eta \rightarrow \bar{K}^*(892)^+ K^-, \bar{K}^{*+} \rightarrow K_S^0 \pi^+)/\Gamma(K_S^0 K^- 2\pi^+)$ Γ_{81}/Γ_{77}

VALUE (units 10^{-2})	EVTS	DOCUMENT ID	TECN	COMMENT
2.2±0.6±0.2	1.3k	¹ ABLIKIM	21K	BES3 e^+e^- at 4.178–4.226 GeV

¹ $D_S^+ \rightarrow K_S^0 K^- 2\pi^+$ amplitude analysis with 13 components.

 $\Gamma(\eta(1475)\pi^+, \eta \rightarrow a_0(980)^- \pi^+, a_0^- \rightarrow K_S^0 K^-)/\Gamma(K_S^0 K^- 2\pi^+)$ Γ_{82}/Γ_{77}

VALUE (units 10^{-2})	EVTS	DOCUMENT ID	TECN	COMMENT
10.8±2.6±5.2	1.3k	¹ ABLIKIM	21K	BES3 e^+e^- at 4.178–4.226 GeV

¹ $D_S^+ \rightarrow K_S^0 K^- 2\pi^+$ amplitude analysis with 13 components.

 $\Gamma(\bar{K}_1(1285)\pi^+, \bar{K}_1 \rightarrow a_0(980)^- \pi^+, a_0^- \rightarrow K_S^0 K^-)/\Gamma(K_S^0 K^- 2\pi^+)$ Γ_{83}/Γ_{77}

VALUE (units 10^{-2})	EVTS	DOCUMENT ID	TECN	COMMENT
2.2±0.5±0.2	1.3k	¹ ABLIKIM	21K	BES3 e^+e^- at 4.178–4.226 GeV

¹ $D_S^+ \rightarrow K_S^0 K^- 2\pi^+$ amplitude analysis with 13 components.

 $\Gamma(K^+ K_S^0 \pi^+ \pi^-)/\Gamma_{total}$ Γ_{84}/Γ

VALUE (%)	DOCUMENT ID	TECN	COMMENT
0.95±0.08 OUR FIT			Error includes scale factor of 1.1.
1.03±0.06±0.08	ONYISI	13	CLEO e^+e^- at 4.17 GeV

 $\Gamma(K^+ K_S^0 \pi^+ \pi^-)/\Gamma(K_S^0 K^- 2\pi^+)$ Γ_{84}/Γ_{77}

VALUE	EVTS	DOCUMENT ID	TECN	COMMENT
0.62 ± 0.05 OUR FIT				
0.586±0.052±0.043	476	LINK	01c	FOCS $\gamma A, \bar{E}_\gamma \approx 180$ GeV

 $\Gamma(K^+ K^- 2\pi^+ \pi^-)/\Gamma_{total}$ Γ_{85}/Γ

VALUE (units 10^{-3})	EVTS	DOCUMENT ID	TECN	COMMENT
6.60±0.47±0.38	309	ABLIKIM	22AB	BES3 e^+e^- at 4.178–4.226 GeV

 $\Gamma(K^+ K^- 2\pi^+ \pi^-)/\Gamma(K^+ K^- \pi^+)$ Γ_{85}/Γ_{47}

VALUE	EVTS	DOCUMENT ID	TECN	COMMENT
0.160±0.027 OUR AVERAGE				
0.150±0.019±0.025	240	LINK	03D	FOCS $\gamma A, \bar{E}_\gamma \approx 180$ GeV
0.188±0.036±0.040	75	FRABETTI	97c	E687 $\gamma Be, \bar{E}_\gamma \approx 200$ GeV

¹ABLIKIM 21U uses an amplitude analysis of $D_S^+ \rightarrow K^+ K^- \pi^+ \pi^0$ with 9 components.

²ABLIKIM 21U uses an amplitude analysis of $D_S^+ \rightarrow K^+ K^- \pi^+ \pi^0$ with 9 components.

 $\Gamma(\phi 2\pi^+ \pi^-)/\Gamma(\phi\pi^+)$ Γ_{86}/Γ_{48}

VALUE	EVTS	DOCUMENT ID	TECN	COMMENT
0.269±0.027 OUR AVERAGE				
0.249±0.024±0.021	136	LINK	03D	FOCS $\gamma A, \bar{E}_\gamma \approx 180$ GeV
0.28±0.06±0.01	40	FRABETTI	97c	E687 $\gamma Be, \bar{E}_\gamma \approx 200$ GeV
0.58±0.21±0.10	21	FRABETTI	92	E687 γBe
0.42±0.13±0.07	19	ANJOS	88	E691 Photoproduction
1.11±0.37±0.28	62	ALBRECHT	85D	ARG e^+e^- 10 GeV

¹ABLIKIM 21U uses an amplitude analysis of $D_S^+ \rightarrow K^+ K^- \pi^+ \pi^0$ with 9 components.

²ABLIKIM 21U uses an amplitude analysis of $D_S^+ \rightarrow K^+ K^- \pi^+ \pi^0$ with 9 components.

³ABLIKIM 21U uses an amplitude analysis of $D_S^+ \rightarrow K^+ K^- \pi^+ \pi^0$ with 9 components.

 $\Gamma(\phi\rho^0\pi^+, \phi \rightarrow K^+ K^-)/\Gamma(K^+ K^- 2\pi^+ \pi^-)$ Γ_{87}/Γ_{85}

VALUE	DOCUMENT ID	TECN	COMMENT
0.75±0.06±0.04	LINK	03D	FOCS $\gamma A, \bar{E}_\gamma \approx 180$ GeV

$\Gamma(\phi a_1(1260)^+, \phi \rightarrow K^+ K^-, a_1^+ \rightarrow \rho^0 \pi^+)/\Gamma(K^+ K^- \pi^+)$ Γ_{88}/Γ_{47}			
VALUE	DOCUMENT ID	TECN	COMMENT
0.137 ± 0.019 ± 0.011	LINK	03D	FOCS $\gamma A, \bar{E}_\gamma \approx 180$ GeV

$\Gamma(\phi a_1(1260)^+, \phi \rightarrow K^+ K^-, a_1^+ \rightarrow \rho^0 \pi^+)/\Gamma(K^+ K^- 2\pi^+ \pi^-)$ Γ_{88}/Γ_{85}				
VALUE	EVTS	DOCUMENT ID	TECN	COMMENT
0.781 ± 0.029 ± 0.016	235	ABLIKIM	22AB	BES3 $e^+ e^-$ at 4.178-4.226 GeV

$\Gamma(\phi 2\pi^+ \pi^- \text{ non-}\rho, \phi \rightarrow K^+ K^-)/\Gamma(K^+ K^- 2\pi^+ \pi^-)$ Γ_{89}/Γ_{85}			
VALUE	DOCUMENT ID	TECN	COMMENT
0.21 ± 0.05 ± 0.06	LINK	03D	FOCS $\gamma A, \bar{E}_\gamma \approx 180$ GeV

$\Gamma(K^+ K^- \rho^0 \pi^+ \text{ non-}\phi)/\Gamma(K^+ K^- 2\pi^+ \pi^-)$ Γ_{90}/Γ_{85}				
VALUE	CL%	DOCUMENT ID	TECN	COMMENT
<0.03	90	LINK	03D	FOCS $\gamma A, \bar{E}_\gamma \approx 180$ GeV

$\Gamma(K^+ K^- 2\pi^+ \pi^- \text{ nonresonant})/\Gamma(K^+ K^- 2\pi^+ \pi^-)$ Γ_{91}/Γ_{85}				
VALUE	EVTS	DOCUMENT ID	TECN	COMMENT
0.15 ± 0.06 OUR AVERAGE				
0.218 ± 0.029 ± 0.08	235	ABLIKIM	22AB	BES3 $e^+ e^-$ at 4.178-4.226 GeV
0.10 ± 0.06 ± 0.05		LINK	03D	FOCS $\gamma A, \bar{E}_\gamma \approx 180$ GeV

$\Gamma(2K_S^0 2\pi^+ \pi^-)/\Gamma(K_S^0 K^- 2\pi^+)$ Γ_{92}/Γ_{77}				
VALUE	EVTS	DOCUMENT ID	TECN	COMMENT
0.051 ± 0.015 ± 0.015	37 ± 10	LINK	04D	FOCS $\gamma A, \bar{E}_\gamma \approx 180$ GeV

Pionic modes

$\Gamma(\pi^+ \pi^0)/\Gamma_{\text{total}}$ Γ_{93}/Γ				
VALUE	CL%	DOCUMENT ID	TECN	COMMENT
<1.2 × 10⁻⁴	90	1	GUAN	21 BELL $e^+ e^- \rightarrow \Upsilon(4,5S)$
¹ Uses $B(D_s^+ \rightarrow \pi^+ \phi, \phi \rightarrow K^+ K^-) = (2.24 \pm 0.08)\%$.				

$\Gamma(\pi^+ \pi^0)/\Gamma(K^+ K_S^0)$ Γ_{93}/Γ_{44}				
VALUE (units 10 ⁻²)	CL%	DOCUMENT ID	TECN	COMMENT
<2.3	90	MENDEZ	10	CLEO $e^+ e^-$ at 4170 MeV
• • • We do not use the following data for averages, fits, limits, etc. • • •				
<4.1	90	ADAMS	07A	CLEO See MENDEZ 10

$\Gamma(2\pi^+ \pi^-)/\Gamma_{\text{total}}$ Γ_{94}/Γ			
VALUE (%)	DOCUMENT ID	TECN	COMMENT
1.08 ± 0.04 OUR FIT			
1.11 ± 0.04 ± 0.04	ONYISI	13	CLEO $e^+ e^-$ at 4.17 GeV
• • • We do not use the following data for averages, fits, limits, etc. • • •			
1.11 ± 0.07 ± 0.04	1	ALEXANDER	08 CLEO See ONYISI 13
¹ ALEXANDER 08 uses single- and double-tagged events in an overall fit.			

$\Gamma(2\pi^+ \pi^-)/\Gamma(K^+ K^- \pi^+)$ Γ_{94}/Γ_{47}				
VALUE	EVTS	DOCUMENT ID	TECN	COMMENT
0.201 ± 0.007 OUR FIT				
0.199 ± 0.004 ± 0.009	$\approx 10.5k$	AUBERT	09o	BABR $e^+ e^- \approx 10.6$ GeV
• • • We do not use the following data for averages, fits, limits, etc. • • •				
0.265 ± 0.041 ± 0.031	98	FRABETTI	97D	E687 γ Be ≈ 200 GeV

$\Gamma(\rho^0 \pi^+)/\Gamma(2\pi^+ \pi^-)$ Γ_{95}/Γ_{94}			
VALUE (units 10 ⁻²)	DOCUMENT ID	TECN	COMMENT
1.04 ± 0.15 OUR AVERAGE			
1.038 ± 0.054 ± 0.097 ± 0.11	1	AAIJ	23AN LHCB Dalitz fit, 0.7M events
0.9 ± 0.4 ± 0.5		ABLIKIM	22Bi BES3 Dalitz fit, 11.1k events
1.8 ± 0.5 ± 1.0		AUBERT	09o BABR Dalitz fit, $\approx 10.5k$ evts
• • • We do not use the following data for averages, fits, limits, etc. • • •			
not seen		LINK	04 FOCS Dalitz fit, 1475 ± 50 evts
5.8 ± 2.3 ± 3.7		AITALA	01A E791 Dalitz fit, 848 evts
¹ The last error reflects the uncertainty on the amplitude model.			

$\Gamma(\omega \pi^+, \omega \rightarrow \pi^+ \pi^-)/\Gamma(2\pi^+ \pi^-)$ Γ_{111}/Γ_{94}			
VALUE (units 10 ⁻³)	DOCUMENT ID	TECN	COMMENT
3.60 ± 0.16 ± 0.34 ± 0.16	1	AAIJ	23AN LHCB Dalitz fit, 0.7M events
¹ The last error reflects the uncertainty on the amplitude model.			

$\Gamma(\pi^+ (\pi^+ \pi^-)_{S\text{-wave}})/\Gamma(2\pi^+ \pi^-)$ Γ_{96}/Γ_{94}			
This is the "fit fraction" from the Dalitz-plot analysis. See also KLEMP 08, which uses 568 $D_s^+ \rightarrow 3\pi$ decays (over 280 background events) from FNAL E791 to study various parametrizations of the decay amplitudes. The emphasis there is more on S-wave $\pi\pi$ decay products — 20 different solutions are given — than on D_s^+ fit fractions.			
VALUE (units 10 ⁻²)	DOCUMENT ID	TECN	COMMENT
84.7 ± 0.6 OUR AVERAGE			
84.97 ± 0.14 ± 0.30 ± 0.63	1,2	AAIJ	23AN LHCB Dalitz fit, 0.7M events
84.2 ± 0.8 ± 1.2	2	ABLIKIM	22Bi BES3 Dalitz fit, 11.1k events

83.0 ± 0.9 ± 1.9	2	AUBERT	09o BABR Dalitz fit, $\approx 10.5k$ evts
87.04 ± 5.60 ± 4.38	3	LINK	04 FOCS Dalitz fit, 1475 ± 50 evts

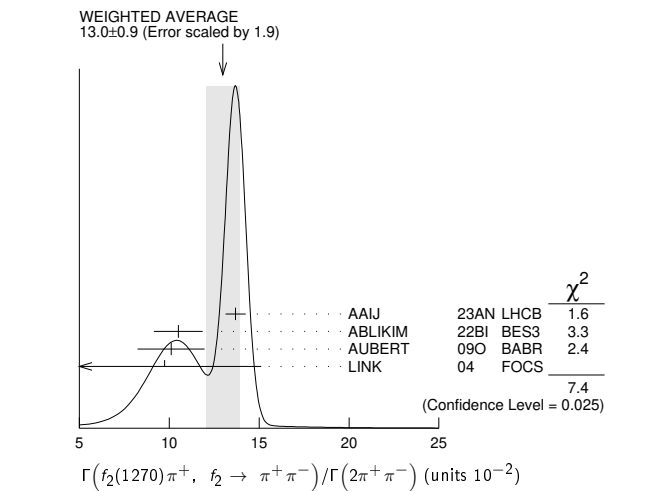
¹ The last error reflects the uncertainty due to the amplitude model.
² AAJ 23AN, ABLIKIM 22Bi, and AUBERT 09o give the amplitude and phase of the $\pi^+ \pi^-$ S-wave in bins of $\pi^+ \pi^-$ invariant-mass. (50 bins for AAJ 23AN, 29 for ABLIKIM 22Bi and AUBERT 09o.)
³ LINK 04 borrows a K-matrix parametrization from ANISOVICH 03 of the full $\pi-\pi$ S-wave isoscalar scattering amplitude to describe the $\pi^+ \pi^-$ S-wave component of the $\pi^+ \pi^+ \pi^-$ state. The fit fraction given above is a sum over five f_0 mesons, the $f_0(980)$, $f_0(1300)$, $f_0(1200-1600)$, $f_0(1500)$, and $f_0(1750)$. See LINK 04 for details and discussion.

$\Gamma(f_0(980) \pi^+, f_0 \rightarrow \pi^+ \pi^-)/\Gamma(2\pi^+ \pi^-)$ Γ_{97}/Γ_{94}			
This is the "fit fraction" from the Dalitz-plot analysis. See above for the full $\pi^+ (\pi^+ \pi^-)_{S\text{-wave}}$ fit fraction.			
VALUE	DOCUMENT ID	TECN	COMMENT
• • • We do not use the following data for averages, fits, limits, etc. • • •			
0.565 ± 0.043 ± 0.047		AITALA	01A E791 Dalitz fit, 848 evts
1.074 ± 0.140 ± 0.043		FRABETTI	97D E687 γ Be ≈ 200 GeV

$\Gamma(f_0(1370) \pi^+, f_0 \rightarrow \pi^+ \pi^-)/\Gamma(2\pi^+ \pi^-)$ Γ_{98}/Γ_{94}			
This is the "fit fraction" from the Dalitz-plot analysis. See above for the full $\pi^+ (\pi^+ \pi^-)_{S\text{-wave}}$ fit fraction.			
VALUE	DOCUMENT ID	TECN	COMMENT
• • • We do not use the following data for averages, fits, limits, etc. • • •			
0.324 ± 0.077 ± 0.017		AITALA	01A E791 Dalitz fit, 848 evts

$\Gamma(f_0(1500) \pi^+, f_0 \rightarrow \pi^+ \pi^-)/\Gamma(2\pi^+ \pi^-)$ Γ_{99}/Γ_{94}			
This is the "fit fraction" from the Dalitz-plot analysis. See above for the full $\pi^+ (\pi^+ \pi^-)_{S\text{-wave}}$ fit fraction.			
VALUE	DOCUMENT ID	TECN	COMMENT
• • • We do not use the following data for averages, fits, limits, etc. • • •			
0.274 ± 0.114 ± 0.019	1	FRABETTI	97D E687 γ Be ≈ 200 GeV
¹ FRABETTI 97D calls this mode $S(1475) \pi^+$, but finds the mass and width of this $S(1475)$ to be in excellent agreement with those of the $f_0(1500)$.			

$\Gamma(f_2(1270) \pi^+, f_2 \rightarrow \pi^+ \pi^-)/\Gamma(2\pi^+ \pi^-)$ Γ_{100}/Γ_{94}			
This is the "fit fraction" from the Dalitz-plot analysis.			
VALUE (units 10 ⁻²)	DOCUMENT ID	TECN	COMMENT
13.0 ± 0.9 OUR AVERAGE			Error includes scale factor of 1.9. See the ideogram below.
13.69 ± 0.14 ± 0.22 ± 0.49	1	AAIJ	23AN LHCB Dalitz fit, 0.7M events
10.5 ± 0.8 ± 1.1		ABLIKIM	22Bi BES3 Dalitz fit, 11.1k events
10.1 ± 1.5 ± 1.1		AUBERT	09o BABR Dalitz fit, $\approx 10.5k$ evts
9.74 ± 4.49 ± 2.94		LINK	04 FOCS Dalitz fit, 1475 ± 50 evts
• • • We do not use the following data for averages, fits, limits, etc. • • •			
19.7 ± 3.3 ± 0.6		AITALA	01A E791 Dalitz fit, 848 evts
12.3 ± 5.6 ± 1.8		FRABETTI	97D E687 γ Be ≈ 200 GeV
¹ The last error reflects the uncertainty on the amplitude model.			



$\Gamma(f_2'(1525)^0 \pi^+, f_2' \rightarrow \pi^+ \pi^-)/\Gamma(2\pi^+ \pi^-)$ Γ_{101}/Γ_{94}			
VALUE (units 10 ⁻⁴)	DOCUMENT ID	TECN	COMMENT
5.28 ± 0.70 ± 1.50 ± 0.87	1	AAIJ	23AN LHCB Dalitz fit, 0.7M events
¹ The last error reflects the uncertainty on the amplitude model.			

$\Gamma(\rho(1450)^0 \pi^+, \rho^0 \rightarrow \pi^+ \pi^-)/\Gamma(2\pi^+ \pi^-)$ Γ_{102}/Γ_{94}			
This is the "fit fraction" from the Dalitz-plot analysis.			
VALUE (units 10 ⁻²)	DOCUMENT ID	TECN	COMMENT
1.7 ± 0.6 OUR AVERAGE			
3.86 ± 0.15 ± 0.14 ± 2.0	1	AAIJ	23AN LHCB Dalitz fit, 0.7M events
1.3 ± 0.4 ± 0.5		ABLIKIM	22Bi BES3 Dalitz fit, 11.1k events
2.3 ± 0.8 ± 1.7		AUBERT	09o BABR Dalitz fit, $\approx 10.5k$ evts
6.56 ± 3.43 ± 4.40		LINK	04 FOCS Dalitz fit, 1475 ± 50 evts

Meson Particle Listings

 D_S^\pm

• • • We do not use the following data for averages, fits, limits, etc. • • •

4.4 ± 2.1 ± 0.2 AITALA 01A E791 Dalitz fit, 848 evts

¹ The last error reflects the uncertainty on the amplitude model.

$\Gamma(\rho(1700)^0 \pi^+, \rho^0 \rightarrow \pi^+ \pi^-) / \Gamma(2\pi^+ \pi^-)$ $\Gamma_{103} / \Gamma_{94}$

VALUE (units 10 ⁻³)	DOCUMENT ID	TECN	COMMENT
3.65 ± 0.50 ± 0.45 ± 3.40	¹ AAIJ	23AN	LHCB Dalitz fit, 0.7M events

¹ The last error reflects the uncertainty on the amplitude model.

$\Gamma(\pi^+ 2\pi^0) / \Gamma_{total}$ Γ_{104} / Γ

VALUE (%)	EVTs	DOCUMENT ID	TECN	COMMENT
0.52 ± 0.05 OUR AVERAGE				Error includes scale factor of 1.1.
0.50 ± 0.04 ± 0.02	590	ABLIKIM	22Z	BES3 e ⁺ e ⁻ at 4.178–4.226 GeV
0.65 ± 0.13 ± 0.03	72 ± 16	NAIK	09A	CLEO e ⁺ e ⁻ at 4170 MeV

$\Gamma(f_0(980)\pi^+, f_0 \rightarrow \pi^0 \pi^0) / \Gamma(\pi^+ 2\pi^0)$ $\Gamma_{105} / \Gamma_{104}$

This is a "fit fraction" from an amplitude analysis.

VALUE (units 10 ⁻²)	DOCUMENT ID	TECN	COMMENT
55.4 ± 6.8 ± 7.3	ABLIKIM	22Z	BES3 Dalitz plot fit, 440 evts

$\Gamma(f_0(1370)\pi^+, f_0 \rightarrow \pi^0 \pi^0) / \Gamma(\pi^+ 2\pi^0)$ $\Gamma_{106} / \Gamma_{104}$

This is a "fit fraction" from an amplitude analysis.

VALUE (units 10 ⁻²)	DOCUMENT ID	TECN	COMMENT
25.5 ± 5.1 ± 9.3	ABLIKIM	22Z	BES3 Dalitz plot fit, 440 evts

$\Gamma(f_2(1270)\pi^+, f_2 \rightarrow \pi^0 \pi^0) / \Gamma(\pi^+ 2\pi^0)$ $\Gamma_{107} / \Gamma_{104}$

This is a "fit fraction" from an amplitude analysis.

VALUE (units 10 ⁻²)	DOCUMENT ID	TECN	COMMENT
9.7 ± 2.9 ± 6.0	ABLIKIM	22Z	BES3 Dalitz plot fit, 440 evts

$\Gamma(2\pi^+ \pi^- \pi^0) / \Gamma(\phi \pi^+)$ $\Gamma_{108} / \Gamma_{48}$

VALUE	CL%	DOCUMENT ID	TECN	COMMENT
<3.3	90	ANJOS	89E	E691 Photoproduction

• • • We do not use the following data for averages, fits, limits, etc. • • •

$\Gamma(\eta \pi^+) / \Gamma_{total}$ Γ_{109} / Γ

Unseen decay modes of the η are included.

VALUE (%)	EVTs	DOCUMENT ID	TECN	COMMENT
1.67 ± 0.09 OUR FIT				Error includes scale factor of 1.1.
1.71 ± 0.08 OUR AVERAGE				
1.67 ± 0.08 ± 0.06		ONYISI	13	CLEO e ⁺ e ⁻ at 4.17 GeV
1.82 ± 0.14 ± 0.07	0.8k	ZUPANC	13	BELL e ⁺ e ⁻ at $\Upsilon(4S)$, $\Upsilon(5S)$

• • • We do not use the following data for averages, fits, limits, etc. • • •

1.58 ± 0.11 ± 0.18 ¹ALEXANDER 08 CLEO See ONYISI 13

¹ALEXANDER 08 uses single- and double-tagged events in an overall fit.

$\Gamma(\eta \pi^+) / \Gamma(K^+ K_S^0)$ $\Gamma_{109} / \Gamma_{44}$

Unseen decay modes of the η are included.

VALUE	EVTs	DOCUMENT ID	TECN	COMMENT
1.15 ± 0.07 OUR FIT				Error includes scale factor of 1.1.

• • • We do not use the following data for averages, fits, limits, etc. • • •

1.236 ± 0.043 ± 0.063 2587 ± 89 MENDEZ 10 CLEO See ONYISI 13

$\Gamma(\eta \pi^+) / \Gamma(K^+ K^- \pi^+)$ $\Gamma_{109} / \Gamma_{47}$

VALUE (units 10 ⁻²)	EVTs	DOCUMENT ID	TECN	COMMENT
31.94 ± 0.33 ± 0.49	19.5k	ABLIKIM	20R	BES3 e ⁺ e ⁻ , 4178 ~ 4226 MeV

$\Gamma(\eta \pi^+) / \Gamma(\phi \pi^+)$ $\Gamma_{109} / \Gamma_{48}$

Unseen decay modes of the resonances are included.

VALUE	EVTs	DOCUMENT ID	TECN	COMMENT
0.48 ± 0.03 ± 0.04	920	JESSOP	98	CLE2 e ⁺ e ⁻ ≈ $\Upsilon(4S)$
0.54 ± 0.09 ± 0.06	165	ALEXANDER	92	CLE2 See JESSOP 98

• • • We do not use the following data for averages, fits, limits, etc. • • •

$\Gamma(\eta \pi^+) / \Gamma(\phi \pi^+, \phi \rightarrow K^+ K^-)$ $\Gamma_{109} / \Gamma_{49}$

VALUE (%)	EVTs	DOCUMENT ID	TECN	COMMENT
84.80 ± 0.47 ± 2.64	22k	GUAN	21	BELL e ⁺ e ⁻ ≈ $\Upsilon(4,5S)$

$\Gamma(\omega \pi^+) / \Gamma_{total}$ Γ_{110} / Γ

Unseen decay modes of the ω are included.

VALUE (%)	EVTs	DOCUMENT ID	TECN	COMMENT
0.192 ± 0.030 OUR FIT				
0.181 ± 0.032 OUR AVERAGE				
0.177 ± 0.032 ± 0.013	65 ± 12	ABLIKIM	19AH	BES3 e ⁺ e ⁻ at 4.178 GeV
0.21 ± 0.09 ± 0.01	6 ± 2.4	GE	09A	CLEO e ⁺ e ⁻ at 4170 MeV

$\Gamma(\omega \pi^+) / \Gamma(\eta \pi^+)$ $\Gamma_{110} / \Gamma_{109}$

Unseen decay modes of the resonances are included.

VALUE	DOCUMENT ID	TECN	COMMENT
0.115 ± 0.018 OUR FIT			
0.16 ± 0.04 ± 0.03	BALEST	97	CLE2 e ⁺ e ⁻ ≈ $\Upsilon(4S)$

$\Gamma(3\pi^+ 2\pi^-) / \Gamma(K^+ K^- \pi^+)$ $\Gamma_{112} / \Gamma_{47}$

VALUE	EVTs	DOCUMENT ID	TECN	COMMENT
0.146 ± 0.014 OUR AVERAGE				
0.145 ± 0.011 ± 0.010	671	LINK	03D	FOCS γ A, $\overline{E}_\gamma \approx 180$ GeV
0.158 ± 0.042 ± 0.031	37	FRABETTI	97C	E687 γ Be, $\overline{E}_\gamma \approx 200$ GeV

$\Gamma(\eta \rho^+) / \Gamma_{total}$ Γ_{114} / Γ

Unseen decay modes of the η are included.

VALUE (%)	EVTs	DOCUMENT ID	TECN	COMMENT
8.9 ± 0.6 ± 0.5	328 ± 22	NAIK	09A	CLEO $\eta \rightarrow 2\gamma$

$\Gamma(\eta \rho^+) / \Gamma(\phi \pi^+)$ $\Gamma_{114} / \Gamma_{48}$

Unseen decay modes of the resonances are included.

VALUE	EVTs	DOCUMENT ID	TECN	COMMENT
2.98 ± 0.20 ± 0.39	447	JESSOP	98	CLE2 e ⁺ e ⁻ ≈ $\Upsilon(4S)$
2.86 ± 0.38 ± 0.36	217	AVERY	92	CLE2 See JESSOP 98

• • • We do not use the following data for averages, fits, limits, etc. • • •

$\Gamma(\eta \rho^+) / \Gamma(\eta \pi^+ \pi^0)$ $\Gamma_{114} / \Gamma_{115}$

VALUE (units 10 ⁻²)	EVTs	DOCUMENT ID	TECN	COMMENT
78.3 ± 5.0 ± 2.1	1.2k	ABLIKIM	19BE	BES3 $\eta \pi^+ \pi^0$ amplitude analysis

$\Gamma(\eta \pi^+ \pi^0) / \Gamma_{total}$ Γ_{115} / Γ

VALUE (%)	EVTs	DOCUMENT ID	TECN	COMMENT
9.5 ± 0.5 OUR AVERAGE				
9.50 ± 0.28 ± 0.41	2.6k	ABLIKIM	19BE	BES3 e ⁺ e ⁻ at 4.178 GeV
9.2 ± 0.4 ± 1.1		ONYISI	13	CLEO e ⁺ e ⁻ at 4.17 GeV

$\Gamma(\eta(\pi^+ \pi^0)_{P-wave}) / \Gamma(\eta \pi^+ \pi^0)$ $\Gamma_{116} / \Gamma_{115}$

VALUE (units 10 ⁻²)	EVTs	DOCUMENT ID	TECN	COMMENT
5.4 ± 2.1 ± 2.5	1.2k	ABLIKIM	19BE	BES3 $\eta \pi^+ \pi^0$ amplitude analysis

$\Gamma(a_0(980)^+ \pi^0, a_0(980)^+ \rightarrow \eta \pi^+) / \Gamma(\eta \pi^+ \pi^0)$ $\Gamma_{117} / \Gamma_{115}$

VALUE (units 10 ⁻²)	EVTs	DOCUMENT ID	TECN	COMMENT
23.2 ± 2.3 ± 3.3	1.2k	¹ ABLIKIM	19BE	BES3 $\eta \pi^+ \pi^0$ amplitude analysis

¹ Coherent sum of $D_S^+ \rightarrow a_0^+ \pi^0 \rightarrow \eta \pi^+ \pi^0$ and $D_S^+ \rightarrow a_0^0 \pi^+ \rightarrow \eta \pi^+ \pi^0$. ABLIKIM19BE find $a_0(980)^0 - f(980)$ mixing effects negligibly small in this $D_S^+ \rightarrow \eta \pi^+ \pi^0$ Dalitz plot analysis.

$\Gamma(\omega \pi^+ \pi^0) / \Gamma_{total}$ Γ_{118} / Γ

Unseen decay modes of the ω are included.

VALUE (%)	EVTs	DOCUMENT ID	TECN	COMMENT
2.78 ± 0.65 ± 0.25	34 ± 7.9	GE	09A	CLEO e ⁺ e ⁻ at 4170 MeV

$\Gamma(2\pi^+ \pi^- \eta) / \Gamma_{total}$ Γ_{119} / Γ

VALUE (units 10 ⁻²)	EVTs	DOCUMENT ID	TECN	COMMENT
3.12 ± 0.13 ± 0.09	2.1k	ABLIKIM	21AR	BES3 e ⁺ e ⁻ at 4.178–4.226 GeV

$\Gamma(a_1(1260)^+ \eta, a_1^+ \rightarrow \rho(770)^0 \pi^+, \rho^0 \rightarrow \pi^+ \pi^-) / \Gamma(2\pi^+ \pi^- \eta)$ $\Gamma_{120} / \Gamma_{119}$

VALUE (units 10 ⁻²)	DOCUMENT ID	TECN	COMMENT
55.4 ± 3.9 ± 2.0	¹ ABLIKIM	21AR	BES3 e ⁺ e ⁻ at 4.178–4.226 GeV

¹ $D_S^+ \rightarrow 2\pi^+ \pi^- \eta$ amplitude analysis with 11 components.

$\Gamma(a_1(1260)^+ \eta, a_1^+ \rightarrow f_0(500)\pi^+, f_0 \rightarrow \pi^+ \pi^-) / \Gamma(2\pi^+ \pi^- \eta)$ $\Gamma_{121} / \Gamma_{119}$

VALUE (units 10 ⁻²)	DOCUMENT ID	TECN	COMMENT
8.1 ± 1.9 ± 2.1	¹ ABLIKIM	21AR	BES3 e ⁺ e ⁻ at 4.178–4.226 GeV

¹ $D_S^+ \rightarrow 2\pi^+ \pi^- \eta$ amplitude analysis with 11 components.

$\Gamma(a_0(980)^+ \rho(770)^0, a_0^+ \rightarrow \eta \pi^+) / \Gamma(2\pi^+ \pi^- \eta)$ $\Gamma_{122} / \Gamma_{119}$

VALUE (units 10 ⁻²)	DOCUMENT ID	TECN	COMMENT
6.7 ± 2.5 ± 1.5	¹ ABLIKIM	21AR	BES3 e ⁺ e ⁻ at 4.178–4.226 GeV

¹ $D_S^+ \rightarrow 2\pi^+ \pi^- \eta$ amplitude analysis with 11 components.

$\Gamma(\eta(1405)\pi^+, \eta(1405) \rightarrow a_0(980)^- \pi^+, a_0^- \rightarrow \eta \pi^-) / \Gamma(2\pi^+ \pi^- \eta)$ $\Gamma_{123} / \Gamma_{119}$

VALUE (units 10 ⁻²)	DOCUMENT ID	TECN	COMMENT
0.7 ± 0.2 ± 0.1	¹ ABLIKIM	21AR	BES3 e ⁺ e ⁻ at 4.178–4.226 GeV

¹ $D_S^+ \rightarrow 2\pi^+ \pi^- \eta$ amplitude analysis with 11 components.

$\Gamma(\eta(1405)\pi^+, \eta(1405) \rightarrow a_0(980)^+ \pi^-, a_0^+ \rightarrow \eta \pi^+) / \Gamma(2\pi^+ \pi^- \eta)$ $\Gamma_{124} / \Gamma_{119}$

VALUE (units 10 ⁻²)	DOCUMENT ID	TECN	COMMENT
0.7 ± 0.2 ± 0.1	¹ ABLIKIM	21AR	BES3 e ⁺ e ⁻ at 4.178–4.226 GeV

¹ $D_S^+ \rightarrow 2\pi^+ \pi^- \eta$ amplitude analysis with 11 components.

$\Gamma(f_1(1420)\pi^+, f_1 \rightarrow a_0(980)^-\pi^+, a_0^- \rightarrow \eta\pi^-)/\Gamma(2\pi^+\pi^-\eta)$ $\Gamma_{125}/\Gamma_{119}$

VALUE (units 10^{-2})	DOCUMENT ID	TECN	COMMENT
1.9 ± 0.5 ± 0.3	¹ ABLIKIM	21AR	BES3 e^+e^- at 4.178–4.226 GeV
¹ $D_s^+ \rightarrow 2\pi^+\pi^-\eta$ amplitude analysis with 11 components.			

 $\Gamma(f_1(1420)\pi^+, f_1 \rightarrow a_0(980)^+\pi^-, a_0^0 \rightarrow \eta\pi^+)/\Gamma(2\pi^+\pi^-\eta)$ $\Gamma_{126}/\Gamma_{119}$

VALUE (units 10^{-2})	DOCUMENT ID	TECN	COMMENT
1.7 ± 0.5 ± 0.3	¹ ABLIKIM	21AR	BES3 e^+e^- at 4.178–4.226 GeV
¹ $D_s^+ \rightarrow 2\pi^+\pi^-\eta$ amplitude analysis with 11 components.			

 $\Gamma(3\pi^+2\pi^-\pi^0)/\Gamma_{total}$ Γ_{127}/Γ

VALUE	DOCUMENT ID	TECN	COMMENT
0.049 ± 0.033 -0.030	BARLAG	92c	ACCM π^- 230 GeV

 $\Gamma(\omega(2\pi^+\pi^-))/\Gamma_{total}$ Γ_{128}/Γ

VALUE (%)	EVTS	DOCUMENT ID	TECN	COMMENT
1.58 ± 0.45 ± 0.09	29 ± 8.2	GE	09A	CLEO e^+e^- at 4170 MeV

 $\Gamma(\eta'(958)\pi^+)/\Gamma_{total}$ Γ_{129}/Γ

VALUE (%)	DOCUMENT ID	TECN	COMMENT
3.94 ± 0.15 ± 0.20	ONYISI	13	CLEO e^+e^- at 4.17 GeV
• • • We do not use the following data for averages, fits, limits, etc. • • •			
3.77 ± 0.25 ± 0.30	¹ ALEXANDER	08	CLEO See ONYISI 13
¹ ALEXANDER 08 uses single- and double-tagged events in an overall fit.			

 $\Gamma(\eta'(958)\pi^+)/\Gamma(K^+K_S^0)$ Γ_{129}/Γ_{44}

VALUE	EVTS	DOCUMENT ID	TECN	COMMENT
2.654 ± 0.088 ± 0.139	1436 ± 47	MENDEZ	10	CLEO See ONYISI 13

 $\Gamma(\eta'(958)\pi^+)/\Gamma(K^+K^-\pi^+)$ Γ_{129}/Γ_{47}

VALUE (units 10^{-2})	EVTS	DOCUMENT ID	TECN	COMMENT
69.4 ± 0.8 ± 3.8	9.9k	ABLIKIM	20R	BES3 e^+e^- , 4178 ~ 4226 MeV

 $\Gamma(\eta'(958)\pi^+)/\Gamma(\phi\pi^+)$ Γ_{129}/Γ_{48}

VALUE	EVTS	DOCUMENT ID	TECN	COMMENT
• • • We do not use the following data for averages, fits, limits, etc. • • •				
1.03 ± 0.06 ± 0.07	537	JESSOP	98	CLE2 $e^+e^- \approx \Upsilon(4S)$
1.20 ± 0.15 ± 0.11	281	ALEXANDER	92	CLE2 See JESSOP 98
2.5 ± 1.0 ^{+1.5} _{-0.4}	22	ALVAREZ	91	NA14 Photoproduction
2.5 ± 0.5 ± 0.3	215	ALBRECHT	90d	ARG $e^+e^- \approx 10.4$ GeV

 $\Gamma(\omega\eta\pi^+)/\Gamma_{total}$ Γ_{131}/Γ

VALUE (units 10^{-3})	CL%	EVTS	DOCUMENT ID	TECN	COMMENT
5.4 ± 1.2 ± 0.4		78	ABLIKIM	23AL	BES3 e^+e^- at 4.128–4.226 GeV
• • • We do not use the following data for averages, fits, limits, etc. • • •					
<21.3		90	GE	09A	CLEO e^+e^- at 4170 MeV

 $\Gamma(\eta'(958)\rho^+)/\Gamma_{total}$ Γ_{132}/Γ

VALUE (%)	DOCUMENT ID	TECN	COMMENT
5.8 ± 1.4 ± 0.4	ABLIKIM	15Z	BES3 482 pb ⁻¹ , 4009 MeV

 $\Gamma(\eta'(958)\rho^+)/\Gamma(\phi\pi^+)$ Γ_{132}/Γ_{48}

VALUE	EVTS	DOCUMENT ID	TECN	COMMENT
• • • We do not use the following data for averages, fits, limits, etc. • • •				
2.78 ± 0.28 ± 0.30	137	¹ JESSOP	98	CLE2 $e^+e^- \approx \Upsilon(4S)$
3.44 ± 0.62 ^{+0.44} _{-0.46}	68	AVERY	92	CLE2 See JESSOP 98

¹ This JESSOP 98 fraction, when combined with other η' fractions, greatly overshoots the inclusive η' fraction. See the measurement just above, which fits nicely.

 $\Gamma(\eta'(958)\rho^+)/\Gamma(\eta'(958)\pi^+\pi^0)$ $\Gamma_{132}/\Gamma_{133}$

VALUE	EVTS	DOCUMENT ID	TECN	COMMENT
• • • We do not use the following data for averages, fits, limits, etc. • • •				
≈ 1	395	¹ ABLIKIM	22AA	BES3 e^+e^- at 4.178–4.226 GeV

¹ Result of an amplitude analysis of $D_s^+ \rightarrow \pi^+\pi^0\eta'$ which found that $D_s^+ \rightarrow \rho^+\eta'$ is the dominant decay mode, with other contributions negligible. No uncertainty is assigned to this 100% fit fraction; however, the fit fractions of non-resonant contributions are shown to be below 1%.

 $\Gamma(\eta'(958)\pi^+\pi^0)/\Gamma_{total}$ Γ_{133}/Γ

VALUE (%)	EVTS	DOCUMENT ID	TECN	COMMENT
6.08 ± 0.29 OUR AVERAGE				
6.15 ± 0.25 ± 0.18	837	¹ ABLIKIM	22AA	BES3 e^+e^- at 4.178–4.226 GeV
5.6 ± 0.5 ± 0.6		ONYISI	13	CLEO e^+e^- at 4.17 GeV

¹ An amplitude analysis in the same publication finds that $D_s^+ \rightarrow \rho^+\eta'$ is the only statistically significant contribution to this decay.

 $\Gamma(\eta'(958)\pi^+\pi^0 \text{ nonresonant})/\Gamma_{total}$ Γ_{134}/Γ

VALUE	CL%	DOCUMENT ID	TECN	COMMENT
<5.1 × 10⁻²	90	ABLIKIM	15Z	BES3 482 pb ⁻¹ , 4009 MeV

Modes with one or three K's

 $\Gamma(K^+\pi^0)/\Gamma(K^+K_S^0)$ Γ_{135}/Γ_{44}

VALUE (units 10^{-2})	EVTS	DOCUMENT ID	TECN	COMMENT
4.2 ± 1.4 ± 0.2	202 ± 70	MENDEZ	10	CLEO e^+e^- at 4170 MeV
• • • We do not use the following data for averages, fits, limits, etc. • • •				
5.5 ± 1.3 ± 0.7	141 ± 34	ADAMS	07A	CLEO See MENDEZ 10

 $\Gamma(K^+\pi^0)/\Gamma(K^+K^-\pi^+)$ Γ_{135}/Γ_{47}

VALUE (units 10^{-3})	EVTS	DOCUMENT ID	TECN	COMMENT
13.73 ± 0.90 ± 0.33	2.3k	ABLIKIM	20R	BES3 e^+e^- , 4178 ~ 4226 MeV

 $\Gamma(K^+\pi^0)/\Gamma(\phi\pi^+, \phi \rightarrow K^+K^-)$ Γ_{135}/Γ_{49}

VALUE (%)	EVTS	DOCUMENT ID	TECN	COMMENT
3.28 ± 0.23 ± 0.13	12k	GUAN	21	BELL $e^+e^- \approx \Upsilon(4,5S)$

 $\Gamma(K_S^0\pi^+)/\Gamma(K^+K_S^0)$ Γ_{136}/Γ_{44}

VALUE (units 10^{-2})	EVTS	DOCUMENT ID	TECN	COMMENT
8.12 ± 0.28 OUR AVERAGE				
8.5 ± 0.7 ± 0.2	393 ± 33	MENDEZ	10	CLEO e^+e^- at 4170 MeV
8.03 ± 0.24 ± 0.19	17.6k ± 481	WON	09	BELL e^+e^- at $\Upsilon(4S)$
10.4 ± 2.4 ± 1.4	113 ± 26	LINK	08	FOCS γA , $E_\gamma \approx 180$ GeV
• • • We do not use the following data for averages, fits, limits, etc. • • •				
8.2 ± 0.9 ± 0.2	206 ± 22	ADAMS	07A	CLEO See MENDEZ 10

 $\Gamma(K_S^0\pi^+)/\Gamma(K^+K^-\pi^+)$ Γ_{136}/Γ_{47}

VALUE (units 10^{-3})	EVTS	DOCUMENT ID	TECN	COMMENT
20.35 ± 0.62 ± 0.42	2.7k	ABLIKIM	20R	BES3 e^+e^- , 4178 ~ 4226 MeV

 $\Gamma(K^+\eta)/\Gamma(K^+K_S^0)$ Γ_{137}/Γ_{44}

VALUE (units 10^{-2})	EVTS	DOCUMENT ID	TECN	COMMENT
Unseen decay modes of the η are included.				
11.8 ± 2.2 ± 0.6	222 ± 41	MENDEZ	10	CLEO e^+e^- at 4170 MeV

 $\Gamma(K^+\eta)/\Gamma(K^+K^-\pi^+)$ Γ_{137}/Γ_{47}

VALUE (units 10^{-2})	EVTS	DOCUMENT ID	TECN	COMMENT
2.97 ± 0.18 ± 0.06	1.8k	ABLIKIM	20R	BES3 e^+e^- , 4178 ~ 4226 MeV

 $\Gamma(K^+\eta)/\Gamma(\phi\pi^+, \phi \rightarrow K^+K^-)$ Γ_{137}/Γ_{49}

VALUE (%)	EVTS	DOCUMENT ID	TECN	COMMENT
7.81 ± 0.22 ± 0.24	14k	GUAN	21	BELL $e^+e^- \approx \Upsilon(4,5S)$

 $\Gamma(K^+\eta)/\Gamma(\eta\pi^+)$ $\Gamma_{137}/\Gamma_{109}$

VALUE (units 10^{-2})	EVTS	DOCUMENT ID	TECN	COMMENT
• • • We do not use the following data for averages, fits, limits, etc. • • •				
8.9 ± 1.5 ± 0.4	113 ± 18	ADAMS	07A	CLEO See MENDEZ 10

 $\Gamma(K^+\omega)/\Gamma_{total}$ Γ_{138}/Γ

VALUE (units 10^{-4})	CL%	EVTS	DOCUMENT ID	TECN	COMMENT
Unseen decay modes of the ω are included.					
9.9 ± 1.5 OUR FIT					
8.7 ± 2.4 ± 0.8		29	¹ ABLIKIM	19AH	BES3 e^+e^- at 4.178 GeV
• • • We do not use the following data for averages, fits, limits, etc. • • •					
<24		90	GE	09A	CLEO e^+e^- at 4170 MeV

¹ Evidence for mode at 4.4 σ .

 $\Gamma(K^+\omega)/\Gamma(K^+\pi^+\pi^-\pi^0)$ $\Gamma_{138}/\Gamma_{158}$

VALUE (units 10^{-2})	DOCUMENT ID	TECN	COMMENT
10.3 ± 1.5 OUR FIT			
10.9 ± 1.8 ± 0.1	¹ ABLIKIM	22BL	BES3 PWA, 550 $D_s^\pm \rightarrow K^\pm\pi^\pm\pi^0\pi^0$
¹ ABLIKIM 22BL reports $[\Gamma(D_s^+ \rightarrow K^+\omega)/\Gamma(D_s^+ \rightarrow K^+\pi^+\pi^-\pi^0)] \times [B(\omega(782) \rightarrow \pi^+\pi^-\pi^0)] = (9.7 \pm 1.5 \pm 0.6) \times 10^{-2}$ which we divide by our best value $B(\omega(782) \rightarrow \pi^+\pi^-\pi^0) = (89.2 \pm 0.7) \times 10^{-2}$. Our first error is their experiment's error and our second error is the systematic error from using our best value.			

 $\Gamma(K^+\eta'(958))/\Gamma(K^+K_S^0)$ Γ_{139}/Γ_{44}

VALUE (units 10^{-2})	EVTS	DOCUMENT ID	TECN	COMMENT
Unseen decay modes of the $\eta'(958)$ are included.				
11.8 ± 3.6 ± 0.7	56 ± 17	MENDEZ	10	CLEO e^+e^- at 4170 MeV

 $\Gamma(K^+\eta'(958))/\Gamma(K^+K^-\pi^+)$ Γ_{139}/Γ_{47}

VALUE (units 10^{-2})	EVTS	DOCUMENT ID	TECN	COMMENT
4.91 ± 0.31 ± 0.31	675	ABLIKIM	20R	BES3 e^+e^- , 4178 ~ 4226 MeV

Meson Particle Listings

 D_S^\pm $\Gamma(K^+\eta'(958))/\Gamma(\eta'(958)\pi^+)$ $\Gamma_{139}/\Gamma_{129}$

VALUE (units 10^{-2})	EVTS	DOCUMENT ID	TECN	COMMENT
$4.2 \pm 1.3 \pm 0.3$	28 ± 9	ADAMS	07A	CLEO See MENDEZ 10

 $\Gamma(K^+\pi^+\pi^-)/\Gamma_{\text{total}}$ Γ_{140}/Γ

VALUE (units 10^{-3})	EVTS	DOCUMENT ID	TECN	COMMENT
6.20 ± 0.19 OUR FIT				
6.20 ± 0.19 OUR AVERAGE				
$6.11 \pm 0.18 \pm 0.11$	1.3k	ABLIKIM	22Ac	BES3 e^+e^- at 4.178–4.226 GeV
$6.54 \pm 0.33 \pm 0.25$		ONYISI	13	CLEO e^+e^- at 4.17 GeV
$6.9 \pm 0.5 \pm 0.3$		¹ ALEXANDER	08	CLEO See ONYISI 13
		¹ ALEXANDER	08	uses single- and double-tagged events in an overall fit.

 $\Gamma(K^+\pi^+\pi^-)/\Gamma(K^+K^-\pi^+)$ Γ_{140}/Γ_{47}

VALUE	EVTS	DOCUMENT ID	TECN	COMMENT
0.115 ± 0.004 OUR FIT				Error includes scale factor of 1.1.
$0.127 \pm 0.007 \pm 0.014$	567 ± 31	LINK	04F	FOCS $\gamma A, \bar{E}_\gamma \approx 180$ GeV

 $\Gamma(K^+\rho^0)/\Gamma(K^+\pi^+\pi^-)$ $\Gamma_{141}/\Gamma_{140}$

VALUE	DOCUMENT ID	TECN	COMMENT
0.35 ± 0.04 OUR AVERAGE			
$0.321 \pm 0.037 \pm 0.037$	ABLIKIM	22Ac	BES3 Dalitz plot fit, 1.3k evts
$0.388 \pm 0.053 \pm 0.026$	LINK	04F	FOCS Dalitz plot fit, 567 evts

 $\Gamma(K^+\rho(1450)^0, \rho^0 \rightarrow \pi^+\pi^-)/\Gamma(K^+\pi^+\pi^-)$ $\Gamma_{142}/\Gamma_{140}$

VALUE	DOCUMENT ID	TECN	COMMENT
0.117 ± 0.028 OUR AVERAGE			
$0.131 \pm 0.031 \pm 0.029$	ABLIKIM	22Ac	BES3 Dalitz plot fit, 1.3k evts
$0.106 \pm 0.035 \pm 0.010$	LINK	04F	FOCS Dalitz plot fit, 567 evts

 $\Gamma(K^+f_0(500), f_0 \rightarrow \pi^+\pi^-)/\Gamma(K^+\pi^+\pi^-)$ $\Gamma_{143}/\Gamma_{140}$

VALUE (units 10^{-2})	DOCUMENT ID	TECN	COMMENT
$7.2 \pm 2.1 \pm 4.4$	ABLIKIM	22Ac	BES3 Dalitz plot fit, 1.3k evts

 $\Gamma(K^+f_0(980), f_0 \rightarrow \pi^+\pi^-)/\Gamma(K^+\pi^+\pi^-)$ $\Gamma_{144}/\Gamma_{140}$

VALUE (units 10^{-2})	DOCUMENT ID	TECN	COMMENT
$4.5 \pm 1.3 \pm 1.2$	ABLIKIM	22Ac	BES3 Dalitz plot fit, 1.3k evts

 $\Gamma(K^+f_0(1370), f_0 \rightarrow \pi^+\pi^-)/\Gamma(K^+\pi^+\pi^-)$ $\Gamma_{145}/\Gamma_{140}$

VALUE (units 10^{-2})	DOCUMENT ID	TECN	COMMENT
$19.9 \pm 2.9 \pm 9.3$	ABLIKIM	22Ac	BES3 Dalitz plot fit, 1.3k evts

 $\Gamma(K^*(892)^0\pi^+, K^*0 \rightarrow K^+\pi^-)/\Gamma(K^+\pi^+\pi^-)$ $\Gamma_{146}/\Gamma_{140}$

VALUE	DOCUMENT ID	TECN	COMMENT
0.27 ± 0.04 OUR AVERAGE			Error includes scale factor of 2.0.
$0.302 \pm 0.018 \pm 0.020$	ABLIKIM	22Ac	BES3 Dalitz plot fit, 1.3k evts
$0.2164 \pm 0.0321 \pm 0.0114$	LINK	04F	FOCS Dalitz plot fit, 567 evts

 $\Gamma(K^*(1410)^0\pi^+, K^*0 \rightarrow K^+\pi^-)/\Gamma(K^+\pi^+\pi^-)$ $\Gamma_{147}/\Gamma_{140}$

VALUE	DOCUMENT ID	TECN	COMMENT
0.10 ± 0.07 OUR AVERAGE			Error includes scale factor of 2.7.
$0.045 \pm 0.021 \pm 0.025$	ABLIKIM	22Ac	BES3 Dalitz plot fit, 1.3k evts
$0.1882 \pm 0.0403 \pm 0.0122$	LINK	04F	FOCS Dalitz plot fit, 567 evts

 $\Gamma(K^*(1430)^0\pi^+, K^*0 \rightarrow K^+\pi^-)/\Gamma(K^+\pi^+\pi^-)$ $\Gamma_{148}/\Gamma_{140}$

VALUE	DOCUMENT ID	TECN	COMMENT
0.15 ± 0.05 OUR AVERAGE			Error includes scale factor of 1.7.
$0.185 \pm 0.025 \pm 0.026$	ABLIKIM	22Ac	BES3 Dalitz plot fit, 1.3k evts
$0.0765 \pm 0.0500 \pm 0.0170$	LINK	04F	FOCS Dalitz plot fit, 567 evts

 $\Gamma(K^+\pi^+\pi^- \text{ nonresonant})/\Gamma(K^+\pi^+\pi^-)$ $\Gamma_{149}/\Gamma_{140}$

VALUE	DOCUMENT ID	TECN	COMMENT
$0.1588 \pm 0.0492 \pm 0.0153$	LINK	04F	FOCS Dalitz fit, 567 evts

 $\Gamma(K_S^0\pi^+\pi^0)/\Gamma_{\text{total}}$ Γ_{151}/Γ

VALUE (units 10^{-3})	EVTS	DOCUMENT ID	TECN	COMMENT
5.38 ± 0.32 OUR AVERAGE				
$5.43 \pm 0.30 \pm 0.15$	666	¹ ABLIKIM	21AB	BES3 e^+e^- at 4.178–4.226 GeV
$5.0 \pm 0.9 \pm 0.2$	44	² NAIK	09A	CLEO e^+e^- at 4170 MeV

¹ABLIKIM 21AB uses an amplitude analysis with 5 resonant modes plus one background component.

²NAIK 09A reports $B(D_S^+ \rightarrow K^0\pi^+\pi^-) = (1.00 \pm 0.18 \pm 0.04) \times 10^{-2}$ which we have divided by 2.

 $\Gamma(K_S^0\rho(770)^+, \rho^+ \rightarrow \pi^+\pi^0)/\Gamma(K_S^0\pi^+\pi^0)$ $\Gamma_{152}/\Gamma_{151}$

VALUE (units 10^{-2})	EVTS	DOCUMENT ID	TECN	COMMENT
$50.2 \pm 7.2 \pm 3.9$	666	¹ ABLIKIM	21AB	BES3 e^+e^- at 4.178–4.226 GeV

¹ABLIKIM 21AB uses an amplitude analysis with 5 resonant modes plus one background component.

 $\Gamma(K_S^0\rho(1450)^+, \rho^+ \rightarrow \pi^+\pi^0)/\Gamma(K_S^0\pi^+\pi^0)$ $\Gamma_{153}/\Gamma_{151}$

VALUE (units 10^{-2})	EVTS	DOCUMENT ID	TECN	COMMENT
$20.4 \pm 4.3 \pm 4.4$	666	¹ ABLIKIM	21AB	BES3 e^+e^- at 4.178–4.226 GeV
		¹ ABLIKIM	21AB	uses an amplitude analysis with 5 resonant modes plus one background component.

 $\Gamma(K^*(892)^0\pi^+, K^*0 \rightarrow K_S^0\pi^0)/\Gamma(K_S^0\pi^+\pi^0)$ $\Gamma_{154}/\Gamma_{151}$

VALUE (units 10^{-2})	EVTS	DOCUMENT ID	TECN	COMMENT
$8.4 \pm 2.2 \pm 0.9$	666	¹ ABLIKIM	21AB	BES3 e^+e^- at 4.178–4.226 GeV
		¹ ABLIKIM	21AB	uses an amplitude analysis with 5 resonant modes plus one background component.

 $\Gamma(K^*(892)^+\pi^0, K^{*+} \rightarrow K_S^0\pi^+)/\Gamma(K_S^0\pi^+\pi^0)$ $\Gamma_{155}/\Gamma_{151}$

VALUE (units 10^{-2})	EVTS	DOCUMENT ID	TECN	COMMENT
$4.6 \pm 1.4 \pm 0.4$	666	¹ ABLIKIM	21AB	BES3 e^+e^- at 4.178–4.226 GeV
		¹ ABLIKIM	21AB	uses an amplitude analysis with 5 resonant modes plus one background component.

 $\Gamma(K^*(1410)^0\pi^+, K^*0 \rightarrow K_S^0\pi^0)/\Gamma(K_S^0\pi^+\pi^0)$ $\Gamma_{156}/\Gamma_{151}$

VALUE (units 10^{-2})	EVTS	DOCUMENT ID	TECN	COMMENT
$3.3 \pm 1.6 \pm 0.5$	666	¹ ABLIKIM	21AB	BES3 e^+e^- at 4.178–4.226 GeV
		¹ ABLIKIM	21AB	uses an amplitude analysis with 5 resonant modes plus one background component.

 $\Gamma(K_S^02\pi^+\pi^-)/\Gamma(K_S^0K^-2\pi^+)$ Γ_{157}/Γ_{77}

VALUE	EVTS	DOCUMENT ID	TECN	COMMENT
$0.18 \pm 0.04 \pm 0.05$	179 ± 36	LINK	08	FOCS $\gamma A, \bar{E}_\gamma \approx 180$ GeV

 $\Gamma(K^+\pi^+\pi^-\pi^0)/\Gamma(K^+K^-\pi^+\pi^0)$ Γ_{158}/Γ_{68}

VALUE (units 10^{-2})	EVTS	DOCUMENT ID	TECN	COMMENT
$17.13 \pm 0.62 \pm 0.51$	26k	LI	23G	BELL e^+e^- at/near $\Upsilon(nS)$, $n=1, \dots, 5$

 $\Gamma(K^+\pi^+\pi^-\pi^0)/\Gamma_{\text{total}}$ Γ_{158}/Γ

VALUE (units 10^{-3})	EVTS	DOCUMENT ID	TECN	COMMENT
9.7 ± 0.6 OUR FIT				
$9.75 \pm 0.54 \pm 0.17$	776	ABLIKIM	22BL	BES3 e^+e^- at 4.178–4.226 GeV

 $\Gamma(K^*(892)^0\rho^+, K^*0 \rightarrow K^+\pi^-)/\Gamma(K^+\pi^+\pi^-)$ $\Gamma_{159}/\Gamma_{158}$

VALUE (units 10^{-2})	DOCUMENT ID	TECN	COMMENT
$40.5 \pm 2.8 \pm 1.5$	ABLIKIM	22BL	BES3 PWA, 550 $D_S^\pm \rightarrow K^\pm\pi^\pm\pi^+\pi^0$

 $\Gamma(K^*(892)^+\rho^0, K^{*+} \rightarrow K^+\pi^0)/\Gamma(K^+\pi^+\pi^-)$ $\Gamma_{160}/\Gamma_{158}$

VALUE (units 10^{-2})	DOCUMENT ID	TECN	COMMENT
$4.3 \pm 1.1 \pm 0.6$	ABLIKIM	22BL	BES3 PWA, 550 $D_S^\pm \rightarrow K^\pm\pi^\pm\pi^+\pi^0$

 $\Gamma(K_1(1270)^0\pi^+, K_1^0 \rightarrow K^+\rho^-)/\Gamma(K^+\pi^+\pi^-)$ $\Gamma_{161}/\Gamma_{158}$

VALUE (units 10^{-2})	DOCUMENT ID	TECN	COMMENT
$4.0 \pm 1.2 \pm 0.6$	ABLIKIM	22BL	BES3 PWA, 550 $D_S^\pm \rightarrow K^\pm\pi^\pm\pi^+\pi^0$

 $\Gamma(K_1(1400)^0\pi^+, K_1^0 \rightarrow K^*(890)^+\pi^-, K^{*+} \rightarrow K^+\pi^0)/\Gamma(K^+\pi^+\pi^-)$ $\Gamma_{162}/\Gamma_{158}$

VALUE (units 10^{-2})	DOCUMENT ID	TECN	COMMENT
$5.6 \pm 0.9 \pm 0.2$	ABLIKIM	22BL	BES3 PWA, 550 $D_S^\pm \rightarrow K^\pm\pi^\pm\pi^+\pi^0$

 $\Gamma(K_1(1400)^0\pi^+, K_1^0 \rightarrow K^*(890)^0\pi^0, K^*0 \rightarrow K^+\pi^-)/\Gamma(K^+\pi^+\pi^-)$ $\Gamma_{163}/\Gamma_{158}$

VALUE (units 10^{-2})	DOCUMENT ID	TECN	COMMENT
$6.1 \pm 0.9 \pm 0.2$	ABLIKIM	22BL	BES3 PWA, 550 $D_S^\pm \rightarrow K^\pm\pi^\pm\pi^+\pi^0$

 $\Gamma(K^+a_1(1260)^0, a_1 \rightarrow \rho^+\pi^-)/\Gamma(K^+\pi^+\pi^-)$ $\Gamma_{164}/\Gamma_{158}$

VALUE (units 10^{-2})	DOCUMENT ID	TECN	COMMENT
$1.9 \pm 0.7 \pm 0.9$	ABLIKIM	22BL	BES3 PWA, 550 $D_S^\pm \rightarrow K^\pm\pi^\pm\pi^+\pi^0$

 $\Gamma(K^+a_1(1260)^0, a_1 \rightarrow \rho^-\pi^+)/\Gamma(K^+\pi^+\pi^-)$ $\Gamma_{165}/\Gamma_{158}$

VALUE (units 10^{-2})	DOCUMENT ID	TECN	COMMENT
$1.9 \pm 0.7 \pm 0.9$	ABLIKIM	22BL	BES3 PWA, 550 $D_S^\pm \rightarrow K^\pm\pi^\pm\pi^+\pi^0$

 $\Gamma(K^+\pi^+\pi^-\pi^0 \text{ nonresonant})/\Gamma(K^+\pi^+\pi^-)$ $\Gamma_{166}/\Gamma_{158}$

VALUE (units 10^{-2})	DOCUMENT ID	TECN	COMMENT
$9.5 \pm 2.2 \pm 0.9$	ABLIKIM	22BL	BES3 PWA, 550 $D_S^\pm \rightarrow K^\pm\pi^\pm\pi^+\pi^0$

 $\Gamma((K^+\pi^0)_P \text{-wave } \rho^0)/\Gamma(K^+\pi^+\pi^-)$ $\Gamma_{167}/\Gamma_{158}$

VALUE (units 10^{-2})	DOCUMENT ID	TECN	COMMENT
$10.4 \pm 2.0 \pm 0.6$	ABLIKIM	22BL	BES3 PWA, 550 $D_S^\pm \rightarrow K^\pm\pi^\pm\pi^+\pi^0$

$\Gamma(K^+\omega\pi^0)/\Gamma_{total}$ Γ_{168}/Γ
 Unseen decay modes of the ω are included.

VALUE (%)	CL%	DOCUMENT ID	TECN	COMMENT
<0.82	90	GE	09A	CLEO e^+e^- at 4170 MeV

$\Gamma(K^+\omega\pi^+\pi^-)/\Gamma_{total}$ Γ_{169}/Γ
 Unseen decay modes of the ω are included.

VALUE (%)	CL%	DOCUMENT ID	TECN	COMMENT
<0.54	90	GE	09A	CLEO e^+e^- at 4170 MeV

$\Gamma(K^+\omega\eta)/\Gamma_{total}$ Γ_{170}/Γ
 Unseen decay modes of the ω and η are included.

VALUE (%)	CL%	DOCUMENT ID	TECN	COMMENT
<0.79	90	GE	09A	CLEO e^+e^- at 4170 MeV

$\Gamma(2K^+K^-)/\Gamma(K^+K^-\pi^+)$ Γ_{171}/Γ_{47}

VALUE (units 10^{-3})	EVTS	DOCUMENT ID	TECN	COMMENT
$4.0 \pm 0.3 \pm 0.2$	748 ± 60	DEL-AMO-SA...11G	BABR	$e^+e^- \approx \mathcal{T}(4S)$
••• We do not use the following data for averages, fits, limits, etc. •••				
$8.95 \pm 2.12 \pm 2.24$	31	LINK	02i	FOCS $\gamma A, \approx 180$ GeV

$\Gamma(\phi K^+, \phi \rightarrow K^+K^-)/\Gamma(2K^+K^-)$ $\Gamma_{172}/\Gamma_{171}$

VALUE	DOCUMENT ID	TECN	COMMENT
$0.41 \pm 0.08 \pm 0.03$	DEL-AMO-SA...11G	BABR	$e^+e^- \approx \mathcal{T}(4S)$

———— Doubly Cabibbo-suppressed modes ————

$\Gamma(2K^+\pi^-)/\Gamma(K^+K^-\pi^+)$ Γ_{173}/Γ_{47}

VALUE (units 10^{-3})	EVTS	DOCUMENT ID	TECN	COMMENT
2.371 ± 0.034 OUR AVERAGE				
$2.372 \pm 0.024 \pm 0.025$	67k	AAIJ	19G	LHCB pp at 8 TeV
$2.3 \pm 0.3 \pm 0.2$	356 ± 52	DEL-AMO-SA...11G	BABR	$e^+e^- \approx \mathcal{T}(4S)$
$2.29 \pm 0.28 \pm 0.12$	281 ± 34	KO	09	BELL e^+e^- at $\mathcal{T}(4S)$
$5.2 \pm 1.7 \pm 1.1$	27 ± 9	LINK	05k	FOCS $<0.78\%$, CL = 90%

$\Gamma(K^+K^*(892)^0, K^{*0} \rightarrow K^+\pi^-)/\Gamma(2K^+\pi^-)$ $\Gamma_{174}/\Gamma_{173}$

VALUE	DOCUMENT ID	TECN	COMMENT
$0.47 \pm 0.22 \pm 0.15$	DEL-AMO-SA...11G	BABR	$e^+e^- \approx \mathcal{T}(4S)$

———— Baryon-antibaryon mode ————

$\Gamma(p\bar{p})/\Gamma_{total}$ Γ_{175}/Γ
 This is the only baryonic mode allowed kinematically.

VALUE (units 10^{-3})	EVTS	DOCUMENT ID	TECN	COMMENT
1.22 ± 0.11 OUR AVERAGE				
$1.21 \pm 0.10 \pm 0.05$	193 ± 17	ABLIKIM	19o	BES3 $e^+e^-, E_{cm} = 4178$ MeV
$1.30 \pm 0.36 \pm 0.12$	13.0 ± 3.6	ATHAR	08	CLEO $e^+e^-, E_{cm} \approx 4170$ MeV

$\Gamma(p\bar{p}e^+\nu_e)/\Gamma_{total}$ Γ_{176}/Γ

VALUE	CL%	DOCUMENT ID	TECN	COMMENT
< 2.0×10^{-4}	90	ABLIKIM	19bD	BES3 e^+e^- at 4178 MeV

———— Rare or forbidden modes ————

$\Gamma(\pi^+e^+e^-)/\Gamma_{total}$ Γ_{177}/Γ
 This mode is not a useful test for a $\Delta C=1$ weak neutral current because both quarks must change flavor in this decay.

VALUE	CL%	DOCUMENT ID	TECN	COMMENT
< 5.5×10^{-6}	90	AAIJ	21T	LHCB $1.6 \text{ fb}^{-1} pp$
••• We do not use the following data for averages, fits, limits, etc. •••				
< 13×10^{-6}	90	LEES	11G	BABR $e^+e^- \approx \mathcal{T}(4S)$
< 2.2×10^{-5}	90	RUBIN	10	CLEO e^+e^- at 4170 MeV
< 27×10^{-5}	90	AITALA	99G	E791 $\pi^- N$ 500 GeV

¹ This RUBIN 10 limit is for the e^+e^- mass in the continuum away from the $\phi(1020)$. See the next data block.

$\Gamma(\pi^+\phi, \phi \rightarrow e^+e^-)/\Gamma_{total}$ Γ_{178}/Γ
 This is not a test for the $\Delta C = 1$ weak neutral current, but leads to the $\pi^+e^+e^-$ final state.

VALUE	EVTS	DOCUMENT ID	TECN	COMMENT
$(6 \pm 8 \pm 1) \times 10^{-6}$	3	RUBIN	10	CLEO e^+e^- at 4170 MeV

$\Gamma(\pi^+\mu^+\mu^-)/\Gamma_{total}$ Γ_{179}/Γ
 This mode is not a useful test for a $\Delta C=1$ weak neutral current because both quarks must change flavor in this decay.

VALUE	CL%	DOCUMENT ID	TECN	COMMENT
< 1.8×10^{-7}	90	AAIJ	21T	LHCB $1.6 \text{ fb}^{-1} pp$
••• We do not use the following data for averages, fits, limits, etc. •••				
< 4.1×10^{-7}	90	AAIJ	13Af	LHCB pp at 7 TeV
< 4.3×10^{-5}	90	LEES	11G	BABR $e^+e^- \approx \mathcal{T}(4S)$
< 2.6×10^{-5}	90	LINK	03F	FOCS $\gamma A, \bar{E}_\gamma \approx 180$ GeV
< 1.4×10^{-4}	90	AITALA	99G	E791 $\pi^- N$ 500 GeV
< 4.3×10^{-4}	90	KODAMA	95	E653 π^- emulsion 600 GeV

$\Gamma(K^+e^+e^-)/\Gamma_{total}$ Γ_{180}/Γ
 A test for the $\Delta C=1$ weak neutral current. Allowed by higher-order electroweak interactions.

VALUE	CL%	DOCUMENT ID	TECN	COMMENT
< 3.7×10^{-6}	90	LEES	11G	BABR $e^+e^- \approx \mathcal{T}(4S)$
••• We do not use the following data for averages, fits, limits, etc. •••				
< 4.9×10^{-6}	90	AAIJ	21T	LHCB $1.6 \text{ fb}^{-1} pp$
< 5.2×10^{-5}	90	RUBIN	10	CLEO e^+e^- at 4170 MeV
< 1.6×10^{-3}	90	AITALA	99G	E791 $\pi^- N$ 500 GeV

$\Gamma(K^+\mu^+\mu^-)/\Gamma_{total}$ Γ_{181}/Γ
 A test for the $\Delta C=1$ weak neutral current. Allowed by higher-order electroweak interactions.

VALUE	CL%	DOCUMENT ID	TECN	COMMENT
< 1.4×10^{-7}	90	AAIJ	21T	LHCB $1.6 \text{ fb}^{-1} pp$
••• We do not use the following data for averages, fits, limits, etc. •••				
< 21×10^{-6}	90	LEES	11G	BABR $e^+e^- \approx \mathcal{T}(4S)$
< 3.6×10^{-5}	90	LINK	03F	FOCS $\gamma A, \bar{E}_\gamma \approx 180$ GeV
< 1.4×10^{-4}	90	AITALA	99G	E791 $\pi^- N$ 500 GeV
< 5.9×10^{-4}	90	KODAMA	95	E653 π^- emulsion 600 GeV

$\Gamma(K^*(892)^+\mu^+\mu^-)/\Gamma_{total}$ Γ_{182}/Γ
 A test for the $\Delta C=1$ weak neutral current. Allowed by higher-order electroweak interactions.

VALUE	CL%	DOCUMENT ID	TECN	COMMENT
< 1.4×10^{-3}	90	KODAMA	95	E653 π^- emulsion 600 GeV

$\Gamma(\pi^+e^+\mu^-)/\Gamma_{total}$ Γ_{183}/Γ
 A test of lepton-family-number conservation.

VALUE	CL%	DOCUMENT ID	TECN	COMMENT
< 1.1×10^{-6}	90	AAIJ	21T	LHCB $1.6 \text{ fb}^{-1} pp$
••• We do not use the following data for averages, fits, limits, etc. •••				
< 12×10^{-6}	90	LEES	11G	BABR $e^+e^- \approx \mathcal{T}(4S)$

$\Gamma(\pi^+e^-\mu^+)/\Gamma_{total}$ Γ_{184}/Γ
 A test of lepton-family-number conservation.

VALUE	CL%	DOCUMENT ID	TECN	COMMENT
< 9.4×10^{-7}	90	AAIJ	21T	LHCB $1.6 \text{ fb}^{-1} pp$
••• We do not use the following data for averages, fits, limits, etc. •••				
< 20×10^{-6}	90	LEES	11G	BABR $e^+e^- \approx \mathcal{T}(4S)$

$\Gamma(K^+e^+\mu^-)/\Gamma_{total}$ Γ_{185}/Γ
 A test of lepton-family-number conservation.

VALUE	CL%	DOCUMENT ID	TECN	COMMENT
< 7.9×10^{-7}	90	AAIJ	21T	LHCB $1.6 \text{ fb}^{-1} pp$
••• We do not use the following data for averages, fits, limits, etc. •••				
< 14×10^{-6}	90	LEES	11G	BABR $e^+e^- \approx \mathcal{T}(4S)$

$\Gamma(K^+e^-\mu^+)/\Gamma_{total}$ Γ_{186}/Γ
 A test of lepton-family-number conservation.

VALUE	CL%	DOCUMENT ID	TECN	COMMENT
< 5.6×10^{-7}	90	AAIJ	21T	LHCB $1.6 \text{ fb}^{-1} pp$
••• We do not use the following data for averages, fits, limits, etc. •••				
< 9.7×10^{-6}	90	LEES	11G	BABR $e^+e^- \approx \mathcal{T}(4S)$

$\Gamma(\pi^-2e^+)/\Gamma_{total}$ Γ_{187}/Γ
 A test of lepton-number conservation.

VALUE	CL%	DOCUMENT ID	TECN	COMMENT
< 1.4×10^{-6}	90	AAIJ	21T	LHCB $1.6 \text{ fb}^{-1} pp$
••• We do not use the following data for averages, fits, limits, etc. •••				
< 4.1×10^{-6}	90	LEES	11G	BABR $e^+e^- \approx \mathcal{T}(4S)$
< 1.8×10^{-5}	90	RUBIN	10	CLEO e^+e^- at 4170 MeV
< 69×10^{-5}	90	AITALA	99G	E791 $\pi^- N$ 500 GeV

$\Gamma(\pi^-2\mu^+)/\Gamma_{total}$ Γ_{188}/Γ
 A test of lepton-number conservation.

VALUE	CL%	DOCUMENT ID	TECN	COMMENT
< 8.6×10^{-8}	90	AAIJ	21T	LHCB $1.6 \text{ fb}^{-1} pp$
••• We do not use the following data for averages, fits, limits, etc. •••				
< 1.2×10^{-7}	90	AAIJ	13Af	LHCB pp at 7 TeV
< 1.4×10^{-5}	90	LEES	11G	BABR $e^+e^- \approx \mathcal{T}(4S)$
< 2.9×10^{-5}	90	LINK	03F	FOCS $\gamma A, \bar{E}_\gamma \approx 180$ GeV
< 8.2×10^{-5}	90	AITALA	99G	E791 $\pi^- N$ 500 GeV
< 4.3×10^{-4}	90	KODAMA	95	E653 π^- emulsion 600 GeV

$\Gamma(\pi^-e^+\mu^+)/\Gamma_{total}$ Γ_{189}/Γ
 A test of lepton-number conservation.

VALUE	CL%	DOCUMENT ID	TECN	COMMENT
< 6.3×10^{-7}	90	AAIJ	21T	LHCB $1.6 \text{ fb}^{-1} pp$
••• We do not use the following data for averages, fits, limits, etc. •••				
< 8.4×10^{-6}	90	LEES	11G	BABR $e^+e^- \approx \mathcal{T}(4S)$
< 7.3×10^{-4}	90	AITALA	99G	E791 $\pi^- N$ 500 GeV

Meson Particle Listings

 D_s^\pm $\Gamma(K^- 2e^+)/\Gamma_{\text{total}}$

A test of lepton-number conservation.

VALUE	CL%	DOCUMENT ID	TECN	COMMENT
$< 2.6 \times 10^{-7}$	90	AAIJ	21T LHCb	$1.6 \text{ fb}^{-1} pp$
••• We do not use the following data for averages, fits, limits, etc. •••				
$< 5.2 \times 10^{-6}$	90	LEES	11G BABR	$e^+ e^- \approx \Upsilon(4S)$
$< 1.7 \times 10^{-5}$	90	RUBIN	10 CLEO	$e^+ e^-$ at 4170 MeV
$< 63 \times 10^{-5}$	90	AITALA	99G E791	$\pi^- N$ 500 GeV

 Γ_{190}/Γ $\Gamma(K^- 2\mu^+)/\Gamma_{\text{total}}$

A test of lepton-number conservation.

VALUE	CL%	DOCUMENT ID	TECN	COMMENT
$< 2.6 \times 10^{-8}$	90	AAIJ	21T LHCb	$1.6 \text{ fb}^{-1} pp$
••• We do not use the following data for averages, fits, limits, etc. •••				
$< 1.3 \times 10^{-5}$	90	LEES	11G BABR	$e^+ e^- \approx \Upsilon(4S)$
$< 1.3 \times 10^{-5}$	90	LINK	03F FOCUS	$\gamma A, \bar{E}_\gamma \approx 180 \text{ GeV}$
$< 1.8 \times 10^{-4}$	90	AITALA	99G E791	$\pi^- N$ 500 GeV
$< 5.9 \times 10^{-4}$	90	KODAMA	95 E653	π^- emulsion 600 GeV

 Γ_{191}/Γ $\Gamma(K^- e^+ \mu^+)/\Gamma_{\text{total}}$

A test of lepton-number conservation.

VALUE	CL%	DOCUMENT ID	TECN	COMMENT
$< 2.6 \times 10^{-7}$	90	AAIJ	21T LHCb	$1.6 \text{ fb}^{-1} pp$
••• We do not use the following data for averages, fits, limits, etc. •••				
$< 6.1 \times 10^{-6}$	90	LEES	11G BABR	$e^+ e^- \approx \Upsilon(4S)$
$< 6.8 \times 10^{-4}$	90	AITALA	99G E791	$\pi^- N$ 500 GeV

 Γ_{192}/Γ $\Gamma(K^*(892) 2\mu^+)/\Gamma_{\text{total}}$

A test of lepton-number conservation.

VALUE	CL%	DOCUMENT ID	TECN	COMMENT
$< 1.4 \times 10^{-3}$	90	KODAMA	95 E653	π^- emulsion 600 GeV

 Γ_{193}/Γ D_s^\pm Amplitude Analyses $D_s^+ \rightarrow K^+ K^- \pi^+$ partial wave analysesAmplitude analyses of D_s^+ decays to the $K^+ K^- \pi^+$ final state, fitting simultaneously different partial wave components.

VALUE	EVTS	DOCUMENT ID	TECN	COMMENT
seen	18.6k	¹ ABLIKIM	21AE BES3	$e^+ e^-$ at 4.178 GeV
seen	96k	¹ DEL-AMO-SA..11G	BABR	$e^+ e^-$ at $\Upsilon(4S)$
seen	12k	¹ MITCHELL	09A CLEO	$e^+ e^-$ at 4.17 GeV
seen	701	² FRABETTI	95B E687	

¹ Amplitude analysis with 6 components.² Amplitude analysis with 5 components. $D_s^+ \rightarrow K^+ K_S^0 \pi^0$ partial wave analyses

VALUE	EVTS	DOCUMENT ID	TECN	COMMENT
	990	¹ ABLIKIM	22AH BES3	$e^+ e^-$ at 4.178–4.226 GeV

¹ Amplitude analysis with 5 components. $D_s^+ \rightarrow 2\pi^+ \pi^-$ partial wave analyses

VALUE	EVTS	DOCUMENT ID	TECN	COMMENT
	0.7M	¹ AAIJ	23AN LHCb	Dalitz fit, 0.7M events
	11.1k	² ABLIKIM	22BI BES3	Dalitz fit
	10.5k	² AUBERT	09O BABR	Dalitz fit
	1.5k	³ LINK	04 FOCUS	Dalitz fit
	848	⁴ AITALA	01A E791	Dalitz fit

¹ Amplitude analysis with 7 components, one of which is a model-independent $\pi^+ \pi^- S$ -wave parametrisation as complex numbers in 50 $\pi^+ \pi^-$ mass bins.² Amplitude analysis with 4 components, one of which is a model-independent $\pi^+ \pi^- S$ -wave parametrisation as complex numbers in 29 $\pi^+ \pi^-$ mass bins.³ Amplitude analysis with 5 components.⁴ Amplitude analysis with 6 components. $D_s^+ \rightarrow 2\pi^+ \pi^- \eta$ partial wave analysesAmplitude analyses of D_s^+ decays to the $\pi^+ \pi^+ \pi^- \eta$ final state, fitting simultaneously different partial wave components.

VALUE	EVTS	DOCUMENT ID	TECN	COMMENT
seen	2.1k	¹ ABLIKIM	21AR BES3	$e^+ e^-$ at 4.178–4.226 GeV

¹ Amplitude analysis with 11 components. $D_s^+ \rightarrow \pi^+ \pi^0 \eta'$ partial wave analyses.

VALUE	EVTS	DOCUMENT ID	TECN	COMMENT
	395	¹ ABLIKIM	22AA BES3	$e^+ e^-$ at 4.178–4.226 GeV

¹ The only significant contribution found in this analysis is $D_s^+ \rightarrow \rho^+ \eta'$. $D_s^+ \rightarrow \pi^+ 2\pi^0$ partial wave analyses.

VALUE	EVTS	DOCUMENT ID	TECN	COMMENT
	440	ABLIKIM	22Z BES3	$e^+ e^-$ at 4.178–4.226 GeV

 $D_s^+ \rightarrow K^+ \pi^+ \pi^-$ partial wave analyses

VALUE	EVTS	DOCUMENT ID	TECN	COMMENT
	1.3k	¹ ABLIKIM	22AC BES3	$e^+ e^-$ at 4.178–4.226 GeV

¹ ABLIKIM 22AC uses an amplitude analysis with 8 components. $D_s^+ \rightarrow K_S^0 \pi^+ \pi^0$ partial wave analyses

VALUE	EVTS	DOCUMENT ID	TECN	COMMENT
	666	¹ ABLIKIM	21AB BES3	$e^+ e^-$ at 4.178–4.226 GeV

¹ ABLIKIM 21AB uses an amplitude analysis with 5 resonant modes plus one background component. $D_s^+ \rightarrow K^+ \pi^+ \pi^- \pi^0$ partial wave analyses

VALUE	EVTS	DOCUMENT ID	TECN	COMMENT
seen	550	¹ ABLIKIM	22BL BES3	$e^+ e^-$ at 4.178–4.226 GeV

¹ Amplitude analysis with 11 components. $D_s^+ \rightarrow 2K_S^0 \pi^+$ partial wave analyses

VALUE	EVTS	DOCUMENT ID	TECN	COMMENT
	400	¹ ABLIKIM	22F BES3	$e^+ e^-$ at 4.178–4.226 GeV

¹ Amplitude analysis with 2 components. $D_s^+ \rightarrow (KS)^0 K^- 2\pi^+$ partial wave analysesAmplitude analyses of D_s^+ decays to the $K_S^0 K^- 2\pi^+$ final state, fitting simultaneously different partial wave components.

VALUE	EVTS	DOCUMENT ID	TECN	COMMENT
seen	1.3k	¹ ABLIKIM	21K BES3	$e^+ e^-$ at 4.178–4.226 GeV

¹ Amplitude analysis with 13 components. $D_s^+ \rightarrow K^- K^+ \pi^+ \pi^0$ partial wave analysesAmplitude analyses of D_s^+ decays to the $K^- K^+ \pi^+ \pi^0$ final state, fitting simultaneously different partial wave components.

VALUE	EVTS	DOCUMENT ID	TECN	COMMENT
seen	3k	¹ ABLIKIM	21U BES3	$e^+ e^-$ at 4.178–4.226 GeV

¹ ABLIKIM 21U uses an amplitude analysis with 9 components. $D_s^+ \rightarrow K^- K^+ 2\pi^+ \pi^-$ partial wave analyses

VALUE	EVTS	DOCUMENT ID	TECN	COMMENT
	309	ABLIKIM	22AB BES3	$e^+ e^-$ at 4.178–4.226 GeV

 $D_s^+ - D_s^-$ CP-VIOLATING DECAY-RATE ASYMMETRIESThis is the difference between D_s^+ and D_s^- partial widths for the decay to state r , divided by the sum of the widths:

$$A_{CP}(r) = [\Gamma(D_s^+ \rightarrow r) - \Gamma(D_s^- \rightarrow \bar{r})] / [\Gamma(D_s^+ \rightarrow r) + \Gamma(D_s^- \rightarrow \bar{r})].$$

 $A_{CP}(\mu^\pm \nu)$ in $D_s^+ \rightarrow \mu^+ \nu$, $D_s^- \rightarrow \mu^- \bar{\nu}_\mu$

VALUE (%)	EVTS	DOCUMENT ID	TECN	COMMENT
-0.2 ± 2.5 OUR AVERAGE				
$-1.2 \pm 2.5 \pm 1.0$	2.2k	ABLIKIM	21BE BES3	$e^+ e^-$ at 4.178, 4.226 GeV
4.8 ± 6.1		ALEXANDER	09 CLEO	$e^+ e^-$ at 4170 MeV

 $A_{CP}(\tau^\pm \nu)$ in $D_s^+ \rightarrow \tau^+ \nu_\tau$, $D_s^- \rightarrow \tau^- \bar{\nu}_\tau$

VALUE (%)	EVTS	DOCUMENT ID	TECN	COMMENT
$2.9 \pm 4.8 \pm 1.0$	950	¹ ABLIKIM	21BE BES3	$e^+ e^-$ at 4.178, 4.226 GeV

¹ ABLIKIM 21BE also reports that when constrained by the Standard Model ratio of $\Gamma(D_s^+ \rightarrow \tau^+ \nu_\tau) / \Gamma(D_s^+ \rightarrow \mu^+ \nu_\mu) = 9.75$, the result is $(-0.1 \pm 1.9 \pm 1.0)\%$. $A_{CP}(K^\pm K_S^0)$ in $D_s^\pm \rightarrow K^\pm K_S^0$

VALUE (%)	EVTS	DOCUMENT ID	TECN	COMMENT
0.09 ± 0.26 OUR AVERAGE				
$0.6 \pm 2.8 \pm 0.6$	1.8k	ABLIKIM	19AMBES3	$e^+ e^-$ at 4178 MeV
$-0.05 \pm 0.23 \pm 0.24$	288k	¹ LEES	13E BABR	$e^+ e^-$ at $\Upsilon(4S)$
$2.6 \pm 1.5 \pm 0.6$		ONYISI	13 CLEO	$e^+ e^-$ at 4.17 GeV
$0.12 \pm 0.36 \pm 0.22$		KO	10 BELL	$e^+ e^- \approx \Upsilon(4S)$

••• We do not use the following data for averages, fits, limits, etc. •••

$4.7 \pm 1.8 \pm 0.9$	4.0k	MENDEZ	10 CLEO	See ONYISI 13
$4.9 \pm 2.1 \pm 0.9$		ALEXANDER	08 CLEO	See MENDEZ 10

¹ LEES 13E finds that after subtracting the contribution due to $K^0 - \bar{K}^0$ mixing, the CP asymmetry is $(+0.28 \pm 0.23 \pm 0.24)\%$. $A_{CP}(K^\pm K_L^0)$ in $D_s^\pm \rightarrow K^\pm K_L^0$

VALUE (units 10^{-2})	EVTS	DOCUMENT ID	TECN	COMMENT
$-1.1 \pm 2.6 \pm 0.6$	2.3k	ABLIKIM	19AMBES3	$e^+ e^-$ at 4178 MeV

 $A_{CP}(K^+ K^- \pi^\pm)$ in $D_s^\pm \rightarrow K^\pm K^- \pi^\pm$

VALUE (%)	DOCUMENT ID	TECN	COMMENT
$-0.5 \pm 0.8 \pm 0.4$	ONYISI	13 CLEO	$e^+ e^-$ at 4.17 GeV

••• We do not use the following data for averages, fits, limits, etc. •••

$0.3 \pm 1.1 \pm 0.8$	ALEXANDER	08 CLEO	See ONYISI 13
-----------------------	-----------	---------	---------------

$A_{CP}(\phi\pi^\pm)$ in $D_s^\pm \rightarrow \phi\pi^\pm$

VALUE (%)	DOCUMENT ID	TECN	COMMENT
$-0.38 \pm 0.26 \pm 0.08$	ABAZOV	14b	D0 $p\bar{p}$ at 1.96 TeV

 $A_{CP}(K^\pm K_S^0 \pi^0)$ in $D_s^\pm \rightarrow K^\pm K_S^0 \pi^0$

VALUE (%)	DOCUMENT ID	TECN	COMMENT
$-1.6 \pm 6.0 \pm 1.1$	ONYISI	13	CLEO e^+e^- at 4.17 GeV

 $A_{CP}(2K_S^0 \pi^\pm)$ in $D_s^\pm \rightarrow 2K_S^0 \pi^\pm$

VALUE (%)	DOCUMENT ID	TECN	COMMENT
$3.1 \pm 5.2 \pm 0.6$	ONYISI	13	CLEO e^+e^- at 4.17 GeV

 $A_{CP}(K^+ K^- \pi^\pm \pi^0)$ in $D_s^\pm \rightarrow K^+ K^- \pi^\pm \pi^0$

VALUE (%)	DOCUMENT ID	TECN	COMMENT
$0.0 \pm 2.7 \pm 1.2$	ONYISI	13	CLEO e^+e^- at 4.17 GeV

••• We do not use the following data for averages, fits, limits, etc. •••

$-5.9 \pm 4.2 \pm 1.2$	ALEXANDER	08	CLEO See ONYISI 13
------------------------	-----------	----	--------------------

 $A_{CP}(K^\pm K_S^0 \pi^+ \pi^-)$ in $D_s^\pm \rightarrow K^\pm K_S^0 \pi^+ \pi^-$

VALUE (%)	DOCUMENT ID	TECN	COMMENT
$-5.7 \pm 5.3 \pm 0.9$	ONYISI	13	CLEO e^+e^- at 4.17 GeV

 $A_{CP}(K_S^0 K^\mp 2\pi^\pm)$ in $D_s^\pm \rightarrow K_S^0 K^\mp 2\pi^\pm$

VALUE (%)	DOCUMENT ID	TECN	COMMENT
$4.1 \pm 2.7 \pm 0.9$	ONYISI	13	CLEO e^+e^- at 4.17 GeV

••• We do not use the following data for averages, fits, limits, etc. •••

$-0.7 \pm 3.6 \pm 1.1$	ALEXANDER	08	CLEO See ONYISI 13
------------------------	-----------	----	--------------------

 $A_{CP}(\pi^+ \pi^- \pi^\pm)$ in $D_s^\pm \rightarrow \pi^+ \pi^- \pi^\pm$

VALUE (%)	DOCUMENT ID	TECN	COMMENT
$-0.7 \pm 3.0 \pm 0.6$	ONYISI	13	CLEO e^+e^- at 4.17 GeV

••• We do not use the following data for averages, fits, limits, etc. •••

$2.0 \pm 4.6 \pm 0.7$	ALEXANDER	08	CLEO See ONYISI 13
-----------------------	-----------	----	--------------------

 $A_{CP}(\pi^\pm \eta)$ in $D_s^\pm \rightarrow \pi^\pm \eta$

VALUE (%)	EVTS	DOCUMENT ID	TECN	COMMENT
0.32 ± 0.31 OUR AVERAGE	136k			

$0.32 \pm 0.51 \pm 0.12$	136k	AAIJ	23E	LHCB 6 fb^{-1} , $p\bar{p}$ at 13 TeV, $\eta \rightarrow \gamma\pi\pi$
$0.8 \pm 0.7 \pm 0.5$	38k	AAIJ	21u	LHCB $p\bar{p}$ at 7, 8 TeV
$0.2 \pm 0.3 \pm 0.3$	22k	GUAN	21	BELL $e^+e^- \approx \gamma(4,5S)$

••• We do not use the following data for averages, fits, limits, etc. •••

$1.1 \pm 3.0 \pm 0.8$	2.5k	ONYISI	13	CLEO e^+e^- at 4.17 GeV
$-4.6 \pm 2.9 \pm 0.3$		MENDEZ	10	CLEO See ONYISI 13
$-8.2 \pm 5.2 \pm 0.8$		ALEXANDER	08	CLEO See MENDEZ 10

 $A_{CP}(\pi^\pm \eta')$ in $D_s^\pm \rightarrow \pi^\pm \eta'$

VALUE (%)	EVTS	DOCUMENT ID	TECN	COMMENT
-0.06 ± 0.22 OUR AVERAGE	Error includes scale factor of 1.6			

$0.01 \pm 0.12 \pm 0.08$	1M	AAIJ	23E	LHCB 6 fb^{-1} , $p\bar{p}$ at 13 TeV, $\eta \rightarrow \gamma\pi\pi$
$-0.82 \pm 0.36 \pm 0.35$	152k	AAIJ	17AF	LHCB $p\bar{p}$ at 7, 8 TeV
$-2.2 \pm 2.2 \pm 0.6$		ONYISI	13	CLEO e^+e^- at 4.17 GeV

••• We do not use the following data for averages, fits, limits, etc. •••

$-6.1 \pm 3.0 \pm 0.3$	1.4k	MENDEZ	10	CLEO See ONYISI 13
$-5.5 \pm 3.7 \pm 1.2$		ALEXANDER	08	CLEO See MENDEZ 10

 $A_{CP}(\eta\pi^\pm\pi^0)$ in $D_s^\pm \rightarrow \eta\pi^\pm\pi^0$

VALUE (%)	DOCUMENT ID	TECN	COMMENT
$-0.5 \pm 3.9 \pm 2.0$	ONYISI	13	CLEO e^+e^- at 4.17 GeV

 $A_{CP}(\eta'\pi^\pm\pi^0)$ in $D_s^\pm \rightarrow \eta'\pi^\pm\pi^0$

VALUE (%)	DOCUMENT ID	TECN	COMMENT
$-0.4 \pm 7.4 \pm 1.9$	ONYISI	13	CLEO e^+e^- at 4.17 GeV

 $A_{CP}(K^\pm\pi^0)$ in $D_s^\pm \rightarrow K^\pm\pi^0$

VALUE (%)	EVTS	DOCUMENT ID	TECN	COMMENT
2 ± 4 OUR AVERAGE	Error includes scale factor of 1.2			

$-0.8 \pm 3.9 \pm 1.2$	2.8k	AAIJ	21u	LHCB $p\bar{p}$ at 7, 8, 13 TeV
$6.4 \pm 4.4 \pm 1.1$	12k	GUAN	21	BELL $e^+e^- \approx \gamma(4,5S)$

••• We do not use the following data for averages, fits, limits, etc. •••

$-26.6 \pm 23.8 \pm 0.9$	202	MENDEZ	10	CLEO e^+e^- at 4170 MeV
2 ± 29		ADAMS	07A	CLEO See MENDEZ 10

 $A_{CP}(K^0/K^+\pi^\pm)$ in $D_s^\pm \rightarrow K^0/K^+\pi^\pm$

VALUE (%)	EVTS	DOCUMENT ID	TECN	COMMENT
0.4 ± 0.5 OUR AVERAGE				

$0.38 \pm 0.46 \pm 0.17$	121k	¹ AAIJ	14BD	LHCB $p\bar{p}$ at 7, 8 TeV
$0.3 \pm 2.0 \pm 0.3$	14k	LEES	13E	BABR e^+e^- at $\gamma(4S)$

••• We do not use the following data for averages, fits, limits, etc. •••

$0.61 \pm 0.83 \pm 0.14$	26k	AAIJ	13W	LHCB See AAJ14BD
--------------------------	-----	------	-----	------------------

¹AAIJ 14BD reports its result as $A_{CP}(D_s^\pm \rightarrow K_S^0 K^\pm)$ with CP -violation effects in the $K^0 - \bar{K}^0$ system subtracted. It also measures $A_{CP}(D^\pm \rightarrow \bar{K}^0/K^0 K^\pm)$ + $A_{CP}(D_s^\pm \rightarrow \bar{K}^0/K^0 \pi^\pm) = (0.41 \pm 0.49 \pm 0.26)\%$.

 $A_{CP}(K_S^0 \pi^\pm)$ in $D_s^\pm \rightarrow K_S^0 \pi^\pm$

VALUE (%)	EVTS	DOCUMENT ID	TECN	COMMENT
0.20 ± 0.18 OUR AVERAGE				

$0.16 \pm 0.17 \pm 0.05$	721k	AAIJ	19T	LHCB $p\bar{p}$ at 7, 8, 13 TeV
$0.6 \pm 2.0 \pm 0.3$	14k	LEES	13E	BABR e^+e^- at $\gamma(4S)$

$5.45 \pm 2.50 \pm 0.33$		KO	10	BELL $e^+e^- \approx \gamma(4S)$
$16.3 \pm 7.3 \pm 0.3$	0.4k	MENDEZ	10	CLEO e^+e^- at 4170 MeV

••• We do not use the following data for averages, fits, limits, etc. •••

27 ± 11		ADAMS	07A	CLEO See MENDEZ 10
-------------	--	-------	-----	--------------------

 $A_{CP}(K^\pm \pi^+ \pi^-)$ in $D_s^\pm \rightarrow K^\pm \pi^+ \pi^-$

VALUE (%)	EVTS	DOCUMENT ID	TECN	COMMENT
3.7 ± 2.7 OUR AVERAGE				

$3.3 \pm 3.0 \pm 1.3$	1.3k	ABLIKIM	22Ac	BES3 e^+e^- at 4.178–4.226 GeV
$4.5 \pm 4.8 \pm 0.6$		ONYISI	13	CLEO e^+e^- at 4.17 GeV

••• We do not use the following data for averages, fits, limits, etc. •••

$11.2 \pm 7.0 \pm 0.9$		ALEXANDER	08	CLEO See ONYISI 13
------------------------	--	-----------	----	--------------------

 $A_{CP}(K_S^0 \pi^+ \pi^0)$ in $D_s^\pm \rightarrow K_S^0 \pi^+ \pi^0$

VALUE (%)	EVTS	DOCUMENT ID	TECN	COMMENT
2.7 ± 5.5 ± 0.9	666	¹ ABLIKIM	21AB	BES3 e^+e^- at 4.178–4.226 GeV

¹ABLIKIM 21AB uses an amplitude analysis with 5 resonant modes plus one background component.

 $A_{CP}(K^\pm \pi^+ \pi^- \pi^0)$ in $D_s^\pm \rightarrow K^\pm \pi^+ \pi^- \pi^0$

VALUE (units 10 ⁻²)	EVTS	DOCUMENT ID	TECN	COMMENT
6.6 ± 5.4 ± 0.7	776	ABLIKIM	22BL	BES3 e^+e^- at 4.178–4.226 GeV

 $A_{CP}(K^\pm \eta)$ in $D_s^\pm \rightarrow K^\pm \eta$

VALUE (%)	EVTS	DOCUMENT ID	TECN	COMMENT
1.8 ± 1.9 OUR AVERAGE				

$0.9 \pm 3.7 \pm 1.1$	2.5k	AAIJ	21u	LHCB $p\bar{p}$ at 13 TeV
$2.1 \pm 2.1 \pm 0.4$	14k	GUAN	21	BELL $e^+e^- \approx \gamma(4,5S)$

••• We do not use the following data for averages, fits, limits, etc. •••

$9.3 \pm 15.2 \pm 0.9$	222	MENDEZ	10	CLEO e^+e^- at 4170 MeV
-20 ± 18		ADAMS	07A	CLEO See MENDEZ 10

 $A_{CP}(K^\pm \eta'(958))$ in $D_s^\pm \rightarrow K^\pm \eta'(958)$

VALUE (%)	EVTS	DOCUMENT ID	TECN	COMMENT
6.0 ± 18.9 ± 0.9	56 ± 17	MENDEZ	10	CLEO e^+e^- at 4170 MeV

••• We do not use the following data for averages, fits, limits, etc. •••

-17 ± 37		ADAMS	07A	CLEO See MENDEZ 10
--------------	--	-------	-----	--------------------

 $D_s^\pm \chi^2$ TESTS OF CP -VIOLATION (CPV)

We list model-independent searches for local CP violation in phase-space distributions of multi-body decays.

Most of these searches divide phase space (Dalitz plot for 3-body decays, five-dimensional equivalent for 4-body decays) into bins, and perform a χ^2 test comparing normalised yields N_i, \bar{N}_i in CP -conjugate bin pairs i : $\chi^2 = \sum_i (N_i - \alpha \bar{N}_i) / \sigma(N_i - \alpha \bar{N}_i)$. The factor $\alpha = (\sum_j N_j) / (\sum_j \bar{N}_j)$ removes the dependence on phase-space-integrated rate asymmetries. The result is used to obtain the probability (p-value) to obtain the measured χ^2 or larger under the assumption of CP conservation [AUBERT 08A0, BEDIAGA 09]. Alternative methods obtain p-values from other test variables based on unbinned analyses [WILLIAMS 11, AAJ14C]. Results can be combined using Fisher's method [MOSTELLER 48].

Local CPV in $D_s^\pm \rightarrow K^+ K^- K^\pm$

VALUE	EVTS	DOCUMENT ID	TECN	COMMENT
0.133	970k	AAIJ	23L	LHCB χ^2

 CP VIOLATING ASYMMETRIES OF P -ODD (T -ODD) MOMENTS $A_{Tviol}(K_S^0 K^\pm \pi^+ \pi^-)$ in $D_s^\pm \rightarrow K_S^0 K^\pm \pi^+ \pi^-$

$C_T \equiv \bar{p}_{K^+} \cdot (\bar{p}_{\pi^+} \times \bar{p}_{\pi^-})$ is a parity-odd correlation of the K^+ , π^+ , and π^- momenta for the D_s^+ . $\bar{C}_T \equiv \bar{p}_{K^-} \cdot (\bar{p}_{\pi^-} \times \bar{p}_{\pi^+})$ is the corresponding quantity for the D_s^- . Then

$A_T \equiv [\Gamma(C_T > 0) - \Gamma(C_T < 0)] / [\Gamma(C_T > 0) + \Gamma(C_T < 0)]$, and
 $\bar{A}_T \equiv [\Gamma(-\bar{C}_T > 0) - \Gamma(-\bar{C}_T < 0)] / [\Gamma(-\bar{C}_T > 0) + \Gamma(-\bar{C}_T < 0)]$, and
 $A_{Tviol} \equiv \frac{1}{2}(A_T - \bar{A}_T)$. C_T and \bar{C}_T are commonly referred to as T -odd moments, because they are odd under T reversal. However, the T -conjugate process $K_S^0 K^\pm \pi^+ \pi^- \rightarrow D_s^\pm$ is not accessible, while the P -conjugate process is.

VALUE (units 10 ⁻³)	EVTS	DOCUMENT ID	TECN	COMMENT
-8 ± 6 OUR AVERAGE				

$-4.6 \pm 6.3 \pm 3.8$	70k	MOON	23	BELL 980 fb ⁻¹ at $\sim \gamma(4S)$
$-13.6 \pm 7.7 \pm 3.4$	29.8k	LEES	11E	BABR $e^+e^- \approx \gamma(4S)$

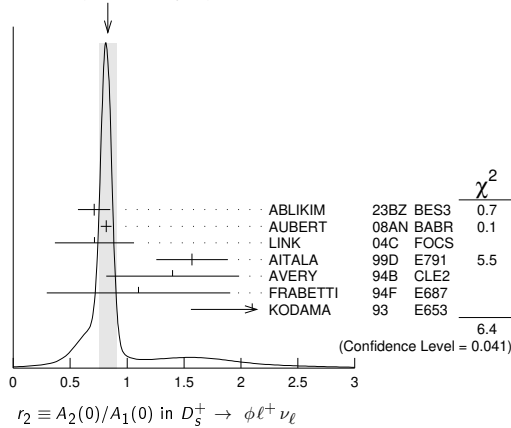
••• We do not use the following data for averages, fits, limits, etc. •••

$-36 \pm 67 \pm 23$	508	LINK	05E	FOCS $\gamma A, \bar{E}_\gamma \approx 180 \text{ GeV}$
---------------------	-----	------	-----	---

Meson Particle Listings

 D_s^\pm D_s^+ Semileptonic Form Factors and Decay Constants $r_2 \equiv A_2(0)/A_1(0)$ in $D_s^+ \rightarrow \phi \ell^+ \nu_\ell$

VALUE	EVTS	DOCUMENT ID	TECN	COMMENT
0.83 ± 0.08 OUR AVERAGE		Error includes scale factor of 1.8. See the ideogram below.		
0.71 ± 0.14 ± 0.02		¹ ABLIKIM	23Bz BES3	$D_s^+ \rightarrow K^+ K^- \mu^+ \nu_\mu$
0.816 ± 0.036 ± 0.030	25k	² AUBERT	08AN BABR	$\phi e^+ \nu_e$
0.713 ± 0.202 ± 0.284	793	LINK	04c FOCS	$\phi \mu^+ \nu_\mu$
1.57 ± 0.25 ± 0.19	271	AITALA	99D E791	$\phi e^+ \nu_e, \phi \mu^+ \nu_\mu$
1.4 ± 0.5 ± 0.3	308	AVERY	94B CLE2	$\phi e^+ \nu_e$
1.1 ± 0.8 ± 0.1	90	FRABETTI	94F E687	$\phi \mu^+ \nu_\mu$
2.1 $^{+0.6}_{-0.5}$ ± 0.2	19	KODAMA	93 E653	$\phi \mu^+ \nu_\mu$

¹ Partial wave analysis of 939 $D_s^+ \rightarrow K^+ K^- \mu^+ \nu_\mu$ events.² To compare with previous measurements, this AUBERT 08AN value is from a fit that fixes the pole masses at $m_A = 2.5$ GeV/c² and $m_V = 2.1$ GeV/c². A simultaneous fit to r_2, r_V, r_0 (a significant s-wave contribution) and m_A , gives $r_2 = 0.763 \pm 0.071 \pm 0.065$.WEIGHTED AVERAGE
0.83 ± 0.08 (Error scaled by 1.8) $r_V \equiv V(0)/A_1(0)$ in $D_s^+ \rightarrow \phi \ell^+ \nu_\ell$

VALUE	EVTS	DOCUMENT ID	TECN	COMMENT
1.76 ± 0.07 OUR AVERAGE		Error includes scale factor of 1.1.		
1.58 ± 0.17 ± 0.02		¹ ABLIKIM	23Bz BES3	$D_s^+ \rightarrow K^+ K^- \mu^+ \nu_\mu$
1.807 ± 0.046 ± 0.065	25k	² AUBERT	08AN BABR	$\phi e^+ \nu_e$
1.549 ± 0.250 ± 0.148	793	LINK	04c FOCS	$\phi \mu^+ \nu_\mu$
2.27 ± 0.35 ± 0.22	271	AITALA	99D E791	$\phi e^+ \nu_e, \phi \mu^+ \nu_\mu$
0.9 ± 0.6 ± 0.3	308	AVERY	94B CLE2	$\phi e^+ \nu_e$
1.8 ± 0.9 ± 0.2	90	FRABETTI	94F E687	$\phi \mu^+ \nu_\mu$
2.3 $^{+1.1}_{-0.9}$ ± 0.4	19	KODAMA	93 E653	$\phi \mu^+ \nu_\mu$

¹ Partial wave analysis of 939 $D_s^+ \rightarrow K^+ K^- \mu^+ \nu_\mu$ events.² To compare with previous measurements, this AUBERT 08AN value is from a fit that fixes the pole masses at $m_A = 2.5$ GeV/c² and $m_V = 2.1$ GeV/c². A simultaneous fit to r_2, r_V, r_0 (a significant s-wave contribution) and m_A , gives $r_V = 1.849 \pm 0.060 \pm 0.095$. Γ_L/Γ_T in $D_s^+ \rightarrow \phi \ell^+ \nu_\ell$

VALUE	EVTS	DOCUMENT ID	TECN	COMMENT
0.72 ± 0.18 OUR AVERAGE				
1.0 ± 0.3 ± 0.2	308	AVERY	94B CLE2	$\phi e^+ \nu_e$
1.0 ± 0.5 ± 0.1	90	¹ FRABETTI	94F E687	$\phi \mu^+ \nu_\mu$
0.54 ± 0.21 ± 0.10	19	¹ KODAMA	93 E653	$\phi \mu^+ \nu_\mu$

¹ FRABETTI 94F and KODAMA 93 evaluate Γ_L/Γ_T for a lepton mass of zero. $f_+(0)$ in $D_s^+ \rightarrow \eta e^+ \nu_e$

VALUE	EVTS	DOCUMENT ID	TECN	COMMENT
0.4519 ± 0.0071 ± 0.0065	4k	ABLIKIM	23Bz BES3	$e^+ e^-$ at 4128–4226 MeV
• • • We do not use the following data for averages, fits, limits, etc. • • •				
0.445 ± 0.0053 ± 0.0044	1.8k	¹ ABLIKIM	19s BES3	$e^+ e^-$ at 4178 MeV

¹ Superseded by ABLIKIM 23Bz $f_+(0) |V_{cs}|$ in $D_s^+ \rightarrow \eta' e^+ \nu_e$

VALUE	EVTS	DOCUMENT ID	TECN	COMMENT
0.525 ± 0.024 ± 0.009	675	ABLIKIM	23Bz BES3	$e^+ e^-$ at 4128–4226 MeV
• • • We do not use the following data for averages, fits, limits, etc. • • •				
0.47 ± 0.049 ± 0.011	261	¹ ABLIKIM	19s BES3	$e^+ e^-$ at 4178 MeV

¹ Superseded by ABLIKIM 23Bz $f_+(0) |V_{cd}|$ in $D_s^+ \rightarrow K^0 e^+ \nu_e$

VALUE	EVTS	DOCUMENT ID	TECN	COMMENT
0.162 ± 0.019 ± 0.003	117	¹ ABLIKIM	19D BES3	$K_S^0 e^+ \nu_e$

¹ Using a two parameter fit in the z expansion. $r_V \equiv V(0)/A_1(0)$ in $D_s^+ \rightarrow K^*(892)^0 e^+ \nu_e$

VALUE	EVTS	DOCUMENT ID	TECN	COMMENT
1.67 ± 0.34 ± 0.16	155	ABLIKIM	19D BES3	$e^+ e^-$ at 4178 MeV

 $r_2 \equiv A_2(0)/A_1(0)$ in $D_s^+ \rightarrow K^*(892)^0 e^+ \nu_e$

VALUE	EVTS	DOCUMENT ID	TECN	COMMENT
0.77 ± 0.28 ± 0.07	155	ABLIKIM	19D BES3	$e^+ e^-$ at 4178 MeV

 $f_{D_s^+} |V_{cs}|$ in $D_s^+ \rightarrow \mu^+ \nu_\mu$

VALUE (MeV)	EVTS	DOCUMENT ID	TECN	COMMENT
241.8 ± 2.5 ± 2.2	2.5k	ABLIKIM	23BR BES3	$e^+ e^-$ at 4.128–4.226 GeV

• • • We do not use the following data for averages, fits, limits, etc. • • •

243.1 ± 3.0 ± 3.6 ± 1.0	2.2K	^{1,2} ABLIKIM	21BE BES3	$e^+ e^-$ at 4.178, 4.226 GeV
246.2 ± 3.6 ± 3.5	1.1k	² ABLIKIM	19E BES3	$e^+ e^-$ at 4178 MeV

¹ The third uncertainty is dominated by the uncertainty of the D_s^+ lifetime.² Superseded by ABLIKIM 23BR. $f_{D_s^+} |V_{cd}|$ in $D_s^+ \rightarrow \tau^+ \nu_\tau$

VALUE (MeV)	EVTS	DOCUMENT ID	TECN	COMMENT
246.6 ± 2.5 OUR AVERAGE				

248.3 ± 3.9 ± 3.1 ± 1.0	2.4k	¹ ABLIKIM	23BP BES3	$e^+ e^-$ at 4.128–4.226 GeV
246.7 ± 3.9 ± 3.6	2.3k	² ABLIKIM	23BX BES3	$e^+ e^-$ at 4.128–4.226 GeV
251.6 ± 5.9 ± 4.9	1.7k	³ ABLIKIM	21AF BES3	$e^+ e^-$ at 4.178, 4.226 GeV
244.4 ± 2.3 ± 2.9	4.9k	⁴ ABLIKIM	21AZ BES3	$e^+ e^-$ at 4.178, 4.226 GeV

• • • We do not use the following data for averages, fits, limits, etc. • • •

243.0 ± 5.8 ± 4.0 ± 1.0	950	^{5,6} ABLIKIM	21BE BES3	$e^+ e^-$ at 4.178, 4.226 GeV
-------------------------	-----	------------------------	-----------	-------------------------------

¹ ABLIKIM 23BP uses $\tau^+ \rightarrow \pi^+ \bar{\nu}_\tau$ decays. The third uncertainty is due to the input parameters, mainly the D_s^+ lifetime.² ABLIKIM 23BX uses $\tau^+ \rightarrow \mu^+ \nu_\mu \bar{\nu}_\tau$ decays.³ ABLIKIM 21AF uses $\tau^+ \rightarrow \pi^+ \pi^0 \bar{\nu}_\tau$ decays.⁴ ABLIKIM 21AZ uses $\tau^+ \rightarrow e^+ \nu_e \bar{\nu}_\tau$ decays.⁵ ABLIKIM 21BE uses $\tau^+ \rightarrow \pi^+ \bar{\nu}_\tau$ decays. When constrained by the Standard Model ratio of $\Gamma(D_s^+ \rightarrow \tau^+ \nu_\tau)/\Gamma(D_s^+ \rightarrow \mu^+ \nu_\mu) = 9.75$, the result is $243.2 \pm 2.3 \pm 3.3 \pm 1.0$.⁶ The third uncertainty is dominated by the uncertainty of the D_s^+ lifetime. Superseded by ABLIKIM 23BP. D_s^\pm REFERENCES

AAIJ	23AN JHEP 2307 204	R. Aaij et al.	(LHCb Collab.)
AAIJ	23E JHEP 2304 081	R. Aaij et al.	(LHCb Collab.)
AAIJ	23L JHEP 2307 067	R. Aaij et al.	(LHCb Collab.)
ABLIKIM	23AL PR D107 052010	M. Ablikim et al.	(BESIII Collab.)
ABLIKIM	23AV PR D108 032001	M. Ablikim et al.	(BESIII Collab.)
ABLIKIM	23BQ PR D108 092003	M. Ablikim et al.	(BESIII Collab.)
ABLIKIM	23BP PR D108 092014	M. Ablikim et al.	(BESIII Collab.)
ABLIKIM	23BR PR D108 112001	M. Ablikim et al.	(BESIII Collab.)
ABLIKIM	23BS PR D108 112002	M. Ablikim et al.	(BESIII Collab.)
ABLIKIM	23BX JHEP 2309 124	M. Ablikim et al.	(BESIII Collab.)
ABLIKIM	23BZ JHEP 2312 072	M. Ablikim et al.	(BESIII Collab.)
ADACHI	23G PRL 131 171803	I. Adachi et al.	(BELLE II Collab.)
LI	23G PR D107 033003	L.K. Li et al.	(BELLE Collab.)
MOON	23 PR D108 L111102	H.K. Moon et al.	(BELLE Collab.)
ABLIKIM	22AA JHEP 2204 058	M. Ablikim et al.	(BESIII Collab.)
ABLIKIM	22AB JHEP 2207 051	M. Ablikim et al.	(BESIII Collab.)
ABLIKIM	22AC JHEP 2208 196	M. Ablikim et al.	(BESIII Collab.)
ABLIKIM	22AH PRL 129 182001	M. Ablikim et al.	(BESIII Collab.)
ABLIKIM	22BH PR D106 112004	M. Ablikim et al.	(BESIII Collab.)
ABLIKIM	22BI PR D106 112006	M. Ablikim et al.	(BESIII Collab.)
ABLIKIM	22BL JHEP 2209 242	M. Ablikim et al.	(BESIII Collab.)
ABLIKIM	22F PR D105 L051103	M. Ablikim et al.	(BESIII Collab.)
ABLIKIM	22J PR D105 L031101	M. Ablikim et al.	(BESIII Collab.)
ABLIKIM	22Z JHEP 2201 052	M. Ablikim et al.	(BESIII Collab.)
AAIJ	21T JHEP 2106 044	R. Aaij et al.	(LHCb Collab.)
AAIJ	21U JHEP 2106 019	R. Aaij et al.	(LHCb Collab.)
ABLIKIM	21AB JHEP 2106 181	M. Ablikim et al.	(BESIII Collab.)
ABLIKIM	21AC PR D104 012003	M. Ablikim et al.	(BESIII Collab.)
ABLIKIM	21AE PR D104 012016	M. Ablikim et al.	(BESIII Collab.)
ABLIKIM	21AF PR D104 032001	M. Ablikim et al.	(BESIII Collab.)
ABLIKIM	21AR PR D104 L071101	M. Ablikim et al.	(BESIII Collab.)
ABLIKIM	21AZ PRL 127 171801	M. Ablikim et al.	(BESIII Collab.)
ABLIKIM	21BE PR D104 052009	M. Ablikim et al.	(BESIII Collab.)
ABLIKIM	21K PR D103 092006	M. Ablikim et al.	(BESIII Collab.)
ABLIKIM	21U PR D104 032011	M. Ablikim et al.	(BESIII Collab.)
ABLIKIM	21Y PR D103 092004	M. Ablikim et al.	(BESIII Collab.)
GUAN	21 PR D103 112005	Y. Guan et al.	(BELLE Collab.)
LEES	21A PR D104 072002	J.P. Lees et al.	(BABAR Collab.)
ABLIKIM	20R JHEP 2008 146	M. Ablikim et al.	(BESIII Collab.)
AAIJ	19G JHEP 1903 176	R. Aaij et al.	(LHCb Collab.)
AAIJ	19T PRL 122 191803	R. Aaij et al.	(LHCb Collab.)
ABLIKIM	19AD PR D99 072002	M. Ablikim et al.	(BESIII Collab.)
ABLIKIM	19AH PR D99 091101	M. Ablikim et al.	(BESIII Collab.)
ABLIKIM	19AM PR D99 112005	M. Ablikim et al.	(BESIII Collab.)
ABLIKIM	19BD PR D100 112008	M. Ablikim et al.	(BESIII Collab.)
ABLIKIM	19BE PRL 123 112001	M. Ablikim et al.	(BESIII Collab.)
ABLIKIM	19D PRL 122 061801	M. Ablikim et al.	(BESIII Collab.)
ABLIKIM	19E PRL 122 071802	M. Ablikim et al.	(BESIII Collab.)
ABLIKIM	19O PR D99 031101	M. Ablikim et al.	(BESIII Collab.)
ABLIKIM	19S PRL 122 121801	M. Ablikim et al.	(BESIII Collab.)
ABLIKIM	18A PR D97 012006	M. Ablikim et al.	(BESIII Collab.)
AAIJ	17AF PL B771 21	R. Aaij et al.	(LHCb Collab.)
AAIJ	17AM PRL 119 101801	R. Aaij et al.	(LHCb Collab.)
ABLIKIM	16O PR D94 072004	M. Ablikim et al.	(BESIII Collab.)
ABLIKIM	16T PR D94 112003	M. Ablikim et al.	(BESIII Collab.)
ABLIKIM	15Z PL B750 466	M. Ablikim et al.	(BESIII Collab.)
HIETALA	15 PR D92 012009	J. Hietala et al.	(MINN., LUTH., OXF)
LEES	15D PR D91 019901 (errata.)	J.P. Lees et al.	(BABAR Collab.)
AAIJ	14BD JHEP 1410 025	R. Aaij et al.	(LHCb Collab.)
AAIJ	14C PL B728 585	R. Aaij et al.	(LHCb Collab.)
ABAZOV	14B PRL 112 111804	V.M. Abazov et al.	(DO Collab.)

AAUJ	13AF	PL B724 203	R. Aaij et al.	(LHCb Collab.)
AAUJ	13V	JHEP 1306 065	R. Aaij et al.	(LHCb Collab.)
AAUJ	13W	JHEP 1306 112	R. Aaij et al.	(LHCb Collab.)
LEES	13E	PR D87 052012	J.P. Lees et al.	(BABAR Collab.)
ONYISI	13	PR D88 032009	P.U.E. Onyisi et al.	(CLEO Collab.)
ZUPANIC	13	JHEP 1309 139	A. Zupanic et al.	(BELLE Collab.)
DEL-AMO-SA...	11G	PR D83 052001	P. del Amo Sanchez et al.	(BABAR Collab.)
LEES	11E	PR D84 031103	J.P. Lees et al.	(BABAR Collab.)
LEES	11G	PR D84 072006	J.P. Lees et al.	(BABAR Collab.)
MARTIN	11	PR D84 012005	L. Martin et al.	(CLEO Collab.)
WILLIAMS	11	PR D84 054015	M. Williams	(CLEO Collab.)
ASNER	10	PR D81 052007	D.M. Asner et al.	(CLEO Collab.)
DEL-AMO-SA...	10J	PR D82 091103	P. del Amo Sanchez et al.	(BABAR Collab.)
Also		PR D91 019901 (errata.)	J.P. Lees et al.	(BABAR Collab.)
KO	10	PRL 104 181602	B.R. Ko et al.	(BELLE Collab.)
MENDEZ	10	PR D81 052013	H. Mendez et al.	(CLEO Collab.)
RUBIN	10	PR D82 092007	P. Rubin et al.	(CLEO Collab.)
ALEXANDER	09	PR D79 052001	J.P. Alexander et al.	(CLEO Collab.)
AUBERT	09O	PR D79 032003	B. Aubert et al.	(BABAR Collab.)
BEDIAGA	09	PR D80 096006	I. Bediaga et al.	(CBPF, NDAM Collab.)
DOBBS	09	PR D79 112008	S. Dobbs et al.	(CLEO Collab.)
ECKLUND	09	PR D80 052009	S.M. Ecklund et al.	(CLEO Collab.)
GE	09A	PR D80 051102	J.Y. Ge et al.	(CLEO Collab.)
KO	09	PRL 102 221802	B.R. Ko et al.	(BELLE Collab.)
MITCHELL	09A	PR D79 072008	R.E. Mitchell et al.	(CLEO Collab.)
NAIK	09A	PR D80 112004	P. Naik et al.	(CLEO Collab.)
ONYISI	09	PR D79 052002	P.U.E. Onyisi et al.	(CLEO Collab.)
WON	09	PR D80 111101	E. Won et al.	(BELLE Collab.)
YELTON	09	PR D80 052007	J. Yelton et al.	(CLEO Collab.)
ALEXANDER	08	PRL 100 161804	J.P. Alexander et al.	(CLEO Collab.)
ATHAR	08	PRL 100 161802	S.B. Athar et al.	(CLEO Collab.)
AUBERT	08AN	PR D78 051101	B. Aubert et al.	(BABAR Collab.)
AUBERT	08AO	PR D78 051102	B. Aubert et al.	(BABAR Collab.)
ECKLUND	08	PRL 100 161801	K.M. Ecklund et al.	(CLEO Collab.)
KLEMPPT	08	EPJ C55 39	E. Klempf, M. Matveev, A.V. Sarantsev	(BONN+ Collab.)
LINK	08	PL B660 147	J.M. Link et al.	(FNAL FOCUS Collab.)
WIDHALM	08	PRL 100 241801	L. Widhalm et al.	(BELLE Collab.)
ADAMS	07A	PRL 99 191805	G.S. Adams et al.	(CLEO Collab.)
AUBERT	07V	PRL 98 141801	B. Aubert et al.	(BABAR Collab.)
PEDLAR	07A	PR D76 072002	T.K. Pedlar et al.	(CLEO Collab.)
Also		PRL 99 071802	M. Artuso et al.	(CLEO Collab.)
AUBERT	06N	PR D74 031103	B. Aubert et al.	(BABAR Collab.)
HUANG	06B	PR D74 112005	H. Huang et al.	(CLEO Collab.)
PDG	06	IP G33 1	W.-M. Yao et al.	(PDG Collab.)
AUBERT	05V	PR D71 091104	B. Aubert et al.	(BABAR Collab.)
LINK	05E	PL B622 239	J.M. Link et al.	(FNAL FOCUS Collab.)
LINK	05J	PRL 95 052003	J.M. Link et al.	(FNAL FOCUS Collab.)
LINK	05K	PL B624 166	J.M. Link et al.	(FNAL FOCUS Collab.)
LINK	04	PL B585 200	J.M. Link et al.	(FNAL FOCUS Collab.)
LINK	04C	PL B586 183	J.M. Link et al.	(FNAL FOCUS Collab.)
LINK	04D	PL B586 191	J.M. Link et al.	(FNAL FOCUS Collab.)
LINK	04F	PL B601 10	J.M. Link et al.	(FNAL FOCUS Collab.)
ACOSTA	03D	PR D68 072004	D. Acosta et al.	(FNAL CDF-II Collab.)
ANISOVICH	03	EPJ A16 229	V.V. Anisovich et al.	(FNAL FOCUS Collab.)
LINK	03D	PL B561 225	J.M. Link et al.	(FNAL FOCUS Collab.)
LINK	03F	PL B572 21	J.M. Link et al.	(FNAL FOCUS Collab.)
AUBERT	02G	PR D65 091104	B. Aubert et al.	(BABAR Collab.)
HEISTER	02I	PL B528 1	A. Heister et al.	(ALEPH Collab.)
LINK	02I	PL B541 227	J.M. Link et al.	(FNAL FOCUS Collab.)
LINK	02J	PL B541 243	J.M. Link et al.	(FNAL FOCUS Collab.)
ABBBIENDI	01L	PL B516 236	G. Abbiendi et al.	(OPAL Collab.)
AITALA	01A	PRL 86 765	E.M. Aitala et al.	(FNAL E791 Collab.)
IORI	01	PL B523 22	M. Iori et al.	(FNAL SELEX Collab.)
LINK	01C	PRL 87 162001	J.M. Link et al.	(FNAL FOCUS Collab.)
ALEXANDROV	00	PL B478 31	Y. Alexandrov et al.	(CERN BEATRICE Collab.)
AITALA	99	PL B465 449	E.M. Aitala et al.	(FNAL E791 Collab.)
AITALA	99D	PL B450 294	E.M. Aitala et al.	(FNAL E791 Collab.)
AITALA	99G	PL B462 401	E.M. Aitala et al.	(FNAL E791 Collab.)
BONVICINI	99	PRL 82 4586	G. Bonvicini et al.	(CLEO Collab.)
CHADHA	98	PR D58 032002	M. Chada et al.	(CLEO Collab.)
JESSOP	98	PR D58 052002	C.P. Jessop et al.	(CLEO Collab.)
ACCIARRI	97F	PL B396 327	M. Acciarri et al.	(L3 Collab.)
BALEST	97	PRL 79 1436	R. Balest et al.	(CLEO Collab.)
FRABETTI	97C	PL B401 131	P.L. Frabetti et al.	(FNAL E687 Collab.)
FRABETTI	97D	PL B407 79	P.L. Frabetti et al.	(FNAL E687 Collab.)
ARTUSO	96	PL B378 364	M. Artuso et al.	(CLEO Collab.)
BAI	95C	PR D52 3781	H. Bai et al.	(BES Collab.)
BRANDENB...	95	PRL 75 3804	G.W. Brandenburg et al.	(CLEO Collab.)
FRABETTI	95B	PL B351 591	P.L. Frabetti et al.	(FNAL E687 Collab.)
KODAMA	95	PL B345 85	K. Kodama et al.	(FNAL E653 Collab.)
ACOSTA	94	PR D49 5690	D. Acosta et al.	(CLEO Collab.)
AVERY	94B	PL B337 405	P. Avery et al.	(CLEO Collab.)
BROWN	94	PR D50 1884	D. Brown et al.	(CLEO Collab.)
BUTLER	94	PL B324 255	F. Butler et al.	(CLEO Collab.)
FRABETTI	94F	PL B328 187	P.L. Frabetti et al.	(FNAL E687 Collab.)
FRABETTI	95F	PRL 71 827	P.L. Frabetti et al.	(FNAL E687 Collab.)
FRABETTI	93G	PL B313 253	P.L. Frabetti et al.	(FNAL E687 Collab.)
KODAMA	93	PL B309 483	K. Kodama et al.	(FNAL E653 Collab.)
ALBRECHT	92B	ZPHY C53 361	H. Albrecht et al.	(ARGUS Collab.)
ALEXANDER	92	PRL 68 1275	J. Alexander et al.	(CLEO Collab.)
AVERY	92	PRL 68 1279	P. Avery et al.	(CLEO Collab.)
BARLAG	92C	ZPHY C55 383	S. Barlag et al.	(ACCMOR Collab.)
Also		ZPHY C48 29	S. Barlag et al.	(ACCMOR Collab.)
FRABETTI	92	PL B281 167	P.L. Frabetti et al.	(FNAL E687 Collab.)
ALBRECHT	91	PL B255 634	H. Albrecht et al.	(ARGUS Collab.)
ALVAREZ	91	PL B255 639	M.P. Alvarez et al.	(CERN NA14/2 Collab.)
ALBRECHT	90D	PL B245 315	H. Albrecht et al.	(ARGUS Collab.)
ALEXANDER	90B	PRL 65 1531	J. Alexander et al.	(CLEO Collab.)
BARLAG	90C	ZPHY C46 563	S. Barlag et al.	(ACCMOR Collab.)
FRABETTI	90	PL B251 639	P.L. Frabetti et al.	(FNAL E687 Collab.)
ANJOS	89E	PL B223 267	J.C. Anjos et al.	(FNAL E691 Collab.)
CHEN	89	PL B226 192	W.Y. Chen et al.	(CLEO Collab.)
ALBRECHT	88	PL B207 349	H. Albrecht et al.	(ARGUS Collab.)
ANJOS	88	PRL 60 897	J.C. Anjos et al.	(FNAL E691 Collab.)
RAAB	88	PR D37 2391	J.R. Raab et al.	(FNAL E691 Collab.)
BECKER	87B	PL B184 277	H. Becker et al.	(NA11 and NA32 Collabs.)
BLAYLOCK	87	PRL 58 2171	G.T. Blaylock et al.	(Mark III Collab.)
USHIDA	86	PRL 56 1767	N. Ushida et al.	(FNAL E531 Collab.)
ALBRECHT	85D	PL B538 343	H. Albrecht et al.	(ARGUS Collab.)
DERICK	85B	PRL 54 2568	H. Derrick et al.	(HRS Collab.)
AIHARA	84D	PRL 53 2465	H. Aihara et al.	(TPC Collab.)
ALTHOFF	84	PL B366 130	M. Althoff et al.	(TASSO Collab.)
BAILEY	84	PL B398 320	R. Bailey et al.	(ACCMOR Collab.)
CHEN	83C	PRL 51 634	A. Chen et al.	(CLEO Collab.)
MOSTELLER	48	Am.Stat. 3 No.5 30	R.A. Fisher, F. Mosteller	

$D_s^{*\pm}$

$I(J^P) = 0(1^-)$

$J^P = 1^-$ established by ABLIKIM 23AZ.

$D_s^{*\pm}$ MASS

The fit includes $D^\pm, D^0, D_s^\pm, D^{*\pm}, D^{*0}, D_s^{*\pm}, D_1(2420)^0, D_{s1}^{*0}(2460)^0$, and $D_{s1}(2536)^\pm$ mass and mass difference measurements.

VALUE (MeV)	DOCUMENT ID	TECN	COMMENT
2112.2 ± 0.4 OUR FIT			
2106.6 ± 2.1 ± 2.7	¹ BLAYLOCK 87 MRK3		$e^+e^- \rightarrow D_s^{*\pm}\gamma X$

¹ Assuming $D_s^{*\pm}$ mass = 1968.7 ± 0.9 MeV.

$m_{D_s^{*\pm}} - m_{D_s^\pm}$

The fit includes $D^\pm, D^0, D_s^\pm, D^{*\pm}, D^{*0}, D_s^{*\pm}, D_1(2420)^0, D_{s1}^{*0}(2460)^0$, and $D_{s1}(2536)^\pm$ mass and mass difference measurements.

VALUE (MeV)	EVTS	DOCUMENT ID	TECN	COMMENT
143.8 ± 0.4 OUR FIT				
143.9 ± 0.4 OUR AVERAGE				
143.76 ± 0.39 ± 0.40		GRONBERG 95 CLE2		e^+e^-
144.22 ± 0.47 ± 0.37		BROWN 94 CLE2		e^+e^-
142.5 ± 0.8 ± 1.5		² ALBRECHT 88 ARG		$e^+e^- \rightarrow D_s^{*\pm}\gamma X$
139.5 ± 8.3 ± 9.7	60	AIHARA 84D	TPC	$e^+e^- \rightarrow$ hadrons
143.0 ± 18.0	8	ASRATYAN 85 HLBC	FNAL 15-ft, μ^-2H	
110 ± 46		BRANDELIK 79 DASP		$e^+e^- \rightarrow D_s^{*\pm}\gamma X$

² Result includes data of ALBRECHT 84b.

$D_s^{*\pm}$ WIDTH

VALUE (MeV)	CL%	DOCUMENT ID	TECN	COMMENT
< 1.9	90	GRONBERG 95 CLE2		e^+e^-
< 4.5	90	ALBRECHT 88 ARG		$E_{cm}^{ee} = 10.2$ GeV
< 4.9	90	BROWN 94 CLE2		e^+e^-
< 22	90	BLAYLOCK 87 MRK3		$e^+e^- \rightarrow D_s^{*\pm}\gamma X$

• • • We do not use the following data for averages, fits, limits, etc. • • •

D_s^{*+} DECAY MODES

D_s^{*+} modes are charge conjugates of the modes below.

Mode	Fraction (Γ_i/Γ)
$\Gamma_1 D_s^{*+}\gamma$	(93.6 ± 0.4) %
$\Gamma_2 D_s^{*+}\pi^0$	(5.77 ± 0.35) %
$\Gamma_3 D_s^{*+}e^+e^-$	(6.7 ± 1.6) × 10 ⁻³
$\Gamma_4 e^+\nu_e$	(2.1 $\frac{+1.2}{-0.9}$) × 10 ⁻⁵

CONSTRAINED FIT INFORMATION

An overall fit to 2 branching ratios uses 4 measurements and one constraint to determine 3 parameters. The overall fit has a $\chi^2 = 0.0$ for 2 degrees of freedom.

The following off-diagonal array elements are the correlation coefficients $\langle \delta x_i \delta x_j \rangle / (\delta x_i \delta x_j)$, in percent, from the fit to the branching fractions, $x_i \equiv \Gamma_i/\Gamma_{total}$. The fit constrains the x_i (argus labels appear in this array to sum to one).

x_2	-91	
x_3	-38	-4
	x_1	x_2

D_s^{*+} BRANCHING RATIOS

$\Gamma(D_s^{*+}\gamma)/\Gamma_{total}$	VALUE (%)	DOCUMENT ID	TECN	COMMENT
				• • • We do not use the following data for averages, fits, limits, etc. • • •
seen		ASRATYAN 91 HLBC		$\bar{\nu}_\mu Ne$
seen		ALBRECHT 88 ARG		$e^+e^- \rightarrow D_s^{*\pm}\gamma X$
seen		AIHARA 84D		
seen		ALBRECHT 84B		
seen		BRANDELIK 79		

OTHER RELATED PAPERS

RICHMAN	95	RMP 67 893	J.D. Richman, P.R. Burchat	(UCSB, STAN)
---------	----	------------	----------------------------	--------------

Meson Particle Listings

$D_s^{*\pm}, D_{s0}^*(2317)^\pm$

$\Gamma(D_s^+ \pi^0)/\Gamma(D_s^+ \gamma)$		Γ_2/Γ_1	
VALUE (units 10^{-2})	DOCUMENT ID	TECN	COMMENT
6.2 ± 0.4 OUR FIT			
6.2 ± 0.4 OUR AVERAGE			
6.16 ± 0.43 ± 0.18	ABLIKIM	23P BES3	$e^+ e^-$
6.2 ± 0.5 ± 0.6	AUBERT, BE	05G BABR	10.6 $e^+ e^- \rightarrow$ hadrons
6.2 $^{+2.0}_{-1.8} \pm 2.2$	GRONBERG	95 CLE2	$e^+ e^-$

$\Gamma(D_s^+ e^+ e^-)/\Gamma(D_s^+ \gamma)$		Γ_3/Γ_1	
VALUE (units 10^{-3})	EVTS	DOCUMENT ID	TECN COMMENT
7.2 ± 1.7 OUR FIT			
7.2 $^{+1.5}_{-1.3} \pm 1.0$	38	CRONIN-HEN.12	CLEO 4.17 $e^+ e^- \rightarrow$ hadrons

$\Gamma(e^+ \nu_e)/\Gamma_{total}$		Γ_4/Γ	
VALUE (units 10^{-5})	DOCUMENT ID	TECN	COMMENT
2.1 $^{+1.2}_{-0.9} \pm 0.2$	ABLIKIM	23BF BES3	$e^+ e^- \rightarrow D_s^- D_s^{*+}$

••• We do not use the following data for averages, fits, limits, etc. •••

349.6 ± 0.4 ± 3.0	1267	^{8,9} AUBERT	03G BABR	10.6 $e^+ e^-$
350.2 ± 1.3	273	^{10,11} AUBERT	03G BABR	10.6 $e^+ e^-$

⁷ Recalculated by us using $m_{D_s^+} = 1968.5 \pm 0.6$ MeV.

⁸ From $D_s^+ \rightarrow K^+ K^- \pi^+$ decay.

⁹ Recalculated by us using $m_{D_s^+} = 1967.20 \pm 0.03$ MeV.

¹⁰ From $D_s^+ \rightarrow K^+ K^- \pi^+ \pi^0$ decay.

¹¹ Recalculated by us using $m_{D_s^+} = 1967.4 \pm 0.2$ MeV. Systematic errors not estimated.

$D_{s0}^*(2317)^\pm$ WIDTH

VALUE (MeV)	CL%	EVTS	DOCUMENT ID	TECN	COMMENT
< 3.8	95	3180	AUBERT	06P BABR	10.6 $e^+ e^- \rightarrow D_s^+ \pi^0 X$
••• We do not use the following data for averages, fits, limits, etc. •••					
< 4.6	90	761	MIKAMI	04 BELL	10.6 $e^+ e^-$
< 10			AUBERT	03G BABR	10.6 $e^+ e^-$
< 7	90	135	BESSION	03 CLE2	10.6 $e^+ e^-$

$D_{s0}^*(2317)^\pm$ DECAY MODES

$D_{s0}^*(2317)^-$ modes are charge conjugates of modes below.

Mode	Fraction (Γ_i/Γ)	Confidence level
$\Gamma_1 D_s^+ \pi^0$	(100 $^{+0}_{-20}$) %	
$\Gamma_2 D_s^+ \gamma$	< 5 %	90%
$\Gamma_3 D_s^*(2112)^+ \gamma$	< 6 %	90%
$\Gamma_4 D_s^+ \gamma \gamma$	< 18 %	95%
$\Gamma_5 D_s^*(2112)^+ \pi^0$	< 11 %	90%
$\Gamma_6 D_s^+ \pi^+ \pi^-$	< 4 $\times 10^{-3}$	90%
$\Gamma_7 D_s^+ \pi^0 \pi^0$	not seen	

$D_{s0}^*(2317)^\pm$ BRANCHING RATIOS

$\Gamma(D_s^+ \pi^0)/\Gamma_{total}$		Γ_1/Γ	
VALUE	EVTS	DOCUMENT ID	TECN COMMENT
1.00 $^{+0.00+0.00}_{-0.14-0.14}$	47	ABLIKIM	18J BES3 4.6 $e^+ e^- \rightarrow D_s^+ \pi^0 X$
••• We do not use the following data for averages, fits, limits, etc. •••			
seen	1.5k	AUBERT	03G BABR 10.6 $e^+ e^-$

$\Gamma(D_s^+ \gamma)/\Gamma(D_s^+ \pi^0)$		Γ_2/Γ_1	
VALUE	CL%	DOCUMENT ID	TECN COMMENT
< 0.05	90	MIKAMI	04 BELL 10.6 $e^+ e^-$
••• We do not use the following data for averages, fits, limits, etc. •••			
< 0.14	95	AUBERT	06P BABR 10.6 $e^+ e^-$
< 0.052	90	BESSION	03 CLE2 10.6 $e^+ e^-$

$\Gamma(D_s^*(2112)^+ \gamma)/\Gamma(D_s^+ \pi^0)$		Γ_3/Γ_1	
VALUE	CL%	DOCUMENT ID	TECN COMMENT
< 0.059	90	BESSION	03 CLE2 10.6 $e^+ e^-$
••• We do not use the following data for averages, fits, limits, etc. •••			
< 0.16	95	AUBERT	06P BABR 10.6 $e^+ e^-$
< 0.18	90	MIKAMI	04 BELL 10.6 $e^+ e^-$

$\Gamma(D_s^+ \gamma \gamma)/\Gamma(D_s^+ \pi^0)$		Γ_4/Γ_1	
VALUE	CL%	DOCUMENT ID	TECN COMMENT
< 0.18	95	AUBERT	06P BABR 10.6 $e^+ e^-$
••• We do not use the following data for averages, fits, limits, etc. •••			
not seen		AUBERT	03G BABR 10.6 $e^+ e^-$

$\Gamma(D_s^*(2112)^+ \pi^0)/\Gamma(D_s^+ \pi^0)$		Γ_5/Γ_1	
VALUE	CL%	DOCUMENT ID	TECN COMMENT
< 0.11	90	BESSION	03 CLE2 10.6 $e^+ e^-$

$\Gamma(D_s^+ \pi^+ \pi^-)/\Gamma(D_s^+ \pi^0)$		Γ_6/Γ_1	
VALUE	CL%	DOCUMENT ID	TECN COMMENT
< 0.004	90	MIKAMI	04 BELL 10.6 $e^+ e^-$
••• We do not use the following data for averages, fits, limits, etc. •••			
< 0.005	95	AUBERT	06P BABR 10.6 $e^+ e^-$
< 0.019	90	BESSION	03 CLE2 10.6 $e^+ e^-$

$\Gamma(D_s^+ \pi^0 \pi^0)/\Gamma(D_s^+ \pi^0)$		Γ_7/Γ_1	
VALUE	CL%	DOCUMENT ID	TECN COMMENT
< 0.25	95	AUBERT	06P BABR 10.6 $e^+ e^-$

$D_s^{*\pm}$ REFERENCES

ABLIKIM	23AZ	PL B846	138245	M. Ablikim et al.	(BESIII Collab.) JP
ABLIKIM	23BF	PRL 131	141802	M. Ablikim et al.	(BESIII Collab.)
ABLIKIM	23P	PR D107	032011	M. Ablikim et al.	(BESIII Collab.)
CRONIN-HEN.12	12	PR D86	072005	D. Cronin-Hennessey et al.	(CLEO Collab.)
AUBERT, BE	05G	PR D72	091101	B. Aubert et al.	(BABAR Collab.)
GRONBERG	95	PRL 75	3232	J. Gronberg et al.	(CLEO Collab.)
BROWN	94	PR D50	1884	D. Brown et al.	(CLEO Collab.)
ASRATYAN	91	PL B257	525	A.E. Asratyan et al.	(ITEP, BELG, SACL+)
ALBRECHT	88	PL B207	349	H. Albrecht et al.	(ARGUS Collab.)
BLAYLOCK	87	PRL 58	2171	G.T. Blaylock et al.	(Mark III Collab.)
ASRATYAN	85	PL 156B	441	A.E. Asratyan et al.	(ITEP, SERP)
AIHARA	84D	PRL 53	2465	H. Aihara et al.	(TPC Collab.)
ALBRECHT	84B	PL 146B	111	H. Albrecht et al.	(ARGUS Collab.)
BRANDELIC	79	PL 80B	412	R. Brandelik et al.	(DASP Collab.)

$D_{s0}^*(2317)^\pm$

$I(J^P) = 0(0^+)$
 J, P need confirmation.

AUBERT 06P and CHOI 15A do not observe neutral and doubly charged partners of the $D_{s0}^*(2317)^+$. See the review on "Heavy Non- $q\bar{q}$ Mesons."

$D_{s0}^*(2317)^\pm$ MASS

The fit includes $D_s^\pm, D^0, D_s^\pm, D^{*±}, D^{*0}, D_s^{*±}, D_1(2420)^0, D_2^*(2460)^0$, and $D_{s1}(2536)^\pm$ mass and mass difference measurements.

VALUE (MeV)	EVTS	DOCUMENT ID	TECN	COMMENT
2317.8 ± 0.5 OUR FIT				
2318.0 ± 0.7 OUR AVERAGE				
2318.3 ± 1.2 ± 1.2	115	¹ ABLIKIM	18J BES3	4.6 $e^+ e^- \rightarrow D_s^{*\pm} D_{s0}^*(2317)^\mp$
2319.6 ± 0.2 ± 1.4	3.1k	AUBERT	06P BABR	10.6 $e^+ e^- \rightarrow D_s^+ \pi^0 X$
2317.3 ± 0.4 ± 0.8	1.0k	² AUBERT	04E BABR	10.6 $e^+ e^-$
••• We do not use the following data for averages, fits, limits, etc. •••				
2317.2 ± 1.3	88	³ AUBERT, B	04S BABR	$B \rightarrow D_{s0}^*(2317) + \bar{D}^*(*)$
2317.2 ± 0.5 ± 0.9	761	⁴ MIKAMI	04 BELL	10.6 $e^+ e^-$
2316.8 ± 0.4 ± 3.0	1.2k	^{4,5} AUBERT	03G BABR	10.6 $e^+ e^-$
2317.6 ± 1.3	273	^{4,6} AUBERT	03G BABR	10.6 $e^+ e^-$
2319.8 ± 2.1 ± 2.0	24	⁴ KROKOVNY	03B BELL	10.6 $e^+ e^-$

¹ From a fit of the D_s^* recoil mass where the $D_{s0}^*(2317)$ signal is described with a Crystal Ball function convolved with a Gaussian function.

² Supersedes AUBERT 03c.

³ Systematic errors not evaluated.

⁴ Not independent of the corresponding $m_{D_{s0}^*(2317)} - m_{D_s^*}$.

⁵ From $D_s^+ \rightarrow K^+ K^- \pi^+$ decay.

⁶ From $D_s^+ \rightarrow K^+ K^- \pi^+ \pi^0$ decay.

$m_{D_{s0}^*(2317)^\pm} - m_{D_s^\pm}$

The fit includes $D_s^\pm, D^0, D_s^\pm, D^{*±}, D^{*0}, D_s^{*±}, D_1(2420)^0, D_2^*(2460)^0$, and $D_{s1}(2536)^\pm$ mass and mass difference measurements.

VALUE (MeV)	EVTS	DOCUMENT ID	TECN	COMMENT
349.4 ± 0.5 OUR FIT				
349.2 ± 0.7 OUR AVERAGE				
348.7 ± 0.5 ± 0.7	761	MIKAMI	04 BELL	10.6 $e^+ e^-$
350.0 ± 1.2 ± 1.0	135	BESSION	03 CLE2	10.6 $e^+ e^-$
351.3 ± 2.1 ± 1.9	24	⁷ KROKOVNY	03B BELL	10.6 $e^+ e^-$

$D_{s0}^*(2317)^\pm$ REFERENCES

ABLIKIM	18J	PR D97 051103	M. Ablikim <i>et al.</i>	(BESIII Collab.)
CHOI	15A	PR D91 092011	S.-K. Choi <i>et al.</i>	(BELLE Collab.)
AUBERT	06P	PR D74 032007	B. Aubert <i>et al.</i>	(BABAR Collab.)
AUBERT	04E	PR D69 031101	B. Aubert <i>et al.</i>	(BABAR Collab.)
AUBERT,B	04S	PRL 93 181801	B. Aubert <i>et al.</i>	(BABAR Collab.)
MIKAMI	04	PRL 92 012002	Y. Mikami <i>et al.</i>	(BELLE Collab.)
AUBERT	03G	PRL 90 242001	B. Aubert <i>et al.</i>	(BABAR Collab.)
BESSION	03	PR D68 032002	D. Besson <i>et al.</i>	(CLEO Collab.)
KROKOVNY	03B	PRL 91 262002	P. Krokovny <i>et al.</i>	(BELLE Collab.)

$D_{s1}(2460)^\pm$

$I(J^P) = 0(1^+)$

See the review on "Heavy Non- $q\bar{q}$ Mesons."

$D_{s1}(2460)^\pm$ MASS

The fit includes $D^\pm, D^0, D_s^\pm, D^{*\pm}, D^{*0}, D_{s1}(2420)^0, D_{s2}^*(2460)^0$, and $D_{s1}(2536)^\pm$ mass and mass difference measurements.

VALUE (MeV)	EVTS	DOCUMENT ID	TECN	COMMENT
2459.5 ± 0.6 OUR FIT				Error includes scale factor of 1.1.
2459.6 ± 0.9 OUR AVERAGE				Error includes scale factor of 1.3.
2460.1 ± 0.2 ± 0.8	1	AUBERT 06P BABR		10.6 e ⁺ e ⁻
2458.0 ± 1.0 ± 1.0	195	AUBERT 04E BABR		10.6 e ⁺ e ⁻
• • • We do not use the following data for averages, fits, limits, etc. • • •				
2459.5 ± 1.2 ± 3.7	920	AUBERT 06P BABR		10.6 e ⁺ e ⁻ → D _s ⁺ γX
2458.6 ± 1.0 ± 2.5	560	AUBERT 06P BABR		10.6 e ⁺ e ⁻ → D _s ⁺ π ⁰ γX
2460.2 ± 0.2 ± 0.8	123	AUBERT 06P BABR		10.6 e ⁺ e ⁻ → D _s ⁺ π ⁺ π ⁻ X
2458.9 ± 1.5	112	² AUBERT,B 04S BABR		B → D _{s1} (2460) ⁺ $\bar{D}^{(*)}$
2461.1 ± 1.6	139	³ AUBERT,B 04S BABR		B → D _{s1} (2460) ⁺ $\bar{D}^{(*)}$
2456.5 ± 1.3 ± 1.3	126	^{4,5} MIKAMI 04 BELL		10.6 e ⁺ e ⁻
2459.5 ± 1.3 ± 2.0	152	^{6,7} MIKAMI 04 BELL		10.6 e ⁺ e ⁻
2459.9 ± 0.9 ± 1.6	60	^{6,7} MIKAMI 04 BELL		10.6 e ⁺ e ⁻
2459.2 ± 1.6 ± 2.0	57	KROKOVNY 03B BELL		10.6 e ⁺ e ⁻

- The average of the values obtained from the $D_s^+ \gamma, D_s^+ \pi^0 \gamma, D_s^+ \pi^+ \pi^-$ final state.
- Systematic errors not evaluated. From the decay to $D_s^{*+} \pi^0$.
- Systematic errors not evaluated. From the decay to $D_s^+ \gamma$.
- Not independent of the corresponding $m_{D_{s1}(2460)^\pm} - m_{D_s^{*\pm}}$.
- Using $m_{D_s^{*+}} = 2112.4 \pm 0.7$ MeV.
- Not independent of the corresponding $m_{D_{s1}(2460)^\pm} - m_{D_s^\pm}$.
- Using $m_{D_s^\pm} = 1968.5 \pm 0.6$ MeV.

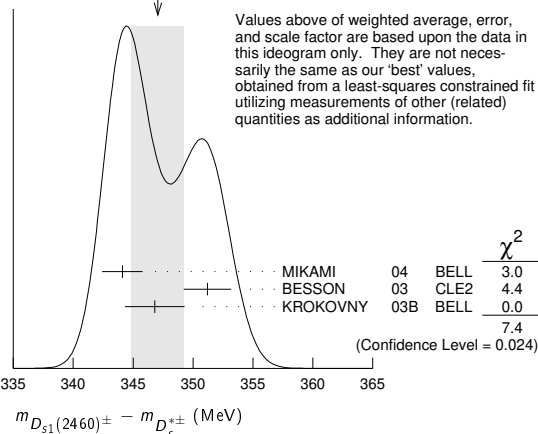
$m_{D_{s1}(2460)^\pm} - m_{D_s^{*\pm}}$

The fit includes $D^\pm, D^0, D_s^\pm, D^{*\pm}, D^{*0}, D_{s1}(2420)^0, D_{s2}^*(2460)^0$, and $D_{s1}(2536)^\pm$ mass and mass difference measurements.

VALUE (MeV)	EVTS	DOCUMENT ID	TECN	COMMENT
347.3 ± 0.7 OUR FIT				Error includes scale factor of 1.2.
347.1 ± 2.2 OUR AVERAGE				Error includes scale factor of 1.9. See the ideogram below.
344.1 ± 1.3 ± 1.1	126	MIKAMI 04 BELL		10.6 e ⁺ e ⁻
351.2 ± 1.7 ± 1.0	41	BESSION 03 CLE2		10.6 e ⁺ e ⁻
346.8 ± 1.6 ± 1.9	57	⁸ KROKOVNY 03B BELL		10.6 e ⁺ e ⁻

⁸ Recalculated by us using $m_{D_s^{*+}} = 2112.4 \pm 0.7$ MeV.

WEIGHTED AVERAGE
347.1 ± 2.2 (Error scaled by 1.9)



$m_{D_{s1}(2460)^\pm} - m_{D_s^\pm}$

The fit includes $D^\pm, D^0, D_s^\pm, D^{*\pm}, D^{*0}, D_s^{*\pm}, D_1(2420)^0, D_{s2}^*(2460)^0$, and $D_{s1}(2536)^\pm$ mass and mass difference measurements.

VALUE (MeV)	EVTS	DOCUMENT ID	TECN	COMMENT
491.1 ± 0.6 OUR FIT				Error includes scale factor of 1.1.
491.3 ± 1.4 OUR AVERAGE				
491.0 ± 1.3 ± 1.9	152	⁹ MIKAMI 04 BELL		10.6 e ⁺ e ⁻
491.4 ± 0.9 ± 1.5	60	¹⁰ MIKAMI 04 BELL		10.6 e ⁺ e ⁻

⁹ From the decay to $D_s^\pm \gamma$.
¹⁰ From the decay to $D_s^\pm \pi^+ \pi^-$.

$D_{s1}(2460)^\pm$ WIDTH

VALUE (MeV)	CL%	EVTS	DOCUMENT ID	TECN	COMMENT
< 3.5	95	123	AUBERT 06P BABR		10.6 e ⁺ e ⁻ → D _s ⁺ π ⁺ π ⁻ X
• • • We do not use the following data for averages, fits, limits, etc. • • •					
< 6.3	95	560	AUBERT 06P BABR		10.6 e ⁺ e ⁻ → D _s ⁺ π ⁰ γX
< 10		195	AUBERT 04E BABR		10.6 e ⁺ e ⁻
< 5.5	90	126	MIKAMI 04 BELL		10.6 e ⁺ e ⁻
< 7	90	41	BESSION 03 CLE2		10.6 e ⁺ e ⁻

$D_{s1}(2460)^\pm$ DECAY MODES

$D_{s1}(2460)^\pm$ modes are charge conjugates of the modes below.

Mode	Fraction (Γ_i/Γ)	Scale factor / Confidence level
$\Gamma_1 D_s^{*+} \pi^0$	(48 ± 11) %	
$\Gamma_2 D_s^+ \gamma$	(18 ± 4) %	
$\Gamma_3 D_s^+ \pi^+ \pi^-$	(4.3 ± 1.3) %	S=1.1
$\Gamma_4 D_s^+ \gamma$	< 8 %	CL=90%
$\Gamma_5 D_{s0}^*(2317)^+ \gamma$	(3.7 ^{+5.0} _{-2.4}) %	
$\Gamma_6 D_s^+ \pi^0$		
$\Gamma_7 D_s^+ \pi^0 \pi^0$		
$\Gamma_8 D_s^+ \gamma \gamma$		

CONSTRAINED FIT INFORMATION

An overall fit to 7 branching ratios uses 8 measurements and one constraint to determine 5 parameters. The overall fit has a $\chi^2 = 3.4$ for 4 degrees of freedom.

The following *off-diagonal* array elements are the correlation coefficients $\langle \delta x_i \delta x_j \rangle / (\delta x_i \delta x_j)$, in percent, from the fit to the branching fractions, $x_i \equiv \Gamma_i / \Gamma_{\text{total}}$. The fit constrains the x_i whose labels appear in this array to sum to one.

x_2	80		
x_3	68	62	
x_5	-3	25	26
	x_1	x_2	x_3

$D_{s1}(2460)^\pm$ BRANCHING RATIOS

$\Gamma(D_s^{*+} \pi^0) / \Gamma_{\text{total}}$	EVTS	DOCUMENT ID	TECN	COMMENT	Γ_1/Γ	
0.48 ± 0.11 OUR FIT						
0.56 ± 0.13 ± 0.09						
• • • We do not use the following data for averages, fits, limits, etc. • • •						
seen	41	BESSION 03 CLE2		10.6 e ⁺ e ⁻		
¹¹ Evaluated in AUBERT 06N including measurements from AUBERT,B 04S.						
$\Gamma(D_s^+ \gamma) / \Gamma_{\text{total}}$	DOCUMENT ID	TECN	COMMENT	Γ_2/Γ		
0.18 ± 0.04 OUR FIT						
0.16 ± 0.04 ± 0.03						
¹² Evaluated in AUBERT 06N including measurements from AUBERT,B 04S.						
$\Gamma(D_s^+ \gamma) / \Gamma(D_s^{*+} \pi^0)$	CL%	EVTS	DOCUMENT ID	TECN	COMMENT	Γ_2/Γ_1
0.38 ± 0.05 OUR FIT						
0.44 ± 0.09 OUR AVERAGE						
0.55 ± 0.13 ± 0.08	152	MIKAMI 04 BELL			10.6 e ⁺ e ⁻	
0.38 ± 0.11 ± 0.04	38	KROKOVNY 03B BELL			10.6 e ⁺ e ⁻	

Meson Particle Listings

$D_{s1}(2460)^\pm, D_{s1}(2536)^\pm$

••• We do not use the following data for averages, fits, limits, etc. •••

0.274±0.045±0.020	251	¹³ AUBERT,B	04s	BABR	$B \rightarrow D_{s1}(2460)^+ \bar{D}^{(*)}$
< 0.49	90	BESSON	03	CLE2	10.6 e ⁺ e ⁻

¹³Used by AUBERT 06N in their measurement of B($D_s^{*-} \pi^0$) and B($D_s^- \gamma$).

$\Gamma(D_s^+ \pi^+ \pi^-) / \Gamma(D_s^{*+} \pi^0)$ Γ_3/Γ_1

VALUE	CL%	EVTS	DOCUMENT ID	TECN	COMMENT
0.090±0.020 OUR FIT					Error includes scale factor of 1.2.
0.14 ± 0.04 ± 0.02		60	MIKAMI	04	BELL 10.6 e ⁺ e ⁻

••• We do not use the following data for averages, fits, limits, etc. •••

<0.08	90	BESSON	03	CLE2	10.6 e ⁺ e ⁻
-------	----	--------	----	------	------------------------------------

$\Gamma(D_s^{*+} \gamma) / \Gamma(D_s^{*+} \pi^0)$ Γ_4/Γ_1

VALUE	CL%	DOCUMENT ID	TECN	COMMENT	
<0.16		90	BESSON	03	CLE2 10.6 e ⁺ e ⁻
<0.31	90	MIKAMI	04	BELL 10.6 e ⁺ e ⁻	

••• We do not use the following data for averages, fits, limits, etc. •••

<0.58	90	BESSON	03	CLE2	10.6 e ⁺ e ⁻
-------	----	--------	----	------	------------------------------------

$\Gamma(D_{s0}^* (2317)^+ \gamma) / \Gamma(D_s^{*+} \pi^0)$ Γ_5/Γ_1

VALUE	CL%	DOCUMENT ID	TECN	COMMENT	
<0.22		95	AUBERT	04E	BABR 10.6 e ⁺ e ⁻

••• We do not use the following data for averages, fits, limits, etc. •••

<0.58	90	BESSON	03	CLE2	10.6 e ⁺ e ⁻
-------	----	--------	----	------	------------------------------------

$\Gamma(D_s^{*+} \pi^0) / [\Gamma(D_s^{*+} \pi^0) + \Gamma(D_{s0}^* (2317)^+ \gamma)]$ $\Gamma_1/(\Gamma_1+\Gamma_5)$

VALUE	CL%	DOCUMENT ID	TECN	COMMENT	
0.93±0.09 OUR FIT					
0.97±0.09±0.05			AUBERT	06P	BABR 10.6 e ⁺ e ⁻

$\Gamma(D_s^+ \gamma) / [\Gamma(D_s^{*+} \pi^0) + \Gamma(D_{s0}^* (2317)^+ \gamma)]$ $\Gamma_2/(\Gamma_1+\Gamma_5)$

VALUE	CL%	DOCUMENT ID	TECN	COMMENT	
0.35 ± 0.04 OUR FIT					
0.337±0.036±0.038			AUBERT	06P	BABR 10.6 e ⁺ e ⁻

$\Gamma(D_s^+ \pi^+ \pi^-) / [\Gamma(D_s^{*+} \pi^0) + \Gamma(D_{s0}^* (2317)^+ \gamma)]$ $\Gamma_3/(\Gamma_1+\Gamma_5)$

VALUE	CL%	DOCUMENT ID	TECN	COMMENT	
0.083±0.017 OUR FIT				Error includes scale factor of 1.2.	
0.077±0.013±0.008			AUBERT	06P	BABR 10.6 e ⁺ e ⁻

$\Gamma(D_s^{*+} \gamma) / [\Gamma(D_s^{*+} \pi^0) + \Gamma(D_{s0}^* (2317)^+ \gamma)]$ $\Gamma_4/(\Gamma_1+\Gamma_5)$

VALUE	CL%	DOCUMENT ID	TECN	COMMENT	
<0.24		95	AUBERT	06P	BABR 10.6 e ⁺ e ⁻

$\Gamma(D_{s0}^* (2317)^+ \gamma) / [\Gamma(D_s^{*+} \pi^0) + \Gamma(D_{s0}^* (2317)^+ \gamma)]$ $\Gamma_5/(\Gamma_1+\Gamma_5)$

VALUE	CL%	DOCUMENT ID	TECN	COMMENT	
<0.25		95	AUBERT	06P	BABR 10.6 e ⁺ e ⁻

$\Gamma(D_s^+ \pi^0) / [\Gamma(D_s^{*+} \pi^0) + \Gamma(D_{s0}^* (2317)^+ \gamma)]$ $\Gamma_6/(\Gamma_1+\Gamma_5)$

VALUE	CL%	DOCUMENT ID	TECN	COMMENT	
<0.042		95	AUBERT	06P	BABR 10.6 e ⁺ e ⁻

$\Gamma(D_s^+ \pi^0 \pi^0) / [\Gamma(D_s^{*+} \pi^0) + \Gamma(D_{s0}^* (2317)^+ \gamma)]$ $\Gamma_7/(\Gamma_1+\Gamma_5)$

VALUE	CL%	DOCUMENT ID	TECN	COMMENT	
<0.68		95	AUBERT	06P	BABR 10.6 e ⁺ e ⁻

$\Gamma(D_s^+ \gamma \gamma) / [\Gamma(D_s^{*+} \pi^0) + \Gamma(D_{s0}^* (2317)^+ \gamma)]$ $\Gamma_8/(\Gamma_1+\Gamma_5)$

VALUE	CL%	DOCUMENT ID	TECN	COMMENT	
<0.33		95	AUBERT	06P	BABR 10.6 e ⁺ e ⁻

$D_{s1}(2460)^\pm$ REFERENCES

AUBERT 06N PR D74 031103	B. Aubert et al.	(BABAR Collab.)
AUBERT 06P PR D74 032007	B. Aubert et al.	(BABAR Collab.)
AUBERT 04E PR D69 031101	B. Aubert et al.	(BABAR Collab.)
AUBERT,B 04s PRL 93 181901	B. Aubert et al.	(BABAR Collab.)
MIKAMI 04 PRL 92 012002	Y. Mikami et al.	(BELLE Collab.)
BESSON 03 PR D68 032002	D. Besson et al.	(CLEO Collab.)
KROKOVNY 03B PRL 91 262002	P. Krokovny et al.	(BELLE Collab.)

$D_{s1}(2536)^\pm$

$$J(J^P) = 0(1^+)$$

J, P need confirmation.

Seen in $D^*(2010)^+ K^0, D^*(2007)^0 K^+,$ and $D_s^+ \pi^+ \pi^-$. Not seen in $D^+ K^0$ or $D^0 K^+$. $J^P = 1^+$ assignment strongly favored.

$D_{s1}(2536)^\pm$ MASS

The fit includes $D^\pm, D^0, D_s^\pm, D^{*\pm}, D^{*0}, D_s^{*\pm}, D_1(2420)^0, D_2^*(2460)^0,$ and $D_{s1}(2536)^\pm$ mass and mass difference measurements.

VALUE (MeV)	CL%	EVTS	DOCUMENT ID	TECN	COMMENT
2535.11±0.06 OUR FIT					
2535.21±0.28 OUR AVERAGE					
2537.7 ± 0.5 ± 3.1	24		¹ ABLIKIM	19P	BES3 4.6 e ⁺ e ⁻ → $D_s^+ \bar{D}^0 K^-$
2535.7 ± 0.6 ± 0.5	46		² ABAZOV	09G	D0 $B_s^0 \rightarrow D_{s1}^- \mu^+ \nu_\mu X$

2534.78±0.31±0.40	182	AUBERT	08B	BABR	$B \rightarrow \bar{D}^{(*)} D^* K$
2534.6 ± 0.3 ± 0.7	193	AUBERT	06P	BABR	10.6 e ⁺ e ⁻ → $D_s^+ \pi^+ \pi^- X$

2535.3 ± 0.7	92	³ HEISTER	02B	ALEP	e ⁺ e ⁻ → $D^{*+} K^0 X,$ $D^{*0} K^+ X$
--------------	----	----------------------	-----	------	---

2534.2 ± 1.2	9	ASRATYAN	94	BEBC	$\nu N \rightarrow D^{*+} K^0 X, D^{*0} K^\pm X$
--------------	---	----------	----	------	--

2535 ± 0.6 ± 1	75	FRABETTI	94B	E687	$\gamma Be \rightarrow D^{*+} K^0 X,$ $D^{*0} K^+ X$
----------------	----	----------	-----	------	---

2535.2 ± 0.5 ± 1.5	28	ALBRECHT	92R	ARG	10.4 e ⁺ e ⁻ → $D^{*0} K^+ X$
--------------------	----	----------	-----	-----	---

2536.6 ± 0.7 ± 0.4		AVERY	90	CLEO	e ⁺ e ⁻ → $D^{*+} K^0 X$
--------------------	--	-------	----	------	--

2535.9 ± 0.6 ± 2.0		ALBRECHT	89E	ARG	$D_{s1}^+ \rightarrow D^*(2010) K^0$
--------------------	--	----------	-----	-----	--------------------------------------

••• We do not use the following data for averages, fits, limits, etc. •••

2534.1 ± 0.6	116	⁴ AUSHEV	11	BELL	$B \rightarrow D_{s1}(2536) + D^{(*)}$
--------------	-----	---------------------	----	------	--

2535.08±0.01±0.15	8038	⁵ LEES	11B	BABR	10.6 e ⁺ e ⁻ → $D^{*+} K_S^0 X$
-------------------	------	-------------------	-----	------	---

2535.57 ^{+0.44} _{-0.41} ±0.10	236	⁶ CHEKANOV	09	ZEUS	e [±] p → $D^{*+} K_S^0 X,$ $D^{*0} K^+ X$
---	-----	-----------------------	----	------	--

2535.3 ± 0.2 ± 0.5	134	⁷ ALEXANDER	93	CLE2	e ⁺ e ⁻ → $D^{*0} K^+ X$
--------------------	-----	------------------------	----	------	--

2534.8 ± 0.6 ± 0.6	44	⁸ ALEXANDER	93	CLE2	e ⁺ e ⁻ → $D^{*+} K^0 X$
--------------------	----	------------------------	----	------	--

2535 ± 28		⁹ ASRATYAN	88	HLBC	$\nu N \rightarrow D_s \gamma \gamma X$
-----------	--	-----------------------	----	------	---

¹ From a fit of the D_s^+ recoil mass distribution with an incoherent sum of the S-wave and D-wave Breit-Wigner line shapes.
² Using the $D^*(2010)^\pm$ mass of 2010.0 ± 0.4 MeV from PDG 06.
³ Calculated using $m(D^*(2010)^\pm) = 2010.0 \pm 0.5$ MeV, $m(D^*(2007)^0) = 2006.7 \pm 0.5$ MeV, and the mass difference below.
⁴ Systematic uncertainties not evaluated.
⁵ Calculated using the mass difference $m(D_{s1}^+) - m(D^{*+})_{PDG}$ below and $m(D^{*+})_{PDG} = 2010.25 \pm 0.14$ MeV. Assuming S-wave decay of the $D_{s1}(2536)$ to $D^{*+} K_S^0$, using a Breit-Wigner line shape corresponding to L=0.
⁶ Calculated using the mass difference $m(D_{s1}^+) - m(D^{*+})_{PDG}$ reported below and $m(D^{*+})_{PDG} = 2010.27 \pm 0.17$ MeV.
⁷ Calculated using $m(D^*(2007)^0) = 2006.6 \pm 0.5$ MeV and the mass difference below.
⁸ Calculated using $m(D^*(2010)^\pm) = 2010.1 \pm 0.6$ MeV and the mass difference below.
⁹ Not seen in $D^* K$.

$m_{D_{s1}(2536)^\pm} - m_{D_s^*(2111)}$

The fit includes $D^\pm, D^0, D_s^\pm, D^{*\pm}, D^{*0}, D_s^{*\pm}, D_1(2420)^0, D_2^*(2460)^0,$ and $D_{s1}(2536)^\pm$ mass and mass difference measurements.

VALUE (MeV)	CL%	EVTS	DOCUMENT ID	TECN	COMMENT
422.9 ± 0.4 OUR FIT					
424 ± 28			ASRATYAN	88	HLBC $D_s^{*\pm} \gamma$

$m_{D_{s1}(2536)^\pm} - m_{D^*(2010)^\pm}$

The fit includes $D^\pm, D^0, D_s^\pm, D^{*\pm}, D^{*0}, D_s^{*\pm}, D_1(2420)^0, D_2^*(2460)^0,$ and $D_{s1}(2536)^\pm$ mass and mass difference measurements.

VALUE (MeV)	CL%	EVTS	DOCUMENT ID	TECN	COMMENT
524.85 ± 0.04 OUR FIT					
524.84 ± 0.04 OUR AVERAGE					

524.83±0.01±0.04	8038	¹⁰ LEES	11B	BABR	10.6 e ⁺ e ⁻ → $D^{*+} K_S^0 X$
------------------	------	--------------------	-----	------	---

525.30 ^{+0.44} _{-0.41} ±0.10	236 ± 30	CHEKANOV	09	ZEUS	e [±] p → $D^{*+} K_S^0 X,$ $D^{*0} K^+ X$
--	----------	----------	----	------	--

525.3 ± 0.6 ± 0.1	41	HEISTER	02B	ALEP	e ⁺ e ⁻ → $D^{*+} K^0 X$
-------------------	----	---------	-----	------	--

524.7 ± 0.6 ± 0.2	44	ALEXANDER93	CLE2		e ⁺ e ⁻ → $D^{*+} K_S^0 X$
-------------------	----	-------------	------	--	--

¹⁰ Assuming S-wave decay of the $D_{s1}(2536)$ to $D^{*+} K_S^0$, using a Breit-Wigner line shape corresponding to L=0.

$m_{D_{s1}(2536)^\pm} - m_{D^*(2007)^0}$

The fit includes $D^\pm, D^0, D_s^\pm, D^{*\pm}, D^{*0}, D_s^{*\pm}, D_1(2420)^0, D_2^*(2460)^0,$ and $D_{s1}(2536)^\pm$ mass and mass difference measurements.

VALUE (MeV)	CL%	EVTS	DOCUMENT ID	TECN	COMMENT
528.26 ± 0.05 OUR FIT					Error includes scale factor of 1.1.
528.68 ± 0.28 OUR AVERAGE					

528.7 ± 1.9 ± 0.5	51	HEISTER	02B	ALEP	e ⁺ e ⁻ → $D^{*0} K^+ X$
-------------------	----	---------	-----	------	--

527.3 ± 2.2	29	ACKERSTAFF	97W	OPAL	e ⁺ e ⁻ → $D^{*0} K^+ X$
-------------	----	------------	-----	------	--

528.7 ± 0.2 ± 0.2	134	ALEXANDER	93	CLE2	e ⁺ e ⁻ → $D^{*0} K^+ X$
-------------------	-----	-----------	----	------	--

$D_{s1}(2536)^\pm$ WIDTH

VALUE (MeV)	CL%	EVTS	DOCUMENT ID	TECN	COMMENT
0.92 ± 0.05 OUR AVERAGE					
1.7 ± 1.2 ± 0.6	24		¹¹ ABLIKIM	19P	BES3 4.6 e ⁺ e ⁻ → $D_s^+ \bar{D}^0 K^-$
0.92±0.03±0.04	8038		¹² LEES	11B	BABR 10.6 e ⁺ e ⁻ → $D^{*+} K_S^0 X$

See key on page 1171

Meson Particle Listings

$D_{s1}(2536)^\pm, D_{s2}^*(2573)$

••• We do not use the following data for averages, fits, limits, etc. •••

VALUE	EVTS	DOCUMENT ID	TECN	COMMENT
0.75 ± 0.23	116	13 AUSHEV	11 BELL	$B \rightarrow D_{s1}(2536) + D^{(*)}$
< 2.5	95 193	AUBERT	06P BABR	$10.6 e^+ e^- \rightarrow D_{s1}^+ \pi^+ \pi^- X$
< 3.2	90 75	FRABETTI	94B E687	$\gamma Be \rightarrow D^{*+} K^0 X, D^{*0} K^+ X$
< 2.3	90	ALEXANDER	93 CLEO	$e^+ e^- \rightarrow D^{*0} K^+ X$
< 3.9	90	ALBRECHT	92R ARG	$10.4 e^+ e^- \rightarrow D^{*0} K^+ X$
< 5.44	90	AVERY	90 CLEO	$e^+ e^- \rightarrow D^{*+} K^0 X$
< 4.6	90	ALBRECHT	89E ARG	$D_{s1}^* \rightarrow D^*(2010) K^0$

¹¹ From a fit of the D_s^+ recoil mass distribution with an incoherent sum of the S-wave and S-wave Breit-Wigner line shapes.
¹² Assuming S-wave decay of the $D_{s1}(2536)$ to $D^{*+} K_S^0$, using a Breit-Wigner line shape corresponding to L=0.
¹³ Systematic uncertainties not evaluated.

$D_{s1}(2536)^+$ DECAY MODES

Branching fractions are given relative to the one DEFINED AS 1.
 $D_{s1}(2536)^-$ modes are charge conjugates of the modes below.

Mode	Fraction (Γ_i/Γ)	Confidence level
Γ_1 $D^*(2010)^+ K^0$	0.85 ± 0.12	
Γ_2 $(D^*(2010)^+ K^0)_{S-wave}$	0.61 ± 0.09	
Γ_3 $(D^*(2010)^+ K^0)_{D-wave}$		
Γ_4 $K_S^0 D^*(2010)^+$	0.48 ± 0.07	
Γ_5 $D^+ \pi^- K^+$	0.028 ± 0.005	
Γ_6 $D^*(2007)^0 K^+$	DEFINED AS 1	
Γ_7 $D^+ K^0$	< 0.34	90%
Γ_8 $D^0 K^+$	< 0.12	90%
Γ_9 $D_s^{*+} \gamma$	possibly seen	
Γ_{10} $D_s^+ \pi^+ \pi^-$	seen	

$D_{s1}(2536)^+$ BRANCHING RATIOS

$\Gamma(D^*(2007)^0 K^+)/\Gamma(D^*(2010)^+ K^0)$ Γ_6/Γ_1

VALUE	EVTS	DOCUMENT ID	TECN	COMMENT
1.18 ± 0.16 OUR AVERAGE				
0.88 ± 0.24 ± 0.08	116	AUSHEV	11 BELL	$B \rightarrow D_{s1}(2536) + D^{(*)}$
2.3 ± 0.6 ± 0.3	236 ± 30	CHEKANOV	09 ZEUS	$e^\pm p \rightarrow D^{*+} K_S^0 X, D^{*0} K^+ X$
1.32 ± 0.47 ± 0.23	92	14 HEISTER	02B ALEP	$e^+ e^- \rightarrow D^{*+} K^0 X, D^{*0} K^+ X$
1.9 $^{+1.1}_{-0.9}$ ± 0.4	35	14 ACKERSTAFF	97W OPAL	$e^+ e^- \rightarrow D^{*0} K^+ X, D^{*+} K^0 X$
1.1 ± 0.3		ALEXANDER	93 CLEO	$e^+ e^- \rightarrow D^{*0} K^+ X, D^{*+} K^0 X$
1.4 ± 0.3 ± 0.2	15	ALBRECHT	92R ARG	$10.4 e^+ e^- \rightarrow D^{*0} K^+ X, D^{*+} K^0 X$

¹⁴ Ratio of the production rates measured in Z^0 decays.
¹⁵ Evaluated by us from published inclusive cross-sections.

$\Gamma(K_S^0 D^*(2010)^+)/\Gamma(D^*(2007)^0 K^+)$ Γ_4/Γ_6

VALUE	DOCUMENT ID	TECN	COMMENT
0.48 ± 0.07 ± 0.02	GAO	23 BELL	$e^+ e^-$ at 10.52 GeV

$\Gamma((D^*(2010)^+ K^0)_{S-wave})/\Gamma(D^*(2010)^+ K^0)$ Γ_2/Γ_1

VALUE	EVTS	DOCUMENT ID	TECN	COMMENT
0.72 ± 0.05 ± 0.01	5485	BALAGURA	08 BELL	$10.6 e^+ e^- \rightarrow D^{*+} K^0 X$

$\Gamma(D^+ \pi^- K^+)/\Gamma(D^*(2010)^+ K^0)$ Γ_5/Γ_1

VALUE (units 10^{-2})	EVTS	DOCUMENT ID	TECN	COMMENT
3.27 ± 0.18 ± 0.37	1264	BALAGURA	08 BELL	$10.6 e^+ e^- \rightarrow D^+ \pi^- K^+ X$

$\Gamma(D^+ K^0)/\Gamma(D^*(2010)^+ K^0)$ Γ_7/Γ_1

VALUE	CL%	DOCUMENT ID	TECN	COMMENT
< 0.40	90	ALEXANDER	93 CLEO	$e^+ e^- \rightarrow D^{*+} K^0 X$

••• We do not use the following data for averages, fits, limits, etc. •••

< 0.43	90	ALBRECHT	89E ARG	$D_{s1}^* \rightarrow D^*(2010) K^0$
--------	----	----------	---------	--------------------------------------

$\Gamma(D^0 K^+)/\Gamma(D^*(2007)^0 K^+)$ Γ_8/Γ_6

VALUE	CL%	DOCUMENT ID	TECN	COMMENT
< 0.12	90	ALEXANDER	93 CLEO	$e^+ e^- \rightarrow D^{*0} K^+ X$

$\Gamma(D_s^{*+} \gamma)/\Gamma_{total}$ Γ_9/Γ

VALUE	DOCUMENT ID	TECN	COMMENT
possibly seen	ASRATYAN	88 HLBC	$\nu N \rightarrow D_s \gamma \gamma X$

$\Gamma(D_s^{*+} \gamma)/\Gamma(D^*(2007)^0 K^+)$ Γ_9/Γ_6

VALUE	CL%	DOCUMENT ID	TECN	COMMENT
< 0.42	90	ALEXANDER	93 CLEO	$e^+ e^- \rightarrow D^{*0} K^+ X$

$\Gamma(D_s^+ \pi^+ \pi^-)/\Gamma_{total}$ Γ_{10}/Γ

VALUE	DOCUMENT ID	TECN	COMMENT
seen	AUBERT	06P BABR	$10.6 e^+ e^- \rightarrow D_s^+ \pi^+ \pi^- X$

$D_{s1}(2536)^\pm$ REFERENCES

GAO	23	PR D108 112015	B.S. Gao <i>et al.</i>	(BELLE Collab.)
ABLIKIM	19P	CP C43 031001	M. Ablikim <i>et al.</i>	(BESIII Collab.)
AUSHEV	11	PR D83 051102	T. Aushev <i>et al.</i>	(BELLE Collab.)
LEES	11B	PR D83 072003	J.P. Lees <i>et al.</i>	(BABAR Collab.)
ABAZOV	09G	PRL 102 051801	V.M. Abazov <i>et al.</i>	(DO Collab.)
CHEKANOV	09	EPL C60 25	S. Chekanov <i>et al.</i>	(ZEUS Collab.)
AUBERT	08B	PR D77 011102	B. Aubert <i>et al.</i>	(BABAR Collab.)
BALAGURA	08	PR D77 032001	V. Balagura <i>et al.</i>	(BELLE Collab.)
AUBERT	06P	PR D74 032007	B. Aubert <i>et al.</i>	(BABAR Collab.)
PDG	06	JP G33 1	W.-M. Yao <i>et al.</i>	(PDG Collab.)
HEISTER	02B	PL B526 34	A. Heister <i>et al.</i>	(ALEPH Collab.)
ACKERSTAFF	97W	ZPHY C76 425	K. Ackerstaff <i>et al.</i>	(OPAL Collab.)
ASRATYAN	94	ZPHY C61 563	A.E. Asratyan <i>et al.</i>	(BIRM, BELG, CERN+)
FRABETTI	94B	PRL 72 324	P.L. Frabetti <i>et al.</i>	(FNAL E687 Collab.)
ALEXANDER	93	PL B303 377	J. Alexander <i>et al.</i>	(CLEO Collab.)
ALBRECHT	92R	PL B297 425	H. Albrecht <i>et al.</i>	(ARGUS Collab.)
AVERY	90	PR D41 774	P. Avery, D. Besson	(CLEO Collab.)
ALBRECHT	89E	PL B230 162	H. Albrecht <i>et al.</i>	(ARGUS Collab.)
ASRATYAN	88	ZPHY C40 483	A.E. Asratyan <i>et al.</i>	(ITEP, SERP)

$D_{s2}^*(2573)$

$J(P) = 0(2^+)$

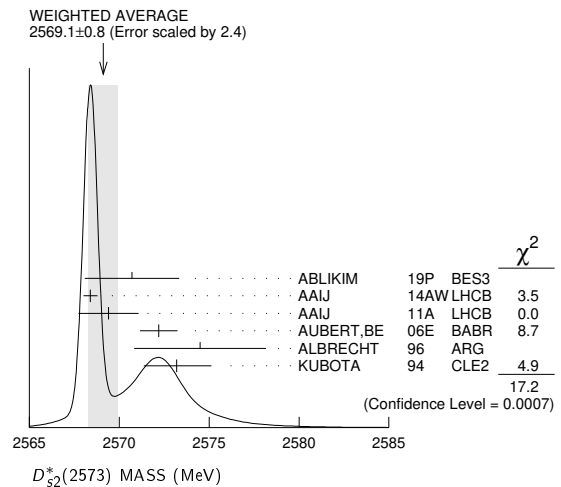
$D_{s2}^*(2573)$ MASS

VALUE (MeV)	EVTS	DOCUMENT ID	TECN	COMMENT
2569.1 ± 0.8 OUR AVERAGE				Error includes scale factor of 2.4. See the ideogram below.
2570.7 ± 2.0 ± 1.7	62	¹ ABLIKIM	19P BES3	$4.6 e^+ e^- \rightarrow D^+ \bar{D}^0 K^-$
2568.39 ± 0.29 ± 0.26		AAIJ	14AWLHCB	$B_S^0 \rightarrow \bar{D}^0 K^- \pi^+$
2569.4 ± 1.6 ± 0.5	82	AAIJ	11A LHCB	$B_S \rightarrow D_{s2}^*(2573) \mu \bar{\nu} X$
2572.2 ± 0.3 ± 1.0		AUBERT, BE	06E BABR	$e^+ e^- \rightarrow D K X$
2574.5 ± 3.3 ± 1.6		ALBRECHT	96 ARG	$e^+ e^- \rightarrow D^0 K^+ X$
2573.2 $^{+1.7}_{-1.6}$ ± 0.9	217	KUBOTA	94 CLE2	$e^+ e^- \sim 10.5$ GeV

••• We do not use the following data for averages, fits, limits, etc. •••

2570.0 ± 4.3	25	² EVDOKIMOV	04 SELX	$600 \Sigma^- A \rightarrow D^0 K^+ X$
2568.6 ± 3.2	64	³ HEISTER	02B ALEP	$e^+ e^- \rightarrow D^0 K^+ X$

¹ From a fit of the D_s^+ recoil mass distribution.
² Not independent of the mass difference below.
³ Calculated using $m_{D^0} = 1864.5 \pm 0.5$ MeV and the mass difference below.



$m_{D_{s2}^*(2573)} - m_{D^0}$

VALUE (MeV)	EVTS	DOCUMENT ID	TECN	COMMENT
704 ± 3 ± 1	64	HEISTER	02B ALEP	$e^+ e^- \rightarrow D^0 K^+ X$
705.4 ± 4.3	25	¹ EVDOKIMOV	04 SELX	$600 \Sigma^- A \rightarrow D^0 K^+ X$

¹ Systematic errors not estimated.

$D_{s2}^*(2573)$ WIDTH

VALUE (MeV)	EVTS	DOCUMENT ID	TECN	COMMENT
16.9 ± 0.7 OUR AVERAGE				
17.2 ± 3.6 ± 1.1	62	¹ ABLIKIM	19P BES3	$4.6 e^+ e^- \rightarrow D_s^+ \bar{D}^0 K^-$
16.9 ± 0.5 ± 0.6		AAIJ	14AWLHCB	$B_S^0 \rightarrow \bar{D}^0 K^- \pi^+$
12.1 ± 4.5 ± 1.6	82	AAIJ	11A LHCB	$B_S \rightarrow D_{s2}^*(2573) \mu \bar{\nu} X$

Meson Particle Listings

$D_{s2}^*(2573)$, $D_{s0}(2590)^+$, $D_{s1}^*(2700)^\pm$

27.1 ± 0.6 ± 5.6	AUBERT, BE	06E	BABR	$e^+e^- \rightarrow DKX$
10.4 ± 8.3 ± 3.0	ALBRECHT	96	ARG	$e^+e^- \rightarrow D^0 K^+ X$
16 $^{+5}_{-4}$ ± 3	217	KUBOTA	94	CLE2 $e^+e^- \sim 10.5$ GeV
• • •	We do not use the following data for averages, fits, limits, etc. • • •			
14 $^{+9}_{-6}$	25	EVDOKIMOV	04	SELX $600 \Sigma^- A \rightarrow D^0 K^+ X$

¹ From a fit of the D_s^+ recoil mass distribution.
² Systematic errors not estimated.

$D_{s2}^*(2573)^+$ DECAY MODES

$D_{s2}^*(2573)^-$ modes are charge conjugates of the modes below.

Mode	Fraction (Γ_i/Γ)
Γ_1 $D^0 K^+$	seen
Γ_2 $D^*(2007)^0 K^+$	not seen
Γ_3 $D^+ K_S^0$	seen
Γ_4 $D^{*+} K_S^0$	seen

$D_{s2}^*(2573)^+$ BRANCHING RATIOS

$\Gamma(D^0 K^+)/\Gamma_{\text{total}}$						Γ_1/Γ
VALUE	EVTS	DOCUMENT ID	TECN	CHG	COMMENT	
seen	217	KUBOTA	94	CLE2	\pm	$e^+e^- \sim 10.5$ GeV

$\Gamma(D^*(2007)^0 K^+)/\Gamma(D^0 K^+)$						Γ_2/Γ_1
VALUE	CL%	DOCUMENT ID	TECN	CHG	COMMENT	
<0.33	90	KUBOTA	94	CLE2	+	$e^+e^- \sim 10.5$ GeV

$\Gamma(D^+ K_S^0)/\Gamma(D^0 K^+)$						Γ_3/Γ_1
VALUE	DOCUMENT ID	TECN	COMMENT			
0.49 ± 0.10 ± 0.02	GAO	23	BELL	e^+e^-	at 10.52 GeV	

$\Gamma(D^{*+} K_S^0)/\Gamma(D^+ K_S^0)$						Γ_4/Γ_3
VALUE	EVTS	DOCUMENT ID	TECN	COMMENT		
0.044 ± 0.005 ± 0.011	2000	1 AAIJ	16AW	LHCB	$pp \rightarrow D^{*+} K_S^0 X$	at 7, 8 TeV

¹ First observation of the $D_{s2}^*(2573)^+ \rightarrow D^{*+} K_S^0$ decay with a significance of 6.9 σ .

$D_{s2}^*(2573)$ REFERENCES

GAO	23	PR D108 112015	B.S. Gao et al.	(BELLE Collab.)
ABLIKIM	19P	CP C43 031001	M. Ablikim et al.	(BESIII Collab.)
AAIJ	16AW	JHEP 1602 133	R. Aaij et al.	(LHCb Collab.)
AAIJ	14AW	PRL 113 162001	R. Aaij et al.	(LHCb Collab.) JP
AAIJ	11A	PL B698 14	R. Aaij et al.	(LHCb Collab.)
AUBERT, BE	06E	PRL 97 222001	B. Aubert et al.	(BABAR Collab.)
EVDOKIMOV	04	PRL 93 242001	A.V. Evdokimov et al.	(SLEX Collab.)
HEISTER	02B	PL B526 34	A. Heister et al.	(ALPH Collab.)
ALBRECHT	96	ZPHY C69 405	H. Albrecht et al.	(ARGUS Collab.)
KUBOTA	94	PRL 72 1972	Y. Kubota et al.	(CLEO Collab.)

$D_{s0}(2590)^+$ $I(J^P) = 0(0^-)$

OMITTED FROM SUMMARY TABLE

$D_{s0}(2590)^+$ MASS

VALUE (MeV)	EVTS	DOCUMENT ID	TECN	COMMENT
2591 ± 6 ± 7	444	1 AAIJ	21A	LHCB $B^0 \rightarrow D^-(D^+ K^+ \pi^-)$

¹ The mass is calculated from the position of the T-matrix pole

$D_{s0}(2590)^+$ WIDTH

VALUE (MeV)	EVTS	DOCUMENT ID	TECN	COMMENT
89 ± 16 ± 12	444	1 AAIJ	21A	LHCB $B^0 \rightarrow D^-(D^+ K^+ \pi^-)$

¹ The width is calculated from the position of the T-matrix pole

$D_{s0}(2590)^+$ DECAY MODES

Mode	Fraction (Γ_i/Γ)
Γ_1 $D^+ K^+ \pi^-$	seen

$\Gamma(D^+ K^+ \pi^-)/\Gamma_{\text{total}}$						Γ_1/Γ
VALUE	EVTS	DOCUMENT ID	TECN	COMMENT		
seen	444	AAIJ	21A	LHCB	$B^0 \rightarrow D^-(D^+ K^+ \pi^-)$	

$D_{s0}(2590)^+$ REFERENCES

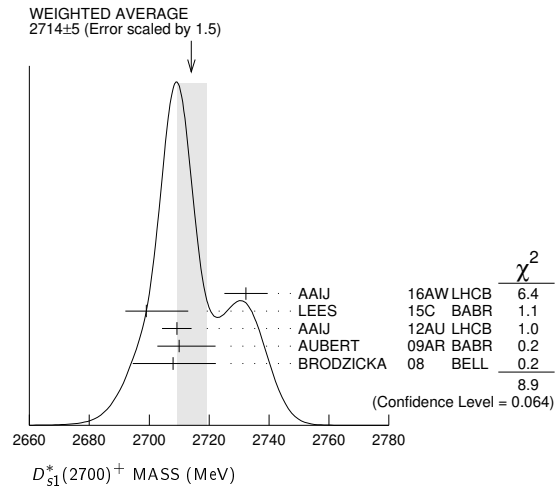
AAIJ	21A	PRL 126 122002	R. Aaij et al.	(LHCb Collab.)
------	-----	----------------	----------------	----------------

$D_{s1}^*(2700)^\pm$ $I(J^P) = 0(1^-)$

$D_{s1}^*(2700)^+$ MASS

VALUE (MeV)	EVTS	DOCUMENT ID	TECN	COMMENT
2714 ± 5	OUR AVERAGE			
2732.3 ± 4.3 ± 5.8	15.7k	AAIJ	16AW	LHCB $pp \rightarrow D^{*+} K_S^0 X$ at 7, 8 TeV
2699 $^{+14}_{-7}$		1 LEES	15c	BABR $B \rightarrow D D^0 K^+$
2709.2 ± 1.9 ± 4.5	52k	2 AAIJ	12AU	LHCB $pp \rightarrow (DK)^+ X$ at 7 TeV
2710 ± 2 $^{+12}_{-7}$	10.4k	3 AUBERT	09AR	BABR $e^+e^- \rightarrow D^{(*)} K X$
2708 ± 9 $^{+11}_{-10}$	182	BRODZICKA	08	BELL $B^+ \rightarrow D^0 \bar{D}^0 K^+$
• • •	We do not use the following data for averages, fits, limits, etc. • • •			
2694 ± 8 $^{+13}_{-3}$		LEES	15c	BABR $B^0 \rightarrow D^- D^0 K^+$
2707 ± 8 ± 8		LEES	15c	BABR $B^+ \rightarrow \bar{D}^0 D^0 K^+$
2688 ± 4 ± 3		4 AUBERT, BE	06E	BABR $10.6 e^+e^- \rightarrow DKX$

¹ From a combined analysis of $B^0 \rightarrow D^- D^0 K^+$ and $B^+ \rightarrow \bar{D}^0 D^0 K^+$.
² From the combined fit of the $D^+ K_S^0$ and $D^0 K^+$ modes in the model including the $D_{s2}^*(2573)^+$, $D_{s1}^*(2700)^+$ and spin-0 $D_{sJ}^*(2860)^+$.
³ From simultaneous fits to the two DK mass spectra and to the total $D^* K$ mass spectrum.
⁴ Superseded by AUBERT 09AR.



$D_{s1}^*(2700)^+$ WIDTH

VALUE (MeV)	EVTS	DOCUMENT ID	TECN	COMMENT
122 ± 10	OUR AVERAGE			
136 ± 19 ± 24	15.7k	AAIJ	16AW	LHCB $pp \rightarrow D^{*+} K_S^0 X$ at 7, 8 TeV
127 $^{+24}_{-19}$		1 LEES	15c	BABR $B \rightarrow D D^0 K^+$
115.8 ± 7.3 ± 12.1	52k	2 AAIJ	12AU	LHCB $pp \rightarrow (DK)^+ X$ at 7 TeV
149 ± 7 $^{+39}_{-52}$	10.4k	3 AUBERT	09AR	BABR $e^+e^- \rightarrow D^{(*)} K X$
108 ± 23 $^{+36}_{-31}$	182	BRODZICKA	08	BELL $B^+ \rightarrow D^0 \bar{D}^0 K^+$
• • •	We do not use the following data for averages, fits, limits, etc. • • •			
145 ± 24 $^{+22}_{-14}$		LEES	15c	BABR $B^0 \rightarrow D^- D^0 K^+$
113 ± 21 $^{+20}_{-16}$		LEES	15c	BABR $B^+ \rightarrow \bar{D}^0 D^0 K^+$
112 ± 7 ± 36		4 AUBERT, BE	06E	BABR $10.6 e^+e^- \rightarrow DKX$

¹ From a combined analysis of $B^0 \rightarrow D^- D^0 K^+$ and $B^+ \rightarrow \bar{D}^0 D^0 K^+$.
² From the combined fit of the $D^+ K_S^0$ and $D^0 K^+$ modes in the model including the $D_{s2}^*(2573)^+$, $D_{s1}^*(2700)^+$ and spin-0 $D_{sJ}^*(2860)^+$.
³ From simultaneous fits to the two DK mass spectra and to the total $D^* K$ mass spectrum.
⁴ Superseded by AUBERT 09AR.

See key on page 1171

Meson Particle Listings

 $D_{s1}^*(2700)^\pm, D_{s1}^*(2860)^\pm, D_{s3}^*(2860)^\pm$ $D_{s1}^*(2700)^\pm$ DECAY MODES

Mode	Fraction (Γ_i/Γ)
Γ_1 DK	
Γ_2 $D^0 K^+$	seen
Γ_3 $D^+ K_S^0$	seen
Γ_4 $D^* K$	
Γ_5 $D^{*0} K^+$	seen
Γ_6 $D^{*+} K_S^0$	seen

 $D_{s1}^*(2700)^\pm$ BRANCHING RATIOS

$\Gamma(D^* K)/\Gamma(DK)$	Γ_4/Γ_1			
VALUE	EVTS	DOCUMENT ID	TECN	COMMENT
$0.91 \pm 0.13 \pm 0.12$	10.4k	¹ AUBERT	09AR BABR	$e^+ e^- \rightarrow D^{(*)} K X$

¹ From the average of the corresponding ratios with $D^{(*)0} K^+$ and $D^{(*)+} K_S^0$.

$\Gamma(D^{*0} K^+)/\Gamma(D^0 K^+)$	Γ_5/Γ_2			
VALUE	EVTS	DOCUMENT ID	TECN	COMMENT
$0.88 \pm 0.14 \pm 0.14$	7716	¹ AUBERT	09AR BABR	$e^+ e^- \rightarrow D^{(*)} K X$

¹ From the $D^{*0} K^+$ and $D^0 K^+$, where $D^{*0} \rightarrow D^0 \pi^0$.

$\Gamma(D^{*+} K_S^0)/\Gamma(D^+ K_S^0)$	Γ_6/Γ_3			
VALUE	EVTS	DOCUMENT ID	TECN	COMMENT
$1.14 \pm 0.39 \pm 0.23$	2700	¹ AUBERT	09AR BABR	$e^+ e^- \rightarrow D^{(*)} K X$

¹ From the $D^{*+} K_S^0$ and $D^+ K_S^0$, where $D^{*+} \rightarrow D^+ \pi^0$.

 $D_{s1}^*(2700)^\pm$ REFERENCES

AAIJ	16AW JHEP 1602 133	R. Aaij et al.	(LHCb Collab.)
LEES	15C PR D91 052002	J.P. Lees et al.	(BABAR Collab.)
AAIJ	12AU JHEP 1210 151	R. Aaij et al.	(LHCb Collab.)
AUBERT	09AR PR D80 092003	B. Aubert et al.	(BABAR Collab.)
BRODZICKA	08 PRL 100 092001	J. Brodzicka et al.	(BELLE Collab.)
AUBERT,BE	06E PRL 97 222001	B. Aubert et al.	(BABAR Collab.)

 $D_{s1}^*(2860)^\pm$

$$I(J^P) = 0(1^-)$$

OMITTED FROM SUMMARY TABLE

was $D_{s1}^{*J}(2860)$ J^P consistent with 1^- from angular analysis of AAIJ 14AW. $D_{s1}^*(2860)^+$ MASS

VALUE (MeV)	DOCUMENT ID	TECN	COMMENT
$2859 \pm 12 \pm 24$	¹ AAIJ	14AW LHCb	$B_S^0 \rightarrow \bar{D}^0 K^- \pi^+$

¹ Separated from the spin-3 component $D_{s3}^*(2860)^-$ by a fit of the helicity angle of the $\bar{D}^0 K^-$ system, with a statistical significance of the spin-3 and spin-1 components in excess of 10σ .

 $D_{s1}^*(2860)^+$ WIDTH

VALUE (MeV)	DOCUMENT ID	TECN	COMMENT
$159 \pm 23 \pm 77$	¹ AAIJ	14AW LHCb	$B_S^0 \rightarrow \bar{D}^0 K^- \pi^+$

¹ Separated from the spin-3 component $D_{s3}^*(2860)^-$ by a fit of the helicity angle of the $\bar{D}^0 K^-$ system, with a statistical significance of the spin-3 and spin-1 components in excess of 10σ .

 $D_{s1}^*(2860)^\pm$ REFERENCES

AAIJ	14AW PRL 113 162001	R. Aaij et al.	(LHCb Collab.) JP
------	---------------------	----------------	-------------------

 $D_{s3}^*(2860)^\pm$

$$I(J^P) = 0(3^-)$$

J^P consistent with 3^- from angular analysis of AAIJ 14AW. Observed by AUBERT, BE 06E and AUBERT 09AR in inclusive production of DK and $D^* K$ in $e^+ e^-$ annihilation.

 $D_{s3}^*(2860)^+$ MASS

VALUE (MeV)	EVTS	DOCUMENT ID	TECN	COMMENT
$2860.5 \pm 2.6 \pm 6.5$		¹ AAIJ	14AW LHCb	$B_S^0 \rightarrow \bar{D}^0 K^- \pi^+$

••• We do not use the following data for averages, fits, limits, etc. •••

$2867.1 \pm 4.3 \pm 1.9$	3.1k	AAIJ	16AW LHCb	$pp \rightarrow D^{*+} K_S^0 X$ at 7, 8 TeV
$2866.1 \pm 1.0 \pm 6.3$	36k	^{2,3} AAIJ	12AU LHCb	$pp \rightarrow (DK)^+ X$ at 7 TeV
$2862 \pm 2 \pm 5_2$	3122	^{2,4} AUBERT	09AR BABR	$e^+ e^- \rightarrow D^{(*)} K X$
$2856.6 \pm 1.5 \pm 5.0$		⁵ AUBERT,BE	06E BABR	$e^+ e^- \rightarrow DKX$

¹ Separated from the spin-1 component $D_{s1}^*(2860)^-$ by a fit of the helicity angle of the $\bar{D}^0 K^-$ system, with a statistical significance of the spin-3 and spin-1 components in excess of 10σ .

² Possible contribution from the $D_{s1}^*(2860)$ state.

³ From the combined fit of the $D^+ K_S^0$ and $D^0 K^+$ modes in the model including the $D_{s2}^*(2573)^+$, $D_{s1}^*(2700)^+$ and spin-0 $D_{s,J}^*(2860)^+$.

⁴ From simultaneous fits to the two DK mass spectra and to the total $D^* K$ mass spectrum.

⁵ Superseded by AUBERT 09AR.

 $D_{s3}^*(2860)^+$ WIDTH

VALUE (MeV)	EVTS	DOCUMENT ID	TECN	COMMENT
$53 \pm 7 \pm 7$		¹ AAIJ	14AW LHCb	$B_S^0 \rightarrow \bar{D}^0 K^- \pi^+$

••• We do not use the following data for averages, fits, limits, etc. •••

$50 \pm 11 \pm 13$	3.1k	AAIJ	16AW LHCb	$pp \rightarrow D^{*+} K_S^0 X$ at 7, 8 TeV
$69.9 \pm 3.2 \pm 6.6$	36k	^{2,3} AAIJ	12AU LHCb	$pp \rightarrow (DK)^+ X$ at 7 TeV
$48 \pm 3 \pm 6$	3122	^{2,4} AUBERT	09AR BABR	$e^+ e^- \rightarrow D^{(*)} K X$
$47 \pm 7 \pm 10$		⁵ AUBERT,BE	06E BABR	$e^+ e^- \rightarrow DKX$

¹ Separated from the spin-1 component $D_{s1}^*(2860)^-$ by a fit of the helicity angle of the $\bar{D}^0 K^-$ system, with a statistical significance of the spin-3 and spin-1 components in excess of 10σ .

² Possible contribution from the $D_{s1}^*(2860)$ state.

³ From the combined fit of the $D^+ K_S^0$ and $D^0 K^+$ modes in the model including the $D_{s2}^*(2573)^+$, $D_{s1}^*(2700)^+$ and spin-0 $D_{s,J}^*(2860)^+$.

⁴ From simultaneous fits to the two DK mass spectra and to the total $D^* K$ mass spectrum.

⁵ Superseded by AUBERT 09AR.

 $D_{s3}^*(2860)^\pm$ DECAY MODES

Mode	Fraction (Γ_i/Γ)
Γ_1 DK	
Γ_2 $D^0 K^+$	seen
Γ_3 $D^+ K_S^0$	seen
Γ_4 $D^* K$	
Γ_5 $D^{*0} K^+$	seen
Γ_6 $D^{*+} K_S^0$	seen

 $D_{s3}^*(2860)^\pm$ BRANCHING RATIOS

$\Gamma(D^* K)/\Gamma(DK)$	Γ_4/Γ_1			
VALUE	EVTS	DOCUMENT ID	TECN	COMMENT
$1.10 \pm 0.15 \pm 0.19$	3122	¹ AUBERT	09AR BABR	$e^+ e^- \rightarrow D^{(*)} K X$

¹ From the average of the corresponding ratios with $D^{(*)0} K^+$ and $D^{(*)+} K_S^0$.

$\Gamma(D^{*0} K^+)/\Gamma(D^0 K^+)$	Γ_5/Γ_2			
VALUE	EVTS	DOCUMENT ID	TECN	COMMENT
$1.04 \pm 0.17 \pm 0.20$	2241	¹ AUBERT	09AR BABR	$e^+ e^- \rightarrow D^{(*)} K X$

¹ From the $D^{*0} K^+$ and $D^0 K^+$, where $D^{*0} \rightarrow D^0 \pi^0$.

$\Gamma(D^{*+} K_S^0)/\Gamma(D^+ K_S^0)$	Γ_6/Γ_3			
VALUE	EVTS	DOCUMENT ID	TECN	COMMENT
$1.38 \pm 0.35 \pm 0.49$	881	¹ AUBERT	09AR BABR	$e^+ e^- \rightarrow D^{(*)} K X$

¹ From the $D^{*+} K_S^0$ and $D^+ K_S^0$, where $D^{*+} \rightarrow D^+ \pi^0$.

 $D_{s3}^*(2860)^\pm$ REFERENCES

AAIJ	16AW JHEP 1602 133	R. Aaij et al.	(LHCb Collab.)
AAIJ	14AW PRL 113 162001	R. Aaij et al.	(LHCb Collab.) JP
AAIJ	12AU JHEP 1210 151	R. Aaij et al.	(LHCb Collab.)
AUBERT	09AR PR D80 092003	B. Aubert et al.	(BABAR Collab.)
AUBERT,BE	06E PRL 97 222001	B. Aubert et al.	(BABAR Collab.)

Meson Particle Listings

 $D_{sJ}(3040)^\pm$ $D_{sJ}(3040)^\pm$

$$I(J^P) = 0(?^?)$$

OMITTED FROM SUMMARY TABLE

Observed by AUBERT 09AR in inclusive production of $D^* K$ in e^+e^- annihilation. $D_{sJ}(3040)^+$ MASS

VALUE (MeV)	DOCUMENT ID	TECN	COMMENT
$3044 \pm 8^{+30}_{-5}$	AUBERT	09AR BABR	$e^+e^- \rightarrow D^* K X$

 $D_{sJ}(3040)^+$ WIDTH

VALUE (MeV)	DOCUMENT ID	TECN	COMMENT
$239 \pm 35^{+46}_{-42}$	AUBERT	09AR BABR	$e^+e^- \rightarrow D^* K X$

 $D_{sJ}(3040)^\pm$ DECAY MODES

Mode	
Γ_1	$D^* K$
Γ_2	$D^{*0} K^+$
Γ_3	$D^{*+} K_S^0$

 $D_{sJ}(3040)^\pm$ REFERENCESAUBERT 09AR PR D80 092003 B. Aubert *et al.* (BABAR Collab.)

BOTTOM MESONS**($B = \pm 1$)** $B^+ = u\bar{b}$, $B^0 = d\bar{b}$, $\bar{B}^0 = \bar{d}b$, $B^- = \bar{u}b$, similarly for B^{*} 's***B*-particle organization**

Many measurements of *B* decays involve admixtures of *B* hadrons. Previously we arbitrarily included such admixtures in the B^\pm section, but because of their importance we have created two new sections: " B^\pm/B^0 Admixture" for $\mathcal{T}(4S)$ results and " $B^\pm/B^0/B_S^0/b$ -baryon Admixture" for results at higher energies. Most inclusive decay branching fractions and χ_b at high energy are found in the Admixture sections. $B^0\text{-}\bar{B}^0$ mixing data are found in the B^0 section, while $B_S^0\text{-}\bar{B}_S^0$ mixing data and $B\text{-}\bar{B}$ mixing data for a B^0/B_S^0 admixture are found in the B_S^0 section. CP -violation data are found in the B^\pm , B^0 , and B^\pm/B^0 Admixture sections. *b*-baryons are found near the end of the Baryon section. Recently, we also created a new section: " V_{cb} and V_{ub} CKM Matrix Elements."

The organization of the *B* sections is now as follows, where bullets indicate particle sections and brackets indicate reviews.

[Production and Decay of *b*-flavored Hadrons]

[A Short Note on HFLAV Activities]

- B^\pm
 - mass, mean life
 - branching fractions
 - polarization in B^\pm decay
 - CP violation
- B^0
 - mass, mean life
 - branching fractions
 - [Polarization in *B* decay]
 - polarization in B^0 decay
 - [$B\text{-}\bar{B}$ Mixing]
 - $B^0\text{-}\bar{B}^0$ mixing
 - CP violation
- B^\pm/B^0 Admixture
 - branching fractions, CP violation
 - CP violation
- $B^\pm/B^0/B_S^0/b$ -baryon Admixture
 - mean life
 - production fractions
 - branching fractions
 - χ_b at high energy
 - production fractions in hadronic *Z* decay
- V_{cb} and V_{ub} CKM Matrix Elements
 - [Determination of V_{cb} and V_{ub}]
- B^* , $B_1(5721)$, $B_J^*(5732)$, $B_2^*(5747)$, $B_J(5840)$, $B_J(5970)$
 - mass, width, branching fractions
- B_S^0
 - mass, mean life
 - branching fractions
 - polarization in B_S^0 decay
 - $B_S^0\text{-}\bar{B}_S^0$ mixing
- B_S^* , $B_{S1}(5830)^0$, $B_{S2}^*(5840)^0$, $B_{S^*J}(5850)$, $B_{sJ}(6063)^0$, $B_{sJ}(6114)^0$
 - mass, width, branching fractions
- B_c^\pm
 - mass, mean life
 - branching fractions
- $B_c(2S)^\pm$
 - mass, branching fractions

At the end of Baryon Listings:

- Λ_b
 - mass, mean life
 - branching fractions
- $\Lambda_b(5912)^0$, $\Lambda_b(5920)^0$, $\Lambda_b(6070)^0$, $\Lambda_b(6146)^0$, $\Lambda_b(6152)^0$
 - mass, width, branching fractions
- Σ_b
 - mass, width, branching fractions

- Σ_b^* , $\Sigma_b(6097)^+$, $\Sigma_b(6097)^-$
 - mass, width, branching fractions
- Ξ_b^0 , Ξ_b^-
 - mass, mean life
 - branching fractions, P , CP violation
- $\Xi_b'(5935)^-$, $\Xi_b(5945)^0$, $\Xi_b(5955)^-$, $\Xi_b(6100)^-$, $\Xi_b(6227)^-$, $\Xi_b(6227)^0$, $\Xi_b(6327)^0$, $\Xi_b(6333)^0$
 - mass, width, branching fractions
- Ω_b^-
 - mass, mean life
 - branching fractions
- $\Omega_b(6316)^-$, $\Omega_b(6330)^-$, $\Omega_b(6340)^-$, $\Omega_b(6350)^-$
 - mass, width, branching fractions
- *b*-baryon Admixture
 - mean life
 - branching fractions

See the related review(s):

[Production and Decay of *b*-flavored Hadrons](#)**HEAVY FLAVOR AVERAGING GROUP**

Revised February 2024 by U. Egede (Monash University) and A. Soffer (Tel Aviv University)

The Heavy Flavor Averaging Group (HFLAV) is an international collaboration of physicists from experiments measuring properties of heavy flavored particles, *i.e.*, hadrons containing *b* and *c* quarks, and τ leptons. HFLAV calculates and publishes [1] world average values of quantities such as lifetimes, branching fractions, form factors, mixing parameters, and CP -violating asymmetries. Most parameters concern decays of *B* and *D* mesons, and many are related to elements of the Cabibbo-Kobayashi-Maskawa (CKM) quark mixing matrix [2], [3].

HFLAV was originally formed in 2002 to continue the activities of the LEP Heavy Flavor Steering group. Since its inception, a wide range of results have become available from increasingly larger data sets. Consequently, HFLAV has expanded to include eight subgroups:

- *b*-hadron lifetimes and oscillations, including parameters of CP violation in *b* mixing;
- decay-time-dependent CP violation in *B* decays, and angles of the CKM Unitarity Triangle;
- semileptonic decays of *b*-hadrons ($B \rightarrow X\ell\nu$, $\ell = e, \mu, \tau$), including determinations of the CKM matrix elements $|V_{cb}|$ and $|V_{ub}|$;
- *b*-hadron decays to hadronic final states containing *c*-quarks (open charm and charmonium);
- (rarer) *b*-hadron decays to final states not containing *c*-quarks, including fully hadronic, semileptonic ($B \rightarrow X\ell\ell, X\nu\bar{\nu}$), leptonic, and radiative decays;
- CP - and T -violating asymmetries of *D* mesons and $D^0\text{-}\bar{D}^0$ mixing;
- *c*-hadron decays (hadronic, semileptonic, leptonic), properties of excited *D* states and charm baryons and determination of $|V_{cs}|$ and $|V_{cd}|$;
- τ -lepton physics including branching fractions, tests of lepton universality, determination of $|V_{us}|$, and searches for lepton flavor violation.

Meson Particle Listings

b -flavored hadrons, B^\pm

Each subgroup has one or two conveners and typically a half-dozen members representing experiments that conduct measurements in that area. Most groups contain representatives from the Belle II and LHCb experiments, and some groups have representatives from the ATLAS, BABAR, Belle, BESIII and CMS experiments. Members of HFLAV are appointed by their respective experimental collaborations. HFLAV has two co-leaders, who are appointed by the managements of Belle II and LHCb.

The averaging procedures used by HFLAV are similar to those of the PDG [4]. When sufficient information is available in publications when calculating world averages, common parameters used for different input measurements are adjusted (rescaled) to common values. The p -value of the fit is provided to indicate the consistency of the measurements included in the average. However, unlike the PDG, when obtaining a world average with a low p -value (*i.e.*, a large χ^2 per degree of freedom), HFLAV does not usually scale the resulting uncertainty. Rather, the systematic uncertainties of the measurements are reviewed with experts from the experiments to understand the discrepancy. Unless inconsistencies among measurements are found, no correction is made to the calculated uncertainty. Close communication between representatives of the experiments and HFLAV members who perform averages helps ensure that measurement uncertainties, known correlations, and systematic effects are properly accounted for. If a special treatment is needed to calculate an average, or if an approximation used in an average calculation might not be sufficiently accurate (*e.g.*, assuming Gaussian uncertainties when the likelihood function is non-Gaussian), a note is included in the HFLAV publication and online documentation to describe this.

In general, HFLAV uses all publicly available results that have written documentation such as a journal publication, preprint, or conference note. These include preliminary results presented at conferences and workshops. However, preliminary results that remain unpublished for an extended period of time, or for which no publication is planned, are not included. A special subset of HFLAV averages are included in the PDG listings; for these averages, only measurements that are published or accepted for publication are used. The averages provided by HFLAV are listed by the PDG as “Produced by HFLAV”.

All HFLAV averages and input measurements are documented in an approximately biennial journal paper or preprint; the most recent version is Ref. [1]. The latest results and plots are posted on an extensive set of webpages that are updated several times per year; these are available at

<https://hflav.web.cern.ch>.

References:

1. Y. S. Amhis *et al.* (Heavy Flavor Averaging Group), Phys. Rev. **D107**, 052008 (2023) [arXiv:2206.07501], doi:10.1103/PhysRevD.107.052008, updated results and plots available at [https://hflav.web.cern.ch/..](https://hflav.web.cern.ch/)
2. N. Cabibbo, Phys. Rev. Lett. **10**, 531 (1963).

3. M. Kobayashi and T. Maskawa, Prog. Theor. Phys. **49**, 652 (1973).
4. See Section 5 of the “Introduction” to this *Review*.

B^\pm

$$J(P) = \frac{1}{2}(0^-)$$

Quantum numbers not measured. Values shown are quark-model predictions.

See also the B^\pm/B^0 ADMIXTURE and $B^\pm/B^0/B_s^0/b$ -baryon ADMIXTURE sections.

B^\pm MASS

The fit uses m_{B^\pm} , ($m_{B^0} - m_{B^\pm}$), and m_{B^0} to determine m_{B^\pm} , m_{B^0} , and the mass difference.

VALUE (MeV)	EVTs	DOCUMENT ID	TECN	COMMENT
5279.41 ± 0.07 OUR FIT				
5279.42 ± 0.08 OUR AVERAGE				
5279.44 ± 0.05 ± 0.07		¹ AAIJ	23Q	LHCb $p\bar{p}$ at 7, 8, 13 TeV
5279.38 ± 0.11 ± 0.33		² AAIJ	12E	LHCb $p\bar{p}$ at 7 TeV
5279.10 ± 0.41 ± 0.36		³ ACOSTA	06	CDF $p\bar{p}$ at 1.96 TeV
5279.1 ± 0.4 ± 0.4	526	⁴ CSORNA	00	CLE2 $e^+e^- \rightarrow \Upsilon(4S)$
5279.1 ± 1.7 ± 1.4	147	ABE	96B	CDF $p\bar{p}$ at 1.8 TeV
5278.8 ± 0.54 ± 2.0	362	ALAM	94	CLE2 $e^+e^- \rightarrow \Upsilon(4S)$
5278.3 ± 0.4 ± 2.0		BORTOLETTI	092	CLEO $e^+e^- \rightarrow \Upsilon(4S)$
5280.5 ± 1.0 ± 2.0		⁵ ALBRECHT	90J	ARG $e^+e^- \rightarrow \Upsilon(4S)$
5275.8 ± 1.3 ± 3.0	32	ALBRECHT	87c	ARG $e^+e^- \rightarrow \Upsilon(4S)$
5278.2 ± 1.8 ± 3.0	12	⁶ ALBRECHT	87D	ARG $e^+e^- \rightarrow \Upsilon(4S)$
5278.6 ± 0.8 ± 2.0		BEBEK	87	CLEO $e^+e^- \rightarrow \Upsilon(4S)$

¹ Uses $B^+ \rightarrow J/\psi \bar{p}$ decays.

² Uses $B^+ \rightarrow J/\psi K^+$ fully reconstructed decays.

³ Uses exclusively reconstructed final states containing a $J/\psi \rightarrow \mu^+ \mu^-$ decays.

⁴ CSORNA 00 uses fully reconstructed 526 $B^+ \rightarrow J/\psi(\Upsilon) K^+$ events and invariant masses without beam constraint.

⁵ ALBRECHT 90J assumes 10580 for $\Upsilon(4S)$ mass. Supersedes ALBRECHT 87c and ALBRECHT 87D.

⁶ Found using fully reconstructed decays with $J/\psi(1S)$. ALBRECHT 87D assume $m_{\Upsilon(4S)} = 10577$ MeV.

B^\pm MEAN LIFE

See $B^\pm/B^0/B_s^0/b$ -baryon ADMIXTURE section for data on B -hadron mean life averaged over species of bottom particles.

VALUE (10^{-12} s)	EVTs	DOCUMENT ID	TECN	COMMENT
1.638 ± 0.004 OUR EVALUATION				(Produced by HFLAV)
1.637 ± 0.004 ± 0.003		AAIJ	14E	LHCb $p\bar{p}$ at 7 TeV
1.639 ± 0.009 ± 0.009		¹ AALTONEN	11	CDF $p\bar{p}$ at 1.96 TeV
1.663 ± 0.023 ± 0.015		² AALTONEN	11B	CDF $p\bar{p}$ at 1.96 TeV
1.635 ± 0.011 ± 0.011		³ ABE	05B	BELL $e^+e^- \rightarrow \Upsilon(4S)$
1.624 ± 0.014 ± 0.018		⁴ ABDALLAH	04E	DLPH $e^+e^- \rightarrow Z$
1.636 ± 0.058 ± 0.025		⁵ ACOSTA	02C	CDF $p\bar{p}$ at 1.8 TeV
1.673 ± 0.032 ± 0.023		⁶ AUBERT	01F	BABR $e^+e^- \rightarrow \Upsilon(4S)$
1.648 ± 0.049 ± 0.035		⁷ BARATE	00R	ALEP $e^+e^- \rightarrow Z$
1.643 ± 0.037 ± 0.025		⁸ ABBIENDI	99J	OPAL $e^+e^- \rightarrow Z$
1.637 ± 0.058 ^{+0.045} _{-0.043}		⁷ ABE	98Q	CDF $p\bar{p}$ at 1.8 TeV
1.66 ± 0.06 ± 0.03		⁸ ACCIARRI	98s	L3 $e^+e^- \rightarrow Z$
1.66 ± 0.06 ± 0.05		⁸ ABE	97J	SLD $e^+e^- \rightarrow Z$
1.58 ^{+0.21} _{-0.18} ^{+0.04} _{-0.03}	94	⁵ BUSKULIC	96J	ALEP $e^+e^- \rightarrow Z$
1.61 ± 0.16 ± 0.12		^{7,9} ABREU	95Q	DLPH $e^+e^- \rightarrow Z$
1.72 ± 0.08 ± 0.06		¹⁰ ADAM	95	DLPH $e^+e^- \rightarrow Z$
1.52 ± 0.14 ± 0.09		⁷ AKERS	95T	OPAL $e^+e^- \rightarrow Z$
1.695 ± 0.026 ± 0.015		⁶ ABE	02H	BELL Repl. by ABE 05b
1.68 ± 0.07 ± 0.02		⁵ ABE	98B	CDF Repl. by ACOSTA 02c
1.56 ± 0.13 ± 0.06		⁷ ABE	96c	CDF Repl. by ABE 98q
1.58 ± 0.09 ± 0.03		¹¹ BUSKULIC	96j	ALEP $e^+e^- \rightarrow Z$
1.58 ± 0.09 ± 0.04		⁷ BUSKULIC	96j	ALEP Repl. by BARATE 00r
1.70 ± 0.09		¹² ADAM	95	DLPH $e^+e^- \rightarrow Z$
1.61 ± 0.16 ± 0.05	148	⁵ ABE	94D	CDF Repl. by ABE 98b
1.30 ^{+0.33} _{-0.29} ± 0.16	92	⁷ ABREU	93D	DLPH Sup. by ABREU 95q
1.56 ± 0.19 ± 0.13	134	¹⁰ ABREU	93G	DLPH Sup. by ADAM 95
1.51 ^{+0.30} _{-0.28} ^{+0.12} _{-0.14}	59	⁷ ACTON	93c	OPAL Sup. by AKERS 95t
1.47 ^{+0.22} _{-0.19} ^{+0.15} _{-0.14}	77	⁷ BUSKULIC	93D	ALEP Sup. by BUSKULIC 96j

¹ Measured mean life using fully reconstructed decays ($J/\psi K^{(*)}$).

- ² Measured using $B^- \rightarrow D^0 \pi^-$ with $D^0 \rightarrow K^- \pi^+$ events that were selected using a silicon vertex trigger.
- ³ Measurement performed using a combined fit of CP -violation, mixing and lifetimes.
- ⁴ Measurement performed using an inclusive reconstruction and B flavor identification technique.
- ⁵ Measured mean life using fully reconstructed decays.
- ⁶ Events are selected in which one B meson is fully reconstructed while the second B meson is reconstructed inclusively.
- ⁷ Data analyzed using $D/D^* \ell X$ event vertices.
- ⁸ Data analyzed using charge of secondary vertex.
- ⁹ ABREU 95Q assumes $B(B^0 \rightarrow D^{*-} \ell^+ \nu_\ell) = 3.2 \pm 1.7\%$.
- ¹⁰ Data analyzed using vertex-charge technique to tag B charge.
- ¹¹ Combined result of $D/D^* \ell X$ analysis and fully reconstructed B analysis.
- ¹² Combined ABREU 95Q and ADAM 95 result.

τ_{B^\pm}/τ_{B^-}	VALUE	DOCUMENT ID	TECN	COMMENT
	$1.002 \pm 0.004 \pm 0.002$	¹ AAIJ	14E LHCb	pp at 7 TeV
	¹ Measured using $B^\pm \rightarrow J/\psi K^\pm$ decays.			

B^+ DECAY MODES

B^- modes are charge conjugates of the modes below. Modes which do not identify the charge state of the B are listed in the B^\pm/B^0 ADMIXTURE section.

The branching fractions listed below assume 50% $B^0 \bar{B}^0$ and 50% $B^+ B^-$ production at the $T(4S)$. We have attempted to bring older measurements up to date by rescaling their assumed $T(4S)$ production ratio to 50:50 and their assumed D, D_s, D^* , and ψ branching ratios to current values whenever this would affect our averages and best limits significantly.

Indentation is used to indicate a subchannel of a previous reaction. All resonant subchannels have been corrected for resonance branching fractions to the final state so the sum of the subchannel branching fractions can exceed that of the final state.

For inclusive branching fractions, e.g., $B \rightarrow D^\pm X$, the values usually are multiplicities, not branching fractions. They can be greater than one.

Mode	Fraction (Γ_i/Γ)	Scale factor/ Confidence level
Semileptonic and leptonic modes		
Γ_1 $\ell^+ \nu_\ell X$	[a] (10.99 ± 0.28) %	
Γ_2 $e^+ \nu_e X_c$	(10.8 ± 0.4) %	
Γ_3 $\ell^+ \nu_\ell X_u$	[a] (1.65 ± 0.21) × 10 ⁻³	
Γ_4 $D \ell^+ \nu_\ell X$	[a] (9.5 ± 0.7) %	
Γ_5 $\bar{D}^0 \ell^+ \nu_\ell$	[a] (2.21 ± 0.06) %	
Γ_6 $\bar{D}^0 \tau^+ \nu_\tau$	(7.7 ± 2.5) × 10 ⁻³	
Γ_7 $\bar{D}^*(2007)^0 \ell^+ \nu_\ell$	[a] (5.53 ± 0.22) %	
Γ_8 $\bar{D}^*(2007)^0 e^+ \nu_e$		
Γ_9 $\bar{D}^*(2007)^0 \mu^+ \nu_\mu$		
Γ_{10} $\bar{D}^*(2007)^0 \tau^+ \nu_\tau$	(1.88 ± 0.20) %	
Γ_{11} $D^{(*)} n \pi \ell^+ \nu_\ell (n \geq 1)$	[a] (1.83 ± 0.25) %	
Γ_{12} $D^- \pi^+ \ell^+ \nu_\ell$	[a] (3.82 ± 0.20) × 10 ⁻³	
Γ_{13} $\bar{D}_2^-(2460)^0 \ell^+ \nu_\ell, \bar{D}_2^{*0} \rightarrow$	[a] (1.59 ± 0.10) × 10 ⁻³	
Γ_{14} $\bar{D}_0^-(2420)^0 \ell^+ \nu_\ell, \bar{D}_0^{*0} \rightarrow$	[a] (9 ± 5) × 10 ⁻⁴	S=2.6
Γ_{15} $D^{*-} \pi^+ \ell^+ \nu_\ell$	[a] (5.42 ± 0.28) × 10 ⁻³	
Γ_{16} $\bar{D}_1^-(2420)^0 \ell^+ \nu_\ell, \bar{D}_1^0 \rightarrow$	[a] (2.84 ± 0.17) × 10 ⁻³	S=1.1
Γ_{17} $\bar{D}_1^{*-} \pi^+ \ell^+ \nu_\ell, \bar{D}_1^{*0} \rightarrow$	[a] (1.7 ± 0.6) × 10 ⁻³	S=1.8
Γ_{18} $\bar{D}_2^{*-} \pi^+ \ell^+ \nu_\ell, \bar{D}_2^{*0} \rightarrow$	[a] (1.06 ± 0.18) × 10 ⁻³	S=1.7
Γ_{19} $\bar{D}^0 \pi^+ \pi^- \ell^+ \nu_\ell$	[a] (1.73 ± 0.19) × 10 ⁻³	
Γ_{20} $\bar{D}_1^-(2420)^0 \ell^+ \nu_\ell, \bar{D}_1^0 \rightarrow$	[a] (1.05 ± 0.14) × 10 ⁻³	
Γ_{21} $\bar{D}^{*0} \pi^+ \pi^- \ell^+ \nu_\ell$	[a] (7.0 ± 1.7) × 10 ⁻⁴	
Γ_{22} $D_s^{(*)-} K^+ \ell^+ \nu_\ell$	[a] (6.1 ± 1.0) × 10 ⁻⁴	
Γ_{23} $D_s^- K^+ \ell^+ \nu_\ell$	[a] (3.0 ± 1.4) × 10 ⁻⁴	
Γ_{24} $D_s^{*-} K^+ \ell^+ \nu_\ell$	[a] (2.9 ± 1.9) × 10 ⁻⁴	
Γ_{25} $\pi^0 \ell^+ \nu_\ell$	[a] (7.80 ± 0.27) × 10 ⁻⁵	
Γ_{26} $\pi^0 e^+ \nu_e$		
Γ_{27} $\eta \ell^+ \nu_\ell$	[a] (3.5 ± 0.4) × 10 ⁻⁵	
Γ_{28} $\eta' \ell^+ \nu_\ell$	[a] (2.4 ± 0.7) × 10 ⁻⁵	
Γ_{29} $\omega \ell^+ \nu_\ell$	[a] (1.19 ± 0.09) × 10 ⁻⁴	
Γ_{30} $\omega \mu^+ \nu_\mu$		
Γ_{31} $\rho^0 \ell^+ \nu_\ell$	[a] (1.58 ± 0.11) × 10 ⁻⁴	

Γ_{32} $\pi^+ \pi^- \ell^+ \nu_\ell$	[a] (2.3 ± 0.4) × 10 ⁻⁴	
Γ_{33} $\rho \bar{D} \ell^+ \nu_\ell$	[a] (5.8 ± 2.6) × 10 ⁻⁶	
Γ_{34} $\rho \bar{D} \mu^+ \nu_\mu$	(5.32 ± 0.34) × 10 ⁻⁶	
Γ_{35} $\rho \bar{D} e^+ \nu_e$	(8.2 ± 4.0) × 10 ⁻⁶	
Γ_{36} $e^+ \nu_e$	< 9.8	× 10 ⁻⁷ CL=90%
Γ_{37} $\mu^+ \nu_\mu$	< 8.6	× 10 ⁻⁷ CL=90%
Γ_{38} $\tau^+ \nu_\tau$	(1.09 ± 0.24) × 10 ⁻⁴	S=1.2
Γ_{39} $\ell^+ \nu_\ell \gamma$	[a] < 3.0	× 10 ⁻⁶ CL=90%
Γ_{40} $e^+ \nu_e \gamma$	< 4.3	× 10 ⁻⁶ CL=90%
Γ_{41} $\mu^+ \nu_\mu \gamma$	< 3.4	× 10 ⁻⁶ CL=90%
Γ_{42} $\mu^+ \mu^- \mu^+ \nu_\mu$	< 1.6	× 10 ⁻⁸ CL=95%

Inclusive modes

Γ_{43} $D^0 X$	(8.6 ± 0.7) %
Γ_{44} $\bar{D}^0 X$	(79 ± 4) %
Γ_{45} $D^+ X$	(2.5 ± 0.5) %
Γ_{46} $D^- X$	(9.9 ± 1.2) %
Γ_{47} $D_s^+ X$	(7.9 ± 1.4) %
Γ_{48} $D_s^- X$	(1.10 ± 0.40) %
Γ_{49} $A_c^+ X$	(2.1 ± 0.9) %
Γ_{50} $\bar{A}_c^- X$	(2.8 ± 1.1) %
Γ_{51} $\bar{c} X$	(97 ± 4) %
Γ_{52} $c X$	(23.4 ± 2.2) %
Γ_{53} $c/\bar{c} X$	(120 ± 6) %

$D, D^*,$ or D_s modes

Γ_{54} $\bar{D}^0 \pi^+$	(4.61 ± 0.10) × 10 ⁻³
Γ_{55} $D_{CP(+1)} \pi^+$	[b] (2.03 ± 0.19) × 10 ⁻³
Γ_{56} $D_{CP(-1)} \pi^+$	[b] (2.0 ± 0.4) × 10 ⁻³
Γ_{57} $\bar{D}^0 \rho^+$	(1.34 ± 0.18) %
Γ_{58} $\bar{D}^0 K^+$	(3.64 ± 0.15) × 10 ⁻⁴
Γ_{59} $D_{CP(+1)} K^+$	[b] (1.80 ± 0.08) × 10 ⁻⁴
Γ_{60} $D_{CP(-1)} K^+$	[b] (1.96 ± 0.18) × 10 ⁻⁴
Γ_{61} $D^0 K^+$	(3.60 ± 0.24) × 10 ⁻⁶
Γ_{62} $[K^- \pi^+]_D K^+$	[c] < 2.8
Γ_{63} $[K^+ \pi^-]_D K^+$	[c] < 2.0
Γ_{64} $[K^- \pi^+ \pi^0]_D K^+$	seen
Γ_{65} $[K^+ \pi^- \pi^0]_D K^+$	seen
Γ_{66} $[K^- \pi^+ \pi^+ \pi^-]_D K^+$	seen
Γ_{67} $[K^+ \pi^- \pi^+ \pi^-]_D K^+$	seen
Γ_{68} $[\pi^+ \pi^+ \pi^- \pi^-] K^+$	
Γ_{69} $[\pi^+ \pi^- \pi^+ \pi^-]_D K^*(892)^+$	
Γ_{70} $[K^- \pi^+]_D K^*(892)^+$	[c]
Γ_{71} $[K^+ \pi^-]_D K^*(892)^+$	[c]
Γ_{72} $[K^- \pi^+ \pi^- \pi^+]_D K^*(892)^+$	
Γ_{73} $[K^+ \pi^- \pi^+ \pi^-]_D K^*(892)^+$	
Γ_{74} $[K^- \pi^+]_D \pi^+$	[c] (6.3 ± 1.1) × 10 ⁻⁷
Γ_{75} $[K^+ \pi^-]_D \pi^+$	(1.7 ± 0.4) × 10 ⁻⁴
Γ_{76} $[K^- \pi^+ \pi^0]_D \pi^+$	seen
Γ_{77} $[K^+ \pi^- \pi^0]_D \pi^+$	seen
Γ_{78} $[K^- \pi^+ \pi^+ \pi^-]_D \pi^+$	seen
Γ_{79} $[K^+ \pi^- \pi^+ \pi^-]_D \pi^+$	seen
Γ_{80} $[K^- \pi^+]_{(D\pi)} \pi^+$	
Γ_{81} $[K^+ \pi^-]_{(D\pi)} \pi^+$	
Γ_{82} $[K^- \pi^+]_{(D\gamma)} \pi^+$	
Γ_{83} $[K^+ \pi^-]_{(D\gamma)} \pi^+$	
Γ_{84} $[K^- \pi^+]_{(D\pi)} K^+$	
Γ_{85} $[K^+ \pi^-]_{(D\pi)} K^+$	
Γ_{86} $[K^- \pi^+]_{(D\gamma)} K^+$	
Γ_{87} $[K^+ \pi^-]_{(D\gamma)} K^+$	
Γ_{88} $[\pi^+ \pi^- \pi^0]_D K^-$	(4.6 ± 0.9) × 10 ⁻⁶
Γ_{89} $[K_S^0 K^+ \pi^-]_D K^+$	seen
Γ_{90} $[K^*(892)^- K^+]_D K^+$	
Γ_{91} $[K_S^0 K^- \pi^+]_D K^+$	seen
Γ_{92} $[K^*(892)^+ K^-]_D K^+$	seen
Γ_{93} $[K_S^0 K^- \pi^+]_D \pi^+$	seen
Γ_{94} $[K^*(892)^+ K^-]_D \pi^+$	seen
Γ_{95} $[K_S^0 K^+ \pi^-]_D \pi^+$	seen
Γ_{96} $[K^*(892)^- K^+]_D \pi^+$	seen

Meson Particle Listings

 B^\pm

Γ_{97}	$[K^+ K^- \pi^0]_D K^+$		Γ_{159}	$\bar{D}_2^*(2462)^0 \pi^+, \bar{D}_2^{*0} \rightarrow$	$(2.2 \pm 1.0) \times 10^{-4}$
Γ_{98}	$[K^+ K^- \pi^0]_D \pi^+$		Γ_{160}	$\bar{D}_2^*(2462)^0 \pi^+, \bar{D}_2^{*0} \rightarrow$	$< 1.6 \times 10^{-4}$ CL=90%
Γ_{99}	$[\pi^+ \pi^- \pi^0]_D K^+$			$\bar{D}^0 \pi^- \pi^+$ (nonresonant)	
Γ_{100}	$[\pi^+ \pi^- \pi^0]_D \pi^+$		Γ_{161}	$\bar{D}_2^*(2462)^0 \pi^+, \bar{D}_2^{*0} \rightarrow$	$(2.1 \pm 1.0) \times 10^{-4}$
Γ_{101}	$\bar{D}^0 K^*(892)^+$	$(5.3 \pm 0.4) \times 10^{-4}$		$D^*(2010)^- \pi^+$	
Γ_{102}	$D_{CP(-)} K^*(892)^+$	[b] $(2.7 \pm 0.8) \times 10^{-4}$		$\bar{D}_0^*(2400)^0 \pi^+$	$(6.4 \pm 1.4) \times 10^{-4}$
Γ_{103}	$D_{CP(+)} K^*(892)^+$	[b] $(6.2 \pm 0.7) \times 10^{-4}$		$\times B(\bar{D}_0^*(2400)^0 \rightarrow D^- \pi^+)$	
Γ_{104}	$D^0 K^*(892)^+$	$(5.4 \pm 1.8) \times 10^{-6}$		$\bar{D}_1^*(2421)^0 \pi^+, \bar{D}_1^0 \rightarrow D^{*-} \pi^+$	$(7.4 \pm 1.0) \times 10^{-4}$
Γ_{105}	$\bar{D}^0 K^+ \pi^+ \pi^-$	$(5.2 \pm 2.1) \times 10^{-4}$		$\bar{D}_2^*(2462)^0 \pi^+, \bar{D}_2^{*0} \rightarrow D^{*-} \pi^+$	$(1.98 \pm 0.30) \times 10^{-4}$
Γ_{106}	$[K^+ \pi^-]_D K^+ \pi^- \pi^+$		Γ_{165}	$\bar{D}_1^*(2427)^0 \pi^+, \bar{D}_1^0 \rightarrow D^{*-} \pi^+$	$(3.5 \pm 0.9) \times 10^{-4}$ S=1.5
Γ_{107}	$[K^- \pi^+]_D K^+ \pi^- \pi^+$		Γ_{166}	$\bar{D}_1^*(2420)^0 \pi^+ \times B(\bar{D}_1^0 \rightarrow$	$< 6 \times 10^{-6}$ CL=90%
Γ_{108}	$D_{CP(+)} K^+ \pi^- \pi^+$			$\bar{D}^{*0} \pi^+ \pi^-)$	
Γ_{109}	$\bar{D}^0 K^+ \bar{K}^0$	$(5.5 \pm 1.6) \times 10^{-4}$	Γ_{167}	$\bar{D}_1^*(2420)^0 \rho^+$	$< 1.4 \times 10^{-3}$ CL=90%
Γ_{110}	$\bar{D}^0 K^+ \bar{K}^*(892)^0$	$(7.5 \pm 1.7) \times 10^{-4}$	Γ_{168}	$\bar{D}_2^*(2460)^0 \pi^+$	$< 1.3 \times 10^{-3}$ CL=90%
Γ_{111}	$\bar{D}^0 \pi^+ \pi^+ \pi^-$	$(5.5 \pm 2.0) \times 10^{-3}$ S=3.6	Γ_{169}	$\bar{D}_2^*(2460)^0 \pi^+ \times B(\bar{D}_2^{*0} \rightarrow$	$< 2.2 \times 10^{-5}$ CL=90%
Γ_{112}	$[K^- \pi^+]_D \pi^+ \pi^- \pi^+$			$\bar{D}^{*0} \pi^+ \pi^-)$	
Γ_{113}	$\bar{D}^0 \pi^+ \pi^+ \pi^-$ nonresonant	$(5 \pm 4) \times 10^{-3}$	Γ_{170}	$\bar{D}_1^*(2680)^0 \pi^+, \bar{D}_1^*(2680)^0 \rightarrow$	$(8.4 \pm 2.1) \times 10^{-5}$
Γ_{114}	$\bar{D}^0 \pi^+ \rho^0$	$(4.2 \pm 3.0) \times 10^{-3}$		$D^- \pi^+$	
Γ_{115}	$\bar{D}^0 a_1(1260)^+$	$(4 \pm 4) \times 10^{-3}$	Γ_{171}	$\bar{D}(2740)^0 \pi^+, \bar{D}^0 \rightarrow$	$(3.3 \pm 1.5) \times 10^{-5}$
Γ_{116}	$\bar{D}^0 \omega \pi^+$	$(4.1 \pm 0.9) \times 10^{-3}$		$D^*(2010)^- \pi^+$	
Γ_{117}	$D^*(2010)^- \pi^+ \pi^+$	$(1.35 \pm 0.22) \times 10^{-3}$	Γ_{172}	$\bar{D}_3^*(2750)^0 \pi^+, \bar{D}_3^{*0} \rightarrow$	$(1.10 \pm 0.32) \times 10^{-5}$
Γ_{118}	$D^*(2010)^- K^+ \pi^+$	$(8.2 \pm 1.4) \times 10^{-5}$		$D^*(2010)^- \pi^+$	
Γ_{119}	$\bar{D}_1(2420)^0 \pi^+, \bar{D}_1^0 \rightarrow$	$(8.4 \pm 1.5) \times 10^{-4}$	Γ_{173}	$\bar{D}_3^*(2760)^0 \pi^+,$	$(1.00 \pm 0.22) \times 10^{-5}$
	$D^*(2010)^- \pi^+$			$\bar{D}_3^*(2760)^0 \pi^+ \rightarrow D^- \pi^+$	
Γ_{120}	$D^- \pi^+ \pi^+$	$(1.07 \pm 0.05) \times 10^{-3}$	Γ_{174}	$\bar{D}_2^*(3000)^0 \pi^+,$	$(2.0 \pm 1.4) \times 10^{-6}$
Γ_{121}	$D^- K^+ \pi^+$	$(7.7 \pm 0.5) \times 10^{-5}$		$\bar{D}_2^*(3000)^0 \pi^+ \rightarrow D^- \pi^+$	
Γ_{122}	$D_0^*(2300)^0 K^+, D_0^{*0} \rightarrow$	$(6.1 \pm 2.4) \times 10^{-6}$	Γ_{175}	$\bar{D}_2^*(2460)^0 \rho^+$	$< 4.7 \times 10^{-3}$ CL=90%
	$D^- \pi^+$		Γ_{176}	$\bar{D}^0 D_s^+$	$(9.0 \pm 0.9) \times 10^{-3}$
Γ_{123}	$D_2^*(2460)^0 K^+, D_2^{*0} \rightarrow$	$(2.32 \pm 0.23) \times 10^{-5}$	Γ_{177}	$D_{s0}^*(2317)^+ \bar{D}^0, D_{s0}^{*+} \rightarrow$	$(8.0 \pm 1.6) \times 10^{-4}$
	$D^- \pi^+$			$D_s^+ \pi^0$	$(1.3) \times 10^{-4}$
Γ_{124}	$D_1^*(2760)^0 K^+, D_1^{*0} \rightarrow$	$(3.6 \pm 1.2) \times 10^{-6}$	Γ_{178}	$D_{s0}(2317)^+ \bar{D}^0 \times$	$< 7.6 \times 10^{-4}$ CL=90%
	$D^- \pi^+$			$B(D_{s0}(2317)^+ \rightarrow D_s^{*+} \gamma)$	
Γ_{125}	$D^+ K^0$	$< 2 \times 10^{-6}$ CL=90%	Γ_{179}	$D_{s0}(2317)^+ \bar{D}^*(2007)^0 \times$	$(9 \pm 7) \times 10^{-4}$
Γ_{126}	$D^+ K^+ \pi^-$	$(5.6 \pm 1.1) \times 10^{-6}$		$B(D_{s0}(2317)^+ \rightarrow D_s^+ \pi^0)$	
Γ_{127}	$D^+ \eta$	$< 1.2 \times 10^{-5}$ CL=90%	Γ_{180}	$D_{s,J}(2457)^+ \bar{D}^0$	$(3.1 \pm 1.0) \times 10^{-3}$
Γ_{128}	$D_2^*(2460)^0 K^+, D_2^{*0} \rightarrow$	$< 6.3 \times 10^{-7}$ CL=90%		$D_{s,J}(2457)^+ \bar{D}^0 \times$	$(4.6 \pm 1.3) \times 10^{-4}$
	$D^+ \pi^-$			$B(D_{s,J}(2457)^+ \rightarrow D_s^+ \gamma)$	
Γ_{129}	$D^+ K^{*0}$	$< 4.9 \times 10^{-7}$ CL=90%	Γ_{181}	$D_{s,J}(2457)^+ \bar{D}^0 \times$	$< 2.2 \times 10^{-4}$ CL=90%
Γ_{130}	$D^+ \bar{K}^{*0}$	$< 1.4 \times 10^{-6}$ CL=90%		$B(D_{s,J}(2457)^+ \rightarrow D_s^+ \pi^-)$	
Γ_{131}	$\bar{D}^*(2007)^0 \pi^+$	$(5.17 \pm 0.15) \times 10^{-3}$	Γ_{182}	$D_{s,J}(2457)^+ \bar{D}^0 \times$	$< 2.7 \times 10^{-4}$ CL=90%
Γ_{132}	$\bar{D}_{CP(+)}^{*0} \pi^+$	[d] $(2.9 \pm 0.6) \times 10^{-3}$		$B(D_{s,J}(2457)^+ \rightarrow D_s^+ \pi^+ \pi^-)$	
Γ_{133}	$D_{CP(-)}^{*0} \pi^+$	[d] $(2.6 \pm 1.0) \times 10^{-3}$	Γ_{183}	$D_{s,J}(2457)^+ \bar{D}^0 \times$	$< 9.8 \times 10^{-4}$ CL=90%
Γ_{134}	$\bar{D}^*(2007)^0 \omega \pi^+$	$(4.5 \pm 1.2) \times 10^{-3}$		$B(D_{s,J}(2457)^+ \rightarrow D_s^+ \pi^0)$	
Γ_{135}	$\bar{D}^*(2007)^0 \rho^+$	$(9.8 \pm 1.7) \times 10^{-3}$	Γ_{184}	$D_{s,J}(2457)^+ \bar{D}^0 \times$	$< 9.8 \times 10^{-4}$ CL=90%
Γ_{136}	$\bar{D}^*(2007)^0 K^+$	$(4.19 \pm 0.31) \times 10^{-4}$		$B(D_{s,J}(2457)^+ \rightarrow D_s^{*+} \gamma)$	
Γ_{137}	$\bar{D}_{CP(+)}^{*0} K^+$	[d] $(2.75 \pm 0.35) \times 10^{-4}$	Γ_{185}	$D_{s,J}(2457)^+ \bar{D}^*(2007)^0$	$(1.20 \pm 0.30) \%$
Γ_{138}	$\bar{D}_{CP(-)}^{*0} K^+$	[d] $(2.31 \pm 0.31) \times 10^{-4}$	Γ_{186}	$D_{s,J}(2457)^+ \bar{D}^*(2007)^0 \times$	$(1.4 \pm 0.7) \times 10^{-3}$
Γ_{139}	$D^*(2007)^0 K^+$	$(4.5 \pm 1.2) \times 10^{-6}$		$B(D_{s,J}(2457)^+ \rightarrow D_s^+ \gamma)$	
Γ_{140}	$\bar{D}^*(2007)^0 K^*(892)^+$	$(8.1 \pm 1.4) \times 10^{-4}$	Γ_{187}	$\bar{D}^0 D_{s1}(2536)^+ \times$	$(4.0 \pm 1.0) \times 10^{-4}$
Γ_{141}	$\bar{D}^*(2007)^0 K^+ \bar{K}^0$	$< 1.06 \times 10^{-3}$ CL=90%		$B(D_{s1}(2536)^+ \rightarrow$	
Γ_{142}	$\bar{D}^*(2007)^0 K^+ \bar{K}^*(892)^0$	$(1.5 \pm 0.4) \times 10^{-3}$		$D^*(2007)^0 K^+ +$	
Γ_{143}	$\bar{D}^*(2007)^0 \pi^+ \pi^+ \pi^-$	$(1.03 \pm 0.12) \%$		$D^*(2010)^+ K^0)$	
Γ_{144}	$\bar{D}^*(2007)^0 a_1(1260)^+$	$(1.9 \pm 0.5) \%$	Γ_{188}	$\bar{D}^0 D_{s1}(2536)^+ \times$	$(2.2 \pm 0.7) \times 10^{-4}$
Γ_{145}	$\bar{D}^*(2007)^0 \pi^- \pi^+ \pi^+ \pi^0$	$(1.8 \pm 0.4) \%$		$B(D_{s1}(2536)^+ \rightarrow$	
Γ_{146}	$\bar{D}^{*0} 3\pi^+ 2\pi^-$	$(5.7 \pm 1.2) \times 10^{-3}$		$D^*(2007)^0 K^+)$	
Γ_{147}	$D^*(2010)^+ \pi^0$	$< 3.6 \times 10^{-6}$	Γ_{189}	$\bar{D}^*(2007)^0 D_{s1}(2536)^+ \times$	$(5.5 \pm 1.6) \times 10^{-4}$
Γ_{148}	$D^*(2010)^+ K^0$	$< 9.0 \times 10^{-6}$ CL=90%		$B(D_{s1}(2536)^+ \rightarrow$	
Γ_{149}	$D^*(2010)^- \pi^+ \pi^+ \pi^0$	$(1.5 \pm 0.7) \%$		$D^*(2007)^0 K^+)$	
Γ_{150}	$D^*(2010)^- \pi^+ \pi^+ \pi^+ \pi^-$	$(2.6 \pm 0.4) \times 10^{-3}$	Γ_{190}	$\bar{D}^0 D_{s1}(2536)^+ \times$	$(2.3 \pm 1.1) \times 10^{-4}$
Γ_{151}	$\bar{D}^{*0} \pi^+$	[e] $(5.6 \pm 1.2) \times 10^{-3}$		$B(D_{s1}(2536)^+ \rightarrow D^{*+} K^0)$	
Γ_{152}	$\bar{D}_1^*(2420)^0 \pi^+$	$(1.5 \pm 0.6) \times 10^{-3}$ S=1.3	Γ_{191}	$\bar{D}^0 D_{s,J}(2700)^+ \times$	$(5.6 \pm 1.8) \times 10^{-4}$ S=1.7
Γ_{153}	$\bar{D}_1(2420)^0 \pi^+ \times B(\bar{D}_1^0 \rightarrow$	$(2.5 \pm 1.6) \times 10^{-4}$ S=3.8		$B(D_{s,J}(2700)^+ \rightarrow D^0 K^+)$	
	$\bar{D}^0 \pi^+ \pi^-)$		Γ_{192}	$\bar{D}^{*0} D_{s1}(2536)^+, D_{s1}^+ \rightarrow$	$(3.9 \pm 2.6) \times 10^{-4}$
Γ_{154}	$\bar{D}_1(2420)^0 \pi^+ \times B(\bar{D}_1^0 \rightarrow$	$(2.2 \pm 0.9) \times 10^{-4}$		$D^{*+} K^0$	
	$\bar{D}^0 \pi^+ \pi^-$ (nonresonant))		Γ_{193}	$\bar{D}^0 D_{s,J}(2573)^+, D_{s,J}^+ \rightarrow$	$(8 \pm 15) \times 10^{-6}$
Γ_{155}	$\bar{D}_1(2430)^0 \pi^+, \bar{D}_1^0 \rightarrow$	$(3.5 \pm 0.6) \times 10^{-4}$		$D^0 K^+$	
	$D^*(2010)^- \pi^+$		Γ_{194}	$\bar{D}^{*0} D_{s,J}(2573), D_{s,J}^+ \rightarrow D^0 K^+$	$< 2 \times 10^{-4}$ CL=90%
Γ_{156}	$\bar{D}(2550)^0 \pi^+, \bar{D}^0 \rightarrow$	$(7.2 \pm 1.4) \times 10^{-5}$	Γ_{195}	$\bar{D}^*(2007)^0 D_{s,J}(2573), D_{s,J}^+ \rightarrow$	$< 5 \times 10^{-4}$ CL=90%
	$D^*(2010)^- \pi^+$			$D^0 K^+$	
Γ_{157}	$\bar{D}_J^*(2600)^0 \pi^+, \bar{D}_J^{*0} \rightarrow$	$(6.8 \pm 1.3) \times 10^{-5}$	Γ_{196}	$\bar{D}^0 D_s^{*+}$	$(7.6 \pm 1.6) \times 10^{-3}$
	$D^*(2010)^- \pi^+$				
Γ_{158}	$\bar{D}_2^*(2462)^0 \pi^+, \bar{D}_2^{*0} \rightarrow D^- \pi^+$	$(3.56 \pm 0.24) \times 10^{-4}$			

Γ ₁₉₇	$D^- D_s^+ \pi^+$			Γ ₂₆₁	$\eta_c(2S) K^+, \eta_c \rightarrow p\bar{p}$	$(3.5 \pm 0.8) \times 10^{-8}$	
Γ ₁₉₈	$\bar{D}^*(2007)^0 D_s^+$	$(8.2 \pm 1.7) \times 10^{-3}$		Γ ₂₆₂	$\eta_c(2S) K^+, \eta_c \rightarrow K_S^0 K^\mp \pi^\pm$	$(3.4 \pm_{-1.6}^{2.3}) \times 10^{-6}$	
Γ ₁₉₉	$\bar{D}^*(2007)^0 D_s^+, \bar{D}^{*0} \rightarrow$			Γ ₂₆₃	$\eta_c(2S) K^+, \eta_c \rightarrow p\bar{p}\pi^+\pi^-$	$(1.12 \pm 0.18) \times 10^{-6}$	
Γ ₂₀₀	$\bar{D}^*(2007)^0 D_s^{*+}$	$(1.71 \pm 0.24) \%$		Γ ₂₆₄	$h_c(1P) K^+, h_c \rightarrow J/\psi \pi^+ \pi^-$	$< 3.4 \times 10^{-6}$	CL=90%
Γ ₂₀₁	$\bar{D}_2^*(2460)^0 D_s^+, \bar{D}_2^* \rightarrow D^- \pi^+$			Γ ₂₆₅	$X(3730)^0 K^+, X^0 \rightarrow \eta_c \eta$	$< 4.6 \times 10^{-5}$	CL=90%
Γ ₂₀₂	$\bar{D}_1^*(2600)^0 D_s^+, \bar{D}_1^{*0} \rightarrow D^- \pi^+$			Γ ₂₆₆	$X(3730)^0 K^+, X^0 \rightarrow \eta_c \pi^0$	$< 5.7 \times 10^{-6}$	CL=90%
Γ ₂₀₃	$\bar{D}_3^*(2750)^0 D_s^+, \bar{D}_3^{*0} \rightarrow D^- \pi^+$			Γ ₂₆₇	$\eta_{c2}(1D) K^+, \eta_{c2} \rightarrow h_c \gamma$	$< 3.7 \times 10^{-5}$	CL=90%
Γ ₂₀₄	$\bar{D}_1^*(2760)^0 D_s^+, \bar{D}_1^{*0} \rightarrow D^- \pi^+$			Γ ₂₆₈	$\eta_{c2}(1D) \pi^+ K_S^0, \eta_{c2} \rightarrow h_c \gamma$	$< 1.1 \times 10^{-4}$	CL=90%
Γ ₂₀₅	$\bar{D}_J^*(3000)^0 D_s^+, \bar{D}_J^{*0} \rightarrow D^- \pi^+$			Γ ₂₆₉	$\psi_2(3823) K^+, \psi_2 \rightarrow$	$(2.8 \pm 0.6) \times 10^{-7}$	
Γ ₂₀₆	$T_{cs0}^*(2900)^{++} D^-, T_{cs0}^{*++} \rightarrow$				$J/\psi \pi^+ \pi^-$		
Γ ₂₀₇	$D_s^{(*)+} \bar{D}^{*0}$	$(2.7 \pm 1.2) \%$		Γ ₂₇₀	$\psi_2(3823) K^+, \psi_2 \rightarrow J/\psi \eta$	$(1.2 \pm_{-0.5}^{0.7}) \times 10^{-6}$	
Γ ₂₀₈	$\bar{D}^*(2007)^0 D^*(2010)^+$	$(8.1 \pm 1.7) \times 10^{-4}$		Γ ₂₇₁	$\psi_3(3842) K^+, \psi_3 \rightarrow J/\psi \eta$	$< 6.1 \times 10^{-7}$	CL=90%
Γ ₂₀₉	$\bar{D}^0 D^*(2010)^+ + \bar{D}^*(2007)^0 D^+$	$< 1.30 \%$	CL=90%	Γ ₂₇₂	$\chi_{c1}(3872) K^+$	$(2.3 \pm 0.6) \times 10^{-4}$	
Γ ₂₁₀	$\bar{D}^0 D^*(2010)^+$	$(3.9 \pm 0.5) \times 10^{-4}$		Γ ₂₇₃	$\chi_{c0}(3915) K^+$	$< 2.8 \times 10^{-4}$	CL=90%
Γ ₂₁₁	$\bar{D}^0 D^+$	$(3.8 \pm 0.4) \times 10^{-4}$		Γ ₂₇₄	$\chi_{c0}(3915) K^+, \chi_{c0} \rightarrow D^+ D^-$	$(8.1 \pm 3.3) \times 10^{-6}$	
Γ ₂₁₂	$\bar{D}^0 D^+ K^0$	$(1.55 \pm 0.21) \times 10^{-3}$		Γ ₂₇₅	$\chi_{c0}(3915) K^+, \chi_{c0} \rightarrow \eta_c \eta$	$< 4.7 \times 10^{-5}$	CL=90%
Γ ₂₁₃	$D^+ \bar{D}^*(2007)^0$	$(6.3 \pm 1.7) \times 10^{-4}$		Γ ₂₇₆	$\chi_{c0}(3915) K^+, \chi_{c0} \rightarrow \eta_c \pi^0$	$< 1.7 \times 10^{-5}$	CL=90%
Γ ₂₁₄	$\bar{D}^*(2007)^0 D^+ K^0$	$(2.1 \pm 0.5) \times 10^{-3}$		Γ ₂₇₇	$X(4014)^0 K^+, X^0 \rightarrow \eta_c \eta$	$< 3.9 \times 10^{-5}$	CL=90%
Γ ₂₁₅	$\bar{D}^0 D^*(2010)^+ K^0$	$(3.8 \pm 0.4) \times 10^{-3}$		Γ ₂₇₈	$X(4014)^0 K^+, X^0 \rightarrow \eta_c \pi^0$	$< 1.2 \times 10^{-5}$	CL=90%
Γ ₂₁₆	$\bar{D}^*(2007)^0 D^*(2010)^+ K^0$	$(9.2 \pm 1.2) \times 10^{-3}$		Γ ₂₇₉	$T_{c\bar{c}1}(3900)^0 K^+, T_{c\bar{c}1}^0 \rightarrow$	$< 4.7 \times 10^{-5}$	CL=90%
Γ ₂₁₇	$\bar{D}^0 D^0 K^+$	$(1.45 \pm 0.33) \times 10^{-3}$	S=2.6		$J/\psi \eta$		
Γ ₂₁₈	$\bar{D}^*(2007)^0 D^0 K^+$	$(2.26 \pm 0.23) \times 10^{-3}$		Γ ₂₈₀	$T_{c\bar{c}1}(3900)^0 K^+, T_{c\bar{c}1}^0 \rightarrow$	$< 4.3 \times 10^{-7}$	CL=90%
Γ ₂₁₉	$\bar{D}^0 D^*(2007)^0 K^+$	$(6.3 \pm 0.5) \times 10^{-3}$			$J/\psi \eta$		
Γ ₂₂₀	$\bar{D}^*(2007)^0 D^*(2007)^0 K^+$	$(1.12 \pm 0.13) \%$		Γ ₂₈₁	$T_{c\bar{c}1}(4020)^0 K^+, T_{c\bar{c}1}^0 \rightarrow$	$< 1.6 \times 10^{-5}$	CL=90%
Γ ₂₂₁	$D^- D^+ K^+$	$(2.2 \pm 0.7) \times 10^{-4}$			$\eta_c \pi^+ \pi^-$		
Γ ₂₂₂	$T_{cs0}^*(2870)^0 D^+, T_{cs0}^{*0} \rightarrow$	$(1.2 \pm 0.5) \times 10^{-5}$		Γ ₂₈₂	$\chi_{c1}(3872) K^*(892)^+$	$< 6 \times 10^{-4}$	CL=90%
	$D^- K^+$			Γ ₂₈₃	$\chi_{c1}(3872)^+ K^0, \chi_{c1}^+ \rightarrow$	$[f] < 6.1 \times 10^{-6}$	CL=90%
Γ ₂₂₃	$T_{cs1}^*(2900)^0 D^+, T_{cs1}^{*0} \rightarrow$	$(6.7 \pm 2.3) \times 10^{-5}$			$J/\psi(1S) \pi^+ \pi^0$		
	$D^- K^+$			Γ ₂₈₄	$\chi_{c1}(3872) K^0 \pi^+$	$(3.0 \pm 1.2) \times 10^{-4}$	
Γ ₂₂₄	$D^- D^+ K^+$ nonresonant	$(5.3 \pm 1.8) \times 10^{-5}$		Γ ₂₈₅	$T_{c\bar{c}1}(4430)^+ K^0, T_{c\bar{c}1}^+ \rightarrow$	$< 1.5 \times 10^{-5}$	CL=95%
Γ ₂₂₅	$D^- D^*(2010)^+ K^+$	$(6.3 \pm 1.1) \times 10^{-4}$			$J/\psi \pi^+$		
Γ ₂₂₆	$D^*(2010)^- D^+ K^+$	$(6.0 \pm 1.3) \times 10^{-4}$		Γ ₂₈₆	$T_{c\bar{c}1}(4430)^+ K^0, T_{c\bar{c}1}^+ \rightarrow$	$< 4.7 \times 10^{-5}$	CL=95%
Γ ₂₂₇	$D^*(2010)^- D^*(2010)^+ K^+$	$(1.32 \pm 0.18) \times 10^{-3}$			$\psi(2S) \pi^+$		
Γ ₂₂₈	$(\bar{D} + \bar{D}^*)(D + D^*) K$	$(4.05 \pm 0.30) \%$		Γ ₂₈₇	$T_{c\bar{c}1}(4430)^0 K^+, T_{c\bar{c}1}^0 \rightarrow$	$< 1.27 \times 10^{-6}$	CL=90%
Γ ₂₂₉	$D_s^- D_s^+ K^+$	$(1.2 \pm 0.4) \times 10^{-4}$			$J/\psi \eta$		
Γ ₂₃₀	$D_s^+ \pi^0$	$(1.6 \pm 0.5) \times 10^{-5}$		Γ ₂₈₈	$\psi(4230)^0 K^+, \psi^0 \rightarrow$	$< 1.56 \times 10^{-5}$	CL=95%
Γ ₂₃₁	$D_s^{*+} \pi^0$	$< 2.6 \times 10^{-4}$	CL=90%		$J/\psi \pi^+ \pi^-$		
Γ ₂₃₂	$D_s^+ \eta$	$< 1.4 \times 10^{-5}$	CL=90%	Γ ₂₈₉	$\psi(4230) K^+, \psi \rightarrow J/\psi \eta$	$< 3.9 \times 10^{-7}$	CL=90%
Γ ₂₃₃	$D_s^{*+} \eta$	$< 1.7 \times 10^{-5}$	CL=90%	Γ ₂₉₀	$\psi(4360) K^+, \psi \rightarrow J/\psi \eta$	$< 1.24 \times 10^{-6}$	CL=90%
Γ ₂₃₄	$D_s^+ \rho^0$	$< 3.0 \times 10^{-4}$	CL=90%	Γ ₂₉₁	$\psi(4390) K^+, \psi \rightarrow J/\psi \eta$	$< 2.41 \times 10^{-6}$	CL=90%
Γ ₂₃₅	$D_s^{*+} \rho^0$	$< 4 \times 10^{-4}$	CL=90%	Γ ₂₉₂	$\chi_{c0}(3915) K^+, \chi_{c0} \rightarrow J/\psi \gamma$	$< 1.4 \times 10^{-5}$	CL=90%
Γ ₂₃₆	$D_s^+ \omega$	$< 4 \times 10^{-4}$	CL=90%	Γ ₂₉₃	$\chi_{c0}(3915) K^+, \chi_{c0} \rightarrow$	$< 3.8 \times 10^{-5}$	CL=90%
Γ ₂₃₇	$D_s^{*+} \omega$	$< 6 \times 10^{-4}$	CL=90%		$\chi_{c1}(1P) \pi^0$		
Γ ₂₃₈	$D_s^+ a_1(1260)^0$	$< 1.8 \times 10^{-3}$	CL=90%	Γ ₂₉₄	$X(3930)^0 K^+, X^0 \rightarrow J/\psi \gamma$	$< 2.5 \times 10^{-6}$	CL=90%
Γ ₂₃₉	$D_s^{*+} a_1(1260)^0$	$< 1.3 \times 10^{-3}$	CL=90%	Γ ₂₉₅	$J/\psi(1S) K^+$	$(1.020 \pm 0.019) \times 10^{-3}$	
Γ ₂₄₀	$D_s^+ K^+ K^-$	$(7.2 \pm 1.1) \times 10^{-6}$		Γ ₂₉₆	$J/\psi(1S) K^0 \pi^+$	$(1.14 \pm 0.11) \times 10^{-3}$	
Γ ₂₄₁	$D_s^+ \phi$	$< 4.2 \times 10^{-7}$	CL=90%	Γ ₂₉₇	$J/\psi(1S) K^+ \pi^+ \pi^-$	$(8.1 \pm 1.3) \times 10^{-4}$	S=2.5
Γ ₂₄₂	$D_s^{*+} \phi$	$< 1.2 \times 10^{-5}$	CL=90%	Γ ₂₉₈	$J/\psi(1S) K^+ K^- K^+$	$(3.37 \pm 0.29) \times 10^{-5}$	
Γ ₂₄₃	$D_s^+ \bar{K}^0$	$< 3 \times 10^{-6}$	CL=90%	Γ ₂₉₉	$\chi_{c0}(3915) K^+, \chi_{c0} \rightarrow p\bar{p}$	$< 7.1 \times 10^{-8}$	CL=95%
Γ ₂₄₄	$D_s^{*+} \bar{K}^0$	$< 6 \times 10^{-6}$	CL=90%	Γ ₃₀₀	$J/\psi(1S) K^*(892)^+$	$(1.43 \pm 0.08) \times 10^{-3}$	
Γ ₂₄₅	$D_s^+ \bar{K}^*(892)^0$	$< 4.4 \times 10^{-6}$	CL=90%	Γ ₃₀₁	$J/\psi(1S) K(1270)^+$	$(1.8 \pm 0.5) \times 10^{-3}$	
Γ ₂₄₆	$D_s^+ K^*0$	$< 3.5 \times 10^{-6}$	CL=90%	Γ ₃₀₂	$J/\psi(1S) K(1400)^+$	$< 5 \times 10^{-4}$	CL=90%
Γ ₂₄₇	$D_s^{*+} \bar{K}^*(892)^0$	$< 3.5 \times 10^{-4}$	CL=90%	Γ ₃₀₃	$J/\psi(1S) \eta K^+$	$(1.24 \pm 0.14) \times 10^{-4}$	
Γ ₂₄₈	$D_{cs}^- \pi^+ K^+$	$(1.80 \pm 0.22) \times 10^{-4}$		Γ ₃₀₄	$\chi_{c1-odd}(3872) K^+, \chi_{c1-odd} \rightarrow J/\psi \eta$	$< 3.8 \times 10^{-6}$	CL=90%
Γ ₂₄₉	$D_{cs}^* \pi^+ K^+$	$(1.45 \pm 0.24) \times 10^{-4}$			$\psi(4160) K^+, \psi \rightarrow J/\psi \eta$	$< 8.7 \times 10^{-7}$	CL=90%
Γ ₂₅₀	$D_{cs}^- \pi^+ K^*(892)^+$	$< 5 \times 10^{-3}$	CL=90%	Γ ₃₀₅	$J/\psi(1S) \eta' K^+$	$(3.1 \pm 0.4) \times 10^{-5}$	
Γ ₂₅₁	$D_{cs}^* \pi^+ K^*(892)^+$	$< 7 \times 10^{-3}$	CL=90%	Γ ₃₀₆	$J/\psi(1S) \phi K^+$	$(5.0 \pm 0.4) \times 10^{-5}$	
Γ ₂₅₂	$D_s^- K^+ K^+$	$(9.7 \pm 2.1) \times 10^{-6}$		Γ ₃₀₇	$J/\psi(1S) \phi K^+$	$(5.0 \pm 0.4) \times 10^{-5}$	
Γ ₂₅₃	$D_s^{*-} K^+ K^+$	$< 1.5 \times 10^{-5}$	CL=90%	Γ ₃₀₈	$J/\psi(1S) K_1(1650), K_1 \rightarrow$	$(6 \pm_{-6}^{10}) \times 10^{-6}$	
					ϕK^+		
Γ ₂₅₄	$\eta_c K^+$	$(1.10 \pm 0.07) \times 10^{-3}$	S=1.1	Γ ₃₀₉	$J/\psi(1S) K^*(1680)^+, K^* \rightarrow$	$(3.4 \pm_{-2.2}^{1.9}) \times 10^{-6}$	
Γ ₂₅₅	$\eta_c K^*(892)^+$	$(1.2 \pm_{-0.4}^{0.5}) \times 10^{-3}$			ϕK^+		
Γ ₂₅₆	$\eta_c K^+ \pi^+ \pi^-$	$< 3.9 \times 10^{-4}$	CL=90%	Γ ₃₁₀	$J/\psi(1S) K_2^*(1980), K_2^* \rightarrow$	$(1.5 \pm_{-0.5}^{0.9}) \times 10^{-6}$	
Γ ₂₅₇	$\eta_c K^+ \omega(782)$	$< 5.3 \times 10^{-4}$	CL=90%		ϕK^+		
Γ ₂₅₈	$\eta_c K^+ \eta$	$< 2.2 \times 10^{-4}$	CL=90%	Γ ₃₁₁	$J/\psi(1S) K(1830)^+, K(1830)^+ \rightarrow \phi K^+$	$(1.3 \pm_{-1.1}^{1.3}) \times 10^{-6}$	
Γ ₂₅₉	$\eta_c K^+ \pi^0$	$< 6.2 \times 10^{-5}$	CL=90%	Γ ₃₁₂	$\chi_{c1}(4140) K^+, \chi_{c1} \rightarrow$	$(10 \pm 4) \times 10^{-6}$	
Γ ₂₆₀	$\eta_c(2S) K^+$	$(4.4 \pm 1.0) \times 10^{-4}$			$J/\psi(1S) \phi$		
				Γ ₃₁₃	$\chi_{c1}(4274) K^+, \chi_{c1} \rightarrow$	$(3.6 \pm_{-1.8}^{2.2}) \times 10^{-6}$	
					$J/\psi(1S) \phi$		
				Γ ₃₁₄	$\chi_{c0}(4500) K^+, \chi_{c0} \rightarrow$	$(3.3 \pm_{-1.7}^{2.1}) \times 10^{-6}$	
					$J/\psi(1S) \phi$		

Charmonium modes

Meson Particle Listings

B^\pm

Γ ₃₁₅	$\chi_{c0}(4700)K^+, \chi_{c0} \rightarrow J/\psi(1S)\phi$	$(6 \pm \frac{5}{4}) \times 10^{-6}$	Γ ₃₈₂	$\eta(1405)K^+ \times B(\eta(1405) \rightarrow K^*K)$	$< 1.2 \times 10^{-6}$ CL=90%
Γ ₃₁₆	$J/\psi(1S)\omega K^+$	$(3.20 \pm \frac{0.60}{0.32}) \times 10^{-4}$	Γ ₃₈₃	$\eta(1475)K^+ \times B(\eta(1475) \rightarrow K^*K)$	$(1.38 \pm \frac{0.21}{0.18}) \times 10^{-5}$
Γ ₃₁₇	$\chi_{c0}(3915)K^+, \chi_{c0} \rightarrow J/\psi\omega$	$(3.0 \pm \frac{0.9}{0.7}) \times 10^{-5}$	Γ ₃₈₄	$f_1(1285)K^+$	$< 2.0 \times 10^{-6}$ CL=90%
Γ ₃₁₈	$J/\psi(1S)\pi^+$	$(3.92 \pm 0.09) \times 10^{-5}$	Γ ₃₈₅	$f_1(1420)K^+ \times B(f_1(1420) \rightarrow \eta\pi\pi)$	$< 2.9 \times 10^{-6}$ CL=90%
Γ ₃₁₉	$J/\psi(1S)\pi^+\pi^+\pi^-\pi^-\pi^-$	$(1.17 \pm 0.13) \times 10^{-5}$	Γ ₃₈₆	$f_1(1420)K^+ \times B(f_1(1420) \rightarrow K^*K)$	$< 4.1 \times 10^{-6}$ CL=90%
Γ ₃₂₀	$\psi(2S)\pi^+\pi^+\pi^-$	$(1.9 \pm 0.4) \times 10^{-5}$	Γ ₃₈₇	$\phi(1680)K^+ \times B(\phi(1680) \rightarrow K^*K)$	$< 3.4 \times 10^{-6}$ CL=90%
Γ ₃₂₁	$J/\psi(1S)\rho^+$	$(4.1 \pm 0.5) \times 10^{-5}$ S=1.4	Γ ₃₈₈	$f_0(1500)K^+$	$(3.7 \pm 2.2) \times 10^{-6}$
Γ ₃₂₂	$J/\psi(1S)\pi^+\pi^0$ nonresonant	$< 7.3 \times 10^{-6}$ CL=90%	Γ ₃₈₉	ωK^+	$(6.5 \pm 0.4) \times 10^{-6}$
Γ ₃₂₃	$J/\psi(1S)a_1(1260)^+$	$< 1.2 \times 10^{-3}$ CL=90%	Γ ₃₉₀	$\omega K^*(892)^+$	$< 7.4 \times 10^{-6}$ CL=90%
Γ ₃₂₄	$J/\psi(1S)p\bar{p}\pi^+$	$< 5.0 \times 10^{-7}$ CL=90%	Γ ₃₉₁	$\omega(K\pi)_0^{*+}$	$(2.8 \pm 0.4) \times 10^{-5}$
Γ ₃₂₅	$J/\psi(1S)p\bar{\Lambda}$	$(1.46 \pm 0.12) \times 10^{-5}$	Γ ₃₉₂	$\omega K_0^*(1430)^+$	$(2.4 \pm 0.5) \times 10^{-5}$
Γ ₃₂₆	$J/\psi(1S)\Sigma^0\rho$	$< 1.1 \times 10^{-5}$ CL=90%	Γ ₃₉₃	$\omega K_2^*(1430)^+$	$(2.1 \pm 0.4) \times 10^{-5}$
Γ ₃₂₇	$J/\psi(1S)D^+$	$< 1.2 \times 10^{-4}$ CL=90%	Γ ₃₉₄	$a_0(980)^+K^0 \times B(a_0(980)^+ \rightarrow \eta\pi^+)$	$< 3.9 \times 10^{-6}$ CL=90%
Γ ₃₂₈	$J/\psi(1S)\bar{D}^0\pi^+$	$< 2.5 \times 10^{-5}$ CL=90%	Γ ₃₉₅	$a_0(980)^0K^+ \times B(a_0(980)^0 \rightarrow \eta\pi^0)$	$< 2.5 \times 10^{-6}$ CL=90%
Γ ₃₂₉	$\psi(2S)\pi^+$	$(2.44 \pm 0.30) \times 10^{-5}$	Γ ₃₉₆	$K^*(892)^0\pi^+$	$(1.01 \pm 0.08) \times 10^{-5}$
Γ ₃₃₀	$\psi(2S)K^+$	$(6.24 \pm 0.21) \times 10^{-4}$	Γ ₃₉₇	$K^*(892)^+\pi^0$	$(6.8 \pm 0.9) \times 10^{-6}$
Γ ₃₃₁	$\psi(2S)K^*(892)^+$	$(6.7 \pm 1.4) \times 10^{-4}$ S=1.3	Γ ₃₉₈	$K^+\pi^-\pi^+$	$(5.10 \pm 0.29) \times 10^{-5}$
Γ ₃₃₂	$\psi(2S)K^0\pi^+$		Γ ₃₉₉	$K^+\pi^-\pi^+$ nonresonant	$(1.63 \pm \frac{0.21}{0.15}) \times 10^{-5}$
Γ ₃₃₃	$\psi(2S)K^+\pi^+\pi^-$	$(4.3 \pm 0.5) \times 10^{-4}$	Γ ₄₀₀	$\omega(782)K^+$	$(6 \pm 9) \times 10^{-6}$
Γ ₃₃₄	$\psi(2S)\phi(1020)K^+$	$(4.0 \pm 0.7) \times 10^{-6}$	Γ ₄₀₁	$K^+f_0(980) \times B(f_0(980) \rightarrow \pi^+\pi^-)$	$(9.4 \pm \frac{1.0}{1.2}) \times 10^{-6}$
Γ ₃₃₅	$\psi(3770)K^+$	$(4.3 \pm 1.1) \times 10^{-4}$	Γ ₄₀₂	$f_2(1270)^0K^+$	$(1.07 \pm 0.27) \times 10^{-6}$
Γ ₃₃₆	$\psi(3770)K^+, \psi \rightarrow D^0\bar{D}^0$	$(1.5 \pm 0.5) \times 10^{-4}$ S=1.4	Γ ₄₀₃	$f_0(1370)^0K^+ \times B(f_0(1370)^0 \rightarrow \pi^+\pi^-)$	$< 1.07 \times 10^{-5}$ CL=90%
Γ ₃₃₇	$\psi(3770)K^+, \psi \rightarrow D^+D^-$	$(9.4 \pm 3.5) \times 10^{-5}$	Γ ₄₀₄	$\rho(14500)K^+ \times B(\rho(1450)^0 \rightarrow \pi^+\pi^-)$	$< 1.17 \times 10^{-5}$ CL=90%
Γ ₃₃₈	$\psi(3770)K^+, \psi \rightarrow p\bar{p}$	$< 2 \times 10^{-7}$ CL=95%	Γ ₄₀₅	$f_2'(1525)K^+ \times B(f_2'(1525) \rightarrow \pi^+\pi^-)$	$< 3.4 \times 10^{-6}$ CL=90%
Γ ₃₃₉	$\psi(3770)K^+, \psi \rightarrow J/\psi\eta$	$< 4.6 \times 10^{-7}$ CL=90%	Γ ₄₀₆	$K^+\rho^0$	$(3.7 \pm 0.5) \times 10^{-6}$
Γ ₃₄₀	$\psi(4040)K^+$	$(1.6 \pm 0.5) \times 10^{-3}$	Γ ₄₀₇	$K_0^*(1430)^0\pi^+$	$(3.9 \pm \frac{0.6}{0.5}) \times 10^{-5}$ S=1.4
Γ ₃₄₁	$\psi(4040)K^+, \psi \rightarrow D^+D^-$	$(1.1 \pm 0.5) \times 10^{-5}$	Γ ₄₀₈	$K_2^*(1430)^0\pi^+$	$(5.6 \pm \frac{2.2}{1.5}) \times 10^{-6}$
Γ ₃₄₂	$\psi(4160)K^+$	$(5.1 \pm 2.7) \times 10^{-4}$	Γ ₄₀₉	$K^*(1410)^0\pi^+$	$< 4.5 \times 10^{-5}$ CL=90%
Γ ₃₄₃	$\psi(4160)K^+, \psi \rightarrow \bar{D}^0D^0$	$(8 \pm 5) \times 10^{-5}$	Γ ₄₁₀	$K^*(1680)^0\pi^+$	$< 1.2 \times 10^{-5}$ CL=90%
Γ ₃₄₄	$\psi(4160)K^+, \psi \rightarrow D^+D^-$	$(1.5 \pm 0.6) \times 10^{-5}$	Γ ₄₁₁	$K^+\pi^0\pi^0$	$(1.62 \pm 0.19) \times 10^{-5}$
Γ ₃₄₅	$\psi(4415)K^+, \psi \rightarrow D^+D^-$	$(2.0 \pm 0.8) \times 10^{-5}$	Γ ₄₁₂	$f_0(980)K^+ \times B(f_0 \rightarrow \pi^0\pi^0)$	$(2.8 \pm 0.8) \times 10^{-6}$
Γ ₃₄₆	$\psi(4415)K^+, \psi \rightarrow J/\psi\eta$	$< 9.6 \times 10^{-7}$ CL=90%	Γ ₄₁₃	$K^-\pi^+\pi^+$	$< 4.6 \times 10^{-8}$ CL=90%
Γ ₃₄₇	$\chi_{c0}\pi^+, \chi_{c0} \rightarrow \pi^+\pi^-$	$< 1 \times 10^{-7}$ CL=90%	Γ ₄₁₄	$K^-\pi^+\pi^+$ nonresonant	$< 5.6 \times 10^{-5}$ CL=90%
Γ ₃₄₈	$\chi_{c0}\pi^+, \chi_{c0} \rightarrow \pi^0\pi^0$	$< 5 \times 10^{-7}$ CL=90%	Γ ₄₁₅	$K_1(1270)^0\pi^+$	$< 4.0 \times 10^{-5}$ CL=90%
Γ ₃₄₉	$\chi_{c0}K^+$	$(1.51 \pm \frac{0.15}{0.13}) \times 10^{-4}$	Γ ₄₁₆	$K_1(1400)^0\pi^+$	$< 3.9 \times 10^{-5}$ CL=90%
Γ ₃₅₀	$\chi_{c0}K^0\pi^+$	$(1.45 \pm 0.21) \times 10^{-3}$	Γ ₄₁₇	$K^0\pi^+\pi^0$	$< 6.6 \times 10^{-5}$ CL=90%
Γ ₃₅₁	$\chi_{c0}K^*(892)^+$	$< 2.1 \times 10^{-4}$ CL=90%	Γ ₄₁₈	$K_0^*(1430)^+\pi^0$	$(1.19 \pm \frac{0.20}{0.23}) \times 10^{-5}$
Γ ₃₅₂	$\chi_{c1}(1P)\pi^+$	$(2.2 \pm 0.5) \times 10^{-5}$	Γ ₄₁₉	$K^0\rho^+$	$(7.3 \pm \frac{1.0}{1.2}) \times 10^{-6}$
Γ ₃₅₃	$\chi_{c1}(1P)K^+$	$(4.74 \pm 0.22) \times 10^{-4}$	Γ ₄₂₀	$K^*(892)^+\pi^+\pi^-$	$(7.5 \pm 1.0) \times 10^{-5}$
Γ ₃₅₄	$\chi_{c1}(1P)K^*(892)^+$	$(3.0 \pm 0.6) \times 10^{-4}$ S=1.1	Γ ₄₂₁	$K^*(892)^+\rho^0$	$(4.6 \pm 1.1) \times 10^{-6}$
Γ ₃₅₅	$\chi_{c1}(1P)K^0\pi^+$	$(5.8 \pm 0.4) \times 10^{-4}$	Γ ₄₂₂	$K^*(892)^+f_0(980)$	$(4.2 \pm 0.7) \times 10^{-6}$
Γ ₃₅₆	$\chi_{c1}(1P)K^+\pi^0$	$(3.29 \pm 0.35) \times 10^{-4}$	Γ ₄₂₃	$a_1^+K^0$	$(3.5 \pm 0.7) \times 10^{-5}$
Γ ₃₅₇	$\chi_{c1}(1P)K^+\pi^+\pi^-$	$(3.74 \pm 0.30) \times 10^{-4}$	Γ ₄₂₄	$b_1^+K^0 \times B(b_1^+ \rightarrow \omega\pi^+)$	$(9.6 \pm 1.9) \times 10^{-6}$
Γ ₃₅₈	$\chi_{c1}(2P)K^+, \chi_{c1}(2P) \rightarrow \pi^+\pi^-\chi_{c1}(1P)$	$< 1.1 \times 10^{-5}$ CL=90%	Γ ₄₂₅	$K^*(892)^0\rho^+$	$(9.2 \pm 1.5) \times 10^{-6}$
Γ ₃₅₉	$\chi_{c2}\pi^+, \chi_{c2} \rightarrow \pi^0\pi^0$	$< 7 \times 10^{-7}$ CL=90%	Γ ₄₂₆	$K_1(1400)^+\rho^0$	$< 7.8 \times 10^{-4}$ CL=90%
Γ ₃₆₀	$\chi_{c2}K^+$	$(1.1 \pm 0.4) \times 10^{-5}$	Γ ₄₂₇	$K_2^*(1430)^+\rho^0$	$< 1.5 \times 10^{-3}$ CL=90%
Γ ₃₆₁	$\chi_{c2}K^+, \chi_{c2} \rightarrow p\bar{p}\pi^+\pi^-$	$< 1.9 \times 10^{-7}$	Γ ₄₂₈	$b_1^0K^+ \times B(b_1^0 \rightarrow \omega\pi^0)$	$(9.1 \pm 2.0) \times 10^{-6}$
Γ ₃₆₂	$\chi_{c2}K^*(892)^+$	$< 1.2 \times 10^{-4}$ CL=90%	Γ ₄₂₉	$b_1^+K^*0 \times B(b_1^+ \rightarrow \omega\pi^+)$	$< 5.9 \times 10^{-6}$ CL=90%
Γ ₃₆₃	$\chi_{c2}K^0\pi^+$	$(1.24 \pm 0.25) \times 10^{-4}$	Γ ₄₃₀	$b_1^0K^*+ \times B(b_1^0 \rightarrow \omega\pi^0)$	$< 6.7 \times 10^{-6}$ CL=90%
Γ ₃₆₄	$\chi_{c2}K^+\pi^0$	$< 6.2 \times 10^{-5}$ CL=90%	Γ ₄₃₁	$K^+\bar{K}^0$	$(1.32 \pm 0.17) \times 10^{-6}$ S=1.2
Γ ₃₆₅	$\chi_{c2}K^+\pi^+\pi^-$	$(1.34 \pm 0.19) \times 10^{-4}$	Γ ₄₃₂	$\bar{K}^0K^+\pi^0$	$< 2.4 \times 10^{-5}$ CL=90%
Γ ₃₆₆	$\chi_{c2}(3930)K^+, \chi_{c2} \rightarrow D^+D^-$	$(1.6 \pm 0.6) \times 10^{-5}$	Γ ₄₃₃	$K^+K_S^0K_S^0$	$(1.05 \pm 0.04) \times 10^{-5}$
Γ ₃₆₇	$\chi_{c2}(3930)\pi^+, \chi_{c2} \rightarrow \pi^+\pi^-$	$< 1 \times 10^{-7}$ CL=90%	Γ ₄₃₄	$f_0(980)K^+, f_0 \rightarrow K_S^0K_S^0$	$(1.47 \pm 0.33) \times 10^{-5}$
Γ ₃₆₈	$h_c(1P)K^+$	$(3.7 \pm 1.2) \times 10^{-5}$	Γ ₄₃₅	$f_0(1710)K^+, f_0 \rightarrow K_S^0K_S^0$	$(4.8 \pm \frac{4.0}{2.6}) \times 10^{-7}$
Γ ₃₆₉	$h_c(1P)K^+, h_c \rightarrow p\bar{p}$	$< 6.4 \times 10^{-8}$ CL=95%	Γ ₄₃₆	$K^+K_S^0K_S^0$ nonresonant	$(2.0 \pm 0.4) \times 10^{-5}$
K or K^* modes					
Γ ₃₇₀	$K^0\pi^+$	$(2.39 \pm 0.06) \times 10^{-5}$	Γ ₄₃₇	$K_S^0K_S^0\pi^+$	$< 5.1 \times 10^{-7}$ CL=90%
Γ ₃₇₁	$K^+\pi^0$	$(1.32 \pm 0.04) \times 10^{-5}$	Γ ₄₃₈	$K^+K^-\pi^+$	$(5.2 \pm 0.4) \times 10^{-6}$
Γ ₃₇₂	$\eta'K^+$	$(7.04 \pm 0.25) \times 10^{-5}$	Γ ₄₃₉	$K^+K^-\pi^+$ nonresonant	$(1.68 \pm 0.26) \times 10^{-6}$
Γ ₃₇₃	$\eta'K^*(892)^+$	$(4.8 \pm \frac{1.8}{1.6}) \times 10^{-6}$	Γ ₄₄₀	$K^+\bar{K}^*(892)^0$	$(5.9 \pm 0.8) \times 10^{-7}$
Γ ₃₇₄	$\eta'K_0^*(1430)^+$	$(5.2 \pm 2.1) \times 10^{-6}$			
Γ ₃₇₅	$\eta'K_2^*(1430)^+$	$(2.8 \pm 0.5) \times 10^{-5}$			
Γ ₃₇₆	ηK^+	$(2.4 \pm 0.4) \times 10^{-6}$ S=1.7			
Γ ₃₇₇	$\eta K^*(892)^+$	$(1.93 \pm 0.16) \times 10^{-5}$			
Γ ₃₇₈	$\eta K_0^*(1430)^+$	$(1.8 \pm 0.4) \times 10^{-5}$			
Γ ₃₇₉	$\eta K_2^*(1430)^+$	$(9.1 \pm 3.0) \times 10^{-6}$			
Γ ₃₈₀	$\eta(1295)K^+ \times B(\eta(1295) \rightarrow \eta\pi\pi)$	$(2.9 \pm \frac{0.8}{0.7}) \times 10^{-6}$			
Γ ₃₈₁	$\eta(1405)K^+ \times B(\eta(1405) \rightarrow \eta\pi\pi)$	$< 1.3 \times 10^{-6}$ CL=90%			

Γ441	$K^+ \bar{K}_0^*(1430)^0$	(3.8 ± 1.3) × 10 ⁻⁷	
Γ442	$\pi^+ (K^+ K^-)_{s\text{-wave}}$	(8.5 ± 0.9) × 10 ⁻⁷	
Γ443	$\pi^+ K^+ K^-, m_{K^+ K^-} < 1.1$ GeV	(5.4 ± 0.5) × 10 ⁻⁶	
Γ444	$K^+ K^+ \pi^-$	< 1.1 × 10 ⁻⁸	CL=90%
Γ445	$K^+ K^+ \pi^-$ nonresonant	< 8.79 × 10 ⁻⁵	CL=90%
Γ446	$f_2'(1525) K^+$	(1.8 ± 0.5) × 10 ⁻⁶	S=1.1
Γ447	$K^+ f_J(2220)$		
Γ448	$K^{*+} \pi^+ K^-$	< 1.18 × 10 ⁻⁵	CL=90%
Γ449	$K^*(892)^+ K^*(892)^0$	(9.1 ± 2.9) × 10 ⁻⁷	
Γ450	$K^{*+} K^+ \pi^-$	< 6.1 × 10 ⁻⁶	CL=90%
Γ451	$K^+ K^- K^+$	(3.40 ± 0.14) × 10 ⁻⁵	S=1.4
Γ452	$K^+ \phi$	(8.8 ± 0.7) × 10 ⁻⁶	S=1.1
Γ453	$f_0(980) K^+ \times B(f_0(980) \rightarrow$ $K^+ K^-)$	(9.4 ± 3.2) × 10 ⁻⁶	
Γ454	$a_2(1320) K^+ \times B(a_2(1320) \rightarrow$ $K^+ K^-)$	< 1.1 × 10 ⁻⁶	CL=90%
Γ455	$X_0(1550) K^+ \times$ $B(X_0(1550) \rightarrow K^+ K^-)$	(4.3 ± 0.7) × 10 ⁻⁶	
Γ456	$\phi(1680) K^+ \times B(\phi(1680) \rightarrow$ $K^+ K^-)$	< 8 × 10 ⁻⁷	CL=90%
Γ457	$f_0(1710) K^+ \times B(f_0(1710) \rightarrow$ $K^+ K^-)$	(1.1 ± 0.6) × 10 ⁻⁶	
Γ458	$K^+ K^- K^+$ nonresonant	(2.38 ± 0.28) × 10 ⁻⁵	
Γ459	$K^*(892)^+ K^+ K^-$	(3.6 ± 0.5) × 10 ⁻⁵	
Γ460	$K^*(892)^+ \phi$	(10.0 ± 2.0) × 10 ⁻⁶	S=1.7
Γ461	$K^0 K^+ K^- \pi^+$	(3.40 ± 0.33) × 10 ⁻⁴	
Γ462	$J/\psi K^+, J/\psi \rightarrow K^0 K^- \pi^+$	(5.4 ± 1.2) × 10 ⁻⁶	
Γ463	$\chi_{c1} K^+, \chi_{c1} \rightarrow K^0 K^- \pi^+$	(2.25 ± 0.25) × 10 ⁻⁶	
Γ464	$\eta_c K^+, \eta_c \rightarrow K^0 K^- \pi^+$	(2.83 ± 0.30) × 10 ⁻⁵	
Γ465	$\eta_c(2S) K^+, \eta_c(2S) \rightarrow$ $K^0 K^- \pi^+$	(3.3 ± 0.4) × 10 ⁻⁶	
Γ466	$K^0 K^+ K^+ \pi^-$	(2.80 ± 0.30) × 10 ⁻⁴	
Γ467	$J/\psi K^+, J/\psi \rightarrow K^0 K^+ \pi^-$	(5.4 ± 1.3) × 10 ⁻⁶	
Γ468	$\chi_{c1} K^+, \chi_{c1} \rightarrow K^0 K^+ \pi^-$	(2.06 ± 0.32) × 10 ⁻⁶	
Γ469	$\eta_c K^+, \eta_c \rightarrow K^0 K^+ \pi^-$	(3.00 ± 0.34) × 10 ⁻⁵	
Γ470	$\eta_c(2S) K^+, \eta_c(2S) \rightarrow$ $K^0 K^+ \pi^-$	(3.1 ± 0.6) × 10 ⁻⁶	
Γ471	$\phi(K\pi)_0^{*+}$	(8.3 ± 1.6) × 10 ⁻⁶	
Γ472	$\phi K_1(1270)^+$	(6.1 ± 1.9) × 10 ⁻⁶	
Γ473	$\phi K_1(1400)^+$	< 3.2 × 10 ⁻⁶	CL=90%
Γ474	$\phi K^*(1410)^+$	< 4.3 × 10 ⁻⁶	CL=90%
Γ475	$\phi K_0^*(1430)^+$	(7.0 ± 1.6) × 10 ⁻⁶	
Γ476	$\phi K_2^*(1430)^+$	(8.4 ± 2.1) × 10 ⁻⁶	
Γ477	$\phi K_2^*(1770)^+$	< 1.50 × 10 ⁻⁵	CL=90%
Γ478	$\phi K_2^*(1820)^+$	< 1.63 × 10 ⁻⁵	CL=90%
Γ479	$a_1^+ K^{*0}$	< 3.6 × 10 ⁻⁶	CL=90%
Γ480	$K^+ \phi \phi$	(4.2 ± 0.8) × 10 ⁻⁶	S=2.2
Γ481	$\eta' \eta' K^+$	< 2.5 × 10 ⁻⁵	CL=90%
Γ482	$\omega \phi K^+$	< 1.9 × 10 ⁻⁶	CL=90%
Γ483	$X(1812) K^+ \times B(X \rightarrow \omega \phi)$	< 3.2 × 10 ⁻⁷	CL=90%
Γ484	$K^*(892)^+ \gamma$	(3.92 ± 0.22) × 10 ⁻⁵	S=1.7
Γ485	$K_1(1270)^+ \gamma$	(4.4 ± 0.7) × 10 ⁻⁵	
Γ486	$\eta K^+ \gamma$	(7.9 ± 0.9) × 10 ⁻⁶	
Γ487	$\eta' K^+ \gamma$	(2.9 ± 1.0) × 10 ⁻⁶	
Γ488	$\phi K^+ \gamma$	(2.7 ± 0.4) × 10 ⁻⁶	S=1.2
Γ489	$K^+ \pi^- \pi^+ \gamma$	(2.58 ± 0.15) × 10 ⁻⁵	S=1.3
Γ490	$K^*(892)^0 \pi^+ \gamma$	(2.33 ± 0.12) × 10 ⁻⁵	
Γ491	$K^+ \rho^0 \gamma$	(8.2 ± 0.9) × 10 ⁻⁶	
Γ492	$(K^+ \pi^-)_{NR} \pi^+ \gamma$	(9.9 ± 1.7) × 10 ⁻⁶	
Γ493	$K^0 \pi^+ \pi^0 \gamma$	(4.6 ± 0.5) × 10 ⁻⁵	
Γ494	$K_1(1400)^+ \gamma$	(10 ± 5) × 10 ⁻⁶	
Γ495	$K^*(1410)^+ \gamma$	(2.7 ± 0.8) × 10 ⁻⁵	
Γ496	$K_0^*(1430)^0 \pi^+ \gamma$	(1.32 ± 0.26) × 10 ⁻⁶	
Γ497	$K_2^*(1430)^+ \gamma$	(1.4 ± 0.4) × 10 ⁻⁵	
Γ498	$K^*(1680)^+ \gamma$	(6.7 ± 1.7) × 10 ⁻⁵	
Γ499	$K_3^*(1780)^+ \gamma$	< 3.9 × 10 ⁻⁵	CL=90%
Γ500	$K_4^*(2045)^+ \gamma$	< 9.9 × 10 ⁻³	CL=90%

Light unflavored meson modes

Γ501	$\rho^+ \gamma$	(9.8 ± 2.5) × 10 ⁻⁷	
Γ502	$\pi^+ \pi^0$	(5.31 ± 0.26) × 10 ⁻⁶	
Γ503	$\pi^+ \pi^+ \pi^-$	(1.52 ± 0.14) × 10 ⁻⁵	
Γ504	$\rho^0 \pi^+$	(8.3 ± 1.2) × 10 ⁻⁶	
Γ505	$\pi^+ f_0(980), f_0 \rightarrow \pi^+ \pi^-$	< 1.5 × 10 ⁻⁶	CL=90%
Γ506	$\pi^+ f_2(1270)$	(2.2 ± 0.7) × 10 ⁻⁶	
Γ507	$\rho(1450)^0 \pi^+, \rho^0 \rightarrow \pi^+ \pi^-$	(1.4 ± 0.6) × 10 ⁻⁶	
Γ508	$\rho(1450)^0 \pi^+, \rho^0 \rightarrow K^+ K^-$	(1.60 ± 0.14) × 10 ⁻⁶	
Γ509	$f_0(1370) \pi^+, f_0 \rightarrow \pi^+ \pi^-$	< 4.0 × 10 ⁻⁶	CL=90%
Γ510	$f_0(1370) \pi^+, f_0 \rightarrow \pi^0 \pi^0$	< 1.1 × 10 ⁻⁶	CL=90%
Γ511	$f_0(500) \pi^+, f_0 \rightarrow \pi^+ \pi^-$	< 4.1 × 10 ⁻⁶	CL=90%
Γ512	$\pi^+ \pi^- \pi^+$ nonresonant	(5.3 ± 1.5) × 10 ⁻⁶	
Γ513	$\pi^+ \pi^0 \pi^0$	(1.90 ± 0.21) × 10 ⁻⁵	
Γ514	$\rho^+ \pi^0$	(1.06 ± 0.12) × 10 ⁻⁵	
Γ515	$\rho(1450)^+ \pi^0, \rho^+ \rightarrow \pi^+ \pi^0$	(1.2 ± 0.6) × 10 ⁻⁶	
Γ516	$\pi^+ \pi^0 \pi^0$ nonresonant	< 6 × 10 ⁻⁷	CL=90%
Γ517	$X \rho i^+, X \rightarrow \pi^0 \pi^0$	(6.9 ± 1.1) × 10 ⁻⁶	
Γ518	$\pi^+ \pi^- \pi^+ \pi^0$	< 4.0 × 10 ⁻³	CL=90%
Γ519	$\rho^+ \rho^0$	(2.40 ± 0.19) × 10 ⁻⁵	
Γ520	$\rho^+ f_0(980), f_0 \rightarrow \pi^+ \pi^-$	< 2.0 × 10 ⁻⁶	CL=90%
Γ521	$a_1(1260)^+ \pi^0$	(2.6 ± 0.7) × 10 ⁻⁵	
Γ522	$a_1(1260)^0 \pi^+$	(2.0 ± 0.6) × 10 ⁻⁵	
Γ523	$\omega \pi^+$	(6.9 ± 0.5) × 10 ⁻⁶	
Γ524	$\omega \rho^+$	(1.59 ± 0.21) × 10 ⁻⁵	
Γ525	$\eta \pi^+$	(4.02 ± 0.27) × 10 ⁻⁶	
Γ526	$\eta \rho^+$	(7.0 ± 2.9) × 10 ⁻⁶	S=2.8
Γ527	$\eta' \pi^+$	(2.7 ± 0.9) × 10 ⁻⁶	S=1.9
Γ528	$\eta' \rho^+$	(9.7 ± 2.2) × 10 ⁻⁶	
Γ529	$\phi \pi^+$	(3.2 ± 1.5) × 10 ⁻⁸	
Γ530	$\phi \rho^+$	< 3.0 × 10 ⁻⁶	CL=90%
Γ531	$a_0(980)^0 \pi^+, a_0^0 \rightarrow \eta \pi^0$	< 5.8 × 10 ⁻⁶	CL=90%
Γ532	$a_0(980)^+ \pi^0, a_0^+ \rightarrow \eta \pi^+$	< 1.4 × 10 ⁻⁶	CL=90%
Γ533	$\pi^+ \pi^+ \pi^+ \pi^-$	< 8.6 × 10 ⁻⁴	CL=90%
Γ534	$\rho^0 a_1(1260)^+$	< 6.2 × 10 ⁻⁴	CL=90%
Γ535	$\rho^0 a_2(1320)^+$	< 7.2 × 10 ⁻⁴	CL=90%
Γ536	$b_1^0 \pi^+, b_1^0 \rightarrow \omega \pi^0$	(6.7 ± 2.0) × 10 ⁻⁶	
Γ537	$b_1^+ \pi^0, b_1^+ \rightarrow \omega \pi^+$	< 3.3 × 10 ⁻⁶	CL=90%
Γ538	$\pi^+ \pi^+ \pi^+ \pi^- \pi^0$	< 6.3 × 10 ⁻³	CL=90%
Γ539	$b_1^+ \rho^0, b_1^+ \rightarrow \omega \pi^+$	< 5.2 × 10 ⁻⁶	CL=90%
Γ540	$a_1(1260)^+ a_1(1260)^0$	< 1.3 %	CL=90%
Γ541	$b_1^0 \rho^+, b_1^0 \rightarrow \omega \pi^0$	< 3.3 × 10 ⁻⁶	CL=90%

Charged particle (h±) modes

$h^\pm = K^\pm \text{ or } \pi^\pm$

Γ542	$h^+ \pi^0$	(1.6 ± 0.7) × 10 ⁻⁵	
Γ543	ωh^+	(1.38 ± 0.27) × 10 ⁻⁵	
Γ544	$h^+ X^0$ (Familon)	< 4.9 × 10 ⁻⁵	CL=90%
Γ545	$K^+ X^0, X^0 \rightarrow \mu^+ \mu^-$	< 1 × 10 ⁻⁷	CL=95%

Baryon modes

Γ546	$p \bar{p} \pi^+$	(1.62 ± 0.20) × 10 ⁻⁶	
Γ547	$p \bar{p} \pi^+$ nonresonant	< 5.3 × 10 ⁻⁵	CL=90%
Γ548	$p \bar{p} \pi^+ \pi^0$	(4.6 ± 1.3) × 10 ⁻⁶	
Γ549	$p \bar{p} \pi^+ \pi^+ \pi^-$		
Γ550	$p \bar{p} K^+$	(5.9 ± 0.5) × 10 ⁻⁶	S=1.5
Γ551	$\Theta(1710)^{++} \bar{p}, \Theta^{++} \rightarrow$ $p K^+$	[g] < 9.1 × 10 ⁻⁸	CL=90%
Γ552	$f_J(2220) K^+, f_J \rightarrow p \bar{p}$	[g] < 4.1 × 10 ⁻⁷	CL=90%
Γ553	$p \bar{n} \pi^0$	< 6.3 × 10 ⁻⁶	CL=90%
Γ554	$p \bar{\Lambda}(1520)$	(3.1 ± 0.6) × 10 ⁻⁷	
Γ555	$p \bar{p} K^+$ nonresonant	< 8.9 × 10 ⁻⁵	CL=90%
Γ556	$p \bar{p} K^*(892)^+$	(3.6 ± 0.8) × 10 ⁻⁶	
Γ557	$f_J(2220) K^{*+}, f_J \rightarrow p \bar{p}$	< 7.7 × 10 ⁻⁷	CL=90%
Γ558	$p \bar{\Lambda}$	(2.4 ± 1.0) × 10 ⁻⁷	
Γ559	$p \bar{\Lambda} \gamma$	(2.4 ± 0.5) × 10 ⁻⁶	
Γ560	$p \bar{\Lambda} \pi^0$	(3.0 ± 0.7) × 10 ⁻⁶	
Γ561	$p \bar{\Sigma}(1385)^0$	< 4.7 × 10 ⁻⁷	CL=90%
Γ562	$\Delta^+ \bar{\Lambda}$	< 8.2 × 10 ⁻⁷	CL=90%

x_{617}	0	
x_{624}	0	0
	x_{431}	x_{617}

FIT INFORMATION

A multiparticle fit to $\eta_c(1S)$, $J/\psi(1S)$, $\psi(2S)$, $h_c(1P)$, and B^\pm with the total width, 10 combinations of partial widths obtained from integrated cross section, and 38 branching ratios uses 113 measurements to determine 19 parameters. The overall fit has a $\chi^2 = 184.6$ for 94 degrees of freedom.

B^+ BRANCHING RATIOS

$\Gamma(\ell^+ \nu_\ell X)/\Gamma_{total}$	Γ_1/Γ		
VALUE (units 10^{-2})	DOCUMENT ID	TECN	COMMENT
10.99 ± 0.28 OUR EVALUATION	(Produced by HFLAV)		
10.76 ± 0.32 OUR AVERAGE	Error includes scale factor of 1.1.		
11.17 ± 0.25 ± 0.28	¹ URQUIJO	07	BELL $e^+e^- \rightarrow \Upsilon(4S)$
10.28 ± 0.26 ± 0.39	² AUBERT,B	06Y	BABR $e^+e^- \rightarrow \Upsilon(4S)$
10.25 ± 0.57 ± 0.65	³ ARTUSO	97	CLE2 $e^+e^- \rightarrow \Upsilon(4S)$
• • • We do not use the following data for averages, fits, limits, etc. • • •			
11.15 ± 0.26 ± 0.41	⁴ OKABE	05	BELL Repl. by URQUIJO 07
10.1 ± 1.8 ± 1.5	ATHANAS	94	CLE2 Sup. by ARTUSO 97

- ¹ URQUIJO 07 report a measurement of $(10.34 \pm 0.23 \pm 0.25)\%$ for the partial branching fraction of $B^+ \rightarrow e^+ \nu_e X_C$ decay with electron energy above 0.6 GeV. We converted the result to $B^+ \rightarrow e^+ \nu_e X$ branching fraction.
- ² The measurements are obtained for charged and neutral B mesons partial rates of semileptonic decay to electrons with momentum above 0.6 GeV/c in the B rest frame. The best precision on the ratio is achieved for a momentum threshold of 1.0 GeV: $B(B^+ \rightarrow e^+ \nu_e X) / B(B^0 \rightarrow e^+ \nu_e X) = 1.074 \pm 0.041 \pm 0.026$.
- ³ ARTUSO 97 uses partial reconstruction of $B \rightarrow D^* \ell \nu_\ell$ and inclusive semileptonic branching ratio from BARISH 96b $(0.1049 \pm 0.0017 \pm 0.0043)$.
- ⁴ The measurements are obtained for charged and neutral B mesons partial rates of semileptonic decay to electrons with momentum above 0.6 GeV/c in the B rest frame, and their ratio of $B(B^+ \rightarrow e^+ \nu_e X)/B(B^0 \rightarrow e^+ \nu_e X) = 1.08 \pm 0.05 \pm 0.02$.

$\Gamma(e^+ \nu_e X_C)/\Gamma_{total}$	Γ_2/Γ		
VALUE (units 10^{-2})	DOCUMENT ID	TECN	COMMENT
10.79 ± 0.25 ± 0.27	¹ URQUIJO	07	BELL $e^+e^- \rightarrow \Upsilon(4S)$

- ¹ Measure the independent B^+ and B^0 partial branching fractions with electron threshold energies of 0.4 GeV.

$\Gamma(\ell^+ \nu_\ell X_\mu)/\Gamma_{total}$	Γ_3/Γ		
VALUE (units 10^{-3})	DOCUMENT ID	TECN	COMMENT
1.65 ± 0.10 ± 0.18	¹ CAO	21A	BELL $e^+e^- \rightarrow \Upsilon(4S)$

Requires $E_\ell^* > 1$ GeV, where E_ℓ^* is lepton energy in B rest frame.

- ¹ The correlation of 50% with $B(B^0 \rightarrow \ell^+ \nu_\ell X_\mu)$ (lepton energy in B rest frame $E_\ell^* > 1$ GeV) was reported.

$\Gamma(D^0 \ell^+ \nu_\ell)/\Gamma_{total}$	Γ_5/Γ		
VALUE (%)	DOCUMENT ID	TECN	COMMENT
2.21 ± 0.06 OUR EVALUATION	(Produced by HFLAV)		
2.29 ± 0.08 OUR AVERAGE			
2.29 ± 0.08 ± 0.09	¹ AUBERT	10	BABR $e^+e^- \rightarrow \Upsilon(4S)$
2.34 ± 0.03 ± 0.13	AUBERT	09A	BABR $e^+e^- \rightarrow \Upsilon(4S)$
2.21 ± 0.13 ± 0.19	² BARTELT	99	CLE2 $e^+e^- \rightarrow \Upsilon(4S)$
1.6 ± 0.6 ± 0.3	³ FULTON	91	CLEO $e^+e^- \rightarrow \Upsilon(4S)$
• • • We do not use the following data for averages, fits, limits, etc. • • •			
2.33 ± 0.09 ± 0.09	¹ AUBERT	08Q	BABR Repl. by AUBERT 09A
1.94 ± 0.15 ± 0.34	⁴ ATHANAS	97	CLE2 Repl. by BARTELT 99

- ¹ Uses a fully reconstructed B meson as a tag on the recoil side.
- ² Assumes equal production of B^+ and B^0 at the $\Upsilon(4S)$.
- ³ FULTON 91 assumes equal production of $B^0 \bar{B}^0$ and $B^+ B^-$ at the $\Upsilon(4S)$.
- ⁴ ATHANAS 97 uses missing energy and missing momentum to reconstruct neutrino.

$\Gamma(D^0 \ell^+ \nu_\ell)/\Gamma(\ell^+ \nu_\ell X)$	Γ_5/Γ_1		
VALUE	DOCUMENT ID	TECN	COMMENT
0.255 ± 0.009 ± 0.009	¹ AUBERT	10	BABR $e^+e^- \rightarrow \Upsilon(4S)$

- ¹ Uses a fully reconstructed B meson on the recoil side.

$\Gamma(D^0 \ell^+ \nu_\ell)/\Gamma(D \ell^+ \nu_\ell X)$	Γ_5/Γ_4		
VALUE	DOCUMENT ID	TECN	COMMENT
0.230 ± 0.020 OUR AVERAGE			
0.25 ± 0.06	¹ AAIJ	19AC	LHCB pp at 7 and 8 TeV
0.227 ± 0.014 ± 0.016	² AUBERT	07AN	BABR $e^+e^- \rightarrow \Upsilon(4S)$

- ¹ The relative branching fractions of $B^- \rightarrow D^0, D^{*0}, D^{**0}$ in the $B^- \rightarrow D^0 X \mu^- \bar{\nu}$ channel are determined by fitting the distribution of the missing mass in $\bar{B}^{*0} \rightarrow B^- K^+$ decays.
- ² Uses a fully reconstructed B meson on the recoil side.

$\Gamma(D^0 \tau^+ \nu_\tau)/\Gamma_{total}$	Γ_6/Γ		
VALUE (units 10^{-2})	DOCUMENT ID	TECN	COMMENT
0.77 ± 0.22 ± 0.12	¹ BOZEK	10	BELL $e^+e^- \rightarrow \Upsilon(4S)$
0.67 ± 0.37 ± 0.13	² AUBERT	08N	BABR Repl. by AUBERT 09s

- • • We do not use the following data for averages, fits, limits, etc. • • •
- ¹ Assumes equal production of B^+ and B^0 at the $\Upsilon(4S)$.
- ² Uses a fully reconstructed B meson as a tag on the recoil side.

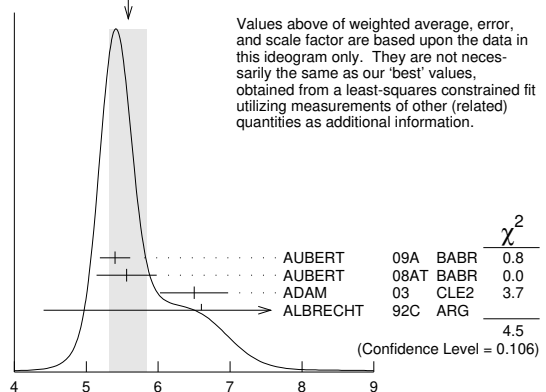
$\Gamma(D^0 \tau^+ \nu_\tau)/\Gamma(D^0 \ell^+ \nu_\ell)$	Γ_6/Γ_5		
VALUE	DOCUMENT ID	TECN	COMMENT
0.44 ± 0.07 OUR AVERAGE			
0.441 ± 0.060 ± 0.066	¹ AAIJ	23AR	LHCB pp at 7 and 8 TeV
0.429 ± 0.082 ± 0.052	^{2,3} LEES	12D	BABR $e^+e^- \rightarrow \Upsilon(4S)$
0.314 ± 0.170 ± 0.049	² AUBERT	09s	BABR Repl. by LEES 12D

- • • We do not use the following data for averages, fits, limits, etc. • • •
- ¹ Uses $\tau^+ \rightarrow \mu^+ \nu_\mu \bar{\nu}_\tau$ and μ^+ as ℓ^+ .
- ² Uses a fully reconstructed B meson as a tag on the recoil side.
- ³ Uses $\tau^+ \rightarrow e^+ \nu_e \bar{\nu}_\tau$ and $\tau^+ \rightarrow \mu^+ \nu_\mu \bar{\nu}_\tau$ and e^+ or μ^+ as ℓ^+ .

$\Gamma(D^{*0} \ell^+ \nu_\ell)/\Gamma_{total}$	Γ_7/Γ		
VALUE (%)	DOCUMENT ID	TECN	COMMENT
5.53 ± 0.22 OUR EVALUATION	(Produced by HFLAV)		
5.60 ± 0.26 OUR FIT	Error includes scale factor of 1.5.		
5.58 ± 0.26 OUR AVERAGE	Error includes scale factor of 1.5. See the ideogram below.		
5.40 ± 0.02 ± 0.21	AUBERT	09A	BABR $e^+e^- \rightarrow \Upsilon(4S)$
5.56 ± 0.08 ± 0.41	¹ AUBERT	08AT	BABR $e^+e^- \rightarrow \Upsilon(4S)$
6.50 ± 0.20 ± 0.43	² ADAM	03	CLE2 $e^+e^- \rightarrow \Upsilon(4S)$
6.6 ± 1.6 ± 1.5	³ ALBRECHT	92C	ARG $e^+e^- \rightarrow \Upsilon(4S)$
• • • We do not use the following data for averages, fits, limits, etc. • • •			
5.83 ± 0.15 ± 0.30	⁴ AUBERT	08Q	BABR Repl. by AUBERT 09A
6.50 ± 0.20 ± 0.43	⁵ BRIERE	02	CLE2 $e^+e^- \rightarrow \Upsilon(4S)$
5.13 ± 0.54 ± 0.64	⁶ BARISH	95	CLE2 Repl. by ADAM 03
seen	⁷ SANGHERA	93	CLE2 $e^+e^- \rightarrow \Upsilon(4S)$
4.1 ± 0.8 ^{+0.8} _{-0.9}	⁸ FULTON	91	CLEO $e^+e^- \rightarrow \Upsilon(4S)$
7.0 ± 1.8 ± 1.4	⁹ ANTREASYAN	90B	CBAL $e^+e^- \rightarrow \Upsilon(4S)$

- ¹ Measured using the dependence of $B^- \rightarrow D^{*0} e^- \bar{\nu}_e$ decay differential rate and the form factor description by CAPRINI 98.
- ² Simultaneous measurements of both $B^0 \rightarrow D^{*0} \ell^+ \nu_\ell$ and $B^+ \rightarrow \bar{D}^0(2007)^0 \ell^+ \nu_\ell$.
- ³ ALBRECHT 92c reports $0.058 \pm 0.014 \pm 0.013$. We rescale using the method described in STONE 94 but with the updated PDG 94 $B(D^0 \rightarrow K^- \pi^+)$. Assumes equal production of $B^0 \bar{B}^0$ and $B^+ B^-$ at the $\Upsilon(4S)$.
- ⁴ Uses a fully reconstructed B meson as a tag on the recoil side.
- ⁵ The results are based on the same analysis and data sample reported in ADAM 03.
- ⁶ BARISH 95 use $B(D^0 \rightarrow K^- \pi^+) = (3.91 \pm 0.08 \pm 0.17)\%$ and $B(D^{*0} \rightarrow D^0 \pi^0) = (63.6 \pm 2.3 \pm 3.3)\%$.
- ⁷ Combining $\bar{D}^{*0} \ell^+ \nu_\ell$ and $\bar{D}^{*0} \ell^+ \nu_\ell$ SANGHERA 93 test $V-A$ structure and fit the decay angular distributions to obtain $A_{FB} = 3/4 * (\Gamma^- - \Gamma^+) / \Gamma = 0.14 \pm 0.06 \pm 0.03$. Assuming a value of V_{cb} , they measure $V, A_1,$ and A_2 , the three form factors for the $D^* \ell \nu_\ell$ decay, where results are slightly dependent on model assumptions.
- ⁸ Assumes equal production of $B^0 \bar{B}^0$ and $B^+ B^-$ at the $\Upsilon(4S)$. Uncorrected for D and D^* branching ratio assumptions.
- ⁹ ANTREASYAN 90b is average over B and $\bar{D}^*(2010)$ charge states.

WEIGHTED AVERAGE
5.58±0.26 (Error scaled by 1.5)



$\Gamma(\bar{D}^{*0} \ell^+ \nu_\ell)/\Gamma_{total}$ Γ_7/Γ

Meson Particle Listings

B^\pm

$\Gamma(\overline{D}^*(2007)^0 \ell^+ \nu_\ell) / \Gamma(D \ell^+ \nu_\ell X)$				Γ_7 / Γ_4
VALUE	DOCUMENT ID	TECN	COMMENT	
0.582 ± 0.018 ± 0.030	¹ AUBERT	07AN	BABR $e^+ e^- \rightarrow \Upsilon(4S)$	

¹ Uses a fully reconstructed B meson on the recoil side.

$\Gamma(\overline{D}^*(2007)^0 e^+ \nu_e) / \Gamma(\overline{D}^*(2007)^0 \mu^+ \nu_\mu)$				Γ_8 / Γ_9
VALUE	DOCUMENT ID	TECN	COMMENT	
0.976 ± 0.029 ± 0.023	PRIM	23	BELL $e^+ e^- \rightarrow \Upsilon(4S)$	

$\Gamma(\overline{D}^*(2007)^0 \tau^+ \nu_\tau) / \Gamma_{\text{total}}$				Γ_{10} / Γ
VALUE (units 10^{-2})	DOCUMENT ID	TECN	COMMENT	
1.88 ± 0.20 OUR FIT				
2.12 ± 0.29 ± 0.29	¹ BOZEK	10	BELL $e^+ e^- \rightarrow \Upsilon(4S)$	

• • • We do not use the following data for averages, fits, limits, etc. • • •
 2.25 ± 0.48 ± 0.28 ² AUBERT 08N BABR Repl. by AUBERT 09s
¹ Assumes equal production of B^+ and B^0 at the $\Upsilon(4S)$.
² Uses a fully reconstructed B meson as a tag on the recoil side.

$\Gamma(\overline{D}^*(2007)^0 \tau^+ \nu_\tau) / \Gamma(\overline{D}^*(2007)^0 \ell^+ \nu_\ell)$				Γ_{10} / Γ_7
VALUE	DOCUMENT ID	TECN	COMMENT	
0.335 ± 0.034 OUR FIT				
0.322 ± 0.032 ± 0.022	^{1,2} LEES	12D	BABR $e^+ e^- \rightarrow \Upsilon(4S)$	

• • • We do not use the following data for averages, fits, limits, etc. • • •
 0.346 ± 0.073 ± 0.034 ¹ AUBERT 09s BABR Repl. by LEES 12D
¹ Uses a fully reconstructed B meson as a tag on the recoil side.
² Uses $\tau^+ \rightarrow e^+ \nu_e \overline{\nu}_\tau$ and $\tau^+ \rightarrow \mu^+ \nu_\mu \overline{\nu}_\tau$ and e^+ or μ^+ as ℓ^+ .

$\Gamma(D^{(*)n} \pi \ell^+ \nu_\ell (n \geq 1)) / \Gamma(D \ell^+ \nu_\ell X)$				Γ_{11} / Γ_4
VALUE	DOCUMENT ID	TECN	COMMENT	
0.193 ± 0.022 OUR AVERAGE				
0.21 ± 0.07	^{1,2} AAIJ	19AC	LHCb pp at 7 and 8 TeV	
0.191 ± 0.013 ± 0.019	³ AUBERT	07AN	BABR $e^+ e^- \rightarrow \Upsilon(4S)$	

¹ The relative branching fractions of $B^- \rightarrow D^0, D^{*0}, D^{**0}$ in the $B^- \rightarrow D^0 X \mu^- \overline{\nu}$ channel are determined by fitting the distribution of the missing mass in $\overline{B}^{*0} \rightarrow B^- K^+$ decays.
² In this measurement of $f_{D^{**0}} = B(B^- \rightarrow (D^{**0} \rightarrow D^0 X) \mu^- \overline{\nu}) / B(B^- \rightarrow D^0 X \mu^- \overline{\nu})$, D^{**0} refers collectively to $L = 1$ states $D_0^*(2400), D_1(2420), D_1(2430)$, and $D_2^*(2460)$, as well as other resonances such as radially excited D mesons, and to nonresonant contributions with additional pions.
³ Uses a fully reconstructed B meson on the recoil side.

$\Gamma(D^- \pi^+ \ell^+ \nu_\ell) / \Gamma_{\text{total}}$				Γ_{12} / Γ
VALUE (units 10^{-3})	DOCUMENT ID	TECN	COMMENT	
3.82 ± 0.20 OUR AVERAGE				
3.78 ± 0.13 ± 0.17	MEIER	23	BELL $e^+ e^- \rightarrow \Upsilon(4S)$	
4.2 ± 0.6 ± 0.3	¹ AUBERT	08Q	BABR $e^+ e^- \rightarrow \Upsilon(4S)$	

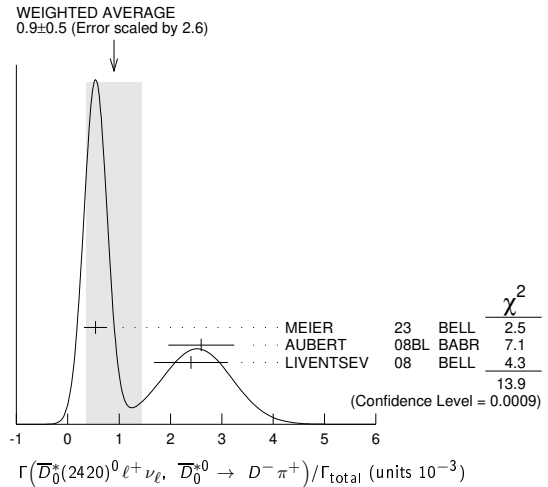
• • • We do not use the following data for averages, fits, limits, etc. • • •
 4.55 ± 0.27 ± 0.39 VOSSEN 18 BELL Repl. by MEIER 23
 4.1 ± 0.6 ± 0.1 ^{1,2} LIVENTSEV 08 BELL Repl. by VOSSEN 18
 5.3 ± 0.9 ± 0.1 ³ LIVENTSEV 05 BELL Repl. by LIVENTSEV 08
¹ Uses a fully reconstructed B meson as a tag on the recoil side.
² LIVENTSEV 08 reports $(4.0 \pm 0.4 \pm 0.6) \times 10^{-3}$ from a measurement of $[\Gamma(B^+ \rightarrow D^- \pi^+ \ell^+ \nu_\ell) / \Gamma_{\text{total}}] / [B(B^+ \rightarrow \overline{D}^0 \ell^+ \nu_\ell)]$ assuming $B(B^+ \rightarrow \overline{D}^0 \ell^+ \nu_\ell) = (2.15 \pm 0.22) \times 10^{-2}$, which we rescale to our best value $B(B^+ \rightarrow \overline{D}^0 \ell^+ \nu_\ell) = (2.21 \pm 0.06) \times 10^{-2}$. Our first error is their experiment's error and our second error is the systematic error from using our best value.
³ LIVENTSEV 05 reports $[\Gamma(B^+ \rightarrow D^- \pi^+ \ell^+ \nu_\ell) / \Gamma_{\text{total}}] / [B(B^0 \rightarrow D^- \ell^+ \nu_\ell)] = 0.25 \pm 0.03 \pm 0.03$ which we multiply by our best value $B(B^0 \rightarrow D^- \ell^+ \nu_\ell) = (2.12 \pm 0.06) \times 10^{-2}$. Our first error is their experiment's error and our second error is the systematic error from using our best value.

$\Gamma(\overline{D}_2^*(2460)^0 \ell^+ \nu_\ell, \overline{D}_2^{*0} \rightarrow D^- \pi^+) / \Gamma_{\text{total}}$				Γ_{13} / Γ
VALUE (units 10^{-3})	DOCUMENT ID	TECN	COMMENT	
1.59 ± 0.10 OUR AVERAGE				
1.63 ± 0.11 ± 0.07	MEIER	23	BELL $e^+ e^- \rightarrow \Upsilon(4S)$	
1.42 ± 0.15 ± 0.15	¹ AUBERT	09Y	BABR $e^+ e^- \rightarrow \Upsilon(4S)$	
1.5 ± 0.2 ± 0.2	² AUBERT	08BL	BABR $e^+ e^- \rightarrow \Upsilon(4S)$	
2.2 ± 0.3 ± 0.4	² LIVENTSEV	08	BELL $e^+ e^- \rightarrow \Upsilon(4S)$	

¹ Uses a simultaneous fit of all B semileptonic decays without full reconstruction of events. AUBERT 09Y reports $B(B^+ \rightarrow \overline{D}_2^*(2460)^0 \ell^+ \nu_\ell) \cdot B(\overline{D}_2^*(2460)^0 \rightarrow D^+ \pi^-) = (2.29 \pm 0.23 \pm 0.21) \times 10^{-3}$ and the authors have provided us the individual measurement.
² Uses a fully reconstructed B meson as a tag on the recoil side.

$\Gamma(\overline{D}_0^*(2420)^0 \ell^+ \nu_\ell, \overline{D}_0^{*0} \rightarrow D^- \pi^+) / \Gamma_{\text{total}}$				Γ_{14} / Γ
VALUE (units 10^{-3})	DOCUMENT ID	TECN	COMMENT	
0.9 ± 0.5 OUR AVERAGE				
0.54 ± 0.22 ± 0.05	MEIER	23	BELL $e^+ e^- \rightarrow \Upsilon(4S)$	
2.6 ± 0.5 ± 0.4	¹ AUBERT	08BL	BABR $e^+ e^- \rightarrow \Upsilon(4S)$	

2.4 ± 0.4 ± 0.6 ¹ LIVENTSEV 08 BELL $e^+ e^- \rightarrow \Upsilon(4S)$
¹ Uses a fully reconstructed B meson as a tag on the recoil side.



$\Gamma(D^{*-} \pi^+ \ell^+ \nu_\ell) / \Gamma_{\text{total}}$				Γ_{15} / Γ
VALUE (units 10^{-3})	DOCUMENT ID	TECN	COMMENT	
5.42 ± 0.28 OUR AVERAGE				
5.30 ± 0.19 ± 0.25	MEIER	23	BELL $e^+ e^- \rightarrow \Upsilon(4S)$	
5.9 ± 0.5 ± 0.4	¹ AUBERT	08Q	BABR $e^+ e^- \rightarrow \Upsilon(4S)$	

• • • We do not use the following data for averages, fits, limits, etc. • • •
 6.03 ± 0.43 ± 0.38 VOSSEN 18 BELL Repl. by MEIER 23
 6.6 ± 1.0 ± 0.2 ^{1,2} LIVENTSEV 08 BELL Repl. by VOSSEN 18
 5.9 ± 1.4 ± 0.1 ^{3,4} LIVENTSEV 05 BELL Repl. by LIVENTSEV 08
¹ Uses a fully reconstructed B meson as a tag on the recoil side.
² LIVENTSEV 08 reports $(6.4 \pm 0.8 \pm 0.9) \times 10^{-3}$ from a measurement of $[\Gamma(B^+ \rightarrow D^{*-} \pi^+ \ell^+ \nu_\ell) / \Gamma_{\text{total}}] / [B(B^+ \rightarrow \overline{D}^0 \ell^+ \nu_\ell)]$ assuming $B(B^+ \rightarrow \overline{D}^0 \ell^+ \nu_\ell) = (2.15 \pm 0.22) \times 10^{-2}$, which we rescale to our best value $B(B^+ \rightarrow \overline{D}^0 \ell^+ \nu_\ell) = (2.21 \pm 0.06) \times 10^{-2}$. Our first error is their experiment's error and our second error is the systematic error from using our best value.
³ Excludes D^{*+} contribution to $D \pi$ modes.
⁴ LIVENTSEV 05 reports $[\Gamma(B^+ \rightarrow D^{*-} \pi^+ \ell^+ \nu_\ell) / \Gamma_{\text{total}}] / [B(B^0 \rightarrow D^* (2010)^- \ell^+ \nu_\ell)] = 0.12 \pm 0.02 \pm 0.02$ which we multiply by our best value $B(B^0 \rightarrow D^* (2010)^- \ell^+ \nu_\ell) = (4.90 \pm 0.12) \times 10^{-2}$. Our first error is their experiment's error and our second error is the systematic error from using our best value.

$\Gamma(\overline{D}_1(2420)^0 \ell^+ \nu_\ell, \overline{D}_1^0 \rightarrow D^{*-} \pi^+) / \Gamma_{\text{total}}$				Γ_{16} / Γ
VALUE (units 10^{-3})	DOCUMENT ID	TECN	COMMENT	
2.84 ± 0.17 OUR AVERAGE				
2.49 ± 0.23 ± 0.14	MEIER	23	BELL $e^+ e^- \rightarrow \Upsilon(4S)$	
2.97 ± 0.17 ± 0.17	¹ AUBERT	09Y	BABR $e^+ e^- \rightarrow \Upsilon(4S)$	
2.9 ± 0.3 ± 0.3	² AUBERT	08BL	BABR $e^+ e^- \rightarrow \Upsilon(4S)$	
4.2 ± 0.7 ± 0.7	² LIVENTSEV	08	BELL $e^+ e^- \rightarrow \Upsilon(4S)$	
3.73 ± 0.85 ± 0.57	³ ANASTASSOV	98	CLE2 $e^+ e^- \rightarrow \Upsilon(4S)$	

Error includes scale factor of 1.1.
¹ Uses a simultaneous measurement of all B semileptonic decays without full reconstruction of events.
² Uses a fully reconstructed B meson as a tag on the recoil side.
³ Assumes equal production of B^+ and B^0 at the $\Upsilon(4S)$.

$\Gamma(\overline{D}_1^*(2430)^0 \ell^+ \nu_\ell, \overline{D}_1^{*0} \rightarrow D^{*-} \pi^+) / \Gamma_{\text{total}}$				Γ_{17} / Γ
VALUE (units 10^{-3})	CL%	DOCUMENT ID	TECN	COMMENT
1.7 ± 0.6 OUR AVERAGE				Error includes scale factor of 1.8.
1.38 ± 0.36 ± 0.08		MEIER	23	BELL $e^+ e^- \rightarrow \Upsilon(4S)$
2.7 ± 0.4 ± 0.5		¹ AUBERT	08BL	BABR $e^+ e^- \rightarrow \Upsilon(4S)$

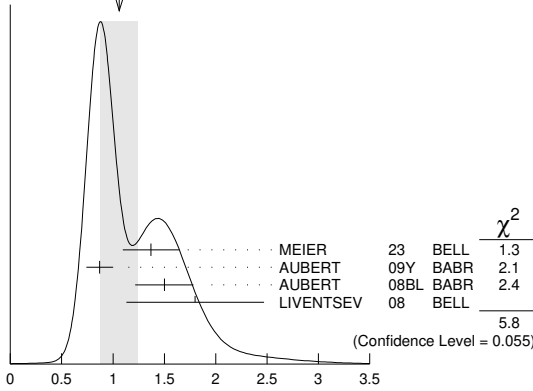
• • • We do not use the following data for averages, fits, limits, etc. • • •
 <0.7 ¹ LIVENTSEV 90 ¹ LIVENTSEV 08 BELL $e^+ e^- \rightarrow \Upsilon(4S)$
¹ Uses a fully reconstructed B meson as a tag on the recoil side.

$\Gamma(\overline{D}_2^*(2460)^0 \ell^+ \nu_\ell, \overline{D}_2^{*0} \rightarrow D^{*-} \pi^+) / \Gamma_{\text{total}}$				Γ_{18} / Γ
VALUE (units 10^{-3})	CL%	DOCUMENT ID	TECN	COMMENT
1.06 ± 0.18 OUR AVERAGE				Error includes scale factor of 1.7. See the ideogram below.
1.37 ± 0.26 ± 0.09		MEIER	23	BELL $e^+ e^- \rightarrow \Upsilon(4S)$
0.87 ± 0.11 ± 0.07		¹ AUBERT	09Y	BABR $e^+ e^- \rightarrow \Upsilon(4S)$
1.5 ± 0.2 ± 0.2		² AUBERT	08BL	BABR $e^+ e^- \rightarrow \Upsilon(4S)$
1.8 ± 0.6 ± 0.3		² LIVENTSEV	08	BELL $e^+ e^- \rightarrow \Upsilon(4S)$

• • • We do not use the following data for averages, fits, limits, etc. • • •
 <1.6 ¹ ANASTASSOV 98 CLE2 $e^+ e^- \rightarrow \Upsilon(4S)$
¹ Uses a simultaneous fit of all B semileptonic decays without full reconstruction of events. AUBERT 09Y reports $B(B^+ \rightarrow \overline{D}_2^*(2460)^0 \ell^+ \nu_\ell) \cdot B(\overline{D}_2^*(2460)^0 \rightarrow D^+ \pi^-) = (2.29 \pm 0.23 \pm 0.21) \times 10^{-3}$ and the authors have provided us the individual measurement.

See key on page 1171

Meson Particle Listings

 B^{\pm} ² Uses a fully reconstructed B meson as a tag on the recoil side.³ Assumes equal production of B^+ and B^0 at the $\Upsilon(4S)$.WEIGHTED AVERAGE
1.06±0.18 (Error scaled by 1.7) $\Gamma(\overline{D}_s^{*0}(2460)^0 \ell^+ \nu_\ell, \overline{D}_s^{*0} \rightarrow D^{*0} \pi^+)/\Gamma_{\text{total}}$ (units 10^{-3}) $\Gamma(\overline{D}^0 \pi^+ \pi^- \ell^+ \nu_\ell)/\Gamma_{\text{total}}$ Γ_{19}/Γ

VALUE (units 10^{-3})	DOCUMENT ID	TECN	COMMENT
1.73 ± 0.14 ± 0.13	MEIER	23	BELL $e^+ e^- \rightarrow \Upsilon(4S)$

 $\Gamma(\overline{D}^0 \pi^+ \pi^- \ell^+ \nu_\ell)/\Gamma(\overline{D}^0 \ell^+ \nu_\ell)$ Γ_{19}/Γ_5

VALUE (units 10^{-2})	DOCUMENT ID	TECN	COMMENT
7.1 ± 1.3 ± 0.8	1 LEES	16	BABR $e^+ e^- \rightarrow \Upsilon(4S)$

¹ Measurement used electrons and muons as leptons. $\Gamma(\overline{D}_1^-(2420)^0 \ell^+ \nu_\ell, \overline{D}_1^0 \rightarrow \overline{D}^0 \pi^+ \pi^-)/\Gamma_{\text{total}}$ Γ_{20}/Γ

VALUE (units 10^{-3})	DOCUMENT ID	TECN	COMMENT
1.05 ± 0.11 ± 0.08	MEIER	23	BELL $e^+ e^- \rightarrow \Upsilon(4S)$

 $\Gamma(\overline{D}^{*0} \pi^+ \pi^- \ell^+ \nu_\ell)/\Gamma(\overline{D}^{*0}(2007)^0 \ell^+ \nu_\ell)$ Γ_{21}/Γ_7

VALUE (units 10^{-2})	DOCUMENT ID	TECN	COMMENT
1.4 ± 0.7 ± 0.4	1 LEES	16	BABR $e^+ e^- \rightarrow \Upsilon(4S)$

¹ Measurement used electrons and muons as leptons. $\Gamma(\overline{D}^{*0} \pi^+ \pi^- \ell^+ \nu_\ell)/\Gamma_{\text{total}}$ Γ_{21}/Γ

VALUE (units 10^{-4})	DOCUMENT ID	TECN	COMMENT
7.0 ± 1.5 ± 0.8	MEIER	23	BELL $e^+ e^- \rightarrow \Upsilon(4S)$

 $\Gamma(D_s^{*-} K^+ \ell^+ \nu_\ell)/\Gamma_{\text{total}}$ Γ_{22}/Γ

VALUE (units 10^{-4})	DOCUMENT ID	TECN	COMMENT
6.1 ± 1.0 OUR AVERAGE			

5.9 ± 1.2 ± 1.5	1 STYPULA	12	BELL $e^+ e^- \rightarrow \Upsilon(4S)$
6.13 ^{+1.04} _{-1.03} ± 0.67	1 DEL-AMO-SA...11L	BABR	$e^+ e^- \rightarrow \Upsilon(4S)$

¹ Assumes equal production of B^+ and B^0 at the $\Upsilon(4S)$. $\Gamma(D_s^- K^+ \ell^+ \nu_\ell)/\Gamma_{\text{total}}$ Γ_{23}/Γ

VALUE (units 10^{-4})	DOCUMENT ID	TECN	COMMENT
3.0 ± 0.9^{+1.1}_{-0.8}	1 STYPULA	12	BELL $e^+ e^- \rightarrow \Upsilon(4S)$

¹ Assumes equal production of B^+ and B^0 at the $\Upsilon(4S)$. $\Gamma(D_s^{*-} K^+ \ell^+ \nu_\ell)/\Gamma_{\text{total}}$ Γ_{24}/Γ

VALUE (units 10^{-4})	DOCUMENT ID	TECN	COMMENT
2.9 ± 1.6^{+1.1}_{-1.0}	1,2 STYPULA	12	BELL $e^+ e^- \rightarrow \Upsilon(4S)$

¹ Assumes equal production of B^+ and B^0 at the $\Upsilon(4S)$.² STYPULA 12 provides also an upper limit of 0.56×10^{-3} at 90% CL for the same data. Also measures branching fraction of the combined modes of $D_s^- K^+ \ell^+ \nu_\ell$ and $D_s^{*-} K^+ \ell^+ \nu_\ell$ as $B(B^+ \rightarrow D_s^{*-} K^+ \ell^+ \nu_\ell) = (5.9 \pm 1.2 \pm 1.5) \times 10^{-4}$. $\Gamma(\pi^0 \ell^+ \nu_\ell)/\Gamma_{\text{total}}$ Γ_{25}/Γ

VALUE (units 10^{-4})	DOCUMENT ID	TECN	COMMENT
0.780 ± 0.027 OUR EVALUATION			
0.748 ± 0.029 OUR AVERAGE			

0.80 ± 0.08 ± 0.04	1 SIBIDANOV	13	BELL $e^+ e^- \rightarrow \Upsilon(4S)$
0.77 ± 0.04 ± 0.03	2 LEES	12AA	BABR $e^+ e^- \rightarrow \Upsilon(4S)$
0.705 ± 0.025 ± 0.035	3 DEL-AMO-SA...11c	BABR	$e^+ e^- \rightarrow \Upsilon(4S)$
0.82 ± 0.09 ± 0.05	3 AUBERT	08AV	BABR $e^+ e^- \rightarrow \Upsilon(4S)$
0.77 ± 0.14 ± 0.08	4 HOKUUE	07	BELL $e^+ e^- \rightarrow \Upsilon(4S)$

• • • We do not use the following data for averages, fits, limits, etc. • • •

0.74 ± 0.05 ± 0.10	5 AUBERT,B	05o	BABR Repl. by DEL-AMO-SANCHEZ 11c
--------------------	------------	-----	-----------------------------------

¹ The signal events are tagged by a second B meson reconstructed in the fully hadronic decays.² Uses loose neutrino reconstruction technique. Assumes $B(\Upsilon(4S) \rightarrow B^+ B^-) = (51.6 \pm 0.6)\%$ and $B(\Upsilon(4S) \rightarrow B^0 \overline{B}^0) = (48.4 \pm 0.6)\%$.³ Using the isospin symmetry relation, B^+ and B^0 branching fractions are combined.⁴ The signal events are tagged by a second B meson reconstructed in the semileptonic mode $B \rightarrow D^{(*)} \ell \nu_\ell$.⁵ B^+ and B^0 decays combined assuming isospin symmetry. Systematic errors include both experimental and form-factor uncertainties. $\Gamma(\pi^0 e^+ \nu_e)/\Gamma_{\text{total}}$ Γ_{26}/Γ

VALUE (units 10^{-4})	CL%	DOCUMENT ID	TECN	COMMENT
--------------------------	-----	-------------	------	---------

• • • We do not use the following data for averages, fits, limits, etc. • • •

0.9 ± 0.2 ± 0.2		1 ALEXANDER	96T	CLE2 $e^+ e^- \rightarrow \Upsilon(4S)$
<22	90	ANTREASNYAN	90B	CBAL $e^+ e^- \rightarrow \Upsilon(4S)$

¹ Derived based in the reported B^0 result by assuming isospin symmetry: $\Gamma(B^0 \rightarrow \pi^- \ell^+ \nu) = 2\Gamma(B^+ \rightarrow \pi^0 \ell^+ \nu)$. $\Gamma(\eta \ell^+ \nu_\ell)/\Gamma_{\text{total}}$ Γ_{27}/Γ

VALUE (units 10^{-4})	CL%	DOCUMENT ID	TECN	COMMENT
--------------------------	-----	-------------	------	---------

0.35 ± 0.04 OUR AVERAGE

0.283 ± 0.055 ± 0.034	1	GEBAUER	22	BELL $e^+ e^- \rightarrow \Upsilon(4S)$
0.42 ± 0.11 ± 0.03	2	BELENO	17	BELL $e^+ e^- \rightarrow \Upsilon(4S)$
0.38 ± 0.05 ± 0.05	3	LEES	12AA	BABR $e^+ e^- \rightarrow \Upsilon(4S)$
0.31 ± 0.06 ± 0.08	3	AUBERT	09Q	BABR $e^+ e^- \rightarrow \Upsilon(4S)$
0.64 ± 0.20 ± 0.03	4	AUBERT	08AV	BABR $e^+ e^- \rightarrow \Upsilon(4S)$

• • • We do not use the following data for averages, fits, limits, etc. • • •

0.36 ± 0.05 ± 0.04	3	DEL-AMO-SA...11F	BABR	Repl. by LEES 12AA
<1.01	90	5 ADAM	07	CLE2 $e^+ e^- \rightarrow \Upsilon(4S)$
0.84 ± 0.31 ± 0.18	6	ATHAR	03	CLE2 Repl. by ADAM 07

¹ Assumes $B(\Upsilon(4S) \rightarrow B^+ B^-) = (51.3 \pm 0.6)\%$.² Uses missing-mass technique by fully reconstructing the hadronic decay chain of the accompanying B .³ Uses loose neutrino reconstruction technique. Assumes $B(\Upsilon(4S) \rightarrow B^+ B^-) = (51.6 \pm 0.6)\%$ and $B(\Upsilon(4S) \rightarrow B^0 \overline{B}^0) = (48.4 \pm 0.6)\%$.⁴ Assumes equal production of B^+ and B^0 at the $\Upsilon(4S)$.⁵ The B^0 and B^+ results are combined assuming the isospin, B lifetimes, and relative charged/neutral B production at the $\Upsilon(4S)$.⁶ ATHAR 03 reports systematic errors 0.16 ± 0.09 , which are experimental systematic and systematic due to model dependence. We combine these in quadrature. $\Gamma(\eta' \ell^+ \nu_\ell)/\Gamma_{\text{total}}$ Γ_{28}/Γ

VALUE (units 10^{-4})	CL%	DOCUMENT ID	TECN	COMMENT
--------------------------	-----	-------------	------	---------

0.24 ± 0.07 OUR AVERAGE

0.279 ± 0.129 ± 0.030	1	GEBAUER	22	BELL $e^+ e^- \rightarrow \Upsilon(4S)$
0.24 ± 0.08 ± 0.03	2	LEES	12AA	BABR $e^+ e^- \rightarrow \Upsilon(4S)$
0.04 ± 0.22 ^{+0.05} _{-0.02}	3	AUBERT	08AV	BABR $e^+ e^- \rightarrow \Upsilon(4S)$
2.66 ± 0.80 ± 0.56	4	ADAM	07	CLE2 $e^+ e^- \rightarrow \Upsilon(4S)$

• • • We do not use the following data for averages, fits, limits, etc. • • •

<0.72	90	5 BELENO	17	BELL $e^+ e^- \rightarrow \Upsilon(4S)$
0.24 ± 0.08 ± 0.03	2	DEL-AMO-SA...11F	BABR	Repl. by LEES 12AA

¹ Assumes $B(\Upsilon(4S) \rightarrow B^+ B^-) = (51.3 \pm 0.6)\%$.² Uses loose neutrino reconstruction technique. Assumes $B(\Upsilon(4S) \rightarrow B^+ B^-) = (51.6 \pm 0.6)\%$ and $B(\Upsilon(4S) \rightarrow B^0 \overline{B}^0) = (48.4 \pm 0.6)\%$.³ Assumes equal production of B^+ and B^0 at the $\Upsilon(4S)$.⁴ The B^0 and B^+ results are combined assuming the isospin, B lifetimes, and relative charged/neutral B production at the $\Upsilon(4S)$. Corresponds to 90% CL interval $(1.20-4.46) \times 10^{-4}$.⁵ Uses missing-mass technique by fully reconstructing the hadronic decay chain of the accompanying B . $\Gamma(\omega \ell^+ \nu_\ell)/\Gamma_{\text{total}}$ Γ_{29}/Γ $\ell = e$ or μ , not sum over e and μ modes.

VALUE (units 10^{-4})	CL%	DOCUMENT ID	TECN	COMMENT
--------------------------	-----	-------------	------	---------

1.19 ± 0.09 OUR AVERAGE

1.21 ± 0.14 ± 0.08	1,2	LEES	13A	BABR $e^+ e^- \rightarrow \Upsilon(4S)$
1.35 ± 0.21 ± 0.11	3	LEES	13T	BABR $e^+ e^- \rightarrow \Upsilon(4S)$
1.07 ± 0.16 ± 0.07	4	SIBIDANOV	13	BELL $e^+ e^- \rightarrow \Upsilon(4S)$
1.19 ± 0.16 ± 0.09	2,5	LEES	12AA	BABR $e^+ e^- \rightarrow \Upsilon(4S)$
1.3 ± 0.4 ± 0.4	6	SCHWANDA	04	BELL $e^+ e^- \rightarrow \Upsilon(4S)$

• • • We do not use the following data for averages, fits, limits, etc. • • •

1.14 ± 0.16 ± 0.08	2	AUBERT	09Q	BABR Repl. by LEES 13A
<2.1	90	7 BEAN	93B	CLE2 $e^+ e^- \rightarrow \Upsilon(4S)$

¹ LEES 13A reports $(1.21 \pm 0.14 \pm 0.08) \times 10^{-4}$ from a measurement of $[\Gamma(B^+ \rightarrow \omega \ell^+ \nu_\ell)/\Gamma_{\text{total}}] \times [B(\omega(782) \rightarrow \pi^+ \pi^- \pi^0)]$ assuming $B(\omega(782) \rightarrow \pi^+ \pi^- \pi^0) = (89.2 \pm 0.7) \times 10^{-2}$.² Uses $B(\Upsilon(4S) \rightarrow B^+ B^-) = (51.6 \pm 0.6)\%$ and $B(\Upsilon(4S) \rightarrow B^0 \overline{B}^0) = (48.4 \pm 0.6)\%$.³ Uses semileptonic tagging. Assumes $B(\omega \rightarrow \pi^+ \pi^- \pi^0) = (89.2 \pm 0.7)\%$ and that the production ratio of $B^+ B^-$ to $B^0 \overline{B}^0$ from $\Upsilon(4S)$ is 1.056 ± 0.028 . The partial branching fractions in three bins of q^2 are also reported.⁴ The signal events are tagged by a second B meson reconstructed in the fully hadronic decays.⁵ Uses loose neutrino reconstruction technique.

Meson Particle Listings

B^\pm

⁶ Assumes equal production of B^+ and B^0 at the $\mathcal{T}(4S)$.
⁷ BEAN 93B limit set using ISGW Model. Using isospin and the quark model to combine $\Gamma(\rho^0 \ell^+ \nu_\ell)$ and $\Gamma(\rho^- \ell^+ \nu_\ell)$ with this result, they obtain a limit $<(1.6-2.7) \times 10^{-4}$ at 90% CL for $B^+ \rightarrow \omega \ell^+ \nu_\ell$. The range corresponds to the ISGW, WSB, and KS models. An upper limit on $|V_{ub}/V_{cb}| < 0.8-0.13$ at 90% CL is derived as well.

$\Gamma(\omega \mu^+ \nu_\mu)/\Gamma_{total}$ Γ_{30}/Γ

VALUE DOCUMENT ID TECN COMMENT
 • • • We do not use the following data for averages, fits, limits, etc. • • •
 seen ¹ ALBRECHT 91c ARG

¹ In ALBRECHT 91c, one event is fully reconstructed providing evidence for the $b \rightarrow u$ transition.

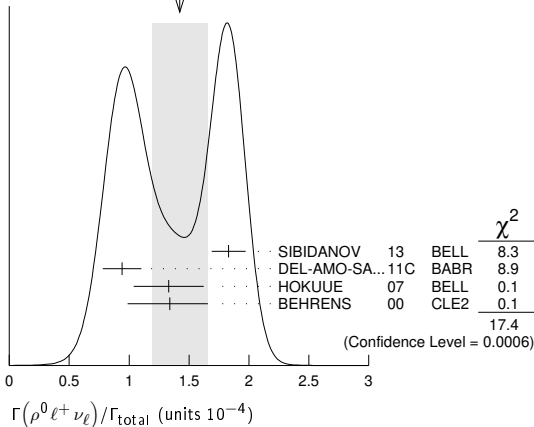
$\Gamma(\rho^0 \ell^+ \nu_\ell)/\Gamma_{total}$ Γ_{31}/Γ

$\ell = e \text{ or } \mu$, not sum over e and μ modes.
 VALUE (units 10^{-4}) CL% DOCUMENT ID TECN COMMENT
1.58 ± 0.11 OUR EVALUATION (Produced by HFLAV)
1.42 ± 0.23 OUR AVERAGE Error includes scale factor of 2.4. See the ideogram below.

1.83 ± 0.10 ± 0.10	¹ SIBIDANOV	13	BELL	$e^+ e^- \rightarrow \mathcal{T}(4S)$
0.94 ± 0.08 ± 0.14	² DEL-AMO-SA...	11c	BABR	$e^+ e^- \rightarrow \mathcal{T}(4S)$
1.33 ± 0.23 ± 0.18	³ HOKUUE	07	BELL	$e^+ e^- \rightarrow \mathcal{T}(4S)$
1.34 ± 0.15 +0.28 -0.32	⁴ BEHRENS	00	CLE2	$e^+ e^- \rightarrow \mathcal{T}(4S)$
• • • We do not use the following data for averages, fits, limits, etc. • • •				
1.16 ± 0.11 ± 0.30	² AUBERT,B	05o	BABR	Repl. by DEL-AMO-SANCHEZ 11c
1.40 ± 0.21 +0.32 -0.33	⁴ BEHRENS	00	CLE2	$e^+ e^- \rightarrow \mathcal{T}(4S)$
1.2 ± 0.2 +0.3 -0.4	⁴ ALEXANDER	96T	CLE2	$e^+ e^- \rightarrow \mathcal{T}(4S)$
<2.1	⁵ BEAN	93B	CLE2	$e^+ e^- \rightarrow \mathcal{T}(4S)$

- ¹ The signal events are tagged by a second B meson reconstructed in the fully hadronic decays.
- ² B^+ and B^0 decays combined assuming isospin symmetry. Systematic errors include both experimental and form-factor uncertainties.
- ³ The signal events are tagged by a second B meson reconstructed in the semileptonic mode $B \rightarrow D^{(*)} \ell \nu_\ell$.
- ⁴ Derived based in the reported B^0 result by assuming isospin symmetry: $\Gamma(B^0 \rightarrow \rho^- \ell^+ \nu) = 2\Gamma(B^+ \rightarrow \rho^0 \ell^+ \nu) \approx 2\Gamma(B^+ \rightarrow \omega \ell^+ \nu)$.
- ⁵ BEAN 93B limit set using ISGW Model. Using isospin and the quark model to combine $\Gamma(\omega \ell^+ \nu_\ell)$ and $\Gamma(\rho^- \ell^+ \nu_\ell)$ with this result, they obtain a limit $<(1.6-2.7) \times 10^{-4}$ at 90% CL for $B^+ \rightarrow \rho^0 \ell^+ \nu_\ell$. The range corresponds to the ISGW, WSB, and KS models. An upper limit on $|V_{ub}/V_{cb}| < 0.8-0.13$ at 90% CL is derived as well.

WEIGHTED AVERAGE
 1.42±0.23 (Error scaled by 2.4)



$\Gamma(\pi^+ \pi^- \ell^+ \nu_\ell)/\Gamma_{total}$ Γ_{32}/Γ

VALUE (units 10^{-5}) DOCUMENT ID TECN COMMENT
22.7 ± 1.9 ± 3.5 BELENO 21 BELL $e^+ e^- \rightarrow \mathcal{T}(4S)$

$\Gamma(\rho \bar{p} \ell^+ \nu_\ell)/\Gamma_{total}$ Γ_{33}/Γ

VALUE (units 10^{-6}) DOCUMENT ID TECN COMMENT
5.8 ± 2.4 ± 0.9 ¹ TIEN 14 BELL $e^+ e^- \rightarrow \mathcal{T}(4S)$

¹ Assumes equal production of B^+ and B^0 at the $\mathcal{T}(4S)$.

$\Gamma(\rho \bar{p} \mu^+ \nu_\mu)/\Gamma_{total}$ Γ_{34}/Γ

VALUE (units 10^{-6}) CL% DOCUMENT ID TECN COMMENT
 • • • We do not use the following data for averages, fits, limits, etc. • • •
 <8.5 90 ¹ TIEN 14 BELL $e^+ e^- \rightarrow \mathcal{T}(4S)$
¹ Assumes equal production of B^+ and B^0 at the $\mathcal{T}(4S)$.

$\Gamma(\rho \bar{p} \mu^+ \nu_\mu)/\Gamma(J/\psi(1S) K^+)$ Γ_{34}/Γ_{295}

VALUE (units 10^{-3}) DOCUMENT ID TECN COMMENT
5.22 ± 0.31 ± 0.03 ¹ AAIJ 20k LHCB pp at 7, 8 and 13 TeV

¹ AAIJ 20k reports $[\Gamma(B^+ \rightarrow \rho \bar{p} \mu^+ \nu_\mu)/\Gamma(B^+ \rightarrow J/\psi(1S) K^+)] / [B(J/\psi(1S) \rightarrow \mu^+ \mu^-)] = (8.75 \pm 0.39 \pm 0.35) \times 10^{-2}$ which we multiply by our best value $B(J/\psi(1S) \rightarrow \mu^+ \mu^-) = (5.961 \pm 0.033) \times 10^{-2}$. Our first error is their experiment's error and our second error is the systematic error from using our best value.

$\Gamma(\rho \bar{p} e^+ \nu_e)/\Gamma_{total}$ Γ_{35}/Γ

VALUE (units 10^{-6}) CL% DOCUMENT ID TECN COMMENT
8.2 ± 3.7 ± 3.2 ± 0.6 ¹ TIEN 14 BELL $e^+ e^- \rightarrow \mathcal{T}(4S)$

• • • We do not use the following data for averages, fits, limits, etc. • • •
 <5200 90 ² ADAM 03B CLE2 $e^+ e^- \rightarrow \mathcal{T}(4S)$
¹ Assumes equal production of B^+ and B^0 at the $\mathcal{T}(4S)$.
² Based on phase-space model; if $V-A$ model is used, the 90% CL upper limit becomes $< 1.2 \times 10^{-3}$.

$\Gamma(e^+ \nu_e)/\Gamma_{total}$ Γ_{36}/Γ

VALUE (units 10^{-6}) CL% DOCUMENT ID TECN COMMENT
< 0.98 90 ¹ SATOYAMA 07 BELL $e^+ e^- \rightarrow \mathcal{T}(4S)$

• • • We do not use the following data for averages, fits, limits, etc. • • •
 < 3.5 90 ² YOOK 15 BELL $e^+ e^- \rightarrow \mathcal{T}(4S)$
 < 8 90 ¹ AUBERT 10E BABR $e^+ e^- \rightarrow \mathcal{T}(4S)$
 < 9 90 ¹ AUBERT 09V BABR $e^+ e^- \rightarrow \mathcal{T}(4S)$
 < 5.2 90 ¹ AUBERT 08AD BABR $e^+ e^- \rightarrow \mathcal{T}(4S)$
 < 15 90 ARTUSO 95 CLE2 $e^+ e^- \rightarrow \mathcal{T}(4S)$

¹ Assumes equal production of B^+ and B^0 at the $\mathcal{T}(4S)$.
² Assumes $B(\mathcal{T}(4S) \rightarrow B^+ B^-) = 0.513 \pm 0.006$.

$\Gamma(\mu^+ \nu_\mu)/\Gamma_{total}$ Γ_{37}/Γ

VALUE (units 10^{-6}) CL% DOCUMENT ID TECN COMMENT
< 0.86 90 ¹ PRIM 20 BELL $e^+ e^- \rightarrow \mathcal{T}(4S)$

• • • We do not use the following data for averages, fits, limits, etc. • • •
 0.29 to 1.07 90 ² SIBIDANOV 18 BELL $e^+ e^- \rightarrow \mathcal{T}(4S)$
 < 2.7 90 ³ YOOK 15 BELL $e^+ e^- \rightarrow \mathcal{T}(4S)$
 < 11 90 ⁴ AUBERT 10E BABR $e^+ e^- \rightarrow \mathcal{T}(4S)$
 < 1.0 90 ⁴ AUBERT 09V BABR $e^+ e^- \rightarrow \mathcal{T}(4S)$
 < 5.6 90 ⁴ AUBERT 08AD BABR $e^+ e^- \rightarrow \mathcal{T}(4S)$
 < 1.7 90 ^{4,5} SATOYAMA 07 BELL $e^+ e^- \rightarrow \mathcal{T}(4S)$
 < 6.6 90 AUBERT 04o BABR Repl. by AUBERT 09V
 < 21 90 ARTUSO 95 CLE2 $e^+ e^- \rightarrow \mathcal{T}(4S)$

- ¹ This is a 90% C.L. upper limit in the frequentist approach. The corresponding upper limit in the Bayesian approach is $< 8.9 \times 10^{-7}$. A 2.8 standard deviation signal above the background is found, with a measured branching fraction $(5.3 \pm 2.0 \pm 0.9) \times 10^{-7}$.
- ² This is a 90% confidence interval in the frequentist approach. A 2.4 standard deviation signal above the background is found, with a measured branching fraction $(6.46 \pm 2.22 \pm 1.60) \times 10^{-7}$.
- ³ Assumes $B(\mathcal{T}(4S) \rightarrow B^+ B^-) = 0.513 \pm 0.006$.
- ⁴ Assumes equal production of B^+ and B^0 at the $\mathcal{T}(4S)$.
- ⁵ Superseded by SIBIDANOV 18.

$\Gamma(\tau^+ \nu_\tau)/\Gamma_{total}$ Γ_{38}/Γ

See the note on "Decay Constants of Charged Pseudoscalar Mesons" in the D_s^+ Listings.

VALUE (units 10^{-4}) CL% DOCUMENT ID TECN COMMENT
1.09 ± 0.24 OUR AVERAGE Error includes scale factor of 1.2.

1.25 ± 0.28 ± 0.27	^{1,2} KRONENBIT...	15	BELL	$e^+ e^- \rightarrow \mathcal{T}(4S)$
0.72 ± 0.27 ± 0.25 ± 0.11	³ HARA	13	BELL	$e^+ e^- \rightarrow \mathcal{T}(4S)$
1.83 ± 0.53 ± 0.49 ± 0.24	^{2,4} LEES	13k	BABR	$e^+ e^- \rightarrow \mathcal{T}(4S)$
1.7 ± 0.8 ± 0.2	^{2,5} AUBERT	10E	BABR	$e^+ e^- \rightarrow \mathcal{T}(4S)$
• • • We do not use the following data for averages, fits, limits, etc. • • •				
1.54 ± 0.38 ± 0.37 ± 0.31	^{2,6} HARA	10	BELL	Repl. by KRONENBIT-TER 15
1.8 ± 0.9 ± 0.8 ± 0.45	^{2,7} AUBERT	08D	BABR	Repl. by LEES 13k
0.9 ± 0.6 ± 0.1	^{2,5} AUBERT	07AL	BABR	Repl. by AUBERT 10E
< 2.6	90 ² AUBERT	06k	BABR	$e^+ e^- \rightarrow \mathcal{T}(4S)$
1.79 ± 0.56 ± 0.49 ± 0.51	^{2,7} IKADO	06	BELL	Repl. by HARA 13
< 4.2	90 ² AUBERT,B	05B	BABR	Repl. by AUBERT 06k
< 8.3	90 ⁸ BARATE	01E	ALEP	$e^+ e^- \rightarrow Z$
< 8.4	90 ² BROWDER	01	CLE2	$e^+ e^- \rightarrow \mathcal{T}(4S)$
< 5.7	90 ⁹ ACCIARRI	97F	L3	$e^+ e^- \rightarrow Z$
< 104	90 ¹⁰ ALBRECHT	95D	ARG	$e^+ e^- \rightarrow \mathcal{T}(4S)$
< 22	90 ARTUSO	95	CLE2	$e^+ e^- \rightarrow \mathcal{T}(4S)$
< 18	90 ¹¹ BUSKULIC	95	ALEP	$e^+ e^- \rightarrow Z$

- ¹ Requires one reconstructed semileptonic B decay $B^- \rightarrow D^{(*)0} \ell^- \bar{\nu}_\ell$ in the recoil.
- ² Assumes equal production of B^+ and B^0 at the $\mathcal{T}(4S)$.
- ³ The authors combine their result with that from HARA 10 obtaining $B(B^- \rightarrow \tau^- \bar{\nu}_\tau) = (0.96 \pm 0.26) \times 10^{-4}$ and deriving $f_B |V_{ub}| = (7.4 \pm 0.8 \pm 0.5) \times 10^{-4}$ GeV.

See key on page 1171

Meson Particle Listings

 B^\pm

⁴ Requires a fully reconstructed hadronic B -decay in the recoil. Reports that this result combined with AUBERT 10E value gives $B(B^- \rightarrow \tau^- \bar{\nu}_\tau) = (1.79 \pm 0.48) \times 10^{-4}$.

⁵ Requires one reconstructed semileptonic B decay $B^- \rightarrow D^0 \ell^- \bar{\nu}_\ell X$ in the recoil.

⁶ Requires one reconstructed semileptonic B decay $B^- \rightarrow D^{(*)0} \ell^- \bar{\nu}_\ell X$ in the recoil.

⁷ The analysis is based on a sample of events with one fully reconstructed tag B in a hadronic decay mode $B^- \rightarrow D^{(*)0} X^-$.

⁸ The energy-flow and b -tagging algorithms were used.

⁹ ACCIARRI 97F uses missing-energy technique and $f(b \rightarrow B^-) = (38.2 \pm 2.5)\%$.

¹⁰ ALBRECHT 95D uses full reconstruction of one B decay as tag.

¹¹ BUSKULIC 95 uses same missing-energy technique as in $\bar{B} \rightarrow \tau^+ \nu_\tau X$, but analysis is restricted to endpoint region of missing-energy distribution.

$\Gamma(\ell^+ \nu_\ell \gamma)/\Gamma_{\text{total}}$ Γ_{39}/Γ

VALUE	CL%	DOCUMENT ID	TECN	COMMENT
$< 3.0 \times 10^{-6}$	90	1,2 GELB	18 BELL	$e^+ e^- \rightarrow \Upsilon(4S)$
• • • We do not use the following data for averages, fits, limits, etc. • • •				
$< 3.5 \times 10^{-6}$	90	2,3 HELLER	15 BELL	$e^+ e^- \rightarrow \Upsilon(4S)$
$< 15.6 \times 10^{-6}$	90	2 AUBERT	09AT BABR	$e^+ e^- \rightarrow \Upsilon(4S)$

¹ Supersedes HELLER 15.

² Assumes equal production of B^+ and B^0 at the $\Upsilon(4S)$.

³ Superseded by GELB 18.

$\Gamma(e^+ \nu_e \gamma)/\Gamma_{\text{total}}$ Γ_{40}/Γ

VALUE	CL%	DOCUMENT ID	TECN	COMMENT
$< 4.3 \times 10^{-6}$	90	1,2 GELB	18 BELL	$e^+ e^- \rightarrow \Upsilon(4S)$
• • • We do not use the following data for averages, fits, limits, etc. • • •				
$< 6.1 \times 10^{-6}$	90	2,3 HELLER	15 BELL	$e^+ e^- \rightarrow \Upsilon(4S)$
$< 17 \times 10^{-6}$	90	2 AUBERT	09AT BABR	$e^+ e^- \rightarrow \Upsilon(4S)$
$< 200 \times 10^{-6}$	90	4 BROWDER	97 CLE2	$e^+ e^- \rightarrow \Upsilon(4S)$

¹ Supersedes HELLER 15.

² Assumes equal production of B^+ and B^0 at the $\Upsilon(4S)$.

³ Superseded by GELB 18.

⁴ BROWDER 97 uses the hermiticity of the CLEOII detector to reconstruct the neutrino energy and momentum.

$\Gamma(\mu^+ \nu_\mu \gamma)/\Gamma_{\text{total}}$ Γ_{41}/Γ

VALUE	CL%	DOCUMENT ID	TECN	COMMENT
$< 3.4 \times 10^{-6}$	90	1,2 GELB	18 BELL	$e^+ e^- \rightarrow \Upsilon(4S)$
• • • We do not use the following data for averages, fits, limits, etc. • • •				
$< 3.4 \times 10^{-6}$	90	2,3 HELLER	15 BELL	$e^+ e^- \rightarrow \Upsilon(4S)$
$< 24 \times 10^{-6}$	90	2,4 AUBERT	09AT BABR	$e^+ e^- \rightarrow \Upsilon(4S)$
$< 52 \times 10^{-6}$	90	5 BROWDER	97 CLE2	$e^+ e^- \rightarrow \Upsilon(4S)$

¹ Supersedes HELLER 15.

² Assumes equal production of B^+ and B^0 at the $\Upsilon(4S)$.

³ Superseded by GELB 18.

⁴ Note that the value given by AUBERT 09AT is 24×10^{-6} in the paper abstract, and 26×10^{-6} in the paper itself (Table I).

⁵ BROWDER 97 uses the hermiticity of the CLEOII detector to reconstruct the neutrino energy and momentum.

$\Gamma(\mu^+ \mu^- \mu^+ \nu_\mu)/\Gamma_{\text{total}}$ Γ_{42}/Γ

VALUE	CL%	DOCUMENT ID	TECN	COMMENT
$< 1.6 \times 10^{-8}$	95	1 AAIJ	19P LHCb	pp at 7, 8, 13 TeV

¹ AAIJ 19P limit established for the kinematic region where the lower of the two $M(\mu^+ \mu^-)$ is less than $980 \text{ MeV}/c^2$.

$\Gamma(D^0 X)/\Gamma_{\text{total}}$ Γ_{43}/Γ

VALUE	DOCUMENT ID	TECN	COMMENT
$0.086 \pm 0.006 \pm 0.004$	¹ AUBERT 07N BABR	$e^+ e^- \rightarrow \Upsilon(4S)$	
• • • We do not use the following data for averages, fits, limits, etc. • • •			
$0.098 \pm 0.009 \pm 0.006$	¹ AUBERT, BE 04B BABR	Repl. by AUBERT 07N	

¹ Events are selected by completely reconstructing one B and searching for a reconstructed charmed particle in the rest of the event. The last error includes systematic and charm branching ratio uncertainties.

$\Gamma(\bar{D}^0 X)/\Gamma_{\text{total}}$ Γ_{44}/Γ

VALUE	DOCUMENT ID	TECN	COMMENT
$0.786 \pm 0.016 \pm_{-0.033}^{+0.034}$	¹ AUBERT 07N BABR	$e^+ e^- \rightarrow \Upsilon(4S)$	
• • • We do not use the following data for averages, fits, limits, etc. • • •			
$0.793 \pm 0.025 \pm_{-0.044}^{+0.045}$	¹ AUBERT, BE 04B BABR	Repl. by AUBERT 07N	

¹ Events are selected by completely reconstructing one B and searching for a reconstructed charmed particle in the rest of the event. The last error includes systematic and charm branching ratio uncertainties.

$\Gamma(D^0 X)/[\Gamma(D^0 X) + \Gamma(\bar{D}^0 X)]$ $\Gamma_{43}/(\Gamma_{43} + \Gamma_{44})$

VALUE	DOCUMENT ID	TECN	COMMENT
$0.098 \pm 0.007 \pm 0.001$	AUBERT 07N BABR	$e^+ e^- \rightarrow \Upsilon(4S)$	
• • • We do not use the following data for averages, fits, limits, etc. • • •			
$0.110 \pm 0.010 \pm 0.003$	AUBERT, BE 04B BABR	Repl. by AUBERT 07N	

$\Gamma(D^+ X)/\Gamma_{\text{total}}$ Γ_{45}/Γ

VALUE	DOCUMENT ID	TECN	COMMENT
$0.025 \pm 0.005 \pm 0.002$	¹ AUBERT 07N BABR	$e^+ e^- \rightarrow \Upsilon(4S)$	
• • • We do not use the following data for averages, fits, limits, etc. • • •			
$0.038 \pm 0.009 \pm 0.005$	¹ AUBERT, BE 04B BABR	Repl. by AUBERT 07N	

¹ Events are selected by completely reconstructing one B and searching for a reconstructed charmed particle in the rest of the event. The last error includes systematic and charm branching ratio uncertainties.

$\Gamma(D^- X)/\Gamma_{\text{total}}$ Γ_{46}/Γ

VALUE	DOCUMENT ID	TECN	COMMENT
$0.099 \pm 0.008 \pm 0.009$	¹ AUBERT 07N BABR	$e^+ e^- \rightarrow \Upsilon(4S)$	
• • • We do not use the following data for averages, fits, limits, etc. • • •			
$0.098 \pm 0.012 \pm 0.014$	¹ AUBERT, BE 04B BABR	Repl. by AUBERT 07N	

¹ Events are selected by completely reconstructing one B and searching for a reconstructed charmed particle in the rest of the event. The last error includes systematic and charm branching ratio uncertainties.

$\Gamma(D^+ X)/[\Gamma(D^+ X) + \Gamma(D^- X)]$ $\Gamma_{45}/(\Gamma_{45} + \Gamma_{46})$

VALUE	DOCUMENT ID	TECN	COMMENT
$0.204 \pm 0.035 \pm 0.001$	AUBERT 07N BABR	$e^+ e^- \rightarrow \Upsilon(4S)$	
• • • We do not use the following data for averages, fits, limits, etc. • • •			
$0.278 \pm 0.052 \pm 0.009$	AUBERT, BE 04B BABR	Repl. by AUBERT 07N	

$\Gamma(D_s^+ X)/\Gamma_{\text{total}}$ Γ_{47}/Γ

VALUE	DOCUMENT ID	TECN	COMMENT
$0.079 \pm 0.006 \pm_{-0.011}^{+0.013}$	¹ AUBERT 07N BABR	$e^+ e^- \rightarrow \Upsilon(4S)$	
• • • We do not use the following data for averages, fits, limits, etc. • • •			
$0.143 \pm 0.016 \pm_{-0.034}^{+0.051}$	¹ AUBERT, BE 04B BABR	Repl. by AUBERT 07N	

¹ Events are selected by completely reconstructing one B and searching for a reconstructed charmed particle in the rest of the event. The last error includes systematic and charm branching ratio uncertainties.

$\Gamma(D_s^- X)/\Gamma_{\text{total}}$ Γ_{48}/Γ

VALUE	CL%	DOCUMENT ID	TECN	COMMENT
$0.011 \pm_{-0.003}^{+0.004} \pm_{-0.001}^{+0.002}$		¹ AUBERT 07N BABR	$e^+ e^- \rightarrow \Upsilon(4S)$	
• • • We do not use the following data for averages, fits, limits, etc. • • •				
< 0.022	90	¹ AUBERT, BE 04B BABR	Repl. by AUBERT 07N	

¹ Events are selected by completely reconstructing one B and searching for a reconstructed charmed particle in the rest of the event. The last error includes systematic and charm branching ratio uncertainties.

$\Gamma(D_s^+ X)/[\Gamma(D_s^+ X) + \Gamma(D_s^- X)]$ $\Gamma_{47}/(\Gamma_{47} + \Gamma_{48})$

VALUE	DOCUMENT ID	TECN	COMMENT
$0.884 \pm 0.038 \pm 0.002$	AUBERT 07N BABR	$e^+ e^- \rightarrow \Upsilon(4S)$	
• • • We do not use the following data for averages, fits, limits, etc. • • •			
$0.966 \pm 0.039 \pm 0.012$	AUBERT, BE 04B BABR	Repl. by AUBERT 07N	

$\Gamma(D_s^- X)/[\Gamma(D_s^+ X) + \Gamma(D_s^- X)]$ $\Gamma_{48}/(\Gamma_{47} + \Gamma_{48})$

VALUE	CL%	DOCUMENT ID	TECN	COMMENT
< 0.126	90	AUBERT, BE 04B BABR	$e^+ e^- \rightarrow \Upsilon(4S)$	

$\Gamma(A_c^+ X)/\Gamma_{\text{total}}$ Γ_{49}/Γ

VALUE	DOCUMENT ID	TECN	COMMENT
$0.021 \pm 0.005 \pm_{-0.004}^{+0.008}$	¹ AUBERT 07N BABR	$e^+ e^- \rightarrow \Upsilon(4S)$	
• • • We do not use the following data for averages, fits, limits, etc. • • •			
$0.029 \pm 0.008 \pm_{-0.007}^{+0.011}$	¹ AUBERT, BE 04B BABR	Repl. by AUBERT 07N	

¹ Events are selected by completely reconstructing one B and searching for a reconstructed charmed particle in the rest of the event. The last error includes systematic and charm branching ratio uncertainties.

$\Gamma(\bar{A}_c^- X)/\Gamma_{\text{total}}$ Γ_{50}/Γ

VALUE	DOCUMENT ID	TECN	COMMENT
$0.028 \pm 0.005 \pm_{-0.007}^{+0.010}$	¹ AUBERT 07N BABR	$e^+ e^- \rightarrow \Upsilon(4S)$	
• • • We do not use the following data for averages, fits, limits, etc. • • •			
$0.035 \pm 0.008 \pm_{-0.009}^{+0.013}$	¹ AUBERT, BE 04B BABR	Repl. by AUBERT 07N	

¹ Events are selected by completely reconstructing one B and searching for a reconstructed charmed particle in the rest of the event. The last error includes systematic and charm branching ratio uncertainties.

$\Gamma(A_c^+ X)/[\Gamma(A_c^+ X) + \Gamma(\bar{A}_c^- X)]$ $\Gamma_{49}/(\Gamma_{49} + \Gamma_{50})$

VALUE	DOCUMENT ID	TECN	COMMENT
$0.427 \pm 0.071 \pm 0.001$	AUBERT 07N BABR	$e^+ e^- \rightarrow \Upsilon(4S)$	
• • • We do not use the following data for averages, fits, limits, etc. • • •			
$0.452 \pm 0.090 \pm 0.003$	AUBERT, BE 04B BABR	Repl. by AUBERT 07N	

Meson Particle Listings

 B^\pm $\Gamma(\tau X)/\Gamma_{\text{total}}$ Γ_{51}/Γ

VALUE	DOCUMENT ID	TECN	COMMENT
0.968 ± 0.019^{+0.041}_{-0.039}	1 AUBERT	07N	BABR $e^+e^- \rightarrow \Upsilon(4S)$

• • • We do not use the following data for averages, fits, limits, etc. • • •

0.983 ± 0.030 ^{+0.054} _{-0.051}	1 AUBERT, BE	04B	BABR Repl. by AUBERT 07N
---	--------------	-----	--------------------------

¹ Events are selected by completely reconstructing one B and searching for a reconstructed charmed particle in the rest of the event. The last error includes systematic and charm branching ratio uncertainties.

 $\Gamma(cX)/\Gamma_{\text{total}}$ Γ_{52}/Γ

VALUE	DOCUMENT ID	TECN	COMMENT
0.234 ± 0.012^{+0.018}_{-0.014}	1 AUBERT	07N	BABR $e^+e^- \rightarrow \Upsilon(4S)$

• • • We do not use the following data for averages, fits, limits, etc. • • •

0.330 ± 0.022 ^{+0.055} _{-0.037}	1 AUBERT, BE	04B	BABR Repl. by AUBERT 07N
---	--------------	-----	--------------------------

¹ Events are selected by completely reconstructing one B and searching for a reconstructed charmed particle in the rest of the event. The last error includes systematic and charm branching ratio uncertainties.

 $\Gamma(c/\bar{c}X)/\Gamma_{\text{total}}$ Γ_{53}/Γ

VALUE	DOCUMENT ID	TECN	COMMENT
1.202 ± 0.023^{+0.053}_{-0.049}	1 AUBERT	07N	BABR $e^+e^- \rightarrow \Upsilon(4S)$

• • • We do not use the following data for averages, fits, limits, etc. • • •

1.313 ± 0.037 ^{+0.088} _{-0.075}	1 AUBERT, BE	04B	BABR Repl. by AUBERT 07N
---	--------------	-----	--------------------------

¹ Events are selected by completely reconstructing one B and searching for a reconstructed charmed particle in the rest of the event. The last error includes systematic and charm branching ratio uncertainties.

 $\Gamma(\bar{D}^0\pi^+)/\Gamma_{\text{total}}$ Γ_{54}/Γ

VALUE (units 10^{-3})	EVTS	DOCUMENT ID	TECN	COMMENT
4.61 ± 0.10 OUR FIT				
4.63 ± 0.10 OUR AVERAGE				

4.53 ± 0.02 ± 0.15		BLOOMFIELD 22	BELL	$e^+e^- \rightarrow \Upsilon(4S)$
4.34 ± 0.10 ± 0.23		1 KATO 18	BELL	$e^+e^- \rightarrow \Upsilon(4S)$
4.90 ± 0.07 ± 0.22		2 AUBERT 07H	BABR	$e^+e^- \rightarrow \Upsilon(4S)$
4.9 ± 0.6 ± 0.2		3 ABULENCIA 06J	CDF	$p\bar{p}$ at 1.96 TeV
4.49 ± 0.21 ± 0.23		4 AUBERT, BE 06J	BABR	$e^+e^- \rightarrow \Upsilon(4S)$
4.97 ± 0.12 ± 0.29		2,5 AHMED 02B	CLE2	$e^+e^- \rightarrow \Upsilon(4S)$
5.0 ± 0.7 ± 0.6	54	6 BORTOLETTO 92	CLEO	$e^+e^- \rightarrow \Upsilon(4S)$
5.4 ^{+1.8} _{-1.5} ± 1.2 ^{+1.2} _{-0.9}	14	7 BEBEK 87	CLEO	$e^+e^- \rightarrow \Upsilon(4S)$

• • • We do not use the following data for averages, fits, limits, etc. • • •

4.68 ± 0.26 ± 0.04		8 AUBERT, B 04P	BABR	Repl. by AUBERT 07H
5.5 ± 0.4 ± 0.5	304	9 ALAM 94	CLE2	Repl. by AHMED 02B
2.0 ± 0.8 ± 0.6	12	6 ALBRECHT 90J	ARG	$e^+e^- \rightarrow \Upsilon(4S)$
1.9 ± 1.0 ± 0.6	7	10 ALBRECHT 88K	ARG	$e^+e^- \rightarrow \Upsilon(4S)$

- ¹ Measures absolute branching fractions using a missing-mass technique.
² Assumes equal production of B^+ and B^0 at the $\Upsilon(4S)$.
³ ABULENCIA 06J reports $[\Gamma(B^+ \rightarrow \bar{D}^0\pi^+)/\Gamma_{\text{total}}] / [B(B^0 \rightarrow D^-\pi^+)] = 1.97 \pm 0.10 \pm 0.21$ which we multiply by our best value $B(B^0 \rightarrow D^-\pi^+) = (2.51 \pm 0.08) \times 10^{-3}$. Our first error is their experiment's error and our second error is the systematic error from using our best value.
⁴ Uses a missing-mass method. Does not depend on D branching fractions or B^-/B^0 production rates.
⁵ AHMED 02B reports an additional uncertainty on the branching ratios to account for 4.5% uncertainty on relative production of B^0 and B^+ , which is not included here.
⁶ Assumes equal production of B^+ and B^0 at the $\Upsilon(4S)$ and uses the MarkIII branching fractions for the D .
⁷ BEBEK 87 value has been updated in BERKELMAN 91 to use same assumptions as noted for BORTOLETTO 92.
⁸ AUBERT, B 04P reports $[\Gamma(B^+ \rightarrow \bar{D}^0\pi^+)/\Gamma_{\text{total}}] \times [B(D^0 \rightarrow K^-\pi^+)] = (1.846 \pm 0.032 \pm 0.097) \times 10^{-4}$ which we divide by our best value $B(D^0 \rightarrow K^-\pi^+) = (3.947 \pm 0.030) \times 10^{-2}$. Our first error is their experiment's error and our second error is the systematic error from using our best value.
⁹ ALAM 94 assume equal production of B^+ and B^0 at the $\Upsilon(4S)$ and use the CLEOII absolute $B(D^0 \rightarrow K^-\pi^+)$ and the PDG 1992 $B(D^0 \rightarrow K^-\pi^+\pi^0)/B(D^0 \rightarrow K^-\pi^+)$ and $B(D^0 \rightarrow K^-\pi^+\pi^-)/B(D^0 \rightarrow K^-\pi^+)$.
¹⁰ ALBRECHT 88K assumes $B^0\bar{B}^0:B^+B^-$ ratio is 45:55. Superseded by ALBRECHT 90J.

 $\Gamma(\bar{D}^0\rho^+)/\Gamma_{\text{total}}$ Γ_{57}/Γ

VALUE	EVTS	DOCUMENT ID	TECN	COMMENT
0.0134 ± 0.0018 OUR AVERAGE				

0.0135 ± 0.0012 ± 0.0015	212	1 ALAM 94	CLE2	$e^+e^- \rightarrow \Upsilon(4S)$
0.013 ± 0.004 ± 0.004	19	2 ALBRECHT 90J	ARG	$e^+e^- \rightarrow \Upsilon(4S)$

• • • We do not use the following data for averages, fits, limits, etc. • • •

- 0.021 ± 0.008 ± 0.009 10 3 ALBRECHT 88K ARG $e^+e^- \rightarrow \Upsilon(4S)$
¹ ALAM 94 assume equal production of B^+ and B^0 at the $\Upsilon(4S)$ and use the CLEOII absolute $B(D^0 \rightarrow K^-\pi^+)$ and the PDG 1992 $B(D^0 \rightarrow K^-\pi^+\pi^0)/B(D^0 \rightarrow K^-\pi^+)$ and $B(D^0 \rightarrow K^-\pi^+\pi^-)/B(D^0 \rightarrow K^-\pi^+)$.
² Assumes equal production of B^+ and B^0 at the $\Upsilon(4S)$ and uses the MarkIII branching fractions for the D .
³ ALBRECHT 88K assumes $B^0\bar{B}^0:B^+B^-$ ratio is 45:55.

 $\Gamma(\bar{D}^0K^+)/\Gamma(\bar{D}^0\pi^+)$ Γ_{58}/Γ_{54}

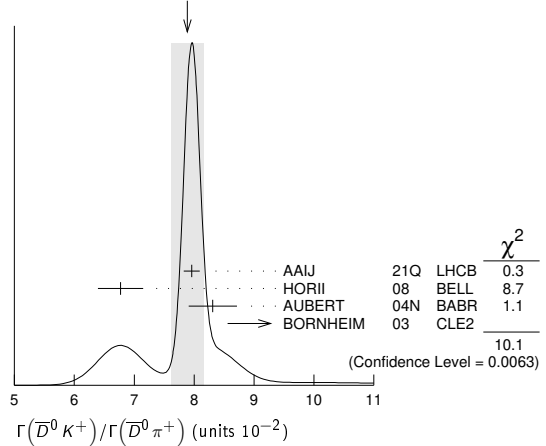
VALUE (units 10^{-2})	DOCUMENT ID	TECN	COMMENT
7.89 ± 0.27 OUR AVERAGE			Error includes scale factor of 2.3. See the ideogram below.

7.96 ± 0.03 ± 0.13	AAIJ	21Q	LHCB pp at 7, 8, 13 TeV
6.77 ± 0.23 ± 0.30	HORII	08	BELL $e^+e^- \rightarrow \Upsilon(4S)$
8.31 ± 0.35 ± 0.20	AUBERT	04N	BABR $e^+e^- \rightarrow \Upsilon(4S)$
9.9 ^{+1.4} _{-1.2} ± 0.7 ^{+0.7} _{-0.6}	BORNHEIM	03	CLE2 $e^+e^- \rightarrow \Upsilon(4S)$

7.768 ± 0.038 ± 0.066	1,2 AAIJ	18A	LHCB pp at 7, 8, 13 TeV
7.79 ± 0.06 ± 0.19	AAIJ	16L	LHCB pp at 7, 8 TeV
7.93 ± 0.10 ± 0.18	3 AAIJ	16L	LHCB pp at 7, 8 TeV
7.71 ± 0.17 ± 0.26	3 AAIJ	13AE	LHCB Repl. by AAIJ 16L
7.74 ± 0.12 ± 0.19	AAIJ	12M	LHCB Repl. by AAIJ 16L
9.4 ± 0.9 ± 0.7	ABE	03D	BELL Repl. by SWAIN 03
7.7 ± 0.5 ± 0.6	SWAIN	03	BELL Repl. by HORII 08
7.9 ± 0.9 ± 0.6	ABE	01I	BELL Repl. by ABE 03D
5.5 ± 1.4 ± 0.5	ATHANAS	98	CLE2 Repl. by BORNHEIM 03

- ¹ Supersedes AAIJ 16L.
² Superseded by AAIJ 21Q.
³ Uses $B^\pm \rightarrow [K^\pm\pi^\mp\pi^\pm\pi^-]_D h^\pm$ mode.

WEIGHTED AVERAGE
7.89±0.27 (Error scaled by 2.3)

 $\Gamma(D_{CP(+)}K^+)/\Gamma(D_{CP(+)}\pi^+)$ Γ_{59}/Γ_{55}

VALUE	DOCUMENT ID	TECN	COMMENT
0.089 ± 0.008 OUR AVERAGE			

0.089 ± 0.008 ± 0.003	1,2 ABE	06	BELL $e^+e^- \rightarrow \Upsilon(4S)$
0.088 ± 0.016 ± 0.005	3 AUBERT	04N	BABR $e^+e^- \rightarrow \Upsilon(4S)$
0.125 ± 0.036 ± 0.010	3 ABE	03D	BELL Repl. by SWAIN 03
0.093 ± 0.018 ± 0.008	3 SWAIN	03	BELL Repl. by ABE 06

- ¹ Reports a double ratio of $B(B^+ \rightarrow D_{CP(+)}K^+)/B(B^+ \rightarrow D_{CP(+)}\pi^+)$ and $B(B^+ \rightarrow \bar{D}^0K^+)/B(B^+ \rightarrow \bar{D}^0\pi^+)$, $1.13 \pm 0.16 \pm 0.08$. We multiply by our best value of $B(B^+ \rightarrow \bar{D}^0K^+)/B(B^+ \rightarrow \bar{D}^0\pi^+) = 0.083 \pm 0.006$. Our first error is their experiment's error and the second error is systematic error from using our best value.
² ABE 06 reports $[\Gamma(B^+ \rightarrow D_{CP(+)}K^+)/\Gamma(B^+ \rightarrow D_{CP(+)}\pi^+)] / [\Gamma(B^+ \rightarrow \bar{D}^0K^+)/\Gamma(B^+ \rightarrow \bar{D}^0\pi^+)] = 1.13 \pm 0.06 \pm 0.08$ which we multiply by our best value $[\Gamma(B^+ \rightarrow \bar{D}^0K^+)/\Gamma(B^+ \rightarrow \bar{D}^0\pi^+)] = 0.0789 \pm 0.0027$. Our first error is their experiment's error and our second error is the systematic error from using our best value.
³ $CP=+1$ eigenstate of $D^0\bar{D}^0$ system is reconstructed via K^+K^- and $\pi^+\pi^-$.

 $\Gamma(D_{CP(+)}K^+)/\Gamma(\bar{D}^0K^+)$ Γ_{59}/Γ_{58}

VALUE	DOCUMENT ID	TECN	COMMENT
0.495 ± 0.007 OUR AVERAGE			

0.494 ± 0.008 ± 0.006	1 AAIJ	18A	LHCB pp at 7, 8, 13 TeV
0.496 ± 0.014 ± 0.008	2 AAIJ	18A	LHCB pp at 7, 8, 13 TeV
0.489 ± 0.010 ± 0.009	3 AAIJ	16L	LHCB pp at 7, 8 TeV
0.65 ± 0.12 ± 0.06	4 AALTONEN	10A	CDF $p\bar{p}$ at 1.96 TeV
0.590 ± 0.045 ± 0.025	5 DEL-AMO-SA..10G	BABR	$e^+e^- \rightarrow \Upsilon(4S)$

0.504 ± 0.019 ± 0.006	6 AAIJ	12M	LHCB Repl. by AAIJ 16L
0.53 ± 0.05 ± 0.025	AUBERT	08AA	BABR Repl. by DEL-AMO-SANCHEZ 10G
0.45 ± 0.06 ± 0.02	AUBERT	06J	BABR Repl. by AUBERT 08AA

- ¹ Uses $D \rightarrow K^+K^-$ decay mode and reports $R_{CP+} = 0.988 \pm 0.015 \pm 0.011$ which we have divided by 2.
² Uses $D \rightarrow \pi^+\pi^-$ decay mode and reports $R_{CP+} = 0.992 \pm 0.027 \pm 0.015$ which we have divided by 2.
³ AAIJ 16L reports $R_{CP+} = 0.978 \pm 0.019 \pm 0.018$ which we have divided by 2.
⁴ Reports $R_{CP+} = 2 (B(B^- \rightarrow D_{CP(+)}K^-) + B(B^+ \rightarrow D_{CP(+)}K^+)) / (B(B^- \rightarrow D^0K^-) + B(B^+ \rightarrow \bar{D}^0K^+)) = 1.30 \pm 0.24 \pm 0.12$ that we have divided by 2.
⁵ Reports $R_{CP+} = 1.18 \pm 0.09 \pm 0.05$ that we have divided by 2.
⁶ AAIJ 12M reports $R_{CP+} = 1.007 \pm 0.038 \pm 0.012$ which we have divided by 2.

See key on page 1171

Meson Particle Listings

 B^\pm $\Gamma(D_{CP(-1)}K^+)/\Gamma(D_{CP(-1)}\pi^+)$ Γ_{60}/Γ_{56}

VALUE	DOCUMENT ID	TECN	COMMENT
0.097 ± 0.016 ± 0.007	¹ ABE	06	BELL $e^+e^- \rightarrow \Upsilon(4S)$
0.119 ± 0.028 ± 0.006	² ABE	03D	BELL Repl. by SWAIN 03
0.108 ± 0.019 ± 0.007	² SWAIN	03	BELL Repl. by ABE 06

¹ Reports a double ratio of $B(B^+ \rightarrow D_{CP(-1)}K^+)/B(B^+ \rightarrow D_{CP(-1)}\pi^+)$ and $B(B^+ \rightarrow \bar{D}^0K^+)/B(B^+ \rightarrow \bar{D}^0\pi^+)$, $1.17 \pm 0.14 \pm 0.14$. We multiply by our best value of $B(B^+ \rightarrow \bar{D}^0K^+)/B(B^+ \rightarrow \bar{D}^0\pi^+) = 0.083 \pm 0.006$. Our first error is their experiment's error and the second error is systematic error from using our best value.

² $CP=-1$ eigenstate of $D^0\bar{D}^0$ system is reconstructed via $K_S^0\pi^0$, $K_S^0\omega$, $K_S^0\phi$, $K_S^0\eta$, and $K_S^0\eta'$.

 $\Gamma(D_{CP(-1)}K^+)/\Gamma(\bar{D}^0K^+)$ Γ_{60}/Γ_{58}

VALUE	DOCUMENT ID	TECN	COMMENT
0.54 ± 0.04 ± 0.02	¹ DEL-AMO-SA..10G	BABR	$e^+e^- \rightarrow \Upsilon(4S)$
0.515 ± 0.05 ± 0.025	AUBERT	08AA	BABR Repl. by DEL-AMO-SANCHEZ 10G
0.43 ± 0.05 ± 0.02	AUBERT	06J	BABR Repl. by AUBERT 08AA

¹ Reports $R_{CP+} = 1.07 \pm 0.08 \pm 0.04$ that we have divided by 2.

 $\Gamma(D^0K^+)/\Gamma(\bar{D}^0K^+)$ Γ_{61}/Γ_{58}

VALUE (units 10^{-3})	DOCUMENT ID	TECN	COMMENT
9.88 ± 0.52 OUR EVALUATION	(Produced by HFLAV)		

 $\Gamma([K^-\pi^+]_D K^+)/\Gamma_{total}$ Γ_{62}/Γ

VALUE	CL%	DOCUMENT ID	TECN	COMMENT
<2.8 × 10⁻⁷	90	HORII	08	BELL $e^+e^- \rightarrow \Upsilon(4S)$
<6.3 × 10 ⁻⁷	90	SAIGO	05	BELL $e^+e^- \rightarrow \Upsilon(4S)$

 $\Gamma([K^-\pi^+]_D K^+)/\Gamma([K^+\pi^-]_D K^+)$ Γ_{62}/Γ_{63}

VALUE (units 10^{-3})	CL%	DOCUMENT ID	TECN	COMMENT
14 ± 7 OUR AVERAGE		Error includes scale factor of 14.7.		
9.5 ± 0.5 ± 0.3		¹ AAIJ	21Q	LHCB pp at 7, 8, 13 TeV
25.2 ± 0.8 ± 0.4		² AAIJ	21Q	LHCB pp at 7, 8, 13 TeV
22.0 ± 8.6 ± 2.6		³ AALTONEN	11AJ	CDF $p\bar{p}$ at 1.96 TeV
16.3 ^{+4.4+0.7} _{-4.1-1.3}		HORII	11	BELL $e^+e^- \rightarrow \Upsilon(4S)$
11 ± 6 ± 2		DEL-AMO-SA..10H	BABR	$e^+e^- \rightarrow \Upsilon(4S)$
18.8 ± 1.1 ± 1.0		⁴ AAIJ	16L	LHCB pp at 7, 8 TeV
15.2 ± 2.0 ± 0.4		AAIJ	12M	LHCB Repl. by AAIJ 16L
7.8 ^{+6.2+2.0} _{-5.7-2.8}		HORII	08	BELL Repl. by HORII 11
<29	90	⁵ AUBERT	05G	BABR Repl. by DEL-AMO-SANCHEZ 10H
<44	90	⁶ SAIGO	05	BELL $e^+e^- \rightarrow \Upsilon(4S)$
<26	90	⁷ AUBERT,B	04L	BABR Repl. by AUBERT 05G

¹ Uses the ratio of $B^- \rightarrow [K^+\pi^-]_D K^-$ and $B^- \rightarrow [K^-\pi^+]_D K^-$. AAIJ 21Q gives the charge-averaged rate as 0.0173 ± 0.0006 , where the statistical and systematic uncertainties have been combined according to the correlations between the observables.

² Uses the ratio of $B^+ \rightarrow [K^-\pi^+]_D K^+$ and $B^+ \rightarrow [K^+\pi^-]_D K^+$. AAIJ 21Q gives the charge-averaged rate as 0.0173 ± 0.0006 , where the statistical and systematic uncertainties have been combined according to the correlations between the observables.

³ AALTONEN 11AJ also measures the ratio separately for B^+ ($R^+(K)$) and B^- ($R^-(K)$) and obtains: $R^+(K) = (42.6 \pm 13.7 \pm 2.8) \times 10^{-3}$, $R^-(K) = (3.8 \pm 10.3 \pm 2.7) \times 10^{-3}$.

⁴ Superseded by AAIJ 21Q.

⁵ AUBERT 05G extract a constraint on the magnitude of the ratio of amplitudes $|A(B^+ \rightarrow D^0K^+)/A(B^+ \rightarrow \bar{D}^0K^+)| < 0.23$ at 90% CL (Bayesian). Similar measurements from $B^+ \rightarrow D^{*0}K^+$ are also reported.

⁶ SAIGO 05 extract a constraint on the magnitude of the ratio of amplitudes $|A(B^+ \rightarrow D^0K^+)/A(B^+ \rightarrow \bar{D}^0K^+)| < 0.27$ at 90% CL.

⁷ AUBERT,B 04L extract a constraint on the magnitude of the ratio of amplitudes $|A(B^+ \rightarrow D^0K^+)/A(B^+ \rightarrow \bar{D}^0K^+)| < 0.22$ at 90% CL.

 $\Gamma([K^-\pi^+]_D K^+)/\Gamma([K^+\pi^-]_D K^+)$ Γ_{64}/Γ_{65}

VALUE (units 10^{-3})	CL%	DOCUMENT ID	TECN	COMMENT
13.1 ± 1.6 OUR AVERAGE				
12.7 ± 1.6 ± 0.2		AAIJ	22T	LHCB pp at 7, 8, 13 TeV
19.8 ± 6.2 ± 2.4		NAYAK	13	BELL $e^+e^- \rightarrow \Upsilon(4S)$
14.0 ± 4.7 ± 2.1		¹ AAIJ	15W	LHCB Repl. by AAIJ 22T
<21	90	² LEES	11D	BABR $e^+e^- \rightarrow \Upsilon(4S)$
<39	95	³ AUBERT	07BN	BABR Repl. by LEES 11D

¹ Uses $D^0 \rightarrow K^-\pi^+\pi^0$ for the favored mode, and $D^0 \rightarrow K^+\pi^-\pi^0$ for the suppressed mode.

² Extracts a constraint on the magnitude of the ratio of amplitudes $|A(B^+ \rightarrow D^0K^+)/A(B^+ \rightarrow \bar{D}^0K^+)| < 0.13$ at 95% CL.

³ Extracts a constraint on the magnitude of the ratio of amplitudes $|A(B^+ \rightarrow D^0K^+)/A(B^+ \rightarrow \bar{D}^0K^+)| < 0.19$ at 95% CL.

 $\Gamma([K^-\pi^+\pi^-\pi^-]_D K^+)/\Gamma([K^+\pi^-\pi^-\pi^-]_D K^+)$ Γ_{66}/Γ_{67}

VALUE (units 10^{-2})	DOCUMENT ID	TECN	COMMENT
1.333 ± 0.055 ± 0.008	AAIJ	23I	LHCB pp at 7, 8, 13 TeV
1.40 ± 0.15 ± 0.06	¹ AAIJ	16L	LHCB pp at 7, 8 TeV
1.24 ± 0.27	AAIJ	13AE	LHCB Repl. by AAIJ 16L

¹ Superseded by AAIJ 23I.

 $\Gamma([K^+\pi^+\pi^-\pi^-]_D K^+)/\Gamma([K^+\pi^-\pi^-\pi^-]_D K^+)$ Γ_{68}/Γ_{67}

VALUE	DOCUMENT ID	TECN	COMMENT
0.975 ± 0.037 ± 0.019	AAIJ	16L	LHCB pp at 7, 8 TeV

 $\Gamma([K^-\pi^+]_D K^*(892)^+)/\Gamma([K^+\pi^-]_D K^*(892)^+)$ Γ_{70}/Γ_{71}

VALUE	DOCUMENT ID	TECN	COMMENT
0.012 ± 0.004 OUR AVERAGE			
0.011 ± 0.004 ± 0.001	AAIJ	17Bo	LHCB pp at 7, 8, 13 TeV
0.066 ± 0.031 ± 0.010	AUBERT	09AJ	BABR $e^+e^- \rightarrow \Upsilon(4S)$
0.046 ± 0.031 ± 0.008	AUBERT,B	05V	BABR Repl. by AUBERT 09AJ

 $\Gamma([K^-\pi^+\pi^-\pi^+]_D K^*(892)^+)/\Gamma([K^+\pi^-\pi^+\pi^-]_D K^*(892)^+)$ Γ_{72}/Γ_{73}

VALUE	DOCUMENT ID	TECN	COMMENT
0.011 ± 0.005 ± 0.003	AAIJ	17Bo	LHCB pp at 7, 8, 13 TeV

 $\Gamma([K^+\pi^-\pi^+\pi^-]_D K^*(892)^+)/\Gamma([K^+\pi^-\pi^-\pi^-]_D K^*(892)^+)$ Γ_{69}/Γ_{73}

VALUE	DOCUMENT ID	TECN	COMMENT
1.08 ± 0.13 ± 0.03	AAIJ	17Bo	LHCB pp at 7, 8, 13 TeV

 $\Gamma([K^-\pi^+]_D \pi^+)/\Gamma_{total}$ Γ_{74}/Γ

VALUE (units 10^{-7})	DOCUMENT ID	TECN	COMMENT
6.29^{+1.02+0.37}_{-0.98-0.48}	HORII	08	BELL $e^+e^- \rightarrow \Upsilon(4S)$
6.6 ^{+1.9} _{-1.7} ± 0.5	SAIGO	05	BELL Repl. by HORII 08

 $\Gamma([K^-\pi^+]_D \pi^+)/\Gamma([K^+\pi^-]_D \pi^+)$ Γ_{74}/Γ_{75}

VALUE (units 10^{-3})	DOCUMENT ID	TECN	COMMENT
3.6 ± 0.5 OUR AVERAGE		Error includes scale factor of 7.9.	
4.15 ± 0.08 ± 0.04	¹ AAIJ	21Q	LHCB pp at 7, 8, 13 TeV
3.20 ± 0.07 ± 0.04	² AAIJ	21Q	LHCB pp at 7, 8, 13 TeV
2.8 ± 0.7 ± 0.4	³ AALTONEN	11AJ	CDF $p\bar{p}$ at 1.96 TeV
3.28 ^{+0.38+0.12} _{-0.36-0.18}	HORII	11	BELL $e^+e^- \rightarrow \Upsilon(4S)$
3.3 ± 0.6 ± 0.4	DEL-AMO-SA..10H	BABR	$e^+e^- \rightarrow \Upsilon(4S)$
3.60 ± 0.12 ± 0.09	⁴ AAIJ	16L	LHCB pp at 7, 8 TeV
4.10 ± 0.25 ± 0.05	AAIJ	12M	LHCB Repl. by AAIJ 16L
3.40 ^{+0.55+0.15} _{-0.53-0.22}	HORII	08	BELL Repl. by HORII 11
3.5 ^{+1.0} _{-0.9} ± 0.2	SAIGO	05	BELL Repl. by HORII 08

¹ Uses the ratio of $B^- \rightarrow [K^+\pi^-]_D K^-$ and $B^- \rightarrow [K^-\pi^+]_D K^-$. AAIJ 21Q gives the charge-averaged rate as 0.00368 ± 0.00007 , where the statistical and systematic uncertainties have been combined according to the correlations between the observables.

² Uses the ratio of $B^+ \rightarrow [K^-\pi^+]_D \pi^+$ and $B^+ \rightarrow [K^+\pi^-]_D \pi^+$. AAIJ 21Q gives the charge-averaged rate as 0.00368 ± 0.00007 , where the statistical and systematic uncertainties have been combined according to the correlations between the observables.

³ AALTONEN 11AJ also measures the ratio separately for B^+ ($R^+(\pi)$) and B^- ($R^-(\pi)$) and obtains: $R^+(\pi) = (2.4 \pm 1.0 \pm 0.4) \times 10^{-3}$, $R^-(\pi) = (3.1 \pm 1.1 \pm 0.4) \times 10^{-3}$.

⁴ Superseded by AAIJ 21Q.

 $\Gamma([K^-\pi^+\pi^0]_D \pi^+)/\Gamma([K^+\pi^-\pi^0]_D \pi^+)$ Γ_{76}/Γ_{77}

VALUE (units 10^{-3})	DOCUMENT ID	TECN	COMMENT
2.05 ± 0.19 OUR AVERAGE			
2.07 ± 0.20 ± 0.03	AAIJ	22T	LHCB pp at 7, 8, 13 TeV
1.89 ± 0.54 ^{+0.22} _{-0.25}	NAYAK	13	BELL $e^+e^- \rightarrow \Upsilon(4S)$
2.35 ± 0.49 ± 0.06	¹ AAIJ	15W	LHCB Repl. by AAIJ 22T

¹ Uses $D^0 \rightarrow K^-\pi^+\pi^0$ for the favored mode, and $D^0 \rightarrow K^+\pi^-\pi^0$ for the suppressed mode.

 $\Gamma([K^-\pi^+\pi^+\pi^-]_D \pi^+)/\Gamma([K^+\pi^-\pi^+\pi^-]_D \pi^+)$ Γ_{78}/Γ_{79}

VALUE (units 10^{-3})	DOCUMENT ID	TECN	COMMENT
3.45 ± 0.07 ± 0.01	AAIJ	23I	LHCB pp at 7, 8, 13 TeV
3.77 ± 0.18 ± 0.06	¹ AAIJ	16L	LHCB pp at 7, 8 TeV
3.7 ± 0.4	AAIJ	13AE	LHCB Repl. by AAIJ 16L

¹ Superseded by AAIJ 23I.

Meson Particle Listings

B^\pm

$$\Gamma([K^-\pi^+](D\pi)\pi^+)/\Gamma([K^-\pi^-](D\pi)\pi^+) \quad \Gamma_{80}/\Gamma_{81}$$

VALUE (units 10^{-3})	DOCUMENT ID	TECN	COMMENT
4.4 ± 0.6 OUR AVERAGE	Error includes scale factor of 1.1.		
4.05 ± 0.56 ± 0.59	¹ AAIJ	21Q LHCb	pp at 7, 8, 13 TeV
5.36 ± 0.56 ± 0.58	² AAIJ	21Q LHCb	pp at 7, 8, 13 TeV
3.2 ± 0.9 ± 0.8	DEL-AMO-SA...10H	BABR	$e^+e^- \rightarrow \Upsilon(4S)$

¹ Uses the ratio of $B^- \rightarrow ([K^+\pi^-]D\pi^0)_{D^*}K^-$ and $B^- \rightarrow ([K^-\pi^+]D\pi^0)_{D^*}K^-$, without inclusion of the neutral pion in the reconstruction. AAIJ 21Q gives the charge-averaged rate as 0.00471 ± 0.00077, where the statistical and systematic uncertainties have been combined according to the correlations between the observables.

² Uses the ratio of $B^+ \rightarrow ([K^+\pi^-]D\pi^0)_{D^*}K^+$ and $B^+ \rightarrow ([K^-\pi^+]D\pi^0)_{D^*}K^+$, without inclusion of the neutral pion in the reconstruction. AAIJ 21Q gives the charge-averaged rate as 0.00471 ± 0.00077, where the statistical and systematic uncertainties have been combined according to the correlations between the observables.

$$\Gamma([K^-\pi^+](D\gamma)\pi^+)/\Gamma([K^+\pi^-](D\gamma)\pi^+) \quad \Gamma_{82}/\Gamma_{83}$$

VALUE (units 10^{-3})	DOCUMENT ID	TECN	COMMENT
4.1 ± 1.0 OUR AVERAGE	Error includes scale factor of 1.1.		
4.72 ± 0.92 ± 1.18	¹ AAIJ	21Q LHCb	pp at 7, 8, 13 TeV
4.03 ± 0.91 ± 1.14	² AAIJ	21Q LHCb	pp at 7, 8, 13 TeV
2.7 ± 1.4 ± 2.2	DEL-AMO-SA...10H	BABR	$e^+e^- \rightarrow \Upsilon(4S)$

¹ Uses the ratio of $B^- \rightarrow ([K^+\pi^-]D\gamma)_{D^*}K^-$ and $B^- \rightarrow ([K^-\pi^+]D\gamma)_{D^*}K^-$, without inclusion of the photon in the reconstruction. AAIJ 21Q gives the charge-averaged rate as 0.00420 ± 0.00138, where the statistical and systematic uncertainties have been combined according to the correlations between the observables.

² Uses the ratio of $B^+ \rightarrow ([K^+\pi^-]D\gamma)_{D^*}K^+$ and $B^+ \rightarrow ([K^-\pi^+]D\gamma)_{D^*}K^+$, without inclusion of the photon in the reconstruction. AAIJ 21Q gives the charge-averaged rate as 0.00420 ± 0.00138, where the statistical and systematic uncertainties have been combined according to the correlations between the observables.

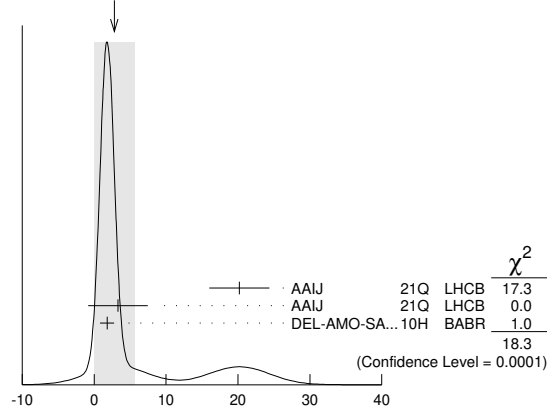
$$\Gamma([K^-\pi^+](D\pi)K^+)/\Gamma([K^+\pi^-](D\pi)K^+) \quad \Gamma_{84}/\Gamma_{85}$$

VALUE (units 10^{-3})	DOCUMENT ID	TECN	COMMENT
2.8 ± 2.8 OUR AVERAGE	Error includes scale factor of 3.0. See the ideogram below.		
20.2 ± 3.5 ± 2.3	¹ AAIJ	21Q LHCb	pp at 7, 8, 13 TeV
3.3 ± 3.5 ± 2.2	² AAIJ	21Q LHCb	pp at 7, 8, 13 TeV
1.8 ± 0.9 ± 0.4	DEL-AMO-SA...10H	BABR	$e^+e^- \rightarrow \Upsilon(4S)$

¹ Uses the ratio of $B^- \rightarrow ([K^+\pi^-]D\pi^0)_{D^*}K^-$ and $B^- \rightarrow ([K^-\pi^+]D\pi^0)_{D^*}K^-$, without inclusion of the neutral pion in the reconstruction. AAIJ 21Q gives the charge-averaged rate as 0.0118 ± 0.0034, where the statistical and systematic uncertainties have been combined according to the correlations between the observables.

² Uses the ratio of $B^+ \rightarrow ([K^+\pi^-]D\pi^0)_{D^*}K^+$ and $B^+ \rightarrow ([K^-\pi^+]D\pi^0)_{D^*}K^+$, without inclusion of the neutral pion in the reconstruction. AAIJ 21Q gives the charge-averaged rate as 0.0118 ± 0.0034, where the statistical and systematic uncertainties have been combined according to the correlations between the observables.

WEIGHTED AVERAGE
2.8±2.8 (Error scaled by 3.0)



$\Gamma([K^-\pi^+](D\pi)K^+)/\Gamma([K^+\pi^-](D\pi)K^+) \text{ (units } 10^{-3}\text{)}$

$$\Gamma([K^-\pi^+](D\gamma)K^+)/\Gamma([K^+\pi^-](D\gamma)K^+) \quad \Gamma_{86}/\Gamma_{87}$$

VALUE (units 10^{-3})	DOCUMENT ID	TECN	COMMENT
1.4 ± 1.6 OUR AVERAGE	Error includes scale factor of 1.1.		
11.7 ± 21.5 ± 31.3	¹ AAIJ	21Q LHCb	pp at 7, 8, 13 TeV
29.2 ± 21.4 ± 31.2	² AAIJ	21Q LHCb	pp at 7, 8, 13 TeV
1.3 ± 1.4 ± 0.8	DEL-AMO-SA...10H	BABR	$e^+e^- \rightarrow \Upsilon(4S)$

¹ Uses the ratio of $B^- \rightarrow ([K^+\pi^-]D\gamma)_{D^*}K^-$ and $B^- \rightarrow ([K^-\pi^+]D\gamma)_{D^*}K^-$, without inclusion of the photon in the reconstruction. AAIJ 21Q gives the charge-averaged rate as 0.0163 ± 0.0373, where the statistical and systematic uncertainties have been combined according to the correlations between the observables.

² Uses the ratio of $B^+ \rightarrow ([K^+\pi^-]D\gamma)_{D^*}K^+$ and $B^+ \rightarrow ([K^-\pi^+]D\gamma)_{D^*}K^+$, without inclusion of the photon in the reconstruction. AAIJ 21Q gives the charge-averaged rate as 0.0163 ± 0.0373, where the statistical and systematic uncertainties have been combined according to the correlations between the observables.

$$\Gamma([\pi^+\pi^-\pi^0]DK^-)/\Gamma_{total} \quad \Gamma_{88}/\Gamma$$

VALUE (units 10^{-6})	DOCUMENT ID	TECN	COMMENT
4.6 ± 0.8 ± 0.4	¹ AUBERT	07Bj BABR	$e^+e^- \rightarrow \Upsilon(4S)$
••• We do not use the following data for averages, fits, limits, etc. •••			
5.5 ± 1.0 ± 0.7	¹ AUBERT,B	05T BABR	Repl. by AUBERT 07Bj

¹ Assumes equal production of B^+ and B^0 at the $\Upsilon(4S)$.

$$\Gamma([K_S^0 K^+\pi^-]DK^+)/\Gamma([K_S^0 K^+\pi^-]D\pi^+) \quad \Gamma_{89}/\Gamma_{95}$$

VALUE	DOCUMENT ID	TECN	COMMENT
0.103 ± 0.015 OUR AVERAGE	Error includes scale factor of 1.9.		
0.122 ± 0.012 ± 0.004	¹ ADACHI	23L BELL	$e^+e^- \rightarrow \Upsilon(4S)$
0.092 ± 0.009 ± 0.004	¹ AAIJ	14V LHCb	pp at 7, 8 TeV
••• We do not use the following data for averages, fits, limits, etc. •••			
0.081 ± 0.008 ± 0.004	² AAIJ	20N LHCb	pp at 7, 8, 13 TeV

¹ The analysis uses all of $D \rightarrow K_S^0 K\pi$ Dalitz decays.

² The analysis uses $D \rightarrow K_S^0 K\pi$ Dalitz decays with K^*K^+ region excluded.

$$\Gamma([K_S^0 K^-\pi^+]DK^+)/\Gamma([K_S^0 K^-\pi^+]D\pi^+) \quad \Gamma_{91}/\Gamma_{93}$$

VALUE	DOCUMENT ID	TECN	COMMENT
0.075 ± 0.013 OUR AVERAGE	Error includes scale factor of 1.7.		
0.093 ± 0.013 ± 0.003	¹ ADACHI	23L BELL	$e^+e^- \rightarrow \Upsilon(4S)$
0.066 ± 0.009 ± 0.002	¹ AAIJ	14V LHCb	pp at 7, 8 TeV
••• We do not use the following data for averages, fits, limits, etc. •••			
0.073 ± 0.006 ± 0.002	² AAIJ	20N LHCb	pp at 7, 8, 13 TeV

¹ The analysis uses all of $D \rightarrow K_S^0 K\pi$ Dalitz decays.

² The analysis uses $D \rightarrow K_S^0 K\pi$ Dalitz decays with K^*K^+ region excluded.

$$\Gamma([K^*(892)^-K^-]DK^+)/\Gamma([K^*(892)^-K^-]D\pi^+) \quad \Gamma_{90}/\Gamma_{96}$$

VALUE	DOCUMENT ID	TECN	COMMENT
0.080 ± 0.004 OUR AVERAGE	Error includes scale factor of 1.7.		
0.093 ± 0.012 ± 0.005	¹ ADACHI	23L BELL	$e^+e^- \rightarrow \Upsilon(4S)$
0.079 ± 0.004 ± 0.002	¹ AAIJ	20N LHCb	pp at 7, 8, 13 TeV
••• We do not use the following data for averages, fits, limits, etc. •••			
0.084 ± 0.011 ± 0.003	¹ AAIJ	14V LHCb	Repl. by AAIJ 20N

¹ The Analysis uses $D \rightarrow K^*(892)K \rightarrow K_S^0 K\pi$ decays.

$$\Gamma([K^*(892)^+K^-]DK^+)/\Gamma([K^*(892)^+K^-]D\pi^+) \quad \Gamma_{92}/\Gamma_{94}$$

VALUE	DOCUMENT ID	TECN	COMMENT
0.066 ± 0.012 OUR AVERAGE	Error includes scale factor of 1.9.		
0.103 ± 0.020 ± 0.006	¹ ADACHI	23L BELL	$e^+e^- \rightarrow \Upsilon(4S)$
0.062 ± 0.006 ± 0.003	¹ AAIJ	20N LHCb	pp at 7, 8, 13 TeV
••• We do not use the following data for averages, fits, limits, etc. •••			
0.056 ± 0.013 ± 0.002	¹ AAIJ	14V LHCb	Repl. by AAIJ 20N

¹ The Analysis uses $D \rightarrow K^*(892)K \rightarrow K_S^0 K\pi$ decays.

$$\Gamma([K_S^0 K^+\pi^-]DK^+)/\Gamma([K_S^0 K^+\pi^-]D\pi^+) \quad \Gamma_{95}/\Gamma_{93}$$

VALUE	DOCUMENT ID	TECN	COMMENT
1.47 ± 0.05 OUR AVERAGE	Error includes scale factor of 1.2.		
1.428 ± 0.057 ± 0.002	¹ ADACHI	23L BELL	$e^+e^- \rightarrow \Upsilon(4S)$
1.528 ± 0.058 ± 0.025	¹ AAIJ	14V LHCb	pp at 7, 8 TeV
••• We do not use the following data for averages, fits, limits, etc. •••			
0.706 ± 0.019 ± 0.009	² AAIJ	20N LHCb	pp at 7, 8, 13 TeV

¹ The analysis uses all of $D \rightarrow K_S^0 K\pi$ Dalitz decays.

² The analysis uses $D \rightarrow K_S^0 K\pi$ Dalitz decays with K^*K^+ region excluded.

$$\Gamma([K^+K^-\pi^0]DK^+)/\Gamma([K^+K^-\pi^0]D\pi^+) \quad \Gamma_{97}/\Gamma_{98}$$

VALUE	DOCUMENT ID	TECN	COMMENT
0.95 ± 0.22 ± 0.05	¹ AAIJ	15W LHCb	pp at 7, 8 TeV

¹ Uses $D \rightarrow K^+K^-\pi^0$ mode.

$$\Gamma([\pi^+\pi^-\pi^0]DK^+)/\Gamma([\pi^+\pi^-\pi^0]D\pi^+) \quad \Gamma_{99}/\Gamma_{100}$$

VALUE	DOCUMENT ID	TECN	COMMENT
0.98 ± 0.11 ± 0.05	¹ AAIJ	15W LHCb	pp at 7, 8 TeV

¹ Uses $D \rightarrow \pi^+\pi^-\pi^0$ mode.

$$\Gamma([K^*(892)^-K^+]DK^+)/\Gamma([K^*(892)^-K^+]D\pi^+) \quad \Gamma_{96}/\Gamma_{94}$$

VALUE	DOCUMENT ID	TECN	COMMENT
2.56 ± 0.06 OUR AVERAGE	Error includes scale factor of 1.2.		
2.412 ± 0.132 ± 0.019	¹ ADACHI	23L BELL	$e^+e^- \rightarrow \Upsilon(4S)$
2.585 ± 0.057 ± 0.019	¹ AAIJ	20N LHCb	pp at 7, 8, 13 TeV
••• We do not use the following data for averages, fits, limits, etc. •••			
2.57 ± 0.13 ± 0.06	¹ AAIJ	14V LHCb	Repl. by AAIJ 20N

¹ The Analysis uses $D \rightarrow K^*(892)K \rightarrow K_S^0 K\pi$ decays.

$$\Gamma(D^0 K^*(892)^+)/\Gamma_{total} \quad \Gamma_{101}/\Gamma$$

VALUE (units 10^{-4})	DOCUMENT ID	TECN	COMMENT
5.3 ± 0.4 OUR AVERAGE	Error includes scale factor of 1.2.		
5.29 ± 0.30 ± 0.34	¹ AUBERT	06z BABR	$e^+e^- \rightarrow \Upsilon(4S)$
6.1 ± 1.6 ± 1.7	¹ MAHAPATRA	02 CLE2	$e^+e^- \rightarrow \Upsilon(4S)$
••• We do not use the following data for averages, fits, limits, etc. •••			
6.3 ± 0.7 ± 0.5	¹ AUBERT	04Q BABR	Repl. by AUBERT 06z

¹ Assumes equal production of B^+ and B^0 at the $\Upsilon(4S)$.

$\Gamma(D_{CP(-)} K^*(892)^+)/\Gamma(D^0 K^*(892)^+)$ $\Gamma_{102}/\Gamma_{101}$

VALUE	DOCUMENT ID	TECN	COMMENT
0.515 ± 0.135 ± 0.065	¹ AUBERT	09AJ	BABR $e^+e^- \rightarrow \Upsilon(4S)$

• • • We do not use the following data for averages, fits, limits, etc. • • •

0.325 ± 0.13 ± 0.04 ² AUBERT,B 05U BABR Repl. by AUBERT 09AJ

¹ The authors report $R_{CP-} = 1.03 \pm 0.27 \pm 0.13$ which is, assuming CP conservation, twice the value of the quoted above branching ratio,
² The authors report $R_{CP-} = 0.65 \pm 0.26 \pm 0.08$ which is, assuming CP conservation, twice the value of the quoted above branching ratio.

 $\Gamma(D_{CP(+)} K^*(892)^+)/\Gamma(D^0 K^*(892)^+)$ $\Gamma_{103}/\Gamma_{101}$

VALUE	DOCUMENT ID	TECN	COMMENT
1.16 ± 0.08 OUR AVERAGE			
1.18 ± 0.08 ± 0.02	¹ AAIJ	18X	LHCb pp at 7, 8, 13 TeV
1.085 ± 0.175 ± 0.045	² AUBERT	09AJ	BABR $e^+e^- \rightarrow \Upsilon(4S)$

• • • We do not use the following data for averages, fits, limits, etc. • • •

1.18 ± 0.08 ± 0.01 ³ AAIJ 17Bo LHCb Repl. by AAIJ 18X
0.98 ± 0.20 ± 0.055 ⁴ AUBERT,B 05U BABR Repl. by AUBERT 09AJ

¹ Measures the ratio separately for K^+K^- and $\pi^+\pi^-$ final states, $R_{KK} = 1.22 \pm 0.09 \pm 0.02$ and $R_{\pi\pi} = 1.08 \pm 0.14 \pm 0.03$, and combines the two results.
² The authors report $R_{CP+} = 2.17 \pm 0.35 \pm 0.09$ which is, assuming CP conservation, twice the value of the quoted above branching ratio,
³ Measures the ratio separately for K^+K^- and $\pi^+\pi^-$ final states, $R_{KK} = 1.22 \pm 0.09 \pm 0.01$ and $R_{\pi\pi} = 1.08 \pm 0.14 \pm 0.03$, and combines the two results.
⁴ The authors report $R_{CP+} = 1.96 \pm 0.40 \pm 0.11$ which is, assuming CP conservation, twice the value of the quoted above branching ratio.

 $\Gamma(D^0 K^*(892)^+)/\Gamma(D^0 K^*(892)^+)$ $\Gamma_{104}/\Gamma_{101}$

VALUE (units 10^{-3})	DOCUMENT ID	TECN	COMMENT
10.2 ± 3.2 ± 6.9 OUR EVALUATION			(Produced by HFLAV)

 $\Gamma(D^0 K^+ \pi^+ \pi^-)/\Gamma(D^0 \pi^+ \pi^+ \pi^-)$ $\Gamma_{105}/\Gamma_{111}$

VALUE (units 10^{-2})	DOCUMENT ID	TECN	COMMENT
9.4 ± 1.3 ± 0.9	AAIJ	12T	LHCb pp at 7 TeV

 $\Gamma(D_{CP(+)} K^+ \pi^- \pi^+)/\Gamma(K^+ \pi^- \pi^+)_D K^+ \pi^- \pi^+)$ $\Gamma_{108}/\Gamma_{106}$

VALUE	DOCUMENT ID	TECN	COMMENT
1.040 ± 0.064	AAIJ	15Bc	LHCb pp at 7, 8 TeV

 $\Gamma([K^+ \pi^-]_D K^+ \pi^- \pi^+)/\Gamma([K^+ \pi^-]_D K^+ \pi^- \pi^+)$ $\Gamma_{107}/\Gamma_{106}$

VALUE (units 10^{-4})	DOCUMENT ID	TECN	COMMENT
85 +36 -33	AAIJ	15Bc	LHCb pp at 7, 8 TeV

 $\Gamma(D^0 K^+ \bar{K}^0)/\Gamma_{total}$ Γ_{109}/Γ

VALUE (units 10^{-4})	DOCUMENT ID	TECN	COMMENT
5.5 ± 1.4 ± 0.8	¹ DRUTSKOY	02	BELL $e^+e^- \rightarrow \Upsilon(4S)$

¹ Assumes equal production of B^+ and B^0 at the $\Upsilon(4S)$.

 $\Gamma(D^0 K^+ \bar{K}^*(892)^0)/\Gamma_{total}$ Γ_{110}/Γ

VALUE (units 10^{-4})	DOCUMENT ID	TECN	COMMENT
7.5 ± 1.3 ± 1.1	¹ DRUTSKOY	02	BELL $e^+e^- \rightarrow \Upsilon(4S)$

¹ Assumes equal production of B^+ and B^0 at the $\Upsilon(4S)$.

 $\Gamma(D^0 \pi^+ \pi^+ \pi^-)/\Gamma_{total}$ Γ_{111}/Γ

VALUE	DOCUMENT ID	TECN	COMMENT
0.0055 ± 0.0020 OUR FIT			Error includes scale factor of 3.6.
0.0115 ± 0.0029 ± 0.0021	¹ BORTOLETTO92	CLEO	$e^+e^- \rightarrow \Upsilon(4S)$

¹ BORTOLETTO 92 assumes equal production of B^+ and B^0 at the $\Upsilon(4S)$ and uses MarkIII branching fractions for the D .

 $\Gamma(D^0 \pi^+ \pi^+ \pi^-)/\Gamma(D^0 \pi^+)$ Γ_{111}/Γ_{54}

VALUE	DOCUMENT ID	TECN	COMMENT
1.2 ± 0.4 OUR FIT			Error includes scale factor of 3.6.
1.27 ± 0.06 ± 0.11	AAIJ	11E	LHCb pp at 7 TeV

 $\Gamma([K^+ \pi^-]_D \pi^+ \pi^- \pi^+)/\Gamma([K^+ \pi^-]_D K^+ \pi^- \pi^+)$ $\Gamma_{112}/\Gamma_{106}$

VALUE (units 10^{-4})	DOCUMENT ID	TECN	COMMENT
42.7 ± 5.6	AAIJ	15Bc	LHCb pp at 7, 8 TeV

 $\Gamma(D^0 \pi^+ \pi^+ \pi^- \text{ nonresonant})/\Gamma_{total}$ Γ_{113}/Γ

VALUE	DOCUMENT ID	TECN	COMMENT
0.0051 ± 0.0034 ± 0.0023	¹ BORTOLETTO92	CLEO	$e^+e^- \rightarrow \Upsilon(4S)$

¹ BORTOLETTO 92 assumes equal production of B^+ and B^0 at the $\Upsilon(4S)$ and uses MarkIII branching fractions for the D .

 $\Gamma(D^0 \pi^+ \rho^0)/\Gamma_{total}$ Γ_{114}/Γ

VALUE	DOCUMENT ID	TECN	COMMENT
0.0042 ± 0.0023 ± 0.0020	¹ BORTOLETTO92	CLEO	$e^+e^- \rightarrow \Upsilon(4S)$

¹ BORTOLETTO 92 assumes equal production of B^+ and B^0 at the $\Upsilon(4S)$ and uses MarkIII branching fractions for the D .

 $\Gamma(D^0 a_1(1260)^+)/\Gamma_{total}$ Γ_{115}/Γ

VALUE	DOCUMENT ID	TECN	COMMENT
0.0045 ± 0.0019 ± 0.0031	¹ BORTOLETTO92	CLEO	$e^+e^- \rightarrow \Upsilon(4S)$

¹ BORTOLETTO 92 assumes equal production of B^+ and B^0 at the $\Upsilon(4S)$ and uses MarkIII branching fractions for the D .

 $\Gamma(D^0 \omega \pi^+)/\Gamma_{total}$ Γ_{116}/Γ

VALUE	DOCUMENT ID	TECN	COMMENT
0.0041 ± 0.0007 ± 0.0006	¹ ALEXANDER	01B	CLE2 $e^+e^- \rightarrow \Upsilon(4S)$

¹ Assumes equal production of B^+ and B^0 at the $\Upsilon(4S)$. The signal is consistent with all observed $\omega \pi^+$ having proceeded through the ρ^+ resonance at mass $1349 \pm 25 \pm 10$ MeV and width $547 \pm 86 \pm 46$ MeV.

 $\Gamma(D^*(2010)^- \pi^+ \pi^+)/\Gamma_{total}$ Γ_{117}/Γ

VALUE (units 10^{-3})	CL%	EVTS	DOCUMENT ID	TECN	COMMENT
1.35 ± 0.22 OUR AVERAGE					
1.25 ± 0.08 ± 0.22			¹ ABE	04D	BELL $e^+e^- \rightarrow \Upsilon(4S)$
1.9 ± 0.7 ± 0.3	14		² ALAM	94	CLE2 $e^+e^- \rightarrow \Upsilon(4S)$
2.6 ± 1.4 ± 0.7	11		³ ALBRECHT	90J	ARG $e^+e^- \rightarrow \Upsilon(4S)$
2.4 +1.7 +1.0 -1.6 -0.6	3		⁴ BEBEK	87	CLEO $e^+e^- \rightarrow \Upsilon(4S)$

• • • We do not use the following data for averages, fits, limits, etc. • • •

<.4. 90 ⁵ BORTOLETTO92 CLEO $e^+e^- \rightarrow \Upsilon(4S)$
5. ± 2. ± 3. 7 ⁶ ALBRECHT 87C ARG $e^+e^- \rightarrow \Upsilon(4S)$

¹ Assumes equal production of B^+ and B^0 at the $\Upsilon(4S)$.
² ALAM 94 assume equal production of B^+ and B^0 at the $\Upsilon(4S)$ and use the CLEOII $B(D^*(2010)^+ \rightarrow D^0 \pi^+)$ and absolute $B(D^0 \rightarrow K^- \pi^+)$ and the PDG 1992 $B(D^0 \rightarrow K^- \pi^+ \pi^0)/B(D^0 \rightarrow K^- \pi^+)$ and $B(D^0 \rightarrow K^- 2\pi^+ \pi^-)/B(D^0 \rightarrow K^- \pi^+)$.
³ Assumes equal production of B^+ and B^0 at the $\Upsilon(4S)$ and uses the MarkIII branching fractions for the D .
⁴ BEBEK 87 value has been updated in BERKELMAN 91 to use same assumptions as noted for BORTOLETTO 92.
⁵ BORTOLETTO 92 assumes equal production of B^+ and B^0 at the $\Upsilon(4S)$ and uses MarkIII branching fractions for the D and $D^*(2010)$. The authors also find the product branching fraction into $D^{**} \pi$ followed by $D^{**} \rightarrow D^*(2010) \pi$ to be $0.0014 \pm 0.0008 \pm 0.0003$ where D^{**} represents all orbitally excited D mesons.
⁶ ALBRECHT 87C use PDG 86 branching ratios for D and $D^*(2010)$ and assume $B(\Upsilon(4S) \rightarrow B^+ B^-) = 55\%$ and $B(\Upsilon(4S) \rightarrow B^0 \bar{B}^0) = 45\%$. Superseded by ALBRECHT 90J.

 $\Gamma(D^*(2010)^- K^+ \pi^+)/\Gamma_{total}$ Γ_{118}/Γ

VALUE (units 10^{-5})	DOCUMENT ID	TECN	COMMENT
8.2 ± 0.3 ± 1.4	¹ AAIJ	17AR	LHCb pp at 7, 8 TeV

¹ The branching fraction of the normalization mode $B^+ \rightarrow D^{*-} \pi^+ \pi^+$ is rescaled to the updated ratio of $\Upsilon(4S) \rightarrow B^+ B^-$ to $\Upsilon(4S) \rightarrow B^0 \bar{B}^0$ decay rates of 1.058 ± 0.024 .

 $\Gamma(D^*(2010)^- K^+ \pi^+)/\Gamma(D^*(2010)^- \pi^+ \pi^+)$ $\Gamma_{118}/\Gamma_{117}$

VALUE (units 10^{-2})	DOCUMENT ID	TECN	COMMENT
6.39 ± 0.27 ± 0.48	¹ AAIJ	17AR	LHCb pp at 7, 8 TeV

¹ Uses $D^{*-} \rightarrow \bar{D}^0 \pi^-$ and $\bar{D}^0 \rightarrow K^+ \pi^-$ decays.

 $\Gamma(\bar{D}_1(2420)^0 \pi^+, \bar{D}_1^0 \rightarrow D^*(2010)^- \pi^+)/\Gamma_{total}$ Γ_{119}/Γ

VALUE (units 10^{-4})	DOCUMENT ID	TECN	COMMENT
8.42 ± 0.08 ± 1.46	¹ AAIJ	20D	LHCb pp at 7, 8, 13 TeV

¹ AAIJ 20D used a 4-body amplitude analysis of $B^- \rightarrow D^{*+} \pi^- \pi^-$ decays.

 $\Gamma(\bar{D}_1(2420)^0 \pi^+, \bar{D}_1^0 \rightarrow D^*(2010)^- \pi^+)/\Gamma(D^0 \pi^+ \pi^+ \pi^-)$ $\Gamma_{119}/\Gamma_{111}$

VALUE (units 10^{-2})	DOCUMENT ID	TECN	COMMENT
9.3 ± 1.6 ± 0.9	¹ AAIJ	11E	LHCb pp at 7 TeV

¹ AAIJ 11E reports $(9.3 \pm 1.6 \pm 0.9) \times 10^{-2}$ from a measurement of $[\Gamma(B^+ \rightarrow \bar{D}_1(2420)^0 \pi^+, \bar{D}_1^0 \rightarrow D^*(2010)^- \pi^+)/\Gamma(B^+ \rightarrow \bar{D}^0 \pi^+ \pi^+ \pi^-)] \times [B(D^*(2010)^+ \rightarrow D^0 \pi^+)]$ assuming $B(D^*(2010)^+ \rightarrow D^0 \pi^+) = (67.7 \pm 0.5) \times 10^{-2}$.

 $\Gamma(D^- \pi^+ \pi^+)/\Gamma_{total}$ Γ_{120}/Γ

VALUE (units 10^{-3})	CL%	EVTS	DOCUMENT ID	TECN	COMMENT
1.07 ± 0.05 OUR AVERAGE					
1.08 ± 0.03 ± 0.05			¹ AUBERT	09AB	BABR $e^+e^- \rightarrow \Upsilon(4S)$
1.02 ± 0.04 ± 0.15			¹ ABE	04D	BELL $e^+e^- \rightarrow \Upsilon(4S)$
<1.4	90		² ALAM	94	CLE2 $e^+e^- \rightarrow \Upsilon(4S)$
<7	90		³ BORTOLETTO92	CLEO	$e^+e^- \rightarrow \Upsilon(4S)$
2.5 +4.1 +2.4 -2.3 -0.8	1		⁴ BEBEK	87	CLEO $e^+e^- \rightarrow \Upsilon(4S)$

¹ Assumes equal production of B^+ and B^0 at the $\Upsilon(4S)$.
² ALAM 94 assume equal production of B^+ and B^0 at the $\Upsilon(4S)$ and use the MarkIII $B(D^+ \rightarrow K^- 2\pi^+)$.
³ BORTOLETTO 92 assumes equal production of B^+ and B^0 at the $\Upsilon(4S)$ and uses MarkIII branching fractions for the D . The product branching fraction into $D_1^*(2340) \pi$ followed by $D_1^*(2340) \rightarrow D \pi$ is < 0.005 at 90%CL and into $D_2^*(2460)$ followed by $D_2^*(2460) \rightarrow D \pi$ is < 0.004 at 90%CL.
⁴ BEBEK 87 assume the $\Upsilon(4S)$ decays 43% to $B^0 \bar{B}^0$. $B(D^- \rightarrow K^+ \pi^- \pi^-) = (9.1 \pm 1.3 \pm 0.4)\%$ is assumed.

Meson Particle Listings

 B^\pm $\Gamma(D^- K^+ \pi^+)/\Gamma(D^- \pi^+ \pi^+)$ $\Gamma_{121}/\Gamma_{120}$

VALUE (units 10^{-2})	DOCUMENT ID	TECN	COMMENT
$7.20 \pm 0.19 \pm 0.21$	AAIJ	15v	LHCB pp at 7, 8 TeV

 $\Gamma(D_0^*(2300)^0 K^+, D_0^{*0} \rightarrow D^- \pi^+)/\Gamma_{\text{total}}$ Γ_{122}/Γ

VALUE (units 10^{-6})	DOCUMENT ID	TECN	COMMENT
$6.1 \pm 1.9 \pm 1.5$	¹ AAIJ	15v	LHCB pp at 7, 8 TeV

¹ Performs the amplitude analysis by fitting the square-Dalitz-plot distribution. $\Gamma(D_2^*(2460)^0 K^+, D_2^{*0} \rightarrow D^- \pi^+)/\Gamma_{\text{total}}$ Γ_{123}/Γ

VALUE (units 10^{-6})	DOCUMENT ID	TECN	COMMENT
$23.2 \pm 1.1 \pm 2.0$	¹ AAIJ	15v	LHCB pp at 7, 8 TeV

¹ Performs the amplitude analysis by fitting the square-Dalitz-plot distribution. $\Gamma(D_1^*(2760)^0 K^+, D_1^{*0} \rightarrow D^- \pi^+)/\Gamma_{\text{total}}$ Γ_{124}/Γ

VALUE (units 10^{-6})	DOCUMENT ID	TECN	COMMENT
$3.6 \pm 0.9 \pm 0.8$	¹ AAIJ	15v	LHCB pp at 7, 8 TeV

¹ Performs the amplitude analysis by fitting the square-Dalitz-plot distribution. $\Gamma(D^+ K^0)/\Gamma_{\text{total}}$ Γ_{125}/Γ

VALUE	CL%	DOCUMENT ID	TECN	COMMENT
$< 2 \times 10^{-6}$	90	KUMAR	23	BELL $e^+ e^- \rightarrow \Upsilon(4S)$
•••		We do not use the following data for averages, fits, limits, etc. •••		
$< 2.9 \times 10^{-6}$	90	¹ DEL-AMO-SA..10k	BABR	$e^+ e^- \rightarrow \Upsilon(4S)$
$< 5.0 \times 10^{-6}$	90	¹ AUBERT,B	05E	BABR Repl. by DEL-AMO-SANCHEZ 10k

¹ Assumes equal production of B^+ and B^0 at the $\Upsilon(4S)$. $\Gamma(D^+ K^+ \pi^-)/\Gamma(D^- K^+ \pi^+)$ $\Gamma_{126}/\Gamma_{121}$

VALUE (units 10^{-2})	DOCUMENT ID	TECN	COMMENT
$7.3 \pm 1.2 \pm 0.7$	AAIJ	16m	LHCB pp at 7, 8 TeV

 $\Gamma(D^+ \eta)/\Gamma_{\text{total}}$ Γ_{127}/Γ

VALUE	CL%	DOCUMENT ID	TECN	COMMENT
$< 1.2 \times 10^{-5}$	90	KUMAR	23	BELL $e^+ e^- \rightarrow \Upsilon(4S)$

 $\Gamma(D_2^*(2460)^0 K^+, D_2^{*0} \rightarrow D^+ \pi^-)/\Gamma_{\text{total}}$ Γ_{128}/Γ

VALUE	CL%	DOCUMENT ID	TECN	COMMENT
$< 6.3 \times 10^{-7}$	90	AAIJ	16r	LHCB pp at 7, 8 TeV

 $\Gamma(D^+ K^{*0})/\Gamma_{\text{total}}$ Γ_{129}/Γ

VALUE	CL%	DOCUMENT ID	TECN	COMMENT
$< 4.9 \times 10^{-7}$	90	AAIJ	16m	LHCB pp at 7, 8 TeV
•••		We do not use the following data for averages, fits, limits, etc. •••		
$< 1.8 \times 10^{-6}$	90	AAIJ	13r	LHCB Repl. by AAIJ 16m
$< 3.0 \times 10^{-6}$	90	¹ DEL-AMO-SA..10k	BABR	$e^+ e^- \rightarrow \Upsilon(4S)$

¹ Assumes equal production of B^+ and B^0 at the $\Upsilon(4S)$. $\Gamma(D^+ \bar{K}^{*0})/\Gamma_{\text{total}}$ Γ_{130}/Γ

VALUE (units 10^{-6})	CL%	DOCUMENT ID	TECN	COMMENT
< 1.4	90	AAIJ	13r	LHCB pp at 7 TeV

 $\Gamma(\bar{D}^*(2007)^0 \pi^+)/\Gamma_{\text{total}}$ Γ_{131}/Γ

VALUE (units 10^{-3})	EVS	DOCUMENT ID	TECN	COMMENT
$5.17 \pm 0.15 \pm 0.48$	OUR AVERAGE			
$5.35 \pm 0.04 \pm 0.22$		AAIJ	21q	LHCB pp at 7, 8, 13 TeV
$4.82 \pm 0.12 \pm 0.35$		¹ KATO	18	BELL $e^+ e^- \rightarrow \Upsilon(4S)$
$5.52 \pm 0.17 \pm 0.42$		² AUBERT	07H	BABR $e^+ e^- \rightarrow \Upsilon(4S)$
$5.3 \pm 0.4 \pm 0.1$		^{3,4} AUBERT,BE	06j	BABR $e^+ e^- \rightarrow \Upsilon(4S)$
$4.34 \pm 0.47 \pm 0.18$		⁵ BRANDENB...	98	CLE2 $e^+ e^- \rightarrow \Upsilon(4S)$
$5.2 \pm 0.7 \pm 0.7$	71	⁶ ALAM	94	CLE2 $e^+ e^- \rightarrow \Upsilon(4S)$
$7.2 \pm 1.8 \pm 1.6$		⁷ BORTOLETTO	092	CLEO $e^+ e^- \rightarrow \Upsilon(4S)$
$4.0 \pm 1.4 \pm 1.2$	9	⁷ ALBRECHT	90j	ARG $e^+ e^- \rightarrow \Upsilon(4S)$
•••		We do not use the following data for averages, fits, limits, etc. •••		
$4.664 \pm 0.029 \pm 0.268$		⁸ AAIJ	18A	LHCB pp at 7, 8, 13 TeV
2.7 ± 4.4		⁹ BEBEK	87	CLEO $e^+ e^- \rightarrow \Upsilon(4S)$

¹ Measures absolute branching fractions using a missing-mass technique.² Assumes equal production of B^+ and B^0 at the $\Upsilon(4S)$.³ AUBERT,BE 06j reports $[\Gamma(B^+ \rightarrow \bar{D}^*(2007)^0 \pi^+)/\Gamma_{\text{total}}] / [B(B^+ \rightarrow \bar{D}^0 \pi^+)] = 1.14 \pm 0.07 \pm 0.04$ which we multiply by our best value $B(B^+ \rightarrow \bar{D}^0 \pi^+) = (4.61 \pm 0.10) \times 10^{-3}$. Our first error is their experiment's error and our second error is the systematic error from using our best value.⁴ Uses a missing-mass method. Does not depend on D branching fractions or B^+/\bar{B}^0 production rates.⁵ BRANDENBURG 98 assume equal production of B^+ and B^0 at $\Upsilon(4S)$ and use the D^* reconstruction technique. The first error is their experiment's error and the second error is the systematic error from the PDG 96 value of $B(D^* \rightarrow D \pi)$.⁶ ALAM 94 assume equal production of B^+ and B^0 at the $\Upsilon(4S)$ and use the CLEO II $B(D^*(2007)^0 \rightarrow D^0 \pi^0)$ and absolute $B(D^0 \rightarrow K^- \pi^+)$ and the PDG 1992 $B(D^0 \rightarrow K^- \pi^+ \pi^0)/B(D^0 \rightarrow K^- \pi^+)$ and $B(D^0 \rightarrow K^- 2\pi^+ \pi^-)/B(D^0 \rightarrow K^- \pi^+)$.⁷ Assumes equal production of B^+ and B^0 at the $\Upsilon(4S)$ and uses Mark III branching fractions for the D and $D^*(2010)$.⁸ Superseded by AAIJ 21q.⁹ This is a derived branching ratio, using the inclusive pion spectrum and other two-body B decays. BEBEK 87 assume the $\Upsilon(4S)$ decays 43% to $B^0 \bar{B}^0$. $\Gamma(\bar{D}^*(2007)^0 \omega \pi^+)/\Gamma_{\text{total}}$ Γ_{134}/Γ

VALUE	DOCUMENT ID	TECN	COMMENT
$0.0045 \pm 0.0010 \pm 0.0007$	¹ ALEXANDER	01B	CLE2 $e^+ e^- \rightarrow \Upsilon(4S)$

¹ Assumes equal production of B^+ and B^0 at the $\Upsilon(4S)$. The signal is consistent with all observed $\omega \pi^+$ having proceeded through the ρ^{*+} resonance at mass $1349 \pm 25 \pm 10$ MeV and width $547 \pm 86 \pm 46$ MeV. $\Gamma(\bar{D}^*(2007)^0 \rho^+)/\Gamma_{\text{total}}$ Γ_{135}/Γ

VALUE	EVS	DOCUMENT ID	TECN	COMMENT
0.0098 ± 0.0017	OUR AVERAGE			
$0.0098 \pm 0.0006 \pm 0.0017$		¹ CSORNA	03	CLE2 $e^+ e^- \rightarrow \Upsilon(4S)$
$0.010 \pm 0.006 \pm 0.004$	7	² ALBRECHT	90j	ARG $e^+ e^- \rightarrow \Upsilon(4S)$
•••		We do not use the following data for averages, fits, limits, etc. •••		
$0.0168 \pm 0.0021 \pm 0.0028$	86	³ ALAM	94	CLE2 $e^+ e^- \rightarrow \Upsilon(4S)$

¹ Assumes equal production of B^0 and B^+ at the $\Upsilon(4S)$ resonance. The second error combines the systematic and theoretical uncertainties in quadrature. CSORNA 03 includes data used in ALAM 94. A full angular fit to three complex helicity amplitudes is performed.² Assumes equal production of B^+ and B^0 at the $\Upsilon(4S)$ and uses Mark III branching fractions for the D and $D^*(2010)$.³ ALAM 94 assume equal production of B^+ and B^0 at the $\Upsilon(4S)$ and use the CLEO II $B(D^*(2007)^0 \rightarrow D^0 \pi^0)$ and absolute $B(D^0 \rightarrow K^- \pi^+)$ and the PDG 1992 $B(D^0 \rightarrow K^- \pi^+ \pi^0)/B(D^0 \rightarrow K^- \pi^+)$ and $B(D^0 \rightarrow K^- 2\pi^+ \pi^-)/B(D^0 \rightarrow K^- \pi^+)$. The nonresonant $\pi^+ \pi^-$ contribution under the ρ^+ is negligible. $\Gamma(\bar{D}^*(2007)^0 K^+)/\Gamma_{\text{total}}$ Γ_{136}/Γ

VALUE (units 10^{-4})	DOCUMENT ID	TECN	COMMENT
$4.19 \pm 0.31 \pm 0.28$	OUR AVERAGE		

$4.21 \pm 0.30 \pm 0.12$	¹ AUBERT	05N	BABR $e^+ e^- \rightarrow \Upsilon(4S)$
$4.0 \pm 1.1 \pm 0.1$	² ABE	01i	BELL $e^+ e^- \rightarrow \Upsilon(4S)$

¹ AUBERT 05N reports $[\Gamma(B^+ \rightarrow \bar{D}^*(2007)^0 K^+)/\Gamma_{\text{total}}] / [B(B^+ \rightarrow \bar{D}^*(2007)^0 \pi^+)] = 0.0813 \pm 0.0040 \pm 0.0042$ which we multiply by our best value $B(B^+ \rightarrow \bar{D}^*(2007)^0 \pi^+) = (5.17 \pm 0.15) \times 10^{-3}$. Our first error is their experiment's error and our second error is the systematic error from using our best value.² ABE 01i reports $[\Gamma(B^+ \rightarrow \bar{D}^*(2007)^0 K^+)/\Gamma_{\text{total}}] / [B(B^+ \rightarrow \bar{D}^*(2007)^0 \pi^+)] = 0.078 \pm 0.019 \pm 0.009$ which we multiply by our best value $B(B^+ \rightarrow \bar{D}^*(2007)^0 \pi^+) = (5.17 \pm 0.15) \times 10^{-3}$. Our first error is their experiment's error and our second error is the systematic error from using our best value. $\Gamma(\bar{D}_{CP(1)}^{*0} K^+)/\Gamma_{\text{total}}$ Γ_{137}/Γ

VALUE (units 10^{-4})	DOCUMENT ID	TECN	COMMENT
$2.75 \pm 0.29 \pm 0.21 \pm 0.18$	¹ AUBERT	08BF	BABR $e^+ e^- \rightarrow \Upsilon(4S)$

¹ AUBERT 08BF reports $[\Gamma(B^+ \rightarrow \bar{D}_{CP(1)}^{*0} K^+)/\Gamma_{\text{total}}] / [B(B^+ \rightarrow \bar{D}^*(2007)^0 K^+)] = 0.655 \pm 0.065 \pm 0.020$ which we multiply by our best value $B(B^+ \rightarrow \bar{D}^*(2007)^0 K^+) = (4.19 \pm 0.31 \pm 0.28) \times 10^{-4}$. Our first error is their experiment's error and our second error is the systematic error from using our best value. $\Gamma(\bar{D}^*(2007)^0 K^+)/\Gamma(\bar{D}^*(2007)^0 \pi^+)$ $\Gamma_{136}/\Gamma_{131}$

VALUE (units 10^{-2})	DOCUMENT ID	TECN	COMMENT	
$8.51 \pm 0.12 \pm 0.48$	¹ AAIJ	21q	LHCB pp at 7, 8, 13 TeV	
•••		We do not use the following data for averages, fits, limits, etc. •••		
$7.930 \pm 0.110 \pm 0.560$	² AAIJ	18A	LHCB pp at 7, 8, 13 TeV	

¹ Uses semi-inclusive reconstruction of $B^+ \rightarrow ([K^+ \pi^-]_{D^*} / \pi^0)_{D^*} K^+ / \pi^+$. Decays of $D^* \rightarrow D \gamma / \pi^0$ are reconstructed without inclusion of π^0 or γ .² Superseded by AAIJ 21q. $\Gamma(\bar{D}_{CP(1)}^{*0} K^+)/\Gamma(\bar{D}_{CP(1)}^{*0} \pi^+)$ $\Gamma_{137}/\Gamma_{132}$

VALUE	DOCUMENT ID	TECN	COMMENT
0.095 ± 0.017	OUR AVERAGE		
$0.11 \pm 0.02 \pm 0.02$	¹ ABE	06	BELL $e^+ e^- \rightarrow \Upsilon(4S)$
$0.086 \pm 0.021 \pm 0.007$	² AUBERT	05N	BABR $e^+ e^- \rightarrow \Upsilon(4S)$

¹ Reports a double ratio of $B(B^+ \rightarrow D_{CP(1)}^{*0} K^+)/B(B^+ \rightarrow D_{CP(1)}^{*0} \pi^+)$ and $B(B^+ \rightarrow \bar{D}^0 K^+)/B(B^+ \rightarrow \bar{D}^0 \pi^+)$, $1.41 \pm 0.25 \pm 0.06$. We multiply by our best value of $B(B^+ \rightarrow \bar{D}^0 K^+)/B(B^+ \rightarrow \bar{D}^0 \pi^+) = 0.080 \pm 0.011$. Our first error is their experiment's error and the second error is systematic error from using our best value.² Uses $D^{*0} \rightarrow D^0 \pi^0$ with D^0 reconstructed in the CP -even eigenstates $K^+ K^-$ and $\pi^+ \pi^-$. $\Gamma(\bar{D}_{CP(1)}^{*0} K^-)/\Gamma_{\text{total}}$ Γ_{138}/Γ

VALUE (units 10^{-4})	DOCUMENT ID	TECN	COMMENT
$2.31 \pm 0.27 \pm 0.17 \pm 0.16$	¹ AUBERT	08BF	BABR $e^+ e^- \rightarrow \Upsilon(4S)$

¹ AUBERT 08BF reports $[\Gamma(B^+ \rightarrow \bar{D}_{CP(1)}^{*0} K^-)/\Gamma_{\text{total}}] / [B(B^+ \rightarrow \bar{D}^*(2007)^0 K^+)] = 0.55 \pm 0.06 \pm 0.02$ which we multiply by our best value $B(B^+ \rightarrow \bar{D}^*(2007)^0 K^+) = (4.19 \pm 0.31 \pm 0.28) \times 10^{-4}$. Our first error is their experiment's error and our second error is the systematic error from using our best value.

See key on page 1171

Meson Particle Listings

B^\pm

$\Gamma(\overline{D}^{*0}_{CP(-1)} K^+)/\Gamma(D^{*0}_{CP(-1)} \pi^+)$ $\Gamma_{138}/\Gamma_{133}$

VALUE	DOCUMENT ID	TECN	COMMENT
0.09 ± 0.03 ± 0.01	¹ ABE 06	BELL	$e^+e^- \rightarrow \Upsilon(4S)$

¹ Reports a double ratio of $B(B^+ \rightarrow D^{*0}_{CP(-1)} K^+)/B(B^+ \rightarrow D^{*0}_{CP(-1)} \pi^+)$ and $B(B^+ \rightarrow \overline{D}^{*0} K^+)/B(B^+ \rightarrow \overline{D}^{*0} \pi^+)$, $1.15 \pm 0.31 \pm 0.12$. We multiply by our best value of $B(B^+ \rightarrow \overline{D}^{*0} K^+)/B(B^+ \rightarrow \overline{D}^{*0} \pi^+) = 0.080 \pm 0.011$. Our first error is their experiment's error and the second error is systematic error from using our best value.

$\Gamma(D^*(2007)^0 K^+)/\Gamma(\overline{D}^*(2007)^0 K^+)$ $\Gamma_{139}/\Gamma_{136}$

VALUE (units 10^{-2})	DOCUMENT ID	TECN	COMMENT
1.08 ± 0.27 OUR EVALUATION	(Produced by HFLAV)		

$\Gamma(\overline{D}^*(2007)^0 K^*(892)^+)/\Gamma_{total}$ Γ_{140}/Γ

VALUE (units 10^{-4})	DOCUMENT ID	TECN	COMMENT
8.1 ± 1.4 OUR AVERAGE			
8.3 ± 1.1 ± 1.0	¹ AUBERT 04k	BABR	$e^+e^- \rightarrow \Upsilon(4S)$
7.2 ± 2.2 ± 2.6	² MAHAPATRA 02	CLE2	$e^+e^- \rightarrow \Upsilon(4S)$

¹ Assumes equal production of B^+ and B^0 at the $\Upsilon(4S)$.
² Assumes equal production of B^+ and B^0 at the $\Upsilon(4S)$ and an unpolarized final state.

$\Gamma(\overline{D}^*(2007)^0 K^+ \overline{K}^0)/\Gamma_{total}$ Γ_{141}/Γ

VALUE (units 10^{-4})	CL%	DOCUMENT ID	TECN	COMMENT
<10.6	90	¹ DRUTSKOY 02	BELL	$e^+e^- \rightarrow \Upsilon(4S)$

¹ Assumes equal production of B^+ and B^0 at the $\Upsilon(4S)$.

$\Gamma(\overline{D}^*(2007)^0 K^+ \overline{K}^*(892)^0)/\Gamma_{total}$ Γ_{142}/Γ

VALUE (units 10^{-4})	DOCUMENT ID	TECN	COMMENT
15.3 ± 3.1 ± 2.9	¹ DRUTSKOY 02	BELL	$e^+e^- \rightarrow \Upsilon(4S)$

¹ Assumes equal production of B^+ and B^0 at the $\Upsilon(4S)$.

$\Gamma(\overline{D}^*(2007)^0 \pi^+ \pi^+ \pi^-)/\Gamma_{total}$ Γ_{143}/Γ

VALUE (units 10^{-2})	EVTs	DOCUMENT ID	TECN	COMMENT
1.03 ± 0.12 OUR AVERAGE				
1.055 ± 0.047 ± 0.129	¹ MAJUMDER 04	BELL	$e^+e^- \rightarrow \Upsilon(4S)$	
0.94 ± 0.20 ± 0.17	48 ^{2,3} ALAM 94	CLE2	$e^+e^- \rightarrow \Upsilon(4S)$	

¹ Assumes equal production of B^+ and B^0 at the $\Upsilon(4S)$.
² ALAM 94 assume equal production of B^+ and B^0 at the $\Upsilon(4S)$ and use the CLEOII $B(D^*(2007)^0 \rightarrow D^0 \pi^0)$ and absolute $B(D^0 \rightarrow K^- \pi^+)$ and the PDG 1992 $B(D^0 \rightarrow K^- \pi^+ \pi^0)/B(D^0 \rightarrow K^- \pi^+)$ and $B(D^0 \rightarrow K^- 2\pi^+ \pi^-)/B(D^0 \rightarrow K^- \pi^+)$.
³ The three pion mass is required to be between 1.0 and 1.6 GeV consistent with an a_1 meson. (If this channel is dominated by a_1^+ , the branching ratio for $\overline{D}^{*0} a_1^+$ is twice that for $\overline{D}^{*0} \pi^+ \pi^+ \pi^-$.)

$\Gamma(\overline{D}^*(2007)^0 a_1(1260)^+)/\Gamma_{total}$ Γ_{144}/Γ

VALUE	DOCUMENT ID	TECN	COMMENT
0.0188 ± 0.0040 ± 0.0034	^{1,2} ALAM 94	CLE2	$e^+e^- \rightarrow \Upsilon(4S)$

¹ ALAM 94 value is twice their $\Gamma(\overline{D}^*(2007)^0 \pi^+ \pi^+ \pi^-)/\Gamma_{total}$ value based on their observation that the three pions are dominantly in the $a_1(1260)$ mass range 1.0 to 1.6 GeV.
² ALAM 94 assume equal production of B^+ and B^0 at the $\Upsilon(4S)$ and use the CLEOII $B(D^*(2007)^0 \rightarrow D^0 \pi^0)$ and absolute $B(D^0 \rightarrow K^- \pi^+)$ and the PDG 1992 $B(D^0 \rightarrow K^- \pi^+ \pi^0)/B(D^0 \rightarrow K^- \pi^+)$ and $B(D^0 \rightarrow K^- 2\pi^+ \pi^-)/B(D^0 \rightarrow K^- \pi^+)$.

$\Gamma(\overline{D}^*(2007)^0 \pi^- \pi^+ \pi^0)/\Gamma_{total}$ Γ_{145}/Γ

VALUE	DOCUMENT ID	TECN	COMMENT
0.0180 ± 0.0024 ± 0.0027	¹ ALEXANDER 01b	CLE2	$e^+e^- \rightarrow \Upsilon(4S)$

¹ Assumes equal production of B^+ and B^0 at the $\Upsilon(4S)$. The signal is consistent with all observed $\omega \pi^+$ having proceeded through the ρ^+ resonance at mass $1349 \pm 25 \pm 10$ MeV and width $547 \pm 86 \pm 46$ MeV.

$\Gamma(\overline{D}^{*0} 3\pi^+ 2\pi^-)/\Gamma_{total}$ Γ_{146}/Γ

VALUE (units 10^{-3})	DOCUMENT ID	TECN	COMMENT
5.67 ± 0.91 ± 0.85	¹ MAJUMDER 04	BELL	$e^+e^- \rightarrow \Upsilon(4S)$

¹ Assumes equal production of B^+ and B^0 at the $\Upsilon(4S)$.

$\Gamma(D^*(2010)^+ \pi^0)/\Gamma_{total}$ Γ_{147}/Γ

VALUE	CL%	DOCUMENT ID	TECN	COMMENT
<3.6 × 10⁻⁶		¹ IWABUCHI 08	BELL	$e^+e^- \rightarrow \Upsilon(4S)$
<1.7 × 10⁻⁴	90	² BRANDENB... 98	CLE2	$e^+e^- \rightarrow \Upsilon(4S)$

••• We do not use the following data for averages, fits, limits, etc. **•••**
¹ Assumes equal production of B^+ and B^0 at the $\Upsilon(4S)$.
² BRANDENBURG 98 assume equal production of B^+ and B^0 at $\Upsilon(4S)$ and use the D^* partial reconstruction technique. The first error is their experiment's error and the second error is the systematic error from the PDG 96 value of $B(D^* \rightarrow D\pi)$.

$\Gamma(D^*(2010)^+ K^0)/\Gamma_{total}$ Γ_{148}/Γ

VALUE	CL%	DOCUMENT ID	TECN	COMMENT
<9.0 × 10⁻⁶	90	¹ AUBERT,B 05E	BABR	$e^+e^- \rightarrow \Upsilon(4S)$
<9.5 × 10⁻⁵	90	¹ GRITSAN 01	CLE2	$e^+e^- \rightarrow \Upsilon(4S)$

••• We do not use the following data for averages, fits, limits, etc. **•••**
¹ Assumes equal production of B^+ and B^0 at the $\Upsilon(4S)$.

$\Gamma(D^*(2010)^- \pi^+ \pi^+ \pi^0)/\Gamma_{total}$ Γ_{149}/Γ

VALUE	EVTs	DOCUMENT ID	TECN	COMMENT
0.0152 ± 0.0071 ± 0.0001	26	¹ ALBRECHT 90j	ARG	$e^+e^- \rightarrow \Upsilon(4S)$
0.043 ± 0.013 ± 0.026	24	² ALBRECHT 87c	ARG	$e^+e^- \rightarrow \Upsilon(4S)$

••• We do not use the following data for averages, fits, limits, etc. **•••**
¹ ALBRECHT 90j reports $0.018 \pm 0.007 \pm 0.005$ from a measurement of $[\Gamma(B^+ \rightarrow D^*(2010)^- \pi^+ \pi^+ \pi^0)/\Gamma_{total}] \times [B(D^*(2010)^+ \rightarrow D^0 \pi^+)]$ assuming $B(D^*(2010)^+ \rightarrow D^0 \pi^+) = 0.57 \pm 0.06$, which we rescale to our best value $B(D^*(2010)^+ \rightarrow D^0 \pi^+) = (67.7 \pm 0.5) \times 10^{-2}$. Our first error is their experiment's error and our second error is the systematic error from using our best value. Assumes equal production of B^+ and B^0 at the $\Upsilon(4S)$ and uses MarkIII branching fractions for the D .
² ALBRECHT 87c use PDG 86 branching ratios for D and $D^*(2010)$ and assume $B(\Upsilon(4S) \rightarrow B^+ B^-) = 55\%$ and $B(\Upsilon(4S) \rightarrow B^0 \overline{B}^0) = 45\%$. Superseded by ALBRECHT 90j.

$\Gamma(D^*(2010)^- \pi^+ \pi^+ \pi^+ \pi^-)/\Gamma_{total}$ Γ_{150}/Γ

VALUE (units 10^{-3})	CL%	DOCUMENT ID	TECN	COMMENT
2.56 ± 0.26 ± 0.33		¹ MAJUMDER 04	BELL	$e^+e^- \rightarrow \Upsilon(4S)$
<10	90	² ALBRECHT 90j	ARG	$e^+e^- \rightarrow \Upsilon(4S)$

••• We do not use the following data for averages, fits, limits, etc. **•••**
¹ Assumes equal production of B^+ and B^0 at the $\Upsilon(4S)$.
² Assumes equal production of B^+ and B^0 at the $\Upsilon(4S)$ and uses MarkIII branching fractions for the D and $D^*(2010)$.

$\Gamma(\overline{D}^{*0} \pi^+)/\Gamma_{total}$ Γ_{151}/Γ

D^{*0} represents an excited state with mass $2.2 < M < 2.8$ GeV/ c^2 .

VALUE (units 10^{-3})	DOCUMENT ID	TECN	COMMENT
5.6 ± 1.2 ± 0.1	^{1,2} AUBERT, BE 06j	BABR	$e^+e^- \rightarrow \Upsilon(4S)$

¹ AUBERT, BE 06j reports $[\Gamma(B^+ \rightarrow \overline{D}^{*0} \pi^+)/\Gamma_{total}] / [B(B^+ \rightarrow \overline{D}^0 \pi^+)] = 1.22 \pm 0.13 \pm 0.23$ which we multiply by our best value $B(B^+ \rightarrow \overline{D}^0 \pi^+) = (4.61 \pm 0.10) \times 10^{-3}$. Our first error is their experiment's error and our second error is the systematic error from using our best value.
² Uses a missing-mass method. Does not depend on D branching fractions or B^+/B^0 production rates.

$\Gamma(\overline{D}^*_1(2420)^0 \pi^+)/\Gamma_{total}$ Γ_{152}/Γ

VALUE	EVTs	DOCUMENT ID	TECN	COMMENT
0.0015 ± 0.0006 OUR AVERAGE				Error includes scale factor of 1.3.
0.0011 ± 0.0005 ± 0.0002	8	¹ ALAM 94	CLE2	$e^+e^- \rightarrow \Upsilon(4S)$
0.0025 ± 0.0007 ± 0.0006		² ALBRECHT 94D	ARG	$e^+e^- \rightarrow \Upsilon(4S)$

¹ ALAM 94 assume equal production of B^+ and B^0 at the $\Upsilon(4S)$ and use the CLEOII $B(D^*(2010)^+ \rightarrow D^0 \pi^+)$ and absolute $B(D^0 \rightarrow K^- \pi^+)$ and the PDG 1992 $B(D^0 \rightarrow K^- \pi^+ \pi^0)/B(D^0 \rightarrow K^- \pi^+)$ and assuming $B(D_1(2420)^0 \rightarrow D^*(2010)^+ \pi^-) = 67\%$.
² ALBRECHT 94D assume equal production of B^+ and B^0 at the $\Upsilon(4S)$ and use the CLEOII $B(D^*(2010)^+ \rightarrow D^0 \pi^+)$ assuming $B(D_1(2420)^0 \rightarrow D^*(2010)^+ \pi^-) = 67\%$.

$\Gamma(\overline{D}_1(2420)^0 \pi^+ \times B(\overline{D}_1^0 \rightarrow \overline{D}^0 \pi^+ \pi^-))/\Gamma_{total}$ Γ_{153}/Γ

VALUE (units 10^{-4})	DOCUMENT ID	TECN	COMMENT
2.5 ^{+1.6} _{-1.4} OUR FIT			Error includes scale factor of 3.8.
1.85 ± 0.29 ^{+0.35} _{-0.55}	¹ ABE 05A	BELL	$e^+e^- \rightarrow \Upsilon(4S)$

¹ Assumes equal production of B^+ and B^0 at the $\Upsilon(4S)$.

$\Gamma(\overline{D}_1(2420)^0 \pi^+ \times B(\overline{D}_1^0 \rightarrow \overline{D}^0 \pi^+ \pi^-))/\Gamma(\overline{D}^0 \pi^+ \pi^+ \pi^-)$ $\Gamma_{153}/\Gamma_{111}$

VALUE (units 10^{-2})	DOCUMENT ID	TECN	COMMENT
4.6 ^{+3.3} _{-2.7} OUR FIT			Error includes scale factor of 3.9.
10.3 ± 1.5 ± 0.9	AAIJ 11E	LHCB	pp at 7 TeV

$\Gamma(\overline{D}_1(2420)^0 \pi^+ \times B(\overline{D}_1^0 \rightarrow \overline{D}^0 \pi^+ \pi^- (\text{nonresonant}))/\Gamma(\overline{D}^0 \pi^+ \pi^+ \pi^-)$ $\Gamma_{154}/\Gamma_{111}$

VALUE (units 10^{-2})	DOCUMENT ID	TECN	COMMENT
4.0 ± 0.7 ± 0.5	¹ AAIJ 11E	LHCB	pp at 7 TeV

¹ Excludes decays where $\overline{D}_1(2420)^0 \rightarrow D^*(2010)^- \pi^+$.

$\Gamma(\overline{D}_1(2430)^0 \pi^+, \overline{D}_1^0 \rightarrow D^*(2010)^- \pi^+)/\Gamma_{total}$ Γ_{155}/Γ

VALUE (units 10^{-4})	DOCUMENT ID	TECN	COMMENT
3.51 ± 0.06 ± 0.61	¹ AAIJ 20D	LHCB	pp at 7, 8, 13 TeV

¹ AAIJ 20D used a 4-body amplitude analysis of $B^- \rightarrow D^{*+} \pi^- \pi^-$ decays.

Meson Particle Listings

 B^\pm $\Gamma(\overline{D}_2^*(2462)^0 \pi^+, \overline{D}_2^{*0} \rightarrow D^- \pi^+)/\Gamma_{\text{total}}$ Γ_{158}/Γ

VALUE (units 10^{-4})	DOCUMENT ID	TECN	COMMENT
3.56 ± 0.24 OUR AVERAGE			
3.62 ± 0.06 ± 0.30	¹ AAIJ	16AH LHCb	pp at 7, 8 TeV
3.5 ± 0.2 ± 0.4	² AUBERT	09AB BABR	$e^+e^- \rightarrow \Upsilon(4S)$
3.4 ± 0.3 ± 0.72	² ABE	04D BELL	$e^+e^- \rightarrow \Upsilon(4S)$

¹ Measured using a Dalitz plot analysis of $B^- \rightarrow D^+ \pi^- \pi^-$ decays.² Assumes equal production of B^+ and B^0 at the $\Upsilon(4S)$. $\Gamma(\overline{D}_2^*(2462)^0 \pi^+, \overline{D}_2^{*0} \rightarrow \overline{D}^0 \pi^- \pi^+)/\Gamma(\overline{D}^0 \pi^+ \pi^+ \pi^-)$ $\Gamma_{159}/\Gamma_{111}$

VALUE (units 10^{-2})	DOCUMENT ID	TECN	COMMENT
4.0 ± 1.0 ± 0.4	AAIJ	11E LHCb	pp at 7 TeV

 $\Gamma(\overline{D}_2^*(2462)^0 \pi^+, \overline{D}_2^{*0} \rightarrow \overline{D}^0 \pi^- \pi^+ (\text{nonresonant}))/\Gamma(\overline{D}^0 \pi^+ \pi^+ \pi^-)$ $\Gamma_{160}/\Gamma_{111}$

VALUE	CL%	DOCUMENT ID	TECN	COMMENT
<3.0 × 10⁻²	90	¹ AAIJ	11E LHCb	pp at 7 TeV

¹ Excludes decays where $\overline{D}_2^*(2462)^0 \rightarrow D^*(2010)^- \pi^+$. $\Gamma(\overline{D}_2^*(2462)^0 \pi^+, \overline{D}_2^{*0} \rightarrow D^*(2010)^- \pi^+)/\Gamma(\overline{D}^0 \pi^+ \pi^+ \pi^-)$ $\Gamma_{161}/\Gamma_{111}$

VALUE (units 10^{-2})	DOCUMENT ID	TECN	COMMENT
3.9 ± 1.2 ± 0.4	¹ AAIJ	11E LHCb	pp at 7 TeV

¹ Uses $B(D^*(2010)^+ \rightarrow D^0 \pi^+) = (67.7 \pm 0.5)\%$. $\Gamma(\overline{D}_0^*(2400)^0 \pi^+ \times B(\overline{D}_0^*(2400)^0 \rightarrow D^- \pi^+)/\Gamma_{\text{total}}$ Γ_{162}/Γ

VALUE (units 10^{-4})	DOCUMENT ID	TECN	COMMENT
6.4 ± 1.4 OUR AVERAGE			
6.8 ± 0.3 ± 2.0	¹ AUBERT	09AB BABR	$e^+e^- \rightarrow \Upsilon(4S)$
6.1 ± 0.6 ± 1.8	¹ ABE	04D BELL	$e^+e^- \rightarrow \Upsilon(4S)$

¹ Assumes equal production of B^+ and B^0 at the $\Upsilon(4S)$. $\Gamma(\overline{D}_1^*(2421)^0 \pi^+, \overline{D}_1^{*0} \rightarrow D^{*-} \pi^+)/\Gamma_{\text{total}}$ Γ_{163}/Γ

VALUE (units 10^{-4})	DOCUMENT ID	TECN	COMMENT
7.4 ± 1.0 OUR AVERAGE			
7.95 ± 0.09 ± 1.34	¹ AAIJ	20D LHCb	pp at 7, 8, 13 TeV
6.8 ± 0.7 ± 1.3	² ABE	04D BELL	$e^+e^- \rightarrow \Upsilon(4S)$

¹ AAIJ 20D used a 4-body amplitude analysis of $B^- \rightarrow D^{*+} \pi^- \pi^-$ decays.² Assumes equal production of B^+ and B^0 at the $\Upsilon(4S)$. $\Gamma(\overline{D}_2^*(2462)^0 \pi^+, \overline{D}_2^{*0} \rightarrow D^{*-} \pi^+)/\Gamma_{\text{total}}$ Γ_{164}/Γ

VALUE (units 10^{-4})	DOCUMENT ID	TECN	COMMENT
1.98 ± 0.30 OUR AVERAGE			
2.08 ± 0.03 ± 0.37	¹ AAIJ	20D LHCb	pp at 7, 8, 13 TeV
1.8 ± 0.3 ± 0.4	² ABE	04D BELL	$e^+e^- \rightarrow \Upsilon(4S)$

¹ AAIJ 20D used a 4-body amplitude analysis of $B^- \rightarrow D^{*+} \pi^- \pi^-$ decays.² Assumes equal production of B^+ and B^0 at the $\Upsilon(4S)$. $\Gamma(\overline{D}_1^*(2427)^0 \pi^+, \overline{D}_1^{*0} \rightarrow D^{*-} \pi^+)/\Gamma_{\text{total}}$ Γ_{165}/Γ

VALUE (units 10^{-4})	DOCUMENT ID	TECN	COMMENT
3.5 ± 0.9 OUR AVERAGE	Error includes scale factor of 1.5.		
2.96 ± 0.30 ± 0.63	¹ AAIJ	20D LHCb	pp at 7, 8, 13 TeV
5.0 ± 0.4 ± 1.1	² ABE	04D BELL	$e^+e^- \rightarrow \Upsilon(4S)$

¹ AAIJ 20D used a 4-body amplitude analysis of $B^- \rightarrow D^{*+} \pi^- \pi^-$ decays.² Assumes equal production of B^+ and B^0 at the $\Upsilon(4S)$. $\Gamma(\overline{D}_1^*(2420)^0 \pi^+ \times B(\overline{D}_1^{*0} \rightarrow \overline{D}^{*0} \pi^+ \pi^-))/\Gamma_{\text{total}}$ Γ_{166}/Γ

VALUE (units 10^{-4})	CL%	DOCUMENT ID	TECN	COMMENT
<0.06	90	¹ ABE	05A BELL	$e^+e^- \rightarrow \Upsilon(4S)$

¹ Assumes equal production of B^+ and B^0 at the $\Upsilon(4S)$. $\Gamma(\overline{D}_1^*(2420)^0 \rho^+)/\Gamma_{\text{total}}$ Γ_{167}/Γ

VALUE	CL%	DOCUMENT ID	TECN	COMMENT
<0.0014	90	¹ ALAM	94 CLE2	$e^+e^- \rightarrow \Upsilon(4S)$

¹ ALAM 94 assume equal production of B^+ and B^0 at the $\Upsilon(4S)$ and use the CLEOII $B(D^*(2010)^+ \rightarrow D^0 \pi^+)$ assuming $B(D_1^*(2420)^0 \rightarrow D^*(2010)^+ \pi^-) = 67\%$. $\Gamma(\overline{D}_2^*(2460)^0 \pi^+)/\Gamma_{\text{total}}$ Γ_{168}/Γ

VALUE	CL%	DOCUMENT ID	TECN	COMMENT
<0.0013	90	¹ ALAM	94 CLE2	$e^+e^- \rightarrow \Upsilon(4S)$
•••	•••	•••	•••	•••
<0.0028	90	² ALAM	94 CLE2	$e^+e^- \rightarrow \Upsilon(4S)$
<0.0023	90	³ ALBRECHT	94D ARG	$e^+e^- \rightarrow \Upsilon(4S)$

¹ ALAM 94 assume equal production of B^+ and B^0 at the $\Upsilon(4S)$ and use the MarkIII $B(D^+ \rightarrow K^- 2\pi^+)$ and $B(D_2^*(2460)^0 \rightarrow D^+ \pi^-) = 30\%$.² ALAM 94 assume equal production of B^+ and B^0 at the $\Upsilon(4S)$ and use the MarkIII $B(D^+ \rightarrow K^- 2\pi^+)$, the CLEOII $B(D^*(2010)^+ \rightarrow D^0 \pi^+)$ and $B(D_2^*(2460)^0 \rightarrow D^*(2010)^+ \pi^-) = 20\%$.³ ALBRECHT 94D assume equal production of B^+ and B^0 at the $\Upsilon(4S)$ and use the CLEOII $B(D^*(2010)^+ \rightarrow D^0 \pi^+)$ and $B(D_2^*(2460)^0 \rightarrow D^*(2010)^+ \pi^-) = 30\%$. $\Gamma(\overline{D}_2^*(2460)^0 \pi^+ \times B(\overline{D}_2^{*0} \rightarrow \overline{D}^{*0} \pi^+ \pi^-))/\Gamma_{\text{total}}$ Γ_{169}/Γ

VALUE (units 10^{-4})	CL%	DOCUMENT ID	TECN	COMMENT
<0.22	90	¹ ABE	05A BELL	$e^+e^- \rightarrow \Upsilon(4S)$

¹ Assumes equal production of B^+ and B^0 at the $\Upsilon(4S)$. $\Gamma(\overline{D}_2^*(2460)^0 \rho^+)/\Gamma_{\text{total}}$ Γ_{175}/Γ

VALUE	CL%	DOCUMENT ID	TECN	COMMENT
<0.0047	90	¹ ALAM	94 CLE2	$e^+e^- \rightarrow \Upsilon(4S)$
<0.005	90	² ALAM	94 CLE2	$e^+e^- \rightarrow \Upsilon(4S)$

¹ ALAM 94 assume equal production of B^+ and B^0 at the $\Upsilon(4S)$ and use the MarkIII $B(D^+ \rightarrow K^- 2\pi^+)$ and $B(D_2^*(2460)^0 \rightarrow D^+ \pi^-) = 30\%$.² ALAM 94 assume equal production of B^+ and B^0 at the $\Upsilon(4S)$ and use the MarkIII $B(D^+ \rightarrow K^- 2\pi^+)$, the CLEOII $B(D^*(2010)^+ \rightarrow D^0 \pi^+)$ and $B(D_2^*(2460)^0 \rightarrow D^*(2010)^+ \pi^-) = 20\%$. $\Gamma(\overline{D}(2550)^0 \pi^+, \overline{D}^0 \rightarrow D^*(2010)^- \pi^+)/\Gamma_{\text{total}}$ Γ_{156}/Γ

VALUE (units 10^{-4})	DOCUMENT ID	TECN	COMMENT
0.72 ± 0.01 ± 0.14	¹ AAIJ	20D LHCb	pp at 7, 8, 13 TeV

¹ AAIJ 20D used a 4-body amplitude analysis of $B^- \rightarrow D^{*+} \pi^- \pi^-$ decays. $\Gamma(\overline{D}_2^*(2600)^0 \pi^+, \overline{D}_2^{*0} \rightarrow D^*(2010)^- \pi^+)/\Gamma_{\text{total}}$ Γ_{157}/Γ

VALUE (units 10^{-4})	DOCUMENT ID	TECN	COMMENT
0.68 ± 0.01 ± 0.13	¹ AAIJ	20D LHCb	pp at 7, 8, 13 TeV

¹ AAIJ 20D used a 4-body amplitude analysis of $B^- \rightarrow D^{*+} \pi^- \pi^-$ decays. $\Gamma(\overline{D}_1^*(2680)^0 \pi^+, \overline{D}_1^{*0} \rightarrow D^- \pi^+)/\Gamma_{\text{total}}$ Γ_{170}/Γ

VALUE (units 10^{-4})	DOCUMENT ID	TECN	COMMENT
0.84 ± 0.06 ± 0.20	¹ AAIJ	16AH LHCb	pp at 7, 8 TeV

¹ Measured using a Dalitz plot analysis of $B^+ \rightarrow D^- \pi^+ \pi^+$ decays. $\Gamma(\overline{D}(2740)^0 \pi^+, \overline{D}^0 \rightarrow D^*(2010)^- \pi^+)/\Gamma_{\text{total}}$ Γ_{171}/Γ

VALUE (units 10^{-4})	DOCUMENT ID	TECN	COMMENT
0.33 ± 0.02 ± 0.15	¹ AAIJ	20D LHCb	pp at 7, 8, 13 TeV

¹ AAIJ 20D used a 4-body amplitude analysis of $B^- \rightarrow D^{*+} \pi^- \pi^-$ decays. $\Gamma(\overline{D}_3^*(2750)^0 \pi^+, \overline{D}_3^{*0} \rightarrow D^*(2010)^- \pi^+)/\Gamma_{\text{total}}$ Γ_{172}/Γ

VALUE (units 10^{-4})	DOCUMENT ID	TECN	COMMENT
0.11 ± 0.01 ± 0.03	¹ AAIJ	20D LHCb	pp at 7, 8, 13 TeV

¹ AAIJ 20D used a 4-body amplitude analysis of $B^- \rightarrow D^{*+} \pi^- \pi^-$ decays. $\Gamma(\overline{D}_3^*(2760)^0 \pi^+, \overline{D}_3^{*0} \rightarrow D^- \pi^+)/\Gamma_{\text{total}}$ Γ_{173}/Γ

VALUE (units 10^{-5})	DOCUMENT ID	TECN	COMMENT
1.0 ± 0.1 ± 0.2	¹ AAIJ	16AH LHCb	pp at 7, 8 TeV

¹ Measured using a Dalitz plot analysis of $B^+ \rightarrow D^- \pi^+ \pi^+$ decays. $\Gamma(\overline{D}_2^*(3000)^0 \pi^+, \overline{D}_2^{*0} \rightarrow D^- \pi^+)/\Gamma_{\text{total}}$ Γ_{174}/Γ

VALUE (units 10^{-6})	DOCUMENT ID	TECN	COMMENT
2 ± 1 ± 1	¹ AAIJ	16AH LHCb	pp at 7, 8 TeV

¹ Measured using a Dalitz plot analysis of $B^+ \rightarrow D^- \pi^+ \pi^+$ decays. $\Gamma(\overline{D}^0 D_s^+)/\Gamma_{\text{total}}$ Γ_{176}/Γ

VALUE (units 10^{-3})	DOCUMENT ID	TECN	COMMENT
9.0 ± 0.9 OUR AVERAGE			
8.6 ± 0.2 ± 1.1	¹ AAIJ	13AP LHCb	pp at 7 TeV
9.5 ± 2.0 ± 0.8	² AUBERT	06N BABR	$e^+e^- \rightarrow \Upsilon(4S)$
9.8 ± 2.6 ± 0.9	³ GIBAUT	96 CLE2	$e^+e^- \rightarrow \Upsilon(4S)$
14 ± 8 ± 1	⁴ ALBRECHT	92G ARG	$e^+e^- \rightarrow \Upsilon(4S)$
13 ± 6 ± 1	⁵ BORTOLETTO90	CLEO	$e^+e^- \rightarrow \Upsilon(4S)$

¹ Uses $B(B^0 \rightarrow D^- D_s^+) = (7.2 \pm 0.8) \times 10^{-3}$.² AUBERT 06N reports $(0.92 \pm 0.14 \pm 0.18) \times 10^{-2}$ from a measurement of $[\Gamma(B^+ \rightarrow \overline{D}^0 D_s^+)/\Gamma_{\text{total}}] \times [B(D_s^+ \rightarrow \phi \pi^+)]$ assuming $B(D_s^+ \rightarrow \phi \pi^+) = 0.0462 \pm 0.0062$, which we rescale to our best value $B(D_s^+ \rightarrow \phi \pi^+) = (4.5 \pm 0.4) \times 10^{-2}$. Our first error is their experiment's error and our second error is the systematic error from using our best value.³ GIBAUT 96 reports $0.0126 \pm 0.0022 \pm 0.0025$ from a measurement of $[\Gamma(B^+ \rightarrow \overline{D}^0 D_s^+)/\Gamma_{\text{total}}] \times [B(D_s^+ \rightarrow \phi \pi^+)]$ assuming $B(D_s^+ \rightarrow \phi \pi^+) = 0.035$, which we rescale to our best value $B(D_s^+ \rightarrow \phi \pi^+) = (4.5 \pm 0.4) \times 10^{-2}$. Our first error is their experiment's error and our second error is the systematic error from using our best value.⁴ ALBRECHT 92G reports $0.024 \pm 0.012 \pm 0.004$ from a measurement of $[\Gamma(B^+ \rightarrow \overline{D}^0 D_s^+)/\Gamma_{\text{total}}] \times [B(D_s^+ \rightarrow \phi \pi^+)]$ assuming $B(D_s^+ \rightarrow \phi \pi^+) = 0.027$, which we rescale to our best value $B(D_s^+ \rightarrow \phi \pi^+) = (4.5 \pm 0.4) \times 10^{-2}$. Our first error is their experiment's error and our second error is the systematic error from using our best value. Assumes PDG 1990 D^0 branching ratios, e.g., $B(D^0 \rightarrow K^- \pi^+) = 3.71 \pm 0.25\%$.⁵ BORTOLETTO 90 reports 0.029 ± 0.013 from a measurement of $[\Gamma(B^+ \rightarrow \overline{D}^0 D_s^+)/\Gamma_{\text{total}}] \times [B(D_s^+ \rightarrow \phi \pi^+)]$ assuming $B(D_s^+ \rightarrow \phi \pi^+) = 0.02$, which we rescale to our best value $B(D_s^+ \rightarrow \phi \pi^+) = (4.5 \pm 0.4) \times 10^{-2}$. Our first error is their experiment's error and our second error is the systematic error from using our best value.

$\Gamma(\bar{D}^0 D^+)/\Gamma(\bar{D}^0 D_s^+)$	$\Gamma_{211}/\Gamma_{176}$		
VALUE (units 10^{-2})	DOCUMENT ID	TECN	COMMENT
$7.25 \pm 0.09 \pm 0.09$	AAIJ	23AX	LHCB pp at 7, 8, 13 TeV

$\Gamma(D_{s0}^*(2317)^+ \bar{D}^0, D_{s0}^{*+} \rightarrow D_s^+ \pi^0)/\Gamma_{total}$	Γ_{177}/Γ		
VALUE (units 10^{-3})	DOCUMENT ID	TECN	COMMENT

$0.80^{+0.16}_{-0.13}$ OUR AVERAGE

$0.80 \pm 0.17 \pm 0.02$	1,2	CHOI	15A	BELL	$e^+ e^- \rightarrow \Upsilon(4S)$
$0.80^{+0.35}_{-0.21} \pm 0.07$	2,3	AUBERT,B	04s	BABR	$e^+ e^- \rightarrow \Upsilon(4S)$

• • • We do not use the following data for averages, fits, limits, etc. • • •

$0.65^{+0.26}_{-0.24} \pm 0.06$	2,4	KROKOVNY	03B	BELL	Repl. by CHOI 15A
---------------------------------	-----	----------	-----	------	-------------------

¹ CHOI 15A reports $(8.0^{+1.3}_{-1.2} \pm 1.1 \pm 0.4) \times 10^{-4}$ from a measurement of $[\Gamma(B^+ \rightarrow D_{s0}^*(2317)^+ \bar{D}^0, D_{s0}^{*+} \rightarrow D_s^+ \pi^0)/\Gamma_{total}] \times [B(D_s^+ \rightarrow K^+ K^- \pi^+)]$ assuming $B(D_s^+ \rightarrow K^+ K^- \pi^+) = (5.39 \pm 0.21) \times 10^{-2}$, which we rescale to our best value $B(D_s^+ \rightarrow K^+ K^- \pi^+) = (5.37 \pm 0.10) \times 10^{-2}$. Our first error is their experiment's error and our second error is the systematic error from using our best value.

² Assumes equal production of B^+ and B^0 at the $\Upsilon(4S)$.

³ AUBERT,B 04s reports $(1.0 \pm 0.3^{+0.2}_{-0.2}) \times 10^{-3}$ from a measurement of $[\Gamma(B^+ \rightarrow D_{s0}^*(2317)^+ \bar{D}^0, D_{s0}^{*+} \rightarrow D_s^+ \pi^0)/\Gamma_{total}] \times [B(D_s^+ \rightarrow \phi \pi^+)]$ assuming $B(D_s^+ \rightarrow \phi \pi^+) = 0.036 \pm 0.009$, which we rescale to our best value $B(D_s^+ \rightarrow \phi \pi^+) = (4.5 \pm 0.4) \times 10^{-2}$. Our first error is their experiment's error and our second error is the systematic error from using our best value.

⁴ KROKOVNY 03B reports $(0.81^{+0.30}_{-0.27} \pm 0.24) \times 10^{-3}$ from a measurement of $[\Gamma(B^+ \rightarrow D_{s0}^*(2317)^+ \bar{D}^0, D_{s0}^{*+} \rightarrow D_s^+ \pi^0)/\Gamma_{total}] \times [B(D_s^+ \rightarrow \phi \pi^+)]$ assuming $B(D_s^+ \rightarrow \phi \pi^+) = 0.036 \pm 0.009$, which we rescale to our best value $B(D_s^+ \rightarrow \phi \pi^+) = (4.5 \pm 0.4) \times 10^{-2}$. Our first error is their experiment's error and our second error is the systematic error from using our best value.

$\Gamma(D_{s0}(2317)^+ \bar{D}^0 \times B(D_{s0}(2317)^+ \rightarrow D_s^{*+} \gamma))/\Gamma_{total}$	Γ_{178}/Γ				
VALUE (units 10^{-3})	CL%	DOCUMENT ID	TECN	COMMENT	
<0.76	90	1	KROKOVNY	03B	BELL $e^+ e^- \rightarrow \Upsilon(4S)$

¹ Assumes equal production of B^+ and B^0 at the $\Upsilon(4S)$.

$\Gamma(D_{s0}(2317)^+ \bar{D}^*(2007)^0 \times B(D_{s0}(2317)^+ \rightarrow D_s^{*+} \pi^0))/\Gamma_{total}$	Γ_{179}/Γ		
VALUE (units 10^{-3})	DOCUMENT ID	TECN	COMMENT

$0.9 \pm 0.6^{+0.4}_{-0.3}$	1	AUBERT,B	04s	BABR	$e^+ e^- \rightarrow \Upsilon(4S)$
-----------------------------	---	----------	-----	------	------------------------------------

¹ Assumes equal production of B^+ and B^0 at the $\Upsilon(4S)$.

$\Gamma(D_{sJ}(2457)^+ \bar{D}^0)/\Gamma_{total}$	Γ_{180}/Γ		
VALUE (units 10^{-3})	DOCUMENT ID	TECN	COMMENT

$3.1^{+1.0}_{-0.9}$ OUR AVERAGE

$4.3 \pm 1.6 \pm 1.3$	1	AUBERT	06N	BABR	$e^+ e^- \rightarrow \Upsilon(4S)$
$4.6^{+1.8}_{-1.6} \pm 1.0$	2,3	AUBERT,B	04s	BABR	$e^+ e^- \rightarrow \Upsilon(4S)$
$2.1^{+1.1}_{-0.9} \pm 0.5$	2,4	KROKOVNY	03B	BELL	$e^+ e^- \rightarrow \Upsilon(4S)$

¹ Uses a missing-mass method in the events that one of the B mesons is fully reconstructed.

² Assumes equal production of B^+ and B^0 at the $\Upsilon(4S)$.

³ AUBERT,B 04s reports $[\Gamma(B^+ \rightarrow D_{sJ}(2457)^+ \bar{D}^0)/\Gamma_{total}] \times [B(D_{s1}(2460)^+ \rightarrow D_s^{*+} \pi^0)] = (2.2^{+0.8}_{-0.7} \pm 0.3) \times 10^{-3}$ which we divide by our best value $B(D_{s1}(2460)^+ \rightarrow D_s^{*+} \pi^0) = (48 \pm 11) \times 10^{-2}$. Our first error is their experiment's error and our second error is the systematic error from using our best value.

⁴ KROKOVNY 03B reports $[\Gamma(B^+ \rightarrow D_{sJ}(2457)^+ \bar{D}^0)/\Gamma_{total}] \times [B(D_{s1}(2460)^+ \rightarrow D_s^{*+} \pi^0)] = (1.0^{+0.5}_{-0.4} \pm 0.1) \times 10^{-3}$ which we divide by our best value $B(D_{s1}(2460)^+ \rightarrow D_s^{*+} \pi^0) = (48 \pm 11) \times 10^{-2}$. Our first error is their experiment's error and our second error is the systematic error from using our best value.

$\Gamma(D_{sJ}(2457)^+ \bar{D}^0 \times B(D_{sJ}(2457)^+ \rightarrow D_s^{*+} \gamma))/\Gamma_{total}$	Γ_{181}/Γ		
VALUE (units 10^{-3})	DOCUMENT ID	TECN	COMMENT

$0.46^{+0.13}_{-0.11}$ OUR AVERAGE

$0.48^{+0.19}_{-0.13} \pm 0.04$	1,2	AUBERT,B	04s	BABR	$e^+ e^- \rightarrow \Upsilon(4S)$
$0.45^{+0.15}_{-0.14} \pm 0.04$	1,3	KROKOVNY	03B	BELL	$e^+ e^- \rightarrow \Upsilon(4S)$

¹ Assumes equal production of B^+ and B^0 at the $\Upsilon(4S)$.

² AUBERT,B 04s reports $(0.6 \pm 0.2^{+0.2}_{-0.1}) \times 10^{-3}$ from a measurement of $[\Gamma(B^+ \rightarrow D_{sJ}(2457)^+ \bar{D}^0 \times B(D_{sJ}(2457)^+ \rightarrow D_s^{*+} \gamma))/\Gamma_{total}] \times [B(D_s^+ \rightarrow \phi \pi^+)]$ assuming $B(D_s^+ \rightarrow \phi \pi^+) = 0.036 \pm 0.009$, which we rescale to our best value $B(D_s^+ \rightarrow \phi \pi^+) = (4.5 \pm 0.4) \times 10^{-2}$. Our first error is their experiment's error and our second error is the systematic error from using our best value.

³ KROKOVNY 03B reports $(0.56^{+0.16}_{-0.15} \pm 0.17) \times 10^{-3}$ from a measurement of $[\Gamma(B^+ \rightarrow D_{sJ}(2457)^+ \bar{D}^0 \times B(D_{sJ}(2457)^+ \rightarrow D_s^{*+} \gamma))/\Gamma_{total}] \times [B(D_s^+ \rightarrow \phi \pi^+)]$ assuming $B(D_s^+ \rightarrow \phi \pi^+) = 0.036 \pm 0.009$, which we rescale to our best value $B(D_s^+ \rightarrow \phi \pi^+) = (4.5 \pm 0.4) \times 10^{-2}$. Our first error is their experiment's error and our second error is the systematic error from using our best value.

$\Gamma(D_{sJ}(2457)^+ \bar{D}^0 \times B(D_{sJ}(2457)^+ \rightarrow D_s^{*+} \pi^-))/\Gamma_{total}$	Γ_{182}/Γ			
VALUE (units 10^{-3})	CL%	DOCUMENT ID	TECN	COMMENT

<0.22	90	1	KROKOVNY	03B	BELL $e^+ e^- \rightarrow \Upsilon(4S)$
---------	----	---	----------	-----	---

¹ Assumes equal production of B^+ and B^0 at the $\Upsilon(4S)$.

$\Gamma(D_{sJ}(2457)^+ \bar{D}^0 \times B(D_{sJ}(2457)^+ \rightarrow D_s^{*+} \pi^0))/\Gamma_{total}$	Γ_{183}/Γ			
VALUE (units 10^{-3})	CL%	DOCUMENT ID	TECN	COMMENT

<0.27	90	1	KROKOVNY	03B	BELL $e^+ e^- \rightarrow \Upsilon(4S)$
---------	----	---	----------	-----	---

¹ Assumes equal production of B^+ and B^0 at the $\Upsilon(4S)$.

$\Gamma(D_{sJ}(2457)^+ \bar{D}^0 \times B(D_{sJ}(2457)^+ \rightarrow D_s^{*+} \gamma))/\Gamma_{total}$	Γ_{184}/Γ			
VALUE (units 10^{-3})	CL%	DOCUMENT ID	TECN	COMMENT

<0.98	90	1	KROKOVNY	03B	BELL $e^+ e^- \rightarrow \Upsilon(4S)$
---------	----	---	----------	-----	---

¹ Assumes equal production of B^+ and B^0 at the $\Upsilon(4S)$.

$\Gamma(D_{sJ}(2457)^+ \bar{D}^*(2007)^0)/\Gamma_{total}$	Γ_{185}/Γ		
VALUE (units 10^{-3})	DOCUMENT ID	TECN	COMMENT

12.0 ± 3.0 OUR AVERAGE					
$11.2 \pm 2.6 \pm 2.0$	1	AUBERT	06N	BABR	$e^+ e^- \rightarrow \Upsilon(4S)$

$16^{+8}_{-6} \pm 4$	2,3	AUBERT,B	04s	BABR	$e^+ e^- \rightarrow \Upsilon(4S)$
----------------------	-----	----------	-----	------	------------------------------------

¹ Uses a missing-mass method in the events that one of the B mesons is fully reconstructed.

² AUBERT,B 04s reports $[\Gamma(B^+ \rightarrow D_{sJ}(2457)^+ \bar{D}^*(2007)^0)/\Gamma_{total}] \times [B(D_{s1}(2460)^+ \rightarrow D_s^{*+} \pi^0)] = (7.6 \pm 1.7^{+3.2}_{-2.4}) \times 10^{-3}$ which we divide by our best value $B(D_{s1}(2460)^+ \rightarrow D_s^{*+} \pi^0) = (48 \pm 11) \times 10^{-2}$. Our first error is their experiment's error and our second error is the systematic error from using our best value.

³ Assumes equal production of B^+ and B^0 at the $\Upsilon(4S)$.

$\Gamma(D_{sJ}(2457)^+ \bar{D}^*(2007)^0 \times B(D_{sJ}(2457)^+ \rightarrow D_s^{*+} \gamma))/\Gamma_{total}$	Γ_{186}/Γ		
VALUE (units 10^{-3})	DOCUMENT ID	TECN	COMMENT

$1.4 \pm 0.4^{+0.6}_{-0.4}$	1	AUBERT,B	04s	BABR	$e^+ e^- \rightarrow \Upsilon(4S)$
-----------------------------	---	----------	-----	------	------------------------------------

¹ Assumes equal production of B^+ and B^0 at the $\Upsilon(4S)$.

$\Gamma(\bar{D}^0 D_{s1}(2536)^+ \times B(D_{s1}(2536)^+ \rightarrow D^*(2007)^0 K^+))/\Gamma_{total}$	Γ_{188}/Γ			
VALUE (units 10^{-4})	CL%	DOCUMENT ID	TECN	COMMENT

$2.16 \pm 0.52 \pm 0.45$	1	AUBERT	08B	BABR	$e^+ e^- \rightarrow \Upsilon(4S)$
--------------------------	---	--------	-----	------	------------------------------------

• • • We do not use the following data for averages, fits, limits, etc. • • •

<2	90	AUBERT	03X	BABR	Repl. by AUBERT 08B
------	----	--------	-----	------	---------------------

¹ Assumes equal production of B^+ and B^0 at the $\Upsilon(4S)$.

$\Gamma(\bar{D}^0 D_{s1}(2536)^+ \times B(D_{s1}(2536)^+ \rightarrow D^*(2007)^0 K^+ + D^*(2010)^+ K^0))/\Gamma_{total}$	Γ_{187}/Γ		
VALUE (units 10^{-4})	DOCUMENT ID	TECN	COMMENT

$3.97 \pm 0.85 \pm 0.56$	1,2	AUSHEV	11	BELL	$e^+ e^- \rightarrow \Upsilon(4S)$
--------------------------	-----	--------	----	------	------------------------------------

¹ Uses $\Gamma(D^*(2007)^0 \rightarrow D^0 \pi^0) / \Gamma(D^*(2007)^0 \rightarrow D^0 \gamma) = 1.74 \pm 0.13$ and

$\Gamma(D_{s1}(2536)^+ \rightarrow D^*(2007)^0 K^+) / \Gamma(D_{s1}(2536)^+ \rightarrow D^*(2010)^+ K^0) = 1.36 \pm 0.2$.

² Assumes equal production of B^+ and B^0 at the $\Upsilon(4S)$.

$\Gamma(\bar{D}^*(2007)^0 D_{s1}(2536)^+ \times B(D_{s1}(2536)^+ \rightarrow D^*(2007)^0 K^+))/\Gamma_{total}$	Γ_{189}/Γ			
VALUE (units 10^{-4})	CL%	DOCUMENT ID	TECN	COMMENT

$5.46 \pm 1.17 \pm 1.04$	1	AUBERT	08B	BABR	$e^+ e^- \rightarrow \Upsilon(4S)$
--------------------------	---	--------	-----	------	------------------------------------

• • • We do not use the following data for averages, fits, limits, etc. • • •

<7	90	AUBERT	03X	BABR	Repl. by AUBERT 08B
------	----	--------	-----	------	---------------------

¹ Assumes equal production of B^+ and B^0 at the $\Upsilon(4S)$.

$\Gamma(\bar{D}^0 D_{s1}(2536)^+ \times B(D_{s1}(2536)^+ \rightarrow D^{*+} K^0))/\Gamma_{total}$	Γ_{190}/Γ		
VALUE (units 10^{-4})	DOCUMENT ID	TECN	COMMENT

$2.30 \pm 0.98 \pm 0.43$	1	AUBERT	08B	BABR	$e^+ e^- \rightarrow \Upsilon(4S)$
--------------------------	---	--------	-----	------	------------------------------------

¹ Assumes equal production of B^+ and B^0 at the $\Upsilon(4S)$.

$\Gamma(\bar{D}^0 D_{sJ}(2700)^+ \times B(D_{sJ}(2700)^+ \rightarrow D^0 K^+))/\Gamma_{total}$	Γ_{191}/Γ		
VALUE (units 10^{-4})	DOCUMENT ID	TECN	COMMENT

5.6 ± 1.8 OUR AVERAGE	Error	includes scale factor of 1.7.			
$5.02 \pm 0.71 \pm 0.93$	1	LEES	15c	BABR	$e^+ e^- \rightarrow \Upsilon(4S)$

$11.3 \pm 2.2^{+1.4}_{-2.8}$	1	BRODZICKA	08	BELL	$e^+ e^- \rightarrow \Upsilon(4S)$
------------------------------	---	-----------	----	------	------------------------------------

¹ Assumes equal production of B^+ and B^0 at the $\Upsilon(4S)$.

$\Gamma(\bar{D}^{*0} D_{s1}(2536)^+, D_{s1}^+ \rightarrow D^{*+} K^0)/\Gamma_{total}$	Γ_{192}/Γ		
VALUE (units 10^{-4})	DOCUMENT ID	TECN	COMMENT

$3.92 \pm 2.46 \pm 0.83$	1	AUBERT	08B	BABR	$e^+ e^- \rightarrow \Upsilon(4S)$
--------------------------	---	--------	-----	------	------------------------------------

¹ Assumes equal production of B^+ and B^0 at the $\Upsilon(4S)$.

$\Gamma(\bar{D}^0 D_{sJ}(2573)^+, D_{sJ}^+ \rightarrow D^0 K^+)/\Gamma_{total}$	Γ_{193}/Γ		
VALUE (units 10^{-4})	DOCUMENT ID	TECN	COMMENT

$0.08 \pm 0.14 \pm 0.05$	1	LEES	15c	BABR	$e^+ e^- \rightarrow \Upsilon(4S)$
--------------------------	---	------	-----	------	------------------------------------

¹ Assumes equal production of B^+ and B^0 at the $\Upsilon(4S)$.

Meson Particle Listings

 B^\pm

$\Gamma(\overline{D}^{*0} D_{sJ}(2573), D_{sJ}^+ \rightarrow D^0 K^+)/\Gamma_{\text{total}}$				Γ_{194}/Γ
VALUE (units 10^{-4})	CL%	DOCUMENT ID	TECN COMMENT	
<2	90	AUBERT	03x BABR $e^+e^- \rightarrow \Upsilon(4S)$	

$\Gamma(\overline{D}^*(2007)^0 D_{sJ}(2573), D_{sJ}^+ \rightarrow D^0 K^+)/\Gamma_{\text{total}}$				Γ_{195}/Γ
VALUE (units 10^{-4})	CL%	DOCUMENT ID	TECN COMMENT	
<5	90	AUBERT	03x BABR $e^+e^- \rightarrow \Upsilon(4S)$	

$\Gamma(\overline{D}^0 D_s^{*+})/\Gamma_{\text{total}}$				Γ_{196}/Γ
VALUE		DOCUMENT ID	TECN COMMENT	
0.0076 ± 0.0016 OUR AVERAGE				
0.0079 ± 0.0017 ± 0.0007		¹ AUBERT	06N BABR $e^+e^- \rightarrow \Upsilon(4S)$	
0.0068 ± 0.0025 ± 0.0006		² GIBAUT	96 CLE2 $e^+e^- \rightarrow \Upsilon(4S)$	
0.010 ± 0.007 ± 0.001		³ ALBRECHT	92G ARG $e^+e^- \rightarrow \Upsilon(4S)$	

- ¹ AUBERT 06N reports $(0.77 \pm 0.15 \pm 0.13) \times 10^{-2}$ from a measurement of $[\Gamma(B^+ \rightarrow \overline{D}^0 D_s^{*+})/\Gamma_{\text{total}}] \times [B(D_s^+ \rightarrow \phi\pi^+)]$ assuming $B(D_s^+ \rightarrow \phi\pi^+) = 0.0462 \pm 0.0062$, which we rescale to our best value $B(D_s^+ \rightarrow \phi\pi^+) = (4.5 \pm 0.4) \times 10^{-2}$. Our first error is their experiment's error and our second error is the systematic error from using our best value.
- ² GIBAUT 96 reports $0.0087 \pm 0.0027 \pm 0.0017$ from a measurement of $[\Gamma(B^+ \rightarrow \overline{D}^0 D_s^{*+})/\Gamma_{\text{total}}] \times [B(D_s^+ \rightarrow \phi\pi^+)]$ assuming $B(D_s^+ \rightarrow \phi\pi^+) = 0.035$, which we rescale to our best value $B(D_s^+ \rightarrow \phi\pi^+) = (4.5 \pm 0.4) \times 10^{-2}$. Our first error is their experiment's error and our second error is the systematic error from using our best value.
- ³ ALBRECHT 92G reports $0.016 \pm 0.012 \pm 0.003$ from a measurement of $[\Gamma(B^+ \rightarrow \overline{D}^0 D_s^{*+})/\Gamma_{\text{total}}] \times [B(D_s^+ \rightarrow \phi\pi^+)]$ assuming $B(D_s^+ \rightarrow \phi\pi^+) = 0.027$, which we rescale to our best value $B(D_s^+ \rightarrow \phi\pi^+) = (4.5 \pm 0.4) \times 10^{-2}$. Our first error is their experiment's error and our second error is the systematic error from using our best value. Assumes PDG 1990 D^0 branching ratios, e.g., $B(D^0 \rightarrow K^-\pi^+) = 3.71 \pm 0.25\%$.

$\Gamma(\overline{D}^*(2007)^0 D_s^+, \overline{D}^{*0} \rightarrow D^-\pi^+)/\Gamma(D^- D_s^+ \pi^+)$				$\Gamma_{199}/\Gamma_{197}$
VALUE (units 10^{-2})		DOCUMENT ID	TECN COMMENT	
14.7 ± 1.3 ± 2.7		¹ AAIJ	23B LHCb pp at 7, 8, 13 TeV	

- ¹ Uses simultaneous fits of $\overline{B}^0 \rightarrow \overline{D}^0 D_s^+ \pi^-$ and $B^+ \rightarrow D^- D_s^+ \pi^+$ amplitudes assuming isospin symmetry.

$\Gamma(\overline{D}^*(2007)^0 D_s^+)/\Gamma_{\text{total}}$				Γ_{198}/Γ
VALUE		DOCUMENT ID	TECN COMMENT	
0.0082 ± 0.0017 OUR AVERAGE				
0.0078 ± 0.0018 ± 0.0007		¹ AUBERT	06N BABR $e^+e^- \rightarrow \Upsilon(4S)$	
0.011 ± 0.004 ± 0.001		² GIBAUT	96 CLE2 $e^+e^- \rightarrow \Upsilon(4S)$	
0.008 ± 0.006 ± 0.001		³ ALBRECHT	92G ARG $e^+e^- \rightarrow \Upsilon(4S)$	

- ¹ AUBERT 06N reports $(0.76 \pm 0.15 \pm 0.13) \times 10^{-2}$ from a measurement of $[\Gamma(B^+ \rightarrow \overline{D}^*(2007)^0 D_s^+)/\Gamma_{\text{total}}] \times [B(D_s^+ \rightarrow \phi\pi^+)]$ assuming $B(D_s^+ \rightarrow \phi\pi^+) = 0.0462 \pm 0.0062$, which we rescale to our best value $B(D_s^+ \rightarrow \phi\pi^+) = (4.5 \pm 0.4) \times 10^{-2}$. Our first error is their experiment's error and our second error is the systematic error from using our best value.
- ² GIBAUT 96 reports $0.0140 \pm 0.0043 \pm 0.0035$ from a measurement of $[\Gamma(B^+ \rightarrow \overline{D}^*(2007)^0 D_s^+)/\Gamma_{\text{total}}] \times [B(D_s^+ \rightarrow \phi\pi^+)]$ assuming $B(D_s^+ \rightarrow \phi\pi^+) = 0.035$, which we rescale to our best value $B(D_s^+ \rightarrow \phi\pi^+) = (4.5 \pm 0.4) \times 10^{-2}$. Our first error is their experiment's error and our second error is the systematic error from using our best value.
- ³ ALBRECHT 92G reports $0.013 \pm 0.009 \pm 0.002$ from a measurement of $[\Gamma(B^+ \rightarrow \overline{D}^*(2007)^0 D_s^+)/\Gamma_{\text{total}}] \times [B(D_s^+ \rightarrow \phi\pi^+)]$ assuming $B(D_s^+ \rightarrow \phi\pi^+) = 0.027$, which we rescale to our best value $B(D_s^+ \rightarrow \phi\pi^+) = (4.5 \pm 0.4) \times 10^{-2}$. Our first error is their experiment's error and our second error is the systematic error from using our best value. Assumes PDG 1990 D^0 and $D^*(2007)^0$ branching ratios, e.g., $B(D^0 \rightarrow K^-\pi^+) = 3.71 \pm 0.25\%$ and $B(D^*(2007)^0 \rightarrow D^0 \pi^0) = 55 \pm 6\%$.

$\Gamma(\overline{D}^*(2007)^0 D_s^{*+})/\Gamma_{\text{total}}$				Γ_{200}/Γ
VALUE		DOCUMENT ID	TECN COMMENT	
0.0171 ± 0.0024 OUR AVERAGE				
0.0167 ± 0.0019 ± 0.0015		¹ AUBERT	06N BABR $e^+e^- \rightarrow \Upsilon(4S)$	
0.024 ± 0.009 ± 0.002		² GIBAUT	96 CLE2 $e^+e^- \rightarrow \Upsilon(4S)$	
0.019 ± 0.010 ± 0.002		³ ALBRECHT	92G ARG $e^+e^- \rightarrow \Upsilon(4S)$	

- ¹ AUBERT 06N reports $(1.62 \pm 0.22 \pm 0.18) \times 10^{-2}$ from a measurement of $[\Gamma(B^+ \rightarrow \overline{D}^*(2007)^0 D_s^{*+})/\Gamma_{\text{total}}] \times [B(D_s^+ \rightarrow \phi\pi^+)]$ assuming $B(D_s^+ \rightarrow \phi\pi^+) = 0.0462 \pm 0.0062$, which we rescale to our best value $B(D_s^+ \rightarrow \phi\pi^+) = (4.5 \pm 0.4) \times 10^{-2}$. Our first error is their experiment's error and our second error is the systematic error from using our best value.
- ² GIBAUT 96 reports $0.0310 \pm 0.0088 \pm 0.0065$ from a measurement of $[\Gamma(B^+ \rightarrow \overline{D}^*(2007)^0 D_s^{*+})/\Gamma_{\text{total}}] \times [B(D_s^+ \rightarrow \phi\pi^+)]$ assuming $B(D_s^+ \rightarrow \phi\pi^+) = 0.035$, which we rescale to our best value $B(D_s^+ \rightarrow \phi\pi^+) = (4.5 \pm 0.4) \times 10^{-2}$. Our first error is their experiment's error and our second error is the systematic error from using our best value.
- ³ ALBRECHT 92G reports $0.031 \pm 0.016 \pm 0.005$ from a measurement of $[\Gamma(B^+ \rightarrow \overline{D}^*(2007)^0 D_s^{*+})/\Gamma_{\text{total}}] \times [B(D_s^+ \rightarrow \phi\pi^+)]$ assuming $B(D_s^+ \rightarrow \phi\pi^+) = 0.027$, which we rescale to our best value $B(D_s^+ \rightarrow \phi\pi^+) = (4.5 \pm 0.4) \times 10^{-2}$. Our first error is their experiment's error and our second error is the systematic error from using our best value. Assumes PDG 1990 D^0 and $D^*(2007)^0$ branching ratios, e.g., $B(D^0 \rightarrow K^-\pi^+) = 3.71 \pm 0.25\%$ and $B(D^*(2007)^0 \rightarrow D^0 \pi^0) = 55 \pm 6\%$.

$\Gamma(\overline{D}_2^{*0}(2460)^0 D_s^+, \overline{D}_2^{*0} \rightarrow D^-\pi^+)/\Gamma(D^- D_s^+ \pi^+)$				$\Gamma_{201}/\Gamma_{197}$
VALUE (units 10^{-2})		DOCUMENT ID	TECN COMMENT	
22.35 ± 0.91 ± 0.71		¹ AAIJ	23B LHCb pp at 7, 8, 13 TeV	

- ¹ Uses simultaneous fits of $\overline{B}^0 \rightarrow \overline{D}^0 D_s^+ \pi^-$ and $B^+ \rightarrow D^- D_s^+ \pi^+$ amplitudes assuming isospin symmetry.

$\Gamma(\overline{D}_1^{*0}(2600)^0 D_s^+, \overline{D}_1^{*0} \rightarrow D^-\pi^+)/\Gamma(D^- D_s^+ \pi^+)$				$\Gamma_{202}/\Gamma_{197}$
VALUE (units 10^{-2})		DOCUMENT ID	TECN COMMENT	
1.37 ± 0.42 ± 0.62		¹ AAIJ	23B LHCb pp at 7, 8, 13 TeV	

- ¹ Uses simultaneous fits of $\overline{B}^0 \rightarrow \overline{D}^0 D_s^+ \pi^-$ and $B^+ \rightarrow D^- D_s^+ \pi^+$ amplitudes assuming isospin symmetry.

$\Gamma(\overline{D}_3^{*0}(2750)^0 D_s^+, \overline{D}_3^{*0} \rightarrow D^-\pi^+)/\Gamma(D^- D_s^+ \pi^+)$				$\Gamma_{203}/\Gamma_{197}$
VALUE (units 10^{-2})		DOCUMENT ID	TECN COMMENT	
0.31 ± 0.15 ± 0.17		¹ AAIJ	23B LHCb pp at 7, 8, 13 TeV	

- ¹ Uses simultaneous fits of $\overline{B}^0 \rightarrow \overline{D}^0 D_s^+ \pi^-$ and $B^+ \rightarrow D^- D_s^+ \pi^+$ amplitudes assuming isospin symmetry.

$\Gamma(\overline{D}_1^{*0}(2760)^0 D_s^+, \overline{D}_1^{*0} \rightarrow D^-\pi^+)/\Gamma(D^- D_s^+ \pi^+)$				$\Gamma_{204}/\Gamma_{197}$
VALUE (units 10^{-2})		DOCUMENT ID	TECN COMMENT	
0.28 ± 0.26 ± 1.53		¹ AAIJ	23B LHCb pp at 7, 8, 13 TeV	

- ¹ Uses simultaneous fits of $\overline{B}^0 \rightarrow \overline{D}^0 D_s^+ \pi^-$ and $B^+ \rightarrow D^- D_s^+ \pi^+$ amplitudes assuming isospin symmetry.

$\Gamma(\overline{D}_2^{*0}(3000)^0 D_s^+, \overline{D}_2^{*0} \rightarrow D^-\pi^+)/\Gamma(D^- D_s^+ \pi^+)$				$\Gamma_{205}/\Gamma_{197}$
VALUE (units 10^{-2})		DOCUMENT ID	TECN COMMENT	
0.45 ± 0.16 ± 0.37		¹ AAIJ	23B LHCb pp at 7, 8, 13 TeV	

- ¹ Uses simultaneous fits of $\overline{B}^0 \rightarrow \overline{D}^0 D_s^+ \pi^-$ and $B^+ \rightarrow D^- D_s^+ \pi^+$ amplitudes assuming isospin symmetry.

$\Gamma(T_{\text{CS}}^{*0}(2900)^{++} D^-, T_{\text{CS}}^{*++} \rightarrow D_s^+ \pi^+)/\Gamma(D^- D_s^+ \pi^+)$				$\Gamma_{206}/\Gamma_{197}$
VALUE (units 10^{-2})		DOCUMENT ID	TECN COMMENT	
2.25 ± 0.67 ± 0.77		¹ AAIJ	23B LHCb pp at 7, 8, 13 TeV	

- ¹ Uses simultaneous fits of $\overline{B}^0 \rightarrow \overline{D}^0 D_s^+ \pi^-$ and $B^+ \rightarrow D^- D_s^+ \pi^+$ amplitudes assuming isospin symmetry.

$\Gamma(D_s^{*+} \overline{D}^{*0})/\Gamma_{\text{total}}$				Γ_{207}/Γ
VALUE		DOCUMENT ID	TECN COMMENT	
(2.73 ± 0.93 ± 0.68) × 10⁻²		¹ AHMED	00B CLE2 $e^+e^- \rightarrow \Upsilon(4S)$	

- ¹ AHMED 00B reports their experiment's uncertainties $(\pm 0.78 \pm 0.48 \pm 0.68)\%$, where the first error is statistical, the second is systematic, and the third is the uncertainty in the $D_s \rightarrow \phi\pi$ branching fraction. We combine the first two in quadrature.

$\Gamma(\overline{D}^*(2007)^0 D^*(2010)^+)/\Gamma_{\text{total}}$				Γ_{208}/Γ
VALUE (units 10^{-4})	CL%	DOCUMENT ID	TECN COMMENT	
8.1 ± 1.2 ± 1.2		¹ AUBERT,B	06A BABR $e^+e^- \rightarrow \Upsilon(4S)$	

- • • We do not use the following data for averages, fits, limits, etc. • • •
- | VALUE | CL% | DOCUMENT ID | TECN COMMENT |
|-------|-----|-------------|---------------------------------|
| <110 | 90 | BARATE | 98Q ALEP $e^+e^- \rightarrow Z$ |

- ¹ Assumes equal production of B^+ and B^0 at the $\Upsilon(4S)$.

$[\Gamma(\overline{D}^0 D^*(2010)^+) + \Gamma(\overline{D}^*(2007)^0 D^+)]/\Gamma_{\text{total}}$				Γ_{209}/Γ
VALUE (units 10^{-4})	CL%	DOCUMENT ID	TECN COMMENT	
<130	90	BARATE	98Q ALEP $e^+e^- \rightarrow Z$	

$\Gamma(\overline{D}^0 D^*(2010)^+)/\Gamma_{\text{total}}$				Γ_{210}/Γ
VALUE (units 10^{-4})		DOCUMENT ID	TECN COMMENT	
3.9 ± 0.5 OUR AVERAGE				
3.6 ± 0.5 ± 0.4		¹ AUBERT,B	06A BABR $e^+e^- \rightarrow \Upsilon(4S)$	
4.57 ± 0.71 ± 0.56		¹ MAJUMDER	05 BELL $e^+e^- \rightarrow \Upsilon(4S)$	

- ¹ Assumes equal production of B^+ and B^0 at the $\Upsilon(4S)$.

$\Gamma(\overline{D}^0 D^+)/\Gamma_{\text{total}}$				Γ_{211}/Γ
VALUE (units 10^{-4})	CL%	DOCUMENT ID	TECN COMMENT	
3.8 ± 0.4 OUR AVERAGE				
3.85 ± 0.31 ± 0.38		¹ ADACHI	08 BELL $e^+e^- \rightarrow \Upsilon(4S)$	
3.8 ± 0.6 ± 0.5		¹ AUBERT,B	06A BABR $e^+e^- \rightarrow \Upsilon(4S)$	

- • • We do not use the following data for averages, fits, limits, etc. • • •
- | VALUE | CL% | DOCUMENT ID | TECN COMMENT |
|--------------------|-----|-----------------------|---------------------------------|
| 4.83 ± 0.78 ± 0.58 | | ¹ MAJUMDER | 05 BELL Repl. by ADACHI 08 |
| <67 | 90 | BARATE | 98Q ALEP $e^+e^- \rightarrow Z$ |

- ¹ Assumes equal production of B^+ and B^0 at the $\Upsilon(4S)$.

$\Gamma(\overline{D}^0 D^*(2010)^+)/\Gamma(\overline{D}^0 D^+)$				$\Gamma_{210}/\Gamma_{211}$
VALUE		DOCUMENT ID	TECN COMMENT	
0.271 ± 0.007 ± 0.005		AAIJ	23Ax LHCb pp at 7, 8, 13 TeV	

$\Gamma(\overline{D}^0 D^+ K^0)/\Gamma_{\text{total}}$				Γ_{212}/Γ
VALUE (units 10^{-3})	CL%	DOCUMENT ID	TECN COMMENT	
1.55 ± 0.17 ± 0.13		¹ DEL-AMO-SA...11B	BABR $e^+e^- \rightarrow \Upsilon(4S)$	

• • • We do not use the following data for averages, fits, limits, etc. • • •

<2.8 90 ¹AUBERT 03x BABR Repl. by DEL-AMO-SANCHEZ 11B

¹ Assumes equal production of B^+ and B^0 at the $\Upsilon(4S)$.

$\Gamma(D^+ \bar{D}^*(2007)^0)/\Gamma_{\text{total}}$ Γ_{213}/Γ

VALUE (units 10^{-4}) DOCUMENT ID TECN COMMENT
6.3 ± 1.4 ± 1.0 ¹AUBERT,B 06A BABR $e^+e^- \rightarrow \Upsilon(4S)$

¹ Assumes equal production of B^+ and B^0 at the $\Upsilon(4S)$.

$\Gamma(\bar{D}^*(2007)^0 D^+ K^0)/\Gamma_{\text{total}}$ Γ_{214}/Γ

VALUE (units 10^{-3}) CL% DOCUMENT ID TECN COMMENT
2.06 ± 0.38 ± 0.30 ¹DEL-AMO-SA...11B BABR $e^+e^- \rightarrow \Upsilon(4S)$

• • • We do not use the following data for averages, fits, limits, etc. • • •

<6.1 90 ¹AUBERT 03x BABR Repl. by DEL-AMO-SANCHEZ 11B

¹ Assumes equal production of B^+ and B^0 at the $\Upsilon(4S)$.

$\Gamma(\bar{D}^0 D^*(2010)^+ K^0)/\Gamma_{\text{total}}$ Γ_{215}/Γ

VALUE (units 10^{-3}) DOCUMENT ID TECN COMMENT
3.81 ± 0.31 ± 0.23 ¹DEL-AMO-SA...11B BABR $e^+e^- \rightarrow \Upsilon(4S)$

• • • We do not use the following data for averages, fits, limits, etc. • • •

5.2 $^{+2.3}_{-0.9} \pm 0.7$ ¹AUBERT 03x BABR Repl. by DEL-AMO-SANCHEZ 11B

¹ Assumes equal production of B^+ and B^0 at the $\Upsilon(4S)$.

$\Gamma(\bar{D}^*(2007)^0 D^*(2010)^+ K^0)/\Gamma_{\text{total}}$ Γ_{216}/Γ

VALUE (units 10^{-3}) DOCUMENT ID TECN COMMENT
9.17 ± 0.83 ± 0.90 ¹DEL-AMO-SA...11B BABR $e^+e^- \rightarrow \Upsilon(4S)$

• • • We do not use the following data for averages, fits, limits, etc. • • •

7.8 $^{+2.3}_{-2.1} \pm 1.4$ ¹AUBERT 03x BABR Repl. by DEL-AMO-SANCHEZ 11B

¹ Assumes equal production of B^+ and B^0 at the $\Upsilon(4S)$.

$\Gamma(\bar{D}^0 D^0 K^+)/\Gamma_{\text{total}}$ Γ_{217}/Γ

VALUE (units 10^{-3}) DOCUMENT ID TECN COMMENT
1.45 ± 0.33 OUR AVERAGE Error includes scale factor of 2.6.

1.31 ± 0.07 ± 0.12 ¹DEL-AMO-SA...11B BABR $e^+e^- \rightarrow \Upsilon(4S)$

2.22 ± 0.22 ± 0.26 ¹BRODZICKA 08 BELL $e^+e^- \rightarrow \Upsilon(4S)$

• • • We do not use the following data for averages, fits, limits, etc. • • •

1.17 ± 0.21 ± 0.15 ¹CHISTOV 04 BELL Repl. by BRODZICKA 08

1.9 ± 0.3 ± 0.3 ¹AUBERT 03x BABR Repl. by DEL-AMO-SANCHEZ 11B

¹ Assumes equal production of B^+ and B^0 at the $\Upsilon(4S)$.

$\Gamma(\bar{D}^*(2007)^0 D^0 K^+)/\Gamma_{\text{total}}$ Γ_{218}/Γ

VALUE (units 10^{-3}) CL% DOCUMENT ID TECN COMMENT
2.26 ± 0.16 ± 0.17 ¹DEL-AMO-SA...11B BABR $e^+e^- \rightarrow \Upsilon(4S)$

• • • We do not use the following data for averages, fits, limits, etc. • • •

<3.8 90 ¹AUBERT 03x BABR Repl. by DEL-AMO-SANCHEZ 11B

¹ Assumes equal production of B^+ and B^0 at the $\Upsilon(4S)$.

$\Gamma(\bar{D}^0 D^*(2007)^0 K^+)/\Gamma_{\text{total}}$ Γ_{219}/Γ

VALUE (units 10^{-3}) DOCUMENT ID TECN COMMENT
6.32 ± 0.19 ± 0.45 ¹DEL-AMO-SA...11B BABR $e^+e^- \rightarrow \Upsilon(4S)$

• • • We do not use the following data for averages, fits, limits, etc. • • •

4.7 ± 0.7 ± 0.7 ¹AUBERT 03x BABR Repl. by DEL-AMO-SANCHEZ 11B

¹ Assumes equal production of B^+ and B^0 at the $\Upsilon(4S)$.

$\Gamma(\bar{D}^*(2007)^0 D^*(2007)^0 K^+)/\Gamma_{\text{total}}$ Γ_{220}/Γ

VALUE (units 10^{-3}) DOCUMENT ID TECN COMMENT
11.23 ± 0.36 ± 1.26 ¹DEL-AMO-SA...11B BABR $e^+e^- \rightarrow \Upsilon(4S)$

• • • We do not use the following data for averages, fits, limits, etc. • • •

5.3 $^{+1.1}_{-1.0} \pm 1.2$ ¹AUBERT 03x BABR Repl. by DEL-AMO-SANCHEZ 11B

¹ Assumes equal production of B^+ and B^0 at the $\Upsilon(4S)$.

$\Gamma(D^- D^+ K^+)/\Gamma_{\text{total}}$ Γ_{221}/Γ

VALUE (units 10^{-3}) CL% DOCUMENT ID TECN COMMENT
0.22 ± 0.05 ± 0.05 ¹DEL-AMO-SA...11B BABR $e^+e^- \rightarrow \Upsilon(4S)$

• • • We do not use the following data for averages, fits, limits, etc. • • •

<0.90 90 ¹CHISTOV 04 BELL $e^+e^- \rightarrow \Upsilon(4S)$

<0.4 90 ¹AUBERT 03x BABR Repl. by DEL-AMO-SANCHEZ 11B

¹ Assumes equal production of B^+ and B^0 at the $\Upsilon(4S)$.

$\Gamma(T_{cs0}^*(2870)^0 D^+, T_{cs0}^{*0} \rightarrow D^- K^+)/\Gamma(D^- D^+ K^+)$ $\Gamma_{222}/\Gamma_{221}$

VALUE (units 10^{-2}) DOCUMENT ID TECN COMMENT
5.6 ± 1.4 ± 0.5 ¹AAIJ 20Al LHCB pp at 7, 8, 13 TeV

¹ Measured in Dalitz plot analysis of $B^+ \rightarrow D^- D^+ K^+$ decays.

$\Gamma(T_{cs1}^*(2900)^0 D^+, T_{cs1}^{*0} \rightarrow D^- K^+)/\Gamma(D^- D^+ K^+)$ $\Gamma_{223}/\Gamma_{221}$

VALUE (units 10^{-2}) DOCUMENT ID TECN COMMENT
30.6 ± 2.4 ± 2.1 ¹AAIJ 20Al LHCB pp at 7, 8, 13 TeV

¹ Measured in Dalitz plot analysis of $B^+ \rightarrow D^- D^+ K^+$ decays.

$\Gamma(D^- D^+ K^+ \text{ nonresonant})/\Gamma(D^- D^+ K^+)$ $\Gamma_{224}/\Gamma_{221}$

VALUE (units 10^{-2}) DOCUMENT ID TECN COMMENT
24.2 ± 2.2 ± 0.5 ¹AAIJ 20Al LHCB pp at 7, 8, 13 TeV

¹ Measured in Dalitz plot analysis of $B^+ \rightarrow D^- D^+ K^+$ decays.

$\Gamma(D^- D^*(2010)^+ K^+)/\Gamma_{\text{total}}$ Γ_{225}/Γ

VALUE (units 10^{-3}) CL% DOCUMENT ID TECN COMMENT
0.63 ± 0.09 ± 0.06 ¹DEL-AMO-SA...11B BABR $e^+e^- \rightarrow \Upsilon(4S)$

• • • We do not use the following data for averages, fits, limits, etc. • • •

<0.7 90 ¹AUBERT 03x BABR Repl. by DEL-AMO-SANCHEZ 11B

¹ Assumes equal production of B^+ and B^0 at the $\Upsilon(4S)$.

$\Gamma(D^- D^*(2010)^+ K^+)/\Gamma(\bar{D}^0 D^0 K^+)$ $\Gamma_{225}/\Gamma_{217}$

VALUE DOCUMENT ID TECN COMMENT
0.517 ± 0.015 ± 0.017 ¹AAIJ 20AN LHCB pp at 7, 8, 13 TeV

¹ Uses $D^+ \rightarrow K^- \pi^+ \pi^+$, $D^0 \rightarrow K^- \pi^+$ and $D^0 \rightarrow K^- \pi^+ \pi^+ \pi^-$ decays.

$\Gamma(D^*(2010)^- D^+ K^+)/\Gamma_{\text{total}}$ Γ_{226}/Γ

VALUE (units 10^{-3}) DOCUMENT ID TECN COMMENT
0.60 ± 0.10 ± 0.08 ¹DEL-AMO-SA...11B BABR $e^+e^- \rightarrow \Upsilon(4S)$

• • • We do not use the following data for averages, fits, limits, etc. • • •

1.5 ± 0.3 ± 0.2 ¹AUBERT 03x BABR Repl. by DEL-AMO-SANCHEZ 11B

¹ Assumes equal production of B^+ and B^0 at the $\Upsilon(4S)$.

$\Gamma(D^*(2010)^- D^+ K^+)/\Gamma(\bar{D}^0 D^0 K^+)$ $\Gamma_{226}/\Gamma_{217}$

VALUE DOCUMENT ID TECN COMMENT
0.577 ± 0.016 ± 0.018 ¹AAIJ 20AN LHCB pp at 7, 8, 13 TeV

¹ Uses $D^+ \rightarrow K^- \pi^+ \pi^+$, $D^0 \rightarrow K^- \pi^+$ and $D^0 \rightarrow K^- \pi^+ \pi^+ \pi^-$ decays.

$\Gamma(D^- D^*(2010)^+ K^+)/\Gamma(D^*(2010)^- D^+ K^+)$ $\Gamma_{225}/\Gamma_{226}$

VALUE DOCUMENT ID TECN COMMENT
0.907 ± 0.033 ± 0.014 ¹AAIJ 20AN LHCB pp at 7, 8, 13 TeV

¹ Uses $D^+ \rightarrow K^- \pi^+ \pi^+$, $D^0 \rightarrow K^- \pi^+$ and $D^0 \rightarrow K^- \pi^+ \pi^+ \pi^-$ decays.

$\Gamma(D^*(2010)^- D^*(2010)^+ K^+)/\Gamma_{\text{total}}$ Γ_{227}/Γ

VALUE (units 10^{-3}) CL% DOCUMENT ID TECN COMMENT
1.32 ± 0.13 ± 0.12 ¹DEL-AMO-SA...11B BABR $e^+e^- \rightarrow \Upsilon(4S)$

• • • We do not use the following data for averages, fits, limits, etc. • • •

<1.8 90 ¹AUBERT 03x BABR Repl. by DEL-AMO-SANCHEZ 11B

¹ Assumes equal production of B^+ and B^0 at the $\Upsilon(4S)$.

$\Gamma((\bar{D}^+ \bar{D}^*)(D^+ D^*) K^+)/\Gamma_{\text{total}}$ Γ_{228}/Γ

VALUE (units 10^{-2}) DOCUMENT ID TECN COMMENT
4.05 ± 0.11 ± 0.28 ¹DEL-AMO-SA...11B BABR $e^+e^- \rightarrow \Upsilon(4S)$

• • • We do not use the following data for averages, fits, limits, etc. • • •

3.5 ± 0.3 ± 0.5 ¹AUBERT 03x BABR Repl. by DEL-AMO-SANCHEZ 11B

¹ Assumes equal production of B^+ and B^0 at the $\Upsilon(4S)$.

$\Gamma(D_s^- D_s^+ K^+)/\Gamma(D^- D^+ K^+)$ $\Gamma_{229}/\Gamma_{221}$

VALUE DOCUMENT ID TECN COMMENT
0.525 ± 0.033 ± 0.027 ± 0.034 ¹AAIJ 23Al LHCB pp at 7, 8, 13 TeV

¹ AAJ 23Al report that the last error is due to the uncertainties on the branching fractions of the $D_s^\pm \rightarrow K^\mp K^\pm \pi^\pm$ and $D^\pm \rightarrow K^\mp \pi^\pm \pi^\pm$ decays.

$\Gamma(D_s^+ \pi^0)/\Gamma_{\text{total}}$ Γ_{230}/Γ

VALUE (units 10^{-5}) CL% DOCUMENT ID TECN COMMENT
1.6 $^{+0.6}_{-0.5} \pm 0.1$ ¹AUBERT 07M BABR $e^+e^- \rightarrow \Upsilon(4S)$

• • • We do not use the following data for averages, fits, limits, etc. • • •

<16 90 ²ALEXANDER 93B CLE2 $e^+e^- \rightarrow \Upsilon(4S)$

¹ AUBERT 07M reports $[\Gamma(B^+ \rightarrow D_s^+ \pi^0)/\Gamma_{\text{total}}] \times [B(D_s^+ \rightarrow \phi \pi^+)] = (7.0^{+2.4+0.6}_{-2.1-0.8}) \times 10^{-7}$ which we divide by our best value $B(D_s^+ \rightarrow \phi \pi^+) = (4.5 \pm 0.4) \times 10^{-2}$. Our first error is their experiment's error and our second error is the systematic error from using our best value.

² ALEXANDER 93B reports $< 2.0 \times 10^{-4}$ from a measurement of $[\Gamma(B^+ \rightarrow D_s^+ \pi^0)/\Gamma_{\text{total}}] \times [B(D_s^+ \rightarrow \phi \pi^+)]$ assuming $B(D_s^+ \rightarrow \phi \pi^+) = 0.037$, which we rescale to our best value $B(D_s^+ \rightarrow \phi \pi^+) = 4.5 \times 10^{-2}$.

Meson Particle Listings

 B^\pm $(\Gamma(D_S^+ \pi^0) + \Gamma(D_S^{*+} \pi^0))/\Gamma_{\text{total}}$ ($\Gamma_{230} + \Gamma_{231}$)/ Γ

VALUE	CL%	DOCUMENT ID	TECN	COMMENT
$< 5 \times 10^{-4}$	90	¹ ALBRECHT 93E	ARG	$e^+e^- \rightarrow \Upsilon(4S)$
¹ ALBRECHT 93E reports $< 0.9 \times 10^{-3}$ from a measurement of $[\Gamma(B^+ \rightarrow D_S^+ \pi^0) + \Gamma(B^+ \rightarrow D_S^{*+} \pi^0)]/\Gamma_{\text{total}} \times [B(D_S^+ \rightarrow \phi\pi^+)]$ assuming $B(D_S^+ \rightarrow \phi\pi^+) = 0.027$, which we rescale to our best value $B(D_S^+ \rightarrow \phi\pi^+) = 4.5 \times 10^{-2}$.				

 $\Gamma(D_S^{*+} \pi^0)/\Gamma_{\text{total}}$ Γ_{231}/Γ

VALUE	CL%	DOCUMENT ID	TECN	COMMENT
$< 2.6 \times 10^{-4}$	90	¹ ALEXANDER 93B	CLE2	$e^+e^- \rightarrow \Upsilon(4S)$
¹ ALEXANDER 93B reports $< 3.2 \times 10^{-4}$ from a measurement of $[\Gamma(B^+ \rightarrow D_S^{*+} \pi^0)/\Gamma_{\text{total}}] \times [B(D_S^+ \rightarrow \phi\pi^+)]$ assuming $B(D_S^+ \rightarrow \phi\pi^+) = 0.037$, which we rescale to our best value $B(D_S^+ \rightarrow \phi\pi^+) = 4.5 \times 10^{-2}$.				

 $\Gamma(D_S^+ \eta)/\Gamma_{\text{total}}$ Γ_{232}/Γ

VALUE	CL%	DOCUMENT ID	TECN	COMMENT
$< 1.4 \times 10^{-5}$	90	KUMAR 23	BELL	$e^+e^- \rightarrow \Upsilon(4S)$
••• We do not use the following data for averages, fits, limits, etc. •••				
$< 4 \times 10^{-4}$	90	¹ ALEXANDER 93B	CLE2	$e^+e^- \rightarrow \Upsilon(4S)$
¹ ALEXANDER 93B reports $< 4.6 \times 10^{-4}$ from a measurement of $[\Gamma(B^+ \rightarrow D_S^+ \eta)/\Gamma_{\text{total}}] \times [B(D_S^+ \rightarrow \phi\pi^+)]$ assuming $B(D_S^+ \rightarrow \phi\pi^+) = 0.037$, which we rescale to our best value $B(D_S^+ \rightarrow \phi\pi^+) = 4.5 \times 10^{-2}$.				

 $\Gamma(D_S^{*+} \eta)/\Gamma_{\text{total}}$ Γ_{233}/Γ

VALUE	CL%	DOCUMENT ID	TECN	COMMENT
$< 1.7 \times 10^{-5}$	90	KUMAR 23	BELL	$e^+e^- \rightarrow \Upsilon(4S)$
••• We do not use the following data for averages, fits, limits, etc. •••				
$< 6 \times 10^{-4}$	90	¹ ALEXANDER 93B	CLE2	$e^+e^- \rightarrow \Upsilon(4S)$
¹ ALEXANDER 93B reports $< 7.5 \times 10^{-4}$ from a measurement of $[\Gamma(B^+ \rightarrow D_S^{*+} \eta)/\Gamma_{\text{total}}] \times [B(D_S^+ \rightarrow \phi\pi^+)]$ assuming $B(D_S^+ \rightarrow \phi\pi^+) = 0.037$, which we rescale to our best value $B(D_S^+ \rightarrow \phi\pi^+) = 4.5 \times 10^{-2}$.				

 $\Gamma(D_S^+ \rho^0)/\Gamma_{\text{total}}$ Γ_{234}/Γ

VALUE	CL%	DOCUMENT ID	TECN	COMMENT
$< 3.0 \times 10^{-4}$	90	¹ ALEXANDER 93B	CLE2	$e^+e^- \rightarrow \Upsilon(4S)$
¹ ALEXANDER 93B reports $< 3.7 \times 10^{-4}$ from a measurement of $[\Gamma(B^+ \rightarrow D_S^+ \rho^0)/\Gamma_{\text{total}}] \times [B(D_S^+ \rightarrow \phi\pi^+)]$ assuming $B(D_S^+ \rightarrow \phi\pi^+) = 0.037$, which we rescale to our best value $B(D_S^+ \rightarrow \phi\pi^+) = 4.5 \times 10^{-2}$.				

 $(\Gamma(D_S^+ \rho^0) + \Gamma(D_S^{*+} \bar{K}^*(892)^0))/\Gamma_{\text{total}}$ ($\Gamma_{234} + \Gamma_{245}$)/ Γ

VALUE	CL%	DOCUMENT ID	TECN	COMMENT
$< 2.0 \times 10^{-3}$	90	¹ ALBRECHT 93E	ARG	$e^+e^- \rightarrow \Upsilon(4S)$
¹ ALBRECHT 93E reports $< 3.4 \times 10^{-3}$ from a measurement of $[\Gamma(B^+ \rightarrow D_S^+ \rho^0) + \Gamma(B^+ \rightarrow D_S^{*+} \bar{K}^*(892)^0)]/\Gamma_{\text{total}} \times [B(D_S^+ \rightarrow \phi\pi^+)]$ assuming $B(D_S^+ \rightarrow \phi\pi^+) = 0.027$, which we rescale to our best value $B(D_S^+ \rightarrow \phi\pi^+) = 4.5 \times 10^{-2}$.				

 $\Gamma(D_S^{*+} \rho^0)/\Gamma_{\text{total}}$ Γ_{235}/Γ

VALUE	CL%	DOCUMENT ID	TECN	COMMENT
$< 4 \times 10^{-4}$	90	¹ ALEXANDER 93B	CLE2	$e^+e^- \rightarrow \Upsilon(4S)$
¹ ALEXANDER 93B reports $< 4.8 \times 10^{-4}$ from a measurement of $[\Gamma(B^+ \rightarrow D_S^{*+} \rho^0)/\Gamma_{\text{total}}] \times [B(D_S^+ \rightarrow \phi\pi^+)]$ assuming $B(D_S^+ \rightarrow \phi\pi^+) = 0.037$, which we rescale to our best value $B(D_S^+ \rightarrow \phi\pi^+) = 4.5 \times 10^{-2}$.				

 $(\Gamma(D_S^{*+} \rho^0) + \Gamma(D_S^{*+} \bar{K}^*(892)^0))/\Gamma_{\text{total}}$ ($\Gamma_{235} + \Gamma_{247}$)/ Γ

VALUE	CL%	DOCUMENT ID	TECN	COMMENT
$< 1.2 \times 10^{-3}$	90	¹ ALBRECHT 93E	ARG	$e^+e^- \rightarrow \Upsilon(4S)$
¹ ALBRECHT 93E reports $< 2.0 \times 10^{-3}$ from a measurement of $[\Gamma(B^+ \rightarrow D_S^{*+} \rho^0) + \Gamma(B^+ \rightarrow D_S^{*+} \bar{K}^*(892)^0)]/\Gamma_{\text{total}} \times [B(D_S^+ \rightarrow \phi\pi^+)]$ assuming $B(D_S^+ \rightarrow \phi\pi^+) = 0.027$, which we rescale to our best value $B(D_S^+ \rightarrow \phi\pi^+) = 4.5 \times 10^{-2}$.				

 $\Gamma(D_S^+ \omega)/\Gamma_{\text{total}}$ Γ_{236}/Γ

VALUE	CL%	DOCUMENT ID	TECN	COMMENT
$< 4 \times 10^{-4}$	90	¹ ALEXANDER 93B	CLE2	$e^+e^- \rightarrow \Upsilon(4S)$
••• We do not use the following data for averages, fits, limits, etc. •••				
$< 2.0 \times 10^{-3}$	90	² ALBRECHT 93E	ARG	$e^+e^- \rightarrow \Upsilon(4S)$
¹ ALEXANDER 93B reports $< 4.8 \times 10^{-4}$ from a measurement of $[\Gamma(B^+ \rightarrow D_S^+ \omega)/\Gamma_{\text{total}}] \times [B(D_S^+ \rightarrow \phi\pi^+)]$ assuming $B(D_S^+ \rightarrow \phi\pi^+) = 0.037$, which we rescale to our best value $B(D_S^+ \rightarrow \phi\pi^+) = 4.5 \times 10^{-2}$.				
² ALBRECHT 93E reports $< 3.4 \times 10^{-3}$ from a measurement of $[\Gamma(B^+ \rightarrow D_S^+ \omega)/\Gamma_{\text{total}}] \times [B(D_S^+ \rightarrow \phi\pi^+)]$ assuming $B(D_S^+ \rightarrow \phi\pi^+) = 0.027$, which we rescale to our best value $B(D_S^+ \rightarrow \phi\pi^+) = 4.5 \times 10^{-2}$.				

 $\Gamma(D_S^{*+} \omega)/\Gamma_{\text{total}}$ Γ_{237}/Γ

VALUE	CL%	DOCUMENT ID	TECN	COMMENT
$< 6 \times 10^{-4}$	90	¹ ALEXANDER 93B	CLE2	$e^+e^- \rightarrow \Upsilon(4S)$
••• We do not use the following data for averages, fits, limits, etc. •••				
$< 1.1 \times 10^{-3}$	90	² ALBRECHT 93E	ARG	$e^+e^- \rightarrow \Upsilon(4S)$
¹ ALEXANDER 93B reports $< 6.8 \times 10^{-4}$ from a measurement of $[\Gamma(B^+ \rightarrow D_S^{*+} \omega)/\Gamma_{\text{total}}] \times [B(D_S^+ \rightarrow \phi\pi^+)]$ assuming $B(D_S^+ \rightarrow \phi\pi^+) = 0.037$, which we rescale to our best value $B(D_S^+ \rightarrow \phi\pi^+) = 4.5 \times 10^{-2}$.				
² ALBRECHT 93E reports $< 1.9 \times 10^{-3}$ from a measurement of $[\Gamma(B^+ \rightarrow D_S^{*+} \omega)/\Gamma_{\text{total}}] \times [B(D_S^+ \rightarrow \phi\pi^+)]$ assuming $B(D_S^+ \rightarrow \phi\pi^+) = 0.027$, which we rescale to our best value $B(D_S^+ \rightarrow \phi\pi^+) = 4.5 \times 10^{-2}$.				

 $\Gamma(D_S^+ a_1(1260)^0)/\Gamma_{\text{total}}$ Γ_{238}/Γ

VALUE	CL%	DOCUMENT ID	TECN	COMMENT
$< 1.8 \times 10^{-3}$	90	¹ ALBRECHT 93E	ARG	$e^+e^- \rightarrow \Upsilon(4S)$
¹ ALBRECHT 93E reports $< 3.0 \times 10^{-3}$ from a measurement of $[\Gamma(B^+ \rightarrow D_S^+ a_1(1260)^0)/\Gamma_{\text{total}}] \times [B(D_S^+ \rightarrow \phi\pi^+)]$ assuming $B(D_S^+ \rightarrow \phi\pi^+) = 0.027$, which we rescale to our best value $B(D_S^+ \rightarrow \phi\pi^+) = 4.5 \times 10^{-2}$.				

 $\Gamma(D_S^{*+} a_1(1260)^0)/\Gamma_{\text{total}}$ Γ_{239}/Γ

VALUE	CL%	DOCUMENT ID	TECN	COMMENT
$< 1.3 \times 10^{-3}$	90	¹ ALBRECHT 93E	ARG	$e^+e^- \rightarrow \Upsilon(4S)$
¹ ALBRECHT 93E reports $< 2.2 \times 10^{-3}$ from a measurement of $[\Gamma(B^+ \rightarrow D_S^{*+} a_1(1260)^0)/\Gamma_{\text{total}}] \times [B(D_S^+ \rightarrow \phi\pi^+)]$ assuming $B(D_S^+ \rightarrow \phi\pi^+) = 0.027$, which we rescale to our best value $B(D_S^+ \rightarrow \phi\pi^+) = 4.5 \times 10^{-2}$.				

 $\Gamma(D_S^+ K^+ K^-)/\Gamma(\bar{D}^0 D_S^+)$ $\Gamma_{240}/\Gamma_{176}$

VALUE (units 10^{-4})	CL%	DOCUMENT ID	TECN	COMMENT
$8.0 \pm 0.9 \pm 0.1$		¹ AAJ 18B	LHCb	pp at 7, 8, 13 TeV
¹ AAJ 18B reports $[\Gamma(B^+ \rightarrow D_S^+ K^+ K^-)/\Gamma(B^+ \rightarrow \bar{D}^0 D_S^+)] / [B(D^0 \rightarrow K^+ K^-)] = 0.197 \pm 0.015 \pm 0.017$ which we multiply by our best value $B(D^0 \rightarrow K^+ K^-) = (4.08 \pm 0.06) \times 10^{-3}$. Our first error is their experiment's error and our second error is the systematic error from using our best value.				

 $\Gamma(D_S^+ \phi)/\Gamma_{\text{total}}$ Γ_{241}/Γ

VALUE (units 10^{-6})	CL%	DOCUMENT ID	TECN	COMMENT
< 0.42	90	¹ AAJ 18B	LHCb	pp at 7, 8, 13 TeV
••• We do not use the following data for averages, fits, limits, etc. •••				
$1.7^{+1.1}_{-0.7} \pm 0.2$		² AAJ 13R	LHCb	Repl. by AAJ 18B
< 1.9	90	³ AUBERT 06F	BABR	$e^+e^- \rightarrow \Upsilon(4S)$
< 1000	90	⁴ ALBRECHT 93E	ARG	$e^+e^- \rightarrow \Upsilon(4S)$
< 260	90	⁵ ALEXANDER 93B	CLE2	$e^+e^- \rightarrow \Upsilon(4S)$

¹ AAJ 18B uses $B^+ \rightarrow D_S^+ \bar{D}^0$ decays for normalization.

² AAJ 13R reports $(1.87^{+1.25}_{-0.73} \pm 0.19 \pm 0.32) \times 10^{-6}$ from a measurement of $[\Gamma(B^+ \rightarrow D_S^+ \phi)/\Gamma_{\text{total}}] / [B(B^+ \rightarrow \bar{D}^0 D_S^+)]$ assuming $B(B^+ \rightarrow \bar{D}^0 D_S^+) = (10.0 \pm 1.7) \times 10^{-3}$, which we rescale to our best value $B(B^+ \rightarrow \bar{D}^0 D_S^+) = (9.0 \pm 0.9) \times 10^{-3}$. Our first error is their experiment's error and our second error is the systematic error from using our best value.

³ Assumes equal production of B^+ and B^0 at the $\Upsilon(4S)$.

⁴ ALBRECHT 93E reports $< 1.7 \times 10^{-3}$ from a measurement of $[\Gamma(B^+ \rightarrow D_S^+ \phi)/\Gamma_{\text{total}}] \times [B(D_S^+ \rightarrow \phi\pi^+)]$ assuming $B(D_S^+ \rightarrow \phi\pi^+) = 0.027$, which we rescale to our best value $B(D_S^+ \rightarrow \phi\pi^+) = 4.5 \times 10^{-2}$.

⁵ ALEXANDER 93B reports $< 3.1 \times 10^{-4}$ from a measurement of $[\Gamma(B^+ \rightarrow D_S^+ \phi)/\Gamma_{\text{total}}] \times [B(D_S^+ \rightarrow \phi\pi^+)]$ assuming $B(D_S^+ \rightarrow \phi\pi^+) = 0.037$, which we rescale to our best value $B(D_S^+ \rightarrow \phi\pi^+) = 4.5 \times 10^{-2}$.

 $\Gamma(D_S^{*+} \phi)/\Gamma_{\text{total}}$ Γ_{242}/Γ

VALUE	CL%	DOCUMENT ID	TECN	COMMENT
$< 1.2 \times 10^{-5}$	90	¹ AUBERT 06F	BABR	$e^+e^- \rightarrow \Upsilon(4S)$
••• We do not use the following data for averages, fits, limits, etc. •••				
$< 1.3 \times 10^{-3}$	90	² ALBRECHT 93E	ARG	$e^+e^- \rightarrow \Upsilon(4S)$
$< 3.5 \times 10^{-4}$	90	³ ALEXANDER 93B	CLE2	$e^+e^- \rightarrow \Upsilon(4S)$

¹ Assumes equal production of B^+ and B^0 at the $\Upsilon(4S)$.

² ALBRECHT 93E reports $< 2.1 \times 10^{-3}$ from a measurement of $[\Gamma(B^+ \rightarrow D_S^{*+} \phi)/\Gamma_{\text{total}}] \times [B(D_S^+ \rightarrow \phi\pi^+)]$ assuming $B(D_S^+ \rightarrow \phi\pi^+) = 0.027$, which we rescale to our best value $B(D_S^+ \rightarrow \phi\pi^+) = 4.5 \times 10^{-2}$.

³ ALEXANDER 93B reports $< 4.2 \times 10^{-4}$ from a measurement of $[\Gamma(B^+ \rightarrow D_S^{*+} \phi)/\Gamma_{\text{total}}] \times [B(D_S^+ \rightarrow \phi\pi^+)]$ assuming $B(D_S^+ \rightarrow \phi\pi^+) = 0.037$, which we rescale to our best value $B(D_S^+ \rightarrow \phi\pi^+) = 4.5 \times 10^{-2}$.

 $\Gamma(D_S^+ \bar{K}^0)/\Gamma_{\text{total}}$ Γ_{243}/Γ

VALUE	CL%	DOCUMENT ID	TECN	COMMENT
$< 3 \times 10^{-6}$	90	KUMAR 23	BELL	$e^+e^- \rightarrow \Upsilon(4S)$

- • • We do not use the following data for averages, fits, limits, etc. • • •
- $<1.5 \times 10^{-3}$ 90 ¹ ALBRECHT 93E ARG $e^+e^- \rightarrow \Upsilon(4S)$
- $<8 \times 10^{-4}$ 90 ² ALEXANDER 93B CLE2 $e^+e^- \rightarrow \Upsilon(4S)$
- ¹ ALBRECHT 93E reports $< 2.5 \times 10^{-3}$ from a measurement of $[\Gamma(B^+ \rightarrow D_s^+ \bar{K}^0)/\Gamma_{\text{total}}] \times [B(D_s^+ \rightarrow \phi\pi^+)]$ assuming $B(D_s^+ \rightarrow \phi\pi^+) = 0.027$, which we rescale to our best value $B(D_s^+ \rightarrow \phi\pi^+) = 4.5 \times 10^{-2}$.
- ² ALEXANDER 93B reports $< 10.3 \times 10^{-4}$ from a measurement of $[\Gamma(B^+ \rightarrow D_s^+ \bar{K}^0)/\Gamma_{\text{total}}] \times [B(D_s^+ \rightarrow \phi\pi^+)]$ assuming $B(D_s^+ \rightarrow \phi\pi^+) = 0.037$, which we rescale to our best value $B(D_s^+ \rightarrow \phi\pi^+) = 4.5 \times 10^{-2}$.

$\Gamma(D_s^+ \bar{K}^0)/\Gamma_{\text{total}}$		Γ_{244}/Γ		
VALUE	CL%	DOCUMENT ID	TECN	COMMENT
$<6 \times 10^{-6}$	90	KUMAR 23	BELL	$e^+e^- \rightarrow \Upsilon(4S)$

- • • We do not use the following data for averages, fits, limits, etc. • • •
- $<1.9 \times 10^{-3}$ 90 ¹ ALBRECHT 93E ARG $e^+e^- \rightarrow \Upsilon(4S)$
- $<9 \times 10^{-4}$ 90 ² ALEXANDER 93B CLE2 $e^+e^- \rightarrow \Upsilon(4S)$
- ¹ ALBRECHT 93E reports $< 3.1 \times 10^{-3}$ from a measurement of $[\Gamma(B^+ \rightarrow D_s^+ \bar{K}^0)/\Gamma_{\text{total}}] \times [B(D_s^+ \rightarrow \phi\pi^+)]$ assuming $B(D_s^+ \rightarrow \phi\pi^+) = 0.027$, which we rescale to our best value $B(D_s^+ \rightarrow \phi\pi^+) = 4.5 \times 10^{-2}$.
- ² ALEXANDER 93B reports $< 10.9 \times 10^{-4}$ from a measurement of $[\Gamma(B^+ \rightarrow D_s^+ \bar{K}^0)/\Gamma_{\text{total}}] \times [B(D_s^+ \rightarrow \phi\pi^+)]$ assuming $B(D_s^+ \rightarrow \phi\pi^+) = 0.037$, which we rescale to our best value $B(D_s^+ \rightarrow \phi\pi^+) = 4.5 \times 10^{-2}$.

$\Gamma(D_s^+ \bar{K}^*(892)^0)/\Gamma_{\text{total}}$		Γ_{245}/Γ		
VALUE	CL%	DOCUMENT ID	TECN	COMMENT
$<4.4 \times 10^{-6}$	90	AAIJ 13R	LHCB	pp at 7 TeV

- • • We do not use the following data for averages, fits, limits, etc. • • •
- $<4 \times 10^{-4}$ 90 ¹ ALEXANDER 93B CLE2 $e^+e^- \rightarrow \Upsilon(4S)$
- ¹ ALEXANDER 93B reports $< 4.4 \times 10^{-4}$ from a measurement of $[\Gamma(B^+ \rightarrow D_s^+ \bar{K}^*(892)^0)/\Gamma_{\text{total}}] \times [B(D_s^+ \rightarrow \phi\pi^+)]$ assuming $B(D_s^+ \rightarrow \phi\pi^+) = 0.037$, which we rescale to our best value $B(D_s^+ \rightarrow \phi\pi^+) = 4.5 \times 10^{-2}$.

$\Gamma(D_s^+ K^*0)/\Gamma_{\text{total}}$		Γ_{246}/Γ		
VALUE (units 10^{-6})	CL%	DOCUMENT ID	TECN	COMMENT
<3.5	90	AAIJ 13R	LHCB	pp at 7 TeV

$\Gamma(D_s^+ \bar{K}^*(892)^0)/\Gamma_{\text{total}}$		Γ_{247}/Γ		
VALUE	CL%	DOCUMENT ID	TECN	COMMENT
$<3.5 \times 10^{-4}$	90	ALEXANDER 93B	CLE2	$e^+e^- \rightarrow \Upsilon(4S)$

- ¹ ALEXANDER 93B reports $< 4.3 \times 10^{-4}$ from a measurement of $[\Gamma(B^+ \rightarrow D_s^+ \bar{K}^*(892)^0)/\Gamma_{\text{total}}] \times [B(D_s^+ \rightarrow \phi\pi^+)]$ assuming $B(D_s^+ \rightarrow \phi\pi^+) = 0.037$, which we rescale to our best value $B(D_s^+ \rightarrow \phi\pi^+) = 4.5 \times 10^{-2}$.

$\Gamma(D_s^- \pi^+ K^+)/\Gamma_{\text{total}}$		Γ_{248}/Γ		
VALUE (units 10^{-4})	CL%	DOCUMENT ID	TECN	COMMENT
1.80 ± 0.22 OUR AVERAGE				
$1.71^{+0.08}_{-0.07} \pm 0.25$		WIECHCZYN...09	BELL	$e^+e^- \rightarrow \Upsilon(4S)$
$2.02 \pm 0.13 \pm 0.38$		AUBERT 08G	BABR	$e^+e^- \rightarrow \Upsilon(4S)$

- • • We do not use the following data for averages, fits, limits, etc. • • •
- <7 90 ² ALBRECHT 93E ARG $e^+e^- \rightarrow \Upsilon(4S)$
- ¹ Assumes equal production of B^+ and B^0 at the $\Upsilon(4S)$.
- ² ALBRECHT 93E reports $< 1.1 \times 10^{-3}$ from a measurement of $[\Gamma(B^+ \rightarrow D_s^- \pi^+ K^+)/\Gamma_{\text{total}}] \times [B(D_s^+ \rightarrow \phi\pi^+)]$ assuming $B(D_s^+ \rightarrow \phi\pi^+) = 0.027$, which we rescale to our best value $B(D_s^+ \rightarrow \phi\pi^+) = 4.5 \times 10^{-2}$.

$\Gamma(D_s^- \pi^+ K^+)/\Gamma_{\text{total}}$		Γ_{249}/Γ		
VALUE (units 10^{-4})	CL%	DOCUMENT ID	TECN	COMMENT
1.45 ± 0.24 OUR AVERAGE				
$1.31^{+0.13}_{-0.12} \pm 0.28$		WIECHCZYN...09	BELL	$e^+e^- \rightarrow \Upsilon(4S)$
$1.67 \pm 0.16 \pm 0.35$		AUBERT 08G	BABR	$e^+e^- \rightarrow \Upsilon(4S)$

- • • We do not use the following data for averages, fits, limits, etc. • • •
- <10 90 ² ALBRECHT 93E ARG $e^+e^- \rightarrow \Upsilon(4S)$
- ¹ Assumes equal production of B^+ and B^0 at the $\Upsilon(4S)$.
- ² ALBRECHT 93E reports $< 1.6 \times 10^{-3}$ from a measurement of $[\Gamma(B^+ \rightarrow D_s^- \pi^+ K^+)/\Gamma_{\text{total}}] \times [B(D_s^+ \rightarrow \phi\pi^+)]$ assuming $B(D_s^+ \rightarrow \phi\pi^+) = 0.027$, which we rescale to our best value $B(D_s^+ \rightarrow \phi\pi^+) = 4.5 \times 10^{-2}$.

$\Gamma(D_s^- \pi^+ K^*(892)^+)/\Gamma_{\text{total}}$		Γ_{250}/Γ		
VALUE	CL%	DOCUMENT ID	TECN	COMMENT
$<5 \times 10^{-3}$	90	ALBRECHT 93E	ARG	$e^+e^- \rightarrow \Upsilon(4S)$

- ¹ ALBRECHT 93E reports $< 8.6 \times 10^{-3}$ from a measurement of $[\Gamma(B^+ \rightarrow D_s^- \pi^+ K^*(892)^+)/\Gamma_{\text{total}}] \times [B(D_s^+ \rightarrow \phi\pi^+)]$ assuming $B(D_s^+ \rightarrow \phi\pi^+) = 0.027$, which we rescale to our best value $B(D_s^+ \rightarrow \phi\pi^+) = 4.5 \times 10^{-2}$.

$\Gamma(D_s^- \pi^+ K^*(892)^+)/\Gamma_{\text{total}}$		Γ_{251}/Γ		
VALUE	CL%	DOCUMENT ID	TECN	COMMENT
$<7 \times 10^{-3}$	90	ALBRECHT 93E	ARG	$e^+e^- \rightarrow \Upsilon(4S)$

- ¹ ALBRECHT 93E reports $< 1.1 \times 10^{-2}$ from a measurement of $[\Gamma(B^+ \rightarrow D_s^- \pi^+ K^*(892)^+)/\Gamma_{\text{total}}] \times [B(D_s^+ \rightarrow \phi\pi^+)]$ assuming $B(D_s^+ \rightarrow \phi\pi^+) = 0.027$, which we rescale to our best value $B(D_s^+ \rightarrow \phi\pi^+) = 4.5 \times 10^{-2}$.

$\Gamma(D_s^- K^+ K^+)/\Gamma_{\text{total}}$		Γ_{252}/Γ		
VALUE (units 10^{-5})	CL%	DOCUMENT ID	TECN	COMMENT
0.97 ± 0.21 OUR AVERAGE				
$0.93 \pm 0.22 \pm 0.10$		WIECHCZYN...15	BELL	$e^+e^- \rightarrow \Upsilon(4S)$
$1.1 \pm 0.4 \pm 0.2$		AUBERT 08G	BABR	$e^+e^- \rightarrow \Upsilon(4S)$

- ¹ Assumes equal production of B^+ and B^0 at the $\Upsilon(4S)$.

$\Gamma(D_s^- K^+ K^+)/\Gamma(D_s^- \pi^+ K^+)$		$\Gamma_{252}/\Gamma_{248}$		
VALUE	CL%	DOCUMENT ID	TECN	COMMENT
0.054 ± 0.013 ± 0.006				
		WIECHCZYN...15	BELL	$e^+e^- \rightarrow \Upsilon(4S)$

$\Gamma(D_s^- K^+ K^+)/\Gamma_{\text{total}}$		Γ_{253}/Γ		
VALUE (units 10^{-4})	CL%	DOCUMENT ID	TECN	COMMENT
<0.15	90	AUBERT 08G	BABR	$e^+e^- \rightarrow \Upsilon(4S)$

- ¹ Assumes equal production of B^+ and B^0 at the $\Upsilon(4S)$.

$\Gamma(\eta_c K^+)/\Gamma_{\text{total}}$		Γ_{254}/Γ		
VALUE (units 10^{-3})	CL%	DOCUMENT ID	TECN	COMMENT
1.10 ± 0.07 OUR FIT				Error includes scale factor of 1.1.
1.11 ± 0.12 OUR AVERAGE				Error includes scale factor of 1.4.
$0.96 \pm 0.12 \pm 0.06 \pm 0.03$		LEES 20c	BABR	$e^+e^- \rightarrow \Upsilon(4S)$
$1.20 \pm 0.08 \pm 0.07$		KATO 18	BELL	$e^+e^- \rightarrow \Upsilon(4S)$

- • • We do not use the following data for averages, fits, limits, etc. • • •
- $1.08^{+0.13+0.13}_{-0.12-0.14}$ ³ CHILIKIN 19 BELL $e^+e^- \rightarrow \Upsilon(4S)$
- 0.87 ± 0.15 ⁴ AUBERT 06E BABR Repl. by LEES 20c
- $1.35^{+0.27}_{-0.21} \pm 0.11$ ⁵ AUBERT,B 05L BABR $e^+e^- \rightarrow \Upsilon(4S)$
- $1.04 \pm 0.12 \pm 0.06$ ^{4,6} AUBERT,B 04B BABR $e^+e^- \rightarrow \Upsilon(4S)$
- $1.25 \pm 0.14^{+0.39}_{-0.40}$ ⁷ FANG 03 BELL $e^+e^- \rightarrow \Upsilon(4S)$
- $0.69^{+0.26}_{-0.21} \pm 0.22$ ⁸ EDWARDS 01 CLE2 $e^+e^- \rightarrow \Upsilon(4S)$

- ¹ Measures absolute branching fractions using a missing-mass technique.
- ² LEES 20c measurement's last uncertainty is due to the used $B(B^{\pm} \rightarrow K^{\pm} J/\psi)$ value.
- ³ CHILIKIN 19 reports $[\Gamma(B^+ \rightarrow \eta_c K^+)/\Gamma_{\text{total}}] \times [B(\eta_c(1S) \rightarrow p\bar{p}\pi^+\pi^-)] = (39.4^{+4.1+2.2}_{-3.9-1.8}) \times 10^{-7}$ which we divide by our best value $B(\eta_c(1S) \rightarrow p\bar{p}\pi^+\pi^-) = (3.7 \pm 0.5) \times 10^{-3}$. Our first error is their experiment's error and our second error is the systematic error from using our best value.
- ⁴ The ratio of $B(B^{\pm} \rightarrow K^{\pm} \eta_c) B(\eta_c \rightarrow K\bar{K}\pi) = (7.4 \pm 0.5 \pm 0.7) \times 10^{-5}$ reported in AUBERT,B 04B and $B(B^{\pm} \rightarrow K^{\pm} \eta_c) = (8.7 \pm 1.5) \times 10^{-3}$ reported in AUBERT 06E contribute to the determination of $B(\eta_c \rightarrow K\bar{K}\pi)$, which is used by others for normalization.
- ⁵ AUBERT,B 05L reports $[\Gamma(B^+ \rightarrow \eta_c K^+)/\Gamma_{\text{total}}] \times [B(\eta_c(1S) \rightarrow p\bar{p})] = (1.8^{+0.3}_{-0.2}) \times 10^{-6}$ which we divide by our best value $B(\eta_c(1S) \rightarrow p\bar{p}) = (1.33 \pm 0.11) \times 10^{-3}$. Our first error is their experiment's error and our second error is the systematic error from using our best value.
- ⁶ AUBERT,B 04B reports $[\Gamma(B^+ \rightarrow \eta_c K^+)/\Gamma_{\text{total}}] \times [B(\eta_c(1S) \rightarrow K\bar{K}\pi)] = (0.074 \pm 0.005 \pm 0.007) \times 10^{-3}$ which we divide by our best value $B(\eta_c(1S) \rightarrow K\bar{K}\pi) = (7.1 \pm 0.4) \times 10^{-2}$. Our first error is their experiment's error and our second error is the systematic error from using our best value.
- ⁷ Assumes equal production of B^+ and B^0 at the $\Upsilon(4S)$.
- ⁸ EDWARDS 01 assumes equal production of B^0 and B^+ at the $\Upsilon(4S)$. The correlated uncertainties (28.3)% from $B(J/\psi(1S) \rightarrow \gamma\eta_c)$ in those modes have been accounted for.

$\Gamma(B^+ \rightarrow \eta_c K^+)/\Gamma_{\text{total}} \times \Gamma(\eta_c(1S) \rightarrow \gamma\gamma)/\Gamma_{\text{total}}$		$\Gamma_{254}/\Gamma \times \Gamma_{59}^{\eta_c(1S)}/\Gamma_{\eta_c(1S)}$		
VALUE (units 10^{-6})	CL%	DOCUMENT ID	TECN	COMMENT
0.22 ± 0.09 ± 0.04				
$0.22^{+0.09}_{-0.07} \pm 0.02$		WICHT 08	BELL	$e^+e^- \rightarrow \Upsilon(4S)$

- ¹ Assumes equal production of B^+ and B^0 at the $\Upsilon(4S)$.

$\Gamma(\eta_c K^*(892)^+)/\Gamma_{\text{total}}$		Γ_{255}/Γ		
VALUE (units 10^{-3})	CL%	DOCUMENT ID	TECN	COMMENT
1.2 ± 0.5 ± 0.1				
$1.2^{+0.5}_{-0.4} \pm 0.1$		AUBERT 07AV	BABR	$e^+e^- \rightarrow \Upsilon(4S)$

- ¹ AUBERT 07AV reports $[\Gamma(B^+ \rightarrow \eta_c K^*(892)^+)/\Gamma_{\text{total}}] \times [B(\eta_c(1S) \rightarrow p\bar{p})] = (1.57^{+0.56+0.45}_{-0.46-0.36}) \times 10^{-6}$ which we divide by our best value $B(\eta_c(1S) \rightarrow p\bar{p}) = (1.33 \pm 0.11) \times 10^{-3}$. Our first error is their experiment's error and our second error is the systematic error from using our best value.
- ² Assumes equal production of B^+ and B^0 at the $\Upsilon(4S)$.

$\Gamma(\eta_c K^+ \pi^+ \pi^-)/\Gamma_{\text{total}}$		Γ_{256}/Γ		
VALUE	CL%	DOCUMENT ID	TECN	COMMENT
$<3.9 \times 10^{-4}$	90	VINOKUROVA 15	BELL	$e^+e^- \rightarrow \Upsilon(4S)$

- ¹ ALBRECHT 93E reports $< 8.6 \times 10^{-3}$ from a measurement of $[\Gamma(B^+ \rightarrow D_s^- \pi^+ K^*(892)^+)/\Gamma_{\text{total}}] \times [B(D_s^+ \rightarrow \phi\pi^+)]$ assuming $B(D_s^+ \rightarrow \phi\pi^+) = 0.027$, which we rescale to our best value $B(D_s^+ \rightarrow \phi\pi^+) = 4.5 \times 10^{-2}$.

Meson Particle Listings

B^\pm

$\Gamma(\eta_c K^+ \omega(782))/\Gamma_{total}$				Γ_{257}/Γ
VALUE	CL%	DOCUMENT ID	TECN	COMMENT
$<3.3 \times 10^{-4}$	90	VINOKUROVA 15	BELL	$e^+e^- \rightarrow \Upsilon(4S)$

$\Gamma(\eta_c K^+ \eta)/\Gamma_{total}$				Γ_{258}/Γ
VALUE	CL%	DOCUMENT ID	TECN	COMMENT
$<2.2 \times 10^{-4}$	90	VINOKUROVA 15	BELL	$e^+e^- \rightarrow \Upsilon(4S)$

$\Gamma(\eta_c K^+ \pi^0)/\Gamma_{total}$				Γ_{259}/Γ
VALUE	CL%	DOCUMENT ID	TECN	COMMENT
$<6.2 \times 10^{-5}$	90	VINOKUROVA 15	BELL	$e^+e^- \rightarrow \Upsilon(4S)$

$\Gamma(\eta_c(2S) K^+)/\Gamma_{total}$				Γ_{260}/Γ
VALUE (units 10^{-7})	CL%	DOCUMENT ID	TECN	COMMENT
4.4 ± 1.0 OUR AVERAGE				
$3.5 \pm 1.7 \pm 0.5 \pm 0.1$		1,2 LEES 20c	BABR	$e^+e^- \rightarrow \Upsilon(4S)$
$4.8 \pm 1.1 \pm 0.3$		2 KATO 18	BELL	$e^+e^- \rightarrow \Upsilon(4S)$
• • • We do not use the following data for averages, fits, limits, etc. • • •				
$3.4 \pm 1.8 \pm 0.3$		2 AUBERT 06E	BABR	Repl. by LEES 20c
1 LEES 20c measurement's last uncertainty is due to the used $B(B^\pm \rightarrow K^\pm J/\psi)$ value.				
2 Measures absolute branching fractions using a missing-mass technique.				

$\Gamma(\eta_c(2S) K^+, \eta_c \rightarrow p\bar{p})/\Gamma_{total}$				Γ_{261}/Γ
VALUE (units 10^{-8})	CL%	DOCUMENT ID	TECN	COMMENT
$3.47 \pm 0.72 \pm 0.26$		1 AAIJ 17AD	LHCB	pp at 7 and 8 TeV
• • • We do not use the following data for averages, fits, limits, etc. • • •				
<10.6	95	2 AAIJ 13s	LHCB	Repl. by AAIJ 17AD

1 Measured relative to $B^+ \rightarrow J/\psi K^+$ decay with charmonia reconstructed in $p\bar{p}$ final state and using $B(B^+ \rightarrow J/\psi K^+) \times B(J/\psi \rightarrow p\bar{p}) = (2.17 \pm 0.08) \times 10^{-6}$. The last uncertainty includes the uncertainty of $B(B^+ \rightarrow J/\psi K^+) \times B(J/\psi \rightarrow p\bar{p})$.

2 Measured relative to $B^+ \rightarrow J/\psi K^+$ decay with charmonia reconstructed in $p\bar{p}$ final state and using $B(B^+ \rightarrow J/\psi K^+) = (1.013 \pm 0.034) \times 10^{-3}$ and $B(J/\psi \rightarrow p\bar{p}) = (2.17 \pm 0.07) \times 10^{-3}$.

$\Gamma(\eta_c(2S) K^+, \eta_c \rightarrow p\bar{p}\pi^+\pi^-)/\Gamma_{total}$				Γ_{263}/Γ
VALUE (units 10^{-7})	CL%	DOCUMENT ID	TECN	COMMENT
$11.2^{+1.8+0.5}_{-1.6-0.7}$		CHILIKIN 19	BELL	$e^+e^- \rightarrow \Upsilon(4S)$

$\Gamma(B^+ \rightarrow h_c(1P) K^+)/\Gamma_{total} \times \Gamma(h_c(1P) \rightarrow \gamma \eta_c(1S))/\Gamma_{total}$				$\Gamma_{368}/\Gamma \times \Gamma_{25}^{h_c(1P)}/\Gamma_{h_c(1P)}$
VALUE (units 10^{-4})	CL%	DOCUMENT ID	TECN	COMMENT
<0.48	90	1 AUBERT 08AB	BABR	$e^+e^- \rightarrow \Upsilon(4S)$
1 Uses the production ratio of $(B^+ B^-)/(B^0 \bar{B}^0) = 1.026 \pm 0.032$ at $\Upsilon(4S)$.				

$\Gamma(B^+ \rightarrow \eta_c(2S) K^+)/\Gamma_{total} \times \Gamma(\eta_c(2S) \rightarrow \gamma \gamma)/\Gamma_{total}$				$\Gamma_{260}/\Gamma \times \Gamma_{16}^{\eta_c(2S)}/\Gamma_{\eta_c(2S)}$
VALUE (units 10^{-6})	CL%	DOCUMENT ID	TECN	COMMENT
<0.18	90	1 WICHT 08	BELL	$e^+e^- \rightarrow \Upsilon(4S)$
1 Assumes equal production of B^+ and B^0 at the $\Upsilon(4S)$.				

$\Gamma(\eta_c(2S) K^+, \eta_c \rightarrow K_S^0 K^\mp \pi^\pm)/\Gamma_{total}$				Γ_{262}/Γ
VALUE (units 10^{-6})	CL%	DOCUMENT ID	TECN	COMMENT
$3.4^{+2.2+0.5}_{-1.5-0.4}$		1,2 VINOKUROVA 11	BELL	$e^+e^- \rightarrow \Upsilon(4S)$
1 Assumes equal production of B^0 and B^+ from Upsilon(4S) decays.				
2 The first uncertainty includes both statistical and interference effects while the second is due to systematics.				

$\Gamma(J/\psi(1S) K^+)/\Gamma_{total}$				Γ_{295}/Γ
VALUE (units 10^{-4})	CL%	DOCUMENT ID	TECN	COMMENT
10.20 ± 0.19 OUR FIT				
10.18 ± 0.20 OUR AVERAGE				
$10.32 \pm 0.07 \pm 0.24$		1 CHOUDHURY 21	BELL	$e^+e^- \rightarrow \Upsilon(4S)$
$9.4 \pm 0.7 \pm 0.8$		2 CHILIKIN 19	BELL	$e^+e^- \rightarrow \Upsilon(4S)$
$8.9 \pm 0.6 \pm 0.5$		3 KATO 18	BELL	$e^+e^- \rightarrow \Upsilon(4S)$
$8.1 \pm 1.3 \pm 0.7$		3 AUBERT 06E	BABR	$e^+e^- \rightarrow \Upsilon(4S)$
$10.61 \pm 0.15 \pm 0.48$		4 AUBERT 05J	BABR	$e^+e^- \rightarrow \Upsilon(4S)$
$10.4 \pm 1.1 \pm 0.1$		5 AUBERT,B 05L	BABR	$e^+e^- \rightarrow \Upsilon(4S)$
$10.2 \pm 0.8 \pm 0.7$		4 JESSOP 97	CLE2	$e^+e^- \rightarrow \Upsilon(4S)$
$9.24 \pm 3.04 \pm 0.05$		6 BORTOLETTO92	CLEO	$e^+e^- \rightarrow \Upsilon(4S)$
$8.09 \pm 3.50 \pm 0.04$	6	7 ALBRECHT 90J	ARG	$e^+e^- \rightarrow \Upsilon(4S)$
• • • We do not use the following data for averages, fits, limits, etc. • • •				
$10.1 \pm 0.2 \pm 0.7$		4 ABE 03B	BELL	Repl. by CHOUDHURY 21
$10.1 \pm 0.3 \pm 0.5$		4 AUBERT 02	BABR	Repl. by AUBERT 05J
$11.0 \pm 1.5 \pm 0.9$	59	4 ALAM 94	CLE2	Repl. by JESSOP 97
$22 \pm 10 \pm 2$		BUSKULIC 92G	ALEP	$e^+e^- \rightarrow Z$
7 ± 4	3	8 ALBRECHT 87D	ARG	$e^+e^- \rightarrow \Upsilon(4S)$
$10 \pm 7 \pm 2$	3	9 BEBEK 87	CLEO	$e^+e^- \rightarrow \Upsilon(4S)$
9 ± 5	3	10 ALAM 86	CLEO	$e^+e^- \rightarrow \Upsilon(4S)$

1 CHOUDHURY 21 uses the relative production fraction of charged (f^{\pm}) to neutral (f^0) B mesons at $\Upsilon(4S)$ value of $f^+/f^0 = 1.058 \pm 0.024$.

2 CHILIKIN 19 reports $[\Gamma(B^+ \rightarrow J/\psi(1S) K^+)/\Gamma_{total}] \times [B(J/\psi(1S) \rightarrow p\bar{p}\pi^+\pi^-)] = (56.4^{+3.3+2.7}_{-3.2-2.5}) \times 10^{-7}$ which we divide by our best value $B(J/\psi(1S) \rightarrow p\bar{p}\pi^+\pi^-) = (6.0 \pm 0.5) \times 10^{-3}$. Our first error is their experiment's error and our second error is the systematic error from using our best value.

3 Measures absolute branching fractions using a missing-mass technique.

4 Assumes equal production of B^+ and B^0 at the $\Upsilon(4S)$.

5 AUBERT,B 05L reports $[\Gamma(B^+ \rightarrow J/\psi(1S) K^+)/\Gamma_{total}] \times [B(J/\psi(1S) \rightarrow p\bar{p})] = (2.2 \pm 0.2 \pm 0.1) \times 10^{-6}$ which we divide by our best value $B(J/\psi(1S) \rightarrow p\bar{p}) = (2.120 \pm 0.029) \times 10^{-3}$. Our first error is their experiment's error and our second error is the systematic error from using our best value.

6 BORTOLETTO 92 reports $(8 \pm 2 \pm 2) \times 10^{-4}$ from a measurement of $[\Gamma(B^+ \rightarrow J/\psi(1S) K^+)/\Gamma_{total}] \times [B(J/\psi(1S) \rightarrow e^+e^-)]$ assuming $B(J/\psi(1S) \rightarrow e^+e^-) = 0.069 \pm 0.009$, which we rescale to our best value $B(J/\psi(1S) \rightarrow e^+e^-) = (5.971 \pm 0.032) \times 10^{-2}$. Our first error is their experiment's error and our second error is the systematic error from using our best value. Assumes equal production of B^+ and B^0 at the $\Upsilon(4S)$.

7 ALBRECHT 90J reports $(7 \pm 3 \pm 1) \times 10^{-4}$ from a measurement of $[\Gamma(B^+ \rightarrow J/\psi(1S) K^+)/\Gamma_{total}] \times [B(J/\psi(1S) \rightarrow e^+e^-)]$ assuming $B(J/\psi(1S) \rightarrow e^+e^-) = 0.069 \pm 0.009$, which we rescale to our best value $B(J/\psi(1S) \rightarrow e^+e^-) = (5.971 \pm 0.032) \times 10^{-2}$. Our first error is their experiment's error and our second error is the systematic error from using our best value. Assumes equal production of B^+ and B^0 at the $\Upsilon(4S)$.

8 ALBRECHT 87D assume $B^+ B^-/B^0 \bar{B}^0$ ratio is 55/45. Superseded by ALBRECHT 90J.

9 BEBEK 87 value has been updated in BERKELMAN 91 to use same assumptions as noted for BORTOLETTO 92.

10 ALAM 86 assumes B^\pm/B^0 ratio is 60/40.

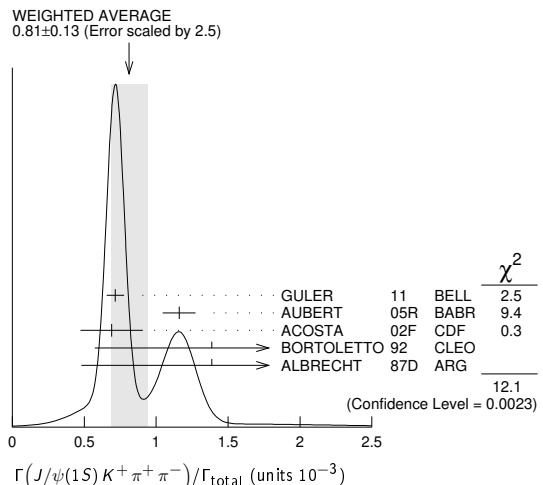
$\Gamma(\eta_c K^+)/\Gamma(J/\psi(1S) K^+)$				$\Gamma_{254}/\Gamma_{295}$
VALUE	CL%	DOCUMENT ID	TECN	COMMENT
0.94 ± 0.10 OUR AVERAGE				
$0.92 \pm 0.07 \pm 0.08$		1 AAIJ 13s	LHCB	pp at 7 TeV
$1.33 \pm 0.10 \pm 0.43$		2 AUBERT,B 04B	BABR	$e^+e^- \rightarrow \Upsilon(4S)$

1 AAIJ 13s reports $[\Gamma(B^+ \rightarrow \eta_c K^+)/\Gamma(B^+ \rightarrow J/\psi(1S) K^+)] \times [B(\eta_c(1S) \rightarrow p\bar{p})] / [B(J/\psi(1S) \rightarrow p\bar{p})] = 0.578 \pm 0.035 \pm 0.026$ which we multiply or divide by our best values $B(\eta_c(1S) \rightarrow p\bar{p}) = (1.33 \pm 0.11) \times 10^{-3}$, $B(J/\psi(1S) \rightarrow p\bar{p}) = (2.120 \pm 0.029) \times 10^{-3}$. Our first error is their experiment's error and our second error is the systematic error from using our best values.

2 Uses BABAR measurement of $B(B^+ \rightarrow J/\psi K^+) = (10.1 \pm 0.3 \pm 0.5) \times 10^{-4}$.

$\Gamma(B^+ \rightarrow J/\psi(1S) K^+)/\Gamma_{total} \times \Gamma(J/\psi(1S) \rightarrow \gamma \gamma)/\Gamma_{total}$				$\Gamma_{295}/\Gamma \times \Gamma_{373}^{J/\psi(1S)}/\Gamma_{J/\psi(1S)}$
VALUE (units 10^{-6})	CL%	DOCUMENT ID	TECN	COMMENT
<0.16	90	1 WICHT 08	BELL	$e^+e^- \rightarrow \Upsilon(4S)$
1 Assumes equal production of B^+ and B^0 at the $\Upsilon(4S)$.				

$\Gamma(J/\psi(1S) K^+ \pi^+ \pi^-)/\Gamma_{total}$				Γ_{297}/Γ	
VALUE (units 10^{-3})	CL%	EVTS	DOCUMENT ID	TECN	COMMENT
0.81 ± 0.13 OUR AVERAGE					Error includes scale factor of 2.5. See the ideogram below.
$0.716 \pm 0.010 \pm 0.060$			1 GULER 11	BELL	$e^+e^- \rightarrow \Upsilon(4S)$
$1.16 \pm 0.07 \pm 0.09$			1 AUBERT 05R	BABR	$e^+e^- \rightarrow \Upsilon(4S)$
$0.69 \pm 0.18 \pm 0.12$			2 ACOSTA 02F	CDF	$p\bar{p}$ 1.8 TeV
$1.39 \pm 0.81 \pm 0.01$			3 BORTOLETTO92	CLEO	$e^+e^- \rightarrow \Upsilon(4S)$
$1.39 \pm 0.91 \pm 0.01$		6	4 ALBRECHT 87D	ARG	$e^+e^- \rightarrow \Upsilon(4S)$
• • • We do not use the following data for averages, fits, limits, etc. • • •					
<1.8	90		5 ALBRECHT 90J	ARG	$e^+e^- \rightarrow \Upsilon(4S)$



1 Assumes equal production of B^+ and B^0 at the $\Upsilon(4S)$.

See key on page 1171

Meson Particle Listings

 B^\pm

² ACOSTA 02F uses as reference of $B(B \rightarrow J/\psi(1S) K^+) = (10.1 \pm 0.6) \times 10^{-4}$. The second error includes the systematic error and the uncertainties of the branching ratio.

³ BORTOLETTO 92 reports $(1.2 \pm 0.6 \pm 0.4) \times 10^{-3}$ from a measurement of $[\Gamma(B^+ \rightarrow J/\psi(1S) K^+ \pi^+ \pi^-)/\Gamma_{\text{total}}] \times [B(J/\psi(1S) \rightarrow e^+ e^-)]$ assuming $B(J/\psi(1S) \rightarrow e^+ e^-) = 0.069 \pm 0.009$, which we rescale to our best value $B(J/\psi(1S) \rightarrow e^+ e^-) = (5.971 \pm 0.032) \times 10^{-2}$. Our first error is their experiment's error and our second error is the systematic error from using our best value. Assumes equal production of B^+ and B^0 at the $\Upsilon(4S)$.

⁴ ALBRECHT 87D reports $(1.2 \pm 0.8) \times 10^{-3}$ from a measurement of $[\Gamma(B^+ \rightarrow J/\psi(1S) K^+ \pi^+ \pi^-)/\Gamma_{\text{total}}] \times [B(J/\psi(1S) \rightarrow e^+ e^-)]$ assuming $B(J/\psi(1S) \rightarrow e^+ e^-) = 0.069 \pm 0.009$, which we rescale to our best value $B(J/\psi(1S) \rightarrow e^+ e^-) = (5.971 \pm 0.032) \times 10^{-2}$. Our first error is their experiment's error and our second error is the systematic error from using our best value. They actually report 0.0011 ± 0.0007 assuming $B^+ B^-/B^0 \bar{B}^0$ ratio is 55/45. We rescale to 50/50. Analysis explicitly removes $B^+ \rightarrow \psi(2S) K^+$.

⁵ ALBRECHT 90I reports $< 1.6 \times 10^{-3}$ from a measurement of $[\Gamma(B^+ \rightarrow J/\psi(1S) K^+ \pi^+ \pi^-)/\Gamma_{\text{total}}] \times [B(J/\psi(1S) \rightarrow e^+ e^-)]$ assuming $B(J/\psi(1S) \rightarrow e^+ e^-) = 0.069$, which we rescale to our best value $B(J/\psi(1S) \rightarrow e^+ e^-) = (5.971 \pm 0.032) \times 10^{-2}$. Assumes equal production of B^+ and B^0 at the $\Upsilon(4S)$.

$\Gamma(J/\psi(1S) K^+ K^- K^+)/\Gamma_{\text{total}}$		Υ_{298}/Γ			
VALUE (units 10^{-6})	CL%	DOCUMENT ID	TECN	COMMENT	
$33.7 \pm 2.5 \pm 1.4$	90	LEES	15	BABR	$e^+ e^- \rightarrow \Upsilon(4S)$

$\Gamma(h_c(1P) K^+, h_c \rightarrow J/\psi \pi^+ \pi^-)/\Gamma_{\text{total}}$		Υ_{264}/Γ			
VALUE	CL%	DOCUMENT ID	TECN	COMMENT	
$< 3.4 \times 10^{-6}$	90	¹ AUBERT	05R	BABR	$e^+ e^- \rightarrow \Upsilon(4S)$

¹ Assumes equal production of B^+ and B^0 at the $\Upsilon(4S)$.

$\Gamma(X(3730)^0 K^+, X^0 \rightarrow \eta_c \eta)/\Gamma_{\text{total}}$		Υ_{265}/Γ			
VALUE	CL%	DOCUMENT ID	TECN	COMMENT	
$< 4.6 \times 10^{-5}$	90	VINOKUROVA	15	BELL	$e^+ e^- \rightarrow \Upsilon(4S)$

$\Gamma(X(3730)^0 K^+, X^0 \rightarrow \eta_c \pi^0)/\Gamma_{\text{total}}$		Υ_{266}/Γ			
VALUE	CL%	DOCUMENT ID	TECN	COMMENT	
$< 5.7 \times 10^{-6}$	90	VINOKUROVA	15	BELL	$e^+ e^- \rightarrow \Upsilon(4S)$

$\Gamma(\eta_{c2}(1D) K^+, \eta_{c2} \rightarrow h_c \gamma)/\Gamma_{\text{total}}$		Υ_{267}/Γ			
VALUE	CL%	DOCUMENT ID	TECN	COMMENT	
$< 3.7 \times 10^{-5}$	90	CHILIKIN	20	BELL	$e^+ e^- \rightarrow \Upsilon(4S)$

$\Gamma(\eta_{c2}(1D) \pi^+ K_S^0, \eta_{c2} \rightarrow h_c \gamma)/\Gamma_{\text{total}}$		Υ_{268}/Γ			
VALUE	CL%	DOCUMENT ID	TECN	COMMENT	
$< 1.1 \times 10^{-4}$	90	CHILIKIN	20	BELL	$e^+ e^- \rightarrow \Upsilon(4S)$

$\Gamma(\psi_2(3823) K^+, \psi_2 \rightarrow J/\psi \pi^+ \pi^-)/\Gamma_{\text{total}}$		Υ_{269}/Γ			
VALUE (units 10^{-7})	CL%	DOCUMENT ID	TECN	COMMENT	
$2.82 \pm 0.54 \pm 0.13$	90	¹ AAIJ	20S	LHCB	pp at 7, 8, 13 TeV

¹ The first error is statistic; the second error is the total systematic error.

$\Gamma(\psi_2(3823) K^+, \psi_2 \rightarrow J/\psi \eta)/\Gamma_{\text{total}}$		Υ_{270}/Γ			
VALUE (units 10^{-6})	CL%	DOCUMENT ID	TECN	COMMENT	
$1.25^{+0.71}_{-0.53} \pm 0.04$	90	AAIJ	22D	LHCB	pp at 7, 8, 13 TeV

$\Gamma(\psi_3(3842) K^+, \psi_3 \rightarrow J/\psi \eta)/\Gamma_{\text{total}}$		Υ_{271}/Γ			
VALUE	CL%	DOCUMENT ID	TECN	COMMENT	
$< 6.1 \times 10^{-7}$	90	AAIJ	22D	LHCB	pp at 7, 8, 13 TeV

$\Gamma(\chi_{c1}(3872) K^+)/\Gamma_{\text{total}}$		Υ_{272}/Γ			
VALUE (units 10^{-4})	CL%	DOCUMENT ID	TECN	COMMENT	
2.3 ± 0.6 OUR AVERAGE					
$2.9^{+0.7}_{-0.6} \pm 1.0$	90	¹ HIRATA	23	BELL	$e^+ e^- \rightarrow \Upsilon(4S)$
$2.1 \pm 0.6 \pm 0.3 \pm 0.1$	90	^{2,3} LEES	20C	BABR	$e^+ e^- \rightarrow \Upsilon(4S)$
< 2.6	90	² KATO	18	BELL	$e^+ e^- \rightarrow \Upsilon(4S)$
$2.9 \pm 0.8^{+0.7}_{-0.8}$	90	^{4,5} AUBERT	06	BABR	Repl. by AUBERT 08Y
< 3.2	90	² AUBERT	06E	BABR	$e^+ e^- \rightarrow \Upsilon(4S)$
$3.6 \pm 1.2^{+0.9}_{-1.0}$	90	^{4,6} AUBERT	05R	BABR	Repl. by AUBERT 06
$3.9 \pm 0.9 \pm 1.0$	90	⁷ CHOI	03	BELL	Repl. by CHOI 11

¹ HIRATA 23 reports $[\Gamma(B^+ \rightarrow \chi_{c1}(3872) K^+)/\Gamma_{\text{total}}] \times [B(\chi_{c1}(3872) \rightarrow \bar{D}^{*0} D^0)] = (0.97^{+0.21}_{-0.18} \pm 0.10) \times 10^{-4}$ which we divide by our best value $B(\chi_{c1}(3872) \rightarrow \bar{D}^{*0} D^0) = (34 \pm 12) \times 10^{-2}$. Our first error is their experiment's error and our second error is the systematic error from using our best value.

² Measures absolute branching fractions using a missing-mass technique.

³ LEES 20C measurement's last uncertainty is due to the used $B(B^{\pm} \rightarrow K^{\pm} J/\psi)$ value.

⁴ Assumes equal production of B^+ and B^0 at the $\Upsilon(4S)$.

⁵ AUBERT 06 reports $[\Gamma(B^+ \rightarrow \chi_{c1}(3872) K^+)/\Gamma_{\text{total}}] \times [B(\chi_{c1}(3872) \rightarrow \pi^+ \pi^- J/\psi(1S))] = (10.1 \pm 2.5 \pm 1.0) \times 10^{-6}$ which we divide by our best value

$B(\chi_{c1}(3872) \rightarrow \pi^+ \pi^- J/\psi(1S)) = (3.5 \pm 0.9) \times 10^{-2}$. Our first error is their experiment's error and our second error is the systematic error from using our best value.

⁶ AUBERT 05R reports $[\Gamma(B^+ \rightarrow \chi_{c1}(3872) K^+)/\Gamma_{\text{total}}] \times [B(\chi_{c1}(3872) \rightarrow \pi^+ \pi^- J/\psi(1S))] = (12.8 \pm 4.1) \times 10^{-6}$ which we divide by our best value $B(\chi_{c1}(3872) \rightarrow \pi^+ \pi^- J/\psi(1S)) = (3.5 \pm 0.9) \times 10^{-2}$. Our first error is their experiment's error and our second error is the systematic error from using our best value.

⁷ CHOI 03 reports $[\Gamma(B^+ \rightarrow \chi_{c1}(3872) K^+)/\Gamma_{\text{total}}] \times [B(\chi_{c1}(3872) \rightarrow \pi^+ \pi^- J/\psi(1S))] = (13.6 \pm 3.0 \pm 0.5) \times 10^{-6}$ which we divide by our best value $B(\chi_{c1}(3872) \rightarrow \pi^+ \pi^- J/\psi(1S)) = (3.5 \pm 0.9) \times 10^{-2}$. Our first error is their experiment's error and our second error is the systematic error from using our best value.

$\Gamma(\chi_{c0}(3915) K^+)/\Gamma_{\text{total}}$		Υ_{273}/Γ			
VALUE	CL%	DOCUMENT ID	TECN	COMMENT	
$< 2.8 \times 10^{-4}$	90	¹ KATO	18	BELL	$e^+ e^- \rightarrow \Upsilon(4S)$

¹ Measures absolute branching fractions using a missing-mass technique.

$\Gamma(\chi_{c0}(3915) K^+, \chi_{c0} \rightarrow D^+ D^-)/\Gamma(D^- D^+ K^+)$		$\Upsilon_{274}/\Gamma_{221}$			
VALUE (units 10^{-2})	CL%	DOCUMENT ID	TECN	COMMENT	
$3.7 \pm 0.9 \pm 0.2$	90	¹ AAIJ	20A1	LHCB	pp at 7, 8, 13 TeV

¹ Measured in Dalitz plot analysis of $B^+ \rightarrow D^- D^+ K^+$ decays.

$\Gamma(\chi_{c0}(3915) K^+, \chi_{c0} \rightarrow \eta_c \eta)/\Gamma_{\text{total}}$		Υ_{275}/Γ			
VALUE	CL%	DOCUMENT ID	TECN	COMMENT	
$< 4.7 \times 10^{-5}$	90	¹ VINOKUROVA	15	BELL	$e^+ e^- \rightarrow \Upsilon(4S)$

¹ Upper limit is corrected in the Erratum.

$\Gamma(\chi_{c0}(3915) K^+, \chi_{c0} \rightarrow \eta_c \pi^0)/\Gamma_{\text{total}}$		Υ_{276}/Γ			
VALUE	CL%	DOCUMENT ID	TECN	COMMENT	
$< 1.7 \times 10^{-5}$	90	¹ VINOKUROVA	15	BELL	$e^+ e^- \rightarrow \Upsilon(4S)$

¹ Upper limit is corrected in the Erratum.

$\Gamma(X(4014)^0 K^+, X^0 \rightarrow \eta_c \eta)/\Gamma_{\text{total}}$		Υ_{277}/Γ			
VALUE	CL%	DOCUMENT ID	TECN	COMMENT	
$< 3.9 \times 10^{-5}$	90	VINOKUROVA	15	BELL	$e^+ e^- \rightarrow \Upsilon(4S)$

$\Gamma(X(4014)^0 K^+, X^0 \rightarrow \eta_c \pi^0)/\Gamma_{\text{total}}$		Υ_{278}/Γ			
VALUE	CL%	DOCUMENT ID	TECN	COMMENT	
$< 1.2 \times 10^{-5}$	90	VINOKUROVA	15	BELL	$e^+ e^- \rightarrow \Upsilon(4S)$

$\Gamma(T_{c\bar{c}1}(3900)^0 K^+, T_{c\bar{c}1}^0 \rightarrow \eta_c \pi^+ \pi^-)/\Gamma_{\text{total}}$		Υ_{279}/Γ			
VALUE	CL%	DOCUMENT ID	TECN	COMMENT	
$< 4.7 \times 10^{-5}$	90	VINOKUROVA	15	BELL	$e^+ e^- \rightarrow \Upsilon(4S)$

$\Gamma(T_{c\bar{c}1}(3900)^0 K^+, T_{c\bar{c}1}^0 \rightarrow J/\psi \eta)/\Gamma_{\text{total}}$		Υ_{280}/Γ			
VALUE	CL%	DOCUMENT ID	TECN	COMMENT	
$< 4.3 \times 10^{-7}$	90	AAIJ	22D	LHCB	pp at 7, 8, 13 TeV

$\Gamma(T_{c\bar{c}1}(4020)^0 K^+, T_{c\bar{c}1}^0 \rightarrow \eta_c \pi^+ \pi^-)/\Gamma_{\text{total}}$		Υ_{281}/Γ			
VALUE	CL%	DOCUMENT ID	TECN	COMMENT	
$< 1.6 \times 10^{-5}$	90	VINOKUROVA	15	BELL	$e^+ e^- \rightarrow \Upsilon(4S)$

$\Gamma(\chi_{c1}(3872) K^*(892)^+)/\Gamma_{\text{total}}$		Υ_{282}/Γ			
VALUE	CL%	DOCUMENT ID	TECN	COMMENT	
$< 6 \times 10^{-4}$	90	^{1,2} AUBERT	09B	BABR	$e^+ e^- \rightarrow \Upsilon(4S)$

••• We do not use the following data for averages, fits, limits, etc. •••

¹ AUBERT 09B reports $[\Gamma(B^+ \rightarrow \chi_{c1}(3872) K^*(892)^+)/\Gamma_{\text{total}}] \times [B(\chi_{c1}(3872) \rightarrow \gamma J/\psi)] < 4.8 \times 10^{-6}$ which we divide by our best value $B(\chi_{c1}(3872) \rightarrow \gamma J/\psi) = 7.8 \times 10^{-3}$.

² Uses $B(\Upsilon(4S) \rightarrow B^+ B^-) = (51.6 \pm 0.6)\%$ and $B(\Upsilon(4S) \rightarrow B^0 \bar{B}^0) = (48.4 \pm 0.6)\%$.

³ AUBERT 09B reports $[\Gamma(B^+ \rightarrow \chi_{c1}(3872) K^*(892)^+)/\Gamma_{\text{total}}] \times [B(\chi_{c1}(3872) \rightarrow \gamma \psi(2S))] < 28 \times 10^{-6}$ which we divide by our best value $B(\chi_{c1}(3872) \rightarrow \gamma \psi(2S)) = 0 \times 10^{-2}$.

$\Gamma(\chi_{c1}(3872)^+ K^0, \chi_{c1}^+ \rightarrow J/\psi(1S) \pi^+ \pi^0)/\Gamma_{\text{total}}$		Υ_{283}/Γ			
VALUE (units 10^{-6})	CL%	DOCUMENT ID	TECN	COMMENT	
< 6.1	90	^{1,2} CHOI	11	BELL	$e^+ e^- \rightarrow \Upsilon(4S)$

••• We do not use the following data for averages, fits, limits, etc. •••

¹ Assumes $\pi^+ \pi^0$ originates from ρ^+ .

² Assumes equal production of B^+ and B^0 at the $\Upsilon(4S)$.

³ Assumes equal production of B^+ and B^0 at the $\Upsilon(4S)$. The isovector-X hypothesis is excluded with a likelihood test at 1×10^{-4} level.

$\Gamma(\chi_{c1}(3872) K^0 \pi^+)/\Gamma_{\text{total}}$		Υ_{284}/Γ			
VALUE (units 10^{-4})	CL%	DOCUMENT ID	TECN	COMMENT	
$3.0 \pm 0.9 \pm 0.8$	90	¹ BALA	15	BELL	$e^+ e^- \rightarrow \Upsilon(4S)$

¹ BALA 15 reports $[\Gamma(B^+ \rightarrow \chi_{c1}(3872) K^0 \pi^+)/\Gamma_{\text{total}}] \times [B(\chi_{c1}(3872) \rightarrow \pi^+ \pi^- J/\psi(1S))] = (10.6 \pm 3.0 \pm 0.9) \times 10^{-6}$ which we divide by our best value $B(\chi_{c1}(3872) \rightarrow \pi^+ \pi^- J/\psi(1S)) = (3.5 \pm 0.9) \times 10^{-2}$. Our first error is their experiment's error and our second error is the systematic error from using our best value.

Meson Particle Listings

 B^\pm $\Gamma(T_{c\bar{c}1}(4430)^+ K^0, T_{c\bar{c}1}^+ \rightarrow J/\psi \pi^+)/\Gamma_{\text{total}}$ Γ_{285}/Γ

VALUE (units 10^{-5})	CL%	DOCUMENT ID	TECN	COMMENT
<1.5	95	¹ AUBERT 09AA BABR		$e^+e^- \rightarrow \Upsilon(4S)$

¹ Assumes equal production of B^+ and B^0 at the $\Upsilon(4S)$. $\Gamma(T_{c\bar{c}1}(4430)^+ K^0, T_{c\bar{c}1}^+ \rightarrow \psi(2S) \pi^+)/\Gamma_{\text{total}}$ Γ_{286}/Γ

VALUE (units 10^{-5})	CL%	DOCUMENT ID	TECN	COMMENT
<4.7	95	¹ AUBERT 09AA BABR		$e^+e^- \rightarrow \Upsilon(4S)$

¹ Assumes equal production of B^+ and B^0 at the $\Upsilon(4S)$. $\Gamma(T_{c\bar{c}1}(4430)^0 K^+, T_{c\bar{c}1}^0 \rightarrow J/\psi \eta)/\Gamma_{\text{total}}$ Γ_{287}/Γ

VALUE	CL%	DOCUMENT ID	TECN	COMMENT
<12.7 $\times 10^{-7}$	90	AAIJ 22D LHCb		pp at 7, 8, 13 TeV

 $\Gamma(\psi(4230)^0 K^+, \psi^0 \rightarrow J/\psi \pi^+ \pi^-)/\Gamma_{\text{total}}$ Γ_{288}/Γ

VALUE (units 10^{-6})	CL%	DOCUMENT ID	TECN	COMMENT
<15.6	95	^{1,2} GARG 19 BELL		$e^+e^- \rightarrow \Upsilon(4S)$

••• We do not use the following data for averages, fits, limits, etc. •••

<29 95 ²AUBERT 06 BABR $e^+e^- \rightarrow \Upsilon(4S)$ ¹ Corresponds to a 90% CL upper limit of $< 14 \times 10^{-6}$.² Assumes equal production of B^+ and B^0 at the $\Upsilon(4S)$. $\Gamma(\psi(4230) K^+, \psi \rightarrow J/\psi \eta)/\Gamma_{\text{total}}$ Γ_{289}/Γ

VALUE	CL%	DOCUMENT ID	TECN	COMMENT
<3.9 $\times 10^{-7}$	90	AAIJ 22D LHCb		pp at 7, 8, 13 TeV

 $\Gamma(\psi(4360) K^+, \psi \rightarrow J/\psi \eta)/\Gamma_{\text{total}}$ Γ_{290}/Γ

VALUE	CL%	DOCUMENT ID	TECN	COMMENT
<12.4 $\times 10^{-7}$	90	AAIJ 22D LHCb		pp at 7, 8, 13 TeV

 $\Gamma(\psi(4390) K^+, \psi \rightarrow J/\psi \eta)/\Gamma_{\text{total}}$ Γ_{291}/Γ

VALUE	CL%	DOCUMENT ID	TECN	COMMENT
<24.1 $\times 10^{-7}$	90	AAIJ 22D LHCb		pp at 7, 8, 13 TeV

 $\Gamma(\chi_{c0}(3915) K^+, \chi_{c0} \rightarrow J/\psi \gamma)/\Gamma_{\text{total}}$ Γ_{292}/Γ

VALUE (units 10^{-6})	CL%	DOCUMENT ID	TECN	COMMENT
<14	90	¹ AUBERT, BE 06M BABR		$e^+e^- \rightarrow \Upsilon(4S)$

¹ Assumes equal production of B^+ and B^0 at the $\Upsilon(4S)$. $\Gamma(\chi_{c0}(3915) K^+, \chi_{c0} \rightarrow \chi_{c1}(1P) \pi^0)/\Gamma_{\text{total}}$ Γ_{293}/Γ

VALUE	CL%	DOCUMENT ID	TECN	COMMENT
<3.8 $\times 10^{-5}$	90	¹ BHARDWAJ 19 BELL		$e^+e^- \rightarrow \Upsilon(4S)$

¹ Assumes equal production of B^+ and B^0 at the $\Upsilon(4S)$. $\Gamma(\chi(3930)^0 K^+, \chi^0 \rightarrow J/\psi \gamma)/\Gamma_{\text{total}}$ Γ_{294}/Γ

VALUE (units 10^{-6})	CL%	DOCUMENT ID	TECN	COMMENT
<2.5	90	¹ AUBERT, BE 06M BABR		$e^+e^- \rightarrow \Upsilon(4S)$

¹ Assumes equal production of B^+ and B^0 at the $\Upsilon(4S)$. $\Gamma(J/\psi(1S) K^0 \pi^+)/\Gamma_{\text{total}}$ Γ_{296}/Γ

VALUE (units 10^{-3})	DOCUMENT ID	TECN	COMMENT
1.101 ± 0.021	¹ AUBERT 09AA BABR		$e^+e^- \rightarrow \Upsilon(4S)$

••• We do not use the following data for averages, fits, limits, etc. •••

¹ Does not report systematic uncertainties. $\Gamma(J/\psi(1S) K^*(892)^+)/\Gamma_{\text{total}}$ Γ_{300}/Γ For polarization information see the Listings at the end of the " B^0 Branching Ratios" section.

VALUE (units 10^{-3})	EVTS	DOCUMENT ID	TECN	COMMENT
1.43 ± 0.08 OUR FIT				
1.43 ± 0.08 OUR AVERAGE				

1.78 $\pm 0.36_{-0.32} \pm 0.02$ ^{1,2}AUBERT 07AV BABR $e^+e^- \rightarrow \Upsilon(4S)$ 1.454 $\pm 0.047 \pm 0.097$ ²AUBERT 05J BABR $e^+e^- \rightarrow \Upsilon(4S)$ 1.28 $\pm 0.07 \pm 0.14$ ²ABE 02N BELL $e^+e^- \rightarrow \Upsilon(4S)$ 1.41 $\pm 0.23 \pm 0.24$ ²JESSOP 97 CLE2 $e^+e^- \rightarrow \Upsilon(4S)$ 1.58 $\pm 0.47 \pm 0.27$ ³ABE 96H CDF $p\bar{p}$ at 1.8 TeV1.50 $\pm 1.08 \pm 0.01$ ⁴BORTOLETTO92 CLEO $e^+e^- \rightarrow \Upsilon(4S)$ 1.85 $\pm 1.30 \pm 0.01$ ²ALBRECHT 90J ARG $e^+e^- \rightarrow \Upsilon(4S)$

••• We do not use the following data for averages, fits, limits, etc. •••

1.37 $\pm 0.09 \pm 0.11$ ²AUBERT 02 BABR Repl. by AUBERT 05J1.78 $\pm 0.51 \pm 0.23$ ²ALAM 94 CLE2 Sup. by JESSOP 97¹ AUBERT 07AV reports $[\Gamma(B^+ \rightarrow J/\psi(1S) K^*(892)^+)/\Gamma_{\text{total}}] \times [B(J/\psi(1S) \rightarrow p\bar{p})] = (3.78^{+0.72+0.28}_{-0.64-0.23}) \times 10^{-6}$ which we divide by our best value $B(J/\psi(1S) \rightarrow p\bar{p}) = (2.120 \pm 0.029) \times 10^{-3}$. Our first error is their experiment's error and our second error is the systematic error from using our best value.² Assumes equal production of B^+ and B^0 at the $\Upsilon(4S)$.³ ABE 96H assumes that $B(B^+ \rightarrow J/\psi K^+) = (1.02 \pm 0.14) \times 10^{-3}$.⁴ BORTOLETTO 92 reports $(1.3 \pm 0.9 \pm 0.3) \times 10^{-3}$ from a measurement of $[\Gamma(B^+ \rightarrow J/\psi(1S) K^*(892)^+)/\Gamma_{\text{total}}] \times [B(J/\psi(1S) \rightarrow e^+e^-)]$ assuming $B(J/\psi(1S) \rightarrow$ $e^+e^-) = 0.069 \pm 0.009$, which we rescale to our best value $B(J/\psi(1S) \rightarrow e^+e^-) = (5.971 \pm 0.032) \times 10^{-2}$. Our first error is their experiment's error and our second error is the systematic error from using our best value. Assumes equal production of B^+ and B^0 at the $\Upsilon(4S)$.⁵ ALBRECHT 90J reports $(1.6 \pm 1.1 \pm 0.3) \times 10^{-3}$ from a measurement of $[\Gamma(B^+ \rightarrow J/\psi(1S) K^*(892)^+)/\Gamma_{\text{total}}] \times [B(J/\psi(1S) \rightarrow e^+e^-)]$ assuming $B(J/\psi(1S) \rightarrow e^+e^-) = 0.069 \pm 0.009$, which we rescale to our best value $B(J/\psi(1S) \rightarrow e^+e^-) = (5.971 \pm 0.032) \times 10^{-2}$. Our first error is their experiment's error and our second error is the systematic error from using our best value. Assumes equal production of B^+ and B^0 at the $\Upsilon(4S)$. $\Gamma(J/\psi(1S) K^*(892)^+)/\Gamma(J/\psi(1S) K^+)$ $\Gamma_{300}/\Gamma_{295}$

VALUE	DOCUMENT ID	TECN	COMMENT
1.39 ± 0.09 OUR AVERAGE			

1.37 $\pm 0.05 \pm 0.08$ AUBERT 05J BABR $e^+e^- \rightarrow \Upsilon(4S)$ 1.45 $\pm 0.20 \pm 0.17$ ¹JESSOP 97 CLE2 $e^+e^- \rightarrow \Upsilon(4S)$ 1.92 $\pm 0.60 \pm 0.17$ ABE 96Q CDF $p\bar{p}$

••• We do not use the following data for averages, fits, limits, etc. •••

1.37 $\pm 0.10 \pm 0.08$ ²AUBERT 02 BABR Repl. by AUBERT 05J¹ JESSOP 97 assumes equal production of B^+ and B^0 at the $\Upsilon(4S)$. The measurement is actually measured as an average over kaon charged and neutral states.² Assumes equal production of B^+ and B^0 at the $\Upsilon(4S)$. $\Gamma(J/\psi(1S) K(1270)^+)/\Gamma_{\text{total}}$ Γ_{301}/Γ

VALUE (units 10^{-3})	DOCUMENT ID	TECN	COMMENT
1.80 $\pm 0.34 \pm 0.39$	¹ ABE 01L BELL		$e^+e^- \rightarrow \Upsilon(4S)$

¹ Uses the PDG value of $B(B^+ \rightarrow J/\psi(1S) K^+) = (1.00 \pm 0.10) \times 10^{-3}$. $\Gamma(J/\psi(1S) K(1400)^+)/\Gamma(J/\psi(1S) K(1270)^+)$ $\Gamma_{302}/\Gamma_{301}$

VALUE	CL%	DOCUMENT ID	TECN	COMMENT
<0.30	90	ABE 01L BELL		$e^+e^- \rightarrow \Upsilon(4S)$

 $\Gamma(J/\psi(1S) \eta K^+)/\Gamma_{\text{total}}$ Γ_{303}/Γ

VALUE (units 10^{-5})	DOCUMENT ID	TECN	COMMENT
12.4 ± 1.4 OUR AVERAGE			

12.7 $\pm 1.1 \pm 1.1$ ¹IWASHITA 14 BELL $e^+e^- \rightarrow \Upsilon(4S)$ 10.8 $\pm 2.3 \pm 2.4$ ¹AUBERT 04Y BABR $e^+e^- \rightarrow \Upsilon(4S)$ ¹ Assumes equal production of B^+ and B^0 at the $\Upsilon(4S)$. $\Gamma(\chi_{c1-odd}(3872) K^+, \chi_{c1-odd} \rightarrow J/\psi \eta)/\Gamma_{\text{total}}$ Γ_{304}/Γ

VALUE	CL%	DOCUMENT ID	TECN	COMMENT
<3.8 $\times 10^{-6}$	90	IWASHITA 14 BELL		$e^+e^- \rightarrow \Upsilon(4S)$

 $\Gamma(\psi(4160) K^+, \psi \rightarrow J/\psi \eta)/\Gamma_{\text{total}}$ Γ_{305}/Γ

VALUE	CL%	DOCUMENT ID	TECN	COMMENT
<8.7 $\times 10^{-7}$	90	AAIJ 22D LHCb		pp at 7, 8, 13 TeV

••• We do not use the following data for averages, fits, limits, etc. •••

<7.4 $\times 10^{-6}$ 90 IWASHITA 14 BELL $e^+e^- \rightarrow \Upsilon(4S)$ $\Gamma(J/\psi(1S) \eta' K^+)/\Gamma_{\text{total}}$ Γ_{306}/Γ

VALUE (units 10^{-5})	CL%	DOCUMENT ID	TECN	COMMENT
<8.8	90	¹ XIE 07 BELL		$e^+e^- \rightarrow \Upsilon(4S)$

¹ Assumes equal production of B^+ and B^0 at the $\Upsilon(4S)$. $\Gamma(J/\psi(1S) \eta' K^+)/\Gamma(\psi(2S) K^+)$ $\Gamma_{306}/\Gamma_{330}$

VALUE (units 10^{-2})	DOCUMENT ID	TECN	COMMENT
4.91 $\pm 0.47 \pm 0.30$	¹ AAIJ 23AK LHCb		pp at 7, 8 and 13 TeV

¹ AAIJ 23AK measurements last uncertainty includes ± 0.07 uncertainties on the branching fractions of the intermediate resonances. $\Gamma(J/\psi(1S) \phi K^+)/\Gamma_{\text{total}}$ Γ_{307}/Γ

VALUE (units 10^{-5})	DOCUMENT ID	TECN	COMMENT
5.0 ± 0.4 OUR AVERAGE			

5.00 $\pm 0.37 \pm 0.15$ LEES 15 BABR $e^+e^- \rightarrow \Upsilon(4S)$ 4.4 $\pm 1.4 \pm 0.5$ ¹AUBERT 03O BABR $e^+e^- \rightarrow \Upsilon(4S)$ 8.8 $\pm 3.5_{-3.0} \pm 1.3$ ²ANASTASSOV 00 CLE2 $e^+e^- \rightarrow \Upsilon(4S)$ ¹ Assumes equal production of B^+ and B^0 at the $\Upsilon(4S)$.² ANASTASSOV 00 finds 10 events on a background of 0.5 ± 0.2 . Assumes equal production of B^0 and B^+ at the $\Upsilon(4S)$, a uniform Dalitz plot distribution, isotropic $J/\psi(1S)$ and ϕ decays, and $B(B^+ \rightarrow J/\psi(1S) \phi K^+) = B(B^0 \rightarrow J/\psi(1S) \phi K^0)$. $\Gamma(J/\psi(1S) K_1(1650), K_1 \rightarrow \phi K^+)/\Gamma(J/\psi(1S) \phi K^+)$ $\Gamma_{308}/\Gamma_{307}$

VALUE	DOCUMENT ID	TECN	COMMENT
0.12 $\pm 0.10 \pm 0.17_{-0.06}$	¹ AAIJ 17 LHCb		pp at 7, 8 TeV

¹ Measured in amplitude analysis of $B^+ \rightarrow J/\psi(1S) \phi K^+$. $\Gamma(J/\psi(1S) K^*(1680)^+, K^* \rightarrow \phi K^+)/\Gamma(J/\psi(1S) \phi K^+)$ $\Gamma_{309}/\Gamma_{307}$

VALUE (units 10^{-2})	DOCUMENT ID	TECN	COMMENT
6.7 $\pm 1.9 \pm 3.2_{-3.9}$	¹ AAIJ 17 LHCb		pp at 7, 8 TeV

¹ Measured in amplitude analysis of $B^+ \rightarrow J/\psi(1S) \phi K^+$.

$\Gamma(J/\psi(1S)K_2^*(1980), K_2^* \rightarrow \phi K^+)/\Gamma(J/\psi(1S)\phi K^+)$ $\Gamma_{310}/\Gamma_{307}$

VALUE (units 10^{-2})	DOCUMENT ID	TECN	COMMENT
$2.9 \pm 0.8^{+1.7}_{-0.7}$	¹ AAIJ	17	LHCB pp at 7, 8 TeV

¹ Measured in amplitude analysis of $B^+ \rightarrow J/\psi(1S)\phi K^+$.

$\Gamma(J/\psi(1S)K(1830)^+, K(1830)^+ \rightarrow \phi K^+)/\Gamma(J/\psi(1S)\phi K^+)$ $\Gamma_{311}/\Gamma_{307}$

VALUE (units 10^{-2})	DOCUMENT ID	TECN	COMMENT
$2.6 \pm 1.1^{+2.3}_{-1.8}$	¹ AAIJ	17	LHCB pp at 7, 8 TeV

¹ Measured in amplitude analysis of $B^+ \rightarrow J/\psi(1S)\phi K^+$.

$\Gamma(\chi_{c1}(4140)K^+, \chi_{c1} \rightarrow J/\psi(1S)\phi)/\Gamma(J/\psi(1S)\phi K^+)$ $\Gamma_{312}/\Gamma_{307}$

VALUE	CL%	DOCUMENT ID	TECN	COMMENT
0.19 ± 0.08 OUR AVERAGE				
0.13 ± 0.032 ^{+4.8} _{-2.0}		¹ AAIJ	17	LHCB pp at 7, 8 TeV
0.19 ± 0.07 ± 0.04		² ABAZOV	14A	D0 $p\bar{p}$ at 1.96 TeV
••• We do not use the following data for averages, fits, limits, etc. •••				
<0.133	90	LEES	15	BABR $e^+e^- \rightarrow \Upsilon(4S)$
<0.07	90	³ AAIJ	12AA	LHCB pp at 7 TeV

¹ Measured in amplitude analysis of $B^+ \rightarrow J/\psi(1S)\phi K^+$.

² Reported a threshold enhancement in the $J/\psi\phi$ mass distribution consistent with the $\chi_{c1}(4140)$ state with a statistical significance of 3.1 standard deviations.

³ Branching fractions are normalized to 382 ± 22 events of $B^+ \rightarrow J/\psi\phi K^+$.

$\Gamma(\chi_{c1}(4274)K^+, \chi_{c1} \rightarrow J/\psi(1S)\phi)/\Gamma(J/\psi(1S)\phi K^+)$ $\Gamma_{313}/\Gamma_{307}$

VALUE (units 10^{-2})	CL%	DOCUMENT ID	TECN	COMMENT
7.1 ± 2.5^{+3.5}_{-2.4}		¹ AAIJ	17	LHCB pp at 7, 8 TeV
••• We do not use the following data for averages, fits, limits, etc. •••				
<18.1	90	LEES	15	BABR $e^+e^- \rightarrow \Upsilon(4S)$
< 8	90	² AAIJ	12AA	LHCB Repl. by AAJ17

¹ Measured in amplitude analysis of $B^+ \rightarrow J/\psi(1S)\phi K^+$.

² Branching fractions are normalized to 382 ± 22 events of $B^+ \rightarrow J/\psi\phi K^+$.

$\Gamma(\chi_{c0}(4500)K^+, \chi_{c0} \rightarrow J/\psi(1S)\phi)/\Gamma(J/\psi(1S)\phi K^+)$ $\Gamma_{314}/\Gamma_{307}$

VALUE (units 10^{-2})	DOCUMENT ID	TECN	COMMENT
$6.6 \pm 2.4^{+3.5}_{-2.3}$	¹ AAIJ	17	LHCB pp at 7, 8 TeV

¹ Measured in amplitude analysis of $B^+ \rightarrow J/\psi(1S)\phi K^+$.

$\Gamma(\chi_{c0}(4700)K^+, \chi_{c0} \rightarrow J/\psi(1S)\phi)/\Gamma(J/\psi(1S)\phi K^+)$ $\Gamma_{315}/\Gamma_{307}$

VALUE	DOCUMENT ID	TECN	COMMENT
$0.12 \pm 0.05^{+0.09}_{-0.05}$	¹ AAIJ	17	LHCB pp at 7, 8 TeV

¹ Measured in amplitude analysis of $B^+ \rightarrow J/\psi(1S)\phi K^+$.

$\Gamma(J/\psi(1S)\omega K^+)/\Gamma_{total}$ Γ_{316}/Γ

VALUE (units 10^{-4})	DOCUMENT ID	TECN	COMMENT
$3.2 \pm 0.1^{+0.6}_{-0.3}$	¹ DEL-AMO-SA...10B	BABR	$e^+e^- \rightarrow \Upsilon(4S)$
••• We do not use the following data for averages, fits, limits, etc. •••			
$3.5 \pm 0.2 \pm 0.4$	¹ AUBERT	08W	BABR Repl. by DEL-AMO-SANCHEZ 10B

¹ Assumes equal production of B^+ and B^0 at the $\Upsilon(4S)$.

$\Gamma(\chi_{c0}(3915)K^+, \chi_{c0} \rightarrow J/\psi\omega)/\Gamma_{total}$ Γ_{317}/Γ

VALUE (units 10^{-5})	DOCUMENT ID	TECN	COMMENT
$3.0^{+0.7+0.5}_{-0.6-0.3}$	¹ DEL-AMO-SA...10B	BABR	$e^+e^- \rightarrow \Upsilon(4S)$

••• We do not use the following data for averages, fits, limits, etc. •••

$4.9^{+1.0}_{-0.9} \pm 0.5$	¹ AUBERT	08W	BABR Repl. by DEL-AMO-SANCHEZ 10B
-----------------------------	---------------------	-----	-----------------------------------

¹ Assumes equal production of B^+ and B^0 at the $\Upsilon(4S)$.

$\Gamma(\chi_{c0}(3915)K^+, \chi_{c0} \rightarrow p\bar{p})/\Gamma_{total}$ Γ_{299}/Γ

VALUE	CL%	DOCUMENT ID	TECN	COMMENT
$<7.1 \times 10^{-8}$	95	¹ AAIJ	13S	LHCB pp at 7 TeV

¹ Measured relative to $B^+ \rightarrow J/\psi K^+$ decay with charmonia reconstructed in $p\bar{p}$ final state and using $B(B^+ \rightarrow J/\psi K^+) = (1.013 \pm 0.034) \times 10^{-3}$ and $B(J/\psi \rightarrow p\bar{p}) = (2.17 \pm 0.07) \times 10^{-3}$.

$\Gamma(J/\psi(1S)\pi^+)/\Gamma_{total}$ Γ_{318}/Γ

VALUE	DOCUMENT ID	TECN	COMMENT
$(3.92 \pm 0.09) \times 10^{-5}$ OUR FIT			
$(3.8 \pm 0.6 \pm 0.3) \times 10^{-5}$	¹ ABE	03B	BELL $e^+e^- \rightarrow \Upsilon(4S)$

¹ Assumes equal production of B^+ and B^0 at the $\Upsilon(4S)$.

$\Gamma(J/\psi(1S)\pi^+)/\Gamma(J/\psi(1S)K^+)$ $\Gamma_{318}/\Gamma_{295}$

VALUE (units 10^{-2})	EVTS	DOCUMENT ID	TECN	COMMENT
3.85 ± 0.04 OUR FIT				
3.85 ± 0.04 OUR AVERAGE				
$3.83 \pm 0.03 \pm 0.03$		AAIJ	17O	LHCB pp at 7, 8 TeV

$3.5 \pm 0.3 \pm 1.2$	AABOUD	16L	ATLS pp at 7, 8 TeV
$4.86 \pm 0.82 \pm 0.15$	ABULENCIA	09	CDF $p\bar{p}$ at 1.96 TeV
$5.37 \pm 0.45 \pm 0.11$	AUBERT	04P	BABR $e^+e^- \rightarrow \Upsilon(4S)$
$5.0^{+1.9}_{-1.7} \pm 0.1$	ABE	96R	CDF $p\bar{p}$ 1.8 TeV
5.2 ± 2.4	BISHAI	96	CLE2 $e^+e^- \rightarrow \Upsilon(4S)$

••• We do not use the following data for averages, fits, limits, etc. •••

$3.83 \pm 0.11 \pm 0.07$	AAIJ	12AC	LHCB Repl. by AAJ17O
$3.91 \pm 0.78 \pm 0.19$	AUBERT	02F	BABR Repl. by AUBERT 04P
4.3 ± 2.3	5	¹ ALEXANDER	95 CLE2 Sup. by BISHAI 96

¹ Assumes equal production of B^+B^- and $B^0\bar{B}^0$ on $\Upsilon(4S)$.

$\Gamma(J/\psi(1S)\pi^+\pi^+\pi^-\pi^-)/\Gamma(\psi(2S)K^+)$ $\Gamma_{319}/\Gamma_{330}$

VALUE (units 10^{-2})	DOCUMENT ID	TECN	COMMENT
1.88 ± 0.17 ± 0.09	¹ AAIJ	17K	LHCB pp at 7 and 8 TeV

¹ Contains also the contribution from $B^+ \rightarrow \psi(2S)[\rightarrow J/\psi\pi^+\pi^-]\pi^+\pi^+\pi^-$ decays.

$\Gamma(\psi(2S)\pi^+\pi^-\pi^-)/\Gamma(\psi(2S)K^+)$ $\Gamma_{320}/\Gamma_{330}$

VALUE (units 10^{-2})	DOCUMENT ID	TECN	COMMENT
3.04 ± 0.50 ± 0.26	AAIJ	17K	LHCB pp at 7 and 8 TeV

$\Gamma(J/\psi(1S)\rho^+)/\Gamma_{total}$ Γ_{321}/Γ

VALUE (units 10^{-5})	CL%	DOCUMENT ID	TECN	COMMENT
4.1 ± 0.5 OUR AVERAGE				Error includes scale factor of 1.4.
$3.81^{+0.25}_{-0.24} \pm 0.35$		AAIJ	19O	LHCB pp at 7 and 8 TeV
$5.0 \pm 0.7 \pm 0.3$		¹ AUBERT	07AC	BABR $e^+e^- \rightarrow \Upsilon(4S)$

••• We do not use the following data for averages, fits, limits, etc. •••

<77	90	BISHAI	96	CLE2 $e^+e^- \rightarrow \Upsilon(4S)$
-----	----	--------	----	--

¹ Assumes equal production of B^+ and B^0 at the $\Upsilon(4S)$.

$\Gamma(J/\psi(1S)\pi^+\pi^0 \text{ nonresonant})/\Gamma_{total}$ Γ_{322}/Γ

VALUE (units 10^{-5})	CL%	DOCUMENT ID	TECN	COMMENT
<0.73	90	¹ AUBERT	07AC	BABR $e^+e^- \rightarrow \Upsilon(4S)$

¹ Assumes equal production of B^+ and B^0 at the $\Upsilon(4S)$.

$\Gamma(J/\psi(1S)a_1(1260)^+)/\Gamma_{total}$ Γ_{323}/Γ

VALUE	CL%	DOCUMENT ID	TECN	COMMENT
<1.2 × 10⁻³	90	BISHAI	96	CLE2 $e^+e^- \rightarrow \Upsilon(4S)$

$\Gamma(J/\psi(1S)p\bar{p}\pi^+)/\Gamma_{total}$ Γ_{324}/Γ

VALUE	CL%	DOCUMENT ID	TECN	COMMENT
<5.0 × 10⁻⁷	90	¹ AAIJ	13Z	LHCB pp at 7 TeV

¹ Uses $B(B_S^0 \rightarrow J/\psi(1S)\pi^+\pi^-) = (1.98 \pm 0.20) \times 10^{-4}$.

$\Gamma(J/\psi(1S)\rho\bar{\rho})/\Gamma_{total}$ Γ_{325}/Γ

VALUE (units 10^{-6})	CL%	DOCUMENT ID	TECN	COMMENT
14.6 ± 1.2 OUR AVERAGE				
$15.1 \pm 0.8 \pm 1.0$		¹ SIRUNYAN	19CM	CMS pp at 8 TeV
$11.7 \pm 2.8^{+1.8}_{-2.3}$		² XIE	05	BELL $e^+e^- \rightarrow \Upsilon(4S)$
12^{+9}_{-6}		² AUBERT	03K	BABR $e^+e^- \rightarrow \Upsilon(4S)$

••• We do not use the following data for averages, fits, limits, etc. •••

<41 90 ZANG 04 BELL $e^+e^- \rightarrow \Upsilon(4S)$

¹ SIRUNYAN 19CM reports $B(B^+ \rightarrow J/\psi\bar{\Lambda}p)/B(B^+ \rightarrow J/\psi K^*(892)) = (1.054 \pm 0.057 \pm 0.035 \pm 0.011) \times 10^{-2}$ and rescaled with the best value of $B(B^+ \rightarrow J/\psi K^*(892)) = (1.43 \pm 0.08) \times 10^{-3}$, where the last uncertainty is the uncertainty from the branching fractions of $\bar{\Lambda}$ and $K^*(892)$ to reconstructed final states.

² Assumes equal production of B^+ and B^0 at the $\Upsilon(4S)$.

$\Gamma(J/\psi(1S)\Sigma^0 p)/\Gamma_{total}$ Γ_{326}/Γ

VALUE	CL%	DOCUMENT ID	TECN	COMMENT
<1.1 × 10⁻⁵	90	¹ XIE	05	BELL $e^+e^- \rightarrow \Upsilon(4S)$

¹ Assumes equal production of B^+ and B^0 at the $\Upsilon(4S)$.

$\Gamma(J/\psi(1S)D^+)/\Gamma_{total}$ Γ_{327}/Γ

VALUE (units 10^{-5})	CL%	DOCUMENT ID	TECN	COMMENT
<12	90	¹ AUBERT	05U	BABR $e^+e^- \rightarrow \Upsilon(4S)$

¹ Assumes equal production of B^+ and B^0 at the $\Upsilon(4S)$.

$\Gamma(J/\psi(1S)\bar{D}^0\pi^+)/\Gamma_{total}$ Γ_{328}/Γ

VALUE (units 10^{-5})	CL%	DOCUMENT ID	TECN	COMMENT
<2.5	90	¹ ZHANG	05B	BELL $e^+e^- \rightarrow \Upsilon(4S)$

••• We do not use the following data for averages, fits, limits, etc. •••

<5.2	90	¹ AUBERT	05R	BABR $e^+e^- \rightarrow \Upsilon(4S)$
------	----	---------------------	-----	--

¹ Assumes equal production of B^+ and B^0 at the $\Upsilon(4S)$.

$\Gamma(\psi(2S)\pi^+)/\Gamma_{total}$ Γ_{329}/Γ

VALUE (units 10^{-5})	DOCUMENT ID	TECN	COMMENT
2.44 ± 0.22 ± 0.20	¹ BHARDWAJ	08	BELL $e^+e^- \rightarrow \Upsilon(4S)$

¹ Assumes equal production of B^+ and B^0 at the $\Upsilon(4S)$.

Meson Particle Listings

 B^\pm $\Gamma(\psi(2S)\pi^+)/\Gamma(\psi(2S)K^+)$

VALUE (units 10^{-2})	DOCUMENT ID	TECN	COMMENT
3.97 ± 0.29 OUR AVERAGE			
3.95 ± 0.40 ± 0.12	AAIJ	12AC	LHCB pp at 7 TeV
3.99 ± 0.36 ± 0.17	BHARDWAJ	08	BELL $e^+e^- \rightarrow \Upsilon(4S)$

 $\Gamma(\psi(2S)K^+)/\Gamma_{total}$

VALUE (units 10^{-4})	EVTs	DOCUMENT ID	TECN	COMMENT
6.24 ± 0.21 OUR FIT				
6.40 ± 0.34 OUR AVERAGE				
4.6 ± 1.0 ± 0.7		1	LEES	20c BABR $e^+e^- \rightarrow \Upsilon(4S)$
6.4 ± 1.0 ± 0.4		1	KATO	18 BELL $e^+e^- \rightarrow \Upsilon(4S)$
6.65 ± 0.17 ± 0.55		2	GULER	11 BELL $e^+e^- \rightarrow \Upsilon(4S)$
6.17 ± 0.32 ± 0.44		2	AUBERT	05J BABR $e^+e^- \rightarrow \Upsilon(4S)$
7.8 ± 0.7 ± 0.9		2	RICHICHI	01 CLE2 $e^+e^- \rightarrow \Upsilon(4S)$
18 ± 8 ± 4	5	2	ALBRECHT	90J ARG $e^+e^- \rightarrow \Upsilon(4S)$

• • • We do not use the following data for averages, fits, limits, etc. • • •

4.9 ± 1.6 ± 0.4		1	AUBERT	06E BABR Repl. by LEES 20c
6.9 ± 0.6		2	ABE	03B BELL Repl. by GULER 11
6.4 ± 0.5 ± 0.8		2	AUBERT	02 BABR Repl. by AUBERT 05J
6.1 ± 2.3 ± 0.9	7	2	ALAM	94 CLE2 Repl. by RICHICHI 01
<5 at 90% CL		2	BORTOLETTO	92 CLEO $e^+e^- \rightarrow \Upsilon(4S)$
22 ± 17	3	3	ALBRECHT	87D ARG $e^+e^- \rightarrow \Upsilon(4S)$

¹ Measures absolute branching fractions using a missing-mass technique.

² Assumes equal production of B^+ and B^0 at the $\Upsilon(4S)$.

³ ALBRECHT 87D assume $B^+B^-/B^0\bar{B}^0$ ratio is 55/45. Superseded by ALBRECHT 90J.

 $\Gamma(\psi(2S)K^+)/\Gamma(J/\psi(1S)K^+)$

VALUE	DOCUMENT ID	TECN	COMMENT
0.612 ± 0.019 OUR FIT			
0.605 ± 0.023 OUR AVERAGE			
0.58 ± 0.11 ± 0.02	1	AAIJ	13s LHCB pp at 7 TeV
0.608 ± 0.018 ± 0.017	2,3	AAIJ	12L LHCB pp at 7 TeV
0.63 ± 0.05 ± 0.08		ABAZOV	09Y D0 $p\bar{p}$ at 1.96 TeV
0.558 ± 0.082 ± 0.056		ABE	98O CDF $p\bar{p}$ 1.8 TeV

• • • We do not use the following data for averages, fits, limits, etc. • • •

0.64 ± 0.06 ± 0.07 ⁴ AUBERT 02 BABR $e^+e^- \rightarrow \Upsilon(4S)$

¹ AAIJ 13s reports $[\Gamma(B^+ \rightarrow \psi(2S)K^+)/\Gamma(B^+ \rightarrow J/\psi(1S)K^+)] \times [B(\psi(2S) \rightarrow p\bar{p}) / B(J/\psi(1S) \rightarrow p\bar{p})] = 0.080 \pm 0.012 \pm 0.009$ which we multiply or divide by our best values $B(\psi(2S) \rightarrow p\bar{p}) = (2.94 \pm 0.09) \times 10^{-4}$, $B(J/\psi(1S) \rightarrow p\bar{p}) = (2.120 \pm 0.029) \times 10^{-3}$. Our first error is their experiment's error and our second error is the systematic error from using our best values.

² AAIJ 12L reports $0.594 \pm 0.006 \pm 0.016 \pm 0.015$ from a measurement of $[\Gamma(B^+ \rightarrow \psi(2S)K^+)/\Gamma(B^+ \rightarrow J/\psi(1S)K^+)] \times [B(J/\psi(1S) \rightarrow e^+e^-)] / [B(\psi(2S) \rightarrow e^+e^-)]$ assuming $B(J/\psi(1S) \rightarrow e^+e^-) = (5.94 \pm 0.06) \times 10^{-2}$, $B(\psi(2S) \rightarrow e^+e^-) = (7.72 \pm 0.17) \times 10^{-3}$, which we rescale to our best values $B(J/\psi(1S) \rightarrow e^+e^-) = (5.971 \pm 0.032) \times 10^{-2}$, $B(\psi(2S) \rightarrow e^+e^-) = (7.94 \pm 0.22) \times 10^{-3}$. Our first error is their experiment's error and our second error is the systematic error from using our best values.

³ Assumes $B(J/\psi \rightarrow \mu^+\mu^-) / B(\psi(2S) \rightarrow \mu^+\mu^-) = B(J/\psi \rightarrow e^+e^-) / B(\psi(2S) \rightarrow e^+e^-) = 7.69 \pm 0.19$.

⁴ Assumes equal production of B^+ and B^0 at the $\Upsilon(4S)$.

 $\Gamma(\psi(2S)K^*(892)^+)/\Gamma_{total}$

VALUE (units 10^{-4})	CL%	DOCUMENT ID	TECN	COMMENT
6.7 ± 1.4 OUR AVERAGE				Error includes scale factor of 1.3.
5.92 ± 0.85 ± 0.89		1	AUBERT	05J BABR $e^+e^- \rightarrow \Upsilon(4S)$
9.2 ± 1.9 ± 1.2		1	RICHICHI	01 CLE2 $e^+e^- \rightarrow \Upsilon(4S)$

• • • We do not use the following data for averages, fits, limits, etc. • • •

<30	90	1	ALAM	94 CLE2 Repl. by RICHICHI 01
<35	90	1	BORTOLETTO	92 CLEO $e^+e^- \rightarrow \Upsilon(4S)$
<49	90	1	ALBRECHT	90J ARG $e^+e^- \rightarrow \Upsilon(4S)$

¹ Assumes equal production of B^+ and B^0 at the $\Upsilon(4S)$.

 $\Gamma(\psi(2S)K^*(892)^+)/\Gamma(\psi(2S)K^+)$

VALUE	DOCUMENT ID	TECN	COMMENT
0.96 ± 0.15 ± 0.09	AUBERT	05J	BABR $e^+e^- \rightarrow \Upsilon(4S)$

 $\Gamma(\psi(2S)K^0\pi^+)/\Gamma_{total}$

VALUE (units 10^{-3})	DOCUMENT ID	TECN	COMMENT
0.588 ± 0.034	1	AUBERT	09AA BABR $e^+e^- \rightarrow \Upsilon(4S)$

¹ Does not report systematic uncertainties.

 $\Gamma(\psi(2S)K^+\pi^+\pi^-)/\Gamma_{total}$

VALUE (units 10^{-4})	EVTs	DOCUMENT ID	TECN	COMMENT
4.3 ± 0.5 OUR AVERAGE				
4.31 ± 0.20 ± 0.50		1	GULER	11 BELL $e^+e^- \rightarrow \Upsilon(4S)$
19 ± 11 ± 4	3	1	ALBRECHT	90J ARG $e^+e^- \rightarrow \Upsilon(4S)$

¹ Assumes equal production of B^+ and B^0 at the $\Upsilon(4S)$.

 $\Gamma(\psi(2S)\phi(1020)K^+)/\Gamma_{total}$

VALUE (units 10^{-6})	DOCUMENT ID	TECN	COMMENT
4.0 ± 0.4 ± 0.6	1,2	KHACHATRYAN	17C CMS pp at 8 TeV

¹ Measured using $B^+ \rightarrow \psi(2S)K^+$ as a normalization channel. The second error represents total systematic uncertainties including those from branching fractions which were taken from PDG 16 as $B(\phi \rightarrow K^+K^-) = 0.489 \pm 0.005$ and $B(B^+ \rightarrow \psi(2S)K^+) = (6.26 \pm 0.24) \times 10^{-4}$.

² An upper limit on the fraction of the non- ϕ component in $B^+ \rightarrow \psi(2S)K^+K^-K^+$ decays is set as 0.26 at the 95% confidence level.

 $\Gamma(\psi(3770)K^+)/\Gamma_{total}$

VALUE (units 10^{-3})	CL%	DOCUMENT ID	TECN	COMMENT
0.43 ± 0.11 OUR AVERAGE				
0.32 ± 0.20 ± 0.05 ± 0.01		1,2	LEES	20c BABR $e^+e^- \rightarrow \Upsilon(4S)$
0.48 ± 0.11 ± 0.07		3	CHISTOV	04 BELL $e^+e^- \rightarrow \Upsilon(4S)$

• • • We do not use the following data for averages, fits, limits, etc. • • •

<0.23 ⁹⁰ 2 KATO ² KATO 02 BELL $e^+e^- \rightarrow \Upsilon(4S)$

3.5 ± 2.5 ± 0.3 ² AUBERT 06E BABR Repl. by LEES 20c

¹ LEES 20c measurement's last uncertainty is due to the used $B(B^\pm \rightarrow K^\pm J/\psi)$ value.

² Measures absolute branching fractions using a missing-mass technique.

³ Assumes equal production of B^+ and B^0 at the $\Upsilon(4S)$.

 $\Gamma(\psi(3770)K^+)/\Gamma(D^-D^+K^+)$

VALUE	DOCUMENT ID	TECN	COMMENT
0.352 ± 0.035 +0.034 -0.031	1,2	AAIJ	20AI LHCB pp at 7, 8, 13 TeV

¹ AAIJ 20AI reports $[\Gamma(B^+ \rightarrow \psi(3770)K^+)/\Gamma(B^+ \rightarrow D^-D^+K^+)] \times [B(\psi(3770) \rightarrow D^+D^-)] = (14.5 \pm 1.2 \pm 0.8) \times 10^{-2}$ which we divide by our best value $B(\psi(3770) \rightarrow D^+D^-) = (41 \pm 4) \times 10^{-2}$. Our first error is their experiment's error and our second error is the systematic error from using our best value.

² Measured in Dalitz plot analysis of $B^+ \rightarrow D^-D^+K^+$ decays.

 $\Gamma(\psi(3770)K^+, \psi \rightarrow D^0\bar{D}^0)/\Gamma_{total}$

VALUE (units 10^{-4})	DOCUMENT ID	TECN	COMMENT
1.5 ± 0.5 OUR AVERAGE			Error includes scale factor of 1.4.
1.18 ± 0.41 ± 0.15	1	LEES	15c BABR $e^+e^- \rightarrow \Upsilon(4S)$
2.2 ± 0.5 ± 0.3	1	BRODZICKA	08 BELL $e^+e^- \rightarrow \Upsilon(4S)$

• • • We do not use the following data for averages, fits, limits, etc. • • •

1.41 ± 0.30 ± 0.22 ¹ AUBERT 08B BABR Repl. by LEES 15c

3.4 ± 0.8 ± 0.5 ¹ CHISTOV 04 BELL Repl. by BRODZICKA 08

¹ Assumes equal production of B^+ and B^0 at the $\Upsilon(4S)$.

 $\Gamma(\psi(3770)K^+, \psi \rightarrow D^+D^-)/\Gamma_{total}$

VALUE (units 10^{-4})	DOCUMENT ID	TECN	COMMENT
0.94 ± 0.35 OUR AVERAGE			
0.84 ± 0.32 ± 0.21	1	AUBERT	08B BABR $e^+e^- \rightarrow \Upsilon(4S)$
1.4 ± 0.8 ± 0.2	1	CHISTOV	04 BELL $e^+e^- \rightarrow \Upsilon(4S)$

¹ Assumes equal production of B^+ and B^0 at the $\Upsilon(4S)$.

 $\Gamma(\psi(3770)K^+, \psi \rightarrow p\bar{p})/\Gamma_{total}$

VALUE	CL%	DOCUMENT ID	TECN	COMMENT
<2 × 10⁻⁷	95	1	AAIJ	17AD LHCB pp at 7 and 8 TeV

¹ Measured relative to $B^+ \rightarrow J/\psi K^+$ decay with charmonia reconstructed in $p\bar{p}$ final state and using $B(B^+ \rightarrow J/\psi K^+) \times B(J/\psi \rightarrow p\bar{p}) = (2.17 \pm 0.08) \times 10^{-6}$.

 $\Gamma(\psi(3770)K^+, \psi \rightarrow J/\psi\eta)/\Gamma_{total}$

VALUE	CL%	DOCUMENT ID	TECN	COMMENT
<4.6 × 10⁻⁷	90	AAIJ	22D	LHCB pp at 7, 8, 13 TeV

 $\Gamma(\psi(4040)K^+)/\Gamma_{total}$

VALUE (units 10^{-3})	CL%	DOCUMENT ID	TECN	COMMENT
1.6 ± 0.5 ± 0.2		1	AAIJ	22D LHCB pp at 7, 8, 13 TeV

• • • We do not use the following data for averages, fits, limits, etc. • • •

<3.0 ⁹⁰ 2 IWASHITA 14 BELL $e^+e^- \rightarrow \Upsilon(4S)$

<0.13 ⁹⁰ AAIJ 13Bc LHCB pp at 7, 8 TeV

¹ AAIJ 22D reports $[\Gamma(B^+ \rightarrow \psi(4040)K^+)/\Gamma_{total}] \times [B(\psi(4040) \rightarrow J/\psi\eta)] = (8.53 \pm 2.35 \pm 0.30) \times 10^{-6}$ which we divide by our best value $B(\psi(4040) \rightarrow J/\psi\eta) = (5.2 \pm 0.7) \times 10^{-3}$. Our first error is their experiment's error and our second error is the systematic error from using our best value.

² IWASHITA 14 reports $[\Gamma(B^+ \rightarrow \psi(4040)K^+)/\Gamma_{total}] \times [B(\psi(4040) \rightarrow J/\psi\eta)] < 15.5 \times 10^{-6}$ which we divide by our best value $B(\psi(4040) \rightarrow J/\psi\eta) = 5.2 \times 10^{-3}$.

 $\Gamma(\psi(4040)K^+, \psi \rightarrow D^+D^-)/\Gamma(D^-D^+K^+)$

VALUE (units 10^{-2})	DOCUMENT ID	TECN	COMMENT
5.0 ± 1.3 ± 0.4	1	AAIJ	20AI LHCB pp at 7, 8, 13 TeV

¹ Measured in Dalitz plot analysis of $B^+ \rightarrow D^-D^+K^+$ decays.

 $\Gamma(\psi(4160)K^+)/\Gamma_{total}$

VALUE (units 10^{-4})	DOCUMENT ID	TECN	COMMENT
5.1 ± 1.3 ± 2.4	1	AAIJ	13Bc LHCB pp at 7, 8 TeV

¹ AAIJ 13bC reports $[\Gamma(B^+ \rightarrow \psi(4160) K^+)/\Gamma_{\text{total}}] \times \text{B}(\psi(4160) \rightarrow \mu^+ \mu^-) = (3.5_{-0.8}^{+0.9}) \times 10^{-9}$ which we divide by our best value $\text{B}(\psi(4160) \rightarrow e^+ e^-) = (6.9 \pm 3.3) \times 10^{-6}$ assuming lepton universality. Our first error is their experiment's error and our second error is the systematic error from using our best value.

$\Gamma(\psi(4160) K^+, \psi \rightarrow \bar{D}^0 D^0)/\Gamma_{\text{total}}$					Γ_{343}/Γ
VALUE (units 10^{-4})		DOCUMENT ID	TECN	COMMENT	
0.84 ± 0.41 ± 0.33		¹ LEES	15c	BABR $e^+ e^- \rightarrow \Upsilon(4S)$	

¹ Assumes equal production of B⁺ and B⁰ at the $\Upsilon(4S)$.

$\Gamma(\psi(4160) K^+, \psi \rightarrow D^+ D^-)/\Gamma(D^- D^+ K^+)$					$\Gamma_{344}/\Gamma_{221}$
VALUE (units 10^{-2})		DOCUMENT ID	TECN	COMMENT	
6.6 ± 1.5 ± 1.2		¹ AAIJ	20aI	LHCB pp at 7, 8, 13 TeV	

¹ Measured in Dalitz plot analysis of B⁺ → D⁻ D⁺ K⁺ decays.

$\Gamma(\psi(4415) K^+, \psi \rightarrow D^+ D^-)/\Gamma(D^- D^+ K^+)$					$\Gamma_{345}/\Gamma_{221}$
VALUE (units 10^{-2})		DOCUMENT ID	TECN	COMMENT	
9.2 ± 1.4 ± 1.5		¹ AAIJ	20aI	LHCB pp at 7, 8, 13 TeV	

¹ Measured in Dalitz plot analysis of B⁺ → D⁻ D⁺ K⁺ decays.

$\Gamma(\psi(4415) K^+, \psi \rightarrow J/\psi \eta)/\Gamma_{\text{total}}$					Γ_{346}/Γ
VALUE	CL%	DOCUMENT ID	TECN	COMMENT	
< 9.6 × 10⁻⁷	90	AAIJ	22d	LHCB pp at 7, 8, 13 TeV	

$\Gamma(\chi_{c0} \pi^+, \chi_{c0} \rightarrow \pi^+ \pi^-)/\Gamma_{\text{total}}$					Γ_{347}/Γ
VALUE (units 10^{-6})	CL%	DOCUMENT ID	TECN	COMMENT	
< 0.1	90	¹ AUBERT	09L	BABR $e^+ e^- \rightarrow \Upsilon(4S)$	
• • •		• • • We do not use the following data for averages, fits, limits, etc. • • •			
< 0.3	90	¹ AUBERT,B	05G	BABR Repl. by AUBERT 09L	
		¹ Assumes equal production of B ⁺ and B ⁰ at the $\Upsilon(4S)$.			

$\Gamma(\chi_{c0} \pi^+, \chi_{c0} \rightarrow \pi^0 \pi^0)/\Gamma_{\text{total}}$					Γ_{348}/Γ
VALUE	CL%	DOCUMENT ID	TECN	COMMENT	
< 5 × 10⁻⁷	90	LAI	23	BELL $e^+ e^- \rightarrow \Upsilon(4S)$	

$\Gamma(\chi_{c0} K^+)/\Gamma_{\text{total}}$					Γ_{349}/Γ
VALUE (units 10^{-4})	CL%	DOCUMENT ID	TECN	COMMENT	

1.51 ± 0.15 OUR AVERAGE

2.0 ± 1.3 ± 0.3 ± 0.1		^{1,2} LEES	20c	BABR $e^+ e^- \rightarrow \Upsilon(4S)$	
1.8 ± 0.6 ± 0.5		³ CHILIKIN	19	BELL $e^+ e^- \rightarrow \Upsilon(4S)$	
1.84 ± 0.25 ± 0.14		^{4,5} LEES	12o	BABR $e^+ e^- \rightarrow \Upsilon(4S)$	
1.68 ± 0.32 ± 0.16		^{4,6} LEES	12o	BABR $e^+ e^- \rightarrow \Upsilon(4S)$	
1.8 ± 0.8 ± 0.1		⁷ LEES	11i	BABR $e^+ e^- \rightarrow \Upsilon(4S)$	
1.23 ± 0.27 ± 0.25 ± 0.06		^{4,8} AUBERT	08aI	BABR $e^+ e^- \rightarrow \Upsilon(4S)$	
4.3 ± 2.0 ± 0.3		⁹ AUBERT,BE	06M	BABR $e^+ e^- \rightarrow \Upsilon(4S)$	
1.12 ± 0.12 ± 0.30 ± 0.20		⁴ GARMASH	06	BELL $e^+ e^- \rightarrow \Upsilon(4S)$	
• • •		• • • We do not use the following data for averages, fits, limits, etc. • • •			
< 3.3	90	² KATO	18	BELL $e^+ e^- \rightarrow \Upsilon(4S)$	
< 2.7	95	¹⁰ AAIJ	13s	LHCB pp at 7 TeV	
< 5	90	^{4,11} WICHT	08	BELL $e^+ e^- \rightarrow \Upsilon(4S)$	
< 1.8	90	² AUBERT	06E	BABR $e^+ e^- \rightarrow \Upsilon(4S)$	
1.84 ± 0.32 ± 0.31		^{4,12} AUBERT	06o	BABR Repl. by LEES 12o	
< 8.9	90	⁴ AUBERT	05K	BABR $e^+ e^- \rightarrow \Upsilon(4S)$	
1.39 ± 0.49 ± 0.11		¹³ AUBERT,B	05N	BABR Repl. by AUBERT 08aI	
1.96 ± 0.35 ± 2.00 ± 0.42		⁴ GARMASH	05	BELL Repl. by GARMASH 06	
2.7 ± 0.7		¹⁴ AUBERT	04T	BABR Repl. by AUBERT,B 04P	
3.0 ± 0.8 ± 0.3		¹⁵ AUBERT,B	04P	BABR Repl. by AUBERT,B 05N	
6.0 ± 2.1 ± 1.1		¹⁶ ABE	02B	BELL Repl. by GARMASH 05	
< 4.8	90	¹⁷ EDWARDS	01	CLE2 $e^+ e^- \rightarrow \Upsilon(4S)$	

¹ LEES 20c measurement's last uncertainty is due to the used $\text{B}(B^{\pm} \rightarrow K^{\pm} J/\psi)$ value.
² Measures absolute branching fractions using a missing-mass technique.
³ CHILIKIN 19 reports $[\Gamma(B^+ \rightarrow \chi_{c0} K^+)/\Gamma_{\text{total}}] \times [\text{B}(\chi_{c0}(1P) \rightarrow p\bar{p}\pi^+\pi^-)] = (3.7_{-1.0}^{+1.2} \pm 0.2) \times 10^{-7}$ which we divide by our best value $\text{B}(\chi_{c0}(1P) \rightarrow p\bar{p}\pi^+\pi^-) = (2.1 \pm 0.7) \times 10^{-3}$. Our first error is their experiment's error and our second error is the systematic error from using our best value.
⁴ Assumes equal production of B⁺ and B⁰ at the $\Upsilon(4S)$.
⁵ Measured in the B⁺ → K⁺ K⁻ K⁺ decay.
⁶ Measured in the B⁺ → K⁺ K_S⁰ K_S⁰ decay.
⁷ LEES 11i reports $[\Gamma(B^+ \rightarrow \chi_{c0} K^+)/\Gamma_{\text{total}}] \times [\text{B}(\chi_{c0}(1P) \rightarrow \pi\pi)] = (1.53 \pm 0.66 \pm 0.27) \times 10^{-6}$ which we divide by our best value $\text{B}(\chi_{c0}(1P) \rightarrow \pi\pi) = (8.5 \pm 0.4) \times 10^{-3}$. Our first error is their experiment's error and our second error is the systematic error from using our best value.
⁸ AUBERT 08aI reports $(0.70 \pm 0.10 \pm 0.12 \pm 0.16) \times 10^{-6}$ for $\text{B}(B^+ \rightarrow \chi_{c0} K^+) \times \text{B}(\chi_{c0} \rightarrow \pi^+ \pi^-)$. We compute $\text{B}(B^+ \rightarrow \chi_{c0} K^+)$ using the PDG value $\text{B}(\chi_{c0} \rightarrow \pi\pi) = (8.5 \pm 0.4) \times 10^{-3}$ and 2/3 for the $\pi^+ \pi^-$ fraction. Our first error is their experiment's error and the second error is systematic error from using our best value.

⁹ AUBERT,BE 06M reports $[\Gamma(B^+ \rightarrow \chi_{c0} K^+)/\Gamma_{\text{total}}] \times [\text{B}(\chi_{c0}(1P) \rightarrow \gamma J/\psi(1S))] = (6.1 \pm 2.6 \pm 1.1) \times 10^{-6}$ which we divide by our best value $\text{B}(\chi_{c0}(1P) \rightarrow \gamma J/\psi(1S)) = (1.41 \pm 0.09) \times 10^{-2}$. Our first error is their experiment's error and our second error is the systematic error from using our best value. The significance of the observed signal is 2.4 σ .

¹⁰ AAIJ 13s reports $[\Gamma(B^+ \rightarrow \chi_{c0} K^+)/\Gamma_{\text{total}}] \times [\text{B}(\chi_{c0}(1P) \rightarrow p\bar{p})] < 6 \times 10^{-8}$ which we divide by our best value $\text{B}(\chi_{c0}(1P) \rightarrow p\bar{p}) = 2.21 \times 10^{-4}$.
¹¹ WICHT 08 reports $[\Gamma(B^+ \rightarrow \chi_{c0} K^+)/\Gamma_{\text{total}}] \times [\text{B}(\chi_{c0}(1P) \rightarrow \gamma\gamma)] < 0.11 \times 10^{-6}$ which we divide by our best value $\text{B}(\chi_{c0}(1P) \rightarrow \gamma\gamma) = 2.04 \times 10^{-4}$.
¹² Measured in the B⁺ → K⁺ K⁻ K⁺ decay.
¹³ AUBERT,B 05N reports $(0.66 \pm 0.22 \pm 0.08) \times 10^{-6}$ for $\text{B}(B^+ \rightarrow \chi_{c0}^0 K^+) \times \text{B}(\chi_{c0}^0 \rightarrow \pi^+ \pi^-)$. We compute $\text{B}(B^+ \rightarrow \chi_{c0}^0 K^+)$ using the PDG value $\text{B}(\chi_{c0}^0 \rightarrow \pi^+ \pi^-) = (7.1 \pm 0.6) \times 10^{-3}$ and 2/3 for the $\pi^+ \pi^-$ fraction.
¹⁴ The measurement performed using decay channels $\chi_{c0} \rightarrow \pi^+ \pi^-$ and $\chi_{c0} \rightarrow K^+ K^-$. The ratio of the branching ratios for these channels is found to be consistent with world average.
¹⁵ AUBERT 04P reports $\text{B}(B^+ \rightarrow \chi_{c0} K^+) \times \text{B}(\chi_{c0} \rightarrow \pi^+ \pi^-) = (1.5 \pm 0.4 \pm 0.1) \times 10^{-6}$ and used PDG value of $\text{B}(\chi_{c0} \rightarrow \pi\pi) = (7.4 \pm 0.8) \times 10^{-3}$ and Clebsch-Gordan coefficient to compute $\text{B}(B^{\pm} \rightarrow \chi_{c0} K^{\pm})$.
¹⁶ ABE 02b measures the ratio of $\text{B}(B^+ \rightarrow \chi_{c0} K^+)/\text{B}(B^+ \rightarrow J/\psi(1S) K^+) = 0.60 + 0.21 - 0.18 \pm 0.05 \pm 0.08$, where the third error is due to the uncertainty in the $\text{B}(\chi_{c0} \rightarrow \pi^+ \pi^-)$, and uses $\text{B}(B^+ \rightarrow J/\psi(1S) K^+) = (10.0 \pm 1.0) \times 10^{-4}$ to obtain the result.
¹⁷ EDWARDS 01 assumes equal production of B⁰ and B⁺ at the $\Upsilon(4S)$. The correlated uncertainties (28.3%) from $\text{B}(J/\psi(1S) \rightarrow \gamma\eta_c)$ in those modes have been accounted for.

$\Gamma(\chi_{c0} K^0 \pi^+)/\Gamma_{\text{total}}$					Γ_{350}/Γ
VALUE (units 10^{-3})		DOCUMENT ID	TECN	COMMENT	
1.45 ± 0.08 ± 0.19		¹ AAIJ	23aH	LHCB pp at 7, 8 and 13 TeV	
		¹ The second uncertainty includes systematic and reference branching reaction of B ⁺ → J/ψ K ⁺ uncertainties.			

$\Gamma(\chi_{c0} K^*(892^+)/\Gamma_{\text{total}}$					Γ_{351}/Γ
VALUE (units 10^{-4})	CL%	DOCUMENT ID	TECN	COMMENT	
< 2.1	90	¹ AUBERT	08bD	BABR $e^+ e^- \rightarrow \Upsilon(4S)$	
• • •		• • • We do not use the following data for averages, fits, limits, etc. • • •			
< 28.6	90	¹ AUBERT	05K	BABR Repl. by AUBERT 08bD	
		¹ Assumes equal production of B ⁺ and B ⁰ at the $\Upsilon(4S)$.			

$\Gamma(\chi_{c1}(1P) \pi^+)/\Gamma_{\text{total}}$					Γ_{352}/Γ
VALUE (units 10^{-5})		DOCUMENT ID	TECN	COMMENT	
2.2 ± 0.4 ± 0.3		¹ KUMAR	06	BELL $e^+ e^- \rightarrow \Upsilon(4S)$	
		¹ Assumes equal production of B ⁺ and B ⁰ at the $\Upsilon(4S)$.			

$\Gamma(\chi_{c1}(1P) K^+)/\Gamma_{\text{total}}$					Γ_{353}/Γ
VALUE (units 10^{-4})		DOCUMENT ID	TECN	COMMENT	
4.74 ± 0.22 OUR AVERAGE					
4.0 ± 0.8 ± 0.6 ± 0.1		^{1,2} LEES	20c	BABR $e^+ e^- \rightarrow \Upsilon(4S)$	
9 ± 2 ± 4		³ CHILIKIN	19	BELL $e^+ e^- \rightarrow \Upsilon(4S)$	
5.8 ± 0.9 ± 0.5		¹ KATO	18	BELL $e^+ e^- \rightarrow \Upsilon(4S)$	
4.94 ± 0.11 ± 0.33		⁴ BHARDWAJ	11	BELL $e^+ e^- \rightarrow \Upsilon(4S)$	
4.5 ± 0.1 ± 0.3		⁵ AUBERT	09b	BABR $e^+ e^- \rightarrow \Upsilon(4S)$	
15.5 ± 5.4 ± 2.0		⁶ ACOSTA	02f	CDF $p\bar{p}$ 1.8 TeV	
• • •		• • • We do not use the following data for averages, fits, limits, etc. • • •			
8.1 ± 1.4 ± 0.7		¹ AUBERT	06E	BABR Repl. by LEES 20c	
5.1 ± 0.4 ± 0.2		⁷ AUBERT,BE	06M	BABR Repl. by AUBERT 09b	
4.49 ± 0.19 ± 0.53		⁴ SONI	06	BELL Repl. by BHARDWAJ 11	
5.79 ± 0.26 ± 0.65		⁴ AUBERT	05J	BABR Repl. by AUBERT,BE 06M	
6.0 ± 0.9 ± 0.2		⁸ AUBERT	02	BABR Repl. by AUBERT 05J	
9.7 ± 4.0 ± 0.9		⁴ ALAM	94	CLE2 $e^+ e^- \rightarrow \Upsilon(4S)$	
19 ± 13 ± 6		⁹ ALBRECHT	92E	ARG $e^+ e^- \rightarrow \Upsilon(4S)$	

¹ Measures absolute branching fractions using a missing-mass technique.
² LEES 20c measurement's last uncertainty is due to the used $\text{B}(B^{\pm} \rightarrow K^{\pm} J/\psi)$ value.
³ CHILIKIN 19 reports $[\Gamma(B^+ \rightarrow \chi_{c1}(1P) K^+)/\Gamma_{\text{total}}] \times [\text{B}(\chi_{c1}(1P) \rightarrow p\bar{p}\pi^+\pi^-)] = (4.7_{-1.2}^{+1.3} \pm 0.4) \times 10^{-7}$ which we divide by our best value $\text{B}(\chi_{c1}(1P) \rightarrow p\bar{p}\pi^+\pi^-) = (5.0 \pm 1.9) \times 10^{-4}$. Our first error is their experiment's error and our second error is the systematic error from using our best value.
⁴ Assumes equal production of B⁺ and B⁰ at the $\Upsilon(4S)$.
⁵ Uses $\chi_{c1,2} \rightarrow J/\psi \gamma$. Assumes $\text{B}(\Upsilon(4S) \rightarrow B^+ B^-) = (51.6 \pm 0.6)\%$ and $\text{B}(\Upsilon(4S) \rightarrow B^0 \bar{B}^0) = (48.4 \pm 0.6)\%$.
⁶ ACOSTA 02f uses as reference of $\text{B}(B \rightarrow J/\psi(1S) K^+) = (10.1 \pm 0.6) \times 10^{-4}$. The second error includes the systematic error and the uncertainties of the branching ratio.
⁷ AUBERT,BE 06M reports $[\Gamma(B^+ \rightarrow \chi_{c1}(1P) K^+)/\Gamma_{\text{total}}] \times [\text{B}(\chi_{c1}(1P) \rightarrow \gamma J/\psi(1S))] = (1.76 \pm 0.07 \pm 0.12) \times 10^{-4}$ which we divide by our best value $\text{B}(\chi_{c1}(1P) \rightarrow \gamma J/\psi(1S)) = (34.3 \pm 1.3) \times 10^{-2}$. Our first error is their experiment's error and our second error is the systematic error from using our best value.
⁸ AUBERT 02 reports $(7.5 \pm 0.9 \pm 0.8) \times 10^{-4}$ from a measurement of $[\Gamma(B^+ \rightarrow \chi_{c1}(1P) K^+)/\Gamma_{\text{total}}] \times [\text{B}(\chi_{c1}(1P) \rightarrow \gamma J/\psi(1S))] \times [\text{B}(\chi_{c1}(1P) \rightarrow \gamma J/\psi(1S))] = 0.273 \pm 0.016$, which we rescale to our best value $\text{B}(\chi_{c1}(1P) \rightarrow \gamma J/\psi(1S)) = (34.3 \pm 1.3) \times 10^{-2}$. Our first error is their experiment's error and our second error is the systematic error from using our best value. Assumes equal production of B⁺ and B⁰ at the $\Upsilon(4S)$.
⁹ ALBRECHT 92E assumes no $\chi_{c2}(1P)$ production and $\text{B}(\Upsilon(4S) \rightarrow B^+ B^-) = 50\%$.

Meson Particle Listings

 B^\pm $\Gamma(\chi_{c1}(1P)K^+)/\Gamma(J/\psi(1S)K^+)$ $\Gamma_{353}/\Gamma_{295}$

VALUE	DOCUMENT ID	TECN	COMMENT
0.60 ± 0.07 ± 0.02	¹ AUBERT 02	BABR	$e^+e^- \rightarrow \Upsilon(4S)$

¹AUBERT 02 reports $0.75 \pm 0.08 \pm 0.05$ from a measurement of $[\Gamma(B^+ \rightarrow \chi_{c1}(1P)K^+)/\Gamma(B^+ \rightarrow J/\psi(1S)K^+)] \times [B(\chi_{c1}(1P) \rightarrow \gamma J/\psi(1S))]$ assuming $B(\chi_{c1}(1P) \rightarrow \gamma J/\psi(1S)) = 0.273 \pm 0.016$, which we rescale to our best value $B(\chi_{c1}(1P) \rightarrow \gamma J/\psi(1S)) = (34.3 \pm 1.3) \times 10^{-2}$. Our first error is their experiment's error and our second error is the systematic error from using our best value. Assumes equal production of B^+ and B^0 at the $\Upsilon(4S)$.

 $\Gamma(\chi_{c1}(1P)\pi^+)/\Gamma(\chi_{c1}(1P)K^+)$ $\Gamma_{352}/\Gamma_{353}$

VALUE	DOCUMENT ID	TECN	COMMENT
0.043 ± 0.008 ± 0.003	¹ KUMAR 06	BELL	$e^+e^- \rightarrow \Upsilon(4S)$

¹Assumes equal production of B^+ and B^0 at the $\Upsilon(4S)$.

 $\Gamma(\chi_{c1}(1P)K^*(892)^+)/\Gamma_{total}$ Γ_{354}/Γ

VALUE (units 10^{-4})	CL%	DOCUMENT ID	TECN	COMMENT
3.0 ± 0.6 OUR AVERAGE				Error includes scale factor of 1.1.

¹AUBERT 09B BABR $e^+e^- \rightarrow \Upsilon(4S)$
²SONI 06 BELL $e^+e^- \rightarrow \Upsilon(4S)$

• • • We do not use the following data for averages, fits, limits, etc. • • •

2.94 ± 0.95 ± 0.98		² AUBERT 05J	BABR	Repl. by AUBERT 09B
<21	90	² ALAM 94	CLE2	$e^+e^- \rightarrow \Upsilon(4S)$

¹Uses $\chi_{c1,2} \rightarrow J/\psi\gamma$. Assumes $B(\Upsilon(4S) \rightarrow B^+B^-) = (51.6 \pm 0.6)\%$ and $B(\Upsilon(4S) \rightarrow B^0\bar{B}^0) = (48.4 \pm 0.6)\%$.

²Assumes equal production of B^+ and B^0 at the $\Upsilon(4S)$.

 $\Gamma(\chi_{c1}(1P)K^*(892)^+)/\Gamma(\chi_{c1}(1P)K^+)$ $\Gamma_{354}/\Gamma_{353}$

VALUE	DOCUMENT ID	TECN	COMMENT
0.51 ± 0.17 ± 0.16	AUBERT 05J	BABR	$e^+e^- \rightarrow \Upsilon(4S)$

 $\Gamma(\chi_{c1}(1P)K^0\pi^+)/\Gamma_{total}$ Γ_{355}/Γ

VALUE (units 10^{-4})	DOCUMENT ID	TECN	COMMENT
5.75 ± 0.26 ± 0.32	¹ BHARDWAJ 16	BELL	$e^+e^- \rightarrow \Upsilon(4S)$

¹Assumes equal production of B^+ and B^0 at the $\Upsilon(4S)$.

 $\Gamma(\chi_{c1}(1P)K^0\pi^+)/\Gamma(J/\psi(1S)K^0\pi^+)$ $\Gamma_{355}/\Gamma_{296}$

VALUE	DOCUMENT ID	TECN	COMMENT
0.503 ± 0.030 ± 0.019	¹ LEES 12B	BABR	$e^+e^- \rightarrow \Upsilon(4S)$

¹LEES 12B reports $0.501 \pm 0.024 \pm 0.028$ from a measurement of $[\Gamma(B^+ \rightarrow \chi_{c1}(1P)K^0\pi^+)/\Gamma(B^+ \rightarrow J/\psi(1S)K^0\pi^+)] \times [B(\chi_{c1}(1P) \rightarrow \gamma J/\psi(1S))]$ assuming $B(\chi_{c1}(1P) \rightarrow \gamma J/\psi(1S)) = (34.4 \pm 1.5) \times 10^{-2}$, which we rescale to our best value $B(\chi_{c1}(1P) \rightarrow \gamma J/\psi(1S)) = (34.3 \pm 1.3) \times 10^{-2}$. Our first error is their experiment's error and our second error is the systematic error from using our best value.

 $\Gamma(\chi_{c1}(1P)K^+\pi^0)/\Gamma_{total}$ Γ_{356}/Γ

VALUE (units 10^{-4})	DOCUMENT ID	TECN	COMMENT
3.29 ± 0.29 ± 0.19	¹ BHARDWAJ 16	BELL	$e^+e^- \rightarrow \Upsilon(4S)$

¹Assumes equal production of B^+ and B^0 at the $\Upsilon(4S)$.

 $\Gamma(\chi_{c1}(1P)K^+\pi^-\pi^-)/\Gamma_{total}$ Γ_{357}/Γ

VALUE (units 10^{-4})	DOCUMENT ID	TECN	COMMENT
3.74 ± 0.18 ± 0.24	¹ BHARDWAJ 16	BELL	$e^+e^- \rightarrow \Upsilon(4S)$

¹Assumes equal production of B^+ and B^0 at the $\Upsilon(4S)$.

 $\Gamma(\chi_{c1}(2P)K^+, \chi_{c1}(2P) \rightarrow \pi^+\pi^-\chi_{c1}(1P))/\Gamma_{total}$ Γ_{358}/Γ

VALUE	CL%	DOCUMENT ID	TECN	COMMENT
<1.1 × 10⁻⁵	90	^{1,2} BHARDWAJ 16	BELL	$e^+e^- \rightarrow \Upsilon(4S)$

¹BHARDWAJ 16 analysis fixes mass and width of the $\chi_{c1}(2P)$ state to 3920 MeV and 20 MeV.

²Assumes equal production of B^+ and B^0 at the $\Upsilon(4S)$.

 $\Gamma(\chi_{c2}\pi^+, \chi_{c2} \rightarrow \pi^0\pi^0)/\Gamma_{total}$ Γ_{359}/Γ

VALUE	CL%	DOCUMENT ID	TECN	COMMENT
<7 × 10⁻⁷	90	LAI 23	BELL	$e^+e^- \rightarrow \Upsilon(4S)$

 $\Gamma(\chi_{c2}K^+)/\Gamma_{total}$ Γ_{360}/Γ

VALUE (units 10^{-3})	CL%	DOCUMENT ID	TECN	COMMENT
1.11 + 0.36 - 0.34 ± 0.09		¹ BHARDWAJ 11	BELL	$e^+e^- \rightarrow \Upsilon(4S)$

• • • We do not use the following data for averages, fits, limits, etc. • • •

< 1.8	90	² AUBERT 09B	BABR	$e^+e^- \rightarrow \Upsilon(4S)$
< 20	90	³ AUBERT 06E	BABR	$e^+e^- \rightarrow \Upsilon(4S)$
< 2.9	90	¹ SONI 06	BELL	Repl. by BHARDWAJ 11
< 3.0	90	¹ AUBERT 05K	BABR	Repl. by AUBERT 06E

¹Assumes equal production of B^+ and B^0 at the $\Upsilon(4S)$.

²Uses $\chi_{c1,2} \rightarrow J/\psi\gamma$. Assumes $B(\Upsilon(4S) \rightarrow B^+B^-) = (51.6 \pm 0.6)\%$ and $B(\Upsilon(4S) \rightarrow B^0\bar{B}^0) = (48.4 \pm 0.6)\%$.

³Perform measurements of absolute branching fractions using a missing mass technique.

 $\Gamma(\chi_{c2}K^+, \chi_{c2} \rightarrow p\bar{p}\pi^+\pi^-)/\Gamma_{total}$ Γ_{361}/Γ

VALUE	DOCUMENT ID	TECN	COMMENT
<1.9 × 10⁻⁷	CHILIKIN 19	BELL	$e^+e^- \rightarrow \Upsilon(4S)$

 $\Gamma(B^+ \rightarrow \chi_{c2}K^+)/\Gamma_{total} \times \Gamma(\chi_{c2}(1P) \rightarrow \gamma\gamma)/\Gamma_{total}$ $\Gamma_{360}/\Gamma \times \Gamma_{98}^{\chi_{c2}(1P)}/\Gamma_{\chi_{c2}(1P)}$

VALUE (units 10^{-6})	CL%	DOCUMENT ID	TECN	COMMENT
<0.09	90	¹ WICHT 08	BELL	$e^+e^- \rightarrow \Upsilon(4S)$

¹Assumes equal production of B^+ and B^0 at the $\Upsilon(4S)$.

 $\Gamma(\chi_{c2}K^*(892)^+)/\Gamma_{total}$ Γ_{362}/Γ

VALUE	CL%	DOCUMENT ID	TECN	COMMENT
<12 × 10⁻⁵	90	¹ AUBERT 09B	BABR	$e^+e^- \rightarrow \Upsilon(4S)$

• • • We do not use the following data for averages, fits, limits, etc. • • •

<12.7 × 10 ⁻⁵	90	² SONI 06	BELL	$e^+e^- \rightarrow \Upsilon(4S)$
< 1.2 × 10 ⁻⁵	90	² AUBERT 05K	BABR	Repl. by AUBERT 09B

¹Uses $\chi_{c1,2} \rightarrow J/\psi\gamma$. Assumes $B(\Upsilon(4S) \rightarrow B^+B^-) = (51.6 \pm 0.6)\%$ and $B(\Upsilon(4S) \rightarrow B^0\bar{B}^0) = (48.4 \pm 0.6)\%$.

²Assumes equal production of B^+ and B^0 at the $\Upsilon(4S)$.

 $\Gamma(\chi_{c2}K^0\pi^+)/\Gamma_{total}$ Γ_{363}/Γ

VALUE (units 10^{-4})	DOCUMENT ID	TECN	COMMENT
1.24 ± 0.25 OUR AVERAGE			

¹AAIJ 23AH LHCB pp at 7, 8 and 13 TeV
²BHARDWAJ 16 BELL $e^+e^- \rightarrow \Upsilon(4S)$

¹The second uncertainty includes systematic and reference branching reaction of $B^+ \rightarrow J/\psi K^+$ uncertainties.

²Assumes equal production of B^+ and B^0 at the $\Upsilon(4S)$.

 $\Gamma(\chi_{c2}K^+\pi^0)/\Gamma_{total}$ Γ_{364}/Γ

VALUE	CL%	DOCUMENT ID	TECN	COMMENT
<0.62 × 10⁻⁴	90	¹ BHARDWAJ 16	BELL	$e^+e^- \rightarrow \Upsilon(4S)$

¹Assumes equal production of B^+ and B^0 at the $\Upsilon(4S)$.

 $\Gamma(\chi_{c2}K^+\pi^-\pi^-)/\Gamma_{total}$ Γ_{365}/Γ

VALUE (units 10^{-4})	DOCUMENT ID	TECN	COMMENT
1.34 ± 0.17 ± 0.09	¹ BHARDWAJ 16	BELL	$e^+e^- \rightarrow \Upsilon(4S)$

¹Assumes equal production of B^+ and B^0 at the $\Upsilon(4S)$.

 $\Gamma(\chi_{c2}(3930)K^+, \chi_{c2} \rightarrow D^+D^-)/\Gamma(D^-D^+K^+)$ $\Gamma_{366}/\Gamma_{221}$

VALUE (units 10^{-2})	DOCUMENT ID	TECN	COMMENT
7.2 ± 1.2 ± 0.3	¹ AAIJ 20AI	LHCB	pp at 7, 8, 13 TeV

¹Measured in Dalitz plot analysis of $B^+ \rightarrow D^-D^+K^+$ decays.

 $\Gamma(\chi_{c2}(3930)\pi^+, \chi_{c2} \rightarrow \pi^+\pi^-)/\Gamma_{total}$ Γ_{367}/Γ

VALUE (units 10^{-6})	CL%	DOCUMENT ID	TECN	COMMENT
<0.1	90	¹ AUBERT 09L	BABR	$e^+e^- \rightarrow \Upsilon(4S)$

¹Assumes equal production of B^+ and B^0 at the $\Upsilon(4S)$.

 $\Gamma(h_c(1P)K^+)/\Gamma_{total}$ Γ_{368}/Γ

VALUE (units 10^{-5})	CL%	DOCUMENT ID	TECN	COMMENT
3.7 + 1.0 + 0.8 - 0.9 - 0.8		CHILIKIN 19	BELL	$e^+e^- \rightarrow \Upsilon(4S)$

• • • We do not use the following data for averages, fits, limits, etc. • • •

<3.8 90 ¹FANG 06 BELL $e^+e^- \rightarrow \Upsilon(4S)$

¹Assumes equal production of B^+ and B^0 at the $\Upsilon(4S)$ and $B(h_c \rightarrow \eta_c\gamma) = 50\%$.

 $\Gamma(h_c(1P)K^+, h_c \rightarrow p\bar{p})/\Gamma_{total}$ Γ_{369}/Γ

VALUE	CL%	DOCUMENT ID	TECN	COMMENT
<6.4 × 10⁻⁸	95	¹ AAIJ 13S	LHCB	pp at 7 TeV

¹Measured relative to $B^+ \rightarrow J/\psi K^+$ decay with charmonia reconstructed in $p\bar{p}$ final state and using $B(B^+ \rightarrow J/\psi K^+) = (1.013 \pm 0.034) \times 10^{-3}$ and $B(J/\psi \rightarrow p\bar{p}) = (2.17 \pm 0.07) \times 10^{-3}$.

 $\Gamma(K^0\pi^+)/\Gamma_{total}$ Γ_{370}/Γ

VALUE (units 10^{-6})	CL%	DOCUMENT ID	TECN	COMMENT
23.9 ± 0.6 OUR FIT				

24.0 ± 0.6 OUR AVERAGE				
24.37 ± 0.71 ± 0.86		ADACHI 24	BELL	$e^+e^- \rightarrow \Upsilon(4S)$
23.97 ± 0.53 ± 0.71		¹ DUH 13	BELL	$e^+e^- \rightarrow \Upsilon(4S)$
23.9 ± 1.1 ± 1.0		¹ AUBERT, BE 06C	BABR	$e^+e^- \rightarrow \Upsilon(4S)$
18.8 ± 3.7 + 2.1 - 3.3 - 1.8		¹ BORNHEIM 03	CLE2	$e^+e^- \rightarrow \Upsilon(4S)$

• • • We do not use the following data for averages, fits, limits, etc. • • •

22.8 ± 0.8 ± 1.3		¹ LIN 07	BELL	Repl. by DUH 13
26.0 ± 1.3 ± 1.0		¹ AUBERT, BE 05E	BABR	Repl. by AUBERT, BE 06C
22.3 ± 1.7 ± 1.1		¹ AUBERT 04M	BABR	Repl. by AUBERT, BE 05E
22.0 ± 1.9 ± 1.1		¹ CHAO 04	BELL	Repl. by LIN 07
19.4 ± 3.1 ± 1.6		¹ CASEY 02	BELL	Repl. by CHAO 04

13.7	± 5.7	$+1.9$	-1.8	1 ABE	01H	BELL	Repl. by CASEY 02
18.2	± 3.3	± 2.0		1 AUBERT	01E	BABR	Repl. by AUBERT 04M
18.2	± 4.6	± 1.6		1 CRONIN-HEN..00	CLE2	Repl. by BORNHEIM 03	
23	± 11	± 3.6		GODANG	98	CLE2	Repl. by CRONIN-HENNESSY 00
< 48	90			ASNER	96	CLE2	Repl. by GODANG 98
<190	90			ALBRECHT	91B	ARG	$e^+e^- \rightarrow \Upsilon(4S)$
<100	90			2 AVERY	89B	CLEO	$e^+e^- \rightarrow \Upsilon(4S)$
<680	90			AVERY	87	CLEO	$e^+e^- \rightarrow \Upsilon(4S)$

¹ Assumes equal production of B^+ and B^0 at the $\Upsilon(4S)$.
² AVERY 89B reports $< 9 \times 10^{-5}$ assuming the $\Upsilon(4S)$ decays 43% to $B^0\bar{B}^0$. We rescale to 50%.

$\Gamma(K^+\pi^0)/\Gamma_{total}$ Γ_{371}/Γ

VALUE (units 10^{-6})	CL%	DOCUMENT ID	TECN	COMMENT
13.2 ± 0.4 OUR AVERAGE				
13.93 $\pm 0.38 \pm 0.71$		ADACHI	24	BELL $e^+e^- \rightarrow \Upsilon(4S)$
12.62 $\pm 0.31 \pm 0.56$		1 DUH	13	BELL $e^+e^- \rightarrow \Upsilon(4S)$
13.6 $\pm 0.6 \pm 0.7$		1 AUBERT	07bc	BABR $e^+e^- \rightarrow \Upsilon(4S)$
12.9 ± 2.4	± 1.2	1 BORNHEIM	03	CLE2 $e^+e^- \rightarrow \Upsilon(4S)$
12.4 ± 0.5	± 0.6	1 LIN	07A	BELL Repl. by DUH 13
12.0 ± 0.7	± 0.6	1 AUBERT	05L	BABR Repl. by AUBERT 07bc
12.0 ± 1.3	± 1.3	1 CHAO	04	BELL Repl. by LIN 07A
12.8 ± 1.2	± 1.0	1 AUBERT	03L	BABR Repl. by AUBERT 05L
13.0 ± 2.5	± 1.3	1 CASEY	02	BELL Repl. by CHAO 04
16.3 ± 3.5	± 1.6	1 ABE	01H	BELL Repl. by CASEY 02
10.8 ± 2.1	± 1.0	1 AUBERT	01E	BABR Repl. by AUBERT 03L
11.6 ± 3.0	± 1.4	1 CRONIN-HEN..00	CLE2	Repl. by BORNHEIM 03
<16	90	GODANG	98	CLE2 Repl. by CRONIN-HENNESSY 00
<14	90	ASNER	96	CLE2 Repl. by GODANG 98

¹ Assumes equal production of B^+ and B^0 at the $\Upsilon(4S)$.

$\Gamma(K^+\pi^0)/\Gamma(K^0\pi^+)$ $\Gamma_{371}/\Gamma_{370}$

VALUE	DOCUMENT ID	TECN	COMMENT
0.54 $\pm 0.03 \pm 0.04$	LIN	07A	BELL $e^+e^- \rightarrow \Upsilon(4S)$
2.38 ± 0.98	ABE	01H	BELL Repl. by LIN 07A

$\Gamma(\eta'K^+)/\Gamma_{total}$ Γ_{372}/Γ

VALUE (units 10^{-6})	DOCUMENT ID	TECN	COMMENT
70.5 ± 2.5 OUR AVERAGE			
71.5 $\pm 1.3 \pm 3.2$	1 AUBERT	09AV	BABR $e^+e^- \rightarrow \Upsilon(4S)$
61 ± 10	1,2 WICHT	08	BELL $e^+e^- \rightarrow \Upsilon(4S)$
69.2 $\pm 2.2 \pm 3.7$	1 SCHUEMANN	06	BELL $e^+e^- \rightarrow \Upsilon(4S)$
80 ± 10	1 RICHICHI	00	CLE2 $e^+e^- \rightarrow \Upsilon(4S)$
70.0 $\pm 1.5 \pm 2.8$	1 AUBERT	07AE	BABR Repl. by AUBERT 09AV
68.9 $\pm 2.0 \pm 3.2$	1 AUBERT	05M	BABR Repl. by AUBERT 07AE
76.9 $\pm 3.5 \pm 4.4$	1 AUBERT	03W	BABR Repl. by AUBERT 05M
79 ± 12	1 ABE	01M	BELL Repl. by SCHUEMANN 06
70 ± 8	1 AUBERT	01G	BABR Repl. by AUBERT 03W
65 ± 15	BEHRENS	98	CLE2 Repl. by RICHICHI 00

¹ Assumes equal production of B^+ and B^0 at the $\Upsilon(4S)$.
² WICHT 08 reports $[\Gamma(B^+ \rightarrow \eta'K^+)/\Gamma_{total}] \times [B(\eta'(958) \rightarrow \gamma\gamma)] = (1.40^{+0.16+0.15}_{-0.15-0.12}) \times 10^{-6}$ which we divide by our best value $B(\eta'(958) \rightarrow \gamma\gamma) = (2.307 \pm 0.033) \times 10^{-2}$. Our first error is their experiment's error and our second error is the systematic error from using our best value.

$\Gamma(\eta'K^*(892)^+)/\Gamma_{total}$ Γ_{373}/Γ

VALUE (units 10^{-6})	CL%	DOCUMENT ID	TECN	COMMENT
4.8 $\pm 1.6 \pm 0.8$		1 DEL-AMO-SA..10A	BABR	$e^+e^- \rightarrow \Upsilon(4S)$
4.9 ± 1.9	± 0.8	1 AUBERT	07E	BABR Repl. by DEL-AMO-SANCHEZ 10A
< 2.9	90	1 SCHUEMANN	07	BELL $e^+e^- \rightarrow \Upsilon(4S)$
<14	90	1 AUBERT,B	04D	BABR Repl. by AUBERT 07E
<35	90	1 RICHICHI	00	CLE2 $e^+e^- \rightarrow \Upsilon(4S)$
<13	90	BEHRENS	98	CLE2 Repl. by RICHICHI 00

¹ Assumes equal production of B^+ and B^0 at the $\Upsilon(4S)$.

$\Gamma(\eta'K^*_2(1430)^+)/\Gamma_{total}$ Γ_{374}/Γ

VALUE (units 10^{-6})	DOCUMENT ID	TECN	COMMENT
5.2 $\pm 1.9 \pm 1.0$	1 DEL-AMO-SA..10A	BABR	$e^+e^- \rightarrow \Upsilon(4S)$
¹ Assumes equal production of B^+ and B^0 at the $\Upsilon(4S)$.			

$\Gamma(\eta'K^*_2(1430)^+)/\Gamma_{total}$ Γ_{375}/Γ

VALUE (units 10^{-6})	DOCUMENT ID	TECN	COMMENT
28.0 $\pm 4.6 \pm 2.6$	1 DEL-AMO-SA..10A	BABR	$e^+e^- \rightarrow \Upsilon(4S)$
¹ Assumes equal production of B^+ and B^0 at the $\Upsilon(4S)$.			

$\Gamma(\eta K^+)/\Gamma_{total}$ Γ_{376}/Γ

VALUE (units 10^{-6})	CL%	DOCUMENT ID	TECN	COMMENT
2.4 ± 0.4 OUR AVERAGE				Error includes scale factor of 1.7.
2.12 $\pm 0.23 \pm 0.11$		1 HOI	12	BELL $e^+e^- \rightarrow \Upsilon(4S)$
2.94 ± 0.39	± 0.21	1 AUBERT	09AV	BABR $e^+e^- \rightarrow \Upsilon(4S)$
2.2 ± 2.8	± 2.2	1 RICHICHI	00	CLE2 $e^+e^- \rightarrow \Upsilon(4S)$
• • • We do not use the following data for averages, fits, limits, etc. • • •				
2.21 ± 0.48	± 0.01	1,2 WICHT	08	BELL Repl. by HOI 12
3.7 ± 0.4	± 0.1	1 AUBERT	07AE	BABR Repl. by AUBERT 09AV
1.9 ± 0.3	± 0.2	1 CHANG	07B	BELL Repl. by HOI 12
3.3 ± 0.6	± 0.3	1 AUBERT,B	05K	BABR Repl. by AUBERT 07AE
2.1 ± 0.6	± 0.2	1 CHANG	05A	BELL Repl. by CHANG 07B
3.4 ± 0.8	± 0.2	1 AUBERT	04H	BABR Repl. by AUBERT,B 05K
<14	90	BEHRENS	98	CLE2 Repl. by RICHICHI 00

¹ Assumes equal production of B^+ and B^0 at the $\Upsilon(4S)$.
² WICHT 08 reports $[\Gamma(B^+ \rightarrow \eta K^+)/\Gamma_{total}] \times [B(\eta \rightarrow 2\gamma)] = (0.87^{+0.16+0.10}_{-0.15-0.07}) \times 10^{-6}$ which we divide by our best value $B(\eta \rightarrow 2\gamma) = (39.36 \pm 0.18) \times 10^{-2}$. Our first error is their experiment's error and our second error is the systematic error from using our best value.

$\Gamma(\eta K^*(892)^+)/\Gamma_{total}$ Γ_{377}/Γ

VALUE (units 10^{-6})	CL%	DOCUMENT ID	TECN	COMMENT
19.3 ± 1.6 OUR AVERAGE				
19.3 ± 2.0	± 1.5	1 WANG	07b	BELL $e^+e^- \rightarrow \Upsilon(4S)$
18.9 $\pm 1.8 \pm 1.3$		1 AUBERT,B	06H	BABR $e^+e^- \rightarrow \Upsilon(4S)$
26.4 ± 9.6	± 3.3	1 RICHICHI	00	CLE2 $e^+e^- \rightarrow \Upsilon(4S)$
25.6 $\pm 4.0 \pm 2.4$		1 AUBERT,B	04d	BABR Repl. by AUBERT,B 06H
<30	90	BEHRENS	98	CLE2 Repl. by RICHICHI 00

$\Gamma(\eta K^*_0(1430)^+)/\Gamma_{total}$ Γ_{378}/Γ

VALUE (units 10^{-6})	DOCUMENT ID	TECN	COMMENT
18.2 $\pm 2.6 \pm 2.6$	1 AUBERT,B	06H	BABR $e^+e^- \rightarrow \Upsilon(4S)$
¹ Assumes equal production of B^+ and B^0 at the $\Upsilon(4S)$.			

$\Gamma(\eta K^*_2(1430)^+)/\Gamma_{total}$ Γ_{379}/Γ

VALUE (units 10^{-6})	DOCUMENT ID	TECN	COMMENT
9.1 $\pm 2.7 \pm 1.4$	1 AUBERT,B	06H	BABR $e^+e^- \rightarrow \Upsilon(4S)$
¹ Assumes equal production of B^+ and B^0 at the $\Upsilon(4S)$.			

$\Gamma(\eta(1295)K^+ \times B(\eta(1295) \rightarrow \eta\pi\pi))/\Gamma_{total}$ Γ_{380}/Γ

VALUE (units 10^{-6})	DOCUMENT ID	TECN	COMMENT
2.9 $\pm 0.8 \pm 0.2$	1 AUBERT	08x	BABR $e^+e^- \rightarrow \Upsilon(4S)$
¹ Assumes equal production of B^+ and B^0 at the $\Upsilon(4S)$.			

$\Gamma(\eta(1405)K^+ \times B(\eta(1405) \rightarrow \eta\pi\pi))/\Gamma_{total}$ Γ_{381}/Γ

VALUE (units 10^{-6})	CL%	DOCUMENT ID	TECN	COMMENT
<1.3	90	1 AUBERT	08x	BABR $e^+e^- \rightarrow \Upsilon(4S)$
¹ Assumes equal production of B^+ and B^0 at the $\Upsilon(4S)$.				

$\Gamma(\eta(1405)K^+ \times B(\eta(1405) \rightarrow K^*K))/\Gamma_{total}$ Γ_{382}/Γ

VALUE (units 10^{-6})	CL%	DOCUMENT ID	TECN	COMMENT
<1.2	90	1 AUBERT	08x	BABR $e^+e^- \rightarrow \Upsilon(4S)$
¹ Assumes equal production of B^+ and B^0 at the $\Upsilon(4S)$.				

$\Gamma(\eta(1475)K^+ \times B(\eta(1475) \rightarrow K^*K))/\Gamma_{total}$ Γ_{383}/Γ

VALUE (units 10^{-6})	DOCUMENT ID	TECN	COMMENT
13.8 $\pm 1.8 \pm 1.0$	1 AUBERT	08x	BABR $e^+e^- \rightarrow \Upsilon(4S)$
¹ Assumes equal production of B^+ and B^0 at the $\Upsilon(4S)$.			

$\Gamma(f_1(1285)K^+)/\Gamma_{total}$ Γ_{384}/Γ

VALUE (units 10^{-6})	CL%	DOCUMENT ID	TECN	COMMENT
<2.0	90	1 AUBERT	08x	BABR $e^+e^- \rightarrow \Upsilon(4S)$
¹ Assumes equal production of B^+ and B^0 at the $\Upsilon(4S)$.				

Meson Particle Listings

 B^\pm $\Gamma(\bar{f}_1(1420)K^+ \times B(\bar{f}_1(1420) \rightarrow \eta\pi\pi))/\Gamma_{\text{total}}$ Γ_{385}/Γ

VALUE (units 10^{-6})	CL%	DOCUMENT ID	TECN	COMMENT
<2.9	90	¹ AUBERT	08x BABR	$e^+e^- \rightarrow \Upsilon(4S)$

¹ Assumes equal production of B^+ and B^0 at the $\Upsilon(4S)$. $\Gamma(\bar{f}_1(1420)K^+ \times B(\bar{f}_1(1420) \rightarrow K^*K))/\Gamma_{\text{total}}$ Γ_{386}/Γ

VALUE (units 10^{-6})	CL%	DOCUMENT ID	TECN	COMMENT
<4.1	90	¹ AUBERT	08x BABR	$e^+e^- \rightarrow \Upsilon(4S)$

¹ Assumes equal production of B^+ and B^0 at the $\Upsilon(4S)$. $\Gamma(\phi(1680)K^+ \times B(\phi(1680) \rightarrow K^*K))/\Gamma_{\text{total}}$ Γ_{387}/Γ

VALUE (units 10^{-6})	CL%	DOCUMENT ID	TECN	COMMENT
<3.4	90	¹ AUBERT	08x BABR	$e^+e^- \rightarrow \Upsilon(4S)$

¹ Assumes equal production of B^+ and B^0 at the $\Upsilon(4S)$. $\Gamma(f_0(1500)K^+)/\Gamma_{\text{total}}$ Γ_{388}/Γ

VALUE (units 10^{-6})	CL%	DOCUMENT ID	TECN	COMMENT
3.7 ± 2.2 OUR AVERAGE				
17 ± 4 ± 12		¹ LEES	12o BABR	$e^+e^- \rightarrow \Upsilon(4S)$
20 ± 10 ± 27		² LEES	12o BABR	$e^+e^- \rightarrow \Upsilon(4S)$
3.2 ⁺ _{-1.9} ± 0.2		^{3,4} AUBERT	08AI BABR	$e^+e^- \rightarrow \Upsilon(4S)$

• • • We do not use the following data for averages, fits, limits, etc. • • •

<19	90	^{4,5} AUBERT,B	05N BABR	Repl. by AUBERT 08AI
-----	----	-------------------------	----------	----------------------

¹ Measured in the $B^+ \rightarrow K^+K^-K^+$ decay.² Measured in the $B^+ \rightarrow K^+K_S^0K^0$ decay.

³ AUBERT 08AI reports $B(B^+ \rightarrow f_0(1500)K^+) \cdot B(f_0(1500) \rightarrow \pi^+\pi^-) = (0.73 \pm 0.21_{-0.47}^{+0.47}) \times 10^{-6}$. We divide this result by our best value of $B(f_0(1500) \rightarrow \pi\pi) = (34.5 \pm 2.2) \times 10^{-2}$ multiplied by 2/3 to account for the $\pi^+\pi^-$ fraction. Our first quoted uncertainty is the combined experiment's uncertainty and our second is the systematic uncertainty from using our best value.

⁴ Assumes equal production of B^+ and B^0 at the $\Upsilon(4S)$.

⁵ AUBERT,B 05N reports $B(B^+ \rightarrow f_0(1500)K^+) \cdot B(f_0(1500) \rightarrow \pi^+\pi^-) < 4.4 \times 10^{-6}$. We divide this result by our best value of $B(f_0(1500) \rightarrow \pi\pi) = (34.5 \pm 2.2) \times 10^{-2}$ multiplied by 2/3 to account for the $\pi^+\pi^-$ fraction. Our first quoted uncertainty is the combined experiment's uncertainty and our second is the systematic uncertainty from using our best value.

 $\Gamma(\omega K^+)/\Gamma_{\text{total}}$ Γ_{389}/Γ

VALUE (units 10^{-6})	CL%	DOCUMENT ID	TECN	COMMENT
6.5 ± 0.4 OUR AVERAGE				
6.8 ± 0.4 ± 0.4		¹ CHOBANOVA	14 BELL	$e^+e^- \rightarrow \Upsilon(4S)$
6.3 ± 0.5 ± 0.3		¹ AUBERT	07AE BABR	$e^+e^- \rightarrow \Upsilon(4S)$
3.2 ⁺ _{-1.9} ± 0.8		¹ JESSOP	00 CLE2	$e^+e^- \rightarrow \Upsilon(4S)$

• • • We do not use the following data for averages, fits, limits, etc. • • •

6.1 ± 0.6 ± 0.4		¹ AUBERT,B	06E BABR	AUBERT 07AE
8.1 ± 0.6 ± 0.6		¹ JEN	06 BELL	Repl. by CHOBANOVA 14
4.8 ± 0.8 ± 0.4		¹ AUBERT	04H BABR	Repl. by AUBERT,B 06E
6.5 ⁺ _{-1.2} ± 0.6		¹ WANG	04A BELL	Repl. by JEN 06
9.2 ⁺ _{-2.3} ± 1.0		¹ LU	02 BELL	Repl. by WANG 04A
<4	90	¹ AUBERT	01G BABR	$e^+e^- \rightarrow \Upsilon(4S)$
1.5 ⁺ _{-0.6} ± 2		¹ BERGFELD	98 CLE2	Repl. by JESSOP 00

¹ Assumes equal production of B^+ and B^0 at the $\Upsilon(4S)$. $\Gamma(\omega K^*(892)^+)/\Gamma_{\text{total}}$ Γ_{390}/Γ

VALUE (units 10^{-6})	CL%	DOCUMENT ID	TECN	COMMENT
< 7.4	90	¹ AUBERT	09H BABR	$e^+e^- \rightarrow \Upsilon(4S)$

• • • We do not use the following data for averages, fits, limits, etc. • • •

< 3.4	90	¹ AUBERT,B	06T BABR	Repl. by AUBERT 09H
< 7.4	90	¹ AUBERT	05o BABR	Repl. by AUBERT,B 06T
< 87	90	¹ BERGFELD	98 CLE2	

¹ Assumes equal production of B^+ and B^0 at the $\Upsilon(4S)$. $\Gamma(\omega(K\pi)_0^{*+})/\Gamma_{\text{total}}$ Γ_{391}/Γ

($K\pi$)₀^{*+} is the total S-wave composed of $K_S^0(1430)$ and nonresonant that are described using LASS shape.

VALUE (units 10^{-6})	CL%	DOCUMENT ID	TECN	COMMENT
27.5 ± 3.0 ± 2.6				
		¹ AUBERT	09H BABR	$e^+e^- \rightarrow \Upsilon(4S)$

¹ Assumes equal production of B^+ and B^0 at the $\Upsilon(4S)$. $\Gamma(\omega K_S^0(1430)^+)/\Gamma_{\text{total}}$ Γ_{392}/Γ

VALUE (units 10^{-6})	CL%	DOCUMENT ID	TECN	COMMENT
24.0 ± 2.6 ± 4.4				
		¹ AUBERT	09H BABR	$e^+e^- \rightarrow \Upsilon(4S)$

¹ Assumes equal production of B^+ and B^0 at the $\Upsilon(4S)$. $\Gamma(\omega K_S^2(1430)^+)/\Gamma_{\text{total}}$ Γ_{393}/Γ

VALUE (units 10^{-6})	CL%	DOCUMENT ID	TECN	COMMENT
21.5 ± 3.6 ± 2.4				
		¹ AUBERT	09H BABR	$e^+e^- \rightarrow \Upsilon(4S)$

¹ Assumes equal production of B^+ and B^0 at the $\Upsilon(4S)$. $\Gamma(\bar{a}_0(980)^0 K^+ \times B(\bar{a}_0(980)^0 \rightarrow \eta\pi^0))/\Gamma_{\text{total}}$ Γ_{395}/Γ

VALUE (units 10^{-6})	CL%	DOCUMENT ID	TECN	COMMENT
<2.5	90	¹ AUBERT,BE	04 BABR	$e^+e^- \rightarrow \Upsilon(4S)$

¹ Assumes equal production of charged and neutral B mesons from $\Upsilon(4S)$ decays. $\Gamma(\bar{a}_0(980)^+ K^0 \times B(\bar{a}_0(980)^+ \rightarrow \eta\pi^+))/\Gamma_{\text{total}}$ Γ_{394}/Γ

VALUE (units 10^{-6})	CL%	DOCUMENT ID	TECN	COMMENT
<3.9	90	¹ AUBERT,BE	04 BABR	$e^+e^- \rightarrow \Upsilon(4S)$

¹ Assumes equal production of charged and neutral B mesons from $\Upsilon(4S)$ decays. $\Gamma(K^*(892)^0\pi^+)/\Gamma_{\text{total}}$ Γ_{396}/Γ

VALUE (units 10^{-6})	CL%	DOCUMENT ID	TECN	COMMENT
10.1 ± 0.8 OUR AVERAGE				
10.1 ± 1.7 ± 1.0		¹ LEES	17G BABR	$e^+e^- \rightarrow \Upsilon(4S)$
10.8 ± 0.6 ⁺ _{-1.4}		² AUBERT	08AI BABR	$e^+e^- \rightarrow \Upsilon(4S)$
9.67 ± 0.64 ⁺ _{-0.89}		² GARMASH	06 BELL	$e^+e^- \rightarrow \Upsilon(4S)$

• • • We do not use the following data for averages, fits, limits, etc. • • •

13.5 ± 1.2 ⁺ _{-0.9}		² AUBERT,B	05N BABR	Repl. by AUBERT 08AI
9.8 ± 0.9 ⁺ _{-1.2}		² GARMASH	05 BELL	Repl. by GARMASH 06
15.5 ± 1.8 ⁺ _{-4.0}		^{2,3} AUBERT,B	04P BABR	Repl. by AUBERT,B 05N
19.4 ± 4.2 ⁺ _{-3.9} ± 4.1		⁴ GARMASH	02 BELL	Repl. by GARMASH 05
<119	90	⁵ ABE	00c SLD	$e^+e^- \rightarrow Z$
< 16	90	² JESSOP	00 CLE2	$e^+e^- \rightarrow \Upsilon(4S)$
<390	90	⁶ ADAM	96D DLPH	$e^+e^- \rightarrow Z$
< 41	90	⁶ ASNER	96 CLE2	Repl. by JESSOP 00
<480	90	⁶ ABREU	95N DLPH	Sup. by ADAM 96D
<170	90	⁷ ALBRECHT	91B ARG	$e^+e^- \rightarrow \Upsilon(4S)$
<150	90	⁷ AVERY	89B CLEO	$e^+e^- \rightarrow \Upsilon(4S)$
<260	90	⁷ AVERY	87 CLEO	$e^+e^- \rightarrow \Upsilon(4S)$

¹ Obtains the result from a Dalitz analysis of $B^+ \rightarrow K_S^0\pi^+\pi^0$ decays. The first error is statistical, the second combines all the systematic uncertainties reported in the paper, including signal modelling.

² Assumes equal production of B^+ and B^0 at the $\Upsilon(4S)$.

³ AUBERT 04P also report a branching ratio for $B^+ \rightarrow$ "higher K^* resonances" π^+ , $K^* \rightarrow K^+\pi^-$, $(25.1 \pm 2.0_{-5.7}^{+11.0}) \times 10^{-6}$.

⁴ Uses a reference decay mode $B^+ \rightarrow \bar{D}^0\pi^+$ and $\bar{D}^0 \rightarrow K^+\pi^-$ with $B(B^+ \rightarrow \bar{D}^0\pi^+) \cdot B(\bar{D}^0 \rightarrow K^+\pi^-) = (20.3 \pm 2.0) \times 10^{-5}$.

⁵ ABE 00c assumes $B(Z \rightarrow b\bar{b}) = (21.7 \pm 0.1)\%$ and the B fractions $f_{B^+} = (39.7_{-2.2}^{+1.8})\%$ and $f_{B^0} = (10.5_{-2.2}^{+1.8})\%$.

⁶ Assumes a B^0 , B^- production fraction of 0.39 and a B_S production fraction of 0.12.

⁷ AVERY 89B reports $< 1.3 \times 10^{-4}$ assuming the $\Upsilon(4S)$ decays 43% to $B^0\bar{B}^0$. We rescale to 50%.

 $\Gamma(K^*(892)^+\pi^0)/\Gamma_{\text{total}}$ Γ_{397}/Γ

VALUE (units 10^{-6})	CL%	DOCUMENT ID	TECN	COMMENT
6.8 ± 0.9 OUR AVERAGE				
6.4 ± 0.9 ⁺ _{-0.5}		¹ LEES	17G BABR	$e^+e^- \rightarrow \Upsilon(4S)$
8.2 ± 1.5 ± 1.1		² LEES	11I BABR	$e^+e^- \rightarrow \Upsilon(4S)$

• • • We do not use the following data for averages, fits, limits, etc. • • •

6.9 ± 2.0 ± 1.3		² AUBERT	05x BABR	Repl. by LEES 11I
<31	90	² JESSOP	00 CLE2	$e^+e^- \rightarrow \Upsilon(4S)$
<99	90	² ASNER	96 CLE2	Repl. by JESSOP 00

¹ Obtains the result from a Dalitz analysis of $B^+ \rightarrow K_S^0\pi^+\pi^0$ decays. The first error is statistical, the second combines all the systematic uncertainties reported in the paper, including signal modelling.

² Assumes equal production of B^+ and B^0 at the $\Upsilon(4S)$.

 $\Gamma(K^+\pi^-\pi^+)/\Gamma(K^+K^-K^+)$ $\Gamma_{398}/\Gamma_{451}$

VALUE	DOCUMENT ID	TECN	COMMENT
1.703 ± 0.011 ± 0.022	AAIJ	20AJ LHCB	pp at 7 and 8 TeV

 $\Gamma(K^+\pi^-\pi^+)/\Gamma_{\text{total}}$ Γ_{398}/Γ

VALUE (units 10^{-6})	DOCUMENT ID	TECN	COMMENT
51.0 ± 2.9 OUR AVERAGE			
54.4 ± 1.1 ± 4.6	¹ AUBERT	08AI BABR	$e^+e^- \rightarrow \Upsilon(4S)$
48.8 ± 1.1 ± 3.6	¹ GARMASH	06 BELL	$e^+e^- \rightarrow \Upsilon(4S)$

• • • We do not use the following data for averages, fits, limits, etc. • • •

64.1 ± 2.4 ± 4.0	¹ AUBERT,B	05N BABR	Repl. by AUBERT 08AI
46.6 ± 2.1 ± 4.3	¹ GARMASH	05 BELL	Repl. by GARMASH 06
53.6 ± 3.1 ± 5.1	¹ GARMASH	04 BELL	Repl. by GARMASH 05
59.1 ± 3.8 ± 3.2	² AUBERT	03M BABR	Repl. by AUBERT,B 05N
55.6 ± 5.8 ± 7.7	³ GARMASH	02 BELL	Repl. by GARMASH 04

¹ Assumes equal production of B^+ and B^0 at the $\Upsilon(4S)$.

² Assumes equal production of B^0 and B^+ at the $\Upsilon(4S)$; charm and charmonium contributions are subtracted, otherwise no assumptions about intermediate resonances.

³ Uses a reference decay mode $B^+ \rightarrow \bar{D}^0\pi^+$ and $\bar{D}^0 \rightarrow K^+\pi^-$ with $B(B^+ \rightarrow \bar{D}^0\pi^+) \cdot B(\bar{D}^0 \rightarrow K^+\pi^-) = (20.3 \pm 2.0) \times 10^{-5}$.

See key on page 1171

Meson Particle Listings

B^\pm

$\Gamma(K^+\pi^-\pi^+\text{ nonresonant})/\Gamma_{\text{total}}$ Γ_{399}/Γ

VALUE (units 10^{-6})	CL%	DOCUMENT ID	TECN	COMMENT
16.3$^{+2.1}_{-1.5}$		OUR AVERAGE		
9.3 ± 1.0 $^{+6.9}_{-1.7}$		1,2 AUBERT	08AI BABR	$e^+e^- \rightarrow \Upsilon(4S)$
16.9 ± 1.3 $^{+1.7}_{-1.6}$		1 GARMASH	06 BELL	$e^+e^- \rightarrow \Upsilon(4S)$
• • • We do not use the following data for averages, fits, limits, etc. • • •				
2.9 ± 0.6 $^{+0.8}_{-0.5}$		1 AUBERT,B	05N BABR	Repl. by AUBERT 08AI
17.3 ± 1.7 $^{+17.2}_{-8.0}$		1 GARMASH	05 BELL	Repl. by GARMASH 06
< 17	90	1 AUBERT,B	04P BABR	Repl. by AUBERT,B 05N
< 330	90	3 ADAM	96D DLPH	$e^+e^- \rightarrow Z$
< 28	90	BERGFELD	96B CLE2	$e^+e^- \rightarrow \Upsilon(4S)$
< 400	90	3 ABREU	95N DLPH	Sup. by ADAM 96D
< 330	90	ALBRECHT	91E ARG	$e^+e^- \rightarrow \Upsilon(4S)$
< 190	90	4 AVERY	89B CLEO	$e^+e^- \rightarrow \Upsilon(4S)$

- Assumes equal production of B^+ and B^0 at the $\Upsilon(4S)$.
- Calculate the total nonresonant contribution by combining the S-wave composed of $K_0^*(1430)$ and nonresonant that are described using LASS shape.
- Assumes a B^0, B^- production fraction of 0.39 and a B_S production fraction of 0.12.
- AVERY 89B reports $< 1.7 \times 10^{-4}$ assuming the $\Upsilon(4S)$ decays 43% to $B^0\bar{B}^0$. We rescale to 50%.

$\Gamma(\omega(782)K^+)/\Gamma_{\text{total}}$ Γ_{400}/Γ

VALUE (units 10^{-6})	DOCUMENT ID	TECN	COMMENT
5.9$^{+8.8}_{-9.0} \pm 0.5$	1,2 AUBERT	08AI BABR	$e^+e^- \rightarrow \Upsilon(4S)$

- Assumes equal production of B^+ and B^0 at the $\Upsilon(4S)$.
- AUBERT 08AI reports $[\Gamma(B^+ \rightarrow \omega(782)K^+)/\Gamma_{\text{total}}] \times [B(\omega(782) \rightarrow \pi^+\pi^-)] = (0.09 \pm 0.13^{+0.036}_{-0.045}) \times 10^{-6}$ which we divide by our best value $B(\omega(782) \rightarrow \pi^+\pi^-) = (1.53 \pm 0.12) \times 10^{-2}$. Our first error is their experiment's error and our second error is the systematic error from using our best value.

$\Gamma(K^+f_0(980) \times B(f_0(980) \rightarrow \pi^+\pi^-))/\Gamma_{\text{total}}$ Γ_{401}/Γ

VALUE (units 10^{-6})	CL%	DOCUMENT ID	TECN	COMMENT
9.4$^{+1.0}_{-1.2}$		OUR AVERAGE		
10.3 ± 0.5 $^{+2.0}_{-1.4}$		1 AUBERT	08AI BABR	$e^+e^- \rightarrow \Upsilon(4S)$
8.78 ± 0.82 $^{+0.85}_{-1.76}$		1 GARMASH	06 BELL	$e^+e^- \rightarrow \Upsilon(4S)$
• • • We do not use the following data for averages, fits, limits, etc. • • •				
9.47 ± 0.97 $^{+0.62}_{-0.88}$		1 AUBERT,B	05N BABR	Repl. by AUBERT 08AI
7.55 ± 1.24 $^{+1.63}_{-1.18}$		1 GARMASH	05 BELL	Repl. by GARMASH 06
9.2 ± 1.2 $^{+2.1}_{-2.6}$		2 AUBERT,B	04P BABR	Repl. by AUBERT,B 05N
9.6 $^{+2.5}_{-2.3}$ $^{+3.7}_{-1.7}$		3 GARMASH	02 BELL	Repl. by GARMASH 05
< 80	90	4 AVERY	89B CLEO	$e^+e^- \rightarrow \Upsilon(4S)$

- Assumes equal production of B^+ and B^0 at the $\Upsilon(4S)$.
- AUBERT,B 04P also reports $B(B^+ \rightarrow \text{"higher } f^0 \text{ resonances"} \pi^+, f(980)^0 \rightarrow \pi^+\pi^-) = (3.2 \pm 1.2^{+6.9}_{-2.9}) \times 10^{-6}$.
- Uses a reference decay mode $B^+ \rightarrow \bar{D}^0\pi^+$ and $\bar{D}^0 \rightarrow K^+\pi^-$ with $B(B^+ \rightarrow \bar{D}^0\pi^+) \times B(\bar{D}^0 \rightarrow K^+\pi^-) = (20.3 \pm 2.0) \times 10^{-5}$. Only charged pions from the $f_0(980)$ are used.
- AVERY 89B reports $< 7 \times 10^{-5}$ assuming the $\Upsilon(4S)$ decays 43% to $B^0\bar{B}^0$. We rescale to 50%.

$\Gamma(f_2(1270)^0K^+)/\Gamma_{\text{total}}$ Γ_{402}/Γ

VALUE (units 10^{-6})	CL%	DOCUMENT ID	TECN	COMMENT
1.07$^{+0.27}_{-0.27}$		OUR AVERAGE		
0.89 $^{+0.38}_{-0.33}$ $^{+0.01}_{-0.03}$		1,2 AUBERT	08AI BABR	$e^+e^- \rightarrow \Upsilon(4S)$
1.33 ± 0.30 $^{+0.23}_{-0.34}$		1 GARMASH	06 BELL	$e^+e^- \rightarrow \Upsilon(4S)$
• • • We do not use the following data for averages, fits, limits, etc. • • •				
< 16	90	3 AUBERT,B	05N BABR	Repl. by AUBERT 08AI
< 2.3	90	4 GARMASH	05 BELL	Repl. by GARMASH 06

- Assumes equal production of B^+ and B^0 at the $\Upsilon(4S)$.
- AUBERT 08AI reports $(0.50 \pm 0.15^{+0.15}_{-0.11}) \times 10^{-6}$ for $B(B^+ \rightarrow f_2(1270)K^+) \times B(f_2 \rightarrow \pi^+\pi^-)$. We compute $B(B^+ \rightarrow f_2(1270)K^+)$ using the PDG value $B(f_2(1270) \rightarrow \pi\pi) = (84.3 \pm 2.8^{+1.0}_{-1.0}) \times 10^{-2}$ and 2/3 for the $\pi^+\pi^-$ fraction. Our first error is their experiment's error and the second error is systematic error from using our best value.
- AUBERT,B 05N reports 8.9×10^{-6} at 90% CL for $B(B^+ \rightarrow f_2(1270)K^+) \times B(f_2(1270) \rightarrow \pi^+\pi^-)$. We rescaled it using the PDG value $B(f_2(1270) \rightarrow \pi\pi) = 84.7\%$ and 2/3 for the $\pi^+\pi^-$ fraction.
- GARMASH 05 reports 1.3×10^{-6} at 90% CL for $B(B^+ \rightarrow f_2(1270)K^+) \times B(f_2(1270) \rightarrow \pi^+\pi^-)$. We rescaled it using the PDG value $B(f_2(1270) \rightarrow \pi\pi) = 84.7\%$ and 2/3 for the $\pi^+\pi^-$ fraction.

$\Gamma(f_0(1370)^0K^+ \times B(f_0(1370)^0 \rightarrow \pi^+\pi^-))/\Gamma_{\text{total}}$ Γ_{403}/Γ

VALUE	CL%	DOCUMENT ID	TECN	COMMENT
< 11.7 $\times 10^{-6}$	90	1 AUBERT,B	05N BABR	$e^+e^- \rightarrow \Upsilon(4S)$

¹ Assumes equal production of B^+ and B^0 at the $\Upsilon(4S)$.

$\Gamma(\rho(1450)K^+ \times B(\rho(1450)^0 \rightarrow \pi^+\pi^-))/\Gamma_{\text{total}}$ Γ_{404}/Γ

VALUE	CL%	DOCUMENT ID	TECN	COMMENT
< 11.7 $\times 10^{-6}$	90	1 AUBERT,B	05N BABR	$e^+e^- \rightarrow \Upsilon(4S)$

¹ Assumes equal production of B^+ and B^0 at the $\Upsilon(4S)$.

$\Gamma(f_2'(1525)K^+ \times B(f_2'(1525) \rightarrow \pi^+\pi^-))/\Gamma_{\text{total}}$ Γ_{405}/Γ

VALUE	CL%	DOCUMENT ID	TECN	COMMENT
< 3.4 $\times 10^{-6}$	90	1 AUBERT,B	05N BABR	$e^+e^- \rightarrow \Upsilon(4S)$

¹ Assumes equal production of B^+ and B^0 at the $\Upsilon(4S)$.

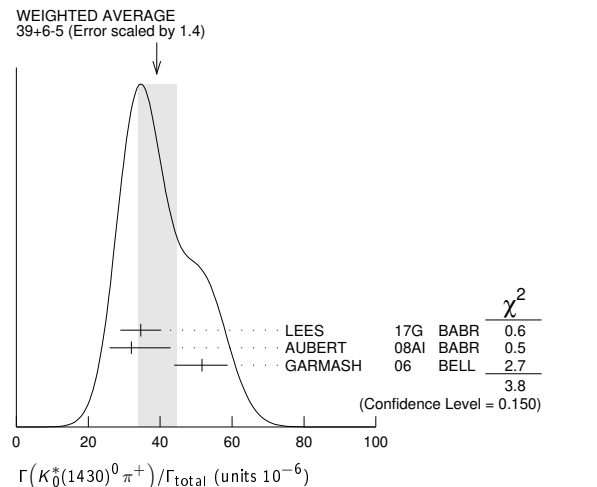
$\Gamma(K^+\rho^0)/\Gamma_{\text{total}}$ Γ_{406}/Γ

VALUE (units 10^{-6})	CL%	DOCUMENT ID	TECN	COMMENT
3.7 ± 0.5		OUR AVERAGE		
3.56 ± 0.45 $^{+0.57}_{-0.46}$		1 AUBERT	08AI BABR	$e^+e^- \rightarrow \Upsilon(4S)$
3.89 ± 0.47 $^{+0.43}_{-0.41}$		1 GARMASH	06 BELL	$e^+e^- \rightarrow \Upsilon(4S)$
• • • We do not use the following data for averages, fits, limits, etc. • • •				
5.07 ± 0.75 $^{+0.55}_{-0.88}$		1 AUBERT,B	05N BABR	Repl. by AUBERT 08AI
4.78 ± 0.75 $^{+1.01}_{-0.97}$		1 GARMASH	05 BELL	Repl. by GARMASH 06
< 6.2	90	2 AUBERT,B	04P BABR	Repl. by AUBERT,B 05N
< 12	90	3 GARMASH	02 BELL	$e^+e^- \rightarrow \Upsilon(4S)$
< 86	90	4 ABE	00C SLD	$e^+e^- \rightarrow Z$
< 17	90	1 JESSOP	00 CLE2	$e^+e^- \rightarrow \Upsilon(4S)$
< 120	90	5 ADAM	96D DLPH	$e^+e^- \rightarrow Z$
< 19	90	ASNER	96 CLE2	Repl. by JESSOP 00
< 190	90	5 ABREU	95N DLPH	Sup. by ADAM 96D
< 180	90	ALBRECHT	91B ARG	$e^+e^- \rightarrow \Upsilon(4S)$
< 80	90	6 AVERY	89B CLEO	$e^+e^- \rightarrow \Upsilon(4S)$
< 260	90	AVERY	87 CLEO	$e^+e^- \rightarrow \Upsilon(4S)$

- Assumes equal production of B^+ and B^0 at the $\Upsilon(4S)$.
- AUBERT 04P reports a central value of $(3.9 \pm 1.2^{+1.3}_{-3.5}) \times 10^{-6}$ for this branching ratio.
- Uses a reference decay mode $B^+ \rightarrow \bar{D}^0\pi^+$ and $\bar{D}^0 \rightarrow K^+\pi^-$ with $B(B^+ \rightarrow \bar{D}^0\pi^+) \times B(\bar{D}^0 \rightarrow K^+\pi^-) = (20.3 \pm 2.0) \times 10^{-5}$.
- ABE 00c assumes $B(Z \rightarrow b\bar{b}) = (21.7 \pm 0.1)\%$ and the B fractions $f_{B^0} = f_{B^+} = (39.7^{+1.8}_{-2.2})\%$ and $f_{B_S} = (10.5^{+1.8}_{-2.2})\%$.
- Assumes production fractions $f_{B^0} = f_{B^-} = 0.39$ and $f_{B_S} = 0.12$.
- AVERY 89B reports $< 7 \times 10^{-5}$ assuming the $\Upsilon(4S)$ decays 43% to $B^0\bar{B}^0$. We rescale to 50%.

$\Gamma(K_0^*(1430)^0\pi^+)/\Gamma_{\text{total}}$ Γ_{407}/Γ

VALUE (units 10^{-6})	DOCUMENT ID	TECN	COMMENT
39$^{+6}_{-5}$	OUR AVERAGE Error includes scale factor of 1.4. See the ideogram below.		
34.6 ± 3.3 ± 4.6	1 LEES	17G BABR	$e^+e^- \rightarrow \Upsilon(4S)$
32.0 ± 1.2 $^{+10.8}_{-6.0}$	2 AUBERT	08AI BABR	$e^+e^- \rightarrow \Upsilon(4S)$
51.6 ± 1.7 $^{+7.0}_{-7.5}$	2 GARMASH	06 BELL	$e^+e^- \rightarrow \Upsilon(4S)$
• • • We do not use the following data for averages, fits, limits, etc. • • •			
44.4 ± 2.2 ± 5.3	2,3 AUBERT,B	05N BABR	Repl. by AUBERT 08AI
45.0 ± 2.9 $^{+15.0}_{-10.7}$	2 GARMASH	05 BELL	Repl. by GARMASH 06



Meson Particle Listings

 B^\pm

¹ Obtains the result from a Dalitz analysis of $B^+ \rightarrow K_S^0 \pi^+ \pi^0$ decays. The first error is statistical, the second combines all the systematic uncertainties reported in the paper, including signal modelling.

² Assumes equal production of B^+ and B^0 at the $\mathcal{T}(4S)$.

³ See erratum: AUBERT_BE 06A.

$\Gamma(K_2^*(1430)^0 \pi^+)/\Gamma_{\text{total}}$		Γ_{408}/Γ			
VALUE (units 10^{-6})	CL%	DOCUMENT ID	TECN	COMMENT	
$5.6^{+2.2}_{-1.5} \pm 0.1$		1,2 AUBERT	08A1	BABR	$e^+ e^- \rightarrow \mathcal{T}(4S)$

• • • We do not use the following data for averages, fits, limits, etc. • • •

< 23	90	³ AUBERT,B	05N	BABR	Repl. by AUBERT 08A1
< 6.9	90	⁴ GARMASH	05	BELL	$e^+ e^- \rightarrow \mathcal{T}(4S)$
< 680	90	ALBRECHT	91B	ARG	$e^+ e^- \rightarrow \mathcal{T}(4S)$

¹ Assumes equal production of B^+ and B^0 at the $\mathcal{T}(4S)$.

² AUBERT 08A1 reports $(1.85 \pm 0.41^{+0.61}_{-0.29}) \times 10^{-6}$ for $B(B^+ \rightarrow K_2^*(1430)^0 \pi^+) \times B(K_2^*(1430)^0 \rightarrow K^+ \pi^-)$. We compute $B(B^+ \rightarrow K_2^*(1430)^0 \pi^+)$ using the PDG value $B(K_2^*(1430)^0 \rightarrow K\pi) = (49.9 \pm 1.2) \times 10^{-2}$ and 2/3 for the $K^+ \pi^-$ fraction. Our first error is their experiment's error and the second error is systematic error from using our best value.

³ AUBERT,B 05N reports 7.7×10^{-6} at 90% CL for $B(B^+ \rightarrow K_2^*(1430)^0 \pi^+) \times B(K_2^*(1430)^0 \rightarrow K^+ \pi^-)$. We rescaled it using the PDG value $B(K_2^*(1430)^0 \rightarrow K\pi) = 49.9\%$ and 2/3 for the $K^+ \pi^-$ fraction.

⁴ GARMASH 05 reports 2.3×10^{-6} at 90% CL for $B(B^+ \rightarrow K_2^*(1430)^0 \pi^+) \times B(K_2^*(1430)^0 \rightarrow K^+ \pi^-)$. We rescaled it using the PDG value $B(K_2^*(1430)^0 \rightarrow K\pi) = 49.9\%$ and 2/3 for the $K^+ \pi^-$ mode.

$\Gamma(K^*(1410)^0 \pi^+)/\Gamma_{\text{total}}$		Γ_{409}/Γ			
VALUE (units 10^{-6})	CL%	DOCUMENT ID	TECN	COMMENT	
< 45	90	¹ GARMASH	05	BELL	$e^+ e^- \rightarrow \mathcal{T}(4S)$

¹ GARMASH 05 reports 2.0×10^{-6} at 90% CL for $B(B^+ \rightarrow K^*(1410)^0 \pi^+) \times B(K^*(1410)^0 \rightarrow K^+ \pi^-)$. We rescaled it using the PDG value $B(K^*(1410)^0 \rightarrow K\pi) = 6.6\%$ and 2/3 for the $K^+ \pi^-$ mode.

$\Gamma(K^*(1680)^0 \pi^+)/\Gamma_{\text{total}}$		Γ_{410}/Γ			
VALUE (units 10^{-6})	CL%	DOCUMENT ID	TECN	COMMENT	
< 12	90	¹ GARMASH	05	BELL	$e^+ e^- \rightarrow \mathcal{T}(4S)$

• • • We do not use the following data for averages, fits, limits, etc. • • •

< 15	90	² AUBERT,B	05N	BABR	$e^+ e^- \rightarrow \mathcal{T}(4S)$
------	----	-----------------------	-----	------	---------------------------------------

¹ GARMASH 05 reports 3.1×10^{-6} at 90% CL for $B(B^+ \rightarrow K^*(1680)^0 \pi^+) \times B(K^*(1680)^0 \rightarrow K^+ \pi^-)$. We rescaled it using the PDG value $B(K^*(1680)^0 \rightarrow K\pi) = 38.7\%$ and 2/3 for the $K^+ \pi^-$ mode.

² AUBERT,B 05N reports 3.8×10^{-6} at 90% CL for $B(B^+ \rightarrow K^*(1680)^0 \pi^+) \times B(K^*(1680)^0 \rightarrow K^+ \pi^-)$. We rescaled it using the PDG value $B(K^*(1680)^0 \rightarrow K\pi) = 38.7\%$ and 2/3 for the $K^+ \pi^-$ fraction.

$\Gamma(K^+ \pi^0 \pi^0)/\Gamma_{\text{total}}$		Γ_{411}/Γ			
VALUE (units 10^{-6})	CL%	DOCUMENT ID	TECN	COMMENT	
$16.2 \pm 1.2 \pm 1.5$		¹ LEES	11i	BABR	$e^+ e^- \rightarrow \mathcal{T}(4S)$

¹ Assumes equal production of B^+ and B^0 at the $\mathcal{T}(4S)$.

$\Gamma(f_0(980) K^+ \times B(f_0 \rightarrow \pi^0 \pi^0))/\Gamma_{\text{total}}$		Γ_{412}/Γ			
VALUE (units 10^{-6})	CL%	DOCUMENT ID	TECN	COMMENT	
$2.8 \pm 0.6 \pm 0.5$		¹ LEES	11i	BABR	$e^+ e^- \rightarrow \mathcal{T}(4S)$

¹ Assumes equal production of B^+ and B^0 at the $\mathcal{T}(4S)$.

$\Gamma(K^- \pi^+ \pi^+)/\Gamma_{\text{total}}$		Γ_{413}/Γ			
VALUE	CL%	DOCUMENT ID	TECN	COMMENT	
$< 4.6 \times 10^{-8}$	90	AAIJ	17E	LHCB	pp at 7, 8 TeV

• • • We do not use the following data for averages, fits, limits, etc. • • •

< 9.5×10^{-7}	90	¹ AUBERT	08BE	BABR	$e^+ e^- \rightarrow \mathcal{T}(4S)$
< 4.5×10^{-6}	90	¹ GARMASH	04	BELL	$e^+ e^- \rightarrow \mathcal{T}(4S)$
< 1.8×10^{-6}	90	² AUBERT	03M	BABR	Repl. by AUBERT 08BE
< 7.0×10^{-6}	90	³ GARMASH	02	BELL	$e^+ e^- \rightarrow \mathcal{T}(4S)$

¹ Assumes equal production of B^+ and B^0 at the $\mathcal{T}(4S)$.

² Assumes equal production of B^0 and B^+ at the $\mathcal{T}(4S)$; charm and charmonium contributions are subtracted, otherwise no assumptions about intermediate resonances.

³ Uses a reference decay mode $B^+ \rightarrow \overline{D}^0 \pi^+$ and $\overline{D}^0 \rightarrow K^+ \pi^-$ with $B(B^+ \rightarrow \overline{D}^0 \pi^+) \cdot B(\overline{D}^0 \rightarrow K^+ \pi^-) = (20.3 \pm 2.0) \times 10^{-5}$.

$\Gamma(K^- \pi^+ \pi^+ \text{nonresonant})/\Gamma_{\text{total}}$		Γ_{414}/Γ			
VALUE (units 10^{-6})	CL%	DOCUMENT ID	TECN	COMMENT	
< 56	90	BERGFELD	96B	CLE2	$e^+ e^- \rightarrow \mathcal{T}(4S)$

$\Gamma(K_1(1270)^0 \pi^+)/\Gamma_{\text{total}}$		Γ_{415}/Γ			
VALUE	CL%	DOCUMENT ID	TECN	COMMENT	
< 4.0×10^{-5}	90	¹ AUBERT	10D	BABR	$e^+ e^- \rightarrow \mathcal{T}(4S)$

¹ Assumes equal production of B^+ and B^0 at the $\mathcal{T}(4S)$.

$\Gamma(K_1(1400)^0 \pi^+)/\Gamma_{\text{total}}$		Γ_{416}/Γ			
VALUE	CL%	DOCUMENT ID	TECN	COMMENT	
< 3.9×10^{-5}	90	¹ AUBERT	10D	BABR	$e^+ e^- \rightarrow \mathcal{T}(4S)$
• • •		We do not use the following data for averages, fits, limits, etc. • • •			
< 2.6×10^{-3}	90	ALBRECHT	91B	ARG	$e^+ e^- \rightarrow \mathcal{T}(4S)$

¹ Assumes equal production of B^+ and B^0 at the $\mathcal{T}(4S)$.

$\Gamma(K^0 \pi^+ \pi^0)/\Gamma_{\text{total}}$		Γ_{417}/Γ			
VALUE (units 10^{-6})	CL%	DOCUMENT ID	TECN	COMMENT	
$31.8 \pm 1.8^{+6.3}_{-2.1}$		¹ LEES	17G	BABR	$e^+ e^- \rightarrow \mathcal{T}(4S)$
< 66	90	² ECKHART	02	CLE2	$e^+ e^- \rightarrow \mathcal{T}(4S)$

¹ Obtains the result from a Dalitz analysis of $B^+ \rightarrow K_S^0 \pi^+ \pi^0$ decays. The first error is statistical, the second combines all the systematic uncertainties reported in the paper, including signal modelling.

² Assumes equal production of B^+ and B^0 at the $\mathcal{T}(4S)$.

$\Gamma(K^0 \rho^+)/\Gamma_{\text{total}}$		Γ_{419}/Γ			
VALUE (units 10^{-6})	CL%	DOCUMENT ID	TECN	COMMENT	
$7.3^{+1.0}_{-1.2}$ OUR AVERAGE					
$6.5 \pm 1.1^{+0.8}_{-1.9}$		¹ LEES	17G	BABR	$e^+ e^- \rightarrow \mathcal{T}(4S)$
$8.0^{+1.4}_{-1.3} \pm 0.6$		AUBERT	07Z	BABR	$e^+ e^- \rightarrow \mathcal{T}(4S)$

• • • We do not use the following data for averages, fits, limits, etc. • • •

< 48	90	ASNER	96	CLE2	$e^+ e^- \rightarrow \mathcal{T}(4S)$
------	----	-------	----	------	---------------------------------------

¹ Obtains the result from a Dalitz analysis of $B^+ \rightarrow K_S^0 \pi^+ \pi^0$ decays. The first error is statistical, the second combines all the systematic uncertainties reported in the paper, including signal modelling.

$\Gamma(K_0^*(1430)^+ \pi^0)/\Gamma_{\text{total}}$		Γ_{418}/Γ			
VALUE (units 10^{-6})	CL%	DOCUMENT ID	TECN	COMMENT	
$11.9 \pm 1.7^{+1.0}_{-1.6}$		¹ LEES	17G	BABR	$e^+ e^- \rightarrow \mathcal{T}(4S)$

¹ Obtains the result from a Dalitz analysis of $B^+ \rightarrow K_S^0 \pi^+ \pi^0$ decays. The first error is statistical, the second combines all the systematic uncertainties reported in the paper, including signal modelling.

$\Gamma(K^*(892)^+ \pi^+ \pi^-)/\Gamma_{\text{total}}$		Γ_{420}/Γ			
VALUE (units 10^{-6})	CL%	DOCUMENT ID	TECN	COMMENT	
$75.3 \pm 6.0 \pm 8.1$		¹ AUBERT,B	06U	BABR	$e^+ e^- \rightarrow \mathcal{T}(4S)$

• • • We do not use the following data for averages, fits, limits, etc. • • •

< 1100	90	ALBRECHT	91E	ARG	$e^+ e^- \rightarrow \mathcal{T}(4S)$
--------	----	----------	-----	-----	---------------------------------------

¹ Assumes equal production of B^+ and B^0 at the $\mathcal{T}(4S)$.

$\Gamma(K^*(892)^+ \rho^0)/\Gamma_{\text{total}}$		Γ_{421}/Γ			
VALUE (units 10^{-6})	CL%	DOCUMENT ID	TECN	COMMENT	
$4.6 \pm 1.0 \pm 0.4$		¹ DEL-AMO-SA...11D	BABR	$e^+ e^- \rightarrow \mathcal{T}(4S)$	

• • • We do not use the following data for averages, fits, limits, etc. • • •

< 6.1	90	¹ AUBERT,B	06G	BABR	Repl. by DEL-AMO-SANCHEZ 11D
-------	----	-----------------------	-----	------	------------------------------

¹ Assumes equal production of B^+ and B^0 at the $\mathcal{T}(4S)$.

² Assumes a helicity 00 configuration. For a helicity 11 configuration, the limit decreases to 4.9×10^{-5} .

$10.6^{+3.0}_{-2.6} \pm 2.4$		¹ AUBERT	03v	BABR	Repl. by AUBERT,B 06G
------------------------------	--	---------------------	-----	------	-----------------------

< 74
 90 | ² GODANG | 02 | CLE2 | $e^+ e^- \rightarrow \mathcal{T}(4S)$ |

< 90
 90 | ALBRECHT | 91B | ARG | $e^+ e^- \rightarrow \mathcal{T}(4S)$ |

¹ Assumes equal production of B^+ and B^0 at the $\mathcal{T}(4S)$.

² Assumes a helicity 00 configuration. For a helicity 11 configuration, the limit decreases to 4.9×10^{-5} .

$\Gamma(K^*(892)^+ f_0(980))/\Gamma_{\text{total}}$		Γ_{422}/Γ			
VALUE (units 10^{-6})	CL%	DOCUMENT ID	TECN	COMMENT	
$4.2 \pm 0.6 \pm 0.3$		¹ DEL-AMO-SA...11D	BABR	$e^+ e^- \rightarrow \mathcal{T}(4S)$	

• • • We do not use the following data for averages, fits, limits, etc. • • •

$5.2 \pm 1.2 \pm 0.5$		¹ AUBERT,B	06G	BABR	Repl. by DEL-AMO-SANCHEZ 11D
-----------------------	--	-----------------------	-----	------	------------------------------

¹ Assumes equal production of B^+ and B^0 at the $\mathcal{T}(4S)$.

$\Gamma(a_1^+ K^0)/\Gamma_{\text{total}}$		Γ_{423}/Γ			
VALUE (units 10^{-6})	CL%	DOCUMENT ID	TECN	COMMENT	
$34.9 \pm 5.0 \pm 4.4$		^{1,2} AUBERT	08F	BABR	$e^+ e^- \rightarrow \mathcal{T}(4S)$

¹ Assumes equal production of B^+ and B^0 at the $\mathcal{T}(4S)$.

² Assumes a_1^\pm decays only to 3π and $B(a_1^\pm \rightarrow \pi^\pm \pi^\mp \pi^\pm) = 0.5$.

$\Gamma(b_1^+ K^0 \times B(b_1^+ \rightarrow \omega \pi^+))/\Gamma_{\text{total}}$		Γ_{424}/Γ			
VALUE (units 10^{-6})	CL%	DOCUMENT ID	TECN	COMMENT	
$9.6 \pm 1.7 \pm 0.9$		¹ AUBERT	08AG	BABR	$e^+ e^- \rightarrow \mathcal{T}(4S)$

¹ Assumes equal production of B^+ and B^0 at the $\mathcal{T}(4S)$.

$\Gamma(K^*(892)^0 \rho^+)/\Gamma_{total}$ Γ_{425}/Γ

VALUE (units 10^{-6})	DOCUMENT ID	TECN	COMMENT
9.2 ± 1.5 OUR AVERAGE			
9.6 ± 1.7 ± 1.5	¹ AUBERT,B	06G	BABR $e^+e^- \rightarrow \Upsilon(4S)$
8.9 ± 1.7 ± 1.2	¹ ZHANG	05D	BELL $e^+e^- \rightarrow \Upsilon(4S)$

¹ Assumes equal production of B^+ and B^0 at the $\Upsilon(4S)$.

$\Gamma(K_1^+(1400)^+ \rho^+)/\Gamma_{total}$ Γ_{426}/Γ

VALUE	CL%	DOCUMENT ID	TECN	COMMENT
< 7.8 × 10⁻⁴	90	ALBRECHT	91B	ARG $e^+e^- \rightarrow \Upsilon(4S)$

$\Gamma(K_2^+(1430)^+ \rho^+)/\Gamma_{total}$ Γ_{427}/Γ

VALUE	CL%	DOCUMENT ID	TECN	COMMENT
< 1.5 × 10⁻³	90	ALBRECHT	91B	ARG $e^+e^- \rightarrow \Upsilon(4S)$

$\Gamma(b_1^0 K^+ \times B(b_1^0 \rightarrow \omega \pi^0))/\Gamma_{total}$ Γ_{428}/Γ

VALUE (units 10^{-6})	DOCUMENT ID	TECN	COMMENT
9.1 ± 1.7 ± 1.0	¹ AUBERT	07B1	BABR $e^+e^- \rightarrow \Upsilon(4S)$

¹ Assumes equal production of B^+ and B^0 at the $\Upsilon(4S)$.

$\Gamma(b_1^+ K^{*0} \times B(b_1^+ \rightarrow \omega \pi^+))/\Gamma_{total}$ Γ_{429}/Γ

VALUE	CL%	DOCUMENT ID	TECN	COMMENT
< 5.9 × 10⁻⁶	90	¹ AUBERT	09AF	BABR $e^+e^- \rightarrow \Upsilon(4S)$

¹ Assumes equal production of B^+ and B^0 at the $\Upsilon(4S)$.

$\Gamma(b_1^0 K^{*+} \times B(b_1^0 \rightarrow \omega \pi^0))/\Gamma_{total}$ Γ_{430}/Γ

VALUE	CL%	DOCUMENT ID	TECN	COMMENT
< 6.7 × 10⁻⁶	90	¹ AUBERT	09AF	BABR $e^+e^- \rightarrow \Upsilon(4S)$

¹ Assumes equal production of B^+ and B^0 at the $\Upsilon(4S)$.

$\Gamma(K^+ \bar{K}^0)/\Gamma_{total}$ Γ_{431}/Γ

VALUE (units 10^{-6})	CL%	DOCUMENT ID	TECN	COMMENT
1.32 ± 0.17 OUR FIT		Error includes scale factor of 1.2.		
1.19 ± 0.18 OUR AVERAGE				
1.11 ± 0.19 ± 0.05		¹ DUH	13	BELL $e^+e^- \rightarrow \Upsilon(4S)$
1.61 ± 0.44 ± 0.09		¹ AUBERT, BE	06c	BABR $e^+e^- \rightarrow \Upsilon(4S)$
••• We do not use the following data for averages, fits, limits, etc. •••				
1.22 ± 0.32 ± 0.13		¹ LIN	07	BELL Repl. by DUH 13
1.0 ± 0.4 ± 0.1		¹ ABE	05G	BELL Repl. by LIN 07
1.5 ± 0.5 ± 0.1		¹ AUBERT, BE	05E	BABR Repl. by AUBERT, BE 06c
< 2.5	90	¹ AUBERT	04M	BABR Repl. by AUBERT, BE 05E
< 3.3	90	¹ CHAO	04	BELL $e^+e^- \rightarrow \Upsilon(4S)$
< 3.3	90	¹ BORNHEIM	03	CLE2 $e^+e^- \rightarrow \Upsilon(4S)$
< 2.0	90	¹ CASEY	02	BELL Repl. by CHAO 04
< 5.0	90	¹ ABE	01H	BELL $e^+e^- \rightarrow \Upsilon(4S)$
< 2.4	90	¹ AUBERT	01E	BABR $e^+e^- \rightarrow \Upsilon(4S)$
< 5.1	90	¹ CRONIN-HEN..00	CLE2	$e^+e^- \rightarrow \Upsilon(4S)$
< 21	90	GODANG	98	CLE2 Repl. by CRONIN-HENNESSY 00

¹ Assumes equal production of B^+ and B^0 at the $\Upsilon(4S)$.

$\Gamma(K^+ \bar{K}^0)/\Gamma(K^0 \pi^+)$ $\Gamma_{431}/\Gamma_{370}$

VALUE	DOCUMENT ID	TECN	COMMENT
0.055 ± 0.007 OUR FIT	Error includes scale factor of 1.2.		
0.064 ± 0.009 ± 0.004	AAIJ	13Bs	LHCB pp at 7 TeV

$\Gamma(\bar{K}^0 K^+ \pi^0)/\Gamma_{total}$ Γ_{432}/Γ

VALUE	CL%	DOCUMENT ID	TECN	COMMENT
< 24 × 10⁻⁶	90	¹ ECKHART	02	CLE2 $e^+e^- \rightarrow \Upsilon(4S)$

¹ Assumes equal production of B^+ and B^0 at the $\Upsilon(4S)$.

$\Gamma(K^+ K_S^0 K_S^0)/\Gamma_{total}$ Γ_{433}/Γ

VALUE (units 10^{-6})	DOCUMENT ID	TECN	COMMENT	
10.5 ± 0.4 OUR AVERAGE				
10.42 ± 0.43 ± 0.22	¹ KALIYAR	19	BELL $e^+e^- \rightarrow \Upsilon(4S)$	
10.6 ± 0.5 ± 0.3	^{1,2} LEES	120	BABR $e^+e^- \rightarrow \Upsilon(4S)$	
••• We do not use the following data for averages, fits, limits, etc. •••				
10.7 ± 1.2 ± 1.0	¹ AUBERT,B	04v	BABR Repl. by LEES 120	
13.4 ± 1.9 ± 1.5	¹ GARMASH	04	BELL Repl. by KALIYAR 19	

¹ Assumes equal production of B^+ and B^0 at the $\Upsilon(4S)$.
² All intermediate charmonium and charm resonances are removed, except of χ_{c0} .

$\Gamma(f_0(980) K^+, f_0 \rightarrow K_S^0 K_S^0)/\Gamma_{total}$ Γ_{434}/Γ

VALUE (units 10^{-6})	DOCUMENT ID	TECN	COMMENT
14.7 ± 2.8 ± 1.8	¹ LEES	120	BABR $e^+e^- \rightarrow \Upsilon(4S)$

¹ Assumes equal production of B^+ and B^0 at the $\Upsilon(4S)$.

$\Gamma(f_0(1710) K^+, f_0 \rightarrow K_S^0 K_S^0)/\Gamma_{total}$ Γ_{435}/Γ

VALUE (units 10^{-6})	DOCUMENT ID	TECN	COMMENT
0.48^{+0.40}_{-0.24} ± 0.11	¹ LEES	120	BABR $e^+e^- \rightarrow \Upsilon(4S)$

¹ Assumes equal production of B^+ and B^0 at the $\Upsilon(4S)$.

$\Gamma(K^+ K_S^0 K_S^0 \text{ nonresonant})/\Gamma_{total}$ Γ_{436}/Γ

VALUE (units 10^{-6})	DOCUMENT ID	TECN	COMMENT
19.8 ± 3.7 ± 2.5	¹ LEES	120	BABR $e^+e^- \rightarrow \Upsilon(4S)$

¹ Assumes equal production of B^+ and B^0 at the $\Upsilon(4S)$.

$\Gamma(K_S^0 K_S^0 \pi^+)/\Gamma_{total}$ Γ_{437}/Γ

VALUE	CL%	DOCUMENT ID	TECN	COMMENT
< 5.1 × 10⁻⁷	90	¹ AUBERT	09j	BABR $e^+e^- \rightarrow \Upsilon(4S)$
••• We do not use the following data for averages, fits, limits, etc. •••				
< 8.7 × 10 ⁻⁷		¹ KALIYAR	19	BELL $e^+e^- \rightarrow \Upsilon(4S)$
< 3.2 × 10 ⁻⁶	90	¹ GARMASH	04	BELL $e^+e^- \rightarrow \Upsilon(4S)$

¹ Assumes equal production of B^+ and B^0 at the $\Upsilon(4S)$.

$\Gamma(K^+ K^- \pi^+)/\Gamma(K^+ K^- K^+)$ $\Gamma_{438}/\Gamma_{451}$

VALUE	DOCUMENT ID	TECN	COMMENT
0.151 ± 0.004 ± 0.008	AAIJ	20AJ	LHCB pp at 7 and 8 TeV

$\Gamma(K^+ K^- \pi^+)/\Gamma_{total}$ Γ_{438}/Γ

VALUE (units 10^{-6})	CL%	DOCUMENT ID	TECN	COMMENT
5.2 ± 0.4 OUR AVERAGE				
5.38 ± 0.40 ± 0.35		^{1,2} HSU	17	BELL $e^+e^- \rightarrow \Upsilon(4S)$
5.0 ± 0.5 ± 0.5		² AUBERT	07Bb	BABR $e^+e^- \rightarrow \Upsilon(4S)$
••• We do not use the following data for averages, fits, limits, etc. •••				
< 13	90	² GARMASH	04	BELL $e^+e^- \rightarrow \Upsilon(4S)$
< 6.3	90	^{2,3} AUBERT	03M	BABR Repl. by AUBERT 07Bb
< 12	90	⁴ GARMASH	02	BELL $e^+e^- \rightarrow \Upsilon(4S)$

¹ HSU 17 provides also measurement as a function of $K^+ K^-$ invariant mass.
² Assumes equal production of B^+ and B^0 at the $\Upsilon(4S)$.
³ Charm and charmonium contributions are subtracted, otherwise no assumptions about intermediate resonances.
⁴ Uses a reference decay mode $B^+ \rightarrow \bar{D}^0 \pi^+$ and $\bar{D}^0 \rightarrow K^+ \pi^-$ with $B(B^+ \rightarrow \bar{D}^0 \pi^+) \cdot B(\bar{D}^0 \rightarrow K^+ \pi^-) = (20.3 \pm 2.0) \times 10^{-5}$.

$\Gamma(K^+ K^- \pi^+ \text{ nonresonant})/\Gamma_{total}$ Γ_{439}/Γ

VALUE (units 10^{-6})	CL%	DOCUMENT ID	TECN	COMMENT
1.68 ± 0.23 ± 0.13		¹ AAIJ	19AL	LHCB pp at 7, 8 TeV
••• We do not use the following data for averages, fits, limits, etc. •••				
< 75	90	BERGFELD	96B	CLE2 $e^+e^- \rightarrow \Upsilon(4S)$

¹ AAIJ 19AL reports $0.323 \pm 0.015 \pm 0.041$ fit fraction for $B^+ \rightarrow K^+ K^- \pi^+$ nonresonant from the amplitude analysis of $B^\pm \rightarrow \pi^\pm K^+ K^-$ decays. We use the PDG 19 value $B(B^+ \rightarrow K^+ K^- \pi^+) = (5.2 \pm 0.4) \times 10^{-6}$ to obtain $B(B^+ \rightarrow K^+ K^- \pi^+ \text{ nonresonant})$. Our first error is the experiment's error and the second error is systematic error from using our best value.

$\Gamma(K^+ \bar{K}^*(892)^0)/\Gamma_{total}$ Γ_{440}/Γ

VALUE (units 10^{-7})	CL%	DOCUMENT ID	TECN	COMMENT
5.9 ± 0.6 ± 0.5		¹ AAIJ	19AL	LHCB pp at 7, 8 TeV
••• We do not use the following data for averages, fits, limits, etc. •••				
< 11	90	² AUBERT	07AR	BABR $e^+e^- \rightarrow \Upsilon(4S)$
< 1290	90	ABBIENDI	00B	OPAL $e^+e^- \rightarrow Z$
< 1380	90	³ ABE	00c	SLD $e^+e^- \rightarrow Z$
< 53	90	² JESSOP	00	CLE2 $e^+e^- \rightarrow \Upsilon(4S)$

¹ AAIJ 19AL reports $(7.5 \pm 0.6 \pm 0.5) \times 10^{-2}$ fit fraction for $B^+ \rightarrow K^+ \bar{K}^*(892)^0$ from the amplitude analysis of $B^\pm \rightarrow \pi^\pm K^+ K^-$ decays. We use the PDG 19 value $B(B^+ \rightarrow K^+ K^- \pi^+) = (5.2 \pm 0.4) \times 10^{-6}$ to obtain $B(B^+ \rightarrow K^+ \bar{K}^*(892)^0, \bar{K}^*(892)^0 \rightarrow K^+ \pi^-)$. We compute $B(B^+ \rightarrow K^+ \bar{K}^*(892)^0)$ using 2/3 of $B(\bar{K}^*(892)^0 \rightarrow (K \pi)^0) = (99.754 \pm 0.021)\%$ for the $K^+ \pi^-$ fraction. Our first error is the experiment's error and the second error is systematic error from using our best value.
² Assumes equal production of B^+ and B^0 at the $\Upsilon(4S)$.
³ ABE 00c assumes $B(Z \rightarrow b\bar{b}) = (21.7 \pm 0.1)\%$ and the B fractions $f_{B^0} = f_{B^+} = (39.7 \pm 1.8)_-2.2\%$ and $f_{B_s} = (10.5 \pm 1.8)_-2.2\%$.

$\Gamma(K^+ \bar{K}_0^*(1430)^0)/\Gamma_{total}$ Γ_{441}/Γ

VALUE (units 10^{-6})	CL%	DOCUMENT ID	TECN	COMMENT
0.38 ± 0.12 ± 0.05		¹ AAIJ	19AL	LHCB pp at 7, 8 TeV
••• We do not use the following data for averages, fits, limits, etc. •••				
< 2.2	90	² AUBERT	07AR	BABR $e^+e^- \rightarrow \Upsilon(4S)$

¹ AAIJ 19AL reports $(4.5 \pm 0.7 \pm 1.2) \times 10^{-2}$ fit fraction for $B^+ \rightarrow K^+ \bar{K}_0^*(1430)^0$ from the amplitude analysis of $B^\pm \rightarrow \pi^\pm K^+ K^-$ decays. We use the PDG 19 value $B(B^+ \rightarrow K^+ K^- \pi^+) = (5.2 \pm 0.4) \times 10^{-6}$ to obtain $B(B^+ \rightarrow K^+ \bar{K}_0^*(1430)^0, \bar{K}_0^*(1430)^0 \rightarrow K^+ \pi^-)$. We compute $B(B^+ \rightarrow K^+ \bar{K}_0^*(1430)^0)$ using 2/3 of PDG 19 value $B(K_0^*(1430)^0 \rightarrow K^+ \pi^-) = (93 \pm 10)\%$ for the $K^+ \pi^-$ fraction. Our first error is the experiment's error and the second error is systematic error from using our best value.
² Assumes equal production of B^+ and B^0 at the $\Upsilon(4S)$.

$\Gamma(\rho(1450)^0 \pi^+, \rho^0 \rightarrow K^+ K^-)/\Gamma_{total}$ Γ_{508}/Γ

VALUE (units 10^{-6})	DOCUMENT ID	TECN	COMMENT
1.60 ± 0.08 ± 0.12	¹ AAIJ	19AL	LHCB pp at 7, 8 TeV

¹ AAIJ 19AL reports $0.307 \pm 0.012 \pm 0.009$ fit fraction for $B^+ \rightarrow \rho(1450)^0 \pi^+$ from the amplitude analysis of $B^\pm \rightarrow \pi^\pm K^+ K^-$ decays. We use the PDG 19 value $B(B^+ \rightarrow K^+ K^- \pi^+) = (5.2 \pm 0.4) \times 10^{-6}$ to obtain $B(B^+ \rightarrow \rho(1450)^0 \pi^+, \rho(1450)^0 \rightarrow K^+ K^-)$. Our first error is the experiment's error and the second error is systematic error from using our best value.

Meson Particle Listings

 B^\pm $\Gamma(\pi^+(K^+K^-)_{S-wave})/\Gamma_{total}$ Γ_{442}/Γ

VALUE (units 10^{-7})	DOCUMENT ID	TECN	COMMENT
8.53 ± 0.67 ± 0.66	¹ AAIJ	19AL	LHCB $p\bar{p}$ at 7, 8 TeV

¹AAIJ 19AL reports $0.164 \pm 0.008 \pm 0.01$ fit fraction for $B^+ \rightarrow \pi^+(K^+K^-)_{S-wave}$ in the region of $0.95 < m(K^+K^-) < 1.42$ GeV/ c^2 from the amplitude analysis of $B^\pm \rightarrow \pi^\pm K^+ K^-$ decays. We use the PDG 19 value $B(B^+ \rightarrow K^+ K^- \pi^+) = (5.2 \pm 0.4) \times 10^{-6}$ to obtain $B(B^+ \rightarrow \pi^+(K^+K^-)_{S-wave})$. Our first error is the experiment's error and the second error is systematic error from using our best value.

 $\Gamma(\pi^+ K^+ K^-, m_{K^+ K^-} < 1.1 \text{ GeV})/\Gamma_{total}$ Γ_{443}/Γ

VALUE (units 10^{-6})	DOCUMENT ID	TECN	COMMENT
5.38 ± 0.40 ± 0.35	¹ HSU	23	BELL $e^+e^- \rightarrow \Upsilon(4S)$

¹Investigated the angular distribution of K^+K^- pairs with invariant mass below 1.1 GeV/ c^2 , which exhibits both a strong enhancement in signal and very large direct CP violation.

 $\Gamma(K^+ K^+ \pi^-)/\Gamma_{total}$ Γ_{444}/Γ

VALUE	CL%	DOCUMENT ID	TECN	COMMENT
<1.1 × 10⁻⁸	90	AAIJ	17E	LHCB $p\bar{p}$ at 7, 8 TeV

• • • We do not use the following data for averages, fits, limits, etc. • • •

<1.6 × 10 ⁻⁷	90	¹ AUBERT	08BE	BABR $e^+e^- \rightarrow \Upsilon(4S)$
<2.4 × 10 ⁻⁶	90	¹ GARMASH	04	BELL $e^+e^- \rightarrow \Upsilon(4S)$
<1.3 × 10 ⁻⁶	90	² AUBERT	03M	BABR Repl. by AUBERT 08BE
<3.2 × 10 ⁻⁶	90	³ GARMASH	02	BELL $e^+e^- \rightarrow \Upsilon(4S)$

¹Assumes equal production of B^+ and B^0 at the $\Upsilon(4S)$.
²Assumes equal production of B^0 and B^+ at the $\Upsilon(4S)$; charm and charmonium contributions are subtracted, otherwise no assumptions about intermediate resonances.
³Uses a reference decay mode $B^+ \rightarrow \bar{D}^0 \pi^+$ and $\bar{D}^0 \rightarrow K^+ \pi^-$ with $B(B^+ \rightarrow \bar{D}^0 \pi^+) \cdot B(\bar{D}^0 \rightarrow K^+ \pi^-) = (20.3 \pm 2.0) \times 10^{-5}$.

 $\Gamma(K^+ K^+ \pi^- \text{ nonresonant})/\Gamma_{total}$ Γ_{445}/Γ

VALUE (units 10^{-6})	CL%	DOCUMENT ID	TECN	COMMENT
<87.9	90	ABBIENDI	00B	OPAL $e^+e^- \rightarrow Z$

 $\Gamma(f_2'(1525) K^+)/\Gamma_{total}$ Γ_{446}/Γ

VALUE (units 10^{-6})	CL%	DOCUMENT ID	TECN	COMMENT
1.8 ± 0.5 OUR AVERAGE				Error includes scale factor of 1.1.
1.56 ± 0.36 ± 0.30		^{1,2} LEES	12o	BABR $e^+e^- \rightarrow \Upsilon(4S)$
2.8 ± 0.9 $^{+0.5}_{-0.4}$		^{1,3} LEES	12o	BABR $e^+e^- \rightarrow \Upsilon(4S)$

• • • We do not use the following data for averages, fits, limits, etc. • • •

<8	90	^{1,4} GARMASH	05	BELL $e^+e^- \rightarrow \Upsilon(4S)$
----	----	------------------------	----	--

¹Assumes equal production of B^+ and B^0 at the $\Upsilon(4S)$.
²Measured in the $B^+ \rightarrow K^+ K^- K^+$ decay.
³Measured in the $B^+ \rightarrow K^+ K_S^0 K_S^0$ decay.
⁴GARMASH 05 reports $B(B^+ \rightarrow f_2'(1525) K^+) \cdot B(f_2'(1525) \rightarrow K^+ K^-) < 4.9 \times 10^{-6}$ at 90% CL. We divide this result by our best value of $B(f_2'(1525) \rightarrow K^+ K^-) = 88.8 \times 10^{-2}$ multiplied by 2/3 to account for the $K^+ K^-$ fraction.

 $\Gamma(K^+ f_J(2220))/\Gamma_{total}$ Γ_{447}/Γ

VALUE (units 10^{-6})	DOCUMENT ID	TECN	COMMENT
not seen	¹ HUANG	03	BELL $e^+e^- \rightarrow \Upsilon(4S)$

¹No evidence is found for such decay and set a limit on $B(B^+ \rightarrow f_J(2220)) \times B(f_J(2220) \rightarrow \phi\phi) < 1.2 \times 10^{-6}$ at 90% CL where the $f_J(2220)$ is a possible glueball state.

 $\Gamma(K^* K^+ K^-)/\Gamma_{total}$ Γ_{448}/Γ

VALUE (units 10^{-6})	CL%	DOCUMENT ID	TECN	COMMENT
<11.8	90	¹ AUBERT,B	06U	BABR $e^+e^- \rightarrow \Upsilon(4S)$

¹Assumes equal production of B^+ and B^0 at the $\Upsilon(4S)$.

 $\Gamma(K^*(892)^+ K^*(892)^0)/\Gamma_{total}$ Γ_{449}/Γ

VALUE (units 10^{-6})	CL%	DOCUMENT ID	TECN	COMMENT
0.91 ± 0.29 OUR AVERAGE				
0.77 $^{+0.35}_{-0.30}$ ± 0.12		¹ GOH	15	BELL $e^+e^- \rightarrow \Upsilon(4S)$
1.2 ± 0.5 ± 0.1		² AUBERT	09F	BABR $e^+e^- \rightarrow \Upsilon(4S)$

• • • We do not use the following data for averages, fits, limits, etc. • • •

<71	90	³ GODANG	02	CLE2 $e^+e^- \rightarrow \Upsilon(4S)$
-----	----	---------------------	----	--

¹Signal significance is 2.7 standard deviations. This measurement corresponds to an upper limit of $< 1.31 \times 10^{-6}$ at 90% CL.
²Signal significance is 3.7 standard deviations.
³Assumes a helicity 00 configuration. For a helicity 11 configuration, the limit decreases to 4.8×10^{-5} .

 $\Gamma(K^* K^+ \pi^-)/\Gamma_{total}$ Γ_{450}/Γ

VALUE (units 10^{-6})	CL%	DOCUMENT ID	TECN	COMMENT
<6.1	90	¹ AUBERT,B	06U	BABR $e^+e^- \rightarrow \Upsilon(4S)$

¹Assumes equal production of B^+ and B^0 at the $\Upsilon(4S)$.

 $\Gamma(K^+ K^- K^+)/\Gamma_{total}$ Γ_{451}/Γ

VALUE (units 10^{-6})	CL%	DOCUMENT ID	TECN	COMMENT
34.0 ± 1.4 OUR AVERAGE				Error includes scale factor of 1.4.
34.6 ± 0.6 ± 0.9		^{1,2} LEES	12o	BABR $e^+e^- \rightarrow \Upsilon(4S)$
30.6 ± 1.2 ± 2.3		¹ GARMASH	05	BELL $e^+e^- \rightarrow \Upsilon(4S)$

• • • We do not use the following data for averages, fits, limits, etc. • • •

35.2 ± 0.9 ± 1.6		¹ AUBERT	06o	BABR Repl. by LEES 12o
32.8 ± 1.8 ± 2.8		¹ GARMASH	04	BELL Repl. by GARMASH 05
29.6 ± 2.1 ± 1.6		³ AUBERT	03M	BABR Repl. by AUBERT 06o
35.3 ± 3.7 ± 4.5		⁴ GARMASH	02	BELL Repl. by GARMASH 04
<200	90	⁵ ADAM	96D	DLPH $e^+e^- \rightarrow Z$
<320	90	⁵ ABREU	95N	DLPH Sup. by ADAM 96D
<350	90	ALBRECHT	91E	ARG $e^+e^- \rightarrow \Upsilon(4S)$

¹Assumes equal production of B^+ and B^0 at the $\Upsilon(4S)$.
²All intermediate charmonium and charm resonances are removed, except of χ_{c0} .
³Assumes equal production of B^0 and B^+ at the $\Upsilon(4S)$; charm and charmonium contributions are subtracted, otherwise no assumptions about intermediate resonances.
⁴Uses a reference decay mode $B^+ \rightarrow \bar{D}^0 \pi^+$ and $\bar{D}^0 \rightarrow K^+ \pi^-$ with $B(B^+ \rightarrow \bar{D}^0 \pi^+) \cdot B(\bar{D}^0 \rightarrow K^+ \pi^-) = (20.3 \pm 2.0) \times 10^{-5}$.
⁵Assumes B^0 and B^- production fractions of 0.39, and B_S production fraction of 0.12.

 $\Gamma(K^+ \phi)/\Gamma_{total}$ Γ_{452}/Γ

VALUE (units 10^{-6})	CL%	DOCUMENT ID	TECN	COMMENT
8.8 $^{+0.7}_{-0.6}$ OUR AVERAGE				Error includes scale factor of 1.1.
9.2 ± 0.4 $^{+0.7}_{-0.5}$		¹ LEES	12o	BABR $e^+e^- \rightarrow \Upsilon(4S)$
7.6 ± 1.3 ± 0.6		² ACOSTA	05J	CDF $p\bar{p}$ at 1.96 TeV
9.60 ± 0.92 $^{+1.05}_{-0.85}$		¹ GARMASH	05	BELL $e^+e^- \rightarrow \Upsilon(4S)$
5.5 $^{+2.1}_{-1.8}$ ± 0.6		¹ BRIERE	01	CLE2 $e^+e^- \rightarrow \Upsilon(4S)$

• • • We do not use the following data for averages, fits, limits, etc. • • •

8.4 ± 0.7 ± 0.7		¹ AUBERT	06o	BABR Repl. by LEES 12o
10.0 $^{+0.9}_{-0.8}$ ± 0.5		¹ AUBERT	04A	BABR Repl. by AUBERT 06o
9.4 ± 1.1 ± 0.7		¹ CHEN	03B	BELL Repl. by GARMASH 05
14.6 $^{+3.0}_{-2.8}$ ± 2.0		³ GARMASH	02	BELL Repl. by CHEN 03B
7.7 $^{+1.6}_{-1.4}$ ± 0.8		¹ AUBERT	01D	BABR $e^+e^- \rightarrow \Upsilon(4S)$
<144	90	⁴ ABE	00c	SLD $e^+e^- \rightarrow Z$
< 5	90	¹ BERGFELD	98	CLE2
<280	90	⁵ ADAM	96D	DLPH $e^+e^- \rightarrow Z$
< 12	90	ASNER	96	CLE2 $e^+e^- \rightarrow \Upsilon(4S)$
<440	90	⁶ ABREU	95N	DLPH Sup. by ADAM 96D
<180	90	ALBRECHT	91B	ARG $e^+e^- \rightarrow \Upsilon(4S)$
< 90	90	⁷ AVERY	89B	CLEO $e^+e^- \rightarrow \Upsilon(4S)$
<210	90	AVERY	87	CLEO $e^+e^- \rightarrow \Upsilon(4S)$

¹Assumes equal production of B^+ and B^0 at the $\Upsilon(4S)$.
²Uses $B(B^+ \rightarrow J/\psi K^+) = (1.00 \pm 0.04) \times 10^{-3}$ and $B(J/\psi \rightarrow \mu^+ \mu^-) = 0.0588 \pm 0.0010$.
³Uses a reference decay mode $B^+ \rightarrow \bar{D}^0 \pi^+$ and $\bar{D}^0 \rightarrow K^+ \pi^-$ with $B(B^+ \rightarrow \bar{D}^0 \pi^+) \cdot B(\bar{D}^0 \rightarrow K^+ \pi^-) = (20.3 \pm 2.0) \times 10^{-5}$.
⁴ABE 00c assumes $B(Z \rightarrow b\bar{b}) = (21.7 \pm 0.1)\%$ and the B fractions $f_{B^0} = f_{B^+} = (39.7 \pm 2.2)\%$ and $f_{B_S} = (10.5 \pm 1.8)\%$.
⁵ADAM 96D assumes $f_{B^0} = f_{B^-} = 0.39$ and $f_{B_S} = 0.12$.
⁶Assumes a B^0 , B^- production fraction of 0.39 and a B_S production fraction of 0.12.
⁷AVERY 89B reports $< 8 \times 10^{-5}$ assuming the $\Upsilon(4S)$ decays 43% to $B^0 \bar{B}^0$. We rescale to 50%.

 $\Gamma(f_0(980) K^+ \times B(f_0(980) \rightarrow K^+ K^-))/\Gamma_{total}$ Γ_{453}/Γ

VALUE (units 10^{-6})	CL%	DOCUMENT ID	TECN	COMMENT
9.4 ± 1.6 ± 2.8		¹ LEES	12o	BABR $e^+e^- \rightarrow \Upsilon(4S)$

• • • We do not use the following data for averages, fits, limits, etc. • • •

6.5 ± 2.5 ± 1.6		¹ AUBERT	06o	BABR $e^+e^- \rightarrow \Upsilon(4S)$
<2.9	90	¹ GARMASH	05	BELL $e^+e^- \rightarrow \Upsilon(4S)$

¹Assumes equal production of B^+ and B^0 at the $\Upsilon(4S)$.

 $\Gamma(a_2(1320) K^+ \times B(a_2(1320) \rightarrow K^+ K^-))/\Gamma_{total}$ Γ_{454}/Γ

VALUE	CL%	DOCUMENT ID	TECN	COMMENT
<1.1 × 10⁻⁶	90	¹ GARMASH	05	BELL $e^+e^- \rightarrow \Upsilon(4S)$

¹Assumes equal production of B^+ and B^0 at the $\Upsilon(4S)$.

 $\Gamma(X_0(1550) K^+ \times B(X_0(1550) \rightarrow K^+ K^-))/\Gamma_{total}$ Γ_{455}/Γ

VALUE (units 10^{-6})	DOCUMENT ID	TECN	COMMENT
4.3 ± 0.6 ± 0.3	¹ AUBERT	06o	BABR $e^+e^- \rightarrow \Upsilon(4S)$

¹Assumes equal production of B^+ and B^0 at the $\Upsilon(4S)$.

 $\Gamma(\phi(1680) K^+ \times B(\phi(1680) \rightarrow K^+ K^-))/\Gamma_{total}$ Γ_{456}/Γ

VALUE	CL%	DOCUMENT ID	TECN	COMMENT
<0.8 × 10⁻⁶	90	¹ GARMASH	05	BELL $e^+e^- \rightarrow \Upsilon(4S)$

¹Assumes equal production of B^+ and B^0 at the $\Upsilon(4S)$.

$\Gamma(f_0(1710)K^+ \times B(f_0(1710) \rightarrow K^+ K^-))/\Gamma_{\text{total}}$ Γ_{457}/Γ

VALUE (units 10^{-6})	DOCUMENT ID	TECN	COMMENT
1.12 ± 0.25 ± 0.50	¹ LEES	120	BABR $e^+ e^- \rightarrow \Upsilon(4S)$
• • • We do not use the following data for averages, fits, limits, etc. • • •			
1.7 ± 1.0 ± 0.3	¹ AUBERT	060	BABR Repl. by LEES 120
¹ Assumes equal production of B^+ and B^0 at the $\Upsilon(4S)$.			

 $\Gamma(K^+ K^- K^+ \text{ nonresonant})/\Gamma_{\text{total}}$ Γ_{458}/Γ

VALUE (units 10^{-6})	CL%	DOCUMENT ID	TECN	COMMENT
23.8^{+2.8}_{-5.0} OUR AVERAGE				
22.8 ± 2.7 ± 7.6		¹ LEES	120	BABR $e^+ e^- \rightarrow \Upsilon(4S)$
24.0 ± 1.5 ^{+2.6} _{-6.0}		¹ GARMASH	05	BELL $e^+ e^- \rightarrow \Upsilon(4S)$
• • • We do not use the following data for averages, fits, limits, etc. • • •				
50.0 ± 6.0 ± 4.0		¹ AUBERT	060	BABR Repl. by LEES 120
< 38	90	BERGFELD	96B	CLE2 $e^+ e^- \rightarrow \Upsilon(4S)$
¹ Assumes equal production of B^+ and B^0 at the $\Upsilon(4S)$.				

 $\Gamma(K^*(892)^+ K^+ K^-)/\Gamma_{\text{total}}$ Γ_{459}/Γ

VALUE (units 10^{-6})	CL%	DOCUMENT ID	TECN	COMMENT
36.2 ± 3.3 ± 3.6		¹ AUBERT,B	06U	BABR $e^+ e^- \rightarrow \Upsilon(4S)$
• • • We do not use the following data for averages, fits, limits, etc. • • •				
< 1600	90	ALBRECHT	91E	ARG $e^+ e^- \rightarrow \Upsilon(4S)$
¹ Assumes equal production of B^+ and B^0 at the $\Upsilon(4S)$.				

 $\Gamma(K^*(892)^+ \phi)/\Gamma_{\text{total}}$ Γ_{460}/Γ

VALUE (units 10^{-6})	CL%	DOCUMENT ID	TECN	COMMENT
10.0 ± 2.0 OUR AVERAGE		Error includes scale factor of 1.7.		
11.2 ± 1.0 ± 0.9		¹ AUBERT	07BA	BABR $e^+ e^- \rightarrow \Upsilon(4S)$
6.7 ^{+2.1+0.7} _{-1.9-1.0}		¹ CHEN	03B	BELL $e^+ e^- \rightarrow \Upsilon(4S)$
• • • We do not use the following data for averages, fits, limits, etc. • • •				
12.7 ^{+2.2} _{-2.0} ± 1.1		¹ AUBERT	03V	BABR Repl. by AUBERT 07BA
9.7 ^{+4.2} _{-3.4} ± 1.7		¹ AUBERT	01D	BABR Repl. by AUBERT 03v
< 22.5	90	¹ BRIERE	01	CLE2 $e^+ e^- \rightarrow \Upsilon(4S)$
< 41	90	¹ BERGFELD	98	CLE2
< 70	90	ASNER	96	CLE2 $e^+ e^- \rightarrow \Upsilon(4S)$
< 1300	90	ALBRECHT	91B	ARG $e^+ e^- \rightarrow \Upsilon(4S)$
¹ Assumes equal production of B^+ and B^0 at the $\Upsilon(4S)$.				

 $\Gamma(K^0 K^+ K^- \pi^+)/\Gamma_{\text{total}}$ Γ_{461}/Γ

VALUE (units 10^{-5})	DOCUMENT ID	TECN	COMMENT
34.01 ± 0.74 ± 3.23	¹ AAIJ	23AH	LHCB pp at 7, 8 and 13 TeV
¹ The second uncertainty includes systematic and reference branching reaction of $B^+ \rightarrow J/\psi K^+$ uncertainties.			

 $\Gamma(J/\psi K^+, J/\psi \rightarrow K^0 K^- \pi^+)/\Gamma_{\text{total}}$ Γ_{462}/Γ

VALUE (units 10^{-6})	DOCUMENT ID	TECN	COMMENT
5.43 ± 0.12 ± 1.23	¹ AAIJ	23AH	LHCB pp at 7, 8 and 13 TeV
¹ The second uncertainty includes systematic and reference branching reaction of $B^+ \rightarrow \eta_c K^+$ uncertainties.			

 $\Gamma(\chi_{c1} K^+, \chi_{c1} \rightarrow K^0 K^- \pi^+)/\Gamma_{\text{total}}$ Γ_{463}/Γ

VALUE (units 10^{-6})	DOCUMENT ID	TECN	COMMENT
2.25 ± 0.11 ± 0.22	¹ AAIJ	23AH	LHCB pp at 7, 8 and 13 TeV
¹ The second uncertainty includes systematic and reference branching reaction of $B^+ \rightarrow J/\psi K^+$ uncertainties.			

 $\Gamma(\eta_c K^+, \eta_c \rightarrow K^0 K^- \pi^+)/\Gamma_{\text{total}}$ Γ_{464}/Γ

VALUE (units 10^{-5})	DOCUMENT ID	TECN	COMMENT
2.83 ± 0.07 ± 0.29	¹ AAIJ	23AH	LHCB pp at 7, 8 and 13 TeV
¹ The second uncertainty includes systematic and reference branching reaction of $B^+ \rightarrow J/\psi K^+$ uncertainties.			

 $\Gamma(\eta_c(2S) K^+, \eta_c(2S) \rightarrow K^0 K^- \pi^+)/\Gamma_{\text{total}}$ Γ_{465}/Γ

VALUE (units 10^{-6})	DOCUMENT ID	TECN	COMMENT
3.27 ± 0.17 ± 0.34	¹ AAIJ	23AH	LHCB pp at 7, 8 and 13 TeV
¹ The second uncertainty includes systematic and reference branching reaction of $B^+ \rightarrow J/\psi K^+$ uncertainties.			

 $\Gamma(K^0 K^+ K^+ \pi^-)/\Gamma_{\text{total}}$ Γ_{466}/Γ

VALUE (units 10^{-5})	DOCUMENT ID	TECN	COMMENT
28.01 ± 0.68 ± 2.89	¹ AAIJ	23AH	LHCB pp at 7, 8 and 13 TeV
¹ The second uncertainty includes systematic and reference branching reaction of $B^+ \rightarrow J/\psi K^+$ uncertainties.			

 $\Gamma(J/\psi K^+, J/\psi \rightarrow K^0 K^+ \pi^-)/\Gamma_{\text{total}}$ Γ_{467}/Γ

VALUE (units 10^{-6})	DOCUMENT ID	TECN	COMMENT
5.41 ± 0.14 ± 1.25	¹ AAIJ	23AH	LHCB pp at 7, 8 and 13 TeV
¹ The second uncertainty includes systematic and reference branching reaction of $B^+ \rightarrow \eta_c K^+$ uncertainties.			

 $\Gamma(\chi_{c1} K^+, \chi_{c1} \rightarrow K^0 K^+ \pi^-)/\Gamma_{\text{total}}$ Γ_{468}/Γ

VALUE (units 10^{-6})	DOCUMENT ID	TECN	COMMENT
2.06 ± 0.12 ± 0.30	¹ AAIJ	23AH	LHCB pp at 7, 8 and 13 TeV
¹ The second uncertainty includes systematic and reference branching reaction of $B^+ \rightarrow J/\psi K^+$ uncertainties.			

 $\Gamma(\eta_c K^+, \eta_c \rightarrow K^0 K^+ \pi^-)/\Gamma_{\text{total}}$ Γ_{469}/Γ

VALUE (units 10^{-5})	DOCUMENT ID	TECN	COMMENT
3.00 ± 0.14 ± 0.31	¹ AAIJ	23AH	LHCB pp at 7, 8 and 13 TeV
¹ The second uncertainty includes systematic and reference branching reaction of $B^+ \rightarrow J/\psi K^+$ uncertainties.			

 $\Gamma(\eta_c(2S) K^+, \eta_c(2S) \rightarrow K^0 K^+ \pi^-)/\Gamma_{\text{total}}$ Γ_{470}/Γ

VALUE (units 10^{-6})	DOCUMENT ID	TECN	COMMENT
3.13 ± 0.21 ± 0.52	¹ AAIJ	23AH	LHCB pp at 7, 8 and 13 TeV
¹ The second uncertainty includes systematic and reference branching reaction of $B^+ \rightarrow J/\psi K^+$ uncertainties.			

 $\Gamma(\phi(K\pi)_0^{*+})/\Gamma_{\text{total}}$ Γ_{471}/Γ

VALUE (units 10^{-6})	DOCUMENT ID	TECN	COMMENT
8.3 ± 1.4 ± 0.8	¹ AUBERT	08B1	BABR $e^+ e^- \rightarrow \Upsilon(4S)$
¹ Assumes equal production of B^+ and B^0 at the $\Upsilon(4S)$.			

($K\pi)_0^{*+}$ is the total S-wave composed of $K_0^*(1430)$ and nonresonant that are described using LASS shape.

 $\Gamma(\phi K_1(1270)^+)/\Gamma_{\text{total}}$ Γ_{472}/Γ

VALUE (units 10^{-6})	DOCUMENT ID	TECN	COMMENT
6.1 ± 1.6 ± 1.1	¹ AUBERT	08B1	BABR $e^+ e^- \rightarrow \Upsilon(4S)$
¹ Assumes equal production of B^+ and B^0 at the $\Upsilon(4S)$.			

 $\Gamma(\phi K_1(1400)^+)/\Gamma_{\text{total}}$ Γ_{473}/Γ

VALUE (units 10^{-6})	CL%	DOCUMENT ID	TECN	COMMENT
< 3.2	90	¹ AUBERT	08B1	BABR $e^+ e^- \rightarrow \Upsilon(4S)$
• • • We do not use the following data for averages, fits, limits, etc. • • •				
< 1100	90	ALBRECHT	91B	ARG $e^+ e^- \rightarrow \Upsilon(4S)$
¹ Assumes equal production of B^+ and B^0 at the $\Upsilon(4S)$.				

 $\Gamma(\phi K^*(1410)^+)/\Gamma_{\text{total}}$ Γ_{474}/Γ

VALUE (units 10^{-6})	CL%	DOCUMENT ID	TECN	COMMENT
< 4.3	90	¹ AUBERT	08B1	BABR $e^+ e^- \rightarrow \Upsilon(4S)$
¹ Assumes equal production of B^+ and B^0 at the $\Upsilon(4S)$.				

 $\Gamma(\phi K_0^*(1430)^+)/\Gamma_{\text{total}}$ Γ_{475}/Γ

VALUE (units 10^{-6})	DOCUMENT ID	TECN	COMMENT
7.0 ± 1.3 ± 0.9	¹ AUBERT	08B1	BABR $e^+ e^- \rightarrow \Upsilon(4S)$
¹ Assumes equal production of B^+ and B^0 at the $\Upsilon(4S)$.			

 $\Gamma(\phi K_2^*(1430)^+)/\Gamma_{\text{total}}$ Γ_{476}/Γ

VALUE (units 10^{-6})	CL%	DOCUMENT ID	TECN	COMMENT
8.4 ± 1.8 ± 1.0		¹ AUBERT	08B1	BABR $e^+ e^- \rightarrow \Upsilon(4S)$
• • • We do not use the following data for averages, fits, limits, etc. • • •				
< 3400	90	ALBRECHT	91B	ARG $e^+ e^- \rightarrow \Upsilon(4S)$
¹ Assumes equal production of B^+ and B^0 at the $\Upsilon(4S)$.				

 $\Gamma(\phi K_2^*(1770)^+)/\Gamma_{\text{total}}$ Γ_{477}/Γ

VALUE (units 10^{-6})	CL%	DOCUMENT ID	TECN	COMMENT
< 15.0	90	¹ AUBERT	08B1	BABR $e^+ e^- \rightarrow \Upsilon(4S)$
¹ Assumes equal production of B^+ and B^0 at the $\Upsilon(4S)$.				

 $\Gamma(\phi K_2^*(1820)^+)/\Gamma_{\text{total}}$ Γ_{478}/Γ

VALUE (units 10^{-6})	CL%	DOCUMENT ID	TECN	COMMENT
< 16.3	90	¹ AUBERT	08B1	BABR $e^+ e^- \rightarrow \Upsilon(4S)$
¹ Assumes equal production of B^+ and B^0 at the $\Upsilon(4S)$.				

 $\Gamma(a_1^+ K^0)/\Gamma_{\text{total}}$ Γ_{479}/Γ

VALUE (units 10^{-6})	CL%	DOCUMENT ID	TECN	COMMENT
< 3.6	90	^{1,2} DEL-AMO-SA...101	BABR	$e^+ e^- \rightarrow \Upsilon(4S)$
¹ Assumes $B(a_1^\pm \rightarrow \pi^\pm \pi^\mp \pi^\pm) = 0.5$				
² Assumes equal production of B^+ and B^0 at the $\Upsilon(4S)$.				

Meson Particle Listings

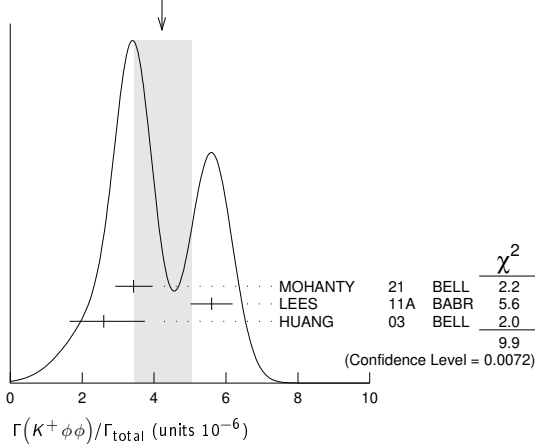
B^\pm

$\Gamma(K^+ \phi \phi) / \Gamma_{total}$

VALUE (units 10^{-6})	DOCUMENT ID	TECN	COMMENT
4.2 ± 0.8 OUR AVERAGE	Error includes scale factor of 2.2. See the ideogram below.		
3.43 ^{+0.48} _{-0.46} ± 0.22	1 MOHANTY	21 BELL	$e^+ e^- \rightarrow \Upsilon(4S)$
5.6 ± 0.5 ± 0.3	1 LEES	11A BABR	$e^+ e^- \rightarrow \Upsilon(4S)$
2.6 ^{+1.1} _{-0.9} ± 0.3	1 HUANG	03 BELL	$e^+ e^- \rightarrow \Upsilon(4S)$

- • • We do not use the following data for averages, fits, limits, etc. • • •
- 7.5 ± 1.0 ± 0.7¹ AUBERT,BE 06H BABR Repl. by LEES 11A
- ¹ Assumes equal production of B^0 and B^+ at the $\Upsilon(4S)$ and the $\phi\phi$ invariant mass below 2.85 GeV/c².

WEIGHTED AVERAGE
4.2±0.8 (Error scaled by 2.2)



$\Gamma(\eta' \eta' K^+) / \Gamma_{total}$

VALUE (units 10^{-6})	CL%	DOCUMENT ID	TECN	COMMENT
<25	90	1 AUBERT,B	06P BABR	$e^+ e^- \rightarrow \Upsilon(4S)$

¹ Assumes equal production of B^+ and B^0 at the $\Upsilon(4S)$.

$\Gamma(\omega \phi K^+) / \Gamma_{total}$

VALUE (units 10^{-6})	CL%	DOCUMENT ID	TECN	COMMENT
<1.9	90	1 LIU	09 BELL	$e^+ e^- \rightarrow \Upsilon(4S)$

¹ Assumes equal production of B^+ and B^0 at the $\Upsilon(4S)$.

$\Gamma(X(1812) K^+ \times B(X \rightarrow \omega \phi)) / \Gamma_{total}$

VALUE (units 10^{-6})	CL%	DOCUMENT ID	TECN	COMMENT
<0.32	90	1 LIU	09 BELL	$e^+ e^- \rightarrow \Upsilon(4S)$

¹ Assumes equal production of B^+ and B^0 at the $\Upsilon(4S)$.

$\Gamma(K^*(892)^+ \gamma) / \Gamma_{total}$

VALUE (units 10^{-5})	CL%	DOCUMENT ID	TECN	COMMENT
3.92 ± 0.22 OUR AVERAGE	Error includes scale factor of 1.7.			
3.76 ± 0.10 ± 0.12		1 HORIGUCHI	17 BELL	$e^+ e^- \rightarrow \Upsilon(4S)$
4.22 ± 0.14 ± 0.16		2 AUBERT	09A0 BABR	$e^+ e^- \rightarrow \Upsilon(4S)$
3.76 ^{+0.89} _{-0.83} ± 0.28		3 COAN	00 CLE2	$e^+ e^- \rightarrow \Upsilon(4S)$

- • • We do not use the following data for averages, fits, limits, etc. • • •
- 3.87 ± 0.28 ± 0.26⁴ AUBERT,BE 04A BABR Repl. by AUBERT 09A0
- 4.25 ± 0.31 ± 0.24³ NAKAO 04 BELL Repl. by HORIGUCHI 17
- 3.83 ± 0.62 ± 0.22³ AUBERT 02C BABR Repl. by AUBERT,BE 04A
- 5.7 ± 3.1 ± 1.1⁵ AMMAR 93 CLE2 Repl. by COAN 00
- < 55⁹⁰ ALBRECHT 89G ARG $e^+ e^- \rightarrow \Upsilon(4S)$
- < 55⁹⁰ AVERY 89B CLEO $e^+ e^- \rightarrow \Upsilon(4S)$
- < 180⁹⁰ AVERY 87 CLEO $e^+ e^- \rightarrow \Upsilon(4S)$
- ¹ Uses $B(\Upsilon(4S) \rightarrow B^+ B^-) = (51.4 \pm 0.6)\%$ and $B(\Upsilon(4S) \rightarrow B^0 \bar{B}^0) = (48.6 \pm 0.6)\%$.
- ² Uses $B(\Upsilon(4S) \rightarrow B^+ B^-) = (51.6 \pm 0.6)\%$ and $B(\Upsilon(4S) \rightarrow B^0 \bar{B}^0) = (48.4 \pm 0.6)\%$.
- ³ Assumes equal production of B^+ and B^0 at the $\Upsilon(4S)$.
- ⁴ Uses the production ratio of charged and neutral B from $\Upsilon(4S)$ decays $R^{+0} = 1.006 \pm 0.048$.
- ⁵ AMMAR 93 observed 4.1 ± 2.3 events above background.
- ⁶ Assumes the $\Upsilon(4S)$ decays 43% to $B^0 \bar{B}^0$.

$\Gamma(K_1(1270)^+ \gamma) / \Gamma_{total}$

VALUE (units 10^{-5})	CL%	DOCUMENT ID	TECN	COMMENT
4.4^{+0.7}_{-0.6} OUR AVERAGE				
4.41 ^{+0.63} _{-0.44} ± 0.58		1,2 DEL-AMO-SA...16	BABR	$e^+ e^- \rightarrow \Upsilon(4S)$
4.3 ± 0.9 ± 0.9		3 YANG	05 BELL	$e^+ e^- \rightarrow \Upsilon(4S)$

• • • We do not use the following data for averages, fits, limits, etc. • • •

< 9.9	90	3 NISHIDA	02 BELL	Repl. by YANG 05
< 730	90	4 ALBRECHT	89G ARG	$e^+ e^- \rightarrow \Upsilon(4S)$

- ¹ Requires $M_{K\pi\pi} < 1.8$ GeV/c².
- ² Uses $B(\Upsilon(4S) \rightarrow B^+ B^-) = 0.513 \pm 0.006$.
- ³ Assumes equal production of B^+ and B^0 at the $\Upsilon(4S)$.
- ⁴ ALBRECHT 89G reports < 0.0066 assuming the $\Upsilon(4S)$ decays 45% to $B^0 \bar{B}^0$. We rescale to 50%.

$\Gamma(\eta K^+ \gamma) / \Gamma_{total}$

VALUE (units 10^{-6})	DOCUMENT ID	TECN	COMMENT
7.9 ± 0.9 OUR AVERAGE			
7.7 ± 1.0 ± 0.4	1,2 AUBERT	09 BABR	$e^+ e^- \rightarrow \Upsilon(4S)$
8.4 ± 1.5 ^{+1.2} _{-0.9}	2,3 NISHIDA	05 BELL	$e^+ e^- \rightarrow \Upsilon(4S)$

- • • We do not use the following data for averages, fits, limits, etc. • • •
- 10.0 ± 1.3 ± 0.5^{1,2} AUBERT,B 06M BABR Repl. by AUBERT 09
- ¹ $m_{\eta K} < 3.25$ GeV/c².
- ² Assumes equal production of B^+ and B^0 at the $\Upsilon(4S)$.
- ³ $m_{\eta K} < 2.4$ GeV/c²

$\Gamma(\eta' K^+ \gamma) / \Gamma_{total}$

VALUE (units 10^{-6})	DOCUMENT ID	TECN	COMMENT
2.9 ± 1.0 OUR AVERAGE			
3.6 ± 1.2 ± 0.4	1,2 WEDD	10 BELL	$e^+ e^- \rightarrow \Upsilon(4S)$
1.9 ± 1.5 ^{+1.2} _{-1.2} ± 0.1	1,3 AUBERT,B	06M BABR	$e^+ e^- \rightarrow \Upsilon(4S)$

- ¹ Assumes equal production of B^+ and B^0 at the $\Upsilon(4S)$.
- ² $m_{\eta' K} < 3.4$ GeV/c².
- ³ Set the upper limit of 4.2×10^{-6} at 90% CL with $m_{\eta' K} < 3.25$ GeV/c².

$\Gamma(\phi K^+ \gamma) / \Gamma_{total}$

VALUE (units 10^{-6})	DOCUMENT ID	TECN	COMMENT
2.7 ± 0.4 OUR AVERAGE	Error includes scale factor of 1.2.		
2.48 ± 0.30 ± 0.24	1 SAHOO	11A BELL	$e^+ e^- \rightarrow \Upsilon(4S)$
3.5 ± 0.6 ± 0.4	1 AUBERT	07Q BABR	$e^+ e^- \rightarrow \Upsilon(4S)$

• • • We do not use the following data for averages, fits, limits, etc. • • •

3.4 ± 0.9 ± 0.4	1 DRUTSKOY	04 BELL	Repl. by SAHOO 11A
-----------------	------------	---------	--------------------

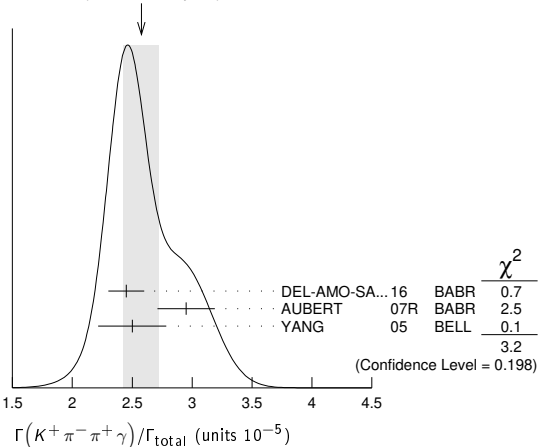
¹ Assumes equal production of B^+ and B^0 at $\Upsilon(4S)$.

$\Gamma(K^+ \pi^- \pi^+ \gamma) / \Gamma_{total}$

VALUE (units 10^{-5})	DOCUMENT ID	TECN	COMMENT
2.58 ± 0.15 OUR AVERAGE	Error includes scale factor of 1.3. See the ideogram below.		
2.45 ± 0.09 ± 0.12	1,2 DEL-AMO-SA...16	BABR	$e^+ e^- \rightarrow \Upsilon(4S)$
2.95 ± 0.13 ± 0.20	1,3 AUBERT	07R BABR	$e^+ e^- \rightarrow \Upsilon(4S)$
2.50 ± 0.18 ± 0.22	3,4 YANG	05 BELL	$e^+ e^- \rightarrow \Upsilon(4S)$

- • • We do not use the following data for averages, fits, limits, etc. • • •
- 2.4 ± 0.5^{+0.4}_{-0.2}^{3,5} NISHIDA 02 BELL Repl. by YANG 05
- ¹ $M_{K\pi\pi} < 1.8$ GeV/c².
- ² Uses $B(\Upsilon(4S) \rightarrow B^+ B^-) = 0.513 \pm 0.006$.
- ³ Assumes equal production of B^+ and B^0 at the $\Upsilon(4S)$.
- ⁴ $M_{K\pi\pi} < 2.0$ GeV/c².
- ⁵ $M_{K\pi\pi} < 2.4$ GeV/c².

WEIGHTED AVERAGE
2.58±0.15 (Error scaled by 1.3)



$\Gamma(K^*(892)^0 \pi^+ \gamma) / \Gamma_{total}$

VALUE (units 10^{-5})	DOCUMENT ID	TECN	COMMENT
2.33 ± 0.12 OUR AVERAGE			
2.34 ± 0.09 ^{+0.08} _{-0.07} ± 0.2	1,2 DEL-AMO-SA...16	BABR	$e^+ e^- \rightarrow \Upsilon(4S)$
2.0 ± 0.7 ^{+0.7} _{-0.6} ± 0.2	3,4 NISHIDA	02 BELL	$e^+ e^- \rightarrow \Upsilon(4S)$

See key on page 1171

Meson Particle Listings

 B^\pm ¹ Requires $M_{K\pi\pi} < 1.8 \text{ GeV}/c^2$.² Uses $B(\Upsilon(4S) \rightarrow B^+B^-) = 0.513 \pm 0.006$.³ Assumes equal production of B^+ and B^0 at the $\Upsilon(4S)$.⁴ $M_{K\pi\pi} < 2.4 \text{ GeV}/c^2$. $\Gamma(K^+\rho^0\gamma)/\Gamma_{\text{total}}$ Γ_{491}/Γ

VALUE (units 10^{-6})	CL%	DOCUMENT ID	TECN	COMMENT
$8.2 \pm 0.4 \pm 0.8$		1,2 DEL-AMO-SA..16	BABR	$e^+e^- \rightarrow \Upsilon(4S)$
••• We do not use the following data for averages, fits, limits, etc. •••				
<20	90	3,4 NISHIDA	02 BELL	$e^+e^- \rightarrow \Upsilon(4S)$

¹ Requires $M_{K\pi\pi} < 1.8 \text{ GeV}/c^2$.² Uses $B(\Upsilon(4S) \rightarrow B^+B^-) = 0.513 \pm 0.006$.³ Assumes equal production of B^+ and B^0 at the $\Upsilon(4S)$.⁴ $M_{K\pi\pi} < 2.4 \text{ GeV}/c^2$. $\Gamma((K^+\pi^-)_{NR}\pi^+\gamma)/\Gamma_{\text{total}}$ Γ_{492}/Γ

VALUE (units 10^{-6})	CL%	DOCUMENT ID	TECN	COMMENT
$9.9 \pm 0.7 \pm 1.5$ 1.9		1,2 DEL-AMO-SA..16	BABR	$e^+e^- \rightarrow \Upsilon(4S)$
••• We do not use the following data for averages, fits, limits, etc. •••				
<9.2	90	3,4 NISHIDA	02 BELL	$e^+e^- \rightarrow \Upsilon(4S)$

¹ Requires $M_{K\pi\pi} < 1.8 \text{ GeV}/c^2$.² Uses $B(\Upsilon(4S) \rightarrow B^+B^-) = 0.513 \pm 0.006$.³ Assumes equal production of B^+ and B^0 at the $\Upsilon(4S)$.⁴ $M_{K\pi\pi} < 2.4 \text{ GeV}/c^2$. $\Gamma(K^0\pi^+\pi^0\gamma)/\Gamma_{\text{total}}$ Γ_{493}/Γ

VALUE (units 10^{-5})	DOCUMENT ID	TECN	COMMENT
$4.56 \pm 0.42 \pm 0.31$	1,2 AUBERT 07R	BABR	$e^+e^- \rightarrow \Upsilon(4S)$

¹ $M_{K\pi\pi} < 1.8 \text{ GeV}/c^2$.² Assumes equal production of B^+ and B^0 at the $\Upsilon(4S)$. $\Gamma(K_1(1400)^+\gamma)/\Gamma_{\text{total}}$ Γ_{494}/Γ

VALUE (units 10^{-6})	CL%	DOCUMENT ID	TECN	COMMENT
$9.7 \pm 4.6 \pm 2.9$ 2.4		1,2 DEL-AMO-SA..16	BABR	$e^+e^- \rightarrow \Upsilon(4S)$
••• We do not use the following data for averages, fits, limits, etc. •••				
< 15	90	3 YANG	05 BELL	$e^+e^- \rightarrow \Upsilon(4S)$
< 50	90	3 NISHIDA	02 BELL	Repl. by YANG 05
<2200	90	4 ALBRECHT	89G ARG	$e^+e^- \rightarrow \Upsilon(4S)$

¹ Requires $M_{K\pi\pi} < 1.8 \text{ GeV}/c^2$.² Uses $B(\Upsilon(4S) \rightarrow B^+B^-) = 0.513 \pm 0.006$.³ Assumes equal production of B^+ and B^0 at the $\Upsilon(4S)$.⁴ ALBRECHT 89G reports < 0.0020 assuming the $\Upsilon(4S)$ decays 45% to $B^0\bar{B}^0$. We rescale to 50%. $\Gamma(K^*(1410)^+\gamma)/\Gamma_{\text{total}}$ Γ_{495}/Γ

VALUE (units 10^{-5})	DOCUMENT ID	TECN	COMMENT
$2.71 \pm 0.54 \pm 0.59$ $0.48 - 0.37$	1,2 DEL-AMO-SA..16	BABR	$e^+e^- \rightarrow \Upsilon(4S)$

¹ Requires $M_{K\pi\pi} < 1.8 \text{ GeV}/c^2$.² Uses $B(\Upsilon(4S) \rightarrow B^+B^-) = 0.513 \pm 0.006$. $\Gamma(K_0^*(1430)^0\pi^+\gamma)/\Gamma_{\text{total}}$ Γ_{496}/Γ

VALUE (units 10^{-6})	DOCUMENT ID	TECN	COMMENT
$1.32 \pm 0.09 \pm 0.24$ $0.10 - 0.30$	1,2 DEL-AMO-SA..16	BABR	$e^+e^- \rightarrow \Upsilon(4S)$

¹ Requires $M_{K\pi\pi} < 1.8 \text{ GeV}/c^2$.² Uses $B(\Upsilon(4S) \rightarrow B^+B^-) = 0.513 \pm 0.006$. $\Gamma(K_2^*(1430)^+\gamma)/\Gamma_{\text{total}}$ Γ_{497}/Γ

VALUE (units 10^{-5})	CL%	DOCUMENT ID	TECN	COMMENT
1.4 ± 0.4 OUR AVERAGE				
$0.87 \pm 0.70 \pm 0.87$ $-0.53 - 1.04$		1,2 DEL-AMO-SA..16	BABR	$e^+e^- \rightarrow \Upsilon(4S)$
$1.45 \pm 0.40 \pm 0.15$		3 AUBERT,B	04U BABR	$e^+e^- \rightarrow \Upsilon(4S)$
••• We do not use the following data for averages, fits, limits, etc. •••				
<140	90	4 ALBRECHT	89G ARG	$e^+e^- \rightarrow \Upsilon(4S)$

¹ Requires $M_{K\pi\pi} < 1.8 \text{ GeV}/c^2$.² Uses $B(\Upsilon(4S) \rightarrow B^+B^-) = 0.513 \pm 0.006$.³ Assumes equal production of B^+ and B^0 at the $\Upsilon(4S)$.⁴ ALBRECHT 89G reports < 0.0013 assuming the $\Upsilon(4S)$ decays 45% to $B^0\bar{B}^0$. We rescale to 50%. $\Gamma(K^*(1680)^+\gamma)/\Gamma_{\text{total}}$ Γ_{498}/Γ

VALUE (units 10^{-5})	CL%	DOCUMENT ID	TECN	COMMENT
$6.67 \pm 0.93 \pm 1.44$ $-0.78 - 1.14$		1,2 DEL-AMO-SA..16	BABR	$e^+e^- \rightarrow \Upsilon(4S)$
••• We do not use the following data for averages, fits, limits, etc. •••				
<190	90	3 ALBRECHT	89G ARG	$e^+e^- \rightarrow \Upsilon(4S)$

¹ Requires $M_{K\pi\pi} < 1.8 \text{ GeV}/c^2$.² Uses $B(\Upsilon(4S) \rightarrow B^+B^-) = 0.513 \pm 0.006$.³ ALBRECHT 89G reports < 0.0017 assuming the $\Upsilon(4S)$ decays 45% to $B^0\bar{B}^0$. We rescale to 50%. $\Gamma(K_3^*(1780)^+\gamma)/\Gamma_{\text{total}}$ Γ_{499}/Γ

VALUE (units 10^{-6})	CL%	DOCUMENT ID	TECN	COMMENT
< 39	90	1,2 NISHIDA	05 BELL	$e^+e^- \rightarrow \Upsilon(4S)$
••• We do not use the following data for averages, fits, limits, etc. •••				
<5500	90	3 ALBRECHT	89G ARG	$e^+e^- \rightarrow \Upsilon(4S)$

¹ Assumes equal production of B^+ and B^0 at the $\Upsilon(4S)$.² Uses $B(K_3^*(1780) \rightarrow \eta K) = 0.11 \pm 0.05$.³ ALBRECHT 89G reports < 0.005 assuming the $\Upsilon(4S)$ decays 45% to $B^0\bar{B}^0$. We rescale to 50%. $\Gamma(K_4^*(2045)^+\gamma)/\Gamma_{\text{total}}$ Γ_{500}/Γ

VALUE (units 10^{-6})	CL%	DOCUMENT ID	TECN	COMMENT
<0.0099	90	1 ALBRECHT	89G ARG	$e^+e^- \rightarrow \Upsilon(4S)$

¹ ALBRECHT 89G reports < 0.0090 assuming the $\Upsilon(4S)$ decays 45% to $B^0\bar{B}^0$. We rescale to 50%. $\Gamma(\rho^+\gamma)/\Gamma_{\text{total}}$ Γ_{501}/Γ

VALUE (units 10^{-6})	CL%	DOCUMENT ID	TECN	COMMENT
0.98 ± 0.25 OUR AVERAGE				
$1.20 \pm 0.42 \pm 0.20$ -0.37		1 AUBERT	08BH BABR	$e^+e^- \rightarrow \Upsilon(4S)$
$0.87 \pm 0.29 \pm 0.09$ $-0.27 - 0.11$		1 TANIGUCHI	08 BELL	$e^+e^- \rightarrow \Upsilon(4S)$
••• We do not use the following data for averages, fits, limits, etc. •••				
1.10 ± 0.37 -0.33 ± 0.09		1 AUBERT	07L BABR	Repl. by AUBERT 08BH
$0.55 \pm 0.42 \pm 0.09$ $-0.36 - 0.08$		1 MOHAPATRA	06 BELL	Repl. by TANIGUCHI 08
$0.9 \pm 0.6 \pm 0.1$	90	1 AUBERT	05 BABR	Repl. by AUBERT 07L
< 2.2	90	1 MOHAPATRA	05 BELL	$e^+e^- \rightarrow \Upsilon(4S)$
< 2.1	90	1 AUBERT	04c BABR	$e^+e^- \rightarrow \Upsilon(4S)$
<13	90	1,2 COAN	00 CLE2	$e^+e^- \rightarrow \Upsilon(4S)$

¹ Assumes equal production of B^+ and B^0 at $\Upsilon(4S)$.² No evidence for a nonresonant $K\pi\gamma$ contamination was seen; the central value assumes no contamination. $\Gamma(\pi^+\pi^0)/\Gamma_{\text{total}}$ Γ_{502}/Γ

VALUE (units 10^{-6})	CL%	DOCUMENT ID	TECN	COMMENT
5.31 ± 0.26 OUR AVERAGE				
$5.10 \pm 0.29 \pm 0.27$		ADACHI	24 BELL	$e^+e^- \rightarrow \Upsilon(4S)$
$5.86 \pm 0.26 \pm 0.38$		1 DUH	13 BELL	$e^+e^- \rightarrow \Upsilon(4S)$
$5.02 \pm 0.46 \pm 0.29$		1 AUBERT	07bC BABR	$e^+e^- \rightarrow \Upsilon(4S)$
$4.6 \pm 1.8 \pm 0.6$ $-1.6 - 0.7$		1 BORNHEIM	03 CLE2	$e^+e^- \rightarrow \Upsilon(4S)$
••• We do not use the following data for averages, fits, limits, etc. •••				
$6.5 \pm 0.4 \pm 0.4$		1 LIN	07A BELL	Repl. by DUH 13
$5.8 \pm 0.6 \pm 0.4$		1 AUBERT	05L BABR	Repl. by AUBERT 07bC
$5.0 \pm 1.2 \pm 0.5$		1 CHAO	04 BELL	Repl. by LIN 07A
$5.5 \pm 1.0 \pm 0.6$ -1.9		1 AUBERT	03L BABR	Repl. by AUBERT 05L
$7.4 \pm 2.3 \pm 0.9$ -2.2		1 CASEY	02 BELL	Repl. by CHAO 04
< 13.4	90	1 ABE	01H BELL	$e^+e^- \rightarrow \Upsilon(4S)$
< 9.6	90	1 AUBERT	01E BABR	$e^+e^- \rightarrow \Upsilon(4S)$
< 12.7	90	1 CRONIN-HEN.	00 CLE2	$e^+e^- \rightarrow \Upsilon(4S)$
< 20	90	1 GONDANG	98 CLE2	Repl. by CRONIN-HENNESSY 00
< 17	90	1 ASNER	96 CLE2	Repl. by GONDANG 98
< 240	90	1 ALBRECHT	90B ARG	$e^+e^- \rightarrow \Upsilon(4S)$
<2300	90	2 BEBEK	87 CLEO	$e^+e^- \rightarrow \Upsilon(4S)$

¹ Assumes equal production of B^+ and B^0 at the $\Upsilon(4S)$.² BEBEK 87 assume the $\Upsilon(4S)$ decays 43% to $B^0\bar{B}^0$. $\Gamma(\pi^+\pi^0)/\Gamma(K^0\pi^+)$ $\Gamma_{502}/\Gamma_{370}$

VALUE	DOCUMENT ID	TECN	COMMENT
$0.285 \pm 0.02 \pm 0.02$	LIN	07A BELL	$e^+e^- \rightarrow \Upsilon(4S)$

 $\Gamma(\pi^+\pi^+\pi^-)/\Gamma(K^+K^-K^+)$ $\Gamma_{503}/\Gamma_{451}$

VALUE	DOCUMENT ID	TECN	COMMENT
$0.488 \pm 0.005 \pm 0.009$	AAIJ	20AJ LHCb	pp at 7 and 8 TeV

 $\Gamma(\pi^+\pi^+\pi^-)/\Gamma_{\text{total}}$ Γ_{503}/Γ

VALUE (units 10^{-6})	CL%	DOCUMENT ID	TECN	COMMENT
$15.2 \pm 0.6 \pm 1.3$ 1.2		1 AUBERT	09L BABR	$e^+e^- \rightarrow \Upsilon(4S)$
••• We do not use the following data for averages, fits, limits, etc. •••				
$16.2 \pm 1.2 \pm 0.9$		1 AUBERT,B	05G BABR	Repl. by AUBERT 09L
$10.9 \pm 3.3 \pm 1.6$		1 AUBERT	03M BABR	Repl. by AUBERT 05G
<130	90	2 ADAM	96D DLPH	$e^+e^- \rightarrow Z$
<220	90	3 ABREU	95N DLPH	Sup. by ADAM 96D
<450	90	4 ALBRECHT	90B ARG	$e^+e^- \rightarrow \Upsilon(4S)$
<190	90	5 BORTOLETTO	089 CLEO	$e^+e^- \rightarrow \Upsilon(4S)$

¹ Assumes equal production of B^0 and B^+ at the $\Upsilon(4S)$; charm and charmonium contributions are subtracted, otherwise no assumptions about intermediate resonances.² ADAM 96D assumes $f_{B^0} = f_{B^-} = 0.39$ and $f_{B_s} = 0.12$.

Meson Particle Listings

 B^\pm

³ Assumes a B^0 , B^- production fraction of 0.39 and a B_S production fraction of 0.12.

⁴ ALBRECHT 90B limit assumes equal production of $B^0\bar{B}^0$ and B^+B^- at $\Upsilon(4S)$.

⁵ BORTOLETTO 89 reports $< 1.7 \times 10^{-4}$ assuming the $\Upsilon(4S)$ decays 43% to $B^0\bar{B}^0$. We rescale to 50%.

$\Gamma(\rho^0\pi^+)/\Gamma_{\text{total}}$		Γ_{504}/Γ		
VALUE (units 10^{-6})	CL%	DOCUMENT ID	TECN	COMMENT
8.3 ± 1.2 OUR AVERAGE				
$8.1 \pm 0.7^{+1.3}_{-1.6}$		¹ AUBERT	09L BABR	$e^+e^- \rightarrow \Upsilon(4S)$
$8.0^{+2.3}_{-2.0} \pm 0.7$		¹ GORDON	02 BELL	$e^+e^- \rightarrow \Upsilon(4S)$
$10.4^{+3.3}_{-3.4} \pm 2.1$		¹ JESSOP	00 CLE2	$e^+e^- \rightarrow \Upsilon(4S)$
• • • We do not use the following data for averages, fits, limits, etc. • • •				
$8.8 \pm 1.0^{+0.6}_{-0.9}$		¹ AUBERT,B	05G BABR	Repl. by AUBERT 09L
$9.5 \pm 1.1 \pm 0.9$		¹ AUBERT	04Z BABR	Repl. by AUBERT 05G
< 83	90	² ABE	00C SLD	$e^+e^- \rightarrow Z$
< 160	90	³ ADAM	96D DLPH	$e^+e^- \rightarrow Z$
< 43	90	ASNER	96 CLE2	Repl. by JESSOP 00
< 260	90	⁴ ABREU	95N DLPH	Sup. by ADAM 96D
< 150	90	¹ ALBRECHT	90B ARG	$e^+e^- \rightarrow \Upsilon(4S)$
< 170	90	⁵ BORTOLETTO89	CLEO	$e^+e^- \rightarrow \Upsilon(4S)$
< 230	90	⁵ BEBEK	87 CLEO	$e^+e^- \rightarrow \Upsilon(4S)$
< 600	90	GILES	84 CLEO	Repl. by BEBEK 87

¹ Assumes equal production of B^+ and B^0 at the $\Upsilon(4S)$.

² ABE 00C assumes $B(Z \rightarrow b\bar{b}) = (21.7 \pm 0.1)\%$ and the B fractions $f_{B^0} = f_{B^+} = (39.7^{+1.8}_{-2.2})\%$ and $f_{B_S} = (10.5^{+1.8}_{-2.2})\%$.

³ ADAM 96D assumes $f_{B^0} = f_{B^-} = 0.39$ and $f_{B_S} = 0.12$.

⁴ Assumes a B^0 , B^- production fraction of 0.39 and a B_S production fraction of 0.12.

⁵ Papers assume the $\Upsilon(4S)$ decays 43% to $B^0\bar{B}^0$. We rescale to 50%.

$[\Gamma(K^*(892)^0\pi^+) + \Gamma(\rho^0\pi^+)]/\Gamma_{\text{total}}$		$(\Gamma_{396} + \Gamma_{504})/\Gamma$		
VALUE (units 10^{-6})		DOCUMENT ID	TECN	COMMENT
$170^{+120}_{-80} \pm 20$		¹ ADAM	96D DLPH	$e^+e^- \rightarrow Z$
¹ ADAM 96D assumes $f_{B^0} = f_{B^-} = 0.39$ and $f_{B_S} = 0.12$.				

$\Gamma(\pi^+ f_0(980), f_0 \rightarrow \pi^+\pi^-)/\Gamma_{\text{total}}$		Γ_{505}/Γ		
VALUE (units 10^{-6})	CL%	DOCUMENT ID	TECN	COMMENT
< 1.5	90	¹ AUBERT	09L BABR	$e^+e^- \rightarrow \Upsilon(4S)$
• • • We do not use the following data for averages, fits, limits, etc. • • •				
< 3.0	90	¹ AUBERT,B	05G BABR	Repl. by AUBERT 09L
< 140	90	² BORTOLETTO89	CLEO	$e^+e^- \rightarrow \Upsilon(4S)$

¹ Assumes equal production of B^+ and B^0 at the $\Upsilon(4S)$.

² BORTOLETTO 89 reports $< 1.2 \times 10^{-4}$ assuming the $\Upsilon(4S)$ decays 43% to $B^0\bar{B}^0$. We rescale to 50%.

$\Gamma(\pi^+ f_2(1270))/\Gamma_{\text{total}}$		Γ_{506}/Γ		
VALUE (units 10^{-6})	CL%	DOCUMENT ID	TECN	COMMENT
$2.2^{+0.7}_{-0.4}$ OUR AVERAGE				
$17.0 \pm 2.4 \pm 2.1$		¹ AAIJ	19AL LHCB	pp at 7, 8 TeV
$1.60^{+0.67+0.02}_{-0.44-0.05}$		^{2,3} AUBERT	09L BABR	$e^+e^- \rightarrow \Upsilon(4S)$
• • • We do not use the following data for averages, fits, limits, etc. • • •				
$4.09 \pm 1.28^{+0.05}_{-0.14}$		^{3,4} AUBERT,B	05G BABR	Repl. by AUBERT 09L
< 240	90	⁵ BORTOLETTO89	CLEO	$e^+e^- \rightarrow \Upsilon(4S)$

¹ AAIJ 19AL reports $0.075 \pm 0.008 \pm 0.007$ fit fraction for $B^+ \rightarrow f_2(1270)\pi^+$ from the amplitude analysis of $B^\pm \rightarrow \pi^\pm K^+ K^-$ decays. We use the PDG 19 value $B(B^+ \rightarrow K^+ K^- \pi^+) = (5.2 \pm 0.4) \times 10^{-6}$ to obtain $B(B^+ \rightarrow f_2(1270)\pi^+, f_2(1270) \rightarrow K^+ K^-)$. We compute $B(B^+ \rightarrow f_2(1270)\pi^+)$ using 1/2 of PDG 19 value of $B(f_2(1270) \rightarrow K^+ K^-) = (4.6^{+0.5}_{-0.4})\%$ for $K^+ K^-$ fraction. Our first error is the experiment's error and the second error is systematic error from using our best value.

² AUBERT 09L reports $[\Gamma(B^+ \rightarrow \pi^+ f_2(1270))/\Gamma_{\text{total}}] \times [B(f_2(1270) \rightarrow \pi^+\pi^-)] = (0.9 \pm 0.2 \pm 0.1^{+0.3}_{-0.1}) \times 10^{-6}$ which we divide by our best value $B(f_2(1270) \rightarrow \pi^+\pi^-) = (56.2^{+1.9}_{-0.6}) \times 10^{-2}$. Our first error is their experiment's error and our second error is the systematic error from using our best value.

³ Assumes equal production of B^+ and B^0 at the $\Upsilon(4S)$.

⁴ AUBERT,B 05G reports $[\Gamma(B^+ \rightarrow \pi^+ f_2(1270))/\Gamma_{\text{total}}] \times [B(f_2(1270) \rightarrow \pi^+\pi^-)] = (2.3 \pm 0.6 \pm 0.4) \times 10^{-6}$ which we divide by our best value $B(f_2(1270) \rightarrow \pi^+\pi^-) = (56.2^{+1.9}_{-0.6}) \times 10^{-2}$. Our first error is their experiment's error and our second error is the systematic error from using our best value.

⁵ BORTOLETTO 89 reports $< 2.1 \times 10^{-4}$ assuming the $\Upsilon(4S)$ decays 43% to $B^0\bar{B}^0$. We rescale to 50%.

$\Gamma(\rho(1450)^0\pi^+, \rho^0 \rightarrow \pi^+\pi^-)/\Gamma_{\text{total}}$		Γ_{507}/Γ		
VALUE (units 10^{-6})	CL%	DOCUMENT ID	TECN	COMMENT

$1.4 \pm 0.4^{+0.5}_{-0.8}$ ¹ AUBERT 09L BABR $e^+e^- \rightarrow \Upsilon(4S)$

• • • We do not use the following data for averages, fits, limits, etc. • • •

< 2.3 90 ¹ AUBERT,B 05G BABR Repl. by AUBERT 09L

¹ Assumes equal production of B^+ and B^0 at the $\Upsilon(4S)$.

$\Gamma(f_0(1370)\pi^+, f_0 \rightarrow \pi^+\pi^-)/\Gamma_{\text{total}}$		Γ_{509}/Γ		
VALUE (units 10^{-6})	CL%	DOCUMENT ID	TECN	COMMENT

< 4.0 90 ¹ AUBERT 09L BABR $e^+e^- \rightarrow \Upsilon(4S)$

• • • We do not use the following data for averages, fits, limits, etc. • • •

< 3.0 90 ¹ AUBERT,B 05G BABR Repl. by AUBERT 09L

¹ Assumes equal production of B^+ and B^0 at the $\Upsilon(4S)$.

$\Gamma(f_0(1370)\pi^+, f_0 \rightarrow \pi^0\pi^0)/\Gamma_{\text{total}}$		Γ_{510}/Γ		
VALUE	CL%	DOCUMENT ID	TECN	COMMENT

< **1.1×10^{-6}** 90 LAI 23 BELL $e^+e^- \rightarrow \Upsilon(4S)$

$\Gamma(f_0(500)\pi^+, f_0 \rightarrow \pi^+\pi^-)/\Gamma_{\text{total}}$		Γ_{511}/Γ		
VALUE (units 10^{-6})	CL%	DOCUMENT ID	TECN	COMMENT

< 4.1 90 ¹ AUBERT,B 05G BABR $e^+e^- \rightarrow \Upsilon(4S)$

¹ Assumes equal production of B^+ and B^0 at the $\Upsilon(4S)$.

$\Gamma(\pi^+\pi^-\pi^+\text{nonresonant})/\Gamma_{\text{total}}$		Γ_{512}/Γ		
VALUE (units 10^{-6})	CL%	DOCUMENT ID	TECN	COMMENT

$5.3 \pm 0.7^{+1.3}_{-0.8}$ ¹ AUBERT 09L BABR $e^+e^- \rightarrow \Upsilon(4S)$

• • • We do not use the following data for averages, fits, limits, etc. • • •

< 4.6 90 ¹ AUBERT,B 05G BABR Repl. by AUBERT 09L

< 41 90 BERGFELD 96B CLE2 $e^+e^- \rightarrow \Upsilon(4S)$

¹ Assumes equal production of B^+ and B^0 at the $\Upsilon(4S)$.

$\Gamma(\pi^+\pi^0\pi^0)/\Gamma_{\text{total}}$		Γ_{513}/Γ		
VALUE (units 10^{-5})	CL%	DOCUMENT ID	TECN	COMMENT

$1.90 \pm 0.15 \pm 0.14$ LAI 23 BELL $e^+e^- \rightarrow \Upsilon(4S)$

• • • We do not use the following data for averages, fits, limits, etc. • • •

< 89 90 ¹ ALBRECHT 90B ARG $e^+e^- \rightarrow \Upsilon(4S)$

¹ ALBRECHT 90B limit assumes equal production of $B^0\bar{B}^0$ and B^+B^- at $\Upsilon(4S)$.

$\Gamma(\pi^+\pi^0)/\Gamma_{\text{total}}$		Γ_{514}/Γ		
VALUE (units 10^{-5})	CL%	DOCUMENT ID	TECN	COMMENT

$1.06^{+0.12}_{-0.13}$ OUR AVERAGE

$1.12 \pm 0.11^{+0.12}_{-0.18}$ ¹ LAI 23 BELL $e^+e^- \rightarrow \Upsilon(4S)$

$1.02 \pm 0.14 \pm 0.09$ ² AUBERT 07X BABR $e^+e^- \rightarrow \Upsilon(4S)$

• • • We do not use the following data for averages, fits, limits, etc. • • •

$1.32 \pm 0.23^{+0.14}_{-0.19}$ ² ZHANG 05A BELL Repl. by LAI 23

$1.09 \pm 0.19 \pm 0.19$ ² AUBERT 04Z BABR Repl. by AUBERT 07X

< 4.3 90 ^{2,3} JESSOP 00 CLE2 $e^+e^- \rightarrow \Upsilon(4S)$

< 7.7 90 ASNER 96 CLE2 Repl. by JESSOP 00

< 55 90 ² ALBRECHT 90B ARG $e^+e^- \rightarrow \Upsilon(4S)$

¹ The second uncertainty includes both systematics ($(\pm 0.09) \times 10^{-5}$) and possible interference with $B^+ \rightarrow \rho(1450)^+\pi^0 ((\pm 0.08) \times 10^{-5})$.

² Assumes equal production of B^+ and B^0 at the $\Upsilon(4S)$.

³ Assumes no nonresonant contributions of $B^+ \rightarrow \pi^+\pi^0\pi^0$.

$\Gamma(\rho(1450)^+\pi^0, \rho^+ \rightarrow \pi^+\pi^0)/\Gamma_{\text{total}}$		Γ_{515}/Γ		
VALUE (units 10^{-6})		DOCUMENT ID	TECN	COMMENT

$1.2 \pm 0.6 \pm 0.2$ LAI 23 BELL $e^+e^- \rightarrow \Upsilon(4S)$

$\Gamma(\pi^+\pi^0\pi^0\text{nonresonant})/\Gamma_{\text{total}}$		Γ_{516}/Γ		
VALUE	CL%	DOCUMENT ID	TECN	COMMENT

< **6×10^{-7}** 90 LAI 23 BELL $e^+e^- \rightarrow \Upsilon(4S)$

$\Gamma(X\pi^+, X \rightarrow \pi^0\pi^0)/\Gamma_{\text{total}}$		Γ_{517}/Γ		
VALUE (units 10^{-6})		DOCUMENT ID	TECN	COMMENT

$6.9 \pm 0.9 \pm 0.6$ LAI 23 BELL $e^+e^- \rightarrow \Upsilon(4S)$

$\Gamma(\pi^+\pi^-\pi^+\pi^0)/\Gamma_{\text{total}}$		Γ_{518}/Γ		
VALUE	CL%	DOCUMENT ID	TECN	COMMENT

< **4.0×10^{-3}** 90 ¹ ALBRECHT 90B ARG $e^+e^- \rightarrow \Upsilon(4S)$

¹ ALBRECHT 90B limit assumes equal production of $B^0\bar{B}^0$ and B^+B^- at $\Upsilon(4S)$.

$\Gamma(\rho^+\rho^0)/\Gamma_{\text{total}}$ Γ_{519}/Γ

VALUE (units 10^{-6})	CL%	DOCUMENT ID	TECN	COMMENT
24.0±1.9 OUR AVERAGE				
23.7±1.4±1.4		¹ AUBERT	09G BABR	$e^+e^- \rightarrow \Upsilon(4S)$
31.7±7.1+ ^{3.8} / _{-6.7}		^{1,2} ZHANG	03B BELL	$e^+e^- \rightarrow \Upsilon(4S)$

• • • We do not use the following data for averages, fits, limits, etc. • • •

16.8±2.2±2.3		¹ AUBERT,BE	06G BABR	Repl. by AUBERT 09G
22.5+ ^{5.7} / _{-5.4} ±5.8		¹ AUBERT	03V BABR	Repl. by AUBERT,BE 06G
< 1000	90	¹ ALBRECHT	90B ARG	$e^+e^- \rightarrow \Upsilon(4S)$

¹ Assumes equal production of B^+ and B^0 at the $\Upsilon(4S)$.
² The systematic error includes the error associated with the helicity-mix uncertainty.

 $\Gamma(\rho^+\rho_0(980), \rho_0 \rightarrow \pi^+\pi^-)/\Gamma_{\text{total}}$ Γ_{520}/Γ

VALUE (units 10^{-6})	CL%	DOCUMENT ID	TECN	COMMENT
<2.0	90	¹ AUBERT	09G BABR	$e^+e^- \rightarrow \Upsilon(4S)$

• • • We do not use the following data for averages, fits, limits, etc. • • •

<1.9	90	¹ AUBERT,BE	06G BABR	Repl. by AUBERT 09G
------	----	------------------------	----------	---------------------

¹ Assumes equal production of B^+ and B^0 at the $\Upsilon(4S)$.

 $\Gamma(a_1(1260)^+\pi^0)/\Gamma_{\text{total}}$ Γ_{521}/Γ

VALUE (units 10^{-6})	CL%	DOCUMENT ID	TECN	COMMENT
26.4±5.4±4.1		^{1,2} AUBERT	07BL BABR	$e^+e^- \rightarrow \Upsilon(4S)$

• • • We do not use the following data for averages, fits, limits, etc. • • •

<1700	90	¹ ALBRECHT	90B ARG	$e^+e^- \rightarrow \Upsilon(4S)$
-------	----	-----------------------	---------	-----------------------------------

¹ Assumes equal production of B^+ and B^0 at the $\Upsilon(4S)$.
² Assumes a_1^+ decays only to 3π and $B(a_1^+ \rightarrow \pi^+\pi^-\pi^+) = 0.5$.

 $\Gamma(a_1(1260)^0\pi^+)/\Gamma_{\text{total}}$ Γ_{522}/Γ

VALUE (units 10^{-6})	CL%	DOCUMENT ID	TECN	COMMENT
20.4±4.7±3.4		^{1,2} AUBERT	07BL BABR	$e^+e^- \rightarrow \Upsilon(4S)$

• • • We do not use the following data for averages, fits, limits, etc. • • •

<900	90	¹ ALBRECHT	90B ARG	$e^+e^- \rightarrow \Upsilon(4S)$
------	----	-----------------------	---------	-----------------------------------

¹ Assumes equal production of B^+ and B^0 at the $\Upsilon(4S)$.
² Assumes a_1^0 decays only to 3π and $B(a_1^0 \rightarrow \pi^+\pi^-\pi^0) = 1.0$.

 $\Gamma(\omega\pi^+)/\Gamma_{\text{total}}$ Γ_{523}/Γ

VALUE (units 10^{-6})	CL%	DOCUMENT ID	TECN	COMMENT
6.9±0.5 OUR AVERAGE				
6.7±0.5±0.4		¹ AUBERT	07AE BABR	$e^+e^- \rightarrow \Upsilon(4S)$
6.9±0.6±0.5		¹ JEN	06 BELL	$e^+e^- \rightarrow \Upsilon(4S)$
11.3+ ^{3.3} / _{-2.9} ±1.4		¹ JESSOP	00 CLE2	$e^+e^- \rightarrow \Upsilon(4S)$

• • • We do not use the following data for averages, fits, limits, etc. • • •

6.1±0.7±0.4		¹ AUBERT,B	06E BABR	Repl. by AUBERT 07AE
5.5±0.9±0.5		¹ AUBERT	04H BABR	Repl. by AUBERT,B 06E
5.7+ ^{1.4} / _{-1.3} ±0.6		¹ WANG	04A BELL	Repl. by JEN 06
4.2+ ^{2.0} / _{-1.8} ±0.5		¹ LU	02 BELL	Repl. by WANG 04A
6.6+ ^{2.1} / _{-1.8} ±0.7		¹ AUBERT	01G BABR	Repl. by AUBERT 04H
< 23	90	¹ BERGFELD	98 CLE2	Repl. by JESSOP 00
<400	90	¹ ALBRECHT	90B ARG	$e^+e^- \rightarrow \Upsilon(4S)$

¹ Assumes equal production of B^+ and B^0 at the $\Upsilon(4S)$.

 $\Gamma(\omega\rho^+)/\Gamma_{\text{total}}$ Γ_{524}/Γ

VALUE (units 10^{-6})	CL%	DOCUMENT ID	TECN	COMMENT
15.9±1.6±1.4		¹ AUBERT	09H BABR	$e^+e^- \rightarrow \Upsilon(4S)$

• • • We do not use the following data for averages, fits, limits, etc. • • •

10.6±2.1+ ^{1.6} / _{-1.0}		¹ AUBERT,B	06T BABR	Repl. by AUBERT 09H
12.6+ ^{3.7} / _{-3.3} ±1.6		¹ AUBERT	05O BABR	Repl. by AUBERT,B 06T
<61	90	¹ BERGFELD	98 CLE2	

¹ Assumes equal production of B^+ and B^0 at the $\Upsilon(4S)$.

 $\Gamma(\eta\pi^+)/\Gamma_{\text{total}}$ Γ_{525}/Γ

VALUE (units 10^{-6})	CL%	DOCUMENT ID	TECN	COMMENT
4.02±0.27 OUR AVERAGE				
4.07±0.26±0.21		¹ HOI	12 BELL	$e^+e^- \rightarrow \Upsilon(4S)$
4.00±0.40±0.24		¹ AUBERT	09AV BABR	$e^+e^- \rightarrow \Upsilon(4S)$
1.2+ ^{2.8} / _{-1.2}		¹ RICHICHI	00 CLE2	$e^+e^- \rightarrow \Upsilon(4S)$

• • • We do not use the following data for averages, fits, limits, etc. • • •

5.0±0.5±0.3		¹ AUBERT	07AE BABR	Repl. by AUBERT 09AV
4.2±0.4±0.2		¹ CHANG	07B BELL	Repl. by HOI 12
5.1±0.6±0.3		¹ AUBERT,B	05K BABR	Repl. by AUBERT 07AE
4.8±0.7±0.3		¹ CHANG	05A BELL	Repl. by CHANG 07B
5.3±1.0±0.3		¹ AUBERT	04H BABR	Repl. by AUBERT,B 05K
< 15	90	BEHRENS	98 CLE2	Repl. by RICHICHI 00
<700	90	ALBRECHT	90B ARG	$e^+e^- \rightarrow \Upsilon(4S)$

¹ Assumes equal production of B^+ and B^0 at the $\Upsilon(4S)$.

 $\Gamma(\eta\rho^+)/\Gamma_{\text{total}}$ Γ_{526}/Γ

VALUE (units 10^{-6})	CL%	DOCUMENT ID	TECN	COMMENT
7.0±2.9 OUR AVERAGE				Error includes scale factor of 2.8.
9.9±1.2±0.8		¹ AUBERT	08AH BABR	$e^+e^- \rightarrow \Upsilon(4S)$
4.1+ ^{1.4} / _{-1.3} ±0.4		¹ WANG	07B BELL	$e^+e^- \rightarrow \Upsilon(4S)$

• • • We do not use the following data for averages, fits, limits, etc. • • •

8.4±1.9±1.1		¹ AUBERT,B	05K BABR	Repl. by AUBERT 08AH
<14	90	¹ AUBERT,B	04D BABR	Repl. by AUBERT,B 05K
<15	90	¹ RICHICHI	00 CLE2	$e^+e^- \rightarrow \Upsilon(4S)$
<32	90	BEHRENS	98 CLE2	Repl. by RICHICHI 00

¹ Assumes equal production of B^+ and B^0 at the $\Upsilon(4S)$.

 $\Gamma(\eta'\pi^+)/\Gamma_{\text{total}}$ Γ_{527}/Γ

VALUE (units 10^{-6})	CL%	DOCUMENT ID	TECN	COMMENT
2.7 ±0.9 OUR AVERAGE				Error includes scale factor of 1.9.
3.5 ±0.6 ±0.2		¹ AUBERT	09AV BABR	$e^+e^- \rightarrow \Upsilon(4S)$
1.76+ ^{0.67+0.15} / _{-0.62-0.14}		¹ SCHUEMANN	06 BELL	$e^+e^- \rightarrow \Upsilon(4S)$

• • • We do not use the following data for averages, fits, limits, etc. • • •

3.9 ±0.7 ±0.3		¹ AUBERT	07AE BABR	Repl. by AUBERT 09AV
4.0 ±0.8 ±0.4		¹ AUBERT,B	05K BABR	Repl. by AUBERT 07AE
< 4.5	90	¹ AUBERT	04H BABR	Repl. by AUBERT,B 05K
< 7.0	90	¹ ABE	01M BELL	$e^+e^- \rightarrow \Upsilon(4S)$
<12	90	¹ AUBERT	01G BABR	$e^+e^- \rightarrow \Upsilon(4S)$
<12	90	¹ RICHICHI	00 CLE2	$e^+e^- \rightarrow \Upsilon(4S)$
<31	90	BEHRENS	98 CLE2	Repl. by RICHICHI 00

¹ Assumes equal production of B^+ and B^0 at the $\Upsilon(4S)$.

 $\Gamma(\eta'\rho^+)/\Gamma_{\text{total}}$ Γ_{528}/Γ

VALUE (units 10^{-6})	CL%	DOCUMENT ID	TECN	COMMENT
9.7+^{1.9}/_{-1.8}±1.1		¹ DEL-AMO-SA...	10A BABR	$e^+e^- \rightarrow \Upsilon(4S)$

• • • We do not use the following data for averages, fits, limits, etc. • • •

8.7+ ^{3.1+2.3} / _{-2.8-1.3}		¹ AUBERT	07E BABR	Repl. by DEL-AMO-SANCHEZ 10A
< 5.8	90	¹ SCHUEMANN	07 BELL	$e^+e^- \rightarrow \Upsilon(4S)$
<22	90	¹ AUBERT,B	04D BABR	Repl. by AUBERT 07E
<33	90	¹ RICHICHI	00 CLE2	$e^+e^- \rightarrow \Upsilon(4S)$
<47	90	BEHRENS	98 CLE2	Repl. by RICHICHI 00

¹ Assumes equal production of B^+ and B^0 at the $\Upsilon(4S)$.

 $\Gamma(\phi\pi^+)/\Gamma_{\text{total}}$ Γ_{529}/Γ

VALUE (units 10^{-6})	CL%	DOCUMENT ID	TECN	COMMENT
3.2±1.5±0.3		¹ AAIJ	19AL LHCB	pp at 7, 8 TeV

• • • We do not use the following data for averages, fits, limits, etc. • • •

< 15	90	² AAIJ	14A LHCB	Repl. by AAIJ 19AL
< 33	90	³ KIM	12A BELL	$e^+e^- \rightarrow \Upsilon(4S)$
< 24	90	³ AUBERT,B	06C BABR	$e^+e^- \rightarrow \Upsilon(4S)$
< 41	90	³ AUBERT	04A BABR	Repl. by AUBERT,B 06C
< 140	90	³ AUBERT	01D BABR	$e^+e^- \rightarrow \Upsilon(4S)$
<15300	90	⁴ ABE	00C CLE2	$e^+e^- \rightarrow Z$
< 500	90	³ BERGFELD	98 CLE2	

¹ AAIJ 19AL reports $(0.3 \pm 0.1 \pm 0.1) \times 10^{-2}$ fit fraction for $B^+ \rightarrow \phi(1020)\pi^+$ from the amplitude analysis of $B^\pm \rightarrow \pi^\pm K^+ K^-$ decays. We use the PDG 19 value $B(B^+ \rightarrow K^+ K^- \pi^+) = (5.2 \pm 0.4) \times 10^{-6}$ to obtain $B(B^+ \rightarrow \phi(1020)\pi^+) = \phi(1020)\pi^+, \phi(1020) \rightarrow K^+ K^-)$. We compute $B(B^+ \rightarrow \phi(1020)\pi^+)$ using the PDG 19 value of $B(\phi(1020) \rightarrow K^+ K^-) = (49.2 \pm 0.5)\%$. Our first error is the experiment's error and the second error is systematic error from using our best value.
² Measures $B(B^+ \rightarrow \phi\pi^+)/B(B^+ \rightarrow \phi K^+) < 0.018$ at 90% C.L. and assumes $B(B^+ \rightarrow \phi K^+) = (8.8+^{0.7}/_{-0.6}) \times 10^{-6}$.
³ Assumes equal production of B^+ and B^0 at the $\Upsilon(4S)$.
⁴ ABE 00c assumes $B(Z \rightarrow b\bar{b}) = (21.7 \pm 0.1)\%$ and the B fractions $f_{B^0} = f_{B^+} = (39.7+^{1.8}/_{-2.2})\%$ and $f_{B_s} = (10.5+^{1.8}/_{-2.2})\%$.

 $\Gamma(\phi\rho^+)/\Gamma_{\text{total}}$ Γ_{530}/Γ

VALUE (units 10^{-6})	CL%	DOCUMENT ID	TECN	COMMENT
< 3.0	90	¹ AUBERT	08BK BABR	$e^+e^- \rightarrow \Upsilon(4S)$

• • • We do not use the following data for averages, fits, limits, etc. • • •

<16		¹ BERGFELD	98 CLE2	
-----	--	-----------------------	---------	--

¹ Assumes equal production of B^+ and B^0 at the $\Upsilon(4S)$.

 $\Gamma(a_0(980)^0\pi^+, a_0^0 \rightarrow \eta\pi^0)/\Gamma_{\text{total}}$ Γ_{531}/Γ

VALUE (units 10^{-6})	CL%	DOCUMENT ID	TECN	COMMENT
<5.8	90	¹ AUBERT,BE	04 BABR	$e^+e^- \rightarrow \Upsilon(4S)$

¹ Assumes equal production of charged and neutral B mesons from $\Upsilon(4S)$ decays.

 $\Gamma(a_0(980)^+\pi^0, a_0^+ \rightarrow \eta\pi^+)/\Gamma_{\text{total}}$ Γ_{532}/Γ

VALUE (units 10^{-6})	CL%	DOCUMENT ID	TECN	COMMENT
<1.4	90	¹ AUBERT	08A BABR	$e^+e^- \rightarrow \Upsilon(4S)$

¹ Assumes equal production of B^+ and B^0 at the $\Upsilon(4S)$.

Meson Particle Listings

 B^\pm $\Gamma(\pi^+\pi^+\pi^-\pi^-\pi^-)/\Gamma_{\text{total}}$ Γ_{533}/Γ

VALUE	CL%	DOCUMENT ID	TECN	COMMENT
$<8.6 \times 10^{-4}$	90	¹ ALBRECHT 90B	ARG	$e^+e^- \rightarrow \Upsilon(4S)$
¹ ALBRECHT 90B limit assumes equal production of $B^0\bar{B}^0$ and B^+B^- at $\Upsilon(4S)$.				

 $\Gamma(\rho^0 a_1(1260)^+)/\Gamma_{\text{total}}$ Γ_{534}/Γ

VALUE	CL%	DOCUMENT ID	TECN	COMMENT
$<6.2 \times 10^{-4}$	90	¹ BORTOLETTO89	CLEO	$e^+e^- \rightarrow \Upsilon(4S)$
••• We do not use the following data for averages, fits, limits, etc. •••				
$<6.0 \times 10^{-4}$	90	² ALBRECHT 90B	ARG	$e^+e^- \rightarrow \Upsilon(4S)$
$<3.2 \times 10^{-3}$	90	¹ BEBEK 87	CLEO	$e^+e^- \rightarrow \Upsilon(4S)$
¹ BORTOLETTO 89 reports $<5.4 \times 10^{-4}$ assuming the $\Upsilon(4S)$ decays 43% to $B^0\bar{B}^0$. We rescale to 50%.				
² ALBRECHT 90B limit assumes equal production of $B^0\bar{B}^0$ and B^+B^- at $\Upsilon(4S)$.				

 $\Gamma(\rho^0 a_2(1320)^+)/\Gamma_{\text{total}}$ Γ_{535}/Γ

VALUE	CL%	DOCUMENT ID	TECN	COMMENT
$<7.2 \times 10^{-4}$	90	¹ BORTOLETTO89	CLEO	$e^+e^- \rightarrow \Upsilon(4S)$
••• We do not use the following data for averages, fits, limits, etc. •••				
$<2.6 \times 10^{-3}$	90	² BEBEK 87	CLEO	$e^+e^- \rightarrow \Upsilon(4S)$
¹ BORTOLETTO 89 reports $<6.3 \times 10^{-4}$ assuming the $\Upsilon(4S)$ decays 43% to $B^0\bar{B}^0$. We rescale to 50%.				
² BEBEK 87 reports $<2.3 \times 10^{-3}$ assuming the $\Upsilon(4S)$ decays 43% to $B^0\bar{B}^0$. We rescale to 50%.				

 $\Gamma(b_1^0\pi^+, b_1^0 \rightarrow \omega\pi^0)/\Gamma_{\text{total}}$ Γ_{536}/Γ

VALUE (units 10^{-6})	CL%	DOCUMENT ID	TECN	COMMENT
$6.7 \pm 1.7 \pm 1.0$		¹ AUBERT 07B1	BABR	$e^+e^- \rightarrow \Upsilon(4S)$
¹ Assumes equal production of B^+ and B^0 at the $\Upsilon(4S)$.				

 $\Gamma(b_1^+\pi^0, b_1^+ \rightarrow \omega\pi^+)/\Gamma_{\text{total}}$ Γ_{537}/Γ

VALUE (units 10^{-6})	CL%	DOCUMENT ID	TECN	COMMENT
<3.3	90	¹ AUBERT 08A9	BABR	$e^+e^- \rightarrow \Upsilon(4S)$
¹ Assumes equal production of B^+ and B^0 at the $\Upsilon(4S)$.				

 $\Gamma(\pi^+\pi^+\pi^-\pi^-\pi^0)/\Gamma_{\text{total}}$ Γ_{538}/Γ

VALUE	CL%	DOCUMENT ID	TECN	COMMENT
$<6.3 \times 10^{-3}$	90	¹ ALBRECHT 90B	ARG	$e^+e^- \rightarrow \Upsilon(4S)$
¹ ALBRECHT 90B limit assumes equal production of $B^0\bar{B}^0$ and B^+B^- at $\Upsilon(4S)$.				

 $\Gamma(b_1^+\rho^0, b_1^+ \rightarrow \omega\pi^+)/\Gamma_{\text{total}}$ Γ_{539}/Γ

VALUE	CL%	DOCUMENT ID	TECN	COMMENT
$<5.2 \times 10^{-6}$	90	¹ AUBERT 09AF	BABR	$e^+e^- \rightarrow \Upsilon(4S)$
¹ Assumes equal production of B^+ and B^0 at the $\Upsilon(4S)$.				

 $\Gamma(b_1^0\rho^+, b_1^0 \rightarrow \omega\pi^0)/\Gamma_{\text{total}}$ Γ_{541}/Γ

VALUE	CL%	DOCUMENT ID	TECN	COMMENT
$<3.3 \times 10^{-6}$	90	¹ AUBERT 09AF	BABR	$e^+e^- \rightarrow \Upsilon(4S)$
¹ Assumes equal production of B^+ and B^0 at the $\Upsilon(4S)$.				

 $\Gamma(a_1(1260)^+ a_1(1260)^0)/\Gamma_{\text{total}}$ Γ_{540}/Γ

VALUE	CL%	DOCUMENT ID	TECN	COMMENT
$<1.3 \times 10^{-2}$	90	¹ ALBRECHT 90B	ARG	$e^+e^- \rightarrow \Upsilon(4S)$
¹ ALBRECHT 90B limit assumes equal production of $B^0\bar{B}^0$ and B^+B^- at $\Upsilon(4S)$.				

 $\Gamma(h^+\pi^0)/\Gamma_{\text{total}}$ Γ_{542}/Γ

VALUE (units 10^{-6})	CL%	DOCUMENT ID	TECN	COMMENT
$16 \pm 6 \pm 3.6$		GODANG 98	CLE2	$e^+e^- \rightarrow \Upsilon(4S)$
$h^+ = K^+$ or π^+				

 $\Gamma(\omega h^+)/\Gamma_{\text{total}}$ Γ_{543}/Γ

VALUE (units 10^{-6})	CL%	DOCUMENT ID	TECN	COMMENT
13.8 ± 2.4		OUR AVERAGE		

VALUE	CL%	DOCUMENT ID	TECN	COMMENT
$13.4 \pm 3.3 \pm 1.1$		¹ LU 02	BELL	$e^+e^- \rightarrow \Upsilon(4S)$
$14.3 \pm 3.6 \pm 2.0$		¹ JESSOP 00	CLE2	$e^+e^- \rightarrow \Upsilon(4S)$
••• We do not use the following data for averages, fits, limits, etc. •••				
$25 \pm 8 \pm 3$		¹ BERGFELD 98	CLE2	Repl. by JESSOP 00
¹ Assumes equal production of B^+ and B^0 at the $\Upsilon(4S)$.				

 $\Gamma(h^+X^0(\text{Familon}))/\Gamma_{\text{total}}$ Γ_{544}/Γ

VALUE (units 10^{-6})	CL%	DOCUMENT ID	TECN	COMMENT
<49	90	¹ AMMAR 01B	CLE2	$e^+e^- \rightarrow \Upsilon(4S)$
¹ AMMAR 01B searched for the two-body decay of the B meson to a massless neutral feebly-interacting particle X^0 such as the familon, the Nambu-Goldstone boson associated with a spontaneously broken global family symmetry.				

 $\Gamma(K^+X^0, X^0 \rightarrow \mu^+\mu^-)/\Gamma_{\text{total}}$ Γ_{545}/Γ

VALUE	CL%	DOCUMENT ID	TECN	COMMENT
$<1 \times 10^{-7}$	95	¹ AAIJ 17AQ	LHCB	pp at 7, 8 TeV
X^0 stands here for a long-lived scalar particle.				
¹ AAIJ 17AQ searched for a long-lived scalar particle $X^0 \rightarrow \mu^+\mu^-$ in the mass range 250–4700 MeV and lifetime range 0.1–1000 ps. The limit is between 10^{-7} and 2×10^{-10} in these ranges except in vetoed mass regions around $K_S^0, J/\psi, \psi(2S)$, and $\psi(3770)$.				

 $\Gamma(p\bar{p}\pi^+)/\Gamma_{\text{total}}$ Γ_{546}/Γ

VALUE (units 10^{-6})	CL%	DOCUMENT ID	TECN	COMMENT
1.62 ± 0.20		OUR AVERAGE		
$1.60 \pm 0.22 \pm 0.15 \pm 0.12$		^{1,2,3} WEI 08	BELL	$e^+e^- \rightarrow \Upsilon(4S)$
$1.69 \pm 0.29 \pm 0.26$		¹ AUBERT 07AV	BABR	$e^+e^- \rightarrow \Upsilon(4S)$
••• We do not use the following data for averages, fits, limits, etc. •••				
$1.07 \pm 0.11 \pm 0.11$		⁴ AAIJ 14AF	LHCB	pp at 7, 8 TeV
$3.06 \pm 0.73 \pm 0.62 \pm 0.37$		^{1,3} WANG 04	BELL	Repl. by WEI 08
<3.7	90	^{1,2} ABE 02K	BELL	Repl. by WANG 04
<500	90	⁵ ABREU 95N	DLPH	Repl. by ADAM 96D
<160	90	⁶ BEBEK 89	CLEO	$e^+e^- \rightarrow \Upsilon(4S)$
$570 \pm 150 \pm 210$		⁷ ALBRECHT 88F	ARG	$e^+e^- \rightarrow \Upsilon(4S)$
¹ Assumes equal production of B^+ and B^0 at the $\Upsilon(4S)$.				
² Explicitly vetoes resonant production of $p\bar{p}$ from Charmonium states.				
³ Also provides results with $m_{p\bar{p}} < 2.85 \text{ GeV}/c^2$ and angular asymmetry of $p\bar{p}$ system.				
⁴ Requires $m_{p\bar{p}} < 2.85 \text{ GeV}/c^2$.				
⁵ Assumes a B^0, B^- production fraction of 0.39 and a B_S production fraction of 0.12.				
⁶ BEBEK 89 reports $<1.4 \times 10^{-4}$ assuming the $\Upsilon(4S)$ decays 43% to $B^0\bar{B}^0$. We rescale to 50%.				
⁷ ALBRECHT 88F reports $(5.2 \pm 1.4 \pm 1.9) \times 10^{-4}$ assuming the $\Upsilon(4S)$ decays 45% to $B^0\bar{B}^0$. We rescale to 50%.				

 $\Gamma(p\bar{p}\pi^+\text{nonresonant})/\Gamma_{\text{total}}$ Γ_{547}/Γ

VALUE (units 10^{-6})	CL%	DOCUMENT ID	TECN	COMMENT
<53	90	BERGFELD 96B	CLE2	$e^+e^- \rightarrow \Upsilon(4S)$

 $\Gamma(p\bar{p}\pi^+\pi^0)/\Gamma_{\text{total}}$ Γ_{548}/Γ

VALUE (units 10^{-6})	CL%	DOCUMENT ID	TECN	COMMENT
$4.58 \pm 1.17 \pm 0.67$		¹ CHU 20	BELL	$e^+e^- \rightarrow \Upsilon(4S)$
¹ Assumes equal production of B^0 and B^+ from $\Upsilon(4S)$ decays. This measurement is quoted for $M(\pi^+\pi^0) < 1.3 \text{ GeV}$.				

 $\Gamma(p\bar{p}\pi^+\pi^-\pi^0)/\Gamma_{\text{total}}$ Γ_{549}/Γ

VALUE	CL%	DOCUMENT ID	TECN	COMMENT
$<5.2 \times 10^{-4}$	90	¹ ALBRECHT 88F	ARG	$e^+e^- \rightarrow \Upsilon(4S)$
¹ ALBRECHT 88F reports $<4.7 \times 10^{-4}$ assuming the $\Upsilon(4S)$ decays 45% to $B^0\bar{B}^0$. We rescale to 50%.				

 $\Gamma(p\bar{p}K^+)/\Gamma_{\text{total}}$ Γ_{550}/Γ

VALUE (units 10^{-6})	CL%	DOCUMENT ID	TECN	COMMENT
5.9 ± 0.5		OUR AVERAGE		
Error includes scale factor of 1.5.				
$5.54 \pm 0.27 \pm 0.25 \pm 0.36$		^{1,2,3} WEI 08	BELL	$e^+e^- \rightarrow \Upsilon(4S)$
$6.7 \pm 0.5 \pm 0.4$		^{1,3} AUBERT,B 05L	BABR	$e^+e^- \rightarrow \Upsilon(4S)$
••• We do not use the following data for averages, fits, limits, etc. •••				
$4.59 \pm 0.38 \pm 0.34 \pm 0.50$		^{1,2,3} WANG 05A	BELL	Repl. by WEI 08
$5.66 \pm 0.67 \pm 0.57 \pm 0.62$		^{1,2,3} WANG 04	BELL	Repl. by WANG 05A
$4.3 \pm 1.1 \pm 0.9 \pm 0.5$		^{1,2} ABE 02K	BELL	Repl. by WANG 04
¹ Assumes equal production of B^+ and B^0 at the $\Upsilon(4S)$.				
² Explicitly vetoes resonant production of $p\bar{p}$ from Charmonium states.				
³ Provides also results with $m_{p\bar{p}} < 2.85 \text{ GeV}/c^2$ and angular asymmetry of $p\bar{p}$ system.				

 $\Gamma(p\bar{p}K^+)/\Gamma(J/\psi(1S)K^+)$ $\Gamma_{550}/\Gamma_{295}$

VALUE	CL%	DOCUMENT ID	TECN	COMMENT
$0.0104 \pm 0.0005 \pm 0.0001$		^{1,2} AAIJ 13s	LHCB	pp at 7 TeV
¹ AAIJ 13s reports $[\Gamma(B^+ \rightarrow p\bar{p}K^+)/\Gamma(B^+ \rightarrow J/\psi(1S)K^+)] / [B(J/\psi(1S) \rightarrow p\bar{p})] = 4.91 \pm 0.19 \pm 0.14$ which we multiply by our best value $B(J/\psi(1S) \rightarrow p\bar{p}) = (2.120 \pm 0.029) \times 10^{-3}$. Our first error is their experiment's error and our second error is the systematic error from using our best value.				
² Measurement includes contribution where $p\bar{p}$ is produced in charmonia decays.				

 $\Gamma(\Theta(1710)^{++}\bar{p}, \Theta^{++} \rightarrow pK^+)/\Gamma_{\text{total}}$ Γ_{551}/Γ

VALUE (units 10^{-6})	CL%	DOCUMENT ID	TECN	COMMENT
<0.091	90	¹ WANG 05A	BELL	$e^+e^- \rightarrow \Upsilon(4S)$
••• We do not use the following data for averages, fits, limits, etc. •••				
<0.1	90	^{1,2} AUBERT,B 05L	BABR	$e^+e^- \rightarrow \Upsilon(4S)$
¹ Assumes equal production of B^+ and B^0 at the $\Upsilon(4S)$.				
² Provides upper limits depending on the pentaquark masses between 1.43 to 2.0 GeV/c^2 .				

$\Gamma(f_J(2220)K^+, f_J \rightarrow p\bar{p})/\Gamma_{\text{total}}$ Γ_{552}/Γ

VALUE (units 10^{-6})	CL%	DOCUMENT ID	TECN	COMMENT
<0.41	90	¹ WANG	05A BELL	$e^+e^- \rightarrow \Upsilon(4S)$

¹ Assumes equal production of B^+ and B^0 at the $\Upsilon(4S)$.

 $\Gamma(\rho\pi\pi^0)/\Gamma_{\text{total}}$ Γ_{553}/Γ

VALUE	CL%	DOCUMENT ID	TECN	COMMENT
<6.3 $\times 10^{-6}$	90	CHU	23 BELL	$e^+e^- \rightarrow \Upsilon(4S)$

 $\Gamma(\rho\bar{\Lambda}(1520))/\Gamma_{\text{total}}$ Γ_{554}/Γ

VALUE (units 10^{-7})	CL%	DOCUMENT ID	TECN	COMMENT
3.15 $\pm 0.48 \pm 0.27$		¹ AAIJ	14AF LHCB	pp at 7, 8 TeV

• • • We do not use the following data for averages, fits, limits, etc. • • •

3.9 $^{+1.0}_{-0.9} \pm 0.3$		¹ AAIJ	13AU LHCB	Repl. by AAIJ 14AF
<15	90	² AUBERT,B	05L BABR	$e^+e^- \rightarrow \Upsilon(4S)$

¹ Uses $B(B^+ \rightarrow J/\psi K^+) = (1.016 \pm 0.033) \times 10^{-3}$, $B(J/\psi \rightarrow p\bar{p}) = (2.17 \pm 0.07) \times 10^{-3}$ and $B(\Lambda(1520) \rightarrow K^- p) = 0.234 \pm 0.016$.

² Assumes equal production of B^+ and B^0 at the $\Upsilon(4S)$.

 $\Gamma(\rho\bar{p}K^+ \text{ nonresonant})/\Gamma_{\text{total}}$ Γ_{555}/Γ

VALUE (units 10^{-6})	CL%	DOCUMENT ID	TECN	COMMENT
<89	90	BERGFELD	96B CLE2	$e^+e^- \rightarrow \Upsilon(4S)$

 $\Gamma(\rho\bar{p}K^*(892^+)/\Gamma_{\text{total}}$ Γ_{556}/Γ

VALUE (units 10^{-6})	CL%	DOCUMENT ID	TECN	COMMENT
3.6 $^{+0.9}_{-0.7}$ OUR AVERAGE				

3.38 $^{+0.73}_{-0.60} \pm 0.39$		^{1,2} CHEN	08c BELL	$e^+e^- \rightarrow \Upsilon(4S)$
----------------------------------	--	---------------------	----------	-----------------------------------

5.3 $\pm 1.5 \pm 1.3$		² AUBERT	07AV BABR	$e^+e^- \rightarrow \Upsilon(4S)$
-----------------------	--	---------------------	-----------	-----------------------------------

• • • We do not use the following data for averages, fits, limits, etc. • • •

10.3 $^{+3.6}_{-2.8} \pm 1.3$		^{2,3} WANG	04 BELL	Repl. by CHEN 08c
-------------------------------	--	---------------------	---------	-------------------

¹ Explicitly vetoes resonant production of $\rho\bar{p}$ from charmonium states.

² Assumes equal production of B^+ and B^0 at the $\Upsilon(4S)$.

³ Explicitly vetoes resonant production of $\rho\bar{p}$ from charmonium states. The branching fraction for $M_{\rho\bar{p}} < 2.85 \text{ GeV}/c^2$ is also reported.

 $\Gamma(f_J(2220)K^{*+}, f_J \rightarrow p\bar{p})/\Gamma_{\text{total}}$ Γ_{557}/Γ

VALUE (units 10^{-6})	CL%	DOCUMENT ID	TECN	COMMENT
<0.77	90	¹ AUBERT	07AV BABR	$e^+e^- \rightarrow \Upsilon(4S)$

¹ Assumes equal production of B^+ and B^0 at the $\Upsilon(4S)$.

 $\Gamma(\rho\bar{\Lambda})/\Gamma_{\text{total}}$ Γ_{558}/Γ

VALUE (units 10^{-6})	CL%	DOCUMENT ID	TECN	COMMENT
0.24 $^{+0.10}_{-0.08} \pm 0.03$		¹ AAIJ	17R LHCB	pp at 7, 8 TeV

• • • We do not use the following data for averages, fits, limits, etc. • • •

< 0.32	90	² TSAI	07 BELL	$e^+e^- \rightarrow \Upsilon(4S)$
--------	----	-------------------	---------	-----------------------------------

< 0.49	90	² CHANG	05 BELL	Repl. by TSAI 07
--------	----	--------------------	---------	------------------

< 1.5	90	² BORNHEIM	03 CLE2	$e^+e^- \rightarrow \Upsilon(4S)$
-------	----	-----------------------	---------	-----------------------------------

< 2.2	90	² ABE	02o BELL	$e^+e^- \rightarrow \Upsilon(4S)$
-------	----	------------------	----------	-----------------------------------

< 2.6	90	² COAN	99 CLE2	$e^+e^- \rightarrow \Upsilon(4S)$
-------	----	-------------------	---------	-----------------------------------

<60	90	³ AVERY	89B CLEO	$e^+e^- \rightarrow \Upsilon(4S)$
-----	----	--------------------	----------	-----------------------------------

<93	90	⁴ ALBRECHT	88F ARG	$e^+e^- \rightarrow \Upsilon(4S)$
-----	----	-----------------------	---------	-----------------------------------

¹ Statistical significance of the signal is 4.1 standard deviations where the the normalisation is based on $B(B^+ \rightarrow K_S^0 \pi^+) = (11.895 \pm 0.375) \times 10^{-6}$.

² Assumes equal production of B^+ and B^0 at the $\Upsilon(4S)$.

³ AVERY 89B reports $< 5 \times 10^{-5}$ assuming the $\Upsilon(4S)$ decays 43% to $B^0\bar{B}^0$. We rescale to 50%.

⁴ ALBRECHT 88F reports $< 8.5 \times 10^{-5}$ assuming the $\Upsilon(4S)$ decays 45% to $B^0\bar{B}^0$. We rescale to 50%.

 $\Gamma(\rho\bar{\Lambda}\gamma)/\Gamma_{\text{total}}$ Γ_{559}/Γ

VALUE (units 10^{-6})	CL%	DOCUMENT ID	TECN	COMMENT
2.45 $^{+0.44}_{-0.38} \pm 0.22$		¹ WANG	07c BELL	$e^+e^- \rightarrow \Upsilon(4S)$

• • • We do not use the following data for averages, fits, limits, etc. • • •

2.16 $^{+0.58}_{-0.53} \pm 0.20$		¹ LEE	05 BELL	Repl. by WANG 07c
----------------------------------	--	------------------	---------	-------------------

<3.9	90	² EDWARDS	03 CLE2	$e^+e^- \rightarrow \Upsilon(4S)$
------	----	----------------------	---------	-----------------------------------

¹ Assumes equal production of B^+ and B^0 at the $\Upsilon(4S)$.

² Corresponds to $E_\gamma > 1.5 \text{ GeV}$. The limit changes to 3.3×10^{-6} for $E_\gamma > 2.0 \text{ GeV}$.

 $\Gamma(\rho\bar{\Lambda}\pi^0)/\Gamma_{\text{total}}$ Γ_{560}/Γ

VALUE (units 10^{-6})	CL%	DOCUMENT ID	TECN	COMMENT
3.00 $^{+0.61}_{-0.53} \pm 0.33$		¹ WANG	07c BELL	$e^+e^- \rightarrow \Upsilon(4S)$

¹ Assumes equal production of B^+ and B^0 at the $\Upsilon(4S)$.

 $\Gamma(\rho\bar{\Sigma}(1385)^0)/\Gamma_{\text{total}}$ Γ_{561}/Γ

VALUE (units 10^{-6})	CL%	DOCUMENT ID	TECN	COMMENT
<0.47	90	¹ WANG	07c BELL	$e^+e^- \rightarrow \Upsilon(4S)$

¹ Assumes equal production of B^+ and B^0 at the $\Upsilon(4S)$.

 $\Gamma(\Delta^+\bar{\Lambda})/\Gamma_{\text{total}}$ Γ_{562}/Γ

VALUE (units 10^{-6})	CL%	DOCUMENT ID	TECN	COMMENT
<0.82	90	¹ WANG	07c BELL	$e^+e^- \rightarrow \Upsilon(4S)$

¹ Assumes equal production of B^+ and B^0 at the $\Upsilon(4S)$.

 $\Gamma(\rho\bar{\Sigma}\gamma)/\Gamma_{\text{total}}$ Γ_{563}/Γ

VALUE (units 10^{-6})	CL%	DOCUMENT ID	TECN	COMMENT
<4.6	90	¹ LEE	05 BELL	$e^+e^- \rightarrow \Upsilon(4S)$

• • • We do not use the following data for averages, fits, limits, etc. • • •

<7.9	90	² EDWARDS	03 CLE2	$e^+e^- \rightarrow \Upsilon(4S)$
------	----	----------------------	---------	-----------------------------------

¹ Assumes equal production of B^+ and B^0 at the $\Upsilon(4S)$.

² Corresponds to $E_\gamma > 1.5 \text{ GeV}$. The limit changes to 6.4×10^{-6} for $E_\gamma > 2.0 \text{ GeV}$.

 $\Gamma(\rho\bar{\Lambda}\pi^+\pi^-)/\Gamma_{\text{total}}$ Γ_{564}/Γ

VALUE (units 10^{-6})	CL%	DOCUMENT ID	TECN	COMMENT
11.28 $^{+0.91}_{-0.72} \pm 1.03$		¹ CHEN	09c BELL	$e^+e^- \rightarrow \Upsilon(4S)$

• • • We do not use the following data for averages, fits, limits, etc. • • •

<200	90	² ALBRECHT	88F ARG	$e^+e^- \rightarrow \Upsilon(4S)$
------	----	-----------------------	---------	-----------------------------------

¹ Assumes equal production of B^+ and B^0 at the $\Upsilon(4S)$.

² ALBRECHT 88F reports $< 1.8 \times 10^{-4}$ assuming the $\Upsilon(4S)$ decays 45% to $B^0\bar{B}^0$. We rescale to 50%.

 $\Gamma(\rho\bar{\Lambda}\pi^+\pi^- \text{ nonresonant})/\Gamma_{\text{total}}$ Γ_{565}/Γ

VALUE (units 10^{-6})	CL%	DOCUMENT ID	TECN	COMMENT
5.92 $^{+0.88}_{-0.84} \pm 0.69$		¹ CHEN	09c BELL	$e^+e^- \rightarrow \Upsilon(4S)$

¹ Assumes equal production of B^+ and B^0 at the $\Upsilon(4S)$.

 $\Gamma(\rho\bar{\Lambda}\rho^0, \rho^0 \rightarrow \pi^+\pi^-)/\Gamma_{\text{total}}$ Γ_{566}/Γ

VALUE (units 10^{-6})	CL%	DOCUMENT ID	TECN	COMMENT
4.78 $^{+0.67}_{-0.64} \pm 0.60$		¹ CHEN	09c BELL	$e^+e^- \rightarrow \Upsilon(4S)$

¹ Assumes equal production of B^+ and B^0 at the $\Upsilon(4S)$.

 $\Gamma(\rho\bar{\Lambda}\rho^0, \rho^0 \rightarrow \pi^+\pi^-)/\Gamma_{\text{total}}$ Γ_{567}/Γ

VALUE (units 10^{-6})	CL%	DOCUMENT ID	TECN	COMMENT
2.03 $^{+0.77}_{-0.72} \pm 0.27$		¹ CHEN	09c BELL	$e^+e^- \rightarrow \Upsilon(4S)$

¹ Assumes equal production of B^+ and B^0 at the $\Upsilon(4S)$.

 $\Gamma(\rho\bar{\Lambda}K^+K^-)/\Gamma_{\text{total}}$ Γ_{568}/Γ

VALUE (units 10^{-6})	CL%	DOCUMENT ID	TECN	COMMENT
4.10 $^{+0.45}_{-0.43} \pm 0.50$		¹ LU	19 BELL	$e^+e^- \rightarrow \Upsilon(4S)$

¹ Assumes equal production of B^+ and B^0 at the $\Upsilon(4S)$.

 $\Gamma(\rho\bar{\Lambda}\phi)/\Gamma_{\text{total}}$ Γ_{569}/Γ

VALUE (units 10^{-6})	CL%	DOCUMENT ID	TECN	COMMENT
0.795 $\pm 0.209 \pm 0.077$		¹ LU	19 BELL	$e^+e^- \rightarrow \Upsilon(4S)$

¹ Assumes equal production of B^+ and B^0 at the $\Upsilon(4S)$.

 $\Gamma(\bar{p}\Lambda K^+K^-)/\Gamma_{\text{total}}$ Γ_{570}/Γ

VALUE (units 10^{-6})	CL%	DOCUMENT ID	TECN	COMMENT
3.70 $^{+0.39}_{-0.37} \pm 0.44$		¹ LU	19 BELL	$e^+e^- \rightarrow \Upsilon(4S)$

¹ Assumes equal production of B^+ and B^0 at the $\Upsilon(4S)$.

 $\Gamma(\Lambda\bar{\Lambda}\pi^+)/\Gamma_{\text{total}}$ Γ_{571}/Γ

VALUE (units 10^{-6})	CL%	DOCUMENT ID	TECN	COMMENT
<0.94	90	^{1,2} CHANG	09 BELL	Repl. by CHANG 09

• • • We do not use the following data for averages, fits, limits, etc. • • •

<2.8	90	² LEE	04 BELL	$e^+e^- \rightarrow \Upsilon(4S)$
------	----	------------------	---------	-----------------------------------

¹ For $m_{\Lambda\bar{\Lambda}} < 2.85 \text{ GeV}/c^2$.

² Assumes equal production of B^+ and B^0 at the $\Upsilon(4S)$.

 $\Gamma(\Lambda\bar{\Lambda}K^+)/\Gamma_{\text{total}}$ Γ_{572}/Γ

VALUE (units 10^{-6})	CL%	DOCUMENT ID	TECN	COMMENT
3.38 $^{+0.41}_{-0.36} \pm 0.41$		^{1,2} CHANG	09 BELL	$e^+e^- \rightarrow \Upsilon(4S)$

• • • We do not use the following data for averages, fits, limits, etc. • • •

2.91 $^{+0.9}_{-0.70} \pm 0.38$		² LEE	04 BELL	Repl. by CHANG 09
---------------------------------	--	------------------	---------	-------------------

¹ Excluding charmonium events in $2.85 < m_{\Lambda\bar{\Lambda}} < 3.128 \text{ GeV}/c^2$ and $3.315 < m_{\Lambda\bar{\Lambda}} < 3.735 \text{ GeV}/c^2$. Measurements in various $m_{\Lambda\bar{\Lambda}}$ bins are also reported.

² Assumes equal production of B^+ and B^0 at the $\Upsilon(4S)$.

Meson Particle Listings

 B^\pm $\Gamma(\Lambda\bar{\Lambda}K^{*+})/\Gamma_{\text{total}}$ Γ_{573}/Γ

VALUE (units 10^{-6})	DOCUMENT ID	TECN	COMMENT
$2.19^{+1.13}_{-0.88} \pm 0.33$	1,2 CHANG 09	BELL	$e^+e^- \rightarrow \Upsilon(4S)$

¹ For $m_{\Lambda\bar{\Lambda}} < 2.85 \text{ GeV}/c^2$.² Assumes equal production of B^+ and B^0 at the $\Upsilon(4S)$. $\Gamma(\Lambda(1520)\bar{\Lambda}K^+)/\Gamma_{\text{total}}$ Γ_{574}/Γ

VALUE (units 10^{-6})	DOCUMENT ID	TECN	COMMENT
$2.23 \pm 0.63 \pm 0.25$	1 LU 19	BELL	$e^+e^- \rightarrow \Upsilon(4S)$

¹ Assumes equal production of B^+ and B^0 at the $\Upsilon(4S)$. $\Gamma(\Lambda\bar{\Lambda}(1520)K^+)/\Gamma_{\text{total}}$ Γ_{575}/Γ

VALUE	DOCUMENT ID	TECN	COMMENT
$< 2.08 \times 10^{-6}$	1 LU 19	BELL	$e^+e^- \rightarrow \Upsilon(4S)$

¹ Assumes equal production of B^+ and B^0 at the $\Upsilon(4S)$. $\Gamma(\bar{D}^0 \rho)/\Gamma_{\text{total}}$ Γ_{576}/Γ

VALUE (units 10^{-6})	CL%	DOCUMENT ID	TECN	COMMENT
< 1.38	90	1 WEI 08	BELL	$e^+e^- \rightarrow \Upsilon(4S)$

• • • We do not use the following data for averages, fits, limits, etc. • • •

 < 380 90 2 BORTOLETTO89 CLEO $e^+e^- \rightarrow \Upsilon(4S)$ ¹ Assumes equal production of B^+ and B^0 at the $\Upsilon(4S)$.² BORTOLETTO 89 reports $< 3.3 \times 10^{-4}$ assuming the $\Upsilon(4S)$ decays 43% to $B^0\bar{B}^0$. We rescale to 50%. $\Gamma(\Delta^{++}\bar{p})/\Gamma_{\text{total}}$ Γ_{577}/Γ

VALUE (units 10^{-6})	CL%	DOCUMENT ID	TECN	COMMENT
< 0.14	90	1 WEI 08	BELL	$e^+e^- \rightarrow \Upsilon(4S)$

• • • We do not use the following data for averages, fits, limits, etc. • • •

 < 150 90 2 BORTOLETTO89 CLEO $e^+e^- \rightarrow \Upsilon(4S)$ ¹ Assumes equal production of B^+ and B^0 at the $\Upsilon(4S)$.² BORTOLETTO 89 reports $< 1.3 \times 10^{-4}$ assuming the $\Upsilon(4S)$ decays 43% to $B^0\bar{B}^0$. We rescale to 50%. $\Gamma(D^+ p\bar{p})/\Gamma_{\text{total}}$ Γ_{578}/Γ

VALUE	CL%	DOCUMENT ID	TECN	COMMENT
$< 1.5 \times 10^{-5}$	90	1 ABE 02W	BELL	$e^+e^- \rightarrow \Upsilon(4S)$

¹ Assumes equal production of B^+ and B^0 at the $\Upsilon(4S)$. $\Gamma(D^*(2010)^+ p\bar{p})/\Gamma_{\text{total}}$ Γ_{579}/Γ

VALUE	CL%	DOCUMENT ID	TECN	COMMENT
$< 1.5 \times 10^{-5}$	90	1 ABE 02W	BELL	$e^+e^- \rightarrow \Upsilon(4S)$

¹ Assumes equal production of B^+ and B^0 at the $\Upsilon(4S)$. $\Gamma(\bar{D}^0 \rho\bar{p}\pi^+)/\Gamma_{\text{total}}$ Γ_{580}/Γ

VALUE (units 10^{-4})	DOCUMENT ID	TECN	COMMENT
$3.72 \pm 0.11 \pm 0.25$	1,2 DEL-AMO-SA..12	BABR	$e^+e^- \rightarrow \Upsilon(4S)$

¹ Uses the values of D and D^* branching fractions from PDG 08.² Assumes equal production of B^+ and B^0 at the $\Upsilon(4S)$. $\Gamma(\bar{D}^{*0} \rho\bar{p}\pi^+)/\Gamma_{\text{total}}$ Γ_{581}/Γ

VALUE (units 10^{-4})	DOCUMENT ID	TECN	COMMENT
$3.73 \pm 0.17 \pm 0.27$	1,2 DEL-AMO-SA..12	BABR	$e^+e^- \rightarrow \Upsilon(4S)$

¹ Uses the values of D and D^* branching fractions from PDG 08.² Assumes equal production of B^+ and B^0 at the $\Upsilon(4S)$. $\Gamma(D^- \rho\bar{p}\pi^+\pi^-)/\Gamma_{\text{total}}$ Γ_{582}/Γ

VALUE (units 10^{-4})	DOCUMENT ID	TECN	COMMENT
$1.66 \pm 0.13 \pm 0.27$	1,2 DEL-AMO-SA..12	BABR	$e^+e^- \rightarrow \Upsilon(4S)$

¹ Uses the values of D and D^* branching fractions from PDG 08.² Assumes equal production of B^+ and B^0 at the $\Upsilon(4S)$. $\Gamma(D^{*-} \rho\bar{p}\pi^+\pi^-)/\Gamma_{\text{total}}$ Γ_{583}/Γ

VALUE (units 10^{-4})	DOCUMENT ID	TECN	COMMENT
$1.86 \pm 0.16 \pm 0.19$	1,2 DEL-AMO-SA..12	BABR	$e^+e^- \rightarrow \Upsilon(4S)$

¹ Uses the values of D and D^* branching fractions from PDG 08.² Assumes equal production of B^+ and B^0 at the $\Upsilon(4S)$. $\Gamma(\rho\bar{\Lambda}^0\bar{D}^0)/\Gamma_{\text{total}}$ Γ_{584}/Γ

VALUE (units 10^{-5})	DOCUMENT ID	TECN	COMMENT
$1.43^{+0.28}_{-0.25} \pm 0.18$	1,2 CHEN 11F	BELL	$e^+e^- \rightarrow \Upsilon(4S)$

¹ Uses $B(\Lambda \rightarrow p\pi^-) = 63.9 \pm 0.5\%$, $B(D^0 \rightarrow K^-\pi^+) = 3.89 \pm 0.05\%$, and $B(D^0 \rightarrow K^-\pi^+\pi^0) = 13.9 \pm 0.5\%$.² Assumes equal production of B^0 and B^+ from Upsilon(4S) decays. $\Gamma(\rho\bar{\Lambda}^0\bar{D}^*(2007)^0)/\Gamma_{\text{total}}$ Γ_{585}/Γ

VALUE (units 10^{-5})	CL%	DOCUMENT ID	TECN	COMMENT
< 5	90	1,2,3 CHEN 11F	BELL	$e^+e^- \rightarrow \Upsilon(4S)$

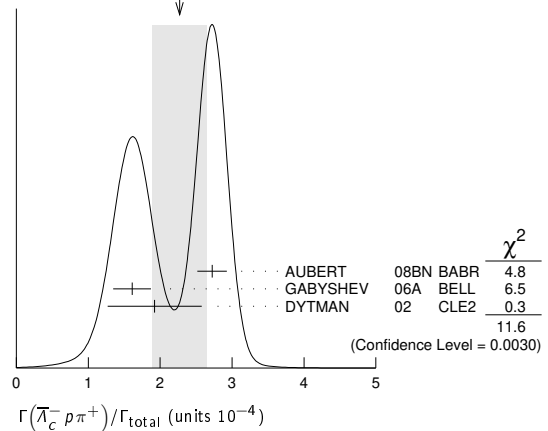
¹ CHEN 11F reports $< 4.8 \times 10^{-5}$ from a measurement of $[\Gamma(B^+ \rightarrow \rho\bar{\Lambda}^0\bar{D}^*(2007)^0)/\Gamma_{\text{total}}] / [B(D^*(2007)^0 \rightarrow D^0\pi^0)]$ assuming $B(D^*(2007)^0 \rightarrow D^0\pi^0) = (61.9 \pm 2.9) \times 10^{-2}$, which we rescale to our best value $B(D^*(2007)^0 \rightarrow D^0\pi^0) = 64.7 \times 10^{-2}$.² Uses $B(\Lambda \rightarrow p\pi^-) = 63.9 \pm 0.5\%$ and $B(D^0 \rightarrow K^-\pi^+) = 3.89 \pm 0.05\%$.³ Assumes equal production of B^0 and B^+ from Upsilon(4S) decays. $\Gamma(\bar{\Lambda}_c^- \rho\pi^+)/\Gamma_{\text{total}}$ Γ_{586}/Γ

VALUE (units 10^{-4})	DOCUMENT ID	TECN	COMMENT
2.3 ± 0.4	OUR AVERAGE		Error includes scale factor of 2.4. See the ideogram below.

2.72 ± 0.16 ± 0.12 1,2 AUBERT 08BN BABR $e^+e^- \rightarrow \Upsilon(4S)$ 1.61 ± 0.20 ± 0.07 1,3 GABYSHEV 06A BELL $e^+e^- \rightarrow \Upsilon(4S)$ 1.9 ± 0.5 ± 0.1 1,4 DYTMAN 02 CLE2 $e^+e^- \rightarrow \Upsilon(4S)$

• • • We do not use the following data for averages, fits, limits, etc. • • •

1.5 ± 0.4 ± 0.1 1,5 GABYSHEV 02 BELL Repl. by GABYSHEV 06A

6.2 $\pm_{-2.0}^{+2.3}$ ± 1.6 1,6 FU 97 CLE2 Repl. by DYTMAN 02¹ Assumes equal production of B^+ and B^0 at the $\Upsilon(4S)$.² AUBERT 08BN reports $(3.4 \pm 0.1 \pm 0.9) \times 10^{-4}$ from a measurement of $[\Gamma(B^+ \rightarrow \bar{\Lambda}_c^- \rho\pi^+)/\Gamma_{\text{total}}] \times [B(\Lambda_c^+ \rightarrow pK^-\pi^+)]$ assuming $B(\Lambda_c^+ \rightarrow pK^-\pi^+) = (5.0 \pm 1.3) \times 10^{-2}$, which we rescale to our best value $B(\Lambda_c^+ \rightarrow pK^-\pi^+) = (6.24 \pm 0.28) \times 10^{-2}$. Our first error is their experiment's error and our second error is the systematic error from using our best value.³ GABYSHEV 06A reports $(2.01 \pm 0.15 \pm 0.20) \times 10^{-4}$ from a measurement of $[\Gamma(B^+ \rightarrow \bar{\Lambda}_c^- \rho\pi^+)/\Gamma_{\text{total}}] \times [B(\Lambda_c^+ \rightarrow pK^-\pi^+)]$ assuming $B(\Lambda_c^+ \rightarrow pK^-\pi^+) = 0.05$, which we rescale to our best value $B(\Lambda_c^+ \rightarrow pK^-\pi^+) = (6.24 \pm 0.28) \times 10^{-2}$. Our first error is their experiment's error and our second error is the systematic error from using our best value.⁴ DYTMAN 02 reports $(2.4^{+0.63}_{-0.62}) \times 10^{-4}$ from a measurement of $[\Gamma(B^+ \rightarrow \bar{\Lambda}_c^- \rho\pi^+)/\Gamma_{\text{total}}] \times [B(\Lambda_c^+ \rightarrow pK^-\pi^+)]$ assuming $B(\Lambda_c^+ \rightarrow pK^-\pi^+) = 0.05$, which we rescale to our best value $B(\Lambda_c^+ \rightarrow pK^-\pi^+) = (6.24 \pm 0.28) \times 10^{-2}$. Our first error is their experiment's error and our second error is the systematic error from using our best value.⁵ GABYSHEV 02 reports $(1.87^{+0.51}_{-0.49}) \times 10^{-4}$ from a measurement of $[\Gamma(B^+ \rightarrow \bar{\Lambda}_c^- \rho\pi^+)/\Gamma_{\text{total}}] \times [B(\Lambda_c^+ \rightarrow pK^-\pi^+)]$ assuming $B(\Lambda_c^+ \rightarrow pK^-\pi^+) = 0.05$, which we rescale to our best value $B(\Lambda_c^+ \rightarrow pK^-\pi^+) = (6.24 \pm 0.28) \times 10^{-2}$. Our first error is their experiment's error and our second error is the systematic error from using our best value.⁶ FU 97 uses PDG 96 values of Λ_c branching fraction.WEIGHTED AVERAGE
2.3±0.4 (Error scaled by 2.4) $\Gamma(\bar{\Lambda}_c^- \Delta(1232)^+)/\Gamma_{\text{total}}$ Γ_{587}/Γ

VALUE (units 10^{-5})	CL%	DOCUMENT ID	TECN	COMMENT
< 1.9	90	GABYSHEV 06A	BELL	$e^+e^- \rightarrow \Upsilon(4S)$

 $\Gamma(\bar{\Lambda}_c^- \Delta_X(1600)^+)/\Gamma_{\text{total}}$ Γ_{588}/Γ

VALUE (units 10^{-5})	DOCUMENT ID	TECN	COMMENT
$4.7 \pm 0.9 \pm 0.2$	1 GABYSHEV 06A	BELL	$e^+e^- \rightarrow \Upsilon(4S)$

¹ GABYSHEV 06A reports $(5.9 \pm 1.0 \pm 0.6) \times 10^{-5}$ from a measurement of $[\Gamma(B^+ \rightarrow \bar{\Lambda}_c^- \Delta_X(1600)^+)/\Gamma_{\text{total}}] \times [B(\Lambda_c^+ \rightarrow pK^-\pi^+)]$ assuming $B(\Lambda_c^+ \rightarrow pK^-\pi^+) = 0.05$, which we rescale to our best value $B(\Lambda_c^+ \rightarrow pK^-\pi^+) = (6.24 \pm 0.28) \times 10^{-2}$. Our first error is their experiment's error and our second error is the systematic error from using our best value.

$\Gamma(\overline{\Lambda}_c^- \Delta_X(2420)^+)/\Gamma_{\text{total}}$ Γ_{589}/Γ
 VALUE (units 10^{-5}) DOCUMENT ID TECN COMMENT

$3.8 \pm_{-0.8}^{+0.9} \pm 0.2$

¹ GABYSHEV 06A BELL $e^+e^- \rightarrow \Upsilon(4S)$

¹ GABYSHEV 06A reports $(4.7 \pm_{-0.9}^{+1.0} \pm 0.4) \times 10^{-5}$ from a measurement of $[\Gamma(B^+ \rightarrow \overline{\Lambda}_c^- \Delta_X(2420)^+)/\Gamma_{\text{total}}] \times [B(\Lambda_c^+ \rightarrow pK^-\pi^+)]$ assuming $B(\Lambda_c^+ \rightarrow pK^-\pi^+) = 0.05$, which we rescale to our best value $B(\Lambda_c^+ \rightarrow pK^-\pi^+) = (6.24 \pm 0.28) \times 10^{-2}$. Our first error is their experiment's error and our second error is the systematic error from using our best value.

$\Gamma((\overline{\Lambda}_c^- p)_s \pi^+)/\Gamma_{\text{total}}$ Γ_{590}/Γ
 $(\overline{\Lambda}_c^- p)_s$ denotes a low-mass enhancement near 3.35 GeV/c².
 VALUE (units 10^{-5}) DOCUMENT ID TECN COMMENT

$3.1 \pm_{-0.6}^{+0.7} \pm 0.1$

¹ GABYSHEV 06A BELL $e^+e^- \rightarrow \Upsilon(4S)$

¹ GABYSHEV 06A reports $(3.9 \pm_{-0.7}^{+0.8} \pm 0.4) \times 10^{-5}$ from a measurement of $[\Gamma(B^+ \rightarrow (\overline{\Lambda}_c^- p)_s \pi^+)/\Gamma_{\text{total}}] \times [B(\Lambda_c^+ \rightarrow pK^-\pi^+)]$ assuming $B(\Lambda_c^+ \rightarrow pK^-\pi^+) = 0.05$, which we rescale to our best value $B(\Lambda_c^+ \rightarrow pK^-\pi^+) = (6.24 \pm 0.28) \times 10^{-2}$. Our first error is their experiment's error and our second error is the systematic error from using our best value.

$\Gamma(\overline{\Sigma}_c(2520)^0 p)/\Gamma_{\text{total}}$ Γ_{591}/Γ
 VALUE (units 10^{-5}) CL% DOCUMENT ID TECN COMMENT

<0.3

90 ^{1,2} AUBERT 08BN BABR $e^+e^- \rightarrow \Upsilon(4S)$

• • • We do not use the following data for averages, fits, limits, etc. • • •

<2.7

90 ^{1,2} GABYSHEV 06A BELL $e^+e^- \rightarrow \Upsilon(4S)$

<4.6

90 ^{1,2} GABYSHEV 02 BELL Repl. by GABYSHEV 06A

¹ Assumes equal production of B^+ and B^0 at the $\Upsilon(4S)$.

² Uses the value for $\Lambda_c \rightarrow pK^-\pi^+$ branching ratio $(5.0 \pm 1.3)\%$.

$\Gamma(\overline{\Sigma}_c(2520)^0 p)/\Gamma(\overline{\Lambda}_c^- p \pi^+)$ $\Gamma_{591}/\Gamma_{586}$
 VALUE (units 10^{-3}) CL% DOCUMENT ID TECN COMMENT

<9

90 AUBERT 08BN BABR $e^+e^- \rightarrow \Upsilon(4S)$

$\Gamma(\overline{\Sigma}_c(2800)^0 p)/\Gamma_{\text{total}}$ Γ_{592}/Γ
 VALUE (units 10^{-5}) DOCUMENT ID TECN COMMENT

$2.7 \pm_{-0.8}^{+0.8} \pm 0.4$

¹ AUBERT 08BN BABR $e^+e^- \rightarrow \Upsilon(4S)$

¹ AUBERT 08BN reports $[\Gamma(B^+ \rightarrow \overline{\Sigma}_c(2800)^0 p)/\Gamma_{\text{total}}] / [B(B^+ \rightarrow \overline{\Lambda}_c^- p \pi^+)] = 0.117 \pm 0.023 \pm 0.024$ which we multiply by our best value $B(B^+ \rightarrow \overline{\Lambda}_c^- p \pi^+) = (2.3 \pm 0.4) \times 10^{-4}$. Our first error is their experiment's error and our second error is the systematic error from using our best value.

$\Gamma(\overline{\Lambda}_c^- p \pi^+ \pi^0)/\Gamma_{\text{total}}$ Γ_{593}/Γ
 VALUE (units 10^{-3}) CL% DOCUMENT ID TECN COMMENT

$1.81 \pm_{-0.50}^{+0.29} \pm 0.52$

^{1,2} DYTMAN 02 CLE2 $e^+e^- \rightarrow \Upsilon(4S)$

• • • We do not use the following data for averages, fits, limits, etc. • • •

<3.12

90 ³ FU 97 CLE2 $e^+e^- \rightarrow \Upsilon(4S)$

¹ Assumes equal production of B^+ and B^0 at the $\Upsilon(4S)$.

² DYTMAN 02 measurement uses $B(\Lambda_c^- \rightarrow \overline{p}K^+\pi^-) = 5.0 \pm 1.3\%$. The second error includes the systematic and the uncertainty of the branching ratio.

³ FU 97 uses PDG 96 values of Λ_c branching ratio.

$\Gamma(\overline{\Lambda}_c^- p \pi^+ \pi^+ \pi^-)/\Gamma_{\text{total}}$ Γ_{594}/Γ
 VALUE (units 10^{-3}) CL% DOCUMENT ID TECN COMMENT

$2.25 \pm_{-0.61}^{+0.25} \pm 0.63$

^{1,2} DYTMAN 02 CLE2 $e^+e^- \rightarrow \Upsilon(4S)$

• • • We do not use the following data for averages, fits, limits, etc. • • •

<1.46

90 ³ FU 97 CLE2 $e^+e^- \rightarrow \Upsilon(4S)$

¹ Assumes equal production of B^+ and B^0 at the $\Upsilon(4S)$.

² DYTMAN 02 measurement uses $B(\Lambda_c^- \rightarrow \overline{p}K^+\pi^-) = 5.0 \pm 1.3\%$. The second error includes the systematic and the uncertainty of the branching ratio.

³ FU 97 uses PDG 96 values of Λ_c branching ratio.

$\Gamma(\overline{\Lambda}_c^- p \pi^+ \pi^+ \pi^- \pi^0)/\Gamma_{\text{total}}$ Γ_{595}/Γ
 VALUE CL% DOCUMENT ID TECN COMMENT

$<1.34 \times 10^{-2}$

¹ FU 97 uses PDG 96 values of Λ_c branching ratio.

$\Gamma(\Lambda_c^+ \Lambda_c^- K^+)/\Gamma_{\text{total}}$ Γ_{596}/Γ
 VALUE (units 10^{-4}) DOCUMENT ID TECN COMMENT

4.9 ± 0.7 OUR AVERAGE

$4.80 \pm 0.43 \pm 0.60$

LI 18A BELL $e^+e^- \rightarrow \Upsilon(4S)$

$9.1 \pm 4.5 \pm 0.4$

^{1,2} AUBERT 08H BABR $e^+e^- \rightarrow \Upsilon(4S)$

• • • We do not use the following data for averages, fits, limits, etc. • • •

$6.3 \pm 2.5 \pm 0.3$

^{2,3} GABYSHEV 06 BELL Repl. by LI 18A.

¹ AUBERT 08H reports $(1.14 \pm 0.15 \pm 0.62) \times 10^{-3}$ from a measurement of $[\Gamma(B^+ \rightarrow \Lambda_c^+ \Lambda_c^- K^+)/\Gamma_{\text{total}}] \times [B(\Lambda_c^+ \rightarrow pK^-\pi^+)]$ assuming $B(\Lambda_c^+ \rightarrow pK^-\pi^+) = (5.0 \pm 1.3) \times 10^{-2}$, which we rescale to our best value $B(\Lambda_c^+ \rightarrow pK^-\pi^+) = (6.24 \pm 0.28) \times 10^{-2}$. Our first error is their experiment's error and our second error is the systematic error from using our best value.

² Assumes equal production of B^+ and B^0 at the $\Upsilon(4S)$.

³ GABYSHEV 06 reports $(7.9 \pm_{-0.9}^{+1.0} \pm 3.6) \times 10^{-4}$ from a measurement of $[\Gamma(B^+ \rightarrow \Lambda_c^+ \Lambda_c^- K^+)/\Gamma_{\text{total}}] \times [B(\Lambda_c^+ \rightarrow pK^-\pi^+)]$ assuming $B(\Lambda_c^+ \rightarrow pK^-\pi^+) = (5.0 \pm 1.3) \times 10^{-2}$, which we rescale to our best value $B(\Lambda_c^+ \rightarrow pK^-\pi^+) = (6.24 \pm 0.28) \times 10^{-2}$. Our first error is their experiment's error and our second error is the systematic error from using our best value.

$\Gamma(\Lambda_c^+ \Lambda_c^- K^+)/\Gamma(D^- D^+ K^+)$ $\Gamma_{596}/\Gamma_{221}$
 VALUE DOCUMENT ID TECN COMMENT

2.36 ± 0.11 ± 0.33

¹ AAIJ 23X LHCb pp at 13 TeV

¹ The second uncertainty includes both systematic (± 0.22) and the charm decay branching fraction (± 0.25).

$\Gamma(\Xi_c(2930)\Lambda_c^+, \Xi_c \rightarrow K^+\Lambda_c^-)/\Gamma_{\text{total}}$ Γ_{597}/Γ
 VALUE (units 10^{-4}) DOCUMENT ID TECN COMMENT

1.73 ± 0.45 ± 0.21

¹ LI 18A BELL $e^+e^- \rightarrow \Upsilon(4S)$

¹ The $\Xi_c(2930)$ is found in its decay to $K^-\Lambda_c^+$ in $B^- \rightarrow K^-\Lambda_c^+\Lambda_c^+$ with a significance more than 5 sigma.

$\Gamma(\overline{\Sigma}_c(2455)^0 p)/\Gamma_{\text{total}}$ Γ_{598}/Γ
 VALUE (units 10^{-5}) CL% DOCUMENT ID TECN COMMENT

3.0 ± 0.6 ± 0.1

^{1,2} GABYSHEV 06A BELL $e^+e^- \rightarrow \Upsilon(4S)$

• • • We do not use the following data for averages, fits, limits, etc. • • •

<8

90 ^{1,3} DYTMAN 02 CLE2 $e^+e^- \rightarrow \Upsilon(4S)$

<9.3

90 ^{1,4} GABYSHEV 02 BELL Repl. by GABYSHEV 06A

¹ Assumes equal production of B^+ and B^0 at the $\Upsilon(4S)$.

² GABYSHEV 06A reports $(3.7 \pm 0.7 \pm 0.4) \times 10^{-5}$ from a measurement of $[\Gamma(B^+ \rightarrow \overline{\Sigma}_c(2455)^0 p)/\Gamma_{\text{total}}] \times [B(\Lambda_c^+ \rightarrow pK^-\pi^+)]$ assuming $B(\Lambda_c^+ \rightarrow pK^-\pi^+) = 0.05$, which we rescale to our best value $B(\Lambda_c^+ \rightarrow pK^-\pi^+) = (6.24 \pm 0.28) \times 10^{-2}$. Our first error is their experiment's error and our second error is the systematic error from using our best value.

³ DYTMAN 02 measurement uses $B(\Lambda_c^- \rightarrow \overline{p}K^+\pi^-) = 5.0 \pm 1.3\%$. The second error includes the systematic and the uncertainty of the branching ratio.

⁴ Uses the value for $\Lambda_c \rightarrow pK^-\pi^+$ branching ratio $(5.0 \pm 1.3)\%$.

$\Gamma(\overline{\Sigma}_c(2455)^0 p)/\Gamma(\overline{\Lambda}_c^- p \pi^+)$ $\Gamma_{598}/\Gamma_{586}$
 VALUE DOCUMENT ID TECN COMMENT

0.123 ± 0.012 ± 0.008

¹ AUBERT 08BN BABR $e^+e^- \rightarrow \Upsilon(4S)$

¹ Assumes equal production of B^+ and B^0 at the $\Upsilon(4S)$.

$\Gamma(\overline{\Sigma}_c(2455)^0 p \pi^0)/\Gamma_{\text{total}}$ Γ_{599}/Γ
 VALUE (units 10^{-4}) DOCUMENT ID TECN COMMENT

3.5 ± 1.1 ± 0.2

^{1,2} DYTMAN 02 CLE2 $e^+e^- \rightarrow \Upsilon(4S)$

¹ DYTMAN 02 reports $(4.4 \pm 1.4) \times 10^{-4}$ from a measurement of $[\Gamma(B^+ \rightarrow \overline{\Sigma}_c(2455)^0 p \pi^0)/\Gamma_{\text{total}}] \times [B(\Lambda_c^+ \rightarrow pK^-\pi^+)]$ assuming $B(\Lambda_c^+ \rightarrow pK^-\pi^+) = 0.05$, which we rescale to our best value $B(\Lambda_c^+ \rightarrow pK^-\pi^+) = (6.24 \pm 0.28) \times 10^{-2}$. Our first error is their experiment's error and our second error is the systematic error from using our best value.

² Assumes equal production of B^+ and B^0 at the $\Upsilon(4S)$.

$\Gamma(\overline{\Sigma}_c(2455)^0 p \pi^- \pi^+)/\Gamma_{\text{total}}$ Γ_{600}/Γ
 VALUE (units 10^{-4}) DOCUMENT ID TECN COMMENT

3.5 ± 1.0 ± 0.2

^{1,2} DYTMAN 02 CLE2 $e^+e^- \rightarrow \Upsilon(4S)$

¹ DYTMAN 02 reports $(4.4 \pm 1.3) \times 10^{-4}$ from a measurement of $[\Gamma(B^+ \rightarrow \overline{\Sigma}_c(2455)^0 p \pi^- \pi^+)/\Gamma_{\text{total}}] \times [B(\Lambda_c^+ \rightarrow pK^-\pi^+)]$ assuming $B(\Lambda_c^+ \rightarrow pK^-\pi^+) = 0.05$, which we rescale to our best value $B(\Lambda_c^+ \rightarrow pK^-\pi^+) = (6.24 \pm 0.28) \times 10^{-2}$. Our first error is their experiment's error and our second error is the systematic error from using our best value.

² Assumes equal production of B^+ and B^0 at the $\Upsilon(4S)$.

$\Gamma(\overline{\Sigma}_c(2455)^- p \pi^+ \pi^+)/\Gamma_{\text{total}}$ Γ_{601}/Γ
 VALUE (units 10^{-4}) DOCUMENT ID TECN COMMENT

2.38 ± 0.19 OUR AVERAGE

$2.39 \pm 0.16 \pm_{-0.10}^{+0.11}$

^{1,2} LEES 12Z BABR $e^+e^- \rightarrow \Upsilon(4S)$

$2.2 \pm 0.8 \pm 0.1$

^{1,3} DYTMAN 02 CLE2 $e^+e^- \rightarrow \Upsilon(4S)$

¹ Assumes equal production of B^+ and B^0 at the $\Upsilon(4S)$.

² LEES 12Z reports $(2.98 \pm 0.16 \pm 0.15 \pm 0.77) \times 10^{-4}$ from a measurement of $[\Gamma(B^+ \rightarrow \overline{\Sigma}_c(2455)^- p \pi^+ \pi^+)/\Gamma_{\text{total}}] \times [B(\Lambda_c^+ \rightarrow pK^-\pi^+)]$ assuming $B(\Lambda_c^+ \rightarrow pK^-\pi^+) = (5.0 \pm 1.3) \times 10^{-2}$, which we rescale to our best value $B(\Lambda_c^+ \rightarrow pK^-\pi^+) = (6.24 \pm 0.28) \times 10^{-2}$. Our first error is their experiment's error and our second error is the systematic error from using our best value.

³ DYTMAN 02 reports $(2.8 \pm 0.9 \pm 0.5 \pm 0.7) \times 10^{-4}$ from a measurement of $[\Gamma(B^+ \rightarrow \overline{\Sigma}_c(2455)^- p \pi^+ \pi^+)/\Gamma_{\text{total}}] \times [B(\Lambda_c^+ \rightarrow pK^-\pi^+)]$ assuming $B(\Lambda_c^+ \rightarrow pK^-\pi^+) = (5.0 \pm 1.3) \times 10^{-2}$, which we rescale to our best value $B(\Lambda_c^+ \rightarrow pK^-\pi^+) = (6.24 \pm 0.28) \times 10^{-2}$. Our first error is their experiment's error and our second error is the systematic error from using our best value.

Meson Particle Listings

 B^\pm $\Gamma(\Lambda_c(2593)^-/\Lambda_c(2625)^- p\pi^+)/\Gamma_{\text{total}}$ Γ_{602}/Γ

VALUE	CL%	DOCUMENT ID	TECN	COMMENT
$<1.9 \times 10^{-4}$	90	1,2 DYTMAN	02	CLE2 $e^+e^- \rightarrow \Upsilon(4S)$

¹ Assumes equal production of B^+ and B^0 at the $\Upsilon(4S)$.

² DYTMAN 02 measurement uses $B(\Lambda_c^- \rightarrow \bar{p}K^+\pi^-) = 5.0 \pm 1.3\%$. The second error includes the systematic and the uncertainty of the branching ratio.

 $\Gamma(\Xi_c^0\Lambda_c^+)/\Gamma_{\text{total}}$ Γ_{603}/Γ

VALUE (units 10^{-4})	DOCUMENT ID	TECN	COMMENT
$9.51 \pm 2.10 \pm 0.88$	1 LI	19A	BELL $e^+e^- \rightarrow \Upsilon(4S)$

¹ First measured the absolute branching fraction using a missing-mass technique.

 $\Gamma(\Xi_c^0\Lambda_c^+, \Xi_c^0 \rightarrow \Xi^+\pi^-)/\Gamma_{\text{total}}$ Γ_{604}/Γ

VALUE (units 10^{-3})	DOCUMENT ID	TECN	COMMENT
1.76 ± 0.29 OUR AVERAGE			

1.71 ± 0.28 ± 0.15	1 LI	19A	BELL $e^+e^- \rightarrow \Upsilon(4S)$
2.0 ± 0.7 ± 0.1	2,3 AUBERT	08H	BABR $e^+e^- \rightarrow \Upsilon(4S)$

• • • We do not use the following data for averages, fits, limits, etc. • • •

4.5 $^{+1.8}_{-1.5} \pm 0.2$	3,4 CHISTOV	06A	BELL Repl. by LI 19A
------------------------------	-------------	-----	----------------------

¹ Using a hadronic B -tagging method based on a full reconstruction.

² AUBERT 08H reports $(2.51 \pm 0.89 \pm 0.61) \times 10^{-5}$ from a measurement of $[\Gamma(B^+ \rightarrow \Xi_c^0\Lambda_c^+, \Xi_c^0 \rightarrow \Xi^+\pi^-)/\Gamma_{\text{total}}] \times [B(\Lambda_c^+ \rightarrow pK^-\pi^+)]$ assuming $B(\Lambda_c^+ \rightarrow pK^-\pi^+) = (5.0 \pm 1.3) \times 10^{-2}$, which we rescale to our best value $B(\Lambda_c^+ \rightarrow pK^-\pi^+) = (6.24 \pm 0.28) \times 10^{-2}$. Our first error is their experiment's error and our second error is the systematic error from using our best value.

³ Assumes equal production of B^+ and B^0 at the $\Upsilon(4S)$.

⁴ CHISTOV 06A reports $(5.6^{+1.9}_{-1.5} \pm 1.9) \times 10^{-5}$ from a measurement of $[\Gamma(B^+ \rightarrow \Xi_c^0\Lambda_c^+, \Xi_c^0 \rightarrow \Xi^+\pi^-)/\Gamma_{\text{total}}] \times [B(\Lambda_c^+ \rightarrow pK^-\pi^+)]$ assuming $B(\Lambda_c^+ \rightarrow pK^-\pi^+) = (5.0 \pm 1.3) \times 10^{-2}$, which we rescale to our best value $B(\Lambda_c^+ \rightarrow pK^-\pi^+) = (6.24 \pm 0.28) \times 10^{-2}$. Our first error is their experiment's error and our second error is the systematic error from using our best value.

 $\Gamma(\Xi_c^0\Lambda_c^+, \Xi_c^0 \rightarrow \Lambda K^+\pi^-)/\Gamma_{\text{total}}$ Γ_{605}/Γ

VALUE (units 10^{-5})	DOCUMENT ID	TECN	COMMENT
1.14 ± 0.26 OUR AVERAGE			

1.11 ± 0.26 ± 0.10	1 LI	19A	BELL $e^+e^- \rightarrow \Upsilon(4S)$
1.4 ± 0.8 ± 0.1	2,3 AUBERT	08H	BABR $e^+e^- \rightarrow \Upsilon(4S)$

• • • We do not use the following data for averages, fits, limits, etc. • • •

3.2 $^{+1.1}_{-1.0} \pm 0.1$	3,4 CHISTOV	06A	BELL Repl. by LI 19A
------------------------------	-------------	-----	----------------------

¹ Using a hadronic B -tagging method based on a full reconstruction.

² AUBERT 08H reports $(1.70 \pm 0.93 \pm 0.53) \times 10^{-5}$ from a measurement of $[\Gamma(B^+ \rightarrow \Xi_c^0\Lambda_c^+, \Xi_c^0 \rightarrow \Lambda K^+\pi^-)/\Gamma_{\text{total}}] \times [B(\Lambda_c^+ \rightarrow pK^-\pi^+)]$ assuming $B(\Lambda_c^+ \rightarrow pK^-\pi^+) = (5.0 \pm 1.3) \times 10^{-2}$, which we rescale to our best value $B(\Lambda_c^+ \rightarrow pK^-\pi^+) = (6.24 \pm 0.28) \times 10^{-2}$. Our first error is their experiment's error and our second error is the systematic error from using our best value.

³ Assumes equal production of B^+ and B^0 at the $\Upsilon(4S)$.

⁴ CHISTOV 06A reports $(4.0^{+1.1}_{-0.9} \pm 1.3) \times 10^{-5}$ from a measurement of $[\Gamma(B^+ \rightarrow \Xi_c^0\Lambda_c^+, \Xi_c^0 \rightarrow \Lambda K^+\pi^-)/\Gamma_{\text{total}}] \times [B(\Lambda_c^+ \rightarrow pK^-\pi^+)]$ assuming $B(\Lambda_c^+ \rightarrow pK^-\pi^+) = (5.0 \pm 1.3) \times 10^{-2}$, which we rescale to our best value $B(\Lambda_c^+ \rightarrow pK^-\pi^+) = (6.24 \pm 0.28) \times 10^{-2}$. Our first error is their experiment's error and our second error is the systematic error from using our best value.

 $\Gamma(\Xi_c^0\Lambda_c^+, \Xi_c^0 \rightarrow pK^-K^-\pi^+)/\Gamma_{\text{total}}$ Γ_{606}/Γ

VALUE (units 10^{-6})	DOCUMENT ID	TECN	COMMENT
5.47 ± 1.78 ± 0.57	1 LI	19A	BELL $e^+e^- \rightarrow \Upsilon(4S)$

¹ Using a hadronic B -tagging method based on a full reconstruction.

 $\Gamma(\Lambda_c^+\Xi_c^0)/\Gamma_{\text{total}}$ Γ_{607}/Γ

VALUE	CL%	DOCUMENT ID	TECN	COMMENT
$<6.5 \times 10^{-4}$	90	1 LI	19G	BELL $e^+e^- \rightarrow \Upsilon(4S)$

¹ Uses fully reconstructed B^+ meson on tag side and recoil against Λ_c^+ on signal side.

 $\Gamma(\Lambda_c^+\Xi_c(2645)^0)/\Gamma_{\text{total}}$ Γ_{608}/Γ

VALUE	CL%	DOCUMENT ID	TECN	COMMENT
$<7.9 \times 10^{-4}$	90	1 LI	19G	BELL $e^+e^- \rightarrow \Upsilon(4S)$

¹ Uses fully reconstructed B^+ meson on tag side and recoil against Λ_c^+ on signal side.

 $\Gamma(\Lambda_c^+\Xi_c(2790)^0)/\Gamma_{\text{total}}$ Γ_{609}/Γ

VALUE (units 10^{-3})	DOCUMENT ID	TECN	COMMENT
1.1 ± 0.4 ± 0.2	1 LI	19G	BELL $e^+e^- \rightarrow \Upsilon(4S)$

¹ Uses fully reconstructed B^+ meson on tag side and recoil against Λ_c^+ on signal side.

 $\Gamma(p\psi_{DS})/\Gamma_{\text{total}}$ Γ_{610}/Γ

VALUE	CL%	DOCUMENT ID	TECN	COMMENT
$<10^{-7-10^{-5}}$	90	1 LEES	23c	BABR $e^+e^- \rightarrow \Upsilon(4S)$

¹ LEES 23c searched for ψ_{DS} , where ψ_{DS} is a dark sector antibaryon, in the recoil mass against p and the fully reconstructed accompanying B meson. The cited upper limit is for $m_{\psi_{DS}}$ between 1 and 4.3 GeV/ c^2 .

 $\Gamma(\pi^+\ell^+\ell^-)/\Gamma_{\text{total}}$ Γ_{611}/Γ

VALUE	CL%	DOCUMENT ID	TECN	COMMENT
$<4.9 \times 10^{-8}$	90	1 WEI	08A	BELL $e^+e^- \rightarrow \Upsilon(4S)$

• • • We do not use the following data for averages, fits, limits, etc. • • •

$<6.6 \times 10^{-8}$	90	1 LEES	13M	BABR $e^+e^- \rightarrow \Upsilon(4S)$
$<1.2 \times 10^{-7}$	90	1 AUBERT	07AG	BABR $e^+e^- \rightarrow \Upsilon(4S)$

¹ Assumes equal production of B^+ and B^0 at the $\Upsilon(4S)$.

 $\Gamma(\pi^+e^+e^-)/\Gamma_{\text{total}}$ Γ_{612}/Γ

Test for $\Delta B=1$ weak neutral current. Allowed by higher-order electroweak interactions.

VALUE	CL%	DOCUMENT ID	TECN	COMMENT
$<8.0 \times 10^{-8}$	90	1 WEI	08A	BELL $e^+e^- \rightarrow \Upsilon(4S)$

• • • We do not use the following data for averages, fits, limits, etc. • • •

$<12.5 \times 10^{-8}$	90	1 LEES	13M	BABR $e^+e^- \rightarrow \Upsilon(4S)$
$<18 \times 10^{-8}$	90	1 AUBERT	07AG	BABR $e^+e^- \rightarrow \Upsilon(4S)$

¹ Assumes equal production of B^+ and B^0 at the $\Upsilon(4S)$.

² WEIR 90B assumes B^+ production cross section from LUND.

 $\Gamma(\pi^+\mu^+\mu^-)/\Gamma_{\text{total}}$ Γ_{613}/Γ

Test for $\Delta B=1$ weak neutral current. Allowed by higher-order electroweak interactions.

VALUE (units 10^{-8})	CL%	DOCUMENT ID	TECN	COMMENT
1.78 ± 0.22 ± 0.03		1 AAIJ	15AR	LHCB pp at 7, 8 TeV

• • • We do not use the following data for averages, fits, limits, etc. • • •

<5.5	90	2 LEES	13M	BABR $e^+e^- \rightarrow \Upsilon(4S)$
$2.3 \pm 0.6 \pm 0.1$		AAIJ	12AY	LHCB Repl. by AAIJ 15AR

<6.9	90	2 WEI	08A	BELL $e^+e^- \rightarrow \Upsilon(4S)$
<28	90	2 AUBERT	07AG	BABR $e^+e^- \rightarrow \Upsilon(4S)$

¹ AAIJ 15AR reports $(1.83 \pm 0.24 \pm 0.05) \times 10^{-8}$ from a measurement of $[\Gamma(B^+ \rightarrow \pi^+\mu^+\mu^-)/\Gamma_{\text{total}}] / [B(B^+ \rightarrow J/\psi(1S)K^+)] / [B(J/\psi(1S) \rightarrow \mu^+\mu^-)]$ assuming $B(B^+ \rightarrow J/\psi(1S)K^+) = (1.05 \pm 0.05) \times 10^{-3}$, $B(J/\psi(1S) \rightarrow \mu^+\mu^-) = (5.961 \pm 0.033) \times 10^{-2}$, which we rescale to our best values $B(B^+ \rightarrow J/\psi(1S)K^+) = (1.020 \pm 0.019) \times 10^{-3}$, $B(J/\psi(1S) \rightarrow \mu^+\mu^-) = (5.961 \pm 0.033) \times 10^{-2}$. Our first error is their experiment's error and our second error is the systematic error from using our best values.

² Assumes equal production of B^+ and B^0 at the $\Upsilon(4S)$.

 $\Gamma(\pi^+\mu^+\mu^-)/\Gamma(K^+\mu^+\mu^-)$ $\Gamma_{613}/\Gamma_{617}$

VALUE	DOCUMENT ID	TECN	COMMENT
$0.053 \pm 0.014 \pm 0.001$	AAIJ	12AY	LHCB Repl. by AAIJ 15AR

• • • We do not use the following data for averages, fits, limits, etc. • • •

¹ AAIJ 15AR reports $(1.83 \pm 0.24 \pm 0.05) \times 10^{-8}$ from a measurement of $[\Gamma(B^+ \rightarrow \pi^+\mu^+\mu^-)/\Gamma_{\text{total}}] / [B(B^+ \rightarrow J/\psi(1S)K^+)] / [B(J/\psi(1S) \rightarrow \mu^+\mu^-)]$ assuming $B(B^+ \rightarrow J/\psi(1S)K^+) = (1.05 \pm 0.05) \times 10^{-3}$, $B(J/\psi(1S) \rightarrow \mu^+\mu^-) = (5.961 \pm 0.033) \times 10^{-2}$, which we rescale to our best values $B(B^+ \rightarrow J/\psi(1S)K^+) = (1.020 \pm 0.019) \times 10^{-3}$, $B(J/\psi(1S) \rightarrow \mu^+\mu^-) = (5.961 \pm 0.033) \times 10^{-2}$. Our first error is their experiment's error and our second error is the systematic error from using our best values.

² Assumes equal production of B^+ and B^0 at the $\Upsilon(4S)$.

 $\Gamma(\pi^+\nu\bar{\nu})/\Gamma_{\text{total}}$ Γ_{614}/Γ

Test for $\Delta B=1$ weak neutral current. Allowed by higher-order electroweak interactions.

VALUE	CL%	DOCUMENT ID	TECN	COMMENT
$<1.4 \times 10^{-5}$	90	1 GRYGIER	17	BELL $e^+e^- \rightarrow \Upsilon(4S)$

• • • We do not use the following data for averages, fits, limits, etc. • • •

$<9.8 \times 10^{-5}$	90	1 LUTZ	13	BELL $e^+e^- \rightarrow \Upsilon(4S)$
$<1.7 \times 10^{-4}$	90	1 CHEN	07D	BELL $e^+e^- \rightarrow \Upsilon(4S)$
$<1.0 \times 10^{-4}$	90	1 AUBERT	05H	BABR $e^+e^- \rightarrow \Upsilon(4S)$

¹ Assumes equal production of B^+ and B^0 at the $\Upsilon(4S)$.

 $\Gamma(K^+\ell^+\ell^-)/\Gamma_{\text{total}}$ Γ_{615}/Γ

Test for $\Delta B=1$ weak neutral current. Allowed by higher-order electroweak interactions.

VALUE (units 10^{-7})	DOCUMENT ID	TECN	COMMENT
4.7 ± 0.5 OUR AVERAGE			Error includes scale factor of 2.3. See the ideogram below.

$5.99^{+0.45}_{-0.43} \pm 0.14$	CHOUDHURY	21	BELL $e^+e^- \rightarrow \Upsilon(4S)$
$4.36 \pm 0.15 \pm 0.18$	1 AAIJ	13H	LHCB pp at 7 TeV
$4.8 \pm 0.9 \pm 0.2$	2 AUBERT	09T	BABR $e^+e^- \rightarrow \Upsilon(4S)$

• • • We do not use the following data for averages, fits, limits, etc. • • •

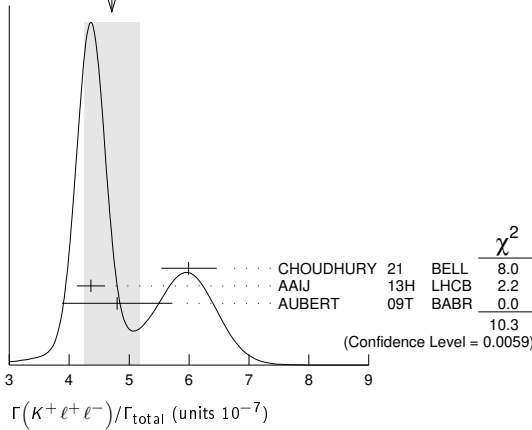
$5.3^{+0.6}_{-0.5} \pm 0.3$	2,3 WEI	09A	BELL $e^+e^- \rightarrow \Upsilon(4S)$
$3.8^{+0.9}_{-0.8} \pm 0.2$	2 AUBERT,B	06J	BABR Repl. by AUBERT 09T
$5.3^{+1.1}_{-1.0} \pm 0.3$	2 ISHIKAWA	03	BELL Repl. by WEI 09A

¹ Uses $B(B^+ \rightarrow J/\psi K^+ \rightarrow \mu^+\mu^- K^+) = (6.01 \pm 0.21) \times 10^{-5}$.

² Assumes equal production of B^+ and B^0 at the $\Upsilon(4S)$.

³ Superseded by CHOUDHURY 21.

WEIGHTED AVERAGE
4.7±0.5 (Error scaled by 2.3)



$\Gamma(K^+ e^+ e^-)/\Gamma_{total}$ Γ_{616}/Γ

Test for $\Delta B=1$ weak neutral current. Allowed by higher-order electroweak interactions.

VALUE (units 10^{-7})	CL%	DOCUMENT ID	TECN	COMMENT
5.6 ± 0.6 OUR AVERAGE				
5.75 ^{+0.64} _{-0.61} ± 0.15		CHOUDHURY 21	BELL	$e^+ e^- \rightarrow \Upsilon(4S)$
5.1 ^{+1.2} _{-1.1} ± 0.2		¹ AUBERT 09T	BABR	$e^+ e^- \rightarrow \Upsilon(4S)$
• • • We do not use the following data for averages, fits, limits, etc. • • •				
5.7 ^{+0.9} _{-0.8} ± 0.3		^{1,2} WEI 09A	BELL	$e^+ e^- \rightarrow \Upsilon(4S)$
4.2 ^{+1.2} _{-1.1} ± 0.2		¹ AUBERT,B 06J	BABR	Repl. by AUBERT 09T
10.5 ^{+2.5} _{-2.2} ± 0.7		¹ AUBERT 03U	BABR	Repl. by AUBERT,B 06J
6.3 ^{+1.9} _{-1.7} ± 0.3		³ ISHIKAWA 03	BELL	Repl. by WEI 09A
<14	90	¹ ABE 02	BELL	$e^+ e^- \rightarrow \Upsilon(4S)$
<9	90	¹ AUBERT 02L	BABR	$e^+ e^- \rightarrow \Upsilon(4S)$
<24	90	⁴ ANDERSON 01B	CLE2	$e^+ e^- \rightarrow \Upsilon(4S)$

¹ Assumes equal production of B^+ and B^0 at the $\Upsilon(4S)$.
² Superseded by CHOUDHURY 21.
³ Assumes equal production of B^0 and B^+ at $\Upsilon(4S)$. The second error is a total of systematic uncertainties including model dependence.
⁴ The result is for di-lepton masses above 0.5 GeV.

$\Gamma(K^+ \mu^+ \mu^-)/\Gamma_{total}$ Γ_{617}/Γ

Test for $\Delta B=1$ weak neutral current. Allowed by higher-order electroweak interactions.

VALUE (units 10^{-7})	CL%	DOCUMENT ID	TECN	COMMENT
4.53 ± 0.35 OUR FIT				Error includes scale factor of 1.8.
4.5 ± 0.6 OUR AVERAGE				Error includes scale factor of 2.9.
6.24 ^{+0.65} _{-0.61} ± 0.16		CHOUDHURY 21	BELL	$e^+ e^- \rightarrow \Upsilon(4S)$
4.29 ± 0.07 ± 0.21		¹ AAIJ 14M	LHCB	pp at 7, 8 TeV
4.1 ^{+1.6} _{-1.5} ± 0.2		² AUBERT 09T	BABR	$e^+ e^- \rightarrow \Upsilon(4S)$
• • • We do not use the following data for averages, fits, limits, etc. • • •				
4.36 ± 0.15 ± 0.18		³ AAIJ 13H	LHCB	Repl. by AAIJ 14M
5.3 ^{+0.8} _{-0.7} ± 0.3		^{2,4} WEI 09A	BELL	$e^+ e^- \rightarrow \Upsilon(4S)$
3.1 ^{+1.5} _{-1.2} ± 0.3		² AUBERT,B 06J	BABR	Repl. by AUBERT 09T
0.7 ^{+1.9} _{-1.1} ± 0.2		² AUBERT 03U	BABR	Repl. by AUBERT,B 06J
4.5 ^{+1.4} _{-1.2} ± 0.3		⁵ ISHIKAWA 03	BELL	Repl. by WEI 09A
9.8 ^{+4.6} _{-3.6} ± 1.6		² ABE 02	BELL	Repl. by ISHIKAWA 03
< 12	90	² AUBERT 02L	BABR	$e^+ e^- \rightarrow \Upsilon(4S)$
< 36.8	90	⁶ ANDERSON 01B	CLE2	$e^+ e^- \rightarrow \Upsilon(4S)$
< 52	90	⁷ AFFOLDER 99B	CDF	$p\bar{p}$ at 1.8 TeV
< 100	90	⁸ ABE 96L	CDF	Repl. by AFFOLDER 99B
< 2400	90	⁹ ALBRECHT 91E	ARG	$e^+ e^- \rightarrow \Upsilon(4S)$
< 64000	90	¹⁰ WEIR 90B	MRK2	$e^+ e^-$ 29 GeV
< 1700	90	¹¹ AVERY 89B	CLEO	$e^+ e^- \rightarrow \Upsilon(4S)$
< 3800	90	¹² AVERY 87	CLEO	$e^+ e^- \rightarrow \Upsilon(4S)$

¹ Uses $B(B^+ \rightarrow J/\psi(1S) K^+) = (0.998 \pm 0.014 \pm 0.040) \times 10^{-3}$ for normalization.
² Assumes equal production of B^+ and B^0 at the $\Upsilon(4S)$.
³ Uses $B(B^+ \rightarrow J/\psi K^+ \rightarrow \mu^+ \mu^- K^+) = (6.01 \pm 0.21) \times 10^{-5}$.
⁴ Superseded by CHOUDHURY 21.
⁵ Assumes equal production of B^0 and B^+ at $\Upsilon(4S)$. The second error is a total of systematic uncertainties including model dependence.
⁶ The result is for di-lepton masses above 0.5 GeV.
⁷ AFFOLDER 99B measured relative to $B^+ \rightarrow J/\psi(1S) K^+$.
⁸ ABE 96L measured relative to $B^+ \rightarrow J/\psi(1S) K^+$ using PDG 94 branching ratios.

⁹ ALBRECHT 91E reports $< 2.2 \times 10^{-4}$ assuming the $\Upsilon(4S)$ decays 45% to $B^0 \bar{B}^0$. We rescale to 50%.
¹⁰ WEIR 90B assumes B^+ production cross section from LUND.
¹¹ AVERY 89B reports $< 1.5 \times 10^{-4}$ assuming the $\Upsilon(4S)$ decays 43% to $B^0 \bar{B}^0$. We rescale to 50%.
¹² AVERY 87 reports $< 3.2 \times 10^{-4}$ assuming the $\Upsilon(4S)$ decays 40% to $B^0 \bar{B}^0$. We rescale to 50%.

$\Gamma(K^+ \mu^+ \mu^- \text{ nonresonant})/\Gamma_{total}$ Γ_{618}/Γ

VALUE (units 10^{-7})	CL%	DOCUMENT ID	TECN	COMMENT
4.37 ± 0.15 ± 0.23		¹ AAIJ 17Y	LHCB	pp at 7, 8 TeV
• • • We do not use the following data for averages, fits, limits, etc. • • •				
¹ Measured in amplitude analysis using model including short-distance $K^+ \mu^+ \mu^-$ and $\rho(770)$, $\omega(782)$, $\phi(1020)$, J/ψ , $\psi(2S)$, $\psi(3770)$, $\psi(4040)$, $\psi(4160)$, and $\psi(4415)$ contributions.				

$\Gamma(K^+ \tau^+ \tau^-)/\Gamma_{total}$ Γ_{619}/Γ

VALUE	CL%	DOCUMENT ID	TECN	COMMENT
< 2.25 × 10⁻³	90	^{1,2} LEES 17	BABR	$e^+ e^- \rightarrow \Upsilon(4S)$
• • • We do not use the following data for averages, fits, limits, etc. • • •				
¹ Uses only leptonic decays of τ and the quoted limit combines the final states $K^+ e^+ e^-$, $K^+ \mu^+ \mu^-$, and $K^+ e^\pm \mu^\mp$. ² If observed events are interpreted as a signal the branching fraction measurement becomes $(1.31^{+0.66+0.35}_{-0.61-0.25}) \times 10^{-3}$.				

$\Gamma(K^+ \mu^+ \mu^-)/\Gamma(J/\psi(1S) K^+)$ Γ_{617}/Γ_{95}

VALUE (units 10^{-3})	CL%	DOCUMENT ID	TECN	COMMENT
0.44 ± 0.034 OUR FIT				Error includes scale factor of 1.7.
0.46 ± 0.04 ± 0.02		AALTONEN 11A	CDF	$p\bar{p}$ at 1.96 TeV
• • • We do not use the following data for averages, fits, limits, etc. • • •				
0.38 ± 0.05 ± 0.02		AALTONEN 11L	CDF	Repl. by AALTONEN 11A
0.59 ± 0.15 ± 0.03		AALTONEN 09B	CDF	Repl. by AALTONEN 11L

$\Gamma(K^+ \nu \bar{\nu})/\Gamma_{total}$ Γ_{620}/Γ

Test for $\Delta B=1$ weak neutral current. Allowed by higher-order electroweak interactions.

VALUE	CL%	DOCUMENT ID	TECN	COMMENT
< 1.6 × 10⁻⁵	90	^{1,2} LEES 13i	BABR	$e^+ e^- \rightarrow \Upsilon(4S)$
• • • We do not use the following data for averages, fits, limits, etc. • • •				
< 4.1 × 10 ⁻⁵	90	³ ABUDINEN 21	BEL2	$e^+ e^- \rightarrow \Upsilon(4S)$
< 1.9 × 10 ⁻⁵	90	^{1,4} GRYGIER 17	BELL	$e^+ e^- \rightarrow \Upsilon(4S)$
< 5.5 × 10 ⁻⁵	90	¹ LUTZ 13	BELL	$e^+ e^- \rightarrow \Upsilon(4S)$
< 1.3 × 10 ⁻⁵	90	¹ DEL-AMO-SAI10q	BABR	Repl. by LEES 13i
< 1.4 × 10 ⁻⁵	90	¹ CHEN 07D	BELL	$e^+ e^- \rightarrow \Upsilon(4S)$
< 5.2 × 10 ⁻⁵	90	¹ AUBERT 05H	BABR	$e^+ e^- \rightarrow \Upsilon(4S)$
< 2.4 × 10 ⁻⁴	90	¹ BROWDER 01	CLE2	$e^+ e^- \rightarrow \Upsilon(4S)$
• • • We do not use the following data for averages, fits, limits, etc. • • •				
¹ Assumes equal production of B^+ and B^0 at the $\Upsilon(4S)$. ² Also reported a limit $< 3.7 \times 10^{-5}$ at 90% CL obtained using a fully reconstructed hadronic B -tag events. ³ Using an inclusive tagging method that exploits not only the properties of the $B^+ \rightarrow K^+ \nu \bar{\nu}$ decay, but also the inclusive properties of the other B meson in the event. ⁴ The result was reported in arXiv:1702.03224, but missing from the publication by mistake.				

$\Gamma(\rho^+ \nu \bar{\nu})/\Gamma_{total}$ Γ_{621}/Γ

Test for $\Delta B=1$ weak neutral current. Allowed by higher-order electroweak interaction.

VALUE	CL%	DOCUMENT ID	TECN	COMMENT
< 3.0 × 10⁻⁵	90	¹ GRYGIER 17	BELL	$e^+ e^- \rightarrow \Upsilon(4S)$
• • • We do not use the following data for averages, fits, limits, etc. • • •				
< 2.13 × 10 ⁻⁴	90	¹ LUTZ 13	BELL	$e^+ e^- \rightarrow \Upsilon(4S)$
< 1.5 × 10 ⁻⁴	90	¹ CHEN 07D	BELL	Repl. by LUTZ 13
• • • We do not use the following data for averages, fits, limits, etc. • • •				
¹ Assumes equal production of B^+ and B^0 at the $\Upsilon(4S)$.				

$\Gamma(K^*(892)^+ \ell^+ \ell^-)/\Gamma_{total}$ Γ_{622}/Γ

Test for $\Delta B=1$ weak neutral current. Allowed by higher-order electroweak interactions.

VALUE (units 10^{-7})	CL%	DOCUMENT ID	TECN	COMMENT
10.1 ± 1.1 OUR AVERAGE				Error includes scale factor of 1.1.
9.24 ± 0.93 ± 0.67		AAIJ 14M	LHCB	pp at 7, 8 TeV
14.0 ^{+4.0} _{-3.7} ± 0.9		¹ AUBERT 09T	BABR	$e^+ e^- \rightarrow \Upsilon(4S)$
12.4 ^{+2.3} _{-2.1} ± 1.3		¹ WEI 09A	BELL	$e^+ e^- \rightarrow \Upsilon(4S)$
• • • We do not use the following data for averages, fits, limits, etc. • • •				
11.6 ± 1.9		² AAIJ 12AH	LHCB	Repl. by AAIJ 14M
7.3 ^{+5.0} _{-4.2} ± 2.1		¹ AUBERT,B 06J	BABR	Repl. by AUBERT 09T
< 22	90	¹ ISHIKAWA 03	BELL	$e^+ e^- \rightarrow \Upsilon(4S)$
• • • We do not use the following data for averages, fits, limits, etc. • • •				
¹ Assumes equal production of B^+ and B^0 at the $\Upsilon(4S)$. ² Measured in $B^+ \rightarrow K^*(892)^+ \mu^+ \mu^-$ decays.				

$\Gamma(K^*(892)^+ e^+ e^-)/\Gamma_{total}$ Γ_{623}/Γ

Test for $\Delta B=1$ weak neutral current. Allowed by higher-order electroweak interactions.

VALUE (units 10^{-7})	CL%	DOCUMENT ID	TECN	COMMENT
15.5 ± 4.0 OUR AVERAGE				
13.8 ^{+4.7} _{-4.2} ± 0.8		¹ AUBERT 09T	BABR	$e^+ e^- \rightarrow \Upsilon(4S)$
17.3 ^{+5.0} _{-4.2} ± 2.0		¹ WEI 09A	BELL	$e^+ e^- \rightarrow \Upsilon(4S)$

Meson Particle Listings

 B^\pm

• • • We do not use the following data for averages, fits, limits, etc. • • •

$7.5 \pm 7.6 \pm 3.8$	1	AUBERT,B	06J	BABR	Repl. by AUBERT 09T
$2.0 \pm 13.4 \pm 2.8$	1	AUBERT	03U	BABR	$e^+e^- \rightarrow \Upsilon(4S)$
< 46	90	2	ISHIKAWA	03	BELL $e^+e^- \rightarrow \Upsilon(4S)$
< 89	90	1	ABE	02	BELL Repl. by ISHIKAWA 03
< 95	90	1	AUBERT	02L	BABR $e^+e^- \rightarrow \Upsilon(4S)$
< 6900	90	3	ALBRECHT	91E	ARG $e^+e^- \rightarrow \Upsilon(4S)$

- ¹ Assumes equal production of B^+ and B^0 at the $\Upsilon(4S)$.
² Assumes equal production of B^0 and B^+ at $\Upsilon(4S)$. The second error is a total of systematic uncertainties including model dependence.
³ ALBRECHT 91E reports $< 6.3 \times 10^{-4}$ assuming the $\Upsilon(4S)$ decays 45% to $B^0\bar{B}^0$. We rescale to 50%.

$\Gamma(K^*(892)^+\mu^+\mu^-)/\Gamma_{\text{total}}$ Γ_{624}/Γ
 Test for $\Delta B=1$ weak neutral current. Allowed by higher-order electroweak interactions.

VALUE (units 10^{-7})	CL%	DOCUMENT ID	TECN	COMMENT
9.6 ± 1.0 OUR FIT				
9.6 ± 1.1 OUR AVERAGE				
$9.24 \pm 0.93 \pm 0.67$		1	AAIJ	14M LHCb pp at 7, 8 TeV
$14.6 \pm 7.9 \pm 1.2$		2	AUBERT	09T BABR $e^+e^- \rightarrow \Upsilon(4S)$
$11.1 \pm 3.2 \pm 1.0$		2	WEI	09A BELL $e^+e^- \rightarrow \Upsilon(4S)$

• • • We do not use the following data for averages, fits, limits, etc. • • •

11.6 ± 1.9			AAIJ	12AH LHCb Repl. by AAIJ 14M
$9.7 \pm 9.4 \pm 1.4$		2	AUBERT,B	06J BABR Repl. by AUBERT 09T
$30.7 \pm 25.8 \pm 4.2$		2	AUBERT	03U BABR $e^+e^- \rightarrow \Upsilon(4S)$
$6.5 \pm 6.9 \pm 1.5$ $-5.3 -1.6$		3	ISHIKAWA	03 BELL Repl. by WEI 09A
< 39	90	2	ABE	02L BELL Repl. by ISHIKAWA 03
< 170	90	2	AUBERT	02L BABR $e^+e^- \rightarrow \Upsilon(4S)$

- ¹ Uses $B(B^+ \rightarrow J/\psi(1S)K^*(892)^+) = (1.431 \pm 0.027 \pm 0.090) \times 10^{-3}$ for normalization.
² Assumes equal production of B^+ and B^0 at the $\Upsilon(4S)$.
³ Assumes equal production of B^0 and B^+ at $\Upsilon(4S)$. The second error is a total of systematic uncertainties including model dependence. The 90% C.L. upper limit is 2.2×10^{-6} .

$\Gamma(K^*(892)^+\mu^+\mu^-)/\Gamma(J/\psi(1S)K^*(892)^+)$ $\Gamma_{624}/\Gamma_{300}$

VALUE (units 10^{-3})	DOCUMENT ID	TECN	COMMENT
0.67 ± 0.08 OUR FIT			
$0.67 \pm 0.22 \pm 0.04$	AALTONEN	11A1	CDF $p\bar{p}$ at 1.96 TeV

$\Gamma(K^*(892)^+\nu\bar{\nu})/\Gamma_{\text{total}}$ Γ_{625}/Γ
 Test for $\Delta B=1$ weak neutral current. Allowed by higher-order electroweak interaction.

VALUE	CL%	DOCUMENT ID	TECN	COMMENT
$< 4.0 \times 10^{-5}$	90	1	LUTZ	13 BELL $e^+e^- \rightarrow \Upsilon(4S)$
$< 6.1 \times 10^{-5}$	90	1	GRYGIER	17 BELL $e^+e^- \rightarrow \Upsilon(4S)$
$< 6.4 \times 10^{-5}$	90	1,2	LEES	13I BABR $e^+e^- \rightarrow \Upsilon(4S)$
$< 8 \times 10^{-5}$	90		AUBERT	08Bc BABR Repl. by LEES 13I
$< 1.4 \times 10^{-4}$	90	1	CHEN	07D BELL $e^+e^- \rightarrow \Upsilon(4S)$

- ¹ Assumes equal production of B^+ and B^0 at the $\Upsilon(4S)$.
² Also reported a limit $< 11.6 \times 10^{-5}$ at 90% CL obtained using a fully reconstructed hadronic B -tag events.

$\Gamma(K^+\pi^+\pi^-\mu^+\mu^-)/\Gamma(\psi(2S)K^+)$ $\Gamma_{626}/\Gamma_{330}$

VALUE (units 10^{-4})	DOCUMENT ID	TECN	COMMENT
$6.95 \pm 0.46 \pm 0.34$	AAIJ	14AZ	LHCb pp at 7, 8 TeV

$\Gamma(\phi K^+\mu^+\mu^-)/\Gamma(J/\psi(1S)\phi K^+)$ $\Gamma_{627}/\Gamma_{307}$

VALUE (units 10^{-3})	DOCUMENT ID	TECN	COMMENT
$1.58 \pm 0.36 \pm 0.19$ $-0.32 -0.07$	AAIJ	14AZ	LHCb pp at 7, 8 TeV

$\Gamma(\bar{\Lambda}p\nu\bar{\nu})/\Gamma_{\text{total}}$ Γ_{628}/Γ

VALUE	CL%	DOCUMENT ID	TECN	COMMENT
$< 3.0 \times 10^{-5}$	90	1	LEES	19c BABR $e^+e^- \rightarrow \Upsilon(4S)$

- ¹ Signal candidates are identified by first fully reconstructing B^+ in one of many possible exclusive decays to hadronic final states.

$\Gamma(\pi^+e^+\mu^-)/\Gamma_{\text{total}}$ Γ_{629}/Γ
 Test of lepton family number conservation.

VALUE	CL%	DOCUMENT ID	TECN	COMMENT
< 0.0064	90	1	WEIR	90B MRK2 e^+e^- 29 GeV

- ¹ WEIR 90B assumes B^+ production cross section from LUND.

$\Gamma(\pi^+e^-\mu^+)/\Gamma_{\text{total}}$ Γ_{630}/Γ
 Test of lepton family number conservation.

VALUE	CL%	DOCUMENT ID	TECN	COMMENT
< 0.0064	90	1	WEIR	90B MRK2 e^+e^- 29 GeV

- ¹ WEIR 90B assumes B^+ production cross section from LUND.

$\Gamma(\pi^+e^\pm\mu^\mp)/\Gamma_{\text{total}}$ Γ_{631}/Γ

VALUE	CL%	DOCUMENT ID	TECN	COMMENT
$< 1.7 \times 10^{-7}$	90	1	AUBERT	07Ag BABR $e^+e^- \rightarrow \Upsilon(4S)$

- ¹ Assumes equal production of B^+ and B^0 at the $\Upsilon(4S)$.

$\Gamma(\pi^+e^+\tau^-)/\Gamma_{\text{total}}$ Γ_{632}/Γ

Test of lepton family number conservation.

VALUE (units 10^{-6})	CL%	DOCUMENT ID	TECN	COMMENT
< 74	90	1	LEES	12P BABR $e^+e^- \rightarrow \Upsilon(4S)$

- ¹ Uses a fully reconstructed hadronic B decay as a tag on the recoil side.

$\Gamma(\pi^+e^-\tau^-)/\Gamma_{\text{total}}$ Γ_{633}/Γ

Test of lepton family number conservation.

VALUE (units 10^{-6})	CL%	DOCUMENT ID	TECN	COMMENT
< 20	90	1	LEES	12P BABR $e^+e^- \rightarrow \Upsilon(4S)$

- ¹ Uses a fully reconstructed hadronic B decay as a tag on the recoil side.

$\Gamma(\pi^+e^\pm\tau^\mp)/\Gamma_{\text{total}}$ Γ_{634}/Γ

Test of lepton family number conservation.

VALUE (units 10^{-6})	CL%	DOCUMENT ID	TECN	COMMENT
< 75	90	1,2	LEES	12P BABR $e^+e^- \rightarrow \Upsilon(4S)$

- ¹ Assumes $B(B^+ \rightarrow h^+\ell^+\tau^-) = B(B^+ \rightarrow h^+\ell^-\tau^+)$.
² Uses a fully reconstructed hadronic B decay as a tag on the recoil side.

$\Gamma(\pi^+\mu^+\tau^-)/\Gamma_{\text{total}}$ Γ_{635}/Γ

Test of lepton family number conservation.

VALUE (units 10^{-6})	CL%	DOCUMENT ID	TECN	COMMENT
< 62	90	1	LEES	12P BABR $e^+e^- \rightarrow \Upsilon(4S)$

- ¹ Uses a fully reconstructed hadronic B decay as a tag on the recoil side.

$\Gamma(\pi^+\mu^-\tau^+)/\Gamma_{\text{total}}$ Γ_{636}/Γ

Test of lepton family number conservation.

VALUE (units 10^{-6})	CL%	DOCUMENT ID	TECN	COMMENT
< 45	90	1	LEES	12P BABR $e^+e^- \rightarrow \Upsilon(4S)$

- ¹ Uses a fully reconstructed hadronic B decay as a tag on the recoil side.

$\Gamma(\pi^+\mu^\pm\tau^\mp)/\Gamma_{\text{total}}$ Γ_{637}/Γ

Test of lepton family number conservation.

VALUE (units 10^{-6})	CL%	DOCUMENT ID	TECN	COMMENT
< 72	90	1,2	LEES	12P BABR $e^+e^- \rightarrow \Upsilon(4S)$

- ¹ Assumes $B(B^+ \rightarrow h^+\ell^+\tau^-) = B(B^+ \rightarrow h^+\ell^-\tau^+)$.
² Uses a fully reconstructed hadronic B decay as a tag on the recoil side.

$\Gamma(K^+e^+\mu^-)/\Gamma_{\text{total}}$ Γ_{638}/Γ

Test of lepton family number conservation.

VALUE	CL%	DOCUMENT ID	TECN	COMMENT
$< 7.0 \times 10^{-9}$	90	AAIJ	19AM	LHCb pp at 7, 8 TeV

• • • We do not use the following data for averages, fits, limits, etc. • • •

$< 3.0 \times 10^{-8}$	90		CHOUDHURY 21	BELL $e^+e^- \rightarrow \Upsilon(4S)$
$< 0.91 \times 10^{-7}$	90	1	AUBERT,B	06J BABR $e^+e^- \rightarrow \Upsilon(4S)$
$< 8 \times 10^{-7}$	90	1	AUBERT	02L BABR Repl. by AUBERT,B 06J
$< 6.4 \times 10^{-3}$	90	2	WEIR	90B MRK2 e^+e^- 29 GeV

- ¹ Assumes equal production of B^+ and B^0 at the $\Upsilon(4S)$.
² WEIR 90B assumes B^+ production cross section from LUND.

$\Gamma(K^+e^-\mu^+)/\Gamma_{\text{total}}$ Γ_{639}/Γ

Test of lepton family number conservation.

VALUE	CL%	DOCUMENT ID	TECN	COMMENT
$< 6.4 \times 10^{-9}$	90	AAIJ	19AM	LHCb pp at 7, 8 TeV

• • • We do not use the following data for averages, fits, limits, etc. • • •

$< 8.5 \times 10^{-8}$	90		CHOUDHURY 21	BELL $e^+e^- \rightarrow \Upsilon(4S)$
$< 1.3 \times 10^{-7}$	90	1	AUBERT,B	06J BABR $e^+e^- \rightarrow \Upsilon(4S)$
$< 6.4 \times 10^{-3}$	90	2	WEIR	90B MRK2 e^+e^- 29 GeV

- ¹ Assumes equal production of B^+ and B^0 at the $\Upsilon(4S)$.
² WEIR 90B assumes B^+ production cross section from LUND.

$\Gamma(K^+e^\pm\mu^\mp)/\Gamma_{\text{total}}$ Γ_{640}/Γ

VALUE (units 10^{-7})	CL%	DOCUMENT ID	TECN	COMMENT
< 0.91	90	1	AUBERT,B	06J BABR $e^+e^- \rightarrow \Upsilon(4S)$

- ¹ Assumes equal production of B^+ and B^0 at the $\Upsilon(4S)$.

$\Gamma(K^+e^+\tau^-)/\Gamma_{\text{total}}$ Γ_{641}/Γ

Test of lepton family number conservation.

VALUE	CL%	DOCUMENT ID	TECN	COMMENT
$< 1.53 \times 10^{-5}$	90	1	WATANUKI 23	BELL $e^+e^- \rightarrow \Upsilon(4S)$

• • • We do not use the following data for averages, fits, limits, etc. • • •

$< 4.3 \times 10^{-5}$	90	2	LEES	12P BABR $e^+e^- \rightarrow \Upsilon(4S)$
------------------------	----	---	------	--

- ¹ Uses a fully reconstructed hadronic B^- decay as a tag on the recoil side.
² Uses a fully reconstructed hadronic B decay as a tag on the recoil side.

$\Gamma(K^+ e^- \tau^+)/\Gamma_{\text{total}}$ Γ_{642}/Γ

Test of lepton family number conservation.

VALUE	CL%	DOCUMENT ID	TECN	COMMENT
$<1.51 \times 10^{-5}$	90	¹ WATA NUKI 23	BELL	$e^+ e^- \rightarrow \Upsilon(4S)$
$<1.5 \times 10^{-5}$	90	² LEES	12P BABR	$e^+ e^- \rightarrow \Upsilon(4S)$

- ¹ Uses a fully reconstructed hadronic B^- decay as a tag on the recoil side.
² Uses a fully reconstructed hadronic B decay as a tag on the recoil side.

 $\Gamma(K^+ e^{\pm} \tau^{\mp})/\Gamma_{\text{total}}$ Γ_{643}/Γ

Test of lepton family number conservation.

VALUE (units 10^{-6})	CL%	DOCUMENT ID	TECN	COMMENT
<30	90	^{1,2} LEES	12P BABR	$e^+ e^- \rightarrow \Upsilon(4S)$

- ¹ Assumes $B(B^+ \rightarrow h^+ \ell^+ \tau^-) = B(B^+ \rightarrow h^+ \ell^- \tau^+)$.
² Uses a fully reconstructed hadronic B decay as a tag on the recoil side.

 $\Gamma(K^+ \mu^+ \tau^-)/\Gamma_{\text{total}}$ Γ_{644}/Γ

Test of lepton family number conservation.

VALUE	CL%	DOCUMENT ID	TECN	COMMENT
$<2.45 \times 10^{-5}$	90	¹ WATA NUKI 23	BELL	$e^+ e^- \rightarrow \Upsilon(4S)$
••• We do not use the following data for averages, fits, limits, etc. •••				
$<4.5 \times 10^{-5}$	90	² LEES	12P BABR	$e^+ e^- \rightarrow \Upsilon(4S)$

- ¹ Uses a fully reconstructed hadronic B^- decay as a tag on the recoil side.
² Uses a fully reconstructed hadronic B decay as a tag on the recoil side.

 $\Gamma(K^+ \mu^- \tau^+)/\Gamma_{\text{total}}$ Γ_{645}/Γ

Test of lepton family number conservation.

VALUE	CL%	DOCUMENT ID	TECN	COMMENT
$<0.59 \times 10^{-5}$	90	¹ WATA NUKI 23	BELL	$e^+ e^- \rightarrow \Upsilon(4S)$
••• We do not use the following data for averages, fits, limits, etc. •••				
$<3.9 \times 10^{-5}$	90	² AAIJ	20P LHCB	pp at 7, 8, 13 TeV
$<2.8 \times 10^{-5}$	90	³ LEES	12P BABR	$e^+ e^- \rightarrow \Upsilon(4S)$

- ¹ Uses a fully reconstructed hadronic B^- decay as a tag on the recoil side.
² Uses the $B_{s2}^0 \rightarrow B^+ K^-$ decays for kinematic constraints.
³ Uses a fully reconstructed hadronic B decay as a tag on the recoil side.

 $\Gamma(K^+ \mu^{\pm} \tau^{\mp})/\Gamma_{\text{total}}$ Γ_{646}/Γ

Test of lepton family number conservation.

VALUE (units 10^{-6})	CL%	DOCUMENT ID	TECN	COMMENT
<48	90	^{1,2} LEES	12P BABR	$e^+ e^- \rightarrow \Upsilon(4S)$
••• We do not use the following data for averages, fits, limits, etc. •••				
<77	90	¹ AUBERT	07AZ BABR	Repl. by LEES 12P

- ¹ Uses a fully reconstructed hadronic B decay as a tag on the recoil side.
² Assumes $B(B^+ \rightarrow h^+ \ell^+ \tau^-) = B(B^+ \rightarrow h^+ \ell^- \tau^+)$.

 $\Gamma(K^*(892)^+ e^+ \mu^-)/\Gamma_{\text{total}}$ Γ_{647}/Γ

VALUE (units 10^{-7})	CL%	DOCUMENT ID	TECN	COMMENT
<13	90	¹ AUBERT,B 06J	BABR	$e^+ e^- \rightarrow \Upsilon(4S)$

- ¹ Assumes equal production of B^+ and B^0 at the $\Upsilon(4S)$.

 $\Gamma(K^*(892)^+ e^- \mu^+)/\Gamma_{\text{total}}$ Γ_{648}/Γ

VALUE (units 10^{-7})	CL%	DOCUMENT ID	TECN	COMMENT
<9.9	90	¹ AUBERT,B 06J	BABR	$e^+ e^- \rightarrow \Upsilon(4S)$

- ¹ Assumes equal production of B^+ and B^0 at the $\Upsilon(4S)$.

 $\Gamma(K^*(892)^+ e^{\pm} \mu^{\mp})/\Gamma_{\text{total}}$ Γ_{649}/Γ

Test of lepton family number conservation.

VALUE	CL%	DOCUMENT ID	TECN	COMMENT
$<1.4 \times 10^{-6}$	90	¹ AUBERT,B 06J	BABR	$e^+ e^- \rightarrow \Upsilon(4S)$
••• We do not use the following data for averages, fits, limits, etc. •••				
$<7.9 \times 10^{-6}$	90	¹ AUBERT	02L BABR	Repl. by AUBERT,B 06J

- ¹ Assumes equal production of B^+ and B^0 at the $\Upsilon(4S)$.

 $\Gamma(\pi^- e^+ e^+)/\Gamma_{\text{total}}$ Γ_{650}/Γ

Test of total lepton number conservation.

VALUE	CL%	DOCUMENT ID	TECN	COMMENT
$<2.3 \times 10^{-8}$	90	¹ LEES	12J BABR	$e^+ e^- \rightarrow \Upsilon(4S)$
••• We do not use the following data for averages, fits, limits, etc. •••				
$<1.6 \times 10^{-6}$	90	¹ EDWARDS	02B CLE2	$e^+ e^- \rightarrow \Upsilon(4S)$
<0.0039	90	² WEIR	90B MRK2	$e^+ e^-$ 29 GeV

- ¹ Assumes equal production of B^+ and B^0 at the $\Upsilon(4S)$.
² WEIR 90B assumes B^+ production cross section from LUND.

 $\Gamma(\pi^- \mu^+ \mu^+)/\Gamma_{\text{total}}$ Γ_{651}/Γ

Test of total lepton number conservation.

VALUE	CL%	DOCUMENT ID	TECN	COMMENT
$<4.0 \times 10^{-9}$	95	¹ AAIJ	14AC LHCB	pp at 7, 8 TeV
••• We do not use the following data for averages, fits, limits, etc. •••				
$<1.3 \times 10^{-8}$	95	² AAIJ	12AD LHCB	Repl. by AAIJ 14AC
$<4.4 \times 10^{-8}$	90	¹ AAIJ	12C LHCB	pp at 7 TeV
$<10.7 \times 10^{-8}$	90	³ LEES	12J BABR	$e^+ e^- \rightarrow \Upsilon(4S)$
$<1.4 \times 10^{-6}$	90	³ EDWARDS	02B CLE2	$e^+ e^- \rightarrow \Upsilon(4S)$
$<9.1 \times 10^{-3}$	90	⁴ WEIR	90B MRK2	$e^+ e^-$ 29 GeV

- ¹ Uses $B^+ \rightarrow J/\psi K^+$, $J/\psi \rightarrow \mu^+ \mu^-$ mode for normalization. Obtains neutrino-mass-dependent upper limits in the range 0.4–4.0 $\times 10^{-9}$. This limit is applicable for Majorana neutrino lifetime < 1 ps.
² Uses $B^+ \rightarrow J/\psi K^+$, $J/\psi \rightarrow \mu^+ \mu^-$ mode for normalization. Obtains neutrino-mass-dependent upper limits in the range 0.4–1.0 $\times 10^{-8}$.
³ Assumes equal production of B^+ and B^0 at the $\Upsilon(4S)$.
⁴ WEIR 90B assumes B^+ production cross section from LUND.

 $\Gamma(\pi^- e^+ \mu^+)/\Gamma_{\text{total}}$ Γ_{652}/Γ

Test of total lepton number conservation.

VALUE	CL%	DOCUMENT ID	TECN	COMMENT
$<1.5 \times 10^{-7}$	90	¹ LEES	14A BABR	$e^+ e^- \rightarrow \Upsilon(4S)$
••• We do not use the following data for averages, fits, limits, etc. •••				
$<1.3 \times 10^{-6}$	90	¹ EDWARDS	02B CLE2	$e^+ e^- \rightarrow \Upsilon(4S)$
<0.0064	90	² WEIR	90B MRK2	$e^+ e^-$ 29 GeV

- ¹ Assumes equal production of B^+ and B^0 at the $\Upsilon(4S)$.
² WEIR 90B assumes B^+ production cross section from LUND.

 $\Gamma(\rho^- e^+ e^+)/\Gamma_{\text{total}}$ Γ_{653}/Γ

Test of total lepton number conservation.

VALUE (units 10^{-6})	CL%	DOCUMENT ID	TECN	COMMENT
<0.17	90	¹ LEES	14A BABR	$e^+ e^- \rightarrow \Upsilon(4S)$
••• We do not use the following data for averages, fits, limits, etc. •••				
<2.6	90	¹ EDWARDS	02B CLE2	$e^+ e^- \rightarrow \Upsilon(4S)$

- ¹ Assumes equal production of B^+ and B^0 at the $\Upsilon(4S)$.

 $\Gamma(\rho^- \mu^+ \mu^+)/\Gamma_{\text{total}}$ Γ_{654}/Γ

Test of total lepton number conservation.

VALUE (units 10^{-6})	CL%	DOCUMENT ID	TECN	COMMENT
<0.42	90	LEES	14A BABR	$e^+ e^- \rightarrow \Upsilon(4S)$
••• We do not use the following data for averages, fits, limits, etc. •••				
<5.0	90	¹ EDWARDS	02B CLE2	$e^+ e^- \rightarrow \Upsilon(4S)$

- ¹ Assumes equal production of B^+ and B^0 at the $\Upsilon(4S)$.

 $\Gamma(\rho^- e^+ \mu^+)/\Gamma_{\text{total}}$ Γ_{655}/Γ

Test of total lepton number conservation.

VALUE (units 10^{-6})	CL%	DOCUMENT ID	TECN	COMMENT
<0.47	90	¹ LEES	14A BABR	$e^+ e^- \rightarrow \Upsilon(4S)$
••• We do not use the following data for averages, fits, limits, etc. •••				
<3.3	90	¹ EDWARDS	02B CLE2	$e^+ e^- \rightarrow \Upsilon(4S)$

- ¹ Assumes equal production of B^+ and B^0 at the $\Upsilon(4S)$.

 $\Gamma(K^- e^+ e^+)/\Gamma_{\text{total}}$ Γ_{656}/Γ

Test of total lepton number conservation.

VALUE	CL%	DOCUMENT ID	TECN	COMMENT
$<3.0 \times 10^{-8}$	90	¹ LEES	12I BABR	$e^+ e^- \rightarrow \Upsilon(4S)$
••• We do not use the following data for averages, fits, limits, etc. •••				
$<1.0 \times 10^{-6}$	90	¹ EDWARDS	02B CLE2	$e^+ e^- \rightarrow \Upsilon(4S)$
<0.0039	90	² WEIR	90B MRK2	$e^+ e^-$ 29 GeV

- ¹ Assumes equal production of B^+ and B^0 at the $\Upsilon(4S)$.
² WEIR 90B assumes B^+ production cross section from LUND.

 $\Gamma(K^- \mu^+ \mu^+)/\Gamma_{\text{total}}$ Γ_{657}/Γ

Test of total lepton number conservation.

VALUE	CL%	DOCUMENT ID	TECN	COMMENT
$<4.1 \times 10^{-8}$	90	AAIJ	12C LHCB	pp at 7 TeV
••• We do not use the following data for averages, fits, limits, etc. •••				
$<6.7 \times 10^{-8}$	90	¹ LEES	12J BABR	$e^+ e^- \rightarrow \Upsilon(4S)$
$<1.8 \times 10^{-6}$	90	¹ EDWARDS	02B CLE2	$e^+ e^- \rightarrow \Upsilon(4S)$
$<9.1 \times 10^{-3}$	90	² WEIR	90B MRK2	$e^+ e^-$ 29 GeV

- ¹ Assumes equal production of B^+ and B^0 at the $\Upsilon(4S)$.
² WEIR 90B assumes B^+ production cross section from LUND.

 $\Gamma(K^- e^+ \mu^+)/\Gamma_{\text{total}}$ Γ_{658}/Γ

Test of total lepton number conservation.

VALUE	CL%	DOCUMENT ID	TECN	COMMENT
$<1.6 \times 10^{-7}$	90	¹ LEES	14A BABR	$e^+ e^- \rightarrow \Upsilon(4S)$
••• We do not use the following data for averages, fits, limits, etc. •••				
$<2.0 \times 10^{-6}$	90	¹ EDWARDS	02B CLE2	$e^+ e^- \rightarrow \Upsilon(4S)$
<0.0064	90	² WEIR	90B MRK2	$e^+ e^-$ 29 GeV

- ¹ Assumes equal production of B^+ and B^0 at the $\Upsilon(4S)$.
² WEIR 90B assumes B^+ production cross section from LUND.

 $\Gamma(K^*(892)^- e^+ e^+)/\Gamma_{\text{total}}$ Γ_{659}/Γ

Test of total lepton number conservation.

VALUE (units 10^{-6})	CL%	DOCUMENT ID	TECN	COMMENT
<0.40	90	¹ LEES	14A BABR	$e^+ e^- \rightarrow \Upsilon(4S)$
••• We do not use the following data for averages, fits, limits, etc. •••				
<2.8	90	¹ EDWARDS	02B CLE2	$e^+ e^- \rightarrow \Upsilon(4S)$

- ¹ Assumes equal production of B^+ and B^0 at the $\Upsilon(4S)$.

Meson Particle Listings

 B^\pm

$\Gamma(K^*(892)^-\mu^+\mu^-)/\Gamma_{\text{total}}$ Γ_{660}/Γ
Test of total lepton number conservation.

VALUE (units 10^{-6})	CL%	DOCUMENT ID	TECN	COMMENT
<0.59	90	¹ LEES	14A	BABR $e^+e^- \rightarrow \Upsilon(4S)$
••• We do not use the following data for averages, fits, limits, etc. •••				
<8.3	90	¹ EDWARDS	02B	CLE2 $e^+e^- \rightarrow \Upsilon(4S)$

¹ Assumes equal production of B^+ and B^0 at the $\Upsilon(4S)$.

$\Gamma(K^*(892)^-e^+\mu^-)/\Gamma_{\text{total}}$ Γ_{661}/Γ
Test of total lepton number conservation.

VALUE (units 10^{-6})	CL%	DOCUMENT ID	TECN	COMMENT
<0.30	90	¹ LEES	14A	BABR $e^+e^- \rightarrow \Upsilon(4S)$
••• We do not use the following data for averages, fits, limits, etc. •••				
<4.4	90	¹ EDWARDS	02B	CLE2 $e^+e^- \rightarrow \Upsilon(4S)$

¹ Assumes equal production of B^+ and B^0 at the $\Upsilon(4S)$.

$\Gamma(D^-e^+e^-)/\Gamma_{\text{total}}$ Γ_{662}/Γ

VALUE	CL%	DOCUMENT ID	TECN	COMMENT
<2.6 $\times 10^{-6}$	90	¹ LEES	14A	BABR $e^+e^- \rightarrow \Upsilon(4S)$
<2.6 $\times 10^{-6}$	90	^{1,2} SEON	11B	BELL $e^+e^- \rightarrow \Upsilon(4S)$

¹ Assumes equal production of B^0 and B^+ from Upsilon(4S) decays.

² Uses $D^- \rightarrow K^+\pi^-\pi^-$ mode and 3-body phase-space hypothesis for the signal decays.

$\Gamma(D^-e^+\mu^-)/\Gamma_{\text{total}}$ Γ_{663}/Γ

VALUE	CL%	DOCUMENT ID	TECN	COMMENT
<1.8 $\times 10^{-6}$	90	^{1,2} SEON	11	BELL $e^+e^- \rightarrow \Upsilon(4S)$
••• We do not use the following data for averages, fits, limits, etc. •••				
<2.1 $\times 10^{-6}$	90	¹ LEES	14A	BABR $e^+e^- \rightarrow \Upsilon(4S)$

¹ Assumes equal production of B^0 and B^+ from Upsilon(4S) decays.

² Uses $D^- \rightarrow K^+\pi^-\pi^-$ mode and 3-body phase-space hypothesis for the signal decays.

$\Gamma(D^-\mu^+\mu^-)/\Gamma_{\text{total}}$ Γ_{664}/Γ

VALUE	CL%	DOCUMENT ID	TECN	COMMENT
< 6.9 $\times 10^{-7}$	95	¹ AAJ	12AD	LHCB pp at 7 TeV
••• We do not use the following data for averages, fits, limits, etc. •••				
<17 $\times 10^{-7}$	90	² LEES	14A	BABR $e^+e^- \rightarrow \Upsilon(4S)$
< 1.1 $\times 10^{-6}$	90	^{2,3} SEON	11	BELL $e^+e^- \rightarrow \Upsilon(4S)$

¹ Uses $B^+ \rightarrow \psi(2S)K^+$, $\psi(2S) \rightarrow J/\psi\pi^+\pi^-$ mode for normalization.

² Assumes equal production of B^0 and B^+ from Upsilon(4S) decays.

³ Uses $D^- \rightarrow K^+\pi^-\pi^-$ mode and 3-body phase-space hypothesis for the signal decays.

$\Gamma(D^{*-}\mu^+\mu^-)/\Gamma_{\text{total}}$ Γ_{665}/Γ

VALUE	CL%	DOCUMENT ID	TECN	COMMENT
<2.4 $\times 10^{-6}$	95	¹ AAJ	12AD	LHCB pp at 7 TeV

¹ Uses $B^+ \rightarrow \psi(2S)K^+$, $\psi(2S) \rightarrow J/\psi\pi^+\pi^-$ mode for normalization.

$\Gamma(D_s^-\mu^+\mu^-)/\Gamma_{\text{total}}$ Γ_{666}/Γ

VALUE	CL%	DOCUMENT ID	TECN	COMMENT
<5.8 $\times 10^{-7}$	95	¹ AAJ	12AD	LHCB pp at 7 TeV

¹ Uses $B^+ \rightarrow \psi(2S)K^+$, $\psi(2S) \rightarrow J/\psi\pi^+\pi^-$ mode for normalization. Obtains neutrino-mass-dependent upper limits in the range $1.5\text{--}8.0 \times 10^{-7}$.

$\Gamma(\bar{D}^0\pi^-\mu^+\mu^-)/\Gamma_{\text{total}}$ Γ_{667}/Γ

VALUE	CL%	DOCUMENT ID	TECN	COMMENT
<1.5 $\times 10^{-6}$	95	¹ AAJ	12AD	LHCB pp at 7 TeV

¹ Uses $B^+ \rightarrow \psi(2S)K^+$, $\psi(2S) \rightarrow J/\psi\pi^+\pi^-$ mode for normalization. Obtains neutrino-mass-dependent upper limits in the range $0.3\text{--}1.5 \times 10^{-6}$.

$\Gamma(\Lambda^0\mu^+)/\Gamma_{\text{total}}$ Γ_{668}/Γ

VALUE	CL%	DOCUMENT ID	TECN	COMMENT
<6 $\times 10^{-8}$	90	^{1,2} DEL-AMO-SA..11k	BABR	$e^+e^- \rightarrow \Upsilon(4S)$

¹ DEL-AMO-SANCHEZ 11k reports $< 6.1 \times 10^{-8}$ from a measurement of $[\Gamma(B^+ \rightarrow \Lambda^0\mu^+)/\Gamma_{\text{total}}] \times [B(\Lambda \rightarrow p\pi^-)]$ assuming $B(\Lambda \rightarrow p\pi^-) = (63.9 \pm 0.5) \times 10^{-2}$, which we rescale to our best value $B(\Lambda \rightarrow p\pi^-) = 64.1 \times 10^{-2}$.

² Uses $B(\Upsilon(4S) \rightarrow B^0\bar{B}^0) = (51.6 \pm 0.6)\%$ and $B(\Upsilon(4S) \rightarrow B^+B^-) = (48.4 \pm 0.6)\%$.

$\Gamma(\Lambda^0e^+)/\Gamma_{\text{total}}$ Γ_{669}/Γ

VALUE	CL%	DOCUMENT ID	TECN	COMMENT
<3.2 $\times 10^{-8}$	90	^{1,2} DEL-AMO-SA..11k	BABR	$e^+e^- \rightarrow \Upsilon(4S)$

¹ DEL-AMO-SANCHEZ 11k reports $< 3.2 \times 10^{-8}$ from a measurement of $[\Gamma(B^+ \rightarrow \Lambda^0e^+)/\Gamma_{\text{total}}] \times [B(\Lambda \rightarrow p\pi^-)]$ assuming $B(\Lambda \rightarrow p\pi^-) = (63.9 \pm 0.5) \times 10^{-2}$, which we rescale to our best value $B(\Lambda \rightarrow p\pi^-) = 64.1 \times 10^{-2}$.

² Uses $B(\Upsilon(4S) \rightarrow B^0\bar{B}^0) = (51.6 \pm 0.6)\%$ and $B(\Upsilon(4S) \rightarrow B^+B^-) = (48.4 \pm 0.6)\%$.

$\Gamma(\bar{\Lambda}^0\mu^+)/\Gamma_{\text{total}}$ Γ_{670}/Γ

VALUE	CL%	DOCUMENT ID	TECN	COMMENT
<6 $\times 10^{-8}$	90	^{1,2} DEL-AMO-SA..11k	BABR	$e^+e^- \rightarrow \Upsilon(4S)$

¹ DEL-AMO-SANCHEZ 11k reports $< 6.2 \times 10^{-8}$ from a measurement of $[\Gamma(B^+ \rightarrow \bar{\Lambda}^0\mu^+)/\Gamma_{\text{total}}] \times [B(\Lambda \rightarrow p\pi^-)]$ assuming $B(\Lambda \rightarrow p\pi^-) = (63.9 \pm 0.5) \times 10^{-2}$, which we rescale to our best value $B(\Lambda \rightarrow p\pi^-) = 64.1 \times 10^{-2}$.

² Uses $B(\Upsilon(4S) \rightarrow B^0\bar{B}^0) = (51.6 \pm 0.6)\%$ and $B(\Upsilon(4S) \rightarrow B^+B^-) = (48.4 \pm 0.6)\%$.

$\Gamma(\bar{\Lambda}^0e^+)/\Gamma_{\text{total}}$ Γ_{671}/Γ

VALUE	CL%	DOCUMENT ID	TECN	COMMENT
<8 $\times 10^{-8}$	90	^{1,2} DEL-AMO-SA..11k	BABR	$e^+e^- \rightarrow \Upsilon(4S)$

¹ DEL-AMO-SANCHEZ 11k reports $< 8.1 \times 10^{-8}$ from a measurement of $[\Gamma(B^+ \rightarrow \bar{\Lambda}^0e^+)/\Gamma_{\text{total}}] \times [B(\Lambda \rightarrow p\pi^-)]$ assuming $B(\Lambda \rightarrow p\pi^-) = (63.9 \pm 0.5) \times 10^{-2}$, which we rescale to our best value $B(\Lambda \rightarrow p\pi^-) = 64.1 \times 10^{-2}$.

² Uses $B(\Upsilon(4S) \rightarrow B^0\bar{B}^0) = (51.6 \pm 0.6)\%$ and $B(\Upsilon(4S) \rightarrow B^+B^-) = (48.4 \pm 0.6)\%$.

POLARIZATION IN B^+ DECAY

In decays involving two vector mesons, one can distinguish among the states in which meson polarizations are both longitudinal (L) or both are transverse and parallel (\parallel) or perpendicular (\perp) to each other with the parameters Γ_L/Γ , Γ_{\perp}/Γ , and the relative phases ϕ_{\parallel} and ϕ_{\perp} . See the definitions in the note on "Polarization in B Decays" review in the B^0 Particle Listings.

Γ_L/Γ in $B^+ \rightarrow \bar{D}^{*0}\rho^+$

VALUE	DOCUMENT ID	TECN	COMMENT
0.892 ± 0.018 ± 0.016	CSORNA	03	CLE2 $e^+e^- \rightarrow \Upsilon(4S)$

Γ_L/Γ in $B^+ \rightarrow \bar{D}^{*0}K^{*+}$

VALUE	DOCUMENT ID	TECN	COMMENT
0.86 ± 0.06 ± 0.03	AUBERT	04k	BABR $e^+e^- \rightarrow \Upsilon(4S)$

Γ_L/Γ in $B^+ \rightarrow \bar{D}^{*0}\ell^+\nu_{\ell}$

VALUE	DOCUMENT ID	TECN	COMMENT
0.514 ± 0.018 ± 0.005	PRIM	23	BELL $e^+e^- \rightarrow \Upsilon(4S)$

Γ_L/Γ in $B^+ \rightarrow \bar{D}^{*0}e^+\nu_e$

VALUE	DOCUMENT ID	TECN	COMMENT
0.505 ± 0.027 ± 0.006	PRIM	23	BELL $e^+e^- \rightarrow \Upsilon(4S)$

Γ_L/Γ in $B^+ \rightarrow \bar{D}^{*0}\mu^+\nu_{\mu}$

VALUE	DOCUMENT ID	TECN	COMMENT
0.522 ± 0.025 ± 0.007	PRIM	23	BELL $e^+e^- \rightarrow \Upsilon(4S)$

$\Delta(\Gamma_L/\Gamma)$ in $B^+ \rightarrow \bar{D}^{*0}\ell^+\nu_{\ell}$

VALUE	DOCUMENT ID	TECN	COMMENT
0.017 ± 0.037 ± 0.009	PRIM	23	BELL $e^+e^- \rightarrow \Upsilon(4S)$

Γ_L/Γ in $B^+ \rightarrow J/\psi K^{*+}$

VALUE	DOCUMENT ID	TECN	COMMENT
0.604 ± 0.015 ± 0.018	ITOH	05	BELL $e^+e^- \rightarrow \Upsilon(4S)$

Γ_{\perp}/Γ in $B^+ \rightarrow J/\psi K^{*+}$

VALUE	DOCUMENT ID	TECN	COMMENT
0.180 ± 0.014 ± 0.010	ITOH	05	BELL $e^+e^- \rightarrow \Upsilon(4S)$

Γ_L/Γ in $B^+ \rightarrow \omega K^{*+}$

VALUE	DOCUMENT ID	TECN	COMMENT
0.41 ± 0.18 ± 0.05	AUBERT	09H	BABR $e^+e^- \rightarrow \Upsilon(4S)$

Γ_L/Γ in $B^+ \rightarrow \omega K_2^*(1430)^+$

VALUE	DOCUMENT ID	TECN	COMMENT
0.56 ± 0.10 ± 0.04	AUBERT	09H	BABR $e^+e^- \rightarrow \Upsilon(4S)$

Γ_L/Γ in $B^+ \rightarrow K^{*+}\bar{K}^{*0}$

VALUE	DOCUMENT ID	TECN	COMMENT
0.82 ± 0.15 ± 0.21 OUR AVERAGE			
1.06 ± 0.30 ± 0.14	¹ GOH	15	BELL $e^+e^- \rightarrow \Upsilon(4S)$
0.75 ± 0.19 ± 0.26 ± 0.03	^{2,3} AUBERT	09F	BABR $e^+e^- \rightarrow \Upsilon(4S)$

¹ Signal significance 2.7 standard deviations.

² Signal significance 3.7 standard deviations.

³ Assumes equal production of B^+ and B^0 at the $\Upsilon(4S)$.

Γ_L/Γ in $B^+ \rightarrow \phi K^*(892)^+$

VALUE	DOCUMENT ID	TECN	COMMENT
0.50 ± 0.05 OUR AVERAGE			
0.49 ± 0.05 ± 0.03	AUBERT	07BA	BABR $e^+e^- \rightarrow \Upsilon(4S)$
0.52 ± 0.08 ± 0.03	CHEN	05A	BELL $e^+e^- \rightarrow \Upsilon(4S)$
••• We do not use the following data for averages, fits, limits, etc. •••			
0.46 ± 0.12 ± 0.03	AUBERT	03v	BABR Repl. by AUBERT 07BA

Γ_{\perp}/Γ in $B^+ \rightarrow \phi K^{*+}$

VALUE	DOCUMENT ID	TECN	COMMENT
0.20 ± 0.05 OUR AVERAGE			
0.21 ± 0.05 ± 0.02	AUBERT	07BA	BABR $e^+e^- \rightarrow \Upsilon(4S)$
0.19 ± 0.08 ± 0.02	CHEN	05A	BELL $e^+e^- \rightarrow \Upsilon(4S)$

ϕ_{\parallel} in $B^+ \rightarrow \phi K^{*+}$

VALUE (°)	DOCUMENT ID	TECN	COMMENT
2.34 ± 0.18 OUR AVERAGE			
2.47 ± 0.20 ± 0.07	AUBERT	07BA BABR	$e^+e^- \rightarrow \Upsilon(4S)$
2.10 ± 0.28 ± 0.04	CHEN	05A BELL	$e^+e^- \rightarrow \Upsilon(4S)$

ϕ_{\perp} in $B^+ \rightarrow \phi K^{*+}$

VALUE (°)	DOCUMENT ID	TECN	COMMENT
2.58 ± 0.17 OUR AVERAGE			
2.69 ± 0.20 ± 0.03	AUBERT	07BA BABR	$e^+e^- \rightarrow \Upsilon(4S)$
2.31 ± 0.30 ± 0.07	CHEN	05A BELL	$e^+e^- \rightarrow \Upsilon(4S)$

$\delta_0(B^+ \rightarrow \phi K^{*+})$

VALUE (rad)	DOCUMENT ID	TECN	COMMENT
3.07 ± 0.18 ± 0.06	AUBERT	07BA BABR	$e^+e^- \rightarrow \Upsilon(4S)$

$A_{CP}^0(B^+ \rightarrow \phi K^{*+})$

VALUE	DOCUMENT ID	TECN	COMMENT
0.17 ± 0.11 ± 0.02	AUBERT	07BA BABR	$e^+e^- \rightarrow \Upsilon(4S)$

$A_{CP}^1(B^+ \rightarrow \phi K^{*+})$

VALUE	DOCUMENT ID	TECN	COMMENT
0.22 ± 0.24 ± 0.08	AUBERT	07BA BABR	$e^+e^- \rightarrow \Upsilon(4S)$

$\Delta\phi_{\parallel}(B^+ \rightarrow \phi K^{*+})$

VALUE (rad)	DOCUMENT ID	TECN	COMMENT
0.07 ± 0.20 ± 0.05	AUBERT	07BA BABR	$e^+e^- \rightarrow \Upsilon(4S)$

$\Delta\phi_{\perp}(B^+ \rightarrow \phi K^{*+})$

VALUE (rad)	DOCUMENT ID	TECN	COMMENT
0.19 ± 0.20 ± 0.07	AUBERT	07BA BABR	$e^+e^- \rightarrow \Upsilon(4S)$

$\Delta\delta_0(B^+ \rightarrow \phi K^{*+})$

VALUE (rad)	DOCUMENT ID	TECN	COMMENT
0.20 ± 0.18 ± 0.03	AUBERT	07BA BABR	$e^+e^- \rightarrow \Upsilon(4S)$

Γ_L/Γ in $B^+ \rightarrow \phi K_1(1270)^+$

VALUE	DOCUMENT ID	TECN	COMMENT
0.46^{+0.12+0.06}_{-0.13-0.07}	AUBERT	08BI BABR	$e^+e^- \rightarrow \Upsilon(4S)$

Γ_L/Γ in $B^+ \rightarrow \phi K_2^*(1430)^+$

VALUE	DOCUMENT ID	TECN	COMMENT
0.80^{+0.09}_{-0.10} ± 0.03	AUBERT	08BI BABR	$e^+e^- \rightarrow \Upsilon(4S)$

$\delta_0(B^+ \rightarrow \phi K_2^*(1430)^+)$

VALUE (rad)	DOCUMENT ID	TECN	COMMENT
3.59 ± 0.19 ± 0.12	AUBERT	08BI BABR	$e^+e^- \rightarrow \Upsilon(4S)$

$\Delta\delta_0(B^+ \rightarrow \phi K_2^*(1430)^+)$

VALUE (rad)	DOCUMENT ID	TECN	COMMENT
-0.05 ± 0.19 ± 0.06	AUBERT	08BI BABR	$e^+e^- \rightarrow \Upsilon(4S)$

Γ_L/Γ in $B^+ \rightarrow \rho^0 K^*(892)^+$

VALUE	DOCUMENT ID	TECN	COMMENT
0.78 ± 0.12 ± 0.03	DEL-AMO-SA...11D	BABR	$e^+e^- \rightarrow \Upsilon(4S)$
0.96 ^{+0.04} _{-0.15} ± 0.04	AUBERT	03V BABR	Repl. by DEL-AMO-SANCHEZ 11D

$\Gamma_L/\Gamma(B^+ \rightarrow K^*(892)^0 \rho^+)$

VALUE	DOCUMENT ID	TECN	COMMENT
0.48 ± 0.08 OUR AVERAGE			
0.52 ± 0.10 ± 0.04	AUBERT,B	06G BABR	$e^+e^- \rightarrow \Upsilon(4S)$
0.43 ± 0.11 ^{+0.05} _{-0.02}	ZHANG	05D BELL	$e^+e^- \rightarrow \Upsilon(4S)$

Γ_L/Γ in $B^+ \rightarrow \mu^+ \mu^- K^*(892)^+ (1.0 < q^2 < 8.68 \text{ GeV}^2/c^4)$

VALUE	DOCUMENT ID	TECN	COMMENT
0.60^{+0.31}_{-0.25} ± 0.13	¹ SIRUNYAN	21AC CMS	pp at 8 TeV

¹ SIRUNYAN 21AC measurement is performed in $1.0 < q^2 < 8.68 \text{ GeV}^2/c^4$. Reports also measurements in several other q^2 intervals.

Γ_L/Γ in $B^+ \rightarrow \mu^+ \mu^- K^*(892)^+ (1.1 < q^2 < 6.0 \text{ GeV}^2/c^4)$

VALUE	DOCUMENT ID	TECN	COMMENT
0.59 ± 0.09 ± 0.03	¹ AAIJ	21J LHCb	pp at 7, 8, 13 TeV

¹ The full set of CP-averaged angular observables is measured as a function of the q^2 . The measured Γ_L is related to the polarisation of the $K^*(892)^+$.

Γ_L/Γ in $B^+ \rightarrow \mu^+ \mu^- K^*(892)^+ (10.09 < q^2 < 12.86 \text{ GeV}^2/c^4)$

VALUE	DOCUMENT ID	TECN	COMMENT
0.88^{+0.10}_{-0.13} ± 0.05	¹ SIRUNYAN	21AC CMS	pp at 8 TeV

¹ SIRUNYAN 21AC measurement is performed in $10.09 < q^2 < 12.86 \text{ GeV}^2/c^4$. Reports also measurements in several other q^2 intervals.

Γ_L/Γ in $B^+ \rightarrow \mu^+ \mu^- K^*(892)^+ (14.18 < q^2 < 19.0 \text{ GeV}^2/c^4)$

VALUE	DOCUMENT ID	TECN	COMMENT
0.55^{+0.13}_{-0.10} ± 0.06	¹ SIRUNYAN	21AC CMS	pp at 8 TeV

¹ SIRUNYAN 21AC measurement is performed in $14.18 < q^2 < 19.0 \text{ GeV}^2/c^4$. Reports also measurements in several other q^2 intervals.

Γ_L/Γ in $B^+ \rightarrow \mu^+ \mu^- K^*(892)^+ (15.0 < q^2 < 19.0 \text{ GeV}^2/c^4)$

VALUE	DOCUMENT ID	TECN	COMMENT
0.40^{+0.13}_{-0.11} ± 0.03	¹ AAIJ	21J LHCb	pp at 7, 8, 13 TeV

¹ The full set of CP-averaged angular observables is measured as a function of the q^2 . The measured Γ_L is related to the polarisation of the $K^*(892)^+$.

Γ_L/Γ in $B^+ \rightarrow \rho^+ \rho^0$

VALUE	DOCUMENT ID	TECN	COMMENT
0.950 ± 0.016 OUR AVERAGE			
0.950 ± 0.015 ± 0.006	AUBERT	09G BABR	$e^+e^- \rightarrow \Upsilon(4S)$
0.948 ± 0.106 ± 0.021	ZHANG	03B BELL	$e^+e^- \rightarrow \Upsilon(4S)$
0.905 ± 0.042 ^{+0.023} _{-0.027}	AUBERT,BE	06G BABR	Repl. by AUBERT 09G
0.97 ^{+0.03} _{-0.07} ± 0.04	AUBERT	03V BABR	Repl. by AUBERT,BE 06G

Γ_L/Γ in $B^+ \rightarrow \omega \rho^+$

VALUE	DOCUMENT ID	TECN	COMMENT
0.90 ± 0.05 ± 0.03	AUBERT	09H BABR	$e^+e^- \rightarrow \Upsilon(4S)$
0.82 ± 0.11 ± 0.02	AUBERT,B	06T BABR	Repl. by AUBERT 09H
0.88 ^{+0.12} _{-0.15} ± 0.03	AUBERT	05O BABR	Repl. by AUBERT,B 06T

Γ_L/Γ in $B^+ \rightarrow \rho^+ \bar{p} K^*(892)^+$

VALUE	DOCUMENT ID	TECN	COMMENT
0.32 ± 0.17 ± 0.09	CHEN	08C BELL	$e^+e^- \rightarrow \Upsilon(4S)$

CP VIOLATION

A_{CP} is defined as

$$\frac{B(B^- \rightarrow \bar{f}) - B(B^+ \rightarrow f)}{B(B^- \rightarrow \bar{f}) + B(B^+ \rightarrow f)}$$

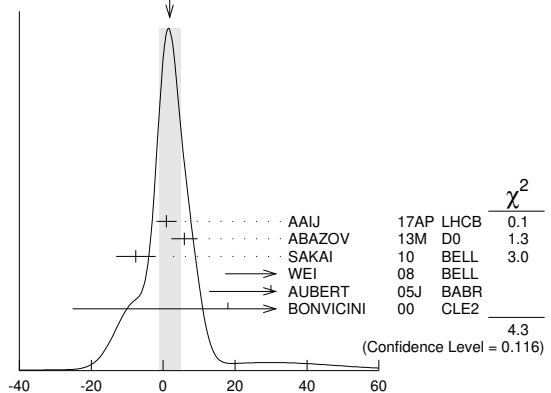
the CP-violation charge asymmetry of exclusive B^- and B^+ decay.

$A_{CP}(B^+ \rightarrow J/\psi(1S)K^+)$

VALUE (units 10^{-3})	DOCUMENT ID	TECN	COMMENT
1.8 ± 3.0 OUR AVERAGE			Error includes scale factor of 1.5. See the ideogram below.
0.9 ± 2.7 ± 0.7	AAIJ	17AP LHCb	pp at 7, 8 TeV
5.9 ± 3.6 ± 0.7	ABAZOV	13M D0	$p\bar{p}$ at 1.96 TeV
-7.6 ± 5.0 ± 2.2	SAKAI	10 BELL	$e^+e^- \rightarrow \Upsilon(4S)$
90 ± 70 ± 20	¹ WEI	08 BELL	$e^+e^- \rightarrow \Upsilon(4S)$
30 ± 14 ± 10	² AUBERT	05J BABR	$e^+e^- \rightarrow \Upsilon(4S)$
18 ± 43 ± 4	³ BONVICINI	00 CLE2	$e^+e^- \rightarrow \Upsilon(4S)$
7.5 ± 6.1 ± 3.0	⁴ ABAZOV	08O D0	Repl. by ABAZOV 13M
30 ± 15 ± 6	AUBERT	04P BABR	Repl. by AUBERT 05J
-26 ± 22 ± 17	ABE	03B BELL	Repl. by SAKAI 10
3 ± 30 ± 4	AUBERT	02F BABR	Repl. by AUBERT 04P

• • • We do not use the following data for averages, fits, limits, etc. • • •
¹ Uses $B^+ \rightarrow J/\psi K^+$, where $J/\psi \rightarrow p\bar{p}$.
² The result reported corresponds to $-A_{CP}$.
³ A +0.3% correction is applied due to a slightly higher reconstruction efficiency for the positive kaons.
⁴ Uses $J/\psi \rightarrow \mu^+ \mu^-$ decay.

WEIGHTED AVERAGE
1.8 ± 3.0 (Error scaled by 1.5)



$A_{CP}(B^+ \rightarrow J/\psi(1S)K^+)$ (units 10^{-3})

Meson Particle Listings

B^\pm

$A_{CP}(B^+ \rightarrow J/\psi(1S)\pi^+)$

VALUE (units 10^{-2})	DOCUMENT ID	TECN	COMMENT
1.8 ± 1.2 OUR AVERAGE	Error includes scale factor of 1.3.		
1.91 ± 0.89 ± 0.16	¹ AAIJ	17o	LHCB pp at 7, 8 TeV
-4.2 ± 4.4 ± 0.9	ABAZOV	13m	D0 $p\bar{p}$ at 1.96 TeV
12.3 ± 8.5 ± 0.4	AUBERT	04P	BABR $e^+e^- \rightarrow \Upsilon(4S)$
-2.3 ± 16.4 ± 1.5	ABE	03B	BELL $e^+e^- \rightarrow \Upsilon(4S)$
••• We do not use the following data for averages, fits, limits, etc. •••			
0.5 ± 2.7 ± 1.1	² AAIJ	12Ac	LHCB Repl. by AAIJ 17o
-9 ± 8 ± 3	³ ABAZOV	08o	D0 Repl. by ABAZOV 13m
1 ± 22 ± 1	AUBERT	02F	BABR Repl. by AUBERT 04P

¹ Obtained by using LHCb measurement of $A_{CP}(B^+ \rightarrow J/\psi K^+) = (0.09 \pm 0.27 \pm 0.07) \times 10^{-2}$ of AAIJ 17AP.
² Uses $A_{CP}(B^+ \rightarrow J/\psi K^+) = 0.001 \pm 0.007$ to extract production asymmetry.
³ Uses $J/\psi \rightarrow \mu^+\mu^-$ decay.

$A_{CP}(B^+ \rightarrow J/\psi\rho^+)$

VALUE	DOCUMENT ID	TECN	COMMENT
-0.05 ± 0.05 OUR AVERAGE			
-0.045 ± 0.056 ± 0.008	AAIJ	19o	LHCB pp at 7 and 8 TeV
-0.11 ± 0.12 ± 0.08	AUBERT	07Ac	BABR $e^+e^- \rightarrow \Upsilon(4S)$

$A_{CP}(B^+ \rightarrow J/\psi K^*(892)^+)$

VALUE	DOCUMENT ID	TECN	COMMENT
-0.048 ± 0.029 ± 0.016	¹ AUBERT	05j	BABR $e^+e^- \rightarrow \Upsilon(4S)$

¹ The result reported corresponds to $-A_{CP}$.

$A_{CP}(B^+ \rightarrow \eta_c K^+)$

VALUE	DOCUMENT ID	TECN	COMMENT
0.01 ± 0.07 OUR AVERAGE	Error includes scale factor of 2.2.		
0.040 ± 0.034 ± 0.004	¹ AAIJ	14AF	LHCB pp at 7, 8 TeV
-0.16 ± 0.08 ± 0.02	¹ WEI	08	BELL $e^+e^- \rightarrow \Upsilon(4S)$
••• We do not use the following data for averages, fits, limits, etc. •••			
0.046 ± 0.057 ± 0.007	¹ AAIJ	13AU	LHCB Repl. by AAIJ 14AF

¹ Uses $B^+ \rightarrow \eta_c K^+$, where $\eta_c \rightarrow p\bar{p}$.

$A_{CP}(B^+ \rightarrow \psi(2S)\pi^+)$

VALUE	DOCUMENT ID	TECN	COMMENT
0.03 ± 0.06 OUR AVERAGE			
0.048 ± 0.090 ± 0.011	¹ AAIJ	12Ac	LHCB pp at 7 TeV
0.022 ± 0.085 ± 0.016	BHARDWAJ	08	BELL $e^+e^- \rightarrow \Upsilon(4S)$

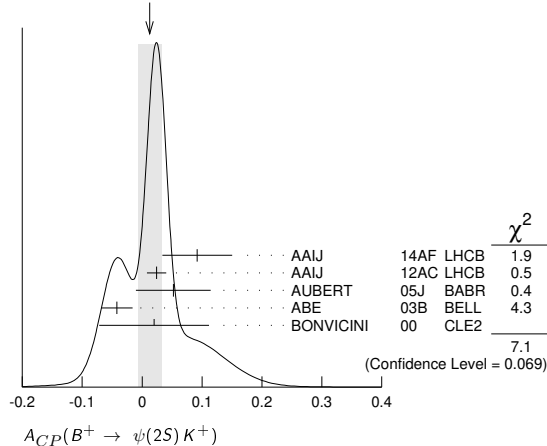
¹ Uses $A_{CP}(B^+ \rightarrow J/\psi K^+) = 0.001 \pm 0.007$ to extract production asymmetry.

$A_{CP}(B^+ \rightarrow \psi(2S)K^+)$

VALUE	DOCUMENT ID	TECN	COMMENT
0.012 ± 0.020 OUR AVERAGE	Error includes scale factor of 1.5. See the ideogram below.		
0.092 ± 0.058 ± 0.004	¹ AAIJ	14AF	LHCB pp at 7, 8 TeV
0.024 ± 0.014 ± 0.008	² AAIJ	12Ac	LHCB pp at 7 TeV
0.052 ± 0.059 ± 0.020	AUBERT	05j	BABR $e^+e^- \rightarrow \Upsilon(4S)$
-0.042 ± 0.020 ± 0.017	ABE	03B	BELL $e^+e^- \rightarrow \Upsilon(4S)$
0.02 ± 0.091 ± 0.01	³ BONVICINI	00	CLE2 $e^+e^- \rightarrow \Upsilon(4S)$
••• We do not use the following data for averages, fits, limits, etc. •••			
-0.002 ± 0.123 ± 0.012	^{1,2} AAIJ	13AU	LHCB Repl. by AAIJ 14AF

¹ Uses $\psi(2S) \rightarrow p\bar{p}$ decays.
² Uses $A_{CP}(B^+ \rightarrow J/\psi K^+) = 0.001 \pm 0.007$ to extract production asymmetry.
³ A +0.3% correction is applied due to a slightly higher reconstruction efficiency for the positive kaons.

WEIGHTED AVERAGE
0.012±0.020 (Error scaled by 1.5)



$A_{CP}(B^+ \rightarrow \psi(2S)K^*(892)^+)$

VALUE	DOCUMENT ID	TECN	COMMENT
0.077 ± 0.207 ± 0.051	¹ AUBERT	05j	BABR $e^+e^- \rightarrow \Upsilon(4S)$

¹ The result reported corresponds to $-A_{CP}$.

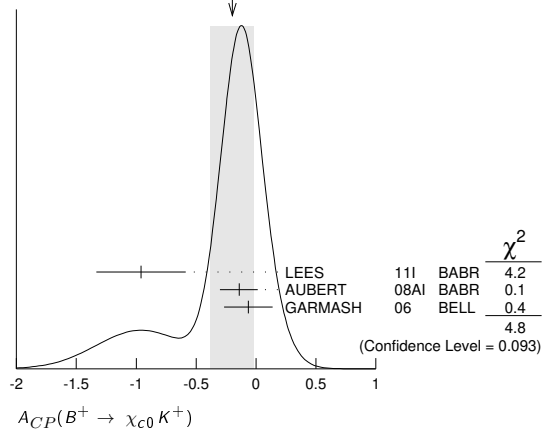
$A_{CP}(B^+ \rightarrow \chi_{c1}(1P)\pi^+)$

VALUE	DOCUMENT ID	TECN	COMMENT
0.07 ± 0.18 ± 0.02	KUMAR	06	BELL $e^+e^- \rightarrow \Upsilon(4S)$

$A_{CP}(B^+ \rightarrow \chi_{c0} K^+)$

VALUE	DOCUMENT ID	TECN	COMMENT
-0.20 ± 0.18 OUR AVERAGE	Error includes scale factor of 1.5. See the ideogram below.		
-0.96 ± 0.37 ± 0.04	LEES	11i	BABR $e^+e^- \rightarrow \Upsilon(4S)$
-0.14 ± 0.15 ± 0.03 ± 0.06	AUBERT	08Ai	BABR $e^+e^- \rightarrow \Upsilon(4S)$
-0.065 ± 0.20 ± 0.035 ± 0.024	GARMASH	06	BELL $e^+e^- \rightarrow \Upsilon(4S)$

WEIGHTED AVERAGE
-0.20±0.18 (Error scaled by 1.5)



$A_{CP}(B^+ \rightarrow \chi_{c1} K^+)$

VALUE	DOCUMENT ID	TECN	COMMENT
-0.009 ± 0.033 OUR AVERAGE			
-0.01 ± 0.03 ± 0.02	KUMAR	06	BELL $e^+e^- \rightarrow \Upsilon(4S)$
-0.003 ± 0.076 ± 0.017	¹ AUBERT	05j	BABR $e^+e^- \rightarrow \Upsilon(4S)$

¹ The result reported corresponds to $-A_{CP}$.

$A_{CP}(B^+ \rightarrow \chi_{c1} K^*(892)^+)$

VALUE	DOCUMENT ID	TECN	COMMENT
0.471 ± 0.378 ± 0.268	¹ AUBERT	05j	BABR $e^+e^- \rightarrow \Upsilon(4S)$

¹ The result reported corresponds to $-A_{CP}$.

$A_{CP}(B^+ \rightarrow D^0 \ell^+ \nu_\ell)$

VALUE (units 10^{-2})	DOCUMENT ID	TECN	COMMENT
-0.14 ± 0.14 ± 0.14	¹ ABAZOV	17A	D0 $p\bar{p}$ at 1.96 TeV

¹ Uses $D^0 \rightarrow K^-\pi^+$ decays and $f(B^+) = 0.56 \pm 0.01$ from 10.4 fb⁻¹ of Run II data.

$A_{CP}(B^+ \rightarrow D^0 \pi^+)$

VALUE (units 10^{-3})	DOCUMENT ID	TECN	COMMENT
-3 ± 5 OUR AVERAGE			
1.9 ± 3.6 ± 5.7	BLOOMFIELD	22	BELL $e^+e^- \rightarrow \Upsilon(4S)$
-6 ± 5 ± 10	¹ AAIJ	13AE	LHCB pp at 7 TeV
-8 ± 8	ABE	06	BELL $e^+e^- \rightarrow \Upsilon(4S)$

¹ Uses $B^\pm \rightarrow [K^\pm \pi^\mp \pi^\pm \pi^\mp]_D h^\pm$ mode.

$A_{CP}(B^+ \rightarrow D_{CP(+)} \pi^+)$

VALUE	DOCUMENT ID	TECN	COMMENT
-0.0080 ± 0.0024 OUR AVERAGE			
-0.008 ± 0.002 ± 0.002	¹ AAIJ	21Q	LHCB pp at 7, 8, 13 TeV
-0.0098 ± 0.0043 ± 0.0021	AAIJ	16L	LHCB pp at 7, 8 TeV
0.035 ± 0.024	ABE	06	BELL $e^+e^- \rightarrow \Upsilon(4S)$

••• We do not use the following data for averages, fits, limits, etc. •••
-0.008 ± 0.003 ± 0.002 ^{2,3} AAIJ 18A LHCB pp at 7, 8, 13 TeV
-0.008 ± 0.006 ± 0.002 ^{3,4} AAIJ 18A LHCB pp at 7, 8, 13 TeV
¹ Uses $D \rightarrow K^+ K^-$ and $D \rightarrow \pi^+ \pi^-$ decay modes.
² Uses $D \rightarrow K^+ K^-$ decay mode.
³ Superseded by AAIJ 21Q.
⁴ Uses $D \rightarrow \pi^+ \pi^-$ decay mode.

$A_{CP}(B^+ \rightarrow D_{CP(-)} \pi^+)$

VALUE	DOCUMENT ID	TECN	COMMENT
0.017 ± 0.026	ABE	06	BELL $e^+e^- \rightarrow \Upsilon(4S)$

$A_{CP}([K^\mp \pi^\pm \pi^\mp \pi^-]_D \pi^+)$

VALUE	DOCUMENT ID	TECN	COMMENT
$0.070 \pm 0.019 \pm 0.006$	AAIJ	23i LHCb	pp at 7, 8, 13 TeV
••• We do not use the following data for averages, fits, limits, etc. •••			
$0.023 \pm 0.048 \pm 0.005$	¹ AAIJ	16L LHCb	pp at 7, 8 TeV
0.13 ± 0.10	AAIJ	13Ae LHCb	Repl. by AAIJ 16L

¹ Superseded by AAIJ 23i. $A_{CP}(B^+ \rightarrow [\pi^+ \pi^+ \pi^- \pi^-]_D K^+)$

VALUE	DOCUMENT ID	TECN	COMMENT
$0.061 \pm 0.013 \pm 0.002$	AAIJ	23N LHCb	pp at 7, 8, 13 TeV
••• We do not use the following data for averages, fits, limits, etc. •••			
$0.100 \pm 0.034 \pm 0.018$	¹ AAIJ	16L LHCb	pp at 7, 8 TeV

¹ Superseded by AAIJ 23N. $A_{CP}(B^+ \rightarrow [\pi^+ \pi^- \pi^+ \pi^-]_D K^*(892)^+)$

VALUE	DOCUMENT ID	TECN	COMMENT
$0.02 \pm 0.11 \pm 0.01$	AAIJ	17Bo LHCb	pp at 7, 8, 13 TeV

 $A_{CP}(B^+ \rightarrow [K^+ K^- \pi^+ \pi^-]_D K^+)$

VALUE	DOCUMENT ID	TECN	COMMENT
$0.095 \pm 0.023 \pm 0.002$	AAIJ	23N LHCb	pp at 7, 8, 13 TeV

 $A_{CP}(B^+ \rightarrow [K^+ K^- \pi^+ \pi^-]_D \pi^+)$

VALUE	DOCUMENT ID	TECN	COMMENT
$-0.009 \pm 0.006 \pm 0.001$	AAIJ	23N LHCb	pp at 7, 8, 13 TeV

 $A_{CP}(B^+ \rightarrow \bar{D}^0 K^+)$

VALUE	DOCUMENT ID	TECN	COMMENT
-0.017 ± 0.005 OUR AVERAGE			
$-0.019 \pm 0.005 \pm 0.002$	AAIJ	18A LHCb	pp at 7, 8, 13 TeV
$-0.0194 \pm 0.0072 \pm 0.0060$	AAIJ	16L LHCb	pp at 7, 8 TeV
$0.010 \pm 0.026 \pm 0.005$	² AAIJ	15W LHCb	pp at 7, 8 TeV
0.066 ± 0.036	ABE	06 BELL	$e^+ e^- \rightarrow \Upsilon(4S)$
••• We do not use the following data for averages, fits, limits, etc. •••			
$0.000 \pm 0.012 \pm 0.002$	³ AAIJ	16L LHCb	pp at 7, 8 TeV
$-0.029 \pm 0.020 \pm 0.018$	³ AAIJ	13Ae LHCb	Repl. by AAIJ 16L
$0.003 \pm 0.080 \pm 0.037$	⁴ ABE	03D BELL	Repl. by SWAIN 03
$0.04 \pm 0.06 \pm 0.03$	⁵ SWAIN	03 BELL	Repl. by ABE 06

¹ Supersedes AAIJ 16L.² Uses $D^0 \rightarrow K^- \pi^+ \pi^0$ for the favored mode, and $D^0 \rightarrow K^+ \pi^- \pi^0$ for the suppressed mode.³ Uses $B^\pm \rightarrow [K^\pm \pi^\mp \pi^\pm \pi^\mp]_D h^\pm$ mode.⁴ Corresponds to 90% confidence range $-0.15 < A_{CP} < 0.16$.⁵ Corresponds to 90% confidence range $-0.07 < A_{CP} < 0.15$. $A_{CP}([K^\mp \pi^\pm \pi^\mp \pi^-]_D K^+)$

VALUE	DOCUMENT ID	TECN	COMMENT
$-0.321 \pm 0.039 \pm 0.005$	AAIJ	23i LHCb	pp at 7, 8, 13 TeV
••• We do not use the following data for averages, fits, limits, etc. •••			
$-0.313 \pm 0.102 \pm 0.038$	¹ AAIJ	16L LHCb	pp at 7, 8 TeV
-0.42 ± 0.22	AAIJ	13Ae LHCb	Repl. by AAIJ 16L

¹ Superseded by AAIJ 23i. $A_{CP}(B^+ \rightarrow [\pi^+ \pi^+ \pi^- \pi^-]_D \pi^+)$

VALUE (units 10^{-3})	DOCUMENT ID	TECN	COMMENT
$-8.2 \pm 3.1 \pm 0.7$	AAIJ	23N LHCb	pp at 7, 8, 13 TeV
••• We do not use the following data for averages, fits, limits, etc. •••			
$-4.1 \pm 7.9 \pm 2.4$	¹ AAIJ	16L LHCb	pp at 7, 8 TeV

¹ Superseded by AAIJ 23N. $A_{CP}(B^+ \rightarrow [K^- \pi^+]_D K^+)$

VALUE	DOCUMENT ID	TECN	COMMENT
-0.58 ± 0.21 OUR AVERAGE			
$-0.82 \pm 0.44 \pm 0.09$	AALTONEN	11Aj CDF	$p\bar{p}$ at 1.96 TeV
$-0.39 \pm 0.26 \pm 0.04$	HORII	11 BELL	$e^+ e^- \rightarrow \Upsilon(4S)$
$-0.86 \pm 0.47 \pm 0.12$	DEL-AMO-SA...10H	BABR	$e^+ e^- \rightarrow \Upsilon(4S)$
••• We do not use the following data for averages, fits, limits, etc. •••			
$-0.1 \pm 0.8 \pm 0.4$	HORII	08 BELL	Repl. by HORII 11
$+0.88 \pm 0.77 \pm 0.06$	SAIGO	05 BELL	Repl. by HORII 08

 $A_{CP}(B^+ \rightarrow [K^- \pi^+ \pi^0]_D K^+)$

VALUE	DOCUMENT ID	TECN	COMMENT
-0.27 ± 0.27 OUR AVERAGE	Error	includes scale factor of 2.4.	
$-0.38 \pm 0.12 \pm 0.02$	AAIJ	22T LHCb	pp at 7, 8, 13 TeV
$0.41 \pm 0.30 \pm 0.05$	NAYAK	13 BELL	$e^+ e^- \rightarrow \Upsilon(4S)$
••• We do not use the following data for averages, fits, limits, etc. •••			
$-0.20 \pm 0.27 \pm 0.04$	¹ AAIJ	15W LHCb	Repl. by AAIJ 22T

¹ Uses $D^0 \rightarrow K^- \pi^+ \pi^0$ for the favored mode, and $D^0 \rightarrow K^+ \pi^- \pi^0$ for the suppressed mode. $A_{CP}(B^+ \rightarrow [K^+ \pi^- \pi^0]_D K^+)$

VALUE	DOCUMENT ID	TECN	COMMENT
$-0.024 \pm 0.013 \pm 0.002$	AAIJ	22T LHCb	pp at 7, 8, 13 TeV

 $A_{CP}(B^+ \rightarrow [K^+ K^- \pi^0]_D K^+)$

VALUE	DOCUMENT ID	TECN	COMMENT
$0.067 \pm 0.073 \pm 0.003$	AAIJ	22T LHCb	pp at 7, 8, 13 TeV
••• We do not use the following data for averages, fits, limits, etc. •••			
$0.30 \pm 0.20 \pm 0.02$	¹ AAIJ	15W LHCb	Repl. by AAIJ 22T

¹ Uses $D \rightarrow K^+ K^- \pi^0$ mode. $A_{CP}(B^+ \rightarrow [\pi^+ \pi^- \pi^0]_D K^+)$

VALUE	DOCUMENT ID	TECN	COMMENT
$0.109 \pm 0.043 \pm 0.003$	AAIJ	22T LHCb	pp at 7, 8, 13 TeV
••• We do not use the following data for averages, fits, limits, etc. •••			
$0.054 \pm 0.091 \pm 0.011$	¹ AAIJ	15W LHCb	Repl. by AAIJ 22T

¹ Uses $D \rightarrow \pi^+ \pi^- \pi^0$ mode. $A_{CP}(B^+ \rightarrow \bar{D}^0 K^*(892)^+)$

VALUE	DOCUMENT ID	TECN	COMMENT
-0.007 ± 0.019 OUR AVERAGE			
$-0.004 \pm 0.023 \pm 0.008$	¹ AAIJ	17Bo LHCb	pp at 7, 8, 13 TeV
$-0.013 \pm 0.031 \pm 0.009$	² AAIJ	17Bo LHCb	pp at 7, 8, 13 TeV

¹ Uses $B^\pm \rightarrow [K^\pm \pi^\mp]_D K^*(892)^\pm$ decay mode.² Uses $B^\pm \rightarrow [K^\pm \pi^\mp \pi^\pm \pi^\mp]_D K^*(892)^\pm$ decay mode. $A_{CP}(B^+ \rightarrow [K^- \pi^+]_D K^*(892)^+)$

VALUE	DOCUMENT ID	TECN	COMMENT
-0.75 ± 0.16 OUR AVERAGE			
$-0.81 \pm 0.17 \pm 0.04$	AAIJ	17Bo LHCb	pp at 7, 8, 13 TeV
$-0.34 \pm 0.43 \pm 0.16$	AUBERT	09Aj BABR	$e^+ e^- \rightarrow \Upsilon(4S)$
••• We do not use the following data for averages, fits, limits, etc. •••			
$-0.22 \pm 0.61 \pm 0.17$	AUBERT,B	05v BABR	Repl. by AUBERT 09Aj

 $A_{CP}(B^+ \rightarrow [K^- \pi^+ \pi^- \pi^+]_D K^*(892)^+)$

VALUE	DOCUMENT ID	TECN	COMMENT
$-0.45 \pm 0.21 \pm 0.14$	AAIJ	17Bo LHCb	pp at 7, 8, 13 TeV

 $A_{CP}(B^+ \rightarrow [K^- \pi^+]_D \pi^+)$

VALUE	DOCUMENT ID	TECN	COMMENT
0.00 ± 0.09 OUR AVERAGE			
$0.13 \pm 0.25 \pm 0.02$	AALTONEN	11Aj CDF	$p\bar{p}$ at 1.96 TeV
$-0.04 \pm 0.11 \pm 0.01$	HORII	11 BELL	$e^+ e^- \rightarrow \Upsilon(4S)$
$0.03 \pm 0.17 \pm 0.04$	DEL-AMO-SA...10H	BABR	$e^+ e^- \rightarrow \Upsilon(4S)$
••• We do not use the following data for averages, fits, limits, etc. •••			
$-0.02 \pm 0.15 \pm 0.16 \pm 0.04$	HORII	08 BELL	Repl. by HORII 11
$+0.30 \pm 0.29 \pm 0.25 \pm 0.06$	SAIGO	05 BELL	Repl. by HORII 08

 $A_{CP}(B^+ \rightarrow [K^- \pi^+ \pi^0]_D \pi^+)$

VALUE	DOCUMENT ID	TECN	COMMENT
0.08 ± 0.09 OUR AVERAGE			
$0.069 \pm 0.094 \pm 0.016$	AAIJ	22T LHCb	pp at 7, 8, 13 TeV
$0.16 \pm 0.27 \pm 0.03 \pm 0.04$	NAYAK	13 BELL	$e^+ e^- \rightarrow \Upsilon(4S)$
••• We do not use the following data for averages, fits, limits, etc. •••			
$0.438 \pm 0.190 \pm 0.011$	¹ AAIJ	15W LHCb	Repl. by AAIJ 22T

¹ Uses $D^0 \rightarrow K^- \pi^+ \pi^0$ for the favored mode, and $D^0 \rightarrow K^+ \pi^- \pi^0$ for the suppressed mode. $A_{CP}(B^+ \rightarrow [K^+ K^- \pi^0]_D \pi^+)$

VALUE	DOCUMENT ID	TECN	COMMENT
$-0.001 \pm 0.019 \pm 0.002$	AAIJ	22T LHCb	pp at 7, 8, 13 TeV
••• We do not use the following data for averages, fits, limits, etc. •••			
$-0.030 \pm 0.040 \pm 0.005$	¹ AAIJ	15W LHCb	Repl. by AAIJ 22T

¹ Uses $D \rightarrow K^+ K^- \pi^0$ mode. $A_{CP}(B^+ \rightarrow [\pi^+ \pi^- \pi^0]_D \pi^+)$

VALUE	DOCUMENT ID	TECN	COMMENT
$0.001 \pm 0.010 \pm 0.002$	AAIJ	22T LHCb	pp at 7, 8, 13 TeV
••• We do not use the following data for averages, fits, limits, etc. •••			
$-0.016 \pm 0.020 \pm 0.004$	¹ AAIJ	15W LHCb	Repl. by AAIJ 22T

¹ Uses $D \rightarrow \pi^+ \pi^- \pi^0$ mode. $A_{CP}(B^+ \rightarrow [K^- \pi^+]_D \pi^+)$

VALUE	DOCUMENT ID	TECN	COMMENT
$-0.09 \pm 0.27 \pm 0.05$	DEL-AMO-SA...10H	BABR	$e^+ e^- \rightarrow \Upsilon(4S)$

 $A_{CP}(B^+ \rightarrow [K^- \pi^+]_D \gamma \pi^+)$

VALUE	DOCUMENT ID	TECN	COMMENT
$-0.65 \pm 0.55 \pm 0.22$	DEL-AMO-SA...10H	BABR	$e^+ e^- \rightarrow \Upsilon(4S)$

Meson Particle Listings

 B^\pm $A_{CP}(B^+ \rightarrow [K^-\pi^+]_D K^+)$

VALUE	DOCUMENT ID	TECN	COMMENT
0.77 ± 0.35 ± 0.12	DEL-AMO-SA...10H	BABR	$e^+e^- \rightarrow \Upsilon(4S)$

 $A_{CP}(B^+ \rightarrow [K^-\pi^+]_{D\gamma} K^+)$

VALUE	DOCUMENT ID	TECN	COMMENT
0.36 ± 0.94 ± 0.25 -0.41	DEL-AMO-SA...10H	BABR	$e^+e^- \rightarrow \Upsilon(4S)$

 $A_{CP}(B^+ \rightarrow [\pi^+\pi^-\pi^0]_D K^+)$

VALUE	DOCUMENT ID	TECN	COMMENT
-0.02 ± 0.15 ± 0.03	¹ AUBERT 07BJ	BABR	$e^+e^- \rightarrow \Upsilon(4S)$
••• We do not use the following data for averages, fits, limits, etc. •••			
-0.02 ± 0.16 ± 0.03	AUBERT,B 05T	BABR	Repl. by AUBERT 07BJ
¹ Uses a Dalitz plot analysis of $D^0 \rightarrow \pi^+\pi^-\pi^0$. Also reports the one-sigma regions: $0.06 < r_B < 0.78$, $-30^\circ < \gamma < 76^\circ$, and $-27^\circ < \delta < 78^\circ$.			

 $A_{CP}(B^+ \rightarrow [K_S^0 K^+\pi^-]_D K^+)$

VALUE	DOCUMENT ID	TECN	COMMENT
0.00 ± 0.09 OUR AVERAGE	Error includes scale factor of 1.4.		
-0.089 ± 0.091 ± 0.011	¹ ADACHI 23L	BELL	$e^+e^- \rightarrow \Upsilon(4S)$
0.095 ± 0.089 ± 0.018	² AAIJ 20N	LHCb	pp at 7, 8, 13 TeV
••• We do not use the following data for averages, fits, limits, etc. •••			
0.040 ± 0.091 ± 0.018	¹ AAIJ 14V	LHCb	Repl. by AAIJ 20N
¹ The analysis uses all of $D \rightarrow K_S^0 K\pi$ Dalitz decays.			
² The analysis uses $D \rightarrow K_S^0 K\pi$ Dalitz decays with $K^* K^+$ region excluded.			

 $A_{CP}(B^+ \rightarrow [K_S^0 K^-\pi^+]_D K^+)$

VALUE	DOCUMENT ID	TECN	COMMENT
0.00 ± 0.07 OUR AVERAGE			
0.109 ± 0.133 ± 0.013	¹ ADACHI 23L	BELL	$e^+e^- \rightarrow \Upsilon(4S)$
-0.038 ± 0.075 ± 0.011	² AAIJ 20N	LHCb	pp at 7, 8, 13 TeV
••• We do not use the following data for averages, fits, limits, etc. •••			
0.233 ± 0.129 ± 0.024	¹ AAIJ 14V	LHCb	Repl. by AAIJ 20N
¹ The analysis uses all of $D \rightarrow K_S^0 K\pi$ Dalitz decays.			
² The analysis uses $D \rightarrow K_S^0 K\pi$ Dalitz decays with $K^* K^+$ region excluded.			

 $A_{CP}(B^+ \rightarrow [K_S^0 K^-\pi^+]_D \pi^+)$

VALUE	DOCUMENT ID	TECN	COMMENT
-0.003 ± 0.014 OUR AVERAGE			
-0.028 ± 0.031 ± 0.009	¹ ADACHI 23L	BELL	$e^+e^- \rightarrow \Upsilon(4S)$
0.003 ± 0.015 ± 0.003	² AAIJ 20N	LHCb	pp at 7, 8, 13 TeV
••• We do not use the following data for averages, fits, limits, etc. •••			
-0.052 ± 0.029 ± 0.017	¹ AAIJ 14V	LHCb	Repl. by AAIJ 20N
¹ The analysis uses all of $D \rightarrow K_S^0 K\pi$ Dalitz decays.			
² The analysis uses $D \rightarrow K_S^0 K\pi$ Dalitz decays with $K^* K^+$ region excluded.			

 $A_{CP}(B^+ \rightarrow [K_S^0 K^+\pi^-]_D \pi^+)$

VALUE	DOCUMENT ID	TECN	COMMENT
-0.016 ± 0.025 OUR AVERAGE	Error includes scale factor of 1.5.		
-0.018 ± 0.026 ± 0.009	¹ ADACHI 23L	BELL	$e^+e^- \rightarrow \Upsilon(4S)$
-0.034 ± 0.020 ± 0.003	² AAIJ 20N	LHCb	pp at 7, 8, 13 TeV
••• We do not use the following data for averages, fits, limits, etc. •••			
-0.025 ± 0.024 ± 0.010	¹ AAIJ 14V	LHCb	Repl. by AAIJ 20N
¹ The analysis uses all of $D \rightarrow K_S^0 K\pi$ Dalitz decays.			
² The analysis uses $D \rightarrow K_S^0 K\pi$ Dalitz decays with $K^* K^+$ region excluded.			

 $A_{CP}(B^+ \rightarrow [K^*(892)^- K^+]_D K^+)$

VALUE	DOCUMENT ID	TECN	COMMENT
0.08 ± 0.05 OUR AVERAGE			
0.055 ± 0.119 ± 0.020	¹ ADACHI 23L	BELL	$e^+e^- \rightarrow \Upsilon(4S)$
0.084 ± 0.049 ± 0.008	¹ AAIJ 20N	LHCb	pp at 7, 8, 13 TeV
••• We do not use the following data for averages, fits, limits, etc. •••			
0.026 ± 0.109 ± 0.029	¹ AAIJ 14V	LHCb	Repl. by AAIJ 20N
¹ The Analysis uses $D \rightarrow K^*(892) K \rightarrow K_S^0 K\pi$ decays.			

 $A_{CP}(B^+ \rightarrow [K^*(892)^+ K^-]_D K^+)$

VALUE	DOCUMENT ID	TECN	COMMENT
0.07 ± 0.09 OUR AVERAGE			
0.231 ± 0.184 ± 0.014	¹ ADACHI 23L	BELL	$e^+e^- \rightarrow \Upsilon(4S)$
0.021 ± 0.094 ± 0.017	¹ AAIJ 20N	LHCb	pp at 7, 8, 13 TeV
••• We do not use the following data for averages, fits, limits, etc. •••			
0.336 ± 0.208 ± 0.026	¹ AAIJ 14V	LHCb	Repl. by AAIJ 20N
¹ The Analysis uses $D \rightarrow K^*(892) K \rightarrow K_S^0 K\pi$ decays.			

 $A_{CP}(B^+ \rightarrow [K^*(892)^+ K^-]_D \pi^+)$

VALUE	DOCUMENT ID	TECN	COMMENT
0.007 ± 0.016 OUR AVERAGE			
0.009 ± 0.046 ± 0.009	¹ ADACHI 23L	BELL	$e^+e^- \rightarrow \Upsilon(4S)$
0.007 ± 0.017 ± 0.003	¹ AAIJ 20N	LHCb	pp at 7, 8, 13 TeV
••• We do not use the following data for averages, fits, limits, etc. •••			
-0.054 ± 0.043 ± 0.017	¹ AAIJ 14V	LHCb	Repl. by AAIJ 20N
¹ The Analysis uses $D \rightarrow K^*(892) K \rightarrow K_S^0 K\pi$ decays.			

 $A_{CP}(B^+ \rightarrow [K^*(892)^- K^+]_D \pi^+)$

VALUE	DOCUMENT ID	TECN	COMMENT
-0.013 ± 0.020 OUR AVERAGE	Error includes scale factor of 1.9.		
0.046 ± 0.029 ± 0.016	¹ ADACHI 23L	BELL	$e^+e^- \rightarrow \Upsilon(4S)$
-0.020 ± 0.011 ± 0.003	¹ AAIJ 20N	LHCb	pp at 7, 8, 13 TeV
••• We do not use the following data for averages, fits, limits, etc. •••			
-0.012 ± 0.028 ± 0.010	¹ AAIJ 14V	LHCb	Repl. by AAIJ 20N
¹ The Analysis uses $D \rightarrow K^*(892) K \rightarrow K_S^0 K\pi$ decays.			

 $A_{CP}(B^+ \rightarrow D_{CP(+)} K^+)$

VALUE	DOCUMENT ID	TECN	COMMENT
0.132 ± 0.015 OUR AVERAGE	Error includes scale factor of 1.8.		
0.136 ± 0.009 ± 0.001	¹ AAIJ 21Q	LHCb	pp at 7, 8, 13 TeV
0.097 ± 0.018 ± 0.009	AAIJ 16L	LHCb	pp at 7, 8 TeV
0.39 ± 0.17 ± 0.04	AALTONEN 10A	CDF	$p\bar{p}$ at 1.96 TeV
0.25 ± 0.06 ± 0.02	² DEL-AMO-SA...10G	BABR	$e^+e^- \rightarrow \Upsilon(4S)$
0.06 ± 0.14 ± 0.05	ABE 06	BELL	$e^+e^- \rightarrow \Upsilon(4S)$
••• We do not use the following data for averages, fits, limits, etc. •••			
0.126 ± 0.014 ± 0.002	^{3,4} AAIJ 18A	LHCb	pp at 7, 8, 13 TeV
0.115 ± 0.025 ± 0.007	^{4,5} AAIJ 18A	LHCb	pp at 7, 8, 13 TeV
0.145 ± 0.032 ± 0.010	⁶ AAIJ 12M	LHCb	Repl. by AAIJ 16L
0.27 ± 0.09 ± 0.04	AUBERT 08AA	BABR	Repl. by DEL-AMO-SANCHEZ 10G
0.35 ± 0.13 ± 0.04	AUBERT 06J	BABR	Repl. by AUBERT 08AA
0.07 ± 0.17 ± 0.06	AUBERT 04N	BABR	Repl. by AUBERT 06J
0.29 ± 0.26 ± 0.05	⁷ ABE 03D	BELL	Repl. by SWAIN 03
0.06 ± 0.19 ± 0.04	⁸ SWAIN 03	BELL	Repl. by ABE 06

¹ Uses $D \rightarrow K^+ K^-$ and $D \rightarrow \pi^+ \pi^-$ decay modes.

² Reports the first evidence for direct CP violation in $B \rightarrow DK$ decays with 3.6 standard deviations.

³ Uses $D \rightarrow K^+ K^-$ decay mode.

⁴ Superseded by AAIJ 21Q.

⁵ Uses $D \rightarrow \pi^+ \pi^-$ decay mode.

⁶ AAIJ 12M reports an evidence of direct CP violation in $B^\pm \rightarrow DK^\pm$ decays with a total significance of 5.8 σ .

⁷ Corresponds to 90% confidence range $-0.14 < A_{CP} < 0.73$.

⁸ Corresponds to 90% confidence range $-0.26 < A_{CP} < 0.38$.

 $A_{ADS}(B^+ \rightarrow DK^+)$

$$A_{ADS}(B^+ \rightarrow DK^+) = \frac{(R_K^- - R_K^+)}{(R_K^- + R_K^+)}$$
 where

$$R_K^- = \Gamma(B^- \rightarrow [K^+\pi^-]_D K^-) / \Gamma(B^- \rightarrow [K^-\pi^+]_D K^-)$$
 and

$$R_K^+ = \Gamma(B^+ \rightarrow [K^-\pi^+]_D K^+) / \Gamma(B^+ \rightarrow [K^+\pi^-]_D K^+)$$

VALUE	DOCUMENT ID	TECN	COMMENT
-0.451 ± 0.026	¹ AAIJ 21Q	LHCb	pp at 7, 8, 13 TeV
••• We do not use the following data for averages, fits, limits, etc. •••			
-0.403 ± 0.056 ± 0.011	² AAIJ 16L	LHCb	pp at 7, 8 TeV
-0.52 ± 0.15 ± 0.02	AAIJ 12M	LHCb	Repl. by AAIJ 16L

¹ The statistical and systematic uncertainties have been combined according to the correlations between the R_K^- and R_K^+ observables.

² Superseded by AAIJ 21Q.

 $A_{ADS}(B^+ \rightarrow D\pi^+)$

$$A_{ADS}(B^+ \rightarrow D\pi^+) = \frac{(R_\pi^- - R_\pi^+)}{(R_\pi^- + R_\pi^+)}$$
 where

$$R_\pi^- = \Gamma(B^- \rightarrow [K^+\pi^-]_D \pi^-) / \Gamma(B^- \rightarrow [K^-\pi^+]_D \pi^-)$$
 and

$$R_\pi^+ = \Gamma(B^+ \rightarrow [K^-\pi^+]_D \pi^+) / \Gamma(B^+ \rightarrow [K^+\pi^-]_D \pi^+)$$

VALUE	DOCUMENT ID	TECN	COMMENT
0.129 ± 0.014	¹ AAIJ 21Q	LHCb	pp at 7, 8, 13 TeV
••• We do not use the following data for averages, fits, limits, etc. •••			
0.100 ± 0.031 ± 0.009	² AAIJ 16L	LHCb	pp at 7, 8 TeV
0.143 ± 0.062 ± 0.011	AAIJ 12M	LHCb	Repl. by AAIJ 16L

¹ The statistical and systematic uncertainties have been combined according to the correlations between the R_π^- and R_π^+ observables.

² Superseded by AAIJ 21Q.

 $A_{ADS}(B^+ \rightarrow D^*(D\gamma) K^+)$

$$A_{ADS}(B^+ \rightarrow D^*(D\gamma) K^+) = (R_K^- - R_K^+) / (R_K^- + R_K^+),$$
 where

$$R_K^- = \Gamma(B^- \rightarrow (\gamma[K^+\pi^-]_D)_{D^*} K^-) / \Gamma(B^- \rightarrow (\gamma[K^-\pi^+]_D)_{D^*} K^-)$$
 and

$$R_K^+ = \Gamma(B^+ \rightarrow (\gamma[K^-\pi^+]_D)_{D^*} K^+) / \Gamma(B^+ \rightarrow (\gamma[K^+\pi^-]_D)_{D^*} K^+)$$

VALUE	DOCUMENT ID	TECN	COMMENT
-0.558 ± 1.349	¹ AAIJ 21Q	LHCb	pp at 7, 8, 13 TeV
¹ The statistical and systematic uncertainties have been combined according to the correlations between the R_K^- and R_K^+ observables.			

A_{ADS}(B⁺ → D*⁰(Dπ⁰)K⁺)

$A_{ADS}(B^+ \rightarrow D^*(D\pi^0)K^+) = (R_K^- - R_K^+) / (R_K^- + R_K^+)$, where
 $R_K^- = \Gamma(B^- \rightarrow ([K^+\pi^-]_D\pi^0)_{D^*}K^-) / \Gamma(B^- \rightarrow ([K^-\pi^+]_D\pi^0)_{D^*}K^-)$ and
 $R_K^+ = \Gamma(B^+ \rightarrow ([K^-\pi^+]_D\pi^0)_{D^*}K^+) / \Gamma(B^+ \rightarrow ([K^+\pi^-]_D\pi^0)_{D^*}K^+)$

VALUE	DOCUMENT ID	TECN	COMMENT
0.717 ± 0.286	¹ AAIJ	21q	LHCB pp at 7, 8, 13 TeV

¹ The statistical and systematic uncertainties have been combined according to the correlations between the R_K⁻ and R_K⁺ observables.

A_{ADS}(B⁺ → D*(Dγ)π⁺)

$A_{ADS}(B^+ \rightarrow D^*(D\gamma)\pi^+) = (R_\pi^- - R_\pi^+) / (R_\pi^- + R_\pi^+)$, where
 $R_\pi^- = \Gamma(B^- \rightarrow (\gamma[K^+\pi^-]_D)_{D^*}\pi^-) / \Gamma(B^- \rightarrow (\gamma[K^-\pi^+]_D)_{D^*}\pi^-)$ and
 $R_\pi^+ = \Gamma(B^+ \rightarrow (\gamma[K^-\pi^+]_D)_{D^*}\pi^+) / \Gamma(B^+ \rightarrow (\gamma[K^+\pi^-]_D)_{D^*}\pi^+)$

VALUE	DOCUMENT ID	TECN	COMMENT
0.079 ± 0.128	¹ AAIJ	21q	LHCB pp at 7, 8, 13 TeV

¹ The statistical and systematic uncertainties have been combined according to the correlations between the R_π⁻ and R_π⁺ observables.

A_{ADS}(B⁺ → D*(Dπ⁰)π⁺)

$A_{ADS}(B^+ \rightarrow D^*(D\pi^0)\pi^+) = (R_\pi^- - R_\pi^+) / (R_\pi^- + R_\pi^+)$, where
 $R_\pi^- = \Gamma(B^- \rightarrow ([K^+\pi^-]_D\pi^0)_{D^*}\pi^-) / \Gamma(B^- \rightarrow ([K^-\pi^+]_D\pi^0)_{D^*}\pi^-)$ and
 $R_\pi^+ = \Gamma(B^+ \rightarrow ([K^-\pi^+]_D\pi^0)_{D^*}\pi^+) / \Gamma(B^+ \rightarrow ([K^+\pi^-]_D\pi^0)_{D^*}\pi^+)$

VALUE	DOCUMENT ID	TECN	COMMENT
-0.140 ± 0.059	¹ AAIJ	21q	LHCB pp at 7, 8, 13 TeV

¹ The statistical and systematic uncertainties have been combined according to the correlations between the R_π⁻ and R_π⁺ observables.

A_{ADS}(B⁺ → [K⁻π⁺]D K⁺π⁺π⁺)

VALUE	DOCUMENT ID	TECN	COMMENT
-0.33^{+0.36}_{-0.34}	AAIJ	15bc	LHCB pp at 7, 8 TeV

A_{ADS}(B⁺ → [K⁻π⁺]D π⁺π⁺π⁺)

VALUE	DOCUMENT ID	TECN	COMMENT
-0.013 ± 0.087	AAIJ	15bc	LHCB pp at 7, 8 TeV

A_{CP}(B⁺ → D_{CP(-1)}K⁺)

VALUE	DOCUMENT ID	TECN	COMMENT
-0.10 ± 0.07 OUR AVERAGE			
-0.09 ± 0.07 ± 0.02	DEL-AMO-SA...10G	BABR	e ⁺ e ⁻ → T(4S)
-0.12 ± 0.14 ± 0.05	ABE	06	BELL e ⁺ e ⁻ → T(4S)
••• We do not use the following data for averages, fits, limits, etc. •••			
-0.09 ± 0.09 ± 0.02	AUBERT	08AA	BABR Repl. by DEL-AMO-SANCHEZ 10G
-0.06 ± 0.13 ± 0.04	AUBERT	06J	BABR Repl. by AUBERT 08AA
-0.22 ± 0.24 ± 0.04	¹ ABE	03D	BELL Repl. by SWAIN 03
-0.19 ± 0.17 ± 0.05	² SWAIN	03	BELL Repl. by ABE 06

¹ Corresponds to 90% confidence range -0.62 < A_{CP} < 0.18.
² Corresponds to 90% confidence range -0.47 < A_{CP} < 0.11.

A_{CP}(B⁺ → [K⁺K⁻]D K⁺π⁻π⁺)

VALUE	DOCUMENT ID	TECN	COMMENT
-0.045 ± 0.064 ± 0.011	AAIJ	15bc	LHCB pp at 7, 8 TeV

A_{CP}(B⁺ → [π⁺π⁻]D K⁺π⁻π⁺)

VALUE	DOCUMENT ID	TECN	COMMENT
-0.054 ± 0.101 ± 0.011	AAIJ	15bc	LHCB pp at 7, 8 TeV

A_{CP}(B⁺ → [K⁻π⁺]D K⁺π⁻π⁺)

VALUE	DOCUMENT ID	TECN	COMMENT
0.013 ± 0.019 ± 0.013	AAIJ	15bc	LHCB pp at 7, 8 TeV

A_{CP}(B⁺ → [K⁺K⁻]D π⁺π⁻π⁺)

VALUE	DOCUMENT ID	TECN	COMMENT
-0.019 ± 0.011 ± 0.010	AAIJ	15bc	LHCB pp at 7, 8 TeV

A_{CP}(B⁺ → [π⁺π⁻]D π⁺π⁻π⁺)

VALUE	DOCUMENT ID	TECN	COMMENT
-0.013 ± 0.016 ± 0.010	AAIJ	15bc	LHCB pp at 7, 8 TeV

A_{CP}(B⁺ → [K⁻π⁺]D π⁺π⁻π⁺)

VALUE	DOCUMENT ID	TECN	COMMENT
-0.002 ± 0.003 ± 0.011	AAIJ	15bc	LHCB pp at 7, 8 TeV

A_{CP}(B⁺ → D⁰π⁺)

VALUE	DOCUMENT ID	TECN	COMMENT
-0.0004 ± 0.0021 OUR AVERAGE			Error includes scale factor of 1.1.
-0.004 ± 0.004 ± 0.001	¹ AAIJ	21q	LHCB pp at 7, 8, 13 TeV
0.001 ± 0.002 ± 0.001	² AAIJ	21q	LHCB pp at 7, 8, 13 TeV
-0.014 ± 0.015	ABE	06	BELL e ⁺ e ⁻ → T(4S)
••• We do not use the following data for averages, fits, limits, etc. •••			
0.000 ± 0.006 ± 0.001	^{1,3} AAIJ	18A	LHCB pp at 7, 8, 13 TeV
0.002 ± 0.003 ± 0.001	^{2,3} AAIJ	18A	LHCB pp at 7, 8, 13 TeV

¹ Uses D⁰ → D⁰γ decay mode.

² Uses D⁰ → D⁰π⁰ decay mode.
³ Superseded by AAIJ 21q.

A_{CP}(B⁺ → D⁰_{CP(+1)}π⁺)

VALUE	DOCUMENT ID	TECN	COMMENT
0.010 ± 0.007 OUR AVERAGE			
0.000 ± 0.014 ± 0.006	¹ AAIJ	21q	LHCB pp at 7, 8, 13 TeV
0.013 ± 0.007 ± 0.003	² AAIJ	21q	LHCB pp at 7, 8, 13 TeV
-0.021 ± 0.045	ABE	06	BELL e ⁺ e ⁻ → T(4S)
••• We do not use the following data for averages, fits, limits, etc. •••			
-0.003 ± 0.017 ± 0.002	^{1,3} AAIJ	18A	LHCB pp at 7, 8, 13 TeV
0.025 ± 0.010 ± 0.003	^{2,3} AAIJ	18A	LHCB pp at 7, 8, 13 TeV

¹ Uses D⁰ → D⁰γ decay mode.
² Uses D⁰ → D⁰π⁰ decay mode.
³ Superseded by AAIJ 21q.

A_{CP}(B⁺ → D⁰_{CP(-1)}π⁺)

VALUE	DOCUMENT ID	TECN	COMMENT
-0.090 ± 0.051	ABE	06	BELL e ⁺ e ⁻ → T(4S)

A_{CP}(B⁺ → D⁰K⁺)

VALUE	DOCUMENT ID	TECN	COMMENT
0.012 ± 0.010 OUR AVERAGE			Error includes scale factor of 1.5.
-0.004 ± 0.014 ± 0.003	¹ AAIJ	21q	LHCB pp at 7, 8, 13 TeV
0.020 ± 0.007 ± 0.003	² AAIJ	21q	LHCB pp at 7, 8, 13 TeV
-0.06 ± 0.04 ± 0.01	AUBERT	08BF	BABR e ⁺ e ⁻ → T(4S)
-0.089 ± 0.086	ABE	06	BELL e ⁺ e ⁻ → T(4S)
••• We do not use the following data for averages, fits, limits, etc. •••			
0.001 ± 0.021 ± 0.007	^{1,3} AAIJ	18A	LHCB pp at 7, 8, 13 TeV
0.006 ± 0.012 ± 0.004	^{2,3} AAIJ	18A	LHCB pp at 7, 8, 13 TeV

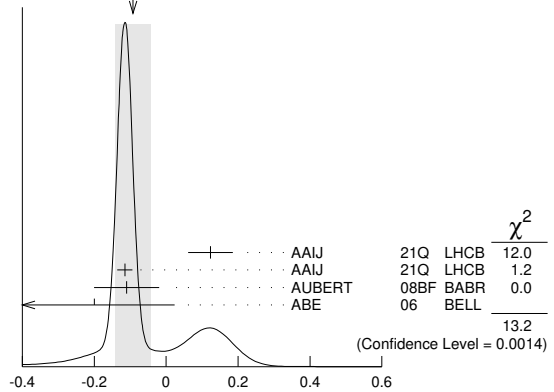
¹ Uses D⁰ → D⁰γ decay mode.
² Uses D⁰ → D⁰π⁰ decay mode.
³ Superseded by AAIJ 21q.

A_{CP}(B⁺ → D⁰_{CP(+1)}K⁺)

VALUE	DOCUMENT ID	TECN	COMMENT
-0.09 ± 0.05 OUR AVERAGE			Error includes scale factor of 2.6. See the ideogram below.
0.123 ± 0.054 ± 0.031	¹ AAIJ	21q	LHCB pp at 7, 8, 13 TeV
-0.115 ± 0.019 ± 0.009	² AAIJ	21q	LHCB pp at 7, 8, 13 TeV
-0.11 ± 0.09 ± 0.01	AUBERT	08BF	BABR e ⁺ e ⁻ → T(4S)
-0.20 ± 0.22 ± 0.04	ABE	06	BELL e ⁺ e ⁻ → T(4S)
••• We do not use the following data for averages, fits, limits, etc. •••			
0.276 ± 0.094 ± 0.047	^{1,3} AAIJ	18A	LHCB pp at 7, 8, 13 TeV
-0.151 ± 0.033 ± 0.011	^{2,3} AAIJ	18A	LHCB pp at 7, 8, 13 TeV
-0.10 ± 0.23 ± 0.03	AUBERT	05N	BABR Repl. by AUBERT 08BF

¹ Uses D⁰ → D⁰γ decay mode.
² Uses D⁰ → D⁰π⁰ decay mode.
³ Superseded by AAIJ 21q.

WEIGHTED AVERAGE
 -0.09 ± 0.05 (Error scaled by 2.6)



A_{CP}(B⁺ → D⁰_{CP(-1)}K⁺)

VALUE	DOCUMENT ID	TECN	COMMENT
0.07 ± 0.10 OUR AVERAGE			
+0.06 ± 0.10 ± 0.02	AUBERT	08BF	BABR e ⁺ e ⁻ → T(4S)
+0.13 ± 0.30 ± 0.08	ABE	06	BELL e ⁺ e ⁻ → T(4S)

Meson Particle Listings

 B^\pm $A_{CP}(B^+ \rightarrow D_{CP(+)} K^*(892)^+)$

VALUE	DOCUMENT ID	TECN	COMMENT
0.08 ± 0.06 OUR AVERAGE			
0.08 ± 0.06 ± 0.01	¹ AAIJ	17B0	LHCB pp at 7, 8, 13 TeV
0.09 ± 0.13 ± 0.06	AUBERT	09AJ	BABR $e^+e^- \rightarrow \Upsilon(4S)$

• • • We do not use the following data for averages, fits, limits, etc. • • •
 -0.08 ± 0.19 ± 0.08 AUBERT,B 05U BABR Repl. by AUBERT 09AJ

¹ Measures the asymmetry separately for K^+K^- and $\pi^+\pi^-$ final states, $A(KK) = 0.06 \pm 0.07 \pm 0.01$ and $A(\pi\pi) = 0.15 \pm 0.13 \pm 0.01$, and combines the two results. The value of $A(\pi\pi)$ was updated in AAIJ 18X.

 $A_{CP}(B^+ \rightarrow D_{CP(-)} K^*(892)^+)$

VALUE	DOCUMENT ID	TECN	COMMENT
-0.23 ± 0.21 ± 0.07			
-0.23 ± 0.21 ± 0.07	AUBERT	09AJ	BABR $e^+e^- \rightarrow \Upsilon(4S)$
-0.26 ± 0.40 ± 0.12	AUBERT,B	05U	BABR Repl. by AUBERT 09AJ

• • • We do not use the following data for averages, fits, limits, etc. • • •

 $A_{CP}(B^+ \rightarrow D_s^+ \phi)$

VALUE	DOCUMENT ID	TECN	COMMENT
-0.01 ± 0.41 ± 0.03			
-0.01 ± 0.41 ± 0.03	AAIJ	13R	LHCB pp at 7 TeV

 $A_{CP}(B^+ \rightarrow D_s^+ \bar{D}^0)$

VALUE (%)	DOCUMENT ID	TECN	COMMENT
0.5 ± 0.2 ± 0.6			
0.5 ± 0.2 ± 0.6	¹ AAIJ	23AX	LHCB pp at 7, 8, 13 TeV
-0.4 ± 0.5 ± 0.5	AAIJ	18W	LHCB Repl. by AAIJ 23AX

• • • We do not use the following data for averages, fits, limits, etc. • • •

¹ The last error includes the uncertainty from $A_{CP}(B^+ \rightarrow J/\psi K^+)$.

 $A_{CP}(B^+ \rightarrow D_s^+ \bar{D}^0)$

VALUE (units 10^{-2})	DOCUMENT ID	TECN	COMMENT
-0.5 ± 1.1 ± 1.0			
-0.5 ± 1.1 ± 1.0	¹ AAIJ	23AX	LHCB pp at 7, 8, 13 TeV

¹ The last error includes the uncertainty from $A_{CP}(B^+ \rightarrow J/\psi K^+)$.

 $A_{CP}(B^+ \rightarrow D_s^+ \bar{D}^{*0})$

VALUE (units 10^{-2})	DOCUMENT ID	TECN	COMMENT
1.1 ± 0.8 ± 0.7			
1.1 ± 0.8 ± 0.7	¹ AAIJ	23AX	LHCB pp at 7, 8, 13 TeV

¹ The last error includes the uncertainty from $A_{CP}(B^+ \rightarrow J/\psi K^+)$.

 $A_{CP}(B^+ \rightarrow D^{*+} \bar{D}^{*0})$

VALUE (units 10^{-2})	DOCUMENT ID	TECN	COMMENT
1.3 ± 2.6 OUR AVERAGE			
2.3 ± 2.1 ± 1.7	¹ AAIJ	23AX	LHCB pp at 7, 8, 13 TeV
-15 ± 11 ± 2	AUBERT,B	06A	BABR $e^+e^- \rightarrow \Upsilon(4S)$

¹ The last error includes the uncertainty from $A_{CP}(B^+ \rightarrow J/\psi K^+)$.

 $A_{CP}(B^+ \rightarrow D^{*+} \bar{D}^0)$

VALUE (units 10^{-2})	DOCUMENT ID	TECN	COMMENT
3.1 ± 1.7 OUR AVERAGE			
3.3 ± 1.6 ± 0.7	¹ AAIJ	23AX	LHCB pp at 7, 8, 13 TeV
-6 ± 13 ± 2	AUBERT,B	06A	BABR $e^+e^- \rightarrow \Upsilon(4S)$

¹ The last error includes the uncertainty from $A_{CP}(B^+ \rightarrow J/\psi K^+)$.

 $A_{CP}(B^+ \rightarrow D^+ \bar{D}^{*0})$

VALUE (units 10^{-2})	DOCUMENT ID	TECN	COMMENT
0.0 ± 2.4 OUR AVERAGE			
-0.2 ± 2.0 ± 1.4	¹ AAIJ	23AX	LHCB pp at 7, 8, 13 TeV
13 ± 18 ± 4	AUBERT,B	06A	BABR $e^+e^- \rightarrow \Upsilon(4S)$

¹ The last error includes the uncertainty from $A_{CP}(B^+ \rightarrow J/\psi K^+)$.

 $A_{CP}(B^+ \rightarrow D^+ \bar{D}^0)$

VALUE (units 10^{-2})	DOCUMENT ID	TECN	COMMENT
2.4 ± 1.1 OUR AVERAGE			
2.5 ± 1.0 ± 0.5	¹ AAIJ	23AX	LHCB pp at 7, 8, 13 TeV
0 ± 8 ± 2	ADACHI	08	BELL $e^+e^- \rightarrow \Upsilon(4S)$
-13 ± 14 ± 2	AUBERT,B	06A	BABR $e^+e^- \rightarrow \Upsilon(4S)$

• • • We do not use the following data for averages, fits, limits, etc. • • •

2.3 ± 2.7 ± 0.4 AAIJ 18W LHCB Repl. by AAIJ 23AX
¹ The last error includes the uncertainty from $A_{CP}(B^+ \rightarrow J/\psi K^+)$.

 $A_{CP}(B^+ \rightarrow K_S^0 \pi^+)$

VALUE	DOCUMENT ID	TECN	COMMENT
-0.003 ± 0.015 OUR AVERAGE			
-0.046 ± 0.029 ± 0.007	ADACHI	24	BELL $e^+e^- \rightarrow \Upsilon(4S)$
-0.022 ± 0.025 ± 0.010	AAIJ	13Bs	LHCB pp at 7 TeV
-0.011 ± 0.021 ± 0.006	DUH	13	BELL $e^+e^- \rightarrow \Upsilon(4S)$
-0.029 ± 0.039 ± 0.010	¹ AUBERT, BE	06c	BABR $e^+e^- \rightarrow \Upsilon(4S)$
0.18 ± 0.24	² CHEN	00	CLE2 $e^+e^- \rightarrow \Upsilon(4S)$

Error includes scale factor of 1.1.

• • • We do not use the following data for averages, fits, limits, etc. • • •

0.03 ± 0.03 ± 0.01	LIN	07	BELL Repl. by DUH 13
-0.09 ± 0.05 ± 0.01	³ AUBERT, BE	05E	BABR Repl. by AUBERT, BE 06c
0.05 ± 0.05 ± 0.01	⁴ CHAO	05A	BELL Repl. by LIN 07
-0.05 ± 0.08 ± 0.01	⁵ AUBERT	04M	BABR Repl. by AUBERT, BE 05E
0.07 +0.09 +0.01 -0.08 -0.03	⁶ UNNO	03	BELL Repl. by CHAO 05A
0.46 ± 0.15 ± 0.02	⁷ CASEY	02	BELL Repl. by UNNO 03
0.098 +0.430 +0.020 -0.343 -0.063	⁸ ABE	01K	BELL Repl. by CASEY 02
-0.21 ± 0.18 ± 0.03	⁹ AUBERT	01E	BABR Repl. by AUBERT 04M

¹ Corresponds to 90% confidence range $-0.092 < A_{CP} < 0.036$.

² Corresponds to 90% confidence range $-0.22 < A_{CP} < 0.56$.

³ Corresponds to 90% confidence range $-0.16 < A_{CP} < -0.02$.

⁴ Corresponds to 90% confidence range $-0.04 < A_{CP} < 0.13$.

⁵ Corresponds to 90% confidence range $-0.18 < A_{CP} < 0.08$.

⁶ Corresponds to 90% confidence range $-0.10 < A_{CP} < +0.22$.

⁷ Corresponds to 90% confidence range $+0.19 < A_{CP} < +0.72$.

⁸ Corresponds to 90% confidence range $-0.53 < A_{CP} < 0.82$.

⁹ Corresponds to 90% confidence range $-0.51 < A_{CP} < 0.09$.

 $A_{CP}(B^+ \rightarrow K^+ \pi^0)$

VALUE	DOCUMENT ID	TECN	COMMENT
0.027 ± 0.012 OUR AVERAGE			
0.013 ± 0.027 ± 0.005	ADACHI	24	BELL $e^+e^- \rightarrow \Upsilon(4S)$
0.025 ± 0.015 ± 0.007	AAIJ	21H	LHCB pp at 13 TeV
0.043 ± 0.024 ± 0.002	DUH	13	BELL $e^+e^- \rightarrow \Upsilon(4S)$
0.030 ± 0.039 ± 0.010	AUBERT	07Bc	BABR $e^+e^- \rightarrow \Upsilon(4S)$
-0.29 ± 0.23	¹ CHEN	00	CLE2 $e^+e^- \rightarrow \Upsilon(4S)$

• • • We do not use the following data for averages, fits, limits, etc. • • •

0.07 ± 0.03 ± 0.01	LIN	08	BELL Repl. by DUH 13
0.06 ± 0.06 ± 0.01	² AUBERT	05L	BABR Repl. by AUBERT 07Bc
0.06 ± 0.06 ± 0.02	² CHAO	05A	BELL Repl. by CHAO 04B
0.04 ± 0.05 ± 0.02	³ CHAO	04B	BELL Repl. by LIN 08
-0.09 ± 0.09 ± 0.01	⁴ AUBERT	03L	BABR Repl. by AUBERT 05L
-0.02 ± 0.19 ± 0.02	⁵ CASEY	02	BELL Repl. by CHAO 04B
-0.059 +0.222 +0.055 -0.196 -0.017	⁶ ABE	01K	BELL Repl. by CASEY 02
0.00 ± 0.18 ± 0.04	⁷ AUBERT	01E	BABR Repl. by AUBERT 03L

¹ Corresponds to 90% confidence range $-0.67 < A_{CP} < 0.09$.

² Corresponds to a 90% CL interval of $-0.06 < A_{CP} < 0.18$.

³ Corresponds to 90% CL interval of $-0.05 < A_{CP} < 0.13$.

⁴ Corresponds to 90% confidence range $-0.24 < A_{CP} < 0.06$.

⁵ Corresponds to 90% confidence range $-0.35 < A_{CP} < +0.30$.

⁶ Corresponds to 90% confidence range $-0.40 < A_{CP} < 0.36$.

⁷ Corresponds to 90% confidence range $-0.30 < A_{CP} < +0.30$.

 $A_{CP}(B^+ \rightarrow \eta' K^+)$

VALUE	DOCUMENT ID	TECN	COMMENT
0.004 ± 0.011 OUR AVERAGE			
-0.002 ± 0.012 ± 0.006	¹ AAIJ	15o	LHCB pp at 7, 8 TeV
0.008 +0.017 -0.018	AUBERT	09AV	BABR $e^+e^- \rightarrow \Upsilon(4S)$
0.028 ± 0.028 ± 0.021	SCHUEMANN	06	BELL $e^+e^- \rightarrow \Upsilon(4S)$
0.03 ± 0.12	² CHEN	00	CLE2 $e^+e^- \rightarrow \Upsilon(4S)$

• • • We do not use the following data for averages, fits, limits, etc. • • •

0.010 ± 0.022 ± 0.006	AUBERT	07A	BABR Repl. by AUBERT 09AV
0.033 ± 0.028 ± 0.005	³ AUBERT	05M	BABR Repl. by AUBERT 07AE
0.037 ± 0.045 ± 0.011	⁴ AUBERT	03W	BABR Repl. by AUBERT 05M
-0.11 ± 0.11 ± 0.02	⁵ AUBERT	02E	BABR Repl. by AUBERT 05M
-0.015 ± 0.070 ± 0.009	⁶ CHEN	02b	BELL Repl. by SCHUEMANN 06
0.06 ± 0.15 ± 0.01	⁷ ABE	01M	BELL Repl. by CHEN 02B

¹ Obtained using $A_{CP}(B^\pm \rightarrow J/\psi K^\pm) = (0.3 \pm 0.6) \times 10^{-2}$.

² Corresponds to 90% confidence range $-0.17 < A_{CP} < 0.23$.

³ Corresponds to 90% confidence range $-0.012 < A_{CP} < 0.078$.

⁴ Corresponds to 90% confidence range $-0.04 < A_{CP} < 0.11$.

⁵ Corresponds to 90% confidence range $-0.28 < A_{CP} < 0.07$.

⁶ Corresponds to 90% confidence range $-0.13 < A_{CP} < 0.10$.

⁷ Corresponds to 90% confidence range $-0.20 < A_{CP} < 0.32$.

 $A_{CP}(B^+ \rightarrow \eta' K^*(892)^+)$

VALUE	DOCUMENT ID	TECN	COMMENT
-0.26 ± 0.27 ± 0.02			
-0.26 ± 0.27 ± 0.02	DEL-AMO-SA...	10A	BABR $e^+e^- \rightarrow \Upsilon(4S)$
-0.30 +0.33 -0.37	¹ AUBERT	07E	BABR Repl. by DEL-AMO-SANCHEZ 10A

¹ Reports A_{CP} with the opposite sign convention.

 $A_{CP}(B^+ \rightarrow \eta' K_S^0(1430)^+)$

VALUE	DOCUMENT ID	TECN	COMMENT
0.06 ± 0.20 ± 0.02			
0.06 ± 0.20 ± 0.02	DEL-AMO-SA...	10A	BABR $e^+e^- \rightarrow \Upsilon(4S)$

$A_{CP}(B^+ \rightarrow \eta' K_S^0(1430)^+)$

VALUE	DOCUMENT ID	TECN	COMMENT
$0.15 \pm 0.13 \pm 0.02$	DEL-AMO-SA...10A	BABR	$e^+ e^- \rightarrow \Upsilon(4S)$

 $A_{CP}(B^+ \rightarrow \eta K^+)$

VALUE	DOCUMENT ID	TECN	COMMENT
-0.37 ± 0.08 OUR AVERAGE			
$-0.38 \pm 0.11 \pm 0.01$	HOI	12	BELL $e^+ e^- \rightarrow \Upsilon(4S)$
$-0.36 \pm 0.11 \pm 0.03$	AUBERT	09AV	BABR $e^+ e^- \rightarrow \Upsilon(4S)$
• • • We do not use the following data for averages, fits, limits, etc. • • •			
$-0.22 \pm 0.11 \pm 0.01$	AUBERT	07AE	BABR Repl. by AUBERT 09AV
$-0.39 \pm 0.16 \pm 0.03$	CHANG	07B	BELL Repl. by HOI 12
$-0.20 \pm 0.15 \pm 0.01$	AUBERT,B	05K	BABR Repl. by AUBERT 07AE
$-0.49 \pm 0.31 \pm 0.07$	CHANG	05A	BELL Repl. by CHANG 07B
$-0.52 \pm 0.24 \pm 0.01$	AUBERT	04H	BABR Repl. by AUBERT,B 05K

 $A_{CP}(B^+ \rightarrow \eta K^*(892)^+)$

VALUE	DOCUMENT ID	TECN	COMMENT
0.02 ± 0.06 OUR AVERAGE			
$0.03 \pm 0.10 \pm 0.01$	WANG	07B	BELL $e^+ e^- \rightarrow \Upsilon(4S)$
$0.01 \pm 0.08 \pm 0.02$	AUBERT,B	06H	BABR $e^+ e^- \rightarrow \Upsilon(4S)$
• • • We do not use the following data for averages, fits, limits, etc. • • •			
$0.13 \pm 0.14 \pm 0.02$	AUBERT,B	04D	BABR Repl. by AUBERT,B 06H

 $A_{CP}(B^+ \rightarrow \eta K_0^0(1430)^+)$

VALUE	DOCUMENT ID	TECN	COMMENT
$0.05 \pm 0.13 \pm 0.02$	AUBERT,B	06H	BABR $e^+ e^- \rightarrow \Upsilon(4S)$

 $A_{CP}(B^+ \rightarrow \eta K_S^0(1430)^+)$

VALUE	DOCUMENT ID	TECN	COMMENT
$-0.45 \pm 0.30 \pm 0.02$	AUBERT,B	06H	BABR $e^+ e^- \rightarrow \Upsilon(4S)$

 $A_{CP}(B^+ \rightarrow \omega K^+)$

VALUE	DOCUMENT ID	TECN	COMMENT
-0.02 ± 0.04 OUR AVERAGE			
$-0.03 \pm 0.04 \pm 0.01$	CHOBANOVA	14	BELL $e^+ e^- \rightarrow \Upsilon(4S)$
$-0.01 \pm 0.07 \pm 0.01$	AUBERT	07AE	BABR $e^+ e^- \rightarrow \Upsilon(4S)$
• • • We do not use the following data for averages, fits, limits, etc. • • •			
$0.05 \pm 0.09 \pm 0.01$	AUBERT,B	06E	BABR Repl. by AUBERT 07AE
$0.05 \pm 0.08 \pm 0.01$	JEN	06	BELL Repl. by CHOBANOVA 14
$-0.09 \pm 0.17 \pm 0.01$	AUBERT	04H	BABR Repl. by AUBERT,B 06E
$0.06 \pm 0.21 \pm 0.01$	¹ WANG	04A	BELL Repl. by JEN 06
$-0.21 \pm 0.28 \pm 0.03$	² LU	02	BELL Repl. by WANG 04A

¹ Corresponds to 90% CL interval $0.15 < A_{CP} < 0.90$

² Corresponds to 90% confidence range $-0.70 < A_{CP} < +0.38$.

 $A_{CP}(B^+ \rightarrow \omega K^{*+})$

VALUE	DOCUMENT ID	TECN	COMMENT
$+0.29 \pm 0.35 \pm 0.02$	AUBERT	09H	BABR $e^+ e^- \rightarrow \Upsilon(4S)$

 $A_{CP}(B^+ \rightarrow \omega(K\pi)_0^{*+})$

VALUE	DOCUMENT ID	TECN	COMMENT
$-0.10 \pm 0.09 \pm 0.02$	AUBERT	09H	BABR $e^+ e^- \rightarrow \Upsilon(4S)$

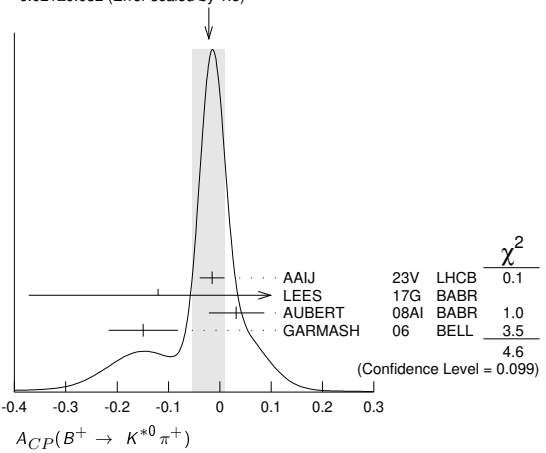
 $A_{CP}(B^+ \rightarrow \omega K_S^0(1430)^+)$

VALUE	DOCUMENT ID	TECN	COMMENT
$+0.14 \pm 0.15 \pm 0.02$	AUBERT	09H	BABR $e^+ e^- \rightarrow \Upsilon(4S)$

 $A_{CP}(B^+ \rightarrow K^{*0} \pi^+)$

VALUE	DOCUMENT ID	TECN	COMMENT
-0.021 ± 0.032 OUR AVERAGE			Error includes scale factor of 1.5. See the ideogram below.
$-0.015 \pm 0.021 \pm 0.012$	AAIJ	23V	LHCB pp at 13 TeV
$-0.12 \pm 0.21 \pm 0.08$	¹ LEES	17G	BABR $e^+ e^- \rightarrow \Upsilon(4S)$
$0.032 \pm 0.052 \pm 0.016$	AUBERT	08AI	BABR $e^+ e^- \rightarrow \Upsilon(4S)$
$-0.149 \pm 0.064 \pm 0.022$	GARMASH	06	BELL $e^+ e^- \rightarrow \Upsilon(4S)$
• • • We do not use the following data for averages, fits, limits, etc. • • •			
$0.068 \pm 0.078 \pm 0.070$	AUBERT,B	05N	BABR Repl. by AUBERT 08AI

¹ Obtains the result from a Dalitz analysis of $B^+ \rightarrow K_S^0 \pi^+ \pi^0$ decays. The first error is statistical, the second combines all the systematic uncertainties reported in the paper, including signal modelling.

WEIGHTED AVERAGE
 -0.021 ± 0.032 (Error scaled by 1.5) $A_{CP}(B^+ \rightarrow K^*(892)^+ \pi^0)$

VALUE	DOCUMENT ID	TECN	COMMENT
-0.39 ± 0.21 OUR AVERAGE			Error includes scale factor of 1.6.
$-0.52 \pm 0.14 \pm 0.06$	¹ LEES	17G	BABR $e^+ e^- \rightarrow \Upsilon(4S)$
$-0.06 \pm 0.24 \pm 0.04$	LEES	11I	BABR $e^+ e^- \rightarrow \Upsilon(4S)$
$0.04 \pm 0.29 \pm 0.05$	AUBERT	05X	BABR Repl. by LEES 11I

¹ Obtains the result from a Dalitz analysis of $B^+ \rightarrow K_S^0 \pi^+ \pi^0$ decays. The first error is statistical, the second combines all the systematic uncertainties reported in the paper, including signal modelling.

 $A_{CP}(B^+ \rightarrow K^+ \pi^- \pi^+)$

VALUE	DOCUMENT ID	TECN	COMMENT
0.015 ± 0.006 OUR AVERAGE			Error includes scale factor of 1.4.
$0.011 \pm 0.002 \pm 0.004$	¹ AAIJ	23U	LHCB pp at 13 TeV
$0.025 \pm 0.004 \pm 0.008$	¹ AAIJ	14B0	LHCB pp at 7, 8 TeV
$0.028 \pm 0.020 \pm 0.023$	AUBERT	08AI	BABR $e^+ e^- \rightarrow \Upsilon(4S)$
$0.049 \pm 0.026 \pm 0.020$	GARMASH	06	BELL $e^+ e^- \rightarrow \Upsilon(4S)$
• • • We do not use the following data for averages, fits, limits, etc. • • •			
$0.032 \pm 0.008 \pm 0.008$	AAIJ	13AZ	LHCB Repl. by AAIJ 14B0
$-0.013 \pm 0.037 \pm 0.011$	AUBERT,B	05N	BABR Repl. by AUBERT 08AI
$0.01 \pm 0.07 \pm 0.03$	AUBERT	03M	BABR Repl. by AUBERT,B 05N

¹ The second error includes both systematics and the uncertainties from CP asymmetries in restricted regions of phase space.

 $A_{CP}(B^+ \rightarrow K^+ K^- K^+ \text{ nonresonant})$

VALUE	DOCUMENT ID	TECN	COMMENT
$0.060 \pm 0.044 \pm 0.019$	LEES	120	BABR $e^+ e^- \rightarrow \Upsilon(4S)$

 $A_{CP}(B^+ \rightarrow f(980)^0 K^+)$

VALUE	DOCUMENT ID	TECN	COMMENT
$-0.08 \pm 0.08 \pm 0.04$	¹ LEES	120	BABR $e^+ e^- \rightarrow \Upsilon(4S)$

¹ Measured in the $B^+ \rightarrow K^+ K^- K^+$ decay.

 $A_{CP}(B^+ \rightarrow f_2(1270) K^+)$

VALUE	DOCUMENT ID	TECN	COMMENT
-0.68 ± 0.19 OUR AVERAGE			
$-0.85 \pm 0.22 \pm 0.26$	AUBERT	08AI	BABR $e^+ e^- \rightarrow \Upsilon(4S)$
$-0.59 \pm 0.22 \pm 0.036$	GARMASH	06	BELL $e^+ e^- \rightarrow \Upsilon(4S)$

 $A_{CP}(B^+ \rightarrow f_0(1500) K^+)$

VALUE	DOCUMENT ID	TECN	COMMENT
$0.28 \pm 0.26 \pm 0.15$ OUR AVERAGE			
$0.28 \pm 0.26 \pm 0.14$	AUBERT	08AI	BABR $e^+ e^- \rightarrow \Upsilon(4S)$

 $A_{CP}(B^+ \rightarrow f_2'(1525)^0 K^+)$

VALUE	DOCUMENT ID	TECN	COMMENT
-0.08 ± 0.05 OUR AVERAGE			
$0.18 \pm 0.18 \pm 0.04$	¹ LEES	11I	BABR $e^+ e^- \rightarrow \Upsilon(4S)$
$-0.106 \pm 0.050 \pm 0.036$	AUBERT	08AI	BABR $e^+ e^- \rightarrow \Upsilon(4S)$
$-0.077 \pm 0.065 \pm 0.046$	GARMASH	06	BELL $e^+ e^- \rightarrow \Upsilon(4S)$
• • • We do not use the following data for averages, fits, limits, etc. • • •			
$0.14 \pm 0.10 \pm 0.04$	² LEES	120	BABR $e^+ e^- \rightarrow \Upsilon(4S)$
$-0.31 \pm 0.25 \pm 0.08$	³ AUBERT	060	BABR Repl. by LEES 120
$0.088 \pm 0.095 \pm 0.097$	AUBERT,B	05N	BABR Repl. by AUBERT 08AI

¹ Measured in $B^+ \rightarrow f_0 K^+$ with $f_0 \rightarrow \pi^0 \pi^0$ decay.

² Measured in the $B^+ \rightarrow K^+ K^- K^+$ decay assuming $A_{CP}(B^+ \rightarrow f_2'(1525)^0 K^+) =$

$A_{CP}(B^+ \rightarrow f_0(1500)^0 K^+) = A_{CP}(B^+ \rightarrow f_0(1710)^0 K^+)$

³ Measured in the $B^+ \rightarrow K^+ K^- K^+$ decay.

Meson Particle Listings

 B^\pm $A_{CP}(B^+ \rightarrow \rho^0 K^+)$

VALUE	DOCUMENT ID	TECN	COMMENT
0.160 ± 0.021 OUR AVERAGE			
0.150 ± 0.019 ± 0.011	AAIJ	23v	LHCB pp at 13 TeV
0.44 ± 0.10 $^{+0.06}_{-0.14}$	AUBERT	08aI	BABR $e^+e^- \rightarrow \Upsilon(4S)$
0.30 ± 0.11 $^{+0.11}_{-0.04}$	GARMASH	06	BELL $e^+e^- \rightarrow \Upsilon(4S)$
• • • We do not use the following data for averages, fits, limits, etc. • • •			
0.32 ± 0.13 $^{+0.10}_{-0.08}$	AUBERT,B	05N	BABR Repl. by AUBERT 08aI

 $A_{CP}(B^+ \rightarrow K^0 \pi^+ \pi^0)$

VALUE	DOCUMENT ID	TECN	COMMENT
0.07 ± 0.05 ± 0.04	¹ LEES	17G	BABR $e^+e^- \rightarrow \Upsilon(4S)$
¹ Obtains the result from a Dalitz analysis of $B^+ \rightarrow K_S^0 \pi^+ \pi^0$ decays. The first error is statistical, the second combines all the systematic uncertainties reported in the paper, including signal modelling.			

 $A_{CP}(B^+ \rightarrow K_S^0(1430)^0 \pi^+)$

VALUE	DOCUMENT ID	TECN	COMMENT
0.061 ± 0.032 OUR AVERAGE			
0.14 ± 0.10 $^{+0.14}_{-0.06}$	¹ LEES	17G	BABR $e^+e^- \rightarrow \Upsilon(4S)$
0.032 ± 0.035 $^{+0.034}_{-0.028}$	AUBERT	08aI	BABR $e^+e^- \rightarrow \Upsilon(4S)$
0.076 ± 0.038 $^{+0.028}_{-0.022}$	GARMASH	06	BELL $e^+e^- \rightarrow \Upsilon(4S)$
• • • We do not use the following data for averages, fits, limits, etc. • • •			
-0.064 ± 0.032 $^{+0.023}_{-0.026}$	AUBERT,B	05N	BABR Repl. by AUBERT 08aI

¹ Obtains the result from a Dalitz analysis of $B^+ \rightarrow K_S^0 \pi^+ \pi^0$ decays. The first error is statistical, the second combines all the systematic uncertainties reported in the paper, including signal modelling.

 $A_{CP}(B^+ \rightarrow K_S^0(1430)^+ \pi^0)$

VALUE	DOCUMENT ID	TECN	COMMENT
0.26 ± 0.12 $^{+0.14}_{-0.08}$	¹ LEES	17G	BABR $e^+e^- \rightarrow \Upsilon(4S)$

¹ Obtains the result from a Dalitz analysis of $B^+ \rightarrow K_S^0 \pi^+ \pi^0$ decays. The first error is statistical, the second combines all the systematic uncertainties reported in the paper, including signal modelling.

 $A_{CP}(B^+ \rightarrow K_2^+(1430)^0 \pi^+)$

VALUE	DOCUMENT ID	TECN	COMMENT
0.05 ± 0.23 $^{+0.18}_{-0.08}$	AUBERT	08aI	BABR $e^+e^- \rightarrow \Upsilon(4S)$

 $A_{CP}(B^+ \rightarrow K^+ \pi^0 \pi^0)$

VALUE	DOCUMENT ID	TECN	COMMENT
-0.06 ± 0.06 ± 0.04	LEES	11i	BABR $e^+e^- \rightarrow \Upsilon(4S)$

 $A_{CP}(B^+ \rightarrow K^0 \rho^+)$

VALUE	DOCUMENT ID	TECN	COMMENT
-0.03 ± 0.15 OUR AVERAGE			
0.21 ± 0.19 $^{+0.24}_{-0.20}$	¹ LEES	17G	BABR $e^+e^- \rightarrow \Upsilon(4S)$
-0.12 ± 0.17 ± 0.02	AUBERT	07z	BABR $e^+e^- \rightarrow \Upsilon(4S)$

¹ Obtains the result from a Dalitz analysis of $B^+ \rightarrow K_S^0 \pi^+ \pi^0$ decays. The first error is statistical, the second combines all the systematic uncertainties reported in the paper, including signal modelling.

 $A_{CP}(B^+ \rightarrow K^{*+} \pi^+ \pi^-)$

VALUE	DOCUMENT ID	TECN	COMMENT
0.07 ± 0.07 ± 0.04	AUBERT,B	06u	BABR $e^+e^- \rightarrow \Upsilon(4S)$

 $A_{CP}(B^+ \rightarrow \rho^0 K^*(892)^+)$

VALUE	DOCUMENT ID	TECN	COMMENT
0.31 ± 0.13 ± 0.03	DEL-AMO-SA...11d	BABR	$e^+e^- \rightarrow \Upsilon(4S)$
• • • We do not use the following data for averages, fits, limits, etc. • • •			
0.20 $^{+0.32}_{-0.29}$ ± 0.04	AUBERT	03v	BABR Repl. by DEL-AMO-SANCHEZ 11d

 $A_{CP}(B^+ \rightarrow K^*(892)^+ f_0(980))$

VALUE	DOCUMENT ID	TECN	COMMENT
-0.15 ± 0.12 ± 0.03	DEL-AMO-SA...11d	BABR	$e^+e^- \rightarrow \Upsilon(4S)$
• • • We do not use the following data for averages, fits, limits, etc. • • •			
-0.34 ± 0.21 ± 0.03	AUBERT,B	06g	BABR Repl. by DEL-AMO-SANCHEZ 11d

 $A_{CP}(B^+ \rightarrow a_1^+ K^0)$

VALUE	DOCUMENT ID	TECN	COMMENT
+0.12 ± 0.11 ± 0.02	AUBERT	08f	BABR $e^+e^- \rightarrow \Upsilon(4S)$

 $A_{CP}(B^+ \rightarrow b_1^+ K^0)$

VALUE	DOCUMENT ID	TECN	COMMENT
-0.03 ± 0.15 ± 0.02	AUBERT	08aG	BABR $e^+e^- \rightarrow \Upsilon(4S)$

 $A_{CP}(B^+ \rightarrow K^*(892)^0 \rho^+)$

VALUE	DOCUMENT ID	TECN	COMMENT
-0.01 ± 0.16 ± 0.02	AUBERT,B	06g	BABR $e^+e^- \rightarrow \Upsilon(4S)$

 $A_{CP}(B^+ \rightarrow b_1^0 K^+)$

VALUE	DOCUMENT ID	TECN	COMMENT
-0.46 ± 0.20 ± 0.02	AUBERT	07Bi	BABR $e^+e^- \rightarrow \Upsilon(4S)$

 $A_{CP}(B^+ \rightarrow K^0 K^+)$

VALUE	DOCUMENT ID	TECN	COMMENT
0.04 ± 0.14 OUR AVERAGE			
0.014 ± 0.168 ± 0.002	DUH	13	BELL $e^+e^- \rightarrow \Upsilon(4S)$
0.10 ± 0.26 ± 0.03	¹ AUBERT,BE	06c	BABR $e^+e^- \rightarrow \Upsilon(4S)$
• • • We do not use the following data for averages, fits, limits, etc. • • •			
0.13 $^{+0.23}_{-0.24}$ ± 0.02	LIN	07	BELL Repl. by DUH 13
0.15 ± 0.33 ± 0.03	² AUBERT,BE	05E	BABR Repl. by AUBERT,BE 06c
¹ Corresponds to 90% confidence range $-0.31 < A_{CP} < 0.54$.			
² Corresponds to 90% confidence range $-0.43 < A_{CP} < 0.68$.			

 $A_{CP}(B^+ \rightarrow K_S^0 K^+)$

VALUE	DOCUMENT ID	TECN	COMMENT
-0.21 ± 0.14 ± 0.01	AAIJ	13Bs	LHCB pp at 7 TeV

 $A_{CP}(B^+ \rightarrow K^+ K_S^0 K_S^0)$

VALUE	DOCUMENT ID	TECN	COMMENT
0.025 ± 0.031 OUR AVERAGE			
0.016 ± 0.039 ± 0.009	KALIYAR	19	BELL $e^+e^- \rightarrow \Upsilon(4S)$
0.04 $^{+0.04}_{-0.05}$ ± 0.02	LEES	12o	BABR $e^+e^- \rightarrow \Upsilon(4S)$
• • • We do not use the following data for averages, fits, limits, etc. • • •			
-0.04 ± 0.11 ± 0.02	¹ AUBERT,B	04v	BABR Repl. by LEES 12o
¹ Corresponds to 90% confidence range $-0.23 < A_{CP} < 0.15$.			

 $A_{CP}(B^+ \rightarrow K^+ K^- \pi^+)$

VALUE	DOCUMENT ID	TECN	COMMENT
-0.115 ± 0.008 OUR AVERAGE			
-0.114 ± 0.007 ± 0.004	¹ AAIJ	23u	LHCB pp at 13 TeV
-0.170 ± 0.073 ± 0.017	² HSU	17	BELL $e^+e^- \rightarrow \Upsilon(4S)$
-0.123 ± 0.017 ± 0.014	¹ AAIJ	14Bo	LHCB pp at 7, 8 TeV
0.00 ± 0.10 ± 0.03	AUBERT	07Bb	BABR $e^+e^- \rightarrow \Upsilon(4S)$
• • • We do not use the following data for averages, fits, limits, etc. • • •			
-0.141 ± 0.040 ± 0.019	³ AAIJ	14	LHCB Repl. by AAIJ 14Bo

¹ The second error includes both systematics and the uncertainties from CP asymmetries in restricted regions of phase space.
² HSU 17 provides also measurement as a function of $K^+ K^-$ invariant mass.
³ AAIJ 14 reports $A_{CP}(B^+ \rightarrow K^+ K^- \pi^+) = -0.648 \pm 0.070 \pm 0.013 \pm 0.007$ in the Dalitz plot region of $m_{K^+ K^-}^2 < 1.5 \text{ GeV}^2/c^4$. The third uncertainty is due to the CP asymmetry of the $B^\pm \rightarrow J/\psi K^\pm$ reference mode uncertainty.

 $A_{CP}(B^+ \rightarrow K^+ K^- \pi^+ \text{ nonresonant})$

VALUE	DOCUMENT ID	TECN	COMMENT
-0.107 ± 0.053 ± 0.035	¹ AAIJ	19AL	LHCB pp at 7, 8 TeV
¹ Uses amplitude analysis of $B^\pm \rightarrow \pi^\pm K^+ K^-$ decays.			

 $A_{CP}(B^+ \rightarrow \pi^+ K^+ K^-, m_{K^+ K^-} < 1.1 \text{ GeV})$

VALUE	DOCUMENT ID	TECN	COMMENT
-0.170 ± 0.073 ± 0.017	¹ HSU	23	BELL $e^+e^- \rightarrow \Upsilon(4S)$
¹ Investigated the angular distribution of $K^+ K^-$ pairs with invariant mass below 1.1 GeV/c^2 , which exhibits both a strong enhancement in signal and very large direct CP violation.			

 $A_{CP}(B^+ \rightarrow K^+ \bar{K}^*(892)^0)$

VALUE	DOCUMENT ID	TECN	COMMENT
0.04 ± 0.05 OUR AVERAGE			
0.007 ± 0.054 ± 0.032	AAIJ	23v	LHCB pp at 13 TeV
0.123 ± 0.087 ± 0.045	¹ AAIJ	19AL	LHCB pp at 7, 8 TeV
¹ Uses amplitude analysis of $B^\pm \rightarrow \pi^\pm K^+ K^-$ decays.			

 $A_{CP}(B^+ \rightarrow K^+ \bar{K}_0^*(1430)^0)$

VALUE	DOCUMENT ID	TECN	COMMENT
0.104 ± 0.149 ± 0.088	¹ AAIJ	19AL	LHCB pp at 7, 8 TeV
¹ Uses amplitude analysis of $B^\pm \rightarrow \pi^\pm K^+ K^-$ decays.			

 $A_{CP}(B^+ \rightarrow \phi \pi^+)$

VALUE	DOCUMENT ID	TECN	COMMENT
0.098 ± 0.436 ± 0.266	¹ AAIJ	19AL	LHCB pp at 7, 8 TeV
¹ Uses amplitude analysis of $B^\pm \rightarrow \pi^\pm K^+ K^-$ decays.			

 $A_{CP}(B^+ \rightarrow \pi^+ (K^+ K^-)_{S\text{-wave}})$

VALUE	DOCUMENT ID	TECN	COMMENT
-0.664 ± 0.038 ± 0.019	¹ AAIJ	19AL	LHCB pp at 7, 8 TeV
¹ Uses amplitude analysis of $B^\pm \rightarrow \pi^\pm K^+ K^-$ decays in the $\pi\pi - KK$ rescattering mass region of $0.95 < m(K^+ K^-) < 1.42 \text{ GeV}/c^2$.			

$A_{CP}(B^+ \rightarrow K^+ K^- K^+)$

VALUE	DOCUMENT ID	TECN	COMMENT
-0.036 ± 0.004 OUR AVERAGE			
$-0.037 \pm 0.002 \pm 0.004$	¹ AAIJ	23u LHCb	pp at 13 TeV
$-0.036 \pm 0.004 \pm 0.007$	¹ AAIJ	14Bo LHCb	pp at 7, 8 TeV
$-0.017 \pm 0.019 \pm 0.014$	² LEES	12o BABR	$e^+ e^- \rightarrow \Upsilon(4S)$

• • • We do not use the following data for averages, fits, limits, etc. • • •

$-0.043 \pm 0.009 \pm 0.008$	AAIJ	13Az LHCb	Repl. by AAIJ 14Bo
$-0.017 \pm 0.026 \pm 0.015$	AUBERT	06o BABR	Repl. by LEES 12o
$0.02 \pm 0.07 \pm 0.03$	AUBERT	03M BABR	Repl. by AUBERT 06o

¹ The second error includes both systematics and the uncertainties from CP asymmetries in restricted regions of phase space.
² All intermediate charmonium and charm resonances are removed, except of χ_{c0} .

 $A_{CP}(B^+ \rightarrow \phi K^+)$

VALUE	DOCUMENT ID	TECN	COMMENT
0.017 ± 0.017 OUR AVERAGE	Error includes scale factor of 1.8. See the ideogram below.		
$0.004 \pm 0.014 \pm 0.007$	AAIJ	23v LHCb	pp at 13 TeV
$0.017 \pm 0.011 \pm 0.006$	¹ AAIJ	15o LHCb	pp at 7, 8 TeV
$0.128 \pm 0.044 \pm 0.013$	LEES	12o BABR	$e^+ e^- \rightarrow \Upsilon(4S)$
$-0.07 \pm 0.17 \pm 0.03$	ACOSTA	05J CDF	$p\bar{p}$ at 1.96 TeV
$0.01 \pm 0.12 \pm 0.05$	² CHEN	03B BELL	$e^+ e^- \rightarrow \Upsilon(4S)$

• • • We do not use the following data for averages, fits, limits, etc. • • •

$0.022 \pm 0.021 \pm 0.009$	AAIJ	14A LHCb	Repl. by AAIJ 15o
$0.00 \pm 0.08 \pm 0.02$	AUBERT	06o BABR	Repl. by LEES 12o
$0.04 \pm 0.09 \pm 0.01$	³ AUBERT	04A BABR	Repl. by AUBERT 06o
$-0.05 \pm 0.20 \pm 0.03$	⁴ AUBERT	02E BABR	$e^+ e^- \rightarrow \Upsilon(4S)$

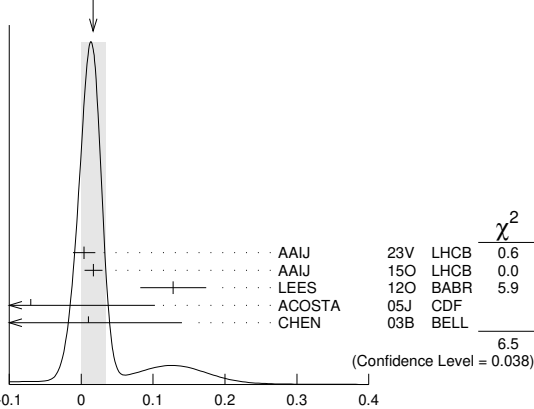
¹ Obtained using $A_{CP}(B^\pm \rightarrow J/\psi K^\pm) = (0.3 \pm 0.6) \times 10^{-2}$.

² Corresponds to 90% confidence range $-0.20 < A_{CP} < 0.22$.

³ Corresponds to 90% confidence range $-0.10 < A_{CP} < 0.18$.

⁴ Corresponds to 90% confidence range $-0.37 < A_{CP} < 0.28$.

WEIGHTED AVERAGE
 0.017 ± 0.017 (Error scaled by 1.8)



$A_{CP}(B^+ \rightarrow \phi K^+)$

 $A_{CP}(B^+ \rightarrow X_0(1550) K^+)$

VALUE	DOCUMENT ID	TECN	COMMENT
$-0.04 \pm 0.07 \pm 0.02$	¹ AUBERT	06o BABR	$e^+ e^- \rightarrow \Upsilon(4S)$

¹ Measured in the $B^+ \rightarrow K^+ K^- K^+$ decay.

 $A_{CP}(B^+ \rightarrow K^{*+} K^+ K^-)$

VALUE	DOCUMENT ID	TECN	COMMENT
$0.11 \pm 0.08 \pm 0.03$	AUBERT,B	06u BABR	$e^+ e^- \rightarrow \Upsilon(4S)$

 $A_{CP}(B^+ \rightarrow \phi K^*(892)^+)$

VALUE	DOCUMENT ID	TECN	COMMENT
-0.01 ± 0.08 OUR AVERAGE			
$0.00 \pm 0.09 \pm 0.04$	AUBERT	07Ba BABR	$e^+ e^- \rightarrow \Upsilon(4S)$
$-0.02 \pm 0.14 \pm 0.03$	¹ CHEN	05A BELL	$e^+ e^- \rightarrow \Upsilon(4S)$

• • • We do not use the following data for averages, fits, limits, etc. • • •

$0.16 \pm 0.17 \pm 0.03$	AUBERT	03v BABR	Repl. by AUBERT 07Ba
$-0.13 \pm 0.29 \pm 0.08$	² CHEN	03B BELL	Repl. by CHEN 05A
$-0.43 \pm 0.30 \pm 0.06$	³ AUBERT	02E BABR	Repl. by AUBERT 03v

¹ Corresponds to 90% confidence range $-0.25 < A_{CP} < 0.22$.

² Corresponds to 90% confidence range $-0.64 < A_{CP} < 0.36$.

³ Corresponds to 90% confidence range $-0.88 < A_{CP} < 0.18$.

 $A_{CP}(B^+ \rightarrow \phi(K\pi)_0^{*+})$

VALUE	DOCUMENT ID	TECN	COMMENT
$0.04 \pm 0.15 \pm 0.04$	AUBERT	08Bi BABR	$e^+ e^- \rightarrow \Upsilon(4S)$

 $A_{CP}(B^+ \rightarrow \phi K_1(1270)^+)$

VALUE	DOCUMENT ID	TECN	COMMENT
$0.15 \pm 0.19 \pm 0.05$	AUBERT	08Bi BABR	$e^+ e^- \rightarrow \Upsilon(4S)$

 $A_{CP}(B^+ \rightarrow \phi K_2^*(1430)^+)$

VALUE	DOCUMENT ID	TECN	COMMENT
$-0.23 \pm 0.19 \pm 0.06$	AUBERT	08Bi BABR	$e^+ e^- \rightarrow \Upsilon(4S)$

 $A_{CP}(B^+ \rightarrow K^+ \phi\phi)$

VALUE	DOCUMENT ID	TECN	COMMENT
-0.08 ± 0.07 OUR AVERAGE			
$0.12 \pm 0.12 \pm 0.11$	¹ MOHANTY	21 BELL	$e^+ e^- \rightarrow \Upsilon(4S)$
$-0.10 \pm 0.08 \pm 0.02$	¹ LEES	11A BABR	$e^+ e^- \rightarrow \Upsilon(4S)$

¹ Assumes $m_{\phi\phi} < 2.85$ GeV/ c^2 .

 $A_{CP}(B^+ \rightarrow K^+[\phi\phi]\eta_c)$

VALUE	DOCUMENT ID	TECN	COMMENT
0.10 ± 0.08 OUR AVERAGE			
$0.12 \pm 0.12 \pm 0.01$	¹ MOHANTY	21 BELL	$e^+ e^- \rightarrow \Upsilon(4S)$
$0.09 \pm 0.10 \pm 0.02$	¹ LEES	11A BABR	$e^+ e^- \rightarrow \Upsilon(4S)$

¹ $m_{\phi\phi}$ is consistent with η_c mass in [2.94, 3.02] GeV/ c^2 .

 $A_{CP}(B^+ \rightarrow K^*(892)^+ \gamma)$

VALUE	DOCUMENT ID	TECN	COMMENT
0.014 ± 0.018 OUR AVERAGE			
$0.011 \pm 0.023 \pm 0.003$	¹ HORIGUCHI	17 BELL	$e^+ e^- \rightarrow \Upsilon(4S)$
$0.018 \pm 0.028 \pm 0.007$	AUBERT	09Ao BABR	$e^+ e^- \rightarrow \Upsilon(4S)$

¹ Uses $B(\Upsilon(4S) \rightarrow B^+ B^-) = (51.4 \pm 0.6)\%$ and $B(\Upsilon(4S) \rightarrow B^0 \bar{B}^0) = (48.6 \pm 0.6)\%$.

 $A_{CP}(B^+ \rightarrow X_s \gamma)$

VALUE	DOCUMENT ID	TECN	COMMENT
$0.0275 \pm 0.0184 \pm 0.0032$	¹ WATANUKI	19 BELL	$e^+ e^- \rightarrow \Upsilon(4S)$

¹ Using a sum-of-exclusive technique with $m_{X_s} < 2.8$ GeV/ c^2 .

 $A_{CP}(B^+ \rightarrow \eta K^+ \gamma)$

VALUE	DOCUMENT ID	TECN	COMMENT
-0.12 ± 0.07 OUR AVERAGE			
$-0.09 \pm 0.10 \pm 0.01$	¹ AUBERT	09 BABR	$e^+ e^- \rightarrow \Upsilon(4S)$
$-0.16 \pm 0.09 \pm 0.06$	² NISHIDA	05 BELL	$e^+ e^- \rightarrow \Upsilon(4S)$

• • • We do not use the following data for averages, fits, limits, etc. • • •

$-0.09 \pm 0.12 \pm 0.01$	¹ AUBERT,B	06M BABR	Repl. by AUBERT 09
---------------------------	-----------------------	----------	--------------------

¹ $m_{\eta K} < 3.25$ GeV/ c^2 .

² $m_{\eta K} < 2.4$ GeV/ c^2 .

 $A_{CP}(B^+ \rightarrow \phi K^+ \gamma)$

VALUE	DOCUMENT ID	TECN	COMMENT
-0.13 ± 0.11 OUR AVERAGE	Error includes scale factor of 1.1.		
$-0.03 \pm 0.11 \pm 0.08$	SAHOO	11A BELL	$e^+ e^- \rightarrow \Upsilon(4S)$
$-0.26 \pm 0.14 \pm 0.05$	AUBERT	07Q BABR	$e^+ e^- \rightarrow \Upsilon(4S)$

 $A_{CP}(B^+ \rightarrow \rho^+ \gamma)$

VALUE	DOCUMENT ID	TECN	COMMENT
$-0.11 \pm 0.32 \pm 0.09$	TANIGUCHI	08 BELL	$e^+ e^- \rightarrow \Upsilon(4S)$

 $A_{CP}(B^+ \rightarrow \pi^+ \pi^0)$

VALUE	DOCUMENT ID	TECN	COMMENT
-0.01 ± 0.04 OUR AVERAGE	Error includes scale factor of 1.1.		
$-0.081 \pm 0.054 \pm 0.008$	ADACHI	24 BELL	$e^+ e^- \rightarrow \Upsilon(4S)$
$0.025 \pm 0.043 \pm 0.007$	DUH	13 BELL	$e^+ e^- \rightarrow \Upsilon(4S)$
$0.03 \pm 0.08 \pm 0.01$	AUBERT	07Bc BABR	$e^+ e^- \rightarrow \Upsilon(4S)$

• • • We do not use the following data for averages, fits, limits, etc. • • •

$0.07 \pm 0.06 \pm 0.01$	LIN	08 BELL	Repl. by DUH 13
$-0.01 \pm 0.10 \pm 0.02$	¹ AUBERT	05L BABR	Repl. by AUBERT 07Bc
$0.00 \pm 0.10 \pm 0.02$	² CHAO	05A BELL	Repl. by CHAO 04B
$-0.02 \pm 0.10 \pm 0.01$	³ CHAO	04B BELL	Repl. by LIN 08
$-0.03 \pm 0.18 \pm 0.02$	⁴ AUBERT	03L BABR	Repl. by AUBERT 05L
$0.30 \pm 0.30 \pm 0.06$	⁵ CASEY	02 BELL	Repl. by CHAO 04B

¹ Corresponds to a 90% CL interval of $-0.19 < A_{CP} < 0.21$.

² Corresponds to a 90% CL interval of $-0.17 < A_{CP} < 0.16$.

³ This corresponds to 90% CL interval of $-0.18 < A_{CP} < 0.14$.

⁴ Corresponds to 90% confidence range $-0.32 < A_{CP} < 0.27$.

⁵ Corresponds to 90% confidence range $-0.23 < A_{CP} < +0.86$.

Meson Particle Listings

 B^\pm $A_{CP}(B^+ \rightarrow \pi^+ \pi^- \pi^+)$

VALUE	DOCUMENT ID	TECN	COMMENT
0.076 ± 0.008 OUR AVERAGE	Error includes scale factor of 1.5.		
0.080 ± 0.004 ± 0.004	¹ AAIJ	23u	LHCb pp at 13 TeV
0.058 ± 0.008 ± 0.011	¹ AAIJ	14Bo	LHCb pp at 7, 8 TeV
0.032 ± 0.044 $^{+0.040}_{-0.037}$	AUBERT	09L	BABR $e^+e^- \rightarrow \Upsilon(4S)$

••• We do not use the following data for averages, fits, limits, etc. •••

0.117 ± 0.021 ± 0.011	² AAIJ	14	LHCb Repl. by AAJ 14Bo
-0.007 ± 0.077 ± 0.025	AUBERT,B	05G	BABR Repl. by AUBERT 09L
-0.39 ± 0.33 ± 0.12	AUBERT	03M	BABR Repl. by AUBERT 05G

¹The second error includes both systematics and the uncertainties from CP asymmetries in restricted regions of phase space.

²AAIJ 14 reports $A_{CP}(B^+ \rightarrow \pi^+ \pi^- \pi^+) = 0.584 \pm 0.082 \pm 0.027 \pm 0.007$ in the Dalitz plot region of $m^2_{\pi^+ \pi^-} > 15 \text{ GeV}^2/c^4$ or $m^2_{\pi^+ \pi^-} < 0.4 \text{ GeV}^2/c^4$. The third uncertainty is due to the CP asymmetry of the $B^\pm \rightarrow J/\psi K^\pm$ reference mode uncertainty.

 $A_{CP}(B^+ \rightarrow \pi^+ \pi^0 \pi^0)$

VALUE (units 10^{-2})	DOCUMENT ID	TECN	COMMENT
9.2 ± 6.8 ± 0.7	LAI	23	BELL $e^+e^- \rightarrow \Upsilon(4S)$

 $A_{CP}(B^+ \rightarrow \rho^0 \pi^+)$

VALUE	DOCUMENT ID	TECN	COMMENT
0.003 ± 0.014 OUR AVERAGE			
-0.004 ± 0.017 ± 0.009	AAIJ	23v	LHCb pp at 13 TeV
0.007 ± 0.011 ± 0.016	¹ AAIJ	20A	LHCb pp at 7, 8 TeV
0.18 ± 0.07 $^{+0.05}_{-0.15}$	AUBERT	09L	BABR $e^+e^- \rightarrow \Upsilon(4S)$

••• We do not use the following data for averages, fits, limits, etc. •••

-0.074 ± 0.120 $^{+0.035}_{-0.055}$	AUBERT,B	05G	BABR Repl. by AUBERT 09L
-0.19 ± 0.11 ± 0.02	AUBERT	04z	BABR Repl. by AUBERT,B 05G

¹This result is obtained with an amplitude analysis of $B^+ \rightarrow \pi^+ \pi^+ \pi^-$ decays, using the isobar model within the mass range $1.0 < m(\pi^+ \pi^-) < 1.5 \text{ GeV}$ to describe the $\pi^+ \pi^-$ S -wave contribution.

 $A_{CP}(B^+ \rightarrow f_2(1270) \pi^+)$

VALUE	DOCUMENT ID	TECN	COMMENT
0.40 ± 0.06 OUR AVERAGE			
0.468 ± 0.061 ± 0.046	¹ AAIJ	20A	LHCb pp at 7, 8 TeV
0.267 ± 0.102 ± 0.048	² AAIJ	19AL	LHCb pp at 7, 8 TeV
0.41 ± 0.25 $^{+0.18}_{-0.15}$	AUBERT	09L	BABR $e^+e^- \rightarrow \Upsilon(4S)$

••• We do not use the following data for averages, fits, limits, etc. •••

-0.004 ± 0.247 $^{+0.028}_{-0.032}$	AUBERT,B	05G	BABR Repl. by AUBERT 09L
-------------------------------------	----------	-----	--------------------------

¹This result is obtained with an amplitude analysis of $B^+ \rightarrow \pi^+ \pi^+ \pi^-$ decays, using the isobar model within the mass range $1.0 < m(\pi^+ \pi^-) < 1.5 \text{ GeV}$ to describe the $\pi^+ \pi^-$ S -wave contribution.

²Uses amplitude analysis of $B^\pm \rightarrow \pi^\pm K^+ K^-$ decays.

 $A_{CP}(B^+ \rightarrow \rho^0(1450) \pi^+)$

VALUE	DOCUMENT ID	TECN	COMMENT
-0.11 ± 0.05 OUR AVERAGE			
-0.129 ± 0.033 ± 0.359	¹ AAIJ	20A	LHCb pp at 7, 8 TeV
-0.109 ± 0.044 ± 0.024	² AAIJ	19AL	LHCb pp at 7, 8 TeV
-0.06 ± 0.28 $^{+0.23}_{-0.40}$	AUBERT	09L	BABR $e^+e^- \rightarrow \Upsilon(4S)$

¹This result is obtained with an amplitude analysis of $B^+ \rightarrow \pi^+ \pi^+ \pi^-$ decays, using the isobar model within the mass range $1.0 < m(\pi^+ \pi^-) < 1.5 \text{ GeV}$ to describe the $\pi^+ \pi^-$ S -wave contribution.

²Uses amplitude analysis of $B^\pm \rightarrow \pi^\pm K^+ K^-$ decays.

 $A_{CP}(B^+ \rightarrow \rho_3(1690) \pi^+)$

VALUE	DOCUMENT ID	TECN	COMMENT
-0.801 ± 0.114 ± 0.253	¹ AAIJ	20A	LHCb pp at 7, 8 TeV

¹This result is obtained with an amplitude analysis of $B^+ \rightarrow \pi^+ \pi^+ \pi^-$ decays, using the isobar model within the mass range $1.0 < m(\pi^+ \pi^-) < 1.5 \text{ GeV}$ to describe the $\pi^+ \pi^-$ S -wave contribution.

 $A_{CP}(B^+ \rightarrow f_0(1370) \pi^+)$

VALUE	DOCUMENT ID	TECN	COMMENT
0.72 ± 0.15 ± 0.16	AUBERT	09L	BABR $e^+e^- \rightarrow \Upsilon(4S)$

 $A_{CP}(B^+ \rightarrow \pi^+ \pi^- \pi^+ \text{ nonresonant})$

VALUE	DOCUMENT ID	TECN	COMMENT
-0.14 ± 0.14 $^{+0.18}_{-0.08}$	AUBERT	09L	BABR $e^+e^- \rightarrow \Upsilon(4S)$

 $A_{CP}(B^+ \rightarrow \rho^+ \pi^0)$

VALUE	DOCUMENT ID	TECN	COMMENT
0.03 ± 0.10 OUR AVERAGE			
0.080 ± 0.150 $^{+0.023}_{-0.075}$	LAI	23	BELL $e^+e^- \rightarrow \Upsilon(4S)$
-0.01 ± 0.13 ± 0.02	AUBERT	07X	BABR $e^+e^- \rightarrow \Upsilon(4S)$

••• We do not use the following data for averages, fits, limits, etc. •••

0.06 ± 0.17 $^{+0.04}_{-0.05}$	ZHANG	05A	BELL Repl. by LAI 23
0.24 ± 0.16 ± 0.06	AUBERT	04z	BABR Repl. by AUBERT 07X

 $A_{CP}(B^+ \rightarrow X \pi^+, X \rightarrow \pi^0 \pi^0)$

VALUE	DOCUMENT ID	TECN	COMMENT
0.182 ± 0.116 ± 0.007	LAI	23	BELL $e^+e^- \rightarrow \Upsilon(4S)$

 $A_{CP}(B^+ \rightarrow \rho^+ \rho^0)$

VALUE	DOCUMENT ID	TECN	COMMENT
-0.05 ± 0.05 OUR AVERAGE			
-0.054 ± 0.055 ± 0.010	AUBERT	09G	BABR $e^+e^- \rightarrow \Upsilon(4S)$
0.00 ± 0.22 ± 0.03	ZHANG	03B	BELL $e^+e^- \rightarrow \Upsilon(4S)$

••• We do not use the following data for averages, fits, limits, etc. •••

-0.12 ± 0.13 ± 0.10	AUBERT,BE	06G	BABR Repl. by AUBERT 09G
-0.19 ± 0.23 ± 0.03	AUBERT	03v	BABR Repl. by AUBERT,BE 06G

 $A_{CP}(B^+ \rightarrow \omega \pi^+)$

VALUE	DOCUMENT ID	TECN	COMMENT
-0.04 ± 0.05 OUR AVERAGE			
-0.048 ± 0.065 ± 0.038	¹ AAIJ	20A	LHCb pp at 7, 8 TeV
-0.02 ± 0.08 ± 0.01	AUBERT	07AE	BABR $e^+e^- \rightarrow \Upsilon(4S)$
-0.02 ± 0.09 ± 0.01	JEN	06	BELL $e^+e^- \rightarrow \Upsilon(4S)$
-0.34 ± 0.25	² CHEN	00	CLE2 $e^+e^- \rightarrow \Upsilon(4S)$

••• We do not use the following data for averages, fits, limits, etc. •••

-0.01 ± 0.10 ± 0.01	AUBERT,B	06E	BABR Repl. by AUBERT 07AE
0.03 ± 0.16 ± 0.01	AUBERT	04H	BABR Repl. by AUBERT,B 06E
0.50 $^{+0.23}_{-0.20}$ ± 0.02	³ WANG	04A	BELL Repl. by JEN 06
-0.01 $^{+0.29}_{-0.31}$ ± 0.03	⁴ AUBERT	02E	BABR Repl. by AUBERT 04H

¹This result is obtained with an amplitude analysis of $B^+ \rightarrow \pi^+ \pi^+ \pi^-$ decays, using the isobar model within the mass range $1.0 < m(\pi^+ \pi^-) < 1.5 \text{ GeV}$ to describe the $\pi^+ \pi^-$ S -wave contribution.

²Corresponds to 90% confidence range $-0.75 < A_{CP} < 0.07$.

³Corresponds to 90% CL interval $-0.25 < A_{CP} < 0.41$

⁴Corresponds to 90% confidence range $-0.50 < A_{CP} < 0.46$.

 $A_{CP}(B^+ \rightarrow \omega \rho^+)$

VALUE	DOCUMENT ID	TECN	COMMENT
-0.20 ± 0.09 ± 0.02	AUBERT	09H	BABR $e^+e^- \rightarrow \Upsilon(4S)$

••• We do not use the following data for averages, fits, limits, etc. •••

0.04 ± 0.18 ± 0.02	AUBERT,B	06T	BABR Repl. by AUBERT 09H
0.05 ± 0.26 ± 0.02	AUBERT	05o	BABR Repl. by AUBERT,B 06T

 $A_{CP}(B^+ \rightarrow \eta \pi^+)$

VALUE	DOCUMENT ID	TECN	COMMENT
-0.14 ± 0.07 OUR AVERAGE	Error includes scale factor of 1.4.		
-0.19 ± 0.06 ± 0.01	HOI	12	BELL $e^+e^- \rightarrow \Upsilon(4S)$
-0.03 ± 0.09 ± 0.03	AUBERT	09AV	BABR $e^+e^- \rightarrow \Upsilon(4S)$

••• We do not use the following data for averages, fits, limits, etc. •••

-0.08 ± 0.10 ± 0.01	AUBERT	07AE	BABR Repl. by AUBERT 09AV
-0.23 ± 0.09 ± 0.02	CHANG	07B	BELL Repl. by HOI 12
-0.13 ± 0.12 ± 0.01	AUBERT,B	05K	BABR Repl. by AUBERT 07AE
0.07 ± 0.15 ± 0.03	CHANG	05A	BELL Repl. by CHANG 07B
-0.44 ± 0.18 ± 0.01	AUBERT	04H	BABR Repl. by AUBERT,B 05K

 $A_{CP}(B^+ \rightarrow \eta \rho^+)$

VALUE	DOCUMENT ID	TECN	COMMENT
0.11 ± 0.11 OUR AVERAGE			
0.13 ± 0.11 ± 0.02	AUBERT	08AH	BABR $e^+e^- \rightarrow \Upsilon(4S)$
-0.04 $^{+0.34}_{-0.32}$ ± 0.01	WANG	07B	BELL $e^+e^- \rightarrow \Upsilon(4S)$

••• We do not use the following data for averages, fits, limits, etc. •••

0.02 ± 0.18 ± 0.02	AUBERT,B	05K	BABR Repl. by AUBERT 08AH
--------------------	----------	-----	---------------------------

 $A_{CP}(B^+ \rightarrow \eta' \pi^+)$

VALUE	DOCUMENT ID	TECN	COMMENT
0.06 ± 0.16 OUR AVERAGE			
0.03 ± 0.17 ± 0.02	AUBERT	09AV	BABR $e^+e^- \rightarrow \Upsilon(4S)$
0.20 $^{+0.37}_{-0.36}$ ± 0.04	SCHUEMANN	06	BELL $e^+e^- \rightarrow \Upsilon(4S)$

••• We do not use the following data for averages, fits, limits, etc. •••

0.21 ± 0.17 ± 0.01	AUBERT	07AE	BABR Repl. by AUBERT 09AV
0.14 ± 0.16 ± 0.01	AUBERT,B	05K	BABR Repl. by AUBERT 07AE

 $A_{CP}(B^+ \rightarrow \eta' \rho^+)$

VALUE	DOCUMENT ID	TECN	COMMENT
0.26 ± 0.17 ± 0.02	DEL-AMO-SA...	10A	BABR $e^+e^- \rightarrow \Upsilon(4S)$

••• We do not use the following data for averages, fits, limits, etc. •••

0.04 ± 0.28 ± 0.02	¹ AUBERT	07E	BABR Repl. by DEL-AMO-SANCHEZ 10A
--------------------	---------------------	-----	-----------------------------------

¹Reports A_{CP} with the opposite sign convention.

 $A_{CP}(B^+ \rightarrow b_1^0 \pi^+)$

VALUE	DOCUMENT ID	TECN	COMMENT
+0.05 ± 0.16 ± 0.02	AUBERT	07B1	BABR $e^+e^- \rightarrow \Upsilon(4S)$

See key on page 1171

Meson Particle Listings

B^\pm

$A_{CP}(B^+ \rightarrow p\bar{p}\pi^+)$

VALUE	DOCUMENT ID	TECN	COMMENT
0.00 ± 0.04 OUR AVERAGE			
-0.02 ± 0.05 ± 0.02	¹ WEI 08	BELL	$e^+e^- \rightarrow \Upsilon(4S)$
+0.04 ± 0.07 ± 0.04	AUBERT 07AV	BABR	$e^+e^- \rightarrow \Upsilon(4S)$
••• We do not use the following data for averages, fits, limits, etc. •••			
-0.16 ± 0.22 ± 0.01	WANG 04	BELL	Repl. by WEI 08
¹ Requires $m_{p\bar{p}} < 2.85 \text{ GeV}/c^2$.			

$A_{CP}(B^+ \rightarrow p\bar{p}K^+)$

VALUE	DOCUMENT ID	TECN	COMMENT
0.00 ± 0.04 OUR AVERAGE			Error includes scale factor of 2.2.
0.021 ± 0.020 ± 0.004	¹ AAIJ 14AF	LHCB	pp at 7, 8 TeV
-0.17 ± 0.10 ± 0.02	¹ WEI 08	BELL	$e^+e^- \rightarrow \Upsilon(4S)$
-0.16 $\begin{smallmatrix} +0.07 \\ -0.08 \end{smallmatrix}$ ± 0.04	¹ AUBERT,B 05L	BABR	$e^+e^- \rightarrow \Upsilon(4S)$
••• We do not use the following data for averages, fits, limits, etc. •••			
-0.047 ± 0.036 ± 0.007	¹ AAIJ 13AU	LHCB	Repl. by AAIJ 14AF
-0.05 ± 0.11 ± 0.01	WANG 04	BELL	Repl. by WEI 08
¹ Requires $m_{p\bar{p}} < 2.85 \text{ GeV}/c^2$.			

$A_{CP}(B^+ \rightarrow p\bar{p}K^*(892)^+)$

VALUE	DOCUMENT ID	TECN	COMMENT
0.21 ± 0.16 OUR AVERAGE			Error includes scale factor of 1.4.
-0.01 ± 0.19 ± 0.02	CHEN 08c	BELL	$e^+e^- \rightarrow \Upsilon(4S)$
+0.32 ± 0.13 ± 0.05	AUBERT 07AV	BABR	$e^+e^- \rightarrow \Upsilon(4S)$

$A_{CP}(B^+ \rightarrow p\bar{p}\gamma)$

VALUE	DOCUMENT ID	TECN	COMMENT
+0.17 ± 0.16 ± 0.05	WANG 07c	BELL	$e^+e^- \rightarrow \Upsilon(4S)$

$A_{CP}(B^+ \rightarrow p\bar{p}\pi^0)$

VALUE	DOCUMENT ID	TECN	COMMENT
+0.01 ± 0.17 ± 0.04	WANG 07c	BELL	$e^+e^- \rightarrow \Upsilon(4S)$

$A_{CP}(B^+ \rightarrow K^+\ell^+\ell^-)$

VALUE	DOCUMENT ID	TECN	COMMENT
-0.02 ± 0.08 OUR AVERAGE			
-0.03 ± 0.14 ± 0.01	¹ LEES 12s	BABR	$e^+e^- \rightarrow \Upsilon(4S)$
-0.18 ± 0.18 ± 0.01	AUBERT 09T	BABR	$e^+e^- \rightarrow \Upsilon(4S)$
+0.04 ± 0.10 ± 0.02	WEI 09A	BELL	$e^+e^- \rightarrow \Upsilon(4S)$
••• We do not use the following data for averages, fits, limits, etc. •••			
-0.07 ± 0.22 ± 0.02	AUBERT,B 06j	BABR	Repl. by AUBERT 09T
¹ Measured in the union of $0.10 < q^2 < 8.12 \text{ GeV}^2/c^4$ and $q^2 > 10.11 \text{ GeV}^2/c^4$. LEES 12s reports also individual measurements $A_{CP}(B^+ \rightarrow K^+\ell^+\ell^-) = 0.02 \pm 0.18 \pm 0.01$ for $0.10 < q^2 < 8.12 \text{ GeV}^2/c^4$ and $A_{CP}(B^+ \rightarrow K^+\ell^+\ell^-) = -0.06 \pm 0.22 \pm 0.01$ for $q^2 > 10.11 \text{ GeV}^2/c^4$.			

$A_{CP}(B^+ \rightarrow K^+e^+e^-)$

VALUE	DOCUMENT ID	TECN	COMMENT
+0.14 ± 0.14 ± 0.03	WEI 09A	BELL	$e^+e^- \rightarrow \Upsilon(4S)$

$A_{CP}(B^+ \rightarrow K^+\mu^+\mu^-)$

VALUE	DOCUMENT ID	TECN	COMMENT
0.01 ± 0.017 OUR AVERAGE			
0.012 ± 0.017 ± 0.001	AAIJ 14AN	LHCB	pp at 7, 8 TeV
-0.05 ± 0.13 ± 0.03	WEI 09A	BELL	$e^+e^- \rightarrow \Upsilon(4S)$
••• We do not use the following data for averages, fits, limits, etc. •••			
0.000 ± 0.033 ± 0.009	AAIJ 13BN	LHCB	Repl. by AAIJ 14AN

$A_{CP}(B^+ \rightarrow \pi^+\mu^+\mu^-)$

VALUE	DOCUMENT ID	TECN	COMMENT
-0.11 ± 0.12 ± 0.01	AAIJ 15AR	LHCB	pp at 7, 8 TeV

$A_{CP}(B^+ \rightarrow K^*\ell^+\ell^-)$

VALUE	DOCUMENT ID	TECN	COMMENT
-0.09 ± 0.14 OUR AVERAGE			
0.01 $\begin{smallmatrix} +0.26 \\ -0.24 \end{smallmatrix}$ ± 0.02	AUBERT 09T	BABR	$e^+e^- \rightarrow \Upsilon(4S)$
-0.13 $\begin{smallmatrix} +0.17 \\ -0.16 \end{smallmatrix}$ ± 0.01	WEI 09A	BELL	$e^+e^- \rightarrow \Upsilon(4S)$
••• We do not use the following data for averages, fits, limits, etc. •••			
0.03 ± 0.23 ± 0.03	AUBERT,B 06j	BABR	Repl. by AUBERT 09T

$A_{CP}(B^+ \rightarrow K^*e^+e^-)$

VALUE	DOCUMENT ID	TECN	COMMENT
-0.14 $\begin{smallmatrix} +0.23 \\ -0.22 \end{smallmatrix}$ ± 0.02	WEI 09A	BELL	$e^+e^- \rightarrow \Upsilon(4S)$

$A_{CP}(B^+ \rightarrow K^*\mu^+\mu^-)$

VALUE	DOCUMENT ID	TECN	COMMENT
-0.12 ± 0.24 ± 0.02	WEI 09A	BELL	$e^+e^- \rightarrow \Upsilon(4S)$

CP VIOLATION PARAMETERS IN $B^+ \rightarrow DK^+$ AND SIMILAR DECAYS

The parameters r_{B^+} and δ_{B^+} are the magnitude ratio and strong phase difference between the amplitudes of $A(B^+ \rightarrow \bar{D}^{(*)0}K^{(*)+})$ and $A(B^+ \rightarrow D^{(*)0}K^{(*)+})$. The measured observables are defined as $x_\pm = r_{B^+} \cos(\delta_{B^+} \pm \gamma)$ and $y_\pm = r_{B^+} \sin(\delta_{B^+} \pm \gamma)$, and can be used to measure the CKM angle γ .

"OUR EVALUATION" is provided by the Heavy Flavor Averaging Group (HFLAV). It is derived from combinations of their results on $B^+ \rightarrow DK^+$ and related processes.

γ

For angle $\gamma(\phi_3)$ of the CKM unitarity triangle, see the review on "CP Violation" in the Reviews section.

VALUE (°)	CL%	DOCUMENT ID	TECN	COMMENT
-----------	-----	-------------	------	---------

65.9 $\begin{smallmatrix} +2.9 \\ -3.1 \end{smallmatrix}$ OUR EVALUATION (Produced by HFLAV)

••• We do not use the following data for averages, fits, limits, etc. •••

69 $\begin{smallmatrix} +13 \\ -14 \end{smallmatrix}$		¹ AAIJ	23BA	LHCB	pp at 7, 8, 13 TeV
54.8 $\begin{smallmatrix} +6.0+6.7 \\ -5.8-4.3 \end{smallmatrix}$		² AAIJ	23i	LHCB	pp at 7, 8, 13 TeV
116 $\begin{smallmatrix} +12 \\ -14 \end{smallmatrix}$		³ AAIJ	23N	LHCB	pp at 7, 8, 13 TeV
78.4 ± 11.4 ± 1.1		^{4,5} ABUDINEN	22	BELL	$e^+e^- \rightarrow \Upsilon(4S)$
65.4 $\begin{smallmatrix} +3.8 \\ -4.2 \end{smallmatrix}$		⁶ AAIJ	21AM	LHCB	pp at 7, 8, 13 TeV
68.7 $\begin{smallmatrix} +5.2 \\ -5.1 \end{smallmatrix}$		⁴ AAIJ	21L	LHCB	pp at 7, 8, 13 TeV
44 ± 12		^{7,8} AAIJ	21M	LHCB	pp at 7, 8, 13 TeV
5.7 $\begin{smallmatrix} +10.2 \\ -8.8 \end{smallmatrix}$ ± 6.7		⁹ RESMI	19	BELL	$e^+e^- \rightarrow \Upsilon(4S)$
87 $\begin{smallmatrix} +11 \\ -12 \end{smallmatrix}$		¹⁰ AAIJ	18AD	LHCB	Repl. by AAIJ 21L
128 $\begin{smallmatrix} +17 \\ -22 \end{smallmatrix}$		¹¹ AAIJ	18U	LHCB	pp at 7, 8 TeV
5-86 or 185-266		¹² AAIJ	18Z	LHCB	pp at 7, 8 TeV
80 $\begin{smallmatrix} +21 \\ -22 \end{smallmatrix}$		¹³ AAIJ	16AA	LHCB	Repl. by AAIJ 16Z
72.2 $\begin{smallmatrix} +6.8 \\ -7.3 \end{smallmatrix}$		¹⁴ AAIJ	16AQ	LHCB	Repl. by AAIJ 21AM
71 ± 20		^{15,16} AAIJ	16Z	LHCB	pp at 7, 8 TeV
74 $\begin{smallmatrix} +20 \\ -19 \end{smallmatrix}$		AAIJ	15BC	LHCB	pp at 7, 8 TeV
63.5 $\begin{smallmatrix} +7.2 \\ -6.7 \end{smallmatrix}$		^{17,18} AAIJ	15K	LHCB	pp at 7, 8 TeV
62 $\begin{smallmatrix} +15 \\ -14 \end{smallmatrix}$		¹⁹ AAIJ	14BA	LHCB	Repl. by AAIJ 21L
84 $\begin{smallmatrix} +49 \\ -42 \end{smallmatrix}$		²⁰ AAIJ	14BE	LHCB	Repl. by AAIJ 14BA
115 $\begin{smallmatrix} +28 \\ -43 \end{smallmatrix}$		²¹ AAIJ	14BF	LHCB	Repl. by AAIJ 18U
72.6 $\begin{smallmatrix} +9.7 \\ -17.2 \end{smallmatrix}$		²² AAIJ	13AK	LHCB	Repl. by AAIJ 21AM
69 $\begin{smallmatrix} +17 \\ -16 \end{smallmatrix}$		²³ LEES	13B	BABR	$e^+e^- \rightarrow \Upsilon(4S)$
44 $\begin{smallmatrix} +43 \\ -38 \end{smallmatrix}$		^{24,25} AAIJ	12AQ	LHCB	Repl. by AAIJ 13AK
77.3 $\begin{smallmatrix} +15.1 \\ -14.9 \end{smallmatrix}$ ± 5.9		^{25,26} AIHARA	12	BELL	$e^+e^- \rightarrow \Upsilon(4S)$.
68 ± 14 ± 5		²⁷ DEL-AMO-SA-10F	BABR		Repl. by LEES 13B
7 to 173		²⁸ DEL-AMO-SA-10G	BABR		$e^+e^- \rightarrow \Upsilon(4S)$
78.4 $\begin{smallmatrix} +10.8 \\ -11.6 \end{smallmatrix}$ ± 9.6		²⁹ POLUEKTOV	10	BELL	$e^+e^- \rightarrow \Upsilon(4S)$
162 ± 56		³⁰ AUBERT	09R	BABR	$e^+e^- \rightarrow \Upsilon(4S)$
76 $\begin{smallmatrix} +22 \\ -23 \end{smallmatrix}$ ± 7.1		³¹ AUBERT	08AL	BABR	Repl. by DEL-AMO-SANCHEZ 10F
53 $\begin{smallmatrix} +15 \\ -18 \end{smallmatrix}$ ± 10		³² POLUEKTOV	06	BELL	Repl. by POLUEKTOV 10
70 ± 31 $\begin{smallmatrix} +18 \\ -15 \end{smallmatrix}$		³³ AUBERT,B	05Y	BABR	Repl. by AUBERT 08AL
77 $\begin{smallmatrix} +17 \\ -19 \end{smallmatrix}$ ± 17		³⁴ POLUEKTOV	04	BELL	Repl. by POLUEKTOV 06

¹ Measured using $B^\pm \rightarrow D^*K^\pm$ and $B^\pm \rightarrow D^*\pi^\pm$ decays analysing the signal yield variation with the fully reconstructed $D^* \rightarrow D\pi^0/\gamma$, $D \rightarrow (KS)^0\pi^+\pi^-/(KS)^0K^+K^-$ decays. The model-independent approach uses external strong phase input from BESIII and CLEO collaborations.

² Measured using $B^\pm \rightarrow D[K^\mp\pi^\pm\pi^\pm\pi^\mp]h^\pm$ decays in bins of the phase space of the D decay. The third uncertainty includes systematic and finite knowledge of the D -meson decay parameters.

³ A model-dependent binned analysis of the decays $B^\pm \rightarrow [K^+K^-\pi^+\pi^-]_D h^\pm$ is used.

⁴ Uses binned Dalitz plot analysis of $D \rightarrow K_S^0\pi^+\pi^-$ and $K_S^0K^+K^-$ from $B^\pm \rightarrow DK^\pm$ modes. Strong phase measurements from CLEO-c and BES-III of the D decay over the Dalitz plot are used as input. Value is modulo 180° .

⁵ Supersedes AIHARA 12.

⁶ AAIJ 21AM presents a combination of existing measurements from LHCB collaboration. It includes also charm mixing parameters.

⁷ Measured in $B_S^0 \rightarrow D_S^\pm K^\mp\pi^\pm\pi^\mp$ decays in restricted phase space with $m(K^+\pi^-) < 1950 \text{ MeV}$, $m(K^+\pi^-) < 1200 \text{ MeV}$ and $m(\pi^+\pi^-) < 1200 \text{ MeV}$. The value is modulo 180° .

⁸ A model-independent coherence factor for the decay $B_S \rightarrow D_S K\pi$ (in the restricted phase space region) is also reported.

Meson Particle Listings

 B^\pm

- ⁹ Uses binned analysis of $D \rightarrow K_S^0 \pi^+ \pi^- \pi^0$ from $B^\pm \rightarrow DK^\pm$ modes over the phase space. Strong phase measurements from RESMI 18 analysis of CLEO-c data of the D decay over the phase space binning are used as input.
- ¹⁰ Uses binned Dalitz plot analysis of $D \rightarrow K_S^0 \pi^+ \pi^-$ and $K_S^0 K^+ K^-$ from $B^\pm \rightarrow DK^\pm$ modes. Strong phase measurements from CLEO-c of the D decay over the Dalitz plot are used as input.
- ¹¹ Measured in $B_S^0 \rightarrow D_S^\mp K^\pm$ decays, constraining $-2\beta_S$ by the measurement of $\phi_S = 0.030 \pm 0.033$ from HFLAV. The value is modulo 180° .
- ¹² AAIJ 18z reports the intervals $(5-86)^\circ$ or $(185-266)^\circ$ at 68% C.L. The extraction uses the time dependent CP violation measurement in $B^0 \rightarrow D^\mp \pi^\pm$ decays with external input and some theoretical assumptions.
- ¹³ Uses Dalitz plot analysis of $D \rightarrow K_S^0 \pi^+ \pi^-$ decays coming from $B^0 \rightarrow DK^*(892)^0$ modes. Measures $r_{B^0} = 0.39 \pm 0.13$, and $\delta_{B^0} = 197^{+24}_{-20}$ degrees.
- ¹⁴ A combination of measurements from analyses of time-integrated $B^+ \rightarrow DK^+$, $B^0 \rightarrow DK^*(*)^0$, $B^0 \rightarrow DK^+ \pi^-$, and $B^+ \rightarrow DK^+ \pi^+ \pi^-$ tree-level decays. In addition, results from a time-dependent analysis of $B_S^0 \rightarrow D_S K$ decays are included.
- ¹⁵ A model-independent binned Dalitz plot analysis of the decays $B^0 \rightarrow DK^{*0}$, with $D \rightarrow K_S^0 \pi^+ \pi^-$ and $D \rightarrow K_S^0 K^+ K^-$. The results cannot be combined with the model-dependent analysis of the same dataset reported in AAIJ 16AA.
- ¹⁶ Angle γ required to satisfy $0 < \gamma < 180$ degrees.
- ¹⁷ Obtained by measuring time-dependent CP asymmetry in $B_S^0 \rightarrow K^+ K^-$ and using a U-spin relation between $B_S^0 \rightarrow K^+ K^-$ and $B^0 \rightarrow \pi^+ \pi^-$.
- ¹⁸ Results are also presented using additional inputs on $B^0 \rightarrow \pi^0 \pi^0$ and $B^+ \rightarrow \pi^+ \pi^0$ decays from other experiments and isospin symmetry assumptions. The dependence of the results on the maximum allowed amount of U-spin breaking up to 50% is also included.
- ¹⁹ Uses binned Dalitz plot analysis of $B^+ \rightarrow DK^+$ decays, with $D \rightarrow K_S^0 \pi^+ \pi^-$ and $D \rightarrow K_S^0 K^+ K^-$. Strong phase measurements from CLEO-c (LIBBY 10) of the D decay over the Dalitz plot are used as input. Solution that satisfies $0 < \gamma < 180$ is chosen.
- ²⁰ AAIJ 14BE uses model-dependent analysis of $D \rightarrow K_S^0 \pi^+ \pi^-$ amplitudes. The model is the same as in DEL-AMO-SANCHEZ 10F.
- ²¹ Measured in $B^0 \rightarrow D^\mp K^\pm$ decays, constraining $-2\beta_S$ by the measurement of $\phi_S = 0.01 \pm 0.07 \pm 0.0$ from AAIJ 13AR. The value is modulo 180° at 68% CL.
- ²² Presents a confidence region $55.4^\circ < \gamma < 82.3^\circ$ at 68% CL with best fit value 72.6° and includes both statistical and systematic uncertainties. The corresponding 95% CL is $40.2^\circ < \gamma < 92.7^\circ$. The value is determined from combination of measurements using D meson decaying to $K^+ K^-$, $\pi^+ \pi^-$, $K^\pm \pi^\mp$, $K_S^0 \pi^+ \pi^-$, $K_S^0 K^+ K^-$, and $K^\pm \pi^\mp \pi^\pm \pi^\mp$. Combines $B^\pm \rightarrow DK^\pm$ and $B^\pm \rightarrow D\pi^\pm$.
- ²³ Reports combination of published measurements using GGSZ, GLW, and ADS methods. Reports also 2σ range of $41-102^\circ$ and a 5.9σ significance for $\gamma(B^+ \rightarrow D^*(*)^0 K^+)$ $\neq 0$ hypothesis.
- ²⁴ Reports combined statistical and systematic uncertainties.
- ²⁵ Uses binned Dalitz plot of $\bar{D}^0 \rightarrow K_S^0 \pi^+ \pi^-$ decays from $B^+ \rightarrow \bar{D}^0 K^+$. Measurement of strong phases in $\bar{D}^0 \rightarrow K_S^0 \pi^+ \pi^-$ Dalitz plot from LIBBY 10 is used as input.
- ²⁶ We combined the systematics in quadrature. The authors report separately the contribution to the systematic uncertainty due to the uncertainty on the bin-averaged strong phase difference between D^0 and \bar{D}^0 amplitudes. Superseded by ABUDINEN 22.
- ²⁷ Uses Dalitz plot analysis of $\bar{D}^0 \rightarrow K_S^0 \pi^+ \pi^-$, $K_S^0 K^+ K^-$ decays from $B^+ \rightarrow D^*(*)^+ K^+$, DK^{*+} modes. The corresponding two standard deviation interval for γ is $39^\circ < \gamma < 98^\circ$. CP conservation in the combined result is ruled out with a significance of 3.5 standard deviations.
- ²⁸ Reports confidence intervals for the CKM angle γ from the measured values of the GLW parameters using $B^\pm \rightarrow DK^\pm$ decays with D mesons decaying to non-CP($K\pi$), CP-even ($K^+ K^-$, $\pi^+ \pi^-$), and CP-odd ($K_S^0 \pi^+ \pi^-$, $K_S^0 \omega$) states.
- ²⁹ Uses Dalitz plot analysis of $\bar{D}^0 \rightarrow K_S^0 \pi^+ \pi^-$ decays from $B^+ \rightarrow D^*(*)^+ K^+$ modes. The corresponding two standard deviation interval for γ is $54.2^\circ < \gamma < 100.5^\circ$. CP conservation in the combined result is ruled out with a significance of 3.5 standard deviations.
- ³⁰ Uses Dalitz plot analysis of $D^0 \rightarrow K_S^0 \pi^+ \pi^-$ decays coming from $B^0 \rightarrow D^0 K^{*0}$ modes. The corresponding 95% CL interval is $77^\circ < \gamma < 247^\circ$. A 180 degree ambiguity is implied.
- ³¹ Uses Dalitz plot analysis of $\bar{D}^0 \rightarrow K_S^0 \pi^+ \pi^-$ and $\bar{D}^0 \rightarrow K_S^0 K^+ K^-$ decays coming from $B^\pm \rightarrow D^*(*)^+ K^+$ modes. The corresponding two standard deviation interval is $29^\circ < \gamma < 122^\circ$.
- ³² Uses a Dalitz plot analysis of the $\bar{D}^0 \rightarrow K_S^0 \pi^+ \pi^-$ decays; Combines the DK^+ , $D^* K^+$ and DK^{*+} modes. The corresponding two standard deviations interval for gamma is $8^\circ < \gamma < 111^\circ$.
- ³³ Uses a Dalitz plot analysis of neutral $D \rightarrow K_S^0 \pi^+ \pi^-$ decays coming from $B^\pm \rightarrow DK^\pm$ and $B^\pm \rightarrow D^*(*)^+ K^\pm$ followed by $D^*(*)^0 \rightarrow D\pi^0, D\gamma$. The corresponding two standard deviations interval for gamma is $12^\circ < \gamma < 137^\circ$. AUBERT,B 05Y also reports the amplitude ratios and the strong phases.
- ³⁴ Uses a Dalitz plot analysis of the 3-body $D \rightarrow K_S^0 \pi^+ \pi^-$ decays coming from $B^\pm \rightarrow DK^\pm$ and $B^\pm \rightarrow D^*(*)^+ K^\pm$ followed by $D^*(*)^0 \rightarrow D\pi^0$; here we use D to denote that the neutral D meson produced in the decay is an admixture of D^0 and \bar{D}^0 . The corresponding two standard deviations interval for γ is $26^\circ < \gamma < 126^\circ$. POLUEKTOV 04 also reports the amplitude ratios and the strong phases.

 $r_B(B^+ \rightarrow D^0 K^+)$

r_B and δ_B are the amplitude ratio and relative strong phase between the amplitudes of $A(B^+ \rightarrow D^0 K^+)$ and $A(B^+ \rightarrow \bar{D}^0 K^+)$,

VALUE (units 10^{-2})	CL%	DOCUMENT ID	TECN	COMMENT
9.94 ± 0.26	OUR EVALUATION	(Produced by HFLAV)		

• • • We do not use the following data for averages, fits, limits, etc. • • •

9.46 ± 0.31	$^{+0.30}_{-0.24}$	1 AAIJ	23i	LHCB	pp at 7, 8, 13 TeV
-------------	--------------------	--------	-----	------	----------------------

11.0 ± 2.0		2 AAIJ	23N	LHCB	pp at 7, 8, 13 TeV	
12.9 ± 2.4 ± 0.2		3 ABUDINEN	22	BELL	$e^+ e^- \rightarrow \Upsilon(4S)$	
9.04 $^{+0.77}_{-0.75}$		4 AAIJ	21L	LHCB	pp at 7, 8, 13 TeV	
32.3 ± 14.7 ± 5.6		5 RESMI	19	BELL	$e^+ e^- \rightarrow \Upsilon(4S)$	
8.6 $^{+1.3}_{-1.4}$		6 AAIJ	18AD	LHCB	Repl. by AAIJ 21L	
8.0 $^{+1.9}_{-2.1}$		3 AAIJ	14BA	LHCB	Repl. by AAIJ 21L	
6 ± 4		7 AAIJ	14BE	LHCB	Repl. by AAIJ 14BA	
9.7 ± 1.1		8 AAIJ	13AE	LHCB	pp at 7 TeV	
9.2 $^{+1.3}_{-1.2}$		9 LEES	13B	BABR	$e^+ e^- \rightarrow \Upsilon(4S)$	
7 ± 4		10,11 AAIJ	12AQ	LHCB	pp at 7 TeV	
14.5 ± 3.0 ± 1.5		11,12 AIHARA	12	BELL	$e^+ e^- \rightarrow \Upsilon(4S)$.	
<13		13 LEES	11D	BABR	$e^+ e^- \rightarrow \Upsilon(4S)$	
9.6 ± 2.9 ± 0.6		14 DEL-AMO-SA..10F	BABR	Repl. by LEES 13B		
9.5 $^{+5.1}_{-4.1}$		15 DEL-AMO-SA..10H	BABR	Repl. by LEES 13B		
16.0 $^{+4.0}_{-3.8}$ $^{+5.1}_{-1.5}$		16 POLUEKTOV	10	BELL	$e^+ e^- \rightarrow \Upsilon(4S)$	
8.6 ± 3.2 ± 1.5		17 AUBERT	08AL	BABR	Repl. by DEL-AMO-SANCHEZ 10F	
<19		90	HORII	08	BELL	$e^+ e^- \rightarrow \Upsilon(4S)$
15.9 $^{+5.4}_{-5.0}$ ± 5.0		18 POLUEKTOV	06	BELL	Repl. by POLUEKTOV 10	
12 ± 8 ± 5		19 AUBERT,B	05Y	BABR	Repl. by AUBERT 08AL	

¹ Measured using $B^\pm \rightarrow D[K^\mp \pi^\pm \pi^\pm \pi^\mp] h^\pm$ decays in bins of the phase space of the D decay. The third uncertainty includes systematic and finite knowledge of the D -meson decay parameters.

² A model-dependent binned analysis of the decays $B^\pm \rightarrow [K^+ K^- \pi^+ \pi^-]_D h^\pm$ is used.

³ Uses binned Dalitz plot analysis of $B^+ \rightarrow DK^+$ decays, with $D \rightarrow K_S^0 \pi^+ \pi^-$ and $D \rightarrow K_S^0 K^+ K^-$. Strong phase measurements from CLEO-c (LIBBY 10) of the D decay over the Dalitz plot are used as input. Supersedes AIHARA 12.

⁴ Uses binned analysis of $D \rightarrow K_S^0 \pi^+ \pi^- \pi^0$ from $B^\pm \rightarrow DK^\pm$ modes over the phase space. Strong phase measurements from CLEO-c and BES-III data of the D decay over the phase space binning are used as input.

⁵ Uses binned analysis of $D \rightarrow K_S^0 \pi^+ \pi^- \pi^0$ from $B^\pm \rightarrow DK^\pm$ modes over the phase space. Strong phase measurements from RESMI 18 analysis of CLEO-c data of the D decay over the phase space binning are used as input.

⁶ Uses binned Dalitz plot analysis of $D \rightarrow K_S^0 \pi^+ \pi^-$ and $K_S^0 K^+ K^-$ from $B^\pm \rightarrow DK^\pm$ modes. Strong phase measurements from CLEO-c of the D decay over the Dalitz plot are used as input.

⁷ AAIJ 14BE uses model-dependent analysis of $D \rightarrow K_S^0 \pi^+ \pi^-$ amplitudes. The model is the same as in DEL-AMO-SANCHEZ 10F.

⁸ Uses $B^\pm \rightarrow [K^\pm \pi^\mp \pi^+ \pi^-]_D h^\pm$ mode.

⁹ Reports combination of published measurements using GGSZ, GLW, and ADS methods. ¹⁰ Reports combined statistical and systematic uncertainties.

¹¹ Uses binned Dalitz plot of $\bar{D}^0 \rightarrow K_S^0 \pi^+ \pi^-$ decays from $B^+ \rightarrow \bar{D}^0 K^+$. Measurement of strong phases in $\bar{D}^0 \rightarrow K_S^0 \pi^+ \pi^-$ Dalitz plot from LIBBY 10 is used as input.

¹² We combined the systematics in quadrature. The authors report separately the contribution to the systematic uncertainty due to the uncertainty on the bin-averaged strong phase difference between D^0 and \bar{D}^0 amplitudes. Superseded by ABUDINEN 22.

¹³ Uses decays of neutral D to $K^- \pi^+ \pi^0$.

¹⁴ Uses Dalitz plot analysis of $\bar{D}^0 \rightarrow K_S^0 \pi^+ \pi^-$, $K_S^0 K^+ K^-$ decays from $B^+ \rightarrow D^*(*)^+ K^+$ modes. The corresponding two standard deviation interval is $0.037 < r_B < 0.155$.

¹⁵ Uses the Cabibbo suppressed decay of $B^+ \rightarrow \bar{D}^0 K^+$ followed by $\bar{D}^0 \rightarrow K^- \pi^+$.

¹⁶ Uses Dalitz plot analysis of $\bar{D}^0 \rightarrow K_S^0 \pi^+ \pi^-$ decays from $B^+ \rightarrow D^0 K^+$ modes. The corresponding two standard deviation interval is $0.084 < r_B < 0.239$.

¹⁷ Uses Dalitz plot analysis of $\bar{D}^0 \rightarrow K_S^0 \pi^+ \pi^-$ and $\bar{D}^0 \rightarrow K_S^0 K^+ K^-$ decays coming from $B^\pm \rightarrow D^*(*)^+ K^\pm$ modes.

¹⁸ Uses a Dalitz plot analysis of the $\bar{D}^0 \rightarrow K_S^0 \pi^+ \pi^-$ decays; Combines the DK^+ , $D^* K^+$ and DK^{*+} modes.

¹⁹ Uses a Dalitz analysis of neutral D decays to $K_S^0 \pi^+ \pi^-$ in the processes $B^\pm \rightarrow D^*(*)^+ K^\pm$, $D^* \rightarrow D\pi^0, D\gamma$.

 $\delta_B(B^+ \rightarrow D^0 K^+)$

VALUE (°)	DOCUMENT ID	TECN	COMMENT
127.7 $^{+3.6}_{-3.9}$	OUR EVALUATION	(Produced by HFLAV)	

• • • We do not use the following data for averages, fits, limits, etc. • • •

134.6 ± 6.0	$^{+8.6}_{-8.7}$	1 AAIJ	23i	LHCB	pp at 7, 8, 13 TeV
81	$^{+14}_{-13}$	2 AAIJ	23N	LHCB	pp at 7, 8, 13 TeV
124.8 ± 12.9 ± 1.8		3,4 ABUDINEN	22	BELL	$e^+ e^- \rightarrow \Upsilon(4S)$
118.3 $^{+5.5}_{-5.6}$		5 AAIJ	21L	LHCB	pp at 7, 8, 13 TeV
83.4 $^{+18.3}_{-16.6}$ ± 5.1		6 RESMI	19	BELL	$e^+ e^- \rightarrow \Upsilon(4S)$
101 ± 11		7 AAIJ	18AD	LHCB	Repl. by AAIJ 21L
134	$^{+14}_{-15}$	3 AAIJ	14BA	LHCB	Repl. by AAIJ 21L
115	$^{+41}_{-51}$	8 AAIJ	14BE	LHCB	Repl. by AAIJ 14BA
105	$^{+16}_{-17}$	9 LEES	13B	BABR	$e^+ e^- \rightarrow \Upsilon(4S)$

137	$\begin{smallmatrix} +35 \\ -46 \end{smallmatrix}$	10,11	AAIJ	12Aq	LHCB	pp	at 7 TeV
129.9	$\pm 15.0 \pm 6.0$	11,12	AIHARA	12	BELL	e^+e^-	$\rightarrow \Upsilon(4S)$
119	$\begin{smallmatrix} +19 \\ -20 \end{smallmatrix} \pm 4$	13	DEL-AMO-SA...10F	BABR	Repl. by	LEES	13B
136.7	$\begin{smallmatrix} +13.0 \\ -15.8 \end{smallmatrix} \pm 23.2$	14	POLUEKTOV	10	BELL	e^+e^-	$\rightarrow \Upsilon(4S)$
109	$\begin{smallmatrix} +27 \\ -30 \end{smallmatrix} \pm 8$	15	AUBERT	08AL	BABR	Repl. by	DEL-AMO-SANCHEZ 10F
145.7	$\begin{smallmatrix} +19.0 \\ -19.7 \end{smallmatrix} \pm 23.1$	16	POLUEKTOV	06	BELL	Repl. by	POLUEKTOV 10
104	$\begin{smallmatrix} +45 \\ -32 \end{smallmatrix} \pm 23$	17	AUBERT,B	05Y	BABR	Repl. by	AUBERT 08AL

¹ Measured using $B^\pm \rightarrow D[K^\mp \pi^\pm \pi^\pm \pi^\mp] h^\pm$ decays in bins of the phase space of the D decay. The third uncertainty includes systematic and finite knowledge of the D -meson decay parameters.

² A model-dependent binned analysis of the decays $B^\pm \rightarrow [K^+ K^- \pi^+ \pi^-]_D h^\pm$ is used.

³ Uses binned Dalitz plot analysis of $B^+ \rightarrow DK^+$ decays, with $D \rightarrow K_S^0 \pi^+ \pi^-$ and $D \rightarrow K_S^0 K^+ K^-$. Strong phase measurements from CLEO-c (LIBBY 10) of the D decay over the Dalitz plot are used as input.

⁴ Supersedes AIHARA 12.

⁵ Uses binned Dalitz plot analysis of $D \rightarrow K_S^0 \pi^+ \pi^-$ and $K_S^0 K^+ K^-$ from $B^\pm \rightarrow DK^\pm$ modes. Strong phase measurements from CLEO-c and BES-III of the D decay over the Dalitz plot are used as input. Value is modulo 180° .

⁶ Uses binned analysis of $D \rightarrow K_S^0 \pi^+ \pi^- \pi^0$ from $B^\pm \rightarrow DK^\pm$ modes over the phase space. Strong phase measurements from RESMI 18 analysis of CLEO-c data of the D decay over the phase space binning are used as input.

⁷ Uses binned Dalitz plot analysis of $D \rightarrow K_S^0 \pi^+ \pi^-$ and $K_S^0 K^+ K^-$ from $B^\pm \rightarrow DK^\pm$ modes. Strong phase measurements from CLEO-c of the D decay over the Dalitz plot are used as input.

⁸ AAIJ 148E uses model-dependent analysis of $D \rightarrow K_S^0 \pi^+ \pi^-$ amplitudes. The model is the same as in DEL-AMO-SANCHEZ 10F.

⁹ Reports combination of published measurements using GGSZ, GLW, and ADS methods.

¹⁰ Reports combined statistical and systematic uncertainties.

¹¹ Uses binned Dalitz plot of $\overline{D}^0 \rightarrow K_S^0 \pi^+ \pi^-$ decays from $B^+ \rightarrow \overline{D}^0 K^+$. Measurement of strong phases in $\overline{D}^0 \rightarrow K_S^0 \pi^+ \pi^-$ Dalitz plot from LIBBY 10 is used as input.

¹² We combined the systematics in quadrature. The authors report separately the contribution to the systematic uncertainty due to the uncertainty on the bin-averaged strong phase difference between D^0 and \overline{D}^0 amplitudes. Superseded by ABUDINEN 22.

¹³ Uses Dalitz plot analysis of $\overline{D}^0 \rightarrow K_S^0 \pi^+ \pi^-$ and $K_S^0 K^+ K^-$ decays from $B^+ \rightarrow D^*(*) K^+$ modes. The corresponding two standard deviation interval is $75^\circ < \delta_B < 157^\circ$.

¹⁴ Uses Dalitz plot analysis of $\overline{D}^0 \rightarrow K_S^0 \pi^+ \pi^-$ decays from $B^+ \rightarrow \overline{D}^0 K^+$ modes. The corresponding two standard deviation interval is $102.2^\circ < \delta_B < 162.3^\circ$.

¹⁵ Uses Dalitz plot analysis of $\overline{D}^0 \rightarrow K_S^0 \pi^+ \pi^-$ and $\overline{D}^0 \rightarrow K_S^0 K^+ K^-$ decays coming from $B^\pm \rightarrow D^*(*) K^{\pm}$ modes.

¹⁶ Uses a Dalitz plot analysis of the $\overline{D}^0 \rightarrow K_S^0 \pi^+ \pi^-$ decays; Combines the DK^+ , $D^* K^+$ and DK^{*+} modes.

¹⁷ Uses a Dalitz analysis of neutral D decays to $K_S^0 \pi^+ \pi^-$ in the processes $B^\pm \rightarrow D^*(*) K^\pm$, $D^* \rightarrow D\pi^0, D\gamma$.

$r_B(B^+ \rightarrow D^0 \pi^+)$

VALUE (units 10^{-3})	DOCUMENT ID	TECN	COMMENT
$4.5 \begin{smallmatrix} +1.1+0.5 \\ -1.0-0.4 \end{smallmatrix}$	1	AAIJ	23i LHCB pp at 7, 8, 13 TeV
$4.1 \begin{smallmatrix} +5.4 \\ -4.1 \end{smallmatrix}$	2	AAIJ	23N LHCB pp at 7, 8, 13 TeV
$17 \pm 6 \pm 1$	3	ABUDINEN	22 BELL $e^+e^- \rightarrow \Upsilon(4S)$
5.0 ± 1.7	3	AAIJ	21L LHCB pp at 7, 8, 13 TeV

¹ Measured using $B^\pm \rightarrow D[K^\mp \pi^\pm \pi^\pm \pi^\mp] h^\pm$ decays in bins of the phase space of the D decay. The third uncertainty includes systematic and finite knowledge of the D -meson decay parameters.

² A model-dependent binned analysis of the decays $B^\pm \rightarrow [K^+ K^- \pi^+ \pi^-]_D h^\pm$ is used.

³ Uses binned Dalitz plot analysis of $D \rightarrow K_S^0 \pi^+ \pi^-$ and $K_S^0 K^+ K^-$ from $B^\pm \rightarrow D\pi^\pm$ modes. Strong phase measurements from CLEO-c and BES-III of the D decay over the Dalitz plot are used as input.

$\delta_B(B^+ \rightarrow D^0 \pi^+)$

VALUE ($^\circ$)	DOCUMENT ID	TECN	COMMENT
$311.8 \begin{smallmatrix} +14.7+15.0 \\ -15.0-15.2 \end{smallmatrix}$	1	AAIJ	23i LHCB pp at 7, 8, 13 TeV
$298 \begin{smallmatrix} +62 \\ -118 \end{smallmatrix}$	2	AAIJ	23N LHCB pp at 7, 8, 13 TeV
$341.0 \pm 17.0 \pm 2.9$	3	ABUDINEN	22 BELL $e^+e^- \rightarrow \Upsilon(4S)$
$291 \begin{smallmatrix} +24 \\ -26 \end{smallmatrix}$	3	AAIJ	21L LHCB pp at 7, 8, 13 TeV

¹ Measured using $B^\pm \rightarrow D[K^\mp \pi^\pm \pi^\pm \pi^\mp] h^\pm$ decays in bins of the phase space of the D decay. The third uncertainty includes systematic and finite knowledge of the D -meson decay parameters.

² A model-dependent binned analysis of the decays $B^\pm \rightarrow [K^+ K^- \pi^+ \pi^-]_D h^\pm$ is used.

³ Uses binned Dalitz plot analysis of $D \rightarrow K_S^0 \pi^+ \pi^-$ and $K_S^0 K^+ K^-$ from $B^\pm \rightarrow D\pi^\pm$ modes. Strong phase measurements from CLEO-c and BES-III of the D decay over the Dalitz plot are used as input. Value is modulo 180° .

$r_B(B^+ \rightarrow D^0 K^{*+})$

r_B and δ_B are the amplitude ratio and relative strong phase between the amplitudes of $ACP(B^+ \rightarrow D^0 K^{*+})$ and $ACP(B^+ \rightarrow \overline{D}^0 K^{*+})$.

VALUE	DOCUMENT ID	TECN	COMMENT
-------	-------------	------	---------

0.101 \pm 0.016 \pm 0.034 OUR EVALUATION (Produced by HFLAV)

• • • We do not use the following data for averages, fits, limits, etc. • • •

$0.143 \begin{smallmatrix} +0.048 \\ -0.049 \end{smallmatrix}$	1	LEES	13B BABR $e^+e^- \rightarrow \Upsilon(4S)$
$0.166 \begin{smallmatrix} +0.073 \\ -0.069 \end{smallmatrix}$	2	DEL-AMO-SA...10F	BABR Repl. by LEES 13B
0.31 ± 0.07	3	AUBERT	09AJ BABR Repl. by LEES 13B
$0.181 \begin{smallmatrix} +0.088 \\ -0.108 \end{smallmatrix} \pm 0.042$	4	AUBERT	08AL BABR Repl. by AUBERT 09AJ
$0.564 \begin{smallmatrix} +0.216 \\ -0.155 \end{smallmatrix} \pm 0.093$	5	POLUEKTOV	06 BELL $e^+e^- \rightarrow \Upsilon(4S)$

¹ Reports combination of published measurements using GGSZ, GLW, and ADS methods.

² DEL-AMO-SANCHEZ 10F reports $r_B \cdot k = 0.149 \begin{smallmatrix} +0.066 \\ -0.062 \end{smallmatrix}$ for $k = 0.9$.

³ Obtained by combining the GLW and ADS methods. The 2-sigma range corresponds to [0.17, 0.43].

⁴ Uses Dalitz plot analysis of $\overline{D}^0 \rightarrow K_S^0 \pi^+ \pi^-$ and $\overline{D}^0 \rightarrow K_S^0 K^+ K^-$ decays coming from $B^\pm \rightarrow D^*(*) K^{\pm}$ modes.

⁵ Uses a Dalitz plot analysis of the $\overline{D}^0 \rightarrow K_S^0 \pi^+ \pi^-$ decays; Combines the DK^+ , $D^* K^+$ and DK^{*+} modes.

$\delta_B(B^+ \rightarrow D^0 K^{*+})$

VALUE ($^\circ$)	DOCUMENT ID	TECN	COMMENT
--------------------	-------------	------	---------

48 \pm 59 \pm 16 OUR EVALUATION (Produced by HFLAV)

• • • We do not use the following data for averages, fits, limits, etc. • • •

101 ± 43	1	LEES	13B BABR $e^+e^- \rightarrow \Upsilon(4S)$
111 ± 32		DEL-AMO-SA...10F	BABR Repl. by LEES 13B
$104 \begin{smallmatrix} +39 \\ -37 \end{smallmatrix} \pm 18$	2	AUBERT	08AL BABR Repl. by LEES 13B
$242.6 \begin{smallmatrix} +20.2 \\ -23.2 \end{smallmatrix} \pm 49.4$	3	POLUEKTOV	06 BELL $e^+e^- \rightarrow \Upsilon(4S)$

¹ Reports combination of published measurements using GGSZ, GLW, and ADS methods.

² Uses Dalitz plot analysis of $\overline{D}^0 \rightarrow K_S^0 \pi^+ \pi^-$ and $\overline{D}^0 \rightarrow K_S^0 K^+ K^-$ decays coming from $B^\pm \rightarrow D^*(*) K^{\pm}$ modes.

³ Uses a Dalitz plot analysis of the $\overline{D}^0 \rightarrow K_S^0 \pi^+ \pi^-$ decays; Combines the DK^+ , $D^* K^+$ and DK^{*+} modes.

$r_B(B^+ \rightarrow D^{*0} K^+)$

r_B and δ_B are the amplitude ratio and relative strong phase between the amplitudes of $A(B^+ \rightarrow D^{*0} K^+)$ and $A(B^+ \rightarrow \overline{D}^{*0} K^+)$.

VALUE	DOCUMENT ID	TECN	COMMENT
-------	-------------	------	---------

0.104 \pm 0.013 \pm 0.014 OUR EVALUATION (Produced by HFLAV)

• • • We do not use the following data for averages, fits, limits, etc. • • •

0.15 ± 0.03	1	AAIJ	23BA LHCB pp at 7, 8, 13 TeV
$0.106 \begin{smallmatrix} +0.019 \\ -0.036 \end{smallmatrix}$	2	LEES	13B BABR $e^+e^- \rightarrow \Upsilon(4S)$
$0.133 \begin{smallmatrix} +0.042 \\ -0.035 \end{smallmatrix} \pm 0.013$	3	DEL-AMO-SA...10F	BABR Repl. by LEES 13B
$0.096 \begin{smallmatrix} +0.035 \\ -0.051 \end{smallmatrix}$	4	DEL-AMO-SA...10H	BABR Repl. by LEES 13B
$0.196 \begin{smallmatrix} +0.072+0.064 \\ -0.069-0.017 \end{smallmatrix}$	5	POLUEKTOV	10 BELL $e^+e^- \rightarrow \Upsilon(4S)$
$0.135 \pm 0.050 \pm 0.012$	6	AUBERT	08AL BABR Repl. by DEL-AMO-SANCHEZ 10F
$0.175 \begin{smallmatrix} +0.108 \\ -0.099 \end{smallmatrix} \pm 0.050$	7	POLUEKTOV	06 BELL Repl. by POLUEKTOV 10
$0.17 \pm 0.10 \pm 0.04$	8	AUBERT,B	05Y BABR Repl. by AUBERT 08AL

¹ Measured using $B^\pm \rightarrow D^* K^\pm$ decays analysing the signal yield variation with the fully reconstructed $D^* \rightarrow D\pi^0/\gamma$, $D \rightarrow (KS)^0 \pi^+ \pi^- / (KS)^0 K^+ K^-$ decays. The model-independent approach uses external strong phase input from BESIII and CLEO collaborations.

² Reports combination of published measurements using GGSZ, GLW, and ADS methods.

³ Uses Dalitz plot analysis of $\overline{D}^0 \rightarrow K_S^0 \pi^+ \pi^-$, $K_S^0 K^+ K^-$ decays from $B^+ \rightarrow D^*(*) K^+$ modes. The corresponding two standard deviation interval is $0.049 < r_B^* < 0.215$.

⁴ Uses the Cabibbo suppressed decay of $B^+ \rightarrow \overline{D}^* K^+$ followed by $\overline{D}^* \rightarrow \overline{D}\pi^0$ or $\overline{D}\gamma$, and $\overline{D} \rightarrow K^- \pi^+$.

⁵ Uses Dalitz plot analysis of $\overline{D}^0 \rightarrow K_S^0 \pi^+ \pi^-$ decays from $B^+ \rightarrow D^{*0} K^+$ modes. The corresponding two standard deviation interval is $0.061 < r_B^* < 0.271$.

⁶ Uses Dalitz plot analysis of $\overline{D}^0 \rightarrow K_S^0 \pi^+ \pi^-$ and $\overline{D}^0 \rightarrow K_S^0 K^+ K^-$ decays coming from $B^\pm \rightarrow D^*(*) K^{\pm}$ modes.

⁷ Uses a Dalitz plot analysis of the $\overline{D}^0 \rightarrow K_S^0 \pi^+ \pi^-$ decays; Combines the DK^+ , $D^* K^+$ and DK^{*+} modes.

⁸ Uses a Dalitz analysis of neutral D decays to $K_S^0 \pi^+ \pi^-$ in the processes $B^\pm \rightarrow D^*(*) K^\pm$, $D^* \rightarrow D\pi^0, D\gamma$.

$\delta_B(B^+ \rightarrow D^{*0} K^+)$

VALUE ($^\circ$)	DOCUMENT ID	TECN	COMMENT
--------------------	-------------	------	---------

314.8 \pm 7.9 \pm 9.9 OUR EVALUATION (Produced by HFLAV)

Meson Particle Listings

 B^\pm

• • • We do not use the following data for averages, fits, limits, etc. • • •

311 ± 14	¹ AAIJ	23BA LHCb	pp at 7, 8, 13 TeV
294 $\begin{smallmatrix} +21 \\ -31 \end{smallmatrix}$	² LEES	13B BABR	$e^+e^- \rightarrow \Upsilon(4S)$
278 $\pm 21 \pm 6$	³ DEL-AMO-SA...10F	BABR	Repl. by LEES 13B
341.9 $\begin{smallmatrix} +18.0 \\ -19.6 \end{smallmatrix} \pm 23.1$	⁴ POLUEKTOV	10 BELL	$e^+e^- \rightarrow \Upsilon(4S)$
297 $\begin{smallmatrix} +27 \\ -29 \end{smallmatrix} \pm 6.4$	⁵ AUBERT	08AL BABR	Repl. by DEL-AMO-SANCHEZ 10F
302.0 $\begin{smallmatrix} +33.8 \\ -35.1 \end{smallmatrix} \pm 23.7$	⁶ POLUEKTOV	06 BELL	Repl. by POLUEKTOV 10
296 $\pm 41 \begin{smallmatrix} +20 \\ -19 \end{smallmatrix}$	⁷ AUBERT,B	05Y BABR	Repl. by AUBERT 08AL

¹ Measured using $B^\pm \rightarrow D^* K^\pm$ decays analysing the signal yield variation with the fully reconstructed $D^* \rightarrow D\pi^0/\gamma$, $D \rightarrow (KS)^0\pi^+\pi^-/(KS)^0K^+K^-$ decays. The model-independent approach uses external strong phase input from BESIII and CLEO collaborations.

² Reports combination of published measurements using GGSZ, GLW, and ADS methods. We added 360° to the value of $(-66 \pm 21)^\circ$ quoted by LEES 13B.

³ Uses Dalitz plot analysis of $\overline{D}^0 \rightarrow K_S^0\pi^+\pi^-$, $K_S^0 K^+K^-$ decays from $B^+ \rightarrow D^{(*)}K^{(*)}$ modes. The corresponding two standard deviation interval is $236^\circ < \delta_B^* < 322^\circ$.

⁴ Uses Dalitz plot analysis of $\overline{D}^0 \rightarrow K_S^0\pi^+\pi^-$ decays from $B^+ \rightarrow D^*K^+$ modes. The corresponding two standard deviation interval is $296.5^\circ < \delta_B^* < 382.7^\circ$.

⁵ Uses Dalitz plot analysis of $\overline{D}^0 \rightarrow K_S^0\pi^+\pi^-$ and $\overline{D}^0 \rightarrow K_S^0K^+K^-$ decays coming from $B^\pm \rightarrow D^{(*)}K^{(*)}$ modes.

⁶ Uses a Dalitz plot analysis of the $\overline{D}^0 \rightarrow K_S^0\pi^+\pi^-$ decays; Combines the $D K^+$, $D^* K^+$ and $D K^{*+}$ modes.

⁷ Uses a Dalitz analysis of neutral D decays to $K_S^0\pi^+\pi^-$ in the processes $B^\pm \rightarrow D^{(*)}K^\pm$, $D^* \rightarrow D\pi^0$, $D\gamma$.

 $r_B(B^+ \rightarrow D^{*0}\pi^+)$

r_B and δ_B are the amplitude ratio and relative strong phase between the amplitudes of $A(B^+ \rightarrow D^{*0}\pi^+)$ and $A(B^+ \rightarrow \overline{D}^{*0}\pi^+)$.

VALUE	DOCUMENT ID	TECN	COMMENT
0.01 ± 0.01	¹ AAIJ	23BA LHCb	pp at 7, 8, 13 TeV

• • • We do not use the following data for averages, fits, limits, etc. • • •

¹ Measured using $B^\pm \rightarrow D^*\pi^\pm$ decays analysing the signal yield variation with the fully reconstructed $D^* \rightarrow D\pi^0/\gamma$, $D \rightarrow (KS)^0\pi^+\pi^-/(KS)^0K^+K^-$ decays. The model-independent approach uses external strong phase input from BESIII and CLEO collaborations.

 $\delta_B(B^+ \rightarrow D^{*0}\pi^+)$

VALUE ($^\circ$)	DOCUMENT ID	TECN	COMMENT
--------------------	-------------	------	---------

• • • We do not use the following data for averages, fits, limits, etc. • • •

37 ± 37	¹ AAIJ	23BA LHCb	pp at 7, 8, 13 TeV
-------------	-------------------	-----------	----------------------

¹ Measured using $B^\pm \rightarrow D^*\pi^\pm$ decays analysing the signal yield variation with the fully reconstructed $D^* \rightarrow D\pi^0/\gamma$, $D \rightarrow (KS)^0\pi^+\pi^-/(KS)^0K^+K^-$ decays. The model-independent approach uses external strong phase input from BESIII and CLEO collaborations.

PARTIAL BRANCHING FRACTIONS

 $B(B^+ \rightarrow K^{*+}\ell^+\ell^-) (q^2 < 2.0 \text{ GeV}^2/c^4)$

VALUE (units 10^{-7})	DOCUMENT ID	TECN	COMMENT
1.4 ± 0.5 OUR AVERAGE			
1.37 $\begin{smallmatrix} +0.60 \\ -0.58 \end{smallmatrix}$	AAIJ	12AH LHCb	pp at 7 TeV
1.30 $\pm 0.98 \pm 0.14$	AALTONEN	11AI CDF	$p\overline{p}$ at 1.96 TeV

 $B(B^+ \rightarrow K^{*+}\ell^+\ell^-) (2.0 < q^2 < 4.3 \text{ GeV}^2/c^4)$

VALUE (units 10^{-7})	DOCUMENT ID	TECN	COMMENT
1.1 ± 0.5 OUR AVERAGE			
1.24 $\begin{smallmatrix} +0.60 \\ -0.55 \end{smallmatrix}$	AAIJ	12AH LHCb	pp at 7 TeV
0.71 $\pm 1.00 \pm 0.15$	AALTONEN	11AI CDF	$p\overline{p}$ at 1.96 TeV

 $B(B^+ \rightarrow K^{*+}\ell^+\ell^-) (4.3 < q^2 < 8.68 \text{ GeV}^2/c^4)$

VALUE (units 10^{-7})	DOCUMENT ID	TECN	COMMENT
2.4 $\begin{smallmatrix} +0.8 \\ -0.7 \end{smallmatrix}$ OUR AVERAGE			
2.50 $\begin{smallmatrix} +0.88 \\ -0.74 \end{smallmatrix}$	AAIJ	12AH LHCb	pp at 7 TeV
1.71 $\pm 1.58 \pm 0.49$	AALTONEN	11AI CDF	$p\overline{p}$ at 1.96 TeV

 $B(B^+ \rightarrow K^{*+}\ell^+\ell^-) (10.09 < q^2 < 12.86 \text{ GeV}^2/c^4)$

VALUE (units 10^{-7})	DOCUMENT ID	TECN	COMMENT
2.1 ± 0.6 OUR AVERAGE			
2.13 $\begin{smallmatrix} +0.72 \\ -0.66 \end{smallmatrix}$	AAIJ	12AH LHCb	pp at 7 TeV
1.97 $\pm 0.99 \pm 0.22$	AALTONEN	11AI CDF	$p\overline{p}$ at 1.96 TeV

 $B(B^+ \rightarrow K^{*+}\ell^+\ell^-) (14.18 < q^2 < 16.0 \text{ GeV}^2/c^4)$

VALUE (units 10^{-7})	DOCUMENT ID	TECN	COMMENT
0.86 $\begin{smallmatrix} +0.40 \\ -0.32 \end{smallmatrix}$ OUR AVERAGE			
1.00 $\begin{smallmatrix} +0.47 \\ -0.38 \end{smallmatrix}$	AAIJ	12AH LHCb	pp at 7 TeV
0.52 $\pm 0.61 \pm 0.09$	AALTONEN	11AI CDF	$p\overline{p}$ at 1.96 TeV

 $B(B^+ \rightarrow K^{*+}\ell^+\ell^-) (15.0 < q^2 < 19.0 \text{ GeV}^2/c^4)$

VALUE (units 10^{-7})	DOCUMENT ID	TECN	COMMENT
1.78 $\begin{smallmatrix} +0.32 \\ -0.25 \end{smallmatrix}$ OUR AVERAGE			
2.9 $\begin{smallmatrix} +1.0 \\ -0.8 \end{smallmatrix} \pm 0.3$	¹ WEHLE	21 BELL	$e^+e^- \rightarrow \Upsilon(4S)$
2.1 $\begin{smallmatrix} +1.2 \\ -1.0 \end{smallmatrix} \pm 0.2$	² WEHLE	21 BELL	$e^+e^- \rightarrow \Upsilon(4S)$
1.58 $\begin{smallmatrix} +0.32 \\ -0.29 \end{smallmatrix} \pm 0.11$	³ AAIJ	14M LHCb	pp at 7, 8 TeV

¹ Measured with $\mu^+\mu^-$ as lepton pair.

² Measured with e^+e^- as lepton pair.

³ Uses $B(B^+ \rightarrow J/\psi(1S)K^*(892)^+) = (1.431 \pm 0.027 \pm 0.090) \times 10^{-3}$ for normalization and $\mu^+\mu^-$ as a lepton pair.

 $B(B^+ \rightarrow K^{*+}\ell^+\ell^-) (q^2 > 16.0 \text{ GeV}^2/c^4)$

VALUE (units 10^{-7})	DOCUMENT ID	TECN	COMMENT
1.3 ± 0.4 OUR AVERAGE			
1.25 ± 0.46	AAIJ	12AH LHCb	pp at 7 TeV
1.57 $\pm 0.96 \pm 0.17$	AALTONEN	11AI CDF	$p\overline{p}$ at 1.96 TeV

 $B(B^+ \rightarrow K^{*+}\ell^+\ell^-) (1.0 < q^2 < 6.0 \text{ GeV}^2/c^4)$

VALUE (units 10^{-7})	DOCUMENT ID	TECN	COMMENT
1.72 $\begin{smallmatrix} +0.40 \\ -0.32 \end{smallmatrix}$ OUR AVERAGE			
1.2 $\begin{smallmatrix} +0.9 \\ -0.7 \end{smallmatrix} \pm 0.2$	^{1,2} WEHLE	21 BELL	$e^+e^- \rightarrow \Upsilon(4S)$
1.7 $\begin{smallmatrix} +1.0 \\ -1.0 \end{smallmatrix} \pm 0.2$	^{2,3} WEHLE	21 BELL	$e^+e^- \rightarrow \Upsilon(4S)$
1.79 $\begin{smallmatrix} +0.41 \\ -0.37 \end{smallmatrix} \pm 0.13$	⁴ AAIJ	14M LHCb	pp at 7, 8 TeV
2.57 $\pm 1.61 \pm 0.40$	AALTONEN	11AI CDF	$p\overline{p}$ at 1.96 TeV
• • • We do not use the following data for averages, fits, limits, etc. • • •			
2.90 $\begin{smallmatrix} +0.90 \\ -0.85 \end{smallmatrix}$	AAIJ	12AH LHCb	Repl. by AAIJ 14M

¹ Measured with $\mu^+\mu^-$ as lepton pair.

² Result is determined for the range $1.1 < q^2 < 6.0 \text{ GeV}^4/c^2$.

³ Measured with e^+e^- as lepton pair.

⁴ Uses $B(B^+ \rightarrow J/\psi(1S)K^*(892)^+) = (1.431 \pm 0.027 \pm 0.090) \times 10^{-3}$ for normalization and $\mu^+\mu^-$ as a lepton pair. Measured in $1.1 < q^2 < 6.0 \text{ GeV}^2/c^4$.

 $B(B^+ \rightarrow K^{*+}\ell^+\ell^-) (0.0 < q^2 < 4.3 \text{ GeV}^2/c^4)$

VALUE (units 10^{-7})	DOCUMENT ID	TECN	COMMENT
2.01 $\pm 1.39 \pm 0.27$			
	AALTONEN	11AI CDF	$p\overline{p}$ at 1.96 TeV

 $B(B^+ \rightarrow K^{*+}e^+e^-) (0.045 < q^2 < 6.0 \text{ GeV}^2/c^4)$

VALUE (units 10^{-8})	DOCUMENT ID	TECN	COMMENT
55 $\pm 11 \begin{smallmatrix} +5 \\ -4 \end{smallmatrix}$	¹ AAIJ	22I LHCb	pp at 7, 8, 13 TeV

¹ The reported value is converted from the measured $dB/dq^2 = (9.2 \pm 1.9 + 0.8) \times 10^{-8} (\text{GeV}^2/c^4)^{-1}$ by multiplying by the $\Delta q^2 = 5.955 \text{ GeV}^2/c^4$ range.

 $B(B^+ \rightarrow K^{*+}\mu^+\mu^-) / B(B^+ \rightarrow K^{*+}e^+e^-) (0.045 < q^2 < 1.1 \text{ GeV}^2/c^4)$

VALUE	DOCUMENT ID	TECN	COMMENT
0.62 $\begin{smallmatrix} +0.60 \\ -0.36 \end{smallmatrix} \pm 0.07$	WEHLE	21 BELL	$e^+e^- \rightarrow \Upsilon(4S)$

 $B(B^+ \rightarrow K^{*+}\mu^+\mu^-) / B(B^+ \rightarrow K^{*+}e^+e^-) (1.1 < q^2 < 6.0 \text{ GeV}^2/c^4)$

VALUE	DOCUMENT ID	TECN	COMMENT
0.72 $\begin{smallmatrix} +0.99 \\ -0.44 \end{smallmatrix} \pm 0.14$	WEHLE	21 BELL	$e^+e^- \rightarrow \Upsilon(4S)$

 $B(B^+ \rightarrow K^{*+}\mu^+\mu^-) / B(B^+ \rightarrow K^{*+}e^+e^-) (0.045 < q^2 < 6.0 \text{ GeV}^2/c^4)$

VALUE	DOCUMENT ID	TECN	COMMENT
0.70 $\begin{smallmatrix} +0.18 + 0.03 \\ -0.13 - 0.04 \end{smallmatrix}$	AAIJ	22I LHCb	pp at 7, 8, 13 TeV

 $B(B^+ \rightarrow K^{*+}\mu^+\mu^-) / B(B^+ \rightarrow K^{*+}e^+e^-) (15.0 < q^2 < 19.0 \text{ GeV}^2/c^4)$

VALUE	DOCUMENT ID	TECN	COMMENT
1.40 $\begin{smallmatrix} +1.99 \\ -0.68 \end{smallmatrix} \pm 0.11$	WEHLE	21 BELL	$e^+e^- \rightarrow \Upsilon(4S)$

 $B(B^+ \rightarrow K^+\ell^+\ell^-) (q^2 < 2.0 \text{ GeV}^2/c^4)$

VALUE (units 10^{-7})	DOCUMENT ID	TECN	COMMENT
0.51 ± 0.08 OUR AVERAGE			Error includes scale factor of 1.5.
0.556 $\pm 0.053 \pm 0.027$	¹ AAIJ	13H LHCb	pp at 7 TeV
0.36 $\pm 0.11 \pm 0.03$	AALTONEN	11AI CDF	$p\overline{p}$ at 1.96 TeV

¹ Measured in $0.05 < q^2 < 2.0 \text{ GeV}^2/c^4$ range.

B(B⁺ → K⁺ℓ⁺ℓ⁻) (2.0 < q² < 4.3 GeV²/c⁴)

VALUE (units 10 ⁻⁷)	DOCUMENT ID	TECN	COMMENT
0.60 ± 0.07 OUR AVERAGE	Error includes scale factor of 1.3.		
0.573 ± 0.053 ± 0.023	AAIJ	13H LHCb	pp at 7 TeV
0.80 ± 0.15 ± 0.05	AALTONEN	11A1 CDF	p \bar{p} at 1.96 TeV

B(B⁺ → K⁺ℓ⁺ℓ⁻) (4.3 < q² < 8.68 GeV²/c⁴)

VALUE (units 10 ⁻⁷)	DOCUMENT ID	TECN	COMMENT
1.03 ± 0.07 OUR AVERAGE			
1.003 ± 0.070 ± 0.039	AAIJ	13H LHCb	pp at 7 TeV
1.18 ± 0.19 ± 0.09	AALTONEN	11A1 CDF	p \bar{p} at 1.96 TeV

B(B⁺ → K⁺ℓ⁺ℓ⁻) (10.09 < q² < 12.86 GeV²/c⁴)

VALUE (units 10 ⁻⁷)	DOCUMENT ID	TECN	COMMENT
0.58 ± 0.05 OUR AVERAGE			
0.565 ± 0.050 ± 0.022	AAIJ	13H LHCb	pp at 7 TeV
0.68 ± 0.12 ± 0.05	AALTONEN	11A1 CDF	p \bar{p} at 1.96 TeV

B(B⁺ → K⁺ℓ⁺ℓ⁻) (14.18 < q² < 16.0 GeV²/c⁴)

VALUE (units 10 ⁻⁷)	DOCUMENT ID	TECN	COMMENT
0.40 ± 0.05 OUR AVERAGE	Error includes scale factor of 1.4.		
0.377 ± 0.036 ± 0.015	AAIJ	13H LHCb	pp at 7 TeV
0.53 ± 0.10 ± 0.03	AALTONEN	11A1 CDF	p \bar{p} at 1.96 TeV

B(B⁺ → K⁺ℓ⁺ℓ⁻) (16.0 < q² < 18.0 GeV²/c⁴)

VALUE (units 10 ⁻⁷)	DOCUMENT ID	TECN	COMMENT
0.354 ± 0.036 ± 0.018	AAIJ	13H LHCb	pp at 7 TeV

B(B⁺ → K⁺ℓ⁺ℓ⁻) (18.0 < q² < 22.0 GeV²/c⁴)

F_H is a fractional contribution of (pseudo) scalar and tensor amplitudes to the decay width in the massless muon approximation.

VALUE (units 10 ⁻⁷)	DOCUMENT ID	TECN	COMMENT
0.312 ± 0.040 ± 0.016	AAIJ	13H LHCb	pp at 7 TeV

B(B⁺ → K⁺ℓ⁺ℓ⁻) (15.0 < q² < 22.0 GeV²/c⁴)

VALUE (units 10 ⁻⁷)	DOCUMENT ID	TECN	COMMENT
0.85 ± 0.03 ± 0.04	¹ AAIJ	14M LHCb	pp at 7, 8 TeV

¹ Uses B(B⁺ → J/ψ(1S) K⁺) = (0.998 ± 0.014 ± 0.040) × 10⁻³ for normalization and μ⁺μ⁻ as a lepton pair.

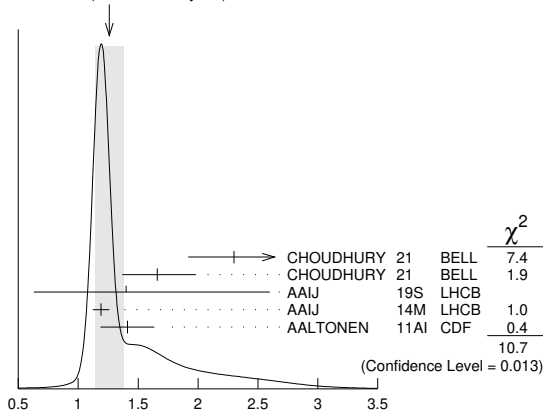
B(B⁺ → K⁺ℓ⁺ℓ⁻) (16.0 < q² < 22.0 GeV²/c⁴)

VALUE (units 10 ⁻⁷)	DOCUMENT ID	TECN	COMMENT
0.48 ± 0.11 ± 0.03	AALTONEN	11A1 CDF	p \bar{p} at 1.96 TeV

B(B⁺ → K⁺ℓ⁺ℓ⁻) (1.0 < q² < 6.0 GeV²/c⁴)

VALUE (units 10 ⁻⁷)	DOCUMENT ID	TECN	COMMENT
1.26 ± 0.12 OUR AVERAGE	Error includes scale factor of 1.9. See the ideogram below.		
2.30 ^{+0.41} / _{-0.38} ± 0.05	¹ CHOUDHURY	21 BELL	e ⁺ e ⁻ → γ(4S)
1.66 ^{+0.32} / _{-0.29} ± 0.04	² CHOUDHURY	21 BELL	e ⁺ e ⁻ → γ(4S)
1.40 ^{+0.98} / _{-0.34} ± 0.69	³ AAIJ	19S LHCb	pp at 7, 8, 13 TeV
1.19 ± 0.034 ± 0.059	⁴ AAIJ	14M LHCb	pp at 7, 8 TeV
1.41 ± 0.20 ± 0.10	AALTONEN	11A1 CDF	p \bar{p} at 1.96 TeV
• • • We do not use the following data for averages, fits, limits, etc. • • •			
1.56 ^{+0.19} / _{-0.15} ± 0.06	⁵ AAIJ	14AR LHCb	pp at 7, 8 TeV
1.205 ± 0.085 ± 0.070	AAIJ	13H LHCb	Repl. by AAIJ 14M

WEIGHTED AVERAGE
1.26±0.12 (Error scaled by 1.9)



B(B⁺ → K⁺ℓ⁺ℓ⁻) (1.0 < q² < 6.0 GeV²/c⁴) (units 10⁻⁷)

¹ Measured for B⁺ → K⁺μ⁺μ⁻ decays. Measurements in other q² bins are also reported.

² Measured for B⁺ → K⁺e⁺e⁻ decays. Measurements in other q² bins are also reported.

³ Measured by taking the ratio of the branching fraction from B⁺ → K⁺e⁺e⁻ and B⁺ → J/ψ(e⁺e⁻)K⁺ decays and multiplying it by the measured value of B⁺ → J/ψK⁺ and J/ψ → e⁺e⁻ as in PDG 18. The branching fraction of B⁺ → K⁺e⁺e⁻ is determined in the region 1.1 < q² < 6 GeV²/c⁴.

⁴ Uses B(B⁺ → J/ψ(1S) K⁺) = (0.998 ± 0.014 ± 0.040) × 10⁻³ for normalization and μ⁺μ⁻ for leptons. Measured for 1.1 < q² < 6.0 GeV²/c⁴.

⁵ Measured by taking the ratio of the branching fraction from B⁺ → K⁺e⁺e⁻ and B⁺ → J/ψ(e⁺e⁻)K⁺ decays and multiplying it by the measured value of B⁺ → J/ψK⁺ and J/ψ → e⁺e⁻ as in PDG 12. The branching fraction of B⁺ → K⁺e⁺e⁻ is determined in the region 1 < q² < 6 GeV²/c⁴.

B(B⁺ → K⁺μ⁺μ⁻) / B(B⁺ → K⁺e⁺e⁻) (0.1 < q² < 1.1 GeV²/c⁴)

VALUE	DOCUMENT ID	TECN	COMMENT
0.994^{+0.090}/_{-0.082} ± 0.029	AAIJ	23AB LHCb	pp at 7, 8, 13 TeV

B(B⁺ → K⁺μ⁺μ⁻) / B(B⁺ → K⁺e⁺e⁻) (1.0 < q² < 6.0 GeV²/c⁴)

VALUE	DOCUMENT ID	TECN	COMMENT
0.96 ± 0.05 OUR AVERAGE			
0.949 ^{+0.042} / _{-0.041} ± 0.022	¹ AAIJ	23AB LHCb	pp at 7, 8, 13 TeV
1.39 ^{+0.36} / _{-0.33} ± 0.02	² CHOUDHURY	21 BELL	e ⁺ e ⁻ → γ(4S)

• • • We do not use the following data for averages, fits, limits, etc. • • •

0.846 ^{+0.042} / _{-0.039} ± 0.013	^{3,4} AAIJ	22v LHCb	pp at 7, 8, 13 TeV
0.846 ^{+0.060} / _{-0.054} ± 0.016	^{3,5} AAIJ	19S LHCb	pp at 7, 8, 13 TeV
0.745 ^{+0.090} / _{-0.074} ± 0.036	³ AAIJ	14AR LHCb	pp at 7, 8 TeV

¹ Measured for the region 1.1 < q² < 6.0 GeV²/c⁴.

² Measurements in other q² bins are also reported.

³ The ratio is determined using the relative branching fractions of the decays B⁺ → K⁺ℓ⁺ℓ⁻ and B⁺ → J/ψ(→ ℓ⁺ℓ⁻)K⁺, with ℓ = e, μ. Measured for the region 1.1 < q² < 6.0 GeV²/c⁴.

⁴ Superseded by AAIJ 23AB.

⁵ Superseded by AAIJ 22v.

B(B⁺ → K⁺ℓ⁺ℓ⁻) (0.0 < q² < 4.3 GeV²/c⁴)

VALUE (units 10 ⁻⁷)	DOCUMENT ID	TECN	COMMENT
1.13 ± 0.19 ± 0.08	AALTONEN	11A1 CDF	p \bar{p} at 1.96 TeV

B(B⁺ → K⁺π⁺π⁻μ⁺μ⁻) (1.00 < q² < 6.00 GeV²/c⁴)

VALUE (units 10 ⁻⁷)	DOCUMENT ID	TECN	COMMENT
1.38^{+0.15}/_{-0.14} ± 0.08	AAIJ	14AZ LHCb	pp at 7, 8 TeV

B(B⁺ → K⁺π⁺π⁻μ⁺μ⁻) (0.10 < q² < 2.00 GeV²/c⁴)

VALUE (units 10 ⁻⁷)	DOCUMENT ID	TECN	COMMENT
1.33^{+0.13}/_{-0.12} ± 0.09	AAIJ	14AZ LHCb	pp at 7, 8 TeV

B(B⁺ → K⁺π⁺π⁻μ⁺μ⁻) (2.00 < q² < 4.30 GeV²/c⁴)

VALUE (units 10 ⁻⁸)	DOCUMENT ID	TECN	COMMENT
5.38^{+0.94}/_{-0.87} ± 0.35	AAIJ	14AZ LHCb	pp at 7, 8 TeV

B(B⁺ → K⁺π⁺π⁻μ⁺μ⁻) (4.30 < q² < 8.68 GeV²/c⁴)

VALUE (units 10 ⁻⁷)	DOCUMENT ID	TECN	COMMENT
1.01^{+0.12}/_{-0.13} ± 0.09	AAIJ	14AZ LHCb	pp at 7, 8 TeV

B(B⁺ → K⁺π⁺π⁻μ⁺μ⁻) (10.09 < q² < 12.86 GeV²/c⁴)

VALUE (units 10 ⁻⁸)	DOCUMENT ID	TECN	COMMENT
5.07^{+0.94}/_{-0.89} ± 0.47	AAIJ	14AZ LHCb	pp at 7, 8 TeV

B(B⁺ → K⁺π⁺π⁻μ⁺μ⁻) (14.18 < q² < 19.00 GeV²/c⁴)

VALUE (units 10 ⁻⁸)	DOCUMENT ID	TECN	COMMENT
0.48^{+0.39}/_{-0.29} ± 0.05	AAIJ	14AZ LHCb	pp at 7, 8 TeV

B(B⁺ → π⁺μ⁺μ⁻)/B(B⁺ → K⁺μ⁺μ⁻) (1.00 < q² < 6.00 GeV²/c⁴)

VALUE (units 10 ⁻²)	DOCUMENT ID	TECN	COMMENT
3.8 ± 0.9 ± 0.1	AAIJ	15AR LHCb	pp at 7, 8 TeV

B(B⁺ → π⁺μ⁺μ⁻) (1.00 < q² < 6.00 GeV²/c⁴)

VALUE (units 10 ⁻³)	DOCUMENT ID	TECN	COMMENT
4.55^{+1.05}/_{-1.00} ± 0.15	AAIJ	15AR LHCb	pp at 7, 8 TeV

B(B⁺ → π⁺μ⁺μ⁻) (15.00 < q² < 22.00 GeV²/c⁴)

VALUE (units 10 ⁻³)	DOCUMENT ID	TECN	COMMENT
3.29^{+0.84}/_{-0.70} ± 0.07	AAIJ	15AR LHCb	pp at 7, 8 TeV

Meson Particle Listings

 B^\pm $A_{FB}(B^\pm \rightarrow \pi^+ \mu^+ \mu^-) / A_{FB}(B^\pm \rightarrow K^+ \mu^+ \mu^-)$ ($15.0 < q^2 < 22.0 \text{ GeV}^2/c^4$)

VALUE (units 10^{-2})	DOCUMENT ID	TECN	COMMENT
$3.7 \pm 0.8 \pm 0.1$	AAIJ	15AR	LHCb pp at 7, 8 TeV

 $A_{FB}(B^\pm \rightarrow K^+ \mu^+ \mu^-)$ ($1.1 < q^2 < 6.0 \text{ GeV}^2/c^4$)

A_{FB} is the forward-backward angular asymmetry of the lepton pair in $B \rightarrow K^{(*)} \ell^+ \ell^-$ decay as defined in B^\pm, B^0 admixture particle listings.

VALUE	DOCUMENT ID	TECN	COMMENT
-0.003 ± 0.017 OUR AVERAGE			
$-0.14^{+0.07}_{-0.06} \pm 0.03$	¹ SIRUNYAN	18DX	CMS pp at 8 TeV
$0.005 \pm 0.015 \pm 0.010$	² AAIJ	14o	LHCb pp at 7, 8 TeV
$0.02^{+0.05}_{-0.03} \pm 0.02$	AAIJ	13H	LHCb Repl. by AAIJ 14o

¹ Measurement is performed in $1.0 < q^2 < 6.0 \text{ GeV}^2/c^4$. SIRUNYAN 18DX reports also measurements in several other q^2 intervals.

² AAIJ 14o reports 68% C.L. interval, which we encode as midpoint with uncertainty as half of the width of interval.

 $A_{FB}(B^\pm \rightarrow K^+ \mu^+ \mu^-)$ ($15.0 < q^2 < 22.0 \text{ GeV}^2/c^4$)

VALUE	DOCUMENT ID	TECN	COMMENT
$-0.015 \pm 0.015 \pm 0.01$	¹ AAIJ	14o	LHCb pp at 7, 8 TeV

¹ AAIJ 14o reports 68% C.L. interval, which we encode as midpoint with uncertainty as half of the width of interval.

 $F_H(B^\pm \rightarrow K^+ \mu^+ \mu^-)$ ($1.1 < q^2 < 6.0 \text{ GeV}^2/c^4$)

F_H is a fractional contribution of (pseudo) scalar and tensor amplitudes to the decay width in the massless muon approximation.

VALUE	DOCUMENT ID	TECN	COMMENT
0.04 ± 0.04 OUR AVERAGE			
$0.38^{+0.17}_{-0.21} \pm 0.09$	¹ SIRUNYAN	18DX	CMS pp at 8 TeV
$0.03 \pm 0.03 \pm 0.02$	² AAIJ	14o	LHCb pp at 7, 8 TeV
$0.05^{+0.08}_{-0.05} \pm 0.04$	AAIJ	13H	LHCb Repl. by AAIJ 14o

¹ Measurement is performed in $1.0 < q^2 < 6.0 \text{ GeV}^2/c^4$. SIRUNYAN 18DX reports also measurements in several other q^2 intervals.

² AAIJ 14o reports 68% C.L. interval, which we encode as midpoint with uncertainty as half of the width of interval.

 $F_H(B^\pm \rightarrow K^+ \mu^+ \mu^-)$ ($15.0 < q^2 < 22.0 \text{ GeV}^2/c^4$)

F_H is a fractional contribution of (pseudo) scalar and tensor amplitudes to the decay width in the massless muon approximation.

VALUE	DOCUMENT ID	TECN	COMMENT
$0.035 \pm 0.035 \pm 0.02$	¹ AAIJ	14o	LHCb pp at 7, 8 TeV

¹ AAIJ 14o reports 68% C.L. interval, which we encode as midpoint with uncertainty as half of the width of interval.

FORWARD-BACKWARD ASYMMETRIES

The forward-backward asymmetry is defined as $A_{FB} = [N(q_{FB} > 0) - N(q_{FB} < 0)] / [N(q_{FB} > 0) + N(q_{FB} < 0)]$, where $q_{FB} = -q_B \cdot \text{sgn}(\eta_B)$ with q_B as the B hadron electric charge, η_B as its pseudorapidity, and $\text{sgn}(\eta_B)$ as a sign function of η_B .

 $A_{FB}(B^\pm \rightarrow J/\psi K^\pm)$

VALUE (units 10^{-2})	DOCUMENT ID	TECN	COMMENT
$-0.24 \pm 0.41 \pm 0.19$	ABAZOV	15	D0 $p\bar{p}$ at 1.96 TeV

 A_{FB} in $B^+ \rightarrow \bar{D}^{*0} e^+ \nu_e$

VALUE	DOCUMENT ID	TECN	COMMENT
$0.234 \pm 0.026 \pm 0.006$	PRIM	23	BELL $e^+ e^- \rightarrow \Upsilon(4S)$

 A_{FB} in $B^+ \rightarrow \bar{D}^{*0} \mu^+ \nu_\mu$

VALUE	DOCUMENT ID	TECN	COMMENT
$0.243 \pm 0.026 \pm 0.006$	PRIM	23	BELL $e^+ e^- \rightarrow \Upsilon(4S)$

 $\Delta(A_{FB}) = (A_{FB}^\mu - A_{FB}^e)$ in $B^+ \rightarrow \bar{D}^{*0} \ell^+ \nu_\ell$

VALUE	DOCUMENT ID	TECN	COMMENT
$0.008 \pm 0.037 \pm 0.009$	PRIM	23	BELL $e^+ e^- \rightarrow \Upsilon(4S)$

 $A_{FB}(B^\pm \rightarrow K^*(892)^+ \mu^+ \mu^-)$ ($1.0 < q^2 < 8.68 \text{ GeV}^2/c^4$)

VALUE	DOCUMENT ID	TECN	COMMENT
$-0.14^{+0.32}_{-0.35} \pm 0.17$	^{1,2} SIRUNYAN	21AC	CMS pp at 8 TeV

¹ SIRUNYAN 21AC measurement is performed in $1.0 < q^2 < 8.68 \text{ GeV}^2/c^4$. Reports also measurements in several other q^2 intervals.

² A_{FB} is defined with respect to $\mu^+ \mu^-$ direction and not the B direction.

 $A_{FB}(B^\pm \rightarrow K^*(892)^+ \mu^+ \mu^-)$ ($1.1 < q^2 < 6.0 \text{ GeV}^2/c^4$)

VALUE	DOCUMENT ID	TECN	COMMENT
$-0.08^{+0.07}_{-0.06} \pm 0.02$	¹ AAIJ	21J	LHCb pp at 7, 8, 13 TeV

¹ The full set of CP-averaged angular observables is measured as a function of the q^2 . The A_{FB} is measured related to the dimuon system.

 $A_{FB}(B^\pm \rightarrow K^*(892)^+ \mu^+ \mu^-)$ ($10.09 < q^2 < 12.86 \text{ GeV}^2/c^4$)

VALUE	DOCUMENT ID	TECN	COMMENT
$0.09^{+0.16}_{-0.11} \pm 0.04$	^{1,2} SIRUNYAN	21AC	CMS pp at 8 TeV

¹ SIRUNYAN 21AC measurement is performed in $10.09 < q^2 < 12.86 \text{ GeV}^2/c^4$. Reports also measurements in several other q^2 intervals.

² A_{FB} is defined with respect to $\mu^+ \mu^-$ direction and not the B direction.

 $A_{FB}(B^\pm \rightarrow K^*(892)^+ \mu^+ \mu^-)$ ($14.18 < q^2 < 19.0 \text{ GeV}^2/c^4$)

VALUE	DOCUMENT ID	TECN	COMMENT
$0.33^{+0.11}_{-0.07} \pm 0.05$	^{1,2} SIRUNYAN	21AC	CMS pp at 8 TeV

¹ SIRUNYAN 21AC measurement is performed in $14.18 < q^2 < 19.0 \text{ GeV}^2/c^4$. Reports also measurements in several other q^2 intervals.

² A_{FB} is defined with respect to $\mu^+ \mu^-$ direction and not the B direction.

 $A_{FB}(B^\pm \rightarrow K^*(892)^+ \mu^+ \mu^-)$ ($15.0 < q^2 < 19.0 \text{ GeV}^2/c^4$)

VALUE	DOCUMENT ID	TECN	COMMENT
$0.31 \pm 0.06 \pm 0.04$	¹ AAIJ	21J	LHCb pp at 7, 8, 13 TeV

¹ The full set of CP-averaged angular observables is measured as a function of the q^2 . The A_{FB} is measured related to the dimuon system.

 $A_{FB}(B^\pm) = [\sigma(B^-) - \sigma(B^+)] / [\sigma(B^-) + \sigma(B^+)]$

VALUE (units 10^{-3})	DOCUMENT ID	TECN	COMMENT
-5.7 ± 1.7 OUR AVERAGE			
$-7.0 \pm 0.8 \pm 3.1$	¹ AAIJ	23U	LHCb pp at 13 TeV
$-4.1 \pm 4.9 \pm 1.0$	² AAIJ	17AP	LHCb pp at 7 TeV
$-5.3 \pm 3.1 \pm 1.0$	² AAIJ	17AP	LHCb pp at 8 TeV
$-2.3 \pm 2.4 \pm 3.7$	³ AAIJ	17BF	LHCb pp at 7 TeV
$-7.4 \pm 1.5 \pm 3.2$	³ AAIJ	17BF	LHCb pp at 8 TeV

¹ The second error includes the uncertainties from $A_{CP}(B^+ \rightarrow J/\psi K^+) = 0.0018 \pm 0.0030$.

² AAIJ 17AP uses $B^+ \rightarrow \bar{D}^0 \pi^+$ decays with B^+ transverse momenta p_T and rapidities y in the region of $2 < p_T < 30 \text{ GeV}/c$ and $2.1 < y < 4.5$.

³ AAIJ 17BF uses $B^+ \rightarrow J/\psi K^+$ decays with B^+ transverse momenta p_T and rapidities y in the region of $0 < p_T < 30 \text{ GeV}/c$ and $2.1 < y < 4.5$.

 B^\pm REFERENCES

ADACHI	24	PR D109 012001	I. Adachi <i>et al.</i>	(BELLE II Collab.)
AAIJ	23AB	PRL 131 051803	R. Aaij <i>et al.</i>	(LHCb Collab.)
Also		PR D108 032002	R. Aaij <i>et al.</i>	(LHCb Collab.)
AAIJ	23AH	PR D108 032010	R. Aaij <i>et al.</i>	(LHCb Collab.)
AAIJ	23AI	PR D108 034012	R. Aaij <i>et al.</i>	(LHCb Collab.)
AAIJ	23AK	JHEP 2308 174	R. Aaij <i>et al.</i>	(LHCb Collab.)
Also		JHEP 2308 174	R. Aaij <i>et al.</i>	(LHCb Collab.)
AAIJ	23AR	PRL 131 111802	R. Aaij <i>et al.</i>	(LHCb Collab.)
AAIJ	23AX	JHEP 2309 202	R. Aaij <i>et al.</i>	(LHCb Collab.)
AAIJ	23B	PR D108 012017	R. Aaij <i>et al.</i>	(LHCb Collab.)
AAIJ	23BA	JHEP 2312 013	R. Aaij <i>et al.</i>	(LHCb Collab.)
AAIJ	23I	JHEP 2307 138	R. Aaij <i>et al.</i>	(LHCb Collab.)
AAIJ	23N	EPJ C83 547	R. Aaij <i>et al.</i>	(LHCb Collab.)
Also		EPJ C83 672 (errat.)	R. Aaij <i>et al.</i>	(LHCb Collab.)
AAIJ	23Q	PRL 131 031901	R. Aaij <i>et al.</i>	(LHCb Collab.)
AAIJ	23U	PR D108 012008	R. Aaij <i>et al.</i>	(LHCb Collab.)
AAIJ	23V	PR D108 012013	R. Aaij <i>et al.</i>	(LHCb Collab.)
AAIJ	23X	PR D108 012020	R. Aaij <i>et al.</i>	(LHCb Collab.)
ADACHI	23L	JHEP 2309 146	I. Adachi <i>et al.</i>	(BELLE II Collab.)
CHU	23	PR D108 112007	K.-M. Chu <i>et al.</i>	(BELLE Collab.)
HIRATA	23	PR D107 112011	H. Hirata <i>et al.</i>	(BELLE Collab.)
HSU	23	PR D107 032013	C.-L. Hsu <i>et al.</i>	(BELLE Collab.)
KUMAR	23	PR D107 L031101	M. Kumar <i>et al.</i>	(BELLE Collab.)
LAI	23	PRL 130 181804	Y.-T. Lai <i>et al.</i>	(BELLE Collab.)
LEES	23C	PRL 131 201801	J.P. Lees <i>et al.</i>	(BABAR Collab.)
MEIER	23	PR D107 092003	F. Meier <i>et al.</i>	(BELLE Collab.)
PRIM	23	PR D108 012002	M.T. Prim <i>et al.</i>	(BELLE Collab.)
WATANUKI	23	PRL 130 261802	S. Watanuki <i>et al.</i>	(BELLE Collab.)
AAIJ	22D	JHEP 2204 046	R. Aaij <i>et al.</i>	(LHCb Collab.)
AAIJ	22J	PRL 128 191802	R. Aaij <i>et al.</i>	(LHCb Collab.)
AAIJ	22T	JHEP 2207 099	R. Aaij <i>et al.</i>	(LHCb Collab.)
AAIJ	22V	NATP 18 277	R. Aaij <i>et al.</i>	(LHCb Collab.)
ABUDINEN	22	JHEP 2202 063	F. Abudinen <i>et al.</i>	(BELLE and BELLE II Collab.)
BLOOMFIELD	22	PR D105 072007	T. Bloomfield <i>et al.</i>	(BELLE Collab.)
GEBAUER	22	PR D106 032013	U. Gebauer <i>et al.</i>	(BELLE Collab.)
AAIJ	21AM	JHEP 2112 141	R. Aaij <i>et al.</i>	(LHCb Collab.)
AAIJ	21H	PRL 126 091802	R. Aaij <i>et al.</i>	(LHCb Collab.)
AAIJ	21J	PRL 126 161802	R. Aaij <i>et al.</i>	(LHCb Collab.)
AAIJ	21L	JHEP 2102 169	R. Aaij <i>et al.</i>	(LHCb Collab.)
AAIJ	21M	JHEP 2103 137	R. Aaij <i>et al.</i>	(LHCb Collab.)
AAIJ	21Q	JHEP 2104 081	R. Aaij <i>et al.</i>	(LHCb Collab.)
ABUDINEN	21	PRL 127 181802	F. Abudinen <i>et al.</i>	(BELLE II Collab.)
BELENO	21	PR D103 112001	C. Belenko <i>et al.</i>	(BELLE Collab.)
CAO	21A	PR D104 012008	L. Cao <i>et al.</i>	(BELLE Collab.)
CHOUHURY	21	JHEP 2103 105	S. Choudhury <i>et al.</i>	(BELLE Collab.)
MOHANTY	21	PR D103 052013	S. Mohanty <i>et al.</i>	(BELLE Collab.)
SIRUNYAN	21AC	JHEP 2104 124	A.M. Sirunyan <i>et al.</i>	(CMS Collab.)
WEHLE	21	PRL 126 161801	S. Wehle <i>et al.</i>	(BELLE Collab.)
AAIJ	20A	PRL 124 031801	R. Aaij <i>et al.</i>	(LHCb Collab.)
Also		PR D101 012006	R. Aaij <i>et al.</i>	(LHCb Collab.)
AAIJ	20AI	PR D102 112003	R. Aaij <i>et al.</i>	(LHCb Collab.)
AAIJ	20AJ	PR D102 112010	R. Aaij <i>et al.</i>	(LHCb Collab.)
AAIJ	20AN	JHEP 2012 139	R. Aaij <i>et al.</i>	(LHCb Collab.)
AAIJ	20D	PR D101 032005	R. Aaij <i>et al.</i>	(LHCb Collab.)
AAIJ	20K	JHEP 2003 146	R. Aaij <i>et al.</i>	(LHCb Collab.)
AAIJ	20N	JHEP 2006 058	R. Aaij <i>et al.</i>	(LHCb Collab.)
AAIJ	20P	JHEP 2006 129	R. Aaij <i>et al.</i>	(LHCb Collab.)
AAIJ	20S	JHEP 2008 123	R. Aaij <i>et al.</i>	(LHCb Collab.)
CHILIKIN	20	JHEP 2005 034	K. Chilikin <i>et al.</i>	(BELLE Collab.)
CHU	20	PR D101 052012	K. Chu <i>et al.</i>	(BELLE Collab.)
LEES	20C	PRL 124 152001	J.P. Lees <i>et al.</i>	(BABAR Collab.)
PRIM	20	PRL D101 032007	M.T. Prim <i>et al.</i>	(BELLE Collab.)
AAIJ	19AC	PR D99 092009	R. Aaij <i>et al.</i>	(LHCb Collab.)
AAIJ	19AL	PRL 123 231802	R. Aaij <i>et al.</i>	(LHCb Collab.)
AAIJ	19AM	PRL 123 241802	R. Aaij <i>et al.</i>	(LHCb Collab.)

GODANG	02	PRL 88 021802	R. Godang et al.	(CLEO Collab.)
GORDON	02	PL B542 183	A. Gordon et al.	(BELLE Collab.)
LU	02	PRL 89 191801	R.-S. Lu et al.	(BELLE Collab.)
MAHAPATRA	02	PRL 88 101803	R. Mahapatra et al.	(CLEO Collab.)
NISHIDA	02	PRL 89 231801	S. Nishida et al.	(BELLE Collab.)
ABE	01H	PRL 87 101801	K. ABE et al.	(BELLE Collab.)
ABE	01I	PRL 87 111801	K. ABE et al.	(BELLE Collab.)
ABE	01K	PR D64 071101	K. ABE et al.	(BELLE Collab.)
ABE	01L	PRL 87 161401	K. ABE et al.	(BELLE Collab.)
ABE	01M	PL B517 309	K. ABE et al.	(BELLE Collab.)
ALEXANDER	01B	PR D64 092001	J.P. Alexander et al.	(CLEO Collab.)
AMMAR	01B	PRL 87 271801	R. Ammar et al.	(CLEO Collab.)
ANDERSON	01B	PRL 87 181803	S. Anderson et al.	(CLEO Collab.)
AUBERT	01D	PRL 87 151801	B. Aubert et al.	(BABAR Collab.)
AUBERT	01E	PRL 87 151802	B. Aubert et al.	(BABAR Collab.)
AUBERT	01F	PRL 87 201803	B. Aubert et al.	(BABAR Collab.)
AUBERT	01G	PRL 87 221802	B. Aubert et al.	(BABAR Collab.)
BARATE	01E	EPJ C19 213	R. Barate et al.	(ALEPH Collab.)
BIERE	01	PRL 86 3718	R.A. Biere et al.	(CLEO Collab.)
BROWDER	01	PRL 86 2950	T.E. Browder et al.	(CLEO Collab.)
EDWARDS	01	PRL 86 30	K.W. Edwards et al.	(CLEO Collab.)
GRITSAN	01	PR D64 077501	A. Gritsan et al.	(CLEO Collab.)
RICHICHI	01	PR D63 031103	S.J. Richichi et al.	(CLEO Collab.)
ABBIENDI	00B	PL B476 233	G. Abbiendi et al.	(OPAL Collab.)
ABE	00C	PR D62 071101	K. ABE et al.	(SLD Collab.)
AHMED	00B	PR D62 112003	S. Ahmed et al.	(CLEO Collab.)
ANASTASSOV	00	PRL 84 1393	A. Anastassov et al.	(CLEO Collab.)
BARATE	00R	PL B492 275	R. Barate et al.	(ALEPH Collab.)
BEHRENS	00	PR D61 052001	B.H. Behrens et al.	(CLEO Collab.)
BONVICINI	00	PRL 84 5940	G. Bonvicini et al.	(CLEO Collab.)
CHEM	00	PRL 85 525	S. Chen et al.	(CLEO Collab.)
COAN	00	PRL 84 5283	T.E. Coan et al.	(CLEO Collab.)
CRONIN-HEN...	00	PRL 85 515	D. Cronin-Hennessy et al.	(CLEO Collab.)
CSORNA	00	PR D61 111101	S.E. Csorna et al.	(CLEO Collab.)
JESSOP	00	PRL 85 2881	C.P. Jessop et al.	(CLEO Collab.)
RICHICHI	00	PRL 85 520	S.J. Richichi et al.	(CLEO Collab.)
ABBIENDI	99J	EPJ C12 609	G. Abbiendi et al.	(OPAL Collab.)
AFFOLDER	99B	PRL 83 3378	T. Affolder et al.	(CDF Collab.)
BARTELT	99	PRL 82 3746	J. Bartelt et al.	(CLEO Collab.)
COAN	99	PR D59 111101	T.E. Coan et al.	(CLEO Collab.)
ABE	98B	PR D57 5382	F. ABE et al.	(CDF Collab.)
ABE	98O	PR D58 072001	F. ABE et al.	(CDF Collab.)
ABE	98Q	PR D58 092002	F. ABE et al.	(CDF Collab.)
ACCIARRI	98S	PL B438 417	M. Acciari et al.	(L3 Collab.)
ANASTASSOV	98	PRL 80 4127	A. Anastassov et al.	(CLEO Collab.)
ATHANAS	98	PRL 80 5493	M. Athanas et al.	(CLEO Collab.)
BARATE	98Q	EPJ C4 387	R. Barate et al.	(ALEPH Collab.)
BEHRENS	98	PRL 80 3710	B.H. Behrens et al.	(CLEO Collab.)
BERGFELD	98	PRL 81 272	T. Bergfeld et al.	(CLEO Collab.)
BRANDENB...	98	PRL 80 2762	G. Brandenburger et al.	(BCIP, CERN)
CAPRINI	98	NP B530 153	I. Caprini, L. Lelouch, M. Neubert	(CLEO Collab.)
GODANG	98	PRL 80 3456	R. Godang et al.	(CLEO Collab.)
ABE	97J	PRL 79 590	K. ABE et al.	(SLD Collab.)
ACCIARRI	97F	PL B396 327	M. Acciari et al.	(L3 Collab.)
ARTUSO	97	PL B399 321	M. Artuso et al.	(CLEO Collab.)
ATHANAS	97	PRL 79 2208	M. Athanas et al.	(CLEO Collab.)
BROWDER	97	PR D56 11	T. Browder et al.	(CLEO Collab.)
FU	97	PRL 79 3125	X. Fu et al.	(CLEO Collab.)
JESSOP	97	PRL 79 4533	C.P. Jessop et al.	(CLEO Collab.)
ABE	96B	PR D53 3496	F. ABE et al.	(CDF Collab.)
ABE	96C	PRL 76 4462	F. ABE et al.	(CDF Collab.)
ABE	96H	PRL 76 2015	F. ABE et al.	(CDF Collab.)
ABE	96L	PRL 76 4675	F. ABE et al.	(CDF Collab.)
ABE	96Q	PR D54 6596	F. ABE et al.	(CDF Collab.)
ABE	96R	PRL 77 5176	F. ABE et al.	(CDF Collab.)
ADAM	96D	ZPHY C72 207	W. Adam et al.	(DELPHI Collab.)
ALEXANDER	96T	PRL 77 5000	J.P. Alexander et al.	(CLEO Collab.)
ASNER	96	PR D53 1039	D.M. Asner et al.	(CLEO Collab.)
BARISH	96B	PRL 76 1570	B.C. Barish et al.	(CLEO Collab.)
BERGFELD	96B	PRL 77 4503	T. Bergfeld et al.	(CLEO Collab.)
BISHAI	96	PL B369 186	M. Bishai et al.	(CLEO Collab.)
BUSKULIC	96J	ZPHY C71 31	D. Buskulic et al.	(ALEPH Collab.)
GIBAUT	96	PR D53 4734	D. Gibaut et al.	(CLEO Collab.)
PDG	96	PR D54 1	R. M. Barnett et al.	(PDG Collab.)
ABREU	95N	PL B357 255	P. Abreu et al.	(DELPHI Collab.)
ABREU	95Q	ZPHY C68 13	P. Abreu et al.	(DELPHI Collab.)
ADAM	95	ZPHY C68 363	W. Adam et al.	(DELPHI Collab.)
AKERS	95T	ZPHY C67 379	R. Akers et al.	(OPAL Collab.)
ALBRECHT	95D	PL B353 554	H. Albrecht et al.	(ARGUS Collab.)
ALEXANDER	95	PL B341 435	J. Alexander et al.	(CLEO Collab.)
Also		PL B347 469 (errata)	J. Alexander et al.	(CLEO Collab.)
ARTUSO	95	PRL 75 785	M. Artuso et al.	(CLEO Collab.)
BARISH	95	PR D51 1014	B.C. Barish et al.	(CLEO Collab.)
BUSKULIC	95	PL B343 444	D. Buskulic et al.	(ALEPH Collab.)
ABE	94D	PRL 72 3456	F. ABE et al.	(CDF Collab.)
ALAM	94	PR D50 43	M.S. Alam et al.	(CLEO Collab.)
ALBRECHT	94D	PL B335 526	H. Albrecht et al.	(ARGUS Collab.)
ATHANAS	94	PRL 73 3503	M. Athanas et al.	(CLEO Collab.)
Also		PRL 74 3090 (errata)	M. Athanas et al.	(CLEO Collab.)
PDG	94	PR D50 1173	L. Montanet et al.	(CERN, LBL, BOST+)
STONE	94	HEPSY 93-11	S. Stone	(CERN, LBL, BOST+)
Published in B Decays, 2nd Edition, World Scientific, Singapore				
ABREU	93D	ZPHY C57 181	P. Abreu et al.	(DELPHI Collab.)
ABREU	93G	PL B312 253	P. Abreu et al.	(DELPHI Collab.)
ACTON	93C	PL B307 247	P.D. Acton et al.	(OPAL Collab.)
ALBRECHT	93E	ZPHY C60 11	H. Albrecht et al.	(ARGUS Collab.)
ALEXANDER	93B	PL B319 365	J. Alexander et al.	(CLEO Collab.)
AMMAR	93	PRL 71 674	R. Ammar et al.	(CLEO Collab.)
BEAN	93B	PRL 70 2681	A. Bean et al.	(CLEO Collab.)
BUSKULIC	93D	PL B307 194	D. Buskulic et al.	(ALEPH Collab.)
Also		PL B325 537 (errata)	D. Buskulic et al.	(ALEPH Collab.)
SANGHERA	93	PR D47 791	S. Sanghera et al.	(CLEO Collab.)
ALBRECHT	92C	PL B275 195	H. Albrecht et al.	(ARGUS Collab.)
ALBRECHT	92E	PL B277 209	H. Albrecht et al.	(ARGUS Collab.)
ALBRECHT	92G	ZPHY C54 1	H. Albrecht et al.	(ARGUS Collab.)
BORTOLETTO	92	PR D45 21	D. Bortoletto et al.	(CLEO Collab.)
BUSKULIC	92G	PL B295 396	D. Buskulic et al.	(ALEPH Collab.)
ALBRECHT	91B	PL B254 288	H. Albrecht et al.	(ARGUS Collab.)
ALBRECHT	91C	PL B255 297	H. Albrecht et al.	(ARGUS Collab.)
ALBRECHT	91E	PL B262 148	H. Albrecht et al.	(ARGUS Collab.)
BERKELMAN	91	ARNPS 41 1	K. Berkelman, S. Stone	(CORN, SYRA)
"Decays of B Mesons"				
FULTON	91	PR D43 651	R. Fulton et al.	(CLEO Collab.)
ALBRECHT	90B	PL B241 278	H. Albrecht et al.	(ARGUS Collab.)
ALBRECHT	90J	ZPHY C48 543	H. Albrecht et al.	(ARGUS Collab.)
ANTREASYAN	90B	ZPHY C48 553	D. Antreasyan et al.	(Crystal Ball Collab.)
BORTOLETTO	90	PR D44 2117	D. Bortoletto et al.	(CLEO Collab.)
Also		PR D45 21	D. Bortoletto et al.	(CLEO Collab.)
WEIR	90B	PR D41 1384	A.J. Weir et al.	(Mark II Collab.)
ALBRECHT	89G	PL B229 304	H. Albrecht et al.	(ARGUS Collab.)
AVERY	89B	PL B223 470	P. Avery et al.	(CLEO Collab.)

BEBEK	89	PRL 62 8	C. Bebek et al.	(CLEO Collab.)
BORTOLETTO	89	PRL 62 2436	D. Bortoletto et al.	(CLEO Collab.)
ALBRECHT	88F	PL B209 119	H. Albrecht et al.	(ARGUS Collab.)
ALBRECHT	88K	PL B215 424	H. Albrecht et al.	(ARGUS Collab.)
ALBRECHT	87C	PL B185 218	H. Albrecht et al.	(ARGUS Collab.)
ALBRECHT	87D	PL B199 451	H. Albrecht et al.	(ARGUS Collab.)
AVERY	87	PL B183 429	P. Avery et al.	(CLEO Collab.)
BEBEK	87	PR D36 1289	C. Bebek et al.	(CLEO Collab.)
ALAM	86	PR D34 3279	M.S. Alam et al.	(CLEO Collab.)
PDG	86	PL 170B 1	M. Aguilar-Benitez et al.	(CERN, CIT+)
GILES	84	PR D30 2279	R. Giles et al.	(CLEO Collab.)

B^0

$$I(J^P) = \frac{1}{2}(0^-)$$

Quantum numbers not measured. Values shown are quark-model predictions.

See also the B^\pm/B^0 ADMIXTURE and $B^\pm/B^0/B_s^0/b$ -baryon ADMIXTURE sections.

See the Note "Production and Decay of b -flavored Hadrons" at the beginning of the B^\pm Particle Listings and the Note on " $B^0-\bar{B}^0$ Mixing" near the end of the B^0 Particle Listings.

B^0 MASS

The fit uses m_{B^\pm} , ($m_{B^0} - m_{B^\pm}$), and m_{B^0} to determine m_{B^\pm} , m_{B^0} , and the mass difference.

VALUE (MeV)	EVTS	DOCUMENT ID	TECN	COMMENT
5279.72 ± 0.08 OUR FIT				
5279.63 ± 0.20 OUR AVERAGE				
5279.74 ± 0.30 ± 0.10		1 AAIJ	19U LHCb	pp at 7, 8, 13 TeV
5279.6 ± 0.2 ± 1.0		2 AAD	13U ATLAS	pp at 7 TeV
5279.58 ± 0.15 ± 0.28		3 AAIJ	12E LHCb	pp at 7 TeV
5279.63 ± 0.53 ± 0.33		4 ACOSTA	06 CDF	$p\bar{p}$ at 1.96 TeV
5279.1 ± 0.7 ± 0.3	135	5 CSORNA	00 CLE2	$e^+e^- \rightarrow \Upsilon(4S)$
5281.3 ± 2.2 ± 1.4	51	ABE	96B CDF	$p\bar{p}$ at 1.8 TeV
• • • We do not use the following data for averages, fits, limits, etc. • • •				
5279.2 ± 0.54 ± 2.0	340	ALAM	94 CLE2	$e^+e^- \rightarrow \Upsilon(4S)$
5278.0 ± 0.4 ± 2.0		BORTOLETTO92	CLEO	$e^+e^- \rightarrow \Upsilon(4S)$
5279.6 ± 0.7 ± 2.0	40	6 ALBRECHT	90J ARG	$e^+e^- \rightarrow \Upsilon(4S)$
5278.2 ± 1.0 ± 3.0	40	ALBRECHT	87C ARG	$e^+e^- \rightarrow \Upsilon(4S)$
5279.5 ± 1.6 ± 3.0	7	7 ALBRECHT	87D ARG	$e^+e^- \rightarrow \Upsilon(4S)$
5280.6 ± 0.8 ± 2.0		BEBEK	87 CLEO	$e^+e^- \rightarrow \Upsilon(4S)$

- 1 Uses $B^0 \rightarrow J/\psi p\bar{p}$ decays.
- 2 Measured with $B^0 \rightarrow J/\psi(\mu^+\mu^-) K_S^0(\pi^+\pi^-)$ decays.
- 3 Uses $B^0 \rightarrow J/\psi K^0$ fully reconstructed decays.
- 4 Uses exclusively reconstructed final states containing a $J/\psi \rightarrow \mu^+\mu^-$ decays.
- 5 CSORNA 00 uses fully reconstructed 135 $B^0 \rightarrow J/\psi(\ell^+) K_S^0$ events and invariant masses without beam constraint.
- 6 ALBRECHT 90J assumes 10580 for $\Upsilon(4S)$ mass. Supersedes ALBRECHT 87C and ALBRECHT 87D.
- 7 Found using fully reconstructed decays with J/ψ . ALBRECHT 87D assume $m_{\Upsilon(4S)} = 10577$ MeV.

$m_{B^0} - m_{B^\pm}$

VALUE (MeV)	DOCUMENT ID	TECN	COMMENT
0.31 ± 0.05 OUR FIT			
0.33 ± 0.05 OUR AVERAGE			
0.57 ± 0.49 ± 0.10	1 SIRUNYAN	18DF CMS	pp at 8 TeV
0.20 ± 0.17 ± 0.11	1 AAIJ	12E LHCb	pp at 7 TeV
0.33 ± 0.05 ± 0.03	2 AUBERT	08AF BABR	$e^+e^- \rightarrow \Upsilon(4S)$
0.53 ± 0.67 ± 0.14	1 ACOSTA	06 CDF	$p\bar{p}$ at 1.96 TeV
0.41 ± 0.25 ± 0.19	ALAM	94 CLE2	$e^+e^- \rightarrow \Upsilon(4S)$
-0.4 ± 0.6 ± 0.5	BORTOLETTO92	CLEO	$e^+e^- \rightarrow \Upsilon(4S)$
-0.9 ± 1.2 ± 0.5	ALBRECHT	90J ARG	$e^+e^- \rightarrow \Upsilon(4S)$
2.0 ± 1.1 ± 0.3	3 BEBEK	87 CLEO	$e^+e^- \rightarrow \Upsilon(4S)$

- 1 Uses exclusively reconstructed final states containing a $J/\psi \rightarrow \mu^+\mu^-$ decay.
- 2 Uses the B -momentum distributions in the e^+e^- rest frame.
- 3 BEBEK 87 actually measure the difference between half of E_{cm} and the B^\pm or B^0 mass, so the $m_{B^0} - m_{B^\pm}$ is more accurate. Assume $m_{\Upsilon(4S)} = 10580$ MeV.

$m_{B_H^0} - m_{B_L^0}$

See the $B^0-\bar{B}^0$ MIXING PARAMETERS section near the end of these B^0 Listings.

Meson Particle Listings

 B^0 B^0 MEAN LIFE

See $B^\pm/B^0/B_s^0/b$ -baryon ADMIXTURE section for data on B -hadron mean life averaged over species of bottom particles.

VALUE (10^{-12} s)	EVTS	DOCUMENT ID	TECN	COMMENT
1.517 ± 0.004 OUR EVALUATION		(Produced by HFLAV)		
1.499 ± 0.013 ± 0.008	1	ABUDINEN 23D	BELL	$e^+e^- \rightarrow \Upsilon(4S)$
1.515 ± 0.005 ± 0.006	2	SIRUNYAN 18BY	CMS	pp at 8 TeV
1.534 ± 0.019 ± 0.021	3	ABAZOV 15A	D0	$p\bar{p}$ at 1.96 TeV
1.499 ± 0.013 ± 0.005	4	AAIJ 14E	LHCB	pp at 7 TeV
1.524 ± 0.006 ± 0.004	5	AAIJ 14E	LHCB	pp at 7 TeV
1.524 ± 0.011 ± 0.004	6	AAIJ 14R	LHCB	pp at 7 TeV
1.509 ± 0.012 ± 0.018	7	AAD 13U	ATLS	pp at 7 TeV
1.508 ± 0.025 ± 0.043	8	ABAZOV 12U	D0	$p\bar{p}$ at 1.96 TeV
1.507 ± 0.010 ± 0.008	9	AALTONEN 11	CDF	$p\bar{p}$ at 1.96 TeV
1.414 ± 0.018 ± 0.034	9	ABAZOV 09E	D0	$p\bar{p}$ at 1.96 TeV
1.504 ± 0.013 ± 0.013	10	AUBERT 06G	BABR	$e^+e^- \rightarrow \Upsilon(4S)$
1.534 ± 0.008 ± 0.010	11	ABE 05B	BELL	$e^+e^- \rightarrow \Upsilon(4S)$
1.531 ± 0.021 ± 0.031	12	ABDALLAH 04E	DLPH	$e^+e^- \rightarrow Z$
1.523 +0.024 -0.023 ± 0.022	13	AUBERT 03C	BABR	$e^+e^- \rightarrow \Upsilon(4S)$
1.533 ± 0.034 ± 0.038	14	AUBERT 03H	BABR	$e^+e^- \rightarrow \Upsilon(4S)$
1.497 ± 0.073 ± 0.032	15	ACOSTA 02C	CDF	$p\bar{p}$ at 1.8 TeV
1.529 ± 0.012 ± 0.029	16	AUBERT 02H	BABR	$e^+e^- \rightarrow \Upsilon(4S)$
1.546 ± 0.032 ± 0.022	17	AUBERT 01F	BABR	$e^+e^- \rightarrow \Upsilon(4S)$
1.541 ± 0.028 ± 0.023	16	ABBIENDI,G 00B	OPAL	$e^+e^- \rightarrow Z$
1.518 ± 0.053 ± 0.034	18	BARATE 00R	ALEP	$e^+e^- \rightarrow Z$
1.523 ± 0.057 ± 0.053	19	ABBIENDI 99J	OPAL	$e^+e^- \rightarrow Z$
1.474 ± 0.039 ± 0.052 -0.051	18	ABE 98Q	CDF	$p\bar{p}$ at 1.8 TeV
1.52 ± 0.06 ± 0.04	19	ACCIARRI 98S	L3	$e^+e^- \rightarrow Z$
1.64 ± 0.08 ± 0.08	19	ABE 97J	SLD	$e^+e^- \rightarrow Z$
1.532 ± 0.041 ± 0.040	20	ABREU 97F	DLPH	$e^+e^- \rightarrow Z$
1.25 +0.15 -0.13 ± 0.05	121	15 BUSKULIC 96J	ALEP	$e^+e^- \rightarrow Z$
1.49 +0.17 -0.15 ± 0.08 -0.06	21	BUSKULIC 96J	ALEP	$e^+e^- \rightarrow Z$
1.61 +0.14 -0.13 ± 0.08	18,22	ABREU 95Q	DLPH	$e^+e^- \rightarrow Z$
1.63 ± 0.14 ± 0.13	23	ADAM 95	DLPH	$e^+e^- \rightarrow Z$
1.53 ± 0.12 ± 0.08	18,24	AKERS 95T	OPAL	$e^+e^- \rightarrow Z$
• • • We do not use the following data for averages, fits, limits, etc. • • •				
1.501 +0.078 -0.074 ± 0.050	4	ABAZOV 07S	D0	Repl. by ABAZOV 12U
1.524 ± 0.030 ± 0.016	4	ABULENCIA 07A	CDF	Repl. by AALTONEN 11
1.473 +0.052 -0.050 ± 0.023	9	ABAZOV 05B	D0	Repl. by ABAZOV 05W
1.40 +0.11 -0.10 ± 0.03	4	ABAZOV 05C	D0	Repl. by ABAZOV 07S
1.530 ± 0.043 ± 0.023	9	ABAZOV 05W	D0	Repl. by ABAZOV 09E
1.54 ± 0.05 ± 0.02	25	ACOSTA 05	CDF	Repl. by AALTONEN 11
1.554 ± 0.030 ± 0.019	17	ABE 02H	BELL	Repl. by ABE 05B
1.58 ± 0.09 ± 0.02	15	ABE 98B	CDF	Repl. by ACOSTA 02C
1.54 ± 0.08 ± 0.06	18	ABE 96C	CDF	Repl. by ABE 98Q
1.55 ± 0.06 ± 0.03	26	BUSKULIC 96J	ALEP	$e^+e^- \rightarrow Z$
1.61 ± 0.07 ± 0.04	18	BUSKULIC 96J	ALEP	Repl. by BARATE 00R
1.62 ± 0.12	27	ADAM 95	DLPH	$e^+e^- \rightarrow Z$
1.57 ± 0.18 ± 0.08	121	15 ABE 94D	CDF	Repl. by ABE 98B
1.17 +0.29 -0.23 ± 0.16	96	18 ABREU 93D	DLPH	Sup. by ABREU 95Q
1.55 ± 0.25 ± 0.18	76	23 ABREU 93G	DLPH	Sup. by ADAM 95
1.51 +0.24 -0.23 ± 0.12 -0.14	78	18 ACTON 93C	OPAL	Sup. by AKERS 95T
1.52 +0.20 -0.18 ± 0.07 -0.13	77	18 BUSKULIC 93D	ALEP	Sup. by BUSKULIC 96J
1.20 +0.52 -0.36 ± 0.16 -0.14	15	28 WAGNER 90	MRK2	$E_{\text{cm}}^{\text{ee}} = 29$ GeV
0.82 +0.57 -0.37 ± 0.27	29	AVERILL 89	HRS	$E_{\text{cm}}^{\text{ee}} = 29$ GeV

- Measured using $B^0 \rightarrow D^{(*)-}\pi^+$ decays.
- Measured using $B^0 \rightarrow J/\psi K^*(892)^0$ and $B^0 \rightarrow J/\psi K_S^0$ decays.
- Measured using $B^0 \rightarrow D^{*-}\mu^+\nu X$ decays.
- Measured mean life using $B^0 \rightarrow J/\psi K_S^0$ decays.
- Measured using $B^0 \rightarrow J/\psi K^*0$ decays.
- Measured using $B^0 \rightarrow K^+\pi^-$ decays.
- Measured with $B_d^0 \rightarrow J/\psi(\mu^+\mu^-)K_S^0(\pi^+\pi^-)$ decays.
- Measured mean life using fully reconstructed decays ($J/\psi K^{(*)}$).
- Measured mean life using $B^0 \rightarrow J/\psi K^*0$ decays.
- Measured using a simultaneous fit of the B^0 lifetime and $\bar{B}^0 B^0$ oscillation frequency Δm_d in the partially reconstructed $B^0 \rightarrow D^{*-}\ell\nu$ decays.
- Measurement performed using a combined fit of CP -violation, mixing and lifetimes.
- Measurement performed using an inclusive reconstruction and B flavor identification technique.
- AUBERT 03C uses a sample of approximately 14,000 exclusively reconstructed $B^0 \rightarrow D^*(2010)^-\ell\nu$ and simultaneously measures the lifetime and oscillation frequency.
- Measurement performed with decays $B^0 \rightarrow D^{*-}\pi^+$ and $B^0 \rightarrow D^{*-}\rho^+$ using a partial reconstruction technique.
- Measured mean life using fully reconstructed decays.

- Data analyzed using partially reconstructed $\bar{B}^0 \rightarrow D^{*-}\pi^+\nu$ decays.
- Events are selected in which one B meson is fully reconstructed while the second B meson is reconstructed inclusively.
- Data analyzed using $D/D^* \ell X$ event vertices.
- Data analyzed using charge of secondary vertex.
- Data analyzed using inclusive $D/D^* \ell X$.
- Measured mean life using partially reconstructed $D^{*-}\pi^+ X$ vertices.
- ABREU 95Q assumes $B(B^0 \rightarrow D^{*-}\ell^+\nu_\ell) = 3.2 \pm 1.7\%$.
- Data analyzed using vertex-charge technique to tag B charge.
- AKERS 95T assumes $B(B^0 \rightarrow D_s^{(*)}D^{0(*)}) = 5.0 \pm 0.9\%$ to find B^+/B^0 yield.
- Measured using the time-dependent angular analysis of $B_d^0 \rightarrow J/\psi K^*0$ decays.
- Combined result of $D/D^* \ell X$ analysis, fully reconstructed B analysis, and partially reconstructed $D^{*-}\pi^+ X$ analysis.
- Combined ABREU 95Q and ADAM 95 result.
- WAGNER 90 tagged B^0 mesons by their decays into $D^{*-}e^+\nu$ and $D^{*-}\mu^+\nu$ where the D^{*-} is tagged by its decay into $\pi^-\bar{D}^0$.
- AVERILL 89 is an estimate of the B^0 mean lifetime assuming that $B^0 \rightarrow D^{*+} X$ always.

 τ_{B^0}/τ_{B^+}

VALUE	DOCUMENT ID	TECN	COMMENT
1.000 ± 0.008 ± 0.009	1	AAIJ 14E	LHCB pp at 7 TeV

- Measured using $B^0 \rightarrow J/\psi K^*0$ decays.

MEAN LIFE RATIO τ_{B^+}/τ_{B^0} τ_{B^+}/τ_{B^0} (direct measurements)

VALUE	EVTS	DOCUMENT ID	TECN	COMMENT	
1.076 ± 0.004 OUR EVALUATION		(Produced by HFLAV)			
1.074 ± 0.005 ± 0.003	1	AAIJ 14E	LHCB	pp at 7 TeV	
1.088 ± 0.009 ± 0.004	2	AALTONEN 11	CDF	$p\bar{p}$ at 1.96 TeV	
1.080 ± 0.016 ± 0.014	3	ABAZOV 05D	D0	$p\bar{p}$ at 1.96 TeV	
1.066 ± 0.008 ± 0.008	4	ABE 05B	BELL	$e^+e^- \rightarrow \Upsilon(4S)$	
1.060 ± 0.021 ± 0.024	5	ABDALLAH 04E	DLPH	$e^+e^- \rightarrow Z$	
1.093 ± 0.066 ± 0.028	6	ACOSTA 02C	CDF	$p\bar{p}$ at 1.8 TeV	
1.082 ± 0.026 ± 0.012	7	AUBERT 01F	BABR	$e^+e^- \rightarrow \Upsilon(4S)$	
1.085 ± 0.059 ± 0.018	3	BARATE 00R	ALEP	$e^+e^- \rightarrow Z$	
1.079 ± 0.064 ± 0.041	8	ABBIENDI 99J	OPAL	$e^+e^- \rightarrow Z$	
1.110 ± 0.056 ± 0.033 -0.030	3	ABE 98Q	CDF	$p\bar{p}$ at 1.8 TeV	
1.09 ± 0.07 ± 0.03	8	ACCIARRI 98S	L3	$e^+e^- \rightarrow Z$	
1.01 ± 0.07 ± 0.06	8	ABE 97J	SLD	$e^+e^- \rightarrow Z$	
1.27 +0.23 -0.19 ± 0.03 -0.02	6	BUSKULIC 96J	ALEP	$e^+e^- \rightarrow Z$	
1.00 +0.17 -0.15 ± 0.10	3,9	ABREU 95Q	DLPH	$e^+e^- \rightarrow Z$	
1.06 +0.13 -0.11 ± 0.10	10	ADAM 95	DLPH	$e^+e^- \rightarrow Z$	
0.99 ± 0.14 ± 0.05 -0.04	3,11	AKERS 95T	OPAL	$e^+e^- \rightarrow Z$	
• • • We do not use the following data for averages, fits, limits, etc. • • •					
1.091 ± 0.023 ± 0.014	7	ABE 02H	BELL	Repl. by ABE 05B	
1.06 ± 0.07 ± 0.02	6	ABE 98B	CDF	Repl. by ACOSTA 02C	
1.01 ± 0.11 ± 0.02	3	ABE 96C	CDF	Repl. by ABE 98Q	
1.03 ± 0.08 ± 0.02	12	BUSKULIC 96J	ALEP	$e^+e^- \rightarrow Z$	
0.98 ± 0.08 ± 0.03	3	BUSKULIC 96J	ALEP	Repl. by BARATE 00R	
1.02 ± 0.16 ± 0.05	269	6	ABE 94D	CDF	Repl. by ABE 98B
1.11 +0.51 -0.39 ± 0.11	188	3	ABREU 93D	DLPH	Sup. by ABREU 95Q
1.01 +0.29 -0.22 ± 0.12	253	10	ABREU 93G	DLPH	Sup. by ADAM 95
1.0 +0.33 -0.25 ± 0.08	130	ACTON 93C	OPAL	Sup. by AKERS 95T	
0.96 +0.19 -0.15 ± 0.18 -0.12	154	3	BUSKULIC 93D	ALEP	Sup. by BUSKULIC 96J

- Measured using $B \rightarrow J/\psi K^{(*)}$ decays.
- Measured mean life using fully reconstructed decays ($J/\psi K^{(*)}$).
- Data analyzed using $D/D^* \mu X$ vertices.
- Measurement performed using a combined fit of CP -violation, mixing and lifetimes.
- Measurement performed using an inclusive reconstruction and B flavor identification technique.
- Measured using fully reconstructed decays.
- Events are selected in which one B meson is fully reconstructed while the second B meson is reconstructed inclusively.
- Data analyzed using charge of secondary vertex.
- ABREU 95Q assumes $B(B^0 \rightarrow D^{*-}\ell^+\nu_\ell) = 3.2 \pm 1.7\%$.
- Data analyzed using vertex-charge technique to tag B charge.
- AKERS 95T assumes $B(B^0 \rightarrow D_s^{(*)}D^{0(*)}) = 5.0 \pm 0.9\%$ to find B^+/B^0 yield.
- Combined result of $D/D^* \ell X$ analysis and fully reconstructed B analysis.

 τ_{B^+}/τ_{B^0} (inferred from branching fractions)

These measurements are inferred from the branching fractions for semileptonic decay or other spectator-dominated decays by assuming that the rates for such decays are equal for B^0 and B^+ . We do not use measurements which assume equal production of B^0 and B^+ because of the large uncertainty in the production ratio.

VALUE	CL%	EVTS	DOCUMENT ID	TECN	COMMENT
1.07 ± 0.04 OUR AVERAGE					
1.07 ± 0.04 ± 0.03			URQUIJO 07	BELL	$e^+e^- \rightarrow \Upsilon(4S)$
1.067 ± 0.041 ± 0.033			AUBERT,B 06Y	BABR	$e^+e^- \rightarrow \Upsilon(4S)$

- • • We do not use the following data for averages, fits, limits, etc. • • •
- 0.95 ^{+0.117}/_{-0.080} ± 0.091 1 ARTUSO 97 CLE2 e⁺e⁻ → $\Upsilon(4S)$
- 1.15 ± 0.17 ± 0.06 2 JESSOP 97 CLE2 e⁺e⁻ → $\Upsilon(4S)$
- 0.93 ± 0.18 ± 0.12 3 ATHANAS 94 CLE2 Sup. by ARTUSO 97
- 0.91 ± 0.27 ± 0.21 4 ALBRECHT 92c ARG e⁺e⁻ → $\Upsilon(4S)$
- 1.0 ± 0.4 29 4.5 ALBRECHT 92G ARG e⁺e⁻ → $\Upsilon(4S)$
- 0.89 ± 0.19 ± 0.13 4 FULTON 91 CLEO e⁺e⁻ → $\Upsilon(4S)$
- 1.00 ± 0.23 ± 0.14 4 ALBRECHT 89L ARG e⁺e⁻ → $\Upsilon(4S)$
- 0.49 to 2.3 90 6 BEAN 87B CLEO e⁺e⁻ → $\Upsilon(4S)$

¹ ARTUSO 97 uses partial reconstruction of $B \rightarrow D^* \ell \nu_\ell$ and independent of B^0 and B^+ production fraction.
² Assumes equal production of B^+ and B^0 at the $\Upsilon(4S)$.
³ ATHANAS 94 uses events tagged by fully reconstructed B^- decays and partially or fully reconstructed B^0 decays.
⁴ Assumes equal production of B^0 and B^+ .
⁵ ALBRECHT 92G data analyzed using $B \rightarrow D_s \bar{D}, D_s \bar{D}^*, D_s^* \bar{D}, D_s^* \bar{D}^*$ events.
⁶ BEAN 87B assume the fraction of $B^0 \bar{B}^0$ events at the $\Upsilon(4S)$ is 0.41.

$\Delta\Gamma_{B_d^0} / \Gamma_{B_d^0}$

$\Gamma_{B_d^0}$ and $\Delta\Gamma_{B_d^0}$ are the decay rate average and difference between two B_d^0 CP eigenstates (light - heavy). The λ_{CP} characterizes B^0 and \bar{B}^0 decays to states of charmonium plus K_L^0 , see the review on "CP Violation" in the reviews section.

VALUE (units 10 ⁻²)	CL%	DOCUMENT ID	TECN	COMMENT
0.1 ± 1.0 OUR EVALUATION (Produced by HFLAV)				
0.1 ± 1.0 OUR AVERAGE				
3.4 ± 2.3 ± 2.4		1 SIRUNYAN	18BY CMS	pp at 8 TeV
- 0.1 ± 1.1 ± 0.9		2 AABOUD	16G ATLS	pp at 7, 8 TeV
- 4.4 ± 2.5 ± 1.1		3 AAIJ	14E LHCb	pp at 7 TeV
1.7 ± 1.8 ± 1.1		4 HIGUCHI	12 BELL	e ⁺ e ⁻ → $\Upsilon(4S)$
0.8 ± 3.7 ± 1.8		5 AUBERT,B	04c BABR	e ⁺ e ⁻ → $\Upsilon(4S)$
0 ± 9		6 ABDALLAH	03B DLPH	e ⁺ e ⁻ → Z
0.50 ± 1.38		7 ABAZOV	14 D0	p \bar{p} at 1.96 TeV
< 80	95	7 BEHRENS	00B CLE2	e ⁺ e ⁻ → $\Upsilon(4S)$

¹ Measured using $B^0 \rightarrow J/\psi K^*(892)^0$ and $B^0 \rightarrow J/\psi K_S^0$ decays, and assuming $\beta = 21.9 \pm 0.7$ degrees.
² Measured from the ratio of decay time distributions of $B^0 \rightarrow J/\psi K_S^0$ and $B^0 \rightarrow J/\psi K^{*0}$ decays.
³ Measured using the effective lifetimes of $B^0 \rightarrow J/\psi K_S^0$ and $B^0 \rightarrow J/\psi K^{*0}$ decays.
⁴ Reports $-\Delta\Gamma_d/\Gamma_d$ using $B^0 \rightarrow J/\psi K_S^0, J/\psi K_L^0, D^- \pi^+, D^{*-} \pi^+, D^{*-} \rho^+$, and $D^{*-} \ell^+ \nu$ decays.
⁵ Corresponds to 90% confidence range [-0.084, 0.068].
⁶ Used the measured $\tau_{B^0} = 1.55 \pm 0.03$ ps. Corresponds to an upper limit of < 0.18 at 95% C.L.
⁷ BEHRENS 00B uses high-momentum lepton tags and partially reconstructed $\bar{B}^0 \rightarrow D^{*+} \pi^-, \rho^-$ decays to determine the flavor of the B meson. Assumes $\Delta_{md} = 0.478 \pm 0.018$ ps⁻¹ and $\tau_{B^0} = 1.548 \pm 0.032$ ps.

B⁰ DECAY MODES

\bar{B}^0 modes are charge conjugates of the modes below. Reactions indicate the weak decay vertex and do not include mixing. Modes which do not identify the charge state of the B are listed in the B^\pm/B^0 ADMIXTURE section.

The branching fractions listed below assume 50% $B^0 \bar{B}^0$ and 50% $B^+ B^-$ production at the $\Upsilon(4S)$. We have attempted to bring older measurements up to date by rescaling their assumed $\Upsilon(4S)$ production ratio to 50:50 and their assumed D, D_s, D^* , and ψ branching ratios to current values whenever this would affect our averages and best limits significantly.

Indentation is used to indicate a subchannel of a previous reaction. All resonant subchannels have been corrected for resonance branching fractions to the final state so the sum of the subchannel branching fractions can exceed that of the final state.

For inclusive branching fractions, e.g., $B \rightarrow D^\pm X$, the values usually are multiplicities, not branching fractions. They can be greater than one.

Mode	Fraction (Γ_i/Γ)	Scale factor/ Confidence level
Γ_1 $\ell^+ \nu_\ell X$	[a] (10.33 ± 0.28) %	
Γ_2 $e^+ \nu_e X_c$	(10.1 ± 0.4) %	
Γ_3 $\ell^+ \nu_\ell X_H$	[a] (1.51 ± 0.19) × 10 ⁻³	
Γ_4 $D \ell^+ \nu_\ell X$	[a] (9.1 ± 0.8) %	
Γ_5 $D^- \ell^+ \nu_\ell$	[a] (2.12 ± 0.06) %	
Γ_6 $D^- \tau^+ \nu_\tau$	(9.9 ± 2.1) × 10 ⁻³	
Γ_7 $D^*(2010)^- \ell^+ \nu_\ell$	[a] (4.90 ± 0.12) %	
Γ_8 $D^*(2010)^- e^+ \nu_e$		

Γ_9 $D^*(2010)^- \mu^+ \nu_\mu$		
Γ_{10} $D^*(2010)^- \tau^+ \nu_\tau$	(1.45 ± 0.10) %	S=1.3
Γ_{11} $\bar{D}^{(*)0} n \pi \ell^+ \nu_\ell (n \geq 1)$	[a] (2.3 ± 0.5) %	
Γ_{12} $\bar{D}^0 \pi^- \ell^+ \nu_\ell$	[a] (3.64 ± 0.20) × 10 ⁻³	
Γ_{13} $D_0^{*0} \pi^- \ell^+ \nu_\ell$	[a] < 4.4 × 10 ⁻⁴	CL=90%
	$D_0^{*0} \rightarrow \bar{D}^0 \pi^-$	
Γ_{14} $D_2^{*0} (2460)^- \ell^+ \nu_\ell$	[a] (1.41 ± 0.20) × 10 ⁻³	S=1.7
	$D_2^{*0} \rightarrow \bar{D}^0 \pi^-$	
Γ_{15} $\bar{D}^{*0} \pi^- \ell^+ \nu_\ell$	[a] (5.44 ± 0.28) × 10 ⁻³	
Γ_{16} $D_1 (2420)^- \ell^+ \nu_\ell, D_1^- \rightarrow \bar{D}^{*0} \pi^-$	[a] (2.85 ± 0.25) × 10 ⁻³	
Γ_{17} $D_1 (2420)^- \ell^+ \nu_\ell, D_1^- \rightarrow D_1^- \pi^+ \pi^-$	[a] (1.02 ± 0.16) × 10 ⁻³	
Γ_{18} $D_1' (2430)^- \ell^+ \nu_\ell, D_1'^- \rightarrow \bar{D}^{*0} \pi^-$	[a] (2.5 ± 0.6) × 10 ⁻³	
Γ_{19} $D_2^* (2460)^- \ell^+ \nu_\ell, D_2^{*-} \rightarrow \bar{D}^{*0} \pi^-$	[a] (6.6 ± 1.1) × 10 ⁻⁴	
	$D^- \pi^+ \pi^- \ell^+ \nu_\ell$	[a] (1.45 ± 0.22) × 10 ⁻³
Γ_{21} $D^{*-} \pi^+ \pi^- \ell^+ \nu_\ell$	[a] (5.1 ± 2.3) × 10 ⁻⁴	
Γ_{22} $\rho^- \ell^+ \nu_\ell$	[a] (2.94 ± 0.21) × 10 ⁻⁴	
Γ_{23} $\pi^- \ell^+ \nu_\ell$	[a] (1.50 ± 0.06) × 10 ⁻⁴	
Γ_{24} $\pi^- \mu^+ \nu_\mu$		
Γ_{25} $\pi^- \tau^+ \nu_\tau$	< 2.5 × 10 ⁻⁴	CL=90%

Inclusive modes

Γ_{26} $K^\pm X$	(78 ± 8) %	
Γ_{27} $D^0 X$	(8.1 ± 1.5) %	
Γ_{28} $\bar{D}^0 X$	(47.4 ± 2.8) %	
Γ_{29} $D^+ X$	< 3.9 %	CL=90%
Γ_{30} $D^- X$	(36.9 ± 3.3) %	
Γ_{31} $D_s^+ X$	(10.3 ± 2.1) %	
	(1.8 ± 1.8) %	
Γ_{32} $D_s^- X$	< 2.6 %	CL=90%
Γ_{33} $\Lambda_c^+ X$	< 3.1 %	CL=90%
Γ_{34} $\bar{\Lambda}_c^- X$	(5.0 ± 2.1) %	
	(1.5 ± 1.5) %	
Γ_{35} $\bar{c} X$	(95 ± 5) %	
Γ_{36} $c X$	(24.6 ± 3.1) %	
Γ_{37} $\bar{c}/c X$	(119 ± 6) %	

D, D*, or D_s modes

Γ_{38} $D^- \pi^+$	(2.51 ± 0.08) × 10 ⁻³	
Γ_{39} $D^- \rho^+$	(7.6 ± 1.2) × 10 ⁻³	
Γ_{40} $D^- K^0 \pi^+$	(4.9 ± 0.9) × 10 ⁻⁴	
Γ_{41} $D^- K^*(892)^+$	(4.5 ± 0.7) × 10 ⁻⁴	
Γ_{42} $D^- \omega \pi^+$	(2.8 ± 0.6) × 10 ⁻³	
Γ_{43} $D^- K^+$	(2.05 ± 0.08) × 10 ⁻⁴	
Γ_{44} $D^- K^+ \pi^+ \pi^-$	(3.5 ± 0.8) × 10 ⁻⁴	
Γ_{45} $D^- K^+ \bar{K}^0$	< 3.1 × 10 ⁻⁴	CL=90%
Γ_{46} $D^- K^+ \bar{K}^*(892)^0$	(8.8 ± 1.9) × 10 ⁻⁴	
Γ_{47} $\bar{D}^0 \pi^+ \pi^-$	(8.8 ± 0.5) × 10 ⁻⁴	
Γ_{48} $D^*(2010)^- \pi^+$	(2.66 ± 0.07) × 10 ⁻³	
Γ_{49} $\bar{D}^0 K^+ K^-$	(6.1 ± 0.5) × 10 ⁻⁵	
Γ_{50} $D^- \pi^+ \pi^+ \pi^-$	(6.0 ± 0.6) × 10 ⁻³	
Γ_{51} $(D^- \pi^+ \pi^+ \pi^-)$ nonresonant	(3.9 ± 1.9) × 10 ⁻³	
Γ_{52} $D^- \pi^+ \rho^0$	(1.1 ± 1.0) × 10 ⁻³	
Γ_{53} $D^- a_1(1260)^+$	(6.0 ± 3.3) × 10 ⁻³	
Γ_{54} $D^*(2010)^- \pi^+ \pi^0$	(1.5 ± 0.5) %	
Γ_{55} $D^*(2010)^- \rho^+$	(6.8 ± 0.9) × 10 ⁻³	
Γ_{56} $D^*(2010)^- K^+$	(2.16 ± 0.08) × 10 ⁻⁴	
Γ_{57} $D^*(2010)^- K^0 \pi^+$	(3.0 ± 0.8) × 10 ⁻⁴	
Γ_{58} $D^*(2010)^- K^*(892)^+$	(3.3 ± 0.6) × 10 ⁻⁴	
Γ_{59} $D^*(2010)^- K^+ \bar{K}^0$	< 4.7 × 10 ⁻⁴	CL=90%
Γ_{60} $D^*(2010)^- K^+ \bar{K}^*(892)^0$	(1.29 ± 0.33) × 10 ⁻³	
Γ_{61} $D^*(2010)^- \pi^+ \pi^+ \pi^-$	(7.21 ± 0.29) × 10 ⁻³	
Γ_{62} $(D^*(2010)^- \pi^+ \pi^+ \pi^-)$ non-resonant	(0.0 ± 2.5) × 10 ⁻³	
Γ_{63} $D^*(2010)^- \pi^+ \rho^0$	(5.7 ± 3.2) × 10 ⁻³	
Γ_{64} $D^*(2010)^- a_1(1260)^+$	(1.30 ± 0.27) %	
Γ_{65} $\bar{D}_1 (2420)^0 \pi^- \pi^+, \bar{D}_1^0 \rightarrow D^{*-} \pi^+$	(1.47 ± 0.35) × 10 ⁻⁴	
	$D^{*-} \pi^+$	
Γ_{66} $D^*(2010)^- K^+ \pi^- \pi^+$	(4.7 ± 0.4) × 10 ⁻⁴	
Γ_{67} $D^*(2010)^- \pi^+ \pi^+ \pi^- \pi^0$	(1.76 ± 0.27) %	
Γ_{68} $D^{*-} 3\pi^+ 2\pi^-$	(4.7 ± 0.9) × 10 ⁻³	
Γ_{69} $D^*(2010)^- \omega \pi^+$	(2.46 ± 0.18) × 10 ⁻³	S=1.2
Γ_{70} $\bar{D}_1 (2430)^0 \omega, \bar{D}_1^0 \rightarrow D^{*-} \pi^+$	(2.7 ± 0.8) × 10 ⁻⁴	
	(0.4 ± 0.4) × 10 ⁻⁴	

Meson Particle Listings

 B^0

Γ_{71}	$D^{*-}\rho(1450)^+, \rho^+ \rightarrow \omega\pi^+$	$(1.07^{+0.40}_{-0.34}) \times 10^{-3}$		Γ_{119}	$D^*(2010)^- D_{s1}(2536)^+, D_{s1}^+ \rightarrow D^{*0}K^+$	$(3.3 \pm 1.1) \times 10^{-4}$	
Γ_{72}	$\bar{D}_1(2420)^0\omega, \bar{D}_1^0 \rightarrow D^{*-}\pi^+$	$(7.0 \pm 2.2) \times 10^{-5}$		Γ_{120}	$D^{*-}D_{s1}(2536)^+, D_{s1}^+ \rightarrow D^{*+}K^0$	$(5.0 \pm 1.7) \times 10^{-4}$	
Γ_{73}	$\bar{D}_2^*(2460)^0\omega, \bar{D}_2^0 \rightarrow D^{*-}\pi^+$	$(4.0 \pm 1.4) \times 10^{-5}$		Γ_{121}	$D^- D_{sJ}(2573)^+, D_{sJ}^+ \rightarrow D^0K^+$	$(3.4 \pm 1.8) \times 10^{-5}$	
Γ_{74}	$D^{*-}b_1(1235)^+, b_1^+ \rightarrow \omega\pi^+$	< 7	$\times 10^{-5}$	Γ_{122}	$D^*(2010)^- D_{sJ}(2573)^+, D_{sJ}^+ \rightarrow D^0K^+$	< 2	$\times 10^{-4}$
Γ_{75}	$\bar{D}^{*-}\pi^+$	[b] $(1.9 \pm 0.9) \times 10^{-3}$		Γ_{123}	$D^- D_{sJ}(2700)^+, D_{sJ}^+ \rightarrow D^0K^+$	$(7.1 \pm 1.2) \times 10^{-4}$	CL=90%
Γ_{76}	$D_1(2420)^-\pi^+, D_1^- \rightarrow D^0\pi^-$	$(9.9 \pm \frac{2.0}{2.5}) \times 10^{-5}$		Γ_{124}	$D^+\pi^-$	$(7.3 \pm 1.2) \times 10^{-7}$	
Γ_{77}	$D_1(2420)^-\pi^+, D_1^- \rightarrow D^0\pi^-$	< 3.3	$\times 10^{-5}$	Γ_{125}	$D_s^+\pi^-$	$(2.03 \pm 0.18) \times 10^{-5}$	
Γ_{78}	$\bar{D}_2^*(2460)^-\pi^+, D_2^{*-} \rightarrow D^0\pi^-$	$(2.38 \pm 0.16) \times 10^{-4}$		Γ_{126}	$D_s^+\pi^-$	$(2.1 \pm 0.4) \times 10^{-5}$	S=1.4
Γ_{79}	$\bar{D}_2^*(2400)^-\pi^+, D_2^{*-} \rightarrow D^0\pi^-$	$(7.6 \pm 0.8) \times 10^{-5}$		Γ_{127}	$D_s^+\rho^-$	< 2.4	$\times 10^{-5}$
Γ_{80}	$D_2^*(2460)^-\pi^+, D_2^{*-} \rightarrow D^0\pi^-$	< 2.4	$\times 10^{-5}$	Γ_{128}	$D_s^+\rho^-$	$(4.1 \pm 1.3) \times 10^{-5}$	CL=90%
Γ_{81}	$\bar{D}_2^*(2460)^-\rho^+$	< 4.9	$\times 10^{-3}$	Γ_{129}	$D_s^+a_0^-$	< 1.9	$\times 10^{-5}$
Γ_{82}	$D^0\bar{D}^0$	$(1.4 \pm 0.7) \times 10^{-5}$		Γ_{130}	$D_s^+a_0^-$	< 3.6	$\times 10^{-5}$
Γ_{83}	$D^{*0}\bar{D}^0$	< 2.9	$\times 10^{-4}$	Γ_{131}	$D_s^+a_1(1260)^-$	< 2.1	$\times 10^{-3}$
Γ_{84}	D^-D^+	$(2.11 \pm 0.18) \times 10^{-4}$		Γ_{132}	$D_s^+a_1(1260)^-$	< 1.7	$\times 10^{-3}$
Γ_{85}	$D^\pm D^{*\mp}$ (CP-averaged)	$(6.1 \pm 0.6) \times 10^{-4}$		Γ_{133}	$D_s^+a_2^-$	< 1.9	$\times 10^{-4}$
Γ_{86}	$D^-D_s^+$	$(7.2 \pm 0.8) \times 10^{-3}$		Γ_{134}	$D_s^+a_2^-$	< 2.0	$\times 10^{-4}$
Γ_{87}	$\bar{D}^0 D_s^+ \pi^-, m(\bar{D}^0 \pi^-) > 2.05$ GeV			Γ_{135}	$D_s^- K^+$	$(2.7 \pm 0.5) \times 10^{-5}$	S=2.7
Γ_{88}	$D^*(2010)^- D_s^+$	$(8.0 \pm 1.1) \times 10^{-3}$		Γ_{136}	$D_s^- K^+$	$(2.19 \pm 0.30) \times 10^{-5}$	
Γ_{89}	$D^*(2010)^- D_s^+, D^{*-} \rightarrow \bar{D}^0 \pi^-, m(\bar{D}^0 \pi^-) > 2.05$ GeV			Γ_{137}	$D_{s1}(2536)^{\mp} K^\pm, D_{s1}^- \rightarrow \bar{D}^*(2007)^0 K^-$	$(5.1 \pm 0.6) \times 10^{-6}$	
Γ_{90}	$D_2^*(2460)^- D_s^+, D_2^{*-} \rightarrow \bar{D}^0 \pi^-$			Γ_{138}	$D_s^- K^*(892)^+$	$(3.5 \pm 1.0) \times 10^{-5}$	
Γ_{91}	$D_1^*(2600)^- D_s^+, D_1^{*-} \rightarrow \bar{D}^0 \pi^-$			Γ_{139}	$D_s^- K^*(892)^+$	$(3.2 \pm \frac{1.5}{1.3}) \times 10^{-5}$	
Γ_{92}	$D_3^*(2750)^- D_s^+, D_3^{*-} \rightarrow \bar{D}^0 \pi^-$			Γ_{140}	$D_s^- \pi^+ K^0$	$(9.7 \pm 1.4) \times 10^{-5}$	
Γ_{93}	$D_1^*(2760)^- D_s^+, D_1^{*-} \rightarrow \bar{D}^0 \pi^-$			Γ_{141}	$D_s^- \pi^+ K^0$	< 1.10	$\times 10^{-4}$
Γ_{94}	$D_J^*(3000)^- D_s^+, D_J^{*-} \rightarrow \bar{D}^0 \pi^-$			Γ_{142}	$D_s^- K^+ \pi^+ \pi^-$	$(1.7 \pm 0.5) \times 10^{-4}$	
Γ_{95}	$T_{cs0}^*(2870)^0 \bar{D}^0, T_{cs0}^* \rightarrow D_s^+ \pi^-$			Γ_{143}	$D_s^- \pi^+ K^*(892)^0$	< 3.0	$\times 10^{-3}$
Γ_{96}	$D^- D_s^+$	$(7.4 \pm 1.6) \times 10^{-3}$		Γ_{144}	$D_s^- \pi^+ K^*(892)^0$	< 1.6	$\times 10^{-3}$
Γ_{97}	$D^*(2010)^- D_s^+$	$(1.77 \pm 0.14) \%$		Γ_{145}	$\bar{D}^0 K^0$	$(5.5 \pm 0.4) \times 10^{-5}$	
Γ_{98}	$D_{s0}(2317)^- K^+, D_{s0}^- \rightarrow D_s^- \pi^0$	$(4.2 \pm 1.4) \times 10^{-5}$		Γ_{146}	$\bar{D}^0 K^+ \pi^-$	$(8.8 \pm 1.7) \times 10^{-5}$	
Γ_{99}	$D_{s0}(2317)^- \pi^+, D_{s0}^- \rightarrow D_s^- \pi^0$	< 2.5	$\times 10^{-5}$	Γ_{147}	$\bar{D}^0 K^*(892)^0$	$(4.5 \pm 0.6) \times 10^{-5}$	
Γ_{100}	$D_{sJ}(2457)^- K^+, D_{sJ}^- \rightarrow D_s^- \pi^0$	< 9.4	$\times 10^{-6}$	Γ_{148}	$\bar{D}^0 K^*(1410)^0$	< 6.7	$\times 10^{-5}$
Γ_{101}	$D_{sJ}(2457)^- \pi^+, D_{sJ}^- \rightarrow D_s^- \pi^0$	< 4.0	$\times 10^{-6}$	Γ_{149}	$\bar{D}^0 K_0^*(1430)^0$	$(7 \pm 7) \times 10^{-6}$	
Γ_{102}	$D_s^- D_s^+$	< 3.6	$\times 10^{-5}$	Γ_{150}	$\bar{D}^0 K_2^*(1430)^0$	$(2.1 \pm 0.9) \times 10^{-5}$	
Γ_{103}	$D_s^- D_s^+$	< 1.3	$\times 10^{-4}$	Γ_{151}	$D_0^*(2300)^- K^+, D_0^{*-} \rightarrow \bar{D}^0 \pi^-$	$(1.9 \pm 0.9) \times 10^{-5}$	
Γ_{104}	$D_s^{*-} D_s^+$	< 2.4	$\times 10^{-4}$	Γ_{152}	$D_2^*(2460)^- K^+, D_2^{*-} \rightarrow \bar{D}^0 \pi^-$	$(2.03 \pm 0.35) \times 10^{-5}$	
Γ_{105}	$D_{s0}^*(2317)^+ D^-, D_{s0}^{*+} \rightarrow D_s^+ \pi^0$	$(1.06 \pm 0.16) \times 10^{-3}$	S=1.1	Γ_{153}	$D_3^*(2760)^- K^+, D_3^{*-} \rightarrow \bar{D}^0 \pi^-$	< 1.0	$\times 10^{-6}$
Γ_{106}	$D_{s0}(2317)^+ D^-, D_{s0}^+ \rightarrow D_s^+ \gamma$	< 9.5	$\times 10^{-4}$	Γ_{154}	$\bar{D}^0 K^+ \pi^-$ nonresonant	< 3.7	$\times 10^{-5}$
Γ_{107}	$D_{s0}(2317)^+ D^*(2010)^-, D_{s0}^+ \rightarrow D_s^+ \pi^0$	$(1.5 \pm 0.6) \times 10^{-3}$		Γ_{155}	$[K^+ K^-]_D K^*(892)^0$	$(4.2 \pm 0.7) \times 10^{-5}$	
Γ_{108}	$D_{sJ}(2457)^+ D^-$	$(3.5 \pm 1.1) \times 10^{-3}$		Γ_{156}	$[\pi^+ \pi^-]_D K^*(892)^0$	$(6.0 \pm 1.1) \times 10^{-5}$	
Γ_{109}	$D_{sJ}(2457)^+ D^-, D_{sJ}^+ \rightarrow D_s^+ \gamma$	$(6.5 \pm \frac{1.7}{1.4}) \times 10^{-4}$		Γ_{157}	$[\pi^+ K^-]_D K^*(892)^0$		
Γ_{110}	$D_{sJ}(2457)^+ D^-, D_{sJ}^+ \rightarrow D_s^+ \gamma$	< 6.0	$\times 10^{-4}$	Γ_{158}	$[K^+ \pi^-]_D K^*(892)^0$		
Γ_{111}	$D_{sJ}(2457)^+ D^-, D_{sJ}^+ \rightarrow D_s^+ \pi^+ \pi^-$	< 2.0	$\times 10^{-4}$	Γ_{159}	$[\pi^+ \pi^- \pi^+ \pi^-]_D K^{*0}$	$(4.6 \pm 0.9) \times 10^{-5}$	
Γ_{112}	$D_{sJ}(2457)^+ D^-, D_{sJ}^+ \rightarrow D_s^+ \pi^0$	< 3.6	$\times 10^{-4}$	Γ_{160}	$[\pi^+ K^- \pi^+ \pi^-]_D K^{*0}$		
Γ_{113}	$D^*(2010)^- D_{sJ}(2457)^+$	$(9.3 \pm 2.2) \times 10^{-3}$		Γ_{161}	$[K^+ \pi^- \pi^+ \pi^-]_D K^{*0}$		
Γ_{114}	$D_{sJ}(2457)^+ D^*(2010), D_{sJ}^+ \rightarrow D_s^+ \gamma$	$(2.3 \pm \frac{0.9}{0.7}) \times 10^{-3}$		Γ_{162}	$\bar{D}^0 \pi^0$	$(2.67 \pm 0.09) \times 10^{-4}$	
Γ_{115}	$D^- D_{s1}(2536)^+, D_{s1}^+ \rightarrow D^{*0} K^+ + D^{*+} K^0$	$(2.8 \pm 0.7) \times 10^{-4}$		Γ_{163}	$\bar{D}^0 \rho^0$	$(3.21 \pm 0.21) \times 10^{-4}$	
Γ_{116}	$D^- D_{s1}(2536)^+, D_{s1}^+ \rightarrow D^{*0} K^+ + D^{*+} K^0$	$(1.7 \pm 0.6) \times 10^{-4}$		Γ_{164}	$\bar{D}^0 f_2$	$(1.56 \pm 0.21) \times 10^{-4}$	
Γ_{117}	$D^- D_{s1}(2536)^+, D_{s1}^+ \rightarrow D^{*0} K^+ + D^{*+} K^0$	$(2.6 \pm 1.1) \times 10^{-4}$		Γ_{165}	$\bar{D}^0 \eta$	$(2.56 \pm 0.12) \times 10^{-4}$	
Γ_{118}	$D^*(2010)^- D_{s1}(2536)^+, D_{s1}^+ \rightarrow D^{*0} K^+ + D^{*+} K^0$	$(5.0 \pm 1.4) \times 10^{-4}$		Γ_{166}	$\bar{D}^0 \eta'$	$(1.38 \pm 0.16) \times 10^{-4}$	S=1.3
				Γ_{167}	$\bar{D}^0 \omega$	$(2.54 \pm 0.16) \times 10^{-4}$	
				Γ_{168}	$\bar{D}^0 \phi$	$(7.7 \pm 2.3) \times 10^{-7}$	
				Γ_{169}	$D^0 K^+ \pi^-$	$(5.3 \pm 3.2) \times 10^{-6}$	
				Γ_{170}	$D^0 K^*(892)^0$	$(3.0 \pm 0.6) \times 10^{-6}$	
				Γ_{171}	$\bar{D}^{*0} \gamma$	< 2.5	$\times 10^{-5}$
				Γ_{172}	$\bar{D}^*(2007)^0 \pi^0$	$(2.2 \pm 0.6) \times 10^{-4}$	CL=90%
				Γ_{173}	$\bar{D}^*(2007)^0 \rho^0$	< 5.1	$\times 10^{-4}$
				Γ_{174}	$\bar{D}^*(2007)^0 \eta$	$(2.3 \pm 0.6) \times 10^{-4}$	S=2.8
				Γ_{175}	$\bar{D}^*(2007)^0 \eta'$	$(1.40 \pm 0.22) \times 10^{-4}$	
				Γ_{176}	$\bar{D}^*(2007)^0 \pi^+ \pi^-$	$(6.2 \pm 2.2) \times 10^{-4}$	
				Γ_{177}	$\bar{D}^*(2007)^0 K^+ \pi^-$	$(5.2 \pm 1.9) \times 10^{-5}$	
				Γ_{178}	$\bar{D}^*(2007)^0 K^0$	$(3.6 \pm 1.2) \times 10^{-5}$	
				Γ_{179}	$\bar{D}^*(2007)^0 K^*(892)^0$	< 6.9	$\times 10^{-5}$
				Γ_{180}	$\bar{D}^*(2007)^0 \phi$	$(2.2 \pm 0.6) \times 10^{-6}$	CL=90%
				Γ_{181}	$D^*(2007)^0 K^*(892)^0$	< 4.0	$\times 10^{-5}$

Γ_{182}	$D^*(2007)^0 \pi^+ \pi^+ \pi^- \pi^-$	$(2.7 \pm 0.5) \times 10^{-3}$		Γ_{244}	$J/\psi(1S) \pi^+ \pi^- \pi^+ \pi^-$	$(1.44 \pm 0.12) \times 10^{-5}$	
Γ_{183}	$D^*(2010)^+ D^*(2010)^-$	$(8.0 \pm 0.6) \times 10^{-4}$		Γ_{245}	$J/\psi(1S) f_1(1285)$	$(8.4 \pm 2.1) \times 10^{-6}$	
Γ_{184}	$\bar{D}^*(2007)^0 \omega$	$(3.6 \pm 1.1) \times 10^{-4}$	S=3.1	Γ_{246}	$J/\psi(1S) K^*(892)^0 \pi^+ \pi^-$	$(6.6 \pm 2.2) \times 10^{-4}$	
Γ_{185}	$D^*(2010)^+ D^-$	$(6.1 \pm 1.5) \times 10^{-4}$	S=1.6	Γ_{247}	$\eta_{c2}(1D) K_S^0, \eta_{c2} \rightarrow h_c \gamma$	< 3.5	CL=90%
Γ_{186}	$D^*(2007)^0 \bar{D}^*(2007)^0$	< 9	CL=90%	Γ_{248}	$\eta_{c2}(1D) \pi^- K^+, \eta_{c2} \rightarrow h_c \gamma$	< 1.0	CL=90%
Γ_{187}	$D^- D^0 K^+$	$(1.07 \pm 0.11) \times 10^{-3}$		Γ_{249}	$\chi_{c1}(3872)^- K^+$	< 5	CL=90%
Γ_{188}	$D^- D^*(2007)^0 K^+$	$(3.5 \pm 0.4) \times 10^{-3}$		Γ_{250}	$\chi_{c1}(3872)^- K^+,$ $\chi_{c1}(3872)^- \rightarrow$ $J/\psi(1S) \pi^- \pi^0$	$[c] < 4.2$	CL=90%
Γ_{189}	$D^*(2010)^- D^0 K^+$	$(2.47 \pm 0.21) \times 10^{-3}$		Γ_{251}	$\chi_{c1}(3872) K^0$	$(1.4 \pm 0.4) \times 10^{-4}$	S=1.1
Γ_{190}	$D^*(2010)^- D^*(2007)^0 K^+$	$(1.06 \pm 0.09) \%$		Γ_{252}	$\chi_{c1}(3872) K^*(892)^0$	$(1.1 \pm 0.5) \times 10^{-4}$	
Γ_{191}	$D^- D^+ K^0$	$(7.5 \pm 1.7) \times 10^{-4}$		Γ_{253}	$\chi_{c1}(3872) K^+ \pi^-$	$(2.2 \pm 0.7) \times 10^{-4}$	
Γ_{192}	$D^*(2010)^- D^+ K^0 +$ $D^- D^*(2010)^+ K^0$	$(6.4 \pm 0.5) \times 10^{-3}$		Γ_{254}	$\chi_{c1}(3872) \gamma$	< 1.5	CL=90%
Γ_{193}	$D^*(2010)^- D^*(2010)^+ K^0$	$(8.1 \pm 0.7) \times 10^{-3}$		Γ_{255}	$T_{c\bar{c}1}(4430)^\pm K^\mp, T_{c\bar{c}1}^\pm \rightarrow$ $\psi(2S) \pi^\pm$	(6.0 ± 3.0) $- 2.4$	$\times 10^{-5}$
Γ_{194}	$D^{*-} D_{s1}(2536)^+, D_{s1}^+ \rightarrow$ $D^{*+} K^0$	$(8.0 \pm 2.4) \times 10^{-4}$		Γ_{256}	$T_{c\bar{c}1}(4430)^\pm K^\mp, T_{c\bar{c}1}^\pm \rightarrow$ $J/\psi \pi^\pm$	(5.4 ± 4.0) $- 1.2$	$\times 10^{-6}$
Γ_{195}	$\bar{D}^0 D^0 K^0$	$(2.7 \pm 1.1) \times 10^{-4}$		Γ_{257}	$T_{c\bar{c}1}(3900)^\pm K^\mp, T_{c\bar{c}1}^\pm \rightarrow$ $J/\psi \pi^\pm$	< 9	$\times 10^{-7}$
Γ_{196}	$D^0 \bar{D}^0 K^+ \pi^-$	$(3.5 \pm 0.5) \times 10^{-4}$		Γ_{258}	$T_{c\bar{c}1}(4200)^\pm K^\mp, T_{c\bar{c}1}^\pm \rightarrow$ $J/\psi \pi^\pm$	(2.2 ± 1.3) $- 0.8$	$\times 10^{-5}$
Γ_{197}	$\bar{D}^0 D^*(2007)^0 K^0 +$ $\bar{D}^*(2007)^0 D^0 K^0$	$(1.1 \pm 0.5) \times 10^{-3}$		Γ_{259}	$J/\psi(1S) p \bar{p}$	$(4.5 \pm 0.6) \times 10^{-7}$	
Γ_{198}	$\bar{D}^*(2007)^0 D^*(2007)^0 K^0$	$(2.4 \pm 0.9) \times 10^{-3}$		Γ_{260}	$J/\psi(1S) \gamma$	< 1.5	CL=90%
Γ_{199}	$(\bar{D} + \bar{D}^*)(D + D^*) K$	$(3.68 \pm 0.26) \%$		Γ_{261}	$J/\psi \mu^+ \mu^-, J/\psi \rightarrow \mu^+ \mu^-$	< 1.0	CL=95%
Charmonium modes				Γ_{262}	$J/\psi(1S) \bar{D}^0$	< 1.3	CL=90%
Γ_{200}	$\eta_c K^0$	$(9.0 \pm 1.1) \times 10^{-4}$		Γ_{263}	$\psi(2S) \pi^0$	$(1.17 \pm 0.19) \times 10^{-5}$	
Γ_{201}	$\eta_c(1S) K^+ \pi^-$	$(6.5 \pm 0.7) \times 10^{-4}$		Γ_{264}	$\psi(2S) K^0$	$(5.8 \pm 0.5) \times 10^{-4}$	
Γ_{202}	$\eta_c(1S) K^+ \pi^-$ (NR)	$(6.7 \pm 1.4) \times 10^{-5}$		Γ_{265}	$\psi(2S) K^0 \pi^+ \pi^-$	$(2.81 \pm 0.30) \times 10^{-4}$	
Γ_{203}	$T_{c\bar{c}}(4100)^- K^+, T_{c\bar{c}}^- \rightarrow$ $\eta_c \pi^-$	$(2.2 \pm 1.1) \times 10^{-5}$		Γ_{266}	$\psi(3770) K^0, \psi \rightarrow \bar{D}^0 D^0$	< 1.23	CL=90%
Γ_{204}	$\eta_c(1S) K^*(1410)^0$	$(2.1 \pm 1.6) \times 10^{-4}$		Γ_{267}	$\psi(3770) K^0, \psi \rightarrow D^- D^+$	< 1.88	CL=90%
Γ_{205}	$\eta_c(1S) K_0^*(1430)^0$	$(1.8 \pm 0.4) \times 10^{-4}$		Γ_{268}	$\psi(2S) \pi^+ \pi^-$	$(2.24 \pm 0.35) \times 10^{-5}$	
Γ_{206}	$\eta_c(1S) K_2^*(1430)^0$	(5.4 ± 2.4) $- 2.9$	$\times 10^{-5}$	Γ_{269}	$\psi(2S) K^+ \pi^-$	$(5.8 \pm 0.4) \times 10^{-4}$	
Γ_{207}	$\eta_c(1S) K^*(1680)^0$	(4 ± 4)	$\times 10^{-5}$	Γ_{270}	$\psi(2S) K^*(892)^0$	$(5.9 \pm 0.4) \times 10^{-4}$	
Γ_{208}	$\eta_c(1S) K_0^*(1950)^0$	(4.8 ± 3.2) $- 4.0$	$\times 10^{-5}$	Γ_{271}	$\chi_{c0} K^0$	$(1.9 \pm 0.4) \times 10^{-4}$	
Γ_{209}	$\eta_c K^*(892)^0$	(5.3 ± 0.8) $- 0.9$	$\times 10^{-4}$	Γ_{272}	$\chi_{c0} K^*(892)^0$	$(1.7 \pm 0.4) \times 10^{-4}$	
Γ_{210}	$\eta_c(2S) K_S^0, \eta_c \rightarrow p \bar{p} \pi^+ \pi^-$	(4.2 ± 1.4) $- 1.2$	$\times 10^{-7}$	Γ_{273}	$\chi_{c1} \pi^0$	$(1.12 \pm 0.28) \times 10^{-5}$	
Γ_{211}	$\eta_c(2S) K^{*0}$	< 3.9	$\times 10^{-4}$	Γ_{274}	$\chi_{c1} K^0$	$(3.95 \pm 0.27) \times 10^{-4}$	
Γ_{212}	$h_c(1P) K_S^0$	< 1.4	$\times 10^{-5}$	Γ_{275}	$\chi_{c1} \pi^- K^+$	$(4.97 \pm 0.30) \times 10^{-4}$	
Γ_{213}	$h_c(1P) K^{*0}$	< 4	$\times 10^{-4}$	Γ_{276}	$\chi_{c1} K^*(892)^0$	$(2.38 \pm 0.19) \times 10^{-4}$	S=1.2
Γ_{214}	$J/\psi(1S) K^0$	$(8.91 \pm 0.21) \times 10^{-4}$		Γ_{277}	$T_{c\bar{c}}(4050)^- K^+, T_{c\bar{c}}^- \rightarrow$ $\chi_{c1} \pi^-$	(3.0 ± 4.0) $- 1.8$	$\times 10^{-5}$
Γ_{215}	$J/\psi(1S) K^+ \pi^-$	$(1.15 \pm 0.05) \times 10^{-3}$		Γ_{278}	$T_{c\bar{c}}(4250)^- K^+, T_{c\bar{c}}^- \rightarrow$ $\chi_{c1} \pi^-$	(4.0 ± 20.0) $- 1.0$	$\times 10^{-5}$
Γ_{216}	$J/\psi(1S) K^*(892)^0$	$(1.27 \pm 0.05) \times 10^{-3}$		Γ_{279}	$\chi_{c1} \pi^+ \pi^- K^0$	$(3.2 \pm 0.5) \times 10^{-4}$	
Γ_{217}	$J/\psi(1S) \eta K_S^0$	$(5.4 \pm 0.9) \times 10^{-5}$		Γ_{280}	$\chi_{c1} \pi^- \pi^0 K^+$	$(3.5 \pm 0.6) \times 10^{-4}$	
Γ_{218}	$J/\psi(1S) \eta' K_S^0$	< 2.5	$\times 10^{-5}$	Γ_{281}	$\chi_{c2} K^0$	< 1.5	CL=90%
Γ_{219}	$J/\psi(1S) \phi K^0$	$(4.9 \pm 1.0) \times 10^{-5}$	S=1.3	Γ_{282}	$\chi_{c2} K^*(892)^0$	$(4.9 \pm 1.2) \times 10^{-5}$	S=1.1
Γ_{220}	$J/\psi(1S) \omega K^0$	$(2.3 \pm 0.4) \times 10^{-4}$		Γ_{283}	$\chi_{c2} \pi^- K^+$	$(7.2 \pm 1.0) \times 10^{-5}$	
Γ_{221}	$\chi_{c0}(3915), \chi_{c0} \rightarrow J/\psi \omega$	$(2.1 \pm 0.9) \times 10^{-5}$		Γ_{284}	$\chi_{c2} \pi^+ \pi^- K^0$	< 1.70	$\times 10^{-4}$
Γ_{222}	$J/\psi(1S) K(1270)^0$	$(1.3 \pm 0.5) \times 10^{-3}$		Γ_{285}	$\chi_{c2} \pi^- \pi^0 K^+$	< 7.4	$\times 10^{-5}$
Γ_{223}	$J/\psi(1S) \pi^0$	$(1.66 \pm 0.10) \times 10^{-5}$		Γ_{286}	$\psi(4660) K^0, \psi \rightarrow \Lambda_c^+ \Lambda_c^-$	< 2.3	$\times 10^{-4}$
Γ_{224}	$J/\psi(1S) \eta$	$(1.08 \pm 0.23) \times 10^{-5}$	S=1.5	Γ_{287}	$\psi(4230)^0 K^0, \psi^0 \rightarrow$ $J/\psi \pi^+ \pi^-$	< 1.7	$\times 10^{-5}$
Γ_{225}	$J/\psi(1S) \pi^+ \pi^-$	$(3.99 \pm 0.15) \times 10^{-5}$		K or K* modes			
Γ_{226}	$J/\psi(1S) \pi^+ \pi^-$ nonresonant	< 1.2	$\times 10^{-5}$	Γ_{288}	$K^+ \pi^-$	$(2.00 \pm 0.04) \times 10^{-5}$	
Γ_{227}	$J/\psi(1S) f_0(500), f_0 \rightarrow \pi \pi$	(8.8 ± 1.2) $- 1.6$	$\times 10^{-6}$	Γ_{289}	$K^0 \pi^0$	$(1.01 \pm 0.04) \times 10^{-5}$	
Γ_{228}	$J/\psi(1S) f_2$	(3.3 ± 0.5) $- 0.6$	$\times 10^{-6}$	Γ_{290}	$\eta' K^0$	$(6.6 \pm 0.4) \times 10^{-5}$	S=1.4
Γ_{229}	$J/\psi(1S) \rho^0$	(2.55 ± 0.18) $- 0.16$	$\times 10^{-5}$	Γ_{291}	$\eta' K^*(892)^0$	$(2.8 \pm 0.6) \times 10^{-6}$	
Γ_{230}	$J/\psi(1S) f_0(980), f_0 \rightarrow$ $\pi^+ \pi^-$	< 1.1	$\times 10^{-6}$	Γ_{292}	$\eta' K_0^*(1430)^0$	$(6.3 \pm 1.6) \times 10^{-6}$	
Γ_{231}	$J/\psi(1S) \rho(1450)^0, \rho^0 \rightarrow \pi \pi$	(2.9 ± 1.6) $- 0.7$	$\times 10^{-6}$	Γ_{293}	$\eta' K_2^*(1430)^0$	$(1.37 \pm 0.32) \times 10^{-5}$	
Γ_{232}	$J/\psi \rho(1700)^0, \rho^0 \rightarrow \pi^+ \pi^-$	$(2.0 \pm 1.3) \times 10^{-6}$		Γ_{294}	ηK^0	(1.23 ± 0.27) $- 0.24$	$\times 10^{-6}$
Γ_{233}	$J/\psi(1S) \omega$	(1.8 ± 0.7) $- 0.5$	$\times 10^{-5}$	Γ_{295}	$\eta K^*(892)^0$	$(1.59 \pm 0.10) \times 10^{-5}$	
Γ_{234}	$J/\psi(1S) K^+ K^-$	$(2.53 \pm 0.35) \times 10^{-6}$		Γ_{296}	$\eta K_0^*(1430)^0$	$(1.10 \pm 0.22) \times 10^{-5}$	
Γ_{235}	$J/\psi(1S) a_0(980), a_0 \rightarrow$ $K^+ K^-$	$(4.7 \pm 3.4) \times 10^{-7}$		Γ_{297}	$\eta K_2^*(1430)^0$	$(9.6 \pm 2.1) \times 10^{-6}$	
Γ_{236}	$J/\psi(1S) \phi$	< 1.1	$\times 10^{-7}$	Γ_{298}	ωK^0	$(4.8 \pm 0.4) \times 10^{-6}$	
Γ_{237}	$J/\psi(1S) \eta'(958)$	$(7.6 \pm 2.4) \times 10^{-6}$		Γ_{299}	$a_0(980)^0 K^0, a_0^0 \rightarrow \eta \pi^0$	< 7.8	$\times 10^{-6}$
Γ_{238}	$J/\psi(1S) K^0 \pi^+ \pi^-$	$(4.5 \pm 0.4) \times 10^{-4}$		Γ_{300}	$b_1^0 K^0, b_1^0 \rightarrow \omega \pi^0$	< 7.8	$\times 10^{-6}$
Γ_{239}	$J/\psi(1S) K^0 K^- \pi^+ + c.c.$	< 2.1	$\times 10^{-5}$	Γ_{301}	$a_0(980)^\pm K^\mp, a_0^\pm \rightarrow \eta \pi^\pm$	< 1.9	$\times 10^{-6}$
Γ_{240}	$J/\psi(1S) K^0 K^+ K^-$	$(2.5 \pm 0.7) \times 10^{-5}$	S=1.8	Γ_{302}	$b_1^- K^+, b_1^- \rightarrow \omega \pi^-$	$(7.4 \pm 1.4) \times 10^{-6}$	
Γ_{241}	$J/\psi(1S) K^0 K^\pm \pi^\mp$	$(2.5 \pm 0.7) \times 10^{-5}$		Γ_{303}	$b_1^0 K^{*0}, b_1^0 \rightarrow \omega \pi^0$	< 8.0	$\times 10^{-6}$
Γ_{242}	$J/\psi(1S) K^0 \rho^0$	$(5.4 \pm 3.0) \times 10^{-4}$		Γ_{304}	$b_1^- K^{*+}, b_1^- \rightarrow \omega \pi^-$	< 5.0	$\times 10^{-6}$
Γ_{243}	$J/\psi(1S) K^*(892)^+ \pi^-$	$(8 \pm 4) \times 10^{-4}$					

Meson Particle Listings

 B^0

Γ ₃₀₅	$a_0(1450)^\pm K^\mp, a_0^\pm \rightarrow \eta\pi^\pm$	< 3.1	$\times 10^{-6}$	CL=90%	Γ ₃₇₀	$K_S^0 K_S^0 K_S^0$	(6.0 ± 0.5)	$\times 10^{-6}$	S=1.1
Γ ₃₀₆	$K_S^0 X^0$ (Familon)	< 5.3	$\times 10^{-5}$	CL=90%	Γ ₃₇₁	$f_0(980) K^0, f_0 \rightarrow K_S^0 K_S^0$	(2.7 ± 1.8)	$\times 10^{-6}$	
Γ ₃₀₇	$\omega K^*(892)^0$	(2.0 ± 0.5)	$\times 10^{-6}$		Γ ₃₇₂	$f_0(1710) K^0, f_0 \rightarrow K_S^0 K_S^0$	(5.0 ± 5.0)	$\times 10^{-7}$	
Γ ₃₀₈	$\omega(K\pi)_0^{*0}$	(1.84 ± 0.25)	$\times 10^{-5}$		Γ ₃₇₃	$f_2(2010) K^0, f_2 \rightarrow K_S^0 K_S^0$	(5 ± 6)	$\times 10^{-7}$	
Γ ₃₀₉	$\omega K_0^*(1430)^0$	(1.60 ± 0.34)	$\times 10^{-5}$		Γ ₃₇₄	$K_S^0 K_S^0 K_S^0$ nonresonant	(1.33 ± 0.31)	$\times 10^{-5}$	
Γ ₃₁₀	$\omega K_2^*(1430)^0$	(1.01 ± 0.23)	$\times 10^{-5}$		Γ ₃₇₅	$K_S^0 K_S^0 K_L^0$	< 1.6	$\times 10^{-5}$	CL=90%
Γ ₃₁₁	$\omega K^+ \pi^-$ nonresonant	(5.1 ± 1.0)	$\times 10^{-6}$		Γ ₃₇₆	$K^*(892)^0 K^+ K^-$	(2.75 ± 0.26)	$\times 10^{-5}$	
Γ ₃₁₂	$K^+ \pi^- \pi^0$	(3.78 ± 0.32)	$\times 10^{-5}$		Γ ₃₇₇	$K^*(892)^0 \phi$	(1.00 ± 0.05)	$\times 10^{-5}$	
Γ ₃₁₃	$K^+ \rho^-$	(7.0 ± 0.9)	$\times 10^{-6}$		Γ ₃₇₈	$K^+ K^- \pi^+ \pi^-$ nonresonant	< 7.17	$\times 10^{-5}$	CL=90%
Γ ₃₁₄	$K^+ \rho(1450)^-$	(2.4 ± 1.2)	$\times 10^{-6}$		Γ ₃₇₉	$K^*(892)^0 K^- \pi^+$	(4.5 ± 1.3)	$\times 10^{-6}$	
Γ ₃₁₅	$K^+ \rho(1700)^-$	(6 ± 7)	$\times 10^{-7}$		Γ ₃₈₀	$K^*(892)^0 \bar{K}^*(892)^0$	(8.3 ± 2.4)	$\times 10^{-7}$	S=1.5
Γ ₃₁₆	$(K^+ \pi^- \pi^0)$ nonresonant	(2.8 ± 0.6)	$\times 10^{-6}$		Γ ₃₈₁	$K^+ K^+ \pi^- \pi^-$ nonresonant	< 6.0	$\times 10^{-6}$	CL=90%
Γ ₃₁₇	$(K\pi)_0^{*+} \pi^-, (K\pi)_0^{*+} \rightarrow$	(3.4 ± 0.5)	$\times 10^{-5}$		Γ ₃₈₂	$K^*(892)^0 K^+ \pi^-$	< 2.2	$\times 10^{-6}$	CL=90%
Γ ₃₁₈	$(K\pi)_0^{*0} \pi^0, (K\pi)_0^{*0} \rightarrow$	(8.6 ± 1.7)	$\times 10^{-6}$		Γ ₃₈₃	$K^*(892)^0 K^*(892)^0$	< 2	$\times 10^{-7}$	CL=90%
Γ ₃₁₉	$K_2^*(1430)^0 \pi^0$	< 4.0	$\times 10^{-6}$	CL=90%	Γ ₃₈₄	$K^*(892)^+ K^*(892)^-$	< 2.0	$\times 10^{-6}$	CL=90%
Γ ₃₂₀	$K^*(1680)^0 \pi^0$	< 7.5	$\times 10^{-6}$	CL=90%	Γ ₃₈₅	$K_1(1400)^0 \phi$	< 5.0	$\times 10^{-3}$	CL=90%
Γ ₃₂₁	$K_x^{*0} \pi^0$	[d] (6.1 ± 1.6)	$\times 10^{-6}$		Γ ₃₈₆	$\phi(K\pi)_0^{*0}$	(4.3 ± 0.4)	$\times 10^{-6}$	
Γ ₃₂₂	$K^0 \pi^+ \pi^-$	(4.97 ± 0.18)	$\times 10^{-5}$		Γ ₃₈₇	$\phi(K\pi)_0^{*0} (1.60 < m_{K\pi} < 2.15)$ [f]	< 1.7	$\times 10^{-6}$	CL=90%
Γ ₃₂₃	$K^0 \pi^+ \pi^-$ nonresonant	(1.39 ± 0.26)	$\times 10^{-5}$	S=1.6	Γ ₃₈₈	$K_0^*(1430)^0 K^- \pi^+$	< 3.18	$\times 10^{-5}$	CL=90%
Γ ₃₂₄	$K^0 \rho^0$	(3.4 ± 1.1)	$\times 10^{-6}$	S=2.3	Γ ₃₈₉	$K_0^*(1430)^0 \bar{K}^*(892)^0$	< 3.3	$\times 10^{-6}$	CL=90%
Γ ₃₂₅	$K^*(892)^+ \pi^-$	(7.5 ± 0.4)	$\times 10^{-6}$		Γ ₃₉₀	$K_0^*(1430)^0 \bar{K}_0^*(1430)^0$	< 8.4	$\times 10^{-6}$	CL=90%
Γ ₃₂₆	$K_0^*(1430)^+ \pi^-$	(3.3 ± 0.7)	$\times 10^{-5}$	S=2.0	Γ ₃₉₁	$K_0^*(1430)^0 \phi$	(3.9 ± 0.8)	$\times 10^{-6}$	
Γ ₃₂₇	$K_x^{*+} \pi^-$	[d] (5.1 ± 1.6)	$\times 10^{-6}$		Γ ₃₉₂	$K_0^*(1430)^0 K^*(892)^0$	< 1.7	$\times 10^{-6}$	CL=90%
Γ ₃₂₈	$K^*(1410)^+ \pi^-, K^{*+} \rightarrow$	< 3.8	$\times 10^{-6}$	CL=90%	Γ ₃₉₃	$K_0^*(1430)^0 K_0^*(1430)^0$	< 4.7	$\times 10^{-6}$	CL=90%
Γ ₃₂₉	$(K\pi)_0^{*+} \pi^-, (K\pi)_0^{*+} \rightarrow$	(1.62 ± 0.13)	$\times 10^{-5}$		Γ ₃₉₄	$K^*(1680)^0 \phi$	< 3.5	$\times 10^{-6}$	CL=90%
Γ ₃₃₀	$f_0(980) K^0, f_0 \rightarrow \pi^+ \pi^-$	(8.1 ± 0.8)	$\times 10^{-6}$	S=1.3	Γ ₃₉₅	$K^*(1780)^0 \phi$	< 2.7	$\times 10^{-6}$	CL=90%
Γ ₃₃₁	$K^0 f_0(500)$	(1.6 ± 2.5)	$\times 10^{-7}$		Γ ₃₉₆	$K^*(2045)^0 \phi$	< 1.53	$\times 10^{-5}$	CL=90%
Γ ₃₃₂	$K^0 f_0(1500)$	(1.3 ± 0.8)	$\times 10^{-6}$		Γ ₃₉₇	$K_2^*(1430)^0 \rho^0$	< 1.1	$\times 10^{-3}$	CL=90%
Γ ₃₃₃	$f_2(1270) K^0$	(2.7 ± 1.3)	$\times 10^{-6}$		Γ ₃₉₈	$K_2^*(1430)^0 \phi$	(6.8 ± 0.9)	$\times 10^{-6}$	S=1.2
Γ ₃₃₄	$f_x(1300) K^0, f_x \rightarrow \pi^+ \pi^-$	(1.8 ± 0.7)	$\times 10^{-6}$		Γ ₃₉₉	$K^0 \phi \phi$	(3.7 ± 0.7)	$\times 10^{-6}$	S=1.3
Γ ₃₃₅	$K^*(892)^0 \pi^0$	(3.3 ± 0.6)	$\times 10^{-6}$		Γ ₄₀₀	$\eta' \eta' K^0$	< 3.1	$\times 10^{-5}$	CL=90%
Γ ₃₃₆	$K_2^*(1430)^+ \pi^-$	(3.65 ± 0.34)	$\times 10^{-6}$		Γ ₄₀₁	$\eta K^0 \gamma$	(7.6 ± 1.8)	$\times 10^{-6}$	
Γ ₃₃₇	$K^*(1680)^+ \pi^-$	(1.41 ± 0.10)	$\times 10^{-5}$		Γ ₄₀₂	$\eta' K^0 \gamma$	< 6.4	$\times 10^{-6}$	CL=90%
Γ ₃₃₈	$K^+ \pi^- \pi^+ \pi^-$	[e] < 2.3	$\times 10^{-4}$	CL=90%	Γ ₄₀₃	$K^0 \phi \gamma$	(2.7 ± 0.7)	$\times 10^{-6}$	
Γ ₃₃₉	$\rho^0 K^+ \pi^-$	(2.8 ± 0.7)	$\times 10^{-6}$		Γ ₄₀₄	$K^+ \pi^- \gamma$	(4.6 ± 1.4)	$\times 10^{-6}$	
Γ ₃₄₀	$f_0(980) K^+ \pi^-, f_0 \rightarrow \pi\pi$	(1.4 ± 0.5)	$\times 10^{-6}$		Γ ₄₀₅	$K^*(892)^0 \gamma$	(4.18 ± 0.25)	$\times 10^{-5}$	S=2.1
Γ ₃₄₁	$K^+ \pi^- \pi^+ \pi^-$ nonresonant	< 2.1	$\times 10^{-6}$	CL=90%	Γ ₄₀₆	$K^*(1410) \gamma$	< 1.3	$\times 10^{-4}$	CL=90%
Γ ₃₄₂	$K^*(892)^0 \pi^+ \pi^-$	(5.5 ± 0.5)	$\times 10^{-5}$		Γ ₄₀₇	$K^+ \pi^- \gamma$ nonresonant	< 2.6	$\times 10^{-6}$	CL=90%
Γ ₃₄₃	$K^*(892)^0 \rho^0$	(3.9 ± 1.3)	$\times 10^{-6}$	S=1.9	Γ ₄₀₈	$K^*(892)^0 X(214), X \rightarrow \mu^+ \mu^-$ [g]	< 2.26	$\times 10^{-8}$	CL=90%
Γ ₃₄₄	$K^*(892)^0 f_0(980), f_0 \rightarrow \pi\pi$	(3.9 ± 2.1)	$\times 10^{-6}$	S=3.9	Γ ₄₀₉	$K^0 \pi^+ \pi^- \gamma$	(1.99 ± 0.18)	$\times 10^{-5}$	
Γ ₃₄₅	$K_1(1270)^+ \pi^-$	< 3.0	$\times 10^{-5}$	CL=90%	Γ ₄₁₀	$K^+ \pi^- \pi^0 \gamma$	(4.1 ± 0.4)	$\times 10^{-5}$	
Γ ₃₄₆	$K_1(1400)^+ \pi^-$	< 2.7	$\times 10^{-5}$	CL=90%	Γ ₄₁₁	$K_1(1270)^0 \gamma$	< 5.8	$\times 10^{-5}$	CL=90%
Γ ₃₄₇	$a_1(1260)^- K^+$	[e] (1.6 ± 0.4)	$\times 10^{-5}$		Γ ₄₁₂	$K_1(1400)^0 \gamma$	< 1.2	$\times 10^{-5}$	CL=90%
Γ ₃₄₈	$K^*(892)^+ \rho^-$	(1.03 ± 0.26)	$\times 10^{-5}$		Γ ₄₁₃	$K_2^*(1430)^0 \gamma$	(1.24 ± 0.24)	$\times 10^{-5}$	
Γ ₃₄₉	$K_0^*(1430)^+ \rho^-$	(2.8 ± 1.2)	$\times 10^{-5}$		Γ ₄₁₄	$K_2^*(1680)^0 \gamma$	< 2.0	$\times 10^{-3}$	CL=90%
Γ ₃₅₀	$K_1(1400)^0 \rho^0$	< 3.0	$\times 10^{-3}$	CL=90%	Γ ₄₁₅	$K_3^*(1780)^0 \gamma$	< 8.3	$\times 10^{-5}$	CL=90%
Γ ₃₅₁	$K_0^*(1430)^0 \rho^0$	(2.7 ± 0.6)	$\times 10^{-5}$		Γ ₄₁₆	$K_4^*(2045)^0 \gamma$	< 4.3	$\times 10^{-3}$	CL=90%
Γ ₃₅₂	$K_0^*(1430)^0 f_0(980), f_0 \rightarrow \pi\pi$	(2.7 ± 0.9)	$\times 10^{-6}$		Light unflavored meson modes				
Γ ₃₅₃	$K_2^*(1430)^0 f_0(980), f_0 \rightarrow \pi\pi$	(8.6 ± 2.0)	$\times 10^{-6}$		Γ ₄₁₇	$\rho^0 \gamma$	(8.6 ± 1.5)	$\times 10^{-7}$	
Γ ₃₅₄	$K^+ K^-$	(7.8 ± 1.5)	$\times 10^{-8}$		Γ ₄₁₈	$\rho^0 X(214), X \rightarrow \mu^+ \mu^-$ [g]	< 1.73	$\times 10^{-8}$	CL=90%
Γ ₃₅₅	$K^0 \bar{K}^0$	(1.21 ± 0.16)	$\times 10^{-6}$		Γ ₄₁₉	$\omega \gamma$	(4.4 ± 1.8)	$\times 10^{-7}$	
Γ ₃₅₆	$K^0 K^- \pi^+$	(6.7 ± 0.5)	$\times 10^{-6}$		Γ ₄₂₀	$\phi \gamma$	< 1.0	$\times 10^{-7}$	CL=90%
Γ ₃₅₇	$K^*(892)^\pm K^\mp$	< 4	$\times 10^{-7}$	CL=90%	Γ ₄₂₁	$f_2(1270) \gamma, f_2 \rightarrow (KS)^0 (KS)^0$	< 3.1	$\times 10^{-7}$	
Γ ₃₅₈	$\bar{K}^{*0} K^0 + K^{*0} \bar{K}^0$	< 9.6	$\times 10^{-7}$	CL=90%	Γ ₄₂₂	$f_2'(1525) \gamma, f_2' \rightarrow$ $(KS)^0 (KS)^0$	< 2.1	$\times 10^{-7}$	
Γ ₃₅₉	$K^+ K^- \pi^0$	(2.2 ± 0.6)	$\times 10^{-6}$		Γ ₄₂₃	$\pi^+ \pi^-$	(5.37 ± 0.20)	$\times 10^{-6}$	S=1.3
Γ ₃₆₀	$K_S^0 K_S^0 \pi^0$	< 9	$\times 10^{-7}$	CL=90%	Γ ₄₂₄	$\pi^0 \pi^0$	(1.55 ± 0.17)	$\times 10^{-6}$	S=1.1
Γ ₃₆₁	$K_S^0 K_S^0 \eta$	< 1.0	$\times 10^{-6}$	CL=90%	Γ ₄₂₅	$\eta \pi^0$	(4.1 ± 1.7)	$\times 10^{-7}$	
Γ ₃₆₂	$K_S^0 K_S^0 \eta'$	< 2.0	$\times 10^{-6}$	CL=90%	Γ ₄₂₆	$\eta \eta$	< 1.0	$\times 10^{-6}$	CL=90%
Γ ₃₆₃	$K^0 K^+ K^-$	(2.68 ± 0.11)	$\times 10^{-5}$		Γ ₄₂₇	$\eta' \pi^0$	(1.2 ± 0.6)	$\times 10^{-6}$	S=1.7
Γ ₃₆₄	$K^0 \phi$	(7.3 ± 0.7)	$\times 10^{-6}$		Γ ₄₂₈	$\eta' \eta'$	< 1.7	$\times 10^{-6}$	CL=90%
Γ ₃₆₅	$f_0(980) K^0, f_0 \rightarrow K^+ K^-$	(7.0 ± 3.5)	$\times 10^{-6}$		Γ ₄₂₉	$\eta' \eta$	< 1.2	$\times 10^{-6}$	CL=90%
Γ ₃₆₆	$f_0(1500) K^0$	(1.3 ± 0.7)	$\times 10^{-5}$		Γ ₄₃₀	$\eta' \rho^0$	< 1.3	$\times 10^{-6}$	CL=90%
Γ ₃₆₇	$f_2'(1525)^0 K^0$	(3 ± 5)	$\times 10^{-7}$		Γ ₄₃₁	$\eta' f_0(980), f_0 \rightarrow \pi^+ \pi^-$	< 9	$\times 10^{-7}$	CL=90%
Γ ₃₆₈	$f_0(1710) K^0, f_0 \rightarrow K^+ K^-$	(4.4 ± 0.9)	$\times 10^{-6}$		Γ ₄₃₂	$\eta \rho^0$	< 1.5	$\times 10^{-6}$	CL=90%
Γ ₃₆₉	$K^0 K^+ K^-$ nonresonant	(3.3 ± 1.0)	$\times 10^{-5}$		Γ ₄₃₃	$\eta f_0(980), f_0 \rightarrow \pi^+ \pi^-$	< 4	$\times 10^{-7}$	CL=90%
					Γ ₄₃₄	$\omega \eta$	(9.4 ± 4.0)	$\times 10^{-7}$	
					Γ ₄₃₅	$\omega \eta'$	(1.0 ± 0.5)	$\times 10^{-6}$	
					Γ ₄₃₆	$\omega \rho^0$	< 1.6	$\times 10^{-6}$	CL=90%
					Γ ₄₃₇	$\omega f_0(980), f_0 \rightarrow \pi^+ \pi^-$	< 1.5	$\times 10^{-6}$	CL=90%
					Γ ₄₃₈	$\omega \omega$	(1.2 ± 0.4)	$\times 10^{-6}$	

Γ439	$\phi\pi^0$	< 1.5	$\times 10^{-7}$	CL=90%
Γ440	$\phi\eta$	< 5	$\times 10^{-7}$	CL=90%
Γ441	$\phi\eta'$	< 5	$\times 10^{-7}$	CL=90%
Γ442	$\phi\pi^+\pi^-$	(1.8 ± 0.5)	$\times 10^{-7}$	
Γ443	$\phi\rho^0$	< 3.3	$\times 10^{-7}$	CL=90%
Γ444	$\phi f_0(980), f_0 \rightarrow \pi^+\pi^-$	< 3.8	$\times 10^{-7}$	CL=90%
Γ445	$\phi\omega$	< 7	$\times 10^{-7}$	CL=90%
Γ446	$\phi\phi$	< 2.7	$\times 10^{-8}$	CL=90%
Γ447	$a_0(980)\pi^+\pi^-, a_0^\pm \rightarrow \eta\pi^\pm$	< 3.1	$\times 10^{-6}$	CL=90%
Γ448	$a_0(1450)\pi^+\pi^-, a_0^\pm \rightarrow \eta\pi^\pm$	< 2.3	$\times 10^{-6}$	CL=90%
Γ449	$\pi^+\pi^-\pi^0$	< 7.2	$\times 10^{-4}$	CL=90%
Γ450	$\rho^0\pi^0$	(2.0 ± 0.5)	$\times 10^{-6}$	
Γ451	$\rho^\mp\pi^\pm$	[h] (2.30 ± 0.23)	$\times 10^{-5}$	
Γ452	$\pi^+\pi^-\pi^+\pi^-$	< 1.12	$\times 10^{-5}$	CL=90%
Γ453	$\rho^0\pi^+\pi^-$	< 8.8	$\times 10^{-6}$	CL=90%
Γ454	$\rho^0\rho^0$	(9.6 ± 1.5)	$\times 10^{-7}$	
Γ455	$f_0(980)\pi^+\pi^-, f_0 \rightarrow \pi^+\pi^-$	< 3.0	$\times 10^{-6}$	CL=90%
Γ456	$\rho^0 f_0(980), f_0 \rightarrow \pi^+\pi^-$	(7.8 ± 2.5)	$\times 10^{-7}$	
Γ457	$f_0(980) f_0(980), f_0 \rightarrow \pi^+\pi^-, f_0 \rightarrow \pi^+\pi^-$	< 1.9	$\times 10^{-7}$	CL=90%
Γ458	$f_0(980) f_0(980), f_0 \rightarrow \pi^+\pi^-, f_0 \rightarrow K^+K^-$	< 2.3	$\times 10^{-7}$	CL=90%
Γ459	$a_1(1260)\pi^+\pi^-$	[h] (2.6 ± 0.5)	$\times 10^{-5}$	S=1.9
Γ460	$a_2(1320)\pi^+\pi^-$	[h] < 6.3	$\times 10^{-6}$	CL=90%
Γ461	$\pi^+\pi^-\pi^0\pi^0$	< 3.1	$\times 10^{-3}$	CL=90%
Γ462	$\rho^+\rho^-$	(2.77 ± 0.19)	$\times 10^{-5}$	
Γ463	$a_1(1260)^0\pi^0$	< 1.1	$\times 10^{-3}$	CL=90%
Γ464	$\omega\pi^0$	< 5	$\times 10^{-7}$	CL=90%
Γ465	$\pi^+\pi^+\pi^-\pi^-\pi^0$	< 9.0	$\times 10^{-3}$	CL=90%
Γ466	$a_1(1260)^+\rho^-$	< 6.1	$\times 10^{-5}$	CL=90%
Γ467	$a_1(1260)^0\rho^0$	< 2.4	$\times 10^{-3}$	CL=90%
Γ468	$b_1^\mp\pi^\pm, b_1^\mp \rightarrow \omega\pi^\mp$	(1.09 ± 0.15)	$\times 10^{-5}$	
Γ469	$b_1^0\pi^0, b_1^0 \rightarrow \omega\pi^0$	< 1.9	$\times 10^{-6}$	CL=90%
Γ470	$b_1^-\rho^+, b_1^- \rightarrow \omega\pi^-$	< 1.4	$\times 10^{-6}$	CL=90%
Γ471	$b_1^0\rho^0, b_1^0 \rightarrow \omega\pi^0$	< 3.4	$\times 10^{-6}$	CL=90%
Γ472	$\pi^+\pi^+\pi^+\pi^-\pi^-\pi^-$	< 3.0	$\times 10^{-3}$	CL=90%
Γ473	$a_1(1260)^+ a_1(1260)^-, a_1^+ \rightarrow 2\pi^+\pi^-, a_1^- \rightarrow 2\pi^-\pi^+$	(1.18 ± 0.31)	$\times 10^{-5}$	
Γ474	$\pi^+\pi^+\pi^+\pi^-\pi^-\pi^-\pi^0$	< 1.1	%	CL=90%

Baryon modes

Γ475	$\rho\bar{p}$	(1.27 ± 0.14)	$\times 10^{-8}$	
Γ476	$\rho\bar{p}\pi^+\pi^-$	(2.87 ± 0.19)	$\times 10^{-6}$	
Γ477	$\rho\bar{p}K^+\pi^-$	(6.3 ± 0.5)	$\times 10^{-6}$	
Γ478	$\rho\bar{p}K^0$	(2.66 ± 0.32)	$\times 10^{-6}$	
Γ479	$\Theta(1540)^+\bar{p}, \Theta^+ \rightarrow \rho K_S^0$	[i] < 5	$\times 10^{-8}$	CL=90%
Γ480	$f_J(2220)K^0, f_J \rightarrow \rho\bar{p}$	< 4.5	$\times 10^{-7}$	CL=90%
Γ481	$\rho\bar{p}K^*(892)^0$	(1.24 ± 0.28 / 0.25)	$\times 10^{-6}$	
Γ482	$f_J(2220)K_0^*, f_J \rightarrow \rho\bar{p}$	< 1.5	$\times 10^{-7}$	CL=90%
Γ483	$\rho\bar{p}K^+K^-$	(1.21 ± 0.32)	$\times 10^{-7}$	
Γ484	$\rho\bar{p}\pi^0$	(5.0 ± 1.9)	$\times 10^{-7}$	
Γ485	$\rho\bar{p}\rho\bar{p}$	(2.2 ± 0.4)	$\times 10^{-8}$	
Γ486	$\rho\bar{\Lambda}\pi^-$	(3.16 ± 0.24)	$\times 10^{-6}$	
Γ487	$\rho\bar{\Lambda}\pi^-\gamma$	< 6.5	$\times 10^{-7}$	CL=90%
Γ488	$\rho\bar{\Sigma}^-(1385)^-$	< 2.6	$\times 10^{-7}$	CL=90%
Γ489	$\Delta(1232)^+\bar{p} + \Delta(1232)^-\rho$	< 1.6	$\times 10^{-6}$	
Γ490	$\Delta^0\bar{\Lambda}$	< 9.3	$\times 10^{-7}$	CL=90%
Γ491	$\rho\bar{\Lambda}K^-$	< 8.2	$\times 10^{-7}$	CL=90%
Γ492	$\rho\bar{\Lambda}D^-$	(2.5 ± 0.4)	$\times 10^{-5}$	
Γ493	$\rho\bar{\Lambda}D^{*-}$	(3.4 ± 0.8)	$\times 10^{-5}$	
Γ494	$\rho\bar{\Sigma}^0\pi^-$	(1.2 ± 0.4)	$\times 10^{-6}$	
Γ495	$\bar{\Lambda}\Lambda$	< 3.2	$\times 10^{-7}$	CL=90%
Γ496	$\bar{\Lambda}\Lambda K^0$	(4.8 ± 1.0 / 0.9)	$\times 10^{-6}$	
Γ497	$\bar{\Lambda}\Lambda K^{*0}$	(2.5 ± 0.9 / 0.8)	$\times 10^{-6}$	
Γ498	$\bar{\Lambda}\Lambda D^0$	(1.00 ± 0.30 / 0.26)	$\times 10^{-5}$	
Γ499	$D^0\bar{\Sigma}^0\bar{\Lambda} + c.c.$	< 3.1	$\times 10^{-5}$	CL=90%
Γ500	$\Delta^0\bar{\Delta}^0$	< 1.5	$\times 10^{-3}$	CL=90%
Γ501	$\Delta^{++}\bar{\Delta}^{--}$	< 1.1	$\times 10^{-4}$	CL=90%
Γ502	$\bar{D}^0\rho\bar{p}$	(1.04 ± 0.07)	$\times 10^{-4}$	
Γ503	$D_s^-\bar{\Lambda}\rho$	(2.8 ± 0.9)	$\times 10^{-5}$	
Γ504	$\bar{D}_s^*(2007)^0\rho\bar{p}$	(9.9 ± 1.1)	$\times 10^{-5}$	
Γ505	$D^*(2010)^-\rho\bar{p}$	(1.4 ± 0.4)	$\times 10^{-3}$	

Γ506	$D^-\rho\bar{p}\pi^+$	(3.32 ± 0.31)	$\times 10^{-4}$	
Γ507	$D^*(2010)^-\rho\bar{p}\pi^+$	(4.7 ± 0.5)	$\times 10^{-4}$	S=1.2
Γ508	$\bar{D}^0\rho\bar{p}\pi^+\pi^-$	(3.0 ± 0.5)	$\times 10^{-4}$	
Γ509	$\bar{D}^{*0}\rho\bar{p}\pi^+\pi^-$	(1.9 ± 0.5)	$\times 10^{-4}$	
Γ510	$\Theta_c\bar{p}\pi^+, \Theta_c \rightarrow D^-\rho$	< 9	$\times 10^{-6}$	CL=90%
Γ511	$\Theta_c\bar{p}\pi^+, \Theta_c \rightarrow D^{*-}\rho$	< 1.4	$\times 10^{-5}$	CL=90%
Γ512	$\bar{\Sigma}_c^{--}\Delta^{++}$	< 8	$\times 10^{-4}$	CL=90%
Γ513	$\bar{\Lambda}_c^-\rho\pi^+\pi^-$	(1.02 ± 0.14)	$\times 10^{-3}$	S=1.3
Γ514	$\bar{\Lambda}_c^-\rho$	(1.55 ± 0.17)	$\times 10^{-5}$	
Γ515	$\bar{\Lambda}_c^-\rho\pi^0$	(1.55 ± 0.18)	$\times 10^{-4}$	
Γ516	$\bar{\Sigma}_c(2455)^-\rho$	< 2.4	$\times 10^{-5}$	
Γ517	$\bar{\Lambda}_c^-\rho\pi^+\pi^-\pi^0$	< 5.07	$\times 10^{-3}$	CL=90%
Γ518	$\bar{\Lambda}_c^-\rho\pi^+\pi^-\pi^+\pi^-$	< 2.74	$\times 10^{-3}$	CL=90%
Γ519	$\bar{\Lambda}_c^-\rho\pi^+\pi^-$ (nonresonant)	(5.5 ± 1.0)	$\times 10^{-4}$	S=1.3
Γ520	$\bar{\Sigma}_c(2520)^-\rho\pi^+$	(1.02 ± 0.18)	$\times 10^{-4}$	
Γ521	$\bar{\Sigma}_c(2520)^0\rho\pi^-$	< 3.1	$\times 10^{-5}$	CL=90%
Γ522	$\bar{\Sigma}_c(2455)^0\rho\pi^-$	(1.08 ± 0.09)	$\times 10^{-4}$	
Γ523	$\bar{\Sigma}_c(2455)^0N^0, N^0 \rightarrow \rho\pi^-$	(6.4 ± 1.7)	$\times 10^{-5}$	
Γ524	$\bar{\Sigma}_c(2455)^-\rho\pi^+$	(1.89 ± 0.15)	$\times 10^{-4}$	
Γ525	$\bar{\Lambda}_c^-pK^+\pi^-$	(3.5 ± 0.7)	$\times 10^{-5}$	
Γ526	$\bar{\Sigma}_c(2455)^-\rho K^+, \bar{\Sigma}_c^{--} \rightarrow \bar{\Lambda}_c^-\pi^-$	(8.9 ± 2.6)	$\times 10^{-6}$	
Γ527	$\bar{\Lambda}_c^-pK^*(892)^0$	< 2.42	$\times 10^{-5}$	CL=90%
Γ528	$\bar{\Lambda}_c^-pK^+K^-$	(2.0 ± 0.4)	$\times 10^{-5}$	
Γ529	$\bar{\Lambda}_c^-\rho\phi$	< 1.0	$\times 10^{-5}$	CL=90%
Γ530	$\bar{\Lambda}_c^-\rho\bar{p}\rho$	< 2.8	$\times 10^{-6}$	
Γ531	$\bar{\Lambda}_c^-\Lambda K^+$	(4.8 ± 1.1)	$\times 10^{-5}$	
Γ532	$\bar{\Lambda}_c^-\Lambda_c^+$	< 1.6	$\times 10^{-5}$	CL=95%
Γ533	$\bar{\Lambda}_c^-(2593)^- / \bar{\Lambda}_c^-(2625)^-\rho$	< 1.1	$\times 10^{-4}$	CL=90%
Γ534	$\bar{\Xi}_c^-\Lambda_c^+$	(1.2 ± 0.8)	$\times 10^{-3}$	
Γ535	$\bar{\Xi}_c^-\Lambda_c^+, \bar{\Xi}_c^- \rightarrow \Xi^-\pi^-\pi^-$	(2.4 ± 1.1)	$\times 10^{-5}$	S=1.8
Γ536	$\bar{\Xi}_c^-\Lambda_c^+, \bar{\Xi}_c^- \rightarrow \bar{p}K^+\pi^-$	(5.3 ± 1.7)	$\times 10^{-6}$	
Γ537	$\Lambda_c^+\Lambda_c^-K^0$	(4.0 ± 0.9)	$\times 10^{-4}$	
Γ538	$\bar{\Lambda}_c^-(2910)^-\rho, \bar{\Lambda}_c^- \rightarrow \bar{\Sigma}_c(2455)^-\pi^+$	(1.2 ± 0.4)	$\times 10^{-5}$	
Γ539	$\bar{\Lambda}_c^-(2910)^-\rho, \bar{\Lambda}_c^- \rightarrow \bar{\Sigma}_c(2455)^0\pi^-$	(10 ± 4)	$\times 10^{-6}$	
Γ540	$\bar{\Xi}_c^-(2930)^-\Lambda_c^+, \bar{\Xi}_c^- \rightarrow \bar{\Lambda}_c^-K^0$	(2.4 ± 0.6)	$\times 10^{-4}$	
Γ541	$\Lambda\psi_{DS}$	[j] < 0.13-5.2	$\times 10^{-5}$	

Lepton Family number (LF) or Lepton number (L) or Baryon number (B) violating modes, or/and $\Delta B = 1$ weak neutral current (BI) modes

Γ542	$\gamma\gamma$	B1	< 3.2	$\times 10^{-7}$	CL=90%
Γ543	e^+e^-	B1	< 2.5	$\times 10^{-9}$	CL=90%
Γ544	$e^+e^-\gamma$	B1	< 1.2	$\times 10^{-7}$	CL=90%
Γ545	$\mu^+\mu^-$	B1	< 1.5	$\times 10^{-10}$	CL=90%
Γ546	$\mu^+\mu^-\gamma$	B1			
Γ547	$\mu^+\mu^-\mu^+\mu^-$	B1	< 1.8	$\times 10^{-10}$	CL=95%
Γ548	$SP, S \rightarrow \mu^+\mu^-, P \rightarrow \mu^+\mu^-$	B1 [k]	< 6.0	$\times 10^{-10}$	CL=95%
Γ549	$a\bar{a}, a \rightarrow \mu^+\mu^-$	B1	< 2.3	$\times 10^{-10}$	CL=95%
Γ550	$\tau^+\tau^-$	B1	< 2.1	$\times 10^{-3}$	CL=95%
Γ551	$\pi^0\ell^+\ell^-$	B1 [a]	< 5.3	$\times 10^{-8}$	CL=90%
Γ552	$\pi^0e^+e^-$	B1	< 8.4	$\times 10^{-8}$	CL=90%
Γ553	$\pi^0\mu^+\mu^-$	B1	< 6.9	$\times 10^{-8}$	CL=90%
Γ554	$\eta\ell^+\ell^-$	B1 [a]	< 6.4	$\times 10^{-8}$	CL=90%
Γ555	ηe^+e^-	B1	< 1.08	$\times 10^{-7}$	CL=90%
Γ556	$\eta\mu^+\mu^-$	B1	< 1.12	$\times 10^{-7}$	CL=90%
Γ557	$\pi^0\nu\bar{\nu}$	B1	< 9	$\times 10^{-6}$	CL=90%
Γ558	$K^0\ell^+\ell^-$	B1 [a]	(3.3 ± 0.6)	$\times 10^{-7}$	
Γ559	$K^0e^+e^-$	B1	(2.5 ± 1.1 / 0.9)	$\times 10^{-7}$	S=1.3
Γ560	$K^0\mu^+\mu^-$	B1	(3.39 ± 0.35)	$\times 10^{-7}$	S=1.1
Γ561	$K^0\nu\bar{\nu}$	B1	< 2.6	$\times 10^{-5}$	CL=90%
Γ562	$\rho^0\nu\bar{\nu}$	B1	< 4.0	$\times 10^{-5}$	CL=90%
Γ563	$K^*(892)^0\ell^+\ell^-$	B1 [a]	(9.9 ± 1.2 / 1.1)	$\times 10^{-7}$	
Γ564	$K^*(892)^0e^+e^-$	B1	(1.03 ± 0.19 / 0.17)	$\times 10^{-6}$	
Γ565	$K^*(892)^0\mu^+\mu^-$	B1	(9.4 ± 0.5)	$\times 10^{-7}$	
Γ566	$K^*(892)^0\chi, \chi \rightarrow \mu^+\mu^-$	B1			
Γ567	$K^*(892)^0\tau^+\tau^-$	B1	< 3.1	$\times 10^{-3}$	CL=90%

Meson Particle Listings

B^0

Γ_{568}	$\pi^+ \pi^- \mu^+ \mu^-$	$B1$	$(2.1 \pm 0.5) \times 10^{-8}$
Γ_{569}	$K^*(892)^0 \nu \bar{\nu}$	$B1$	$< 1.8 \times 10^{-5}$ CL=90%
Γ_{570}	invisible	$B1$	$< 2.4 \times 10^{-5}$ CL=90%
Γ_{571}	$\nu \bar{\nu} \gamma$	$B1$	$< 1.6 \times 10^{-5}$ CL=90%
Γ_{572}	$\phi \mu^+ \mu^-$	$B1$	$< 3.2 \times 10^{-9}$
Γ_{573}	$\phi \nu \bar{\nu}$	$B1$	$< 1.27 \times 10^{-4}$ CL=90%
Γ_{574}	$e^\pm \mu^\mp$	LF	$[h] < 1.0 \times 10^{-9}$ CL=90%
Γ_{575}	$\pi^0 e^\pm \mu^\mp$	LF	$< 1.4 \times 10^{-7}$ CL=90%
Γ_{576}	$K^0 e^\pm \mu^\mp$	LF	$< 3.8 \times 10^{-8}$ CL=90%
Γ_{577}	$K^*(892)^0 e^+ \mu^-$	LF	$< 6.8 \times 10^{-9}$ CL=90%
Γ_{578}	$K^*(892)^0 e^- \mu^+$	LF	$< 5.7 \times 10^{-9}$ CL=90%
Γ_{579}	$K^*(892)^0 e^\pm \mu^\mp$	LF	$< 1.01 \times 10^{-8}$ CL=90%
Γ_{580}	$K^*(892)^0 \tau^+ \mu^-$	LF	$< 1.0 \times 10^{-5}$ CL=90%
Γ_{581}	$K^*(892)^0 \tau^- \mu^+$	LF	$< 8.2 \times 10^{-6}$ CL=90%
Γ_{582}	$e^\pm \tau^\mp$	LF	$[h] < 1.6 \times 10^{-5}$ CL=90%
Γ_{583}	$\mu^\pm \tau^\mp$	LF	$[h] < 1.4 \times 10^{-5}$ CL=95%
Γ_{584}	$\rho \mu^-$	L, B	$< 2.6 \times 10^{-9}$ CL=90%
Γ_{585}	$\Lambda_c^+ \mu^-$	L, B	$< 1.4 \times 10^{-6}$ CL=90%
Γ_{586}	$\Lambda_c^+ e^-$	L, B	$< 4 \times 10^{-6}$ CL=90%

- [a] An ℓ indicates an e or a μ mode, not a sum over these modes.
- [b] \bar{D}^{**} represents an excited state with mass $2.2 < M < 2.8 \text{ GeV}/c^2$.
- [c] $\chi_{c1}(3872)^+$ is a hypothetical charged partner of the $\chi_{c1}(3872)$.
- [d] Stands for the possible candidates of $K^*(1410)$, $K_0^*(1430)$ and $K_2^*(1430)$.
- [e] B^0 and B_s^0 contributions not separated. Limit is on weighted average of the two decay rates.
- [f] This decay refers to the coherent sum of resonant and nonresonant $J^P = 0^+ K \pi$ components with $1.60 < m_{K\pi} < 2.15 \text{ GeV}/c^2$.
- [g] $X(214)$ is a hypothetical particle of mass $214 \text{ MeV}/c^2$ reported by the HyperCP experiment, Physical Review Letters **94** 021801 (2005)
- [h] The value is for the sum of the charge states or particle/antiparticle states indicated.
- [i] $\Theta(1540)^+$ denotes a possible narrow pentaquark state.
- [j] ψ_{DS} is a GeV-scale dark sector antibaryon (mass range 1–4 GeV/c^2).
- [k] Here S and P are the hypothetical scalar and pseudoscalar particles with masses of $2.5 \text{ GeV}/c^2$ and $214.3 \text{ MeV}/c^2$, respectively.

FIT INFORMATION

An overall fit to 36 branching ratios uses 95 measurements to determine 22 parameters. The overall fit has a $\chi^2 = 72.1$ for 73 degrees of freedom.

The following *off-diagonal* array elements are the correlation coefficients $\langle \delta x_i \delta x_j \rangle / (\delta x_i \delta x_j)$, in percent, from the fit to the branching fractions, $x_i \equiv \Gamma_i / \Gamma_{\text{total}}$.

x_{10}	26																			
x_{38}	0	0																		
x_{50}	0	0	28																	
x_{76}	0	0	4	13																
x_{125}	0	0	19	6	1															
x_{135}	0	0	7	2	0	1														
x_{214}	0	0	0	0	0	0	0													
x_{216}	0	0	0	0	0	0	0	0												
x_{264}	0	0	0	0	0	0	0	0	0											
x_{270}	0	0	0	0	0	0	0	0	0	0										19
x_{276}	0	0	0	0	0	0	0	0	0	0	29									0
x_{282}	0	0	0	0	0	0	0	0	0	0	0	6								0
x_{288}	0	0	0	0	0	0	0	0	0	0	0	0	0							0
x_{322}	0	0	0	0	0	0	0	0	0	0	0	0	0	0						0
x_{356}	0	0	0	0	0	0	0	0	0	0	0	0	0	0	0					0
x_{363}	0	0	0	0	0	0	0	0	0	0	0	0	0	0	0					0
x_{377}	0	0	0	0	0	0	0	0	0	0	0	0	0	0	0					0
x_{423}	0	0	0	0	0	0	0	0	0	0	0	0	0	0	0					0
x_{454}	0	0	0	0	0	0	0	0	0	0	0	0	0	0	0					0
x_{560}	0	0	0	0	0	0	0	0	0	0	0	0	0	0	0					0
x_{565}	0	0	0	0	0	0	0	0	0	0	0	0	15							0

x_{276}	0																			
x_{282}	0	22																		
x_{288}	0	0	0																	
x_{322}	0	0	0	0																
x_{356}	0	0	0	0	16															
x_{363}	0	0	0	0	0	27	4													
x_{377}	0	0	0	0	0	0	0	0												
x_{423}	0	0	0	24	0	0	0	0	0											
x_{454}	0	0	0	0	0	0	0	0	20	0										
x_{560}	0	0	0	0	0	0	0	0	0	0	0									
x_{565}	0	4	1	0	0	0	0	0	0	0	0	0								

B^0 BRANCHING RATIOS

For branching ratios in which the charge of the decaying B is not determined, see the B^\pm section.

$\Gamma(\ell^+ \nu_\ell X) / \Gamma_{\text{total}}$	VALUE (units 10^{-2})	DOCUMENT ID	TECN	COMMENT	Γ_1 / Γ
10.33 ± 0.28 OUR EVALUATION	(Produced by HFLAV)				
10.14 ± 0.30 OUR AVERAGE	Error includes scale factor of 1.1.				
10.46 ± 0.30 ± 0.23		1 URQUIJO	07 BELL	$e^+ e^- \rightarrow T(4S)$	
9.64 ± 0.27 ± 0.33		2 AUBERT,B	06Y BABR	$e^+ e^- \rightarrow T(4S)$	
10.78 ± 0.60 ± 0.69		3 ARTUSO	97 CLE2	$e^+ e^- \rightarrow T(4S)$	
9.3 ± 1.1 ± 1.5		ALBRECHT	94 ARG	$e^+ e^- \rightarrow T(4S)$	
9.9 ± 3.0 ± 0.9		HENDERSON	92 CLEO	$e^+ e^- \rightarrow T(4S)$	
• • • We do not use the following data for averages, fits, limits, etc. • • •					
10.32 ± 0.36 ± 0.35		4 OKABE	05 BELL	Repl. by URQUIJO 07	
10.9 ± 0.7 ± 1.1		ATHANAS	94 CLE2	Sup. by ARTUSO 97	

- 1 URQUIJO 07 report a measurement of $(9.80 \pm 0.29 \pm 0.21)\%$ for the partial branching fraction of $B \rightarrow e \nu_e X_c$ decay with electron energy above 0.6 GeV. We converted the result to $B \rightarrow e \nu_e X$ branching fraction.
- 2 The measurements are obtained for charged and neutral B mesons partial rates of semi-leptonic decay to electrons with momentum above 0.6 GeV/c in the B rest frame. The best precision on the ratio is achieved for a momentum threshold of 1.0 GeV: $B(B^+ \rightarrow e^+ \nu_e X) / B(B^0 \rightarrow e^+ \nu_e X) = 1.074 \pm 0.041 \pm 0.026$.
- 3 ARTUSO 97 uses partial reconstruction of $B \rightarrow D^* \ell \nu_\ell$ and inclusive semileptonic branching ratio from BARISH 96b $(0.1049 \pm 0.0017 \pm 0.0043)$.
- 4 The measurements are obtained for charged and neutral B mesons partial rates of semi-leptonic decay to electrons with momentum above 0.6 GeV/c in the B rest frame, and their ratio of $B(B^+ \rightarrow e^+ \nu_e X) / B(B^0 \rightarrow e^+ \nu_e X) = 1.08 \pm 0.05 \pm 0.02$.

$\Gamma(e^+ \nu_e X_c) / \Gamma_{\text{total}}$	VALUE (units 10^{-2})	DOCUMENT ID	TECN	COMMENT	Γ_2 / Γ
10.08 ± 0.30 ± 0.22		1 URQUIJO	07 BELL	$e^+ e^- \rightarrow T(4S)$	

- 1 Measure the independent B^+ and B^0 partial branching fractions with electron threshold energies of 0.4 GeV.

$\Gamma(\ell^+ \nu_\ell X_u) / \Gamma_{\text{total}}$	Requires $E_\ell^* > 1 \text{ GeV}$, where E_ℓ^* is lepton energy in B rest frame.	VALUE (units 10^{-3})	DOCUMENT ID	TECN	COMMENT	Γ_3 / Γ
1.51 ± 0.10 ± 0.16			1 CAO	21A BELL	$e^+ e^- \rightarrow T(4S)$	

- 1 The correlation of 50% with $B(B^+ \rightarrow \ell^+ \nu_\ell X_u)$ (lepton energy in B rest frame $E_\ell^* > 1 \text{ GeV}$) was reported.

$\Gamma(D^- \ell^+ \nu_\ell) / \Gamma_{\text{total}}$	ℓ denotes e or μ , not the sum.	VALUE (%)	DOCUMENT ID	TECN	COMMENT	Γ_5 / Γ
2.12 ± 0.06 OUR EVALUATION	(Produced by HFLAV)					
2.25 ± 0.08 OUR AVERAGE						
2.31 ± 0.03 ± 0.11			1 GLATTAUER	16 BELL	$e^+ e^- \rightarrow T(4S)$	
2.21 ± 0.11 ± 0.11			2 AUBERT	10 BABR	$e^+ e^- \rightarrow T(4S)$	
2.09 ± 0.13 ± 0.18			3 BARTELT	99 CLE2	$e^+ e^- \rightarrow T(4S)$	
2.35 ± 0.20 ± 0.44			4 BUSKULIC	97 ALEP	$e^+ e^- \rightarrow Z$	
• • • We do not use the following data for averages, fits, limits, etc. • • •						
2.21 ± 0.11 ± 0.12			2 AUBERT	08Q BABR	Repl. by AUBERT 10	
2.13 ± 0.12 ± 0.39			ABE	02E BELL	Repl. by GLATTAUER 16	
1.87 ± 0.15 ± 0.32			5 ATHANAS	97 CLE2	Repl. by BARTELT 99	
1.8 ± 0.6 ± 0.3			6 FULTON	91 CLEO	$e^+ e^- \rightarrow T(4S)$	
2.0 ± 0.7 ± 0.6			7 ALBRECHT	89J ARG	$e^+ e^- \rightarrow T(4S)$	

- 1 Uses a fully reconstructed B meson as a tag on the recoil side while the other, on the signal side, is partially reconstructed from $B \rightarrow D \ell \nu$.
- 2 Uses a fully reconstructed B meson as a tag on the recoil side.
- 3 Assumes equal production of B^+ and B^0 at the $T(4S)$.
- 4 BUSKULIC 97 assumes fraction $(B^+) = \text{fraction}(B^0) = (37.8 \pm 2.2)\%$ and PDG 96 values for B lifetime and branching ratio of D^* and D decays.

- ⁵ ATHANAS 97 uses missing energy and missing momentum to reconstruct neutrino.
- ⁶ FULTON 91 assumes assuming equal production of B⁰ and B⁺ at the T(4S) and uses Mark III D and D* branching ratios.
- ⁷ ALBRECHT 89J reports 0.018 ± 0.006 ± 0.005. We rescale using the method described in STONE 94 but with the updated PDG 94 B(D⁰ → K⁻π⁺).

$\Gamma(D^-\ell^+\nu_\ell)/\Gamma(\ell^+\nu_\ell X)$	DOCUMENT ID	TECN	COMMENT	Γ_5/Γ_1
0.230 ± 0.011 ± 0.011	¹ AUBERT 10	BABR	e ⁺ e ⁻ → T(4S)	

¹ Uses a fully reconstructed B meson on the recoil side.

$\Gamma(D^-\ell^+\nu_\ell)/\Gamma(D\ell^+\nu_\ell X)$	DOCUMENT ID	TECN	COMMENT	Γ_5/Γ_4
0.215 ± 0.016 ± 0.013	¹ AUBERT 07AN	BABR	e ⁺ e ⁻ → T(4S)	

¹ Uses a fully reconstructed B meson on the recoil side.

$\Gamma(D^-\tau^+\nu_\tau)/\Gamma_{total}$	DOCUMENT ID	TECN	COMMENT	Γ_6/Γ
1.04 ± 0.35 ± 0.18	¹ AUBERT 08N	BABR	Repl. by AUBERT 09s	

• • • We do not use the following data for averages, fits, limits, etc. • • •

¹ Uses a fully reconstructed B meson as a tag on the recoil side.

$\Gamma(D^-\tau^+\nu_\tau)/\Gamma(D^-\ell^+\nu_\ell)$	DOCUMENT ID	TECN	COMMENT	Γ_6/Γ_5
0.469 ± 0.084 ± 0.053	^{1,2} LEES 12D	BABR	e ⁺ e ⁻ → T(4S)	

• • • We do not use the following data for averages, fits, limits, etc. • • •

¹ AUBERT 09s BABR Repl. by LEES 12D

¹ Uses a fully reconstructed B meson as a tag on the recoil side.

² Uses τ⁺ → e⁺ν_eν̄_τ and τ⁺ → μ⁺ν_μν̄_τ and e⁺ or μ⁺ as ℓ⁺.

$\Gamma(D^*(2010)^-\ell^+\nu_\ell)/\Gamma_{total}$	DOCUMENT ID	TECN	COMMENT	Γ_7/Γ
4.90 ± 0.12 OUR EVALUATION	(Produced by HFLAV) This value assumes isospin symmetry.			

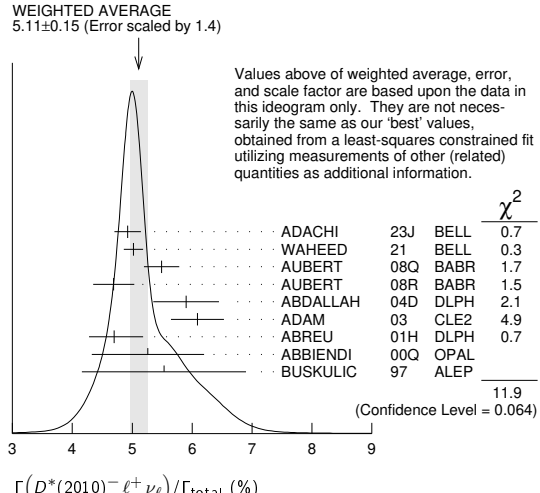
5.11 ± 0.14 OUR FIT Error includes scale factor of 1.4.

5.11 ± 0.15 OUR AVERAGE Error includes scale factor of 1.4. See the ideogram below.

4.922 ± 0.023 ± 0.220	¹ ADACHI 23J	BELL	e ⁺ e ⁻ → T(4S)
5.02 ± 0.02 ± 0.16	² WAHEED 21	BELL	e ⁺ e ⁻ → T(4S)
5.49 ± 0.16 ± 0.25	³ AUBERT 08Q	BABR	e ⁺ e ⁻ → T(4S)
4.69 ± 0.04 ± 0.34	⁴ AUBERT 08R	BABR	e ⁺ e ⁻ → T(4S)
5.90 ± 0.22 ± 0.50	⁵ ABDALLAH 04D	DLPH	e ⁺ e ⁻ → Z ⁰
6.09 ± 0.19 ± 0.40	⁶ ADAM 03	CLE2	e ⁺ e ⁻ → T(4S)
4.70 ± 0.13 ± 0.36 -0.31	⁷ ABREU 01H	DLPH	e ⁺ e ⁻ → Z
5.26 ± 0.20 ± 0.46	⁸ ABBIENDI 00Q	OPAL	e ⁺ e ⁻ → Z
5.53 ± 0.26 ± 0.52	⁹ BUSKULIC 97	ALEP	e ⁺ e ⁻ → Z
• • • We do not use the following data for averages, fits, limits, etc. • • •			
4.917 ± 0.032 ± 0.216	¹⁰ ADACHI 23J	BELL	e ⁺ e ⁻ → T(4S)
4.926 ± 0.032 ± 0.231	¹¹ ADACHI 23J	BELL	e ⁺ e ⁻ → T(4S)
4.90 ± 0.02 ± 0.16	² WAHEED 19	BELL	Repl. by WAHEED 21
4.58 ± 0.03 ± 0.26	² DUNGEL 10	BELL	Repl. by WAHEED 19
4.90 ± 0.07 ± 0.36 -0.35	⁵ AUBERT 05E	BABR	Repl. by AUBERT 08R
5.39 ± 0.11 ± 0.34	¹² ABDALLAH 04D	DLPH	e ⁺ e ⁻ → Z ⁰
4.59 ± 0.23 ± 0.40	¹³ ABE 02F	BELL	Repl. by DUNGEL 10
6.09 ± 0.19 ± 0.40	¹⁴ BRIERE 02	CLE2	e ⁺ e ⁻ → T(4S)
5.08 ± 0.21 ± 0.66	¹⁵ ACKERSTAFF 97G	OPAL	Repl. by ABBIENDI 00Q
5.52 ± 0.17 ± 0.68	¹⁶ ABREU 96P	DLPH	Repl. by ABREU 01H
4.49 ± 0.32 ± 0.39	¹⁷ BARISH 95	CLE2	Repl. by ADAM 03
5.18 ± 0.30 ± 0.62	¹⁸ BUSKULIC 95N	ALEP	Sup. by BUSKULIC 97
4.5 ± 0.3 ± 0.4	¹⁹ ALBRECHT 94	ARG	e ⁺ e ⁻ → T(4S)
4.7 ± 0.5 ± 0.5	²⁰ ALBRECHT 93	ARG	e ⁺ e ⁻ → T(4S)
seen	²¹ SANGHERA 93	CLE2	e ⁺ e ⁻ → T(4S)
7.0 ± 1.8 ± 1.4	²² ANTREASAYAN 90B	CBAL	e ⁺ e ⁻ → T(4S)
	²³ ALBRECHT 89C	ARG	e ⁺ e ⁻ → T(4S)
6.0 ± 1.0 ± 1.4	²⁴ ALBRECHT 89J	ARG	e ⁺ e ⁻ → T(4S)
4.0 ± 0.4 ± 0.6	²⁵ BORTOLETTO89B	CLEO	e ⁺ e ⁻ → T(4S)
7.0 ± 1.2 ± 1.9	²⁶ ALBRECHT 87J	ARG	e ⁺ e ⁻ → T(4S)

- ¹ Uses fully reconstructed D*⁻ℓ⁺ν events with ℓ = e or μ.
- ² WAHEED 21 uses fully reconstructed D*⁻ℓ⁺ν events (ℓ = e or μ).
- ³ Uses a fully reconstructed B meson as a tag on the recoil side.
- ⁴ Measured using fully reconstructed D* sample and a simultaneous fit to the Caprin-Lellouch-Neubert form factor parameters: ρ² = 1.191 ± 0.048 ± 0.028, R₁(1) = 1.429 ± 0.061 ± 0.044, and R₂(1) = 0.827 ± 0.038 ± 0.022.
- ⁵ Measured using fully reconstructed D* sample.
- ⁶ Uses the combined fit of both B⁰ → D*(2010)⁻ℓν and B⁺ → D̄(2007)⁰ℓν samples.
- ⁷ ABREU 01H measured using about 5000 partial reconstructed D* sample.
- ⁸ ABBIENDI 00Q assumes the fraction B(B → B⁰) = (39.7^{+1.8}_{-2.2})%. This result is an average of two methods using exclusive and partial D* reconstruction.
- ⁹ BUSKULIC 97 assumes fraction (B⁺) = fraction (B⁰) = (37.8 ± 2.2)% and PDG 96 values for B lifetime and D* and D branching fractions.
- ¹⁰ Uses fully reconstructed D*⁻e⁺ν events.
- ¹¹ Uses fully reconstructed D*⁻μ⁺ν events.

- ¹² Combines with previous partial reconstructed D* measurement.
- ¹³ Assumes equal production of B⁺ and B⁰ at the T(4S).
- ¹⁴ The results are based on the same analysis and data sample reported in ADAM 03.
- ¹⁵ ACKERSTAFF 97G assumes fraction (B⁺) = fraction (B⁰) = (37.8 ± 2.2)% and PDG 96 values for B lifetime and branching ratio of D* and D decays.
- ¹⁶ ABREU 96P result is the average of two methods using exclusive and partial D* reconstruction.
- ¹⁷ BARISH 95 use B(D⁰ → K⁻π⁺) = (3.91 ± 0.08 ± 0.17)% and B(D*⁺ → D⁰π⁺) = (68.1 ± 1.0 ± 1.3)%.
- ¹⁸ BUSKULIC 95N assumes fraction (B⁺) = fraction (B⁰) = 38.2 ± 1.3 ± 2.2% and τ_{B⁰} = 1.58 ± 0.06 ps. Γ(D*⁻ℓ⁺ν_ℓ)/total = [5.18 - 0.13(fraction(B⁰) - 38.2) - 1.5(τ_{B⁰} - 1.58)]%.
- ¹⁹ ALBRECHT 94 assumes B(D*⁺ → D⁰π⁺) = 68.1 ± 1.0 ± 1.3%. Uses partial reconstruction of D*⁺ and is independent of D⁰ branching ratios.
- ²⁰ ALBRECHT 93 reports 0.052 ± 0.005 ± 0.006. We rescale using the method described in STONE 94 but with the updated PDG 94 B(D⁰ → K⁻π⁺). We have taken their average e and μ value. They also obtain α = 2*Γ⁰/(Γ⁻ + Γ⁺) - 1 = 1.1 ± 0.4 ± 0.2, A_{AF} = 3/4*(Γ⁻ - Γ⁺)/Γ = 0.2 ± 0.08 ± 0.06 and a value of |V_{cb}| = 0.036 - 0.045 depending on model assumptions.
- ²¹ Combining D*⁰ℓ⁺ν_ℓ and D*⁻ℓ⁺ν_ℓ SANGHERA 93 test V-A structure and fit the decay angular distributions to obtain A_{FB} = 3/4*(Γ⁻ - Γ⁺)/Γ = 0.14 ± 0.06 ± 0.03. Assuming a value of V_{cb}, they measure V, A₁, and A₂, the three form factors for the D*ℓν_ℓ decay, where results are slightly dependent on model assumptions.
- ²² ANTREASAYAN 90B is average over B and D*(2010) charge states.
- ²³ The measurement of ALBRECHT 89c suggests a D* polarization γ_L/γ_T of 0.85 ± 0.45, or α = 0.7 ± 0.9.
- ²⁴ ALBRECHT 89J is ALBRECHT 87J value rescaled using B(D*(2010)⁻ → D⁰π⁻) = 0.57 ± 0.04 ± 0.04. Superseded by ALBRECHT 93.
- ²⁵ We have taken average of the the BORTOLETTO 89b values for electrons and muons, 0.046 ± 0.005 ± 0.007. We rescale using the method described in STONE 94 but with the updated PDG 94 B(D⁰ → K⁻π⁺). The measurement suggests a D* polarization parameter value α = 0.65 ± 0.66 ± 0.25.
- ²⁶ ALBRECHT 87J assume μ-e universality, the B(T(4S) → B⁰B̄⁰) = 0.45, the B(D⁰ → K⁻π⁺) = (0.042 ± 0.004 ± 0.004), and the B(D*(2010)⁻ → D⁰π⁻) = 0.49 ± 0.08. Superseded by ALBRECHT 89J.



$\Gamma(D^*(2010)^-\ell^+\nu_\ell)/\Gamma(D\ell^+\nu_\ell X)$	DOCUMENT ID	TECN	COMMENT	Γ_7/Γ_4
0.537 ± 0.031 ± 0.036	¹ AUBERT 07AN	BABR	e ⁺ e ⁻ → T(4S)	

¹ Uses a fully reconstructed B meson on the recoil side.

$\Gamma(D^*(2010)^-e^+\nu_e)/\Gamma(D^*(2010)^-\mu^+\nu_\mu)$	DOCUMENT ID	TECN	COMMENT	Γ_8/Γ_9
1.001 ± 0.019 OUR AVERAGE				
0.998 ± 0.009 ± 0.020	ADACHI 23J	BELL	e ⁺ e ⁻ → T(4S)	
1.011 ± 0.035 ± 0.024	PRIM 23	BELL	e ⁺ e ⁻ → T(4S)	

$\Gamma(D^*(2010)^-\tau^+\nu_\tau)/\Gamma_{total}$	DOCUMENT ID	TECN	COMMENT	Γ_{10}/Γ
1.45 ± 0.10 OUR FIT	Error includes scale factor of 1.3.			

$1.48 ± 0.18 OUR AVERAGE$	DOCUMENT ID	TECN	COMMENT
1.42 ± 0.094 ± 0.140	¹ AAIJ 18D	LHCb	pp at 7, 8 TeV
2.02 ^{+0.40} _{-0.37} ± 0.37	² MATYJA 07	BELL	e ⁺ e ⁻ → T(4S)

- • • We do not use the following data for averages, fits, limits, etc. • • •
- 1.11 ± 0.51 ± 0.06 ³ AUBERT 08N BABR Repl. by AUBERT 09s
- ¹ Normalizes to B(B⁰ → D*(2010)⁻π⁺π⁻π⁺) = (7.214 ± 0.28) × 10⁻³.
- ² Observed in the recoil of the accompanying B meson.
- ³ Uses a fully reconstructed B meson as a tag on the recoil side.

Meson Particle Listings

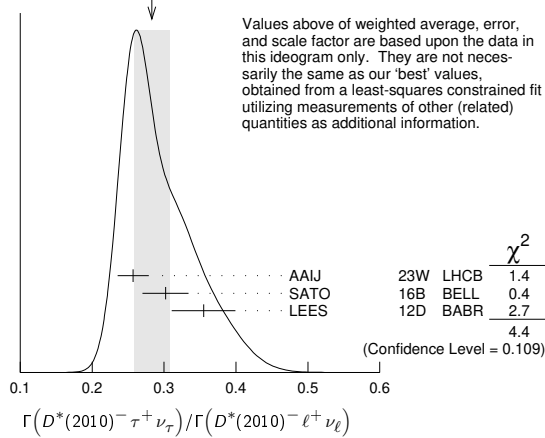
B^0

$$\Gamma(D^{*}(2010)^{-}\tau^{+}\nu_{\tau})/\Gamma(D^{*}(2010)^{-}\ell^{+}\nu_{\ell}) \quad \Gamma_{10}/\Gamma_7$$

VALUE	DOCUMENT ID	TECN	COMMENT
0.284±0.019 OUR FIT	Error includes scale factor of 1.3.		
0.283±0.025 OUR AVERAGE	Error includes scale factor of 1.5. See the ideogram below.		
0.257±0.012±0.018	^{1,2} AAIJ	23W LHCb	pp at 7, 8, 13 TeV
0.302±0.030±0.011	³ SATO	16B BELL	$e^{+}e^{-} \rightarrow \Upsilon(4S)$
0.355±0.039±0.021	^{4,5} LEES	12D BABR	$e^{+}e^{-} \rightarrow \Upsilon(4S)$
••• We do not use the following data for averages, fits, limits, etc. •••			
0.247±0.015±0.019	¹ AAIJ	23W LHCb	pp at 13 TeV
0.291±0.019±0.029	¹ AAIJ	18D LHCb	Repl. by AAJ 23W
0.336±0.027±0.030	⁶ AAIJ	15Q LHCb	Repl. by AAJ 23AR
0.207±0.095±0.008	⁴ AUBERT	09S BABR	Repl. by LEES 12D

- Uses $\tau^{+} \rightarrow \pi^{+}\pi^{-}\pi^{+}\bar{\nu}_{\tau}$ and $\tau^{+} \rightarrow \pi^{+}\pi^{-}\pi^{+}\pi^{0}\bar{\nu}_{\tau}$, and μ^{+} as ℓ^{+} .
- Combination with measurement from AAJ 18D.
- Uses semileptonic B decay events for tagging and $\tau^{+} \rightarrow \ell^{+}\nu_{\ell}\bar{\nu}_{\tau}$ mode.
- Uses a fully reconstructed B meson as a tag on the recoil side.
- Uses $\tau^{+} \rightarrow e^{+}\nu_e\bar{\nu}_{\tau}$ and $\tau^{+} \rightarrow \mu^{+}\nu_{\mu}\bar{\nu}_{\tau}$ and e^{+} or μ^{+} as ℓ^{+} .
- Uses $\tau^{+} \rightarrow \mu^{+}\nu_{\mu}\bar{\nu}_{\tau}$ and μ^{+} as ℓ^{+} .

WEIGHTED AVERAGE
0.283±0.025 (Error scaled by 1.5)



$$\Gamma(D^{*}(2010)^{-}\tau^{+}\nu_{\tau})/\Gamma(D^{*}(2010)^{-}\pi^{+}\pi^{+}\pi^{-}) \quad \Gamma_{10}/\Gamma_{61}$$

VALUE	DOCUMENT ID	TECN	COMMENT
1.77±0.08±0.10	^{1,2} AAIJ	23W LHCb	pp at 7, 8, 13 TeV
••• We do not use the following data for averages, fits, limits, etc. •••			
1.70±0.10±0.10	¹ AAIJ	23W LHCb	pp at 13 TeV
1.97±0.13±0.18	¹ AAIJ	18D LHCb	Repl. by AAJ 23W
1 Uses $\tau^{+} \rightarrow \pi^{+}\pi^{-}\pi^{+}\bar{\nu}_{\tau}$ and $\tau^{+} \rightarrow \pi^{+}\pi^{-}\pi^{+}\pi^{0}\bar{\nu}_{\tau}$ modes.			
2 Combination with result from AAJ 18D.			

$$\Gamma(\bar{D}^{*0}\pi^{-}\ell^{+}\nu_{\ell})/\Gamma(D\ell^{+}\nu_{\ell}X) \quad \Gamma_{11}/\Gamma_4$$

VALUE	DOCUMENT ID	TECN	COMMENT
0.248±0.032±0.030	¹ AUBERT	07AN BABR	$e^{+}e^{-} \rightarrow \Upsilon(4S)$
1 Uses a fully reconstructed B meson on the recoil side.			

$$\Gamma(\bar{D}^0\pi^{-}\ell^{+}\nu_{\ell})/\Gamma_{\text{total}} \quad \Gamma_{12}/\Gamma$$

VALUE (units 10^{-3})	DOCUMENT ID	TECN	COMMENT
3.64±0.20 OUR AVERAGE			
3.60±0.18±0.11	MEIER	23 BELL	$e^{+}e^{-} \rightarrow \Upsilon(4S)$
4.3 ± 0.8 ± 0.3	¹ AUBERT	08Q BABR	$e^{+}e^{-} \rightarrow \Upsilon(4S)$
••• We do not use the following data for averages, fits, limits, etc. •••			
4.05±0.36±0.41	VOSSEN	18 BELL	Repl. by MEIER 23
4.2 ± 0.8 ± 0.1	^{1,2} LIVENTSEV	08 BELL	Repl. by VOSSEN 18
3.3 ± 0.9 ± 0.1	³ LIVENTSEV	05 BELL	Repl. by LIVENTSEV 08

- Uses a fully reconstructed B meson as a tag on the recoil side.
- LIVENTSEV 08 reports $(4.2 \pm 0.7 \pm 0.6) \times 10^{-3}$ from a measurement of $[\Gamma(B^0 \rightarrow \bar{D}^0\pi^{-}\ell^{+}\nu_{\ell})/\Gamma_{\text{total}}] / [B(B^0 \rightarrow D^{-}\ell^{+}\nu_{\ell})]$ assuming $B(B^0 \rightarrow D^{-}\ell^{+}\nu_{\ell}) = (2.12 \pm 0.20) \times 10^{-2}$, which we rescale to our best value $B(B^0 \rightarrow D^{-}\ell^{+}\nu_{\ell}) = (2.12 \pm 0.06) \times 10^{-2}$. Our first error is their experiment's error and our second error is the systematic error from using our best value.
- LIVENTSEV 05 reports $[\Gamma(B^0 \rightarrow \bar{D}^0\pi^{-}\ell^{+}\nu_{\ell})/\Gamma_{\text{total}}] / [B(B^+ \rightarrow \bar{D}^0\ell^{+}\nu_{\ell})] = 0.15 \pm 0.03 \pm 0.03$ which we multiply by our best value $B(B^+ \rightarrow \bar{D}^0\ell^{+}\nu_{\ell}) = (2.21 \pm 0.06) \times 10^{-2}$. Our first error is their experiment's error and our second error is the systematic error from using our best value.

$$\Gamma(D_0^{*}(2300)^{-}\ell^{+}\nu_{\ell}, D_0^{*-} \rightarrow \bar{D}^0\pi^{-})/\Gamma_{\text{total}} \quad \Gamma_{13}/\Gamma$$

VALUE (units 10^{-4})	CL%	DOCUMENT ID	TECN	COMMENT
< 4.4	90	MEIER	23 BELL	$e^{+}e^{-} \rightarrow \Upsilon(4S)$
••• We do not use the following data for averages, fits, limits, etc. •••				
44 ± 8 ± 6		¹ AUBERT	08BL BABR	$e^{+}e^{-} \rightarrow \Upsilon(4S)$
20 ± 7 ± 5		¹ LIVENTSEV	08 BELL	$e^{+}e^{-} \rightarrow \Upsilon(4S)$

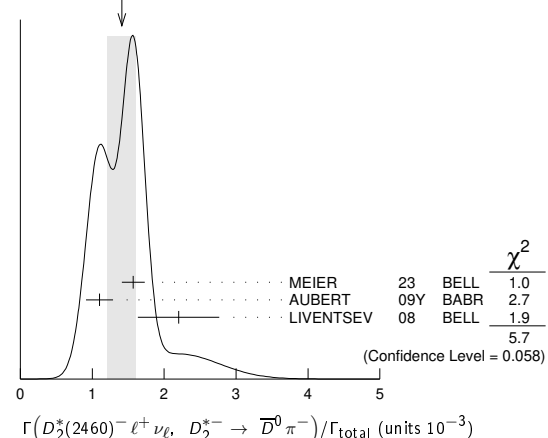
- Uses a fully reconstructed B meson as a tag on the recoil side.

$$\Gamma(D_2^{*}(2460)^{-}\ell^{+}\nu_{\ell}, D_2^{*-} \rightarrow \bar{D}^0\pi^{-})/\Gamma_{\text{total}} \quad \Gamma_{14}/\Gamma$$

VALUE (units 10^{-3})	DOCUMENT ID	TECN	COMMENT
1.41±0.20 OUR AVERAGE	Error includes scale factor of 1.7. See the ideogram below.		
1.57±0.15±0.05	MEIER	23 BELL	$e^{+}e^{-} \rightarrow \Upsilon(4S)$
1.10±0.17±0.08	¹ AUBERT	09Y BABR	$e^{+}e^{-} \rightarrow \Upsilon(4S)$
2.2 ± 0.4 ± 0.4	² LIVENTSEV	08 BELL	$e^{+}e^{-} \rightarrow \Upsilon(4S)$

- Uses a simultaneous fit of all B semileptonic decays without full reconstruction of events. AUBERT 09Y reports $B(B^0 \rightarrow \bar{D}_2^{*}(2460)^{-}\ell^{+}\nu_{\ell}) \cdot B(\bar{D}_2^{*}(2460)^{-} \rightarrow \bar{D}^{*0}\pi^{-}) = (1.77 \pm 0.26 \pm 0.11) \times 10^{-3}$ and the authors have provided us the individual measurement.
- Uses a fully reconstructed B meson as a tag on the recoil side.

WEIGHTED AVERAGE
1.41±0.20 (Error scaled by 1.7)



$$\Gamma(\bar{D}^{*0}\pi^{-}\ell^{+}\nu_{\ell})/\Gamma_{\text{total}} \quad \Gamma_{15}/\Gamma$$

VALUE (units 10^{-3})	DOCUMENT ID	TECN	COMMENT
5.44±0.28 OUR AVERAGE			
5.51±0.24±0.17	MEIER	23 BELL	$e^{+}e^{-} \rightarrow \Upsilon(4S)$
4.8 ± 0.8 ± 0.4	¹ AUBERT	08Q BABR	$e^{+}e^{-} \rightarrow \Upsilon(4S)$
••• We do not use the following data for averages, fits, limits, etc. •••			
6.46±0.53±0.52	VOSSEN	18 BELL	Repl. by MEIER 23
5.6 ± 2.2 ± 0.2	^{1,2} LIVENTSEV	08 BELL	Repl. by VOSSEN 18
5.5 ± 1.2 ± 0.2	^{3,4} LIVENTSEV	05 BELL	Repl. by LIVENTSEV 08

- Uses a fully reconstructed B meson as a tag on the recoil side.
- LIVENTSEV 08 reports $(5.6 \pm 2.1 \pm 0.8) \times 10^{-3}$ from a measurement of $[\Gamma(B^0 \rightarrow \bar{D}^{*0}\pi^{-}\ell^{+}\nu_{\ell})/\Gamma_{\text{total}}] / [B(B^0 \rightarrow D^{-}\ell^{+}\nu_{\ell})]$ assuming $B(B^0 \rightarrow D^{-}\ell^{+}\nu_{\ell}) = (2.12 \pm 0.20) \times 10^{-2}$, which we rescale to our best value $B(B^0 \rightarrow D^{-}\ell^{+}\nu_{\ell}) = (2.12 \pm 0.06) \times 10^{-2}$. Our first error is their experiment's error and our second error is the systematic error from using our best value.
- Excludes D^{*+} contribution to $D\pi$ modes.
- LIVENTSEV 05 reports $[\Gamma(B^0 \rightarrow \bar{D}^{*0}\pi^{-}\ell^{+}\nu_{\ell})/\Gamma_{\text{total}}] / [B(B^+ \rightarrow \bar{D}^{*}(2007)^0\ell^{+}\nu_{\ell})] = 0.10 \pm 0.02 \pm 0.01$ which we multiply by our best value $B(B^+ \rightarrow \bar{D}^{*}(2007)^0\ell^{+}\nu_{\ell}) = (5.53 \pm 0.22) \times 10^{-2}$. Our first error is their experiment's error and our second error is the systematic error from using our best value.

$$\Gamma(D_1(2420)^{-}\ell^{+}\nu_{\ell}, D_1^{-} \rightarrow \bar{D}^0\pi^{-})/\Gamma_{\text{total}} \quad \Gamma_{16}/\Gamma$$

VALUE (units 10^{-3})	DOCUMENT ID	TECN	COMMENT
2.85±0.25 OUR AVERAGE			
3.06±0.50±0.28	MEIER	23 BELL	$e^{+}e^{-} \rightarrow \Upsilon(4S)$
2.78±0.24±0.25	¹ AUBERT	09Y BABR	$e^{+}e^{-} \rightarrow \Upsilon(4S)$
2.7 ± 0.4 ± 0.3	² AUBERT	08BL BABR	$e^{+}e^{-} \rightarrow \Upsilon(4S)$
5.4 ± 1.9 ± 0.9	² LIVENTSEV	08 BELL	$e^{+}e^{-} \rightarrow \Upsilon(4S)$

- Uses a simultaneous measurement of all B semileptonic decays without full reconstruction of events.
- Uses a fully reconstructed B meson as a tag on the recoil side.

$$\Gamma(D_1(2420)^{-}\ell^{+}\nu_{\ell}, D_1^{-} \rightarrow D^{-}\pi^{+}\pi^{-})/\Gamma_{\text{total}} \quad \Gamma_{17}/\Gamma$$

VALUE (units 10^{-3})	DOCUMENT ID	TECN	COMMENT
1.02±0.13±0.09	MEIER	23 BELL	$e^{+}e^{-} \rightarrow \Upsilon(4S)$

$\Gamma(D_1^{*0}(2430)^- \ell^+ \nu_\ell, D_1^{*-} \rightarrow \bar{D}^{*0} \pi^-) / \Gamma_{\text{total}}$ Γ_{18} / Γ

VALUE (units 10 ⁻³)	CL%	DOCUMENT ID	TECN	COMMENT
2.5 ± 0.6 OUR AVERAGE				
2.06 ± 0.68 ± 0.25		MEIER 23	BELL	e ⁺ e ⁻ → T(4S)
3.1 ± 0.7 ± 0.5		¹ AUBERT 08BL	BABR	e ⁺ e ⁻ → T(4S)
<5.0	90	¹ LIVENTSEV 08	BELL	e ⁺ e ⁻ → T(4S)

¹ Uses a fully reconstructed B meson as a tag on the recoil side.

$\Gamma(D_2^{*0}(2460)^- \ell^+ \nu_\ell, D_2^{*-} \rightarrow \bar{D}^{*0} \pi^-) / \Gamma_{\text{total}}$ Γ_{19} / Γ

VALUE (units 10 ⁻⁴)	CL%	DOCUMENT ID	TECN	COMMENT
6.6 ± 1.1 OUR AVERAGE				
5.1 ± 4.0 ± 1.0		MEIER 23	BELL	e ⁺ e ⁻ → T(4S)
6.7 ± 1.2 ± 0.5		¹ AUBERT 09Y	BABR	e ⁺ e ⁻ → T(4S)
7 ± 2 ± 2		² AUBERT 08BL	BABR	e ⁺ e ⁻ → T(4S)
<30	90	² LIVENTSEV 08	BELL	e ⁺ e ⁻ → T(4S)

¹ Uses a simultaneous fit of all B semileptonic decays without full reconstruction of events. AUBERT 09Y reports B(B⁰ → D₂^{*(2460)⁻ ℓ⁺ ν_ℓ) · B(D₂^{*(2460)⁻ → D^{(*)0} π⁻) = (1.77 ± 0.26 ± 0.11) × 10⁻³ and the authors have provided us the individual measurement.}}

² Uses a fully reconstructed B meson as a tag on the recoil side.

$\Gamma(D^- \pi^+ \pi^- \ell^+ \nu_\ell) / \Gamma_{\text{total}}$ Γ_{20} / Γ

VALUE (units 10 ⁻³)	DOCUMENT ID	TECN	COMMENT
1.45 ± 0.18 ± 0.13	MEIER 23	BELL	e ⁺ e ⁻ → T(4S)

$\Gamma(D^- \pi^+ \pi^- \ell^+ \nu_\ell) / \Gamma(D^- \ell^+ \nu_\ell)$ Γ_{20} / Γ_5

VALUE (units 10 ⁻²)	DOCUMENT ID	TECN	COMMENT
5.8 ± 1.8 ± 1.2	¹ LEES 16	BABR	e ⁺ e ⁻ → T(4S)

¹ Measurement used electrons and muons as leptons.

$\Gamma(D^{*-} \pi^+ \pi^- \ell^+ \nu_\ell) / \Gamma_{\text{total}}$ Γ_{21} / Γ

VALUE (units 10 ⁻⁴)	DOCUMENT ID	TECN	COMMENT
5.1 ± 2.1 ± 0.9	MEIER 23	BELL	e ⁺ e ⁻ → T(4S)

$\Gamma(D^{*-} \pi^+ \pi^- \ell^+ \nu_\ell) / \Gamma(D^{*0}(2010)^- \ell^+ \nu_\ell)$ Γ_{21} / Γ_7

VALUE (units 10 ⁻²)	DOCUMENT ID	TECN	COMMENT
2.8 ± 0.8 ± 0.6	¹ LEES 16	BABR	e ⁺ e ⁻ → T(4S)

¹ Measurement used electrons and muons as leptons.

$\Gamma(\rho^- \ell^+ \nu_\ell) / \Gamma_{\text{total}}$ Γ_{22} / Γ

ℓ = e or μ, not sum over e and μ modes.

“OUR EVALUATION” includes both B⁰ and B⁺ decays. The average assumes equality of the semileptonic decay width for these isospin conjugate states.

VALUE (units 10 ⁻⁴)	CL%	DOCUMENT ID	TECN	COMMENT
2.94 ± 0.11 ± 0.18 OUR EVALUATION		(Produced by HFLAV)		
2.45 ± 0.32 OUR AVERAGE		Error includes scale factor of 1.6. See the ideogram below.		

3.22 ± 0.27 ± 0.24		¹ SIBIDANOV 13	BELL	e ⁺ e ⁻ → T(4S)
1.75 ± 0.15 ± 0.27		² DEL-AMO-SA...11c	BABR	e ⁺ e ⁻ → T(4S)
2.93 ± 0.37 ± 0.37		³ ADAM 07	CLE2	e ⁺ e ⁻ → T(4S)
2.17 ± 0.54 ± 0.32		⁴ HOKUUE 07	BELL	e ⁺ e ⁻ → T(4S)
2.57 ± 0.29 ± 0.53		⁵ BEHRENS 00	CLE2	e ⁺ e ⁻ → T(4S)
2.14 ± 0.21 ± 0.56		² AUBERT,B 05o	BABR	Repl. by DEL-AMO-SANCHEZ 11c
2.17 ± 0.34 ± 0.62		⁶ ATHAR 03	CLE2	Repl. by ADAM 07
3.29 ± 0.42 ± 0.72		⁷ AUBERT 03E	BABR	Repl. by AUBERT,B 05o
2.69 ± 0.41 ± 0.61		⁸ BEHRENS 00	CLE2	e ⁺ e ⁻ → T(4S)
2.5 ± 0.4 ± 0.7		⁹ ALEXANDER 96T	CLE2	Repl. by BEHRENS 00
<4.1	90	¹⁰ BEAN 93B	CLE2	e ⁺ e ⁻ → T(4S)

¹ The signal events are tagged by a second B meson reconstructed in the fully hadronic decays.

² B⁺ and B⁰ decays combined assuming isospin symmetry. Systematic errors include both experimental and form-factor uncertainties.

³ The B⁰ and B⁺ results are combined assuming the isospin, B lifetimes, and relative charged/neutral B production at the T(4S).

⁴ The signal events are tagged by a second B meson reconstructed in the semileptonic mode B → D^(*) ℓ ν_ℓ.

⁵ Averaging with ALEXANDER 96T results including experimental and theoretical correlations considered, BEHRENS 00 reports systematic errors +0.33 ± 0.41, where the second error is theoretical model dependence. We combine these in quadrature.

⁶ ATHAR 03 reports systematic errors +0.47 ± 0.41 ± 0.01, which are experimental systematic, systematic due to residual form-factor uncertainties in the signal, and systematic due to residual form-factor uncertainties in the cross-feed modes, respectively. We combine these in quadrature.

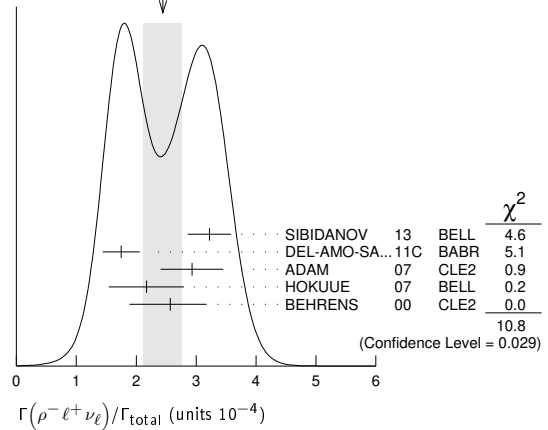
⁷ Uses isospin constraints and extrapolation to all electron energies according to five different form-factor calculations. The second error combines the systematic and theoretical uncertainties in quadrature.

⁸ BEHRENS 00 reports +0.35 ± 0.50, where the second error is the theoretical model dependence. We combine these in quadrature. B⁺ and B⁰ decays combined using isospin symmetry: Γ(B⁰ → ρ⁻ ℓ⁺ ν) = 2Γ(B⁺ → ρ⁰ ℓ⁺ ν) ≈ 2Γ(B⁺ → ω ℓ⁺ ν). No evidence for ω ℓ ν is reported.

⁹ ALEXANDER 96T reports +0.5 ± 0.5 where the second error is the theoretical model dependence. We combine these in quadrature. B⁺ and B⁰ decays combined using isospin symmetry: Γ(B⁰ → ρ⁻ ℓ⁺ ν) = 2Γ(B⁺ → ρ⁰ ℓ⁺ ν) ≈ 2Γ(B⁺ → ω ℓ⁺ ν). No evidence for ω ℓ ν is reported.

¹⁰ BEAN 93B limit set using ISGW Model. Using isospin and the quark model to combine Γ(ρ⁰ ℓ⁺ ν_ℓ) and Γ(ω ℓ⁺ ν_ℓ) with this result, they obtain a limit <(1.6-2.7) × 10⁻⁴ at 90% CL for B⁺ → (ω or ρ⁰) ℓ⁺ ν_ℓ. The range corresponds to the ISGW, WSB, and KS models. An upper limit on |V_{ub}/V_{cb}| < 0.08-0.13 at 90% CL is derived as well.

WEIGHTED AVERAGE
2.45 ± 0.32 (Error scaled by 1.6)



$\Gamma(\pi^- \ell^+ \nu_\ell) / \Gamma_{\text{total}}$ Γ_{23} / Γ

VALUE (units 10 ⁻⁴)	DOCUMENT ID	TECN	COMMENT
1.50 ± 0.06 OUR EVALUATION	(Produced by HFLAV)		
1.46 ± 0.04 OUR AVERAGE			

1.49 ± 0.09 ± 0.07	¹ SIBIDANOV 13	BELL	e ⁺ e ⁻ → T(4S)
1.47 ± 0.05 ± 0.06	^{2,3} LEES 12AA	BABR	e ⁺ e ⁻ → T(4S)
1.41 ± 0.05 ± 0.07	⁴ DEL-AMO-SA...11c	BABR	e ⁺ e ⁻ → T(4S)
1.49 ± 0.04 ± 0.07	² HA 11	BELL	e ⁺ e ⁻ → T(4S)
1.54 ± 0.17 ± 0.09	⁴ AUBERT 08AV	BABR	e ⁺ e ⁻ → T(4S)
1.37 ± 0.15 ± 0.11	^{5,6} ADAM 07	CLE2	e ⁺ e ⁻ → T(4S)
1.38 ± 0.19 ± 0.14	⁷ HOKUUE 07	BELL	e ⁺ e ⁻ → T(4S)
1.53 ± 0.18 ± 0.12	^{1,8} CAO 23	BELL	e ⁺ e ⁻ → T(4S)
1.42 ± 0.05 ± 0.08	² DEL-AMO-SA...11F	BABR	Repl. by LEES 12AA
1.46 ± 0.07 ± 0.08	⁹ AUBERT 07J	BABR	Repl. by DEL-AMO-SANCHEZ 11F
1.33 ± 0.17 ± 0.11	¹⁰ AUBERT,B 06K	BABR	Repl. by AUBERT 08AV
1.38 ± 0.10 ± 0.18	¹¹ AUBERT,B 05o	BABR	Repl. by DEL-AMO-SANCHEZ 11c
1.33 ± 0.18 ± 0.13	¹² ATHAR 03	CLE2	Repl. by ADAM 07
1.8 ± 0.4 ± 0.4	¹³ ALEXANDER 96T	CLE2	Repl. by ATHAR 03

¹ The signal events are tagged by a second B meson reconstructed in the fully hadronic decays.

² Uses loose neutrino reconstruction technique. Assumes B(T(4S) → B⁺ B⁻) = (51.6 ± 0.6)% and B(T(4S) → B⁰ B⁰) = (48.4 ± 0.6)%.

³ Reports also a branching fraction value B(B⁰ → π⁻ ℓ⁺ ν) = (1.45 ± 0.04 ± 0.06) × 10⁻⁴ from the decays of B⁺ and B⁰ that are combined using the isospin symmetry relation.

⁴ Using the isospin symmetry relation, B⁺ and B⁰ branching fractions are combined.

⁵ The B⁰ and B⁺ results are combined assuming the isospin, B lifetimes, and relative charged/neutral B production at the T(4S).

⁶ Also report the rate for q² > 16 GeV² of (0.41 ± 0.08 ± 0.04) × 10⁻⁴ from which they obtain |V_{ub}| = 3.6 ± 0.4 ± 0.2 ± 0.6 (last error is from theory).

⁷ The signal events are tagged by a second B meson reconstructed in the semileptonic mode B → D^(*) ℓ ν_ℓ.

⁸ This analysis provides the inclusive and exclusive measurement of |V_{ub}|.

⁹ The analysis uses events in which the signal B decays are reconstructed with an innovative loose neutrino reconstruction technique.

¹⁰ The signals are tagged by a second B meson reconstructed in a semileptonic or hadronic decay. The B⁰ and B⁺ results are combined assuming the isospin symmetry.

¹¹ B⁺ and B⁰ decays combined assuming isospin symmetry. Systematic errors include both experimental and form-factor uncertainties.

¹² ATHAR 03 reports systematic errors 0.11 ± 0.01 ± 0.07, which are experimental systematic, systematic due to residual form-factor uncertainties in the signal, and systematic due to residual form-factor uncertainties in the cross-feed modes, respectively. We combine these in quadrature.

¹³ ALEXANDER 96T gives systematic errors ±0.3 ± 0.2 where the second error reflects the estimated model dependence. We combine these in quadrature. Assumes isospin symmetry: Γ(B⁰ → π⁻ ℓ⁺ ν) = 2 × Γ(B⁺ → π⁰ ℓ⁺ ν).

Meson Particle Listings

 B^0 $\Gamma(\pi^- \mu^+ \nu_\mu)/\Gamma_{\text{total}}$ Γ_{24}/Γ

VALUE DOCUMENT ID TECN COMMENT
 ••• We do not use the following data for averages, fits, limits, etc. •••
 seen ¹ALBRECHT 91c ARG

¹In ALBRECHT 91c, one event is fully reconstructed providing evidence for the $b \rightarrow u$ transition.

 $\Gamma(\pi^- \tau^+ \nu_\tau)/\Gamma_{\text{total}}$ Γ_{25}/Γ

VALUE CL% DOCUMENT ID TECN COMMENT
 $<2.5 \times 10^{-4}$ 90 ¹HAMER 16 BELL $e^+ e^- \rightarrow \Upsilon(4S)$

¹Assumes equal production of B^+ and B^0 at the $\Upsilon(4S)$.

 $\Gamma(K^\pm X)/\Gamma_{\text{total}}$ Γ_{26}/Γ

VALUE DOCUMENT ID TECN COMMENT
 0.78 ± 0.08 ¹ALBRECHT 96D ARG $e^+ e^- \rightarrow \Upsilon(4S)$

¹Average multiplicity.

 $\Gamma(D^0 X)/\Gamma_{\text{total}}$ Γ_{27}/Γ

VALUE DOCUMENT ID TECN COMMENT
 $0.081 \pm 0.014 \pm 0.005$ ¹AUBERT 07N BABR $e^+ e^- \rightarrow \Upsilon(4S)$

••• We do not use the following data for averages, fits, limits, etc. •••
 $0.063 \pm 0.019 \pm 0.005$ ¹AUBERT,BE 04B BABR Repl. by AUBERT 07N

¹Events are selected by completely reconstructing one B and searching for a reconstructed charmed particle in the rest of the event. The last error includes systematic and charm branching ratio uncertainties.

 $\Gamma(\overline{D}^0 X)/\Gamma_{\text{total}}$ Γ_{28}/Γ

VALUE DOCUMENT ID TECN COMMENT
 $0.474 \pm 0.020 \pm 0.020$ ¹AUBERT 07N BABR $e^+ e^- \rightarrow \Upsilon(4S)$

••• We do not use the following data for averages, fits, limits, etc. •••
 $0.511 \pm 0.031 \pm 0.028$ ¹AUBERT,BE 04B BABR Repl. by AUBERT 07N

¹Events are selected by completely reconstructing one B and searching for a reconstructed charmed particle in the rest of the event. The last error includes systematic and charm branching ratio uncertainties.

 $\Gamma(D^0 X)/[\Gamma(D^0 X) + \Gamma(\overline{D}^0 X)]$ $\Gamma_{27}/(\Gamma_{27} + \Gamma_{28})$

VALUE DOCUMENT ID TECN COMMENT
 $0.146 \pm 0.022 \pm 0.006$ AUBERT 07N BABR $e^+ e^- \rightarrow \Upsilon(4S)$

••• We do not use the following data for averages, fits, limits, etc. •••
 $0.110 \pm 0.031 \pm 0.008$ AUBERT,BE 04B BABR Repl. by AUBERT 07N

 $\Gamma(D^+ X)/\Gamma_{\text{total}}$ Γ_{29}/Γ

VALUE CL% DOCUMENT ID TECN COMMENT
 <0.039 90 ¹AUBERT 07N BABR $e^+ e^- \rightarrow \Upsilon(4S)$

••• We do not use the following data for averages, fits, limits, etc. •••
 <0.051 90 ¹AUBERT,BE 04B BABR Repl. by AUBERT 07N

¹Events are selected by completely reconstructing one B and searching for a reconstructed charmed particle in the rest of the event. The last error includes systematic and charm branching ratio uncertainties.

 $\Gamma(D^- X)/\Gamma_{\text{total}}$ Γ_{30}/Γ

VALUE DOCUMENT ID TECN COMMENT
 $0.369 \pm 0.016 \pm 0.030$ ¹AUBERT 07N BABR $e^+ e^- \rightarrow \Upsilon(4S)$

••• We do not use the following data for averages, fits, limits, etc. •••
 $0.397 \pm 0.030 \pm 0.040$ ¹AUBERT,BE 04B BABR Repl. by AUBERT 07N

¹Events are selected by completely reconstructing one B and searching for a reconstructed charmed particle in the rest of the event. The last error includes systematic and charm branching ratio uncertainties.

 $\Gamma(D^+ X)/[\Gamma(D^+ X) + \Gamma(D^- X)]$ $\Gamma_{29}/(\Gamma_{29} + \Gamma_{30})$

VALUE DOCUMENT ID TECN COMMENT
 $0.058 \pm 0.028 \pm 0.006$ AUBERT 07N BABR $e^+ e^- \rightarrow \Upsilon(4S)$

••• We do not use the following data for averages, fits, limits, etc. •••
 $0.055 \pm 0.040 \pm 0.006$ AUBERT,BE 04B BABR Repl. by AUBERT 07N

 $\Gamma(D_s^+ X)/\Gamma_{\text{total}}$ Γ_{31}/Γ

VALUE DOCUMENT ID TECN COMMENT
 $0.103 \pm 0.012 \pm 0.017$ ¹AUBERT 07N BABR $e^+ e^- \rightarrow \Upsilon(4S)$

••• We do not use the following data for averages, fits, limits, etc. •••
 $0.109 \pm 0.021 \pm 0.039$ ¹AUBERT,BE 04B BABR Repl. by AUBERT 07N

¹Events are selected by completely reconstructing one B and searching for a reconstructed charmed particle in the rest of the event. The last error includes systematic and charm branching ratio uncertainties.

 $\Gamma(D_s^- X)/\Gamma_{\text{total}}$ Γ_{32}/Γ

VALUE CL% DOCUMENT ID TECN COMMENT
 <0.026 90 ¹AUBERT 07N BABR $e^+ e^- \rightarrow \Upsilon(4S)$

••• We do not use the following data for averages, fits, limits, etc. •••
 <0.087 90 ¹AUBERT,BE 04B BABR Repl. by AUBERT 07N

¹Events are selected by completely reconstructing one B and searching for a reconstructed charmed particle in the rest of the event. The last error includes systematic and charm branching ratio uncertainties.

 $\Gamma(D_s^+ X)/[\Gamma(D_s^+ X) + \Gamma(D_s^- X)]$ $\Gamma_{31}/(\Gamma_{31} + \Gamma_{32})$

VALUE DOCUMENT ID TECN COMMENT
 $0.879 \pm 0.066 \pm 0.005$ AUBERT 07N BABR $e^+ e^- \rightarrow \Upsilon(4S)$

••• We do not use the following data for averages, fits, limits, etc. •••
 $0.733 \pm 0.092 \pm 0.010$ AUBERT,BE 04B BABR Repl. by AUBERT 07N

 $\Gamma(A_c^+ X)/\Gamma_{\text{total}}$ Γ_{33}/Γ

VALUE CL% DOCUMENT ID TECN COMMENT
 <0.031 90 ¹AUBERT 07N BABR $e^+ e^- \rightarrow \Upsilon(4S)$

••• We do not use the following data for averages, fits, limits, etc. •••
 <0.038 90 ¹AUBERT,BE 04B BABR Repl. by AUBERT 07N

¹Events are selected by completely reconstructing one B and searching for a reconstructed charmed particle in the rest of the event. The last error includes systematic and charm branching ratio uncertainties.

 $\Gamma(\overline{A}_c^- X)/\Gamma_{\text{total}}$ Γ_{34}/Γ

VALUE DOCUMENT ID TECN COMMENT
 $0.05 \pm 0.010 \pm 0.019$ ¹AUBERT 07N BABR $e^+ e^- \rightarrow \Upsilon(4S)$

••• We do not use the following data for averages, fits, limits, etc. •••
 $0.049 \pm 0.017 \pm 0.018$ ¹AUBERT,BE 04B BABR Repl. by AUBERT 07N

¹Events are selected by completely reconstructing one B and searching for a reconstructed charmed particle in the rest of the event. The last error includes systematic and charm branching ratio uncertainties.

 $\Gamma(A_c^+ X)/[\Gamma(A_c^+ X) + \Gamma(\overline{A}_c^- X)]$ $\Gamma_{33}/(\Gamma_{33} + \Gamma_{34})$

VALUE DOCUMENT ID TECN COMMENT
 $0.243 \pm 0.119 \pm 0.003$ AUBERT 07N BABR $e^+ e^- \rightarrow \Upsilon(4S)$

••• We do not use the following data for averages, fits, limits, etc. •••
 $0.286 \pm 0.142 \pm 0.007$ AUBERT,BE 04B BABR Repl. by AUBERT 07N

 $\Gamma(\overline{C} X)/\Gamma_{\text{total}}$ Γ_{35}/Γ

VALUE DOCUMENT ID TECN COMMENT
 $0.947 \pm 0.030 \pm 0.045$ ¹AUBERT 07N BABR $e^+ e^- \rightarrow \Upsilon(4S)$

••• We do not use the following data for averages, fits, limits, etc. •••
 $1.039 \pm 0.051 \pm 0.063$ ¹AUBERT,BE 04B BABR Repl. by AUBERT 07N

¹Events are selected by completely reconstructing one B and searching for a reconstructed charmed particle in the rest of the event. The last error includes systematic and charm branching ratio uncertainties.

 $\Gamma(C X)/\Gamma_{\text{total}}$ Γ_{36}/Γ

VALUE DOCUMENT ID TECN COMMENT
 $0.246 \pm 0.024 \pm 0.021$ ¹AUBERT 07N BABR $e^+ e^- \rightarrow \Upsilon(4S)$

••• We do not use the following data for averages, fits, limits, etc. •••
 $0.237 \pm 0.036 \pm 0.041$ ¹AUBERT,BE 04B BABR Repl. by AUBERT 07N

¹Events are selected by completely reconstructing one B and searching for a reconstructed charmed particle in the rest of the event. The last error includes systematic and charm branching ratio uncertainties.

 $\Gamma(\overline{C}/c X)/\Gamma_{\text{total}}$ Γ_{37}/Γ

VALUE DOCUMENT ID TECN COMMENT
 $1.193 \pm 0.030 \pm 0.053$ ¹AUBERT 07N BABR $e^+ e^- \rightarrow \Upsilon(4S)$

••• We do not use the following data for averages, fits, limits, etc. •••
 $1.276 \pm 0.062 \pm 0.088$ ¹AUBERT,BE 04B BABR Repl. by AUBERT 07N

¹Events are selected by completely reconstructing one B and searching for a reconstructed charmed particle in the rest of the event. The last error includes systematic and charm branching ratio uncertainties.

 $\Gamma(D^- \pi^+)/\Gamma_{\text{total}}$ Γ_{38}/Γ

VALUE (units 10^{-3}) EVTS DOCUMENT ID TECN COMMENT
 2.51 ± 0.08 OUR FIT

2.56 ± 0.08 OUR AVERAGE

$2.48 \pm 0.01 \pm 0.10$ WAHEED 22 BELL $e^+ e^- \rightarrow \Upsilon(4S)$

$2.55 \pm 0.05 \pm 0.16$ ¹AUBERT 07H BABR $e^+ e^- \rightarrow \Upsilon(4S)$

$3.03 \pm 0.23 \pm 0.23$ ²AUBERT,BE 06J BABR $e^+ e^- \rightarrow \Upsilon(4S)$

$2.68 \pm 0.12 \pm 0.24$ ^{1,3}AHMED 02B CLE2 $e^+ e^- \rightarrow \Upsilon(4S)$

$2.7 \pm 0.6 \pm 0.5$ ⁴BORTOLETTO92 CLEO $e^+ e^- \rightarrow \Upsilon(4S)$

$4.8 \pm 1.1 \pm 1.1$ ⁵ALBRECHT 90J ARG $e^+ e^- \rightarrow \Upsilon(4S)$

$5.1 \pm 2.8 \pm 1.3$ ⁶BEBEK 87 CLEO $e^+ e^- \rightarrow \Upsilon(4S)$

-2.5 ± 1.2 ⁶BEBEK 87 CLEO $e^+ e^- \rightarrow \Upsilon(4S)$

••• We do not use the following data for averages, fits, limits, etc. •••

$2.73 \pm 0.19 \pm 0.05$ ^{1,7}AUBERT,B 04o BABR Repl. by AUBERT 07H

$2.83 \pm 0.42 \pm 0.05$ ⁸ALAM 94 CLE2 Repl. by AHMED 02B

$3.1 \pm 1.3 \pm 1.0$ ⁵ALBRECHT 88k ARG $e^+ e^- \rightarrow \Upsilon(4S)$

¹Assumes equal production of B^+ and B^0 at the $\Upsilon(4S)$.

²Uses a missing-mass method. Does not depend on D branching fractions or B^+/B^0 production rates.

³AHMED 02B reports an additional uncertainty on the branching ratios to account for 4.5% uncertainty on relative production of B^0 and B^+ , which is not included here.

⁴BORTOLETTO 92 assumes equal production of B^+ and B^0 at the $\Upsilon(4S)$ and uses Mark III branching fractions for the D .

⁵ALBRECHT 88k assumes $B^0\bar{B}^0:B^+B^-$ production ratio is 45:55. Superseded by ALBRECHT 90i which assumes 50:50.

⁶BEBEK 87 value has been updated in BERKELMAN 91 to use same assumptions as noted for BORTOLETTO 92.

⁷AUBERT,B 04o reports $[\Gamma(B^0 \rightarrow D^-\pi^+)/\Gamma_{\text{total}}] \times [B(D^+ \rightarrow K_S^0\pi^+)] = (42.7 \pm 2.1 \pm 2.2) \times 10^{-6}$ which we divide by our best value $B(D^+ \rightarrow K_S^0\pi^+) = (1.562 \pm 0.031) \times 10^{-2}$. Our first error is their experiment's error and our second error is the systematic error from using our best value.

⁸ALAM 94 reports $[\Gamma(B^0 \rightarrow D^-\pi^+)/\Gamma_{\text{total}}] \times [B(D^+ \rightarrow K^-2\pi^+)] = (0.265 \pm 0.032 \pm 0.023) \times 10^{-3}$ which we divide by our best value $B(D^+ \rightarrow K^-2\pi^+) = (9.38 \pm 0.16) \times 10^{-2}$. Our first error is their experiment's error and our second error is the systematic error from using our best value. Assumes equal production of B^+ and B^0 at the $\Upsilon(4S)$.

 $\Gamma(D^-\ell^+\nu_\ell)/\Gamma(D^-\pi^+)$ Γ_5/Γ_{38}

VALUE	DOCUMENT ID	TECN	COMMENT
9.9 ± 1.0 ± 0.9	AALTONEN 09E	CDF	$p\bar{p}$ at 1.96 TeV

 $\Gamma(D^-\rho^+)/\Gamma_{\text{total}}$ Γ_{39}/Γ

VALUE	EVS	DOCUMENT ID	TECN	COMMENT
0.0076 ± 0.0012 OUR AVERAGE				

0.0075 ± 0.0013 ± 0.0001	79	¹ ALAM	94	CLE2	$e^+e^- \rightarrow \Upsilon(4S)$
0.009 ± 0.005 ± 0.003	9	² ALBRECHT	90j	ARG	$e^+e^- \rightarrow \Upsilon(4S)$

• • • We do not use the following data for averages, fits, limits, etc. • • •

0.022 ± 0.012 ± 0.009	6	² ALBRECHT	88k	ARG	$e^+e^- \rightarrow \Upsilon(4S)$
-----------------------	---	-----------------------	-----	-----	-----------------------------------

¹ALAM 94 reports $[\Gamma(B^0 \rightarrow D^-\rho^+)/\Gamma_{\text{total}}] \times [B(D^+ \rightarrow K^-2\pi^+)] = 0.000704 \pm 0.000096 \pm 0.000070$ which we divide by our best value $B(D^+ \rightarrow K^-2\pi^+) = (9.38 \pm 0.16) \times 10^{-2}$. Our first error is their experiment's error and our second error is the systematic error from using our best value. Assumes equal production of B^+ and B^0 at the $\Upsilon(4S)$.

²ALBRECHT 88k assumes $B^0\bar{B}^0:B^+B^-$ production ratio is 45:55. Superseded by ALBRECHT 90i which assumes 50:50.

 $\Gamma(D^-K^0\pi^+)/\Gamma_{\text{total}}$ Γ_{40}/Γ

VALUE (units 10^{-4})	DOCUMENT ID	TECN	COMMENT
4.9 ± 0.7 ± 0.5	¹ AUBERT,BE 05B	BABR	$e^+e^- \rightarrow \Upsilon(4S)$

¹Assumes equal production of B^+ and B^0 at the $\Upsilon(4S)$.

 $\Gamma(D^-K^*(892)^+)/\Gamma_{\text{total}}$ Γ_{41}/Γ

VALUE (units 10^{-4})	DOCUMENT ID	TECN	COMMENT
4.5 ± 0.7 OUR AVERAGE			

4.6 ± 0.6 ± 0.5	¹ AUBERT,BE 05B	BABR	$e^+e^- \rightarrow \Upsilon(4S)$
3.7 ± 1.5 ± 1.0	¹ MAHAPATRA 02	CLE2	$e^+e^- \rightarrow \Upsilon(4S)$

¹Assumes equal production of B^+ and B^0 at the $\Upsilon(4S)$.

 $\Gamma(D^-\omega\pi^+)/\Gamma_{\text{total}}$ Γ_{42}/Γ

VALUE	DOCUMENT ID	TECN	COMMENT
0.0028 ± 0.0005 ± 0.0004	¹ ALEXANDER 01B	CLE2	$e^+e^- \rightarrow \Upsilon(4S)$

¹Assumes equal production of B^+ and B^0 at the $\Upsilon(4S)$. The signal is consistent with all observed $\omega\pi^+$ having proceeded through the ρ^+ resonance at mass $1349 \pm 25^{+10}_{-5}$ MeV and width $547 \pm 86^{+46}_{-45}$ MeV.

 $\Gamma(D^-K^+)/\Gamma(D^-\pi^+)$ Γ_{43}/Γ_{38}

VALUE (units 10^{-2})	DOCUMENT ID	TECN	COMMENT
8.19 ± 0.20 OUR AVERAGE			

8.19 ± 0.20 ± 0.23	WAHEED 22	BELL	$e^+e^- \rightarrow \Upsilon(4S)$
8.22 ± 0.11 ± 0.25	AAIJ 13P	LHCB	pp at 7 TeV
6.8 ± 1.5 ± 0.7	ABE 01i	BELL	$e^+e^- \rightarrow \Upsilon(4S)$

 $\Gamma(D^-K^+\pi^+\pi^-)/\Gamma(D^-\pi^+\pi^+\pi^-)$ Γ_{44}/Γ_{50}

VALUE (units 10^{-2})	DOCUMENT ID	TECN	COMMENT
5.9 ± 1.1 ± 0.5	AAIJ 12T	LHCB	pp at 7 TeV

 $\Gamma(D^-K^+\bar{K}^0)/\Gamma_{\text{total}}$ Γ_{45}/Γ

VALUE (units 10^{-4})	CL%	DOCUMENT ID	TECN	COMMENT
<3.1	90	¹ DRUTSKOY 02	BELL	$e^+e^- \rightarrow \Upsilon(4S)$

¹Assumes equal production of B^+ and B^0 at the $\Upsilon(4S)$.

 $\Gamma(D^-K^+\bar{K}^*(892)^0)/\Gamma_{\text{total}}$ Γ_{46}/Γ

VALUE (units 10^{-4})	DOCUMENT ID	TECN	COMMENT
8.8 ± 1.1 ± 1.5	¹ DRUTSKOY 02	BELL	$e^+e^- \rightarrow \Upsilon(4S)$

¹Assumes equal production of B^+ and B^0 at the $\Upsilon(4S)$.

 $\Gamma(\bar{D}^0\pi^+\pi^-)/\Gamma_{\text{total}}$ Γ_{47}/Γ

VALUE (units 10^{-4})	CL%	EVS	DOCUMENT ID	TECN	COMMENT
8.8 ± 0.5 OUR AVERAGE					

8.95 ± 0.15 ± 0.52			¹ AAIJ 15Y	LHCB	pp at 7, 8 TeV
8.4 ± 0.4 ± 0.8			² KUZMIN 07	BELL	$e^+e^- \rightarrow \Upsilon(4S)$

• • • We do not use the following data for averages, fits, limits, etc. • • •

8.0 ± 0.6 ± 1.5	2,3	SATPATHY 03	BELL	Repl. by KUZMIN 07
< 16	90	² ALAM 94	CLE2	$e^+e^- \rightarrow \Upsilon(4S)$
< 70	90	⁴ BORTOLETTO92	CLEO	$e^+e^- \rightarrow \Upsilon(4S)$
< 340	90	⁵ BEBEK 87	CLEO	$e^+e^- \rightarrow \Upsilon(4S)$
700 ± 500	5	⁶ BEHREND 83	CLEO	$e^+e^- \rightarrow \Upsilon(4S)$

¹The second uncertainty combines in quadrature all systematic uncertainties quoted in the paper. AAIJ 15Y reports $B(\bar{D}^0\pi^+\pi^-) = (8.46 \pm 0.14 \pm 0.49) \times 10^{-4}$ in the kinematic region $m(\bar{D}^0\pi^\pm) > 2.1$ GeV which we corrected to the full phase-space dividing by 0.945 from Belle.

²Assumes equal production of B^+ and B^0 at the $\Upsilon(4S)$.

³No assumption about the intermediate mechanism is made in the analysis.

⁴BORTOLETTO 92 assumes equal production of B^+ and B^0 at the $\Upsilon(4S)$ and uses Mark III branching fractions for the D . The product branching fraction into $D_S^*(2340)\pi$ followed by $D_S^*(2340) \rightarrow D^0\pi$ is < 0.0001 at 90% CL and into $D_S^*(2460)$ followed by $D_S^*(2460) \rightarrow D^0\pi$ is < 0.0004 at 90% CL.

⁵BEBEK 87 assume the $\Upsilon(4S)$ decays 43% to $B^0\bar{B}^0$. We rescale to 50%. $B(\bar{D}^0 \rightarrow K^-\pi^+) = (4.2 \pm 0.4 \pm 0.4)\%$ and $B(\bar{D}^0 \rightarrow K^-\pi^+\pi^-\pi^-) = (9.1 \pm 0.8 \pm 0.8)\%$ were used.

⁶Corrected by us using assumptions: $B(\bar{D}^0 \rightarrow K^-\pi^+) = (0.042 \pm 0.006)$ and $B(\Upsilon(4S) \rightarrow B^0\bar{B}^0) = 50\%$. The product branching ratio is $B(\bar{D}^0 \rightarrow \bar{D}^0\pi^+\pi^-)B(\bar{D}^0 \rightarrow K^+\pi^-) = (0.39 \pm 0.26) \times 10^{-2}$.

 $\Gamma(D^*(2010)^-\pi^+)/\Gamma_{\text{total}}$ Γ_{48}/Γ

VALUE (units 10^{-3})	EVS	DOCUMENT ID	TECN	COMMENT
2.66 ± 0.07 OUR AVERAGE				

2.62 ± 0.02 ± 0.09		¹ KROHN 23	BELL	$e^+e^- \rightarrow \Upsilon(4S)$
2.79 ± 0.08 ± 0.17		² AUBERT 07H	BABR	$e^+e^- \rightarrow \Upsilon(4S)$
2.48 ± 0.34 ± 0.08		^{3,4} AUBERT,BE 06j	BABR	$e^+e^- \rightarrow \Upsilon(4S)$
2.81 ± 0.24 ± 0.05		⁵ BRANDENB... 98	CLE2	$e^+e^- \rightarrow \Upsilon(4S)$
2.6 ± 0.3 ± 0.4	82	⁶ ALAM 94	CLE2	$e^+e^- \rightarrow \Upsilon(4S)$
3.37 ± 0.96 ± 0.02		⁷ BORTOLETTO92	CLEO	$e^+e^- \rightarrow \Upsilon(4S)$
2.36 ± 0.88 ± 0.02	12	⁸ ALBRECHT 90j	ARG	$e^+e^- \rightarrow \Upsilon(4S)$
2.36 $^{+1.50}_{-1.10} \pm 0.02$	5	⁹ BEBEK 87	CLEO	$e^+e^- \rightarrow \Upsilon(4S)$

• • • We do not use the following data for averages, fits, limits, etc. • • •

10 ± 4 ± 1	8	¹⁰ AKERS 94j	OPAL	$e^+e^- \rightarrow Z$
2.7 ± 1.4 ± 1.0	5	¹¹ ALBRECHT 87c	ARG	$e^+e^- \rightarrow \Upsilon(4S)$
3.5 ± 2 ± 2		¹² ALBRECHT 86f	ARG	$e^+e^- \rightarrow \Upsilon(4S)$
17 ± 5 ± 5	41	¹³ GILES 84	CLEO	$e^+e^- \rightarrow \Upsilon(4S)$

¹KROHN 23 reports $(2.623 \pm 0.016 \pm 0.086) \times 10^{-3}$ from a measurement of $[\Gamma(B^0 \rightarrow D^*(2010)^-\pi^+)/\Gamma_{\text{total}}] / [B(\Upsilon(4S) \rightarrow B^0\bar{B}^0)]$ assuming $B(\Upsilon(4S) \rightarrow B^0\bar{B}^0) = 0.486 \pm 0.006$.

²Assumes equal production of B^+ and B^0 at the $\Upsilon(4S)$.

³AUBERT,BE 06j reports $[\Gamma(B^0 \rightarrow D^*(2010)^-\pi^+)/\Gamma_{\text{total}}] / [B(B^0 \rightarrow D^-\pi^+)] = 0.99 \pm 0.11 \pm 0.08$ which we multiply by our best value $B(B^0 \rightarrow D^-\pi^+) = (2.51 \pm 0.08) \times 10^{-3}$. Our first error is their experiment's error and our second error is the systematic error from using our best value.

⁴Uses a missing-mass method. Does not depend on D branching fractions or B^+/B^0 production rates.

⁵BRANDENBURG 98 assume equal production of B^+ and B^0 at $\Upsilon(4S)$ and use the D^* reconstruction technique. The first error is their experiment's error and the second error is the systematic error from the PDG 96 value of $B(D^* \rightarrow D\pi)$.

⁶ALAM 94 assume equal production of B^+ and B^0 at the $\Upsilon(4S)$ and use the CLEO II $B(D^*(2010)^+ \rightarrow D^0\pi^+)$ and absolute $B(D^0 \rightarrow K^-\pi^+)$ and the PDG 1992 $B(D^0 \rightarrow K^-\pi^+\pi^0)/B(D^0 \rightarrow K^-\pi^+)$ and $B(D^0 \rightarrow K^-2\pi^+\pi^-)/B(D^0 \rightarrow K^-\pi^+)$.

⁷BORTOLETTO 92 reports $(4.0 \pm 1.0 \pm 0.7) \times 10^{-3}$ from a measurement of $[\Gamma(B^0 \rightarrow D^*(2010)^-\pi^+)/\Gamma_{\text{total}}] \times [B(D^*(2010)^+ \rightarrow D^0\pi^+)]$ assuming $B(D^*(2010)^+ \rightarrow D^0\pi^+) = 0.57 \pm 0.06$, which we rescale to our best value $B(D^*(2010)^+ \rightarrow D^0\pi^+) = (67.7 \pm 0.5) \times 10^{-2}$. Our first error is their experiment's error and our second error is the systematic error from using our best value. Assumes equal production of B^+ and B^0 at the $\Upsilon(4S)$ and uses Mark III branching fractions for the D .

⁸ALBRECHT 90j reports $(2.8 \pm 0.9 \pm 0.6) \times 10^{-3}$ from a measurement of $[\Gamma(B^0 \rightarrow D^*(2010)^-\pi^+)/\Gamma_{\text{total}}] \times [B(D^*(2010)^+ \rightarrow D^0\pi^+)]$ assuming $B(D^*(2010)^+ \rightarrow D^0\pi^+) = 0.57 \pm 0.06$, which we rescale to our best value $B(D^*(2010)^+ \rightarrow D^0\pi^+) = (67.7 \pm 0.5) \times 10^{-2}$. Our first error is their experiment's error and our second error is the systematic error from using our best value. Assumes equal production of B^+ and B^0 at the $\Upsilon(4S)$ and uses Mark III branching fractions for the D .

⁹BEBEK 87 reports $(2.8^{+1.5+1.0}_{-1.2-0.6}) \times 10^{-3}$ from a measurement of $[\Gamma(B^0 \rightarrow D^*(2010)^-\pi^+)/\Gamma_{\text{total}}] \times [B(D^*(2010)^+ \rightarrow D^0\pi^+)]$ assuming $B(D^*(2010)^+ \rightarrow D^0\pi^+) = 0.57 \pm 0.06$, which we rescale to our best value $B(D^*(2010)^+ \rightarrow D^0\pi^+) = (67.7 \pm 0.5) \times 10^{-2}$. Our first error is their experiment's error and our second error is the systematic error from using our best value. Updated in BERKELMAN 91 to use same assumptions as noted for BORTOLETTO 92 and ALBRECHT 90j.

¹⁰Assumes $B(Z \rightarrow b\bar{b}) = 0.217$ and 38% B_d production fraction.

¹¹ALBRECHT 87c use PDG 86 branching ratios for D and $D^*(2010)$ and assume $B(\Upsilon(4S) \rightarrow B^+B^-) = 55\%$ and $B(\Upsilon(4S) \rightarrow B^0\bar{B}^0) = 45\%$. Superseded by ALBRECHT 90j.

¹²ALBRECHT 86f uses pseudomass that is independent of D^0 and D^+ branching ratios.

¹³Assumes $B(D^*(2010)^+ \rightarrow D^0\pi^+) = 0.60^{+0.08}_{-0.15}$. Assumes $B(\Upsilon(4S) \rightarrow B^0\bar{B}^0) = 0.40 \pm 0.02$. Does not depend on D branching ratios.

Meson Particle Listings

 B^0

$\Gamma(D^*(2010)^- \ell^+ \nu_\ell) / \Gamma(D^*(2010)^- \pi^+)$				Γ_7 / Γ_{48}
VALUE	DOCUMENT ID	TECN	COMMENT	
$16.5 \pm 2.3 \pm 1.1$	AALTONEN	09E	CDF $p\bar{p}$ at 1.96 TeV	

$\Gamma(D^0 K^+ K^-) / \Gamma(D^0 \pi^+ \pi^-)$				$\Gamma_{49} / \Gamma_{47}$
VALUE	DOCUMENT ID	TECN	COMMENT	
$0.069 \pm 0.004 \pm 0.003$	AAIJ	18AZ	LHCB pp at 7, 8 TeV	
• • • We do not use the following data for averages, fits, limits, etc. • • •				
$0.056 \pm 0.011 \pm 0.007$	AAIJ	12AMLHCB	pp at 7 TeV, Repl. by AAIJ 18AZ	

$\Gamma(D^- \pi^+ \pi^+ \pi^-) / \Gamma_{\text{total}}$				Γ_{50} / Γ
VALUE	DOCUMENT ID	TECN	COMMENT	
0.0060 ± 0.0006 OUR FIT				
$0.0080 \pm 0.0021 \pm 0.0014$	¹ BORTOLETTO92	CLEO	$e^+e^- \rightarrow \Upsilon(4S)$	
¹ BORTOLETTO 92 assumes equal production of B^+ and B^0 at the $\Upsilon(4S)$ and uses Mark III branching fractions for the D .				

$\Gamma(D^- \pi^+ \pi^+ \pi^-) / \Gamma(D^- \pi^+)$				$\Gamma_{50} / \Gamma_{38}$
VALUE	DOCUMENT ID	TECN	COMMENT	
2.39 ± 0.23 OUR FIT				
$2.38 \pm 0.11 \pm 0.21$	AAIJ	11E	LHCB pp at 7 TeV	

$\Gamma((D^- \pi^+ \pi^+ \pi^-) \text{ nonresonant}) / \Gamma_{\text{total}}$				Γ_{51} / Γ
VALUE	DOCUMENT ID	TECN	COMMENT	
$0.0039 \pm 0.0014 \pm 0.0013$	¹ BORTOLETTO92	CLEO	$e^+e^- \rightarrow \Upsilon(4S)$	
¹ BORTOLETTO 92 assumes equal production of B^+ and B^0 at the $\Upsilon(4S)$ and uses Mark III branching fractions for the D .				

$\Gamma(D^- \pi^+ \rho^0) / \Gamma_{\text{total}}$				Γ_{52} / Γ
VALUE	DOCUMENT ID	TECN	COMMENT	
$0.0011 \pm 0.0009 \pm 0.0004$	¹ BORTOLETTO92	CLEO	$e^+e^- \rightarrow \Upsilon(4S)$	
¹ BORTOLETTO 92 assumes equal production of B^+ and B^0 at the $\Upsilon(4S)$ and uses Mark III branching fractions for the D .				

$\Gamma(D^- a_1(1260)^+) / \Gamma_{\text{total}}$				Γ_{53} / Γ
VALUE	DOCUMENT ID	TECN	COMMENT	
$0.0060 \pm 0.0022 \pm 0.0024$	¹ BORTOLETTO92	CLEO	$e^+e^- \rightarrow \Upsilon(4S)$	
¹ BORTOLETTO 92 assumes equal production of B^+ and B^0 at the $\Upsilon(4S)$ and uses Mark III branching fractions for the D .				

$\Gamma(D^*(2010)^- \pi^+ \pi^0) / \Gamma_{\text{total}}$				Γ_{54} / Γ
VALUE	EVTS	DOCUMENT ID	TECN	COMMENT
$0.0152 \pm 0.0052 \pm 0.0001$	51	¹ ALBRECHT 90j	ARG	$e^+e^- \rightarrow \Upsilon(4S)$
• • • We do not use the following data for averages, fits, limits, etc. • • •				
$0.015 \pm 0.008 \pm 0.008$	8	² ALBRECHT 87c	ARG	$e^+e^- \rightarrow \Upsilon(4S)$
¹ ALBRECHT 90j reports $0.018 \pm 0.004 \pm 0.005$ from a measurement of $[\Gamma(B^0 \rightarrow D^*(2010)^- \pi^+ \pi^0) / \Gamma_{\text{total}}] \times [B(D^*(2010)^+ \rightarrow D^0 \pi^+)]$ assuming $B(D^*(2010)^+ \rightarrow D^0 \pi^+) = 0.57 \pm 0.06$, which we rescale to our best value $B(D^*(2010)^+ \rightarrow D^0 \pi^+) = (67.7 \pm 0.5) \times 10^{-2}$. Our first error is their experiment's error and our second error is the systematic error from using our best value. Assumes equal production of B^+ and B^0 at the $\Upsilon(4S)$ and uses Mark III branching fractions for the D .				
² ALBRECHT 87c use PDG 86 branching ratios for D and $D^*(2010)$ and assume $B(\Upsilon(4S) \rightarrow B^+ B^-) = 55\%$ and $B(\Upsilon(4S) \rightarrow B^0 \bar{B}^0) = 45\%$. Superseded by ALBRECHT 90j.				

$\Gamma(D^*(2010)^- \rho^+) / \Gamma_{\text{total}}$				Γ_{55} / Γ
VALUE (units 10^{-3})	EVTS	DOCUMENT ID	TECN	COMMENT
6.8 ± 0.9 OUR AVERAGE				
$6.8 \pm 0.3 \pm 0.9$		^{1,2} CSORNA 03	CLE2	$e^+e^- \rightarrow \Upsilon(4S)$
$16.0 \pm 11.3 \pm 0.1$		³ BORTOLETTO92	CLEO	$e^+e^- \rightarrow \Upsilon(4S)$
$5.89 \pm 3.52 \pm 0.04$	19	⁴ ALBRECHT 90j	ARG	$e^+e^- \rightarrow \Upsilon(4S)$
• • • We do not use the following data for averages, fits, limits, etc. • • •				
$7.4 \pm 1.0 \pm 1.4$	76	^{2,5} MATVIENKO 15	BELL	$e^+e^- \rightarrow \Upsilon(4S)$
		^{6,7} ALAM 94	CLE2	$e^+e^- \rightarrow \Upsilon(4S)$
$81 \pm 29 \pm 24$	19	⁸ CHEN 85	CLEO	$e^+e^- \rightarrow \Upsilon(4S)$

- ¹ The second error combines the systematic and theoretical uncertainties in quadrature. CSORNA 03 includes data used in ALAM 94. A full angular fit to three complex helicity amplitudes is performed.
- ² Assumes equal production of B^0 and B^+ at the $\Upsilon(4S)$ resonance.
- ³ BORTOLETTO 92 reports $0.019 \pm 0.008 \pm 0.011$ from a measurement of $[\Gamma(B^0 \rightarrow D^*(2010)^- \rho^+) / \Gamma_{\text{total}}] \times [B(D^*(2010)^+ \rightarrow D^0 \pi^+)]$ assuming $B(D^*(2010)^+ \rightarrow D^0 \pi^+) = 0.57 \pm 0.06$, which we rescale to our best value $B(D^*(2010)^+ \rightarrow D^0 \pi^+) = (67.7 \pm 0.5) \times 10^{-2}$. Our first error is their experiment's error and our second error is the systematic error from using our best value. Assumes equal production of B^+ and B^0 at the $\Upsilon(4S)$ and uses Mark III branching fractions for the D .
- ⁴ ALBRECHT 90j reports $0.007 \pm 0.003 \pm 0.003$ from a measurement of $[\Gamma(B^0 \rightarrow D^*(2010)^- \rho^+) / \Gamma_{\text{total}}] \times [B(D^*(2010)^+ \rightarrow D^0 \pi^+)]$ assuming $B(D^*(2010)^+ \rightarrow D^0 \pi^+) = 0.57 \pm 0.06$, which we rescale to our best value $B(D^*(2010)^+ \rightarrow D^0 \pi^+) = (67.7 \pm 0.5) \times 10^{-2}$. Our first error is their experiment's error and our second error is the systematic error from using our best value. Assumes equal production of B^+ and B^0 at the $\Upsilon(4S)$ and uses Mark III branching fractions for the D .

⁵ MATVIENKO 15 reports $B(B^0 \rightarrow D^*(2010)^- \rho^+, \rho^+ \rightarrow \omega \pi^+) = (1.48 \pm 0.27 + 0.15 + 0.21) \times 10^{-3}$. The last uncertainty is a model one.

⁶ ALAM 94 assume equal production of B^+ and B^0 at the $\Upsilon(4S)$ and use the CLEO II $B(D^*(2010)^+ \rightarrow D^0 \pi^+)$ and absolute $B(D^0 \rightarrow K^- \pi^+)$ and the PDG 1992 $B(D^0 \rightarrow K^- \pi^+ \pi^0) / B(D^0 \rightarrow K^- \pi^+)$ and $B(D^0 \rightarrow K^- 2\pi^+ \pi^-) / B(D^0 \rightarrow K^- \pi^+)$.

⁷ This decay is nearly completely longitudinally polarized, $\Gamma_L / \Gamma = (93 \pm 5 \pm 5)\%$, as expected from the factorization hypothesis (ROSNER 90). The nonresonant $\pi^+ \pi^0$ contribution under the ρ^+ is less than 9% at 90% CL.

⁸ Uses $B(D^* \rightarrow D^0 \pi^+) = 0.6 \pm 0.15$ and $B(\Upsilon(4S) \rightarrow B^0 \bar{B}^0) = 0.4$. Does not depend on D branching ratios.

$\Gamma(D^*(2010)^- K^+) / \Gamma_{\text{total}}$				Γ_{56} / Γ
VALUE (units 10^{-4})	DOCUMENT ID	TECN	COMMENT	
2.16 ± 0.08 OUR AVERAGE				
$2.22 \pm 0.06 \pm 0.08$	¹ KROHN 23	BELL	$e^+e^- \rightarrow \Upsilon(4S)$	
$2.06 \pm 0.12 \pm 0.06$	² AUBERT 06A	BABR	$e^+e^- \rightarrow \Upsilon(4S)$	
• • • We do not use the following data for averages, fits, limits, etc. • • •				
$2.0 \pm 0.4 \pm 0.1$	³ ABE 01i	BELL	Repl. by KROHN 23	

¹ KROHN 23 reports $(2.221 \pm 0.063 \pm 0.077) \times 10^{-4}$ from a measurement of $[\Gamma(B^0 \rightarrow D^*(2010)^- K^+) / \Gamma_{\text{total}}] / [B(\Upsilon(4S) \rightarrow B^0 \bar{B}^0)]$ assuming $B(\Upsilon(4S) \rightarrow B^0 \bar{B}^0) = 0.486 \pm 0.006$.

² AUBERT 06A reports $[\Gamma(B^0 \rightarrow D^*(2010)^- K^+) / \Gamma_{\text{total}}] / [B(B^0 \rightarrow D^*(2010)^- \pi^+)] = 0.0776 \pm 0.0034 \pm 0.0029$ which we multiply by our best value $B(B^0 \rightarrow D^*(2010)^- \pi^+) = (2.66 \pm 0.07) \times 10^{-3}$. Our first error is their experiment's error and our second error is the systematic error from using our best value.

³ ABE 01i reports $[\Gamma(B^0 \rightarrow D^*(2010)^- K^+) / \Gamma_{\text{total}}] / [B(B^0 \rightarrow D^*(2010)^- \pi^+)] = 0.074 \pm 0.015 \pm 0.006$ which we multiply by our best value $B(B^0 \rightarrow D^*(2010)^- \pi^+) = (2.66 \pm 0.07) \times 10^{-3}$. Our first error is their experiment's error and our second error is the systematic error from using our best value.

$\Gamma(D^*(2010)^- K^+) / \Gamma(D^*(2010)^- \pi^+)$				$\Gamma_{56} / \Gamma_{48}$
VALUE (units 10^{-2})	DOCUMENT ID	TECN	COMMENT	
8.22 ± 0.29 OUR AVERAGE			Error includes scale factor of 1.3.	
$8.41 \pm 0.24 \pm 0.13$	KROHN 23	BELL	$e^+e^- \rightarrow \Upsilon(4S)$	
$7.76 \pm 0.34 \pm 0.26$	AAIJ	13A0	LHCB pp at 7 TeV	

$\Gamma(D^*(2010)^- K^0 \pi^+) / \Gamma_{\text{total}}$				Γ_{57} / Γ
VALUE (units 10^{-4})	DOCUMENT ID	TECN	COMMENT	
$3.0 \pm 0.7 \pm 0.3$	¹ AUBERT, BE 05B	BABR	$e^+e^- \rightarrow \Upsilon(4S)$	
¹ Assumes equal production of B^+ and B^0 at the $\Upsilon(4S)$.				

$\Gamma(D^*(2010)^- K^*(892)^+) / \Gamma_{\text{total}}$				Γ_{58} / Γ
VALUE (units 10^{-4})	DOCUMENT ID	TECN	COMMENT	
3.3 ± 0.6 OUR AVERAGE				
$3.2 \pm 0.6 \pm 0.3$	¹ AUBERT, BE 05B	BABR	$e^+e^- \rightarrow \Upsilon(4S)$	
$3.8 \pm 1.3 \pm 0.8$	² MAHAPATRA 02	CLE2	$e^+e^- \rightarrow \Upsilon(4S)$	
¹ Assumes equal production of B^+ and B^0 at the $\Upsilon(4S)$.				
² Assumes equal production of B^+ and B^0 at the $\Upsilon(4S)$ and an unpolarized final state.				

$\Gamma(D^*(2010)^- K^+ \bar{K}^0) / \Gamma_{\text{total}}$				Γ_{59} / Γ
VALUE (units 10^{-4})	CL%	DOCUMENT ID	TECN	COMMENT
< 4.7	90	¹ DRUTSKOY 02	BELL	$e^+e^- \rightarrow \Upsilon(4S)$
¹ Assumes equal production of B^+ and B^0 at the $\Upsilon(4S)$.				

$\Gamma(D^*(2010)^- K^+ \bar{K}^*(892)^0) / \Gamma_{\text{total}}$				Γ_{60} / Γ
VALUE (units 10^{-4})	DOCUMENT ID	TECN	COMMENT	
$12.9 \pm 2.2 \pm 2.5$	¹ DRUTSKOY 02	BELL	$e^+e^- \rightarrow \Upsilon(4S)$	
¹ Assumes equal production of B^+ and B^0 at the $\Upsilon(4S)$.				

$\Gamma(D^*(2010)^- \pi^+ \pi^+ \pi^-) / \Gamma_{\text{total}}$				Γ_{61} / Γ
VALUE (units 10^{-3})	CL%	DOCUMENT ID	TECN	COMMENT
7.21 ± 0.29 OUR AVERAGE				
$7.26 \pm 0.11 \pm 0.31$		¹ LEES 16H	BABR	$e^+e^- \rightarrow \Upsilon(4S)$
$6.81 \pm 0.23 \pm 0.72$		² MAJUMDER 04	BELL	$e^+e^- \rightarrow \Upsilon(4S)$
$6.3 \pm 1.0 \pm 1.1$		^{3,4} ALAM 94	CLE2	$e^+e^- \rightarrow \Upsilon(4S)$
$13.4 \pm 3.6 \pm 0.1$		⁵ BORTOLETTO92	CLEO	$e^+e^- \rightarrow \Upsilon(4S)$
$10.1 \pm 4.1 \pm 0.1$		⁶ ALBRECHT 90j	ARG	$e^+e^- \rightarrow \Upsilon(4S)$
• • • We do not use the following data for averages, fits, limits, etc. • • •				
$33 \pm 9 \pm 16$		⁷ ALBRECHT 87c	ARG	$e^+e^- \rightarrow \Upsilon(4S)$
< 42	90	⁸ BEBEK 87	CLEO	$e^+e^- \rightarrow \Upsilon(4S)$

¹ Assumes $B(\Upsilon(4S) \rightarrow B^0 \bar{B}^0) = 0.486 \pm 0.006$.

² Assumes equal production of B^+ and B^0 at the $\Upsilon(4S)$.

³ ALAM 94 assume equal production of B^+ and B^0 at the $\Upsilon(4S)$ and use the CLEO II $B(D^*(2010)^+ \rightarrow D^0 \pi^+)$ and absolute $B(D^0 \rightarrow K^- \pi^+)$ and the PDG 1992 $B(D^0 \rightarrow K^- \pi^+ \pi^0) / B(D^0 \rightarrow K^- \pi^+)$ and $B(D^0 \rightarrow K^- 2\pi^+ \pi^-) / B(D^0 \rightarrow K^- \pi^+)$.

⁴ The three pion mass is required to be between 1.0 and 1.6 GeV consistent with an a_1 meson. (If this channel is dominated by a_1^+ , the branching ratio for $D^* \rightarrow a_1^+$ is twice that for $D^* \rightarrow \pi^+ \pi^+ \pi^-$.)

⁵ BORTOLETTO 92 reports $0.0159 \pm 0.0028 \pm 0.0037$ from a measurement of $[\Gamma(B^0 \rightarrow D^*(2010)^- \pi^+ \pi^+ \pi^-) / \Gamma_{\text{total}}] \times [B(D^*(2010)^+ \rightarrow D^0 \pi^+)]$ assuming $B(D^*(2010)^+ \rightarrow D^0 \pi^+) = 0.57 \pm 0.06$, which we rescale to our best value

$B(D^*(2010)^+ \rightarrow D^0 \pi^+) = (67.7 \pm 0.5) \times 10^{-2}$. Our first error is their experiment's error and our second error is the systematic error from using our best value. Assumes equal production of B^+ and B^0 at the $\Upsilon(4S)$ and uses MarkIII branching fractions for the D .

⁶ALBRECHT 90i reports $0.012 \pm 0.003 \pm 0.004$ from a measurement of $[\Gamma(B^0 \rightarrow D^*(2010)^- \pi^+ \pi^+ \pi^-)/\Gamma_{\text{total}}] \times [B(D^*(2010)^+ \rightarrow D^0 \pi^+)]$ assuming $B(D^*(2010)^+ \rightarrow D^0 \pi^+) = 0.57 \pm 0.06$, which we rescale to our best value $B(D^*(2010)^+ \rightarrow D^0 \pi^+) = (67.7 \pm 0.5) \times 10^{-2}$. Our first error is their experiment's error and our second error is the systematic error from using our best value. Assumes equal production of B^+ and B^0 at the $\Upsilon(4S)$ and uses MarkIII branching fractions for the D .

⁷ALBRECHT 87c use PDG 86 branching ratios for D and $D^*(2010)$ and assume $B(\Upsilon(4S) \rightarrow B^+ B^-) = 55\%$ and $B(\Upsilon(4S) \rightarrow B^0 \bar{B}^0) = 45\%$. Superseded by ALBRECHT 90i.

⁸BEBEK 87 value has been updated in BERKELMAN 91 to use same assumptions as noted for BORTOLETTO 92.

$\Gamma((D^*(2010)^- \pi^+ \pi^+ \pi^-) \text{ nonresonant})/\Gamma_{\text{total}}$ Γ_{62}/Γ

VALUE	DOCUMENT ID	TECN	COMMENT
0.0000 ± 0.0019 ± 0.0016	¹ BORTOLETTO92	CLEO	$e^+ e^- \rightarrow \Upsilon(4S)$

¹BORTOLETTO 92 assumes equal production of B^+ and B^0 at the $\Upsilon(4S)$ and uses Mark III branching fractions for the D and $D^*(2010)$.

$\Gamma(D^*(2010)^- \pi^+ \rho^0)/\Gamma_{\text{total}}$ Γ_{63}/Γ

VALUE	DOCUMENT ID	TECN	COMMENT
0.00573 ± 0.00317 ± 0.00004	¹ BORTOLETTO92	CLEO	$e^+ e^- \rightarrow \Upsilon(4S)$

¹BORTOLETTO 92 reports $0.0068 \pm 0.0032 \pm 0.0021$ from a measurement of $[\Gamma(B^0 \rightarrow D^*(2010)^- \pi^+ \rho^0)/\Gamma_{\text{total}}] \times [B(D^*(2010)^+ \rightarrow D^0 \pi^+)]$ assuming $B(D^*(2010)^+ \rightarrow D^0 \pi^+) = 0.57 \pm 0.06$, which we rescale to our best value $B(D^*(2010)^+ \rightarrow D^0 \pi^+) = (67.7 \pm 0.5) \times 10^{-2}$. Our first error is their experiment's error and our second error is the systematic error from using our best value. Assumes equal production of B^+ and B^0 at the $\Upsilon(4S)$ and uses MarkIII branching fractions for the D .

$\Gamma(D^*(2010)^- a_1(1260)^+)/\Gamma_{\text{total}}$ Γ_{64}/Γ

VALUE	DOCUMENT ID	TECN	COMMENT
0.0130 ± 0.0027 OUR AVERAGE			
0.0126 ± 0.0020 ± 0.0022	^{1,2} ALAM 94	CLE2	$e^+ e^- \rightarrow \Upsilon(4S)$
0.0152 ± 0.0070 ± 0.0001	³ BORTOLETTO92	CLEO	$e^+ e^- \rightarrow \Upsilon(4S)$

¹ALAM 94 value is twice their $\Gamma(D^*(2010)^- \pi^+ \pi^+ \pi^-)/\Gamma_{\text{total}}$ value based on their observation that the three pions are dominantly in the $a_1(1260)$ mass range 1.0 to 1.6 GeV.

²ALAM 94 assume equal production of B^+ and B^0 at the $\Upsilon(4S)$ and use the CLEOII $B(D^*(2010)^+ \rightarrow D^0 \pi^+)$ and absolute $B(D^0 \rightarrow K^- \pi^+)$ and the PDG 1992 $B(D^0 \rightarrow K^- \pi^+ \pi^0)/B(D^0 \rightarrow K^- \pi^+)$ and $B(D^0 \rightarrow K^- 2\pi^+ \pi^-)/B(D^0 \rightarrow K^- \pi^+)$.

³BORTOLETTO 92 reports $0.018 \pm 0.006 \pm 0.006$ from a measurement of $[\Gamma(B^0 \rightarrow D^*(2010)^- a_1(1260)^+)/\Gamma_{\text{total}}] \times [B(D^*(2010)^+ \rightarrow D^0 \pi^+)]$ assuming $B(D^*(2010)^+ \rightarrow D^0 \pi^+) = 0.57 \pm 0.06$, which we rescale to our best value $B(D^*(2010)^+ \rightarrow D^0 \pi^+) = (67.7 \pm 0.5) \times 10^{-2}$. Our first error is their experiment's error and our second error is the systematic error from using our best value. Assumes equal production of B^+ and B^0 at the $\Upsilon(4S)$ and uses MarkIII branching fractions for the D .

$\Gamma(\bar{D}_1(2420)^0 \pi^- \pi^+, \bar{D}_1^0 \rightarrow D^{*-} \pi^+)/\Gamma(D^*(2010)^- \pi^+ \pi^+ \pi^-)$ Γ_{65}/Γ_{61}

VALUE	DOCUMENT ID	TECN	COMMENT
(2.04 ± 0.42 ± 0.22) × 10⁻²	AALJ	13A0 LHCb	pp at 7 TeV

$\Gamma(D^*(2010)^- K^+ \pi^- \pi^+)/\Gamma(D^*(2010)^- \pi^+ \pi^+ \pi^-)$ Γ_{66}/Γ_{61}

VALUE	DOCUMENT ID	TECN	COMMENT
(6.47 ± 0.37 ± 0.35) × 10⁻²	AALJ	13A0 LHCb	pp at 7 TeV

$\Gamma(D^*(2010)^- \pi^+ \pi^+ \pi^- \pi^0)/\Gamma_{\text{total}}$ Γ_{67}/Γ

VALUE	EVTs	DOCUMENT ID	TECN	COMMENT
0.0176 ± 0.0027 OUR AVERAGE				
0.0172 ± 0.0014 ± 0.0024		¹ ALEXANDER 01B	CLE2	$e^+ e^- \rightarrow \Upsilon(4S)$
0.0345 ± 0.0181 ± 0.0003	28	² ALBRECHT 90j	ARG	$e^+ e^- \rightarrow \Upsilon(4S)$

¹Assumes equal production of B^+ and B^0 at the $\Upsilon(4S)$. The signal is consistent with all observed $\omega \pi^+$ having proceeded through the ρ^+ resonance at mass $1349 \pm 25 \pm 10$ MeV and width $547 \pm 86 \pm 46$ MeV.

²ALBRECHT 90j reports $0.041 \pm 0.015 \pm 0.016$ from a measurement of $[\Gamma(B^0 \rightarrow D^*(2010)^- \pi^+ \pi^+ \pi^- \pi^0)/\Gamma_{\text{total}}] \times [B(D^*(2010)^+ \rightarrow D^0 \pi^+)]$ assuming $B(D^*(2010)^+ \rightarrow D^0 \pi^+) = 0.57 \pm 0.06$, which we rescale to our best value $B(D^*(2010)^+ \rightarrow D^0 \pi^+) = (67.7 \pm 0.5) \times 10^{-2}$. Our first error is their experiment's error and our second error is the systematic error from using our best value. Assumes equal production of B^+ and B^0 at the $\Upsilon(4S)$ and uses MarkIII branching fractions for the D .

$\Gamma(D^{*-} 3\pi^+ 2\pi^-)/\Gamma_{\text{total}}$ Γ_{68}/Γ

VALUE (units 10 ⁻³)	DOCUMENT ID	TECN	COMMENT
4.72 ± 0.59 ± 0.71	¹ MAJUMDER 04	BELL	$e^+ e^- \rightarrow \Upsilon(4S)$

¹Assumes equal production of B^+ and B^0 at the $\Upsilon(4S)$.

$\Gamma(D^*(2010)^- \omega \pi^+)/\Gamma_{\text{total}}$ Γ_{69}/Γ

VALUE (units 10 ⁻³)	DOCUMENT ID	TECN	COMMENT
2.46 ± 0.18 OUR AVERAGE			Error includes scale factor of 1.2.
2.31 ± 0.11 ± 0.14	¹ MATVIENKO 15	BELL	$e^+ e^- \rightarrow \Upsilon(4S)$
2.88 ± 0.21 ± 0.31	¹ AUBERT 06L	BABR	$e^+ e^- \rightarrow \Upsilon(4S)$
2.9 ± 0.3 ± 0.4	^{1,2} ALEXANDER 01B	CLE2	$e^+ e^- \rightarrow \Upsilon(4S)$

¹Assumes equal production of B^+ and B^0 at the $\Upsilon(4S)$.

²The signal is consistent with all observed $\omega \pi^+$ having proceeded through the ρ^+ resonance at mass $1349 \pm 25 \pm 10$ MeV and width $547 \pm 86 \pm 46$ MeV.

$\Gamma(\bar{D}_1(2430)^0 \omega, \bar{D}_1^0 \rightarrow D^{*-} \pi^+)/\Gamma_{\text{total}}$ Γ_{70}/Γ

VALUE (units 10 ⁻⁴)	DOCUMENT ID	TECN	COMMENT
2.7 ± 0.8 OUR AVERAGE			
2.5 ± 0.4 ± 0.8	^{1,2} MATVIENKO 15	BELL	$e^+ e^- \rightarrow \Upsilon(4S)$
4.1 ± 1.2 ± 1.1	³ AUBERT 06L	BABR	$e^+ e^- \rightarrow \Upsilon(4S)$

¹Assumes equal production of B^+ and B^0 .

²The measurement is obtained by amplitude analysis of $B^0 \rightarrow D^{*-} \omega \pi^+$. The second uncertainty combines in quadrature experimental systematic and model uncertainties.

³Obtained by fitting the events with $\cos \theta_{D^*} < 0.5$ and scaling up the result by a factor of 4/3. No interference effects between $B^0 \rightarrow D_1^0 \omega$ and $D^* \omega \pi^+$ are assumed.

$\Gamma(D^{*-} \rho(1450)^+, \rho^+ \rightarrow \omega \pi^+)/\Gamma_{\text{total}}$ Γ_{71}/Γ

VALUE (units 10 ⁻³)	DOCUMENT ID	TECN	COMMENT
1.07 ± 0.15 ± 0.40	^{1,2} MATVIENKO 15	BELL	$e^+ e^- \rightarrow \Upsilon(4S)$
-0.31 ± 0.13			

¹Obtained by amplitude analysis of $\bar{B}^0 \rightarrow D^{*-} \omega \pi^+$. The second uncertainty combines in quadrature experimental systematic and model uncertainties.

²Assumes equal production of B^0 and B^+ at $\Upsilon(4S)$.

$\Gamma(\bar{D}_1(2420)^0 \omega, \bar{D}_1^0 \rightarrow D^{*-} \pi^+)/\Gamma_{\text{total}}$ Γ_{72}/Γ

VALUE (units 10 ⁻⁴)	DOCUMENT ID	TECN	COMMENT
0.7 ± 0.2 ± 0.1	^{1,2} MATVIENKO 15	BELL	$e^+ e^- \rightarrow \Upsilon(4S)$

¹Obtained by amplitude analysis of $\bar{B}^0 \rightarrow D^{*-} \omega \pi^+$. The second uncertainty combines in quadrature experimental systematic and model uncertainties.

²Assumes equal production of B^0 and B^+ at $\Upsilon(4S)$.

$\Gamma(\bar{D}_2^0(2460)^0 \omega, \bar{D}_2^0 \rightarrow D^{*-} \pi^+)/\Gamma_{\text{total}}$ Γ_{73}/Γ

VALUE (units 10 ⁻⁴)	DOCUMENT ID	TECN	COMMENT
0.4 ± 0.1 ± 0.1	^{1,2} MATVIENKO 15	BELL	$e^+ e^- \rightarrow \Upsilon(4S)$

¹Obtained by amplitude analysis of $\bar{B}^0 \rightarrow D^{*-} \omega \pi^+$. The second uncertainty combines in quadrature experimental systematic and model uncertainties.

²Assumes equal production of B^0 and B^+ at $\Upsilon(4S)$.

$\Gamma(D^{*-} b_1(1235)^+, b_1^+ \rightarrow \omega \pi^+)/\Gamma_{\text{total}}$ Γ_{74}/Γ

VALUE	CL%	DOCUMENT ID	TECN	COMMENT
< 0.7 × 10⁻⁴	90	¹ MATVIENKO 15	BELL	$e^+ e^- \rightarrow \Upsilon(4S)$

¹Assumes equal production of B^0 and B^+ at $\Upsilon(4S)$.

$\Gamma(\bar{D}^{*-} \pi^+)/\Gamma_{\text{total}}$ Γ_{75}/Γ

D^{*-} represents an excited state with mass $2.2 < M < 2.8$ GeV/ c^2 .

VALUE (units 10 ⁻³)	DOCUMENT ID	TECN	COMMENT
1.9 ± 0.9 ± 0.1	^{1,2} AUBERT, BE 06j	BABR	$e^+ e^- \rightarrow \Upsilon(4S)$

¹AUBERT, BE 06j reports $[\Gamma(B^0 \rightarrow \bar{D}^{*-} \pi^+)/\Gamma_{\text{total}}] / [B(B^0 \rightarrow D^- \pi^+)] = 0.77 \pm 0.22 \pm 0.29$ which we multiply by our best value $B(B^0 \rightarrow D^- \pi^+) = (2.51 \pm 0.08) \times 10^{-3}$. Our first error is their experiment's error and our second error is the systematic error from using our best value.

²Uses a missing-mass method. Does not depend on D branching fractions or B^+/B^0 production rates.

$\Gamma(D_1(2420)^- \pi^+, D_1^- \rightarrow D^- \pi^+ \pi^-)/\Gamma_{\text{total}}$ Γ_{76}/Γ

VALUE (units 10 ⁻⁴)	DOCUMENT ID	TECN	COMMENT
0.99 ± 0.20 OUR FIT			
0.89 ± 0.15 ± 0.17	¹ ABE 05A	BELL	$e^+ e^- \rightarrow \Upsilon(4S)$
-0.32			

¹Assumes equal production of B^+ and B^0 at the $\Upsilon(4S)$.

$\Gamma(D_1(2420)^- \pi^+, D_1^- \rightarrow D^- \pi^+ \pi^-)/\Gamma(D^- \pi^+ \pi^-)$ Γ_{76}/Γ_{50}

VALUE (units 10 ⁻²)	DOCUMENT ID	TECN	COMMENT
1.7 ± 0.4 OUR FIT			
2.1 ± 0.5 ± 0.3	AALJ	11E LHCb	pp at 7 TeV

$\Gamma(D_1(2420)^- \pi^+, D_1^- \rightarrow D^{*-} \pi^+ \pi^-)/\Gamma_{\text{total}}$ Γ_{77}/Γ

VALUE (units 10 ⁻⁴)	CL%	DOCUMENT ID	TECN	COMMENT
< 0.33	90	¹ ABE 05A	BELL	$e^+ e^- \rightarrow \Upsilon(4S)$

¹Assumes equal production of B^+ and B^0 at the $\Upsilon(4S)$.

Meson Particle Listings

 B^0

$\Gamma(D^{*0}(2010)^- \pi^+ \pi^+ \pi^-)/\Gamma(D^{*0}(2010)^- \pi^+)$				Γ_{61}/Γ_{48}
VALUE	DOCUMENT ID	TECN	COMMENT	
2.64 ± 0.04 ± 0.13	AAIJ	13A0	LHCB pp at 7 TeV	

$\Gamma(\overline{D}_2^*(2460)^- \pi^+, D_2^{*-} \rightarrow D^0 \pi^-)/\Gamma_{total}$				Γ_{78}/Γ
VALUE (units 10^{-4})	CL%	DOCUMENT ID	TECN	COMMENT
2.38 ± 0.16 OUR AVERAGE				
2.44 ± 0.07 ± 0.16		¹ AAIJ	15Y	LHCB pp at 7, 8 TeV
2.15 ± 0.17 ± 0.31		^{2,3} KUZMIN	07	BELL $e^+e^- \rightarrow \Upsilon(4S)$

• • • We do not use the following data for averages, fits, limits, etc. • • •

<14.7 90 ²ALAM 94 CLE2 $e^+e^- \rightarrow \Upsilon(4S)$

¹ Result obtained using the isobar formalism. The second uncertainty combines in quadrature all systematic uncertainties quoted in the paper.

² Assumes equal production of B^+ and B^0 at the $\Upsilon(4S)$.

³ Our second uncertainty combines systematics and model errors quoted in the paper.

$\Gamma(\overline{D}_0^*(2400)^- \pi^+, D_0^{*-} \rightarrow D^0 \pi^-)/\Gamma_{total}$				Γ_{79}/Γ
VALUE (units 10^{-4})	DOCUMENT ID	TECN	COMMENT	
0.76 ± 0.08 OUR AVERAGE				
0.77 ± 0.05 ± 0.06		¹ AAIJ	15Y	LHCB pp at 7, 8 TeV
0.60 ± 0.13 ± 0.27		^{2,3} KUZMIN	07	BELL $e^+e^- \rightarrow \Upsilon(4S)$

¹ Result obtained using the isobar formalism. The second uncertainty combines in quadrature all systematic uncertainties quoted in the paper.

² Assumes equal production of B^+ and B^0 at the $\Upsilon(4S)$.

³ Our second uncertainty combines systematics and model errors quoted in the paper.

$\Gamma(D_2^*(2460)^- \pi^+, D_2^{*-} \rightarrow D^{*-} \pi^+ \pi^-)/\Gamma_{total}$				Γ_{80}/Γ
VALUE (units 10^{-4})	CL%	DOCUMENT ID	TECN	COMMENT
<0.24	90	¹ ABE	05A	BELL $e^+e^- \rightarrow \Upsilon(4S)$

¹ Assumes equal production of B^+ and B^0 at the $\Upsilon(4S)$.

$\Gamma(\overline{D}_2^*(2460)^- \rho^+)/\Gamma_{total}$				Γ_{81}/Γ
VALUE	CL%	DOCUMENT ID	TECN	COMMENT
<0.0049	90	¹ ALAM	94	CLE2 $e^+e^- \rightarrow \Upsilon(4S)$

¹ ALAM 94 assumes equal production of B^+ and B^0 at the $\Upsilon(4S)$ and use the CLEOII absolute $B(D^0 \rightarrow K^- \pi^+)$ and $B(D_2^*(2460)^+ \rightarrow D^0 \pi^+) = 30\%$.

$\Gamma(D^0 \overline{D}^0)/\Gamma_{total}$				Γ_{82}/Γ
VALUE (units 10^{-4})	CL%	DOCUMENT ID	TECN	COMMENT
0.14 ± 0.06 ± 0.03				
<0.43	90	² ADACHI	08	BELL $e^+e^- \rightarrow \Upsilon(4S)$
<0.6	90	² AUBERT,B	06A	BABR $e^+e^- \rightarrow \Upsilon(4S)$

• • • We do not use the following data for averages, fits, limits, etc. • • •

<0.43 90 ²ADACHI 08 BELL $e^+e^- \rightarrow \Upsilon(4S)$

<0.6 90 ²AUBERT,B 06A BABR $e^+e^- \rightarrow \Upsilon(4S)$

¹ Uses $B(B^0 \rightarrow D^- D^+) = (2.11 \pm 0.31) \times 10^{-4}$ and $B(B^+ \rightarrow \overline{D}^0 D_s^+) = (10.1 \pm 1.7) \times 10^{-3}$.

² Assumes equal production of B^+ and B^0 at the $\Upsilon(4S)$.

$\Gamma(D^{*0} \overline{D}^0)/\Gamma_{total}$				Γ_{83}/Γ
VALUE (units 10^{-4})	CL%	DOCUMENT ID	TECN	COMMENT
<2.9	90	¹ AUBERT,B	06A	BABR $e^+e^- \rightarrow \Upsilon(4S)$

¹ Assumes equal production of B^+ and B^0 at the $\Upsilon(4S)$.

$\Gamma(D^- D^+)/\Gamma_{total}$				Γ_{84}/Γ
VALUE (units 10^{-4})	CL%	DOCUMENT ID	TECN	COMMENT
2.11 ± 0.18 OUR AVERAGE				
2.12 ± 0.16 ± 0.18		¹ ROHRKEN	12	BELL $e^+e^- \rightarrow \Upsilon(4S)$
1.97 ± 0.20 ± 0.20		¹ FRATINA	07	BELL $e^+e^- \rightarrow \Upsilon(4S)$
2.8 ± 0.4 ± 0.5		¹ AUBERT,B	06A	BABR $e^+e^- \rightarrow \Upsilon(4S)$

• • • We do not use the following data for averages, fits, limits, etc. • • •

1.91 ± 0.51 ± 0.30

< 9.4 90 ¹MAJUMDER 05 BELL Repl. by FRATINA 07

<59 90 ¹LIPELES 00 CLE2 $e^+e^- \rightarrow \Upsilon(4S)$

<12 90 ¹BARATE 98Q ALEP $e^+e^- \rightarrow Z$

<12 90 ¹ASNER 97 CLE2 $e^+e^- \rightarrow \Upsilon(4S)$

¹ Assumes equal production of B^+ and B^0 at the $\Upsilon(4S)$.

$\Gamma(D^\pm D^{*\mp}(CP\text{-averaged}))/\Gamma_{total}$				Γ_{85}/Γ
VALUE (units 10^{-4})	DOCUMENT ID	TECN	COMMENT	
6.14 ± 0.29 ± 0.50				
	¹ ROHRKEN	12	BELL $e^+e^- \rightarrow \Upsilon(4S)$	

¹ Assumes equal production of B^+ and B^0 at the $\Upsilon(4S)$.

$\Gamma(D^- D_s^+)/\Gamma_{total}$				Γ_{86}/Γ
VALUE	EVTs	DOCUMENT ID	TECN	COMMENT
0.0072 ± 0.0008 OUR AVERAGE				
0.0073 ± 0.0004 ± 0.0007		¹ ZUPANC	07	BELL $e^+e^- \rightarrow \Upsilon(4S)$
0.0066 ± 0.0014 ± 0.0006		² AUBERT	06N	BABR $e^+e^- \rightarrow \Upsilon(4S)$
0.0068 ± 0.0024 ± 0.0006		³ GIBAUT	96	CLE2 $e^+e^- \rightarrow \Upsilon(4S)$
0.010 ± 0.009 ± 0.001		⁴ ALBRECHT	92G	ARG $e^+e^- \rightarrow \Upsilon(4S)$
0.0053 ± 0.0030 ± 0.0005		⁵ BORTOLETTO92	CLEO	$e^+e^- \rightarrow \Upsilon(4S)$

• • • We do not use the following data for averages, fits, limits, etc. • • •

0.012 ± 0.007 3 ⁶BORTOLETTO90 CLEO $e^+e^- \rightarrow \Upsilon(4S)$

¹ ZUPANC 07 reports $(7.5 \pm 0.2 \pm 1.1) \times 10^{-3}$ from a measurement of $[\Gamma(B^0 \rightarrow D^- D_s^+)/\Gamma_{total}] \times [B(D_s^+ \rightarrow \phi \pi^+)]$ assuming $B(D_s^+ \rightarrow \phi \pi^+) = (4.4 \pm 0.6) \times 10^{-2}$, which we rescale to our best value $B(D_s^+ \rightarrow \phi \pi^+) = (4.5 \pm 0.4) \times 10^{-2}$. Our first error is their experiment's error and our second error is the systematic error from using our best value.

² AUBERT 06N reports $(0.64 \pm 0.13 \pm 0.10) \times 10^{-2}$ from a measurement of $[\Gamma(B^0 \rightarrow D^- D_s^+)/\Gamma_{total}] \times [B(D_s^+ \rightarrow \phi \pi^+)]$ assuming $B(D_s^+ \rightarrow \phi \pi^+) = 0.0462 \pm 0.0062$, which we rescale to our best value $B(D_s^+ \rightarrow \phi \pi^+) = (4.5 \pm 0.4) \times 10^{-2}$. Our first error is their experiment's error and our second error is the systematic error from using our best value.

³ GIBAUT 96 reports $0.0087 \pm 0.0024 \pm 0.0020$ from a measurement of $[\Gamma(B^0 \rightarrow D^- D_s^+)/\Gamma_{total}] \times [B(D_s^+ \rightarrow \phi \pi^+)]$ assuming $B(D_s^+ \rightarrow \phi \pi^+) = 0.035$, which we rescale to our best value $B(D_s^+ \rightarrow \phi \pi^+) = (4.5 \pm 0.4) \times 10^{-2}$. Our first error is their experiment's error and our second error is the systematic error from using our best value.

⁴ ALBRECHT 92G reports $0.017 \pm 0.013 \pm 0.006$ from a measurement of $[\Gamma(B^0 \rightarrow D^- D_s^+)/\Gamma_{total}] \times [B(D_s^+ \rightarrow \phi \pi^+)]$ assuming $B(D_s^+ \rightarrow \phi \pi^+) = 0.027$, which we rescale to our best value $B(D_s^+ \rightarrow \phi \pi^+) = (4.5 \pm 0.4) \times 10^{-2}$. Our first error is their experiment's error and our second error is the systematic error from using our best value. Assumes PDG 1990 D^+ branching ratios, e.g., $B(D^+ \rightarrow K^- 2\pi^+) = 7.7 \pm 1.0\%$.

⁵ BORTOLETTO 92 reports $0.0080 \pm 0.0045 \pm 0.0030$ from a measurement of $[\Gamma(B^0 \rightarrow D^- D_s^+)/\Gamma_{total}] \times [B(D_s^+ \rightarrow \phi \pi^+)]$ assuming $B(D_s^+ \rightarrow \phi \pi^+) = 0.030 \pm 0.011$, which we rescale to our best value $B(D_s^+ \rightarrow \phi \pi^+) = (4.5 \pm 0.4) \times 10^{-2}$. Our first error is their experiment's error and our second error is the systematic error from using our best value. Assumes equal production of B^+ and B^0 at the $\Upsilon(4S)$ and use MarkIII branching fractions for the D .

⁶ BORTOLETTO 90 assume $B(D_s \rightarrow \phi \pi^+) = 2\%$. Superseded by BORTOLETTO 92.

⁶ BORTOLETTO 90 assume $B(D_s \rightarrow \phi \pi^+) = 2\%$. Superseded by BORTOLETTO 92.

⁶ BORTOLETTO 90 assume $B(D_s \rightarrow \phi \pi^+) = 2\%$. Superseded by BORTOLETTO 92.

⁶ BORTOLETTO 90 assume $B(D_s \rightarrow \phi \pi^+) = 2\%$. Superseded by BORTOLETTO 92.

⁶ BORTOLETTO 90 assume $B(D_s \rightarrow \phi \pi^+) = 2\%$. Superseded by BORTOLETTO 92.

⁶ BORTOLETTO 90 assume $B(D_s \rightarrow \phi \pi^+) = 2\%$. Superseded by BORTOLETTO 92.

⁶ BORTOLETTO 90 assume $B(D_s \rightarrow \phi \pi^+) = 2\%$. Superseded by BORTOLETTO 92.

⁶ BORTOLETTO 90 assume $B(D_s \rightarrow \phi \pi^+) = 2\%$. Superseded by BORTOLETTO 92.

⁶ BORTOLETTO 90 assume $B(D_s \rightarrow \phi \pi^+) = 2\%$. Superseded by BORTOLETTO 92.

⁶ BORTOLETTO 90 assume $B(D_s \rightarrow \phi \pi^+) = 2\%$. Superseded by BORTOLETTO 92.

⁶ BORTOLETTO 90 assume $B(D_s \rightarrow \phi \pi^+) = 2\%$. Superseded by BORTOLETTO 92.

⁶ BORTOLETTO 90 assume $B(D_s \rightarrow \phi \pi^+) = 2\%$. Superseded by BORTOLETTO 92.

⁶ BORTOLETTO 90 assume $B(D_s \rightarrow \phi \pi^+) = 2\%$. Superseded by BORTOLETTO 92.

⁶ BORTOLETTO 90 assume $B(D_s \rightarrow \phi \pi^+) = 2\%$. Superseded by BORTOLETTO 92.

⁶ BORTOLETTO 90 assume $B(D_s \rightarrow \phi \pi^+) = 2\%$. Superseded by BORTOLETTO 92.

⁶ BORTOLETTO 90 assume $B(D_s \rightarrow \phi \pi^+) = 2\%$. Superseded by BORTOLETTO 92.

⁶ BORTOLETTO 90 assume $B(D_s \rightarrow \phi \pi^+) = 2\%$. Superseded by BORTOLETTO 92.

⁶ BORTOLETTO 90 assume $B(D_s \rightarrow \phi \pi^+) = 2\%$. Superseded by BORTOLETTO 92.

⁶ BORTOLETTO 90 assume $B(D_s \rightarrow \phi \pi^+) = 2\%$. Superseded by BORTOLETTO 92.

⁶ BORTOLETTO 90 assume $B(D_s \rightarrow \phi \pi^+) = 2\%$. Superseded by BORTOLETTO 92.

⁶ BORTOLETTO 90 assume $B(D_s \rightarrow \phi \pi^+) = 2\%$. Superseded by BORTOLETTO 92.

⁶ BORTOLETTO 90 assume $B(D_s \rightarrow \phi \pi^+) = 2\%$. Superseded by BORTOLETTO 92.

⁶ BORTOLETTO 90 assume $B(D_s \rightarrow \phi \pi^+) = 2\%$. Superseded by BORTOLETTO 92.

⁶ BORTOLETTO 90 assume $B(D_s \rightarrow \phi \pi^+) = 2\%$. Superseded by BORTOLETTO 92.

⁶ BORTOLETTO 90 assume $B(D_s \rightarrow \phi \pi^+) = 2\%$. Superseded by BORTOLETTO 92.

⁶ BORTOLETTO 90 assume $B(D_s \rightarrow \phi \pi^+) = 2\%$. Superseded by BORTOLETTO 92.

⁶ BORTOLETTO 90 assume $B(D_s \rightarrow \phi \pi^+) = 2\%$. Superseded by BORTOLETTO 92.

⁶ BORTOLETTO 90 assume $B(D_s \rightarrow \phi \pi^+) = 2\%$. Superseded by BORTOLETTO 92.

⁶ BORTOLETTO 90 assume $B(D_s \rightarrow \phi \pi^+) = 2\%$. Superseded by BORTOLETTO 92.

⁶ BORTOLETTO 90 assume $B(D_s \rightarrow \phi \pi^+) = 2\%$. Superseded by BORTOLETTO 92.

⁶ BORTOLETTO 90 assume $B(D_s \rightarrow \phi \pi^+) = 2\%$. Superseded by BORTOLETTO 92.

⁶ BORTOLETTO 90 assume $B(D_s \rightarrow \phi \pi^+) = 2\%$. Superseded by BORTOLETTO 92.

⁶ BORTOLETTO 90 assume $B(D_s \rightarrow \phi \pi^+) = 2\%$. Superseded by BORTOLETTO 92.

⁶ BORTOLETTO 90 assume $B(D_s \rightarrow \phi \pi^+) = 2\%$. Superseded by BORTOLETTO 92.

⁶ BORTOLETTO 90 assume $B(D_s \rightarrow \phi \pi^+) = 2\%$. Superseded by BORTOLETTO 92.

⁶ BORTOLETTO 90 assume $B(D_s \rightarrow \phi \pi^+) = 2\%$. Superseded by BORTOLETTO 92.

⁶ BORTOLETTO 90 assume $B(D_s \rightarrow \phi \pi^+) = 2\%$. Superseded by BORTOLETTO 92.

⁶ BORTOLETTO 90 assume $B(D_s \rightarrow \phi \pi^+) = 2\%$. Superseded by BORTOLETTO 92.

⁶ BORTOLETTO 90 assume $B(D_s \rightarrow \phi \pi^+) = 2\%$. Superseded by BORTOLETTO 92.

⁶ BORTOLETTO 90 assume $B(D_s \rightarrow \phi \pi^+) = 2\%$. Superseded by BORTOLETTO 92.

⁶ BORTOLETTO 90 assume $B(D_s \rightarrow \phi \pi^+) = 2\%$. Superseded by BORTOLETTO 92.

⁶ BORTOLETTO 90 assume $B(D_s \rightarrow \phi \pi^+) = 2\%$. Superseded by BORTOLETTO 92.

⁶ BORTOLETTO 90 assume $B(D_s \rightarrow \phi \pi^+) = 2\%$. Superseded by BORTOLETTO 92.

⁶ BORTOLETTO 90 assume $B(D_s \rightarrow \phi \pi^+) = 2\%$. Superseded by BORTOLETTO 92.

⁶ BORTOLETTO 90 assume $B(D_s \rightarrow \phi \pi^+) = 2\%$. Superseded by BORTOLETTO 92.

⁶ BORTOLETTO 90 assume $B(D_s \rightarrow \phi \pi^+) = 2\%$. Superseded by BORTOLETTO 92.

⁶ BORTOLETTO 90 assume $B(D_s \rightarrow \phi \pi^+) = 2\%$. Superseded by BORTOLETTO 92.

⁶ BORTOLETTO 90 assume $B(D_s \rightarrow \phi \pi^+) = 2\%$. Superseded by BORTOLETTO 92.

⁶ BORTOLETTO 90 assume $B(D_s \rightarrow \phi \pi^+) = 2\%$. Superseded by BORTOLETTO 92.

⁶ BORTOLETTO 90 assume $B(D_s \rightarrow \phi \pi^+) = 2\%$. Superseded by BORTOLETTO 92.

⁶ BORTOLETTO 90 assume $B(D_s \rightarrow \phi \pi^+) = 2\%$. Superseded by BORTOLETTO 92.

⁶ BORTOLETTO 90 assume $B(D_s \rightarrow \phi \pi^+) = 2\%$. Superseded by BORTOLETTO 92.

⁶ BORTOLETTO 90 assume $B(D_s \rightarrow \phi \pi^+) = 2\%$. Superseded by BORTOLETTO 92.

⁶ BORTOLETTO 90 assume $B(D_s \rightarrow \phi \pi^+) = 2\%$. Superseded by BORTOLETTO 92.

⁶ BORTOLETTO 90 assume $B(D_s \rightarrow \phi \pi^+) = 2\%$. Superseded by BORTOLETTO 92.

⁶ BORTOLETTO 90 assume $B(D_s \rightarrow \phi \pi^+) = 2\%$. Superseded by BORTOLETTO 92.

⁶ BORTOLETTO 90 assume $B(D_s \rightarrow \phi \pi^+) = 2\%$. Superseded by BORTOLETTO 92.

⁶ BORTOLETTO 90 assume $B(D_s \rightarrow \phi \pi^+) = 2\%$. Superseded by BORTOLETTO 92.

⁶ BORTOLETTO 90 assume $B(D_s \rightarrow \phi \pi^+) = 2\%$. Superseded by BORTOLETTO 92.

⁶ BORTOLETTO 90 assume $B(D_s \rightarrow \phi \pi^+) = 2\%$. Superseded by BORTOLETTO 92.

⁶ BORTOLETTO 90 assume $B(D_s \rightarrow \phi \pi^+) = 2\%$. Superseded by BORTOLETTO 92.

⁶ BORTOLETTO 90 assume $B(D_s \rightarrow \phi \pi^+) = 2\%$. Superseded by BORTOLETTO 92.

⁶ BORTOLETTO 90 assume $B(D_s \rightarrow \phi \pi^+) = 2\%$. Superseded by BORTOLETTO 92.

⁶ BORTOLETTO 90 assume $B(D_s \rightarrow \phi \pi^+) = 2\%$. Superseded by BORTOLETTO 92.

⁶ BORTOLETTO 90 assume $B(D_s \rightarrow \phi \pi^+) = 2\%$. Superseded by BORTOLETTO 92.

⁶ BORTOLETTO 90 assume $B(D_s \rightarrow \phi \pi^+) = 2\%$. Superseded by BORTOLETTO 92.

⁶ BORTOLETTO 90 assume $B(D_s \rightarrow \phi \pi^+) = 2\%$. Superseded by BORTOLETTO 92.

$\Gamma(D^*(2010)^- D_s^+, D^{*-} \rightarrow \bar{D}^0 \pi^-, m(\bar{D}^0 \pi^-) > 2.05 \text{ GeV}) / \Gamma(\bar{D}^0 D_s^+ \pi^-, m(\bar{D}^0 \pi^-) > 2.05 \text{ GeV})$ $\Gamma_{89} / \Gamma_{87}$

VALUE (units 10^{-2})	DOCUMENT ID	TECN	COMMENT
15.8 ± 1.3 ± 2.4	¹ AAIJ	23B	LHCB pp at 7, 8, 13 TeV

¹ Uses simultaneous fits of $\bar{B}^0 \rightarrow \bar{D}^0 D_s^+ \pi^-$ and $B^+ \rightarrow D^- D_s^+ \pi^+$ amplitudes assuming isospin symmetry.

$\Gamma(D_s^*(2460)^- D_s^+, D_2^{*-} \rightarrow \bar{D}^0 \pi^-) / \Gamma(\bar{D}^0 D_s^+ \pi^-, m(\bar{D}^0 \pi^-) > 2.05 \text{ GeV})$ $\Gamma_{90} / \Gamma_{87}$

VALUE (units 10^{-2})	DOCUMENT ID	TECN	COMMENT
22.38 ± 0.88 ± 0.60	¹ AAIJ	23B	LHCB pp at 7, 8, 13 TeV

¹ Uses simultaneous fits of $\bar{B}^0 \rightarrow \bar{D}^0 D_s^+ \pi^-$ and $B^+ \rightarrow D^- D_s^+ \pi^+$ amplitudes assuming isospin symmetry.

$\Gamma(D_s^*(2600)^- D_s^+, D_1^{*-} \rightarrow \bar{D}^0 \pi^-) / \Gamma(\bar{D}^0 D_s^+ \pi^-, m(\bar{D}^0 \pi^-) > 2.05 \text{ GeV})$ $\Gamma_{91} / \Gamma_{87}$

VALUE (units 10^{-2})	DOCUMENT ID	TECN	COMMENT
1.35 ± 0.40 ± 0.59	¹ AAIJ	23B	LHCB pp at 7, 8, 13 TeV

¹ Uses simultaneous fits of $\bar{B}^0 \rightarrow \bar{D}^0 D_s^+ \pi^-$ and $B^+ \rightarrow D^- D_s^+ \pi^+$ amplitudes assuming isospin symmetry.

$\Gamma(D_s^*(2750)^- D_s^+, D_3^{*-} \rightarrow \bar{D}^0 \pi^-) / \Gamma(\bar{D}^0 D_s^+ \pi^-, m(\bar{D}^0 \pi^-) > 2.05 \text{ GeV})$ $\Gamma_{92} / \Gamma_{87}$

VALUE (units 10^{-2})	DOCUMENT ID	TECN	COMMENT
0.31 ± 0.14 ± 0.17	¹ AAIJ	23B	LHCB pp at 7, 8, 13 TeV

¹ Uses simultaneous fits of $\bar{B}^0 \rightarrow \bar{D}^0 D_s^+ \pi^-$ and $B^+ \rightarrow D^- D_s^+ \pi^+$ amplitudes assuming isospin symmetry.

$\Gamma(D_s^*(2760)^- D_s^+, D_1^{*-} \rightarrow \bar{D}^0 \pi^-) / \Gamma(\bar{D}^0 D_s^+ \pi^-, m(\bar{D}^0 \pi^-) > 2.05 \text{ GeV})$ $\Gamma_{93} / \Gamma_{87}$

VALUE (units 10^{-2})	DOCUMENT ID	TECN	COMMENT
0.28 ± 0.25 ± 1.48	¹ AAIJ	23B	LHCB pp at 7, 8, 13 TeV

¹ Uses simultaneous fits of $\bar{B}^0 \rightarrow \bar{D}^0 D_s^+ \pi^-$ and $B^+ \rightarrow D^- D_s^+ \pi^+$ amplitudes assuming isospin symmetry.

$\Gamma(D_s^*(3000)^- D_s^+, D_{J^*}^{*-} \rightarrow \bar{D}^0 \pi^-) / \Gamma(\bar{D}^0 D_s^+ \pi^-, m(\bar{D}^0 \pi^-) > 2.05 \text{ GeV})$ $\Gamma_{94} / \Gamma_{87}$

VALUE (units 10^{-2})	DOCUMENT ID	TECN	COMMENT
0.45 ± 0.16 ± 0.38	¹ AAIJ	23B	LHCB pp at 7, 8, 13 TeV

¹ Uses simultaneous fits of $\bar{B}^0 \rightarrow \bar{D}^0 D_s^+ \pi^-$ and $B^+ \rightarrow D^- D_s^+ \pi^+$ amplitudes assuming isospin symmetry.

$\Gamma(T_{cs0}^*(2870)^0 \bar{D}^0, T_{cs0}^{*0} \rightarrow D_s^+ \pi^-) / \Gamma(\bar{D}^0 D_s^+ \pi^-, m(\bar{D}^0 \pi^-) > 2.05 \text{ GeV})$ $\Gamma_{95} / \Gamma_{87}$

VALUE (units 10^{-2})	DOCUMENT ID	TECN	COMMENT
2.48 ± 0.67 ± 0.77	¹ AAIJ	23B	LHCB pp at 7, 8, 13 TeV

¹ Uses simultaneous fits of $\bar{B}^0 \rightarrow \bar{D}^0 D_s^+ \pi^-$ and $B^+ \rightarrow D^- D_s^+ \pi^+$ amplitudes assuming isospin symmetry.

$\Gamma(D^- D_s^{*+}) / \Gamma_{\text{total}}$ Γ_{96} / Γ

VALUE	DOCUMENT ID	TECN	COMMENT
0.0074 ± 0.0016 OUR AVERAGE			
0.0071 ± 0.0016 ± 0.0006	¹ AUBERT	06N	BABR $e^+ e^- \rightarrow \Upsilon(4S)$
0.0078 ± 0.0032 ± 0.0007	² GIBAUT	96	CLE2 $e^+ e^- \rightarrow \Upsilon(4S)$
0.016 ± 0.012 ± 0.001	³ ALBRECHT	92G	ARG $e^+ e^- \rightarrow \Upsilon(4S)$

¹ AUBERT 06N reports $(0.69 \pm 0.16 \pm 0.09) \times 10^{-2}$ from a measurement of $[\Gamma(B^0 \rightarrow D^- D_s^{*+}) / \Gamma_{\text{total}}] \times [B(D_s^+ \rightarrow \phi \pi^+)]$ assuming $B(D_s^+ \rightarrow \phi \pi^+) = 0.0462 \pm 0.0062$, which we rescale to our best value $B(D_s^+ \rightarrow \phi \pi^+) = (4.5 \pm 0.4) \times 10^{-2}$. Our first error is their experiment's error and our second error is the systematic error from using our best value.

² GIBAUT 96 reports $0.0100 \pm 0.0035 \pm 0.0022$ from a measurement of $[\Gamma(B^0 \rightarrow D^- D_s^{*+}) / \Gamma_{\text{total}}] \times [B(D_s^+ \rightarrow \phi \pi^+)]$ assuming $B(D_s^+ \rightarrow \phi \pi^+) = 0.035$, which we rescale to our best value $B(D_s^+ \rightarrow \phi \pi^+) = (4.5 \pm 0.4) \times 10^{-2}$. Our first error is their experiment's error and our second error is the systematic error from using our best value.

³ ALBRECHT 92G reports $0.027 \pm 0.017 \pm 0.009$ from a measurement of $[\Gamma(B^0 \rightarrow D^- D_s^{*+}) / \Gamma_{\text{total}}] \times [B(D_s^+ \rightarrow \phi \pi^+)]$ assuming $B(D_s^+ \rightarrow \phi \pi^+) = 0.027$, which we rescale to our best value $B(D_s^+ \rightarrow \phi \pi^+) = (4.5 \pm 0.4) \times 10^{-2}$. Our first error is their experiment's error and our second error is the systematic error from using our best value. Assumes PDG 1990 D^+ branching ratios, e.g., $B(D^+ \rightarrow K^- 2\pi^+) = 7.7 \pm 1.0\%$.

$\Gamma(D^*(2010)^- D_s^{*+}) / \Gamma_{\text{total}}$ Γ_{97} / Γ

VALUE	DOCUMENT ID	TECN	COMMENT
0.0177 ± 0.0014 OUR AVERAGE			
0.0173 ± 0.0018 ± 0.0015	¹ AUBERT	06N	BABR $e^+ e^- \rightarrow \Upsilon(4S)$
0.0188 ± 0.0009 ± 0.0017	² AUBERT	05V	BABR $e^+ e^- \rightarrow \Upsilon(4S)$
0.0158 ± 0.0027 ± 0.0014	³ AUBERT	03i	BABR $e^+ e^- \rightarrow \Upsilon(4S)$
0.015 ± 0.004 ± 0.001	⁴ AHMED	00B	CLE2 $e^+ e^- \rightarrow \Upsilon(4S)$
0.016 ± 0.009 ± 0.001	⁵ ALBRECHT	92G	ARG $e^+ e^- \rightarrow \Upsilon(4S)$

• • • We do not use the following data for averages, fits, limits, etc. • • •

0.016 ± 0.005 ± 0.001 ⁶ GIBAUT 96 CLE2 Repl. by AHMED 00B

¹ AUBERT 06N reports $(1.68 \pm 0.21 \pm 0.19) \times 10^{-2}$ from a measurement of $[\Gamma(B^0 \rightarrow D^*(2010)^- D_s^{*+}) / \Gamma_{\text{total}}] \times [B(D_s^+ \rightarrow \phi \pi^+)]$ assuming $B(D_s^+ \rightarrow \phi \pi^+) = 0.0462 \pm 0.0062$, which we rescale to our best value $B(D_s^+ \rightarrow \phi \pi^+) = (4.5 \pm 0.4) \times 10^{-2}$. Our first error is their experiment's error and our second error is the systematic error from using our best value.

² A partial reconstruction technique is used and the result is independent of the particle decay rate of D_s^+ meson. It also provides a model-independent determination of $B(D_s^+ \rightarrow \phi \pi^+) = (4.81 \pm 0.52 \pm 0.38)\%$.

³ AUBERT 03i reports $0.0197 \pm 0.0015 \pm 0.0030$ from a measurement of $[\Gamma(B^0 \rightarrow D^*(2010)^- D_s^{*+}) / \Gamma_{\text{total}}] \times [B(D_s^+ \rightarrow \phi \pi^+)]$ assuming $B(D_s^+ \rightarrow \phi \pi^+) = 0.036$, which we rescale to our best value $B(D_s^+ \rightarrow \phi \pi^+) = (4.5 \pm 0.4) \times 10^{-2}$. Our first error is their experiment's error and our second error is the systematic error from using our best value.

⁴ AHMED 00B reports $0.0182 \pm 0.0037 \pm 0.0025$ from a measurement of $[\Gamma(B^0 \rightarrow D^*(2010)^- D_s^{*+}) / \Gamma_{\text{total}}] \times [B(D_s^+ \rightarrow \phi \pi^+)]$ assuming $B(D_s^+ \rightarrow \phi \pi^+) = 0.036$, which we rescale to our best value $B(D_s^+ \rightarrow \phi \pi^+) = (4.5 \pm 0.4) \times 10^{-2}$. Our first error is their experiment's error and our second error is the systematic error from using our best value.

⁵ ALBRECHT 92G reports $0.026 \pm 0.014 \pm 0.006$ from a measurement of $[\Gamma(B^0 \rightarrow D^*(2010)^- D_s^{*+}) / \Gamma_{\text{total}}] \times [B(D_s^+ \rightarrow \phi \pi^+)]$ assuming $B(D_s^+ \rightarrow \phi \pi^+) = 0.027$, which we rescale to our best value $B(D_s^+ \rightarrow \phi \pi^+) = (4.5 \pm 0.4) \times 10^{-2}$. Our first error is their experiment's error and our second error is the systematic error from using our best value. Assumes PDG 1990 D^+ and $D^*(2010)^+$ branching ratios, e.g., $B(D^0 \rightarrow K^- \pi^+) = 3.71 \pm 0.25\%$, $B(D^+ \rightarrow K^- 2\pi^+) = 7.1 \pm 1.0\%$, and $B(D^*(2010)^+ \rightarrow D^0 \pi^+) = 55 \pm 4\%$.

⁶ GIBAUT 96 reports $0.0203 \pm 0.0050 \pm 0.0036$ from a measurement of $[\Gamma(B^0 \rightarrow D^*(2010)^- D_s^{*+}) / \Gamma_{\text{total}}] \times [B(D_s^+ \rightarrow \phi \pi^+)]$ assuming $B(D_s^+ \rightarrow \phi \pi^+) = 0.035$, which we rescale to our best value $B(D_s^+ \rightarrow \phi \pi^+) = (4.5 \pm 0.4) \times 10^{-2}$. Our first error is their experiment's error and our second error is the systematic error from using our best value.

$\Gamma(D^*(2010)^- D_s^{*+}) / \Gamma(D^*(2010)^- D_s^+)$ $\Gamma_{97} / \Gamma_{88}$

VALUE	DOCUMENT ID	TECN	COMMENT
2.19 ± 0.08 ± 0.01	¹ AAIJ	21s	LHCB pp at 13 TeV

¹ AAIJ 21s reports $[\Gamma(B^0 \rightarrow D^*(2010)^- D_s^{*+}) / \Gamma(B^0 \rightarrow D^*(2010)^- D_s^+)] \times [B(D_s^+ \rightarrow D_s^+ \gamma)] = 2.045 \pm 0.022 \pm 0.071$ which we divide by our best value $B(D_s^+ \rightarrow D_s^+ \gamma) = (93.6 \pm 0.4) \times 10^{-2}$. Our first error is their experiment's error and our second error is the systematic error from using our best value.

$[\Gamma(D^*(2010)^- D_s^+) + \Gamma(D^*(2010)^- D_s^{*+})] / \Gamma_{\text{total}}$ $(\Gamma_{88} + \Gamma_{97}) / \Gamma$

VALUE (units 10^{-2})	EVTS	DOCUMENT ID	TECN	COMMENT
2.5 ± 0.4 OUR AVERAGE				
2.40 ± 0.35 ± 0.22		¹ AUBERT	03i	BABR $e^+ e^- \rightarrow \Upsilon(4S)$
3.3 ± 0.9 ± 0.3	22	² BORTOLETTO	90	CLEO $e^+ e^- \rightarrow \Upsilon(4S)$

¹ AUBERT 03i reports $(3.00 \pm 0.19 \pm 0.39) \times 10^{-2}$ from a measurement of $[\Gamma(B^0 \rightarrow D^*(2010)^- D_s^+) + \Gamma(B^0 \rightarrow D^*(2010)^- D_s^{*+})] / \Gamma_{\text{total}}] \times [B(D_s^+ \rightarrow \phi \pi^+)]$ assuming $B(D_s^+ \rightarrow \phi \pi^+) = 0.036$, which we rescale to our best value $B(D_s^+ \rightarrow \phi \pi^+) = (4.5 \pm 0.4) \times 10^{-2}$. Our first error is their experiment's error and our second error is the systematic error from using our best value.

² BORTOLETTO 90 reports $(7.5 \pm 2.0) \times 10^{-2}$ from a measurement of $[\Gamma(B^0 \rightarrow D^*(2010)^- D_s^+) + \Gamma(B^0 \rightarrow D^*(2010)^- D_s^{*+})] / \Gamma_{\text{total}}] \times [B(D_s^+ \rightarrow \phi \pi^+)]$ assuming $B(D_s^+ \rightarrow \phi \pi^+) = 0.02$, which we rescale to our best value $B(D_s^+ \rightarrow \phi \pi^+) = (4.5 \pm 0.4) \times 10^{-2}$. Our first error is their experiment's error and our second error is the systematic error from using our best value.

$\Gamma(D_{s0}(2317)^- K^+, D_{s0}^- \rightarrow D_s^- \pi^0) / \Gamma_{\text{total}}$ Γ_{98} / Γ

VALUE (units 10^{-5})	DOCUMENT ID	TECN	COMMENT
4.2 ± 1.4 ± 0.4	¹ DRUTSKOY	05	BELL $e^+ e^- \rightarrow \Upsilon(4S)$

¹ DRUTSKOY 05 reports $(5.3^{+1.5}_{-1.3} \pm 1.6) \times 10^{-5}$ from a measurement of $[\Gamma(B^0 \rightarrow D_{s0}(2317)^- K^+, D_{s0}^- \rightarrow D_s^- \pi^0) / \Gamma_{\text{total}}] \times [B(D_s^+ \rightarrow \phi \pi^+)]$ assuming $B(D_s^+ \rightarrow \phi \pi^+) = 0.036 \pm 0.009$, which we rescale to our best value $B(D_s^+ \rightarrow \phi \pi^+) = (4.5 \pm 0.4) \times 10^{-2}$. Our first error is their experiment's error and our second error is the systematic error from using our best value.

$\Gamma(D_{s0}(2317)^- \pi^+, D_{s0}^- \rightarrow D_s^- \pi^0) / \Gamma_{\text{total}}$ Γ_{99} / Γ

VALUE (units 10^{-5})	CL%	DOCUMENT ID	TECN	COMMENT
<2.5	90	¹ DRUTSKOY	05	BELL $e^+ e^- \rightarrow \Upsilon(4S)$

¹ Assumes equal production of B^+ and B^0 at the $\Upsilon(4S)$.

$\Gamma(D_{sJ}(2457)^- K^+, D_{sJ}^- \rightarrow D_s^- \pi^0) / \Gamma_{\text{total}}$ Γ_{100} / Γ

VALUE (units 10^{-5})	CL%	DOCUMENT ID	TECN	COMMENT
<0.94	90	¹ DRUTSKOY	05	BELL $e^+ e^- \rightarrow \Upsilon(4S)$

¹ Assumes equal production of B^+ and B^0 at the $\Upsilon(4S)$.

Meson Particle Listings

 B^0 $\Gamma(D_{sJ}(2457)^- \pi^+, D_{sJ}^- \rightarrow D_s^- \pi^0)/\Gamma_{\text{total}}$ Γ_{101}/Γ

VALUE (units 10^{-5})	CL%	DOCUMENT ID	TECN	COMMENT
<0.40	90	¹ DRUTSKOY 05	BELL	$e^+ e^- \rightarrow \Upsilon(4S)$

¹ Assumes equal production of B^+ and B^0 at the $\Upsilon(4S)$. $\Gamma(D_s^- D_s^+)/\Gamma_{\text{total}}$ Γ_{102}/Γ

VALUE	CL%	DOCUMENT ID	TECN	COMMENT
< 3.6 $\times 10^{-5}$	90	¹ ZUPANC 07	BELL	$e^+ e^- \rightarrow \Upsilon(4S)$

• • • We do not use the following data for averages, fits, limits, etc. • • •

<10 $\times 10^{-5}$	90	¹ AUBERT,BE 05F	BABR	$e^+ e^- \rightarrow \Upsilon(4S)$
---	----	----------------------------	------	------------------------------------

¹ Assumes equal production of B^+ and B^0 at the $\Upsilon(4S)$. $\Gamma(D_s^{*-} D_s^+)/\Gamma_{\text{total}}$ Γ_{103}/Γ

VALUE	CL%	DOCUMENT ID	TECN	COMMENT
<1.3 $\times 10^{-4}$	90	¹ AUBERT,BE 05F	BABR	$e^+ e^- \rightarrow \Upsilon(4S)$

¹ Assumes equal production of B^+ and B^0 at the $\Upsilon(4S)$. $\Gamma(D_s^{*-} D_s^{*+})/\Gamma_{\text{total}}$ Γ_{104}/Γ

VALUE	CL%	DOCUMENT ID	TECN	COMMENT
<2.4 $\times 10^{-4}$	90	¹ AUBERT,BE 05F	BABR	$e^+ e^- \rightarrow \Upsilon(4S)$

¹ Assumes equal production of B^+ and B^0 at the $\Upsilon(4S)$. $\Gamma(D_{s0}^*(2317)^+ D^-, D_{s0}^{*+} \rightarrow D_s^+ \pi^0)/\Gamma_{\text{total}}$ Γ_{105}/Γ

VALUE (units 10^{-3})	DOCUMENT ID	TECN	COMMENT
1.06 \pm 0.16 OUR AVERAGE	Error includes scale factor of 1.1.		

1.00 $^{+0.16}_{-0.15} \pm 0.03$	^{1,2} CHOI 15A	BELL	$e^+ e^- \rightarrow \Upsilon(4S)$
----------------------------------	-------------------------	------	------------------------------------

1.4 $^{+0.5}_{-0.4} \pm 0.1$	^{2,3} AUBERT,B 04s	BABR	$e^+ e^- \rightarrow \Upsilon(4S)$
------------------------------	-----------------------------	------	------------------------------------

• • • We do not use the following data for averages, fits, limits, etc. • • •

0.69 $^{+0.29}_{-0.24} \pm 0.06$	^{2,4} KROKOVNY 03B	BELL	Repl. by CHOI 15A
----------------------------------	-----------------------------	------	-------------------

¹ CHOI 15A reports $(10.2 \pm 1.3 \pm 1.0 \pm 0.4) \times 10^{-4}$ from a measurement of $[\Gamma(B^0 \rightarrow D_{s0}^*(2317)^+ D^-, D_{s0}^{*+} \rightarrow D_s^+ \pi^0)/\Gamma_{\text{total}}] \times [B(D_s^+ \rightarrow K^+ K^- \pi^+)] \times [B(D^+ \rightarrow K^- 2\pi^+)]$ assuming $B(D_s^+ \rightarrow K^+ K^- \pi^+) = (5.39 \pm 0.21) \times 10^{-2}$, $B(D^+ \rightarrow K^- 2\pi^+) = (9.13 \pm 0.19) \times 10^{-2}$, which we rescale to our best values $B(D_s^+ \rightarrow K^+ K^- \pi^+) = (5.37 \pm 0.10) \times 10^{-2}$, $B(D^+ \rightarrow K^- 2\pi^+) = (9.38 \pm 0.16) \times 10^{-2}$. Our first error is their experiment's error and our second error is the systematic error from using our best values.

² Assumes equal production of B^+ and B^0 at the $\Upsilon(4S)$.

³ AUBERT,B 04s reports $(1.8 \pm 0.4 \pm 0.7) \times 10^{-3}$ from a measurement of $[\Gamma(B^0 \rightarrow D_{s0}^*(2317)^+ D^-, D_{s0}^{*+} \rightarrow D_s^+ \pi^0)/\Gamma_{\text{total}}] \times [B(D_s^+ \rightarrow \phi \pi^+)]$ assuming $B(D_s^+ \rightarrow \phi \pi^+) = 0.036 \pm 0.009$, which we rescale to our best value $B(D_s^+ \rightarrow \phi \pi^+) = (4.5 \pm 0.4) \times 10^{-2}$. Our first error is their experiment's error and our second error is the systematic error from using our best value.

⁴ KROKOVNY 03B reports $(0.86 \pm 0.33 \pm 0.26) \times 10^{-3}$ from a measurement of $[\Gamma(B^0 \rightarrow D_{s0}^*(2317)^+ D^-, D_{s0}^{*+} \rightarrow D_s^+ \pi^0)/\Gamma_{\text{total}}] \times [B(D_s^+ \rightarrow \phi \pi^+)]$ assuming $B(D_s^+ \rightarrow \phi \pi^+) = 0.036 \pm 0.009$, which we rescale to our best value $B(D_s^+ \rightarrow \phi \pi^+) = (4.5 \pm 0.4) \times 10^{-2}$. Our first error is their experiment's error and our second error is the systematic error from using our best value.

 $\Gamma(D_{s0}(2317)^+ D^-, D_{s0}^+ \rightarrow D_s^{*+} \gamma)/\Gamma_{\text{total}}$ Γ_{106}/Γ

VALUE (units 10^{-3})	CL%	DOCUMENT ID	TECN	COMMENT
<0.95	90	¹ KROKOVNY 03B	BELL	$e^+ e^- \rightarrow \Upsilon(4S)$

¹ Assumes equal production of B^+ and B^0 at the $\Upsilon(4S)$. $\Gamma(D_{s0}(2317)^+ D^*(2010)^-, D_{s0}^+ \rightarrow D_s^+ \pi^0)/\Gamma_{\text{total}}$ Γ_{107}/Γ

VALUE (units 10^{-3})	DOCUMENT ID	TECN	COMMENT
1.5 \pm 0.4 $^{+0.5}_{-0.4}$	¹ AUBERT,B 04s	BABR	$e^+ e^- \rightarrow \Upsilon(4S)$

¹ Assumes equal production of B^+ and B^0 at the $\Upsilon(4S)$. $\Gamma(D_{sJ}(2457)^+ D^-)/\Gamma_{\text{total}}$ Γ_{108}/Γ

VALUE (units 10^{-3})	DOCUMENT ID	TECN	COMMENT
3.5 \pm 1.1 OUR AVERAGE			

2.6 \pm 1.5 \pm 0.7	¹ AUBERT 06N	BABR	$e^+ e^- \rightarrow \Upsilon(4S)$
-------------------------	-------------------------	------	------------------------------------

4.8 $^{+2.2}_{-1.6} \pm 1.1$	^{2,3} AUBERT,B 04s	BABR	$e^+ e^- \rightarrow \Upsilon(4S)$
------------------------------	-----------------------------	------	------------------------------------

3.9 $^{+1.5}_{-1.3} \pm 0.9$	^{2,4} KROKOVNY 03B	BELL	$e^+ e^- \rightarrow \Upsilon(4S)$
------------------------------	-----------------------------	------	------------------------------------

¹ Uses a missing-mass method in the events that one of the B mesons is fully reconstructed.² Assumes equal production of B^+ and B^0 at the $\Upsilon(4S)$.

³ AUBERT,B 04s reports $[\Gamma(B^0 \rightarrow D_{sJ}(2457)^+ D^-)/\Gamma_{\text{total}}] \times [B(D_{s1}(2460)^+ \rightarrow D_s^+ \pi^0)] = (2.3 \pm 1.0 \pm 0.3) \times 10^{-3}$ which we divide by our best value $B(D_{s1}(2460)^+ \rightarrow D_s^+ \pi^0) = (48 \pm 11) \times 10^{-2}$. Our first error is their experiment's error and our second error is the systematic error from using our best value.

⁴ KROKOVNY 03B reports $[\Gamma(B^0 \rightarrow D_{sJ}(2457)^+ D^-)/\Gamma_{\text{total}}] \times [B(D_{s1}(2460)^+ \rightarrow D_s^+ \pi^0)] = (1.9 \pm 0.7 \pm 0.2) \times 10^{-3}$ which we divide by our best value $B(D_{s1}(2460)^+ \rightarrow D_s^+ \pi^0) = (48 \pm 11) \times 10^{-2}$. Our first error is their experiment's error and our second error is the systematic error from using our best value.

 $\Gamma(D_{sJ}(2457)^+ D^-, D_{sJ}^+ \rightarrow D_s^+ \gamma)/\Gamma_{\text{total}}$ Γ_{109}/Γ

VALUE (units 10^{-3})	DOCUMENT ID	TECN	COMMENT
0.65 $^{+0.17}_{-0.14}$ OUR AVERAGE			

0.64 $^{+0.24}_{-0.16} \pm 0.06$	^{1,2} AUBERT,B 04s	BABR	$e^+ e^- \rightarrow \Upsilon(4S)$
----------------------------------	-----------------------------	------	------------------------------------

0.66 $^{+0.21}_{-0.19} \pm 0.06$	^{1,3} KROKOVNY 03B	BELL	$e^+ e^- \rightarrow \Upsilon(4S)$
----------------------------------	-----------------------------	------	------------------------------------

¹ Assumes equal production of B^+ and B^0 at the $\Upsilon(4S)$.

² AUBERT,B 04s reports $(0.8 \pm 0.2 \pm 0.3) \times 10^{-3}$ from a measurement of $[\Gamma(B^0 \rightarrow D_{sJ}(2457)^+ D^-, D_{sJ}^+ \rightarrow D_s^+ \gamma)/\Gamma_{\text{total}}] \times [B(D_s^+ \rightarrow \phi \pi^+)]$ assuming $B(D_s^+ \rightarrow \phi \pi^+) = 0.036 \pm 0.009$, which we rescale to our best value $B(D_s^+ \rightarrow \phi \pi^+) = (4.5 \pm 0.4) \times 10^{-2}$. Our first error is their experiment's error and our second error is the systematic error from using our best value.

³ KROKOVNY 03B reports $(0.82 \pm 0.22 \pm 0.25) \times 10^{-3}$ from a measurement of $[\Gamma(B^0 \rightarrow D_{sJ}(2457)^+ D^-, D_{sJ}^+ \rightarrow D_s^+ \gamma)/\Gamma_{\text{total}}] \times [B(D_s^+ \rightarrow \phi \pi^+)]$ assuming $B(D_s^+ \rightarrow \phi \pi^+) = 0.036 \pm 0.009$, which we rescale to our best value $B(D_s^+ \rightarrow \phi \pi^+) = (4.5 \pm 0.4) \times 10^{-2}$. Our first error is their experiment's error and our second error is the systematic error from using our best value.

 $\Gamma(D_{sJ}(2457)^+ D^-, D_{sJ}^+ \rightarrow D_s^{*+} \gamma)/\Gamma_{\text{total}}$ Γ_{110}/Γ

VALUE (units 10^{-3})	CL%	DOCUMENT ID	TECN	COMMENT
<0.60	90	¹ KROKOVNY 03B	BELL	$e^+ e^- \rightarrow \Upsilon(4S)$

¹ Assumes equal production of B^+ and B^0 at the $\Upsilon(4S)$. $\Gamma(D_{sJ}(2457)^+ D^-, D_{sJ}^+ \rightarrow D_s^+ \pi^+ \pi^-)/\Gamma_{\text{total}}$ Γ_{111}/Γ

VALUE (units 10^{-3})	CL%	DOCUMENT ID	TECN	COMMENT
<0.20	90	¹ KROKOVNY 03B	BELL	$e^+ e^- \rightarrow \Upsilon(4S)$

¹ Assumes equal production of B^+ and B^0 at the $\Upsilon(4S)$. $\Gamma(D_{sJ}(2457)^+ D^-, D_{sJ}^+ \rightarrow D_s^+ \pi^0)/\Gamma_{\text{total}}$ Γ_{112}/Γ

VALUE (units 10^{-3})	CL%	DOCUMENT ID	TECN	COMMENT
<0.36	90	¹ KROKOVNY 03B	BELL	$e^+ e^- \rightarrow \Upsilon(4S)$

¹ Assumes equal production of B^+ and B^0 at the $\Upsilon(4S)$. $\Gamma(D^*(2010)^- D_{sJ}(2457)^+)/\Gamma_{\text{total}}$ Γ_{113}/Γ

VALUE (units 10^{-3})	DOCUMENT ID	TECN	COMMENT
9.3 \pm 2.2 OUR AVERAGE			

8.8 \pm 2.0 \pm 1.4	¹ AUBERT 06N	BABR	$e^+ e^- \rightarrow \Upsilon(4S)$
-------------------------	-------------------------	------	------------------------------------

11 $^{+5}_{-4} \pm 3$	^{2,3} AUBERT,B 04s	BABR	$e^+ e^- \rightarrow \Upsilon(4S)$
-----------------------	-----------------------------	------	------------------------------------

¹ Uses a missing-mass method in the events that one of the B mesons is fully reconstructed.

² AUBERT,B 04s reports $[\Gamma(B^0 \rightarrow D^*(2010)^- D_{sJ}(2457)^+)/\Gamma_{\text{total}}] \times [B(D_{s1}(2460)^+ \rightarrow D_s^+ \pi^0)] = (5.5 \pm 1.2 \pm 2.2) \times 10^{-3}$ which we divide by our best value $B(D_{s1}(2460)^+ \rightarrow D_s^+ \pi^0) = (48 \pm 11) \times 10^{-2}$. Our first error is their experiment's error and our second error is the systematic error from using our best value.

³ Assumes equal production of B^+ and B^0 at the $\Upsilon(4S)$. $\Gamma(D_{sJ}(2457)^+ D^*(2010), D_{sJ}^+ \rightarrow D_s^+ \gamma)/\Gamma_{\text{total}}$ Γ_{114}/Γ

VALUE (units 10^{-3})	DOCUMENT ID	TECN	COMMENT
2.3 \pm 0.3 $^{+0.9}_{-0.6}$	¹ AUBERT,B 04s	BABR	$e^+ e^- \rightarrow \Upsilon(4S)$

¹ Assumes equal production of B^+ and B^0 at the $\Upsilon(4S)$. $[\Gamma(D^- D_{s1}(2536)^+, D_{s1}^+ \rightarrow D^{*0} K^+) + \Gamma(D^{*+} K^0)]/\Gamma_{\text{total}}$ $\Gamma_{115}/\Gamma = (\Gamma_{116} + \Gamma_{117})/\Gamma$

VALUE (units 10^{-4})	DOCUMENT ID	TECN	COMMENT
2.75 \pm 0.62 \pm 0.36	^{1,2} AUSHEV 11	BELL	$e^+ e^- \rightarrow \Upsilon(4S)$

¹ Uses $\Gamma(D^*(2007)^0 \rightarrow D^0 \pi^0) / \Gamma(D^*(2007)^0 \rightarrow D^0 \gamma) = 1.74 \pm 0.13$ and $\Gamma(D_{s1}(2536)^+ \rightarrow D^*(2007)^0 K^+) / \Gamma(D_{s1}(2536)^+ \rightarrow D^*(2010)^+ K^0) = 1.36 \pm 0.2$.

² Assumes equal production of B^+ and B^0 at the $\Upsilon(4S)$. $\Gamma(D^- D_{s1}(2536)^+, D_{s1}^+ \rightarrow D^{*0} K^+)/\Gamma_{\text{total}}$ Γ_{116}/Γ

VALUE (units 10^{-4})	CL%	DOCUMENT ID	TECN	COMMENT
1.71 \pm 0.48 \pm 0.32		¹ AUBERT 08B	BABR	$e^+ e^- \rightarrow \Upsilon(4S)$

• • • We do not use the following data for averages, fits, limits, etc. • • •

<5	90	AUBERT 03X	BABR	Repl. by AUBERT 08B
----	----	------------	------	---------------------

¹ Assumes equal production of B^+ and B^0 at the $\Upsilon(4S)$. $\Gamma(D^- D_{s1}(2536)^+, D_{s1}^+ \rightarrow D^{*+} K^0)/\Gamma_{\text{total}}$ Γ_{117}/Γ

VALUE (units 10^{-4})	DOCUMENT ID	TECN	COMMENT
2.61 \pm 1.03 \pm 0.31	¹ AUBERT 08B	BABR	$e^+ e^- \rightarrow \Upsilon(4S)$

¹ Assumes equal production of B^+ and B^0 at the $\Upsilon(4S)$.

$$\frac{\Gamma(D^*(2010) - D_{s1}(2536)^+, D_{s1}^+ \rightarrow D^{*0} K^+) + \Gamma(D^{*+} K^0)}{\Gamma_{118}/\Gamma = (\Gamma_{119} + \Gamma_{120})/\Gamma}$$

VALUE (units 10^{-4})	DOCUMENT ID	TECN	COMMENT
5.01 ± 1.21 ± 0.70	1,2 AUSHEV	11	BELL $e^+ e^- \rightarrow \Upsilon(4S)$

¹ Uses $\Gamma(D^*(2007)^0 \rightarrow D^0 \pi^0) / \Gamma(D^*(2007)^0 \rightarrow D^0 \gamma) = 1.74 \pm 0.13$ and $\Gamma(D_{s1}(2536)^+ \rightarrow D^*(2007)^0 K^+) / \Gamma(D_{s1}(2536)^+ \rightarrow D^*(2010)^+ K^0) = 1.36 \pm 0.2$.

² Assumes equal production of B^+ and B^0 at the $\Upsilon(4S)$.

$$\Gamma(D^*(2010) - D_{s1}(2536)^+, D_{s1}^+ \rightarrow D^{*0} K^+)/\Gamma_{119}/\Gamma$$

VALUE (units 10^{-4})	CL%	DOCUMENT ID	TECN	COMMENT
3.32 ± 0.88 ± 0.66		1 AUBERT	08B	BABR $e^+ e^- \rightarrow \Upsilon(4S)$

• • • We do not use the following data for averages, fits, limits, etc. • • •

<7	90	AUBERT	03X	BABR Repl. by AUBERT 08B
----	----	--------	-----	--------------------------

¹ Assumes equal production of B^+ and B^0 at the $\Upsilon(4S)$.

$$\Gamma(D^* - D_{s1}(2536)^+, D_{s1}^+ \rightarrow D^{*+} K^0)/\Gamma_{120}/\Gamma$$

VALUE (units 10^{-4})	DOCUMENT ID	TECN	COMMENT
5.00 ± 1.51 ± 0.67	1 AUBERT	08B	BABR $e^+ e^- \rightarrow \Upsilon(4S)$

¹ Assumes equal production of B^+ and B^0 at the $\Upsilon(4S)$.

$$\Gamma(D^- D_{sJ}(2573)^+, D_{sJ}^+ \rightarrow D^0 K^+)/\Gamma_{121}/\Gamma$$

VALUE (units 10^{-5})	CL%	DOCUMENT ID	TECN	COMMENT
3.4 ± 1.7 ± 0.5		1 LEES	15C	BABR $e^+ e^- \rightarrow \Upsilon(4S)$

• • • We do not use the following data for averages, fits, limits, etc. • • •

<10	90	AUBERT	03X	BABR $e^+ e^- \rightarrow \Upsilon(4S)$
-----	----	--------	-----	---

¹ Assumes equal production of B^+ and B^0 at the $\Upsilon(4S)$.

$$\Gamma(D^*(2010) - D_{sJ}(2573)^+, D_{sJ}^+ \rightarrow D^0 K^+)/\Gamma_{122}/\Gamma$$

VALUE (units 10^{-4})	CL%	DOCUMENT ID	TECN	COMMENT	
<2		90	AUBERT	03X	BABR $e^+ e^- \rightarrow \Upsilon(4S)$

$$\Gamma(D^- D_{sJ}(2700)^+, D_{sJ}^+ \rightarrow D^0 K^+)/\Gamma_{123}/\Gamma$$

VALUE (units 10^{-4})	DOCUMENT ID	TECN	COMMENT
7.14 ± 0.96 ± 0.69	1 LEES	15C	BABR $e^+ e^- \rightarrow \Upsilon(4S)$

¹ Assumes equal production of B^+ and B^0 at the $\Upsilon(4S)$.

$$\Gamma(D^+ \pi^-)/\Gamma_{124}/\Gamma$$

VALUE (units 10^{-7})	DOCUMENT ID	TECN	COMMENT
7.3 ± 1.2 ± 0.2	1,2 DAS	10	BELL $e^+ e^- \rightarrow \Upsilon(4S)$

¹ DAS 10 reports $[\Gamma(B^0 \rightarrow D^+ \pi^-)/\Gamma_{\text{total}}] / [B(B^0 \rightarrow D^- \pi^+)] = (2.92 \pm 0.38 \pm 0.31) \times 10^{-4}$ which we multiply by our best value $B(B^0 \rightarrow D^- \pi^+) = (2.51 \pm 0.08) \times 10^{-3}$. Our first error is their experiment's error and our second error is the systematic error from using our best value.

² Derived using $\tan(\theta_C) f_D/f_{D_s} \sqrt{B(B^0 \rightarrow D_s^+ \pi^-)/B(B^0 \rightarrow D^- \pi^+)}$ by assuming the flavor SU(3) symmetry, where θ_C is the Cabibbo angle, f_D (f_{D_s}) is the D (D_s) meson decay constant.

$$\Gamma(D_s^+ \pi^-)/\Gamma_{125}/\Gamma$$

VALUE (units 10^{-6})	CL%	DOCUMENT ID	TECN	COMMENT
20.3 ± 1.8 OUR FIT				
21.6 ± 2.6 OUR AVERAGE				

19.9 ± 2.6 ± 1.8	1 DAS	10	BELL	$e^+ e^- \rightarrow \Upsilon(4S)$
25 ± 4 ± 2	1 AUBERT	08AJ	BABR	$e^+ e^- \rightarrow \Upsilon(4S)$

• • • We do not use the following data for averages, fits, limits, etc. • • •

14.0 ± 3.5 ± 1.3	2 AUBERT	07K	BABR	Repl. by AUBERT 08AJ
------------------	----------	-----	------	----------------------

25 ± 9 ± 2	3 AUBERT	03D	BABR	Repl. by AUBERT 07K
------------	----------	-----	------	---------------------

19 ± 9 ± 2	4 KROKOVNY	02	BELL	Repl. by DAS 10
------------	------------	----	------	-----------------

< 220	90	5 ALEXANDER	93B	CLE2 $e^+ e^- \rightarrow \Upsilon(4S)$
-------	----	-------------	-----	---

< 1300	90	6 BORTOLETTO	090	CLEO $e^+ e^- \rightarrow \Upsilon(4S)$
--------	----	--------------	-----	---

¹ Assumes equal production of B^+ and B^0 at the $\Upsilon(4S)$.

² AUBERT 07K reports $[\Gamma(B^0 \rightarrow D_s^+ \pi^-)/\Gamma_{\text{total}}] \times [B(D_s^+ \rightarrow \phi \pi^+)] = (0.63 \pm 0.15 \pm 0.05) \times 10^{-6}$ which we divide by our best value $B(D_s^+ \rightarrow \phi \pi^+) = (4.5 \pm 0.4) \times 10^{-2}$. Our first error is their experiment's error and our second error is the systematic error from using our best value.

³ AUBERT 03D reports $[\Gamma(B^0 \rightarrow D_s^+ \pi^-)/\Gamma_{\text{total}}] \times [B(D_s^+ \rightarrow \phi \pi^+)] = (1.13 \pm 0.33 \pm 0.21) \times 10^{-6}$ which we divide by our best value $B(D_s^+ \rightarrow \phi \pi^+) = (4.5 \pm 0.4) \times 10^{-2}$. Our first error is their experiment's error and our second error is the systematic error from using our best value.

⁴ KROKOVNY 02 reports $[\Gamma(B^0 \rightarrow D_s^+ \pi^-)/\Gamma_{\text{total}}] \times [B(D_s^+ \rightarrow \phi \pi^+)] = (0.86^{+0.37}_{-0.30} \pm 0.11) \times 10^{-6}$ which we divide by our best value $B(D_s^+ \rightarrow \phi \pi^+) = (4.5 \pm 0.4) \times 10^{-2}$. Our first error is their experiment's error and our second error is the systematic error from using our best value.

⁵ ALEXANDER 93B reports $< 270 \times 10^{-6}$ from a measurement of $[\Gamma(B^0 \rightarrow D_s^+ \pi^-)/\Gamma_{\text{total}}] \times [B(D_s^+ \rightarrow \phi \pi^+)]$ assuming $B(D_s^+ \rightarrow \phi \pi^+) = 0.037$, which we rescale to our best value $B(D_s^+ \rightarrow \phi \pi^+) = 4.5 \times 10^{-2}$.

⁶ BORTOLETTO 90 assume $B(D_s \rightarrow \phi \pi^+) = 2\%$.

$$\frac{\Gamma(D_s^+ \pi^-) + \Gamma(D_s^- K^+)}{\Gamma_{\text{total}}} / \Gamma_{125} + \Gamma_{135} / \Gamma$$

VALUE	CL%	DOCUMENT ID	TECN	COMMENT
< 1.0 × 10⁻³		90	1 ALBRECHT	93E ARG $e^+ e^- \rightarrow \Upsilon(4S)$

¹ ALBRECHT 93E reports $< 1.7 \times 10^{-3}$ from a measurement of $[\Gamma(B^0 \rightarrow D_s^+ \pi^-) + \Gamma(B^0 \rightarrow D_s^- K^+)]/\Gamma_{\text{total}} \times [B(D_s^+ \rightarrow \phi \pi^+)]$ assuming $B(D_s^+ \rightarrow \phi \pi^+) = 0.027$, which we rescale to our best value $B(D_s^+ \rightarrow \phi \pi^+) = 4.5 \times 10^{-2}$.

$$\Gamma(D_s^+ \pi^-)/\Gamma(D^- \pi^+) \Gamma_{125}/\Gamma_{38}$$

VALUE (units 10^{-3})	DOCUMENT ID	TECN	COMMENT
8.1 ± 0.7 OUR FIT			
7.7 ± 0.7 ± 0.6	AAIJ	21W	LHCb pp at 7, 8, 13 TeV

$$\Gamma(D_s^{*+} \pi^-)/\Gamma_{126}/\Gamma$$

VALUE (units 10^{-5})	CL%	DOCUMENT ID	TECN	COMMENT
2.1 ± 0.4 OUR AVERAGE				Error includes scale factor of 1.4.

1.75 ± 0.34 ± 0.20	1 JOSHI	10	BELL	$e^+ e^- \rightarrow \Upsilon(4S)$
--------------------	---------	----	------	------------------------------------

2.6 ^{+0.5} _{-0.4} ± 0.2	1 AUBERT	08AJ	BABR	$e^+ e^- \rightarrow \Upsilon(4S)$
---	----------	------	------	------------------------------------

• • • We do not use the following data for averages, fits, limits, etc. • • •

2.9 ± 0.7 ± 0.3	2 AUBERT	07K	BABR	Repl. by AUBERT 08AJ
-----------------	----------	-----	------	----------------------

< 4.1	90	AUBERT	03D	BABR Repl. by AUBERT 07K
-------	----	--------	-----	--------------------------

< 40	90	3 ALEXANDER	93B	CLE2 $e^+ e^- \rightarrow \Upsilon(4S)$
------	----	-------------	-----	---

¹ Assumes equal production of B^+ and B^0 at the $\Upsilon(4S)$.

² AUBERT 07K reports $[\Gamma(B^0 \rightarrow D_s^{*+} \pi^-)/\Gamma_{\text{total}}] \times [B(D_s^+ \rightarrow \phi \pi^+)] = (1.32 \pm 0.27 \pm 0.15) \times 10^{-6}$ which we divide by our best value $B(D_s^+ \rightarrow \phi \pi^+) = (4.5 \pm 0.4) \times 10^{-2}$. Our first error is their experiment's error and our second error is the systematic error from using our best value.

³ ALEXANDER 93B reports $< 44 \times 10^{-5}$ from a measurement of $[\Gamma(B^0 \rightarrow D_s^{*+} \pi^-)/\Gamma_{\text{total}}] \times [B(D_s^+ \rightarrow \phi \pi^+)]$ assuming $B(D_s^+ \rightarrow \phi \pi^+) = 0.037$, which we rescale to our best value $B(D_s^+ \rightarrow \phi \pi^+) = 4.5 \times 10^{-2}$.

$$\frac{\Gamma(D_s^{*+} \pi^-) + \Gamma(D_s^{*+} K^+)}{\Gamma_{\text{total}}} / \Gamma_{126} + \Gamma_{136} / \Gamma$$

VALUE	CL%	DOCUMENT ID	TECN	COMMENT
< 7 × 10⁻⁴		90	1 ALBRECHT	93E ARG $e^+ e^- \rightarrow \Upsilon(4S)$

¹ ALBRECHT 93E reports $< 1.2 \times 10^{-3}$ from a measurement of $[\Gamma(B^0 \rightarrow D_s^{*+} \pi^-) + \Gamma(B^0 \rightarrow D_s^{*+} K^+)]/\Gamma_{\text{total}} \times [B(D_s^+ \rightarrow \phi \pi^+)]$ assuming $B(D_s^+ \rightarrow \phi \pi^+) = 0.027$, which we rescale to our best value $B(D_s^+ \rightarrow \phi \pi^+) = 4.5 \times 10^{-2}$.

$$\Gamma(D_s^+ \rho^-)/\Gamma_{127}/\Gamma$$

VALUE (units 10^{-9})	CL%	DOCUMENT ID	TECN	COMMENT	
< 2.4		90	1 AUBERT	08AJ	BABR $e^+ e^- \rightarrow \Upsilon(4S)$

• • • We do not use the following data for averages, fits, limits, etc. • • •

< 130	90	2 ALBRECHT	93E	ARG $e^+ e^- \rightarrow \Upsilon(4S)$
-------	----	------------	-----	--

< 50	90	3 ALEXANDER	93B	CLE2 $e^+ e^- \rightarrow \Upsilon(4S)$
------	----	-------------	-----	---

¹ Assumes equal production of B^+ and B^0 at the $\Upsilon(4S)$.

² ALBRECHT 93E reports $< 2.2 \times 10^{-3}$ from a measurement of $[\Gamma(B^0 \rightarrow D_s^+ \rho^-)/\Gamma_{\text{total}}] \times [B(D_s^+ \rightarrow \phi \pi^+)]$ assuming $B(D_s^+ \rightarrow \phi \pi^+) = 0.027$, which we rescale to our best value $B(D_s^+ \rightarrow \phi \pi^+) = 4.5 \times 10^{-2}$.

³ ALEXANDER 93B reports $< 6.6 \times 10^{-4}$ from a measurement of $[\Gamma(B^0 \rightarrow D_s^+ \rho^-)/\Gamma_{\text{total}}] \times [B(D_s^+ \rightarrow \phi \pi^+)]$ assuming $B(D_s^+ \rightarrow \phi \pi^+) = 0.037$, which we rescale to our best value $B(D_s^+ \rightarrow \phi \pi^+) = 4.5 \times 10^{-2}$.

$$\Gamma(D_s^{*+} \rho^-)/\Gamma_{128}/\Gamma$$

VALUE (units 10^{-9})	CL%	DOCUMENT ID	TECN	COMMENT
4.1 ± 1.3 ± 0.4		1 AUBERT	08AJ	BABR $e^+ e^- \rightarrow \Upsilon(4S)$

• • • We do not use the following data for averages, fits, limits, etc. • • •

< 150	90	2 ALBRECHT	93E	ARG $e^+ e^- \rightarrow \Upsilon(4S)$
-------	----	------------	-----	--

< 60	90	3 ALEXANDER	93B	CLE2 $e^+ e^- \rightarrow \Upsilon(4S)$
------	----	-------------	-----	---

¹ Assumes equal production of B^+ and B^0 at the $\Upsilon(4S)$.

² ALBRECHT 93E reports $< 2.5 \times 10^{-3}$ from a measurement of $[\Gamma(B^0 \rightarrow D_s^{*+} \rho^-)/\Gamma_{\text{total}}] \times [B(D_s^+ \rightarrow \phi \pi^+)]$ assuming $B(D_s^+ \rightarrow \phi \pi^+) = 0.027$, which we rescale to our best value $B(D_s^+ \rightarrow \phi \pi^+) = 4.5 \times 10^{-2}$.

³ ALEXANDER 93B reports $< 7.4 \times 10^{-4}$ from a measurement of $[\Gamma(B^0 \rightarrow D_s^{*+} \rho^-)/\Gamma_{\text{total}}] \times [B(D_s^+ \rightarrow \phi \pi^+)]$ assuming $B(D_s^+ \rightarrow \phi \pi^+) = 0.037$, which we rescale to our best value $B(D_s^+ \rightarrow \phi \pi^+) = 4.5 \times 10^{-2}$.

$$\Gamma(D_s^+ \phi_0)/\Gamma_{129}/\Gamma$$

VALUE (units 10^{-9})	CL%	DOCUMENT ID	TECN	COMMENT	
< 1.9		90	1 AUBERT	06X	BABR $e^+ e^- \rightarrow \Upsilon(4S)$

¹ Assumes equal production of B^+ and B^0 at the $\Upsilon(4S)$.

Meson Particle Listings

 B^0

$\Gamma(D_s^{*+} a_0^-)/\Gamma_{\text{total}}$		Γ_{130}/Γ			
VALUE (units 10^{-5})	CL%	DOCUMENT ID	TECN	COMMENT	
<3.6	90	¹ AUBERT	06x	BABR	$e^+e^- \rightarrow \Upsilon(4S)$

¹ Assumes equal production of B^+ and B^0 at the $\Upsilon(4S)$.

$\Gamma(D_s^{*+} a_1(1260)^-)/\Gamma_{\text{total}}$		Γ_{131}/Γ			
VALUE	CL%	DOCUMENT ID	TECN	COMMENT	
<2.1 $\times 10^{-3}$	90	¹ ALBRECHT	93E	ARG	$e^+e^- \rightarrow \Upsilon(4S)$

¹ ALBRECHT 93E reports $< 3.5 \times 10^{-3}$ from a measurement of $[\Gamma(B^0 \rightarrow D_s^{*+} a_1(1260)^-)/\Gamma_{\text{total}}] \times [B(D_s^+ \rightarrow \phi\pi^+)]$ assuming $B(D_s^+ \rightarrow \phi\pi^+) = 0.027$, which we rescale to our best value $B(D_s^+ \rightarrow \phi\pi^+) = 4.5 \times 10^{-2}$.

$\Gamma(D_s^{*+} a_1(1260)^-)/\Gamma_{\text{total}}$		Γ_{132}/Γ			
VALUE	CL%	DOCUMENT ID	TECN	COMMENT	
<1.7 $\times 10^{-3}$	90	¹ ALBRECHT	93E	ARG	$e^+e^- \rightarrow \Upsilon(4S)$

¹ ALBRECHT 93E reports $< 2.9 \times 10^{-3}$ from a measurement of $[\Gamma(B^0 \rightarrow D_s^{*+} a_1(1260)^-)/\Gamma_{\text{total}}] \times [B(D_s^+ \rightarrow \phi\pi^+)]$ assuming $B(D_s^+ \rightarrow \phi\pi^+) = 0.027$, which we rescale to our best value $B(D_s^+ \rightarrow \phi\pi^+) = 4.5 \times 10^{-2}$.

$\Gamma(D_s^{*+} a_2^-)/\Gamma_{\text{total}}$		Γ_{133}/Γ			
VALUE (units 10^{-5})	CL%	DOCUMENT ID	TECN	COMMENT	
<1.9	90	¹ AUBERT	06x	BABR	$e^+e^- \rightarrow \Upsilon(4S)$

¹ Assumes equal production of B^+ and B^0 at the $\Upsilon(4S)$.

$\Gamma(D_s^{*+} a_2^-)/\Gamma_{\text{total}}$		Γ_{134}/Γ			
VALUE (units 10^{-5})	CL%	DOCUMENT ID	TECN	COMMENT	
<2.0	90	¹ AUBERT	06x	BABR	$e^+e^- \rightarrow \Upsilon(4S)$

¹ Assumes equal production of B^+ and B^0 at the $\Upsilon(4S)$.

$\Gamma(D_s^- K^+)/\Gamma_{\text{total}}$		Γ_{135}/Γ			
VALUE (units 10^{-6})	CL%	DOCUMENT ID	TECN	COMMENT	
27 \pm 5 OUR FIT		Error includes scale factor of 2.7.			
22 \pm 5 OUR AVERAGE		Error includes scale factor of 1.8.			
19.1 \pm 2.4 \pm 1.7		¹ DAS	10	BELL	$e^+e^- \rightarrow \Upsilon(4S)$
29 \pm 4 \pm 2		¹ AUBERT	08AJ	BABR	$e^+e^- \rightarrow \Upsilon(4S)$
• • • We do not use the following data for averages, fits, limits, etc. • • •					
27 \pm 5 \pm 2		² AUBERT	07K	BABR	Repl. by AUBERT 08AJ
26 \pm 10 \pm 2		³ AUBERT	03D	BABR	Repl. by AUBERT 07K
36 \pm 11 \pm 3		⁴ KROKOVNY	02	BELL	Repl. by DAS 10
< 190	90	⁵ ALEXANDER	93B	CLE2	$e^+e^- \rightarrow \Upsilon(4S)$
<1300	90	⁶ BORTOLETTO	090	CLEO	$e^+e^- \rightarrow \Upsilon(4S)$

¹ Assumes equal production of B^+ and B^0 at the $\Upsilon(4S)$.

² AUBERT 07K reports $[\Gamma(B^0 \rightarrow D_s^- K^+)/\Gamma_{\text{total}}] \times [B(D_s^+ \rightarrow \phi\pi^+)] = (1.21 \pm 0.17 \pm 0.11) \times 10^{-6}$ which we divide by our best value $B(D_s^+ \rightarrow \phi\pi^+) = (4.5 \pm 0.4) \times 10^{-2}$. Our first error is their experiment's error and our second error is the systematic error from using our best value.

³ AUBERT 03D reports $[\Gamma(B^0 \rightarrow D_s^- K^+)/\Gamma_{\text{total}}] \times [B(D_s^+ \rightarrow \phi\pi^+)] = (1.16 \pm 0.36 \pm 0.24) \times 10^{-6}$ which we divide by our best value $B(D_s^+ \rightarrow \phi\pi^+) = (4.5 \pm 0.4) \times 10^{-2}$. Our first error is their experiment's error and our second error is the systematic error from using our best value.

⁴ KROKOVNY 02 reports $[\Gamma(B^0 \rightarrow D_s^- K^+)/\Gamma_{\text{total}}] \times [B(D_s^+ \rightarrow \phi\pi^+)] = (1.61 \pm 0.45 \pm 0.21) $\times 10^{-6}$ which we divide by our best value $B(D_s^+ \rightarrow \phi\pi^+) = (4.5 \pm 0.4) \times 10^{-2}$. Our first error is their experiment's error and our second error is the systematic error from using our best value.$

⁵ ALEXANDER 93B reports $< 230 \times 10^{-6}$ from a measurement of $[\Gamma(B^0 \rightarrow D_s^- K^+)/\Gamma_{\text{total}}] \times [B(D_s^+ \rightarrow \phi\pi^+)]$ assuming $B(D_s^+ \rightarrow \phi\pi^+) = 0.037$, which we rescale to our best value $B(D_s^+ \rightarrow \phi\pi^+) = 4.5 \times 10^{-2}$.

⁶ BORTOLETTO 90 assume $B(D_s \rightarrow \phi\pi^+) = 2\%$.

$\Gamma(D_s^- K^+)/\Gamma(D^- \pi^+)$		Γ_{135}/Γ_{38}			
VALUE (units 10^{-2})	CL%	DOCUMENT ID	TECN	COMMENT	
1.09 \pm 0.19 OUR FIT		Error includes scale factor of 2.7.			
1.29 \pm 0.05 \pm 0.08		AAIJ	15AC	LHCb	pp at 7, 8 TeV

$\Gamma(D_s^{*-} K^+)/\Gamma_{\text{total}}$		Γ_{136}/Γ			
VALUE (units 10^{-5})	CL%	DOCUMENT ID	TECN	COMMENT	
2.19 \pm 0.30 OUR AVERAGE					
2.02 \pm 0.33 \pm 0.22		¹ JOSHI	10	BELL	$e^+e^- \rightarrow \Upsilon(4S)$
2.4 \pm 0.4 \pm 0.2		¹ AUBERT	08AJ	BABR	$e^+e^- \rightarrow \Upsilon(4S)$
• • • We do not use the following data for averages, fits, limits, etc. • • •					
2.2 \pm 0.6 \pm 0.2		² AUBERT	07K	BABR	Repl. by AUBERT 08AJ
< 2.5	90	AUBERT	03D	BABR	Repl. by AUBERT 07K
<14	90	³ ALEXANDER	93B	CLE2	$e^+e^- \rightarrow \Upsilon(4S)$

¹ Assumes equal production of B^+ and B^0 at the $\Upsilon(4S)$.

² AUBERT 07K reports $[\Gamma(B^0 \rightarrow D_s^{*-} K^+)/\Gamma_{\text{total}}] \times [B(D_s^+ \rightarrow \phi\pi^+)] = (0.97 \pm 0.24 \pm 0.12) \times 10^{-6}$ which we divide by our best value $B(D_s^+ \rightarrow \phi\pi^+) = (4.5 \pm 0.4) \times 10^{-2}$. Our first error is their experiment's error and our second error is the systematic error from using our best value.

³ ALEXANDER 93B reports $< 17 \times 10^{-5}$ from a measurement of $[\Gamma(B^0 \rightarrow D_s^{*-} K^+)/\Gamma_{\text{total}}] \times [B(D_s^+ \rightarrow \phi\pi^+)]$ assuming $B(D_s^+ \rightarrow \phi\pi^+) = 0.037$, which we rescale to our best value $B(D_s^+ \rightarrow \phi\pi^+) = 4.5 \times 10^{-2}$.

$\Gamma(D_{s1}(2536)^{\mp} K^{\pm}, D_{s1}^- \rightarrow \bar{D}^*(2007)^0 K^-)/\Gamma(\bar{D}^0 K^+ K^-)$		Γ_{137}/Γ_{49}			
VALUE (units 10^{-2})	CL%	DOCUMENT ID	TECN	COMMENT	
8.4 \pm 0.3 \pm 0.6		AAIJ	23AY	LHCb	pp at 7, 8, 13 TeV

$\Gamma(D_s^- K^*(892)^+)/\Gamma_{\text{total}}$		Γ_{138}/Γ			
VALUE (units 10^{-5})	CL%	DOCUMENT ID	TECN	COMMENT	
3.5 \pm 1.0 \pm 0.4		¹ AUBERT	08AJ	BABR	$e^+e^- \rightarrow \Upsilon(4S)$
• • • We do not use the following data for averages, fits, limits, etc. • • •					
<280	90	² ALBRECHT	93E	ARG	$e^+e^- \rightarrow \Upsilon(4S)$
< 80	90	³ ALEXANDER	93B	CLE2	$e^+e^- \rightarrow \Upsilon(4S)$

¹ Assumes equal production of B^+ and B^0 at the $\Upsilon(4S)$.

² ALBRECHT 93E reports $< 4.6 \times 10^{-3}$ from a measurement of $[\Gamma(B^0 \rightarrow D_s^- K^*(892)^+)/\Gamma_{\text{total}}] \times [B(D_s^+ \rightarrow \phi\pi^+)]$ assuming $B(D_s^+ \rightarrow \phi\pi^+) = 0.027$, which we rescale to our best value $B(D_s^+ \rightarrow \phi\pi^+) = 4.5 \times 10^{-2}$.

³ ALEXANDER 93B reports $< 9.7 \times 10^{-4}$ from a measurement of $[\Gamma(B^0 \rightarrow D_s^- K^*(892)^+)/\Gamma_{\text{total}}] \times [B(D_s^+ \rightarrow \phi\pi^+)]$ assuming $B(D_s^+ \rightarrow \phi\pi^+) = 0.037$, which we rescale to our best value $B(D_s^+ \rightarrow \phi\pi^+) = 4.5 \times 10^{-2}$.

$\Gamma(D_s^{*-} K^*(892)^+)/\Gamma_{\text{total}}$		Γ_{139}/Γ			
VALUE (units 10^{-5})	CL%	DOCUMENT ID	TECN	COMMENT	
3.2 \pm 1.4 \pm 0.4		¹ AUBERT	08AJ	BABR	$e^+e^- \rightarrow \Upsilon(4S)$

• • • We do not use the following data for averages, fits, limits, etc. • • •

<350 90 ² ALBRECHT 93E ARG $e^+e^- \rightarrow \Upsilon(4S)$

< 90 90 ³ ALEXANDER 93B CLE2 $e^+e^- \rightarrow \Upsilon(4S)$

¹ Assumes equal production of B^+ and B^0 at the $\Upsilon(4S)$.

² ALBRECHT 93E reports $< 5.8 \times 10^{-3}$ from a measurement of $[\Gamma(B^0 \rightarrow D_s^{*-} K^*(892)^+)/\Gamma_{\text{total}}] \times [B(D_s^+ \rightarrow \phi\pi^+)]$ assuming $B(D_s^+ \rightarrow \phi\pi^+) = 0.027$, which we rescale to our best value $B(D_s^+ \rightarrow \phi\pi^+) = 4.5 \times 10^{-2}$.

³ ALEXANDER 93B reports $< 11.0 \times 10^{-4}$ from a measurement of $[\Gamma(B^0 \rightarrow D_s^{*-} K^*(892)^+)/\Gamma_{\text{total}}] \times [B(D_s^+ \rightarrow \phi\pi^+)]$ assuming $B(D_s^+ \rightarrow \phi\pi^+) = 0.037$, which we rescale to our best value $B(D_s^+ \rightarrow \phi\pi^+) = 4.5 \times 10^{-2}$.

$\Gamma(D_s^- \pi^+ K^0)/\Gamma_{\text{total}}$		Γ_{140}/Γ			
VALUE (units 10^{-4})	CL%	DOCUMENT ID	TECN	COMMENT	
0.97 \pm 0.14 OUR AVERAGE					
0.94 \pm 0.12 \pm 0.10		¹ WIEHCZYN...	15	BELL	$e^+e^- \rightarrow \Upsilon(4S)$
1.10 \pm 0.26 \pm 0.20		¹ AUBERT	08G	BABR	$e^+e^- \rightarrow \Upsilon(4S)$

• • • We do not use the following data for averages, fits, limits, etc. • • •

<40 90 ² ALBRECHT 93E ARG $e^+e^- \rightarrow \Upsilon(4S)$

¹ Assumes equal production of B^+ and B^0 at the $\Upsilon(4S)$.

² ALBRECHT 93E reports $< 7.3 \times 10^{-3}$ from a measurement of $[\Gamma(B^0 \rightarrow D_s^- \pi^+ K^0)/\Gamma_{\text{total}}] \times [B(D_s^+ \rightarrow \phi\pi^+)]$ assuming $B(D_s^+ \rightarrow \phi\pi^+) = 0.027$, which we rescale to our best value $B(D_s^+ \rightarrow \phi\pi^+) = 4.5 \times 10^{-2}$.

$\Gamma(D_s^{*-} \pi^+ K^0)/\Gamma_{\text{total}}$		Γ_{141}/Γ			
VALUE (units 10^{-4})	CL%	DOCUMENT ID	TECN	COMMENT	
< 1.10	90	¹ AUBERT	08G	BABR	$e^+e^- \rightarrow \Upsilon(4S)$

• • • We do not use the following data for averages, fits, limits, etc. • • •

<25 90 ² ALBRECHT 93E ARG $e^+e^- \rightarrow \Upsilon(4S)$

¹ Assumes equal production of B^+ and B^0 at the $\Upsilon(4S)$.

² ALBRECHT 93E reports $< 4.2 \times 10^{-3}$ from a measurement of $[\Gamma(B^0 \rightarrow D_s^{*-} \pi^+ K^0)/\Gamma_{\text{total}}] \times [B(D_s^+ \rightarrow \phi\pi^+)]$ assuming $B(D_s^+ \rightarrow \phi\pi^+) = 0.027$, which we rescale to our best value $B(D_s^+ \rightarrow \phi\pi^+) = 4.5 \times 10^{-2}$.

$\Gamma(D_s^- K^+ \pi^+ \pi^-)/\Gamma_{\text{total}}$		Γ_{142}/Γ			
VALUE (units 10^{-4})	CL%	DOCUMENT ID	TECN	COMMENT	
1.71 \pm 0.31 \pm 0.34		¹ AAIJ	12AX	LHCb	pp at 7 TeV

¹ AAIJ 12AX reports $[\Gamma(B^0 \rightarrow D_s^- K^+ \pi^+ \pi^-)/\Gamma_{\text{total}}] / [B(B^0 \rightarrow D_s^- K^+ \pi^+ \pi^-)] = 0.54 \pm 0.07 \pm 0.07$ which we multiply by our best value $B(B^0 \rightarrow D_s^- K^+ \pi^+ \pi^-) = (3.2 \pm 0.6) \times 10^{-4}$. Our first error is their experiment's error and our second error is the systematic error from using our best value.

$\Gamma(D_s^- \pi^+ K^*(892)^0)/\Gamma_{\text{total}}$ Γ_{143}/Γ

VALUE	CL%	DOCUMENT ID	TECN	COMMENT
$<3.0 \times 10^{-3}$	90	¹ ALBRECHT 93E	ARG	$e^+e^- \rightarrow \Upsilon(4S)$
¹ ALBRECHT 93E reports $< 5.0 \times 10^{-3}$ from a measurement of $[\Gamma(B^0 \rightarrow D_s^- \pi^+ K^*(892)^0)/\Gamma_{\text{total}}] \times [B(D_s^+ \rightarrow \phi\pi^+)]$ assuming $B(D_s^+ \rightarrow \phi\pi^+) = 0.027$, which we rescale to our best value $B(D_s^+ \rightarrow \phi\pi^+) = 4.5 \times 10^{-2}$.				

$\Gamma(D_s^{*-} \pi^+ K^*(892)^0)/\Gamma_{\text{total}}$ Γ_{144}/Γ

VALUE	CL%	DOCUMENT ID	TECN	COMMENT
$<1.6 \times 10^{-3}$	90	¹ ALBRECHT 93E	ARG	$e^+e^- \rightarrow \Upsilon(4S)$
¹ ALBRECHT 93E reports $< 2.7 \times 10^{-3}$ from a measurement of $[\Gamma(B^0 \rightarrow D_s^{*-} \pi^+ K^*(892)^0)/\Gamma_{\text{total}}] \times [B(D_s^+ \rightarrow \phi\pi^+)]$ assuming $B(D_s^+ \rightarrow \phi\pi^+) = 0.027$, which we rescale to our best value $B(D_s^+ \rightarrow \phi\pi^+) = 4.5 \times 10^{-2}$.				

$\Gamma(\bar{D}^0 K^0)/\Gamma_{\text{total}}$ Γ_{145}/Γ

VALUE (units 10^{-5})	DOCUMENT ID	TECN	COMMENT
5.5 ± 0.4 OUR AVERAGE			
5.6 ± 0.5 ± 0.2	KUMAR 23	BELL	$e^+e^- \rightarrow \Upsilon(4S)$
5.3 ± 0.7 ± 0.3	¹ AUBERT,B 06L	BABR	$e^+e^- \rightarrow \Upsilon(4S)$
• • • We do not use the following data for averages, fits, limits, etc. • • •			
5.0 ± $^{+1.3}_{-1.2}$ ± 0.6	¹ KROKOVNY 03	BELL	Repl. by KUMAR 23
¹ Assumes equal production of B^+ and B^0 at the $\Upsilon(4S)$.			

$\Gamma(\bar{D}^0 K^+ \pi^-)/\Gamma_{\text{total}}$ Γ_{146}/Γ

VALUE (units 10^{-6})	DOCUMENT ID	TECN	COMMENT
88 ± 15 ± 9			
	¹ AUBERT 06A	BABR	$e^+e^- \rightarrow \Upsilon(4S)$
¹ Assumes equal production of B^+ and B^0 at the $\Upsilon(4S)$.			

$\Gamma(\bar{D}^0 K^+ \pi^-)/\Gamma(\bar{D}^0 \pi^+ \pi^-)$ Γ_{146}/Γ_{47}

VALUE	DOCUMENT ID	TECN	COMMENT
0.106 ± 0.007 ± 0.008	AAIJ 13Aq	LHCB	pp at 7 TeV

$\Gamma(\bar{D}^0 K^*(892)^0)/\Gamma_{\text{total}}$ Γ_{147}/Γ

VALUE (units 10^{-5})	DOCUMENT ID	TECN	COMMENT
4.5 ± 0.6 OUR AVERAGE			
5.4 ± 0.3 ± 1.1	^{1,2} AAIJ 15x	LHCB	pp at 7, 8 TeV
4.0 ± 0.7 ± 0.3	³ AUBERT,B 06L	BABR	$e^+e^- \rightarrow \Upsilon(4S)$
4.8 ± $^{+1.1}_{-1.0}$ ± 0.5	³ KROKOVNY 03	BELL	$e^+e^- \rightarrow \Upsilon(4S)$
• • • We do not use the following data for averages, fits, limits, etc. • • •			
5.7 ± 0.9 ± 0.6	³ AUBERT 06A	BABR	Repl. by AUBERT,B 06L
¹ AAIJ 15x reports $(5.13 \pm 0.20 \pm 0.15 \pm 0.24 \pm 0.60) \times 10^{-5}$ from a measurement of $[\Gamma(B^0 \rightarrow \bar{D}^0 K^*(892)^0)/\Gamma_{\text{total}}] \times [B(B^0 \rightarrow \bar{D}^0 K^+ \pi^-)]$ assuming $B(B^0 \rightarrow \bar{D}^0 K^+ \pi^-) = (9.2 \pm 0.6 \pm 0.7 \pm 0.6) \times 10^{-5}$, which we rescale to our best value $B(B^0 \rightarrow \bar{D}^0 K^+ \pi^-) = (8.8 \pm 1.7) \times 10^{-5}$. Our first error is their experiment's error and our second error is the systematic error from using our best value.			
² Measured via amplitude analysis of $B^0 \rightarrow \bar{D}^0 K^+ \pi^-$, which excludes contribution from decay via $D^*(2010)^-$ resonance.			
³ Assumes equal production of B^+ and B^0 at the $\Upsilon(4S)$.			

$\Gamma(\bar{D}^0 K^*(1410)^0)/\Gamma_{\text{total}}$ Γ_{148}/Γ

VALUE	CL%	DOCUMENT ID	TECN	COMMENT
$<6.7 \times 10^{-5}$	90	¹ AAIJ 15x	LHCB	pp at 7, 8 TeV
¹ Measured via amplitude analysis of $B^0 \rightarrow \bar{D}^0 K^+ \pi^-$, which excludes contribution from decay via $D^*(2010)^-$ resonance.				

$\Gamma(\bar{D}^0 K_0^*(1430)^0)/\Gamma_{\text{total}}$ Γ_{149}/Γ

VALUE (units 10^{-5})	DOCUMENT ID	TECN	COMMENT
0.7 ± 0.7 ± 0.1			
	^{1,2} AAIJ 15x	LHCB	pp at 7, 8 TeV
¹ AAIJ 15x reports $(0.71 \pm 0.27 \pm 0.33 \pm 0.47 \pm 0.08) \times 10^{-5}$ from a measurement of $[\Gamma(B^0 \rightarrow \bar{D}^0 K_0^*(1430)^0)/\Gamma_{\text{total}}] \times [B(B^0 \rightarrow \bar{D}^0 K^+ \pi^-)]$ assuming $B(B^0 \rightarrow \bar{D}^0 K^+ \pi^-) = (9.2 \pm 0.6 \pm 0.7 \pm 0.6) \times 10^{-5}$, which we rescale to our best value $B(B^0 \rightarrow \bar{D}^0 K^+ \pi^-) = (8.8 \pm 1.7) \times 10^{-5}$. Our first error is their experiment's error and our second error is the systematic error from using our best value.			
² Measured via amplitude analysis of $B^0 \rightarrow \bar{D}^0 K^+ \pi^-$, which excludes contribution from decay via $D^*(2010)^-$ resonance.			

$\Gamma(\bar{D}^0 K_2^*(1430)^0)/\Gamma_{\text{total}}$ Γ_{150}/Γ

VALUE (units 10^{-5})	DOCUMENT ID	TECN	COMMENT
2.1 ± 0.8 ± 0.4			
	^{1,2} AAIJ 15x	LHCB	pp at 7, 8 TeV
¹ AAIJ 15x reports $(2.04 \pm 0.45 \pm 0.30 \pm 0.54 \pm 0.25) \times 10^{-5}$ from a measurement of $[\Gamma(B^0 \rightarrow \bar{D}^0 K_2^*(1430)^0)/\Gamma_{\text{total}}] \times [B(B^0 \rightarrow \bar{D}^0 K^+ \pi^-)]$ assuming $B(B^0 \rightarrow \bar{D}^0 K^+ \pi^-) = (9.2 \pm 0.6 \pm 0.7 \pm 0.6) \times 10^{-5}$, which we rescale to our best value $B(B^0 \rightarrow \bar{D}^0 K^+ \pi^-) = (8.8 \pm 1.7) \times 10^{-5}$. Our first error is their experiment's error and our second error is the systematic error from using our best value.			
² Measured via amplitude analysis of $B^0 \rightarrow \bar{D}^0 K^+ \pi^-$, which excludes contribution from decay via $D^*(2010)^-$ resonance.			

$\Gamma(D_0^*(2300)^- K^+, D_0^{*-} \rightarrow \bar{D}^0 \pi^-)/\Gamma_{\text{total}}$ Γ_{151}/Γ

VALUE (units 10^{-5})	DOCUMENT ID	TECN	COMMENT
1.9 ± 0.8 ± 0.4			
	^{1,2} AAIJ 15x	LHCB	pp at 7, 8 TeV
¹ AAIJ 15x reports $(1.77 \pm 0.26 \pm 0.19 \pm 0.67 \pm 0.20) \times 10^{-5}$ from a measurement of $[\Gamma(B^0 \rightarrow D_0^*(2300)^- K^+, D_0^{*-} \rightarrow \bar{D}^0 \pi^-)/\Gamma_{\text{total}}] \times [B(B^0 \rightarrow \bar{D}^0 K^+ \pi^-)]$ assuming $B(B^0 \rightarrow \bar{D}^0 K^+ \pi^-) = (9.2 \pm 0.6 \pm 0.7 \pm 0.6) \times 10^{-5}$, which we rescale to our best value $B(B^0 \rightarrow \bar{D}^0 K^+ \pi^-) = (8.8 \pm 1.7) \times 10^{-5}$. Our first error is their experiment's error and our second error is the systematic error from using our best value.			
² Measured via amplitude analysis of $B^0 \rightarrow \bar{D}^0 K^+ \pi^-$, which excludes contribution from decay via $D^*(2010)^-$ resonance.			

$\Gamma(D_2^*(2460)^- K^+, D_2^{*-} \rightarrow \bar{D}^0 \pi^-)/\Gamma_{\text{total}}$ Γ_{152}/Γ

VALUE (units 10^{-6})	DOCUMENT ID	TECN	COMMENT
20.3 ± 3.5 OUR AVERAGE			
22 ± 2 ± 4	^{1,2} AAIJ 15x	LHCB	pp at 7, 8 TeV
18.3 ± 4.0 ± 3.1	³ AUBERT 06A	BABR	$e^+e^- \rightarrow \Upsilon(4S)$
¹ AAIJ 15x reports $(2.12 \pm 0.10 \pm 0.11 \pm 0.11 \pm 0.25) \times 10^{-5}$ from a measurement of $[\Gamma(B^0 \rightarrow D_2^*(2460)^- K^+, D_2^{*-} \rightarrow \bar{D}^0 \pi^-)/\Gamma_{\text{total}}] \times [B(B^0 \rightarrow \bar{D}^0 K^+ \pi^-)]$ assuming $B(B^0 \rightarrow \bar{D}^0 K^+ \pi^-) = (9.2 \pm 0.6 \pm 0.7 \pm 0.6) \times 10^{-5}$, which we rescale to our best value $B(B^0 \rightarrow \bar{D}^0 K^+ \pi^-) = (8.8 \pm 1.7) \times 10^{-5}$. Our first error is their experiment's error and our second error is the systematic error from using our best value.			
² Measured via amplitude analysis of $B^0 \rightarrow \bar{D}^0 K^+ \pi^-$, which excludes contribution from decay via $D^*(2010)^-$ resonance.			
³ Assumes equal production of B^+ and B^0 at the $\Upsilon(4S)$.			

$\Gamma(D_3^*(2760)^- K^+, D_3^{*-} \rightarrow \bar{D}^0 \pi^-)/\Gamma_{\text{total}}$ Γ_{153}/Γ

VALUE	CL%	DOCUMENT ID	TECN	COMMENT
$<0.10 \times 10^{-5}$	90	¹ AAIJ 15x	LHCB	pp at 7, 8 TeV
¹ Measured via amplitude analysis of $B^0 \rightarrow \bar{D}^0 K^+ \pi^-$, which excludes contribution from decay via $D^*(2010)^-$ resonance.				

$\Gamma(\bar{D}^0 K^+ \pi^- \text{ nonresonant})/\Gamma_{\text{total}}$ Γ_{154}/Γ

VALUE (units 10^{-6})	CL%	DOCUMENT ID	TECN	COMMENT
<37	90	¹ AUBERT 06A	BABR	$e^+e^- \rightarrow \Upsilon(4S)$
¹ Assumes equal production of B^+ and B^0 at the $\Upsilon(4S)$.				

$\Gamma([\bar{K}^+ K^-]_D K^*(892)^0)/\Gamma(\bar{D}^0 K^*(892)^0)$ $\Gamma_{155}/\Gamma_{147}$

VALUE	DOCUMENT ID	TECN	COMMENT
0.92 ± 0.10 ± 0.02	AAIJ 19N	LHCB	pp at 7, 8, 13 TeV
• • • We do not use the following data for averages, fits, limits, etc. • • •			
1.05 ± $^{+0.17}_{-0.15}$ ± 0.04	AAIJ 14BN	LHCB	Repl. by AAIJ 16s
1.36 ± $^{+0.37}_{-0.32}$ ± 0.07	AAIJ 13L	LHCB	Repl. by AAIJ 14BN

$\Gamma([\pi^+ \pi^-]_D K^*(892)^0)/\Gamma(\bar{D}^0 K^*(892)^0)$ $\Gamma_{156}/\Gamma_{147}$

VALUE	DOCUMENT ID	TECN	COMMENT
1.32 ± 0.19 ± 0.03	AAIJ 19N	LHCB	pp at 7, 8, 13 TeV
• • • We do not use the following data for averages, fits, limits, etc. • • •			
1.21 ± $^{+0.28}_{-0.25}$ ± 0.05	AAIJ 14BN	LHCB	Repl. by AAIJ 16s

$\Gamma([\pi^+ K^-]_D K^*(892)^0)/\Gamma([\bar{K}^+ \pi^-]_D K^*(892)^0)$ $\Gamma_{157}/\Gamma_{158}$

VALUE	DOCUMENT ID	TECN	COMMENT
0.080 ± 0.015 ± 0.002	AAIJ 19N	LHCB	pp at 7, 8, 13 TeV

$\Gamma([\pi^+ \pi^- \pi^+ \pi^-]_D K^*(892)^0)/\Gamma(\bar{D}^0 K^*(892)^0)$ $\Gamma_{159}/\Gamma_{147}$

VALUE	DOCUMENT ID	TECN	COMMENT
1.01 ± 0.16 ± 0.04	AAIJ 19N	LHCB	pp at 7, 8, 13 TeV

$\Gamma([\pi^+ K^- \pi^+ \pi^-]_D K^*(892)^0)/\Gamma([\bar{K}^+ \pi^- \pi^+ \pi^-]_D K^*(892)^0)$ $\Gamma_{160}/\Gamma_{161}$

VALUE	DOCUMENT ID	TECN	COMMENT
0.073 ± 0.018 ± 0.002	AAIJ 19N	LHCB	pp at 7, 8, 13 TeV

$\Gamma(\bar{D}^0 \pi^0)/\Gamma_{\text{total}}$ Γ_{162}/Γ

VALUE (units 10^{-4})	CL%	DOCUMENT ID	TECN	COMMENT
2.67 ± 0.09 OUR AVERAGE				
2.70 ± 0.06 ± 0.10		BLOOMFIELD 22	BELL	$e^+e^- \rightarrow \Upsilon(4S)$
2.69 ± 0.09 ± 0.13	¹	LEES 11M	BABR	$e^+e^- \rightarrow \Upsilon(4S)$
2.25 ± 0.14 ± 0.35	¹	BLYTH 06	BELL	$e^+e^- \rightarrow \Upsilon(4S)$
2.74 ± $^{+0.36}_{-0.32}$ ± 0.55	¹	COAN 02	CLE2	$e^+e^- \rightarrow \Upsilon(4S)$
• • • We do not use the following data for averages, fits, limits, etc. • • •				
2.9 ± 0.2 ± 0.3	¹	AUBERT 04B	BABR	Repl. by LEES 11M
3.1 ± 0.4 ± 0.5	¹	ABE 02J	BELL	Repl. by BLYTH 06
<1.2	90	² NEMAT 98	CLE2	Repl. by COAN 02
<4.8	90	³ ALAM 94	CLE2	Repl. by NEMAT 98
¹ Assumes equal production of B^+ and B^0 at the $\Upsilon(4S)$.				
² NEMAT 98 assumes equal production of B^+ and B^0 at the $\Upsilon(4S)$ and use the PDG 96 values for D^0, D^{*0}, η, η' , and ω branching fractions.				
³ ALAM 94 assume equal production of B^+ and B^0 at the $\Upsilon(4S)$ and use the CLEO II absolute $B(D^0 \rightarrow K^-\pi^+)/B(D^0 \rightarrow K^-\pi^+\pi^0)/B(D^0 \rightarrow K^-\pi^+)$ and $B(D^0 \rightarrow K^-\pi^+\pi^-)/B(D^0 \rightarrow K^-\pi^+)$.				

Meson Particle Listings

 B^0 $\Gamma(\overline{D}^0 \rho^0)/\Gamma_{\text{total}}$ Γ_{163}/Γ

VALUE (units 10^{-4})	CL%	DOCUMENT ID	TECN	COMMENT
3.21 ± 0.21 OUR AVERAGE				
3.21 ± 0.10 ± 0.21		¹ AAIJ	15Y	LHCB pp at 7, 8 TeV
3.19 ± 0.20 ± 0.45		^{2,3} KUZMIN	07	BELL $e^+e^- \rightarrow \Upsilon(4S)$
• • • We do not use the following data for averages, fits, limits, etc. • • •				
2.9 ± 1.0 ± 0.4		² SATPATHY	03	BELL Repl. by KUZMIN 07
< 3.9	90	⁴ NEMAT1	98	CLE2 $e^+e^- \rightarrow \Upsilon(4S)$
< 5.5	90	⁵ ALAM	94	CLE2 Repl. by NEMAT1 98
< 6.0	90	⁶ BORTOLETTO92	CLEO	$e^+e^- \rightarrow \Upsilon(4S)$
< 27.0	90	⁷ ALBRECHT	88k	ARG $e^+e^- \rightarrow \Upsilon(4S)$

¹ Measured using isobar formalism in the decay chain $B^0 \rightarrow \overline{D}^0 \rho(770)$, $\rho \rightarrow \pi^+ \pi^-$ assuming $B(\rho(770) \rightarrow \pi^+ \pi^-) = 1$. The second uncertainty combines in quadrature all systematic uncertainties quoted in the paper.

² Assumes equal production of B^+ and B^0 at the $\Upsilon(4S)$.

³ Our second uncertainty combines systematics and model errors quoted in the paper.

⁴ NEMAT1 98 assumes equal production of B^+ and B^0 at the $\Upsilon(4S)$ and use the PDG 96 values for D^0 , D^{*0} , η , η' , and ω branching fractions.

⁵ ALAM 94 assume equal production of B^+ and B^0 at the $\Upsilon(4S)$ and use the CLEO11 absolute $B(D^0 \rightarrow K^- \pi^+)$ and the PDG 1992 $B(D^0 \rightarrow K^- \pi^+ \pi^0)/B(D^0 \rightarrow K^- \pi^+)$ and $B(D^0 \rightarrow K^- 2\pi^+ \pi^-)/B(D^0 \rightarrow K^- \pi^+)$.

⁶ BORTOLETTO 92 assumes equal production of B^+ and B^0 at the $\Upsilon(4S)$ and uses Mark III branching fractions for the D .

⁷ ALBRECHT 88k reports < 0.003 assuming $B^0 \overline{D}^0 : B^+ B^-$ production ratio is 45:55. We rescale to 50%.

 $\Gamma(\overline{D}^0 f_2)/\Gamma_{\text{total}}$ Γ_{164}/Γ

VALUE (units 10^{-4})	DOCUMENT ID	TECN	COMMENT
1.56 ± 0.21 OUR AVERAGE			
1.68 ± 0.11 ± 0.21	¹ AAIJ	15Y	LHCB pp at 7, 8 TeV
1.20 ± 0.18 ± 0.38	^{2,3} KUZMIN	07	BELL $e^+e^- \rightarrow \Upsilon(4S)$

¹ Result obtained using the isobar formalism. The second uncertainty combines in quadrature all systematic uncertainties quoted in the paper. Measured in the decay chain $B^0 \rightarrow \overline{D}^0 f_2(1270)$, $f_2 \rightarrow \pi^+ \pi^-$.

² Assumes equal production of B^+ and B^0 at the $\Upsilon(4S)$.

³ Our second uncertainty combines systematics and model errors quoted in the paper.

 $\Gamma(\overline{D}^0 \eta)/\Gamma_{\text{total}}$ Γ_{165}/Γ

VALUE (units 10^{-4})	CL%	DOCUMENT ID	TECN	COMMENT
2.56 ± 0.12 OUR AVERAGE				
2.66 ± 0.12 ± 0.21		KUMAR	23	BELL $e^+e^- \rightarrow \Upsilon(4S)$
2.53 ± 0.09 ± 0.11		¹ LEES	11M	BABR $e^+e^- \rightarrow \Upsilon(4S)$
• • • We do not use the following data for averages, fits, limits, etc. • • •				
1.77 ± 0.16 ± 0.21		¹ BLYTH	06	BELL Repl. by KUMAR 23
2.5 ± 0.2 ± 0.3		¹ AUBERT	04B	BABR Repl. by LEES 11M
1.4 $^{+0.5}_{-0.4}$ ± 0.3		¹ ABE	02J	BELL Repl. by BLYTH 06
< 1.3	90	² NEMAT1	98	CLE2 $e^+e^- \rightarrow \Upsilon(4S)$
< 6.8	90	³ ALAM	94	CLE2 Repl. by NEMAT1 98

¹ Assumes equal production of B^+ and B^0 at the $\Upsilon(4S)$.

² NEMAT1 98 assumes equal production of B^+ and B^0 at the $\Upsilon(4S)$ and use the PDG 96 values for D^0 , D^{*0} , η , η' , and ω branching fractions.

³ ALAM 94 assume equal production of B^+ and B^0 at the $\Upsilon(4S)$ and use the CLEO11 absolute $B(D^0 \rightarrow K^- \pi^+)$ and the PDG 1992 $B(D^0 \rightarrow K^- \pi^+ \pi^0)/B(D^0 \rightarrow K^- \pi^+)$ and $B(D^0 \rightarrow K^- 2\pi^+ \pi^-)/B(D^0 \rightarrow K^- \pi^+)$.

 $\Gamma(\overline{D}^0 \eta')/\Gamma_{\text{total}}$ Γ_{166}/Γ

VALUE (units 10^{-4})	CL%	DOCUMENT ID	TECN	COMMENT
1.38 ± 0.16 OUR AVERAGE				
1.48 ± 0.13 ± 0.07		¹ LEES	11M	BABR $e^+e^- \rightarrow \Upsilon(4S)$
1.14 ± 0.20 $^{+0.10}_{-0.13}$		¹ SCHUMANN	05	BELL $e^+e^- \rightarrow \Upsilon(4S)$
• • • We do not use the following data for averages, fits, limits, etc. • • •				
1.7 ± 0.4 ± 0.2		¹ AUBERT	04B	BABR Repl. by LEES 11M
< 9.4	90	² NEMAT1	98	CLE2 $e^+e^- \rightarrow \Upsilon(4S)$
< 8.6	90	³ ALAM	94	CLE2 Repl. by NEMAT1 98

¹ Assumes equal production of B^+ and B^0 at the $\Upsilon(4S)$.

² NEMAT1 98 assumes equal production of B^+ and B^0 at the $\Upsilon(4S)$ and use the PDG 96 values for D^0 , D^{*0} , η , η' , and ω branching fractions.

³ ALAM 94 assume equal production of B^+ and B^0 at the $\Upsilon(4S)$ and use the CLEO11 absolute $B(D^0 \rightarrow K^- \pi^+)$ and the PDG 1992 $B(D^0 \rightarrow K^- \pi^+ \pi^0)/B(D^0 \rightarrow K^- \pi^+)$ and $B(D^0 \rightarrow K^- 2\pi^+ \pi^-)/B(D^0 \rightarrow K^- \pi^+)$.

 $\Gamma(\overline{D}^0 \eta')/\Gamma(\overline{D}^0 \eta)$ $\Gamma_{166}/\Gamma_{165}$

VALUE	DOCUMENT ID	TECN	COMMENT
0.54 ± 0.07 ± 0.01	LEES	11M	BABR $e^+e^- \rightarrow \Upsilon(4S)$
• • • We do not use the following data for averages, fits, limits, etc. • • •			
0.7 ± 0.2 ± 0.1	AUBERT	04B	BABR Repl. by LEES 11M

 $\Gamma(\overline{D}^0 \omega)/\Gamma_{\text{total}}$ Γ_{167}/Γ

VALUE (units 10^{-4})	CL%	DOCUMENT ID	TECN	COMMENT
2.54 ± 0.16 OUR AVERAGE				
2.75 ± 0.72 ± 0.35		¹ AAIJ	15Y	LHCB pp at 7, 8 TeV
2.57 ± 0.11 ± 0.14		² LEES	11M	BABR $e^+e^- \rightarrow \Upsilon(4S)$
2.37 ± 0.23 ± 0.28		² BLYTH	06	BELL $e^+e^- \rightarrow \Upsilon(4S)$
• • • We do not use the following data for averages, fits, limits, etc. • • •				
3.0 ± 0.3 ± 0.4		² AUBERT	04B	BABR Repl. by LEES 11M
1.8 ± 0.5 $^{+0.4}_{-0.3}$		² ABE	02J	BELL Repl. by BLYTH 06
< 5.1	90	³ NEMAT1	98	CLE2 $e^+e^- \rightarrow \Upsilon(4S)$
< 6.3	90	⁴ ALAM	94	CLE2 Repl. by NEMAT1 98

¹ Result obtained using the isobar model. The second uncertainty combines in quadrature all systematic uncertainties quoted in the paper.

² Assumes equal production of B^+ and B^0 at the $\Upsilon(4S)$.

³ NEMAT1 98 assumes equal production of B^+ and B^0 at the $\Upsilon(4S)$ and use the PDG 96 values for D^0 , D^{*0} , η , η' , and ω branching fractions.

⁴ ALAM 94 assume equal production of B^+ and B^0 at the $\Upsilon(4S)$ and use the CLEO11 absolute $B(D^0 \rightarrow K^- \pi^+)$ and the PDG 1992 $B(D^0 \rightarrow K^- \pi^+ \pi^0)/B(D^0 \rightarrow K^- \pi^+)$ and $B(D^0 \rightarrow K^- 2\pi^+ \pi^-)/B(D^0 \rightarrow K^- \pi^+)$.

 $\Gamma(\overline{D}^0 \phi)/\Gamma_{\text{total}}$ Γ_{168}/Γ

VALUE (units 10^{-7})	CL%	DOCUMENT ID	TECN	COMMENT
7.7 ± 2.1 ± 1.0		¹ AAIJ	23AZ	LHCB pp at 7, 8, 13 TeV
• • • We do not use the following data for averages, fits, limits, etc. • • •				
< 23	95	AAIJ	18AY	LHCB Repl. by AAIJ 23AZ
< 116	90	² AUBERT	07A0	BABR $e^+e^- \rightarrow \Upsilon(4S)$

¹ The last uncertainty includes the uncertainties of the branching fractions $B(B^0 \rightarrow \overline{D}^0 K^+ K^-)$ and $B(\phi \rightarrow K^+ K^-)$.

² Assumes equal production of B^+ and B^0 at the $\Upsilon(4S)$.

 $\Gamma(D^0 K^+ \pi^-)/\Gamma_{\text{total}}$ Γ_{169}/Γ

VALUE (units 10^{-6})	CL%	DOCUMENT ID	TECN	COMMENT
• • • We do not use the following data for averages, fits, limits, etc. • • •				
< 19	90	¹ AUBERT	06A	BABR Repl. by AUBERT 09AE

¹ Assumes equal production of B^+ and B^0 at the $\Upsilon(4S)$.

 $\Gamma(D^0 K^+ \pi^-)/\Gamma(\overline{D}^0 K^+ \pi^-)$ $\Gamma_{169}/\Gamma_{146}$

VALUE	DOCUMENT ID	TECN	COMMENT
0.060 ± 0.034 OUR AVERAGE			
0.045 $^{+0.056}_{-0.050}$ $^{+0.028}_{-0.018}$	^{1,2} NEGISHI	12	BELL $e^+e^- \rightarrow \Upsilon(4S)$
0.068 ± 0.042	³ AUBERT	09AE	BABR $e^+e^- \rightarrow \Upsilon(4S)$

¹ Assumes equal production of B^0 and B^+ at $\Upsilon(4S)$.

² Uses $D^0 \rightarrow K^- \pi^+$ mode. Restricts $K^+ \pi^-$ mass within ± 50 MeV of the nominal K^*0 mass. Corresponds to the upper limit, < 0.16 at 95% CL.

³ Reports a signal at the level of 2.5 standard deviations after combining results from $D^0 \rightarrow K^+ \pi^-$, $K^+ \pi^- \pi^0$, and $K^+ \pi^- \pi^+ \pi^-$.

 $\Gamma(D^0 K^*(892)^0)/\Gamma_{\text{total}}$ Γ_{170}/Γ

VALUE (units 10^{-5})	CL%	DOCUMENT ID	TECN	COMMENT
• • • We do not use the following data for averages, fits, limits, etc. • • •				
< 1.1	90	¹ AUBERT,B	06L	BABR $e^+e^- \rightarrow \Upsilon(4S)$
< 1.8	90	¹ KROKOVNY	03	BELL $e^+e^- \rightarrow \Upsilon(4S)$

¹ Assumes equal production of B^+ and B^0 at the $\Upsilon(4S)$.

 $\Gamma(D^0 K^*(892)^0)/\Gamma(\overline{D}^0 K^*(892)^0)$ $\Gamma_{170}/\Gamma_{147}$

"OUR EVALUATION" is derived from $r_{B^0}(B^0 \rightarrow D K^{*0})$ data block listed in "CP violation parameters" section.

VALUE (units 10^{-2})	DOCUMENT ID
6.6 $^{+1.1}_{-1.2}$ OUR EVALUATION	(Produced by HFLAV)

 $\Gamma(\overline{D}^{*0} \gamma)/\Gamma_{\text{total}}$ Γ_{171}/Γ

VALUE	CL%	DOCUMENT ID	TECN	COMMENT
< 2.5 × 10⁻⁵	90	¹ AUBERT,B	05Q	BABR $e^+e^- \rightarrow \Upsilon(4S)$
• • • We do not use the following data for averages, fits, limits, etc. • • •				
< 5.0 × 10 ⁻⁵	90	¹ ARTUSO	00	CLE2 $e^+e^- \rightarrow \Upsilon(4S)$

¹ Assumes equal production of B^+ and B^0 at the $\Upsilon(4S)$.

 $\Gamma(\overline{D}^*(2007)^0 \pi^0)/\Gamma_{\text{total}}$ Γ_{172}/Γ

VALUE (units 10^{-4})	CL%	DOCUMENT ID	TECN	COMMENT
2.2 ± 0.6 OUR AVERAGE				
3.05 ± 0.14 ± 0.28		¹ LEES	11M	BABR $e^+e^- \rightarrow \Upsilon(4S)$
1.39 ± 0.18 ± 0.26		¹ BLYTH	06	BELL $e^+e^- \rightarrow \Upsilon(4S)$
2.20 $^{+0.59}_{-0.52}$ ± 0.79		¹ COAN	02	CLE2 $e^+e^- \rightarrow \Upsilon(4S)$
• • • We do not use the following data for averages, fits, limits, etc. • • •				
2.9 ± 0.4 ± 0.5		¹ AUBERT	04B	BABR Repl. by LEES 11M
2.7 $^{+0.8}_{-0.7}$ $^{+0.5}_{-0.6}$		¹ ABE	02J	BELL Repl. by BLYTH 06
< 4.4	90	² NEMAT1	98	CLE2 Repl. by COAN 02
< 9.7	90	³ ALAM	94	CLE2 Repl. by NEMAT1 98

Error includes scale factor of 2.6. See the ideogram below.

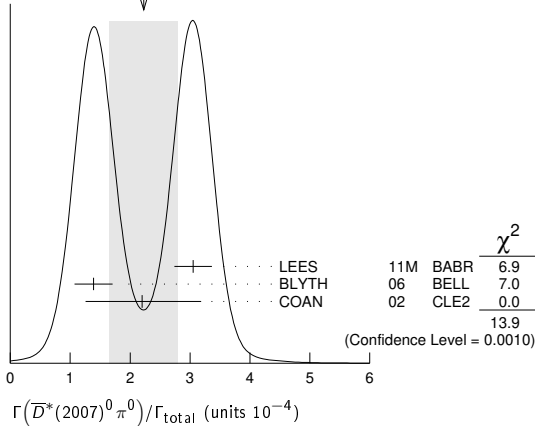
See key on page 1171

Meson Particle Listings

B^0

- ¹ Assumes equal production of B^+ and B^0 at the $\Upsilon(4S)$.
² NEMATI 98 assumes equal production of B^+ and B^0 at the $\Upsilon(4S)$ and use the PDG 96 values for D^0 , D^{*0} , η , η' , and ω branching fractions.
³ ALAM 94 assume equal production of B^+ and B^0 at the $\Upsilon(4S)$ and use the CLEOII $B(D^*(2007)^0 \rightarrow D^0 \pi^0)$ and absolute $B(D^0 \rightarrow K^- \pi^+)$ and the PDG 1992 $B(D^0 \rightarrow K^- \pi^+ \pi^0)/B(D^0 \rightarrow K^- \pi^+)$ and $B(D^0 \rightarrow K^- 2\pi^+ \pi^-)/B(D^0 \rightarrow K^- \pi^+)$.

WEIGHTED AVERAGE
 2.2 ± 0.6 (Error scaled by 2.6)



$\Gamma(D^0 \pi^0)/\Gamma(D^*(2007)^0 \pi^0)$ $\Gamma_{162}/\Gamma_{172}$

VALUE	DOCUMENT ID	TECN	COMMENT
0.90 ± 0.08 OUR AVERAGE			
$0.88 \pm 0.05 \pm 0.06$	LEES	11M BABR	$e^+ e^- \rightarrow \Upsilon(4S)$
$1.62 \pm 0.23 \pm 0.35$	BLYTH	06 BELL	$e^+ e^- \rightarrow \Upsilon(4S)$
••• We do not use the following data for averages, fits, limits, etc. •••			
$1.0 \pm 0.1 \pm 0.2$	AUBERT	04B BABR	Repl. by LEES 11M

$\Gamma(D^*(2007)^0 \rho^0)/\Gamma_{total}$ Γ_{173}/Γ

VALUE	CL%	DOCUMENT ID	TECN	COMMENT
$<5.1 \times 10^{-4}$	90	¹ SATPATHY	03 BELL	$e^+ e^- \rightarrow \Upsilon(4S)$
••• We do not use the following data for averages, fits, limits, etc. •••				
<0.00056	90	² NEMATI	98 CLE2	$e^+ e^- \rightarrow \Upsilon(4S)$
<0.00117	90	³ ALAM	94 CLE2	Repl. by NEMATI 98

- ¹ Assumes equal production of B^+ and B^0 at the $\Upsilon(4S)$.
² NEMATI 98 assumes equal production of B^+ and B^0 at the $\Upsilon(4S)$ and use the PDG 96 values for D^0 , D^{*0} , η , η' , and ω branching fractions.
³ ALAM 94 assume equal production of B^+ and B^0 at the $\Upsilon(4S)$ and use the CLEOII $B(D^*(2007)^0 \rightarrow D^0 \pi^0)$ and absolute $B(D^0 \rightarrow K^- \pi^+)$ and the PDG 1992 $B(D^0 \rightarrow K^- \pi^+ \pi^0)/B(D^0 \rightarrow K^- \pi^+)$ and $B(D^0 \rightarrow K^- 2\pi^+ \pi^-)/B(D^0 \rightarrow K^- \pi^+)$.

$\Gamma(D^*(2007)^0 \eta)/\Gamma_{total}$ Γ_{174}/Γ

VALUE (units 10^{-4})	CL%	DOCUMENT ID	TECN	COMMENT
2.3 ± 0.6 OUR AVERAGE				Error includes scale factor of 2.8.
$2.69 \pm 0.14 \pm 0.23$		¹ LEES	11M BABR	$e^+ e^- \rightarrow \Upsilon(4S)$
$1.40 \pm 0.28 \pm 0.26$		¹ BLYTH	06 BELL	$e^+ e^- \rightarrow \Upsilon(4S)$
••• We do not use the following data for averages, fits, limits, etc. •••				
$2.6 \pm 0.4 \pm 0.4$		^{1,2} AUBERT	04B BABR	Repl. by LEES 11M
<4.6	90	¹ ABE	02J BELL	$e^+ e^- \rightarrow \Upsilon(4S)$
<2.6	90	² NEMATI	98 CLE2	$e^+ e^- \rightarrow \Upsilon(4S)$
<6.9	90	³ ALAM	94 CLE2	Repl. by NEMATI 98

- ¹ Assumes equal production of B^+ and B^0 at the $\Upsilon(4S)$.
² NEMATI 98 assumes equal production of B^+ and B^0 at the $\Upsilon(4S)$ and use the PDG 96 values for D^0 , D^{*0} , η , η' , and ω branching fractions.
³ ALAM 94 assume equal production of B^+ and B^0 at the $\Upsilon(4S)$ and use the CLEOII $B(D^*(2007)^0 \rightarrow D^0 \pi^0)$ and absolute $B(D^0 \rightarrow K^- \pi^+)$ and the PDG 1992 $B(D^0 \rightarrow K^- \pi^+ \pi^0)/B(D^0 \rightarrow K^- \pi^+)$ and $B(D^0 \rightarrow K^- 2\pi^+ \pi^-)/B(D^0 \rightarrow K^- \pi^+)$.

$\Gamma(D^0 \eta)/\Gamma(D^*(2007)^0 \eta)$ $\Gamma_{165}/\Gamma_{174}$

VALUE	DOCUMENT ID	TECN	COMMENT
0.99 ± 0.10 OUR AVERAGE			
$0.97 \pm 0.07 \pm 0.07$	LEES	11M BABR	$e^+ e^- \rightarrow \Upsilon(4S)$
$1.27 \pm 0.29 \pm 0.25$	BLYTH	06 BELL	$e^+ e^- \rightarrow \Upsilon(4S)$
••• We do not use the following data for averages, fits, limits, etc. •••			
$0.9 \pm 0.2 \pm 0.1$	AUBERT	04B BABR	Repl. by LEES 11M

$\Gamma(D^*(2007)^0 \eta)/\Gamma(D^*(2007)^0 \eta)$ $\Gamma_{175}/\Gamma_{174}$

VALUE	DOCUMENT ID	TECN	COMMENT
$0.61 \pm 0.14 \pm 0.02$	LEES	11M BABR	$e^+ e^- \rightarrow \Upsilon(4S)$
••• We do not use the following data for averages, fits, limits, etc. •••			
$0.5 \pm 0.3 \pm 0.1$	AUBERT	04B BABR	Repl. by LEES 11M

$\Gamma(D^*(2007)^0 \eta)/\Gamma_{total}$ Γ_{175}/Γ

VALUE (units 10^{-4})	CL%	DOCUMENT ID	TECN	COMMENT
1.40 ± 0.22 OUR AVERAGE				
$1.48 \pm 0.22 \pm 0.13$		¹ LEES	11M BABR	$e^+ e^- \rightarrow \Upsilon(4S)$
$1.21 \pm 0.34 \pm 0.22$		¹ SCHUMANN	05 BELL	$e^+ e^- \rightarrow \Upsilon(4S)$
••• We do not use the following data for averages, fits, limits, etc. •••				
$1.3 \pm 0.7 \pm 0.2$		^{1,2} AUBERT	04B BABR	Repl. by LEES 11M
<14	90	BRANDENB...	98 CLE2	$e^+ e^- \rightarrow \Upsilon(4S)$
<19	90	³ NEMATI	98 CLE2	$e^+ e^- \rightarrow \Upsilon(4S)$
<27	90	⁴ ALAM	94 CLE2	Repl. by NEMATI 98

- ¹ Assumes equal production of B^+ and B^0 at the $\Upsilon(4S)$.
² Reports an upper limit $< 2.6 \times 10^{-4}$ at 90% CL.
³ NEMATI 98 assumes equal production of B^+ and B^0 at the $\Upsilon(4S)$ and use the PDG 96 values for D^0 , D^{*0} , η , η' , and ω branching fractions.
⁴ ALAM 94 assume equal production of B^+ and B^0 at the $\Upsilon(4S)$ and use the CLEOII $B(D^*(2007)^0 \rightarrow D^0 \pi^0)$ and absolute $B(D^0 \rightarrow K^- \pi^+)$ and the PDG 1992 $B(D^0 \rightarrow K^- \pi^+ \pi^0)/B(D^0 \rightarrow K^- \pi^+)$ and $B(D^0 \rightarrow K^- 2\pi^+ \pi^-)/B(D^0 \rightarrow K^- \pi^+)$.

$\Gamma(D^0 \eta)/\Gamma(D^*(2007)^0 \eta)$ $\Gamma_{166}/\Gamma_{175}$

VALUE	DOCUMENT ID	TECN	COMMENT
$0.96 \pm 0.18 \pm 0.06$	LEES	11M BABR	$e^+ e^- \rightarrow \Upsilon(4S)$
••• We do not use the following data for averages, fits, limits, etc. •••			
$1.3 \pm 0.8 \pm 0.2$	AUBERT	04B BABR	Repl. by LEES 11M

$\Gamma(D^*(2007)^0 \pi^+ \pi^-)/\Gamma_{total}$ Γ_{176}/Γ

VALUE	DOCUMENT ID	TECN	COMMENT
$(6.2 \pm 1.2 \pm 1.8) \times 10^{-4}$	^{1,2} SATPATHY	03 BELL	$e^+ e^- \rightarrow \Upsilon(4S)$
¹ Assumes equal production of B^+ and B^0 at the $\Upsilon(4S)$. ² No assumption about the intermediate mechanism is made in the analysis.			

$\Gamma(D^*(2007)^0 K^+ \pi^-)/\Gamma(D^*(2007)^0 \pi^+ \pi^-)$ $\Gamma_{177}/\Gamma_{176}$

VALUE (units 10^{-2})	DOCUMENT ID	TECN	COMMENT
$8.36 \pm 0.43 \pm 0.61$	AAIJ	22N LHCB	pp at 13 TeV

$\Gamma(D^*(2007)^0 K^0)/\Gamma_{total}$ Γ_{178}/Γ

VALUE (units 10^{-5})	CL%	DOCUMENT ID	TECN	COMMENT
$3.6 \pm 1.2 \pm 0.3$		¹ AUBERT,B	06L BABR	$e^+ e^- \rightarrow \Upsilon(4S)$
••• We do not use the following data for averages, fits, limits, etc. •••				
<6.6	90	¹ KROKOVNY	03 BELL	$e^+ e^- \rightarrow \Upsilon(4S)$
¹ Assumes equal production of B^+ and B^0 at the $\Upsilon(4S)$.				

$\Gamma(D^*(2007)^0 K^*(892)^0)/\Gamma_{total}$ Γ_{179}/Γ

VALUE	CL%	DOCUMENT ID	TECN	COMMENT
$<6.9 \times 10^{-5}$	90	¹ KROKOVNY	03 BELL	$e^+ e^- \rightarrow \Upsilon(4S)$
¹ Assumes equal production of B^+ and B^0 at the $\Upsilon(4S)$.				

$\Gamma(D^*(2007)^0 \phi)/\Gamma_{total}$ Γ_{180}/Γ

VALUE (units 10^{-6})	DOCUMENT ID	TECN	COMMENT
$2.2 \pm 0.5 \pm 0.3$	¹ AAIJ	23az LHCB	pp at 7, 8, 13 TeV
¹ The last uncertainty includes the uncertainties of the branching fraction $B(B^0 \rightarrow \bar{D}^0 K^+ K^-)$ and $B(\phi \rightarrow K^+ K^-)$.			

$\Gamma(D^*(2007)^0 K^*(892)^0)/\Gamma_{total}$ Γ_{181}/Γ

VALUE	CL%	DOCUMENT ID	TECN	COMMENT
$<4.0 \times 10^{-5}$	90	¹ KROKOVNY	03 BELL	$e^+ e^- \rightarrow \Upsilon(4S)$
¹ Assumes equal production of B^+ and B^0 at the $\Upsilon(4S)$.				

$\Gamma(D^*(2007)^0 \pi^+ \pi^+ \pi^- \pi^-)/\Gamma_{total}$ Γ_{182}/Γ

VALUE (units 10^{-3})	DOCUMENT ID	TECN	COMMENT
2.7 ± 0.5 OUR AVERAGE			
$2.60 \pm 0.47 \pm 0.37$	¹ MAJUMDER	04 BELL	$e^+ e^- \rightarrow \Upsilon(4S)$
$3.0 \pm 0.7 \pm 0.6$	¹ EDWARDS	02 CLE2	$e^+ e^- \rightarrow \Upsilon(4S)$
¹ Assumes equal production of B^+ and B^0 at the $\Upsilon(4S)$.			

$\Gamma(D^*(2007)^0 \pi^+ \pi^+ \pi^- \pi^-)/\Gamma(D^*(2010)^- \pi^+ \pi^+ \pi^- \pi^0)$ Γ_{182}/Γ_{67}

VALUE	DOCUMENT ID	TECN	COMMENT
$0.17 \pm 0.04 \pm 0.02$	¹ EDWARDS	02 CLE2	$e^+ e^- \rightarrow \Upsilon(4S)$
¹ Assumes equal production of B^+ and B^0 at the $\Upsilon(4S)$.			

$\Gamma(D^*(2010)^+ D^*(2010)^-)/\Gamma_{total}$ Γ_{183}/Γ

VALUE (units 10^{-4})	CL%	DOCUMENT ID	TECN	COMMENT
8.0 ± 0.6 OUR AVERAGE				
$7.82 \pm 0.38 \pm 0.63$		¹ KRONENBIT...	12 BELL	$e^+ e^- \rightarrow \Upsilon(4S)$
$8.1 \pm 0.6 \pm 1.0$		¹ AUBERT,B	06A BABR	$e^+ e^- \rightarrow \Upsilon(4S)$
$9.9 \pm 4.2 \pm 1.2$		¹ LIPELES	00 CLE2	$e^+ e^- \rightarrow \Upsilon(4S)$
••• We do not use the following data for averages, fits, limits, etc. •••				
$8.1 \pm 0.8 \pm 1.1$		¹ MIYAKE	05 BELL	Repl. by KRONENBIT-TER 12
$8.3 \pm 1.6 \pm 1.2$		^{1,2} AUBERT	02M BABR	Repl. by AUBERT,B 06B
$6.2 \pm 4.0 \pm 1.0$		³ ARTUSO	99 CLE2	Repl. by LIPELES 00
<61	90	⁴ BARATE	98Q ALEP	$e^+ e^- \rightarrow Z$
<22	90	⁵ ASNER	97 CLE2	Repl. by ARTUSO 99

Meson Particle Listings

 B^0

- ¹ Assumes equal production of B^+ and B^0 at the $\Upsilon(4S)$.
² AUBERT 02M also assumes the measured CP -odd fraction of the final states is $0.22 \pm 0.18 \pm 0.03$.
³ ARTUSO 99 uses $B(\Upsilon(4S) \rightarrow B^0 \bar{B}^0) = (48 \pm 4)\%$.
⁴ BARATE 98Q (ALEPH) observes 2 events with an expected background of 0.10 ± 0.03 which corresponds to a branching ratio of $(2.3^{+1.9}_{-1.2} \pm 0.4) \times 10^{-3}$.
⁵ ASNER 97 at CLEO observes 1 event with an expected background of 0.022 ± 0.011 . This corresponds to a branching ratio of $(5.3^{+7.1}_{-3.7} \pm 1.0) \times 10^{-4}$.

 $\Gamma(\bar{D}^*(2007)^0 \omega) / \Gamma_{\text{total}}$ Γ_{184} / Γ

VALUE (units 10^{-4})	CL%	DOCUMENT ID	TECN	COMMENT
3.6 ± 1.1	OUR AVERAGE	Error includes scale factor of 3.1.		
$4.55 \pm 0.24 \pm 0.39$		¹ LEES	11M	BABR $e^+ e^- \rightarrow \Upsilon(4S)$
$2.29 \pm 0.39 \pm 0.40$		¹ BLYTH	06	BELL $e^+ e^- \rightarrow \Upsilon(4S)$
• • • We do not use the following data for averages, fits, limits, etc. • • •				
$4.2 \pm 0.7 \pm 0.9$	90	¹ AUBERT	04B	BABR Repl. by LEES 11M
< 7.9	90	¹ ABE	02J	BELL $e^+ e^- \rightarrow \Upsilon(4S)$
< 7.4	90	² NEMAT1	98	CLE2 $e^+ e^- \rightarrow \Upsilon(4S)$
< 21	90	³ ALAM	94	CLE2 Repl. by NEMAT1 98

- ¹ Assumes equal production of B^+ and B^0 at the $\Upsilon(4S)$.
² NEMAT1 98 assumes equal production of B^+ and B^0 at the $\Upsilon(4S)$ and use the PDG 96 values for D^0 , D^{*0} , η , η' , and ω branching fractions.
³ ALAM 94 assume equal production of B^+ and B^0 at the $\Upsilon(4S)$ and use the CLEO II $B(D^*(2007)^0 \rightarrow D^0 \pi^0)$ and absolute $B(D^0 \rightarrow K^- \pi^+)$ and the PDG 1992 $B(D^0 \rightarrow K^- \pi^+ \pi^0) / B(D^0 \rightarrow K^- \pi^+)$ and $B(D^0 \rightarrow K^- 2\pi^+ \pi^-) / B(D^0 \rightarrow K^- \pi^+)$.

 $\Gamma(\bar{D}^0 \omega) / \Gamma(\bar{D}^*(2007)^0 \omega)$ $\Gamma_{167} / \Gamma_{184}$

VALUE	DOCUMENT ID	TECN	COMMENT
0.58 ± 0.06	OUR AVERAGE		
$0.56 \pm 0.04 \pm 0.04$	LEES	11M	BABR $e^+ e^- \rightarrow \Upsilon(4S)$
$1.04 \pm 0.20 \pm 0.17$	BLYTH	06	BELL $e^+ e^- \rightarrow \Upsilon(4S)$
• • • We do not use the following data for averages, fits, limits, etc. • • •			
$0.7 \pm 0.1 \pm 0.1$	AUBERT	04B	BABR Repl. by LEES 11M

 $\Gamma(D^*(2010)^+ D^-) / \Gamma_{\text{total}}$ Γ_{185} / Γ

VALUE (units 10^{-4})	CL%	DOCUMENT ID	TECN	COMMENT
6.1 ± 1.5	OUR AVERAGE	Error includes scale factor of 1.6.		
$5.7 \pm 0.7 \pm 0.7$		¹ AUBERT,B	06A	BABR $e^+ e^- \rightarrow \Upsilon(4S)$
$11.7 \pm 2.6^{+2.2}_{-2.5}$		^{1,2} ABE	02Q	BELL $e^+ e^- \rightarrow \Upsilon(4S)$
• • • We do not use the following data for averages, fits, limits, etc. • • •				
$8.8 \pm 1.0 \pm 1.3$		¹ AUBERT	03J	BABR Repl. by AUBERT,B 06B
$14.8 \pm 3.8^{+2.8}_{-3.1}$		^{1,3} ABE	02Q	BELL $e^+ e^- \rightarrow \Upsilon(4S)$
< 6.3	90	¹ LIPELES	00	CLE2 $e^+ e^- \rightarrow \Upsilon(4S)$
< 56	90	BARATE	98Q	ALEP $e^+ e^- \rightarrow Z$
< 18	90	ASNER	97	CLE2 $e^+ e^- \rightarrow \Upsilon(4S)$

- ¹ Assumes equal production of B^+ and B^0 at the $\Upsilon(4S)$.
² The measurement is performed using fully reconstructed D^* and D^+ decays.
³ The measurement is performed using a partial reconstruction technique for the D^* and fully reconstructed D^+ decays as a cross check.

 $\Gamma(D^*(2007)^0 \bar{D}^*(2007)^0) / \Gamma_{\text{total}}$ Γ_{186} / Γ

VALUE (units 10^{-4})	CL%	DOCUMENT ID	TECN	COMMENT
< 0.9	90	¹ AUBERT,B	06A	BABR $e^+ e^- \rightarrow \Upsilon(4S)$
• • • We do not use the following data for averages, fits, limits, etc. • • •				
< 270	90	BARATE	98Q	ALEP $e^+ e^- \rightarrow Z$

- ¹ Assumes equal production of B^+ and B^0 at the $\Upsilon(4S)$.

 $\Gamma(D^- D^0 K^+) / \Gamma_{\text{total}}$ Γ_{187} / Γ

VALUE (units 10^{-3})	DOCUMENT ID	TECN	COMMENT
$1.07 \pm 0.07 \pm 0.09$	¹ DEL-AMO-SA..11B	BABR	$e^+ e^- \rightarrow \Upsilon(4S)$
• • • We do not use the following data for averages, fits, limits, etc. • • •			
$1.7 \pm 0.3 \pm 0.3$	¹ AUBERT	03X	BABR Repl. by DEL-AMO-SANCHEZ 11B

- ¹ Assumes equal production of B^+ and B^0 at the $\Upsilon(4S)$.

 $\Gamma(D^- D^*(2007)^0 K^+) / \Gamma_{\text{total}}$ Γ_{188} / Γ

VALUE (units 10^{-3})	DOCUMENT ID	TECN	COMMENT
$3.46 \pm 0.18 \pm 0.37$	¹ DEL-AMO-SA..11B	BABR	$e^+ e^- \rightarrow \Upsilon(4S)$
• • • We do not use the following data for averages, fits, limits, etc. • • •			
$4.6 \pm 0.7 \pm 0.7$	¹ AUBERT	03X	BABR Repl. by DEL-AMO-SANCHEZ 11B

- ¹ Assumes equal production of B^+ and B^0 at the $\Upsilon(4S)$.

 $\Gamma(D^*(2010)^- D^0 K^+) / \Gamma_{\text{total}}$ Γ_{189} / Γ

VALUE (units 10^{-3})	DOCUMENT ID	TECN	COMMENT
$2.47 \pm 0.10 \pm 0.18$	¹ DEL-AMO-SA..11B	BABR	$e^+ e^- \rightarrow \Upsilon(4S)$
• • • We do not use the following data for averages, fits, limits, etc. • • •			
$3.1^{+0.4}_{-0.3} \pm 0.4$	¹ AUBERT	03X	BABR Repl. by DEL-AMO-SANCHEZ 11B

- ¹ Assumes equal production of B^+ and B^0 at the $\Upsilon(4S)$.

 $\Gamma(D^*(2010)^- D^0 K^+) / \Gamma(D^- D^0 K^+)$ $\Gamma_{189} / \Gamma_{187}$

VALUE	DOCUMENT ID	TECN	COMMENT
$1.754 \pm 0.028 \pm 0.038$	¹ AAIJ	20AN	LHCB pp at 7, 8, 13 TeV
¹ Uses $D^+ \rightarrow K^- \pi^+ \pi^+$, $D^0 \rightarrow K^- \pi^+$ and $D^0 \rightarrow K^- \pi^+ \pi^+ \pi^-$ decays.			

 $\Gamma(D^*(2010)^- D^*(2007)^0 K^+) / \Gamma_{\text{total}}$ Γ_{190} / Γ

VALUE (units 10^{-3})	DOCUMENT ID	TECN	COMMENT
$10.6 \pm 0.33 \pm 0.86$	¹ DEL-AMO-SA..11B	BABR	$e^+ e^- \rightarrow \Upsilon(4S)$
• • • We do not use the following data for averages, fits, limits, etc. • • •			
$11.8 \pm 1.0 \pm 1.7$	¹ AUBERT	03X	BABR Repl. by DEL-AMO-SANCHEZ 11B

- ¹ Assumes equal production of B^+ and B^0 at the $\Upsilon(4S)$.

 $\Gamma(D^- D^+ K^0) / \Gamma_{\text{total}}$ Γ_{191} / Γ

VALUE (units 10^{-3})	CL%	DOCUMENT ID	TECN	COMMENT
$0.75 \pm 0.12 \pm 0.12$		¹ DEL-AMO-SA..11B	BABR	$e^+ e^- \rightarrow \Upsilon(4S)$
• • • We do not use the following data for averages, fits, limits, etc. • • •				
< 1.7	90	¹ AUBERT	03X	BABR Repl. by DEL-AMO-SANCHEZ 11B

- ¹ Assumes equal production of B^+ and B^0 at the $\Upsilon(4S)$.

 $[\Gamma(D^*(2010)^- D^+ K^0) + \Gamma(D^- D^*(2010)^+ K^0)] / \Gamma_{\text{total}}$ Γ_{192} / Γ

VALUE (units 10^{-3})	DOCUMENT ID	TECN	COMMENT
$6.41 \pm 0.36 \pm 0.39$	¹ DEL-AMO-SA..11B	BABR	$e^+ e^- \rightarrow \Upsilon(4S)$
• • • We do not use the following data for averages, fits, limits, etc. • • •			
$6.5 \pm 1.2 \pm 1.0$	¹ AUBERT	03X	BABR Repl. by DEL-AMO-SANCHEZ 11B

- ¹ Assumes equal production of B^+ and B^0 at the $\Upsilon(4S)$.

 $\Gamma(D^*(2010)^- D^*(2010)^+ K^0) / \Gamma_{\text{total}}$ Γ_{193} / Γ

VALUE (units 10^{-3})	DOCUMENT ID	TECN	COMMENT
8.1 ± 0.7	OUR AVERAGE		
$8.26 \pm 0.43 \pm 0.67$	¹ DEL-AMO-SA..11B	BABR	$e^+ e^- \rightarrow \Upsilon(4S)$
$6.8 \pm 0.8 \pm 1.4$	^{1,2} DALSENO	07	BELL $e^+ e^- \rightarrow \Upsilon(4S)$
$8.8 \pm 0.8 \pm 1.4$	^{1,2} AUBERT,B	06Q	BABR $e^+ e^- \rightarrow \Upsilon(4S)$
• • • We do not use the following data for averages, fits, limits, etc. • • •			
$8.8^{+1.5}_{-1.4} \pm 1.3$	¹ AUBERT	03X	BABR Repl. by AUBERT,B 06Q

- ¹ Assumes equal production of B^+ and B^0 at the $\Upsilon(4S)$.
² The result is rescaled by a factor of 2 to convert from K_S^0 to K^0 .

 $\Gamma(D^{*-} D_{s1}(2536)^+, D_{s1}^+ \rightarrow D^{*+} K^0) / \Gamma_{\text{total}}$ Γ_{194} / Γ

VALUE (units 10^{-4})	DOCUMENT ID	TECN	COMMENT
8.0 ± 2.4	OUR AVERAGE		
$7.6^{+4.8+1.6}_{-4.2-1.4}$	^{1,2} DALSENO	07	BELL $e^+ e^- \rightarrow \Upsilon(4S)$
$8.2 \pm 2.6 \pm 1.2$	^{1,2} AUBERT,B	06Q	BABR $e^+ e^- \rightarrow \Upsilon(4S)$

- ¹ Assumes equal production of B^+ and B^0 at the $\Upsilon(4S)$.
² The result is rescaled by a factor of 2 to convert from K_S^0 to K^0 .

 $\Gamma(\bar{D}^0 D^0 K^0) / \Gamma_{\text{total}}$ Γ_{195} / Γ

VALUE (units 10^{-3})	CL%	DOCUMENT ID	TECN	COMMENT
$0.27 \pm 0.10 \pm 0.05$		¹ DEL-AMO-SA..11B	BABR	$e^+ e^- \rightarrow \Upsilon(4S)$
• • • We do not use the following data for averages, fits, limits, etc. • • •				
< 1.4	90	¹ AUBERT	03X	BABR Repl. by DEL-AMO-SANCHEZ 11B

- ¹ Assumes equal production of B^+ and B^0 at the $\Upsilon(4S)$.

 $\Gamma(D^0 D^0 K^+ \pi^-) / \Gamma(D^*(2010)^- D^0 K^+)$ $\Gamma_{196} / \Gamma_{189}$

VALUE (%)	DOCUMENT ID	TECN	COMMENT
$14.2 \pm 1.1 \pm 1.0$	¹ AAIJ	20AG	LHCB pp at 7, 8, and 13 TeV
¹ AAIJ 20AG excluded contributions from $B^0 \rightarrow D^{*-} D^0 K^+$ transitions with $D^{*-} \rightarrow \bar{D}^0 \pi^-$.			

 $[\Gamma(\bar{D}^0 D^*(2007)^0 K^0) + \Gamma(\bar{D}^*(2007)^0 D^0 K^0)] / \Gamma_{\text{total}}$ Γ_{197} / Γ

VALUE (units 10^{-3})	CL%	DOCUMENT ID	TECN	COMMENT
$1.08 \pm 0.32 \pm 0.36$		¹ DEL-AMO-SA..11B	BABR	$e^+ e^- \rightarrow \Upsilon(4S)$
• • • We do not use the following data for averages, fits, limits, etc. • • •				
< 3.7	90	¹ AUBERT	03X	BABR Repl. by DEL-AMO-SANCHEZ 11B

- ¹ Assumes equal production of B^+ and B^0 at the $\Upsilon(4S)$.

 $\Gamma(\bar{D}^*(2007)^0 D^*(2007)^0 K^0) / \Gamma_{\text{total}}$ Γ_{198} / Γ

VALUE (units 10^{-3})	CL%	DOCUMENT ID	TECN	COMMENT
$2.40 \pm 0.55 \pm 0.67$		¹ DEL-AMO-SA..11B	BABR	$e^+ e^- \rightarrow \Upsilon(4S)$
• • • We do not use the following data for averages, fits, limits, etc. • • •				
< 6.6	90	¹ AUBERT	03X	BABR Repl. by DEL-AMO-SANCHEZ 11B

- ¹ Assumes equal production of B^+ and B^0 at the $\Upsilon(4S)$.

$\Gamma((\bar{D} + \bar{D}^*)(D + D^*)K)/\Gamma_{\text{total}}$	Γ_{199}/Γ		
VALUE (units 10 ⁻²)	DOCUMENT ID	TECN	COMMENT
3.68 ± 0.10 ± 0.24	¹ DEL-AMO-SA...11B	BABR	e ⁺ e ⁻ → $\Upsilon(4S)$
• • • We do not use the following data for averages, fits, limits, etc. • • •			
4.3 ± 0.3 ± 0.6	¹ AUBERT	03x BABR	Repl. by DEL-AMO-SANCHEZ 11B

¹ Assumes equal production of B⁺ and B⁰ at the $\Upsilon(4S)$.

$\Gamma(\eta_c K^0)/\Gamma_{\text{total}}$	Γ_{200}/Γ		
VALUE (units 10 ⁻³)	DOCUMENT ID	TECN	COMMENT
0.90 ± 0.11 OUR AVERAGE			
1.04 ^{+0.18} _{-0.15} ± 0.13	¹ CHILIKIN	19 BELL	e ⁺ e ⁻ → $\Upsilon(4S)$
0.62 ^{+0.21} _{-0.20} ± 0.05	^{2,3} AUBERT	07AV BABR	e ⁺ e ⁻ → $\Upsilon(4S)$
0.91 ± 0.16 ± 0.05	^{2,4} AUBERT,B	04B BABR	e ⁺ e ⁻ → $\Upsilon(4S)$
1.23 ± 0.23 ^{+0.40} _{-0.41}	² FANG	03 BELL	e ⁺ e ⁻ → $\Upsilon(4S)$
1.09 ^{+0.55} _{-0.42} ± 0.33	⁵ EDWARDS	01 CLE2	e ⁺ e ⁻ → $\Upsilon(4S)$

¹ CHILIKIN 19 reports $[\Gamma(B^0 \rightarrow \eta_c K^0)/\Gamma_{\text{total}}] \times [B(\eta_c(1S) \rightarrow p\bar{p}\pi^+\pi^-)] = (38.0^{+6.4+1.3}_{-2.9-4.7}) \times 10^{-7}$ which we divide by our best value $B(\eta_c(1S) \rightarrow p\bar{p}\pi^+\pi^-) = (3.7 \pm 0.5) \times 10^{-3}$. Our first error is their experiment's error and our second error is the systematic error from using our best value.

² Assumes equal production of B⁺ and B⁰ at the $\Upsilon(4S)$.

³ AUBERT 07AV reports $[\Gamma(B^0 \rightarrow \eta_c K^0)/\Gamma_{\text{total}}] \times [B(\eta_c(1S) \rightarrow p\bar{p})] = (0.83^{+0.28}_{-0.26} \pm 0.05) \times 10^{-6}$ which we divide by our best value $B(\eta_c(1S) \rightarrow p\bar{p}) = (1.33 \pm 0.11) \times 10^{-3}$. Our first error is their experiment's error and our second error is the systematic error from using our best value.

⁴ AUBERT,B 04B reports $[\Gamma(B^0 \rightarrow \eta_c K^0)/\Gamma_{\text{total}}] \times [B(\eta_c(1S) \rightarrow K\bar{K}\pi)] = (0.0648 \pm 0.0085 \pm 0.0071) \times 10^{-3}$ which we divide by our best value $B(\eta_c(1S) \rightarrow K\bar{K}\pi) = (7.1 \pm 0.4) \times 10^{-2}$. Our first error is their experiment's error and our second error is the systematic error from using our best value.

⁵ EDWARDS 01 assumes equal production of B⁰ and B⁺ at the $\Upsilon(4S)$. The correlated uncertainties (28.3)% from $B(J/\psi(1S) \rightarrow \gamma\eta_c)$ in those modes have been accounted for.

$\Gamma(\eta_c K^0)/\Gamma(J/\psi(1S)K^0)$	$\Gamma_{200}/\Gamma_{214}$		
VALUE	DOCUMENT ID	TECN	COMMENT
1.39 ± 0.20 ± 0.45	¹ AUBERT,B	04B BABR	e ⁺ e ⁻ → $\Upsilon(4S)$
¹ Uses BABAR measurement of $B(B^0 \rightarrow J/\psi K^0) = (8.5 \pm 0.5 \pm 0.6) \times 10^{-4}$.			

$\Gamma(\eta_c(1S)K^+\pi^-)/\Gamma(J/\psi(1S)K^+\pi^-)$	$\Gamma_{201}/\Gamma_{215}$		
VALUE	DOCUMENT ID	TECN	COMMENT
0.57 ± 0.03 ± 0.05	¹ AAIJ	18AN LHCB	pp at 7, 8, 13 TeV
¹ AAIJ 18AN reports $[\Gamma(B^0 \rightarrow \eta_c(1S)K^+\pi^-)/\Gamma(B^0 \rightarrow J/\psi(1S)K^+\pi^-)] \times [B(\eta_c(1S) \rightarrow p\bar{p})] / [B(J/\psi(1S) \rightarrow p\bar{p})] = 0.357 \pm 0.015 \pm 0.008$ which we multiply or divide by our best values $B(\eta_c(1S) \rightarrow p\bar{p}) = (1.33 \pm 0.11) \times 10^{-3}$, $B(J/\psi(1S) \rightarrow p\bar{p}) = (2.120 \pm 0.029) \times 10^{-3}$. Our first error is their experiment's error and our second error is the systematic error from using our best values.			

$\Gamma(\eta_c(1S)K^*(1410)^0)/\Gamma(\eta_c(1S)K^+\pi^-)$	$\Gamma_{204}/\Gamma_{201}$		
VALUE (units 10 ⁻²)	DOCUMENT ID	TECN	COMMENT
32 ± 24 ± 6	¹ AAIJ	18AN LHCB	pp at 7, 8, 13 TeV
¹ AAIJ 18AN reports $[\Gamma(B^0 \rightarrow \eta_c(1S)K^*(1410)^0)/\Gamma(B^0 \rightarrow \eta_c(1S)K^+\pi^-)] \times [B(K^*(1410) \rightarrow K\pi)] = 0.021 \pm 0.011 \pm 0.011$ which we divide by our best value $B(K^*(1410) \rightarrow K\pi) = (6.6 \pm 1.3) \times 10^{-2}$. Our first error is their experiment's error and our second error is the systematic error from using our best value.			

$\Gamma(\eta_c(1S)K^+\pi^-(NR))/\Gamma(\eta_c(1S)K^+\pi^-)$	$\Gamma_{202}/\Gamma_{201}$		
VALUE (units 10 ⁻²)	DOCUMENT ID	TECN	COMMENT
10.3 ± 1.4^{+1.0}_{-1.2}	AAIJ	18AN LHCB	pp at 7, 8, 13 TeV

$\Gamma(\eta_c(1S)K_0^*(1430)^0)/\Gamma(\eta_c(1S)K^+\pi^-)$	$\Gamma_{205}/\Gamma_{201}$		
VALUE (units 10 ⁻²)	DOCUMENT ID	TECN	COMMENT
27 ± 5 ± 3	¹ AAIJ	18AN LHCB	pp at 7, 8, 13 TeV
¹ AAIJ 18AN reports $[\Gamma(B^0 \rightarrow \eta_c(1S)K_0^*(1430)^0)/\Gamma(B^0 \rightarrow \eta_c(1S)K^+\pi^-)] \times [B(K_0^*(1430) \rightarrow K\pi)] = 0.253 \pm 0.035^{+0.035}_{-0.028}$ which we divide by our best value $B(K_0^*(1430) \rightarrow K\pi) = (93 \pm 10) \times 10^{-2}$. Our first error is their experiment's error and our second error is the systematic error from using our best value.			

$\Gamma(\eta_c(1S)K_2^*(1430)^0)/\Gamma(\eta_c(1S)K^+\pi^-)$	$\Gamma_{206}/\Gamma_{201}$		
VALUE (units 10 ⁻²)	DOCUMENT ID	TECN	COMMENT
8.2^{+3.6}_{-4.4} ± 0.2	¹ AAIJ	18AN LHCB	pp at 7, 8, 13 TeV
¹ AAIJ 18AN reports $[\Gamma(B^0 \rightarrow \eta_c(1S)K_2^*(1430)^0)/\Gamma(B^0 \rightarrow \eta_c(1S)K^+\pi^-)] \times [B(K_2^*(1430) \rightarrow K\pi)] = 0.041 \pm 0.015^{+0.010}_{-0.016}$ which we divide by our best value $B(K_2^*(1430) \rightarrow K\pi) = (49.9 \pm 1.2) \times 10^{-2}$. Our first error is their experiment's error and our second error is the systematic error from using our best value.			

$\Gamma(\eta_c(1S)K^*(1680)^0)/\Gamma(\eta_c(1S)K^+\pi^-)$	$\Gamma_{207}/\Gamma_{201}$		
VALUE (units 10 ⁻²)	DOCUMENT ID	TECN	COMMENT
5.7^{+6.5}_{-6.8} ± 0.4	¹ AAIJ	18AN LHCB	pp at 7, 8, 13 TeV
¹ AAIJ 18AN reports $[\Gamma(B^0 \rightarrow \eta_c(1S)K^*(1680)^0)/\Gamma(B^0 \rightarrow \eta_c(1S)K^+\pi^-)] \times [B(K^*(1680) \rightarrow K\pi)] = 0.022 \pm 0.020^{+0.015}_{-0.017}$ which we divide by our best value $B(K^*(1680) \rightarrow K\pi) = (38.7 \pm 2.5) \times 10^{-2}$. Our first error is their experiment's error and our second error is the systematic error from using our best value.			

$\Gamma(\eta_c(1S)K_0^*(1950)^0)/\Gamma(\eta_c(1S)K^+\pi^-)$	$\Gamma_{208}/\Gamma_{201}$		
VALUE (units 10 ⁻²)	DOCUMENT ID	TECN	COMMENT
7⁺⁴₋₆ ± 2	¹ AAIJ	18AN LHCB	pp at 7, 8, 13 TeV
¹ AAIJ 18AN reports $[\Gamma(B^0 \rightarrow \eta_c(1S)K_0^*(1950)^0)/\Gamma(B^0 \rightarrow \eta_c(1S)K^+\pi^-)] \times [B(K_0^*(1950) \rightarrow K^-\pi^+)] = 0.038 \pm 0.018^{+0.014}_{-0.025}$ which we divide by our best value $B(K_0^*(1950) \rightarrow K^-\pi^+) = (52 \pm 14) \times 10^{-2}$. Our first error is their experiment's error and our second error is the systematic error from using our best value.			

$\Gamma(T_{cc}^-(4100)^-K^+, T_{cc}^-(4100)^-\eta_c\pi^-)/\Gamma(\eta_c(1S)K^+\pi^-)$	$\Gamma_{203}/\Gamma_{201}$		
VALUE (units 10 ⁻²)	DOCUMENT ID	TECN	COMMENT
3.3 ± 1.1^{+1.2}_{-1.1}	AAIJ	18AN LHCB	pp at 7, 8, 13 TeV

$\Gamma(\eta_c K^*(892)^0)/\Gamma_{\text{total}}$	Γ_{209}/Γ		
VALUE (units 10 ⁻⁴)	DOCUMENT ID	TECN	COMMENT
5.3^{+0.8}_{-0.9} OUR AVERAGE			Error includes scale factor of 1.7. See the ideogram below.
4.42 ± 0.24 ^{+0.54} _{-0.66}	¹ AAIJ	18AN LHCB	pp at 7, 8, 13 TeV
6.8 ± 0.9 ± 0.4	^{2,3} AUBERT	08AB BABR	e ⁺ e ⁻ → $\Upsilon(4S)$
7.7 ^{+2.4} _{-2.2} ± 0.7	^{4,5} AUBERT	07AV BABR	e ⁺ e ⁻ → $\Upsilon(4S)$
16.2 ± 3.2 ^{+5.5} _{-6.0}	⁵ FANG	03 BELL	e ⁺ e ⁻ → $\Upsilon(4S)$

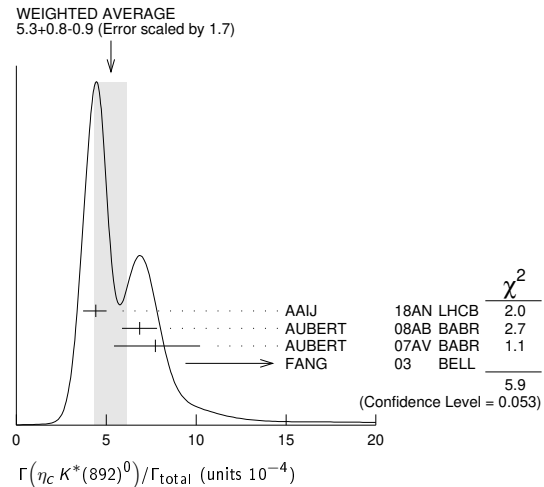
¹ AAIJ 18AN reports $B(B^0 \rightarrow \eta_c K^*(892)^0)$, $K^*(892)^0 \rightarrow K^+\pi^- = (2.95 \pm 0.16^{+0.36}_{-0.44}) \times 10^{-4}$ using the fitted fraction of $0.514 \pm 0.019^{+0.017}_{-0.048}$ from Dalitz decay of $B(B^0 \rightarrow \eta_c K^+\pi^-) = (5.73 \pm 0.24 \pm 0.67) \times 10^{-4}$ and corrected for $B(K^*(892)^0 \rightarrow K^+\pi^-) = 2/3$.

² AUBERT 08AB reports $[\Gamma(B^0 \rightarrow \eta_c K^*(892)^0)/\Gamma_{\text{total}}] / [B(B^+ \rightarrow \eta_c K^+)] = 0.62 \pm 0.06 \pm 0.05$ which we multiply by our best value $B(B^+ \rightarrow \eta_c K^+) = (1.10 \pm 0.07) \times 10^{-3}$. Our first error is their experiment's error and our second error is the systematic error from using our best value.

³ Uses the production ratio of $(B^+B^-)/(B^0\bar{B}^0) = 1.026 \pm 0.032$ at $\Upsilon(4S)$.

⁴ AUBERT 07AV reports $[\Gamma(B^0 \rightarrow \eta_c K^*(892)^0)/\Gamma_{\text{total}}] \times [B(\eta_c(1S) \rightarrow p\bar{p})] = (1.03^{+0.27}_{-0.24} \pm 0.17) \times 10^{-6}$ which we divide by our best value $B(\eta_c(1S) \rightarrow p\bar{p}) = (1.33 \pm 0.11) \times 10^{-3}$. Our first error is their experiment's error and our second error is the systematic error from using our best value.

⁵ Assumes equal production of B⁺ and B⁰ at the $\Upsilon(4S)$.



$\Gamma(\eta_c(2S)K_0^0, \eta_c \rightarrow p\bar{p}\pi^+\pi^-)/\Gamma_{\text{total}}$	Γ_{210}/Γ		
VALUE (units 10 ⁻⁷)	DOCUMENT ID	TECN	COMMENT
4.2 ± 1.4 ± 0.3	CHILIKIN	19 BELL	e ⁺ e ⁻ → $\Upsilon(4S)$

$\Gamma(\eta_c(2S)K^*0)/\Gamma_{\text{total}}$	Γ_{211}/Γ			
VALUE (units 10 ⁻⁴)	CL%	DOCUMENT ID	TECN	COMMENT
<3.9	90	¹ AUBERT	08AB BABR	e ⁺ e ⁻ → $\Upsilon(4S)$
¹ Uses the production ratio of $(B^+B^-)/(B^0\bar{B}^0) = 1.026 \pm 0.032$ at $\Upsilon(4S)$.				

Meson Particle Listings

 B^0

$\Gamma(h_c(1P) K_S^0)/\Gamma_{\text{total}}$	Γ_{212}/Γ		
VALUE	DOCUMENT ID	TECN	COMMENT
$<1.4 \times 10^{-5}$	CHILIKIN	19	BELL $e^+e^- \rightarrow \Upsilon(4S)$

$\Gamma(B^0 \rightarrow h_c(1P) K^{*0})/\Gamma_{\text{total}} \times \Gamma(h_c(1P) \rightarrow \gamma \eta_c(1S))/\Gamma_{\text{total}}$	$\Gamma_{213}/\Gamma \times \Gamma_{25}^{h_c(1P)}/\Gamma_{h_c(1P)}$		
VALUE (units 10^{-4})	DOCUMENT ID	TECN	COMMENT
<2.2	90	1	AUBERT 08AB BABR $e^+e^- \rightarrow \Upsilon(4S)$

¹ Uses the production ratio of $(B^+B^-)/(B^0\bar{B}^0) = 1.026 \pm 0.032$ at $\Upsilon(4S)$.

$\Gamma(\eta_c K^*(892)^0)/\Gamma(\eta_c K^0)$	$\Gamma_{209}/\Gamma_{200}$		
VALUE	DOCUMENT ID	TECN	COMMENT
$1.33 \pm 0.36^{+0.24}_{-0.33}$	FANG	03	BELL $e^+e^- \rightarrow \Upsilon(4S)$

$\Gamma(J/\psi(1S) K^0)/\Gamma_{\text{total}}$	Γ_{214}/Γ		
VALUE (units 10^{-4})	DOCUMENT ID	TECN	COMMENT
8.91 ± 0.21 OUR FIT			
8.91 ± 0.21 OUR AVERAGE			

VALUE (units 10^{-4})	CL%	EVTS	DOCUMENT ID	TECN	COMMENT
9.02 ± 0.10 ± 0.26			1	CHOUDHURY 21	BELL $e^+e^- \rightarrow \Upsilon(4S)$
8.1 ± 0.9 ± 0.6			2	CHILIKIN 19	BELL $e^+e^- \rightarrow \Upsilon(4S)$
8.8 $^{+1.4}_{-1.3} \pm 0.1$			3,4	AUBERT 07AV	BABR $e^+e^- \rightarrow \Upsilon(4S)$
8.69 ± 0.22 ± 0.30			4	AUBERT 05J	BABR $e^+e^- \rightarrow \Upsilon(4S)$
9.5 ± 0.8 ± 0.6			4	VERY 00	CLE2 $e^+e^- \rightarrow \Upsilon(4S)$
11.5 ± 2.3 ± 1.7			5	ABE 96H	CDF $p\bar{p}$ at 1.8 TeV
6.93 ± 4.07 ± 0.04			6	BORTOLETTO 92	CLEO $e^+e^- \rightarrow \Upsilon(4S)$
9.24 ± 7.21 ± 0.05		2	7	ALBRECHT 90J	ARG $e^+e^- \rightarrow \Upsilon(4S)$
• • • We do not use the following data for averages, fits, limits, etc. • • •					
7.9 ± 0.4 ± 0.9			4	ABE 03B	BELL Repl. by CHOUDHURY 21
8.3 ± 0.4 ± 0.5			4	AUBERT 02	BABR Repl. by AUBERT 05J
8.5 $^{+1.4}_{-1.2} \pm 0.6$			4	JESSOP 97	CLE2 Repl. by AVERY 00
7.5 ± 2.4 ± 0.8		10	6	ALAM 94	CLE2 Sup. by JESSOP 97
<50	90		6	ALAM 86	CLEO $e^+e^- \rightarrow \Upsilon(4S)$

¹ CHOUDHURY 21 uses the relative production fraction of charged (f^{\pm}) to neutral (f^0) B mesons at $\Upsilon(4S)$ value of $f^{\pm}/f^0 = 1.058 \pm 0.024$.

² CHILIKIN 19 reports $[\Gamma(B^0 \rightarrow J/\psi(1S) K^0)/\Gamma_{\text{total}}] \times [B(J/\psi(1S) \rightarrow p\bar{p}\pi^+\pi^-)] = (48.6^{+4.6+2.4}_{-4.4-2.6}) \times 10^{-7}$ which we divide by our best value $B(J/\psi(1S) \rightarrow p\bar{p}\pi^+\pi^-) = (6.0 \pm 0.5) \times 10^{-3}$. Our first error is their experiment's error and our second error is the systematic error from using our best value.

³ AUBERT 07AV reports $[\Gamma(B^0 \rightarrow J/\psi(1S) K^0)/\Gamma_{\text{total}}] \times [B(J/\psi(1S) \rightarrow p\bar{p})] = (1.87^{+0.28}_{-0.26} \pm 0.07) \times 10^{-6}$ which we divide by our best value $B(J/\psi(1S) \rightarrow p\bar{p}) = (2.120 \pm 0.029) \times 10^{-3}$. Our first error is their experiment's error and our second error is the systematic error from using our best value.

⁴ Assumes equal production of B^+ and B^0 at the $\Upsilon(4S)$.

⁵ ABE 96H assumes that $B(B^+ \rightarrow J/\psi K^+) = (1.02 \pm 0.14) \times 10^{-3}$.

⁶ BORTOLETTO 92 reports $(6 \pm 3 \pm 2) \times 10^{-4}$ from a measurement of $[\Gamma(B^0 \rightarrow J/\psi(1S) K^0)/\Gamma_{\text{total}}] \times [B(J/\psi(1S) \rightarrow e^+e^-)]$ assuming $B(J/\psi(1S) \rightarrow e^+e^-) = 0.069 \pm 0.009$, which we rescale to our best value $B(J/\psi(1S) \rightarrow e^+e^-) = (5.971 \pm 0.032) \times 10^{-2}$. Our first error is their experiment's error and our second error is the systematic error from using our best value. Assumes equal production of B^+ and B^0 at the $\Upsilon(4S)$.

⁷ ALBRECHT 90J reports $(8 \pm 6 \pm 2) \times 10^{-4}$ from a measurement of $[\Gamma(B^0 \rightarrow J/\psi(1S) K^0)/\Gamma_{\text{total}}] \times [B(J/\psi(1S) \rightarrow e^+e^-)]$ assuming $B(J/\psi(1S) \rightarrow e^+e^-) = 0.069 \pm 0.009$, which we rescale to our best value $B(J/\psi(1S) \rightarrow e^+e^-) = (5.971 \pm 0.032) \times 10^{-2}$. Our first error is their experiment's error and our second error is the systematic error from using our best value. Assumes equal production of B^+ and B^0 at the $\Upsilon(4S)$.

$\Gamma(J/\psi(1S) K^+\pi^-)/\Gamma_{\text{total}}$	Γ_{215}/Γ		
VALUE (units 10^{-3})	DOCUMENT ID	TECN	COMMENT
1.15 ± 0.05 OUR AVERAGE			
1.15 ± 0.01 ± 0.05	CHILIKIN	14	BELL $\bar{B}^0 \rightarrow J/\psi K^-\pi^+$
1.16 ± 0.56 ± 0.01	1	BORTOLETTO 92	CLEO $e^+e^- \rightarrow \Upsilon(4S)$

• • • We do not use the following data for averages, fits, limits, etc. • • •

1.079 ± 0.011	2	AUBERT 09AA	BABR $e^+e^- \rightarrow \Upsilon(4S)$	
<1.3	90	3	ALBRECHT 87D	ARG $e^+e^- \rightarrow \Upsilon(4S)$
<6.3	90		GILES 84	CLEO $e^+e^- \rightarrow \Upsilon(4S)$

¹ BORTOLETTO 92 reports $(1.0 \pm 0.4 \pm 0.3) \times 10^{-3}$ from a measurement of $[\Gamma(B^0 \rightarrow J/\psi(1S) K^+\pi^-)/\Gamma_{\text{total}}] \times [B(J/\psi(1S) \rightarrow e^+e^-)]$ assuming $B(J/\psi(1S) \rightarrow e^+e^-) = 0.069 \pm 0.009$, which we rescale to our best value $B(J/\psi(1S) \rightarrow e^+e^-) = (5.971 \pm 0.032) \times 10^{-2}$. Our first error is their experiment's error and our second error is the systematic error from using our best value. Assumes equal production of B^+ and B^0 at the $\Upsilon(4S)$.

² Does not report systematic uncertainties.

³ ALBRECHT 87D assume $B^+B^-/B^0\bar{B}^0$ ratio is 55/45. $K\pi$ system is specifically selected as nonresonant.

$\Gamma(J/\psi(1S) K^*(892)^0)/\Gamma_{\text{total}}$	Γ_{216}/Γ		
VALUE (units 10^{-3})	DOCUMENT ID	TECN	COMMENT
1.27 ± 0.05 OUR FIT			
1.28 ± 0.05 OUR AVERAGE			

VALUE (units 10^{-3})	EVTS	DOCUMENT ID	TECN	COMMENT
1.19 ± 0.01 ± 0.08		CHILIKIN	14	BELL $\bar{B}^0 \rightarrow J/\psi K^-\pi^+$
1.33 $^{+0.22}_{-0.21} \pm 0.02$		1,2	AUBERT 07AV	BABR $e^+e^- \rightarrow \Upsilon(4S)$
1.309 ± 0.026 ± 0.077		2	AUBERT 05J	BABR $e^+e^- \rightarrow \Upsilon(4S)$
1.29 ± 0.05 ± 0.13		2	ABE 02N	BELL $e^+e^- \rightarrow \Upsilon(4S)$
1.74 ± 0.20 ± 0.18		3	ABE 98O	CDF $p\bar{p}$ 1.8 TeV
1.32 ± 0.17 ± 0.17		4	JESSOP 97	CLE2 $e^+e^- \rightarrow \Upsilon(4S)$
1.27 ± 0.65 ± 0.01		5	BORTOLETTO 92	CLEO $e^+e^- \rightarrow \Upsilon(4S)$
1.27 ± 0.60 ± 0.01	6	6	ALBRECHT 90J	ARG $e^+e^- \rightarrow \Upsilon(4S)$
4.04 ± 1.81 ± 0.02	5	7	BEBEK 87	CLEO $e^+e^- \rightarrow \Upsilon(4S)$

• • • We do not use the following data for averages, fits, limits, etc. • • •

1.24 ± 0.05 ± 0.09	2	AUBERT 02	BABR	Repl. by AUBERT 05J
1.36 ± 0.27 ± 0.22	8	ABE 96H	CDF	Sup. by ABE 98O
1.69 ± 0.31 ± 0.18	29	9	ALAM 94	CLE2 Sup. by JESSOP 97
		10	ALBRECHT 94G	ARG $e^+e^- \rightarrow \Upsilon(4S)$
4.0 ± 0.30		11	ALBAJAR 91E	UA1 $E_{\text{cm}}^{\text{pp}}$ = 630 GeV
3.3 ± 0.18	5	12	ALBRECHT 87D	ARG $e^+e^- \rightarrow \Upsilon(4S)$
4.1 ± 0.18	5	13	ALAM 86	CLEO Repl. by BEBEK 87

¹ AUBERT 07AV reports $[\Gamma(B^0 \rightarrow J/\psi(1S) K^*(892)^0)/\Gamma_{\text{total}}] \times [B(J/\psi(1S) \rightarrow p\bar{p})] = (2.82^{+0.30+0.36}_{-0.28-0.35}) \times 10^{-6}$ which we divide by our best value $B(J/\psi(1S) \rightarrow p\bar{p}) = (2.120 \pm 0.029) \times 10^{-3}$. Our first error is their experiment's error and our second error is the systematic error from using our best value.

² Assumes equal production of B^+ and B^0 at the $\Upsilon(4S)$.

³ ABE 98O reports $[B(B^0 \rightarrow J/\psi(1S) K^*(892)^0)]/[B(B^+ \rightarrow J/\psi(1S) K^+)] = 1.76 \pm 0.14 \pm 0.15$. We multiply by our best value $B(B^+ \rightarrow J/\psi(1S) K^+) = (9.9 \pm 1.0) \times 10^{-4}$. Our first error is their experiment's error and our second error is the systematic error from using our best value.

⁴ Assumes equal production of B^+ and B^0 at the $\Upsilon(4S)$.

⁵ BORTOLETTO 92 reports $(1.1 \pm 0.5 \pm 0.3) \times 10^{-3}$ from a measurement of $[\Gamma(B^0 \rightarrow J/\psi(1S) K^*(892)^0)/\Gamma_{\text{total}}] \times [B(J/\psi(1S) \rightarrow e^+e^-)]$ assuming $B(J/\psi(1S) \rightarrow e^+e^-) = 0.069 \pm 0.009$, which we rescale to our best value $B(J/\psi(1S) \rightarrow e^+e^-) = (5.971 \pm 0.032) \times 10^{-2}$. Our first error is their experiment's error and our second error is the systematic error from using our best value. Assumes equal production of B^+ and B^0 at the $\Upsilon(4S)$.

⁶ ALBRECHT 90J reports $(1.1 \pm 0.5 \pm 0.2) \times 10^{-3}$ from a measurement of $[\Gamma(B^0 \rightarrow J/\psi(1S) K^*(892)^0)/\Gamma_{\text{total}}] \times [B(J/\psi(1S) \rightarrow e^+e^-)]$ assuming $B(J/\psi(1S) \rightarrow e^+e^-) = 0.069 \pm 0.009$, which we rescale to our best value $B(J/\psi(1S) \rightarrow e^+e^-) = (5.971 \pm 0.032) \times 10^{-2}$. Our first error is their experiment's error and our second error is the systematic error from using our best value. Assumes equal production of B^+ and B^0 at the $\Upsilon(4S)$.

⁷ BEBEK 87 reports $(3.5 \pm 1.6 \pm 0.3) \times 10^{-3}$ from a measurement of $[\Gamma(B^0 \rightarrow J/\psi(1S) K^*(892)^0)/\Gamma_{\text{total}}] \times [B(J/\psi(1S) \rightarrow e^+e^-)]$ assuming $B(J/\psi(1S) \rightarrow e^+e^-) = 0.069 \pm 0.009$, which we rescale to our best value $B(J/\psi(1S) \rightarrow e^+e^-) = (5.971 \pm 0.032) \times 10^{-2}$. Our first error is their experiment's error and our second error is the systematic error from using our best value. Updated in BORTOLETTO 92 to use the same assumptions.

⁸ ABE 96H assumes that $B(B^+ \rightarrow J/\psi K^+) = (1.02 \pm 0.14) \times 10^{-3}$.

⁹ The neutral and charged B events together are predominantly longitudinally polarized, $\Gamma_{\perp}/\Gamma = 0.080 \pm 0.08 \pm 0.05$. This can be compared with a prediction using HQET, 0.73 (KRAMER 92). This polarization indicates that the $B \rightarrow \psi K^*$ decay is dominated by the $CP = -1$ CP eigenstate. Assumes equal production of B^+ and B^0 at the $\Upsilon(4S)$.

¹⁰ ALBRECHT 94G measures the polarization in the vector-vector decay to be predominantly longitudinal, $\Gamma_{\perp}/\Gamma = 0.03 \pm 0.16 \pm 0.15$ making the neutral decay a CP eigenstate when the K^*0 decays through $K_S^0 \pi^0$.

¹¹ ALBAJAR 91E assumes B_d^0 production fraction of 36%.

¹² ALBRECHT 87D assume $B^+B^-/B^0\bar{B}^0$ ratio is 55/45. Superseded by ALBRECHT 90J.

¹³ ALAM 86 assumes B^{\pm}/B^0 ratio is 60/40. The observation of the decay $B^+ \rightarrow J/\psi K^*(892)^+$ (HAAS 85) has been retracted in this paper.

$\Gamma(J/\psi(1S) K^*(892)^0)/\Gamma(J/\psi(1S) K^0)$	$\Gamma_{216}/\Gamma_{214}$		
VALUE	DOCUMENT ID	TECN	COMMENT
1.50 ± 0.09 OUR AVERAGE			
1.51 ± 0.05 ± 0.08	AUBERT	05J	BABR $e^+e^- \rightarrow \Upsilon(4S)$
1.39 ± 0.36 ± 0.10	ABE	96Q	CDF $p\bar{p}$

• • • We do not use the following data for averages, fits, limits, etc. • • •

1.49 ± 0.10 ± 0.08	1	AUBERT 02	BABR	Repl. by AUBERT 05J
--------------------	---	-----------	------	---------------------

¹ Assumes equal production of B^+ and B^0 at the $\Upsilon(4S)$.

$\Gamma(J/\psi(1S) \eta K_S^0)/\Gamma_{\text{total}}$	Γ_{217}/Γ		
VALUE (units 10^{-5})	DOCUMENT ID	TECN	COMMENT
5.4 ± 0.9 OUR AVERAGE			
5.22 ± 0.78 ± 0.49	1	IWASHITA 14	BELL $e^+e^- \rightarrow \Upsilon(4S)$
8.4 ± 2.6 ± 2.7	1	AUBERT 04Y	BABR $e^+e^- \rightarrow \Upsilon(4S)$

¹ Assumes equal production of B^+ and B^0 at the $\Upsilon(4S)$.

$\Gamma(J/\psi(1S) \eta' K_S^0)/\Gamma_{\text{total}}$	Γ_{218}/Γ			
VALUE (units 10^{-5})	DOCUMENT ID	TECN	COMMENT	
<2.5	90	1	XIE 07	BELL $e^+e^- \rightarrow \Upsilon(4S)$

¹ Assumes equal production of B^+ and B^0 at the $\Upsilon(4S)$.

See key on page 1171

Meson Particle Listings

 B^0 $\Gamma(J/\psi(1S)\omega K^0)/\Gamma_{\text{total}}$ Γ_{220}/Γ

VALUE (units 10^{-4})	DOCUMENT ID	TECN	COMMENT
2.3 ± 0.3 ± 0.3	¹ DEL-AMO-SA..10B	BABR	$e^+e^- \rightarrow \Upsilon(4S)$
• • • We do not use the following data for averages, fits, limits, etc. • • •			
3.1 ± 0.6 ± 0.3	¹ AUBERT 08W	BABR	Repl. by DEL-A MO-SANCHEZ 10B
¹ Assumes equal production of B^+ and B^0 at the $\Upsilon(4S)$.			

 $\Gamma(\chi_{c0}(3915), \chi_{c0} \rightarrow J/\psi\omega)/\Gamma_{\text{total}}$ Γ_{221}/Γ

VALUE (units 10^{-5})	DOCUMENT ID	TECN	COMMENT
2.1 ± 0.9 ± 0.3	¹ DEL-AMO-SA..10B	BABR	$e^+e^- \rightarrow \Upsilon(4S)$
• • • We do not use the following data for averages, fits, limits, etc. • • •			
1.3 ± $^{+1.3}_{-1.1}$ ± 0.2	^{1,2} AUBERT 08W	BABR	Repl. by DEL-A MO-SANCHEZ 10B
¹ Assumes equal production of B^+ and B^0 at the $\Upsilon(4S)$.			
² Corresponds to upper limit of 3.9×10^{-5} at 90% CL.			

 $\Gamma(J/\psi(1S)\phi K^0)/\Gamma_{\text{total}}$ Γ_{219}/Γ

VALUE (units 10^{-5})	DOCUMENT ID	TECN	COMMENT
4.9 ± 1.0 OUR AVERAGE	Error includes scale factor of 1.3.		
4.43 ± 0.76 ± 0.19	LEES 15	BABR	$e^+e^- \rightarrow \Upsilon(4S)$
10.2 ± 3.8 ± 1.0	¹ AUBERT 03o	BABR	$e^+e^- \rightarrow \Upsilon(4S)$
8.8 $^{+3.5}_{-3.0}$ ± 1.3	² ANASTASSOV 00	CLE2	$e^+e^- \rightarrow \Upsilon(4S)$
¹ Assumes equal production of B^+ and B^0 at the $\Upsilon(4S)$.			
² ANASTASSOV 00 finds 10 events on a background of 0.5 ± 0.2 . Assumes equal production of B^0 and B^+ at the $\Upsilon(4S)$, a uniform Dalitz plot distribution, isotropic $J/\psi(1S)$ and ϕ decays, and $B(B^+ \rightarrow J/\psi(1S)\phi K^+) = B(B^0 \rightarrow J/\psi(1S)\phi K^0)$.			

 $\Gamma(J/\psi(1S)K(1270)^0)/\Gamma_{\text{total}}$ Γ_{222}/Γ

VALUE (units 10^{-3})	DOCUMENT ID	TECN	COMMENT
1.30 ± 0.34 ± 0.32	¹ ABE 01L	BELL	$e^+e^- \rightarrow \Upsilon(4S)$
¹ Assumes equal production of B^+ and B^0 at the $\Upsilon(4S)$ and uses the PDG value of $B(B^+ \rightarrow J/\psi(1S)K^+) = (1.00 \pm 0.10) \times 10^{-3}$.			

 $\Gamma(J/\psi(1S)\pi^0)/\Gamma_{\text{total}}$ Γ_{223}/Γ

VALUE (units 10^{-5})	CL%	DOCUMENT ID	TECN	COMMENT
1.66 ± 0.10 OUR AVERAGE				
1.62 ± 0.11 ± 0.06		¹ PAL 18	BELL	$e^+e^- \rightarrow \Upsilon(4S)$
1.69 ± 0.14 ± 0.07		¹ AUBERT 08AU	BABR	$e^+e^- \rightarrow \Upsilon(4S)$
2.5 $^{+1.1}_{-0.9}$ ± 0.2		¹ AVERY 00	CLE2	$e^+e^- \rightarrow \Upsilon(4S)$
• • • We do not use the following data for averages, fits, limits, etc. • • •				
1.94 ± 0.22 ± 0.17		¹ AUBERT,B 06B	BABR	Repl. by AUBERT 08AU
2.3 ± 0.5 ± 0.2		¹ ABE 03B	BELL	Repl. by PAL 18
2.0 ± 0.6 ± 0.2		¹ AUBERT 02	BABR	Repl. by AUBERT,B 06B
< 32	90	² ACCIARRI 97C	L3	
< 5.8	90	BISHAI 96	CLE2	Sup. by AVERY 00
< 690	90	¹ ALEXANDER 95	CLE2	Sup. by BISHAI 96
¹ Assumes equal production of B^+ and B^0 at the $\Upsilon(4S)$.				
² ACCIARRI 97C assumes B^0 production fraction (39.5 ± 4.0)% and B_S (12.0 ± 3.0)%.				

 $\Gamma(J/\psi(1S)\eta)/\Gamma_{\text{total}}$ Γ_{224}/Γ

VALUE (units 10^{-6})	CL%	DOCUMENT ID	TECN	COMMENT
10.8 ± 2.3 OUR AVERAGE				Error includes scale factor of 1.5.
7.3 ± 2.5 ± 1.3		¹ AAIJ 15D	LHCB	pp at 7, 8 TeV
12.3 $^{+1.8}_{-1.7}$ ± 0.7		^{2,3} CHANG 12	BELL	$e^+e^- \rightarrow \Upsilon(4S)$
• • • We do not use the following data for averages, fits, limits, etc. • • •				
9.5 ± 1.7 ± 0.8		³ CHANG 07A	BELL	Repl. by CHANG 12
< 27	90	³ AUBERT 03o	BABR	$e^+e^- \rightarrow \Upsilon(4S)$
< 1200	90	⁴ ACCIARRI 97C	L3	
¹ AAIJ 15D reports $[\Gamma(B^0 \rightarrow J/\psi(1S)\eta)/\Gamma_{\text{total}}] / [B(B^0 \rightarrow J/\psi(1S)\eta)] = (1.85 \pm 0.61 \pm 0.14) \times 10^{-2}$ which we multiply by our best value $B(B^0_S \rightarrow J/\psi(1S)\eta) = (4.0 \pm 0.7) \times 10^{-4}$. Our first error is their experiment's error and our second error is the systematic error from using our best value.				
² Reconstructs η in $\gamma\gamma$ and $\pi^+\pi^-\pi^0$ decays.				
³ Assumes equal production of B^+ and B^0 at the $\Upsilon(4S)$.				
⁴ ACCIARRI 97C assumes B^0 production fraction (39.5 ± 4.0)% and B_S (12.0 ± 3.0)%.				

 $\Gamma(J/\psi(1S)\pi^+\pi^-)/\Gamma_{\text{total}}$ Γ_{225}/Γ

VALUE (units 10^{-5})	DOCUMENT ID	TECN	COMMENT
3.99 ± 0.15 OUR AVERAGE			
3.98 ± 0.14 ± 0.07	^{1,2} AAIJ 13M	LHCB	pp at 7 TeV
4.6 ± 0.7 ± 0.6	³ AUBERT 03B	BABR	$e^+e^- \rightarrow \Upsilon(4S)$
¹ AAIJ 13M reports $(3.97 \pm 0.09 \pm 0.11 \pm 0.16) \times 10^{-5}$ from a measurement of $[\Gamma(B^0 \rightarrow J/\psi(1S)\pi^+\pi^-)/\Gamma_{\text{total}}] / [B(B^0 \rightarrow J/\psi(1S)K^+)]$ assuming $B(B^+ \rightarrow J/\psi(1S)K^+) = (1.018 \pm 0.042) \times 10^{-3}$, which we rescale to our best value $B(B^+ \rightarrow J/\psi(1S)K^+) = (1.020 \pm 0.019) \times 10^{-3}$. Our first error is their experiment's error and our second error is the systematic error from using our best value.			
² AAIJ 13M does not report correlations between various measurements of the $J/\psi\pi\pi$ final state.			
³ Assumes equal production of B^+ and B^0 at the $\Upsilon(4S)$.			

 $\Gamma(J/\psi(1S)\pi^+\pi^- \text{ nonresonant})/\Gamma_{\text{total}}$ Γ_{226}/Γ

VALUE (units 10^{-5})	CL%	DOCUMENT ID	TECN	COMMENT
< 1.2	90	¹ AUBERT 07AC	BABR	$e^+e^- \rightarrow \Upsilon(4S)$
¹ Assumes equal production of B^+ and B^0 at the $\Upsilon(4S)$.				

 $\Gamma(J/\psi(1S)f_0(500), f_0 \rightarrow \pi\pi)/\Gamma_{\text{total}}$ Γ_{227}/Γ

VALUE (units 10^{-6})	DOCUMENT ID	TECN	COMMENT
8.8 ± 0.5 $^{+1.1}_{-1.5}$	¹ AAIJ 14X	LHCB	pp at 7, 8 TeV
• • • We do not use the following data for averages, fits, limits, etc. • • •			
6.4 $^{+2.5}_{-1.1}$ ± 0.2	^{2,3} AAIJ 13M	LHCB	Repl. by AAIJ 14X
¹ AAIJ 14X uses Dalitz plot analysis of $B^0 \rightarrow J/\psi\pi^+\pi^-$.			
² AAIJ 13M reports $(6.4 \pm 0.8 ^{+2.4}_{-0.8}) \times 10^{-6}$ from a measurement of $[\Gamma(B^0 \rightarrow J/\psi(1S)f_0(500), f_0 \rightarrow \pi\pi)/\Gamma_{\text{total}}] / [B(B^0 \rightarrow J/\psi(1S)\pi^+\pi^-)]$ assuming $B(B^0 \rightarrow J/\psi(1S)\pi^+\pi^-) = (3.97 \pm 0.09 \pm 0.11 \pm 0.16) \times 10^{-5}$, which we rescale to our best value $B(B^0 \rightarrow J/\psi(1S)\pi^+\pi^-) = (3.99 \pm 0.15) \times 10^{-5}$. Our first error is their experiment's error and our second error is the systematic error from using our best value.			
³ AAIJ 13M does not report correlations between various measurements of the $J/\psi\pi\pi$ final state. Measured in Dalitz plot like analysis of $B^0 \rightarrow J/\psi\pi^+\pi^-$.			

 $\Gamma(J/\psi(1S)f_2)/\Gamma_{\text{total}}$ Γ_{228}/Γ

VALUE (units 10^{-5})	CL%	DOCUMENT ID	TECN	COMMENT
0.33 $^{+0.05}_{-0.06}$ OUR AVERAGE				Error includes scale factor of 1.5.
0.30 ± 0.03 $^{+0.02}_{-0.03}$		¹ AAIJ 14X	LHCB	pp at 7, 8 TeV
0.42 ± 0.06 ± 0.02		^{2,3} AAIJ 13M	LHCB	pp at 7 TeV
• • • We do not use the following data for averages, fits, limits, etc. • • •				
< 0.5	90	^{4,5} AUBERT 07AC	BABR	$e^+e^- \rightarrow \Upsilon(4S)$
¹ AAIJ 14X uses Dalitz plot analysis of $B^0 \rightarrow J/\psi\pi^+\pi^-$.				
² AAIJ 13M reports $[\Gamma(B^0 \rightarrow J/\psi(1S)f_2)/\Gamma_{\text{total}}] \times [B(f_2(1270) \rightarrow \pi\pi)] = (3.5 \pm 0.4 \pm 0.4) \times 10^{-6}$ from a measurement of $[\Gamma(B^0 \rightarrow J/\psi(1S)f_2)/\Gamma_{\text{total}}] \times [B(f_2(1270) \rightarrow \pi\pi)] / [B(B^0 \rightarrow J/\psi(1S)\pi^+\pi^-)]$ assuming $B(B^0 \rightarrow J/\psi(1S)\pi^+\pi^-) = (3.97 \pm 0.09 \pm 0.11 \pm 0.16) \times 10^{-5}$, which we rescale to our best values $B(f_2(1270) \rightarrow \pi\pi) = (84.3 ^{+2.8}_{-1.0}) \times 10^{-2}$, $B(B^0 \rightarrow J/\psi(1S)\pi^+\pi^-) = (3.99 \pm 0.15) \times 10^{-5}$. Our first error is their experiment's error and our second error is the systematic error from using our best values.				
³ AAIJ 13M does not report correlations between various measurements of the $J/\psi\pi\pi$ final state. Measured in Dalitz plot like analysis of $B^0 \rightarrow J/\psi\pi^+\pi^-$.				
⁴ AUBERT 07AC reports $[\Gamma(B^0 \rightarrow J/\psi(1S)f_2)/\Gamma_{\text{total}}] \times [B(f_2(1270) \rightarrow \pi\pi)] < 0.46 \times 10^{-5}$ which we divide by our best value $B(f_2(1270) \rightarrow \pi\pi) = 84.3 \times 10^{-2}$.				
⁵ Assumes equal production of B^+ and B^0 at the $\Upsilon(4S)$.				

VALUE (units 10^{-5})	CL%	DOCUMENT ID	TECN	COMMENT
2.55 $^{+0.18}_{-0.16}$ OUR AVERAGE				
2.50 ± 0.10 $^{+0.18}_{-0.15}$		¹ AAIJ 14X	LHCB	pp at 7, 8 TeV
2.7 ± 0.3 ± 0.2		² AUBERT 07AC	BABR	$e^+e^- \rightarrow \Upsilon(4S)$
• • • We do not use the following data for averages, fits, limits, etc. • • •				
2.51 $^{+0.22}_{-0.23}$ ± 0.10		^{3,4} AAIJ 13M	LHCB	Repl. by AAIJ 14X
1.6 ± 0.6 ± 0.4		² AUBERT 03B	BABR	Repl. by AUBERT 07AC
< 25	90	BISHAI 96	CLE2	$e^+e^- \rightarrow \Upsilon(4S)$
¹ AAIJ 14X uses Dalitz plot analysis of $B^0 \rightarrow J/\psi\pi^+\pi^-$. We assume $B(\rho(770)^0 \rightarrow \pi^+\pi^-) = 100\%$.				
² Assumes equal production of B^+ and B^0 at the $\Upsilon(4S)$.				
³ AAIJ 13M reports $(2.49 ^{+0.20}_{-0.13} ^{+0.16}_{-0.23}) \times 10^{-5}$ from a measurement of $[\Gamma(B^0 \rightarrow J/\psi(1S)\rho^0)/\Gamma_{\text{total}}] / [B(B^0 \rightarrow J/\psi(1S)\pi^+\pi^-)]$ assuming $B(B^0 \rightarrow J/\psi(1S)\pi^+\pi^-) = (3.97 \pm 0.09 \pm 0.11 \pm 0.16) \times 10^{-5}$, which we rescale to our best value $B(B^0 \rightarrow J/\psi(1S)\pi^+\pi^-) = (3.99 \pm 0.15) \times 10^{-5}$. Our first error is their experiment's error and our second error is the systematic error from using our best value.				
⁴ AAIJ 13M does not report correlations between various measurements of the $J/\psi\pi\pi$ final state. Measured in Dalitz plot like analysis of $B^0 \rightarrow J/\psi\pi^+\pi^-$. Assumes $B(\rho(770)^0 \rightarrow \pi\pi) = 100\%$.				

 $\Gamma(J/\psi(1S)\rho^0)/\Gamma_{\text{total}}$ Γ_{229}/Γ

VALUE (units 10^{-5})	CL%	DOCUMENT ID	TECN	COMMENT
2.55 $^{+0.18}_{-0.16}$ OUR AVERAGE				
2.50 ± 0.10 $^{+0.18}_{-0.15}$		¹ AAIJ 14X	LHCB	pp at 7, 8 TeV
2.7 ± 0.3 ± 0.2		² AUBERT 07AC	BABR	$e^+e^- \rightarrow \Upsilon(4S)$
• • • We do not use the following data for averages, fits, limits, etc. • • •				
2.51 $^{+0.22}_{-0.23}$ ± 0.10		^{3,4} AAIJ 13M	LHCB	Repl. by AAIJ 14X
1.6 ± 0.6 ± 0.4		² AUBERT 03B	BABR	Repl. by AUBERT 07AC
< 25	90	BISHAI 96	CLE2	$e^+e^- \rightarrow \Upsilon(4S)$
¹ AAIJ 14X uses Dalitz plot analysis of $B^0 \rightarrow J/\psi\pi^+\pi^-$. We assume $B(\rho(770)^0 \rightarrow \pi^+\pi^-) = 100\%$.				
² Assumes equal production of B^+ and B^0 at the $\Upsilon(4S)$.				
³ AAIJ 13M reports $(2.49 ^{+0.20}_{-0.13} ^{+0.16}_{-0.23}) \times 10^{-5}$ from a measurement of $[\Gamma(B^0 \rightarrow J/\psi(1S)\rho^0)/\Gamma_{\text{total}}] / [B(B^0 \rightarrow J/\psi(1S)\pi^+\pi^-)]$ assuming $B(B^0 \rightarrow J/\psi(1S)\pi^+\pi^-) = (3.97 \pm 0.09 \pm 0.11 \pm 0.16) \times 10^{-5}$, which we rescale to our best value $B(B^0 \rightarrow J/\psi(1S)\pi^+\pi^-) = (3.99 \pm 0.15) \times 10^{-5}$. Our first error is their experiment's error and our second error is the systematic error from using our best value.				
⁴ AAIJ 13M does not report correlations between various measurements of the $J/\psi\pi\pi$ final state. Measured in Dalitz plot like analysis of $B^0 \rightarrow J/\psi\pi^+\pi^-$. Assumes $B(\rho(770)^0 \rightarrow \pi\pi) = 100\%$.				

 $\Gamma(J/\psi(1S)f_0(980), f_0 \rightarrow \pi^+\pi^-)/\Gamma_{\text{total}}$ Γ_{230}/Γ

VALUE	CL%	DOCUMENT ID	TECN	COMMENT
< 1.1 × 10⁻⁶	90	¹ AAIJ 13M	LHCB	pp at 7 TeV
¹ AAIJ 13M does not provide correlations between various measurements of the $J/\psi\pi^+\pi^-$ final state. The measurements were obtained from a Dalitz plot like analysis of $B^0 \rightarrow J/\psi\pi^+\pi^-$. Also reports $\Gamma(J/\psi(1S)f_0(980), f_0 \rightarrow \pi^+\pi^-)/\Gamma_{\text{total}} = (6.1 ^{+3.1}_{-2.0} ^{+1.7}_{-1.4}) \times 10^{-6}$.				

 $\Gamma(J/\psi(1S)\rho(1450)^0, \rho^0 \rightarrow \pi\pi)/\Gamma_{\text{total}}$ Γ_{231}/Γ

VALUE (units 10^{-6})	DOCUMENT ID	TECN	COMMENT
2.9 $^{+1.6}_{-0.7}$ OUR AVERAGE			
4.6 ± 1.1 ± 1.9	¹ AAIJ 14X	LHCB	pp at 7, 8 TeV
2.1 $^{+2.4}_{-0.7}$ ± 0.1	^{2,3} AAIJ 13M	LHCB	pp at 7 TeV

Meson Particle Listings

 B^0 ¹ AAIJ 14x uses Dalitz plot analysis of $B^0 \rightarrow J/\psi \pi^+ \pi^-$.² AAIJ 13M reports $(2.1^{+1.0+2.2}_{-0.6-0.4}) \times 10^{-6}$ from a measurement of $[\Gamma(B^0 \rightarrow J/\psi(1S) \rho(1450)^0, \rho^0 \rightarrow \pi\pi)/\Gamma_{\text{total}}] / [B(B^0 \rightarrow J/\psi(1S) \pi^+ \pi^-)]$ assuming $B(B^0 \rightarrow J/\psi(1S) \pi^+ \pi^-) = (3.97 \pm 0.09 \pm 0.11 \pm 0.16) \times 10^{-5}$, which we rescale to our best value $B(B^0 \rightarrow J/\psi(1S) \pi^+ \pi^-) = (3.99 \pm 0.15) \times 10^{-5}$. Our first error is their experiment's error and our second error is the systematic error from using our best value.³ AAIJ 13M does not report correlations between various measurements of the $J/\psi \pi \pi$ final state. Measured in Dalitz plot like analysis of $B^0 \rightarrow J/\psi \pi^+ \pi^-$.

VALUE (units 10^{-6})	DOCUMENT ID	TECN	COMMENT	Γ_{232}/Γ
$2.0 \pm 0.5 \pm 1.2$	¹ AAIJ	14x	LHCB $p\bar{p}$ at 7, 8 TeV	

¹ AAIJ 14x uses Dalitz plot analysis of $B^0 \rightarrow J/\psi \pi^+ \pi^-$.

VALUE (units 10^{-5})	CL%	DOCUMENT ID	TECN	COMMENT	Γ_{233}/Γ
$1.8^{+0.7}_{-0.5} \pm 0.1$		¹ AAIJ	14x	LHCB $p\bar{p}$ at 7, 8 TeV	

• • • We do not use the following data for averages, fits, limits, etc. • • •

< 27 90 BISHAI 96 CLE2 $e^+ e^- \rightarrow \Upsilon(4S)$ ¹ AAIJ 14x reports $[\Gamma(B^0 \rightarrow J/\psi(1S) \omega)/\Gamma_{\text{total}}] \times [B(\omega(782) \rightarrow \pi^+ \pi^-)] = (2.7^{+0.8+0.7}_{-0.6-0.5}) \times 10^{-7}$ which we divide by our best value $B(\omega(782) \rightarrow \pi^+ \pi^-) = (1.53 \pm 0.12) \times 10^{-2}$. Our first error is their experiment's error and our second error is the systematic error from using our best value.

VALUE	DOCUMENT ID	TECN	COMMENT	$\Gamma_{233}/\Gamma_{229}$
$0.61^{+0.39}_{-0.21} \pm 0.05$	^{1,2} AAIJ	13M	LHCB $p\bar{p}$ at 7 TeV	

¹ AAIJ 13M reports $0.61^{+0.24+0.31}_{-0.14-0.16}$ from a measurement of $[\Gamma(B^0 \rightarrow J/\psi(1S) \omega)/\Gamma(B^0 \rightarrow J/\psi(1S) \rho^0)] \times [B(\omega(782) \rightarrow \pi^+ \pi^-)]$ assuming $B(\omega(782) \rightarrow \pi^+ \pi^-) = (1.53^{+0.11}_{-0.13}) \times 10^{-2}$, which we rescale to our best value $B(\omega(782) \rightarrow \pi^+ \pi^-) = (1.53 \pm 0.12) \times 10^{-2}$. Our first error is their experiment's error and our second error is the systematic error from using our best value.² AAIJ 13M does not report correlations between various measurements of the $J/\psi \pi \pi$ final state. Measured in Dalitz plot like analysis of $B^0 \rightarrow J/\psi \pi^+ \pi^-$. Assumes $B(\rho(770)^0 \rightarrow \pi\pi) = 100\%$.

VALUE	DOCUMENT ID	TECN	COMMENT	$\Gamma_{233}/\Gamma_{229}$
$0.89 \pm 0.19 \pm 0.07_{-0.13}$	AAIJ	13A	LHCB $p\bar{p}$ at 7 TeV	

VALUE (units 10^{-6})	DOCUMENT ID	TECN	COMMENT	Γ_{234}/Γ
$2.53 \pm 0.35 \pm 0.05$	¹ AAIJ	13BT	LHCB $p\bar{p}$ at 7 TeV	

¹ AAIJ 13BT reports $(2.53 \pm 0.31 \pm 0.19) \times 10^{-6}$ from a measurement of $[\Gamma(B^0 \rightarrow J/\psi(1S) K^+ K^-)/\Gamma_{\text{total}}] / [B(B^+ \rightarrow J/\psi(1S) K^+)]$ assuming $B(B^+ \rightarrow J/\psi(1S) K^+) = (1.018 \pm 0.042) \times 10^{-3}$, which we rescale to our best value $B(B^+ \rightarrow J/\psi(1S) K^+) = (1.020 \pm 0.019) \times 10^{-3}$. Our first error is their experiment's error and our second error is the systematic error from using our best value.

VALUE (units 10^{-6})	DOCUMENT ID	TECN	COMMENT	Γ_{235}/Γ
$0.470 \pm 0.331 \pm 0.072$	¹ AAIJ	13BT	LHCB $p\bar{p}$ at 7 TeV	

¹ AAIJ 13BT uses $B(B^0 \rightarrow J/\psi K^+ K^-) = (2.53 \pm 0.31 \pm 0.19) \times 10^{-6}$ to derive this result. It also reports the equivalent upper limit of $< 9.0 \times 10^{-7}$ at 90% CL.

VALUE	CL%	DOCUMENT ID	TECN	COMMENT	Γ_{236}/Γ
$< 1.1 \times 10^{-7}$	90	AAIJ	21K	LHCB $p\bar{p}$ at 7, 8, 13 TeV	

• • • We do not use the following data for averages, fits, limits, etc. • • •

< 1.1×10^{-7} 90 LEES 15 BABR $e^+ e^- \rightarrow \Upsilon(4S)$ < 1.9×10^{-7} 90 ¹ AAIJ 13BT LHCB $p\bar{p}$ at 7 TeV< 9.4×10^{-7} 90 2 LIU 08I BELL $e^+ e^- \rightarrow \Upsilon(4S)$ < 9.2×10^{-6} 90 2 AUBERT 03O BABR $e^+ e^- \rightarrow \Upsilon(4S)$ ¹ AAIJ 13BT uses $B(B^0 \rightarrow J/\psi(1S) K^+ K^-) = (2.53 \pm 0.31 \pm 0.19) \times 10^{-6}$ and $B(\phi \rightarrow K^+ K^-) = (48.9 \pm 0.5)\%$ to obtain this result.² Assumes equal production of B^+ and B^0 at the $\Upsilon(4S)$.

VALUE (units 10^{-6})	CL%	DOCUMENT ID	TECN	COMMENT	Γ_{237}/Γ
$7.6 \pm 2.2 \pm 1.0$		¹ AAIJ	15D	LHCB $p\bar{p}$ at 7, 8 TeV	

• • • We do not use the following data for averages, fits, limits, etc. • • •

< 7.4 90 ^{2,3} CHANG 12 BELL $e^+ e^- \rightarrow \Upsilon(4S)$ < 63 90 ³ AUBERT 03O BABR $e^+ e^- \rightarrow \Upsilon(4S)$ ¹ AAIJ 15D reports $[\Gamma(B^0 \rightarrow J/\psi(1S) \eta(958))/\Gamma_{\text{total}}] / [B(B_S^0 \rightarrow J/\psi(1S) \eta)] = (2.28 \pm 0.65 \pm 0.16) \times 10^{-2}$ which we multiply by our best value $B(B_S^0 \rightarrow J/\psi(1S) \eta) = (3.3 \pm 0.4) \times 10^{-4}$. Our first error is their experiment's error and our second error is the systematic error from using our best value.² Reconstructs $\eta(958)$ in $(\eta\pi^+ + \pi^0)$ and $\rho(770)$ decays.³ Assumes equal production of B^+ and B^0 at the $\Upsilon(4S)$.

VALUE	DOCUMENT ID	TECN	COMMENT	$\Gamma_{224}/\Gamma_{237}$
$1.111 \pm 0.475 \pm 0.062$	¹ AAIJ	15D	LHCB $p\bar{p}$ at 7, 8 TeV	

¹ Uses $J/\psi \rightarrow \mu^+ \mu^-$, $\eta' \rightarrow \rho^0 \gamma$, and $\eta' \rightarrow \eta \pi^+ \pi^-$ decays.

VALUE	DOCUMENT ID	TECN	COMMENT	$\Gamma_{238}/\Gamma_{214}$
0.50 ± 0.04 OUR AVERAGE				
$0.493 \pm 0.034 \pm 0.027$	AAIJ	14L	LHCB $p\bar{p}$ at 7 TeV	
$1.24 \pm 0.40 \pm 0.15$	AFFOLDER	02B	CDF $p\bar{p}$ 1.8 TeV	

VALUE (units 10^{-6})	DOCUMENT ID	TECN	COMMENT	Γ_{240}/Γ
25 ± 7 OUR AVERAGE			Error includes scale factor of 1.8.	
$34.9 \pm 6.7 \pm 1.5$	LEES	15	BABR $e^+ e^- \rightarrow \Upsilon(4S)$	
$20.2 \pm 4.3 \pm 1.9$	¹ AAIJ	14L	LHCB $p\bar{p}$ at 7 TeV	

¹ Measured with $B(B^0 \rightarrow J/\psi K_S^0 K^+ K^-) / B(B^0 \rightarrow J/\psi K_S^0)$ using PDG 12 for the involved branching fractions.

VALUE	CL%	DOCUMENT ID	TECN	COMMENT	Γ_{239}/Γ
$< 21 \times 10^{-6}$	90	¹ AAIJ	14L	LHCB $p\bar{p}$ at 7 TeV	

¹ Measured with $B(B^0 \rightarrow J/\psi K_S^0 K^{\pm} K^{\mp}) / B(B^0 \rightarrow J/\psi K_S^0 \pi^+ \pi^-)$ using PDG 12 values for the involved branching fractions.

VALUE (units 10^{-4})	DOCUMENT ID	TECN	COMMENT	Γ_{242}/Γ
$5.4 \pm 2.9 \pm 0.9$	¹ AFFOLDER	02B	CDF $p\bar{p}$ 1.8 TeV	

¹ Uses $B^0 \rightarrow J/\psi(1S) K_S^0$ decay as a reference and $B(B^0 \rightarrow J/\psi(1S) K^0) = 8.3 \times 10^{-4}$.

VALUE (units 10^{-4})	DOCUMENT ID	TECN	COMMENT	Γ_{243}/Γ
$7.7 \pm 4.1 \pm 1.3$	¹ AFFOLDER	02B	CDF $p\bar{p}$ 1.8 TeV	

¹ Uses $B^0 \rightarrow J/\psi(1S) K_S^0$ decay as a reference and $B(B^0 \rightarrow J/\psi(1S) K^0) = 8.3 \times 10^{-4}$.

VALUE	DOCUMENT ID	TECN	COMMENT	$\Gamma_{244}/\Gamma_{225}$
$0.361 \pm 0.017 \pm 0.021$	¹ AAIJ	14Y	LHCB $p\bar{p}$ at 7, 8 TeV	

¹ Excludes contributions from $\psi(2S)$ and $\chi_{c1}(3872)$ decaying to $J/\psi(1S) \pi^+ \pi^-$.

VALUE (units 10^{-6})	DOCUMENT ID	TECN	COMMENT	Γ_{245}/Γ
$8.4^{+2.1}_{-2.0} \pm 0.5$	¹ AAIJ	14Y	LHCB $p\bar{p}$ at 7, 8 TeV	

¹ AAIJ 14Y reports $(8.37 \pm 1.95^{+0.71}_{-0.66} \pm 0.35) \times 10^{-6}$ from a measurement of $[\Gamma(B^0 \rightarrow J/\psi(1S) f_1(1285))/\Gamma_{\text{total}}] \times [B(f_1(1285) \rightarrow 2\pi^+ 2\pi^-)]$ assuming $B(f_1(1285) \rightarrow 2\pi^+ 2\pi^-) = 0.11^{+0.007}_{-0.006}$, which we rescale to our best value $B(f_1(1285) \rightarrow 2\pi^+ 2\pi^-) = (10.9 \pm 0.6) \times 10^{-2}$. Our first error is their experiment's error and our second error is the systematic error from using our best value.

VALUE (units 10^{-4})	DOCUMENT ID	TECN	COMMENT	Γ_{246}/Γ
$6.6 \pm 1.9 \pm 1.1$	¹ AFFOLDER	02B	CDF $p\bar{p}$ 1.8 TeV	

¹ Uses $B^0 \rightarrow J/\psi(1S) K^*(892)^0$ decay as a reference and $B(B^0 \rightarrow J/\psi(1S) K^0) = 12.4 \times 10^{-4}$.

VALUE	CL%	DOCUMENT ID	TECN	COMMENT	Γ_{247}/Γ
$< 3.5 \times 10^{-5}$	90	CHILIKIN	20	BELL $e^+ e^- \rightarrow \Upsilon(4S)$	

VALUE	CL%	DOCUMENT ID	TECN	COMMENT	Γ_{248}/Γ
$< 1.0 \times 10^{-4}$	90	CHILIKIN	20	BELL $e^+ e^- \rightarrow \Upsilon(4S)$	

VALUE (units 10^{-4})	CL%	DOCUMENT ID	TECN	COMMENT	Γ_{251}/Γ
1.4 ± 0.4 OUR AVERAGE				Error includes scale factor of 1.1.	

¹ HIRATA 23 BELL $e^+ e^- \rightarrow \Upsilon(4S)$ ² CHOI 11 BELL $e^+ e^- \rightarrow \Upsilon(4S)$ ³ DEL-AMO-SA...10B BABR $e^+ e^- \rightarrow \Upsilon(4S)$

< 3.1	90	^{4,5} BHARDWAJ	11	BELL $e^+ e^- \rightarrow \Upsilon(4S)$	
$2.9 \pm 1.4 \pm 1.0$		^{5,6} AUSHEV	10	BELL $e^+ e^- \rightarrow \Upsilon(4S)$	
< 6	90	^{7,8} AUBERT	09B	BABR $e^+ e^- \rightarrow \Upsilon(4S)$	
$6.6 \pm 3.4^{+2.3}_{-2.4}$		^{5,7,9} AUBERT	08B	BABR $e^+ e^- \rightarrow \Upsilon(4S)$	
< 1.7	90	¹⁰ AUBERT	08Y	BABR $e^+ e^- \rightarrow \Upsilon(4S)$	
< 2.9	90	¹¹ AUBERT	06	BABR Repl. by AUBERT 08Y	
$3.7^{+1.7+1.8}_{-1.8-1.7}$		^{12,13} GOKHROO	06	BELL $e^+ e^- \rightarrow \Upsilon(4S)$	

- ¹HIRATA 23 reports $[\Gamma(B^0 \rightarrow \chi_{c1}(3872) K^0)/\Gamma_{\text{total}}] \times [B(\chi_{c1}(3872) \rightarrow \bar{D}^{*0} D^0)] = (1.30^{+0.36+0.12}_{-0.31-0.07}) \times 10^{-4}$ which we divide by our best value $B(\chi_{c1}(3872) \rightarrow \bar{D}^{*0} D^0) = (34 \pm 12) \times 10^{-2}$. Our first error is their experiment's error and our second error is the systematic error from using our best value.
- ²CHOI 11 reports $[\Gamma(B^0 \rightarrow \chi_{c1}(3872) K^0)/\Gamma_{\text{total}}] / [B(B^+ \rightarrow \chi_{c1}(3872) K^+)] = 0.50 \pm 0.14 \pm 0.04$ which we multiply by our best value $B(B^+ \rightarrow \chi_{c1}(3872) K^+) = (2.3 \pm 0.6) \times 10^{-4}$. Our first error is their experiment's error and our second error is the systematic error from using our best value.
- ³DEL-AMO-SANCHEZ 10B reports $[\Gamma(B^0 \rightarrow \chi_{c1}(3872) K^0)/\Gamma_{\text{total}}] \times [B(\chi_{c1}(3872) \rightarrow \omega J/\psi(1S))] = (6 \pm 3 \pm 1) \times 10^{-6}$ which we divide by our best value $B(\chi_{c1}(3872) \rightarrow \omega J/\psi(1S)) = (4.1 \pm 1.4) \times 10^{-2}$. Our first error is their experiment's error and our second error is the systematic error from using our best value.
- ⁴BHARDWAJ 11 reports $[\Gamma(B^0 \rightarrow \chi_{c1}(3872) K^0)/\Gamma_{\text{total}}] \times [B(\chi_{c1}(3872) \rightarrow \gamma J/\psi)] < 2.4 \times 10^{-6}$ which we divide by our best value $B(\chi_{c1}(3872) \rightarrow \gamma J/\psi) = 7.8 \times 10^{-3}$.
- ⁵Assumes equal production of B^+ and B^0 at the $\Upsilon(4S)$.
- ⁶AUSHEV 10 reports $[\Gamma(B^0 \rightarrow \chi_{c1}(3872) K^0)/\Gamma_{\text{total}}] \times [B(\chi_{c1}(3872) \rightarrow \bar{D}^{*0} D^0)] = (0.97 \pm 0.46 \pm 0.13) \times 10^{-4}$ which we divide by our best value $B(\chi_{c1}(3872) \rightarrow \bar{D}^{*0} D^0) = (34 \pm 12) \times 10^{-2}$. Our first error is their experiment's error and our second error is the systematic error from using our best value.
- ⁷Uses $B(\Upsilon(4S) \rightarrow B^+ B^-) = (51.6 \pm 0.6)\%$ and $B(\Upsilon(4S) \rightarrow B^0 \bar{B}^0) = (48.4 \pm 0.6)\%$.
- ⁸AUBERT 09b reports $[\Gamma(B^0 \rightarrow \chi_{c1}(3872) K^0)/\Gamma_{\text{total}}] \times [B(\chi_{c1}(3872) \rightarrow \gamma J/\psi)] < 4.9 \times 10^{-6}$ which we divide by our best value $B(\chi_{c1}(3872) \rightarrow \gamma J/\psi) = 7.8 \times 10^{-3}$.
- ⁹AUBERT 08b reports $[\Gamma(B^0 \rightarrow \chi_{c1}(3872) K^0)/\Gamma_{\text{total}}] \times [B(\chi_{c1}(3872) \rightarrow \bar{D}^{*0} D^0)] = (2.22 \pm 1.05 \pm 0.42) \times 10^{-4}$ which we divide by our best value $B(\chi_{c1}(3872) \rightarrow \bar{D}^{*0} D^0) = (34 \pm 12) \times 10^{-2}$. Our first error is their experiment's error and our second error is the systematic error from using our best value.
- ¹⁰AUBERT 08y reports $[\Gamma(B^0 \rightarrow \chi_{c1}(3872) K^0)/\Gamma_{\text{total}}] \times [B(\chi_{c1}(3872) \rightarrow \pi^+ \pi^- J/\psi(1S))] < 6.0 \times 10^{-6}$ which we divide by our best value $B(\chi_{c1}(3872) \rightarrow \pi^+ \pi^- J/\psi(1S)) = 3.5 \times 10^{-2}$.
- ¹¹AUBERT 06 reports $[\Gamma(B^0 \rightarrow \chi_{c1}(3872) K^0)/\Gamma_{\text{total}}] \times [B(\chi_{c1}(3872) \rightarrow \pi^+ \pi^- J/\psi(1S))] < 10.3 \times 10^{-6}$ which we divide by our best value $B(\chi_{c1}(3872) \rightarrow \pi^+ \pi^- J/\psi(1S)) = 3.5 \times 10^{-2}$.
- ¹²GOKHROO 06 reports $[\Gamma(B^0 \rightarrow \chi_{c1}(3872) K^0)/\Gamma_{\text{total}}] \times [B(\chi_{c1}(3872) \rightarrow D^0 \bar{D}^0 \pi^0)] = (1.66 \pm 0.70^{+0.32}_{-0.37}) \times 10^{-4}$ which we divide by our best value $B(\chi_{c1}(3872) \rightarrow D^0 \bar{D}^0 \pi^0) = (45 \pm 21) \times 10^{-2}$. Our first error is their experiment's error and our second error is the systematic error from using our best value.
- ¹³Measure the near-threshold enhancements in the $(D^0 \bar{D}^0 \pi^0)$ system at a mass $3875.2 \pm 0.7^{+0.3}_{-1.6} \pm 0.8$ MeV/ c^2 .

$\Gamma(\chi_{c1}(3872) K^+) / \Gamma_{\text{total}}$		Γ_{249} / Γ		
VALUE	CL%	DOCUMENT ID	TECN	COMMENT
$< 5 \times 10^{-4}$	90	¹ AUBERT 06E	BABR	$e^+ e^- \rightarrow \Upsilon(4S)$

¹ Perform measurements of absolute branching fractions using a missing mass technique.

$\Gamma(\chi_{c1}(3872) K^+, \chi_{c1}(3872) K^- \rightarrow J/\psi(1S) \pi^+ \pi^0) / \Gamma_{\text{total}}$		Γ_{250} / Γ		
VALUE (units 10^{-6})	CL%	DOCUMENT ID	TECN	COMMENT
< 4.2	90	^{1,2} CHOI 11	BELL	$e^+ e^- \rightarrow \Upsilon(4S)$

- • • We do not use the following data for averages, fits, limits, etc. • • •
 - < 5.4 90 ^{2,3}AUBERT 05B BABR $e^+ e^- \rightarrow \Upsilon(4S)$
- ¹ Assumes $\pi^+ \pi^0$ originates from ρ^+ .
- ² Assumes equal production of B^+ and B^0 at the $\Upsilon(4S)$.
- ³ The isovector- X hypothesis is excluded with a likelihood test at 1×10^{-4} level.

$\Gamma(\chi_{c1}(3872) K^*(892)^0) / \Gamma_{\text{total}}$		Γ_{252} / Γ		
VALUE (units 10^{-4})	CL%	DOCUMENT ID	TECN	COMMENT
$1.1 \pm 0.4 \pm 0.3$		¹ BALA 15	BELL	$e^+ e^- \rightarrow \Upsilon(4S)$

- • • We do not use the following data for averages, fits, limits, etc. • • •
 - < 4 90 ^{2,3}AUBERT 09B BABR $e^+ e^- \rightarrow \Upsilon(4S)$
 - < 4 90 ^{3,4}AUBERT 09B BABR $e^+ e^- \rightarrow \Upsilon(4S)$
- ¹ BALA 15 reports $[\Gamma(B^0 \rightarrow \chi_{c1}(3872) K^*(892)^0) / \Gamma_{\text{total}}] \times [B(\chi_{c1}(3872) \rightarrow \pi^+ \pi^- J/\psi(1S))] = (4.0 \pm 1.5 \pm 0.3) \times 10^{-6}$ which we divide by our best value $B(\chi_{c1}(3872) \rightarrow \pi^+ \pi^- J/\psi(1S)) = (3.5 \pm 0.9) \times 10^{-2}$. Our first error is their experiment's error and our second error is the systematic error from using our best value.
- ² AUBERT 09B reports $[\Gamma(B^0 \rightarrow \chi_{c1}(3872) K^*(892)^0) / \Gamma_{\text{total}}] \times [B(\chi_{c1}(3872) \rightarrow \gamma J/\psi)] < 2.8 \times 10^{-6}$ which we divide by our best value $B(\chi_{c1}(3872) \rightarrow \gamma J/\psi) = 7.8 \times 10^{-3}$.
- ³ Uses $B(\Upsilon(4S) \rightarrow B^+ B^-) = (51.6 \pm 0.6)\%$ and $B(\Upsilon(4S) \rightarrow B^0 \bar{B}^0) = (48.4 \pm 0.6)\%$.
- ⁴ AUBERT 09B reports $[\Gamma(B^0 \rightarrow \chi_{c1}(3872) K^*(892)^0) / \Gamma_{\text{total}}] \times [B(\chi_{c1}(3872) \rightarrow \gamma \psi(2S))] < 4.4 \times 10^{-6}$ at 90% CL.

$\Gamma(\chi_{c1}(3872) K^+ \pi^-) / \Gamma_{\text{total}}$		Γ_{253} / Γ		
VALUE (units 10^{-4})	CL%	DOCUMENT ID	TECN	COMMENT
$2.2 \pm 0.4 \pm 0.6$		^{1,2} BALA 15	BELL	$e^+ e^- \rightarrow \Upsilon(4S)$

- ¹ BALA 15 reports $[\Gamma(B^0 \rightarrow \chi_{c1}(3872) K^+ \pi^-) / \Gamma_{\text{total}}] \times [B(\chi_{c1}(3872) \rightarrow \pi^+ \pi^- J/\psi(1S))] = (7.9 \pm 1.3 \pm 0.4) \times 10^{-6}$ which we divide by our best value $B(\chi_{c1}(3872) \rightarrow \pi^+ \pi^- J/\psi(1S)) = (3.5 \pm 0.9) \times 10^{-2}$. Our first error is their experiment's error and our second error is the systematic error from using our best value.
- ² Assumes equal production of B^+ and B^0 at the $\Upsilon(4S)$.

$\Gamma(\chi_{c1}(3872) \gamma) / \Gamma_{\text{total}}$		Γ_{254} / Γ		
VALUE	CL%	DOCUMENT ID	TECN	COMMENT
$< 1.5 \times 10^{-5}$	90	^{1,2} CHOU 19	BELL	$e^+ e^- \rightarrow \Upsilon(4S)$

- ¹ Assumes equal production of B^+ and B^0 at $\Upsilon(4S)$.
- ² CHOU 19 reports $[\Gamma(B^0 \rightarrow \chi_{c1}(3872) \gamma) / \Gamma_{\text{total}}] \times [B(\chi_{c1}(3872) \rightarrow \pi^+ \pi^- J/\psi(1S))] < 5.1 \times 10^{-7}$ which we divide by our best value $B(\chi_{c1}(3872) \rightarrow \pi^+ \pi^- J/\psi(1S)) = 3.5 \times 10^{-2}$.

$\Gamma(T_{c\bar{c}1}(4430) \pm K^\mp, T_{c\bar{c}1}^\pm \rightarrow \psi(2S) \pi^\pm) / \Gamma_{\text{total}}$		Γ_{255} / Γ		
VALUE (units 10^{-5})	CL%	DOCUMENT ID	TECN	COMMENT
$6.0^{+1.7+2.5}_{-2.0-1.4}$		CHILIKIN 13	BELL	$e^+ e^- \rightarrow \Upsilon(4S)$

- • • We do not use the following data for averages, fits, limits, etc. • • •
 - < 3.1 95 ¹AUBERT 09AA BABR $e^+ e^- \rightarrow \Upsilon(4S)$
 - $3.2^{+1.8+5.3}_{-0.9-1.6}$ ¹MIZUK 09 BELL $e^+ e^- \rightarrow \Upsilon(4S)$
 - $1.1 \pm 1.0 \pm 1.4$ ^{1,2}CHOI 08 BELL Repl. by MIZUK 09
- ¹ Assumes equal production of B^+ and B^0 at the $\Upsilon(4S)$.
- ² Establishes the $(Z_c 4430)^+$ with a significance of 6.5 sigma. Needs confirmation.

$\Gamma(T_{c\bar{c}1}(4430) \pm K^\mp, T_{c\bar{c}1}^\pm \rightarrow J/\psi \pi^\pm) / \Gamma_{\text{total}}$		Γ_{256} / Γ		
VALUE (units 10^{-6})	CL%	DOCUMENT ID	TECN	COMMENT
$5.4^{+4.0+0.1}_{-1.0-0.6}$		CHILIKIN 14	BELL	$\bar{B}^0 \rightarrow J/\psi K^- \pi^+$

- • • We do not use the following data for averages, fits, limits, etc. • • •
 - < 4 95 ¹AUBERT 09AA BABR $e^+ e^- \rightarrow \Upsilon(4S)$
- ¹ Assumes equal production of B^+ and B^0 at the $\Upsilon(4S)$.

$\Gamma(T_{c\bar{c}1}(3900) \pm K^\mp, T_{c\bar{c}1}^\pm \rightarrow J/\psi \pi^\pm) / \Gamma_{\text{total}}$		Γ_{257} / Γ		
VALUE	CL%	DOCUMENT ID	TECN	COMMENT
$< 9 \times 10^{-7}$		CHILIKIN 14	BELL	$\bar{B}^0 \rightarrow J/\psi K^- \pi^+$

$\Gamma(T_{c\bar{c}1}(4200) \pm K^\mp, T_{c\bar{c}1}^\pm \rightarrow J/\psi \pi^\pm) / \Gamma_{\text{total}}$		Γ_{258} / Γ		
VALUE (units 10^{-5})	CL%	DOCUMENT ID	TECN	COMMENT
$2.2^{+0.7+1.1}_{-0.5-0.6}$		CHILIKIN 14	BELL	$\bar{B}^0 \rightarrow J/\psi K^- \pi^+$

$\Gamma(T_{c\bar{c}1}(3900) \pm K^\mp, T_{c\bar{c}1}^\pm \rightarrow J/\psi \pi^\pm) / \Gamma(J/\psi(1S) K^*(892)^0)$		$\Gamma_{257} / \Gamma_{216}$		
VALUE	CL%	DOCUMENT ID	TECN	COMMENT
$< 1.5 \times 10^{-2}$	90	ABAZOV 18B	D0	$p\bar{p}$ at 1.96 TeV

$\Gamma(J/\psi(1S) \rho\bar{\rho}) / \Gamma_{\text{total}}$		Γ_{259} / Γ		
VALUE (units 10^{-7})	CL%	DOCUMENT ID	TECN	COMMENT
$4.51 \pm 0.40 \pm 0.44$		¹ AAIJ 19U	LHCB	pp at 7, 8, 13 TeV

- • • We do not use the following data for averages, fits, limits, etc. • • •
 - < 5.2 90 ²AAIJ 13Z LHCB Repl. by AAIJ 19U
 - < 8.3 90 ³XIE 05 BELL $e^+ e^- \rightarrow \Upsilon(4S)$
 - < 19 90 ³AUBERT 03K BABR $e^+ e^- \rightarrow \Upsilon(4S)$
- ¹ Measured relative to $B_S^0 \rightarrow J/\psi \phi$ assuming $B(B_S^0 \rightarrow J/\psi \phi) = (10.5 \pm 0.13 \pm 0.64) \times 10^{-4}$ and taking into account small $K^+ K^- S$ -wave contribution. Measurement assumes $f_s/f_d = 0.259 \pm 0.015$ for 7, 8 TeV data and f_s/f_d multiplied by 1.068 ± 0.046 for 13 TeV data.
- ² Uses $B(B_S^0 \rightarrow J/\psi(1S) \pi^+ \pi^-) = (1.98 \pm 0.20) \times 10^{-4}$.
- ³ Assumes equal production of B^+ and B^0 at the $\Upsilon(4S)$.

$\Gamma(J/\psi(1S) \gamma) / \Gamma_{\text{total}}$		Γ_{260} / Γ		
VALUE (units 10^{-6})	CL%	DOCUMENT ID	TECN	COMMENT
< 1.5	90	¹ AAIJ 15BB	LHCB	pp at 7, 8 TeV

- • • We do not use the following data for averages, fits, limits, etc. • • •
 - < 1.6 90 ²AUBERT.B 04T BABR $e^+ e^- \rightarrow \Upsilon(4S)$
- ¹ Branching fractions of normalization modes $B^0 \rightarrow J/\psi \gamma X$ taken from PDG 14. Uses $f_s/f_d = 0.259 \pm 0.015$.
- ² Assumes equal production of B^+ and B^0 at the $\Upsilon(4S)$.

$\Gamma(J/\psi \mu^+ \mu^-, J/\psi \rightarrow \mu^+ \mu^-) / \Gamma_{\text{total}}$		Γ_{261} / Γ		
VALUE	CL%	DOCUMENT ID	TECN	COMMENT
$< 1.0 \times 10^{-9}$	95	AAIJ 22Q	LHCB	pp at 7, 8, 13 TeV

$\Gamma(J/\psi(1S) \bar{D}^0) / \Gamma_{\text{total}}$		Γ_{262} / Γ		
VALUE (units 10^{-5})	CL%	DOCUMENT ID	TECN	COMMENT
< 1.3	90	¹ AUBERT 05U	BABR	$e^+ e^- \rightarrow \Upsilon(4S)$

- • • We do not use the following data for averages, fits, limits, etc. • • •
 - < 2.0 90 ¹ZHANG 05B BELL $e^+ e^- \rightarrow \Upsilon(4S)$
- ¹ Assumes equal production of B^+ and B^0 at the $\Upsilon(4S)$.

$\Gamma(\psi(2S) \pi^0) / \Gamma_{\text{total}}$		Γ_{263} / Γ		
VALUE (units 10^{-5})	CL%	DOCUMENT ID	TECN	COMMENT
$1.17 \pm 0.17 \pm 0.08$		¹ CHOBANOVA 16	BELL	$e^+ e^- \rightarrow \Upsilon(4S)$

- ¹ Assumes equal production of B^+ and B^0 at the $\Upsilon(4S)$.

Meson Particle Listings

 B^0 $\Gamma(\psi(2S) K^0)/\Gamma_{\text{total}}$ Γ_{264}/Γ

VALUE (units 10^{-4})	CL%	DOCUMENT ID	TECN	COMMENT
5.8 ± 0.5 OUR FIT				
5.8 ± 0.5 OUR AVERAGE				
4.7 ± 0.7 ± 0.7		¹ AAIJ	14L LHCb	pp at 7 TeV
6.46 ± 0.65 ± 0.51		² AUBERT	05J BABR	$e^+e^- \rightarrow \Upsilon(4S)$
6.7 ± 1.1		² ABE	03B BELL	$e^+e^- \rightarrow \Upsilon(4S)$
5.0 ± 1.1 ± 0.6		² RICHICHI	01 CLE2	$e^+e^- \rightarrow \Upsilon(4S)$
6.9 ± 1.1 ± 1.1		² AUBERT	02 BABR	Repl. by AUBERT 05J
< 8	90	² ALAM	94 CLE2	$e^+e^- \rightarrow \Upsilon(4S)$
<15	90	² BORTOLETTO	92 CLEO	$e^+e^- \rightarrow \Upsilon(4S)$
<28	90	² ALBRECHT	90J ARG	$e^+e^- \rightarrow \Upsilon(4S)$

¹ Measured with $B(B^0 \rightarrow \psi(2S) K_S^0) \times B(\psi(2S) \rightarrow J/\psi \pi^+ \pi^-) / B(B^0 \rightarrow J/\psi K_S^0)$ using PDG 12 values for the involved branching fractions.
² Assumes equal production of B^+ and B^0 at the $\Upsilon(4S)$.

 $\Gamma(\psi(2S) K^0 \pi^+ \pi^-)/\Gamma(\psi(2S) K^0)$ $\Gamma_{265}/\Gamma_{264}$

VALUE	DOCUMENT ID	TECN	COMMENT
0.480 ± 0.013 ± 0.032	TUMASYAN	22A1	CMS pp at 13 TeV

 $\Gamma(\psi(2S) K^0)/\Gamma(J/\psi(1S) K^0)$ $\Gamma_{264}/\Gamma_{214}$

VALUE	DOCUMENT ID	TECN	COMMENT
0.82 ± 0.13 ± 0.12	¹ AUBERT	02	BABR $e^+e^- \rightarrow \Upsilon(4S)$

¹ Assumes equal production of B^+ and B^0 at the $\Upsilon(4S)$.

 $\Gamma(\psi(3770) K^0, \psi \rightarrow \bar{D}^0 D^0)/\Gamma_{\text{total}}$ Γ_{266}/Γ

VALUE (units 10^{-4})	CL%	DOCUMENT ID	TECN	COMMENT
<1.23	90	¹ AUBERT	08B BABR	$e^+e^- \rightarrow \Upsilon(4S)$

¹ Assumes equal production of B^+ and B^0 at the $\Upsilon(4S)$.

 $\Gamma(\psi(3770) K^0, \psi \rightarrow D^- D^+)/\Gamma_{\text{total}}$ Γ_{267}/Γ

VALUE (units 10^{-4})	CL%	DOCUMENT ID	TECN	COMMENT
<1.88	90	¹ AUBERT	08B BABR	$e^+e^- \rightarrow \Upsilon(4S)$

¹ Assumes equal production of B^+ and B^0 at the $\Upsilon(4S)$.

 $\Gamma(\psi(2S) \pi^+ \pi^-)/\Gamma(J/\psi(1S) \pi^+ \pi^-)$ $\Gamma_{268}/\Gamma_{225}$

VALUE	DOCUMENT ID	TECN	COMMENT
0.56 ± 0.07 ± 0.05	¹ AAIJ	13AA	LHCb pp at 7 TeV

¹ Assuming lepton universality for dimuon decay modes of J/ψ and $\psi(2S)$ mesons, the ratio $B(J/\psi \rightarrow \mu^+ \mu^-)/B(\psi(2S) \rightarrow \mu^+ \mu^-) = B(J/\psi \rightarrow e^+ e^-)/B(\psi(2S) \rightarrow e^+ e^-) = 7.69 \pm 0.19$ was used.

 $\Gamma(\psi(2S) K^+ \pi^-)/\Gamma_{\text{total}}$ Γ_{269}/Γ

VALUE (units 10^{-4})	CL%	DOCUMENT ID	TECN	COMMENT
5.80 ± 0.39		^{1,2} CHILIKIN	13 BELL	$e^+e^- \rightarrow \Upsilon(4S)$

• • • We do not use the following data for averages, fits, limits, etc. • • •

5.57 ± 0.16		³ AUBERT	09AA BABR	$e^+e^- \rightarrow \Upsilon(4S)$
5.68 ± 0.13 ± 0.42		² MIZUK	09 BELL	$e^+e^- \rightarrow \Upsilon(4S)$
<10	90	² ALBRECHT	90J ARG	$e^+e^- \rightarrow \Upsilon(4S)$

¹ Combines measurements with $\psi(2S) \rightarrow \ell^+ \ell^-$ with measurement from MIZUK 09 which uses $\psi(2S) \rightarrow J/\psi \pi^+ \pi^-$.

² Assumes equal production of B^+ and B^0 at the $\Upsilon(4S)$.

³ Does not report systematic uncertainties.

 $\Gamma(\psi(2S) K^*(892)^0)/\Gamma_{\text{total}}$ Γ_{270}/Γ

VALUE (units 10^{-4})	CL%	DOCUMENT ID	TECN	COMMENT
5.9 ± 0.4 OUR FIT				
6.0 ± 0.5 OUR AVERAGE				Error includes scale factor of 1.1.

5.55 ± 0.22 ± 0.41 -0.23 - 0.84		¹ CHILIKIN	13 BELL	$e^+e^- \rightarrow \Upsilon(4S)$
6.49 ± 0.59 ± 0.97		¹ AUBERT	05J BABR	$e^+e^- \rightarrow \Upsilon(4S)$
7.6 ± 1.1 ± 1.0		¹ RICHICHI	01 CLE2	$e^+e^- \rightarrow \Upsilon(4S)$
9.0 ± 2.2 ± 0.9		² ABE	98o CDF	$p\bar{p}$ 1.8 TeV

• • • We do not use the following data for averages, fits, limits, etc. • • •

5.52 ± 0.35 ± 0.53 -0.32 - 0.58		¹ MIZUK	09 BELL	$e^+e^- \rightarrow \Upsilon(4S)$
<19	90	¹ ALAM	94 CLE2	Repl. by RICHICHI 01
14 ± 8 ± 4		¹ BORTOLETTO	92 CLEO	$e^+e^- \rightarrow \Upsilon(4S)$
<23	90	¹ ALBRECHT	90J ARG	$e^+e^- \rightarrow \Upsilon(4S)$

¹ Assumes equal production of B^+ and B^0 at the $\Upsilon(4S)$.

² ABE 98o reports $[B(B^0 \rightarrow \psi(2S) K^*(892)^0)]/[B(B^+ \rightarrow J/\psi(1S) K^+)] = 0.908 \pm 0.194 \pm 0.10$. We multiply by our best value $B(B^+ \rightarrow J/\psi(1S) K^+) = (9.9 \pm 1.0) \times 10^{-4}$. Our first error is their experiment's error and our second error is the systematic error from using our best value.

 $\Gamma(\psi(2S) K^*(892)^0)/\Gamma(J/\psi(1S) K^*(892)^0)$ $\Gamma_{270}/\Gamma_{216}$

VALUE	DOCUMENT ID	TECN	COMMENT
0.487 ± 0.018 ± 0.014	^{1,2} AAIJ	12L	LHCb pp at 7 TeV

¹ AAIJ 12L reports $0.476 \pm 0.014 \pm 0.010 \pm 0.012$ from a measurement of $[\Gamma(B^0 \rightarrow \psi(2S) K^*(892)^0)/\Gamma(B^0 \rightarrow J/\psi(1S) K^*(892)^0)] \times [B(J/\psi(1S) \rightarrow e^+ e^-)] /$

$[B(\psi(2S) \rightarrow e^+ e^-)]$ assuming $B(J/\psi(1S) \rightarrow e^+ e^-) = (5.94 \pm 0.06) \times 10^{-2}$, $B(\psi(2S) \rightarrow e^+ e^-) = (7.72 \pm 0.17) \times 10^{-3}$, which we rescale to our best values $B(J/\psi(1S) \rightarrow e^+ e^-) = (5.971 \pm 0.032) \times 10^{-2}$, $B(\psi(2S) \rightarrow e^+ e^-) = (7.94 \pm 0.22) \times 10^{-3}$. Our first error is their experiment's error and our second error is the systematic error from using our best values.
² Assumes $B(J/\psi \rightarrow \mu^+ \mu^-) / B(\psi(2S) \rightarrow \mu^+ \mu^-) = B(J/\psi \rightarrow e^+ e^-) / B(\psi(2S) \rightarrow e^+ e^-) = 7.69 \pm 0.19$.

 $\Gamma(\psi(2S) K^*(892)^0)/\Gamma(\psi(2S) K^0)$ $\Gamma_{270}/\Gamma_{264}$

VALUE	DOCUMENT ID	TECN	COMMENT
1.02 ± 0.10 OUR FIT			
1.00 ± 0.14 ± 0.09	AUBERT	05J	BABR $e^+e^- \rightarrow \Upsilon(4S)$

 $\Gamma(\chi_{c0} K^0)/\Gamma_{\text{total}}$ Γ_{271}/Γ

VALUE (units 10^{-6})	CL%	DOCUMENT ID	TECN	COMMENT
195 ± 42 ± 11		¹ AAIJ	18F	LHCb pp at 7, 8 TeV

• • • We do not use the following data for averages, fits, limits, etc. • • •

145 ± 103 ± 85 ± 9		^{2,3} LEES	12i	BABR $e^+e^- \rightarrow \Upsilon(4S)$
148 ± 30 ± 13		^{2,4} LEES	12o	BABR $e^+e^- \rightarrow \Upsilon(4S)$
142 ± 55 ± 44 ± 22		^{2,5} AUBERT	09AU	BABR $e^+e^- \rightarrow \Upsilon(4S)$
< 113	90	⁵ GARMASH	07	BELL $e^+e^- \rightarrow \Upsilon(4S)$
<1240	90	² AUBERT	05K	BABR $e^+e^- \rightarrow \Upsilon(4S)$
< 500	90	⁶ EDWARDS	01	CLE2 $e^+e^- \rightarrow \Upsilon(4S)$

¹ AAIJ 18F uses Dalitz plot analysis of the $B^0 \rightarrow K_S^0 \pi^+ \pi^-$ final state decays. For the branching fraction of the reference mode, the PDG 18 average $B(B^0 \rightarrow K_S^0 \pi^+ \pi^-) = (4.96 \pm 0.20) \times 10^{-5}$ is used. We compute $B(B^0 \rightarrow \chi_{c0} K^0)$ using the PDG value $B(\chi_{c0} \rightarrow \pi\pi) = (8.51 \pm 0.33) \times 10^{-3}$ and 2/3 for the $\pi^+ \pi^-$ fraction. Our first error is their experiment's error and the second error is systematic error from using our best value.

² Assumes equal production of B^+ and B^0 at the $\Upsilon(4S)$.

³ LEES 12i reports $[\Gamma(B^0 \rightarrow \chi_{c0} K^0)/\Gamma_{\text{total}}] \times [B(\chi_{c0}(1P) \rightarrow K_S^0 K_S^0)] = (0.46 \pm 0.25 \pm 0.21) \times 10^{-6}$ which we divide by our best value $B(\chi_{c0}(1P) \rightarrow K_S^0 K_S^0) = (3.17 \pm 0.19) \times 10^{-3}$. Our first error is their experiment's error and our second error is the systematic error from using our best value.

⁴ Measured in the $B^0 \rightarrow K_S^0 K^+ K^-$ decay.

⁵ Uses Dalitz plot analysis of the $B^0 \rightarrow K^0 \pi^+ \pi^-$ final state decays.

⁶ EDWARDS 01 assumes equal production of B^0 and B^+ at the $\Upsilon(4S)$. The correlated uncertainties (28.3%) from $B(J/\psi(1S) \rightarrow \gamma \eta_c)$ in those modes have been accounted for.

 $\Gamma(\chi_{c0} K^*(892)^0)/\Gamma_{\text{total}}$ Γ_{272}/Γ

VALUE (units 10^{-4})	CL%	DOCUMENT ID	TECN	COMMENT
1.7 ± 0.3 ± 0.2		¹ AUBERT	08BD	BABR $e^+e^- \rightarrow \Upsilon(4S)$

• • • We do not use the following data for averages, fits, limits, etc. • • •

<7.7	90	¹ AUBERT	05K	BABR Repl. by AUBERT 08BD
------	----	---------------------	-----	---------------------------

¹ Assumes equal production of B^+ and B^0 at the $\Upsilon(4S)$.

 $\Gamma(\chi_{c1} \pi^0)/\Gamma_{\text{total}}$ Γ_{273}/Γ

VALUE (units 10^{-5})	DOCUMENT ID	TECN	COMMENT
1.12 ± 0.25 ± 0.12	¹ KUMAR	08	BELL $e^+e^- \rightarrow \Upsilon(4S)$

¹ Assumes equal production of B^+ and B^0 at the $\Upsilon(4S)$.

 $\Gamma(\chi_{c1} K^0)/\Gamma_{\text{total}}$ Γ_{274}/Γ

VALUE (units 10^{-4})	CL%	DOCUMENT ID	TECN	COMMENT
3.95 ± 0.27 OUR AVERAGE				

15 ± 5 ± 4 ± 6		¹ CHILIKIN	19 BELL	$e^+e^- \rightarrow \Upsilon(4S)$
3.78 ± 0.17 ± 0.16 ± 0.33		² BHARDWAJ	11 BELL	$e^+e^- \rightarrow \Upsilon(4S)$
4.2 ± 0.3 ± 0.3		³ AUBERT	09B	BABR $e^+e^- \rightarrow \Upsilon(4S)$
3.1 ± 1.5 ± 1.1 ± 0.1		⁴ AVERY	00	CLE2 $e^+e^- \rightarrow \Upsilon(4S)$

• • • We do not use the following data for averages, fits, limits, etc. • • •

3.51 ± 0.33 ± 0.45		² SONI	06	BELL Repl. by BHARDWAJ 11
4.53 ± 0.41 ± 0.51		² AUBERT	05J	BABR Repl. by AUBERT 09b
4.3 ± 1.4 ± 0.2		⁵ AUBERT	02	BABR Repl. by AUBERT 05J
<27	90	² ALAM	94	CLE2 $e^+e^- \rightarrow \Upsilon(4S)$

¹ CHILIKIN 19 reports $[\Gamma(B^0 \rightarrow \chi_{c1} K^0)/\Gamma_{\text{total}}] \times [B(\chi_{c1}(1P) \rightarrow p\bar{p}\pi^+\pi^-)] = (7.4 \pm 2.0 \pm 0.4) \times 10^{-7}$ which we divide by our best value $B(\chi_{c1}(1P) \rightarrow p\bar{p}\pi^+\pi^-) = (5.0 \pm 1.9) \times 10^{-4}$. Our first error is their experiment's error and our second error is the systematic error from using our best value.

² Assumes equal production of B^+ and B^0 at the $\Upsilon(4S)$.

³ Uses $\chi_{c1,2} \rightarrow J/\psi \gamma$. Assumes $B(\Upsilon(4S) \rightarrow B^+ B^-) = (51.6 \pm 0.6)\%$ and $B(\Upsilon(4S) \rightarrow B^0 \bar{B}^0) = (48.4 \pm 0.6)\%$.

⁴ AVERY 00 reports $(3.9 \pm 1.3 \pm 0.4) \times 10^{-4}$ from a measurement of $[\Gamma(B^0 \rightarrow \chi_{c1} K^0)/\Gamma_{\text{total}}] \times [B(\chi_{c1}(1P) \rightarrow \gamma J/\psi(1S))] \times [B(\chi_{c1}(1P) \rightarrow \gamma J/\psi(1S))] = 0.273 \pm 0.016$, which we rescale to our best value $B(\chi_{c1}(1P) \rightarrow \gamma J/\psi(1S)) = (34.3 \pm 1.3) \times 10^{-2}$. Our first error is their experiment's error and our second error is the systematic error from using our best value. Assumes equal production of B^+ and B^0 at the $\Upsilon(4S)$.

⁵ AUBERT 02 reports $(5.4 \pm 1.4 \pm 1.1) \times 10^{-4}$ from a measurement of $[\Gamma(B^0 \rightarrow \chi_{c1} K^0)/\Gamma_{\text{total}}] \times [B(\chi_{c1}(1P) \rightarrow \gamma J/\psi(1S))] \times [B(\chi_{c1}(1P) \rightarrow \gamma J/\psi(1S))] = 0.273 \pm 0.016$, which we rescale to our best value $B(\chi_{c1}(1P) \rightarrow \gamma J/\psi(1S)) = (34.3 \pm 1.3) \times 10^{-2}$. Our first error is their experiment's error and our second error is the systematic error from using our best value. Assumes equal production of B^+ and B^0 at the $\Upsilon(4S)$.

$\Gamma(\chi_{c1} K^0)/\Gamma(J/\psi(1S) K^0)$ $\Gamma_{274}/\Gamma_{214}$

VALUE	DOCUMENT ID	TECN	COMMENT
0.53 ± 0.16 ± 0.02	¹ AUBERT 02	BABR	$e^+e^- \rightarrow \Upsilon(4S)$
¹ AUBERT 02 reports $0.66 \pm 0.11 \pm 0.17$ from a measurement of $[\Gamma(B^0 \rightarrow \chi_{c1} K^0)/\Gamma(B^0 \rightarrow J/\psi(1S) K^0)] \times [B(\chi_{c1}(1P) \rightarrow \gamma J/\psi(1S))]$ assuming $B(\chi_{c1}(1P) \rightarrow \gamma J/\psi(1S)) = 0.273 \pm 0.016$, which we rescale to our best value $B(\chi_{c1}(1P) \rightarrow \gamma J/\psi(1S)) = (34.3 \pm 1.3) \times 10^{-2}$. Our first error is their experiment's error and our second error is the systematic error from using our best value. Assumes equal production of B^+ and B^0 at the $\Upsilon(4S)$.			

 $\Gamma(\chi_{c1} \pi^- K^+)/\Gamma_{total}$ Γ_{275}/Γ

VALUE (units 10^{-4})	DOCUMENT ID	TECN	COMMENT
4.97 ± 0.12 ± 0.28	¹ BHARDWAJ 16	BELL	$e^+e^- \rightarrow \Upsilon(4S)$
• • • We do not use the following data for averages, fits, limits, etc. • • •			
$3.83 \pm 0.10 \pm 0.39$	¹ MIZUK 08	BELL	Repl. by BHARDWAJ 16
¹ Assumes equal production of B^+ and B^0 at the $\Upsilon(4S)$.			

 $\Gamma(\chi_{c1} \pi^- K^+)/\Gamma(J/\psi(1S) K^+ \pi^-)$ $\Gamma_{275}/\Gamma_{215}$

VALUE	DOCUMENT ID	TECN	COMMENT
0.476 ± 0.021 ± 0.018	¹ LEES 12b	BABR	
¹ LEES 12b reports $0.474 \pm 0.013 \pm 0.026$ from a measurement of $[\Gamma(B^0 \rightarrow \chi_{c1} \pi^- K^+)/\Gamma(B^0 \rightarrow J/\psi(1S) K^+ \pi^-)] \times [B(\chi_{c1}(1P) \rightarrow \gamma J/\psi(1S))]$ assuming $B(\chi_{c1}(1P) \rightarrow \gamma J/\psi(1S)) = (34.4 \pm 1.5) \times 10^{-2}$, which we rescale to our best value $B(\chi_{c1}(1P) \rightarrow \gamma J/\psi(1S)) = (34.3 \pm 1.3) \times 10^{-2}$. Our first error is their experiment's error and our second error is the systematic error from using our best value.			

 $\Gamma(\chi_{c1} K^*(892)^0)/\Gamma_{total}$ Γ_{276}/Γ

VALUE (units 10^{-4})	CL%	DOCUMENT ID	TECN	COMMENT
2.38 ± 0.19 OUR FIT		Error includes scale factor of 1.2.		
2.22^{+0.40}_{-0.31} OUR AVERAGE		Error includes scale factor of 1.6.		
$2.5 \pm 0.2 \pm 0.2$		¹ AUBERT 09b	BABR	$e^+e^- \rightarrow \Upsilon(4S)$
$1.73^{+0.15+0.34}$ -0.12 ± 0.22		² MIZUK 08	BELL	$e^+e^- \rightarrow \Upsilon(4S)$
• • • We do not use the following data for averages, fits, limits, etc. • • •				
$3.14 \pm 0.34 \pm 0.72$		² SONI 06	BELL	Repl. by MIZUK 08
$3.27 \pm 0.42 \pm 0.64$		² AUBERT 05j	BABR	Repl. by AUBERT 09b
$3.8 \pm 1.3 \pm 0.1$		³ AUBERT 02	BABR	Repl. by AUBERT 05j
<21	90	⁴ ALAM 94	CLE2	$e^+e^- \rightarrow \Upsilon(4S)$

¹ Uses $\chi_{c1,2} \rightarrow J/\psi\gamma$. Assumes $B(\Upsilon(4S) \rightarrow B^+ B^-) = (51.6 \pm 0.6)\%$ and $B(\Upsilon(4S) \rightarrow B^0 \bar{B}^0) = (48.4 \pm 0.6)\%$.

² Assumes equal production of B^+ and B^0 at the $\Upsilon(4S)$.

³ AUBERT 02 reports $(4.8 \pm 1.4 \pm 0.9) \times 10^{-4}$ from a measurement of $[\Gamma(B^0 \rightarrow \chi_{c1} K^*(892)^0)/\Gamma_{total}] \times [B(\chi_{c1}(1P) \rightarrow \gamma J/\psi(1S))]$ assuming $B(\chi_{c1}(1P) \rightarrow \gamma J/\psi(1S)) = 0.273 \pm 0.016$, which we rescale to our best value $B(\chi_{c1}(1P) \rightarrow \gamma J/\psi(1S)) = (34.3 \pm 1.3) \times 10^{-2}$. Our first error is their experiment's error and our second error is the systematic error from using our best value. Assumes equal production of B^+ and B^0 at the $\Upsilon(4S)$.

⁴ BORTOLETTO 92 assumes equal production of B^+ and B^0 at the $\Upsilon(4S)$.

 $\Gamma(\chi_{c1} K^*(892)^0)/\Gamma(J/\psi(1S) K^*(892)^0)$ $\Gamma_{276}/\Gamma_{216}$

VALUE (units 10^{-2})	DOCUMENT ID	TECN	COMMENT
18.8 ± 1.5 OUR FIT	Error includes scale factor of 1.1.		
19.8 ± 1.1 ± 1.5	¹ AAIJ 13a	LHCB	pp at 7 TeV
¹ Uses $B(\chi_{c1} \rightarrow J/\psi\gamma) = (34.4 \pm 1.5)\%$.			

 $\Gamma(\chi_{c1} K^*(892)^0)/\Gamma(\chi_{c1} K^0)$ $\Gamma_{276}/\Gamma_{274}$

VALUE	DOCUMENT ID	TECN	COMMENT
0.72 ± 0.11 ± 0.12	AUBERT 05j	BABR	$e^+e^- \rightarrow \Upsilon(4S)$
• • • We do not use the following data for averages, fits, limits, etc. • • •			
$0.89 \pm 0.34 \pm 0.17$	¹ AUBERT 02	BABR	Repl. by AUBERT 05j
¹ Assumes equal production of B^+ and B^0 at the $\Upsilon(4S)$.			

 $\Gamma(T_{c\bar{c}}(4050)^- K^+, T_{c\bar{c}}^- \rightarrow \chi_{c1} \pi^-)/\Gamma_{total}$ Γ_{277}/Γ

VALUE (units 10^{-5})	CL%	DOCUMENT ID	TECN	COMMENT
3.0^{+1.5+3.7}_{-0.8-1.6}		¹ MIZUK 08	BELL	$e^+e^- \rightarrow \Upsilon(4S)$
• • • We do not use the following data for averages, fits, limits, etc. • • •				
<4.0	90	^{1,2} LEES 12b	BABR	
¹ Assumes equal production of B^+ and B^0 at the $\Upsilon(4S)$.				
² Uses $\chi_{c1} \rightarrow J/\psi\gamma$ mode. Uses $\chi_{c1} \rightarrow J/\psi\gamma$ mode. Finds a good description of the data without this $B^0 \rightarrow X(4051)^+ K^-$ decay mode in a fit.				

 $\Gamma(T_{c\bar{c}}(4250)^- K^+, T_{c\bar{c}}^- \rightarrow \chi_{c1} \pi^-)/\Gamma_{total}$ Γ_{278}/Γ

VALUE (units 10^{-5})	CL%	DOCUMENT ID	TECN	COMMENT
4.0^{+2.3+19.7}_{-0.9-0.5}		¹ MIZUK 08	BELL	$e^+e^- \rightarrow \Upsilon(4S)$
• • • We do not use the following data for averages, fits, limits, etc. • • •				
<4.0	90	^{1,2} LEES 12b	BABR	
¹ Assumes equal production of B^+ and B^0 at the $\Upsilon(4S)$.				
² Uses $\chi_{c1} \rightarrow J/\psi\gamma$ mode. Finds a good description of the data without this $B^0 \rightarrow X(4248)^+ K^-$ decay mode in a fit.				

 $\Gamma(\chi_{c1} \pi^+ \pi^- K^0)/\Gamma_{total}$ Γ_{279}/Γ

VALUE (units 10^{-4})	DOCUMENT ID	TECN	COMMENT
3.16 ± 0.35 ± 0.32	¹ BHARDWAJ 16	BELL	$e^+e^- \rightarrow \Upsilon(4S)$
¹ Assumes equal production of B^+ and B^0 at the $\Upsilon(4S)$.			

 $\Gamma(\chi_{c1} \pi^- \pi^0 K^+)/\Gamma_{total}$ Γ_{280}/Γ

VALUE (units 10^{-4})	DOCUMENT ID	TECN	COMMENT
3.52 ± 0.52 ± 0.24	¹ BHARDWAJ 16	BELL	$e^+e^- \rightarrow \Upsilon(4S)$
¹ Assumes equal production of B^+ and B^0 at the $\Upsilon(4S)$.			

 $\Gamma(\chi_{c2} K^0)/\Gamma_{total}$ Γ_{281}/Γ

VALUE	CL%	DOCUMENT ID	TECN	COMMENT
<1.5 × 10⁻⁵	90	¹ BHARDWAJ 11	BELL	$e^+e^- \rightarrow \Upsilon(4S)$
• • • We do not use the following data for averages, fits, limits, etc. • • •				
<2.8 × 10 ⁻⁵	90	² AUBERT 09b	BABR	$e^+e^- \rightarrow \Upsilon(4S)$
<2.6 × 10 ⁻⁵	90	¹ SONI 06	BELL	Repl. by BHARDWAJ 11
<4.1 × 10 ⁻⁵	90	¹ AUBERT 05k	BABR	$e^+e^- \rightarrow \Upsilon(4S)$

¹ Assumes equal production of B^+ and B^0 at the $\Upsilon(4S)$.

² Uses $\chi_{c1,2} \rightarrow J/\psi\gamma$. Assumes $B(\Upsilon(4S) \rightarrow B^+ B^-) = (51.6 \pm 0.6)\%$ and $B(\Upsilon(4S) \rightarrow B^0 \bar{B}^0) = (48.4 \pm 0.6)\%$.

 $\Gamma(\chi_{c2} K^*(892)^0)/\Gamma_{total}$ Γ_{282}/Γ

VALUE (units 10^{-5})	CL%	DOCUMENT ID	TECN	COMMENT
4.9 ± 1.2 OUR FIT		Error includes scale factor of 1.1.		
6.6 ± 1.8 ± 0.5		¹ AUBERT 09b	BABR	$e^+e^- \rightarrow \Upsilon(4S)$
• • • We do not use the following data for averages, fits, limits, etc. • • •				
<7.1	90	² SONI 06	BELL	$e^+e^- \rightarrow \Upsilon(4S)$
<3.6	90	² AUBERT 05k	BABR	Repl. by AUBERT 09b

¹ Uses $\chi_{c1,2} \rightarrow J/\psi\gamma$. Assumes $B(\Upsilon(4S) \rightarrow B^+ B^-) = (51.6 \pm 0.6)\%$ and $B(\Upsilon(4S) \rightarrow B^0 \bar{B}^0) = (48.4 \pm 0.6)\%$.

² Assumes equal production of B^+ and B^0 at the $\Upsilon(4S)$.

 $\Gamma(\chi_{c2} K^*(892)^0)/\Gamma(\chi_{c1} K^*(892)^0)$ $\Gamma_{282}/\Gamma_{276}$

VALUE (units 10^{-2})	DOCUMENT ID	TECN	COMMENT
20 ± 5 OUR FIT	Error includes scale factor of 1.1.		
17.1 ± 5.0 ± 2.0	¹ AAIJ 13a	LHCB	pp at 7 TeV
¹ Uses $B(\chi_{c1} \rightarrow J/\psi\gamma)/B(\chi_{c2} \rightarrow J/\psi\gamma) = 1.76 \pm 0.11$.			

 $\Gamma(\chi_{c2} \pi^- K^+)/\Gamma_{total}$ Γ_{283}/Γ

VALUE (units 10^{-4})	DOCUMENT ID	TECN	COMMENT
0.72 ± 0.09 ± 0.05	¹ BHARDWAJ 16	BELL	$e^+e^- \rightarrow \Upsilon(4S)$
¹ Assumes equal production of B^+ and B^0 at the $\Upsilon(4S)$.			

 $\Gamma(\chi_{c2} \pi^+ \pi^- K^0)/\Gamma_{total}$ Γ_{284}/Γ

VALUE	CL%	DOCUMENT ID	TECN	COMMENT
<1.70 × 10⁻⁴	90	¹ BHARDWAJ 16	BELL	$e^+e^- \rightarrow \Upsilon(4S)$
¹ Assumes equal production of B^+ and B^0 at the $\Upsilon(4S)$.				

 $\Gamma(\chi_{c2} \pi^- \pi^0 K^+)/\Gamma_{total}$ Γ_{285}/Γ

VALUE	CL%	DOCUMENT ID	TECN	COMMENT
<0.74 × 10⁻⁴	90	¹ BHARDWAJ 16	BELL	$e^+e^- \rightarrow \Upsilon(4S)$
¹ Assumes equal production of B^+ and B^0 at the $\Upsilon(4S)$.				

 $\Gamma(\psi(4660) K^0, \psi \rightarrow \Lambda_c^+ \Lambda_c^-)/\Gamma_{total}$ Γ_{286}/Γ

VALUE	CL%	DOCUMENT ID	TECN	COMMENT
<2.3 × 10⁻⁴	90	¹ LI 18d	BELL	$e^+e^- \rightarrow \Upsilon(4S)$
¹ Assumes $B(\Upsilon(4S) \rightarrow B^0 \bar{B}^0) = 48.6 \pm 0.6\%$ and $B(\Lambda_c^+ \rightarrow p K^- \pi^+) = 6.23 \pm 0.33\%$.				

 $\Gamma(\psi(4230)^0 K^0, \psi^0 \rightarrow J/\psi \pi^+ \pi^-)/\Gamma_{total}$ Γ_{287}/Γ

VALUE	CL%	DOCUMENT ID	TECN	COMMENT
<17 × 10⁻⁶	90	¹ GARG 19	BELL	$e^+e^- \rightarrow \Upsilon(4S)$
¹ Assumes equal production of B^0 and B^+ at the $\Upsilon(4S)$.				

 $\Gamma(K^+ \pi^-)/\Gamma_{total}$ Γ_{288}/Γ

VALUE (units 10^{-6})	CL%	DOCUMENT ID	TECN	COMMENT
20.0 ± 0.4 OUR FIT				
20.0 ± 0.4 OUR AVERAGE				
$20.67 \pm 0.37 \pm 0.62$		ADACHI 24	BELL	$e^+e^- \rightarrow \Upsilon(4S)$
$20.00 \pm 0.34 \pm 0.60$		¹ DUH 13	BELL	$e^+e^- \rightarrow \Upsilon(4S)$
$19.1 \pm 0.6 \pm 0.6$		¹ AUBERT 07b	BABR	$e^+e^- \rightarrow \Upsilon(4S)$
$18.0 \pm 2.3 \pm 1.2$ $-2.1 - 0.9$		¹ BORNHEIM 03	CLE2	$e^+e^- \rightarrow \Upsilon(4S)$
• • • We do not use the following data for averages, fits, limits, etc. • • •				
$19.9 \pm 0.4 \pm 0.8$		¹ LIN 07a	BELL	Repl. by DUH 13
$18.5 \pm 1.0 \pm 0.7$		¹ CHAO 04	BELL	Repl. by LIN 07a
$17.9 \pm 0.9 \pm 0.7$		¹ AUBERT 02q	BABR	Repl. by AUBERT 07b
$22.5 \pm 1.9 \pm 1.8$		¹ CASEY 02	BELL	Repl. by CHAO 04
$19.3 \pm 3.4 \pm 1.5$ $-3.2 - 0.6$		¹ ABE 01h	BELL	Repl. by CASEY 02
$16.7 \pm 1.6 \pm 1.3$		¹ AUBERT 01e	BABR	Repl. by AUBERT 02q

Meson Particle Listings

 B^0

VALUE	DOCUMENT ID	TECN	COMMENT
< 66	90	2 ABE	00c SLD $e^+e^- \rightarrow Z$
$17.2 \pm 2.5 \pm 1.2$	1 CRONIN-HEN..00	CLE2	Repl. by BORNHEIM 03
$15 \pm 5 \pm 1.4$	GODANG	98 CLE2	Repl. by CRONIN-HENNESSY 00
$24 \pm 17 \pm 2$	3 ADAM	96d DLPH	$e^+e^- \rightarrow Z$
< 17	90	ASNER	96 CLE2 Sup. by ADAM 96d
< 30	90	4 BUSKULIC	96v ALEP $e^+e^- \rightarrow Z$
< 90	90	5 ABREU	95n DLPH Sup. by ADAM 96d
< 81	90	6 AKERS	94L OPAL $e^+e^- \rightarrow Z$
< 26	90	7 BATTLE	93 CLE2 $e^+e^- \rightarrow \Upsilon(4S)$
< 180	90	ALBRECHT	91B ARG $e^+e^- \rightarrow \Upsilon(4S)$
< 90	90	8 AVERY	89B CLEO $e^+e^- \rightarrow \Upsilon(4S)$
< 320	90	AVERY	87 CLEO $e^+e^- \rightarrow \Upsilon(4S)$

- ¹ Assumes equal production of B^+ and B^0 at the $\Upsilon(4S)$.
² ABE 00c assumes $B(Z \rightarrow b\bar{b}) = (21.7 \pm 0.1)\%$ and the B fractions $f_{B^0} = f_{B^+} = (39.7 \pm 1.8)\%$ and $f_{B_s} = (10.5 \pm 1.3)\%$.
³ ADAM 96d assumes $f_{B^0} = f_{B^-} = 0.39$ and $f_{B_s} = 0.12$. Contributions from B^0 and B_s decays cannot be separated. Limits are given for the weighted average of the decay rates for the two neutral B mesons.
⁴ BUSKULIC 96v assumes PDG 96 production fractions for B^0 , B^+ , B_s , b baryons.
⁵ Assumes a B^0 , B^- production fraction of 0.39 and a B_s production fraction of 0.12. Contributions from B^0 and B_s decays cannot be separated. Limits are given for the weighted average of the decay rates for the two neutral B mesons.
⁶ Assumes $B(Z \rightarrow b\bar{b}) = 0.217$ and B_s^0 (B_s^+) fraction 39.5% (12%).
⁷ BATTLE 93 assumes equal production of $B^0\bar{B}^0$ and B^+B^- at $\Upsilon(4S)$.
⁸ Assumes the $\Upsilon(4S)$ decays 43% to $B^0\bar{B}^0$.

 $\Gamma(K^+\pi^-)/\Gamma(K^0\pi^0)$ $\Gamma_{288}/\Gamma_{289}$

VALUE	DOCUMENT ID	TECN	COMMENT
$2.16 \pm 0.16 \pm 0.16$	LIN	07A BELL	$e^+e^- \rightarrow \Upsilon(4S)$

••• We do not use the following data for averages, fits, limits, etc. •••

$1.20 \pm 0.50 \pm 0.22$ $-0.58 - 0.32$	1 ABE	01H BELL	Repl. by LIN 07A
--	-------	----------	------------------

¹ Assumes equal production of B^+ and B^0 at the $\Upsilon(4S)$.

 $[\Gamma(K^+\pi^-) + \Gamma(\pi^+\pi^-)]/\Gamma_{total}$ $(\Gamma_{288} + \Gamma_{423})/\Gamma$

VALUE (units 10^{-6})	EVTS	DOCUMENT ID	TECN	COMMENT
19 ± 6 OUR AVERAGE				

$28 \pm 15 \pm 20$	1 ADAM	96d DLPH	$e^+e^- \rightarrow Z$
$18 \pm 6 \pm 3$ -5 ± 4	17.2 ASNER	96 CLE2	$e^+e^- \rightarrow \Upsilon(4S)$

••• We do not use the following data for averages, fits, limits, etc. •••

$24 \pm 8 \pm 2$	2 BATTLE	93 CLE2	$e^+e^- \rightarrow \Upsilon(4S)$
------------------	----------	---------	-----------------------------------

- ¹ ADAM 96d assumes $f_{B^0} = f_{B^-} = 0.39$ and $f_{B_s} = 0.12$. Contributions from B^0 and B_s decays cannot be separated. Limits are given for the weighted average of the decay rates for the two neutral B mesons.
² BATTLE 93 assumes equal production of $B^0\bar{B}^0$ and B^+B^- at $\Upsilon(4S)$.

 $\Gamma(K^0\pi^0)/\Gamma_{total}$ Γ_{289}/Γ

VALUE (units 10^{-6})	CL%	DOCUMENT ID	TECN	COMMENT
10.1 ± 0.4 OUR AVERAGE				

$10.73 \pm 0.63 \pm 0.62$	1 ADACHI	24 BELL	$e^+e^- \rightarrow \Upsilon(4S)$
$9.68 \pm 0.46 \pm 0.50$	2 DUH	13 BELL	$e^+e^- \rightarrow \Upsilon(4S)$
$10.1 \pm 0.6 \pm 0.4$	2 LEES	13d BABR	$e^+e^- \rightarrow \Upsilon(4S)$
$12.8 \pm 4.0 \pm 1.7$ $-3.3 - 1.4$	2 BORNHEIM	03 CLE2	$e^+e^- \rightarrow \Upsilon(4S)$

••• We do not use the following data for averages, fits, limits, etc. •••

$8.7 \pm 0.5 \pm 0.6$	2 FUJIKAWA	10A BELL	Repl. by DUH 13
$10.3 \pm 0.7 \pm 0.6$	2 AUBERT	08E BABR	Repl. by LEES 13d
$9.2 \pm 0.7 \pm 0.6$	2 LIN	07A BELL	Repl. by FUJIKAWA 10A
$11.4 \pm 0.9 \pm 0.6$	2 AUBERT	05Y BABR	Repl. by AUBERT 08E
$11.4 \pm 1.7 \pm 0.8$	2 AUBERT	04M BABR	Repl. by AUBERT 05Y
$11.7 \pm 2.3 \pm 1.2$ -1.3	2 CHAO	04 BELL	Repl. by LIN 07A
$8.0 \pm 3.3 \pm 1.6$ -3.1	2 CASEY	02 BELL	Repl. by CHAO 04
$16.0 \pm 7.2 \pm 2.5$ $-5.9 - 2.7$	2 ABE	01H BELL	Repl. by CASEY 02
$8.2 \pm 3.1 \pm 1.2$ -2.7	2 AUBERT	01E BABR	Repl. by AUBERT 04M
$14.6 \pm 5.9 \pm 2.4$ $-5.1 - 3.3$	2 CRONIN-HEN..00	CLE2	Repl. by BORNHEIM 03

< 41	90	GODANG	98 CLE2 Repl. by CRONIN-HENNESSY 00
< 40	90	ASNER	96 CLE2 Repl. by GODANG 98

¹ This is the combined result of this analysis (ADACHI 24) and the updated analysis of ADACHI 23E. The individual results are $(10.40 \pm 0.66 \pm 0.60) \times 10^{-6}$ and $(11.15 \pm 0.68 \pm 0.62) \times 10^{-6}$, respectively.

² Assumes equal production of B^+ and B^0 at the $\Upsilon(4S)$.

 $\Gamma(\eta'K^0)/\Gamma_{total}$ Γ_{290}/Γ

VALUE (units 10^{-6})	DOCUMENT ID	TECN	COMMENT
66 ± 4 OUR AVERAGE			Error includes scale factor of 1.4.

$68.5 \pm 2.2 \pm 3.1$	1 AUBERT	09AV BABR	$e^+e^- \rightarrow \Upsilon(4S)$
$58.9 \pm 3.6 \pm 4.3$	1 SCHUEMANN 06	BELL	$e^+e^- \rightarrow \Upsilon(4S)$

$89 \pm 18 \pm 9$	1 RICHICHI	00 CLE2	$e^+e^- \rightarrow \Upsilon(4S)$
-------------------	------------	---------	-----------------------------------

••• We do not use the following data for averages, fits, limits, etc. •••

$66.6 \pm 2.6 \pm 2.8$	1 AUBERT	07AE BABR	Repl. by AUBERT 09AV
$67.4 \pm 3.3 \pm 3.2$	1 AUBERT	05M BABR	AUBERT 07AE
$60.6 \pm 5.6 \pm 4.6$	1 AUBERT	03W BABR	Repl. by AUBERT 05M

$55 \pm 19 \pm 8$	1 ABE	01M BELL	Repl. by SCHUEMANN 06
-------------------	-------	----------	-----------------------

$42 \pm 13 \pm 4$	1 AUBERT	01G BABR	Repl. by AUBERT 03W
-------------------	----------	----------	---------------------

$47 \pm 27 \pm 9$	BEHRENS	98 CLE2	Repl. by RICHICHI 00
-------------------	---------	---------	----------------------

¹ Assumes equal production of B^+ and B^0 at the $\Upsilon(4S)$.

 $\Gamma(\eta'K^*(892)^0)/\Gamma_{total}$ Γ_{291}/Γ

VALUE (units 10^{-6})	CL%	DOCUMENT ID	TECN	COMMENT
2.8 ± 0.6 OUR AVERAGE				

$2.6 \pm 0.7 \pm 0.2$	1 SATO	14 BELL	$e^+e^- \rightarrow \Upsilon(4S)$
$3.1 \pm 0.9 \pm 0.3$ -0.8 ± 0.3	1 DEL-AMO-SA..10A	BABR	$e^+e^- \rightarrow \Upsilon(4S)$

••• We do not use the following data for averages, fits, limits, etc. •••

$3.8 \pm 1.1 \pm 0.5$	1 AUBERT	07E BABR	Repl. by DEL-AMO-SANCHEZ 10A
< 2.6	90	1 SCHUEMANN 07	BELL $e^+e^- \rightarrow \Upsilon(4S)$
< 7.6	90	1 AUBERT,B	04D BABR Repl. by AUBERT 07E
< 24	90	1 RICHICHI	00 CLE2 $e^+e^- \rightarrow \Upsilon(4S)$
< 39	90	BEHRENS	98 CLE2 Repl. by RICHICHI 00

¹ Assumes equal production of B^+ and B^0 at the $\Upsilon(4S)$.

 $\Gamma(\eta'K_0^*(1430)^0)/\Gamma_{total}$ Γ_{292}/Γ

VALUE (units 10^{-6})	DOCUMENT ID	TECN	COMMENT
$6.3 \pm 1.3 \pm 0.9$	1 DEL-AMO-SA..10A	BABR	$e^+e^- \rightarrow \Upsilon(4S)$

¹ Assumes equal production of B^+ and B^0 at the $\Upsilon(4S)$.

 $\Gamma(\eta'K_2^*(1430)^0)/\Gamma_{total}$ Γ_{293}/Γ

VALUE (units 10^{-6})	DOCUMENT ID	TECN	COMMENT
$13.7 \pm 3.0 \pm 1.2$	1 DEL-AMO-SA..10A	BABR	$e^+e^- \rightarrow \Upsilon(4S)$

¹ Assumes equal production of B^+ and B^0 at the $\Upsilon(4S)$.

 $\Gamma(\eta K^0)/\Gamma_{total}$ Γ_{294}/Γ

VALUE (units 10^{-6})	DOCUMENT ID	TECN	COMMENT
$1.23 \pm 0.27 \pm 0.24$ OUR AVERAGE			

$1.27 \pm 0.33 \pm 0.08$ -0.29	1 HOI	12 BELL	$e^+e^- \rightarrow \Upsilon(4S)$
$1.15 \pm 0.43 \pm 0.09$ -0.38	1 AUBERT	09AV BABR	$e^+e^- \rightarrow \Upsilon(4S)$

••• We do not use the following data for averages, fits, limits, etc. •••

< 1.9	90	1 CHANG	07B BELL Repl. by HOI 12
< 2.9	90	1 AUBERT,B	06V BABR $e^+e^- \rightarrow \Upsilon(4S)$
< 2.5	90	1 AUBERT,B	05K BABR $e^+e^- \rightarrow \Upsilon(4S)$
< 2.0	90	1 CHANG	05A BELL Repl. by CHANG 07B
< 5.2	90	1 AUBERT	04H BABR Repl. by AUBERT,B 05K
< 9.3	90	1 RICHICHI	00 CLE2 $e^+e^- \rightarrow \Upsilon(4S)$
< 33	90	BEHRENS	98 CLE2 Repl. by RICHICHI 00

¹ Assumes equal production of B^+ and B^0 at the $\Upsilon(4S)$.

 $\Gamma(\eta K^*(892)^0)/\Gamma_{total}$ Γ_{295}/Γ

VALUE (units 10^{-6})	CL%	DOCUMENT ID	TECN	COMMENT
15.9 ± 1.0 OUR AVERAGE				

$15.2 \pm 1.2 \pm 1.0$	1 WANG	07B BELL	$e^+e^- \rightarrow \Upsilon(4S)$
$16.5 \pm 1.1 \pm 0.8$	1 AUBERT,B	06H BABR	$e^+e^- \rightarrow \Upsilon(4S)$
$13.8 \pm 5.5 \pm 1.6$ -4.6	1 RICHICHI	00 CLE2	$e^+e^- \rightarrow \Upsilon(4S)$

••• We do not use the following data for averages, fits, limits, etc. •••

$18.6 \pm 2.3 \pm 1.2$	1 AUBERT,B	04D BABR	Repl. by AUBERT,B 06H
< 30	90	BEHRENS	98 CLE2 Repl. by RICHICHI 00

¹ Assumes equal production of B^+ and B^0 at the $\Upsilon(4S)$.

 $\Gamma(\eta K_0^*(1430)^0)/\Gamma_{total}$ Γ_{296}/Γ

VALUE (units 10^{-6})	DOCUMENT ID	TECN	COMMENT
$11.0 \pm 1.6 \pm 1.5$	1 AUBERT,B	06H BABR	$e^+e^- \rightarrow \Upsilon(4S)$

¹ Assumes equal production of B^+ and B^0 at the $\Upsilon(4S)$.

 $\Gamma(\eta K_2^*(1430)^0)/\Gamma_{total}$ Γ_{297}/Γ

VALUE (units 10^{-6})	DOCUMENT ID	TECN	COMMENT
$9.6 \pm 1.8 \pm 1.1$	1 AUBERT,B	06H BABR	$e^+e^- \rightarrow \Upsilon(4S)$

¹ Assumes equal production of B^+ and B^0 at the $\Upsilon(4S)$.

$\Gamma(\omega K^0)/\Gamma_{\text{total}}$		Γ_{298}/Γ
VALUE (units 10^{-6})	CL%	DOCUMENT ID
4.8 ± 0.4 OUR AVERAGE		
4.5 ± 0.4 ± 0.3		¹ CHOBANOVA 14 BELL $e^+e^- \rightarrow \Upsilon(4S)$
5.4 ± 0.8 ± 0.3		¹ AUBERT 07AE BABR $e^+e^- \rightarrow \Upsilon(4S)$
10.0 ^{+5.4} _{-4.2} ± 1.4		¹ JESSOP 00 CLE2 $e^+e^- \rightarrow \Upsilon(4S)$
• • • We do not use the following data for averages, fits, limits, etc. • • •		
6.2 ± 1.0 ± 0.4		¹ AUBERT,B 06E BABR Repl. by AUBERT 07AE
4.4 ^{+0.8} _{-0.7} ± 0.4		¹ JEN 06 BELL Repl. by CHOBANOVA 14
5.9 ^{+1.6} _{-1.3} ± 0.5		¹ AUBERT 04H BABR Repl. by AUBERT,B 06E
4.0 ^{+1.9} _{-1.6} ± 0.5		¹ WANG 04A BELL Repl. by JEN 06
<13	90	¹ AUBERT 01G BABR Repl. by AUBERT 04H
<57	90	¹ BERGFELD 98 CLE2 Repl. by JESSOP 00
¹ Assumes equal production of B^+ and B^0 at the $\Upsilon(4S)$.		

$\Gamma(a_0(980)^0 K^0, a_0^0 \rightarrow \eta\pi^0)/\Gamma_{\text{total}}$		Γ_{299}/Γ
VALUE (units 10^{-6})	CL%	DOCUMENT ID
<7.8	90	¹ AUBERT,BE 04 BABR $e^+e^- \rightarrow \Upsilon(4S)$
¹ Assumes equal production of charged and neutral B mesons at $\Upsilon(4S)$.		

$\Gamma(b_1^0 K^0, b_1^0 \rightarrow \omega\pi^0)/\Gamma_{\text{total}}$		Γ_{300}/Γ
VALUE (units 10^{-6})	CL%	DOCUMENT ID
<7.8	90	¹ AUBERT 08AQ BABR $e^+e^- \rightarrow \Upsilon(4S)$
¹ Assumes equal production of B^+ and B^0 at the $\Upsilon(4S)$.		

$\Gamma(a_0(980)^\pm K^\mp, a_0^\pm \rightarrow \eta\pi^\pm)/\Gamma_{\text{total}}$		Γ_{301}/Γ
VALUE (units 10^{-6})	CL%	DOCUMENT ID
<1.9	90	¹ AUBERT 07Y BABR $e^+e^- \rightarrow \Upsilon(4S)$
• • • We do not use the following data for averages, fits, limits, etc. • • •		
<2.1	90	¹ AUBERT,BE 04 BABR Repl. by AUBERT 07Y
¹ Assumes equal production of B^+ and B^0 at the $\Upsilon(4S)$.		

$\Gamma(b_1^- K^+, b_1^- \rightarrow \omega\pi^-)/\Gamma_{\text{total}}$		Γ_{302}/Γ
VALUE (units 10^{-6})	CL%	DOCUMENT ID
7.4 ± 1.0 ± 1.0		¹ AUBERT 07BI BABR $e^+e^- \rightarrow \Upsilon(4S)$
¹ Assumes equal production of B^+ and B^0 at the $\Upsilon(4S)$.		

$\Gamma(b_1^0 K^0, b_1^0 \rightarrow \omega\pi^0)/\Gamma_{\text{total}}$		Γ_{303}/Γ
VALUE	CL%	DOCUMENT ID
<8.0 × 10⁻⁶	90	¹ AUBERT 09AF BABR $e^+e^- \rightarrow \Upsilon(4S)$
¹ Assumes equal production of B^+ and B^0 at the $\Upsilon(4S)$.		

$\Gamma(b_1^- K^{*+}, b_1^- \rightarrow \omega\pi^-)/\Gamma_{\text{total}}$		Γ_{304}/Γ
VALUE	CL%	DOCUMENT ID
<5.0 × 10⁻⁶	90	¹ AUBERT 09AF BABR $e^+e^- \rightarrow \Upsilon(4S)$
¹ Assumes equal production of B^+ and B^0 at the $\Upsilon(4S)$.		

$\Gamma(a_0(1450)^\pm K^\mp, a_0^\pm \rightarrow \eta\pi^\pm)/\Gamma_{\text{total}}$		Γ_{305}/Γ
VALUE (units 10^{-6})	CL%	DOCUMENT ID
<3.1	90	¹ AUBERT 07Y BABR $e^+e^- \rightarrow \Upsilon(4S)$
¹ Assumes equal production of B^+ and B^0 at the $\Upsilon(4S)$.		

$\Gamma(K_S^0 X^0 (\text{Familon}))/\Gamma_{\text{total}}$		Γ_{306}/Γ
VALUE (units 10^{-6})	CL%	DOCUMENT ID
<53	90	¹ AMMAR 01B CLE2 $e^+e^- \rightarrow \Upsilon(4S)$
¹ AMMAR 01B searched for the two-body decay of the B meson to a massless neutral feebly-interacting particle X^0 such as the familon, the Nambu-Goldstone boson associated with a spontaneously broken global family symmetry.		

$\Gamma(\omega K^*(892)^0)/\Gamma_{\text{total}}$		Γ_{307}/Γ
VALUE (units 10^{-6})	CL%	DOCUMENT ID
2.0 ± 0.5 OUR AVERAGE		
2.2 ± 0.6 ± 0.2		¹ AUBERT 09H BABR $e^+e^- \rightarrow \Upsilon(4S)$
1.8 ± 0.7 ± 0.3		¹ GOLDENZWE..08 BELL $e^+e^- \rightarrow \Upsilon(4S)$
• • • We do not use the following data for averages, fits, limits, etc. • • •		
< 4.2	90	¹ AUBERT,B 06T BABR Repl. by AUBERT 09H
< 6.0	90	¹ AUBERT 05o BABR Repl. by AUBERT,B 06T
< 23	90	¹ BERGFELD 98 CLE2
¹ Assumes equal production of B^+ and B^0 at the $\Upsilon(4S)$.		

$\Gamma(\omega(K\pi)_0^{*0})/\Gamma_{\text{total}}$		Γ_{308}/Γ
VALUE (units 10^{-6})	CL%	DOCUMENT ID
18.4 ± 1.8 ± 1.7		¹ AUBERT 09H BABR $e^+e^- \rightarrow \Upsilon(4S)$
¹ Assumes equal production of B^+ and B^0 at the $\Upsilon(4S)$.		

$\Gamma(\omega K_0^*(1430)^0)/\Gamma_{\text{total}}$		Γ_{309}/Γ
VALUE (units 10^{-6})	DOCUMENT ID	TECN
16.0 ± 1.6 ± 3.0	¹ AUBERT 09H BABR	$e^+e^- \rightarrow \Upsilon(4S)$
¹ Assumes equal production of B^+ and B^0 at the $\Upsilon(4S)$.		

$\Gamma(\omega K_2^*(1430)^0)/\Gamma_{\text{total}}$		Γ_{310}/Γ
VALUE (units 10^{-6})	DOCUMENT ID	TECN
10.1 ± 2.0 ± 1.1	¹ AUBERT 09H BABR	$e^+e^- \rightarrow \Upsilon(4S)$
¹ Assumes equal production of B^+ and B^0 at the $\Upsilon(4S)$.		

$\Gamma(\omega K^+ \pi^- \text{ nonresonant})/\Gamma_{\text{total}}$		Γ_{311}/Γ
VALUE (units 10^{-6})	DOCUMENT ID	TECN
5.1 ± 0.7 ± 0.7	^{1,2} GOLDENZWE..08 BELL	$e^+e^- \rightarrow \Upsilon(4S)$
¹ Assumes equal production of B^+ and B^0 at the $\Upsilon(4S)$.		
² For the $K\pi$ mass range 0.755–1.250 GeV/ c^2 , excluding $K^*(892)$.		

$\Gamma(K^+ \pi^- \pi^0)/\Gamma_{\text{total}}$		Γ_{312}/Γ
VALUE (units 10^{-6})	DOCUMENT ID	TECN
37.8 ± 3.2 OUR AVERAGE		
38.5 ± 1.0 ± 3.9	^{1,2} LEES 11 BABR	$e^+e^- \rightarrow \Upsilon(4S)$
36.6 ^{+4.2} _{-4.3} ± 3.0	¹ CHANG 04 BELL	$e^+e^- \rightarrow \Upsilon(4S)$
• • • We do not use the following data for averages, fits, limits, etc. • • •		
35.7 ^{+2.6} _{-1.5} ± 2.2	¹ AUBERT 08AQ BABR	Repl. by LEES 11
<40	90	¹ ECKHART 02 CLE2 $e^+e^- \rightarrow \Upsilon(4S)$
¹ Assumes equal production of B^+ and B^0 at the $\Upsilon(4S)$.		
² Uses Dalitz plot analysis of $B^0 \rightarrow K^+ \pi^- \pi^0$ decays.		

$\Gamma(K^+ \rho^-)/\Gamma_{\text{total}}$		Γ_{313}/Γ
VALUE (units 10^{-6})	CL%	DOCUMENT ID
7.0 ± 0.9 OUR AVERAGE		
6.6 ± 0.5 ± 0.8		^{1,2} LEES 11 BABR $e^+e^- \rightarrow \Upsilon(4S)$
15.1 ^{+3.4} _{-3.3} ± 2.4		¹ CHANG 04 BELL $e^+e^- \rightarrow \Upsilon(4S)$
• • • We do not use the following data for averages, fits, limits, etc. • • •		
8.0 ^{+0.8} _{-1.3} ± 0.6		¹ AUBERT 08AQ BABR Repl. by LEES 11
7.3 ^{+1.3} _{-1.2} ± 1.3		¹ AUBERT 03T BABR Repl. by AUBERT 08AQ
<32	90	¹ JESSOP 00 CLE2 $e^+e^- \rightarrow \Upsilon(4S)$
<35	90	ASNER 96 CLE2 Repl. by JESSOP 00
¹ Assumes equal production of B^+ and B^0 at the $\Upsilon(4S)$.		
² Uses Dalitz plot analysis of $B^0 \rightarrow K^+ \pi^- \pi^0$ decays.		

$\Gamma(K^+ \rho(1450)^-)/\Gamma_{\text{total}}$		Γ_{314}/Γ
VALUE (units 10^{-6})	CL%	DOCUMENT ID
2.4 ± 1.0 ± 0.6		^{1,2} LEES 11 BABR $e^+e^- \rightarrow \Upsilon(4S)$
• • • We do not use the following data for averages, fits, limits, etc. • • •		
<2.1	90	¹ AUBERT 08AQ BABR Repl. by LEES 11
¹ Assumes equal production of B^+ and B^0 at the $\Upsilon(4S)$.		
² Uses Dalitz plot analysis of $B^0 \rightarrow K^+ \pi^- \pi^0$ decays.		

$\Gamma(K^+ \rho(1700)^-)/\Gamma_{\text{total}}$		Γ_{315}/Γ
VALUE (units 10^{-6})	CL%	DOCUMENT ID
0.6 ± 0.6 ± 0.4		^{1,2} LEES 11 BABR $e^+e^- \rightarrow \Upsilon(4S)$
• • • We do not use the following data for averages, fits, limits, etc. • • •		
<1.1	90	¹ AUBERT 08AQ BABR Repl. by LEES 11
¹ Assumes equal production of B^+ and B^0 at the $\Upsilon(4S)$.		
² Uses Dalitz plot analysis of $B^0 \rightarrow K^+ \pi^- \pi^0$ decays.		

$\Gamma((K^+ \pi^- \pi^0) \text{ nonresonant})/\Gamma_{\text{total}}$		Γ_{316}/Γ
VALUE (units 10^{-6})	CL%	DOCUMENT ID
2.8 ± 0.5 ± 0.4		^{1,2} LEES 11 BABR $e^+e^- \rightarrow \Upsilon(4S)$
• • • We do not use the following data for averages, fits, limits, etc. • • •		
4.4 ± 0.9 ± 0.5		¹ AUBERT 08AQ BABR Repl. by LEES 11
<9.4	90	¹ CHANG 04 BELL $e^+e^- \rightarrow \Upsilon(4S)$
¹ Assumes equal production of B^+ and B^0 at the $\Upsilon(4S)$.		
² Uses Dalitz plot analysis of $B^0 \rightarrow K^+ \pi^- \pi^0$ decays. The quoted value is only for the flat part of the non-resonant component.		

$\Gamma((K\pi)_0^{*+} \pi^-, (K\pi)_0^{*+} \rightarrow K^+ \pi^0)/\Gamma_{\text{total}}$		Γ_{317}/Γ
VALUE (units 10^{-6})	DOCUMENT ID	TECN
34.2 ± 2.4 ± 4.1	^{1,2} LEES 11 BABR	$e^+e^- \rightarrow \Upsilon(4S)$
• • • We do not use the following data for averages, fits, limits, etc. • • •		
9.4 ^{+1.1} _{-1.3} ± 2.3	¹ AUBERT 08AQ BABR	Repl. by LEES 11
¹ Assumes equal production of B^+ and B^0 at the $\Upsilon(4S)$.		
² Uses Dalitz plot analysis of $B^0 \rightarrow K^+ \pi^- \pi^0$ decays.		

Meson Particle Listings

B^0

$\Gamma((K\pi)_0^0 \pi^0, (K\pi)_0^0 \rightarrow K^+ \pi^-) / \Gamma_{\text{total}}$ Γ_{318} / Γ

$(K\pi)_0^0$ is the total S-wave composed of $K_0^*(1430)$ and nonresonant that are described using LA S S shape.

VALUE (units 10^{-6})	DOCUMENT ID	TECN	COMMENT
$8.6 \pm 1.1 \pm 1.3$	1,2 LEES	11	BABR $e^+ e^- \rightarrow \Upsilon(4S)$
$8.7^{+1.1+2.8}_{-0.9-2.6}$	1 AUBERT	08AQ	BABR Repl. by LEES 11

• • • We do not use the following data for averages, fits, limits, etc. • • •

¹ Assumes equal production of B^+ and B^0 at the $\Upsilon(4S)$.
² Uses Dalitz plot analysis of $B^0 \rightarrow K^+ \pi^- \pi^0$ decays.

$\Gamma(K_2^*(1430)^0 \pi^0) / \Gamma_{\text{total}}$ Γ_{319} / Γ

VALUE (units 10^{-6})	CL%	DOCUMENT ID	TECN	COMMENT
<4.0	90	1 AUBERT	08AQ	BABR $e^+ e^- \rightarrow \Upsilon(4S)$

¹ Assumes equal production of B^+ and B^0 at the $\Upsilon(4S)$.

$\Gamma(K^*(1680)^0 \pi^0) / \Gamma_{\text{total}}$ Γ_{320} / Γ

VALUE (units 10^{-6})	CL%	DOCUMENT ID	TECN	COMMENT
<7.5	90	1 AUBERT	08AQ	BABR $e^+ e^- \rightarrow \Upsilon(4S)$

¹ Assumes equal production of B^+ and B^0 at the $\Upsilon(4S)$.

$\Gamma(K_x^{*0} \pi^0) / \Gamma_{\text{total}}$ Γ_{321} / Γ

K_x^{*0} stands for the possible candidates of $K^*(1410)$, $K_0^*(1430)$ and $K_2^*(1430)$.

VALUE (units 10^{-6})	DOCUMENT ID	TECN	COMMENT
$6.1^{+1.6+0.5}_{-1.5-0.6}$	1 CHANG	04	BELL $e^+ e^- \rightarrow \Upsilon(4S)$

¹ Assumes equal production of B^+ and B^0 at the $\Upsilon(4S)$.

$\Gamma(K^0 \pi^+ \pi^-) / \Gamma_{\text{total}}$ Γ_{322} / Γ

VALUE (units 10^{-6})	CL%	DOCUMENT ID	TECN	COMMENT
49.7 ± 1.8 OUR FIT				
49.6 ± 2.0 OUR AVERAGE				
$50.2 \pm 1.5 \pm 1.8$		1 AUBERT	09AU	BABR $e^+ e^- \rightarrow \Upsilon(4S)$
$47.5 \pm 2.4 \pm 3.7$		2 GARMASH	07	BELL $e^+ e^- \rightarrow \Upsilon(4S)$
$50^{+10}_{-9} \pm 7$		1 ECKHART	02	CLE2 $e^+ e^- \rightarrow \Upsilon(4S)$

$43.0 \pm 2.3 \pm 2.3$		1 AUBERT	06i	BABR Repl. by AUBERT 09AU
$43.7 \pm 3.8 \pm 3.4$		1 AUBERT,B	04o	BABR Repl. by AUBERT 06i
$45.4 \pm 5.2 \pm 5.9$		1 GARMASH	04	BELL Repl. by GARMASH 07
<440	90	ALBRECHT	91E	ARG $e^+ e^- \rightarrow \Upsilon(4S)$

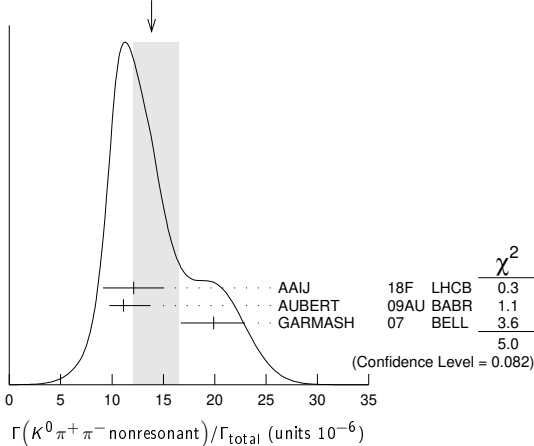
¹ Assumes equal production of B^+ and B^0 at the $\Upsilon(4S)$.
² Uses Dalitz plot analysis of the $B^0 \rightarrow K^0 \pi^+ \pi^-$ final state decays.

$\Gamma(K^0 \pi^+ \pi^- \text{ nonresonant}) / \Gamma_{\text{total}}$ Γ_{323} / Γ

VALUE (units 10^{-6})	DOCUMENT ID	TECN	COMMENT
$13.9^{+2.6}_{-1.8}$ OUR AVERAGE	Error includes scale factor of 1.6. See the ideogram below.		
$12.1 \pm 0.6 \pm 2.9$	1 AAIJ	18F	LHCB pp at 7, 8 TeV
$11.1^{+2.5}_{-1.0} \pm 0.9$	2 AUBERT	09AU	BABR $e^+ e^- \rightarrow \Upsilon(4S)$
$19.9 \pm 2.5^{+1.7}_{-2.0}$	3 GARMASH	07	BELL $e^+ e^- \rightarrow \Upsilon(4S)$

¹ Uses Dalitz plot analysis of the $B^0 \rightarrow K_S^0 \pi^+ \pi^-$ final state decays. For the branching fraction of the reference mode, the PDG 18 average $B(B^0 \rightarrow K_S^0 \pi^+ \pi^-) = (4.96 \pm 0.20) \times 10^{-5}$ is used.
² Assumes equal production of B^+ and B^0 at the $\Upsilon(4S)$.
³ Uses Dalitz plot analysis of the $B^0 \rightarrow K^0 \pi^+ \pi^-$ final state decays.

WEIGHTED AVERAGE
 $13.9^{+2.6-1.8}$ (Error scaled by 1.6)



$\Gamma(K^0 \rho^0) / \Gamma_{\text{total}}$ Γ_{324} / Γ

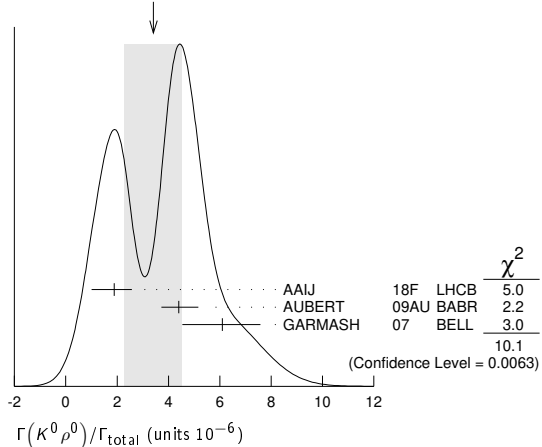
3.4 ± 1.1 OUR AVERAGE Error includes scale factor of 2.3. See the ideogram below.

VALUE (units 10^{-6})	CL%	DOCUMENT ID	TECN	COMMENT
$1.89^{+0.55}_{-0.79} \pm 0.40$		1 AAIJ	18F	LHCB pp at 7, 8 TeV
$4.4^{+0.7}_{-0.6} \pm 0.3$		2 AUBERT	09AU	BABR $e^+ e^- \rightarrow \Upsilon(4S)$
$6.1 \pm 1.0^{+1.1}_{-1.2}$		3 GARMASH	07	BELL $e^+ e^- \rightarrow \Upsilon(4S)$

$4.9 \pm 0.8 \pm 0.9$		2 AUBERT	07F	BABR Repl. by AUBERT 09AU
<39	90	ASNER	96	CLEO $e^+ e^- \rightarrow \Upsilon(4S)$
<320	90	ALBRECHT	91B	ARG $e^+ e^- \rightarrow \Upsilon(4S)$
<500	90	4 AVERY	89B	CLEO $e^+ e^- \rightarrow \Upsilon(4S)$

¹ Uses Dalitz plot analysis of the $B^0 \rightarrow K_S^0 \pi^+ \pi^-$ final state decays. For the branching fraction of the reference mode, the PDG 18 average $B(B^0 \rightarrow K_S^0 \pi^+ \pi^-) = (4.96 \pm 0.20) \times 10^{-5}$ is used.
² Assumes equal production of B^+ and B^0 at the $\Upsilon(4S)$.
³ Uses Dalitz plot analysis of the $B^0 \rightarrow K^0 \pi^+ \pi^-$ final state decays.
⁴ AVERY 89B reports $< 5.8 \times 10^{-4}$ assuming the $\Upsilon(4S)$ decays 43% to $B^0 \bar{B}^0$. We rescale to 50%.

WEIGHTED AVERAGE
 3.4 ± 1.1 (Error scaled by 2.3)



$\Gamma(K^*(892)^+ \pi^-) / \Gamma_{\text{total}}$ Γ_{325} / Γ

VALUE (units 10^{-6})	CL%	DOCUMENT ID	TECN	COMMENT
7.5 ± 0.4 OUR AVERAGE				
$7.02 \pm 0.30 \pm 0.45$		1 AAIJ	18F	LHCB pp at 7, 8 TeV
$8.0 \pm 1.1 \pm 0.8$		2,3 LEES	11	BABR $e^+ e^- \rightarrow \Upsilon(4S)$
$8.3^{+0.9}_{-0.8} \pm 0.8$		3,4 AUBERT	09AU	BABR $e^+ e^- \rightarrow \Upsilon(4S)$
$8.4 \pm 1.1^{+1.0}_{-0.9}$		4 GARMASH	07	BELL $e^+ e^- \rightarrow \Upsilon(4S)$
$16^{+6}_{-5} \pm 2$		3 ECKHART	02	CLE2 $e^+ e^- \rightarrow \Upsilon(4S)$

$12.6^{+2.7}_{-1.6} \pm 0.9$		2,3 AUBERT	08AQ	BABR Repl. by LEES 11
$11.0 \pm 1.5 \pm 0.71$		3 AUBERT	06i	BABR Repl. by AUBERT 09AU
$12.9 \pm 2.4 \pm 1.4$		3 AUBERT,B	04o	BABR Repl. by AUBERT 06i
$14.8^{+4.6+2.8}_{-4.4-1.3}$		3 CHANG	04	BELL Repl. by GARMASH 07

<72	90	ASNER	96	CLE2 $e^+ e^- \rightarrow \Upsilon(4S)$
<620	90	ALBRECHT	91B	ARG $e^+ e^- \rightarrow \Upsilon(4S)$
<380	90	5 AVERY	89B	CLEO $e^+ e^- \rightarrow \Upsilon(4S)$
<560	90	6 AVERY	87	CLEO $e^+ e^- \rightarrow \Upsilon(4S)$

¹ Uses Dalitz plot analysis of the $B^0 \rightarrow K_S^0 \pi^+ \pi^-$ final state decays. For the branching fraction of the reference mode, the PDG 18 average $B(B^0 \rightarrow K_S^0 \pi^+ \pi^-) = (4.96 \pm 0.20) \times 10^{-5}$ is used.
² Uses Dalitz plot analysis of $B^0 \rightarrow K^+ \pi^- \pi^0$ decays.
³ Assumes equal production of B^+ and B^0 at the $\Upsilon(4S)$.
⁴ Uses Dalitz plot analysis of the $B^0 \rightarrow K^0 \pi^+ \pi^-$ final state decays.
⁵ AVERY 89B reports $< 4.4 \times 10^{-4}$ assuming the $\Upsilon(4S)$ decays 43% to $B^0 \bar{B}^0$. We rescale to 50%.
⁶ AVERY 87 reports $< 7 \times 10^{-4}$ assuming the $\Upsilon(4S)$ decays 40% to $B^0 \bar{B}^0$. We rescale to 50%.

$\Gamma(K_0^*(1430)^+ \pi^-) / \Gamma_{\text{total}}$ Γ_{326} / Γ

VALUE (units 10^{-6})	DOCUMENT ID	TECN	COMMENT
33 ± 7 OUR AVERAGE	Error includes scale factor of 2.0.		
$29.9^{+2.3}_{-1.7} \pm 3.6$	1,2 AUBERT	09AU	BABR $e^+ e^- \rightarrow \Upsilon(4S)$
$49.7 \pm 3.8^{+6.8}_{-8.2}$	2 GARMASH	07	BELL $e^+ e^- \rightarrow \Upsilon(4S)$

See key on page 1171

Meson Particle Listings

B^0

¹ Assumes equal production of B^+ and B^0 at the $\Upsilon(4S)$.
² Uses Dalitz plot analysis of the $B^0 \rightarrow K^0 \pi^+ \pi^-$ final state decays.

$\Gamma(K_x^{*+} \pi^-)/\Gamma_{\text{total}}$ Γ_{327}/Γ
 K_x^{*+} stands for the possible candidates of $K^*(1410)$, $K_0^*(1430)$ and $K_2^*(1430)$.

VALUE (units 10^{-6})	DOCUMENT ID	TECN	COMMENT
$5.1 \pm 1.5 \pm 0.6$	1 CHANG	04 BELL	$e^+ e^- \rightarrow \Upsilon(4S)$

¹ Assumes equal production of B^+ and B^0 at the $\Upsilon(4S)$.

$\Gamma(K^*(1410)^+ \pi^-, K^{*+} \rightarrow K^0 \pi^+)/\Gamma_{\text{total}}$ Γ_{328}/Γ

VALUE (units 10^{-6})	CL%	DOCUMENT ID	TECN	COMMENT
< 3.8	90	1 GARMASH	07 BELL	$e^+ e^- \rightarrow \Upsilon(4S)$

¹ Uses Dalitz plot analysis of the $B^0 \rightarrow K^0 \pi^+ \pi^-$ final state decays.

$\Gamma((K\pi)_0^+ \pi^-, (K\pi)_0^+ \rightarrow K^0 \pi^+)/\Gamma_{\text{total}}$ Γ_{329}/Γ

VALUE (units 10^{-6})	DOCUMENT ID	TECN	COMMENT
$16.2 \pm 0.69 \pm 1.15$	1 AAIJ	18F LHCb	pp at 7, 8 TeV

¹ Uses Dalitz plot analysis of the $B^0 \rightarrow K_S^0 \pi^+ \pi^-$ final state decays. $(K\pi)_0^+$ is the S-wave component of $K^0 \pi^+$. For the branching fraction of the reference mode, the PDG 18 average $B(B^0 \rightarrow K_S^0 \pi^+ \pi^-) = (4.96 \pm 0.20) \times 10^{-5}$ is used.

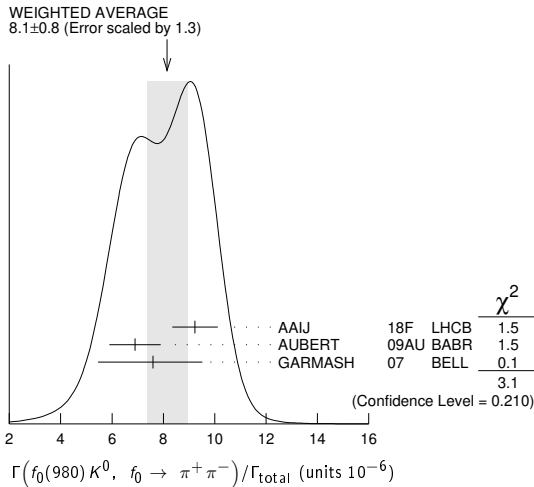
$\Gamma(f_0(980) K^0, f_0 \rightarrow \pi^+ \pi^-)/\Gamma_{\text{total}}$ Γ_{330}/Γ

VALUE (units 10^{-6})	CL%	DOCUMENT ID	TECN	COMMENT
8.1 ± 0.8	OUR AVERAGE	Error includes scale factor of 1.3. See the ideogram below.		

9.23 ± 0.40 ± 0.79	1 AAIJ	18F LHCb	pp at 7, 8 TeV
6.9 ± 0.8 ± 0.6	2 AUBERT	09AU BABR	$e^+ e^- \rightarrow \Upsilon(4S)$
7.6 ± 1.7 ± 0.9	3 GARMASH	07 BELL	$e^+ e^- \rightarrow \Upsilon(4S)$
5.5 ± 0.7 ± 0.6	2 AUBERT	06i BABR	Repl. by AUBERT 09AU
<360	4 AVERY	89B CLEO	$e^+ e^- \rightarrow \Upsilon(4S)$

¹ Uses Dalitz plot analysis of the $B^0 \rightarrow K_S^0 \pi^+ \pi^-$ final state decays. For the branching fraction of the reference mode, the PDG 18 average $B(B^0 \rightarrow K_S^0 \pi^+ \pi^-) = (4.96 \pm 0.20) \times 10^{-5}$ is used.

² Assumes equal production of B^+ and B^0 at the $\Upsilon(4S)$.
³ Uses Dalitz plot analysis of the $B^0 \rightarrow K^0 \pi^+ \pi^-$ final state decays.
⁴ AVERY 89B reports $< 4.2 \times 10^{-4}$ assuming the $\Upsilon(4S)$ decays 43% to $B^0 \bar{B}^0$. We rescale to 50%.



$\Gamma(K^0 f_0(500))/\Gamma_{\text{total}}$ Γ_{331}/Γ

VALUE (units 10^{-6})	DOCUMENT ID	TECN	COMMENT
$0.16 \pm 0.20 \pm 0.15$	1 AAIJ	18F LHCb	pp at 7, 8 TeV

¹ Uses Dalitz plot analysis of the $B^0 \rightarrow K_S^0 \pi^+ \pi^-$ final state decays. For the branching fraction of the reference mode, the PDG 18 average $B(B^0 \rightarrow K_S^0 \pi^+ \pi^-) = (4.96 \pm 0.20) \times 10^{-5}$ is used.

$\Gamma(K^0 f_0(1500))/\Gamma_{\text{total}}$ Γ_{332}/Γ

VALUE (units 10^{-6})	DOCUMENT ID	TECN	COMMENT
$1.29 \pm 0.27 \pm 0.70$	1 AAIJ	18F LHCb	pp at 7, 8 TeV

¹ Uses Dalitz plot analysis of the $B^0 \rightarrow K_S^0 \pi^+ \pi^-$ final state decays. For the branching fraction of the reference mode, the PDG 18 average $B(B^0 \rightarrow K_S^0 \pi^+ \pi^-) = (4.96 \pm 0.20) \times 10^{-5}$ is used.

$\Gamma(f_2(1270) K^0)/\Gamma_{\text{total}}$ Γ_{333}/Γ

VALUE (units 10^{-6})	CL%	DOCUMENT ID	TECN	COMMENT
$2.7 \pm 1.0 \pm 0.9$		1 AUBERT	09AU BABR	$e^+ e^- \rightarrow \Upsilon(4S)$

• • • We do not use the following data for averages, fits, limits, etc. • • •
 < 2.5 90 2 GARMASH 07 BELL $e^+ e^- \rightarrow \Upsilon(4S)$
¹ Assumes equal production of B^+ and B^0 at the $\Upsilon(4S)$.
² GARMASH 07 reports $B(B^0 \rightarrow f_2(1270) K^0) \times B(f_2(1270) \rightarrow \pi^+ \pi^-) < 1.4 \times 10^{-6}$ using Dalitz plot analysis. We compute $B(B^0 \rightarrow f_2(1270) K^0)$ using the PDG value $B(f_2(1270) \rightarrow \pi\pi) = 84.3 \times 10^{-2}$ and 2/3 for the $\pi^+ \pi^-$ fraction.

$\Gamma(f_x(1300) K^0, f_x \rightarrow \pi^+ \pi^-)/\Gamma_{\text{total}}$ Γ_{334}/Γ

VALUE (units 10^{-6})	DOCUMENT ID	TECN	COMMENT
$1.81 \pm 0.55 \pm 0.48$	1 AUBERT	09AU BABR	$e^+ e^- \rightarrow \Upsilon(4S)$

¹ Assumes equal production of B^+ and B^0 at the $\Upsilon(4S)$.

$\Gamma(K^*(892)^0 \pi^0)/\Gamma_{\text{total}}$ Γ_{335}/Γ

VALUE (units 10^{-6})	CL%	DOCUMENT ID	TECN	COMMENT
$3.3 \pm 0.5 \pm 0.4$		1,2 LEES	11 BABR	$e^+ e^- \rightarrow \Upsilon(4S)$
3.6 ± 0.7 ± 0.4		1,2 AUBERT	08AQ BABR	Repl. by LEES 11
< 3.5	90	2 CHANG	04 BELL	$e^+ e^- \rightarrow \Upsilon(4S)$
< 3.6	90	JESSOP	00 CLE2	$e^+ e^- \rightarrow \Upsilon(4S)$
<28	90	ASNER	96 CLE2	Repl. by JESSOP 00

¹ Uses Dalitz plot analysis of $B^0 \rightarrow K^+ \pi^- \pi^0$ decays.
² Assumes equal production of B^+ and B^0 at the $\Upsilon(4S)$.

$\Gamma(K_2^*(1430)^+ \pi^-)/\Gamma_{\text{total}}$ Γ_{336}/Γ

VALUE (units 10^{-6})	CL%	DOCUMENT ID	TECN	COMMENT
$3.65 \pm 0.15 \pm 0.31$		1 AAIJ	18F LHCb	pp at 7, 8 TeV

• • • We do not use the following data for averages, fits, limits, etc. • • •
 < 16.2 90 2,3 AUBERT 08AQ BABR $e^+ e^- \rightarrow \Upsilon(4S)$
 < 6 90 4 GARMASH 07 BELL $e^+ e^- \rightarrow \Upsilon(4S)$
 < 18 90 3 GARMASH 04 BELL Repl. by GARMASH 07
 < 2600 90 ALBRECHT 91B ARG $e^+ e^- \rightarrow \Upsilon(4S)$

¹ Uses Dalitz plot analysis of the $B^0 \rightarrow K_S^0 \pi^+ \pi^-$ final state decays. We compute $B(B^0 \rightarrow K_2^*(1430)^+ \pi^-)$ using the PDG 18 value $B(K_2^*(1430) \rightarrow K\pi) = 49.9 \times 10^{-2}$ and 2/3 for the $K^0 \pi^+$ fraction. For the branching fraction of the reference mode, the PDG 18 average $B(B^0 \rightarrow K_S^0 \pi^+ \pi^-) = (4.96 \pm 0.20) \times 10^{-5}$ is used.

² Uses Dalitz plot analysis of $B^0 \rightarrow K^+ \pi^- \pi^0$ decays.
³ Assumes equal production of B^+ and B^0 at the $\Upsilon(4S)$.
⁴ GARMASH 07 reports $B(B^0 \rightarrow K_2^*(1430)^+ \pi^-) \times B(K_2^* \rightarrow K^0 \pi^+) < 2.1 \times 10^{-6}$ using Dalitz plot analysis. We compute $B(B^0 \rightarrow K_2^*(1430)^+ \pi^-)$ using the PDG value $B(K_2^*(1430) \rightarrow K\pi) = 49.9 \times 10^{-2}$ and 2/3 for the $K^0 \pi^+$ fraction.

$\Gamma(K^*(1680)^+ \pi^-)/\Gamma_{\text{total}}$ Γ_{337}/Γ

VALUE (units 10^{-6})	CL%	DOCUMENT ID	TECN	COMMENT
$14.1 \pm 0.58 \pm 0.84$		1 AAIJ	18F LHCb	pp at 7, 8 TeV

• • • We do not use the following data for averages, fits, limits, etc. • • •
 < 25 90 2,3 AUBERT 08AQ BABR $e^+ e^- \rightarrow \Upsilon(4S)$
 < 10 90 4 GARMASH 07 BELL $e^+ e^- \rightarrow \Upsilon(4S)$

¹ Uses Dalitz plot analysis of the $B^0 \rightarrow K_S^0 \pi^+ \pi^-$ final state decays. We compute $B(B^0 \rightarrow K_2^*(1430)^+ \pi^-)$ using the PDG 18 value $B(K_2^*(1430) \rightarrow K\pi) = (49.9 \pm 1.2) \times 10^{-2}$ and 2/3 for the $K^0 \pi^+$ fraction. For the branching fraction of the reference mode, the PDG 18 average $B(B^0 \rightarrow K_S^0 \pi^+ \pi^-) = (4.96 \pm 0.20) \times 10^{-5}$ is used.
² Uses Dalitz plot analysis of $B^0 \rightarrow K^+ \pi^- \pi^0$ decays.
³ Assumes equal production of B^+ and B^0 at the $\Upsilon(4S)$.
⁴ GARMASH 07 reports $B(B^0 \rightarrow K^*(1680)^+ \pi^-) \times B(K^* \rightarrow K^0 \pi^+) < 2.6 \times 10^{-6}$ using Dalitz plot analysis. We compute $B(B^0 \rightarrow K^*(1680)^+ \pi^-)$ using the PDG value $B(K^*(1680) \rightarrow K\pi) = 38.7 \times 10^{-2}$ and 2/3 for the $K^0 \pi^+$ fraction.

$\Gamma(K^+ \pi^- \pi^+ \pi^-)/\Gamma_{\text{total}}$ Γ_{338}/Γ

VALUE	CL%	DOCUMENT ID	TECN	COMMENT
$< 2.3 \times 10^{-4}$	90	1 ADAM	96D DLPH	$e^+ e^- \rightarrow Z$

• • • We do not use the following data for averages, fits, limits, etc. • • •
 $< 2.1 \times 10^{-4}$ 90 2 ABREU 95N DLPH Sup. by ADAM 96D
¹ ADAM 96D assumes $f_{B^0} = f_{B^-} = 0.39$ and $f_{B_s} = 0.12$. Contributions from B^0 and B_s decays cannot be separated. Limits are given for the weighted average of the decay rates for the two neutral B mesons.
² Assumes a B^0, B^- production fraction of 0.39 and a B_s production fraction of 0.12. Contributions from B^0 and B_s decays cannot be separated. Limits are given for the weighted average of the decay rates for the two neutral B mesons.

$\Gamma(\rho^0 K^+ \pi^-)/\Gamma_{\text{total}}$ Γ_{339}/Γ

VALUE (units 10^{-6})	DOCUMENT ID	TECN	COMMENT
$2.8 \pm 0.5 \pm 0.5$	1,2 KYEONG	09 BELL	$e^+ e^- \rightarrow \Upsilon(4S)$

¹ Assumes equal production of B^+ and B^0 at the $\Upsilon(4S)$.
² Required $0.75 < m_{K^+ \pi^-} < 1.20$ GeV/ c^2 .

Meson Particle Listings

 B^0 $\Gamma(f_0(980)K^+\pi^-, f_0 \rightarrow \pi\pi)/\Gamma_{\text{total}}$ Γ_{340}/Γ

VALUE (units 10^{-6})	CL%	DOCUMENT ID	TECN	COMMENT
$1.4 \pm 0.4 \pm 0.3$ 0.4		1,2 KYEONG	09 BELL	$e^+e^- \rightarrow \Upsilon(4S)$

- ¹ Assumes equal production of B^+ and B^0 at the $\Upsilon(4S)$.
² Required $0.75 < m_{K^+K^-} < 1.2$ GeV/ c^2 .

 $\Gamma(K^+\pi^-\pi^+\pi^-\text{ nonresonant})/\Gamma_{\text{total}}$ Γ_{341}/Γ

VALUE	CL%	DOCUMENT ID	TECN	COMMENT
$< 2.1 \times 10^{-6}$	90	1,2 KYEONG	09 BELL	$e^+e^- \rightarrow \Upsilon(4S)$

- ¹ Assumes equal production of B^+ and B^0 at the $\Upsilon(4S)$.
² Required $0.55 < m_{\pi^+\pi^-} < 1.42$ and $0.75 < m_{K^+\pi^-} < 1.20$ GeV/ c^2 .

 $\Gamma(K^*(892)^0\pi^+\pi^-)/\Gamma_{\text{total}}$ Γ_{342}/Γ

VALUE (units 10^{-6})	CL%	DOCUMENT ID	TECN	COMMENT
$54.5 \pm 2.9 \pm 4.3$		1 AUBERT	07As BABR	$e^+e^- \rightarrow \Upsilon(4S)$
$4.5 \pm 1.1 \pm 0.9$ $-1.0 - 1.6$		1,2 KYEONG	09 BELL	$e^+e^- \rightarrow \Upsilon(4S)$
< 1400	90	ALBRECHT	91E ARG	$e^+e^- \rightarrow \Upsilon(4S)$

- ¹ Assumes equal production of B^+ and B^0 at the $\Upsilon(4S)$.
² Required $0.55 < m_{\pi^+\pi^-} < 1.42$ GeV/ c^2 .

 $\Gamma(K^*(892)^0\rho^0)/\Gamma_{\text{total}}$ Γ_{343}/Γ

VALUE (units 10^{-6})	CL%	DOCUMENT ID	TECN	COMMENT
3.9 ± 1.3 OUR AVERAGE		Error includes scale factor of 1.9.		
$5.1 \pm 0.6 \pm 0.6$ 0.8		1 LEES	12k BABR	$e^+e^- \rightarrow \Upsilon(4S)$
$2.1 \pm 0.8 \pm 0.9$ $-0.7 - 0.5$		1 KYEONG	09 BELL	$e^+e^- \rightarrow \Upsilon(4S)$
$5.6 \pm 0.9 \pm 1.3$		1 AUBERT,B	06G BABR	Repl. by LEES 12k
< 34	90	2 GODANG	02 CLE2	$e^+e^- \rightarrow \Upsilon(4S)$
< 286	90	3 ABE	00c SLD	$e^+e^- \rightarrow Z$
< 460	90	ALBRECHT	91B ARG	$e^+e^- \rightarrow \Upsilon(4S)$
< 580	90	4 AVERY	89B CLEO	$e^+e^- \rightarrow \Upsilon(4S)$
< 960	90	5 AVERY	87 CLEO	$e^+e^- \rightarrow \Upsilon(4S)$

- ¹ Assumes equal production of B^+ and B^0 at the $\Upsilon(4S)$.
² Assumes a helicity 00 configuration. For a helicity 11 configuration, the limit decreases to 2.4×10^{-5} .
³ ABE 00c assumes $B(Z \rightarrow b\bar{b}) = (21.7 \pm 0.1)\%$ and the B fractions $f_{B^0} = f_{B^+} = (39.7 \pm 1.8) \pm 2.2\%$ and $f_{B_s} = (10.5 \pm 1.8) \pm 2.2\%$.
⁴ AVERY 89B reports $< 6.7 \times 10^{-4}$ assuming the $\Upsilon(4S)$ decays 43% to $B^0\bar{B}^0$. We rescale to 50%.
⁵ AVERY 87 reports $< 1.2 \times 10^{-3}$ assuming the $\Upsilon(4S)$ decays 40% to $B^0\bar{B}^0$. We rescale to 50%.

 $\Gamma(K^*(892)^0 f_0(980), f_0 \rightarrow \pi\pi)/\Gamma_{\text{total}}$ Γ_{344}/Γ

VALUE (units 10^{-6})	CL%	DOCUMENT ID	TECN	COMMENT
3.9 ± 2.1 -1.8 OUR AVERAGE		Error includes scale factor of 3.9.		
$5.7 \pm 0.6 \pm 0.4$		1 LEES	12k BABR	$e^+e^- \rightarrow \Upsilon(4S)$
$1.4 \pm 0.6 \pm 0.6$ $-0.5 - 0.4$		1,2 KYEONG	09 BELL	$e^+e^- \rightarrow \Upsilon(4S)$

- ¹ Assumes equal production of B^+ and B^0 at the $\Upsilon(4S)$.
² The upper limit is 2.2×10^{-6} at 90% CL.
³ AVERY 89B reports $< 2.0 \times 10^{-4}$ assuming the $\Upsilon(4S)$ decays 43% to $B^0\bar{B}^0$. We rescale to 50%.

 $\Gamma(K_1(1270)^+\pi^-)/\Gamma_{\text{total}}$ Γ_{345}/Γ

VALUE	CL%	DOCUMENT ID	TECN	COMMENT
$< 3.0 \times 10^{-5}$	90	1 AUBERT	10D BABR	$e^+e^- \rightarrow \Upsilon(4S)$

- ¹ Assumes equal production of B^+ and B^0 at the $\Upsilon(4S)$.

 $\Gamma(K_1(1400)^+\pi^-)/\Gamma_{\text{total}}$ Γ_{346}/Γ

VALUE	CL%	DOCUMENT ID	TECN	COMMENT
$< 2.7 \times 10^{-5}$	90	1 AUBERT	10D BABR	$e^+e^- \rightarrow \Upsilon(4S)$
$< 1.1 \times 10^{-3}$	90	ALBRECHT	91B ARG	$e^+e^- \rightarrow \Upsilon(4S)$

- ¹ Assumes equal production of B^+ and B^0 at the $\Upsilon(4S)$.

 $\Gamma(a_1(1260)^-K^+)/\Gamma_{\text{total}}$ Γ_{347}/Γ

VALUE (units 10^{-6})	CL%	DOCUMENT ID	TECN	COMMENT
$16.3 \pm 2.9 \pm 2.3$		1,2 AUBERT	08F BABR	$e^+e^- \rightarrow \Upsilon(4S)$
< 230	90	3 ADAM	96D DLPH	$e^+e^- \rightarrow Z$
< 390	90	4 ABREU	95N DLPH	Sup. by ADAM 96D

- ¹ Supercedes results of AAIJ 12AR.

- ¹ Assumes equal production of B^+ and B^0 at the $\Upsilon(4S)$.

- ² Assumes a_1^\pm decays only to 3π and $B(a_1^\pm \rightarrow \pi^\pm\pi^\mp\pi^\pm) = 0.5$.

- ³ ADAM 96D assumes $f_{B^0} = f_{B^-} = 0.39$ and $f_{B_s} = 0.12$. Contributions from B^0 and B_s decays cannot be separated. Limits are given for the weighted average of the decay rates for the two neutral B mesons.

- ⁴ Assumes a B^0, B^- production fraction of 0.39 and a B_s production fraction of 0.12. Contributions from B^0 and B_s^0 decays cannot be separated. Limits are given for the weighted average of the decay rates for the two neutral B mesons.

 $\Gamma(K^*(892)^+\rho^-)/\Gamma_{\text{total}}$ Γ_{348}/Γ

VALUE (units 10^{-6})	CL%	DOCUMENT ID	TECN	COMMENT
$10.3 \pm 2.3 \pm 1.3$		1 LEES	12k BABR	$e^+e^- \rightarrow \Upsilon(4S)$
< 12.0	90	1 AUBERT,B	06G BABR	Repl. by LEES 12k

- ¹ Assumes equal production of B^+ and B^0 at the $\Upsilon(4S)$.

 $\Gamma(K_0^*(1430)^+\rho^-)/\Gamma_{\text{total}}$ Γ_{349}/Γ

VALUE (units 10^{-6})	CL%	DOCUMENT ID	TECN	COMMENT
$28 \pm 10 \pm 6$		1 LEES	12k BABR	$e^+e^- \rightarrow \Upsilon(4S)$

- ¹ Assumes equal production of B^+ and B^0 at the $\Upsilon(4S)$.

 $\Gamma(K_1(1400)^0\rho^0)/\Gamma_{\text{total}}$ Γ_{350}/Γ

VALUE	CL%	DOCUMENT ID	TECN	COMMENT
$< 3.0 \times 10^{-3}$	90	ALBRECHT	91B ARG	$e^+e^- \rightarrow \Upsilon(4S)$

 $\Gamma(K_0^*(1430)^0\rho^0)/\Gamma_{\text{total}}$ Γ_{351}/Γ

VALUE (units 10^{-6})	CL%	DOCUMENT ID	TECN	COMMENT
$27 \pm 4 \pm 4$		1 LEES	12k BABR	$e^+e^- \rightarrow \Upsilon(4S)$

- ¹ Assumes equal production of B^+ and B^0 at the $\Upsilon(4S)$.

 $\Gamma(K_0^*(1430)^0 f_0(980), f_0 \rightarrow \pi\pi)/\Gamma_{\text{total}}$ Γ_{352}/Γ

VALUE (units 10^{-6})	CL%	DOCUMENT ID	TECN	COMMENT
$2.7 \pm 0.7 \pm 0.6$		1 LEES	12k BABR	$e^+e^- \rightarrow \Upsilon(4S)$

- ¹ Assumes equal production of B^+ and B^0 at the $\Upsilon(4S)$.

 $\Gamma(K_2^*(1430)^0 f_0(980), f_0 \rightarrow \pi\pi)/\Gamma_{\text{total}}$ Γ_{353}/Γ

VALUE (units 10^{-6})	CL%	DOCUMENT ID	TECN	COMMENT
$8.6 \pm 1.7 \pm 1.0$		1 LEES	12k BABR	$e^+e^- \rightarrow \Upsilon(4S)$

- ¹ Assumes equal production of B^+ and B^0 at the $\Upsilon(4S)$.

 $\Gamma(K^+K^-)/\Gamma_{\text{total}}$ Γ_{354}/Γ

VALUE (units 10^{-3})	CL%	DOCUMENT ID	TECN	COMMENT
$7.80 \pm 1.27 \pm 0.84$		1 AAIJ	17G LHCB	pp at 7 and 8 TeV
$10 \pm 8 \pm 4$		2,3 DUH	13 BELL	$e^+e^- \rightarrow \Upsilon(4S)$
$12 \pm 8 \pm 2$		4 AAIJ	12AR LHCB	Repl. by AAIJ 17G
$23 \pm 10 \pm 10$		5 AALTONEN	12L CDF	$p\bar{p}$ at 1.96 TeV
< 70	90	6 AALTONEN	09c CDF	Repl. by AALTONEN 12L
< 50	90	3 AUBERT	07B BABR	$e^+e^- \rightarrow \Upsilon(4S)$
< 41	90	3 LIN	07B BELL	Repl. by DUH 13
< 180	90	7 ABULENCIA,A	06D CDF	Repl. by AALTONEN 09c
< 37	90	ABE	05G BELL	Repl. by LIN 07
< 70	90	CHAO	04 BELL	$e^+e^- \rightarrow \Upsilon(4S)$
< 80	90	3 BORNHEIM	03 CLE2	$e^+e^- \rightarrow \Upsilon(4S)$
< 60	90	3 AUBERT	02Q BABR	$e^+e^- \rightarrow \Upsilon(4S)$
< 90	90	3 CASEY	02 BELL	$e^+e^- \rightarrow \Upsilon(4S)$
< 270	90	3 ABE	01H BELL	$e^+e^- \rightarrow \Upsilon(4S)$
< 250	90	3 AUBERT	01E BABR	$e^+e^- \rightarrow \Upsilon(4S)$
< 6600	90	8 ABE	00c SLD	$e^+e^- \rightarrow Z$
< 190	90	3 CRONIN-HEN.	00 CLE2	$e^+e^- \rightarrow \Upsilon(4S)$
< 430	90	GODANG	98 CLE2	Repl. by CRONIN-HENNESSY 00
< 4600		9 ADAM	96D DLPH	$e^+e^- \rightarrow Z$
< 400	90	ASNER	96 CLE2	Repl. by GODANG 98
< 1800	90	10 BUSKULIC	96V ALEP	$e^+e^- \rightarrow Z$
< 12000	90	11 ABREU	95N DLPH	Sup. by ADAM 96D
< 700	90	3 BATTLE	93 CLE2	$e^+e^- \rightarrow \Upsilon(4S)$

- ¹ Supercedes results of AAIJ 12AR.
² DUH 13 reports also for the same data $B(B^0 \rightarrow K^+K^-) < 0.20 \times 10^{-6}$ at 90% CL.
³ Assumes equal production of B^+ and B^0 at the $\Upsilon(4S)$.
⁴ AAIJ 12AR reports $[B(B^0 \rightarrow K^+K^-)/\Gamma_{\text{total}}] / [B(B_s^0 \rightarrow K^+K^-) / \Gamma(\bar{B} \rightarrow B_s^0)] = 0.018 \pm 0.008 \pm 0.009$ which we multiply by our best values $B(B_s^0 \rightarrow K^+K^-) = (2.72 \pm 0.23) \times 10^{-5}$, $\Gamma(\bar{B} \rightarrow B_s^0) / \Gamma(\bar{B} \rightarrow B^0) = 0.246 \pm 0.023$. Our first error is their experiment's error and our second error is the systematic error from using our best values.
⁵ Reported a central value of $(0.23 \pm 0.10 \pm 0.10) \times 10^{-6}$ using $B(B^0 \rightarrow K^+\pi^-) = (19.4 \pm 0.6) \times 10^{-6}$.
⁶ Obtains this result from $B(K^+K^-)/B(K^+\pi^-) = 0.020 \pm 0.008 \pm 0.006$, assuming $B(B^0 \rightarrow K^+\pi^-) = (19.4 \pm 0.6) \times 10^{-6}$.

⁷ ABULENCIA, A 06D obtains this from $\Gamma(K^+K^-)/\Gamma(K^+\pi^-) < 0.10$ at 90% CL, assuming $B(B^0 \rightarrow K^+\pi^-) = (18.9 \pm 0.7) \times 10^{-6}$.

⁸ ABE 00c assumes $B(Z \rightarrow b\bar{b}) = (21.7 \pm 0.1)\%$ and the B fractions $f_{B^0} = f_{B^+} = (39.7^{+1.8}_{-2.2})\%$ and $f_{B_s} = (10.5^{+1.8}_{-2.2})\%$.

⁹ ADAM 96D assumes $f_{B^0} = f_{B^-} = 0.39$ and $f_{B_s} = 0.12$. Contributions from B^0 and B_s decays cannot be separated. Limits are given for the weighted average of the decay rates for the two neutral B mesons.

¹⁰ BUSKULIC 96V assumes PDG 96 production fractions for B^0, B^+, B_s, b baryons.

¹¹ Assumes a B^0, B^- production fraction of 0.39 and a B_s production fraction of 0.12. Contributions from B^0 and B_s decays cannot be separated. Limits are given for the weighted average of the decay rates for the two neutral B mesons.

$\Gamma(K^0\bar{K}^0)/\Gamma_{\text{total}}$ Γ_{355}/Γ

VALUE (units 10^{-6})	CL%	DOCUMENT ID	TECN	COMMENT
1.21 ± 0.16 OUR AVERAGE				
1.26 ± 0.19 ± 0.05		¹ DUH 13	BELL	$e^+e^- \rightarrow \Upsilon(4S)$
1.08 ± 0.28 ± 0.11		¹ AUBERT, BE 06c	BABR	$e^+e^- \rightarrow \Upsilon(4S)$
• • • We do not use the following data for averages, fits, limits, etc. • • •				
0.87 ^{+0.25} _{-0.20} ± 0.09		¹ LIN 07	BELL	Repl. by DUH 13
0.8 ± 0.3 ± 0.9		¹ ABE 05G	BELL	Repl. by LIN 07
1.19 ^{+0.40} _{-0.35} ± 0.13		¹ AUBERT, BE 05E	BABR	Repl. by AUBERT, BE 06c
< 1.8	90	¹ AUBERT 04M	BABR	$e^+e^- \rightarrow \Upsilon(4S)$
< 1.5	90	¹ CHAO 04	BELL	Repl. by ABE 05G
< 3.3	90	¹ BORNHEIM 03	CLE2	$e^+e^- \rightarrow \Upsilon(4S)$
< 4.1	90	¹ CASEY 02	BELL	$e^+e^- \rightarrow \Upsilon(4S)$
< 17	90	GODANG 98	CLE2	$e^+e^- \rightarrow \Upsilon(4S)$
¹ Assumes equal production of B^+ and B^0 at the $\Upsilon(4S)$.				

$\Gamma(K^0\bar{K}^0)/\Gamma(K^0\phi)$ $\Gamma_{355}/\Gamma_{364}$

VALUE	DOCUMENT ID	TECN	COMMENT
0.17 ± 0.08 ± 0.02	¹ AAIJ 20F	LHCB	pp at 7, 8, 13 TeV

¹ Observed signal with a significance of 3.5 σ .

$\Gamma(K^0K^-\pi^+)/\Gamma_{\text{total}}$ Γ_{356}/Γ

VALUE (units 10^{-6})	CL%	DOCUMENT ID	TECN	COMMENT
6.7 ± 0.5 OUR FIT				
7.0 ± 0.6 OUR AVERAGE				
7.2 ± 0.7 ± 0.3		¹ LAI 19	BELL	$e^+e^- \rightarrow \Upsilon(4S)$
6.4 ± 1.0 ± 0.6		¹ DEL-AMO-SA..10E	BABR	$e^+e^- \rightarrow \Upsilon(4S)$
• • • We do not use the following data for averages, fits, limits, etc. • • •				
< 18	90	¹ GARMASH 04	BELL	$e^+e^- \rightarrow \Upsilon(4S)$
< 21	90	¹ ECKHART 02	CLE2	$e^+e^- \rightarrow \Upsilon(4S)$
¹ Assumes equal production of B^+ and B^0 at the $\Upsilon(4S)$.				

$\Gamma(K^*(892)^\pm K^\mp)/\Gamma_{\text{total}}$ Γ_{357}/Γ

VALUE	CL%	DOCUMENT ID	TECN	COMMENT
< 0.4 × 10⁻⁶	90	AAIJ 14BMLHCB		pp at 7 TeV

$\Gamma(K^0K^-\pi^+)/\Gamma(K^0\pi^+\pi^-)$ $\Gamma_{356}/\Gamma_{322}$

VALUE	DOCUMENT ID	TECN	COMMENT
0.134 ± 0.011 OUR FIT			
0.123 ± 0.009 ± 0.015	AAIJ 17BP LHCB		pp at 7, 8 TeV
• • • We do not use the following data for averages, fits, limits, etc. • • •			
0.128 ± 0.017 ± 0.009	AAIJ 13BP LHCB		Repl. by AAIJ 17BP

$[\Gamma(\bar{K}^{*0}K^0) + \Gamma(K^{*0}\bar{K}^0)]/\Gamma_{\text{total}}$ Γ_{358}/Γ

VALUE (units 10^{-6})	CL%	DOCUMENT ID	TECN	COMMENT
< 0.96	90	¹ AAIJ 16	LHCB	pp at 7 TeV
• • • We do not use the following data for averages, fits, limits, etc. • • •				
< 1.9	90	² AUBERT, BE 06N	BABR	$e^+e^- \rightarrow \Upsilon(4S)$
¹ Assumes $B(B^0 \rightarrow K^0\pi^+\pi^-) = (4.96 \pm 0.20) \times 10^{-5}$.				
² Assumes equal production of B^+ and B^0 at the $\Upsilon(4S)$.				

$\Gamma(K^+K^-\pi^0)/\Gamma_{\text{total}}$ Γ_{359}/Γ

VALUE (units 10^{-6})	CL%	DOCUMENT ID	TECN	COMMENT
2.17 ± 0.60 ± 0.24		¹ GAUR 13	BELL	$e^+e^- \rightarrow \Upsilon(4S)$
• • • We do not use the following data for averages, fits, limits, etc. • • •				
< 19	90	¹ ECKHART 02	CLE2	$e^+e^- \rightarrow \Upsilon(4S)$
¹ Assumes equal production of B^+ and B^0 at the $\Upsilon(4S)$.				

$\Gamma(K_S^0 K_S^0 \pi^0)/\Gamma_{\text{total}}$ Γ_{360}/Γ

VALUE	CL%	DOCUMENT ID	TECN	COMMENT
< 0.9 × 10⁻⁶	90	¹ AUBERT 09AD	BABR	$e^+e^- \rightarrow \Upsilon(4S)$

¹ Assumes equal production of B^+ and B^0 at the $\Upsilon(4S)$.

$\Gamma(K_S^0 K_S^0 \eta)/\Gamma_{\text{total}}$ Γ_{361}/Γ

VALUE	CL%	DOCUMENT ID	TECN	COMMENT
< 1.0 × 10⁻⁶	90	¹ AUBERT 09AD	BABR	$e^+e^- \rightarrow \Upsilon(4S)$

¹ Assumes equal production of B^+ and B^0 at the $\Upsilon(4S)$.

$\Gamma(K_S^0 K_S^0 \eta)/\Gamma_{\text{total}}$ Γ_{362}/Γ

VALUE	CL%	DOCUMENT ID	TECN	COMMENT
< 2.0 × 10⁻⁶	90	¹ AUBERT 09AD	BABR	$e^+e^- \rightarrow \Upsilon(4S)$

¹ Assumes equal production of B^+ and B^0 at the $\Upsilon(4S)$.

$\Gamma(K^0K^+K^-)/\Gamma_{\text{total}}$ Γ_{363}/Γ

VALUE (units 10^{-6})	CL%	DOCUMENT ID	TECN	COMMENT
26.8 ± 1.1 OUR FIT				
26.6 ± 1.2 OUR AVERAGE				
26.5 ± 0.9 ± 0.8		^{1,2} LEES 12o	BABR	$e^+e^- \rightarrow \Upsilon(4S)$
28.3 ± 3.3 ± 4.0		¹ GARMASH 04	BELL	$e^+e^- \rightarrow \Upsilon(4S)$
• • • We do not use the following data for averages, fits, limits, etc. • • •				
23.8 ± 2.0 ± 1.6		¹ AUBERT, B 04V	BABR	Repl. by LEES 12o
< 1300	90	ALBRECHT 91E	ARG	$e^+e^- \rightarrow \Upsilon(4S)$
¹ Assumes equal production of B^+ and B^0 at the $\Upsilon(4S)$.				
² All intermediate charmonium and charm resonances are removed, except of χ_{c0} .				

$\Gamma(K^0K^+K^-)/\Gamma(K^0\pi^+\pi^-)$ $\Gamma_{363}/\Gamma_{322}$

VALUE	DOCUMENT ID	TECN	COMMENT
0.539 ± 0.025 OUR FIT			
0.549 ± 0.018 ± 0.033	AAIJ 17BP LHCB		pp at 7, 8 TeV
• • • We do not use the following data for averages, fits, limits, etc. • • •			
0.385 ± 0.031 ± 0.023	AAIJ 13BP LHCB		Repl. by AAIJ 17BP

$\Gamma(K^0\phi)/\Gamma_{\text{total}}$ Γ_{364}/Γ

VALUE (units 10^{-6})	CL%	DOCUMENT ID	TECN	COMMENT
7.3 ± 0.7 OUR AVERAGE				
7.1 ± 0.6 ^{+0.4} _{-0.3}		¹ LEES 12o	BABR	$e^+e^- \rightarrow \Upsilon(4S)$
9.0 ^{+2.2} _{-1.8} ± 0.7		¹ CHEN 03B	BELL	$e^+e^- \rightarrow \Upsilon(4S)$
• • • We do not use the following data for averages, fits, limits, etc. • • •				
8.4 ^{+1.5} _{-1.3} ± 0.5		¹ AUBERT 04A	BABR	Repl. by LEES 12o
8.1 ^{+3.1} _{-2.5} ± 0.8		¹ AUBERT 01D	BABR	$e^+e^- \rightarrow \Upsilon(4S)$
< 12.3	90	¹ BRIERE 01	CLE2	$e^+e^- \rightarrow \Upsilon(4S)$
< 31	90	¹ BERGFELD 98	CLE2	
< 88	90	ASNER 96	CLE2	$e^+e^- \rightarrow \Upsilon(4S)$
< 720	90	ALBRECHT 91B	ARG	$e^+e^- \rightarrow \Upsilon(4S)$
< 420	90	² AVERY 89B	CLEO	$e^+e^- \rightarrow \Upsilon(4S)$
< 1000	90	³ AVERY 87	CLEO	$e^+e^- \rightarrow \Upsilon(4S)$

¹ Assumes equal production of B^+ and B^0 at the $\Upsilon(4S)$.

² AVERY 89B reports $< 4.9 \times 10^{-4}$ assuming the $\Upsilon(4S)$ decays 43% to $B^0\bar{B}^0$. We rescale to 50%.

³ AVERY 87 reports $< 1.3 \times 10^{-3}$ assuming the $\Upsilon(4S)$ decays 40% to $B^0\bar{B}^0$. We rescale to 50%.

$\Gamma(f_0(980)K^0, f_0 \rightarrow K^+K^-)/\Gamma_{\text{total}}$ Γ_{365}/Γ

VALUE (units 10^{-6})	DOCUMENT ID	TECN	COMMENT
7.0^{+2.6}_{-1.8} ± 2.4	¹ LEES 12o	BABR	$e^+e^- \rightarrow \Upsilon(4S)$

¹ Assumes equal production of B^+ and B^0 at the $\Upsilon(4S)$.

$\Gamma(f_0(1500)K^0)/\Gamma_{\text{total}}$ Γ_{366}/Γ

VALUE (units 10^{-6})	DOCUMENT ID	TECN	COMMENT
13.3^{+5.8}_{-4.8} ± 3.2	¹ LEES 12o	BABR	$e^+e^- \rightarrow \Upsilon(4S)$

¹ Assumes equal production of B^+ and B^0 at the $\Upsilon(4S)$.

$\Gamma(f_2'(1525)K^0)/\Gamma_{\text{total}}$ Γ_{367}/Γ

VALUE (units 10^{-6})	DOCUMENT ID	TECN	COMMENT
0.29^{+0.27}_{-0.18} ± 0.36	¹ LEES 12o	BABR	$e^+e^- \rightarrow \Upsilon(4S)$

¹ Assumes equal production of B^+ and B^0 at the $\Upsilon(4S)$.

$\Gamma(f_0(1710)K^0, f_0 \rightarrow K^+K^-)/\Gamma_{\text{total}}$ Γ_{368}/Γ

VALUE (units 10^{-6})	DOCUMENT ID	TECN	COMMENT
4.4 ± 0.7 ± 0.5	¹ LEES 12o	BABR	$e^+e^- \rightarrow \Upsilon(4S)$

¹ Assumes equal production of B^+ and B^0 at the $\Upsilon(4S)$.

$\Gamma(K^0K^+K^- \text{ nonresonant})/\Gamma_{\text{total}}$ Γ_{369}/Γ

VALUE (units 10^{-6})	DOCUMENT ID	TECN	COMMENT
33 ± 5 ± 9	¹ LEES 12o	BABR	$e^+e^- \rightarrow \Upsilon(4S)$

¹ Assumes equal production of B^+ and B^0 at the $\Upsilon(4S)$.

$\Gamma(K_S^0 K_S^0 \pi^0)/\Gamma_{\text{total}}$ Γ_{370}/Γ

VALUE (units 10^{-6})	DOCUMENT ID	TECN	COMMENT
6.0 ± 0.5 OUR AVERAGE	Error includes scale factor of 1.1.		
6.19 ± 0.48 ± 0.19	¹ LEES 12i	BABR	$e^+e^- \rightarrow \Upsilon(4S)$
4.2 ^{+1.6} _{-1.3} ± 0.8	¹ GARMASH 04	BELL	$e^+e^- \rightarrow \Upsilon(4S)$
• • • We do not use the following data for averages, fits, limits, etc. • • •			
6.9 ^{+0.9} _{-0.8} ± 0.6	¹ AUBERT, B 05	BABR	Repl. by LEES 12i
¹ Assumes equal production of B^+ and B^0 at the $\Upsilon(4S)$.			

Meson Particle Listings

B^0

$\Gamma(f_0(980)K^0, f_0 \rightarrow K_S^0 K_S^0)/\Gamma_{total}$ Γ_{371}/Γ

VALUE (units 10^{-6})	DOCUMENT ID	TECN	COMMENT
$2.7^{+1.3}_{-1.2} \pm 1.3$	1,2 LEES	12i	BABR $e^+e^- \rightarrow \Upsilon(4S)$

¹ Assumes equal production of B^+ and B^0 at the $\Upsilon(4S)$.
² Uses Dalitz plot analysis of the $B^0 \rightarrow K_S^0 K_S^0$ decay.

$\Gamma(f_0(1710)K^0, f_0 \rightarrow K_S^0 K_S^0)/\Gamma_{total}$ Γ_{372}/Γ

VALUE (units 10^{-6})	DOCUMENT ID	TECN	COMMENT
$0.50^{+0.46}_{-0.24} \pm 0.11$	1,2 LEES	12i	BABR $e^+e^- \rightarrow \Upsilon(4S)$

¹ Assumes equal production of B^+ and B^0 at the $\Upsilon(4S)$.
² Uses Dalitz plot analysis of the $B^0 \rightarrow K_S^0 K_S^0$ decay.

$\Gamma(f_2(2010)K^0, f_2 \rightarrow K_S^0 K_S^0)/\Gamma_{total}$ Γ_{373}/Γ

VALUE (units 10^{-6})	DOCUMENT ID	TECN	COMMENT
$0.54^{+0.21}_{-0.20} \pm 0.52$	1,2 LEES	12i	BABR $e^+e^- \rightarrow \Upsilon(4S)$

¹ Assumes equal production of B^+ and B^0 at the $\Upsilon(4S)$.
² Uses Dalitz plot analysis of the $B^0 \rightarrow K_S^0 K_S^0$ decay.

$\Gamma(K_S^0 K_S^0 K_S^0 \text{ nonresonant})/\Gamma_{total}$ Γ_{374}/Γ

VALUE (units 10^{-6})	DOCUMENT ID	TECN	COMMENT
$13.3^{+2.2}_{-2.3} \pm 2.2$	1,2 LEES	12i	BABR $e^+e^- \rightarrow \Upsilon(4S)$

¹ Assumes equal production of B^+ and B^0 at the $\Upsilon(4S)$.
² Uses Dalitz plot analysis of the $B^0 \rightarrow K_S^0 K_S^0 K_S^0$ decay.

$\Gamma(K_S^0 K_S^0 K_L^0)/\Gamma_{total}$ Γ_{375}/Γ

VALUE (units 10^{-6})	CL%	DOCUMENT ID	TECN	COMMENT
<16	90	¹ AUBERT,B	06R	BABR $e^+e^- \rightarrow \Upsilon(4S)$

¹ Assumes equal production of B^+ and B^0 at the $\Upsilon(4S)$.

$\Gamma(K^*(892)^0 K^+ K^-)/\Gamma_{total}$ Γ_{376}/Γ

VALUE (units 10^{-6})	CL%	DOCUMENT ID	TECN	COMMENT
$27.5 \pm 1.3 \pm 2.2$		¹ AUBERT	07As	BABR $e^+e^- \rightarrow \Upsilon(4S)$
<610	90	ALBRECHT	91E	ARG $e^+e^- \rightarrow \Upsilon(4S)$

¹ Assumes equal production of B^+ and B^0 at the $\Upsilon(4S)$.

$\Gamma(K^*(892)^0 \phi)/\Gamma_{total}$ Γ_{377}/Γ

VALUE (units 10^{-6})	CL%	DOCUMENT ID	TECN	COMMENT
10.0 ± 0.5 OUR FIT				
10.0 ± 0.5 OUR AVERAGE				
$10.4 \pm 0.5 \pm 0.6$		¹ PRIM	13	BELL $e^+e^- \rightarrow \Upsilon(4S)$
$9.7 \pm 0.5 \pm 0.5$		¹ AUBERT	08Bg	BABR $e^+e^- \rightarrow \Upsilon(4S)$
$11.5^{+4.5+1.8}_{-3.7-1.7}$		¹ BRIERE	01	CLE2 $e^+e^- \rightarrow \Upsilon(4S)$
$9.2 \pm 0.7 \pm 0.6$		¹ AUBERT	07D	BABR Repl. by AUBERT 08Bg
$9.2 \pm 0.9 \pm 0.5$		¹ AUBERT,B	04W	BABR Repl. by AUBERT 07D
$11.2 \pm 1.3 \pm 0.8$		¹ AUBERT	03V	BABR Repl. by AUBERT,B 04W
$10.0^{+1.6+0.7}_{-1.5-0.8}$		¹ CHEN	03B	BELL Repl. by PRIM 13
$8.7^{+2.5}_{-2.1} \pm 1.1$		¹ AUBERT	01D	BABR Repl. by AUBERT 03V
<384	90	² ABE	00c	SLD $e^+e^- \rightarrow Z$
<21	90	¹ BERGFELD	98	CLE2
<43	90	ASNER	96	CLE2 $e^+e^- \rightarrow \Upsilon(4S)$
<320	90	ALBRECHT	91B	ARG $e^+e^- \rightarrow \Upsilon(4S)$
<380	90	³ AVERY	89B	CLEO $e^+e^- \rightarrow \Upsilon(4S)$
<380	90	⁴ AVERY	87	CLEO $e^+e^- \rightarrow \Upsilon(4S)$

¹ Assumes equal production of B^+ and B^0 at the $\Upsilon(4S)$.
² ABE 00c assumes $B(Z \rightarrow b\bar{b})=(21.7 \pm 0.1)\%$ and the B fractions $f_{B^0}=f_{B^+}=(39.7^{+1.8}_{-2.2})\%$ and $f_{B_s}=(10.5^{+1.8}_{-2.2})\%$.
³ AVERY 89B reports $< 4.4 \times 10^{-4}$ assuming the $\Upsilon(4S)$ decays 43% to $B^0 \bar{B}^0$. We rescale to 50%.
⁴ AVERY 87 reports $< 4.7 \times 10^{-4}$ assuming the $\Upsilon(4S)$ decays 40% to $B^0 \bar{B}^0$. We rescale to 50%.

$\Gamma(K^+ K^- \pi^+ \pi^- \text{ nonresonant})/\Gamma_{total}$ Γ_{378}/Γ

VALUE (units 10^{-6})	CL%	DOCUMENT ID	TECN	COMMENT
<71.7	90	1,2 CHIANG	10	BELL $e^+e^- \rightarrow \Upsilon(4S)$

¹ Measured in the range $0.7 < m_{K\pi} < 1.7$ and corrected using PS assumption for the full $K\pi$ mass range.
² Assumes equal production of B^+ and B^0 at the $\Upsilon(4S)$.

$\Gamma(K^*(892)^0 K^- \pi^+)/\Gamma_{total}$ Γ_{379}/Γ

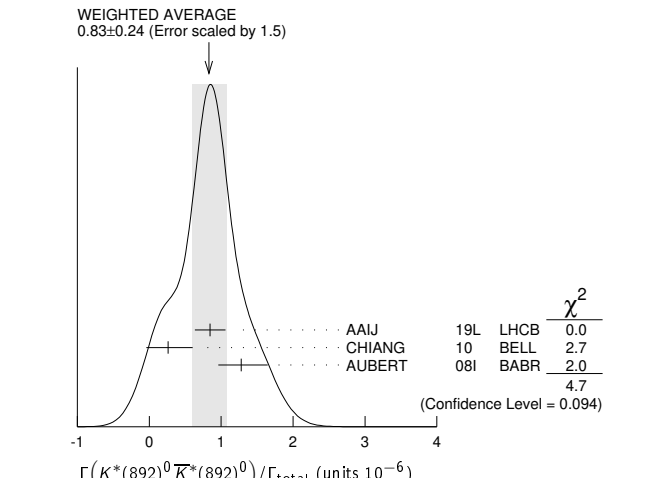
VALUE (units 10^{-6})	DOCUMENT ID	TECN	COMMENT
4.5 ± 1.3 OUR AVERAGE			
$2.11^{+5.63+4.85}_{-5.26-4.75}$	1,2 CHIANG	10	BELL $e^+e^- \rightarrow \Upsilon(4S)$
$4.6 \pm 1.1 \pm 0.8$	² AUBERT	07As	BABR $e^+e^- \rightarrow \Upsilon(4S)$

¹ Measured in the range $0.7 < m_{K\pi} < 1.7$ and corrected using PS assumption for the full $K\pi$ mass range. The quoted result is equivalent to the upper limit of $< 13.9 \times 10^{-6}$ at 90% CL.
² Assumes equal production of B^+ and B^0 at the $\Upsilon(4S)$.

$\Gamma(K^*(892)^0 \bar{K}^*(892)^0)/\Gamma_{total}$ Γ_{380}/Γ

VALUE (units 10^{-6})	CL%	DOCUMENT ID	TECN	COMMENT
0.83 ± 0.24 OUR AVERAGE				Error includes scale factor of 1.5. See the ideogram below.
$0.85 \pm 0.07 \pm 0.20$		¹ AAIJ	19L	LHCB pp at 7 and 8 TeV
$0.26^{+0.33+0.10}_{-0.29-0.08}$		^{2,3} CHIANG	10	BELL $e^+e^- \rightarrow \Upsilon(4S)$
$1.28^{+0.35}_{-0.30} \pm 0.11$		³ AUBERT	08i	BABR $e^+e^- \rightarrow \Upsilon(4S)$
<22	90	⁴ GODANG	02	CLE2 $e^+e^- \rightarrow \Upsilon(4S)$
<469	90	⁵ ABE	00c	SLD $e^+e^- \rightarrow Z$

¹ AAIJ 19L reports $[\Gamma(B^0 \rightarrow K^*(892)^0 \bar{K}^*(892)^0)/\Gamma_{total}] / [B(B_s^0 \rightarrow \bar{K}^*(892)^0 K^*(892)^0)] = 0.0758 \pm 0.0057 \pm 0.0030$ which we multiply by our best value $B(B_s^0 \rightarrow \bar{K}^*(892)^0 K^*(892)^0) = (1.11 \pm 0.27) \times 10^{-5}$. Our first error is their experiment's error and our second error is the systematic error from using our best value.
² Measured in the range $0.7 < m_{K\pi} < 1.7$ and corrected using PS assumption for the full $K\pi$ mass range. The quoted result is equivalent to the upper limit of $< 0.8 \times 10^{-6}$ at 90% CL.
³ Assumes equal production of B^+ and B^0 at the $\Upsilon(4S)$.
⁴ Assumes a helicity 00 configuration. For a helicity 11 configuration, the limit decreases to 1.9×10^{-5} .
⁵ ABE 00c assumes $B(Z \rightarrow b\bar{b})=(21.7 \pm 0.1)\%$ and the B fractions $f_{B^0}=f_{B^+}=(39.7^{+1.8}_{-2.2})\%$ and $f_{B_s}=(10.5^{+1.8}_{-2.2})\%$.



$\Gamma(K^+ K^+ \pi^- \pi^- \text{ nonresonant})/\Gamma_{total}$ Γ_{381}/Γ

VALUE (units 10^{-6})	CL%	DOCUMENT ID	TECN	COMMENT
<6.0	90	¹ CHIANG	10	BELL $e^+e^- \rightarrow \Upsilon(4S)$

¹ Assumes equal production of B^+ and B^0 at the $\Upsilon(4S)$.

$\Gamma(K^*(892)^0 K^+ \pi^-)/\Gamma_{total}$ Γ_{382}/Γ

VALUE (units 10^{-6})	CL%	DOCUMENT ID	TECN	COMMENT
<2.2	90	¹ AUBERT	07As	BABR $e^+e^- \rightarrow \Upsilon(4S)$
<7.6	90	¹ CHIANG	10	BELL $e^+e^- \rightarrow \Upsilon(4S)$

¹ Assumes equal production of B^+ and B^0 at the $\Upsilon(4S)$.

$\Gamma(K^*(892)^0 K^*(892)^0)/\Gamma_{total}$ Γ_{383}/Γ

VALUE (units 10^{-6})	CL%	DOCUMENT ID	TECN	COMMENT
<0.2	90	¹ CHIANG	10	BELL $e^+e^- \rightarrow \Upsilon(4S)$
<0.41	90	¹ AUBERT	08i	BABR $e^+e^- \rightarrow \Upsilon(4S)$
<37	90	² GODANG	02	CLE2 $e^+e^- \rightarrow \Upsilon(4S)$

¹ Assumes equal production of B^+ and B^0 at the $\Upsilon(4S)$.
² Assumes a helicity 00 configuration. For a helicity 11 configuration, the limit decreases to 2.9×10^{-5} .

$\Gamma(K^*(892)^+ K^*(892)^-)/\Gamma_{total}$ Γ_{384}/Γ

VALUE (units 10^{-6})	CL%	DOCUMENT ID	TECN	COMMENT
<2.0	90	¹ AUBERT	08AP	BABR $e^+e^- \rightarrow \Upsilon(4S)$
<141	90	² GODANG	02	CLE2 $e^+e^- \rightarrow \Upsilon(4S)$

¹ Assumes equal production of B^+ and B^0 at the $\Upsilon(4S)$.
² Assumes a helicity 00 configuration. For a helicity 11 configuration, the limit decreases to 8.9×10^{-5} .

See key on page 1171

Meson Particle Listings

 B^0

$\Gamma(K_1(1400)^0 \phi)/\Gamma_{\text{total}}$		Γ_{385}/Γ	
VALUE	CL%	DOCUMENT ID	TECN COMMENT
$<5.0 \times 10^{-3}$	90	ALBRECHT 91B ARG	$e^+e^- \rightarrow \Upsilon(4S)$

$\Gamma(\phi(K\pi)_0^{*0})/\Gamma_{\text{total}}$		Γ_{386}/Γ	
This decay refers to the coherent sum of resonant and nonresonant $J^P = 0^+ K\pi$ components with $1.13 < m_{K\pi} < 1.53 \text{ GeV}/c^2$.			
VALUE (units 10^{-6})	CL%	DOCUMENT ID	TECN COMMENT

4.3 ± 0.4 OUR AVERAGE			
4.3 ± 0.4 ± 0.4		¹ PRIM 13 BELL	$e^+e^- \rightarrow \Upsilon(4S)$
4.3 ± 0.6 ± 0.4		¹ AUBERT 08BG BABR	$e^+e^- \rightarrow \Upsilon(4S)$
• • • We do not use the following data for averages, fits, limits, etc. • • •			
5.0 ± 0.8 ± 0.3		¹ AUBERT 07D BABR	Repl. by AUBERT 08BG
¹ Assumes equal production of B^+ and B^0 at the $\Upsilon(4S)$.			

$\Gamma(\phi(K\pi)_0^{*0}(1.60 < m_{K\pi} < 2.15))/\Gamma_{\text{total}}$		Γ_{387}/Γ	
This decay refers to the coherent sum of resonant and nonresonant $J^P = 0^+ K\pi$ components with $1.60 < m_{K\pi} < 2.15 \text{ GeV}/c^2$.			
VALUE (units 10^{-6})	CL%	DOCUMENT ID	TECN COMMENT

<1.7	90	¹ AUBERT 07A0 BABR	$e^+e^- \rightarrow \Upsilon(4S)$
¹ Assumes equal production of B^+ and B^0 at the $\Upsilon(4S)$.			

$\Gamma(K_0^*(1430)^0 K^- \pi^+)/\Gamma_{\text{total}}$		Γ_{388}/Γ	
VALUE (units 10^{-6})	CL%	DOCUMENT ID	TECN COMMENT
<31.8	90	^{1,2} CHIANG 10 BELL	$e^+e^- \rightarrow \Upsilon(4S)$

¹ Measured in the range $0.7 < m_{K\pi} < 1.7$ and corrected using PS assumption for the full $K\pi$ mass range.			
² Assumes equal production of B^+ and B^0 at the $\Upsilon(4S)$.			

$\Gamma(K_0^*(1430)^0 \bar{K}^*(892)^0)/\Gamma_{\text{total}}$		Γ_{389}/Γ	
VALUE (units 10^{-6})	CL%	DOCUMENT ID	TECN COMMENT
<3.3	90	^{1,2} CHIANG 10 BELL	$e^+e^- \rightarrow \Upsilon(4S)$

¹ Measured in the range $0.7 < m_{K\pi} < 1.7$ and corrected using PS assumption for the full $K\pi$ mass range.			
² Assumes equal production of B^+ and B^0 at the $\Upsilon(4S)$.			

$\Gamma(K_0^*(1430)^0 \bar{K}_0^*(1430)^0)/\Gamma_{\text{total}}$		Γ_{390}/Γ	
VALUE (units 10^{-6})	CL%	DOCUMENT ID	TECN COMMENT
<8.4	90	^{1,2} CHIANG 10 BELL	$e^+e^- \rightarrow \Upsilon(4S)$

¹ Measured in the range $0.7 < m_{K\pi} < 1.7$ and corrected using PS assumption for the full $K\pi$ mass range.			
² Assumes equal production of B^+ and B^0 at the $\Upsilon(4S)$.			

$\Gamma(K_0^*(1430)^0 \phi)/\Gamma_{\text{total}}$		Γ_{391}/Γ	
VALUE (units 10^{-6})	CL%	DOCUMENT ID	TECN COMMENT
3.9 ± 0.5 ± 0.6		¹ AUBERT 08BG BABR	$e^+e^- \rightarrow \Upsilon(4S)$
• • • We do not use the following data for averages, fits, limits, etc. • • •			
4.6 ± 0.7 ± 0.6		¹ AUBERT 07D BABR	Repl. by AUBERT 08BG
seen		² AUBERT,B 04W BABR	Repl. by AUBERT 07D

¹ Assumes equal production of B^+ and B^0 at the $\Upsilon(4S)$.			
² Observed 181 ± 17 events with statistical significance greater than 10 σ .			

$\Gamma(K_0^*(1430)^0 K^*(892)^0)/\Gamma_{\text{total}}$		Γ_{392}/Γ	
VALUE (units 10^{-6})	CL%	DOCUMENT ID	TECN COMMENT
<1.7	90	¹ CHIANG 10 BELL	$e^+e^- \rightarrow \Upsilon(4S)$

¹ Assumes equal production of B^+ and B^0 at the $\Upsilon(4S)$.			
--	--	--	--

$\Gamma(K_0^*(1430)^0 K_0^*(1430)^0)/\Gamma_{\text{total}}$		Γ_{393}/Γ	
VALUE (units 10^{-6})	CL%	DOCUMENT ID	TECN COMMENT
<4.7	90	¹ CHIANG 10 BELL	$e^+e^- \rightarrow \Upsilon(4S)$

¹ Assumes equal production of B^+ and B^0 at the $\Upsilon(4S)$.			
--	--	--	--

$\Gamma(K^*(1680)^0 \phi)/\Gamma_{\text{total}}$		Γ_{394}/Γ	
VALUE (units 10^{-6})	CL%	DOCUMENT ID	TECN COMMENT
<3.5	90	¹ AUBERT 07A0 BABR	$e^+e^- \rightarrow \Upsilon(4S)$

¹ Assumes equal production of B^+ and B^0 at the $\Upsilon(4S)$.			
--	--	--	--

$\Gamma(K^*(1780)^0 \phi)/\Gamma_{\text{total}}$		Γ_{395}/Γ	
VALUE (units 10^{-6})	CL%	DOCUMENT ID	TECN COMMENT
<2.7	90	¹ AUBERT 07A0 BABR	$e^+e^- \rightarrow \Upsilon(4S)$

¹ Assumes equal production of B^+ and B^0 at the $\Upsilon(4S)$.			
--	--	--	--

$\Gamma(K^*(2045)^0 \phi)/\Gamma_{\text{total}}$		Γ_{396}/Γ	
VALUE (units 10^{-6})	CL%	DOCUMENT ID	TECN COMMENT
<15.3	90	¹ AUBERT 07A0 BABR	$e^+e^- \rightarrow \Upsilon(4S)$

¹ Assumes equal production of B^+ and B^0 at the $\Upsilon(4S)$.			
--	--	--	--

$\Gamma(K_2^*(1430)^0 \rho^0)/\Gamma_{\text{total}}$		Γ_{397}/Γ	
VALUE (units 10^{-6})	CL%	DOCUMENT ID	TECN COMMENT
$<1.1 \times 10^3$	90	ALBRECHT 91B ARG	$e^+e^- \rightarrow \Upsilon(4S)$

$\Gamma(K_2^*(1430)^0 \phi)/\Gamma_{\text{total}}$		Γ_{398}/Γ	
VALUE (units 10^{-6})	CL%	DOCUMENT ID	TECN COMMENT
6.8 ± 0.9 OUR AVERAGE		Error includes scale factor of 1.2.	

5.5 $^{+0.9}_{-0.7} \pm 1.0$		¹ PRIM 13 BELL	$e^+e^- \rightarrow \Upsilon(4S)$
7.5 ± 0.9 ± 0.5		¹ AUBERT 08BG BABR	$e^+e^- \rightarrow \Upsilon(4S)$
• • • We do not use the following data for averages, fits, limits, etc. • • •			
7.8 ± 1.1 ± 0.6		¹ AUBERT 07D BABR	Repl. by AUBERT 08BG
seen		² AUBERT,B 04W BABR	Repl. by AUBERT 07D
<1400	90	ALBRECHT 91B ARG	$e^+e^- \rightarrow \Upsilon(4S)$

¹ Assumes equal production of B^+ and B^0 at the $\Upsilon(4S)$.			
² The angular distribution of $B \rightarrow \phi K^*(1430)$ provides evidence with statistical significance of 3.2 σ .			

$\Gamma(K^0 \phi \phi)/\Gamma_{\text{total}}$		Γ_{399}/Γ	
VALUE (units 10^{-6})	CL%	DOCUMENT ID	TECN COMMENT
3.7 ± 0.7 OUR AVERAGE		Error includes scale factor of 1.3.	

3.02 $^{+0.75}_{-0.66} \pm 0.20$		¹ MOHANTY 21 BELL	$e^+e^- \rightarrow \Upsilon(4S)$
4.5 ± 0.8 ± 0.3		¹ LEES 11A BABR	$e^+e^- \rightarrow \Upsilon(4S)$
• • • We do not use the following data for averages, fits, limits, etc. • • •			
4.1 $^{+1.7}_{-1.4} \pm 0.4$		¹ AUBERT,BE 06H BABR	Repl. by LEES 11A
¹ Assumes equal production of B^0 and B^+ at the $\Upsilon(4S)$ and the $\phi\phi$ invariant mass below 2.85 GeV/c^2 .			

$\Gamma(\eta'/\eta' K^0)/\Gamma_{\text{total}}$		Γ_{400}/Γ	
VALUE (units 10^{-6})	CL%	DOCUMENT ID	TECN COMMENT
<31	90	¹ AUBERT,B 06P BABR	$e^+e^- \rightarrow \Upsilon(4S)$

¹ Assumes equal production of B^+ and B^0 at the $\Upsilon(4S)$.			
--	--	--	--

$\Gamma(\eta K^0 \gamma)/\Gamma_{\text{total}}$		Γ_{401}/Γ	
VALUE (units 10^{-6})	CL%	DOCUMENT ID	TECN COMMENT
7.6 ± 1.8 OUR AVERAGE			

7.1 $^{+2.1}_{-2.0} \pm 0.4$		^{1,2} AUBERT 09 BABR	$e^+e^- \rightarrow \Upsilon(4S)$
8.7 $^{+3.1+1.9}_{-2.7-1.6}$		^{2,3} NISHIDA 05 BELL	$e^+e^- \rightarrow \Upsilon(4S)$
• • • We do not use the following data for averages, fits, limits, etc. • • •			
11.3 $^{+2.8}_{-1.6} \pm 0.6$		^{1,2} AUBERT,B 06M BABR	Repl. by AUBERT 09
¹ $m_{\eta K} < 3.25 \text{ GeV}/c^2$.			
² Assumes equal production of B^+ and B^0 at the $\Upsilon(4S)$.			
³ $m_{\eta' K} < 2.4 \text{ GeV}/c^2$.			

$\Gamma(\eta' K^0 \gamma)/\Gamma_{\text{total}}$		Γ_{402}/Γ	
VALUE (units 10^{-6})	CL%	DOCUMENT ID	TECN COMMENT
<6.4	90	^{1,2} WEDD 10 BELL	$e^+e^- \rightarrow \Upsilon(4S)$

• • • We do not use the following data for averages, fits, limits, etc. • • •			
<6.6	90	^{1,3} AUBERT,B 06M BABR	$e^+e^- \rightarrow \Upsilon(4S)$
¹ Assumes equal production of B^+ and B^0 at the $\Upsilon(4S)$.			
² $m_{\eta' K} < 3.4 \text{ GeV}/c^2$.			
³ $m_{\eta' K} < 3.25 \text{ GeV}/c^2$.			

$\Gamma(K^0 \phi \gamma)/\Gamma_{\text{total}}$		Γ_{403}/Γ	
VALUE (units 10^{-6})	CL%	DOCUMENT ID	TECN COMMENT
2.74 ± 0.60 ± 0.32		¹ SAHOO 11A BELL	$e^+e^- \rightarrow \Upsilon(4S)$

• • • We do not use the following data for averages, fits, limits, etc. • • •			
<2.7	90	¹ AUBERT 07Q BABR	$e^+e^- \rightarrow \Upsilon(4S)$
<8.3	90	¹ DRUTSKOY 04 BELL	$e^+e^- \rightarrow \Upsilon(4S)$
¹ Assumes equal production of B^+ and B^0 at $\Upsilon(4S)$.			

$\Gamma(K^+ \pi^- \pi^-)/\Gamma_{\text{total}}$		Γ_{404}/Γ	
VALUE	CL%	DOCUMENT ID	TECN COMMENT
(4.6 $^{+1.3+0.5}_{-1.2-0.7}$) × 10⁻⁶		^{1,2} NISHIDA 02 BELL	$e^+e^- \rightarrow \Upsilon(4S)$

¹ Assumes equal production of B^+ and B^0 at the $\Upsilon(4S)$.			
² 1.25 $\text{GeV}/c^2 < m_{K\pi} < 1.6 \text{ GeV}/c^2$			

$\Gamma(K^*(892)^0 \gamma)/\Gamma_{\text{total}}$		Γ_{405}/Γ	
VALUE (units 10^{-6})	CL%	DOCUMENT ID	TECN COMMENT
41.8 ± 2.5 OUR AVERAGE		Error includes scale factor of 2.1.	

39.6 ± 0.7 ± 1.4		¹ HORIGUCHI 17 BELL	$e^+e^- \rightarrow \Upsilon(4S)$
44.7 ± 1.0 ± 1.6		² AUBERT 09A0 BABR	$e^+e^- \rightarrow \Upsilon(4S)$
45.5 $^{+7.2}_{-6.8} \pm 3.4$		³ COAN 00 CLE2	$e^+e^- \rightarrow \Upsilon(4S)$
• • • We do not use the following data for averages, fits, limits, etc. • • •			
39.2 ± 2.0 ± 2.4		⁴ AUBERT,BE 04A BABR	Repl. by AUBERT 09A0
40.1 ± 2.1 ± 1.7		⁵ NAKAO 04 BELL	Repl. by HORIGUCHI 17
< 110	90	⁵ ACOSTA 02G CDF	$p\bar{p}$ at 1.8 TeV
42.3 ± 4.0 ± 2.2		⁵ AUBERT 02C BABR	Repl. by AUBERT,BE 04A
< 210	90	⁶ ADAM 96D DLPH	$e^+e^- \rightarrow Z$
40 ± 17 ± 8		⁷ AMMAR 93 CLE2	Repl. by COAN 00
< 420	90	ALBRECHT 89G ARG	$e^+e^- \rightarrow \Upsilon(4S)$
< 240	90	⁸ AVERY 89B CLEO	$e^+e^- \rightarrow \Upsilon(4S)$
< 2100	90	AVERY 87 CLEO	$e^+e^- \rightarrow \Upsilon(4S)$

Meson Particle Listings

 B^0

- 1 Uses $B(\Upsilon(4S) \rightarrow B^+ B^-) = (51.4 \pm 0.6)\%$ and $B(\Upsilon(4S) \rightarrow B^0 \bar{B}^0) = (48.6 \pm 0.6)\%$.
 2 Uses $B(\Upsilon(4S) \rightarrow B^+ B^-) = (51.6 \pm 0.6)\%$ and $B(\Upsilon(4S) \rightarrow B^0 \bar{B}^0) = (48.4 \pm 0.6)\%$.
 3 Assumes equal production of B^+ and B^0 at the $\Upsilon(4S)$. No evidence for a nonresonant $K\pi\gamma$ contamination was seen; the central value assumes no contamination.
 4 Uses the production ratio of charged and neutral B from $\Upsilon(4S)$ decays $R^{+0} = 1.006 \pm 0.048$.
 5 Assumes equal production of B^+ and B^0 at the $\Upsilon(4S)$.
 6 ADAM 96D assumes $f_{B^0} = f_{B^-} = 0.39$ and $f_{B_s} = 0.12$.
 7 AMMAR 93 observed 6.6 ± 2.8 events above background.
 8 AVERY 89B reports $< 2.8 \times 10^{-4}$ assuming the $\Upsilon(4S)$ decays 43% to $B^0 \bar{B}^0$. We rescale to 50%.

 $\Gamma(K^*(1410)\gamma)/\Gamma_{\text{total}}$ Γ_{406}/Γ

VALUE	CL%	DOCUMENT ID	TECN	COMMENT
$< 1.3 \times 10^{-4}$	90	1 NISHIDA	02	BELL $e^+ e^- \rightarrow \Upsilon(4S)$

- 1 Assumes equal production of B^+ and B^0 at the $\Upsilon(4S)$.

 $\Gamma(K^+ \pi^- \gamma \text{ nonresonant})/\Gamma_{\text{total}}$ Γ_{407}/Γ

VALUE	CL%	DOCUMENT ID	TECN	COMMENT
$< 2.6 \times 10^{-6}$	90	1,2 NISHIDA	02	BELL $e^+ e^- \rightarrow \Upsilon(4S)$

- 1 Assumes equal production of B^+ and B^0 at the $\Upsilon(4S)$.
 2 $1.25 \text{ GeV}/c^2 < M_{K\pi} < 1.6 \text{ GeV}/c^2$

 $\Gamma(K^*(892)^0 X(214), X \rightarrow \mu^+ \mu^-)/\Gamma_{\text{total}}$ Γ_{408}/Γ

$X(214)$ is a hypothetical particle of mass $214 \text{ MeV}/c^2$ reported by the HyperCP experiment (PARK 05)

VALUE (units 10^{-8})	CL%	DOCUMENT ID	TECN	COMMENT
< 2.26	90	1,2 HYUN	10	BELL $e^+ e^- \rightarrow \Upsilon(4S)$

- 1 Assumes equal production of B^+ and B^0 at the $\Upsilon(4S)$.
 2 Based on scalar nature of X particle. With a vector X assumption, the upper limit is 2.27×10^{-8} .

 $\Gamma(K^0 \pi^+ \pi^- \gamma)/\Gamma_{\text{total}}$ Γ_{409}/Γ

VALUE (units 10^{-5})	CL%	DOCUMENT ID	TECN	COMMENT
1.99 \pm 0.18 OUR AVERAGE				

$2.05 \pm 0.20 \pm 0.26$		1,2 DEL-AMO-SA..16	BABR	$e^+ e^- \rightarrow \Upsilon(4S)$
$1.85 \pm 0.21 \pm 0.12$		1,3 AUBERT	07R	BABR $e^+ e^- \rightarrow \Upsilon(4S)$
$2.40 \pm 0.4 \pm 0.3$		3,4 YANG	05	BELL $e^+ e^- \rightarrow \Upsilon(4S)$

- 1 $M_{K\pi\pi} < 1.8 \text{ GeV}/c^2$.
 2 Uses $B(\Upsilon(4S) \rightarrow B^+ B^-) = 0.513 \pm 0.006$.
 3 Assumes equal production of B^+ and B^0 at the $\Upsilon(4S)$.
 4 $M_{K\pi\pi} < 2.0 \text{ GeV}/c^2$.

 $\Gamma(K^+ \pi^- \pi^0 \gamma)/\Gamma_{\text{total}}$ Γ_{410}/Γ

VALUE (units 10^{-5})	CL%	DOCUMENT ID	TECN	COMMENT
4.07 \pm 0.22 \pm 0.31		1,2 AUBERT	07R	BABR $e^+ e^- \rightarrow \Upsilon(4S)$

- 1 $M_{K\pi\pi} < 1.8 \text{ GeV}/c^2$.
 2 Assumes equal production of B^+ and B^0 at the $\Upsilon(4S)$.

 $\Gamma(K_1(1270)^0 \gamma)/\Gamma_{\text{total}}$ Γ_{411}/Γ

VALUE (units 10^{-5})	CL%	DOCUMENT ID	TECN	COMMENT
< 5.8	90	1 YANG	05	BELL $e^+ e^- \rightarrow \Upsilon(4S)$

- • • We do not use the following data for averages, fits, limits, etc. • • •
 < 700 90 2 ALBRECHT 89G ARG $e^+ e^- \rightarrow \Upsilon(4S)$

- 1 Assumes equal production of B^+ and B^0 at the $\Upsilon(4S)$.
 2 ALBRECHT 89G reports < 0.0078 assuming the $\Upsilon(4S)$ decays 45% to $B^0 \bar{B}^0$. We rescale to 50%.

 $\Gamma(K_1(1400)^0 \gamma)/\Gamma_{\text{total}}$ Γ_{412}/Γ

VALUE (units 10^{-5})	CL%	DOCUMENT ID	TECN	COMMENT
< 1.2	90	1 YANG	05	BELL $e^+ e^- \rightarrow \Upsilon(4S)$

- • • We do not use the following data for averages, fits, limits, etc. • • •
 < 430 90 2 ALBRECHT 89G ARG $e^+ e^- \rightarrow \Upsilon(4S)$

- 1 Assumes equal production of B^+ and B^0 at the $\Upsilon(4S)$.
 2 ALBRECHT 89G reports < 0.0048 assuming the $\Upsilon(4S)$ decays 45% to $B^0 \bar{B}^0$. We rescale to 50%.

 $\Gamma(K_2^*(1430)^0 \gamma)/\Gamma_{\text{total}}$ Γ_{413}/Γ

VALUE (units 10^{-5})	CL%	DOCUMENT ID	TECN	COMMENT
1.24 \pm 0.24 OUR AVERAGE				

$1.22 \pm 0.25 \pm 0.10$		1 AUBERT,B	04u	BABR $e^+ e^- \rightarrow \Upsilon(4S)$
$1.3 \pm 0.5 \pm 0.1$		1 NISHIDA	02	BELL $e^+ e^- \rightarrow \Upsilon(4S)$

- • • We do not use the following data for averages, fits, limits, etc. • • •
 < 40 90 2 ALBRECHT 89G ARG $e^+ e^- \rightarrow \Upsilon(4S)$
- 1 Assumes equal production of B^+ and B^0 at the $\Upsilon(4S)$.
 2 ALBRECHT 89G reports $< 4.4 \times 10^{-4}$ assuming the $\Upsilon(4S)$ decays 45% to $B^0 \bar{B}^0$. We rescale to 50%.

 $\Gamma(K^*(1680)^0 \gamma)/\Gamma_{\text{total}}$ Γ_{414}/Γ

VALUE	CL%	DOCUMENT ID	TECN	COMMENT
< 0.0020	90	1 ALBRECHT	89G	ARG $e^+ e^- \rightarrow \Upsilon(4S)$

- 1 ALBRECHT 89G reports < 0.0022 assuming the $\Upsilon(4S)$ decays 45% to $B^0 \bar{B}^0$. We rescale to 50%.

 $\Gamma(K_3^*(1780)^0 \gamma)/\Gamma_{\text{total}}$ Γ_{415}/Γ

VALUE (units 10^{-6})	CL%	DOCUMENT ID	TECN	COMMENT
< 83	90	1,2 NISHIDA	05	BELL $e^+ e^- \rightarrow \Upsilon(4S)$

- • • We do not use the following data for averages, fits, limits, etc. • • •
 < 10000 90 3 ALBRECHT 89G ARG $e^+ e^- \rightarrow \Upsilon(4S)$

- 1 Assumes equal production of B^+ and B^0 at the $\Upsilon(4S)$.
 2 Uses $B(K_3^*(1780) \rightarrow \eta K) = 0.11 \pm 0.05$.
 3 ALBRECHT 89G reports < 0.011 assuming the $\Upsilon(4S)$ decays 45% to $B^0 \bar{B}^0$. We rescale to 50%.

 $\Gamma(K_4^*(2045)^0 \gamma)/\Gamma_{\text{total}}$ Γ_{416}/Γ

VALUE	CL%	DOCUMENT ID	TECN	COMMENT
< 0.0043	90	1 ALBRECHT	89G	ARG $e^+ e^- \rightarrow \Upsilon(4S)$

- 1 ALBRECHT 89G reports < 0.0048 assuming the $\Upsilon(4S)$ decays 45% to $B^0 \bar{B}^0$. We rescale to 50%.

 $\Gamma(\rho^0 \gamma)/\Gamma_{\text{total}}$ Γ_{417}/Γ

VALUE (units 10^{-6})	CL%	DOCUMENT ID	TECN	COMMENT
0.86 \pm 0.15 OUR AVERAGE				

$0.97 \pm 0.24 \pm 0.06$		1 AUBERT	08BH	BABR $e^+ e^- \rightarrow \Upsilon(4S)$
--------------------------	--	----------	------	---

$0.78 \pm 0.17 \pm 0.09$		1 TANIGUCHI	08	BELL $e^+ e^- \rightarrow \Upsilon(4S)$
--------------------------	--	-------------	----	---

- • • We do not use the following data for averages, fits, limits, etc. • • •
 $0.79 \pm 0.22 \pm 0.06$ 1 AUBERT 07L BABR Repl. by AUBERT 08BH

$1.25 \pm 0.37 \pm 0.07$		1 MOHAPATRA	06	BELL Repl. by TANIGUCHI 08
--------------------------	--	-------------	----	----------------------------

$0.0 \pm 0.2 \pm 0.1$	90	1 AUBERT	05	BABR Repl. by AUBERT 07L
-----------------------	----	----------	----	--------------------------

< 0.8	90	1 MOHAPATRA	05	BELL $e^+ e^- \rightarrow \Upsilon(4S)$
---------	----	-------------	----	---

< 1.2	90	1 AUBERT	04c	BABR $e^+ e^- \rightarrow \Upsilon(4S)$
---------	----	----------	-----	---

< 17	90	1 COAN	00	CLE2 $e^+ e^- \rightarrow \Upsilon(4S)$
--------	----	--------	----	---

- 1 Assumes equal production of B^+ and B^0 at the $\Upsilon(4S)$.

 $\Gamma(\rho^0 X(214), X \rightarrow \mu^+ \mu^-)/\Gamma_{\text{total}}$ Γ_{418}/Γ

$X(214)$ is a hypothetical particle of mass $214 \text{ MeV}/c^2$ reported by the HyperCP experiment (PARK 05)

VALUE (units 10^{-8})	CL%	DOCUMENT ID	TECN	COMMENT
< 1.73	90	1,2 HYUN	10	BELL $e^+ e^- \rightarrow \Upsilon(4S)$

- 1 Assumes equal production of B^+ and B^0 at the $\Upsilon(4S)$.
 2 The result is the same for a scalar or vector X particle.

 $\Gamma(\rho^0 \gamma)/\Gamma(K^*(892)^0 \gamma)$ $\Gamma_{417}/\Gamma_{405}$

VALUE (units 10^{-2})	DOCUMENT ID	TECN	COMMENT
2.06 \pm 0.45 \pm 0.14	TANIGUCHI	08	BELL $e^+ e^- \rightarrow \Upsilon(4S)$

$2.06 \pm 0.45 \pm 0.14$			
--------------------------	--	--	--

- • • We do not use the following data for averages, fits, limits, etc. • • •
 $0.40 \pm 0.19 \pm 0.13$ 1 TANIGUCHI 08 BELL $e^+ e^- \rightarrow \Upsilon(4S)$

$0.40 \pm 0.24 \pm 0.05$		1 AUBERT	07L	BABR Repl. by AUBERT 08BH
--------------------------	--	----------	-----	---------------------------

$0.56 \pm 0.34 \pm 0.05$		1 MOHAPATRA	06	BELL Repl. by TANIGUCHI 08
--------------------------	--	-------------	----	----------------------------

< 1.0	90	1 AUBERT	05	BABR Repl. by AUBERT 07L
---------	----	----------	----	--------------------------

< 0.8	90	1 MOHAPATRA	05	BELL Repl. by MOHAPATRA 06
---------	----	-------------	----	----------------------------

< 1.0	90	1 AUBERT	04c	BABR $e^+ e^- \rightarrow \Upsilon(4S)$
---------	----	----------	-----	---

< 9.2	90	1 COAN	00	CLE2 $e^+ e^- \rightarrow \Upsilon(4S)$
---------	----	--------	----	---

- 1 Assumes equal production of B^+ and B^0 at the $\Upsilon(4S)$.

 $\Gamma(\phi \gamma)/\Gamma_{\text{total}}$ Γ_{420}/Γ

VALUE	CL%	DOCUMENT ID	TECN	COMMENT
$< 1.0 \times 10^{-7}$	90	1 KING	16	BELL $e^+ e^- \rightarrow \Upsilon(4S)$

- • • We do not use the following data for averages, fits, limits, etc. • • •
 $< 8.5 \times 10^{-7}$ 90 1 AUBERT,BE 05c BABR $e^+ e^- \rightarrow \Upsilon(4S)$
 $< 3.3 \times 10^{-6}$ 90 1 COAN 00 CLE2 $e^+ e^- \rightarrow \Upsilon(4S)$

- 1 Assumes equal production of B^+ and B^0 at the $\Upsilon(4S)$.

 $\Gamma(\tilde{h}_2(1270)\gamma, \tilde{h}_2 \rightarrow (KS)^0(KS)^0)/\Gamma_{\text{total}}$ Γ_{421}/Γ

VALUE	DOCUMENT ID	TECN	COMMENT
$< 3.1 \times 10^{-7}$	JEON	22	BELL $e^+ e^- \rightarrow \Upsilon(4S)$

$\Gamma(f_2'(1525)\gamma, f_2' \rightarrow (KS)^0(KS^0)^0)/\Gamma_{total}$				Γ_{422}/Γ
VALUE	DOCUMENT ID	TECN	COMMENT	
$<2.1 \times 10^{-7}$	JEON	22	BELL $e^+e^- \rightarrow \Upsilon(4S)$	

$\Gamma(\pi^+\pi^-)/\Gamma_{total}$				Γ_{423}/Γ
VALUE (units 10^{-6})	CL%	DOCUMENT ID	TECN	COMMENT
5.37±0.20 OUR FIT	Error includes scale factor of 1.3.			
5.43±0.26 OUR AVERAGE	Error includes scale factor of 1.4. See the ideogram below.			

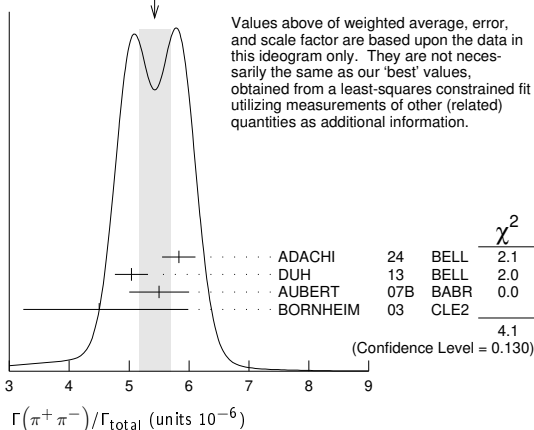
5.83±0.22±0.17		ADACHI	24	BELL	$e^+e^- \rightarrow \Upsilon(4S)$
5.04±0.21±0.18		¹ DUH	13	BELL	$e^+e^- \rightarrow \Upsilon(4S)$
5.5±0.4±0.3		¹ AUBERT	07B	BABR	$e^+e^- \rightarrow \Upsilon(4S)$
4.5±1.4±0.5		¹ BORNHEIM	03	CLE2	$e^+e^- \rightarrow \Upsilon(4S)$
4.5	-1.2	-0.4			

• • • We do not use the following data for averages, fits, limits, etc. • • •

5.1±0.2±0.2		¹ LIN	07A	BELL	Repl. by DUH 13
4.4±0.6±0.3		¹ CHAO	04	BELL	Repl. by LIN 07A
4.7±0.6±0.2		¹ AUBERT	02Q	BABR	Repl. by AUBERT 07B
5.4±1.2±0.5		¹ CASEY	02	BELL	Repl. by CHAO 04
5.6	+2.3	+0.4			
	-2.0	-0.5			
4.1±1.0±0.7		¹ AUBERT	01E	BABR	Repl. by AUBERT 02Q
< 67	90	² ABE	00C	SLD	$e^+e^- \rightarrow Z$
4.3	+1.6	±0.5			
	-1.4				
< 15	90	GODANG	98	CLE2	Repl. by CRONIN-HENNESSY 00
< 45	90	³ ADAM	96D	DLPH	$e^+e^- \rightarrow Z$
< 20	90	ASNER	96	CLE2	Repl. by GODANG 98
< 41	90	⁴ BUSKULIC	96V	ALEP	$e^+e^- \rightarrow Z$
< 55	90	⁵ ABREU	95N	DLPH	Sup. by ADAM 96D
< 47	90	⁶ AKERS	94L	OPAL	$e^+e^- \rightarrow Z$
< 29	90	¹ BATTLE	93	CLE2	$e^+e^- \rightarrow \Upsilon(4S)$
< 130	90	¹ ALBRECHT	90B	ARG	$e^+e^- \rightarrow \Upsilon(4S)$
< 77	90	⁷ BORTOLETTO	89	CLEO	$e^+e^- \rightarrow \Upsilon(4S)$
< 260	90	⁷ BEBEK	87	CLEO	$e^+e^- \rightarrow \Upsilon(4S)$
< 500	90	GILES	84	CLEO	$e^+e^- \rightarrow \Upsilon(4S)$

- Assumes equal production of B⁺ and B⁰ at the $\Upsilon(4S)$.
- ABE 00C assumes $B(Z \rightarrow b\bar{b}) = (21.7 \pm 0.1)\%$ and the B fractions $f_{B^0} = f_{B^+} = (39.7 \pm 1.8)\%$ and $f_{B_s} = (10.5 \pm 1.8)\%$.
- ADAM 96D assumes $f_{B^0} = f_{B^-} = 0.39$ and $f_{B_s} = 0.12$.
- BUSKULIC 96V assumes PDG 96 production fractions for B⁰, B⁺, B_s, b baryons.
- Assumes a B⁰, B⁻ production fraction of 0.39 and a B_s production fraction of 0.12.
- Assumes $B(Z \rightarrow b\bar{b}) = 0.217$ and $B_d^0(B_s^0)$ fraction 39.5% (12%).
- Paper assumes the $\Upsilon(4S)$ decays 43% to B⁰ \bar{B}^0 . We rescale to 50%.

WEIGHTED AVERAGE
5.43±0.26 (Error scaled by 1.4)



$\Gamma(\pi^+\pi^-)/\Gamma(K^+\pi^-)$				$\Gamma_{423}/\Gamma_{288}$
VALUE	DOCUMENT ID	TECN	COMMENT	
0.268±0.010 OUR FIT	Error includes scale factor of 1.2.			
0.261±0.015 OUR AVERAGE				

0.262±0.009±0.017	AAIJ	12AR	LHCB	pp at 7 TeV
0.259±0.017±0.016	AALTONEN	11N	CDF	$p\bar{p}$ at 1.96 TeV
0.21±0.05±0.03	ABULENCIA,A	06D	CDF	Repl. by AALTONEN 11N

• • • We do not use the following data for averages, fits, limits, etc. • • •

$\Gamma(\pi^0\pi^0)/\Gamma_{total}$				Γ_{424}/Γ
VALUE (units 10^{-6})	CL%	DOCUMENT ID	TECN	COMMENT
1.55±0.17 OUR AVERAGE	Error includes scale factor of 1.1.			
1.38±0.27±0.22		ABUDINEN	23E	BELL $e^+e^- \rightarrow \Upsilon(4S)$
1.31±0.19±0.19		¹ JULIUS	17	BELL $e^+e^- \rightarrow \Upsilon(4S)$
1.83±0.21±0.13		¹ LEES	13D	BABR $e^+e^- \rightarrow \Upsilon(4S)$

• • • We do not use the following data for averages, fits, limits, etc. • • •

1.47±0.25±0.12		¹ AUBERT	07Bc	BABR	Repl. by LEES 13D
1.17±0.32±0.10		¹ AUBERT	05L	BABR	Repl. by AUBERT 07Bc
2.3	+0.4	+0.2			
	-0.5	-0.3			
< 3.6	90	¹ CHAO	05	BELL	Repl. by JULIUS 17
2.1±0.6±0.3		¹ AUBERT	03L	BABR	$e^+e^- \rightarrow \Upsilon(4S)$
< 4.4	90	¹ AUBERT	03s	BABR	Repl. by AUBERT 05L
1.7±0.6±0.2		¹ BORNHEIM	03	CLE2	$e^+e^- \rightarrow \Upsilon(4S)$
< 5.7	90	¹ LEE	03	BELL	Repl. by CHAO 05
< 6.4	90	¹ ASNER	02	CLE2	$e^+e^- \rightarrow \Upsilon(4S)$
< 9.3	90	¹ CASEY	02	BELL	$e^+e^- \rightarrow \Upsilon(4S)$
< 9.1	90	GODANG	98	CLE2	Repl. by ASNER 02
< 60	90	ASNER	96	CLE2	Repl. by GODANG 98
		² ACCIARRI	95H	L3	$e^+e^- \rightarrow Z$

- Assumes equal production of B⁺ and B⁰ at the $\Upsilon(4S)$.
- ACCIARRI 95H assumes $f_{B^0} = 39.5 \pm 4.0$ and $f_{B_s} = 12.0 \pm 3.0\%$.

$\Gamma(\eta\pi^0)/\Gamma_{total}$				Γ_{425}/Γ
VALUE (units 10^{-6})	CL%	DOCUMENT ID	TECN	COMMENT
0.41±0.17±0.05	Error includes scale factor of 1.3.			
-0.15±0.07				
1.2	PAL	15	BELL	$e^+e^- \rightarrow \Upsilon(4S)$

• • • We do not use the following data for averages, fits, limits, etc. • • •

< 1.5	90	² AUBERT	08AH	BABR	$e^+e^- \rightarrow \Upsilon(4S)$
< 1.3	90	² AUBERT	06W	BABR	Repl. by AUBERT 08AH
< 2.5	90	² CHANG	05A	BELL	Repl. by PAL 15
< 2.5	90	² AUBERT,B	04D	BABR	Repl. by AUBERT 06W
< 2.9	90	² RICHICHI	00	CLE2	$e^+e^- \rightarrow \Upsilon(4S)$
< 8	90	BEHRENS	98	CLE2	Repl. by RICHICHI 00
< 250	90	³ ACCIARRI	95H	L3	$e^+e^- \rightarrow Z$
< 1800	90	² ALBRECHT	90B	ARG	$e^+e^- \rightarrow \Upsilon(4S)$

- PAL 15 signal significance is 3.0 standard deviations. The measurement corresponds to 90% CL upper limit of $< 6.5 \times 10^{-7}$.
- Assumes equal production of B⁺ and B⁰ at the $\Upsilon(4S)$.
- ACCIARRI 95H assumes $f_{B^0} = 39.5 \pm 4.0$ and $f_{B_s} = 12.0 \pm 3.0\%$.

$\Gamma(\eta\eta)/\Gamma_{total}$				Γ_{426}/Γ	
VALUE (units 10^{-6})	CL%	DOCUMENT ID	TECN	COMMENT	
< 1.0	90	¹ AUBERT	09AV	BABR	$e^+e^- \rightarrow \Upsilon(4S)$

• • • We do not use the following data for averages, fits, limits, etc. • • •

< 1.8	90	¹ AUBERT,B	06V	BABR	Repl. by AUBERT 09AV
< 2.0	90	¹ CHANG	05A	BELL	$e^+e^- \rightarrow \Upsilon(4S)$
< 2.8	90	¹ AUBERT,B	04X	BABR	$e^+e^- \rightarrow \Upsilon(4S)$
< 18	90	BEHRENS	98	CLE2	$e^+e^- \rightarrow \Upsilon(4S)$
< 410	90	² ACCIARRI	95H	L3	$e^+e^- \rightarrow Z$

- Assumes equal production of B⁺ and B⁰ at the $\Upsilon(4S)$.
- ACCIARRI 95H assumes $f_{B^0} = 39.5 \pm 4.0$ and $f_{B_s} = 12.0 \pm 3.0\%$.

$\Gamma(\eta'\pi^0)/\Gamma_{total}$				Γ_{427}/Γ	
VALUE (units 10^{-6})	CL%	DOCUMENT ID	TECN	COMMENT	
1.2±0.6 OUR AVERAGE	Error includes scale factor of 1.7.				
0.9±0.4±0.1		¹ AUBERT	08AH	BABR	$e^+e^- \rightarrow \Upsilon(4S)$
2.8±1.0±0.3		¹ SCHUEMANN	06	BELL	$e^+e^- \rightarrow \Upsilon(4S)$

• • • We do not use the following data for averages, fits, limits, etc. • • •

0.8	+0.8	±0.1			
	-0.6				
1.0	+1.4	±0.8			
	-1.0				
< 5.7	90	¹ AUBERT,B	06W	BABR	Repl. by AUBERT 08AH
< 11	90	¹ AUBERT,B	04D	BABR	Repl. by AUBERT 06W
< 5.7	90	¹ RICHICHI	00	CLE2	$e^+e^- \rightarrow \Upsilon(4S)$
< 11	90	BEHRENS	98	CLE2	Repl. by RICHICHI 00

- Assumes equal production of B⁺ and B⁰ at the $\Upsilon(4S)$.

$\Gamma(\eta'\eta)/\Gamma_{total}$				Γ_{428}/Γ	
VALUE (units 10^{-6})	CL%	DOCUMENT ID	TECN	COMMENT	
< 1.7	90	¹ AUBERT	09AV	BABR	$e^+e^- \rightarrow \Upsilon(4S)$

• • • We do not use the following data for averages, fits, limits, etc. • • •

< 6.5	90	¹ SCHUEMANN	07	BELL	$e^+e^- \rightarrow \Upsilon(4S)$
< 2.4	90	¹ AUBERT,B	06V	BABR	Repl. by AUBERT 09AV
< 10	90	¹ AUBERT,B	04X	BABR	Repl. by AUBERT,B 06V
< 47	90	BEHRENS	98	CLE2	$e^+e^- \rightarrow \Upsilon(4S)$

- Assumes equal production of B⁺ and B⁰ at the $\Upsilon(4S)$.

$\Gamma(\eta'\eta')/\Gamma_{total}$				Γ_{429}/Γ	
VALUE (units 10^{-6})	CL%	DOCUMENT ID	TECN	COMMENT	
< 1.2	90	¹ AUBERT	08AH	BABR	$e^+e^- \rightarrow \Upsilon(4S)$

• • • We do not use the following data for averages, fits, limits, etc. • • •

< 4.5	90	¹ SCHUEMANN	07	BELL	$e^+e^- \rightarrow \Upsilon(4S)$
< 1.7	90	¹ AUBERT	06W	BABR	Repl. by AUBERT 08AH
< 4.6	90	¹ AUBERT,B	04X	BABR	$e^+e^- \rightarrow \Upsilon(4S)$
< 27	90	BEHRENS	98	CLE2	$e^+e^- \rightarrow \Upsilon(4S)$

- Assumes equal production of B⁺ and B⁰ at the $\Upsilon(4S)$.

Meson Particle Listings

 B^0 $\Gamma(\eta' \rho^0)/\Gamma_{\text{total}}$ Γ_{430}/Γ

VALUE (units 10^{-6})	CL%	DOCUMENT ID	TECN	COMMENT
< 1.3	90	¹ SCHUEMANN 07	BELL	$e^+e^- \rightarrow \Upsilon(4S)$
••• We do not use the following data for averages, fits, limits, etc. •••				
< 2.8	90	¹ DEL-AMO-SA...10A	BABR	$e^+e^- \rightarrow \Upsilon(4S)$
< 3.7	90	AUBERT 07E	BABR	Repl. by DEL-AMO-SANCHEZ 10A
< 4.3	90	¹ AUBERT,B 04D	BABR	Repl. by AUBERT 07E
<12	90	¹ RICHICHI 00	CLE2	$e^+e^- \rightarrow \Upsilon(4S)$
<23	90	BEHRENS 98	CLE2	Repl. by RICHICHI 00
¹ Assumes equal production of B^+ and B^0 at the $\Upsilon(4S)$.				

 $\Gamma(\eta' f_0(980), f_0 \rightarrow \pi^+ \pi^-)/\Gamma_{\text{total}}$ Γ_{431}/Γ

VALUE (units 10^{-6})	CL%	DOCUMENT ID	TECN	COMMENT
<0.9	90	¹ DEL-AMO-SA...10A	BABR	$e^+e^- \rightarrow \Upsilon(4S)$
••• We do not use the following data for averages, fits, limits, etc. •••				
<1.5	90	AUBERT 07E	BABR	Repl. by DEL-AMO-SANCHEZ 10A
¹ Assumes equal production of B^+ and B^0 at the $\Upsilon(4S)$.				

 $\Gamma(\eta \rho^0)/\Gamma_{\text{total}}$ Γ_{432}/Γ

VALUE (units 10^{-6})	CL%	DOCUMENT ID	TECN	COMMENT
< 1.5	90	¹ AUBERT 07Y	BABR	$e^+e^- \rightarrow \Upsilon(4S)$
••• We do not use the following data for averages, fits, limits, etc. •••				
< 1.9	90	¹ WANG 07B	BELL	$e^+e^- \rightarrow \Upsilon(4S)$
< 1.5	90	¹ AUBERT,B 04D	BABR	Repl. by AUBERT 07Y
<10	90	¹ RICHICHI 00	CLE2	$e^+e^- \rightarrow \Upsilon(4S)$
<13	90	BEHRENS 98	CLE2	Repl. by RICHICHI 00
¹ Assumes equal production of B^+ and B^0 at the $\Upsilon(4S)$.				

 $\Gamma(\eta f_0(980), f_0 \rightarrow \pi^+ \pi^-)/\Gamma_{\text{total}}$ Γ_{433}/Γ

VALUE (units 10^{-6})	CL%	DOCUMENT ID	TECN	COMMENT
<0.4	90	¹ AUBERT 07Y	BABR	$e^+e^- \rightarrow \Upsilon(4S)$
¹ Assumes equal production of B^+ and B^0 at the $\Upsilon(4S)$.				

 $\Gamma(\omega \eta)/\Gamma_{\text{total}}$ Γ_{434}/Γ

VALUE (units 10^{-6})	CL%	DOCUMENT ID	TECN	COMMENT
$0.94 \pm 0.35 \pm 0.09$		¹ AUBERT 09AV	BABR	$e^+e^- \rightarrow \Upsilon(4S)$
••• We do not use the following data for averages, fits, limits, etc. •••				
< 1.9	90	¹ AUBERT,B 05K	BABR	Repl. by AUBERT 09AV
$4.0 \pm 1.3 \pm 0.4$		¹ AUBERT,B 04X	BABR	Repl. by AUBERT,B 05K
<12	90	¹ BERGFELD 98	CLE2	
¹ Assumes equal production of B^+ and B^0 at the $\Upsilon(4S)$.				

 $\Gamma(\omega \eta')/\Gamma_{\text{total}}$ Γ_{435}/Γ

VALUE (units 10^{-6})	CL%	DOCUMENT ID	TECN	COMMENT
$1.01 \pm 0.46 \pm 0.09$		¹ AUBERT 09AV	BABR	$e^+e^- \rightarrow \Upsilon(4S)$
••• We do not use the following data for averages, fits, limits, etc. •••				
< 2.2	90	¹ SCHUEMANN 07	BELL	$e^+e^- \rightarrow \Upsilon(4S)$
< 2.8	90	¹ AUBERT,B 04X	BABR	$e^+e^- \rightarrow \Upsilon(4S)$
<60	90	¹ BERGFELD 98	CLE2	
¹ Assumes equal production of B^+ and B^0 at the $\Upsilon(4S)$.				

 $\Gamma(\omega \rho^0)/\Gamma_{\text{total}}$ Γ_{436}/Γ

VALUE (units 10^{-6})	CL%	DOCUMENT ID	TECN	COMMENT
< 1.6	90	¹ AUBERT 09H	BABR	$e^+e^- \rightarrow \Upsilon(4S)$
••• We do not use the following data for averages, fits, limits, etc. •••				
< 1.5	90	¹ AUBERT,B 06T	BABR	Repl. by AUBERT 09H
< 3.3	90	¹ AUBERT 05O	BABR	Repl. by AUBERT,B 06T
<11	90	¹ BERGFELD 98	CLE2	
¹ Assumes equal production of B^+ and B^0 at the $\Upsilon(4S)$.				

 $\Gamma(\omega f_0(980), f_0 \rightarrow \pi^+ \pi^-)/\Gamma_{\text{total}}$ Γ_{437}/Γ

VALUE (units 10^{-6})	CL%	DOCUMENT ID	TECN	COMMENT
<1.5	90	¹ AUBERT 09H	BABR	$e^+e^- \rightarrow \Upsilon(4S)$
••• We do not use the following data for averages, fits, limits, etc. •••				
<1.5	90	¹ AUBERT,B 06T	BABR	Repl. by AUBERT 09H
¹ Assumes equal production of B^+ and B^0 at the $\Upsilon(4S)$.				

 $\Gamma(\omega \omega)/\Gamma_{\text{total}}$ Γ_{438}/Γ

VALUE (units 10^{-6})	CL%	DOCUMENT ID	TECN	COMMENT
$1.2 \pm 0.3 \pm 0.3$		¹ LEES 14	BABR	$e^+e^- \rightarrow \Upsilon(4S)$
••• We do not use the following data for averages, fits, limits, etc. •••				
< 4.0	90	¹ AUBERT,B 06T	BABR	Repl. by LEES 14
<19	90	¹ BERGFELD 98	CLE2	
¹ Assumes equal production of B^+ and B^0 at the $\Upsilon(4S)$.				

 $\Gamma(\phi \pi^0)/\Gamma_{\text{total}}$ Γ_{439}/Γ

VALUE (units 10^{-6})	CL%	DOCUMENT ID	TECN	COMMENT
<0.15	90	¹ KIM 12A	BELL	$e^+e^- \rightarrow \Upsilon(4S)$
••• We do not use the following data for averages, fits, limits, etc. •••				
<0.28	90	¹ AUBERT,B 06c	BABR	$e^+e^- \rightarrow \Upsilon(4S)$
<1.0	90	¹ AUBERT,B 04D	BABR	Repl. by AUBERT,B 06c
<5	90	¹ BERGFELD 98	CLE2	
¹ Assumes equal production of B^+ and B^0 at the $\Upsilon(4S)$.				

 $\Gamma(\phi \eta)/\Gamma_{\text{total}}$ Γ_{440}/Γ

VALUE (units 10^{-6})	CL%	DOCUMENT ID	TECN	COMMENT
<0.5	90	¹ AUBERT 09AV	BABR	$e^+e^- \rightarrow \Upsilon(4S)$
••• We do not use the following data for averages, fits, limits, etc. •••				
<0.6	90	¹ AUBERT,B 06V	BABR	Repl. by AUBERT 09AV
<1.0	90	¹ AUBERT,B 04X	BABR	Repl. by AUBERT,B 06V
<9	90	¹ BERGFELD 98	CLE2	
¹ Assumes equal production of B^+ and B^0 at the $\Upsilon(4S)$.				

 $\Gamma(\phi \eta')/\Gamma_{\text{total}}$ Γ_{441}/Γ

VALUE (units 10^{-6})	CL%	DOCUMENT ID	TECN	COMMENT
< 0.5	90	¹ SCHUEMANN 07	BELL	$e^+e^- \rightarrow \Upsilon(4S)$
••• We do not use the following data for averages, fits, limits, etc. •••				
< 1.1	90	¹ AUBERT 09AV	BABR	$e^+e^- \rightarrow \Upsilon(4S)$
< 1.0	90	¹ AUBERT,B 06V	BABR	Repl. by AUBERT 09AV
< 4.5	90	¹ AUBERT,B 04X	BABR	Repl. by AUBERT,B 06V
<31	90	¹ BERGFELD 98	CLE2	
¹ Assumes equal production of B^+ and B^0 at the $\Upsilon(4S)$.				

 $\Gamma(\phi \pi^+ \pi^-)/\Gamma_{\text{total}}$ Γ_{442}/Γ

VALUE (units 10^{-7})	DOCUMENT ID	TECN	COMMENT
$1.82 \pm 0.25 \pm 0.43$	¹ AAIJ 17A	LHCb	pp at 7, 8 TeV
¹ Signal evidence is 4.5 standard deviations.			

 $\Gamma(\phi \rho^0)/\Gamma_{\text{total}}$ Γ_{443}/Γ

VALUE (units 10^{-6})	CL%	DOCUMENT ID	TECN	COMMENT
< 0.33	90	¹ AUBERT 08Bk	BABR	$e^+e^- \rightarrow \Upsilon(4S)$
••• We do not use the following data for averages, fits, limits, etc. •••				
<156	90	² ABE 00c	SLD	$e^+e^- \rightarrow Z$
< 13	90	¹ BERGFELD 98	CLE2	
¹ Assumes equal production of B^+ and B^0 at the $\Upsilon(4S)$.				
² ABE 00c assumes $B(Z \rightarrow b\bar{b}) = (21.7 \pm 0.1)\%$ and the B fractions $f_{B^0} = f_{B^+} = (39.7 \pm 1.8, 2.2)\%$ and $f_{B_s} = (10.5 \pm 1.8, -2.2)\%$.				

 $\Gamma(\phi f_0(980), f_0 \rightarrow \pi^+ \pi^-)/\Gamma_{\text{total}}$ Γ_{444}/Γ

VALUE (units 10^{-6})	CL%	DOCUMENT ID	TECN	COMMENT
<0.38	90	¹ AUBERT 08Bk	BABR	$e^+e^- \rightarrow \Upsilon(4S)$
¹ Assumes equal production of B^+ and B^0 at the $\Upsilon(4S)$.				

 $\Gamma(\phi \omega)/\Gamma_{\text{total}}$ Γ_{445}/Γ

VALUE (units 10^{-6})	CL%	DOCUMENT ID	TECN	COMMENT
< 0.7	90	¹ LEES 14	BABR	$e^+e^- \rightarrow \Upsilon(4S)$
••• We do not use the following data for averages, fits, limits, etc. •••				
< 1.2	90	¹ AUBERT,B 06T	BABR	Repl. by LEES 14
<21	90	¹ BERGFELD 98	CLE2	
¹ Assumes equal production of B^+ and B^0 at the $\Upsilon(4S)$.				

 $\Gamma(\phi \phi)/\Gamma_{\text{total}}$ Γ_{446}/Γ

VALUE	CL%	DOCUMENT ID	TECN	COMMENT
< 2.7×10^{-8}	90	AAIJ 19AP	LHCb	pp at 7, 8 and 13 TeV
••• We do not use the following data for averages, fits, limits, etc. •••				
< 2.8×10^{-8}	90	AAIJ 15AS	LHCb	Repl. by AAJJ 19AP
< 2×10^{-7}	90	¹ AUBERT 08Bk	BABR	$e^+e^- \rightarrow \Upsilon(4S)$
< 1.5×10^{-6}	90	¹ AUBERT,B 04X	BABR	Repl. by AUBERT 08Bk
< 3.21×10^{-4}	90	² ABE 00c	SLD	$e^+e^- \rightarrow Z$
< 1.2×10^{-5}	90	¹ BERGFELD 98	CLE2	
< 3.9×10^{-5}	90	ASNER 96	CLE2	$e^+e^- \rightarrow \Upsilon(4S)$
¹ Assumes equal production of B^+ and B^0 at the $\Upsilon(4S)$.				
² ABE 00c assumes $B(Z \rightarrow b\bar{b}) = (21.7 \pm 0.1)\%$ and the B fractions $f_{B^0} = f_{B^+} = (39.7 \pm 1.8, 2.2)\%$ and $f_{B_s} = (10.5 \pm 1.8, -2.2)\%$.				

 $\Gamma(a_0(980) \pm \pi^\mp, a_0^\pm \rightarrow \eta \pi^\pm)/\Gamma_{\text{total}}$ Γ_{447}/Γ

VALUE (units 10^{-6})	CL%	DOCUMENT ID	TECN	COMMENT
<3.1	90	¹ AUBERT 07Y	BABR	$e^+e^- \rightarrow \Upsilon(4S)$
••• We do not use the following data for averages, fits, limits, etc. •••				
<5.1	90	¹ AUBERT,BE 04	BABR	Repl. by AUBERT 07Y
¹ Assumes equal production of B^+ and B^0 at the $\Upsilon(4S)$.				

$\Gamma(a_0(1450)^\pm \pi^\mp, a_0^\pm \rightarrow \eta \pi^\pm)/\Gamma_{\text{total}}$ Γ_{448}/Γ

VALUE (units 10^{-6})	CL%	DOCUMENT ID	TECN	COMMENT
< 2.3	90	¹ AUBERT 07Y BABR		$e^+e^- \rightarrow \Upsilon(4S)$

¹ Assumes equal production of B^+ and B^0 at the $\Upsilon(4S)$.

 $\Gamma(\pi^+ \pi^- \pi^0)/\Gamma_{\text{total}}$ Γ_{449}/Γ

VALUE	CL%	DOCUMENT ID	TECN	COMMENT
$< 7.2 \times 10^{-4}$	90	¹ ALBRECHT 90B ARG		$e^+e^- \rightarrow \Upsilon(4S)$

¹ ALBRECHT 90B limit assumes equal production of $B^0 \bar{B}^0$ and $B^+ B^-$ at $\Upsilon(4S)$.

 $\Gamma(\rho^0 \pi^0)/\Gamma_{\text{total}}$ Γ_{450}/Γ

VALUE (units 10^{-6})	CL%	DOCUMENT ID	TECN	COMMENT
2.0 ± 0.5 OUR AVERAGE				
$3.0 \pm 0.5 \pm 0.7$		^{1,2} KUSAKA 08 BELL		$e^+e^- \rightarrow \Upsilon(4S)$
$1.4 \pm 0.6 \pm 0.3$		¹ AUBERT 04Z BABR		$e^+e^- \rightarrow \Upsilon(4S)$
$1.6 \pm 2.0 \pm 0.8$		¹ JESSOP 00 CLEO		$e^+e^- \rightarrow \Upsilon(4S)$
$3.12 \pm 0.88 \pm 0.60$		¹ DRAGIC 06 BELL		Repl. by KUSAKA 08
$5.1 \pm 1.6 \pm 0.9$		¹ DRAGIC 04 BELL		Repl. by DRAGIC 06
< 5.3	90	¹ GORDON 02 BELL		Repl. by DRAGIC 04
< 24	90	ASNER 96 CLEO		Repl. by JESSOP 00
< 400	90	¹ ALBRECHT 90B ARG		$e^+e^- \rightarrow \Upsilon(4S)$

¹ Assumes equal production of B^+ and B^0 at the $\Upsilon(4S)$.
² This is the first measurement that excludes contributions from $\rho(1450)$ and $\rho(1570)$ resonances.

 $\Gamma(\rho^\mp \pi^\pm)/\Gamma_{\text{total}}$ Γ_{451}/Γ

VALUE (units 10^{-6})	CL%	DOCUMENT ID	TECN	COMMENT
23.0 ± 2.3 OUR AVERAGE				
$22.6 \pm 1.1 \pm 4.4$		^{1,2} KUSAKA 08 BELL		$e^+e^- \rightarrow \Upsilon(4S)$
$22.6 \pm 1.8 \pm 2.2$		¹ AUBERT 03T BABR		$e^+e^- \rightarrow \Upsilon(4S)$
$27.6 \pm 8.4 \pm 4.2$		¹ JESSOP 00 CLE2		$e^+e^- \rightarrow \Upsilon(4S)$
$20.8 \pm 6.0 \pm 2.8$		¹ GORDON 02 BELL		Repl. by KUSAKA 08
< 88	90	ASNER 96 CLE2		Repl. by JESSOP 00
< 520	90	¹ ALBRECHT 90B ARG		$e^+e^- \rightarrow \Upsilon(4S)$
< 5200	90	³ BEBEK 87 CLEO		$e^+e^- \rightarrow \Upsilon(4S)$

¹ Assumes equal production of B^+ and B^0 at the $\Upsilon(4S)$.
² This is the first measurement that excludes contributions from $\rho(1450)$ and $\rho(1570)$ resonances.
³ BEBEK 87 reports $< 6.1 \times 10^{-3}$ assuming the $\Upsilon(4S)$ decays 43% to $B^0 \bar{B}^0$. We rescale to 50%.

 $\Gamma(\pi^+ \pi^- \pi^+ \pi^-)/\Gamma_{\text{total}}$ Γ_{452}/Γ

VALUE	CL%	DOCUMENT ID	TECN	COMMENT
$< 11.2 \times 10^{-6}$	90	¹ VANHOEFER 14 BELL		$e^+e^- \rightarrow \Upsilon(4S)$
$< 23.1 \times 10^{-6}$	90	¹ AUBERT 08BB BABR		$e^+e^- \rightarrow \Upsilon(4S)$
$< 19.3 \times 10^{-6}$	90	¹ CHIANG 08 BELL		Repl. by VANHOEFER 14
$< 2.3 \times 10^{-4}$	90	² ADAM 96D DLPH		$e^+e^- \rightarrow Z$
$< 2.8 \times 10^{-4}$	90	³ ABREU 95N DLPH		Sup. by ADAM 96D
$< 6.7 \times 10^{-4}$	90	¹ ALBRECHT 90B ARG		$e^+e^- \rightarrow \Upsilon(4S)$

¹ Assumes equal production of B^+ and B^0 at the $\Upsilon(4S)$.
² ADAM 96D assumes $f_{B^0} = f_{B^-} = 0.39$ and $f_{B_s} = 0.12$.
³ Assumes a B^0, B^- production fraction of 0.39 and a B_s production fraction of 0.12.

 $\Gamma(\rho^0 \pi^+ \pi^-)/\Gamma_{\text{total}}$ Γ_{453}/Γ

VALUE (units 10^{-6})	CL%	DOCUMENT ID	TECN	COMMENT
< 8.8	90	¹ AUBERT 08BB BABR		$e^+e^- \rightarrow \Upsilon(4S)$
< 12.0	90	¹ VANHOEFER 14 BELL		$e^+e^- \rightarrow \Upsilon(4S)$
< 12.0	90	¹ CHIANG 08 BELL		Repl. by VANHOEFER 14

¹ Assumes equal production of B^+ and B^0 at the $\Upsilon(4S)$.

 $\Gamma(\rho^0 \rho^0)/\Gamma_{\text{total}}$ Γ_{454}/Γ

VALUE (units 10^{-6})	CL%	DOCUMENT ID	TECN	COMMENT
0.96 ± 0.15 OUR FIT				
0.97 ± 0.24 OUR AVERAGE				
$1.02 \pm 0.30 \pm 0.15$		^{1,2} VANHOEFER 14 BELL		$e^+e^- \rightarrow \Upsilon(4S)$
$0.92 \pm 0.32 \pm 0.14$		² AUBERT 08BB BABR		$e^+e^- \rightarrow \Upsilon(4S)$
$0.4 \pm 0.4 \pm 0.2$		² CHIANG 08 BELL		Repl. by VANHOEFER 14
$1.07 \pm 0.33 \pm 0.19$		² AUBERT 07G BABR		Repl. by AUBERT 08BB
< 1.1	90	² AUBERT 05I BABR		Repl. by AUBERT 07G
< 2.1	90	² AUBERT 03V BABR		Repl. by AUBERT 05I
< 18	90	³ GODANG 02 CLE2		$e^+e^- \rightarrow \Upsilon(4S)$
< 136	90	⁴ ABE 00C SLD		$e^+e^- \rightarrow Z$
< 280	90	² ALBRECHT 90B ARG		$e^+e^- \rightarrow \Upsilon(4S)$
< 290	90	⁵ BORTOLETTO89 CLEO		$e^+e^- \rightarrow \Upsilon(4S)$
< 430	90	⁵ BEBEK 87 CLEO		$e^+e^- \rightarrow \Upsilon(4S)$

¹ Signal significance 3.4 standard deviations.

² Assumes equal production of B^+ and B^0 at the $\Upsilon(4S)$.

³ Assumes a helicity 00 configuration. For a helicity 11 configuration, the limit decreases to 1.4×10^{-5} .

⁴ ABE 00C assumes $B(Z \rightarrow b\bar{b}) = (21.7 \pm 0.1)\%$ and the B fractions $f_{B^0} = f_{B^+} = (39.7 \pm 1.8)\%$ and $f_{B_s} = (10.5 \pm 1.8)\%$.

⁵ Paper assumes the $\Upsilon(4S)$ decays 43% to $B^0 \bar{B}^0$. We rescale to 50%.

 $\Gamma(\rho^0 \rho^0)/\Gamma(K^*(892)^0 \phi)$ $\Gamma_{454}/\Gamma_{377}$

VALUE (units 10^{-2})	DOCUMENT ID	TECN	COMMENT
9.5 ± 1.5 OUR FIT			
$9.4 \pm 1.7 \pm 0.9$	AAIJ 15T LHCB		pp at 7, 8 TeV

 $\Gamma(f_0(980) \pi^+ \pi^-, f_0 \rightarrow \pi^+ \pi^-)/\Gamma_{\text{total}}$ Γ_{455}/Γ

VALUE	CL%	DOCUMENT ID	TECN	COMMENT
$< 3.0 \times 10^{-6}$	90	¹ VANHOEFER 14 BELL		$e^+e^- \rightarrow \Upsilon(4S)$
$< 3.8 \times 10^{-6}$	90	¹ CHIANG 08 BELL		$e^+e^- \rightarrow \Upsilon(4S)$

¹ We do not use the following data for averages, fits, limits, etc. $\bullet \bullet \bullet$

¹ Assumes equal production of B^+ and B^0 at the $\Upsilon(4S)$.

 $\Gamma(\rho^0 f_0(980), f_0 \rightarrow \pi^+ \pi^-)/\Gamma_{\text{total}}$ Γ_{456}/Γ

VALUE (units 10^{-7})	CL%	DOCUMENT ID	TECN	COMMENT
$7.8 \pm 2.2 \pm 1.1$		^{1,2} VANHOEFER 14 BELL		$e^+e^- \rightarrow \Upsilon(4S)$
< 8.1	90	AAIJ 15T LHCB		pp at 7, 8 TeV
< 4.0	90	² AUBERT 08BB BABR		$e^+e^- \rightarrow \Upsilon(4S)$
< 3	90	² CHIANG 08 BELL		Repl. by VANHOEFER 14
< 5.3	90	² AUBERT 07G BABR		Repl. by AUBERT 08BB

¹ Signal significance of 3.1 standard deviations.
² Assumes equal production of B^+ and B^0 at the $\Upsilon(4S)$.

 $\Gamma(f_0(980) f_0(980), f_0 \rightarrow \pi^+ \pi^-, f_0 \rightarrow \pi^+ \pi^-)/\Gamma_{\text{total}}$ Γ_{457}/Γ

VALUE (units 10^{-6})	CL%	DOCUMENT ID	TECN	COMMENT
< 0.19	90	¹ AUBERT 08BB BABR		$e^+e^- \rightarrow \Upsilon(4S)$
< 0.2	90	¹ VANHOEFER 14 BELL		$e^+e^- \rightarrow \Upsilon(4S)$
< 0.1	90	¹ CHIANG 08 BELL		Repl. by VANHOEFER 14
< 0.16	90	¹ AUBERT 07G BABR		Repl. by AUBERT 08BB

¹ Assumes equal production of B^+ and B^0 at the $\Upsilon(4S)$.

 $\Gamma(f_0(980) f_0(980), f_0 \rightarrow \pi^+ \pi^-, f_0 \rightarrow K^+ K^-)/\Gamma_{\text{total}}$ Γ_{458}/Γ

VALUE (units 10^{-6})	CL%	DOCUMENT ID	TECN	COMMENT
< 0.23	90	¹ AUBERT 08BK BABR		$e^+e^- \rightarrow \Upsilon(4S)$

¹ Assumes equal production of B^+ and B^0 at the $\Upsilon(4S)$.

 $\Gamma(a_1(1260)^\mp \pi^\pm)/\Gamma_{\text{total}}$ Γ_{459}/Γ

VALUE (units 10^{-6})	CL%	DOCUMENT ID	TECN	COMMENT
26 ± 5 OUR AVERAGE				Error includes scale factor of 1.9.
$22.2 \pm 2.0 \pm 2.8$		^{1,2} DALSENO 12 BELL		$e^+e^- \rightarrow \Upsilon(4S)$
$33.2 \pm 3.8 \pm 3.0$		^{2,3} AUBERT 06V BABR		$e^+e^- \rightarrow \Upsilon(4S)$
< 630	90	² ALBRECHT 90B ARG		$e^+e^- \rightarrow \Upsilon(4S)$
< 490	90	⁴ BORTOLETTO89 CLEO		$e^+e^- \rightarrow \Upsilon(4S)$
< 1000	90	⁴ BEBEK 87 CLEO		$e^+e^- \rightarrow \Upsilon(4S)$

¹ DALSENO 12 reports $B(B^0 \rightarrow a_1^\pm \pi^\mp) B(a_1^\pm \rightarrow \pi^\pm \pi^+ \pi^-) = (11.1 \pm 1.0 \pm 1.4) \times 10^{-6}$ which we rescaled assuming $a_1(1260)$ decays only to 3π and $B(a_1^\pm \rightarrow \pi^\pm \pi^+ \pi^-) = 0.5$.
² Assumes equal production of B^+ and B^0 at the $\Upsilon(4S)$.
³ Assumes $a_1(1260)$ decays only to 3π and $B(a_1^\pm \rightarrow \pi^\pm \pi^+ \pi^-) = 0.5$.
⁴ Paper assumes the $\Upsilon(4S)$ decays 43% to $B^0 \bar{B}^0$. We rescale to 50%.

 $\Gamma(a_2(1320)^\mp \pi^\pm)/\Gamma_{\text{total}}$ Γ_{460}/Γ

VALUE	CL%	DOCUMENT ID	TECN	COMMENT
$< 6.3 \times 10^{-6}$	90	¹ DALSENO 12 BELL		$e^+e^- \rightarrow \Upsilon(4S)$
$< 3.0 \times 10^{-4}$	90	² BORTOLETTO89 CLEO		$e^+e^- \rightarrow \Upsilon(4S)$
$< 1.4 \times 10^{-3}$	90	² BEBEK 87 CLEO		$e^+e^- \rightarrow \Upsilon(4S)$

¹ DALSENO 12 reports $B(B^0 \rightarrow a_2^\pm \pi^\mp) B(a_2^\pm \rightarrow \pi^\pm \pi^+ \pi^-) < 2.2 \times 10^{-6}$ which we rescaled using $B(a_2^\pm \rightarrow \pi^\pm \pi^+ \pi^-) = 1/2 B(a_2^\pm \rightarrow 3\pi) = 0.35 \pm 0.013$.
² Paper assumes the $\Upsilon(4S)$ decays 43% to $B^0 \bar{B}^0$. We rescale to 50%.

 $\Gamma(\pi^+ \pi^- \pi^0 \pi^0)/\Gamma_{\text{total}}$ Γ_{461}/Γ

VALUE	CL%	DOCUMENT ID	TECN	COMMENT
$< 3.1 \times 10^{-3}$	90	¹ ALBRECHT 90B ARG		$e^+e^- \rightarrow \Upsilon(4S)$

¹ ALBRECHT 90B limit assumes equal production of $B^0 \bar{B}^0$ and $B^+ B^-$ at $\Upsilon(4S)$.

Meson Particle Listings

 B^0 $\Gamma(\rho^+\rho^-)/\Gamma_{\text{total}}$ Γ_{462}/Γ

VALUE (units 10^{-6})	CL%	DOCUMENT ID	TECN	COMMENT
27.7±1.9 OUR AVERAGE				
28.3±1.5±1.5		¹ VANHOFER 16	BELL	$e^+e^- \rightarrow \Upsilon(4S)$
25.5±2.1± $\frac{3.6}{-3.9}$		¹ AUBERT 07Bf	BABR	$e^+e^- \rightarrow \Upsilon(4S)$
• • • We do not use the following data for averages, fits, limits, etc. • • •				
22.8±3.8± $\frac{2.3}{-2.6}$		¹ SOMOV 06	BELL	Repl. by VANHOFER 16
25 $\frac{+7}{-6}$ $\frac{+5}{-6}$		¹ AUBERT 04G	BABR	Repl. by AUBERT,B 04R
30 ±4 ±5		^{1,2} AUBERT,B	04R	BABR Repl. by AUBERT 07Bf
<2200	90	¹ ALBRECHT 90B	ARG	$e^+e^- \rightarrow \Upsilon(4S)$

- ¹ Assumes equal production of B^+ and B^0 at the $\Upsilon(4S)$.
² The quoted result is obtained after combining with AUBERT 04G result by AUBERT 04R alone gives $(33 \pm 4 \pm 5) \times 10^{-6}$.

 $\Gamma(a_1(1260)^0\pi^0)/\Gamma_{\text{total}}$ Γ_{463}/Γ

VALUE	CL%	DOCUMENT ID	TECN	COMMENT
<1.1 × 10⁻³	90	¹ ALBRECHT 90B	ARG	$e^+e^- \rightarrow \Upsilon(4S)$

- ¹ ALBRECHT 90B limit assumes equal production of $B^0\bar{B}^0$ and B^+B^- at $\Upsilon(4S)$.

 $\Gamma(\omega\pi^0)/\Gamma_{\text{total}}$ Γ_{464}/Γ

VALUE (units 10^{-6})	CL%	DOCUMENT ID	TECN	COMMENT
< 0.5	90	¹ AUBERT 08AH	BABR	$e^+e^- \rightarrow \Upsilon(4S)$
• • • We do not use the following data for averages, fits, limits, etc. • • •				
< 2.0	90	¹ JEN 06	BELL	$e^+e^- \rightarrow \Upsilon(4S)$
< 1.2	90	¹ AUBERT,B 04D	BABR	Repl. by AUBERT 08AH
< 1.9	90	¹ WANG 04A	BELL	$e^+e^- \rightarrow \Upsilon(4S)$
< 3	90	¹ AUBERT 01G	BABR	$e^+e^- \rightarrow \Upsilon(4S)$
< 5.5	90	¹ JESSOP 00	CLE2	$e^+e^- \rightarrow \Upsilon(4S)$
< 14	90	¹ BERGFELD 98	CLE2	Repl. by JESSOP 00
<460	90	² ALBRECHT 90B	ARG	$e^+e^- \rightarrow \Upsilon(4S)$

- ¹ Assumes equal production of B^+ and B^0 at the $\Upsilon(4S)$.
² ALBRECHT 90B limit assumes equal production of $B^0\bar{B}^0$ and B^+B^- at $\Upsilon(4S)$.

 $\Gamma(\pi^+\pi^+\pi^-\pi^-\pi^0)/\Gamma_{\text{total}}$ Γ_{465}/Γ

VALUE	CL%	DOCUMENT ID	TECN	COMMENT
<9.0 × 10⁻³	90	¹ ALBRECHT 90B	ARG	$e^+e^- \rightarrow \Upsilon(4S)$

- ¹ ALBRECHT 90B limit assumes equal production of $B^0\bar{B}^0$ and B^+B^- at $\Upsilon(4S)$.

 $\Gamma(a_1(1260)^+\rho^-)/\Gamma_{\text{total}}$ Γ_{466}/Γ

VALUE (units 10^{-6})	CL%	DOCUMENT ID	TECN	COMMENT
< 61	90	^{1,2} AUBERT,B 06o	BABR	$e^+e^- \rightarrow \Upsilon(4S)$
• • • We do not use the following data for averages, fits, limits, etc. • • •				
<3400	90	¹ ALBRECHT 90B	ARG	$e^+e^- \rightarrow \Upsilon(4S)$

- ¹ Assumes equal production of B^+ and B^0 at the $\Upsilon(4S)$.
² Assumes $a_1(1260)$ decays only to 3π and $B(a_1^\pm \rightarrow \pi^\pm\pi^\mp\pi^\pm) = 0.5$.

 $\Gamma(a_1(1260)^0\rho^0)/\Gamma_{\text{total}}$ Γ_{467}/Γ

VALUE	CL%	DOCUMENT ID	TECN	COMMENT
<2.4 × 10⁻³	90	¹ ALBRECHT 90B	ARG	$e^+e^- \rightarrow \Upsilon(4S)$

- ¹ ALBRECHT 90B limit assumes equal production of $B^0\bar{B}^0$ and B^+B^- at $\Upsilon(4S)$.

 $\Gamma(b_1^-\pi^\pm, b_1^-\pi^\mp \rightarrow \omega\pi^\mp)/\Gamma_{\text{total}}$ Γ_{468}/Γ

VALUE (units 10^{-6})	CL%	DOCUMENT ID	TECN	COMMENT
10.9±1.2±0.9		¹ AUBERT 07Bi	BABR	$e^+e^- \rightarrow \Upsilon(4S)$

- ¹ Assumes equal production of B^+ and B^0 at the $\Upsilon(4S)$.

 $\Gamma(b_1^0\pi^0, b_1^0 \rightarrow \omega\pi^0)/\Gamma_{\text{total}}$ Γ_{469}/Γ

VALUE (units 10^{-6})	CL%	DOCUMENT ID	TECN	COMMENT
<1.9	90	¹ AUBERT 08AG	BABR	$e^+e^- \rightarrow \Upsilon(4S)$

- ¹ Assumes equal production of B^+ and B^0 at the $\Upsilon(4S)$.

 $\Gamma(b_1^-\rho^+, b_1^-\rho^- \rightarrow \omega\pi^-)/\Gamma_{\text{total}}$ Γ_{470}/Γ

VALUE	CL%	DOCUMENT ID	TECN	COMMENT
<1.4 × 10⁻⁶	90	¹ AUBERT 09AF	BABR	$e^+e^- \rightarrow \Upsilon(4S)$

- ¹ Assumes equal production of B^+ and B^0 at the $\Upsilon(4S)$.

 $\Gamma(b_1^0\rho^0, b_1^0 \rightarrow \omega\pi^0)/\Gamma_{\text{total}}$ Γ_{471}/Γ

VALUE	CL%	DOCUMENT ID	TECN	COMMENT
<3.4 × 10⁻⁶	90	¹ AUBERT 09AF	BABR	$e^+e^- \rightarrow \Upsilon(4S)$

- ¹ Assumes equal production of B^+ and B^0 at the $\Upsilon(4S)$.

 $\Gamma(\pi^+\pi^+\pi^+\pi^-\pi^-\pi^0)/\Gamma_{\text{total}}$ Γ_{472}/Γ

VALUE	CL%	DOCUMENT ID	TECN	COMMENT
<3.0 × 10⁻³	90	¹ ALBRECHT 90B	ARG	$e^+e^- \rightarrow \Upsilon(4S)$

- ¹ ALBRECHT 90B limit assumes equal production of $B^0\bar{B}^0$ and B^+B^- at $\Upsilon(4S)$.

 $\Gamma(a_1(1260)^+a_1(1260)^-, a_1^\pm \rightarrow 2\pi^+\pi^-, a_1^\mp \rightarrow 2\pi^-\pi^+)/\Gamma_{\text{total}}$ Γ_{473}/Γ

VALUE (units 10^{-6})	CL%	DOCUMENT ID	TECN	COMMENT
11.8±2.6±1.6		¹ AUBERT 09AL	BABR	$e^+e^- \rightarrow \Upsilon(4S)$
• • • We do not use the following data for averages, fits, limits, etc. • • •				
<6000	90	¹ ALBRECHT 90B	ARG	$e^+e^- \rightarrow \Upsilon(4S)$
<2800	90	² BORTOLETTO89	CLEO	$e^+e^- \rightarrow \Upsilon(4S)$

- ¹ Assumes equal production of $B^0\bar{B}^0$ and B^+B^- at $\Upsilon(4S)$.
² BORTOLETTO 89 reports $< 3.2 \times 10^{-3}$ assuming the $\Upsilon(4S)$ decays 43% to $B^0\bar{B}^0$. We rescale to 50%.

 $\Gamma(\pi^+\pi^+\pi^+\pi^-\pi^-\pi^0)/\Gamma_{\text{total}}$ Γ_{474}/Γ

VALUE	CL%	DOCUMENT ID	TECN	COMMENT
<1.1 × 10⁻²	90	¹ ALBRECHT 90B	ARG	$e^+e^- \rightarrow \Upsilon(4S)$

- ¹ ALBRECHT 90B limit assumes equal production of $B^0\bar{B}^0$ and B^+B^- at $\Upsilon(4S)$.

 $\Gamma(\rho\bar{\rho})/\Gamma_{\text{total}}$ Γ_{475}/Γ

VALUE (units 10^{-8})	CL%	DOCUMENT ID	TECN	COMMENT
1.27±0.13±0.06		¹ AAIJ 23T	LHCB	pp at 7, 8 and 13 TeV
• • • We do not use the following data for averages, fits, limits, etc. • • •				
1.25±0.27±0.18		¹ AAIJ 17Bj	LHCB	Repl. by AAJ 23T
1.47 $\frac{+0.62}{-0.51}$ $\frac{+0.35}{-0.14}$		² AAIJ 13BQ	LHCB	Repl. by AAJ 17Bj
< 11	90	³ TSAI 07	BELL	$e^+e^- \rightarrow \Upsilon(4S)$
< 41	90	³ CHANG 05	BELL	$e^+e^- \rightarrow \Upsilon(4S)$
< 27	90	³ AUBERT 04U	BABR	$e^+e^- \rightarrow \Upsilon(4S)$
< 140	90	³ BORNHEIM 03	CLE2	$e^+e^- \rightarrow \Upsilon(4S)$
< 120	90	³ ABE 02o	BELL	$e^+e^- \rightarrow \Upsilon(4S)$
< 700	90	³ COAN 99	CLE2	$e^+e^- \rightarrow \Upsilon(4S)$
< 1800	90	⁴ BUSKULIC 96v	ALEP	$e^+e^- \rightarrow Z$
<35000	90	⁵ ABREU 95N	DLPH	Sup. by ADAM 96D
< 3400	90	⁶ BORTOLETTO89	CLEO	$e^+e^- \rightarrow \Upsilon(4S)$
<12000	90	⁷ ALBRECHT 88F	ARG	$e^+e^- \rightarrow \Upsilon(4S)$
<17000	90	⁶ BEBEK 87	CLEO	$e^+e^- \rightarrow \Upsilon(4S)$

- ¹ Uses normalization mode $B(B^0 \rightarrow K^+\pi^-) = (19.6 \pm 0.5) \times 10^{-6}$.
² Uses normalization mode $B(B^0 \rightarrow K^+\pi^-) = (19.55 \pm 0.54) \times 10^{-6}$.
³ Assumes equal production of B^+ and B^0 at the $\Upsilon(4S)$.
⁴ BUSKULIC 96v assumes PDG 96 production fractions for B^0, B^+, B_s, b baryons.
⁵ Assumes a B^0, B^- production fraction of 0.39 and a B_s production fraction of 0.12.
⁶ Paper assumes the $\Upsilon(4S)$ decays 43% to $B^0\bar{B}^0$. We rescale to 50%.
⁷ ALBRECHT 88F reports $< 1.3 \times 10^{-4}$ assuming the $\Upsilon(4S)$ decays 45% to $B^0\bar{B}^0$. We rescale to 50%.

 $\Gamma(\rho\bar{\rho}\pi^+\pi^-)/\Gamma_{\text{total}}$ Γ_{476}/Γ

VALUE (units 10^{-6})	CL%	DOCUMENT ID	TECN	COMMENT
2.87±0.15±0.11		^{1,2} AAIJ 17Bd	LHCB	pp at 7, 8 TeV
• • • We do not use the following data for averages, fits, limits, etc. • • •				
0.83±0.17±0.17		³ CHU 20	BELL	$e^+e^- \rightarrow \Upsilon(4S)$
<950	90	⁴ ABREU 95N	DLPH	Sup. by ADAM 96D
<250	90	⁵ BEBEK 89	CLEO	$e^+e^- \rightarrow \Upsilon(4S)$
540 ±180 ±200		⁶ ALBRECHT 88F	ARG	$e^+e^- \rightarrow \Upsilon(4S)$

- ¹ AAJ 17Bd reports $[\Gamma(B^0 \rightarrow \rho\bar{\rho}\pi^+\pi^-)/\Gamma_{\text{total}}] / [B(B^0 \rightarrow J/\psi(1S)K^*(892)^0)] / [B(J/\psi(1S) \rightarrow p\bar{p})] / [B(K^*(892) \rightarrow (K\pi)^\pm)] = 1.07 \pm 0.04 \pm 0.04$ which we multiply by our best values $B(B^0 \rightarrow J/\psi(1S)K^*(892)^0) = (1.27 \pm 0.05) \times 10^{-3}$, $B(J/\psi(1S) \rightarrow p\bar{p}) = (2.120 \pm 0.029) \times 10^{-3}$, $B(K^*(892) \rightarrow (K\pi)^\pm) = (99.902 \pm 0.009) \times 10^{-2}$. Our first error is their experiment's error and our second error is the systematic error from using our best values.
² The branching ratio is given for $m_{\rho\bar{\rho}} < 2.85$ GeV.
³ Assumes equal production of B^0 and B^+ from $\Upsilon(4S)$ decays. This measurement is quoted for $M(\pi^+\pi^-) < 1.22$ GeV excluding the $0.46 < M(\pi^+\pi^-) < 0.53$ GeV region.
⁴ Assumes a B^0, B^- production fraction of 0.39 and a B_s production fraction of 0.12.
⁵ BEBEK 89 reports $< 2.9 \times 10^{-4}$ assuming the $\Upsilon(4S)$ decays 43% to $B^0\bar{B}^0$. We rescale to 50%.
⁶ ALBRECHT 88F reports $6.0 \pm 2.0 \pm 2.2$ assuming the $\Upsilon(4S)$ decays 45% to $B^0\bar{B}^0$. We rescale to 50%.

 $\Gamma(\rho\bar{\rho}\pi^+\pi^-)/\Gamma(\rho\bar{\rho}K^+\pi^-)$ $\Gamma_{476}/\Gamma_{477}$

VALUE	CL%	DOCUMENT ID	TECN	COMMENT
0.46±0.02±0.02		¹ AAIJ 17Bd	LHCB	pp at 7, 8 TeV

- ¹ The ratio is given for $m_{\rho\bar{\rho}} < 2.85$ GeV.

 $\Gamma(\rho\bar{\rho}K^0)/\Gamma_{\text{total}}$ Γ_{478}/Γ

VALUE (units 10^{-6})	CL%	DOCUMENT ID	TECN	COMMENT
2.66±0.32 OUR AVERAGE				
2.51 $\frac{+0.35}{-0.29}$ ±0.21		^{1,2} CHEN 08c	BELL	$e^+e^- \rightarrow \Upsilon(4S)$
3.0 ±0.5 ±0.3		² AUBERT 07Av	BABR	$e^+e^- \rightarrow \Upsilon(4S)$
• • • We do not use the following data for averages, fits, limits, etc. • • •				
2.40 $\frac{+0.64}{-0.44}$ ±0.28		^{2,3} WANG 05A	BELL	Repl. by CHEN 08c
1.88 $\frac{+0.77}{-0.60}$ ±0.23		^{2,3,5} WANG 04	BELL	Repl. by WANG 05A
<7.2	90	^{2,3} ABE 02k	BELL	Repl. by WANG 04

See key on page 1171

Meson Particle Listings
 B^0

- 1 Explicitly vetoes resonant production of $p\bar{p}$ from charmonium states.
 2 Assumes equal production of B^+ and B^0 at the $\mathcal{T}(4S)$.
 3 Explicitly vetoes resonant production of $p\bar{p}$ from charmonium states and ρK^0 production from Λ_c .
 4 Provides also results with $M_{p\bar{p}} < 2.85$ GeV/ c^2 and angular asymmetry of $p\bar{p}$ system.
 5 The branching fraction for $M_{p\bar{p}} < 2.85$ is also reported.

 $\Gamma(\Theta(1540)^+\bar{p}, \Theta^+ \rightarrow \rho K_S^0)/\Gamma_{\text{total}}$ Γ_{479}/Γ

VALUE (units 10^{-6})	CL%	DOCUMENT ID	TECN	COMMENT
<0.05	90	1 AUBERT	07AV BABR	$e^+e^- \rightarrow \mathcal{T}(4S)$
••• We do not use the following data for averages, fits, limits, etc. •••				
<0.23	90	1 WANG	05A BELL	$e^+e^- \rightarrow \mathcal{T}(4S)$
1 Assumes equal production of B^+ and B^0 at the $\mathcal{T}(4S)$.				

 $\Gamma(f_J(2220)K^0, f_J \rightarrow p\bar{p})/\Gamma_{\text{total}}$ Γ_{480}/Γ

VALUE (units 10^{-6})	CL%	DOCUMENT ID	TECN	COMMENT
<0.45	90	1 AUBERT	07AV BABR	$e^+e^- \rightarrow \mathcal{T}(4S)$
1 Assumes equal production of B^+ and B^0 at the $\mathcal{T}(4S)$.				

 $\Gamma(p\bar{p}K^+\pi^-)/\Gamma_{\text{total}}$ Γ_{477}/Γ

VALUE (units 10^{-6})	CL%	DOCUMENT ID	TECN	COMMENT
$6.3 \pm 0.5 \pm 0.2$		1,2 AAIJ	17BD LHCB	pp at 7, 8 TeV
1 AAIJ 17BD reports $[\Gamma(B^0 \rightarrow p\bar{p}K^+\pi^-)/\Gamma_{\text{total}}] / [B(B^0 \rightarrow J/\psi(1S)K^*(892)^0)] / [B(J/\psi(1S) \rightarrow p\bar{p})] / [B(K^*(892) \rightarrow (K\pi)^\pm)] = 2.34 \pm 0.12 \pm 0.12$ which we multiply by our best values $B(B^0 \rightarrow J/\psi(1S)K^*(892)^0) = (1.27 \pm 0.05) \times 10^{-3}$, $B(J/\psi(1S) \rightarrow p\bar{p}) = (2.120 \pm 0.029) \times 10^{-3}$, $B(K^*(892) \rightarrow (K\pi)^\pm) = (99.902 \pm 0.009) \times 10^{-2}$. Our first error is their experiment's error and our second error is the systematic error from using our best values.				
2 The branching ratio is given for $m_{p\bar{p}} < 2.85$ GeV.				

 $\Gamma(p\bar{p}K^*(892)^0)/\Gamma_{\text{total}}$ Γ_{481}/Γ

VALUE (units 10^{-6})	CL%	DOCUMENT ID	TECN	COMMENT
1.24 ± 0.28		OUR AVERAGE		
$1.18 \pm 0.29 \pm 0.11$		1,2 CHEN	08c BELL	$e^+e^- \rightarrow \mathcal{T}(4S)$
$1.47 \pm 0.45 \pm 0.40$		2 AUBERT	07AV BABR	$e^+e^- \rightarrow \mathcal{T}(4S)$
••• We do not use the following data for averages, fits, limits, etc. •••				
<7.6	90	2 WANG	04 BELL	$e^+e^- \rightarrow \mathcal{T}(4S)$
1 Explicitly vetoes resonant production of $p\bar{p}$ from charmonium states. 2 Assumes equal production of B^+ and B^0 at the $\mathcal{T}(4S)$.				

 $\Gamma(p\bar{p}\pi^0)/\Gamma_{\text{total}}$ Γ_{484}/Γ

VALUE (units 10^{-7})	CL%	DOCUMENT ID	TECN	COMMENT
$5.0 \pm 1.8 \pm 0.6$		PAL	19 BELL	$e^+e^- \rightarrow \mathcal{T}(4S)$

 $\Gamma(f_J(2220)K_S^0, f_J \rightarrow p\bar{p})/\Gamma_{\text{total}}$ Γ_{482}/Γ

VALUE (units 10^{-6})	CL%	DOCUMENT ID	TECN	COMMENT
<0.15	90	1 AUBERT	07AV BABR	$e^+e^- \rightarrow \mathcal{T}(4S)$
1 Assumes equal production of B^+ and B^0 at the $\mathcal{T}(4S)$.				

 $\Gamma(p\bar{p}K^+K^-)/\Gamma_{\text{total}}$ Γ_{483}/Γ

VALUE (units 10^{-8})	CL%	DOCUMENT ID	TECN	COMMENT
$12.1 \pm 3.1 \pm 0.5$		1,2 AAIJ	17BD LHCB	pp at 7, 8 TeV
1 AAIJ 17BD reports $[\Gamma(B^0 \rightarrow p\bar{p}K^+K^-)/\Gamma_{\text{total}}] / [B(B^0 \rightarrow J/\psi(1S)K^*(892)^0)] / [B(J/\psi(1S) \rightarrow p\bar{p})] / [B(K^*(892) \rightarrow (K\pi)^\pm)] = 0.045 \pm 0.011 \pm 0.004$ which we multiply by our best values $B(B^0 \rightarrow J/\psi(1S)K^*(892)^0) = (1.27 \pm 0.05) \times 10^{-3}$, $B(J/\psi(1S) \rightarrow p\bar{p}) = (2.120 \pm 0.029) \times 10^{-3}$, $B(K^*(892) \rightarrow (K\pi)^\pm) = (99.902 \pm 0.009) \times 10^{-2}$. Our first error is their experiment's error and our second error is the systematic error from using our best values.				
2 The branching ratio is given for $m_{p\bar{p}} < 2.85$ GeV.				

 $\Gamma(p\bar{p}K^+K^-)/\Gamma(p\bar{p}K^+\pi^-)$ $\Gamma_{483}/\Gamma_{477}$

VALUE (%)	CL%	DOCUMENT ID	TECN	COMMENT
••• We do not use the following data for averages, fits, limits, etc. •••				
$1.9 \pm 0.5 \pm 0.2$		1 AAIJ	17BD LHCB	pp at 7, 8 TeV
1 The ratio is given for $m_{p\bar{p}} < 2.85$ GeV.				

 $\Gamma(p\bar{p}p\bar{p})/\Gamma_{\text{total}}$ Γ_{485}/Γ

VALUE (units 10^{-8})	CL%	DOCUMENT ID	TECN	COMMENT
$2.2 \pm 0.4 \pm 0.1$		1 AAIJ	23AD LHCB	pp at 7, 8, 13 TeV
••• We do not use the following data for averages, fits, limits, etc. •••				
<20	90	2 LEES	18c BABR	$e^+e^- \rightarrow \mathcal{T}(4S)$
1 AAIJ 23AD reports $(2.2 \pm 0.4 \pm 0.1 \pm 0.1) \times 10^{-8}$ from a measurement of $[\Gamma(B^0 \rightarrow p\bar{p}p\bar{p})/\Gamma_{\text{total}}] / [B(B^0 \rightarrow J/\psi(1S)K^*(892)^0)] / [B(J/\psi(1S) \rightarrow p\bar{p})]$ assuming $B(B^0 \rightarrow J/\psi(1S)K^*(892)^0) = (1.27 \pm 0.05) \times 10^{-3}$, $B(J/\psi(1S) \rightarrow p\bar{p}) = (2.120 \pm 0.029) \times 10^{-3}$. It also includes $B(K^*(892)^0 \rightarrow K^+\pi^-) = 2/3$.				
2 Assumes equal production of B^+ and B^0 at the $\mathcal{T}(4S)$.				

 $\Gamma(p\bar{\Lambda}\pi^-)/\Gamma_{\text{total}}$ Γ_{486}/Γ

VALUE (units 10^{-6})	CL%	DOCUMENT ID	TECN	COMMENT
3.16 ± 0.24		OUR AVERAGE		
$3.21 \pm 0.28 \pm 0.16$		1 CHANG	23 BELL	$e^+e^- \rightarrow \mathcal{T}(4S)$
$3.07 \pm 0.31 \pm 0.23$		1 AUBERT	09AC BABR	$e^+e^- \rightarrow \mathcal{T}(4S)$
••• We do not use the following data for averages, fits, limits, etc. •••				
$3.23 \pm 0.33 \pm 0.29$		1 WANG	07c BELL	$e^+e^- \rightarrow \mathcal{T}(4S)$
$2.62 \pm 0.44 \pm 0.31$		1,2 WANG	05A BELL	Repl. by WANG 07c
$3.97 \pm 1.00 \pm 0.56$		1 WANG	03 BELL	Repl. by WANG 05A
<13	90	1 COAN	99 CLE2	$e^+e^- \rightarrow \mathcal{T}(4S)$
<180	90	3 ALBRECHT	88F ARG	$e^+e^- \rightarrow \mathcal{T}(4S)$
1 Assumes equal production of B^+ and B^0 at the $\mathcal{T}(4S)$. 2 Provides also results with $M_{p\bar{p}} < 2.85$ GeV/ c^2 and angular asymmetry of $p\bar{\Lambda}$ system. 3 ALBRECHT 88F reports $< 2.0 \times 10^{-4}$ assuming the $\mathcal{T}(4S)$ decays 45% to $B^0\bar{B}^0$. We rescale to 50%.				

 $\Gamma(p\bar{\Lambda}\pi^-\gamma)/\Gamma_{\text{total}}$ Γ_{487}/Γ

VALUE	CL%	DOCUMENT ID	TECN	COMMENT
<6.5 $\times 10^{-7}$	90	1 LAI	14 BELL	$e^+e^- \rightarrow \mathcal{T}(4S)$
1 Assumes equal production of B^+ and B^0 at the $\mathcal{T}(4S)$.				

 $\Gamma(p\bar{\Sigma}^-(1385)^-)/\Gamma_{\text{total}}$ Γ_{488}/Γ

VALUE (units 10^{-6})	CL%	DOCUMENT ID	TECN	COMMENT
<0.26	90	1 WANG	07c BELL	$e^+e^- \rightarrow \mathcal{T}(4S)$
1 Assumes equal production of B^+ and B^0 at the $\mathcal{T}(4S)$.				

 $[\Gamma(\Delta(1232)^+\bar{p}) + \Gamma(\Delta(1232)^-\bar{p})]/\Gamma_{\text{total}}$ Γ_{489}/Γ

VALUE	CL%	DOCUMENT ID	TECN	COMMENT
<1.6 $\times 10^{-6}$		PAL	19 BELL	$e^+e^- \rightarrow \mathcal{T}(4S)$

 $\Gamma(\Delta^0\bar{\Lambda})/\Gamma_{\text{total}}$ Γ_{490}/Γ

VALUE (units 10^{-6})	CL%	DOCUMENT ID	TECN	COMMENT
<0.93	90	1 WANG	07c BELL	$e^+e^- \rightarrow \mathcal{T}(4S)$
1 Assumes equal production of B^+ and B^0 at the $\mathcal{T}(4S)$.				

 $\Gamma(p\bar{\Lambda}K^-)/\Gamma_{\text{total}}$ Γ_{491}/Γ

VALUE (units 10^{-6})	CL%	DOCUMENT ID	TECN	COMMENT
<0.82	90	1 WANG	03 BELL	$e^+e^- \rightarrow \mathcal{T}(4S)$
1 Assumes equal production of B^+ and B^0 at the $\mathcal{T}(4S)$.				

 $\Gamma(p\bar{\Lambda}D^-)/\Gamma_{\text{total}}$ Γ_{492}/Γ

VALUE (units 10^{-6})	CL%	DOCUMENT ID	TECN	COMMENT
$25.1 \pm 2.6 \pm 3.5$		1 CHANG	15 BELL	$e^+e^- \rightarrow \mathcal{T}(4S)$
1 Assumes equal production of B^+ and B^0 at the $\mathcal{T}(4S)$.				

 $\Gamma(p\bar{\Lambda}D^{*-})/\Gamma_{\text{total}}$ Γ_{493}/Γ

VALUE (units 10^{-6})	CL%	DOCUMENT ID	TECN	COMMENT
$33.6 \pm 6.3 \pm 4.4$		1 CHANG	15 BELL	$e^+e^- \rightarrow \mathcal{T}(4S)$
1 Assumes equal production of B^+ and B^0 at the $\mathcal{T}(4S)$.				

 $\Gamma(p\bar{\Sigma}^0\pi^-)/\Gamma_{\text{total}}$ Γ_{494}/Γ

VALUE (units 10^{-6})	CL%	DOCUMENT ID	TECN	COMMENT
1.17 ± 0.43		1 CHANG	23 BELL	$e^+e^- \rightarrow \mathcal{T}(4S)$
••• We do not use the following data for averages, fits, limits, etc. •••				
<3.8	90	1 WANG	03 BELL	$e^+e^- \rightarrow \mathcal{T}(4S)$
1 Assumes equal production of B^+ and B^0 at the $\mathcal{T}(4S)$.				

 $\Gamma(\bar{\Lambda}\Lambda)/\Gamma_{\text{total}}$ Γ_{495}/Γ

VALUE (units 10^{-6})	CL%	DOCUMENT ID	TECN	COMMENT
<0.32	90	1 TSAI	07 BELL	$e^+e^- \rightarrow \mathcal{T}(4S)$
••• We do not use the following data for averages, fits, limits, etc. •••				
<0.69	90	1 CHANG	05 BELL	Repl. by TSAI 07
<1.2	90	1 BORNHEIM	03 CLE2	$e^+e^- \rightarrow \mathcal{T}(4S)$
<1.0	90	1 ABE	020 BELL	Repl. by CHANG 05
<3.9	90	1 COAN	99 CLE2	$e^+e^- \rightarrow \mathcal{T}(4S)$
1 Assumes equal production of B^+ and B^0 at the $\mathcal{T}(4S)$.				

 $\Gamma(\bar{\Lambda}\Lambda K^0)/\Gamma_{\text{total}}$ Γ_{496}/Γ

VALUE (units 10^{-6})	CL%	DOCUMENT ID	TECN	COMMENT
4.76 ± 0.84		1,2 CHANG	09 BELL	$e^+e^- \rightarrow \mathcal{T}(4S)$
1 Excluding charmonium events in $2.85 < m_{\Lambda\bar{\Lambda}} < 3.128$ GeV/ c^2 and $3.315 < m_{\Lambda\bar{\Lambda}} < 3.735$ GeV/ c^2 . Measurements in various $m_{\Lambda\bar{\Lambda}}$ bins are also reported. 2 Assumes equal production of B^+ and B^0 at the $\mathcal{T}(4S)$.				

Meson Particle Listings

 B^0 $\Gamma(\Lambda\Lambda K^0)/\Gamma_{\text{total}}$ Γ_{497}/Γ

VALUE (units 10^{-6})	DOCUMENT ID	TECN	COMMENT
$2.46^{+0.87}_{-0.72} \pm 0.34$	1,2 CHANG 09	BELL	$e^+e^- \rightarrow \Upsilon(4S)$

¹ Excluding charmonium events in $2.85 < m_{\Lambda\Lambda} < 3.128$ GeV/c² and $3.315 < m_{\Lambda\Lambda} < 3.735$ GeV/c². Measurements in various $m_{\Lambda\Lambda}$ bins are also reported.

² Assumes equal production of B^+ and B^0 at the $\Upsilon(4S)$.

 $\Gamma(\Lambda\Lambda D^0)/\Gamma_{\text{total}}$ Γ_{498}/Γ

VALUE (units 10^{-5})	DOCUMENT ID	TECN	COMMENT
$1.00^{+0.30}_{-0.26}$ OUR AVERAGE			

$0.96^{+0.29}_{-0.26} \pm 0.19$	1,2 LEES 14B	BABR	$e^+e^- \rightarrow \Upsilon(4S)$
---------------------------------	--------------	------	-----------------------------------

$1.05^{+0.57}_{-0.44} \pm 0.14$	2 CHANG 09	BELL	$e^+e^- \rightarrow \Upsilon(4S)$
---------------------------------	------------	------	-----------------------------------

¹ Evidence for 3.4 st. dev. signal significance.

² Assumes equal production of B^+ and B^0 at the $\Upsilon(4S)$.

 $\Gamma(D^0 \Sigma^0 \bar{\Lambda} + \text{c.c.})/\Gamma_{\text{total}}$ Γ_{499}/Γ

VALUE	CL%	DOCUMENT ID	TECN	COMMENT
$< 3.1 \times 10^{-5}$	90	1,2 LEES 14B	BABR	$e^+e^- \rightarrow \Upsilon(4S)$

¹ Here $\Sigma^0 \rightarrow \Lambda\gamma$.

² Assumes equal production of B^+ and B^0 at the $\Upsilon(4S)$.

 $\Gamma(\Delta^0 \bar{D}^0)/\Gamma_{\text{total}}$ Γ_{500}/Γ

VALUE	CL%	DOCUMENT ID	TECN	COMMENT
< 0.0015	90	1 BORTOLETTO89	CLEO	$e^+e^- \rightarrow \Upsilon(4S)$

¹ BORTOLETTO 89 reports < 0.0018 assuming $\Upsilon(4S)$ decays 43% to $B^0\bar{B}^0$. We rescale to 50%.

 $\Gamma(\Delta^{++} \bar{D}^{--})/\Gamma_{\text{total}}$ Γ_{501}/Γ

VALUE	CL%	DOCUMENT ID	TECN	COMMENT
$< 1.1 \times 10^{-4}$	90	1 BORTOLETTO89	CLEO	$e^+e^- \rightarrow \Upsilon(4S)$

¹ BORTOLETTO 89 reports $< 1.3 \times 10^{-4}$ assuming $\Upsilon(4S)$ decays 43% to $B^0\bar{B}^0$. We rescale to 50%.

 $\Gamma(\bar{D}^0 p\bar{p})/\Gamma_{\text{total}}$ Γ_{502}/Γ

VALUE (units 10^{-4})	DOCUMENT ID	TECN	COMMENT
1.04 ± 0.07 OUR AVERAGE			

$1.02 \pm 0.04 \pm 0.06$	1,2 DEL-AMO-SA...12	BABR	$e^+e^- \rightarrow \Upsilon(4S)$
--------------------------	---------------------	------	-----------------------------------

$1.18 \pm 0.15 \pm 0.16$	2 ABE 02w	BELL	$e^+e^- \rightarrow \Upsilon(4S)$
--------------------------	-----------	------	-----------------------------------

• • • We do not use the following data for averages, fits, limits, etc. • • •

$1.13 \pm 0.06 \pm 0.08$	2 AUBERT,B 06s	BABR	Repl. by DEL-AMO-SANCHEZ 12
--------------------------	----------------	------	-----------------------------

¹ Uses the values of D and D^* branching fractions from PDG 08.

² Assumes equal production of B^+ and B^0 at the $\Upsilon(4S)$.

 $\Gamma(D_s^- \bar{\Lambda} p)/\Gamma_{\text{total}}$ Γ_{503}/Γ

VALUE (units 10^{-5})	DOCUMENT ID	TECN	COMMENT
$2.8 \pm 0.8 \pm 0.3$	1,2 MEDVEDEVA 07	BELL	$e^+e^- \rightarrow \Upsilon(4S)$

¹ Assumes equal production of B^+ and B^0 at the $\Upsilon(4S)$.

² MEDVEDEVA 07 reports $(2.9 \pm 0.7 \pm 0.5 \pm 0.4) \times 10^{-5}$ from a measurement of $[\Gamma(B^0 \rightarrow D_s^- \bar{\Lambda} p)/\Gamma_{\text{total}}] \times [B(D_s^+ \rightarrow \phi\pi^+)]$ assuming $B(D_s^+ \rightarrow \phi\pi^+) = (4.4 \pm 0.6) \times 10^{-2}$, which we rescale to our best value $B(D_s^+ \rightarrow \phi\pi^+) = (4.5 \pm 0.4) \times 10^{-2}$. Our first error is their experiment's error and our second error is the systematic error from using our best value.

 $\Gamma(\bar{D}^*(2007)^0 p\bar{p})/\Gamma_{\text{total}}$ Γ_{504}/Γ

VALUE (units 10^{-4})	DOCUMENT ID	TECN	COMMENT
0.99 ± 0.11 OUR AVERAGE			

$0.97 \pm 0.07 \pm 0.09$	1,2 DEL-AMO-SA...12	BABR	$e^+e^- \rightarrow \Upsilon(4S)$
--------------------------	---------------------	------	-----------------------------------

$1.20^{+0.33}_{-0.29} \pm 0.21$	2 ABE 02w	BELL	$e^+e^- \rightarrow \Upsilon(4S)$
---------------------------------	-----------	------	-----------------------------------

• • • We do not use the following data for averages, fits, limits, etc. • • •

$1.01 \pm 0.10 \pm 0.09$	2 AUBERT,B 06s	BABR	Repl. by DEL-AMO-SANCHEZ 12
--------------------------	----------------	------	-----------------------------

¹ Uses the values of D and D^* branching fractions from PDG 08.

² Assumes equal production of B^+ and B^0 at the $\Upsilon(4S)$.

 $\Gamma(D^*(2010)^- p\bar{p})/\Gamma_{\text{total}}$ Γ_{505}/Γ

VALUE (units 10^{-4})	DOCUMENT ID	TECN	COMMENT
$14.5^{+3.4}_{-3.0} \pm 2.7$	1 ANDERSON 01	CLE2	$e^+e^- \rightarrow \Upsilon(4S)$

¹ Assumes equal production of B^+ and B^0 at the $\Upsilon(4S)$.

 $\Gamma(D^- p\bar{p}\pi^+)/\Gamma_{\text{total}}$ Γ_{506}/Γ

VALUE (units 10^{-4})	DOCUMENT ID	TECN	COMMENT
$3.32 \pm 0.10 \pm 0.29$	1,2 DEL-AMO-SA...12	BABR	$e^+e^- \rightarrow \Upsilon(4S)$

• • • We do not use the following data for averages, fits, limits, etc. • • •

$3.38 \pm 0.14 \pm 0.29$	2 AUBERT,B 06s	BABR	Repl. by DEL-AMO-SANCHEZ 12
--------------------------	----------------	------	-----------------------------

¹ Uses the values of D and D^* branching fractions from PDG 08.

² Assumes equal production of B^+ and B^0 at the $\Upsilon(4S)$.

 $\Gamma(D^*(2010)^- p\bar{p}\pi^+)/\Gamma_{\text{total}}$ Γ_{507}/Γ

VALUE (units 10^{-4})	DOCUMENT ID	TECN	COMMENT
4.7 ± 0.5 OUR AVERAGE			Error includes scale factor of 1.2.

$4.55 \pm 0.16 \pm 0.39$	1,2 DEL-AMO-SA...12	BABR	$e^+e^- \rightarrow \Upsilon(4S)$
--------------------------	---------------------	------	-----------------------------------

$6.5^{+1.3}_{-1.2} \pm 1.0$	2 ANDERSON 01	CLE2	$e^+e^- \rightarrow \Upsilon(4S)$
-----------------------------	---------------	------	-----------------------------------

• • • We do not use the following data for averages, fits, limits, etc. • • •

$4.81 \pm 0.22 \pm 0.44$	2 AUBERT,B 06s	BABR	Repl. by DEL-AMO-SANCHEZ 12
--------------------------	----------------	------	-----------------------------

¹ Uses the values of D and D^* branching fractions from PDG 08.

² Assumes equal production of B^+ and B^0 at the $\Upsilon(4S)$.

 $\Gamma(\bar{D}^0 p\bar{p}\pi^+\pi^-)/\Gamma_{\text{total}}$ Γ_{508}/Γ

VALUE (units 10^{-4})	DOCUMENT ID	TECN	COMMENT
$2.99 \pm 0.21 \pm 0.45$	1,2 DEL-AMO-SA...12	BABR	$e^+e^- \rightarrow \Upsilon(4S)$

¹ Uses the values of D and D^* branching fractions from PDG 08.

² Assumes equal production of B^+ and B^0 at the $\Upsilon(4S)$.

 $\Gamma(\bar{D}^{*0} p\bar{p}\pi^+\pi^-)/\Gamma_{\text{total}}$ Γ_{509}/Γ

VALUE (units 10^{-4})	DOCUMENT ID	TECN	COMMENT
$1.91 \pm 0.36 \pm 0.29$	1,2 DEL-AMO-SA...12	BABR	$e^+e^- \rightarrow \Upsilon(4S)$

¹ Uses the values of D and D^* branching fractions from PDG 08.

² Assumes equal production of B^+ and B^0 at the $\Upsilon(4S)$.

 $\Gamma(\Theta_c \bar{p}\pi^+, \Theta_c \rightarrow D^- p)/\Gamma_{\text{total}}$ Γ_{510}/Γ

VALUE (units 10^{-6})	CL%	DOCUMENT ID	TECN	COMMENT
< 9	90	1 AUBERT,B 06s	BABR	$e^+e^- \rightarrow \Upsilon(4S)$

¹ Assumes equal production of B^+ and B^0 at the $\Upsilon(4S)$.

 $\Gamma(\Theta_c \bar{p}\pi^+, \Theta_c \rightarrow D^{*-} p)/\Gamma_{\text{total}}$ Γ_{511}/Γ

VALUE (units 10^{-6})	CL%	DOCUMENT ID	TECN	COMMENT
< 14	90	1 AUBERT,B 06s	BABR	$e^+e^- \rightarrow \Upsilon(4S)$

¹ Assumes equal production of B^+ and B^0 at the $\Upsilon(4S)$.

 $\Gamma(\Sigma_c^- \Delta^{++})/\Gamma_{\text{total}}$ Γ_{512}/Γ

VALUE	CL%	DOCUMENT ID	TECN	COMMENT
$< 8 \times 10^{-4}$	90	1 PROCARIO 94	CLE2	$e^+e^- \rightarrow \Upsilon(4S)$

¹ PROCARIO 94 reports < 0.0012 from a measurement of $[\Gamma(B^0 \rightarrow \Sigma_c^- \Delta^{++})/\Gamma_{\text{total}}] \times [B(\Lambda_c^+ \rightarrow pK^- \pi^+)]$ assuming $B(\Lambda_c^+ \rightarrow pK^- \pi^+) = 0.043$, which we rescale to our best value $B(\Lambda_c^+ \rightarrow pK^- \pi^+) = 6.24 \times 10^{-2}$.

 $\Gamma(\bar{\Lambda}_c^- p\pi^+\pi^-)/\Gamma_{\text{total}}$ Γ_{513}/Γ

VALUE (units 10^{-3})	DOCUMENT ID	TECN	COMMENT
1.02 ± 0.14 OUR AVERAGE			Error includes scale factor of 1.3. See the ideogram below.

$1.23 \pm 0.05 \pm 0.33$	1,2 LEES 13H	BABR	$e^+e^- \rightarrow \Upsilon(4S)$
--------------------------	--------------	------	-----------------------------------

$0.90 \pm 0.11 \pm 0.04$	1,3 PARK 07	BELL	$e^+e^- \rightarrow \Upsilon(4S)$
--------------------------	-------------	------	-----------------------------------

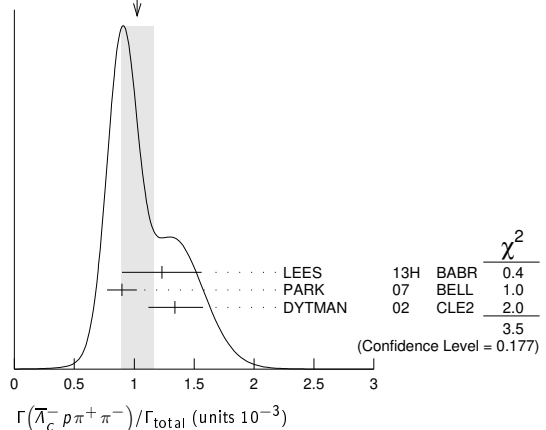
$1.34^{+0.22}_{-0.20} \pm 0.06$	4 DYTMAN 02	CLE2	$e^+e^- \rightarrow \Upsilon(4S)$
---------------------------------	-------------	------	-----------------------------------

• • • We do not use the following data for averages, fits, limits, etc. • • •

$0.88 \pm 0.16 \pm 0.04$	5 GABYSHEV 02	BELL	Repl. by PARK 07
--------------------------	---------------	------	------------------

$1.33^{+0.46}_{-0.42} \pm 0.37$	6 FU 97	CLE2	Repl. by DYTMAN 02
---------------------------------	---------	------	--------------------

WEIGHTED AVERAGE
1.02±0.14 (Error scaled by 1.3)



¹ Assumes equal production of B^+ and B^0 at the $\Upsilon(4S)$.

² Uses $\Lambda_c^+ \rightarrow pK^- \pi^+$ mode. The second error includes the uncertainty of the branching fraction of the Λ_c decay, $B(\Lambda_c^+ \rightarrow pK^- \pi^+) = (5.0 \pm 1.3)\%$.

³ PARK 07 reports $(11.2 \pm 0.5 \pm 3.2) \times 10^{-4}$ from a measurement of $[\Gamma(B^0 \rightarrow \bar{\Lambda}_c^- p\pi^+\pi^-)/\Gamma_{\text{total}}] \times [B(\Lambda_c^+ \rightarrow pK^- \pi^+)]$ assuming $B(\Lambda_c^+ \rightarrow pK^- \pi^+) =$

See key on page 1171

Meson Particle Listings

 B^0

$(5.0 \pm 1.3) \times 10^{-2}$, which we rescale to our best value $B(\Lambda_c^+ \rightarrow pK^-\pi^+) = (6.24 \pm 0.28) \times 10^{-2}$. Our first error is their experiment's error and our second error is the systematic error from using our best value.

⁴ DYTMAN 02 reports $(1.67^{+0.27}_{-0.25}) \times 10^{-3}$ from a measurement of $[\Gamma(B^0 \rightarrow \bar{\Lambda}_c^- p\pi^+\pi^-)/\Gamma_{\text{total}}] \times [B(\Lambda_c^+ \rightarrow pK^-\pi^+)]$ assuming $B(\Lambda_c^+ \rightarrow pK^-\pi^+) = 0.05$, which we rescale to our best value $B(\Lambda_c^+ \rightarrow pK^-\pi^+) = (6.24 \pm 0.28) \times 10^{-2}$. Our first error is their experiment's error and our second error is the systematic error from using our best value.

⁵ GABYSHEV 02 reports $(1.1 \pm 0.2) \times 10^{-3}$ from a measurement of $[\Gamma(B^0 \rightarrow \bar{\Lambda}_c^- p\pi^+\pi^-)/\Gamma_{\text{total}}] \times [B(\Lambda_c^+ \rightarrow pK^-\pi^+)]$ assuming $B(\Lambda_c^+ \rightarrow pK^-\pi^+) = 0.05$, which we rescale to our best value $B(\Lambda_c^+ \rightarrow pK^-\pi^+) = (6.24 \pm 0.28) \times 10^{-2}$. Our first error is their experiment's error and our second error is the systematic error from using our best value.

⁶ FU 97 uses PDG 96 values of Λ_c branching fraction.

$\Gamma(\bar{\Lambda}_c^- p)/\Gamma_{\text{total}}$		Γ_{514}/Γ			
VALUE (units 10^{-5})	CL%	DOCUMENT ID	TECN	COMMENT	
1.55 ± 0.17 OUR AVERAGE					
$1.51 \pm 0.17 \pm 0.07$		^{1,2} AUBERT	08BN BABR	$e^+e^- \rightarrow \Upsilon(4S)$	
$2.19^{+0.56}_{-0.49} \pm 0.65$		^{1,3} GABYSHEV	03 BELL	$e^+e^- \rightarrow \Upsilon(4S)$	
• • • We do not use the following data for averages, fits, limits, etc. • • •					
$2.10^{+0.67+0.77}_{-0.55-0.46}$		^{1,4} AUBERT	07AV BABR	Repl. by AUBERT 08BN	
< 9	90	^{1,5} DYTMAN	02 CLE2	$e^+e^- \rightarrow \Upsilon(4S)$	
< 3.1	90	^{1,4} GABYSHEV	02 BELL	$e^+e^- \rightarrow \Upsilon(4S)$	
< 21	90	⁶ FU	97 CLE2	$e^+e^- \rightarrow \Upsilon(4S)$	

¹ Assumes equal production of B^+ and B^0 at the $\Upsilon(4S)$.

² AUBERT 08BN reports $(1.89 \pm 0.21 \pm 0.49) \times 10^{-5}$ from a measurement of $[\Gamma(B^0 \rightarrow \bar{\Lambda}_c^- p)/\Gamma_{\text{total}}] \times [B(\Lambda_c^+ \rightarrow pK^-\pi^+)]$ assuming $B(\Lambda_c^+ \rightarrow pK^-\pi^+) = (5.0 \pm 1.3) \times 10^{-2}$, which we rescale to our best value $B(\Lambda_c^+ \rightarrow pK^-\pi^+) = (6.24 \pm 0.28) \times 10^{-2}$. Our first error is their experiment's error and our second error is the systematic error from using our best value.

³ The second error for GABYSHEV 03 includes the systematic and the error of $\Lambda_c \rightarrow \bar{p}K^+\pi^-$ decay branching fraction.

⁴ Uses the value for $\Lambda_c \rightarrow pK^-\pi^+$ branching ratio $(5.0 \pm 1.3)\%$.

⁵ DYTMAN 02 measurement uses $B(\Lambda_c^- \rightarrow \bar{p}K^+\pi^-) = 5.0 \pm 1.3\%$. The second error includes the systematic and the uncertainty of the branching ratio.

⁶ FU 97 uses PDG 96 values of Λ_c branching ratio.

$\Gamma(\bar{\Lambda}_c^- p\pi^0)/\Gamma_{\text{total}}$		Γ_{515}/Γ			
VALUE (units 10^{-4})	CL%	DOCUMENT ID	TECN	COMMENT	
1.55 ± 0.17 ± 0.07					
		^{1,2} AUBERT	10H BABR	$e^+e^- \rightarrow \Upsilon(4S)$	
• • • We do not use the following data for averages, fits, limits, etc. • • •					
< 5.9	90	³ FU	97 CLE2	$e^+e^- \rightarrow \Upsilon(4S)$	
¹ AUBERT 10H reports $(1.94 \pm 0.17 \pm 0.52) \times 10^{-4}$ from a measurement of $[\Gamma(B^0 \rightarrow \bar{\Lambda}_c^- p\pi^0)/\Gamma_{\text{total}}] \times [B(\Lambda_c^+ \rightarrow pK^-\pi^+)]$ assuming $B(\Lambda_c^+ \rightarrow pK^-\pi^+) = (5.0 \pm 1.3) \times 10^{-2}$, which we rescale to our best value $B(\Lambda_c^+ \rightarrow pK^-\pi^+) = (6.24 \pm 0.28) \times 10^{-2}$. Our first error is their experiment's error and our second error is the systematic error from using our best value.					
² Assumes equal production of B^+ and B^0 at the $\Upsilon(4S)$.					
³ FU 97 uses PDG 96 values of Λ_c branching ratio.					

$\Gamma(\bar{\Lambda}_c^- pK^+K^-)/\Gamma_{\text{total}}$		Γ_{528}/Γ			
VALUE (units 10^{-5})	CL%	DOCUMENT ID	TECN	COMMENT	
2.0 ± 0.4 ± 0.1					
		^{1,2} LEES	15B BABR	$e^+e^- \rightarrow \Upsilon(4S)$	
¹ LEES 15B reports $[\Gamma(B^0 \rightarrow \bar{\Lambda}_c^- pK^+K^-)/\Gamma_{\text{total}}] \times [B(\Lambda_c^+ \rightarrow pK^-\pi^+)] = (12.5 \pm 2.0 \pm 1.0) \times 10^{-7}$ which we divide by our best value $B(\Lambda_c^+ \rightarrow pK^-\pi^+) = (6.24 \pm 0.28) \times 10^{-2}$. Our first error is their experiment's error and our second error is the systematic error from using our best value.					
² Assumes equal production of B^+ and B^0 at the $\Upsilon(4S)$.					

$\Gamma(\bar{\Lambda}_c^- p\phi)/\Gamma_{\text{total}}$		Γ_{529}/Γ			
VALUE	CL%	DOCUMENT ID	TECN	COMMENT	
< 1.0 × 10⁻⁵					
	90	^{1,2} LEES	15B BABR	$e^+e^- \rightarrow \Upsilon(4S)$	
¹ LEES 15B reports $< 1.2 \times 10^{-5}$ from a measurement of $[\Gamma(B^0 \rightarrow \bar{\Lambda}_c^- p\phi)/\Gamma_{\text{total}}] \times [B(\Lambda_c^+ \rightarrow pK^-\pi^+)]$ assuming $B(\Lambda_c^+ \rightarrow pK^-\pi^+) = (5.0 \pm 1.3) \times 10^{-2}$, which we rescale to our best value $B(\Lambda_c^+ \rightarrow pK^-\pi^+) = 6.24 \times 10^{-2}$.					
² Assumes equal production of B^+ and B^0 at the $\Upsilon(4S)$.					

$\Gamma(\Sigma_c(2455)^- p)/\Gamma_{\text{total}}$		Γ_{516}/Γ			
VALUE (units 10^{-6})	CL%	DOCUMENT ID	TECN	COMMENT	
< 24					
		^{1,2} AUBERT	10H BABR	$e^+e^- \rightarrow \Upsilon(4S)$	
¹ AUBERT 10H reports $[\Gamma(B^0 \rightarrow \Sigma_c(2455)^- p)/\Gamma_{\text{total}}] \times [B(\Lambda_c^+ \rightarrow pK^-\pi^+)] < 1.5 \times 10^{-6}$ which we divide by our best value $B(\Lambda_c^+ \rightarrow pK^-\pi^+) = 6.24 \times 10^{-2}$.					
² Assumes equal production of B^+ and B^0 at the $\Upsilon(4S)$.					

$\Gamma(\bar{\Lambda}_c^- p\pi^+\pi^-)/\Gamma_{\text{total}}$		Γ_{517}/Γ			
VALUE	CL%	DOCUMENT ID	TECN	COMMENT	
< 5.07 × 10⁻³					
	90	¹ FU	97 CLE2	$e^+e^- \rightarrow \Upsilon(4S)$	
¹ FU 97 uses PDG 96 values of Λ_c branching ratio.					

$\Gamma(\bar{\Lambda}_c^- p\pi^+\pi^-\pi^-)/\Gamma_{\text{total}}$		Γ_{518}/Γ			
VALUE	CL%	DOCUMENT ID	TECN	COMMENT	
< 2.74 × 10⁻³					
	90	¹ FU	97 CLE2	$e^+e^- \rightarrow \Upsilon(4S)$	
¹ FU 97 uses PDG 96 values of Λ_c branching ratio.					

$\Gamma(\bar{\Lambda}_c^- p\pi^+\pi^- (\text{nonresonant}))/\Gamma_{\text{total}}$		Γ_{519}/Γ			
VALUE (units 10^{-4})	CL%	DOCUMENT ID	TECN	COMMENT	
5.5 ± 1.0 OUR AVERAGE Error includes scale factor of 1.3.					
$7.9 \pm 0.4 \pm 2.0$		^{1,2} LEES	13H BABR	$e^+e^- \rightarrow \Upsilon(4S)$	
$5.1 \pm 0.8 \pm 0.2$		^{1,3} PARK	07 BELL	$e^+e^- \rightarrow \Upsilon(4S)$	
¹ Assumes equal production of B^+ and B^0 at the $\Upsilon(4S)$.					
² Uses $\Lambda_c^+ \rightarrow pK^-\pi^+$ mode. The second error includes the uncertainty of the branching fraction of the Λ_c decay, $B(\Lambda_c^+ \rightarrow pK^-\pi^+) = (5.0 \pm 1.3)\%$.					
³ PARK 07 reports $(6.4 \pm 0.4 \pm 1.9) \times 10^{-4}$ from a measurement of $[\Gamma(B^0 \rightarrow \bar{\Lambda}_c^- p\pi^+\pi^- (\text{nonresonant}))/\Gamma_{\text{total}}] \times [B(\Lambda_c^+ \rightarrow pK^-\pi^+)]$ assuming $B(\Lambda_c^+ \rightarrow pK^-\pi^+) = (5.0 \pm 1.3) \times 10^{-2}$, which we rescale to our best value $B(\Lambda_c^+ \rightarrow pK^-\pi^+) = (6.24 \pm 0.28) \times 10^{-2}$. Our first error is their experiment's error and our second error is the systematic error from using our best value.					

$\Gamma(\Sigma_c(2520)^- p\pi^+)/\Gamma_{\text{total}}$		Γ_{520}/Γ			
VALUE (units 10^{-4})	CL%	DOCUMENT ID	TECN	COMMENT	
1.02 ± 0.18 OUR AVERAGE					
$1.15 \pm 0.10 \pm 0.30$		^{1,2} LEES	13H BABR	$e^+e^- \rightarrow \Upsilon(4S)$	
$0.96 \pm 0.22 \pm 0.04$		^{1,3} PARK	07 BELL	$e^+e^- \rightarrow \Upsilon(4S)$	
• • • We do not use the following data for averages, fits, limits, etc. • • •					
$1.3 \pm 0.5 \pm 0.1$		⁴ GABYSHEV	02 BELL	Repl. by PARK 07	
¹ Assumes equal production of B^+ and B^0 at the $\Upsilon(4S)$.					
² Uses $\Lambda_c^+ \rightarrow pK^-\pi^+$ mode. The second error includes the uncertainty of the branching fraction of the Λ_c decay, $B(\Lambda_c^+ \rightarrow pK^-\pi^+) = (5.0 \pm 1.3)\%$.					
³ PARK 07 reports $(1.2 \pm 0.1 \pm 0.4) \times 10^{-4}$ from a measurement of $[\Gamma(B^0 \rightarrow \Sigma_c(2520)^- p\pi^+)/\Gamma_{\text{total}}] \times [B(\Lambda_c^+ \rightarrow pK^-\pi^+)]$ assuming $B(\Lambda_c^+ \rightarrow pK^-\pi^+) = (5.0 \pm 1.3) \times 10^{-2}$, which we rescale to our best value $B(\Lambda_c^+ \rightarrow pK^-\pi^+) = (6.24 \pm 0.28) \times 10^{-2}$. Our first error is their experiment's error and our second error is the systematic error from using our best value.					
⁴ GABYSHEV 02 reports $(1.63^{+0.64}_{-0.58}) \times 10^{-4}$ from a measurement of $[\Gamma(B^0 \rightarrow \Sigma_c(2520)^- p\pi^+)/\Gamma_{\text{total}}] \times [B(\Lambda_c^+ \rightarrow pK^-\pi^+)]$ assuming $B(\Lambda_c^+ \rightarrow pK^-\pi^+) = 0.05$, which we rescale to our best value $B(\Lambda_c^+ \rightarrow pK^-\pi^+) = (6.24 \pm 0.28) \times 10^{-2}$. Our first error is their experiment's error and our second error is the systematic error from using our best value.					

$\Gamma(\Sigma_c(2520)^0 p\pi^-)/\Gamma_{\text{total}}$		Γ_{521}/Γ			
VALUE	CL%	DOCUMENT ID	TECN	COMMENT	
< 0.31 × 10⁻⁴					
	90	^{1,2} LEES	13H BABR	$e^+e^- \rightarrow \Upsilon(4S)$	
• • • We do not use the following data for averages, fits, limits, etc. • • •					
$< 0.38 \times 10^{-4}$	90	¹ PARK	07 BELL	$e^+e^- \rightarrow \Upsilon(4S)$	
$< 1.21 \times 10^{-4}$	90	^{1,2} GABYSHEV	02 BELL	Repl. by PARK 07	
¹ Assumes equal production of B^+ and B^0 at the $\Upsilon(4S)$.					
² Uses the value for $\Lambda_c \rightarrow pK^-\pi^+$ branching ratio $(5.0 \pm 1.3)\%$.					

$\Gamma(\Sigma_c(2455)^0 N^0, N^0 \rightarrow p\pi^-)/\Gamma_{\text{total}}$		Γ_{523}/Γ			
VALUE (units 10^{-4})	CL%	DOCUMENT ID	TECN	COMMENT	
0.64 ± 0.16 ± 0.03					
		^{1,2} KIM	08 BELL	$e^+e^- \rightarrow \Upsilon(4S)$	
¹ Assumes equal production of B^+ and B^0 at the $\Upsilon(4S)$.					
² KIM 08 reports $(0.80 \pm 0.15 \pm 0.25) \times 10^{-4}$ from a measurement of $[\Gamma(B^0 \rightarrow \Sigma_c(2455)^0 N^0, N^0 \rightarrow p\pi^-)/\Gamma_{\text{total}}] \times [B(\Lambda_c^+ \rightarrow pK^-\pi^+)]$ assuming $B(\Lambda_c^+ \rightarrow pK^-\pi^+) = (5.0 \pm 1.3) \times 10^{-2}$, which we rescale to our best value $B(\Lambda_c^+ \rightarrow pK^-\pi^+) = (6.24 \pm 0.28) \times 10^{-2}$. Our first error is their experiment's error and our second error is the systematic error from using our best value.					

$\Gamma(\Sigma_c(2455)^0 p\pi^-)/\Gamma_{\text{total}}$		Γ_{522}/Γ			
VALUE (units 10^{-4})	CL%	DOCUMENT ID	TECN	COMMENT	
1.08 ± 0.09 OUR AVERAGE					
$1.09 \pm 0.06 \pm 0.07$		LI	23E BELL	$e^+e^- \rightarrow \Upsilon(4S)$	
$0.91 \pm 0.07 \pm 0.24$		^{1,2} LEES	13H BABR	$e^+e^- \rightarrow \Upsilon(4S)$	
$1.8 \pm 0.6 \pm 0.1$		³ DYTMAN	02 CLE2	$e^+e^- \rightarrow \Upsilon(4S)$	
• • • We do not use the following data for averages, fits, limits, etc. • • •					
$1.12 \pm 0.21 \pm 0.05$		^{1,4} PARK	07 BELL	Repl. by LI 23E.	
$0.38^{+0.37}_{-0.33} \pm 0.02$	90	⁵ GABYSHEV	02 BELL	Repl. by PARK 07	

Meson Particle Listings

 B^0

- ¹ Assumes equal production of B^+ and B^0 at the $\Upsilon(4S)$.
² Uses $\Lambda_c^+ \rightarrow p K^- \pi^+$ mode. The second error includes the uncertainty of the branching fraction of the Λ_c decay, $B(\Lambda_c^+ \rightarrow p K^- \pi^+) = (5.0 \pm 1.3)\%$.
³ DYTMAN 02 reports $(2.2 \pm 0.7) \times 10^{-4}$ from a measurement of $[\Gamma(B^0 \rightarrow \bar{\Sigma}_c(2455)^0 p \pi^-) / \Gamma_{\text{total}}] \times [B(\Lambda_c^+ \rightarrow p K^- \pi^+)]$ assuming $B(\Lambda_c^+ \rightarrow p K^- \pi^+) = 0.05$, which we rescale to our best value $B(\Lambda_c^+ \rightarrow p K^- \pi^+) = (6.24 \pm 0.28) \times 10^{-2}$. Our first error is their experiment's error and our second error is the systematic error from using our best value.
⁴ PARK 07 reports $(1.4 \pm 0.2 \pm 0.4) \times 10^{-4}$ from a measurement of $[\Gamma(B^0 \rightarrow \bar{\Sigma}_c(2455)^0 p \pi^-) / \Gamma_{\text{total}}] \times [B(\Lambda_c^+ \rightarrow p K^- \pi^+)]$ assuming $B(\Lambda_c^+ \rightarrow p K^- \pi^+) = (5.0 \pm 1.3) \times 10^{-2}$, which we rescale to our best value $B(\Lambda_c^+ \rightarrow p K^- \pi^+) = (6.24 \pm 0.28) \times 10^{-2}$. Our first error is their experiment's error and our second error is the systematic error from using our best value.
⁵ GABYSHEV 02 reports $(0.48^{+0.46}_{-0.41}) \times 10^{-4}$ from a measurement of $[\Gamma(B^0 \rightarrow \bar{\Sigma}_c(2455)^0 p \pi^-) / \Gamma_{\text{total}}] \times [B(\Lambda_c^+ \rightarrow p K^- \pi^+)]$ assuming $B(\Lambda_c^+ \rightarrow p K^- \pi^+) = 0.05$, which we rescale to our best value $B(\Lambda_c^+ \rightarrow p K^- \pi^+) = (6.24 \pm 0.28) \times 10^{-2}$. Our first error is their experiment's error and our second error is the systematic error from using our best value.

 $\Gamma(\bar{\Sigma}_c(2455)^- \rightarrow p \pi^+) / \Gamma_{\text{total}}$ Γ_{524} / Γ

VALUE (units 10^{-4})	DOCUMENT ID	TECN	COMMENT
1.89 ± 0.15 OUR AVERAGE			
1.84 ± 0.11 ± 0.12	LI	23E	BELL $e^+ e^- \rightarrow \Upsilon(4S)$
2.13 ± 0.10 ± 0.56	1,2 LEES	13H	BABR $e^+ e^- \rightarrow \Upsilon(4S)$
3.0 ± 0.9 ± 0.1	3 DYTMAN	02	CLE2 $e^+ e^- \rightarrow \Upsilon(4S)$
••• We do not use the following data for averages, fits, limits, etc. •••			
1.68 ± 0.26 ± 0.08	1,4 PARK	07	BELL Repl. by LI 23E.
1.9 ± 0.6 ± 0.1	5 GABYSHEV	02	BELL Repl. by PARK 07

- ¹ Assumes equal production of B^+ and B^0 at the $\Upsilon(4S)$.
² Uses $\Lambda_c^+ \rightarrow p K^- \pi^+$ mode. The second error includes the uncertainty of the branching fraction of the Λ_c decay, $B(\Lambda_c^+ \rightarrow p K^- \pi^+) = (5.0 \pm 1.3)\%$.
³ DYTMAN 02 reports $(3.7 \pm 1.1) \times 10^{-4}$ from a measurement of $[\Gamma(B^0 \rightarrow \bar{\Sigma}_c(2455)^- p \pi^+) / \Gamma_{\text{total}}] \times [B(\Lambda_c^+ \rightarrow p K^- \pi^+)]$ assuming $B(\Lambda_c^+ \rightarrow p K^- \pi^+) = 0.05$, which we rescale to our best value $B(\Lambda_c^+ \rightarrow p K^- \pi^+) = (6.24 \pm 0.28) \times 10^{-2}$. Our first error is their experiment's error and our second error is the systematic error from using our best value.
⁴ PARK 07 reports $(2.1 \pm 0.2 \pm 0.6) \times 10^{-4}$ from a measurement of $[\Gamma(B^0 \rightarrow \bar{\Sigma}_c(2455)^- p \pi^+) / \Gamma_{\text{total}}] \times [B(\Lambda_c^+ \rightarrow p K^- \pi^+)]$ assuming $B(\Lambda_c^+ \rightarrow p K^- \pi^+) = (5.0 \pm 1.3) \times 10^{-2}$, which we rescale to our best value $B(\Lambda_c^+ \rightarrow p K^- \pi^+) = (6.24 \pm 0.28) \times 10^{-2}$. Our first error is their experiment's error and our second error is the systematic error from using our best value.
⁵ GABYSHEV 02 reports $(2.38^{+0.75}_{-0.69}) \times 10^{-4}$ from a measurement of $[\Gamma(B^0 \rightarrow \bar{\Sigma}_c(2455)^- p \pi^+) / \Gamma_{\text{total}}] \times [B(\Lambda_c^+ \rightarrow p K^- \pi^+)]$ assuming $B(\Lambda_c^+ \rightarrow p K^- \pi^+) = 0.05$, which we rescale to our best value $B(\Lambda_c^+ \rightarrow p K^- \pi^+) = (6.24 \pm 0.28) \times 10^{-2}$. Our first error is their experiment's error and our second error is the systematic error from using our best value.

 $\Gamma(\Lambda_c^- \rightarrow p K^+ \pi^-) / \Gamma_{\text{total}}$ Γ_{525} / Γ

VALUE (units 10^{-5})	DOCUMENT ID	TECN	COMMENT
3.5 ± 0.7 ± 0.2	1,2 AUBERT	09AG	BABR $e^+ e^- \rightarrow \Upsilon(4S)$
¹ AUBERT 09AG reports $(4.33 \pm 0.82 \pm 0.33 \pm 1.13) \times 10^{-5}$ from a measurement of $[\Gamma(B^0 \rightarrow \Lambda_c^- p K^+ \pi^-) / \Gamma_{\text{total}}] \times [B(\Lambda_c^+ \rightarrow p K^- \pi^+)]$ assuming $B(\Lambda_c^+ \rightarrow p K^- \pi^+) = (5.0 \pm 1.3) \times 10^{-2}$, which we rescale to our best value $B(\Lambda_c^+ \rightarrow p K^- \pi^+) = (6.24 \pm 0.28) \times 10^{-2}$. Our first error is their experiment's error and our second error is the systematic error from using our best value. ² Assumes equal production of B^+ and B^0 at the $\Upsilon(4S)$.			

 $\Gamma(\bar{\Sigma}_c(2455)^- \rightarrow p K^+, \bar{\Sigma}_c^- \rightarrow \bar{\Lambda}_c^- \pi^-) / \Gamma_{\text{total}}$ Γ_{526} / Γ

VALUE (units 10^{-5})	DOCUMENT ID	TECN	COMMENT
0.89 ± 0.25 ± 0.04	1,2 AUBERT	09AG	BABR $e^+ e^- \rightarrow \Upsilon(4S)$
¹ AUBERT 09AG reports $(1.11 \pm 0.30 \pm 0.09 \pm 0.29) \times 10^{-5}$ from a measurement of $[\Gamma(B^0 \rightarrow \bar{\Sigma}_c(2455)^- p K^+, \bar{\Sigma}_c^- \rightarrow \bar{\Lambda}_c^- \pi^-) / \Gamma_{\text{total}}] \times [B(\Lambda_c^+ \rightarrow p K^- \pi^+)]$ assuming $B(\Lambda_c^+ \rightarrow p K^- \pi^+) = (5.0 \pm 1.3) \times 10^{-2}$, which we rescale to our best value $B(\Lambda_c^+ \rightarrow p K^- \pi^+) = (6.24 \pm 0.28) \times 10^{-2}$. Our first error is their experiment's error and our second error is the systematic error from using our best value. ² Assumes equal production of B^+ and B^0 at the $\Upsilon(4S)$.			

 $\Gamma(\Lambda_c^- \rightarrow p K^*(892)^0) / \Gamma_{\text{total}}$ Γ_{527} / Γ

VALUE (units 10^{-5})	CL%	DOCUMENT ID	TECN	COMMENT
<2.42	90	1 AUBERT	09AG	BABR $e^+ e^- \rightarrow \Upsilon(4S)$
¹ Assumes equal production of B^+ and B^0 at the $\Upsilon(4S)$.				

 $\Gamma(\Lambda_c^- \rightarrow p \bar{p} p) / \Gamma_{\text{total}}$ Γ_{530} / Γ

VALUE (units 10^{-6})	DOCUMENT ID	TECN	COMMENT
<2.8	1 LEES	14C	BABR $e^+ e^- \rightarrow \Upsilon(4S)$
¹ Assumes equal production of B^+ and B^0 at the $\Upsilon(4S)$ and $B(\Lambda_c^+ \rightarrow p K^- \pi^+) = 0.050 \pm 0.013$.			

 $\Gamma(\bar{\Lambda}_c^- \Lambda K^+) / \Gamma_{\text{total}}$ Γ_{531} / Γ

VALUE (units 10^{-5})	DOCUMENT ID	TECN	COMMENT
4.8 ± 1.0 ± 0.2	1,2 LEES	11F	BABR $e^+ e^- \rightarrow \Upsilon(4S)$
¹ Assumes equal production of B^0 and B^+ from Upsilon(4S) decays. ² LEES 11F reports $(3.8 \pm 0.8 \pm 0.2 \pm 1.0) \times 10^{-5}$ from a measurement of $[\Gamma(B^0 \rightarrow \bar{\Lambda}_c^- \Lambda K^+) / \Gamma_{\text{total}}] / [B(\Lambda_c^+ \rightarrow p K^- \pi^+)] / [B(\Lambda \rightarrow p \pi^-)]$ assuming $B(\Lambda_c^+ \rightarrow p K^- \pi^+) = (5.0 \pm 1.3) \times 10^{-2}$, $B(\Lambda \rightarrow p \pi^-) = (63.9 \pm 0.5) \times 10^{-2}$, which we rescale to our best values $B(\Lambda_c^+ \rightarrow p K^- \pi^+) = (6.24 \pm 0.28) \times 10^{-2}$, $B(\Lambda \rightarrow p \pi^-) = (64.1 \pm 0.5) \times 10^{-2}$. Our first error is their experiment's error and our second error is the systematic error from using our best values. The reported uncertainties are statistical, systematic, and Λ_c^- branching fraction uncertainty.			

 $\Gamma(\bar{\Lambda}_c^- \Lambda_c^+) / \Gamma_{\text{total}}$ Γ_{532} / Γ

VALUE (units 10^{-5})	CL%	DOCUMENT ID	TECN	COMMENT
<1.6	95	1 AAIJ	14AA	LHCB pp at 7 TeV
••• We do not use the following data for averages, fits, limits, etc. •••				
<6.2	90	2 UCHIDA	08	BELL $e^+ e^- \rightarrow \Upsilon(4S)$
¹ Uses $B(\bar{B}^0 \rightarrow D^+ D_s^-) = (7.2 \pm 0.8) \times 10^{-3}$. ² Assumes equal production of B^+ and B^0 at the $\Upsilon(4S)$.				

 $\Gamma(\bar{\Lambda}_c(2593)^- / \bar{\Lambda}_c(2625)^- p) / \Gamma_{\text{total}}$ Γ_{533} / Γ

VALUE	CL%	DOCUMENT ID	TECN	COMMENT
<1.1 × 10⁻⁴	90	1,2 DYTMAN	02	CLE2 $e^+ e^- \rightarrow \Upsilon(4S)$
¹ Assumes equal production of B^+ and B^0 at the $\Upsilon(4S)$. ² DYTMAN 02 measurement uses $B(\Lambda_c^- \rightarrow \bar{p} K^+ \pi^-) = 5.0 \pm 1.3\%$. The second error includes the systematic and the uncertainty of the branching ratio.				

 $\Gamma(\bar{\Xi}_c^- \Lambda_c^+) / \Gamma_{\text{total}}$ Γ_{534} / Γ

VALUE (units 10^{-3})	DOCUMENT ID	TECN	COMMENT
1.2 ± 0.8 ± 0.1	1,2 LI	19C	BELL $e^+ e^- \rightarrow \Upsilon(4S)$
¹ Uses fully reconstructed B^0 on tag side with recoil against Λ_c^+ . ² LI 19C reports $(1.16 \pm 0.74 \pm 0.33) \times 10^{-3}$ from a measurement of $[\Gamma(B^0 \rightarrow \bar{\Xi}_c^- \Lambda_c^+) / \Gamma_{\text{total}}] \times [B(\Lambda_c^+ \rightarrow p K^- \pi^+)]$ assuming $B(\Lambda_c^+ \rightarrow p K^- \pi^+) = (6.28 \pm 0.32) \times 10^{-2}$, which we rescale to our best value $B(\Lambda_c^+ \rightarrow p K^- \pi^+) = (6.24 \pm 0.28) \times 10^{-2}$. Our first error is their experiment's error and our second error is the systematic error from using our best value.			

 $\Gamma(\bar{\Xi}_c^- \Lambda_c^+, \bar{\Xi}_c^- \rightarrow \bar{\Xi}^+ \pi^- \pi^-) / \Gamma_{\text{total}}$ Γ_{535} / Γ

VALUE (units 10^{-5})	DOCUMENT ID	TECN	COMMENT
2.4 ± 1.1 OUR AVERAGE			Error includes scale factor of 1.8.
3.3 ± 0.8 ± 0.2	1 LI	19C	BELL $e^+ e^- \rightarrow \Upsilon(4S)$
1.2 ± 0.9 ± 0.1	2,3 AUBERT	08H	BABR $e^+ e^- \rightarrow \Upsilon(4S)$
••• We do not use the following data for averages, fits, limits, etc. •••			
7.5 ± 3.3 ± 0.3	3,4 CHISTOV	06A	BELL Repl. by LI 19C

- ¹ LI 19C reports $(3.32 \pm 0.74 \pm 0.33) \times 10^{-5}$ from a measurement of $[\Gamma(B^0 \rightarrow \bar{\Xi}_c^- \Lambda_c^+, \bar{\Xi}_c^- \rightarrow \bar{\Xi}^+ \pi^- \pi^-) / \Gamma_{\text{total}}] \times [B(\Lambda_c^+ \rightarrow p K^- \pi^+)]$ assuming $B(\Lambda_c^+ \rightarrow p K^- \pi^+) = (6.28 \pm 0.32) \times 10^{-2}$, which we rescale to our best value $B(\Lambda_c^+ \rightarrow p K^- \pi^+) = (6.24 \pm 0.28) \times 10^{-2}$. Our first error is their experiment's error and our second error is the systematic error from using our best value.
² AUBERT 08H reports $(1.5 \pm 1.07 \pm 0.44) \times 10^{-5}$ from a measurement of $[\Gamma(B^0 \rightarrow \bar{\Xi}_c^- \Lambda_c^+, \bar{\Xi}_c^- \rightarrow \bar{\Xi}^+ \pi^- \pi^-) / \Gamma_{\text{total}}] \times [B(\Lambda_c^+ \rightarrow p K^- \pi^+)]$ assuming $B(\Lambda_c^+ \rightarrow p K^- \pi^+) = (5.0 \pm 1.3) \times 10^{-2}$, which we rescale to our best value $B(\Lambda_c^+ \rightarrow p K^- \pi^+) = (6.24 \pm 0.28) \times 10^{-2}$. Our first error is their experiment's error and our second error is the systematic error from using our best value.
³ Assumes equal production of B^+ and B^0 at the $\Upsilon(4S)$.
⁴ CHISTOV 06A reports $(9.3^{+3.7}_{-2.8} \pm 3.1) \times 10^{-5}$ from a measurement of $[\Gamma(B^0 \rightarrow \bar{\Xi}_c^- \Lambda_c^+, \bar{\Xi}_c^- \rightarrow \bar{\Xi}^+ \pi^- \pi^-) / \Gamma_{\text{total}}] \times [B(\Lambda_c^+ \rightarrow p K^- \pi^+)]$ assuming $B(\Lambda_c^+ \rightarrow p K^- \pi^+) = (5.0 \pm 1.3) \times 10^{-2}$, which we rescale to our best value $B(\Lambda_c^+ \rightarrow p K^- \pi^+) = (6.24 \pm 0.28) \times 10^{-2}$. Our first error is their experiment's error and our second error is the systematic error from using our best value.

 $\Gamma(\bar{\Xi}_c^- \Lambda_c^+, \bar{\Xi}_c^- \rightarrow \bar{p} K^+ \pi^-) / \Gamma_{\text{total}}$ Γ_{536} / Γ

VALUE (units 10^{-6})	DOCUMENT ID	TECN	COMMENT
5.3 ± 1.6 ± 0.2	1 LI	19C	BELL $e^+ e^- \rightarrow \Upsilon(4S)$
¹ LI 19C reports $(5.27 \pm 1.51 \pm 0.69) \times 10^{-6}$ from a measurement of $[\Gamma(B^0 \rightarrow \bar{\Xi}_c^- \Lambda_c^+, \bar{\Xi}_c^- \rightarrow \bar{p} K^+ \pi^-) / \Gamma_{\text{total}}] \times [B(\Lambda_c^+ \rightarrow p K^- \pi^+)]$ assuming $B(\Lambda_c^+ \rightarrow p K^- \pi^+) = (6.28 \pm 0.32) \times 10^{-2}$, which we rescale to our best value $B(\Lambda_c^+ \rightarrow p K^- \pi^+) = (6.24 \pm 0.28) \times 10^{-2}$. Our first error is their experiment's error and our second error is the systematic error from using our best value.			

 $\Gamma(\Lambda_c^+ \Lambda_c^- K^0) / \Gamma_{\text{total}}$ Γ_{537} / Γ

VALUE (units 10^{-4})	DOCUMENT ID	TECN	COMMENT
4.0 ± 0.9 OUR AVERAGE			
3.99 ± 0.76 ± 0.51	1 LI	18D	BELL $e^+ e^- \rightarrow \Upsilon(4S)$
3.8 ± 3.1 ± 2.1	2,3 AUBERT	08H	BABR $e^+ e^- \rightarrow \Upsilon(4S)$
••• We do not use the following data for averages, fits, limits, etc. •••			
7.9 ± 2.9 ± 4.3	2,3 GABYSHEV	06	BELL Repl. by LI 18D

¹ Assumes $B(\Upsilon(4S) \rightarrow B^0 \bar{B}^0) = 48.6 \pm 0.6\%$ and $B(\Lambda_c^+ \rightarrow p K^- \pi^+) = 6.23 \pm 0.33\%$.

² Assumes $B(\Lambda_c^+ \rightarrow p K^- \pi^+) = 5.0 \pm 1.3\%$.

³ Assumes equal production of B^+ and B^0 at the $\Upsilon(4S)$.

$\Gamma(\Lambda_c(2910)^- p, \bar{\Lambda}_c^- \rightarrow \Sigma_c(2455)^- \pi^+)/\Gamma_{\text{total}}$				Γ_{538}/Γ
VALUE (units 10^{-5})	CL%	DOCUMENT ID	TECN COMMENT	
$1.24 \pm 0.35 \pm 0.10$		LI	23E BELL $e^+ e^- \rightarrow \Upsilon(4S)$	

$\Gamma(\Lambda_c(2910)^- p, \bar{\Lambda}_c^- \rightarrow \Sigma_c(2455)^0 \pi^-)/\Gamma_{\text{total}}$				Γ_{539}/Γ
VALUE (units 10^{-6})	CL%	DOCUMENT ID	TECN COMMENT	
$9.5 \pm 3.6 \pm 1.6$		LI	23E BELL $e^+ e^- \rightarrow \Upsilon(4S)$	

$\Gamma(\Xi_c(2930)^- \Lambda_c^+, \Xi_c^- \rightarrow \Lambda_c^0 K^0)/\Gamma_{\text{total}}$				Γ_{540}/Γ
VALUE (units 10^{-4})	CL%	DOCUMENT ID	TECN COMMENT	
$2.37 \pm 0.51 \pm 0.31$		1 LI	18D BELL $e^+ e^- \rightarrow \Upsilon(4S)$	

¹ Assumes $B(\Upsilon(4S) \rightarrow B^0 \bar{B}^0) = 48.6 \pm 0.6\%$ and $B(\Lambda_c^+ \rightarrow p K^- \pi^+) = 6.23 \pm 0.33\%$.

$\Gamma(\Lambda\psi_{DS})/\Gamma_{\text{total}}$				Γ_{541}/Γ
VALUE	CL%	DOCUMENT ID	TECN COMMENT	
$< 0.13\text{--}5.2 \times 10^{-5}$	90	1 LEES	23B BABR $e^+ e^- \rightarrow \Upsilon(4S)$	
$< 2.1 \times 10^{-5}$	90	2 HADJIVASILIOU22	BELL $e^+ e^- \rightarrow \Upsilon(4S)$	

••• We do not use the following data for averages, fits, limits, etc. •••

¹ LEES 23B searched for ψ_{DS} in the recoil mass against Λ and the fully reconstructed accompanying B meson. The cited upper limit is for $m(\psi_{DS})$ between 1 and 4.1 GeV/ c^2 .

² HADJIVASILIOU 22 searched for ψ_{DS} , in the mass range 1–3.9 GeV/ c^2 , in the recoil mass against Λ and the accompanying B meson. The cited upper limit is for $m(\psi_{DS}) = 2.0$ GeV/ c^2 and is the most stringent. The least stringent limit is $< 3.8 \times 10^{-5}$ at $m(\psi_{DS}) = 3.9$ GeV/ c^2 .

$\Gamma(\gamma\gamma)/\Gamma_{\text{total}}$				Γ_{542}/Γ
Test for $\Delta B=1$ weak neutral current. Allowed by higher-order electroweak interactions.				
VALUE	CL%	DOCUMENT ID	TECN COMMENT	
$< 3.2 \times 10^{-7}$	90	1 DEL-AMO-SA...11A	BABR $e^+ e^- \rightarrow \Upsilon(4S)$	
$< 6.2 \times 10^{-7}$	90	1 VILLA	06 BELL $e^+ e^- \rightarrow \Upsilon(4S)$	
$< 1.7 \times 10^{-6}$	90	1 AUBERT	01I BABR $e^+ e^- \rightarrow \Upsilon(4S)$	
$< 3.9 \times 10^{-5}$	90	2 ACCIARRI	95I L3 $e^+ e^- \rightarrow Z$	

¹ Assumes equal production of B^+ and B^0 at the $\Upsilon(4S)$.

² ACCIARRI 95I assumes $f_{B^0} = 39.5 \pm 4.0$ and $f_{B_s} = 12.0 \pm 3.0\%$.

$\Gamma(e^+ e^-)/\Gamma_{\text{total}}$				Γ_{543}/Γ
Test for $\Delta B=1$ weak neutral current. Allowed by higher-order electroweak interactions.				
VALUE	CL%	DOCUMENT ID	TECN COMMENT	
$< 2.5 \times 10^{-9}$	90	1 AAIJ	20W LHCb pp at 7, 8, 13 TeV	
$< 8.3 \times 10^{-8}$	90	AALTONEN	09P CDF $p\bar{p}$ at 1.96 TeV	
$< 11.3 \times 10^{-8}$	90	2 AUBERT	08P BABR $e^+ e^- \rightarrow \Upsilon(4S)$	
$< 6.1 \times 10^{-8}$	90	2 AUBERT	05W BABR Repl. by AUBERT 08P	
$< 1.9 \times 10^{-7}$	90	2 CHANG	03 BELL $e^+ e^- \rightarrow \Upsilon(4S)$	
$< 8.3 \times 10^{-7}$	90	2 BERGFELD	00B CLE2 $e^+ e^- \rightarrow \Upsilon(4S)$	
$< 1.4 \times 10^{-5}$	90	3 ACCIARRI	97B L3 $e^+ e^- \rightarrow Z$	
$< 5.9 \times 10^{-6}$	90	4 AMMAR	94 CLE2 Repl. by BERGFELD 00B	
$< 2.6 \times 10^{-5}$	90	4 AVERY	89B CLEO $e^+ e^- \rightarrow \Upsilon(4S)$	
$< 7.6 \times 10^{-5}$	90	5 ALBRECHT	87D ARG $e^+ e^- \rightarrow \Upsilon(4S)$	
$< 6.4 \times 10^{-5}$	90	6 AVERY	87 CLEO $e^+ e^- \rightarrow \Upsilon(4S)$	
$< 3 \times 10^{-4}$	90	GILES	84 CLEO Repl. by AVERY 87	

¹ Assumes no contribution from $B_s^0 \rightarrow e^+ e^-$ decays.

² Assumes equal production of B^+ and B^0 at the $\Upsilon(4S)$.

³ ACCIARRI 97B assume PDG 96 production fractions for B^+ , B^0 , B_s , and Λ_b .

⁴ AVERY 89B reports $< 3 \times 10^{-5}$ assuming the $\Upsilon(4S)$ decays 43% to $B^0 \bar{B}^0$. We rescale to 50%.

⁵ ALBRECHT 87D reports $< 8.5 \times 10^{-5}$ assuming the $\Upsilon(4S)$ decays 45% to $B^0 \bar{B}^0$. We rescale to 50%.

⁶ AVERY 87 reports $< 8 \times 10^{-5}$ assuming the $\Upsilon(4S)$ decays 40% to $B^0 \bar{B}^0$. We rescale to 50%.

$\Gamma(e^+ e^- \gamma)/\Gamma_{\text{total}}$				Γ_{544}/Γ
Test for $\Delta B=1$ weak neutral current. Allowed by higher-order electroweak interactions.				
VALUE	CL%	DOCUMENT ID	TECN COMMENT	
$< 1.2 \times 10^{-7}$	90	AUBERT	08C BABR $e^+ e^- \rightarrow \Upsilon(4S)$	

$\Gamma(\mu^+ \mu^-)/\Gamma_{\text{total}}$				Γ_{545}/Γ
Test for $\Delta B=1$ weak neutral current. Allowed by higher-order electroweak interactions.				
VALUE (units 10^{-10})	CL%	DOCUMENT ID	TECN COMMENT	
< 1.5	90	1,2 TUMASYAN	23A CMS pp at 13 TeV	
$1.2 \pm 0.8 \pm 0.1$		3 AAIJ	22 LHCb pp at 7, 8, 13 TeV	
< 3.6	95	4 SIRUNYAN	20AG pp at 7, 8, 13 TeV	
$- 1.9 \pm 1.6$		5,6 AABOUD	19L ATLAS pp at 7, 8, 13 TeV	

••• We do not use the following data for averages, fits, limits, etc. •••

$1.5 \pm 1.2 \pm 0.2$ $- 1.0 \pm 0.1$	7	AAIJ	17AI LHCb	Repl. by AAIJ 22
$- 2.5 \pm 2.0$	8	AABOUD	16L ATLAS	Repl. by AABOUD 19L
3.9 ± 1.6 $- 1.4$	9	KHACHATRY...	15BE LHC	pp at 7, 8 TeV
< 8.0	90	10	AAIJ	13B LHCb Repl. by AAIJ 13BA
< 6.3	90	11	AAIJ	13BA LHCb Repl. by KHACHA- TRYAN 15BE
< 38	90	12	AALTONEN	13F CDF $p\bar{p}$ at 1.96 TeV
3.5 ± 2.1 $- 1.8$	90	13	CHATRCHYAN	13AW CMS Repl. by SIRUN- YAN 20AG
< 26	90	10	AAIJ	12A LHCb Repl. by AAIJ 12W
< 8.1	90	14	AAIJ	12W LHCb Repl. by AAIJ 13B
< 14	90	14	CHATRCHYAN	12A CMS pp at 7 TeV
< 120	90	15	AAIJ	11B LHCb Repl. by AAIJ 12A
< 50	90	14	AALTONEN	11AG CDF $p\bar{p}$ at 1.96 TeV
< 37	90	14	CHATRCHYAN	11T CMS Repl. by CHA- TRCHYAN 12A

¹ Corresponds to a 95% CL upper limit of $< 1.9 \times 10^{-10}$.

² Uses normalization mode $B(B^+ \rightarrow J/\psi K^+) = (1.020 \pm 0.019) \times 10^{-3}$, $B(J/\psi \rightarrow \mu^+ \mu^-) = (5.961 \pm 0.033) \times 10^{-2}$.

³ Corresponds to a 95% CL upper limit of $< 2.6 \times 10^{-10}$.

⁴ Uses normalization mode $B(B^+ \rightarrow J/\psi K^+) = (1.01 \pm 0.03) \times 10^{-3}$.

⁵ Corresponds to a 95% CL upper limit of $< 2.1 \times 10^{-10}$.

⁶ Uses normalization mode $B(B^+ \rightarrow J/\psi K^+) = (1.010 \pm 0.029) \times 10^{-3}$ and B production ratio $f(b \rightarrow B_s^0)/f(b \rightarrow B^0) = 0.256 \pm 0.013$.

⁷ Corresponds to a 95% CL upper limit of $< 3.4 \times 10^{-10}$.

⁸ This value is obtained from a profile-likelihood fit, see Fig. 9. It corresponds to an upper limit of $< 0.42 \times 10^{-9}$ at 95% C.L.

⁹ Derived from the combined fit to CMS and LHCb data. Uncertainty includes both statistical and systematic component. Also reports $B(B^0 \rightarrow \mu^+ \mu^-)/B(B_s \rightarrow \mu^+ \mu^-) = 0.14 \pm 0.08$.

¹⁰ Uses $B(B^+ \rightarrow J/\psi K^+ \rightarrow \mu^+ \mu^- K^+) = (6.01 \pm 0.21) \times 10^{-5}$ and $B(B^0 \rightarrow K^+ \pi^-) = (1.94 \pm 0.06) \times 10^{-5}$ for normalization.

¹¹ Reports also a limit of $< 7.4 \times 10^{-10}$ at 95% CL. Uses normalization modes $B^+ \rightarrow J/\psi K^+ \rightarrow \mu^+ \mu^- K^+$ and $B^0 \rightarrow K^+ \pi^-$.

¹² Uses normalization mode $B(B^+ \rightarrow J/\psi K^+) = (10.22 \pm 0.35) \times 10^{-4}$.

¹³ Reports also a limit of $< 9.2 \times 10^{-10}$ at 90% CL. Uses $B(B^+ \rightarrow J/\psi K^+ \rightarrow \mu^+ \mu^- K^+) = (6.0 \pm 0.2) \times 10^{-5}$ for normalization.

¹⁴ Uses $B(B^+ \rightarrow J/\psi K^+ \rightarrow \mu^+ \mu^- K^+) = (6.01 \pm 0.21) \times 10^{-5}$.

¹⁵ Uses B production ratio $f(\bar{b} \rightarrow B^+)/f(\bar{b} \rightarrow B_s^0) = 3.71 \pm 0.47$ and three normalization modes.

$\Gamma(\mu^+ \mu^- \gamma)/\Gamma_{\text{total}}$				Γ_{546}/Γ
Test for $\Delta B=1$ weak neutral current. Allowed by higher-order electroweak interactions.				
VALUE	CL%	DOCUMENT ID	TECN COMMENT	
$< 1.6 \times 10^{-7}$	90	AUBERT	08C BABR $e^+ e^- \rightarrow \Upsilon(4S)$	

$\Gamma(\tau^+ \tau^-)/\Gamma_{\text{total}}$				Γ_{550}/Γ
Test for $\Delta B=1$ weak neutral current. Allowed by higher-order electroweak interactions.				
VALUE	CL%	DOCUMENT ID	TECN COMMENT	
$< 2.1 \times 10^{-3}$	95	1 AAIJ	17AJ LHCb pp at 7, 8 TeV	
$< 4.1 \times 10^{-3}$	90	2 AUBERT	06S BABR $e^+ e^- \rightarrow \Upsilon(4S)$	

¹ Assuming no contribution from $B_s^0 \rightarrow \tau^+ \tau^-$.

² Assumes equal production of B^+ and B^0 at the $\Upsilon(4S)$.

$\Gamma(\mu^+ \mu^- \mu^+ \mu^-)/\Gamma_{\text{total}}$				Γ_{547}/Γ
VALUE	CL%	DOCUMENT ID	TECN COMMENT	
$< 1.8 \times 10^{-10}$	95	AAIJ	22Q LHCb pp at 7, 8, 13 TeV	
$< 6.9 \times 10^{-10}$	95	AAIJ	17N LHCb pp at 7, 8 TeV	
$< 6.6 \times 10^{-9}$	95	1 AAIJ	13AW LHCb Repl. by AAIJ 17N	

¹ Also reports a limit of $< 5.3 \times 10^{-9}$ at 90% CL.

$\Gamma(SP, S \rightarrow \mu^+ \mu^-, P \rightarrow \mu^+ \mu^-)/\Gamma_{\text{total}}$				Γ_{548}/Γ
Here S and P are the hypothetical scalar and pseudoscalar particles with masses of 2.5 GeV/ c^2 and 214.3 MeV/ c^2 , respectively.				
VALUE	CL%	DOCUMENT ID	TECN COMMENT	
$< 6.0 \times 10^{-10}$	95	AAIJ	17N LHCb pp at 7, 8 TeV	
$< 5.1 \times 10^{-9}$	90	1 AAIJ	13AW LHCb Repl. by AAIJ 17N	

¹ Also reports a limit of $< 6.3 \times 10^{-9}$ at 95% CL.

$\Gamma(a a, a \rightarrow \mu^+ \mu^-)/\Gamma_{\text{total}}$				Γ_{549}/Γ
Here particle a is a scalar with a mass of 1 GeV/ c^2 .				
VALUE	CL%	DOCUMENT ID	TECN COMMENT	
$< 2.3 \times 10^{-10}$	95	AAIJ	22Q LHCb pp at 7, 8, 13 TeV	

$\Gamma(\pi^0 \ell^+ \ell^-)/\Gamma_{\text{total}}$				Γ_{551}/Γ
VALUE	CL%	DOCUMENT ID	TECN COMMENT	
$< 5.3 \times 10^{-8}$	90	1 LEES	13M BABR $e^+ e^- \rightarrow \Upsilon(4S)$	
$< 1.5 \times 10^{-7}$	90	1 WEI	08A BELL $e^+ e^- \rightarrow \Upsilon(4S)$	
$< 1.2 \times 10^{-7}$	90	1 AUBERT	07AG BABR Repl. by LEES 13M	

¹ Assumes equal production of B^+ and B^0 at the $\Upsilon(4S)$.

Meson Particle Listings

 B^0

$\Gamma(\pi^0 \nu \bar{\nu})/\Gamma_{\text{total}}$ Γ_{557}/Γ
 Test for $\Delta B = 1$ weak neutral current. Allowed by higher-order electroweak interaction.

VALUE	CL%	DOCUMENT ID	TECN	COMMENT
$<0.9 \times 10^{-5}$	90	¹ GRYGIER 17	BELL	$e^+ e^- \rightarrow \Upsilon(4S)$
$<6.9 \times 10^{-5}$	90	¹ LUTZ 13	BELL	$e^+ e^- \rightarrow \Upsilon(4S)$
$<2.2 \times 10^{-4}$	90	¹ CHEN 07D	BELL	Repl. by LUTZ 13

• • • We do not use the following data for averages, fits, limits, etc. • • •

¹ Assumes equal production of B^+ and B^0 at the $\Upsilon(4S)$.

$\Gamma(\pi^0 e^+ e^-)/\Gamma_{\text{total}}$ Γ_{552}/Γ

VALUE	CL%	DOCUMENT ID	TECN	COMMENT
$<8.4 \times 10^{-8}$	90	¹ LEES 13M	BABR	$e^+ e^- \rightarrow \Upsilon(4S)$
$<2.3 \times 10^{-7}$	90	¹ WEI 08A	BELL	$e^+ e^- \rightarrow \Upsilon(4S)$
$<1.4 \times 10^{-7}$	90	¹ AUBERT 07AG	BABR	Repl. by LEES 13M

• • • We do not use the following data for averages, fits, limits, etc. • • •

¹ Assumes equal production of B^+ and B^0 at the $\Upsilon(4S)$.

$\Gamma(\pi^0 \mu^+ \mu^-)/\Gamma_{\text{total}}$ Γ_{553}/Γ

VALUE	CL%	DOCUMENT ID	TECN	COMMENT
$<6.9 \times 10^{-8}$	90	¹ LEES 13M	BABR	$e^+ e^- \rightarrow \Upsilon(4S)$
$<1.8 \times 10^{-7}$	90	¹ WEI 08A	BELL	$e^+ e^- \rightarrow \Upsilon(4S)$
$<5.1 \times 10^{-7}$	90	¹ AUBERT 07AG	BABR	$e^+ e^- \rightarrow \Upsilon(4S)$

• • • We do not use the following data for averages, fits, limits, etc. • • •

¹ Assumes equal production of B^+ and B^0 at the $\Upsilon(4S)$.

$\Gamma(\eta e^+ e^-)/\Gamma_{\text{total}}$ Γ_{554}/Γ

VALUE	CL%	DOCUMENT ID	TECN	COMMENT
$<6.4 \times 10^{-8}$	90	¹ LEES 13M	BABR	$e^+ e^- \rightarrow \Upsilon(4S)$

¹ Assumes equal production of B^+ and B^0 at the $\Upsilon(4S)$.

$\Gamma(\eta e^+ e^-)/\Gamma_{\text{total}}$ Γ_{555}/Γ

VALUE	CL%	DOCUMENT ID	TECN	COMMENT
$<10.8 \times 10^{-8}$	90	¹ LEES 13M	BABR	$e^+ e^- \rightarrow \Upsilon(4S)$

¹ Assumes equal production of B^+ and B^0 at the $\Upsilon(4S)$.

$\Gamma(\eta \mu^+ \mu^-)/\Gamma_{\text{total}}$ Γ_{556}/Γ

VALUE	CL%	DOCUMENT ID	TECN	COMMENT
$<11.2 \times 10^{-8}$	90	¹ LEES 13M	BABR	$e^+ e^- \rightarrow \Upsilon(4S)$

¹ Assumes equal production of B^+ and B^0 at the $\Upsilon(4S)$.

$\Gamma(K^0 e^+ e^-)/\Gamma_{\text{total}}$ Γ_{558}/Γ

VALUE (units 10^{-7})	CL%	DOCUMENT ID	TECN	COMMENT
3.3 ± 0.6 OUR AVERAGE				
$3.51^{+0.69}_{-0.60} \pm 0.10$		CHOUDHURY 21	BELL	$e^+ e^- \rightarrow \Upsilon(4S)$
$2.1^{+1.5}_{-1.3} \pm 0.2$		¹ AUBERT 09T	BABR	$e^+ e^- \rightarrow \Upsilon(4S)$
• • • We do not use the following data for averages, fits, limits, etc. • • •				
$3.4^{+0.9}_{-0.8} \pm 0.2$		^{1,2} WEI 09A	BELL	$e^+ e^- \rightarrow \Upsilon(4S)$
$2.9^{+1.6}_{-1.3} \pm 0.3$		¹ AUBERT,B 06J	BABR	Repl. by AUBERT 09T
<6.8	90	¹ ISHIKAWA 03	BELL	$e^+ e^- \rightarrow \Upsilon(4S)$

¹ Assumes equal production of B^0 and B^+ at $\Upsilon(4S)$.
² Superseded by CHOUDHURY 21.

$\Gamma(K^0 e^+ e^-)/\Gamma_{\text{total}}$ Γ_{559}/Γ

VALUE (units 10^{-7})	CL%	DOCUMENT ID	TECN	COMMENT
$2.5^{+1.1}_{-0.9}$ OUR AVERAGE				Error includes scale factor of 1.3.
$3.1^{+1.0}_{-0.9} \pm 0.08$		CHOUDHURY 21	BELL	$e^+ e^- \rightarrow \Upsilon(4S)$
$0.8^{+1.5}_{-1.2} \pm 0.1$		¹ AUBERT 09T	BABR	$e^+ e^- \rightarrow \Upsilon(4S)$
• • • We do not use the following data for averages, fits, limits, etc. • • •				
$2.0^{+1.4}_{-1.0} \pm 0.1$		^{1,2} WEI 09A	BELL	$e^+ e^- \rightarrow \Upsilon(4S)$
$1.3^{+1.6}_{-1.1} \pm 0.2$		¹ AUBERT,B 06J	BABR	Repl. by AUBERT 09T
$-2.1^{+2.3}_{-1.6} \pm 0.8$		¹ AUBERT 03U	BABR	$e^+ e^- \rightarrow \Upsilon(4S)$
< 5.4	90	³ ISHIKAWA 03	BELL	$e^+ e^- \rightarrow \Upsilon(4S)$
< 27	90	¹ ABE 02	BELL	Repl. by ISHIKAWA 03
< 38	90	¹ AUBERT 02L	BABR	$e^+ e^- \rightarrow \Upsilon(4S)$
< 84.5	90	⁴ ANDERSON 01B	CLE2	$e^+ e^- \rightarrow \Upsilon(4S)$
< 3000	90	ALBRECHT 91E	ARG	$e^+ e^- \rightarrow \Upsilon(4S)$
< 5200	90	⁵ AVERY 87	CLEO	$e^+ e^- \rightarrow \Upsilon(4S)$

¹ Assumes equal production of B^+ and B^0 at the $\Upsilon(4S)$.
² Superseded by CHOUDHURY 21.
³ Assumes equal production of B^0 and B^+ at $\Upsilon(4S)$.
⁴ The result is for di-lepton masses above 0.5 GeV.
⁵ AVERY 87 reports $< 6.5 \times 10^{-4}$ assuming the $\Upsilon(4S)$ decays 40% to $B^0 \bar{B}^0$. We rescale to 50%.

$\Gamma(K^0 \nu \bar{\nu})/\Gamma_{\text{total}}$ Γ_{561}/Γ
 Test for $\Delta B = 1$ weak neutral current. Allowed by higher-order electroweak interaction.

VALUE	CL%	DOCUMENT ID	TECN	COMMENT
$< 2.6 \times 10^{-5}$	90	¹ GRYGIER 17	BELL	$e^+ e^- \rightarrow \Upsilon(4S)$
$< 4.9 \times 10^{-5}$	90	^{1,2} LEES 13I	BABR	$e^+ e^- \rightarrow \Upsilon(4S)$
$< 19.4 \times 10^{-5}$	90	¹ LUTZ 13	BELL	$e^+ e^- \rightarrow \Upsilon(4S)$
$< 5.6 \times 10^{-5}$	90	¹ DEL-AMO-SA.10Q	BABR	Repl. by LEES 13I
$< 1.6 \times 10^{-4}$	90	¹ CHEN 07D	BELL	$e^+ e^- \rightarrow \Upsilon(4S)$

• • • We do not use the following data for averages, fits, limits, etc. • • •

¹ Assumes equal production of B^+ and B^0 at the $\Upsilon(4S)$.
² Also reported a limit $< 8.1 \times 10^{-5}$ at 90% CL obtained using a fully reconstructed hadronic B -tag evnets.

$\Gamma(\rho^0 \nu \bar{\nu})/\Gamma_{\text{total}}$ Γ_{562}/Γ
 Test for $\Delta B = 1$ weak neutral current. Allowed by higher-order electroweak interaction.

VALUE	CL%	DOCUMENT ID	TECN	COMMENT
$< 4.0 \times 10^{-5}$	90	¹ GRYGIER 17	BELL	$e^+ e^- \rightarrow \Upsilon(4S)$
$< 2.08 \times 10^{-4}$	90	¹ LUTZ 13	BELL	$e^+ e^- \rightarrow \Upsilon(4S)$
$< 4.4 \times 10^{-4}$	90	¹ CHEN 07D	BELL	Repl. by LUTZ 13

• • • We do not use the following data for averages, fits, limits, etc. • • •

¹ Assumes equal production of B^+ and B^0 at the $\Upsilon(4S)$.

$\Gamma(K^0 \mu^+ \mu^-)/\Gamma_{\text{total}}$ Γ_{560}/Γ
 Test for $\Delta B = 1$ weak neutral current. Allowed by higher-order electroweak interactions.

VALUE (units 10^{-7})	CL%	DOCUMENT ID	TECN	COMMENT
3.39 ± 0.35 OUR FIT				Error includes scale factor of 1.1.
3.39 ± 0.35 OUR AVERAGE				
$3.9^{+1.0}_{-0.8} \pm 0.3$		CHOUDHURY 21	BELL	$e^+ e^- \rightarrow \Upsilon(4S)$
$3.27 \pm 0.34 \pm 0.17$		¹ AAIJ 14M	LHCB	$p\bar{p}$ at 7, 8 TeV
$4.9^{+2.9}_{-2.5} \pm 0.3$		² AUBERT 09T	BABR	$e^+ e^- \rightarrow \Upsilon(4S)$
• • • We do not use the following data for averages, fits, limits, etc. • • •				
$3.1^{+0.7}_{-0.6}$		AAIJ	12AH LHCB	Repl. by AAIJ 14M
$4.4^{+1.3}_{-1.1} \pm 0.3$		^{2,3} WEI 09A	BELL	$e^+ e^- \rightarrow \Upsilon(4S)$
$5.9^{+3.3}_{-2.6} \pm 0.7$		² AUBERT,B 06J	BABR	Repl. by AUBERT 09T
$1.63^{+0.82}_{-0.63} \pm 0.14$		² AUBERT 03U	BABR	Repl. by AUBERT,B 06J
$5.6^{+2.9}_{-2.3} \pm 0.5$		⁴ ISHIKAWA 03	BELL	Repl. by WEI 09A
< 33	90	² ABE 02	BELL	Repl. by ISHIKAWA 03
< 36	90	AUBERT 02L	BABR	$e^+ e^- \rightarrow \Upsilon(4S)$
< 66.4	90	⁵ ANDERSON 01B	CLE2	$e^+ e^- \rightarrow \Upsilon(4S)$
< 5200	90	ALBRECHT 91E	ARG	$e^+ e^- \rightarrow \Upsilon(4S)$
< 3600	90	⁶ AVERY 87	CLEO	$e^+ e^- \rightarrow \Upsilon(4S)$

¹ Uses $B(B^0 \rightarrow J/\psi(1S) K^0) = (0.928 \pm 0.013 \pm 0.037) \times 10^{-3}$ for normalization.
² Assumes equal production of B^+ and B^0 at the $\Upsilon(4S)$.
³ Superseded by CHOUDHURY 21.
⁴ Assumes equal production of B^0 and B^+ at $\Upsilon(4S)$. The second error is a total of systematic uncertainties including model dependence.
⁵ The result is for di-lepton masses above 0.5 GeV.
⁶ AVERY 87 reports $< 4.5 \times 10^{-4}$ assuming the $\Upsilon(4S)$ decays 40% to $B^0 \bar{B}^0$. We rescale to 50%.

$\Gamma(K^0 \mu^+ \mu^-)/\Gamma(J/\psi(1S) K^0)$ $\Gamma_{560}/\Gamma_{214}$

VALUE (units 10^{-3})	CL%	DOCUMENT ID	TECN	COMMENT
0.38 ± 0.04 OUR FIT				Error includes scale factor of 1.1.
$0.37 \pm 0.12 \pm 0.02$		AALTONEN 11AI	CDF	$p\bar{p}$ at 1.96 TeV

$\Gamma(K^*(892)^0 e^+ e^-)/\Gamma_{\text{total}}$ Γ_{563}/Γ
 Test for $\Delta B = 1$ weak neutral current. Allowed by higher-order electroweak interactions.

VALUE (units 10^{-7})	CL%	DOCUMENT ID	TECN	COMMENT
$9.9^{+1.2}_{-1.1}$ OUR AVERAGE				
$10.3^{+2.2}_{-2.1} \pm 0.7$		¹ AUBERT 09T	BABR	$e^+ e^- \rightarrow \Upsilon(4S)$
$9.7^{+1.3}_{-1.1} \pm 0.7$		¹ WEI 09A	BELL	$e^+ e^- \rightarrow \Upsilon(4S)$
• • • We do not use the following data for averages, fits, limits, etc. • • •				
$8.1^{+2.1}_{-1.9} \pm 0.9$		¹ AUBERT,B 06J	BABR	Repl. by AUBERT 09T
$11.7^{+3.0}_{-2.7} \pm 0.9$		¹ ISHIKAWA 03	BELL	Repl. by WEI 09A

¹ Assumes equal production of B^0 and B^+ at $\Upsilon(4S)$.

$\Gamma(K^*(892)^0 e^+ e^-)/\Gamma_{\text{total}}$ Γ_{564}/Γ
 Test for $\Delta B = 1$ weak neutral current. Allowed by higher-order electroweak interactions.

VALUE (units 10^{-7})	CL%	DOCUMENT ID	TECN	COMMENT
$10.3^{+1.9}_{-1.7}$ OUR AVERAGE				
$8.6^{+2.6}_{-2.4} \pm 0.5$		¹ AUBERT 09T	BABR	$e^+ e^- \rightarrow \Upsilon(4S)$
$11.8^{+2.7}_{-2.2} \pm 0.9$		¹ WEI 09A	BELL	$e^+ e^- \rightarrow \Upsilon(4S)$

See key on page 1171

Meson Particle Listings

 B^0

• • • We do not use the following data for averages, fits, limits, etc. • • •

$10.4^{+3.3}_{-2.9} \pm 1.1$		¹ AUBERT,B	06J	BABR	Repl. by AUBERT 09T
$11.1^{+5.6}_{-4.7} \pm 1.1$		¹ AUBERT	03U	BABR	$e^+e^- \rightarrow \Upsilon(4S)$
< 24	90	² ISHIKAWA	03	BELL	$e^+e^- \rightarrow \Upsilon(4S)$
< 64	90	¹ ABE	02	BELL	Repl. by ISHIKAWA 03
< 67	90	¹ AUBERT	02L	BABR	$e^+e^- \rightarrow \Upsilon(4S)$
< 2900	90	ALBRECHT	91E	ARG	$e^+e^- \rightarrow \Upsilon(4S)$

¹ Assumes equal production of B^+ and B^0 at the $\Upsilon(4S)$.² Assumes equal production of B^0 and B^+ at $\Upsilon(4S)$.

$\Gamma(K^*(892)^0 \mu^+ \mu^-) / \Gamma_{\text{total}}$ Γ_{565} / Γ
 Test for $\Delta B=1$ weak neutral current. Allowed by higher-order electroweak interactions.

VALUE (units 10^{-7})	CL%	DOCUMENT ID	TECN	COMMENT
9.4 ± 0.5 OUR FIT				
9.4 ± 0.6 OUR AVERAGE				
$9.04^{+0.16}_{-0.15} \pm 0.62$		¹ AAIJ	17Q	LHCB pp at 7, 8 TeV
$13.5^{+4.0}_{-3.7} \pm 1.0$		² AUBERT	09T	BABR $e^+e^- \rightarrow \Upsilon(4S)$
$10.6^{+1.9}_{-1.4} \pm 0.7$		² WEI	09A	BELL $e^+e^- \rightarrow \Upsilon(4S)$
$10.36^{+0.18}_{-0.17} \pm 0.71$		¹ AAIJ	16A0	LHCB Repl. by AAIJ 17Q
$8.7^{+3.8}_{-3.3} \pm 1.2$		² AUBERT,B	06J	BABR Repl. by AUBERT 09T
$8.6^{+7.9}_{-5.8} \pm 1.1$		² AUBERT	03U	BABR Repl. by AUBERT,B 06J
$13.3^{+4.2}_{-3.7} \pm 1.1$		³ ISHIKAWA	03	BELL Repl. by WEI 09A
< 42	90	² ABE	02	BELL $e^+e^- \rightarrow \Upsilon(4S)$
< 33	90	AUBERT	02L	BABR $e^+e^- \rightarrow \Upsilon(4S)$
< 40	90	⁴ AFFOLDER	99B	CDF $p\bar{p}$ at 1.8 TeV

¹ Uses $B(B^0 \rightarrow J/\psi K^*(892)^0) = (1.19 \pm 0.01 \pm 0.08) \times 10^{-3}$. The second error is the total systematic uncertainty.² Assumes equal production of B^+ and B^0 at the $\Upsilon(4S)$.³ Assumes equal production of B^0 and B^+ at $\Upsilon(4S)$. The second error is a total of systematic uncertainties including model dependence.⁴ AFFOLDER 99B measured relative to $B^0 \rightarrow J/\psi(1S) K^*(892)^0$.

$\Gamma(K^*(892)^0 \mu^+ \mu^-) / \Gamma(J/\psi(1S) K^*(892)^0)$ $\Gamma_{565} / \Gamma_{216}$

VALUE (units 10^{-3})	DOCUMENT ID	TECN	COMMENT
0.75 ± 0.05 OUR FIT			
0.77 ± 0.08 ± 0.03			
$0.80 \pm 0.10 \pm 0.06$	AALTONEN 11L	CDF	Repl. by AALTONEN 11A1
$0.61 \pm 0.23 \pm 0.07$	AALTONEN 09B	CDF	Repl. by AALTONEN 11L

$\Gamma(K^*(892)^0 \chi, \chi \rightarrow \mu^+ \mu^-) / \Gamma_{\text{total}}$ Γ_{566} / Γ

VALUE	CL%	DOCUMENT ID	TECN	COMMENT
< $\sim 10^{-9}$	95	¹ AAIJ	15A2	LHCB pp at 7, 8 TeV

¹ The limit is obtained as a function of di-muon mass. A normalizing mode branching fraction value of $B(B^0 \rightarrow K^{*0} \mu^+ \mu^-) = (1.6 \pm 0.3) \times 10^{-7}$ is used.

$\Gamma(K^*(892)^0 \tau^+ \tau^-) / \Gamma_{\text{total}}$ Γ_{567} / Γ

VALUE	CL%	DOCUMENT ID	TECN	COMMENT
< 3.1×10^{-3}	90	¹ DONG	23	BELL $e^+e^- \rightarrow \Upsilon(4S)$

¹ Uses full reconstruction of companion neutral B .

$\Gamma(\pi^+ \pi^- \mu^+ \mu^-) / \Gamma_{\text{total}}$ Γ_{568} / Γ

VALUE (units 10^{-8})	DOCUMENT ID	TECN	COMMENT
2.1 ± 0.5 ± 0.1	¹ AAIJ	15s	LHCB pp at 7, 8 TeV

¹ AAIJ 15s reports $(2.11 \pm 0.51 \pm 0.15 \pm 0.16) \times 10^{-8}$ from a measurement of $\Gamma(B^0 \rightarrow \pi^+ \pi^- \mu^+ \mu^-) / \Gamma_{\text{total}} / [B(B^0 \rightarrow J/\psi(1S) K^*(892)^0)]$ assuming $B(B^0 \rightarrow J/\psi(1S) K^*(892)^0) = (1.3 \pm 0.1) \times 10^{-3}$, which we rescale to our best value $B(B^0 \rightarrow J/\psi(1S) K^*(892)^0) = (1.27 \pm 0.05) \times 10^{-3}$. Our first error is their experiment's error and our second error is the systematic error from using our best value.

$\Gamma(K^*(892)^0 \nu \bar{\nu}) / \Gamma_{\text{total}}$ Γ_{569} / Γ

VALUE	CL%	DOCUMENT ID	TECN	COMMENT
< 1.8×10^{-5}	90	¹ GRYGIER	17	BELL $e^+e^- \rightarrow \Upsilon(4S)$

• • • We do not use the following data for averages, fits, limits, etc. • • •

< 1.2×10^{-4}	90	^{1,2} LEES	13i	BABR $e^+e^- \rightarrow \Upsilon(4S)$
< 5.5×10^{-5}	90	¹ LUTZ	13	BELL $e^+e^- \rightarrow \Upsilon(4S)$
< 1.2×10^{-4}	90	AUBERT	08Bc	BABR Repl. by LEES 13i
< 3.4×10^{-4}	90	¹ CHEN	07D	BELL $e^+e^- \rightarrow \Upsilon(4S)$
< 1.0×10^{-3}	90	³ ADAM	96D	DLPH $e^+e^- \rightarrow Z$

¹ Assumes equal production of B^+ and B^0 at the $\Upsilon(4S)$.² Also reported a limit $< 9.3 \times 10^{-5}$ at 90% CL obtained using a fully reconstructed hadronic B -tag events.³ ADAM 96D assumes $f_{B^0} = f_{B^-} = 0.39$ and $f_{B_s} = 0.12$.

$\Gamma(\text{invisible}) / \Gamma_{\text{total}}$ Γ_{570} / Γ

VALUE (units 10^{-5})	CL%	DOCUMENT ID	TECN	COMMENT
< 2.4	90	¹ LEES	12T	BABR $e^+e^- \rightarrow \Upsilon(4S)$
< 7.8	90	² KU	20	BELL $e^+e^- \rightarrow \Upsilon(4S)$
< 13	90	³ HSU	12	BELL $e^+e^- \rightarrow \Upsilon(4S)$
< 22	90	¹ AUBERT,B	04J	BABR $e^+e^- \rightarrow \Upsilon(4S)$

¹ Uses the fully reconstructed $B^0 \rightarrow D^{(*)-} \ell^+ \nu_\ell$ events as a tag.² Identified by fully reconstructing a hadronic decay of the accompanying B meson.³ Identified by fully reconstructing a hadronic decay of the accompanying B meson and requiring no other particles in the event.

$\Gamma(\nu \bar{\nu} \gamma) / \Gamma_{\text{total}}$ Γ_{571} / Γ

VALUE (units 10^{-5})	CL%	DOCUMENT ID	TECN	COMMENT
< 1.6	90	¹ KU	20	BELL $e^+e^- \rightarrow \Upsilon(4S)$
< 1.7	90	² LEES	12T	BABR $e^+e^- \rightarrow \Upsilon(4S)$
< 4.7	90	² AUBERT,B	04J	BABR Repl. by LEES 12T

¹ Identified by fully reconstructing a hadronic decay of the accompanying B meson.² Uses the fully reconstructed $B^0 \rightarrow D^{(*)-} \ell^+ \nu_\ell$ events as a tag.

$\Gamma(\phi \mu^+ \mu^-) / \Gamma_{\text{total}}$ Γ_{572} / Γ

VALUE	CL%	DOCUMENT ID	TECN	COMMENT
< 3.2×10^{-9}	90	¹ AAIJ	22s	LHCB pp at 7, 8, 13 TeV

¹ Using $B(B_s^0 \rightarrow \phi \mu^+ \mu^-)$ as normalization. The limit is set for the full q^2 phase space.

$\Gamma(\phi \nu \bar{\nu}) / \Gamma_{\text{total}}$ Γ_{573} / Γ

VALUE	CL%	DOCUMENT ID	TECN	COMMENT
< 1.27×10^{-4}	90	¹ LUTZ	13	BELL $e^+e^- \rightarrow \Upsilon(4S)$
< 5.8×10^{-5}	90	¹ CHEN	07D	BELL Repl. by LUTZ 13

• • • We do not use the following data for averages, fits, limits, etc. • • •

¹ Assumes equal production of B^+ and B^0 at the $\Upsilon(4S)$.

$\Gamma(e^\pm \mu^\mp) / \Gamma_{\text{total}}$ Γ_{574} / Γ

Test of lepton family number conservation. Allowed by higher-order electroweak interactions.

VALUE	CL%	DOCUMENT ID	TECN	COMMENT
< 1.0×10^{-9}	90	¹ AAIJ	18T	LHCB pp at 7, 8 TeV
< 2.8×10^{-9}	90	² AAIJ	13BMLHCB	Repl. by AAIJ 18T
< 6.4×10^{-8}	90	AALTONEN	09P	CDF $p\bar{p}$ at 1.96 TeV
< 9.2×10^{-8}	90	³ AUBERT	08P	BABR $e^+e^- \rightarrow \Upsilon(4S)$
< 1.8×10^{-7}	90	³ AUBERT	05W	BABR $e^+e^- \rightarrow \Upsilon(4S)$
< 1.7×10^{-7}	90	³ CHANG	03	BELL $e^+e^- \rightarrow \Upsilon(4S)$
< 15×10^{-7}	90	³ BERGFELD	00B	CLE2 $e^+e^- \rightarrow \Upsilon(4S)$
< 3.5×10^{-6}	90	ABE	98V	CDF $p\bar{p}$ at 1.8 TeV
< 1.6×10^{-5}	90	⁴ ACCIARRI	97B	L3 $e^+e^- \rightarrow Z$
< 5.9×10^{-6}	90	AMMAR	94	CLE2 $e^+e^- \rightarrow \Upsilon(4S)$
< 3.4×10^{-5}	90	⁵ AVERY	89B	CLEO $e^+e^- \rightarrow \Upsilon(4S)$
< 4.5×10^{-5}	90	⁶ ALBRECHT	87D	ARG $e^+e^- \rightarrow \Upsilon(4S)$
< 7.7×10^{-5}	90	⁷ AVERY	87	CLEO $e^+e^- \rightarrow \Upsilon(4S)$
< 3×10^{-4}	90	GILES	84	CLEO Repl. by AVERY 87

¹ AAIJ 18T uses normalization modes $B(B^0 \rightarrow K^+ \pi^-) = (19.6 \pm 0.5) \times 10^{-6}$ and $B(B^+ \rightarrow J/\psi K^+) = (1.026 \pm 0.031) \times 10^{-3}$.² Uses normalization mode $B(B^0 \rightarrow K^+ \pi^-) = (19.4 \pm 0.6) \times 10^{-6}$.³ Assumes equal production of B^+ and B^0 at the $\Upsilon(4S)$.⁴ ACCIARRI 97B assume PDG 96 production fractions for B^+ , B^0 , B_s , and Λ_b .⁵ Paper assumes the $\Upsilon(4S)$ decays 43% to $B^0 \bar{B}^0$. We rescale to 50%.⁶ ALBRECHT 87D reports $< 5 \times 10^{-5}$ assuming the $\Upsilon(4S)$ decays 45% to $B^0 \bar{B}^0$. We rescale to 50%.⁷ AVERY 87 reports $< 9 \times 10^{-5}$ assuming the $\Upsilon(4S)$ decays 40% to $B^0 \bar{B}^0$. We rescale to 50%.

$\Gamma(\pi^0 e^\pm \mu^\mp) / \Gamma_{\text{total}}$ Γ_{575} / Γ

VALUE	CL%	DOCUMENT ID	TECN	COMMENT
< 1.4×10^{-7}	90	¹ AUBERT	07AG	BABR $e^+e^- \rightarrow \Upsilon(4S)$

¹ Assumes equal production of B^+ and B^0 at the $\Upsilon(4S)$.

$\Gamma(K^0 e^\pm \mu^\mp) / \Gamma_{\text{total}}$ Γ_{576} / Γ

VALUE	CL%	DOCUMENT ID	TECN	COMMENT
< 3.8×10^{-8}	90	CHOUDHURY 21	BELL	$e^+e^- \rightarrow \Upsilon(4S)$

• • • We do not use the following data for averages, fits, limits, etc. • • •

< 2.7×10^{-7}	90	¹ AUBERT,B	06J	BABR $e^+e^- \rightarrow \Upsilon(4S)$
< 40×10^{-7}	90	¹ AUBERT	02L	BABR Repl. by AUBERT,B 06J

¹ Assumes equal production of B^+ and B^0 at the $\Upsilon(4S)$.

Meson Particle Listings

 B^0

$\Gamma(K^*(892)^0 e^+ \mu^-)/\Gamma_{\text{total}}$ Γ_{577}/Γ

VALUE	CL%	DOCUMENT ID	TECN	COMMENT
$<6.8 \times 10^{-9}$	90	1 AAIJ	23G LHCB	pp at 7, 8, 13 TeV
$<1.6 \times 10^{-7}$	90	2 SANDILYA	18 BELL	$e^+ e^- \rightarrow \Upsilon(4S)$
$<5.3 \times 10^{-7}$	90	3 AUBERT,B	06J BABR	$e^+ e^- \rightarrow \Upsilon(4S)$

- • • We do not use the following data for averages, fits, limits, etc. • • •
- ¹ Uses the uniform phase space model for the signal decays.
- ² Uses $B(\Upsilon(4S) \rightarrow B^0 \bar{B}^0) = 0.486 \pm 0.006$.
- ³ Assumes equal production of B^0 and B^+ at $\Upsilon(4S)$.

$\Gamma(K^*(892)^0 e^- \mu^+)/\Gamma_{\text{total}}$ Γ_{578}/Γ

VALUE	CL%	DOCUMENT ID	TECN	COMMENT
$<5.7 \times 10^{-9}$	90	1 AAIJ	23G LHCB	pp at 7, 8, 13 TeV
$<1.2 \times 10^{-7}$	90	2 SANDILYA	18 BELL	$e^+ e^- \rightarrow \Upsilon(4S)$
$<3.4 \times 10^{-7}$	90	3 AUBERT,B	06J BABR	$e^+ e^- \rightarrow \Upsilon(4S)$

- • • We do not use the following data for averages, fits, limits, etc. • • •
- ¹ Uses the uniform phase space model for the signal decays.
- ² Uses $B(\Upsilon(4S) \rightarrow B^0 \bar{B}^0) = 0.486 \pm 0.006$.
- ³ Assumes equal production of B^0 and B^+ at $\Upsilon(4S)$.

$\Gamma(K^*(892)^0 e^\pm \mu^\mp)/\Gamma_{\text{total}}$ Γ_{579}/Γ

Test of lepton family number conservation.

VALUE	CL%	DOCUMENT ID	TECN	COMMENT
$<1.01 \times 10^{-8}$	90	1 AAIJ	23G LHCB	pp at 7, 8, 13 TeV
$<1.8 \times 10^{-7}$	90	2 SANDILYA	18 BELL	$e^+ e^- \rightarrow \Upsilon(4S)$
$<5.8 \times 10^{-7}$	90	3 AUBERT,B	06J BABR	$e^+ e^- \rightarrow \Upsilon(4S)$
$<34 \times 10^{-7}$	90	3 AUBERT	02L BABR	Repl. by AUBERT,B 06J

- • • We do not use the following data for averages, fits, limits, etc. • • •
- ¹ Uses the uniform phase space model for the signal decays.
- ² Uses $B(\Upsilon(4S) \rightarrow B^0 \bar{B}^0) = 0.486 \pm 0.006$.
- ³ Assumes equal production of B^+ and B^0 at the $\Upsilon(4S)$.

$\Gamma(K^*(892)^0 \tau^+ \mu^-)/\Gamma_{\text{total}}$ Γ_{580}/Γ

VALUE	CL%	DOCUMENT ID	TECN	COMMENT
$<1.0 \times 10^{-5}$	90	1 AAIJ	23F LHCB	pp at 7, 8, 13 TeV

- ¹ Using $B^0 \rightarrow D^- D_s^+$ as normalisation decay.

$\Gamma(K^*(892)^0 \tau^- \mu^+)/\Gamma_{\text{total}}$ Γ_{581}/Γ

VALUE	CL%	DOCUMENT ID	TECN	COMMENT
$<8.2 \times 10^{-6}$	90	1 AAIJ	23F LHCB	pp at 7, 8, 13 TeV

- ¹ Using $B^0 \rightarrow D^- D_s^+$ as normalisation decay.

$\Gamma(e^\pm \tau^\mp)/\Gamma_{\text{total}}$ Γ_{582}/Γ

Test of lepton family number conservation. Allowed by higher-order electroweak interactions.

VALUE	CL%	DOCUMENT ID	TECN	COMMENT
$<1.6 \times 10^{-5}$	90	1 ATMACAN	21 BELL	$e^+ e^- \rightarrow \Upsilon(4S)$
$<2.8 \times 10^{-5}$	90	2 AUBERT	08AD BABR	$e^+ e^- \rightarrow \Upsilon(4S)$
$<1.1 \times 10^{-4}$	90	BORNHEIM	04 CLE2	$e^+ e^- \rightarrow \Upsilon(4S)$
$<5.3 \times 10^{-4}$	90	AMMAR	94 CLE2	Repl. by BORNHEIM 04

- ¹ Uses events in which one B meson is fully reconstructed in a hadronic decay mode.
- ² Assumes equal production of B^+ and B^0 at the $\Upsilon(4S)$.

$\Gamma(\mu^\pm \tau^\mp)/\Gamma_{\text{total}}$ Γ_{583}/Γ

Test of lepton family number conservation. Allowed by higher-order electroweak interactions.

VALUE	CL%	DOCUMENT ID	TECN	COMMENT
$<1.4 \times 10^{-5}$	95	1 AAIJ	19AK LHCB	pp at 7, 8 TeV
$<1.5 \times 10^{-5}$	90	2 ATMACAN	21 BELL	$e^+ e^- \rightarrow \Upsilon(4S)$
$<2.2 \times 10^{-5}$	90	3 AUBERT	08AD BABR	$e^+ e^- \rightarrow \Upsilon(4S)$
$<3.8 \times 10^{-5}$	90	BORNHEIM	04 CLE2	$e^+ e^- \rightarrow \Upsilon(4S)$
$<8.3 \times 10^{-4}$	90	AMMAR	94 CLE2	Repl. by BORNHEIM 04

- ¹ Assuming no contribution from $B_s^0 \rightarrow \mu^\pm \tau^\mp$.
- ² Uses events in which one B meson is fully reconstructed in a hadronic decay mode.
- ³ Assumes equal production of B^+ and B^0 at the $\Upsilon(4S)$.

$\Gamma(p \mu^-)/\Gamma_{\text{total}}$ Γ_{584}/Γ

VALUE	CL%	DOCUMENT ID	COMMENT
$<2.6 \times 10^{-9}$	90	1 AAIJ	23Y pp at 7, 8, 13 TeV

- ¹ Assumes that B^0 decay branching fractions to $p \mu^-$ and $\bar{p} \mu^+$ are the same.

$\Gamma(\Lambda_c^+ \mu^-)/\Gamma_{\text{total}}$ Γ_{585}/Γ

VALUE	CL%	DOCUMENT ID	TECN	COMMENT
$<1.4 \times 10^{-6}$	90	1,2 DEL-AMO-SA..11k	BABR	$e^+ e^- \rightarrow \Upsilon(4S)$

- ¹ DEL-AMO-SANCHEZ 11k reports $<180 \times 10^{-8}$ from a measurement of $[\Gamma(B^0 \rightarrow \Lambda_c^+ \mu^-)/\Gamma_{\text{total}}] \times [B(\Lambda_c^+ \rightarrow p K^- \pi^+)]$ assuming $B(\Lambda_c^+ \rightarrow p K^- \pi^+) = (5.0 \pm 1.3) \times 10^{-2}$, which we rescale to our best value $B(\Lambda_c^+ \rightarrow p K^- \pi^+) = 6.24 \times 10^{-2}$.
- ² Uses $B(\Upsilon(4S) \rightarrow B^0 \bar{B}^0) = (51.6 \pm 0.6)\%$ and $B(\Upsilon(4S) \rightarrow B^+ B^-) = (48.4 \pm 0.6)\%$.

$\Gamma(\Lambda_c^+ e^-)/\Gamma_{\text{total}}$ Γ_{586}/Γ

VALUE	CL%	DOCUMENT ID	TECN	COMMENT
$<4 \times 10^{-6}$	90	1,2 DEL-AMO-SA..11k	BABR	$e^+ e^- \rightarrow \Upsilon(4S)$

- ¹ DEL-AMO-SANCHEZ 11k reports $<520 \times 10^{-8}$ from a measurement of $[\Gamma(B^0 \rightarrow \Lambda_c^+ e^-)/\Gamma_{\text{total}}] \times [B(\Lambda_c^+ \rightarrow p K^- \pi^+)]$ assuming $B(\Lambda_c^+ \rightarrow p K^- \pi^+) = (5.0 \pm 1.3) \times 10^{-2}$, which we rescale to our best value $B(\Lambda_c^+ \rightarrow p K^- \pi^+) = 6.24 \times 10^{-2}$.

- ² Uses $B(\Upsilon(4S) \rightarrow B^0 \bar{B}^0) = (51.6 \pm 0.6)\%$ and $B(\Upsilon(4S) \rightarrow B^+ B^-) = (48.4 \pm 0.6)\%$.

 B_s^0 CROSS-PARTICLE BRANCHING RATIOS

$\Gamma([K^+ K^-]_D K^*(892)^0)/\Gamma_{\text{total}} \times B(B_s^0 \rightarrow [K^+ K^-]_D K^*(892)^0)$ $\Gamma_{155}/\Gamma \times B$

VALUE	DOCUMENT ID	TECN	COMMENT
$0.10 \pm 0.02 \pm 0.01$	AAIJ	14BN LHCB	pp at 7, 8 TeV

$\Gamma([\pi^+ \pi^-]_D K^*(892)^0)/\Gamma_{\text{total}} \times B(B_s^0 \rightarrow [\pi^+ \pi^-]_D K^*(892)^0)$ $\Gamma_{156}/\Gamma \times B$

VALUE	DOCUMENT ID	TECN	COMMENT
$0.15 \pm 0.04 \pm 0.01$	AAIJ	14BN LHCB	pp at 7, 8 TeV

See the related review(s):

[Polarization in B Decays](#)

POLARIZATION IN B^0 DECAY

In decays involving two vector mesons, one can distinguish among the states in which meson polarizations are both longitudinal (L) or both are transverse and parallel (\parallel) or perpendicular (\perp) to each other with the parameters Γ_L/Γ , Γ_\perp/Γ , and the relative phases ϕ_\parallel and ϕ_\perp . See the definitions in the note on "Polarization in B Decays" review in the B^0 Particle Listings.

Γ_L/Γ in $B^0 \rightarrow J/\psi(1S) K^*(892)^0$

VALUE	EVTS	DOCUMENT ID	TECN	COMMENT
0.571 ± 0.007 OUR AVERAGE				
$0.572 \pm 0.006 \pm 0.014$		1 AAIJ	13AT LHCB	pp at 7 TeV
$0.587 \pm 0.011 \pm 0.013$		2 ABAZOV	09E D0	$p\bar{p}$ at 1.96 TeV
$0.556 \pm 0.009 \pm 0.010$		3 AUBERT	07AD BABR	$e^+ e^- \rightarrow \Upsilon(4S)$
$0.562 \pm 0.026 \pm 0.018$		ACOSTA	05 CDF	$p\bar{p}$ at 1.96 TeV
$0.574 \pm 0.012 \pm 0.009$		ITOH	05 BELL	$e^+ e^- \rightarrow \Upsilon(4S)$
$0.59 \pm 0.06 \pm 0.01$		4 AFFOLDER	00N CDF	$p\bar{p}$ at 1.8 TeV
$0.52 \pm 0.07 \pm 0.04$		5 JESSOP	97 CLE2	$e^+ e^- \rightarrow \Upsilon(4S)$
$0.65 \pm 0.10 \pm 0.04$	65	ABE	95Z CDF	$p\bar{p}$ at 1.8 TeV
$0.97 \pm 0.16 \pm 0.15$	13	6 ALBRECHT	94G ARG	$e^+ e^- \rightarrow \Upsilon(4S)$
$0.566 \pm 0.012 \pm 0.005$		3 AUBERT	05P BABR	Repl. by AUBERT 07AD
$0.62 \pm 0.02 \pm 0.03$		7 ABE	02N BELL	Repl. by ITOH 05
$0.597 \pm 0.028 \pm 0.024$		8 AUBERT	01H BABR	Repl. by AUBERT 07AD
$0.80 \pm 0.08 \pm 0.05$	42	6 ALAM	94 CLE2	Sup. by JESSOP 97

- • • We do not use the following data for averages, fits, limits, etc. • • •
- ¹ AAIJ 13AT obtains $\Gamma_\parallel/\Gamma = 0.227 \pm 0.004 \pm 0.011$. The relation $1 = (\Gamma_L + \Gamma_\perp + \Gamma_\parallel)/\Gamma$ is used to obtain Γ_L/Γ .

- ² Measured the angular and lifetime parameters for the time-dependent angular untagged decays $B_d^0 \rightarrow J/\psi K^{*0}$ and $B_s^0 \rightarrow J/\psi \phi$.

- ³ Obtained by combining the B^0 and B^+ modes.

- ⁴ AFFOLDER 00N measurements are based on 190 B^0 candidates obtained from a data sample of 89 pb^{-1} . The P -wave fraction is found to be $0.13^{+0.12}_{-0.09} \pm 0.06$.

- ⁵ JESSOP 97 is the average over a mixture of B^0 and B^+ decays. The P -wave fraction is found to be $0.16 \pm 0.08 \pm 0.04$.

- ⁶ Averaged over an admixture of B^0 and B^+ decays.

- ⁷ Averaged over an admixture of B^0 and B^+ decays and the P wave fraction is $(19 \pm 2 \pm 3)\%$.

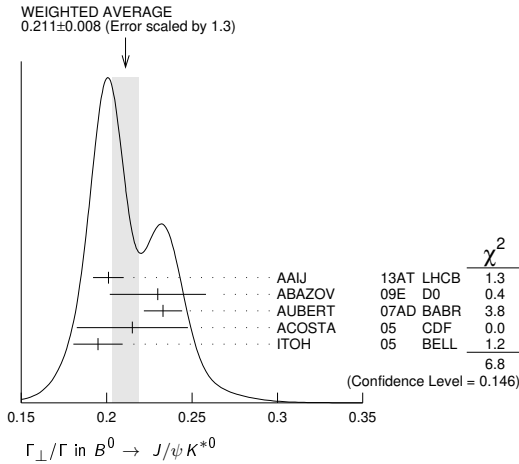
- ⁸ Averaged over an admixture of B^0 and B^- decays and the P wave fraction is $(16.0 \pm 3.2 \pm 1.4) \times 10^{-2}$.

Γ_L/Γ in $B^0 \rightarrow J/\psi K^{*0}$

VALUE	DOCUMENT ID	TECN	COMMENT
0.211 ± 0.008 OUR AVERAGE			Error includes scale factor of 1.3. See the ideogram below.
$0.201 \pm 0.004 \pm 0.008$	AAIJ	13AT LHCB	pp at 7 TeV
$0.230 \pm 0.013 \pm 0.025$	1 ABAZOV	09E D0	$p\bar{p}$ at 1.96 TeV
$0.233 \pm 0.010 \pm 0.005$	2 AUBERT	07AD BABR	$e^+ e^- \rightarrow \Upsilon(4S)$
$0.215 \pm 0.032 \pm 0.006$	ACOSTA	05 CDF	$p\bar{p}$ at 1.96 TeV
$0.195 \pm 0.012 \pm 0.008$	ITOH	05 BELL	$e^+ e^- \rightarrow \Upsilon(4S)$

- ¹ Measured the angular and lifetime parameters for the time-dependent angular untagged decays $B_d^0 \rightarrow J/\psi K^{*0}$ and $B_s^0 \rightarrow J/\psi \phi$.

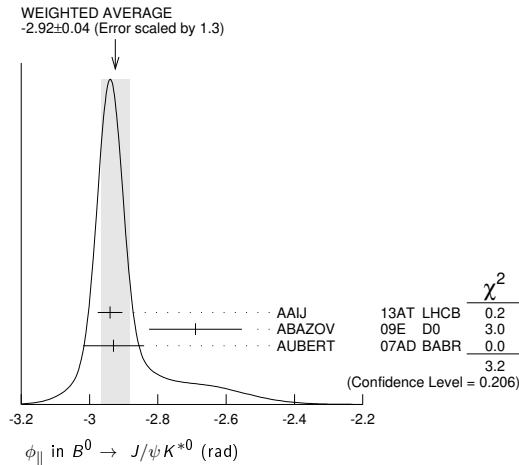
- ² Obtained by combining the B^0 and B^+ modes.



φ_{||} in B⁰ → J/ψK*⁰

VALUE (rad)	DOCUMENT ID	TECN	COMMENT
-2.92±0.04 OUR AVERAGE	Error includes scale factor of 1.3. See the ideogram below.		
-2.94±0.02±0.03	AAIJ	13AT	LHCB pp at 7 TeV
-2.69±0.08±0.11	¹ ABAZOV	09E	D0 p \bar{p} at 1.96 TeV
-2.93±0.08±0.04	² AUBERT	07AD	BABR e ⁺ e ⁻ → T(4S)

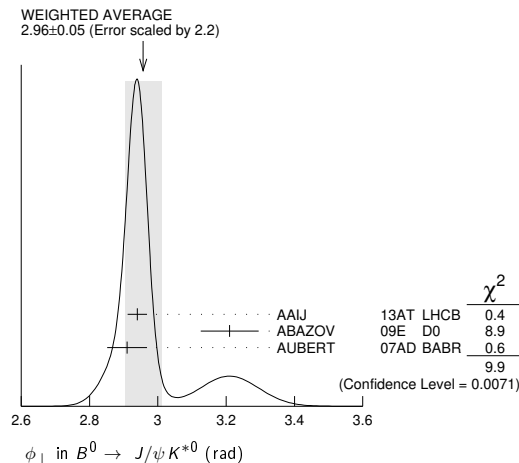
¹ Obtained by combining φ_{||} as δ₂ - δ₁, assuming they are uncorrelated.
² Obtained by combining the B⁰ and B⁺ modes.



φ_⊥ in B⁰ → J/ψK*⁰

VALUE (rad)	DOCUMENT ID	TECN	COMMENT
2.96±0.05 OUR AVERAGE	Error includes scale factor of 2.2. See the ideogram below.		
2.94±0.02±0.02	AAIJ	13AT	LHCB pp at 7 TeV
3.21±0.06±0.06	ABAZOV	09E	D0 p \bar{p} at 1.96 TeV
2.91±0.05±0.03	¹ AUBERT	07AD	BABR e ⁺ e ⁻ → T(4S)

¹ Obtained by combining the B⁰ and B⁺ modes.



Γ_⊥/Γ in B⁰ → ψ(2S)K*(892)⁰

VALUE	DOCUMENT ID	TECN	COMMENT
0.463^{+0.028}_{-0.040} OUR AVERAGE			
0.455 ^{+0.031+0.014} _{-0.029-0.049}	CHILIKIN	13	BELL e ⁺ e ⁻ → T(4S)
0.48 ± 0.05 ± 0.02	¹ AUBERT	07AD	BABR e ⁺ e ⁻ → T(4S)
0.45 ± 0.11 ± 0.04	² RICHICHI	01	CLE2 e ⁺ e ⁻ → T(4S)
••• We do not use the following data for averages, fits, limits, etc. •••			
0.448 ^{+0.040+0.040} _{-0.027-0.053}	MIZUK	09	BELL e ⁺ e ⁻ → T(4S)

¹ Obtained by combining the B⁰ and B⁺ modes.
² Averages between charged and neutral B mesons.

Γ_⊥/Γ in B⁰ → ψ(2S)K*⁰

VALUE	DOCUMENT ID	TECN	COMMENT
0.30±0.06±0.02	¹ AUBERT	07AD	BABR e ⁺ e ⁻ → T(4S)

¹ Obtained by combining the B⁰ and B⁺ modes.

φ_{||} in B⁰ → ψ(2S)K*⁰

VALUE (rad)	DOCUMENT ID	TECN	COMMENT
-2.8±0.4±0.1	¹ AUBERT	07AD	BABR e ⁺ e ⁻ → T(4S)

¹ Obtained by combining the B⁰ and B⁺ modes.

φ_⊥ in B⁰ → ψ(2S)K*⁰

VALUE (rad)	DOCUMENT ID	TECN	COMMENT
2.8±0.3±0.1	¹ AUBERT	07AD	BABR e ⁺ e ⁻ → T(4S)

¹ Obtained by combining the B⁰ and B⁺ modes.

Γ_⊥/Γ in B⁰ → χ_{c1}K*(892)⁰

VALUE	DOCUMENT ID	TECN	COMMENT
0.83^{+0.06}_{-0.08} OUR AVERAGE	Error includes scale factor of 1.3.		
0.947 ^{+0.038+0.046} _{-0.048-0.099}	MIZUK	08	BELL e ⁺ e ⁻ → T(4S)
0.77 ± 0.07 ± 0.04	¹ AUBERT	07AD	BABR e ⁺ e ⁻ → T(4S)

¹ Obtained by combining the B⁰ and B⁺ modes.

Γ_⊥/Γ in B⁰ → χ_{c1}K*(892)⁰

VALUE	DOCUMENT ID	TECN	COMMENT
0.03±0.04±0.02	¹ AUBERT	07AD	BABR e ⁺ e ⁻ → T(4S)

¹ Obtained by combining the B⁰ and B⁺ modes.

φ_{||} in B⁰ → χ_{c1}K*(892)⁰

VALUE (rad)	DOCUMENT ID	TECN	COMMENT
0.0±0.3±0.1	¹ AUBERT	07AD	BABR e ⁺ e ⁻ → T(4S)

¹ Obtained by combining the B⁰ and B⁺ modes.

Γ_⊥/Γ in B⁰ → D*⁻ℓ⁺ν_ℓ

VALUE	DOCUMENT ID	TECN	COMMENT
0.487±0.017±0.005	PRIM	23	BELL e ⁺ e ⁻ → T(4S)

Γ_⊥/Γ in B⁰ → D*⁻e⁺ν_e

VALUE	DOCUMENT ID	TECN	COMMENT
0.516±0.013 OUR AVERAGE	Error includes scale factor of 1.9.		
0.520±0.005±0.005	ADACHI	23j	BELL e ⁺ e ⁻ → T(4S)
0.471±0.024±0.007	PRIM	23	BELL e ⁺ e ⁻ → T(4S)

Γ_⊥/Γ in B⁰ → D*⁻μ⁺ν_μ

VALUE	DOCUMENT ID	TECN	COMMENT
0.525±0.007 OUR AVERAGE			
0.527±0.005±0.005	ADACHI	23j	BELL e ⁺ e ⁻ → T(4S)
0.504±0.023±0.007	PRIM	23	BELL e ⁺ e ⁻ → T(4S)

Δ(Γ_⊥/Γ) in B⁰ → D*⁻ℓ⁺ν_ℓ

$$\Delta(\Gamma_{\perp}/\Gamma) = (\Gamma_{\perp}/\Gamma)^{\mu} - (\Gamma_{\perp}/\Gamma)^e$$

VALUE	DOCUMENT ID	TECN	COMMENT
0.008±0.008 OUR AVERAGE			
0.006±0.007±0.005	ADACHI	23j	BELL e ⁺ e ⁻ → T(4S)
0.033±0.033±0.010	PRIM	23	BELL e ⁺ e ⁻ → T(4S)

Γ_⊥/Γ in B⁰ → D_s⁺D*⁻

VALUE	DOCUMENT ID	TECN	COMMENT
0.574±0.014 OUR AVERAGE			
0.578±0.010±0.011	¹ AAIJ	21s	LHCB pp at 13 TeV
0.519±0.050±0.028	² AUBERT	03i	BABR e ⁺ e ⁻ → T(4S)
0.506±0.139±0.036	AHMED	00b	CLE2 e ⁺ e ⁻ → T(4S)

¹ AAJ 21s uses D_s⁺ → D_s⁺γ decays.

² Measurement performed using partial reconstruction of D*⁻ decay.

Meson Particle Listings

 B^0 $|H_+|$ in $B^0 \rightarrow D_s^{*+} D^{*-}$

H_+, H_- define parity-even (\parallel) and parity-odd (\perp) polarization transversity amplitudes
 $A_{\parallel,\perp} = (H_+ \pm H_-)/\sqrt{2}$.

VALUE	DOCUMENT ID	TECN	COMMENT
$0.195 \pm 0.022 \pm 0.032$	¹ AAIJ	21s	BELL pp at 13 TeV

¹ AAIJ 21s uses $D_s^{*+} \rightarrow D_s^+ \gamma$ decays.

 $|H_-|$ in $B^0 \rightarrow D_s^{*+} D^{*-}$

H_+, H_- define parity-even (\parallel) and parity-odd (\perp) polarization transversity amplitudes
 $A_{\parallel,\perp} = (H_+ \pm H_-)/\sqrt{2}$.

VALUE	DOCUMENT ID	TECN	COMMENT
$0.620 \pm 0.011 \pm 0.013$	¹ AAIJ	21s	LHCB pp at 13 TeV

¹ AAIJ 21s uses $D_s^{*+} \rightarrow D_s^+ \gamma$ decays.

 ϕ_+ in $B^0 \rightarrow D_s^{*+} D^{*-}$

VALUE	DOCUMENT ID	TECN	COMMENT
$-0.046 \pm 0.102 \pm 0.020$	¹ AAIJ	21s	LHCB pp at 13 TeV

¹ AAIJ 21s uses $D_s^{*+} \rightarrow D_s^+ \gamma$ decays.

 ϕ_- in $B^0 \rightarrow D_s^{*+} D^{*-}$

VALUE	DOCUMENT ID	TECN	COMMENT
$0.108 \pm 0.170 \pm 0.051$	¹ AAIJ	21s	LHCB pp at 13 TeV

¹ AAIJ 21s uses $D_s^{*+} \rightarrow D_s^+ \gamma$ decays.

 Γ_L/Γ in $B^0 \rightarrow D^{*-} \rho^+$

VALUE	DOCUMENT ID	TECN	COMMENT
$0.895 \pm 0.016 \pm 0.012$	CSORNA	03	CLE2 $e^+ e^- \rightarrow \Upsilon(4S)$

• • • We do not use the following data for averages, fits, limits, etc. • • •

$0.93 \pm 0.05 \pm 0.05$	76	ALAM	94	CLE2	$e^+ e^- \rightarrow \Upsilon(4S)$
--------------------------	----	------	----	------	------------------------------------

 Γ_L/Γ in $B^0 \rightarrow D_s^{*+} \rho^-$

VALUE	DOCUMENT ID	TECN	COMMENT
$0.84 \pm 0.26 \pm 0.13$	¹ AUBERT	08AJ	BABR $e^+ e^- \rightarrow \Upsilon(4S)$

¹ Assumes equal production of B^+ and B^0 at the $\Upsilon(4S)$.

 Γ_L/Γ in $B^0 \rightarrow D_s^{*+} K^{*-}$

VALUE	DOCUMENT ID	TECN	COMMENT
$0.92 \pm 0.37 \pm 0.07$	¹ AUBERT	08AJ	BABR $e^+ e^- \rightarrow \Upsilon(4S)$

¹ Assumes equal production of B^+ and B^0 at the $\Upsilon(4S)$.

 Γ_L/Γ in $B^0 \rightarrow D^{*+} D^{*-}$

VALUE	DOCUMENT ID	TECN	COMMENT
$0.624 \pm 0.029 \pm 0.011$	KRONENBIT...12	BELL	$e^+ e^- \rightarrow \Upsilon(4S)$

• • • We do not use the following data for averages, fits, limits, etc. • • •

$0.57 \pm 0.08 \pm 0.02$	MIYAKE	05	BELL	Repl. by KRONENBITTER 12
--------------------------	--------	----	------	--------------------------

 Γ_{\perp}/Γ in $B^0 \rightarrow D^{*+} D^{*-}$

VALUE	DOCUMENT ID	TECN	COMMENT
0.147 ± 0.019 OUR AVERAGE			

$0.138 \pm 0.024 \pm 0.006$	KRONENBIT...12	BELL	$e^+ e^- \rightarrow \Upsilon(4S)$
-----------------------------	----------------	------	------------------------------------

$0.158 \pm 0.028 \pm 0.006$	AUBERT	09c	BABR $e^+ e^- \rightarrow \Upsilon(4S)$
-----------------------------	--------	-----	---

• • • We do not use the following data for averages, fits, limits, etc. • • •

$0.125 \pm 0.043 \pm 0.023$	VERVINK	09	BELL	Repl. by KRONENBITTER 12
-----------------------------	---------	----	------	--------------------------

$0.143 \pm 0.034 \pm 0.008$	AUBERT	07Bo	BABR	Repl. by AUBERT 09c
-----------------------------	--------	------	------	---------------------

$0.125 \pm 0.044 \pm 0.007$	AUBERT, BE	05A	BABR	Repl. by AUBERT 07Bo
-----------------------------	------------	-----	------	----------------------

$0.19 \pm 0.08 \pm 0.01$	MIYAKE	05	BELL	Repl. by VERVINK 09
--------------------------	--------	----	------	---------------------

$0.063 \pm 0.055 \pm 0.009$	AUBERT	03q	BABR	Repl. by AUBERT, BE 05A
-----------------------------	--------	-----	------	-------------------------

 Γ_L/Γ in $B^0 \rightarrow \bar{D}^{*0} \omega$

VALUE	DOCUMENT ID	TECN	COMMENT
$0.665 \pm 0.047 \pm 0.015$	LEES	11M	BABR $e^+ e^- \rightarrow \Upsilon(4S)$

 Γ_L/Γ in $B^0 \rightarrow \bar{D}_1(2430)^0 \omega$

VALUE (%)	DOCUMENT ID	TECN	COMMENT
$63.0 \pm 9.1 \pm 6.5$ -6.0	^{1,2} MATVIENKO	15	BELL $e^+ e^- \rightarrow \Upsilon(4S)$

¹ Obtained by amplitude analysis of $\bar{B}^0 \rightarrow D^{*-} \omega \pi^+$. The second uncertainty combines in quadrature experimental systematic and model uncertainties.

² Assumes equal production of B^0 and B^+ at $\Upsilon(4S)$.

 Γ_L/Γ in $B^0 \rightarrow \bar{D}_1(2420)^0 \omega$

VALUE (%)	DOCUMENT ID	TECN	COMMENT
$67.1 \pm 11.7 \pm 2.3$ -5.0	^{1,2} MATVIENKO	15	BELL $e^+ e^- \rightarrow \Upsilon(4S)$

¹ Obtained by amplitude analysis of $\bar{B}^0 \rightarrow D^{*-} \omega \pi^+$. The second uncertainty combines in quadrature experimental systematic and model uncertainties.

² Assumes equal production of B^0 and B^+ at $\Upsilon(4S)$.

 Γ_L/Γ in $B^0 \rightarrow \bar{D}_2^*(2460)^0 \omega$

VALUE (%)	DOCUMENT ID	TECN	COMMENT
$76.0 \pm 18.3 \pm 3.5$ $-8.5 - 2.8$	^{1,2} MATVIENKO	15	BELL $e^+ e^- \rightarrow \Upsilon(4S)$

¹ Obtained by amplitude analysis of $\bar{B}^0 \rightarrow D^{*-} \omega \pi^+$. The second uncertainty combines in quadrature experimental systematic and model uncertainties.

² Assumes equal production of B^0 and B^+ at $\Upsilon(4S)$.

 Γ_L/Γ in $B^0 \rightarrow D^{*-} \omega \pi^+$

VALUE	DOCUMENT ID	TECN	COMMENT
$0.654 \pm 0.042 \pm 0.016$	¹ AUBERT	06L	BABR $e^+ e^- \rightarrow \Upsilon(4S)$

¹ Invariant mass of the $[\omega \pi]$ system is restricted in the region 1.1 and 1.9 GeV.

 Γ_L/Γ in $B^0 \rightarrow \omega K^{*0}$

VALUE	DOCUMENT ID	TECN	COMMENT
0.69 ± 0.11 OUR AVERAGE			
$0.68 \pm 0.17 \pm 0.16$	AAIJ	19J	LHCB pp at 7, 8 TeV
$0.72 \pm 0.14 \pm 0.02$	AUBERT	09H	BABR $e^+ e^- \rightarrow \Upsilon(4S)$
$0.56 \pm 0.29 \pm 0.18$ -0.08	GOLDENZWE...08	BELL	$e^+ e^- \rightarrow \Upsilon(4S)$

 Γ_L/Γ in $B^0 \rightarrow \omega K^*(892)^0$

VALUE	DOCUMENT ID	TECN	COMMENT
$0.10 \pm 0.09 \pm 0.09$	AAIJ	19J	LHCB pp at 7, 8 TeV

 A_{CP}^0 in $B^0 \rightarrow \omega K^*(892)^0$

VALUE	DOCUMENT ID	TECN	COMMENT
$-0.13 \pm 0.27 \pm 0.13$	AAIJ	19J	LHCB pp at 7, 8 TeV

 A_{CP}^{\perp} in $B^0 \rightarrow \omega K^*(892)^0$

VALUE	DOCUMENT ID	TECN	COMMENT
$0.3 \pm 0.8 \pm 0.4$	AAIJ	19J	LHCB pp at 7, 8 TeV

 A_{CP}^{\parallel} in $B^0 \rightarrow \omega K^*(892)^0$

VALUE	DOCUMENT ID	TECN	COMMENT
$0.26 \pm 0.55 \pm 0.22$	AAIJ	19J	LHCB pp at 7, 8 TeV

 ϕ_0 in $B^0 \rightarrow \omega K^*(892)^0$

VALUE	DOCUMENT ID	TECN	COMMENT
$-0.86 \pm 0.29 \pm 0.71$	AAIJ	19J	LHCB pp at 7, 8 TeV

 ϕ_{\perp} in $B^0 \rightarrow \omega K^*(892)^0$

VALUE	DOCUMENT ID	TECN	COMMENT
$1.6 \pm 0.4 \pm 0.6$	AAIJ	19J	LHCB pp at 7, 8 TeV

 ϕ_{\parallel} in $B^0 \rightarrow \omega K^*(892)^0$

VALUE	DOCUMENT ID	TECN	COMMENT
$-1.83 \pm 0.29 \pm 0.32$	AAIJ	19J	LHCB pp at 7, 8 TeV

 Γ_L/Γ in $B^0 \rightarrow \omega K_2^*(1430)^0$

VALUE	DOCUMENT ID	TECN	COMMENT
$0.45 \pm 0.12 \pm 0.02$	AUBERT	09H	BABR $e^+ e^- \rightarrow \Upsilon(4S)$

 Γ_L/Γ in $B^0 \rightarrow K^{*0} \bar{K}^{*0}$

VALUE	DOCUMENT ID	TECN	COMMENT
0.74 ± 0.05 OUR AVERAGE			

$0.724 \pm 0.051 \pm 0.016$	¹ AAIJ	19L	LHCB pp at 7 and 8 TeV
-----------------------------	-------------------	-----	--------------------------

$0.80 \pm 0.10 \pm 0.06$ -0.12	AUBERT	08i	BABR $e^+ e^- \rightarrow \Upsilon(4S)$
-------------------------------------	--------	-----	---

¹ Untagged and time-integrated analysis within 150 MeV of the K^{*0} mass.

 Γ_L/Γ in $B^0 \rightarrow \phi K^*(892)^0$

VALUE	DOCUMENT ID	TECN	COMMENT
0.497 ± 0.017 OUR AVERAGE			

$0.497 \pm 0.019 \pm 0.015$	AAIJ	14AM	LHCB pp at 7 TeV
-----------------------------	------	------	--------------------

$0.499 \pm 0.030 \pm 0.018$	PRIM	13	BELL $e^+ e^- \rightarrow \Upsilon(4S)$
-----------------------------	------	----	---

$0.494 \pm 0.034 \pm 0.013$	AUBERT	08BG	BABR $e^+ e^- \rightarrow \Upsilon(4S)$
-----------------------------	--------	------	---

• • • We do not use the following data for averages, fits, limits, etc. • • •

$0.506 \pm 0.040 \pm 0.015$	AUBERT	07D	BABR	Repl. by AUBERT 08BG
-----------------------------	--------	-----	------	----------------------

$0.45 \pm 0.05 \pm 0.02$	CHEN	05A	BELL	Repl. by PRIM 13
--------------------------	------	-----	------	------------------

$0.52 \pm 0.05 \pm 0.02$	¹ AUBERT, B	04W	BABR	Repl. by AUBERT 07D
--------------------------	------------------------	-----	------	---------------------

$0.65 \pm 0.07 \pm 0.02$	AUBERT	03V	BABR	Repl. by AUBERT, B 04W
--------------------------	--------	-----	------	------------------------

$0.41 \pm 0.10 \pm 0.04$	CHEN	03B	BELL	Repl. by CHEN 05A
--------------------------	------	-----	------	-------------------

¹ AUBERT, B 04W also measures the fraction of parity-odd transverse contribution $f_{\perp} = 0.22 \pm 0.05 \pm 0.02$ and the phases of the parity-even and parity-odd transverse amplitudes relative to the longitudinal amplitude.

 Γ_{\perp}/Γ in $B^0 \rightarrow \phi K^*(892)^0$

VALUE	DOCUMENT ID	TECN	COMMENT
0.224 ± 0.015 OUR AVERAGE			

$0.221 \pm 0.016 \pm 0.013$	AAIJ	14AM	LHCB pp at 7 TeV
-----------------------------	------	------	--------------------

$0.238 \pm 0.026 \pm 0.008$	PRIM	13	BELL $e^+ e^- \rightarrow \Upsilon(4S)$
-----------------------------	------	----	---

$0.212 \pm 0.032 \pm 0.013$	AUBERT	08BG	BABR $e^+ e^- \rightarrow \Upsilon(4S)$
-----------------------------	--------	------	---

• • • We do not use the following data for averages, fits, limits, etc. • • •

$0.227 \pm 0.038 \pm 0.013$	AUBERT	07D	BABR	Repl. by AUBERT 08BG
-----------------------------	--------	-----	------	----------------------

$0.31 \pm 0.06 \pm 0.02$ -0.05	¹ CHEN	05A	BELL	Repl. by PRIM 13
-------------------------------------	-------------------	-----	------	------------------

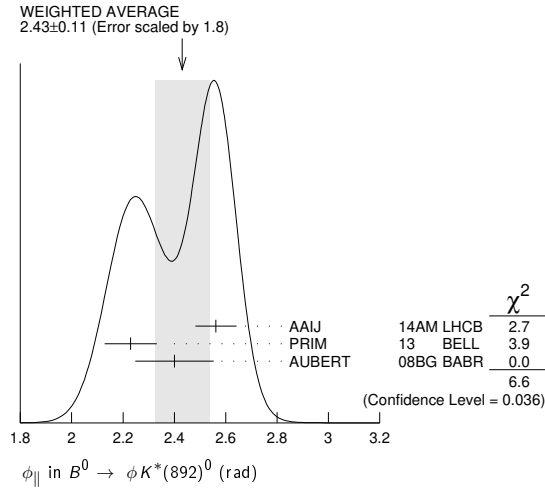
$0.22 \pm 0.05 \pm 0.02$	AUBERT, B	04W	BABR	Repl. by AUBERT 07D
--------------------------	-----------	-----	------	---------------------

¹ This quantity was recalculated by the BELLE authors from numbers in the original paper.

ϕ_{\parallel} in $B^0 \rightarrow \phi K^*(892)^0$

VALUE (rad)	DOCUMENT ID	TECN	COMMENT
2.43 ± 0.11 OUR AVERAGE	Error includes scale factor of 1.8. See the ideogram below.		
2.562 ± 0.069 ± 0.040	AAIJ	14AMLHCB	pp at 7 TeV
2.23 ± 0.10 ± 0.02	PRIM	13 BELL	e ⁺ e ⁻ → $\Upsilon(4S)$
2.40 ± 0.13 ± 0.08	AUBERT	08BG BABR	e ⁺ e ⁻ → $\Upsilon(4S)$
••• We do not use the following data for averages, fits, limits, etc. •••			
2.31 ± 0.14 ± 0.08	AUBERT	07D BABR	Repl. by AUBERT 08Bg
2.40 +0.28 -0.24 ± 0.07	¹ CHEN	05A BELL	Repl. by PRIM 13
2.34 +0.23 -0.20 ± 0.05	AUBERT,B	04W BABR	Repl. by AUBERT 07D

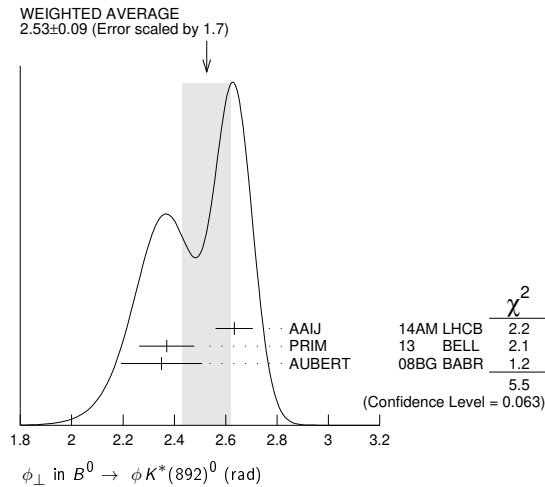
¹ This quantity was recalculated by the BELLE authors from numbers in the original paper.



ϕ_{\perp} in $B^0 \rightarrow \phi K^*(892)^0$

VALUE (rad)	DOCUMENT ID	TECN	COMMENT
2.53 ± 0.09 OUR AVERAGE	Error includes scale factor of 1.7. See the ideogram below.		
2.633 ± 0.062 ± 0.037	AAIJ	14AM LHCB	pp at 7 TeV
2.37 ± 0.10 ± 0.04	PRIM	13 BELL	e ⁺ e ⁻ → $\Upsilon(4S)$
2.35 ± 0.13 ± 0.09	AUBERT	08BG BABR	e ⁺ e ⁻ → $\Upsilon(4S)$
••• We do not use the following data for averages, fits, limits, etc. •••			
2.24 ± 0.15 ± 0.09	AUBERT	07D BABR	Repl. by AUBERT 08Bg
2.51 ± 0.25 ± 0.06	¹ CHEN	05A BELL	Repl. by PRIM 13
2.47 ± 0.25 ± 0.05	AUBERT,B	04W BABR	Repl. by AUBERT 07D

¹ This quantity was recalculated by the BELLE authors from numbers in the original paper.



$\delta_0(B^0 \rightarrow \phi K^*(892)^0)$

VALUE (rad)	DOCUMENT ID	TECN	COMMENT
2.88 ± 0.10 OUR AVERAGE	Error includes scale factor of 1.1.		
2.91 ± 0.10 ± 0.08	PRIM	13 BELL	e ⁺ e ⁻ → $\Upsilon(4S)$
2.82 ± 0.15 ± 0.09	AUBERT	08BG BABR	e ⁺ e ⁻ → $\Upsilon(4S)$
••• We do not use the following data for averages, fits, limits, etc. •••			
2.78 ± 0.17 ± 0.09	AUBERT	07D BABR	Repl. by AUBERT 08Bg

A_{CP}^0 in $B^0 \rightarrow \phi K^*(892)^0$

VALUE	DOCUMENT ID	TECN	COMMENT
-0.007 ± 0.030 OUR AVERAGE			
-0.003 ± 0.038 ± 0.005	AAIJ	14AM LHCB	pp at 7 TeV
-0.030 ± 0.061 ± 0.007	PRIM	13 BELL	e ⁺ e ⁻ → $\Upsilon(4S)$
0.01 ± 0.07 ± 0.02	AUBERT	08BG BABR	e ⁺ e ⁻ → $\Upsilon(4S)$
••• We do not use the following data for averages, fits, limits, etc. •••			
-0.03 ± 0.08 ± 0.02	AUBERT	07D BABR	Repl. by AUBERT 08Bg
0.13 ± 0.12 ± 0.04	¹ CHEN	05A BELL	Repl. by PRIM 13
-0.06 ± 0.10 ± 0.01	AUBERT,B	04W BABR	Repl. by AUBERT 07D

¹ This quantity was recalculated by the BELLE authors from numbers in the original paper.

A_{CP}^{\perp} in $B^0 \rightarrow \phi K^*(892)^0$

VALUE	DOCUMENT ID	TECN	COMMENT
-0.02 ± 0.06 OUR AVERAGE			
0.047 ± 0.074 ± 0.009	AAIJ	14AM LHCB	pp at 7 TeV
-0.14 ± 0.11 ± 0.01	PRIM	13 BELL	e ⁺ e ⁻ → $\Upsilon(4S)$
-0.04 ± 0.15 ± 0.06	AUBERT	08BG BABR	e ⁺ e ⁻ → $\Upsilon(4S)$
••• We do not use the following data for averages, fits, limits, etc. •••			
-0.03 ± 0.16 ± 0.05	AUBERT	07D BABR	Repl. by AUBERT 08Bg
-0.20 ± 0.18 ± 0.04	¹ CHEN	05A BELL	Repl. by PRIM 13
-0.10 ± 0.24 ± 0.05	AUBERT,B	04W BABR	Repl. by AUBERT 07D

¹ This quantity was recalculated by the BELLE authors from numbers in the original paper.

$\Delta\phi_{\parallel}$ in $B^0 \rightarrow \phi K^*(892)^0$

VALUE (rad)	DOCUMENT ID	TECN	COMMENT
0.05 ± 0.05 OUR AVERAGE			
0.045 ± 0.069 ± 0.015	AAIJ	14AM LHCB	pp at 7 TeV
-0.02 ± 0.10 ± 0.01	PRIM	13 BELL	e ⁺ e ⁻ → $\Upsilon(4S)$
0.22 ± 0.12 ± 0.08	AUBERT	08BG BABR	e ⁺ e ⁻ → $\Upsilon(4S)$
••• We do not use the following data for averages, fits, limits, etc. •••			
0.24 ± 0.14 ± 0.08	AUBERT	07D BABR	Repl. by AUBERT 08Bg
-0.32 ± 0.27 ± 0.07	¹ CHEN	05A BELL	Repl. by PRIM 13
0.27 +0.20 -0.23 ± 0.05	AUBERT,B	04W BABR	Repl. by AUBERT 07D

¹ This quantity was recalculated by the BELLE authors from numbers in the original paper.

$\Delta\phi_{\perp}$ in $B^0 \rightarrow \phi K^*(892)^0$

VALUE (rad)	DOCUMENT ID	TECN	COMMENT
0.08 ± 0.05 OUR AVERAGE			
0.062 ± 0.062 ± 0.005	AAIJ	14AM LHCB	pp at 7 TeV
0.05 ± 0.10 ± 0.02	PRIM	13 BELL	e ⁺ e ⁻ → $\Upsilon(4S)$
0.21 ± 0.13 ± 0.08	AUBERT	08BG BABR	e ⁺ e ⁻ → $\Upsilon(4S)$
••• We do not use the following data for averages, fits, limits, etc. •••			
0.19 ± 0.15 ± 0.08	AUBERT	07D BABR	Repl. by AUBERT 08Bg
-0.30 ± 0.25 ± 0.06	¹ CHEN	05A BELL	Repl. by PRIM 13
0.36 ± 0.25 ± 0.05	AUBERT,B	04W BABR	Repl. by AUBERT 07D

¹ This quantity was recalculated by the BELLE authors from numbers in the original paper.

$\Delta\delta_0(B^0 \rightarrow \phi K^*(892)^0)$

VALUE (rad)	DOCUMENT ID	TECN	COMMENT
0.13 ± 0.09 OUR AVERAGE			
0.08 ± 0.10 ± 0.01	PRIM	13 BELL	e ⁺ e ⁻ → $\Upsilon(4S)$
0.27 ± 0.14 ± 0.08	AUBERT	08BG BABR	e ⁺ e ⁻ → $\Upsilon(4S)$
••• We do not use the following data for averages, fits, limits, etc. •••			
0.21 ± 0.17 ± 0.08	AUBERT	07D BABR	Repl. by AUBERT 08Bg

$\Delta\phi_{00}(B^0 \rightarrow \phi K_0^*(1430)^0)$

VALUE (rad)	DOCUMENT ID	TECN	COMMENT
0.28 ± 0.42 ± 0.04	AUBERT	08BG BABR	e ⁺ e ⁻ → $\Upsilon(4S)$

Γ_{\perp}/Γ in $B^0 \rightarrow \phi K_2^*(1430)^0$

VALUE	DOCUMENT ID	TECN	COMMENT
0.913 +0.028 -0.050 OUR AVERAGE			
0.918 +0.029 -0.060 ± 0.012	PRIM	13 BELL	e ⁺ e ⁻ → $\Upsilon(4S)$
0.901 +0.046 -0.058 ± 0.037	AUBERT	08BG BABR	e ⁺ e ⁻ → $\Upsilon(4S)$
••• We do not use the following data for averages, fits, limits, etc. •••			
0.853 +0.061 -0.069 ± 0.036	AUBERT	07D BABR	Repl. by AUBERT 08Bg

Γ_{\perp}/Γ in $B^0 \rightarrow \phi K_2^*(1430)^0$

VALUE	DOCUMENT ID	TECN	COMMENT
0.027 +0.031 -0.025 OUR AVERAGE	Error includes scale factor of 1.1.		
0.056 +0.050 -0.035 ± 0.009	PRIM	13 BELL	e ⁺ e ⁻ → $\Upsilon(4S)$
0.002 +0.018 -0.002 ± 0.031	AUBERT	08BG BABR	e ⁺ e ⁻ → $\Upsilon(4S)$
••• We do not use the following data for averages, fits, limits, etc. •••			
0.045 +0.049 -0.040 ± 0.013	AUBERT	07D BABR	Repl. by AUBERT 08Bg

Meson Particle Listings

 B^0 ϕ_{\parallel} in $B^0 \rightarrow \phi K_2^*(1430)^0$

VALUE (rad)	DOCUMENT ID	TECN	COMMENT
4.0 ± 0.4 OUR AVERAGE			
3.76 ± 2.88 ± 1.32	PRIM	13	BELL $e^+e^- \rightarrow \Upsilon(4S)$
3.96 ± 0.38 ± 0.06	AUBERT	08BG	BABR $e^+e^- \rightarrow \Upsilon(4S)$
••• We do not use the following data for averages, fits, limits, etc. •••			
2.90 ± 0.39 ± 0.06	AUBERT	07D	BABR Repl. by AUBERT 08BG

 ϕ_{\perp} in $B^0 \rightarrow \phi K_2^*(1430)^0$

VALUE (rad)	DOCUMENT ID	TECN	COMMENT
4.45^{+0.43}_{-0.38} ± 0.13			
••• We do not use the following data for averages, fits, limits, etc. •••			
5.72 ^{+0.55} _{-0.87} ± 0.11	AUBERT	07D	BABR Repl. by AUBERT 08BG

 $\delta_0(B^0 \rightarrow \phi K_2^*(1430)^0)$

VALUE (rad)	DOCUMENT ID	TECN	COMMENT
3.46 ± 0.14 OUR AVERAGE			
3.53 ± 0.11 ± 0.19	PRIM	13	BELL $e^+e^- \rightarrow \Upsilon(4S)$
3.41 ± 0.13 ± 0.13	AUBERT	08BG	BABR $e^+e^- \rightarrow \Upsilon(4S)$
••• We do not use the following data for averages, fits, limits, etc. •••			
3.54 ^{+0.12} _{-0.14} ± 0.06	AUBERT	07D	BABR Repl. by AUBERT 08BG

 A_{CP}^0 in $B^0 \rightarrow \phi K_2^*(1430)^0$

VALUE	DOCUMENT ID	TECN	COMMENT
-0.03 ± 0.04 OUR AVERAGE			
-0.016 ^{+0.066} _{-0.051} ± 0.008	PRIM	13	BELL $e^+e^- \rightarrow \Upsilon(4S)$
-0.05 ± 0.06 ± 0.01	AUBERT	08BG	BABR $e^+e^- \rightarrow \Upsilon(4S)$

 A_{CP}^{\perp} in $B^0 \rightarrow \phi K_2^*(1430)^0$

VALUE	DOCUMENT ID	TECN	COMMENT
-0.01^{+0.85}_{-0.67} ± 0.09	PRIM	13	BELL $e^+e^- \rightarrow \Upsilon(4S)$

 $\Delta\phi_{\parallel}(B^0 \rightarrow \phi K_2^*(1430)^0)$

VALUE (rad)	DOCUMENT ID	TECN	COMMENT
-0.9 ± 0.4 OUR AVERAGE			
-0.02 ± 1.08 ± 1.01	PRIM	13	BELL $e^+e^- \rightarrow \Upsilon(4S)$
-1.00 ± 0.38 ± 0.09	AUBERT	08BG	BABR $e^+e^- \rightarrow \Upsilon(4S)$

 $\Delta\phi_{\perp}(B^0 \rightarrow \phi K_2^*(1430)^0)$

VALUE	DOCUMENT ID	TECN	COMMENT
-0.19 ± 0.42 ± 0.11	PRIM	13	BELL $e^+e^- \rightarrow \Upsilon(4S)$

 $\Delta\delta_0$ in $B^0 \rightarrow \phi K_2^*(1430)^0$

VALUE (rad)	DOCUMENT ID	TECN	COMMENT
0.08 ± 0.09 OUR AVERAGE			
0.06 ± 0.11 ± 0.02	PRIM	13	BELL $e^+e^- \rightarrow \Upsilon(4S)$
0.11 ± 0.13 ± 0.06	AUBERT	08BG	BABR $e^+e^- \rightarrow \Upsilon(4S)$

 Γ_L/Γ in $B^0 \rightarrow K^*(892)^0 \rho^0$

VALUE	DOCUMENT ID	TECN	COMMENT
0.173 ± 0.026 OUR AVERAGE			
0.164 ± 0.015 ± 0.022	AAIJ	19J	LHCB pp at 7, 8 TeV
0.40 ± 0.08 ± 0.11	LEES	12K	BABR $e^+e^- \rightarrow \Upsilon(4S)$
••• We do not use the following data for averages, fits, limits, etc. •••			
0.57 ± 0.09 ± 0.08	AUBERT,B	06G	BABR Repl. by LEES 12K

 Γ_{\perp}/Γ in $B^0 \rightarrow K^*(892)^0 \rho^0$

VALUE	DOCUMENT ID	TECN	COMMENT
0.401 ± 0.016 ± 0.037	AAIJ	19J	LHCB pp at 7, 8 TeV

 A_{CP}^0 in $B^0 \rightarrow K^*(892)^0 \rho^0$

VALUE	DOCUMENT ID	TECN	COMMENT
-0.62 ± 0.09 ± 0.09	AAIJ	19J	LHCB pp at 7, 8 TeV

 A_{CP}^{\perp} in $B^0 \rightarrow K^*(892)^0 \rho^0$

VALUE	DOCUMENT ID	TECN	COMMENT
0.050 ± 0.039 ± 0.015	AAIJ	19J	LHCB pp at 7, 8 TeV

 A_{CP}^{\parallel} in $B^0 \rightarrow K^*(892)^0 \rho^0$

VALUE	DOCUMENT ID	TECN	COMMENT
0.188 ± 0.037 ± 0.022	AAIJ	19J	LHCB pp at 7, 8 TeV

 ϕ_0 in $B^0 \rightarrow K^*(892)^0 \rho^0$

VALUE	DOCUMENT ID	TECN	COMMENT
1.57 ± 0.08 ± 0.18	AAIJ	19J	LHCB pp at 7, 8 TeV

 ϕ_{\perp} in $B^0 \rightarrow K^*(892)^0 \rho^0$

VALUE	DOCUMENT ID	TECN	COMMENT
-2.365 ± 0.032 ± 0.054	AAIJ	19J	LHCB pp at 7, 8 TeV

 ϕ_{\parallel} in $B^0 \rightarrow K^*(892)^0 \rho^0$

VALUE	DOCUMENT ID	TECN	COMMENT
0.795 ± 0.030 ± 0.068	AAIJ	19J	LHCB pp at 7, 8 TeV

 Γ_L/Γ in $B^0 \rightarrow K^{*+} \rho^-$

VALUE	DOCUMENT ID	TECN	COMMENT
0.38 ± 0.13 ± 0.03	LEES	12K	BABR $e^+e^- \rightarrow \Upsilon(4S)$

 Γ_L/Γ in $B^0 \rightarrow \rho^+ \rho^-$

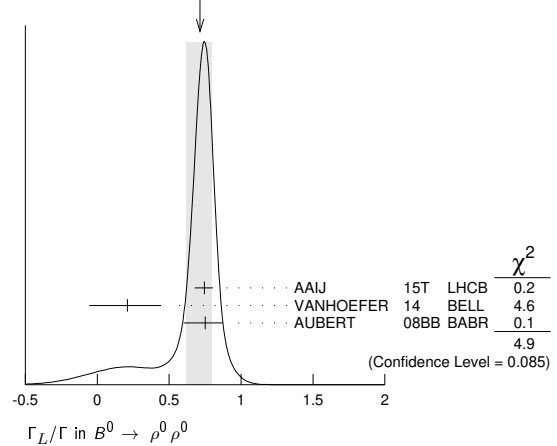
VALUE	DOCUMENT ID	TECN	COMMENT
0.990^{+0.021}_{-0.019} OUR AVERAGE			

0.988 ± 0.012 ± 0.023	VANHOEFER	16	BELL $e^+e^- \rightarrow \Upsilon(4S)$
0.992 ± 0.024 ^{+0.026} _{-0.013}	AUBERT	07BF	BABR $e^+e^- \rightarrow \Upsilon(4S)$
••• We do not use the following data for averages, fits, limits, etc. •••			
0.941 ^{+0.034} _{-0.040} ± 0.030	SOMOV	06	BELL Repl. by VANHOEFER 16
0.978 ± 0.014 ^{+0.021} _{-0.029}	AUBERT,B	05C	BABR Repl. by AUBERT 07BF
0.98 ^{+0.02} _{-0.08} ± 0.03	AUBERT	04G	BABR Repl. by AUBERT,B 04R
0.99 ± 0.03 ^{+0.04} _{-0.03}	AUBERT,B	04R	BABR Repl. by AUBERT,B 05C

 Γ_L/Γ in $B^0 \rightarrow \rho^0 \rho^0$

VALUE	DOCUMENT ID	TECN	COMMENT
0.71^{+0.08}_{-0.09} OUR AVERAGE			Error includes scale factor of 1.6. See the ideogram below.

0.745 ^{+0.048} _{-0.058} ± 0.034	AAIJ	15T	LHCB pp at 7, 8 TeV
0.21 ^{+0.18} _{-0.22} ± 0.15	VANHOEFER	14	BELL $e^+e^- \rightarrow \Upsilon(4S)$
0.75 ^{+0.11} _{-0.14} ± 0.05	AUBERT	08BB	BABR $e^+e^- \rightarrow \Upsilon(4S)$
••• We do not use the following data for averages, fits, limits, etc. •••			
0.87 ± 0.13 ± 0.04	AUBERT	07G	BABR Repl. by AUBERT 08BB

WEIGHTED AVERAGE
0.71±0.08-0.09 (Error scaled by 1.6) Γ_L/Γ in $B^0 \rightarrow a_1(1260)^+ a_1(1260)^-$

VALUE	DOCUMENT ID	TECN	COMMENT
0.31 ± 0.22 ± 0.10	AUBERT	09AL	BABR $e^+e^- \rightarrow \Upsilon(4S)$

 Γ_L/Γ in $B^0 \rightarrow \rho^0 \bar{p} K^*(892)^0$

VALUE	DOCUMENT ID	TECN	COMMENT
1.01 ± 0.13 ± 0.03	CHEN	08c	BELL $e^+e^- \rightarrow \Upsilon(4S)$

 Γ_L/Γ in $B^0 \rightarrow \Lambda \bar{\Lambda} K^*(892)^0$

VALUE	DOCUMENT ID	TECN	COMMENT
0.60 ± 0.22 ± 0.08	CHANG	09	BELL $e^+e^- \rightarrow \Upsilon(4S)$

 Γ_L/Γ in $B^0 \rightarrow K^*(892)^0 \mu^+ \mu^-$ ($0.04 < q^2 < 6.0 \text{ GeV}^2/c^4$)

VALUE	DOCUMENT ID	TECN	COMMENT
0.50 ± 0.06 ± 0.04	¹ AABOUD	18BY	ATLS pp at 8 TeV

¹ A set of angular parameters obtained for this decay is also presented. Γ_L/Γ in $B^0 \rightarrow K^*(892)^0 e^+ e^-$ (at low q^2)

VALUE	DOCUMENT ID	TECN	COMMENT
0.044 ± 0.026 ± 0.014	¹ AAIJ	20A0	LHCB pp at 7, 8, 13 TeV

••• We do not use the following data for averages, fits, limits, etc. •••

0.16 ± 0.06 ± 0.03	² AAIJ	15z	LHCB Repl. by AAIJ 20A0
--------------------	-------------------	-----	-------------------------

¹ Determined in the effective dielectron invariant mass range $0.0008 < q^2 < 0.257 \text{ GeV}^2/c^4$.² Determined in the effective dielectron invariant mass range $0.002 < q^2 < 1.120 \text{ GeV}^2/c^4$.

A_T⁽²⁾ in B⁰ → K*(892)⁰ e⁺ e⁻ (at low q²)

VALUE	DOCUMENT ID	TECN	COMMENT
0.11 ± 0.10 ± 0.02	¹ AAIJ	20A0 LHCb	pp at 7, 8, 13 TeV
• • • We do not use the following data for averages, fits, limits, etc. • • •			
-0.23 ± 0.23 ± 0.05	² AAIJ	15z LHCb	Repl. by AAIJ 20A0
¹ Determined in the effective dielectron invariant mass range 0.0008 < q ² < 0.257 GeV ² /c ⁴ .			
² Determined in the effective dielectron invariant mass range 0.002 < q ² < 1.120 GeV ² /c ⁴ .			

A_T^{Im} in B⁰ → K*(892)⁰ e⁺ e⁻ (at low q²)

VALUE	DOCUMENT ID	TECN	COMMENT
0.02 ± 0.10 ± 0.01	¹ AAIJ	20A0 LHCb	pp at 7, 8, 13 TeV
• • • We do not use the following data for averages, fits, limits, etc. • • •			
0.14 ± 0.22 ± 0.05	² AAIJ	15z LHCb	Repl. by AAIJ 20A0
¹ Determined in the effective dielectron invariant mass range 0.0008 < q ² < 0.257 GeV ² /c ⁴ .			
² Determined in the effective dielectron invariant mass range 0.002 < q ² < 1.120 GeV ² /c ⁴ .			

A_T^{Re} in B⁰ → K*(892)⁰ e⁺ e⁻ (at low q²)

Related to A_{FB}, F_L by A_T^{Re} = (4/3) A_{FB} / (1 - F_L).

VALUE	DOCUMENT ID	TECN	COMMENT
-0.06 ± 0.08 ± 0.02	¹ AAIJ	20A0 LHCb	pp at 7, 8, 13 TeV
• • • We do not use the following data for averages, fits, limits, etc. • • •			
0.10 ± 0.18 ± 0.05	² AAIJ	15z LHCb	Repl. by AAIJ 20A0
¹ Determined in the effective dielectron invariant mass range 0.0008 < q ² < 0.257 GeV ² /c ⁴ .			
² Determined in the effective dielectron invariant mass range 0.002 < q ² < 1.120 GeV ² /c ⁴ .			

See the related review(s):

B⁰ - B⁰ Mixing

B⁰-B⁰ MIXING PARAMETERS

For a discussion of B⁰-B⁰ mixing see the note on "B⁰-B⁰ Mixing" in the B⁰ Particle Listings above.

χ_d is a measure of the time-integrated B⁰-B⁰ mixing probability that a produced B⁰(B⁰) decays as a B⁰(B⁰). Mixing violates ΔB ≠ 2 rule.

$$\chi_d = \frac{x_d^2}{2(1+x_d^2)}$$

$$x_d = \frac{\Delta m_{B^0}}{\Gamma_{B^0}} = (m_{B_H^0} - m_{B_L^0}) \tau_{B^0}$$

where H, L stand for heavy and light states of two B⁰ CP eigenstates and $\tau_{B^0} = \frac{1}{0.5(\Gamma_{B_H^0} + \Gamma_{B_L^0})}$.

χ_d

This B⁰-B⁰ mixing parameter is the probability (integrated over time) that a produced B⁰ (or B⁰) decays as a B⁰ (or B⁰), e.g. for inclusive lepton decays

$$\chi_d = \frac{\Gamma(B^0 \rightarrow \ell^- X \text{ (via } \bar{B}^0)) / \Gamma(B^0 \rightarrow \ell^\pm X)}{\Gamma(\bar{B}^0 \rightarrow \ell^- X \text{ (via } B^0)) / \Gamma(\bar{B}^0 \rightarrow \ell^\pm X)}$$

Where experiments have measured the parameter r = χ/(1-χ), we have converted to χ. Mixing violates the ΔB ≠ 2 rule.

Note that the measurement of χ at energies higher than the Υ(4S) have not separated χ_d from χ_s where the subscripts indicate B⁰(B⁰d) or B_s⁰(B_s⁰s). They are listed in the B[±]/B_s⁰/B_s⁻/b-baryon ADMIXTURE section.

The experiments at Υ(4S) make an assumption about the B⁰-B⁰ fraction and about the ratio of the B[±] and B⁰ semileptonic branching ratios (usually that it equals one).

"OUR EVALUATION" is an average using rescaled values of the data listed below. The averaging/rescaling procedure takes into account correlations between the measurements, includes χ_d calculated from Δm_{B⁰} and τ_{B⁰}.

VALUE	CL%	DOCUMENT ID	TECN	COMMENT
0.1860 ± 0.0011 OUR EVALUATION		(Produced by HFLAV)		
0.182 ± 0.015 OUR AVERAGE				
0.198 ± 0.013 ± 0.014		¹ BEHRENS	00b CLE2	e ⁺ e ⁻ → Υ(4S)
0.16 ± 0.04 ± 0.04		² ALBRECHT	94 ARG	e ⁺ e ⁻ → Υ(4S)
0.149 ± 0.023 ± 0.022		³ BARTELT	93 CLE2	e ⁺ e ⁻ → Υ(4S)
0.171 ± 0.048		⁴ ALBRECHT	92L ARG	e ⁺ e ⁻ → Υ(4S)
• • • We do not use the following data for averages, fits, limits, etc. • • •				
0.20 ± 0.13 ± 0.12		⁵ ALBRECHT	96D ARG	e ⁺ e ⁻ → Υ(4S)
0.19 ± 0.07 ± 0.09		⁶ ALBRECHT	96D ARG	e ⁺ e ⁻ → Υ(4S)
0.24 ± 0.12		⁷ ELSEN	90 JADE	e ⁺ e ⁻ 35-44 GeV
0.158 ^{+0.052} / _{-0.059}		ARTUSO	89 CLEO	e ⁺ e ⁻ → Υ(4S)
0.17 ± 0.05		⁸ ALBRECHT	87I ARG	e ⁺ e ⁻ → Υ(4S)
<0.19	90	⁹ BEAN	87B CLEO	e ⁺ e ⁻ → Υ(4S)
<0.27	90	¹⁰ AVERY	84 CLEO	e ⁺ e ⁻ → Υ(4S)

¹ BEHRENS 00b uses high-momentum lepton tags and partially reconstructed B⁰ → D*⁺π⁻, ρ⁻ decays to determine the flavor of the B meson.

- ² ALBRECHT 94 reports r=0.194 ± 0.062 ± 0.054. We convert to χ for comparison. Uses tagged events (lepton + pion from D*⁺).
- ³ BARTELT 93 analysis performed using tagged events (lepton+pion from D*⁺). Using dilepton events they obtain 0.157 ± 0.016 ^{+0.033}/_{-0.028}.
- ⁴ ALBRECHT 92L is a combined measurement employing several lepton-based techniques. It uses all previous ARGUS data in addition to new data and therefore supersedes ALBRECHT 87I. A value of r = 20.6 ± 7.0% is directly measured. The value can be used to measure x = ΔM/Γ = 0.72 ± 0.15 for the B_d meson. Assumes f₊/f₀ = 1.0 ± 0.05 and uses τ_{B[±]}/τ_{B⁰} = (0.95 ± 0.14) (f₊/f₀).
- ⁵ Uses D*⁺ K[±] correlations.
- ⁶ Uses (D*⁺ℓ⁻) K[±] correlations.
- ⁷ These experiments see a combination of B_s and B_d mesons.
- ⁸ ALBRECHT 87I is inclusive measurement with like-sign dileptons, with tagged B decays plus leptons, and one fully reconstructed event. Measures r=0.21 ± 0.08. We convert to χ for comparison. Superseded by ALBRECHT 92L.
- ⁹ BEAN 87B measured r < 0.24; we converted to χ.
- ¹⁰ Same-sign dilepton events. Limit assumes semileptonic BR for B⁺ and B⁰ equal. If B⁰/B[±] ratio < 0.58, no limit exists. The limit was corrected in BEAN 87B from r < 0.30 to r < 0.37. We converted this limit to χ.

Δm_{B⁰} = m_{B_H⁰} - m_{B_L⁰}

Δm_{B⁰} is a measure of 2π times the B⁰-B⁰ oscillation frequency in time-dependent mixing experiments.

"OUR EVALUATION" is an average using rescaled values of the data listed below. The averaging/rescaling procedure takes into account correlations between the measurements and includes Δm_d calculated from χ_d measured at Υ(4S).

VALUE (10 ¹² h s ⁻¹)	DOCUMENT ID	TECN	COMMENT
0.5069 ± 0.0019 OUR EVALUATION	(Produced by HFLAV)		
0.516 ± 0.008 ± 0.005	¹ ABUDINEN	23D BELL	e ⁺ e ⁻ → Υ(4S)
0.5050 ± 0.0021 ± 0.0010	² AAIJ	16AV LHCb	pp at 7, 8 TeV
0.503 ± 0.011 ± 0.013	³ AAIJ	13CF LHCb	pp at 7 TeV
0.5156 ± 0.0051 ± 0.0033	⁴ AAIJ	13F LHCb	pp at 7 TeV
0.499 ± 0.032 ± 0.003	⁵ AAIJ	12I LHCb	pp at 7 TeV
0.506 ± 0.020 ± 0.016	⁶ ABZOV	06W D0	pp at 1.96 TeV
0.511 ± 0.007 ^{+0.007} / _{-0.006}	⁷ AUBERT	06G BABR	e ⁺ e ⁻ → Υ(4S)
0.511 ± 0.005 ± 0.006	⁸ ABE	05B BELL	e ⁺ e ⁻ → Υ(4S)
0.531 ± 0.025 ± 0.007	⁹ ABDALLAH	03B DLPH	e ⁺ e ⁻ → Z
0.492 ± 0.018 ± 0.013	¹⁰ AUBERT	03C BABR	e ⁺ e ⁻ → Υ(4S)
0.503 ± 0.008 ± 0.010	¹¹ HASTINGS	03 BELL	e ⁺ e ⁻ → Υ(4S)
0.509 ± 0.017 ± 0.020	¹² ZHENG	03 BELL	e ⁺ e ⁻ → Υ(4S)
0.516 ± 0.016 ± 0.010	¹³ AUBERT	02I BABR	e ⁺ e ⁻ → Υ(4S)
0.493 ± 0.012 ± 0.009	¹⁴ AUBERT	02I BABR	e ⁺ e ⁻ → Υ(4S)
0.497 ± 0.024 ± 0.025	¹⁵ ABBIENDI,G	00B OPAL	e ⁺ e ⁻ → Z
0.503 ± 0.064 ± 0.071	¹⁶ ABE	99K CDF	pp at 1.8 TeV
0.500 ± 0.052 ± 0.043	¹⁷ ABE	99Q CDF	pp at 1.8 TeV
0.516 ± 0.099 ^{+0.029} / _{-0.035}	¹⁸ AFFOLDER	99C CDF	pp at 1.8 TeV
0.471 ^{+0.078} / _{-0.068} ^{+0.033} / _{-0.034}	¹⁹ ABE	98C CDF	pp at 1.8 TeV
0.458 ± 0.046 ± 0.032	²⁰ ACCIARRI	98D L3	e ⁺ e ⁻ → Z
0.437 ± 0.043 ± 0.044	²¹ ACCIARRI	98D L3	e ⁺ e ⁻ → Z
0.472 ± 0.049 ± 0.053	²² ACCIARRI	98D L3	e ⁺ e ⁻ → Z
0.523 ± 0.072 ± 0.043	²³ ABREU	97N DLPH	e ⁺ e ⁻ → Z
0.493 ± 0.042 ± 0.027	²¹ ABREU	97N DLPH	e ⁺ e ⁻ → Z
0.499 ± 0.053 ± 0.015	²⁴ ABREU	97N DLPH	e ⁺ e ⁻ → Z
0.480 ± 0.040 ± 0.051	²⁰ ABREU	97N DLPH	e ⁺ e ⁻ → Z
0.444 ± 0.029 ^{+0.020} / _{-0.017}	²¹ ACKERSTAFF	97U OPAL	e ⁺ e ⁻ → Z
0.430 ± 0.043 ^{+0.028} / _{-0.030}	²⁰ ACKERSTAFF	97V OPAL	e ⁺ e ⁻ → Z
0.482 ± 0.044 ± 0.024	²⁵ BUSKULIC	97D ALEP	e ⁺ e ⁻ → Z
0.404 ± 0.045 ± 0.027	²¹ BUSKULIC	97D ALEP	e ⁺ e ⁻ → Z
0.452 ± 0.039 ± 0.044	²⁰ BUSKULIC	97D ALEP	e ⁺ e ⁻ → Z
0.539 ± 0.060 ± 0.024	²⁶ ALEXANDER	96V OPAL	e ⁺ e ⁻ → Z
0.567 ± 0.089 ^{+0.029} / _{-0.023}	²⁷ ALEXANDER	96V OPAL	e ⁺ e ⁻ → Z
• • • We do not use the following data for averages, fits, limits, etc. • • •			
0.516 ± 0.016 ± 0.010	²⁸ AUBERT	02N BABR	e ⁺ e ⁻ → Υ(4S)
0.494 ± 0.012 ± 0.015	²⁹ HARA	02 BELL	Repl. by ABE 05B
0.528 ± 0.017 ± 0.011	³⁰ TOMURA	02 BELL	Repl. by ABE 05B
0.463 ± 0.008 ± 0.016	¹⁴ ABE	01D BELL	Repl. by HASTINGS 03
0.444 ± 0.028 ± 0.028	³¹ ACCIARRI	98D L3	e ⁺ e ⁻ → Z
0.497 ± 0.035	³² ABREU	97N DLPH	e ⁺ e ⁻ → Z
0.467 ± 0.022 ^{+0.017} / _{-0.015}	³³ ACKERSTAFF	97V OPAL	e ⁺ e ⁻ → Z
0.446 ± 0.032	³⁴ BUSKULIC	97D ALEP	e ⁺ e ⁻ → Z
0.531 ^{+0.050} / _{-0.046} ± 0.078	³⁵ ABREU	96Q DLPH	Sup. by ABREU 97N
0.496 ^{+0.055} / _{-0.051} ± 0.043	²⁰ ACCIARRI	96E L3	Repl. by ACCIARRI 98D
0.548 ± 0.050 ^{+0.023} / _{-0.019}	³⁶ ALEXANDER	96V OPAL	e ⁺ e ⁻ → Z
0.496 ± 0.046	³⁷ AKERS	95J OPAL	Repl. by ACKERSTAFF 97V
0.462 ^{+0.040} / _{-0.053} ^{+0.052} / _{-0.035}	²⁰ AKERS	95J OPAL	Repl. by ACKERSTAFF 97V

Meson Particle Listings

 B^0

0.50	± 0.12	± 0.06	23	ABREU	94M	DLPH	Sup. by ABREU 97N
0.508	± 0.075	± 0.025	26	AKERS	94C	OPAL	Repl. by ALEXANDER 96V
0.57	± 0.11	± 0.02	27	AKERS	94H	OPAL	Repl. by ALEXANDER 96V
0.50	± 0.07	± 0.11	20	BUSKULIC	94B	ALEP	Sup. by BUSKULIC 97D
0.52	± 0.10	± 0.04	27	BUSKULIC	93K	ALEP	Sup. by BUSKULIC 97D
	-0.06	-0.10					
	-0.11	-0.03					

- Measured using $B^0 \rightarrow D^{(*)-} \pi^+$ decays.
- Uses semileptonic decays of $B^0 \rightarrow D^- \mu^+ \nu_\mu X$ and $B^0 \rightarrow D^{(*)-} \mu^+ \nu_\mu X$, where the D mesons are reconstructed in $D^- \rightarrow K^+ \pi^- \pi^-$ and $D^{(*)-} \rightarrow \bar{D}^0 \pi^-$ with $\bar{D}^0 \rightarrow K^+ \pi^-$.
- Uses semileptonic decays of $B^0 \rightarrow D^- \mu^+ \nu_\mu X$ where the D^- mesons are reconstructed in $D^- \rightarrow K^+ K^- \pi^-$.
- Measured using $B^0 \rightarrow D^- \pi^+$ and $B^0 \rightarrow J/\psi K^*(892)^0$ decays.
- Measured using $B^0 \rightarrow D^- \pi^+$.
- Uses opposite-side flavor-tagging with $B \rightarrow D^{(*)} \mu \nu_\mu X$ events.
- Measured using a simultaneous fit of the B^0 lifetime and $\bar{B}^0 B^0$ oscillation frequency Δm_d in the partially reconstructed $B^0 \rightarrow D^{*-} \ell^+ \nu$ decays.
- Measurement performed using a combined fit of CP -violation, mixing and lifetimes.
- Events with a high transverse momentum lepton were removed and an inclusively reconstructed vertex was required.
- AUBERT 03c uses a sample of approximately 14,000 exclusively reconstructed $B^0 \rightarrow D^{*}(2010)^- \ell \nu$ and simultaneously measures the lifetime and oscillation frequency.
- HASTINGS 03 measurement based on the time evolution of dilepton events. It also reports $f_+/f_0 = 1.01 \pm 0.03 \pm 0.09$ and CPT violation parameters in B^0 - \bar{B}^0 mixing.
- ZHENG 03 data analyzed using partially reconstructed $\bar{B}^0 \rightarrow D^{*-} \pi^+$ decay and a flavor tag based on the charge of the lepton from the accompanying B decay.
- Uses a tagged sample of fully-reconstructed neutral B decays at $\Upsilon(4S)$.
- Measured based on the time evolution of dilepton events in $\Upsilon(4S)$ decays.
- Data analyzed using partially reconstructed $\bar{B}^0 \rightarrow D^{*+} \ell^- \bar{\nu}$ decay and a combination of flavor tags from the rest of the event.
- Uses di-muon events.
- Uses jet-charge and lepton-flavor tagging.
- Uses $\ell^- D^{*+} - \ell$ events.
- Uses $\pi^- B$ in the same side.
- Uses ℓ - ℓ .
- Uses ℓ - Q_{hem} .
- Uses ℓ - ℓ with impact parameters.
- Uses $D^{*\pm} Q_{\text{hem}}$.
- Uses $\pi_s^\pm \ell$ - Q_{hem} .
- Uses $D^{*\pm} \ell$ / Q_{hem} .
- Uses $D^{*\pm} \ell$ - Q_{hem} .
- Uses $D^{*\pm} \ell$.
- AUBERT 02N result based on the same analysis and data sample reported in AUBERT 02I.
- Uses a tagged sample of B^0 decays reconstructed in the mode $B^0 \rightarrow D^{*} \ell \nu$.
- Uses a tagged sample of fully-reconstructed hadronic B^0 decays at $\Upsilon(4S)$.
- ACCARI 98D combines results from ℓ - ℓ , ℓ - Q_{hem} , and ℓ - ℓ with impact parameters.
- ABREU 97N combines results from $D^{*\pm} Q_{\text{hem}}$, ℓ - Q_{hem} , $\pi_s^\pm \ell$ - Q_{hem} , and ℓ - ℓ .
- ACKERSTAFF 97V combines results from ℓ - ℓ , ℓ - Q_{hem} , $D^{*-} \ell$, and $D^{*\pm} Q_{\text{hem}}$.
- BUSKULIC 97D combines results from $D^{*\pm} \ell$ / Q_{hem} , ℓ - Q_{hem} , and ℓ - ℓ .
- ABREU 96Q analysis performed using lepton, kaon, and jet-charge tags.
- ALEXANDER 96V combines results from $D^{*\pm} \ell$ and $D^{*\pm} \ell$ - Q_{hem} .
- AKERS 95J combines results from charge measurement, $D^{*\pm} \ell$ - Q_{hem} and ℓ - ℓ .

 $\chi_d = \Delta m_{B^0} / \Gamma_{B^0}$

"OUR EVALUATION" is an average using rescaled values of the data listed below. The averaging/rescaling procedure takes into account correlations between the measurements and includes Δm_d calculated from χ_d measured at $\Upsilon(4S)$.

VALUE	DOCUMENT ID
0.7697 \pm 0.0035 OUR EVALUATION	(Produced by HFLAV)

 $\text{Re}(\lambda_{CP} / |\lambda_{CP}|) \text{Re}(z)$

The λ_{CP} characterizes B^0 and \bar{B}^0 decays to states of charmonium plus K^0 . Parameter z is used to describe CPT violation in mixing, see the review on "CP Violation" in the reviews section.

VALUE	DOCUMENT ID	TECN	COMMENT
0.047 \pm 0.022 \pm 0.003	1 LEES	16E	BABR $e^+ e^- \rightarrow \Upsilon(4S)$
0.014 \pm 0.035 \pm 0.034	2 AUBERT,B	04C	BABR Repl. by LEES 16E

- • • We do not use the following data for averages, fits, limits, etc. • • •
- 1 The first uncertainty is the uncertainty from $\text{Re}(z)$ and the second uncertainty is from $\text{Re}(\lambda/|\lambda|)$.
- 2 Corresponds to 90% confidence range $[-0.072, 0.101]$.

 $\Delta \Gamma \text{Re}(z)$

VALUE (ps^{-1})	DOCUMENT ID	TECN	COMMENT
-0.0071 \pm 0.0039 \pm 0.0020	AUBERT	06T	BABR $e^+ e^- \rightarrow \Upsilon(4S)$

 $\text{Re}(z)$

VALUE (units 10^{-2})	DOCUMENT ID	TECN	COMMENT
-4 \pm 4 OUR AVERAGE	Error includes scale factor of 1.4.		
-6.5 \pm 2.8 \pm 1.4	1 LEES	16E	BABR $e^+ e^- \rightarrow \Upsilon(4S)$
1.9 \pm 3.7 \pm 3.3	2 HIGUCHI	12	BELL $e^+ e^- \rightarrow \Upsilon(4S)$

- • • We do not use the following data for averages, fits, limits, etc. • • •

- | | | | | |
|--------------------|---|----|------|---------------------|
| 0 \pm 12 \pm 1 | 3 HASTINGS | 03 | BELL | Repl. by HIGUCHI 12 |
| 1 | Measurement uses decays $B^0/\bar{B}^0 \rightarrow c\bar{c}K_S^0/K_L^0$. | | | |
| 2 | Measured using $B^0 \rightarrow J/\psi K_S^0, J/\psi K_L^0, D^- \pi^+, D^{*-} \pi^+, D^{*-} \rho^+$, and $D^{*-} \ell^+ \nu$ decays. | | | |
| 3 | Measured using inclusive dilepton events from B^0 decay. | | | |

 $\text{Im}(z)$

VALUE (units 10^{-2})	DOCUMENT ID	TECN	COMMENT
-0.8 \pm 0.4 OUR AVERAGE			
1.0 \pm 3.0 \pm 1.3	1 LEES	16E	BABR $e^+ e^- \rightarrow \Upsilon(4S)$
-0.57 \pm 0.33 \pm 0.33	2 HIGUCHI	12	BELL $e^+ e^- \rightarrow \Upsilon(4S)$
-1.39 \pm 0.73 \pm 0.32	3 AUBERT	06T	BABR $e^+ e^- \rightarrow \Upsilon(4S)$
3.8 \pm 2.9 \pm 2.5	4 AUBERT,B	04C	BABR Repl. by AUBERT 06T
-3 \pm 1 \pm 3	5 HASTINGS	03	BELL Repl. by HIGUCHI 12
1	Measurement uses decays $B^0/\bar{B}^0 \rightarrow c\bar{c}K_S^0/K_L^0$.		
2	Measured using $B^0 \rightarrow J/\psi K_S^0, J/\psi K_L^0, D^- \pi^+, D^{*-} \pi^+, D^{*-} \rho^+$, and $D^{*-} \ell^+ \nu$ decays.		
3	Measurement uses $B^0/\bar{B}^0 \rightarrow \ell^+ X/\ell^- X$ decays. Assuming $\Delta \Gamma = 0$, the result becomes $\text{Im}(z) = (-0.37 \pm 0.54) \times 10^{-2}$.		
4	Corresponds to 90% confidence range $[-0.028, 0.104]$.		
5	Measured using inclusive dilepton events from B^0 decay.		

CP VIOLATION PARAMETERS

 $\text{Re}(\epsilon_{B^0}) / (1 + |\epsilon_{B^0}|^2)$

CP impurity in B_d^0 system. It is obtained from either $a_{\ell\ell}$, the charge asymmetry in like-sign dilepton events or a_{CP} , the time-dependent asymmetry of inclusive B^0 and \bar{B}^0 decays.

"OUR EVALUATION" is the result of a fit to B_d and B_s CP asymmetries, which includes the B_d measurements listed below and the B_s measurements listed in the B_s section, taking into account correlations between those measurements.

VALUE (units 10^{-3})	DOCUMENT ID	TECN	COMMENT
-0.5 \pm 0.4 OUR EVALUATION	(Produced by HFLAV)		
-0.1 \pm 0.4 OUR AVERAGE			
-0.05 \pm 0.48 \pm 0.75	1 AAJ	15F	LHCB $p\bar{p}$ at 7, 8 TeV
-0.975 \pm 0.875 \pm 0.475	2 LEES	15A	BABR $e^+ e^- \rightarrow \Upsilon(4S)$
1.55 \pm 1.05	3 ABAZOV	14	D0 $p\bar{p}$ at 1.96 TeV
0.15 \pm 0.42 \pm 0.94	4 LEES	13N	BABR $e^+ e^- \rightarrow \Upsilon(4S)$
-1.7 \pm 1.1 \pm 0.4	5 ABAZOV	12aC	D0 $p\bar{p}$ at 1.96 TeV
0.4 \pm 1.3 \pm 0.9	6 AUBERT	06T	BABR $e^+ e^- \rightarrow \Upsilon(4S)$
-0.3 \pm 2.0 \pm 2.1	7 NAKANO	06	BELL $e^+ e^- \rightarrow \Upsilon(4S)$
3.5 \pm 10.3 \pm 1.5	8 JAFFE	01	CLE2 $e^+ e^- \rightarrow \Upsilon(4S)$
-0.3 \pm 1.3	9 ABAZOV	11U	D0 Repl. by ABAZOV 14
-2.3 \pm 1.1 \pm 0.8	10 ABAZOV	06S	D0 Repl. by ABAZOV 11U
-14.7 \pm 6.7 \pm 5.7	11 AUBERT,B	04C	BABR Repl. by AUBERT 06T
1.2 \pm 2.9 \pm 3.6	2 AUBERT	02K	BABR Repl. by LEES 15A
-3.2 \pm 6.5	12 BARATE	01D	ALEP $e^+ e^- \rightarrow Z$
4 \pm 18 \pm 3	13 BEHRENS	00B	CLE2 Repl. by JAFFE 01
1.2 \pm 13.8 \pm 3.2	14 ABBIENDI	99J	OPAL $e^+ e^- \rightarrow Z$
2 \pm 7 \pm 3	15 ACKERSTAFF	97U	OPAL $e^+ e^- \rightarrow Z$
< 45	16 BARTELT	93	CLE2 $e^+ e^- \rightarrow \Upsilon(4S)$

- • • We do not use the following data for averages, fits, limits, etc. • • •
- 1 AAJ 15F uses semileptonic B^0 decays in the inclusive final states $D^- \mu^+$ and $D^{*-} \mu^+$, where the D^- meson decays into the $K^+ \pi^- \pi^-$ final state, and the D^{*-} meson into the $\bar{D}^0 (\rightarrow K^+ \pi^-) \pi^-$ final state. Reports $A_{SL}^d = (-0.02 \pm 0.19 \pm 0.30)\%$, which equals to $4\text{Re}(\epsilon_{B^0}) / (1 + |\epsilon_{B^0}|^2)$.
- 2 Uses the charge asymmetry in like-sign dilepton events. LEES 15A reports $A_{SL}^d = (-3.9 \pm 3.5 \pm 1.9) \times 10^{-3}$.
- 3 ABAZOV 14 uses the dimuon charge asymmetry with different impact parameters from which it reports $A_{SL}^d = (-0.62 \pm 0.42) \times 10^{-2}$.
- 4 Uses $B^0 \rightarrow D^{*-} X \ell^+ \nu_\ell$ and a kaon-tagged sample which yields measurement of $A_{SL}^d = (0.06 \pm 0.17 \pm 0.38 \pm 0.32)\%$, corresponding to $\Delta_{CP} = 1 - |q/p| = (0.29 \pm 0.84 \pm 1.88 \pm 1.61) \times 10^{-3}$.
- 5 ABAZOV 12aC uses $B^0 \rightarrow D^- \mu^+ X$ and $B^0 \rightarrow D^{*}(2010)^- \mu^+ X$ decays without initial state flavor tagging which yields measurement of $A_{SL}^d = (6.8 \pm 4.5 \pm 1.4) \times 10^{-3}$.
- 6 AUBERT 06T reports $|q/p| - 1 = (-0.8 \pm 2.7 \pm 1.9) \times 10^{-3}$. We convert to $(1 - |q/p|^2)/4$.
- 7 Uses the charge asymmetry in like-sign dilepton events and reports $|q/p| = 1.0005 \pm 0.0040 \pm 0.0043$.
- 8 JAFFE 01 finds $a_{\ell\ell} = 0.013 \pm 0.050 \pm 0.005$ and combines with the previous BEHRENS 00B independent measurement.
- 9 ABAZOV 11U uses the dimuon charge asymmetry with different impact parameters from which it reports $A_{SL}^d = (-1.2 \pm 5.2) \times 10^{-3}$.
- 10 Uses the dimuon charge asymmetry.
- 11 AUBERT 04C reports $|q/p| = 1.029 \pm 0.013 \pm 0.011$ and we converted it to $(1 - |q/p|^2)/4$.
- 12 BARATE 01D measured by investigating time-dependent asymmetries in semileptonic and fully inclusive B_d^0 decays.
- 13 BEHRENS 00B uses high-momentum lepton tags and partially reconstructed $\bar{B}^0 \rightarrow D^{*+} \pi^-, \rho^-$ decays to determine the flavor of the B meson.

¹⁴Data analyzed using the time-dependent asymmetry of inclusive B^0 decay. The production flavor of B^0 mesons is determined using both the jet charge and the charge of secondary vertex in the opposite hemisphere.

¹⁵ACKERSTAFF 97U assumes $CP T$ and is based on measuring the charge asymmetry in a sample of B^0 decays defined by lepton and Q_{hem} tags. If $CP T$ is not invoked, $\text{Re}(\epsilon_B) = -0.006 \pm 0.010 \pm 0.006$ is found. The indirect $CP T$ violation parameter is determined to $\text{Im}(\delta B) = -0.020 \pm 0.016 \pm 0.006$.

¹⁶BARTELT 93 finds $a_{\ell\ell} = 0.031 \pm 0.096 \pm 0.032$ which corresponds to $|a_{\ell\ell}| < 0.18$, which yields the above $|\text{Re}(\epsilon_{B^0})/(1+|\epsilon_{B^0}|^2)|$.

 $A_{T/CP}$

$A_{T/CP}$ is defined as

$$\frac{P(\bar{B}^0 \rightarrow B^0) - P(B^0 \rightarrow \bar{B}^0)}{P(\bar{B}^0 \rightarrow B^0) + P(B^0 \rightarrow \bar{B}^0)}$$

the $CP T$ invariant asymmetry between the oscillation probabilities $P(\bar{B}^0 \rightarrow B^0)$ and $P(B^0 \rightarrow \bar{B}^0)$.

VALUE	DOCUMENT ID	TECN	COMMENT
0.005 ± 0.012 ± 0.014	¹ AUBERT	02K	BABR $e^+e^- \rightarrow \Upsilon(4S)$

¹AUBERT 02K uses the charge asymmetry in like-sign dilepton events.

 $A_{CP}(B^0 \rightarrow D^*(2010)^+ D^-)$

A_{CP} is defined as

$$\frac{B(\bar{B}^0 \rightarrow \bar{D}^+) - B(B^0 \rightarrow D^+)}{B(\bar{B}^0 \rightarrow \bar{D}^+) + B(B^0 \rightarrow D^+)}$$

the CP -violation charge asymmetry of exclusive B^0 and \bar{B}^0 decay.

VALUE	DOCUMENT ID	TECN	COMMENT
0.013 ± 0.014 OUR AVERAGE			
0.008 ± 0.014 ± 0.006	AAIJ	20L	LHCB pp at 7, 8, 13 TeV
-0.12 ± 0.06 ± 0.02	ROHRKEN	12	BELL $e^+e^- \rightarrow \Upsilon(4S)$
0.008 ± 0.048 ± 0.013	AUBERT	09C	BABR $e^+e^- \rightarrow \Upsilon(4S)$
0.07 ± 0.08 ± 0.04	¹ AUSHEV	04	BELL $e^+e^- \rightarrow \Upsilon(4S)$

• • • We do not use the following data for averages, fits, limits, etc. • • •

-0.03 ± 0.10 ± 0.02	AUBERT,B	06A	BABR Repl. by AUBERT 07AI
-0.03 ± 0.11 ± 0.05	AUBERT	03J	BABR Repl. by AUBERT,B 06B

¹Combines results from fully and partially reconstructed $B^0 \rightarrow D^{*\pm} D^\mp$ decays.

 $A_{CP}(B^0 \rightarrow D^0 \pi^0)$

VALUE (units 10^{-2})

VALUE	DOCUMENT ID	TECN	COMMENT
0.42 ± 2.05 ± 1.22	BLOOMFIELD	22	BELL $e^+e^- \rightarrow \Upsilon(4S)$

 $A_{CP}(B^0 \rightarrow [K^+ K^-]_D K^*(892)^0)$

VALUE	DOCUMENT ID	TECN	COMMENT
-0.05 ± 0.10 ± 0.01	AAIJ	19N	LHCB pp at 7, 8, 13 TeV

• • • We do not use the following data for averages, fits, limits, etc. • • •

-0.20 ± 0.15 ± 0.02	AAIJ	14BN	LHCB Repl. by AAIJ 16S
-0.45 ± 0.23 ± 0.02	AAIJ	13L	LHCB Repl. by AAIJ 14BN

 $A_{CP}(B^0 \rightarrow [K^+ \pi^-]_D K^*(892)^0)$

VALUE	DOCUMENT ID	TECN	COMMENT
0.047 ± 0.027 ± 0.010	AAIJ	19N	LHCB pp at 7, 8, 13 TeV

• • • We do not use the following data for averages, fits, limits, etc. • • •

-0.03 ± 0.04 ± 0.02	AAIJ	14BN	LHCB Repl. by AAIJ 19N
-0.08 ± 0.08 ± 0.01	AAIJ	13L	LHCB Repl. by AAIJ 14BN

 $A_{CP}(B^0 \rightarrow [K^+ \pi^- \pi^+ \pi^-]_D K^*(892)^0)$

VALUE	DOCUMENT ID	TECN	COMMENT
0.037 ± 0.032 ± 0.010	AAIJ	19N	LHCB pp at 7, 8, 13 TeV

 $A_{CP}(B^0 \rightarrow [K^- \pi^+]_D K^*(892)^0)$

VALUE	DOCUMENT ID	TECN	COMMENT
0.19 ± 0.19 ± 0.01	AAIJ	19N	LHCB pp at 7, 8, 13 TeV

 $A_{CP}(B^0 \rightarrow [K^- \pi^+ \pi^+ \pi^-]_D K^*(892)^0)$

VALUE	DOCUMENT ID	TECN	COMMENT
-0.01 ± 0.24 ± 0.01	AAIJ	19N	LHCB pp at 7, 8, 13 TeV

 $R_d^+ = \Gamma(B^0 \rightarrow [\pi^+ K^-]_D K^{*0}) / \Gamma(B^0 \rightarrow [\pi^- K^+]_D K^{*0})$

VALUE	DOCUMENT ID	TECN	COMMENT
0.064 ± 0.021 ± 0.002	AAIJ	19N	LHCB pp at 7, 8, 13 TeV

• • • We do not use the following data for averages, fits, limits, etc. • • •

0.06 ± 0.03 ± 0.01	AAIJ	14BN	LHCB Repl. by AAIJ 19N
--------------------	------	------	------------------------

 $R_d^- = \Gamma(\bar{B}^0 \rightarrow [\pi^- K^+]_D K^{*0}) / \Gamma(\bar{B}^0 \rightarrow [\pi^+ K^-]_D K^{*0})$

VALUE	DOCUMENT ID	TECN	COMMENT
0.095 ± 0.021 ± 0.003	AAIJ	19N	LHCB pp at 7, 8, 13 TeV

• • • We do not use the following data for averages, fits, limits, etc. • • •

0.06 ± 0.03 ± 0.01	AAIJ	14BN	LHCB Repl. by AAIJ 19N
--------------------	------	------	------------------------

 $A_{CP}(B^0 \rightarrow [\pi^+ \pi^-]_D K^*(892)^0)$

VALUE	DOCUMENT ID	TECN	COMMENT
-0.18 ± 0.14 ± 0.01	AAIJ	19N	LHCB pp at 7, 8, 13 TeV

• • • We do not use the following data for averages, fits, limits, etc. • • •

-0.09 ± 0.22 ± 0.02	AAIJ	14BN	LHCB Repl. by AAIJ 16S
---------------------	------	------	------------------------

 $A_{CP}(B^0 \rightarrow [\pi^+ \pi^- \pi^+ \pi^-]_D K^*(892)^0)$

VALUE	DOCUMENT ID	TECN	COMMENT
-0.03 ± 0.15 ± 0.01	AAIJ	19N	LHCB pp at 7, 8, 13 TeV

 $R_d^+ = \Gamma(B^0 \rightarrow [\pi^+ K^- \pi^+ \pi^-]_D K^{*0}) / \Gamma(B^0 \rightarrow [\pi^- K^+ \pi^+ \pi^-]_D K^{*0})$

VALUE	DOCUMENT ID	TECN	COMMENT
0.074 ± 0.026 ± 0.002	AAIJ	19N	LHCB pp at 7, 8, 13 TeV

 $R_d^- = \Gamma(\bar{B}^0 \rightarrow [\pi^- K^+ \pi^+ \pi^-]_D K^{*0}) / \Gamma(\bar{B}^0 \rightarrow [\pi^+ K^- \pi^+ \pi^-]_D K^{*0})$

VALUE	DOCUMENT ID	TECN	COMMENT
0.072 ± 0.025 ± 0.003	AAIJ	19N	LHCB pp at 7, 8, 13 TeV

 $A_{CP}(B^0 \rightarrow K^+ \pi^-)$

VALUE	DOCUMENT ID	TECN	COMMENT
-0.0831 ± 0.0031 OUR AVERAGE			

-0.072 ± 0.019 ± 0.007	ADACHI	24	BELL $e^+e^- \rightarrow \Upsilon(4S)$
-0.0824 ± 0.0033 ± 0.0033	AAIJ	21o	LHCB pp at 13 TeV
-0.084 ± 0.004 ± 0.003	AAIJ	18o	LHCB pp at 7, 8 TeV
-0.083 ± 0.013 ± 0.004	AALTONEN	14P	CDF $p\bar{p}$ at 1.96 TeV
-0.069 ± 0.014 ± 0.007	DUH	13	BELL $e^+e^- \rightarrow \Upsilon(4S)$
-0.107 ± 0.016 ± 0.006 -0.004	LEES	13D	BABR $e^+e^- \rightarrow \Upsilon(4S)$
-0.04 ± 0.16	¹ CHEN	00	CLE2 $e^+e^- \rightarrow \Upsilon(4S)$
• • • We do not use the following data for averages, fits, limits, etc. • • •			
-0.080 ± 0.007 ± 0.003	AAIJ	13AX	LHCB Repl. by AAIJ 18o
-0.088 ± 0.011 ± 0.008	AAIJ	12v	LHCB Repl. by AAIJ 13AX
-0.086 ± 0.023 ± 0.009	AALTONEN	11N	CDF Repl. by AALTONEN 14P
-0.094 ± 0.018 ± 0.008	LIN	08	BELL Repl. by DUH 13
-0.107 ± 0.018 ± 0.007 -0.004	AUBERT	07AF	BABR Repl. by LEES 13D
-0.013 ± 0.078 ± 0.012	ABULENCIA,A	06D	CDF Repl. by AALTONEN 11N
-0.088 ± 0.035 ± 0.013	² CHAO	05A	BELL Repl. by CHAO 04B
-0.133 ± 0.030 ± 0.009	³ AUBERT,B	04K	BABR Repl. by AUBERT 07AF
-0.101 ± 0.025 ± 0.005	⁴ CHAO	04B	BELL Repl. by LIN 08
-0.07 ± 0.08 ± 0.02	⁵ AUBERT	02D	BABR Repl. by AUBERT 02q
-0.102 ± 0.050 ± 0.016	⁶ AUBERT	02Q	BABR Repl. by AUBERT,B 04K
-0.06 ± 0.09 ± 0.01 -0.02	⁷ CASEY	02	BELL Repl. by CHAO 04B
0.044 ± 0.186 ± 0.018 -0.167 -0.021	⁸ ABE	01K	BELL Repl. by CASEY 02
-0.19 ± 0.10 ± 0.03	⁹ AUBERT	01E	BABR Repl. by AUBERT 02q

¹Corresponds to 90% confidence range $-0.30 < A_{CP} < 0.22$.

²Corresponds to a 90% CL interval of $-0.15 < A_{CP} < -0.03$.

³Based on a total signal yield of $N(K^- \pi^+) + N(K^+ \pi^-) = 1606 \pm 51$ events.

⁴CHAO 04B reports significance of 3.9 standard deviation for deviation of A_{CP} from zero.

⁵Corresponds to 90% confidence range $-0.21 < A_{CP} < 0.07$.

⁶Corresponds to 90% confidence range $-0.188 < A_{CP} < -0.016$.

⁷Corresponds to 90% confidence range $-0.21 < A_{CP} < +0.09$.

⁸Corresponds to 90% confidence range $-0.25 < A_{CP} < 0.37$.

⁹Corresponds to 90% confidence range $-0.35 < A_{CP} < -0.03$.

 $A_{CP}(B^0 \rightarrow \eta' K^*(892)^0)$

VALUE	DOCUMENT ID	TECN	COMMENT
-0.07 ± 0.18 OUR AVERAGE			

-0.22 ± 0.29 ± 0.07	SATO	14	BELL $e^+e^- \rightarrow \Upsilon(4S)$
0.02 ± 0.23 ± 0.02	DEL-AMO-SA..10A	BABR	$e^+e^- \rightarrow \Upsilon(4S)$

• • • We do not use the following data for averages, fits, limits, etc. • • •

0.08 ± 0.25 ± 0.02	¹ AUBERT	07E	BABR Repl. by DEL-AMO-SANCHEZ 10A
--------------------	---------------------	-----	-----------------------------------

¹Reports A_{CP} with the opposite sign convention.

 $A_{CP}(B^0 \rightarrow \eta' K_0^*(1430)^0)$

VALUE	DOCUMENT ID	TECN	COMMENT
-0.19 ± 0.17 ± 0.02	DEL-AMO-SA..10A	BABR	$e^+e^- \rightarrow \Upsilon(4S)$

 $A_{CP}(B^0 \rightarrow \eta' K_2^*(1430)^0)$

VALUE	DOCUMENT ID	TECN	COMMENT
0.14 ± 0.18 ± 0.02	DEL-AMO-SA..10A	BABR	$e^+e^- \rightarrow \Upsilon(4S)$

 $A_{CP}(B^0 \rightarrow \eta K^*(892)^0)$

VALUE	DOCUMENT ID	TECN	COMMENT
0.19 ± 0.05 OUR AVERAGE			

0.17 ± 0.08 ± 0.01	WANG	07B	BELL $e^+e^- \rightarrow \Upsilon(4S)$
0.21 ± 0.06 ± 0.02	AUBERT,B	06H	BABR $e^+e^- \rightarrow \Upsilon(4S)$

• • • We do not use the following data for averages, fits, limits, etc. • • •

0.02 ± 0.11 ± 0.02	AUBERT,B	04D	BABR Repl. by AUBERT,B 06H
--------------------	----------	-----	----------------------------

 $A_{CP}(B^0 \rightarrow \eta K_0^*(1430)^0)$

VALUE	DOCUMENT ID	TECN	COMMENT
0.06 ± 0.13 ± 0.02	AUBERT,B	06H	BABR $e^+e^- \rightarrow \Upsilon(4S)$

Meson Particle Listings

 B^0 $A_{CP}(B^0 \rightarrow \eta K_2^*(1430)^0)$

VALUE	DOCUMENT ID	TECN	COMMENT
$-0.07 \pm 0.19 \pm 0.02$	AUBERT,B	06H	BABR $e^+e^- \rightarrow \Upsilon(4S)$

 $A_{CP}(B^0 \rightarrow b_1 K^+)$

VALUE	DOCUMENT ID	TECN	COMMENT
$-0.07 \pm 0.12 \pm 0.02$	AUBERT	07B1	BABR $e^+e^- \rightarrow \Upsilon(4S)$

 $A_{CP}(B^0 \rightarrow \omega K^{*0})$

VALUE	DOCUMENT ID	TECN	COMMENT
$0.45 \pm 0.25 \pm 0.02$	AUBERT	09H	BABR $e^+e^- \rightarrow \Upsilon(4S)$

 $A_{CP}(B^0 \rightarrow \omega(K\pi)_0^{*0})$

VALUE	DOCUMENT ID	TECN	COMMENT
$-0.07 \pm 0.09 \pm 0.02$	AUBERT	09H	BABR $e^+e^- \rightarrow \Upsilon(4S)$

 $A_{CP}(B^0 \rightarrow \omega K_2^*(1430)^0)$

VALUE	DOCUMENT ID	TECN	COMMENT
$-0.37 \pm 0.17 \pm 0.02$	AUBERT	09H	BABR $e^+e^- \rightarrow \Upsilon(4S)$

 $A_{CP}(B^0 \rightarrow K^+\pi^-\pi^0)$

VALUE (units 10^{-2})	DOCUMENT ID	TECN	COMMENT
0 ± 6 OUR AVERAGE			

$-3.0 \pm 4.5 \pm 5.5$	¹ AUBERT	08AQ	BABR $e^+e^- \rightarrow \Upsilon(4S)$
$7 \pm 11 \pm 1$	² CHANG	04	BELL $e^+e^- \rightarrow \Upsilon(4S)$

- ¹ Uses Dalitz plot analysis of $B^0 \rightarrow K^+\pi^-\pi^0$ decays.
² Corresponds to 90% confidence range $-0.12 < A_{CP} < 0.26$.

 $A_{CP}(B^0 \rightarrow \rho^- K^+)$

VALUE	DOCUMENT ID	TECN	COMMENT
$0.20 \pm 0.09 \pm 0.08$	¹ LEES	11	BABR $e^+e^- \rightarrow \Upsilon(4S)$
$0.22 \pm 0.22 \pm 0.06$	² CHANG	04	BELL $e^+e^- \rightarrow \Upsilon(4S)$

- • • We do not use the following data for averages, fits, limits, etc. • • •
- | | | | |
|---------------------------|---------------------|------|---------------------------|
| $0.11 \pm 0.14 \pm 0.07$ | ¹ AUBERT | 08AQ | BABR Repl. by LEES 11 |
| $-0.28 \pm 0.17 \pm 0.08$ | ³ AUBERT | 03T | BABR Repl. by AUBERT 08AQ |

- ¹ Uses Dalitz plot analysis of $B^0 \rightarrow K^+\pi^-\pi^0$ decays.
² Corresponds to 90% confidence range $-0.18 < A_{CP} < 0.64$.
³ The result reported corresponds to $-A_{CP}$.

 $A_{CP}(B^0 \rightarrow \rho(1450)^- K^+)$

VALUE	DOCUMENT ID	TECN	COMMENT
$-0.10 \pm 0.32 \pm 0.09$	¹ LEES	11	BABR $e^+e^- \rightarrow \Upsilon(4S)$

- ¹ Uses Dalitz plot analysis of $B^0 \rightarrow K^+\pi^-\pi^0$ decays.

 $A_{CP}(B^0 \rightarrow \rho(1700)^- K^+)$

VALUE	DOCUMENT ID	TECN	COMMENT
$-0.36 \pm 0.57 \pm 0.23$	¹ LEES	11	BABR $e^+e^- \rightarrow \Upsilon(4S)$

- ¹ Uses Dalitz plot analysis of $B^0 \rightarrow K^+\pi^-\pi^0$ decays.

 $A_{CP}(B^0 \rightarrow K^+\pi^-\pi^0 \text{ nonresonant})$

VALUE	DOCUMENT ID	TECN	COMMENT
$0.10 \pm 0.16 \pm 0.08$	¹ LEES	11	BABR $e^+e^- \rightarrow \Upsilon(4S)$

- • • We do not use the following data for averages, fits, limits, etc. • • •

$0.23 \pm 0.19 \pm 0.11$	¹ AUBERT	08AQ	BABR Repl. by LEES 11
--------------------------	---------------------	------	-----------------------

- ¹ Uses Dalitz plot analysis of $B^0 \rightarrow K^+\pi^-\pi^0$ decays. The quoted value is only for the flat part of the non-resonant component.

 $A_{CP}(B^0 \rightarrow K^0\pi^+\pi^-)$

VALUE	DOCUMENT ID	TECN	COMMENT
$-0.01 \pm 0.05 \pm 0.01$	¹ AUBERT	09AU	BABR $e^+e^- \rightarrow \Upsilon(4S)$

- ¹ Uses Dalitz plot analysis of $B^0 \rightarrow K^0\pi^+\pi^-$ decays and the first of two equivalent solutions is used.

 $A_{CP}(B^0 \rightarrow K^*(892)^+\pi^-)$

VALUE	DOCUMENT ID	TECN	COMMENT
-0.27 ± 0.04 OUR AVERAGE			

$-0.308 \pm 0.060 \pm 0.016$	¹ AAIJ	18F	LHCB pp at 7, 8 TeV
$-0.29 \pm 0.11 \pm 0.02$	² LEES	11	BABR $e^+e^- \rightarrow \Upsilon(4S)$
$-0.21 \pm 0.10 \pm 0.02$	^{3,4} AUBERT	09AU	BABR $e^+e^- \rightarrow \Upsilon(4S)$
$-0.21 \pm 0.11 \pm 0.07$	⁵ DALSENO	09	BELL $e^+e^- \rightarrow \Upsilon(4S)$
$0.26 \pm 0.33 \pm 0.10$	⁶ EISENSTEIN	03	CLE2 $e^+e^- \rightarrow \Upsilon(4S)$

- • • We do not use the following data for averages, fits, limits, etc. • • •

$-0.19 \pm 0.20 \pm 0.04$	² AUBERT	08AQ	BABR Repl. by LEES 11
$-0.11 \pm 0.14 \pm 0.05$	³ AUBERT	06I	BABR Repl. by AUBERT 09AU
$0.23 \pm 0.18 \pm 0.09$	AUBERT,B	04O	BABR Repl. by AUBERT 06I

- ¹ Uses Dalitz plot analysis of the $B^0 \rightarrow K_S^0\pi^+\pi^-$ final state decays.
² Uses Dalitz plot analysis of $B^0 \rightarrow K^+\pi^-\pi^0$ decays.
³ Uses Dalitz plot analysis of $B^0 \rightarrow K^0\pi^+\pi^-$ decays.
⁴ The first of two equivalent solutions is used.
⁵ Uses Dalitz plot analysis of $B^0 \rightarrow K^0\pi^+\pi^-$ decays and the first of two consistent solutions that may be preferred.
⁶ Corresponds to 90% confidence range $-0.31 < A_{CP} < 0.78$.

 $A_{CP}(B^0 \rightarrow (K\pi)_0^{*+}\pi^-)$

VALUE	DOCUMENT ID	TECN	COMMENT
0.02 ± 0.04 OUR AVERAGE			

$-0.032 \pm 0.047 \pm 0.031$	¹ AAIJ	18F	LHCB pp at 7, 8 TeV
$0.07 \pm 0.14 \pm 0.01$	² LEES	11	BABR $e^+e^- \rightarrow \Upsilon(4S)$
$0.09 \pm 0.07 \pm 0.03$	³ AUBERT	09AU	BABR $e^+e^- \rightarrow \Upsilon(4S)$

- • • We do not use the following data for averages, fits, limits, etc. • • •

$0.17 \pm 0.11 \pm 0.22$	² AUBERT	08AQ	BABR Repl. by LEES 11
--------------------------	---------------------	------	-----------------------

- ¹ Uses Dalitz plot analysis of the $B^0 \rightarrow K_S^0\pi^+\pi^-$ final state decays.
² Uses Dalitz plot analysis of $B^0 \rightarrow K^+\pi^-\pi^0$ decays.
³ Uses Dalitz plot analysis of $B^0 \rightarrow K^0\pi^+\pi^-$ decays and the first of two equivalent solutions is used.

 $A_{CP}(B^0 \rightarrow K_2^*(1430)^+\pi^-)$

VALUE	DOCUMENT ID	TECN	COMMENT
$-0.29 \pm 0.22 \pm 0.09$	¹ AAIJ	18F	LHCB pp at 7, 8 TeV

- ¹ Uses Dalitz plot analysis of the $B^0 \rightarrow K_S^0\pi^+\pi^-$ final state decays.

 $A_{CP}(B^0 \rightarrow K^*(1680)^+\pi^-)$

VALUE	DOCUMENT ID	TECN	COMMENT
$-0.07 \pm 0.13 \pm 0.04$	¹ AAIJ	18F	LHCB pp at 7, 8 TeV

- ¹ Uses Dalitz plot analysis of the $B^0 \rightarrow K_S^0\pi^+\pi^-$ final state decays.

 $A_{CP}(B^0 \rightarrow f_0(980)K_S^0)$

VALUE	DOCUMENT ID	TECN	COMMENT
$0.28 \pm 0.27 \pm 0.15$	¹ AAIJ	18F	LHCB pp at 7, 8 TeV

- ¹ Uses Dalitz plot analysis of the $B^0 \rightarrow K_S^0\pi^+\pi^-$ final state decays.

 $A_{CP}(B^0 \rightarrow (K\pi)_0^{*0}\pi^0)$

VALUE	DOCUMENT ID	TECN	COMMENT
$-0.15 \pm 0.10 \pm 0.04$	¹ LEES	11	BABR $e^+e^- \rightarrow \Upsilon(4S)$

- • • We do not use the following data for averages, fits, limits, etc. • • •

$-0.22 \pm 0.12 \pm 0.30$	¹ AUBERT	08AQ	BABR Repl. by LEES 11
---------------------------	---------------------	------	-----------------------

- ¹ Uses Dalitz plot analysis of $B^0 \rightarrow K^+\pi^-\pi^0$ decays.

 $A_{CP}(B^0 \rightarrow K^{*0}\pi^0)$

VALUE	DOCUMENT ID	TECN	COMMENT
$-0.15 \pm 0.12 \pm 0.04$	¹ LEES	11	BABR $e^+e^- \rightarrow \Upsilon(4S)$

- • • We do not use the following data for averages, fits, limits, etc. • • •

$-0.09 \pm 0.21 \pm 0.09$	¹ AUBERT	08AQ	BABR Repl. by LEES 11
---------------------------	---------------------	------	-----------------------

- ¹ Uses Dalitz plot analysis of $B^0 \rightarrow K^+\pi^-\pi^0$ decays.

 $A_{CP}(B^0 \rightarrow K^*(892)^0\pi^+\pi^-)$

VALUE	DOCUMENT ID	TECN	COMMENT
$0.07 \pm 0.04 \pm 0.03$	AUBERT	07As	BABR $e^+e^- \rightarrow \Upsilon(4S)$

 $A_{CP}(B^0 \rightarrow K^*(892)^0\rho^0)$

VALUE	DOCUMENT ID	TECN	COMMENT
$-0.06 \pm 0.09 \pm 0.02$	LEES	12K	BABR $e^+e^- \rightarrow \Upsilon(4S)$

- • • We do not use the following data for averages, fits, limits, etc. • • •

$0.09 \pm 0.19 \pm 0.02$	AUBERT,B	06G	BABR Repl. by LEES 12K
--------------------------	----------	-----	------------------------

 $A_{CP}(B^0 \rightarrow K^{*0}f_0(980))$

VALUE	DOCUMENT ID	TECN	COMMENT
$0.07 \pm 0.10 \pm 0.02$	LEES	12K	BABR $e^+e^- \rightarrow \Upsilon(4S)$

- • • We do not use the following data for averages, fits, limits, etc. • • •

$-0.17 \pm 0.28 \pm 0.02$	AUBERT,B	06G	BABR Repl. by LEES 12K
---------------------------	----------	-----	------------------------

 $A_{CP}(B^0 \rightarrow K^{*+}\rho^-)$

VALUE	DOCUMENT ID	TECN	COMMENT
$0.21 \pm 0.15 \pm 0.02$	LEES	12K	BABR $e^+e^- \rightarrow \Upsilon(4S)$

 $A_{CP}(B^0 \rightarrow K^*(892)^0 K^+ K^-)$

VALUE	DOCUMENT ID	TECN	COMMENT
$0.01 \pm 0.05 \pm 0.02$	AUBERT	07As	BABR $e^+e^- \rightarrow \Upsilon(4S)$

 $A_{CP}(B^0 \rightarrow a_1^-\pi^+)$

VALUE	DOCUMENT ID	TECN	COMMENT
$-0.16 \pm 0.12 \pm 0.01$	AUBERT	08F	BABR $e^+e^- \rightarrow \Upsilon(4S)$

 $A_{CP}(B^0 \rightarrow K^0 K^0)$

VALUE	DOCUMENT ID	TECN	COMMENT
$-0.58 \pm 0.73 \pm 0.04$	LIN	07	BELL $e^+e^- \rightarrow \Upsilon(4S)$

 $A_{CP}(B^0 \rightarrow K^*(892)^0\phi)$

VALUE	DOCUMENT ID	TECN	COMMENT
0.00 ± 0.04 OUR AVERAGE			

$-0.007 \pm 0.048 \pm 0.021$	PRIM	13	BELL $e^+e^- \rightarrow \Upsilon(4S)$
$0.01 \pm 0.06 \pm 0.03$	AUBERT	08BG	BABR $e^+e^- \rightarrow \Upsilon(4S)$

• • • We do not use the following data for averages, fits, limits, etc. • • •

VALUE	DOCUMENT ID	TECN	COMMENT
$-0.03 \pm 0.07 \pm 0.03$	AUBERT	07D	BABR Repl. by AUBERT 08Bg
$0.02 \pm 0.09 \pm 0.02$	¹ CHEN	05A	BELL Repl. by PRIM 13
$-0.01 \pm 0.09 \pm 0.02$	AUBERT,B	04W	BABR Repl. by AUBERT 07D
$0.04 \pm 0.12 \pm 0.02$	AUBERT	03V	BABR Repl. by AUBERT 04W
$0.07 \pm 0.15 \pm 0.05$ -0.03	² CHEN	03B	BELL Repl. by CHEN 05A
$0.00 \pm 0.27 \pm 0.03$	³ AUBERT	02E	BABR Repl. by AUBERT 03V

¹ Corresponds to 90% confidence range $-0.14 < A_{CP} < 0.17$.
² Corresponds to 90% confidence range $-0.18 < A_{CP} < 0.33$.
³ Corresponds to 90% confidence range $-0.44 < A_{CP} < 0.44$.

$A_{CP}(B^0 \rightarrow K^*(892)^0 K^- \pi^+)$

VALUE	DOCUMENT ID	TECN	COMMENT
$0.22 \pm 0.33 \pm 0.20$	AUBERT	07As	BABR $e^+ e^- \rightarrow \Upsilon(4S)$

$A_{CP}(B^0 \rightarrow \phi(K\pi)_0^0)$

VALUE	DOCUMENT ID	TECN	COMMENT
0.12 ± 0.08 OUR AVERAGE			
$0.093 \pm 0.094 \pm 0.017$	PRIM	13	BELL $e^+ e^- \rightarrow \Upsilon(4S)$
$0.20 \pm 0.14 \pm 0.06$	AUBERT	08Bg	BABR $e^+ e^- \rightarrow \Upsilon(4S)$

• • • We do not use the following data for averages, fits, limits, etc. • • •

$0.17 \pm 0.15 \pm 0.03$	AUBERT	07D	BABR Repl. by AUBERT 08Bg
--------------------------	--------	-----	---------------------------

$A_{CP}(B^0 \rightarrow \phi K_2^*(1430)^0)$

VALUE	DOCUMENT ID	TECN	COMMENT
-0.11 ± 0.10 OUR AVERAGE			
$-0.155 \pm 0.152 \pm 0.033$ -0.133	PRIM	13	BELL $e^+ e^- \rightarrow \Upsilon(4S)$
$-0.08 \pm 0.12 \pm 0.05$	AUBERT	08Bg	BABR $e^+ e^- \rightarrow \Upsilon(4S)$

• • • We do not use the following data for averages, fits, limits, etc. • • •

$-0.12 \pm 0.14 \pm 0.04$	AUBERT	07D	BABR Repl. by AUBERT 08Bg
---------------------------	--------	-----	---------------------------

$A_{CP}(B^0 \rightarrow K^*(892)^0 \gamma)$

VALUE	DOCUMENT ID	TECN	COMMENT
-0.006 ± 0.011 OUR AVERAGE			
$-0.013 \pm 0.017 \pm 0.004$	¹ HORIGUCHI	17	BELL $e^+ e^- \rightarrow \Upsilon(4S)$
$0.008 \pm 0.017 \pm 0.009$	AAIJ	13	LHCB pp at 7 TeV
$-0.016 \pm 0.022 \pm 0.007$	AUBERT	09A0	BABR $e^+ e^- \rightarrow \Upsilon(4S)$

¹ Uses $B(\Upsilon(4S) \rightarrow B^+ B^-) = (51.4 \pm 0.6)\%$ and $B(\Upsilon(4S) \rightarrow B^0 \bar{B}^0) = (48.6 \pm 0.6)\%$.

$A_{CP}(B^0 \rightarrow K_2^*(1430)^0 \gamma)$

VALUE	DOCUMENT ID	TECN	COMMENT
$-0.08 \pm 0.15 \pm 0.01$	AUBERT,B	04U	BABR $e^+ e^- \rightarrow \Upsilon(4S)$

$A_{CP}(B^0 \rightarrow X_s \gamma)$

VALUE	DOCUMENT ID	TECN	COMMENT
$-0.0094 \pm 0.0174 \pm 0.0047$	¹ WATA NUKI	19	BELL $e^+ e^- \rightarrow \Upsilon(4S)$

¹ Using a sum-of-exclusive technique with $m_{X_s} < 2.8 \text{ GeV}/c^2$.

$A_{CP}(B^0 \rightarrow \rho^+ \pi^-)$

VALUE	DOCUMENT ID	TECN	COMMENT
0.13 ± 0.06 OUR AVERAGE			Error includes scale factor of 1.1.
$0.09 \pm 0.05 \pm 0.04$ -0.06	¹ LEES	13J	BABR $e^+ e^- \rightarrow \Upsilon(4S)$
$0.21 \pm 0.08 \pm 0.04$	¹ KUSAKA	07	BELL $e^+ e^- \rightarrow \Upsilon(4S)$

• • • We do not use the following data for averages, fits, limits, etc. • • •

$0.03 \pm 0.07 \pm 0.04$	AUBERT	07AA	BABR Repl. by LEES 13J
$-0.02 \pm 0.16 \pm 0.05$ -0.02	WANG	05	BELL Repl. by KUSAKA 07
$-0.18 \pm 0.08 \pm 0.03$	AUBERT	03T	BABR Repl. by AUBERT 07AA

¹ Uses time-dependent Dalitz plot analysis of $B^0 \rightarrow \pi^+ \pi^- \pi^0$ decays.

$A_{CP}(B^0 \rightarrow \rho^- \pi^+)$

VALUE	DOCUMENT ID	TECN	COMMENT
-0.08 ± 0.08 OUR AVERAGE			
$-0.12 \pm 0.08 \pm 0.04$ -0.05	¹ LEES	13J	BABR $e^+ e^- \rightarrow \Upsilon(4S)$
$0.08 \pm 0.16 \pm 0.11$	¹ KUSAKA	07	BELL $e^+ e^- \rightarrow \Upsilon(4S)$

• • • We do not use the following data for averages, fits, limits, etc. • • •

$-0.37 \pm 0.16 \pm 0.09$ -0.10	AUBERT	07AA	BABR Repl. by LEES 13J
$-0.53 \pm 0.29 \pm 0.09$ -0.04	WANG	05	BELL Repl. by KUSAKA 07

¹ Uses time-dependent Dalitz plot analysis of $B^0 \rightarrow \pi^+ \pi^- \pi^0$ decays.

$A_{CP}(B^0 \rightarrow a_1(1260)^\pm \pi^\mp)$

VALUE	DOCUMENT ID	TECN	COMMENT
-0.07 ± 0.06 OUR AVERAGE			
$-0.06 \pm 0.05 \pm 0.07$	DALSENO	12	BELL $e^+ e^- \rightarrow \Upsilon(4S)$
$-0.07 \pm 0.07 \pm 0.02$	AUBERT	07o	BABR $e^+ e^- \rightarrow \Upsilon(4S)$

$A_{CP}(B^0 \rightarrow b_1^- \pi^+)$

VALUE	DOCUMENT ID	TECN	COMMENT
$-0.05 \pm 0.10 \pm 0.02$	AUBERT	07Bi	BABR $e^+ e^- \rightarrow \Upsilon(4S)$

$A_{CP}(B^0 \rightarrow \rho \bar{p} K^*(892)^0)$

VALUE	DOCUMENT ID	TECN	COMMENT
0.05 ± 0.12 OUR AVERAGE			
$-0.08 \pm 0.20 \pm 0.02$	CHEN	08c	BELL $e^+ e^- \rightarrow \Upsilon(4S)$
$0.11 \pm 0.13 \pm 0.06$	AUBERT	07AV	BABR $e^+ e^- \rightarrow \Upsilon(4S)$

$A_{CP}(B^0 \rightarrow \rho \bar{\lambda} \pi^-)$

VALUE	DOCUMENT ID	TECN	COMMENT
0.04 ± 0.07 OUR AVERAGE			
$0.10 \pm 0.10 \pm 0.02$	AUBERT	09Ac	BABR $e^+ e^- \rightarrow \Upsilon(4S)$
$-0.02 \pm 0.10 \pm 0.03$	WANG	07c	BELL $e^+ e^- \rightarrow \Upsilon(4S)$

$A_{CP}(B^0 \rightarrow K^{*0} \ell^+ \ell^-)$

VALUE	DOCUMENT ID	TECN	COMMENT
-0.05 ± 0.10 OUR AVERAGE			
$0.02 \pm 0.20 \pm 0.02$	AUBERT	09T	BABR $e^+ e^- \rightarrow \Upsilon(4S)$
$-0.08 \pm 0.12 \pm 0.02$	WEI	09A	BELL $e^+ e^- \rightarrow \Upsilon(4S)$

$A_{CP}(B^0 \rightarrow K^{*0} e^+ e^-)$

VALUE	DOCUMENT ID	TECN	COMMENT
$-0.21 \pm 0.19 \pm 0.02$			
$0.00 \pm 0.15 \pm 0.03$	WEI	09A	BELL $e^+ e^- \rightarrow \Upsilon(4S)$

$A_{CP}(B^0 \rightarrow K^{*0} \mu^+ \mu^-)$

VALUE	DOCUMENT ID	TECN	COMMENT
-0.034 ± 0.024 OUR AVERAGE			
$-0.035 \pm 0.024 \pm 0.003$	AAIJ	14AN	LHCB pp at 7, 8 TeV
$0.00 \pm 0.15 \pm 0.03$	WEI	09A	BELL $e^+ e^- \rightarrow \Upsilon(4S)$

• • • We do not use the following data for averages, fits, limits, etc. • • •

$-0.072 \pm 0.040 \pm 0.005$	AAIJ	13E	LHCB Repl. by AAIJ 14AN
------------------------------	------	-----	-------------------------

$C_{D^*(2010)-D^+}(B^0 \rightarrow D^*(2010)^- D^+)$

VALUE	DOCUMENT ID	TECN	COMMENT
-0.02 ± 0.08 OUR AVERAGE			
$-0.028 \pm 0.130 \pm 0.026$	¹ AAIJ	20L	LHCB pp at 7, 8, 13 TeV
$-0.13 \pm 0.16 \pm 0.05$	² ROHRKEN	12	BELL $e^+ e^- \rightarrow \Upsilon(4S)$
$0.00 \pm 0.17 \pm 0.03$	AUBERT	09c	BABR $e^+ e^- \rightarrow \Upsilon(4S)$
$0.23 \pm 0.25 \pm 0.06$	³ AUSHEV	04	BELL $e^+ e^- \rightarrow \Upsilon(4S)$

• • • We do not use the following data for averages, fits, limits, etc. • • •

$0.23 \pm 0.15 \pm 0.04$	AUBERT	07Ai	BABR Repl. by AUBERT 09c
$0.17 \pm 0.24 \pm 0.04$	AUBERT,B	05z	BABR Repl. by AUBERT 07Ai
$-0.22 \pm 0.37 \pm 0.10$	AUBERT	03J	BABR Repl. by AUBERT,B 05z

¹ AAIJ 20L reports the measurements of $C = -0.059 \pm 0.092 \pm 0.020$ and $\Delta C = -0.031 \pm 0.092 \pm 0.016$ such that $C_{D^*(2010)-D^+} = C - \Delta C$.
² ROHRKEN 12 reports the measurements of $C = -0.01 \pm 0.11 \pm 0.04$ and $\Delta C = 0.12 \pm 0.11 \pm 0.03$ such that $C_{D^*(2010)-D^+} = C - \Delta C$.
³ Combines results from fully and partially reconstructed $B^0 \rightarrow D^{*\pm} D^\mp$ decays.

$S_{D^*(2010)-D^+}(B^0 \rightarrow D^*(2010)^- D^+)$

VALUE	DOCUMENT ID	TECN	COMMENT
-0.83 ± 0.09 OUR AVERAGE			
$-0.880 \pm 0.107 \pm 0.022$	¹ AAIJ	20L	LHCB pp at 7, 8, 13 TeV
$-0.65 \pm 0.22 \pm 0.07$	² ROHRKEN	12	BELL $e^+ e^- \rightarrow \Upsilon(4S)$
$-0.73 \pm 0.23 \pm 0.050$	AUBERT	09c	BABR $e^+ e^- \rightarrow \Upsilon(4S)$
$-0.96 \pm 0.43 \pm 0.12$	³ AUSHEV	04	BELL $e^+ e^- \rightarrow \Upsilon(4S)$

• • • We do not use the following data for averages, fits, limits, etc. • • •

$-0.44 \pm 0.22 \pm 0.06$	AUBERT	07Ai	BABR Repl. by AUBERT 09c
$-0.29 \pm 0.33 \pm 0.07$	AUBERT,B	05z	BABR Repl. by AUBERT 07Ai
$-0.24 \pm 0.69 \pm 0.12$	AUBERT	03J	BABR Repl. by AUBERT,B 05z

¹ AAIJ 20L reports the measurements of $S = -0.861 \pm 0.077 \pm 0.019$ and $\Delta S = 0.019 \pm 0.075 \pm 0.012$ such that $S_{D^*(2010)-D^+} = S - \Delta S$.
² ROHRKEN 12 reports the measurements of $S = -0.78 \pm 0.15 \pm 0.05$ and $\Delta S = -0.13 \pm 0.15 \pm 0.04$ such that $S_{D^*(2010)-D^+} = S - \Delta S$.
³ Combines results from fully and partially reconstructed $B^0 \rightarrow D^{*\pm} D^\mp$ decays.

$C_{D^*(2010)+D^-}(B^0 \rightarrow D^*(2010)^+ D^-)$

VALUE	DOCUMENT ID	TECN	COMMENT
-0.03 ± 0.09 OUR AVERAGE			Error includes scale factor of 1.1.
$-0.090 \pm 0.130 \pm 0.026$	¹ AAIJ	20L	LHCB pp at 7, 8, 13 TeV
$0.11 \pm 0.14 \pm 0.06$	² ROHRKEN	12	BELL $e^+ e^- \rightarrow \Upsilon(4S)$
$0.08 \pm 0.17 \pm 0.04$	AUBERT	09c	BABR $e^+ e^- \rightarrow \Upsilon(4S)$
$-0.37 \pm 0.22 \pm 0.06$	³ AUSHEV	04	BELL $e^+ e^- \rightarrow \Upsilon(4S)$

• • • We do not use the following data for averages, fits, limits, etc. • • •

$0.18 \pm 0.15 \pm 0.04$	AUBERT	07Ai	BABR Repl. by AUBERT 09c
$0.09 \pm 0.25 \pm 0.06$	AUBERT,B	05z	BABR Repl. by AUBERT 07Ai
$-0.47 \pm 0.40 \pm 0.12$	AUBERT	03J	BABR Repl. by AUBERT,B 05z

¹ AAIJ 20L reports the measurements of $C = -0.059 \pm 0.092 \pm 0.020$ and $\Delta C = -0.031 \pm 0.092 \pm 0.016$ such that $C_{D^*(2010)+D^-} = C + \Delta C$.
² ROHRKEN 12 reports the measurements of $C = -0.01 \pm 0.11 \pm 0.04$ and $\Delta C = 0.12 \pm 0.11 \pm 0.03$ such that $C_{D^*(2010)+D^-} = C + \Delta C$.
³ Combines results from fully and partially reconstructed $B^0 \rightarrow D^{*\pm} D^\mp$ decays.

Meson Particle Listings

B^0

$S_{D^{*+}D^-} (B^0 \rightarrow D^{*+}D^-)$

VALUE	DOCUMENT ID	TECN	COMMENT
-0.80 ± 0.09 OUR AVERAGE			
-0.842 ± 0.107 ± 0.022	¹ AAIJ	20L	LHCB pp at 7, 8, 13 TeV
-0.90 ± 0.21 ± 0.07	² ROHRKEN	12	BELL $e^+e^- \rightarrow \Upsilon(4S)$
-0.62 ± 0.21 ± 0.03	AUBERT	09c	BABR $e^+e^- \rightarrow \Upsilon(4S)$
-0.55 ± 0.39 ± 0.12	³ AUSHEV	04	BELL $e^+e^- \rightarrow \Upsilon(4S)$

• • • We do not use the following data for averages, fits, limits, etc. • • •

-0.79 ± 0.21 ± 0.06 AUBERT 07AI BABR Repl. by AUBERT 09c
 -0.54 ± 0.35 ± 0.07 AUBERT,B 05Z BABR Repl. by AUBERT 07AI
 -0.82 ± 0.75 ± 0.14 AUBERT 03J BABR Repl. by AUBERT,B 05Z

¹AAIJ 20L reports the measurements of $S = -0.861 \pm 0.077 \pm 0.019$ and $\Delta S = 0.019 \pm 0.075 \pm 0.012$ such that $S_{D^{*+}D^-} = S + \Delta S$.
²ROHRKEN 12 reports the measurements of $S = -0.78 \pm 0.15 \pm 0.05$ and $\Delta S = -0.13 \pm 0.15 \pm 0.04$ such that $S_{D^{*+}D^-} = S + \Delta S$.
³Combines results from fully and partially reconstructed $B^0 \rightarrow D^{*+}D^\mp$ decays.

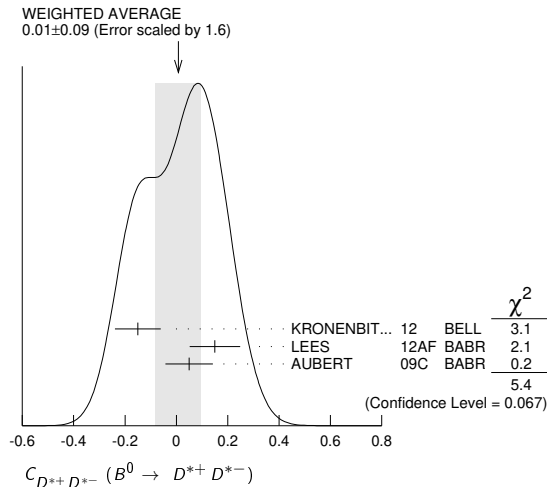
$C_{D^{*+}D^{*-}} (B^0 \rightarrow D^{*+}D^{*-})$

VALUE	DOCUMENT ID	TECN	COMMENT
0.01 ± 0.09 OUR AVERAGE			Error includes scale factor of 1.6. See the ideogram below.
-0.15 ± 0.08 ± 0.04	^{1,2} KRONENBIT...	12	BELL $e^+e^- \rightarrow \Upsilon(4S)$
+0.15 ± 0.09 ± 0.04	³ LEES	12AF	BABR $e^+e^- \rightarrow \Upsilon(4S)$
0.05 ± 0.09 ± 0.02	AUBERT	09c	BABR $e^+e^- \rightarrow \Upsilon(4S)$

• • • We do not use the following data for averages, fits, limits, etc. • • •

-0.15 ± 0.13 ± 0.04 ²VERVINK 09 BELL Repl. by KRONENBITTER 12
 -0.02 ± 0.11 ± 0.02 ¹AUBERT 07Bo BABR Repl. by AUBERT 09c
 0.26 ± 0.26 ± 0.06 ²MIYAKE 05 BELL Repl. by VERVINK 09
 0.28 ± 0.23 ± 0.02 ⁴AUBERT 03q BABR Repl. by AUBERT 07Bo

¹Assumes both CP -even and CP -odd states having the CP asymmetry.
²Belle Collab. quotes $A_{D^{*+}D^{*-}}$ which is equal to $-C_{D^{*+}D^{*-}}$.
³Measured partially reconstructed candidates when one D^0 meson is not explicitly reconstructed. Analysis does not separate CP -even and CP -odd component.
⁴AUBERT 03q reports $|\lambda| = 0.75 \pm 0.19 \pm 0.02$ and $\text{Im}(\lambda) = 0.05 \pm 0.29 \pm 0.10$. We convert them to S and C parameters taking into account correlations.



$S_{D^{*+}D^{*-}} (B^0 \rightarrow D^{*+}D^{*-})$

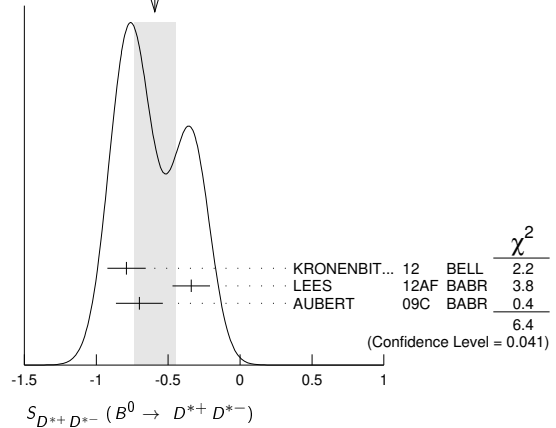
VALUE	DOCUMENT ID	TECN	COMMENT
-0.59 ± 0.14 OUR AVERAGE			Error includes scale factor of 1.8. See the ideogram below.
-0.79 ± 0.13 ± 0.03	¹ KRONENBIT...	12	BELL $e^+e^- \rightarrow \Upsilon(4S)$
-0.34 ± 0.12 ± 0.05	² LEES	12AF	BABR $e^+e^- \rightarrow \Upsilon(4S)$
-0.70 ± 0.16 ± 0.03	¹ AUBERT	09c	BABR $e^+e^- \rightarrow \Upsilon(4S)$

• • • We do not use the following data for averages, fits, limits, etc. • • •

-0.96 ± 0.25 ± 0.13 ¹VERVINK 09 BELL Repl. by KRONENBITTER 12
 -0.66 ± 0.19 ± 0.04 ¹AUBERT 07Bo BABR Repl. by AUBERT 09c
 -0.75 ± 0.56 ± 0.12 ²MIYAKE 05 BELL Repl. by VERVINK 09
 0.06 ± 0.37 ± 0.13 ³AUBERT 03q BABR Repl. by AUBERT 07Bo

¹Assumes both CP -even and CP -odd states having the CP asymmetry.
²Measured partially reconstructed candidates when one D^0 meson is not explicitly reconstructed. Analysis does not separate CP -even and CP -odd component.
³AUBERT 03q reports $|\lambda| = 0.75 \pm 0.19 \pm 0.02$ and $\text{Im}(\lambda) = 0.05 \pm 0.29 \pm 0.10$. We convert them to S and C parameters taking into account correlations.

WEIGHTED AVERAGE -0.59 ± 0.14 (Error scaled by 1.8)



$C_+ (B^0 \rightarrow D^{*+}D^{*-})$

See the note in the $C_{\pi\pi}$ datablock, but for CP even final state.

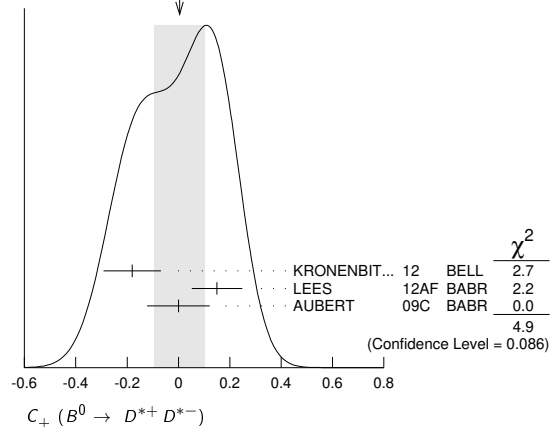
VALUE	DOCUMENT ID	TECN	COMMENT
0.00 ± 0.10 OUR AVERAGE			Error includes scale factor of 1.6. See the ideogram below.
-0.18 ± 0.10 ± 0.05	¹ KRONENBIT...	12	BELL $e^+e^- \rightarrow \Upsilon(4S)$
+0.15 ± 0.09 ± 0.04	² LEES	12AF	BABR $e^+e^- \rightarrow \Upsilon(4S)$
0.00 ± 0.12 ± 0.02	AUBERT	09c	BABR $e^+e^- \rightarrow \Upsilon(4S)$

• • • We do not use the following data for averages, fits, limits, etc. • • •

-0.05 ± 0.14 ± 0.02 AUBERT 07Bo BABR Repl. by AUBERT 09c
 0.06 ± 0.17 ± 0.03 ³AUBERT,BE 05A BABR Repl. by AUBERT 07Bo

¹Belle Collab. quotes $A_{D^{*+}D^{*-}}$ which is equal to $-C_{D^{*+}D^{*-}}$.
²Measured partially reconstructed candidates when one D^0 meson is not explicitly reconstructed. Extracted under assumption of equal C_+ and C_- .
³AUBERT,BE 05A reports a CP -odd fraction $R_\perp = 0.125 \pm 0.044 \pm 0.007$.

WEIGHTED AVERAGE 0.00 ± 0.10 (Error scaled by 1.6)



$S_+ (B^0 \rightarrow D^{*+}D^{*-})$

See the note in the $S_{\pi\pi}$ datablock, but for CP even final state.

VALUE	DOCUMENT ID	TECN	COMMENT
-0.73 ± 0.09 OUR AVERAGE			
-0.81 ± 0.13 ± 0.03	KRONENBIT...	12	BELL $e^+e^- \rightarrow \Upsilon(4S)$
-0.49 ± 0.18 ± 0.08	¹ LEES	12AF	BABR $e^+e^- \rightarrow \Upsilon(4S)$
-0.76 ± 0.16 ± 0.04	AUBERT	09c	BABR $e^+e^- \rightarrow \Upsilon(4S)$

• • • We do not use the following data for averages, fits, limits, etc. • • •

-0.72 ± 0.19 ± 0.05 AUBERT 07Bo BABR Repl. by AUBERT 09c
 -0.75 ± 0.25 ± 0.03 ²AUBERT,BE 05A BABR Repl. by AUBERT 07Bo

¹Measured partially reconstructed candidates when one D^0 meson is not explicitly reconstructed. Analysis does not separate CP -even and CP -odd component. Value is obtained from $S = -0.34 \pm 0.12 \pm 0.05$ using $S = S_+ (1 - 2R_\perp)$ with $R_\perp = 0.158 \pm 0.029$.
²AUBERT,BE 05A reports a CP -odd fraction $R_\perp = 0.125 \pm 0.044 \pm 0.007$.

$C_- (B^0 \rightarrow D^{*+}D^{*-})$

See the note in the $C_{\pi\pi}$ datablock, but for CP odd final state.

VALUE	DOCUMENT ID	TECN	COMMENT
0.19 ± 0.31 OUR AVERAGE			
0.05 ± 0.39 ± 0.08	¹ KRONENBIT...	12	BELL $e^+e^- \rightarrow \Upsilon(4S)$
0.41 ± 0.49 ± 0.08	AUBERT	09c	BABR $e^+e^- \rightarrow \Upsilon(4S)$

• • • We do not use the following data for averages, fits, limits, etc. • • •
 $0.23 \pm 0.67 \pm 0.10$ AUBERT 07B0 BABR Repl. by AUBERT 09c
 $-0.20 \pm 0.96 \pm 0.11$ ² AUBERT, BE 05A BABR Repl. by AUBERT 07B0
¹ Belle Collab. quotes $A_{D^{*+}D^{*-}}$ which is equal to $-C_{D^{*+}D^{*-}}$.
² AUBERT, BE 05A reports a CP-odd fraction $R_{\perp} = 0.125 \pm 0.044 \pm 0.007$.

$S_{-}(B^0 \rightarrow D^{*+}D^{*-})$
 See the note in the $S_{\pi\pi}$ datablock, but for CP odd final state.

VALUE	DOCUMENT ID	TECN	COMMENT
0.1 ± 1.6 OUR AVERAGE	Error includes scale factor of 3.5.		
$1.52 \pm 0.62 \pm 0.12$	KRONENBIT... 12	BELL	$e^+e^- \rightarrow \Upsilon(4S)$
$-1.80 \pm 0.70 \pm 0.16$	AUBERT 09c	BABR	$e^+e^- \rightarrow \Upsilon(4S)$
• • • We do not use the following data for averages, fits, limits, etc. • • •			
$-1.83 \pm 1.04 \pm 0.23$	AUBERT 07B0	BABR	Repl. by AUBERT 09c
$-1.75 \pm 1.78 \pm 0.22$	¹ AUBERT, BE 05A	BABR	Repl. by AUBERT 07B0
¹ AUBERT, BE 05A reports a CP-odd fraction $R_{\perp} = 0.125 \pm 0.044 \pm 0.007$.			

$C(B^0 \rightarrow D^{*}(2010)^+ D^{*}(2010)^- K_S^0)$

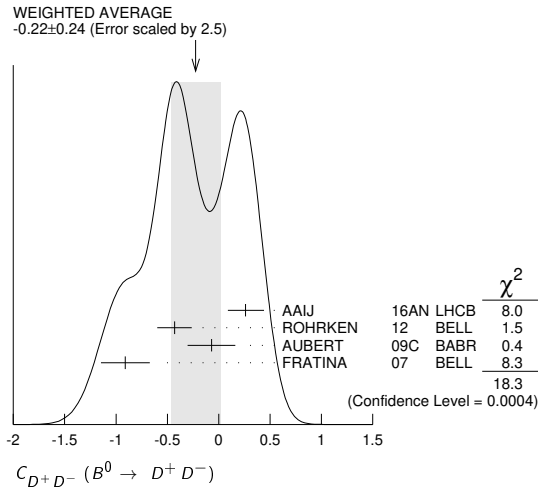
VALUE	DOCUMENT ID	TECN	COMMENT
$0.01 \pm 0.28 \pm 0.09$	¹ DALSENO 07	BELL	$e^+e^- \rightarrow \Upsilon(4S)$
¹ Reports value of A which is equal to $-C$.			

$S(B^0 \rightarrow D^{*}(2010)^+ D^{*}(2010)^- K_S^0)$

VALUE	DOCUMENT ID	TECN	COMMENT
$0.06^{+0.45}_{-0.44} \pm 0.06$	¹ DALSENO 07	BELL	$e^+e^- \rightarrow \Upsilon(4S)$
¹ This value includes an unknown CP dilution factor D due to possible contributions from intermediate resonances and different partial waves.			

$C_{D^+D^-}(B^0 \rightarrow D^+D^-)$

VALUE	DOCUMENT ID	TECN	COMMENT
-0.22 ± 0.24 OUR AVERAGE	Error includes scale factor of 2.5. See the ideogram below.		
$0.26^{+0.18}_{-0.17} \pm 0.02$	AAIJ 16AN	LHCB	pp at 7, 8 TeV
$-0.43 \pm 0.16 \pm 0.05$	ROHRKEN 12	BELL	$e^+e^- \rightarrow \Upsilon(4S)$
$-0.07 \pm 0.23 \pm 0.03$	AUBERT 09c	BABR	$e^+e^- \rightarrow \Upsilon(4S)$
$-0.91 \pm 0.23 \pm 0.06$	¹ FRATINA 07	BELL	$e^+e^- \rightarrow \Upsilon(4S)$
• • • We do not use the following data for averages, fits, limits, etc. • • •			
$0.11 \pm 0.22 \pm 0.07$	AUBERT 07A1	BABR	Repl. by AUBERT 09c
$0.11 \pm 0.35 \pm 0.06$	AUBERT, B 05Z	BABR	Repl. by AUBERT 07A1
¹ The paper reports A, which is equal to $-C$.			



$S_{D^+D^-}(B^0 \rightarrow D^+D^-)$

VALUE	DOCUMENT ID	TECN	COMMENT
$-0.76^{+0.15}_{-0.13} \pm 0.06$ OUR AVERAGE	Error includes scale factor of 1.2.		
$-0.54^{+0.17}_{-0.16} \pm 0.05$	AAIJ 16AN	LHCB	pp at 7, 8 TeV
$-1.06^{+0.21}_{-0.14} \pm 0.08$	ROHRKEN 12	BELL	$e^+e^- \rightarrow \Upsilon(4S)$
$-0.63 \pm 0.36 \pm 0.05$	AUBERT 09c	BABR	$e^+e^- \rightarrow \Upsilon(4S)$
$-1.13 \pm 0.37 \pm 0.09$	FRATINA 07	BELL	$e^+e^- \rightarrow \Upsilon(4S)$
• • • We do not use the following data for averages, fits, limits, etc. • • •			
$-0.54 \pm 0.34 \pm 0.06$	AUBERT 07A1	BABR	Repl. by AUBERT 09c
$-0.29 \pm 0.63 \pm 0.06$	AUBERT, B 05Z	BABR	Repl. by AUBERT 07A1

$C_{J/\psi(1S)\pi^0}(B^0 \rightarrow J/\psi(1S)\pi^0)$

VALUE	DOCUMENT ID	TECN	COMMENT
0.03 ± 0.17 OUR AVERAGE	Error includes scale factor of 1.5.		
$0.15 \pm 0.14^{+0.04}_{-0.03}$	¹ PAL 18	BELL	$e^+e^- \rightarrow \Upsilon(4S)$
$-0.20 \pm 0.19 \pm 0.03$	AUBERT 08AU	BABR	$e^+e^- \rightarrow \Upsilon(4S)$
• • • We do not use the following data for averages, fits, limits, etc. • • •			
$-0.08 \pm 0.16 \pm 0.05$	¹ LEE 08A	BELL	Repl. by PAL 18
$-0.21 \pm 0.26 \pm 0.06$	AUBERT, B 06B	BABR	Repl. by AUBERT 08AU
$0.01 \pm 0.29 \pm 0.03$	¹ KATAOKA 04	BELL	Repl. by LEE 08A
$0.38 \pm 0.41 \pm 0.09$	AUBERT 03N	BABR	Repl. by AUBERT, B 06B
¹ BELLE Collab. quotes $A_{J/\psi\pi^0}$ which is equal to $-C_{J/\psi\pi^0}$.			

$S_{J/\psi(1S)\pi^0}(B^0 \rightarrow J/\psi(1S)\pi^0)$

VALUE	DOCUMENT ID	TECN	COMMENT
-0.88 ± 0.32 OUR AVERAGE	Error includes scale factor of 2.2.		
$-0.59 \pm 0.19 \pm 0.03$	PAL 18	BELL	$e^+e^- \rightarrow \Upsilon(4S)$
$-1.23 \pm 0.21 \pm 0.04$	AUBERT 08AU	BABR	$e^+e^- \rightarrow \Upsilon(4S)$
• • • We do not use the following data for averages, fits, limits, etc. • • •			
$-0.65 \pm 0.21 \pm 0.05$	LEE 08A	BELL	Repl. by PAL 18
$-0.68 \pm 0.30 \pm 0.04$	AUBERT, B 06B	BABR	Repl. by AUBERT 08AU
$-0.72 \pm 0.42 \pm 0.09$	KATAOKA 04	BELL	Repl. by LEE 08A
$0.05 \pm 0.49 \pm 0.16$	AUBERT 03N	BABR	Repl. by AUBERT, B 06B

$C(B^0 \rightarrow J/\psi(1S)\rho^0)$

VALUE	DOCUMENT ID	TECN	COMMENT
$-0.063 \pm 0.056^{+0.019}_{-0.014}$	¹ AAIJ 15J	LHCB	pp at 7, 8 TeV
¹ Time-dependent CP violation is measured in the $B^0 \rightarrow J/\psi\rho^0$ and was used to limit the size of penguin amplitude contributions to ϕ_S in $B_S^0 \rightarrow J/\psi\phi$ decays to be between $[-1.05^\circ, 1.18^\circ]$ at 95% confidence level.			

$S(B^0 \rightarrow J/\psi(1S)\rho^0)$

VALUE	DOCUMENT ID	TECN	COMMENT
$-0.66^{+0.13+0.09}_{-0.12-0.03}$	¹ AAIJ 15J	LHCB	pp at 7, 8 TeV
¹ Time-dependent CP violation is measured in the $B^0 \rightarrow J/\psi\rho^0$ and was used to limit the size of penguin amplitude contributions to ϕ_S in $B_S^0 \rightarrow J/\psi\phi$ decays to be between $[-1.05^\circ, 1.18^\circ]$ at 95% confidence level.			

$C_{D_{CP}^{(*)}h^0}(B^0 \rightarrow D_{CP}^{(*)}h^0)$

VALUE	DOCUMENT ID	TECN	COMMENT
$-0.02 \pm 0.07 \pm 0.03$	¹ ABDESSALAM 15		$e^+e^- \rightarrow \Upsilon(4S)$
• • • We do not use the following data for averages, fits, limits, etc. • • •			
$-0.23 \pm 0.16 \pm 0.04$	AUBERT 07AJ	BABR	Repl. by ABDESSALAM 15
¹ BABAR and BELLE combined analysis uses CP-eigenstate decay modes $D^0 \rightarrow K^+K^-$, $K_S^0\pi^0$, $K_S^0\omega$, and $h^0 = \pi^0, \eta, \omega$.			

$S_{D_{CP}^{(*)}h^0}(B^0 \rightarrow D_{CP}^{(*)}h^0)$

VALUE	DOCUMENT ID	TECN	COMMENT
$-0.66 \pm 0.10 \pm 0.06$	¹ ABDESSALAM 15		$e^+e^- \rightarrow \Upsilon(4S)$
• • • We do not use the following data for averages, fits, limits, etc. • • •			
$-0.56 \pm 0.23 \pm 0.05$	AUBERT 07AJ	BABR	Repl. by ABDESSALAM 15
¹ BABAR and BELLE combined analysis uses CP-eigenstate decay modes $D^0 \rightarrow K^+K^-$, $K_S^0\pi^0$, $K_S^0\omega$, and $h^0 = \pi^0, \eta, \omega$.			

$C_{K^0\pi^0}(B^0 \rightarrow K^0\pi^0)$

VALUE	DOCUMENT ID	TECN	COMMENT
0.00 ± 0.08 OUR AVERAGE			
$-0.01 \pm 0.12 \pm 0.04$	¹ ADACHI 24	BELL	$e^+e^- \rightarrow \Upsilon(4S)$
$-0.14 \pm 0.13 \pm 0.06$	² FUJIKAWA 10A	BELL	$e^+e^- \rightarrow \Upsilon(4S)$
$0.13 \pm 0.13 \pm 0.03$	AUBERT 09I	BABR	$e^+e^- \rightarrow \Upsilon(4S)$
• • • We do not use the following data for averages, fits, limits, etc. • • •			
$-0.06 \pm 0.15 \pm 0.04$	³ ADACHI 24	BELL	$e^+e^- \rightarrow \Upsilon(4S)$
$-0.04^{+0.14}_{-0.15} \pm 0.05$	⁴ ADACHI 23E	BELL	$e^+e^- \rightarrow \Upsilon(4S)$
$0.24 \pm 0.15 \pm 0.03$	AUBERT 08E	BABR	Repl. by AUBERT 09I
$0.05 \pm 0.14 \pm 0.05$	² CHAO 07	BELL	Repl. by FUJIKAWA 10A
$0.06 \pm 0.18 \pm 0.03$	AUBERT 05Y	BABR	Repl. by AUBERT 08E
$-0.16 \pm 0.29 \pm 0.05$	^{2,5} CHAO 05A	BELL	Repl. by CHEN 05B
$0.11 \pm 0.20 \pm 0.09$	² CHEN 05B	BELL	Repl. by CHAO 07
$-0.03 \pm 0.36 \pm 0.11$	² AUBERT 04M	BABR	Repl. by AUBERT, B 04M
$0.40^{+0.27}_{-0.28} \pm 0.09$	⁶ AUBERT, B 04M	BABR	Repl. by AUBERT 05Y
¹ This is the combined result of this analysis (ADACHI 24) and ADACHI 23E.			
² Reports A which is equal to $-C$.			
³ The measurement is using BELL II data reported in ADACHI 24. The combination with ADACHI 23E is also reported.			
⁴ The result has been combined with ADACHI 24.			
⁵ Corresponds to a 90% CL interval of $-0.33 < A_{CP} < 0.64$.			
⁶ Based on a total signal yield of 122 ± 16 events.			

Meson Particle Listings

 B^0 $S_{K^0 \pi^0} (B^0 \rightarrow K^0 \pi^0)$

VALUE	DOCUMENT ID	TECN	COMMENT
0.64 ± 0.13 OUR AVERAGE			
$0.75^{+0.20}_{-0.23} \pm 0.04$	ADACHI	23E	BELL $e^+ e^- \rightarrow \Upsilon(4S)$
$0.67 \pm 0.31 \pm 0.08$	FUJIKAWA	10A	BELL $e^+ e^- \rightarrow \Upsilon(4S)$
$0.55 \pm 0.20 \pm 0.03$	AUBERT	09I	BABR $e^+ e^- \rightarrow \Upsilon(4S)$
• • • We do not use the following data for averages, fits, limits, etc. • • •			
$0.40 \pm 0.23 \pm 0.03$	AUBERT	08E	BABR Repl. by AUBERT 09I
$0.33 \pm 0.35 \pm 0.08$	CHAO	07	BELL Repl. by FUJIKAWA 10A
$0.35^{+0.30}_{-0.33} \pm 0.04$	AUBERT	05Y	BABR Repl. by AUBERT 08E
$0.32 \pm 0.61 \pm 0.13$	CHEN	05B	BELL Repl. by CHAO 07
$0.48^{+0.38}_{-0.47} \pm 0.06$	¹ AUBERT,B	04M	BABR Repl. by AUBERT 05Y

¹ Based on a total signal yield of 122 ± 16 events. $C_{\eta'(958) K_S^0} (B^0 \rightarrow \eta'(958) K_S^0)$ See updated measurements in $C_{\eta' K^0}$

VALUE	DOCUMENT ID	TECN	COMMENT
-0.04 ± 0.20 OUR AVERAGE			Error includes scale factor of 2.5.
$-0.21 \pm 0.10 \pm 0.02$	AUBERT	05M	BABR $e^+ e^- \rightarrow \Upsilon(4S)$
$0.19 \pm 0.11 \pm 0.05$	¹ CHEN	05B	BELL $e^+ e^- \rightarrow \Upsilon(4S)$
• • • We do not use the following data for averages, fits, limits, etc. • • •			
$-0.26 \pm 0.22 \pm 0.03$	¹ ABE	03C	BELL Repl. by ABE 03H
$0.01 \pm 0.16 \pm 0.04$	¹ ABE	03H	BELL Repl. by CHEN 05B
$0.10 \pm 0.22 \pm 0.04$	AUBERT	03W	BABR Repl. by AUBERT 05M
$-0.13 \pm 0.32^{+0.06}_{-0.09}$	¹ CHEN	02B	BELL Repl. by ABE 03C

¹ BELLE Collab. quotes $A_{\eta'(958) K_S^0}$ which is equal to $-C_{\eta'(958) K_S^0}$. $S_{\eta'(958) K_S^0} (B^0 \rightarrow \eta'(958) K_S^0)$ See updated measurements in $S_{\eta' K^0}$

VALUE	DOCUMENT ID	TECN	COMMENT
0.43 ± 0.17 OUR AVERAGE			Error includes scale factor of 1.5.
$0.30 \pm 0.14 \pm 0.02$	AUBERT	05M	BABR $e^+ e^- \rightarrow \Upsilon(4S)$
$0.65 \pm 0.18 \pm 0.04$	CHEN	05B	BELL $e^+ e^- \rightarrow \Upsilon(4S)$
• • • We do not use the following data for averages, fits, limits, etc. • • •			
$0.71 \pm 0.37^{+0.05}_{-0.06}$	ABE	03C	BELL Repl. by ABE 03H
$0.43 \pm 0.27 \pm 0.05$	ABE	03H	BELL Repl. by CHEN 05B
$0.02 \pm 0.34 \pm 0.03$	AUBERT	03W	BABR Repl. by AUBERT 05M
$0.28 \pm 0.55^{+0.07}_{-0.08}$	CHEN	02B	BELL Repl. by ABE 03C

 $C_{\eta' K^0} (B^0 \rightarrow \eta' K^0)$

VALUE	DOCUMENT ID	TECN	COMMENT
-0.06 ± 0.04 OUR AVERAGE			
$-0.03 \pm 0.05 \pm 0.04$	¹ SANTELJ	14	BELL $e^+ e^- \rightarrow \Upsilon(4S)$
$-0.08 \pm 0.06 \pm 0.02$	AUBERT	09I	BABR $e^+ e^- \rightarrow \Upsilon(4S)$
• • • We do not use the following data for averages, fits, limits, etc. • • •			
$-0.16 \pm 0.07 \pm 0.03$	² AUBERT	07A	BABR Repl. by AUBERT 09I
$0.01 \pm 0.07 \pm 0.05$	^{1,2} CHEN	07	BELL Repl. by SANTELJ 14

¹ The paper reports A , which is equal to $-C$.² The mixing-induced CP violation is reported with a significance of more than 5 standard deviations in this $b \rightarrow s$ penguin dominated mode. $S_{\eta' K^0} (B^0 \rightarrow \eta' K^0)$

VALUE	DOCUMENT ID	TECN	COMMENT
0.63 ± 0.06 OUR AVERAGE			
$0.68 \pm 0.07 \pm 0.03$	SANTELJ	14	BELL $e^+ e^- \rightarrow \Upsilon(4S)$
$0.57 \pm 0.08 \pm 0.02$	AUBERT	09I	BABR $e^+ e^- \rightarrow \Upsilon(4S)$
• • • We do not use the following data for averages, fits, limits, etc. • • •			
$0.58 \pm 0.10 \pm 0.03$	¹ AUBERT	07A	BABR Repl. by AUBERT 09I
$0.64 \pm 0.10 \pm 0.04$	¹ CHEN	07	BELL Repl. by SANTELJ 14

¹ The mixing-induced CP violation is reported with a significance of more than 5 standard deviations in this $b \rightarrow s$ penguin dominated mode. $C_{\omega K_S^0} (B^0 \rightarrow \omega K_S^0)$

VALUE	DOCUMENT ID	TECN	COMMENT
0.0 ± 0.4 OUR AVERAGE			Error includes scale factor of 3.0.
$0.36 \pm 0.19 \pm 0.05$	¹ CHOBANOVA	14	BELL $e^+ e^- \rightarrow \Upsilon(4S)$
$-0.52^{+0.22}_{-0.20} \pm 0.03$	AUBERT	09I	BABR $e^+ e^- \rightarrow \Upsilon(4S)$
• • • We do not use the following data for averages, fits, limits, etc. • • •			
$0.09 \pm 0.29 \pm 0.06$	¹ CHAO	07	BELL Repl. by CHOBANOVA 14
$-0.55^{+0.28}_{-0.26} \pm 0.03$	AUBERT,B	06E	BABR Repl. by AUBERT 09I
$-0.27 \pm 0.48 \pm 0.15$	¹ CHEN	05B	BELL Repl. by CHAO 07

¹ Belle Collab. quotes $A_{\omega K_S^0}$ which is equal to $-C_{\omega K_S^0}$. $S_{\omega K_S^0} (B^0 \rightarrow \omega K_S^0)$

VALUE	DOCUMENT ID	TECN	COMMENT
0.70 ± 0.21 OUR AVERAGE			
$0.91 \pm 0.32 \pm 0.05$	CHOBANOVA	14	BELL $e^+ e^- \rightarrow \Upsilon(4S)$
$0.55^{+0.26}_{-0.29} \pm 0.02$	AUBERT	09I	BABR $e^+ e^- \rightarrow \Upsilon(4S)$
• • • We do not use the following data for averages, fits, limits, etc. • • •			
$0.11 \pm 0.46 \pm 0.07$	CHAO	07	BELL Repl. by CHOBANOVA 14
$0.51^{+0.35}_{-0.39} \pm 0.02$	AUBERT,B	06E	BABR Repl. by AUBERT 09I
$0.76 \pm 0.65^{+0.13}_{-0.16}$	CHEN	05B	BELL Repl. by CHAO 07

 $C (B^0 \rightarrow K_S^0 \pi^0 \pi^0)$

VALUE	DOCUMENT ID	TECN	COMMENT
-0.21 ± 0.20 OUR AVERAGE			
$-0.28 \pm 0.21 \pm 0.04$	¹ YUSA	19	BELL $e^+ e^- \rightarrow \Upsilon(4S)$
$0.23 \pm 0.52 \pm 0.13$	AUBERT	07AQ	BABR $e^+ e^- \rightarrow \Upsilon(4S)$
¹ Reports value of A which is equal to $-C$.			

 $S (B^0 \rightarrow K_S^0 \pi^0 \pi^0)$

VALUE	DOCUMENT ID	TECN	COMMENT
0.89 ± 0.27 OUR AVERAGE			
$0.92^{+0.27}_{-0.31} \pm 0.11$	YUSA	19	BELL $e^+ e^- \rightarrow \Upsilon(4S)$
$0.72 \pm 0.71 \pm 0.08$	AUBERT	07AQ	BABR $e^+ e^- \rightarrow \Upsilon(4S)$

 $C_{\rho^0 K_S^0} (B^0 \rightarrow \rho^0 K_S^0)$

VALUE	DOCUMENT ID	TECN	COMMENT
-0.04 ± 0.20 OUR AVERAGE			
$-0.05 \pm 0.26 \pm 0.10$	¹ AUBERT	09AU	BABR $e^+ e^- \rightarrow \Upsilon(4S)$
$-0.03^{+0.24}_{-0.23} \pm 0.15$	^{2,3} DALSENO	09	BELL $e^+ e^- \rightarrow \Upsilon(4S)$
• • • We do not use the following data for averages, fits, limits, etc. • • •			
$0.64 \pm 0.41 \pm 0.20$	AUBERT	07F	BABR Repl. by AUBERT 09AU
¹ Uses Dalitz plot analysis of $B^0 \rightarrow K^0 \pi^+ \pi^-$ decays and the first of two equivalent solutions is used.			
² Quotes $A_{\rho^0 (KS^0)}$ which is equal to $-C_{\rho^0 K_S^0}$.			
³ Uses Dalitz plot analysis of $B^0 \rightarrow K^0 \pi^+ \pi^-$ decays and the first of two consistent solutions that may be preferred.			

 $S_{\rho^0 K_S^0} (B^0 \rightarrow \rho^0 K_S^0)$

VALUE	DOCUMENT ID	TECN	COMMENT
0.50 ± 0.17 OUR AVERAGE			
$0.35^{+0.26}_{-0.31} \pm 0.07$	¹ AUBERT	09AU	BABR $e^+ e^- \rightarrow \Upsilon(4S)$
$0.64^{+0.19}_{-0.25} \pm 0.13$	² DALSENO	09	BELL $e^+ e^- \rightarrow \Upsilon(4S)$
• • • We do not use the following data for averages, fits, limits, etc. • • •			
$0.20 \pm 0.52 \pm 0.24$	AUBERT	07F	BABR Repl. by AUBERT 09AU
¹ Uses Dalitz plot analysis of $B^0 \rightarrow K^0 \pi^+ \pi^-$ decays and the first of two equivalent solutions is used.			
² Uses Dalitz plot analysis of $B^0 \rightarrow K^0 \pi^+ \pi^-$ decays and the first of two consistent solutions that may be preferred.			

 $C_{f_0(980) K_S^0} (B^0 \rightarrow f_0(980) K_S^0)$

VALUE	DOCUMENT ID	TECN	COMMENT
0.29 ± 0.20 OUR AVERAGE			
$0.28 \pm 0.24 \pm 0.09$	¹ LEES	12o	BABR $e^+ e^- \rightarrow \Upsilon(4S)$
$0.30 \pm 0.29 \pm 0.14$	^{2,3} NAKAHAMA	10	BELL $e^+ e^- \rightarrow \Upsilon(4S)$
• • • We do not use the following data for averages, fits, limits, etc. • • •			
$0.08 \pm 0.19 \pm 0.05$	⁴ AUBERT	09AU	BABR Repl. by LEES 12o
$0.06 \pm 0.17 \pm 0.11$	^{2,5} DALSENO	09	BELL Repl. by NAKAHAMA 10
$-0.41 \pm 0.23 \pm 0.07$	² AUBERT	07AX	BABR Repl. by AUBERT 09AU
$0.15 \pm 0.15 \pm 0.07$	² CHAO	07	BELL Repl. by DALSENO 09
$0.39 \pm 0.27 \pm 0.09$	² CHEN	05B	BELL Repl. by CHAO 07
¹ Uses Dalitz plot analysis of the $B^0 \rightarrow K_S^0 K^+ K^-$ decay.			
² Quotes $A_{f_0(980) K_S^0}$ which is equal to $-C_{f_0(980) K_S^0}$.			
³ Uses Dalitz plot analysis of $B^0 \rightarrow K_S^0 K^+ K^-$ decays and the first of four consistent solutions that may be preferred.			
⁴ Uses Dalitz plot analysis of $B^0 \rightarrow K^0 \pi^+ \pi^-$ decays and the first of two equivalent solutions is used.			
⁵ Uses Dalitz plot analysis of $B^0 \rightarrow K^0 \pi^+ \pi^-$ decays and the first of two consistent solutions that may be preferred.			

 $S_{f_0(980) K_S^0} (B^0 \rightarrow f_0(980) K_S^0)$

VALUE	DOCUMENT ID	TECN	COMMENT
-0.50 ± 0.16 OUR AVERAGE			
$-0.55 \pm 0.18 \pm 0.12$	¹ LEES	12o	BABR $e^+ e^- \rightarrow \Upsilon(4S)$
$-0.43^{+0.22}_{-0.20} \pm 0.14$	² DALSENO	09	BELL $e^+ e^- \rightarrow \Upsilon(4S)$

See key on page 1171

Meson Particle Listings

 B^0

• • • We do not use the following data for averages, fits, limits, etc. • • •

$-0.96^{+0.21}_{-0.04} \pm 0.04$	³ AUBERT	09AU BABR	Repl. by LEES 12o
$-0.25 \pm 0.26 \pm 0.10$	⁴ AUBERT	07AX BABR	Repl. by AUBERT 09AU
$0.18 \pm 0.23 \pm 0.11$	CHAO	07 BELL	Repl. by DALSENO 09
$0.47 \pm 0.41 \pm 0.08$	CHEN	05B BELL	Repl. by CHAO 07

¹ Uses Dalitz plot analysis of the $B^0 \rightarrow K_S^0 K^+ K^-$ decay.² Uses Dalitz plot analysis of $B^0 \rightarrow K^0 \pi^+ \pi^-$ decays and the first of two consistent solutions that may be preferred.³ Uses Dalitz plot analysis of $B^0 \rightarrow K^0 \pi^+ \pi^-$ decays and the first of two equivalent solutions is used.⁴ Reports β_{eff} . We quote S obtained from epaps: E-PRLTAO-99-076741. $S_{f_2(1270) K_S^0} (B^0 \rightarrow f_2(1270) K_S^0)$

VALUE	DOCUMENT ID	TECN	COMMENT
$-0.48 \pm 0.52 \pm 0.12$	¹ AUBERT	09AU BABR	$e^+ e^- \rightarrow \Upsilon(4S)$

¹ Uses Dalitz plot analysis of $B^0 \rightarrow K^0 \pi^+ \pi^-$ decays and the first of two equivalent solutions is used. $C_{f_2(1270) K_S^0} (B^0 \rightarrow f_2(1270) K_S^0)$

VALUE	DOCUMENT ID	TECN	COMMENT
$0.28^{+0.35}_{-0.40} \pm 0.11$	¹ AUBERT	09AU BABR	$e^+ e^- \rightarrow \Upsilon(4S)$

¹ Uses Dalitz plot analysis of $B^0 \rightarrow K^0 \pi^+ \pi^-$ decays and the first of two equivalent solutions is used. $S_{f_x(1300) K_S^0} (B^0 \rightarrow f_x(1300) K_S^0)$

VALUE	DOCUMENT ID	TECN	COMMENT
$-0.20 \pm 0.52 \pm 0.10$	¹ AUBERT	09AU BABR	$e^+ e^- \rightarrow \Upsilon(4S)$

¹ Uses Dalitz plot analysis of $B^0 \rightarrow K^0 \pi^+ \pi^-$ decays and the first of two equivalent solutions is used. $C_{f_x(1300) K_S^0} (B^0 \rightarrow f_x(1300) K_S^0)$

VALUE	DOCUMENT ID	TECN	COMMENT
$0.13^{+0.33}_{-0.35} \pm 0.10$	¹ AUBERT	09AU BABR	$e^+ e^- \rightarrow \Upsilon(4S)$

¹ Uses Dalitz plot analysis of $B^0 \rightarrow K^0 \pi^+ \pi^-$ decays and the first of two equivalent solutions is used. $S_{K^0 \pi^+ \pi^-} (B^0 \rightarrow K^0 \pi^+ \pi^- \text{ nonresonant})$

VALUE	DOCUMENT ID	TECN	COMMENT
$-0.01 \pm 0.31 \pm 0.10$	¹ AUBERT	09AU BABR	$e^+ e^- \rightarrow \Upsilon(4S)$

¹ Uses Dalitz plot analysis of $B^0 \rightarrow K^0 \pi^+ \pi^-$ decays and the first of two equivalent solutions is used. $C_{K^0 \pi^+ \pi^-} (B^0 \rightarrow K^0 \pi^+ \pi^- \text{ nonresonant})$

VALUE	DOCUMENT ID	TECN	COMMENT
$0.01 \pm 0.25 \pm 0.08$	¹ AUBERT	09AU BABR	$e^+ e^- \rightarrow \Upsilon(4S)$

¹ Uses Dalitz plot analysis of $B^0 \rightarrow K^0 \pi^+ \pi^-$ decays and the first of two equivalent solutions is used. $C_{K_S^0 K_S^0} (B^0 \rightarrow K_S^0 K_S^0)$

VALUE	DOCUMENT ID	TECN	COMMENT
0.0 \pm 0.4 OUR AVERAGE			Error includes scale factor of 1.4.
$0.38 \pm 0.38 \pm 0.05$	¹ NAKAHAMA	08 BELL	$e^+ e^- \rightarrow \Upsilon(4S)$
$-0.40 \pm 0.41 \pm 0.06$	AUBERT, BE	06c BABR	$e^+ e^- \rightarrow \Upsilon(4S)$

¹ Reports $A_{K_S^0 K_S^0}$ which equals to $-C_{K_S^0 K_S^0}$. $S_{K_S^0 K_S^0} (B^0 \rightarrow K_S^0 K_S^0)$

VALUE	DOCUMENT ID	TECN	COMMENT
-0.8 \pm 0.5 OUR AVERAGE			
$-0.38^{+0.69}_{-0.77} \pm 0.09$	NAKAHAMA	08 BELL	$e^+ e^- \rightarrow \Upsilon(4S)$
$-1.28^{+0.80}_{-0.73} \pm 0.11$	AUBERT, BE	06c BABR	$e^+ e^- \rightarrow \Upsilon(4S)$

 $C_{K^+ K^- K_S^0} (B^0 \rightarrow K^+ K^- K_S^0 \text{ nonresonant})$

VALUE	DOCUMENT ID	TECN	COMMENT
0.06 \pm 0.08 OUR AVERAGE			
$0.02 \pm 0.09 \pm 0.03$	^{1,2} LEES	12o BABR	$e^+ e^- \rightarrow \Upsilon(4S)$
$0.14 \pm 0.11 \pm 0.09$	^{3,4} NAKAHAMA	10 BELL	$e^+ e^- \rightarrow \Upsilon(4S)$

• • • We do not use the following data for averages, fits, limits, etc. • • •

$0.054 \pm 0.102 \pm 0.060$	^{3,5} AUBERT	07AX BABR	Repl. by LEES 12o
$0.09 \pm 0.10 \pm 0.05$	^{3,5} CHAO	07 BELL	Repl. by NAKAHAMA 10
$0.10 \pm 0.14 \pm 0.04$	⁵ AUBERT	05T BABR	Repl. by AUBERT 07AX
$0.09 \pm 0.12 \pm 0.07$	³ CHEN	05B BELL	Repl. by CHAO 07
$-0.10 \pm 0.19 \pm 0.10$	⁵ AUBERT, B	04V BABR	Repl. by AUBERT 05T
$0.40 \pm 0.33^{+0.28}_{-0.10}$	³ ABE	03c BELL	Repl. by ABE 03H
$0.17 \pm 0.16 \pm 0.04$	^{3,5} ABE	03H BELL	Repl. by CHEN 05B

¹ Uses Dalitz plot analysis of the $B^0 \rightarrow K_S^0 K^+ K^-$ decay.² This measurement is performed on all the isobar components, excluding ϕK_S^0 and $\eta(980) K_S^0$.³ Quotes $A_{K^+ K^- K_S^0}$ which is equal to $-C_{K^+ K^- K_S^0}$.⁴ Uses Dalitz plot analysis of $B^0 \rightarrow K_S^0 K^+ K^-$ decays and the first of four consistent solutions that may be preferred.⁵ Excludes the events from $B^0 \rightarrow \phi K_S^0$ decay. The results are derived from a combined sample of $K^+ K^- K_S^0$ and $K^+ K^- K_L^0$ decays. $S_{K^+ K^- K_S^0} (B^0 \rightarrow K^+ K^- K_S^0 \text{ nonresonant})$

VALUE	DOCUMENT ID	TECN	COMMENT
-0.66 \pm 0.11 OUR AVERAGE			
$-0.65 \pm 0.12 \pm 0.03$	^{1,2} LEES	12o BABR	$e^+ e^- \rightarrow \Upsilon(4S)$
$-0.68 \pm 0.15^{+0.21}_{-0.13}$	³ CHAO	07 BELL	$e^+ e^- \rightarrow \Upsilon(4S)$

• • • We do not use the following data for averages, fits, limits, etc. • • •

$-0.764 \pm 0.111^{+0.071}_{-0.040}$	^{3,4} AUBERT	07AX BABR	Repl. by LEES 12o
$-0.42 \pm 0.17 \pm 0.03$	^{3,5} AUBERT	05T BABR	Repl. by AUBERT 07AX
$-0.49 \pm 0.18 \pm 0.04$	CHEN	05B BELL	Repl. by CHAO 07
$-0.56 \pm 0.25 \pm 0.04$	^{3,6} AUBERT, B	04V BABR	Repl. by AUBERT 05T
$-0.49 \pm 0.43 \pm 0.11$	ABE	03c BELL	Repl. by ABE 03H
$-0.51 \pm 0.26 \pm 0.05$	^{3,7} ABE	03H BELL	Repl. by CHEN 05B

¹ Uses Dalitz plot analysis of the $B^0 \rightarrow K_S^0 K^+ K^-$ decay.² This measurement is performed on all the isobar components, excluding ϕK_S^0 and $\eta(980) K_S^0$. Note that the nonresonant component is not a CP eigenstate.³ Excludes events from $B^0 \rightarrow \phi K_S^0$ decay. The results are derived from a combined sample of $K^+ K^- K_S^0$ and $K^+ K^- K_L^0$ decays.⁴ Reports β_{eff} . We quote S obtained from epaps: E-PRLTAO-99-076741.⁵ The measured CP -even final states fraction is $0.89 \pm 0.08 \pm 0.06$.⁶ The measured CP -even final states fraction is $0.98 \pm 0.15 \pm 0.04$.⁷ The measured CP -even final states fraction is $1.03 \pm 0.15 \pm 0.05$. $C_{K^+ K^- K_S^0} (B^0 \rightarrow K^+ K^- K_S^0 \text{ inclusive})$

VALUE	DOCUMENT ID	TECN	COMMENT
0.015 \pm 0.077 \pm 0.053	^{1,2} AUBERT	07AX BABR	$e^+ e^- \rightarrow \Upsilon(4S)$

¹ Measured using full Dalitz plot fit including ϕ component.² The results are derived from a combined sample of $K^+ K^- K_S^0$ and $K^+ K^- K_L^0$ decays. $S_{K^+ K^- K_S^0} (B^0 \rightarrow K^+ K^- K_S^0 \text{ inclusive})$

VALUE	DOCUMENT ID	TECN	COMMENT
-0.647 \pm 0.116 \pm 0.040	¹ AUBERT	07AX BABR	$e^+ e^- \rightarrow \Upsilon(4S)$

¹ Measured using full Dalitz plot fit including ϕ component. $C_{\phi K_S^0} (B^0 \rightarrow \phi K_S^0)$

VALUE	DOCUMENT ID	TECN	COMMENT
-0.09 \pm 0.12 OUR AVERAGE			
$-0.31 \pm 0.20 \pm 0.05$	ADACHI	23i BELL	$e^+ e^- \rightarrow \Upsilon(4S)$
$0.05 \pm 0.18 \pm 0.05$	¹ LEES	12o BABR	$e^+ e^- \rightarrow \Upsilon(4S)$
$-0.04 \pm 0.20 \pm 0.10$	^{2,3} NAKAHAMA	10 BELL	$e^+ e^- \rightarrow \Upsilon(4S)$

• • • We do not use the following data for averages, fits, limits, etc. • • •

$0.08 \pm 0.18 \pm 0.04$	^{2,4} AUBERT	07AX BABR	Repl. by LEES 12o
$-0.07 \pm 0.15 \pm 0.05$	^{2,4} CHEN	07 BELL	Repl. by NAKAHAMA 10
$0.00 \pm 0.23 \pm 0.05$	⁴ AUBERT	05T BABR	Repl. by AUBERT 07AX
$-0.08 \pm 0.22 \pm 0.09$	^{2,4} CHEN	05B BELL	Repl. by CHEN 07
$0.01 \pm 0.33 \pm 0.10$	⁴ AUBERT, B	04G BABR	Repl. by AUBERT 05T
$0.56 \pm 0.41 \pm 0.16$	² ABE	03c BELL	Repl. by ABE 03H
$0.15 \pm 0.29 \pm 0.07$	² ABE	03H BELL	Repl. by CHEN 05B

¹ Uses Dalitz plot analysis of the $B^0 \rightarrow K_S^0 K^+ K^-$ decay.² Quotes $A_{\phi K_S^0}$ which is equal to $-C_{\phi K_S^0}$.³ Uses Dalitz plot analysis of $B^0 \rightarrow K_S^0 K^+ K^-$ decays and the first of four consistent solutions that may be preferred.⁴ Result combines B -meson final states ϕK_S^0 and ϕK_L^0 by assuming $S_{\phi K_S^0} = -S_{\phi K_L^0}$. $S_{\phi K_S^0} (B^0 \rightarrow \phi K_S^0)$

VALUE	DOCUMENT ID	TECN	COMMENT
0.58 \pm 0.12 OUR AVERAGE			
$0.54 \pm 0.26^{+0.06}_{-0.08}$	ADACHI	23i BELL	$e^+ e^- \rightarrow \Upsilon(4S)$
$0.66 \pm 0.17 \pm 0.07$	¹ LEES	12o BABR	$e^+ e^- \rightarrow \Upsilon(4S)$
$0.50 \pm 0.21 \pm 0.06$	² CHEN	07 BELL	$e^+ e^- \rightarrow \Upsilon(4S)$

• • • We do not use the following data for averages, fits, limits, etc. • • •

$0.21 \pm 0.26 \pm 0.11$	^{2,3} AUBERT	07AX BABR	Repl. by LEES 12o
$0.50 \pm 0.25^{+0.07}_{-0.04}$	² AUBERT	05T BABR	Repl. by AUBERT 07AX
$0.08 \pm 0.33 \pm 0.09$	² CHEN	05B BELL	Repl. by CHEN 07
$0.47 \pm 0.34^{+0.08}_{-0.06}$	² AUBERT, B	04G BABR	Repl. by AUBERT 05T
$-0.73 \pm 0.64 \pm 0.22$	ABE	03c BELL	Repl. by ABE 03H
$-0.96 \pm 0.50^{+0.09}_{-0.11}$	ABE	03H BELL	Repl. by CHEN 05B

¹ Uses Dalitz plot analysis of the $B^0 \rightarrow K_S^0 K^+ K^-$ decay.

Meson Particle Listings

 B^0

²Result combines B -meson final states ϕK_S^0 and ϕK_L^0 by assuming $S_{\phi K_S^0} = -S_{\phi K_L^0}$

³Reports β_{eff} . We quote S obtained from epaps: E-PRLTAO-99-076741.

 $C_{K_S K_S K_S}(B^0 \rightarrow K_S K_S K_S)$

VALUE	DOCUMENT ID	TECN	COMMENT
-0.14 ± 0.12 OUR AVERAGE			
$-0.12 \pm 0.16 \pm 0.05$	¹ KANG 21	BELL	$e^+e^- \rightarrow \Upsilon(4S)$
$-0.17 \pm 0.18 \pm 0.04$	LEES 12i	BABR	$e^+e^- \rightarrow \Upsilon(4S)$
••• We do not use the following data for averages, fits, limits, etc. •••			
$0.02 \pm 0.21 \pm 0.05$	AUBERT 07AT	BABR	Repl. by LEES 12i
$-0.31 \pm 0.20 \pm 0.07$	¹ CHEN 07	BELL	Repl. by KANG 21
$-0.34 \pm 0.28 \pm 0.05$	AUBERT,B 05	BABR	Repl. by AUBERT 07AT
$-0.54 \pm 0.34 \pm 0.09$	¹ SU MISAWA 05	BELL	Repl. by CHEN 07
¹ KANG 21 quotes $A_{K_S^0 K_S^0 K_S^0}$ which is equal to $-C_{K_S^0 K_S^0 K_S^0}$.			

 $S_{K_S K_S K_S}(B^0 \rightarrow K_S K_S K_S)$

VALUE	DOCUMENT ID	TECN	COMMENT
-0.82 ± 0.17 OUR AVERAGE			
$-0.71 \pm 0.23 \pm 0.05$	KANG 21	BELL	$e^+e^- \rightarrow \Upsilon(4S)$
$-0.94 \pm 0.24 \pm 0.06$	LEES 12i	BABR	$e^+e^- \rightarrow \Upsilon(4S)$
••• We do not use the following data for averages, fits, limits, etc. •••			
$-0.71 \pm 0.24 \pm 0.04$	AUBERT 07AT	BABR	Repl. by LEES 12i
$0.30 \pm 0.32 \pm 0.08$	CHEN 07	BELL	Repl. by KANG 21
$-0.71 \pm 0.38 \pm 0.04$	AUBERT,B 05	BABR	Repl. by AUBERT 07AT
$1.26 \pm 0.68 \pm 0.20$	SU MISAWA 05	BELL	Repl. by CHEN 07.

 $C_{K_S^0 \pi^0 \gamma}(B^0 \rightarrow K_S^0 \pi^0 \gamma)$

VALUE	DOCUMENT ID	TECN	COMMENT
$0.36 \pm 0.33 \pm 0.04$	¹ AUBERT 08BA	BABR	$e^+e^- \rightarrow \Upsilon(4S)$
••• We do not use the following data for averages, fits, limits, etc. •••			
$0.20 \pm 0.20 \pm 0.06$	^{2,3} USHIRODA 06	BELL	$e^+e^- \rightarrow \Upsilon(4S)$
$-1.0 \pm 0.5 \pm 0.2$	¹ AUBERT,B 05P	BABR	Repl. by AUBERT 08BA
$-0.03 \pm 0.34 \pm 0.11$	³ USHIRODA 05	BELL	Repl. by USHIRODA 06
¹ Requires $1.1 < M_{K_S^0 \pi^0} < 1.8$ GeV/c ² .			
² Requires $M_{K_S^0 \pi^0} < 1.8$ GeV/c ² .			
³ Reports $A_{K_S^0 \pi^0 \gamma}$, which is $-C_{K_S^0 \pi^0 \gamma}$.			

 $S_{K_S^0 \pi^0 \gamma}(B^0 \rightarrow K_S^0 \pi^0 \gamma)$

VALUE	DOCUMENT ID	TECN	COMMENT
$-0.78 \pm 0.59 \pm 0.09$	¹ AUBERT 08BA	BABR	$e^+e^- \rightarrow \Upsilon(4S)$
••• We do not use the following data for averages, fits, limits, etc. •••			
$-0.10 \pm 0.31 \pm 0.07$	² USHIRODA 06	BELL	$e^+e^- \rightarrow \Upsilon(4S)$
$0.9 \pm 1.0 \pm 0.2$	¹ AUBERT,B 05P	BABR	Repl. by AUBERT 08BA
$-0.58 \pm 0.46 \pm 0.11$	USHIRODA 05	BELL	Repl. by USHIRODA 06
¹ Requires $1.1 < M_{K_S^0 \pi^0} < 1.8$ GeV/c ² .			
² Requires $M_{K_S^0 \pi^0} < 1.8$ GeV/c ² .			

 $C_{K_S^0 \pi^+ \pi^- \gamma}(B^0 \rightarrow K_S^0 \pi^+ \pi^- \gamma)$

VALUE	DOCUMENT ID	TECN	COMMENT
$-0.39 \pm 0.20 \pm 0.03$	¹ DEL-AMO-SA..16	BABR	$e^+e^- \rightarrow \Upsilon(4S)$
¹ Requires $M_{K \pi \pi} < 1.8$ GeV/c ² , 0.6 GeV/c ² $< m_{\pi^+ \pi^-} < 0.9$ GeV/c ² , $m_{K \pi} < 0.845$ GeV/c ² or $m_{K \pi} > 0.945$ GeV/c ² .			

 $S_{K_S^0 \pi^+ \pi^- \gamma}(B^0 \rightarrow K_S^0 \pi^+ \pi^- \gamma)$

VALUE	DOCUMENT ID	TECN	COMMENT
$0.14 \pm 0.25 \pm 0.03$	¹ DEL-AMO-SA..16	BABR	$e^+e^- \rightarrow \Upsilon(4S)$
¹ Requires $M_{K \pi \pi} < 1.8$ GeV/c ² , 0.6 GeV/c ² $< m_{\pi^+ \pi^-} < 0.9$ GeV/c ² , $m_{K \pi} < 0.845$ GeV/c ² or $m_{K \pi} > 0.945$ GeV/c ² .			

 $C_{K^*(892)^0 \gamma}(B^0 \rightarrow K^*(892)^0 \gamma)$

VALUE	DOCUMENT ID	TECN	COMMENT
-0.04 ± 0.16 OUR AVERAGE			
$-0.14 \pm 0.16 \pm 0.03$	¹ AUBERT 08BA	BABR	$e^+e^- \rightarrow \Upsilon(4S)$
$0.20 \pm 0.24 \pm 0.05$	^{1,2} USHIRODA 06	BELL	$e^+e^- \rightarrow \Upsilon(4S)$
••• We do not use the following data for averages, fits, limits, etc. •••			
$-0.40 \pm 0.23 \pm 0.03$	AUBERT,B 05P	BABR	Repl. by AUBERT 08BA
$-0.57 \pm 0.32 \pm 0.09$	³ AUBERT,B 04Z	BABR	Repl. by AUBERT,B 05P
¹ Requires $0.8 < M_{K_S^0 \pi^0} < 1.0$ GeV/c ² .			
² Reports value of A which is equal to $-C$.			
³ Based on a total signal of 105 ± 14 events with $K^*(892)^0 \rightarrow K_S^0 \pi^0$ only.			

 $S_{K^*(892)^0 \gamma}(B^0 \rightarrow K^*(892)^0 \gamma)$

VALUE	DOCUMENT ID	TECN	COMMENT
-0.15 ± 0.22 OUR AVERAGE			
$-0.03 \pm 0.29 \pm 0.03$	¹ AUBERT 08BA	BABR	$e^+e^- \rightarrow \Upsilon(4S)$
$-0.32 \pm 0.36 \pm 0.05$	¹ USHIRODA 06	BELL	$e^+e^- \rightarrow \Upsilon(4S)$
••• We do not use the following data for averages, fits, limits, etc. •••			
$-0.21 \pm 0.40 \pm 0.05$	AUBERT,B 05P	BABR	Repl. by AUBERT 08BA
$-0.79 \pm 0.63 \pm 0.10$	² USHIRODA 05	BELL	Repl. by USHIRODA 06
$0.25 \pm 0.63 \pm 0.14$	³ AUBERT,B 04Z	BABR	Repl. by AUBERT,B 05P
¹ Requires $0.8 < M_{K_S^0 \pi^0} < 1.0$ GeV/c ² .			
² Assumes $C(B^0 \rightarrow K^*(892)^0 \gamma) = 0$.			
³ Based on a total signal of 105 ± 14 events with $K^*(892)^0 \rightarrow K_S^0 \pi^0$ only.			

 $C_{\eta K^0 \gamma}(B^0 \rightarrow \eta K^0 \gamma)$

VALUE	DOCUMENT ID	TECN	COMMENT
0.1 ± 0.4 OUR AVERAGE			
$0.48 \pm 0.41 \pm 0.07$	^{1,2} NA KANO 18	BELL	$e^+e^- \rightarrow \Upsilon(4S)$
$-0.32 \pm 0.40 \pm 0.07$	³ AUBERT 09	BABR	$e^+e^- \rightarrow \Upsilon(4S)$
¹ Assuming $m_{\eta K^0} < 2.1$ GeV.			
² Reversed the sign for $C=-A$.			
³ Assuming $m_{\eta K} < 3.25$ GeV.			

 $S_{\eta K^0 \gamma}(B^0 \rightarrow \eta K^0 \gamma)$

VALUE	DOCUMENT ID	TECN	COMMENT
-0.5 ± 0.5 OUR AVERAGE			
$-1.32 \pm 0.77 \pm 0.36$	¹ NA KANO 18	BELL	$e^+e^- \rightarrow \Upsilon(4S)$
$-0.18 \pm 0.49 \pm 0.12$	² AUBERT 09	BABR	$e^+e^- \rightarrow \Upsilon(4S)$
¹ Assuming $m_{\eta K^0} < 2.1$ GeV.			
² Assuming $m_{\eta K} < 3.25$ GeV.			

 $C_{K^0 \phi \gamma}(B^0 \rightarrow K^0 \phi \gamma)$

VALUE	DOCUMENT ID	TECN	COMMENT
$-0.35 \pm 0.58 \pm 0.23$	¹ SAHOO 11A	BELL	$e^+e^- \rightarrow \Upsilon(4S)$
¹ Reports value of A , which is equal to $-C$.			

 $S_{K^0 \phi \gamma}(B^0 \rightarrow K^0 \phi \gamma)$

VALUE	DOCUMENT ID	TECN	COMMENT
$0.74 \pm 0.72 \pm 0.10$	SAHOO 11A	BELL	$e^+e^- \rightarrow \Upsilon(4S)$
-1.05 ± 0.24			

 $C(B^0 \rightarrow K_S^0 \rho^0 \gamma)$

VALUE	DOCUMENT ID	TECN	COMMENT
$-0.05 \pm 0.18 \pm 0.06$	^{1,2} LI 08F	BELL	$e^+e^- \rightarrow \Upsilon(4S)$
¹ Requires $M_{K_S^0 \pi^+ \pi^-} < 1.8$ GeV/c ² and $0.6 < M_{\pi^+ \pi^-} < 0.9$ GeV/c ² .			
² Reports value of A_{eff} which is equal to $-C$, and includes the non-resonant $\pi^+ \pi^-$ contribution in the ρ^0 region.			

 $S(B^0 \rightarrow K_S^0 \rho^0 \gamma)$

VALUE	DOCUMENT ID	TECN	COMMENT
-0.04 ± 0.23 OUR AVERAGE			
$-0.18 \pm 0.32 \pm 0.06$	¹ DEL-AMO-SA..16	BABR	$e^+e^- \rightarrow \Upsilon(4S)$
$0.11 \pm 0.33 \pm 0.05$	² LI 08F	BELL	$e^+e^- \rightarrow \Upsilon(4S)$
¹ Requires $M_{K \pi \pi} < 1.8$ GeV/c ² , 0.6 GeV/c ² $< m_{\pi^+ \pi^-} < 0.9$ GeV/c ² , $m_{K \pi} < 0.845$ GeV/c ² or $m_{K \pi} > 0.945$ GeV/c ² .			
² Requires $M_{K \pi \pi} < 1.8$ GeV/c ² .			

 $C(B^0 \rightarrow \rho^0 \gamma)$

VALUE	DOCUMENT ID	TECN	COMMENT
$0.44 \pm 0.49 \pm 0.14$	¹ USHIRODA 08	BELL	$e^+e^- \rightarrow \Upsilon(4S)$
¹ Reports value of A which is equal to $-C$.			

 $S(B^0 \rightarrow \rho^0 \gamma)$

VALUE	DOCUMENT ID	TECN	COMMENT
$-0.83 \pm 0.65 \pm 0.18$	USHIRODA 08	BELL	$e^+e^- \rightarrow \Upsilon(4S)$

 $C_{\pi \pi}(B^0 \rightarrow \pi^+ \pi^-)$

$C_{\pi \pi}$ is defined as $(1-|\lambda|^2)/(1+|\lambda|^2)$, where the quantity $\lambda=q/p \bar{A}_f/A_f$ is a phase convention independent observable quantity for the final state f . For details, see the review on "CP Violation" in the Reviews section.

VALUE	DOCUMENT ID	TECN	COMMENT
-0.314 ± 0.030 OUR AVERAGE			
$-0.311 \pm 0.045 \pm 0.015$	AAIJ 21o	LHCB	pp at 13 TeV
$-0.34 \pm 0.06 \pm 0.01$	AAIJ 18o	LHCB	pp at 7, 8 TeV
$-0.33 \pm 0.06 \pm 0.03$	¹ DALSENO 13	BELL	$e^+e^- \rightarrow \Upsilon(4S)$
$-0.25 \pm 0.08 \pm 0.02$	LEES 13D	BABR	$e^+e^- \rightarrow \Upsilon(4S)$

• • • We do not use the following data for averages, fits, limits, etc. • • •

-0.38 ± 0.15 ± 0.02	AAIJ	13Bo	LHCB	Repl. by AAIJ 18o
-0.21 ± 0.09 ± 0.02	AUBERT	07AF	BABR	Repl. by LEES 13D
-0.55 ± 0.08 ± 0.05	¹ ISHINO	07	BELL	Repl. by DALSENO 13
-0.56 ± 0.12 ± 0.06	¹ ABE	05D	BELL	Repl. by ISHINO 07
-0.09 ± 0.15 ± 0.04	AUBERT,BE	05	BABR	Repl. by AUBERT 07AF
-0.58 ± 0.15 ± 0.07	¹ ABE	04E	BELL	Repl. by ABE 05D
-0.77 ± 0.27 ± 0.08	¹ ABE	03G	BELL	Repl. by ABE 04E.
-0.94 ^{+0.31} _{-0.25} ± 0.09	¹ ABE	02M	BELL	Repl. by ABE 03G
-0.25 ^{+0.45} _{-0.47} ± 0.14	² AUBERT	02D	BABR	Repl. by AUBERT 02Q
-0.30 ± 0.25 ± 0.04	³ AUBERT	02Q	BABR	Repl. by AUBERT,BE 05

¹ Paper reports $A_{\pi\pi}$ which equals to $-C_{\pi\pi}$.

² Corresponds to 90% confidence range $-1.0 < C_{\pi\pi} < 0.47$.

³ Corresponds to 90% confidence range $-0.72 < C_{\pi\pi} < 0.12$.

$S_{\pi\pi}(B^0 \rightarrow \pi^+\pi^-)$

$S_{\pi\pi} = 2\text{Im}\lambda/(1+|\lambda|^2)$, see the note in the $C_{\pi\pi}$ datablock above.

VALUE	DOCUMENT ID	TECN	COMMENT
-0.670 ± 0.030 OUR AVERAGE			
-0.706 ± 0.042 ± 0.013	AAIJ	21o	LHCB pp at 13 TeV
-0.63 ± 0.05 ± 0.01	AAIJ	18o	LHCB pp at 7, 8 TeV
-0.64 ± 0.08 ± 0.03	¹ DALSENO	13	BELL $e^+e^- \rightarrow \Upsilon(4S)$
-0.68 ± 0.10 ± 0.03	LEES	13D	BABR $e^+e^- \rightarrow \Upsilon(4S)$
• • • We do not use the following data for averages, fits, limits, etc. • • •			
-0.71 ± 0.13 ± 0.02	AAIJ	13Bo	LHCB Repl. by AAIJ 18o
-0.60 ± 0.11 ± 0.03	AUBERT	07AF	BABR Repl. by LEES 13D
-0.61 ± 0.10 ± 0.04	ISHINO	07	BELL Repl. by DALSENO 13
-0.67 ± 0.16 ± 0.06	² ABE	05D	BELL Repl. by ISHINO 07
-0.30 ± 0.17 ± 0.03	AUBERT,BE	05	BABR Repl. by AUBERT 07AF
-1.00 ± 0.21 ± 0.07	³ ABE	04E	BELL Repl. by ABE 05D
-1.23 ± 0.41 ^{+0.08} _{-0.07}	ABE	03G	BELL Repl. by ABE 04E.
-1.21 ^{+0.38} _{-0.27} ± 0.16 ± 0.13	ABE	02M	BELL Repl. by ABE 03G
0.03 ^{+0.52} _{-0.56} ± 0.11	⁴ AUBERT	02D	BABR Repl. by AUBERT 02Q
0.02 ± 0.34 ± 0.05	⁵ AUBERT	02Q	BABR Repl. by AUBERT,BE 05

¹ An isospin analysis using other BELLE measurements, disfavors the region of $23.8^\circ < \phi_2 < 66.8^\circ$ at 68% CL.

² Rule out the CP -conserving case, $C_{\pi\pi} = S_{\pi\pi} = 0$, at the 5.4 sigma level.

³ Rule out the CP -conserving case, $C_{\pi\pi} = S_{\pi\pi} = 0$, at the 5.2 sigma level.

⁴ Corresponds to 90% confidence range $-0.89 < S_{\pi\pi} < 0.85$.

⁵ Corresponds to 90% confidence range $-0.54 < S_{\pi\pi} < 0.58$.

$C_{\rho^0\pi^0}(B^0 \rightarrow \pi^0\pi^0)$

VALUE	DOCUMENT ID	TECN	COMMENT
-0.30 ± 0.20 OUR AVERAGE			
-0.14 ± 0.46 ± 0.07	¹ ABUDINEN	23E	BELL $e^+e^- \rightarrow \Upsilon(4S)$
-0.14 ± 0.36 ± 0.10	¹ JULIUS	17	BELL $e^+e^- \rightarrow \Upsilon(4S)$
-0.43 ± 0.26 ± 0.05	LEES	13D	BABR $e^+e^- \rightarrow \Upsilon(4S)$
• • • We do not use the following data for averages, fits, limits, etc. • • •			
-0.49 ± 0.35 ± 0.05	AUBERT	07Bc	BABR Repl. by LEES 13D
-0.12 ± 0.56 ± 0.06	² AUBERT	05L	BABR Repl. by AUBERT 07Bc
-0.44 ^{+0.52} _{-0.53} ± 0.17	¹ CHAO	05	BELL Repl. by JULIUS 17

¹ Quotes $A_{\rho^0\pi^0}$ which is equal to $-C_{\rho^0\pi^0}$.

² Corresponds to a 90% CL interval of $-0.88 < A_{CP} < 0.64$.

$C_{\rho\pi}(B^0 \rightarrow \rho^+\pi^-)$

VALUE	DOCUMENT ID	TECN	COMMENT
-0.03 ± 0.07 OUR AVERAGE			Error includes scale factor of 1.2.
0.016 ± 0.059 ± 0.036	¹ LEES	13J	BABR $e^+e^- \rightarrow \Upsilon(4S)$
-0.13 ± 0.09 ± 0.05	¹ KUSAKA	07	BELL $e^+e^- \rightarrow \Upsilon(4S)$
• • • We do not use the following data for averages, fits, limits, etc. • • •			
0.15 ± 0.09 ± 0.05	AUBERT	07AA	BABR Repl. by LEES 13J
0.25 ± 0.17 ^{+0.02} _{-0.06}	WANG	05	BELL Repl. by KUSAKA 07
0.36 ± 0.18 ± 0.04	AUBERT	03T	BABR Repl. by AUBERT 07AA

¹ Uses time-dependent Dalitz plot analysis of $B^0 \rightarrow \pi^+\pi^-\pi^0$ decays.

$S_{\rho\pi}(B^0 \rightarrow \rho^+\pi^-)$

VALUE	DOCUMENT ID	TECN	COMMENT
0.05 ± 0.07 OUR AVERAGE			
0.053 ± 0.081 ± 0.034	¹ LEES	13J	BABR $e^+e^- \rightarrow \Upsilon(4S)$
0.06 ± 0.13 ± 0.05	¹ KUSAKA	07	BELL $e^+e^- \rightarrow \Upsilon(4S)$
• • • We do not use the following data for averages, fits, limits, etc. • • •			
-0.03 ± 0.11 ± 0.04	AUBERT	07AA	BABR Repl. by LEES 13J
-0.28 ± 0.23 ^{+0.10} _{-0.08}	WANG	05	BELL Repl. by KUSAKA 07
0.19 ± 0.24 ± 0.03	AUBERT	03T	BABR Repl. by AUBERT 07AA

¹ Uses time-dependent Dalitz plot analysis of $B^0 \rightarrow \pi^+\pi^-\pi^0$ decays.

$\Delta C_{\rho\pi}(B^0 \rightarrow \rho^+\pi^-)$

$\Delta C_{\rho\pi}$ describes the asymmetry between the rates $\Gamma(B^0 \rightarrow \rho^+\pi^-) + \Gamma(\bar{B}^0 \rightarrow \rho^-\pi^+)$ and $\Gamma(B^0 \rightarrow \rho^-\pi^+) + \Gamma(\bar{B}^0 \rightarrow \rho^+\pi^-)$.

VALUE	DOCUMENT ID	TECN	COMMENT
0.27 ± 0.06 OUR AVERAGE			
0.234 ± 0.061 ± 0.048	¹ LEES	13J	BABR $e^+e^- \rightarrow \Upsilon(4S)$
0.36 ± 0.10 ± 0.05	¹ KUSAKA	07	BELL $e^+e^- \rightarrow \Upsilon(4S)$
• • • We do not use the following data for averages, fits, limits, etc. • • •			
0.39 ± 0.09 ± 0.09	AUBERT	07AA	BABR Repl. by LEES 13J
0.38 ± 0.18 ^{+0.02} _{-0.04}	WANG	05	BELL Repl. by KUSAKA 07
0.28 ^{+0.18} _{-0.19} ± 0.04	AUBERT	03T	BABR Repl. by AUBERT 07AA

¹ Uses time-dependent Dalitz plot analysis of $B^0 \rightarrow \pi^+\pi^-\pi^0$ decays.

$\Delta S_{\rho\pi}(B^0 \rightarrow \rho^+\pi^-)$

$\Delta S_{\rho\pi}$ is related to the strong phase difference between the amplitudes contributing to $B^0 \rightarrow \rho^+\pi^-$.

VALUE	DOCUMENT ID	TECN	COMMENT
0.01 ± 0.08 OUR AVERAGE			
0.054 ± 0.082 ± 0.039	¹ LEES	13J	BABR $e^+e^- \rightarrow \Upsilon(4S)$
-0.08 ± 0.13 ± 0.05	¹ KUSAKA	07	BELL $e^+e^- \rightarrow \Upsilon(4S)$
• • • We do not use the following data for averages, fits, limits, etc. • • •			
-0.01 ± 0.14 ± 0.06	AUBERT	07AA	BABR Repl. by LEES 13J
-0.30 ± 0.24 ± 0.09	WANG	05	BELL Repl. by KUSAKA 07
0.15 ± 0.25 ± 0.03	AUBERT	03T	BABR Repl. by AUBERT 07AA

¹ Uses time-dependent Dalitz plot analysis of $B^0 \rightarrow \pi^+\pi^-\pi^0$ decays.

$C_{\rho^0\pi^0}(B^0 \rightarrow \rho^0\pi^0)$

VALUE	DOCUMENT ID	TECN	COMMENT
0.27 ± 0.24 OUR AVERAGE			
0.19 ± 0.23 ± 0.15	¹ LEES	13J	BABR $e^+e^- \rightarrow \Upsilon(4S)$
0.49 ± 0.36 ± 0.28	^{1,2} KUSAKA	07	BELL $e^+e^- \rightarrow \Upsilon(4S)$
• • • We do not use the following data for averages, fits, limits, etc. • • •			
-0.10 ± 0.40 ± 0.53	AUBERT	07AA	BABR Repl. by LEES 13J
0.53 ^{+0.67} _{-0.84} ± 0.10 ± 0.15	² DRAGIC	06	BELL Repl. by KUSAKA 07

¹ Uses time-dependent Dalitz plot analysis of $B^0 \rightarrow \pi^+\pi^-\pi^0$ decays.

² Quotes $A_{\rho^0\pi^0}$ which is equal to $-C_{\rho^0\pi^0}$.

$S_{\rho^0\pi^0}(B^0 \rightarrow \rho^0\pi^0)$

VALUE	DOCUMENT ID	TECN	COMMENT
-0.23 ± 0.34 OUR AVERAGE			
-0.37 ± 0.34 ± 0.20	¹ LEES	13J	BABR $e^+e^- \rightarrow \Upsilon(4S)$
0.17 ± 0.57 ± 0.35	¹ KUSAKA	07	BELL $e^+e^- \rightarrow \Upsilon(4S)$
• • • We do not use the following data for averages, fits, limits, etc. • • •			
0.04 ± 0.44 ± 0.18	AUBERT	07AA	BABR Repl. by LEES 13J

¹ Uses time-dependent Dalitz plot analysis of $B^0 \rightarrow \pi^+\pi^-\pi^0$ decays.

$C_{a_1\pi}(B^0 \rightarrow a_1(1260)^+\pi^-)$

VALUE	DOCUMENT ID	TECN	COMMENT
-0.05 ± 0.11 OUR AVERAGE			
-0.01 ± 0.11 ± 0.09	DALSENO	12	BELL $e^+e^- \rightarrow \Upsilon(4S)$
-0.10 ± 0.15 ± 0.09	AUBERT	07o	BABR $e^+e^- \rightarrow \Upsilon(4S)$

$S_{a_1\pi}(B^0 \rightarrow a_1(1260)^+\pi^-)$

VALUE	DOCUMENT ID	TECN	COMMENT
-0.2 ± 0.4 OUR AVERAGE			Error includes scale factor of 3.2.
-0.51 ± 0.14 ± 0.08	DALSENO	12	BELL $e^+e^- \rightarrow \Upsilon(4S)$
0.37 ± 0.21 ± 0.07	AUBERT	07o	BABR $e^+e^- \rightarrow \Upsilon(4S)$

$\Delta C_{a_1\pi}(B^0 \rightarrow a_1(1260)^+\pi^-)$

$\Delta C_{a_1\pi}$ describes the asymmetry between the rates $\Gamma(B^0 \rightarrow a_1^+\pi^-) + \Gamma(\bar{B}^0 \rightarrow a_1^-\pi^+)$ and $\Gamma(B^0 \rightarrow a_1^-\pi^+) + \Gamma(\bar{B}^0 \rightarrow a_1^+\pi^-)$.

VALUE	DOCUMENT ID	TECN	COMMENT
0.43 ± 0.14 OUR AVERAGE			Error includes scale factor of 1.3.
0.54 ± 0.11 ± 0.07	DALSENO	12	BELL $e^+e^- \rightarrow \Upsilon(4S)$
0.26 ± 0.15 ± 0.07	AUBERT	07o	BABR $e^+e^- \rightarrow \Upsilon(4S)$

$\Delta S_{a_1\pi}(B^0 \rightarrow a_1(1260)^+\pi^-)$

$\Delta S_{a_1\pi}$ is related to the strong phase difference between the amplitudes contributing to $B^0 \rightarrow a_1\pi$ decays.

VALUE	DOCUMENT ID	TECN	COMMENT
-0.11 ± 0.12 OUR AVERAGE			
-0.09 ± 0.14 ± 0.06	DALSENO	12	BELL $e^+e^- \rightarrow \Upsilon(4S)$
-0.14 ± 0.21 ± 0.06	AUBERT	07o	BABR $e^+e^- \rightarrow \Upsilon(4S)$

$C(B^0 \rightarrow b_1^- K^+)$

VALUE	DOCUMENT ID	TECN	COMMENT
-0.22 ± 0.23 ± 0.05	AUBERT	07Bi	BABR $e^+e^- \rightarrow \Upsilon(4S)$

Meson Particle Listings

 B^0 $\Delta C (B^0 \rightarrow b_1^- \pi^+)$

VALUE	DOCUMENT ID	TECN	COMMENT
$-1.04 \pm 0.23 \pm 0.08$	AUBERT	07B1	BABR $e^+ e^- \rightarrow \Upsilon(4S)$

 $C_{\rho\rho} (B^0 \rightarrow \rho^0 \rho^0)$

VALUE	DOCUMENT ID	TECN	COMMENT
$0.2 \pm 0.8 \pm 0.3$	AUBERT	08B8	BABR $e^+ e^- \rightarrow \Upsilon(4S)$

 $S_{\rho\rho} (B^0 \rightarrow \rho^0 \rho^0)$

VALUE	DOCUMENT ID	TECN	COMMENT
$0.3 \pm 0.7 \pm 0.2$	AUBERT	08B8	BABR $e^+ e^- \rightarrow \Upsilon(4S)$

 $C_{\rho\rho} (B^0 \rightarrow \rho^+ \rho^-)$

VALUE	DOCUMENT ID	TECN	COMMENT
0.00 ± 0.09 OUR AVERAGE			
0.00 ± 0.10 ± 0.06	¹ VANHOEFER	16	BELL $e^+ e^- \rightarrow \Upsilon(4S)$
0.01 ± 0.15 ± 0.06	AUBERT	07BF	BABR $e^+ e^- \rightarrow \Upsilon(4S)$

• • • We do not use the following data for averages, fits, limits, etc. • • •

$-0.16 \pm 0.21 \pm 0.08$	¹ SOMOV	07	BELL Repl. by VANHOEFER 16
$-0.00 \pm 0.30 \pm 0.09$	¹ SOMOV	06	BELL Repl. by SOMOV 07
$-0.03 \pm 0.18 \pm 0.09$	AUBERT,B	05C	BABR Repl. by AUBERT 07BF
$-0.17 \pm 0.27 \pm 0.14$	AUBERT,B	04R	BABR Repl. by AUBERT,B 05C

¹ BELLE Collab. quotes A_{CP} which is equal to $-C$.

 $S_{\rho\rho} (B^0 \rightarrow \rho^+ \rho^-)$

VALUE	DOCUMENT ID	TECN	COMMENT
-0.14 ± 0.13 OUR AVERAGE			
$-0.13 \pm 0.15 \pm 0.05$	VANHOEFER	16	BELL $e^+ e^- \rightarrow \Upsilon(4S)$
$-0.17 \pm 0.20^{+0.05}_{-0.06}$	AUBERT	07BF	BABR $e^+ e^- \rightarrow \Upsilon(4S)$

• • • We do not use the following data for averages, fits, limits, etc. • • •

$0.19 \pm 0.30 \pm 0.08$	SOMOV	07	BELL Repl. by VANHOEFER 16
$0.08 \pm 0.41 \pm 0.09$	SOMOV	06	BELL Repl. by SOMOV 07
$-0.33 \pm 0.24^{+0.08}_{-0.14}$	AUBERT,B	05C	BABR Repl. by AUBERT 07BF
$-0.42 \pm 0.42 \pm 0.14$	AUBERT,B	04R	BABR Repl. by AUBERT,B 05C

 $|\lambda| (B^0 \rightarrow J/\psi K^*(892)^0)$

VALUE	CL%	DOCUMENT ID	TECN	COMMENT
<0.25	95	¹ AUBERT,B	04H	BABR $e^+ e^- \rightarrow \Upsilon(4S)$

¹ Uses the measured cosine coefficients C and \bar{C} and assumes $|q/p| = 1$.

 $\cos 2\beta (B^0 \rightarrow J/\psi K^*(892)^0)$

β (ϕ_1) is one of the angles of CKM unitarity triangle, see the review on "CP" Violation in the Reviews section.

VALUE	DOCUMENT ID	TECN	COMMENT
1.7 $^{+0.7}_{-0.9}$ OUR AVERAGE			Error includes scale factor of 1.6.

$2.72^{+0.50}_{-0.79} \pm 0.27$	¹ AUBERT	05P	BABR $e^+ e^- \rightarrow \Upsilon(4S)$
$0.87 \pm 0.74 \pm 0.12$	² ITOH	05	BELL $e^+ e^- \rightarrow \Upsilon(4S)$

¹ The measurement is obtained when $\sin 2\beta$ is fixed to 0.726 and the sign of $\cos 2\beta$ is positive with 86% confidence level.

² The measurement is obtained with $\sin 2\beta$ fixed to 0.731.

 $\cos 2\beta (B^0 \rightarrow [K_S^0 \pi^+ \pi^-]_{D^*(*)} h^0)$

VALUE	DOCUMENT ID	TECN	COMMENT
0.91 ± 0.22 ± 0.11	¹ ADACHI	18	$e^+ e^- \rightarrow \Upsilon(4S)$

• • • We do not use the following data for averages, fits, limits, etc. • • •

$1.06 \pm 0.33^{+0.21}_{-0.15}$	² VOROBYEV	16	BELL $e^+ e^- \rightarrow \Upsilon(4S)$
$0.42 \pm 0.49 \pm 0.16$	³ AUBERT	07BH	BABR $e^+ e^- \rightarrow \Upsilon(4S)$
$1.87^{+0.40+0.22}_{-0.53-0.32}$	⁴ KROKOVNY	06	BELL Repl. by VOROBYEV 16

¹ Analyzes joint data sample of Belle and BaBar using Dalitz plot analysis of $D \rightarrow K_S^0 \pi^+ \pi^-$; the second error combines experimental systematic uncertainty and the Dalitz plot model uncertainty.

² A model-independent measurement uses the binned Dalitz plot technique.

³ AUBERT 07BH evaluates the likelihoods for the positive and negative solutions assuming $\sin(2\beta_{eff}) = 0.678$. It quotes $L_+ / (L_+ + L_-) = 0.86$ corresponding to a likelihood ratio of $L_+ / L_- = 6.14$ in favor of the positive solution.

⁴ KROKOVNY 06 evaluates the likelihoods for the positive and negative solutions assuming $\sin(2\beta_{eff}) = 0.689$. It quotes $L_+ / (L_+ + L_-) = 0.983$ corresponding to a likelihood ratio of $L_+ / L_- = 57.8$ in favor of the positive solution.

 $(S_+ + S_-)/2 (B^0 \rightarrow D^{*-} \pi^+)$

$S_{\pm} = -\frac{2Im(\lambda_{\pm})}{1+|\lambda_{\pm}|^2}$ where λ_+ and λ_- are defined in the $C_{\pi\pi}$ datablock above for

$B^0 \rightarrow D^{*-} \pi^+$ and $\bar{B}^0 \rightarrow D^{*+} \pi^-$.

VALUE	DOCUMENT ID	TECN	COMMENT
-0.039 ± 0.011 OUR AVERAGE			
$-0.046 \pm 0.013 \pm 0.015$	¹ BAHINIPATI	11	BELL $e^+ e^- \rightarrow \Upsilon(4S)$
$-0.040 \pm 0.023 \pm 0.010$	² AUBERT	06Y	BABR $e^+ e^- \rightarrow \Upsilon(4S)$
$-0.034 \pm 0.014 \pm 0.009$	¹ AUBERT	05Z	BABR $e^+ e^- \rightarrow \Upsilon(4S)$

• • • We do not use the following data for averages, fits, limits, etc. • • •

$-0.039 \pm 0.020 \pm 0.013$	³ RONGA	06	BELL Repl. by BAHINIPATI 11
$-0.030 \pm 0.028 \pm 0.018$	¹ GERSHON	05	BELL Repl. by RONGA 06
$-0.068 \pm 0.038 \pm 0.020$	² AUBERT	04V	BABR Repl. by AUBERT 06Y
$-0.063 \pm 0.024 \pm 0.014$	¹ AUBERT	04W	BABR Repl. by AUBERT 05Z
$0.060 \pm 0.040 \pm 0.019$	² SARANGI	04	BELL Repl. by RONGA 06

¹ Uses partially reconstructed $B^0 \rightarrow D^{*\pm} \pi^\mp$ decays.

² Uses fully reconstructed $B^0 \rightarrow D^{*\pm} \pi^\mp$ decays.

³ Combines the results from fully reconstructed and partially reconstructed $D^* \pi$ events by taking weighted averages. Assumes that systematic errors from physics parameters and fit biases in the two measurements are 100% correlated.

 $(S_- - S_+)/2 (B^0 \rightarrow D^{*-} \pi^+)$

VALUE	DOCUMENT ID	TECN	COMMENT
-0.009 ± 0.015 OUR AVERAGE			
$-0.015 \pm 0.013 \pm 0.015$	¹ BAHINIPATI	11	BELL $e^+ e^- \rightarrow \Upsilon(4S)$
$0.049 \pm 0.042 \pm 0.015$	² AUBERT	06Y	BABR $e^+ e^- \rightarrow \Upsilon(4S)$
$-0.019 \pm 0.022 \pm 0.013$	¹ AUBERT	05Z	BABR $e^+ e^- \rightarrow \Upsilon(4S)$

• • • We do not use the following data for averages, fits, limits, etc. • • •

$-0.011 \pm 0.020 \pm 0.013$	³ RONGA	06	BELL Repl. by BAHINIPATI 11
$-0.005 \pm 0.028 \pm 0.018$	¹ GERSHON	05	BELL Repl. by RONGA 06
$0.031 \pm 0.070 \pm 0.033$	² AUBERT	04V	BABR Repl. by AUBERT 06Y
$-0.004 \pm 0.037 \pm 0.014$	¹ AUBERT	04W	BABR Repl. by AUBERT 05Z
$0.049 \pm 0.040 \pm 0.019$	² SARANGI	04	BELL Repl. by RONGA 06

¹ Uses partially reconstructed $B^0 \rightarrow D^{*\pm} \pi^\mp$ decays.

² Uses fully reconstructed $B^0 \rightarrow D^{*\pm} \pi^\mp$ decays.

³ Combines the results from fully reconstructed and partially reconstructed $D^* \pi$ events by taking weighted averages. Assumes that systematic errors from physics parameters and fit biases in the two measurements are 100% correlated.

 $(S_+ + S_-)/2 (B^0 \rightarrow D^- \pi^+)$

VALUE	DOCUMENT ID	TECN	COMMENT
-0.046 ± 0.023 OUR AVERAGE			
$-0.010 \pm 0.023 \pm 0.07$	¹ AUBERT	06Y	BABR $e^+ e^- \rightarrow \Upsilon(4S)$
$-0.050 \pm 0.021 \pm 0.012$	² RONGA	06	BELL $e^+ e^- \rightarrow \Upsilon(4S)$

• • • We do not use the following data for averages, fits, limits, etc. • • •

$-0.022 \pm 0.038 \pm 0.020$	¹ AUBERT	04V	BABR Repl. by AUBERT 06Y
$-0.062 \pm 0.037 \pm 0.018$	¹ SARANGI	04	BELL Repl. by RONGA 06

¹ Uses fully reconstructed $B^0 \rightarrow D^\pm \pi^\mp$ decays.

² Combines the results from fully reconstructed and partially reconstructed $D \pi$ events by taking weighted averages. Assumes that systematic errors from physics parameters and fit biases in the two measurements are 100% correlated.

 $(S_- - S_+)/2 (B^0 \rightarrow D^- \pi^+)$

VALUE	DOCUMENT ID	TECN	COMMENT
-0.022 ± 0.021 OUR AVERAGE			
$-0.033 \pm 0.042 \pm 0.012$	¹ AUBERT	06Y	BABR $e^+ e^- \rightarrow \Upsilon(4S)$
$-0.019 \pm 0.021 \pm 0.012$	² RONGA	06	BELL $e^+ e^- \rightarrow \Upsilon(4S)$

• • • We do not use the following data for averages, fits, limits, etc. • • •

$0.025 \pm 0.068 \pm 0.033$	¹ AUBERT	04V	BABR Repl. by AUBERT 06Y
$-0.025 \pm 0.037 \pm 0.018$	¹ SARANGI	04	BELL Repl. by RONGA 06

¹ Uses fully reconstructed $B^0 \rightarrow D^\pm \pi^\mp$ decays.

² Combines the results from fully reconstructed and partially reconstructed $D \pi$ events by taking weighted averages. Assumes that systematic errors from physics parameters and fit biases in the two measurements are 100% correlated.

 $S_+ (B^0 \rightarrow D^- \pi^+)$

VALUE	DOCUMENT ID	TECN	COMMENT
0.058 ± 0.020 ± 0.011	¹ AAIJ	18Z	LHCb pp at 7, 8 TeV

¹ Measured in the simultaneous analysis of $B^0 \rightarrow D^\mp \pi^\pm$ decays. AAIJ 18Z reports a statistical (systematic) correlation of 0.6 (-0.41) with the measured value of $S_- (B^0 \rightarrow D^+ \pi^-)$.

 $S_- (B^0 \rightarrow D^+ \pi^-)$

VALUE	DOCUMENT ID	TECN	COMMENT
0.038 ± 0.020 ± 0.007	¹ AAIJ	18Z	LHCb pp at 7, 8 TeV

¹ Measured in the simultaneous analysis of $B^0 \rightarrow D^\mp \pi^\pm$ decays. AAIJ 18Z reports a statistical (systematic) correlation of 0.6 (-0.41) with the measured value of $S_+ (B^0 \rightarrow D^- \pi^+)$.

 $(S_+ + S_-)/2 (B^0 \rightarrow D^- \rho^+)$

VALUE	DOCUMENT ID	TECN	COMMENT
-0.024 ± 0.031 ± 0.009	¹ AUBERT	06Y	BABR $e^+ e^- \rightarrow \Upsilon(4S)$

¹ Uses fully reconstructed $B^0 \rightarrow D^- \rho^+$ decays.

 $(S_- - S_+)/2 (B^0 \rightarrow D^- \rho^+)$

VALUE	DOCUMENT ID	TECN	COMMENT
-0.098 ± 0.055 ± 0.018	¹ AUBERT	06Y	BABR $e^+ e^- \rightarrow \Upsilon(4S)$

¹ Uses fully reconstructed $B^0 \rightarrow D^- \rho^+$ decays.

 $C_{\eta_c K_S^0} (B^0 \rightarrow \eta_c K_S^0)$

VALUE	DOCUMENT ID	TECN	COMMENT
0.080 ± 0.124 ± 0.029	AUBERT	09K	BABR $e^+ e^- \rightarrow \Upsilon(4S)$

See key on page 1171

Meson Particle Listings

B^0

$S_{\eta_c K_S^0}(B^0 \rightarrow \eta_c K_S^0)$

VALUE	DOCUMENT ID	TECN	COMMENT
0.925 ± 0.160 ± 0.057	AUBERT	09K	BABR $e^+e^- \rightarrow \Upsilon(4S)$

$C_{c\bar{c}K^{(*)0}}(B^0 \rightarrow c\bar{c}K^{(*)0})$

VALUE (units 10^{-2})	DOCUMENT ID	TECN	COMMENT
-0.5 ± 1.5 OUR EVALUATION	(Produced by HFLAV)		
0.4 ± 1.2 OUR AVERAGE			

0.4 ± 1.2	1	AAIJ	24	LHCB	pp at 7, 8 and 13 TeV
-0.6 ± 1.6 ± 1.2	2	ADACHI	12A	BELL	$e^+e^- \rightarrow \Upsilon(4S)$
-29 ⁺⁵³ ₋₄₄ ± 6	3	AUBERT	09AU	BABR	$e^+e^- \rightarrow \Upsilon(4S)$
2.4 ± 2.0 ± 1.6	4	AUBERT	09K	BABR	$e^+e^- \rightarrow \Upsilon(4S)$
• • • We do not use the following data for averages, fits, limits, etc. • • •					
0.8 ± 1.2 ± 0.3	5,6	AAIJ	24	LHCB	pp at 13 TeV
-1.7 ± 2.9	5,7	AAIJ	17BN	LHCB	pp at 7, 8 TeV
-4 ± 7 ± 5	8	SAHOO	08	BELL	Repl. by ADACHI 12A
4.9 ± 2.3 ± 1.8	4	AUBERT	07AY	BABR	Repl. by AUBERT 09K
-1.8 ± 2.1 ± 1.4	9	CHEN	07	BELL	Repl. by ADACHI 12A
-0.7 ± 4.1 ± 3.3	10	ABE	05B	BELL	Repl. by CHEN 07
5.1 ± 3.2 ± 1.4	11	AUBERT	05F	BABR	Repl. by AUBERT 07AY
5.1 ± 5.1 ± 2.6	12	ABE	02Z	BELL	Repl. by ABE 05B
5.3 ± 5.4 ± 3.2	13	AUBERT	02P	BABR	Repl. by AUBERT 05F

- A combination of this Run 2 result with the Run 1 result from AAIJ 17BN is reported with a correlation coefficient of 0.40.
- Measurement based on $B^0 \rightarrow J/\psi K_S^0$, $B^0 \rightarrow \psi(2S) K_S^0$, $B^0 \rightarrow J/\psi K_L^0$, and $B^0 \rightarrow \chi_{c1}(1P) K_S^0$ decays.
- Uses Dalitz plot analysis of $B^0 \rightarrow K^0 \pi^+ \pi^-$ decays and the first of two equivalent solutions.
- Measurement based on $B^0 \rightarrow c\bar{c}K^{(*)0}$ decays.
- Measurement based on $B^0 \rightarrow J/\psi K_S^0$, $B^0 \rightarrow \psi(2S) K_S^0$ with $J/\psi \rightarrow \mu^+ \mu^-$, $J/\psi \rightarrow e^+ e^-$ and $\psi(2S) \rightarrow \mu^+ \mu^-$.
- AAIJ 24 provides the correlation coefficient $\rho = 0.441$ between the uncertainties of $\sin(2\beta)$ and $C_{c\bar{c}K^{(*)0}}(B^0 \rightarrow c\bar{c}K^{(*)0})$ measurements.
- AAIJ 17BN provides the correlation coefficient $\rho = 0.42$ between the uncertainties of $S_{B^0 \rightarrow c\bar{c}K^{(*)0}}(B^0 \rightarrow c\bar{c}K^{(*)0})$ and $C_{c\bar{c}K^{(*)0}}(B^0 \rightarrow c\bar{c}K^{(*)0})$ measurements.
- Reports value of A of $B^0 \rightarrow \psi(2S) K^0$ which is equal to $-C$.
- Reports value of A of $B^0 \rightarrow J/\psi K^0$ which is equal to $-C$.
- Measurement based on $152 \times 10^6 B\bar{B}$ pairs.
- Measurement based on $227 \times 10^6 B\bar{B}$ pairs.
- Measured with both $\eta_f = \pm 1$ samples.
- Measured with the high purity of $\eta_f = -1$ samples.

$\sin(2\beta)$

For a discussion of CP violation, see the review on "CP Violation" in the Reviews section. $\sin(2\beta)$ is a measure of the CP-violating amplitude in the $B^0_d \rightarrow J/\psi(1S) K_S^0$.

VALUE	DOCUMENT ID	TECN	COMMENT
0.709 ± 0.011 OUR EVALUATION	(Produced by HFLAV)		
0.708 ± 0.017 OUR AVERAGE	Error includes scale factor of 1.5. See the ideogram below.		

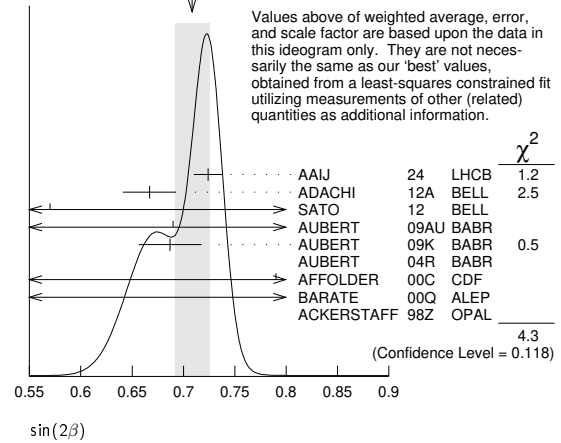
0.724 ± 0.014	1	AAIJ	24	LHCB	pp at 7, 8 and 13 TeV
0.667 ± 0.023 ± 0.012	2	ADACHI	12A	BELL	$e^+e^- \rightarrow \Upsilon(4S)$
0.57 ± 0.58 ± 0.06	3	SATO	12	BELL	$e^+e^- \rightarrow \Upsilon(5S)$
0.69 ± 0.52 ± 0.08	4	AUBERT	09AU	BABR	$e^+e^- \rightarrow \Upsilon(4S)$
0.687 ± 0.028 ± 0.012	5	AUBERT	09K	BABR	$e^+e^- \rightarrow \Upsilon(4S)$
1.56 ± 0.42 ± 0.21	6	AUBERT	04R	BABR	$e^+e^- \rightarrow \Upsilon(4S)$
0.79 ^{+0.41} _{-0.44} ± 0.16	7	AFFOLDER	00C	CDF	$p\bar{p}$ at 1.8 TeV
0.84 ^{+0.82} _{-1.04} ± 0.16	8	BARATE	00Q	ALEP	$e^+e^- \rightarrow Z$
3.2 ^{+1.8} _{-2.0} ± 0.5	9	ACKERSTAFF	98Z	OPAL	$e^+e^- \rightarrow Z$

• • • We do not use the following data for averages, fits, limits, etc. • • •					
0.717 ± 0.013 ± 0.008	10,11	AAIJ	24	LHCB	pp at 13 TeV
0.760 ± 0.034	10,12	AAIJ	17BN	LHCB	pp at 7, 8 TeV
0.72 ± 0.09 ± 0.03	13	SAHOO	08	BELL	Repl. by ADACHI 12A
0.714 ± 0.032 ± 0.018	5	AUBERT	07AY	BABR	Repl. by AUBERT 09K
0.642 ± 0.031 ± 0.017		CHEN	07	BELL	Repl. by ADACHI 12A
0.728 ± 0.056 ± 0.023	14	ABE	05B	BELL	Repl. by CHEN 07
0.722 ± 0.040 ± 0.023	15	AUBERT	05F	BABR	Repl. by AUBERT 07AY
0.99 ± 0.14 ± 0.06	16	ABE	02U	BELL	$e^+e^- \rightarrow \Upsilon(4S)$
0.719 ± 0.074 ± 0.035	17	ABE	02Z	BELL	Repl. by ABE 05B
0.59 ± 0.14 ± 0.05	18	AUBERT	02N	BABR	$e^+e^- \rightarrow \Upsilon(4S)$
0.741 ± 0.067 ± 0.034	19	AUBERT	02P	BABR	Repl. by AUBERT 05F
0.58 ^{+0.32} _{-0.34} ± 0.10		ABASHIAN	01	BELL	Repl. by ABE 01G
0.99 ± 0.14 ± 0.06	20	ABE	01G	BELL	Repl. by ABE 02Z
0.34 ± 0.20 ± 0.05		AUBERT	01	BABR	Repl. by AUBERT 01B
0.59 ± 0.14 ± 0.05	20	AUBERT	01B	BABR	Repl. by AUBERT 02P
1.8 ± 1.1 ± 0.3	21	ABE	98U	CDF	Repl. by AFFOLDER 00C

- A combination of this Run 2 result with the Run 1 result from AAIJ 17BN is reported with a correlation coefficient of 0.40.
- Measurement based on $B^0 \rightarrow J/\psi K_S^0$, $B^0 \rightarrow \psi(2S) K_S^0$, $B^0 \rightarrow J/\psi K_L^0$, and $B^0 \rightarrow \chi_{c1}(1P) K_S^0$ decays.
- SATO 12 uses 121 fb^{-1} data collected on $\Upsilon(5S)$ resonance. Uses the " $B - \pi$ tagging" where $B\pi^+$ and $B\pi^-$ tagged $J/\psi K_S^0$ events are compared.

- Uses Dalitz plot analysis of $B^0 \rightarrow K^0 \pi^+ \pi^-$ decays and the first of two equivalent solutions.
- Measurement based on $B^0 \rightarrow c\bar{c}K^{(*)0}$ decays.
- Measurement in which the J/ψ decays to hadrons or to muons that do not satisfy the standard identification criteria.
- AFFOLDER 00C uses about 400 $B^0 \rightarrow J/\psi(1S) K_S^0$ events. The production flavor of B^0 was determined using three tagging algorithms: a same-side tag, a jet-charge tag, and a soft-lepton tag.
- BARATE 00Q uses 23 candidates for $B^0 \rightarrow J/\psi(1S) K_S^0$ decays. A combination of jet-charge, vertex-charge, and same-side tagging techniques were used to determine the B^0 production flavor.
- ACKERSTAFF 98Z uses 24 candidates for $B^0_d \rightarrow J/\psi(1S) K_S^0$ decay. A combination of jet-charge and vertex-charge techniques were used to tag the B^0_d production flavor.
- Measurement based on $B^0 \rightarrow J/\psi K_S^0$, $B^0 \rightarrow \psi(2S) K_S^0$ with $J/\psi \rightarrow \mu^+ \mu^-$, $J/\psi \rightarrow e^+ e^-$ and $\psi(2S) \rightarrow \mu^+ \mu^-$.
- AAIJ 24 provides the correlation coefficient $\rho = 0.441$ between the uncertainties of $\sin(2\beta)$ and $C_{c\bar{c}K^{(*)0}}(B^0 \rightarrow c\bar{c}K^{(*)0})$ measurements.
- AAIJ 17BN provides the correlation coefficient $\rho = 0.42$ between the uncertainties of $\sin(2\beta)$ and $\cos(2\beta)$ measurements.
- Based on $B^0 \rightarrow \psi(2S) K_S^0$ decays.
- Measurement based on $152 \times 10^6 B\bar{B}$ pairs.
- Measurement based on $227 \times 10^6 B\bar{B}$ pairs.
- ABE 02U result is based on the same analysis and data sample reported in ABE 01G.
- ABE 02Z result is based on $85 \times 10^6 B\bar{B}$ pairs.
- AUBERT 02N result is based on the same analysis and data sample reported in AUBERT 01B.
- AUBERT 02P result is based on $88 \times 10^6 B\bar{B}$ pairs.
- First observation of CP violation in B^0 meson system.
- ABE 98U uses $198 \pm 17 B^0_d \rightarrow J/\psi(1S) K^0$ events. The production flavor of B^0 was determined using the same side tagging technique.

WEIGHTED AVERAGE
0.708 ± 0.017 (Error scaled by 1.5)



$C_{J/\psi(nS) K^0}(B^0 \rightarrow J/\psi(nS) K^0)$

VALUE (units 10^{-2})	DOCUMENT ID	TECN	COMMENT
-0.8 ± 1.7 OUR EVALUATION	(Produced by HFLAV)		
0.3 ± 1.0 OUR AVERAGE			

0.4 ± 1.2	1	AAIJ	24	LHCB	pp at 7, 8 and 13 TeV
1.5 ± 2.1 ^{+2.3} _{-4.5}	2,3	ADACHI	12A	BELL	$e^+e^- \rightarrow \Upsilon(4S)$
-10.4 ± 5.5 ^{+2.7} _{-4.7}	3,4	ADACHI	12A	BELL	$e^+e^- \rightarrow \Upsilon(4S)$
-1.9 ± 2.6 ^{+4.1} _{-1.7}	3,5	ADACHI	12A	BELL	$e^+e^- \rightarrow \Upsilon(4S)$
8.9 ± 7.6 ± 2.0	4	AUBERT	09K	BABR	$e^+e^- \rightarrow \Upsilon(4S)$
1.6 ± 2.3 ± 1.8		AUBERT	09K	BABR	$e^+e^- \rightarrow \Upsilon(4S)$

• • • We do not use the following data for averages, fits, limits, etc. • • •					
0.8 ± 1.2 ± 0.3	6,7	AAIJ	24	LHCB	pp at 13 TeV
-8.7 ± 4.8 ± 0.5	8	AAIJ	24	LHCB	pp at 13 TeV
1.5 ± 1.3 ± 0.3	9	AAIJ	24	LHCB	pp at 13 TeV
-1.7 ± 2.9	6,10	AAIJ	17BN	LHCB	pp at 7, 8 TeV
-1.4 ± 3.0	9	AAIJ	17BN	LHCB	pp at 7, 8 TeV
-5 ± 10 ± 1	8	AAIJ	17BN	LHCB	pp at 7, 8 TeV
-3.8 ± 3.2 ± 0.5	11	AAIJ	15N	LHCB	Repl. by AAIJ 17BN
3 ± 9 ± 1	12	AAIJ	13K	LHCB	Repl. by AAIJ 15N
-4 ± 7 ± 5	3,4	SAHOO	08	BELL	Repl. by ADACHI 12A
-1.8 ± 2.1 ± 1.4	3	CHEN	07	BELL	Repl. by ADACHI 12A

- A combination of this Run 2 result with the Run 1 result from AAIJ 17BN is reported with a correlation coefficient of 0.40.
- Uses $B^0 \rightarrow J/\psi K_S^0$ decays.
- The paper reports A, which is equal to $-C$.

Meson Particle Listings

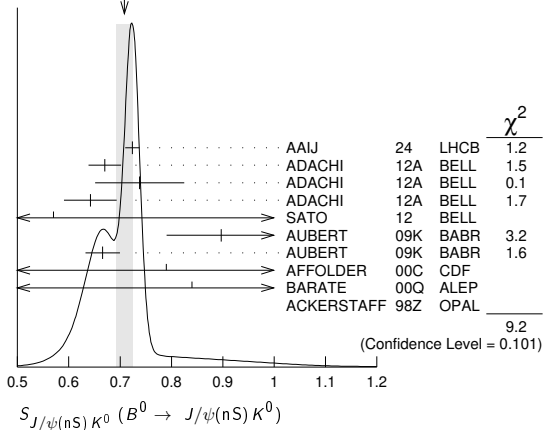
 B^0

- 4 Uses $B^0 \rightarrow \psi(2S) K_S^0$ decays.
 5 Uses $B^0 \rightarrow J/\psi K_S^0$ decays.
 6 Measurement based on $B^0 \rightarrow J/\psi K_S^0$, $B^0 \rightarrow \psi(2S) K_S^0$ with $J/\psi \rightarrow \mu^+ \mu^-$, $J/\psi \rightarrow e^+ e^-$ and $\psi(2S) \rightarrow \mu^+ \mu^-$.
 7 AAIJ 24 provides the correlation coefficient $\rho = 0.441$ between the uncertainties of $C_{J/\psi(nS) K^0}$ ($B^0 \rightarrow J/\psi(nS) K^0$) and $S_{J/\psi(nS) K^0}$ ($B^0 \rightarrow J/\psi(nS) K^0$) measurements.
 8 Measurement based on $B^0 \rightarrow \psi(2S) K_S^0$ with $\psi(2S) \rightarrow \mu^+ \mu^-$.
 9 Measurement based on $B^0 \rightarrow J/\psi K_S^0$ with $J/\psi \rightarrow \mu^+ \mu^-$ and $J/\psi \rightarrow e^+ e^-$.
 10 AAIJ 17BN provides the correlation coefficient $\rho = 0.42$ between the uncertainties of $S_{J/\psi(nS) K^0}$ ($B^0 \rightarrow J/\psi(nS) K^0$) and $C_{J/\psi(nS) K^0}$ ($B^0 \rightarrow J/\psi(nS) K^0$) measurements.
 11 AAIJ 15N uses 41,560 flavor-tagged $B_d \rightarrow J/\psi K_S^0$ events from 3 fb^{-1} of integrated luminosity. Provides the correlation coefficient $\rho = 0.483$ between the statistical uncertainties of and measurements.
 12 AAIJ 13K uses 8200 flavor-tagged $B_d \rightarrow J/\psi K_S^0$ events from 1 fb^{-1} of integrated luminosity. Provides the correlation coefficient $\rho = 0.42$ between the statistical uncertainties of $S_{J/\psi(nS) K^0}$ ($B^0 \rightarrow J/\psi(nS) K^0$) and $C_{J/\psi(nS) K^0}$ ($B^0 \rightarrow J/\psi(nS) K^0$) measurements.

 $S_{J/\psi(nS) K^0}$ ($B^0 \rightarrow J/\psi(nS) K^0$)

VALUE	DOCUMENT ID	TECN	COMMENT
0.701 ± 0.017 OUR EVALUATION	(Produced by HFLAV)		
0.708 ± 0.016 OUR AVERAGE	Error includes scale factor of 1.4. See the ideogram below.		
0.724 ± 0.014	1 AAIJ	24 LHCb	pp at 7, 8 and 13 TeV
$0.670 \pm 0.029 \pm 0.013$	2 ADACHI	12A BELL	$e^+ e^- \rightarrow \Upsilon(4S)$
$0.738 \pm 0.079 \pm 0.036$	3 ADACHI	12A BELL	$e^+ e^- \rightarrow \Upsilon(4S)$
$0.642 \pm 0.047 \pm 0.021$	4 ADACHI	12A BELL	$e^+ e^- \rightarrow \Upsilon(4S)$
$0.57 \pm 0.58 \pm 0.06$	5 SATO	12 BELL	$e^+ e^- \rightarrow \Upsilon(5S)$
$0.897 \pm 0.100 \pm 0.036$	3 AUBERT	09K BABR	$e^+ e^- \rightarrow \Upsilon(4S)$
$0.666 \pm 0.031 \pm 0.013$	AUBERT	09K BABR	$e^+ e^- \rightarrow \Upsilon(4S)$
0.79 ± 0.41 -0.44	6 AFFOLDER	00C CDF	$p\bar{p}$ at 1.8 TeV
0.84 ± 0.82 -1.04	7 BARATE	00Q ALEP	$e^+ e^- \rightarrow Z$
3.2 ± 1.8 -2.0	8 ACKERSTAFF	98Z OPAL	$e^+ e^- \rightarrow Z$
$0.717 \pm 0.013 \pm 0.008$	9,10 AAIJ	24 LHCb	pp at 13 TeV
$0.649 \pm 0.053 \pm 0.018$	11 AAIJ	24 LHCb	pp at 13 TeV
$0.722 \pm 0.014 \pm 0.007$	12 AAIJ	24 LHCb	pp at 13 TeV
0.760 ± 0.034	9,13 AAIJ	17BN LHCb	pp at 7, 8 TeV
0.75 ± 0.04	12 AAIJ	17BN LHCb	pp at 7, 8 TeV
$0.84 \pm 0.10 \pm 0.01$	11 AAIJ	17BN LHCb	pp at 7, 8 TeV
$0.731 \pm 0.035 \pm 0.020$	14 AAIJ	15N LHCb	Repl. by AAIJ 17BN
$0.73 \pm 0.07 \pm 0.04$	15 AAIJ	13K LHCb	Repl. by AAIJ 15N
$0.650 \pm 0.029 \pm 0.018$	16 SAHOO	08 BELL	Repl. by ADACHI 12A
$0.72 \pm 0.09 \pm 0.03$	3 SAHOO	08 BELL	Repl. by ADACHI 12A
$0.642 \pm 0.031 \pm 0.017$	CHEN	07 BELL	Repl. by ADACHI 12A

- 1 A combination of this Run 2 result with the Run 1 result from AAIJ 17BN is reported with a correlation coefficient of 0.40.
 2 Uses $B^0 \rightarrow J/\psi K_S^0$ decays.
 3 Based on $B^0 \rightarrow \psi(2S) K_S^0$ decays.
 4 Uses $B^0 \rightarrow J/\psi K_S^0$ decays.
 5 SATO 12 uses 121 fb^{-1} data collected at $\Upsilon(5S)$ resonance. Uses the " $B - \pi$ tagging" where $B \pi^+$ and $B \pi^-$ tagged $J/\psi K_S^0$ events are compared.
 6 AFFOLDER 00C uses about 400 $B^0 \rightarrow J/\psi(1S) K_S^0$ events. The production flavor of B^0 was determined using three tagging algorithms: a same-side tag, a jet-charge tag, and a soft-lepton tag.
 7 BARATE 00Q uses 23 candidates for $B^0 \rightarrow J/\psi(1S) K_S^0$ decays. A combination of jet-charge, vertex-charge, and same-side tagging techniques were used to determine the B^0 production flavor.
 8 ACKERSTAFF 98Z uses 24 candidates for $B_d^0 \rightarrow J/\psi(1S) K_S^0$ decay. A combination of jet-charge and vertex-charge techniques were used to tag the B_d^0 production flavor.
 9 Measurement based on $B^0 \rightarrow J/\psi K_S^0$, $B^0 \rightarrow \psi(2S) K_S^0$ with $J/\psi \rightarrow \mu^+ \mu^-$, $J/\psi \rightarrow e^+ e^-$ and $\psi(2S) \rightarrow \mu^+ \mu^-$.
 10 AAIJ 24 provides the correlation coefficient $\rho = 0.441$ between the uncertainties of $C_{J/\psi(nS) K^0}$ ($B^0 \rightarrow J/\psi(nS) K^0$) and $S_{J/\psi(nS) K^0}$ ($B^0 \rightarrow J/\psi(nS) K^0$) measurements.
 11 Measurement based on $B^0 \rightarrow \psi(2S) K_S^0$ with $\psi(2S) \rightarrow \mu^+ \mu^-$.
 12 Measurement based on $B^0 \rightarrow J/\psi K_S^0$ with $J/\psi \rightarrow \mu^+ \mu^-$ and $J/\psi \rightarrow e^+ e^-$.
 13 AAIJ 17BN provides the correlation coefficient $\rho = 0.42$ between the uncertainties of $S_{J/\psi(nS) K^0}$ ($B^0 \rightarrow J/\psi(nS) K^0$) and $C_{J/\psi(nS) K^0}$ ($B^0 \rightarrow J/\psi(nS) K^0$) measurements.
 14 AAIJ 15N uses 41,560 flavor-tagged $B_d \rightarrow J/\psi K_S^0$ events from 3 fb^{-1} of integrated luminosity. Provides the correlation coefficient $\rho = 0.483$ between the statistical uncertainties of and measurements.
 15 AAIJ 13K uses 8200 flavor-tagged $B_d \rightarrow J/\psi K_S^0$ events from 1 fb^{-1} of integrated luminosity. Provides the correlation coefficient $\rho = 0.42$ between the statistical uncertainties of $S_{J/\psi(nS) K^0}$ ($B^0 \rightarrow J/\psi(nS) K^0$) and $C_{J/\psi(nS) K^0}$ ($B^0 \rightarrow J/\psi(nS) K^0$) measurements.
 16 Combined result of CHEN 07 and SAHOO 08.

WEIGHTED AVERAGE
0.708±0.016 (Error scaled by 1.4) $C_{J/\psi K^0}$ ($B^0 \rightarrow J/\psi K^0$)

VALUE	DOCUMENT ID	TECN	COMMENT
$0.025 \pm 0.083 \pm 0.054$	1 AUBERT	09K BABR	$e^+ e^- \rightarrow \Upsilon(4S)$
1 Based on $B^0 \rightarrow J/\psi K^0$, $K^0 \rightarrow K_S^0 \pi^0$.			

 $S_{J/\psi K^0}$ ($B^0 \rightarrow J/\psi K^0$)

VALUE	DOCUMENT ID	TECN	COMMENT
$0.601 \pm 0.239 \pm 0.087$	1,2 AUBERT	09K BABR	$e^+ e^- \rightarrow \Upsilon(4S)$
1 Based on $B^0 \rightarrow J/\psi K^0$, $K^0 \rightarrow K_S^0 \pi^0$. 2 This $S_{J/\psi K^0}$ value has been corrected for the dilution of the $\sin(\Delta M \Delta t)$ coefficient of the CP asymmetry by a factor of $1 - R_{\perp}$, which arises from the mixture of CP -even and CP -odd B decay amplitudes.			

 $C_{\chi_{c0} K_S^0}$ ($B^0 \rightarrow \chi_{c0} K_S^0$)

VALUE	DOCUMENT ID	TECN	COMMENT
-0.29 ± 0.53 -0.44 ± 0.06	1 AUBERT	09AU BABR	$e^+ e^- \rightarrow \Upsilon(4S)$
1 Uses Dalitz plot analysis of $B^0 \rightarrow K^0 \pi^+ \pi^-$ decays and the first of two equivalent solutions is used.			

 $S_{\chi_{c0} K_S^0}$ ($B^0 \rightarrow \chi_{c0} K_S^0$)

VALUE	DOCUMENT ID	TECN	COMMENT
$-0.69 \pm 0.52 \pm 0.08$	1 AUBERT	09AU BABR	$e^+ e^- \rightarrow \Upsilon(4S)$
1 Uses Dalitz plot analysis of $B^0 \rightarrow K^0 \pi^+ \pi^-$ decays and the first of two equivalent solutions is used.			

 $C_{\chi_{c1} K_S^0}$ ($B^0 \rightarrow \chi_{c1} K_S^0$)

VALUE	DOCUMENT ID	TECN	COMMENT
0.06 ± 0.07 OUR AVERAGE			
$0.017 \pm 0.083 \pm 0.026$ -0.046	ADACHI	12A BELL	$e^+ e^- \rightarrow \Upsilon(4S)$
$0.129 \pm 0.109 \pm 0.025$	AUBERT	09K BABR	$e^+ e^- \rightarrow \Upsilon(4S)$

 $S_{\chi_{c1} K_S^0}$ ($B^0 \rightarrow \chi_{c1} K_S^0$)

VALUE	DOCUMENT ID	TECN	COMMENT
0.63 ± 0.10 OUR AVERAGE			
$0.640 \pm 0.117 \pm 0.040$	ADACHI	12A BELL	$e^+ e^- \rightarrow \Upsilon(4S)$
$0.614 \pm 0.160 \pm 0.040$	AUBERT	09K BABR	$e^+ e^- \rightarrow \Upsilon(4S)$

 $\sin(2\beta_{\text{eff}})$ ($B^0 \rightarrow \phi K^0$)

VALUE	DOCUMENT ID	TECN	COMMENT
$0.22 \pm 0.27 \pm 0.12$	AUBERT	07AX BABR	$e^+ e^- \rightarrow \Upsilon(4S)$
• • • We do not use the following data for averages, fits, limits, etc. • • •			
$0.50 \pm 0.25 \pm 0.07$ -0.04	1 AUBERT	05T BABR	Repl. by AUBERT 07AX
1 Obtained by constraining $C = 0$.			

 $\sin(2\beta_{\text{eff}})$ ($B^0 \rightarrow \phi K_S^0(1430)^0$)

VALUE	DOCUMENT ID	TECN	COMMENT
0.97 ± 0.03 -0.52	1 AUBERT	08BG BABR	$e^+ e^- \rightarrow \Upsilon(4S)$
1 Measured using the CP -violation phase difference $\Delta\phi_{00}$ between the B and \bar{B} decay amplitude.			

 $\sin(2\beta_{\text{eff}})$ ($B^0 \rightarrow K^+ K^- K_S^0$)

VALUE	DOCUMENT ID	TECN	COMMENT
$0.77 \pm 0.11 \pm 0.07$ -0.04	AUBERT	07AX BABR	$e^+ e^- \rightarrow \Upsilon(4S)$
• • • We do not use the following data for averages, fits, limits, etc. • • •			
$0.55 \pm 0.22 \pm 0.12$	1 AUBERT	05T BABR	Repl. by AUBERT 07AX
1 Obtained by constraining $C = 0$.			

See key on page 1171

Meson Particle Listings
 B^0 $\sin(2\beta_{\text{eff}})(B^0 \rightarrow [K_S^0 \pi^+ \pi^-]_{D^{(*)}} h^0)$

VALUE	DOCUMENT ID	TECN	COMMENT
0.80 ± 0.14 ± 0.07	¹ ADACHI 18		$e^+ e^- \rightarrow \Upsilon(4S)$
0.43 ± 0.27 ± 0.08	² VOROBYEV 16	BELL	$e^+ e^- \rightarrow \Upsilon(4S)$
0.29 ± 0.34 ± 0.06	AUBERT 07BH	BABR	$e^+ e^- \rightarrow \Upsilon(4S)$
0.78 ± 0.44 ± 0.22	KROKOVNY 06	BELL	Repl. by VOROBYEV 16

¹ Analyzes joint data sample of Belle and BaBar using Dalitz plot analysis of $D \rightarrow K_S^0 \pi^+ \pi^-$; the second error combines experimental systematic uncertainty and the Dalitz plot model uncertainty.

² A model-independent measurement uses the binned Dalitz plot technique.

 $\beta_{\text{eff}}(B^0 \rightarrow [K_S^0 \pi^+ \pi^-]_{D^{(*)}} h^0)$

VALUE (°)	DOCUMENT ID	TECN	COMMENT
22.5 ± 4.4 ± 1.3	¹ ADACHI 18		$e^+ e^- \rightarrow \Upsilon(4S)$
11.7 ± 7.8 ± 2.1	² VOROBYEV 16	BELL	$e^+ e^- \rightarrow \Upsilon(4S)$

¹ Analyzes joint data sample of Belle and BaBar using Dalitz plot analysis of $D \rightarrow K_S^0 \pi^+ \pi^-$; the second error combines experimental systematic uncertainty and the Dalitz plot model uncertainty.

² A model-independent measurement uses the binned Dalitz plot technique.

 $2\beta_{\text{eff}}(B^0 \rightarrow J/\psi \rho^0)$

VALUE (°)	DOCUMENT ID	TECN	COMMENT
41.7 ± 9.6 ± 2.8 -6.3	AAIJ 15J	LHCB	pp at 7, 8 TeV

 $|\lambda|(B^0 \rightarrow [K_S^0 \pi^+ \pi^-]_{D^{(*)}} h^0)$

VALUE	DOCUMENT ID	TECN	COMMENT
1.01 ± 0.08 ± 0.02	AUBERT 07BH	BABR	$e^+ e^- \rightarrow \Upsilon(4S)$

 $|\sin(2\beta + \gamma)|$

β (ϕ_1) and γ (ϕ_3) are angles of CKM unitarity triangle, see the review on "CP Violation" in the Reviews section.

VALUE	CL%	DOCUMENT ID	TECN	COMMENT
>0.40	90	¹ AUBERT 06Y	BABR	$e^+ e^- \rightarrow \Upsilon(4S)$
>0.77	68	² AAIJ 18Z	LHCB	pp at 7, 8 TeV
>0.13	95	³ RONGA 06	BELL	$e^+ e^- \rightarrow \Upsilon(4S)$
>0.07	95	³ RONGA 06	BELL	$e^+ e^- \rightarrow \Upsilon(4S)$
>0.35	90	⁴ AUBERT 05Z	BABR	$e^+ e^- \rightarrow \Upsilon(4S)$
>0.69	68	⁵ AUBERT 04V	BABR	$e^+ e^- \rightarrow \Upsilon(4S)$
>0.58	95	⁶ AUBERT 04W	BABR	Repl. by AUBERT 05Z

¹ Uses fully reconstructed $B^0 \rightarrow D^{(*)} \pi^+ \pi^-$ and $D^{\pm} \rho^{\mp}$ decays and some theoretical assumptions.

² Uses a time dependent CP violation measurement in $B^0 \rightarrow D^{\mp} \pi^{\pm}$ decays with external input and some theoretical assumptions.

³ Combines the results from fully reconstructed and partially reconstructed $D^{(*)} \pi$ events by taking weighted averages. Assumes that systematic errors from physics parameters and fit biases in the two measurements are 100% correlated.

⁴ Uses partially reconstructed $B^0 \rightarrow D^{*} \pi^+ \pi^-$ decays and some theoretical assumptions.

⁵ Uses fully reconstructed $B^0 \rightarrow D^{(*)} \pi^+ \pi^-$ decays and some theoretical assumptions, such as the SU(3) symmetry relation.

⁶ Combining this measurement with the results from AUBERT 04v for fully reconstructed $B^0 \rightarrow D^{(*)} \pi^+ \pi^-$ and some theoretical assumptions, such as the SU(3) symmetry relation.

 $2\beta + \gamma$

VALUE (°)	DOCUMENT ID	TECN	COMMENT
83 ± 53 ± 20	¹ AUBERT 08AC	BABR	$e^+ e^- \rightarrow \Upsilon(4S)$

¹ Used a time-dependent Dalitz-plot analysis of $B^0 \rightarrow D^{\mp} K^0 \pi^{\pm}$ assuming the ratio of the $b \rightarrow u$ and $b \rightarrow c$ decay amplitudes to be 0.3.

 α

For angle $\alpha(\phi_2)$ of the CKM unitarity triangle, see the review on "CP violation" in the reviews section.

VALUE (°)	DOCUMENT ID	TECN	COMMENT
84.1 ± 4.5 3.8 OUR EVALUATION	(Produced by HFLAV)		

• • • We do not use the following data for averages, fits, limits, etc. • • •

93.7 ± 10.6	¹ VANHOEFER 16	BELL	$e^+ e^- \rightarrow \Upsilon(4S)$
84.9 ± 13.5	¹ VANHOEFER 14	BELL	Repl. by VANHOEFER 16
79 ± 7 ± 11	² AUBERT 10D	BABR	$e^+ e^- \rightarrow \Upsilon(4S)$
92.4 ± 6.0 -6.5	¹ AUBERT 09G	BABR	$e^+ e^- \rightarrow \Upsilon(4S)$
78.6 ± 7.3	³ AUBERT 07O	BABR	$e^+ e^- \rightarrow \Upsilon(4S)$
88 ± 17	⁴ SOMOV 06	BELL	Repl. by VANHOEFER 14
100 ± 13	⁵ AUBERT,B 05C	BABR	Repl. by AUBERT 09G
102 ± 16 -12	⁶ AUBERT,B 04R	BABR	Repl. by AUBERT,B 05C

¹ Based on an isospin analysis of the $B \rightarrow \rho\rho$ system.

² Obtained using the time dependent analysis of $B^0 \rightarrow a_1(1260) \pi^+ \pi^-$ and branching fraction measurements of $B \rightarrow a_1(1260) K$ and $B \rightarrow K_1 \pi$. Uses SU(3) flavor relations.

³ The angle α_{eff} is obtained using the measured CP parameters of $B^0 \rightarrow a_1(1260) \pi^+ \pi^-$ and choosing one of the four solutions that is compatible with the result of SM-based fits.

⁴ Obtained using isospin relation and selecting a solution closest to the CKM best fit average; the 90% CL allowed interval is $59^\circ < \phi_2 (\equiv \alpha) < 115^\circ$.

⁵ Obtained using isospin relation and selecting a solution closest to the CKM best fit average; 90% CL allowed interval is $79^\circ < \alpha < 123^\circ$.

⁶ Obtained from the measured CP parameters of the longitudinal polarization by selecting the solution closest to the CKM best fit central value of $\alpha = 95^\circ - 98^\circ$.

CP VIOLATION PARAMETERS IN $B^0 \rightarrow D^0 K^{*0}$ DECAY

The parameters r_{B^0} and δ_{B^0} are the magnitude ratio and strong phase difference between the amplitudes of $A(B^0 \rightarrow D^0 K^{*0})$ and $A(B^0 \rightarrow \bar{D}^0 K^{*0})$. The measured observables are defined as $x_{\pm} = r_{B^0} \cos(\delta_{B^0} \pm \gamma)$ and $y_{\pm} = r_{B^0} \sin(\delta_{B^0} \pm \gamma)$ where γ is the CKM angle γ .

"OUR EVALUATION" is provided by the Heavy Flavor Averaging Group (HFLAV). The CKM angle γ is listed in the B^+ section for "CP VIOLATION PARAMETERS IN $B^+ \rightarrow D K^+$ AND SIMILAR DECAYS."

 $x_+(B^0 \rightarrow DK^{*0})$

VALUE	DOCUMENT ID	TECN	COMMENT
0.04 ± 0.17 OUR AVERAGE			
0.04 ± 0.16 ± 0.11	¹ AAIJ 16S	LHCB	pp at 7, 8 TeV
0.05 ± 0.35 ± 0.02	AAIJ 16Z	LHCB	pp at 7, 8 TeV
0.05 ± 0.24 ± 0.04	² AAIJ 16AA	LHCB	Repl. by AAIJ 16Z

• • • We do not use the following data for averages, fits, limits, etc. • • •

¹ Uses Dalitz plot of $B^0 \rightarrow DK^+ \pi^-$ with $D \rightarrow K^+ K^-, \pi^+ \pi^-,$ or $K^+ \pi^-$.

² Uses Dalitz plot analysis of $D \rightarrow K_S^0 \pi^+ \pi^-$ decays coming from $B^0 \rightarrow DK^*(892)^0$ modes.

 $x_-(B^0 \rightarrow DK^{*0})$

VALUE	DOCUMENT ID	TECN	COMMENT
-0.16 ± 0.14 OUR AVERAGE			
-0.02 ± 0.13 ± 0.14	¹ AAIJ 16S	LHCB	pp at 7, 8 TeV
-0.31 ± 0.20 ± 0.04	AAIJ 16Z	LHCB	pp at 7, 8 TeV
-0.15 ± 0.14 ± 0.03	² AAIJ 16AA	LHCB	Repl. by AAIJ 16Z

• • • We do not use the following data for averages, fits, limits, etc. • • •

¹ Uses Dalitz plot of $B^0 \rightarrow DK^+ \pi^-$ with $D \rightarrow K^+ K^-, \pi^+ \pi^-,$ or $K^+ \pi^-$.

² Uses Dalitz plot analysis of $D \rightarrow K_S^0 \pi^+ \pi^-$ decays coming from $B^0 \rightarrow DK^*(892)^0$ modes.

 $y_+(B^0 \rightarrow DK^{*0})$

VALUE	DOCUMENT ID	TECN	COMMENT
-0.68 ± 0.22 OUR AVERAGE			
-0.47 ± 0.28 ± 0.22	¹ AAIJ 16S	LHCB	pp at 7, 8 TeV
-0.81 ± 0.28 ± 0.06	AAIJ 16Z	LHCB	pp at 7, 8 TeV
-0.65 ± 0.24 -0.23 ± 0.08	² AAIJ 16AA	LHCB	Repl. by AAIJ 16Z

• • • We do not use the following data for averages, fits, limits, etc. • • •

¹ Uses Dalitz plot of $B^0 \rightarrow DK^+ \pi^-$ with $D \rightarrow K^+ K^-, \pi^+ \pi^-,$ or $K^+ \pi^-$.

² Uses Dalitz plot analysis of $D \rightarrow K_S^0 \pi^+ \pi^-$ decays coming from $B^0 \rightarrow DK^*(892)^0$ modes.

 $y_-(B^0 \rightarrow DK^{*0})$

VALUE	DOCUMENT ID	TECN	COMMENT
0.20 ± 0.25 OUR AVERAGE	Error includes scale factor of 1.2.		
-0.35 ± 0.26 ± 0.41	¹ AAIJ 16S	LHCB	pp at 7, 8 TeV
0.31 ± 0.21 ± 0.05	AAIJ 16Z	LHCB	pp at 7, 8 TeV
0.25 ± 0.15 ± 0.06	² AAIJ 16AA	LHCB	Repl. by AAIJ 16Z

• • • We do not use the following data for averages, fits, limits, etc. • • •

¹ Uses Dalitz plot of $B^0 \rightarrow DK^+ \pi^-$ with $D \rightarrow K^+ K^-, \pi^+ \pi^-,$ or $K^+ \pi^-$.

² Uses Dalitz plot analysis of $D \rightarrow K_S^0 \pi^+ \pi^-$ decays coming from $B^0 \rightarrow DK^*(892)^0$ modes.

 $r_{B^0}(B^0 \rightarrow DK^{*0})$

VALUE	DOCUMENT ID	TECN	COMMENT
0.257 ± 0.021 -0.023 OUR EVALUATION	(Produced by HFLAV)		
0.39 ± 0.13	¹ AAIJ 16AA	LHCB	Repl. by AAIJ 16Z
0.56 ± 0.17	² AAIJ 16Z	LHCB	pp at 7, 8 TeV

• • • We do not use the following data for averages, fits, limits, etc. • • •

¹ Uses Dalitz plot analysis of $D \rightarrow K_S^0 \pi^+ \pi^-$ decays coming from $B^0 \rightarrow DK^*(892)^0$ modes.

² Measurement is performed with $K^+ \pi^-$ masses within 50 MeV of the K^{*0} mass and an absolute value of the cosine of the K^{*0} helicity angle greater than 0.4. Angle γ is required to satisfy $0 < \gamma < 180$ degrees.

 $\delta_{B^0}(B^0 \rightarrow DK^{*0})$

VALUE (°)	DOCUMENT ID	TECN	COMMENT
194.1 ± 9.6 8.8 OUR EVALUATION	(Produced by HFLAV)		
197 ± 24 -20	¹ AAIJ 16AA	LHCB	Repl. by AAIJ 16Z
204 ± 21 -20	² AAIJ 16Z	LHCB	pp at 7, 8 TeV

• • • We do not use the following data for averages, fits, limits, etc. • • •

Meson Particle Listings

 B^0

¹ Uses Dalitz plot analysis of $D \rightarrow K_S^0 \pi^+ \pi^-$ decays coming from $B^0 \rightarrow DK^*(892)^0$ modes.

² Measurement is performed with $K^+ \pi^-$ masses within 50 MeV of the K^{*0} mass and an absolute value of the cosine of the K^{*0} helicity angle greater than 0.4. Angle γ is required to satisfy $0 < \gamma < 180$ degrees.

 $a_{CP}(B^0 \rightarrow p\bar{p}K^+\pi^-)$

Observable $a_{CP}(B^0 \rightarrow p\bar{p}K^+\pi^-)$ calculated as half of the difference between triple products for B^0 and \bar{B}^0 , which is sensitive to CP violation.

VALUE (%)	DOCUMENT ID	TECN	COMMENT
$0.51 \pm 0.85 \pm 0.08$	¹ AAIJ	23AG LHCb	pp at 7, 8 and 13 TeV

¹ Phase-space integrated asymmetry.

 $a_P(B^0 \rightarrow p\bar{p}K^+\pi^-)$

Observable $a_P(B^0 \rightarrow p\bar{p}K^+\pi^-)$ calculated as the average of the triple products for B^0 and \bar{B}^0 , which is sensitive to parity violation.

VALUE (%)	DOCUMENT ID	TECN	COMMENT
$1.49 \pm 0.85 \pm 0.08$	¹ AAIJ	23AG LHCb	pp at 7, 8 and 13 TeV

¹ Phase-space integrated asymmetry.

T and CPT VIOLATION PARAMETERS

Measured values of the T , CP , and CPT -asymmetry parameters, defined as the differences in $S_{\alpha,\beta}^{\pm}$ and $C_{\alpha,\beta}^{\pm}$ between symmetry-transformed transitions. The indices $\alpha = \ell^+, \ell^-$ and $\beta = K_S^0, K_L^0$ stand for reconstructed the flavor final state and the CP final states from $\Upsilon(4S)$ decay. The sign \pm indicates whether the decay to the flavor final state α occurs before or after the decay to the CP final state.

Alternatively, violations of CPT symmetry and Lorentz invariance are searched for by studying interference effects in B^0 mixing. Results are expressed in terms of the standard model extension parameter Δa , which describes the difference between the couplings of the valence quarks within B^0 meson with the Lorentz-violating fields.

 $\Delta S_T^+(S_{\ell^-,K_S^0}^- - S_{\ell^+,K_S^0}^+)$

VALUE	DOCUMENT ID	TECN	COMMENT
$-1.37 \pm 0.14 \pm 0.06$	LEES	12W BABR	$e^+e^- \rightarrow \Upsilon(4S)$

 $\Delta S_T^-(S_{\ell^-,K_S^0}^+ - S_{\ell^+,K_S^0}^-)$

VALUE	DOCUMENT ID	TECN	COMMENT
$1.17 \pm 0.18 \pm 0.11$	LEES	12W BABR	$e^+e^- \rightarrow \Upsilon(4S)$

 $\Delta C_T^+(C_{\ell^-,K_S^0}^- - C_{\ell^+,K_S^0}^+)$

VALUE	DOCUMENT ID	TECN	COMMENT
$0.10 \pm 0.14 \pm 0.08$	LEES	12W BABR	$e^+e^- \rightarrow \Upsilon(4S)$

 $\Delta C_T^-(C_{\ell^-,K_S^0}^+ - C_{\ell^+,K_S^0}^-)$

VALUE	DOCUMENT ID	TECN	COMMENT
$0.04 \pm 0.14 \pm 0.08$	LEES	12W BABR	$e^+e^- \rightarrow \Upsilon(4S)$

 $\Delta S_{CP}^+(S_{\ell^-,K_S^0}^+ - S_{\ell^+,K_S^0}^+)$

VALUE	DOCUMENT ID	TECN	COMMENT
$-1.30 \pm 0.11 \pm 0.07$	LEES	12W BABR	$e^+e^- \rightarrow \Upsilon(4S)$

 $\Delta S_{CP}^-(S_{\ell^-,K_S^0}^- - S_{\ell^+,K_S^0}^-)$

VALUE	DOCUMENT ID	TECN	COMMENT
$1.33 \pm 0.12 \pm 0.06$	LEES	12W BABR	$e^+e^- \rightarrow \Upsilon(4S)$

 $\Delta C_{CP}^+(C_{\ell^-,K_S^0}^+ - C_{\ell^+,K_S^0}^+)$

VALUE	DOCUMENT ID	TECN	COMMENT
$0.07 \pm 0.09 \pm 0.03$	LEES	12W BABR	$e^+e^- \rightarrow \Upsilon(4S)$

 $\Delta C_{CP}^-(C_{\ell^-,K_S^0}^- - C_{\ell^+,K_S^0}^-)$

VALUE	DOCUMENT ID	TECN	COMMENT
$0.08 \pm 0.10 \pm 0.04$	LEES	12W BABR	$e^+e^- \rightarrow \Upsilon(4S)$

 $\Delta S_{CPT}^+(S_{\ell^+,K_S^0}^- - S_{\ell^+,K_S^0}^+)$

VALUE	DOCUMENT ID	TECN	COMMENT
$0.16 \pm 0.21 \pm 0.09$	LEES	12W BABR	$e^+e^- \rightarrow \Upsilon(4S)$

 $\Delta S_{CPT}^-(S_{\ell^+,K_S^0}^+ - S_{\ell^+,K_S^0}^-)$

VALUE	DOCUMENT ID	TECN	COMMENT
$-0.03 \pm 0.13 \pm 0.06$	LEES	12W BABR	$e^+e^- \rightarrow \Upsilon(4S)$

 $\Delta C_{CPT}^+(C_{\ell^+,K_S^0}^- - C_{\ell^+,K_S^0}^+)$

VALUE	DOCUMENT ID	TECN	COMMENT
$0.14 \pm 0.15 \pm 0.07$	LEES	12W BABR	$e^+e^- \rightarrow \Upsilon(4S)$

 $\Delta C_{CPT}^-(C_{\ell^+,K_S^0}^+ - C_{\ell^+,K_S^0}^-)$

VALUE	DOCUMENT ID	TECN	COMMENT
$0.03 \pm 0.12 \pm 0.08$	LEES	12W BABR	$e^+e^- \rightarrow \Upsilon(4S)$

 Δa_{\parallel} CPT parameter in B^0 mixing

VALUE (10^{-15} GeV)	DOCUMENT ID	TECN	COMMENT
$-0.10 \pm 0.82 \pm 0.54$	¹ AAIJ	16E LHCb	pp at 7, 8 TeV

¹ Uses $B^0 \rightarrow J/\psi K_S^0$ decays.

 Δa_{\perp} CPT parameter in B^0 mixing

VALUE (10^{-13} GeV)	DOCUMENT ID	TECN	COMMENT
$-0.20 \pm 0.22 \pm 0.04$	¹ AAIJ	16E LHCb	pp at 7, 8 TeV

¹ Uses $B^0 \rightarrow J/\psi K_S^0$ decays.

 Δa_{χ} CPT parameter in B^0 mixing

VALUE (10^{-15} GeV)	DOCUMENT ID	TECN	COMMENT
$+1.97 \pm 1.30 \pm 0.29$	¹ AAIJ	16E LHCb	pp at 7, 8 TeV

¹ Uses $B^0 \rightarrow J/\psi K_S^0$ decays.

 Δa_{γ} CPT parameter in B^0 mixing

VALUE (10^{-15} GeV)	DOCUMENT ID	TECN	COMMENT
$+0.44 \pm 1.26 \pm 0.29$	¹ AAIJ	16E LHCb	pp at 7, 8 TeV

¹ Uses $B^0 \rightarrow J/\psi K_S^0$ decays.

 $B^0 \rightarrow D^{*-} \ell^+ \nu_{\ell}$ FORM FACTORS

R_1 (form factor ratio $\sim V/A_1$)

VALUE	DOCUMENT ID	TECN	COMMENT
1.239 ± 0.029 OUR AVERAGE			

$1.229 \pm 0.028 \pm 0.009$	¹ WAHEED	19 BELL	$e^+e^- \rightarrow \Upsilon(4S)$
$1.56 \pm 0.07 \pm 0.15$	AUBERT	09A BABR	$e^+e^- \rightarrow \Upsilon(4S)$
$1.18 \pm 0.30 \pm 0.12$	DUBOSCQ	96 CLE2	$e^+e^- \rightarrow \Upsilon(4S)$

• • • We do not use the following data for averages, fits, limits, etc. • • •

$1.401 \pm 0.034 \pm 0.018$	¹ DUNGEL	10 BELL	Repl. by WAHEED 19
$1.429 \pm 0.061 \pm 0.044$	AUBERT	08R BABR	Repl. by AUBERT 09A
$1.396 \pm 0.060 \pm 0.044$	AUBERT,B	06Z BABR	Repl. by AUBERT 08R

¹ Uses fully reconstructed $D^{*-} \ell^+ \nu$ events ($\ell = e$ or μ).

R_2 (form factor ratio $\sim A_2/A_1$)

VALUE	DOCUMENT ID	TECN	COMMENT
0.84 ± 0.04 OUR AVERAGE			Error includes scale factor of 1.8.

$0.852 \pm 0.021 \pm 0.006$	¹ WAHEED	19 BELL	$e^+e^- \rightarrow \Upsilon(4S)$
$0.66 \pm 0.05 \pm 0.09$	AUBERT	09A BABR	$e^+e^- \rightarrow \Upsilon(4S)$
$0.71 \pm 0.22 \pm 0.07$	DUBOSCQ	96 CLE2	$e^+e^- \rightarrow \Upsilon(4S)$

• • • We do not use the following data for averages, fits, limits, etc. • • •

$0.864 \pm 0.024 \pm 0.008$	¹ DUNGEL	10 BELL	Repl. by WAHEED 19
$0.827 \pm 0.038 \pm 0.022$	AUBERT	08R BABR	Repl. by AUBERT 09A
$0.885 \pm 0.040 \pm 0.026$	AUBERT,B	06Z BABR	Repl. by AUBERT 08R

¹ Uses fully reconstructed $D^{*-} \ell^+ \nu$ events ($\ell = e$ or μ).

$\rho_{A_1}^2$ (form factor slope)

VALUE	DOCUMENT ID	TECN	COMMENT
1.12 ± 0.04 OUR AVERAGE			Error includes scale factor of 1.5.

$1.106 \pm 0.031 \pm 0.007$	¹ WAHEED	19 BELL	$e^+e^- \rightarrow \Upsilon(4S)$
$1.22 \pm 0.02 \pm 0.07$	AUBERT	09A BABR	$e^+e^- \rightarrow \Upsilon(4S)$
$0.91 \pm 0.15 \pm 0.06$	DUBOSCQ	96 CLE2	$e^+e^- \rightarrow \Upsilon(4S)$

• • • We do not use the following data for averages, fits, limits, etc. • • •

$1.214 \pm 0.034 \pm 0.009$	¹ DUNGEL	10 BELL	Repl. by WAHEED 19
$1.191 \pm 0.048 \pm 0.028$	AUBERT	08R BABR	Repl. by AUBERT 09A
$1.145 \pm 0.059 \pm 0.046$	AUBERT,B	06Z BABR	Repl. by AUBERT 08R

¹ Uses fully reconstructed $D^{*-} \ell^+ \nu$ events ($\ell = e$ or μ).

PARTIAL BRANCHING FRACTIONS IN $B^0 \rightarrow K^{(*)0} \ell^+ \ell^-$ $B(B^0 \rightarrow K^{*0} e^+ e^-)$ ($0.0009 < q^2 < 1.0$ GeV²/c⁴)

VALUE (units 10^{-7})	DOCUMENT ID	TECN	COMMENT
$3.1 \pm 0.9 \pm 0.2$ $-0.8 - 0.3 \pm 0.2$	¹ AAIJ	13U LHCb	pp at 7 TeV

¹ The last uncertainty is due to uncertainties of $B(B^0 \rightarrow J/\psi K^{*0})$ and $B(J/\psi \rightarrow e^+ e^-)$ branching fraction measurements.

 $B(B^0 \rightarrow K^{*0} \ell^+ \ell^-)$ ($0.1 < q^2 < 2.0$ GeV²/c⁴)

VALUE (units 10^{-7})	DOCUMENT ID	TECN	COMMENT
1.24 ± 0.23 -0.27 OUR AVERAGE			Error includes scale factor of 1.6.

$1.14 \pm 0.11 \pm 0.11$ -0.15	AAIJ	13Y LHCb	pp at 7 TeV, $K^{*0} \mu^+ \mu^-$
$1.80 \pm 0.36 \pm 0.11$	AALTONEN	11A1 CDF	$p\bar{p}$ at 1.96 TeV

• • • We do not use the following data for averages, fits, limits, etc. • • •

0.48 ± 0.14 -0.12 ± 0.04	¹ CHATRCHYAN13BL	CMS	pp at 7 TeV
$1.16 \pm 0.23 \pm 0.11$	AAIJ	12U LHCb	Repl. by AAIJ 13Y

¹ CHATRCHYAN 13BL uses, for this bin, $1.0 < q^2 < 2.0$ GeV²/c⁴.

B(B⁰ → K*⁰ ℓ⁺ ℓ⁻) (2.0 < q² < 4.3 GeV²/c⁴)

VALUE (units 10 ⁻⁷)	DOCUMENT ID	TECN	COMMENT
0.76 ± 0.07 OUR AVERAGE			
0.759 ± 0.115 ± 0.046	KHACHATRY...16D	CMS	pp at 8 TeV
0.69 ± 0.07 ± 0.09	AAIJ	13Y LHCb	pp at 7 TeV, K* ⁰ μ ⁺ μ ⁻
0.87 ± 0.16 ± 0.07	CHATRCHYAN13BL	CMS	pp at 7 TeV
0.84 ± 0.28 ± 0.06	AALTONEN	11AI CDF	p̄p̄ at 1.96 TeV
••• We do not use the following data for averages, fits, limits, etc. •••			
0.78 ± 0.21 ± 0.05	AAIJ	12U LHCb	Repl. by AAIJ 13Y

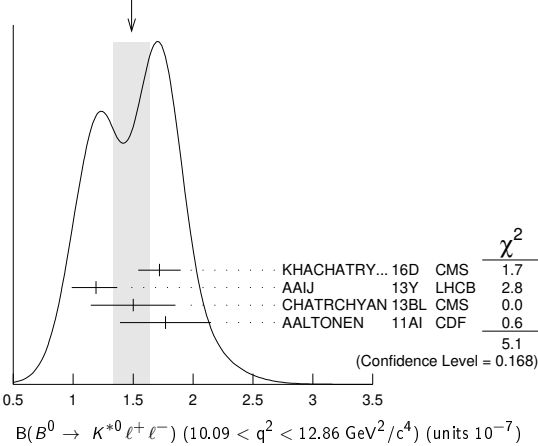
B(B⁰ → K*⁰ ℓ⁺ ℓ⁻) (4.3 < q² < 8.68 GeV²/c⁴)

VALUE (units 10 ⁻⁷)	DOCUMENT ID	TECN	COMMENT
1.87 ± 0.21 OUR AVERAGE			
2.15 ± 0.18 ± 0.22	AAIJ	13Y LHCb	pp at 7 TeV, K* ⁰ μ ⁺ μ ⁻
1.62 ± 0.31 ± 0.18	CHATRCHYAN13BL	CMS	pp at 7 TeV
1.73 ± 0.43 ± 0.15	AALTONEN	11AI CDF	p̄p̄ at 1.96 TeV
••• We do not use the following data for averages, fits, limits, etc. •••			
3.02 ± 0.35 ± 0.22	AAIJ	12U LHCb	Repl. by AAIJ 13Y

B(B⁰ → K*⁰ ℓ⁺ ℓ⁻) (10.09 < q² < 12.86 GeV²/c⁴)

VALUE (units 10 ⁻⁷)	DOCUMENT ID	TECN	COMMENT
1.49 ± 0.15 OUR AVERAGE	Error includes scale factor of 1.3. See the ideogram below.		
1.72 ± 0.11 ± 0.14	KHACHATRY...16D	CMS	pp at 8 TeV
1.19 ± 0.11 ± 0.14	AAIJ	13Y LHCb	pp at 7 TeV, K* ⁰ μ ⁺ μ ⁻
1.50 ± 0.25 ± 0.25	CHATRCHYAN13BL	CMS	pp at 7 TeV
1.77 ± 0.36 ± 0.12	AALTONEN	11AI CDF	p̄p̄ at 1.96 TeV
••• We do not use the following data for averages, fits, limits, etc. •••			
1.52 ± 0.25 ± 0.19	AAIJ	12U LHCb	Repl. by AAIJ 13Y

WEIGHTED AVERAGE
1.49 ± 0.15 (Error scaled by 1.3)



B(B⁰ → K*⁰ ℓ⁺ ℓ⁻) (14.18 < q² < 16.0 GeV²/c⁴)

VALUE (units 10 ⁻⁷)	DOCUMENT ID	TECN	COMMENT
1.09 ± 0.10 OUR AVERAGE	Error includes scale factor of 1.1.		
1.22 ± 0.11 ± 0.09	KHACHATRY...16D	CMS	pp at 8 TeV
1.02 ± 0.11 ± 0.11	AAIJ	13Y LHCb	pp at 7 TeV, K* ⁰ μ ⁺ μ ⁻
0.84 ± 0.16 ± 0.09	CHATRCHYAN13BL	CMS	pp at 7 TeV
1.34 ± 0.26 ± 0.08	AALTONEN	11AI CDF	p̄p̄ at 1.96 TeV
••• We do not use the following data for averages, fits, limits, etc. •••			
1.15 ± 0.20 ± 0.09	AAIJ	12U LHCb	Repl. by AAIJ 13Y

B(B⁰ → K*⁰ ℓ⁺ ℓ⁻) (16.0 < q² < 19.0 GeV²/c⁴)

VALUE (units 10 ⁻⁷)	DOCUMENT ID	TECN	COMMENT
1.27 ± 0.09 OUR AVERAGE			
1.26 ± 0.09 ± 0.09	KHACHATRY...16D	CMS	pp at 8 TeV
1.23 ± 0.12 ± 0.18	AAIJ	13Y LHCb	pp at 7 TeV, K* ⁰ μ ⁺ μ ⁻
1.56 ± 0.18 ± 0.15	CHATRCHYAN13BL	CMS	pp at 7 TeV
0.97 ± 0.26 ± 0.07	AALTONEN	11AI CDF	p̄p̄ at 1.96 TeV
••• We do not use the following data for averages, fits, limits, etc. •••			
1.50 ± 0.24 ± 0.15	AAIJ	12U LHCb	Repl. by AAIJ 13Y

B(B⁰ → K*(892)⁰ ℓ⁺ ℓ⁻) (15.0 < q² < 19.0 GeV²/c⁴)

VALUE (units 10 ⁻⁷)	DOCUMENT ID	TECN	COMMENT
1.80 ± 0.13 OUR AVERAGE			
2.2 ± 0.5 ± 0.2	1 WEHLE	21 BELL	e ⁺ e ⁻ → γ(4S)
2.0 ± 0.6 ± 0.2	2 WEHLE	21 BELL	e ⁺ e ⁻ → γ(4S)
1.744 ± 0.072 ± 0.123	1 AAIJ	17Q LHCb	pp at 7, 8 TeV

••• We do not use the following data for averages, fits, limits, etc. •••

1.95 ± 0.08 ± 0.13	1 AAIJ	16A LHCb	Repl. by AAIJ 17Q
1 Measured with μ ⁺ μ ⁻ as lepton pair.			
2 Measured with e ⁺ e ⁻ as lepton pair.			

B(B⁰ → K*⁰ ℓ⁺ ℓ⁻) (1.0 < q² < 6.0 GeV²/c⁴)

VALUE (units 10 ⁻⁷)	DOCUMENT ID	TECN	COMMENT
1.74 ± 0.11 OUR AVERAGE			
1.9 ± 0.6 ± 0.3	1,2 WEHLE	21 BELL	e ⁺ e ⁻ → γ(4S)
1.8 ± 0.6 ± 0.2	1,3 WEHLE	21 BELL	e ⁺ e ⁻ → γ(4S)
1.68 ± 0.083 ± 0.12	1,2 AAIJ	17Q LHCb	pp at 7, 8 TeV
1.90 ± 0.20	2 KHACHATRY...16D	CMS	pp at 7, 8 TeV
1.42 ± 0.41 ± 0.12	2 AALTONEN	11AI CDF	p̄p̄ at 1.96 TeV
••• We do not use the following data for averages, fits, limits, etc. •••			
1.92 ± 0.10 ± 0.14	AAIJ	16A LHCb	Repl. by AAIJ 17Q
1.70 ± 0.15 ± 0.20	AAIJ	13Y LHCb	Repl. by AAIJ 16A
2.20 ± 0.30 ± 0.25	CHATRCHYAN13BL	CMS	Repl. by KHACHATRYAN 16D
2.10 ± 0.30 ± 0.15	AAIJ	12U LHCb	Repl. by AAIJ 13Y

1 Result is determined for the range 1.1 < q² < 6.0 GeV²/c⁴.

2 Measured with μ⁺ μ⁻ as lepton pair.

3 Measured with e⁺ e⁻ as lepton pair.

B(B⁰ → K*⁰ ℓ⁺ ℓ⁻) (0.0 < q² < 4.3 GeV²/c⁴)

VALUE (units 10 ⁻⁷)	DOCUMENT ID	TECN	COMMENT
2.60 ± 0.45 ± 0.17	AALTONEN	11AI CDF	p̄p̄ at 1.96 TeV

B(B⁰ → K*⁰ μ⁺ μ⁻)/B(B⁰ → K*⁰ e⁺ e⁻) (0.045 < q² < 1.1 GeV²/c⁴)

VALUE	DOCUMENT ID	TECN	COMMENT
0.91 ± 0.09 OUR AVERAGE			
0.927 ± 0.093 ± 0.036	1 AAIJ	23AB LHCb	pp at 7, 8, 13 TeV
0.46 ± 0.55 ± 0.13	WEHLE	21 BELL	e ⁺ e ⁻ → γ(4S)
••• We do not use the following data for averages, fits, limits, etc. •••			
0.66 ± 0.11 ± 0.03	2 AAIJ	17W LHCb	pp at 7, 8 TeV
1 Measured for the region 0.1 < q ² < 1.1 GeV ² /c ⁴ .			
2 Superseded by AAIJ 23AB.			

B(B⁰ → K*⁰ μ⁺ μ⁻)/B(B⁰ → K*⁰ e⁺ e⁻) (1.1 < q² < 6.0 GeV²/c⁴)

VALUE	DOCUMENT ID	TECN	COMMENT
1.03 ± 0.07 OUR AVERAGE			
1.027 ± 0.072 ± 0.027	AAIJ	23AB LHCb	pp at 7, 8, 13 TeV
1.06 ± 0.63 ± 0.13	WEHLE	21 BELL	e ⁺ e ⁻ → γ(4S)
••• We do not use the following data for averages, fits, limits, etc. •••			
0.69 ± 0.11 ± 0.05	1 AAIJ	17W LHCb	pp at 7, 8 TeV
1 Superseded by AAIJ 23AB.			

B(B⁰ → K*⁰ μ⁺ μ⁻)/B(B⁰ → K*⁰ e⁺ e⁻) (15.0 < q² < 19.0 GeV²/c⁴)

VALUE	DOCUMENT ID	TECN	COMMENT
1.12 ± 0.61 ± 0.10	WEHLE	21 BELL	e ⁺ e ⁻ → γ(4S)

B(B⁰ → K⁰ ℓ⁺ ℓ⁻) (q² < 2.0 GeV²/c⁴)

VALUE (units 10 ⁻⁷)	DOCUMENT ID	TECN	COMMENT
0.24 ± 0.22 ± 0.26 OUR AVERAGE			
0.21 ± 0.27 ± 0.23	AAIJ	12AH LHCb	pp at 7 TeV
0.31 ± 0.37 ± 0.02	AALTONEN	11AI CDF	p̄p̄ at 1.96 TeV

B(B⁰ → K⁰ ℓ⁺ ℓ⁻) (2.0 < q² < 4.3 GeV²/c⁴)

VALUE (units 10 ⁻⁷)	DOCUMENT ID	TECN	COMMENT
0.24 ± 0.35 ± 0.30 OUR AVERAGE	Error includes scale factor of 1.6.		
0.07 ± 0.25 ± 0.21	AAIJ	12AH LHCb	pp at 7 TeV
0.93 ± 0.49 ± 0.07	AALTONEN	11AI CDF	p̄p̄ at 1.96 TeV

B(B⁰ → K⁰ ℓ⁺ ℓ⁻) (4.3 < q² < 8.68 GeV²/c⁴)

VALUE (units 10 ⁻⁷)	DOCUMENT ID	TECN	COMMENT
1.08 ± 0.27 OUR AVERAGE			
1.23 ± 0.31	AAIJ	12AH LHCb	pp at 7 TeV
0.66 ± 0.51 ± 0.05	AALTONEN	11AI CDF	p̄p̄ at 1.96 TeV

B(B⁰ → K⁰ ℓ⁺ ℓ⁻) (10.09 < q² < 12.86 GeV²/c⁴)

VALUE (units 10 ⁻⁷)	DOCUMENT ID	TECN	COMMENT
0.27 ± 0.27 OUR AVERAGE	Error includes scale factor of 1.8.		
0.50 ± 0.22 ± 0.19	AAIJ	12AH LHCb	pp at 7 TeV
-0.03 ± 0.22 ± 0.01	AALTONEN	11AI CDF	p̄p̄ at 1.96 TeV

Meson Particle Listings

 B^0 $B(B^0 \rightarrow K^0 \ell^+ \ell^-)$ ($14.18 < q^2 < 16.0 \text{ GeV}^2/c^4$)

VALUE (units 10^{-7})	DOCUMENT ID	TECN	COMMENT
$0.29^{+0.21}_{-0.15}$ OUR AVERAGE			Error includes scale factor of 1.8.
$0.20^{+0.13}_{-0.09}$	AAIJ	12AH LHCb	pp at 7 TeV
$0.73 \pm 0.26 \pm 0.06$	AALTONEN	11AI CDF	$p\bar{p}$ at 1.96 TeV

 $B(B^0 \rightarrow K^0 \ell^+ \ell^-)$ ($q^2 > 16.0 \text{ GeV}^2/c^4$)

VALUE (units 10^{-7})	DOCUMENT ID	TECN	COMMENT
$0.31^{+0.16}_{-0.12}$ OUR AVERAGE			
$0.35^{+0.21}_{-0.14}$	AAIJ	12AH LHCb	pp at 7 TeV
$0.21 \pm 0.18 \pm 0.16$	AALTONEN	11AI CDF	$p\bar{p}$ at 1.96 TeV

 $B(B^0 \rightarrow K^0 \ell^+ \ell^-)$ ($1.0 < q^2 < 6.0 \text{ GeV}^2/c^4$)

VALUE (units 10^{-7})	DOCUMENT ID	TECN	COMMENT
$0.91^{+0.15}_{-0.13}$ OUR AVERAGE			
$0.62^{+0.44}_{-0.32} \pm 0.02$	1 CHOUDHURY 21	BELL	$e^+e^- \rightarrow \Upsilon(4S)$
$1.12^{+0.50}_{-0.40} \pm 0.04$	2 CHOUDHURY 21	BELL	$e^+e^- \rightarrow \Upsilon(4S)$
$0.916^{+0.172}_{-0.157} \pm 0.004$	3 AAIJ	14M LHCb	pp at 7, 8 TeV
$0.98 \pm 0.61 \pm 0.08$	AALTONEN	11AI CDF	$p\bar{p}$ at 1.96 TeV

• • • We do not use the following data for averages, fits, limits, etc. • • •

$0.65^{+0.45}_{-0.35}$	AAIJ	12AH LHCb	Repl. by AAIJ 14M
------------------------	------	-----------	-------------------

1 Measured for $B^0 \rightarrow K_S^0 \mu^+ \mu^-$ decays. Measurements in other q^2 bins are also reported.
 2 Measured for $B^0 \rightarrow K_S^0 e^+ e^-$ decays. Measurements in other q^2 bins are also reported.
 3 Uses $B(B^0 \rightarrow J/\psi(1S) K^0) = (0.928 \pm 0.013 \pm 0.037) \times 10^{-3}$ for normalisation and $\mu^+ \mu^-$ as a lepton pair. Measured in $1.1 < q^2 < 6.0 \text{ GeV}^2/c^4$.

 $B(B^0 \rightarrow K^0 \mu^+ \mu^-) / B(B^0 \rightarrow K^0 e^+ e^-)$ ($1.0 < q^2 < 6.0 \text{ GeV}^2/c^4$)

VALUE	DOCUMENT ID	TECN	COMMENT
$0.64^{+0.18}_{-0.13}$ OUR AVERAGE			
$0.66^{+0.20+0.02}_{-0.14-0.04}$	1 AAIJ	22J LHCb	pp at 7, 8, 13 TeV
$0.55^{+0.46}_{-0.34} \pm 0.01$	2 CHOUDHURY 21	BELL	$e^+e^- \rightarrow \Upsilon(4S)$

1 Measured in the range $1.1 < q^2 < 6.0 \text{ GeV}^2/c^4$.
 2 Measured from the ratio of $K_S^0 \mu^+ \mu^-$ and $K_S^0 e^+ e^-$. Measurements in other q^2 bins are also reported.

 $B(B^0 \rightarrow K^0 \ell^+ \ell^-)$ ($0.0 < q^2 < 4.3 \text{ GeV}^2/c^4$)

VALUE (units 10^{-7})	DOCUMENT ID	TECN	COMMENT
$1.27 \pm 0.62 \pm 0.10$	AALTONEN	11AI CDF	$p\bar{p}$ at 1.96 TeV

 $B(B^0 \rightarrow K^0 \ell^+ \ell^-)$ ($15.0 < q^2 < 22.0 \text{ GeV}^2/c^4$)

VALUE (units 10^{-7})	DOCUMENT ID	TECN	COMMENT
$0.67^{+0.11}_{-0.11} \pm 0.04$	1 AAIJ	14M LHCb	pp at 7, 8 TeV

1 Uses $B(B^0 \rightarrow J/\psi(1S) K^0) = (0.928 \pm 0.013 \pm 0.037) \times 10^{-3}$ for normalisation and $\mu^+ \mu^-$ as a lepton pair.

 $B(B^0 \rightarrow K^0 e^+ e^-)$ ($1.1 < q^2 < 6.0 \text{ GeV}^2/c^4$)

VALUE (units 10^{-8})	DOCUMENT ID	TECN	COMMENT
$13 \pm 3 \pm 1$	1 AAIJ	22J LHCb	pp at 7, 8, 13 TeV

1 The reported value is converted from the measured $dB/dq^2 = (2.6 \pm 0.6 \pm 0.1) \times 10^{-8} (\text{GeV}^2/c^4)^{-1}$ by multiplying by the $\Delta q^2 = 4.9 \text{ GeV}^2/c^4$ range.

 $B(B^0 \rightarrow K_{0,2}^* (1430)^0 \mu^+ \mu^-)$ ($1.10 < q^2 < 6.00 \text{ GeV}^2/c^4$)

VALUE (units 10^{-8})	DOCUMENT ID	TECN	COMMENT
$4.02 \pm 0.44 \pm 0.31$	1,2 AAIJ	16AP LHCb	pp at 7, 8 TeV

1 Measured the differential branching fraction and angular moments of the decay $B^0 \rightarrow K^+ \pi^- \mu^+ \mu^-$ in the $K^+ \pi^-$ invariant mass range $1330 < m(K^+ \pi^-) < 1530 \text{ MeV}/c^2$.
 2 The reported value is converted from the measured $dB/dq^2 = (0.82 \pm 0.09 \pm 0.063) \times 10^{-8} (\text{GeV}^2/c^4)^{-1}$ by multiplying by the $\Delta q^2 = 4.9 \text{ GeV}^2/c^4$ range.

 $F_H(B^0 \rightarrow K^0 \mu^+ \mu^-)$ ($1.1 < q^2 < 6.0 \text{ GeV}^2/c^4$)

F_H is a fractional contribution of (pseudo) scalar and tensor amplitudes to the decay width in the massless muon approximation.

VALUE	DOCUMENT ID	TECN	COMMENT
$0.78 \pm 0.46 \pm 0.09$	1 AAIJ	14O LHCb	pp at 7, 8 TeV

1 AAIJ 14O reports 68% C.L. interval, which we encode as midpoint with uncertainty as half of the width of interval.

 $F_H(B^0 \rightarrow K^0 \mu^+ \mu^-)$ ($15.0 < q^2 < 22.0 \text{ GeV}^2/c^4$)

VALUE	DOCUMENT ID	TECN	COMMENT
$0.34 \pm 0.25 \pm 0.03$	1 AAIJ	14O LHCb	pp at 7, 8 TeV

1 AAIJ 14O reports 68% C.L. interval, which we encode as midpoint with uncertainty as half of the width of interval.

PRODUCTION ASYMMETRIES

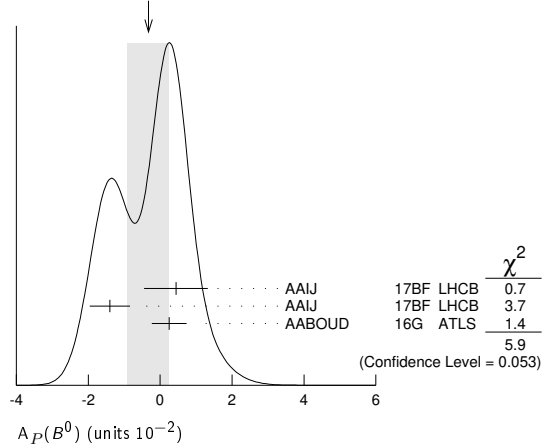
 $A_P(B^0)$

$$A_P(B^0) = [\sigma(\bar{B}^0) - \sigma(B^0)] / [\sigma(\bar{B}^0) + \sigma(B^0)]$$

VALUE (units 10^{-2})	DOCUMENT ID	TECN	COMMENT
-0.3 ± 0.6 OUR AVERAGE			Error includes scale factor of 1.7. See the ideogram below.
$0.44 \pm 0.88 \pm 0.11$	1 AAIJ	17BF LHCb	pp at 7 TeV
$-1.40 \pm 0.55 \pm 0.10$	1 AAIJ	17BF LHCb	pp at 8 TeV
$0.25 \pm 0.48 \pm 0.05$	2 AABOUD	16G ATLS	pp at 7, 8 TeV
$-0.35 \pm 0.76 \pm 0.28$	3 AAIJ	14BP LHCb	Repl. by AAIJ 17BF, pp at 7 TeV

• • • We do not use the following data for averages, fits, limits, etc. • • •

1 AAIJ 17BF uses $B^0 \rightarrow J/\psi K^*0$ decays with B^0 transverse momenta p_T and rapidities y in the region of $0 < p_T < 30 \text{ GeV}/c$ and $2.1 < y < 4.5$.
 2 Based on time-dependent analysis of $B^0 \rightarrow J/\psi K^*0$ decay in kinematic range $p_T > 10 \text{ GeV}/c$ and $|\eta| < 2.5$.
 3 Based on time-dependent analysis of $B^0 \rightarrow J/\psi K^*0$ and $B^0 \rightarrow D^- \pi^+$ in kinematic range $4 < p_T < 30 \text{ GeV}/c$ and $2.5 < \eta < 4.5$.

WEIGHTED AVERAGE
 -0.3 ± 0.6 (Error scaled by 1.7) $A(B^0 + \bar{B}^0)$ in $K_S^0 K^\mp \pi^\pm$

$$A(B^0 + \bar{B}^0) = [n(K_S^0 K^- \pi^+) - n(K_S^0 K^+ \pi^-)] / [n(K_S^0 K^- \pi^+) + n(K_S^0 K^+ \pi^-)]$$

VALUE (units 10^{-2})	DOCUMENT ID	TECN	COMMENT
$-8.5 \pm 8.9 \pm 0.2$	LAI	19 BELL	$e^+e^- \rightarrow \Upsilon(4S)$

FORWARD-BACKWARD ASYMMETRIES

 A_{FB} in $B^0 \rightarrow D^{*-} e^+ \nu_e$

VALUE	DOCUMENT ID	TECN	COMMENT
0.225 ± 0.018 OUR AVERAGE			Error includes scale factor of 1.7.
$0.228 \pm 0.012 \pm 0.018$	ADACHI	23J BELL	$e^+e^- \rightarrow \Upsilon(4S)$
$0.218 \pm 0.030 \pm 0.009$	PRIM	23 BELL	$e^+e^- \rightarrow \Upsilon(4S)$

 A_{FB} in $B^0 \rightarrow D^{*-} \mu^+ \nu_\mu$

VALUE	DOCUMENT ID	TECN	COMMENT
0.235 ± 0.033 OUR AVERAGE			Error includes scale factor of 1.7.
$0.211 \pm 0.011 \pm 0.021$	ADACHI	23J BELL	$e^+e^- \rightarrow \Upsilon(4S)$
$0.281 \pm 0.032 \pm 0.007$	PRIM	23 BELL	$e^+e^- \rightarrow \Upsilon(4S)$

 $\Delta(A_{FB}) = (A_{FB}^{\mu} - A_{FB}^e)$ in $B^0 \rightarrow D^{*-} \ell^+ \nu_\ell$

VALUE	DOCUMENT ID	TECN	COMMENT
-0.018 ± 0.020 OUR AVERAGE			
$-0.024 \pm 0.043 \pm 0.016$	1 ADACHI	23H BELL	$e^+e^- \rightarrow \Upsilon(4S)$
$-0.017 \pm 0.016 \pm 0.016$	ADACHI	23J BELL	$e^+e^- \rightarrow \Upsilon(4S)$
$0.063 \pm 0.044 \pm 0.012$	PRIM	23 BELL	$e^+e^- \rightarrow \Upsilon(4S)$

• • • We do not use the following data for averages, fits, limits, etc. • • •
 1 ADACHI 23H measurement is based on the angular asymmetries of $B^0 \rightarrow D^{*-} \ell^+ \nu_\ell$ decays using explicit reconstruction of the B tag. Other asymmetries from $\Delta(S_3)$, $\Delta(S_5)$, $\Delta(S_7)$, and $\Delta(S_9)$ are also reported.

 B^0 REFERENCES

AAIJ	24	PRL 132 021801	R. Aaij et al.	(LHCb Collab.)
ADACHI	24	PR D109 012001	L. Adachi et al.	(BELLE II Collab.)
AAIJ	23AB	PRL 131 051803	R. Aaij et al.	(LHCb Collab.)
Also		PR D108 032002	R. Aaij et al.	(LHCb Collab.)
AAIJ	23AD	PRL 131 091901	R. Aaij et al.	(LHCb Collab.)
AAIJ	23AG	PR D108 032007	R. Aaij et al.	(LHCb Collab.)
AAIJ	23AR	PRL 131 111802	R. Aaij et al.	(LHCb Collab.)
AAIJ	23AY	JHEP 2310 106	R. Aaij et al.	(LHCb Collab.)
AAIJ	23AZ	JHEP 2310 123	R. Aaij et al.	(LHCb Collab.)
AAIJ	23B	PR D108 012017	R. Aaij et al.	(LHCb Collab.)
AAIJ	23F	JHEP 2306 143	R. Aaij et al.	(LHCb Collab.)
AAIJ	23G	JHEP 2306 073	R. Aaij et al.	(LHCb Collab.)
AAIJ	23T	PR D108 012007	R. Aaij et al.	(LHCb Collab.)
AAIJ	23W	PR D108 012018	R. Aaij et al.	(LHCb Collab.)

See key on page 1171

Meson Particle Listings

B⁰

Table listing meson particles with columns for particle name, mass, production method, and associated experiment/collaboration. Includes entries for various B meson states and decays.

See key on page 1171

Meson Particle Listings

B⁰

Table listing meson particles, organized by meson type (B, D, K, eta, phi, omega, eta', eta''). Each entry includes a code (e.g., AUBERT.B), a particle code (e.g., 06J), a production process (e.g., PR D73 092001), and the discoverer's name (e.g., B. Aubert et al.). Entries are arranged in approximately 10 columns.

Γ ₉	$\overline{D}^* \ell^+ \nu_\ell$	[d]	(4.95 ± 0.11) %		Γ ₇₂	$K_2^*(1430)\gamma$	(1.7 $\begin{smallmatrix} +0.6 \\ -0.5 \end{smallmatrix}$) × 10 ⁻⁵	
Γ ₁₀	$\overline{D}^* e^+ \nu_e$				Γ ₇₃	$K_2(1770)\gamma$	< 1.2 × 10 ⁻³	CL=90%
Γ ₁₁	$\overline{D}^* \mu^+ \nu_\mu$				Γ ₇₄	$K_3^*(1780)\gamma$	< 3.7 × 10 ⁻⁵	CL=90%
Γ ₁₂	$\overline{D}^{**} \ell^+ \nu_\ell$	[b,e]	(2.7 ± 0.7) %		Γ ₇₅	$K_4^*(2045)\gamma$	< 1.0 × 10 ⁻³	CL=90%
Γ ₁₃	$\overline{D}_1(2420)\ell^+ \nu_\ell$ anything		(3.8 ± 1.3) × 10 ⁻³	S=2.4	Γ ₇₆	$K\eta'(958)$	(8.3 ± 1.1) × 10 ⁻⁵	
Γ ₁₄	$\overline{D}\pi\ell^+ \nu_\ell$ anything + $\overline{D}^* \pi\ell^+ \nu_\ell$ anything		(2.6 ± 0.5) %	S=1.5	Γ ₇₇	$K^*(892)\eta'(958)$	(4.1 ± 1.1) × 10 ⁻⁶	
Γ ₁₅	$\overline{D}\pi\ell^+ \nu_\ell$ anything		(1.5 ± 0.6) %		Γ ₇₈	$K\eta$	< 5.2 × 10 ⁻⁶	CL=90%
Γ ₁₆	$\overline{D}^* \pi\ell^+ \nu_\ell$ anything		(1.9 ± 0.4) %		Γ ₇₉	$K^*(892)\eta$	(1.8 ± 0.5) × 10 ⁻⁵	
Γ ₁₇	$\overline{D}_2^*(2460)\ell^+ \nu_\ell$ anything		(4.4 ± 1.6) × 10 ⁻³		Γ ₈₀	$K\phi\phi$	(2.3 ± 0.9) × 10 ⁻⁶	
Γ ₁₈	$\overline{D}^* \pi^+ \ell^+ \nu_\ell$ anything		(1.00 ± 0.34) %		Γ ₈₁	$\overline{b} \rightarrow \overline{s}\gamma$	(3.49 ± 0.19) × 10 ⁻⁴	
Γ ₁₉	$\overline{D}\pi^+ \pi^- \ell^+ \nu_\ell$		(1.62 ± 0.32) × 10 ⁻³		Γ ₈₂	$\overline{b} \rightarrow \overline{d}\gamma$	(9.2 ± 3.0) × 10 ⁻⁶	
Γ ₂₀	$\overline{D}^* \pi^+ \pi^- \ell^+ \nu_\ell$		(9.4 ± 3.2) × 10 ⁻⁴		Γ ₈₃	$\overline{b} \rightarrow \overline{s}$ gluon	< 6.8 %	CL=90%
Γ ₂₁	$D_s^- \ell^+ \nu_\ell$ anything	[b]	< 7 × 10 ⁻³	CL=90%	Γ ₈₄	η anything	(2.6 $\begin{smallmatrix} +0.5 \\ -0.8 \end{smallmatrix}$) × 10 ⁻⁴	
Γ ₂₂	$D_s^- \ell^+ \nu_\ell K^+$ anything	[b]	< 5 × 10 ⁻³	CL=90%	Γ ₈₅	η' anything	(4.2 ± 0.9) × 10 ⁻⁴	
Γ ₂₃	$D_s^- \ell^+ \nu_\ell K^0$ anything	[b]	< 7 × 10 ⁻³	CL=90%	Γ ₈₆	K^+ gluon (charmless)	< 1.87 × 10 ⁻⁴	CL=90%
Γ ₂₄	$X_c \ell^+ \nu_\ell$		(10.63 ± 0.15) %		Γ ₈₇	K^0 gluon (charmless)	(1.9 ± 0.7) × 10 ⁻⁴	
Γ ₂₅	$X_u \ell^+ \nu_\ell$		(1.88 ± 0.27) × 10 ⁻³		Light unflavored meson modes			
Γ ₂₆	$X_u e^+ \nu_e$		(1.57 ± 0.19) × 10 ⁻³		Γ ₈₈	$\rho\gamma$	(1.39 ± 0.25) × 10 ⁻⁶	S=1.2
Γ ₂₇	$X_u \mu^+ \nu_\mu$		(1.62 ± 0.21) × 10 ⁻³		Γ ₈₉	$\rho/\omega\gamma$	(1.30 ± 0.23) × 10 ⁻⁶	S=1.2
Γ ₂₈	$K^+ \ell^+ \nu_\ell$ anything	[b]	(6.3 ± 0.5) %		Γ ₉₀	π^\pm anything	[f] (358 ± 7) %	
Γ ₂₉	$K^- \ell^+ \nu_\ell$ anything	[b]	(10 ± 4) × 10 ⁻³		Γ ₉₁	π^0 anything	(235 ± 11) %	
Γ ₃₀	$K^0/\overline{K}^0 \ell^+ \nu_\ell$ anything	[b]	(4.6 ± 0.5) %		Γ ₉₂	η anything	(17.6 ± 1.6) %	
Γ ₃₁	$\overline{D}^* \tau^+ \nu_\tau$		(8.6 ± 0.8) × 10 ⁻³		Γ ₉₃	ρ^0 anything	(21 ± 5) %	
Γ ₃₂	$\overline{D}^* \tau^+ \nu_\tau$		(1.40 ± 0.07) %		Γ ₉₄	ω anything	< 81 %	CL=90%
D, D*, or D_s modes					Γ ₉₅	ϕ anything	(3.43 ± 0.12) %	
Γ ₃₃	D^\pm anything		(23.1 ± 1.2) %		Γ ₉₆	$\phi K^*(892)$	< 2.2 × 10 ⁻⁵	CL=90%
Γ ₃₄	D^0/\overline{D}^0 anything		(64.6 ± 2.1) %	S=1.5	Γ ₉₇	$\overline{b} \rightarrow \overline{d}$ gluon		
Γ ₃₅	$D^*(2010)^\pm$ anything		(22.5 ± 1.5) %		Γ ₉₈	π^+ gluon (charmless)	(3.7 ± 0.8) × 10 ⁻⁴	
Γ ₃₆	$\overline{D}^*(2007)^0$ anything		(26.0 ± 2.7) %		Baryon modes			
Γ ₃₇	D_s^\pm anything	[f]	(10.6 ± 0.6) %	S=1.7	Γ ₉₉	$\Lambda_c^+/\overline{\Lambda}_c^-$ anything	(3.6 ± 0.4) %	
Γ ₃₈	$D_s^{\pm*}$ anything		(6.3 ± 1.0) %		Γ ₁₀₀	Λ_c^+ anything	< 1.3 %	CL=90%
Γ ₃₉	$D_s^{\pm*}\overline{D}^*$		(3.4 ± 0.6) %		Γ ₁₀₁	$\overline{\Lambda}_c^-$ anything	< 7 %	CL=90%
Γ ₄₀	$\overline{D}D_{s0}(2317)$	seen			Γ ₁₀₂	$\overline{\Lambda}_c^- \ell^+$ anything	< 9 × 10 ⁻⁴	CL=90%
Γ ₄₁	$\overline{D}D_{sJ}(2457)$	seen			Γ ₁₀₃	$\overline{\Lambda}_c^- e^+$ anything	< 1.8 × 10 ⁻³	CL=90%
Γ ₄₂	$D^*(*)\overline{D}^*(*)K^0 + D^*(*)\overline{D}^*(*)K^\pm$ [f,g]		(7.1 $\begin{smallmatrix} +2.7 \\ -1.7 \end{smallmatrix}$) %		Γ ₁₀₄	$\overline{\Lambda}_c^- \mu^+$ anything	< 1.4 × 10 ⁻³	CL=90%
Γ ₄₃	$b \rightarrow c\overline{c}s$		(22 ± 4) %		Γ ₁₀₅	$\overline{\Lambda}_c^- p$ anything	(2.06 ± 0.33) %	
Γ ₄₄	$D_s^*(*)\overline{D}^*(*)$	[f,g]	(5.0 ± 0.4) %		Γ ₁₀₆	$\overline{\Lambda}_c^- p e^+ \nu_e$	< 8 × 10 ⁻⁴	CL=90%
Γ ₄₅	$D^* D^*(2010)^\pm$	[f]	< 5.9 × 10 ⁻³	CL=90%	Γ ₁₀₇	$\overline{\Sigma}_c^-$ anything	(3.4 ± 1.7) × 10 ⁻³	
Γ ₄₆	$D D^*(2010)^\pm + D^* D^\pm$	[f]	< 5.5 × 10 ⁻³	CL=90%	Γ ₁₀₈	$\overline{\Sigma}_c^-$ anything	< 8 × 10 ⁻³	CL=90%
Γ ₄₇	$D D^\pm$	[f]	< 3.1 × 10 ⁻³	CL=90%	Γ ₁₀₉	$\overline{\Sigma}_c^0$ anything	(3.7 ± 1.7) × 10 ⁻³	
Γ ₄₈	$D_s^*(*)\pm\overline{D}^*(*)X(n\pi^\pm)$	[f,g]	(9 $\begin{smallmatrix} +5 \\ -4 \end{smallmatrix}$) %		Γ ₁₁₀	$\overline{\Sigma}_c^0 N(N=p \text{ or } n)$	< 1.2 × 10 ⁻³	CL=90%
Γ ₄₉	$\overline{D}^*(2010)\gamma$		< 1.1 × 10 ⁻³	CL=90%	Γ ₁₁₁	Ξ_c^0 anything, $\Xi_c^0 \rightarrow \Xi^- \pi^+$	(1.93 ± 0.30) × 10 ⁻⁴	S=1.1
Γ ₅₀	$D_s^+ \pi^-, D_s^{*+} \pi^-, D_s^+ \rho^-,$ $D_s^{*+} \rho^-, D_s^+ \pi^0, D_s^{*+} \pi^0,$ $D_s^+ \eta, D_s^{*+} \eta, D_s^+ \rho^0,$ $D_s^{*+} \rho^0, D_s^+ \omega, D_s^{*+} \omega$	[f]	< 4 × 10 ⁻⁴	CL=90%	Γ ₁₁₂	$\Xi_c^+ \pi^+, \Xi_c^+ \rightarrow \Xi^- \pi^+ \pi^+$	(4.5 $\begin{smallmatrix} +1.3 \\ -1.2 \end{smallmatrix}$) × 10 ⁻⁴	
Γ ₅₁	$D_{s1}(2536)^+$ anything		< 9.5 × 10 ⁻³	CL=90%	Γ ₁₁₃	p/\overline{p} anything	[f] (8.0 ± 0.4) %	
Charmonium modes					Γ ₁₁₄	p/\overline{p} (direct) anything	[f] (5.5 ± 0.5) %	
Γ ₅₂	$J/\psi(1S)$ anything		(1.094 ± 0.032) %	S=1.1	Γ ₁₁₅	$\overline{p}e^+ \nu_e$ anything	< 5.9 × 10 ⁻⁴	CL=90%
Γ ₅₃	$J/\psi(1S)$ (direct) anything		(7.8 ± 0.4) × 10 ⁻³	S=1.1	Γ ₁₁₆	$\Lambda/\overline{\Lambda}$ anything	[f] (4.0 ± 0.5) %	
Γ ₅₄	$\psi(2S)$ anything		(3.07 ± 0.21) × 10 ⁻³		Γ ₁₁₇	Λ anything	seen	
Γ ₅₅	$\chi_{c1}(1P)$ anything		(3.55 ± 0.27) × 10 ⁻³	S=1.3	Γ ₁₁₈	$\overline{\Lambda}$ anything	seen	
Γ ₅₆	$\chi_{c1}(1P)$ (direct) anything		(3.08 ± 0.19) × 10 ⁻³		Γ ₁₁₉	Ξ^-/Ξ^+ anything	[f] (2.7 ± 0.6) × 10 ⁻³	
Γ ₅₇	$\chi_{c2}(1P)$ anything		(9.9 ± 1.7) × 10 ⁻⁴	S=1.6	Γ ₁₂₀	baryons anything	(6.8 ± 0.6) %	
Γ ₅₈	$\chi_{c2}(1P)$ (direct) anything		(7.5 ± 1.1) × 10 ⁻⁴		Γ ₁₂₁	$p\overline{p}$ anything	(2.47 ± 0.23) %	
Γ ₅₉	$\eta_c(1S)$ anything		< 9 × 10 ⁻³	CL=90%	Γ ₁₂₂	$\Lambda\overline{p}/\overline{\Lambda}p$ anything	[f] (2.5 ± 0.4) %	
Γ ₆₀	$K\chi_{c1}(3872)$		(2.5 ± 0.9) × 10 ⁻⁴		Γ ₁₂₃	$\Lambda\overline{\Lambda}$ anything	< 5 × 10 ⁻³	CL=90%
Γ ₆₁	$KX(3940), X \rightarrow D^{*0}D^0$		< 6.7 × 10 ⁻⁵	CL=90%	Lepton Family number (LF) violating modes or ΔB = 1 weak neutral current (B1) modes			
Γ ₆₂	$K\chi_{c0}(3915), \chi_{c0} \rightarrow \omega J/\psi$	[h]	(7.1 ± 3.4) × 10 ⁻⁵		Γ ₁₂₄	$s e^+ e^-$	$B1$ (6.7 ± 1.7) × 10 ⁻⁶	S=2.0
K or K* modes					Γ ₁₂₅	$s\mu^+ \mu^-$	$B1$ (4.3 ± 1.0) × 10 ⁻⁶	
Γ ₆₃	K^\pm anything	[f]	(78.9 ± 2.5) %		Γ ₁₂₆	$s\ell^+ \ell^-$	$B1$ [b] (5.8 ± 1.3) × 10 ⁻⁶	S=1.8
Γ ₆₄	K^+ anything		(66 ± 5) %		Γ ₁₂₇	$\pi\ell^+ \ell^-$	$B1$ < 5.9 × 10 ⁻⁸	CL=90%
Γ ₆₅	K^- anything		(13 ± 4) %		Γ ₁₂₈	$\pi e^+ e^-$	$B1$ < 1.10 × 10 ⁻⁷	CL=90%
Γ ₆₆	K^0/\overline{K}^0 anything	[f]	(64 ± 4) %		Γ ₁₂₉	$\pi\mu^+ \mu^-$	$B1$ < 5.0 × 10 ⁻⁸	CL=90%
Γ ₆₇	$K^*(892)^\pm$ anything		(18 ± 6) %		Γ ₁₃₀	$K e^+ e^-$	$B1$ (4.4 ± 0.6) × 10 ⁻⁷	
Γ ₆₈	$K^*(892)^0/\overline{K}^*(892)^0$ anything	[f]	(14.6 ± 2.6) %		Γ ₁₃₁	$K^*(892) e^+ e^-$	$B1$ (1.19 ± 0.20) × 10 ⁻⁶	S=1.2
Γ ₆₉	$K^*(892)\gamma$		(4.2 ± 0.6) × 10 ⁻⁵		Γ ₁₃₂	$K\mu^+ \mu^-$	$B1$ (4.4 ± 0.4) × 10 ⁻⁷	
Γ ₇₀	$\eta K\gamma$		(8.5 $\begin{smallmatrix} +1.8 \\ -1.6 \end{smallmatrix}$) × 10 ⁻⁶		Γ ₁₃₃	$K^*(892)\mu^+ \mu^-$	$B1$ (1.06 ± 0.09) × 10 ⁻⁶	
Γ ₇₁	$K_1(1400)\gamma$		< 1.27 × 10 ⁻⁴	CL=90%	Γ ₁₃₄	$K\ell^+ \ell^-$	$B1$ (4.8 ± 0.4) × 10 ⁻⁷	
					Γ ₁₃₅	$K^*(892)\ell^+ \ell^-$	$B1$ (1.05 ± 0.10) × 10 ⁻⁶	
					Γ ₁₃₆	$K\nu\overline{\nu}$	$B1$ < 1.6 × 10 ⁻⁵	CL=90%

Meson Particle Listings

B^\pm/B^0 ADMIXTURE

Γ_{137}	$K^* \nu \bar{\nu}$	$B1$	<	2.7	$\times 10^{-5}$	CL=90%
Γ_{138}	$\pi \nu \bar{\nu}$	$B1$	<	8	$\times 10^{-6}$	CL=90%
Γ_{139}	$\rho \nu \bar{\nu}$	$B1$	<	2.8	$\times 10^{-5}$	CL=90%
Γ_{140}	$s e^\pm \mu^\mp$	LF	[ℓ]	< 2.2	$\times 10^{-5}$	CL=90%
Γ_{141}	$\pi e^\pm \mu^\mp$	LF	<	9.2	$\times 10^{-8}$	CL=90%
Γ_{142}	$\rho e^\pm \mu^\mp$	LF	<	3.2	$\times 10^{-6}$	CL=90%
Γ_{143}	$K e^\pm \mu^\mp$	LF	<	3.8	$\times 10^{-8}$	CL=90%
Γ_{144}	$K^*(892) e^\pm \mu^\mp$	LF	<	5.1	$\times 10^{-7}$	CL=90%

- 13 YANAGISAWA 91 also measures an average semileptonic branching ratio at the $\Upsilon(5S)$ of 9.6–10.5% depending on assumptions about the relative production of different B meson species.
- 14 ALBRECHT 90H uses the model of ALTARELLI 82 to correct over all lepton momenta. 0.099 ± 0.006 is obtained using ISGUR 89b.
- 15 ALBRECHT 90H uses the model of ALTARELLI 82 to correct over all lepton momenta. 0.097 ± 0.006 is obtained using ISGUR 89b.
- 16 Using data above $p(e) = 2.4$ GeV, WACHS 89 determine $\sigma(B \rightarrow e \nu \mu p) / \sigma(B \rightarrow e \nu \text{charm}) < 0.065$ at 90% CL.
- 17 Ratio $\sigma(b \rightarrow e \nu \mu p) / \sigma(b \rightarrow e \nu \text{charm}) < 0.055$ at CL = 90%.

- [a] These values are model dependent.
- [b] An ℓ indicates an e or a μ mode, not a sum over these modes.
- [c] Here “anything” means at least one particle observed.
- [d] This is a $B(B^0 \rightarrow D^{*-} \ell^+ \nu_\ell)$ value.
- [e] D^{**} stands for the sum of the $D(1^1P_1)$, $D(1^3P_0)$, $D(1^3P_1)$, $D(1^3P_2)$, $D(2^1S_0)$, and $D(2^1S_1)$ resonances.
- [f] The value is for the sum of the charge states or particle/antiparticle states indicated.
- [g] $D^{(*)} \bar{D}^{(*)}$ stands for the sum of $D^* \bar{D}^*$, $D^* \bar{D}$, $D \bar{D}^*$, and $D \bar{D}$.
- [h] $X(3915)$ denotes a near-threshold enhancement in the $\omega J/\psi$ mass spectrum.
- [i] Inclusive branching fractions have a multiplicity definition and can be greater than 100%.

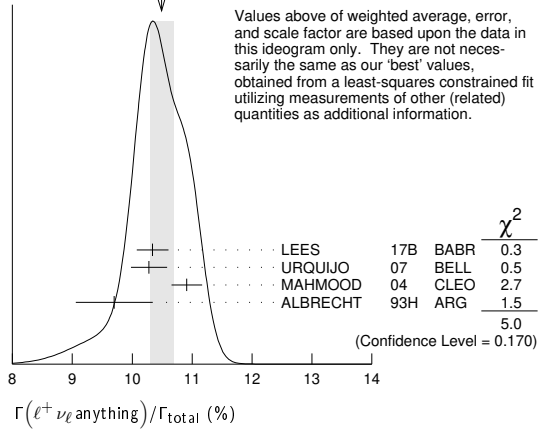
B^\pm/B^0 ADMIXTURE BRANCHING RATIOS

$\Gamma(\ell^+ \nu_\ell \text{anything}) / \Gamma_{\text{total}}$ Γ_3 / Γ
 These branching fraction values are model dependent.

VALUE (%)	DOCUMENT ID	TECN	COMMENT
10.82 ± 0.15 OUR EVALUATION	(Produced by HFLAV)		
10.49 ± 0.20 OUR AVERAGE	Error includes scale factor of 1.3. See the ideogram below.		
10.34 ± 0.04 ± 0.26	1 LEES	17b	BABR $e^+ e^- \rightarrow \Upsilon(4S)$
10.28 ± 0.18 ± 0.24	2 URQUIJO	07	BELL $e^+ e^- \rightarrow \Upsilon(4S)$
10.91 ± 0.09 ± 0.24	3 MAHMOOD	04	CLEO $e^+ e^- \rightarrow \Upsilon(4S)$
9.7 ± 0.5 ± 0.4	4 ALBRECHT	93H	ARG $e^+ e^- \rightarrow \Upsilon(4S)$
• • • We do not use the following data for averages, fits, limits, etc. • • •			
9.96 ± 0.19 ± 0.32	5 AUBERT,B	06Y	BABR Repl. by LEES 17b
10.85 ± 0.21 ± 0.36	6 OKABE	05	BELL Repl. by URQUIJO 07
10.83 ± 0.16 ± 0.06	7 AUBERT	04X	BABR Repl. by AUBERT,B 06Y
10.36 ± 0.06 ± 0.23	8 AUBERT,B	04A	BABR $e^+ e^- \rightarrow \Upsilon(4S)$
10.87 ± 0.18 ± 0.30	9 AUBERT	03	BABR Repl. by AUBERT 04x
10.90 ± 0.12 ± 0.49	10 ABE	02Y	BELL Repl. by OKABE 05
10.49 ± 0.17 ± 0.43	11 BARISH	96B	CLE2 Repl. by MAHMOOD 04
10.80 ± 0.20 ± 0.56	12 HENDERSON	92	CLEO $e^+ e^- \rightarrow \Upsilon(4S)$
10.0 ± 0.4 ± 0.3	13 YANAGISAWA	91	CSB2 $e^+ e^- \rightarrow \Upsilon(4S)$
10.3 ± 0.6 ± 0.2	14 ALBRECHT	90H	ARG Direct e at $\Upsilon(4S)$
10.0 ± 0.6 ± 0.2	15 ALBRECHT	90H	ARG Direct μ at $\Upsilon(4S)$
11.7 ± 0.4 ± 1.0	16 WACHS	89	CBAL Direct e at $\Upsilon(4S)$
12.0 ± 0.7 ± 0.5	CHEN	84	CLEO Direct e at $\Upsilon(4S)$
10.8 ± 0.6 ± 1.0	CHEN	84	CLEO Direct μ at $\Upsilon(4S)$
11.2 ± 0.9 ± 1.0	LEVMAN	84	CUSB Direct e at $\Upsilon(4S)$
13.2 ± 0.8 ± 1.4	17 KLOPFEN...	83b	CUSB Direct e at $\Upsilon(4S)$

- 1 LEES 17b measurement is obtained from semileptonic decays to electrons. The result is averaged over B^\pm and B^0 mesons, assuming lepton universality.
- 2 URQUIJO 07 report a measurement of $(10.07 \pm 0.18 \pm 0.21)\%$ for the partial branching fraction of $B \rightarrow e \nu_e X_c$ decay with electron energy above 0.6 GeV. We converted the result to $B \rightarrow e \nu_e X$ branching fraction.
- 3 Uses charge and angular correlations in $\Upsilon(4S)$ events with a high-momentum lepton and an additional electron.
- 4 ALBRECHT 93H analysis performed using tagged semileptonic decays of the B . This technique is almost model independent for the lepton branching ratio.
- 5 The measurements are obtained for charged and neutral B mesons partial rates of semileptonic decay to electrons with momentum above 0.6 GeV/c in the B rest frame. The best precision on the ratio is achieved for a momentum threshold of 1.0 GeV: $B(B^+ \rightarrow e^+ \nu_e X) / B(B^0 \rightarrow e^+ \nu_e X) = 1.074 \pm 0.041 \pm 0.026$.
- 6 The measurements are obtained for charged and neutral B mesons partial rates of semileptonic decay to electrons with momentum above 0.6 GeV/c in the B rest frame, and their ratio of $B(B^+ \rightarrow e^+ \nu_e X) / B(B^0 \rightarrow e^+ \nu_e X) = 1.08 \pm 0.05 \pm 0.02$.
- 7 The semileptonic branching ratio, $|V_{cb}|$ and other heavy-quark parameters are determined from a simultaneous fit to moments of the hadronic-mass and lepton-energy distribution.
- 8 Uses the high-momentum lepton tag method and requires the electron energy above 0.6 GeV.
- 9 Uses the high-momentum lepton tag method. They also report $|V_{cb}| = 0.0423 \pm 0.0007(\text{exp}) \pm 0.0020(\text{theo.})$.
- 10 Uses the high-momentum lepton tag method. ABE 02Y also reports $|V_{cb}| = 0.0408 \pm 0.0010(\text{exp}) \pm 0.0025(\text{theo.})$. The second error is due to uncertainties of theoretical inputs.
- 11 BARISH 96B analysis performed using tagged semileptonic decays of the B . This technique is almost model independent for the lepton branching ratio.
- 12 HENDERSON 92 measurement employs e and μ . The systematic error contains 0.004 in quadrature from model dependence. The authors average a variation of the Isgur, Scora, Grinstein, and Wise model with that of the Altarelli-Cabibbo-Corbò-Maiani-Martinelli model for semileptonic decays to correct the acceptance.

WEIGHTED AVERAGE
10.49±0.20 (Error scaled by 1.3)



$\Gamma(e^+ \nu_e \text{anything}) / \Gamma(\mu^+ \nu_\mu \text{anything})$ Γ_1 / Γ_2

VALUE	DOCUMENT ID	TECN	COMMENT
1.007 ± 0.009 ± 0.019	1 AGGARWAL	23	BELL $e^+ e^- \rightarrow \Upsilon(4S)$

1 The accompanying B meson is fully reconstructed in its hadronic decay modes.

$\Gamma(D^- \ell^+ \nu_\ell \text{anything}) / \Gamma(\ell^+ \nu_\ell \text{anything})$ Γ_4 / Γ_3
 $\ell = e \text{ or } \mu$

VALUE	DOCUMENT ID	TECN	COMMENT
0.26 ± 0.07 ± 0.04	1 FULTON	91	CLEO $e^+ e^- \rightarrow \Upsilon(4S)$

1 FULTON 91 uses $B(D^+ \rightarrow K^- \pi^+ \pi^+) = (9.1 \pm 1.3 \pm 0.4)\%$ as measured by MARK III.

$\Gamma(D^0 \ell^+ \nu_\ell \text{anything}) / \Gamma(\ell^+ \nu_\ell \text{anything})$ Γ_5 / Γ_3
 $\ell = e \text{ or } \mu$

VALUE	DOCUMENT ID	TECN	COMMENT
0.67 ± 0.09 ± 0.10	1 FULTON	91	CLEO $e^+ e^- \rightarrow \Upsilon(4S)$

1 FULTON 91 uses $B(D^0 \rightarrow K^- \pi^+) = (4.2 \pm 0.4 \pm 0.4)\%$ as measured by MARK III.

$\Gamma(\bar{D} \ell^+ \nu_\ell) / \Gamma(\ell^+ \nu_\ell \text{anything})$ Γ_6 / Γ_3

VALUE	DOCUMENT ID	TECN	COMMENT
0.223 ± 0.006 ± 0.009	1 AUBERT	10	BABR $e^+ e^- \rightarrow \Upsilon(4S)$

1 Uses a fully reconstructed B meson as a tag on the recoil side.

$\Gamma(D^{*-} \ell^+ \nu_\ell \text{anything}) / \Gamma_{\text{total}}$ Γ_7 / Γ

VALUE (units 10^{-2})	DOCUMENT ID	TECN	COMMENT
0.67 ± 0.08 ± 0.10	ABDALLAH	04D	DLPH $e^+ e^- \rightarrow Z^0$

• • • We do not use the following data for averages, fits, limits, etc. • • •

$0.6 \pm 0.3 \pm 0.1$ $\Gamma(4S)$

1 BARISH 95 use $B(D^0 \rightarrow K^- \pi^+) = (3.91 \pm 0.08 \pm 0.17)\%$ and $B(D^{*+} \rightarrow D^0 \pi^+) = (68.1 \pm 1.0 \pm 1.3)\%$.

$\Gamma(D^{*0} \ell^+ \nu_\ell \text{anything}) / \Gamma_{\text{total}}$ Γ_8 / Γ

VALUE (units 10^{-2})	DOCUMENT ID	TECN	COMMENT
0.6 ± 0.6 ± 0.1	1 BARISH	95	CLE2 $e^+ e^- \rightarrow \Upsilon(4S)$

1 BARISH 95 use $B(D^0 \rightarrow K^- \pi^+) = (3.91 \pm 0.08 \pm 0.17)\%$, $B(D^{*+} \rightarrow D^0 \pi^+) = (68.1 \pm 1.0 \pm 1.3)\%$, $B(D^{*0} \rightarrow D^0 \pi^0) = (63.6 \pm 2.3 \pm 3.3)\%$.

$\Gamma(\bar{D}^* e^+ \nu_e) / \Gamma(\bar{D}^* \mu^+ \nu_\mu)$ $\Gamma_{10} / \Gamma_{11}$

VALUE	DOCUMENT ID	TECN	COMMENT
0.993 ± 0.023 ± 0.023	1 PRIM	23	BELL $e^+ e^- \rightarrow \Upsilon(4S)$

1 This is the lepton-flavor universality ratio $R_{e\mu}$ for the $B^+ \rightarrow \bar{D}^{*0} \ell^+ \nu_\ell$ and $B^0 \rightarrow D^{*-} \ell^+ \nu_\ell$ average.

See key on page 1171

Meson Particle Listings
 B^\pm/B^0 ADMIXTURE

$\Gamma(\bar{D}^{**}\ell^+\nu_\ell)/\Gamma_{\text{total}}$ Γ_{12}/Γ
 D^{**} stands for the sum of the $D(1^1P_1)$, $D(1^3P_0)$, $D(1^3P_1)$, $D(1^3P_2)$, $D(2^1S_0)$, and $D(2^1S_1)$ resonances. $\ell = e$ or μ , not sum over e and μ modes.

VALUE	CL%	EVTS	DOCUMENT ID	TECN	COMMENT
0.027 ± 0.005 ± 0.005	63		¹ ALBRECHT 93	ARG	$e^+e^- \rightarrow \Upsilon(4S)$
<0.028	95		² BARISH 95	CLE2	$e^+e^- \rightarrow \Upsilon(4S)$

¹ ALBRECHT 93 assumes the GISW model to correct for unseen modes. Using the BHK model, the result becomes $0.023 \pm 0.006 \pm 0.004$. Assumes $B(D^{**+} \rightarrow D^0\pi^+) = 68.1\%$, $B(D^0 \rightarrow K^-\pi^+) = 3.65\%$, $B(D^0 \rightarrow K^-\pi^+\pi^-\pi^+) = 7.5\%$. We have taken their average e and μ value.
² BARISH 95 use $B(D^0 \rightarrow K^-\pi^+) = (3.91 \pm 0.08 \pm 0.17)\%$, assume all nonresonant channels are zero, and use GISW model for relative abundances of D^{**} states.

$\Gamma(\bar{D}_1(2420)\ell^+\nu_\ell \text{ anything})/\Gamma_{\text{total}}$ Γ_{13}/Γ

VALUE	DOCUMENT ID	TECN	COMMENT
0.0038 ± 0.0013 OUR AVERAGE	Error includes scale factor of 2.4.		
0.0033 ± 0.0006	¹ ABAZOV 05o	D0	$p\bar{p}$ at 1.96 TeV
0.0074 ± 0.0016	² BUSKULIC 97b	ALEP	$e^+e^- \rightarrow Z$
seen	³ BUSKULIC 95b	ALEP	Repl. by BUSKULIC 97b

¹ Assumes $B(D_1 \rightarrow D^*\pi) = 1$, $B(D_1 \rightarrow D^*\pi^\pm) = 2/3$, and $B(b \rightarrow B) = 0.397$.
² BUSKULIC 97b assumes $B(D_1(2420) \rightarrow D^*\pi) = 1$, $B(D_1(2420) \rightarrow D^*\pi^\pm) = 2/3$, and $B(b \rightarrow B) = 0.378 \pm 0.022$.
³ BUSKULIC 95b reports $f_B \times B(B \rightarrow \bar{D}_1(2420)^0\ell^+\nu_\ell \text{ anything}) \times B(\bar{D}_1(2420)^0 \rightarrow \bar{D}^*(2010)^-\pi^+) = (2.04 \pm 0.58 \pm 0.34)10^{-3}$, where f_B is the production fraction for a single B charge state.

$[\Gamma(\bar{D}\pi\ell^+\nu_\ell \text{ anything}) + \Gamma(\bar{D}^*\pi\ell^+\nu_\ell \text{ anything})]/\Gamma_{\text{total}}$ Γ_{14}/Γ

VALUE	DOCUMENT ID	TECN	COMMENT
0.026 ± 0.005 OUR AVERAGE	Error includes scale factor of 1.5.		
0.0340 ± 0.0052 ± 0.0032	¹ ABREU 00R	DLPH	$e^+e^- \rightarrow Z$
0.0226 ± 0.0029 ± 0.0033	² BUSKULIC 97b	ALEP	$e^+e^- \rightarrow Z$

¹ Assumes no contribution from B_s and b baryons. Further assumes contributions from single pion ($D\pi$ and $D^*\pi$) states only, allowing isospin conservation to relate the relative π^0 and π^\pm rates.
² BUSKULIC 97b assumes $B(b \rightarrow B) = 0.378 \pm 0.022$ and uses isospin invariance by assuming that all observed $D^0\pi^+$, $D^{*0}\pi^+$, $D^+\pi^-$, and $D^*\pi^-$ are from D^{**} states. A correction has been applied to account for the production of B_s^0 and Λ_b^0 .

$\Gamma(\bar{D}\pi\ell^+\nu_\ell \text{ anything})/\Gamma_{\text{total}}$ Γ_{15}/Γ

VALUE	DOCUMENT ID	TECN	COMMENT
0.0154 ± 0.0061	ABREU 00R	DLPH	$e^+e^- \rightarrow Z$

$\Gamma(\bar{D}^*\pi\ell^+\nu_\ell \text{ anything})/\Gamma_{\text{total}}$ Γ_{16}/Γ

VALUE	DOCUMENT ID	TECN	COMMENT
0.0186 ± 0.0038	ABREU 00R	DLPH	$e^+e^- \rightarrow Z$

$\Gamma(\bar{D}_2^*(2460)\ell^+\nu_\ell \text{ anything})/\Gamma_{\text{total}}$ Γ_{17}/Γ

VALUE	CL%	DOCUMENT ID	TECN	COMMENT
0.0044 ± 0.0016		¹ ABAZOV 05o	D0	$p\bar{p}$ at 1.96 TeV
<0.0065	95	² BUSKULIC 97b	ALEP	$e^+e^- \rightarrow Z$
not seen		³ BUSKULIC 95b	ALEP	$e^+e^- \rightarrow Z$

¹ Assumes $B(D_2^* \rightarrow D^*\pi^\pm) = 0.30 \pm 0.06$ and $B(b \rightarrow B) = 0.397$.
² A revised number based on BUSKULIC 97b which assumes $B(D_2^*(2460) \rightarrow D^*\pi^\pm) = 0.20$ and $B(b \rightarrow B) = 0.378 \pm 0.022$.
³ BUSKULIC 95b reports $f_B \times B(B \rightarrow \bar{D}_2^*(2460)^0\ell^+\nu_\ell \text{ anything}) \times B(\bar{D}_2^*(2460)^0 \rightarrow \bar{D}^*(2010)^-\pi^+) \leq 0.81 \times 10^{-3}$ at CL=95%, where f_B is the production fraction for a single B charge state.

$\Gamma(B \rightarrow \bar{D}_2^*(2460)\ell^+\nu_\ell \text{ anything}) \times B(D_2^*(2460) \rightarrow D^*\pi^+)$
 $\Gamma(B \rightarrow \bar{D}_1(2420)\ell^+\nu_\ell \text{ anything}) \times B(D_1(2420) \rightarrow D^*\pi^+)$

VALUE	DOCUMENT ID	TECN	COMMENT
0.39 ± 0.09 ± 0.12	ABAZOV 05o	D0	$p\bar{p}$ at 1.96 TeV

$\Gamma(D^-\pi^+\ell^+\nu_\ell \text{ anything})/\Gamma_{\text{total}}$ Γ_{18}/Γ

VALUE (units 10^{-3})	DOCUMENT ID	TECN	COMMENT
10.0 ± 2.7 ± 2.1	¹ BUSKULIC 95b	ALEP	$e^+e^- \rightarrow Z$

¹ BUSKULIC 95b reports $f_B \times B(B \rightarrow \bar{D}^*(2010)^-\pi^+\ell^+\nu_\ell \text{ anything}) = (3.7 \pm 1.0 \pm 0.7)10^{-3}$. Above value assumes $f_B = 0.37 \pm 0.03$.

$\Gamma(\bar{D}\pi^+\pi^-\ell^+\nu_\ell)/\Gamma(\bar{D}\ell^+\nu_\ell)$ Γ_{19}/Γ_6

VALUE (units 10^{-2})	DOCUMENT ID	TECN	COMMENT
6.7 ± 1.0 ± 0.8	¹ LEES 16	BABR	$e^+e^- \rightarrow \Upsilon(4S)$

¹ Measurement used electrons and muons as leptons.

$\Gamma(\bar{D}^*\pi^+\pi^-\ell^+\nu_\ell)/\Gamma(\bar{D}^*\ell^+\nu_\ell)$ Γ_{20}/Γ_9

VALUE (units 10^{-2})	DOCUMENT ID	TECN	COMMENT
1.9 ± 0.5 ± 0.4	¹ LEES 16	BABR	$e^+e^- \rightarrow \Upsilon(4S)$

¹ Measurement used electrons and muons as leptons.

$\Gamma(D_s^-\ell^+\nu_\ell \text{ anything})/\Gamma_{\text{total}}$ Γ_{21}/Γ

VALUE	CL%	DOCUMENT ID	TECN	COMMENT
<7 × 10⁻³	90	¹ ALBRECHT 93E	ARG	$e^+e^- \rightarrow \Upsilon(4S)$

¹ ALBRECHT 93E reports < 0.012 from a measurement of $[\Gamma(B \rightarrow D_s^-\ell^+\nu_\ell \text{ anything})/\Gamma_{\text{total}}] \times [B(D_s^+ \rightarrow \phi\pi^+)]$ assuming $B(D_s^+ \rightarrow \phi\pi^+) = 0.027$, which we rescale to our best value $B(D_s^+ \rightarrow \phi\pi^+) = 4.5 \times 10^{-2}$.

$\Gamma(D_s^-\ell^+\nu_\ell K^+ \text{ anything})/\Gamma_{\text{total}}$ Γ_{22}/Γ

VALUE	CL%	DOCUMENT ID	TECN	COMMENT
<5 × 10⁻³	90	¹ ALBRECHT 93E	ARG	$e^+e^- \rightarrow \Upsilon(4S)$

¹ ALBRECHT 93E reports < 0.008 from a measurement of $[\Gamma(B \rightarrow D_s^-\ell^+\nu_\ell K^+ \text{ anything})/\Gamma_{\text{total}}] \times [B(D_s^+ \rightarrow \phi\pi^+)]$ assuming $B(D_s^+ \rightarrow \phi\pi^+) = 0.027$, which we rescale to our best value $B(D_s^+ \rightarrow \phi\pi^+) = 4.5 \times 10^{-2}$.

$\Gamma(D_s^-\ell^+\nu_\ell K^0 \text{ anything})/\Gamma_{\text{total}}$ Γ_{23}/Γ

VALUE	CL%	DOCUMENT ID	TECN	COMMENT
<7 × 10⁻³	90	¹ ALBRECHT 93E	ARG	$e^+e^- \rightarrow \Upsilon(4S)$

¹ ALBRECHT 93E reports < 0.012 from a measurement of $[\Gamma(B \rightarrow D_s^-\ell^+\nu_\ell K^0 \text{ anything})/\Gamma_{\text{total}}] \times [B(D_s^+ \rightarrow \phi\pi^+)]$ assuming $B(D_s^+ \rightarrow \phi\pi^+) = 0.027$, which we rescale to our best value $B(D_s^+ \rightarrow \phi\pi^+) = 4.5 \times 10^{-2}$.

$\Gamma(X_c\ell^+\nu_\ell)/\Gamma_{\text{total}}$ Γ_{24}/Γ

VALUE (%)	DOCUMENT ID	TECN	COMMENT
10.63 ± 0.15 OUR EVALUATION	(Produced by HFLAV)		
10.29 ± 0.19 OUR AVERAGE			

10.18 ± 0.03 ± 0.24	¹ LEES 17b	BABR	$e^+e^- \rightarrow \Upsilon(4S)$
10.44 ± 0.19 ± 0.22	² URQUIJO 07	BELL	$e^+e^- \rightarrow \Upsilon(4S)$
10.64 ± 0.17 ± 0.06	³ AUBERT 10a	BABR	Repl. by LEES 17b
10.61 ± 0.16 ± 0.06	⁴ AUBERT 04x	BABR	Repl. by AUBERT 10a

¹ The measurement is obtained from semileptonic decays to electrons $B \rightarrow X_c\ell\nu$, and using a theoretical model (GAMBINO 07, GAMBINO 11) to predict the contribution from $B \rightarrow X_c\ell\nu$. The result is averaged over B^\pm and B^0 mesons, assuming lepton universality.

² Measured the independent B^+ and B^0 partial branching fractions with electron energy above 0.4 GeV.

³ Obtained from a combined fit to the moments of observed spectra in inclusive $B \rightarrow X_c\ell^+\nu_\ell$ decay.

⁴ The semileptonic branching ratio, $|V_{cb}|$ and other heavy-quark parameters are determined from a simultaneous fit to moments of the hadronic-mass and lepton-energy distribution.

$\Gamma(X_u\ell^+\nu_\ell)/\Gamma_{\text{total}}$ Γ_{25}/Γ

VALUE (units 10^{-3})	DOCUMENT ID	TECN	COMMENT
1.88 ± 0.27 OUR EVALUATION	(Produced by HFLAV)		
1.85 ± 0.08 ± 0.19			

1.665 ± 0.087 ± 0.103 0.094	² LEES 17b	BABR	$e^+e^- \rightarrow \Upsilon(4S)$
2.01 ± 0.15 ± 0.25	³ LEES 12R	BABR	$e^+e^- \rightarrow \Upsilon(4S)$
2.53 ± 0.24 ± 0.24	⁴ AUBERT,B 05x	BABR	$e^+e^- \rightarrow \Upsilon(4S)$
2.80 ± 0.52 ± 0.41	⁵ LIMOSANI 05	BELL	$e^+e^- \rightarrow \Upsilon(4S)$
1.77 ± 0.29 ± 0.38	⁶ BORNHEIM 02	CLE2	$e^+e^- \rightarrow \Upsilon(4S)$
1.39 ± 0.14 ± 0.22	⁷ CAO 23	BELL	$e^+e^- \rightarrow \Upsilon(4S)$
1.963 ± 0.173 ± 0.159	⁸ URQUIJO 10	BELL	Repl. by CAO 21a
1.18 ± 0.09 ± 0.07	⁹ AUBERT 08a	BABR	Repl. by LEES 12R
2.27 ± 0.26 ± 0.37 -0.33	¹⁰ AUBERT 06H	BABR	Repl. by LEES 17b
2.24 ± 0.27 ± 0.47	^{11,12} AUBERT 04i	BABR	Repl. by AUBERT,B 05x

¹ Measures several partial branching fractions in different phase space regions. The most inclusive result of the full branching fraction is obtained in the region for lepton energy in B rest frame $E_\ell^* > 1$ GeV, where the measured partial branching fraction is $\Delta B = (1.59 \pm 0.07 \pm 0.16) \times 10^{-3}$. The acceptance in that region is reported to be 0.86.

² Obtained from the partial rate $\Delta B = (1.554 \pm 0.082 \pm 0.095 \pm 0.086) \times 10^{-3}$ for the electron momentum interval of 0.8–2.7 GeV/c based on GGOU1 method ($X_c\ell\nu$, m_c constraint fit of SF parameters).

³ Measures several partial branching fractions in different phase space regions. The most precise result on the full branching fraction is obtained in the region for lepton momentum in B rest frame $p_\ell^* > 1$ GeV/c, where the measured partial branching fraction is $\Delta B = (1.80 \pm 0.13 \pm 0.15) \times 10^{-3}$. The acceptance in that region is reported in a private communication by the Authors to be 0.894. The corresponding $|V_{ub}|$ from the BLPN method is $(4.28 \pm 0.15 \pm 0.18 \pm 0.19) \times 10^{-3}$, where the last uncertainty comes from theoretical prediction.

⁴ Determined from the partial rate $\Delta B = (4.41 \pm 0.42 \pm 0.42) \times 10^{-4}$ measured for electron energy > 2 GeV and hadronic mass squared < 3.5 GeV², and calculated acceptance 0.174 in that region. The V_{ub} is measured as $(4.41 \pm 0.30 \pm 0.65 \pm 0.47) \times 10^{-3}$.

⁵ Uses electrons in the momentum interval 1.9–2.6 GeV/c in the center-of-mass frame. The V_{ub} is found to be $(5.08 \pm 0.47 \pm 0.49 \pm 0.48) \times 10^{-3}$.

Meson Particle Listings

 B^\pm/B^0 ADMIXTURE

⁶BORNHEIM 02 uses the observed yield of leptons from semileptonic B decays in the end-point momentum interval 2.2–2.6 GeV/c with recent CLEO-2 data on $B \rightarrow X_S \gamma$. The V_{ub} is found to be $(4.08 \pm 0.34 \pm 0.53) \times 10^{-3}$.

⁷Measurement requires lepton energy $E_\ell^* > 1$ GeV in the B rest frame. It is a part of the inclusive and exclusive $|V_{ub}|$ determination.

⁸Uses a multivariate analysis method and requires lepton momentum in the B rest frame, $p_\ell^* > 1.0$ GeV/c.

⁹Measures several partial branching fractions in different phase space regions. The most precise result is obtained in the region for hadronic mass $M_X < 1.55$ GeV/ c^2 , and is $\Delta B = (1.18 \pm 0.09 \pm 0.07) \times 10^{-3}$. The corresponding $|V_{ub}|$ from the BLNP method is $(4.27 \pm 0.16 \pm 0.13 \pm 0.30) \times 10^{-3}$, where the last uncertainty comes from the theoretical prediction of the partial rate in the given phase-space region.

¹⁰Obtained from the partial rate $\Delta B = (0.572 \pm 0.041 \pm 0.065) \times 10^{-3}$ for the electron momentum interval of 2.0–2.6 GeV/c based on BLNP method.

¹¹Used BaBar measurement of Semileptonic branching fraction $B(B \rightarrow X \ell \nu_\ell) = (10.87 \pm 0.18 \pm 0.30)\%$ to convert the ratio of rates to branching fraction.

¹²The third error includes the systematics and theoretical errors summed in quadrature.

$\Gamma(X_u \ell^+ \nu_\ell)/\Gamma(\ell^+ \nu_\ell \text{ anything})$ Γ_{25}/Γ_3
 ℓ denotes e or μ , not the sum. These experiments measure this ratio in very limited momentum intervals.

VALUE (units 10^{-2})	CL%	EVTS	DOCUMENT ID	TECN	COMMENT
0.26 ± 0.25 ± 0.42			¹ AUBERT 04i	BABR	$e^+ e^- \rightarrow \Upsilon(4S)$
			••• We do not use the following data for averages, fits, limits, etc. •••		
			² ALBRECHT 94c	ARG	$e^+ e^- \rightarrow \Upsilon(4S)$
	107		³ BARTELT 93B	CLE2	$e^+ e^- \rightarrow \Upsilon(4S)$
	77		⁴ ALBRECHT 91c	ARG	$e^+ e^- \rightarrow \Upsilon(4S)$
	41		⁵ ALBRECHT 90	ARG	$e^+ e^- \rightarrow \Upsilon(4S)$
	76		⁶ FULTON 90	CLEO	$e^+ e^- \rightarrow \Upsilon(4S)$
<4.0	90		⁷ BEHRENDIS 87	CLEO	Direct e at $\Upsilon(4S)$
<4.0	90		CHEN 84	CLEO	Direct e at $\Upsilon(4S)$
<5.5	90		KLOPFEN...	83B	CUSB Direct e at $\Upsilon(4S)$

¹The third error includes the systematics and theoretical errors summed in quadrature.

²ALBRECHT 94c find $\Gamma(b \rightarrow c)/\Gamma(b \rightarrow \text{all}) = 0.99 \pm 0.02 \pm 0.04$.

³BARTELT 93B (CLEO II) measures an excess of $107 \pm 15 \pm 11$ leptons in the lepton momentum interval 2.3–2.6 GeV/c which is attributed to $b \rightarrow u \ell \nu_\ell$. This corresponds to a model-dependent partial branching ratio ΔB_{ub} between $(1.15 \pm 0.16 \pm 0.15) \times 10^{-4}$, as evaluated using the KS model (KOERNER 88), and $(1.54 \pm 0.22 \pm 0.20) \times 10^{-4}$ using the ACCMM model (ARTUSO 93). The corresponding values of $|V_{ub}|/|V_{cb}|$ are 0.056 ± 0.006 and 0.076 ± 0.008 , respectively.

⁴ALBRECHT 91c result supersedes ALBRECHT 90. Two events are fully reconstructed providing evidence for the $b \rightarrow u$ transition. Using the model of ALTARELLI 82, they obtain $|V_{ub}|/|V_{cb}| = 0.11 \pm 0.012$ from 77 leptons in the 2.3–2.6 GeV momentum range.

⁵ALBRECHT 90 observes 41 ± 10 excess e and μ (lepton) events in the momentum interval $p = 2.3$ –2.6 GeV signaling the presence of the $b \rightarrow u$ transition. The events correspond to a model-dependent measurement of $|V_{ub}|/|V_{cb}| = 0.10 \pm 0.01$.

⁶FULTON 90 observe 76 ± 20 excess e and μ (lepton) events in the momentum interval $p = 2.4$ –2.6 GeV signaling the presence of the $b \rightarrow u$ transition. The average branching ratio, $(1.8 \pm 0.4 \pm 0.3) \times 10^{-4}$, corresponds to a model-dependent measurement of approximately $|V_{ub}|/|V_{cb}| = 0.1$ using $B(b \rightarrow c \ell \nu) = 10.2 \pm 0.2 \pm 0.7\%$.

⁷The quoted possible limits range from 0.018 to 0.04 for the ratio, depending on which model or momentum range is chosen. We select the most conservative limit they have calculated. This corresponds to a limit on $|V_{ub}|/|V_{cb}| < 0.20$. While the endpoint technique employed is more robust than their previous results in CHEN 84, these results do not provide a numerical improvement in the limit.

$\Gamma(X_u e^+ \nu_e)/\Gamma_{\text{total}}$ Γ_{26}/Γ
 Requires $E_e^* > 1$ GeV, where E_e^* is e^+ energy in B rest frame.

VALUE (units 10^{-3})	DOCUMENT ID	TECN	COMMENT
1.57 ± 0.10 ± 0.16	¹ CAO 21A	BELL	$e^+ e^- \rightarrow \Upsilon(4S)$

¹The correlation of 53% with $B(B \rightarrow X_u \mu^+ \nu_\mu)$ (lepton energy in B rest frame $E_{\mu^+} > 1$ GeV) is reported.

$\Gamma(X_u \mu^+ \nu_\mu)/\Gamma_{\text{total}}$ Γ_{27}/Γ
 Requires $E_\mu^* > 1$ GeV, where E_μ^* is μ^+ energy in B rest frame.

VALUE (units 10^{-3})	DOCUMENT ID	TECN	COMMENT
1.62 ± 0.10 ± 0.18	¹ CAO 21A	BELL	$e^+ e^- \rightarrow \Upsilon(4S)$

¹The correlation of 53% with $B(B \rightarrow X_u e^+ \nu_e)$ (lepton energy in B rest frame $E_{e^+} > 1$ GeV) is reported.

$\Gamma(K^+ \ell^+ \nu_\ell \text{ anything})/\Gamma(\ell^+ \nu_\ell \text{ anything})$ Γ_{28}/Γ_3
 ℓ denotes e or μ , not the sum.

VALUE	DOCUMENT ID	TECN	COMMENT
0.58 ± 0.05 OUR AVERAGE			
0.594 ± 0.021 ± 0.056	¹ ALBRECHT 94c	ARG	$e^+ e^- \rightarrow \Upsilon(4S)$
0.54 ± 0.07 ± 0.06	¹ ALAM 87B	CLEO	$e^+ e^- \rightarrow \Upsilon(4S)$

¹ALAM 87B measurement relies on lepton-kaon correlations.

$\Gamma(K^- \ell^+ \nu_\ell \text{ anything})/\Gamma(\ell^+ \nu_\ell \text{ anything})$ Γ_{29}/Γ_3
 ℓ denotes e or μ , not the sum.

VALUE	DOCUMENT ID	TECN	COMMENT
0.092 ± 0.035 OUR AVERAGE			
0.086 ± 0.011 ± 0.044	¹ ALBRECHT 94c	ARG	$e^+ e^- \rightarrow \Upsilon(4S)$
0.10 ± 0.05 ± 0.02	¹ ALAM 87B	CLEO	$e^+ e^- \rightarrow \Upsilon(4S)$

¹ALAM 87B measurement relies on lepton-kaon correlations.

$\Gamma(K^0/\bar{K}^0 \ell^+ \nu_\ell \text{ anything})/\Gamma(\ell^+ \nu_\ell \text{ anything})$ Γ_{30}/Γ_3
 ℓ denotes e or μ , not the sum. Sum over K^0 and \bar{K}^0 states.

VALUE	DOCUMENT ID	TECN	COMMENT
0.42 ± 0.05 OUR AVERAGE			
0.452 ± 0.038 ± 0.056	¹ ALBRECHT 94c	ARG	$e^+ e^- \rightarrow \Upsilon(4S)$
0.39 ± 0.06 ± 0.04	² ALAM 87B	CLEO	$e^+ e^- \rightarrow \Upsilon(4S)$

¹ALBRECHT 94c assume a K^0/\bar{K}^0 multiplicity twice that of K_S^0 .

²ALAM 87B measurement relies on lepton-kaon correlations.

$\Gamma(\bar{D}^+ \tau^+ \nu_\tau)/\Gamma(\bar{D}^+ \ell^+ \nu_\ell)$ Γ_{31}/Γ_6
 VALUE (units 10^{-2})

VALUE (units 10^{-2})	DOCUMENT ID	TECN	COMMENT
35.8 ± 2.9 OUR EVALUATION	(Produced by HFLAV)		
35 ± 4 OUR AVERAGE	Error includes scale factor of 1.2.		
30.7 ± 3.7 ± 1.6	¹ CARIA 20	BELL	$e^+ e^- \rightarrow \Upsilon(4S)$
37.5 ± 6.4 ± 2.6	^{2,3} HUSCHLE 15	BELL	$e^+ e^- \rightarrow \Upsilon(4S)$
44.0 ± 5.8 ± 4.2	^{2,3} LEES 12D	BABR	$e^+ e^- \rightarrow \Upsilon(4S)$
	••• We do not use the following data for averages, fits, limits, etc. •••		
4.16 ± 11.7 ± 5.2	² AUBERT 08N	BABR	Repl. by LEES 12D

¹The tag-side B meson is reconstructed in a semileptonic decay mode and the signal-side τ is reconstructed in a purely leptonic decay. The Belle combination of HUSCHLE 15 and CARIA 20 yields $R(D) = (32.6 \pm 3.4) \times 10^{-2}$.

²Uses a fully reconstructed B meson as a tag on the recoil side.

³Uses $\tau^+ \rightarrow e^+ \nu_e \bar{\nu}_\tau$ and $\tau^+ \rightarrow \mu^+ \nu_\mu \bar{\nu}_\tau$ and e^+ or μ^+ as ℓ^+ . Obtained from simultaneous fit to B^+ and B^0 assuming isospin symmetry.

$\Gamma(\bar{D}^* \tau^+ \nu_\tau)/\Gamma(\bar{D}^* \ell^+ \nu_\ell)$ Γ_{32}/Γ_9
 VALUE (units 10^{-2})

VALUE (units 10^{-2})	DOCUMENT ID	TECN	COMMENT
28.2 ± 1.2 OUR EVALUATION	(Produced by HFLAV)		
29.3 ± 1.4 OUR AVERAGE			
28.1 ± 1.8 ± 2.4	¹ AAIJ 23AR	LHCB	pp at 7 and 8 TeV
28.3 ± 1.8 ± 1.4	² CARIA 20	BELL	$e^+ e^- \rightarrow \Upsilon(4S)$
27.0 ± 3.5 ± 2.8	³ HIROSE 17	BELL	$e^+ e^- \rightarrow \Upsilon(4S)$
29.3 ± 3.8 ± 1.5	⁴ HUSCHLE 15	BELL	$e^+ e^- \rightarrow \Upsilon(4S)$
33.2 ± 2.4 ± 1.8	⁴ LEES 12D	BABR	$e^+ e^- \rightarrow \Upsilon(4S)$
	••• We do not use the following data for averages, fits, limits, etc. •••		
29.7 ± 5.6 ± 1.8	⁵ AUBERT 08N	BABR	Repl. by LEES 12D

¹Uses $\tau^+ \rightarrow \mu^+ \nu_\mu \bar{\nu}_\tau$ and μ^+ as ℓ^+ . The measurement combines fully reconstructed D^{*+} sample with sample where only D^0 from D^* decays is reconstructed.

²The tag-side B meson is reconstructed in a semileptonic decay mode and the signal-side τ is reconstructed in a purely leptonic decay. The Belle combination of HUSCHLE 15, HIROSE 17, and CARIA 20 yields $R(D^*) = 0.238 \pm 0.018$.

³Uses a fully reconstructed B meson as a tag on the recoil side.

⁴Uses $\tau^+ \rightarrow e^+ \nu_e \bar{\nu}_\tau$ and $\tau^+ \rightarrow \mu^+ \nu_\mu \bar{\nu}_\tau$ and e^+ or μ^+ as ℓ^+ . Obtained from simultaneous fit to B^+ and B^0 assuming isospin symmetry. Uses a fully reconstructed B meson as a tag on the recoil side.

⁵Uses a fully reconstructed B meson as a tag on the recoil side. The results are normalized to the B^+ decay rate.

$\langle \eta_c \rangle$
 VALUE

VALUE	DOCUMENT ID	TECN	COMMENT
1.10 ± 0.05	¹ GIBBONS 97B	CLE2	$e^+ e^- \rightarrow \Upsilon(4S)$
	••• We do not use the following data for averages, fits, limits, etc. •••		
0.98 ± 0.16 ± 0.12	² ALAM 87B	CLEO	$e^+ e^- \rightarrow \Upsilon(4S)$

¹GIBBONS 97B from charm counting using $B(D_s^+ \rightarrow \phi \pi) = 0.036 \pm 0.009$ and $B(\Lambda_c^+ \rightarrow p K^- \pi^+) = 0.044 \pm 0.006$.

²From the difference between K^- and K^+ widths. ALAM 87B measurement relies on lepton-kaon correlations. It does not consider the possibility of $B\bar{B}$ mixing. We have thus removed it from the average.

$\Gamma(D^\pm \text{ anything})/\Gamma_{\text{total}}$ Γ_{33}/Γ
 VALUE

VALUE	EVTS	DOCUMENT ID	TECN	COMMENT
0.231 ± 0.012 OUR AVERAGE				
0.230 ± 0.012 ± 0.004	¹ GIBBONS 97B	CLE2	$e^+ e^- \rightarrow \Upsilon(4S)$	
0.241 ± 0.037 ± 0.004	² BORTOLETTO92	CLEO	$e^+ e^- \rightarrow \Upsilon(4S)$	
0.223 ± 0.051 ± 0.004	³ ALBRECHT 91H	ARG	$e^+ e^- \rightarrow \Upsilon(4S)$	
	••• We do not use the following data for averages, fits, limits, etc. •••			
0.203 ± 0.048 ± 0.003	20k	⁴ BORTOLETTO87	CLEO	Sup. by BORTOLETTO 92

¹GIBBONS 97B reports $[\Gamma(B \rightarrow D^\pm \text{ anything})/\Gamma_{\text{total}}] \times [B(D^+ \rightarrow K^- 2\pi^+)] = (0.0216 \pm 0.0008 \pm 0.00082)$ which we divide by our best value $B(D^+ \rightarrow K^- 2\pi^+) = (9.38 \pm 0.16) \times 10^{-2}$. Our first error is their experiment's error and our second error is the systematic error from using our best value.

²BORTOLETTO 92 reports $[\Gamma(B \rightarrow D^\pm \text{ anything})/\Gamma_{\text{total}}] \times [B(D^+ \rightarrow K^- 2\pi^+)] = 0.0226 \pm 0.0030 \pm 0.0018$ which we divide by our best value $B(D^+ \rightarrow K^- 2\pi^+) = (9.38 \pm 0.16) \times 10^{-2}$. Our first error is their experiment's error and our second error is the systematic error from using our best value.

³ALBRECHT 91H reports $[\Gamma(B \rightarrow D^\pm \text{ anything})/\Gamma_{\text{total}}] \times [B(D^+ \rightarrow K^- 2\pi^+)] = 0.0209 \pm 0.0027 \pm 0.0040$ which we divide by our best value $B(D^+ \rightarrow K^- 2\pi^+) = (9.38 \pm 0.16) \times 10^{-2}$. Our first error is their experiment's error and our second error is the systematic error from using our best value.

⁴BORTOLETTO 87 reports $[\Gamma(B \rightarrow D^\pm \text{ anything})/\Gamma_{\text{total}}] \times [B(D^+ \rightarrow K^- 2\pi^+)] = 0.019 \pm 0.004 \pm 0.002$ which we divide by our best value $B(D^+ \rightarrow K^- 2\pi^+) = (9.38 \pm 0.16) \times 10^{-2}$. Our first error is their experiment's error and our second error is the systematic error from using our best value.

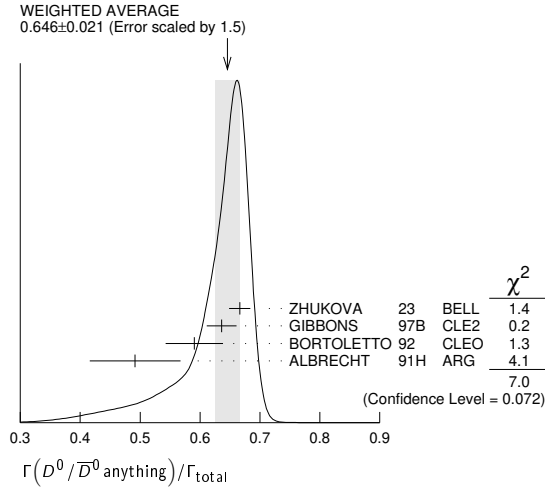
See key on page 1171

Meson Particle Listings

B^\pm/B^0 ADMIXTURE

$\Gamma(D^0/\bar{D}^0 \text{ anything})/\Gamma_{\text{total}}$				Γ_{34}/Γ
VALUE	EVTs	DOCUMENT ID	TECN	COMMENT
0.646 ± 0.021	OUR AVERAGE	Error includes scale factor of 1.5. See the ideogram below.		
0.6663 ± 0.0004 ± 0.0177		ZHUKOVA 23	BELL	$e^+e^- \rightarrow \Upsilon(4S)$
0.636 ± 0.024 ± 0.005		1 GIBBONS 97B	CLE2	$e^+e^- \rightarrow \Upsilon(4S)$
0.590 ± 0.047 ± 0.004		2 BORTOLETTO92	CLEO	$e^+e^- \rightarrow \Upsilon(4S)$
0.492 ± 0.074 ± 0.004		3 ALBRECHT 91H	ARG	$e^+e^- \rightarrow \Upsilon(4S)$
● ● ● We do not use the following data for averages, fits, limits, etc. ● ● ●				
0.532 ± 0.065 ± 0.004		4 BORTOLETTO87	CLEO	$e^+e^- \rightarrow \Upsilon(4S)$
0.608 ± 0.183 ± 0.005		5 GREEN 83	CLEO	Repl. by BORTOLETTO 87

- GIBBONS 97B reports $[\Gamma(B \rightarrow D^0/\bar{D}^0 \text{ anything})/\Gamma_{\text{total}}] \times [B(D^0 \rightarrow K^- \pi^+)] = 0.0251 \pm 0.0006 \pm 0.00075$ which we divide by our best value $B(D^0 \rightarrow K^- \pi^+) = (3.947 \pm 0.030) \times 10^{-2}$. Our first error is their experiment's error and our second error is the systematic error from using our best value.
- BORTOLETTO 92 reports $[\Gamma(B \rightarrow D^0/\bar{D}^0 \text{ anything})/\Gamma_{\text{total}}] \times [B(D^0 \rightarrow K^- \pi^+)] = 0.0233 \pm 0.0012 \pm 0.0014$ which we divide by our best value $B(D^0 \rightarrow K^- \pi^+) = (3.947 \pm 0.030) \times 10^{-2}$. Our first error is their experiment's error and our second error is the systematic error from using our best value.
- ALBRECHT 91H reports $[\Gamma(B \rightarrow D^0/\bar{D}^0 \text{ anything})/\Gamma_{\text{total}}] \times [B(D^0 \rightarrow K^- \pi^+)] = 0.0194 \pm 0.0015 \pm 0.0025$ which we divide by our best value $B(D^0 \rightarrow K^- \pi^+) = (3.947 \pm 0.030) \times 10^{-2}$. Our first error is their experiment's error and our second error is the systematic error from using our best value.
- BORTOLETTO 87 reports $[\Gamma(B \rightarrow D^0/\bar{D}^0 \text{ anything})/\Gamma_{\text{total}}] \times [B(D^0 \rightarrow K^- \pi^+)] = 0.0210 \pm 0.0015 \pm 0.0021$ which we divide by our best value $B(D^0 \rightarrow K^- \pi^+) = (3.947 \pm 0.030) \times 10^{-2}$. Our first error is their experiment's error and our second error is the systematic error from using our best value.
- GREEN 83 reports $[\Gamma(B \rightarrow D^0/\bar{D}^0 \text{ anything})/\Gamma_{\text{total}}] \times [B(D^0 \rightarrow K^- \pi^+)] = 0.024 \pm 0.006 \pm 0.004$ which we divide by our best value $B(D^0 \rightarrow K^- \pi^+) = (3.947 \pm 0.030) \times 10^{-2}$. Our first error is their experiment's error and our second error is the systematic error from using our best value.



$\Gamma(D^- \ell^+ \nu_\ell \text{ anything})/\Gamma(\bar{D}^0 \ell^+ \nu_\ell \text{ anything})$				Γ_4/Γ_5
VALUE	EVTs	DOCUMENT ID	TECN	COMMENT
0.359 ± 0.006 ± 0.009		1 AAIJ 19AD	LHCB	pp at 13 TeV
1 AAIJ 19AD uses $D^0 \rightarrow K^- \pi^+$ and $D^+ \rightarrow K^- \pi^+ \pi^+$ modes.				

$\Gamma(D^*(2010)^\pm \text{ anything})/\Gamma_{\text{total}}$				Γ_{35}/Γ
VALUE	EVTs	DOCUMENT ID	TECN	COMMENT
0.225 ± 0.015	OUR AVERAGE			
0.247 ± 0.019 ± 0.01		1 GIBBONS 97B	CLE2	$e^+e^- \rightarrow \Upsilon(4S)$
0.205 ± 0.019 ± 0.007		2 ALBRECHT 96D	ARG	$e^+e^- \rightarrow \Upsilon(4S)$
0.230 ± 0.028 ± 0.009		3 BORTOLETTO92	CLEO	$e^+e^- \rightarrow \Upsilon(4S)$
● ● ● We do not use the following data for averages, fits, limits, etc. ● ● ●				
0.283 ± 0.053 ± 0.002		4 ALBRECHT 91H	ARG	Sup. by ALBRECHT 96D
0.22 ± 0.04 ± 0.07 ± 0.04	5200	5 BORTOLETTO87	CLEO	$e^+e^- \rightarrow \Upsilon(4S)$
0.27 ± 0.06 ± 0.08 ± 0.06	510	6 CSORNA 85	CLEO	Repl. by BORTOLETTO 87

- GIBBONS 97B reports $B(B \rightarrow D^*(2010)^\pm \text{ anything}) = 0.239 \pm 0.015 \pm 0.014 \pm 0.009$ using CLEO measured D and D^* branching fractions. We rescale to our PDG 96 values of D and D^* branching ratios. Our first error is their experiment's error and our second error is the systematic error from using our best value.
- ALBRECHT 96D reports $B(B \rightarrow D^*(2010)^\pm \text{ anything}) = 0.196 \pm 0.019$ using CLEO measured $B(D^*(2010)^+ \rightarrow D^0 \pi^+) = 0.681 \pm 0.01 \pm 0.013$, $B(D^0 \rightarrow K^- \pi^+) = 0.0401 \pm 0.0014$, $B(D^0 \rightarrow K^- \pi^+ \pi^+ \pi^-) = 0.081 \pm 0.005$. We rescale to our PDG 96 values of D and D^* branching ratios. Our first error is their experiment's error and our second error is the systematic error from using our best value.
- BORTOLETTO 92 reports $B(B \rightarrow D^*(2010)^\pm \text{ anything}) = 0.25 \pm 0.03 \pm 0.04$ using MARK II $B(D^*(2010)^+ \rightarrow D^0 \pi^+) = 0.57 \pm 0.06$ and $B(D^0 \rightarrow K^- \pi^+) = 0.042 \pm$

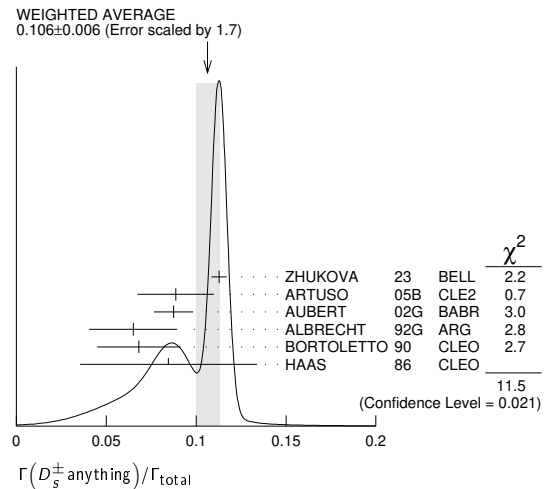
0.008. We rescale to our PDG 96 values of D and D^* branching ratios. Our first error is their experiment's error and our second error is the systematic error from using our best value.

- ALBRECHT 91H reports $0.348 \pm 0.060 \pm 0.035$ from a measurement of $[\Gamma(B \rightarrow D^*(2010)^\pm \text{ anything})/\Gamma_{\text{total}}] \times [B(D^*(2010)^+ \rightarrow D^0 \pi^+)]$ assuming $B(D^*(2010)^+ \rightarrow D^0 \pi^+) = 0.55 \pm 0.04$, which we rescale to our best value $B(D^*(2010)^+ \rightarrow D^0 \pi^+) = (67.7 \pm 0.5) \times 10^{-2}$. Our first error is their experiment's error and our second error is the systematic error from using our best value. Uses the PDG 90 $B(D^0 \rightarrow K^- \pi^+) = 0.0371 \pm 0.0025$.
- BORTOLETTO 87 uses old MARK III (BALTRUSAITIS 86E) branching ratios $B(D^0 \rightarrow K^- \pi^+) = 0.056 \pm 0.004 \pm 0.003$ and also assumes $B(D^*(2010)^+ \rightarrow D^0 \pi^+) = 0.60^{+0.08}_{-0.15}$. The product branching ratio for $B(B \rightarrow D^*(2010)^+) B(D^*(2010)^+ \rightarrow D^0 \pi^+)$ is $0.13 \pm 0.02 \pm 0.012$. Superseded by BORTOLETTO 92.
- $V-A$ momentum spectrum used to extrapolate below $p = 1$ GeV. We correct the value assuming $B(D^0 \rightarrow K^- \pi^+) = 0.042 \pm 0.006$ and $B(D^+ \rightarrow D^0 \pi^+) = 0.6^{+0.08}_{-0.15}$. The product branching fraction is $B(B \rightarrow D^* X) \cdot B(D^* \rightarrow \pi^+ D^0) \cdot B(D^0 \rightarrow K^- \pi^+) = (68 \pm 15 \pm 9) \times 10^{-4}$.

$\Gamma(D_s^*(2007)^0 \text{ anything})/\Gamma_{\text{total}}$				Γ_{36}/Γ
VALUE	EVTs	DOCUMENT ID	TECN	COMMENT
0.260 ± 0.023 ± 0.015		1 GIBBONS 97B	CLE2	$e^+e^- \rightarrow \Upsilon(4S)$

- GIBBONS 97B reports $B(B \rightarrow D_s^*(2007)^0 \text{ anything}) = 0.247 \pm 0.012 \pm 0.018 \pm 0.018$ using CLEO measured D and D^* branching fractions. We rescale to our PDG 96 values of D and D^* branching ratios. Our first error is their experiment's error and our second error is the systematic error from using our best value.

$\Gamma(D_s^\pm \text{ anything})/\Gamma_{\text{total}}$				Γ_{37}/Γ
VALUE	EVTs	DOCUMENT ID	TECN	COMMENT
0.106 ± 0.006	OUR AVERAGE	Error includes scale factor of 1.7. See the ideogram below.		
0.1128 ± 0.0003 ± 0.0043		ZHUKOVA 23	BELL	$e^+e^- \rightarrow \Upsilon(4S)$
0.089 ± 0.010 ± 0.008		1 ARTUSO 05B	CLE2	$e^+e^- \rightarrow \Upsilon(5S)$
0.087 ± 0.005 ± 0.008		2 AUBERT 02G	BABR	$e^+e^- \rightarrow \Upsilon(4S)$
0.065 ± 0.011 ± 0.006		3 ALBRECHT 92G	ARG	$e^+e^- \rightarrow \Upsilon(4S)$
0.068 ± 0.010 ± 0.006	257	4 BORTOLETTO90	CLEO	$e^+e^- \rightarrow \Upsilon(4S)$
0.085 ± 0.022 ± 0.008		5 HAAS 86	CLEO	$e^+e^- \rightarrow \Upsilon(4S)$
● ● ● We do not use the following data for averages, fits, limits, etc. ● ● ●				
0.094 ± 0.007 ± 0.008		6 GIBAUT 96	CLE2	Repl. by ARTUSO 05B
0.094 ± 0.024 ± 0.008		7 ALBRECHT 87H	ARG	$e^+e^- \rightarrow \Upsilon(4S)$



- ARTUSO 05B reports $0.0905 \pm 0.0025 \pm 0.0140$ from a measurement of $[\Gamma(B \rightarrow D_s^\pm \text{ anything})/\Gamma_{\text{total}}] \times [B(D_s^\pm \rightarrow \phi \pi^\pm)]$ assuming $B(D_s^\pm \rightarrow \phi \pi^\pm) = (4.4 \pm 0.5) \times 10^{-2}$, which we rescale to our best value $B(D_s^\pm \rightarrow \phi \pi^\pm) = (4.5 \pm 0.4) \times 10^{-2}$. Our first error is their experiment's error and our second error is the systematic error from using our best value.
- AUBERT 02G reports $[\Gamma(B \rightarrow D_s^\pm \text{ anything})/\Gamma_{\text{total}}] \times [B(D_s^\pm \rightarrow \phi \pi^\pm)] = 0.00393 \pm 0.00007 \pm 0.00021$ which we divide by our best value $B(D_s^\pm \rightarrow \phi \pi^\pm) = (4.5 \pm 0.4) \times 10^{-2}$. Our first error is their experiment's error and our second error is the systematic error from using our best value.
- ALBRECHT 92G reports $[\Gamma(B \rightarrow D_s^\pm \text{ anything})/\Gamma_{\text{total}}] \times [B(D_s^\pm \rightarrow \phi \pi^\pm)] = 0.00292 \pm 0.00039 \pm 0.00031$ which we divide by our best value $B(D_s^\pm \rightarrow \phi \pi^\pm) = (4.5 \pm 0.4) \times 10^{-2}$. Our first error is their experiment's error and our second error is the systematic error from using our best value.
- BORTOLETTO 90 reports $[\Gamma(B \rightarrow D_s^\pm \text{ anything})/\Gamma_{\text{total}}] \times [B(D_s^\pm \rightarrow \phi \pi^\pm)] = 0.00306 \pm 0.00047$ which we divide by our best value $B(D_s^\pm \rightarrow \phi \pi^\pm) = (4.5 \pm 0.4) \times 10^{-2}$. Our first error is their experiment's error and our second error is the systematic error from using our best value.
- HAAS 86 reports $[\Gamma(B \rightarrow D_s^\pm \text{ anything})/\Gamma_{\text{total}}] \times [B(D_s^\pm \rightarrow \phi \pi^\pm)] = 0.0038 \pm 0.0010$ which we divide by our best value $B(D_s^\pm \rightarrow \phi \pi^\pm) = (4.5 \pm 0.4) \times 10^{-2}$. Our first

Meson Particle Listings

 B^\pm/B^0 ADMIXTURE

error is their experiment's error and our second error is the systematic error from using our best value. $64 \pm 22\%$ decays are 2-body.

⁶GIBAUT 96 reports $0.1211 \pm 0.0039 \pm 0.0088$ from a measurement of $[\Gamma(B \rightarrow D_s^\pm \text{ anything})/\Gamma_{\text{total}}] \times [B(D_s^\pm \rightarrow \phi\pi^\pm)]$ assuming $B(D_s^\pm \rightarrow \phi\pi^\pm) = 0.035$, which we rescale to our best value $B(D_s^\pm \rightarrow \phi\pi^\pm) = (4.5 \pm 0.4) \times 10^{-2}$. Our first error is their experiment's error and our second error is the systematic error from using our best value.

⁷ALBRECHT 87H reports $[\Gamma(B \rightarrow D_s^\pm \text{ anything})/\Gamma_{\text{total}}] \times [B(D_s^\pm \rightarrow \phi\pi^\pm)] = 0.0042 \pm 0.0009 \pm 0.0006$ which we divide by our best value $B(D_s^\pm \rightarrow \phi\pi^\pm) = (4.5 \pm 0.4) \times 10^{-2}$. Our first error is their experiment's error and our second error is the systematic error from using our best value. $46 \pm 16\%$ of $B \rightarrow D_s X$ decays are 2-body. Superseded by ALBRECHT 92c.

$\Gamma(D_s^{*\pm} \text{ anything})/\Gamma_{\text{total}}$				Γ_{38}/Γ
VALUE	DOCUMENT ID	TECN	COMMENT	
$0.063 \pm 0.009 \pm 0.006$	¹ AUBERT	02G	BABR $e^+e^- \rightarrow \Upsilon(4S)$	

¹AUBERT 02g reports $[\Gamma(B \rightarrow D_s^{*\pm} \text{ anything})/\Gamma_{\text{total}}] \times [B(D_s^\pm \rightarrow \phi\pi^\pm)] = 0.00284 \pm 0.00029 \pm 0.00025$ which we divide by our best value $B(D_s^\pm \rightarrow \phi\pi^\pm) = (4.5 \pm 0.4) \times 10^{-2}$. Our first error is their experiment's error and our second error is the systematic error from using our best value.

$\Gamma(D_s^{*\pm} \bar{D}^{(*)})/\Gamma(D_s^{*\pm} \text{ anything})$				Γ_{39}/Γ_{38}
Sum over modes				
VALUE	DOCUMENT ID	TECN	COMMENT	
$0.533 \pm 0.037 \pm 0.037$	AUBERT	02G	BABR $e^+e^- \rightarrow \Upsilon(4S)$	

$\Gamma(\bar{D} D_{s0}(2317))/\Gamma_{\text{total}}$				Γ_{40}/Γ
VALUE	DOCUMENT ID	TECN	COMMENT	
seen	¹ KROKOVNY	03B	BELL $e^+e^- \rightarrow \Upsilon(4S)$	

¹The product branching ratio for $B(B \rightarrow \bar{D} D_{s0}(2317)^+) \times B(D_{s0}(2317)^+ \rightarrow D_s \pi^0)$ is measured to be $(8.5_{-1.9}^{+2.1} \pm 2.6) \times 10^{-4}$.

$\Gamma(\bar{D} D_{sJ}(2457))/\Gamma_{\text{total}}$				Γ_{41}/Γ
VALUE	DOCUMENT ID	TECN	COMMENT	
seen	¹ KROKOVNY	03B	BELL $e^+e^- \rightarrow \Upsilon(4S)$	

¹The product branching ratio for $B(B \rightarrow \bar{D} D_{sJ}(2457)^+) \times B(D_{sJ}(2457)^+ \rightarrow D_s^+ \pi^0, D_s^+ \gamma)$ are measured to be $(17.8_{-3.9}^{+4.5} \pm 5.3) \times 10^{-4}$ and $(6.7_{-1.2}^{+1.3} \pm 2.0) \times 10^{-4}$, respectively.

$[\Gamma(D^{(*)} \bar{D}^{(*)} K^0) + \Gamma(D^{(*)} \bar{D}^{(*)} K^\pm)]/\Gamma_{\text{total}}$				Γ_{42}/Γ
VALUE	DOCUMENT ID	TECN	COMMENT	
$0.071 \pm 0.025 \pm 0.010$ -0.015 ± 0.009	¹ BARATE	98Q	ALEP $e^+e^- \rightarrow Z$	

¹The systematic error includes the uncertainties due to the charm branching ratios.

$\Gamma(b \rightarrow c \bar{c} s)/\Gamma_{\text{total}}$				Γ_{43}/Γ
VALUE	DOCUMENT ID	TECN	COMMENT	
0.219 ± 0.037	¹ COAN	98	CLE2 $e^+e^- \rightarrow \Upsilon(4S)$	

¹COAN 98 uses D - ℓ correlation.

$\Gamma(D_s^{(*)} \bar{D}^{(*)})/\Gamma(D_s^{*\pm} \text{ anything})$				Γ_{44}/Γ_{37}
Sum over modes.				
VALUE	DOCUMENT ID	TECN	COMMENT	
0.469 ± 0.017 OUR AVERAGE				
$0.464 \pm 0.013 \pm 0.015$	AUBERT	02G	BABR $e^+e^- \rightarrow \Upsilon(4S)$	
$0.56 \pm 0.21 \pm 0.09$ -0.15 ± 0.08	¹ BARATE	98Q	ALEP $e^+e^- \rightarrow Z$	
$0.457 \pm 0.019 \pm 0.037$	GIBAUT	96	CLE2 $e^+e^- \rightarrow \Upsilon(4S)$	
$0.58 \pm 0.07 \pm 0.09$	ALBRECHT	92G	ARG $e^+e^- \rightarrow \Upsilon(4S)$	
0.56 ± 0.10	BORTOLETTO	09Q	CLEO $e^+e^- \rightarrow \Upsilon(4S)$	

¹BARATE 98Q measures $B(B \rightarrow D_s^{(*)} \bar{D}^{(*)}) = 0.056_{-0.015}^{+0.021} \pm 0.009 \pm 0.019$, where the third error results from the uncertainty on the different D branching ratios and is dominated by the uncertainty on $B(D_s^\pm \rightarrow \phi\pi^\pm)$. We divide $B(B \rightarrow D_s^{(*)} \bar{D}^{(*)})$ by our best value of $B(B \rightarrow D_s \text{ anything}) = 0.1 \pm 0.025$.

$\Gamma(D^* D^*(2010)^\pm)/\Gamma_{\text{total}}$				Γ_{45}/Γ
VALUE	CL%	DOCUMENT ID	TECN	COMMENT
$<5.9 \times 10^{-3}$	90	BARATE	98Q	ALEP $e^+e^- \rightarrow Z$

$[\Gamma(D^* D^*(2010)^\pm) + \Gamma(D^* D^\pm)]/\Gamma_{\text{total}}$				Γ_{46}/Γ
VALUE	CL%	DOCUMENT ID	TECN	COMMENT
$<5.5 \times 10^{-3}$	90	BARATE	98Q	ALEP $e^+e^- \rightarrow Z$

$\Gamma(D D^\pm)/\Gamma_{\text{total}}$				Γ_{47}/Γ
VALUE	CL%	DOCUMENT ID	TECN	COMMENT
$<3.1 \times 10^{-3}$	90	BARATE	98Q	ALEP $e^+e^- \rightarrow Z$

$\Gamma(D_s^{(*)} \pm \bar{D}^{(*)} X (n\pi^\pm))/\Gamma_{\text{total}}$				Γ_{48}/Γ
VALUE	DOCUMENT ID	TECN	COMMENT	
$0.094 \pm 0.040 \pm 0.034$ -0.031 ± 0.024	¹ BARATE	98Q	ALEP $e^+e^- \rightarrow Z$	

¹The systematic error includes the uncertainties due to the charm branching ratios.

$\Gamma(\bar{D}^*(2010)\gamma)/\Gamma_{\text{total}}$				Γ_{49}/Γ
VALUE	CL%	DOCUMENT ID	TECN	COMMENT
$<1.1 \times 10^{-3}$	90	¹ LESIAK	92	CBAL $e^+e^- \rightarrow \Upsilon(4S)$

¹LESIAK 92 set a limit on the inclusive process $B(b \rightarrow s\gamma) < 2.8 \times 10^{-3}$ at 90% CL for the range of masses of 892–2045 MeV, independent of assumptions about s-quark hadronization.

$\Gamma(D_s^+ \pi^-, D_s^+ \pi^0, D_s^+ \rho^-, D_s^+ \rho^0, D_s^+ \pi^0, D_s^+ \pi^0, D_s^+ \eta, D_s^+ \eta, D_s^+ \rho^0, D_s^+ \rho^0, D_s^+ \omega, D_s^+ \omega)/\Gamma_{\text{total}}$				Γ_{50}/Γ
Sum over modes.				
VALUE	CL%	DOCUMENT ID	TECN	COMMENT
$<4 \times 10^{-4}$	90	¹ ALEXANDER	93B	CLE2 $e^+e^- \rightarrow \Upsilon(4S)$

¹ALEXANDER 93B reports $< 4.8 \times 10^{-4}$ from a measurement of $[\Gamma(B \rightarrow D_s^+ \pi^-, D_s^+ \pi^0, D_s^+ \rho^-, D_s^+ \rho^0, D_s^+ \pi^0, D_s^+ \pi^0, D_s^+ \eta, D_s^+ \eta, D_s^+ \rho^0, D_s^+ \rho^0, D_s^+ \omega, D_s^+ \omega)/\Gamma_{\text{total}}] \times [B(D_s^\pm \rightarrow \phi\pi^\pm)]$ assuming $B(D_s^\pm \rightarrow \phi\pi^\pm) = 0.037$, which we rescale to our best value $B(D_s^\pm \rightarrow \phi\pi^\pm) = 4.5 \times 10^{-2}$. This branching ratio limit provides a model-dependent upper limit $|V_{ub}|/|V_{cb}| < 0.16$ at CL=90%.

$\Gamma(D_{s1}(2536)^+ \text{ anything})/\Gamma_{\text{total}}$				Γ_{51}/Γ
$D_{s1}(2536)^+$ is the narrow P -wave D_s^+ meson with $J^P = 1^+$.				
VALUE	CL%	DOCUMENT ID	TECN	COMMENT
<0.0095	90	¹ BISHAI	98	CLE2 $e^+e^- \rightarrow \Upsilon(4S)$

¹Assuming factorization, the decay constant $f_{D_{s1}^+}$ is at least a factor of 2.5 times smaller than $f_{D_s^+}$.

$\Gamma(J/\psi(1S) \text{ anything})/\Gamma_{\text{total}}$				Γ_{52}/Γ
VALUE (units 10^{-2})	EVTs	DOCUMENT ID	TECN	COMMENT
1.094 ± 0.032 OUR AVERAGE				Error includes scale factor of 1.1.
$1.057 \pm 0.012 \pm 0.040$		¹ AUBERT	03F	BABR $e^+e^- \rightarrow \Upsilon(4S)$
$1.121 \pm 0.013 \pm 0.042$		ANDERSON	02	CLE2 $e^+e^- \rightarrow \Upsilon(4S)$
$1.29 \pm 0.45 \pm 0.01$	27	² MASCHMANN	90	CBAL $e^+e^- \rightarrow \Upsilon(4S)$
$1.24 \pm 0.27 \pm 0.01$	120	³ ALBRECHT	87D	ARG $e^+e^- \rightarrow \Upsilon(4S)$
$1.35 \pm 0.24 \pm 0.01$	52	⁴ ALAM	86	CLEO $e^+e^- \rightarrow \Upsilon(4S)$
$1.12 \pm 0.06 \pm 0.01$	1489	⁵ BALEST	95B	CLE2 $e^+e^- \rightarrow \Upsilon(4S)$
1.4 ± 0.6 -0.5	7	⁶ ALBRECHT	85H	ARG $e^+e^- \rightarrow \Upsilon(4S)$
$1.1 \pm 0.21 \pm 0.23$	46	⁷ HAAS	85	CLEO Repl. by ALAM 86

¹AUBERT 03F also reports the momentum distribution and helicity of $J/\psi \rightarrow \ell^+ \ell^-$ in the $\Upsilon(4S)$ center-of-mass frame.

²MASCHMANN 90 reports $(1.12 \pm 0.33 \pm 0.25) \times 10^{-2}$ from a measurement of $[\Gamma(B \rightarrow J/\psi(1S) \text{ anything})/\Gamma_{\text{total}}] \times [B(J/\psi(1S) \rightarrow e^+e^-)]$ assuming $B(J/\psi(1S) \rightarrow e^+e^-) = 0.069 \pm 0.009$, which we rescale to our best value $B(J/\psi(1S) \rightarrow e^+e^-) = (5.971 \pm 0.032) \times 10^{-2}$. Our first error is their experiment's error and our second error is the systematic error from using our best value.

³ALBRECHT 87D reports $(1.07 \pm 0.16 \pm 0.22) \times 10^{-2}$ from a measurement of $[\Gamma(B \rightarrow J/\psi(1S) \text{ anything})/\Gamma_{\text{total}}] \times [B(J/\psi(1S) \rightarrow e^+e^-)]$ assuming $B(J/\psi(1S) \rightarrow e^+e^-) = 0.069 \pm 0.009$, which we rescale to our best value $B(J/\psi(1S) \rightarrow e^+e^-) = (5.971 \pm 0.032) \times 10^{-2}$. Our first error is their experiment's error and our second error is the systematic error from using our best value. ALBRECHT 87D find the branching ratio for J/ψ not from $\psi(2S)$ to be 0.0081 ± 0.0023 .

⁴ALAM 86 reports $(1.09 \pm 0.16 \pm 0.21) \times 10^{-2}$ from a measurement of $[\Gamma(B \rightarrow J/\psi(1S) \text{ anything})/\Gamma_{\text{total}}] \times [B(J/\psi(1S) \rightarrow \mu^+\mu^-)]$ assuming $B(J/\psi(1S) \rightarrow \mu^+\mu^-) = 0.074 \pm 0.012$, which we rescale to our best value $B(J/\psi(1S) \rightarrow \mu^+\mu^-) = (5.961 \pm 0.033) \times 10^{-2}$. Our first error is their experiment's error and our second error is the systematic error from using our best value.

⁵BALEST 95B reports $(1.12 \pm 0.04 \pm 0.06) \times 10^{-2}$ from a measurement of $[\Gamma(B \rightarrow J/\psi(1S) \text{ anything})/\Gamma_{\text{total}}] \times [B(J/\psi(1S) \rightarrow e^+e^-)]$ assuming $B(J/\psi(1S) \rightarrow e^+e^-) = 0.0599 \pm 0.0025$, which we rescale to our best value $B(J/\psi(1S) \rightarrow e^+e^-) = (5.971 \pm 0.032) \times 10^{-2}$. Our first error is their experiment's error and our second error is the systematic error from using our best value. They measure $J/\psi(1S) \rightarrow e^+e^-$ and $\mu^+\mu^-$ and use PDG 1994 values for the branching fractions. The rescaling is the same for either mode so we use e^+e^- .

⁶Statistical and systematic errors were added in quadrature. ALBRECHT 85H also report a CL = 90% limit of 0.007 for $B \rightarrow J/\psi(1S) + X$ where $m_X < 1$ GeV.

⁷Dimuon and dielectron events used.

¹AUBERT 03F also reports the momentum distribution and helicity of $J/\psi \rightarrow \ell^+ \ell^-$ in the $\Upsilon(4S)$ center-of-mass frame.

²MASCHMANN 90 reports $(1.12 \pm 0.33 \pm 0.25) \times 10^{-2}$ from a measurement of $[\Gamma(B \rightarrow J/\psi(1S) \text{ anything})/\Gamma_{\text{total}}] \times [B(J/\psi(1S) \rightarrow e^+e^-)]$ assuming $B(J/\psi(1S) \rightarrow e^+e^-) = 0.069 \pm 0.009$, which we rescale to our best value $B(J/\psi(1S) \rightarrow e^+e^-) = (5.971 \pm 0.032) \times 10^{-2}$. Our first error is their experiment's error and our second error is the systematic error from using our best value.

³ALBRECHT 87D reports $(1.07 \pm 0.16 \pm 0.22) \times 10^{-2}$ from a measurement of $[\Gamma(B \rightarrow J/\psi(1S) \text{ anything})/\Gamma_{\text{total}}] \times [B(J/\psi(1S) \rightarrow e^+e^-)]$ assuming $B(J/\psi(1S) \rightarrow e^+e^-) = 0.069 \pm 0.009$, which we rescale to our best value $B(J/\psi(1S) \rightarrow e^+e^-) = (5.971 \pm 0.032) \times 10^{-2}$. Our first error is their experiment's error and our second error is the systematic error from using our best value. ALBRECHT 87D find the branching ratio for J/ψ not from $\psi(2S)$ to be 0.0081 ± 0.0023 .

⁴ALAM 86 reports $(1.09 \pm 0.16 \pm 0.21) \times 10^{-2}$ from a measurement of $[\Gamma(B \rightarrow J/\psi(1S) \text{ anything})/\Gamma_{\text{total}}] \times [B(J/\psi(1S) \rightarrow \mu^+\mu^-)]$ assuming $B(J/\psi(1S) \rightarrow \mu^+\mu^-) = 0.074 \pm 0.012$, which we rescale to our best value $B(J/\psi(1S) \rightarrow \mu^+\mu^-) = (5.961 \pm 0.033) \times 10^{-2}$. Our first error is their experiment's error and our second error is the systematic error from using our best value.

⁵BALEST 95B reports $(1.12 \pm 0.04 \pm 0.06) \times 10^{-2}$ from a measurement of $[\Gamma(B \rightarrow J/\psi(1S) \text{ anything})/\Gamma_{\text{total}}] \times [B(J/\psi(1S) \rightarrow e^+e^-)]$ assuming $B(J/\psi(1S) \rightarrow e^+e^-) = 0.0599 \pm 0.0025$, which we rescale to our best value $B(J/\psi(1S) \rightarrow e^+e^-) = (5.971 \pm 0.032) \times 10^{-2}$. Our first error is their experiment's error and our second error is the systematic error from using our best value. They measure $J/\psi(1S) \rightarrow e^+e^-$ and $\mu^+\mu^-$ and use PDG 1994 values for the branching fractions. The rescaling is the same for either mode so we use e^+e^- .

⁶Statistical and systematic errors were added in quadrature. ALBRECHT 85H also report a CL = 90% limit of 0.007 for $B \rightarrow J/\psi(1S) + X$ where $m_X < 1$ GeV.

⁷Dimuon and dielectron events used.

$\Gamma(J/\psi(1S) \text{ direct anything})/\Gamma_{\text{total}}$				Γ_{53}/Γ
VALUE	DOCUMENT ID	TECN	COMMENT	
0.0078 ± 0.0004 OUR AVERAGE				Error includes scale factor of 1.1.
$0.00740 \pm 0.00023 \pm 0.00043$	¹ AUBERT	03F	BABR $e^+e^- \rightarrow \Upsilon(4S)$	
$0.00813 \pm 0.00017 \pm 0.00037$	² ANDERSON	02	CLE2 $e^+e^- \rightarrow \Upsilon(4S)$	
0.0080 ± 0.0008	³ BALEST	95B	CLE2 $e^+e^- \rightarrow \Upsilon(4S)$	

¹AUBERT 03F also reports the helicity of $J/\psi \rightarrow \ell^+ \ell^-$ produced directly in B decay.

²Also reports the measurement of $J/\psi \rightarrow \ell^+ \ell^-$ polarization produced directly from B decay.

³BALEST 95B assume PDG 1994 values for sub mode branching ratios. $J/\psi(1S)$ mesons are reconstructed in $J/\psi(1S) \rightarrow e^+e^-$ and $J/\psi(1S) \rightarrow \mu^+\mu^-$. The $B \rightarrow J/\psi(1S) X$ branching ratio contains $J/\psi(1S)$ mesons directly from B decays and also from feeddown through $\psi(2S) \rightarrow J/\psi(1S), \chi_{c1}(1P) \rightarrow J/\psi(1S)$, or $\chi_{c2}(1P) \rightarrow J/\psi(1S)$. Using the measured inclusive rates, BALEST 95B corrects for the feeddown and finds the $B \rightarrow J/\psi(1S)$ (direct) X branching ratio.

$\Gamma(\psi(2S) \text{ anything})/\Gamma_{\text{total}}$ Γ_{54}/Γ

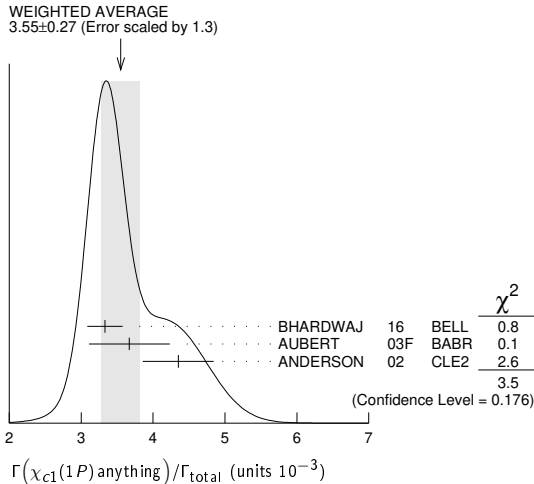
VALUE	EVTs	DOCUMENT ID	TECN	COMMENT
0.00307 ± 0.00021 OUR AVERAGE				
0.00297 ± 0.00020 ± 0.00020		AUBERT	03F BABR	$e^+e^- \rightarrow \Upsilon(4S)$
0.00316 ± 0.00014 ± 0.00028		¹ ANDERSON	02 CLE2	$e^+e^- \rightarrow \Upsilon(4S)$
0.0046 ± 0.0017 ± 0.0011	8	ALBRECHT	87D ARG	$e^+e^- \rightarrow \Upsilon(4S)$
• • • We do not use the following data for averages, fits, limits, etc. • • •				
0.0034 ± 0.0004 ± 0.0003	240	² BALEST	95B CLE2	$e^+e^- \rightarrow \Upsilon(4S)$

¹ Also reports the measurement of $\psi(2S) \rightarrow \ell^+ \ell^-$ polarization produced directly from B decay.
² BALEST 95B assume PDG 1994 values for sub mode branching ratios. They find $B(B \rightarrow \psi(2S)X, \psi(2S) \rightarrow \ell^+ \ell^-) = 0.30 \pm 0.05 \pm 0.04$ and $B(B \rightarrow \psi(2S)X, \psi(2S) \rightarrow J/\psi(1S)\pi^+\pi^-) = 0.37 \pm 0.05 \pm 0.05$. Weighted average is quoted for $B(B \rightarrow \psi(2S)X)$.

$\Gamma(\chi_{c1}(1P) \text{ anything})/\Gamma_{\text{total}}$ Γ_{55}/Γ

VALUE (units 10^{-3})	EVTs	DOCUMENT ID	TECN	COMMENT
3.55 ± 0.27 OUR AVERAGE				Error includes scale factor of 1.3. See the ideogram below.
3.33 ± 0.05 ± 0.24		¹ BHARDWAJ	16 BELL	$e^+e^- \rightarrow \Upsilon(4S)$
3.67 ± 0.35 ± 0.44		AUBERT	03F BABR	$e^+e^- \rightarrow \Upsilon(4S)$
4.35 ± 0.29 ± 0.40		ANDERSON	02 CLE2	$e^+e^- \rightarrow \Upsilon(4S)$
• • • We do not use the following data for averages, fits, limits, etc. • • •				
3.63 ± 0.22 ± 0.34		² ABE	02L BELL	Repl. by BHARDWAJ 16
3.30 ± 0.35 ± 0.12		³ CHEN	01 CLE2	$e^+e^- \rightarrow \Upsilon(4S)$
4.0 ± 0.6 ± 0.4	112	⁴ BALEST	95B CLE2	Repl. by CHEN 01
10.5 ± 3.5 ± 2.5		⁵ ALBRECHT	92E ARG	$e^+e^- \rightarrow \Upsilon(4S)$

- ¹ Assumes equal production of B^+ and B^0 at the $\Upsilon(4S)$.
² ABE 02L uses PDG 01 values for $B(J/\psi(1S) \rightarrow \ell^+ \ell^-)$ and $B(\chi_{c1,c2} \rightarrow J/\psi(1S)\gamma)$.
³ CHEN 01 reports $0.00414 \pm 0.00031 \pm 0.00040$ from a measurement of $[\Gamma(B \rightarrow \chi_{c1}(1P) \text{ anything})/\Gamma_{\text{total}}] \times [B(\chi_{c1}(1P) \rightarrow \gamma J/\psi(1S))]$ assuming $B(\chi_{c1}(1P) \rightarrow \gamma J/\psi(1S)) = 0.273 \pm 0.016$, which we rescale to our best value $B(\chi_{c1}(1P) \rightarrow \gamma J/\psi(1S)) = (34.3 \pm 1.3) \times 10^{-2}$. Our first error is their experiment's error and our second error is the systematic error from using our best value. Assumes equal production of B^+ and B^0 at the $\Upsilon(4S)$.
⁴ BALEST 95B assume $B(\chi_{c1}(1P) \rightarrow J/\psi(1S)\gamma) = (27.3 \pm 1.6) \times 10^{-2}$, the PDG 1994 value. Fit to ψ -photon invariant mass distribution allows for a $\chi_{c1}(1P)$ and a $\chi_{c2}(1P)$ component.
⁵ ALBRECHT 92E assumes no $\chi_{c2}(1P)$ production.



$\Gamma(\chi_{c1}(1P) \text{ (direct) anything})/\Gamma_{\text{total}}$ Γ_{56}/Γ

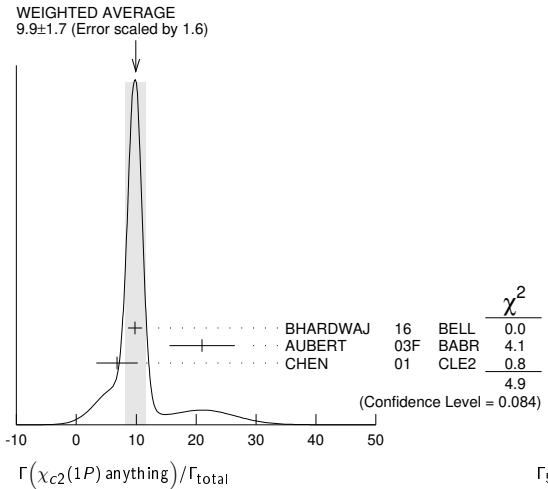
VALUE (units 10^{-3})	DOCUMENT ID	TECN	COMMENT
3.08 ± 0.19 OUR AVERAGE			
3.03 ± 0.05 ± 0.24	¹ BHARDWAJ	16 BELL	$e^+e^- \rightarrow \Upsilon(4S)$
3.41 ± 0.35 ± 0.42	AUBERT	03F BABR	$e^+e^- \rightarrow \Upsilon(4S)$
3.1 ± 0.4 ± 0.1	² CHEN	01 CLE2	$e^+e^- \rightarrow \Upsilon(4S)$
• • • We do not use the following data for averages, fits, limits, etc. • • •			
3.32 ± 0.22 ± 0.34	³ ABE	02L BELL	Repl. by BHARDWAJ 16
3.7 ± 0.7	⁴ BALEST	95B CLE2	Repl. by CHEN 01

- ¹ Assumes equal production of B^+ and B^0 at the $\Upsilon(4S)$.
² CHEN 01 reports $0.00383 \pm 0.00031 \pm 0.00040$ from a measurement of $[\Gamma(B \rightarrow \chi_{c1}(1P) \text{ (direct) anything})/\Gamma_{\text{total}}] \times [B(\chi_{c1}(1P) \rightarrow \gamma J/\psi(1S))]$ assuming $B(\chi_{c1}(1P) \rightarrow \gamma J/\psi(1S)) = 0.273 \pm 0.016$, which we rescale to our best value $B(\chi_{c1}(1P) \rightarrow \gamma J/\psi(1S)) = (34.3 \pm 1.3) \times 10^{-2}$. Our first error is their experiment's error and our second error is the systematic error from using our best value. Assumes equal production of B^+ and B^0 at the $\Upsilon(4S)$.
³ ABE 02L uses PDG 01 values for $B(J/\psi(1S) \rightarrow \ell^+ \ell^-)$ and $B(\chi_{c1,c2} \rightarrow J/\psi(1S)\gamma)$.
⁴ BALEST 95B assume PDG 1994 values. $J/\psi(1S)$ mesons are reconstructed in the e^+e^- and $\mu^+\mu^-$ modes. The $B \rightarrow \chi_{c1}(1P)X$ branching ratio contains $\chi_{c1}(1P)$ mesons directly from B decays and also from feeddown through $\psi(2S) \rightarrow \chi_{c1}(1P)\gamma$. Using the measured inclusive rates, BALEST 95B corrects for the feeddown and finds the $B \rightarrow \chi_{c1}(1P) \text{ (direct) } X$ branching ratio.

$\Gamma(\chi_{c2}(1P) \text{ anything})/\Gamma_{\text{total}}$ Γ_{57}/Γ

VALUE (units 10^{-4})	CL%	DOCUMENT ID	TECN	COMMENT
9.9 ± 1.7 OUR AVERAGE				Error includes scale factor of 1.6. See the ideogram below.
9.8 ± 0.6 ± 1.0		¹ BHARDWAJ	16 BELL	$e^+e^- \rightarrow \Upsilon(4S)$
21.0 ± 4.5 ± 3.1		AUBERT	03F BABR	$e^+e^- \rightarrow \Upsilon(4S)$
6.8 ± 3.4 ± 0.3		² CHEN	01 CLE2	$e^+e^- \rightarrow \Upsilon(4S)$
• • • We do not use the following data for averages, fits, limits, etc. • • •				
18.0 ^{+2.3} _{-2.8} ± 2.6		³ ABE	02L BELL	Repl. by BHARDWAJ 16
<38	90	⁴ BALEST	95B CLE2	Repl. by CHEN 01

- ¹ Assumes equal production of B^+ and B^0 at the $\Upsilon(4S)$.
² CHEN 01 reports $(9.8 \pm 4.8 \pm 1.5) \times 10^{-4}$ from a measurement of $[\Gamma(B \rightarrow \chi_{c2}(1P) \text{ anything})/\Gamma_{\text{total}}] \times [B(\chi_{c2}(1P) \rightarrow \gamma J/\psi(1S))]$ assuming $B(\chi_{c2}(1P) \rightarrow \gamma J/\psi(1S)) = 0.135 \pm 0.011$, which we rescale to our best value $B(\chi_{c2}(1P) \rightarrow \gamma J/\psi(1S)) = (19.5 \pm 0.8) \times 10^{-2}$. Our first error is their experiment's error and our second error is the systematic error from using our best value. Assumes equal production of B^+ and B^0 at the $\Upsilon(4S)$.
³ ABE 02L uses PDG 01 values for $B(J/\psi(1S) \rightarrow \ell^+ \ell^-)$ and $B(\chi_{c1,c2} \rightarrow J/\psi(1S)\gamma)$.
⁴ BALEST 95B assume $B(\chi_{c2}(1P) \rightarrow J/\psi(1S)\gamma) = (13.5 \pm 1.1) \times 10^{-2}$, the PDG 1994 value. $J/\psi(1S)$ mesons are reconstructed in the e^+e^- and $\mu^+\mu^-$ modes, and PDG 1994 branching fractions are used. If interpreted as signal, the 35 ± 13 events correspond to $B(B \rightarrow \chi_{c2}(1P)X) = (0.25 \pm 0.10 \pm 0.03) \times 10^{-2}$.



$\Gamma(\chi_{c2}(1P) \text{ (direct) anything})/\Gamma_{\text{total}}$ Γ_{58}/Γ

VALUE (units 10^{-3})	DOCUMENT ID	TECN	COMMENT
0.75 ± 0.11 OUR AVERAGE			
0.70 ± 0.06 ± 0.10	¹ BHARDWAJ	16 BELL	$e^+e^- \rightarrow \Upsilon(4S)$
1.90 ± 0.45 ± 0.29	AUBERT	03F BABR	$e^+e^- \rightarrow \Upsilon(4S)$
• • • We do not use the following data for averages, fits, limits, etc. • • •			
1.53 ^{+0.23} _{-0.28} ± 0.27	² ABE	02L BELL	Repl. by BHARDWAJ 16

- ¹ Assumes equal production of B^+ and B^0 at the $\Upsilon(4S)$.
² ABE 02L uses PDG 01 values for $B(J/\psi(1S) \rightarrow \ell^+ \ell^-)$ and $B(\chi_{c1,c2} \rightarrow J/\psi(1S)\gamma)$.

$\Gamma(\eta_c(1S) \text{ anything})/\Gamma_{\text{total}}$ Γ_{59}/Γ

VALUE	CL%	DOCUMENT ID	TECN	COMMENT
<0.009	90	¹ BALEST	95B CLE2	$e^+e^- \rightarrow \Upsilon(4S)$

- ¹ BALEST 95B assume PDG 1994 values for sub mode branching ratios. $J/\psi(1S)$ mesons are reconstructed in $J/\psi(1S) \rightarrow e^+e^-$ and $J/\psi(1S) \rightarrow \mu^+\mu^-$. Search region $2960 < m_{\eta_c(1S)} < 3010$ MeV/ c^2 .

$\Gamma(K\chi_{c1}(3872))/\Gamma_{\text{total}}$ Γ_{60}/Γ

VALUE (units 10^{-4})	DOCUMENT ID	TECN	COMMENT
2.5 ± 0.9 OUR AVERAGE			
2.4 ± 0.7 ± 0.8	¹ AUSHEV	10 BELL	$e^+e^- \rightarrow \Upsilon(4S)$
2.7 ^{+0.9} _{-1.0} ± 1.2	^{2,3} GOKHROO	06 BELL	$e^+e^- \rightarrow \Upsilon(4S)$

- ¹ AUSHEV 10 reports $[\Gamma(B \rightarrow K\chi_{c1}(3872))/\Gamma_{\text{total}}] \times [B(\chi_{c1}(3872) \rightarrow \bar{D}^{*0}D^0)] = (0.80 \pm 0.20 \pm 0.10) \times 10^{-4}$ which we divide by our best value $B(\chi_{c1}(3872) \rightarrow \bar{D}^{*0}D^0) = (34 \pm 12) \times 10^{-2}$. Our first error is their experiment's error and our second error is the systematic error from using our best value.
² GOKHROO 06 reports $[\Gamma(B \rightarrow K\chi_{c1}(3872))/\Gamma_{\text{total}}] \times [B(\chi_{c1}(3872) \rightarrow D^0\bar{D}^0\pi^0)] = (1.22 \pm 0.31^{+0.23}_{-0.30}) \times 10^{-4}$ which we divide by our best value $B(\chi_{c1}(3872) \rightarrow D^0\bar{D}^0\pi^0) = (45 \pm 21) \times 10^{-2}$. Our first error is their experiment's error and our second error is the systematic error from using our best value.
³ Measure the near-threshold enhancements in the $(D^0\bar{D}^0\pi^0)$ system at a mass $3875.2 \pm 0.7^{+0.3}_{-1.6} \pm 0.8$ MeV/ c^2 .

Meson Particle Listings

 B^\pm/B^0 ADMIXTURE

$\Gamma(KX(3940), X \rightarrow D^{*0}D^0)/\Gamma_{\text{total}}$					Γ_{61}/Γ
VALUE (units 10^{-4})	CL%	DOCUMENT ID	TECN	COMMENT	
<0.67	90	AUSHEV	10	BELL $e^+e^- \rightarrow \Upsilon(4S)$	

$\Gamma(K\chi_{c0}(3915), \chi_{c0} \rightarrow \omega J/\psi)/\Gamma_{\text{total}}$					Γ_{62}/Γ
VALUE (units 10^{-5})		DOCUMENT ID	TECN	COMMENT	
7.1 ± 1.3 ± 3.1		¹ CHOI	05	BELL $e^+e^- \rightarrow \Upsilon(4S)$	

¹CHOI 05 reports the observation of a near-threshold enhancement in the $\omega J/\psi$ mass spectrum in exclusive $B \rightarrow K\omega J/\psi$. The new state, denoted as $\chi_{c0}(3915)$, is measured to have a mass of $3943 \pm 11 \pm 13$ GeV/ c^2 and a width $\Gamma = 87 \pm 22 \pm 26$ MeV.

$\Gamma(K^\pm \text{ anything})/\Gamma_{\text{total}}$					Γ_{63}/Γ
VALUE		DOCUMENT ID	TECN	COMMENT	
0.789 ± 0.025 OUR AVERAGE					

0.82 ± 0.01 ± 0.05		ALBRECHT	94c	ARG $e^+e^- \rightarrow \Upsilon(4S)$	
0.775 ± 0.015 ± 0.025		¹ ALBRECHT	93i	ARG $e^+e^- \rightarrow \Upsilon(4S)$	
0.85 ± 0.07 ± 0.09		ALAM	87B	CLEO $e^+e^- \rightarrow \Upsilon(4S)$	
• • • We do not use the following data for averages, fits, limits, etc. • • •					
seen		² BRODY	82	CLEO $e^+e^- \rightarrow \Upsilon(4S)$	
seen		³ GIANNINI	82	CUSB $e^+e^- \rightarrow \Upsilon(4S)$	

¹ALBRECHT 93i value is not independent of the sum of $B \rightarrow K^+$ anything and $B \rightarrow K^-$ anything ALBRECHT 94c values.

²Assuming $\Upsilon(4S) \rightarrow B\bar{B}$, a total of $3.38 \pm 0.34 \pm 0.68$ kaons per $\Upsilon(4S)$ decay is found (the second error is systematic). In the context of the standard B -decay model, this defines a value for $(b\text{-quark} \rightarrow c\text{-quark})/(b\text{-quark} \rightarrow \text{all})$ of $1.09 \pm 0.33 \pm 0.13$.

³GIANNINI 82 at CESR-CUSB observed 1.58 ± 0.35 K^0 per hadronic event much higher than 0.82 ± 0.10 below threshold. Consistent with predominant $b \rightarrow cX$ decay.

$\Gamma(K^+ \text{ anything})/\Gamma_{\text{total}}$					Γ_{64}/Γ
VALUE		DOCUMENT ID	TECN	COMMENT	
0.66 ± 0.05		¹ ALBRECHT	94c	ARG $e^+e^- \rightarrow \Upsilon(4S)$	

• • • We do not use the following data for averages, fits, limits, etc. • • •					
0.620 ± 0.013 ± 0.038		² ALBRECHT	94c	ARG $e^+e^- \rightarrow \Upsilon(4S)$	
0.66 ± 0.05 ± 0.07		² ALAM	87B	CLEO $e^+e^- \rightarrow \Upsilon(4S)$	

¹Measurement relies on lepton-kaon correlations. It is for the weak decay vertex and does not include mixing of the neutral B meson. Mixing effects were corrected for by assuming a mixing parameter r of $(18.1 \pm 4.3)\%$.

²Measurement relies on lepton-kaon correlations. It includes production through mixing of the neutral B meson.

$\Gamma(K^- \text{ anything})/\Gamma_{\text{total}}$					Γ_{65}/Γ
VALUE		DOCUMENT ID	TECN	COMMENT	
0.13 ± 0.04		¹ ALBRECHT	94c	ARG $e^+e^- \rightarrow \Upsilon(4S)$	

• • • We do not use the following data for averages, fits, limits, etc. • • •					
0.165 ± 0.011 ± 0.036		² ALBRECHT	94c	ARG $e^+e^- \rightarrow \Upsilon(4S)$	
0.19 ± 0.05 ± 0.02		² ALAM	87B	CLEO $e^+e^- \rightarrow \Upsilon(4S)$	

¹Measurement relies on lepton-kaon correlations. It is for the weak decay vertex and does not include mixing of the neutral B meson. Mixing effects were corrected for by assuming a mixing parameter r of $(18.1 \pm 4.3)\%$.

²Measurement relies on lepton-kaon correlations. It includes production through mixing of the neutral B meson.

$\Gamma(K^0/\bar{K}^0 \text{ anything})/\Gamma_{\text{total}}$					Γ_{66}/Γ
VALUE		DOCUMENT ID	TECN	COMMENT	
0.64 ± 0.04 OUR AVERAGE					

0.642 ± 0.010 ± 0.042		¹ ALBRECHT	94c	ARG $e^+e^- \rightarrow \Upsilon(4S)$	
0.63 ± 0.06 ± 0.06		ALAM	87B	CLEO $e^+e^- \rightarrow \Upsilon(4S)$	

¹ALBRECHT 94c assume a K^0/\bar{K}^0 multiplicity twice that of K_S^0 .

$\Gamma(K^*(892)^\pm \text{ anything})/\Gamma_{\text{total}}$					Γ_{67}/Γ
VALUE		DOCUMENT ID	TECN	COMMENT	
0.182 ± 0.054 ± 0.024		ALBRECHT	94j	ARG $e^+e^- \rightarrow \Upsilon(4S)$	

$\Gamma(K^*(892)^0/\bar{K}^*(892)^0 \text{ anything})/\Gamma_{\text{total}}$					Γ_{68}/Γ
VALUE		DOCUMENT ID	TECN	COMMENT	
0.146 ± 0.016 ± 0.020		ALBRECHT	94j	ARG $e^+e^- \rightarrow \Upsilon(4S)$	

$\Gamma(K^*(892)\gamma)/\Gamma_{\text{total}}$					Γ_{69}/Γ
VALUE (units 10^{-5})	CL%	DOCUMENT ID	TECN	COMMENT	
4.24 ± 0.54 ± 0.32		¹ COAN	00	CLE2 $e^+e^- \rightarrow \Upsilon(4S)$	

• • • We do not use the following data for averages, fits, limits, etc. • • •					
<15.0	90	² LESIK	92	CBAL $e^+e^- \rightarrow \Upsilon(4S)$	
<24	90	ALBRECHT	88H	ARG $e^+e^- \rightarrow \Upsilon(4S)$	

¹An average of $B(B^+ \rightarrow K^*(892)^+\gamma)$ and $B(B^0 \rightarrow K^*(892)^0\gamma)$ measurements reported in COAN 00 by assuming full correlated systematic errors.

²LESIK 92 set a limit on the inclusive process $B(b \rightarrow s\gamma) < 2.8 \times 10^{-3}$ at 90% CL for the range of masses of 892–2045 MeV, independent of assumptions about s-quark hadronization.

$\Gamma(\eta K\gamma)/\Gamma_{\text{total}}$					Γ_{70}/Γ
VALUE (units 10^{-6})		DOCUMENT ID	TECN	COMMENT	
8.5 ± 1.3 ± 1.2 ± 0.9		¹ NISHIDA	05	BELL $e^+e^- \rightarrow \Upsilon(4S)$	

¹ $m_{\eta K} < 2.4$ GeV/ c^2

$\Gamma(K_1(1400)\gamma)/\Gamma_{\text{total}}$					Γ_{71}/Γ
VALUE	CL%	DOCUMENT ID	TECN	COMMENT	
<12.7 × 10 ⁻⁵	90	¹ COAN	00	CLE2 $e^+e^- \rightarrow \Upsilon(4S)$	

• • • We do not use the following data for averages, fits, limits, etc. • • •

< 1.6×10^{-3} 90 ²LESIK 92 CBAL $e^+e^- \rightarrow \Upsilon(4S)$
 < 4.1×10^{-4} 90 ALBRECHT 88H ARG $e^+e^- \rightarrow \Upsilon(4S)$

¹Assumes equal production of B^+ and B^0 at the $\Upsilon(4S)$.

²LESIK 92 set a limit on the inclusive process $B(b \rightarrow s\gamma) < 2.8 \times 10^{-3}$ at 90% CL for the range of masses of 892–2045 MeV, independent of assumptions about s-quark hadronization.

$\Gamma(K_2^*(1430)\gamma)/\Gamma_{\text{total}}$					Γ_{72}/Γ
VALUE (units 10^{-5})	CL%	DOCUMENT ID	TECN	COMMENT	
1.66 ± 0.59 ± 0.13		¹ COAN	00	CLE2 $e^+e^- \rightarrow \Upsilon(4S)$	

• • • We do not use the following data for averages, fits, limits, etc. • • •

<83 90 ALBRECHT 88H ARG $e^+e^- \rightarrow \Upsilon(4S)$

¹COAN 00 obtains a fitted signal yield of $15.9^{+5.7}_{-5.2}$ events. A search for contamination by $K^*(1410)$ yielded a rate consistent with 0; the central value assumes no contamination.

$\Gamma(K_2^*(1770)\gamma)/\Gamma_{\text{total}}$					Γ_{73}/Γ
VALUE	CL%	DOCUMENT ID	TECN	COMMENT	
<1.2 × 10 ⁻³	90	¹ LESIK	92	CBAL $e^+e^- \rightarrow \Upsilon(4S)$	

¹LESIK 92 set a limit on the inclusive process $B(b \rightarrow s\gamma) < 2.8 \times 10^{-3}$ at 90% CL for the range of masses of 892–2045 MeV, independent of assumptions about s-quark hadronization.

$\Gamma(K_3^*(1780)\gamma)/\Gamma_{\text{total}}$					Γ_{74}/Γ
VALUE	CL%	DOCUMENT ID	TECN	COMMENT	
<3.7 × 10 ⁻⁵	90	¹ NISHIDA	05	BELL $e^+e^- \rightarrow \Upsilon(4S)$	

• • • We do not use the following data for averages, fits, limits, etc. • • •

<3.0 × 10⁻³ 90 ALBRECHT 88H ARG $e^+e^- \rightarrow \Upsilon(4S)$

¹Uses $B(K_3^*(1780) \rightarrow \eta K) = 0.11^{+0.05}_{-0.04}$.

$\Gamma(K_4^*(2045)\gamma)/\Gamma_{\text{total}}$					Γ_{75}/Γ
VALUE	CL%	DOCUMENT ID	TECN	COMMENT	
<1.0 × 10 ⁻³	90	¹ LESIK	92	CBAL $e^+e^- \rightarrow \Upsilon(4S)$	

¹LESIK 92 set a limit on the inclusive process $B(b \rightarrow s\gamma) < 2.8 \times 10^{-3}$ at 90% CL for the range of masses of 892–2045 MeV, independent of assumptions about s-quark hadronization.

$\Gamma(K\eta(958))/\Gamma_{\text{total}}$					Γ_{76}/Γ
VALUE		DOCUMENT ID	TECN	COMMENT	
(8.3 ± 0.9 ± 0.7) × 10⁻⁵		¹ RICHICHI	00	CLE2 $e^+e^- \rightarrow \Upsilon(4S)$	

¹Assumes equal production of B^+ and B^0 at the $\Upsilon(4S)$.

$\Gamma(K^*(892)\eta(958))/\Gamma_{\text{total}}$					Γ_{77}/Γ
VALUE (units 10^{-6})	CL%	DOCUMENT ID	TECN	COMMENT	
4.1 ± 1.0 ± 0.5		¹ AUBERT	07E	BABR $e^+e^- \rightarrow \Upsilon(4S)$	

• • • We do not use the following data for averages, fits, limits, etc. • • •

<22 90 ¹RICHICHI 00 CLE2 $e^+e^- \rightarrow \Upsilon(4S)$

¹Assumes equal production of B^+ and B^0 at the $\Upsilon(4S)$.

$\Gamma(K^*(892)\eta)/\Gamma_{\text{total}}$					Γ_{79}/Γ
VALUE		DOCUMENT ID	TECN	COMMENT	
(1.80 ± 0.49 ± 0.18) × 10⁻⁵		¹ RICHICHI	00	CLE2 $e^+e^- \rightarrow \Upsilon(4S)$	

¹Assumes equal production of B^+ and B^0 at the $\Upsilon(4S)$.

$\Gamma(K\phi\phi)/\Gamma_{\text{total}}$					Γ_{80}/Γ
VALUE (units 10^{-5})		DOCUMENT ID	TECN	COMMENT	
2.3 ± 0.9 ± 0.3		¹ HUANG	03	BELL $e^+e^- \rightarrow \Upsilon(4S)$	

¹Assumes equal production of charged and neutral B meson pairs and isospin symmetry.

$\Gamma(\bar{b} \rightarrow \bar{s}\gamma)/\Gamma_{\text{total}}$					Γ_{81}/Γ
VALUE (units 10^{-4})		DOCUMENT ID	TECN	COMMENT	
3.49 ± 0.19 OUR AVERAGE					

3.75 ± 0.18 ± 0.35	^{1,2}	SAITO	15	BELL $e^+e^- \rightarrow \Upsilon(4S)$	
3.52 ± 0.20 ± 0.51	^{1,3}	LEES	12v	BABR $e^+e^- \rightarrow \Upsilon(4S)$	
3.32 ± 0.16 ± 0.31	^{1,4}	LEES	12v	BABR $e^+e^- \rightarrow \Upsilon(4S)$	
3.47 ± 0.15 ± 0.40	^{1,5}	LIMOSANI	09	BELL $e^+e^- \rightarrow \Upsilon(4S)$	
3.90 ± 0.91 ± 0.64	^{1,6}	AUBERT	08o	BABR $e^+e^- \rightarrow \Upsilon(4S)$	
3.29 ± 0.44 ± 0.29	^{1,7}	CHEN	01c	CLE2 $e^+e^- \rightarrow \Upsilon(4S)$	

See key on page 1171

Meson Particle Listings
 B^\pm/B^0 ADMIXTURE

• • • We do not use the following data for averages, fits, limits, etc. • • •

VALUE (units 10^{-6})	DOCUMENT ID	TECN	COMMENT
$2.30 \pm 0.08 \pm 0.30$	⁸ DEL-AMO-SA...10M	BABR	$e^+e^- \rightarrow \Upsilon(4S)$
$4.3 \pm 0.3 \pm 0.7$	⁹ AUBERT	09U	Repl. by DEL-AMO-SANCHEZ 10M
$3.92 \pm 0.31 \pm 0.47$	^{1,10} AUBERT, BE	06B	Repl. by LEES 12v
$3.49 \pm 0.20 \pm 0.59$ -0.46	^{1,11} AUBERT, B	05R	BABR Repl. by LEES 12u
$3.50 \pm 0.32 \pm 0.31$	^{1,12} KOPPENBURG	04	BELL Repl. by LIMOSANI 09
$3.36 \pm 0.53 \pm 0.65$ -0.68	¹³ ABE	01F	BELL Repl. by SAITO 15
$2.32 \pm 0.57 \pm 0.35$	ALAM	95	CLE2 Repl. by CHEN 01c

¹ We extrapolate the measured value to $E_\gamma > 1.6$ GeV using the method of BUCHMUELLER 06 (average of three theoretical models).

² SAITO 15 measured $(3.51 \pm 0.17 \pm 0.33) \times 10^{-4}$ using a sum-of-exclusive approach in which 38 of the hadronic final states with $m_{X_s} < 2.8$ GeV/ c^2 are reconstructed. The cut of minimum photon energy is $E_\gamma > 1.9$ GeV.

³ Reports $(3.29 \pm 0.19 \pm 0.48) \times 10^{-4}$ for $E_\gamma > 1.9$ GeV.

⁴ Reports $(3.21 \pm 0.15 \pm 0.29 \pm 0.08) \times 10^{-4}$ for $1.8 < E_\gamma < 2.8$ GeV, where the last systematic uncertainty is for model dependency. Results with other cutoffs are also reported.

⁵ The measurement reported is $(3.45 \pm 0.15 \pm 0.40) \times 10^{-4}$ for $E_\gamma > 1.7$ GeV.

⁶ Uses a fully reconstructed B meson as a tag on the recoil side. The measurement reported is $(3.66 \pm 0.85 \pm 0.60) \times 10^{-4}$ for $E_\gamma > 1.9$ GeV.

⁷ The measurement reported is $(3.21 \pm 0.43 \pm 0.32) \times 10^{-4}$ for $E_\gamma > 2.0$ GeV.

⁸ Measured using sums of seven exclusive final states $B \rightarrow X_{d(s)}\gamma$ where $X_{d(s)}$ is a nonstrange (strange) charmless hadronic system in mass range 0.5–2.0 GeV/ c^2 .

⁹ Measured using sums of seven exclusive final states $B \rightarrow X_{d(s)}\gamma$ where $X_{d(s)}$ is a nonstrange (strange) charmless hadronic system in mass range 0.6–1.8 GeV/ c^2 .

¹⁰ The measurement reported is $(3.67 \pm 0.29 \pm 0.45) \times 10^{-4}$ for $E_\gamma > 1.9$ GeV.

¹¹ The measurement reported is $(3.27 \pm 0.18 \pm 0.55) \times 10^{-4}$ for $E_\gamma > 1.9$ GeV.

¹² The measurement reported is $(3.55 \pm 0.32 \pm 0.32) \times 10^{-4}$ for $E_\gamma > 1.8$ GeV.

¹³ ABE 01F reports their systematic errors $(\pm 0.42 \pm 0.50) \times 10^{-4}$, where the second error is due to the theoretical uncertainty. We combine them in quadrature.

$\Gamma(\bar{b} \rightarrow \bar{d}\gamma)/\Gamma_{\text{total}}$ Γ_{82}/Γ

VALUE (units 10^{-6})	DOCUMENT ID	TECN	COMMENT
$9.2 \pm 2.0 \pm 2.3$	¹ DEL-AMO-SA...10M	BABR	$e^+e^- \rightarrow \Upsilon(4S)$

• • • We do not use the following data for averages, fits, limits, etc. • • •

$14 \pm 5 \pm 4$	² AUBERT	09U	BABR Repl. by DEL-AMO-SANCHEZ 10M
------------------	---------------------	-----	-----------------------------------

¹ Measured using sums of seven exclusive final states $B \rightarrow X_{d(s)}\gamma$ where $X_{d(s)}$ is a nonstrange (strange) charmless hadronic system in mass range 0.5–2.0 GeV/ c^2 .

² Measured using sums of seven exclusive final states $B \rightarrow X_{d(s)}\gamma$ where $X_{d(s)}$ is a nonstrange (strange) charmless hadronic system in mass range 0.6–1.8 GeV/ c^2 .

$\Gamma(\bar{b} \rightarrow \bar{d}\gamma)/\Gamma(\bar{b} \rightarrow \bar{s}\gamma)$ Γ_{82}/Γ_{81}

VALUE	DOCUMENT ID	TECN	COMMENT
$0.040 \pm 0.009 \pm 0.010$	¹ DEL-AMO-SA...10M	BABR	$e^+e^- \rightarrow \Upsilon(4S)$

• • • We do not use the following data for averages, fits, limits, etc. • • •

$0.033 \pm 0.013 \pm 0.009$	² AUBERT	09U	BABR Repl. by DEL-AMO-SANCHEZ 10M
-----------------------------	---------------------	-----	-----------------------------------

¹ Measured using sums of seven exclusive final states $B \rightarrow X_{d(s)}\gamma$ where $X_{d(s)}$ is a nonstrange (strange) charmless hadronic system in mass range 0.5–2.0 GeV/ c^2 .

² Measured using sums of seven exclusive final states $B \rightarrow X_{d(s)}\gamma$ where $X_{d(s)}$ is a nonstrange (strange) charmless hadronic system in mass range 0.6–1.8 GeV/ c^2 .

$\Gamma(\bar{b} \rightarrow \bar{s}\text{gluon})/\Gamma_{\text{total}}$ Γ_{83}/Γ

VALUE	CL%	EVTS	DOCUMENT ID	TECN	COMMENT
< 0.068	90		¹ COAN	98	CLE2 $e^+e^- \rightarrow \Upsilon(4S)$

• • • We do not use the following data for averages, fits, limits, etc. • • •

< 0.08	2		² ALBRECHT	95D	ARG $e^+e^- \rightarrow \Upsilon(4S)$
----------	---	--	-----------------------	-----	---------------------------------------

¹ COAN 98 uses D - l correlation.

² ALBRECHT 95D use full reconstruction of one B decay as tag. Two candidate events for charmless B decay can be interpreted as either $b \rightarrow \text{sgluon}$ or $b \rightarrow u$ transition. If interpreted as $b \rightarrow \text{sgluon}$ they find a branching ratio of ~ 0.026 and the upper limit quoted above. Result is highly model dependent.

$\Gamma(\eta \text{ anything})/\Gamma_{\text{total}}$ Γ_{84}/Γ

VALUE (units 10^{-4})	CL%	DOCUMENT ID	TECN	COMMENT
$2.61 \pm 0.30 \pm 0.44$ -0.74		¹ NISHIMURA	10	BELL $e^+e^- \rightarrow \Upsilon(4S)$

• • • We do not use the following data for averages, fits, limits, etc. • • •

$1.69 \pm 0.29 \pm 0.36$ -0.62		² NISHIMURA	10	BELL $e^+e^- \rightarrow \Upsilon(4S)$
-------------------------------------	--	------------------------	----	--

< 4.4 90 ³ BROWDER 98 CLE2 $e^+e^- \rightarrow \Upsilon(4S)$

¹ Uses $B \rightarrow \eta X_S$ with $0.4 < m_{X_S} < 2.6$ GeV/ c^2 .

² Uses $B \rightarrow \eta X_S$ with $1.8 < m_{X_S} < 2.6$ GeV/ c^2 .

³ BROWDER 98 search for high momentum $B \rightarrow \eta X_S$ between 2.1 and 2.7 GeV/ c .

 $\Gamma(\eta' \text{ anything})/\Gamma_{\text{total}}$ Γ_{85}/Γ

VALUE (units 10^{-4})	DOCUMENT ID	TECN	COMMENT
4.2 ± 0.9	OUR AVERAGE		

$3.9 \pm 0.8 \pm 0.9$ ¹ AUBERT, B 04F BABR $e^+e^- \rightarrow \Upsilon(4S)$

$4.6 \pm 1.1 \pm 0.6$ ² BONVICINI 03 CLE2 $e^+e^- \rightarrow \Upsilon(4S)$

• • • We do not use the following data for averages, fits, limits, etc. • • •

$6.2 \pm 1.6 \pm 1.3$
 -2.0 ³ BROWDER 98 CLE2 $e^+e^- \rightarrow \Upsilon(4S)$

¹ AUBERT, B 04F reports branching ratio $B \rightarrow \eta' X_S$ for high momentum η' between 2.0 and 2.7 GeV/ c in the $\Upsilon(4S)$ center-of-mass frame. X_S represents a recoil system consisting of a kaon and zero to four pions.

² BONVICINI 03 observed a signal of 61.2 ± 13.9 events in $B \rightarrow \eta' X_{\text{HC}}$ production for high momentum η' between 2.0 and 2.7 GeV/ c in the $\Upsilon(4S)$ center-of-mass frame. The X_{HC} denotes "charmless" hadronic states recoiling against η' . The second error combines systematic and background subtraction uncertainties in quadrature.

³ BROWDER 98 observed a signal of 39.0 ± 11.6 events in high momentum $B \rightarrow \eta' X_S$ production between 2.0 and 2.7 GeV/ c . The branching fraction is based on the interpretation of $b \rightarrow \text{sg}$, where the last error includes additional uncertainties due to the color-suppressed $b \rightarrow$ backgrounds.

 $\Gamma(K^+ \text{ gluon (charmless)})/\Gamma_{\text{total}}$ Γ_{86}/Γ

VALUE (units 10^{-4})	CL%	DOCUMENT ID	TECN	COMMENT
< 1.87	90	¹ DEL-AMO-SA...11	BABR	$e^+e^- \rightarrow \Upsilon(4S)$

¹ $B \rightarrow K^+ X$ with $m_X < 1.69$ GeV/ c^2 .

 $\Gamma(K^0 \text{ gluon (charmless)})/\Gamma_{\text{total}}$ Γ_{87}/Γ

VALUE (units 10^{-4})	DOCUMENT ID	TECN	COMMENT
1.95 ± 0.51 -0.45 ± 0.50	¹ DEL-AMO-SA...11	BABR	$e^+e^- \rightarrow \Upsilon(4S)$

¹ $B \rightarrow K^0 X$ with $m_X < 1.69$ GeV/ c^2 .

 $\Gamma(\rho\gamma)/\Gamma_{\text{total}}$ Γ_{88}/Γ

VALUE (units 10^{-6})	CL%	DOCUMENT ID	TECN	COMMENT
1.39 ± 0.25	OUR AVERAGE Error includes scale factor of 1.2.			

$1.73 \pm 0.34 \pm 0.17$ ^{1,2} AUBERT 08BH BABR $e^+e^- \rightarrow \Upsilon(4S)$

$1.21 \pm 0.24 \pm 0.12$ ^{1,2} TANIGUCHI 08 BELL $e^+e^- \rightarrow \Upsilon(4S)$

• • • We do not use the following data for averages, fits, limits, etc. • • •

$1.36 \pm 0.29 \pm 0.10$ ^{1,3} AUBERT 07L BABR Repl. by AUBERT 08BH

< 1.9 90 ^{1,3} AUBERT 04c BABR Repl. by AUBERT 07L

< 14 90 ^{1,4} COAN 00 CLE2 $e^+e^- \rightarrow \Upsilon(4S)$

¹ Assumes equal production of B^+ and B^0 at the $\Upsilon(4S)$.

² Assumes $\Gamma(B \rightarrow \rho\gamma) = \Gamma(B^+ \rightarrow \rho^+\gamma) = 2\Gamma(B^0 \rightarrow \rho^0\gamma)$ and uses lifetime ratio of $\tau_{B^+}/\tau_{B^0} = 1.071 \pm 0.009$.

³ Assumes $\Gamma(B \rightarrow \rho\gamma) = \Gamma(B^+ \rightarrow \rho^+\gamma) = 2\Gamma(B^0 \rightarrow \rho^0\gamma)$ and uses lifetime ratio of $\tau_{B^+}/\tau_{B^0} = 1.083 \pm 0.017$.

⁴ COAN 00 reports $B(B \rightarrow \rho\gamma)/B(B \rightarrow K^*(892)\gamma) < 0.32$ at 90%CL and scaled by the central value of $B(B \rightarrow K^*(892)\gamma) = (4.24 \pm 0.54 \pm 0.32) \times 10^{-5}$.

 $\Gamma(\rho\gamma)/\Gamma(K^*(892)\gamma)$ Γ_{88}/Γ_{69}

VALUE (units 10^{-2})	DOCUMENT ID	TECN	COMMENT
$3.02 \pm 0.60 \pm 0.26$ -0.55 ± 0.28	TANIGUCHI	08	BELL $e^+e^- \rightarrow \Upsilon(4S)$

 $\Gamma(\rho/\omega\gamma)/\Gamma_{\text{total}}$ Γ_{89}/Γ

VALUE (units 10^{-6})	CL%	DOCUMENT ID	TECN	COMMENT
1.30 ± 0.23	OUR AVERAGE Error includes scale factor of 1.2.			

$1.63 \pm 0.30 \pm 0.16$ ^{1,2,3} AUBERT 08BH BABR $e^+e^- \rightarrow \Upsilon(4S)$

$1.14 \pm 0.20 \pm 0.10$
 -0.12 ^{1,3} TANIGUCHI 08 BELL $e^+e^- \rightarrow \Upsilon(4S)$

• • • We do not use the following data for averages, fits, limits, etc. • • •

$1.25 \pm 0.25 \pm 0.09$ ⁴ AUBERT 07L BABR Repl. by AUBERT 08BH

$1.32 \pm 0.34 \pm 0.10$
 -0.31 ± 0.09 ⁴ MOHAPATRA 06 BELL Repl. by TANIGUCHI 08

$0.6 \pm 0.3 \pm 0.1$ ⁴ AUBERT 05 BABR Repl. by AUBERT 07L

< 1.4 90 ⁴ MOHAPATRA 05 BELL $e^+e^- \rightarrow \Upsilon(4S)$

¹ Assumes $\Gamma(B \rightarrow \rho\gamma) = \Gamma(B^+ \rightarrow \rho^+\gamma) = 2\Gamma(B^0 \rightarrow \rho^0\gamma)$ and uses lifetime ratio of $\tau_{B^+}/\tau_{B^0} = 1.071 \pm 0.009$.

² Also reports $|V_{td}/V_{ts}| = 0.233 \pm 0.025 \pm 0.022$
 -0.024 ± 0.021 .

³ Assumes equal production of B^+ and B^0 at the $\Upsilon(4S)$.

⁴ Assumes $\Gamma(B \rightarrow \rho\gamma) = \Gamma(B^+ \rightarrow \rho^+\gamma) = 2\Gamma(B^0 \rightarrow \rho^0\gamma)$ and uses lifetime ratio of $\tau_{B^+}/\tau_{B^0} = 1.083 \pm 0.017$.

 $\Gamma(\rho/\omega\gamma)/\Gamma(K^*(892)\gamma)$ Γ_{89}/Γ_{69}

VALUE (units 10^{-2})	CL%	DOCUMENT ID	TECN	COMMENT
$2.84 \pm 0.50 \pm 0.27$ -0.29		¹ TANIGUCHI	08	BELL $e^+e^- \rightarrow \Upsilon(4S)$

• • • We do not use the following data for averages, fits, limits, etc. • • •

< 3.5 90 MOHAPATRA 05 BELL Repl. by TANIGUCHI 08

¹ Also reports $|V_{td}/V_{ts}| = 0.195 \pm 0.020 \pm 0.015$.

Meson Particle Listings

 B^\pm/B^0 ADMIXTURE $\Gamma(\pi^\pm \text{ anything})/\Gamma_{\text{total}}$ Γ_{90}/Γ

VALUE	DOCUMENT ID	TECN	COMMENT
$3.585 \pm 0.025 \pm 0.070$	¹ ALBRECHT 93I	ARG	$e^+e^- \rightarrow \Upsilon(4S)$

¹ ALBRECHT 93 excludes π^\pm from K_S^0 and Λ decays. If included, they find $4.105 \pm 0.025 \pm 0.080$.

 $\Gamma(\pi^0 \text{ anything})/\Gamma_{\text{total}}$ Γ_{91}/Γ

VALUE	DOCUMENT ID	TECN	COMMENT
$2.35 \pm 0.02 \pm 0.11$	¹ ABE 01J	BELL	$e^+e^- \rightarrow \Upsilon(4S)$

¹ From fully inclusive π^0 yield with no corrections from decays of K_S^0 or other particles.

 $\Gamma(\eta \text{ anything})/\Gamma_{\text{total}}$ Γ_{92}/Γ

VALUE	DOCUMENT ID	TECN	COMMENT
$0.176 \pm 0.011 \pm 0.012$	KUBOTA 96	CLE2	$e^+e^- \rightarrow \Upsilon(4S)$

 $\Gamma(\rho^0 \text{ anything})/\Gamma_{\text{total}}$ Γ_{93}/Γ

VALUE	DOCUMENT ID	TECN	COMMENT
$0.208 \pm 0.042 \pm 0.032$	ALBRECHT 94J	ARG	$e^+e^- \rightarrow \Upsilon(4S)$

 $\Gamma(\omega \text{ anything})/\Gamma_{\text{total}}$ Γ_{94}/Γ

VALUE	CL%	DOCUMENT ID	TECN	COMMENT
<0.81	90	ALBRECHT 94J	ARG	$e^+e^- \rightarrow \Upsilon(4S)$

 $\Gamma(\phi \text{ anything})/\Gamma_{\text{total}}$ Γ_{95}/Γ

VALUE	DOCUMENT ID	TECN	COMMENT
0.0343 ± 0.0012 OUR AVERAGE			
$0.0353 \pm 0.0005 \pm 0.0030$	HUANG 07	CLEO	$e^+e^- \rightarrow \Upsilon(4S)$
$0.0341 \pm 0.0006 \pm 0.0012$	AUBERT 04s	BABR	$e^+e^- \rightarrow \Upsilon(4S)$
$0.0390 \pm 0.0030 \pm 0.0035$	ALBRECHT 94J	ARG	$e^+e^- \rightarrow \Upsilon(4S)$
$0.023 \pm 0.006 \pm 0.005$	BORTOLETTO86	CLEO	$e^+e^- \rightarrow \Upsilon(4S)$

 $\Gamma(\phi K^*(892))/\Gamma_{\text{total}}$ Γ_{96}/Γ

VALUE	CL%	DOCUMENT ID	TECN	COMMENT
$<2.2 \times 10^{-5}$	90	¹ BERGFELD 98	CLE2	

¹ Assumes equal production of B^+ and B^0 at the $\Upsilon(4S)$.

 $\Gamma(\pi^+ \text{ gluon (charmless)})/\Gamma_{\text{total}}$ Γ_{98}/Γ

VALUE (units 10^{-4})	DOCUMENT ID	TECN	COMMENT
$3.72 \pm 0.50 \pm 0.59$	¹ DEL-AMO-SA...11	BABR	$e^+e^- \rightarrow \Upsilon(4S)$

¹ $B \rightarrow \pi^+ X$ with $m_X < 1.71 \text{ GeV}/c^2$.

 $\Gamma(\Lambda_c^+ / \bar{\Lambda}_c^- \text{ anything})/\Gamma_{\text{total}}$ Γ_{99}/Γ

VALUE (%)	CL%	DOCUMENT ID	TECN	COMMENT
$3.61 \pm 0.32 \pm 0.16$		¹ AUBERT 07c	BABR	$e^+e^- \rightarrow \Upsilon(4S)$
$6.4 \pm 0.8 \pm 0.8$		² CRAWFORD 92	CLEO	$e^+e^- \rightarrow \Upsilon(4S)$
14 ± 9		³ ALBRECHT 88E	ARG	$e^+e^- \rightarrow \Upsilon(4S)$
<11.2	90	⁴ ALAM 87	CLEO	$e^+e^- \rightarrow \Upsilon(4S)$

¹ AUBERT 07c reports $0.045 \pm 0.003 \pm 0.012$ from a measurement of $[\Gamma(B \rightarrow \Lambda_c^+ / \bar{\Lambda}_c^- \text{ anything})/\Gamma_{\text{total}}] \times [B(\Lambda_c^+ \rightarrow pK^- \pi^+)]$ assuming $B(\Lambda_c^+ \rightarrow pK^- \pi^+) = (5.0 \pm 1.3) \times 10^{-2}$, which we rescale to our best value $B(\Lambda_c^+ \rightarrow pK^- \pi^+) = (6.24 \pm 0.28) \times 10^{-2}$. Our first error is their experiment's error and our second error is the systematic error from using our best value.

² CRAWFORD 92 result derived from lepton baryon correlations. Assumes all charmed baryons in B^0 and B^\pm decay are Λ_c .

³ ALBRECHT 88E measured $B(B \rightarrow \Lambda_c^+ X) \cdot B(\Lambda_c^+ \rightarrow pK^- \pi^+) = (0.30 \pm 0.12 \pm 0.06)\%$ and used $B(\Lambda_c^+ \rightarrow pK^- \pi^+) = (2.2 \pm 1.0)\%$ from ABRAMS 80 to obtain above number.

⁴ Assuming all baryons result from charmed baryons, ALAM 86 conclude the branching fraction is $7.4 \pm 2.9\%$. The limit given above is model independent.

 $\Gamma(\Lambda_c^+ \text{ anything})/\Gamma(\bar{\Lambda}_c^- \text{ anything})$ $\Gamma_{100}/\Gamma_{101}$

VALUE	DOCUMENT ID	TECN	COMMENT
$0.19 \pm 0.13 \pm 0.04$	¹ AMMAR 97	CLE2	$e^+e^- \rightarrow \Upsilon(4S)$

¹ AMMAR 97 uses a high-momentum lepton tag ($P_\ell > 1.4 \text{ GeV}/c^2$).

 $\Gamma(\bar{\Lambda}_c^- \mu^+ \text{ anything})/\Gamma(\bar{\Lambda}_c^- \text{ anything})$ $\Gamma_{104}/\Gamma_{101}$

VALUE (units 10^{-2})	DOCUMENT ID	TECN	COMMENT
$-2.0 \pm 2.0 \pm 1.9$	LEES 12	BABR	$e^+e^- \rightarrow \Upsilon(4S)$

 $\Gamma(\bar{\Lambda}_c^- \ell^+ \text{ anything})/\Gamma(\Lambda_c^+ / \bar{\Lambda}_c^- \text{ anything})$ Γ_{102}/Γ_{99}

VALUE	CL%	DOCUMENT ID	TECN	COMMENT
$<2.5 \times 10^{-2}$	90	¹ LEES 12	BABR	$e^+e^- \rightarrow \Upsilon(4S)$

¹ LEES 12 quotes also the measurement $\Gamma(B \rightarrow \bar{\Lambda}_c^- \ell^+ \text{ anything})/\Gamma(B \rightarrow \Lambda_c^+ / \bar{\Lambda}_c^- \text{ anything}) = (1.2 \pm 0.7 \pm 0.4) \times 10^{-2}$.

 $\Gamma(\bar{\Lambda}_c^- e^+ \text{ anything})/\Gamma(\Lambda_c^+ / \bar{\Lambda}_c^- \text{ anything})$ Γ_{103}/Γ_{99}

VALUE	CL%	DOCUMENT ID	TECN	COMMENT
<0.05	90	¹ BONVICINI 98	CLE2	$e^+e^- \rightarrow \Upsilon(4S)$

¹ BONVICINI 98 uses the electron with momentum above $0.6 \text{ GeV}/c$.

 $\Gamma(\bar{\Lambda}_c^- e^+ \text{ anything})/\Gamma(\bar{\Lambda}_c^- \text{ anything})$ $\Gamma_{103}/\Gamma_{101}$

VALUE (units 10^{-2})	DOCUMENT ID	TECN	COMMENT
$2.5 \pm 1.1 \pm 0.6$	¹ LEES 12	BABR	$e^+e^- \rightarrow \Upsilon(4S)$

¹ Uses the full reconstruction of the recoiling B in a hadronic decay as a tag.

 $\Gamma(\bar{\Lambda}_c^- \ell^+ \text{ anything})/\Gamma(\bar{\Lambda}_c^- \text{ anything})$ $\Gamma_{102}/\Gamma_{101}$

VALUE	CL%	DOCUMENT ID	TECN	COMMENT
$<3.5 \times 10^{-2}$	90	¹ LEES 12	BABR	$e^+e^- \rightarrow \Upsilon(4S)$

¹ LEES 12 quotes also the measurement $\Gamma(B \rightarrow \bar{\Lambda}_c^- \ell^+ \text{ anything})/\Gamma(B \rightarrow \bar{\Lambda}_c^- \text{ anything}) = (1.7 \pm 1.0 \pm 0.6) \times 10^{-2}$.

 $\Gamma(\bar{\Lambda}_c^- p \text{ anything})/\Gamma(\Lambda_c^+ / \bar{\Lambda}_c^- \text{ anything})$ Γ_{105}/Γ_{99}

VALUE	DOCUMENT ID	TECN	COMMENT
$0.57 \pm 0.05 \pm 0.05$	BONVICINI 98	CLE2	$e^+e^- \rightarrow \Upsilon(4S)$

 $\Gamma(\bar{\Lambda}_c^- p e^+ \nu_e)/\Gamma(\bar{\Lambda}_c^- p \text{ anything})$ $\Gamma_{106}/\Gamma_{105}$

VALUE	CL%	DOCUMENT ID	TECN	COMMENT
<0.04	90	¹ BONVICINI 98	CLE2	$e^+e^- \rightarrow \Upsilon(4S)$

¹ BONVICINI 98 uses the electron with momentum above $0.6 \text{ GeV}/c$.

 $\Gamma(\bar{\Sigma}_c^- \text{ anything})/\Gamma_{\text{total}}$ Γ_{107}/Γ

VALUE	EVTS	DOCUMENT ID	TECN	COMMENT
$0.0034 \pm 0.0017 \pm 0.0002$	0.0001	77	¹ PROCARIO 94	CLE2 $e^+e^- \rightarrow \Upsilon(4S)$

¹ PROCARIO 94 reports $[\Gamma(B \rightarrow \bar{\Sigma}_c^- \text{ anything})/\Gamma_{\text{total}}] \times [B(\Lambda_c^+ \rightarrow pK^- \pi^+)] = 0.00021 \pm 0.00008 \pm 0.00007$ which we divide by our best value $B(\Lambda_c^+ \rightarrow pK^- \pi^+) = (6.24 \pm 0.28) \times 10^{-2}$. Our first error is their experiment's error and our second error is the systematic error from using our best value.

 $\Gamma(\bar{\Sigma}_c^- \text{ anything})/\Gamma_{\text{total}}$ Γ_{108}/Γ

VALUE	CL%	DOCUMENT ID	TECN	COMMENT
$<8 \times 10^{-3}$	90	¹ PROCARIO 94	CLE2	$e^+e^- \rightarrow \Upsilon(4S)$

¹ PROCARIO 94 reports $[\Gamma(B \rightarrow \bar{\Sigma}_c^- \text{ anything})/\Gamma_{\text{total}}] \times [B(\Lambda_c^+ \rightarrow pK^- \pi^+)] < 0.00048$ which we divide by our best value $B(\Lambda_c^+ \rightarrow pK^- \pi^+) = 6.24 \times 10^{-2}$.

 $\Gamma(\bar{\Xi}_c^0 \text{ anything})/\Gamma_{\text{total}}$ Γ_{109}/Γ

VALUE	EVTS	DOCUMENT ID	TECN	COMMENT
$0.0037 \pm 0.0017 \pm 0.0002$	0.0001	76	¹ PROCARIO 94	CLE2 $e^+e^- \rightarrow \Upsilon(4S)$

¹ PROCARIO 94 reports $[\Gamma(B \rightarrow \bar{\Xi}_c^0 \text{ anything})/\Gamma_{\text{total}}] \times [B(\Lambda_c^+ \rightarrow pK^- \pi^+)] = 0.00023 \pm 0.00008 \pm 0.00007$ which we divide by our best value $B(\Lambda_c^+ \rightarrow pK^- \pi^+) = (6.24 \pm 0.28) \times 10^{-2}$. Our first error is their experiment's error and our second error is the systematic error from using our best value.

 $\Gamma(\bar{\Xi}_c^0 N(N = p \text{ or } n))/\Gamma_{\text{total}}$ Γ_{110}/Γ

VALUE	CL%	DOCUMENT ID	TECN	COMMENT
$<1.2 \times 10^{-3}$	90	¹ PROCARIO 94	CLE2	$e^+e^- \rightarrow \Upsilon(4S)$

¹ PROCARIO 94 reports <0.0017 from a measurement of $[\Gamma(B \rightarrow \bar{\Xi}_c^0 N(N = p \text{ or } n))/\Gamma_{\text{total}}] \times [B(\Lambda_c^+ \rightarrow pK^- \pi^+)]$ assuming $B(\Lambda_c^+ \rightarrow pK^- \pi^+) = 0.043$, which we rescale to our best value $B(\Lambda_c^+ \rightarrow pK^- \pi^+) = 6.24 \times 10^{-2}$.

 $\Gamma(\Xi_c^0 \text{ anything}, \Xi_c^0 \rightarrow \Xi^- \pi^+)/\Gamma_{\text{total}}$ Γ_{111}/Γ

VALUE (units 10^{-3})	DOCUMENT ID	TECN	COMMENT
0.193 ± 0.030 OUR AVERAGE			Error includes scale factor of 1.1.
$0.211 \pm 0.019 \pm 0.025$	¹ AUBERT,B 05M	BABR	$e^+e^- \rightarrow \Upsilon(4S)$
$0.144 \pm 0.048 \pm 0.021$	² BARISH 97	CLE2	$e^+e^- \rightarrow \Upsilon(4S)$

¹ The yield is obtained by requiring the momentum $P < 2.15 \text{ GeV}/c$.

² BARISH 97 find $79 \pm 27 \Xi_c^0$ events.

 $\Gamma(\Xi_c^+, \Xi_c^+ \rightarrow \Xi^- \pi^+ \pi^+)/\Gamma_{\text{total}}$ Γ_{112}/Γ

VALUE (units 10^{-3})	DOCUMENT ID	TECN	COMMENT
$0.453 \pm 0.096 \pm 0.085$	0.065	¹ BARISH 97	CLE2 $e^+e^- \rightarrow \Upsilon(4S)$

¹ BARISH 97 find $125 \pm 28 \Xi_c^+$ events.

 $\Gamma(p/\bar{p} \text{ anything})/\Gamma_{\text{total}}$ Γ_{113}/Γ

VALUE	EVTS	DOCUMENT ID	TECN	COMMENT
0.080 ± 0.004 OUR AVERAGE				
$0.080 \pm 0.005 \pm 0.005$		ALBRECHT 93I	ARG	$e^+e^- \rightarrow \Upsilon(4S)$
$0.080 \pm 0.005 \pm 0.003$		CRAWFORD 92	CLEO	$e^+e^- \rightarrow \Upsilon(4S)$
$0.082 \pm 0.005 \pm 0.013$	0.010	¹ ALBRECHT 89K	ARG	$e^+e^- \rightarrow \Upsilon(4S)$

¹ LEES 12 quotes also the measurement $\Gamma(B \rightarrow \bar{\Lambda}_c^- \ell^+ \text{ anything})/\Gamma(B \rightarrow \bar{\Lambda}_c^- \text{ anything}) = (1.2 \pm 0.7 \pm 0.4) \times 10^{-2}$.

¹ ALBRECHT 89K include direct and nondirect protons.

² ALAM 83B reported their result as $> 0.036 \pm 0.006 \pm 0.009$. Data are consistent with equal yields of p and \bar{p} . Using assumed yields below cut, $B(B \rightarrow p+X) = 0.03$ not including protons from Λ decays.

$\Gamma(p/\bar{p} \text{ (direct) anything})/\Gamma_{\text{total}}$ Γ_{114}/Γ

VALUE	EVTS	DOCUMENT ID	TECN	COMMENT
0.055 ± 0.005 OUR AVERAGE				
0.055 ± 0.005 ± 0.0035		ALBRECHT 93i	ARG	$e^+e^- \rightarrow \Upsilon(4S)$
0.056 ± 0.006 ± 0.005		CRAWFORD 92	CLEO	$e^+e^- \rightarrow \Upsilon(4S)$
0.055 ± 0.016	1220	¹ ALBRECHT 89k	ARG	$e^+e^- \rightarrow \Upsilon(4S)$

¹ALBRECHT 89k subtract contribution of Λ decay from the inclusive proton yield.

 $\Gamma(\bar{p}e^+\nu_e \text{ anything})/\Gamma_{\text{total}}$ Γ_{115}/Γ

VALUE	CL%	DOCUMENT ID	TECN	COMMENT
< 5.9 × 10⁻⁴				
	90	¹ ADAM 03B	CLE2	$e^+e^- \rightarrow \Upsilon(4S)$
• • • We do not use the following data for averages, fits, limits, etc. • • •				
<16 × 10 ⁻⁴	90	ALBRECHT 90H	ARG	$e^+e^- \rightarrow \Upsilon(4S)$

¹Based on $V-A$ model.

 $\Gamma(\Lambda/\bar{\Lambda} \text{ anything})/\Gamma_{\text{total}}$ Γ_{116}/Γ

VALUE	EVTS	DOCUMENT ID	TECN	COMMENT
0.040 ± 0.005 OUR AVERAGE				
0.038 ± 0.004 ± 0.006	2998	CRAWFORD 92	CLEO	$e^+e^- \rightarrow \Upsilon(4S)$
0.042 ± 0.005 ± 0.006	943	ALBRECHT 89k	ARG	$e^+e^- \rightarrow \Upsilon(4S)$
• • • We do not use the following data for averages, fits, limits, etc. • • •				
0.022 ± 0.003 ± 0.0022		¹ ACKERSTAFF 97N	OPAL	$e^+e^- \rightarrow Z$
>0.011		² ALAM 83B	CLEO	$e^+e^- \rightarrow \Upsilon(4S)$

¹ACKERSTAFF 97N assumes $B(b \rightarrow B) = 0.868 \pm 0.041$, i.e., an admixture of B^0 , B^\pm , and B_s .

²ALAM 83B reported their result as $> 0.022 \pm 0.007 \pm 0.004$. Values are for $(B(\Lambda X) + B(\bar{\Lambda} X))/2$. Data are consistent with equal yields of p and \bar{p} . Using assumed yields below cut, $B(B \rightarrow \Lambda X) = 0.03$.

 $\Gamma(\Lambda \text{ anything})/\Gamma(\bar{\Lambda} \text{ anything})$ $\Gamma_{117}/\Gamma_{118}$

VALUE	DOCUMENT ID	TECN	COMMENT
0.43 ± 0.09 ± 0.07			
	¹ AMMAR 97	CLE2	$e^+e^- \rightarrow \Upsilon(4S)$

¹AMMAR 97 uses a high-momentum lepton tag ($P_\ell > 1.4 \text{ GeV}/c^2$).

 $\Gamma(\Xi^-/\Xi^+ \text{ anything})/\Gamma_{\text{total}}$ Γ_{119}/Γ

VALUE	EVTS	DOCUMENT ID	TECN	COMMENT
0.0027 ± 0.0006 OUR AVERAGE				
0.0027 ± 0.0005 ± 0.0004	147	CRAWFORD 92	CLEO	$e^+e^- \rightarrow \Upsilon(4S)$
0.0028 ± 0.0014	54	ALBRECHT 89k	ARG	$e^+e^- \rightarrow \Upsilon(4S)$

 $\Gamma(\text{baryons anything})/\Gamma_{\text{total}}$ Γ_{120}/Γ

VALUE	DOCUMENT ID	TECN	COMMENT
0.068 ± 0.005 ± 0.003			
	¹ ALBRECHT 92o	ARG	$e^+e^- \rightarrow \Upsilon(4S)$
• • • We do not use the following data for averages, fits, limits, etc. • • •			
0.076 ± 0.014	² ALBRECHT 89k	ARG	$e^+e^- \rightarrow \Upsilon(4S)$

¹ALBRECHT 92o result is from simultaneous analysis of p and Λ yields, $p\bar{p}$ and $\Lambda\bar{\Lambda}$ correlations, and various lepton-baryon and lepton-baryon-antibaryon correlations. Supersedes ALBRECHT 89k.

²ALBRECHT 89k obtain this result by adding their measurements (5.5 ± 1.6)% for direct protons and (4.2 ± 0.5 ± 0.6)% for inclusive Λ production. They then assume (5.5 ± 1.6)% for neutron production and add it in also. Since each B decay has two baryons, they divide by 2 to obtain (7.6 ± 1.4)%.

 $\Gamma(p\bar{p} \text{ anything})/\Gamma_{\text{total}}$ Γ_{121}/Γ

VALUE	EVTS	DOCUMENT ID	TECN	COMMENT
0.0247 ± 0.0023 OUR AVERAGE				
0.024 ± 0.001 ± 0.004		CRAWFORD 92	CLEO	$e^+e^- \rightarrow \Upsilon(4S)$
0.025 ± 0.002 ± 0.002	918	ALBRECHT 89k	ARG	$e^+e^- \rightarrow \Upsilon(4S)$

 $\Gamma(p\bar{p} \text{ anything})/\Gamma(p/\bar{p} \text{ anything})$ $\Gamma_{121}/\Gamma_{113}$

VALUE	DOCUMENT ID	TECN	COMMENT
• • • We do not use the following data for averages, fits, limits, etc. • • •			
0.30 ± 0.02 ± 0.05	¹ CRAWFORD 92	CLEO	$e^+e^- \rightarrow \Upsilon(4S)$

¹CRAWFORD 92 value is not independent of their $\Gamma(p\bar{p} \text{ anything})/\Gamma_{\text{total}}$ value.

 $\Gamma(\Lambda\bar{\Lambda}/\Lambda p \text{ anything})/\Gamma_{\text{total}}$ Γ_{122}/Γ

VALUE	EVTS	DOCUMENT ID	TECN	COMMENT
0.025 ± 0.004 OUR AVERAGE				
0.029 ± 0.005 ± 0.005		CRAWFORD 92	CLEO	$e^+e^- \rightarrow \Upsilon(4S)$
0.023 ± 0.004 ± 0.003	165	ALBRECHT 89k	ARG	$e^+e^- \rightarrow \Upsilon(4S)$

 $\Gamma(\Lambda\bar{\Lambda}/\Lambda p \text{ anything})/\Gamma(\Lambda/\bar{\Lambda} \text{ anything})$ $\Gamma_{122}/\Gamma_{116}$

VALUE	DOCUMENT ID	TECN	COMMENT
• • • We do not use the following data for averages, fits, limits, etc. • • •			
0.76 ± 0.11 ± 0.08	¹ CRAWFORD 92	CLEO	$e^+e^- \rightarrow \Upsilon(4S)$

¹CRAWFORD 92 value is not independent of their $[\Gamma(\Lambda\bar{\Lambda} \text{ anything}) + \Gamma(\Lambda p \text{ anything})]/\Gamma_{\text{total}}$ value.

 $\Gamma(\Lambda\bar{\Lambda} \text{ anything})/\Gamma_{\text{total}}$ Γ_{123}/Γ

VALUE	CL%	EVTS	DOCUMENT ID	TECN	COMMENT
< 0.005					
	90		CRAWFORD 92	CLEO	$e^+e^- \rightarrow \Upsilon(4S)$
• • • We do not use the following data for averages, fits, limits, etc. • • •					
<0.0088	90	12	ALBRECHT 89k	ARG	$e^+e^- \rightarrow \Upsilon(4S)$

 $\Gamma(\Lambda\bar{\Lambda} \text{ anything})/\Gamma(\Lambda/\bar{\Lambda} \text{ anything})$ $\Gamma_{123}/\Gamma_{116}$

VALUE	CL%	DOCUMENT ID	TECN	COMMENT
• • • We do not use the following data for averages, fits, limits, etc. • • •				
<0.13	90	¹ CRAWFORD 92	CLEO	$e^+e^- \rightarrow \Upsilon(4S)$

¹CRAWFORD 92 value is not independent of their $\Gamma(\Lambda\bar{\Lambda} \text{ anything})/\Gamma_{\text{total}}$ value.

 $\Gamma(s e^+ e^-)/\Gamma_{\text{total}}$ Γ_{124}/Γ

Test for $\Delta B = 1$ weak neutral current. Allowed by higher-order electroweak interactions.

VALUE (units 10 ⁻⁶)	CL%	DOCUMENT ID	TECN	COMMENT
6.7 ± 1.7 OUR AVERAGE				
Error includes scale factor of 2.0.				
7.69 ^{+0.82+0.71} _{-0.77-0.60}		¹ LEES 14D	BABR	$e^+e^- \rightarrow \Upsilon(4S)$
4.04 ± 1.30 ^{+0.87} _{-0.83}		² IWASAKI 05	BELL	$e^+e^- \rightarrow \Upsilon(4S)$

• • • We do not use the following data for averages, fits, limits, etc. • • •

6.0 ± 1.7 ± 1.3		² AUBERT,B 04i	BABR	Repl. by LEES 14D
5.0 ± 2.3 ± 1.3 ^{+1.3} _{-1.1}		² KANEKO 03	BELL	Repl. by IWASAKI 05
< 57	90	GLENN 98	CLEO	$e^+e^- \rightarrow \Upsilon(4S)$
<50000	90	BEBEK 81	CLEO	$e^+e^- \rightarrow \Upsilon(4S)$

¹Measured from sum of exclusive modes through K^+ , $K^+\pi^0$, $K^+\pi^-$, $K^+\pi^-\pi^0$, $K^+\pi^-\pi^+$, K_S^0 , $K_S^0\pi^0$, $K_S^0\pi^+$, $K_S^0\pi^+\pi^0$, and $K_S^0\pi^+\pi^-$ corrected for unobserved modes.

²Requires $M_{\ell^+\ell^-} > 0.2 \text{ GeV}/c^2$.

 $\Gamma(s\mu^+\mu^-)/\Gamma_{\text{total}}$ Γ_{125}/Γ

Test for $\Delta B = 1$ weak neutral current. Allowed by higher-order electroweak interactions.

VALUE (units 10 ⁻⁶)	CL%	DOCUMENT ID	TECN	COMMENT
4.3 ± 1.0 OUR AVERAGE				
4.41 ^{+1.31+0.63} _{-1.17-0.50}		¹ LEES 14D	BABR	$e^+e^- \rightarrow \Upsilon(4S)$
4.13 ± 1.05 ± 0.85 ^{+0.85} _{-0.81}		² IWASAKI 05	BELL	$e^+e^- \rightarrow \Upsilon(4S)$

• • • We do not use the following data for averages, fits, limits, etc. • • •

5.0 ± 2.8 ± 1.2		AUBERT,B 04i	BABR	Repl. by LEES 14D
7.9 ± 2.1 ± 2.1 ^{+2.1} _{-1.5}		KANEKO 03	BELL	Repl. by IWASAKI 05
< 58	90	GLENN 98	CLEO	$e^+e^- \rightarrow \Upsilon(4S)$
<17000	90	CHADWICK 81	CLEO	$e^+e^- \rightarrow \Upsilon(4S)$

¹Measured from sum of exclusive modes through K^+ , $K^+\pi^0$, $K^+\pi^-$, $K^+\pi^-\pi^0$, $K^+\pi^-\pi^+$, K_S^0 , $K_S^0\pi^0$, $K_S^0\pi^+$, $K_S^0\pi^+\pi^0$, and $K_S^0\pi^+\pi^-$ corrected for unobserved modes.

²Requires $M_{\ell^+\ell^-} > 0.2 \text{ GeV}/c^2$.

 $[\Gamma(s e^+ e^-) + \Gamma(s\mu^+\mu^-)]/\Gamma_{\text{total}}$ $(\Gamma_{124} + \Gamma_{125})/\Gamma$

Test for $\Delta B = 1$ weak neutral current. Allowed by higher-order electroweak interactions.

VALUE	CL%	DOCUMENT ID	TECN	COMMENT
< 4.2 × 10⁻⁵				
	90	GLENN 98	CLEO	$e^+e^- \rightarrow \Upsilon(4S)$
• • • We do not use the following data for averages, fits, limits, etc. • • •				
<0.0024	90	¹ BEAN 87	CLEO	Repl. by GLENN 98
<0.0062	90	² AVERY 84	CLEO	Repl. by BEAN 87

¹BEAN 87 reports $[(\mu^+\mu^-) + (e^+e^-)]/2$ and we converted it.

²Determine ratio of B^+ to B^0 semileptonic decays to be in the range 0.25–2.9.

 $\Gamma(s\ell^+\ell^-)/\Gamma_{\text{total}}$ Γ_{126}/Γ

Test for $\Delta B = 1$ weak neutral current.

VALUE (units 10 ⁻⁶)	DOCUMENT ID	TECN	COMMENT
5.8 ± 1.3 OUR AVERAGE			
Error includes scale factor of 1.8.			
6.73 ^{+0.70+0.60} _{-0.64-0.56}	¹ LEES 14D	BABR	$e^+e^- \rightarrow \Upsilon(4S)$
4.11 ± 0.83 ± 0.85 ^{+0.85} _{-0.81}	² IWASAKI 05	BELL	$e^+e^- \rightarrow \Upsilon(4S)$

• • • We do not use the following data for averages, fits, limits, etc. • • •

5.6 ± 1.5 ± 1.3	³ AUBERT,B 04i	BABR	Repl. by LEES 14D
6.1 ± 1.4 ± 1.4 ^{+1.4} _{-1.1}	³ KANEKO 03	BELL	Repl. by IWASAKI 05

¹Measured from sum of exclusive modes through K^+ , $K^+\pi^0$, $K^+\pi^-$, $K^+\pi^-\pi^0$, $K^+\pi^-\pi^+$, K_S^0 , $K_S^0\pi^0$, $K_S^0\pi^+$, $K_S^0\pi^+\pi^0$, and $K_S^0\pi^+\pi^-$ corrected for unobserved modes.

²Requires $M_{\ell^+\ell^-} > 0.2 \text{ GeV}/c^2$.

³Requires $M_{e^+e^-} > 0.2 \text{ GeV}/c^2$.

 $\Gamma(\pi\ell^+\ell^-)/\Gamma_{\text{total}}$ Γ_{127}/Γ

VALUE	CL%	DOCUMENT ID	TECN	COMMENT
< 5.9 × 10⁻⁸				
	90	¹ LEES 13M	BABR	$e^+e^- \rightarrow \Upsilon(4S)$
• • • We do not use the following data for averages, fits, limits, etc. • • •				
< 6.2 × 10 ⁻⁸	90	¹ WEI 08A	BELL	$e^+e^- \rightarrow \Upsilon(4S)$
< 9.1 × 10 ⁻⁸	90	¹ AUBERT 07AG	BABR	$e^+e^- \rightarrow \Upsilon(4S)$

¹Assumes equal production of B^+ and B^0 at the $\Upsilon(4S)$.

Meson Particle Listings

 B^\pm/B^0 ADMIXTURE

$\Gamma(\pi e^+ e^-)/\Gamma_{\text{total}}$					Γ_{128}/Γ
VALUE	CL%	DOCUMENT ID	TECN	COMMENT	
$<11.0 \times 10^{-8}$	90	¹ LEES	13M BABR	$e^+ e^- \rightarrow \Upsilon(4S)$	
¹ Assumes equal production of B^+ and B^0 at the $\Upsilon(4S)$.					

$\Gamma(\pi \mu^+ \mu^-)/\Gamma_{\text{total}}$					Γ_{129}/Γ
VALUE	CL%	DOCUMENT ID	TECN	COMMENT	
$<5.0 \times 10^{-8}$	90	¹ LEES	13M BABR	$e^+ e^- \rightarrow \Upsilon(4S)$	
¹ Assumes equal production of B^+ and B^0 at the $\Upsilon(4S)$.					

$\Gamma(K e^+ e^-)/\Gamma_{\text{total}}$					Γ_{130}/Γ
Test for $\Delta B = 1$ weak neutral current. Allowed by higher-order electroweak interactions.					
VALUE (units 10^{-7})	CL%	DOCUMENT ID	TECN	COMMENT	
4.4 ± 0.6 OUR AVERAGE					
$3.9^{+0.9}_{-0.8} \pm 0.2$		¹ AUBERT	09T BABR	$e^+ e^- \rightarrow \Upsilon(4S)$	
$4.0^{+0.8}_{-0.7} \pm 0.3$		¹ WEI	09A BELL	$e^+ e^- \rightarrow \Upsilon(4S)$	
• • • We do not use the following data for averages, fits, limits, etc. • • •					
$3.3^{+0.9}_{-0.8} \pm 0.2$		¹ AUBERT,B	06J BABR	Repl. by AUBERT 09T	
$7.4^{+1.8}_{-1.6} \pm 0.5$		¹ AUBERT	03U BABR	Repl. by AUBERT,B 06J	
$4.0^{+1.5}_{-1.3} \pm 0.3$		^{1,2} ISHIKAWA	03 BELL	Repl. by WEI 09A	
<13	90	ABE	02 BELL	Repl. by ISHIKAWA 03	
¹ Assumes equal production of B^+ and B^0 at the $\Upsilon(4S)$.					
² The second error is a total of systematic uncertainties including model dependence.					

$\Gamma(K^*(892) e^+ e^-)/\Gamma_{\text{total}}$					Γ_{131}/Γ
Test for $\Delta B = 1$ weak neutral current. Allowed by higher-order electroweak interactions.					
VALUE (units 10^{-7})	CL%	DOCUMENT ID	TECN	COMMENT	
11.9 ± 2.0 OUR AVERAGE				Error includes scale factor of 1.2.	
$9.9^{+2.3}_{-2.1} \pm 0.6$		¹ AUBERT	09T BABR	$e^+ e^- \rightarrow \Upsilon(4S)$	
$13.9^{+2.3}_{-2.0} \pm 1.2$		¹ WEI	09A BELL	$e^+ e^- \rightarrow \Upsilon(4S)$	
• • • We do not use the following data for averages, fits, limits, etc. • • •					
$9.7^{+3.0}_{-2.7} \pm 1.4$		¹ AUBERT,B	06J BABR	Repl. by AUBERT 09T	
$9.8^{+5.0}_{-4.2} \pm 1.1$		¹ AUBERT	03U BABR	Repl. by AUBERT,B 06J	
$14.9^{+5.2}_{-4.6} \pm 1.2$		² ISHIKAWA	03 BELL	Repl. by WEI 09A	
<56	90	ABE	02 BELL	Repl. by ISHIKAWA 03	
¹ Assumes equal production of B^+ and B^0 at the $\Upsilon(4S)$.					
² Assumes equal production of B^0 and B^+ at $\Upsilon(4S)$. The second error is a total of systematic uncertainties including model dependence.					

$\Gamma(K \mu^+ \mu^-)/\Gamma_{\text{total}}$					Γ_{132}/Γ
Test for $\Delta B = 1$ weak neutral current. Allowed by higher-order electroweak interactions.					
VALUE (units 10^{-7})	CL%	DOCUMENT ID	TECN	COMMENT	
4.2 ± 0.4 OUR AVERAGE					
$4.2 \pm 0.4 \pm 0.2$		AALTONEN	11A CDF	$p\bar{p}$ at 1.96 TeV	
$4.1^{+1.3}_{-1.2} \pm 0.2$		¹ AUBERT	09T BABR	$e^+ e^- \rightarrow \Upsilon(4S)$	
$5.0 \pm 0.6 \pm 0.3$		¹ WEI	09A BELL	$e^+ e^- \rightarrow \Upsilon(4S)$	
• • • We do not use the following data for averages, fits, limits, etc. • • •					
$3.5^{+1.3}_{-1.1} \pm 0.3$		¹ AUBERT,B	06J BABR	Repl. by AUBERT 09T	
$4.5^{+2.3}_{-1.5} \pm 0.4$		¹ AUBERT	03U BABR	Repl. by AUBERT,B 06J	
$4.8^{+1.2}_{-1.1} \pm 0.4$		^{1,2} ISHIKAWA	03 BELL	Repl. by WEI 09A	
$9.9^{+4.0}_{-3.2} \pm 1.0$		ABE	02 BELL	Repl. by ISHIKAWA 03	
¹ Assumes equal production of B^+ and B^0 at the $\Upsilon(4S)$.					
² The second error is a total of systematic uncertainties including model dependence.					

$\Gamma(K \mu^+ \mu^-)/\Gamma(K e^+ e^-)$					$\Gamma_{132}/\Gamma_{130}$
VALUE	CL%	DOCUMENT ID	TECN	COMMENT	
$1.01^{+0.19}_{-0.16}$ OUR AVERAGE					
$1.03^{+0.28}_{-0.24} \pm 0.01$		¹ CHOUDHURY	21 BELL	$e^+ e^- \rightarrow \Upsilon(4S)$	
$1.00^{+0.31}_{-0.25} \pm 0.07$		² LEES	12S BABR	$e^+ e^- \rightarrow \Upsilon(4S)$	
$0.96^{+0.44}_{-0.34} \pm 0.05$		AUBERT	09T BABR	$e^+ e^- \rightarrow \Upsilon(4S)$	
• • • We do not use the following data for averages, fits, limits, etc. • • •					
$1.03 \pm 0.19 \pm 0.06$		³ WEI	09A BELL	$e^+ e^- \rightarrow \Upsilon(4S)$	
$1.06 \pm 0.48 \pm 0.08$		AUBERT,B	06J BABR	Repl. by AUBERT 09T	
¹ For $1.0 < q^2 < 6.0 \text{ GeV}^2/c^4$. Measurements in other q^2 bins are also reported.					
² Measured in the union of $0.10 < q^2 < 8.12 \text{ GeV}^2/c^4$ and $q^2 > 10.11 \text{ GeV}^2/c^4$. LEES 12s reports also individual measurements $\Gamma(B \rightarrow K \mu^+ \mu^-)/\Gamma(B \rightarrow K e^+ e^-) = 0.74^{+0.40}_{-0.31} \pm 0.06$ for $0.10 < q^2 < 8.12 \text{ GeV}^2/c^4$ and $\Gamma(B \rightarrow K \mu^+ \mu^-)/\Gamma(B \rightarrow K e^+ e^-) = 1.43^{+0.65}_{-0.44} \pm 0.12$ for $q^2 > 10.11 \text{ GeV}^2/c^4$.					
³ Superseded by CHOUDHURY 21.					

$\Gamma(K^*(892) \mu^+ \mu^-)/\Gamma_{\text{total}}$					Γ_{133}/Γ
Test for $\Delta B = 1$ weak neutral current. Allowed by higher-order electroweak interactions.					
VALUE (units 10^{-7})	CL%	DOCUMENT ID	TECN	COMMENT	
10.6 ± 0.9 OUR AVERAGE					
$10.1 \pm 1.0 \pm 0.5$		AALTONEN	11A CDF	$p\bar{p}$ at 1.96 TeV	
$13.5^{+3.5}_{-3.3} \pm 1.0$		¹ AUBERT	09T BABR	$e^+ e^- \rightarrow \Upsilon(4S)$	
$11.0^{+1.6}_{-1.4} \pm 0.8$		¹ WEI	09A BELL	$e^+ e^- \rightarrow \Upsilon(4S)$	
• • • We do not use the following data for averages, fits, limits, etc. • • •					
$8.0^{+3.5}_{-3.0} \pm 1.2$		¹ AUBERT,B	06J BABR	Repl. by AUBERT 09T	
$12.7^{+7.6}_{-6.1} \pm 1.6$		¹ AUBERT	03U BABR	Repl. by AUBERT,B 06J	
$11.7^{+3.6}_{-3.1} \pm 1.0$		² ISHIKAWA	03 BELL	Repl. by WEI 09A	
<31	90	ABE	02 BELL	Repl. by ISHIKAWA 03	
¹ Assumes equal production of B^+ and B^0 at the $\Upsilon(4S)$.					
² Assumes equal production of B^0 and B^+ at $\Upsilon(4S)$. The second error is a total of systematic uncertainties including model dependence.					

$\Gamma(K^*(892) \mu^+ \mu^-)/\Gamma(K^*(892) e^+ e^-)$					$\Gamma_{133}/\Gamma_{131}$
VALUE	CL%	DOCUMENT ID	TECN	COMMENT	
0.98 ± 0.15 OUR AVERAGE					
$1.13^{+0.34}_{-0.26} \pm 0.10$		¹ LEES	12S BABR	$e^+ e^- \rightarrow \Upsilon(4S)$	
$1.37^{+0.53}_{-0.40} \pm 0.09$		AUBERT	09T BABR	$e^+ e^- \rightarrow \Upsilon(4S)$	
$0.83 \pm 0.17 \pm 0.08$		WEI	09A BELL	$e^+ e^- \rightarrow \Upsilon(4S)$	
• • • We do not use the following data for averages, fits, limits, etc. • • •					
$0.91 \pm 0.45 \pm 0.06$		AUBERT,B	06J BABR	Repl. by AUBERT 09T	
¹ Measured in the union of $0.10 < q^2 < 8.12 \text{ GeV}^2/c^4$ and $q^2 > 10.11 \text{ GeV}^2/c^4$. LEES 12s reports also individual measurements $\Gamma(B \rightarrow K^*(892) \mu^+ \mu^-)/\Gamma(B \rightarrow K^*(892) e^+ e^-) = 1.06^{+0.48}_{-0.33} \pm 0.08$ for $0.10 < q^2 < 8.12 \text{ GeV}^2/c^4$ and $\Gamma(B \rightarrow K^*(892) \mu^+ \mu^-)/\Gamma(B \rightarrow K^*(892) e^+ e^-) = 1.18^{+0.55}_{-0.37} \pm 0.11$ for $q^2 > 10.11 \text{ GeV}^2/c^4$.					

$\Gamma(K \ell^+ \ell^-)/\Gamma_{\text{total}}$					Γ_{134}/Γ
Test for $\Delta B = 1$ weak neutral current. Allowed by higher-order electroweak interactions.					
VALUE (units 10^{-7})	CL%	DOCUMENT ID	TECN	COMMENT	
4.8 ± 0.4 OUR AVERAGE					
$4.7 \pm 0.6 \pm 0.2$		LEES	12S BABR	$e^+ e^- \rightarrow \Upsilon(4S)$	
$4.8^{+0.5}_{-0.4} \pm 0.3$		WEI	09A BELL	$e^+ e^- \rightarrow \Upsilon(4S)$	
• • • We do not use the following data for averages, fits, limits, etc. • • •					
$3.9 \pm 0.7 \pm 0.2$		¹ AUBERT	09T BABR	Repl. by LEES 12s	
$3.4 \pm 0.7 \pm 0.2$		¹ AUBERT,B	06J BABR	Repl. by AUBERT 09T	
$6.5^{+1.4}_{-1.3} \pm 0.4$		² AUBERT	03U BABR	Repl. by AUBERT,B 06J	
$4.8^{+1.0}_{-0.9} \pm 0.3$		³ ISHIKAWA	03 BELL	Repl. by WEI 09A	
$7.5^{+2.5}_{-2.1} \pm 0.6$		⁴ ABE	02 BELL	Repl. by ISHIKAWA 03	
< 5.1	90	¹ AUBERT	02L BABR	$e^+ e^- \rightarrow \Upsilon(4S)$	
< 17	90	⁵ ANDERSON	01B CLE2	$e^+ e^- \rightarrow \Upsilon(4S)$	
¹ Assumes equal production of B^+ and B^0 at the $\Upsilon(4S)$.					
² Assumes all four $B \rightarrow K \ell^+ \ell^-$ modes having equal partial widths in the fit.					
³ Assumes equal production rate for charge and neutral B meson pairs, isospin invariance, lepton universality for $B \rightarrow K \ell^+ \ell^-$, and $B(B \rightarrow K^*(892) \mu^+ \mu^-) = 1.33$. The second error is total systematic uncertainties including model dependence.					
⁴ Assumes lepton universality.					
⁵ The result is for di-lepton masses above 0.5 GeV.					

$\Gamma(K^*(892) \ell^+ \ell^-)/\Gamma_{\text{total}}$					Γ_{135}/Γ
Test for $\Delta B = 1$ weak neutral current. Allowed by higher-order electroweak interactions.					
VALUE (units 10^{-7})	CL%	DOCUMENT ID	TECN	COMMENT	
10.5 ± 1.0 OUR AVERAGE					
$10.2^{+1.4}_{-1.3} \pm 0.5$		LEES	12S BABR	$e^+ e^- \rightarrow \Upsilon(4S)$	
$10.7^{+1.1}_{-1.0} \pm 0.9$		WEI	09A BELL	$e^+ e^- \rightarrow \Upsilon(4S)$	
• • • We do not use the following data for averages, fits, limits, etc. • • •					
$11.1^{+1.9}_{-1.8} \pm 0.7$		¹ AUBERT	09T BABR	Repl. by LEES 12s	
$7.8^{+1.9}_{-1.7} \pm 1.1$		¹ AUBERT,B	06J BABR	Repl. by AUBERT 09T	
$8.8^{+3.3}_{-2.9} \pm 1.0$		² AUBERT	03U BABR	Repl. by AUBERT,B 06J	
$11.5^{+2.6}_{-2.4} \pm 0.8$		³ ISHIKAWA	03 BELL	Repl. by WEI 09A	
< 31	90	^{1,4} AUBERT	02L BABR	Repl. by AUBERT 03U	
< 33	90	⁵ ANDERSON	01B CLE2	$e^+ e^- \rightarrow \Upsilon(4S)$	
¹ Assumes equal production of B^+ and B^0 at the $\Upsilon(4S)$.					
² Assumes the partial width ratio of electron and muon modes to be $\Gamma(B \rightarrow K^*(892) e^+ e^-)/\Gamma(B \rightarrow K^*(892) \mu^+ \mu^-) = 1.33$.					
³ Assumes equal production rate for charge and neutral B meson pairs, isospin invariance, lepton universality for $B \rightarrow K \ell^+ \ell^-$, and $B(B \rightarrow K^*(892) \mu^+ \mu^-) = 1.33$. The second error is total systematic uncertainties including model dependence.					
⁴ For averaging $K^*(892) \mu^+ \mu^-$ and $K^*(892) e^+ e^-$ modes, AUBERT 02L assumed $B(B \rightarrow K^*(892) e^+ e^-)/B(B \rightarrow K^*(892) \mu^+ \mu^-) = 1.2$.					
⁵ The result is for di-lepton masses above 0.5 GeV.					

Meson Particle Listings

B^\pm/B^0 ADMIXTURE

$\Gamma(K\nu\bar{\nu})/\Gamma_{\text{total}}$ Γ_{136}/Γ

Test for $\Delta B = 1$ weak neutral current.

VALUE	CL%	DOCUMENT ID	TECN	COMMENT
$<1.6 \times 10^{-5}$	90	¹ GRYGIER 17	BELL	$e^+e^- \rightarrow \Upsilon(4S)$
••• We do not use the following data for averages, fits, limits, etc. •••				
$<1.7 \times 10^{-5}$	90	^{1,2} LEES 13i	BABR	$e^+e^- \rightarrow \Upsilon(4S)$
$<1.4 \times 10^{-5}$	90	¹ DEL-AMO-SA...10q	BABR	Repl. by LEES 13i

¹ Assumes equal production of B^+ and B^0 at the $\Upsilon(4S)$.
² Also reported a limit $< 3.2 \times 10^{-5}$ at 90% CL obtained using a fully reconstructed hadronic B -tag evnets.

$\Gamma(K^*\nu\bar{\nu})/\Gamma_{\text{total}}$ Γ_{137}/Γ

Test for $\Delta B = 1$ weak neutral current.

VALUE	CL%	DOCUMENT ID	TECN	COMMENT
$<2.7 \times 10^{-5}$	90	¹ GRYGIER 17	BELL	$e^+e^- \rightarrow \Upsilon(4S)$
••• We do not use the following data for averages, fits, limits, etc. •••				
$<7.6 \times 10^{-5}$	90	^{1,2} LEES 13i	BABR	$e^+e^- \rightarrow \Upsilon(4S)$
$<8 \times 10^{-5}$	90	AUBERT 08bc	BABR	Repl. by LEES 13i

¹ Assumes equal production of B^+ and B^0 at the $\Upsilon(4S)$.
² Also reported a limit $< 7.9 \times 10^{-5}$ at 90% CL obtained using a fully reconstructed hadronic B -tag evnets.

$\Gamma(\pi\nu\bar{\nu})/\Gamma_{\text{total}}$ Γ_{138}/Γ

Test for $\Delta B = 1$ weak neutral current.

VALUE	CL%	DOCUMENT ID	TECN	COMMENT
$<0.8 \times 10^{-5}$	90	¹ GRYGIER 17	BELL	$e^+e^- \rightarrow \Upsilon(4S)$

¹ Assumes equal production of B^+ and B^0 at the $\Upsilon(4S)$.

$\Gamma(\rho\nu\bar{\nu})/\Gamma_{\text{total}}$ Γ_{139}/Γ

Test for $\Delta B = 1$ weak neutral current.

VALUE	CL%	DOCUMENT ID	TECN	COMMENT
$<2.8 \times 10^{-5}$	90	¹ GRYGIER 17	BELL	$e^+e^- \rightarrow \Upsilon(4S)$

¹ Assumes equal production of B^+ and B^0 at the $\Upsilon(4S)$.

$\Gamma(s e^\pm \mu^\mp)/\Gamma_{\text{total}}$ Γ_{140}/Γ

Test for lepton family number conservation. Allowed by higher-order electroweak interactions.

VALUE	CL%	DOCUMENT ID	TECN	COMMENT
$<2.2 \times 10^{-5}$	90	GLENN 98	CLEO	$e^+e^- \rightarrow \Upsilon(4S)$

$\Gamma(\pi e^\pm \mu^\mp)/\Gamma_{\text{total}}$ Γ_{141}/Γ

Test of lepton family number conservation.

VALUE	CL%	DOCUMENT ID	TECN	COMMENT
$<9.2 \times 10^{-8}$	90	¹ AUBERT 07AG	BABR	$e^+e^- \rightarrow \Upsilon(4S)$
••• We do not use the following data for averages, fits, limits, etc. •••				
$<1.6 \times 10^{-6}$	90	¹ EDWARDS 02B	CLE2	$e^+e^- \rightarrow \Upsilon(4S)$

¹ Assumes equal production of B^+ and B^0 at the $\Upsilon(4S)$.

$\Gamma(\rho e^\pm \mu^\mp)/\Gamma_{\text{total}}$ Γ_{142}/Γ

Test of lepton family number conservation.

VALUE	CL%	DOCUMENT ID	TECN	COMMENT
$<3.2 \times 10^{-6}$	90	¹ EDWARDS 02B	CLE2	$e^+e^- \rightarrow \Upsilon(4S)$

¹ Assumes equal production of B^+ and B^0 at the $\Upsilon(4S)$.

$\Gamma(K e^\pm \mu^\mp)/\Gamma_{\text{total}}$ Γ_{143}/Γ

Test of lepton family number conservation.

VALUE (units 10^{-7})	CL%	DOCUMENT ID	TECN	COMMENT
< 0.38	90	¹ AUBERT,B 06j	BABR	$e^+e^- \rightarrow \Upsilon(4S)$
••• We do not use the following data for averages, fits, limits, etc. •••				
<16	90	¹ EDWARDS 02B	CLE2	$e^+e^- \rightarrow \Upsilon(4S)$

¹ Assumes equal production of B^+ and B^0 at the $\Upsilon(4S)$.

$\Gamma(K^*(892) e^\pm \mu^\mp)/\Gamma_{\text{total}}$ Γ_{144}/Γ

Test of lepton family number conservation.

VALUE (units 10^{-7})	CL%	DOCUMENT ID	TECN	COMMENT
< 5.1	90	¹ AUBERT,B 06j	BABR	$e^+e^- \rightarrow \Upsilon(4S)$
••• We do not use the following data for averages, fits, limits, etc. •••				
<62	90	¹ EDWARDS 02B	CLE2	$e^+e^- \rightarrow \Upsilon(4S)$

¹ Assumes equal production of B^+ and B^0 at the $\Upsilon(4S)$.

CP VIOLATION

A_{CP} is defined as

$$\frac{B(\bar{B} \rightarrow \bar{f}) - B(B \rightarrow f)}{B(\bar{B} \rightarrow \bar{f}) + B(B \rightarrow f)}$$

the CP-violation charge asymmetry of inclusive B^\pm and B^0 decay.

$A_{CP}(B \rightarrow K^*(892)\gamma)$

VALUE	DOCUMENT ID	TECN	COMMENT
-0.003 ± 0.011 OUR AVERAGE			
$-0.004 \pm 0.014 \pm 0.003$	¹ HORIGUCHI 17	BELL	$e^+e^- \rightarrow \Upsilon(4S)$
$-0.003 \pm 0.017 \pm 0.007$	² AUBERT 09a0	BABR	$e^+e^- \rightarrow \Upsilon(4S)$
$0.08 \pm 0.13 \pm 0.03$	³ COAN 00	CLE2	$e^+e^- \rightarrow \Upsilon(4S)$

••• We do not use the following data for averages, fits, limits, etc. •••

$-0.013 \pm 0.036 \pm 0.010$	⁴ AUBERT,BE 04A	BABR	Repl. by AUBERT 09a0
$-0.015 \pm 0.044 \pm 0.012$	³ NAKAO 04	BELL	Repl. by HORIGUCHI 17
$-0.044 \pm 0.076 \pm 0.012$	⁵ AUBERT 02c	BABR	Repl. by AUBERT,BE 04A

¹ Uses $B(\Upsilon(4S) \rightarrow B^+B^-) = (51.4 \pm 0.6)\%$ and $B(\Upsilon(4S) \rightarrow B^0\bar{B}^0) = (48.6 \pm 0.6)\%$.
² Corresponds to a 90% CL interval $-0.033 < A_{CP} < 0.028$.
³ Assumes equal production of B^+ and B^0 at the $\Upsilon(4S)$.
⁴ Corresponds to a 90% CL allowed region, $-0.074 < A_{CP} < 0.049$.
⁵ A 90% CL range is $-0.170 < A_{CP} < 0.082$.

$A_{CP}(B \rightarrow s\gamma)$

VALUE	DOCUMENT ID	TECN	COMMENT
0.015 ± 0.011 OUR AVERAGE			
$0.0144 \pm 0.0128 \pm 0.0011$	¹ WATANUKI 19	BELL	$e^+e^- \rightarrow \Upsilon(4S)$
$0.017 \pm 0.019 \pm 0.010$	² LEES 14k	BABR	$e^+e^- \rightarrow \Upsilon(4S)$
••• We do not use the following data for averages, fits, limits, etc. •••			
$-0.011 \pm 0.030 \pm 0.014$	³ AUBERT 08bJ	BABR	Repl. by LEES 14k
$0.025 \pm 0.050 \pm 0.015$	⁴ AUBERT,B 04E	BABR	Repl. by AUBERT 08bJ
$0.002 \pm 0.050 \pm 0.030$	⁵ NISHIDA 04	BELL	Repl. by WATANUKI 19

¹ Using a sum-of-exclusive technique with $m_{X_S} < 2.8 \text{ GeV}/c^2$.
² Measured with 16 exclusively reconstructed $B \rightarrow X_S\gamma$ decays with $0.6 < m_{X_S} < 2.0 \text{ GeV}/c^2$ (ten charged and six neutral self-tagging B modes).
³ Uses a sum of exclusively reconstructed $B \rightarrow X_S$ decay modes, with X_S mass between 0.6 and 2.8 GeV/c^2 .
⁴ Corresponds to $-0.06 < A_{CP} < 0.11$ at 90% CL.
⁵ This measurement is performed inclusively for recoil mass X_S less than 2.1 GeV, which corresponds to $-0.093 < A_{CP} < 0.096$ at 90% CL.

$A_{CP}(B \rightarrow (s+d)\gamma)$

VALUE	DOCUMENT ID	TECN	COMMENT
0.010 ± 0.031 OUR AVERAGE			
$0.022 \pm 0.039 \pm 0.009$	¹ PESANTEZ 15	BELL	$e^+e^- \rightarrow \Upsilon(4S)$
$0.057 \pm 0.060 \pm 0.018$	LEES 12v	BABR	$e^+e^- \rightarrow \Upsilon(4S)$
$-0.10 \pm 0.18 \pm 0.05$	² AUBERT 08b	BABR	$e^+e^- \rightarrow \Upsilon(4S)$
$-0.110 \pm 0.115 \pm 0.017$	AUBERT,BE 06b	BABR	$e^+e^- \rightarrow \Upsilon(4S)$
$-0.079 \pm 0.108 \pm 0.022$	³ COAN 01	CLE2	$e^+e^- \rightarrow \Upsilon(4S)$

¹ Assumes equal production of B^+ and B^0 at the $\Upsilon(4S)$. Uses an opposite side lepton tag. Requires center-of-mass frame $E_\gamma > 2.1 \text{ GeV}$.
² Uses a fully reconstructed B meson as a tag on the recoil side. Requires $E_\gamma > 2.2 \text{ GeV}$.
³ Corresponds to $-0.27 < A_{CP} < 0.10$ at 90% CL.

$A_{CP}(B \rightarrow X_S \ell^+ \ell^-)$

VALUE	DOCUMENT ID	TECN	COMMENT
$0.04 \pm 0.11 \pm 0.01$	¹ LEES 14d	BABR	$e^+e^- \rightarrow \Upsilon(4S)$
••• We do not use the following data for averages, fits, limits, etc. •••			
$-0.22 \pm 0.26 \pm 0.02$	² AUBERT,B 04i	BABR	Repl. by LEES 14d

¹ Measured from sum of exclusive modes through K^+ , $K^+\pi^0$, $K^+\pi^-$, $K^+\pi^-\pi^0$, $K^+\pi^-\pi^+$, $K_S^0\pi^+$, and $K_S^0\pi^+\pi^0$.
² The final state flavor is determined by the kaon and pion charges where modes with $X_S = K_S^0$, $K_S^0\pi^0$ or $K_S^0\pi^+\pi^-$ are not used.

$A_{CP}(B \rightarrow X_S \ell^+ \ell^-) (1.0 < q^2 < 6.0 \text{ GeV}^2/c^4)$

VALUE	DOCUMENT ID	TECN	COMMENT
$-0.06 \pm 0.22 \pm 0.01$	¹ LEES 14d	BABR	$e^+e^- \rightarrow \Upsilon(4S)$

¹ Measured from sum of exclusive modes through K^+ , $K^+\pi^0$, $K^+\pi^-$, $K^+\pi^-\pi^0$, $K^+\pi^-\pi^+$, $K_S^0\pi^+$, and $K_S^0\pi^+\pi^0$.

$A_{CP}(B \rightarrow X_S \ell^+ \ell^-) (10.1 < q^2 < 12.9 \text{ or } q^2 > 14.2 \text{ GeV}^2/c^4)$

VALUE	DOCUMENT ID	TECN	COMMENT
$0.19^{+0.18}_{-0.17} \pm 0.01$	¹ LEES 14d	BABR	$e^+e^- \rightarrow \Upsilon(4S)$

¹ Measured from sum of exclusive modes through K^+ , $K^+\pi^0$, $K^+\pi^-$, $K^+\pi^-\pi^0$, $K^+\pi^-\pi^+$, $K_S^0\pi^+$, and $K_S^0\pi^+(pi^-)^0$.

$A_{CP}(B \rightarrow K^* e^+ e^-)$

VALUE	DOCUMENT ID	TECN	COMMENT
$-0.18 \pm 0.15 \pm 0.01$	WEI 09A	BELL	$e^+e^- \rightarrow \Upsilon(4S)$

$A_{CP}(B \rightarrow K^* \mu^+ \mu^-)$

VALUE	DOCUMENT ID	TECN	COMMENT
$-0.03 \pm 0.13 \pm 0.02$	WEI 09A	BELL	$e^+e^- \rightarrow \Upsilon(4S)$

$A_{CP}(B \rightarrow K^* \ell^+ \ell^-)$

VALUE	DOCUMENT ID	TECN	COMMENT
-0.04 ± 0.07 OUR AVERAGE			
$0.03 \pm 0.13 \pm 0.01$	¹ LEES 12s	BABR	$e^+e^- \rightarrow \Upsilon(4S)$
$+0.01^{+0.16}_{-0.15} \pm 0.01$	AUBERT 09t	BABR	$e^+e^- \rightarrow \Upsilon(4S)$
$-0.10 \pm 0.10 \pm 0.01$	WEI 09A	BELL	$e^+e^- \rightarrow \Upsilon(4S)$

¹ Measured in the union of $0.10 < q^2 < 8.12 \text{ GeV}^2/c^4$ and $q^2 > 10.11 \text{ GeV}^2/c^4$. LEES 12s reports also individual measurements $A_{CP}(B \rightarrow K^* \ell^+ \ell^-) = -0.13^{+0.18}_{-0.19} \pm 0.01$ for $0.10 < q^2 < 8.12 \text{ GeV}^2/c^4$ and $A_{CP}(B \rightarrow K^* \ell^+ \ell^-) = 0.16^{+0.18}_{-0.19} \pm 0.01$ for $q^2 > 10.11 \text{ GeV}^2/c^4$.

Meson Particle Listings

 B^\pm/B^0 ADMIXTURE $A_{CP}(B \rightarrow \eta \text{ anything})$

VALUE	DOCUMENT ID	TECN	COMMENT
$-0.13 \pm 0.04 \pm_{-0.03}^{+0.02}$	¹ NISHIMURA	10	BELL $e^+e^- \rightarrow \Upsilon(4S)$

¹ Uses $B \rightarrow \eta X_s$ with $0.4 < m_{X_s} < 2.6 \text{ GeV}/c^2$.

 $\Delta A_{CP}(X_s \gamma) = A_{CP}(B^\pm \rightarrow X_s \gamma) - A_{CP}(B^0 \rightarrow X_s \gamma)$

This is the isospin difference of the CP asymmetries.

VALUE	DOCUMENT ID	TECN	COMMENT
0.041 ± 0.023 OUR AVERAGE			
$0.0369 \pm 0.0265 \pm 0.0076$	¹ WATANUKI	19	BELL $e^+e^- \rightarrow \Upsilon(4S)$
$0.050 \pm 0.039 \pm 0.015$	² LEES	14k	BABR $e^+e^- \rightarrow \Upsilon(4S)$

¹ Using a sum-of-exclusive technique with $m_{X_s} < 2.8 \text{ GeV}/c^2$.

² Measured with 16 exclusively reconstructed $B \rightarrow X_s \gamma$ decays with $0.6 < m_{X_s} < 2.0 \text{ GeV}/c^2$ (ten charged and six neutral self-tagging B modes).

 $\bar{A}_{CP}(B \rightarrow X_s \gamma) = (A_{CP}(B^+ \rightarrow X_s \gamma) + A_{CP}(B^0 \rightarrow X_s \gamma))/2$

VALUE	DOCUMENT ID	TECN	COMMENT
$0.0091 \pm 0.0121 \pm 0.0013$	¹ WATANUKI	19	BELL $e^+e^- \rightarrow \Upsilon(4S)$

¹ Using a sum-of-exclusive technique with $m_{X_s} < 2.8 \text{ GeV}/c^2$.

 $\Delta A_{CP}(B \rightarrow K^* \gamma) = A_{CP}(B^+ \rightarrow K^* \gamma) - A_{CP}(B^0 \rightarrow K^* \gamma)$

This is the isospin difference of the CP asymmetries.

VALUE	DOCUMENT ID	TECN	COMMENT
$0.024 \pm 0.028 \pm 0.005$	¹ HORIGUCHI	17	BELL $e^+e^- \rightarrow \Upsilon(4S)$

¹ Uses $B(\Upsilon(4S) \rightarrow B^+ B^-) = (51.4 \pm 0.6)\%$ and $B(\Upsilon(4S) \rightarrow B^0 \bar{B}^0) = (48.6 \pm 0.6)\%$.

 $\bar{A}_{CP}(B \rightarrow K^* \gamma) = (A_{CP}(B^+ \rightarrow K^* \gamma) + A_{CP}(B^0 \rightarrow K^* \gamma))/2$

This is the average CP asymmetry.

VALUE	DOCUMENT ID	TECN	COMMENT
$-0.001 \pm 0.014 \pm 0.003$	¹ HORIGUCHI	17	BELL $e^+e^- \rightarrow \Upsilon(4S)$

¹ Uses $B(\Upsilon(4S) \rightarrow B^+ B^-) = (51.4 \pm 0.6)\%$ and $B(\Upsilon(4S) \rightarrow B^0 \bar{B}^0) = (48.6 \pm 0.6)\%$.

POLARIZATION IN B DECAY

In decays involving two vector mesons, one can distinguish among the states in which meson polarizations are both longitudinal (L) or both are transverse and parallel (\parallel) or perpendicular (\perp) to each other with the parameters Γ_L/Γ , Γ_\perp/Γ , and the relative phases ϕ_\parallel and ϕ_\perp . See the definitions in the note on "Polarization in B Decays" review in the B^0 Particle Listings.

 $F_L(B \rightarrow K^* \ell^+ \ell^-) (q^2 > 0.1 \text{ GeV}^2/c^4)$

VALUE	DOCUMENT ID	TECN	COMMENT
$0.63 \pm_{-0.19}^{+0.18} \pm 0.05$	¹ AUBERT.B	06J	BABR $e^+e^- \rightarrow \Upsilon(4S)$

¹ Results with different q^2 cuts are also reported.

 $F_L(B \rightarrow K^* \ell^+ \ell^-) (m_{\ell\ell} < 2.5 \text{ GeV}/c^2)$

VALUE	DOCUMENT ID	TECN	COMMENT
$0.35 \pm 0.16 \pm 0.04$	AUBERT	09N	BABR $e^+e^- \rightarrow \Upsilon(4S)$

 $F_L(B \rightarrow K^* \ell^+ \ell^-) (m_{\ell\ell} > 3.2 \text{ GeV}/c^2)$

VALUE	DOCUMENT ID	TECN	COMMENT
$0.71 \pm_{-0.22}^{+0.20} \pm 0.04$	AUBERT	09N	BABR $e^+e^- \rightarrow \Upsilon(4S)$

 $F_L(B \rightarrow K^* \ell^+ \ell^-) (0.10 < q^2 < 0.98 \text{ GeV}^2/c^4)$

VALUE	DOCUMENT ID	TECN	COMMENT
$0.263 \pm_{-0.044}^{+0.045} \pm 0.017$	AAIJ	16B	LHCB pp at 7, 8 TeV

 $F_L(B \rightarrow K^* \ell^+ \ell^-) (1.1 < q^2 < 2.5 \text{ GeV}^2/c^4)$

VALUE	DOCUMENT ID	TECN	COMMENT
$0.660 \pm_{-0.077}^{+0.083} \pm 0.022$	AAIJ	16B	LHCB pp at 7, 8 TeV

 $F_L(B \rightarrow K^* \ell^+ \ell^-) (0.1 < q^2 < 2.0 \text{ GeV}^2/c^4)$

VALUE	DOCUMENT ID	TECN	COMMENT
$0.34 \pm_{-0.07}^{+0.09}$ OUR AVERAGE			

$0.37 \pm_{-0.09}^{+0.10} \pm 0.04$ AAIJ 13Y LHCB pp at 7 TeV, $K^{*0} \mu^+ \mu^-$

$0.30 \pm 0.16 \pm 0.02$ AALTONEN 12I CDF $p\bar{p}$ at 1.96 TeV

$0.29 \pm_{-0.18}^{+0.21} \pm 0.02$ WEI 09A BELL $e^+e^- \rightarrow \Upsilon(4S)$

• • • We do not use the following data for averages, fits, limits, etc. • • •

$0.60 \pm_{-0.28}^{+0.00} \pm 0.19$ ¹ CHATRCHYAN13BL CMS pp at 7 TeV

$0.00 \pm_{-0.00}^{+0.13} \pm 0.02$ AAIJ 12U LHCB Repl. by AAIJ 13Y

$0.53 \pm_{-0.34}^{+0.32} \pm 0.07$ AALTONEN 11L CDF Repl. by AALTONEN 12I

¹ CHATRCHYAN 13BL uses, for this bin, $1.0 < q^2 < 2.0 \text{ GeV}^2/c^4$.

 $F_L(B \rightarrow K^* \ell^+ \ell^-) (2.0 < q^2 < 4.3 \text{ GeV}^2/c^4)$

VALUE	DOCUMENT ID	TECN	COMMENT
0.77 ± 0.05 OUR AVERAGE			
$0.876 \pm_{-0.097}^{+0.109} \pm 0.017$	¹ AAIJ	16B	LHCB pp at 7, 8 TeV
$0.80 \pm 0.08 \pm 0.06$	KHACHATRY..16D	CMS	pp at 8 TeV
$0.74 \pm_{-0.09}^{+0.10} \pm_{-0.03}^{+0.02}$	AAIJ	13Y	LHCB pp at 7 TeV, $K^{*0} \mu^+ \mu^-$
$0.65 \pm 0.17 \pm 0.03$	CHATRCHYAN13BL	CMS	pp at 7 TeV
$0.37 \pm_{-0.24}^{+0.25} \pm 0.10$	AALTONEN	12I	CDF $p\bar{p}$ at 1.96 TeV
$0.71 \pm 0.24 \pm 0.05$	WEI	09A	BELL $e^+e^- \rightarrow \Upsilon(4S)$
• • • We do not use the following data for averages, fits, limits, etc. • • •			
$0.77 \pm 0.15 \pm 0.03$	AAIJ	12U	LHCB Repl. by AAIJ 13Y
$0.40 \pm_{-0.33}^{+0.32} \pm 0.08$	AALTONEN	11L	CDF Repl. by AALTONEN 12I

¹ Measured in $2.5 < q^2 < 4.0 \text{ GeV}^2/c^4$.

 $F_L(B \rightarrow K^* \ell^+ \ell^-) (4.0 < q^2 < 6.0 \text{ GeV}^2/c^4)$

VALUE	DOCUMENT ID	TECN	COMMENT
$0.611 \pm_{-0.053}^{+0.052} \pm 0.017$	AAIJ	16B	LHCB pp at 7, 8 TeV

 $F_L(B \rightarrow K^* \ell^+ \ell^-) (6.0 < q^2 < 8.0 \text{ GeV}^2/c^4)$

VALUE	DOCUMENT ID	TECN	COMMENT
$0.579 \pm 0.046 \pm 0.015$	AAIJ	16B	LHCB pp at 7, 8 TeV

 $F_L(B \rightarrow K^* \ell^+ \ell^-) (4.3 < q^2 < 8.6 \text{ GeV}^2/c^4)$

VALUE	DOCUMENT ID	TECN	COMMENT
0.64 ± 0.06 OUR AVERAGE			
$0.57 \pm 0.07 \pm 0.03$	AAIJ	13Y	LHCB pp at 7 TeV, $K^{*0} \mu^+ \mu^-$
$0.81 \pm_{-0.12}^{+0.13} \pm 0.05$	CHATRCHYAN13BL	CMS	pp at 7 TeV
$0.68 \pm_{-0.17}^{+0.15} \pm 0.09$	AALTONEN	12I	CDF $p\bar{p}$ at 1.96 TeV
$0.64 \pm_{-0.24}^{+0.23} \pm 0.07$	WEI	09A	BELL $e^+e^- \rightarrow \Upsilon(4S)$
• • • We do not use the following data for averages, fits, limits, etc. • • •			
$0.60 \pm_{-0.07}^{+0.06} \pm 0.01$	AAIJ	12U	LHCB Repl. by AAIJ 13Y
$0.82 \pm_{-0.23}^{+0.19} \pm 0.07$	AALTONEN	11L	CDF Repl. by AALTONEN 12I

• • • We do not use the following data for averages, fits, limits, etc. • • •

 $F_L(B \rightarrow K^* \ell^+ \ell^-) (10.09 < q^2 < 12.86 \text{ GeV}^2/c^4)$

VALUE	DOCUMENT ID	TECN	COMMENT
0.448 ± 0.033 OUR AVERAGE			
$0.493 \pm_{-0.047}^{+0.049} \pm 0.013$	¹ AAIJ	16B	LHCB pp at 7, 8 TeV
$0.39 \pm 0.05 \pm 0.04$	KHACHATRY..16D	CMS	pp at 8 TeV
$0.48 \pm_{-0.09}^{+0.08} \pm 0.03$	AAIJ	13Y	LHCB pp at 7 TeV, $K^{*0} \mu^+ \mu^-$
$0.45 \pm_{-0.11}^{+0.10} \pm 0.04$	CHATRCHYAN13BL	CMS	pp at 7 TeV
$0.47 \pm 0.14 \pm 0.03$	AALTONEN	12I	CDF $p\bar{p}$ at 1.96 TeV
$0.17 \pm_{-0.15}^{+0.17} \pm 0.03$	WEI	09A	BELL $e^+e^- \rightarrow \Upsilon(4S)$
• • • We do not use the following data for averages, fits, limits, etc. • • •			
$0.41 \pm 0.11 \pm 0.03$	AAIJ	12U	LHCB Repl. by AAIJ 13Y
$0.31 \pm_{-0.18}^{+0.19} \pm 0.02$	AALTONEN	11L	CDF Repl. by AALTONEN 12I

¹ Measured in $11.0 < q^2 < 12.5 \text{ GeV}^2/c^4$.

 $F_L(B \rightarrow K^* \ell^+ \ell^-) (15.0 < q^2 < 17.0 \text{ GeV}^2/c^4)$

VALUE	DOCUMENT ID	TECN	COMMENT
$0.349 \pm 0.039 \pm 0.009$	AAIJ	16B	LHCB pp at 7, 8 TeV

 $F_L(B \rightarrow K^* \ell^+ \ell^-) (17.0 < q^2 < 19.0 \text{ GeV}^2/c^4)$

VALUE	DOCUMENT ID	TECN	COMMENT
$0.354 \pm_{-0.048}^{+0.049} \pm 0.025$	AAIJ	16B	LHCB pp at 7, 8 TeV

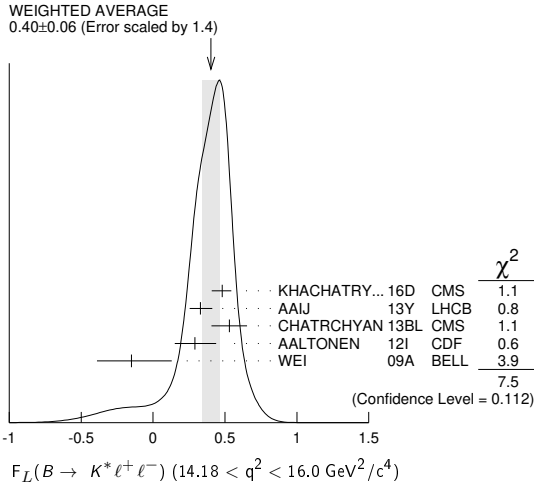
 $F_L(B \rightarrow K^* \ell^+ \ell^-) (14.18 < q^2 < 16.0 \text{ GeV}^2/c^4)$

VALUE	DOCUMENT ID	TECN	COMMENT
0.40 ± 0.06 OUR AVERAGE			Error includes scale factor of 1.4. See the ideogram below.
$0.48 \pm_{-0.06}^{+0.05} \pm 0.04$	KHACHATRY..16D	CMS	pp at 8 TeV
$0.33 \pm_{-0.07}^{+0.08} \pm 0.02$	AAIJ	13Y	LHCB pp at 7 TeV, $K^{*0} \mu^+ \mu^-$
$0.53 \pm 0.12 \pm 0.03$	CHATRCHYAN13BL	CMS	pp at 7 TeV
$0.29 \pm_{-0.13}^{+0.14} \pm 0.05$	AALTONEN	12I	CDF $p\bar{p}$ at 1.96 TeV
$-0.15 \pm_{-0.23}^{+0.27} \pm 0.07$	WEI	09A	BELL $e^+e^- \rightarrow \Upsilon(4S)$
• • • We do not use the following data for averages, fits, limits, etc. • • •			
$0.37 \pm 0.09 \pm 0.05$	AAIJ	12U	LHCB Repl. by AAIJ 13Y
$0.55 \pm_{-0.18}^{+0.17} \pm 0.02$	AALTONEN	11L	CDF Repl. by AALTONEN 12I

See key on page 1171

Meson Particle Listings

B^\pm/B^0 ADMIXTURE



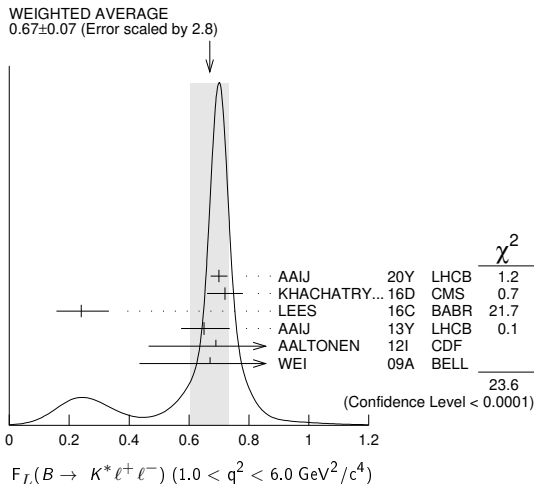
$F_L(B \rightarrow K^* \ell^+ \ell^-)$ (16.0 < q^2 < 19.0 GeV²/c⁴)

VALUE	DOCUMENT ID	TECN	COMMENT
0.350±0.019 OUR AVERAGE			
0.345±0.020±0.007	1 AAIJ	20Y LHCB	pp at 7, 8, 13 TeV
0.38 ^{+0.05} _{-0.06} ±0.04	KHACHATRY...16D	CMS	pp at 8 TeV
0.38 ^{+0.09} _{-0.07} ±0.03	AAIJ	13Y LHCB	pp at 7 TeV, $K^{*0} \mu^+ \mu^-$
0.44±0.07±0.03	CHATRCHYAN13BL	CMS	pp at 7 TeV
0.20 ^{+0.19} _{-0.17} ±0.05	AALTONEN	12I CDF	$p\bar{p}$ at 1.96 TeV
0.12 ^{+0.15} _{-0.13} ±0.02	WEI	09A BELL	$e^+ e^- \rightarrow \Upsilon(4S)$
••• We do not use the following data for averages, fits, limits, etc. •••			
0.344 ^{+0.028} _{-0.030} ±0.008	1 AAIJ	16B LHCB	Repl. by AAIJ 20Y
0.26 ^{+0.10} _{-0.08} ±0.03	AAIJ	12U LHCB	Repl. by AAIJ 13Y
0.09 ^{+0.18} _{-0.14} ±0.03	AALTONEN	11L CDF	Repl. by AALTONEN 12I

¹ Measured in 15.0 < q^2 < 19.0 GeV²/c⁴.

$F_L(B \rightarrow K^* \ell^+ \ell^-)$ (1.0 < q^2 < 6.0 GeV²/c⁴)

VALUE	DOCUMENT ID	TECN	COMMENT
0.67±0.07 OUR AVERAGE			Error includes scale factor of 2.8. See the ideogram below.
0.700±0.025±0.013	1 AAIJ	20Y LHCB	pp at 7, 8, 13 TeV
0.72±0.06	KHACHATRY...16D	CMS	pp at 7, 8 TeV
0.24 ^{+0.09} _{-0.08} ±0.02	2 LEES	16C BABR	$e^+ e^- \rightarrow \Upsilon(4S)$
0.65 ^{+0.08} _{-0.07} ±0.03	AAIJ	13Y LHCB	pp at 7 TeV, $K^{*0} \mu^+ \mu^-$
0.69 ^{+0.19} _{-0.21} ±0.08	AALTONEN	12I CDF	$p\bar{p}$ at 1.96 TeV
0.67±0.23±0.05	WEI	09A BELL	$e^+ e^- \rightarrow \Upsilon(4S)$
••• We do not use the following data for averages, fits, limits, etc. •••			
0.690 ^{+0.035} _{-0.036} ±0.017	1 AAIJ	16B LHCB	Repl. by AAIJ 20Y
0.68±0.10±0.02	CHATRCHYAN13BL	CMS	Repl. by KHACHATRYAN 16D
0.55±0.10±0.03	AAIJ	12U LHCB	Repl. by AAIJ 13Y
0.50 ^{+0.27} _{-0.30} ±0.03	AALTONEN	11L CDF	Repl. by AALTONEN 12I



¹ Measured in 1.1 < q^2 < 6.0 GeV²/c⁴.
² Measured by combining B^0 and B^+ with e and μ as leptons. Results are also provided separately for B^0 and B^+ .

$F_L(B \rightarrow K^* \ell^+ \ell^-)$ (0.0 < q^2 < 4.3 GeV²/c⁴)

VALUE	DOCUMENT ID	TECN	COMMENT
0.33^{+0.14}_{-0.13}±0.03	AALTONEN	12I CDF	$p\bar{p}$ at 1.96 TeV
••• We do not use the following data for averages, fits, limits, etc. •••			
0.47 ^{+0.23} _{-0.24} ±0.03	AALTONEN	11L CDF	Repl. by AALTONEN 12I

$P_\tau(B \rightarrow D^* \tau^+ \nu_\tau)$

Measures difference in decay widths with positive and negative τ^+ helicities normalized to the sum of those decay widths.

VALUE	DOCUMENT ID	TECN	COMMENT
-0.38±0.51^{+0.21}_{-0.16}	1 HIROSE	17 BELL	$e^+ e^- \rightarrow \Upsilon(4S)$
¹ Uses a fully reconstructed B meson as a tag on the recoil side.			

Γ_L/Γ in $B \rightarrow \bar{D}^* \ell^+ \nu_\ell$

VALUE	DOCUMENT ID	TECN	COMMENT
0.502±0.012±0.004	1 PRIM	23 BELL	$e^+ e^- \rightarrow \Upsilon(4S)$
¹ This is the $B^+ \rightarrow \bar{D}^{*0} \ell^+ \nu_\ell$ and $B^0 \rightarrow D^{*-} \ell^+ \nu_\ell$ average.			

Γ_L/Γ in $B \rightarrow \bar{D}^* e^+ \nu_e$

VALUE	DOCUMENT ID	TECN	COMMENT
0.485±0.018±0.005	1 PRIM	23 BELL	$e^+ e^- \rightarrow \Upsilon(4S)$
¹ This is the $B^+ \rightarrow \bar{D}^{*0} e^+ \nu_e$ and $B^0 \rightarrow D^{*-} e^+ \nu_e$ average.			

Γ_L/Γ in $B \rightarrow \bar{D}^* \mu^+ \nu_\mu$

VALUE	DOCUMENT ID	TECN	COMMENT
0.515±0.017±0.005	1 PRIM	23 BELL	$e^+ e^- \rightarrow \Upsilon(4S)$
¹ This is the $B^+ \rightarrow \bar{D}^{*0} \mu^+ \nu_\mu$ and $B^0 \rightarrow D^{*-} \mu^+ \nu_\mu$ average.			

$\Delta(\Gamma_L/\Gamma)$ in $B \rightarrow \bar{D}^*(lepton)^+ \nu_\ell$

$\Delta(\Gamma_L/\Gamma) = (\Gamma_L/\Gamma)^\mu - (\Gamma_L/\Gamma)^e$

VALUE	DOCUMENT ID	TECN	COMMENT
0.030±0.025±0.007	1 PRIM	23 BELL	$e^+ e^- \rightarrow \Upsilon(4S)$
¹ This is the B^+ and B^0 average.			

PARTIAL BRANCHING FRACTIONS IN $B \rightarrow K^*(\ell^+ \ell^-)$

$B(B \rightarrow K^* \ell^+ \ell^-)$ (q^2 < 2.0 GeV²/c⁴)

VALUE (units 10 ⁻⁷)	DOCUMENT ID	TECN	COMMENT
1.68±0.23 OUR AVERAGE			
1.89 ^{+0.52} _{-0.46} ±0.06	1 LEES	12s BABR	$e^+ e^- \rightarrow \Upsilon(4S)$
1.73±0.33±0.10	AALTONEN	11A1 CDF	$p\bar{p}$ at 1.96 TeV
1.46 ^{+0.40} _{-0.35} ±0.11	WEI	09A BELL	$e^+ e^- \rightarrow \Upsilon(4S)$
••• We do not use the following data for averages, fits, limits, etc. •••			
0.98±0.40±0.09	AALTONEN	11L CDF	Repl. by AALTONEN 11A1
¹ The value reported here from LEES 12s refers to 0.1 < q^2 < 2.0 GeV ² /c ⁴ .			

$B(B \rightarrow K^* \ell^+ \ell^-)$ (2.0 < q^2 < 4.3 GeV²/c⁴)

VALUE (units 10 ⁻⁷)	DOCUMENT ID	TECN	COMMENT
0.87±0.17 OUR AVERAGE			
0.95 ^{+0.35} _{-0.30} ±0.04	LEES	12s BABR	$e^+ e^- \rightarrow \Upsilon(4S)$
0.82±0.26±0.06	AALTONEN	11A1 CDF	$p\bar{p}$ at 1.96 TeV
0.86 ^{+0.31} _{-0.27} ±0.07	WEI	09A BELL	$e^+ e^- \rightarrow \Upsilon(4S)$
••• We do not use the following data for averages, fits, limits, etc. •••			
1.00±0.38±0.09	AALTONEN	11L CDF	Repl. by AALTONEN 11A1

$B(B \rightarrow K^* \ell^+ \ell^-)$ (4.3 < q^2 < 8.68 GeV²/c⁴)

VALUE (units 10 ⁻⁷)	DOCUMENT ID	TECN	COMMENT
1.67±0.29 OUR AVERAGE			
1.82 ^{+0.56} _{-0.52} ±0.09	1 LEES	12s BABR	$e^+ e^- \rightarrow \Upsilon(4S)$
1.72±0.41±0.14	AALTONEN	11A1 CDF	$p\bar{p}$ at 1.96 TeV
1.37 ^{+0.47} _{-0.42} ±0.39	WEI	09A BELL	$e^+ e^- \rightarrow \Upsilon(4S)$
••• We do not use the following data for averages, fits, limits, etc. •••			
1.69±0.57±0.15	AALTONEN	11L CDF	Repl. by AALTONEN 11A1
¹ The value reported here from LEES 12s refers to 4.3 < q^2 < 8.12 GeV ² /c ⁴ .			

Meson Particle Listings

B^\pm/B^0 ADMIXTURE

$B(B \rightarrow K^* \ell^+ \ell^-)$ ($10.09 < q^2 < 12.86 \text{ GeV}^2/c^4$)

VALUE (units 10^{-7})	DOCUMENT ID	TECN	COMMENT
1.93 ± 0.25 OUR AVERAGE			
$1.86^{+0.52}_{-0.48} \pm 0.10$	¹ LEES	12s BABR	$e^+ e^- \rightarrow \Upsilon(4S)$
$1.77 \pm 0.34 \pm 0.11$	AALTONEN	11AI CDF	$p\bar{p}$ at 1.96 TeV
$2.24^{+0.44}_{-0.40} \pm 0.19$	WEI	09A BELL	$e^+ e^- \rightarrow \Upsilon(4S)$

• • • We do not use the following data for averages, fits, limits, etc. • • •
 $1.97 \pm 0.47 \pm 0.17$ AALTONEN 11L CDF Repl. by AALTONEN 11AI
¹ The value reported here from LEES 12s refers to $10.11 < q^2 < 12.89 \text{ GeV}^2/c^2$.

$B(B \rightarrow K^* \ell^+ \ell^-)$ ($14.18 < q^2 < 16.0 \text{ GeV}^2/c^4$)

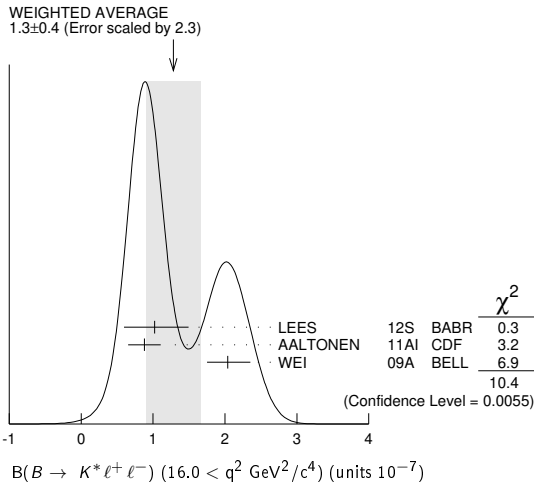
VALUE (units 10^{-7})	DOCUMENT ID	TECN	COMMENT
1.21 ± 0.17 OUR AVERAGE			
$1.46^{+0.41}_{-0.36} \pm 0.06$	¹ LEES	12s BABR	$e^+ e^- \rightarrow \Upsilon(4S)$
$1.21 \pm 0.24 \pm 0.07$	AALTONEN	11AI CDF	$p\bar{p}$ at 1.96 TeV
$1.05^{+0.29}_{-0.26} \pm 0.08$	WEI	09A BELL	$e^+ e^- \rightarrow \Upsilon(4S)$

• • • We do not use the following data for averages, fits, limits, etc. • • •
 $1.51 \pm 0.36 \pm 0.13$ AALTONEN 11L CDF Repl. by AALTONEN 11AI
¹ The value reported here from LEES 12s refers to $14.21 < q^2 < 16.0 \text{ GeV}^2/c^2$.

$B(B \rightarrow K^* \ell^+ \ell^-)$ ($16.0 < q^2 \text{ GeV}^2/c^4$)

VALUE (units 10^{-7})	DOCUMENT ID	TECN	COMMENT
1.3 ± 0.4 OUR AVERAGE			Error includes scale factor of 2.3. See the ideogram below.
$1.02^{+0.47}_{-0.42} \pm 0.06$	LEES	12s BABR	$e^+ e^- \rightarrow \Upsilon(4S)$
$0.88 \pm 0.22 \pm 0.05$	AALTONEN	11AI CDF	$p\bar{p}$ at 1.96 TeV
$2.04^{+0.27}_{-0.24} \pm 0.16$	WEI	09A BELL	$e^+ e^- \rightarrow \Upsilon(4S)$

• • • We do not use the following data for averages, fits, limits, etc. • • •
 $1.35 \pm 0.37 \pm 0.12$ AALTONEN 11L CDF Repl. by AALTONEN 11AI



$B(B \rightarrow K^* \ell^+ \ell^-)$ ($1.0 < q^2 < 6.0 \text{ GeV}^2/c^4$)

VALUE (units 10^{-7})	DOCUMENT ID	TECN	COMMENT
1.64 ± 0.26 OUR AVERAGE			
$2.05^{+0.53}_{-0.48} \pm 0.07$	LEES	12s BABR	$e^+ e^- \rightarrow \Upsilon(4S)$
$1.48 \pm 0.39 \pm 0.12$	AALTONEN	11AI CDF	$p\bar{p}$ at 1.96 TeV
$1.49^{+0.45}_{-0.40} \pm 0.12$	WEI	09A BELL	$e^+ e^- \rightarrow \Upsilon(4S)$

• • • We do not use the following data for averages, fits, limits, etc. • • •
 $1.60 \pm 0.54 \pm 0.14$ AALTONEN 11L CDF Repl. by AALTONEN 11AI

$B(B \rightarrow K^* \ell^+ \ell^-)$ ($0.0 < q^2 < 4.3 \text{ GeV}^2/c^4$)

VALUE (units 10^{-7})	DOCUMENT ID	TECN	COMMENT
$2.53 \pm 0.43 \pm 0.15$	AALTONEN	11AI CDF	$p\bar{p}$ at 1.96 TeV
$1.98 \pm 0.55 \pm 0.18$	AALTONEN	11L CDF	Repl. by AALTONEN 11AI

$B(B^+ \rightarrow K^* \mu^+ \mu^-) / B(B^+ \rightarrow K^* e^+ e^-)$ ($0.045 < q^2 < 1.1 \text{ GeV}^2/c^4$)

VALUE	DOCUMENT ID	TECN	COMMENT
$0.52^{+0.36}_{-0.26} \pm 0.05$	WEHLE	21 BELL	$e^+ e^- \rightarrow \Upsilon(4S)$

$B(B^+ \rightarrow K^* \mu^+ \mu^-) / B(B^+ \rightarrow K^* e^+ e^-)$ ($1.1 < q^2 < 6.0 \text{ GeV}^2/c^4$)

VALUE	DOCUMENT ID	TECN	COMMENT
$0.96^{+0.45}_{-0.29} \pm 0.11$	WEHLE	21 BELL	$e^+ e^- \rightarrow \Upsilon(4S)$

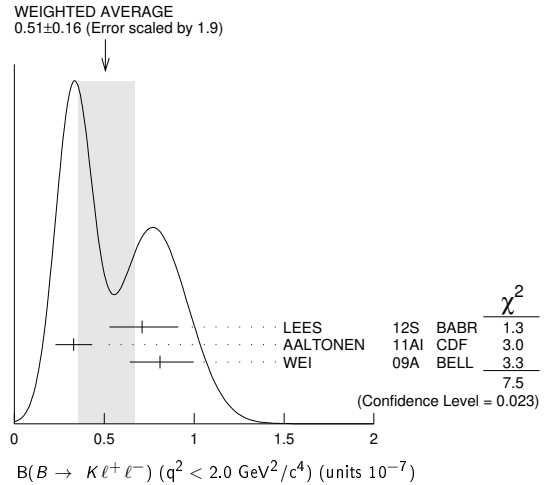
$B(B^+ \rightarrow K^* \mu^+ \mu^-) / B(B^+ \rightarrow K^* e^+ e^-)$ ($15.0 < q^2 < 19.0 \text{ GeV}^2/c^4$)

VALUE	DOCUMENT ID	TECN	COMMENT
$1.18^{+0.52}_{-0.32} \pm 0.10$	WEHLE	21 BELL	$e^+ e^- \rightarrow \Upsilon(4S)$

$B(B \rightarrow K \ell^+ \ell^-)$ ($q^2 < 2.0 \text{ GeV}^2/c^4$)

VALUE (units 10^{-7})	DOCUMENT ID	TECN	COMMENT
0.51 ± 0.16 OUR AVERAGE			Error includes scale factor of 1.9. See the ideogram below.
$0.71^{+0.20}_{-0.18} \pm 0.02$	¹ LEES	12s BABR	$e^+ e^- \rightarrow \Upsilon(4S)$
$0.33 \pm 0.10 \pm 0.02$	AALTONEN	11AI CDF	$p\bar{p}$ at 1.96 TeV
$0.81^{+0.18}_{-0.16} \pm 0.05$	WEI	09A BELL	$e^+ e^- \rightarrow \Upsilon(4S)$

• • • We do not use the following data for averages, fits, limits, etc. • • •
 $0.38 \pm 0.16 \pm 0.03$ AALTONEN 11L CDF Repl. by AALTONEN 11AI
¹ The value reported here from LEES 12s refers to $0.1 < q^2 < 2.0 \text{ GeV}^2/c^2$.



$B(B \rightarrow K \ell^+ \ell^-)$ ($2.0 < q^2 < 4.3 \text{ GeV}^2/c^4$)

VALUE (units 10^{-7})	DOCUMENT ID	TECN	COMMENT
$0.57^{+0.10}_{-0.09}$ OUR AVERAGE			Error includes scale factor of 1.2.
$0.49^{+0.15}_{-0.13} \pm 0.01$	LEES	12s BABR	$e^+ e^- \rightarrow \Upsilon(4S)$
$0.77 \pm 0.14 \pm 0.05$	AALTONEN	11AI CDF	$p\bar{p}$ at 1.96 TeV
$0.46^{+0.14}_{-0.12} \pm 0.03$	WEI	09A BELL	$e^+ e^- \rightarrow \Upsilon(4S)$

• • • We do not use the following data for averages, fits, limits, etc. • • •
 $0.58 \pm 0.19 \pm 0.04$ AALTONEN 11L CDF Repl. by AALTONEN 11AI

$B(B \rightarrow K \ell^+ \ell^-)$ ($4.3 < q^2 < 8.68 \text{ GeV}^2/c^4$)

VALUE (units 10^{-7})	DOCUMENT ID	TECN	COMMENT
1.00 ± 0.11 OUR AVERAGE			
$0.94^{+0.20}_{-0.19} \pm 0.02$	¹ LEES	12s BABR	$e^+ e^- \rightarrow \Upsilon(4S)$
$1.05 \pm 0.17 \pm 0.07$	AALTONEN	11AI CDF	$p\bar{p}$ at 1.96 TeV
$1.00^{+0.19}_{-0.18} \pm 0.06$	WEI	09A BELL	$e^+ e^- \rightarrow \Upsilon(4S)$

• • • We do not use the following data for averages, fits, limits, etc. • • •
 $0.93 \pm 0.25 \pm 0.06$ AALTONEN 11L CDF Repl. by AALTONEN 11AI
¹ The value reported here from LEES 12s refers to $4.3 < q^2 < 8.12 \text{ GeV}^2/c^2$.

$B(B \rightarrow K \ell^+ \ell^-)$ ($10.09 < q^2 < 12.86 \text{ GeV}^2/c^4$)

VALUE (units 10^{-7})	DOCUMENT ID	TECN	COMMENT
0.57 ± 0.11 OUR AVERAGE			Error includes scale factor of 1.4. See the ideogram below.
$0.90^{+0.20}_{-0.19} \pm 0.04$	¹ LEES	12s BABR	$e^+ e^- \rightarrow \Upsilon(4S)$
$0.48 \pm 0.10 \pm 0.03$	AALTONEN	11AI CDF	$p\bar{p}$ at 1.96 TeV
$0.55^{+0.16}_{-0.14} \pm 0.03$	WEI	09A BELL	$e^+ e^- \rightarrow \Upsilon(4S)$

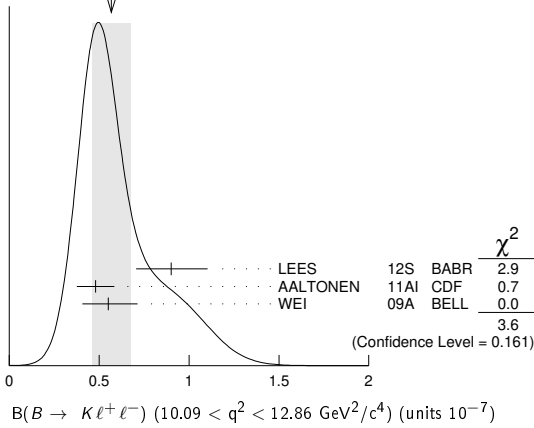
• • • We do not use the following data for averages, fits, limits, etc. • • •
 $0.72 \pm 0.17 \pm 0.05$ AALTONEN 11L CDF Repl. by AALTONEN 11AI
¹ The value reported here from LEES 12s refers to $10.11 < q^2 < 12.89 \text{ GeV}^2/c^2$.

See key on page 1171

Meson Particle Listings

B^\pm/B^0 ADMIXTURE

WEIGHTED AVERAGE
0.57±0.11 (Error scaled by 1.4)



$B(B \to K\ell^+\ell^-)$ (14.18 < q^2 < 16.0 GeV^2/c^4)

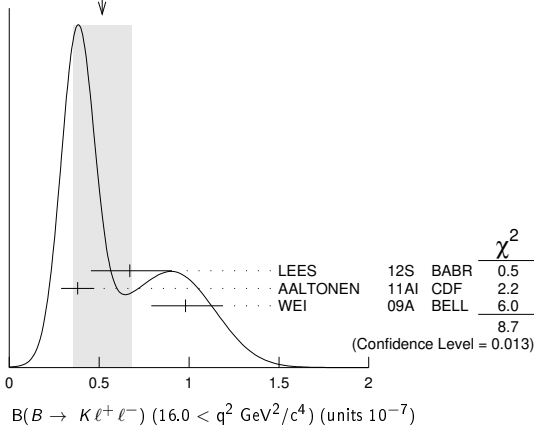
VALUE (units 10^{-7})	DOCUMENT ID	TECN	COMMENT
0.49±0.07 OUR AVERAGE			
0.49 ^{+0.15} _{-0.14} ±0.02	¹ LEES	12s BABR	$e^+e^- \to \Upsilon(4S)$
0.52±0.09±0.03	AALTONEN	11A1 CDF	$p\bar{p}$ at 1.96 TeV
0.38 ^{+0.19} _{-0.12} ±0.02	WEI	09A BELL	$e^+e^- \to \Upsilon(4S)$

• • • We do not use the following data for averages, fits, limits, etc. • • •
0.38±0.12±0.03 AALTONEN 11L CDF Repl. by AALTONEN 11A1
¹ The value reported here from LEES 12s refers to 14.21 < q^2 < 16.0 GeV^2/c^2 .

$B(B \to K\ell^+\ell^-)$ (16.0 < q^2 GeV^2/c^4)

VALUE (units 10^{-7})	DOCUMENT ID	TECN	COMMENT
0.52±0.16 OUR AVERAGE	Error includes scale factor of 2.1. See the ideogram below.		
0.67 ^{+0.23} _{-0.21} ±0.05	LEES	12s BABR	$e^+e^- \to \Upsilon(4S)$
0.38±0.09±0.02	AALTONEN	11A1 CDF	$p\bar{p}$ at 1.96 TeV
0.98 ^{+0.20} _{-0.18} ±0.06	WEI	09A BELL	$e^+e^- \to \Upsilon(4S)$
0.35±0.13±0.02	AALTONEN	11L CDF	Repl. by AALTONEN 11A1

WEIGHTED AVERAGE
0.52±0.16 (Error scaled by 2.1)



$B(B \to K\ell^+\ell^-)$ (1.0 < q^2 < 6.0 GeV^2/c^4)

VALUE (units 10^{-7})	DOCUMENT ID	TECN	COMMENT
1.33±0.13 OUR AVERAGE			
1.36 ^{+0.27} _{-0.24} ±0.03	LEES	12s BABR	$e^+e^- \to \Upsilon(4S)$
1.29±0.18±0.08	AALTONEN	11A1 CDF	$p\bar{p}$ at 1.96 TeV
1.36 ^{+0.23} _{-0.21} ±0.08	WEI	09A BELL	$e^+e^- \to \Upsilon(4S)$
1.01±0.26±0.07	AALTONEN	11L CDF	Repl. by AALTONEN 11A1

$B(B \to K\ell^+\ell^-)$ (0.0 < q^2 < 4.3 GeV^2/c^4)

VALUE (units 10^{-7})	DOCUMENT ID	TECN	COMMENT
1.07±0.17±0.07	AALTONEN	11A1 CDF	$p\bar{p}$ at 1.96 TeV
0.96±0.25±0.06	AALTONEN	11L CDF	Repl. by AALTONEN 11A1

$B(B \to X_s \ell^+ \ell^-)$ (1.0 < q^2 < 6.0 GeV^2/c^4)

VALUE (units 10^{-6})	DOCUMENT ID	TECN	COMMENT
1.60^{+0.41}_{-0.39}±0.25	¹ LEES	14D BABR	$e^+e^- \to \Upsilon(4S)$

¹ Measured from sum of exclusive modes through K^+ , $K^+\pi^0$, $K^+\pi^-$, $K^+\pi^-\pi^0$, $K^+\pi^-\pi^+$, K_S^0 , $K_S^0\pi^0$, $K_S^0\pi^+$, $K_S^0\pi^+\pi^0$, and $K_S^0\pi^+\pi^-$ corrected for unobserved modes.

$B(B \to X_s e^+ e^-)$ (1.0 < q^2 < 6.0 GeV^2/c^4)

VALUE (units 10^{-6})	DOCUMENT ID	TECN	COMMENT
1.93^{+0.47}_{-0.45}±0.28	¹ LEES	14D BABR	$e^+e^- \to \Upsilon(4S)$

¹ Measured from sum of exclusive modes through K^+ , $K^+\pi^0$, $K^+\pi^-$, $K^+\pi^-\pi^0$, $K^+\pi^-\pi^+$, K_S^0 , $K_S^0\pi^0$, $K_S^0\pi^+$, $K_S^0\pi^+\pi^0$, and $K_S^0\pi^+\pi^-$ corrected for unobserved modes.

$B(B \to X_s \mu^+ \mu^-)$ (1.0 < q^2 < 6.0 GeV^2/c^4)

VALUE (units 10^{-6})	DOCUMENT ID	TECN	COMMENT
0.66^{+0.82}_{-0.76}±0.31	¹ LEES	14D BABR	$e^+e^- \to \Upsilon(4S)$

¹ Measured from sum of exclusive modes through K^+ , $K^+\pi^0$, $K^+\pi^-$, $K^+\pi^-\pi^0$, $K^+\pi^-\pi^+$, K_S^0 , $K_S^0\pi^0$, $K_S^0\pi^+$, $K_S^0\pi^+\pi^0$, and $K_S^0\pi^+\pi^-$ corrected for unobserved modes.

$B(B \to X_s \ell^+ \ell^-)$ (14.2 < q^2 GeV^2/c^4)

VALUE (units 10^{-6})	DOCUMENT ID	TECN	COMMENT
0.57^{+0.15}_{-0.15}±0.03	¹ LEES	14D BABR	$e^+e^- \to \Upsilon(4S)$

¹ Measured from sum of exclusive modes through K^+ , $K^+\pi^0$, $K^+\pi^-$, $K^+\pi^-\pi^0$, $K^+\pi^-\pi^+$, K_S^0 , $K_S^0\pi^0$, $K_S^0\pi^+$, $K_S^0\pi^+\pi^0$, and $K_S^0\pi^+\pi^-$ corrected for unobserved modes.

$B(B \to X_s e^+ e^-)$ (14.2 < q^2 GeV^2/c^4)

VALUE (units 10^{-6})	DOCUMENT ID	TECN	COMMENT
0.56^{+0.19}_{-0.18}±0.03	¹ LEES	14D BABR	$e^+e^- \to \Upsilon(4S)$

¹ Measured from sum of exclusive modes through K^+ , $K^+\pi^0$, $K^+\pi^-$, $K^+\pi^-\pi^0$, $K^+\pi^-\pi^+$, K_S^0 , $K_S^0\pi^0$, $K_S^0\pi^+$, $K_S^0\pi^+\pi^0$, and $K_S^0\pi^+\pi^-$ corrected for unobserved modes.

$B(B \to X_s \mu^+ \mu^-)$ (14.2 < q^2 GeV^2/c^4)

VALUE (units 10^{-6})	DOCUMENT ID	TECN	COMMENT
0.60^{+0.31}_{-0.29}±0.05	¹ LEES	14D BABR	$e^+e^- \to \Upsilon(4S)$

¹ Measured from sum of exclusive modes through K^+ , $K^+\pi^0$, $K^+\pi^-$, $K^+\pi^-\pi^0$, $K^+\pi^-\pi^+$, K_S^0 , $K_S^0\pi^0$, $K_S^0\pi^+$, $K_S^0\pi^+\pi^0$, and $K_S^0\pi^+\pi^-$ corrected for unobserved modes.

LEPTON (HADRON) FORWARD-BACKWARD ASYMMETRY IN $B \to K^{(*)} \ell^+ \ell^-$ ($B \to K/\pi h^+ h^-$) DECAY

The forward-backward angular asymmetry of the lepton pair in $B \to K^{(*)} \ell^+ \ell^-$ ($B \to K/\pi h^+ h^-$) decay is defined as

$$A_{FB}(s) = \frac{N(\cos\theta > 0) - N(\cos\theta < 0)}{N(\cos\theta > 0) + N(\cos\theta < 0)}$$

where $s=q^2/m_B^2$, and θ is the angle of the ℓ^- (h^-) with respect to the flight direction of the B meson, measured in the dilepton (dihadron) rest frame. In addition, the fraction of longitudinal polarization F_L of the K^* and F_S , the relative contribution from scalar and pseudoscalar penguin amplitudes in $B \to K\ell^+\ell^-$, can be measured from the angular distribution of its decay products.

$A_{FB}(B \to K^* \ell^+ \ell^-)$ ($q^2 > 0.1 \text{ GeV}^2/c^4$)

VALUE	CL%	DOCUMENT ID	TECN	COMMENT
0.50±0.15±0.02		¹ ISHIKAWA	06 BELL	$e^+e^- \to \Upsilon(4S)$
>0.55	95	² AUBERT,B	06j BABR	$e^+e^- \to \Upsilon(4S)$

• • • We do not use the following data for averages, fits, limits, etc. • • •
¹ Using an unbinned max. likelihood fits to the M_{bc} distribution in five q^2 bins for $\cos\theta > 0$ and $\cos\theta < 0$.
² Results with different q^2 cuts are also reported.

$A_{FB}(B \to K^* \ell^+ \ell^-)$ (0.1 < q^2 < 2.0 GeV^2/c^4)

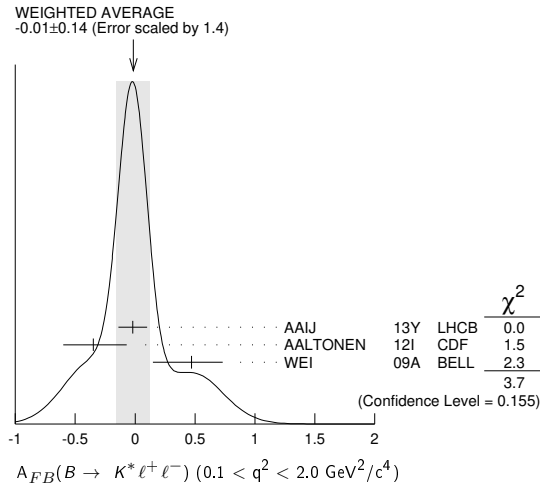
VALUE	DOCUMENT ID	TECN	COMMENT
-0.01±0.14 OUR AVERAGE	Error includes scale factor of 1.4. See the ideogram below.		
-0.02±0.12±0.01	AAIJ	13Y LHCB	$p\bar{p}$ at 7 TeV, $K^{*0} \mu^+ \mu^-$
-0.35 ^{+0.26} _{-0.23} ±0.10	AALTONEN	12i CDF	$p\bar{p}$ at 1.96 TeV
0.47 ^{+0.26} _{-0.32} ±0.03	WEI	09A BELL	$e^+e^- \to \Upsilon(4S)$
-0.29 ^{+0.37} _{-0.00} ±0.18	¹ CHATRCHYAN	13BL CMS	$p\bar{p}$ at 7 TeV
-0.15±0.20±0.06	AAIJ	12u LHCB	Repl. by AAIJ 13Y
0.13 ^{+1.65} _{-0.75} ±0.25	AALTONEN	11L CDF	Repl. by AALTONEN 12i

• • • We do not use the following data for averages, fits, limits, etc. • • •

Meson Particle Listings

B^\pm/B^0 ADMIXTURE

¹ CHATRCHYAN 13BL uses, for this bin, $1.0 < q^2 < 2.0 \text{ GeV}^2/c^4$.



$A_{FB}(B \rightarrow K^* \ell^+ \ell^-) (m_{\ell\ell} < 2.5 \text{ GeV}/c^2)$

VALUE	DOCUMENT ID	TECN	COMMENT
$0.24^{+0.19}_{-0.23} \pm 0.05$	AUBERT	09N BABR	$e^+e^- \rightarrow \Upsilon(4S)$

$A_{FB}(B \rightarrow K^* \ell^+ \ell^-) (m_{\ell\ell} > 3.2 \text{ GeV}/c^2)$

VALUE	DOCUMENT ID	TECN	COMMENT
$0.76^{+0.52}_{-0.32} \pm 0.07$	AUBERT	09N BABR	$e^+e^- \rightarrow \Upsilon(4S)$

$A_{FB}(B \rightarrow K^* \ell^+ \ell^-) (0.10 < q^2 < 0.98 \text{ GeV}^2/c^4)$

VALUE	DOCUMENT ID	TECN	COMMENT
$-0.003^{+0.059}_{-0.057} \pm 0.009$	AAIJ	16B LHC	pp at 7, 8 TeV

$A_{FB}(B \rightarrow K^* \ell^+ \ell^-) (1.1 < q^2 < 2.5 \text{ GeV}^2/c^4)$

VALUE	DOCUMENT ID	TECN	COMMENT
$-0.191^{+0.068}_{-0.080} \pm 0.012$	AAIJ	16B LHC	pp at 7, 8 TeV

$A_{FB}(B \rightarrow K^* \ell^+ \ell^-) (2.0 < q^2 < 4.3 \text{ GeV}^2/c^4)$

VALUE	DOCUMENT ID	TECN	COMMENT
-0.14 ± 0.05 OUR AVERAGE			
$-0.118^{+0.082}_{-0.090} \pm 0.007$	¹ AAIJ	16B LHC	pp at 7, 8 TeV
$-0.12^{+0.15}_{-0.17} \pm 0.05$	KHACHATRY...16D	CMS	pp at 8 TeV
$-0.20 \pm 0.08 \pm 0.01$	AAIJ	13Y LHC	pp at 7 TeV, $K^{*0} \mu^+ \mu^-$
$-0.07 \pm 0.20 \pm 0.02$	CHATRCHYAN13BL	CMS	pp at 7 TeV
$0.29^{+0.32}_{-0.35} \pm 0.15$	AALTONEN	12I CDF	$p\bar{p}$ at 1.96 TeV
$0.11^{+0.31}_{-0.36} \pm 0.07$	WEI	09A BELL	$e^+e^- \rightarrow \Upsilon(4S)$
$0.05^{+0.16}_{-0.20} \pm 0.04$	AAIJ	12U LHC	Repl. by AAIJ 13Y
$0.19^{+0.40}_{-0.41} \pm 0.14$	AALTONEN	11L CDF	Repl. by AALTONEN 12I

¹ Measured in $2.5 < q^2 < 4.0 \text{ GeV}^2/c^4$.

$A_{FB}(B \rightarrow K^* \ell^+ \ell^-) (0.0 < q^2 < 4.3 \text{ GeV}^2/c^4)$

VALUE	DOCUMENT ID	TECN	COMMENT
$-0.08^{+0.21}_{-0.20} \pm 0.05$	AALTONEN	12I CDF	$p\bar{p}$ at 1.96 TeV

$A_{FB}(B \rightarrow K^* \ell^+ \ell^-) (4.0 < q^2 < 6.0 \text{ GeV}^2/c^4)$

VALUE	DOCUMENT ID	TECN	COMMENT
$0.21^{+0.31}_{-0.33} \pm 0.05$	AALTONEN	11L CDF	Repl. by AALTONEN 12I

$A_{FB}(B \rightarrow K^* \ell^+ \ell^-) (4.0 < q^2 < 6.0 \text{ GeV}^2/c^4)$

VALUE	DOCUMENT ID	TECN	COMMENT
$0.025^{+0.051}_{-0.052} \pm 0.004$	AAIJ	16B LHC	pp at 7, 8 TeV

$A_{FB}(B \rightarrow K^* \ell^+ \ell^-) (6.0 < q^2 < 8.0 \text{ GeV}^2/c^4)$

VALUE	DOCUMENT ID	TECN	COMMENT
$0.152^{+0.041}_{-0.040} \pm 0.008$	AAIJ	16B LHC	pp at 7, 8 TeV

$A_{FB}(B \rightarrow K^* \ell^+ \ell^-) (1.0 < q^2 < 6.0 \text{ GeV}^2/c^4)$

VALUE	DOCUMENT ID	TECN	COMMENT
-0.078 ± 0.022 OUR AVERAGE			Error includes scale factor of 1.1.
$-0.073 \pm 0.021 \pm 0.002$	¹ AAIJ	20Y LHC	pp at 7, 8, 13 TeV
-0.12 ± 0.08	KHACHATRY...16D	CMS	pp at 7, 8 TeV
$0.21^{+0.10}_{-0.15} \pm 0.07$	² LEES	16C BABR	$e^+e^- \rightarrow \Upsilon(4S)$

$-0.17 \pm 0.06 \pm 0.01$	AAIJ	13Y LHC	pp at 7 TeV, $K^{*0} \mu^+ \mu^-$
$0.29^{+0.20}_{-0.23} \pm 0.07$	AALTONEN	12I CDF	$p\bar{p}$ at 1.96 TeV
$0.26^{+0.27}_{-0.30} \pm 0.07$	WEI	09A BELL	$e^+e^- \rightarrow \Upsilon(4S)$

• • • We do not use the following data for averages, fits, limits, etc. • • •

$-0.075^{+0.032}_{-0.034} \pm 0.007$	¹ AAIJ	16B LHC	Repl. by AAIJ 20Y
0.55 ± 0.43	³ SATO	16 BELL	$e^+e^- \rightarrow \Upsilon(4S)$
$-0.07 \pm 0.12 \pm 0.01$	CHATRCHYAN13BL	CMS	Repl. by KHACHATRYAN 16D
$-0.06^{+0.13}_{-0.14} \pm 0.07$	AAIJ	12U LHC	Repl. by AAIJ 13Y
$0.43^{+0.36}_{-0.37} \pm 0.06$	AALTONEN	11L CDF	Repl. by AALTONEN 12I

¹ Measured in $1.1 < q^2 < 6.0 \text{ GeV}^2/c^4$.
² Measured by combining B^0 and B^+ with e and μ as leptons. Results are also provided separately for B^0 and B^+ .
³ Uses $K^* \rightarrow K^- \pi^+$, $K^- \pi^0$, $K_S^0 \pi^-$ in the range $M(K\pi) < 1.1 \text{ GeV}/c^2$. Uncertainty is statistical only.

$A_{FB}(B \rightarrow K^* \ell^+ \ell^-) (4.3 < q^2 < 8.6 \text{ GeV}^2/c^4)$

VALUE	DOCUMENT ID	TECN	COMMENT
-------	-------------	------	---------

$0.13^{+0.06}_{-0.05} \pm 0.05$ OUR AVERAGE Error includes scale factor of 1.1.

$0.16^{+0.06}_{-0.05} \pm 0.01$	AAIJ	13Y LHC	pp at 7 TeV, $K^{*0} \mu^+ \mu^-$
$-0.01 \pm 0.11 \pm 0.03$	CHATRCHYAN13BL	CMS	pp at 7 TeV
$0.01 \pm 0.20 \pm 0.09$	AALTONEN	12I CDF	$p\bar{p}$ at 1.96 TeV
$0.45^{+0.15}_{-0.21} \pm 0.15$	WEI	09A BELL	$e^+e^- \rightarrow \Upsilon(4S)$
$0.27^{+0.06}_{-0.08} \pm 0.02$	AAIJ	12U LHC	Repl. by AAIJ 13Y
$-0.06^{+0.30}_{-0.28} \pm 0.05$	AALTONEN	11L CDF	Repl. by AALTONEN 12I

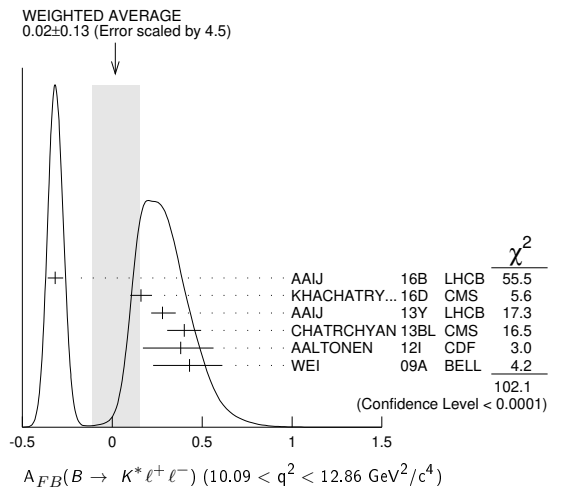
$A_{FB}(B \rightarrow K^* \ell^+ \ell^-) (10.09 < q^2 < 12.86 \text{ GeV}^2/c^4)$

VALUE	DOCUMENT ID	TECN	COMMENT
-------	-------------	------	---------

0.02 ± 0.13 OUR AVERAGE Error includes scale factor of 4.5. See the ideogram below.

$-0.318^{+0.044}_{-0.040} \pm 0.009$	¹ AAIJ	16B LHC	pp at 7, 8 TeV
$0.16 \pm 0.06 \pm 0.01$	KHACHATRY...16D	CMS	pp at 8 TeV
$0.28^{+0.07}_{-0.06} \pm 0.02$	AAIJ	13Y LHC	pp at 7 TeV, $K^{*0} \mu^+ \mu^-$
$0.40 \pm 0.08 \pm 0.05$	CHATRCHYAN13BL	CMS	pp at 7 TeV
$0.38^{+0.16}_{-0.19} \pm 0.09$	AALTONEN	12I CDF	$p\bar{p}$ at 1.96 TeV
$0.43^{+0.18}_{-0.20} \pm 0.03$	WEI	09A BELL	$e^+e^- \rightarrow \Upsilon(4S)$
$0.27^{+0.11}_{-0.13} \pm 0.02$	AAIJ	12U LHC	Repl. by AAIJ 13Y
$0.66^{+0.23}_{-0.20} \pm 0.07$	AALTONEN	11L CDF	Repl. by AALTONEN 12I

¹ Measured in $11.0 < q^2 < 12.5 \text{ GeV}^2/c^4$.



$A_{FB}(B \rightarrow K^* \ell^+ \ell^-) (14.18 < q^2 < 16.0 \text{ GeV}^2/c^4)$

VALUE	DOCUMENT ID	TECN	COMMENT
-------	-------------	------	---------

$0.43^{+0.05}_{-0.06} \pm 0.05$ OUR AVERAGE Error includes scale factor of 1.6. See the ideogram below.

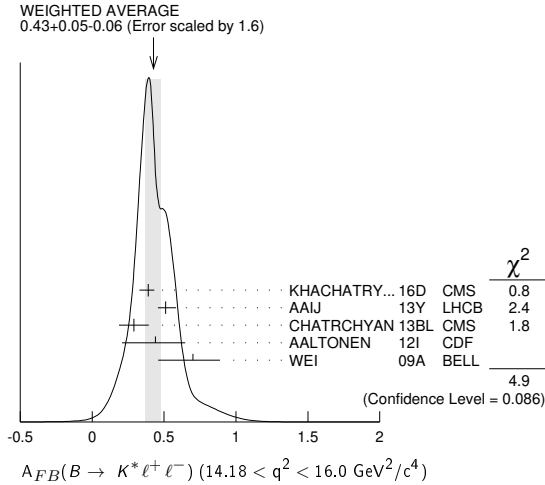
$0.39^{+0.04}_{-0.06} \pm 0.01$	KHACHATRY...16D	CMS	pp at 8 TeV
$0.51^{+0.07}_{-0.05} \pm 0.02$	AAIJ	13Y LHC	pp at 7 TeV, $K^{*0} \mu^+ \mu^-$
$0.29 \pm 0.09 \pm 0.05$	CHATRCHYAN13BL	CMS	pp at 7 TeV

See key on page 1171

Meson Particle Listings

B^\pm/B^0 ADMIXTURE

$0.44^{+0.18}_{-0.21} \pm 0.10$	AALTONEN	12i	CDF	$p\bar{p}$ at 1.96 TeV
$0.70^{+0.16}_{-0.22} \pm 0.10$	WEI	09A	BELL	$e^+e^- \rightarrow \Upsilon(4S)$
••• We do not use the following data for averages, fits, limits, etc. •••				
$0.47^{+0.06}_{-0.08} \pm 0.03$	AAIJ	12u	LHCB	Repl. by AAIJ 13y
$0.42 \pm 0.16 \pm 0.09$	AALTONEN	11L	CDF	Repl. by AALTONEN 12i



$A_{FB}(B \rightarrow K^* \ell^+ \ell^-)$ ($15.0 < q^2 < 17.0 \text{ GeV}^2/c^4$)

VALUE	DOCUMENT ID	TECN	COMMENT
$0.411^{+0.41}_{-0.037} \pm 0.008$	AAIJ	16b	LHCB pp at 7, 8 TeV

$A_{FB}(B \rightarrow K^* \ell^+ \ell^-)$ ($17.0 < q^2 < 19.0 \text{ GeV}^2/c^4$)

VALUE	DOCUMENT ID	TECN	COMMENT
$0.305^{+0.049}_{-0.048} \pm 0.013$	AAIJ	16b	LHCB pp at 7, 8 TeV

$A_{FB}(B \rightarrow K^* \ell^+ \ell^-)$ ($16.0 < q^2 < 19.0 \text{ GeV}^2/c^4$)

VALUE	DOCUMENT ID	TECN	COMMENT
0.362 ± 0.019 OUR AVERAGE			
$0.353 \pm 0.020 \pm 0.010$	¹ AAIJ	20y	LHCB pp at 7, 8, 13 TeV
$0.35 \pm 0.07 \pm 0.01$	KHACHATRY...16d	CMS	pp at 8 TeV
$0.30 \pm 0.08^{+0.01}_{-0.02}$	AAIJ	13y	LHCB pp at 7 TeV, $K^{*0} \mu^+ \mu^-$
$0.41 \pm 0.05 \pm 0.03$	CHATRCHYAN13BL	CMS	pp at 7 TeV
$0.65^{+0.17}_{-0.18} \pm 0.16$	AALTONEN	12i	CDF $p\bar{p}$ at 1.96 TeV
$0.66^{+0.11}_{-0.16} \pm 0.04$	WEI	09A	BELL $e^+e^- \rightarrow \Upsilon(4S)$
••• We do not use the following data for averages, fits, limits, etc. •••			
$0.355 \pm 0.027 \pm 0.009$	¹ AAIJ	16b	LHCB Repl. by AAIJ 20y
$0.16^{+0.11}_{-0.13} \pm 0.06$	AAIJ	12u	LHCB Repl. by AAIJ 13y
$0.70^{+0.16}_{-0.25} \pm 0.10$	AALTONEN	11L	CDF Repl. by AALTONEN 12i

¹ Measured in $15.0 < q^2 < 19.0 \text{ GeV}^2/c^4$.

$A_{FB}(B \rightarrow K \ell^+ \ell^-)$ ($q^2 > 0.1 \text{ GeV}^2/c^4$)

VALUE	DOCUMENT ID	TECN	COMMENT
0.11 ± 0.12 OUR AVERAGE			
$0.15^{+0.21}_{-0.23} \pm 0.08$	¹ AUBERT,B	06j	BABR $e^+e^- \rightarrow \Upsilon(4S)$
$0.10 \pm 0.14 \pm 0.01$	² ISHIKAWA	06	BELL $e^+e^- \rightarrow \Upsilon(4S)$

¹ Results with different q^2 cuts are also reported.

² Using an unbinned max. likelihood fits to the M_{bc} distribution in five q^2 bins for $\cos \theta > 0$ and $\cos \theta < 0$.

$A_{FB}(B \rightarrow K \ell^+ \ell^-)$ ($q^2 < 2.0 \text{ GeV}^2/c^4$)

VALUE	DOCUMENT ID	TECN	COMMENT
0.00 ± 0.06 OUR AVERAGE			
$0.00^{+0.06}_{-0.05} \pm 0.03$	AAIJ	13H	LHCB pp at 7 TeV
$0.13^{+0.42}_{-0.43} \pm 0.07$	AALTONEN	12i	CDF $p\bar{p}$ at 1.96 TeV
$0.06^{+0.32}_{-0.35} \pm 0.02$	WEI	09A	BELL $e^+e^- \rightarrow \Upsilon(4S)$
••• We do not use the following data for averages, fits, limits, etc. •••			
$-0.15^{+0.46}_{-0.39} \pm 0.08$	AALTONEN	11L	CDF Repl. by AALTONEN 12i

$A_{FB}(B \rightarrow K \ell^+ \ell^-)$ ($2.0 < q^2 < 4.3 \text{ GeV}^2/c^4$)

VALUE	DOCUMENT ID	TECN	COMMENT
0.09 ± 0.10 OUR AVERAGE Error includes scale factor of 1.4.			
$0.07^{+0.08}_{-0.05} \pm 0.02$	AAIJ	13H	LHCB pp at 7 TeV
$0.32^{+0.15}_{-0.16} \pm 0.05$	AALTONEN	12i	CDF $p\bar{p}$ at 1.96 TeV
$-0.43^{+0.38}_{-0.40} \pm 0.09$	WEI	09A	BELL $e^+e^- \rightarrow \Upsilon(4S)$
••• We do not use the following data for averages, fits, limits, etc. •••			
$0.72^{+0.40}_{-0.35} \pm 0.07$	AALTONEN	11L	CDF Repl. by AALTONEN 12i

$A_{FB}(B \rightarrow K \ell^+ \ell^-)$ ($0.0 < q^2 < 4.3 \text{ GeV}^2/c^4$)

VALUE	DOCUMENT ID	TECN	COMMENT
0.31 ± 0.16 ± 0.04			
••• We do not use the following data for averages, fits, limits, etc. •••			
$0.36^{+0.24}_{-0.26} \pm 0.06$	AALTONEN	11L	CDF Repl. by AALTONEN 12i

$A_{FB}(B \rightarrow K \ell^+ \ell^-)$ ($1.0 < q^2 < 6.0 \text{ GeV}^2/c^4$)

VALUE	DOCUMENT ID	TECN	COMMENT
0.034 ± 0.040 OUR AVERAGE			
$0.02^{+0.05}_{-0.03} \pm 0.02$	AAIJ	13H	LHCB pp at 7 TeV
$0.13 \pm 0.09 \pm 0.02$	AALTONEN	12i	CDF $p\bar{p}$ at 1.96 TeV
$-0.04^{+0.13}_{-0.16} \pm 0.05$	WEI	09A	BELL $e^+e^- \rightarrow \Upsilon(4S)$
••• We do not use the following data for averages, fits, limits, etc. •••			
0.00 ± 0.13	¹ SATO	16	BELL $e^+e^- \rightarrow \Upsilon(4S)$
$0.08^{+0.27}_{-0.22} \pm 0.07$	AALTONEN	11L	CDF Repl. by AALTONEN 12i

¹ Statistical uncertainty only.

$A_{FB}(B \rightarrow K \ell^+ \ell^-)$ ($4.3 < q^2 < 8.6 \text{ GeV}^2/c^4$)

VALUE	DOCUMENT ID	TECN	COMMENT
-0.04 ± 0.04 OUR AVERAGE			
$-0.02^{+0.03}_{-0.05} \pm 0.03$	AAIJ	13H	LHCB pp at 7 TeV
$0.01^{+0.13}_{-0.10} \pm 0.01$	AALTONEN	12i	CDF $p\bar{p}$ at 1.96 TeV
$-0.20^{+0.12}_{-0.14} \pm 0.03$	WEI	09A	BELL $e^+e^- \rightarrow \Upsilon(4S)$
••• We do not use the following data for averages, fits, limits, etc. •••			
$-0.20^{+0.17}_{-0.28} \pm 0.03$	AALTONEN	11L	CDF Repl. by AALTONEN 12i

$A_{FB}(B \rightarrow K \ell^+ \ell^-)$ ($10.09 < q^2 < 12.86 \text{ GeV}^2/c^4$)

VALUE	DOCUMENT ID	TECN	COMMENT
-0.05 ± 0.06 OUR AVERAGE			
$-0.03 \pm 0.07 \pm 0.01$	AAIJ	13H	LHCB pp at 7 TeV
$-0.03^{+0.11}_{-0.10} \pm 0.04$	AALTONEN	12i	CDF $p\bar{p}$ at 1.96 TeV
$-0.21^{+0.17}_{-0.15} \pm 0.06$	WEI	09A	BELL $e^+e^- \rightarrow \Upsilon(4S)$
••• We do not use the following data for averages, fits, limits, etc. •••			
$-0.10^{+0.17}_{-0.15} \pm 0.07$	AALTONEN	11L	CDF Repl. by AALTONEN 12i

$A_{FB}(B \rightarrow K \ell^+ \ell^-)$ ($14.18 < q^2 < 16.0 \text{ GeV}^2/c^4$)

VALUE	DOCUMENT ID	TECN	COMMENT
-0.02 ± 0.07 OUR AVERAGE			
$-0.01^{+0.12}_{-0.06} \pm 0.01$	AAIJ	13H	LHCB pp at 7 TeV
$-0.05^{+0.09}_{-0.11} \pm 0.03$	AALTONEN	12i	CDF $p\bar{p}$ at 1.96 TeV
$0.04^{+0.32}_{-0.26} \pm 0.05$	WEI	09A	BELL $e^+e^- \rightarrow \Upsilon(4S)$
••• We do not use the following data for averages, fits, limits, etc. •••			
$0.03^{+0.49}_{-0.16} \pm 0.04$	AALTONEN	11L	CDF Repl. by AALTONEN 12i

$A_{FB}(B \rightarrow K \ell^+ \ell^-)$ ($16.0 < q^2 < 18.0 \text{ GeV}^2/c^4$)

VALUE	DOCUMENT ID	TECN	COMMENT
-0.09 ± 0.07 ± 0.02			
$-0.09^{+0.07}_{-0.09} \pm 0.01$	AAIJ	13H	LHCB pp at 7 TeV

$A_{FB}(B \rightarrow K \ell^+ \ell^-)$ ($18.0 < q^2 < 22.0 \text{ GeV}^2/c^4$)

VALUE	DOCUMENT ID	TECN	COMMENT
0.02 ± 0.11 ± 0.01			
$0.02 \pm 0.11 \pm 0.01$	AAIJ	13H	LHCB pp at 7 TeV

$A_{FB}(B \rightarrow K \ell^+ \ell^-)$ ($q^2 > 16.0 \text{ GeV}^2/c^4$)

VALUE	DOCUMENT ID	TECN	COMMENT
0.04 ± 0.09 OUR AVERAGE			
$0.09^{+0.17}_{-0.13} \pm 0.03$	AALTONEN	12i	CDF $p\bar{p}$ at 1.96 TeV
$0.02^{+0.11}_{-0.08} \pm 0.02$	WEI	09A	BELL $e^+e^- \rightarrow \Upsilon(4S)$
••• We do not use the following data for averages, fits, limits, etc. •••			
$0.07^{+0.30}_{-0.23} \pm 0.02$	AALTONEN	11L	CDF Repl. by AALTONEN 12i

Meson Particle Listings

 B^\pm/B^0 ADMIXTURE $A_{FB}(B \rightarrow X_s \ell^+ \ell^-)$ ($1.0 < q^2 < 6.0 \text{ GeV}^2/c^4$)

VALUE	DOCUMENT ID	TECN	COMMENT
0.74 ± 0.54	¹ SATO	16	BELL $e^+ e^- \rightarrow \Upsilon(4S)$

¹ Uses the sum of 10 exclusive X_s modes in the range $M(X_s) > 1.1 \text{ GeV}/c^2$. Uncertainty is statistical only.

 $F_S(B \rightarrow K \ell^+ \ell^-)$ ($q^2 > 0.1 \text{ GeV}^2/c^4$)

VALUE	DOCUMENT ID	TECN	COMMENT
$0.81 \pm 0.58 \pm 0.61 \pm 0.46$	¹ AUBERT,B	06J	BABR $e^+ e^- \rightarrow \Upsilon(4S)$

¹ Results with different q^2 cuts are also reported.

 $A_{FB}(B \rightarrow K \rho \bar{\rho})$ ($m_{\rho \bar{\rho}} < 2.85 \text{ GeV}/c^2$)

VALUE	DOCUMENT ID	TECN	COMMENT
$0.495 \pm 0.012 \pm 0.007$	¹ AAIJ	14AF	LHCB pp at 7, 8 TeV

¹ Measured in $B^+ \rightarrow K^+ \rho \bar{\rho}$ decays.

 $A_{FB}(B \rightarrow \pi \rho \bar{\rho})$ ($m_{\rho \bar{\rho}} < 2.85 \text{ GeV}/c^2$)

VALUE	DOCUMENT ID	TECN	COMMENT
$-0.409 \pm 0.033 \pm 0.006$	¹ AAIJ	14AF	LHCB pp at 7, 8 TeV

¹ Measured in $B^+ \rightarrow \pi^+ \rho \bar{\rho}$ decays.

 A_{FB} in $B \rightarrow \bar{D}^* e^+ \nu_e$

VALUE	DOCUMENT ID	TECN	COMMENT
$0.227 \pm 0.020 \pm 0.006$	¹ PRIM	23	BELL $e^+ e^- \rightarrow \Upsilon(4S)$

¹ This is the B^+ and B^0 average.

 A_{FB} in $B \rightarrow \bar{D}^* \mu^+ \nu_\mu$

VALUE	DOCUMENT ID	TECN	COMMENT
$0.256 \pm 0.020 \pm 0.005$	¹ PRIM	23	BELL $e^+ e^- \rightarrow \Upsilon(4S)$

¹ This is the B^+ and B^0 average.

 $\Delta(A_{FB}) = (A_{FB}^\mu - A_{FB}^e)$ in $B^0 \rightarrow D^{*-} \ell^+ \nu_\ell$

VALUE	DOCUMENT ID	TECN	COMMENT
$0.028 \pm 0.028 \pm 0.008$	¹ PRIM	23	BELL $e^+ e^- \rightarrow \Upsilon(4S)$

¹ This is the B^+ and B^0 average.

ISOSPIN ASYMMETRY

Δ_0^- is defined as

$$\frac{\Gamma(B^0 \rightarrow f_D) - \Gamma(B^- \rightarrow f_D)}{\Gamma(B^0 \rightarrow f_D) + \Gamma(B^- \rightarrow f_D)},$$

the isospin asymmetry of inclusive neutral and charged B decay.

 $\Delta_0^-(B \rightarrow X_s \gamma)$

VALUE	DOCUMENT ID	TECN	COMMENT
-0.005 ± 0.020 OUR AVERAGE			
$-0.0048 \pm 0.0149 \pm 0.0150$	¹ WATA NUKI	19	BELL $e^+ e^- \rightarrow \Upsilon(4S)$
$-0.006 \pm 0.058 \pm 0.026$	AUBERT,B	05R	BABR $e^+ e^- \rightarrow \Upsilon(4S)$

¹ Using a sum-of-exclusive technique with $m_{X_s} < 2.8 \text{ GeV}/c^2$.

 $\Delta_0^-(B \rightarrow X_{s+d} \gamma)$

VALUE	DOCUMENT ID	TECN	COMMENT
$-0.06 \pm 0.15 \pm 0.07$	¹ AUBERT	08o	BABR $e^+ e^- \rightarrow \Upsilon(4S)$

¹ Uses a fully reconstructed B meson as a tag on the recoil side. The result is for $E_\gamma > 2.2 \text{ GeV}$.

 $\Delta_0^+(B \rightarrow K^*(892) \gamma)$

Δ_0^+ describes the isospin asymmetry between $\Gamma(B^0 \rightarrow K^*(892)^0 \gamma)$ and $\Gamma(B^+ \rightarrow K^*(892)^+ \gamma)$.

VALUE	DOCUMENT ID	TECN	COMMENT
0.063 ± 0.017 OUR AVERAGE			
$0.062 \pm 0.015 \pm 0.013$	¹ HORIGUCHI	17	BELL $e^+ e^- \rightarrow \Upsilon(4S)$
$0.066 \pm 0.021 \pm 0.022$	² AUBERT	09A0	BABR $e^+ e^- \rightarrow \Upsilon(4S)$

• • • We do not use the following data for averages, fits, limits, etc. **• • •**

$0.050 \pm 0.045 \pm 0.037$	³ AUBERT,BE	04A	BABR Repl. by AUBERT 09A0
$0.012 \pm 0.044 \pm 0.026$	NAKAO	04	BELL Repl. by HORIGUCHI 17

- ¹ Uses $B(\Upsilon(4S) \rightarrow B^+ B^-) = (51.4 \pm 0.6)\%$ and $B(\Upsilon(4S) \rightarrow B^0 \bar{B}^0) = (48.6 \pm 0.6)\%$.
² Uses the production ratio of charged and neutral B from $\Upsilon(4S)$ decays and the lifetime ratio $\tau_{B^+}/\tau_{B^0} = 1.071 \pm 0.009$. The 90% CL interval is $0.017 < \Delta_0^+ < 0.116$.
³ Uses the production ratio of charged and neutral B from $\Upsilon(4S)$ decays $R^{+0} = 1.006 \pm 0.048$ and the lifetime ratio of $\tau_{B^+}/\tau_{B^0} = 1.083 \pm 0.017$. The 90% CL interval is $-0.046 < \Delta_0^+ < 0.146$.

 $\Delta \rho \gamma = \Gamma(B^+ \rightarrow \rho^+ \gamma) / (2 \cdot \Gamma(B^0 \rightarrow \rho^0 \gamma)) - 1$

VALUE	DOCUMENT ID	TECN	COMMENT
-0.46 ± 0.17 OUR AVERAGE			
$-0.43 \pm 0.25 \pm 0.10$	AUBERT	08BH	BABR $e^+ e^- \rightarrow \Upsilon(4S)$
$-0.48 \pm 0.21 \pm 0.08 \pm 0.19 \pm 0.09$	TANGUCHI	08	BELL $e^+ e^- \rightarrow \Upsilon(4S)$

 $\Delta_0^-(B \rightarrow K \ell^+ \ell^-)$

VALUE	DOCUMENT ID	TECN	COMMENT
-0.15 ± 0.06 OUR AVERAGE			Error includes scale factor of 1.2.
$-0.31 \pm 0.13 \pm 0.01$	¹ CHOUDHURY	21	BELL $e^+ e^- \rightarrow \Upsilon(4S)$
$-0.10 \pm 0.08 \pm 0.02$	² AAIJ	14M	LHCB pp at 7, 8 TeV
$-0.09 \pm 0.08 \pm 0.02$	³ AAIJ	14M	LHCB pp at 7, 8 TeV
$-0.58 \pm 0.29 \pm 0.37 \pm 0.02$	⁴ LEES	12s	BABR $e^+ e^- \rightarrow \Upsilon(4S)$

• • • We do not use the following data for averages, fits, limits, etc. **• • •**

$-0.35 \pm 0.23 \pm 0.27$	⁵ AAIJ	12AH	LHCB Repl. by AAIJ 14M
$-1.43 \pm 0.56 \pm 0.85 \pm 0.05$	^{6,7} AUBERT	09T	BABR Repl. by LEES 12s
$-0.31 \pm 0.17 \pm 0.08$	^{8,9} WEI	09A	BELL $e^+ e^- \rightarrow \Upsilon(4S)$

- ¹ For $1.0 < q^2 < 6.0 \text{ GeV}^2/c^4$ using both $\mu^+ \mu^-$ and $e^+ e^-$ as a lepton pair. Measurements in other q^2 bins are also reported.
² For $1.1 < q^2 < 6.0 \text{ GeV}^2/c^4$ using $\mu^+ \mu^-$ as a lepton pair and assuming isospin symmetry for the $B \rightarrow J/\psi(1S) K$. Measurements in other q^2 bins are also reported.
³ For $15.0 < q^2 < 19.0 \text{ GeV}^2/c^4$ using $\mu^+ \mu^-$ as a lepton pair and assuming isospin symmetry for the $B \rightarrow J/\psi(1S) K$. Measurements in other q^2 bins are also reported.
⁴ For $0.10 < q^2 < 8.12 \text{ GeV}^2/c^4$. Measurements in other q^2 bins are also reported.
⁵ For $1 < q^2 < 6 \text{ GeV}^2/c^4$.
⁶ For $0.1 < m_{\ell^+ \ell^-}^2 < 7.02 \text{ GeV}^2/c^4$.
⁷ Assumes equal production of B^+ and B^0 at the $\Upsilon(4S)$.
⁸ Superseded by CHOUDHURY 21.
⁹ For $q^2 < 8.68 \text{ GeV}^2/c^4$.

 $\Delta_0^-(B \rightarrow K^* \ell^+ \ell^-)$

VALUE	DOCUMENT ID	TECN	COMMENT
$-0.03 \pm 0.08 \pm 0.07$ OUR AVERAGE			Error includes scale factor of 1.2.
$0.00 \pm 0.12 \pm 0.10 \pm 0.02$	¹ AAIJ	14M	LHCB pp at 7, 8 TeV
$0.06 \pm 0.10 \pm 0.09 \pm 0.02$	² AAIJ	14M	LHCB pp at 7, 8 TeV
$-0.25 \pm 0.20 \pm 0.17 \pm 0.03$	³ LEES	12s	BABR $e^+ e^- \rightarrow \Upsilon(4S)$
$-0.29 \pm 0.16 \pm 0.09$	⁴ WEI	09A	BELL $e^+ e^- \rightarrow \Upsilon(4S)$

• • • We do not use the following data for averages, fits, limits, etc. **• • •**

-0.15 ± 0.16	⁵ AAIJ	12AH	LHCB Repl. by AAIJ 14M
$-0.56 \pm 0.17 \pm 0.15 \pm 0.03$	^{6,7} AUBERT	09T	BABR Repl. by LEES 12s

- ¹ For $1.1 < q^2 < 6.0 \text{ GeV}^2/c^4$ using $\mu^+ \mu^-$ as a lepton pair and assuming isospin symmetry for the $B(B \rightarrow J/\psi(1S) K^*(892))$. Measurements in other q^2 bins are also reported.
² For $15.0 < q^2 < 22.0 \text{ GeV}^2/c^4$ using $\mu^+ \mu^-$ as a lepton pair and assuming isospin symmetry for the $B(B \rightarrow J/\psi(1S) K^*(892))$. Measurements in other q^2 bins are also reported.
³ For $0.10 < q^2 < 8.12 \text{ GeV}^2/c^4$. Measurements in other q^2 bins are also reported.
⁴ For $q^2 < 8.68 \text{ GeV}^2/c^4$.
⁵ For $1 < q^2 < 6 \text{ GeV}^2/c^4$.
⁶ For $0.1 < m_{\ell^+ \ell^-}^2 < 7.02 \text{ GeV}^2/c^4$.
⁷ Assumes equal production of B^+ and B^0 at the $\Upsilon(4S)$.

 $\Delta_0^-(B \rightarrow K^*(\ell^+ \ell^-))$

VALUE	DOCUMENT ID	TECN	COMMENT
-0.45 ± 0.17 OUR AVERAGE			Error includes scale factor of 1.7.
$-0.64 \pm 0.15 \pm 0.14 \pm 0.03$	^{1,2} AUBERT	09T	BABR $e^+ e^- \rightarrow \Upsilon(4S)$
$-0.30 \pm 0.12 \pm 0.11 \pm 0.08$	³ WEI	09A	BELL $e^+ e^- \rightarrow \Upsilon(4S)$

- ¹ For $0.1 < m_{\ell^+ \ell^-}^2 < 7.02 \text{ GeV}^2/c^4$.
² Assumes equal production of B^+ and B^0 at the $\Upsilon(4S)$.
³ For $q^2 < 8.68 \text{ GeV}^2/c^2$.

 $B \rightarrow X_c \ell \nu$ HADRONIC MASS MOMENTS $\langle M_X^2 - \bar{M}_D^2 \rangle$ (First Moments)

VALUE (GeV^2)	DOCUMENT ID	TECN	COMMENT
0.36 ± 0.08 OUR AVERAGE			Error includes scale factor of 1.8.
$0.467 \pm 0.038 \pm 0.068$	¹ ACOSTA	05F	CDF $p\bar{p}$ at 1.96 TeV
$0.293 \pm 0.012 \pm 0.058$	² CSORNA	04	CLE2 $e^+ e^- \rightarrow \Upsilon(4S)$

• • • We do not use the following data for averages, fits, limits, etc. **• • •**

$0.251 \pm 0.023 \pm 0.062$	³ CRONIN-HEN..01B	CLE2	$e^+ e^- \rightarrow \Upsilon(4S)$
-----------------------------	------------------------------	------	------------------------------------

- ¹ Moments are measured with a minimum lepton momentum of 0.7 GeV/c in the B rest frame;
² Uses minimum lepton energy of 1.5 GeV and also reports moments with $E_\ell > 1.0 \text{ GeV}$.
³ The leptons are required to have $P_\ell > 1.5 \text{ GeV}/c$.

See key on page 1171

Meson Particle Listings

B^\pm/B^0 ADMIXTURE

$\langle M_X^2 \rangle$ (First Moments)

VALUE (GeV ²)	DOCUMENT ID	TECN	COMMENT
4.156 ± 0.029 OUR AVERAGE			
4.144 ± 0.028 ± 0.022	¹ SCHWA NDA 07	BELL	$e^+e^- \rightarrow \Upsilon(4S)$
4.18 ± 0.04 ± 0.03	¹ AUBERT,B 04	BABR	$e^+e^- \rightarrow \Upsilon(4S)$

¹ The leptons are required to have $E_\ell > 1.5$ GeV/c.

$\langle (M_X^2 - \bar{M}_X^2)^2 \rangle$ (Second Moments)

VALUE (GeV ⁴)	DOCUMENT ID	TECN	COMMENT
0.55 ± 0.08 OUR AVERAGE			
0.515 ± 0.061 ± 0.064	¹ SCHWA NDA 07	BELL	$e^+e^- \rightarrow \Upsilon(4S)$
0.629 ± 0.031 ± 0.143	² CSORNA 04	CLE2	$e^+e^- \rightarrow \Upsilon(4S)$
••• We do not use the following data for averages, fits, limits, etc. •••			
1.05 ± 0.26 ± 0.13	³ ACOSTA 05F	CDF	$p\bar{p}$ at 1.96 TeV
0.576 ± 0.048 ± 0.168	¹ CRONIN-HEN..01B	CLE2	$e^+e^- \rightarrow \Upsilon(4S)$

¹ The leptons are required to have $E_\ell > 1.5$ GeV/c.

² Uses minimum lepton energy of 1.5 GeV and also reports moments with $E_\ell > 1.0$ GeV.

³ Moments are measured with a minimum lepton momentum of 0.7 GeV/c in the B rest frame;

$\langle (M_X^2 - \bar{M}_B^2)^2 \rangle$ (Second Moments)

VALUE (GeV ⁴)	DOCUMENT ID	TECN	COMMENT
0.639 ± 0.056 ± 0.178	¹ CRONIN-HEN..01B	CLE2	$e^+e^- \rightarrow \Upsilon(4S)$

¹ The leptons are required to have $E_\ell > 1.5$ GeV/c.

$B \rightarrow X_c \ell \nu$ LEPTON MOMENTUM MOMENTS

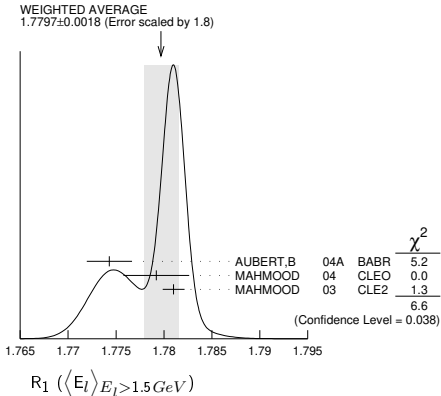
$R_0 (\Gamma_{E_l > 1.7 \text{ GeV}} / \Gamma_{E_l > 1.5 \text{ GeV}})$

VALUE	DOCUMENT ID	TECN	COMMENT
0.6187 ± 0.0014 ± 0.0016	¹ MAHMOOD 03	CLE2	$e^+e^- \rightarrow \Upsilon(4S)$

¹ The leptons are required to have $E_l > 1.5$ GeV in the B rest frame.

$R_1 (\langle E_l \rangle_{E_l > 1.5 \text{ GeV}})$

VALUE	DOCUMENT ID	TECN	COMMENT
1.7797 ± 0.0018 OUR AVERAGE	Error includes scale factor of 1.8. See the ideogram below.		
1.7743 ± 0.0019 ± 0.0014	¹ AUBERT,B 04A	BABR	$e^+e^- \rightarrow \Upsilon(4S)$
1.7792 ± 0.0021 ± 0.0027	² MAHMOOD 04	CLEO	$e^+e^- \rightarrow \Upsilon(4S)$
1.7810 ± 0.0007 ± 0.0009	³ MAHMOOD 03	CLE2	$e^+e^- \rightarrow \Upsilon(4S)$



¹ The leptons are required to have $E_l > 1.5$ GeV in the B rest frame. The result with $E_l > 0.6$ GeV is also given.

² Uses $E_e > 1.5$ GeV and also reports moments with other minimum minimum E_e conditions, as low as $E_e > 0.6$ GeV.

³ The leptons are required to have $E_l > 1.5$ GeV in the B rest frame.

$R_2 (\langle E_l^2 - \bar{E}_l^2 \rangle_{E_l > 1.5 \text{ GeV}})$

VALUE (10 ⁻³ GeV ²)	DOCUMENT ID	TECN	COMMENT
30.8 ± 0.8 OUR AVERAGE			
30.3 ± 0.9 ± 0.5	¹ AUBERT,B 04A	BABR	$e^+e^- \rightarrow \Upsilon(4S)$
31.6 ± 0.8 ± 1.0	² MAHMOOD 04	CLEO	$e^+e^- \rightarrow \Upsilon(4S)$

¹ The leptons are required to have $E_l > 1.5$ GeV in the B rest frame. The result with $E_l > 0.6$ GeV is also given.

² Uses $E_e > 1.5$ GeV and also reports moments with other minimum minimum E_e conditions, as low as $E_e > 0.6$ GeV.

$R_3 (\langle E_l^3 - \bar{E}_l^3 \rangle_{E_l > 1.5 \text{ GeV}})$

VALUE (10 ⁻³ GeV ³)	DOCUMENT ID	TECN	COMMENT
2.12 ± 0.47 ± 0.20	¹ AUBERT,B 04A	BABR	$e^+e^- \rightarrow \Upsilon(4S)$

¹ The leptons are required to have $E_l > 1.5$ GeV in the B rest frame. The result with $E_l > 0.6$ GeV is also given.

$B \rightarrow X_s \gamma$ PHOTON ENERGY MOMENTS

$\langle E_\gamma \rangle$

VALUE (GeV)	DOCUMENT ID	TECN	COMMENT
2.314 ± 0.011 OUR AVERAGE			
2.346 ± 0.018 ± 0.027 ± 0.022	^{1,2} LEES	12U	BABR $e^+e^- \rightarrow \Upsilon(4S)$
2.304 ± 0.014 ± 0.017	^{2,3} LEES	12V	BABR $e^+e^- \rightarrow \Upsilon(4S)$
2.311 ± 0.009 ± 0.015	³ LIMOSANI	09	BELL $e^+e^- \rightarrow \Upsilon(4S)$
2.289 ± 0.058 ± 0.027	^{3,4} AUBERT	08o	BABR $e^+e^- \rightarrow \Upsilon(4S)$
2.309 ± 0.023 ± 0.023	^{2,3} SCHWANDA	08	BELL $e^+e^- \rightarrow \Upsilon(4S)$
••• We do not use the following data for averages, fits, limits, etc. •••			
2.288 ± 0.025 ± 0.023	³ AUBERT,BE	06B	BABR Repl. by LEES 12V

¹ LEES 12U uses $E_\gamma > 1.897$ GeV to calculate the moments; the moments are used to calculate the HQET parameters $m_b = 4.579 \pm 0.032$ GeV/c² and $\mu_\pi^2 = 0.257 \pm 0.034$ GeV² in the shape function model. The same HQET parameters are also determined in the kinetic model.

² Results for different E_γ threshold values are also measured.

³ The result is for $E_\gamma > 1.9$ GeV.

⁴ Uses a fully reconstructed B meson as a tag on the recoil side.

$\langle E_\gamma^2 \rangle - \langle E_\gamma \rangle^2$

VALUE (10 ⁻² GeV ²)	DOCUMENT ID	TECN	COMMENT
3.03 ± 0.25 OUR AVERAGE			
2.11 ± 0.57 ± 0.69	^{1,2} LEES	12U	BABR $e^+e^- \rightarrow \Upsilon(4S)$
3.62 ± 0.33 ± 0.33	^{2,3} LEES	12V	BABR $e^+e^- \rightarrow \Upsilon(4S)$
3.02 ± 0.19 ± 0.30	³ LIMOSANI	09	BELL $e^+e^- \rightarrow \Upsilon(4S)$
3.34 ± 1.24 ± 0.62	^{3,4} AUBERT	08o	BABR $e^+e^- \rightarrow \Upsilon(4S)$
2.17 ± 0.60 ± 0.55	^{2,3} SCHWANDA	08	BELL $e^+e^- \rightarrow \Upsilon(4S)$
••• We do not use the following data for averages, fits, limits, etc. •••			
3.28 ± 0.40 ± 0.43	³ AUBERT,BE	06B	BABR Repl. by LEES 12V

¹ LEES 12U uses $E_\gamma > 1.897$ GeV to calculate the moments; the moments are used to calculate the HQET parameters $m_b = 4.579 \pm 0.032$ GeV/c² and $\mu_\pi^2 = 0.257 \pm 0.034$ GeV² in the shape function model. The same HQET parameters are also determined in the kinetic model.

² Results for different E_γ threshold values are also measured.

³ The result is for $E_\gamma > 1.9$ GeV.

⁴ Uses a fully reconstructed B meson as a tag on the recoil side.

B^\pm/B^0 ADMIXTURE REFERENCES

AAIJ	23AR	PRL 131 111802	R. Aaij et al.	(LHCb Collab.)
AGGARWAL	23	PRL 131 051804	L. Aggarwal et al.	(BELLE II Collab.)
CAO	23	PRL 131 211801	L. Cao et al.	(BELLE Collab.)
PRIM	23	PR D108 012002	M.T. Prim et al.	(BELLE Collab.)
ZHUKOVA	23	JHEP 2308 131	V. Zhukova et al.	(BELLE Collab.)
CAO	21A	PR D104 012008	L. Cao et al.	(BELLE Collab.)
CHOUHURY	21	JHEP 2103 105	S. Choudhury et al.	(BELLE Collab.)
WEHLE	21	PRL 126 161801	S. Wehle et al.	(BELLE Collab.)
AAIJ	20Y	PRL 125 011802	R. Aaij et al.	(LHCb Collab.)
CARIA	20	PRL 124 161803	G. Caria et al.	(BELLE Collab.)
AAIJ	19AD	PR D100 031102	R. Aaij et al.	(LHCb Collab.)
WATANUKI	19	PR D99 032012	S. Watanuki et al.	(BELLE Collab.)
GRYGIER	17	PR D96 091101	J. Grygier et al.	(BELLE Collab.)
HIROSE	17	PRL 118 211801	S. Hirose et al.	(BELLE Collab.)
Also		PR D97 012004	S. Hirose et al.	(BELLE Collab.)
HORIGUCHI	17	PRL 119 191802	T. Horiguchi et al.	(BELLE Collab.)
LEES	17B	PR D95 072001	J.P. Lees et al.	(BABAR Collab.)
AAIJ	16B	JHEP 1602 104	R. Aaij et al.	(LHCb Collab.)
BHARDWAJ	16	PR D93 052016	V. Bhardwaj et al.	(BELLE Collab.)
KHACHATRYAN	16D	PL B753 424	V. Khachatryan et al.	(CMS Collab.)
LEES	16	PRL 116 041801	J.P. Lees et al.	(BABAR Collab.)
LEES	16C	PR D93 052015	J.P. Lees et al.	(BABAR Collab.)
SATO	16	PR D93 032008	Y. Sato et al.	(BELLE Collab.)
Also		PR D93 059901 (err.)	Y. Sato et al.	(BELLE Collab.)
HUSCHLE	15	PR D92 072014	M. Huschle et al.	(BELLE Collab.)
PESANTEZ	15	PRL 114 151601	L. Pesantez et al.	(BELLE Collab.)
SAITO	15	PR D91 052004	T. Saito et al.	(BELLE Collab.)
AAIJ	14AF	PRL 113 141801	R. Aaij et al.	(LHCb Collab.)
AAIJ	14M	JHEP 1406 133	R. Aaij et al.	(LHCb Collab.)
LEES	14D	PRL 112 211802	J.P. Lees et al.	(BABAR Collab.)
LEES	14K	PR D90 092001	J.P. Lees et al.	(BABAR Collab.)
AAIJ	13H	JHEP 1302 105	R. Aaij et al.	(LHCb Collab.)
AAIJ	13Y	JHEP 1308 131	R. Aaij et al.	(LHCb Collab.)
CHATRCHYAN	13BL	PL B727 77	S. Chatrchyan et al.	(CMS Collab.)
LEES	13I	PR D87 112005	J.P. Lees et al.	(BABAR Collab.)
LEES	13M	PR D88 032012	J.P. Lees et al.	(BABAR Collab.)
AAIJ	12AH	JHEP 1207 133	R. Aaij et al.	(LHCb Collab.)
AAIJ	12U	PRL 108 181806	R. Aaij et al.	(LHCb Collab.)
AALTONEN	12I	PRL 108 081807	T. Aaltonen et al.	(CDF Collab.)
LEES	12	PR D85 111102	J.P. Lees et al.	(BABAR Collab.)
LEES	12D	PRL 109 101802	J.P. Lees et al.	(BABAR Collab.)
Also		PR D88 072012	J.P. Lees et al.	(BABAR Collab.)
LEES	12R	PR D86 032004	J.P. Lees et al.	(BABAR Collab.)
LEES	12S	PR D86 032012	J.P. Lees et al.	(BABAR Collab.)
LEES	12U	PR D86 052012	J.P. Lees et al.	(BABAR Collab.)
LEES	12V	PRL 109 191801	J.P. Lees et al.	(BABAR Collab.)
Also		PR D86 112008	J.P. Lees et al.	(BABAR Collab.)
AALTONEN	11AI	PRL 107 201802	T. Aaltonen et al.	(CDF Collab.)
AALTONEN	11L	PRL 106 161801	T. Aaltonen et al.	(CDF Collab.)
DEL-AMO-SA...	11	PR D83 031103	P. del Amo Sanchez et al.	(BABAR Collab.)
GAMBINO	11	JHEP 1109 055	P. Gambino	(LCFT)
AUBERT	10	PRL 104 011802	B. Aubert et al.	(BABAR Collab.)
AUBERT	10A	PR D81 032003	B. Aubert et al.	(BABAR Collab.)
AUSHEV	10	PR D81 031103	T. Aushev et al.	(BELLE Collab.)
DEL-AMO-SA...	10M	PR D82 051101	P. del Amo Sanchez et al.	(BABAR Collab.)
DEL-AMO-SA...	10Q	PR D82 112002	P. del Amo Sanchez et al.	(BABAR Collab.)
NISHIMURA	10	PRL 105 191803	K. Nishimura et al.	(BELLE Collab.)
URQUIJO	10	PRL 104 021801	P. Urquijo et al.	(BELLE Collab.)
AUBERT	09AO	PRL 103 211802	B. Aubert et al.	(BABAR Collab.)
AUBERT	09N	PR D79 031102	B. Aubert et al.	(BABAR Collab.)

Meson Particle Listings

 B^\pm/B^0 ADMIXTURE

AUBERT	09T	PRL 102 091803	B. Aubert <i>et al.</i>	(BABAR Collab.)	ABREU	00R	PL B475 407	P. Abreu <i>et al.</i>	(DELPHI Collab.)
	Also	EPAPS Document No. E-PR/TAO-102-060910		(BABAR Collab.)	COAN	00	PRL 84 5283	T.E. Coan <i>et al.</i>	(CLEO Collab.)
AUBERT	09U	PRL 102 161803	B. Aubert <i>et al.</i>	(BABAR Collab.)	RICHICHI	00	PRL 85 520	S.J. Richichi <i>et al.</i>	(CLEO Collab.)
LIMOSANI	09	PRL 103 241801	A. Limosani <i>et al.</i>	(BELLE Collab.)	BARATE	90Q	EPJ C4 387	R. Barate <i>et al.</i>	(ALEPH Collab.)
WEI	09A	PRL 103 171801	J.-T. Wei <i>et al.</i>	(BELLE Collab.)	BERGFELD	98	PRL 81 272	T. Bergfeld <i>et al.</i>	(CLEO Collab.)
	Also	EPAPS Supplement	J.-T. Wei <i>et al.</i>	(BELLE Collab.)	BISHAI	98	PR D57 3847	M. Bishai <i>et al.</i>	(CLEO Collab.)
AUBERT	08AS	PRL 100 171802	B. Aubert <i>et al.</i>	(BABAR Collab.)	BONVICINI	98	PR D57 6004	G. Bonvicini <i>et al.</i>	(CLEO Collab.)
AUBERT	08BC	PR D78 072007	B. Aubert <i>et al.</i>	(BABAR Collab.)	BROWDER	98	PRL 81 1786	T.E. Browder <i>et al.</i>	(CLEO Collab.)
AUBERT	08BH	PR D78 112001	B. Aubert <i>et al.</i>	(BABAR Collab.)	COAN	98	PRL 80 1150	T.E. Coan <i>et al.</i>	(CLEO Collab.)
AUBERT	08BJ	PRL 101 171804	B. Aubert <i>et al.</i>	(BABAR Collab.)	GLENN	98	PRL 80 2289	S. Glenn <i>et al.</i>	(CLEO Collab.)
AUBERT	08N	PRL 100 021801	B. Aubert <i>et al.</i>	(BABAR Collab.)	ACKERSTAFF	97N	ZPHY C74 423	K. Ackerstaff <i>et al.</i>	(OPAL Collab.)
	Also	PR D79 092002	B. Aubert <i>et al.</i>	(BABAR Collab.)	AMMAR	97	PR D55 13	R. Ammar <i>et al.</i>	(CLEO Collab.)
AUBERT	08O	PR D77 051103	B. Aubert <i>et al.</i>	(BABAR Collab.)	BARISH	97	PRL 79 3599	B. Barish <i>et al.</i>	(CLEO Collab.)
SCHWANDA	08	PR D78 032016	C. Schwanda <i>et al.</i>	(BELLE Collab.)	BUSKULIC	97B	ZPHY C73 601	D. Buskulic <i>et al.</i>	(ALEPH Collab.)
TANIGUCHI	08	PRL 101 111801	N. Taniguchi <i>et al.</i>	(BELLE Collab.)	GIBBONS	97B	PR D56 3783	L. Gibbons <i>et al.</i>	(CLEO Collab.)
WEI	08A	PR D78 011101	J.-T. Wei <i>et al.</i>	(BELLE Collab.)	ALBRECHT	96D	PL B374 256	H. Albrecht <i>et al.</i>	(ARGUS Collab.)
AUBERT	07AG	PRL 99 051801	B. Aubert <i>et al.</i>	(BABAR Collab.)	BARISH	96B	PRL 76 1570	B.C. Barish <i>et al.</i>	(CLEO Collab.)
AUBERT	07C	PR D75 012003	B. Aubert <i>et al.</i>	(BABAR Collab.)	GBAUT	96	PR D53 4734	D. Gibaut <i>et al.</i>	(CLEO Collab.)
AUBERT	07E	PRL 98 051802	B. Aubert <i>et al.</i>	(BABAR Collab.)	KUBOTA	96	PR D53 6033	Y. Kubota <i>et al.</i>	(CLEO Collab.)
AUBERT	07L	PRL 98 151802	B. Aubert <i>et al.</i>	(BABAR Collab.)	PDG	96	PR D54 1	R. M. Barnett <i>et al.</i>	(PDG Collab.)
GAMBINO	07	JHEP 0710 058	P. Gambino <i>et al.</i>	(CLEO Collab.)	ALAM	95	PRL 74 2885	M.S. Alam <i>et al.</i>	(CLEO Collab.)
HUANG	07	PR D75 012002	G.S. Huang <i>et al.</i>	(CLEO Collab.)	ALBRECHT	95D	PL B353 554	H. Albrecht <i>et al.</i>	(ARGUS Collab.)
SCHWANDA	07	PR D75 032005	C. Schwanda <i>et al.</i>	(BELLE Collab.)	BALEST	95B	PR D52 2661	R. Balest <i>et al.</i>	(CLEO Collab.)
URQUIJO	07	PR D75 032001	P. Urquijo <i>et al.</i>	(BELLE Collab.)	BARISH	95	PR D51 1014	B.C. Barish <i>et al.</i>	(CLEO Collab.)
AUBERT	06H	PR D73 012006	B. Aubert <i>et al.</i>	(BABAR Collab.)	BUSKULIC	95B	PL B345 103	D. Buskulic <i>et al.</i>	(ALEPH Collab.)
AUBERT.B	06J	PR D73 092001	B. Aubert <i>et al.</i>	(BABAR Collab.)	ALBRECHT	94C	ZPHY C62 371	H. Albrecht <i>et al.</i>	(ARGUS Collab.)
AUBERT.B	06Y	PR D74 091105	B. Aubert <i>et al.</i>	(BABAR Collab.)	ALBRECHT	94J	ZPHY C61 1	H. Albrecht <i>et al.</i>	(ARGUS Collab.)
AUBERT.BE	06B	PRL 97 171803	B. Aubert <i>et al.</i>	(BABAR Collab.)	PROCARIO	94	PRL 73 1472	M. Procario <i>et al.</i>	(CLEO Collab.)
BUCHMUEL...	06	PR D73 073008	O.L. Buchmüller, H.U. Flacher	(RHBL)	ALBRECHT	93	ZPHY C57 533	H. Albrecht <i>et al.</i>	(ARGUS Collab.)
GOKHROO	06	PRL 97 162002	G. Gokhroo <i>et al.</i>	(BELLE Collab.)	ALBRECHT	93E	ZPHY C60 11	H. Albrecht <i>et al.</i>	(ARGUS Collab.)
ISHIKAWA	06	PRL 96 251801	A. Ishikawa <i>et al.</i>	(BELLE Collab.)	ALBRECHT	93H	PL B318 397	H. Albrecht <i>et al.</i>	(ARGUS Collab.)
MOHAPATRA	06	PRL 96 221801	D. Mohapatra <i>et al.</i>	(BELLE Collab.)	ALBRECHT	93I	ZPHY C58 191	H. Albrecht <i>et al.</i>	(ARGUS Collab.)
ABAZOV	05O	PRL 95 171803	V.M. Abazov <i>et al.</i>	(DD Collab.)	ALEXANDER	93B	PL B319 365	J. Alexander <i>et al.</i>	(CLEO Collab.)
ACOSTA	05F	PR D71 051103	D. Acosta <i>et al.</i>	(CDF Collab.)	ARTUSO	93	PL B311 307	M. Artuso <i>et al.</i>	(SYRA Collab.)
ARTUSO	05B	PRL 95 261801	M. Artuso <i>et al.</i>	(CLEO Collab.)	BARTELT	93B	PRL 71 4111	J.E. Bartelt <i>et al.</i>	(CLEO Collab.)
AUBERT	05	PRL 94 011801	B. Aubert <i>et al.</i>	(BABAR Collab.)	ALBRECHT	92E	PL B277 209	H. Albrecht <i>et al.</i>	(ARGUS Collab.)
AUBERT.B	05M	PRL 95 142003	B. Aubert <i>et al.</i>	(BABAR Collab.)	ALBRECHT	92G	ZPHY C54 1	H. Albrecht <i>et al.</i>	(ARGUS Collab.)
AUBERT.B	05R	PR D72 052004	B. Aubert <i>et al.</i>	(BABAR Collab.)	ALBRECHT	92O	ZPHY C56 1	H. Albrecht <i>et al.</i>	(ARGUS Collab.)
AUBERT.B	05X	PRL 95 111801	B. Aubert <i>et al.</i>	(BABAR Collab.)	BORTOLETTO	92	PR D45 21	D. Bortoletto <i>et al.</i>	(CLEO Collab.)
	Also	PRL 97 019903 (errata.)	B. Aubert <i>et al.</i>	(BABAR Collab.)	CRAWFORD	92	PR D45 752	G. Crawford <i>et al.</i>	(CLEO Collab.)
CHOI	05	PRL 94 182002	S.-K. Choi <i>et al.</i>	(BELLE Collab.)	HENDERSO...	92	PR D45 2212	S. Henderson <i>et al.</i>	(CLEO Collab.)
IWASAKI	05	PR D72 092005	M. Iwasaki <i>et al.</i>	(BELLE Collab.)	LESIAK	92	ZPHY C55 33	T. Lesiak <i>et al.</i>	(Crystal Ball Collab.)
LIMOSANI	05	PL B621 28	A. Limosani <i>et al.</i>	(BELLE Collab.)	ALBRECHT	91C	PL B255 297	H. Albrecht <i>et al.</i>	(ARGUS Collab.)
MOHAPATRA	05	PR D70 011101	D. Mohapatra <i>et al.</i>	(BELLE Collab.)	ALBRECHT	91H	ZPHY C52 353	H. Albrecht <i>et al.</i>	(ARGUS Collab.)
NISHIDA	05	PL B610 23	S. Nishida <i>et al.</i>	(BELLE Collab.)	FULTON	91	PR D43 651	R. Fulton <i>et al.</i>	(CLEO Collab.)
OKABE	05	PL B614 27	T. Okabe <i>et al.</i>	(BELLE Collab.)	YANAGISAWA	91	PRL 66 2436	C. Yanagisawa <i>et al.</i>	(CUSB II Collab.)
ABDALLAH	04D	EPJ C33 213	J. Abdallah <i>et al.</i>	(DELPHI Collab.)	ALBRECHT	90	PL B234 409	H. Albrecht <i>et al.</i>	(ARGUS Collab.)
AUBERT	04C	PRL 92 111801	B. Aubert <i>et al.</i>	(BABAR Collab.)	ALBRECHT	90H	PL B249 359	H. Albrecht <i>et al.</i>	(ARGUS Collab.)
AUBERT	04I	PRL 92 071802	B. Aubert <i>et al.</i>	(BABAR Collab.)	BORTOLETTO	90	PRL 64 2117	D. Bortoletto <i>et al.</i>	(CLEO Collab.)
AUBERT	04S	PR D69 052005	B. Aubert <i>et al.</i>	(BABAR Collab.)		Also	PR D45 21	D. Bortoletto <i>et al.</i>	(CLEO Collab.)
AUBERT	04X	PRL 93 011803	B. Aubert <i>et al.</i>	(BABAR Collab.)	FULTON	90	PRL 64 16	R. Fulton <i>et al.</i>	(CLEO Collab.)
AUBERT.B	04	PR D69 111103	B. Aubert <i>et al.</i>	(BABAR Collab.)	MASCHMANN	90	ZPHY C46 555	W.S. Maschmann <i>et al.</i>	(Crystal Ball Collab.)
AUBERT.B	04A	PR D69 111104	B. Aubert <i>et al.</i>	(BABAR Collab.)	PDG	90	PL B239 1	J.J. Hemandez <i>et al.</i>	(IFIC, BOST, CIT+ Collab.)
AUBERT.B	04E	PRL 93 021804	B. Aubert <i>et al.</i>	(BABAR Collab.)	ALBRECHT	89K	ZPHY C42 519	H. Albrecht <i>et al.</i>	(ARGUS Collab.)
AUBERT.B	04F	PRL 93 061801	B. Aubert <i>et al.</i>	(BABAR Collab.)	IGSUR	89B	PR D39 799	N. Igsur <i>et al.</i>	(TNT, CIT Collab.)
AUBERT.B	04I	PRL 93 081802	B. Aubert <i>et al.</i>	(BABAR Collab.)	WACHS	89	ZPHY C42 33	K. Wachs <i>et al.</i>	(Crystal Ball Collab.)
AUBERT.BE	04A	PR D70 112006	B. Aubert <i>et al.</i>	(BABAR Collab.)	ALBRECHT	88E	PL B210 263	H. Albrecht <i>et al.</i>	(ARGUS Collab.)
CSORNA	04	PR D70 032002	S.E. Csorna <i>et al.</i>	(CLEO Collab.)	ALBRECHT	88H	PL B210 258	H. Albrecht <i>et al.</i>	(ARGUS Collab.)
KOPPENBURG	04	PRL 93 061803	P. Koppenburg <i>et al.</i>	(BELLE Collab.)	KOERNER	88	ZPHY C38 511	J.G. Korner, G.A. Schuler	(MAINZ, DESY Collab.)
MAHMOOD	04	PR D70 032003	A.H. Mahmood <i>et al.</i>	(CLEO Collab.)	ALAM	87	PRL 59 22	M.S. Alam <i>et al.</i>	(CLEO Collab.)
NAKAO	04	PR D69 112001	M. Nakao <i>et al.</i>	(BELLE Collab.)	ALAM	87B	PRL 58 1814	M.S. Alam <i>et al.</i>	(CLEO Collab.)
NISHIDA	04	PRL 93 031803	S. Nishida <i>et al.</i>	(BELLE Collab.)	ALBRECHT	87D	PL B199 451	H. Albrecht <i>et al.</i>	(ARGUS Collab.)
ADAM	03B	PR D68 012004	N.E. Adam <i>et al.</i>	(CLEO Collab.)	ALBRECHT	87H	PL B187 425	H. Albrecht <i>et al.</i>	(ARGUS Collab.)
AUBERT	03	PR D67 031101	B. Aubert <i>et al.</i>	(BABAR Collab.)	BEAN	87	PR D35 3533	A. Bean <i>et al.</i>	(CLEO Collab.)
AUBERT	03F	PR D67 032002	B. Aubert <i>et al.</i>	(BABAR Collab.)	BEHREND...	87	PRL 59 407	S. Behrends <i>et al.</i>	(CLEO Collab.)
AUBERT	03U	PRL 91 221802	B. Aubert <i>et al.</i>	(BABAR Collab.)	BORTOLETTO	87	PR D35 19	D. Bortoletto <i>et al.</i>	(CLEO Collab.)
BONVICINI	03	PR D68 011101	G. Bonvicini <i>et al.</i>	(CLEO Collab.)	ALAM	86	PR D34 3279	M.S. Alam <i>et al.</i>	(CLEO Collab.)
HUANG	03	PRL 91 241802	H.-C. Huang <i>et al.</i>	(BELLE Collab.)	BALTRUSAIT...	86E	PRL 56 2140	R.M. Baltrusaitis <i>et al.</i>	(Mark III Collab.)
ISHIKAWA	03	PRL 91 261601	A. Ishikawa <i>et al.</i>	(BELLE Collab.)	BORTOLETTO	86	PRL 56 800	D. Bortoletto <i>et al.</i>	(CLEO Collab.)
KANEKO	03	PRL 90 021801	J. Kaneko <i>et al.</i>	(BELLE Collab.)	HAAS	86	PRL 56 2781	J. Haas <i>et al.</i>	(CLEO Collab.)
KROKOVNY	03B	PRL 91 262002	P. Krokovny <i>et al.</i>	(BELLE Collab.)	ALBRECHT	85H	PL 162B 395	H. Albrecht <i>et al.</i>	(ARGUS Collab.)
MAHMOOD	03	PR D67 072001	A.H. Mahmood <i>et al.</i>	(CLEO Collab.)	CSORNA	85	PRL 54 1894	S.E. Csorna <i>et al.</i>	(CLEO Collab.)
ABE	02	PRL 88 021801	K. Abe <i>et al.</i>	(BELLE Collab.)	HAAS	85	PRL 55 1248	J. Haas <i>et al.</i>	(CLEO Collab.)
ABE	02L	PRL 89 011803	K. Abe <i>et al.</i>	(BELLE Collab.)	AVERY	84	PRL 53 1309	P. Avery <i>et al.</i>	(CLEO Collab.)
ABE	02Y	PL B547 181	K. Abe <i>et al.</i>	(BELLE Collab.)	CHEN	84	PRL 52 1084	A. Chen <i>et al.</i>	(CLEO Collab.)
ANDERSON	02	PRL 89 282001	S. Anderson <i>et al.</i>	(CLEO Collab.)	LEVMAN	84	PL 141B 271	G.M. Levman <i>et al.</i>	(CUSB Collab.)
AUBERT	02C	PRL 88 101805	B. Aubert <i>et al.</i>	(BABAR Collab.)	ALAM	83B	PRL 51 1143	M.S. Alam <i>et al.</i>	(CLEO Collab.)
AUBERT	02G	PR D65 091104	B. Aubert <i>et al.</i>	(BABAR Collab.)	GREEN	83	PRL 51 347	J. Green <i>et al.</i>	(CLEO Collab.)
AUBERT	02L	PRL 88 241801	B. Aubert <i>et al.</i>	(BABAR Collab.)	KLOPFEN...	83B	PL 130B 444	C. Klopfenstein <i>et al.</i>	(CUSB Collab.)
BORNHEIM	02	PRL 88 231803	A. Bornheim <i>et al.</i>	(CLEO Collab.)	ALTARELLI	82	NP B208 365	G. Altarelli <i>et al.</i>	(ROMA, INFN, FRAS Collab.)
EDWARDS	02B	PR D65 111102	K.W. Edwards <i>et al.</i>	(CLEO Collab.)	BRODY	82	PRL 48 1070	A.D. Brody <i>et al.</i>	(CLEO Collab.)
ABE	01F	PL B511 151	K. Abe <i>et al.</i>	(BELLE Collab.)	GIANNINI	82	NP B206 1	G. Giannini <i>et al.</i>	(CUSB Collab.)
ABE	01J	PR D64 072001	K. Abe <i>et al.</i>	(BELLE Collab.)	BEBEK	81	PRL 46 84	C. Bebek <i>et al.</i>	(CLEO Collab.)
ANDERSON	01B	PRL 87 181803	S. Anderson <i>et al.</i>	(CLEO Collab.)	CHADWICK	81	PRL 46 88	K. Chadwick <i>et al.</i>	(CLEO Collab.)
CHEN	01	PR D63 031102	S. Chen <i>et al.</i>	(CLEO Collab.)	ABRAMS	80	PRL 44 10	G.S. Abrams <i>et al.</i>	(SLAC, LBL Collab.)
CHEN	01C	PRL 87 251807	S. Chen <i>et al.</i>	(CLEO Collab.)					
COAN	01	PRL 86 5661	T.E. Coan <i>et al.</i>	(CLEO Collab.)					
CRONIN-HEN...	01B	PRL 87 251808	D. Cronin-Hennessy <i>et al.</i>	(CLEO Collab.)					
PDG	01	Unofficial 2001 WWW edition							

See key on page 1171

Meson Particle Listings

 $B^\pm/B^0/B_s^0/b$ -baryon ADMIXTURE $B^\pm/B^0/B_s^0/b$ -baryon ADMIXTURE $B^\pm/B^0/B_s^0/b$ -baryon ADMIXTURE MEAN LIFE

Each measurement of the B mean life is an average over an admixture of various bottom mesons and baryons which decay weakly. Different techniques emphasize different admixtures of produced particles, which could result in a different B mean life.

"OUR EVALUATION" is an average using rescaled values of the data listed below. This is a weighted average of the lifetimes of the five main b -hadron species (B^+ , B^0 , B_{sH}^0 , B_{sL}^0 , and Λ_b) that assumes the production fractions in Z decays (given at the end of this section) and equal production fractions of B_{sH}^0 and B_{sL}^0 mesons.

VALUE (10^{-12} s)	EVTs	DOCUMENT ID	TECN	COMMENT
1.5673 ± 0.0029				OUR EVALUATION (Produced by HFLAV)
• • • We do not use the following data for averages, fits, limits, etc. • • •				
1.570 ± 0.005 ± 0.008	1	ABDALLAH 04E	DLPH	$e^+e^- \rightarrow Z$
1.533 ± 0.015 \pm $\begin{smallmatrix} +0.035 \\ -0.031 \end{smallmatrix}$	2	ABE	98b	CDF $p\bar{p}$ at 1.8 TeV
1.549 ± 0.009 ± 0.015	3	ACCIARRI 98	L3	$e^+e^- \rightarrow Z$
1.611 ± 0.010 ± 0.027	4	ACKERSTAFF 97F	OPAL	$e^+e^- \rightarrow Z$
1.582 ± 0.011 ± 0.027	4	ABREU 96E	DLPH	$e^+e^- \rightarrow Z$
1.575 ± 0.010 ± 0.026	5	ABREU 96E	DLPH	$e^+e^- \rightarrow Z$
1.533 ± 0.013 ± 0.022 ^{9,8k}	6	BUSKULIC 96F	ALEP	$e^+e^- \rightarrow Z$
1.564 ± 0.030 ± 0.036	7	ABE,K 95B	SLD	$e^+e^- \rightarrow Z$
1.542 ± 0.021 ± 0.045	8	ABREU 94L	DLPH	$e^+e^- \rightarrow Z$
1.50 $\begin{smallmatrix} +0.24 \\ -0.21 \end{smallmatrix}$ ± 0.03	9	ABREU 94P	DLPH	$e^+e^- \rightarrow Z$
1.46 ± 0.06 ± 0.06 5344	10	ABE 93J	CDF	Repl. by ABE 98B
1.23 $\begin{smallmatrix} +0.14 \\ -0.13 \end{smallmatrix}$ ± 0.15 188	11	ABREU 93D	DLPH	Sup. by ABREU 94L
1.49 ± 0.11 ± 0.12 253	12	ABREU 93C	DLPH	Sup. by ABREU 94L
1.51 $\begin{smallmatrix} +0.16 \\ -0.14 \end{smallmatrix}$ ± 0.11 130	13	ACTON 93C	OPAL	$e^+e^- \rightarrow Z$
1.523 ± 0.034 ± 0.035 ³⁷²	14	ACTON 93L	OPAL	$e^+e^- \rightarrow Z$
1.535 ± 0.035 ± 0.027 ³⁵⁷	14	ADRIANI 93K	L3	Repl. by ACCIARRI 98
1.511 ± 0.022 ± 0.078	15	BUSKULIC 93O	ALEP	$e^+e^- \rightarrow Z$
1.28 ± 0.10	16	ABREU 92	DLPH	Sup. by ABREU 94L
1.37 ± 0.07 ± 0.06 1354	17	ACTON 92	OPAL	Sup. by ACTON 93L
1.49 ± 0.03 ± 0.06	18	BUSKULIC 92F	ALEP	Sup. by BUSKULIC 96F
1.35 $\begin{smallmatrix} +0.19 \\ -0.17 \end{smallmatrix}$ ± 0.05	19	BUSKULIC 92G	ALEP	$e^+e^- \rightarrow Z$
1.32 ± 0.08 ± 0.09 1386	20	ADEVA 91H	L3	Sup. by ADRIANI 93K
1.32 $\begin{smallmatrix} +0.31 \\ -0.25 \end{smallmatrix}$ ± 0.15 37	21	ALEXANDER 91G	OPAL	$e^+e^- \rightarrow Z$
1.29 ± 0.06 ± 0.10 2973	22	DECAMP 91C	ALEP	Sup. by BUSKULIC 92F
1.36 $\begin{smallmatrix} +0.25 \\ -0.23 \end{smallmatrix}$	23	HAGEMANN 90	JADE	$E_{cm}^{ee} = 35$ GeV
1.13 ± 0.15	24	LYONS 90	RVUE	
1.35 ± 0.10 ± 0.24		BRAUNSCH... 89B	TASS	$E_{cm}^{ee} = 35$ GeV
0.98 ± 0.12 ± 0.13		ONG 89	MRK2	$E_{cm}^{ee} = 29$ GeV
1.17 $\begin{smallmatrix} +0.27 \\ -0.22 \end{smallmatrix}$ $\begin{smallmatrix} +0.17 \\ -0.16 \end{smallmatrix}$		KLEM 88	DLCO	$E_{cm}^{ee} = 29$ GeV
1.29 ± 0.20 ± 0.21	25	ASH 87	MAC	$E_{cm}^{ee} = 29$ GeV
1.02 $\begin{smallmatrix} +0.42 \\ -0.39 \end{smallmatrix}$	301	BROM 87	HRS	$E_{cm}^{ee} = 29$ GeV

¹ Measurement performed using an inclusive reconstruction and B flavor identification technique.

² Measured using inclusive $J/\psi(1S) \rightarrow \mu^+\mu^-$ vertex.

³ ACCIARRI 98 uses inclusively reconstructed secondary vertex and lepton impact parameter.

⁴ ACKERSTAFF 97F uses inclusively reconstructed secondary vertices.

⁵ Combines ABREU 96E secondary vertex result with ABREU 94L impact parameter result.

⁶ BUSKULIC 96F analyzed using 3D impact parameter.

⁷ ABE,K 95B uses an inclusive topological technique.

⁸ ABREU 94L uses charged particle impact parameters. Their result from inclusively reconstructed secondary vertices is superseded by ABREU 96E.

⁹ From proper time distribution of $b \rightarrow J/\psi(1S)$ anything.

¹⁰ ABE 93J analyzed using $J/\psi(1S) \rightarrow \mu\mu$ vertices.

¹¹ ABREU 93D data analyzed using D/D^* anything event vertices.

¹² ABREU 93C data analyzed using charged and neutral vertices.

¹³ ACTON 93C analysed using D/D^* anything event vertices.

¹⁴ ACTON 93L and ADRIANI 93K analyzed using lepton (e and μ) impact parameter at Z .

¹⁵ BUSKULIC 93O analyzed using dipole method.

¹⁶ ABREU 92 is combined result of muon and hadron impact parameter analyses. Hadron tracks gave $(12.7 \pm 0.4 \pm 1.2) \times 10^{-13}$ s for an admixture of B species weighted by production fraction and mean charge multiplicity, while muon tracks gave $(13.0 \pm 1.0 \pm 0.8) \times 10^{-13}$ s for an admixture weighted by production fraction and semileptonic branching fraction.

¹⁷ ACTON 92 is combined result of muon and electron impact parameter analyses.

¹⁸ BUSKULIC 92F uses the lepton impact parameter distribution for data from the 1991 run.

¹⁹ BUSKULIC 92G use $J/\psi(1S)$ tags to measure the average b lifetime. This is comparable to other methods only if the $J/\psi(1S)$ branching fractions of the different b -flavored hadrons are in the same ratio.

²⁰ Using $Z \rightarrow e^+X$ or μ^+X , ADEVA 91H determined the average lifetime for an admixture of B hadrons from the impact parameter distribution of the lepton.

²¹ Using $Z \rightarrow J/\psi(1S)X$, $J/\psi(1S) \rightarrow \ell^+\ell^-$, ALEXANDER 91G determined the average lifetime for an admixture of B hadrons from the decay point of the $J/\psi(1S)$.

²² Using $Z \rightarrow eX$ or μX , DECAMP 91C determines the average lifetime for an admixture of B hadrons from the signed impact parameter distribution of the lepton.

²³ HAGEMANN 90 uses electrons and muons in an impact parameter analysis.

²⁴ LYONS 90 combine the results of the B lifetime measurements of ONG 89, BRAUNSCHWEIG 89B, KLEM 88, and ASH 87, and JADE data by private communication. They use statistical techniques which include variation of the error with the mean life, and possible correlations between the systematic errors. This result is not independent of the measured results used in our average.

²⁵ We have combined an overall scale error of 15% in quadrature with the systematic error of ± 0.7 to obtain ± 2.1 systematic error.

²⁶ Statistical and systematic errors were combined by BROM 87.

CHARGED b -HADRON ADMIXTURE MEAN LIFE

VALUE (10^{-12} s)	DOCUMENT ID	TECN	COMMENT
1.72 ± 0.08 ± 0.06	¹ ADAM 95	DLPH	$e^+e^- \rightarrow Z$
	¹ ADAM 95		data analyzed using vertex-charge technique to tag b -hadron charge.

NEUTRAL b -HADRON ADMIXTURE MEAN LIFE

VALUE (10^{-12} s)	DOCUMENT ID	TECN	COMMENT
1.58 ± 0.11 ± 0.09	¹ ADAM 95	DLPH	$e^+e^- \rightarrow Z$
	¹ ADAM 95		data analyzed using vertex-charge technique to tag b -hadron charge.

MEAN LIFE RATIO $\tau_{\text{charged } b\text{-hadron}}/\tau_{\text{neutral } b\text{-hadron}}$

VALUE	DOCUMENT ID	TECN	COMMENT
1.09 $\begin{smallmatrix} +0.11 \\ -0.10 \end{smallmatrix}$ ± 0.08	¹ ADAM 95	DLPH	$e^+e^- \rightarrow Z$
	¹ ADAM 95		data analyzed using vertex-charge technique to tag b -hadron charge.

$$|\Delta\tau_b|/\tau_{b,\bar{b}}$$

$\tau_{b,\bar{b}}$ and $|\Delta\tau_b|$ are the mean life average and difference between b and \bar{b} hadrons.

VALUE	DOCUMENT ID	TECN	COMMENT
-0.001 ± 0.012 ± 0.008	¹ ABBIENDI 99J	OPAL	$e^+e^- \rightarrow Z$
	¹ Data analyzed using both the jet charge and the charge of secondary vertex in the opposite hemisphere.		

 \bar{b} PRODUCTION FRACTIONS AND DECAY MODES

The branching fraction measurements are for an admixture of B mesons and baryons at energies above the $T(4S)$. Only the highest energy results (LHC, LEP, Tevatron, $Sp\bar{p}S$) are used in the branching fraction averages. In the following, we assume that the production fractions are the same at the LHC, LEP, and at the Tevatron.

For inclusive branching fractions, e.g., $B \rightarrow D^\pm$ anything, the values usually are multiplicities, not branching fractions. They can be greater than one.

The modes below are listed for a \bar{b} initial state. b modes are their charge conjugates. Reactions indicate the weak decay vertex and do not include mixing.

Mode	Fraction (Γ_i/Γ)	Scale factor/ Confidence level
------	--------------------------------	-----------------------------------

PRODUCTION FRACTIONS

The production fractions for weakly decaying b -hadrons at high energy have been calculated from the best values of mean lives, mixing parameters, and branching fractions in this edition by the Heavy Flavor Averaging Group (HFLAV) as described in the note " B^0 - \bar{B}^0 Mixing" in the B^0 Particle Listings. We no longer provide world averages of the b -hadron production fractions, where results from LEP, Tevatron and LHC are averaged together; indeed the available data (from CDF and LHCb) shows that the fractions depend on the kinematics (in particular the p_T) of the produced b hadron. Hence we would like to list the fractions in Z decays instead, which are well-defined physics observables. The production fractions in $p\bar{p}$ collisions at the Tevatron are also listed at the end of the section. Values assume

$$\begin{aligned} B(\bar{b} \rightarrow B^+) &= B(\bar{b} \rightarrow B^0) \\ B(\bar{b} \rightarrow B^+) + B(\bar{b} \rightarrow B^0) + B(\bar{b} \rightarrow B_s^0) + B(b \rightarrow b\text{-baryon}) &= 100\%. \end{aligned}$$

The correlation coefficients between production fractions are also reported:

$$\begin{aligned} \text{cor}(B_s^0, b\text{-baryon}) &= 0.064 \\ \text{cor}(B_s^0, B^\pm=B^0) &= -0.633 \\ \text{cor}(b\text{-baryon}, B^\pm=B^0) &= -0.813. \end{aligned}$$

Meson Particle Listings

 $B^\pm/B^0/B_s^0/b$ -baryon ADMIXTURE

The notation for production fractions varies in the literature ($f_d, d_{B^0}, f(b \rightarrow \bar{B}^0), B(b \rightarrow \bar{B}^0)$). We use our own branching fraction notation here, $B(\bar{b} \rightarrow B^0)$.

Note these production fractions are b -hadronization fractions, not the conventional branching fractions of b -quark to a B -hadron, which may have considerable dependence on the initial and final state kinematic and production environment.

Γ_1	B^+	(40.8 ± 0.7) %
Γ_2	B^0	(40.8 ± 0.7) %
Γ_3	B_s^0	(10.0 ± 0.8) %
Γ_4	B_c^+	
Γ_5	b -baryon	(8.4 ± 1.1) %

DECAY MODES

Semileptonic and leptonic modes

Γ_6	ν anything	(23.1 ± 1.5) %	
Γ_7	$\ell^+ \nu_\ell$ anything	[a] (10.69 ± 0.22) %	
Γ_8	$e^+ \nu_e$ anything	(10.86 ± 0.35) %	
Γ_9	$\mu^+ \nu_\mu$ anything	(10.95 ± 0.29) %	
Γ_{10}	$D^- \ell^+ \nu_\ell$ anything	[a] (2.2 ± 0.4) %	S=1.9
Γ_{11}	$D^- \pi^+ \ell^+ \nu_\ell$ anything	(4.9 ± 1.9) × 10 ⁻³	
Γ_{12}	$D^- \pi^- \ell^+ \nu_\ell$ anything	(2.6 ± 1.6) × 10 ⁻³	
Γ_{13}	$\bar{D}^0 \ell^+ \nu_\ell$ anything	[a] (6.79 ± 0.34) %	
Γ_{14}	$\bar{D}^0 \pi^- \ell^+ \nu_\ell$ anything	(1.07 ± 0.27) %	
Γ_{15}	$\bar{D}^0 \pi^+ \ell^+ \nu_\ell$ anything	(2.3 ± 1.6) × 10 ⁻³	
Γ_{16}	$D^{*-} \ell^+ \nu_\ell$ anything	[a] (2.75 ± 0.19) %	
Γ_{17}	$D^{*-} \pi^- \ell^+ \nu_\ell$ anything	(6 ± 7) × 10 ⁻⁴	
Γ_{18}	$D^{*-} \pi^+ \ell^+ \nu_\ell$ anything	(4.8 ± 1.0) × 10 ⁻³	
Γ_{19}	$\bar{D}_j^0 \ell^+ \nu_\ell$ anything × B($\bar{D}_j^0 \rightarrow D^{*+} \pi^-$)	[a,b] (2.6 ± 0.9) × 10 ⁻³	
Γ_{20}	$D_j^- \ell^+ \nu_\ell$ anything × B($D_j^- \rightarrow D^0 \pi^-$)	[a,b] (7.0 ± 2.3) × 10 ⁻³	
Γ_{21}	$\bar{D}_2^*(2460)^0 \ell^+ \nu_\ell$ anything × B($\bar{D}_2^*(2460)^0 \rightarrow D^{*-} \pi^+$)	< 1.4 × 10 ⁻³	CL=90%
Γ_{22}	$D_2^*(2460)^- \ell^+ \nu_\ell$ anything × B($D_2^*(2460)^- \rightarrow D^0 \pi^-$)	(4.2 ± 1.5) × 10 ⁻³	
Γ_{23}	$\bar{D}_2^*(2460)^0 \ell^+ \nu_\ell$ anything × B($\bar{D}_2^*(2460)^0 \rightarrow D^- \pi^+$)	(1.6 ± 0.8) × 10 ⁻³	
Γ_{24}	charmless $\ell \bar{\nu}_\ell$	[a] (1.7 ± 0.5) × 10 ⁻³	
Γ_{25}	$\tau^+ \nu_\tau$ anything	(2.41 ± 0.23) %	
Γ_{26}	$D^{*-} \tau \nu_\tau$ anything	(9 ± 4) × 10 ⁻³	
Γ_{27}	$\bar{c} \rightarrow \ell^- \bar{\nu}_\ell$ anything	[a] (8.02 ± 0.19) %	
Γ_{28}	$c \rightarrow \ell^+ \nu$ anything	(1.6 ± 0.4) %	

Charmed meson and baryon modes

Γ_{29}	\bar{D}^0 anything	(58.7 ± 2.8) %	
Γ_{30}	$D^0 D_s^\pm$ anything	[c] (9.1 ± 4.0) %	
Γ_{31}	$D^\mp D_s^\pm$ anything	[c] (4.0 ± 2.3) %	
Γ_{32}	$\bar{D}^0 D^0$ anything	[c] (5.1 ± 2.0) %	
Γ_{33}	$D^0 D^\pm$ anything	[c] (2.7 ± 1.8) %	
Γ_{34}	$D^\pm D^\mp$ anything	[c] < 9 × 10 ⁻³	CL=90%
Γ_{35}	D^0 anything		
Γ_{36}	D^+ anything		
Γ_{37}	D^- anything	(22.7 ± 1.6) %	
Γ_{38}	$D^*(2010)^+$ anything	(17.3 ± 2.0) %	
Γ_{39}	$D_1(2420)^0$ anything	(5.0 ± 1.5) %	
Γ_{40}	$D^*(2010)^\mp D_s^\pm$ anything	[c] (3.3 ± 1.6) %	
Γ_{41}	$D^0 D^*(2010)^\pm$ anything	[c] (3.0 ± 1.1) %	
Γ_{42}	$D^*(2010)^\pm D^\mp$ anything	[c] (2.5 ± 1.2) %	
Γ_{43}	$D^*(2010)^\pm D^*(2010)^\mp$ anything	[c] (1.2 ± 0.4) %	
Γ_{44}	$\bar{D} D$ anything	(10 ± 11) %	
Γ_{45}	$D_2^*(2460)^0$ anything	(4.7 ± 2.7) %	

Γ_{46}	D_s^- anything	(14.7 ± 2.1) %
Γ_{47}	D_s^+ anything	(10.1 ± 3.1) %
Γ_{48}	Λ_c^+ anything	(7.8 ± 1.1) %
Γ_{49}	\bar{c}/c anything	[d] (116.2 ± 3.2) %

Charmonium modes

Γ_{50}	$J/\psi(1S)$ anything	(1.16 ± 0.10) %	
Γ_{51}	$\psi(2S)$ anything	(3.06 ± 0.30) × 10 ⁻³	
Γ_{52}	$\chi_{c0}(1P)$ anything	(1.4 ± 0.5) %	
Γ_{53}	$\chi_{c1}(1P)$ anything	(1.4 ± 0.4) %	
Γ_{54}	$\chi_{c2}(1P)$ anything	(5.5 ± 2.4) × 10 ⁻³	
Γ_{55}	$\chi_c(2P)$ anything, $\chi_c \rightarrow \phi \phi$	< 2.8 × 10 ⁻⁷	CL=95%
Γ_{56}	$\eta_c(1S)$ anything	(5.6 ± 0.9) × 10 ⁻³	
Γ_{57}	$\eta_c(2S)$ anything, $\eta_c \rightarrow \phi \phi$	(4.1 ± 1.7) × 10 ⁻⁷	
Γ_{58}	$\chi_{c1}(3872)$ anything, $\chi_{c1} \rightarrow \phi \phi$	< 4.5 × 10 ⁻⁷	CL=95%
Γ_{59}	$\chi_{c0}(3915)$ anything, $\chi_{c0} \rightarrow \phi \phi$	< 3.1 × 10 ⁻⁷	CL=95%

K or K* modes

Γ_{60}	$\bar{S} \gamma$	(3.1 ± 1.1) × 10 ⁻⁴	
Γ_{61}	$\bar{S} \bar{\nu} \nu$	B1 < 6.4 × 10 ⁻⁴	CL=90%
Γ_{62}	K^\pm anything	(74 ± 6) %	
Γ_{63}	K_S^0 anything	(29.0 ± 2.9) %	

Pion modes

Γ_{64}	π^\pm anything	(397 ± 21) %
Γ_{65}	π^0 anything	[d] (280 ± 60) %
Γ_{66}	ϕ anything	(2.82 ± 0.23) %

Baryon modes

Γ_{67}	p/\bar{p} anything	(13.1 ± 1.1) %
Γ_{68}	$\Lambda/\bar{\Lambda}$ anything	(5.9 ± 0.6) %
Γ_{69}	b -baryon anything	(10.2 ± 2.8) %
Γ_{70}	$\bar{\Lambda}_b^0$ anything	
Γ_{71}	Ξ_b^\pm anything	

Other modes

Γ_{72}	charged anything	[d] (497 ± 7) %
Γ_{73}	hadron ⁺ hadron ⁻	(1.7 ± 1.0) × 10 ⁻⁵
Γ_{74}	charmless	(7 ± 21) × 10 ⁻³

 $\Delta B = 1$ weak neutral current (B1) modes

Γ_{75}	$e^+ e^-$ anything		
Γ_{76}	$\mu^+ \mu^-$ anything	B1 < 3.2 × 10 ⁻⁴	CL=90%
Γ_{77}	$\nu \bar{\nu}$ anything		

[a] An ℓ indicates an e or a μ mode, not a sum over these modes.

[b] D_j represents an unresolved mixture of pseudoscalar and tensor D^{**} (P -wave) states.

[c] The value is for the sum of the charge states or particle/antiparticle states indicated.

[d] Inclusive branching fractions have a multiplicity definition and can be greater than 100%.

 $B^\pm/B^0/B_s^0/b$ -baryon ADMIXTURE BRANCHING RATIOS

$\Gamma(B^+)/\Gamma_{\text{total}}$	Γ_1/Γ
"OUR EVALUATION" is an average from Z decay.	

VALUE	DOCUMENT ID	TECN	COMMENT
0.408 ± 0.007	OUR EVALUATION		(Produced by HFLAV)
0.4099 ± 0.0082 ± 0.0111	¹ ABDALLAH	03k DLPH	$e^+ e^- \rightarrow Z$

¹ The analysis is based on a neural network, to estimate the charge of the weakly-decaying b hadron by distinguishing its decay products from particles produced at the primary vertex.

$\Gamma(B^+)/\Gamma(B^0)$	Γ_1/Γ_2
---------------------------	---------------------

VALUE	DOCUMENT ID	TECN	COMMENT
1.054 ± 0.018 ± 0.062	AALTONEN	08n CDF	$p\bar{p}$ at 1.96 TeV

$\Gamma(B_s^0)/\Gamma(B^+)$	Γ_3/Γ_1
-----------------------------	---------------------

VALUE	DOCUMENT ID	TECN	COMMENT
•••	•••	•••	•••

0.121 ± 0.002 ± 0.005 ^{1,2} AAIJ 20v LHCb $p\bar{p}$ at 7 TeV

0.124 ± 0.002 ± 0.005 ^{1,3} AAIJ 20v LHCb $p\bar{p}$ at 8 TeV

0.130 ± 0.002 ± 0.005 ^{1,4,5} AAIJ 20v LHCb $p\bar{p}$ at 13 TeV

¹ AAIJ 20v measures the average value using the observed $B_s^0 \rightarrow J/\psi \phi$ and $B^+ \rightarrow J/\psi K^+$ yields, over the ranges b -hadron p_T of 0.5 and 40 GeV and η of 2.0 and 6.5. The value is not used in averages as BR-related systematic uncertainties are not evaluated.

See key on page 1171

Meson Particle Listings

$B^\pm/B^0/B_s^0/b$ -baryon ADMIXTURE

- ² AAIJ 20v reports $[\Gamma(\bar{b} \rightarrow B_s^0)/\Gamma(\bar{b} \rightarrow B^+)] \times [B(B_s^0 \rightarrow J/\psi(1S)\phi)] / [B(B^+ \rightarrow J/\psi(1S)K^+)] = 0.1238 \pm 0.0010 \pm 0.0022$ which we multiply or divide by our best values $B(B_s^0 \rightarrow J/\psi(1S)\phi) = (1.04 \pm 0.04) \times 10^{-3}$, $B(B^+ \rightarrow J/\psi(1S)K^+) = (1.020 \pm 0.019) \times 10^{-3}$. Our first error is their experiment's error and our second error is the systematic error from using our best values.
- ³ AAIJ 20v reports $[\Gamma(\bar{b} \rightarrow B_s^0)/\Gamma(\bar{b} \rightarrow B^+)] \times [B(B_s^0 \rightarrow J/\psi(1S)\phi)] / [B(B^+ \rightarrow J/\psi(1S)K^+)] = 0.1270 \pm 0.0007 \pm 0.0022$ which we multiply or divide by our best values $B(B_s^0 \rightarrow J/\psi(1S)\phi) = (1.04 \pm 0.04) \times 10^{-3}$, $B(B^+ \rightarrow J/\psi(1S)K^+) = (1.020 \pm 0.019) \times 10^{-3}$. Our first error is their experiment's error and our second error is the systematic error from using our best values.
- ⁴ AAIJ 20v reports the results in two different data sets, and we quote here the weighted average.
- ⁵ AAIJ 20v reports $[\Gamma(\bar{b} \rightarrow B_s^0)/\Gamma(\bar{b} \rightarrow B^+)] \times [B(B_s^0 \rightarrow J/\psi(1S)\phi)] / [B(B^+ \rightarrow J/\psi(1S)K^+)] = 0.1326 \pm 0.0007 \pm 0.0023$ which we multiply or divide by our best values $B(B_s^0 \rightarrow J/\psi(1S)\phi) = (1.04 \pm 0.04) \times 10^{-3}$, $B(B^+ \rightarrow J/\psi(1S)K^+) = (1.020 \pm 0.019) \times 10^{-3}$. Our first error is their experiment's error and our second error is the systematic error from using our best values.

$$\Gamma(B_s^0)/[\Gamma(B^+) + \Gamma(B^0)] \quad \Gamma_3/(\Gamma_1 + \Gamma_2)$$

"OUR EVALUATION" is an average from Z decay.

VALUE	DOCUMENT ID	TECN	COMMENT
0.1230 ± 0.0115 OUR EVALUATION	(Produced by HFLAV)		
• • • We do not use the following data for averages, fits, limits, etc. • • •			
0.122 ± 0.006	¹ AAIJ	19AD LHCb	$p\bar{p}$ at 13 TeV
0.134 ± 0.004 ^{+0.011} / _{-0.010}	² AAIJ	12j LHCb	$p\bar{p}$ at 7 TeV
0.1265 ± 0.0085 ± 0.0131	³ AAIJ	11F LHCb	$p\bar{p}$ at 7 TeV
0.128 ^{+0.011} / _{-0.010} ± 0.011	⁴ AALTONEN	08N CDF	$p\bar{p}$ at 1.96 TeV
0.213 ± 0.068	⁵ AFFOLDER	00E CDF	$p\bar{p}$ at 1.8 TeV
0.21 ± 0.036 ^{+0.038} / _{-0.030}	⁶ ABE	99P CDF	$p\bar{p}$ at 1.8 TeV

- ¹ AAIJ 19AD measured the average value using b -hadron semileptonic decays and assuming isospin symmetry for b -hadron p_T of 4 and 25 GeV and η of 2 and 5.
- ² AAIJ 12j measured this value using b -hadron semileptonic decays and assuming isospin symmetry.
- ³ AAIJ 11F measured $f_s/f_d = 0.253 \pm 0.017 \pm 0.017 \pm 0.020$, where the errors are statistical, systematic, and theoretical. We divide their value by 2. Our second error combines systematic and theoretical uncertainties.
- ⁴ AALTONEN 08N reports $[\Gamma(\bar{b} \rightarrow B_s^0)/[\Gamma(\bar{b} \rightarrow B^+) + \Gamma(\bar{b} \rightarrow B^0)]] \times [B(D_s^+ \rightarrow \phi\pi^+)] = (5.76 \pm 0.18 ^{+0.45}/_{-0.42}) \times 10^{-3}$ which we divide by our best value $B(D_s^+ \rightarrow \phi\pi^+) = (4.5 \pm 0.4) \times 10^{-2}$. Our first error is their experiment's error and our second error is the systematic error from using our best value.
- ⁵ AFFOLDER 00E uses several electron-charm final states in $b \rightarrow ce^-X$.
- ⁶ ABE 99P uses the numbers of $K^*(892)^0$, $K^*(892)^+$, and $\phi(1020)$ events produced in association with the double semileptonic decays $b \rightarrow c\mu^-X$ with $c \rightarrow s\mu^+X$.

$$\Gamma(B_s^0)/\Gamma(B^0) \quad \Gamma_3/\Gamma_2$$

VALUE	DOCUMENT ID	TECN	COMMENT
0.246 ± 0.023 OUR EVALUATION	(Produced by HFLAV)		
0.239 ± 0.016 OUR AVERAGE			
0.240 ± 0.004 ± 0.020	¹ AAD	15CM ATLAS	$p\bar{p}$ at 7 TeV
0.238 ± 0.004 ± 0.026	² AAIJ	13P LHCb	$p\bar{p}$ at 7 TeV
• • • We do not use the following data for averages, fits, limits, etc. • • •			
0.2385 ± 0.0075	³ AAIJ	21Y LHCb	$p\bar{p}$ at 8 TeV
0.2539 ± 0.0079	³ AAIJ	21Y LHCb	$p\bar{p}$ at 13 TeV
0.2390 ± 0.0076	³ AAIJ	21Y LHCb	$p\bar{p}$ at 7 TeV

- ¹ AAD 15CM measurement is derived from the observed $B_s^0 \rightarrow J/\psi\phi$ and $B_d^0 \rightarrow J/\psi K^{*0}$ yields and a recent theory prediction of $B(B_s^0 \rightarrow J/\psi\phi)/B(B_d^0 \rightarrow J/\psi K^{*0})$. The second uncertainty combines in quadrature systematic and theoretical uncertainties.
- ² AAIJ 13P studies also separately the $p_T(B)$ and $\eta(B)$ dependency of $\Gamma(\bar{b} \rightarrow B_s^0)/\Gamma(\bar{b} \rightarrow B^0)$, finding $f_s/f_d(p_T) = (0.256 \pm 0.020) + (-2.0 \pm 0.6) 10^{-3} / \text{GeV}/c$ ($p_T - \langle p_T \rangle$) and $f_s/f_d(\eta) = (0.256 \pm 0.020) + (0.005 \pm 0.006)(\eta - \langle \eta \rangle)$, where $\langle p_T \rangle = 10.4 \text{ GeV}/c$ and $\langle \eta \rangle = 3.28$. AAIJ 13P reports the measurement as $0.238 \pm 0.004 \pm 0.015 \pm 0.021$ where the last uncertainty is theoretical.
- ³ AAIJ 21Y uses hadronic decays $B^0 \rightarrow D^-\pi^+$, $B^0 \rightarrow D^-K^+$, $B_s^0 \rightarrow D_s^-\pi^+$ and $B_s^0 \rightarrow J/\psi\phi$ as well as semileptonic B^0 and B_s^0 decays. Measured within the p_T range [0.5,4.0] GeV/c, η range [2, 6.4].

$$\Gamma(B_c^+)/[\Gamma(B^+) + \Gamma(B^0)] \quad \Gamma_4/(\Gamma_1 + \Gamma_2)$$

VALUE (units 10^{-3})	DOCUMENT ID	TECN	COMMENT
3.7 ± 0.6 OUR AVERAGE			
3.63 ± 0.08 ± 0.87	¹ AAIJ	19AI LHCb	$p\bar{p}$ at 7 TeV
3.78 ± 0.04 ± 0.90	¹ AAIJ	19AI LHCb	$p\bar{p}$ at 13 TeV

- ¹ Measured using B_c^+ semileptonic decays.

$$\Gamma(b\text{-baryon})/[\Gamma(B^+) + \Gamma(B^0)] \quad \Gamma_5/(\Gamma_1 + \Gamma_2)$$

"OUR EVALUATION" is an average from Z decay.

VALUE	DOCUMENT ID	TECN	COMMENT
0.103 ± 0.015 OUR EVALUATION	(Produced by HFLAV)		
• • • We do not use the following data for averages, fits, limits, etc. • • •			
0.259 ± 0.018	¹ AAIJ	19AD LHCb	$p\bar{p}$ at 13 TeV

0.305 ± 0.010 ± 0.081	² AAIJ	12j LHCb	$p\bar{p}$ at 7 TeV
0.31 ± 0.11 ^{+0.12} / _{-0.08}	³ AALTONEN	09E CDF	$p\bar{p}$ at 1.8 TeV
0.23 ^{+0.09} / _{-0.07} ± 0.01	⁴ AALTONEN	08N CDF	$p\bar{p}$ at 1.96 TeV
0.118 ± 0.042	^{3,5} AFFOLDER	00E CDF	$p\bar{p}$ at 1.8 TeV

- ¹ AAIJ 19AD measured the average value for Λ_b^0 using semileptonic decays and assuming isospin symmetry for b -hadron p_T of 4 and 25 GeV and η of 2 and 5.
- ² AAIJ 12j measured the ratio to be $(0.404 \pm 0.017 \pm 0.027 \pm 0.105) \times [1 - (0.031 \pm 0.004 \pm 0.003) \times P_T]$ using b -hadron semileptonic decays where the P_T is the momentum of charmed hadron-muon pair in GeV/c. We quote their weighted average value where the second error combines systematic and the error on $B(\Lambda_c^+ \rightarrow pK^-\pi^+)$.
- ³ AALTONEN 09E errata to the measurement reported in AFFOLDER 00E using the p_T spectra from fully reconstructed B^0 and Λ_b decays.
- ⁴ AALTONEN 08N reports $[\Gamma(\bar{b} \rightarrow b\text{-baryon})/[\Gamma(\bar{b} \rightarrow B^+) + \Gamma(\bar{b} \rightarrow B^0)]] \times [B(\Lambda_c^+ \rightarrow pK^-\pi^+)] = (14.1 \pm 0.6 ^{+5.3}/_{-4.4}) \times 10^{-3}$ which we divide by our best value $B(\Lambda_c^+ \rightarrow pK^-\pi^+) = (6.24 \pm 0.28) \times 10^{-2}$. Our first error is their experiment's error and our second error is the systematic error from using our best value.
- ⁵ AFFOLDER 00E uses several electron-charm final states in $b \rightarrow ce^-X$.

$$\Gamma(\nu\text{anything})/\Gamma_{\text{total}} \quad \Gamma_6/\Gamma$$

VALUE	DOCUMENT ID	TECN	COMMENT
0.2308 ± 0.0077 ± 0.0124	^{1,2} ACCIARRI	96c L3	$e^+e^- \rightarrow Z$

- ¹ ACCIARRI 96c assumes relative b semileptonic decay rates $\epsilon:\mu:\tau$ of 1:1:0.25. Based on missing-energy spectrum.
- ² Assumes Standard Model value for R_B .

$$\Gamma(e^+\nu_e\text{anything})/\Gamma_{\text{total}} \quad \Gamma_7/\Gamma$$

"OUR EVALUATION" is an average of the data listed below, excluding all asymmetry measurements, performed by the LEP Electroweak Working Group as described in the "Note on the Z boson" in the Z Particle Listings.

VALUE	DOCUMENT ID	TECN	COMMENT
0.1069 ± 0.0022 OUR EVALUATION			
0.1064 ± 0.0016 OUR AVERAGE			
0.1070 ± 0.0010 ± 0.0035	¹ HEISTER	02G ALEP	$e^+e^- \rightarrow Z$
0.1070 ± 0.0008 ^{+0.0037} / _{-0.0049}	² ABREU	01L DLPH	$e^+e^- \rightarrow Z$
0.1083 ± 0.0010 ^{+0.0028} / _{-0.0024}	³ ABBIENDI	00E OPAL	$e^+e^- \rightarrow Z$
0.1016 ± 0.0013 ± 0.0030	⁴ ACCIARRI	00 L3	$e^+e^- \rightarrow Z$
0.1085 ± 0.0012 ± 0.0047	^{5,6} ACCIARRI	96c L3	$e^+e^- \rightarrow Z$
• • • We do not use the following data for averages, fits, limits, etc. • • •			
0.1106 ± 0.0039 ± 0.0022	⁷ ABREU	95D DLPH	$e^+e^- \rightarrow Z$
0.114 ± 0.003 ± 0.004	⁸ BUSKULIC	94G ALEP	$e^+e^- \rightarrow Z$
0.100 ± 0.007 ± 0.007	⁹ ABREU	93C DLPH	$e^+e^- \rightarrow Z$
0.105 ± 0.006 ± 0.005	¹⁰ AKERS	93B OPAL	Repl. by ABBI- ENDI 00E

- ¹ Uses the combination of lepton transverse momentum spectrum and the correlation between the charge of the lepton and opposite jet charge. The first error is statistic and the second error is the total systematic error including the modeling.
- ² The experimental systematic and model uncertainties are combined in quadrature.
- ³ ABBIENDI 00E result is determined by comparing the distribution of several kinematic variables of leptonic events in a lifetime tagged $Z \rightarrow b\bar{b}$ sample using artificial neural network techniques. The first error is statistic; the second error is the total systematic error.
- ⁴ ACCIARRI 00 result obtained from a combined fit of $R_B = \Gamma(Z \rightarrow b\bar{b})/\Gamma(Z \rightarrow \text{hadrons})$ and $B(b \rightarrow \ell\nu X)$, using double-tagging method.
- ⁵ ACCIARRI 96c result obtained by a fit to the single lepton spectrum.
- ⁶ Assumes Standard Model value for R_B .
- ⁷ ABREU 95D give systematic errors ± 0.0019 (model) and 0.0012 (R_C). We combine these in quadrature.
- ⁸ BUSKULIC 94G uses e and μ events. This value is from a global fit to the lepton p and p_T (relative to jet) spectra which also determines the b and c production fractions, the fragmentation functions, and the forward-backward asymmetries. This branching ratio depends primarily on the ratio of dileptons to single leptons at high p_T , but the lower p_T portion of the lepton spectrum is included in the global fit to reduce the model dependence. The model dependence is ± 0.0026 and is included in the systematic error.
- ⁹ ABREU 93C event count includes ee events. Combining ee , $\mu\mu$, and $e\mu$ events, they obtain $0.100 \pm 0.007 \pm 0.007$.
- ¹⁰ AKERS 93B analysis performed using single and dilepton events.

$$\Gamma(e^+\nu_e\text{anything})/\Gamma_{\text{total}} \quad \Gamma_8/\Gamma$$

VALUE	EVENTS	DOCUMENT ID	TECN	COMMENT
0.1086 ± 0.0035 OUR AVERAGE				
0.1078 ± 0.0008 ^{+0.0050} / _{-0.0046}		¹ ABBIENDI	00E OPAL	$e^+e^- \rightarrow Z$
0.1089 ± 0.0020 ± 0.0051		^{2,3} ACCIARRI	96c L3	$e^+e^- \rightarrow Z$
0.107 ± 0.015 ± 0.007	260	⁴ ABREU	93C DLPH	$e^+e^- \rightarrow Z$
0.138 ± 0.032 ± 0.008		⁵ ADEVA	91c L3	$e^+e^- \rightarrow Z$
• • • We do not use the following data for averages, fits, limits, etc. • • •				
0.086 ± 0.027 ± 0.008		⁶ ABE	93E VNS	$E_{\text{cm}}^{\text{th}} = 58 \text{ GeV}$
0.109 ^{+0.014} / _{-0.013} ± 0.0055	2719	⁷ AKERS	93B OPAL	Repl. by ABBI- ENDI 00E
0.111 ± 0.028 ± 0.026		BEHREND	90D CELL	$E_{\text{cm}}^{\text{th}} = 43 \text{ GeV}$
0.150 ± 0.011 ± 0.022		BEHREND	90D CELL	$E_{\text{cm}}^{\text{th}} = 35 \text{ GeV}$
0.112 ± 0.009 ± 0.011		ONG	88 MRK2	$E_{\text{cm}}^{\text{th}} = 29 \text{ GeV}$

Meson Particle Listings

 $B^\pm/B^0/B_s^0/b$ -baryon ADMIXTURE

0.149 ± 0.022 -0.019	PAL	86	DLCO	$E_{\text{cm}}^{\text{e}} = 29$ GeV
0.110 $\pm 0.018 \pm 0.010$	AIHARA	85	TPC	$E_{\text{cm}}^{\text{e}} = 29$ GeV
0.111 $\pm 0.034 \pm 0.040$	ALTHOFF	84J	TASS	$E_{\text{cm}}^{\text{e}} = 34.6$ GeV
0.146 ± 0.028	KOOP	84	DLCO	Repl. by PAL 86
0.116 $\pm 0.021 \pm 0.017$	NELSON	83	MRK2	$E_{\text{cm}}^{\text{e}} = 29$ GeV

¹ ABBIENDI 00E result is determined by comparing the distribution of several kinematic variables of leptonic events in a lifetime tagged $Z \rightarrow b\bar{b}$ sample using artificial neural network techniques. The first error is statistical; the second error is the total systematic error.

² ACCIARRI 96c result obtained by a fit to the single lepton spectrum.

³ Assumes Standard Model value for R_B .

⁴ ABREU 93c event count includes $e\bar{e}$ events. Combining $e\bar{e}$, $\mu\mu$, and $e\mu$ events, they obtain $0.100 \pm 0.007 \pm 0.007$.

⁵ ADEVA 91c measure the average $B(b \rightarrow eX)$ branching ratio using single and double tagged b enhanced Z events. Combining e and μ results, they obtain $0.113 \pm 0.010 \pm 0.006$. Constraining the initial number of b quarks by the Standard Model prediction (378 ± 3 MeV) for the decay of the Z into $b\bar{b}$, the electron result gives $0.112 \pm 0.004 \pm 0.008$. They obtain $0.119 \pm 0.003 \pm 0.006$ when e and μ results are combined. Used to measure the $b\bar{b}$ width itself, this electron result gives $370 \pm 12 \pm 24$ MeV and combined with the muon result gives $385 \pm 7 \pm 22$ MeV.

⁶ ABE 93E experiment also measures forward-backward asymmetries and fragmentation functions for b and c .

⁷ AKERS 93B analysis performed using single and dilepton events.

$\Gamma(\mu^+ \nu_\mu \text{ anything})/\Gamma_{\text{total}}$ Γ_9/Γ

VALUE	EVTs	DOCUMENT ID	TECN	COMMENT
0.1095 ± 0.0029 -0.0025 OUR AVERAGE				
0.1096 $\pm 0.0008 \pm 0.0034$ -0.0027		¹ ABBIENDI	00E OPAL	$e^+e^- \rightarrow Z$
0.1082 $\pm 0.0015 \pm 0.0059$		^{2,3} ACCIARRI	96c L3	$e^+e^- \rightarrow Z$
0.110 $\pm 0.012 \pm 0.007$	656	⁴ ABREU	93c DLPH	$e^+e^- \rightarrow Z$
0.113 $\pm 0.012 \pm 0.006$		⁵ ADEVA	91c L3	$e^+e^- \rightarrow Z$
• • • We do not use the following data for averages, fits, limits, etc. • • •				
0.122 $\pm 0.006 \pm 0.007$		³ UENO	96 AMY	e^+e^- at 57.9 GeV
0.101 ± 0.010 -0.009 ± 0.0055	4248	⁶ AKERS	93B OPAL	Repl. by ABBIENDI 00E
0.104 $\pm 0.023 \pm 0.016$		BEHREND	90D CELL	$E_{\text{cm}}^{\text{e}} = 43$ GeV
0.148 $\pm 0.010 \pm 0.016$		BEHREND	90D CELL	$E_{\text{cm}}^{\text{e}} = 35$ GeV
0.118 $\pm 0.012 \pm 0.010$		ONG	88 MRK2	$E_{\text{cm}}^{\text{e}} = 29$ GeV
0.117 $\pm 0.016 \pm 0.015$		BARTEL	87 JADE	$E_{\text{cm}}^{\text{e}} = 34.6$ GeV
0.114 $\pm 0.018 \pm 0.025$		BARTEL	85J JADE	Repl. by BARTEL 87
0.117 $\pm 0.028 \pm 0.010$		ALTHOFF	84G TASS	$E_{\text{cm}}^{\text{e}} = 34.5$ GeV
0.105 $\pm 0.015 \pm 0.013$		ADEVA	83B MRKJ	$E_{\text{cm}}^{\text{e}} = 33-38.5$ GeV
0.155 ± 0.054 -0.029		FERNANDEZ	83D MAC	$E_{\text{cm}}^{\text{e}} = 29$ GeV

¹ ABBIENDI 00E result is determined by comparing the distribution of several kinematic variables of leptonic events in a lifetime tagged $Z \rightarrow b\bar{b}$ sample using artificial neural network techniques. The first error is statistical; the second error is the total systematic error.

² ACCIARRI 96c result obtained by a fit to the single lepton spectrum.

³ Assumes Standard Model value for R_B .

⁴ ABREU 93c event count includes $\mu\mu$ events. Combining $e\bar{e}$, $\mu\mu$, and $e\mu$ events, they obtain $0.100 \pm 0.007 \pm 0.007$.

⁵ ADEVA 91c measure the average $B(b \rightarrow eX)$ branching ratio using single and double tagged b enhanced Z events. Combining e and μ results, they obtain $0.113 \pm 0.010 \pm 0.006$. Constraining the initial number of b quarks by the Standard Model prediction (378 ± 3 MeV) for the decay of the Z into $b\bar{b}$, the muon result gives $0.123 \pm 0.003 \pm 0.006$. They obtain $0.119 \pm 0.003 \pm 0.006$ when e and μ results are combined. Used to measure the $b\bar{b}$ width itself, this muon result gives $394 \pm 9 \pm 22$ MeV and combined with the electron result gives $385 \pm 7 \pm 22$ MeV.

⁶ AKERS 93B analysis performed using single and dilepton events.

$\Gamma(D^- \ell^+ \nu_\ell \text{ anything})/\Gamma_{\text{total}}$ Γ_{10}/Γ

VALUE	DOCUMENT ID	TECN	COMMENT
0.022 ± 0.004 OUR AVERAGE			Error includes scale factor of 1.9.
0.0272 $\pm 0.0028 \pm 0.0018$	¹ ABREU	00R DLPH	$e^+e^- \rightarrow Z$
0.0194 $\pm 0.0025 \pm 0.0003$	² AKERS	95Q OPAL	$e^+e^- \rightarrow Z$

¹ ABREU 00R reports their experiment's uncertainties $\pm 0.0019 \pm 0.0016 \pm 0.0018$, where the first error is statistical, the second is systematic, and the third is the uncertainty due to the D branching fraction. We combine first two in quadrature.

² AKERS 95Q reports $[\Gamma(\bar{D}^- \ell^+ \nu_\ell \text{ anything})/\Gamma_{\text{total}}] \times [B(D^+ \rightarrow K^- \pi^+)] = (1.82 \pm 0.20 \pm 0.12) \times 10^{-3}$ which we divide by our best value $B(D^+ \rightarrow K^- \pi^+) = (9.38 \pm 0.16) \times 10^{-2}$. Our first error is their experiment's error and our second error is the systematic error from using our best value.

$\Gamma(D^- \pi^+ \ell^+ \nu_\ell \text{ anything})/\Gamma_{\text{total}}$ Γ_{11}/Γ

VALUE	DOCUMENT ID	TECN	COMMENT
0.0049 $\pm 0.0018 \pm 0.0007$	ABREU	00R DLPH	$e^+e^- \rightarrow Z$

$\Gamma(D^- \pi^- \ell^+ \nu_\ell \text{ anything})/\Gamma_{\text{total}}$ Γ_{12}/Γ

VALUE	DOCUMENT ID	TECN	COMMENT
0.0026 $\pm 0.0015 \pm 0.0004$	ABREU	00R DLPH	$e^+e^- \rightarrow Z$

$\Gamma(\bar{D}^0 \ell^+ \nu_\ell \text{ anything})/\Gamma_{\text{total}}$ Γ_{13}/Γ

VALUE	DOCUMENT ID	TECN	COMMENT
0.0679 ± 0.0034 OUR AVERAGE			
0.0704 $\pm 0.0040 \pm 0.0017$	¹ ABREU	00R DLPH	$e^+e^- \rightarrow Z$
0.0638 $\pm 0.0056 \pm 0.0005$	² AKERS	95Q OPAL	$e^+e^- \rightarrow Z$

¹ ABREU 00R reports their experiment's uncertainties $\pm 0.0034 \pm 0.0036 \pm 0.0017$, where the first error is statistical, the second is systematic, and the third is the uncertainty due to the D branching fraction. We combine first two in quadrature.

² AKERS 95Q reports $[\Gamma(\bar{D}^0 \ell^+ \nu_\ell \text{ anything})/\Gamma_{\text{total}}] \times [B(D^0 \rightarrow K^- \pi^+)] = (2.52 \pm 0.14 \pm 0.17) \times 10^{-3}$ which we divide by our best value $B(D^0 \rightarrow K^- \pi^+) = (3.947 \pm 0.030) \times 10^{-2}$. Our first error is their experiment's error and our second error is the systematic error from using our best value.

$\Gamma(\bar{D}^0 \pi^- \ell^+ \nu_\ell \text{ anything})/\Gamma_{\text{total}}$ Γ_{14}/Γ

VALUE	DOCUMENT ID	TECN	COMMENT
0.0107 $\pm 0.0025 \pm 0.0011$	ABREU	00R DLPH	$e^+e^- \rightarrow Z$

$\Gamma(\bar{D}^0 \pi^+ \ell^+ \nu_\ell \text{ anything})/\Gamma_{\text{total}}$ Γ_{15}/Γ

VALUE	DOCUMENT ID	TECN	COMMENT
0.0023 $\pm 0.0015 \pm 0.0004$	ABREU	00R DLPH	$e^+e^- \rightarrow Z$

$\Gamma(D^{*-} \ell^+ \nu_\ell \text{ anything})/\Gamma_{\text{total}}$ Γ_{16}/Γ

VALUE	DOCUMENT ID	TECN	COMMENT
0.0275 ± 0.0019 OUR AVERAGE			

0.0275 $\pm 0.0021 \pm 0.0009$ ¹ ABREU 00R DLPH $e^+e^- \rightarrow Z$

0.0276 $\pm 0.0027 \pm 0.0011$ ² AKERS 95Q OPAL $e^+e^- \rightarrow Z$

¹ ABREU 00R reports their experiment's uncertainties $\pm 0.0017 \pm 0.0013 \pm 0.0009$, where the first error is statistical, the second is systematic, and the third is the uncertainty due to the D branching fraction. We combine first two in quadrature.

² AKERS 95Q reports $[B(\bar{D}^- \rightarrow D^{*-} \ell^+ \nu_\ell X) \times B(D^{*+} \rightarrow D^0 \pi^+) \times B(D^0 \rightarrow K^- \pi^+)] = ((7.53 \pm 0.47 \pm 0.56) \times 10^{-4})$ and uses $B(D^{*+} \rightarrow D^0 \pi^+) = 0.681 \pm 0.013$ and $B(D^0 \rightarrow K^- \pi^+) = 0.0401 \pm 0.0014$ to obtain the above result. The first error is the experiments error and the second error is the systematic error from the D^{*+} and D^0 branching ratios.

$\Gamma(D^{*-} \pi^- \ell^+ \nu_\ell \text{ anything})/\Gamma_{\text{total}}$ Γ_{17}/Γ

VALUE	DOCUMENT ID	TECN	COMMENT
0.0006 $\pm 0.0007 \pm 0.0002$	ABREU	00R DLPH	$e^+e^- \rightarrow Z$

$\Gamma(D^{*-} \pi^+ \ell^+ \nu_\ell \text{ anything})/\Gamma_{\text{total}}$ Γ_{18}/Γ

VALUE	DOCUMENT ID	TECN	COMMENT
0.0048 $\pm 0.0009 \pm 0.0005$	ABREU	00R DLPH	$e^+e^- \rightarrow Z$

$\Gamma(\bar{D}_j^0 \ell^+ \nu_\ell \text{ anything} \times B(\bar{D}_j^0 \rightarrow D^{*+} \pi^-))/\Gamma_{\text{total}}$ Γ_{19}/Γ

D_j represents an unresolved mixture of pseudoscalar and tensor D^{**} (P -wave) states.

VALUE (units 10^{-3})	DOCUMENT ID	TECN	COMMENT
2.64 $\pm 0.79 \pm 0.39$	ABBIENDI	03M OPAL	$e^+e^- \rightarrow Z$

• • • We do not use the following data for averages, fits, limits, etc. • • •

6.1 $\pm 1.3 \pm 1.3$ AKERS 95Q OPAL Repl. by ABBIENDI 03M

$\Gamma(D_j^- \ell^+ \nu_\ell \text{ anything} \times B(D_j^- \rightarrow D^0 \pi^-))/\Gamma_{\text{total}}$ Γ_{20}/Γ

D_j represents an unresolved mixture of pseudoscalar and tensor D^{**} (P -wave) states.

VALUE (units 10^{-3})	DOCUMENT ID	TECN	COMMENT
7.0 $\pm 1.9 \pm 1.2$ -1.3	AKERS	95Q OPAL	$e^+e^- \rightarrow Z$

$\Gamma(\bar{D}_2^0(2460)^0 \ell^+ \nu_\ell \text{ anything} \times B(\bar{D}_2^{*+}(2460)^0 \rightarrow D^{*-} \pi^+))/\Gamma_{\text{total}}$ Γ_{21}/Γ

VALUE (units 10^{-3})	CL%	DOCUMENT ID	TECN	COMMENT
<1.4	90	ABBIENDI	03M OPAL	$e^+e^- \rightarrow Z$

$\Gamma(D_2^+(2460)^- \ell^+ \nu_\ell \text{ anything} \times B(D_2^{*+}(2460)^- \rightarrow D^0 \pi^-))/\Gamma_{\text{total}}$ Γ_{22}/Γ

VALUE (units 10^{-3})	DOCUMENT ID	TECN	COMMENT
4.2 $\pm 1.3 \pm 0.7$ -1.2	AKERS	95Q OPAL	$e^+e^- \rightarrow Z$

$\Gamma(\bar{D}_2^+(2460)^0 \ell^+ \nu_\ell \text{ anything} \times B(\bar{D}_2^{*+}(2460)^0 \rightarrow D^- \pi^+))/\Gamma_{\text{total}}$ Γ_{23}/Γ

VALUE (units 10^{-3})	DOCUMENT ID	TECN	COMMENT
1.6 $\pm 0.7 \pm 0.3$	AKERS	95Q OPAL	$e^+e^- \rightarrow Z$

$\Gamma(\text{charmless } \ell \bar{\nu}_\ell)/\Gamma_{\text{total}}$ Γ_{24}/Γ

"OUR EVALUATION" is an average of the data listed below performed by the LEP Heavy Flavour Steering Group. The averaging procedure takes into account correlations between the measurements.

VALUE DOCUMENT ID TECN COMMENT

0.00171 ± 0.00052 OUR EVALUATION

0.0017 ± 0.0004 OUR AVERAGE

0.00163 $\pm 0.00053 \pm 0.00055$ ¹ ABBIENDI 01R OPAL $e^+e^- \rightarrow Z$

0.00157 $\pm 0.00035 \pm 0.00055$ ² ABREU 00D DLPH $e^+e^- \rightarrow Z$

0.00173 $\pm 0.00055 \pm 0.00055$ ³ BARATE 99G ALEP $e^+e^- \rightarrow Z$

0.0033 $\pm 0.0010 \pm 0.0017$ ⁴ ACCIARRI 98K L3 $e^+e^- \rightarrow Z$

¹ Obtained from the best fit of the MC simulated events to the data based on the $b \rightarrow X_{\mu} \ell \nu$ neutral network output distributions.

² ABREU 00D result obtained from a fit to the numbers of decays in $b \rightarrow u$ enriched and depleted samples and their lepton spectra, and assuming $|V_{cb}| = 0.0384 \pm 0.0033$ and $\tau_b = 1.564 \pm 0.014$ ps.

³ Uses lifetime tagged $b\bar{b}$ sample.

⁴ ACCIARRI 98K assumes $R_b = 0.2174 \pm 0.0009$ at Z decay.

See key on page 1171

Meson Particle Listings

$B^\pm/B^0/B_s^0/b$ -baryon ADMIXTURE

$\Gamma(\tau^+ \nu_\tau \text{ anything})/\Gamma_{\text{total}}$	Γ_{25}/Γ		
VALUE (units 10^{-2})	DOCUMENT ID	TECN	COMMENT
2.41 ± 0.23 OUR AVERAGE			
$2.76 \pm 0.18 \pm 0.51$	1 ABBIENDI	01Q	OPAL $e^+ e^- \rightarrow Z$
$2.43 \pm 0.20 \pm 0.25$	2 BARATE	01E	ALEP $e^+ e^- \rightarrow Z$
$2.19 \pm 0.24 \pm 0.39$	3 ABREU	00C	DLPH $e^+ e^- \rightarrow Z$
$1.7 \pm 0.5 \pm 1.1$	4,5 ACCIARRI	96C	L3 $e^+ e^- \rightarrow Z$
$2.4 \pm 0.7 \pm 0.8$	1032 6 ACCIARRI	94C	L3 $e^+ e^- \rightarrow Z$
$2.75 \pm 0.30 \pm 0.37$	405 7 BUSKULIC	95	ALEP Repl. by BARATE 01E
$4.08 \pm 0.76 \pm 0.62$		93B	ALEP Repl. by BUSKULIC 95

- • • We do not use the following data for averages, fits, limits, etc. • • •
- ¹ ABBIENDI 01Q uses a missing energy technique.
² The energy-flow and b -tagging algorithms were used.
³ Uses the missing energy in $Z \rightarrow b\bar{b}$ decays without identifying leptons.
⁴ ACCIARRI 96C result obtained from missing energy spectrum.
⁵ Assumes Standard Model value for R_B .
⁶ This is a direct result using tagged $b\bar{b}$ events at the Z, but species are not separated.
⁷ BUSKULIC 95 uses missing-energy technique.

$\Gamma(D^{*-} \tau \nu_\tau \text{ anything})/\Gamma_{\text{total}}$	Γ_{26}/Γ		
VALUE	DOCUMENT ID	TECN	COMMENT
$(0.88 \pm 0.31 \pm 0.28) \times 10^{-2}$	1 BARATE	01E	ALEP $e^+ e^- \rightarrow Z$

- ¹ The energy-flow and b -tagging algorithms were used.

$\Gamma(\bar{D} \rightarrow \tau \rightarrow \ell^- \nu_\ell \text{ anything})/\Gamma_{\text{total}}$	Γ_{27}/Γ		
VALUE	DOCUMENT ID	TECN	COMMENT
0.0802 ± 0.0019 OUR EVALUATION			
0.0817 ± 0.0020 OUR AVERAGE			
$0.0818 \pm 0.0015 \pm 0.0024$	1 HEISTER	02G	ALEP $e^+ e^- \rightarrow Z$
$0.0798 \pm 0.0022 \pm 0.0025$	2 ABREU	01L	DLPH $e^+ e^- \rightarrow Z$
$0.0840 \pm 0.0016 \pm 0.0039$	3 ABBIENDI	00E	OPAL $e^+ e^- \rightarrow Z$
$0.0770 \pm 0.0097 \pm 0.0046$	4 ABREU	95D	DLPH $e^+ e^- \rightarrow Z$
$0.082 \pm 0.003 \pm 0.012$	5 BUSKULIC	94G	ALEP $e^+ e^- \rightarrow Z$
$0.077 \pm 0.004 \pm 0.007$	6 AKERS	93B	OPAL Repl. by ABBI- ENDI 00E

“OUR EVALUATION” is an average of the data listed below, excluding all asymmetry measurements, performed by the LEP Electroweak Working Group as described in the “Note on the Z boson” in the Z Particle Listings.

- ¹ Uses the combination of lepton transverse momentum spectrum and the correlation between the charge of the lepton and opposite jet charge. The first error is statistic and the second error is the total systematic error including the modeling.
² The experimental systematic and model uncertainties are combined in quadrature.
³ ABBIENDI 00E result is determined by comparing the distribution of several kinematic variables of leptonic events in a lifetime tagged $Z \rightarrow b\bar{b}$ sample using artificial neural network techniques. The first error is statistic; the second error is the total systematic error.
⁴ ABREU 95D give systematic errors ± 0.0033 (model) and 0.0032 (R_c). We combine these in quadrature. This result is from the same global fit as their $\Gamma(\bar{D} \rightarrow \ell^+ \nu_\ell X)$ data.
⁵ BUSKULIC 94G uses e and μ events. This value is from the same global fit as their $\Gamma(\bar{D} \rightarrow \ell^+ \nu_\ell \text{ anything})/\Gamma_{\text{total}}$ data.
⁶ AKERS 93B analysis performed using single and dilepton events.

$\Gamma(c \rightarrow \ell^+ \nu \text{ anything})/\Gamma_{\text{total}}$	Γ_{28}/Γ		
VALUE	DOCUMENT ID	TECN	COMMENT
$0.0161 \pm 0.0020 \pm 0.0034$	1 ABREU	01L	DLPH $e^+ e^- \rightarrow Z$

- ¹ The experimental systematic and model uncertainties are combined in quadrature.

$\Gamma(D^0 \text{ anything})/\Gamma_{\text{total}}$	Γ_{29}/Γ		
VALUE	DOCUMENT ID	TECN	COMMENT
$0.587 \pm 0.028 \pm 0.004$	1 BUSKULIC	96Y	ALEP $e^+ e^- \rightarrow Z$

- ¹ BUSKULIC 96Y reports $0.605 \pm 0.024 \pm 0.016$ from a measurement of $[\Gamma(\bar{D} \rightarrow D^0 \text{ anything})/\Gamma_{\text{total}}] \times [B(D^0 \rightarrow K^- \pi^+)]$ assuming $B(D^0 \rightarrow K^- \pi^+) = 0.0383$, which we rescale to our best value $B(D^0 \rightarrow K^- \pi^+) = (3.947 \pm 0.030) \times 10^{-2}$. Our first error is their experiment's error and our second error is the systematic error from using our best value.

$\Gamma(D^0 D_s^\pm \text{ anything})/\Gamma_{\text{total}}$	Γ_{30}/Γ		
VALUE	DOCUMENT ID	TECN	COMMENT
$0.091 \pm 0.020 \pm 0.034$	1 BARATE	98Q	ALEP $e^+ e^- \rightarrow Z$

- ¹ The systematic error includes the uncertainties due to the charm branching ratios.

$\Gamma(D^\mp D_s^\pm \text{ anything})/\Gamma_{\text{total}}$	Γ_{31}/Γ		
VALUE	DOCUMENT ID	TECN	COMMENT
$0.040 \pm 0.017 \pm 0.016$	1 BARATE	98Q	ALEP $e^+ e^- \rightarrow Z$

- ¹ The systematic error includes the uncertainties due to the charm branching ratios.

$[\Gamma(D^0 D_s^\pm \text{ anything}) + \Gamma(D^\mp D_s^\pm \text{ anything})]/\Gamma_{\text{total}}$	$(\Gamma_{30} + \Gamma_{31})/\Gamma$		
VALUE	DOCUMENT ID	TECN	COMMENT
$0.131 \pm 0.026 \pm 0.048$	1 BARATE	98Q	ALEP $e^+ e^- \rightarrow Z$

- ¹ The systematic error includes the uncertainties due to the charm branching ratios.

$\Gamma(D^0 D^0 \text{ anything})/\Gamma_{\text{total}}$	Γ_{32}/Γ		
VALUE	DOCUMENT ID	TECN	COMMENT
$0.051 \pm 0.016 \pm 0.012$	1 BARATE	98Q	ALEP $e^+ e^- \rightarrow Z$

- ¹ The systematic error includes the uncertainties due to the charm branching ratios.

$\Gamma(D^0 D^\pm \text{ anything})/\Gamma_{\text{total}}$	Γ_{33}/Γ		
VALUE	DOCUMENT ID	TECN	COMMENT
$0.027 \pm 0.015 \pm 0.010$	1 BARATE	98Q	ALEP $e^+ e^- \rightarrow Z$

- ¹ The systematic error includes the uncertainties due to the charm branching ratios.

$[\Gamma(D^0 D^0 \text{ anything}) + \Gamma(D^0 D^\pm \text{ anything})]/\Gamma_{\text{total}}$	$(\Gamma_{32} + \Gamma_{33})/\Gamma$		
VALUE	DOCUMENT ID	TECN	COMMENT
$0.078 \pm 0.020 \pm 0.018$	1 BARATE	98Q	ALEP $e^+ e^- \rightarrow Z$

- ¹ The systematic error includes the uncertainties due to the charm branching ratios.

$\Gamma(D^\pm D^\mp \text{ anything})/\Gamma_{\text{total}}$	Γ_{34}/Γ			
VALUE	CL%	DOCUMENT ID	TECN	COMMENT
<0.009	90	BARATE	98Q	ALEP $e^+ e^- \rightarrow Z$

$[\Gamma(D^0 \text{ anything}) + \Gamma(D^+ \text{ anything})]/\Gamma_{\text{total}}$	$(\Gamma_{35} + \Gamma_{36})/\Gamma$		
VALUE	DOCUMENT ID	TECN	COMMENT
$0.093 \pm 0.017 \pm 0.014$	1 ABDALLAH	03E	DLPH $e^+ e^- \rightarrow Z$

- ¹ The second error is the total of systematic uncertainties including the branching fractions used in the measurement.

$\Gamma(D^- \text{ anything})/\Gamma_{\text{total}}$	Γ_{37}/Γ		
VALUE	DOCUMENT ID	TECN	COMMENT
$0.227 \pm 0.016 \pm 0.004$	1 BUSKULIC	96Y	ALEP $e^+ e^- \rightarrow Z$

- ¹ BUSKULIC 96Y reports $0.234 \pm 0.013 \pm 0.010$ from a measurement of $[\Gamma(\bar{D} \rightarrow D^- \text{ anything})/\Gamma_{\text{total}}] \times [B(D^+ \rightarrow K^- 2\pi^+)]$ assuming $B(D^+ \rightarrow K^- 2\pi^+) = 0.091$, which we rescale to our best value $B(D^+ \rightarrow K^- 2\pi^+) = (9.38 \pm 0.16) \times 10^{-2}$. Our first error is their experiment's error and our second error is the systematic error from using our best value.

$\Gamma(D^*(2010)^+ \text{ anything})/\Gamma_{\text{total}}$	Γ_{38}/Γ		
VALUE	DOCUMENT ID	TECN	COMMENT
$0.173 \pm 0.016 \pm 0.012$	1 ACKERSTAFF	98E	OPAL $e^+ e^- \rightarrow Z$

- ¹ Uses lepton tags to select $Z \rightarrow b\bar{b}$ events.

$\Gamma(D_1(2420)^0 \text{ anything})/\Gamma_{\text{total}}$	Γ_{39}/Γ		
VALUE	DOCUMENT ID	TECN	COMMENT
$0.050 \pm 0.014 \pm 0.006$	1 ACKERSTAFF	97W	OPAL $e^+ e^- \rightarrow Z$

- ¹ ACKERSTAFF 97W assumes $B(D_1^*(2460)^0 \rightarrow D^{*+} \pi^-) = 0.21 \pm 0.04$ and $\Gamma_{B\bar{B}}/\Gamma_{\text{hadrons}} = 0.216$ at Z decay.

$\Gamma(D^*(2010)^\mp D_s^\pm \text{ anything})/\Gamma_{\text{total}}$	Γ_{40}/Γ		
VALUE	DOCUMENT ID	TECN	COMMENT
$0.033 \pm 0.010 \pm 0.012$	1 BARATE	98Q	ALEP $e^+ e^- \rightarrow Z$

- ¹ The systematic error includes the uncertainties due to the charm branching ratios.

$\Gamma(D^0 D^*(2010)^\pm \text{ anything})/\Gamma_{\text{total}}$	Γ_{41}/Γ		
VALUE	DOCUMENT ID	TECN	COMMENT
$0.030 \pm 0.009 \pm 0.007$	1 BARATE	98Q	ALEP $e^+ e^- \rightarrow Z$

- ¹ The systematic error includes the uncertainties due to the charm branching ratios.

$\Gamma(D^*(2010)^\pm D^\mp \text{ anything})/\Gamma_{\text{total}}$	Γ_{42}/Γ		
VALUE	DOCUMENT ID	TECN	COMMENT
$0.025 \pm 0.010 \pm 0.006$	1 BARATE	98Q	ALEP $e^+ e^- \rightarrow Z$

- ¹ The systematic error includes the uncertainties due to the charm branching ratios.

$\Gamma(D^*(2010)^\pm D^*(2010)^\mp \text{ anything})/\Gamma_{\text{total}}$	Γ_{43}/Γ		
VALUE	DOCUMENT ID	TECN	COMMENT
$0.012 \pm 0.004 \pm 0.003$	1 BARATE	98Q	ALEP $e^+ e^- \rightarrow Z$

- ¹ The systematic error includes the uncertainties due to the charm branching ratios.

$\Gamma(\bar{D} D \text{ anything})/\Gamma_{\text{total}}$	Γ_{44}/Γ		
VALUE	DOCUMENT ID	TECN	COMMENT
$0.10 \pm 0.032 \pm 0.107$	1 ABBIENDI	04I	OPAL $e^+ e^- \rightarrow Z$

- ¹ Measurement performed using an inclusive identification of B mesons and the D candidates.

Meson Particle Listings

 $B^\pm/B^0/B_s^0/b$ -baryon ADMIXTURE

$\Gamma(D_s^*(2460)^0 \text{ anything})/\Gamma_{\text{total}}$ Γ_{45}/Γ

VALUE	DOCUMENT ID	TECN	COMMENT
0.047 ± 0.024 ± 0.013	¹ ACKERSTAFF 97W	OPAL	$e^+e^- \rightarrow Z$

¹ ACKERSTAFF 97W assumes $B(D_s^*(2460)^0 \rightarrow D^{*+}\pi^-) = 0.21 \pm 0.04$ and $\Gamma_{b\bar{b}}/\Gamma_{\text{hadrons}} = 0.216$ at Z decay.

$\Gamma(D_s^- \text{ anything})/\Gamma_{\text{total}}$ Γ_{46}/Γ

VALUE	DOCUMENT ID	TECN	COMMENT
0.147 ± 0.017 ± 0.013	¹ BUSKULIC 96Y	ALEP	$e^+e^- \rightarrow Z$

¹ BUSKULIC 96Y reports $0.183 \pm 0.019 \pm 0.009$ from a measurement of $[\Gamma(\bar{b} \rightarrow D_s^- \text{ anything})/\Gamma_{\text{total}}] \times [B(D_s^+ \rightarrow \phi\pi^+)]$ assuming $B(D_s^+ \rightarrow \phi\pi^+) = 0.036$, which we rescale to our best value $B(D_s^+ \rightarrow \phi\pi^+) = (4.5 \pm 0.4) \times 10^{-2}$. Our first error is their experiment's error and our second error is the systematic error from using our best value.

$\Gamma(D_s^+ \text{ anything})/\Gamma_{\text{total}}$ Γ_{47}/Γ

VALUE	DOCUMENT ID	TECN	COMMENT
0.101 ± 0.010 ± 0.029	¹ ABDALLAH 03E	DLPH	$e^+e^- \rightarrow Z$

¹ The second error is the total of systematic uncertainties including the branching fractions used in the measurement.

$\Gamma(b \rightarrow \Lambda_c^+ \text{ anything})/\Gamma_{\text{total}}$ Γ_{48}/Γ

VALUE	DOCUMENT ID	TECN	COMMENT
0.078 ± 0.011 ± 0.003	¹ BUSKULIC 96Y	ALEP	$e^+e^- \rightarrow Z$

¹ BUSKULIC 96Y reports $0.110 \pm 0.014 \pm 0.006$ from a measurement of $[\Gamma(b \rightarrow \Lambda_c^+ \text{ anything})/\Gamma_{\text{total}}] \times [B(\Lambda_c^+ \rightarrow pK^-\pi^+)]$ assuming $B(\Lambda_c^+ \rightarrow pK^-\pi^+) = 0.044$, which we rescale to our best value $B(\Lambda_c^+ \rightarrow pK^-\pi^+) = (6.24 \pm 0.28) \times 10^{-2}$. Our first error is their experiment's error and our second error is the systematic error from using our best value.

$\Gamma(\tau/c \text{ anything})/\Gamma_{\text{total}}$ Γ_{49}/Γ

VALUE	DOCUMENT ID	TECN	COMMENT
1.162 ± 0.032 OUR AVERAGE			
1.12 ^{+0.11} _{-0.10}	¹ ABBIENDI 04I	OPAL	$e^+e^- \rightarrow Z$
1.166 ± 0.031 ± 0.080	² ABREU 00	DLPH	$e^+e^- \rightarrow Z$
1.147 ± 0.041	³ ABREU 98D	DLPH	$e^+e^- \rightarrow Z$
1.230 ± 0.036 ± 0.065	⁴ BUSKULIC 96Y	ALEP	$e^+e^- \rightarrow Z$

- ¹ Measurement performed using an inclusive identification of B mesons and the D candidates.
² Evaluated via summation of exclusive and inclusive channels.
³ ABREU 98D results are extracted from a fit to the b -tagging probability distribution based on the impact parameter.
⁴ BUSKULIC 96Y assumes PDG 96 production fractions for B^0, B^+, B_s^0, b baryons, and PDG 96 branching ratios for charm decays. This is sum of their inclusive $\bar{D}^0, D^-, \bar{D}_s$, and Λ_c branching ratios, corrected to include inclusive Ξ_c and charmonium.

$\Gamma(J/\psi(1S) \text{ anything})/\Gamma_{\text{total}}$ Γ_{50}/Γ

VALUE (units 10^{-2})	CL%	EVTS	DOCUMENT ID	TECN	COMMENT
1.16 ± 0.10 OUR AVERAGE					
1.12 ± 0.12 ± 0.10			¹ ABREU 94P	DLPH	$e^+e^- \rightarrow Z$
1.16 ± 0.16 ± 0.14		121	² ADRIANI 93J	L3	$e^+e^- \rightarrow Z$
1.21 ± 0.13 ± 0.08			BUSKULIC 92G	ALEP	$e^+e^- \rightarrow Z$

- • • We do not use the following data for averages, fits, limits, etc. • • •
¹ ABREU 94P is an inclusive measurement from b decays at the Z . Uses $J/\psi(1S) \rightarrow e^+e^-$ and $\mu^+\mu^-$ channels. Assumes $\Gamma(Z \rightarrow b\bar{b})/\Gamma_{\text{hadron}} = 0.22$.
² ADRIANI 93J is an inclusive measurement from b decays at the Z . Uses $J/\psi(1S) \rightarrow \mu^+\mu^-$ and $J/\psi(1S) \rightarrow e^+e^-$ channels.
³ ADRIANI 92 measurement is an inclusive result for $B(Z \rightarrow J/\psi(1S)X) = (4.1 \pm 0.7 \pm 0.3) \times 10^{-3}$ which is used to extract the b -hadron contribution to $J/\psi(1S)$ production.

$\Gamma(\psi(2S) \text{ anything})/\Gamma_{\text{total}}$ Γ_{51}/Γ

VALUE	DOCUMENT ID	TECN	COMMENT
0.0048 ± 0.0022 ± 0.0010	¹ ABREU 94P	DLPH	$e^+e^- \rightarrow Z$

¹ ABREU 94P is an inclusive measurement from b decays at the Z . Uses $\psi(2S) \rightarrow J/\psi(1S)\pi^+\pi^-, J/\psi(1S) \rightarrow \mu^+\mu^-$ channels. Assumes $\Gamma(Z \rightarrow b\bar{b})/\Gamma_{\text{hadron}} = 0.22$.

$\Gamma(\psi(2S) \text{ anything})/\Gamma(J/\psi(1S) \text{ anything})$ Γ_{51}/Γ_{50}

VALUE	DOCUMENT ID	TECN	COMMENT
0.263 ± 0.013 OUR AVERAGE			
0.265 ± 0.002 ± 0.016	¹ AAIJ 20G	LHCB	pp at 13 TeV
0.266 ± 0.06 ± 0.03	^{2,3} AAIJ 12BD	LHCB	pp at 7 TeV
0.257 ± 0.015 ± 0.019	^{4,5} CHATRCHYAN 12AK	CMS	pp at 7 TeV

- ¹ The first error is statistic; the second error is the total systematic error.
² AAIJ 12BD reports $B(b \rightarrow \psi(2S)X) = (3.08 \pm 0.07 \pm 0.36 \pm 0.27) \times 10^{-3}$ and we divided our best value of $B(b \rightarrow \psi(1S)X) = (1.16 \pm 0.10) \times 10^{-2}$ as the ratio listed here.
³ Assumes lepton universality imposing $B(\psi(2S) \rightarrow \mu^+\mu^-) = B(\psi(2S) \rightarrow e^+e^-)$.

⁴ CHATRCHYAN 12AK really reports $\Gamma_{51}/\Gamma = (3.08 \pm 0.12 \pm 0.13 \pm 0.42) \times 10^{-3}$ assuming PDG 10 value of $\Gamma_{50}/\Gamma = (1.16 \pm 0.10) \times 10^{-2}$ which we present as a ratio of $\Gamma_{51}/\Gamma_{50} = (26.5 \pm 1.0 \pm 1.1 \pm 2.8) \times 10^{-2}$.

⁵ CHATRCHYAN 12AK reports $(26.5 \pm 1.0 \pm 1.1 \pm 2.8) \times 10^{-2}$ from a measurement of $[\Gamma(\bar{b} \rightarrow \psi(2S) \text{ anything})/\Gamma(\bar{b} \rightarrow J/\psi(1S) \text{ anything})] \times [B(\psi(2S) \rightarrow \mu^+\mu^-)] / [B(J/\psi(1S) \rightarrow \mu^+\mu^-)]$ assuming $B(\psi(2S) \rightarrow \mu^+\mu^-) = (7.7 \pm 0.8) \times 10^{-3}, B(J/\psi(1S) \rightarrow \mu^+\mu^-) = (5.93 \pm 0.06) \times 10^{-2}$, which we rescale to our best values $B(\psi(2S) \rightarrow \mu^+\mu^-) = (8.0 \pm 0.6) \times 10^{-3}, B(J/\psi(1S) \rightarrow \mu^+\mu^-) = (5.961 \pm 0.033) \times 10^{-2}$. Our first error is their experiment's error and our second error is the systematic error from using our best values.

$\Gamma(\chi_{c0}(1P) \text{ anything})/\Gamma(\eta_c(1S) \text{ anything})$ Γ_{52}/Γ_{56}

VALUE	DOCUMENT ID	TECN	COMMENT
0.32 ± 0.05 ± 0.08	¹ AAIJ 17BB	LHCB	pp at 7, 8 TeV

¹ AAIJ 17BB reports $[\Gamma(\bar{b} \rightarrow \chi_{c0}(1P) \text{ anything})/\Gamma(\bar{b} \rightarrow \eta_c(1S) \text{ anything})] / [B(\eta_c(1S) \rightarrow \phi\phi)] \times [B(\chi_{c0}(1P) \rightarrow \phi\phi)] = 0.147 \pm 0.023 \pm 0.011$ which we multiply or divide by our best values $B(\eta_c(1S) \rightarrow \phi\phi) = (1.8 \pm 0.4) \times 10^{-3}, B(\chi_{c0}(1P) \rightarrow \phi\phi) = (8.48 \pm 0.31) \times 10^{-4}$. Our first error is their experiment's error and our second error is the systematic error from using our best values.

$\Gamma(\chi_{c1}(1P) \text{ anything})/\Gamma_{\text{total}}$ Γ_{53}/Γ

VALUE	EVTS	DOCUMENT ID	TECN	COMMENT
0.014 ± 0.004 OUR AVERAGE				
0.0112 ^{+0.0057} _{-0.0050} ± 0.0004		¹ ABREU 94P	DLPH	$e^+e^- \rightarrow Z$
0.019 ± 0.007 ± 0.001	19	² ADRIANI 93J	L3	$e^+e^- \rightarrow Z$

¹ ABREU 94P reports $0.014 \pm 0.006 \pm 0.004$ from a measurement of $[\Gamma(\bar{b} \rightarrow \chi_{c1}(1P) \text{ anything})/\Gamma_{\text{total}}] \times [B(\chi_{c1}(1P) \rightarrow \gamma J/\psi(1S))] / [B(\chi_{c1}(1P) \rightarrow \gamma J/\psi(1S))] = 0.273 \pm 0.016$, which we rescale to our best value $B(\chi_{c1}(1P) \rightarrow \gamma J/\psi(1S)) = (34.3 \pm 1.3) \times 10^{-2}$. Our first error is their experiment's error and our second error is the systematic error from using our best value. Assumes no $\chi_{c2}(1P)$ and $\Gamma(Z \rightarrow b\bar{b})/\Gamma_{\text{hadron}} = 0.22$.
² ADRIANI 93J reports $0.024 \pm 0.009 \pm 0.002$ from a measurement of $[\Gamma(\bar{b} \rightarrow \chi_{c1}(1P) \text{ anything})/\Gamma_{\text{total}}] \times [B(\chi_{c1}(1P) \rightarrow \gamma J/\psi(1S))] / [B(\chi_{c1}(1P) \rightarrow \gamma J/\psi(1S))] = 0.273 \pm 0.016$, which we rescale to our best value $B(\chi_{c1}(1P) \rightarrow \gamma J/\psi(1S)) = (34.3 \pm 1.3) \times 10^{-2}$. Our first error is their experiment's error and our second error is the systematic error from using our best value.

$\Gamma(\chi_{c1}(1P) \text{ anything})/\Gamma(J/\psi(1S) \text{ anything})$ Γ_{53}/Γ_{50}

VALUE	EVTS	DOCUMENT ID	TECN	COMMENT
• • •				
1.92 ± 0.82	121	¹ ADRIANI 93J	L3	$e^+e^- \rightarrow Z$

¹ ADRIANI 93J is a ratio of inclusive measurements from b decays at the Z using only the $J/\psi(1S) \rightarrow \mu^+\mu^-$ channel since some systematics cancel.

$\Gamma(\chi_{c1}(1P) \text{ anything})/\Gamma(\chi_{c0}(1P) \text{ anything})$ Γ_{53}/Γ_{52}

VALUE	DOCUMENT ID	TECN	COMMENT
1.00 ± 0.22 ± 0.06	¹ AAIJ 17BB	LHCB	pp at 7, 8 TeV

¹ AAIJ 17BB reports $[\Gamma(\bar{b} \rightarrow \chi_{c1}(1P) \text{ anything})/\Gamma(\bar{b} \rightarrow \chi_{c0}(1P) \text{ anything})] / [B(\chi_{c0}(1P) \rightarrow \phi\phi)] \times [B(\chi_{c1}(1P) \rightarrow \phi\phi)] = 0.50 \pm 0.11 \pm 0.01$ which we multiply or divide by our best values $B(\chi_{c0}(1P) \rightarrow \phi\phi) = (8.48 \pm 0.31) \times 10^{-4}, B(\chi_{c1}(1P) \rightarrow \phi\phi) = (4.26 \pm 0.21) \times 10^{-4}$. Our first error is their experiment's error and our second error is the systematic error from using our best values.

$\Gamma(\chi_{c1}(1P) \text{ anything})/\Gamma(\eta_c(1S) \text{ anything})$ Γ_{53}/Γ_{56}

VALUE	DOCUMENT ID	TECN	COMMENT
0.31 ± 0.07 ± 0.08	¹ AAIJ 17BB	LHCB	pp at 7, 8 TeV

¹ AAIJ 17BB reports $[\Gamma(\bar{b} \rightarrow \chi_{c1}(1P) \text{ anything})/\Gamma(\bar{b} \rightarrow \eta_c(1S) \text{ anything})] / [B(\eta_c(1S) \rightarrow \phi\phi)] \times [B(\chi_{c1}(1P) \rightarrow \phi\phi)] = 0.073 \pm 0.016 \pm 0.006$ which we multiply or divide by our best values $B(\eta_c(1S) \rightarrow \phi\phi) = (1.8 \pm 0.4) \times 10^{-3}, B(\chi_{c1}(1P) \rightarrow \phi\phi) = (4.26 \pm 0.21) \times 10^{-4}$. Our first error is their experiment's error and our second error is the systematic error from using our best values.

$\Gamma(\chi_{c2}(1P) \text{ anything})/\Gamma(\chi_{c0}(1P) \text{ anything})$ Γ_{54}/Γ_{52}

VALUE	DOCUMENT ID	TECN	COMMENT
0.39 ± 0.07 ± 0.03	¹ AAIJ 17BB	LHCB	pp at 7, 8 TeV

¹ AAIJ 17BB reports $[\Gamma(\bar{b} \rightarrow \chi_{c2}(1P) \text{ anything})/\Gamma(\bar{b} \rightarrow \chi_{c0}(1P) \text{ anything})] / [B(\chi_{c0}(1P) \rightarrow \phi\phi)] \times [B(\chi_{c2}(1P) \rightarrow \phi\phi)] = 0.56 \pm 0.10 \pm 0.01$ which we multiply or divide by our best values $B(\chi_{c0}(1P) \rightarrow \phi\phi) = (8.48 \pm 0.31) \times 10^{-4}, B(\chi_{c2}(1P) \rightarrow \phi\phi) = (1.23 \pm 0.07) \times 10^{-3}$. Our first error is their experiment's error and our second error is the systematic error from using our best values.

$\Gamma(\chi_{c2}(1P) \text{ anything})/\Gamma(\eta_c(1S) \text{ anything})$ Γ_{54}/Γ_{56}

VALUE	DOCUMENT ID	TECN	COMMENT
0.121 ± 0.021 ± 0.030	¹ AAIJ 17BB	LHCB	pp at 7, 8 TeV

¹ AAIJ 17BB reports $[\Gamma(\bar{b} \rightarrow \chi_{c2}(1P) \text{ anything})/\Gamma(\bar{b} \rightarrow \eta_c(1S) \text{ anything})] / [B(\eta_c(1S) \rightarrow \phi\phi)] \times [B(\chi_{c2}(1P) \rightarrow \phi\phi)] = 0.081 \pm 0.013 \pm 0.005$ which we multiply or divide by our best values $B(\eta_c(1S) \rightarrow \phi\phi) = (1.8 \pm 0.4) \times 10^{-3}, B(\chi_{c2}(1P) \rightarrow \phi\phi) = (1.23 \pm 0.07) \times 10^{-3}$. Our first error is their experiment's error and our second error is the systematic error from using our best values.

$\Gamma(\chi_{c2}(2P) \text{ anything}, \chi_c \rightarrow \phi\phi)/\Gamma_{\text{total}}$ Γ_{55}/Γ

VALUE	CL%	DOCUMENT ID	TECN	COMMENT
< 2.8 × 10⁻⁷	95	AAIJ 17BB	LHCB	pp at 7, 8 TeV

See key on page 1171

Meson Particle Listings

$B^\pm/B^0/B_s^0/b$ -baryon ADMIXTURE

$\Gamma(\eta_c(1S)\text{anything})/\Gamma(J/\psi(1S)\text{anything})$				Γ_{56}/Γ_{50}
VALUE	DOCUMENT ID	TECN	COMMENT	
$0.48 \pm 0.03 \pm 0.06$	AAIJ	20H	LHCB	pp at 13 TeV

$\Gamma(\eta_c(2S)\text{anything}, \eta_c \rightarrow \phi\phi)/\Gamma(\eta_c(1S)\text{anything})$				Γ_{57}/Γ_{56}
VALUE (units 10^{-5})	DOCUMENT ID	TECN	COMMENT	
$7.3 \pm 2.1 \pm 1.7$	1 AAIJ	17Bb	LHCB	pp at 7, 8 TeV

¹AAIJ 17Bb reports $[\Gamma(\bar{b} \rightarrow \eta_c(2S)\text{anything}, \eta_c \rightarrow \phi\phi)/\Gamma(\bar{b} \rightarrow \eta_c(1S)\text{anything})] / [B(\eta_c(1S) \rightarrow \phi\phi)] = 0.040 \pm 0.011 \pm 0.004$ which we multiply by our best value $B(\eta_c(1S) \rightarrow \phi\phi) = (1.8 \pm 0.4) \times 10^{-3}$. Our first error is their experiment's error and our second error is the systematic error from using our best value.

$\Gamma(\chi_{c1}(3872)\text{anything}, \chi_{c1} \rightarrow \phi\phi)/\Gamma_{\text{total}}$				Γ_{58}/Γ	
VALUE	CL%	DOCUMENT ID	TECN	COMMENT	
$<4.5 \times 10^{-7}$	95	AAIJ	17Bb	LHCB	pp at 7, 8 TeV

$\Gamma(\chi_{c0}(3915)\text{anything}, \chi_{c0} \rightarrow \phi\phi)/\Gamma_{\text{total}}$				Γ_{59}/Γ	
VALUE	CL%	DOCUMENT ID	TECN	COMMENT	
$<3.1 \times 10^{-7}$	95	AAIJ	17Bb	LHCB	pp at 7, 8 TeV

$\Gamma(\bar{\Sigma}\gamma)/\Gamma_{\text{total}}$				Γ_{60}/Γ	
VALUE (units 10^{-4})	CL%	DOCUMENT ID	TECN	COMMENT	
$3.11 \pm 0.80 \pm 0.72$		1 BARATE	98i	ALEP	$e^+e^- \rightarrow Z$

• • • We do not use the following data for averages, fits, limits, etc. • • •

<5.4	90	2 ADAM	96D	DLPH	$e^+e^- \rightarrow Z$
<12	90	3 ADRIANI	93L	L3	$e^+e^- \rightarrow Z$

¹BARATE 98i uses lifetime tagged $Z \rightarrow b\bar{b}$ sample.

²ADAM 96D assumes $f_{B^0} = f_{B^-} = 0.39$ and $f_{B_s} = 0.12$.

³ADRIANI 93L result is for $\bar{D} \rightarrow \bar{\Sigma}\gamma$ is performed inclusively.

$\Gamma(\bar{\Sigma}\nu)/\Gamma_{\text{total}}$				Γ_{61}/Γ	
VALUE	CL%	DOCUMENT ID	TECN	COMMENT	
$<6.4 \times 10^{-4}$	90	1 BARATE	01E	ALEP	$e^+e^- \rightarrow Z$

¹The energy-flow and b -tagging algorithms were used.

$\Gamma(K^\pm\text{anything})/\Gamma_{\text{total}}$				Γ_{62}/Γ
VALUE	DOCUMENT ID	TECN	COMMENT	
0.74 ± 0.06 OUR AVERAGE				
$0.72 \pm 0.02 \pm 0.06$	BARATE	98v	ALEP	$e^+e^- \rightarrow Z$
$0.88 \pm 0.05 \pm 0.18$	ABREU	95c	DLPH	$e^+e^- \rightarrow Z$

$\Gamma(K_S^0\text{anything})/\Gamma_{\text{total}}$				Γ_{63}/Γ
VALUE	DOCUMENT ID	TECN	COMMENT	
$0.290 \pm 0.011 \pm 0.027$	ABREU	95c	DLPH	$e^+e^- \rightarrow Z$

$\Gamma(\pi^\pm\text{anything})/\Gamma_{\text{total}}$				Γ_{64}/Γ
VALUE	DOCUMENT ID	TECN	COMMENT	
$3.97 \pm 0.02 \pm 0.21$	BARATE	98v	ALEP	$e^+e^- \rightarrow Z$

$\Gamma(\pi^0\text{anything})/\Gamma_{\text{total}}$				Γ_{65}/Γ
VALUE	DOCUMENT ID	TECN	COMMENT	
$2.78 \pm 0.15 \pm 0.60$	1 ADAM	96	DLPH	$e^+e^- \rightarrow Z$

¹ADAM 96 measurement obtained from a fit to the rapidity distribution of π^0 's in $Z \rightarrow b\bar{b}$ events.

$\Gamma(\phi\text{anything})/\Gamma_{\text{total}}$				Γ_{66}/Γ
VALUE	DOCUMENT ID	TECN	COMMENT	
$0.0282 \pm 0.0013 \pm 0.0019$	ABBIENDI	00z	OPAL	$e^+e^- \rightarrow Z$

$\Gamma(p/\bar{p}\text{anything})/\Gamma_{\text{total}}$				Γ_{67}/Γ
VALUE	DOCUMENT ID	TECN	COMMENT	
0.131 ± 0.011 OUR AVERAGE				
$0.131 \pm 0.004 \pm 0.011$	BARATE	98v	ALEP	$e^+e^- \rightarrow Z$
$0.141 \pm 0.018 \pm 0.056$	ABREU	95c	DLPH	$e^+e^- \rightarrow Z$

$\Gamma(\Lambda/\bar{\Lambda}\text{anything})/\Gamma_{\text{total}}$				Γ_{68}/Γ
VALUE	DOCUMENT ID	TECN	COMMENT	
0.059 ± 0.006 OUR AVERAGE				
$0.0587 \pm 0.0046 \pm 0.0048$	ACKERSTAFF	97N	OPAL	$e^+e^- \rightarrow Z$
$0.059 \pm 0.007 \pm 0.009$	ABREU	95c	DLPH	$e^+e^- \rightarrow Z$

$\Gamma(b\text{-baryon anything})/\Gamma_{\text{total}}$				Γ_{69}/Γ
VALUE	DOCUMENT ID	TECN	COMMENT	
$0.102 \pm 0.007 \pm 0.027$	1 BARATE	98v	ALEP	$e^+e^- \rightarrow Z$

¹BARATE 98v assumes $B(B_{\bar{S}} \rightarrow pX) = 8 \pm 4\%$ and $B(b\text{-baryon} \rightarrow pX) = 58 \pm 6\%$.

$\Gamma(\Xi_b^+\text{anything})/\Gamma(\bar{\Lambda}_b^0\text{anything})$				Γ_{71}/Γ_{70}
VALUE (units 10^{-2})	DOCUMENT ID	TECN	COMMENT	
7.3 ± 1.7 OUR AVERAGE				
$6.7 \pm 0.5 \pm 2.1$	1 AAIJ	19Ab	LHCB	pp at 7 and 8 TeV
$8.2 \pm 0.7 \pm 2.6$	1 AAIJ	19Ab	LHCB	pp at 13 TeV

¹Measured from $R = [B(\bar{D} \rightarrow \Xi_b^+) \times B(\Xi_b^+ \rightarrow J/\psi \Xi^+)] / [B(\bar{D} \rightarrow \bar{\Lambda}_b^0) \times B(\bar{\Lambda}_b^0 \rightarrow J/\psi \bar{\Lambda}^0)]$ and assumes $\Gamma_{\Xi_b^+ \rightarrow J/\psi \Xi^+} / \Gamma_{\bar{\Lambda}_b^0 \rightarrow J/\psi \bar{\Lambda}^0} = 3/2$ related through SU(3) flavor symmetry.

$\Gamma(\text{charged anything})/\Gamma_{\text{total}}$				Γ_{72}/Γ
VALUE	DOCUMENT ID	TECN	COMMENT	
$4.97 \pm 0.03 \pm 0.06$	1 ABREU	98H	DLPH	$e^+e^- \rightarrow Z$

• • • We do not use the following data for averages, fits, limits, etc. • • •

$5.84 \pm 0.04 \pm 0.38$	ABREU	95c	DLPH	Repl. by ABREU 98H
--------------------------	-------	-----	------	--------------------

¹ABREU 98H measurement excludes the contribution from K^0 and Λ decay.

$\Gamma(\text{hadron}^+ \text{hadron}^-)/\Gamma_{\text{total}}$				Γ_{73}/Γ
VALUE (units 10^{-5})	DOCUMENT ID	TECN	COMMENT	
$1.7 \pm 1.0 \pm 0.2$	1,2 BUSKULIC	96v	ALEP	$e^+e^- \rightarrow Z$

¹BUSKULIC 96v assumes PDG 96 production fractions for B^0, B^+, B_s, b baryons.

²Average branching fraction of weakly decaying B hadrons into two long-lived charged hadrons, weighted by their production cross section and lifetimes.

$\Gamma(\text{charmless})/\Gamma_{\text{total}}$				Γ_{74}/Γ
VALUE	DOCUMENT ID	TECN	COMMENT	
0.007 ± 0.021	1 ABREU	98D	DLPH	$e^+e^- \rightarrow Z$

¹ABREU 98D results are extracted from a fit to the b -tagging probability distribution based on the impact parameter. The expected hidden charm contribution of 0.026 ± 0.004 has been subtracted.

$\Gamma(\mu^+ \mu^- \text{anything})/\Gamma_{\text{total}}$				Γ_{76}/Γ
VALUE	CL%	DOCUMENT ID	TECN	COMMENT

Test for $\Delta B = 1$ weak neutral current.

$<3.2 \times 10^{-4}$	90	ABBOTT	98B	D0	$p\bar{p}$ 1.8 TeV
• • • We do not use the following data for averages, fits, limits, etc. • • •					
$<5.0 \times 10^{-5}$	90	1 ALBAJAR	91c	UA1	$E_{\text{cm}}^{p\bar{p}} = 630$ GeV
<0.02	95	ALTHOFF	84G	TASS	$E_{\text{cm}}^{e^+e^-} = 34.5$ GeV
<0.007	95	ADEVA	83	MRKJ	$E_{\text{cm}}^{e^+e^-} = 30\text{--}38$ GeV
<0.007	95	BARTEL	83b	JADE	$E_{\text{cm}}^{e^+e^-} = 33\text{--}37$ GeV

¹Both ABBOTT 98B and GLENN 98 claim that the efficiency quoted in ALBAJAR 91c was overestimated by a large factor.

$[\Gamma(e^+e^- \text{anything}) + \Gamma(\mu^+ \mu^- \text{anything})]/\Gamma_{\text{total}}$				$(\Gamma_{75} + \Gamma_{76})/\Gamma$
VALUE	CL%	DOCUMENT ID	TECN	COMMENT

Test for $\Delta B = 1$ weak neutral current.

• • • We do not use the following data for averages, fits, limits, etc. • • •					
<0.008	90	MATTEUZZI	83	MRK2	$E_{\text{cm}}^{e^+e^-} = 29$ GeV

$\Gamma(\nu\bar{\nu}\text{anything})/\Gamma_{\text{total}}$				Γ_{77}/Γ	
VALUE	DOCUMENT ID	TECN	COMMENT		
• • • We do not use the following data for averages, fits, limits, etc. • • •					
$<3.9 \times 10^{-4}$	1	GROSSMAN	96	RVUE	$e^+e^- \rightarrow Z$

¹GROSSMAN 96 limit is derived from the ALEPH BUSKULIC 95 limit $B(B^+ \rightarrow \tau^+ \nu_\tau) < 1.8 \times 10^{-3}$ at CL=90% using conservative simplifying assumptions.

χ_b AT HIGH ENERGY

χ_b is the average $B\text{--}\bar{B}$ mixing parameter at high-energy $\chi_b = f_d^+ f_d^- \chi_d + f_s^+ f_s^- \chi_s$ where f_d^+ and f_s^+ are the fractions of B^0 and B_s^0 hadrons in an unbiased sample of semileptonic b -hadron decays. We consider here $\bar{\chi}$ for hadrons produced in Z decays.

VALUE (units 10^{-2})	EVTS	DOCUMENT ID	TECN	COMMENT	
12.59 ± 0.42 OUR EVALUATION				(from SCHAEF 06D, eq. 5.39)	
12.6 ± 0.4 OUR AVERAGE					
$13.12 \pm 0.49 \pm 0.42$	1	ABBIENDI	03P	OPAL	$e^+e^- \rightarrow Z$
$12.7 \pm 1.3 \pm 0.6$	2	ABREU	01L	DLPH	$e^+e^- \rightarrow Z$
$11.92 \pm 0.68 \pm 0.51$	3	ACCIARRI	99D	L3	$e^+e^- \rightarrow Z$
$12.1 \pm 1.6 \pm 0.6$	4	ABREU	94J	DLPH	$e^+e^- \rightarrow Z$
$11.4 \pm 1.4 \pm 0.8$	5	BUSKULIC	94G	ALEP	$e^+e^- \rightarrow Z$
12.9 ± 2.2	6	BUSKULIC	92B	ALEP	$e^+e^- \rightarrow Z$
• • • We do not use the following data for averages, fits, limits, etc. • • •					
$13.2 \pm 0.1 \pm 2.4$	7	ABAZOV	06s	D0	$p\bar{p}$ at 1.96 TeV
$15.2 \pm 0.7 \pm 1.1$	8	ACOSTA	04A	CDF	$p\bar{p}$ at 1.8 TeV
$13.1 \pm 2.0 \pm 1.6$	9	ABE	97I	CDF	Repl. by ACOSTA 04A
$11.07 \pm 0.62 \pm 0.55$	10	ALEXANDER	96	OPAL	Repl. by ABBIENDI 03P
$13.6 \pm 3.7 \pm 4.0$	11	UENO	96	AMY	e^+e^- at 57.9 GeV
$14.4 \pm 1.4 \pm 1.7$	12	ABREU	94F	DLPH	Sup. by ABREU 94J
13.1 ± 1.4	13	ABREU	94J	DLPH	$e^+e^- \rightarrow Z$
$12.3 \pm 1.2 \pm 0.8$		ACCIARRI	94D	L3	Repl. by ACCIARRI 99D
$15.7 \pm 2.0 \pm 3.2$	14	ALBAJAR	94	UA1	$\sqrt{s} = 630$ GeV
$12.1 \pm 4.4 \pm 1.7$	15	ABREU	93c	DLPH	Sup. by ABREU 94J
$14.3 \pm 2.2 \pm 0.7$	16	AKERS	93B	OPAL	Sup. by ALEXANDER 96
$14.5 \pm 4.1 \pm 1.8$	17	ACTON	92c	OPAL	$e^+e^- \rightarrow Z$

Meson Particle Listings

 $B^\pm/B^0/B_s^0/b$ -baryon ADMIXTURE

$12.1 \pm 1.7 \pm 0.6$	18	ADEVA	92c	L3	Sup. by ACCIARRI 94d
$17.6 \pm 3.1 \pm 3.2$	1112	19 ABE	91g	CDF	$p\bar{p}$ 1.8 TeV
$14.8 \pm 2.9 \pm 1.7$		20 ALBAJAR	91d	UA1	$p\bar{p}$ 630 GeV
$13.2 \pm 22.0 \pm 1.5$ -1.2	823	21 DECAMP	91	ALEP	$e^+e^- \rightarrow Z$
$17.8 \pm 4.9 \pm 2.0$ -4.0		22 ADEVA	90p	L3	$e^+e^- \rightarrow Z$
17 ± 15 -8	23,24	WEIR	90	MRK2	e^+e^- 29 GeV
21 ± 29 -15		23 BAND	88	MAC	$E_{cm}^{ee} = 29$ GeV
>2 at 90% CL		23 BAND	88	MAC	$E_{cm}^{ee} = 29$ GeV
12.1 ± 4.7	23,25	ALBAJAR	87c	UA1	Repl. by ALBAJAR 91d
<12 at 90% CL	23,26	SCHAAD	85	MRK2	$E_{cm}^{ee} = 29$ GeV

- The average B mixing parameter is determined simultaneously with b and c forward-backward asymmetries in the fit.
- The experimental systematic and model uncertainties are combined in quadrature.
- ACCIARRI 99d uses maximum-likelihood fits to extract χ_b as well as the A_{FB}^b in $Z \rightarrow b\bar{b}$ events containing prompt leptons.
- This ABREU 94J result is from 5182 $\ell\ell$ and 279 $\ell\ell$ events. The systematic error includes 0.004 for model dependence.
- BUSKULIC 94g data analyzed using ee , $e\mu$, and $\mu\mu$ events.
- BUSKULIC 92b uses a jet charge technique combined with electrons and muons.
- Uses the dimuon charge asymmetry. Averaged over the mix of b -flavored hadrons.
- Measurement performed using events containing a dimuon or an e/μ pair.
- Uses di-muon events.
- ALEXANDER 96 uses a maximum likelihood fit to simultaneously extract χ as well as the forward-backward asymmetries in $e^+e^- \rightarrow Z \rightarrow b\bar{b}$ and $c\bar{c}$.
- UENO 96 extracted χ from the energy dependence of the forward-backward asymmetry.
- ABREU 94F uses the average electric charge sum of the jets recoiling against a b -quark jet tagged by a high p_T muon. The result is for $\bar{\chi} = f_d\chi_d + 0.9f_s\chi_s$.
- This ABREU 94J result combines $\ell\ell$, $\ell\ell$, and jet-charge ℓ (ABREU 94F) analyses. It is for $\bar{\chi} = f_d\chi_d + 0.96f_s\chi_s$.
- ALBAJAR 94 uses dimuon events. Not independent of ALBAJAR 91d.
- ABREU 93c data analyzed using ee , $e\mu$, and $\mu\mu$ events.
- AKERS 93b analysis performed using dilepton events.
- ACTON 92c uses electrons and muons. Superseded by AKERS 93b.
- ADEVA 92c uses electrons and muons.
- ABE 91g measurement of χ is done with $e\mu$ and ee events.
- ALBAJAR 91d measurement of χ is done with dimuons.
- DECAMP 91 done with opposite and like-sign dileptons. Superseded by BUSKULIC 92b.
- ADEVA 90p measurement uses ee , $\mu\mu$, and $e\mu$ events from 118k events at the Z. Superseded by ADEVA 92c.
- These experiments are not in the average because the combination of B_s and B_d mesons which they see could differ from those at higher energy.
- The WEIR 90 measurement supersedes the limit obtained in SCHAAD 85. The 90% CL are 0.06 and 0.38.
- ALBAJAR 87c measured $\chi = (\bar{B}^0 \rightarrow B^0 \rightarrow \mu^+X)$ divided by the average production weighted semileptonic branching fraction for B hadrons at 546 and 630 GeV.
- Limit is average probability for hadron containing B quark to produce a positive lepton.

CP VIOLATION PARAMETERS in semileptonic b -hadron decays. $Re(\epsilon_b) / (1 + |\epsilon_b|^2)$ CP impurity in semileptonic b -hadron decays.

VALUE (units 10^{-3})	DOCUMENT ID	TECN	COMMENT
• • • We do not use the following data for averages, fits, limits, etc. • • •			
$-6.2 \pm 5.2 \pm 4.7$	1 AABOUD	17E	ATLS pp at 8 TeV
$-1.24 \pm 0.38 \pm 0.18$	2 ABAZOV	14	D0 $p\bar{p}$ at 1.96 TeV
$-1.97 \pm 0.43 \pm 0.23$	3 ABAZOV	11u	D0 Repl. by ABAZOV 14
$-2.39 \pm 0.63 \pm 0.37$	4 ABAZOV	10H	D0 Repl. by ABAZOV 11u

- AABOUD 17E reports a measurement of charge asymmetry of $A_{SL}^b = (-25 \pm 21 \pm 19) \times 10^{-3}$ in lepton + jets $t\bar{t}$ events in which a b -hadron decays semileptonically to a soft muon.
- ABAZOV 14 reports a measurement of like-sign dimuon charge asymmetry of $A_{SL}^b = (-4.96 \pm 1.53 \pm 0.72) \times 10^{-3}$ in semileptonic b -hadron decays.
- ABAZOV 11u reports a measurement of like-sign dimuon charge asymmetry of $A_{SL}^b = (-7.87 \pm 1.72 \pm 0.93) \times 10^{-3}$ in semileptonic b -hadron decays.
- ABAZOV 10H reports a measurement of like-sign dimuon charge asymmetry of $A_{SL}^b = (-9.57 \pm 2.51 \pm 1.46) \times 10^{-3}$ in semileptonic b -hadron decays. Using the measured production ratio of B_d^0 and B_s^0 , and the asymmetry of $B_d^0 A_{SL}^b = (-4.7 \pm 4.6) \times 10^{-3}$ measured from B -factories, they obtain the asymmetry for $B_s^0 A_{SL}^b = (-14.6 \pm 7.5) \times 10^{-3}$.

B-HADRON PRODUCTION FRACTIONS IN $p\bar{p}$ COLLISIONS AT Tevatron

The production fractions for b -hadrons in $p\bar{p}$ collisions at the Tevatron have been calculated from the best values of mean lifetimes, mixing parameters, and branching fractions in this edition by the Heavy Flavor Averaging Group (HFLAV) (see <https://hflav.web.cern.ch/>).

The values reported below assume:

$$f(\bar{b} \rightarrow B^+) = f(\bar{b} \rightarrow B^0) \\ f(\bar{b} \rightarrow B^+) + f(\bar{b} \rightarrow B^0) + f(\bar{b} \rightarrow B_s^0) + f(b \rightarrow b\text{-baryon}) = 1$$

The values are:

$$f(\bar{b} \rightarrow B^+) = f(\bar{b} \rightarrow B^0) = 0.344 \pm 0.021 \\ f(\bar{b} \rightarrow B_s^0) = 0.115 \pm 0.013$$

$$f(b \rightarrow b\text{-baryon}) = 0.198 \pm 0.046 \\ f(\bar{b} \rightarrow B_s^0) / f(\bar{b} \rightarrow B^0) = 0.334 \pm 0.041$$

and their correlation coefficients are:

$$\text{cor}(B_s^0, b\text{-baryon}) = -0.429$$

$$\text{cor}(B_s^0, B^+ = B^0) = +0.159$$

$$\text{cor}(b\text{-baryon}, B^+ = B^0) = -0.960$$

as obtained with the Tevatron average of time-integrated mixing parameter

$$\bar{\chi} = 0.147 \pm 0.011.$$

PRODUCTION ASYMMETRIES

 $A_{C^b}^{b\bar{b}}$

$$A_{C^b}^{b\bar{b}} = [N(\Delta y > 0) - N(\Delta y < 0)] / [N(\Delta y > 0) + N(\Delta y < 0)] \text{ with } \Delta y = |y_b| - |y_{\bar{b}}|$$

where $y_{b/\bar{b}}$ is rapidity of b or \bar{b} quarks.

VALUE (units 10^{-2})	DOCUMENT ID	TECN	COMMENT
Average is meaningless.			
$0.4 \pm 0.4 \pm 0.3$	1 AAIJ	14As	LHCB pp at 7 TeV
$2.0 \pm 0.9 \pm 0.6$	2 AAIJ	14As	LHCB pp at 7 TeV
$1.6 \pm 1.7 \pm 0.6$	3 AAIJ	14As	LHCB pp at 7 TeV

1 Measured for $40 < M(b\bar{b}) < 75$ GeV/ c^2 .

2 Measured for $75 < M(b\bar{b}) < 105$ GeV/ c^2 .

3 Measured for $M(b\bar{b}) > 105$ GeV/ c^2 .

 $B^\pm/B^0/B_s^0/b$ -baryon ADMIXTURE REFERENCES

AAIJ	21Y	PR D104 032005	R. Aaij et al.	(LHCb Collab.)
AAIJ	20G	EPJ C80 185	R. Aaij et al.	(LHCb Collab.)
AAIJ	20H	EPJ C80 191	R. Aaij et al.	(LHCb Collab.)
AAIJ	20V	PRL 124 122002	R. Aaij et al.	(LHCb Collab.)
AAIJ	19AB	PR D99 052006	R. Aaij et al.	(LHCb Collab.)
AAIJ	19AD	PR D100 031102	R. Aaij et al.	(LHCb Collab.)
AAIJ	19AI	PR D100 112006	R. Aaij et al.	(LHCb Collab.)
AABOUD	17E	JHEP 1702 071	M. Aaboud et al.	(ATLAS Collab.)
AAIJ	17BB	EPJ C77 609	R. Aaij et al.	(LHCb Collab.)
AAD	15CM	PRL 115 262001	G. Aad et al.	(ATLAS Collab.)
AAIJ	14AS	PRL 113 082003	R. Aaij et al.	(LHCb Collab.)
ABAZOV	14	PR D89 012002	V.M. Abazov et al.	(DO Collab.)
AAIJ	13P	JHEP 1304 001	R. Aaij et al.	(LHCb Collab.)
AAIJ	12BD	EPJ C72 2100	R. Aaij et al.	(LHCb Collab.)
Also	EPJ	C80 49 (errata.)	R. Aaij et al.	(LHCb Collab.)
AAIJ	12J	PR D85 032008	R. Aaij et al.	(LHCb Collab.)
CHATRCHYAN	12AK	JHEP 1202 011	S. Chatrchyan et al.	(CMS Collab.)
AAIJ	11F	PRL 107 211801	R. Aaij et al.	(LHCb Collab.)
ABAZOV	11U	PR D84 052007	V.M. Abazov et al.	(DO Collab.)
ABAZOV	10H	PRL 105 081801	V.M. Abazov et al.	(DO Collab.)
Also	PR	D82 032001	V.M. Abazov et al.	(DO Collab.)
PDG	10	JP G37 075021	K. Nakamura et al.	(PDG Collab.)
AALTONEN	09E	PR D79 032001	T. Aaltonen et al.	(CDF Collab.)
AALTONEN	08N	PR D77 072003	T. Aaltonen et al.	(CDF Collab.)
ABAZOV	06S	PR D74 092001	V.M. Abazov et al.	(DO Collab.)
SCHAEL	06D	PRPL 427 257	S. Schael et al.	(LEP, SLD Collabs. and EWWG)
ABBIENDI	04I	EPJ C35 149	G. Abbiendi et al.	(OPAL Collab.)
ABDALLAH	04E	EPJ C33 307	J. Abdallah et al.	(DELPHI Collab.)
ACOSTA	04A	PR D69 012002	D. Acosta et al.	(CDF Collab.)
ABBIENDI	03M	EPJ C30 467	G. Abbiendi et al.	(OPAL Collab.)
ABBIENDI	03P	PL B577 18	G. Abbiendi et al.	(OPAL Collab.)
ABDALLAH	03K	PL B561 26	J. Abdallah et al.	(DELPHI Collab.)
ABDALLAH	03E	PL B576 29	J. Abdallah et al.	(DELPHI Collab.)
HESTER	02G	EPJ C22 613	A. Hester et al.	(ALEPH Collab.)
ABBIENDI	01Q	PL B520 1	G. Abbiendi et al.	(OPAL Collab.)
ABBIENDI	01R	EPJ C21 399	G. Abbiendi et al.	(OPAL Collab.)
ABREU	01L	EPJ C20 455	P. Abreu et al.	(DELPHI Collab.)
BARATE	01E	EPJ C19 213	R. Barate et al.	(ALEPH Collab.)
ABBIENDI	00E	EPJ C13 225	G. Abbiendi et al.	(OPAL Collab.)
ABBIENDI	00Z	PL B492 13	G. Abbiendi et al.	(OPAL Collab.)
ABREU	00	EPJ C12 225	P. Abreu et al.	(DELPHI Collab.)
ABREU	00C	PL B496 43	P. Abreu et al.	(DELPHI Collab.)
ABREU	00D	PL B478 14	P. Abreu et al.	(DELPHI Collab.)
ABREU	00R	PL B475 407	P. Abreu et al.	(DELPHI Collab.)
ACCIARRI	00	EPJ C13 47	M. Acciari et al.	(L3 Collab.)
AFFOLDER	00E	PRL 84 1663	T. Affolder et al.	(CDF Collab.)
ABBIENDI	99J	EPJ C12 609	G. Abbiendi et al.	(OPAL Collab.)
ABE	99P	PR D60 092005	F. Abe et al.	(CDF Collab.)
ACCIARRI	99D	PL B448 152	M. Acciari et al.	(L3 Collab.)
BARATE	99G	EPJ C6 555	R. Barate et al.	(ALEPH Collab.)
ABBOTT	98B	PL B423 419	B. Abbott et al.	(DO Collab.)
ABE	98B	PR D57 5382	F. Abe et al.	(CDF Collab.)
ABREU	98D	PL B426 193	P. Abreu et al.	(DELPHI Collab.)
ABREU	98H	PL B425 399	P. Abreu et al.	(DELPHI Collab.)
ACCIARRI	98	PL B416 220	M. Acciari et al.	(L3 Collab.)
ACCIARRI	98K	PL B436 174	M. Acciari et al.	(L3 Collab.)
ACKERSTAFF	98E	EPJ C1 439	K. Ackerstaff et al.	(CDF Collab.)
BARATE	98I	PL B429 169	R. Barate et al.	(ALEPH Collab.)
BARATE	98Q	EPJ C4 387	R. Barate et al.	(ALEPH Collab.)
BARATE	98V	EPJ C5 205	R. Barate et al.	(ALEPH Collab.)
GLENN	98	PRL 80 2289	S. Glenn et al.	(CLEO Collab.)
ABE	97I	PR D55 2546	F. Abe et al.	(CDF Collab.)
ACKERSTAFF	97F	ZPHY C73 397	K. Ackerstaff et al.	(OPAL Collab.)
ACKERSTAFF	97N	ZPHY C74 423	K. Ackerstaff et al.	(OPAL Collab.)
ACKERSTAFF	97W	ZPHY C76 425	K. Ackerstaff et al.	(OPAL Collab.)
ABREU	96E	PL B377 195	P. Abreu et al.	(DELPHI Collab.)
ACCIARRI	96C	ZPHY C71 379	M. Acciari et al.	(L3 Collab.)
ADAM	96	ZPHY C69 561	W. Adam et al.	(DELPHI Collab.)
ADAM	96D	ZPHY C72 207	W. Adam et al.	(DELPHI Collab.)
ALEXANDER	96	ZPHY C70 357	G. Alexander et al.	(OPAL Collab.)
BUSKULIC	96F	PL B369 151	D. Buskulic et al.	(ALEPH Collab.)
BUSKULIC	96V	PL B384 471	D. Buskulic et al.	(ALEPH Collab.)
BUSKULIC	96Y	PL B388 648	D. Buskulic et al.	(ALEPH Collab.)
GROSSMAN	96	NP B465 369	Y. Grossman, Z. Ligeti, E. Nardi	(REHO, CIT)
Also	NP	B480 753 (errata.)	Y. Grossman, Z. Ligeti, E. Nardi	
PDG	96	PR D54 1	R. M. Barnett et al.	(PDG Collab.)
UENO	96	PL B381 365	K. Ueno et al.	(AMY Collab.)
ABE,K	95B	PRL 75 3624	K. Abe et al.	(SLD Collab.)
ABREU	95C	PL B377 447	P. Abreu et al.	(DELPHI Collab.)
ABREU	95D	ZPHY C66 323	P. Abreu et al.	(DELPHI Collab.)

See key on page 1171

Meson Particle Listings

$B^\pm/B^0/B_s^0/b$ -baryon ADMIXTURE, V_{cb} and V_{ub} CKM Matrix Elements

ADAM	95	ZPHY C68 363	W. Adam et al.	(DELPHI Collab.)
AKERS	95Q	ZPHY C67 57	R. Akers et al.	(OPAL Collab.)
BUSKULIC	95	PL B343 444	D. Buskulić et al.	(ALEPH Collab.)
ABREU	94F	PL B322 459	P. Abreu et al.	(DELPHI Collab.)
ABREU	94J	PL B332 488	P. Abreu et al.	(DELPHI Collab.)
ABREU	94L	ZPHY C63 3	P. Abreu et al.	(DELPHI Collab.)
ABREU	94P	PL B341 109	P. Abreu et al.	(DELPHI Collab.)
ACCIARRI	94C	PL B332 201	M. Acciarrì et al.	(L3 Collab.)
ACCIARRI	94D	PL B335 542	M. Acciarrì et al.	(L3 Collab.)
ALBAJAR	94	ZPHY C61 41	C. Albajar et al.	(UA1 Collab.)
BUSKULIC	94G	ZPHY C62 179	D. Buskulić et al.	(ALEPH Collab.)
ABE	93E	PL B313 288	K. Abe et al.	(VENUS Collab.)
ABE	93J	PRL 71 3421	F. Abe et al.	(CDF Collab.)
ABREU	93C	PL B301 145	P. Abreu et al.	(DELPHI Collab.)
ABREU	93D	ZPHY C57 181	P. Abreu et al.	(DELPHI Collab.)
ABREU	93G	PL B312 253	P. Abreu et al.	(DELPHI Collab.)
ACTON	93C	PL B307 247	P.D. Acton et al.	(OPAL Collab.)
ACTON	93L	ZPHY C60 217	P.D. Acton et al.	(OPAL Collab.)
ADRIANI	93J	PL B317 467	O. Adriani et al.	(L3 Collab.)
ADRIANI	93K	PL B317 474	O. Adriani et al.	(L3 Collab.)
ADRIANI	93L	PL B317 437	O. Adriani et al.	(L3 Collab.)
AKERS	93B	ZPHY C60 199	R. Akers et al.	(OPAL Collab.)
BUSKULIC	93B	PL B298 479	D. Buskulić et al.	(ALEPH Collab.)
BUSKULIC	93O	PL B314 459	D. Buskulić et al.	(ALEPH Collab.)
ABREU	92	ZPHY C53 567	P. Abreu et al.	(DELPHI Collab.)
ACTON	92	PL B274 513	D.P. Acton et al.	(OPAL Collab.)
ACTON	92C	PL B276 379	D.P. Acton et al.	(OPAL Collab.)
ADEVA	92C	PL B288 395	B. Adeva et al.	(L3 Collab.)
ADRIANI	92	PL B288 412	O. Adriani et al.	(L3 Collab.)
BUSKULIC	92B	PL B284 177	D. Buskulić et al.	(ALEPH Collab.)
BUSKULIC	92F	PL B295 174	D. Buskulić et al.	(ALEPH Collab.)
BUSKULIC	92G	PL B295 396	D. Buskulić et al.	(ALEPH Collab.)
ABE	91G	PRL 67 3351	F. Abe et al.	(CDF Collab.)
ADEVA	91C	PL B261 177	B. Adeva et al.	(L3 Collab.)
ADEVA	91H	PL B270 111	B. Adeva et al.	(L3 Collab.)
ALBAJAR	91C	PL B262 163	C. Albajar et al.	(UA1 Collab.)
ALBAJAR	91D	PL B262 171	C. Albajar et al.	(UA1 Collab.)
ALEXANDER	91G	PL B266 485	G. Alexander et al.	(OPAL Collab.)
DECAMP	91	PL B258 236	D. Decamp et al.	(ALEPH Collab.)
DECAMP	91C	PL B257 492	D. Decamp et al.	(ALEPH Collab.)
ADEVA	90P	PL B252 703	B. Adeva et al.	(L3 Collab.)
BEHREND	90D	ZPHY C47 333	H.J. Behrend et al.	(CELLO Collab.)
HAGEMANN	90	ZPHY C48 401	J. Hagemann et al.	(JADE Collab.)
LYONS	90	PR D41 982	J. Lyons, A.J. Martin, D.H. Saxon	(OXF. BRIS+)
WEIR	90	PL B240 289	A.J. Weir et al.	(Mark II Collab.)
BRAUNSCH...	89B	ZPHY C44 1	R. Braunschweig et al.	(TASSO Collab.)
ONG	89	PRL 62 1236	R.A. Ong et al.	(Mark II Collab.)
BAND	88	PL B200 221	H.R. Band et al.	(MAC Collab.)
KLEM	88	PR D37 41	D.E. Klem et al.	(DELCO Collab.)
ONG	88	PRL 60 2587	R.A. Ong et al.	(Mark II Collab.)
ALBAJAR	87C	PL B186 247	C. Albajar et al.	(UA1 Collab.)
ASH	87	PRL 58 640	W.W. Ash et al.	(MAC Collab.)
BARTEL	87	ZPHY C33 339	W. Bartel et al.	(JADE Collab.)
BROM	87	PL B195 301	J.M. Brom et al.	(IRS Collab.)
PAL	86	PR D33 2708	T. Pál et al.	(DELCO Collab.)
AIHARA	85	ZPHY C27 39	H. Aihara et al.	(TPC Collab.)
BARTEL	85J	PL 163B 277	W. Bartel et al.	(JADE Collab.)
SCHAAD	85	PL 160B 188	T. Schaad et al.	(Mark II Collab.)
ALTHOFF	84G	ZPHY C22 219	M. Althoff et al.	(TASSO Collab.)
ALTHOFF	84J	PL 146B 443	M. Althoff et al.	(TASSO Collab.)
KOOP	84	PRL 52 970	D.E. Koop et al.	(DELCO Collab.)
ADEVA	83	PRL 50 799	B. Adeva et al.	(Mark-J Collab.)
ADEVA	83B	PRL 51 443	B. Adeva et al.	(Mark-J Collab.)
BARTEL	83B	PL 132B 241	W. Bartel et al.	(JADE Collab.)
FERNANDEZ	83D	PRL 50 2054	C. Fernandez et al.	(MAC Collab.)
MATTEUZZI	83	PL 129B 141	C. Matteuzzi et al.	(Mark II Collab.)
NELSON	83	PRL 50 1542	M.E. Nelson et al.	(Mark II Collab.)

5	ABDALLAH	04D	DLPH	$e^+e^- \rightarrow Z^0$	
6	ADAM	03	CLE2	$e^+e^- \rightarrow \Upsilon(4S)$	
7	ABREU	01H	DLPH	$e^+e^- \rightarrow Z$	
8	ABBIENDI	00Q	OPAL	$e^+e^- \rightarrow Z$	
9	BUSKULIC	97	ALEP	$e^+e^- \rightarrow Z$	
••• We do not use the following data for averages, fits, limits, etc. •••					
3.483 ± 0.015 ± 0.056	3	WAHEED	19	BELL	Repl. by WAHEED 21
3.46 ± 0.02 ± 0.10	10	DUNDEL	10	BELL	Rep. by WAHEED 19
3.59 ± 0.06 ± 0.14	11	AUBERT	08AT	BABR	Repl. by AUBERT 09A
3.44 ± 0.03 ± 0.11	12	AUBERT	08R	BABR	Repl. by AUBERT 09A
3.55 ± 0.03 ± 0.16	13	AUBERT	05E	BABR	Repl. by AUBERT 08R
3.77 ± 0.11 ± 0.19	14	ABDALLAH	04D	DLPH	$e^+e^- \rightarrow Z^0$
3.54 ± 0.19 ± 0.18	15	ABE	02F	BELL	Repl. by DUNDEL 10
4.31 ± 0.13 ± 0.18	16	BRIERE	02	CLE2	$e^+e^- \rightarrow \Upsilon(4S)$
3.28 ± 0.19 ± 0.22		ACKERSTAFF	97G	OPAL	Repl. by ABBIENDI 00Q
3.50 ± 0.19 ± 0.23	17	ABREU	96P	DLPH	Repl. by ABREU 01H
3.51 ± 0.19 ± 0.20	18	BARISH	95	CLE2	Repl. by ADAM 03
3.14 ± 0.23 ± 0.25		BUSKULIC	95N	ALEP	Repl. by BUSKULIC 97

- Measured from differential shapes of exclusive $B \rightarrow D^* \ell^- \nu_\ell$ ($\ell = e$ or μ) decays. Using CNL form factor parametrization and the zero-recoil lattice QCD point $F(1) = 0.906 \pm 0.013$ ADACHI 23J finds $|V_{cb}|_{CNL} = (40.57 \pm 0.31 \pm 0.95 \pm 0.58) \times 10^{-3}$ where the last uncertainty is due to the prediction of $F(1)$. Also reports a measurement of $|V_{cb}|_{BGL} = (40.13 \pm 0.27 \pm 0.93 \pm 0.58) \times 10^{-3}$ using BGL form factors parametrization.
- Measured from differential shapes of exclusive $B \rightarrow D^* \ell^- \nu_\ell$ decays with hadronic tag-side reconstruction and extracting the CNL and BGL form factor parameters. PRIM 23 finds $|V_{cb}|_{CNL} = (40.2 \pm 0.9) \times 10^{-3}$ with the zero-recoil lattice QCD point $F(1) = 0.906 \pm 0.013$. PRIM 23 provides also a measurement of $|V_{cb}|_{BGL} = (40.7 \pm 1.0) \times 10^{-3}$.
- WAHEED 21 uses fully reconstructed $D^{*-} \ell^+ \nu$ events ($\ell = e$ or μ) and $\eta_{EW} = 1.0066$.
- Obtained from a global fit to $B \rightarrow D^{*+} \ell \nu_\ell$ events, with reconstructed $D^0 \ell$ and $D^+ \ell$ final states and $\rho^2 = 1.22 \pm 0.02 \pm 0.07$.
- Measurement using fully reconstructed D^* sample with a $\rho^2 = 1.32 \pm 0.15 \pm 0.33$.
- Average of the $B^0 \rightarrow D^*(2010)^- \ell^+ \nu$ and $B^+ \rightarrow \bar{D}^*(2007)^+ \ell^+ \nu$ modes with $\rho^2 = 1.61 \pm 0.09 \pm 0.21$ and $f_{+-} = 0.521 \pm 0.012$.
- ABREU 01H measured using about 5000 partial reconstructed D^* sample with a $\rho^2 = 1.34 \pm 0.14 \pm 0.24 \pm 0.22$.
- ABBIENDI 00Q: measured using both inclusively and exclusively reconstructed $D^{*\pm}$ samples with a $\rho^2 = 1.21 \pm 0.12 \pm 0.20$. The statistical and systematic correlations between $|V_{cb}| \times F(1)$ and ρ^2 are 0.90 and 0.54 respectively.
- BUSKULIC 97: measured using exclusively reconstructed $D^{*\pm}$ with a $a^2 = 0.31 \pm 0.17 \pm 0.08$. The statistical correlation is 0.92.
- Uses fully reconstructed $D^{*-} \ell^+ \nu$ events ($\ell = e$ or μ).
- Measured using the dependence of $B^- \rightarrow D^{*0} e^- \bar{\nu}_e$ decay differential rate and the form factor description by CAPRINI 98 with $\rho^2 = 1.16 \pm 0.06 \pm 0.08$.
- Measured using fully reconstructed D^* sample and a simultaneous fit to the Caprini-Lellouch-Neubert form factor parameters: $\rho^2 = 1.191 \pm 0.048 \pm 0.028$, $R_1(1) = 1.429 \pm 0.061 \pm 0.044$, and $R_2(1) = 0.827 \pm 0.038 \pm 0.022$.
- Measurement using fully reconstructed D^* sample with a $\rho^2 = 1.29 \pm 0.03 \pm 0.27$.
- Combines with previous partial reconstructed D^* measurement with a $\rho^2 = 1.39 \pm 0.10 \pm 0.33$.
- Measured using exclusive $B^0 \rightarrow D^*(892)^- e^+ \nu$ decays with $\rho^2 = 1.35 \pm 0.17 \pm 0.19$ and a correlation of 0.91.
- BRIERE 02 result is based on the same analysis and data sample reported in ADAM 03.
- ABREU 96P: measured using both inclusively and exclusively reconstructed $D^{*\pm}$ samples.
- BARISH 95: measured using both exclusive reconstructed $B^0 \rightarrow D^{*-} \ell^+ \nu$ and $B^+ \rightarrow D^{*0} \ell^+ \nu$ samples. They report their experiment's uncertainties $\pm 0.0019 \pm 0.0018 \pm 0.0008$, where the first error is statistical, the second is systematic, and the third is the uncertainty in the lifetimes. We combine the last two in quadrature.

V_{cb} and V_{ub} CKM Matrix Elements

OMITTED FROM SUMMARY TABLE

See the related review(s):

Semileptonic B Hadron Decays, Determination of V_{cb} and V_{ub}

V_{cb} MEASUREMENTS

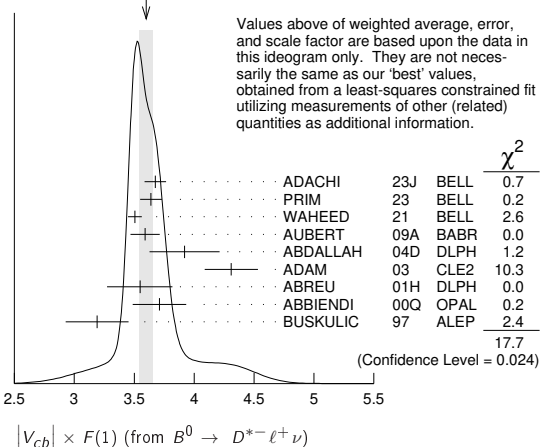
For the discussion of V_{cb} measurements, which is not repeated here, see the review on "Determination of $|V_{cb}|$ and $|V_{ub}|$."

The CKM matrix element $|V_{cb}|$ can be determined by studying the rate of the semileptonic decay $B \rightarrow D^{(*)} \ell \nu$ as a function of the recoil kinematics of $D^{(*)}$ mesons. Taking advantage of theoretical constraints on the normalization and a linear ω dependence of the form factors ($F(\omega)$, $G(\omega)$) provided by Heavy Quark Effective Theory (HQET), the $|V_{cb}| \times F(\omega)$ and ρ^2 can be simultaneously extracted from data, where ω is the scalar product of the two-meson four velocities, $F(1)$ is the form factor at zero recoil ($\omega=1$) and ρ^2 is the slope. Using the theoretical input of $F(1)$, a value of $|V_{cb}|$ can be obtained.

$|V_{cb}| \times F(1)$ (from $B^0 \rightarrow D^{*-} \ell^+ \nu$)

VALUE (units 10^{-2})	DOCUMENT ID	TECN	COMMENT
3.534 ± 0.037 OUR EVALUATION	(Produced by HFLAV) with $\rho^2 = 1.139 \pm 0.020$ and a correlation 0.268. The fitted χ^2 is 63.2 for 27 degrees of freedom.		
3.60 ± 0.06 OUR AVERAGE	Error includes scale factor of 1.5. See the ideogram below.		
3.676 ± 0.028 ± 0.086	1	ADACHI	23J BELL $e^+e^- \rightarrow \Upsilon(4S)$
3.64 ± 0.09	2	PRIM	23 BELL $e^+e^- \rightarrow \Upsilon(4S)$
3.506 ± 0.015 ± 0.056	3	WAHEED	21 BELL $e^+e^- \rightarrow \Upsilon(4S)$
3.59 ± 0.02 ± 0.12	4	AUBERT	09A BABR $e^+e^- \rightarrow \Upsilon(4S)$

WEIGHTED AVERAGE
3.60 ± 0.06 (Error scaled by 1.5)



Meson Particle Listings

V_{cb} and V_{ub} CKM Matrix Elements, B^*

$|V_{cb}| \times G(1)$ (from $B \rightarrow D^- \ell^+ \nu$)

VALUE (units 10^{-2})	DOCUMENT ID	TECN	COMMENT
4.121 ± 0.100 OUR EVALUATION	(Produced by HFLAV) with $\rho^2 = 1.128 \pm 0.033$ and a correlation 0.747. The fitted χ^2 is 4.8 for 8 degrees of freedom.		
4.22 ± 0.10 OUR AVERAGE			
4.229 ± 0.137	1 GLATTAUER	16 BELL	$e^+ e^- \rightarrow \Upsilon(4S)$
4.23 ± 0.19 ± 0.14	2 AUBERT	10 BABR	$e^+ e^- \rightarrow \Upsilon(4S)$
4.31 ± 0.08 ± 0.23	3 AUBERT	09A BABR	$e^+ e^- \rightarrow \Upsilon(4S)$
4.16 ± 0.47 ± 0.37	4 BARTELT	99 CLE2	$e^+ e^- \rightarrow \Upsilon(4S)$
2.78 ± 0.68 ± 0.65	5 BUSKULIC	97 ALEP	$e^+ e^- \rightarrow Z$
• • • We do not use the following data for averages, fits, limits, etc. • • •			
4.11 ± 0.44 ± 0.52	6 ABE	02E BELL	Repl. by GLATTAUER 16
3.37 ± 0.44 ± 0.72 -0.49	7 ATHANAS	97 CLE2	Repl. by BARTELT 99

- 1 Obtained from a fit to the combined partially reconstructed $B \rightarrow \bar{D} \ell \nu_\ell$ sample while tagged by the other fully reconstructed B meson in the event. Also reports fitted $\rho^2 = 1.09 \pm 0.05$.
- 2 Obtained from a fit to the combined $B \rightarrow \bar{D} \ell^+ \nu_\ell$ sample in which a hadronic decay of the second B meson is fully reconstructed and $\rho^2 = 1.20 \pm 0.09 \pm 0.04$.
- 3 Obtained from a global fit to $B \rightarrow D^{(*)} \ell \nu_\ell$ events, with reconstructed $D^0 \ell$ and $D^+ \ell$ final states and $\rho^2 = 1.20 \pm 0.04 \pm 0.07$.
- 4 BARTELT 99: measured using both exclusive reconstructed $B^0 \rightarrow D^- \ell^+ \nu$ and $B^+ \rightarrow D^0 \ell^+ \nu$ samples.
- 5 BUSKULIC 97: measured using exclusively reconstructed D^\pm with a $a^2 = -0.05 \pm 0.53 \pm 0.38$. The statistical correlation is 0.99.
- 6 Using the missing energy and momentum to extract kinematic information about the undetected neutrino in the $B^0 \rightarrow D^- \ell^+ \nu$ decay.
- 7 ATHANAS 97: measured using both exclusive reconstructed $B^0 \rightarrow D^- \ell^+ \nu$ and $B^+ \rightarrow D^0 \ell^+ \nu$ samples with a $\rho^2 = 0.59 \pm 0.22 \pm 0.12^{+0.59}_{-0.0012}$. They report their experiment's uncertainties $\pm 0.0044 \pm 0.0048^{+0.0053}_{-0.0012}$, where the first error is statistical, the second is systematic, and the third is the uncertainty due to the form factor model variations. We combine the last two in quadrature.

$|V_{cb}|$ (from $D_s^{*-} \mu^+ \nu_\mu$)

VALUE (units 10^{-3})	DOCUMENT ID	TECN	COMMENT
41.4 ± 0.6 ± 0.9 ± 1.2	1 AAIJ	20E LHCB	pp at 7, 8 TeV

1 Measured from an inclusive sample of $D_s^{*-} \mu^+$ candidates using CNL parameterization of the form factor. AAIJ 20E provides also measurement of $|V_{cb}| = (42.3 \pm 0.8 \pm 0.9 \pm 1.2) \times 10^{-3}$ using BGL parameterization of the form factor. The third uncertainty is due to the external inputs used in the measurement.

V_{ub} MEASUREMENTS

For the discussion of V_{ub} measurements, which is not repeated here, see the review on "Determination of $|V_{cb}|$ and $|V_{ub}|$."

The CKM matrix element $|V_{ub}|$ can be determined by studying the rate of the charmless semileptonic decay $b \rightarrow u \ell \nu$. The relevant branching ratio measurements based on exclusive and inclusive decays can be found in the B Listings, and are not repeated here.

V_{cb} and V_{ub} CKM Matrix Elements REFERENCES

ADACHI	23J	PR D108 092013	I. Adachi <i>et al.</i>	(BELLE II Collab.)
PRIM	23	PR D108 012002	M.T. Prim <i>et al.</i>	(BELLE Collab.)
WAHEED	21	PR D103 079901	E. Waheed <i>et al.</i>	(BELLE Collab.)
AAIJ	20E	PR D101 072004	R. Aaij <i>et al.</i>	(LHCb Collab.)
WAHEED	19	PR D100 052007	E. Waheed <i>et al.</i>	(BELLE Collab.)
GLATTAUER	16	PR D93 032006	R. Glattauer <i>et al.</i>	(BELLE Collab.)
AUBERT	10	PRL 104 011802	B. Aubert <i>et al.</i>	(BABAR Collab.)
DUNGEL	10	PR D82 112007	W. Dungen <i>et al.</i>	(BELLE Collab.)
AUBERT	09A	PR D79 012002	B. Aubert <i>et al.</i>	(BABAR Collab.)
AUBERT	08AT	PRL 100 231803	B. Aubert <i>et al.</i>	(BABAR Collab.)
AUBERT	08R	PR D77 032002	B. Aubert <i>et al.</i>	(BABAR Collab.)
AUBERT	05E	PR D71 051502	B. Aubert <i>et al.</i>	(BABAR Collab.)
ABDALLAH	04D	EPJ C33 213	J. Abdallah <i>et al.</i>	(DELPHI Collab.)
ADAM	03	PR D67 032001	N.E. Adam <i>et al.</i>	(CLEO Collab.)
ABE	02E	PL B526 258	K. Abe <i>et al.</i>	(BELLE Collab.)
ABE	02F	PL B526 247	K. Abe <i>et al.</i>	(BELLE Collab.)
BRIERE	02	PRL 89 081803	R. Briere <i>et al.</i>	(CLEO Collab.)
ABREU	01H	PL B510 55	P. Abreu <i>et al.</i>	(DELPHI Collab.)
ABBIENDI	00Q	PL B482 15	G. Abbiendi <i>et al.</i>	(OPAL Collab.)
BARTELT	99	PRL 82 3746	J. Bartelt <i>et al.</i>	(CLEO Collab.)
CAPRINI	98	NP B530 153	J. Caprini, L. Lellouch, M. Neubert	(BCIP, CERN)
ACKERSTAFF	97G	PL B395 128	K. Ackerstaff <i>et al.</i>	(OPAL Collab.)
ATHANAS	97	PRL 79 2208	M. Athanas <i>et al.</i>	(CLEO Collab.)
BUSKULIC	97	PL B395 373	D. Buskulic <i>et al.</i>	(ALEPH Collab.)
ABREU	96P	ZPHY C71 539	P. Abreu <i>et al.</i>	(DELPHI Collab.)
BARISH	95	PR D51 1014	B.C. Barish <i>et al.</i>	(CLEO Collab.)
BUSKULIC	95N	PL B359 236	D. Buskulic <i>et al.</i>	(ALEPH Collab.)



$$I(J^P) = \frac{1}{2}(1^-)$$

l, J, P need confirmation.

Quantum numbers shown are quark-model predictions.

B^* MASS

From mass difference below and the average of our B masses ($m_{B^\pm} + m_{B^0}$)/2.

VALUE (MeV)	DOCUMENT ID
5324.75 ± 0.20 OUR FIT	

$m_{B^*} - m_B$

VALUE (MeV)	EVS	DOCUMENT ID	TECN	COMMENT
45.18 ± 0.20 OUR FIT				
45.42 ± 0.26 OUR AVERAGE		Includes data from the datablock that follows this one.		
46.2 ± 0.3 ± 0.8		1 ACKERSTAFF	97M OPAL	$e^+ e^- \rightarrow Z$
45.3 ± 0.35 ± 0.87	4227	1 BUSKULIC	96D ALEP	$E_{cm}^{ee} = 88-94$ GeV
45.5 ± 0.3 ± 0.8		1 ABREU	95R DLPH	$E_{cm}^{ee} = 88-94$ GeV
46.3 ± 1.9	1378	1 ACCIARRI	95B L3	$E_{cm}^{ee} = 88-94$ GeV
46.4 ± 0.3 ± 0.8		2 AKERIB	91 CLE2	$e^+ e^- \rightarrow \gamma X$
45.6 ± 0.8		2 WU	91 CSB2	$e^+ e^- \rightarrow \gamma X, \gamma \ell X$
45.4 ± 1.0		3 LEE-FRANZINI	90 CSB2	$e^+ e^- \rightarrow \Upsilon(5S)$
• • • We do not use the following data for averages, fits, limits, etc. • • •				
52 ± 2 ± 4	1400	4 HAN	85 CUSB	$e^+ e^- \rightarrow \gamma e X$

- 1 u, d, s flavor averaged.
- 2 These papers report E_γ in the B^* center of mass. The $m_{B^*} - m_B$ is 0.2 MeV higher. $E_{cm} = 10.61-10.7$ GeV. Admixture of B^0 and B^+ mesons, but not B_s .
- 3 LEE-FRANZINI 90 value is for an admixture of B^0 and B^+ . They measure $46.7 \pm 0.4 \pm 0.2$ MeV for an admixture of B^0, B^+ , and B_s , and use the shape of the photon line to separate the above value.
- 4 HAN 85 is for $E_{cm} = 10.6-11.2$ GeV, giving an admixture of B^0, B^+ , and B_s .

$m_{B^{*+}} - m_{B^+}$

VALUE (MeV)	DOCUMENT ID	TECN	COMMENT
45.34 ± 0.20 OUR FIT			
45.01 ± 0.30 ± 0.23	5 AAIJ	13O LHCB	pp at 7 TeV

The data in this block is included in the average printed for a previous datablock.

- 5 Obtained the mass difference between $B^{*+} K^-$ and $B^+ K^-$ from $B_{s2}^*(5840)^0$ decay.

$(m_{B^{*+}} - m_{B^+}) - (m_{B^{*0}} - m_{B^0})$

VALUE (MeV)	CL%	DOCUMENT ID	TECN	COMMENT
<6	95	ABREU	95R DLPH	$E_{cm}^{ee} = 88-94$ GeV

$m_{B^{*0}} - m_{B^0}$

VALUE (MeV)	DOCUMENT ID	TECN	COMMENT
0.91 ± 0.24 ± 0.09	6 SIRUNYAN	18DF CMS	pp at 8 TeV

- 6 Uses exclusively reconstructed final states containing a $J/\psi \rightarrow \mu^+ \mu^-$ decay.

B^* DECAY MODES

Mode	Fraction (Γ_i/Γ)
$\Gamma_1 B \gamma$	seen

B^* REFERENCES

SIRUNYAN	18DF	EPJ C78 939	A.M. Sirunyan <i>et al.</i>	(CMS Collab.)
AAIJ	13O	PRL 110 151803	R. Aaij <i>et al.</i>	(LHCb Collab.)
ACKERSTAFF	97M	ZPHY C74 413	K. Ackerstaff <i>et al.</i>	(OPAL Collab.)
BUSKULIC	96D	ZPHY C69 393	D. Buskulic <i>et al.</i>	(ALEPH Collab.)
ABREU	95R	ZPHY C68 353	P. Abreu <i>et al.</i>	(DELPHI Collab.)
ACCIARRI	95B	PL B345 589	M. Acciarri <i>et al.</i>	(L3 Collab.)
AKERIB	91	PRL 67 1692	D.S. Akerib <i>et al.</i>	(CLEO Collab.)
WU	91	PL B273 177	Q.W. Wu <i>et al.</i>	(CUSB II Collab.)
LEE-FRANZINI	90	PRL 65 2947	J. Lee-Franzini <i>et al.</i>	(CUSB II Collab.)
HAN	85	PRL 55 36	K. Han <i>et al.</i>	(COLU, LSU, MPIM, STON)

See key on page 1171

Meson Particle Listings

$B_1(5721), B_J^*(5732)$

$B_1(5721)$

$I(J^P) = \frac{1}{2}(1^+)$
 I, J, P need confirmation.

Quantum numbers shown are quark-model predictions.

$B_1(5721)$ MASS

$B_1(5721)^+$ mass

OUR FIT uses m_{B^+} and $m_{B^+} - m_{B^0}$ to determine $m_{B_1(5721)^+}$.

VALUE (MeV)	DOCUMENT ID
-------------	-------------

5726.0^{+2.5}_{-2.7} OUR FIT

$m_{B_1^+} - m_{B^0}$

VALUE (MeV)	EVTS	DOCUMENT ID	TECN	COMMENT
-------------	------	-------------	------	---------

401.2^{+2.4}_{-2.7} OUR FIT

401.2^{+2.4}_{-2.7} OUR AVERAGE

400.5 ± 1.8 ± 3.1	8k	¹ AAIJ	15AB LHCB	$p\bar{p}$ at 7, 8 TeV
402 ± 3 ⁺¹ ₋₃		² AALTONEN	14i CDF	$p\bar{p}$ at 1.96 TeV

¹ AAIJ 15AB reports $[m_{B_1^+} - m_{B^0}] - (m_{B^+} - m_{B^0}) - m_{\pi^+} = 260.9 \pm 1.8 \pm 3.1$

MeV which we adjust by the π^+ mass and assume $(m_{B^+} - m_{B^0}) = (m_{B^{*+}} - m_{B^+}) = 45.01 \pm 0.30 \pm 0.23$ MeV. The masses inside the square brackets were measured for each candidate event.

² AALTONEN 14i reports $m_{B_1(5721)^+} - m_{B^0} - m_{\pi^+} = 262 \pm 3⁺¹₋₃$ MeV which we adjusted by the π^+ mass.

$B_1(5721)^0$ mass

OUR FIT uses mass differences measurements listed below to determine the mass $m_{B_1(5721)^0}$.

VALUE (MeV)	DOCUMENT ID
-------------	-------------

5726.1 ± 1.2 OUR FIT Error includes scale factor of 1.2.

$m_{B_1^0} - m_{B^+}$

VALUE (MeV)	DOCUMENT ID	TECN	COMMENT
-------------	-------------	------	---------

446.7 ± 1.2 OUR FIT Error includes scale factor of 1.2.

441.5 ± 2.4 ± 1.3 ¹ ABZOV 07T D0 $p\bar{p}$ at 1.96 TeV

• • • We do not use the following data for averages, fits, limits, etc. • • •

446.2 ± 1.9^{+1.0}_{-2.1} ± 1.2 ¹ AALTONEN 09D CDF Repl. by AALTONEN 14i

¹ Observed in $B_1^0 \rightarrow B^{*+} \pi^-$.

$m_{B_1^0} - m_{B^{*+}}$

VALUE (MeV)	EVTS	DOCUMENT ID	TECN	COMMENT
-------------	------	-------------	------	---------

401.4 ± 1.2 OUR FIT Error includes scale factor of 1.2.

402.8 ± 1.1 OUR AVERAGE

403.4 ± 0.7 ± 1.5 35k ¹ AAIJ 15AB LHCB $p\bar{p}$ at 7, 8 TeV

402.3 ± 0.9^{+1.1}_{-1.2} ² AALTONEN 14i CDF $p\bar{p}$ at 1.96 TeV

¹ AAIJ 15AB reports $[m_{B_1^0} - m_{B^+}] - (m_{B^{*+}} - m_{B^+}) - m_{\pi^-} = 263.9 \pm 0.7 \pm 1.4$

MeV which we adjust by the π^- mass and $(m_{B^{*+}} - m_{B^+}) = 45.01 \pm 0.30 \pm 0.23$ MeV. The masses inside the square brackets were measured for each candidate event.

² AALTONEN 14i reports $m_{B_1(5721)^0} - m_{B^{*+}} - m_{\pi^-} = 262.7 \pm 0.9^{+1.1}_{-1.2}$ MeV which we adjusted by the π^- mass.

$B_1(5721)$ WIDTH

$B_1(5721)^+$ width

VALUE (MeV)	EVTS	DOCUMENT ID	TECN	COMMENT
-------------	------	-------------	------	---------

31 ± 6 OUR AVERAGE Error includes scale factor of 1.1.

29.1 ± 3.6 ± 4.3 8k AAIJ 15AB LHCB $p\bar{p}$ at 7, 8 TeV

49⁺¹²₋₁₀ ± 2⁺²₋₁₃ AALTONEN 14i CDF $p\bar{p}$ at 1.96 TeV

$B_1(5721)^0$ width

VALUE (MeV)	EVTS	DOCUMENT ID	TECN	COMMENT
-------------	------	-------------	------	---------

27.5 ± 3.4 OUR AVERAGE Error includes scale factor of 1.1.

30.1 ± 1.5 ± 3.5 35k AAIJ 15AB LHCB $p\bar{p}$ at 7, 8 TeV

23 ± 3 ± 4 AALTONEN 14i CDF $p\bar{p}$ at 1.96 TeV

$B_1(5721)$ DECAY MODES

Mode	Fraction (Γ_i/Γ)
Γ_1 $B^* \pi$	seen

$\Gamma(B^* \pi)/\Gamma_{total}$	Γ_1/Γ
----------------------------------	-------------------

VALUE	DOCUMENT ID	TECN	CHG	COMMENT
-------	-------------	------	-----	---------

seen AAIJ 15AB LHCB ± 0 $p\bar{p}$ at 7, 8 TeV

seen AALTONEN 14i CDF ± $p\bar{p}$ at 1.96 TeV

seen AALTONEN 09D CDF 0 $p\bar{p}$ at 1.96 TeV

seen ¹ ABZOV 07T D0 0 $p\bar{p}$ at 1.96 TeV

¹ Observed in $B_1^0 \rightarrow B^{*+} \pi^-$ with $B^{*+} \rightarrow B^+ \gamma$ and $B^+ \rightarrow J/\psi \pi^+$.

$B_1(5721)$ REFERENCES

AAIJ	15AB	JHEP 1504 024	R. Aaij <i>et al.</i>	(LHCb Collab.)
AALTONEN	14i	PR D90 012013	T. Aaltonen <i>et al.</i>	(CDF Collab.)
AALTONEN	09D	PRL 102 102003	T. Aaltonen <i>et al.</i>	(CDF Collab.)
ABAZOV	07T	PRL 99 172001	V.M. Abazov <i>et al.</i>	(D0 Collab.)

$B_J^*(5732)$

$I(J^P) = ?(?^?)$

OMITTED FROM SUMMARY TABLE

Signal can be interpreted as stemming from several narrow and broad resonances.

$B_J^*(5732)$ MASS

VALUE (MeV)	EVTS	DOCUMENT ID	TECN	COMMENT
-------------	------	-------------	------	---------

5698 ± 8 OUR AVERAGE Error includes scale factor of 1.2.

5710 ± 20 ¹ AFFOLDER 01F CDF $p\bar{p}$ at 1.8 TeV

5695⁺¹⁷₋₁₉ ² BARATE 98L ALEP $e^+e^- \rightarrow Z$

5704 ± 4 ± 10 1944 ³ BUSKULIC 96D ALEP $E_{cm}^{e^+e^-} = 88-94$ GeV

5732 ± 5 ± 20 2157 ABREU 95B DLPH $E_{cm}^{e^+e^-} = 88-94$ GeV

5681 ± 11 1738 AKERS 95E OPAL $E_{cm}^{e^+e^-} = 88-94$ GeV

• • • We do not use the following data for averages, fits, limits, etc. • • •

5713 ± 2 ⁴ ACCIARRI 99N L3 $e^+e^- \rightarrow Z$

¹ AFFOLDER 01F uses the reconstructed B meson through semileptonic decay channels. The fraction of light B mesons that are produced at $L=1$ B^{**} states is measured to be $0.28 \pm 0.06 \pm 0.03$.

² BARATE 98L uses fully reconstructed B mesons to search for B^{**} production in the $B\pi^\pm$ system. In the framework of heavy quark symmetry (HQSS), they also measured the mass of B_J^* to be $5739⁺⁸₋₁₁ + ⁶₋₄ MeV/ c^2 and the relative production rate of $B(b \rightarrow B_J^* \rightarrow B^{(*)} \pi)/B(b \rightarrow B_{u,d}) = (31 \pm 9⁺⁶₋₅)\%$.$

³ Using $m_{B\pi} - m_B = 424 \pm 4 \pm 10$ MeV.

⁴ ACCIARRI 99N uses inclusive reconstructed B mesons to search for B^{**} production in the $B^{(*)} \pi^\pm$ system. In the framework of HQET, they measured the mass of B_1^* and B_J^* to be $5670 \pm 10 \pm 13$ MeV and $5768 \pm 5 \pm 6$ with the $B(b \rightarrow B^{**}) = (32 \pm 3 \pm 6) \times 10^{-2}$. They also reported the evidence for the existence of an excited B -meson state or mixture of states in the region 5.9–6.0 GeV.

$B_J^*(5732)$ WIDTH

VALUE (MeV)	EVTS	DOCUMENT ID	TECN	COMMENT
-------------	------	-------------	------	---------

128 ± 18 OUR AVERAGE

145 ± 28 2157 ABREU 95B DLPH $E_{cm}^{e^+e^-} = 88-94$ GeV

116 ± 24 1738 AKERS 95E OPAL $E_{cm}^{e^+e^-} = 88-94$ GeV

$B_J^*(5732)$ DECAY MODES

Mode	Fraction (Γ_i/Γ)
Γ_1 $B^* \pi + B \pi$	seen
Γ_2 $B^* \pi(X)$	[a] (85 ± 29) %

[a] X refers to decay modes with or without additional accompanying decay particles.

$B_J^*(5732)$ BRANCHING RATIOS

X refers to decay modes with or without additional accompanying decay particles.

$\Gamma(B^* \pi(X))/\Gamma_{total}$	Γ_2/Γ
-------------------------------------	-------------------

VALUE	DOCUMENT ID	TECN	COMMENT
-------	-------------	------	---------

0.85^{+0.26}_{-0.27} ± 0.12 ABBIENDI 02E OPAL $e^+e^- \rightarrow Z$

$B_J^*(5732)$ REFERENCES

ABBIENDI	02E	EPJ C23 437	G. Abbiendi <i>et al.</i>	(OPAL Collab.)
AFFOLDER	01F	PR D64 072002	T. Affolder <i>et al.</i>	(CDF Collab.)
ACCIARRI	99N	PL B465 323	M. Acciarri <i>et al.</i>	(L3 Collab.)
BARATE	98L	PL B425 215	R. Barate <i>et al.</i>	(ALEPH Collab.)
BUSKULIC	96D	ZPHY C69 393	D. Buskulic <i>et al.</i>	(ALEPH Collab.)
ABREU	95B	PL B345 598	P. Abreu <i>et al.</i>	(DELPHI Collab.)
AKERS	95E	ZPHY C66 19	R. Akers <i>et al.</i>	(OPAL Collab.)

Meson Particle Listings

 $B_2^*(5747)$, $B_J(5840)$ $B_2^*(5747)$

$$I(J^P) = \frac{1}{2}(2^+)$$

I, J, P need confirmation.

Quantum numbers shown are quark-model predictions.

 $B_2^*(5747)$ MASS $B_2^*(5747)^+$ massOUR FIT uses m_{B_0} and $m_{B_2^+} - m_{B_0}$ to determine $m_{B_2^*(5747)^+}$.

VALUE (MeV)	DOCUMENT ID
5737.3 ± 0.7 OUR FIT	

 $m_{B_2^+} - m_{B_0}$

VALUE (MeV)	EVTS	DOCUMENT ID	TECN	COMMENT
457.5 ± 0.7 OUR FIT				
457.5 ± 0.7 OUR AVERAGE				
457.62 ± 0.72 ± 0.40	4k	¹ AAIJ	15AB LHCB	$p\bar{p}$ at 7, 8 TeV
457.3 ± 1.3 $^{+0.3}_{-0.9}$		² AALTONEN	14i CDF	$p\bar{p}$ at 1.96 TeV

¹ AAIJ 15AB reports $[m_{B_2^+} - m_{B_0}] - m_{\pi^+} = 318.1 \pm 0.7 \pm 0.4$ MeV which we adjust by the π^+ mass. The masses inside the square brackets were measured for each candidate event.

² AALTONEN 14i reports $m_{B_2^*(5747)^+} - m_{B_0} - m_{\pi^+} = 317.7 \pm 1.2 \pm 0.3 \pm 0.9$ MeV which we adjusted by the π^+ mass.

 $B_2^*(5747)^0$ mass

OUR FIT uses $m_{B_2^+}$, $m_{B_1^0} - m_{B_2^+}$, and mass differences below to determine $m_{B_2^*(5747)^0}$. The -0.659 correlation between statistical uncertainties of $m_{B_1^0} - m_{B_2^+}$ and $m_{B_2^0} - m_{B_1^0}$ measurements reported by ABAZOV 07T is taken into account.

VALUE (MeV)	DOCUMENT ID
5739.6 ± 0.7 OUR FIT	Error includes scale factor of 1.4.

 $m_{B_2^0} - m_{B_1^0}$

VALUE (MeV)	DOCUMENT ID	TECN	COMMENT
13.5 ± 1.4 OUR FIT	Error includes scale factor of 1.3.		
26.2 ± 3.1 ± 0.9	¹ ABAZOV	07T D0	$p\bar{p}$ at 1.96 TeV

• • • We do not use the following data for averages, fits, limits, etc. • • •

14.9 $^{+2.2+1.2}_{-2.5-1.4}$	¹ AALTONEN	09D CDF	Repl. by AALTONEN 14i
-------------------------------	-----------------------	---------	-----------------------

¹ Observed in $B_2^0 \rightarrow B^{*+}\pi^-$ and $B_2^0 \rightarrow B^+\pi^-$.

 $m_{B_2^0} - m_{B^+}$

VALUE (MeV)	EVTS	DOCUMENT ID	TECN	COMMENT
460.2 ± 0.6 OUR FIT				Error includes scale factor of 1.4.
459.9 ± 0.8 OUR AVERAGE				Error includes scale factor of 1.8.
460.18 ± 0.37 ± 0.33	17k	¹ AAIJ	15AB LHCB	$p\bar{p}$ at 7, 8 TeV
457.5 ± 1.2 $^{+0.8}_{-0.9}$		² AALTONEN	14i CDF	$p\bar{p}$ at 1.96 TeV

¹ AAIJ 15AB reports $[m_{B_2^0} - m_{B^+}] - m_{\pi^-} = 320.6 \pm 0.4 \pm 0.3$ MeV which we adjust by the π^- mass. The masses inside the square brackets were measured for each candidate event.

² AALTONEN 14i reports $m_{B_2^*(5747)^0} - m_{B^+} - m_{\pi^-} = 317.9 \pm 1.2 \pm 0.8 \pm 0.9$ MeV which we adjusted by the π^- mass.

 $B_2^*(5747)$ WIDTH $B_2^*(5747)^+$ width

VALUE (MeV)	EVTS	DOCUMENT ID	TECN	COMMENT
20 ± 5 OUR AVERAGE				Error includes scale factor of 2.2.
23.6 ± 2.0 ± 2.1	4k	AAIJ	15AB LHCB	$p\bar{p}$ at 7, 8 TeV
11 $^{+4}_{-3}$ $^{+3}_{-4}$		AALTONEN	14i CDF	$p\bar{p}$ at 1.96 TeV

 $B_2^*(5747)^0$ width

VALUE (MeV)	EVTS	DOCUMENT ID	TECN	COMMENT
24.2 ± 1.7 OUR AVERAGE				
24.5 ± 1.0 ± 1.5	17k	AAIJ	15AB LHCB	$p\bar{p}$ at 7, 8 TeV
22 $^{+3}_{-2}$ $^{+4}_{-5}$		AALTONEN	14i CDF	$p\bar{p}$ at 1.96 TeV

• • • We do not use the following data for averages, fits, limits, etc. • • •

22.7 $^{+3.8+3.2}_{-3.2-10.2}$		AALTONEN	09D CDF	Repl. by AALTONEN 14i
--------------------------------	--	----------	---------	-----------------------

 $B_2^*(5747)$ DECAY MODES

Mode	Fraction (Γ_i/Γ)
Γ_1 $B\pi$	seen
Γ_2 $B^*\pi$	seen

 $\Gamma(B\pi)/\Gamma_{\text{total}}$

VALUE	EVTS	DOCUMENT ID	TECN	CHG	COMMENT	Γ_1/Γ
seen	4k,17k	AAIJ	15AB LHCB	±0	$p\bar{p}$ at 7, 8 TeV	
seen		AALTONEN	14i CDF	±	$p\bar{p}$ at 1.96 TeV	
seen		AALTONEN	09D CDF	0	$p\bar{p}$ at 1.96 TeV	
seen		ABAZOV	07T D0	0	$p\bar{p}$ at 1.96 TeV	

 $\Gamma(B^*\pi)/\Gamma_{\text{total}}$

VALUE	EVTS	DOCUMENT ID	TECN	CHG	COMMENT	Γ_2/Γ
seen	4k,17k	AAIJ	15AB LHCB	±0	$p\bar{p}$ at 7, 8 TeV	
seen		AALTONEN	09D CDF	0	$p\bar{p}$ at 1.96 TeV	
seen		ABAZOV	07T D0	0	$p\bar{p}$ at 1.96 TeV	

 $\Gamma(B^*\pi)/\Gamma(B\pi)$

VALUE	EVTS	DOCUMENT ID	TECN	CHG	COMMENT	Γ_2/Γ_1
0.84 ± 0.27 OUR AVERAGE						
0.71 ± 0.14 ± 0.30	17k	AAIJ	15AB LHCB	0	$p\bar{p}$ at 7, 8 TeV	
1.0 ± 0.5 ± 0.8	4k	AAIJ	15AB LHCB	±	$p\bar{p}$ at 7, 8 TeV	
1.10 ± 0.42 ± 0.31		¹ ABAZOV	07T D0	0	$p\bar{p}$ at 1.96 TeV	

¹ Converted from measured ratio of $R = \text{B}(B_2^0 \rightarrow B^{*+}\pi^-) / \text{B}(B_2^0 \rightarrow B^+\pi^-) = 0.475 \pm 0.095 \pm 0.069$.

 $B_2^*(5747)$ REFERENCES

AAIJ	15AB JHEP 1504 024	R. Aaij et al.	(LHCb Collab.)
AALTONEN	14i PR D90 012013	T. Aaltonen et al.	(CDF Collab.)
AALTONEN	09D PRL 102 102003	T. Aaltonen et al.	(CDF Collab.)
ABAZOV	07T PRL 99 172001	V.M. Abazov et al.	(D0 Collab.)

 $B_J(5840)$

$$I(J^P) = \frac{1}{2}(?)^?$$

I, J, P need confirmation.

OMITTED FROM SUMMARY TABLE

Quantum numbers shown are quark-model predictions.

 $B_J(5840)$ MASS $B_J(5840)^+$ MASSOUR FIT uses m_{B_0} and $m_{B_J(5840)^+} - m_{B_0}$ to determine $m_{B_J(5840)^+}$.

VALUE (MeV)	DOCUMENT ID
5851 ± 19 OUR FIT	

 $m_{B_J(5840)^+} - m_{B_0}$

VALUE (MeV)	EVTS	DOCUMENT ID	TECN	COMMENT
571 ± 19 OUR FIT				
571 ± 13 ± 14	7k	¹ AAIJ	15AB LHCB	$p\bar{p}$ at 7, 8 TeV

• • • We do not use the following data for averages, fits, limits, etc. • • •

595 ± 26 ± 14	7k	² AAIJ	15AB LHCB	$p\bar{p}$ at 7, 8 TeV
---------------	----	-------------------	-----------	------------------------

¹ AAIJ 15AB reports $[m_{B_J^+} - m_{B_0}] - m_{\pi^+} = 431 \pm 13 \pm 14$ MeV which we adjust by

the π^+ mass. The masses inside the square brackets were measured for each candidate event. The result assumes $P = (-1)^J$ and uses two relativistic Breit-Wigner functions in the fit for mass difference.

² AAIJ 15AB reports $[m_{B_J^+} - m_{B_0}] - m_{\pi^+} = 455 \pm 26 \pm 14$ MeV which we adjust by

the π^+ mass. The masses inside the square brackets were measured for each candidate event. The result assumes $P = (-1)^J$ and uses three relativistic Breit-Wigner functions in the fit for mass difference.

 $m_{B_J(5840)^+} - m_{B^0}$

VALUE (MeV)	EVTS	DOCUMENT ID	TECN	COMMENT
• • • We do not use the following data for averages, fits, limits, etc. • • •				
565 ± 15 ± 14	7k	¹ AAIJ	15AB LHCB	$p\bar{p}$ at 7, 8 TeV

¹ AAIJ 15AB reports $[m_{B_J^+} - m_{B^0}] - (m_{B^{*+}} - m_{B^+}) - m_{\pi^+} = 425 \pm 15 \pm 14$

MeV which we adjust by the π^+ mass. The masses inside the square brackets were measured for each candidate event. The result assumes $P = (-1)^J$, $(m_{B^0} - m_{B_0}) = (m_{B^{*+}} - m_{B^+}) = 45.01 \pm 0.30 \pm 0.23$ MeV, and uses three relativistic Breit-Wigner functions in the fit for mass difference.

 $B_J(5840)^0$ MASSOUR FIT uses m_{B^+} and $m_{B_J(5840)^0} - m_{B^+}$ to determine $m_{B_J(5840)^0}$.

VALUE (MeV)	DOCUMENT ID
5863 ± 9 OUR FIT	

See key on page 1171

Meson Particle Listings

$B_J(5840), B_J(5970)$

$m_{B_J(5840)^0} - m_{B^+}$

VALUE (MeV)	EVTS	DOCUMENT ID	TECN	COMMENT
584 ± 9 OUR FIT				
584 ± 5 ± 7	12k	¹ AAIJ	15AB LHCB	pp at 7, 8 TeV
• • • We do not use the following data for averages, fits, limits, etc. • • •				
610 ± 22 ± 7	12k	² AAIJ	15AB LHCB	pp at 7, 8 TeV

¹ AAIJ 15AB reports $[m_{B_J^0} - m_{B^+}] - m_{\pi^-} = 444 \pm 5 \pm 7$ MeV which we adjust by the π^- mass. The masses inside the square brackets were measured for each candidate event. The result assumes $P = (-1)^J$ and uses two relativistic Breit-Wigner functions in the fit for mass difference.

² AAIJ 15AB reports $[m_{B_J^0} - m_{B^+}] - m_{\pi^-} = 471 \pm 22 \pm 7$ MeV which we adjust by the π^- mass. The masses inside the square brackets were measured for each candidate event. The result assumes $P = (-1)^J$ and uses three relativistic Breit-Wigner functions in the fit for mass difference.

$m_{B_J(5840)^0} - m_{B^{*+}}$

VALUE (MeV)	EVTS	DOCUMENT ID	TECN	COMMENT
584 ± 5 ± 7	12k	¹ AAIJ	15AB LHCB	pp at 7, 8 TeV
• • • We do not use the following data for averages, fits, limits, etc. • • •				
¹ AAIJ 15AB reports $[m_{B_J^0} - m_{B^{*+}}] - (m_{B^{*+}} - m_{B^+}) - m_{\pi^-} = 444 \pm 5 \pm 7$ MeV				

which we adjust by the π^- mass. The masses inside the square brackets were measured for each candidate event. The result assumes $P = -(-1)^J$, $(m_{B^{*+}} - m_{B^+}) = 45.01 \pm 0.30 \pm 0.23$ MeV, and uses three relativistic Breit-Wigner functions in the fit for mass difference.

$B_J(5840)$ WIDTH

$B_J(5840)^+$ WIDTH

VALUE (MeV)	EVTS	DOCUMENT ID	TECN	COMMENT
224 ± 24 ± 80	7k	¹ AAIJ	15AB LHCB	pp at 7, 8 TeV
• • • We do not use the following data for averages, fits, limits, etc. • • •				
215 ± 27 ± 80	7k	² AAIJ	15AB LHCB	pp at 7, 8 TeV
229 ± 27 ± 80	7k	³ AAIJ	15AB LHCB	pp at 7, 8 TeV

¹ Assuming $P = (-1)^J$ and using two relativistic Breit-Wigner functions in the fit for mass difference.

² Assuming $P = (-1)^J$ and using three relativistic Breit-Wigner functions in the fit for mass difference.

³ Assuming $P = -(-1)^J$ and using three relativistic Breit-Wigner functions in the fit for mass difference.

$B_J(5840)^0$ WIDTH

VALUE (MeV)	EVTS	DOCUMENT ID	TECN	COMMENT
127 ± 17 ± 34	12k	¹ AAIJ	15AB LHCB	pp at 7, 8 TeV
• • • We do not use the following data for averages, fits, limits, etc. • • •				
107 ± 20 ± 34	12k	² AAIJ	15AB LHCB	pp at 7, 8 TeV
119 ± 17 ± 34	12k	³ AAIJ	15AB LHCB	pp at 7, 8 TeV

¹ Assuming $P = (-1)^J$ and using two relativistic Breit-Wigner functions in the fit for mass difference.

² Assuming $P = (-1)^J$ and using three relativistic Breit-Wigner functions in the fit for mass difference.

³ Assuming $P = -(-1)^J$ and using three relativistic Breit-Wigner functions in the fit for mass difference.

$B_J(5840)$ DECAY MODES

Mode	Fraction (Γ_i/Γ)
Γ_1 $B^* \pi$	seen
Γ_2 $B \pi$	possibly seen

$B_J(5840)$ BRANCHING RATIOS

$\Gamma(B^* \pi)/\Gamma_{\text{total}}$					Γ_1/Γ
VALUE	EVTS	DOCUMENT ID	TECN	CHG	COMMENT
seen	7k	AAIJ	15AB LHCB	\pm	pp at 7, 8 TeV
seen	12k	AAIJ	15AB LHCB	0	pp at 7, 8 TeV

$\Gamma(B \pi)/\Gamma_{\text{total}}$					Γ_2/Γ
VALUE	EVTS	DOCUMENT ID	TECN	CHG	COMMENT
possibly seen	7k	¹ AAIJ	15AB LHCB	\pm	pp at 7, 8 TeV
possibly seen		¹ AAIJ	15AB LHCB	0	pp at 7, 8 TeV

¹ A $B \pi$ decay is forbidden from a $P = -(-1)^J$ parent, whereas $B^* \pi$ is allowed.

$B_J(5840)$ REFERENCES

AAIJ	15AB JHEP 1504 024	R. Aaij <i>et al.</i>	(LHCb Collab.)
------	--------------------	-----------------------	----------------

$B_J(5970)$

$$I(J^P) = \frac{1}{2}(?^?)$$

I, J, P need confirmation.

Quantum numbers shown are quark-model predictions.

$B_J(5970)$ MASS

$B_J(5970)^+$ MASS

OUR FIT uses m_{B^0} and $m_{B_J(5970)^+} - m_{B^0}$ to determine $m_{B_J(5970)^+}$.

VALUE (MeV)	DOCUMENT ID
5965 ± 5 OUR FIT	

$m_{B_J(5970)^+} - m_{B^0}$

VALUE (MeV)	EVTS	DOCUMENT ID	TECN	COMMENT
685 ± 5 OUR FIT				
685 ± 5 OUR AVERAGE				
685.3 ± 4.1 ± 2.5	2k	¹ AAIJ	15AB LHCB	pp at 7, 8 TeV
681 ± 5 ± 12	1.4k	² AALTONEN	14i CDF	$p\bar{p}$ at 1.96 TeV
• • • We do not use the following data for averages, fits, limits, etc. • • •				
686.8 ± 4.5 ± 2.5	2k	³ AAIJ	15AB LHCB	pp at 7, 8 TeV

¹ AAIJ 15AB reports $[m_{B_J^+} - m_{B^0}] - m_{\pi^+} = 545.8 \pm 4.1 \pm 2.5$ MeV which we adjust by the π^+ mass. The masses inside the square brackets were measured for each candidate event. The result assumes $P = (-1)^J$ and uses two relativistic Breit-Wigner functions in the fit for mass difference.

² AALTONEN 14i reports $m_{B_J(5970)^+} - m_{B^0} - m_{\pi^+} = 541 \pm 5 \pm 12$ MeV which we adjust by the π^+ mass.

³ AAIJ 15AB reports $[m_{B_J^+} - m_{B^0}] - m_{\pi^+} = 547 \pm 5 \pm 3$ MeV which we adjust by the π^+ mass. The masses inside the square brackets were measured for each candidate event. The result assumes $P = (-1)^J$ and uses three relativistic Breit-Wigner functions in the fit for mass difference.

$m_{B_J(5970)^+} - m_{B^{*0}}$

VALUE (MeV)	EVTS	DOCUMENT ID	TECN	COMMENT
686.0 ± 4.0 ± 2.5	2k	¹ AAIJ	15AB LHCB	pp at 7, 8 TeV
• • • We do not use the following data for averages, fits, limits, etc. • • •				
¹ AAIJ 15AB reports $[m_{B_J^+} - m_{B^{*0}}] - (m_{B^{*0}} - m_{B^+}) - m_{\pi^+} = 547 \pm 4 \pm 3$ MeV				

we adjust by the π^+ mass. The masses inside the square brackets were measured for each candidate event. The result assumes $P = -(-1)^J$, $(m_{B^{*0}} - m_{B^0}) = (m_{B^{*+}} - m_{B^+}) = 45.01 \pm 0.30 \pm 0.23$ MeV, and uses three relativistic Breit-Wigner functions in the fit for mass difference.

$B_J(5970)^0$ MASS

OUR FIT uses m_{B^+} and $m_{B_J(5970)^0} - m_{B^+}$ to determine $m_{B_J(5970)^0}$.

VALUE (MeV)	DOCUMENT ID
5971 ± 5 OUR FIT	

$m_{B_J(5970)^0} - m_{B^+}$

VALUE (MeV)	EVTS	DOCUMENT ID	TECN	COMMENT
691 ± 5 OUR FIT				
691 ± 5 OUR AVERAGE				
689.9 ± 2.9 ± 5.1	10k	¹ AAIJ	15AB LHCB	pp at 7, 8 TeV
698 ± 5 ± 12	2.6k	² AALTONEN	14i CDF	$p\bar{p}$ at 1.96 TeV
• • • We do not use the following data for averages, fits, limits, etc. • • •				
714.3 ± 6.4 ± 5.1	10k	³ AAIJ	15AB LHCB	pp at 7, 8 TeV

¹ AAIJ 15AB reports $[m_{B_J^0} - m_{B^+}] - m_{\pi^-} = 550.4 \pm 2.9 \pm 5.1$ MeV which we adjust by the π^- mass. The masses inside the square brackets were measured for each candidate event. The result assumes $P = (-1)^J$ and uses two relativistic Breit-Wigner functions in the fit for mass difference.

² AALTONEN 14i reports $m_{B_J(5970)^0} - m_{B^+} - m_{\pi^-} = 558 \pm 5 \pm 12$ MeV which we adjust by the π^- mass.

³ AAIJ 15AB reports $[m_{B_J^0} - m_{B^+}] - m_{\pi^-} = 575 \pm 6 \pm 5$ MeV which we adjust by the π^- mass. The masses inside the square brackets were measured for each candidate event. The result assumes $P = (-1)^J$ and uses three relativistic Breit-Wigner functions in the fit for mass difference.

$m_{B_J(5970)^0} - m_{B^{*+}}$

VALUE (MeV)	EVTS	DOCUMENT ID	TECN	COMMENT
691.6 ± 3.7 ± 5.1	10k	¹ AAIJ	15AB LHCB	pp at 7, 8 TeV
• • • We do not use the following data for averages, fits, limits, etc. • • •				
¹ AAIJ 15AB reports $[m_{B_J^0} - m_{B^{*+}}] - (m_{B^{*+}} - m_{B^+}) - m_{\pi^-} = 552 \pm 4 \pm 5$ MeV				

which we adjust by the π^- mass. The masses inside the square brackets were measured for each candidate event. The result assumes $P = -(-1)^J$, $(m_{B^{*+}} - m_{B^+}) = 45.01 \pm 0.30 \pm 0.23$ MeV, and uses three relativistic Breit-Wigner functions in the fit for mass difference.

Meson Particle Listings

 $B_J(5970)$ $B_J(5970)$ WIDTH $B_J(5970)^+$ WIDTH

VALUE (MeV)	EVTS	DOCUMENT ID	TECN	COMMENT
62±20 OUR AVERAGE				
63±15±17	2k	¹ AAIJ	15AB LHCb	pp at 7, 8 TeV
60 ⁺³⁰ ₋₂₀ ±40	1.4k	AALTONEN	14i CDF	$p\bar{p}$ at 1.96 TeV
61±14±17	2k	² AAIJ	15AB LHCb	pp at 7, 8 TeV
61±15±17	2k	³ AAIJ	15AB LHCb	pp at 7, 8 TeV

• • • We do not use the following data for averages, fits, limits, etc. • • •

¹ Assuming $P = (-1)^J$ and using two relativistic Breit-Wigner functions in the fit for mass difference.

² Assuming $P = (-1)^J$ and using three relativistic Breit-Wigner functions in the fit for mass difference.

³ Assuming $P = -(-1)^J$ and using three relativistic Breit-Wigner functions in the fit for mass difference.

 $B_J(5970)^0$ WIDTH

VALUE (MeV)	EVTS	DOCUMENT ID	TECN	COMMENT
81±12 OUR AVERAGE				
82± 8± 9	10k	¹ AAIJ	15AB LHCb	pp at 7, 8 TeV
70 ⁺³⁰ ₋₂₀ ±30	2.6k	AALTONEN	14i CDF	$p\bar{p}$ at 1.96 TeV
56± 7± 9	10k	² AAIJ	15AB LHCb	pp at 7, 8 TeV
82±10± 9	10k	³ AAIJ	15AB LHCb	pp at 7, 8 TeV

• • • We do not use the following data for averages, fits, limits, etc. • • •

¹ Assuming $P = (-1)^J$ and using two relativistic Breit-Wigner functions in the fit for mass difference.

² Assuming $P = (-1)^J$ and using three relativistic Breit-Wigner functions in the fit for mass difference.

³ Assuming $P = -(-1)^J$ and using three relativistic Breit-Wigner functions in the fit for mass difference.

 $B_J(5970)$ DECAY MODES

Mode	Fraction (Γ_i/Γ)
Γ_1 $B\pi$	possibly seen
Γ_2 $B^*\pi$	seen

 $B_J(5970)$ BRANCHING RATIOS

$\Gamma(B\pi)/\Gamma_{\text{total}}$					Γ_1/Γ
VALUE	EVTS	DOCUMENT ID	TECN	CHG	COMMENT
possibly seen	2k	¹ AAIJ	15AB LHCb	±	pp at 7, 8 TeV
possibly seen	10k	¹ AAIJ	15AB LHCb	0	pp at 7, 8 TeV
possibly seen	2.6k	AALTONEN	14i CDF	0	$p\bar{p}$ at 1.96 TeV
possibly seen	1.4k	AALTONEN	14i CDF	±	$p\bar{p}$ at 1.96 TeV

¹ A $B\pi$ decay is forbidden from a $P = -(-1)^J$ parent, whereas $B^*\pi$ is allowed.

$\Gamma(B^*\pi)/\Gamma_{\text{total}}$					Γ_2/Γ
VALUE	EVTS	DOCUMENT ID	TECN	CHG	COMMENT
seen	10k	AAIJ	15AB LHCb	0	pp at 7, 8 TeV
seen	2k	AAIJ	15AB LHCb	±	pp at 7, 8 TeV
seen	2.6k	AALTONEN	14i CDF	0	$p\bar{p}$ at 1.96 TeV
seen	1.4k	AALTONEN	14i CDF	±	$p\bar{p}$ at 1.96 TeV

 $B_J(5970)$ REFERENCES

AAIJ	15AB JHEP 1504 024	R. Aaij et al.	(LHCb Collab.)
AALTONEN	14i PR D90 012013	T. Aaltonen et al.	(CDF Collab.)

BOTTOM, STRANGE MESONS
($B = \pm 1, S = \mp 1$)

$B_s^0 = s\bar{b}, \bar{B}_s^0 = \bar{s}b$, similarly for B_s^{*0} s

B_s^0

$I(J^P) = 0(0^-)$

I, J, P need confirmation. Quantum numbers shown are quark-model predictions.

B_s^0 MASS

VALUE (MeV)	EVTS	DOCUMENT ID	TECN	COMMENT
5366.93 ± 0.10 OUR FIT				
5366.91 ± 0.11 OUR AVERAGE				
5366.98 ± 0.07 ± 0.13		¹ AAIJ	21c LHCb	pp at 7, 8, 13 TeV
5366.85 ± 0.19 ± 0.13		² AAIJ	19u LHCb	pp at 7, 8, 13 TeV
5366.83 ± 0.25 ± 0.27		³ AAIJ	18Ac LHCb	pp at 7, 8, 13 TeV
5367.08 ± 0.38 ± 0.15	128	⁴ AAIJ	16u LHCb	pp at 7, 8 TeV
5366.90 ± 0.28 ± 0.23		⁵ AAIJ	12E LHCb	pp at 7 TeV
5364.4 ± 1.3 ± 0.7		LOUVOT	09 BELL	$e^+e^- \rightarrow \Upsilon(5S)$
5366.01 ± 0.73 ± 0.33		⁶ ACOSTA	06 CDF	$p\bar{p}$ at 1.96 TeV
5369.9 ± 2.3 ± 1.3	32	⁷ ABE	96B CDF	$p\bar{p}$ at 1.8 TeV
5374 ± 16 ± 2	3	ABREU	94D DLPH	$e^+e^- \rightarrow Z$
5359 ± 19 ± 7	1	⁷ AKERS	94J OPAL	$e^+e^- \rightarrow Z$
5368.6 ± 5.6 ± 1.5	2	BUSKULIC	93G ALEP	$e^+e^- \rightarrow Z$
• • • We do not use the following data for averages, fits, limits, etc. • • •				
5370 ± 1 ± 3		DRUTSKOY	07A BELL	Repl. by LOUVOT 09
5370 ± 4.0	6	⁸ AKERS	94J OPAL	$e^+e^- \rightarrow Z$
5383.3 ± 4.5 ± 5.0	14	ABE	93F CDF	Repl. by ABE 96B

- ¹ Uses $B_s^0 \rightarrow J/\psi \pi^+ \pi^- K^+ K^-$ decays.
- ² Uses $B_s^0 \rightarrow J/\psi p\bar{p}$ decays.
- ³ Uses $B_s \rightarrow \chi_{c1} K^+ K^-$ mode.
- ⁴ Uses $J/\psi \rightarrow \mu^+ \mu^-, \phi \rightarrow K^+ K^-$ decays, and observes 128 ± 13 events of $B_s^0 \rightarrow J/\psi \phi$.
- ⁵ Uses $B_s^0 \rightarrow J/\psi \phi$ fully reconstructed decays.
- ⁶ Uses exclusively reconstructed final states containing a $J/\psi \rightarrow \mu^+ \mu^-$ decays.
- ⁷ From the decay $B_s \rightarrow J/\psi(1S) \phi$.
- ⁸ From the decay $B_s \rightarrow D_s^- \pi^+$.

$m_{B_s^0} - m_B$

m_B is the average of our B masses ($m_{B^\pm} + m_{B^0}$)/2.

VALUE (MeV)	CL%	DOCUMENT ID	TECN	COMMENT
87.37 ± 0.12 OUR FIT				
87.42 ± 0.24 OUR AVERAGE				
87.60 ± 0.44 ± 0.09		¹ AAIJ	15u LHCb	pp at 7, 8 TeV
87.42 ± 0.30 ± 0.09		² AAIJ	12E LHCb	pp at 7 TeV
86.64 ± 0.80 ± 0.08		³ ACOSTA	06 CDF	$p\bar{p}$ at 1.96 TeV

- • • We use the following data for averages but not for fits. • • •
- 89.7 ± 2.7 ± 1.2
- • • We do not use the following data for averages, fits, limits, etc. • • •
- 80 to 130

- ¹ The reported result is $m_{B_s^0} - m_{B^0} = 87.45 \pm 0.44 \pm 0.09$ MeV. We convert it to the mass difference with respect to the average of ($m_{B^\pm} + m_{B^0}$)/2. Uses the mode $B_s^0 \rightarrow \psi(2S) K^- \pi^+$.
- ² The reported result is $m_{B_s^0} - m_{B^+} = 87.52 \pm 0.30 \pm 0.12$ MeV. We convert it to the mass difference with respect to the average of ($m_{B^\pm} + m_{B^0}$)/2.
- ³ The reported result is $m_{B_s^0} - m_{B^0} = 86.38 \pm 0.90 \pm 0.06$ MeV. We convert it to the mass difference with respect to the average of ($m_{B^\pm} + m_{B^0}$)/2.

$m_{B_{SH}^0} - m_{B_{SL}^0}$

See the $B_s^0 - \bar{B}_s^0$ MIXING section near the end of these B_s^0 Listings.

B_s^0 MEAN LIFE

The mean B_s^0 lifetime is defined and computed as $1/\Gamma_{B_s^0}$, where $\Gamma_{B_s^0}$ is the average decay width of the B_s^0 mass eigenstates.

VALUE (10^{-12} s)	EVTS	DOCUMENT ID	TECN	COMMENT
1.520 ± 0.005 OUR EVALUATION				(Produced by HFLAV)

• • • We do not use the following data for averages, fits, limits, etc. • • •

1.518 ± 0.041 ± 0.027		¹ AALTONEN	11AP CDF	$p\bar{p}$ at 1.96 TeV
1.398 ± 0.044 ± 0.028 -0.13 -0.025		² ABAZOV	06V D0	$p\bar{p}$ at 1.96 TeV
1.42 ± 0.14 ± 0.03 -0.13		³ ABREU	00Y DLPH	$e^+e^- \rightarrow Z$
1.53 ± 0.16 ± 0.07 -0.15		⁴ ABREU,P	00G DLPH	$e^+e^- \rightarrow Z$
1.36 ± 0.09 ± 0.06 -0.05		⁵ ABE	99D CDF	$p\bar{p}$ at 1.8 TeV
1.72 ± 0.20 ± 0.18 -0.19 -0.17		⁶ ACKERSTAFF	98F OPAL	$e^+e^- \rightarrow Z$
1.50 ± 0.16 ± 0.04 -0.15		⁵ ACKERSTAFF	98G OPAL	$e^+e^- \rightarrow Z$
1.47 ± 0.14 ± 0.08		⁴ BARATE	98C ALEP	$e^+e^- \rightarrow Z$
1.51 ± 0.11		⁷ BARATE	98C ALEP	$e^+e^- \rightarrow Z$
1.56 ± 0.29 ± 0.08 -0.26 -0.07		⁵ ABREU	96F DLPH	Repl. by ABREU 00Y
1.65 ± 0.34 ± 0.12 -0.31		⁴ ABREU	96F DLPH	Repl. by ABREU 00Y
1.76 ± 0.20 ± 0.15 -0.10		⁸ ABREU	96F DLPH	Repl. by ABREU 00Y
1.60 ± 0.26 ± 0.13 -0.15		⁹ ABREU	96F DLPH	Repl. by ABREU,P 00G
1.67 ± 0.14		¹⁰ ABREU	96F DLPH	$e^+e^- \rightarrow Z$
1.61 ± 0.30 ± 0.18 -0.29 -0.16	90	⁴ BUSKULIC	96E ALEP	Repl. by BARATE 98C
1.54 ± 0.14 ± 0.04 -0.13		⁵ BUSKULIC	96M ALEP	$e^+e^- \rightarrow Z$
1.42 ± 0.27 ± 0.11 -0.23	76	⁵ ABE	95R CDF	Repl. by ABE 99D
1.74 ± 1.08 ± 0.07 -0.69	8	¹¹ ABE	95R CDF	Sup. by ABE 96N
1.54 ± 0.25 ± 0.06 -0.21	79	⁵ AKERS	95G OPAL	Repl. by ACKERSTAFF 98G
1.59 ± 0.17 ± 0.03 -0.15	134	⁵ BUSKULIC	95O ALEP	Sup. by BUSKULIC 96M
0.96 ± 0.37	41	¹² ABREU	94E DLPH	Sup. by ABREU 96F
1.92 ± 0.45 ± 0.04 -0.35	31	⁵ BUSKULIC	94C ALEP	Sup. by BUSKULIC 95O
1.13 ± 0.35 ± 0.09 -0.26	22	⁵ ACTON	93H OPAL	Sup. by AKERS 95G

- ¹ AALTONEN 11AP combines the fully reconstructed $B_s^0 \rightarrow D_s^- \pi^+$ decays and partially reconstructed $B_s^0 \rightarrow D_s X$ decays.
- ² Measured using $D_s \mu^+$ vertices.
- ³ Uses $D_s^- \ell^+$, and $\phi \ell^+$ vertices.
- ⁴ Measured using D_s hadron vertices.
- ⁵ Measured using $D_s^- \ell^+$ vertices.
- ⁶ ACKERSTAFF 98F use fully reconstructed $D_s^- \rightarrow \phi \pi^-$ and $D_s^- \rightarrow K^*0 K^-$ in the inclusive B_s^0 decay.
- ⁷ Combined results from $D_s^- \ell^+$ and D_s hadron.
- ⁸ Measured using $\phi \ell$ vertices.
- ⁹ Measured using inclusive D_s vertices.
- ¹⁰ Combined result for the four ABREU 96F methods.
- ¹¹ Exclusive reconstruction of $B_s \rightarrow \psi \phi$.
- ¹² ABREU 94E uses the flight-distance distribution of D_s vertices, ϕ -lepton vertices, and $D_s \mu$ vertices.

$\Gamma_{B_s^0}$

"OUR EVALUATION" includes the measurements of $\Gamma_{B_s^0}$ and $\Delta\Gamma_{B_s^0}$ listed in this section, as well as constraints from effective lifetimes with pure CP modes and flavor-specific modes.

VALUE (10^{12} s ⁻¹)	DOCUMENT ID	TECN	COMMENT
0.6581 ± 0.0022 OUR EVALUATION			Error includes scale factor of 2.5. (Produced by HFLAV)
0.6611 ± 0.0028 OUR AVERAGE			Error includes scale factor of 2.0. See the ideogram below.
0.6527 ⁺ ± 0.0013 ± 0.0022 -0.0015	¹ AAIJ	24A LHCb	pp at 13 TeV
0.6687 ± 0.0015 ± 0.0022	^{2,3} AAD	21AE ATLS	pp at 13 TeV
0.608 ± 0.018 ± 0.012	⁴ AAIJ	21AN LHCb	pp at 7, 8 TeV
0.6531 ± 0.0042 ± 0.0026	^{3,5} SIRUNYAN	21E CMS	pp at 13 TeV
0.650 ± 0.006 ± 0.004	⁶ AAIJ	17V LHCb	pp at 7, 8 TeV
0.676 ± 0.004 ± 0.004	^{3,7} AAD	16AP ATLS	pp at 8 TeV
0.668 ± 0.011 ± 0.006	⁸ AAIJ	16AK LHCb	pp at 7, 8 TeV
0.6704 ± 0.0043 ± 0.0055	³ KHACHATRY..	16S CMS	pp at 8 TeV
0.6603 ± 0.0027 ± 0.0015	⁹ AAIJ	15I LHCb	pp at 7, 8 TeV
0.677 ± 0.007 ± 0.004	³ AAD	14U ATLS	pp at 7 TeV
0.654 ± 0.008 ± 0.004	³ AALTONEN	12AJ CDF	$p\bar{p}$ at 1.96 TeV
0.693 ± 0.018 ± 0.017	³ ABAZOV	12D D0	$p\bar{p}$ at 1.96 TeV

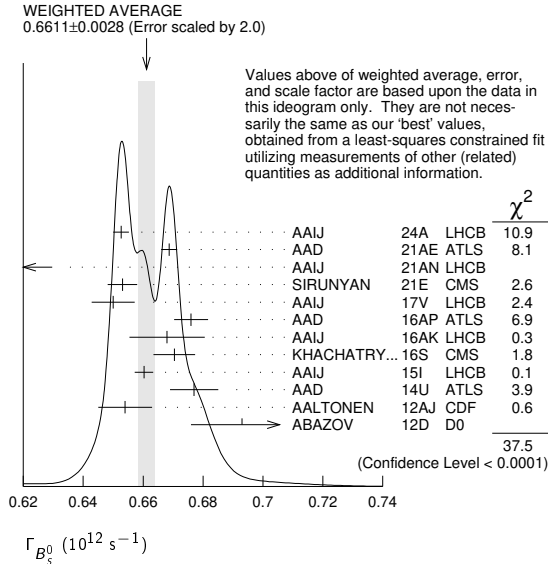
- • • We do not use the following data for averages, fits, limits, etc. • • •
- 0.6531 ± 0.0042 ± 0.0026
- 0.6563 ± 0.0021
- 0.661 ± 0.004 ± 0.006
- 0.677 ± 0.007 ± 0.004
- 0.657 ± 0.009 ± 0.008
- 0.654 ± 0.011 ± 0.005
- ³ SIRUNYAN 21E CMS pp at 13 TeV
- ³ AAIJ 19Q LHCb Repl. by AAIJ 24A
- ¹⁰ AAIJ 13AR LHCb Repl. by AAIJ 15I
- ³ AAD 12CV ATLS Repl. by AAD 14U
- ³ AAIJ 12D LHCb Repl. by AAIJ 13AR
- ^{3,11} AALTONEN 12D CDF Repl. by AALTONEN 12AJ

Meson Particle Listings

B_s^0

0.672 ± 0.027 ± 0.013	³ ABAZOV	09E D0	Repl. by ABAZOV 08AM
0.658 ± 0.017 ± 0.009	^{3,12} AALTONEN	08J CDF	Repl. by AALTONEN 12D
0.658 ± 0.022 ± 0.004	³ ABAZOV	08AMD0	Repl. by ABAZOV 12D
0.658 ± 0.035 ± 0.0130 -0.004	^{3,12} ABAZOV	07 D0	Repl. by ABAZOV 09E
0.714 ± 0.007 ± 0.010 -0.008	^{3,12} ACOSTA	05 CDF	Repl. by AALTONEN 08J

- 1 Reports $\Gamma_s - \Gamma_d = -0.0056^{+0.0013}_{-0.0015} \pm 0.0014 \text{ ps}^{-1}$ using a time-dependent angular analysis of $B_s^0 \rightarrow J/\psi K^+ K^-$ decays and the current B^0 lifetime of $1.517 \pm 0.004 \text{ ps}^{-1}$.
- 2 Reports a combination of $.6703 \pm 0.0014 \pm 0.0018 \text{ ps}^{-1}$ with AAD 16AP.
- 3 Measured using a time-dependent angular analysis of $B_s^0 \rightarrow J/\psi \phi$ decays.
- 4 Measured using a time-dependent angular analysis of $B_s^0 \rightarrow J/\psi \phi$ decays with $J/\psi \rightarrow e^+ e^-$.
- 5 Reports a combination of $0.6590 \pm 0.0032 \pm 0.0023 \text{ ps}^{-1}$ with KHACHATRYAN 16s.
- 6 Measured using time-dependent angular analysis of $B_s^0 \rightarrow J/\psi K^+ K^-$ in the region $m(KK) > 1.05 \text{ GeV}$.
- 7 Reports a combination of $0.675 \pm 0.003 \pm 0.003 \text{ ps}^{-1}$ with AAD 14U.
- 8 Measured using a time-dependent angular analysis of $B_s^0 \rightarrow \psi(2S) \phi$ decays.
- 9 Measured using a time-dependent angular analysis of $B_s^0 \rightarrow J/\psi K^+ K^-$ decays.
- 10 Measured using a combined time-dependent angular analysis of $B_s^0 \rightarrow J/\psi K^+ K^-$ and $B_s^0 \rightarrow J/\psi \pi^+ \pi^-$ decays.
- 11 Assuming CPV phase $\phi_s = -0.04$.
- 12 Assuming CPV phase $\phi_s = 0$.



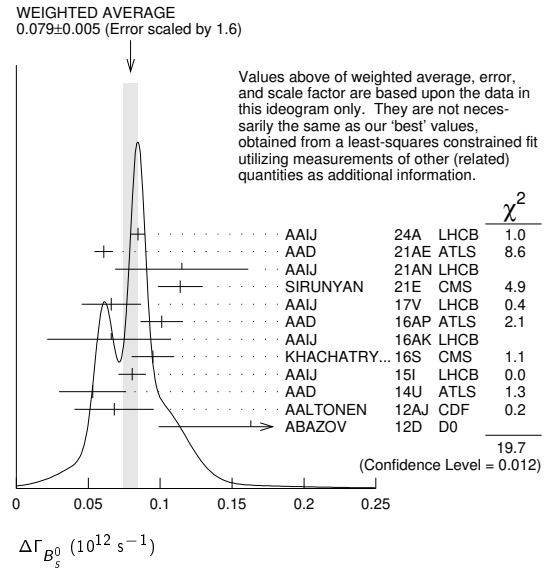
$\Delta\Gamma_{B_s^0}$

"OUR EVALUATION" includes the measurements of $\Gamma_{B_s^0}$ and $\Delta\Gamma_{B_s^0}$ listed in this section, as well as constraints from effective lifetimes with pure CP modes and flavor-specific modes.

VALUE (10^{12} s^{-1})	DOCUMENT ID	TECN	COMMENT
0.083 ± 0.005 OUR EVALUATION	Error includes scale factor of 1.8. (Produced by HFLAV)		
0.079 ± 0.005 OUR AVERAGE	Error includes scale factor of 1.6. See the ideogram below.		
0.0845 ± 0.0044 ± 0.0024	¹ AAIJ	24A LHCb	pp at 13 TeV
0.0607 ± 0.0047 ± 0.0043	^{2,3} AAD	21AE ATLS	pp at 13 TeV
0.115 ± 0.045 ± 0.011	⁴ AAIJ	21AN LHCb	pp at 7, 8 TeV
0.114 ± 0.014 ± 0.007	^{2,5} SIRUNYAN	21E CMS	pp at 13 TeV
0.066 ± 0.018 ± 0.010	⁶ AAIJ	17V LHCb	pp at 7, 8 TeV
0.101 ± 0.013 ± 0.007	^{2,7} AAD	16AP ATLS	pp at 8 TeV
0.066 ± 0.041 ± 0.007 -0.044	⁸ AAIJ	16AK LHCb	pp at 7, 8 TeV
0.095 ± 0.013 ± 0.007	² KHACHATRY... 16s	CMS	pp at 8 TeV
0.0805 ± 0.0091 ± 0.0032	¹ AAIJ	15I LHCb	pp at 7, 8 TeV
0.053 ± 0.021 ± 0.010	² AAD	14U ATLS	pp at 7 TeV
0.068 ± 0.026 ± 0.009	² AALTONEN	12AJ CDF	p \bar{p} at 1.96 TeV
0.163 ± 0.065 ± 0.064 -0.064	^{2,9} ABAZOV	12D D0	p \bar{p} at 1.96 TeV
• • • We do not use the following data for averages, fits, limits, etc. • • •			
0.077 ± 0.008 ± 0.003	¹ AAIJ	19Q LHCb	Repl. by AAIJ 24A
0.106 ± 0.011 ± 0.007	¹⁰ AAIJ	13AR LHCb	Repl. by AAIJ 15I
0.053 ± 0.021 ± 0.010	² AAD	12CV ATLS	Repl. by AAD 14U
0.123 ± 0.029 ± 0.011	² AAIJ	12D LHCb	Repl. by AAIJ 13AR
0.075 ± 0.035 ± 0.006	¹¹ AALTONEN	12D CDF	Repl. by AALTONEN 12AJ

0.085 ± 0.072 ± 0.001 -0.078	¹² ABAZOV	09E D0	Repl. by ABAZOV 08AM
0.076 ± 0.059 ± 0.006 -0.063	¹³ AALTONEN	08J CDF	Repl. by AALTONEN 12D
0.19 ± 0.07 ± 0.01	^{2,14} ABAZOV	08AMD0	Repl. by ABAZOV 12D
0.12 ± 0.08 ± 0.02 -0.10	^{13,15} ABAZOV	07 D0	Repl. by ABAZOV 07N
0.13 ± 0.09	¹⁶ ABAZOV	07N D0	Repl. by ABAZOV 09E
0.47 ± 0.19 ± 0.01 -0.24	¹³ ACOSTA	05 CDF	Repl. by AALTONEN 08J

- 1 Measured using time-dependent angular analysis of $B_s^0 \rightarrow J/\psi K^+ K^-$ decays.
- 2 Measured using the time-dependent angular analysis of $B_s^0 \rightarrow J/\psi \phi$ decays.
- 3 Reports a combination of $0.0657 \pm 0.0043 \pm 0.0037 \text{ ps}^{-1}$ with AAD 16AP.
- 4 Measured using a time-dependent angular analysis of $B_s^0 \rightarrow J/\psi \phi$ decays with $J/\psi \rightarrow e^+ e^-$.
- 5 Reports a combination of $0.1032 \pm 0.0095 \pm 0.0048 \text{ ps}^{-1}$ with KHACHATRYAN 16s.
- 6 Measured using time-dependent angular analysis of $B_s^0 \rightarrow J/\psi K^+ K^-$ in the region $m(KK) > 1.05 \text{ GeV}$.
- 7 Reports a combination of $0.066^{+0.041}_{-0.044} \pm 0.007 \text{ ps}^{-1}$ with AAD 14U.
- 8 Measured using time-dependent angular analysis of $B_s^0 \rightarrow \psi(2S) \phi$ decays.
- 9 The error includes both statistical and systematic uncertainties.
- 10 AAIJ 13AR result comes from a combined fit to $B_s^0 \rightarrow J/\psi K^+ K^-$ and $B_s^0 \rightarrow J/\psi \pi^+ \pi^-$ data sets. Also reports $\Delta\Gamma_s = 0.100 \pm 0.016 \pm 0.003 \text{ ps}^{-1}$ from a fit to $B_s^0 \rightarrow J/\psi K^+ K^-$ decays.
- 11 Uses the time-dependent angular analysis of $B_s^0 \rightarrow J/\psi \phi$ decays and assuming CP-violating angle $\beta_s(B^0 \rightarrow J/\psi \phi) = 0.02$.
- 12 Measured the angular and lifetime parameters for the time-dependent angular untagged decays $B_d^0 \rightarrow J/\psi K^{*0}$ and $B_s^0 \rightarrow J/\psi \phi$.
- 13 Measured using the time-dependent angular analysis of $B_s^0 \rightarrow J/\psi \phi$ decays and assuming CP-violating phase $\phi_s = 0$.
- 14 Obtains 90% CL interval $-0.06 < \Delta\Gamma_s < 0.30$.
- 15 ABAZOV 07 reports $0.17 \pm 0.09 \pm 0.02$ with CP-violating phase ϕ_s as a free parameter.
- 16 Combines D^0 measurements of time-dependent angular distributions in $B_s^0 \rightarrow J/\psi \phi$ and charge asymmetry in semileptonic decays. There is a 4-fold ambiguity in the solution.



$\Delta\Gamma_{B_s^0}/\Gamma_{B_s^0}$

$\Gamma_{B_s^0}$ and $\Delta\Gamma_{B_s^0}$ are the decay rate average and difference between two B_s^0 CP eigenstates (light - heavy). "OUR EVALUATION" is derived from the averages of $\Gamma_{B_s^0}$ and $\Delta\Gamma_{B_s^0}$ (and their correlation).

VALUE	CL%	DOCUMENT ID	TECN	COMMENT
0.127 ± 0.007 OUR EVALUATION		(Produced by HFLAV)		
• • • We do not use the following data for averages, fits, limits, etc. • • •				
0.090 ± 0.009 ± 0.023		¹ ESEN	13 BELL	$e^+ e^- \rightarrow \Upsilon(5S)$
		² AAIJ	12D LHCb	pp at 7 TeV
		³ AALTONEN	12D CDF	p \bar{p} at 1.96 TeV
		⁴ ABAZOV	12D D0	p \bar{p} at 1.96 TeV
0.147 ± 0.036 ± 0.042 -0.030 - 0.041		¹ ESEN	10 BELL	$e^+ e^- \rightarrow \Upsilon(5S)$
0.072 ± 0.021 ± 0.022		⁵ ABAZOV	09I D0	p \bar{p} at 1.96 TeV
> 0.012	95	⁵ AALTONEN	08F CDF	p \bar{p} at 1.96 TeV
0.116 ± 0.09 ± 0.010 -0.10		⁶ AALTONEN	08J CDF	Repl. by AALTONEN 12D

See key on page 1171

Meson Particle Listings

B_s^0

$0.079^{+0.038+0.031}_{-0.035-0.030}$	5	ABAZOV	07Y D0	Repl. by ABAZOV 09I
$0.24^{+0.28+0.03}_{-0.38-0.04}$	6,7	ABAZOV	05W D0	Repl. by ABAZOV 08AM
$0.65^{+0.25}_{-0.33} \pm 0.01$	6	ACOSTA	05 CDF	Repl. by AALTONEN 08J
<0.46	95	8 ABREU	00Y DLPH	$e^+e^- \rightarrow Z$
<0.69	95	9 ABREU,P	00G DLPH	$e^+e^- \rightarrow Z$
$0.25^{+0.21}_{-0.14}$	10	BARATE	00K ALEP	$e^+e^- \rightarrow Z$
<0.83	95	11 ABE	99D CDF	$p\bar{p}$ at 1.8 TeV
<0.67	95	12 ACCIARRI	98S L3	$e^+e^- \rightarrow Z$

- 1 Assumes CP violation is negligible.
- 2 Measured using the time-dependent angular analysis of $B_s^0 \rightarrow J/\psi\phi$ decays.
- 3 Uses the time-dependent angular analysis of $B_s^0 \rightarrow J/\psi\phi$ decays and assuming CP-violating angle $\beta_s(B^0 \rightarrow J/\psi\phi) = 0.02$.
- 4 Measured using fully reconstructed $B_s \rightarrow J/\psi\phi$ decays.
- 5 Assumes $2\text{B}(B_s^0 \rightarrow D_s^{(*)} D_s^{(*)}) \approx \Delta\Gamma_s^{CP} / \Gamma_s$.
- 6 Measured using the time-dependent angular analysis of $B_s^0 \rightarrow J/\psi\phi$ decays.
- 7 Uses $|A_0|^2 - |A_{\parallel}|^2 = 0.355 \pm 0.066$ from ACOSTA 05.
- 8 Uses $D_s^- \ell^+$, and $\phi \ell^+$ vertices.
- 9 Measured using D_s hadron vertices.
- 10 Uses $\phi\phi$ correlations from $B_s^0 \rightarrow D_s^{(*)+} D_s^{(*)-}$.
- 11 ABE 99D assumes $\tau_{B_s^0} = 1.55 \pm 0.05$ ps.
- 12 ACCIARRI 98S assumes $\tau_{B_s^0} = 1.49 \pm 0.06$ ps and PDG 98 values of b production fraction.

B_{sH}^0 MEAN LIFE

B_{sH}^0 is the heavy mass state of two B_s^0 CP eigenstates.

VALUE (10^{-12} s)	DOCUMENT ID	TECN	COMMENT
1.622 ± 0.008 OUR EVALUATION	(Produced by HFLAV)		

• • • We do not use the following data for averages, fits, limits, etc. • • •

$0.99^{+0.42}_{-0.07} \pm 0.17$	1	AAD	23BY ATLS	pp at 13 TeV
$1.83^{+0.23}_{-0.20} \pm 0.04$	1	TUMASYAN	23A CMS	pp at 13 TeV
$2.07 \pm 0.29 \pm 0.03$	1	AAIJ	22 LHCB	pp at 7, 8, 13 TeV
$1.70^{+0.60}_{-0.43} \pm 0.09$	1	SIRUNYAN	20AG CMS	pp at 7, 8, 13 TeV
$1.677 \pm 0.034 \pm 0.011$	2	SIRUNYAN	18BY CMS	pp at 8 TeV
$2.04 \pm 0.44 \pm 0.05$	1	AAIJ	17AI LHCB	pp at 7, 8, 13 TeV
$1.70 \pm 0.14 \pm 0.05$	3	ABAZOV	16C D0	$p\bar{p}$ at 1.96 TeV
$1.75 \pm 0.12 \pm 0.07$	4	AAIJ	13AB LHCB	pp at 7 TeV
$1.652 \pm 0.024 \pm 0.024$	5	AAIJ	13AR LHCB	pp at 7 TeV
$1.700 \pm 0.040 \pm 0.026$	6	AAIJ	12AN LHCB	pp at 7 TeV
	7	AALTONEN	12D CDF	$p\bar{p}$ at 1.96 TeV
$1.70^{+0.12}_{-0.11} \pm 0.03$	6	AALTONEN	11AB CDF	$p\bar{p}$ at 1.96 TeV
$1.613^{+0.123}_{-0.113}$	8,9	AALTONEN	08J CDF	Repl. by AALTONEN 12D
$1.58^{+0.39+0.01}_{-0.42-0.02}$	9	ABAZOV	05W D0	Repl. by ABAZOV 08AM
$2.07^{+0.58}_{-0.46} \pm 0.03$	9	ACOSTA	05 CDF	Repl. by AALTONEN 08J

- 1 Measured using $B_s \rightarrow \mu^+ \mu^-$ decays which, in the Standard Model, correspond to B_{sH}^0 decays. Assumes $-2\text{Re}(\lambda)/(1+|\lambda|^2) = 1$.
- 2 Measured using $B_s^0 \rightarrow J/\psi\pi^+\pi^-$ decays with $0.9240 < m(\pi\pi) < 1.0204$ GeV, which is dominated by the $f_0(980)$ resonance, making it a CP-odd state.
- 3 Measured using $J/\psi\pi^+\pi^-$ mode with $0.880 < m(\pi\pi) < 1.080$ GeV/ c^2 , which is mostly $J/\psi f(0)(980)$ mode, a pure CP-odd final state.
- 4 Measured using a pure CP-odd final state $J/\psi K_S^0$ with the assumption that contributions from penguin diagrams are small.
- 5 Measured using $B_s \rightarrow J/\psi\pi^+\pi^-$ decays which, in the limit of $\phi_s = 0$ and $|\lambda| = 1$, correspond to B_{sH}^0 decays.
- 6 Measured using a pure CP-odd final state $J/\psi f_0(980)$.
- 7 Uses the time-dependent angular analysis of $B_s^0 \rightarrow J/\psi\phi$ decays assuming CP-violating angle $\beta_s(B^0 \rightarrow J/\psi\phi) = 0.02$.
- 8 Obtained from $\Delta\Gamma_s$ and Γ_s fit with a correlation of 0.6.
- 9 Measured using the time-dependent angular analysis of $B_s^0 \rightarrow J/\psi\phi$ decays.

B_{sL}^0 MEAN LIFE

B_{sL}^0 is the light mass state of two B_s^0 CP eigenstates.

VALUE (10^{-12} s)	DOCUMENT ID	TECN	COMMENT
1.429 ± 0.006 OUR EVALUATION	(Produced by HFLAV)		

1.452 ± 0.016 OUR AVERAGE			
$1.445 \pm 0.016 \pm 0.008$	1,2	AAIJ	23P LHCB pp at 7, 8, 13 TeV
$1.479 \pm 0.034 \pm 0.011$	1	AAIJ	16AL LHCB pp at 7, 8 TeV

• • • We do not use the following data for averages, fits, limits, etc. • • •

1.40 ± 0.02	3	SIRUNYAN	18BY CMS	pp at 8 TeV
$1.379 \pm 0.026 \pm 0.017$	4	AAIJ	14F LHCB	pp at 7, 8 TeV
$1.407 \pm 0.016 \pm 0.007$	5	AAIJ	14R LHCB	pp at 7 TeV
$1.440 \pm 0.096 \pm 0.009$	5	AAIJ	12 LHCB	pp at 7 TeV
$1.455 \pm 0.046 \pm 0.006$	5	AAIJ	12R LHCB	Repl. by AAIJ 14R
	6	AALTONEN	12D CDF	$p\bar{p}$ at 1.96 TeV
$1.437^{+0.054}_{-0.047}$	7,8	AALTONEN	08J CDF	Repl. by AALTONEN 12D
$1.24^{+0.14+0.01}_{-0.11-0.02}$	8	ABAZOV	05W D0	Repl. by ABAZOV 08AM
$1.05^{+0.16}_{-0.13} \pm 0.02$	8	ACOSTA	05 CDF	Repl. by AALTONEN 08J
$1.27 \pm 0.33 \pm 0.08$	9	BARATE	00K ALEP	$e^+e^- \rightarrow Z$

- 1 Uses $B_s^0 \rightarrow J/\psi\eta$ decays.
- 2 AAIJ 23P reports a τ_L value combined with AAIJ 16AL result as $\tau_L = 1.452 \pm 0.014 \pm 0.007$ ps.
- 3 Measured using results in SIRUNYAN 18BY for the heavy B_s^0 lifetime obtained from $B_s^0 \rightarrow J/\psi\pi^+\pi^-$ decays and the average effective $B_s^0 \rightarrow J/\psi\phi$ lifetime, and magnitude squared of the CP-odd amplitude $|A_{\perp}|^2 = 0.250 \pm 0.006$. The uncertainty includes all statistical and systematic contributions.
- 4 Measured using $B_s^0 \rightarrow D_s^- D_s^+$. The effective lifetime is translated into a decay width of $\Gamma_L = 0.725 \pm 0.014 \pm 0.009$ ps $^{-1}$.
- 5 Measured using $B_s^0 \rightarrow K^+ K^-$ decays. There may still be CPV in the decay.
- 6 Uses the time-dependent angular analysis of $B_s^0 \rightarrow J/\psi\phi$ decays and assuming CP-violating angle $\beta_s(B^0 \rightarrow J/\psi\phi) = 0.02$.
- 7 Obtained from $\Delta\Gamma_s$ and Γ_s fit with a correlation of 0.6.
- 8 Measured using the time-dependent angular analysis of $B_s^0 \rightarrow J/\psi\phi$ decays.
- 9 Uses $\phi\phi$ correlations from $B_s^0 \rightarrow D_s^{(*)+} D_s^{(*)-}$.

B_s^0 MEAN LIFE (Flavor specific)

VALUE (10^{-12} s)	DOCUMENT ID	TECN	COMMENT
1.527 ± 0.011 OUR EVALUATION	(Produced by HFLAV)		

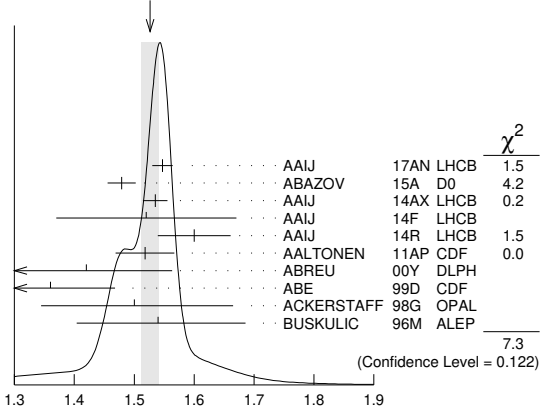
1.526 ± 0.015 OUR AVERAGE Error includes scale factor of 1.3. See the ideogram below.

$1.547 \pm 0.013 \pm 0.011$	1	AAIJ	17AN LHCB	pp at 7, 8 TeV
$1.479 \pm 0.010 \pm 0.021$	2	ABAZOV	15A D0	$p\bar{p}$ at 1.96 TeV
$1.535 \pm 0.015 \pm 0.014$	3	AAIJ	14AX LHCB	pp at 7 TeV
$1.52 \pm 0.15 \pm 0.01$	4	AAIJ	14F LHCB	pp at 7, 8 TeV
$1.60 \pm 0.06 \pm 0.01$	5	AAIJ	14R LHCB	pp at 7 TeV
$1.518 \pm 0.041 \pm 0.027$	6	AALTONEN	11AP CDF	$p\bar{p}$ at 1.96 TeV
$1.42^{+0.14}_{-0.13} \pm 0.03$	7	ABREU	00Y DLPH	$e^+e^- \rightarrow Z$
$1.36 \pm 0.09^{+0.06}_{-0.05}$	8	ABE	99D CDF	$p\bar{p}$ at 1.8 TeV
$1.50^{+0.16}_{-0.15} \pm 0.04$	8	ACKERSTAFF	98G OPAL	$e^+e^- \rightarrow Z$
$1.54^{+0.14}_{-0.13} \pm 0.04$	8	BUSKULIC	96M ALEP	$e^+e^- \rightarrow Z$

• • • We do not use the following data for averages, fits, limits, etc. • • •

$1.398 \pm 0.044^{+0.028}_{-0.025}$	9	ABAZOV	06V D0	Repl. by ABAZOV 15A
-------------------------------------	---	--------	--------	---------------------

WEIGHTED AVERAGE
 1.526 ± 0.015 (Error scaled by 1.3)



B_s^0 MEAN LIFE (Flavor specific)

- 1 AAIJ 17AN value was measured using $B_s^0 \rightarrow D_s^{(*)-} \mu^+ \nu_\mu$ decays relative to $B^0 \rightarrow D^{(*)-} \mu^+ \nu_\mu$ decays.
- 2 Measured using $B_s^0 \rightarrow D_s^- \mu^+ \nu_\mu$ X decays.
- 3 Measured using the $B_s^0 \rightarrow D_s^- \pi^+$ decays.
- 4 Measured using $B_s^0 \rightarrow D^+ D_s^-$.
- 5 Measured using $B_s^0 \rightarrow \pi^+ K^-$ decays.

Meson Particle Listings

 B_S^0

⁶ AALTONEN 11AP combines the fully reconstructed $B_S^0 \rightarrow D_S^- \pi^+$ decays and partially reconstructed $B_S^0 \rightarrow D_S^- X$ decays.

⁷ Uses $D_S^- \ell^+$, and $\phi \ell^+$ vertices.

⁸ Measured using $D_S^- \ell^+$ vertices.

⁹ Measured using $D_S^- \mu^+$ vertices.

 B_S^0 MEAN LIFE (partial) B_S^0 mean life ($B_S \rightarrow D_S^+ D_S^-$)

VALUE (10^{-12} s)	DOCUMENT ID	TECN	COMMENT
1.379 ± 0.031 OUR EVALUATION	(Produced by HFLAV)		
1.379 ± 0.026 ± 0.017	¹ AAIJ	14F LHCb	pp at 7, 8 TeV

¹ Measured using $B_S^0 \rightarrow D_S^- D_S^+$. The effective lifetime is translated into a decay width of $\Gamma_L = 0.725 \pm 0.014 \pm 0.009 \text{ ps}^{-1}$.

 B_S^0 mean life ($B_S \rightarrow J/\psi \phi$)

VALUE (10^{-12} s)	DOCUMENT ID	TECN	COMMENT
1.480 ± 0.007 OUR EVALUATION	(Produced by HFLAV)		
1.480 ± 0.007 OUR AVERAGE			

1.481 ± 0.007 ± 0.005	¹ SIRUNYAN	18BY CMS	pp at 8 TeV
1.480 ± 0.011 ± 0.005	¹ AAIJ	14E LHCb	pp at 7 TeV
1.444 \pm $\frac{+0.098}{-0.090}$ ± 0.020	¹ ABAZOV	05B D0	$p\bar{p}$ at 1.96 TeV

1.34 \pm $\frac{+0.23}{-0.19}$ ± 0.05

• • • We do not use the following data for averages, fits, limits, etc. • • •

1.39 \pm $\frac{+0.13}{-0.16}$ \pm $\frac{+0.01}{-0.02}$

1.34 \pm $\frac{+0.23}{-0.19}$ ± 0.05

¹ Measured using fully reconstructed $B_S \rightarrow J/\psi \phi$ decays.

² Measured using the time-dependent angular analysis of $B_S^0 \rightarrow J/\psi \phi$ decays.

³ ABE 96N uses 58 ± 12 exclusive $B_S \rightarrow J/\psi \phi$ events.

 B_S^0 mean life ($B_S \rightarrow J/\psi \eta$)

VALUE (10^{-12} s)	DOCUMENT ID	TECN	COMMENT
1.452 ± 0.016 OUR EVALUATION	(Produced by HFLAV)		
1.452 ± 0.016 OUR AVERAGE			

1.445 ± 0.016 ± 0.008	^{1,2} AAIJ	23P LHCb	pp at 7, 8, 13 TeV
1.479 ± 0.034 ± 0.011	¹ AAIJ	16L LHCb	pp at 7, 8 TeV

¹ Uses $B_S^0 \rightarrow J/\psi \eta$ decays.

² AAIJ 23P reports a τ_L value combined with AAIJ 16AL result as $\tau_L = 1.452 \pm 0.014 \pm 0.007 \text{ ps}$.

 B_S^0 mean life ($B_S \rightarrow J/\psi K_S^0$)

VALUE (10^{-12} s)	DOCUMENT ID	TECN	COMMENT
1.75 ± 0.14 OUR EVALUATION	(Produced by HFLAV)		
1.75 ± 0.12 ± 0.07	¹ AAIJ	13AB LHCb	pp at 7 TeV

¹ Measured using a pure CP -odd final state $J/\psi K_S^0$ with the assumption that contributions from penguin diagrams are small.

 B_S^0 mean life ($B_S \rightarrow J/\psi \pi^+ \pi^-$)

VALUE (10^{-12} s)	DOCUMENT ID	TECN	COMMENT
1.646 ± 0.013 OUR EVALUATION	(Produced by HFLAV)		
1.660 ± 0.022 OUR AVERAGE			

1.632 ± 0.013 ± 0.05	¹ AAIJ	19AF LHCb	pp at 13 TeV
1.677 ± 0.034 ± 0.011	² SIRUNYAN	18BY CMS	pp at 8 TeV
1.70 ± 0.14 ± 0.05	³ ABAZOV	16C D0	$p\bar{p}$ at 1.96 TeV
1.652 ± 0.024 ± 0.024	⁴ AAIJ	13AR LHCb	pp at 7 TeV
1.70 \pm $\frac{+0.12}{-0.11}$ ± 0.03	⁵ AALTONEN	11AB CDF	$p\bar{p}$ at 1.96 TeV

• • • We do not use the following data for averages, fits, limits, etc. • • •

1.700 ± 0.040 ± 0.026

¹ Based on $\Delta\Gamma = \Gamma_H - \Gamma_{B^0} = -0.05 \pm 0.004 \pm 0.004 \text{ ps}^{-1}$ and $\tau_{B^0} = 1.517 \pm 0.004 \text{ ps}$. The first error is due to the combined $\Delta\Gamma$ uncertainty and the second is from τ_{B^0} uncertainty.

² Measured using $B_S^0 \rightarrow J/\psi \pi^+ \pi^-$ decays with $0.9240 < m(\pi\pi) < 1.0204 \text{ GeV}$, which is dominated by the $f_0(980)$ resonance, making it a CP -odd state.

³ Measured using $J/\psi \pi^+ \pi^-$ mode with $0.880 < m(\pi\pi) < 1.080 \text{ GeV}/c^2$, which is mostly $J/\psi f_0(980)$ mode, a pure CP -odd final state.

⁴ Measured using $B_S \rightarrow J/\psi \pi^+ \pi^-$ decays which, in the limit of $\phi_S = 0$ and $|\lambda| = 1$, correspond to B_{SH}^0 decays.

⁵ Measured using a pure CP -odd final state $J/\psi f_0(980)$.

 B_S^0 mean life ($B_S \rightarrow K^+ K^-$)

VALUE (10^{-12} s)	DOCUMENT ID	TECN	COMMENT
1.408 ± 0.017 OUR EVALUATION	(Produced by HFLAV)		
1.408 ± 0.017 OUR AVERAGE			

1.407 ± 0.016 ± 0.007	¹ AAIJ	14R LHCb	pp at 7 TeV
1.440 ± 0.096 ± 0.009	¹ AAIJ	12 LHCb	pp at 7 TeV

¹ Measured using $B_S^0 \rightarrow K^+ K^-$ decays. There may still be CPV in the decay.

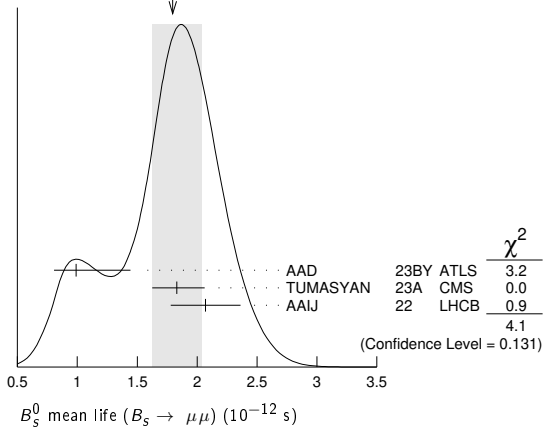
 B_S^0 mean life ($B_S \rightarrow \mu\mu$)

VALUE (10^{-12} s)	DOCUMENT ID	TECN	COMMENT
1.79 ± 0.17 OUR EVALUATION	(Produced by HFLAV)		

1.80 \pm $\frac{+0.24}{-0.18}$ OUR AVERAGE Error includes scale factor of 1.4. See the ideogram below.

0.99 \pm $\frac{+0.42}{-0.07}$ ± 0.17	¹ AAD	23BY ATLS	pp at 13 TeV
1.83 \pm $\frac{+0.23}{-0.20}$ ± 0.04	¹ TUMASYAN	23A CMS	pp at 13 TeV
2.07 ± 0.29 ± 0.03	¹ AAIJ	22 LHCb	pp at 7, 8, 13 TeV
• • •	We do not use the following data for averages, fits, limits, etc. • • •		
1.70 \pm $\frac{+0.60}{-0.43}$ ± 0.09	¹ SIRUNYAN	20AG CMS	Repl. by TUMASYAN 23A
2.04 ± 0.44 ± 0.05	¹ AAIJ	17AI LHCb	Repl. by AAIJ 22

¹ Measured using $B_S \rightarrow \mu^+ \mu^-$ decays which, in the Standard Model, correspond to B_{SH}^0 decays. Assumes $-2 \text{Re}(\lambda)/(1 + |\lambda|^2) = 1$.

WEIGHTED AVERAGE
1.80 ± 0.24 - 0.18 (Error scaled by 1.4) $\tau_{B_S^0}/\tau_{B^0}$ mean life ratio

$\tau_{B_S^0}/\tau_{B^0}$ (direct measurements)

VALUE	DOCUMENT ID	TECN	COMMENT
0.980 ± 0.006 ± 0.003	¹ SIRUNYAN	18BY CMS	pp at 8 TeV

¹ Measured using $B_S^0 \rightarrow J/\psi \phi(1020)$ and $B^0 \rightarrow J/\psi K^*(892)^0$ decays.

 $\Gamma_{B_S^0} - \Gamma_{B^0}$

VALUE (10^{12} s^{-1})	DOCUMENT ID	TECN	COMMENT
-0.0041 ± 0.0024 ± 0.0015	¹ AAIJ	19Q LHCb	pp at 13 TeV

¹ Measured using time-dependent angular analysis of $B_S^0 \rightarrow J/\psi K^+ K^-$ decays.

 $\Gamma_{B_{SH}^0} - \Gamma_{B^0}$

VALUE (10^{12} s^{-1})	DOCUMENT ID	TECN	COMMENT
-0.05 ± 0.004 ± 0.004	¹ AAIJ	19AF LHCb	pp at 7, 8, 13 TeV

¹ Measured in $B_S^0 \rightarrow J/\psi \pi^+ \pi^-$ decays.

 B_S^0 DECAY MODES

These branching fractions all scale with $B(\bar{B} \rightarrow B_S^0)$.

The branching fraction $B(B_S^0 \rightarrow D_S^- \ell^+ \nu_\ell \text{ anything})$ is not a pure measurement since the measured product branching fraction $B(\bar{B} \rightarrow B_S^0) \times B(B_S^0 \rightarrow D_S^- \ell^+ \nu_\ell \text{ anything})$ was used to determine $B(\bar{B} \rightarrow B_S^0)$, as described in the note on " B^0 - \bar{B}^0 Mixing"

For inclusive branching fractions, e.g., $B \rightarrow D^\pm \text{ anything}$, the values usually are multiplicities, not branching fractions. They can be greater than one.

Mode	Fraction (Γ_i/Γ)	Scale factor/ Confidence level
Γ_1 D_S^- anything	(62 ± 6) %	
Γ_2 D_S^\pm anything	(92 ± 11) %	
Γ_3 D^0/\bar{D}^0 anything	(38 ± 10) %	
Γ_4 $\ell \nu_\ell X$	(9.6 ± 0.8) %	
Γ_5 $e^+ \nu X^-$	(9.1 ± 0.8) %	
Γ_6 $\mu^+ \nu X^-$	(10.2 ± 1.0) %	
Γ_7 $D_S^- \ell^+ \nu_\ell$ anything	[a] (8.1 ± 1.3) %	
Γ_8 $D_S^- \ell^+ \nu_\ell$ anything	(5.4 ± 1.1) %	

See key on page 1171

Meson Particle Listings

B_s^0

Γ ₉	$D_s^- \mu^+ \nu_\mu$	(2.31 ± 0.21) %		Γ ₇₀	$J/\psi(1S) \rho, \rho \rightarrow \pi^+ \pi^-$	< 3.4	$\times 10^{-6}$	CL=90%
Γ ₁₀	$D_s^- \mu^+ \nu_\mu$	(5.2 ± 0.5) %		Γ ₇₁	$J/\psi(1S) f_0(980), f_0 \rightarrow$	(1.24 ± 0.15)	$\times 10^{-4}$	S=2.1
Γ ₁₁	$D_{s1}(2536)^- \mu^+ \nu_\mu, D_{s1}^- \rightarrow$ $D^{*-} K_S^0$	(2.7 ± 0.7) $\times 10^{-3}$		Γ ₇₂	$J/\psi(1S) f_2(1270), f_2 \rightarrow$	(1.0 ± 0.4)	$\times 10^{-6}$	
Γ ₁₂	$D_{s1}(2536)^- X \mu^+ \nu, D_{s1}^- \rightarrow$ $\bar{D}^0 K^+$	(4.4 ± 1.3) $\times 10^{-3}$		Γ ₇₃	$J/\psi(1S) f_2(1270)_0, f_2 \rightarrow$	(7.3 ± 1.7)	$\times 10^{-7}$	
Γ ₁₃	$D_{s2}(2573)^- X \mu^+ \nu, D_{s2}^- \rightarrow$ $\bar{D}^0 K^+$	(2.7 ± 1.0) $\times 10^{-3}$		Γ ₇₄	$J/\psi(1S) f_2(1270)_\parallel, f_2 \rightarrow$	(1.05 ± 0.33)	$\times 10^{-6}$	
Γ ₁₄	$K^- \mu^+ \nu_\mu$	(1.06 ± 0.09) $\times 10^{-4}$		Γ ₇₅	$J/\psi(1S) f_2(1270)_\perp, f_2 \rightarrow$	(1.3 ± 0.7)	$\times 10^{-6}$	
Γ ₁₅	$D_s^- \pi^+$	(2.98 ± 0.14) $\times 10^{-3}$		Γ ₇₆	$J/\psi(1S) f_0(1370), f_0 \rightarrow$	(4.4 ± 0.6)	$\times 10^{-5}$	
Γ ₁₆	$D_s^- \rho^+$	(6.8 ± 1.4) $\times 10^{-3}$		Γ ₇₇	$J/\psi(1S) f_0(1500), f_0 \rightarrow$	(2.04 ± 0.32)	$\times 10^{-5}$	
Γ ₁₇	$D_s^- \pi^+ \pi^+ \pi^-$	(6.1 ± 1.0) $\times 10^{-3}$		Γ ₇₈	$J/\psi(1S) f'_2(1525)_0, f'_2 \rightarrow$	(1.03 ± 0.22)	$\times 10^{-6}$	
Γ ₁₈	$D_{s1}(2536)^- \pi^+, D_{s1}^- \rightarrow$ $D_s^- \pi^+ \pi^-$	(2.4 ± 0.8) $\times 10^{-5}$		Γ ₇₉	$J/\psi(1S) f'_2(1525)_\parallel, f'_2 \rightarrow$	(1.2 ± 2.6)	$\times 10^{-7}$	
Γ ₁₉	$D_s^\mp K^\pm$	(2.25 ± 0.12) $\times 10^{-4}$		Γ ₈₀	$J/\psi(1S) f'_2(1525)_\perp, f'_2 \rightarrow$	(5 ± 4)	$\times 10^{-7}$	
Γ ₂₀	$D_{s1}(2536)^\mp K^\pm, D_{s1}^- \rightarrow$ $\bar{D}^*(2007)^0 K^-$	(2.48 ± 0.28) $\times 10^{-5}$		Γ ₈₁	$J/\psi(1S) f_0(1790), f_0 \rightarrow$	(4.9 ± 10.0)	$\times 10^{-6}$	
Γ ₂₁	$D_s^- K^+ \pi^+ \pi^-$	(3.2 ± 0.6) $\times 10^{-4}$		Γ ₈₂	$J/\psi(1S) \pi^+ \pi^-$ (nonresonant)	(1.74 ± 1.10)	$\times 10^{-5}$	
Γ ₂₂	$D_s^+ D_s^-$	(4.4 ± 0.5) $\times 10^{-3}$		Γ ₈₃	$J/\psi(1S) \bar{K}^0 \pi^+ \pi^-$	< 4.4	$\times 10^{-5}$	CL=90%
Γ ₂₃	$D_s^- D^+$	(2.8 ± 0.5) $\times 10^{-4}$		Γ ₈₄	$J/\psi(1S) K^+ K^-$	(7.9 ± 0.7)	$\times 10^{-4}$	
Γ ₂₄	$D^+ D^-$	(2.2 ± 0.6) $\times 10^{-4}$		Γ ₈₅	$J/\psi(1S) K^0 K^- \pi^+ + c.c.$	(9.5 ± 1.3)	$\times 10^{-4}$	
Γ ₂₅	$D^{*+} D^-$			Γ ₈₆	$J/\psi(1S) \bar{K}^0 K^+ K^-$	< 1.2	$\times 10^{-5}$	CL=90%
Γ ₂₆	$D^{*-} D^+$			Γ ₈₇	$J/\psi K^*(892)^0 \bar{K}^*(892)^0$	(1.10 ± 0.09)	$\times 10^{-4}$	
Γ ₂₇	$D^{*+} D^{*-}$	(2.14 ± 0.32) $\times 10^{-4}$		Γ ₈₈	$J/\psi(1S) f'_2(1525)$	(2.6 ± 0.6)	$\times 10^{-4}$	
Γ ₂₈	$D^0 \bar{D}^0$	(1.9 ± 0.5) $\times 10^{-4}$		Γ ₈₉	$J/\psi(1S) p \bar{p}$	(3.6 ± 0.4)	$\times 10^{-6}$	
Γ ₂₉	$D_s^{*-} \pi^+$	(1.9 ± 0.5) $\times 10^{-3}$		Γ ₉₀	$J/\psi(1S) \gamma$	< 7.3	$\times 10^{-6}$	CL=90%
Γ ₃₀	$D_s^{*\mp} K^\pm$	(1.32 ± 0.40) $\times 10^{-4}$		Γ ₉₁	$J/\psi \mu^+ \mu^-, J/\psi \rightarrow \mu^+ \mu^-$	< 2.6	$\times 10^{-9}$	CL=95%
Γ ₃₁	$D_s^{*-} \rho^+$	(9.5 ± 2.0) $\times 10^{-3}$		Γ ₉₂	$J/\psi(1S) \pi^+ \pi^- \pi^+ \pi^-$	(7.5 ± 0.8)	$\times 10^{-5}$	
Γ ₃₂	$D_s^{*+} D_s^- + D_s^{*-} D_s^+$	(1.39 ± 0.17) %		Γ ₉₃	$J/\psi(1S) f_1(1285)$	(7.2 ± 1.4)	$\times 10^{-5}$	
Γ ₃₃	$D_s^+ D_s^{*-}$	(1.44 ± 0.21) %	S=1.1	Γ ₉₄	$\psi(2S) \eta$	(3.3 ± 0.9)	$\times 10^{-4}$	
Γ ₃₄	$D_s^{(*)+} D_s^{*-}$	(4.5 ± 1.4) %		Γ ₉₅	$\psi(2S) \eta'$	(1.29 ± 0.35)	$\times 10^{-4}$	
Γ ₃₅	$D^{*-} D^+$	(3.9 ± 0.8) $\times 10^{-4}$		Γ ₉₆	$\psi(2S) \pi^+ \pi^-$	(6.9 ± 1.2)	$\times 10^{-5}$	
Γ ₃₆	$\bar{D}^{*0} \bar{K}^0$	(2.8 ± 1.1) $\times 10^{-4}$		Γ ₉₇	$\psi(2S) \phi$	(5.3 ± 0.4)	$\times 10^{-4}$	
Γ ₃₇	$\bar{D}^0 \bar{K}^0$	(4.3 ± 0.9) $\times 10^{-4}$		Γ ₉₈	$\psi(2S) K^0$	(1.9 ± 0.5)	$\times 10^{-5}$	
Γ ₃₈	$\bar{D}^0 K^- \pi^+$	(1.04 ± 0.13) $\times 10^{-3}$		Γ ₉₉	$\psi(2S) K^- \pi^+$	(3.1 ± 0.4)	$\times 10^{-5}$	
Γ ₃₉	$\bar{D}^*(2007)^0 K^- \pi^+$	(7.3 ± 2.6) $\times 10^{-4}$		Γ ₁₀₀	$\psi(2S) K^*(892)^0$	(3.3 ± 0.5)	$\times 10^{-5}$	
Γ ₄₀	$\bar{D}^0 \bar{K}^*(892)^0$	(4.4 ± 0.6) $\times 10^{-4}$		Γ ₁₀₁	$\chi_{c1} \phi$	(1.97 ± 0.25)	$\times 10^{-4}$	
Γ ₄₁	$\bar{D}^0 \bar{K}^*(1410)$	(3.9 ± 3.5) $\times 10^{-4}$		Γ ₁₀₂	$\chi_{c1} K^+ K^-$			
Γ ₄₂	$\bar{D}^0 \bar{K}_0^*(1430)$	(3.0 ± 0.7) $\times 10^{-4}$		Γ ₁₀₃	$\chi_{c2} K^+ K^-$			
Γ ₄₃	$\bar{D}^0 \bar{K}_2^*(1430)$	(1.1 ± 0.4) $\times 10^{-4}$		Γ ₁₀₄	$\chi_{c1}(3872) \phi$	(1.22 ± 0.35)	$\times 10^{-4}$	
Γ ₄₄	$\bar{D}^0 \bar{K}^*(1680)$	< 7.8	$\times 10^{-5}$	CL=90%	Γ ₁₀₅	$\chi_{c1}(3872) (K^+ K^-)_{non-\phi}$	(9.4 ± 3.4)	$\times 10^{-5}$
Γ ₄₅	$\bar{D}^0 \bar{K}_0^*(1950)$	< 1.1	$\times 10^{-4}$	CL=90%	Γ ₁₀₆	$\chi_{c1}(3872) \pi^+ \pi^-$	(4.6 ± 1.6)	$\times 10^{-5}$
Γ ₄₆	$\bar{D}^0 \bar{K}_2^*(1780)$	< 2.6	$\times 10^{-5}$	CL=90%	Γ ₁₀₇	$\pi^+ \pi^-$	(7.2 ± 1.0)	$\times 10^{-7}$
Γ ₄₇	$\bar{D}^0 \bar{K}_4^*(2045)$	< 3.1	$\times 10^{-5}$	CL=90%	Γ ₁₀₈	$\pi^0 \pi^0$	< 7.7	$\times 10^{-6}$
Γ ₄₈	$\bar{D}^0 K^- \pi^+$ (non-resonant)	(2.1 ± 0.8) $\times 10^{-4}$		Γ ₁₀₉	$\eta \pi^0$	< 1.0	$\times 10^{-3}$	CL=90%
Γ ₄₉	$D_{s2}^*(2573)^- \pi^+, D_{s2}^- \rightarrow$ $\bar{D}^0 K^-$	(2.6 ± 0.4) $\times 10^{-4}$		Γ ₁₁₀	$\eta \eta$	< 1.43	$\times 10^{-4}$	CL=90%
Γ ₅₀	$D_{s1}^*(2700)^- \pi^+, D_{s1}^- \rightarrow$ $\bar{D}^0 K^-$	(1.6 ± 0.8) $\times 10^{-5}$		Γ ₁₁₁	$\rho^0 \rho^0$	< 3.20	$\times 10^{-4}$	CL=90%
Γ ₅₁	$D_{s1}^*(2860)^- \pi^+, D_{s1}^- \rightarrow$ $\bar{D}^0 K^-$	(5 ± 4) $\times 10^{-5}$		Γ ₁₁₂	$\eta' K_S^0$	< 8.16	$\times 10^{-6}$	CL=90%
Γ ₅₂	$D_{s3}^*(2860)^- \pi^+, D_{s3}^- \rightarrow$ $\bar{D}^0 K^-$	(2.2 ± 0.6) $\times 10^{-5}$		Γ ₁₁₃	$\eta' \eta$	< 6.5	$\times 10^{-5}$	CL=90%
Γ ₅₃	$\bar{D}^0 K^+ K^-$	(5.6 ± 0.9) $\times 10^{-5}$		Γ ₁₁₄	$\eta' \eta'$	(3.3 ± 0.7)	$\times 10^{-5}$	
Γ ₅₄	$\bar{D}^0 f_0(980)$	< 3.1	$\times 10^{-6}$	CL=90%	Γ ₁₁₅	$\eta' \phi$	< 8.2	$\times 10^{-7}$
Γ ₅₅	$\bar{D}^0 \phi$	(2.30 ± 0.25) $\times 10^{-5}$		Γ ₁₁₆	$\phi f_0(980), f_0(980) \rightarrow \pi^+ \pi^-$	(1.12 ± 0.21)	$\times 10^{-6}$	
Γ ₅₆	$\bar{D}^{*0} \phi$	(3.2 ± 0.4) $\times 10^{-5}$		Γ ₁₁₇	$\phi f_2(1270), f_2(1270) \rightarrow$ $\pi^+ \pi^-$	(6.1 ± 1.8)	$\times 10^{-7}$	
Γ ₅₇	$D^{*\mp} \pi^\pm$	< 6.1	$\times 10^{-6}$	CL=90%	Γ ₁₁₈	$\phi \rho^0$	(2.7 ± 0.8)	$\times 10^{-7}$
Γ ₅₈	$\eta_c \phi$	(5.0 ± 0.9) $\times 10^{-4}$		Γ ₁₁₉	$\phi \pi^+ \pi^-$	(3.5 ± 0.5)	$\times 10^{-6}$	
Γ ₅₉	$\eta' X_{s\bar{s}}$			Γ ₁₂₀	$\phi \phi$	(1.85 ± 0.14)	$\times 10^{-5}$	
Γ ₆₀	$\eta_c \pi^+ \pi^-$	(1.8 ± 0.7) $\times 10^{-4}$		Γ ₁₂₁	$\phi \phi \phi$	(2.2 ± 0.6)	$\times 10^{-6}$	
Γ ₆₁	$J/\psi(1S) \phi$	(1.04 ± 0.04) $\times 10^{-3}$		Γ ₁₂₂	$\pi^+ K^-$	(5.9 ± 0.7)	$\times 10^{-6}$	
Γ ₆₂	$J/\psi(1S) \phi \phi$	(1.20 ± 0.14) $\times 10^{-5}$		Γ ₁₂₃	$K^+ K^-$	(2.72 ± 0.23)	$\times 10^{-5}$	
Γ ₆₃	$J/\psi(1S) \pi^0$	< 1.2	$\times 10^{-3}$	CL=90%	Γ ₁₂₄	$K^0 \bar{K}^0$	(1.76 ± 0.31)	$\times 10^{-5}$
Γ ₆₄	$J/\psi(1S) \eta$	(4.0 ± 0.7) $\times 10^{-4}$		Γ ₁₂₅	$K^0 \pi^+ \pi^-$	(9.5 ± 2.1)	$\times 10^{-6}$	
Γ ₆₅	$J/\psi(1S) K_S^0$	(1.92 ± 0.14) $\times 10^{-5}$		Γ ₁₂₆	$K^0 K^\pm \pi^\mp$	(8.4 ± 0.9)	$\times 10^{-5}$	
Γ ₆₆	$J/\psi(1S) \bar{K}^*(892)^0$	(4.1 ± 0.4) $\times 10^{-5}$	S=1.4	Γ ₁₂₇	$K^*(892)^- \pi^+$	(2.9 ± 1.1)	$\times 10^{-6}$	
Γ ₆₇	$J/\psi(1S) \eta'$	(3.3 ± 0.4) $\times 10^{-4}$		Γ ₁₂₈	$K^*(892)^\pm K^\mp$	(1.9 ± 0.5)	$\times 10^{-5}$	
Γ ₆₈	$J/\psi(1S) \pi^+ \pi^-$	(2.02 ± 0.17) $\times 10^{-4}$	S=1.7	Γ ₁₂₉	$K_0^*(1430)^\pm K^\mp$	(3.1 ± 2.5)	$\times 10^{-5}$	
Γ ₆₉	$J/\psi(1S) f_0(500), f_0 \rightarrow$ $\pi^+ \pi^-$	< 4	$\times 10^{-6}$	CL=90%	Γ ₁₃₀	$K_2^*(1430)^\pm K^\mp$	(1.0 ± 1.7)	$\times 10^{-5}$
				Γ ₁₃₁	$K^*(892)^0 \bar{K}^0 + c.c.$	(2.0 ± 0.6)	$\times 10^{-5}$	
				Γ ₁₃₂	$K_0^*(1430) \bar{K}^0 + c.c.$	(3.3 ± 1.0)	$\times 10^{-5}$	

Meson Particle Listings

 B_s^0

Γ_{133}	$K_S^*(1430)^0 \bar{K}^0 + c.c.$	$(1.7 \pm 2.2) \times 10^{-5}$	
Γ_{134}	$K_S^0 \bar{K}^*(892)^0 + c.c.$	$(1.6 \pm 0.4) \times 10^{-5}$	
Γ_{135}	$K_S^0 K^+ K^-$	$(1.3 \pm 0.6) \times 10^{-6}$	
Γ_{136}	$\bar{K}^*(892)^0 \rho^0$	$< 7.67 \times 10^{-4}$	CL=90%
Γ_{137}	$\bar{K}^*(892)^0 K^*(892)^0$	$(1.11 \pm 0.27) \times 10^{-5}$	
Γ_{138}	$K^*(892)^0 \bar{K}_S^*(1430)^0$		
Γ_{139}	$K_S^*(1430)^0 \bar{K}^*(892)^0$		
Γ_{140}	$K_S^*(1430)^0 \bar{K}_S^*(1430)^0$		
Γ_{141}	$\phi K^*(892)^0$	$(1.14 \pm 0.30) \times 10^{-6}$	
Γ_{142}	$\rho \bar{\rho}$	$< 4.4 \times 10^{-9}$	CL=90%
Γ_{143}	$\rho \bar{\rho} K^+ K^-$	$(4.5 \pm 0.5) \times 10^{-6}$	
Γ_{144}	$\rho \bar{\rho} K^+ \pi^-$	$(1.39 \pm 0.26) \times 10^{-6}$	
Γ_{145}	$\rho \bar{\rho} \pi^+ \pi^-$	$(4.3 \pm 2.0) \times 10^{-7}$	
Γ_{146}	$\rho \bar{\rho} \rho \bar{\rho}$	$(2.3 \pm 1.0) \times 10^{-8}$	
Γ_{147}	$\rho \bar{\Lambda} K^- + c.c.$	$(5.5 \pm 1.0) \times 10^{-6}$	
Γ_{148}	$\Lambda_c^- \Lambda \pi^+$	$(3.6 \pm 1.6) \times 10^{-4}$	
Γ_{149}	$\Lambda_c^- \Lambda_c^+$	$< 8.0 \times 10^{-5}$	CL=95%

Lepton Family number (LF) violating modes or $\Delta B = 1$ weak neutral current (BI) modes

Γ_{150}	$\gamma \gamma$	B1	$< 3.1 \times 10^{-6}$	CL=90%
Γ_{151}	$\phi \gamma$	B1	$(3.4 \pm 0.4) \times 10^{-5}$	
Γ_{152}	$\mu^+ \mu^-$	B1	$(3.34 \pm 0.27) \times 10^{-9}$	
Γ_{153}	$e^+ e^-$	B1	$< 9.4 \times 10^{-9}$	CL=90%
Γ_{154}	$\tau^+ \tau^-$	B1	$< 6.8 \times 10^{-3}$	CL=95%
Γ_{155}	$\mu^+ \mu^- \gamma$	B1	$< 2.0 \times 10^{-9}$	
Γ_{156}	$\mu^+ \mu^- \mu^+ \mu^-$	B1	$< 8.6 \times 10^{-10}$	CL=95%
Γ_{157}	$S P, S \rightarrow \mu^+ \mu^-,$ $P \rightarrow \mu^+ \mu^-$	B1	[b] $< 2.2 \times 10^{-9}$	CL=95%
Γ_{158}	$a \bar{a}, \bar{a} \rightarrow \mu^+ \mu^-$	B1	$< 5.8 \times 10^{-10}$	CL=95%
Γ_{159}	$\phi(1020) \mu^+ \mu^-$	B1	$(8.4 \pm 0.4) \times 10^{-7}$	
Γ_{160}	$f_2'(1525) \mu^+ \mu^-$	B1	$(1.62 \pm 0.22) \times 10^{-7}$	
Γ_{161}	$\bar{K}^*(892)^0 \mu^+ \mu^-$	B1	$(2.9 \pm 1.1) \times 10^{-8}$	
Γ_{162}	$\pi^+ \pi^- \mu^+ \mu^-$	B1	$(8.4 \pm 1.7) \times 10^{-8}$	
Γ_{163}	$\phi \nu \bar{\nu}$	B1	$< 5.4 \times 10^{-3}$	CL=90%
Γ_{164}	$e^\pm \mu^\mp$	LF [c]	$< 5.4 \times 10^{-9}$	CL=90%
Γ_{165}	$e^\pm \tau^\mp$	LF	$< 1.4 \times 10^{-3}$	CL=90%
Γ_{166}	$\mu^\pm \tau^\mp$	LF	$< 4.2 \times 10^{-5}$	CL=95%
Γ_{167}	$\phi \mu^\pm e^\mp$	LF	$< 1.6 \times 10^{-8}$	CL=90%
Γ_{168}	$\rho \mu^-$	L,B	$< 1.21 \times 10^{-8}$	CL=90%

- [a] Not a pure measurement. See note at head of B_s^0 Decay Modes.
 [b] Here S and P are the hypothetical scalar and pseudoscalar particles with masses of 2.5 GeV/c² and 214.3 MeV/c², respectively.
 [c] The value is for the sum of the charge states or particle/antiparticle states indicated.

FIT INFORMATION

An overall fit to 12 branching ratios uses 20 measurements to determine 7 parameters. The overall fit has a $\chi^2 = 27.0$ for 13 degrees of freedom.

The following off-diagonal array elements are the correlation coefficients $\langle \delta x_i \delta x_j \rangle / (\delta x_i \delta x_j)$, in percent, from the fit to the branching fractions, $x_i \equiv \Gamma_i / \Gamma_{\text{total}}$.

x_{17}	17					
x_{19}	82	14				
x_{61}	0	0	0			
x_{68}	0	0	0	43		
x_{71}	0	0	0	31	52	
x_{120}	0	0	0	15	6	5
	x_{15}	x_{17}	x_{19}	x_{61}	x_{68}	x_{71}

 B_s^0 BRANCHING RATIOS

$\Gamma(D_s^- \text{ anything}) / \Gamma_{\text{total}}$	Γ_1 / Γ
0.62 ± 0.06 OUR AVERAGE	
0.602 ± 0.058 ± 0.023	1 WANG 22 BELL $e^+ e^- \rightarrow \Upsilon(5S)$
0.91 ± 0.18 ± 0.41	2 DRUTSKOY 07 BELL $e^+ e^- \rightarrow \Upsilon(4S)$
0.81 ± 0.24 ± 0.22	3 BUSKULIC 96E ALEP $e^+ e^- \rightarrow Z$
1.56 ± 0.58 ± 0.44	4 ACTON 92N OPAL $e^+ e^- \rightarrow Z$

¹ WANG 22 selects the B_s events by tagging the accompanying B_s via partial reconstruction of the semileptonic decays $B_s \rightarrow D_s X \ell^+ \nu$.

² The extraction of this result takes into account the correlation between the measurements of $B(\Upsilon(5S) \rightarrow D_s X)$ and $B(\Upsilon(5S) \rightarrow D^0 X)$.

³ BUSKULIC 96E separate $c\bar{c}$ and $b\bar{b}$ sources of D_s^+ mesons using a lifetime tag, subtract generic $\bar{b} \rightarrow W^+ \rightarrow D_s^+$ events, and obtain $B(\bar{b} \rightarrow B_s^0) \times B(B_s^0 \rightarrow D_s^- \text{ anything}) = 0.088 \pm 0.020 \pm 0.020$ assuming $B(D_s \rightarrow \phi\pi) = (3.5 \pm 0.4) \times 10^{-2}$ and PDG 1994 values for the relative partial widths to other D_s channels. We evaluate using our current values $B(\bar{b} \rightarrow B_s^0) = 0.107 \pm 0.014$ and $B(D_s \rightarrow \phi\pi) = 0.036 \pm 0.009$. Our first error is their experiment's and our second error is that due to $B(\bar{b} \rightarrow B_s^0)$ and $B(D_s \rightarrow \phi\pi)$.

⁴ ACTON 92N assume that excess of $147 \pm 48 D_s^0$ events over that expected from $B^0, B^+,$ and $c\bar{c}$ is all from B_s^0 decay. The product branching fraction is measured to be $B(\bar{b} \rightarrow B_s^0) B(B_s^0 \rightarrow D_s^- \text{ anything}) \times B(D_s^- \rightarrow \phi\pi^-) = (5.9 \pm 1.9 \pm 1.1) \times 10^{-3}$. We evaluate using our current values $B(\bar{b} \rightarrow B_s^0) = 0.107 \pm 0.014$ and $B(D_s \rightarrow \phi\pi) = 0.036 \pm 0.009$. Our first error is their experiment's and our second error is that due to $B(\bar{b} \rightarrow B_s^0)$ and $B(D_s \rightarrow \phi\pi)$.

$\Gamma(D_s^\pm \text{ anything}) / \Gamma_{\text{total}}$	Γ_2 / Γ		
0.92 ± 0.11			
VALUE	DOCUMENT ID	TECN	COMMENT
	ZHUKOVA 23	BELL	$e^+ e^- \rightarrow \Upsilon(5S)$

$\Gamma(D^0 / \bar{D}^0 \text{ anything}) / \Gamma(D_s^\pm \text{ anything})$	Γ_3 / Γ_2		
0.416 ± 0.018 ± 0.092			
VALUE	DOCUMENT ID	TECN	COMMENT
	ZHUKOVA 23	BELL	$e^+ e^- \rightarrow \Upsilon(5S)$

$\Gamma(\ell \nu_e X) / \Gamma_{\text{total}}$	Γ_4 / Γ		
9.6 ± 0.8 OUR AVERAGE			
VALUE (units 10^{-2})	DOCUMENT ID	TECN	COMMENT
9.6 ± 0.4 ± 0.7	1 OSWALD 13	BELL	$e^+ e^- \rightarrow \Upsilon(5S)$
9.5 ^{+2.5+1.1} _{-2.0-1.9}	2 LEES 12A	BABR	$e^+ e^-$

¹ The measurement corresponds to the average of the electron and muon branching fractions.

² The measurement corresponds to a branching fraction where the lepton originates from bottom decay and is the average between the electron and muon branching fractions. LEES 12A uses the correlation of the production of ϕ mesons in association with a lepton in $e^+ e^-$ data taken at center-of-mass energies between 10.54 and 11.2 GeV.

$\Gamma(e^+ \nu X^-) / \Gamma_{\text{total}}$	Γ_5 / Γ		
9.1 ± 0.5 ± 0.6			
VALUE (units 10^{-2})	DOCUMENT ID	TECN	COMMENT
	OSWALD 13	BELL	$e^+ e^- \rightarrow \Upsilon(5S)$

$\Gamma(\mu^+ \nu X^-) / \Gamma_{\text{total}}$	Γ_6 / Γ		
10.2 ± 0.6 ± 0.8			
VALUE (units 10^{-2})	DOCUMENT ID	TECN	COMMENT
	OSWALD 13	BELL	$e^+ e^- \rightarrow \Upsilon(5S)$

$\Gamma(D_s^- \ell^+ \nu_\ell \text{ anything}) / \Gamma_{\text{total}}$	Γ_7 / Γ			
8.1 ± 1.3 OUR AVERAGE				
VALUE (units 10^{-2})	EVTS	DOCUMENT ID	TECN	COMMENT
8.2 ± 0.2 ± 1.5	134	1 OSWALD 15	BELL	$e^+ e^- \rightarrow \Upsilon(5S)$
7.6 ± 1.2 ± 2.1		2 BUSKULIC 95o	ALEP	$e^+ e^- \rightarrow Z$
10.7 ± 4.3 ± 2.9		3 ABREU 92M	DLPH	$e^+ e^- \rightarrow Z$
10.3 ± 3.6 ± 2.8	18	4 ACTON 92N	OPAL	$e^+ e^- \rightarrow Z$

• • • We do not use the following data for averages, fits, limits, etc. • • •

- 13 ± 4 ± 4 27 ⁵ BUSKULIC 92E ALEP $e^+ e^- \rightarrow Z$
¹ Obtains $B_s \rightarrow D_s X e \nu$, and $D_s X \mu \nu$ separately, then combines them by assuming systematic uncertainties are fully correlated, except for the one on lepton identification. The third uncertainty adds in quadrature systematic uncertainties from external sources (number of B_s events, and $D_s^{(*)}$ branching fractions). OSWALD 15 also measures the cross-section $\sigma(e^+ e^- \rightarrow B_s^{(*)} \bar{B}_s^{(*)}) = 53.8 \pm 1.4 \pm 5.3$ pb at $\sqrt{s} = 10.86$ GeV.
² BUSKULIC 95o use $D_s \ell$ correlations. The measured product branching ratio is $B(\bar{b} \rightarrow B_s) \times B(B_s \rightarrow D_s^- \ell^+ \nu_\ell \text{ anything}) = (0.82 \pm 0.09^{+0.13}_{-0.14})\%$ assuming $B(D_s \rightarrow \phi\pi) = (3.5 \pm 0.4) \times 10^{-2}$ and PDG 1994 values for the relative partial widths to the six other D_s channels used in this analysis. Combined with results from $\Upsilon(4S)$ experiments this can be used to extract $B(\bar{b} \rightarrow B_s) = (11.0 \pm 1.2^{+2.2}_{-2.6})\%$. We evaluate using our current values $B(\bar{b} \rightarrow B_s^0) = 0.107 \pm 0.014$ and $B(D_s \rightarrow \phi\pi) = 0.036 \pm 0.009$. Our first error is their experiment's and our second error is that due to $B(\bar{b} \rightarrow B_s^0)$ and $B(D_s \rightarrow \phi\pi)$.
³ ABREU 92M measured muons only and obtained product branching ratio $B(Z \rightarrow bor \bar{b}) \times B(\bar{b} \rightarrow B_s) \times B(B_s \rightarrow D_s \mu^+ \nu_\mu \text{ anything}) \times B(D_s \rightarrow \phi\pi) = (18 \pm 8) \times 10^{-5}$. We evaluate using our current values $B(\bar{b} \rightarrow B_s^0) = 0.107 \pm 0.014$ and $B(D_s \rightarrow \phi\pi) = 0.036 \pm 0.009$. Our first error is their experiment's and our second error is that due to $B(\bar{b} \rightarrow B_s^0)$ and $B(D_s \rightarrow \phi\pi)$. We use $B(Z \rightarrow bor \bar{b}) = 2B(Z \rightarrow b \bar{b}) = 2 \times (0.2212 \pm 0.0019)$.
⁴ ACTON 92N is measured using $D_s \rightarrow \phi\pi^+$ and $K^*(892)^0 K^+$ events. The product branching fraction measured is measured to be $B(\bar{b} \rightarrow B_s^0) B(B_s^0 \rightarrow D_s^- \ell^+ \nu_\ell \text{ anything}) \times B(D_s^- \rightarrow \phi\pi^-) = (3.9 \pm 1.1 \pm 0.8) \times 10^{-4}$. We evaluate using our current values

$B(\bar{D} \rightarrow B_s^0) = 0.107 \pm 0.014$ and $B(D_s \rightarrow \phi\pi) = 0.036 \pm 0.009$. Our first error is their experiment's and our second error is that due to $B(\bar{D} \rightarrow B_s^0)$ and $B(D_s \rightarrow \phi\pi)$.

⁵ BUSKULIC 92E is measured using $D_s \rightarrow \phi\pi^+$ and $K^*(892)^0 K^+$ events. They use $2.7 \pm 0.7\%$ for the $\phi\pi^+$ branching fraction. The average product branching fraction is measured to be $B(\bar{D} \rightarrow B_s^0)B(B_s^0 \rightarrow D_s^- \ell^+ \nu_\ell \text{ anything}) = 0.020 \pm 0.0055_{-0.006}^{+0.005}$. We evaluate using our current values $B(\bar{D} \rightarrow B_s^0) = 0.107 \pm 0.014$ and $B(D_s \rightarrow \phi\pi) = 0.036 \pm 0.009$. Our first error is their experiment's and our second error is that due to $B(\bar{D} \rightarrow B_s^0)$ and $B(D_s \rightarrow \phi\pi)$. Superseded by BUSKULIC 950.

$\Gamma(D_s^{*-} \ell^+ \nu_\ell \text{ anything})/\Gamma_{\text{total}}$ Γ_8/Γ

VALUE (units 10^{-2})	DOCUMENT ID	TECN	COMMENT
5.4 ± 0.4 ± 1.0	¹ OSWALD	15	BELL $e^+e^- \rightarrow \Upsilon(5S)$

¹ Obtains $B_s \rightarrow D_s^* X e \nu$, and $D_s^* X \mu \nu$ separately, then combines them by assuming systematic uncertainties are fully correlated, except for the one on lepton identification. The third uncertainty adds in quadrature systematic uncertainties from external sources (number of B_s events, and $D_s^{(*)}$ branching fractions). OSWALD 15 also measures the cross-section $\sigma(e^+e^- \rightarrow B_s^{(*)} \bar{B}_s^{(*)}) = 53.8 \pm 1.4 \pm 5.3$ pb at $\sqrt{s} = 10.86$ GeV.

$\Gamma(D_s^- \mu^+ \nu_\mu)/\Gamma_{\text{total}}$ Γ_9/Γ

VALUE (units 10^{-2})	DOCUMENT ID	TECN	COMMENT
2.31 ± 0.20 ± 0.07	¹ AAIJ	20E	LHCB pp at 7, 8 TeV

¹ AAIJ 20E reports $[\Gamma(B_s^0 \rightarrow D_s^- \mu^+ \nu_\mu)/\Gamma_{\text{total}}] / [B(B^0 \rightarrow D^- \ell^+ \nu_\ell)] = 1.09 \pm 0.05 \pm 0.06 \pm 0.05$ which we multiply by our best value $B(B^0 \rightarrow D^- \ell^+ \nu_\ell) = (2.12 \pm 0.06) \times 10^{-2}$. Our first error is their experiment's error and our second error is the systematic error from using our best value.

$\Gamma(D_s^{*-} \mu^+ \nu_\mu)/\Gamma_{\text{total}}$ Γ_{10}/Γ

VALUE (units 10^{-2})	DOCUMENT ID	TECN	COMMENT
5.2 ± 0.5 ± 0.1	¹ AAIJ	20E	LHCB pp at 7, 8 TeV

¹ AAIJ 20E reports $[\Gamma(B_s^0 \rightarrow D_s^{*-} \mu^+ \nu_\mu)/\Gamma_{\text{total}}] / [B(B^0 \rightarrow D^*(2010)^- \ell^+ \nu_\ell)] = 1.06 \pm 0.05 \pm 0.07 \pm 0.05$ which we multiply by our best value $B(B^0 \rightarrow D^*(2010)^- \ell^+ \nu_\ell) = (4.90 \pm 0.12) \times 10^{-2}$. Our first error is their experiment's error and our second error is the systematic error from using our best value.

$\Gamma(D_s^- \mu^+ \nu_\mu)/\Gamma(D_s^{*-} \mu^+ \nu_\mu)$ Γ_9/Γ_{10}

VALUE	DOCUMENT ID	TECN	COMMENT
0.464 ± 0.013 ± 0.043	¹ AAIJ	20E	LHCB pp at 7, 8 TeV

¹ AAIJ 20E value is not independent of other reported measurements.

$\Gamma(D_{s1}(2536)^- \mu^+ \nu_\mu, D_{s1}^- \rightarrow D^{*-} K_S^0)/\Gamma_{\text{total}}$ Γ_{11}/Γ

VALUE (units 10^{-3})	DOCUMENT ID	TECN	COMMENT
2.7 ± 0.7 ± 0.2	¹ ABAZOV	09G	D0 $p\bar{p}$ at 1.96 TeV

¹ ABAZOV 09G reports $[\Gamma(B_s^0 \rightarrow D_{s1}(2536)^- \mu^+ \nu_\mu, D_{s1}^- \rightarrow D^{*-} K_S^0)/\Gamma_{\text{total}}] \times [B(\bar{D} \rightarrow B_s^0)] = (2.66 \pm 0.52 \pm 0.45) \times 10^{-4}$ which we divide by our best value $B(\bar{D} \rightarrow B_s^0) = (10.0 \pm 0.8) \times 10^{-2}$. Our first error is their experiment's error and our second error is the systematic error from using our best value.

$\Gamma(D_{s1}(2536)^- X \mu^+ \nu, D_{s1}^- \rightarrow \bar{D}^0 K^+)/\Gamma(D_s^- \ell^+ \nu_\ell \text{ anything})$ Γ_{12}/Γ_7

VALUE (units 10^{-2})	DOCUMENT ID	TECN	COMMENT
5.4 ± 1.2 ± 0.5	AAIJ	11A	LHCB pp at 7 TeV

$\Gamma(D_{s2}(2573)^- X \mu^+ \nu, D_{s2}^- \rightarrow \bar{D}^0 K^+)/\Gamma(D_s^- \ell^+ \nu_\ell \text{ anything})$ Γ_{13}/Γ_7

VALUE (units 10^{-2})	DOCUMENT ID	TECN	COMMENT
3.3 ± 1.0 ± 0.4	AAIJ	11A	LHCB pp at 7 TeV

$\Gamma(D_{s1}(2536)^- X \mu^+ \nu, D_{s1}^- \rightarrow \bar{D}^0 K^+)/\Gamma(D_{s2}(2573)^- X \mu^+ \nu, D_{s2}^- \rightarrow \bar{D}^0 K^+)$ Γ_{12}/Γ_{13}

VALUE	DOCUMENT ID	TECN	COMMENT
0.61 ± 0.14 ± 0.05	¹ AAIJ	11A	LHCB pp at 7 TeV

¹ Not independent of other AAIJ 11A measurements.

$\Gamma(K^- \mu^+ \nu_\mu)/\Gamma(D_s^- \mu^+ \nu_\mu)$ Γ_{14}/Γ_9

VALUE (units 10^{-3})	DOCUMENT ID	TECN	COMMENT
4.89 ± 0.21 ± 0.25	^{1,2} AAIJ	21G	LHCB pp at 8 TeV

¹ AAIJ 21G measures $B(B_s^0 \rightarrow K^- \mu^+ \nu_\mu)/B(B_s^0 \rightarrow D_s^- \mu^+ \nu_\mu) = (4.89 \pm 0.21_{-0.21}^{+0.20} \pm 0.14) \times 10^{-3}$ over the whole q^2 range, where the last uncertainty is due to the $D_s^- \rightarrow K^+ K^- \pi^-$ branching fraction.

² AAIJ 21G reports this branching ratio for $q^2 < 7$ GeV² as $(1.66 \pm 0.08 \pm 0.07 \pm 0.05) \times 10^{-3}$ and for $q^2 > 7$ GeV² as $(3.25 \pm 0.21_{-0.17}^{+0.16} \pm 0.09) \times 10^{-3}$.

$\Gamma(K^- \mu^+ \nu_\mu)/\Gamma_{\text{total}}$ Γ_{14}/Γ

VALUE (units 10^{-4})	DOCUMENT ID	TECN	COMMENT
1.06 ± 0.05 ± 0.08	¹ AAIJ	21G	LHCB pp at 8 TeV

¹ The total systematic error includes D_s^- branching fractions, B_s^0 lifetime, $|V_{cb}|$, and $B_s^0 \rightarrow D_s^-$ form factor integral uncertainties.

$\Gamma(D_s^- \pi^+)/\Gamma_{\text{total}}$ Γ_{15}/Γ

VALUE (units 10^{-3})	EVS	DOCUMENT ID	TECN	COMMENT
2.98 ± 0.14 OUR FIT				
2.97 ± 0.13 OUR AVERAGE				

2.96 ± 0.10 ± 0.09 ¹ AAIJ 21Y LHCB pp at 7, 8, 13 TeV
 3.6 ± 0.5 ± 0.5 ² LOUVOT 09 BELL $e^+e^- \rightarrow \Upsilon(5S)$
 2.8 ± 0.6 ± 0.1 ³ ABULENCIA 07C CDF $p\bar{p}$ at 1.96 TeV

• • • We do not use the following data for averages, fits, limits, etc. • • •

2.95 ± 0.05 ± 0.25 -0.28	⁴ AAIJ	12AG	LHCB	Repl. by AAIJ 21Y
6.8 ± 2.2 ± 1.6	DRUTSKOY	07A	BELL	Repl. by LOUVOT 09
3.3 ± 1.1 ± 0.1	⁵ ABULENCIA	06J	CDF	Repl. by ABULENCIA 07C
<130	⁶ AKERS	94J	OPAL	$e^+e^- \rightarrow Z$
seen	¹ BUSKULIC	93G	ALEP	$e^+e^- \rightarrow Z$

¹ AAIJ 21Y reports $[\Gamma(B_s^0 \rightarrow D_s^- \pi^+)/\Gamma_{\text{total}}] / [B(B^0 \rightarrow D^- \pi^+)] = 1.18 \pm 0.04$ which we multiply by our best value $B(B^0 \rightarrow D^- \pi^+) = (2.51 \pm 0.08) \times 10^{-3}$. Our first error is their experiment's error and our second error is the systematic error from using our best value.

² LOUVOT 09 reports $(3.67_{-0.33-0.645}^{+0.35+0.65}) \times 10^{-3}$ from a measurement of $[\Gamma(B_s^0 \rightarrow D_s^- \pi^+)/\Gamma_{\text{total}}] \times [B(\Upsilon(10860) \rightarrow B_s^{(*)} \bar{B}_s^{(*)})]$ assuming $B(\Upsilon(10860) \rightarrow B_s^{(*)} \bar{B}_s^{(*)}) = (19.5 \pm 2.6) \times 10^{-2}$, which we rescale to our best value $B(\Upsilon(10860) \rightarrow B_s^{(*)} \bar{B}_s^{(*)}) = (20.1 \pm 3.1) \times 10^{-2}$. Our first error is their experiment's error and our second error is the systematic error from using our best value.

³ ABULENCIA 07C reports $[\Gamma(B_s^0 \rightarrow D_s^- \pi^+)/\Gamma_{\text{total}}] / [B(B^0 \rightarrow D^- \pi^+)] = 1.13 \pm 0.08 \pm 0.23$ which we multiply by our best value $B(B^0 \rightarrow D^- \pi^+) = (2.51 \pm 0.08) \times 10^{-3}$. Our first error is their experiment's error and our second error is the systematic error from using our best value.

⁴ AAIJ 12AG reports $(2.95 \pm 0.05 \pm 0.17_{-0.22}^{+0.18}) \times 10^{-3}$ where the last uncertainty comes from the semileptonic f_S/f_G measurement. We combined the systematics in quadrature.

⁵ ABULENCIA 06J reports $[\Gamma(B_s^0 \rightarrow D_s^- \pi^+)/\Gamma_{\text{total}}] / [B(B^0 \rightarrow D^- \pi^+)] = 1.32 \pm 0.18 \pm 0.38$ which we multiply by our best value $B(B^0 \rightarrow D^- \pi^+) = (2.51 \pm 0.08) \times 10^{-3}$. Our first error is their experiment's error and our second error is the systematic error from using our best value.

⁶ AKERS 94J sees ≤ 6 events and measures the limit on the product branching fraction $f(\bar{D} \rightarrow B_s^0) \cdot B(B_s^0 \rightarrow D_s^- \pi^+) < 1.3\%$ at CL = 90%. We divide by our current value $B(\bar{D} \rightarrow B_s^0) = 0.105$.

$\Gamma(D_s^- \rho^+)/\Gamma(D_s^- \pi^+)$ Γ_{16}/Γ_{15}

VALUE	DOCUMENT ID	TECN	COMMENT
2.3 ± 0.4 ± 0.2	LOUVOT	10	BELL $e^+e^- \rightarrow \Upsilon(5S)$

$\Gamma(D_s^- \pi^+ \pi^+ \pi^-)/\Gamma_{\text{total}}$ Γ_{17}/Γ

VALUE (units 10^{-3})	DOCUMENT ID	TECN	COMMENT
6.1 ± 1.0 OUR FIT			
6.3 ± 1.4 ± 0.6	¹ ABULENCIA	07C	CDF $p\bar{p}$ at 1.96 TeV

¹ ABULENCIA 07C reports $[\Gamma(B_s^0 \rightarrow D_s^- \pi^+ \pi^+ \pi^-)/\Gamma_{\text{total}}] / [B(B^0 \rightarrow D^- \pi^+ \pi^+ \pi^-)] = 1.05 \pm 0.10 \pm 0.22$ which we multiply by our best value $B(B^0 \rightarrow D^- \pi^+ \pi^+ \pi^-) = (6.0 \pm 0.6) \times 10^{-3}$. Our first error is their experiment's error and our second error is the systematic error from using our best value.

$\Gamma(D_s^- \pi^+ \pi^+ \pi^-)/\Gamma(D_s^- \pi^+)$ Γ_{17}/Γ_{15}

VALUE	DOCUMENT ID	TECN	COMMENT
2.05 ± 0.33 OUR FIT			
2.01 ± 0.37 ± 0.20	AAIJ	11E	LHCB pp at 7 TeV

$\Gamma(D_{s1}(2536)^- \pi^+, D_{s1}^- \rightarrow D_s^- \pi^+ \pi^-)/\Gamma(D_s^- \pi^+ \pi^+ \pi^-)$ Γ_{18}/Γ_{17}

VALUE (units 10^{-3})	DOCUMENT ID	TECN	COMMENT
4.0 ± 1.0 ± 0.4	AAIJ	12Ax	LHCB pp at 7 TeV

$\Gamma(D_s^\mp K^\pm)/\Gamma_{\text{total}}$ Γ_{19}/Γ

VALUE (units 10^{-4})	DOCUMENT ID	TECN	COMMENT
2.25 ± 0.12 OUR FIT			
2.3 $^{+1.2}_{-1.0} \pm 0.4_{-0.3}$	¹ LOUVOT	09	BELL $e^+e^- \rightarrow \Upsilon(5S)$

¹ LOUVOT 09 reports $(2.4_{-1.0}^{+1.2} \pm 0.42) \times 10^{-4}$ from a measurement of $[\Gamma(B_s^0 \rightarrow D_s^\mp K^\pm)/\Gamma_{\text{total}}] \times [B(\Upsilon(10860) \rightarrow B_s^{(*)} \bar{B}_s^{(*)})]$ assuming $B(\Upsilon(10860) \rightarrow B_s^{(*)} \bar{B}_s^{(*)}) = (19.5 \pm 2.6) \times 10^{-2}$, which we rescale to our best value $B(\Upsilon(10860) \rightarrow B_s^{(*)} \bar{B}_s^{(*)}) = (20.1 \pm 3.1) \times 10^{-2}$. Our first error is their experiment's error and our second error is the systematic error from using our best value.

$\Gamma(D_{s1}(2536)^- \bar{K}^\pm, D_{s1}^- \rightarrow \bar{D}^*(2007)^0 K^-)/\Gamma_{\text{total}}$ Γ_{20}/Γ

VALUE (units 10^{-5})	DOCUMENT ID	TECN	COMMENT
2.48 ± 0.18 ± 0.22	¹ AAIJ	23AY	LHCB pp at 7, 8, 13 TeV

¹ AAIJ 23AY reports $[\Gamma(B_s^0 \rightarrow D_{s1}(2536)^- \bar{K}^\pm, D_{s1}^- \rightarrow \bar{D}^*(2007)^0 K^-)/\Gamma_{\text{total}}] / [B(B^0 \rightarrow \bar{D}^0 K^+ K^-)] = 0.409 \pm 0.019 \pm 0.022$ which we multiply by our best value $B(B^0 \rightarrow \bar{D}^0 K^+ K^-) = (6.1 \pm 0.5) \times 10^{-5}$. Our first error is their experiment's error and our second error is the systematic error from using our best value.

Meson Particle Listings

 B_s^0 $\Gamma(D_s^{\mp} K^{\pm})/\Gamma(D_s^{\mp} \pi^{\pm})$ Γ_{19}/Γ_{15}

VALUE (units 10^{-2})	DOCUMENT ID	TECN	COMMENT
7.55 ± 0.24 OUR FIT			
7.55 ± 0.24 OUR AVERAGE			
7.52 ± 0.15 ± 0.19	AAIJ	15AC LHCb	pp at 7, 8 TeV
9.7 ± 1.8 ± 0.9	AALTONEN	09AQ CDF	$p\bar{p}$ at 1.96 TeV
••• We do not use the following data for averages, fits, limits, etc. •••			
6.46 ± 0.43 ± 0.25	AAIJ	12AG LHCb	Repl. by AAIJ 15AC

 $\Gamma(D_s^{\mp} K^+ \pi^+ \pi^-)/\Gamma(D_s^{\mp} \pi^+ \pi^+ \pi^-)$ Γ_{21}/Γ_{17}

VALUE (units 10^{-2})	DOCUMENT ID	TECN	COMMENT
5.2 ± 0.5 ± 0.3	AAIJ	12AX LHCb	pp at 7 TeV

 $\Gamma(D_s^+ D_s^-)/\Gamma_{total}$ Γ_{22}/Γ

VALUE (units 10^{-3})	CL%	DOCUMENT ID	TECN	COMMENT
4.4 ± 0.5 OUR AVERAGE				
4.0 ± 0.2 ± 0.5		1 AAIJ	13AP LHCb	pp at 7 TeV
5.8 ^{+1.1} _{-0.9} ± 1.3		2 ESEN	13 BELL	$e^+e^- \rightarrow \Upsilon(5S)$
5.4 ± 0.8 ± 0.8		3 AALTONEN	12c CDF	$p\bar{p}$ at 1.96 TeV
••• We do not use the following data for averages, fits, limits, etc. •••				
10.3 ^{+3.9+2.6} _{-3.2-2.5}		4 ESEN	10 BELL	Repl. by ESEN 13
10.4 ^{+3.5} _{-3.2} ± 1.1		5 AALTONEN	08F CDF	Repl. by AALTONEN 12c
<67	90	DRUTSKOY	07A BELL	Repl. by ESEN 10

- 1 Uses $B(B^0 \rightarrow D^- D_s^+) = (7.2 \pm 0.8) \times 10^{-3}$.
- 2 Use $\Upsilon(5S) \rightarrow B_s^* \bar{B}_s^*$ decays assuming $B(\Upsilon(5S) \rightarrow B_s^* \bar{B}_s^*) = (17.1 \pm 3.0)\%$ and $\Gamma(\Upsilon(5S) \rightarrow B_s^* \bar{B}_s^*) / \Gamma(\Upsilon(5S) \rightarrow B_s^{(*)} \bar{B}_s^{(*)}) = (87.0 \pm 1.7)\%$.
- 3 AALTONEN 12c reports (f_s/f_d) $(B(B^0 \rightarrow D_s^+ D_s^-) / B(B^0 \rightarrow D^- D_s^+)) = 0.183 \pm 0.021 \pm 0.017$. We multiply this result by our best value of $B(B^0 \rightarrow D^- D_s^+) = (7.2 \pm 0.8) \times 10^{-3}$ and divide by our best value of f_s/f_d , where $1/2 f_s/f_d = 0.1230 \pm 0.0115$. Our first quoted uncertainty is the combined experiment's uncertainty and our second is the systematic uncertainty from using our best values.
- 4 Uses $\Upsilon(10860) \rightarrow B_s^* \bar{B}_s^*$ assuming $B(\Upsilon(10860) \rightarrow B_s^{(*)} \bar{B}_s^{(*)}) = (19.3 \pm 2.9)\%$ and $\Gamma(\Upsilon(10860) \rightarrow B_s^* \bar{B}_s^*) / \Gamma(\Upsilon(10860) \rightarrow B_s^{(*)} \bar{B}_s^{(*)}) = (90.1^{+3.8}_{-4.0})\%$.
- 5 AALTONEN 08F reports $[\Gamma(B^0 \rightarrow D_s^+ D_s^-)/\Gamma_{total}] / [B(B^0 \rightarrow D^- D_s^+)] = 1.44^{+0.48}_{-0.44}$ which we multiply by our best value $B(B^0 \rightarrow D^- D_s^+) = (7.2 \pm 0.8) \times 10^{-3}$. Our first error is their experiment's error and our second error is the systematic error from using our best value.

 $\Gamma(D_s^- D^+)/\Gamma_{total}$ Γ_{23}/Γ

VALUE (units 10^{-4})	DOCUMENT ID	TECN	COMMENT
2.8 ± 0.4 ± 0.3	1 AAIJ	14AA LHCb	pp at 7 TeV
••• We do not use the following data for averages, fits, limits, etc. •••			
3.6 ± 0.6 ± 0.5	2 AAIJ	13AP LHCb	Repl. by AAIJ 14AA

- 1 AAIJ 14AA reports $[\Gamma(B^0 \rightarrow D_s^- D^+)/\Gamma_{total}] / [B(B^0 \rightarrow D^- D_s^+)] = 0.038 \pm 0.004 \pm 0.003$ which we multiply by our best value $B(B^0 \rightarrow D^- D_s^+) = (7.2 \pm 0.8) \times 10^{-3}$. Our first error is their experiment's error and our second error is the systematic error from using our best value..
- 2 Uses $B(B^0 \rightarrow D^- D_s^+) = (7.2 \pm 0.8) \times 10^{-3}$.

 $\Gamma(D^+ D^-)/\Gamma_{total}$ Γ_{24}/Γ

VALUE (units 10^{-4})	DOCUMENT ID	TECN	COMMENT
2.2 ± 0.4 ± 0.4	1 AAIJ	13AP LHCb	pp at 7 TeV
1 Uses $B(B^0 \rightarrow D^- D^+) = (2.11 \pm 0.31) \times 10^{-4}$ and $B(B^+ \rightarrow \bar{D}^0 D_s^+) = (10.1 \pm 1.7) \times 10^{-3}$.			

 $\Gamma(D^0 \bar{D}^0)/\Gamma_{total}$ Γ_{28}/Γ

VALUE (units 10^{-4})	DOCUMENT ID	TECN	COMMENT
1.9 ± 0.3 ± 0.4	1 AAIJ	13AP LHCb	pp at 7 TeV
1 Uses $B(B^0 \rightarrow D^- D^+) = (2.11 \pm 0.31) \times 10^{-4}$ and $B(B^+ \rightarrow \bar{D}^0 D_s^+) = (10.1 \pm 1.7) \times 10^{-3}$.			

 $\Gamma(D^{*+} D^{*-})/\Gamma_{total}$ Γ_{27}/Γ

VALUE (units 10^{-4})	DOCUMENT ID	TECN	COMMENT
2.14 ± 0.28^{+0.17}_{-0.16}	1,2 AAIJ	23J LHCb	pp at 7, 8, 13 TeV

- 1 AAIJ 23J reports $[\Gamma(B^0 \rightarrow D^{*+} D^{*-})/\Gamma_{total}] / [B(B^0 \rightarrow D^* (2010)^+ D^* (2010)^-)] = 0.269 \pm 0.032 \pm 0.011 \pm 0.008$ which we multiply by our best value $B(B^0 \rightarrow D^* (2010)^+ D^* (2010)^-) = (8.0 \pm 0.6) \times 10^{-4}$. Our first error is their experiment's error and our second error is the systematic error from using our best value.
- 2 Uses average B_s^0 lifetime of 1.5215 ps.

 $\Gamma(D_s^{\mp} \pi^+)/\Gamma(D_s^{\mp} \pi^+)$ Γ_{29}/Γ_{15}

VALUE	DOCUMENT ID	TECN	COMMENT
0.65^{+0.15}_{-0.13} ± 0.07	LOUVOT	10 BELL	$e^+e^- \rightarrow \Upsilon(5S)$

 $\Gamma(D_s^{\mp} K^{\pm})/\Gamma(D_s^{\mp} \pi^{\pm})$ Γ_{30}/Γ_{29}

VALUE	DOCUMENT ID	TECN	COMMENT
0.068 ± 0.005^{+0.003}_{-0.002}	AAIJ	15AD LHCb	pp at 7, 8 TeV

 $\Gamma(D_s^{\mp} \rho^+)/\Gamma(D_s^{\mp} \pi^+)$ Γ_{31}/Γ_{15}

VALUE	DOCUMENT ID	TECN	COMMENT
3.2 ± 0.6 ± 0.3	LOUVOT	10 BELL	$e^+e^- \rightarrow \Upsilon(5S)$

 $\Gamma(D_s^{\mp} \rho^+)/\Gamma(D_s^{\mp} \rho^+)$ Γ_{31}/Γ_{16}

VALUE	DOCUMENT ID	TECN	COMMENT
1.4 ± 0.3 ± 0.1	1 LOUVOT	10 BELL	$e^+e^- \rightarrow \Upsilon(5S)$
1 Not independent of other LOUVOT 10 measurements.			

 $[\Gamma(D_s^{*+} D_s^-) + \Gamma(D_s^{\mp} D_s^+)]/\Gamma_{total}$ Γ_{32}/Γ

VALUE (units 10^{-3})	CL%	DOCUMENT ID	TECN	COMMENT
13.9 ± 1.7 OUR AVERAGE				
13.6 ± 1.0 ± 1.4		1 AAIJ	16P LHCb	pp at 7 TeV
17.6 ^{+2.3} _{-2.2} ± 4.0		2 ESEN	13 BELL	$e^+e^- \rightarrow \Upsilon(5S)$
12.5 ± 1.7 ± 1.8		3 AALTONEN	12c CDF	$p\bar{p}$ at 1.96 TeV
••• We do not use the following data for averages, fits, limits, etc. •••				
27.5 ^{+8.3} _{-7.1} ± 6.9		4 ESEN	10 BELL	Repl. by ESEN 13
<121	90	DRUTSKOY	07A BELL	Repl. by ESEN 10

- 1 AAIJ 16P reports $[\Gamma(B^0 \rightarrow D_s^{*+} D_s^-) + \Gamma(D_s^{\mp} D_s^+)]/\Gamma_{total} / [B(B^0 \rightarrow D^- D_s^+)] = 1.88 \pm 0.08 \pm 0.12$ which we multiply by our best value $B(B^0 \rightarrow D^- D_s^+) = (7.2 \pm 0.8) \times 10^{-3}$. Our first error is their experiment's error and our second error is the systematic error from using our best value.
- 2 Use $\Upsilon(5S) \rightarrow B_s^* \bar{B}_s^*$ decays assuming $B(\Upsilon(5S) \rightarrow B_s^* \bar{B}_s^*) = (17.1 \pm 3.0)\%$ and $\Gamma(\Upsilon(5S) \rightarrow B_s^* \bar{B}_s^*) / \Gamma(\Upsilon(5S) \rightarrow B_s^{(*)} \bar{B}_s^{(*)}) = (87.0 \pm 1.7)\%$.
- 3 AALTONEN 12c reports (f_s/f_d) $(B(B^0 \rightarrow D_s^{*+} D_s^- + D_s^{\mp} D_s^+) / B(B^0 \rightarrow D^- D_s^+)) = 0.424 \pm 0.046 \pm 0.035$. We multiply this result by our best value of $B(B^0 \rightarrow D^- D_s^+) = (7.2 \pm 0.8) \times 10^{-3}$ and divide by our best value of f_s/f_d , where $1/2 f_s/f_d = 0.1230 \pm 0.0115$. Our first quoted uncertainty is the combined experiment's uncertainty and our second is the systematic uncertainty from using our best values.
- 4 Uses $\Upsilon(10860) \rightarrow B_s^* \bar{B}_s^*$ assuming $B(\Upsilon(10860) \rightarrow B_s^{(*)} \bar{B}_s^{(*)}) = (19.3 \pm 2.9)\%$ and $\Gamma(\Upsilon(10860) \rightarrow B_s^* \bar{B}_s^*) / \Gamma(\Upsilon(10860) \rightarrow B_s^{(*)} \bar{B}_s^{(*)}) = (90.1^{+3.8}_{-4.0})\%$.

 $\Gamma(D_s^{*+} D_s^{*-})/\Gamma_{total}$ Γ_{33}/Γ

VALUE (units 10^{-3})	CL%	DOCUMENT ID	TECN	COMMENT
14.4 ± 2.1 OUR AVERAGE				Error includes scale factor of 1.1.
12.7 ± 1.3 ± 1.4		1 AAIJ	16P LHCb	pp at 7 TeV
19.8 ^{+3.3+5.2} _{-3.1-5.0}		2 ESEN	13 BELL	$e^+e^- \rightarrow \Upsilon(5S)$
19.2 ± 2.9 ± 2.7		3 AALTONEN	12c CDF	$p\bar{p}$ at 1.96 TeV
••• We do not use the following data for averages, fits, limits, etc. •••				
30.8 ^{+12.2+8.5} _{-10.4-8.6}		4 ESEN	10 BELL	Repl. by ESEN 13
<257	90	DRUTSKOY	07A BELL	Repl. by ESEN 10

- 1 AAIJ 16P reports $[\Gamma(B^0 \rightarrow D_s^{*+} D_s^{*-})/\Gamma_{total}] / [B(B^0 \rightarrow D^- D_s^+)] = 1.76 \pm 0.11 \pm 0.14$ which we multiply by our best value $B(B^0 \rightarrow D^- D_s^+) = (7.2 \pm 0.8) \times 10^{-3}$. Our first error is their experiment's error and our second error is the systematic error from using our best value.
- 2 Use $\Upsilon(5S) \rightarrow B_s^* \bar{B}_s^*$ decays assuming $B(\Upsilon(5S) \rightarrow B_s^* \bar{B}_s^*) = (17.1 \pm 3.0)\%$ and $\Gamma(\Upsilon(5S) \rightarrow B_s^* \bar{B}_s^*) / \Gamma(\Upsilon(5S) \rightarrow B_s^{(*)} \bar{B}_s^{(*)}) = (87.0 \pm 1.7)\%$.
- 3 AALTONEN 12c reports (f_s/f_d) $(B(B^0 \rightarrow D_s^{*+} D_s^{*-}) / B(B^0 \rightarrow D^- D_s^+)) = 0.654 \pm 0.072 \pm 0.065$. We multiply this result by our best value of $B(B^0 \rightarrow D^- D_s^+) = (7.2 \pm 0.8) \times 10^{-3}$ and divide by our best value of f_s/f_d , where $1/2 f_s/f_d = 0.1230 \pm 0.0115$. Our first quoted uncertainty is the combined experiment's uncertainty and our second is the systematic uncertainty from using our best values.
- 4 Uses $\Upsilon(10860) \rightarrow B_s^* \bar{B}_s^*$ assuming $B(\Upsilon(10860) \rightarrow B_s^{(*)} \bar{B}_s^{(*)}) = (19.3 \pm 2.9)\%$ and $\Gamma(\Upsilon(10860) \rightarrow B_s^* \bar{B}_s^*) / \Gamma(\Upsilon(10860) \rightarrow B_s^{(*)} \bar{B}_s^{(*)}) = (90.1^{+3.8}_{-4.0})\%$.

 $\Gamma(D_s^{*+} D_s^{*-})/\Gamma_{total}$ Γ_{34}/Γ

VALUE (%)	CL%	DOCUMENT ID	TECN	COMMENT
4.5 ± 1.4 OUR EVALUATION				(Produced by HFLAV)
3.4 ± 0.4 OUR AVERAGE				
3.07 ± 0.22 ± 0.33		1 AAIJ	16P LHCb	pp at 7 TeV
4.32 ^{+0.42+1.04} _{-0.39-1.03}		2 ESEN	13 BELL	$e^+e^- \rightarrow \Upsilon(5S)$
3.7 ± 0.4 ± 0.5		3 AALTONEN	12c CDF	$p\bar{p}$ at 1.96 TeV
3.5 ± 1.0 ± 1.1		4 ABAZOV	09I D0	$p\bar{p}$ at 1.96 TeV
14 ± 6 ± 3		5,6 BARATE	00K ALEP	$e^+e^- \rightarrow Z$

• • • We do not use the following data for averages, fits, limits, etc. • • •

$6.85^{+1.53+1.79}_{-1.30-1.80}$	7.8 ESEN	10 BELL	Repl. by ESEN 13
$3.9^{+1.9+1.6}_{-1.7-1.5}$	4 ABAZOV	07Y D0	Repl. by ABAZOV 09i
<0.218	90 BARATE	98Q ALEP	$e^+e^- \rightarrow Z$

1 AAIJ 16P reports $[\Gamma(B_S^0 \rightarrow D_S^{(*)+} D_S^{(*)-})/\Gamma_{\text{total}}] / [B(B^0 \rightarrow D^- D_S^+)] = 4.24 \pm 0.14 \pm 0.27$ which we multiply by our best value $B(B^0 \rightarrow D^- D_S^+) = (7.2 \pm 0.8) \times 10^{-3}$. Our first error is their experiment's error and our second error is the systematic error from using our best value.

2 Use $\mathcal{T}(5S) \rightarrow B_S^* \bar{B}_S^*$ decays assuming $B(\mathcal{T}(5S) \rightarrow B_S^* \bar{B}_S^*) = (17.1 \pm 3.0)\%$ and $\Gamma(\mathcal{T}(5S) \rightarrow B_S^* \bar{B}_S^*) / \Gamma(\mathcal{T}(5S) \rightarrow B_S^{(*)+} \bar{B}_S^{(*)-}) = (87.0 \pm 1.7)\%$.

3 AALTONEN 12c reports $(f_S/f_d) (B(B_S^0 \rightarrow D_S^{(*)+} D_S^{(*)-}) / B(B^0 \rightarrow D^- D_S^+)) = 1.261 \pm 0.095 \pm 0.112$. We multiply this result by our best value of $B(B^0 \rightarrow D^- D_S^+) = (7.2 \pm 0.8) \times 10^{-3}$ and divide by our best value of f_S/f_d , where $1/2 f_S/f_d = 0.1230 \pm 0.0115$. Our first quoted uncertainty is the combined experiment's uncertainty and our second is the systematic uncertainty from using our best values.

4 Uses the final states where $D_S^+ \rightarrow \phi \pi^+$ and $D_S^- \rightarrow \phi \mu^- \bar{\nu}_\mu$.

5 Reports $B(B_S^0(\text{short}) \rightarrow D_S^{(*)+} D_S^{(*)-}) = (0.23 \pm 0.10 \pm 0.05) \cdot [0.17/B(D_S \rightarrow \phi \chi)]^2$ assuming $B(B_S^0 \rightarrow B^0(\text{short})) = 50\%$. We use our best value of $B(D_S \rightarrow \phi \chi) = 15.7 \pm 1.0\%$ to obtain the quoted result.

6 Uses $\phi\phi$ correlations from $B_S^0(\text{short}) \rightarrow D_S^{(*)+} D_S^{(*)-}$.

7 Sum of exclusive $B_S \rightarrow D_S^+ D_S^-$, $B_S \rightarrow D_S^{\pm} D_S^{\mp}$ and $B_S \rightarrow D_S^{*+} D_S^{*-}$.

8 Uses $\mathcal{T}(10860) \rightarrow B_S^* \bar{B}_S^*$ assuming $B(\mathcal{T}(10860) \rightarrow B_S^{(*)+} \bar{B}_S^{(*)-}) = (19.3 \pm 2.9)\%$ and $\Gamma(\mathcal{T}(10860) \rightarrow B_S^* \bar{B}_S^*) / \Gamma(\mathcal{T}(10860) \rightarrow B_S^{(*)+} \bar{B}_S^{(*)-}) = (90.1^{+3.8}_{-4.0})\%$.

$\Gamma(D^{*-} D_S^+)/\Gamma_{\text{total}}$				Γ_{35}/Γ
VALUE (units 10^{-4})	DOCUMENT ID	TECN	COMMENT	
$3.9 \pm 0.6 \pm 0.5$	¹ AAIJ	21s LHCb	pp at 13 TeV	

1 AAIJ 21s reports $[\Gamma(B_S^0 \rightarrow D^{*-} D_S^+)/\Gamma_{\text{total}}] / [B(B^0 \rightarrow D^*(2010) D_S^+)] = 0.049 \pm 0.006 \pm 0.0036$ which we multiply by our best value $B(B^0 \rightarrow D^*(2010) D_S^+) = (8.0 \pm 1.1) \times 10^{-3}$. Our first error is their experiment's error and our second error is the systematic error from using our best value.

$[\Gamma(D^{*+} D^-) + \Gamma(D^{*-} D^+)]/\Gamma_{\text{total}}$				$(\Gamma_{25} + \Gamma_{26})/\Gamma$
VALUE (units 10^{-5})	DOCUMENT ID	TECN	COMMENT	
$8.4 \pm 1.1 \pm 0.8$	¹ AAIJ	21N LHCb	pp at 7, 8, 13 TeV	

1 AAIJ 21N reports $[\Gamma(B_S^0 \rightarrow D^{*+} D^-) + \Gamma(B_S^0 \rightarrow D^{*-} D^+)]/\Gamma_{\text{total}}] / [B(B^0 \rightarrow D^{\pm} D^{*\mp} (CP\text{-averaged}))] = 0.137 \pm 0.017 \pm 0.006$ which we multiply by our best value $B(B^0 \rightarrow D^{\pm} D^{*\mp} (CP\text{-averaged})) = (6.1 \pm 0.6) \times 10^{-4}$. Our first error is their experiment's error and our second error is the systematic error from using our best value.

$\Gamma(\bar{D}^{*0} \bar{K}^0)/\Gamma_{\text{total}}$				Γ_{36}/Γ
VALUE (units 10^{-4})	DOCUMENT ID	TECN	COMMENT	
$2.8 \pm 1.0 \pm 0.5$	¹ AAIJ	16c LHCb	pp at 7, 8 TeV	

1 Measured and normalized to the $B_S^0 \rightarrow \bar{D}^{*0} K_S^0$ decay with $f_S/f_d = 0.259 \pm 0.015$. Signal significance is 4.4 standard deviations.

$\Gamma(\bar{D}^0 \bar{K}^0)/\Gamma_{\text{total}}$				Γ_{37}/Γ
VALUE (units 10^{-4})	DOCUMENT ID	TECN	COMMENT	
$4.3 \pm 0.5 \pm 0.7$	¹ AAIJ	16c LHCb	pp at 7, 8 TeV	

1 Measured and normalized to the $B^0 \rightarrow \bar{D}^0 K_S^0$ decay with $f_S/f_d = 0.259 \pm 0.015$.

$\Gamma(\bar{D}^0 K^- \pi^+)/\Gamma_{\text{total}}$				Γ_{38}/Γ
VALUE (units 10^{-4})	DOCUMENT ID	TECN	COMMENT	
$10.4 \pm 1.1 \pm 0.5$	¹ AAIJ	13Aq LHCb	pp at 7 TeV	

1 AAIJ 13Aq reports $[\Gamma(B_S^0 \rightarrow \bar{D}^0 K^- \pi^+)/\Gamma_{\text{total}}] / [B(B^0 \rightarrow \bar{D}^0 \pi^+ \pi^-)] = 1.18 \pm 0.05 \pm 0.12$ which we multiply by our best value $B(B^0 \rightarrow \bar{D}^0 \pi^+ \pi^-) = (8.8 \pm 0.5) \times 10^{-4}$. Our first error is their experiment's error and our second error is the systematic error from using our best value.

$\Gamma(\bar{D}^*(2007)^0 K^- \pi^+)/\Gamma_{\text{total}}$				Γ_{39}/Γ
VALUE (units 10^{-4})	DOCUMENT ID	TECN	COMMENT	
$7.3 \pm 0.6 \pm 2.5$	¹ AAIJ	22N LHCb	pp at 13 TeV	

1 AAIJ 22N reports $[\Gamma(B_S^0 \rightarrow \bar{D}^*(2007)^0 K^- \pi^+)/\Gamma_{\text{total}}] / [B(B^0 \rightarrow \bar{D}^*(2007)^0 \pi^+ \pi^-)] = 1.178 \pm 0.029 \pm 0.091 \pm 0.037$ which we multiply by our best value $B(B^0 \rightarrow \bar{D}^*(2007)^0 \pi^+ \pi^-) = (6.2 \pm 2.2) \times 10^{-4}$. Our first error is their experiment's error and our second error is the systematic error from using our best value.

$\Gamma(\bar{D}^0 \bar{K}^*(892)^0)/\Gamma_{\text{total}}$				Γ_{40}/Γ
VALUE (units 10^{-4})	DOCUMENT ID	TECN	COMMENT	
4.4 ± 0.6 OUR AVERAGE				

4.29 ± 0.09 ± 0.65
4.7 ± 1.2 ± 0.3
• • • We do not use the following data for averages, fits, limits, etc. • • •
3.5 ± 0.4 ± 0.4

¹ AAIJ 14Bh LHCb pp at 7, 8 TeV

² AAIJ 11D LHCb pp at 7 TeV

³ AAIJ 13Bx LHCb Repl. by AAIJ 14Bh

1 Uses Dalitz plot analysis of $B^0 \rightarrow \bar{D}^0 K^- \pi^+$ decays.

2 AAIJ 11D reports $[\Gamma(B_S^0 \rightarrow \bar{D}^0 \bar{K}^*(892)^0)/\Gamma_{\text{total}}] / [B(B^0 \rightarrow \bar{D}^0 \rho^0)] = 1.48 \pm 0.34 \pm 0.19$ which we multiply by our best value $B(B^0 \rightarrow \bar{D}^0 \rho^0) = (3.21 \pm 0.21) \times 10^{-4}$. Our first error is their experiment's error and our second error is the systematic error from using our best value.

3 AAIJ 13Bx reports $[\Gamma(B_S^0 \rightarrow \bar{D}^0 \bar{K}^*(892)^0)/\Gamma_{\text{total}}] / [B(B^0 \rightarrow \bar{D}^0 K^*(892)^0)] = 7.8 \pm 0.7 \pm 0.3 \pm 0.6$ which we multiply by our best value $B(B^0 \rightarrow \bar{D}^0 K^*(892)^0) = (4.5 \pm 0.6) \times 10^{-5}$. Our first error is their experiment's error and our second error is the systematic error from using our best value.

$\Gamma(\bar{D}^0 \bar{K}^*(1410))/\Gamma_{\text{total}}$				Γ_{41}/Γ
VALUE (units 10^{-5})	DOCUMENT ID	TECN	COMMENT	
$38.6 \pm 11.4 \pm 33.3$	¹ AAIJ	14Bh LHCb	pp at 7, 8 TeV	

1 Uses Dalitz plot analysis of $B_S^0 \rightarrow \bar{D}^0 K^- \pi^+$ decays.

$\Gamma(\bar{D}^0 \bar{K}_0^*(1430))/\Gamma_{\text{total}}$				Γ_{42}/Γ
VALUE (units 10^{-5})	DOCUMENT ID	TECN	COMMENT	
$30.0 \pm 2.4 \pm 6.8$	¹ AAIJ	14Bh LHCb	pp at 7, 8 TeV	

1 Uses Dalitz plot analysis of $B_S^0 \rightarrow \bar{D}^0 K^- \pi^+$ decays. Corresponds to the resonant $K_0^*(1430)$ part of LASS parametrization.

$\Gamma(\bar{D}^0 \bar{K}_2^*(1430))/\Gamma_{\text{total}}$				Γ_{43}/Γ
VALUE (units 10^{-5})	DOCUMENT ID	TECN	COMMENT	
$11.1 \pm 1.8 \pm 3.8$	¹ AAIJ	14Bh LHCb	pp at 7, 8 TeV	

1 Uses Dalitz plot analysis of $B_S^0 \rightarrow \bar{D}^0 K^- \pi^+$ decays.

$\Gamma(\bar{D}^0 \bar{K}^*(1680))/\Gamma_{\text{total}}$				Γ_{44}/Γ
VALUE (units 10^{-5})	CL%	DOCUMENT ID	TECN	COMMENT
<7.8	90	¹ AAIJ	14Bh LHCb	pp at 7, 8 TeV

1 Uses Dalitz plot analysis of $B_S^0 \rightarrow \bar{D}^0 K^- \pi^+$ decays.

$\Gamma(\bar{D}^0 \bar{K}_0^*(1950))/\Gamma_{\text{total}}$				Γ_{45}/Γ
VALUE (units 10^{-5})	CL%	DOCUMENT ID	TECN	COMMENT
<11	90	¹ AAIJ	14Bh LHCb	pp at 7, 8 TeV

1 Uses Dalitz plot analysis of $B_S^0 \rightarrow \bar{D}^0 K^- \pi^+$ decays.

$\Gamma(\bar{D}^0 \bar{K}_3^*(1780))/\Gamma_{\text{total}}$				Γ_{46}/Γ
VALUE (units 10^{-5})	CL%	DOCUMENT ID	TECN	COMMENT
<2.6	90	¹ AAIJ	14Bh LHCb	pp at 7, 8 TeV

1 Uses Dalitz plot analysis of $B_S^0 \rightarrow \bar{D}^0 K^- \pi^+$ decays.

$\Gamma(\bar{D}^0 \bar{K}_4^*(2045))/\Gamma_{\text{total}}$				Γ_{47}/Γ
VALUE (units 10^{-5})	CL%	DOCUMENT ID	TECN	COMMENT
<3.1	90	¹ AAIJ	14Bh LHCb	pp at 7, 8 TeV

1 Uses Dalitz plot analysis of $B_S^0 \rightarrow \bar{D}^0 K^- \pi^+$ decays.

$\Gamma(\bar{D}^0 K^- \pi^+ (\text{non-resonant}))/\Gamma_{\text{total}}$				Γ_{48}/Γ
VALUE (units 10^{-5})	DOCUMENT ID	TECN	COMMENT	
$20.6 \pm 3.8 \pm 7.3$	¹ AAIJ	14Bh LHCb	pp at 7, 8 TeV	

1 Uses Dalitz plot analysis of $B_S^0 \rightarrow \bar{D}^0 K^- \pi^+$ decays. Corresponds to the non-resonant part of the LASS parametrization.

$\Gamma(D_{s2}^*(2573)^- \pi^+, D_{s2}^* \rightarrow \bar{D}^0 K^-)/\Gamma_{\text{total}}$				Γ_{49}/Γ
VALUE (units 10^{-5})	DOCUMENT ID	TECN	COMMENT	
$25.7 \pm 0.7 \pm 4.0$	¹ AAIJ	14Bh LHCb	pp at 7, 8 TeV	

1 Uses Dalitz plot analysis of $B_S^0 \rightarrow \bar{D}^0 K^- \pi^+$ decays.

$\Gamma(D_{s1}^*(2700)^- \pi^+, D_{s1}^* \rightarrow \bar{D}^0 K^-)/\Gamma_{\text{total}}$				Γ_{50}/Γ
VALUE (units 10^{-5})	DOCUMENT ID	TECN	COMMENT	
$1.6 \pm 0.4 \pm 0.7$	¹ AAIJ	14Bh LHCb	pp at 7, 8 TeV	

1 Uses Dalitz plot analysis of $B_S^0 \rightarrow \bar{D}^0 K^- \pi^+$ decays.

$\Gamma(D_{s1}^*(2860)^- \pi^+, D_{s1}^* \rightarrow \bar{D}^0 K^-)/\Gamma_{\text{total}}$				Γ_{51}/Γ
VALUE (units 10^{-5})	DOCUMENT ID	TECN	COMMENT	
$5.0 \pm 1.2 \pm 3.4$	¹ AAIJ	14Bh LHCb	pp at 7, 8 TeV	

1 Uses Dalitz plot analysis of $B_S^0 \rightarrow \bar{D}^0 K^- \pi^+$ decays.

$\Gamma(D_{s3}^*(2860)^- \pi^+, D_{s3}^* \rightarrow \bar{D}^0 K^-)/\Gamma_{\text{total}}$				Γ_{52}/Γ
VALUE (units 10^{-5})	DOCUMENT ID	TECN	COMMENT	
$2.2 \pm 0.1 \pm 0.6$	¹ AAIJ	14Bh LHCb	pp at 7, 8 TeV	

1 Uses Dalitz plot analysis of $B_S^0 \rightarrow \bar{D}^0 K^- \pi^+$ decays.

$\Gamma(\bar{D}^0 K^+ K^-)/\Gamma_{\text{total}}$				Γ_{53}/Γ
VALUE (units 10^{-5})	DOCUMENT ID	TECN	COMMENT	
$5.6 \pm 0.7 \pm 0.5$	¹ AAIJ	18Az LHCb	pp at 7, 8 TeV	

Meson Particle Listings

 B_S^0

• • • We do not use the following data for averages, fits, limits, etc. • • •

5.5 ± 2.0 ± 0.5 ^{2,3} AAIJ 12AMLHCB Repl. by AAIJ 18AZ

¹ AAIJ 18AZ reports $[\Gamma(B_S^0 \rightarrow \bar{D}^0 K^+ K^-)/\Gamma_{\text{total}}] / [B(B^0 \rightarrow \bar{D}^0 K^+ K^-)] = 0.930 \pm 0.089 \pm 0.069$ which we multiply by our best value $B(B^0 \rightarrow \bar{D}^0 K^+ K^-) = (6.1 \pm 0.5) \times 10^{-5}$. Our first error is their experiment's error and our second error is the systematic error from using our best value.

² AAIJ 12AM reports $[\Gamma(B_S^0 \rightarrow \bar{D}^0 K^+ K^-)/\Gamma_{\text{total}}] / [B(B^0 \rightarrow \bar{D}^0 K^+ K^-)] = 0.90 \pm 0.27 \pm 0.20$ which we multiply by our best value $B(B^0 \rightarrow \bar{D}^0 K^+ K^-) = (6.1 \pm 0.5) \times 10^{-5}$. Our first error is their experiment's error and our second error is the systematic error from using our best value.

³ Uses $B(b \rightarrow B_S^0)/B(b \rightarrow B^0) = 0.267^{+0.023}_{-0.020}$ measured by the same authors.

$\Gamma(\bar{D}^0 f_0(980))/\Gamma_{\text{total}}$ Γ_{54}/Γ

VALUE	CL%	DOCUMENT ID	TECN	COMMENT
$<3.1 \times 10^{-6}$	90	AAIJ	15AG LHCb	pp at 7, 8 TeV

$\Gamma(\bar{D}^0 \phi)/\Gamma_{\text{total}}$ Γ_{55}/Γ

VALUE (units 10^{-5})	DOCUMENT ID	TECN	COMMENT
2.30 ± 0.10 ± 0.23	¹ AAIJ	23AZ LHCb	pp at 7, 8, 13 TeV

• • • We do not use the following data for averages, fits, limits, etc. • • •

3.0 ± 0.4 ± 0.2 ² AAIJ 18AY LHCb Repl. by AAIJ 23AZ

¹ AAIJ 23AZ result's last uncertainty includes the uncertainty of the branching fraction of $B(B^0 \rightarrow \bar{D}^0 K^+ K^-)$ and of f_s/f_d ratio.

² AAIJ 18AY reports $[\Gamma(B_S^0 \rightarrow \bar{D}^0 \phi)/\Gamma_{\text{total}}] / [B(B^0 \rightarrow \bar{D}^0 \pi^+ \pi^-)] = (3.4 \pm 0.4 \pm 0.3) \times 10^{-2}$ which we multiply by our best value $B(B^0 \rightarrow \bar{D}^0 \pi^+ \pi^-) = (8.8 \pm 0.5) \times 10^{-4}$. Our first error is their experiment's error and our second error is the systematic error from using our best value.

$\Gamma(\bar{D}^0 \phi)/\Gamma(\bar{D}^0 K^*(892)^0)$ Γ_{55}/Γ_{40}

VALUE	DOCUMENT ID	TECN	COMMENT
0.069 ± 0.013 ± 0.007	AAIJ	13Bx LHCb	Repl. by AAIJ 18AY

• • • We do not use the following data for averages, fits, limits, etc. • • •

$\Gamma(\bar{D}^{*0} \phi)/\Gamma_{\text{total}}$ Γ_{56}/Γ

VALUE (units 10^{-5})	DOCUMENT ID	TECN	COMMENT
3.17 ± 0.16 ± 0.32	¹ AAIJ	23AZ LHCb	pp at 7, 8, 13 TeV

• • • We do not use the following data for averages, fits, limits, etc. • • •

3.7 ± 0.6 ± 0.2 ² AAIJ 18AY LHCb Repl. by AAIJ 23AZ

¹ AAIJ 23AZ result's last uncertainty includes the uncertainties of the branching fraction of $B(B^0 \rightarrow \bar{D}^0 K^+ K^-)$ and of f_s/f_d ratio.

² AAIJ 18AY reports $[\Gamma(B_S^0 \rightarrow \bar{D}^{*0} \phi)/\Gamma_{\text{total}}] / [B(B^0 \rightarrow \bar{D}^0 \pi^+ \pi^-)] = (4.2 \pm 0.5 \pm 0.4) \times 10^{-2}$ which we multiply by our best value $B(B^0 \rightarrow \bar{D}^0 \pi^+ \pi^-) = (8.8 \pm 0.5) \times 10^{-4}$. Our first error is their experiment's error and our second error is the systematic error from using our best value.

$\Gamma(D^{*\mp} \pi^\pm)/\Gamma_{\text{total}}$ Γ_{57}/Γ

VALUE	CL%	DOCUMENT ID	TECN	COMMENT
$<6.1 \times 10^{-6}$	90	¹ AAIJ	13AL LHCb	pp at 7 TeV

¹ Uses $f_s/f_d = 0.256 \pm 0.020$ and $B(B^0 \rightarrow D^{*\mp} \pi^\pm) = (2.76 \pm 0.13) \times 10^{-3}$.

$\Gamma(\eta_c \phi)/\Gamma_{\text{total}}$ Γ_{58}/Γ

VALUE (units 10^{-4})	DOCUMENT ID	TECN	COMMENT
5.01 ± 0.53 ± 0.68	¹ AAIJ	17U LHCb	pp at 7, 8 TeV

¹ The last uncertainty includes the limited knowledge of the external branching fractions where the η_c is reconstructed in the $p\bar{p}, K^+ K^- \pi^+ \pi^-, \pi^+ \pi^- \pi^+ \pi^-,$ and $K^+ K^- K^+ K^-$ decays and $\phi(1020) \rightarrow K^+ K^-$.

$\Gamma(\eta_c \pi^+ \pi^-)/\Gamma_{\text{total}}$ Γ_{60}/Γ

VALUE (units 10^{-4})	DOCUMENT ID	TECN	COMMENT
1.76 ± 0.59 ± 0.31	¹ AAIJ	17U LHCb	pp at 7, 8 TeV

¹ The last uncertainty includes the limited knowledge of the external branching fractions where the η_c is reconstructed in the $p\bar{p}, K^+ K^- \pi^+ \pi^-, \pi^+ \pi^- \pi^+ \pi^-,$ and $K^+ K^- K^+ K^-$ decays. The significance of the signal, including systematic uncertainties, is 4.6 standard deviations.

$\Gamma(J/\psi(1S) \phi)/\Gamma_{\text{total}}$ Γ_{61}/Γ

VALUE (units 10^{-3})	EVTS	DOCUMENT ID	TECN	COMMENT
1.04 ± 0.04 OUR FIT				
1.04 ± 0.04 OUR AVERAGE				
1.037 ± 0.032 ± 0.022		¹ AAIJ	21Y LHCb	pp at 7, 8, 13 TeV
1.25 ± 0.07 ± 0.23		² THORNE	13 BELL	$e^+ e^- \rightarrow \Upsilon(5S)$
1.5 ± 0.5 ± 0.1		³ ABE	96Q CDF	$p\bar{p}$

• • • We do not use the following data for averages, fits, limits, etc. • • •

1.050 ± 0.013 ± 0.104 ⁴ AAIJ 13AN LHCb Repl. by AAIJ 21Y

<6 ⁵ AKERS 94J OPAL $e^+ e^- \rightarrow Z$

seen ⁶ ABE 93F CDF $p\bar{p}$ at 1.8 TeV

seen ⁷ ACTON 92N OPAL Sup. by AKERS 94J

¹ AAIJ 21Y reports $[\Gamma(B_S^0 \rightarrow J/\psi(1S) \phi)/\Gamma_{\text{total}}] \times [B(\phi(1020) \rightarrow K^+ K^-)] = (5.01 \pm 0.16 \pm 0.17) \times 10^{-4}$ from a measurement of $[\Gamma(B_S^0 \rightarrow J/\psi(1S) \phi)/\Gamma_{\text{total}}] \times [B(\phi(1020) \rightarrow K^+ K^-)] / [B(B^+ \rightarrow J/\psi(1S) K^+)]$ assuming $B(B^+ \rightarrow J/\psi(1S) K^+) =$

$(1.003 \pm 0.035) \times 10^{-3}$, which we rescale to our best values $B(\phi(1020) \rightarrow K^+ K^-) = (49.1 \pm 0.5) \times 10^{-2}$, $B(B^+ \rightarrow J/\psi(1S) K^+) = (1.020 \pm 0.019) \times 10^{-3}$. Our first error is their experiment's error and our second error is the systematic error from using our best values.

² THORNE 13 uses $f_s = (17.2 \pm 3.0)\%$ as the fraction of $\Upsilon(5S)$ decaying to $B_S^{(*)} \bar{B}_S^{(*)}$.

³ ABE 96Q reports $[\Gamma(B_S^0 \rightarrow J/\psi(1S) \phi)/\Gamma_{\text{total}}] \times [\Gamma(\bar{B} \rightarrow B_S^0)/\Gamma(\bar{B} \rightarrow B^+) + \Gamma(\bar{B} \rightarrow B^0)] = (0.185 \pm 0.055 \pm 0.020) \times 10^{-3}$ which we divide by our best value $\Gamma(\bar{B} \rightarrow B_S^0)/[\Gamma(\bar{B} \rightarrow B^+) + \Gamma(\bar{B} \rightarrow B^0)] = 0.1230 \pm 0.0115$. Our first error is their experiment's error and our second error is the systematic error from using our best value.

⁴ AAIJ 13AN uses $f_s/f_d = 0.256 \pm 0.020$ and $B(B^+ \rightarrow J/\psi K^+) = (10.18 \pm 0.42) \times 10^{-4}$.

⁵ AKERS 94J sees one event and measures the limit on the product branching fraction $f(\bar{B} \rightarrow B_S^0) \cdot B(B_S^0 \rightarrow J/\psi(1S) \phi) < 7 \times 10^{-4}$ at CL = 90%. We divide by $B(\bar{B} \rightarrow B_S^0) = 0.112$.

⁶ ABE 93F measured using $J/\psi(1S) \rightarrow \mu^+ \mu^-$ and $\phi \rightarrow K^+ K^-$.

⁷ In ACTON 92N a limit on the product branching fraction is measured to be $f(\bar{B} \rightarrow B_S^0) \cdot B(B_S^0 \rightarrow J/\psi(1S) \phi) \leq 0.22 \times 10^{-2}$.

$\Gamma(J/\psi(1S) \phi \phi)/\Gamma(J/\psi(1S) \phi)$ Γ_{62}/Γ_{61}

VALUE (units 10^{-2})	EVTS	DOCUMENT ID	TECN	COMMENT
1.15 ± 0.12 ± 0.05	128	¹ AAIJ	16U LHCb	pp at 7, 8 TeV

¹ Uses $J/\psi \rightarrow \mu^+ \mu^-, \phi \rightarrow K^+ K^-$ decays, and observes 128 ± 13 events of $B_S^0 \rightarrow J/\psi \phi \phi$.

$\Gamma(J/\psi(1S) \pi^0)/\Gamma_{\text{total}}$ Γ_{63}/Γ

VALUE	CL%	DOCUMENT ID	TECN
$<1.2 \times 10^{-3}$	90	¹ ACCIARRI	97C L3

¹ ACCIARRI 97C assumes B^0 production fraction (39.5 ± 4.0%) and B_S (12.0 ± 3.0%).

$\Gamma(J/\psi(1S) \eta)/\Gamma_{\text{total}}$ Γ_{64}/Γ

VALUE (units 10^{-4})	CL%	DOCUMENT ID	TECN	COMMENT
4.0 ± 0.7 OUR AVERAGE				Error includes scale factor of 1.4.
3.6 ^{+0.5} _{-0.6} ^{+0.3} _{-0.2}		¹ AAIJ	13A LHCb	pp at 7 TeV
5.10 ± 0.50 ± 1.17 _{-0.83}		² LI	12 BELL	$e^+ e^- \rightarrow \Upsilon(4S)$

• • • We do not use the following data for averages, fits, limits, etc. • • •

<38 ⁹⁰ ³ ACCIARRI 97C L3

¹ AAIJ 13A reports $[\Gamma(B_S^0 \rightarrow J/\psi(1S) \eta)/\Gamma_{\text{total}}] / [B(B^0 \rightarrow J/\psi(1S) \rho^0)] = 14.0 \pm 1.2^{+1.1}_{-1.5} \pm 1.1^{+1.1}_{-1.0}$ which we multiply by our best value $B(B^0 \rightarrow J/\psi(1S) \rho^0) = (2.55^{+0.18}_{-0.16}) \times 10^{-5}$. Our first error is their experiment's error and our second error is the systematic error from using our best value.

² Observed for the first time with significances over 10σ . The second error are total systematic uncertainties including the error on $N(B_S^{(*)} \bar{B}_S^{(*)})$.

³ ACCIARRI 97C assumes B^0 production fraction (39.5 ± 4.0%) and B_S (12.0 ± 3.0%).

$\Gamma(J/\psi(1S) K_S^0)/\Gamma_{\text{total}}$ Γ_{65}/Γ

VALUE (units 10^{-5})	DOCUMENT ID	TECN	COMMENT
1.92 ± 0.14 OUR AVERAGE			
1.92 ± 0.14 ± 0.05	¹ AAIJ	15AL LHCb	pp at 7, 8 TeV
2.0 ± 0.4 ± 0.2	² AALTONEN	11A CDF	$p\bar{p}$ at 1.96 TeV

• • • We do not use the following data for averages, fits, limits, etc. • • •

2.03 ± 0.16 ± 0.20 ³ AAIJ 13AB LHCb Repl. by AAIJ 15AL

2.03 ± 0.26 ± 0.20 ⁴ AAIJ 12O LHCb Repl. by AAIJ 13AB

¹ AAIJ 15AL reports $[\Gamma(B_S^0 \rightarrow J/\psi(1S) K_S^0)/\Gamma_{\text{total}}] / [B(B^0 \rightarrow J/\psi(1S) K_S^0)] = (4.31 \pm 0.17 \pm 0.12 \pm 0.25) \times 10^{-2}$ which we multiply by our best value $B(B^0 \rightarrow J/\psi(1S) K_S^0) = (4.45 \pm 0.11) \times 10^{-4}$. Our first error is their experiment's error and our second error is the systematic error from using our best value.

² AALTONEN 11A reports $[\Gamma(B_S^0 \rightarrow J/\psi(1S) K_S^0)/\Gamma_{\text{total}}] \times [B(\bar{B} \rightarrow B_S^0)] / [B(\bar{B} \rightarrow B^0)] / [B(B^0 \rightarrow J/\psi(1S) K_S^0)] = (1.09 \pm 0.19 \pm 0.11) \times 10^{-2}$ which we multiply or divide by our best values $B(\bar{B} \rightarrow B_S^0) = (10.0 \pm 0.8) \times 10^{-2}$, $B(\bar{B} \rightarrow B^0) = (40.8 \pm 0.7) \times 10^{-2}$, $B(B^0 \rightarrow J/\psi(1S) K_S^0) = 1/2 \times B(B^0 \rightarrow J/\psi(1S) K^0) = 1/2 \times (8.91 \pm 0.21) \times 10^{-4}$. Our first error is their experiment's error and our second error is the systematic error from using our best values.

³ AAIJ 13AB reports $(1.97 \pm 0.14 \pm 0.07 \pm 0.15 \pm 0.08) \times 10^{-5}$ from a measurement of $[\Gamma(B_S^0 \rightarrow J/\psi(1S) K_S^0)/\Gamma_{\text{total}}] / [B(B^0 \rightarrow J/\psi(1S) K^0)] \times [\Gamma(\bar{B} \rightarrow B_S^0)/\Gamma(\bar{B} \rightarrow B^0)]$ assuming $B(B^0 \rightarrow J/\psi(1S) K^0) = (8.98 \pm 0.35) \times 10^{-4}$, $\Gamma(\bar{B} \rightarrow B_S^0)/\Gamma(\bar{B} \rightarrow B^0) = 0.256 \pm 0.020$, which we rescale to our best values $B(B^0 \rightarrow J/\psi(1S) K^0) = (8.91 \pm 0.21) \times 10^{-4}$, $\Gamma(\bar{B} \rightarrow B_S^0)/\Gamma(\bar{B} \rightarrow B^0) = 0.246 \pm 0.023$. Our first error is their experiment's error and our second error is the systematic error from using our best values.

⁴ AAIJ 12O reports $(1.83 \pm 0.21 \pm 0.10 \pm 0.14 \pm 0.07) \times 10^{-5}$ from a measurement of $[\Gamma(B_S^0 \rightarrow J/\psi(1S) K_S^0)/\Gamma_{\text{total}}] / [B(B^0 \rightarrow J/\psi(1S) K^0)] \times [\Gamma(\bar{B} \rightarrow B_S^0)/\Gamma(\bar{B} \rightarrow B^0)]$ assuming $B(B^0 \rightarrow J/\psi(1S) K^0) = (8.71 \pm 0.32) \times 10^{-4}$, $\Gamma(\bar{B} \rightarrow B_S^0)/\Gamma(\bar{B} \rightarrow B^0) = 0.267^{+0.021}_{-0.02}$, which we rescale to our best values $B(B^0 \rightarrow J/\psi(1S) K^0) = (8.91 \pm 0.21) \times 10^{-4}$, $\Gamma(\bar{B} \rightarrow B_S^0)/\Gamma(\bar{B} \rightarrow B^0) = 0.246 \pm 0.023$. Our first error is their experiment's error and our second error is the systematic error from using our best values.

$\Gamma(J/\psi(1S)\bar{K}^*(892)^0)/\Gamma_{total}$ Γ_{66}/Γ

VALUE (units 10^{-5})	DOCUMENT ID	TECN	COMMENT
4.14 ± 0.18 ± 0.35	1 AAIJ	15AV LHCb	pp at 7, 8 TeV
• • • We do not use the following data for averages, fits, limits, etc. • • •			
4.4 $^{+0.5}_{-0.4} \pm 0.8$	2 AAIJ	12AP LHCb	Repl. by AAIJ 15AV
9 $\pm 4 \pm 1$	3 AALTONEN	11A CDF	$p\bar{p}$ at 1.96 TeV

1 AAIJ 15AV result combines two measurements with different normalizing modes of $B^0 \rightarrow J/\psi K^*(892)^0$ and $B_s^0 \rightarrow J/\psi \phi$.

2 AAIJ 12AP reports $B(B_s^0 \rightarrow J/\psi(1S)\bar{K}^*(892)^0)/B(B^0 \rightarrow J/\psi(1S)K^*(892)^0) = (3.43 \pm 0.34 \pm 0.50) \times 10^{-2}$ and $B(B^0 \rightarrow J/\psi(1S)K^*(892)^0) = (1.29 \pm 0.05 \pm 0.13) \times 10^{-3}$ after correcting for the contribution from $K\pi$ S-wave beneath the K^* peak.

3 AALTONEN 11A reports $[\Gamma(B_s^0 \rightarrow J/\psi(1S)\bar{K}^*(892)^0)/\Gamma_{total}] \times [B(\bar{B} \rightarrow B^0)] / [B(\bar{B} \rightarrow B^0)] / [B(B^0 \rightarrow J/\psi(1S)K^*(892)^0)] = 0.0168 \pm 0.0024 \pm 0.0068$ which we multiply or divide by our best values $B(\bar{B} \rightarrow B^0) = (10.0 \pm 0.8) \times 10^{-2}$, $B(\bar{B} \rightarrow B^0) = (40.8 \pm 0.7) \times 10^{-2}$, $B(B^0 \rightarrow J/\psi(1S)K^*(892)^0) = (1.27 \pm 0.05) \times 10^{-3}$. Our first error is their experiment's error and our second error is the systematic error from using our best values.

$\Gamma(J/\psi(1S)\eta')/\Gamma_{total}$ Γ_{67}/Γ

VALUE (units 10^{-4})	DOCUMENT ID	TECN	COMMENT
3.3 ± 0.4 OUR AVERAGE			
3.2 $^{+0.4}_{-0.5} \pm 0.2$	1 AAIJ	13A LHCb	pp at 7 TeV
3.71 ± 0.61 $^{+0.85}_{-0.60}$	2 LI	12 BELL	$e^+e^- \rightarrow \Upsilon(4S)$

1 AAIJ 13A reports $[\Gamma(B_s^0 \rightarrow J/\psi(1S)\eta')/\Gamma_{total}] / [B(B^0 \rightarrow J/\psi(1S)\rho^0)] = 12.7 \pm 1.1 \pm 0.5 \pm 1.0 \pm 1.3 \pm 0.9$ which we multiply by our best value $B(B^0 \rightarrow J/\psi(1S)\rho^0) = (2.55 \pm 0.18 \pm 0.16) \times 10^{-5}$. Our first error is their experiment's error and our second error is the systematic error from using our best value.

2 Observed for the first time with significances over 10σ . The second error are total systematic uncertainties including the error on $N(B_s^{(*)}\bar{B}_s^{(*)})$.

$\Gamma(J/\psi(1S)\eta')/\Gamma(J/\psi(1S)\eta)$ Γ_{67}/Γ_{64}

VALUE	DOCUMENT ID	TECN	COMMENT
0.87 ± 0.06 OUR AVERAGE			
0.902 ± 0.072 ± 0.045	1 AAIJ	15D LHCb	pp at 7, 8 TeV
0.90 ± 0.09 $^{+0.06}_{-0.02}$	2 AAIJ	13A LHCb	pp at 7 TeV
0.73 ± 0.14 ± 0.02	2 LI	12 BELL	$e^+e^- \rightarrow \Upsilon(4S)$

1 Uses $J/\psi \rightarrow \mu^+\mu^-, \eta' \rightarrow \rho^0\gamma$, and $\eta' \rightarrow \eta\pi^+\pi^-$ decays.

2 Strongly correlated with measurements of $\Gamma(J/\psi(1S)\eta)/\Gamma$ and $\Gamma(J/\psi(1S)\eta')/\Gamma$ reported in the same reference.

$\Gamma(J/\psi(1S)\pi^+\pi^-)/\Gamma(J/\psi(1S)\phi)$ Γ_{68}/Γ_{61}

VALUE (units 10^{-2})	DOCUMENT ID	TECN	COMMENT
19.4 ± 1.5 OUR FIT Error includes scale factor of 2.2.			
19.9 ± 0.7 ± 0.2	1 AAIJ	12A0 LHCb	pp at 7 TeV

1 AAIJ 12A0 reports $(19.79 \pm 0.47 \pm 0.52) \times 10^{-2}$ from a measurement of $[\Gamma(B_s^0 \rightarrow J/\psi(1S)\pi^+\pi^-)/\Gamma(B_s^0 \rightarrow J/\psi(1S)\phi)] / [B(\phi(1020) \rightarrow K^+K^-)]$ assuming $B(\phi(1020) \rightarrow K^+K^-) = (48.9 \pm 0.5) \times 10^{-2}$, which we rescale to our best value $B(\phi(1020) \rightarrow K^+K^-) = (49.1 \pm 0.5) \times 10^{-2}$. Our first error is their experiment's error and our second error is the systematic error from using our best value.

$\Gamma(J/\psi(1S)f_0(500), f_0 \rightarrow \pi^+\pi^-)/\Gamma(J/\psi(1S)f_0(980), f_0 \rightarrow \pi^+\pi^-)$ Γ_{69}/Γ_{71}

VALUE	CL%	DOCUMENT ID	TECN	COMMENT
<0.034	90	1 AAIJ	14BR LHCb	pp at 7, 8 TeV

1 Reported first of two solutions using the full Dalitz analysis.

$\Gamma(J/\psi(1S)\rho, \rho \rightarrow \pi^+\pi^-)/\Gamma(J/\psi(1S)\pi^+\pi^-)$ Γ_{70}/Γ_{68}

VALUE	CL%	DOCUMENT ID	TECN	COMMENT
<0.017	90	1 AAIJ	14BR LHCb	pp at 7, 8 TeV

1 Reported first of two solutions using the full Dalitz analysis.

$\Gamma(J/\psi(1S)f_0(980), f_0 \rightarrow \pi^+\pi^-)/\Gamma_{total}$ Γ_{71}/Γ

VALUE (units 10^{-4})	DOCUMENT ID	TECN	COMMENT
1.24 ± 0.15 OUR FIT Error includes scale factor of 2.1.			
1.16 $^{+0.31}_{-0.19} \pm 0.30$	1 LI	11 BELL	$e^+e^- \rightarrow \Upsilon(5S)$

1 The second error includes both the detector systematic and the uncertainty in the number of produced $\Upsilon(5S) \rightarrow B_s^{(*)}\bar{B}_s^{(*)}$ pairs.

$\Gamma(J/\psi(1S)f_0(980), f_0 \rightarrow \pi^+\pi^-)/\Gamma(J/\psi(1S)\phi)$ Γ_{71}/Γ_{61}

VALUE	DOCUMENT ID	TECN	COMMENT
0.119 ± 0.013 OUR FIT Error includes scale factor of 2.4.			
0.110 $^{+0.020}_{-0.018} \pm 0.020$ OUR AVERAGE Error includes scale factor of 2.5. See the ideogram below.			

0.069 ± 0.012 ± 0.001	1 KHACHATRYAN...16Q	CMS	pp at 7 TeV
0.140 $^{+0.026}_{-0.013} \pm 0.001$	2,3 AAIJ	12A0 LHCb	pp at 7 TeV
0.135 ± 0.036 ± 0.001	4 ABAZOV	12C D0	$p\bar{p}$ at 1.96 TeV
0.126 ± 0.012 ± 0.001	5 AALTONEN	11AB CDF	$p\bar{p}$ at 1.96 TeV

• • • We do not use the following data for averages, fits, limits, etc. • • •

0.124 $^{+0.026}_{-0.023} \pm 0.001$ ⁶ AAIJ 11 LHCb Repl. by AAIJ 12A0

1 KHACHATRYAN 16Q reports $[\Gamma(B_s^0 \rightarrow J/\psi(1S)f_0(980), f_0 \rightarrow \pi^+\pi^-)/\Gamma(B_s^0 \rightarrow J/\psi(1S)\phi)] / [B(\phi(1020) \rightarrow K^+K^-)] = 0.140 \pm 0.008 \pm 0.023$ which we multiply by our best value $B(\phi(1020) \rightarrow K^+K^-) = (49.1 \pm 0.5) \times 10^{-2}$. Our first error is their experiment's error and our second error is the systematic error from using our best value.

2 AAIJ 12A0 reports $(13.9 \pm 0.6 \pm 2.5 \pm 1.2) \times 10^{-2}$ from a measurement of $[\Gamma(B_s^0 \rightarrow J/\psi(1S)f_0(980), f_0 \rightarrow \pi^+\pi^-)/\Gamma(B_s^0 \rightarrow J/\psi(1S)\phi)] / [B(\phi(1020) \rightarrow K^+K^-)]$ assuming $B(\phi(1020) \rightarrow K^+K^-) = (48.9 \pm 0.5) \times 10^{-2}$, which we rescale to our best value $B(\phi(1020) \rightarrow K^+K^-) = (49.1 \pm 0.5) \times 10^{-2}$. Our first error is their experiment's error and our second error is the systematic error from using our best value.

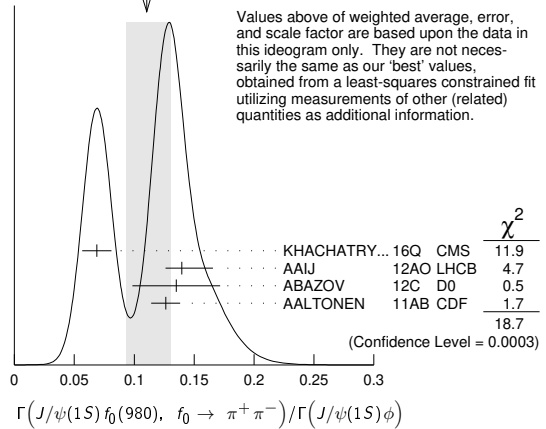
3 Measured in Dalitz plot like analysis of $B_s \rightarrow J/\psi\pi^+\pi^-$ decays.

4 ABAZOV 12C reports $[\Gamma(B_s^0 \rightarrow J/\psi(1S)f_0(980), f_0 \rightarrow \pi^+\pi^-)/\Gamma(B_s^0 \rightarrow J/\psi(1S)\phi)] / [B(\phi(1020) \rightarrow K^+K^-)] = 0.275 \pm 0.041 \pm 0.061$ which we multiply by our best value $B(\phi(1020) \rightarrow K^+K^-) = (49.1 \pm 0.5) \times 10^{-2}$. Our first error is their experiment's error and our second error is the systematic error from using our best value.

5 AALTONEN 11AB reports $[\Gamma(B_s^0 \rightarrow J/\psi(1S)f_0(980), f_0 \rightarrow \pi^+\pi^-)/\Gamma(B_s^0 \rightarrow J/\psi(1S)\phi)] / [B(\phi(1020) \rightarrow K^+K^-)] = 0.257 \pm 0.020 \pm 0.014$ which we multiply by our best value $B(\phi(1020) \rightarrow K^+K^-) = (49.1 \pm 0.5) \times 10^{-2}$. Our first error is their experiment's error and our second error is the systematic error from using our best value.

6 AAIJ 11 reports $[\Gamma(B_s^0 \rightarrow J/\psi(1S)f_0(980), f_0 \rightarrow \pi^+\pi^-)/\Gamma(B_s^0 \rightarrow J/\psi(1S)\phi)] / [B(\phi(1020) \rightarrow K^+K^-)] = 0.252 \pm 0.046 \pm 0.027 \pm 0.032 \pm 0.033$ which we multiply by our best value $B(\phi(1020) \rightarrow K^+K^-) = (49.1 \pm 0.5) \times 10^{-2}$. Our first error is their experiment's error and our second error is the systematic error from using our best value.

WEIGHTED AVERAGE
0.110±0.020-0.018 (Error scaled by 2.5)



$\Gamma(J/\psi(1S)f_0(980), f_0 \rightarrow \pi^+\pi^-)/\Gamma(J/\psi(1S)\pi^+\pi^-)$ Γ_{71}/Γ_{68}

VALUE	DOCUMENT ID	TECN	COMMENT
0.61 ± 0.05 OUR FIT Error includes scale factor of 2.1.			
0.703 ± 0.015 $^{+0.004}_{-0.051}$	1 AAIJ	14BR LHCb	pp at 7, 8 TeV

1 Reported first of two solutions using the full Dalitz analysis.

$\Gamma(J/\psi(1S)f_2(1270), f_2 \rightarrow \pi^+\pi^-)/\Gamma(J/\psi(1S)\phi)$ Γ_{72}/Γ_{61}

VALUE (units 10^{-4})	DOCUMENT ID	TECN	COMMENT
9.8 ± 3.4 ± 0.1	1,2 AAIJ	12A0 LHCb	pp at 7 TeV

1 AAIJ 12A0 reports $(0.098 \pm 0.033 \pm 0.006 \pm 0.015) \times 10^{-2}$ from a measurement of $[\Gamma(B_s^0 \rightarrow J/\psi(1S)f_2(1270), f_2 \rightarrow \pi^+\pi^-)/\Gamma(B_s^0 \rightarrow J/\psi(1S)\phi)] / [B(\phi(1020) \rightarrow K^+K^-)]$ assuming $B(\phi(1020) \rightarrow K^+K^-) = (48.9 \pm 0.5) \times 10^{-2}$, which we rescale to our best value $B(\phi(1020) \rightarrow K^+K^-) = (49.1 \pm 0.5) \times 10^{-2}$. Our first error is their experiment's error and our second error is the systematic error from using our best value.

2 Measured in Dalitz plot like analysis of $B_s \rightarrow J/\psi\pi^+\pi^-$ decays for the f_2 helicity state $\lambda = 0$.

$\Gamma(J/\psi(1S)f_2(1270)_0, f_2 \rightarrow \pi^+\pi^-)/\Gamma(J/\psi(1S)\pi^+\pi^-)$ Γ_{73}/Γ_{68}

VALUE (%)	DOCUMENT ID	TECN	COMMENT
0.36 ± 0.07 ± 0.03	1 AAIJ	14BR LHCb	pp at 7, 8 TeV

1 Reported first of two solutions using the full Dalitz analysis.

$\Gamma(J/\psi(1S)f_2(1270)_\parallel, f_2 \rightarrow \pi^+\pi^-)/\Gamma(J/\psi(1S)\pi^+\pi^-)$ Γ_{74}/Γ_{68}

VALUE (%)	DOCUMENT ID	TECN	COMMENT
0.52 ± 0.15 ± 0.05 OUR FIT			
0.52 $^{+0.15}_{-0.02} \pm 0.02$	1 AAIJ	14BR LHCb	pp at 7, 8 TeV

1 Reported first of two solutions using the full Dalitz analysis.

Meson Particle Listings

$\Gamma(J/\psi(1S) f_2(1270)_\perp, f_2 \rightarrow \pi^+ \pi^-) / \Gamma(J/\psi(1S) \pi^+ \pi^-)$ $\Gamma_{75} / \Gamma_{68}$				$\Gamma(J/\psi(1S) K^0 K^- \pi^+ + \text{c.c.}) / \Gamma_{\text{total}}$ Γ_{85} / Γ				
VALUE (%)	DOCUMENT ID	TECN	COMMENT	VALUE (units 10^{-4})	DOCUMENT ID	TECN	COMMENT	
$0.63 \pm 0.34 \pm 0.16$ -0.08	¹ AAIJ	14BR LHCB	pp at 7, 8 TeV	$9.5 \pm 1.0 \pm 0.8$	¹ AAIJ	14L LHCB	pp at 7 TeV	
¹ Reported first of two solutions using the full Dalitz analysis.				¹ AAIJ 14L reports $[\Gamma(B_S^0 \rightarrow J/\psi(1S) K^0 K^- \pi^+ + \text{c.c.}) / \Gamma_{\text{total}}] / [\Gamma(B^0 \rightarrow J/\psi(1S) K^0 \pi^+ \pi^-)] = 2.12 \pm 0.15 \pm 0.18$ which we multiply by our best value $B(B^0 \rightarrow J/\psi(1S) K^0 \pi^+ \pi^-) = (4.5 \pm 0.4) \times 10^{-4}$. Our first error is their experiment's error and our second error is the systematic error from using our best value. This is an observation of $B_S^0 \rightarrow J/\psi K_S^0 K^\pm \pi^\mp$ with more than 10 standard deviations.				
$\Gamma(J/\psi(1S) f_0(1370), f_0 \rightarrow \pi^+ \pi^-) / \Gamma_{\text{total}}$ Γ_{76} / Γ				$\Gamma(J/\psi(1S) \bar{K}^0 K^+ K^-) / \Gamma_{\text{total}}$ Γ_{86} / Γ				
VALUE (units 10^{-4})	DOCUMENT ID	TECN	COMMENT	VALUE	CL%	DOCUMENT ID	TECN	COMMENT
$0.34 \pm 0.11 + 0.085$ $-0.14 - 0.054$	¹ LI	11 BELL	$e^+ e^- \rightarrow \Upsilon(5S)$	$< 1.2 \times 10^{-6}$	90	¹ AAIJ	14L LHCB	pp at 7 TeV
$\bullet \bullet \bullet$ We do not use the following data for averages, fits, limits, etc. $\bullet \bullet \bullet$				¹ Measured with $B(B_S^0 \rightarrow J/\psi K_S^0 K^+ K^-) / B(B^0 \rightarrow J/\psi K_S^0 \pi^+ \pi^-)$ using PDG 12 values for the involved branching fractions.				
¹ The second error includes both the detector systematic and the uncertainty in the number of produced $\Upsilon(5S) \rightarrow B_S^{(*)} \bar{B}_S^{(*)}$ pairs.				$\Gamma(J/\psi(1S) f_2'(1525)) / \Gamma_{\text{total}}$ Γ_{88} / Γ				
$\Gamma(J/\psi(1S) f_0(1370), f_0 \rightarrow \pi^+ \pi^-) / \Gamma(J/\psi(1S) \phi)$ $\Gamma_{76} / \Gamma_{61}$				$\Gamma(J/\psi(1S) f_2'(1525)) / \Gamma_{\text{total}}$ Γ_{88} / Γ				
VALUE (units 10^{-2})	DOCUMENT ID	TECN	COMMENT	VALUE (units 10^{-4})	DOCUMENT ID	TECN	COMMENT	
$4.21 \pm 0.54 \pm 0.04$ -3.76	^{1,2} AAIJ	12A0 LHCB	pp at 7 TeV	$2.61 \pm 0.20 \pm 0.56$ -0.50	¹ AAIJ	13AN LHCB	pp at 7 TeV	
¹ AAIJ 12A0 reports $(4.19 \pm 0.53 \pm 0.12) \times 10^{-2}$ from a measurement of $[\Gamma(B_S^0 \rightarrow J/\psi(1S) f_0(1370), f_0 \rightarrow \pi^+ \pi^-) / \Gamma(B_S^0 \rightarrow J/\psi(1S) \phi)] / [B(\phi(1020) \rightarrow K^+ K^-)]$ assuming $B(\phi(1020) \rightarrow K^+ K^-) = (48.9 \pm 0.5) \times 10^{-2}$, which we rescale to our best value $B(\phi(1020) \rightarrow K^+ K^-) = (49.1 \pm 0.5) \times 10^{-2}$. Our first error is their experiment's error and our second error is the systematic error from using our best value.				¹ Uses $f_s/f_d = 0.256 \pm 0.020$ and $B(B^+ \rightarrow J/\psi K^+) = (10.18 \pm 0.42) \times 10^{-4}$.				
² Measured in Dalitz plot like analysis of $B_S \rightarrow J/\psi \pi^+ \pi^-$ decays.				$\Gamma(J/\psi(1S) f_2'(1525)) / \Gamma(J/\psi(1S) \phi)$ $\Gamma_{88} / \Gamma_{61}$				
$\Gamma(J/\psi(1S) f_0(1500), f_0 \rightarrow \pi^+ \pi^-) / \Gamma(J/\psi(1S) \pi^+ \pi^-)$ $\Gamma_{77} / \Gamma_{68}$				$\Gamma(J/\psi(1S) f_2'(1525)) / \Gamma(J/\psi(1S) \phi)$ $\Gamma_{88} / \Gamma_{61}$				
VALUE	DOCUMENT ID	TECN	COMMENT	VALUE (units 10^{-2})	DOCUMENT ID	TECN	COMMENT	
$0.101 \pm 0.008 \pm 0.011$ -0.003	¹ AAIJ	14BR LHCB	pp at 7, 8 TeV	21 ± 4 OUR AVERAGE	¹ THORNE	13 BELL	$e^+ e^- \rightarrow \Upsilon(5S)$	
¹ Reported first of two solutions using the full Dalitz analysis.				$21.5 \pm 4.9 \pm 2.6$				
¹ Reported first of two solutions using the full Dalitz analysis.				$21 \pm 7 \pm 1$				
¹ Reported first of two solutions using the full Dalitz analysis.				$27 \pm 4 \pm 1$				
¹ Reported first of two solutions using the full Dalitz analysis.				$\bullet \bullet \bullet$ We do not use the following data for averages, fits, limits, etc. $\bullet \bullet \bullet$				
¹ Reported first of two solutions using the full Dalitz analysis.				¹ Uses $B(f_2'(1525) \rightarrow K^+ K^-) = (44.4 \pm 1.1)\%$.				
¹ Reported first of two solutions using the full Dalitz analysis.				² ABAZOV 12AF reports $[\Gamma(B_S^0 \rightarrow J/\psi(1S) f_2'(1525)) / \Gamma(B_S^0 \rightarrow J/\psi(1S) \phi)] \times B(f_2'(1525) \rightarrow K^+ K^-) / B(\phi(1020) \rightarrow K^+ K^-) = 0.19 \pm 0.05 \pm 0.04$ which we divide and multiply by our best values $B(f_2'(1525) \rightarrow K^+ K^-) = \frac{1}{2} (88.8 \pm 2.2) \times 10^{-2}$, $B(\phi(1020) \rightarrow K^+ K^-) = (49.1 \pm 0.5) \times 10^{-2}$. Our first error is their experiment's error and our second error is the systematic error from using our best values.				
¹ Reported first of two solutions using the full Dalitz analysis.				³ ABAZOV 12AF fits the invariant masses of the $K^+ K^-$ pair in the range $1.35 < M(K^+ K^-) < 2$ GeV.				
¹ Reported first of two solutions using the full Dalitz analysis.				⁴ AAIJ 12s reports $[(26.4 \pm 2.7 \pm 2.4) \times 10^{-2}]$ from a measurement of $\Gamma(B_S^0 \rightarrow J/\psi(1S) f_2'(1525)) / \Gamma(B_S^0 \rightarrow J/\psi(1S) \phi) \times B(f_2'(1525) \rightarrow K^+ K^-) / B(\phi(1020) \rightarrow K^+ K^-)$ assuming $B(f_2'(1525) \rightarrow K^+ K^-) = (44.4 \pm 1.1) \times 10^{-2}$, $B(\phi(1020) \rightarrow K^+ K^-) = (48.9 \pm 0.5) \times 10^{-2}$, which we rescale to our best values $B(f_2'(1525) \rightarrow K^+ K^-) = \frac{1}{2} (88.8 \pm 2.2) \times 10^{-2}$, $B(\phi(1020) \rightarrow K^+ K^-) = (49.1 \pm 0.5) \times 10^{-2}$. Our first error is their experiment's error and our second error is the systematic error from using our best values.				
¹ Reported first of two solutions using the full Dalitz analysis.				$\Gamma(J/\psi(1S) \rho^0) / \Gamma_{\text{total}}$ Γ_{89} / Γ				
VALUE (%)	DOCUMENT ID	TECN	COMMENT	VALUE (units 10^{-6})	CL%	DOCUMENT ID	TECN	COMMENT
$0.51 \pm 0.09 \pm 0.05$ -0.04	¹ AAIJ	14BR LHCB	pp at 7, 8 TeV	$3.58 \pm 0.19 \pm 0.39$		¹ AAIJ	19U LHCB	pp at 7, 8, 13 TeV
¹ Reported first of two solutions using the full Dalitz analysis.				$\bullet \bullet \bullet$ We do not use the following data for averages, fits, limits, etc. $\bullet \bullet \bullet$				
¹ Reported first of two solutions using the full Dalitz analysis.				< 4.8				
¹ Reported first of two solutions using the full Dalitz analysis.				$< 2.6 \times 10^{-9}$				
¹ Reported first of two solutions using the full Dalitz analysis.				¹ Measured relative to $B_S^0 \rightarrow J/\psi \phi$ assuming $B(B_S^0 \rightarrow J/\psi \phi) = (10.5 \pm 0.13 \pm 0.64) \times 10^{-4}$ and taking into account small $K^+ K^- S$ -wave contribution.				
¹ Reported first of two solutions using the full Dalitz analysis.				² Uses $B(B_S^0 \rightarrow J/\psi(1S) \pi^+ \pi^-) = (1.98 \pm 0.20) \times 10^{-4}$.				
$\Gamma(J/\psi(1S) f_2'(1525)_\parallel, f_2' \rightarrow \pi^+ \pi^-) / \Gamma(J/\psi(1S) \pi^+ \pi^-)$ $\Gamma_{79} / \Gamma_{68}$				$\Gamma(J/\psi(1S) \gamma) / \Gamma_{\text{total}}$ Γ_{90} / Γ				
VALUE (%)	DOCUMENT ID	TECN	COMMENT	VALUE	CL%	DOCUMENT ID	TECN	COMMENT
$0.06 \pm 0.13 \pm 0.01$ -0.04	¹ AAIJ	14BR LHCB	pp at 7, 8 TeV	$< 7.3 \times 10^{-6}$	90	¹ AAIJ	15BB LHCB	pp at 7, 8 TeV
¹ Reported first of two solutions using the full Dalitz analysis.				¹ Branching fractions of normalization modes $B_S^0 \rightarrow J/\psi \gamma$ taken from PDG 14. Uses $f_s/f_d = 0.259 \pm 0.015$.				
¹ Reported first of two solutions using the full Dalitz analysis.				$\Gamma(J/\psi \mu^+ \mu^-, J/\psi \rightarrow \mu^+ \mu^-) / \Gamma_{\text{total}}$ Γ_{91} / Γ				
VALUE (%)	DOCUMENT ID	TECN	COMMENT	VALUE	CL%	DOCUMENT ID	TECN	COMMENT
$0.26 \pm 0.18 \pm 0.06$ -0.04	¹ AAIJ	14BR LHCB	pp at 7, 8 TeV	$< 2.6 \times 10^{-9}$	95	AAIJ	22Q LHCB	pp at 7, 8, 13 TeV
¹ Reported first of two solutions using the full Dalitz analysis.				$\Gamma(J/\psi(1S) \pi^+ \pi^- \pi^+ \pi^-) / \Gamma(J/\psi(1S) \pi^+ \pi^-)$ $\Gamma_{92} / \Gamma_{68}$				
VALUE	CL%	DOCUMENT ID	TECN	COMMENT	VALUE	DOCUMENT ID	TECN	COMMENT
$0.024 \pm 0.004 \pm 0.050$ -0.002		¹ AAIJ	14BR LHCB	pp at 7, 8 TeV	$0.371 \pm 0.015 \pm 0.022$	¹ AAIJ	14Y LHCB	pp at 7, 8 TeV
¹ Reported first of two solutions using the full Dalitz analysis.				¹ Excludes contributions from $\psi(2S)$ and $\chi_{c1}(3872)$ decaying to $J/\psi(1S) \pi^+ \pi^-$.				
$\Gamma(J/\psi(1S) \bar{K}^0 \pi^+ \pi^-) / \Gamma_{\text{total}}$ Γ_{83} / Γ				$\Gamma(J/\psi(1S) f_1(1285)) / \Gamma_{\text{total}}$ Γ_{93} / Γ				
VALUE	CL%	DOCUMENT ID	TECN	COMMENT	VALUE (units 10^{-5})	DOCUMENT ID	TECN	COMMENT
$< 4.4 \times 10^{-5}$	90	¹ AAIJ	14L LHCB	pp at 7 TeV	$7.2 \pm 1.3 \pm 0.4$	¹ AAIJ	14Y LHCB	pp at 7, 8 TeV
¹ Measured with $B(B_S^0 \rightarrow J/\psi K_S^0 \pi^+ \pi^-) / B(B^0 \rightarrow J/\psi K_S^0 \pi^+ \pi^-)$ using PDG 12 values for the involved branching fractions.				¹ AAIJ 14Y reports $(7.14 \pm 0.99 \pm 0.83 \pm 0.41) \times 10^{-5}$ from a measurement of $[\Gamma(B_S^0 \rightarrow J/\psi(1S) f_1(1285)) / \Gamma_{\text{total}}] \times [B(f_1(1285) \rightarrow 2\pi^+ 2\pi^-)]$ assuming $B(f_1(1285) \rightarrow 2\pi^+ 2\pi^-) = 0.11 \pm 0.006$, which we rescale to our best value $B(f_1(1285) \rightarrow 2\pi^+ 2\pi^-) = (10.9 \pm 0.6) \times 10^{-2}$. Our first error is their experiment's error and our second error is the systematic error from using our best value.				
$\Gamma(J/\psi(1S) K^+ K^-) / \Gamma_{\text{total}}$ Γ_{84} / Γ								
VALUE (units 10^{-4})	DOCUMENT ID	TECN	COMMENT					
7.9 ± 0.7 OUR AVERAGE								
$7.70 \pm 0.08 \pm 0.72$	¹ AAIJ	13AN LHCB	pp at 7 TeV					
$10.1 \pm 0.9 \pm 2.1$	² THORNE	13 BELL	$e^+ e^- \rightarrow \Upsilon(5S)$					
¹ Uses $f_s/f_d = 0.256 \pm 0.020$ and $B(B^+ \rightarrow J/\psi K^+) = (10.18 \pm 0.42) \times 10^{-4}$.								
² Uses $f_s = (17.2 \pm 3.0)\%$ as the fraction of $\Upsilon(5S)$ decaying to $B_S^{(*)} \bar{B}_S^{(*)}$.								

$\Gamma(\psi(2S)\eta)/\Gamma(J/\psi(1S)\eta)$ Γ_{94}/Γ_{64}

VALUE	DOCUMENT ID	TECN	COMMENT
0.83±0.14±0.12	¹ AAIJ	13AA LHCB	pp at 7 TeV

¹ Assuming lepton universality for dimuon decay modes of J/ψ and $\psi(2S)$ mesons, the ratio $B(J/\psi \rightarrow \mu^+\mu^-)/B(\psi(2S) \rightarrow \mu^+\mu^-) = B(J/\psi \rightarrow e^+e^-)/B(\psi(2S) \rightarrow e^+e^-) = 7.69 \pm 0.19$ was used.

 $\Gamma(\psi(2S)\eta')/\Gamma(J/\psi(1S)\eta')$ Γ_{95}/Γ_{67}

VALUE (units 10^{-2})	DOCUMENT ID	TECN	COMMENT
38.7±9.0±1.6	¹ AAIJ	15D LHCB	pp at 7, 8 TeV

¹ Uses $J/\psi \rightarrow \mu^+\mu^-$, $\eta' \rightarrow \rho^0\gamma$, and $\eta' \rightarrow \eta\pi^+\pi^-$ decays.

 $\Gamma(\psi(2S)\pi^+\pi^-)/\Gamma(J/\psi(1S)\pi^+\pi^-)$ Γ_{96}/Γ_{68}

VALUE	DOCUMENT ID	TECN	COMMENT
0.34±0.04±0.03	¹ AAIJ	13AA LHCB	pp at 7 TeV

¹ Assuming lepton universality for dimuon decay modes of J/ψ and $\psi(2S)$ mesons, the ratio $B(J/\psi \rightarrow \mu^+\mu^-)/B(\psi(2S) \rightarrow \mu^+\mu^-) = B(J/\psi \rightarrow e^+e^-)/B(\psi(2S) \rightarrow e^+e^-) = 7.69 \pm 0.19$ was used.

 $\Gamma(\psi(2S)\phi)/\Gamma_{total}$ Γ_{97}/Γ

VALUE (units 10^{-4})	EVTS	DOCUMENT ID	TECN	COMMENT
• • •	1	BUSKULIC	93G ALEP	$e^+e^- \rightarrow Z$

• • • We do not use the following data for averages, fits, limits, etc. • • •

 $\Gamma(\psi(2S)\phi)/\Gamma(J/\psi(1S)\phi)$ Γ_{97}/Γ_{61}

VALUE	DOCUMENT ID	TECN	COMMENT
0.503±0.035 OUR AVERAGE			

0.500±0.034±0.014 ^{1,2} AAIJ 12L LHCB pp at 7 TeV
 0.53±0.10±0.09 ABYZOV 09Y D0 $p\bar{p}$ at 1.96 TeV
 0.52±0.13±0.07 ABULENCIA 06N CDF $p\bar{p}$ at 1.96 TeV

¹ AAIJ 12L reports $0.489 \pm 0.026 \pm 0.021 \pm 0.012$ from a measurement of $[\Gamma(B_s^0 \rightarrow \psi(2S)\phi)/\Gamma(B_s^0 \rightarrow J/\psi(1S)\phi)] \times [B(J/\psi(1S) \rightarrow e^+e^-)] / [B(\psi(2S) \rightarrow e^+e^-)]$ assuming $B(J/\psi(1S) \rightarrow e^+e^-) = (5.94 \pm 0.06) \times 10^{-2}$, $B(\psi(2S) \rightarrow e^+e^-) = (7.72 \pm 0.17) \times 10^{-3}$, which we rescale to our best values $B(J/\psi(1S) \rightarrow e^+e^-) = (5.971 \pm 0.032) \times 10^{-2}$, $B(\psi(2S) \rightarrow e^+e^-) = (7.94 \pm 0.22) \times 10^{-3}$. Our first error is their experiment's error and our second error is the systematic error from using our best values.

² Assumes $B(J/\psi \rightarrow \mu^+\mu^-) / B(\psi(2S) \rightarrow \mu^+\mu^-) = B(J/\psi \rightarrow e^+e^-) / B(\psi(2S) \rightarrow e^+e^-) = 7.69 \pm 0.19$.

 $\Gamma(\psi(2S)K^0)/\Gamma_{total}$ Γ_{98}/Γ

VALUE (units 10^{-5})	DOCUMENT ID	TECN	COMMENT
1.9±0.5±0.2	¹ TUMASYAN	22Al CMS	pp at 13 TeV

¹ TUMASYAN 22Al reports $[\Gamma(B_s^0 \rightarrow \psi(2S)K^0)/\Gamma_{total}] / [B(B^0 \rightarrow \psi(2S)K^0)] = (3.33 \pm 0.69 \pm 0.11 \pm 0.34) \times 10^{-2}$ which we multiply by our best value $B(B^0 \rightarrow \psi(2S)K^0) = (5.8 \pm 0.5) \times 10^{-4}$. Our first error is their experiment's error and our second error is the systematic error from using our best value.

 $\Gamma(\psi(2S)K^-\pi^+)/\Gamma_{total}$ Γ_{99}/Γ

VALUE (units 10^{-5})	DOCUMENT ID	TECN	COMMENT
3.12±0.30±0.21	¹ AAIJ	15U LHCB	pp at 7, 8 TeV

¹ AAIJ 15U reports $[\Gamma(B_s^0 \rightarrow \psi(2S)K^-\pi^+)/\Gamma_{total}] / [B(B^0 \rightarrow \psi(2S)K^+\pi^-)] = (5.38 \pm 0.36 \pm 0.22 \pm 0.31) \times 10^{-2}$ which we multiply by our best value $B(B^0 \rightarrow \psi(2S)K^+\pi^-) = (5.8 \pm 0.4) \times 10^{-4}$. Our first error is their experiment's error and our second error is the systematic error from using our best value.

 $\Gamma(\psi(2S)\bar{K}^*(892)^0)/\Gamma_{total}$ Γ_{100}/Γ

VALUE (units 10^{-5})	DOCUMENT ID	TECN	COMMENT
3.3±0.5^{+0.2}_{-0.3}	¹ AAIJ	15U LHCB	pp at 7, 8 TeV

¹ AAIJ 15U reports $[\Gamma(B_s^0 \rightarrow \psi(2S)\bar{K}^*(892)^0)/\Gamma_{total}] / [B(B^0 \rightarrow \psi(2S)K^*(892)^0)] = (5.58 \pm 0.57 \pm 0.40 \pm 0.32) \times 10^{-2}$ which we multiply by our best value $B(B^0 \rightarrow \psi(2S)K^*(892)^0) = (5.9 \pm 0.4) \times 10^{-4}$. Our first error is their experiment's error and our second error is the systematic error from using our best value.

 $\Gamma(\chi_{c1}\phi)/\Gamma(J/\psi(1S)\phi)$ Γ_{101}/Γ_{61}

VALUE (units 10^{-2})	DOCUMENT ID	TECN	COMMENT
18.9±1.8±1.5	¹ AAIJ	13Ac LHCB	pp at 7 TeV

¹ Uses $B(\chi_{c1} \rightarrow J/\psi\gamma) = (34.4 \pm 1.5)\%$.

 $\Gamma(\chi_{c2}K^+K^-)/\Gamma(\chi_{c1}K^+K^-)$ $\Gamma_{103}/\Gamma_{102}$

VALUE (units 10^{-2})	DOCUMENT ID	TECN	COMMENT
17.1±3.1±1.0	¹ AAIJ	18Ac LHCB	pp at 7, 8, 13 TeV

¹ Measures the ratio for ± 15 MeV window around ϕ mass.

 $\Gamma(\chi_{c1}(3872)\phi)/\Gamma(\psi(2S)\phi)$ Γ_{104}/Γ_{97}

VALUE	DOCUMENT ID	TECN	COMMENT
0.23±0.06 OUR AVERAGE			

0.24±0.02±0.06 ¹ AAIJ 21c LHCB pp at 7, 8, 13 TeV
 0.22±0.03±0.06 ² SIRUNYAN 20BB CMS pp at 13 TeV

¹ AAIJ 21c reports $[\Gamma(B_s^0 \rightarrow \chi_{c1}(3872)\phi)/\Gamma(B_s^0 \rightarrow \psi(2S)\phi)] \times [B(\chi_{c1}(3872) \rightarrow \pi^+\pi^-J/\psi(1S))] / [B(\psi(2S) \rightarrow J/\psi(1S)\pi^+\pi^-)] = (2.42 \pm 0.23 \pm 0.07) \times 10^{-2}$

which we multiply or divide by our best values $B(\chi_{c1}(3872) \rightarrow \pi^+\pi^-J/\psi(1S)) = (3.5 \pm 0.9) \times 10^{-2}$, $B(\psi(2S) \rightarrow J/\psi(1S)\pi^+\pi^-) = (34.69 \pm 0.34) \times 10^{-2}$. Our first error is their experiment's error and our second error is the systematic error from using our best values.

² SIRUNYAN 20BB reports $[\Gamma(B_s^0 \rightarrow \chi_{c1}(3872)\phi)/\Gamma(B_s^0 \rightarrow \psi(2S)\phi)] \times [B(\chi_{c1}(3872) \rightarrow \pi^+\pi^-J/\psi(1S))] / [B(\psi(2S) \rightarrow J/\psi(1S)\pi^+\pi^-)] = (2.21 \pm 0.29 \pm 0.17) \times 10^{-2}$ which we multiply or divide by our best values $B(\chi_{c1}(3872) \rightarrow \pi^+\pi^-J/\psi(1S)) = (3.5 \pm 0.9) \times 10^{-2}$, $B(\psi(2S) \rightarrow J/\psi(1S)\pi^+\pi^-) = (34.69 \pm 0.34) \times 10^{-2}$. Our first error is their experiment's error and our second error is the systematic error from using our best values.

 $\Gamma(\chi_{c1}(3872)\pi^+\pi^-)/\Gamma(\psi(2S)\pi^+\pi^-)$ Γ_{106}/Γ_{96}

VALUE	DOCUMENT ID	TECN	COMMENT
0.67±0.11±0.18	¹ AAIJ	23AP LHCB	pp at 7, 8, 13 TeV

¹ AAIJ 23AP reports $[\Gamma(B_s^0 \rightarrow \chi_{c1}(3872)\pi^+\pi^-)/\Gamma(B_s^0 \rightarrow \psi(2S)\pi^+\pi^-)] \times [B(\chi_{c1}(3872) \rightarrow \pi^+\pi^-J/\psi(1S))] / [B(\psi(2S) \rightarrow J/\psi(1S)\pi^+\pi^-)] = (6.8 \pm 1.1 \pm 0.2) \times 10^{-2}$ which we multiply or divide by our best values $B(\chi_{c1}(3872) \rightarrow \pi^+\pi^-J/\psi(1S)) = (3.5 \pm 0.9) \times 10^{-2}$, $B(\psi(2S) \rightarrow J/\psi(1S)\pi^+\pi^-) = (34.69 \pm 0.34) \times 10^{-2}$. Our first error is their experiment's error and our second error is the systematic error from using our best values.

 $\Gamma(J/\psi K^*(892)^0\bar{K}^*(892)^0)/\Gamma(\psi(2S)\phi)$ Γ_{87}/Γ_{97}

VALUE	DOCUMENT ID	TECN	COMMENT
0.209±0.006±0.003	¹ AAIJ	21c LHCB	pp at 7, 8, 13 TeV

¹ AAIJ 21c reports $\Gamma(B_s^0 \rightarrow J/\psi K^*(892)^0\bar{K}^*(892)^0)/\Gamma(B_s^0 \rightarrow \psi(2S)\phi) B(K^{*0} \rightarrow K^+\pi^-)/B(\psi(2S) \rightarrow J/\psi\pi^+\pi^-)/B(\phi \rightarrow K^+K^-) = 1.22 \pm 0.03 \pm 0.04$ which we adjust with PDG 20 values of $B(K^{*0} \rightarrow K^+\pi^-) = (99.902 \pm 0.009) \times 10^{-2}$, $B(\psi(2S) \rightarrow J/\psi\pi^+\pi^-) = (34.68 \pm 0.30) \times 10^{-2}$, and $B(\phi \rightarrow K^+K^-) = (49.2 \pm 0.5) \times 10^{-2}$. The first uncertainty is the total experiment's one and the second is due to the adjustment branching fractions.

 $\Gamma(\chi_{c1}(3872)(K^+K^-)_{non-\phi})/\Gamma(\chi_{c1}(3872)\phi)$ $\Gamma_{105}/\Gamma_{104}$

VALUE	DOCUMENT ID	TECN	COMMENT
0.77±0.17±0.01	¹ AAIJ	21c LHCB	pp at 7, 8, 13 TeV

¹ AAIJ 21c reports $[\Gamma(B_s^0 \rightarrow \chi_{c1}(3872)(K^+K^-)_{non-\phi})/\Gamma(B_s^0 \rightarrow \chi_{c1}(3872)\phi)] / [B(\phi(1020) \rightarrow K^+K^-)] = 1.57 \pm 0.32 \pm 0.12$ which we multiply by our best value $B(\phi(1020) \rightarrow K^+K^-) = (49.1 \pm 0.5) \times 10^{-2}$. Our first error is their experiment's error and our second error is the systematic error from using our best value.

 $\Gamma(\pi^+\pi^-)/\Gamma_{total}$ Γ_{107}/Γ

VALUE (units 10^{-7})	CL%	DOCUMENT ID	TECN	COMMENT
7.2±1.0 OUR AVERAGE				

7.5±0.9±0.7 ¹ AAIJ 17G LHCB pp at 7 and 8 TeV
 6.5±1.8±0.6 ² AALTONEN 12L CDF $p\bar{p}$ at 1.96 TeV

• • • We do not use the following data for averages, fits, limits, etc. • • •

10.9^{+2.6}_{-2.2}±1.1 ³ AAIJ 12AR LHCB Repl. by AAIJ 17G

< 120 90 ⁴ PENG 10 BELL $e^+e^- \rightarrow \Upsilon(5S)$
 < 12 90 ⁵ AALTONEN 09c CDF Repl. by AALTONEN 12L
 < 17 90 ⁶ ABULENCIA, A 06c CDF Repl. by AALTONEN 09c
 <2320 90 ⁷ ABE 00c SLD $e^+e^- \rightarrow Z$
 <1700 90 ⁸ BUSKULIC 96v ALEP $e^+e^- \rightarrow Z$

¹ AAIJ 17G reports $[\Gamma(B_s^0 \rightarrow \pi^+\pi^-)/\Gamma_{total}] / [B(B^0 \rightarrow K^+\pi^-)] \times [\Gamma(\bar{b} \rightarrow B_s^0)/\Gamma(\bar{b} \rightarrow B^0)] = (9.15 \pm 0.71 \pm 0.83) \times 10^{-3}$ which we multiply or divide by our best values $B(B^0 \rightarrow K^+\pi^-) = (2.00 \pm 0.04) \times 10^{-5}$, $\Gamma(\bar{b} \rightarrow B_s^0)/\Gamma(\bar{b} \rightarrow B^0) = 0.246 \pm 0.023$. Our first error is their experiment's error and our second error is the systematic error from using our best values.

² AALTONEN 12L reports $[\Gamma(B_s^0 \rightarrow \pi^+\pi^-)/\Gamma_{total}] / [B(B^0 \rightarrow K^+\pi^-)] \times [\Gamma(\bar{b} \rightarrow B_s^0)/\Gamma(\bar{b} \rightarrow B^0)] = 0.008 \pm 0.002 \pm 0.001$ which we multiply or divide by our best values $B(B^0 \rightarrow K^+\pi^-) = (2.00 \pm 0.04) \times 10^{-5}$, $\Gamma(\bar{b} \rightarrow B_s^0)/\Gamma(\bar{b} \rightarrow B^0) = 0.246 \pm 0.023$. Our first error is their experiment's error and our second error is the systematic error from using our best values.

³ AAIJ 12AR reports $[\Gamma(B_s^0 \rightarrow \pi^+\pi^-)/\Gamma_{total}] / [B(B^0 \rightarrow \pi^+\pi^-)] \times [\Gamma(\bar{b} \rightarrow B_s^0)/\Gamma(\bar{b} \rightarrow B^0)] = 0.050^{+0.011}_{-0.009} \pm 0.004$ which we multiply or divide by our best values $B(B^0 \rightarrow \pi^+\pi^-) = (5.37 \pm 0.20) \times 10^{-6}$, $\Gamma(\bar{b} \rightarrow B_s^0)/\Gamma(\bar{b} \rightarrow B^0) = 0.246 \pm 0.023$. Our first error is their experiment's error and our second error is the systematic error from using our best values.

⁴ Uses $\Upsilon(10860) \rightarrow B_s^* \bar{B}_s^*$ and assumes $B(\Upsilon(10860) \rightarrow B_s^* \bar{B}_s^*) = (19.3 \pm 2.9)\%$ and $\Gamma(\Upsilon(10860) \rightarrow B_s^* \bar{B}_s^*) / \Gamma(\Upsilon(10860) \rightarrow B_s^* \bar{B}_s^*) = (90.1 \pm 3.8)_{4.0}\%$.

⁵ Obtains this result from $(f_s/f_d) \cdot B(B_s \rightarrow \pi^+\pi^-)/B(B^0 \rightarrow K^+\pi^-) = 0.007 \pm 0.004 \pm 0.005$, assuming $f_s/f_d = 0.276 \pm 0.034$ and $B(B^0 \rightarrow K^+\pi^-) = (19.4 \pm 0.6) \times 10^{-6}$.

⁶ ABULENCIA, A 06D obtains this from $B(B_s \rightarrow \pi^+\pi^-) / B(B_s \rightarrow K^+K^-) < 0.05$ at 90% CL, assuming $B(B_s \rightarrow K^+K^-) = (33 \pm 6 \pm 7) \times 10^{-6}$.

⁷ ABE 00c assumes $B(Z \rightarrow b\bar{b}) = (21.7 \pm 0.1)\%$ and the B fractions $f_{B^0} = f_{B^+} = (39.7 \pm 1.8)_{2.2}\%$ and $f_{B_s} = (10.5 \pm 1.8)_{2.2}\%$.

⁸ BUSKULIC 96v assumes PDG 96 production fractions for B^0 , B^+ , B_s , b baryons.

Meson Particle Listings

$\Gamma(\pi^0\pi^0)/\Gamma_{\text{total}}$					Γ_{108}/Γ	$\Gamma(\phi\pi^+\pi^-)/\Gamma_{\text{total}}$					Γ_{119}/Γ
VALUE	CL%	DOCUMENT ID	TECN	COMMENT		VALUE (units 10^{-6})	DOCUMENT ID	TECN	COMMENT		
$<7.7 \times 10^{-6}$	90	¹ BORAH	23	BELL $e^+e^- \rightarrow \Upsilon(5S)$		$3.48 \pm 0.23 \pm 0.39$	¹ AAIJ	17A	LHCB pp at 7, 8 TeV		
<ul style="list-style-type: none"> ••• We do not use the following data for averages, fits, limits, etc. ••• $<2.1 \times 10^{-4}$ 90 ²ACCIARRI 95H L3 $e^+e^- \rightarrow Z$ ¹BORAH 23 assumes $f_{B^0} = 20.1 \pm 3.1\%$. ²ACCIARRI 95H assumes $f_{B^0} = 39.5 \pm 4.0$ and $f_{B^s} = 12.0 \pm 3.0\%$. 						<ul style="list-style-type: none"> ¹Inclusive decays in mass range $400 < m(\pi^+\pi^-) < 1600$ MeV/c^2. 					
$\Gamma(\eta\pi^0)/\Gamma_{\text{total}}$					Γ_{109}/Γ	$\Gamma(\phi\phi)/\Gamma_{\text{total}}$					Γ_{120}/Γ
VALUE	CL%	DOCUMENT ID	TECN	COMMENT		VALUE (units 10^{-6})	DOCUMENT ID	TECN	COMMENT		
$<1.0 \times 10^{-3}$	90	¹ ACCIARRI	95H	L3 $e^+e^- \rightarrow Z$		18.5 ± 1.4 OUR FIT	¹ AAIJ	15As	LHCB pp at 7, 8 TeV		
<ul style="list-style-type: none"> ¹ACCIARRI 95H assumes $f_{B^0} = 39.5 \pm 4.0$ and $f_{B^s} = 12.0 \pm 3.0\%$. 						<ul style="list-style-type: none"> ••• We do not use the following data for averages, fits, limits, etc. ••• $14^{+6}_{-5} \pm 6$ ²ACOSTA 05J CDF Repl. by AALTONEN 11AN <1183 90 ³ABE 00c SLD $e^+e^- \rightarrow Z$ ¹AAIJ 15As reports $[\Gamma(B^0 \rightarrow \phi\phi)/\Gamma_{\text{total}}] / [B(B^0 \rightarrow K^*(892)^0\phi)] = 1.84 \pm 0.05 \pm 0.13$ which we multiply by our best value $B(B^0 \rightarrow K^*(892)^0\phi) = (1.00 \pm 0.05) \times 10^{-5}$. Our first error is their experiment's error and our second error is the systematic error from using our best value. ²Uses $B(B^0 \rightarrow J/\psi\phi) = (1.38 \pm 0.49) \times 10^{-3}$ and production cross-section ratio of $\sigma(B_s)/\sigma(B^0) = 0.26 \pm 0.04$. ³ABE 00c assumes $B(Z \rightarrow b\bar{b}) = (21.7 \pm 0.1)\%$ and the B fractions $f_{B^0} = f_{B^+} = (39.7^{+1.8}_{-2.2})\%$ and $f_{B^s} = (10.5^{+1.8}_{-2.2})\%$. 					
$\Gamma(\eta\eta)/\Gamma_{\text{total}}$					Γ_{110}/Γ	$\Gamma(\phi\phi)/\Gamma(J/\psi(1S)\phi)$					Γ_{120}/Γ_{61}
VALUE	CL%	DOCUMENT ID	TECN	COMMENT		VALUE (units 10^{-2})	DOCUMENT ID	TECN	COMMENT		
$<1.43 \times 10^{-4}$	90	BHUYAN	22	BELL $e^+e^- \rightarrow \Upsilon(5S)$		1.77 ± 0.14 OUR FIT					
<ul style="list-style-type: none"> ••• We do not use the following data for averages, fits, limits, etc. ••• $<1.5 \times 10^{-3}$ 90 ¹ACCIARRI 95H L3 $e^+e^- \rightarrow Z$ ¹ACCIARRI 95H assumes $f_{B^0} = 39.5 \pm 4.0$ and $f_{B^s} = 12.0 \pm 3.0\%$. 						<ul style="list-style-type: none"> $1.78 \pm 0.14 \pm 0.20$ AALTONEN 11AN CDF pp at 1.96 TeV 					
$\Gamma(\rho^0\rho^0)/\Gamma_{\text{total}}$					Γ_{111}/Γ	$\Gamma(\phi\phi\phi)/\Gamma(\phi\phi)$					$\Gamma_{121}/\Gamma_{120}$
VALUE	CL%	DOCUMENT ID	TECN	COMMENT		VALUE	DOCUMENT ID	TECN	COMMENT		
$<3.20 \times 10^{-4}$	90	¹ ABE	00c	SLD $e^+e^- \rightarrow Z$		$0.117 \pm 0.030 \pm 0.015$	AAIJ	17Bb	LHCB pp at 7, 8 TeV		
<ul style="list-style-type: none"> ¹ABE 00c assumes $B(Z \rightarrow b\bar{b}) = (21.7 \pm 0.1)\%$ and the B fractions $f_{B^0} = f_{B^+} = (39.7^{+1.8}_{-2.2})\%$ and $f_{B^s} = (10.5^{+1.8}_{-2.2})\%$. 						<ul style="list-style-type: none"> ¹Uses $\Upsilon(10860) \rightarrow B_s^{(*)}\bar{B}_s^{(*)}$ decays and assumes $B(\Upsilon(10860) \rightarrow B_s^{(*)}\bar{B}_s^{(*)}) = (20.1 \pm 3.1)\%$. 					
$\Gamma(\eta'K_S^0)/\Gamma_{\text{total}}$					Γ_{112}/Γ	$\Gamma(\pi^+K^-)/\Gamma_{\text{total}}$					Γ_{122}/Γ
VALUE	CL%	DOCUMENT ID	TECN	COMMENT		VALUE (units 10^{-6})	DOCUMENT ID	TECN	COMMENT		
$<8.16 \times 10^{-6}$	90	¹ PANG	22	BELL $e^+e^- \rightarrow \Upsilon(5S)$		5.9 ± 0.7 OUR AVERAGE	¹ AAIJ	12AR	LHCB pp at 7 TeV		
<ul style="list-style-type: none"> ¹Uses $\Upsilon(10860) \rightarrow B_s^{(*)}\bar{B}_s^{(*)}$ decays and assumes $B(\Upsilon(10860) \rightarrow B_s^{(*)}\bar{B}_s^{(*)}) = (20.1 \pm 3.1)\%$. 						<ul style="list-style-type: none"> ²AALTONEN 09c CDF pp at 1.96 TeV ••• We do not use the following data for averages, fits, limits, etc. ••• <26 90 ³PENG 10 BELL $e^+e^- \rightarrow \Upsilon(5S)$ <5.6 90 ⁴ABULENCIA,A 06D CDF Repl. by AALTONEN 09c <261 90 ⁵ABE 00c SLD $e^+e^- \rightarrow Z$ <210 90 ⁶BUSKULIC 96V ALEP $e^+e^- \rightarrow Z$ <260 90 ⁷AKERS 94L OPAL $e^+e^- \rightarrow Z$ ¹AAIJ 12AR reports $[\Gamma(B^0 \rightarrow \pi^+K^-)/\Gamma_{\text{total}}] / [B(B^0 \rightarrow K^+\pi^-)] \times [\Gamma(\bar{b} \rightarrow B_s^0) / \Gamma(\bar{b} \rightarrow B^0)] = 0.074 \pm 0.006 \pm 0.006$ which we multiply or divide by our best values $B(B^0 \rightarrow K^+\pi^-) = (2.00 \pm 0.04) \times 10^{-5}$; $\Gamma(\bar{b} \rightarrow B_s^0) / \Gamma(\bar{b} \rightarrow B^0) = 0.246 \pm 0.023$. Our first error is their experiment's error and our second error is the systematic error from using our best values. ²AALTONEN 09c reports $[\Gamma(B^0 \rightarrow \pi^+K^-)/\Gamma_{\text{total}}] / [B(B^0 \rightarrow K^+\pi^-)] \times [B(\bar{b} \rightarrow B_s^0) / [B(\bar{b} \rightarrow B^0)]] = 0.071 \pm 0.010 \pm 0.007$ which we multiply or divide by our best values $B(B^0 \rightarrow K^+\pi^-) = (2.00 \pm 0.04) \times 10^{-5}$; $B(\bar{b} \rightarrow B_s^0) = (10.0 \pm 0.8) \times 10^{-2}$; $B(\bar{b} \rightarrow B^0) = (40.8 \pm 0.7) \times 10^{-2}$. Our first error is their experiment's error and our second error is the systematic error from using our best values. ³Uses $\Upsilon(10860) \rightarrow B_s^*\bar{B}_s^*$ and assumes $B(\Upsilon(10860) \rightarrow B_s^*\bar{B}_s^*) = (19.3 \pm 2.9)\%$ and $\Gamma(\Upsilon(10860) \rightarrow B_s^*\bar{B}_s^*) / \Gamma(\Upsilon(10860) \rightarrow B_s^{(*)}\bar{B}_s^{(*)}) = (90.1^{+3.8}_{-4.0})\%$. ⁴ABULENCIA,A 06D obtains this from $(f_s/f_d)(B(B_s \rightarrow \pi^+K^-) / B(B^0 \rightarrow K^+\pi^-)) < 0.08$ at 90% CL, assuming $f_s/f_d = 0.260 \pm 0.039$ and $B(B^0 \rightarrow K^+\pi^-) = (18.9 \pm 0.7) \times 10^{-6}$. ⁵ABE 00c assumes $B(Z \rightarrow b\bar{b}) = (21.7 \pm 0.1)\%$ and the B fractions $f_{B^0} = f_{B^+} = (39.7^{+1.8}_{-2.2})\%$ and $f_{B^s} = (10.5^{+1.8}_{-2.2})\%$. ⁶BUSKULIC 96V assumes PDG 96 production fractions for B^0, B^+, B_s, b baryons. ⁷Assumes $B(Z \rightarrow b\bar{b}) = 0.217$ and $B_d^0(B_s^0)$ fraction 39.5% (12%). 					
$\Gamma(\eta'\eta)/\Gamma_{\text{total}}$					Γ_{113}/Γ	$\Gamma(K^+K^-)/\Gamma_{\text{total}}$					Γ_{123}/Γ
VALUE	CL%	DOCUMENT ID	TECN	COMMENT		VALUE (units 10^{-6})	DOCUMENT ID	TECN	COMMENT		
$<6.5 \times 10^{-5}$	90	¹ NISAR	21	BELL $e^+e^- \rightarrow \Upsilon(5S)$		27.2 ± 2.3 OUR AVERAGE	¹ AAIJ	12AR	LHCB pp at 7 TeV		
<ul style="list-style-type: none"> ¹Uses $\Upsilon(10860) \rightarrow B_s^*\bar{B}_s^*$ decays and assumes $B(\Upsilon(10860) \rightarrow B_s^{(*)}\bar{B}_s^{(*)}) = (20.1 \pm 3.1)\%$. 						<ul style="list-style-type: none"> ²AALTONEN 11N CDF pp at 1.96 TeV ³PENG 10 BELL $e^+e^- \rightarrow \Upsilon(5S)$ ••• We do not use the following data for averages, fits, limits, etc. ••• <310 90 DRUTSKOY 07A BELL $e^+e^- \rightarrow \Upsilon(5S)$ $33 \pm 6 \pm 7$ ⁴ABULENCIA,A 06D CDF Repl. by AALTONEN 11N <283 90 ⁵ABE 00c SLD $e^+e^- \rightarrow Z$ <59 90 ⁶BUSKULIC 96V ALEP $e^+e^- \rightarrow Z$ <140 90 ⁷AKERS 94L OPAL $e^+e^- \rightarrow Z$ ¹AAIJ 12AR reports $[\Gamma(B^0 \rightarrow K^+K^-)/\Gamma_{\text{total}}] / [B(B^0 \rightarrow K^+\pi^-)] \times [\Gamma(\bar{b} \rightarrow B_s^0) / \Gamma(\bar{b} \rightarrow B^0)] = 0.316 \pm 0.009 \pm 0.019$ which we multiply or divide by our best values $B(B^0 \rightarrow K^+\pi^-) = (2.00 \pm 0.04) \times 10^{-5}$; $\Gamma(\bar{b} \rightarrow B_s^0) / \Gamma(\bar{b} \rightarrow B^0) = 0.246 \pm 0.023$. Our first error is their experiment's error and our second error is the systematic error from using our best values. 					
$\Gamma(\eta'K_S^0)/\Gamma_{\text{total}}$					Γ_{114}/Γ	$\Gamma(\phi f_0(980), f_0(980) \rightarrow \pi^+\pi^-)/\Gamma_{\text{total}}$					Γ_{116}/Γ
VALUE (units 10^{-5})	CL%	DOCUMENT ID	TECN	COMMENT		VALUE (units 10^{-6})	DOCUMENT ID	TECN	COMMENT		
$3.3 \pm 0.7 \pm 0.1$	90	¹ AAIJ	15o	LHCB pp at 7, 8 TeV		$1.12 \pm 0.16 \pm 0.14$	¹ AAIJ	17A	LHCB pp at 7, 8 TeV		
<ul style="list-style-type: none"> ¹AAIJ 15o reports $[\Gamma(B^0 \rightarrow \eta'K^+)/\Gamma_{\text{total}}] / [B(B^+ \rightarrow \eta'K^+)] = 0.47 \pm 0.09 \pm 0.04$ which we multiply by our best value $B(B^+ \rightarrow \eta'K^+) = (7.04 \pm 0.25) \times 10^{-5}$. Our first error is their experiment's error and our second error is the systematic error from using our best value. 						<ul style="list-style-type: none"> ¹Signal is observed with 8 standard deviations significance. 					
$\Gamma(\eta'\phi)/\Gamma_{\text{total}}$					Γ_{115}/Γ	$\Gamma(\phi f_2(1270), f_2(1270) \rightarrow \pi^+\pi^-)/\Gamma_{\text{total}}$					Γ_{117}/Γ
VALUE	CL%	DOCUMENT ID	TECN	COMMENT		VALUE (units 10^{-6})	DOCUMENT ID	TECN	COMMENT		
$<0.82 \times 10^{-6}$	90	¹ AAIJ	17Ba	LHCB pp at 7, 8 TeV		$0.61 \pm 0.13^{+0.13}_{-0.08}$	¹ AAIJ	17A	LHCB pp at 7, 8 TeV		
<ul style="list-style-type: none"> ¹Corresponds to the 95% CL upper limit 1.01×10^{-6}. Uses the normalization mode $B^+ \rightarrow \eta'K^+$ with branching fraction $(70.6 \pm 2.5) \times 10^{-6}$ and the ratio of hadronisation fractions $f_s/f_d = 0.259 \pm 0.015$, which is assumed equal to f_s/f_u. 						<ul style="list-style-type: none"> ¹Signal is observed with 5 standard deviations significance. 					
$\Gamma(\eta'X_{S3})/\Gamma_{\text{total}}$					Γ_{59}/Γ	$\Gamma(\phi\rho^0)/\Gamma_{\text{total}}$					Γ_{118}/Γ
VALUE (units 10^{-3})	CL%	DOCUMENT ID	TECN	COMMENT		VALUE (units 10^{-7})	DOCUMENT ID	TECN	COMMENT		
<1.4	90	¹ DUBEY	21	BELL $e^+e^- \rightarrow \Upsilon(4S)$		$2.7 \pm 0.7 \pm 0.3$	¹ AAIJ	17A	LHCB pp at 7, 8 TeV		
<ul style="list-style-type: none"> ¹DUBEY 21 result is for $m(X_{S3}) < 2.85$ GeV/c^2. 						<ul style="list-style-type: none"> ••• We do not use the following data for averages, fits, limits, etc. ••• <6170 90 ²ABE 00c SLD $e^+e^- \rightarrow Z$ ¹Signal evidence is 4 standard deviations. ²ABE 00c assumes $B(Z \rightarrow b\bar{b}) = (21.7 \pm 0.1)\%$ and the B fractions $f_{B^0} = f_{B^+} = (39.7^{+1.8}_{-2.2})\%$ and $f_{B^s} = (10.5^{+1.8}_{-2.2})\%$. 					

See key on page 1171

Meson Particle Listings

 B_S^0

² AALTONEN 11N reports $(f_s/f_d) (B(B_S^0 \rightarrow K^+ K^-) / B(B^0 \rightarrow K^+ \pi^-)) = 0.347 \pm 0.020 \pm 0.021$. We multiply this result by our best value of $B(B^0 \rightarrow K^+ \pi^-) = (2.00 \pm 0.04) \times 10^{-5}$ and divide by our best value of f_s/f_d , where $1/2 f_s/f_d = 0.1230 \pm 0.0115$. Our first quoted uncertainty is the combined experiment's uncertainty and our second is the systematic uncertainty from using our best values.

³ Uses $\Gamma(10860) \rightarrow B_S^* \bar{B}_S^*$ and assumes $B(\Gamma(10860) \rightarrow B_S^{(*)} \bar{B}_S^{(*)}) = (19.3 \pm 2.9)\%$ and $\Gamma(\Gamma(10860) \rightarrow B_S^* \bar{B}_S^*) / \Gamma(\Gamma(10860) \rightarrow B_S^{(*)} \bar{B}_S^{(*)}) = (90.1 \pm 3.8)_{-4.0}^{\pm 3.8}\%$.

⁴ ABULENICA, A 06D obtains this from $(f_s/f_d) (B(B_S \rightarrow K^+ K^-) / B(B^0 \rightarrow K^+ \pi^-)) = 0.46 \pm 0.08 \pm 0.07$, assuming $f_s/f_d = 0.260 \pm 0.039$ and $B(B^0 \rightarrow K^+ \pi^-) = (18.9 \pm 0.7) \times 10^{-6}$.

⁵ ABE 00c assumes $B(Z \rightarrow b \bar{b}) = (21.7 \pm 0.1)\%$ and the B fractions $f_{B^0} = f_{B^+} = (39.7 \pm 1.8)_{-2.2}^{\pm 1.8}\%$ and $f_{B_S} = (10.5 \pm 1.8)_{-2.2}^{\pm 1.8}\%$.

⁶ BUSKULIC 96V assumes PDG 96 production fractions for B^0, B^+, B_S, b baryons.

⁷ Assumes $B(Z \rightarrow b \bar{b}) = 0.217$ and $B_B^0(B_S^0)$ fraction 39.5% (12%).

$\Gamma(K^0 \bar{K}^0) / \Gamma_{\text{total}}$ Γ_{124} / Γ

VALUE (units 10^{-5})	CL%	DOCUMENT ID	TECN	COMMENT
1.76 ± 0.31 OUR AVERAGE				

1.68 ± 0.34 ^{+0.16} _{-0.15}		1 AAIJ	20F LHCb	pp at 7, 8, 13 TeV
---	--	--------	----------	----------------------

1.96 ^{+0.58} _{-0.51} ± 0.10 ± 0.20		2 PAL	16 BELL	$e^+ e^- \rightarrow \Upsilon(5S)$
--	--	-------	---------	------------------------------------

• • • We do not use the following data for averages, fits, limits, etc. • • •

<6.6		90 ³ PENG	10 BELL	Repl. by PAL 16
------	--	----------------------	---------	-----------------

¹ AAIJ 20F reports $[\Gamma(B_S^0 \rightarrow K^0 \bar{K}^0) / \Gamma_{\text{total}}] / [B(B^0 \rightarrow K^0 \phi)] = 2.3 \pm 0.4 \pm 0.2 \pm 0.1$ which we multiply by our best value $B(B^0 \rightarrow K^0 \phi) = (7.3 \pm 0.7) \times 10^{-6}$. Our first error is their experiment's error and our second error is the systematic error from using our best value.

² Observed in $B_S^0 \rightarrow K_S^0 K_S^0$ with significance of 5.1 σ . The last uncertainty is due to the uncertainty of the total number of $B_S^0 \bar{B}_S^0$ pairs.

³ Uses $\Upsilon(10860) \rightarrow B_S^* \bar{B}_S^*$ and assumes $B(\Upsilon(10860) \rightarrow B_S^{(*)} \bar{B}_S^{(*)}) = (19.3 \pm 2.9)\%$ and $\Gamma(\Upsilon(10860) \rightarrow B_S^* \bar{B}_S^*) / \Gamma(\Upsilon(10860) \rightarrow B_S^{(*)} \bar{B}_S^{(*)}) = (90.1 \pm 3.8)_{-4.0}^{\pm 3.8}\%$.

$\Gamma(K^0 \pi^+ \pi^-) / \Gamma_{\text{total}}$ Γ_{125} / Γ

VALUE (units 10^{-5})	DOCUMENT ID	TECN	COMMENT
9.5 ± 2.1 ± 0.3	1,2 AAIJ	17BP LHCb	pp at 7, 8 TeV

• • • We do not use the following data for averages, fits, limits, etc. • • •

14 ± 4 ± 1		3 AAIJ	13BP LHCb	Repl. by AAIJ 17BP
------------	--	--------	-----------	--------------------

¹ AAIJ 17BP reports $[\Gamma(B_S^0 \rightarrow K^0 \pi^+ \pi^-) / \Gamma_{\text{total}}] / [B(B^0 \rightarrow K^0 \pi^+ \pi^-)] = 0.191 \pm 0.027 \pm 0.033$ which we multiply by our best value $B(B^0 \rightarrow K^0 \pi^+ \pi^-) = (4.97 \pm 0.18) \times 10^{-5}$. Our first error is their experiment's error and our second error is the systematic error from using our best value.

² Used $f_s/f_d = 0.259 \pm 0.015$.

³ AAIJ 13BP reports $[\Gamma(B_S^0 \rightarrow K^0 \pi^+ \pi^-) / \Gamma_{\text{total}}] / [B(B^0 \rightarrow K^0 \pi^+ \pi^-)] = 0.29 \pm 0.06 \pm 0.04$ which we multiply by our best value $B(B^0 \rightarrow K^0 \pi^+ \pi^-) = (4.97 \pm 0.18) \times 10^{-5}$. Our first error is their experiment's error and our second error is the systematic error from using our best value.

$\Gamma(K^0 K^\pm \pi^\mp) / \Gamma_{\text{total}}$ Γ_{126} / Γ

VALUE (units 10^{-5})	DOCUMENT ID	TECN	COMMENT
8.4 ± 0.8 ± 0.3	1,2 AAIJ	17BP LHCb	pp at 7, 8 TeV

• • • We do not use the following data for averages, fits, limits, etc. • • •

7.4 ± 0.9 ± 0.3		3 AAIJ	13BP LHCb	Repl. by AAIJ 17BP
-----------------	--	--------	-----------	--------------------

¹ AAIJ 17BP reports $[\Gamma(B_S^0 \rightarrow K^0 K^\pm \pi^\mp) / \Gamma_{\text{total}}] / [B(B^0 \rightarrow K^0 \pi^+ \pi^-)] = 1.70 \pm 0.07 \pm 0.15$ which we multiply by our best value $B(B^0 \rightarrow K^0 \pi^+ \pi^-) = (4.97 \pm 0.18) \times 10^{-5}$. Our first error is their experiment's error and our second error is the systematic error from using our best value.

² Used $f_s/f_d = 0.259 \pm 0.015$.

³ AAIJ 13BP reports $[\Gamma(B_S^0 \rightarrow K^0 K^\pm \pi^\mp) / \Gamma_{\text{total}}] / [B(B^0 \rightarrow K^0 \pi^+ \pi^-)] = 1.48 \pm 0.12 \pm 0.14$ which we multiply by our best value $B(B^0 \rightarrow K^0 \pi^+ \pi^-) = (4.97 \pm 0.18) \times 10^{-5}$. Our first error is their experiment's error and our second error is the systematic error from using our best value.

$\Gamma(K^*(892)^- \pi^+) / \Gamma_{\text{total}}$ Γ_{127} / Γ

VALUE (units 10^{-6})	DOCUMENT ID	TECN	COMMENT
2.9 ± 1.0 ± 0.2	1,2 AAIJ	14BMLHCb	pp at 7 TeV

¹ AAIJ 14BM reports $[\Gamma(B_S^0 \rightarrow K^*(892)^- \pi^+) / \Gamma_{\text{total}}] / [B(B^0 \rightarrow K^*(892)^+ \pi^-)] = 0.39 \pm 0.13 \pm 0.05$ which we multiply by our best value $B(B^0 \rightarrow K^*(892)^+ \pi^-) = (7.5 \pm 0.4) \times 10^{-6}$. Our first error is their experiment's error and our second error is the systematic error from using our best value.

² Uses $f_s/f_d = 0.259 \pm 0.015$.

$\Gamma(K^*(892)^\pm K^\mp) / \Gamma_{\text{total}}$ Γ_{128} / Γ

VALUE (units 10^{-5})	DOCUMENT ID	TECN	COMMENT
1.86 ± 0.12 ± 0.45	1,2 AAIJ	19k LHCb	pp at 7, 8 TeV

• • • We do not use the following data for averages, fits, limits, etc. • • •

1.12 ± 0.21 ^{+0.07} _{-0.06}		3,4 AAIJ	14BMLHCb	Repl. by AAIJ 19k
---	--	----------	----------	-------------------

¹ AAIJ 19k reports $(18.6 \pm 1.2 \pm 0.8 \pm 4.0 \pm 2.0) \times 10^{-6}$ as the measured value. We have combined in quadrature all systematic uncertainties into a single one.

² Measured in Dalitz plot analysis of $B_S^0 \rightarrow K_S^0 K^\pm \pi^\mp$ decays.

³ AAIJ 14BM reports $[\Gamma(B_S^0 \rightarrow K^*(892)^\pm K^\mp) / \Gamma_{\text{total}}] / [B(B^0 \rightarrow K^*(892)^+ \pi^-)] = 1.49 \pm 0.22 \pm 0.18$ which we multiply by our best value $B(B^0 \rightarrow K^*(892)^+ \pi^-) = (7.5 \pm 0.4) \times 10^{-6}$. Our first error is their experiment's error and our second error is the systematic error from using our best value.

⁴ Uses $f_s/f_d = 0.259 \pm 0.015$.

$\Gamma(K_S^0(1430)^\pm K^\mp) / \Gamma_{\text{total}}$ Γ_{129} / Γ

VALUE (units 10^{-5})	DOCUMENT ID	TECN	COMMENT
3.13 ± 0.23 ± 2.53	1,2 AAIJ	19k LHCb	pp at 7, 8 TeV

¹ AAIJ 19k reports $(31.3 \pm 2.3 \pm 0.7 \pm 25.1 \pm 3.3) \times 10^{-6}$ as the measured value. We have combined in quadrature all systematic uncertainties into a single one.

² Measured in Dalitz plot analysis of $B_S^0 \rightarrow K_S^0 K^\pm \pi^\mp$ decays.

$\Gamma(K_S^0(1430)^\pm K^\mp) / \Gamma_{\text{total}}$ Γ_{130} / Γ

VALUE (units 10^{-5})	DOCUMENT ID	TECN	COMMENT
1.03 ± 0.25 ± 1.64	1,2 AAIJ	19k LHCb	pp at 7, 8 TeV

¹ AAIJ 19k reports $(10.3 \pm 2.5 \pm 1.1 \pm 16.3 \pm 1.1) \times 10^{-6}$ as the measured value. We have combined in quadrature all systematic uncertainties into a single one.

² Measured in Dalitz plot analysis of $B_S^0 \rightarrow K_S^0 K^\pm \pi^\mp$ decays.

$\Gamma(K^*(892)^0 \bar{K}^0 + \text{c.c.}) / \Gamma_{\text{total}}$ Γ_{131} / Γ

VALUE (units 10^{-5})	DOCUMENT ID	TECN	COMMENT
1.98 ± 0.28 ± 0.50	1,2 AAIJ	19k LHCb	pp at 7, 8 TeV

¹ AAIJ 19k reports $(19.8 \pm 2.8 \pm 1.2 \pm 4.4 \pm 2.1) \times 10^{-6}$ as the measured value. We have combined in quadrature all systematic uncertainties into a single one.

² Measured in Dalitz plot analysis of $B_S^0 \rightarrow K_S^0 K^\pm \pi^\mp$ decays.

$\Gamma(K_S^0(1430) \bar{K}^0 + \text{c.c.}) / \Gamma_{\text{total}}$ Γ_{132} / Γ

VALUE (units 10^{-5})	DOCUMENT ID	TECN	COMMENT
3.30 ± 0.25 ± 0.98	1,2 AAIJ	19k LHCb	pp at 7, 8 TeV

¹ AAIJ 19k reports $(33.0 \pm 2.5 \pm 0.9 \pm 9.1 \pm 3.5) \times 10^{-6}$ as the measured value. We have combined in quadrature all systematic uncertainties into a single one.

² Measured in Dalitz plot analysis of $B_S^0 \rightarrow K_S^0 K^\pm \pi^\mp$ decays.

$\Gamma(K_S^0(1430) \bar{K}^0 + \text{c.c.}) / \Gamma_{\text{total}}$ Γ_{133} / Γ

VALUE (units 10^{-5})	DOCUMENT ID	TECN	COMMENT
1.68 ± 0.45 ± 2.13	1,2 AAIJ	19k LHCb	pp at 7, 8 TeV

¹ AAIJ 19k reports $(16.8 \pm 4.5 \pm 1.7 \pm 21.2 \pm 1.8) \times 10^{-6}$ as the measured value. We have combined in quadrature all systematic uncertainties into a single one.

² Measured in Dalitz plot analysis of $B_S^0 \rightarrow K_S^0 K^\pm \pi^\mp$ decays.

$\Gamma(K_S^0 \bar{K}^*(892)^0 + \text{c.c.}) / \Gamma_{\text{total}}$ Γ_{134} / Γ

VALUE (units 10^{-6})	DOCUMENT ID	TECN	COMMENT
16.4 ± 3.4 ± 2.3	1 AAIJ	16 LHCb	pp at 7 TeV

¹ Measured relative to $B^0 \rightarrow K_S^0 \pi^+ \pi^-$ using the value of $B(B^0 \rightarrow K^0 \pi^+ \pi^-) = (4.96 \pm 0.2) \times 10^{-5}$.

$\Gamma(K^0 K^+ K^-) / \Gamma_{\text{total}}$ Γ_{135} / Γ

VALUE (units 10^{-7})	CL%	DOCUMENT ID	TECN	COMMENT
12.9 ± 6.5 ± 0.5		1,2,3 AAIJ	17BP LHCb	pp at 7, 8 TeV

• • • We do not use the following data for averages, fits, limits, etc. • • •

<34		90 ⁴ AAIJ	13BP LHCb	Repl. by AAIJ 17BP
-----	--	----------------------	-----------	--------------------

¹ AAIJ 17BP reports $[\Gamma(B_S^0 \rightarrow K^0 K^+ K^-) / \Gamma_{\text{total}}] / [B(B^0 \rightarrow K^0 \pi^+ \pi^-)] = 0.026 \pm 0.011 \pm 0.007$ which we multiply by our best value $B(B^0 \rightarrow K^0 \pi^+ \pi^-) = (4.97 \pm 0.18) \times 10^{-5}$. Our first error is their experiment's error and our second error is the systematic error from using our best value.

² AAIJ 17BP also set the limit range $4-25 \times 10^{-7}$ at 90% CL using the world average value $B(B^0 \rightarrow K^0 \pi^+ \pi^-) = (4.96 \pm 0.20) \times 10^{-5}$.

³ Used $f_s/f_d = 0.259 \pm 0.015$.

⁴ AAIJ 13BP reports $[\Gamma(B_S^0 \rightarrow K^0 K^+ K^-) / \Gamma_{\text{total}}] / [B(B^0 \rightarrow K^0 \pi^+ \pi^-)] < 0.068$ which we multiply by our best value $B(B^0 \rightarrow K^0 \pi^+ \pi^-) = 4.97 \times 10^{-5}$.

$\Gamma(K^*(892)^0 \rho^0) / \Gamma_{\text{total}}$ Γ_{136} / Γ

VALUE	CL%	DOCUMENT ID	TECN	COMMENT
<7.67 × 10⁻⁴	90	1 ABE	00c SLD	$e^+ e^- \rightarrow Z$

¹ ABE 00c assumes $B(Z \rightarrow b \bar{b}) = (21.7 \pm 0.1)\%$ and the B fractions $f_{B^0} = f_{B^+} = (39.7 \pm 1.8)_{-2.2}^{\pm 1.8}\%$ and $f_{B_S} = (10.5 \pm 1.8)_{-2.2}^{\pm 1.8}\%$.

$\Gamma(K^*(892)^0 K^*(892)^0) / \Gamma_{\text{total}}$ Γ_{137} / Γ

VALUE (units 10^{-5})	CL%	DOCUMENT ID	TECN	COMMENT
1.11 ± 0.26 ± 0.06		1 AAIJ	15AF LHCb	pp at 7 TeV

• • • We do not use the following data for averages, fits, limits, etc. • • •

2.81 ± 0.46 ± 0.56		2 AAIJ	12F LHCb	Repl. by AAIJ 15AF
--------------------	--	--------	----------	--------------------

<168.1		90 ³ ABE	00c SLD	$e^+ e^- \rightarrow Z$
--------	--	---------------------	---------	-------------------------

¹ AAIJ 15AF reports $[\Gamma(B_S^0 \rightarrow K^*(892)^0 K^*(892)^0) / \Gamma_{\text{total}}] / [B(B^0 \rightarrow K^*(892)^0 \phi)] = 1.11 \pm 0.22 \pm 0.12 \pm 0.06$ which we multiply by our best value $B(B^0 \rightarrow K^*(892)^0 \phi) = (1.00 \pm 0.05) \times 10^{-5}$. Our first error is their experiment's error and our second error is the systematic error from using our best value.

Meson Particle Listings

 B_S^0

² Uses $B^0 \rightarrow J/\psi K^{*0}$ for normalization and assumes $B(B^0 \rightarrow J/\psi K^{*0}) B(J/\psi \rightarrow \mu^+ \mu^-) B(K^{*0} \rightarrow K^+ \pi^-) = (1.33 \pm 0.06) \times 10^{-3}$ and $f_S/f_d = 0.253 \pm 0.031$. The second quoted error is total uncertainty including the error of 0.34 on f_S/f_d .

³ ABE 00c assumes $B(Z \rightarrow b\bar{b}) = (21.7 \pm 0.1)\%$ and the B fractions $f_{B^0} = f_{B^+} = (39.7 \pm 1.8)_{-2.2}^{\pm 1.8}\%$ and $f_{B_S} = (10.5 \pm 1.8)_{-2.2}^{\pm 1.8}\%$.

 $\Gamma(\phi K^*(892)^0)/\Gamma_{\text{total}}$ Γ_{141}/Γ

VALUE (units 10^{-6})	CL%	DOCUMENT ID	TECN	COMMENT
1.14 ± 0.29 ± 0.06		¹ AAIJ	13BW LHCb	pp at 7 TeV

• • • We do not use the following data for averages, fits, limits, etc. • • •

<1013	90	² ABE	00c SLD	$e^+ e^- \rightarrow Z$
-------	----	------------------	---------	-------------------------

¹ AAIJ 13BW reports $[\Gamma(B_S^0 \rightarrow \phi K^*(892)^0)/\Gamma_{\text{total}}] / [B(B^0 \rightarrow K^*(892)^0 \phi)] = 0.113 \pm 0.024 \pm 0.016$ which we multiply by our best value $B(B^0 \rightarrow K^*(892)^0 \phi) = (1.00 \pm 0.05) \times 10^{-5}$. Our first error is their experiment's error and our second error is the systematic error from using our best value.

² ABE 00c assumes $B(Z \rightarrow b\bar{b}) = (21.7 \pm 0.1)\%$ and the B fractions $f_{B^0} = f_{B^+} = (39.7 \pm 1.8)_{-2.2}^{\pm 1.8}\%$ and $f_{B_S} = (10.5 \pm 1.8)_{-2.2}^{\pm 1.8}\%$.

 $\Gamma(\rho\bar{\rho})/\Gamma_{\text{total}}$ Γ_{142}/Γ

Test for $\Delta B=1$ weak neutral current. Allowed by higher-order electroweak interactions.

VALUE (units 10^{-8})	CL%	DOCUMENT ID	TECN	COMMENT
< 0.44	90	¹ AAIJ	23T LHCb	pp at 13 TeV

• • • We do not use the following data for averages, fits, limits, etc. • • •

< 1.5	90	² AAIJ	17BJ LHCb	Repl. by AAIJ 23T
$2.84 \pm 2.03 + 0.85$ $-1.68 - 0.18$		³ AAIJ	13BQ LHCb	Repl. by AAIJ 17BJ
<5900	90	⁴ BUSKULIC	96v ALEP	$e^+ e^- \rightarrow Z$

¹ Uses normalization mode $B(B^0 \rightarrow K^+ \pi^-) = (19.6 \pm 0.5) \times 10^{-6}$ and B production ratio $f(\bar{D} \rightarrow B_S^0)/f(\bar{D} \rightarrow B_d^0) = 0.2539 \pm 0.0079$.

² Uses normalization mode $B(B^0 \rightarrow K^+ \pi^-) = (19.6 \pm 0.5) \times 10^{-6}$ and B production ratio $f(\bar{D} \rightarrow B_S^0)/f(\bar{D} \rightarrow B_d^0) = 0.259 \pm 0.015$.

³ Uses normalization mode $B(B^0 \rightarrow K^+ \pi^-) = (19.55 \pm 0.54) \times 10^{-6}$ and B production ratio $f(\bar{D} \rightarrow B_S^0)/f(\bar{D} \rightarrow B_d^0) = 0.256 \pm 0.020$.

⁴ BUSKULIC 96v assumes PDG 96 production fractions for B^0, B^+, B_S, b baryons.

 $\Gamma(\rho\bar{\rho}K^+K^-)/\Gamma_{\text{total}}$ Γ_{143}/Γ

VALUE (units 10^{-6})	DOCUMENT ID	TECN	COMMENT
4.5 ± 0.4 ± 0.2	^{1,2} AAIJ	17BD LHCb	pp at 7, 8 TeV

¹ AAIJ 17BD reports $[\Gamma(B_S^0 \rightarrow \rho\bar{\rho}K^+K^-)/\Gamma_{\text{total}}] / [B(B^0 \rightarrow J/\psi(1S) K^*(892)^0)] / [B(J/\psi(1S) \rightarrow \rho\bar{\rho})] / [B(K^*(892) \rightarrow (K\pi)^\pm)] = 1.67 \pm 0.12 \pm 0.11$ which we multiply by our best values $B(B^0 \rightarrow J/\psi(1S) K^*(892)^0) = (1.27 \pm 0.05) \times 10^{-3}$, $B(J/\psi(1S) \rightarrow \rho\bar{\rho}) = (2.120 \pm 0.029) \times 10^{-3}$, $B(K^*(892) \rightarrow (K\pi)^\pm) = (99.902 \pm 0.009) \times 10^{-2}$. Our first error is their experiment's error and our second error is the systematic error from using our best values. Reported value assumes $f_S/f_d = 0.259 \pm 0.015$.

² The branching ratio is given for $m_{\rho\bar{\rho}} < 2.85$ GeV.

 $\Gamma(\rho\bar{\rho}K^+\pi^-)/\Gamma_{\text{total}}$ Γ_{144}/Γ

VALUE (units 10^{-7})	DOCUMENT ID	TECN	COMMENT
13.9 ± 2.5 ± 0.5	^{1,2} AAIJ	17BD LHCb	pp at 7, 8 TeV

¹ AAIJ 17BD reports $[\Gamma(B_S^0 \rightarrow \rho\bar{\rho}K^+\pi^-)/\Gamma_{\text{total}}] / [B(B^0 \rightarrow J/\psi(1S) K^*(892)^0)] / [B(J/\psi(1S) \rightarrow \rho\bar{\rho})] / [B(K^*(892) \rightarrow (K\pi)^\pm)] = 0.52 \pm 0.08 \pm 0.05$ which we multiply by our best values $B(B^0 \rightarrow J/\psi(1S) K^*(892)^0) = (1.27 \pm 0.05) \times 10^{-3}$, $B(J/\psi(1S) \rightarrow \rho\bar{\rho}) = (2.120 \pm 0.029) \times 10^{-3}$, $B(K^*(892) \rightarrow (K\pi)^\pm) = (99.902 \pm 0.009) \times 10^{-2}$. Our first error is their experiment's error and our second error is the systematic error from using our best values. Reported value assumes $f_S/f_d = 0.259 \pm 0.015$.

² The branching ratio is given for $m_{\rho\bar{\rho}} < 2.85$ GeV.

 $\Gamma(\rho\bar{\rho}K^+\pi^-)/\Gamma(\rho\bar{\rho}K^+K^-)$ $\Gamma_{144}/\Gamma_{143}$

VALUE	DOCUMENT ID	TECN	COMMENT
0.31 ± 0.05 ± 0.02	^{1,2} AAIJ	17BD LHCb	pp at 7, 8 TeV

¹ Reports $B(B_S^0 \rightarrow \rho\bar{\rho}K^+\pi^-) / B(B^0 \rightarrow \rho\bar{\rho}K^+K^-) = 0.22 \pm 0.04 \pm 0.02 \pm 0.01$, where the third error is due to f_S/f_d .

² The ratio is given for $m_{\rho\bar{\rho}} < 2.85$ GeV and assuming $f_S/f_d = 0.259 \pm 0.015$.

 $\Gamma(\rho\bar{\rho}\pi^+\pi^-)/\Gamma_{\text{total}}$ Γ_{145}/Γ

VALUE (units 10^{-7})	DOCUMENT ID	TECN	COMMENT
4.3 ± 2.0 ± 0.2	^{1,2} AAIJ	17BD LHCb	pp at 7, 8 TeV

¹ AAIJ 17BD reports $[\Gamma(B_S^0 \rightarrow \rho\bar{\rho}\pi^+\pi^-)/\Gamma_{\text{total}}] / [B(B^0 \rightarrow J/\psi(1S) K^*(892)^0)] / [B(J/\psi(1S) \rightarrow \rho\bar{\rho})] / [B(K^*(892) \rightarrow (K\pi)^\pm)] = 0.16 \pm 0.07 \pm 0.02$ which we multiply by our best values $B(B^0 \rightarrow J/\psi(1S) K^*(892)^0) = (1.27 \pm 0.05) \times 10^{-3}$, $B(J/\psi(1S) \rightarrow \rho\bar{\rho}) = (2.120 \pm 0.029) \times 10^{-3}$, $B(K^*(892) \rightarrow (K\pi)^\pm) = (99.902 \pm 0.009) \times 10^{-2}$. Our first error is their experiment's error and our second error is the systematic error from using our best values. Reported value assumes $f_S/f_d = 0.259 \pm 0.015$.

² The branching ratio is given for $m_{\rho\bar{\rho}} < 2.85$ GeV.

 $\Gamma(\rho\bar{\rho}\rho\bar{\rho})/\Gamma_{\text{total}}$ Γ_{146}/Γ

VALUE (units 10^{-8})	DOCUMENT ID	TECN	COMMENT
2.3 ± 1.0 ± 0.2	¹ AAIJ	23AD LHCb	pp at 7, 8, 13 TeV

¹ AAIJ 23AD reports $(2.3 \pm 1.0 \pm 0.2 \pm 0.1) \times 10^{-8}$ from a measurement of $[\Gamma(B_S^0 \rightarrow \rho\bar{\rho}\rho\bar{\rho})/\Gamma_{\text{total}}] / [B(B_S^0 \rightarrow J/\psi(1S)\phi)] / [B(\phi(1020) \rightarrow K^+ K^-)] / [B(J/\psi(1S) \rightarrow \rho\bar{\rho})]$ assuming $B(B_S^0 \rightarrow J/\psi(1S)\phi) = (1.04 \pm 0.04) \times 10^{-3}$, $B(\phi(1020) \rightarrow K^+ K^-) = 0.491 \pm 0.005$, $B(J/\psi(1S) \rightarrow \rho\bar{\rho}) = (2.120 \pm 0.029) \times 10^{-3}$.

 $\Gamma(\rho\bar{\rho}K^- + c.c.)/\Gamma_{\text{total}}$ Γ_{147}/Γ

VALUE (units 10^{-6})	DOCUMENT ID	TECN	COMMENT
5.5 ± 0.9 ± 0.4	^{1,2} AAIJ	17AL LHCb	pp at 7, 8 TeV

¹ AAIJ 17AL reports $(5.46 \pm 0.61 \pm 0.82) \times 10^{-6}$ from a measurement of $[\Gamma(B_S^0 \rightarrow \rho\bar{\rho}K^- + c.c.)/\Gamma_{\text{total}}] / [B(B^0 \rightarrow \rho\bar{\rho}\pi^-)]$ assuming $B(B^0 \rightarrow \rho\bar{\rho}\pi^-) = (3.14 \pm 0.29) \times 10^{-6}$, which we rescale to our best value $B(B^0 \rightarrow \rho\bar{\rho}\pi^-) = (3.16 \pm 0.24) \times 10^{-6}$. Our first error is their experiment's error and our second error is the systematic error from using our best value.

² AAIJ 17AL value represents the sum of $B_S^0 \rightarrow \rho\bar{\rho}K^-$ and $B_S^0 \rightarrow \bar{\rho}\Lambda K^+$ and assumes the fraction $f_S/f_d = 0.259 \pm 0.015$.

 $\Gamma(\Lambda_c^- \Lambda\pi^+)/\Gamma_{\text{total}}$ Γ_{148}/Γ

VALUE (units 10^{-4})	DOCUMENT ID	TECN	COMMENT
3.6 ± 1.1 ± 1.2	¹ SOLOVIEVA	13 BELL	$e^+ e^- \rightarrow \Upsilon(4S)$

¹ The second error is the total systematic uncertainty including the Λ_c absolute branching fractions and the normalization number of B_S events.

 $\Gamma(\Lambda_c^- \Lambda_c^+)/\Gamma_{\text{total}}$ Γ_{149}/Γ

VALUE	CL%	DOCUMENT ID	TECN	COMMENT
< 8.0 × 10⁻⁵	95	¹ AAIJ	14AA LHCb	pp at 7 TeV

¹ Uses $B(\bar{B}^0 \rightarrow D^+ D_S^-) = (7.2 \pm 0.8) \times 10^{-3}$.

 $\Gamma(\gamma\gamma)/\Gamma_{\text{total}}$ Γ_{150}/Γ

Test for $\Delta B=1$ weak neutral current.

VALUE (units 10^{-6})	CL%	DOCUMENT ID	TECN	COMMENT
< 3.1	90	¹ DUTTA	15 BELL	$e^+ e^- \rightarrow \Upsilon(5S)$

• • • We do not use the following data for averages, fits, limits, etc. • • •

< 8.7	90	² WICHT	08A BELL	Repl. by DUTTA 15
< 5.3	90	² DRUTSKOY	07A BELL	Repl. by WICHT 08A
<148	90	³ ACCIARRI	95i L3	$e^+ e^- \rightarrow Z$

¹ Assumes the fraction of $B_S^{(*)}\bar{B}_S^{(*)}$ in $b\bar{b}$ events is $f_S = (17.2 \pm 3.0)\%$.

² Assumes $\Upsilon(5S) \rightarrow B_S^* \bar{B}_S^* = (19.5 \pm 3.0)_{-2.3}^{\pm 3.0}\%$.

³ ACCIARRI 95i assumes $f_{B^0} = 39.5 \pm 4.0$ and $f_{B_S} = (12.0 \pm 3.0)\%$.

 $\Gamma(\phi\gamma)/\Gamma_{\text{total}}$ Γ_{151}/Γ

VALUE (units 10^{-6})	CL%	DOCUMENT ID	TECN	COMMENT
34 ± 4 OUR AVERAGE				
$36 \pm 5 \pm 7$		¹ DUTTA	15 BELL	$e^+ e^- \rightarrow \Upsilon(5S)$
$33.8 \pm 3.4 \pm 2.0$		² AAIJ	13 LHCb	pp at 7 TeV

• • • We do not use the following data for averages, fits, limits, etc. • • •

39 ± 5		³ AAIJ	12AE LHCb	Repl. by AAIJ 13
$57 \pm 18 \pm 11$		⁴ WICHT	08A BELL	Repl. by DUTTA 15
<390	90	⁵ DRUTSKOY	07A BELL	$e^+ e^- \rightarrow \Upsilon(5S)$
<120	90	⁵ ACOSTA	02G CDF	$\rho\bar{\rho}$ at 1.8 TeV
<700	90	⁵ ADAM	96D DLPH	$e^+ e^- \rightarrow Z$

¹ Assumes the fraction of $B_S^{(*)}\bar{B}_S^{(*)}$ in $b\bar{b}$ events is $f_S = (17.2 \pm 3.0)\%$. The systematic uncertainty from f_S is 0.6×10^{-5} .

² AAIJ 13 reports $[\Gamma(B_S^0 \rightarrow \phi\gamma)/\Gamma_{\text{total}}] / [B(B^0 \rightarrow K^*(892)^0 \gamma)] = 0.81 \pm 0.04 \pm 0.07$ which we multiply by our best value $B(B^0 \rightarrow K^*(892)^0 \gamma) = (4.18 \pm 0.25) \times 10^{-5}$. Our first error is their experiment's error and our second error is the systematic error from using our best value.

³ Measures $B(B^0 \rightarrow K^{*0} \gamma) / B(B_S \rightarrow \phi\gamma) = 1.12 \pm 0.08(\text{stat}) \pm 0.06(\text{sys}) \pm 0.09(f_S/f_d)$ and uses current world-average value of $B(B^0 \rightarrow K^{*0} \gamma) = (4.33 \pm 0.15) \times 10^{-5}$.

⁴ Assumes $\Upsilon(5S) \rightarrow B_S^* \bar{B}_S^* = (19.5 \pm 3.0)_{-2.3}^{\pm 3.0}\%$.

⁵ ADAM 96D assumes $f_{B^0} = f_{B^-} = 0.39$ and $f_{B_S} = 0.12$.

 $\Gamma(\mu^+ \mu^-)/\Gamma_{\text{total}}$ Γ_{152}/Γ

Test for $\Delta B = 1$ weak neutral current.

VALUE (units 10^{-9})	CL%	DOCUMENT ID	TECN	COMMENT
3.34 ± 0.27 OUR AVERAGE				
$3.83 \pm 0.38 \pm 0.24$ $-0.36 - 0.21$		¹ TUMASYAN	23A CMS	pp at 13 TeV
$3.09 \pm 0.46 \pm 0.15$ $-0.43 - 0.11$		AAIJ	22 LHCb	pp at 7, 8, 13 TeV
$2.9 \pm 0.6 \pm 0.4$		² SIRUNYAN	20AG CMS	pp at 7, 8, 13 TeV
2.8 ± 0.8 -0.7		³ AABOUD	19L ATLAS	pp at 7, 8, 13 TeV

••• We do not use the following data for averages, fits, limits, etc. •••

VALUE	CL%	DOCUMENT ID	TECN	COMMENT
$3.0 \pm 0.6 \begin{smallmatrix} +0.3 \\ -0.2 \end{smallmatrix}$		AAIJ 17A1	LHCB	Repl. by AAIJ 22
$0.9 \begin{smallmatrix} +1.1 \\ -0.8 \end{smallmatrix}$		4 AABOUD 16L	ATLS	Repl. by AABOUD 19L
$2.8 \begin{smallmatrix} +0.7 \\ -0.6 \end{smallmatrix}$		5 KHACHATRYAN 15BE	LHC	pp at 7, 8 TeV
$3.2 \begin{smallmatrix} +1.4 \\ -1.2 \\ +0.5 \\ -0.3 \end{smallmatrix}$		6 AAIJ 13B	LHCB	Repl. by AAIJ 13BA
$2.9 \begin{smallmatrix} +1.1 \\ -1.0 \\ +0.3 \\ -0.1 \end{smallmatrix}$		7 AAIJ 13BA	LHCB	Repl. by KHACHATRYAN 15BE
13 $\begin{smallmatrix} +9 \\ -7 \end{smallmatrix}$		8 AALTONEN 13F	CDF	$p\bar{p}$ at 1.96 TeV
<12		9 ABAZOV 13C	D0	$p\bar{p}$ at 1.96 TeV
$3.0 \begin{smallmatrix} +1.0 \\ -0.9 \end{smallmatrix}$		10 CHATRCHYAN 13AW	CMS	Repl. by SIRUNYAN 20Ag
<19		90 11 AAD 12AE	ATLS	pp at 7 TeV
<12		90 12 AAIJ 12A	LHCB	Repl. by AAIJ 12W
< 3.8		90 13 AAIJ 12W	LHCB	Repl. by AAIJ 13B
< 6.4		90 14 CHATRCHYAN 12A	CMS	pp at 7 TeV
<43		90 15 AAIJ 11B	LHCB	Repl. by AAIJ 12A
<35		90 16 AALTONEN 11AG	CDF	$p\bar{p}$ at 1.96 TeV
<16		90 17 CHATRCHYAN 11T	CMS	Repl. by CHATRCHYAN 12A
<42		90 18 ABAZOV 10S	D0	$p\bar{p}$ at 1.96 TeV

- 1 Uses normalization mode $B(B^+ \rightarrow J/\psi K^+) = (1.020 \pm 0.019) \times 10^{-3}$, $B(J/\psi \rightarrow \mu^+ \mu^-) = (5.961 \pm 0.033) \times 10^{-2}$ and B production ratio $f(b \rightarrow B_s^0)/f(b \rightarrow B^+) = 0.231 \pm 0.008$.
- 2 Uses normalization mode $B(B^+ \rightarrow J/\psi K^+) = (1.01 \pm 0.03) \times 10^{-3}$ and B production ratio $f(b \rightarrow B_s^0)/f(b \rightarrow B^+) = 0.252 \pm 0.012 \pm 0.015$.
- 3 Uses normalization mode $B(B^+ \rightarrow J/\psi K^+) = (1.010 \pm 0.029) \times 10^{-3}$ and B production ratio $f(b \rightarrow B_s^0)/f(b \rightarrow B^+) = 0.256 \pm 0.013$.
- 4 This value corresponds to an upper limit of $< 3.0 \times 10^{-9}$ at 95% C.L. It uses $f_s/f_d = 0.24 \pm 0.02$.
- 5 Determined from the joint fit to CMS and LHCB data. Uncertainty includes both statistical and systematic component.
- 6 Uses B production ratio $f(\bar{b} \rightarrow B_s^0)/f(\bar{b} \rightarrow B_d^0) = 0.256 \pm 0.020$ and two normalization modes: $B(B^+ \rightarrow J/\psi K^+ \rightarrow \mu^+ \mu^- K^+) = (6.01 \pm 0.21) \times 10^{-5}$ and $B(B^0 \rightarrow K^+ \pi^-) = (1.94 \pm 0.06) \times 10^{-5}$.
- 7 Uses B production ratio $f(\bar{b} \rightarrow B_s^0)/f(\bar{b} \rightarrow B_d^0) = 0.259 \pm 0.015$ and normalization modes $B^+ \rightarrow J/\psi K^+ \rightarrow \mu^+ \mu^- K^+$ and $B^0 \rightarrow K^+ \pi^-$.
- 8 Uses normalization mode $B(B^+ \rightarrow J/\psi K^+) = (10.22 \pm 0.35) \times 10^{-4}$ and B production ratio $f(\bar{b} \rightarrow B_s^0)/f(\bar{b} \rightarrow B_d^0) = 0.28 \pm 0.04$.
- 9 Uses normalization mode $B(B^+ \rightarrow J/\psi K^+ \rightarrow \mu^+ \mu^- K^+) = (6.01 \pm 0.21) \times 10^{-5}$ and B production ratio $f(\bar{b} \rightarrow B_s^0)/f(\bar{b} \rightarrow B_d^0) = 0.263 \pm 0.017$.
- 10 Uses B production ratio $f(\bar{b} \rightarrow B_s^0)/f(\bar{b} \rightarrow B_d^0) = 0.256 \pm 0.020$ and $B(B^+ \rightarrow J/\psi K^+ \rightarrow \mu^+ \mu^- K^+) = (6.0 \pm 0.2) \times 10^{-5}$ for normalization.
- 11 Uses B production ratio $f(\bar{b} \rightarrow B^+)/f(\bar{b} \rightarrow B_s^0) = 3.75 \pm 0.29$ and $B(B^+ \rightarrow J/\psi K^+ \rightarrow \mu^+ \mu^- K^+) = (6.0 \pm 0.2) \times 10^{-5}$.
- 12 Uses B production ratio $f(\bar{b} \rightarrow B_s^0)/f(\bar{b} \rightarrow B_d^0) = 0.267 \pm \begin{smallmatrix} 0.021 \\ -0.020 \end{smallmatrix}$ and three normalization modes $B(B^+ \rightarrow J/\psi K^+ \rightarrow \mu^+ \mu^- K^+) = (6.01 \pm 0.21) \times 10^{-5}$, $B(B^0 \rightarrow K^+ \pi^-) = (1.94 \pm 0.06) \times 10^{-5}$, and $B(B_s^0 \rightarrow J/\psi \phi \rightarrow \mu^+ \mu^- K^+ K^-) = (3.4 \pm 0.9) \times 10^{-5}$.
- 13 Uses B production ratio $f(\bar{b} \rightarrow B_s^0)/f(\bar{b} \rightarrow B_d^0) = 0.267 \pm \begin{smallmatrix} 0.021 \\ -0.020 \end{smallmatrix}$ and three normalization modes of $B^+ \rightarrow J/\psi K^+$, $B^0 \rightarrow K^+ \pi^-$, and $B_s^0 \rightarrow J/\psi \phi$.
- 14 Uses $f_s/f_d = 0.267 \pm 0.021$ and $B(B^+ \rightarrow J/\psi K^+ \rightarrow \mu^+ \mu^- K^+) = (6.0 \pm 0.2) \times 10^{-5}$.
- 15 Uses B production ratio $f(\bar{b} \rightarrow B^+)/f(\bar{b} \rightarrow B_s^0) = 3.71 \pm 0.47$ and three normalization modes.
- 16 Uses B production ratio $f(\bar{b} \rightarrow B^+)/f(\bar{b} \rightarrow B_s^0) = 3.55 \pm 0.47$ and $B(B^+ \rightarrow J/\psi K^+ \rightarrow \mu^+ \mu^- K^+) = (6.01 \pm 0.21) \times 10^{-5}$.
- 17 Uses B production ratio $f(\bar{b} \rightarrow B^+)/f(\bar{b} \rightarrow B_s^0) = 3.55 \pm 0.42$ and $B(B^+ \rightarrow J/\psi K^+ \rightarrow \mu^+ \mu^- K^+) = (6.0 \pm 0.2) \times 10^{-5}$.
- 18 Uses B production ratio $f(\bar{b} \rightarrow B^+)/f(\bar{b} \rightarrow B_s^0) = 3.86 \pm 0.59$, and the number of $B^+ \rightarrow J/\psi K^+$ decays.

$\Gamma(e^+ e^-)/\Gamma_{total}$ Γ_{153}/Γ
 Test for $\Delta B = 1$ weak neutral current.

VALUE	CL%	DOCUMENT ID	TECN	COMMENT
$<9.4 \times 10^{-9}$		90 1 AAIJ 20W	LHCB	pp at 7, 8, 13 TeV
$<2.8 \times 10^{-7}$		90 AALTONEN 09P	CDF	$p\bar{p}$ at 1.96 TeV
$<5.4 \times 10^{-5}$		90 2 ACCIARRI 97B	L3	$e^+ e^- \rightarrow Z$

••• We do not use the following data for averages, fits, limits, etc. •••

- 1 Assumes no contribution from $B^0 \rightarrow e^+ e^-$ decays.
- 2 ACCIARRI 97B assume PDG 96 production fractions for B^+ , B^0 , B_s , and Λ_b .

$\Gamma(\tau^+ \tau^-)/\Gamma_{total}$ Γ_{154}/Γ

VALUE	CL%	DOCUMENT ID	TECN	COMMENT
$<6.8 \times 10^{-3}$		95 1 AAIJ 17A1	LHCB	pp at 7, 8 TeV

1 Assuming no contribution from $B^0 \rightarrow \tau^+ \tau^-$.

$\Gamma(\mu^+ \mu^- \gamma)/\Gamma_{total}$ Γ_{155}/Γ

VALUE	CL%	DOCUMENT ID	TECN	COMMENT
$<2.0 \times 10^{-9}$		1 AAIJ 22	LHCB	pp at 7, 8, 13 TeV

1 The exclusion is limited to the range $m_{\mu\mu} > 4.9$ GeV/c².

$\Gamma(\mu^+ \mu^- \mu^+ \mu^-)/\Gamma_{total}$ Γ_{156}/Γ

VALUE	CL%	DOCUMENT ID	TECN	COMMENT
$<8.6 \times 10^{-10}$		95 AAIJ 22Q	LHCB	pp at 7, 8, 13 TeV
$<2.5 \times 10^{-9}$		95 AAIJ 17N	LHCB	pp at 7, 8 TeV
$<1.6 \times 10^{-8}$		1 AAIJ 13AW	LHCB	Repl. by AAIJ 17N

1 Also reports a limit of $< 1.2 \times 10^{-8}$ at 90% C.L.

$\Gamma(S P, S \rightarrow \mu^+ \mu^-, P \rightarrow \mu^+ \mu^-)/\Gamma_{total}$ Γ_{157}/Γ
 Here S and P are the hypothetical scalar and pseudoscalar particles with masses of 2.5 GeV/c² and 214.3 MeV/c², respectively.

VALUE	CL%	DOCUMENT ID	TECN	COMMENT
$<2.2 \times 10^{-9}$		95 AAIJ 17N	LHCB	pp at 7, 8 TeV
$<1.2 \times 10^{-8}$		90 1 AAIJ 13AW	LHCB	Repl. by AAIJ 17N

••• We do not use the following data for averages, fits, limits, etc. •••

1 Also reports a limit of $< 1.6 \times 10^{-8}$ at 95% C.L.

$\Gamma(a a, a \rightarrow \mu^+ \mu^-)/\Gamma_{total}$ Γ_{158}/Γ
 Here particle a is a scalar with a mass of 1 GeV/c².

VALUE	CL%	DOCUMENT ID	TECN	COMMENT
$<5.8 \times 10^{-10}$		95 AAIJ 22Q	LHCB	pp at 7, 8, 13 TeV

$\Gamma(\phi(1020) \mu^+ \mu^-)/\Gamma_{total}$ Γ_{159}/Γ
 Test for $\Delta B = 1$ weak neutral current.

VALUE (units 10^{-7})	CL%	DOCUMENT ID	TECN	COMMENT
<32		90 1 ABZOV 06G	D0	$p\bar{p}$ at 1.96 TeV
$< 4.7 \times 10^2$		90 ACOSTA 02D	CDF	$p\bar{p}$ at 1.8 TeV

1 Uses $B(B_s^0 \rightarrow J/\psi \phi) = 9.3 \times 10^{-4}$.

$\Gamma(\phi(1020) \mu^+ \mu^-)/\Gamma(J/\psi(1S) \phi)$ Γ_{159}/Γ_{61}

VALUE (units 10^{-3})	CL%	DOCUMENT ID	TECN	COMMENT
0.806 ± 0.026		OUR AVERAGE		
$0.800 \pm 0.021 \pm 0.016$		AAIJ 21AG	LHCB	pp at 7, 8, 13 TeV
$1.13 \pm 0.19 \pm 0.07$		AALTONEN 11A1	CDF	$p\bar{p}$ at 1.96 TeV
$0.741 \pm \begin{smallmatrix} 0.042 \\ 0.046 \end{smallmatrix} \pm 0.029$		AAIJ 15AQ	LHCB	Repl. by AAIJ 21AG
$0.674 \pm \begin{smallmatrix} 0.061 \\ -0.056 \end{smallmatrix} \pm 0.016$		AAIJ 13X	LHCB	Repl. by AAIJ 15AQ
$1.11 \pm 0.25 \pm 0.09$		AALTONEN 11L	CDF	Repl. by AALTONEN 11A1
< 2.3		90 AALTONEN 09B	CDF	Repl. by AALTONEN 11L

$\Gamma(K^*(892)^0 \mu^+ \mu^-)/\Gamma_{total}$ Γ_{161}/Γ

VALUE (units 10^{-8})	CL%	DOCUMENT ID	TECN	COMMENT
$2.9 \pm 1.0 \pm 0.4$		1 AAIJ 18AB	LHCB	pp at 7, 8, 13 TeV

1 Normalizes to $B(B^0 \rightarrow J/\psi K^*) = 1.19 \pm 0.01 \pm 0.08\%$ and $B(J/\psi \rightarrow \mu^+ \mu^-) = 5.96 \pm 0.03\%$, and uses $f_s/f_d = 0.259 \pm 0.015$.

$\Gamma(f_2'(1525) \mu^+ \mu^-)/\Gamma(J/\psi(1S) \phi)$ Γ_{160}/Γ_{61}

VALUE (units 10^{-4})	CL%	DOCUMENT ID	TECN	COMMENT
$1.55 \pm 0.19 \pm 0.08$		1 AAIJ 21AG	LHCB	pp at 7, 8, 13 TeV

1 Measured by combining the q^2 regions [0.1, 0.98], [1.1, 8.0], and [11.0, 12.5] GeV²/c⁴.

$\Gamma(\pi^+ \pi^- \mu^+ \mu^-)/\Gamma_{total}$ Γ_{162}/Γ

VALUE (units 10^{-8})	CL%	DOCUMENT ID	TECN	COMMENT
$8.4 \pm 1.6 \pm 0.3$		1 AAIJ 15S	LHCB	pp at 7, 8 TeV

1 AAIJ 15S reports $(8.6 \pm 1.5 \pm 0.7 \pm 0.7) \times 10^{-8}$ from a measurement of $[\Gamma(B_s^0 \rightarrow \pi^+ \pi^- \mu^+ \mu^-)/\Gamma_{total}] / [B(B^0 \rightarrow J/\psi(1S) K^*(892)^0)]$ assuming $B(B^0 \rightarrow J/\psi(1S) K^*(892)^0) = (1.3 \pm 0.1) \times 10^{-3}$, which we rescale to our best value $B(B^0 \rightarrow J/\psi(1S) K^*(892)^0) = (1.27 \pm 0.05) \times 10^{-3}$. Our first error is their experiment's error and our second error is the systematic error from using our best value.

$\Gamma(\phi \nu \bar{\nu})/\Gamma_{total}$ Γ_{163}/Γ
 Test for $\Delta B = 1$ weak neutral current.

VALUE	CL%	DOCUMENT ID	TECN	COMMENT
$<5.4 \times 10^{-3}$		90 1 ADAM 96D	DLPH	$e^+ e^- \rightarrow Z$

1 ADAM 96D assumes $f_{B^0} = f_{B^-} = 0.39$ and $f_{B_s} = 0.12$.

$\Gamma(e^\pm \mu^\mp)/\Gamma_{total}$ Γ_{164}/Γ
 Test of lepton family number conservation.

VALUE	CL%	DOCUMENT ID	TECN	COMMENT
$<5.4 \times 10^{-9}$		1 AAIJ 18T	LHCB	pp at 7, 8 TeV
$<1.1 \times 10^{-8}$		2 AAIJ 13B	LHCB	Repl. by AAIJ 18T
$<2.0 \times 10^{-7}$		90 AALTONEN 09P	CDF	$p\bar{p}$ at 1.96 TeV
$<6.1 \times 10^{-6}$		90 ABE 98V	CDF	Repl. by AALTONEN 09P
$<4.1 \times 10^{-5}$		90 3 ACCIARRI 97B	L3	$e^+ e^- \rightarrow Z$

1 AAIJ 18T uses normalization modes $B(B^0 \rightarrow K^+ \pi^-) = (19.6 \pm 0.5) \times 10^{-6}$ and $B(B^+ \rightarrow J/\psi K^+) = (1.026 \pm 0.031) \times 10^{-3}$ with B production ratio $f(\bar{b} \rightarrow B_s^0)/f(\bar{b} \rightarrow B_d^0) = 0.259 \pm 0.015$. The upper limit increases to 6×10^{-9} with the assumption of B_L -dominated decay amplitude.

2 Uses normalization mode $B(B^0 \rightarrow K^+ \pi^-) = (19.4 \pm 0.6) \times 10^{-6}$ and B production ratio $f(\bar{b} \rightarrow B_s^0)/f(\bar{b} \rightarrow B_d^0) = 0.256 \pm 0.020$.

3 ACCIARRI 97B assume PDG 96 production fractions for B^+ , B^0 , B_s , and Λ_b .

Meson Particle Listings

B_s^0

$\Gamma(e^\pm \tau^\mp)/\Gamma_{\text{total}}$				Γ_{165}/Γ
VALUE	CL%	DOCUMENT ID	COMMENT	
$<1.4 \times 10^{-3}$	90	¹ NAYAK 23	$e^+ e^- \rightarrow \Upsilon(4S)$	

¹ Reconstructs the accompanying B_s^0 meson in the semileptonic decay modes.

$\Gamma(\mu^\pm \tau^\mp)/\Gamma_{\text{total}}$				Γ_{166}/Γ
VALUE	CL%	DOCUMENT ID	TECN	COMMENT
$<4.2 \times 10^{-5}$	95	¹ AAIJ 19AK LHCB	pp at 7, 8 TeV	

••• We do not use the following data for averages, fits, limits, etc. •••

$<7.3 \times 10^{-4}$	90	² NAYAK 23	BELL	$e^+ e^- \rightarrow \Upsilon(4S)$
-----------------------	----	-----------------------	------	------------------------------------

¹ Assuming no contribution from $B^0 \rightarrow \mu^\pm \tau^\mp$.
² Reconstructs the accompanying B_s^0 meson in the semileptonic decay modes.

$\Gamma(\phi \mu^\pm e^\mp)/\Gamma_{\text{total}}$				Γ_{167}/Γ
VALUE	CL%	DOCUMENT ID	TECN	COMMENT
$<1.6 \times 10^{-8}$	90	¹ AAIJ 23G LHCB	pp at 7, 8, 13 TeV	

¹ Uses the uniform phase space model for the signal decays.

$\Gamma(\rho \mu^-)/\Gamma_{\text{total}}$				Γ_{168}/Γ
VALUE	CL%	DOCUMENT ID	COMMENT	
$<1.21 \times 10^{-8}$	90	¹ AAIJ 23Y	pp at 7, 8, 13 TeV	

¹ Assumes that B_s^0 decay branching fractions to $\rho \mu^-$ and $\bar{\rho} \mu^+$ are the same.

POLARIZATION IN B_s^0 DECAY

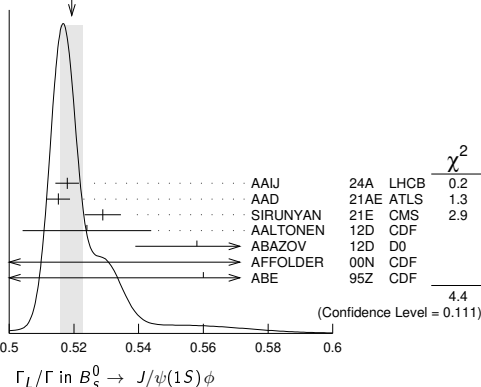
In decays involving two vector mesons, one can distinguish among the states in which meson polarizations are both longitudinal (L), or both are transverse and parallel (\parallel), or perpendicular (\perp) to each other with the parameters Γ_L/Γ , Γ_\perp/Γ , and the relative phases ϕ_\parallel and ϕ_\perp . In decays involving two tensor mesons, the transverse polarization states are described by parameters $\Gamma_{\parallel 1}$, $\Gamma_{\parallel 2}$, $\Gamma_{\perp 1}$, $\Gamma_{\perp 2}$ and their relative phases $\phi_{\parallel 1}$, $\phi_{\parallel 2}$, $\phi_{\perp 1}$, $\phi_{\perp 2}$. See also the review on "Polarization in B Decays."

Γ_L/Γ in $B_s^0 \rightarrow D_s^* \rho^+$			
VALUE	DOCUMENT ID	TECN	COMMENT
$1.05^{+0.08+0.03}_{-0.10-0.04}$	LOUVOT 10	BELL	$e^+ e^- \rightarrow \Upsilon(5S)$

Γ_L/Γ in $B_s^0 \rightarrow J/\psi(1S)\phi$			
VALUE	DOCUMENT ID	TECN	COMMENT
0.5194 ± 0.0034 OUR AVERAGE	Error includes scale factor of 1.5. See the ideogram below.		

$0.5179 \pm 0.0017 \pm 0.0032$	¹ AAIJ 24A	LHCB	pp at 13 TeV
$0.5152 \pm 0.0012 \pm 0.0034$	² AAD 21AE	ATLS	pp at 7, 8, 13 TeV
$0.5289 \pm 0.0038 \pm 0.0041$	³ SIRUNYAN 21E	CMS	pp at 8, 13 TeV
$0.524 \pm 0.013 \pm 0.015$	³ AALTONEN 12D	CDF	$p\bar{p}$ at 1.96 TeV
$0.558^{+0.017}_{-0.019}$	^{3,4} ABAZOV 12D	D0	$p\bar{p}$ at 1.96 TeV
$0.61 \pm 0.14 \pm 0.02$	⁵ AFFOLDER 00N	CDF	$p\bar{p}$ at 1.8 TeV
$0.56 \pm 0.21^{+0.02}_{-0.04}$	ABE 95Z	CDF	$p\bar{p}$ at 1.8 TeV
••• We do not use the following data for averages, fits, limits, etc. •••			
$0.5350 \pm 0.0047 \pm 0.0049$	³ SIRUNYAN 21E	CMS	pp at 13 TeV
$0.5186 \pm 0.0029 \pm 0.0023$	AAIJ 19Q	LHCB	Repl. by AAIJ 24A
$0.522 \pm 0.003 \pm 0.007$	² AAD 16AP	ATLS	Repl. by AAD 21AE
$0.510 \pm 0.005 \pm 0.011$	³ KHACHATRY..16s	CMS	pp at 8 TeV
$0.5241 \pm 0.0034 \pm 0.0067$	AAIJ 15I	LHCB	Repl. by AAIJ 19Q
$0.529 \pm 0.006 \pm 0.012$	² AAD 14U	ATLS	Repl. by AAD 16AP
$0.539 \pm 0.014 \pm 0.016$	³ AAD 12CV	ATLS	Repl. by AAD 14U
$0.555 \pm 0.027 \pm 0.006$	⁶ ABAZOV 09E	D0	Repl. by ABAZOV 12D
$0.531 \pm 0.020 \pm 0.007$	³ AALTONEN 08J	CDF	Repl. by AALTONEN 12D
$0.62 \pm 0.06 \pm 0.01$	ACOSTA 05	CDF	Repl. by AALTONEN 08J

WEIGHTED AVERAGE
 0.5194 ± 0.0034 (Error scaled by 1.5)



¹ Measured using a time-dependent angular analysis of $B_s^0 \rightarrow J/\psi K^+ K^-$ decays.

² Measured using the flavor tagged, time-dependent angular analysis of $B_s^0 \rightarrow J/\psi \phi$ decays.

³ Measured using the time-dependent angular analysis of $B_s^0 \rightarrow J/\psi \phi$ decays.

⁴ The error includes both statistical and systematic uncertainties.

⁵ AFFOLDER 00N measurements are based on 40 B_s^0 candidates obtained from a data sample of 89 pb^{-1} . The P -wave fraction is found to be $0.23 \pm 0.19 \pm 0.04$.

⁶ Measured the angular and lifetime parameters for the time-dependent angular untagged decays $B_d^0 \rightarrow J/\psi K^{*0}$ and $B_s^0 \rightarrow J/\psi \phi$.

Γ_L/Γ in $B_s^0 \rightarrow D_s^{*+} D_s^{*-}$			
VALUE	DOCUMENT ID	TECN	COMMENT
$0.06^{+0.18}_{-0.17} \pm 0.03$	ESEN 13	BELL	$e^+ e^- \rightarrow \Upsilon(5S)$

$\Gamma_{\parallel}/\Gamma$ in $B_s^0 \rightarrow J/\psi(1S)\phi$			
VALUE	DOCUMENT ID	TECN	COMMENT
0.2222 ± 0.0027 OUR AVERAGE			
$0.2220 \pm 0.0017 \pm 0.0021$	¹ AAD 21AE	ATLS	pp at 7, 8, 13 TeV
$0.231 \pm 0.014 \pm 0.015$	² AALTONEN 12D	CDF	$p\bar{p}$ at 1.96 TeV
$0.231^{+0.024}_{-0.030}$	^{2,3} ABAZOV 12D	D0	$p\bar{p}$ at 1.96 TeV

••• We do not use the following data for averages, fits, limits, etc. •••

$0.227 \pm 0.004 \pm 0.006$	¹ AAD 16AP	ATLS	Repl. by AAD 21AE
$0.220 \pm 0.008 \pm 0.009$	¹ AAD 14U	ATLS	Repl. by AAD 16AP
$0.224 \pm 0.010 \pm 0.009$	² AAD 12CV	ATLS	Repl. by AAD 14U
$0.244 \pm 0.032 \pm 0.014$	⁴ ABAZOV 09E	D0	Repl. by ABAZOV 12D
$0.230 \pm 0.029 \pm 0.011$	² AALTONEN 08J	CDF	Repl. by AALTONEN 12D
$0.260 \pm 0.084 \pm 0.013$	ACOSTA 05	CDF	Repl. by AALTONEN 08J

¹ Measured using a tagged, time-dependent angular analysis of $B_s^0 \rightarrow J/\psi \phi$ decays.

² Measured using the time-dependent angular analysis of $B_s^0 \rightarrow J/\psi \phi$ decays.

³ The error includes both statistical and systematic uncertainties.

⁴ Measured the angular and lifetime parameters for the time-dependent angular untagged decays $B_d^0 \rightarrow J/\psi K^{*0}$ and $B_s^0 \rightarrow J/\psi \phi$.

Γ_{\perp}/Γ in $B_s^0 \rightarrow J/\psi(1S)\phi$			
VALUE	DOCUMENT ID	TECN	COMMENT
0.2447 ± 0.0029 OUR AVERAGE			
$0.2463 \pm 0.0023 \pm 0.0024$	¹ AAIJ 24A	LHCB	pp at 13 TeV
$0.2393 \pm 0.0050 \pm 0.0037$	SIRUNYAN 21E	CMS	pp at 8, 13 TeV
••• We do not use the following data for averages, fits, limits, etc. •••			
$0.2337 \pm 0.0063 \pm 0.0045$	SIRUNYAN 21E	CMS	pp at 13 TeV
$0.2456 \pm 0.0040 \pm 0.0019$	AAIJ 19Q	LHCB	Repl. by AAIJ 24A
$0.243 \pm 0.008 \pm 0.012$	KHACHATRY..16s	CMS	pp at 8 TeV
$0.2504 \pm 0.0049 \pm 0.0036$	AAIJ 15I	LHCB	Repl. by AAIJ 19Q

¹ Measured using a time-dependent angular analysis of $B_s^0 \rightarrow J/\psi K^+ K^-$ decays.

ϕ_{\parallel} in $B_s^0 \rightarrow J/\psi(1S)\phi$			
VALUE (rad)	DOCUMENT ID	TECN	COMMENT
3.22 ± 0.05 OUR AVERAGE			
$3.146 \pm 0.061 \pm 0.052$	¹ AAIJ 24A	LHCB	pp at 13 TeV
$3.36 \pm 0.05 \pm 0.09$	² AAD 21AE	ATLS	pp at 7, 8, 13 TeV
$3.19 \pm 0.12 \pm 0.04$	SIRUNYAN 21E	CMS	pp at 8, 13 TeV
3.15 ± 0.22	³ ABAZOV 12D	D0	$p\bar{p}$ at 1.96 TeV

••• We do not use the following data for averages, fits, limits, etc. •••

$3.18 \pm 0.12 \pm 0.003$	SIRUNYAN 21E	CMS	pp at 13 TeV
$3.06^{+0.08}_{-0.07} \pm 0.04$	AAIJ 19Q	LHCB	Repl. by AAIJ 24A
$3.15 \pm 0.10 \pm 0.05$	AAD 16AP	ATLS	Repl. by AAD 21AE
$3.48^{+0.07}_{-0.09} \pm 0.68$	KHACHATRY..16s	CMS	pp at 8 TeV
$3.26^{+0.10+0.06}_{-0.17-0.07}$	AAIJ 15I	LHCB	Repl. by AAIJ 19Q
$2.72^{+1.12}_{-0.27} \pm 0.26$	ABAZOV 09E	D0	Repl. by ABAZOV 12D

¹ Measured using a time-dependent angular analysis of $B_s^0 \rightarrow J/\psi K^+ K^-$ decays.

² The fit found another solution with $\phi_{\parallel} = 2.95 \pm 0.05 \pm 0.09$ rad.

³ The error includes both statistical and systematic uncertainties.

ϕ_{\perp} in $B_s^0 \rightarrow J/\psi(1S)\phi$			
VALUE (rad)	DOCUMENT ID	TECN	COMMENT
2.99 ± 0.12 OUR AVERAGE	Error includes scale factor of 1.9. See the ideogram below.		

$2.903^{+0.075}_{-0.074} \pm 0.048$	¹ AAIJ 24A	LHCB	pp at 13 TeV
$3.22 \pm 0.10 \pm 0.05$	² AAD 21AE	ATLS	pp at 7, 8, 13 TeV
$2.78 \pm 0.15 \pm 0.06$	³ SIRUNYAN 21E	CMS	pp at 8, 13 TeV

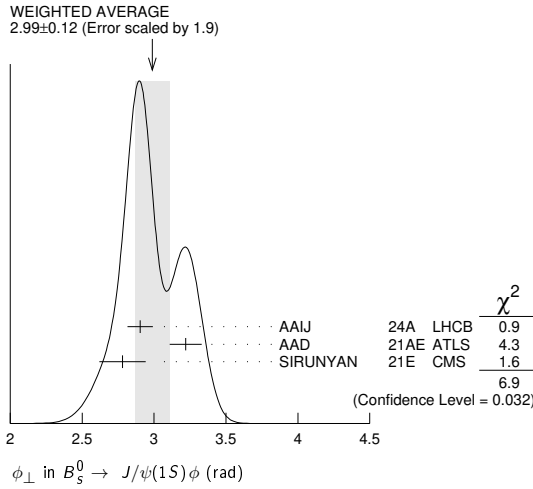
••• We do not use the following data for averages, fits, limits, etc. •••

$2.77 \pm 0.16 \pm 0.05$	³ SIRUNYAN 21E	CMS	pp at 13 TeV
$2.64 \pm 0.13 \pm 0.10$	AAIJ 19Q	LHCB	Repl. by AAIJ 24A
$4.15 \pm 0.32 \pm 0.16$	³ AAD 16AP	ATLS	Repl. by AAD 21AE
$2.98 \pm 0.36 \pm 0.66$	³ KHACHATRY..16s	CMS	pp at 8 TeV
$3.08^{+0.14}_{-0.15} \pm 0.06$	AAIJ 15I	LHCB	Repl. by AAIJ 19Q
$3.89 \pm 0.47 \pm 0.11$	³ AAD 14U	ATLS	Repl. by AAD 16AP

¹ Measured using a time-dependent angular analysis of $B_s^0 \rightarrow J/\psi K^+ K^-$ decays.

² The fit found another solution with $\phi_{\perp} = 3.03 \pm 0.05 \pm 0.09$ rad.

³ Measured using a tagged, time-dependent angular analysis of $B_s^0 \rightarrow J/\psi\phi$ decays.



Γ_{\perp}/Γ in $B_s^0 \rightarrow \psi(2S)\phi$

VALUE	DOCUMENT ID	TECN	COMMENT
$0.264^{+0.024}_{-0.023} \pm 0.002$	¹ AAIJ	16AK LHCb	pp at 7, 8 TeV

¹ Measured using time-dependent angular analysis of $B_s^0 \rightarrow \psi(2S)\phi$ decays.

ϕ_{\parallel} in $B_s^0 \rightarrow \psi(2S)\phi$

VALUE (rad)	DOCUMENT ID	TECN	COMMENT
$3.67^{+0.13}_{-0.18} \pm 0.03$	¹ AAIJ	16AK LHCb	pp at 7, 8 TeV

¹ Measured using time-dependent angular analysis of $B_s^0 \rightarrow \psi(2S)\phi$ decays.

ϕ_{\perp} in $B_s^0 \rightarrow \psi(2S)\phi$

VALUE (rad)	DOCUMENT ID	TECN	COMMENT
$3.29^{+0.43}_{-0.39} \pm 0.04$	¹ AAIJ	16AK LHCb	pp at 7, 8 TeV

¹ Measured using time-dependent angular analysis of $B_s^0 \rightarrow \psi(2S)\phi$ decays.

Γ_{\perp}/Γ for $B_s^0 \rightarrow J/\psi(1S)\bar{K}^*(892)^0$

Longitudinal polarization fraction, equals to $1 - f_{\perp} - f_{\parallel}$ using notation of "Polarization in B decays" review.

VALUE	DOCUMENT ID	TECN	COMMENT
$0.497 \pm 0.025 \pm 0.025$	AAIJ	15AV LHCb	pp at 7, 8 TeV

• • • We do not use the following data for averages, fits, limits, etc. • • •

VALUE	DOCUMENT ID	TECN	COMMENT
$0.50 \pm 0.08 \pm 0.02$	¹ AAIJ	12AP LHCb	Repl. by AAIJ 15AV

¹ The non-resonant $K\pi$ background contributions are subtracted. Also reports an S-wave amplitude $|A_S|^2 = 0.07^{+0.15}_{-0.07}$.

$\Gamma_{\parallel}/\Gamma$ for $B_s^0 \rightarrow J/\psi(1S)\bar{K}^*(892)^0$

Parallel polarization fraction, equals to $1 - f_{\perp} - f_{\parallel}$ using notation of "Polarization in B decays" review.

VALUE	DOCUMENT ID	TECN	COMMENT
$0.179 \pm 0.027 \pm 0.013$	AAIJ	15AV LHCb	pp at 7, 8 TeV

• • • We do not use the following data for averages, fits, limits, etc. • • •

VALUE	DOCUMENT ID	TECN	COMMENT
$0.19^{+0.10}_{-0.08} \pm 0.02$	¹ AAIJ	12AP LHCb	Repl. by AAIJ 15AV

¹ The non-resonant $K\pi$ background contributions are subtracted. Also reports an S-wave amplitude $|A_S|^2 = 0.07^{+0.15}_{-0.07}$.

Γ_{\perp}/Γ of $K^*(892)^0$ in $B_s^0 \rightarrow \psi(2S)\bar{K}^*(892)^0$

VALUE	DOCUMENT ID	TECN	COMMENT
$0.524 \pm 0.056 \pm 0.029$	AAIJ	15U LHCb	pp at 7, 8 TeV

Γ_{\perp}/Γ in $B_s^0 \rightarrow \phi\phi$

VALUE	DOCUMENT ID	TECN	COMMENT
0.379 ± 0.008 OUR AVERAGE	Error includes scale factor of 1.2.		

$0.384 \pm 0.007 \pm 0.003$	AAIJ	23AT LHCb	pp at 13 TeV
$0.364 \pm 0.012 \pm 0.009$	AAIJ	14AE LHCb	pp at 7, 8 TeV
$0.348 \pm 0.041 \pm 0.021$	AALTONEN	11AN CDF	$p\bar{p}$ at 1.96 TeV

• • • We do not use the following data for averages, fits, limits, etc. • • •

$0.381 \pm 0.007 \pm 0.012$	AAIJ	19AP LHCb	pp at 7, 8, partial 13 TeV
$0.365 \pm 0.022 \pm 0.012$	AAIJ	12P LHCb	Repl. by AAIJ 14AE

Γ_{\perp}/Γ in $B_s^0 \rightarrow \phi\phi$

VALUE	DOCUMENT ID	TECN	COMMENT
0.310 ± 0.006 OUR AVERAGE			
$0.310 \pm 0.006 \pm 0.003$	AAIJ	23AT LHCb	pp at 13 TeV
$0.305 \pm 0.013 \pm 0.005$	AAIJ	14AE LHCb	pp at 7, 8 TeV
$0.365 \pm 0.044 \pm 0.027$	AALTONEN	11AN CDF	$p\bar{p}$ at 1.96 TeV
• • • We do not use the following data for averages, fits, limits, etc. • • •			
$0.290 \pm 0.008 \pm 0.005$	¹ AAIJ	19AP LHCb	pp at 7, 8, partial 13 TeV
$0.291 \pm 0.024 \pm 0.010$	AAIJ	12P LHCb	Repl. by AAIJ 14AE

¹ Note: in the summary of AAIJ 19AP the systematic uncertainty is 0.007. We take the systematic uncertainty as given in Table 5 in the paper.

ϕ_{\parallel} in $B_s^0 \rightarrow \phi\phi$

VALUE (rad)	DOCUMENT ID	TECN	COMMENT
2.469 ± 0.029 OUR AVERAGE			
$2.463 \pm 0.029 \pm 0.009$	AAIJ	23AT LHCb	pp at 13 TeV
$2.54 \pm 0.07 \pm 0.09$	¹ AAIJ	14AE LHCb	pp at 7, 8 TeV
$2.71^{+0.31}_{-0.36} \pm 0.22$	² AALTONEN	11AN CDF	$p\bar{p}$ at 1.96 TeV

• • • We do not use the following data for averages, fits, limits, etc. • • •

$2.559 \pm 0.045 \pm 0.033$	AAIJ	19AP LHCb	pp at 7, 8, partial 13 TeV
$2.57 \pm 0.15 \pm 0.06$	³ AAIJ	12P LHCb	Repl. by AAIJ 14AE

¹ AAIJ 14AE reports measurement of ϕ_{\perp} and $\phi_{\perp} - \phi_{\parallel}$, which we convert into ϕ_{\parallel} . Statistical uncertainty includes correlation between measured parameters, while systematic uncertainties are assumed uncorrelated.

² AALTONEN 11AN quotes $\cos\phi_{\parallel} = -0.91^{+0.15}_{-0.13} \pm 0.09$ which we convert to ϕ_{\parallel} taking the smaller solution.

³ AAIJ 12P quotes $\cos\phi_{\parallel} = -0.844 \pm 0.068 \pm 0.029$ which we convert to ϕ_{\parallel} , taking the smaller solution.

ϕ_{\perp} in $B_s^0 \rightarrow \phi\phi$

VALUE (rad)	DOCUMENT ID	TECN	COMMENT
2.75 ± 0.10 OUR AVERAGE			
$2.769 \pm 0.105 \pm 0.011$	AAIJ	23AT LHCb	pp at 13 TeV
$2.67 \pm 0.23 \pm 0.07$	AAIJ	14AE LHCb	pp at 7, 8 TeV
• • • We do not use the following data for averages, fits, limits, etc. • • •			
$2.818 \pm 0.178 \pm 0.073$	AAIJ	19AP LHCb	pp at 7, 8, partial 13 TeV

Γ_{\perp}/Γ in $B_s^0 \rightarrow K^{*0}\bar{K}^{*0}$

VALUE	DOCUMENT ID	TECN	COMMENT
$0.240 \pm 0.031 \pm 0.025$	¹ AAIJ	19L LHCb	pp at 7 and 8 TeV
• • • We do not use the following data for averages, fits, limits, etc. • • •			
$0.208 \pm 0.032 \pm 0.046$	² AAIJ	18S LHCb	Repl. by AAIJ 19L
$0.201 \pm 0.057 \pm 0.040$	³ AAIJ	15AF LHCb	Repl. by AAIJ 18S
$0.31 \pm 0.12 \pm 0.04$	AAIJ	12F LHCb	Repl. by AAIJ 15AF

¹ Untagged and time-integrated analysis within 150 MeV of the K^{*0} mass.

² Measured in angular analysis, which takes into account S-, P- and D-wave contributions.

³ Measured in angular analysis, which takes into account S-wave contributions.

Γ_{\perp}/Γ in $B_s^0 \rightarrow K^{*0}\bar{K}^{*0}$

VALUE	DOCUMENT ID	TECN	COMMENT
$0.38 \pm 0.11 \pm 0.04$	AAIJ	12F LHCb	pp at 7 TeV

$\Gamma_{\parallel}/\Gamma$ in $B_s^0 \rightarrow K^*(892)^0\bar{K}^*(892)^0$

VALUE	DOCUMENT ID	TECN	COMMENT
$0.297 \pm 0.029 \pm 0.042$	¹ AAIJ	18S LHCb	pp at 7, 8 TeV
• • • We do not use the following data for averages, fits, limits, etc. • • •			
$0.215 \pm 0.046 \pm 0.015$	AAIJ	15AF LHCb	Repl. by AAIJ 18S

¹ Measured in angular analysis, which takes into account S-, P- and D-wave contributions.

ϕ_{\parallel} in $B_s^0 \rightarrow K^*(892)^0\bar{K}^*(892)^0$

VALUE	DOCUMENT ID	TECN	COMMENT
$2.40 \pm 0.11 \pm 0.33$	¹ AAIJ	18S LHCb	pp at 7, 8 TeV
• • • We do not use the following data for averages, fits, limits, etc. • • •			
$5.31 \pm 0.24 \pm 0.14$	AAIJ	15AF LHCb	Repl. by AAIJ 18S

¹ Measured in angular analysis, which takes into account S-, P- and D-wave contributions.

ϕ_{\perp} in $B_s^0 \rightarrow K^*(892)^0\bar{K}^*(892)^0$

VALUE (rad)	DOCUMENT ID	TECN	COMMENT
$2.62 \pm 0.26 \pm 0.64$	¹ AAIJ	18S LHCb	pp at 7, 8 TeV

¹ Measured in angular analysis, which takes into account S-, P- and D-wave contributions.

Γ_{\perp}/Γ in $B_s^0 \rightarrow \phi\bar{K}^{*0}$

VALUE	DOCUMENT ID	TECN	COMMENT
$0.51 \pm 0.15 \pm 0.07$	AAIJ	13BW LHCb	pp at 7 TeV

$\Gamma_{\parallel}/\Gamma$ in $B_s^0 \rightarrow \phi\bar{K}^{*0}$

VALUE	DOCUMENT ID	TECN	COMMENT
$0.21 \pm 0.11 \pm 0.02$	AAIJ	13BW LHCb	pp at 7 TeV

Meson Particle Listings

B_s^0

ϕ_{\parallel} in $B_s^0 \rightarrow \phi \bar{K}^{*0}$

VALUE (rad)	DOCUMENT ID	TECN	COMMENT
$1.75 \pm 0.53 \pm 0.29$	¹ AAIJ	13BW	LHCB pp at 7 TeV

¹ Measures $\cos(\phi_{\parallel}) = -0.18 \pm 0.52 \pm 0.29$, which we convert to ϕ_{\parallel} by taking the smaller solution.

Γ_L/Γ in $B_s^0 \rightarrow \bar{D}^{*0} \phi$

VALUE	DOCUMENT ID	TECN	COMMENT
$0.531 \pm 0.060 \pm 0.019$	AAIJ	23AZ	LHCB pp at 7, 8, 13 TeV
$0.73 \pm 0.15 \pm 0.04$	AAIJ	18AY	LHCB Repl. by AAIJ 23AZ

• • • We do not use the following data for averages, fits, limits, etc. • • •

Γ_L/Γ in $B_s^0 \rightarrow K^*(892)^0 \bar{K}_2^*(1430)^0$

VALUE	DOCUMENT ID	TECN	COMMENT
$0.911 \pm 0.020 \pm 0.165$	¹ AAIJ	18s	LHCB pp at 7, 8 TeV

¹ Measured in angular analysis, which takes into account S -, P - and D -wave. contributions.

$\Gamma_{\parallel}/\Gamma$ in $B_s^0 \rightarrow K^*(892)^0 \bar{K}_2^*(1430)^0$

VALUE	DOCUMENT ID	TECN	COMMENT
$0.012 \pm 0.008 \pm 0.053$	¹ AAIJ	18s	LHCB pp at 7, 8 TeV

¹ Measured in angular analysis, which takes into account S -, P - and D -wave. contributions.

Γ_L/Γ in $B_s^0 \rightarrow K_2^*(1430)^0 \bar{K}^*(892)^0$

VALUE	DOCUMENT ID	TECN	COMMENT
$0.62 \pm 0.16 \pm 0.25$	¹ AAIJ	18s	LHCB pp at 7, 8 TeV

¹ Measured in angular analysis, which takes into account S -, P - and D -wave. contributions.

$\Gamma_{\parallel}/\Gamma$ in $B_s^0 \rightarrow K_2^*(1430)^0 \bar{K}^*(892)^0$

VALUE	DOCUMENT ID	TECN	COMMENT
$0.24 \pm 0.10 \pm 0.14$	¹ AAIJ	18s	LHCB pp at 7, 8 TeV

¹ Measured in angular analysis, which takes into account S -, P - and D -wave. contributions.

Γ_L/Γ in $B_s^0 \rightarrow K_2^*(1430)^0 \bar{K}_2^*(1430)^0$

VALUE	DOCUMENT ID	TECN	COMMENT
$0.25 \pm 0.14 \pm 0.18$	¹ AAIJ	18s	LHCB pp at 7, 8 TeV

¹ Measured in angular analysis, which takes into account S -, P - and D -wave. contributions.

$\Gamma_{\parallel 1}/\Gamma$ in $B_s^0 \rightarrow K_2^*(1430)^0 \bar{K}_2^*(1430)^0$

VALUE	DOCUMENT ID	TECN	COMMENT
$0.17 \pm 0.11 \pm 0.14$	¹ AAIJ	18s	LHCB pp at 7, 8 TeV

¹ Measured in angular analysis, which takes into account S -, P - and D -wave. contributions.

$\Gamma_{\perp 1}/\Gamma$ in $B_s^0 \rightarrow K_2^*(1430)^0 \bar{K}_2^*(1430)^0$

VALUE	DOCUMENT ID	TECN	COMMENT
$0.30 \pm 0.18 \pm 0.21$	¹ AAIJ	18s	LHCB pp at 7, 8 TeV

¹ Measured in angular analysis, which takes into account S -, P - and D -wave. contributions.

$\Gamma_{\parallel 2}/\Gamma$ in $B_s^0 \rightarrow K_2^*(1430)^0 \bar{K}_2^*(1430)^0$

VALUE	DOCUMENT ID	TECN	COMMENT
$0.015 \pm 0.033 \pm 0.107$	¹ AAIJ	18s	LHCB pp at 7, 8 TeV

¹ Measured in angular analysis, which takes into account S -, P - and D -wave. contributions.

$F_L(B_s^0 \rightarrow \phi \mu^+ \mu^-)$ ($0.10 < q^2 < 2.00 \text{ GeV}^2/c^4$)

VALUE	DOCUMENT ID	TECN	COMMENT
$0.20 \pm 0.08 \pm 0.02$	AAIJ	15AQ	LHCB pp at 7, 8 TeV
$0.37 \pm 0.19 \pm 0.07$	AAIJ	13x	LHCB Repl. by AAIJ 15AQ

• • • We do not use the following data for averages, fits, limits, etc. • • •

$F_L(B_s^0 \rightarrow \phi \mu^+ \mu^-)$ ($2.00 < q^2 < 5.0 \text{ GeV}^2/c^4$)

VALUE	DOCUMENT ID	TECN	COMMENT
$0.68 \pm 0.16 \pm 0.03$	AAIJ	15AQ	LHCB pp at 7, 8 TeV
$0.53 \pm 0.25 \pm 0.10$	¹ AAIJ	13x	LHCB Repl. by AAIJ 15AQ

¹ Measured in $2.0 < q^2 < 4.3 \text{ GeV}^2/c^4$.

$F_L(B_s^0 \rightarrow \phi \mu^+ \mu^-)$ ($5.0 < q^2 < 8.0 \text{ GeV}^2/c^4$)

VALUE	DOCUMENT ID	TECN	COMMENT
$0.54 \pm 0.10 \pm 0.02$	AAIJ	15AQ	LHCB pp at 7, 8 TeV
$0.81 \pm 0.11 \pm 0.05$	¹ AAIJ	13x	LHCB Repl. by AAIJ 15AQ

¹ Measured in $4.3 < q^2 < 8.68 \text{ GeV}^2/c^4$.

$F_L(B_s^0 \rightarrow \phi \mu^+ \mu^-)$ ($11.0 < q^2 < 12.5 \text{ GeV}^2/c^4$)

VALUE	DOCUMENT ID	TECN	COMMENT
$0.29 \pm 0.11 \pm 0.04$	AAIJ	15AQ	LHCB pp at 7, 8 TeV
$0.33 \pm 0.14 \pm 0.06$	¹ AAIJ	13x	LHCB Repl. by AAIJ 15AQ

¹ Measured in $10.09 < q^2 < 12.90 \text{ GeV}^2/c^4$.

$F_L(B_s^0 \rightarrow \phi \mu^+ \mu^-)$ ($15.0 < q^2 < 17.0 \text{ GeV}^2/c^4$)

VALUE	DOCUMENT ID	TECN	COMMENT
$0.23 \pm 0.09 \pm 0.02$	AAIJ	15AQ	LHCB pp at 7, 8 TeV
$0.34 \pm 0.18 \pm 0.07$	¹ AAIJ	13x	LHCB Repl. by AAIJ 15AQ

• • • We do not use the following data for averages, fits, limits, etc. • • •

¹ Measured in $14.18 < q^2 < 16 \text{ GeV}^2/c^4$.

$F_L(B_s^0 \rightarrow \phi \mu^+ \mu^-)$ ($17.0 < q^2 < 19.0 \text{ GeV}^2/c^4$)

VALUE	DOCUMENT ID	TECN	COMMENT
$0.40 \pm 0.13 \pm 0.02$	AAIJ	15AQ	LHCB pp at 7, 8 TeV
$0.16 \pm 0.17 \pm 0.10$	¹ AAIJ	13x	LHCB Repl. by AAIJ 15AQ

• • • We do not use the following data for averages, fits, limits, etc. • • •

¹ Measured in $16.0 < q^2 < 19.0 \text{ GeV}^2/c^4$.

$F_L(B_s^0 \rightarrow \phi \mu^+ \mu^-)$ ($15.0 < q^2 < 18.9 \text{ GeV}^2/c^4$)

VALUE	DOCUMENT ID	TECN	COMMENT
$0.359 \pm 0.031 \pm 0.019$	AAIJ	21AK	LHCB pp at 7, 8, 13 TeV

$F_L(B_s^0 \rightarrow \phi \mu^+ \mu^-)$ ($1.00 < q^2 < 6.00 \text{ GeV}^2/c^4$)

VALUE	DOCUMENT ID	TECN	COMMENT
$0.715 \pm 0.036 \pm 0.013$	AAIJ	21AK	LHCB pp at 7, 8, 13 TeV
$0.63 \pm 0.09 \pm 0.03$	AAIJ	15AQ	LHCB Repl. by AAIJ 21AK
$0.56 \pm 0.17 \pm 0.16$	AAIJ	13x	LHCB Repl. by AAIJ 15AQ

• • • We do not use the following data for averages, fits, limits, etc. • • •

$B_s^0\text{-}\bar{B}_s^0$ MIXING

For a discussion of $B_s^0\text{-}\bar{B}_s^0$ mixing see the note on “ $B^0\text{-}\bar{B}^0$ Mixing” in the B^0 Particle Listings above.

x_S is a measure of the time-integrated $B_s^0\text{-}\bar{B}_s^0$ mixing probability that produced $B_s^0(\bar{B}_s^0)$ decays as a $\bar{B}_s^0(B_s^0)$. Mixing violates $\Delta B \neq 2$ rule.

$$x_S = \frac{x_S^2}{2(1+x_S^2)}$$

$$x_S = \frac{\Delta m_{B_s^0}}{\Gamma_{B_s^0}} = (m_{B_{sH}^0} - m_{B_{sL}^0}) \tau_{B_s^0}$$

where H, L stand for heavy and light states of two B_s^0 CP eigenstates and

$$\tau_{B_s^0} = \frac{1}{0.5(\Gamma_{B_{sH}^0} + \Gamma_{B_{sL}^0})}$$

$$\Delta m_{B_s^0} = m_{B_{sH}^0} - m_{B_{sL}^0}$$

$\Delta m_{B_s^0}$ is a measure of 2π times the $B_s^0\text{-}\bar{B}_s^0$ oscillation frequency in time-dependent mixing experiments.

VALUE (10^{12} h s^{-1})	CL%	DOCUMENT ID	TECN	COMMENT
17.765 ± 0.006	OUR EVALUATION			(Produced by HFLAV)
17.765 ± 0.005	OUR AVERAGE			
17.743 ± 0.033 ± 0.009		¹ AAIJ	24A	LHCB pp at 13 TeV
17.7683 ± 0.0051 ± 0.0032		² AAIJ	22B	LHCB pp at 13 TeV
17.757 ± 0.007 ± 0.008		³ AAIJ	21M	LHCB pp at 7, 8, 13 TeV
17.51 ± 0.10 ± 0.09		⁴ SIRUNYAN	21E	CMS pp at 13 TeV
17.768 ± 0.023 ± 0.006		² AAIJ	13BI	LHCB pp at 7 TeV
17.93 ± 0.22 ± 0.15		⁵ AAIJ	13CF	LHCB pp at 7 TeV
17.77 ± 0.10 ± 0.07		⁶ ABULENCIA,A	06G	CDF $p\bar{p}$ at 1.96 TeV
• • • We do not use the following data for averages, fits, limits, etc. • • •				
17.703 ± 0.059 ± 0.018		¹ AAIJ	19Q	LHCB Repl. by AAIJ 24A
17.711 ± 0.055 ± 0.057		¹ AAIJ	15I	LHCB Repl. by AAIJ 19Q
17.63 ± 0.11 ± 0.02		⁷ AAIJ	12I	LHCB Repl. by AAIJ 21M
17-21		⁸ ABAZOV	06B	D0 $p\bar{p}$ at 1.96 TeV
17.31 ± 0.33 ± 0.18		⁹ ABULENCIA	06Q	CDF Repl. by ABULENCIA,A 06G
> 8.0	95	10 ABDALLAH	04J	DLPH $e^+e^- \rightarrow Z^0$
> 4.9	95	11 ABDALLAH	04J	DLPH $e^+e^- \rightarrow Z^0$
> 8.5	95	12 ABDALLAH	04J	DLPH $e^+e^- \rightarrow Z^0$
> 5.0	95	13 ABDALLAH	03B	DLPH $e^+e^- \rightarrow Z$
>10.3	95	14 ABE	03	SLD $e^+e^- \rightarrow Z$
>10.9	95	15 HEISTER	03E	ALEP $e^+e^- \rightarrow Z$
> 5.3	95	16 ABE	02V	SLD $e^+e^- \rightarrow Z$
> 1.0	95	17 ABBIENDI	01D	OPAL $e^+e^- \rightarrow Z$
> 7.4	95	18 ABREU	00Y	DLPH Repl. by ABDALLAH 04J
> 4.0	95	19 ABREU,P	00G	DLPH $e^+e^- \rightarrow Z$
> 5.2	95	20 ABBIENDI	99S	OPAL $e^+e^- \rightarrow Z$
<96	95	21 ABE	99D	CDF $p\bar{p}$ at 1.8 TeV
> 5.8	95	22 ABE	99J	CDF $p\bar{p}$ at 1.8 TeV

> 9.6	95	23	BARATE	99J	ALEP	$e^+e^- \rightarrow Z$
> 7.9	95	24	BARATE	98C	ALEP	Repl. by BARATE 99J
> 3.1	95	25	ACKERSTAFF	97U	OPAL	Repl. by ABBIENDI 99s
> 2.2	95	26	ACKERSTAFF	97V	OPAL	Repl. by ABBIENDI 99s
> 6.5	95	27	ADAM	97	DLPH	Repl. by ABREU 00Y
> 6.6	95	28	BUSKULIC	96M	ALEP	Repl. by BARATE 98c
> 2.2	95	26	AKERS	95J	OPAL	Sup. by ACKERSTAFF 97v
> 5.7	95	29	BUSKULIC	95J	ALEP	$e^+e^- \rightarrow Z$
> 1.8	95	26	BUSKULIC	94B	ALEP	$e^+e^- \rightarrow Z$

- 1 Measured using time-dependent angular analysis of $B_s^0 \rightarrow J/\psi K^+ K^-$ decays.
- 2 Measured using $B_s^0 \rightarrow D_s^- \pi^+$ decays.
- 3 Measured using $B_s^0 \rightarrow D_s^- \pi^+ \pi^- \pi^+$ decays.
- 4 Measured using time-dependent angular analysis of $B_s^0 \rightarrow J/\psi \phi$ decays.
- 5 Measured using $B_s^0 \rightarrow D_s^- \mu^+ \nu_\mu X$ decays.
- 6 Significance of oscillation signal is 5.4σ . Also reports $|V_{td} / V_{ts}| = 0.2060 \pm 0.0007^{+0.0081}_{-0.0060}$.
- 7 Measured using $B_s^0 \rightarrow D_s^- \pi^+$ and $D_s^- \pi^+ \pi^- \pi^+$ decays.
- 8 A likelihood scan over the oscillation frequency, Δm_s , gives a most probable value of 19 ps^{-1} and a range of $17 < \Delta m_s < 21 (\text{ps}^{-1})$ at 90% C.L. assuming Gaussian uncertainties. Also excludes $\Delta m_s < 14.8 \text{ ps}^{-1}$ at 95% C.L.
- 9 Significance of oscillation signal is 0.2%. Also reported the value $|V_{td} / V_{ts}| = 0.208^{+0.001+0.008}_{-0.002-0.006}$.
- 10 Uses leptons emitted with large momentum transverse to a jet and improved techniques for vertexing and flavor-tagging.
- 11 Updates of D_s -lepton analysis.
- 12 Combined results from all Delphi analyses.
- 13 Events with a high transverse momentum lepton were removed and an inclusively reconstructed vertex was required.
- 14 ABE 03 uses the novel "charge dipole" technique to reconstruct separate secondary and tertiary vertices originating from the $B \rightarrow D$ decay chain. The analysis excludes $\Delta m_s < 4.9 \text{ ps}^{-1}$ and $7.9 < \Delta m_s < 10.3 \text{ ps}^{-1}$.
- 15 Three analyses based on complementary event selections: (1) fully-reconstructed hadronic decays; (2) semileptonic decays with D_s exclusively reconstructed; (3) inclusive semileptonic decays.
- 16 ABE 02v uses exclusively reconstructed D_s^- mesons and excludes $\Delta m_s < 1.4 \text{ ps}^{-1}$ and $2.4 < \Delta m_s < 5.3 \text{ ps}^{-1}$ at 95% C.L.
- 17 Uses fully or partially reconstructed $D_s \ell$ vertices and a mixing tag as a flavor tagging.
- 18 Replaced by ABDALLAH 04A. Uses $D_s^- \ell^+$, and $\phi \ell^+$ vertices, and a multi-variable discriminant as a flavor tagging.
- 19 Uses inclusive D_s vertices and fully reconstructed B_s decays and a multi-variable discriminant as a flavor tagging.
- 20 Uses ℓ - Q_{hem} and ℓ - ℓ .
- 21 ABE 99D assumes $\tau_{B_s^0} = 1.55 \pm 0.05 \text{ ps}$ and $\Delta\Gamma/\Delta m = (5.6 \pm 2.6) \times 10^{-3}$.
- 22 ABE 99i uses ϕ - ℓ correlation.
- 23 BARATE 99j uses combination of an inclusive lepton and D_s^- -based analyses.
- 24 BARATE 98c combines results from $D_s h\ell/Q_{\text{hem}}$, $D_s h\ell$ in the same side, $D_s \ell/Q_{\text{hem}}$ and $D_s \ell$ - K in the same side.
- 25 Uses ℓ - Q_{hem} .
- 26 Uses ℓ - ℓ .
- 27 ADAM 97 combines results from $D_s \ell$ - Q_{hem} , ℓ - Q_{hem} , and ℓ - ℓ .
- 28 BUSKULIC 96M uses D_s lepton correlations and lepton, kaon, and jet charge tags.
- 29 BUSKULIC 95j uses ℓ - Q_{hem} . They find $\Delta m_s > 5.6$ [> 6.1] for $f_s = 10\%$ [12%]. We interpolate to our central value $f_s = 10.5\%$.

$$x_s = \Delta m_{B_s^0} / \Gamma_{B_s^0}$$

Derived from the results on $\Delta m_{B_s^0}$ and "OUR EVALUATION" of the B_s^0 mean lifetime.

VALUE	DOCUMENT ID
26.99 ± 0.09 OUR EVALUATION	(Produced by HFLAV)

χ_s This is a $B_s^0 \bar{B}_s^0$ integrated mixing parameter derived from x_s above and OUR EVALUATION of $\Delta\Gamma_{B_s^0} / \Gamma_{B_s^0}$.

VALUE	DOCUMENT ID
0.499318 ± 0.000005 OUR EVALUATION	(Produced by HFLAV)

CP VIOLATION PARAMETERS in B_s^0

$$\text{Re}(\epsilon_{B_s^0}) / (1 + |\epsilon_{B_s^0}|^2)$$

CP impurity in B_s^0 system.

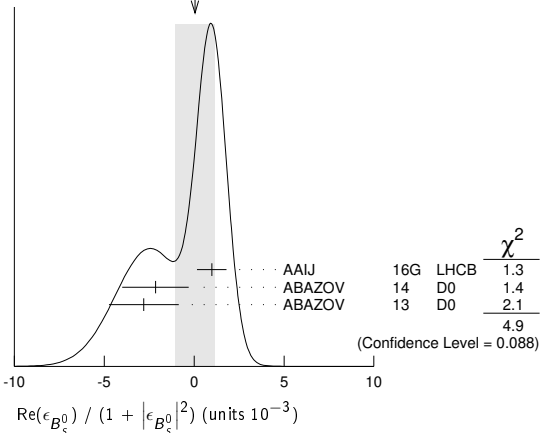
"OUR EVALUATION" is the result of a fit to B_d and B_s CP asymmetries, which includes the B_s measurements listed below and the B_d measurements listed in the B_d section, and takes into account correlations between those measurements.

VALUE (units 10^{-3})	DOCUMENT ID	TECN	COMMENT
-0.15 ± 0.70 OUR EVALUATION	(Produced by HFLAV)		
0.0 ± 1.1 OUR AVERAGE	Error includes scale factor of 1.6.		See the ideogram below.
0.98 ± 0.65 ± 0.5	1 AAIJ	16G LHCb	pp at 7, 8 TeV
-2.15 ± 1.85	2 ABAZOV	14 D0	$p\bar{p}$ at 1.96 TeV
-2.8 ± 1.9 ± 0.4	3 ABAZOV	13 D0	$p\bar{p}$ at 1.96 TeV

• • • We do not use the following data for averages, fits, limits, etc. • • •

- | | | | |
|---------------------|----------|----------|---------------------|
| -0.15 ± 1.25 ± 0.90 | 4 AAIJ | 14D LHCb | Repl. by AAIJ 16G |
| -4.5 ± 2.7 | 5 ABAZOV | 11U D0 | Repl. by ABAZOV 14 |
| -0.4 ± 2.3 ± 0.4 | 6 ABAZOV | 10E D0 | Repl. by ABAZOV 13 |
| -3.6 ± 1.9 | 7 ABAZOV | 10H D0 | Repl. by ABAZOV 11U |
| 6.1 ± 4.8 ± 0.9 | 8 ABAZOV | 07A D0 | Repl. by ABAZOV 10E |
- 1 AAIJ 16G reports a measurement of time-integrated flavor-specific asymmetry in $B_s^0 \rightarrow \mu^+ D_s^- X$ decays, $A_{SL}^s = (0.39 \pm 0.26 \pm 0.20)\%$, which is approximately equal to $4 \times \text{Re}(\epsilon_{B_s^0}) / (1 + |\epsilon_{B_s^0}|^2)$.
 - 2 ABAZOV 14 uses the dimuon charge asymmetry with different impact parameters from which it reports $A_{SL}^s = (-0.86 \pm 0.74) \times 10^{-2}$.
 - 3 ABAZOV 13 reports a measurement of time-integrated flavor-specific asymmetry in mixed semileptonic $B_s^0 \rightarrow \mu^+ D_s^- X$ decays $A_{SL}^s = (-1.12 \pm 0.74 \pm 0.17)\%$ which is approximately equal to $4 \times \text{Re}(\epsilon_{B_s^0}) / (1 + |\epsilon_{B_s^0}|^2)$.
 - 4 AAIJ 14D reports a measurement of time-integrated flavor-specific asymmetry in $B_s^0 \rightarrow \mu^+ D_s^- X$ decays, $A_{SL}^s = (-0.06 \pm 0.50 \pm 0.36)\%$, which is approximately equal to $4 \times \text{Re}(\epsilon_{B_s^0}) / (1 + |\epsilon_{B_s^0}|^2)$.
 - 5 ABAZOV 11U uses the dimuon charge asymmetry with different impact parameters from which it reports $A_{SL}^s = (-18.1 \pm 10.6) \times 10^{-3}$.
 - 6 ABAZOV 10E reports a measurement of flavor-specific asymmetry in $B_s^0 \rightarrow \mu^+ D_s^{*-} X$ decays with a decay-time analysis including initial-state flavor tagging, $A_{SL}^s = (-1.7 \pm 9.1^{+1.4}_{-1.5}) \times 10^{-3}$ which is approximately equal to $4 \times \text{Re}(\epsilon_{B_s^0}) / (1 + |\epsilon_{B_s^0}|^2)$.
 - 7 ABAZOV 10H reports a measurement of like-sign dimuon charge asymmetry of $A_{SL}^s = (-9.57 \pm 2.51 \pm 1.46) \times 10^{-3}$ in semileptonic b -hadron decays. Using the measured production ratio of B_d^0 and B_s^0 , and the asymmetry of B_d^0 , $A_{SL}^s = (-4.7 \pm 4.6) \times 10^{-3}$ measured from B -factories, they obtain the asymmetry for B_s^0 .
 - 8 The first direct measurement of the time integrated flavor untagged charge asymmetry in semileptonic B_s^0 decays is reported as $2 \times A_{SL}^s(\text{untagged}) = A_{SL}^s = (2.45 \pm 1.93 \pm 0.35) \times 10^{-2}$.

WEIGHTED AVERAGE
0.0 ± 1.1 (Error scaled by 1.6)



$C_{KK}(B_s^0 \rightarrow K^+ K^-)$

VALUE	DOCUMENT ID	TECN	COMMENT
0.162 ± 0.035 OUR AVERAGE			
0.164 ± 0.034 ± 0.014	AAIJ	21o LHCb	pp at 13 TeV
0.14 ± 0.11 ± 0.03	AAIJ	13Bo LHCb	pp at 7 TeV

$S_{KK}(B_s^0 \rightarrow K^+ K^-)$

VALUE	DOCUMENT ID	TECN	COMMENT
0.14 ± 0.05 OUR AVERAGE	Error includes scale factor of 1.3.		
0.123 ± 0.034 ± 0.015	AAIJ	21o LHCb	pp at 13 TeV
0.30 ± 0.12 ± 0.04	AAIJ	13Bo LHCb	pp at 7 TeV

$r_B(B_s^0 \rightarrow D_s^\mp K^\pm)$

r_B and δ_B are the amplitude ratio and relative strong phase between the amplitudes of $A(B_s^0 \rightarrow D_s^+ K^-)$ and $A(B_s^0 \rightarrow D_s^- K^+)$,

VALUE	DOCUMENT ID	TECN	COMMENT
0.37 ± 0.10	1 AAIJ	18U LHCb	pp at 7, 8 TeV
-0.09			

• • • We do not use the following data for averages, fits, limits, etc. • • •

- | | | | |
|-------------|--------|-----------|-------------------|
| 0.53 ± 0.17 | 2 AAIJ | 14BF LHCb | Repl. by AAIJ 18U |
| -0.16 | | | |
- 1 Measured in $B_s^0 \rightarrow D_s^\mp K^\pm$ decays, constraining $-2\beta_s$ by the measurement of $\phi_s = -0.030 \pm 0.033$ from HFLAV.
 - 2 Measured in $B_s^0 \rightarrow D_s^\mp K^\pm$ decays, constraining $-2\beta_s$ by the measurement of $\phi_s = 0.01 \pm 0.07 \pm 0.0$ from AAIJ 13AR. At 68% C.L.

Meson Particle Listings

 B_S^0 $r_B(B_S^0 \rightarrow D_s^\mp K^\pm \pi^\pm \pi^\mp)$

VALUE	DOCUMENT ID	TECN	COMMENT
$0.47 \pm 0.08 \pm 0.02$ -0.03	1,2 AAIJ	21M LHCb	pp at 7, 8, 13 TeV

¹ Measured in restricted phase space with $m(K^+\pi^+\pi^-) < 1950$ MeV, $m(K^+\pi^-) < 1200$ MeV and $m(\pi^+\pi^-) < 1200$ MeV.

² A model-independent coherence factor for the decay $B_S \rightarrow D_s K \pi \pi$ (in the restricted phase space region) is also reported.

 $\delta_B(B_S^0 \rightarrow D_s^\pm K^\mp)$

VALUE (°)	DOCUMENT ID	TECN	COMMENT
358_{-14}^{+13}	1 AAIJ	18U LHCb	pp at 7, 8 TeV

• • • We do not use the following data for averages, fits, limits, etc. • • •

3_{-20}^{+19} ² AAIJ 14Bf LHCb Repl. by AAIJ 18U

¹ Measured in $B_S^0 \rightarrow D_s^\mp K^\pm$ decays, constraining $-2\beta_S$ by the measurement of $\phi_S = 0.030 \pm 0.033$ from HFLAV. The value is modulo 180° .

² Measured in $B_S^0 \rightarrow D_s^\mp K^\pm$ decays, constraining $-2\beta_S$ by the measurement of $\phi_S = 0.01 \pm 0.07 \pm 0.0$ from AAIJ 13AR. The value is modulo 180° at 68% CL.

 $\delta_B(B_S^0 \rightarrow D_s^\pm K^\mp \pi^\pm \pi^\mp)$

VALUE (°)	DOCUMENT ID	TECN	COMMENT
-6_{-12-4}^{+10+2}	1,2 AAIJ	21M LHCb	pp at 7, 8, 13 TeV

¹ Measured in restricted phase space with $m(K^+\pi^+\pi^-) < 1950$ MeV, $m(K^+\pi^-) < 1200$ MeV and $m(\pi^+\pi^-) < 1200$ MeV. The value is modulo 180° .

² A model-independent coherence factor for the decay $B_S \rightarrow D_s K \pi \pi$ (in the restricted phase space region) is also reported.

CP Violation phase $\beta_s (b \rightarrow c\bar{c}s)$

$-2\beta_s$ is the weak phase difference between B_S^0 mixing amplitude and the $B_S^0 \rightarrow J/\psi\phi$ decay amplitude driven by the $b \rightarrow c\bar{c}s$ transition (such as $B_S \rightarrow J/\psi\phi$, $J/\psi K^+ K^-$,

$J/\psi\pi^+\pi^-$, and $D_s^+ D_s^-$). The Standard Model value of β_s is $\arg(-\frac{V_{ts}V_{tb}^*}{V_{cs}V_{cb}^*})$ if penguin contributions are neglected.

VALUE (10^{-2} rad)	DOCUMENT ID	TECN	COMMENT
2.0 ± 0.8 OUR EVALUATION	(Produced by HFLAV)		
1.8 ± 0.8 OUR AVERAGE			

$1.9 \pm 1.1 \pm 0.3$	1 AAIJ	24A LHCb	pp at 13 TeV
$4.05 \pm 2.05 \pm 1.10$	2,3 AAD	21AE ATLS	pp at 13 TeV
$0 \pm 14 \pm 4$	4 AAIJ	21AN LHCb	pp at 7, 8 TeV
$0.5 \pm 2.5 \pm 0.5$	5,6 SIRUNYAN	21E CMS	pp at 13 TeV
$2.85 \pm 3.00 \pm 0.55$	7,8 AAIJ	19AF LHCb	pp at 13 TeV
$-5.95 \pm 5.35 \pm 1.70$	9 AAIJ	17V LHCb	pp at 7, 8 TeV
$5.05 \pm 4.05 \pm 2.10$	10,11 AAD	16AP ATLS	pp at 8 TeV
$-11.5_{-14.5}^{+14} \pm 1$	12 AAIJ	16AK LHCb	pp at 7, 8 TeV
$3.75 \pm 4.85 \pm 1.55$	13 KHACHATRYAN	16s CMS	pp at 8 TeV
$2.9 \pm 2.5 \pm 0.3$	14 AAIJ	15I LHCb	pp at 7, 8 TeV
$-6 \pm 13 \pm 3$	15 AAD	14U ATLS	pp at 7 TeV
$-1 \pm 9 \pm 1$	16 AAIJ	14AY LHCb	pp at 7, 8 TeV
$-3.5 \pm 3.4 \pm 0.4$	17 AAIJ	14S LHCb	pp at 7, 8 TeV
	18 AALTONEN	12AJ CDF	$p\bar{p}$ at 1.96 TeV
28_{-19}^{+18}	19 ABAZOV	12D D0	$p\bar{p}$ at 1.96 TeV

• • • We do not use the following data for averages, fits, limits, etc. • • •

$4.15 \pm 2.05 \pm 0.30$	20 AAIJ	19Q LHCb	Repl. by AAIJ 24A
$5.0 \pm 6.5 \pm 7.0$	21 AAIJ	18S LHCb	pp at 7, 8 TeV
6_{-7}^{+8}	22,23 AAIJ	15K LHCb	pp at 7, 8 TeV
$-0.5 \pm 3.5 \pm 0.5$	24 AAIJ	13AR LHCb	Repl. by AAIJ 15I
$-11.0 \pm 20.5 \pm 5.0$	25 AAD	12CV ATLS	Repl. by AAD 14U
$22 \pm 22 \pm 1$	26 AAIJ	12B LHCb	Repl. by AAIJ 12Q
$-8 \pm 9 \pm 3$	27 AAIJ	12D LHCb	Repl. by AAIJ 13AR
$0.95_{-8.65}^{+8.70} \pm 0.15$ -0.20	28 AAIJ	12Q LHCb	Repl. by AAIJ 13AR
	29 AALTONEN	12D CDF	Repl. by AALTONEN 12AJ
	30 AALTONEN	08G CDF	Repl. by AALTONEN 12D
$28_{-15}^{+12} \pm 4$ -1	19,31 ABAZOV	08AMD0	Repl. by ABAZOV 12D
$39.5 \pm 28.0 \pm 0.5$ -7.0	32,33 ABAZOV	07 D0	Repl. by ABAZOV 07N
35_{-24}^{+20}	33,34 ABAZOV	07N D0	Repl. by ABAZOV 08AM

¹ AAIJ 19Q reports $\phi_S = -2\beta_S = -0.039 \pm 0.022 \pm 0.006$ rad. measured using a time-dependent angular analysis of $B_S^0 \rightarrow J/\psi K^+ K^-$ decays.

² Reports a combination of $0.0435 \pm 0.0180 \pm 0.0105$ with AAD 16AP.

³ AAD 21AE measured $\phi_S = -2\beta_S = -0.087 \pm 0.036 \pm 0.021$ rad. using a time-dependent angular analysis of $B_S^0 \rightarrow J/\psi\phi$ decays.

⁴ AAIJ 21AN measured $\phi_S = -2\beta_S = 0.00 \pm 0.28 \pm 0.07$ rad, using a time-dependent angular analysis of $B_S^0 \rightarrow J/\psi\phi$ decays with $J/\psi \rightarrow e^+e^-$.

⁵ Reports a combination of $0.0105 \pm 0.0220 \pm 0.0050$ with KHACHATRYAN 16s.

⁶ SIRUNYAN 21E measured $\phi_S = -2\beta_S = -0.021 \pm 0.044 \pm 0.010$ rad. using a time-dependent angular analysis of $B_S^0 \rightarrow J/\psi\phi$ decays.

⁷ Reports a combination of $-0.001 \pm 0.022 \pm 0.006$ with AAIJ 14S.

⁸ AAIJ 19AF reports $\phi_S = -2\beta_S = 0.002 \pm 0.044 \pm 0.012$ rad. and $|\lambda| = 0.949 \pm 0.036 \pm 0.019$, when direct CP violation is allowed. Measured using a time-dependent fit to $B_S^0 \rightarrow J/\psi\pi^+\pi^-$ decays.

⁹ Measured $\phi_S = -2\beta_S = 0.119 \pm 0.107 \pm 0.034$ rad using time-dependent angular analysis of $B_S^0 \rightarrow J/\psi K^+ K^-$ in the region $m(KK) > 1.05$ GeV.

¹⁰ Reports a combination of $0.0435 \pm 0.0180 \pm 0.0105$ with AAD 14U.

¹¹ AAD 16AP reports $\phi_S = -2\beta_S = -0.090 \pm 0.078 \pm 0.041$ rad. that was measured using a time-dependent angular analysis of $B_S^0 \rightarrow J/\psi\phi$ decays.

¹² AAIJ 16AK reports $\phi_S = -2\beta_S = 0.23_{-0.28}^{+0.29} \pm 0.02$ rad. that was measured using a time-dependent angular analysis of $B_S^0 \rightarrow \psi(2S)\phi$ decays.

¹³ KHACHATRYAN 16s reports $\phi_S = -2\beta_S = -0.075 \pm 0.097 \pm 0.031$ rad. that was measured using a time-dependent angular analysis of $B_S^0 \rightarrow J/\psi\phi$ decays.

¹⁴ AAIJ 15I reports $\phi_S = -2\beta_S = -0.058 \pm 0.049 \pm 0.006$ rad. that was measured using a time-dependent angular analysis of $B_S^0 \rightarrow J/\psi K^+ K^-$ decays. It also combines this result with that of AAIJ 14S and quotes $\phi_S = -2\beta_S = -0.010 \pm 0.039$ rad.

¹⁵ AAD 14U reports $\phi_S = -2\beta_S = 0.12 \pm 0.25 \pm 0.05$ rad. that was measured using a time-dependent angular analysis of $B_S^0 \rightarrow J/\psi\phi$ decays.

¹⁶ AAIJ 14AY reports $\phi_S = -2\beta_S = 0.02 \pm 0.17 \pm 0.02$ rad. in a time-dependent fit to $B_S^0 \rightarrow D_s^+ D_s^-$, while allowing CP violation in decay.

¹⁷ AAIJ 14S reports $\phi_S = -2\beta_S = 0.070 \pm 0.068 \pm 0.008$ rad. and $|\lambda| = 0.89 \pm 0.05 \pm 0.01$, when direct CP violation is allowed. Measured using a time-dependent fit to $B_S^0 \rightarrow J/\psi\pi^+\pi^-$ decays.

¹⁸ AALTONEN 12AJ reports $-\pi/2 < \beta_S < -1.51$ or $-0.06 < \beta_S < 0.30$, or $1.26 < \beta_S < \pi/2$ rad. at 68% CL. Measured using the time-dependent angular analysis of $B_S^0 \rightarrow J/\psi\phi$ decays.

¹⁹ ABAZOV 12D reports $\phi_S = -2\beta_S = -0.55_{-0.36}^{+0.38}$ rad. that was measured using a time-dependent angular analysis of $B_S^0 \rightarrow J/\psi\phi$ decays. A single error includes both statistical and systematic uncertainties.

²⁰ AAIJ 19Q reports $\phi_S = -2\beta_S = -0.083 \pm 0.041 \pm 0.006$ rad. that was measured using a time-dependent angular analysis of $B_S^0 \rightarrow J/\psi K^+ K^-$ decays.

²¹ AAIJ 18S reports $\phi_S = -2\beta_S = -0.10 \pm 0.13 \pm 0.14$ rad measured in $B_S^0 \rightarrow (K^+\pi^-)(K^-\pi^+)$ in the region $0.75 < m(K^\pm\pi^\mp) < 1.6$ GeV. This is a $b \rightarrow d\bar{d}s$ transition with a decay amplitude phase different from that of $b \rightarrow c\bar{c}s$ transition.

²² AAIJ 15K reports $-2\beta_S = -0.12_{-0.16}^{+0.14}$ rad. The value was obtained by measuring time-dependent CP asymmetry in $B_S^0 \rightarrow K^+ K^-$ and using a U-spin relation between $B_S^0 \rightarrow K^+ K^-$ and $B^0 \rightarrow \pi^+ \pi^-$.

²³ Results are also presented using additional inputs on $B^0 \rightarrow \pi^0\pi^0$ and $B^+ \rightarrow \pi^+\pi^0$ decays from other experiments and isospin symmetry assumptions. The dependence of the results on the maximum allowed amount of U-spin breaking up to 50% is also included.

²⁴ AAIJ 13AR reports $\phi_S = -2\beta_S = 0.01 \pm 0.07 \pm 0.01$ rad. obtained from combined fit to $B_S^0 \rightarrow J/\psi K^+ K^-$ and $B_S^0 \rightarrow J/\psi\pi^+\pi^-$ data sets. Also reports separate results of $\phi_S = 0.07 \pm 0.09 \pm 0.01$ rad. from $B_S^0 \rightarrow J/\psi K^+ K^-$ decays and $\phi_S = -0.14_{-0.16}^{+0.17} \pm 0.01$ rad. from $B_S^0 \rightarrow J/\psi\pi^+\pi^-$ decays.

²⁵ AAD 12CV reports $\phi_S = -2\beta_S = 0.22 \pm 0.41 \pm 0.10$ rad. that was measured using a time-dependent angular analysis of $B_S^0 \rightarrow J/\psi\phi$ decays.

²⁶ Reports $\phi_S = -2\beta_S = -0.44 \pm 0.44 \pm 0.02$ rad. that was measured using a time-dependent fit to $B_S^0 \rightarrow J/\psi\eta(980)$ decays.

²⁷ Reports $\phi_S = -2\beta_S = 0.15 \pm 0.18 \pm 0.06$ rad. that was measured using a time-dependent angular analysis of $B_S^0 \rightarrow J/\psi\phi$ decays.

²⁸ Reports $\phi_S = -2\beta_S = -0.019_{-0.174-0.003}^{+0.173+0.004}$ rad. which was measured using a time-dependent fit to $B_S^0 \rightarrow J/\psi\pi^+\pi^-$ decays, with the $\pi^+\pi^-$ mass within 775–1550 MeV. Searches for, but finds no evidence, for direct CP violation in $B_S^0 \rightarrow J/\psi\pi\pi$ decays.

²⁹ Reports $0.02 < \phi_S < 0.52$ or $1.08 < \phi_S < 1.55$ rad. at 68% C.L. confidence regions in the two-dimensional space of ϕ_S and $\Delta\Gamma_{B_S^0}$ from $B_S^0 \rightarrow J/\psi\phi$ decays.

³⁰ Reports $0.32 < 2\beta_S < 2.82$ rad. at 68% C.L. and confidence regions in the two-dimensional space of $2\beta_S$ and $\Delta\Gamma$ from the first measurement of $B_S^0 \rightarrow J/\psi\phi$ decays using flavor tagging. The probability of a deviation from SM prediction as large as the level of observed data is 15%.

³¹ Reports $\phi_S = -2\beta_S$ and obtains 90% CL interval $-0.03 < \beta_S < 0.60$ rad.

³² The first direct measurement of the CP-violating mixing phase is reported from the time-dependent analysis of flavor untagged $B_S^0 \rightarrow J/\psi\phi$ decays.

³³ Reports ϕ_S which equals to $-2\beta_S$.

³⁴ Combines D0 collaboration measurements of time-dependent angular distributions in $B_S^0 \rightarrow J/\psi\phi$ and charge asymmetry in semileptonic decays. There is a 4-fold ambiguity in the solution.

CP Violation phase $\beta_s (b \rightarrow s\bar{s}s)$

VALUE (10^{-2} rad)	DOCUMENT ID	TECN	COMMENT
3.7 ± 3.5	1,2 AAIJ	23AT LHCb	pp at 7, 8, 13 TeV

• • • We do not use the following data for averages, fits, limits, etc. • • •

$2.1 \pm 3.8 \pm 0.5$ ³ AAIJ 23AT LHCb pp at 13 TeV

$3.7 \pm 5.8 \pm 1.4$ ^{4,5} AAIJ 19AP LHCb Repl. by AAIJ 23AT

$0.5 \pm 7.5 \pm 1.5$ ⁶ AAIJ 14AE LHCb Repl. by AAIJ 19AP

8.8 ± 1.23 ⁷ AAIJ 13AY LHCb Repl. by AAIJ 14AE

¹ AAIJ 23AT reports $\phi_s^{S\bar{S}S} = -0.074 \pm 0.069$ rad and $|\lambda| = 1.009 \pm 0.030$. Measured using a time-dependent fit to $B_S^0 \rightarrow \phi\phi$ decays, assuming independence of the helicity of the $\phi\phi$ decay.

See key on page 1171

Meson Particle Listings

 B_s^0

- ² AAIJ 23AT also reports polarisation-dependent results assuming that the longitudinal weak phase is CP -conserving and that there is no direct CP violation.
- ³ Measured using a time-dependent fit to $B_s^0 \rightarrow \phi\phi$ decays, assuming independence of the helicity of the $\phi\phi$ decay.
- ⁴ AAIJ 19AP reports $\phi_s^{S\bar{S}} = -0.073 \pm 0.115 \pm 0.027$ rad and $|\lambda| = 0.99 \pm 0.05 \pm 0.01$. Measured using a time-dependent fit to $B_s^0 \rightarrow \phi\phi$ decays, assuming independence of the helicity of the $\phi\phi$ decay.
- ⁵ AAIJ 19AP reports also polarisation-dependent results assuming that the longitudinal weak phase is CP -conserving and that there is no direct CP violation, giving $\phi_s^{S\bar{S}} = 0.014 \pm 0.055 \pm 0.011$ rad and $\phi_s^{S\bar{S}} = 0.044 \pm 0.059 \pm 0.019$ rad.
- ⁶ AAIJ 14AE value measured in $B_s^0 \rightarrow \phi\phi$ decays. Also reports $\phi_s^{S\bar{S}} = -0.17 \pm 0.15 \pm 0.03$ rad.
- ⁷ AAIJ 13AY uses $B_s^0 \rightarrow \phi\phi$ mode, and reports the 68% CL interval of $\phi_s^{S\bar{S}} = -2 \beta_s^{S\bar{S}}$ as $[-2.46, -0.76]$ rad.

 $|\lambda| (B_s^0 \rightarrow J/\psi(1S)\phi)$

VALUE	DOCUMENT ID	TECN	COMMENT
0.988 ± 0.009 OUR AVERAGE			
0.990 ± 0.010	AAIJ	24A	LHCB pp at 7, 8, 13 TeV
0.972 ± 0.026 ± 0.008	¹ SIRUNYAN	21E	CMS pp at 13 TeV
• • • We do not use the following data for averages, fits, limits, etc. • • •			
0.877 ^{+0.112} _{-0.116} ± 0.031	AAIJ	21AN	LHCB Repl. by AAIJ 24A
1.012 ± 0.016 ± 0.006	AAIJ	19Q	LHCB Repl. by AAIJ 24A
0.964 ± 0.019 ± 0.007	AAIJ	15I	LHCB Repl. by AAIJ 24A
0.93 ± 0.03 ± 0.02	AAIJ	13AR	LHCB Repl. by AAIJ 15I

¹ Measured using time-dependent angular analysis of $B_s^0 \rightarrow J/\psi\phi$ decays.

 $|\lambda| (b \rightarrow c\bar{c}s)$

$\lambda = q/p \cdot A_f/\bar{A}_f$ is a phase-convention-independent observable quantity for the final state f . See the review on " CP Violation in the Quark Sector" for details.

VALUE	DOCUMENT ID	TECN	COMMENT
0.989 ± 0.008 OUR AVERAGE			
0.990 ± 0.010	¹ AAIJ	24A	LHCB pp at 7, 8, 13 TeV
0.972 ± 0.026 ± 0.008	² SIRUNYAN	21E	CMS pp at 13 TeV
0.949 ± 0.036 ± 0.019	³ AAIJ	19AF	LHCB pp at 7, 8, 13 TeV
0.994 ± 0.018 ± 0.006	⁴ AAIJ	17V	LHCB pp at 7, 8 TeV
1.045 ^{+0.069} _{-0.050} ± 0.007	⁵ AAIJ	16AK	LHCB pp at 7, 8 TeV
0.91 ^{+0.18} _{-0.15} ± 0.02	⁶ AAIJ	14AY	LHCB pp at 7, 8 TeV
• • • We do not use the following data for averages, fits, limits, etc. • • •			
1.004 ± 0.030 ± 0.009	⁷ AAIJ	23AT	LHCB pp at 13 TeV
1.009 ± 0.030	⁷ AAIJ	23AT	LHCB pp at 7, 8 and 13 TeV
0.877 ^{+0.112} _{-0.116} ± 0.031	AAIJ	21AN	LHCB Repl. by AAIJ 24A
0.99 ± 0.05 ± 0.01	⁷ AAIJ	19AP	LHCB Repl. by AAIJ 23AT
1.012 ± 0.016 ± 0.006	AAIJ	19Q	LHCB Repl. by AAIJ 24A
1.035 ± 0.034 ± 0.089	⁸ AAIJ	18S	LHCB pp at 7, 8 TeV
0.964 ± 0.019 ± 0.007	AAIJ	15I	LHCB Repl. by AAIJ 24A
1.04 ± 0.07 ± 0.03	⁷ AAIJ	14AE	LHCB Repl. by AAIJ 19AP
0.93 ± 0.03 ± 0.02	AAIJ	13AR	LHCB Repl. by AAIJ 15I

¹ Measured using time-dependent angular analysis of $B_s^0 \rightarrow J/\psi K^+ K^-$ in the region $m(KK)$ in the vicinity of the $\phi(1020)$ resonance.

² Measured using time-dependent angular analysis of $B_s^0 \rightarrow J/\psi\phi$ decays.

³ Measured using time-dependent analysis of $B_s^0 \rightarrow J/\psi\pi^+\pi^-$ decays.

⁴ Measured using time-dependent angular analysis of $B_s^0 \rightarrow J/\psi K^+ K^-$ in the region $m(KK) > 1.05$ GeV.

⁵ Measured using time-dependent angular analysis of $B_s^0 \rightarrow \psi(2S)\phi$ decays.

⁶ Measured in $B_s^0 \rightarrow D_s^+ D_s^-$ decays.

⁷ Measured in $B_s^0 \rightarrow \phi\phi$ decays.

⁸ Measured in $B_s^0 \rightarrow (K^+ \pi^-)(K^- \pi^+)$ in the region $0.75 < m(K^\pm \pi^\mp) < 1.6$ GeV.

A, CP violation parameter

$$A = -2 \operatorname{Re}(\lambda) / (1 + |\lambda|^2)$$

VALUE	DOCUMENT ID	TECN	COMMENT
-0.79 ± 0.08 OUR AVERAGE			
-0.83 ± 0.05 ± 0.09	¹ AAIJ	21O	LHCB pp at 13 TeV
-0.79 ± 0.07 ± 0.10	¹ AAIJ	18O	LHCB pp at 7, 8 TeV
0.49 ^{+0.77} _{-0.65} ± 0.06	² AAIJ	15AL	LHCB pp at 7, 8 TeV

¹ Measured in $B_s^0 \rightarrow K^+ K^-$ decays.

² Measured in $B_s^0 \rightarrow J/\psi K_S^0$ decays.

C, CP violation parameter

$$C = (1 - |\lambda|^2) / (1 + |\lambda|^2)$$

VALUE	DOCUMENT ID	TECN	COMMENT
0.19 ± 0.06 OUR AVERAGE			
0.20 ± 0.06 ± 0.02	¹ AAIJ	18O	LHCB pp at 7, 8 TeV
-0.28 ± 0.41 ± 0.08	² AAIJ	15AL	LHCB pp at 7, 8 TeV

¹ Measured in $B_s^0 \rightarrow K^+ K^-$ decays.

² Measured in $B_s^0 \rightarrow J/\psi K_S^0$ decays.

S, CP violation parameter

$$S = -2 \operatorname{Im}(\lambda) / (1 + |\lambda|^2)$$

VALUE	DOCUMENT ID	TECN	COMMENT
0.17 ± 0.06 OUR AVERAGE			
0.18 ± 0.06 ± 0.02	¹ AAIJ	18O	LHCB pp at 7, 8 TeV
-0.08 ± 0.40 ± 0.08	² AAIJ	15AL	LHCB pp at 7, 8 TeV

¹ Measured in $B_s^0 \rightarrow K^+ K^-$ decays.
² Measured in $B_s^0 \rightarrow J/\psi K_S^0$ decays.

 $A_{CP}^{\perp}(B_s \rightarrow J/\psi \bar{K}^*(892)^0)$

VALUE	DOCUMENT ID	TECN	COMMENT
-0.048 ± 0.057 ± 0.020	AAIJ	15AV	LHCB pp at 7, 8 TeV

 $A_{CP}^{\parallel}(B_s \rightarrow J/\psi \bar{K}^*(892)^0)$

VALUE	DOCUMENT ID	TECN	COMMENT
0.171 ± 0.152 ± 0.028	AAIJ	15AV	LHCB pp at 7, 8 TeV

 $A_{CP}^{\perp}(B_s \rightarrow J/\psi \bar{K}^*(892)^0)$

VALUE	DOCUMENT ID	TECN	COMMENT
-0.049 ± 0.096 ± 0.025	AAIJ	15AV	LHCB pp at 7, 8 TeV

 $A_{CP}(B_s \rightarrow \pi^+ K^-)$

A_{CP} is defined as

$$\frac{B(\bar{B}_s^0 \rightarrow f) - B(B_s^0 \rightarrow \bar{f})}{B(\bar{B}_s^0 \rightarrow f) + B(B_s^0 \rightarrow \bar{f})}$$

the CP -violation asymmetry of exclusive B_s^0 and \bar{B}_s^0 decay.

VALUE	DOCUMENT ID	TECN	COMMENT
0.224 ± 0.012 OUR AVERAGE			
0.236 ± 0.013 ± 0.011	AAIJ	21O	LHCB pp at 13 TeV
0.213 ± 0.015 ± 0.007	AAIJ	18O	LHCB pp at 7, 8 TeV
0.22 ± 0.07 ± 0.02	AALTONEN	14P	CDF $p\bar{p}$ at 1.96 TeV
• • • We do not use the following data for averages, fits, limits, etc. • • •			
0.27 ± 0.04 ± 0.01	AAIJ	13AX	LHCB Repl. by AAIJ 18O
0.27 ± 0.08 ± 0.02	AAIJ	12V	LHCB Repl. by AAIJ 13AX
0.39 ± 0.15 ± 0.08	AALTONEN	11N	CDF Repl. by AALTONEN 14P

 $A_{CP}(B_s^0 \rightarrow [K^+ K^-]_D \bar{K}^*(892)^0)$

VALUE	DOCUMENT ID	TECN	COMMENT
-0.04 ± 0.07 ± 0.02	AAIJ	14BN	LHCB pp at 7, 8 TeV
• • • We do not use the following data for averages, fits, limits, etc. • • •			
0.04 ± 0.16 ± 0.01	AAIJ	13L	LHCB Repl. by AAIJ 14BN

 $A_{CP}(B_s^0 \rightarrow [\pi^+ K^-]_D K^*(892)^0)$

VALUE	DOCUMENT ID	TECN	COMMENT
-0.01 ± 0.03 ± 0.02	AAIJ	14BN	LHCB pp at 7, 8 TeV

 $A_{CP}(B_s^0 \rightarrow [\pi^+ \pi^-]_D K^*(892)^0)$

VALUE	DOCUMENT ID	TECN	COMMENT
0.06 ± 0.13 ± 0.02	AAIJ	14BN	LHCB pp at 7, 8 TeV

 $S(B_s^0 \rightarrow \phi\gamma)$

VALUE	DOCUMENT ID	TECN	COMMENT
0.43 ± 0.30 ± 0.11	¹ AAIJ	19AE	LHCB pp at 7, 8 TeV

¹ Measured in flavor tagged time dependent analysis.

 $C(B_s^0 \rightarrow \phi\gamma)$

VALUE	DOCUMENT ID	TECN	COMMENT
0.11 ± 0.29 ± 0.11	¹ AAIJ	19AE	LHCB pp at 7, 8 TeV

¹ Measured in flavor tagged time dependent analysis.

 $A^{\Delta}(B_s^0 \rightarrow \phi\gamma)$

$A^{\Delta}(B_s \rightarrow \phi\gamma)$ is the multiplicative coefficient of the $\sinh(\Delta\Gamma t/2)$ term in the $B_s \rightarrow \phi\gamma$ decay rate time dependence.

VALUE	DOCUMENT ID	TECN	COMMENT
-0.67^{+0.37}_{-0.41} ± 0.17	¹ AAIJ	19AE	LHCB pp at 7, 8 TeV
• • • We do not use the following data for averages, fits, limits, etc. • • •			
-0.98 ^{+0.46+0.23} _{-0.52-0.20}	² AAIJ	17B	LHCB Repl. by AAIJ 19AE

¹ Measured in flavor tagged time dependent analysis, using tagged and un-tagged events. This result updates AAIJ 17B with better selection efficiency and other analysis improvements.

² Measured in time dependent analysis without initial flavor tagging.

Meson Particle Listings

 B_S^0

CPT VIOLATION PARAMETERS

In the B_S^0 mixing, propagating mass eigenstates can be written as

$$|B_{SL}\rangle \propto p \sqrt{1-\xi} |B_S^0\rangle + q \sqrt{1+\xi} |\bar{B}_S^0\rangle$$

$$|B_{SH}\rangle \propto p \sqrt{1+\xi} |B_S^0\rangle - q \sqrt{1-\xi} |\bar{B}_S^0\rangle$$

where parameter ξ controls CPT violation. If ξ is zero, then CPT is conserved. The parameter ξ can be written as

$$\xi = \frac{2(M_{11}-M_{22})-i(\Gamma_{11}-\Gamma_{22})}{-2\Delta m_S+i\Delta\Gamma_S} \approx \frac{-2\beta^\mu \Delta a_\mu}{2\Delta m_S-i\Delta\Gamma_S},$$

where M_{ii} , Γ_{ii} , Δm_S , and $\Delta\Gamma_S$ are parameters of Hamiltonian governing B_S oscillations, β^μ is the B_S^0 meson velocity and Δa_μ characterizes Lorentz-invariance violation.

 Δa_\perp

VALUE (10^{-12} GeV)	CL%	DOCUMENT ID	TECN	COMMENT
$-0.47 \pm 0.39 \pm 0.08$		1 AAIJ	16E LHCb	pp at 7, 8 TeV
< 1.2	95	2 ABAZOV	15L D0	$p\bar{p}$ at 1.96 TeV

¹ Uses $B_S^0 \rightarrow J/\psi K^+ K^-$ decays.

² Measured in semileptonic $B_S^0 \rightarrow D_S^- \mu^+ X$ decays. Also extracts limit on time and longitudinal components ($-0.8 < \Delta a_T - 0.396 \Delta a_Z < 3.9$) 10^{-13} GeV.

 Δa_\parallel

VALUE (10^{-14} GeV)	DOCUMENT ID	TECN	COMMENT
$-0.89 \pm 1.41 \pm 0.36$	1 AAIJ	16E LHCb	pp at 7, 8 TeV

¹ Uses $B_S^0 \rightarrow J/\psi K^+ K^-$ decays.

 Δa_X

VALUE (10^{-14} GeV)	DOCUMENT ID	TECN	COMMENT
$+1.01 \pm 2.08 \pm 0.71$	1 AAIJ	16E LHCb	pp at 7, 8 TeV

¹ Uses $B_S^0 \rightarrow J/\psi K^+ K^-$ decays.

 Δa_Y

VALUE (10^{-14} GeV)	DOCUMENT ID	TECN	COMMENT
$-3.83 \pm 2.09 \pm 0.71$	1 AAIJ	16E LHCb	pp at 7, 8 TeV

¹ Uses $B_S^0 \rightarrow J/\psi K^+ K^-$ decays.

Re(ξ)

VALUE	DOCUMENT ID	TECN	COMMENT
$-0.022 \pm 0.033 \pm 0.003$	1 AAIJ	16E LHCb	pp at 7, 8 TeV

¹ Uses $B_S^0 \rightarrow J/\psi K^+ K^-$ decays.

Im(ξ)

VALUE	DOCUMENT ID	TECN	COMMENT
$0.004 \pm 0.011 \pm 0.002$	1 AAIJ	16E LHCb	pp at 7, 8 TeV

¹ Uses $B_S^0 \rightarrow J/\psi K^+ K^-$ decays.

PARTIAL BRANCHING FRACTIONS IN $B_S \rightarrow \phi \ell^+ \ell^-$ $B(B_S \rightarrow \phi \ell^+ \ell^-)$ ($0.1 < q^2 < 2.0$ GeV²/c⁴)

VALUE (units 10^{-7})	DOCUMENT ID	TECN	COMMENT
1.14 ± 0.16 OUR AVERAGE			

1.11 $^{+0.14}_{-0.13} \pm 0.09$ ¹ AAIJ 15AQ LHCb pp at 7, 8 TeV

2.78 $\pm 0.95 \pm 0.89$ AALTONEN 11AI CDF $p\bar{p}$ at 1.96 TeV

• • • We do not use the following data for averages, fits, limits, etc. • • •

0.897 $^{+0.207}_{-0.186} \pm 0.097$ ¹ AAIJ 13X LHCb Repl. by AAIJ 15AQ

¹ Measured in $B_S^0 \rightarrow \phi \mu^+ \mu^-$ decays.

 $B(B_S^0 \rightarrow \phi \ell^+ \ell^-)$ ($0.1 < q^2 < 0.98$ GeV²/c⁴)

VALUE (units 10^{-8})	DOCUMENT ID	TECN	COMMENT
6.81 ± 0.47 ± 0.34	1 AAIJ	21AG LHCb	pp at 7, 8, 13 TeV

¹ Measured in $B_S^0 \rightarrow \phi \mu^+ \mu^-$ decays

 $B(B_S^0 \rightarrow \phi \ell^+ \ell^-)$ ($1.1 < q^2 < 2.5$ GeV²/c⁴)

VALUE (units 10^{-8})	DOCUMENT ID	TECN	COMMENT
4.41 ± 0.41 ± 0.24	1 AAIJ	21AG LHCb	pp at 7, 8, 13 TeV

¹ Measured in $B_S^0 \rightarrow \phi \mu^+ \mu^-$ decays

 $B(B_S \rightarrow \phi \ell^+ \ell^-)$ ($2.0 < q^2 < 5.0$ GeV²/c⁴)

VALUE (units 10^{-7})	DOCUMENT ID	TECN	COMMENT
0.77 ± 0.12 ± 0.06	1 AAIJ	15AQ LHCb	pp at 7, 8 TeV

• • • We do not use the following data for averages, fits, limits, etc. • • •

0.529 $^{+0.182}_{-0.159} \pm 0.057$ ^{1,2} AAIJ 13X LHCb Repl. by AAIJ 15AQ

0.58 $\pm 0.55 \pm 0.19$ ² AALTONEN 11AI CDF $p\bar{p}$ at 1.96 TeV

¹ Measured in $B_S^0 \rightarrow \phi \mu^+ \mu^-$ decays.

² Measured in $2 < q^2 < 4.3$ GeV²/c⁴.

 $B(B_S^0 \rightarrow \phi \ell^+ \ell^-)$ ($2.5 < q^2 < 4.0$ GeV²/c⁴)

VALUE (units 10^{-8})	DOCUMENT ID	TECN	COMMENT
3.51 ± 0.39 ± 0.18	1 AAIJ	21AG LHCb	pp at 7, 8, 13 TeV

¹ Measured in $B_S^0 \rightarrow \phi \mu^+ \mu^-$ decays

 $B(B_S^0 \rightarrow \phi \ell^+ \ell^-)$ ($4.0 < q^2 < 6.0$ GeV²/c⁴)

VALUE (units 10^{-8})	DOCUMENT ID	TECN	COMMENT
6.22 ± 0.48 ± 0.32	1 AAIJ	21AG LHCb	pp at 7, 8, 13 TeV

¹ Measured in $B_S^0 \rightarrow \phi \mu^+ \mu^-$ decays

 $B(B_S \rightarrow \phi \ell^+ \ell^-)$ ($5.0 < q^2 < 8.0$ GeV²/c⁴)

VALUE (units 10^{-7})	DOCUMENT ID	TECN	COMMENT
0.96 ± 0.13 ± 0.08	1 AAIJ	15AQ LHCb	pp at 7, 8 TeV

• • • We do not use the following data for averages, fits, limits, etc. • • •

1.38 $^{+0.25}_{-0.23} \pm 0.14$ ^{1,2} AAIJ 13X LHCb Repl. by AAIJ 15AQ

1.34 $\pm 0.83 \pm 0.43$ ² AALTONEN 11AI CDF $p\bar{p}$ at 1.96 TeV

¹ Measured in $B_S^0 \rightarrow \phi \mu^+ \mu^-$ decays.

² Measured in $4.3 < q^2 < 8.68$ GeV²/c⁴.

 $B(B_S^0 \rightarrow \phi \ell^+ \ell^-)$ ($6.0 < q^2 < 8.0$ GeV²/c⁴)

VALUE (units 10^{-8})	DOCUMENT ID	TECN	COMMENT
6.30 ± 0.48 ± 0.32	1 AAIJ	21AG LHCb	pp at 7, 8, 13 TeV

¹ Measured in $B_S^0 \rightarrow \phi \mu^+ \mu^-$ decays

 $B(B_S \rightarrow \phi \ell^+ \ell^-)$ ($11.0 < q^2 < 12.5$ GeV²/c⁴)

VALUE (units 10^{-7})	DOCUMENT ID	TECN	COMMENT
0.717 ± 0.045 ± 0.036	1 AAIJ	21AG LHCb	pp at 7, 8, 13 TeV

• • • We do not use the following data for averages, fits, limits, etc. • • •

0.71 $\pm 0.10 \pm 0.06$ ¹ AAIJ 15AQ LHCb Repl. by AAIJ 21AG

1.18 $^{+0.22}_{-0.21} \pm 0.14$ ^{1,2} AAIJ 13X LHCb Repl. by AAIJ 15AQ

2.98 $\pm 0.95 \pm 0.95$ ² AALTONEN 11AI CDF $p\bar{p}$ at 1.96 TeV

¹ Measured in $B_S^0 \rightarrow \phi \mu^+ \mu^-$ decays.

² Measured in $10.9 < q^2 < 12.86$ GeV²/c⁴.

 $B(B_S^0 \rightarrow \phi \ell^+ \ell^-)$ ($15.0 < q^2 < 19.0$ GeV²/c⁴)

VALUE (units 10^{-8})	DOCUMENT ID	TECN	COMMENT
18.52 ± 0.80 ± 1.00	1 AAIJ	21AG LHCb	pp at 7, 8, 13 TeV

¹ Measured in $B_S^0 \rightarrow \phi \mu^+ \mu^-$ decays

 $B(B_S \rightarrow \phi \ell^+ \ell^-)$ ($15.0 < q^2 < 17.0$ GeV²/c⁴)

VALUE (units 10^{-7})	DOCUMENT ID	TECN	COMMENT
1.050 ± 0.058 ± 0.054	1 AAIJ	21AG LHCb	pp at 7, 8, 13 TeV

• • • We do not use the following data for averages, fits, limits, etc. • • •

0.90 $\pm 0.11 \pm 0.07$ ¹ AAIJ 15AQ LHCb Repl. by AAIJ 21AG

0.760 $^{+0.189}_{-0.169} \pm 0.087$ ^{1,2} AAIJ 13X LHCb Repl. by AAIJ 15AQ

1.86 $\pm 0.66 \pm 0.59$ ² AALTONEN 11AI CDF $p\bar{p}$ at 1.96 TeV

¹ Measured in $B_S^0 \rightarrow \phi \mu^+ \mu^-$ decays.

² Measured in $14.18 < q^2 < 16$ GeV²/c⁴.

 $B(B_S \rightarrow \phi \ell^+ \ell^-)$ ($17.0 < q^2 < 19.0$ GeV²/c⁴)

VALUE (units 10^{-7})	DOCUMENT ID	TECN	COMMENT
0.838 ± 0.058 ± 0.046	1 AAIJ	21AG LHCb	pp at 7, 8, 13 TeV

• • • We do not use the following data for averages, fits, limits, etc. • • •

0.79 $\pm 0.11 \pm 0.07$ ¹ AAIJ 15AQ LHCb Repl. by AAIJ 21AG

1.06 $^{+0.23}_{-0.21} \pm 0.12$ ^{1,2} AAIJ 13X LHCb Repl. by AAIJ 15AQ

2.32 $\pm 0.76 \pm 0.74$ ² AALTONEN 11AI CDF $p\bar{p}$ at 1.96 TeV

¹ Measured in $B_S^0 \rightarrow \phi \mu^+ \mu^-$ decays.

² Measured in $16 < q^2 < 19$ GeV²/c⁴.

 $B(B_S \rightarrow \phi \ell^+ \ell^-)$ ($1.0 < q^2 < 6.0$ GeV²/c⁴)

VALUE (units 10^{-7})	DOCUMENT ID	TECN	COMMENT
1.44 ± 0.11 OUR AVERAGE			

1.440 $\pm 0.075 \pm 0.075$ ¹ AAIJ 21AG LHCb pp at 7, 8, 13 TeV

1.14 $\pm 0.79 \pm 0.36$ AALTONEN 11AI CDF $p\bar{p}$ at 1.96 TeV

• • • We do not use the following data for averages, fits, limits, etc. • • •

1.29 $\pm 0.16 \pm 0.10$ ¹ AAIJ 15AQ LHCb Repl. by AAIJ 21AG

1.14 $^{+0.25}_{-0.23} \pm 0.13$ ¹ AAIJ 13X LHCb Repl. by AAIJ 15AQ

¹ Measured in $B_S^0 \rightarrow \phi \mu^+ \mu^-$ decays.

 $B(B_S \rightarrow \phi \ell^+ \ell^-)$ ($0.0 < q^2 < 4.3$ GeV²/c⁴)

VALUE (units 10^{-7})	DOCUMENT ID	TECN	COMMENT
3.30 ± 1.09 ± 1.05	AALTONEN	11AI CDF	$p\bar{p}$ at 1.96 TeV

PRODUCTION ASYMMETRIES

A_P(B_s⁰)

A_P(B_s⁰) = [σ(B_s⁰) - σ(B_s⁰)] / [σ(B_s⁰) + σ(B_s⁰)]

Table with columns: VALUE (units 10⁻²), DOCUMENT ID, TECN, COMMENT. Includes 'OUR AVERAGE' and various experimental data points with error bars.

B_s⁰ → D_s^{*-} ℓ⁺ ν_ℓ FORM FACTORS

ρ² (form factor slope)

Table with columns: VALUE, DOCUMENT ID, TECN, COMMENT. Includes 'OUR AVERAGE' and detailed comments about reconstruction methods for the form factor slope.

B_s⁰ REFERENCES

Vertical list of references for B_s⁰ production asymmetries and form factors, including author names, journal abbreviations, and years.

Vertical list of references for B_s⁰ production asymmetries and form factors, continuing from the previous section.

Meson Particle Listings

$B_s^0, B_s^*, B_{s1}(5830)^0$

AALTONEN	12AJ	PRL 109 171802	T. Aaltonen et al.	(CDF Collab.)
AALTONEN	12C	PRL 108 201801	T. Aaltonen et al.	(CDF Collab.)
AALTONEN	12D	PR D85 072002	T. Aaltonen et al.	(CDF Collab.)
AALTONEN	12L	PRL 108 211803	T. Aaltonen et al.	(CDF Collab.)
ABAZOV	12AF	PR D86 092011	V.M. Abazov et al.	(DO Collab.)
ABAZOV	12C	PR D85 011103	V.M. Abazov et al.	(DO Collab.)
ABAZOV	12D	PR D85 032006	V.M. Abazov et al.	(DO Collab.)
CHATRCHYAN	12A	JHEP 1204 033	S. Chatrchyan et al.	(CMS Collab.)
LEES	12A	PR D85 011101	J.P. Lees et al.	(BABAR Collab.)
LI	12	PRL 109 181808	J. Li et al.	(BELLE Collab.)
PDG	12	PR D86 010001	J. Beringer et al.	(PDG Collab.)
AAIJ	11	PL B698 115	R. Aaij et al.	(LHCb Collab.)
AAIJ	11A	PL B698 14	R. Aaij et al.	(LHCb Collab.)
AAIJ	11B	PL B699 330	R. Aaij et al.	(LHCb Collab.)
AAIJ	11D	PL B706 32	R. Aaij et al.	(LHCb Collab.)
AAIJ	11E	PR D84 092001	R. Aaij et al.	(LHCb Collab.)
Also		PR D85 039904 (errata.)	R. Aaij et al.	(LHCb Collab.)
AALTONEN	11A	PR D83 052012	T. Aaltonen et al.	(CDF Collab.)
AALTONEN	11AB	PR D84 052012	T. Aaltonen et al.	(CDF Collab.)
AALTONEN	11AG	PRL 107 191801	T. Aaltonen et al.	(CDF Collab.)
Also		PRL 107 239903 (errata.)	T. Aaltonen et al.	(CDF Collab.)
AALTONEN	11AI	PRL 107 201802	T. Aaltonen et al.	(CDF Collab.)
AALTONEN	11AN	PRL 107 261802	T. Aaltonen et al.	(CDF Collab.)
AALTONEN	11AP	PRL 107 272001	T. Aaltonen et al.	(CDF Collab.)
AALTONEN	11L	PRL 106 161801	T. Aaltonen et al.	(CDF Collab.)
AALTONEN	11N	PRL 106 181802	T. Aaltonen et al.	(CDF Collab.)
ABAZOV	11U	PR D84 052007	V.M. Abazov et al.	(DO Collab.)
CHATRCHYAN	11T	PRL 107 191802	S. Chatrchyan et al.	(CMS Collab.)
LI	11	PRL 106 121802	J. Li et al.	(BELLE Collab.)
ABAZOV	10E	PR D82 012003	V.M. Abazov et al.	(DO Collab.)
ABAZOV	10H	PRL 105 081801	V.M. Abazov et al.	(DO Collab.)
Also		PR D82 032001	V.M. Abazov et al.	(DO Collab.)
ABAZOV	10S	PL B693 539	V.M. Abazov et al.	(DO Collab.)
ESEN	10	PRL 105 201802	S. Esen et al.	(BELLE Collab.)
LOUVOT	10	PRL 104 231801	R. LOUVOT et al.	(BELLE Collab.)
PENG	10	PR D82 072007	C.-C. Peng et al.	(BELLE Collab.)
AALTONEN	09AQ	PRL 103 191802	T. Aaltonen et al.	(CDF Collab.)
AALTONEN	09B	PR D79 011104	T. Aaltonen et al.	(CDF Collab.)
AALTONEN	09C	PRL 103 031801	T. Aaltonen et al.	(CDF Collab.)
AALTONEN	09P	PRL 102 201801	T. Aaltonen et al.	(CDF Collab.)
ABAZOV	09E	PRL 102 032001	V.M. Abazov et al.	(DO Collab.)
ABAZOV	09G	PRL 102 051801	V.M. Abazov et al.	(DO Collab.)
ABAZOV	09I	PRL 102 091801	V.M. Abazov et al.	(DO Collab.)
ABAZOV	09Y	PR D79 111102	V.M. Abazov et al.	(DO Collab.)
LOUVOT	09	PRL 102 021801	R. Louvot et al.	(BELLE Collab.)
AALTONEN	08F	PRL 100 021803	T. Aaltonen et al.	(CDF Collab.)
AALTONEN	08G	PRL 100 161802	T. Aaltonen et al.	(CDF Collab.)
AALTONEN	08J	PRL 100 121803	T. Aaltonen et al.	(CDF Collab.)
ABAZOV	08AM	PRL 101 241801	V.M. Abazov et al.	(DO Collab.)
WICHT	08A	PRL 100 121801	J. Wicht et al.	(BELLE Collab.)
ABAZOV	07	PRL 98 121801	V.M. Abazov et al.	(DO Collab.)
ABAZOV	07A	PRL 98 151801	V.M. Abazov et al.	(DO Collab.)
ABAZOV	07N	PR D76 057101	V.M. Abazov et al.	(DO Collab.)
ABAZOV	07Y	PRL 99 241801	V.M. Abazov et al.	(DO Collab.)
ABULENCIA	07C	PRL 98 061802	A. Abulencia et al.	(CDF Collab.)
DRUTSKOY	07	PRL 98 052001	A. Drutskoy et al.	(BELLE Collab.)
DRUTSKOY	07A	PR D76 012002	A. Drutskoy et al.	(BELLE Collab.)
ABAZOV	06B	PRL 97 021802	V.M. Abazov et al.	(DO Collab.)
ABAZOV	06G	PR D74 031107	V.M. Abazov et al.	(DO Collab.)
ABAZOV	06V	PRL 97 241801	V.M. Abazov et al.	(DO Collab.)
ABULENCIA	06J	PRL 96 191801	A. Abulencia et al.	(CDF Collab.)
ABULENCIA	06N	PRL 96 231801	A. Abulencia et al.	(CDF Collab.)
ABULENCIA	06Q	PRL 97 062003	A. Abulencia et al.	(CDF Collab.)
ABULENCIA,A	06D	PRL 97 211802	A. Abulencia et al.	(CDF Collab.)
ABULENCIA,A	06G	PRL 97 242003	A. Abulencia et al.	(CDF Collab.)
ACOSTA	06	PRL 96 202001	D. Acosta et al.	(CDF Collab.)
ABAZOV	05B	PRL 94 042001	V.M. Abazov et al.	(DO Collab.)
ABAZOV	05W	PRL 95 171801	V.M. Abazov et al.	(DO Collab.)
ACOSTA	05	PRL 94 101803	D. Acosta et al.	(CDF Collab.)
ACOSTA	05J	PRL 95 031801	D. Acosta et al.	(CDF Collab.)
ABDALLAH	04A	PL B585 63	J. Abdallah et al.	(DELPHI Collab.)
ABDALLAH	04J	EPJ C35 35	J. Abdallah et al.	(DELPHI Collab.)
ABDALLAH	03B	EPJ C28 155	J. Abdallah et al.	(DELPHI Collab.)
ABE	03	PR D67 012006	K. Abe et al.	(SLD Collab.)
HEISTER	03E	EPJ C29 143	A. Heister et al.	(ALEPH Collab.)
ABE	02V	PR D66 032009	K. Abe et al.	(SLD Collab.)
ACOSTA	02D	PR D65 111101	D. Acosta et al.	(CDF Collab.)
ACOSTA	02G	PR D66 112002	D. Acosta et al.	(CDF Collab.)
ARBIENDI	01D	EPJ C19 241	G. Abbiendi et al.	(OPAL Collab.)
ABE	00C	PR D62 071101	K. Abe et al.	(SLD Collab.)
ABREU	00Y	EPJ C16 555	P. Abreu et al.	(DELPHI Collab.)
ABREU,P	00G	EPJ C18 229	P. Abreu et al.	(DELPHI Collab.)
AFFOLDER	00N	PRL 85 4668	T. Affolder et al.	(CDF Collab.)
BARATE	00K	PL B486 286	R. Barate et al.	(ALEPH Collab.)
ARBIENDI	99S	EPJ C11 587	G. Abbiendi et al.	(OPAL Collab.)
ABE	99D	PR D59 032004	F. Abe et al.	(CDF Collab.)
ABE	99J	PRL 82 3576	F. Abe et al.	(CDF Collab.)
BARATE	99J	EPJ C7 553	R. Barate et al.	(ALEPH Collab.)
Also		EPJ C12 181 (errata.)	R. Barate et al.	(ALEPH Collab.)
ABE	98B	PR D57 5382	F. Abe et al.	(CDF Collab.)
ABE	98V	PRL 81 5742	F. Abe et al.	(CDF Collab.)
ACCIARRI	98S	PL B438 417	M. Acciari et al.	(L3 Collab.)
ACKERSTAFF	98F	EPJ C2 407	K. Ackerstaff et al.	(OPAL Collab.)
ACKERSTAFF	98G	PL B426 161	K. Ackerstaff et al.	(OPAL Collab.)
BARATE	98C	EPJ C4 367	R. Barate et al.	(ALEPH Collab.)
BARATE	98Q	EPJ C4 387	R. Barate et al.	(ALEPH Collab.)
PDG	98	EPJ C3 1	C. Caso et al.	(PDG Collab.)
ACCIARRI	97B	PL B391 474	M. Acciari et al.	(L3 Collab.)
ACCIARRI	97C	PL B391 481	M. Acciari et al.	(L3 Collab.)
ACKERSTAFF	97U	ZPHY C76 401	K. Ackerstaff et al.	(OPAL Collab.)
ACKERSTAFF	97V	ZPHY C76 417	K. Ackerstaff et al.	(OPAL Collab.)
ADAM	97	PL B414 382	W. Adam et al.	(DELPHI Collab.)
ABE	96B	PR D53 3496	F. Abe et al.	(CDF Collab.)
ABE	96N	PRL 77 1945	F. Abe et al.	(CDF Collab.)
ABE	96Q	PR D54 6596	F. Abe et al.	(CDF Collab.)
ABREU	96F	ZPHY C71 11	P. Abreu et al.	(DELPHI Collab.)
ADAM	96D	ZPHY C72 207	W. Adam et al.	(DELPHI Collab.)
BUSKULIC	96E	ZPHY C69 585	D. Buskulić et al.	(ALEPH Collab.)
BUSKULIC	96M	PL B377 205	D. Buskulić et al.	(ALEPH Collab.)
BUSKULIC	96V	PL B384 471	D. Buskulić et al.	(ALEPH Collab.)
PDG	96	PR D54 1	R. M. Barnett et al.	(PDG Collab.)
ABE	95R	PRL 74 4988	F. Abe et al.	(CDF Collab.)
ABE	95Z	PRL 75 3068	F. Abe et al.	(CDF Collab.)
ACCIARRI	95H	PL B363 127	M. Acciari et al.	(L3 Collab.)
ACCIARRI	95I	PL B363 137	M. Acciari et al.	(L3 Collab.)
AKERS	95G	PL B350 273	R. Akers et al.	(OPAL Collab.)
AKERS	95J	ZPHY C66 555	R. Akers et al.	(OPAL Collab.)
BUSKULIC	95J	PL B356 409	D. Buskulić et al.	(ALEPH Collab.)
BUSKULIC	95O	PL B361 221	D. Buskulić et al.	(ALEPH Collab.)
ABREU	94D	PL B324 500	P. Abreu et al.	(DELPHI Collab.)
ABREU	94E	ZPHY C61 407	P. Abreu et al.	(DELPHI Collab.)
Also		PL B289 199	P. Abreu et al.	(DELPHI Collab.)

AKERS	94J	PL B337 196	R. Akers et al.	(OPAL Collab.)
AKERS	94B	PL B337 393	R. Akers et al.	(OPAL Collab.)
BUSKULIC	94B	PL B322 441	D. Buskulić et al.	(ALEPH Collab.)
BUSKULIC	94C	PL B322 275	D. Buskulić et al.	(ALEPH Collab.)
ABE	93F	PRL 71 1685	F. Abe et al.	(CDF Collab.)
ACTON	93H	PL B312 501	P.D. Acton et al.	(OPAL Collab.)
BUSKULIC	93G	PL B311 425	D. Buskulić et al.	(ALEPH Collab.)
ABREU	92M	PL B289 199	P. Abreu et al.	(DELPHI Collab.)
ACTON	92N	PL B295 357	P.D. Acton et al.	(OPAL Collab.)
BUSKULIC	92E	PL B294 145	D. Buskulić et al.	(ALEPH Collab.)
LEE-FRANZINI	90	PRL 65 2947	J. Lee-Franzini et al.	(CUSB II Collab.)

B_s^*

$I(J^P) = 0(1^-)$

I, J, P need confirmation. Quantum numbers shown are quark-model predictions.

B_s^* MASS

From mass difference below and the B_s^0 mass.

VALUE (MeV)	DOCUMENT ID	TECN	COMMENT
5415.4 ± 1.4 OUR FIT	Error includes scale factor of 2.6.		
5415.8 ± 1.5 OUR AVERAGE	Error includes scale factor of 2.6.		
5416.4 ± 0.4 ± 0.5	LOUVOT 09	BELL	$e^+e^- \rightarrow \Upsilon(5S)$
5411.7 ± 1.6 ± 0.6	1 AQUINES 06	CLEO	$e^+e^- \rightarrow \Upsilon(5S)$
• • • We do not use the following data for averages, fits, limits, etc. • • •			
5418 ± 1 ± 3	DRUTSKOY 07A	BELL	Repl. by LOUVOT 09
5414 ± 1 ± 3	2 BONVICINI 06	CLEO	$e^+e^- \rightarrow \Upsilon(5S)$
1 Utilized the beam constrained invariant mass peak positions for B^* and B_s^* to extract the measurement.			
2 Uses 14 candidates consistent with B_s decays into final states with a J/ψ and a $D_s^{(*)-}$.			

$m_{B_s^*} - m_{B_s}$

VALUE (MeV)	DOCUMENT ID	TECN	COMMENT
48.5 ± 1.4 OUR FIT	Error includes scale factor of 2.6.		
46.1 ± 1.5 OUR AVERAGE			
45.7 ± 1.7 ± 0.7	3 AQUINES 06	CLEO	$e^+e^- \rightarrow \Upsilon(5S)$
47.0 ± 2.6	4 LEE-FRANZINI 90	CSB2	$e^+e^- \rightarrow \Upsilon(5S)$
• • • We do not use the following data for averages, fits, limits, etc. • • •			
48 ± 1 ± 3	5 BONVICINI 06	CLEO	Repl. by AQUINES 06
3 Utilized the beam constrained invariant mass peak positions for B^* and B_s^* to extract the measurement.			
4 LEE-FRANZINI 90 measure 46.7 ± 0.4 ± 0.2 MeV for an admixture of $B^0, B^+,$ and B_s^- . They use the shape of the photon line to separate the above value for B_s .			
5 Uses 14 candidates consistent with B_s decays into final states with a J/ψ and a $D_s^{(*)-}$.			

$|(m_{B_s^*} - m_{B_s}) - (m_{B^*} - m_B)|$

VALUE (MeV)	CL%	DOCUMENT ID	TECN	COMMENT
<6	95	ABREU 95R	DLPH	$E_{\text{CM}}^{\text{pl}} = 88-94$ GeV

B_s^* DECAY MODES

Mode	Fraction (Γ_i/Γ)
$\Gamma_1 B_s \gamma$	seen

B_s^* REFERENCES

LOUVOT 09	PRL 102 021801	R. Louvot et al.	(BELLE Collab.)
DRUTSKOY 07A	PR D76 012002	A. Drutskoy et al.	(BELLE Collab.)
AQUINES 06	PRL 96 152001	O. Aquines et al.	(CLEO Collab.)
BONVICINI 06	PRL 96 022002	G. Bonvicini et al.	(CLEO Collab.)
ABREU 95R	ZPHY C68 353	P. Abreu et al.	(DELPHI Collab.)
LEE-FRANZINI 90	PRL 65 2947	J. Lee-Franzini et al.	(CUSB II Collab.)

$B_{s1}(5830)^0$

$I(J^P) = 0(1^+)$

I, J, P need confirmation.

Quantum numbers shown are quark-model predictions.

$B_{s1}(5830)^0$ MASS

VALUE (MeV)	DOCUMENT ID	TECN	COMMENT
5828.73 ± 0.20 OUR FIT			
5828.65 ± 0.24 OUR AVERAGE			
5828.78 ± 0.09 ± 0.29	SIRUNYAN 18DF	CMS	pp at 8 TeV
5828.40 ± 0.04 ± 0.41	1 AAIJ 130	LHCB	pp at 7 TeV
• • • We do not use the following data for averages, fits, limits, etc. • • •			
5829.4 ± 0.7	2 AALTONEN 08K	CDF	Repl. by AALTONEN 14I
1 Uses $B_{s1}(5830)^0 \rightarrow B^* + K^-$ decay.			
2 Uses two-body decays into K^- and B^+ mesons reconstructed as $B^+ \rightarrow J/\psi K^+$, $J/\psi \rightarrow \mu^+ \mu^-$ or $B^+ \rightarrow \bar{D}^0 \pi^+$, $\bar{D}^0 \rightarrow K^+ \pi^-$.			

See key on page 1171

Meson Particle Listings

$B_{s1}(5830)^0, B_{s2}^*(5840)^0, B_{sJ}^*(5850)$

$m_{B_{s1}^0} - m_{B^{++}}$

VALUE (MeV)	DOCUMENT ID	TECN	COMMENT
503.98 ± 0.17 OUR FIT			
504.03 ± 0.12 ± 0.15	¹ AALTONEN 14i CDF		$p\bar{p}$ at 1.96 TeV
• • • We do not use the following data for averages, fits, limits, etc. • • •			
504.41 ± 0.21 ± 0.14	² AALTONEN 08k CDF		Repl. by AALTONEN 14i
¹ AALTONEN 14i reports $m_{B_{s1}(5830)^0} - m_{B^{++}} - m_{K^-} = 10.35 \pm 0.12 \pm 0.15$ MeV which we adjusted by the K^- mass.			
² Uses two-body decays into K^- and B^+ mesons reconstructed as $B^+ \rightarrow J/\psi K^+$, $J/\psi \rightarrow \mu^+ \mu^-$ or $B^+ \rightarrow \bar{D}^0 \pi^+$, $\bar{D}^0 \rightarrow K^+ \pi^-$.			

$B_{s1}(5830)^0$ WIDTH

VALUE (MeV)	DOCUMENT ID	TECN	COMMENT
0.5 ± 0.3 ± 0.3	AALTONEN 14i CDF		$p\bar{p}$ at 1.96 TeV

$B_{s1}(5830)^0$ DECAY MODES

Mode	Fraction (Γ_i/Γ)
Γ_1 $B^{*+} K^-$	seen
Γ_2 $B^{*0} K_S^0$	

$B_{s1}(5830)^0$ BRANCHING RATIOS

$\Gamma(B^{*+} K^-)/\Gamma_{total}$	VALUE	DOCUMENT ID	TECN	COMMENT	Γ_1/Γ
seen		AALTONEN 08k CDF		$p\bar{p}$ at 1.96 TeV	

$\Gamma(B^{*0} K_S^0)/\Gamma(B^{*+} K^-)$	VALUE	DOCUMENT ID	TECN	COMMENT	Γ_2/Γ_1
0.49 ± 0.12 ± 0.07		¹ SIRUNYAN 18DF CMS		pp at 8 TeV	

¹ With the branching fractions $B(B^+ \rightarrow J/\psi K^+) = (1.026 \pm 0.031) \times 10^{-3}$ and $B(B^0 \rightarrow J/\psi K^{*0}) = (1.28 \pm 0.05) \times 10^{-3}$.

$B_{s1}(5830)^0$ REFERENCES

SIRUNYAN 18DF EPJ C78 939	A.M. Sirunyan et al.	(CMS Collab.)
AALTONEN 14i PR D90 012013	T. Aaltonen et al.	(CDF Collab.)
AAIJ 13O PRL 110 151803	R. Aaij et al.	(LHCb Collab.)
AALTONEN 08K PRL 100 082001	T. Aaltonen et al.	(CDF Collab.)

$B_{s2}^*(5840)^0$ $I(J^P) = 0(2^+)$

I, J, P need confirmation.

Quantum numbers shown are quark-model predictions.

$B_{s2}^*(5840)^0$ MASS

VALUE (MeV)	DOCUMENT ID	TECN	COMMENT
5839.88 ± 0.12 OUR FIT			
5839.92 ± 0.14 OUR AVERAGE			
5839.86 ± 0.09 ± 0.17	SIRUNYAN 18DF CMS		pp at 8 TeV
5839.99 ± 0.05 ± 0.20	AAIJ 13O LHCb		pp at 7 TeV
5839.6 ± 1.1 ± 0.7	¹ ABAZOV 08E D0		$p\bar{p}$ at 1.96 TeV
• • • We do not use the following data for averages, fits, limits, etc. • • •			
5839.7 ± 0.7	² AALTONEN 08k CDF		Repl. by AALTONEN 14i
¹ Observed in $B_{s2}^{*0} \rightarrow B^+ K^-$. Measured production rate of B_{s2}^{*0} relative to B^+ to be $(1.15 \pm 0.23 \pm 0.13)\%$.			
² Uses two-body decays into K^- and B^+ mesons reconstructed as $B^+ \rightarrow J/\psi K^+$, $J/\psi \rightarrow \mu^+ \mu^-$ or $B^+ \rightarrow \bar{D}^0 \pi^+$, $\bar{D}^0 \rightarrow K^+ \pi^-$.			

$m_{B_{s2}^0} - m_{B_{s1}^0}$

VALUE (MeV)	DOCUMENT ID	TECN	COMMENT
• • • We do not use the following data for averages, fits, limits, etc. • • •			
10.5 ± 0.6	¹ AALTONEN 08k CDF		Repl. by AALTONEN 14i
¹ Uses two-body decays into K^- and B^+ mesons reconstructed as $B^+ \rightarrow J/\psi K^+$, $J/\psi \rightarrow \mu^+ \mu^-$ or $B^+ \rightarrow \bar{D}^0 \pi^+$, $\bar{D}^0 \rightarrow K^+ \pi^-$.			

$m_{B_{s2}^0} - m_{B^+}$

VALUE (MeV)	DOCUMENT ID	TECN	COMMENT
560.48 ± 0.12 OUR FIT			
560.41 ± 0.13 ± 0.14	¹ AALTONEN 14i CDF		$p\bar{p}$ at 1.96 TeV
¹ AALTONEN 14i reports $m_{B_{s2}(5840)^0} - m_{B^+} - m_{K^-} = 66.73 \pm 0.13 \pm 0.14$ MeV which we adjusted by the K^- mass.			

$B_{s2}^*(5840)^0$ WIDTH

VALUE (MeV)	DOCUMENT ID	TECN	COMMENT
1.49 ± 0.27 OUR AVERAGE			
1.52 ± 0.34 ± 0.30	SIRUNYAN 18DF CMS		pp at 8 TeV
1.4 ± 0.4 ± 0.2	AALTONEN 14i CDF		$p\bar{p}$ at 1.96 TeV
1.56 ± 0.13 ± 0.47	¹ AAIJ 13O LHCb		pp at 7 TeV
¹ Uses $B_{s2}^*(5840)^0 \rightarrow B^{*+} K^-$ decays.			

$B_{s2}^*(5840)^0$ DECAY MODES

Branching fractions are given relative to the one DEFINED AS 1.

Mode	Fraction (Γ_i/Γ)
Γ_1 $B^+ K^-$	DEFINED AS 1
Γ_2 $B^{*+} K^-$	0.093 ± 0.018
Γ_3 $B^0 K_S^0$	0.43 ± 0.11
Γ_4 $B^{*0} K_S^0$	0.04 ± 0.04

$B_{s2}^*(5840)^0$ BRANCHING RATIOS

$\Gamma(B^+ K^-)/\Gamma_{total}$	VALUE	DOCUMENT ID	TECN	COMMENT	Γ_1/Γ
seen		AALTONEN 08k CDF		$p\bar{p}$ at 1.96 TeV	
seen		¹ ABAZOV 08E D0		$p\bar{p}$ at 1.96 TeV	
¹ Measured production rate of B_{s2}^{*0} relative to B^+ to be $(1.15 \pm 0.23 \pm 0.13)\%$.					

$\Gamma(B^{*+} K^-)/\Gamma(B^+ K^-)$	VALUE	DOCUMENT ID	TECN	COMMENT	Γ_2/Γ_1
0.093 ± 0.013 ± 0.012		AAIJ 13O LHCb		pp at 7 TeV	

$\Gamma(B^{*0} K_S^0)/\Gamma(B^0 K_S^0)$	VALUE	DOCUMENT ID	TECN	COMMENT	Γ_4/Γ_3
0.093 ± 0.086 ± 0.014		¹ SIRUNYAN 18DF CMS		pp at 8 TeV	
¹ With the branching fraction $B(B^0 \rightarrow J/\psi K^{*0}) = (1.28 \pm 0.05) \times 10^{-3}$.					

$\Gamma(B^0 K_S^0)/\Gamma(B^+ K^-)$	VALUE	DOCUMENT ID	TECN	COMMENT	Γ_3/Γ_1
0.432 ± 0.077 ± 0.078		¹ SIRUNYAN 18DF CMS		pp at 8 TeV	
¹ With the branching fractions $B(B^+ \rightarrow J/\psi K^+) = (1.026 \pm 0.031) \times 10^{-3}$ and $B(B^0 \rightarrow J/\psi K^{*0}) = (1.28 \pm 0.05) \times 10^{-3}$.					

$\Gamma(B^{*+} K^-)/\Gamma(B^+ K^-)$	VALUE	DOCUMENT ID	TECN	COMMENT	Γ_2/Γ_1
0.081 ± 0.021 ± 0.015		¹ SIRUNYAN 18DF CMS		pp at 8 TeV	
¹ With the branching fraction $B(B^+ \rightarrow J/\psi K^+) = (1.026 \pm 0.031) \times 10^{-3}$.					

$B_{s2}^*(5840)^0$ REFERENCES

SIRUNYAN 18DF EPJ C78 939	A.M. Sirunyan et al.	(CMS Collab.)
AALTONEN 14i PR D90 012013	T. Aaltonen et al.	(CDF Collab.)
AAIJ 13O PRL 110 151803	R. Aaij et al.	(LHCb Collab.)
AALTONEN 08K PRL 100 082001	T. Aaltonen et al.	(CDF Collab.)
ABAZOV 08E PRL 100 082002	V.M. Abazov et al.	(D0 Collab.)

$B_{sJ}^*(5850)$ $I(J^P) = ?(??)$

OMITTED FROM SUMMARY TABLE

Signal can be interpreted as coming from $\bar{D}s$ states. Needs confirmation.

$B_{sJ}^*(5850)$ MASS

VALUE (MeV)	EVTS	DOCUMENT ID	TECN	COMMENT
5853 ± 15	141	AKERS 95E OPAL		$E_{cm}^{6C} = 88-94$ GeV

$B_{sJ}^*(5850)$ WIDTH

VALUE (MeV)	EVTS	DOCUMENT ID	TECN	COMMENT
47 ± 22	141	AKERS 95E OPAL		$E_{cm}^{6C} = 88-94$ GeV

$B_{sJ}^*(5850)$ REFERENCES

AKERS 95E ZPHY C66 19	R. Akers et al.	(OPAL Collab.)
-----------------------	-----------------	----------------

Meson Particle Listings

 $B_{s,J}(6063)^0, B_{s,J}(6114)^0$ $B_{s,J}(6063)^0$ $I(J^P) = 0(?^?)$

OMITTED FROM SUMMARY TABLE

 $B_{s,J}(6063)^0$ MASS

VALUE (MeV)	DOCUMENT ID	TECN	COMMENT
$6063.5 \pm 1.2 \pm 0.8$	¹ AAIJ	21D LHCb	pp at 7, 8, 13 TeV

¹ Seen in the decay channel $B^\pm K^\mp$. Integrated luminosity = 9 fb⁻¹.

 $B_{s,J}(6063)^0$ WIDTH

VALUE (MeV)	DOCUMENT ID	TECN	COMMENT
$26 \pm 4 \pm 4$	¹ AAIJ	21D LHCb	pp at 7, 8, 13 TeV

¹ Seen in the decay channel $B^\pm K^\mp$. Integrated luminosity = 9 fb⁻¹.

 $B_{s,J}(6063)^0$ DECAY MODES

Mode	Fraction (Γ_i/Γ)
Γ_1 $B^+ K^-$	seen

$\Gamma(B^+ K^-)/\Gamma_{\text{total}}$	Γ_1/Γ
seen	

 $B_{s,J}(6063)^0$ REFERENCESAAIJ 21D EPJ C81 601 R. Aaij *et al.* (LHCb Collab.) $B_{s,J}(6114)^0$ $I(J^P) = 0(?^?)$

OMITTED FROM SUMMARY TABLE

 $B_{s,J}(6114)^0$ MASS

VALUE (MeV)	DOCUMENT ID	TECN	COMMENT
$6114 \pm 3 \pm 5$	¹ AAIJ	21D LHCb	pp at 7, 8, 13 TeV

¹ Seen in the decay channel $B^\pm K^\mp$. Integrated luminosity = 9 fb⁻¹.

 $B_{s,J}(6114)^0$ WIDTH

VALUE (MeV)	DOCUMENT ID	TECN	COMMENT
$66 \pm 18 \pm 21$	¹ AAIJ	21D LHCb	pp at 7, 8, 13 TeV

¹ Seen in the decay channel $B^\pm K^\mp$. Integrated luminosity = 9 fb⁻¹.

 $B_{s,J}(6114)^0$ DECAY MODES

Mode	Fraction (Γ_i/Γ)
Γ_1 $B^+ K^-$	seen

$\Gamma(B^+ K^-)/\Gamma_{\text{total}}$	Γ_1/Γ
seen	

 $B_{s,J}(6114)^0$ REFERENCESAAIJ 21D EPJ C81 601 R. Aaij *et al.* (LHCb Collab.)

See key on page 1171

Meson Particle Listings

B_c^+

BOTTOM, CHARMED MESONS
($B = C = \pm 1$)
 $B_c^+ = c\bar{b}, B_c^- = \bar{c}b$, similarly for B_c^{*+} 's

$I(J^P) = 0(0^-)$
 I, J, P need confirmation.
Quantum numbers shown are quark-model predictions.

B_c^+ MASS

VALUE (MeV)	DOCUMENT ID	TECN	COMMENT
6274.47 ± 0.27 ± 0.17	¹ AAIJ	20R LHCb	pp at 7, 8, 13 TeV
• • • We do not use the following data for averages, fits, limits, etc. • • •			
6274.28 ± 1.40 ± 0.32	² AAIJ	17L LHCb	Repl. by AAIJ 20R
6274.0 ± 1.8 ± 0.4	³ AAIJ	14AQ LHCb	Repl. by AAIJ 20R
6276.28 ± 1.44 ± 0.36	⁴ AAIJ	13AS LHCb	Repl. by AAIJ 20R
6273.7 ± 1.3 ± 1.6	⁵ AAIJ	12AV LHCb	Repl. by AAIJ 20R
6275.6 ± 2.9 ± 2.5	⁶ AALTONEN	08M CDF	$p\bar{p}$ at 1.96 TeV
6300 ± 14 ± 5	⁶ ABAZOV	08T D0	$p\bar{p}$ at 1.96 TeV
6285.7 ± 5.3 ± 1.2	⁶ ABULENCIA	06C CDF	Repl. by AALTONEN 08M
6400 ± 390 ± 130	⁷ ABE	98M CDF	$p\bar{p}$ at 1.8 TeV
6320 ± 60	⁸ ACKERSTAFF	98O OPAL	$e^+e^- \rightarrow Z$

- ¹ AAIJ 20R uses the $B_c^+ \rightarrow J/\psi\pi^+, J/\psi\pi^+\pi^-\pi^+, J/\psi p\bar{p}\pi^+, J/\psi D_s^+, J/\psi D^0 K^+$ and $B_s^0\pi^+$ modes.
- ² Measured using $B_c^+ \rightarrow J/\psi D^0 K^+$ decays.
- ³ Uses $B_c^+ \rightarrow J/\psi p\bar{p}\pi^+$ decays.
- ⁴ AAIJ 13AS uses the $B_c^+ \rightarrow J/\psi D_s^+$.
- ⁵ AAIJ 12AV uses the $B_c^+ \rightarrow J/\psi\pi^+$ mode and also measures the mass difference $M(B_c^+) - M(B^+) = 994.6 \pm 1.3 \pm 0.6$ MeV/ c^2 .
- ⁶ Measured using a fully reconstructed decay mode of $B_c \rightarrow J/\psi\pi$.
- ⁷ ABE 98M observed $20.4^{+5.2}_{-5.5}$ events in the $B_c^+ \rightarrow J/\psi(1S)\ell\nu_\ell$ with a significance of > 4.8 standard deviations. The mass value is estimated from $m(J/\psi(1S)\ell)$.
- ⁸ ACKERSTAFF 98O observed 2 candidate events in the $B_c^+ \rightarrow J/\psi(1S)\pi^+$ channel with an estimated background of 0.63 ± 0.20 events.

$m_{B_c^+} - m_{B^0}$

VALUE (MeV)	DOCUMENT ID	TECN	COMMENT
907.75 ± 0.37 ± 0.27	¹ AAIJ	20R LHCb	pp at 7, 8, 13 TeV
¹ AAIJ 20R uses the $B_c^+ \rightarrow J/\psi\pi^+, J/\psi\pi^+\pi^-\pi^+, J/\psi p\bar{p}\pi^+, J/\psi D_s^+, J/\psi D^0 K^+$ and $B_s^0\pi^+$ modes.			

B_c^+ MEAN LIFE

VALUE (10^{-12} s)	DOCUMENT ID	TECN	COMMENT
0.510 ± 0.009 OUR EVALUATION	(Produced by HFLAV)		
0.510 ± 0.009 OUR AVERAGE			
0.541 ± 0.026 ± 0.014	¹ SIRUNYAN	18BY CMS	pp at 8 TeV
0.5134 ± 0.0110 ± 0.0057	^{2,3} AAIJ	15G LHCb	pp at 7, 8 TeV
0.509 ± 0.008 ± 0.012	⁴ AAIJ	14G LHCb	pp at 8 TeV
0.452 ± 0.048 ± 0.027	³ AALTONEN	13 CDF	$p\bar{p}$ at 1.96 TeV
0.448 $^{+0.038}_{-0.036}$ ± 0.032	⁵ ABAZOV	09H D0	$p\bar{p}$ at 1.96 TeV
0.463 $^{+0.073}_{-0.065}$ ± 0.036	⁵ ABULENCIA	06O CDF	$p\bar{p}$ at 1.96 TeV
0.46 $^{+0.18}_{-0.16}$ ± 0.03	⁵ ABE	98M CDF	$p\bar{p}$ 1.8 TeV

- ¹ The lifetime is measured using the decays $B_c^+ \rightarrow J/\psi\pi^+$ and $B^+ \rightarrow J/\psi K^+$.
- ² Also measures the width difference $\Delta\Gamma = \Gamma_{B_c^+} - \Gamma_{B^+} = 4.46 \pm 0.14 \pm 0.07$ $\text{mm}^{-1}c$.
- ³ Uses fully reconstructed $B_c^+ \rightarrow J/\psi\pi^+$ decays.
- ⁴ Measured using $B_c^+ \rightarrow J/\psi\mu^+\nu_\mu X$ decays.
- ⁵ The lifetime is measured from the $J/\psi e$ decay vertices.

B_c^+ DECAY MODES $\times B(\bar{b} \rightarrow B_c)$

The following quantities are not pure branching ratios; rather the fractions $\Gamma_i/\Gamma \times B(\bar{b} \rightarrow B_c)$. B_c^- modes are charge conjugates of the modes below.

Mode	Fraction (Γ_i/Γ)	Confidence level
Γ_1 $J/\psi(1S)\ell^+\nu_\ell$ anything	seen	
Γ_2 $J/\psi(1S)\mu^+\nu_\mu$	seen	
Γ_3 $J/\psi(1S)\tau^+\nu_\tau$	seen	
Γ_4 $J/\psi(1S)\pi^+$	seen	

Γ_5 $J/\psi(1S)K^+$	seen	
Γ_6 $J/\psi(1S)\pi^+\pi^+\pi^-$	seen	
Γ_7 $J/\psi(1S)K^+\pi^-\pi^+$		
Γ_8 $J/\psi(1S)K^+K^-\pi^+$		
Γ_9 $J/\psi(1S)a_1(1260)$	not seen	
Γ_{10} $J/\psi(1S)K^+K^-\pi^+$	seen	
Γ_{11} $J/\psi(1S)\pi^+\pi^+\pi^-\pi^-$	seen	
Γ_{12} $\psi(2S)\pi^+$	seen	
Γ_{13} $\psi(2S)\pi^+\pi^-\pi^+$		
Γ_{14} $\psi(2S)K^+K^-\pi^+$		
Γ_{15} $J/\psi(1S)D^0 K^+$	seen	
Γ_{16} $J/\psi(1S)D^*(2007)^0 K^+$	seen	
Γ_{17} $J/\psi(1S)D^*(2010)^+ K^{*0}$	seen	
Γ_{18} $J/\psi(1S)D^+ K^{*0}$	seen	
Γ_{19} $J/\psi(1S)D_s^{*+}$	seen	
Γ_{20} $J/\psi(1S)D_s^{*+}$	seen	
Γ_{21} $J/\psi(1S)p\bar{p}\pi^+$	seen	
Γ_{22} $\chi_{c0}\pi^+$	$(2.4^{+0.9}_{-0.8}) \times 10^{-5}$	
Γ_{23} $p\bar{p}\pi^+$	not seen	
Γ_{24} $D^0 K^+$	seen	
Γ_{25} $D^0\pi^+$	not seen	
Γ_{26} $D^{*0}\pi^+$	not seen	
Γ_{27} $D^{*0}K^+$	not seen	
Γ_{28} $D_s^+ \bar{D}^0$	$< 7.2 \times 10^{-4}$	90%
Γ_{29} $D_s^+ D^0$	$< 3.0 \times 10^{-4}$	90%
Γ_{30} $D^+ \bar{D}^0$	$< 1.9 \times 10^{-4}$	90%
Γ_{31} $D^+ D^0$	$< 1.4 \times 10^{-4}$	90%
Γ_{32} $D_s^{*+} \bar{D}^0$	$< 5.3 \times 10^{-4}$	90%
Γ_{33} $D_s^+ \bar{D}^*(2007)^0$	$< 4.6 \times 10^{-4}$	90%
Γ_{34} $D_s^{*+} D^0$	$< 9 \times 10^{-4}$	90%
Γ_{35} $D_s^+ D^*(2007)^0$	$< 6.6 \times 10^{-4}$	90%
Γ_{36} $D^*(2010)^+ \bar{D}^0$	$< 3.8 \times 10^{-4}$	90%
Γ_{37} $D^*(2010)^+ \bar{D}^0, D^{*+} \rightarrow D^+\pi^0/\gamma$	not seen	
Γ_{38} $D^+ \bar{D}^*(2007)^0$	$< 6.5 \times 10^{-4}$	90%
Γ_{39} $D^*(2007)^+ D^0$	$< 2.0 \times 10^{-4}$	90%
Γ_{40} $D^*(2010)^+ D^0, D^{*+} \rightarrow D^+\pi^0/\gamma$	not seen	
Γ_{41} $D^+ D^*(2007)^0$	$< 3.7 \times 10^{-4}$	90%
Γ_{42} $D_s^{*+} \bar{D}^*(2007)^0$	$< 1.3 \times 10^{-3}$	90%
Γ_{43} $D_s^{*+} D^*(2007)^0$	$< 1.3 \times 10^{-3}$	90%
Γ_{44} $D^*(2010)^+ \bar{D}^*(2007)^0$	$< 1.0 \times 10^{-3}$	90%
Γ_{45} $D^*(2010)^+ D^*(2007)^0$	$< 7.7 \times 10^{-4}$	90%
Γ_{46} $D^+ K^{*0}$	not seen	
Γ_{47} $D^+ \bar{K}^{*0}$	not seen	
Γ_{48} $D_s^+ K^{*0}$	not seen	
Γ_{49} $D_s^+ \bar{K}^{*0}$	not seen	
Γ_{50} $D_s^+ \phi$	not seen	
Γ_{51} $K^+ K^0$	not seen	
Γ_{52} $B_s^0\pi^+ / B(\bar{b} \rightarrow B_s)$	seen	
Γ_{53} $B_s^0\pi^+$		

B_c^+ BRANCHING RATIOS

VALUE (units 10^{-5})	CL%	DOCUMENT ID	TECN	COMMENT
8.2 ± 1.3 OUR AVERAGE		Error includes scale factor of 1.4.		
$8.8 \pm 1.0 \pm 0.2$		^{1,2} AALTONEN	16A CDF	$p\bar{p}$ at 1.96 TeV
$5.2^{+2.4}_{-2.1}$		³ ABE	98M CDF	$p\bar{p}$ 1.8 TeV
• • • We do not use the following data for averages, fits, limits, etc. • • •				
< 16	90	⁴ ACKERSTAFF	98O OPAL	$e^+e^- \rightarrow Z$
< 19	90	⁵ ABREU	97E DLPH	$e^+e^- \rightarrow Z$
< 12	90	⁶ BARATE	97H ALEP	$e^+e^- \rightarrow Z$

- ¹ AALTONEN 16A reports $[\Gamma(B_c^+ \rightarrow J/\psi(1S)\ell^+\nu_\ell \text{ anything})/\Gamma_{\text{total}} \times B(\bar{b} \rightarrow B_c)] / [B(\bar{b} \rightarrow B^+)] / [B(B^+ \rightarrow J/\psi(1S)K^+)] = 0.211 \pm 0.012^{+0.021}_{-0.020}$ which we multiply by our best values $B(\bar{b} \rightarrow B^+) = (40.8 \pm 0.7) \times 10^{-2}$, $B(B^+ \rightarrow J/\psi(1S)K^+) = (1.020 \pm 0.019) \times 10^{-3}$. Our first error is their experiment's error and our second error is the systematic error from using our best values.
- ² AALTONEN 16A also measures the cross-section $\sigma(B_c) \times B(B_c \rightarrow J/\psi\mu\nu_\mu) = 0.60 \pm 0.09$ nb and estimates the total cross-section $\sigma(B_c)$ to be in the range 25 ± 4 to 52 ± 8 nb for $p_T(B_c) > 6$ GeV/ c and $|y(B_c)| < 1$.
- ³ ABE 98M result is derived from the measurement of $[\sigma(B_c) \times B(B_c \rightarrow J/\psi(1S)\ell\nu_\ell)] / [\sigma(B^+) \times B(B^+ \rightarrow J/\psi(1S)K^+)] = 0.132^{+0.041}_{-0.037} (\text{stat}) \pm 0.031 (\text{sys}) \pm 0.032 (\text{lifetime})$ by using PDG 98 values of $B(b \rightarrow B^+)$ and $B(B^+ \rightarrow J/\psi(1S)K^+)$.

Meson Particle Listings

 B_c^+

⁴ACKERSTAFF 98o reports $B(Z \rightarrow B_c X)/B(Z \rightarrow qq) \times B(B_c \rightarrow J/\psi(1S) \ell \nu_\ell) < 6.95 \times 10^{-5}$ at 90%CL. We rescale to our PDG 98 values of $B(Z \rightarrow b\bar{b})$.

⁵ABREU 97E value listed is for an assumed $\tau_{B_c} = 0.4$ ps and improves to 1.6×10^{-4} for $\tau_{B_c} = 1.4$ ps.

⁶BARATE 97H reports $B(Z \rightarrow B_c X)/B(Z \rightarrow qq) \times B(B_c \rightarrow J/\psi(1S) \ell \nu_\ell) < 5.2 \times 10^{-5}$ at 90%CL. We rescale to our PDG 96 values of $B(Z \rightarrow b\bar{b})$. A $B_c^+ \rightarrow J/\psi(1S) \mu^+ \nu_\mu$ candidate event is found, compared to all the known background sources 2×10^{-3} , which gives $m_{B_c} = 5.96^{+0.25}_{-0.19}$ GeV and $\tau_{B_c} = 1.77 \pm 0.17$ ps.

$\Gamma(J/\psi(1S) \tau^+ \nu_\tau) / \Gamma(J/\psi(1S) \mu^+ \nu_\mu)$ Γ_3 / Γ_2

VALUE	DOCUMENT ID	TECN	COMMENT
0.71 ± 0.17 ± 0.18	¹ AAIJ	18c	LHCB <i>pp</i> at 7, 8 TeV

¹AAIJ 18c uses $\tau^+ \rightarrow \mu^+ \nu_\mu \bar{\nu}_\tau$ mode to obtain the ratio value.

$\Gamma(J/\psi(1S) \pi^+) / \Gamma_{\text{total}} \times B(\bar{B} \rightarrow B_c)$ $\Gamma_4 / \Gamma \times B$

VALUE	CL%	DOCUMENT ID	TECN	COMMENT
seen		¹ AABOUD	21	ATLS <i>pp</i> at 8 TeV
seen		² AAIJ	15M	LHCB <i>pp</i> at 8 TeV
seen		³ KHACHATRYAN...15AA	CMS	<i>pp</i> at 7 TeV
seen		AALTONEN	13	CDF <i>p\bar{p}</i> at 1.96 TeV
seen		⁴ AAIJ	12AV	LHCB <i>pp</i> at 7 TeV
seen		AALTONEN	08M	CDF <i>p\bar{p}</i> at 1.96 TeV
seen		ABAZOV	08T	D0 <i>p\bar{p}</i> at 1.96 TeV

• • • We do not use the following data for averages, fits, limits, etc. • • •

$< 2.4 \times 10^{-4}$	90	⁵ ACKERSTAFF	98o	OPAL $e^+e^- \rightarrow Z$
$< 3.4 \times 10^{-4}$	90	⁶ ABREU	97E	DLPH $e^+e^- \rightarrow Z$
$< 8.2 \times 10^{-5}$	90	⁷ BARATE	97H	ALEP $e^+e^- \rightarrow Z$
$< 2.0 \times 10^{-5}$	95	⁸ ABE	96R	CDF <i>p\bar{p}</i> 1.8 TeV

¹AABOUD 21 reports a measurement of $B(B_c^+ \rightarrow J/\psi \pi^+) / B(B^+ \rightarrow J/\psi K^+) \cdot f_c/f_u = (0.34 \pm 0.04^{+0.06}_{-0.02} \pm 0.01)$ %, at $p_T > 13$ GeV and $|y| < 2.3$.

²AAIJ 15M reports a measurement of $B(B_c^+ \rightarrow J/\psi \pi^+) / B(B^+ \rightarrow J/\psi K^+) \cdot f_c/f_u = (0.683 \pm 0.018 \pm 0.009)$ % at $p_T(B_c) < 20$ GeV and $2.0 < y(B) < 4.5$.

³KHACHATRYAN 15AA reports a measurement of $B(B_c^+ \rightarrow J/\psi \pi^+) / B(B^+ \rightarrow J/\psi K^+) \cdot f_c/f_u = (0.48 \pm 0.05 \pm 0.03 \pm 0.05)$ %, at $p_T > 15$ GeV and $|\eta(B)| < 1.6$.

⁴AAIJ 12AV reports a measurement of $B(B_c^+ \rightarrow J/\psi \pi^+) / B(B^+ \rightarrow J/\psi K^+) \cdot f_c/f_u = (0.68 \pm 0.10 \pm 0.03 \pm 0.05)$ % at $p_T(B) > 4$ GeV and $2.5 < \eta(B) < 4.5$.

⁵ACKERSTAFF 98o reports $B(Z \rightarrow B_c X)/B(Z \rightarrow qq) \times B(B_c \rightarrow J/\psi(1S) \pi^+) < 1.06 \times 10^{-4}$ at 90%CL. We rescale to our PDG 98 values of $B(Z \rightarrow b\bar{b})$.

⁶ABREU 97E value listed is for an assumed $\tau_{B_c} = 0.4$ ps and improves to 2.7×10^{-4} for $\tau_{B_c} = 1.4$ ps.

⁷BARATE 97H reports $B(Z \rightarrow B_c X)/B(Z \rightarrow qq) \times B(B_c \rightarrow J/\psi(1S) \pi) < 3.6 \times 10^{-5}$ at 90%CL. We rescale to our PDG 96 values of $B(Z \rightarrow b\bar{b})$.

⁸ABE 96R reports $B(b \rightarrow B_c X)/B(b \rightarrow B^+ X) \times B(B_c^+ \rightarrow J/\psi(1S) \pi^+) / B(B^+ \rightarrow J/\psi(1S) K^+) < 0.053$ at 95%CL for $\tau_{B_c} = 0.8$ ps. It changes from 0.15 to 0.04 for 0.17 ps $< \tau_{B_c} < 1.6$ ps. We rescale to our PDG 96 values of $B(b \rightarrow B^+) = 0.378 \pm 0.022$ and $B(B^+ \rightarrow J/\psi(1S) K^+) = 0.00101 \pm 0.00014$.

$\Gamma(J/\psi(1S) \pi^+) / \Gamma(J/\psi(1S) \mu^+ \nu_\mu)$ Γ_4 / Γ_2

VALUE (units 10^{-2})	DOCUMENT ID	TECN	COMMENT
4.69 ± 0.28 ± 0.46	¹ AAIJ	14W	LHCB <i>pp</i> at 7 TeV

¹AAIJ 14W reports also a measurement $B(B_c^+ \rightarrow J/\psi \pi^+) / B(B_c^+ \rightarrow J/\psi \mu^+ \nu_\mu) = 0.271 \pm 0.016 \pm 0.016$ in the region $m_{J/\psi \mu^+} > 5.3$ GeV.

$\Gamma(J/\psi(1S) K^+) / \Gamma(J/\psi(1S) \pi^+)$ Γ_5 / Γ_4

VALUE	EVTs	DOCUMENT ID	TECN	COMMENT
0.079 ± 0.007 ± 0.003		AAIJ	16AF	LHCB <i>pp</i> at 7, 8 TeV

• • • We do not use the following data for averages, fits, limits, etc. • • •

$0.069 \pm 0.019 \pm 0.005$	50	AAIJ	13BY	LHCB Repl. by AAIJ 16AF
-----------------------------	----	------	------	-------------------------

$\Gamma(J/\psi(1S) \pi^+ \pi^+ \pi^-) / \Gamma_{\text{total}} \times B(\bar{B} \rightarrow B_c)$ $\Gamma_6 / \Gamma \times B$

VALUE	CL%	DOCUMENT ID	TECN	COMMENT
seen		AAIJ	12Y	LHCB <i>pp</i> at 7 TeV

• • • We do not use the following data for averages, fits, limits, etc. • • •

$< 5.7 \times 10^{-4}$	90	¹ ABREU	97E	DLPH $e^+e^- \rightarrow Z$
------------------------	----	--------------------	-----	-----------------------------

¹ABREU 97E value listed is independent of 0.4 ps $< \tau_{B_c} < 1.4$ ps.

$\Gamma(J/\psi(1S) \pi^+ \pi^+ \pi^-) / \Gamma(J/\psi(1S) \pi^+)$ Γ_6 / Γ_4

VALUE	DOCUMENT ID	TECN	COMMENT
2.4 ± 0.4 OUR AVERAGE			

$2.55 \pm 0.80 \pm 0.33^{+0.04}_{-0.01}$		KHACHATRYAN...15AA	CMS <i>pp</i> at 7 TeV	
$2.41 \pm 0.30 \pm 0.33$		AAIJ	12Y	LHCB <i>pp</i> at 7 TeV

$\Gamma(J/\psi(1S) a_1(1260)) / \Gamma_{\text{total}} \times B(\bar{B} \rightarrow B_c)$ $\Gamma_9 / \Gamma \times B$

VALUE	CL%	DOCUMENT ID	TECN	COMMENT
$< 1.2 \times 10^{-3}$	90	¹ ACKERSTAFF	98o	OPAL $e^+e^- \rightarrow Z$

¹ACKERSTAFF 98o reports $B(Z \rightarrow B_c X)/B(Z \rightarrow qq) \times B(B_c \rightarrow J/\psi(1S) a_1(1260)) < 5.29 \times 10^{-4}$ at 90%CL. We rescale to our PDG 98 values of $B(Z \rightarrow b\bar{b})$.

$\Gamma(J/\psi(1S) K^+ K^- \pi^+) / \Gamma_{\text{total}} \times B(\bar{B} \rightarrow B_c)$ $\Gamma_{10} / \Gamma \times B$

VALUE	DOCUMENT ID	TECN	COMMENT
seen	¹ AAIJ	13CA	LHCB <i>pp</i> at 7, 8 TeV

¹A signal yield of 78 ± 14 decays is reported with a significance of 6.2 standard deviations using an integrated luminosity of 3 fb^{-1} data.

$\Gamma(J/\psi(1S) K^+ K^- \pi^+) / \Gamma(J/\psi(1S) \pi^+)$ Γ_{10} / Γ_4

VALUE	DOCUMENT ID	TECN	COMMENT
0.53 ± 0.10 ± 0.05	¹ AAIJ	13CA	LHCB <i>pp</i> at 7, 8 TeV

¹A signal yield of 78 ± 14 decays is reported with a significance of 6.2 standard deviations using an integrated luminosity of 3 fb^{-1} data.

$\Gamma(J/\psi(1S) \pi^+ \pi^+ \pi^- \pi^-) / \Gamma(J/\psi(1S) \pi^+)$ Γ_{11} / Γ_4

VALUE	DOCUMENT ID	TECN	COMMENT
1.74 ± 0.44 ± 0.24	¹ AAIJ	14P	LHCB <i>pp</i> at 7, 8 TeV

¹A signal yield of 32 ± 8 decays is reported with a significance of 4.5 standard deviations.

$\Gamma(\psi(2S) \pi^+) / \Gamma(J/\psi(1S) \pi^+)$ Γ_{12} / Γ_4

VALUE	DOCUMENT ID	TECN	COMMENT
0.268 ± 0.032 ± 0.007 ± 0.006	¹ AAIJ	15AY	LHCB <i>pp</i> at 7, 8 TeV

• • • We do not use the following data for averages, fits, limits, etc. • • •

$0.250 \pm 0.068 \pm 0.014 \pm 0.006$	¹ AAIJ	13AM	LHCB Repl. by AAIJ 15AY
---------------------------------------	-------------------	------	-------------------------

¹The last uncertainty is due to the uncertainty of the $B(\psi(2S) \rightarrow \mu^+ \mu^-) / B(J/\psi \rightarrow \mu^+ \mu^-)$ ratio measurement.

$\Gamma(\psi(2S) \pi^+) / \Gamma(J/\psi(1S) \pi^+ \pi^+ \pi^-)$ Γ_{12} / Γ_6

VALUE	DOCUMENT ID	TECN	COMMENT
(3.5 ± 0.6 ± 0.2) × 10⁻²	AAIJ	22P	LHCB <i>pp</i> at 7, 8, 13 TeV

$\Gamma(\psi(2S) K^+ K^- \pi^+) / \Gamma(J/\psi(1S) K^+ K^- \pi^+)$ $\Gamma_{14} / \Gamma_{10}$

VALUE	DOCUMENT ID	TECN	COMMENT
(3.7 ± 1.2 ± 0.1) × 10⁻²	AAIJ	22P	LHCB <i>pp</i> at 7, 8, 13 TeV

$\Gamma(J/\psi(1S) K^+ K^- K^+) / \Gamma(J/\psi(1S) K^+ K^- \pi^+)$ Γ_8 / Γ_{10}

VALUE	DOCUMENT ID	TECN	COMMENT
(7.0 ± 1.8 ± 0.2) × 10⁻²	AAIJ	22P	LHCB <i>pp</i> at 7, 8, 13 TeV

$\Gamma(J/\psi(1S) K^+ \pi^- \pi^+) / \Gamma(J/\psi(1S) K^+ K^- \pi^+)$ Γ_7 / Γ_{10}

VALUE	DOCUMENT ID	TECN	COMMENT
0.35 ± 0.06 ± 0.01	AAIJ	22P	LHCB <i>pp</i> at 7, 8, 13 TeV

$\Gamma(J/\psi(1S) K^+ K^- \pi^+) / \Gamma(J/\psi(1S) \pi^+ \pi^+ \pi^-)$ Γ_{10} / Γ_6

VALUE	DOCUMENT ID	TECN	COMMENT
0.185 ± 0.013 ± 0.006	AAIJ	22P	LHCB <i>pp</i> at 7, 8, 13 TeV

$\Gamma(\psi(2S) \pi^+ \pi^- \pi^+) / \Gamma(J/\psi(1S) \pi^+ \pi^+ \pi^-)$ Γ_{13} / Γ_6

VALUE	DOCUMENT ID	TECN	COMMENT
(1.9 ± 0.4 ± 0.1) × 10⁻²	AAIJ	22P	LHCB <i>pp</i> at 7, 8, 13 TeV

$\Gamma(J/\psi(1S) D^0 K^+) / \Gamma(J/\psi(1S) \pi^+)$ Γ_{15} / Γ_4

VALUE	DOCUMENT ID	TECN	COMMENT
0.432 ± 0.136 ± 0.028	AAIJ	17L	LHCB <i>pp</i> at 7, 8 TeV

$\Gamma(J/\psi(1S) D^*(2007)^0 K^+) / \Gamma(J/\psi(1S) D^0 K^+)$ $\Gamma_{16} / \Gamma_{15}$

VALUE	DOCUMENT ID	TECN	COMMENT
5.1 ± 1.8 ± 0.4	AAIJ	17L	LHCB <i>pp</i> at 7, 8 TeV

$\Gamma(J/\psi(1S) D^*(2010)^+ K^0) / \Gamma(J/\psi(1S) D^0 K^+)$ $\Gamma_{17} / \Gamma_{15}$

VALUE	DOCUMENT ID	TECN	COMMENT
2.10 ± 1.08 ± 0.34	AAIJ	17L	LHCB <i>pp</i> at 7, 8 TeV

$\Gamma(J/\psi(1S) D^+ K^0) / \Gamma(J/\psi(1S) D^0 K^+)$ $\Gamma_{18} / \Gamma_{15}$

VALUE	DOCUMENT ID	TECN	COMMENT
0.63 ± 0.39 ± 0.08	AAIJ	17L	LHCB <i>pp</i> at 7, 8 TeV

$\Gamma(J/\psi(1S) D_s^+) / \Gamma(J/\psi(1S) \pi^+)$ Γ_{19} / Γ_4

VALUE	DOCUMENT ID	TECN	COMMENT
2.8 ± 0.4 OUR AVERAGE			

$2.76 \pm 0.33 \pm 0.33$	¹ AAD	22o	ATLS <i>pp</i> at 13 TeV
$2.90 \pm 0.57 \pm 0.24$	AAIJ	13As	LHCB <i>pp</i> at 7, 8 TeV

• • • We do not use the following data for averages, fits, limits, etc. • • •

$3.8 \pm 1.1 \pm 0.4$	AAD	16H	ATLS <i>pp</i> at 7, 8 TeV
-----------------------	-----	-----	----------------------------

¹Supersedes the measurement of AAD 16H.

See key on page 1171

Meson Particle Listings

 B_c^+ $\Gamma(J/\psi(1S)D_s^{*+})/\Gamma(J/\psi(1S)\pi^+)$ Γ_{20}/Γ_4

VALUE	DOCUMENT ID	TECN	COMMENT
$5.33 \pm 0.61 \pm 0.74$	AAD	22o ATLS	pp at 13 TeV
$10.4 \pm 3.1 \pm 1.6$	AAD	16H ATLS	Repl. by AAD 22o

 $\Gamma(J/\psi(1S)D_s^{*+})/\Gamma(J/\psi(1S)D_s^+)$ Γ_{20}/Γ_{19}

VALUE	DOCUMENT ID	TECN	COMMENT
2.00 ± 0.23 OUR AVERAGE			
$1.93 \pm 0.24 \pm 0.09$	¹ AAD	22o ATLS	pp at 13 TeV
$2.37 \pm 0.56 \pm 0.10$	AAIJ	13AS LHCB	pp at 7, 8 TeV
$2.8 \text{ }^{+1.2}_{-0.8} \pm 0.3$	AAD	16H ATLS	pp at 7, 8 TeV

¹ Supersedes the measurement of AAD 16H. $\Gamma(J/\psi(1S)p\bar{p}\pi^+)/\Gamma(J/\psi(1S)\pi^+)$ Γ_{21}/Γ_4

VALUE	DOCUMENT ID	TECN	COMMENT
$0.143 \text{ }^{+0.041}_{-0.036}$	AAIJ	14AQ LHCB	pp at 7, 8 TeV

 $\Gamma(\chi_{c0}\pi^+)/\Gamma_{\text{total}}$ Γ_{22}/Γ

VALUE (units 10^{-6})	DOCUMENT ID	TECN	COMMENT
$24.0 \text{ }^{+8.6}_{-7.6} \pm 0.4$	^{1,2} AAIJ	16AT LHCB	pp at 7 and 8 TeV

¹ AAIJ 16AT reports $[\Gamma(B_c^+ \rightarrow \chi_{c0}\pi^+)/\Gamma_{\text{total}}] \times [\Gamma(\bar{b} \rightarrow B^+)/\Gamma_{\text{total}}] = (9.8 \text{ }^{+3.4}_{-3.0} \pm 0.8) \times 10^{-6}$ which we divide by our best value $\Gamma(\bar{b} \rightarrow B^+)/\Gamma_{\text{total}} = 0.408 \pm 0.007$. Our first error is their experiment's error and our second error is the systematic error from using our best value.

² The significance of the observed signal is 4.0 standard deviations. $\Gamma(p\bar{p}\pi^+)/\Gamma_{\text{total}}$ Γ_{23}/Γ

VALUE	DOCUMENT ID	TECN	COMMENT
not seen	¹ AAIJ	16K LHCB	pp at 7, 8 TeV

¹ Measures the ratio $(f_c/f_u) \times B(B_c^+ \rightarrow p\bar{p}\pi^+) < 3.6 \times 10^{-8}$ at 95% CL, in the region $m(p\bar{p}) < 2.85$ GeV/ c^2 , where f_c (f_u) represents the fragmentation fraction of the b -quark into the B_c^+ (B_u^+) meson.

 $\Gamma(D^0 K^+)/\Gamma_{\text{total}} \times B(\bar{b} \rightarrow B_c)$ $\Gamma_{24}/\Gamma \times B$

VALUE (units 10^{-7})	DOCUMENT ID	TECN	COMMENT
$3.8 \text{ }^{+1.2}_{-1.0} \pm 0.1$	¹ AAIJ	17AG LHCB	pp at 7, 8 TeV

¹ AAIJ 17AG reports $[\Gamma(B_c^+ \rightarrow D^0 K^+)/\Gamma_{\text{total}} \times B(\bar{b} \rightarrow B_c)] / [B(\bar{b} \rightarrow B^+)] = (9.3 \text{ }^{+2.8}_{-2.5} \pm 0.6) \times 10^{-7}$ which we multiply by our best value $B(\bar{b} \rightarrow B^+) = (40.8 \pm 0.7) \times 10^{-2}$. Our first error is their experiment's error and our second error is the systematic error from using our best value.

 $\Gamma(D^0 \pi^+)/\Gamma_{\text{total}} \times B(\bar{b} \rightarrow B_c)$ $\Gamma_{25}/\Gamma \times B$

VALUE	CL%	DOCUMENT ID	TECN	COMMENT
$< 1.6 \times 10^{-7}$	95	¹ AAIJ	17AG LHCB	pp at 7, 8 TeV

¹ AAIJ 17AG reports $[\Gamma(B_c^+ \rightarrow D^0 \pi^+)/\Gamma_{\text{total}} \times B(\bar{b} \rightarrow B_c)] / [B(\bar{b} \rightarrow B^+)] < 3.9 \times 10^{-7}$ which we multiply by our best value $B(\bar{b} \rightarrow B^+) = 40.8 \times 10^{-2}$.

 $\Gamma(D^{*0} \pi^+)/\Gamma_{\text{total}} \times B(\bar{b} \rightarrow B_c)$ $\Gamma_{26}/\Gamma \times B$

VALUE	CL%	DOCUMENT ID	TECN	COMMENT
$< 4 \times 10^{-7}$	95	¹ AAIJ	17AG LHCB	pp at 7, 8 TeV

¹ AAIJ 17AG reports $[\Gamma(B_c^+ \rightarrow D^{*0} \pi^+)/\Gamma_{\text{total}} \times B(\bar{b} \rightarrow B_c)] / [B(\bar{b} \rightarrow B^+)] < 1.1 \times 10^{-6}$ which we multiply by our best value $B(\bar{b} \rightarrow B^+) = 40.8 \times 10^{-2}$.

 $\Gamma(D^{*0} K^+)/\Gamma_{\text{total}} \times B(\bar{b} \rightarrow B_c)$ $\Gamma_{27}/\Gamma \times B$

VALUE	CL%	DOCUMENT ID	TECN	COMMENT
$< 4 \times 10^{-7}$	95	¹ AAIJ	17AG LHCB	pp at 7, 8 TeV

¹ AAIJ 17AG reports $[\Gamma(B_c^+ \rightarrow D^{*0} K^+)/\Gamma_{\text{total}} \times B(\bar{b} \rightarrow B_c)] / [B(\bar{b} \rightarrow B^+)] < 1.1 \times 10^{-6}$ which we multiply by our best value $B(\bar{b} \rightarrow B^+) = 40.8 \times 10^{-2}$.

 $\Gamma(D_s^+ \bar{D}^0)/\Gamma_{\text{total}} \times B(\bar{b} \rightarrow B_c)$ $\Gamma_{28}/\Gamma \times B$

VALUE	CL%	DOCUMENT ID	TECN	COMMENT
$< 1.4 \times 10^{-7}$	90	¹ AAIJ	18P LHCB	pp at 7, 8 TeV

¹ AAIJ 18P reports $[\Gamma(B_c^+ \rightarrow D_s^+ \bar{D}^0)/\Gamma_{\text{total}} \times B(\bar{b} \rightarrow B_c)] / [B(\bar{b} \rightarrow B^+)] / [B(B^+ \rightarrow \bar{D}^0 D^+)] < 0.9 \times 10^{-3}$ which we multiply by our best values $B(\bar{b} \rightarrow B^+) = 40.8 \times 10^{-2}$, $B(B^+ \rightarrow \bar{D}^0 D^+) = 3.8 \times 10^{-4}$.

 $\Gamma(D_s^+ D^0)/\Gamma_{\text{total}} \times B(\bar{b} \rightarrow B_c)$ $\Gamma_{29}/\Gamma \times B$

VALUE	CL%	DOCUMENT ID	TECN	COMMENT
$< 6 \times 10^{-8}$	90	¹ AAIJ	18P LHCB	pp at 7, 8 TeV

¹ AAIJ 18P reports $[\Gamma(B_c^+ \rightarrow D_s^+ D^0)/\Gamma_{\text{total}} \times B(\bar{b} \rightarrow B_c)] / [B(\bar{b} \rightarrow B^+)] / [B(B^+ \rightarrow \bar{D}^0 D^+)] < 3.7 \times 10^{-4}$ which we multiply by our best values $B(\bar{b} \rightarrow B^+) = 40.8 \times 10^{-2}$, $B(B^+ \rightarrow \bar{D}^0 D^+) = 3.8 \times 10^{-4}$.

 $\Gamma(D^+ \bar{D}^0)/\Gamma_{\text{total}} \times B(\bar{b} \rightarrow B_c)$ $\Gamma_{30}/\Gamma \times B$

VALUE	CL%	DOCUMENT ID	TECN	COMMENT
$< 3.0 \times 10^{-6}$	90	¹ AAIJ	18P LHCB	pp at 7, 8 TeV

¹ AAIJ 18P reports $[\Gamma(B_c^+ \rightarrow D^+ \bar{D}^0)/\Gamma_{\text{total}} \times B(\bar{b} \rightarrow B_c)] / [B(\bar{b} \rightarrow B^+)] / [B(B^+ \rightarrow \bar{D}^0 D^+)] < 1.9 \times 10^{-2}$ which we multiply by our best values $B(\bar{b} \rightarrow B^+) = 40.8 \times 10^{-2}$, $B(B^+ \rightarrow \bar{D}^0 D^+) = 3.8 \times 10^{-4}$.

 $\Gamma(D^+ D^0)/\Gamma_{\text{total}} \times B(\bar{b} \rightarrow B_c)$ $\Gamma_{31}/\Gamma \times B$

VALUE	CL%	DOCUMENT ID	TECN	COMMENT
$< 1.9 \times 10^{-6}$	90	¹ AAIJ	18P LHCB	Repl. by AAIJ 21AF

¹ AAIJ 18P reports $[\Gamma(B_c^+ \rightarrow D^+ D^0)/\Gamma_{\text{total}} \times B(\bar{b} \rightarrow B_c)] / [B(\bar{b} \rightarrow B^+)] / [B(B^+ \rightarrow \bar{D}^0 D^+)] < 1.2 \times 10^{-2}$ which we multiply by our best values $B(\bar{b} \rightarrow B^+) = 40.8 \times 10^{-2}$, $B(B^+ \rightarrow \bar{D}^0 D^+) = 3.8 \times 10^{-4}$.

 $[\Gamma(D_s^{*+} \bar{D}^0) + \Gamma(D_s^+ \bar{D}^*(2007^0))]/\Gamma_{\text{total}} \times B(\bar{b} \rightarrow B_c)$ $(\Gamma_{32} + \Gamma_{33})/\Gamma \times B$

VALUE	CL%	DOCUMENT ID	TECN	COMMENT
$< 4 \times 10^{-7}$	90	¹ AAIJ	18P LHCB	Repl. by AAIJ 21AF

¹ AAIJ 18P reports $[\Gamma(B_c^+ \rightarrow D_s^{*+} \bar{D}^0) + \Gamma(B_c^+ \rightarrow D_s^+ \bar{D}^*(2007^0))]/\Gamma_{\text{total}} \times B(\bar{b} \rightarrow B_c)] / [B(\bar{b} \rightarrow B^+)] / [B(B^+ \rightarrow \bar{D}^0 D^+)] < 2.8 \times 10^{-3}$ which we multiply by our best values $B(\bar{b} \rightarrow B^+) = 40.8 \times 10^{-2}$, $B(B^+ \rightarrow \bar{D}^0 D^+) = 3.8 \times 10^{-4}$.

 $[\Gamma(D_s^{*+} D^0) + \Gamma(D_s^+ D^*(2007^0))]/\Gamma_{\text{total}} \times B(\bar{b} \rightarrow B_c)$ $(\Gamma_{34} + \Gamma_{35})/\Gamma \times B$

VALUE	CL%	DOCUMENT ID	TECN	COMMENT
$< 5 \times 10^{-7}$	90	¹ AAIJ	18P LHCB	Repl. by AAIJ 21AF

¹ AAIJ 18P reports $[\Gamma(B_c^+ \rightarrow D_s^{*+} D^0) + \Gamma(B_c^+ \rightarrow D_s^+ D^*(2007^0))]/\Gamma_{\text{total}} \times B(\bar{b} \rightarrow B_c)] / [B(\bar{b} \rightarrow B^+)] / [B(B^+ \rightarrow \bar{D}^0 D^+)] < 3.0 \times 10^{-3}$ which we multiply by our best values $B(\bar{b} \rightarrow B^+) = 40.8 \times 10^{-2}$, $B(B^+ \rightarrow \bar{D}^0 D^+) = 3.8 \times 10^{-4}$.

 $\Gamma(D^*(2010)^+ \bar{D}^0)/\Gamma_{\text{total}} \times B(\bar{b} \rightarrow B_c)$ $\Gamma_{36}/\Gamma \times B$

VALUE	CL%	DOCUMENT ID	TECN	COMMENT
$< 6.2 \times 10^{-3}$	90	¹ BARATE	98Q ALEP	$e^+e^- \rightarrow Z$

¹ BARATE 98Q reports $B(Z \rightarrow B_c X) \times B(B_c \rightarrow D^*(2010)^+ \bar{D}^0) < 1.9 \times 10^{-3}$ at 90%CL. We rescale to our PDG 98 values of $B(Z \rightarrow b\bar{b})$.

 $[\Gamma(D^*(2010)^+ \bar{D}^0, D^{*+} \rightarrow D^+ \pi^0/\gamma) + \Gamma(D^+ \bar{D}^*(2007^0))]/\Gamma_{\text{total}} \times B(\bar{b} \rightarrow B_c)$ $(\Gamma_{37} + \Gamma_{38})/\Gamma \times B$

VALUE	CL%	DOCUMENT ID	TECN	COMMENT
$< 9 \times 10^{-6}$	90	¹ AAIJ	18P LHCB	Repl. by AAIJ 21AF

¹ AAIJ 18P reports $[\Gamma(B_c^+ \rightarrow D^*(2010)^+ \bar{D}^0, D^{*+} \rightarrow D^+ \pi^0/\gamma) + \Gamma(B_c^+ \rightarrow D^+ \bar{D}^*(2007^0))]/\Gamma_{\text{total}} \times B(\bar{b} \rightarrow B_c)] / [B(\bar{b} \rightarrow B^+)] / [B(B^+ \rightarrow \bar{D}^0 D^+)] < 5.5 \times 10^{-2}$ which we multiply by our best values $B(\bar{b} \rightarrow B^+) = 40.8 \times 10^{-2}$, $B(B^+ \rightarrow \bar{D}^0 D^+) = 3.8 \times 10^{-4}$.

 $[\Gamma(D^*(2010)^+ D^0, D^{*+} \rightarrow D^+ \pi^0/\gamma) + \Gamma(D^+ D^*(2007^0))]/\Gamma_{\text{total}} \times B(\bar{b} \rightarrow B_c)$ $(\Gamma_{40} + \Gamma_{41})/\Gamma \times B$

VALUE	CL%	DOCUMENT ID	TECN	COMMENT
$< 3.4 \times 10^{-6}$	90	¹ AAIJ	18P LHCB	Repl. by AAIJ 21AF

¹ AAIJ 18P reports $[\Gamma(B_c^+ \rightarrow D^*(2010)^+ D^0, D^{*+} \rightarrow D^+ \pi^0/\gamma) + \Gamma(B_c^+ \rightarrow D^+ D^*(2007^0))]/\Gamma_{\text{total}} \times B(\bar{b} \rightarrow B_c)] / [B(\bar{b} \rightarrow B^+)] / [B(B^+ \rightarrow \bar{D}^0 D^+)] < 2.2 \times 10^{-2}$ which we multiply by our best values $B(\bar{b} \rightarrow B^+) = 40.8 \times 10^{-2}$, $B(B^+ \rightarrow \bar{D}^0 D^+) = 3.8 \times 10^{-4}$.

 $\Gamma(D_s^{*+} \bar{D}^*(2007^0))/\Gamma_{\text{total}} \times B(\bar{b} \rightarrow B_c)$ $\Gamma_{42}/\Gamma \times B$

VALUE	CL%	DOCUMENT ID	TECN	COMMENT
$< 1.7 \times 10^{-6}$	90	¹ AAIJ	18P LHCB	Repl. by AAIJ 21AF

¹ AAIJ 18P reports $[\Gamma(B_c^+ \rightarrow D_s^{*+} \bar{D}^*(2007^0))/\Gamma_{\text{total}} \times B(\bar{b} \rightarrow B_c)] / [B(\bar{b} \rightarrow B^+)] / [B(B^+ \rightarrow \bar{D}^0 D^+)] < 1.1 \times 10^{-2}$ which we multiply by our best values $B(\bar{b} \rightarrow B^+) = 40.8 \times 10^{-2}$, $B(B^+ \rightarrow \bar{D}^0 D^+) = 3.8 \times 10^{-4}$.

 $\Gamma(D_s^{*+} D^*(2007^0))/\Gamma_{\text{total}} \times B(\bar{b} \rightarrow B_c)$ $\Gamma_{43}/\Gamma \times B$

VALUE	CL%	DOCUMENT ID	TECN	COMMENT
$< 3.1 \times 10^{-6}$	90	¹ AAIJ	18P LHCB	Repl. by AAIJ 21AF

¹ AAIJ 18P reports $[\Gamma(B_c^+ \rightarrow D_s^{*+} D^*(2007^0))/\Gamma_{\text{total}} \times B(\bar{b} \rightarrow B_c)] / [B(\bar{b} \rightarrow B^+)] / [B(B^+ \rightarrow \bar{D}^0 D^+)] < 2.0 \times 10^{-2}$ which we multiply by our best values $B(\bar{b} \rightarrow B^+) = 40.8 \times 10^{-2}$, $B(B^+ \rightarrow \bar{D}^0 D^+) = 3.8 \times 10^{-4}$.

Meson Particle Listings

 B_c^+ $\Gamma(D^*(2010)+\bar{D}^*(2007)^0)/\Gamma_{\text{total}} \times B(\bar{B} \rightarrow B_c)$ $\Gamma_{44}/\Gamma \times B$

VALUE	CL%	DOCUMENT ID	TECN	COMMENT
$<1.0 \times 10^{-4}$	90	¹ AAIJ	18P LHCb	Repl. by AAIJ 21AF

• • • We do not use the following data for averages, fits, limits, etc. • • •

¹ AAIJ 18P reports $[\Gamma(B_c^+ \rightarrow D^*(2010)+\bar{D}^*(2007)^0)/\Gamma_{\text{total}} \times B(\bar{B} \rightarrow B_c)] / [B(\bar{B} \rightarrow B^+) / [B(B^+ \rightarrow \bar{D}^0 D^+)]] < 1.3 \times 10^{-1}$ which we multiply by our best values $B(\bar{B} \rightarrow B^+) = 40.8 \times 10^{-2}$, $B(B^+ \rightarrow \bar{D}^0 D^+) = 3.8 \times 10^{-4}$.

 $\Gamma(D^*(2010)+D^*(2007)^0)/\Gamma_{\text{total}} \times B(\bar{B} \rightarrow B_c)$ $\Gamma_{45}/\Gamma \times B$

VALUE	CL%	DOCUMENT ID	TECN	COMMENT
$<2.0 \times 10^{-5}$	90	¹ AAIJ	18P LHCb	Repl. by AAIJ 21AF

• • • We do not use the following data for averages, fits, limits, etc. • • •

¹ AAIJ 18P reports $[\Gamma(B_c^+ \rightarrow D^*(2010)+D^*(2007)^0)/\Gamma_{\text{total}} \times B(\bar{B} \rightarrow B_c)] / [B(\bar{B} \rightarrow B^+) / [B(B^+ \rightarrow \bar{D}^0 D^+)]] < 1.3 \times 10^{-1}$ which we multiply by our best values $B(\bar{B} \rightarrow B^+) = 40.8 \times 10^{-2}$, $B(B^+ \rightarrow \bar{D}^0 D^+) = 3.8 \times 10^{-4}$.

 $\Gamma(D^+ K^{*0})/\Gamma_{\text{total}} \times B(\bar{B} \rightarrow B_c)$ $\Gamma_{46}/\Gamma \times B$

VALUE	CL%	DOCUMENT ID	TECN	COMMENT
$<2.0 \times 10^{-7}$	90	¹ AAIJ	13R LHCb	<i>pp</i> at 7 TeV

¹ AAIJ 13R reports $[\Gamma(B_c^+ \rightarrow D^+ K^{*0})/\Gamma_{\text{total}} \times B(\bar{B} \rightarrow B_c)] / [B(\bar{B} \rightarrow B^+) < 0.5 \times 10^{-6}$ which we multiply by our best value $B(\bar{B} \rightarrow B^+) = 40.8 \times 10^{-2}$.

 $\Gamma(D^+ \bar{K}^{*0})/\Gamma_{\text{total}} \times B(\bar{B} \rightarrow B_c)$ $\Gamma_{47}/\Gamma \times B$

VALUE	CL%	DOCUMENT ID	TECN	COMMENT
$<1.6 \times 10^{-7}$	90	¹ AAIJ	13R LHCb	<i>pp</i> at 7 TeV

¹ AAIJ 13R reports $[\Gamma(B_c^+ \rightarrow D^+ \bar{K}^{*0})/\Gamma_{\text{total}} \times B(\bar{B} \rightarrow B_c)] / [B(\bar{B} \rightarrow B^+) < 0.4 \times 10^{-6}$ which we multiply by our best value $B(\bar{B} \rightarrow B^+) = 40.8 \times 10^{-2}$.

 $\Gamma(D_s^+ K^{*0})/\Gamma_{\text{total}} \times B(\bar{B} \rightarrow B_c)$ $\Gamma_{48}/\Gamma \times B$

VALUE	CL%	DOCUMENT ID	TECN	COMMENT
$<2.9 \times 10^{-7}$	90	¹ AAIJ	13R LHCb	<i>pp</i> at 7 TeV

¹ AAIJ 13R reports $[\Gamma(B_c^+ \rightarrow D_s^+ K^{*0})/\Gamma_{\text{total}} \times B(\bar{B} \rightarrow B_c)] / [B(\bar{B} \rightarrow B^+) < 0.7 \times 10^{-6}$ which we multiply by our best value $B(\bar{B} \rightarrow B^+) = 40.8 \times 10^{-2}$.

 $\Gamma(D_s^+ \bar{K}^{*0})/\Gamma_{\text{total}} \times B(\bar{B} \rightarrow B_c)$ $\Gamma_{49}/\Gamma \times B$

VALUE	CL%	DOCUMENT ID	TECN	COMMENT
$<4 \times 10^{-7}$	90	¹ AAIJ	13R LHCb	<i>pp</i> at 7 TeV

¹ AAIJ 13R reports $[\Gamma(B_c^+ \rightarrow D_s^+ \bar{K}^{*0})/\Gamma_{\text{total}} \times B(\bar{B} \rightarrow B_c)] / [B(\bar{B} \rightarrow B^+) < 1.1 \times 10^{-6}$ which we multiply by our best value $B(\bar{B} \rightarrow B^+) = 40.8 \times 10^{-2}$.

 $\Gamma(D_s^+ \phi)/\Gamma_{\text{total}} \times B(\bar{B} \rightarrow B_c)$ $\Gamma_{50}/\Gamma \times B$

VALUE	CL%	DOCUMENT ID	TECN	COMMENT
$<3.3 \times 10^{-7}$	90	¹ AAIJ	13R LHCb	<i>pp</i> at 7 TeV

¹ AAIJ 13R reports $[\Gamma(B_c^+ \rightarrow D_s^+ \phi)/\Gamma_{\text{total}} \times B(\bar{B} \rightarrow B_c)] / [B(\bar{B} \rightarrow B^+) < 0.8 \times 10^{-6}$ which we multiply by our best value $B(\bar{B} \rightarrow B^+) = 40.8 \times 10^{-2}$.

 $\Gamma(K^+ K^0)/\Gamma_{\text{total}} \times B(\bar{B} \rightarrow B_c)$ $\Gamma_{51}/\Gamma \times B$

VALUE	CL%	DOCUMENT ID	TECN	COMMENT
$<4.6 \times 10^{-7}$	90	¹ AAIJ	13Bs LHCb	<i>pp</i> at 7 TeV

¹ Derived from $\Gamma(K^+ K^0)/\Gamma \times B(\bar{B} \rightarrow B_c) / (B(B^+ \rightarrow K^0 \pi^+) B(\bar{B} \rightarrow B^+)) < 5.8\%$ at 90% CL using normalization mode $B(B^+ \rightarrow K^0 \pi^+) = (23.97 \pm 0.53 \pm 0.71) \times 10^{-6}$ and assuming a B production ratio $f(\bar{B} \rightarrow B_c^+) = 0.33$.

 $\Gamma(B_s^0 \pi^+ / B(\bar{B} \rightarrow B_s)) / \Gamma_{\text{total}} \times B(\bar{B} \rightarrow B_c)$ $\Gamma_{52}/\Gamma \times B$

VALUE (units 10^{-3})	CL%	DOCUMENT ID	TECN	COMMENT
$2.37 \pm 0.31 \pm 0.11^{+0.17}_{-0.13}$		¹ AAIJ	13Bu LHCb	<i>pp</i> at 7, 8 TeV

¹ The last uncertainty is due to the uncertainty of the B_c^+ lifetime measurement.

 $\Gamma(D_s^+ \bar{D}^0)/\Gamma_{\text{total}}$ Γ_{28}/Γ

VALUE	CL%	DOCUMENT ID	TECN	COMMENT
$<7.2 \times 10^{-4}$	90	¹ AAIJ	21AF LHCb	<i>pp</i> at 13 TeV

¹ Uses $B(\bar{B} \rightarrow B_c)/B(\bar{B} \rightarrow B^+) = 0.76\%$ determined by AAIJ 19AI.

 $\Gamma(D_s^+ D^0)/\Gamma_{\text{total}}$ Γ_{29}/Γ

VALUE	CL%	DOCUMENT ID	TECN	COMMENT
$<3.0 \times 10^{-4}$	90	¹ AAIJ	21AF LHCb	<i>pp</i> at 13 TeV

¹ Uses $B(\bar{B} \rightarrow B_c)/B(\bar{B} \rightarrow B^+) = 0.76\%$ determined by AAIJ 19AI.

 $\Gamma(D^+ \bar{D}^0)/\Gamma_{\text{total}}$ Γ_{30}/Γ

VALUE	CL%	DOCUMENT ID	TECN	COMMENT
$<1.9 \times 10^{-4}$	90	¹ AAIJ	21AF LHCb	<i>pp</i> at 13 TeV

¹ Uses $B(\bar{B} \rightarrow B_c)/B(\bar{B} \rightarrow B^+) = 0.76\%$ determined by AAIJ 19AI.

 $\Gamma(D^+ D^0)/\Gamma_{\text{total}}$ Γ_{31}/Γ

VALUE	CL%	DOCUMENT ID	TECN	COMMENT
$<1.4 \times 10^{-4}$	90	¹ AAIJ	21AF LHCb	<i>pp</i> at 13 TeV

¹ Uses $B(\bar{B} \rightarrow B_c)/B(\bar{B} \rightarrow B^+) = 0.76\%$ determined by AAIJ 19AI.

 $\Gamma(D_s^+ \bar{D}^0)/\Gamma_{\text{total}}$ Γ_{32}/Γ

VALUE	CL%	DOCUMENT ID	TECN	COMMENT
$<5.3 \times 10^{-4}$	90	¹ AAIJ	21AF LHCb	<i>pp</i> at 13 TeV

¹ Uses $B(\bar{B} \rightarrow B_c)/B(\bar{B} \rightarrow B^+) = 0.76\%$ determined by AAIJ 19AI.

 $\Gamma(D_s^+ \bar{D}^*(2007)^0)/\Gamma_{\text{total}}$ Γ_{33}/Γ

VALUE	CL%	DOCUMENT ID	TECN	COMMENT
$<4.6 \times 10^{-4}$	90	¹ AAIJ	21AF LHCb	<i>pp</i> at 13 TeV

¹ Uses $B(\bar{B} \rightarrow B_c)/B(\bar{B} \rightarrow B^+) = 0.76\%$ determined by AAIJ 19AI.

 $\Gamma(D_s^+ D^0)/\Gamma_{\text{total}}$ Γ_{34}/Γ

VALUE	CL%	DOCUMENT ID	TECN	COMMENT
$<0.9 \times 10^{-3}$	90	¹ AAIJ	21AF LHCb	<i>pp</i> at 13 TeV

¹ Uses $B(\bar{B} \rightarrow B_c)/B(\bar{B} \rightarrow B^+) = 0.76\%$ determined by AAIJ 19AI.

 $\Gamma(D_s^+ D^*(2007)^0)/\Gamma_{\text{total}}$ Γ_{35}/Γ

VALUE	CL%	DOCUMENT ID	TECN	COMMENT
$<6.6 \times 10^{-4}$	90	¹ AAIJ	21AF LHCb	<i>pp</i> at 13 TeV

¹ Uses $B(\bar{B} \rightarrow B_c)/B(\bar{B} \rightarrow B^+) = 0.76\%$ determined by AAIJ 19AI.

 $\Gamma(D^*(2010)+\bar{D}^0)/\Gamma_{\text{total}}$ Γ_{36}/Γ

VALUE	CL%	DOCUMENT ID	TECN	COMMENT
$<3.8 \times 10^{-4}$	90	¹ AAIJ	21AF LHCb	<i>pp</i> at 13 TeV

¹ Uses $B(\bar{B} \rightarrow B_c)/B(\bar{B} \rightarrow B^+) = 0.76\%$ determined by AAIJ 19AI.

 $\Gamma(D^*(2007)+D^0)/\Gamma_{\text{total}}$ Γ_{39}/Γ

VALUE	CL%	DOCUMENT ID	TECN	COMMENT
$<2.0 \times 10^{-4}$	90	¹ AAIJ	21AF LHCb	<i>pp</i> at 13 TeV

¹ Uses $B(\bar{B} \rightarrow B_c)/B(\bar{B} \rightarrow B^+) = 0.76\%$ determined by AAIJ 19AI.

 $\Gamma(D^+ \bar{D}^*(2007)^0)/\Gamma_{\text{total}}$ Γ_{38}/Γ

VALUE	CL%	DOCUMENT ID	TECN	COMMENT
$<6.5 \times 10^{-4}$	90	¹ AAIJ	21AF LHCb	<i>pp</i> at 13 TeV

¹ Uses $B(\bar{B} \rightarrow B_c)/B(\bar{B} \rightarrow B^+) = 0.76\%$ determined by AAIJ 19AI.

 $\Gamma(D^+ D^*(2007)^0)/\Gamma_{\text{total}}$ Γ_{41}/Γ

VALUE	CL%	DOCUMENT ID	TECN	COMMENT
$<3.7 \times 10^{-4}$	90	¹ AAIJ	21AF LHCb	<i>pp</i> at 13 TeV

¹ Uses $B(\bar{B} \rightarrow B_c)/B(\bar{B} \rightarrow B^+) = 0.76\%$ determined by AAIJ 19AI.

 $\Gamma(D_s^+ \bar{D}^*(2007)^0)/\Gamma_{\text{total}}$ Γ_{42}/Γ

VALUE	CL%	DOCUMENT ID	TECN	COMMENT
$<1.3 \times 10^{-3}$	90	¹ AAIJ	21AF LHCb	<i>pp</i> at 13 TeV

¹ Uses $B(\bar{B} \rightarrow B_c)/B(\bar{B} \rightarrow B^+) = 0.76\%$ determined by AAIJ 19AI.

 $\Gamma(D_s^+ D^*(2007)^0)/\Gamma_{\text{total}}$ Γ_{43}/Γ

VALUE	CL%	DOCUMENT ID	TECN	COMMENT
$<1.3 \times 10^{-3}$	90	¹ AAIJ	21AF LHCb	<i>pp</i> at 13 TeV

¹ Uses $B(\bar{B} \rightarrow B_c)/B(\bar{B} \rightarrow B^+) = 0.76\%$ determined by AAIJ 19AI.

 $\Gamma(D^*(2010)+\bar{D}^*(2007)^0)/\Gamma_{\text{total}}$ Γ_{44}/Γ

VALUE	CL%	DOCUMENT ID	TECN	COMMENT
$<1.0 \times 10^{-3}$	90	¹ AAIJ	21AF LHCb	<i>pp</i> at 13 TeV

¹ Uses $B(\bar{B} \rightarrow B_c)/B(\bar{B} \rightarrow B^+) = 0.76\%$ determined by AAIJ 19AI.

 $\Gamma(D^*(2010)+D^*(2007)^0)/\Gamma_{\text{total}}$ Γ_{45}/Γ

VALUE	CL%	DOCUMENT ID	TECN	COMMENT
$<7.7 \times 10^{-4}$	90	¹ AAIJ	21AF LHCb	<i>pp</i> at 13 TeV

¹ Uses $B(\bar{B} \rightarrow B_c)/B(\bar{B} \rightarrow B^+) = 0.76\%$ determined by AAIJ 19AI.

 $\Gamma(B_s^0 \pi^+)/\Gamma(J/\psi(1S)\pi^+)$ Γ_{53}/Γ_4

VALUE	DOCUMENT ID	TECN	COMMENT
$91 \pm 10 \pm 8.5$	¹ AAIJ	23M LHCb	<i>pp</i> at 13 TeV

¹ The B_s^0 mesons are reconstructed via the decays $B_s^0 \rightarrow J/\psi \phi$ and $B_s^0 \rightarrow D_s^- \pi^+$. The third uncertainty includes systematic (± 8) and imprecise knowledge of the branching fractions (± 3).

POLARIZATION IN B_c^+ DECAY

In decays involving two vector mesons, one can distinguish among the states in which meson polarizations are both longitudinal (L) or both are transverse and parallel (\parallel) or perpendicular (\perp) to each other with the parameters Γ_L/Γ , Γ_\perp/Γ , and the relative phases ϕ_\parallel and ϕ_\perp . See the definitions in the note on "Polarization in B Decays" review in the B^0 Particle Listings.

 Γ_L/Γ in $B_c^+ \rightarrow J/\psi D_s^{*\pm}$

VALUE	DOCUMENT ID	TECN	COMMENT
0.34 ± 0.09 OUR AVERAGE			

$0.30 \pm 0.10 \pm 0.04$	^{1,2} AAD	22o ATLS	pp at 13 TeV
0.48 ± 0.20	³ AAIJ	13As LHCB	pp at 7, 8 TeV
0.62 ± 0.24	⁴ AAD	16H ATLS	pp at 7, 8 TeV

- ¹ Supersedes the measurement of AAD 16H.
- ² AAD 22o measures $1 - \Gamma_L/\Gamma = 0.70 \pm 0.10 \pm 0.04$.
- ³ AAIJ 13As measures $1 - \Gamma_L/\Gamma = 0.52 \pm 0.20$.
- ⁴ AAD 16H measures $1 - \Gamma_L/\Gamma = 0.38 \pm 0.24$.

 $A_P(B_c^+)$

$$A_P(B_c^+) = [\sigma(B_c^-) - \sigma(B_c^+)] / [\sigma(B_c^-) + \sigma(B_c^+)]$$

VALUE (units 10^{-2})	DOCUMENT ID	TECN	COMMENT
-1.0 ± 1.0 OUR AVERAGE			

$-2.5 \pm 2.1 \pm 0.5$	¹ AAIJ	19Al LHCB	pp at 7 TeV
$-0.5 \pm 1.1 \pm 0.4$	¹ AAIJ	19Al LHCB	pp at 13 TeV

- ¹ Measured using B_c^+ semileptonic decays.

 B_c^+ REFERENCES

AAIJ	23M	JHEP 2307 066	R. Aaij <i>et al.</i>	(LHCb Collab.)
AAD	22O	JHEP 2208 087	G. Aad <i>et al.</i>	(ATLAS Collab.)
AAIJ	22P	JHEP 2201 065	R. Aaij <i>et al.</i>	(LHCb Collab.)
AABOUD	21	PR D104 012010	M. Aaboud <i>et al.</i>	(ATLAS Collab.)
AAIJ	21AF	JHEP 2112 117	R. Aaij <i>et al.</i>	(LHCb Collab.)
AAIJ	20R	JHEP 2007 123	R. Aaij <i>et al.</i>	(LHCb Collab.)
AAIJ	19AI	PR D100 112006	R. Aaij <i>et al.</i>	(LHCb Collab.)
AAIJ	18C	PRL 120 121801	R. Aaij <i>et al.</i>	(LHCb Collab.)
AAIJ	18P	NP B930 563	R. Aaij <i>et al.</i>	(LHCb Collab.)
SIRUNYAN	18BY	EPJ C78 457	A.M. Sirunyan <i>et al.</i>	(CMS Collab.)
AAIJ	17AG	PRL 118 111803	R. Aaij <i>et al.</i>	(LHCb Collab.)
AAIJ	17L	PR D95 032005	R. Aaij <i>et al.</i>	(LHCb Collab.)
AAD	16H	EPJ C76 4	G. Aad <i>et al.</i>	(ATLAS Collab.)
AAIJ	16AF	JHEP 1609 153	R. Aaij <i>et al.</i>	(LHCb Collab.)
AAIJ	16AT	PR D94 091102	R. Aaij <i>et al.</i>	(LHCb Collab.)
AAIJ	16K	PL B759 313	R. Aaij <i>et al.</i>	(LHCb Collab.)
AALTONEN	16A	PR D93 052001	T. Aaltonen <i>et al.</i>	(CDF Collab.)
AAIJ	15AY	PR D92 072007	R. Aaij <i>et al.</i>	(LHCb Collab.)
AAIJ	15G	PL B742 29	R. Aaij <i>et al.</i>	(LHCb Collab.)
AAIJ	15M	PRL 114 132001	R. Aaij <i>et al.</i>	(LHCb Collab.)
KHACHATRYAN...	15AA	JHEP 1501 063	V. Khachatryan <i>et al.</i>	(CMS Collab.)
AAIJ	14AQ	PRL 113 152003	R. Aaij <i>et al.</i>	(LHCb Collab.)
AAIJ	14G	EPJ C74 2839	R. Aaij <i>et al.</i>	(LHCb Collab.)
AAIJ	14P	JHEP 1405 148	R. Aaij <i>et al.</i>	(LHCb Collab.)
AAIJ	14W	PR D90 032009	R. Aaij <i>et al.</i>	(LHCb Collab.)
AAIJ	13AM	PR D87 071103	R. Aaij <i>et al.</i>	(LHCb Collab.)
AAIJ	13AS	PR D87 112012	R. Aaij <i>et al.</i>	(LHCb Collab.)
Also	13BS	PR D89 019901 (err.)	R. Aaij <i>et al.</i>	(LHCb Collab.)
AAIJ	13BU	PRL 111 181801	R. Aaij <i>et al.</i>	(LHCb Collab.)
AAIJ	13BY	JHEP 1309 075	R. Aaij <i>et al.</i>	(LHCb Collab.)
AAIJ	13CA	JHEP 1311 094	R. Aaij <i>et al.</i>	(LHCb Collab.)
AAIJ	13R	JHEP 1302 043	R. Aaij <i>et al.</i>	(LHCb Collab.)
AALTONEN	13	PR D87 011101	T. Aaltonen <i>et al.</i>	(CDF Collab.)
AAIJ	12AV	PRL 109 232001	R. Aaij <i>et al.</i>	(LHCb Collab.)
AAIJ	12Y	PRL 108 251802	R. Aaij <i>et al.</i>	(LHCb Collab.)
ABAZOV	09H	PRL 102 092001	V.M. Abazov <i>et al.</i>	(D0 Collab.)
AALTONEN	08M	PRL 100 182002	T. Aaltonen <i>et al.</i>	(CDF Collab.)
ABAZOV	08T	PRL 101 012001	V.M. Abazov <i>et al.</i>	(D0 Collab.)
ABULENCIA	06C	PRL 96 082002	A. Abulencia <i>et al.</i>	(CDF Collab.)
ABULENCIA	06O	PRL 97 012002	A. Abulencia <i>et al.</i>	(CDF Collab.)
ABE	98M	PRL 81 2432	F. Abe <i>et al.</i>	(CDF Collab.)
Also	98P	PR D58 112004	F. Abe <i>et al.</i>	(CDF Collab.)
ACKERSTAFF	98O	PL B420 157	K. Ackerstaff <i>et al.</i>	(OPAL Collab.)
BARATE	98Q	EPJ C4 387	R. Barate <i>et al.</i>	(ALEPH Collab.)
PDG	98	EPJ C3 1	C. Caso <i>et al.</i>	(PDG Collab.)
ABREU	97E	PL B398 207	P. Abreu <i>et al.</i>	(DELPHI Collab.)
BARATE	97H	PL B402 213	R. Barate <i>et al.</i>	(ALEPH Collab.)
ABE	96R	PRL 77 5176	F. Abe <i>et al.</i>	(CDF Collab.)
PDG	96	PR D54 1	R. M. Barnett <i>et al.</i>	(PDG Collab.)

 $B_c(2S)^\pm$

$$I(J^P) = 0(0^-)$$

Quantum numbers neither measured nor confirmed.

 $B_c(2S)^\pm$ MASS

VALUE (MeV)	EVTS	DOCUMENT ID	TECN	COMMENT
6871.2 ± 1.0 OUR AVERAGE				
$6871.7 \pm 1.3 \pm 0.3$	24	^{1,2} AAIJ	19Y LHCB	pp at 7, 8, 13 TeV
$6870.6 \pm 1.4 \pm 0.3$	51	^{3,4} SIRUNYAN	19M CMS	pp at 13 TeV
not seen		⁵ AAIJ	18AL LHCB	pp at 8 TeV
$6842 \pm 4 \pm 5$	57	^{6,7} AAD	14AQ ATLS	pp at 7, 8 TeV

- • • We do not use the following data for averages, fits, limits, etc. • • •
- not seen
- ¹ AAIJ 19Y observed $B_c(2S)^+$ in the decay mode $B_c(2S)^+ \rightarrow B_c^+ \pi^+ \pi^-$ ($B_c^+ \rightarrow J/\psi \pi^+$) with 2.2 (3.2) global (local) standard deviations significance.
- ² AAIJ 19Y reports mass difference measurement of $M(B_c(2S)^+) - M(B_c^+) = 597.2 \pm 1.3 \pm 0.1$ MeV. We have adjusted this measurement with our best value of $M(B_c^+) = 6274.47 \pm 0.32$ MeV. The first uncertainty of the $M(B_c(2S)^+)$ value is a total of uncertainties reported by the experiment and the second one comes from our best value of $M(B_c^+)$.
- ³ SIRUNYAN 19M observed $B_c(2S)^+$ in the decay mode $B_c(2S)^+ \rightarrow B_c^+ \pi^+ \pi^-$ ($B_c^+ \rightarrow J/\psi \pi^+$) with 6.5 standard deviations significance.
- ⁴ SIRUNYAN 19M reports mass difference measurement of $M(B_c(2S)^+) - M(B_c^+) = 596.1 \pm 1.2 \pm 0.8$ MeV. We have adjusted this measurement with our best value of $M(B_c^+) = 6274.47 \pm 0.32$ MeV. The first uncertainty of the $M(B_c(2S)^+)$ value is a total of uncertainties reported by the experiment and the second one comes from our best value of $M(B_c^+)$.
- ⁵ AAIJ 18AL reports an upper limit on the ratio of production cross sections for $[\sigma(B_c(2S)^+)/\sigma(B_c^+)] \cdot B(B_c(2S)^+ \rightarrow B_c^+ \pi^+ \pi^-) < 0.04-0.09$ at 95% CL for the mass value reported by AAD 14AQ.
- ⁶ Observed in the decay mode $B_c(2S)^+ \rightarrow B_c^+ \pi^+ \pi^-$ ($B_c^+ \rightarrow J/\psi \pi^+$) with 5.2 standard deviations significance.
- ⁷ Might be the $B_c^*(2S)$.

 $B_c(2S)^\pm$ DECAY MODES $\times B(\bar{b} \rightarrow B_c(2S))$

The following quantities are not pure branching ratios; rather the fractions $\Gamma_j/\Gamma \times B(\bar{b} \rightarrow B_c(2S))$.

Mode	Fraction (Γ_j/Γ)
Γ_1 $B_c^+ \pi^+ \pi^-$	seen

 $B_c(2S)^\pm$ BRANCHING RATIOS

$$\Gamma(B_c^+ \pi^+ \pi^-)/\Gamma_{\text{total}} \quad \Gamma_1/\Gamma$$

VALUE	EVTS	DOCUMENT ID	TECN	COMMENT
seen		SIRUNYAN	19M CMS	pp at 13 TeV
seen	57	¹ AAD	14AQ ATLS	pp at 7, 8 TeV
not seen		² AAIJ	18AL LHCB	pp at 8 TeV

- • • We do not use the following data for averages, fits, limits, etc. • • •
- not seen
- ¹ Observed with 5.2 standard deviations significance.
- ² AAIJ 18AL reports an upper limit on the ratio of production cross sections for $[\sigma(B_c(2S)^+)/\sigma(B_c^+)] \cdot B(B_c(2S)^+ \rightarrow B_c^+ \pi^+ \pi^-) < 0.04-0.09$ at 95% CL for the mass value reported by AAD 14AQ.

 $B_c(2S)^\pm$ REFERENCES

AAIJ	19Y	PRL 122 232001	R. Aaij <i>et al.</i>	(LHCb Collab.)
SIRUNYAN	19M	PRL 122 132001	A.M. Sirunyan <i>et al.</i>	(CMS Collab.)
AAIJ	18AL	JHEP 1801 138	R. Aaij <i>et al.</i>	(LHCb Collab.)
AAD	14AQ	PRL 113 212004	G. Aad <i>et al.</i>	(ATLAS Collab.)

See the related review(s):

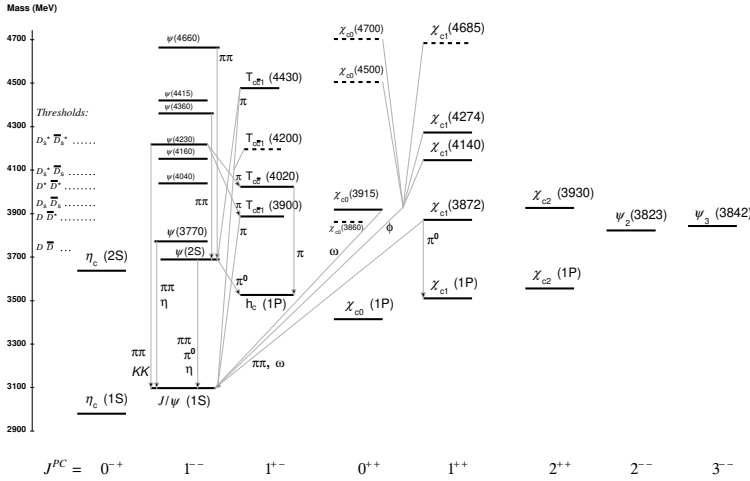
Spectroscopy of Mesons Containing Two Heavy Quarks

Meson Particle Listings

Charmonium, $\eta_c(1S)$

$c\bar{c}$ MESONS (including possibly non- $q\bar{q}$ states)

Updated March 2024.



The level scheme of meson states containing a minimal quark content of $c\bar{c}$ and having $S = C = B = 0$. The name of a state is determined by its quantum numbers $I^G J^{PC}$ (see the review “Naming Scheme for Hadrons”). States included in the Summary Tables are shown with solid lines; selected states not in the Summary Tables, but with assigned quantum numbers, are shown with dotted lines. The arrows indicate the most dominant hadronic transitions. Single photon transitions, including $\psi(nS) \rightarrow \gamma\eta_c(mS)$, $\psi(nS) \rightarrow \gamma\chi_{cJ}(1P)$, and $\chi_{cJ}(1P) \rightarrow \gamma J/\psi$, are omitted for clarity. For orientation, the location of the thresholds related to a pair of ground state open charm mesons is indicated in the figure. The J^P of $T_{cc}(4020)$ is not established. Decays to open flavour final states are not shown in the figure.

$\eta_c(1S)$

$$I^G(J^{PC}) = 0^+(0^{-+})$$

$\eta_c(1S)$ MASS

VALUE (MeV)	EVTS	DOCUMENT ID	TECN	COMMENT
2984.1 ± 0.4	OUR AVERAGE	Error includes scale factor of 1.2.		
2985.01 ± 0.17 ± 0.89	35k	AAIJ	23AH LHCb	$B^+ \rightarrow K^+(K_S^0 K\pi)$
2983.9 ± 0.7 ± 0.1		1 AAIJ	20H LHCb	$pp \rightarrow bX \rightarrow p\bar{p}X$
2985.9 ± 0.7 ± 2.1	1705	ABLIKIM	19AV BES3	$J/\psi \rightarrow \gamma\omega\omega$
2984.6 ± 0.7 ± 2.2	2673	XU	18 BELL	$e^+e^- \rightarrow \eta'\pi^+\pi^-$
2986.7 ± 0.5 ± 0.9	11k	2 AAIJ	17AD LHCb	$pp \rightarrow B^+X \rightarrow p\bar{p}K^+X$
2982.8 ± 1.0 ± 0.5	6.4k	3 AAIJ	17BB LHCb	$pp \rightarrow b\bar{b}X \rightarrow 2(K^+K^-)X$
2982.2 ± 1.5 ± 0.1	2.0k	4 AAIJ	15BI LHCb	$pp \rightarrow \eta_c(1S)X$
2983.5 ± 1.4 ± 1.6 ± 3.6		5 ANASHIN	14 KEDR	$J/\psi \rightarrow \gamma\eta_c$
2979.8 ± 0.8 ± 3.5	4.5k	6,7 LEES	14E BABR	$\gamma\gamma \rightarrow K^+K^-\pi^0$
2984.1 ± 1.1 ± 2.1	900	6,7,8 LEES	14E BABR	$\gamma\gamma \rightarrow K^+K^-\eta$

2984.3 ± 0.6 ± 0.6	9,10	ABLIKIM	12F BES3	$\psi(2S) \rightarrow \gamma\eta_c$
2984.49 ± 1.16 ± 0.52	832	6 ABLIKIM	12N BES3	$\psi(2S) \rightarrow \pi^0\gamma$ hadrons
2982.7 ± 1.8 ± 2.2	486	ZHANG	12A BELL	$e^+e^- \rightarrow e^+e^-\eta'\pi^+\pi^-$
2984.5 ± 0.8 ± 3.1	11k	DEL-AMO-SA...	11M BABR	$\gamma\gamma \rightarrow K^+K^-\pi^+\pi^-\pi^0$
2985.4 ± 1.5 ± 0.5 ± 2.0	920	10 VINOKUROVA	11 BELL	$B^\pm \rightarrow K^\pm(K_S^0 K^\pm\pi^\mp)$
2982.2 ± 0.4 ± 1.6	14k	11 LEES	10 BABR	$10.6 e^+e^- \rightarrow e^+e^-K_S^0 K^\pm\pi^\mp$
2985.8 ± 1.5 ± 3.1	0.9k	AUBERT	08AB BABR	$B \rightarrow \eta_c(1S) K^*(*) \rightarrow K\bar{K}\pi K^*(*)$
2986.1 ± 1.0 ± 2.5	7.5k	UEHARA	08 BELL	$\gamma\gamma \rightarrow \eta_c \rightarrow$ hadrons
2970 ± 5 ± 6	501	12 ABE	07 BELL	$e^+e^- \rightarrow J/\psi(c\bar{c})$
2971 ± 3 ± 2 ± 1	195	WU	06 BELL	$B^+ \rightarrow p\bar{p}K^+$
2974 ± 7 ± 2 ± 1	20	WU	06 BELL	$B^+ \rightarrow \Lambda\bar{\Lambda}K^+$
2981.8 ± 1.3 ± 1.5	592	ASNER	04 CLEO	$\gamma\gamma \rightarrow \eta_c' \rightarrow K_S^0 K^\pm\pi^\mp$
2984.1 ± 2.1 ± 1.0	190	13 AMBROGIANI	03 E835	$\bar{p}p \rightarrow \eta_c \rightarrow \gamma\gamma$
● ● ● We do not use the following data for averages, fits, limits, etc. ● ● ●				
2982.5 ± 0.4 ± 1.4	12k	14 DEL-AMO-SA...	11M BABR	$\gamma\gamma \rightarrow K_S^0 K^\pm\pi^\mp$
2982.2 ± 0.6		15 MITCHELL	09 CLEO	$e^+e^- \rightarrow \gamma X$
2982 ± 5	270	16 AUBERT	06E BABR	$B^\pm \rightarrow K^\pm X_{c\bar{c}}$
2982.5 ± 1.1 ± 0.9	2.5k	17 AUBERT	04D BABR	$\gamma\gamma \rightarrow \eta_c(1S) \rightarrow K\bar{K}\pi$
2977.5 ± 1.0 ± 1.2		15,18 BAI	03 BES	$J/\psi \rightarrow \gamma\eta_c$
2979.6 ± 2.3 ± 1.6	180	19 FANG	03 BELL	$B \rightarrow \eta_c K$
2976.3 ± 2.3 ± 1.2		15,20 BAI	00F BELL	$J/\psi, \psi(2S) \rightarrow \gamma\eta_c$
2976.6 ± 2.9 ± 1.3	140	15,21 BAI	00F BES	$J/\psi \rightarrow \gamma\eta_c$
2980.4 ± 2.3 ± 0.6		22 BRANDENB...	00B CLE2	$\gamma\gamma \rightarrow \eta_c \rightarrow K^\pm K_S^0 \pi^\mp$
2975.8 ± 3.9 ± 1.2		21 BAI	99B BES	Sup. by BAI 00F
2999 ± 8	25	ABREU	98O DLPH	$e^+e^- \rightarrow e^+e^-$ +hadrons
2988.3 ± 3.3 ± 3.1		ARMSTRONG	95F E760	$\bar{p}p \rightarrow \gamma\gamma$
2974.4 ± 1.9		15,23 BISELLO	91 DM2	$J/\psi \rightarrow \eta_c \gamma$
2969 ± 4 ± 4	80	15 BAI	90B MRK3	$J/\psi \rightarrow \gamma K^+K^-K^+K^-$
2956 ± 12 ± 12		15 BAI	90B MRK3	$J/\psi \rightarrow \gamma K^+K^-K_S^0 K_L^0$
2982.6 ± 2.7 ± 2.3		12 BAGLIN	87B SPEC	$\bar{p}p \rightarrow \gamma\gamma$
2980.2 ± 1.6		15,23 BALTRUSAIT...	86 MRK3	$J/\psi \rightarrow \eta_c \gamma$
2984 ± 2.3 ± 4.0		15 GAISER	86 CBAL	$J/\psi \rightarrow \gamma X, \psi(2S) \rightarrow \gamma X$
2976 ± 8		15,24 BALTRUSAIT...	84 MRK3	$J/\psi \rightarrow 2\phi\gamma$
2982 ± 8	18	25 HIMEL	80B MRK2	e^+e^-
2980 ± 9		25 PARTRIDGE	80B CBAL	e^+e^-

1 AAIJ 20H report $m_{J/\psi} - m_{\eta_c(1S)} = 113.0 \pm 0.7 \pm 0.1$ MeV. We use the current value $m_{J/\psi} = 3096.900 \pm 0.006$ MeV to obtain the quoted mass.

2 AAIJ 17AD report $m_{J/\psi} - m_{\eta_c(1S)} = 110.2 \pm 0.5 \pm 0.9$ MeV. We use the current value $m_{J/\psi} = 3096.900 \pm 0.006$ MeV to obtain the quoted mass.

3 From a fit of the $\phi\phi$ invariant mass with the mass and width of $\eta_c(1S)$ as free parameters.

4 AAIJ 15BI reports $m_{J/\psi} - m_{\eta_c(1S)} = 114.7 \pm 1.5 \pm 0.1$ MeV from a sample of $\eta_c(1S)$ and J/ψ produced in b -hadron decays. We have used current value of $m_{J/\psi} = 3096.900 \pm 0.006$ MeV to arrive at the quoted $m_{\eta_c(1S)}$ result.

5 Taking into account an asymmetric photon lineshape.

6 With floating width.

7 Ignoring possible interference with the non-resonant 0^- amplitude.

8 Using both, $\eta \rightarrow \gamma\gamma$ and $\eta \rightarrow \pi^+\pi^-\pi^0$ decays.

9 From a simultaneous fit to six decay modes of the η_c .

10 Accounts for interference with non-resonant continuum.

11 Taking into account interference with the non-resonant $J^P = 0^-$ amplitude.

12 From a fit of the J/ψ recoil mass spectrum. Supersedes ABE,K 02 and ABE 04G.

13 Using mass of $\psi(2S) = 3686.00$ MeV.

14 Not independent from the measurements reported by LEES 10.

15 MITCHELL 09 observes a significant asymmetry in the lineshapes of $\psi(2S) \rightarrow \gamma\eta_c$ and $J/\psi \rightarrow \gamma\eta_c$ transitions. If ignored, this asymmetry could lead to significant bias whenever the mass and width are measured in $\psi(2S)$ or J/ψ radiative decays.

16 From the fit of the kaon momentum spectrum. Systematic errors not evaluated.

17 Superseded by LEES 10.

18 From a simultaneous fit of five decay modes of the η_c .

19 Superseded by VINOKUROVA 11.

20 Weighted average of the $\psi(2S)$ and $J/\psi(1S)$ samples. Using an η_c width of 13.2 MeV.

21 Average of several decay modes. Using an η_c width of 13.2 MeV.

22 Superseded by ASNER 04.

23 Average of several decay modes.

24 $\eta_c \rightarrow \phi\phi$.

25 Mass adjusted by us to correspond to $J/\psi(1S)$ mass = 3097 MeV.

See key on page 1171

Meson Particle Listings

$\eta_c(1S)$

$\eta_c(1S)$ WIDTH

VALUE (MeV)	EVTS	DOCUMENT ID	TECN	COMMENT
30.5 ± 0.5 OUR FIT	Error includes scale factor of 1.2.			
30.5 ± 0.5 OUR AVERAGE	Error includes scale factor of 1.1.			
29.7 ± 0.5 ± 0.2	35k	AAIJ	23AH LHCB	$B^+ \rightarrow K^+(K_S^0 K \pi)$
33.8 ± 1.6 ± 4.1	1705	ABLIKIM	19AV BES3	$J/\psi \rightarrow \gamma \omega \omega$
30.8 ± $\frac{2.3}{2.2} \pm 2.9$	2673	XU	18 BELL	$e^+ e^- \rightarrow e^+ e^- \eta' \pi^+ \pi^-$
34.0 ± 1.9 ± 1.3	11k	AAIJ	17AD LHCB	$pp \rightarrow B^+ X \rightarrow p \bar{p} K^+ X$
31.4 ± 3.5 ± 2.0	6.4k	¹ AAIJ	17BB LHCB	$pp \rightarrow b \bar{b} X \rightarrow 2(K^+ K^-) X$
27.2 ± $\frac{3.1}{2.6} \pm 5.4$		² ANASHIN	14 KEDR	$J/\psi \rightarrow \gamma \eta_c$
25.2 ± 2.6 ± 2.4	4.5k	^{3,4} LEES	14E BABR	$\gamma \gamma \rightarrow K^+ K^- \pi^0$
34.8 ± 3.1 ± 4.0	900	^{3,4,5} LEES	14E BABR	$\gamma \gamma \rightarrow K^+ K^- \eta$
32.0 ± 1.2 ± 1.0		^{6,7} ABLIKIM	12F BES3	$\psi(2S) \rightarrow \gamma \eta_c$
36.4 ± 3.2 ± 1.7	832	³ ABLIKIM	12N BES3	$\psi(2S) \rightarrow \pi^0 \gamma$ hadrons
37.8 ± $\frac{5.8}{5.3} \pm 3.1$	486	ZHANG	12A BELL	$e^+ e^- \rightarrow e^+ e^- \eta' \pi^+ \pi^-$
36.2 ± 2.8 ± 3.0	11k	DEL-AMO-SA...11M	BABR	$\gamma \gamma \rightarrow K^+ K^- \pi^+ \pi^- \pi^0$
35.1 ± $\frac{3.1}{1.6} \pm 1.0$	920	⁷ VINOKUROVA	11 BELL	$B^\pm \rightarrow K^\pm (K_S^0 K^\pm \pi^\mp)$
31.7 ± 1.2 ± 0.8	14k	⁸ LEES	10 BABR	$10.6 e^+ e^- \rightarrow e^+ e^- K_S^0 K^\pm \pi^\mp$
36.3 ± $\frac{3.7}{3.6} \pm 4.4$	0.9k	AUBERT	08AB BABR	$B \rightarrow \eta_c(1S) K^(*) \rightarrow K \bar{K} \pi K^(*)$
28.1 ± 3.2 ± 2.2	7.5k	UEHARA	08 BELL	$\gamma \gamma \rightarrow \eta_c \rightarrow$ hadrons
48 ± $\frac{8}{7} \pm 5$	195	WU	06 BELL	$B^+ \rightarrow p \bar{p} K^+$
40 ± 19 ± 5	20	WU	06 BELL	$B^+ \rightarrow \Lambda \bar{\Lambda} K^+$
24.8 ± 3.4 ± 3.5	592	ASNER	04 CLEO	$\gamma \gamma \rightarrow \eta_c' \rightarrow K_S^0 K^\pm \pi^\mp$
20.4 ± $\frac{7.7}{6.7} \pm 2.0$	190	AMBROGIANI	03 E835	$\bar{p} p \rightarrow \eta_c \rightarrow \gamma \gamma$
23.9 ± $\frac{12.6}{7.1}$		ARMSTRONG	95F E760	$\bar{p} p \rightarrow \gamma \gamma$

• • • We do not use the following data for averages, fits, limits, etc. • • •

¹ From a fit of the $\phi\phi$ invariant mass with the mass and width of $\eta_c(1S)$ as free parameters.
² Taking into account an asymmetric photon lineshape.
³ With floating mass.
⁴ Ignoring possible interference with the non-resonant 0^- amplitude.
⁵ Using both, $\eta \rightarrow \gamma\gamma$ and $\eta \rightarrow \pi^+ \pi^- \pi^0$ decays.
⁶ From a simultaneous fit to six decay modes of the η_c .
⁷ Accounts for interference with non-resonant continuum.
⁸ Taking into account interference with the non-resonant $J^P = 0^-$ amplitude.
⁹ Not independent from the measurements reported by LEES 10.
¹⁰ Superseded by LEES 10.
¹¹ From a simultaneous fit of five decay modes of the η_c .
¹² Superseded by VINOKUROVA 11.
¹³ From a fit to the 4-prong invariant mass in $\psi(2S) \rightarrow \gamma \eta_c$ and $J/\psi(1S) \rightarrow \gamma \eta_c$ decays.
¹⁴ Superseded by ASNER 04.
¹⁵ Positive and negative errors correspond to 90% confidence level.

$\eta_c(1S)$ DECAY MODES

Mode	Fraction (Γ_i/Γ)	Scale factor/ Confidence level
------	--------------------------------	-----------------------------------

Decays involving hadronic resonances

Γ_1	$\eta'(958) \pi \pi$	(2.0 ± 0.4) %	S=1.4
Γ_2	$\eta'(958) K \bar{K}$	(1.73 ± 0.35) %	
Γ_3	$\eta'(958) \eta \eta$	(3.4 ± 0.6) × 10 ⁻³	
Γ_4	$\rho \rho$	(1.8 ± 0.4) %	
Γ_5	$K^*(892)^0 K^- \pi^+ + c.c.$	(1.8 ± 0.5) %	
Γ_6	$K^*(892)^0 \bar{K}^*(892)$	(7.0 ± 1.2) × 10 ⁻³	
Γ_7	$K^*(892)^0 \bar{K}^*(892)^0 \pi^+ \pi^-$	(1.4 ± 0.6) %	
Γ_8	$\phi K^+ K^-$	(3.3 ± $\frac{1.2}{-1.1}$) × 10 ⁻³	
Γ_9	$\phi \phi$	(1.8 ± 0.4) × 10 ⁻³	S=2.3

Γ_{10}	$\phi 2(\pi^+ \pi^-)$	< 4	× 10 ⁻³	CL=90%
Γ_{11}	$a_0(980) \pi$	seen		
Γ_{12}	$a_2(1320) \pi$	seen		
Γ_{13}	$K^*(892) \bar{K} + c.c.$	< 1.28	%	CL=90%
Γ_{14}	$f_2(1270) \eta$	seen		
Γ_{15}	$f_2(1270) \eta'$	seen		
Γ_{16}	$\omega \omega$	(2.7 ± 0.9) × 10 ⁻³		S=2.1
Γ_{17}	$\omega \phi$	< 2.5	× 10 ⁻⁴	CL=90%
Γ_{18}	$f_2(1270) f_2(1270)$	(1.08 ± 0.27) %		
Γ_{19}	$f_2(1270) f_2'(1525)$	(9.7 ± 3.2) × 10 ⁻³		
Γ_{20}	$f_0(500) \eta$	seen		
Γ_{21}	$f_0(500) \eta'$	seen		
Γ_{22}	$f_0(980) \eta$	seen		
Γ_{23}	$f_0(980) \eta'$	seen		
Γ_{24}	$f_0(1500) \eta$	seen		
Γ_{25}	$f_0(1710) \eta'$	seen		
Γ_{26}	$f_0(2100) \eta'$	seen		
Γ_{27}	$f_0(2200) \eta$	seen		
Γ_{28}	$a_0(1320) \pi$	seen		
Γ_{29}	$a_0(1450) \pi$	seen		
Γ_{30}	$a_2(1700) \pi$	seen		
Γ_{31}	$a_0(1710) \pi$	seen		
Γ_{32}	$a_0(1950) \pi$	seen		
Γ_{33}	$K_0^*(1430) \bar{K} + c.c.$	seen		
Γ_{34}	$K_0^*(1430) \bar{K} + c.c.$	seen		
Γ_{35}	$K_0^*(1950) \bar{K} + c.c.$	seen		
Γ_{36}	$K_0^*(2600) \bar{K} + c.c.$	seen		

Decays into stable hadrons

Γ_{37}	$K \bar{K} \pi$	(7.1 ± 0.4) %	S=1.1	
Γ_{38}	$K \bar{K} \eta$	(1.32 ± 0.15) %		
Γ_{39}	$\eta \pi^+ \pi^-$	(1.6 ± 0.4) %		
Γ_{40}	$\eta 2(\pi^+ \pi^-)$	(4.3 ± 1.3) %		
Γ_{41}	$K^+ K^- \pi^+ \pi^-$	(8.3 ± 1.8) × 10 ⁻³	S=1.9	
Γ_{42}	$K^+ K^- \pi^+ \pi^- \pi^0$	(3.4 ± 0.6) %		
Γ_{43}	$K^0 K^- \pi^+ \pi^- \pi^+ + c.c.$	(5.4 ± 1.5) %		
Γ_{44}	$K^+ K^- 2(\pi^+ \pi^-)$	(8.4 ± 2.4) × 10 ⁻³		
Γ_{45}	$2(K^+ K^-)$	(1.4 ± 0.4) × 10 ⁻³	S=1.4	
Γ_{46}	$\pi^+ \pi^- \pi^0$	< 4	× 10 ⁻⁴	CL=90%
Γ_{47}	$\pi^+ \pi^- \pi^0 \pi^0$	(4.6 ± 1.0) %		
Γ_{48}	$2(\pi^+ \pi^-)$	(9.6 ± 1.5) × 10 ⁻³	S=1.4	
Γ_{49}	$2(\pi^+ \pi^- \pi^0)$	(15.9 ± 2.0) %		
Γ_{50}	$3(\pi^+ \pi^-)$	(1.89 ± 0.34) %		
Γ_{51}	$p \bar{p}$	(1.33 ± 0.11) × 10 ⁻³	S=1.1	
Γ_{52}	$p \bar{p} \pi^0$	(3.4 ± 1.3) × 10 ⁻³		
Γ_{53}	$p \bar{p} \pi^+ \pi^-$	(3.7 ± 0.5) × 10 ⁻³		
Γ_{54}	$\Lambda \bar{\Lambda}$	(1.10 ± 0.28) × 10 ⁻³	S=1.5	
Γ_{55}	$K^+ \bar{p} \Lambda + c.c.$	(2.5 ± 0.4) × 10 ⁻³		
Γ_{56}	$\bar{\Lambda}(1520) \Lambda + c.c.$	(3.0 ± 1.3) × 10 ⁻³		
Γ_{57}	$\Sigma^+ \bar{\Sigma}^-$	(2.6 ± 0.5) × 10 ⁻³		
Γ_{58}	$\Xi^- \bar{\Xi}^+$	(1.07 ± 0.24) × 10 ⁻³		

Radiative decays

Γ_{59}	$\gamma \gamma$	(1.66 ± 0.13) × 10 ⁻⁴	S=1.2
---------------	-----------------	------------------------------------	-------

Charge conjugation (C), Parity (P),

Lepton Family number (LF) violating modes

Γ_{60}	$\pi^+ \pi^-$	P, CP	< 1.3	× 10 ⁻⁴	CL=90%
Γ_{61}	$\pi^0 \pi^0$	P, CP	< 4	× 10 ⁻⁵	CL=90%
Γ_{62}	$K^+ K^-$	P, CP	< 7	× 10 ⁻⁴	CL=90%
Γ_{63}	$K_S^0 K_S^0$	P, CP	< 4	× 10 ⁻⁴	CL=90%

FIT INFORMATION

A multiparticle fit to $\eta_c(1S)$, $J/\psi(1S)$, $\psi(2S)$, $h_c(1P)$, and B^\pm with the total width, 10 combinations of partial widths obtained from integrated cross section, and 38 branching ratios uses 113 measurements to determine 19 parameters. The overall fit has a $\chi^2 = 184.6$ for 94 degrees of freedom.

The following off-diagonal array elements are the correlation coefficients $\langle \delta p_i \delta p_j \rangle / (\delta p_i \delta p_j)$, in percent, from the fit to parameters p_i , including the branching fractions, $x_i \equiv \Gamma_i / \Gamma_{\text{total}}$.

Meson Particle Listings

$\eta_c(1S)$

x_6	14									
x_9	11	13								
x_{16}	7	8	8							
x_{18}	9	11	11	7						
x_{37}	25	25	22	12	17					
x_{38}	13	13	11	6	9	51				
x_{41}	7	7	6	4	5	15	8			
x_{45}	5	5	5	2	3	12	6	4		
x_{48}	13	17	17	10	15	26	13	8	5	
x_{51}	19	20	20	11	16	39	20	11	11	24
x_{53}	7	7	8	4	5	22	11	5	10	8
x_{54}	5	7	7	4	6	12	6	3	4	10
x_{59}	-38	-35	-27	-16	-22	-63	-32	-17	-12	-31
Γ	-1	-1	-1	0	-1	-2	-1	0	0	-1
	x_1	x_6	x_9	x_{16}	x_{18}	x_{37}	x_{38}	x_{41}	x_{45}	x_{48}
x_{53}	21									
x_{54}	13	9								
x_{59}	-47	-17	-11							
Γ	1	0	0	-20						
	x_{51}	x_{53}	x_{54}	x_{59}						

$\eta_c(1S)$ PARTIAL WIDTHS

$\Gamma(\gamma\gamma)$					Γ_{59}
VALUE (keV)	EVTS	DOCUMENT ID	TECN	COMMENT	
5.1 ± 0.4 OUR FIT				Error includes scale factor of 1.2.	
• • • We do not use the following data for averages, fits, limits, etc. • • •					
5.8 ± 1.1	486	¹ ZHANG	12A BELL	$e^+e^- \rightarrow e^+e^-\eta'/\pi^+\pi^-$	
5.2 ± 1.2	273 ± 43	^{2,3} AUBERT	06E BABR	$B^\pm \rightarrow K^\pm X_c \bar{c}$	
5.5 ± 1.2 ± 1.8	157 ± 33	⁴ KUO	05 BELL	$\gamma\gamma \rightarrow p\bar{p}$	
7.4 ± 0.4 ± 2.3		⁵ ASNER	04 CLEO	$\gamma\gamma \rightarrow \eta'_c \rightarrow K_S^0 K^\pm \pi^\mp$	
13.9 ± 2.0 ± 3.0	41	⁶ ABDALLAH	03J DLPH	$\gamma\gamma \rightarrow \eta_c$	
3.8 ± 1.1 ± 1.9	190	⁷ AMBROGIANI	03 E835	$\bar{p}p \rightarrow \eta_c \rightarrow \gamma\gamma$	
7.6 ± 0.8 ± 2.3		^{5,8} BRANDENB...	00B CLE2	$\gamma\gamma \rightarrow \eta_c \rightarrow K^\pm K_S^0 \pi^\mp$	
6.9 ± 1.7 ± 2.1	76	⁹ ACCIARRI	99T L3	$e^+e^- \rightarrow e^+e^-\eta_c$	
27 ± 16 ± 10	5	⁵ SHIRAI	98 AMY	58 e^+e^-	
6.7 ± 2.4 ± 2.3		⁴ ARMSTRONG	95F E760	$\bar{p}p \rightarrow \gamma\gamma$	
11.3 ± 4.2		¹⁰ ALBRECHT	94H ARG	$e^+e^- \rightarrow e^+e^-\eta_c$	
8.0 ± 2.3 ± 2.4	17	¹¹ ADRIANI	93N L3	$e^+e^- \rightarrow e^+e^-\eta_c$	
5.9 ± 2.1 ± 1.9		⁷ CHEN	90B CLEO	$e^+e^- \rightarrow e^+e^-\eta_c$	
6.4 ± 5.0 ± 3.4		¹² AIHARA	88D TPC	$e^+e^- \rightarrow e^+e^-X$	
4.3 ± 3.4 ± 3.7 ± 2.4		⁴ BAGLIN	87B SPEC	$\bar{p}p \rightarrow \gamma\gamma$	
28 ± 15		^{5,13} BERGER	86 PLUT	$\gamma\gamma \rightarrow K\bar{K}\pi$	

¹ Assuming there is no interference with the non-resonant background.
² Calculated by us using $\Gamma(\eta_c \rightarrow K\bar{K}\pi) \times \Gamma(\eta_c \rightarrow \gamma\gamma) / \Gamma = 0.44 \pm 0.05$ keV from PDG 06 and $B(\eta_c \rightarrow K\bar{K}\pi) = (8.5 \pm 1.8)\%$ from AUBERT 06E.
³ Systematic errors not evaluated.
⁴ Normalized to $B(\eta_c \rightarrow p\bar{p}) = (1.3 \pm 0.4) \times 10^{-3}$.
⁵ Normalized to $B(\eta_c \rightarrow K^\pm K_S^0 \pi^\mp)$.
⁶ Average of $K_S^0 K^\pm \pi^\mp$, $\pi^+ \pi^- K^+ K^-$, and $2(K^+ K^-)$ decay modes.
⁷ Normalized to the sum of $B(\eta_c \rightarrow K^\pm K_S^0 \pi^\mp)$, $B(\eta_c \rightarrow K^+ K^- \pi^+ \pi^-)$, and $B(\eta_c \rightarrow 2\pi^+ 2\pi^-)$.
⁸ Superseded by ASNER 04.
⁹ Normalized to the sum of 9 branching ratios.
¹⁰ Normalized to the sum of $B(\eta_c \rightarrow K^\pm K_S^0 \pi^\mp)$, $B(\eta_c \rightarrow \phi\phi)$, $B(\eta_c \rightarrow K^+ K^- \pi^+ \pi^-)$, and $B(\eta_c \rightarrow 2\pi^+ 2\pi^-)$.
¹¹ Superseded by ACCIARRI 99T.
¹² Normalized to the sum of $B(\eta_c \rightarrow K^\pm K_S^0 \pi^\mp)$, $B(\eta_c \rightarrow 2K^+ 2K^-)$, $B(\eta_c \rightarrow K^+ K^- \pi^+ \pi^-)$, and $B(\eta_c \rightarrow 2\pi^+ 2\pi^-)$.
¹³ Re-evaluated by AIHARA 88D.

$\eta_c(1S)$ $\Gamma(\eta)\Gamma(\gamma\gamma)/\Gamma(\text{total})$

$\Gamma(\eta'(958)\pi\pi) \times \Gamma(\gamma\gamma)/\Gamma(\text{total})$					Γ_{159}/Γ
VALUE (eV)	EVTS	DOCUMENT ID	TECN	COMMENT	
102 ± 18 OUR FIT				Error includes scale factor of 1.5.	
98.1 ± 3.9 ± 11.7	2673	XU	18 BELL	$e^+e^- \rightarrow e^+e^-\eta'/\pi^+\pi^-$	
• • • We do not use the following data for averages, fits, limits, etc. • • •					
75.8 ± 6.3 ± 8.4	486	¹ ZHANG	12A BELL	$e^+e^- \rightarrow e^+e^-\eta'/\pi^+\pi^-$	

¹ Superseded by XU 18.

$\Gamma(\rho\rho) \times \Gamma(\gamma\gamma)/\Gamma(\text{total})$					Γ_{459}/Γ
VALUE (eV)	CL%	EVTS	DOCUMENT ID	TECN	COMMENT
<39		90	UEHARA	08 BELL	$\gamma\gamma \rightarrow 2(\pi^+ \pi^-)$

• • • We do not use the following data for averages, fits, limits, etc. • • •

$\Gamma(K^*(892)\bar{K}^*(892)) \times \Gamma(\gamma\gamma)/\Gamma(\text{total})$					Γ_{659}/Γ
VALUE (eV)	CL%	EVTS	DOCUMENT ID	TECN	COMMENT
35 ± 6 OUR FIT					
32.4 ± 4.2 ± 5.8		882 ± 115	UEHARA	08 BELL	$\gamma\gamma \rightarrow \pi^+ \pi^- K^+ K^-$

$\Gamma(\phi\phi) \times \Gamma(\gamma\gamma)/\Gamma(\text{total})$					Γ_{959}/Γ
VALUE (eV)	CL%	EVTS	DOCUMENT ID	TECN	COMMENT
9.2 ± 2.2 OUR FIT					Error includes scale factor of 2.7.
7.75 ± 0.66 ± 0.62		386 ± 31	¹ LIU	12B BELL	$\gamma\gamma \rightarrow 2(K^+ K^-)$
• • • We do not use the following data for averages, fits, limits, etc. • • •					
6.8 ± 1.2 ± 1.3		132 ± 23	UEHARA	08 BELL	$\gamma\gamma \rightarrow 2(K^+ K^-)$
¹ Supersedes UEHARA 08. Using $B(\phi \rightarrow K^+ K^-) = (48.9 \pm 0.5)\%$.					

$\Gamma(\omega\omega) \times \Gamma(\gamma\gamma)/\Gamma(\text{total})$					Γ_{1659}/Γ
VALUE (eV)	CL%	EVTS	DOCUMENT ID	TECN	COMMENT
13 ± 5 OUR FIT					Error includes scale factor of 2.2.
8.67 ± 2.86 ± 0.96		85 ± 29	¹ LIU	12B BELL	$\gamma\gamma \rightarrow 2(\pi^+ \pi^- \pi^0)$
¹ Using $B(\omega \rightarrow \pi^+ \pi^- \pi^0) = (89.2 \pm 0.7)\%$.					

$\Gamma(\omega\phi) \times \Gamma(\gamma\gamma)/\Gamma(\text{total})$					Γ_{1759}/Γ
VALUE (eV)	CL%	EVTS	DOCUMENT ID	TECN	COMMENT
<0.49		90	¹ LIU	12B BELL	$\gamma\gamma \rightarrow K^+ K^- \pi^+ \pi^- \pi^0$
¹ Using $B(\phi \rightarrow K^+ K^-) = (48.9 \pm 0.5)\%$ and $B(\omega \rightarrow \pi^+ \pi^- \pi^0) = (89.2 \pm 0.7)\%$.					

$\Gamma(f_2(1270)f_2(1270)) \times \Gamma(\gamma\gamma)/\Gamma(\text{total})$					Γ_{1859}/Γ
VALUE (eV)	CL%	EVTS	DOCUMENT ID	TECN	COMMENT
55 ± 14 OUR FIT					
69 ± 17 ± 12		3182 ± 766	UEHARA	08 BELL	$\gamma\gamma \rightarrow 2(\pi^+ \pi^-)$

$\Gamma(f_2(1270)f_2'(1525)) \times \Gamma(\gamma\gamma)/\Gamma(\text{total})$					Γ_{1959}/Γ
VALUE (eV)	CL%	EVTS	DOCUMENT ID	TECN	COMMENT
49 ± 9 ± 13		1128 ± 206	UEHARA	08 BELL	$\gamma\gamma \rightarrow \pi^+ \pi^- K^+ K^-$

$\Gamma(K\bar{K}\pi) \times \Gamma(\gamma\gamma)/\Gamma(\text{total})$					Γ_{3759}/Γ
VALUE (keV)	CL%	EVTS	DOCUMENT ID	TECN	COMMENT
0.360 ± 0.022 OUR FIT					Error includes scale factor of 1.5.
0.396 ± 0.016 OUR AVERAGE					
0.386 ± 0.008 ± 0.021		12k	DEL-AMO-SA...	11M BABR	$\gamma\gamma \rightarrow K_S^0 K^\pm \pi^\mp$
0.374 ± 0.009 ± 0.031		14k	¹ LEES	10 BABR	10.6 $e^+e^- \rightarrow e^+e^- K_S^0 K^\pm \pi^\mp$
0.407 ± 0.022 ± 0.028			^{2,3} ASNER	04 CLEO	$\gamma\gamma \rightarrow \eta'_c \rightarrow K_S^0 K^\pm \pi^\mp$
0.60 ± 0.12 ± 0.09		41	^{3,4} ABDALLAH	03J DLPH	$\gamma\gamma \rightarrow K_S^0 K^\pm \pi^\mp$
1.47 ± 0.87 ± 0.27			³ SHIRAI	98 AMY	$\gamma\gamma \rightarrow \eta_c \rightarrow K^\pm K_S^0 \pi^\mp$
0.84 ± 0.21			³ ALBRECHT	94H ARG	$\gamma\gamma \rightarrow K^\pm K_S^0 \pi^\mp$
0.60 ± 0.23 ± 0.20			³ CHEN	90B CLEO	$\gamma\gamma \rightarrow \eta_c K^\pm K_S^0 \pi^\mp$
1.06 ± 0.41 ± 0.27		11	³ BRAUNSC...	89 TASS	$\gamma\gamma \rightarrow K\bar{K}\pi$
1.5 ± 0.60 ± 0.3 ± 0.45		7	³ BERGER	86 PLUT	$\gamma\gamma \rightarrow K\bar{K}\pi$
• • • We do not use the following data for averages, fits, limits, etc. • • •					
0.418 ± 0.044 ± 0.022			^{3,5} BRANDENB...	00B CLE2	$\gamma\gamma \rightarrow \eta_c \rightarrow K^\pm K_S^0 \pi^\mp$
<0.63		95	³ BEHREND	89 CELL	$\gamma\gamma \rightarrow K_S^0 K^\pm \pi^\mp$
<4.4		95	ALTHOFF	85B TASS	$\gamma\gamma \rightarrow K\bar{K}\pi$

¹ From the corrected and unfolded mass spectrum.
² Calculated by us from the value reported in ASNER 04 that assumes $B(\eta_c \rightarrow K\bar{K}\pi) = 5.5 \pm 1.7\%$.
³ We have multiplied $K^\pm K_S^0 \pi^\mp$ measurement by 3 to obtain $K\bar{K}\pi$.
⁴ Calculated by us from the value reported in ABDALLAH 03J, which uses $B(\eta_c \rightarrow K_S^0 K^\pm \pi^\mp) = (1.5 \pm 0.4)\%$.
⁵ Superseded by ASNER 04.

$\Gamma(K^+ K^- \pi^+ \pi^-) \times \Gamma(\gamma\gamma)/\Gamma(\text{total})$					Γ_{4159}/Γ
VALUE (eV)	CL%	EVTS	DOCUMENT ID	TECN	COMMENT
42 ± 9 OUR FIT					Error includes scale factor of 2.1.
27 ± 6 OUR AVERAGE					
25.7 ± 3.2 ± 4.9		2019 ± 248	UEHARA	08 BELL	$\gamma\gamma \rightarrow \pi^+ \pi^- K^+ K^-$
280 ± 100 ± 60		42	¹ ABDALLAH	03J DLPH	$\gamma\gamma \rightarrow \pi^+ \pi^- K^+ K^-$
170 ± 80 ± 20		13.9 ± 6.6	ALBRECHT	94H ARG	$\gamma\gamma \rightarrow \pi^+ \pi^- K^+ K^-$
¹ Calculated by us from the value reported in ABDALLAH 03J, which uses $B(\eta_c \rightarrow \pi^+ \pi^- K^+ K^-) = (2.0 \pm 0.7)\%$.					

$\Gamma(K^+ K^- \pi^+ \pi^- \pi^0) \times \Gamma(\gamma\gamma)/\Gamma_{\text{total}}$		$\Gamma_{42}\Gamma_{59}/\Gamma$	
VALUE (keV)	EVTS	DOCUMENT ID	TECN COMMENT
$0.190 \pm 0.006 \pm 0.028$	11k	DEL-AMO-SA...11M	BABR $\gamma\gamma \rightarrow K^+ K^- \pi^+ \pi^- \pi^0$

$\Gamma(2(K^+ K^-)) \times \Gamma(\gamma\gamma)/\Gamma_{\text{total}}$		$\Gamma_{45}\Gamma_{59}/\Gamma$	
VALUE (eV)	EVTS	DOCUMENT ID	TECN COMMENT
7.2 ± 2.1 OUR FIT	Error includes scale factor of 1.5.		
5.8 ± 1.9 OUR AVERAGE			
5.6 ± 1.1 ± 1.6	216 ± 42	UEHARA	08 BELL $\gamma\gamma \rightarrow 2(K^+ K^-)$
350 ± 90 ± 60	46	¹ ABDALLAH	03J DLPH $\gamma\gamma \rightarrow 2(K^+ K^-)$
231 ± 90 ± 23	9.1 ± 3.3	² ALBRECHT	94H ARG $\gamma\gamma \rightarrow 2(K^+ K^-)$

¹ Calculated by us from the value reported in ABDALLAH 03J, which uses $B(\eta_c \rightarrow 2(K^+ K^-)) = (2.1 \pm 1.2)\%$.
² Includes all topological modes except $\eta_c \rightarrow \phi\phi$.

$\Gamma(2(\pi^+ \pi^-)) \times \Gamma(\gamma\gamma)/\Gamma_{\text{total}}$		$\Gamma_{48}\Gamma_{59}/\Gamma$	
VALUE (eV)	EVTS	DOCUMENT ID	TECN COMMENT
48 ± 7 OUR FIT	Error includes scale factor of 1.5.		
42 ± 6 OUR AVERAGE			
40.7 ± 3.7 ± 5.3	5381 ± 492	UEHARA	08 BELL $\gamma\gamma \rightarrow 2(\pi^+ \pi^-)$
180 ± 70 ± 20	21.4 ± 8.6	ALBRECHT	94H ARG $\gamma\gamma \rightarrow 2(\pi^+ \pi^-)$

$\Gamma(\rho\bar{\rho}) \times \Gamma(\gamma\gamma)/\Gamma_{\text{total}}$		$\Gamma_{51}\Gamma_{59}/\Gamma$	
VALUE (eV)	EVTS	DOCUMENT ID	TECN COMMENT
6.7 ± 0.6 OUR FIT	Error includes scale factor of 1.1.		
6.2 ± 1.1 OUR AVERAGE	Error includes scale factor of 1.1.		
7.20 ± 1.53 ± $\frac{0.67}{-0.75}$	157 ± 33	¹ KUO	05 BELL $\gamma\gamma \rightarrow \rho\bar{\rho}$
4.6 ± $\frac{1.3}{-1.1}$ ± 0.4	190	AMBROGIANI	03 E835 $\bar{p}p \rightarrow \gamma\gamma$
8.1 ± $\frac{2.9}{-2.0}$		ARMSTRONG	95F E760 $\bar{p}p \rightarrow \gamma\gamma$

¹ Not independent from the $\Gamma_{\gamma\gamma}$ reported by the same experiment.

 $\eta_c(1S)$ BRANCHING RATIOS

HADRONIC DECAYS

$\Gamma(\eta'(958) K\bar{K})/\Gamma(\eta'(958) \pi\pi)$		Γ_2/Γ_1	
VALUE	DOCUMENT ID	TECN	COMMENT
0.859 ± 0.052 ± 0.043	¹ LEES	21A	BABR $\gamma\gamma \rightarrow \eta' K^+ K^-$, $\eta' \pi^+ \pi^-$

¹ Based on Dalitz-plot analysis of the $\eta_c \rightarrow \eta' K^+ K^-$, $\eta' \pi^+ \pi^-$ final states where the fit fractions and relative phases are determined for numerous two-body intermediate states.

$\Gamma(\eta'(958) \eta\eta)/\Gamma_{\text{total}}$		Γ_3/Γ	
VALUE (units 10^{-3})	DOCUMENT ID	TECN	COMMENT
3.4 ± 0.5 ± 0.3	¹ ABLIKIM	21c	BES3 $J/\psi(1S) \rightarrow \gamma\eta\eta'$

¹ ABLIKIM 21c reports $[\Gamma(\eta_c(1S) \rightarrow \eta'(958) \eta\eta)/\Gamma_{\text{total}}] \times [B(J/\psi(1S) \rightarrow \gamma\eta_c(1S))] = (4.86 \pm 0.62 \pm 0.45) \times 10^{-5}$ which we divide by our best value $B(J/\psi(1S) \rightarrow \gamma\eta_c(1S)) = (1.41 \pm 0.14) \times 10^{-2}$. Our first error is their experiment's error and our second error is the systematic error from using our best value.

$\Gamma(\rho\rho)/\Gamma_{\text{total}}$		Γ_4/Γ	
VALUE (units 10^{-2})	CL% EVTS	DOCUMENT ID	TECN COMMENT
•••	We do not use the following data for averages, fits, limits, etc. •••		
1.1 ± 0.5 ± 0.1	72	¹ ABLIKIM	05L BES2 $J/\psi \rightarrow \pi^+ \pi^- \pi^+ \pi^- \gamma$
2.3 ± 0.5 ± 0.2	113	^{2,3} BISELLO	91 DM2 $J/\psi \rightarrow \gamma\rho^0\rho^0$
2.1 ± 1.0 ± 0.2	32	^{4,5} BISELLO	91 DM2 $J/\psi \rightarrow \gamma\rho^+ \rho^-$
<14	90	⁶ BALTRUSAIT...86	MRK3 $J/\psi \rightarrow \eta_c\gamma$

¹ ABLIKIM 05L reports $[\Gamma(\eta_c(1S) \rightarrow \rho\rho)/\Gamma_{\text{total}}] \times [B(J/\psi(1S) \rightarrow \gamma\eta_c(1S))] = (1.6 \pm 0.6 \pm 0.4) \times 10^{-4}$ which we divide by our best value $B(J/\psi(1S) \rightarrow \gamma\eta_c(1S)) = (1.41 \pm 0.14) \times 10^{-2}$. Our first error is their experiment's error and our second error is the systematic error from using our best value.

² BISELLO 91 reports $[\Gamma(\eta_c(1S) \rightarrow \rho\rho)/\Gamma_{\text{total}}] \times [B(J/\psi(1S) \rightarrow \gamma\eta_c(1S))] = (3.30 \pm 0.30 \pm 0.60) \times 10^{-4}$ which we divide by our best value $B(J/\psi(1S) \rightarrow \gamma\eta_c(1S)) = (1.41 \pm 0.14) \times 10^{-2}$. Our first error is their experiment's error and our second error is the systematic error from using our best value.

³ The value reported by BISELLO 91 has been multiplied by 3 to account for isospin symmetry.

⁴ BISELLO 91 reports $[\Gamma(\eta_c(1S) \rightarrow \rho\rho)/\Gamma_{\text{total}}] \times [B(J/\psi(1S) \rightarrow \gamma\eta_c(1S))] = (3.0 \pm 1.3 \pm 0.6) \times 10^{-4}$ which we divide by our best value $B(J/\psi(1S) \rightarrow \gamma\eta_c(1S)) = (1.41 \pm 0.14) \times 10^{-2}$. Our first error is their experiment's error and our second error is the systematic error from using our best value.

⁵ The value reported by BISELLO 91 has been multiplied by 3/2 to account for isospin symmetry.

⁶ Using $B(J/\psi(1S) \rightarrow \gamma\eta_c(1S)) = 0.0127 \pm 0.0036$.

$\Gamma(K^*(892)^0 K^- \pi^+ + \text{c.c.})/\Gamma_{\text{total}}$		Γ_5/Γ	
VALUE (units 10^{-2})	EVTS	DOCUMENT ID	TECN COMMENT
•••	We do not use the following data for averages, fits, limits, etc. •••		
1.8 ± 0.4 ± 0.2	63	¹ BALTRUSAIT...86	MRK3 $J/\psi \rightarrow \eta_c\gamma$

¹ BALTRUSAITIS 86 reports $[\Gamma(\eta_c(1S) \rightarrow K^*(892)^0 K^- \pi^+ + \text{c.c.})/\Gamma_{\text{total}}] \times [B(J/\psi(1S) \rightarrow \gamma\eta_c(1S))] = (2.6 \pm 0.6) \times 10^{-4}$ which we divide by our best value $B(J/\psi(1S) \rightarrow \gamma\eta_c(1S)) = (1.41 \pm 0.14) \times 10^{-2}$. Our first error is their experiment's error and our second error is the systematic error from using our best value.

$\Gamma(K^*(892)^0 \bar{K}^*(892)^0 \pi^+ \pi^-)/\Gamma_{\text{total}}$		Γ_7/Γ	
VALUE (units 10^{-4})	EVTS	DOCUMENT ID	TECN COMMENT
•••	We do not use the following data for averages, fits, limits, etc. •••		
135 ± 5 ± 13	45	¹ ABLIKIM	06A BES2 $J/\psi \rightarrow K^{*0} \bar{K}^{*0} \pi^+ \pi^- \gamma$

¹ ABLIKIM 06A reports $[\Gamma(\eta_c(1S) \rightarrow K^*(892)^0 \bar{K}^*(892)^0 \pi^+ \pi^-)/\Gamma_{\text{total}}] \times [B(J/\psi(1S) \rightarrow \gamma\eta_c(1S))] = (1.91 \pm 0.64 \pm 0.48) \times 10^{-4}$ which we divide by our best value $B(J/\psi(1S) \rightarrow \gamma\eta_c(1S)) = (1.41 \pm 0.14) \times 10^{-2}$. Our first error is their experiment's error and our second error is the systematic error from using our best value.

$\Gamma(\phi K^+ K^-)/\Gamma_{\text{total}}$		Γ_8/Γ	
VALUE (units 10^{-3})	EVTS	DOCUMENT ID	TECN COMMENT
•••	We do not use the following data for averages, fits, limits, etc. •••		
2.9 ± $\frac{0.9}{-0.8}$ ± 1.1	14.1 ± $\frac{4.4}{-3.7}$	¹ HUANG	03 BELL $B^+ \rightarrow (\phi K^+ K^-) K^+$

¹ Using $B(B^+ \rightarrow \eta_c K^+) = (1.25 \pm 0.12 \pm \frac{0.10}{0.12}) \times 10^{-3}$ from FANG 03 and $B(\eta_c \rightarrow K\bar{K}\pi) = (5.5 \pm 1.7) \times 10^{-2}$.

$\Gamma(\phi 2(\pi^+ \pi^-))/\Gamma_{\text{total}}$		Γ_{10}/Γ	
VALUE (units 10^{-4})	CL%	DOCUMENT ID	TECN COMMENT
<40	90	¹ ABLIKIM	06A BES2 $J/\psi \rightarrow \phi 2(\pi^+ \pi^-) \gamma$

¹ ABLIKIM 06A reports $[\Gamma(\eta_c(1S) \rightarrow \phi 2(\pi^+ \pi^-))/\Gamma_{\text{total}}] \times [B(J/\psi(1S) \rightarrow \gamma\eta_c(1S))] < 0.603 \times 10^{-4}$ which we divide by our best value $B(J/\psi(1S) \rightarrow \gamma\eta_c(1S)) = 1.41 \times 10^{-2}$.

$\Gamma(a_0(980) \pi)/\Gamma_{\text{total}}$		Γ_{11}/Γ	
VALUE	CL%	DOCUMENT ID	TECN COMMENT
seen		AAIJ	23AH LHCB $B^+ \rightarrow K^+(K_S^0 K\pi)$
seen		LEES	21A BABR Dalitz anal. of $\eta_c \rightarrow \pi^+ \pi^- \eta$
seen		LEES	14E BABR Dalitz anal. of $\eta_c \rightarrow K^+ K^- \pi^0$

••• We do not use the following data for averages, fits, limits, etc. •••

<0.02 90 ^{1,2}BALTRUSAIT...86 MRK3 $J/\psi \rightarrow \eta_c\gamma$

¹ The quoted branching ratio uses $B(J/\psi(1S) \rightarrow \gamma\eta_c(1S)) = 0.0127 \pm 0.0036$.

² We are assuming $B(a_0(980) \rightarrow \eta\pi) > 0.5$.

$\Gamma(a_2(1320) \pi)/\Gamma_{\text{total}}$		Γ_{12}/Γ	
VALUE	CL%	DOCUMENT ID	TECN COMMENT
seen		LEES	21A BABR Dalitz anal. of $\eta_c \rightarrow \pi^+ \pi^- \eta$

••• We do not use the following data for averages, fits, limits, etc. •••

<0.02 90 ¹BALTRUSAIT...86 MRK3 $J/\psi \rightarrow \eta_c\gamma$

¹ The quoted branching ratio uses $B(J/\psi(1S) \rightarrow \gamma\eta_c(1S)) = 0.0127 \pm 0.0036$.

$\Gamma(K^*(892) \bar{K} + \text{c.c.})/\Gamma_{\text{total}}$		Γ_{13}/Γ	
VALUE	CL%	DOCUMENT ID	TECN COMMENT
<0.0128	90	BISELLO	91 DM2 $J/\psi \rightarrow \gamma K_S^0 K^\pm \pi^\mp$
<0.0132	90	¹ BISELLO	91 DM2 $J/\psi \rightarrow \gamma K^+ K^- \pi^0$

¹ The quoted branching ratios use $B(J/\psi(1S) \rightarrow \gamma\eta_c(1S)) = 0.0127 \pm 0.0036$.

$\Gamma(f_2(1270) \eta)/\Gamma_{\text{total}}$		Γ_{14}/Γ	
VALUE	CL%	DOCUMENT ID	TECN COMMENT
seen		LEES	21A BABR Dalitz anal. of $\eta_c \rightarrow \pi^+ \pi^- \eta$

••• We do not use the following data for averages, fits, limits, etc. •••

<0.011 90 ¹BALTRUSAIT...86 MRK3 $J/\psi \rightarrow \eta_c\gamma$

¹ The quoted branching ratio uses $B(J/\psi(1S) \rightarrow \gamma\eta_c(1S)) = 0.0127 \pm 0.0036$.

$\Gamma(f_2(1270) \eta')/\Gamma_{\text{total}}$		Γ_{15}/Γ	
VALUE	DOCUMENT ID	TECN	COMMENT
seen	LEES	21A	BABR Dalitz anal. of $\eta_c \rightarrow \pi^+ \pi^- \eta'$; $K^+ K^- \eta'$

••• We do not use the following data for averages, fits, limits, etc. •••

<2.5 × 10⁻⁴ 90 ¹ABLIKIM 17P BES3 $J/\psi \rightarrow \pi^+ \pi^- \pi^0 K^+ K^- \gamma$

••• We do not use the following data for averages, fits, limits, etc. •••

<17 × 10⁻⁴ 90 ²ABLIKIM 05L BES2 $J/\psi \rightarrow \pi^+ \pi^- \pi^0 K^+ K^- \gamma$

¹ Using $B(J/\psi \rightarrow \gamma\eta_c) = 0.017 \pm 0.004$.

² The quoted branching ratio uses $B(J/\psi(1S) \rightarrow \gamma\eta_c(1S)) = 0.0127 \pm 0.0036$.

Meson Particle Listings

 $\eta_c(1S)$

$\Gamma(f_0(500)\eta)/\Gamma_{\text{total}}$	VALUE	DOCUMENT ID	TECN	COMMENT	Γ_{20}/Γ
seen		LEES	21A	BABR Dalitz anal. of $\eta_c \rightarrow \pi^+ \pi^- \eta$	

$\Gamma(f_0(500)\eta')/\Gamma_{\text{total}}$	VALUE	DOCUMENT ID	TECN	COMMENT	Γ_{21}/Γ
seen		LEES	21A	BABR Dalitz anal. of $\eta_c(1S) \rightarrow \pi^+ \pi^- \eta'$	

$\Gamma(f_0(980)\eta)/\Gamma_{\text{total}}$	VALUE	DOCUMENT ID	TECN	COMMENT	Γ_{22}/Γ
seen		LEES	21A	BABR Dalitz anal. of $\eta_c \rightarrow \pi^+ \pi^- \eta$	
seen		LEES	14E	BABR Dalitz anal. of $\eta_c \rightarrow K^+ K^- \eta$	

$\Gamma(f_0(980)\eta')/\Gamma_{\text{total}}$	VALUE	DOCUMENT ID	TECN	COMMENT	Γ_{23}/Γ
seen		LEES	21A	BABR Dalitz anal. of $\eta_c \rightarrow \pi^+ \pi^- \eta'$, $K^+ K^- \eta'$	

$\Gamma(f_0(1500)\eta)/\Gamma_{\text{total}}$	VALUE	DOCUMENT ID	TECN	COMMENT	Γ_{24}/Γ
seen		LEES	21A	BABR Dalitz anal. of $\eta_c \rightarrow \pi^+ \pi^- \eta$	
seen		LEES	14E	BABR Dalitz anal. of $\eta_c \rightarrow K^+ K^- \eta$	

$\Gamma(f_0(1710)\eta')/\Gamma_{\text{total}}$	VALUE	DOCUMENT ID	TECN	COMMENT	Γ_{25}/Γ
seen		LEES	21A	BABR Dalitz anal. of $\eta_c \rightarrow K^+ K^- \eta'$	

$\Gamma(f_0(2100)\eta')/\Gamma_{\text{total}}$	VALUE	DOCUMENT ID	TECN	COMMENT	Γ_{26}/Γ
seen		LEES	21A	BABR Dalitz anal. of $\eta_c \rightarrow \pi^+ \pi^- \eta'$	

$\Gamma(f_0(2200)\eta)/\Gamma_{\text{total}}$	VALUE	DOCUMENT ID	TECN	COMMENT	Γ_{27}/Γ
seen		LEES	14E	BABR Dalitz anal. of $\eta_c \rightarrow K^+ K^- \eta$	

$\Gamma(a_0(1320)\pi)/\Gamma_{\text{total}}$	VALUE	DOCUMENT ID	TECN	COMMENT	Γ_{28}/Γ
seen		AAIJ	23AH LHCB	$B^+ \rightarrow K^+(K_S^0 K \pi)$	
seen		LEES	14E	BABR Dalitz anal. of $\eta_c \rightarrow K^+ K^- \pi^0$	

$\Gamma(a_0(1450)\pi)/\Gamma_{\text{total}}$	VALUE	DOCUMENT ID	TECN	COMMENT	Γ_{29}/Γ
seen		AAIJ	23AH LHCB	$B^+ \rightarrow K^+(K_S^0 K \pi)$	
seen		LEES	21A	BABR Dalitz anal. of $\eta_c \rightarrow \pi^+ \pi^- \eta$	
seen		LEES	14E	BABR Dalitz anal. of $\eta_c \rightarrow K^+ K^- \pi^0$	

$\Gamma(a_2(1700)\pi)/\Gamma_{\text{total}}$	VALUE	DOCUMENT ID	TECN	COMMENT	Γ_{30}/Γ
seen		AAIJ	23AH LHCB	$B^+ \rightarrow K^+(K_S^0 K \pi)$	

$\Gamma(a_0(1710)\pi)/\Gamma_{\text{total}}$	VALUE	DOCUMENT ID	TECN	COMMENT	Γ_{31}/Γ
seen		AAIJ	23AH LHCB	$B^+ \rightarrow K^+(K_S^0 K \pi)$	
seen		LEES	21A	BABR Dalitz anal. of $\eta_c \rightarrow \pi^+ \pi^- \eta'$	

$\Gamma(a_0(1950)\pi)/\Gamma_{\text{total}}$	VALUE	EVTS	DOCUMENT ID	TECN	COMMENT	Γ_{32}/Γ
seen			LEES	21A	BABR Dalitz anal. of $\eta_c(1S) \rightarrow \pi^+ \pi^- \eta'$	
seen	12k	¹	LEES	16A	BABR $\gamma\gamma \rightarrow \eta_c(1S) \rightarrow K \bar{K} \pi$	

¹ From a model-independent partial wave analysis.

$\Gamma(K_2^*(1430)\bar{K} + \text{c.c.})/\Gamma_{\text{total}}$	VALUE	EVTS	DOCUMENT ID	TECN	COMMENT	Γ_{33}/Γ
seen		12k	¹ LEES	16A	BABR $\gamma\gamma \rightarrow \eta_c(1S) \rightarrow K \bar{K} \pi$	
seen			LEES	14E	BABR Dalitz anal. of $\eta_c \rightarrow K^+ K^- \eta/\pi^0$	

¹ From a model-independent partial wave analysis.

$\Gamma(K_2^*(1430)\bar{K} + \text{c.c.})/\Gamma_{\text{total}}$	VALUE	DOCUMENT ID	TECN	COMMENT	Γ_{34}/Γ
seen		AAIJ	23AH LHCB	$B^+ \rightarrow K^+(K_S^0 K \pi)$	
seen		LEES	21A	BABR Dalitz anal. of $\eta_c \rightarrow K^+ K^- \eta'$	
seen		LEES	14E	BABR Dalitz anal. of $\eta_c \rightarrow K^+ K^- \pi^0$	

$\Gamma(K_0^*(1950)\bar{K} + \text{c.c.})/\Gamma_{\text{total}}$	VALUE	EVTS	DOCUMENT ID	TECN	COMMENT	Γ_{35}/Γ
seen			AAIJ	23AH LHCB	$B^+ \rightarrow K^+(K_S^0 K \pi)$	
seen			LEES	21A	BABR Dalitz anal. of $\eta_c \rightarrow K^+ K^- \eta'$	
seen	12k	¹	LEES	16A	BABR $\gamma\gamma \rightarrow \eta_c(1S) \rightarrow K \bar{K} \pi$	
seen			LEES	14E	BABR Dalitz anal. of $\eta_c \rightarrow K^+ K^- \eta/\pi^0$	

¹ From a Dalitz plot analysis using an isobar model.

$\Gamma(K_2^*(2600)\bar{K} + \text{c.c.})/\Gamma_{\text{total}}$	VALUE	DOCUMENT ID	TECN	COMMENT	Γ_{36}/Γ
seen		AAIJ	23AH LHCB	$B^+ \rightarrow K^+(K_S^0 K \pi)$	

$\Gamma(K \bar{K} \pi)/\Gamma_{\text{total}}$	VALUE (units 10^{-2})	EVTS	DOCUMENT ID	TECN	COMMENT	Γ_{37}/Γ
7.1 ± 0.4 OUR FIT					Error includes scale factor of 1.1.	
7.4 ± 0.6 OUR AVERAGE						
6.9 ± 0.7 ± 0.6	146	¹	ABLIKIM	19AP BES3	$h_c \rightarrow \gamma \eta_c$	
7.6 ± 0.6 ± 0.6	267	²	ABLIKIM	19AP BES3	$h_c \rightarrow \gamma \eta_c$	

• • • We do not use the following data for averages, fits, limits, etc. • • •

6.1 ± 1.2 ± 0.6	55	^{3,4}	ABLIKIM	12N BES3	$\psi(2S) \rightarrow \pi^0 \gamma K^+ K^- \pi^0$	
7.6 ± 1.3 ± 0.8	107	^{5,6}	ABLIKIM	12N BES3	$\psi(2S) \rightarrow \pi^0 \gamma K_S^0 K^+ \pi^\pm$	
8.5 ± 1.8		⁷	AUBERT	06E BABR	$B^\pm \rightarrow K^\pm X_{c\bar{c}}$	
4.7 ± 1.2 ± 0.5	0.6k	^{8,9}	BAI	04 BES	$J/\psi \rightarrow \gamma K^\pm \pi^\mp K_S^0$	
6.2 ± 1.7 ± 0.6	33	^{10,11}	BISELLO	91 DM2	$J/\psi \rightarrow \gamma K^+ K^- \pi^0$	
4.9 ± 1.2 ± 0.5	68	^{12,13}	BISELLO	91 DM2	$J/\psi \rightarrow \gamma K^\pm \pi^\mp K_S^0$	
4.8 ± 1.7	95	^{14,15}	BALTRUSAITIS	..86 MRK3	$J/\psi \rightarrow \eta_c \gamma$	
5.5 ± 2.1 ± 0.5	32	^{16,17}	BALTRUSAITIS	..86 MRK3	$J/\psi \rightarrow \gamma K^+ K^- \pi^0$	
4.0 ± 1.1 ± 0.4	63	^{18,19}	BALTRUSAITIS	..86 MRK3	$J/\psi \rightarrow \gamma K^\pm \pi^\mp K_S^0$	
13 $\frac{+7}{-5} \pm 2$		²⁰	HIMEL	80B MRK2	$\psi(2S) \rightarrow \eta_c \gamma$	
< 10.7	90% CL	¹⁵	PARTRIDGE	80B CBAL	$J/\psi \rightarrow \eta_c \gamma$	

¹ ABLIKIM 19AP quotes $B(\eta_c \rightarrow K^+ K^- \pi^0) = (1.15 \pm 0.12 \pm 0.10) \times 10^{-2}$ which we multiply by 6 to account for isospin symmetry.

² ABLIKIM 19AP quotes $B(\eta_c \rightarrow K_S^0 K^\pm \pi^\mp) = (2.60 \pm 0.21 \pm 0.20) \times 10^{-2}$ which we multiply by 3 to account for isospin symmetry.

³ ABLIKIM 12N quotes $B(\psi(2S) \rightarrow \pi^0 h_c) \cdot B(h_c \rightarrow \gamma \eta_c) \cdot B(\eta_c \rightarrow K^+ K^- \pi^0) = (4.54 \pm 0.76 \pm 0.48) \times 10^{-6}$ which we multiply by 6 to account for isospin symmetry.

⁴ ABLIKIM 12N reports $[\Gamma(\eta_c(1S) \rightarrow K \bar{K} \pi)/\Gamma_{\text{total}}] \times [B(\psi(2S) \rightarrow h_c(1P) \pi^0)] \times [B(h_c(1P) \rightarrow \gamma \eta_c(1S))] = (27.24 \pm 4.56 \pm 2.88) \times 10^{-6}$ which we divide by our best values $B(\psi(2S) \rightarrow h_c(1P) \pi^0) = (7.4 \pm 0.5) \times 10^{-4}$, $B(h_c(1P) \rightarrow \gamma \eta_c(1S)) = (60 \pm 4) \times 10^{-2}$. Our first error is their experiment's error and our second error is the systematic error from using our best values.

⁵ ABLIKIM 12N quotes $B(\psi(2S) \rightarrow \pi^0 h_c) \cdot B(h_c \rightarrow \gamma \eta_c) \cdot B(\eta_c \rightarrow K_S^0 K^\pm \pi^\mp) = (11.35 \pm 1.25 \pm 1.50) \times 10^{-6}$ which we multiply by 3 to account for isospin symmetry.

⁶ ABLIKIM 12N reports $[\Gamma(\eta_c(1S) \rightarrow K \bar{K} \pi)/\Gamma_{\text{total}}] \times [B(\psi(2S) \rightarrow h_c(1P) \pi^0)] \times [B(h_c(1P) \rightarrow \gamma \eta_c(1S))] = (34.05 \pm 3.75 \pm 4.50) \times 10^{-6}$ which we divide by our best values $B(\psi(2S) \rightarrow h_c(1P) \pi^0) = (7.4 \pm 0.5) \times 10^{-4}$, $B(h_c(1P) \rightarrow \gamma \eta_c(1S)) = (60 \pm 4) \times 10^{-2}$. Our first error is their experiment's error and our second error is the systematic error from using our best values.

⁷ Determined from the ratio of $B(B^\pm \rightarrow K^\pm \eta_c) \cdot B(\eta_c \rightarrow K \bar{K} \pi) = (7.4 \pm 0.5 \pm 0.7) \times 10^{-5}$ reported in AUBERT, B 04B and $B(B^\pm \rightarrow K^\pm \eta_c) = (8.7 \pm 1.5) \times 10^{-3}$ reported in AUBERT 06E.

⁸ BAI 04 reports $B(J/\psi \rightarrow \gamma \eta_c) \cdot B(\eta_c \rightarrow K^\pm K_S^0 \pi^\mp) = (2.2 \pm 0.3 \pm 0.5) \times 10^{-4}$ which we multiply by 3 to account for isospin symmetry.

⁹ BAI 04 reports $[\Gamma(\eta_c(1S) \rightarrow K \bar{K} \pi)/\Gamma_{\text{total}}] \times [B(J/\psi(1S) \rightarrow \gamma \eta_c(1S))] = (6.6 \pm 0.9 \pm 1.5) \times 10^{-4}$ which we divide by our best value $B(J/\psi(1S) \rightarrow \gamma \eta_c(1S)) = (1.41 \pm 0.14) \times 10^{-2}$. Our first error is their experiment's error and our second error is the systematic error from using our best value.

¹⁰ BISELLO 91 reports $[\Gamma(\eta_c(1S) \rightarrow K \bar{K} \pi)/\Gamma_{\text{total}}] \times [B(J/\psi(1S) \rightarrow \gamma \eta_c(1S))] = (8.76 \pm 1.80 \pm 1.68) \times 10^{-4}$ which we divide by our best value $B(J/\psi(1S) \rightarrow \gamma \eta_c(1S)) = (1.41 \pm 0.14) \times 10^{-2}$. Our first error is their experiment's error and our second error is the systematic error from using our best value.

¹¹ BISELLO 91 reports $B(J/\psi \rightarrow \gamma \eta_c) \cdot B(\eta_c \rightarrow K^+ K^- \pi^0) = (1.46 \pm 0.30 \pm 0.28) \times 10^{-4}$ which we multiply by 6 to account for isospin symmetry.

¹² BISELLO 91 reports $[\Gamma(\eta_c(1S) \rightarrow K \bar{K} \pi)/\Gamma_{\text{total}}] \times [B(J/\psi(1S) \rightarrow \gamma \eta_c(1S))] = (6.9 \pm 1.2 \pm 1.2) \times 10^{-4}$ which we divide by our best value $B(J/\psi(1S) \rightarrow \gamma \eta_c(1S)) = (1.41 \pm 0.14) \times 10^{-2}$. Our first error is their experiment's error and our second error is the systematic error from using our best value.

¹³ BISELLO 91 reports $B(J/\psi \rightarrow \gamma \eta_c) \cdot B(\eta_c \rightarrow K^\pm K_S^0 \pi^\mp) = (2.3 \pm 0.4 \pm 0.4) \times 10^{-4}$ which we multiply by 3 to account for isospin symmetry.

¹⁴ Average from $K^+ K^- \pi^0$ and $K^\pm K_S^0 \pi^\mp$ decay channels.

¹⁵ The quoted branching ratios use $B(J/\psi(1S) \rightarrow \gamma \eta_c(1S)) = 0.0127 \pm 0.0036$. Where relevant, the error in this branching ratio is treated as a common systematic in computing averages.

¹⁶ BALTRUSAITIS 86 reports $[\Gamma(\eta_c(1S) \rightarrow K \bar{K} \pi)/\Gamma_{\text{total}}] \times [B(J/\psi(1S) \rightarrow \gamma \eta_c(1S))] = (7.8 \pm 3.0) \times 10^{-4}$ which we divide by our best value $B(J/\psi(1S) \rightarrow \gamma \eta_c(1S)) = (1.41 \pm 0.14) \times 10^{-2}$. Our first error is their experiment's error and our second error is the systematic error from using our best value.

¹⁷ BALTRUSAITIS 86 reports $B(J/\psi \rightarrow \gamma \eta_c) \cdot B(\eta_c \rightarrow K^+ K^- \pi^0) = (1.3 \pm 0.5) \times 10^{-4}$ which we multiply by 6 to account for isospin symmetry.

¹⁸ BALTRUSAITIS 86 reports $[\Gamma(\eta_c(1S) \rightarrow K \bar{K} \pi)/\Gamma_{\text{total}}] \times [B(J/\psi(1S) \rightarrow \gamma \eta_c(1S))] = (5.7 \pm 1.5) \times 10^{-4}$ which we divide by our best value $B(J/\psi(1S) \rightarrow \gamma \eta_c(1S)) = (1.41 \pm 0.14) \times 10^{-2}$. Our first error is their experiment's error and our second error is the systematic error from using our best value.

¹⁹ BALTRUSAITIS 86 reports $B(J/\psi \rightarrow \gamma \eta_c) \cdot B(\eta_c \rightarrow K^\pm K_S^0 \pi^\mp) = (1.9 \pm 0.5) \times 10^{-4}$ which we multiply by 3 to account for isospin symmetry.

²⁰ HIMEL 80B reports $[\Gamma(\eta_c(1S) \rightarrow K \bar{K} \pi)/\Gamma_{\text{total}}] \times [B(\psi(2S) \rightarrow \gamma \eta_c(1S))] = (4.5 \pm 2.4 \pm 1.8) \times 10^{-4}$ which we divide by our best value $B(\psi(2S) \rightarrow \gamma \eta_c(1S)) = (3.6 \pm 0.5) \times 10^{-3}$. Our first error is their experiment's error and our second error is the systematic error from using our best value.

$\Gamma(\phi K^+ K^-)/\Gamma(K\bar{K}\pi)$ Γ_{8}/Γ_{37}

VALUE	EVTS	DOCUMENT ID	TECN	COMMENT
$0.052 \pm 0.016 \pm 0.014$	7	¹ HUANG	03	BELL $B^\pm \rightarrow K^\pm \phi$

¹ Using $B(B^+ \rightarrow \eta_c K^+) = (1.25 \pm 0.12 \pm 0.10) \times 10^{-3}$ from FANG 03 and $B(\eta_c \rightarrow K\bar{K}\pi) = (5.5 \pm 1.7) \times 10^{-2}$.

$\Gamma(K\bar{K}\eta)/\Gamma_{total}$ Γ_{38}/Γ

VALUE (units 10^{-2})	CL%	EVTS	DOCUMENT ID	TECN	COMMENT
$0.9 \pm 0.5 \pm 0.1$		7	^{1,2} ABLIKIM	12N	BES3 $\psi(2S) \rightarrow \pi^0 \gamma \eta K^+ K^-$
< 3.1	90		³ BALTRUSAITIS..86	MRK3	$J/\psi \rightarrow \eta_c \gamma$

• • • We do not use the following data for averages, fits, limits, etc. • • •

¹ ABLIKIM 12N quotes $B(\psi(2S) \rightarrow \pi^0 h_c) \cdot B(h_c \rightarrow \gamma \eta_c) \cdot B(\eta_c \rightarrow K^+ K^- \eta) = (2.11 \pm 1.01 \pm 0.32) \times 10^{-6}$ which we multiply by 2 to account for isospin symmetry.

² ABLIKIM 12N reports $[\Gamma(\eta_c(1S) \rightarrow K\bar{K}\eta)/\Gamma_{total}] \times [B(\psi(2S) \rightarrow h_c(1P)\pi^0)] \times [B(h_c(1P) \rightarrow \gamma \eta_c(1S))] = (4.22 \pm 2.02 \pm 0.64) \times 10^{-6}$ which we divide by our best values $B(\psi(2S) \rightarrow h_c(1P)\pi^0) = (7.4 \pm 0.5) \times 10^{-4}$, $B(h_c(1P) \rightarrow \gamma \eta_c(1S)) = (60 \pm 4) \times 10^{-2}$. Our first error is their experiment's error and our second error is the systematic error from using our best values.

³ The quoted branching ratios use $B(J/\psi(1S) \rightarrow \gamma \eta_c(1S)) = 0.0127 \pm 0.0036$.

$\Gamma(K\bar{K}\eta)/\Gamma(K\bar{K}\pi)$ Γ_{38}/Γ_{37}

VALUE	EVTS	DOCUMENT ID	TECN	COMMENT
0.186 ± 0.018 OUR FIT				
$0.190 \pm 0.008 \pm 0.017$	5.4k	¹ LEES	14E	BABR $\gamma\gamma \rightarrow K^+ K^- \eta/\pi^0$

¹ LEES 14E reports $B(\eta_c(1S) \rightarrow K^+ K^- \eta)/B(\eta_c(1S) \rightarrow K^+ K^- \pi^0) = 0.571 \pm 0.025 \pm 0.051$, which we divide by 3 to account for isospin symmetry. It uses both $\eta \rightarrow \gamma\gamma$ and $\eta \rightarrow \pi^+ \pi^- \pi^0$ decays.

$\Gamma(\eta\pi^+ \pi^-)/\Gamma_{total}$ Γ_{39}/Γ

VALUE (units 10^{-2})	EVTS	DOCUMENT ID	TECN	COMMENT
$1.6 \pm 0.4 \pm 0.2$	33	¹ ABLIKIM	12N	BES3 $\psi(2S) \rightarrow \pi^0 \gamma \eta \pi^+ \pi^-$

• • • We do not use the following data for averages, fits, limits, etc. • • •

5.4 ± 2.0 ² BALTRUSAITIS..86 MRK3 $J/\psi \rightarrow \eta_c \gamma$

$3.7 \pm 1.3 \pm 2.0$ ² PARTRIDGE 80b CBAL $J/\psi \rightarrow \eta \pi^+ \pi^- \gamma$

¹ ABLIKIM 12N reports $[\Gamma(\eta_c(1S) \rightarrow \eta \pi^+ \pi^-)/\Gamma_{total}] \times [B(\psi(2S) \rightarrow h_c(1P)\pi^0)] \times [B(h_c(1P) \rightarrow \gamma \eta_c(1S))] = (7.22 \pm 1.47 \pm 1.11) \times 10^{-6}$ which we divide by our best values $B(\psi(2S) \rightarrow h_c(1P)\pi^0) = (7.4 \pm 0.5) \times 10^{-4}$, $B(h_c(1P) \rightarrow \gamma \eta_c(1S)) = (60 \pm 4) \times 10^{-2}$. Our first error is their experiment's error and our second error is the systematic error from using our best values.

² The quoted branching ratios use $B(J/\psi(1S) \rightarrow \gamma \eta_c(1S)) = 0.0127 \pm 0.0036$. Where relevant, the error in this branching ratio is treated as a common systematic in computing averages.

$\Gamma(\eta 2(\pi^+ \pi^-))/\Gamma_{total}$ Γ_{40}/Γ

VALUE (units 10^{-2})	EVTS	DOCUMENT ID	TECN	COMMENT
$4.3 \pm 1.2 \pm 0.4$	39	¹ ABLIKIM	12N	BES3 $\psi(2S) \rightarrow \pi^0 \gamma \eta 2(\pi^+ \pi^-)$

¹ ABLIKIM 12N reports $[\Gamma(\eta_c(1S) \rightarrow \eta 2(\pi^+ \pi^-))/\Gamma_{total}] \times [B(\psi(2S) \rightarrow h_c(1P)\pi^0)] \times [B(h_c(1P) \rightarrow \gamma \eta_c(1S))] = (19.17 \pm 3.77 \pm 3.72) \times 10^{-6}$ which we divide by our best values $B(\psi(2S) \rightarrow h_c(1P)\pi^0) = (7.4 \pm 0.5) \times 10^{-4}$, $B(h_c(1P) \rightarrow \gamma \eta_c(1S)) = (60 \pm 4) \times 10^{-2}$. Our first error is their experiment's error and our second error is the systematic error from using our best values.

$\Gamma(K^+ K^- \pi^+ \pi^- \pi^0)/\Gamma(K\bar{K}\pi)$ Γ_{42}/Γ_{37}

VALUE	EVTS	DOCUMENT ID	TECN	COMMENT
$0.477 \pm 0.017 \pm 0.070$	11k	¹ DEL-AMO-SA...11M	BABR	$\gamma\gamma \rightarrow K^+ K^- \pi^+ \pi^- \pi^0$

¹ We have multiplied the value of $\Gamma(K^+ K^- \pi^+ \pi^- \pi^0)/\Gamma(K_S^0 K^\pm \pi^\mp)$ reported in DEL-AMO-SANCHEZ 11M by a factor 1/3 to obtain $\Gamma(K^+ K^- \pi^+ \pi^- \pi^0)/\Gamma(K\bar{K}\pi)$. Not independent from other measurements reported in DEL-AMO-SANCHEZ 11M.

$\Gamma(K^0 K^- \pi^+ \pi^- \pi^+ + c.c.)/\Gamma_{total}$ Γ_{43}/Γ

VALUE (units 10^{-2})	EVTS	DOCUMENT ID	TECN	COMMENT
$5.4 \pm 1.4 \pm 0.5$	43	^{1,2} ABLIKIM	12N	BES3 $\psi(2S) \rightarrow \pi^0 \gamma K_S^0 K^\mp \pi^\mp 2\pi^\pm$

¹ ABLIKIM 12N quotes $B(\psi(2S) \rightarrow \pi^0 h_c) \cdot B(h_c \rightarrow \gamma \eta_c) \cdot B(\eta_c \rightarrow K_S^0 K^- \pi^- 2\pi^+) = (12.01 \pm 2.22 \pm 2.04) \times 10^{-6}$ which we multiply by 2 to take c.c. into account.

² ABLIKIM 12N reports $[\Gamma(\eta_c(1S) \rightarrow K^0 K^- \pi^+ \pi^- \pi^+ + c.c.)/\Gamma_{total}] \times [B(\psi(2S) \rightarrow h_c(1P)\pi^0)] \times [B(h_c(1P) \rightarrow \gamma \eta_c(1S))] = (24.02 \pm 4.44 \pm 4.08) \times 10^{-6}$ which we divide by our best values $B(\psi(2S) \rightarrow h_c(1P)\pi^0) = (7.4 \pm 0.5) \times 10^{-4}$, $B(h_c(1P) \rightarrow \gamma \eta_c(1S)) = (60 \pm 4) \times 10^{-2}$. Our first error is their experiment's error and our second error is the systematic error from using our best values.

$\Gamma(K^+ K^- 2(\pi^+ \pi^-))/\Gamma_{total}$ Γ_{44}/Γ

VALUE (units 10^{-3})	EVTS	DOCUMENT ID	TECN	COMMENT
8.4 ± 2.4 OUR AVERAGE				
8 ± 4	10	¹ ABLIKIM	12N	BES3 $\psi(2S) \rightarrow \pi^0 \gamma K^+ K^- 2(\pi^+ \pi^-)$
$8.6 \pm 2.8 \pm 0.8$	100	² ABLIKIM	06A	BES2 $J/\psi \rightarrow K^+ K^- 2(\pi^+ \pi^-) \gamma$

¹ ABLIKIM 12N reports $[\Gamma(\eta_c(1S) \rightarrow K^+ K^- 2(\pi^+ \pi^-))/\Gamma_{total}] \times [B(\psi(2S) \rightarrow h_c(1P)\pi^0)] \times [B(h_c(1P) \rightarrow \gamma \eta_c(1S))] = (3.60 \pm 1.71 \pm 0.64) \times 10^{-6}$ which we divide by our best values $B(\psi(2S) \rightarrow h_c(1P)\pi^0) = (7.4 \pm 0.5) \times 10^{-4}$, $B(h_c(1P) \rightarrow \gamma \eta_c(1S)) = (60 \pm 4) \times 10^{-2}$. Our first error is their experiment's error and our second error is the systematic error from using our best values.

² ABLIKIM 06A reports $[\Gamma(\eta_c(1S) \rightarrow K^+ K^- 2(\pi^+ \pi^-))/\Gamma_{total}] \times [B(J/\psi(1S) \rightarrow \gamma \eta_c(1S))] = (1.21 \pm 0.32 \pm 0.24) \times 10^{-4}$ which we divide by our best value $B(J/\psi(1S) \rightarrow \gamma \eta_c(1S)) = (1.41 \pm 0.14) \times 10^{-2}$. Our first error is their experiment's error and our second error is the systematic error from using our best value.

$\Gamma(\pi^+ \pi^- \pi^0)/\Gamma_{total}$ Γ_{46}/Γ

VALUE	CL%	DOCUMENT ID	TECN	COMMENT
$< 4 \times 10^{-4}$	90	¹ ABLIKIM	17AJ	BES3 $\psi(2S) \rightarrow \gamma \pi^+ \pi^- \pi^0$

¹ ABLIKIM 17AJ reports $[\Gamma(\eta_c(1S) \rightarrow \pi^+ \pi^- \pi^0)/\Gamma_{total}] \times [B(\psi(2S) \rightarrow \gamma \eta_c(1S))] < 1.6 \times 10^{-6}$ which we divide by our best value $B(\psi(2S) \rightarrow \gamma \eta_c(1S)) = 3.6 \times 10^{-3}$.

$\Gamma(\pi^+ \pi^- \pi^0 \pi^0)/\Gamma_{total}$ Γ_{47}/Γ

VALUE (units 10^{-2})	EVTS	DOCUMENT ID	TECN	COMMENT
$4.6 \pm 0.9 \pm 0.5$	118	¹ ABLIKIM	12N	BES3 $\psi(2S) \rightarrow \pi^0 \gamma \pi^+ \pi^- 2\pi^0$

¹ ABLIKIM 12N reports $[\Gamma(\eta_c(1S) \rightarrow \pi^+ \pi^- \pi^0 \pi^0)/\Gamma_{total}] \times [B(\psi(2S) \rightarrow h_c(1P)\pi^0)] \times [B(h_c(1P) \rightarrow \gamma \eta_c(1S))] = (20.31 \pm 2.20 \pm 3.33) \times 10^{-6}$ which we divide by our best values $B(\psi(2S) \rightarrow h_c(1P)\pi^0) = (7.4 \pm 0.5) \times 10^{-4}$, $B(h_c(1P) \rightarrow \gamma \eta_c(1S)) = (60 \pm 4) \times 10^{-2}$. Our first error is their experiment's error and our second error is the systematic error from using our best values.

$\Gamma(2(\pi^+ \pi^- \pi^0))/\Gamma_{total}$ Γ_{49}/Γ

VALUE (units 10^{-2})	EVTS	DOCUMENT ID	TECN	COMMENT
15.9 ± 2.0 OUR AVERAGE				
$15.3 \pm 1.8 \pm 1.8$	333	ABLIKIM	19AP	BES3 $h_c \rightarrow \gamma \eta_c$
$16.8 \pm 2.8 \pm 1.7$	175	¹ ABLIKIM	12N	BES3 $\psi(2S) \rightarrow \pi^0 \gamma 2(\pi^+ \pi^- \pi^0)$

¹ ABLIKIM 12N reports $[\Gamma(\eta_c(1S) \rightarrow 2(\pi^+ \pi^- \pi^0))/\Gamma_{total}] \times [B(\psi(2S) \rightarrow h_c(1P)\pi^0)] \times [B(h_c(1P) \rightarrow \gamma \eta_c(1S))] = (75.13 \pm 7.42 \pm 9.99) \times 10^{-6}$ which we divide by our best values $B(\psi(2S) \rightarrow h_c(1P)\pi^0) = (7.4 \pm 0.5) \times 10^{-4}$, $B(h_c(1P) \rightarrow \gamma \eta_c(1S)) = (60 \pm 4) \times 10^{-2}$. Our first error is their experiment's error and our second error is the systematic error from using our best values.

$\Gamma(3(\pi^+ \pi^-))/\Gamma_{total}$ Γ_{50}/Γ

VALUE (units 10^{-3})	EVTS	DOCUMENT ID	TECN	COMMENT
18.9 ± 3.4 OUR AVERAGE				
$20 \pm 5 \pm 2$	51	¹ ABLIKIM	12N	BES3 $\psi(2S) \rightarrow \pi^0 \gamma 3(\pi^+ \pi^-)$
$18 \pm 4 \pm 2$	479	² ABLIKIM	06A	BES2 $J/\psi \rightarrow 3(\pi^+ \pi^-) \gamma$

¹ ABLIKIM 12N reports $[\Gamma(\eta_c(1S) \rightarrow 3(\pi^+ \pi^-))/\Gamma_{total}] \times [B(\psi(2S) \rightarrow h_c(1P)\pi^0)] \times [B(h_c(1P) \rightarrow \gamma \eta_c(1S))] = (8.82 \pm 1.57 \pm 1.59) \times 10^{-6}$ which we divide by our best values $B(\psi(2S) \rightarrow h_c(1P)\pi^0) = (7.4 \pm 0.5) \times 10^{-4}$, $B(h_c(1P) \rightarrow \gamma \eta_c(1S)) = (60 \pm 4) \times 10^{-2}$. Our first error is their experiment's error and our second error is the systematic error from using our best values.

² ABLIKIM 06A reports $[\Gamma(\eta_c(1S) \rightarrow 3(\pi^+ \pi^-))/\Gamma_{total}] \times [B(J/\psi(1S) \rightarrow \gamma \eta_c(1S))] = (2.59 \pm 0.32 \pm 0.47) \times 10^{-4}$ which we divide by our best value $B(J/\psi(1S) \rightarrow \gamma \eta_c(1S)) = (1.41 \pm 0.14) \times 10^{-2}$. Our first error is their experiment's error and our second error is the systematic error from using our best value.

$\Gamma(\rho\bar{\rho})/\Gamma_{total}$ Γ_{51}/Γ

VALUE (units 10^{-4})	EVTS	DOCUMENT ID	TECN	COMMENT
13.3 ± 1.1 OUR FIT				Error includes scale factor of 1.1.
$12.0 \pm 2.6 \pm 1.5$	34	ABLIKIM	19AP	BES3 $h_c \rightarrow \gamma \eta_c$

• • • We do not use the following data for averages, fits, limits, etc. • • •

$15 \pm 5 \pm 1$ ¹ ABLIKIM 12N BES3 $\psi(2S) \rightarrow \pi^0 \gamma \rho\bar{\rho}$

$12.9 \pm 2.1 \pm 0.8$ ² WU 06 BELL $B^\pm \rightarrow \rho\bar{\rho} K^\pm$

$13.5 \pm 3.0 \pm 1.3$ ³ BAI 04 BES $J/\psi \rightarrow \gamma \rho\bar{\rho}$

$9.2 \pm 3.5 \pm 0.9$ ⁴ BISELLO 91 DM2 $J/\psi \rightarrow \gamma \rho\bar{\rho}$

$10 \pm 5 \pm 1$ ⁵ BALTRUSAITIS..86 MRK3 $J/\psi \rightarrow \eta_c \gamma$

$22 \pm 11 \pm 3$ ⁶ HIMEL 80B MRK2 $\psi(2S) \rightarrow \eta_c \gamma$

¹ ABLIKIM 12N reports $[\Gamma(\eta_c(1S) \rightarrow \rho\bar{\rho})/\Gamma_{total}] \times [B(\psi(2S) \rightarrow h_c(1P)\pi^0)] \times [B(h_c(1P) \rightarrow \gamma \eta_c(1S))] = (0.65 \pm 0.19 \pm 0.10) \times 10^{-6}$ which we divide by our best values $B(\psi(2S) \rightarrow h_c(1P)\pi^0) = (7.4 \pm 0.5) \times 10^{-4}$, $B(h_c(1P) \rightarrow \gamma \eta_c(1S)) = (60 \pm 4) \times 10^{-2}$. Our first error is their experiment's error and our second error is the systematic error from using our best values.

² WU 06 reports $[\Gamma(\eta_c(1S) \rightarrow \rho\bar{\rho})/\Gamma_{total}] \times [B(B^+ \rightarrow \eta_c K^+)] = (1.42 \pm 0.11 \pm 0.16) \times 10^{-6}$ which we divide by our best value $B(B^+ \rightarrow \eta_c K^+) = (1.10 \pm 0.07) \times 10^{-3}$. Our first error is their experiment's error and our second error is the systematic error from using our best value.

³ BAI 04 reports $[\Gamma(\eta_c(1S) \rightarrow \rho\bar{\rho})/\Gamma_{total}] \times [B(J/\psi(1S) \rightarrow \gamma \eta_c(1S))] = (1.9 \pm 0.3 \pm 0.3) \times 10^{-5}$ which we divide by our best value $B(J/\psi(1S) \rightarrow \gamma \eta_c(1S)) = (1.41 \pm 0.14) \times 10^{-2}$. Our first error is their experiment's error and our second error is the systematic error from using our best value.

⁴ BISELLO 91 reports $[\Gamma(\eta_c(1S) \rightarrow \rho\bar{\rho})/\Gamma_{total}] \times [B(J/\psi(1S) \rightarrow \gamma \eta_c(1S))] = (0.13 \pm 0.04 \pm 0.03) \times 10^{-4}$ which we divide by our best value $B(J/\psi(1S) \rightarrow \gamma \eta_c(1S)) = (1.41 \pm 0.14) \times 10^{-2}$. Our first error is their experiment's error and our second error is the systematic error from using our best value.

⁵ BALTRUSAITIS 86 reports $[\Gamma(\eta_c(1S) \rightarrow \rho\bar{\rho})/\Gamma_{total}] \times [B(J/\psi(1S) \rightarrow \gamma \eta_c(1S))] = (1.4 \pm 0.7) \times 10^{-5}$ which we divide by our best value $B(J/\psi(1S) \rightarrow \gamma \eta_c(1S)) = (1.41 \pm 0.14) \times 10^{-2}$. Our first error is their experiment's error and our second error is the systematic error from using our best value.

⁶ HIMEL 80B reports $[\Gamma(\eta_c(1S) \rightarrow \rho\bar{\rho})/\Gamma_{total}] \times [B(\psi(2S) \rightarrow \gamma \eta_c(1S))] = (8 \pm 4) \times 10^{-6}$ which we divide by our best value $B(\psi(2S) \rightarrow \gamma \eta_c(1S)) = (3.6 \pm 0.5) \times 10^{-3}$. Our first error is their experiment's error and our second error is the systematic error from using our best value.

Meson Particle Listings

 $\eta_c(1S)$ $\Gamma(\rho\bar{\rho})/\Gamma_{\text{total}} \times \Gamma(\phi\phi)/\Gamma_{\text{total}}$ $\Gamma_{51}/\Gamma \times \Gamma_9/\Gamma$

VALUE (units 10^{-5})	DOCUMENT ID	TECN	COMMENT
0.24 ± 0.07 OUR FIT			Error includes scale factor of 1.9.
$4.0 \pm_{-3.2}^{+3.5}$	BAGLIN	89	SPEC $\bar{p}p \rightarrow K^+K^-K^+K^-$

 $\Gamma(\rho\bar{\rho}\pi^0)/\Gamma_{\text{total}}$ Γ_{52}/Γ

VALUE (units 10^{-2})	EVTS	DOCUMENT ID	TECN	COMMENT
$0.34 \pm 0.12 \pm 0.03$	14	¹ ABLIKIM	12N	BES3 $\psi(2S) \rightarrow \pi^0\gamma\bar{p}\pi^0$
$\bullet\bullet\bullet$ We do not use the following data for averages, fits, limits, etc. $\bullet\bullet\bullet$				
¹ ABLIKIM 12N reports $[\Gamma(\eta_c(1S) \rightarrow \rho\bar{\rho}\pi^0)/\Gamma_{\text{total}}] \times [B(\psi(2S) \rightarrow h_c(1P)\pi^0)] \times [B(h_c(1P) \rightarrow \gamma\eta_c(1S))] = (1.53 \pm 0.49 \pm 0.23) \times 10^{-6}$ which we divide by our best values $B(\psi(2S) \rightarrow h_c(1P)\pi^0) = (7.4 \pm 0.5) \times 10^{-4}$, $B(h_c(1P) \rightarrow \gamma\eta_c(1S)) = (60 \pm 4) \times 10^{-2}$. Our first error is their experiment's error and our second error is the systematic error from using our best values.				

 $\Gamma(K^+\bar{p}A + c.c.)/\Gamma_{\text{total}}$ Γ_{55}/Γ

VALUE (units 10^{-3})	EVTS	DOCUMENT ID	TECN	COMMENT
$2.46 \pm_{-0.32}^{+0.33} \pm 0.16$	157	¹ LU	19	BELL $B^+ \rightarrow \bar{p}A K^+ K^+$
$\bullet\bullet\bullet$ We do not use the following data for averages, fits, limits, etc. $\bullet\bullet\bullet$				
¹ LU 19 reports $(2.83 \pm_{-0.34}^{+0.36} \pm 0.35) \times 10^{-3}$ from a measurement of $[\Gamma(\eta_c(1S) \rightarrow K^+\bar{p}A + c.c.)/\Gamma_{\text{total}}] \times [B(B^+ \rightarrow \eta_c K^+)]$ assuming $B(B^+ \rightarrow \eta_c K^+) = (9.6 \pm 1.1) \times 10^{-4}$, which we rescale to our best value $B(B^+ \rightarrow \eta_c K^+) = (1.10 \pm 0.07) \times 10^{-3}$. Our first error is their experiment's error and our second error is the systematic error from using our best value.				

 $\Gamma(\bar{\Lambda}(1520)\Lambda + c.c.)/\Gamma_{\text{total}}$ Γ_{56}/Γ

VALUE (units 10^{-3})	EVTS	DOCUMENT ID	TECN	COMMENT
$3.0 \pm 1.3 \pm 0.2$	43	¹ LU	19	BELL $B^+ \rightarrow \bar{p}A K^+ K^+$
$\bullet\bullet\bullet$ We do not use the following data for averages, fits, limits, etc. $\bullet\bullet\bullet$				
¹ LU 19 reports $(3.48 \pm 1.48 \pm 0.46) \times 10^{-3}$ from a measurement of $[\Gamma(\eta_c(1S) \rightarrow \bar{\Lambda}(1520)\Lambda + c.c.)/\Gamma_{\text{total}}] \times [B(B^+ \rightarrow \eta_c K^+)]$ assuming $B(B^+ \rightarrow \eta_c K^+) = (9.6 \pm 1.1) \times 10^{-4}$, which we rescale to our best value $B(B^+ \rightarrow \eta_c K^+) = (1.10 \pm 0.07) \times 10^{-3}$. Our first error is their experiment's error and our second error is the systematic error from using our best value.				

 $\Gamma(\Sigma^+\bar{\Sigma}^-)/\Gamma_{\text{total}}$ Γ_{57}/Γ

VALUE (units 10^{-3})	EVTS	DOCUMENT ID	TECN	COMMENT
$2.6 \pm 0.4 \pm 0.2$	112	¹ ABLIKIM	13c	BES3 $J/\psi \rightarrow \gamma\rho\bar{p}\pi^0\pi^0$
$\bullet\bullet\bullet$ We do not use the following data for averages, fits, limits, etc. $\bullet\bullet\bullet$				
¹ ABLIKIM 13c reports $[\Gamma(\eta_c(1S) \rightarrow \Sigma^+\bar{\Sigma}^-)/\Gamma_{\text{total}}] \times [B(J/\psi(1S) \rightarrow \gamma\eta_c(1S))] = (3.60 \pm 0.48 \pm 0.31) \times 10^{-5}$ which we divide by our best value $B(J/\psi(1S) \rightarrow \gamma\eta_c(1S)) = (1.41 \pm 0.14) \times 10^{-2}$. Our first error is their experiment's error and our second error is the systematic error from using our best value.				

 $\Gamma(\Xi^-\bar{\Xi}^+)/\Gamma_{\text{total}}$ Γ_{58}/Γ

VALUE (units 10^{-3})	EVTS	DOCUMENT ID	TECN	COMMENT
$1.07 \pm 0.22 \pm 0.10$	78	¹ ABLIKIM	13c	BES3 $J/\psi \rightarrow \gamma\Lambda\bar{\Lambda}\pi^+\pi^-$
$\bullet\bullet\bullet$ We do not use the following data for averages, fits, limits, etc. $\bullet\bullet\bullet$				
¹ ABLIKIM 13c reports $[\Gamma(\eta_c(1S) \rightarrow \Xi^-\bar{\Xi}^+)/\Gamma_{\text{total}}] \times [B(J/\psi(1S) \rightarrow \gamma\eta_c(1S))] = (1.51 \pm 0.27 \pm 0.14) \times 10^{-5}$ which we divide by our best value $B(J/\psi(1S) \rightarrow \gamma\eta_c(1S)) = (1.41 \pm 0.14) \times 10^{-2}$. Our first error is their experiment's error and our second error is the systematic error from using our best value.				

RADIATIVE DECAYS

 $\Gamma(\gamma\gamma)/\Gamma_{\text{total}}$ Γ_{59}/Γ

VALUE (units 10^{-4})	CL%	EVTS	DOCUMENT ID	TECN	COMMENT
1.66 ± 0.13 OUR FIT					Error includes scale factor of 1.2.
$\bullet\bullet\bullet$ We do not use the following data for averages, fits, limits, etc. $\bullet\bullet\bullet$					
$3.2 \pm 1.0 \pm 0.3$			¹ ABLIKIM	13i	BES3
$0.9 \pm_{-0.8}^{+1.9} \pm 0.1$		$1.2 \pm_{-1.1}^{+2.8}$	² ADAMS	08	CLEO $\psi(2S) \rightarrow \pi^+\pi^-\pi^+J/\psi$
$2.0 \pm_{-0.7}^{+0.9} \pm 0.1$		13	³ WICHT	08	BELL $B^\pm \rightarrow K^\pm\gamma\gamma$
$2.80 \pm_{-0.58}^{+0.67} \pm 1.0$			⁴ ARMSTRONG	95F	E760 $\bar{p}p \rightarrow \gamma\gamma$
< 9	90		⁵ BISELLO	91	DM2 $J/\psi \rightarrow \gamma\gamma\gamma$
$6 \pm_{-3}^{+4} \pm 4$			⁴ BAGLIN	87B	SPEC $\bar{p}p \rightarrow \gamma\gamma$
< 18	90		⁶ BLOOM	83	CBAL $J/\psi \rightarrow \eta_c\gamma$
$\bullet\bullet\bullet$ We do not use the following data for averages, fits, limits, etc. $\bullet\bullet\bullet$					
¹ ABLIKIM 13i reports $[\Gamma(\eta_c(1S) \rightarrow \gamma\gamma)/\Gamma_{\text{total}}] \times [B(J/\psi(1S) \rightarrow \gamma\eta_c(1S))] = (4.5 \pm 1.2 \pm 0.6) \times 10^{-6}$ which we divide by our best value $B(J/\psi(1S) \rightarrow \gamma\eta_c(1S)) = (1.41 \pm 0.14) \times 10^{-2}$. Our first error is their experiment's error and our second error is the systematic error from using our best value.					
² ADAMS 08 reports $[\Gamma(\eta_c(1S) \rightarrow \gamma\gamma)/\Gamma_{\text{total}}] \times [B(J/\psi(1S) \rightarrow \gamma\eta_c(1S))] = (1.2 \pm_{-1.1}^{+2.7} \pm 0.3) \times 10^{-6}$ which we divide by our best value $B(J/\psi(1S) \rightarrow \gamma\eta_c(1S)) = (1.41 \pm 0.14) \times 10^{-2}$. Our first error is their experiment's error and our second error is the systematic error from using our best value.					
³ WICHT 08 reports $[\Gamma(\eta_c(1S) \rightarrow \gamma\gamma)/\Gamma_{\text{total}}] \times [B(B^+ \rightarrow \eta_c K^+)] = (2.2 \pm_{-0.7}^{+0.9} \pm 0.4) \times 10^{-7}$ which we divide by our best value $B(B^+ \rightarrow \eta_c K^+) = (1.10 \pm 0.07) \times 10^{-3}$. Our first error is their experiment's error and our second error is the systematic error from using our best value.					
⁴ Not independent from the values of the total and two-photon width quoted by the same experiment.					
⁵ The quoted branching ratios use $B(J/\psi(1S) \rightarrow \gamma\eta_c(1S)) = 0.0127 \pm 0.0036$.					
⁶ Using $B(J/\psi(1S) \rightarrow \gamma\eta_c(1S)) = 0.0127 \pm 0.0036$.					

 $\Gamma(\rho\bar{\rho})/\Gamma_{\text{total}} \times \Gamma(\gamma\gamma)/\Gamma_{\text{total}}$ $\Gamma_{51}/\Gamma \times \Gamma_{59}/\Gamma$

VALUE (units 10^{-6})	EVTS	DOCUMENT ID	TECN	COMMENT
0.221 ± 0.019 OUR FIT				Error includes scale factor of 1.2.
0.26 ± 0.05 OUR AVERAGE				Error includes scale factor of 1.4.
$0.224 \pm_{-0.037}^{+0.038} \pm 0.020$	190	AMBROGIANI	03	E835 $\bar{p}p \rightarrow \eta_c \rightarrow \gamma\gamma$
$0.336 \pm_{-0.070}^{+0.080}$		ARMSTRONG	95F	E760 $\bar{p}p \rightarrow \gamma\gamma$
$0.68 \pm_{-0.31}^{+0.42}$	12	BAGLIN	87B	SPEC $\bar{p}p \rightarrow \gamma\gamma$

Charge conjugation (C), Parity (P),
Lepton family number (LF) violating modes $\Gamma(\pi^+\pi^-)/\Gamma_{\text{total}}$ Γ_{60}/Γ

VALUE (units 10^{-5})	CL%	DOCUMENT ID	TECN	COMMENT
<13	90	¹ ABLIKIM	11G	BES3 $J/\psi \rightarrow \gamma\pi^+\pi^-$
$\bullet\bullet\bullet$ We do not use the following data for averages, fits, limits, etc. $\bullet\bullet\bullet$				
<80	90	² ABLIKIM	06B	BES2 $J/\psi \rightarrow \pi^+\pi^-\gamma$
$\bullet\bullet\bullet$ We do not use the following data for averages, fits, limits, etc. $\bullet\bullet\bullet$				
¹ ABLIKIM 11G reports $[\Gamma(\eta_c(1S) \rightarrow \pi^+\pi^-)/\Gamma_{\text{total}}] \times [B(J/\psi(1S) \rightarrow \gamma\eta_c(1S))] < 1.82 \times 10^{-6}$ which we divide by our best value $B(J/\psi(1S) \rightarrow \gamma\eta_c(1S)) = 1.41 \times 10^{-2}$.				
² ABLIKIM 06B reports $[\Gamma(\eta_c(1S) \rightarrow \pi^+\pi^-)/\Gamma_{\text{total}}] \times [B(J/\psi(1S) \rightarrow \gamma\eta_c(1S))] < 1.1 \times 10^{-5}$ which we divide by our best value $B(J/\psi(1S) \rightarrow \gamma\eta_c(1S)) = 1.41 \times 10^{-2}$.				

 $\Gamma(\pi^0\pi^0)/\Gamma_{\text{total}}$ Γ_{61}/Γ

VALUE (units 10^{-5})	CL%	DOCUMENT ID	TECN	COMMENT
< 4	90	¹ ABLIKIM	11G	BES3 $J/\psi \rightarrow \gamma\pi^0\pi^0$
$\bullet\bullet\bullet$ We do not use the following data for averages, fits, limits, etc. $\bullet\bullet\bullet$				
<50	90	² ABLIKIM	06B	BES2 $J/\psi \rightarrow \pi^0\pi^0\gamma$
$\bullet\bullet\bullet$ We do not use the following data for averages, fits, limits, etc. $\bullet\bullet\bullet$				
¹ ABLIKIM 11G reports $[\Gamma(\eta_c(1S) \rightarrow \pi^0\pi^0)/\Gamma_{\text{total}}] \times [B(J/\psi(1S) \rightarrow \gamma\eta_c(1S))] < 6.0 \times 10^{-7}$ which we divide by our best value $B(J/\psi(1S) \rightarrow \gamma\eta_c(1S)) = 1.41 \times 10^{-2}$.				
² ABLIKIM 06B reports $[\Gamma(\eta_c(1S) \rightarrow \pi^0\pi^0)/\Gamma_{\text{total}}] \times [B(J/\psi(1S) \rightarrow \gamma\eta_c(1S))] < 0.71 \times 10^{-5}$ which we divide by our best value $B(J/\psi(1S) \rightarrow \gamma\eta_c(1S)) = 1.41 \times 10^{-2}$.				

 $\Gamma(K^+K^-)/\Gamma_{\text{total}}$ Γ_{62}/Γ

VALUE (units 10^{-5})	CL%	DOCUMENT ID	TECN	COMMENT
<70	90	¹ ABLIKIM	06B	BES2 $J/\psi \rightarrow K^+K^-\gamma$
$\bullet\bullet\bullet$ We do not use the following data for averages, fits, limits, etc. $\bullet\bullet\bullet$				
¹ ABLIKIM 06B reports $[\Gamma(\eta_c(1S) \rightarrow K^+K^-)/\Gamma_{\text{total}}] \times [B(J/\psi(1S) \rightarrow \gamma\eta_c(1S))] < 0.96 \times 10^{-5}$ which we divide by our best value $B(J/\psi(1S) \rightarrow \gamma\eta_c(1S)) = 1.41 \times 10^{-2}$.				

 $\Gamma(K_S^0 K_S^0)/\Gamma_{\text{total}}$ Γ_{63}/Γ

VALUE (units 10^{-5})	CL%	DOCUMENT ID	TECN	COMMENT
<40	90	¹ ABLIKIM	06B	BES2 $J/\psi \rightarrow K_S^0 K_S^0 \gamma$
$\bullet\bullet\bullet$ We do not use the following data for averages, fits, limits, etc. $\bullet\bullet\bullet$				
<32	90	^{2,3} UEHARA	13	BELL $\gamma\gamma \rightarrow K_S^0 K_S^0$
< 5.6	90	^{4,5} UEHARA	13	BELL $\gamma\gamma \rightarrow K_S^0 K_S^0$
$\bullet\bullet\bullet$ We do not use the following data for averages, fits, limits, etc. $\bullet\bullet\bullet$				
¹ ABLIKIM 06B reports $[\Gamma(\eta_c(1S) \rightarrow K_S^0 K_S^0)/\Gamma_{\text{total}}] \times [B(J/\psi(1S) \rightarrow \gamma\eta_c(1S))] < 0.53 \times 10^{-5}$ which we divide by our best value $B(J/\psi(1S) \rightarrow \gamma\eta_c(1S)) = 1.41 \times 10^{-2}$.				
² Using $\Gamma(\gamma\gamma)(\eta_c) = 5.3 \pm 0.5$ keV. UEHARA 13 reports $\Gamma(\gamma\gamma) \times B(K_S^0 K_S^0) < 1.6$ eV.				
³ Taking into account interference with the non-resonant continuum.				
⁴ Using $\Gamma(\gamma\gamma)(\eta_c) = 5.3 \pm 0.5$ keV. UEHARA 13 reports $\Gamma(\gamma\gamma) \times B(K_S^0 K_S^0) < 0.29$ eV.				
⁵ Neglecting interference with the non-resonant continuum.				

 $\eta_c(1S)$ CROSS-PARTICLE BRANCHING RATIOS $\Gamma(\eta_c(1S) \rightarrow \eta'(958)\pi\pi)/\Gamma_{\text{total}} \times \Gamma(J/\psi(1S) \rightarrow \gamma\eta_c(1S))/\Gamma_{\text{total}}$
 $\Gamma_1/\Gamma \times \Gamma_{237}^{J/\psi(1S)}/\Gamma_{J/\psi(1S)}$

VALUE (units 10^{-4})	EVTS	DOCUMENT ID	TECN	COMMENT
2.8 ± 0.5 OUR FIT				Error includes scale factor of 1.4.
5.25 ± 1.65	14	BALTRUSAITIS..86	MRK3	$J/\psi \rightarrow \eta_c\gamma$
$\bullet\bullet\bullet$ We do not use the following data for averages, fits, limits, etc. $\bullet\bullet\bullet$				
¹ The value reported by BALTRUSAITIS 86 has been multiplied by 3/2 to account for isospin symmetry.				

 $\Gamma(\eta_c(1S) \rightarrow \rho\rho)/\Gamma_{\text{total}} \times \Gamma(J/\psi(1S) \rightarrow \gamma\eta_c(1S))/\Gamma_{\text{total}}$
 $\Gamma_4/\Gamma \times \Gamma_{237}^{J/\psi(1S)}/\Gamma_{J/\psi(1S)}$

VALUE (units 10^{-4})	EVTS	DOCUMENT ID	TECN	COMMENT
2.6 ± 0.6 OUR AVERAGE				Error includes scale factor of 1.2.
$1.6 \pm 0.6 \pm 0.4$	72	ABLIKIM	05L	BES2 $J/\psi \rightarrow \pi^+\pi^-\pi^+\pi^-$
$3.30 \pm 0.30 \pm 0.60$	113	¹ BISELLO	91	DM2 $J/\psi \rightarrow \gamma\rho^0\rho^0$
$3.0 \pm 1.3 \pm 0.6$	32	² BISELLO	91	DM2 $J/\psi \rightarrow \gamma\rho^+\rho^-$
$\bullet\bullet\bullet$ We do not use the following data for averages, fits, limits, etc. $\bullet\bullet\bullet$				
¹ The value reported by BISELLO 91 has been multiplied by 3 to account for isospin symmetry.				
² The value reported by BISELLO 91 has been multiplied by 3/2 to account for isospin symmetry.				

 $\Gamma(\eta_c(1S) \rightarrow K^*(892)^0 K^- \pi^+ + c.c.)/\Gamma_{\text{total}} \times \Gamma(J/\psi(1S) \rightarrow \gamma\eta_c(1S))/\Gamma_{\text{total}}$
 $\Gamma_{\text{total}}/\Gamma \times \Gamma_{237}^{J/\psi(1S)}/\Gamma_{J/\psi(1S)}$

VALUE (units 10^{-4})	EVTS	DOCUMENT ID	TECN	COMMENT
2.6 ± 0.6	63	BALTRUSAITIS..86	MRK3	$J/\psi \rightarrow \eta_c\gamma$

$$\Gamma(\eta_c(1S) \rightarrow K^*(892)\bar{K}^*(892))/\Gamma_{\text{total}} \times \Gamma(J/\psi(1S) \rightarrow \gamma\eta_c(1S))/\Gamma_{\text{total}}$$

$$\Gamma_6/\Gamma \times \Gamma_{237}^{J/\psi(1S)}/\Gamma_{J/\psi(1S)}$$

VALUE (units 10^{-4})	EVTS	DOCUMENT ID	TECN	COMMENT
0.99 ± 0.17 OUR FIT				
1.17 ± 0.29 OUR AVERAGE				
1.4 ± 0.3 ± 0.5	60	ABLIKIM	05L BES2	$J/\psi \rightarrow K^+ K^- \pi^+ \pi^- \gamma$
1.04 ± 0.36 ± 0.18	14	¹ BISELLO	91 DM2	$e^+ e^- \rightarrow \gamma K^+ K^- \pi^+ \pi^-$
1.2 ± 0.6	9	¹ BALTRUSAIT...86	MRK3	$J/\psi \rightarrow \eta_c \gamma$

¹ The reported value has been multiplied by 2 to account for isospin symmetry.

$$\Gamma(\eta_c(1S) \rightarrow K^*(892)^0 \bar{K}^*(892)^0 \pi^+ \pi^-)/\Gamma_{\text{total}} \times \Gamma(J/\psi(1S) \rightarrow \gamma\eta_c(1S))/\Gamma_{\text{total}}$$

$$\Gamma_7/\Gamma \times \Gamma_{237}^{J/\psi(1S)}/\Gamma_{J/\psi(1S)}$$

VALUE (units 10^{-4})	EVTS	DOCUMENT ID	TECN	COMMENT
1.91 ± 0.64 ± 0.48	45	ABLIKIM	06A BES2	$J/\psi \rightarrow K^{*0} \bar{K}^{*0} \pi^+ \pi^- \gamma$

$$\Gamma(\eta_c(1S) \rightarrow \phi K^+ K^-)/\Gamma_{\text{total}} \times \Gamma(B^+ \rightarrow \eta_c K^+)/\Gamma_{\text{total}}$$

$$\Gamma_8/\Gamma \times \Gamma_{253}^{B^+}/\Gamma_{B^+}$$

VALUE (units 10^{-6})	EVTS	DOCUMENT ID	TECN	COMMENT
3.6 ± 1.1 ± 0.8	14.1 ^{+4.4} _{-3.7}	HUANG	03 BELL	$B^+ \rightarrow (\phi K^+ K^-) K^+$

$$\Gamma(\eta_c(1S) \rightarrow \phi\phi)/\Gamma_{\text{total}} \times \Gamma(J/\psi(1S) \rightarrow \gamma\eta_c(1S))/\Gamma_{\text{total}}$$

$$\Gamma_9/\Gamma \times \Gamma_{237}^{J/\psi(1S)}/\Gamma_{J/\psi(1S)}$$

VALUE (units 10^{-5})	EVTS	DOCUMENT ID	TECN	COMMENT
2.6 ± 0.6 OUR FIT				Error includes scale factor of 2.2.
4.1 ± 0.6 OUR AVERAGE				Error includes scale factor of 1.2.
4.3 ± 0.5 ^{+0.5} _{-1.2}	1.2k	ABLIKIM	17P BES3	$J/\psi \rightarrow \gamma K^+ K^- K^+ K^-$
3.3 ± 0.6 ± 0.6	72	ABLIKIM	05L BES2	$J/\psi \rightarrow \gamma K^+ K^- K^+ K^-$
3.9 ± 0.9 ± 0.7	19	BISELLO	91 DM2	$J/\psi \rightarrow \gamma K^+ K^- K^+ K^-$
3.8 ± 2.3 ^{+0.7} _{-1.5}	5	BISELLO	91 DM2	$J/\psi \rightarrow \gamma K^+ K^- K_S^0 K_L^0$
9.3 ± 2.0 ± 1.6	80	BAI	90B MRK3	$J/\psi \rightarrow \gamma K^+ K^- K^+ K^-$
8.5 ± 2.7 ± 1.8		BAI	90B MRK3	$J/\psi \rightarrow \gamma K^+ K^- K_S^0 K_L^0$

• • • We do not use the following data for averages, fits, limits, etc. • • •

3.3 ± 0.6 ± 0.6	357	¹ BAI	04 BES	$J/\psi \rightarrow \gamma K^+ K^- K^+ K^-$
-----------------	-----	------------------	--------	---

¹ Superseded by ABLIKIM 05L.

$$\Gamma(\eta_c(1S) \rightarrow \phi\phi)/\Gamma_{\text{total}} \times \Gamma(B^+ \rightarrow \eta_c K^+)/\Gamma_{\text{total}}$$

$$\Gamma_9/\Gamma \times \Gamma_{253}^{B^+}/\Gamma_{B^+}$$

VALUE (units 10^{-6})	EVTS	DOCUMENT ID	TECN	COMMENT
2.0 ± 0.5 OUR FIT				Error includes scale factor of 2.2.
3.3 ± 1.2 OUR AVERAGE				Error includes scale factor of 1.5.
4.7 ± 1.2 ± 0.5		AUBERT,B	04B BABR	$B^{\pm} \rightarrow K^{\pm} \eta_c$
2.2 ± 1.0 ^{+0.3} _{-0.7} ± 0.5	7	HUANG	03 BELL	$B^{\pm} \rightarrow K^{\pm} \phi$

$$\Gamma(\eta_c(1S) \rightarrow \omega\omega)/\Gamma_{\text{total}} \times \Gamma(J/\psi(1S) \rightarrow \gamma\eta_c(1S))/\Gamma_{\text{total}}$$

$$\Gamma_{16}/\Gamma \times \Gamma_{237}^{J/\psi(1S)}/\Gamma_{J/\psi(1S)}$$

VALUE (units 10^{-5})	EVTS	DOCUMENT ID	TECN	COMMENT
3.7 ± 1.2 OUR FIT				Error includes scale factor of 2.1.
4.90 ± 0.17 ± 0.77	1705	ABLIKIM	19AV BES3	$J/\psi \rightarrow \gamma\omega\omega$

$$\Gamma(\eta_c(1S) \rightarrow f_2(1270) \bar{f}_2(1270))/\Gamma_{\text{total}} \times \Gamma(J/\psi(1S) \rightarrow \gamma\eta_c(1S))/\Gamma_{\text{total}}$$

$$\Gamma_{18}/\Gamma \times \Gamma_{237}^{J/\psi(1S)}/\Gamma_{J/\psi(1S)}$$

VALUE (units 10^{-4})	EVTS	DOCUMENT ID	TECN	COMMENT
1.5 ± 0.4 OUR FIT				
1.3 ± 0.3 ± 0.3 ± 0.4	91.2 ± 19.8	ABLIKIM	04M BES	$J/\psi \rightarrow \gamma 2\pi^+ 2\pi^-$

$$\Gamma(\eta_c(1S) \rightarrow K\bar{K}\pi)/\Gamma_{\text{total}} \times \Gamma(J/\psi(1S) \rightarrow \gamma\eta_c(1S))/\Gamma_{\text{total}}$$

$$\Gamma_{37}/\Gamma \times \Gamma_{237}^{J/\psi(1S)}/\Gamma_{J/\psi(1S)}$$

VALUE (units 10^{-4})	EVTS	DOCUMENT ID	TECN	COMMENT
10.1 ± 0.9 OUR FIT				Error includes scale factor of 1.5.
6.7 ± 0.8 OUR AVERAGE				
6.6 ± 0.9 ± 1.5	0.6k	¹ BAI	04 BES	$J/\psi \rightarrow \gamma K^{\pm} \pi^{\mp} K_S^0$
8.76 ± 1.80 ± 1.68	33	² BISELLO	91 DM2	$J/\psi \rightarrow \gamma K^+ K^- \pi^0$
6.9 ± 1.2 ± 1.2	68	³ BISELLO	91 DM2	$J/\psi \rightarrow \gamma K^{\pm} \pi^{\mp} K_S^0$
7.8 ± 3.0	32	⁴ BALTRUSAIT...86	MRK3	$J/\psi \rightarrow \gamma K^+ K^- \pi^0$
5.7 ± 1.5	63	⁵ BALTRUSAIT...86	MRK3	$J/\psi \rightarrow \gamma K^{\pm} \pi^{\mp} K_S^0$

¹ BAI 04 reports $B(J/\psi \rightarrow \gamma\eta_c) \cdot B(\eta_c \rightarrow K^{\pm} K_S^0 \pi^{\mp}) = (2.2 \pm 0.3 \pm 0.5) \times 10^{-4}$ which we multiply by 3 to account for isospin symmetry.

² BISELLO 91 reports $B(J/\psi \rightarrow \gamma\eta_c) \cdot B(\eta_c \rightarrow K^+ K^- \pi^0) = (1.46 \pm 0.30 \pm 0.28) \times 10^{-4}$ which we multiply by 6 to account for isospin symmetry.

³ BISELLO 91 reports $B(J/\psi \rightarrow \gamma\eta_c) \cdot B(\eta_c \rightarrow K^{\pm} K_S^0 \pi^{\mp}) = (2.3 \pm 0.4 \pm 0.4) \times 10^{-4}$ which we multiply by 3 to account for isospin symmetry.

⁴ BALTRUSAITIS 86 reports $B(J/\psi \rightarrow \gamma\eta_c) \cdot B(\eta_c \rightarrow K^+ K^- \pi^0) = (1.3 \pm 0.5) \times 10^{-4}$ which we multiply by 6 to account for isospin symmetry.

⁵ BALTRUSAITIS 86 reports $B(J/\psi \rightarrow \gamma\eta_c) \cdot B(\eta_c \rightarrow K^{\pm} K_S^0 \pi^{\mp}) = (1.9 \pm 0.5) \times 10^{-4}$ which we multiply by 3 to account for isospin symmetry.

$$\Gamma(\eta_c(1S) \rightarrow K\bar{K}\pi)/\Gamma_{\text{total}} \times \Gamma(B^+ \rightarrow \eta_c K^+)/\Gamma_{\text{total}}$$

$$\Gamma_{37}/\Gamma \times \Gamma_{253}^{B^+}/\Gamma_{B^+}$$

VALUE (units 10^{-5})	DOCUMENT ID	TECN	COMMENT
7.9 ± 0.5 OUR FIT			Error includes scale factor of 1.1.
7.5 ± 0.8 OUR AVERAGE			
8.01 ± 0.42 ± 1.71 ^{+1.71} _{-1.65}	¹ VINOKUROVA 11	BELL	$e^+ e^- \rightarrow \gamma(4S)$
7.4 ± 0.5 ± 0.7	AUBERT,B	04B BABR	$B^{\pm} \rightarrow K^{\pm} \eta_c$

¹ VINOKUROVA 11 reports $B(B^+ \rightarrow \eta_c K^+, \eta_c \rightarrow K_S^0 K^{\pm} \pi^{\mp}) = (26.7 \pm 1.4 \pm 2.9 \pm 4.9) \times 10^{-6}$, where the first uncertainty is statistical, the second is due to systematics, and the third comes from interference of $\eta_c(1S) \rightarrow K_S^0 K^{\pm} \pi^{\mp}$ with nonresonant $K_S^0 K^{\pm} \pi^{\mp}$. We combined both systematic uncertainties to single values. We multiply the reported result by 3 to account for isospin symmetry.

$$\Gamma(\eta_c(1S) \rightarrow K\bar{K}\pi)/\Gamma_{\text{total}} \times \Gamma(\psi(2S) \rightarrow \gamma\eta_c(1S))/\Gamma_{\text{total}}$$

$$\Gamma_{37}/\Gamma \times \Gamma_{182}^{\psi(2S)}/\Gamma_{\psi(2S)}$$

VALUE (units 10^{-4})	DOCUMENT ID	TECN	COMMENT
2.6 ± 0.4 OUR FIT			Error includes scale factor of 1.3.
4.5 ± 2.4 ± 1.8	HIMEL	80B MRK2	$\psi(2S) \rightarrow \eta_c \gamma$

$$\Gamma(\eta_c(1S) \rightarrow K\bar{K}\pi)/\Gamma_{\text{total}} \times \Gamma(h_c(1P) \rightarrow \gamma\eta_c(1S))/\Gamma_{\text{total}}$$

$$\Gamma_{37}/\Gamma \times \Gamma_{25}^{h_c(1P)}/\Gamma_{h_c(1P)}$$

VALUE (units 10^{-2})	EVTS	DOCUMENT ID	TECN	COMMENT
4.28 ± 0.34 OUR FIT				
4.1 ± 0.6 OUR AVERAGE				
3.7 ± 0.7 ± 0.3	55	^{1,2} ABLIKIM	12N BES3	$\psi(2S) \rightarrow \pi^0 \gamma K^+ K^- \pi^0$
4.6 ± 0.8 ± 0.3	107	^{3,4} ABLIKIM	12N BES3	$\psi(2S) \rightarrow \pi^0 \gamma K_S^0 K^{\mp} \pi^{\pm}$

¹ ABLIKIM 12N quotes $B(\psi(2S) \rightarrow \pi^0 h_c) \cdot B(h_c \rightarrow \gamma\eta_c) \cdot B(\eta_c \rightarrow K^+ K^- \pi^0) = (4.54 \pm 0.76 \pm 0.48) \times 10^{-6}$ which we multiply by 6 to account for isospin symmetry.

² ABLIKIM 12N reports $[\Gamma(\eta_c(1S) \rightarrow K\bar{K}\pi)/\Gamma_{\text{total}} \times \Gamma(h_c(1P) \rightarrow \gamma\eta_c(1S))/\Gamma_{\text{total}}] \times [B(\psi(2S) \rightarrow h_c(1P)\pi^0)] = (27.24 \pm 4.56 \pm 2.88) \times 10^{-6}$ which we divide by our best value $B(\psi(2S) \rightarrow h_c(1P)\pi^0) = (7.4 \pm 0.5) \times 10^{-4}$. Our first error is their experiment's error and our second error is the systematic error from using our best value.

³ ABLIKIM 12N quotes $B(\psi(2S) \rightarrow \pi^0 h_c) \cdot B(h_c \rightarrow \gamma\eta_c) \cdot B(\eta_c \rightarrow K_S^0 K^{\pm} \pi^{\mp}) = (11.35 \pm 1.25 \pm 1.50) \times 10^{-6}$ which we multiply by 3 to account for isospin symmetry.

⁴ ABLIKIM 12N reports $[\Gamma(\eta_c(1S) \rightarrow K\bar{K}\pi)/\Gamma_{\text{total}} \times \Gamma(h_c(1P) \rightarrow \gamma\eta_c(1S))/\Gamma_{\text{total}}] \times [B(\psi(2S) \rightarrow h_c(1P)\pi^0)] = (34.05 \pm 3.75 \pm 4.50) \times 10^{-6}$ which we divide by our best value $B(\psi(2S) \rightarrow h_c(1P)\pi^0) = (7.4 \pm 0.5) \times 10^{-4}$. Our first error is their experiment's error and our second error is the systematic error from using our best value.

$$\Gamma(\eta_c(1S) \rightarrow K\bar{K}\pi)/\Gamma_{\text{total}} \times \Gamma(h_c(1P) \rightarrow \gamma\eta_c(1S))/\Gamma_{\text{total}}$$

$$\Gamma_{38}/\Gamma \times \Gamma_{25}^{h_c(1P)}/\Gamma_{h_c(1P)}$$

VALUE (units 10^{-3})	EVTS	DOCUMENT ID	TECN	COMMENT
7.9 ± 1.0 OUR FIT				
5.7 ± 2.9 ± 0.4	7	^{1,2} ABLIKIM	12N BES3	$\psi(2S) \rightarrow \pi^0 \gamma K^+ K^-$

¹ ABLIKIM 12N quotes $B(\psi(2S) \rightarrow \pi^0 h_c) \cdot B(h_c \rightarrow \gamma\eta_c) \cdot B(\eta_c \rightarrow K^+ K^- \eta) = (2.11 \pm 1.01 \pm 0.32) \times 10^{-6}$ which we multiply by 2 to account for isospin symmetry.

² ABLIKIM 12N reports $[\Gamma(\eta_c(1S) \rightarrow K\bar{K}\pi)/\Gamma_{\text{total}} \times \Gamma(h_c(1P) \rightarrow \gamma\eta_c(1S))/\Gamma_{\text{total}}] \times [B(\psi(2S) \rightarrow h_c(1P)\pi^0)] = (4.22 \pm 2.02 \pm 0.64) \times 10^{-6}$ which we divide by our best value $B(\psi(2S) \rightarrow h_c(1P)\pi^0) = (7.4 \pm 0.5) \times 10^{-4}$. Our first error is their experiment's error and our second error is the systematic error from using our best value.

$$\Gamma(\eta_c(1S) \rightarrow \eta\pi^+ \pi^-)/\Gamma_{\text{total}} \times \Gamma(h_c(1P) \rightarrow \gamma\eta_c(1S))/\Gamma_{\text{total}}$$

$$\Gamma_{39}/\Gamma \times \Gamma_{25}^{h_c(1P)}/\Gamma_{h_c(1P)}$$

VALUE (units 10^{-3})	EVTS	DOCUMENT ID	TECN	COMMENT
9.7 ± 2.5 ± 0.7	33	¹ ABLIKIM	12N BES3	$\psi(2S) \rightarrow \pi^0 \gamma \eta \pi^+ \pi^-$

¹ ABLIKIM 12N reports $[\Gamma(\eta_c(1S) \rightarrow \eta\pi^+ \pi^-)/\Gamma_{\text{total}} \times \Gamma(h_c(1P) \rightarrow \gamma\eta_c(1S))/\Gamma_{\text{total}}] \times [B(\psi(2S) \rightarrow h_c(1P)\pi^0)] = (7.22 \pm 1.47 \pm 1.11) \times 10^{-6}$ which we divide by our best value $B(\psi(2S) \rightarrow h_c(1P)\pi^0) = (7.4 \pm 0.5) \times 10^{-4}$. Our first error is their experiment's error and our second error is the systematic error from using our best value.

$$\Gamma(\eta_c(1S) \rightarrow \eta\pi^+ \pi^-)/\Gamma_{\text{total}} \times \Gamma(J/\psi(1S) \rightarrow \gamma\eta_c(1S))/\Gamma_{\text{total}}$$

$$\Gamma_{39}/\Gamma \times \Gamma_{237}^{J/\psi(1S)}/\Gamma_{J/\psi(1S)}$$

VALUE (units 10^{-4})	EVTS	DOCUMENT ID	TECN	COMMENT
4.2 ± 0.9 OUR AVERAGE				
4.6 ± 1.1	75	BALTRUSAIT...86	MRK3	$J/\psi \rightarrow \eta_c \gamma$
3.1 ± 1.1 ± 1.5	18	PARTRIDGE	80B CBAL	$J/\psi \rightarrow \eta \pi^+ \pi^- \gamma$

$$\Gamma(\eta_c(1S) \rightarrow \eta 2(\pi^+ \pi^-))/\Gamma_{\text{total}} \times \Gamma(h_c(1P) \rightarrow \gamma\eta_c(1S))/\Gamma_{\text{total}}$$

$$\Gamma_{40}/\Gamma \times \Gamma_{25}^{h_c(1P)}/\Gamma_{h_c(1P)}$$

VALUE (units 10^{-2})	EVTS	DOCUMENT ID	TECN	COMMENT
2.6 ± 0.7 ± 0.2	39	¹ ABLIKIM	12N BES3	$\psi(2S) \rightarrow \pi^0 \gamma \eta 2(\pi^+ \pi^-)$

¹ ABLIKIM 12N reports $[\Gamma(\eta_c(1S) \rightarrow \eta 2(\pi^+ \pi^-))/\Gamma_{\text{total}} \times \Gamma(h_c(1P) \rightarrow \gamma\eta_c(1S))/\Gamma_{\text{total}}] \times [B(\psi(2S) \rightarrow h_c(1P)\pi^0)] = (19.17 \pm 3.77 \pm 3.72) \times 10^{-6}$ which we divide by our best value $B(\psi(2S) \rightarrow h_c(1P)\pi^0) = (7.4 \pm 0.5) \times 10^{-4}$. Our first error is their experiment's error and our second error is the systematic error from using our best value.

Meson Particle Listings

 $\eta_c(1S)$

$$\Gamma(\eta_c(1S) \rightarrow K^+ K^- \pi^+ \pi^-) / \Gamma_{\text{total}} \times \Gamma(J/\psi(1S) \rightarrow \gamma \eta_c(1S)) / \Gamma_{\text{total}}^{\text{total}}$$

$$\Gamma_{41} / \Gamma \times \Gamma_{237}^{J/\psi(1S)} / \Gamma_{J/\psi(1S)}$$

VALUE (units 10^{-4})	EVTS	DOCUMENT ID	TECN	COMMENT
1.17 ± 0.26 OUR FIT	Error includes scale factor of 2.0.			
1.9 ± 0.6 OUR AVERAGE	Error includes scale factor of 2.4.			
1.5 ± 0.2 ± 0.2	0.4k	BAI	04	BES $J/\psi \rightarrow \gamma K^+ K^- \pi^+ \pi^-$
2.7 ± 0.4	110	BALTRUSAIT...86	MRK3	$J/\psi \rightarrow \eta_c \gamma$

$$\Gamma(\eta_c(1S) \rightarrow K^+ K^- \pi^+ \pi^-) / \Gamma_{\text{total}} \times \Gamma(\psi(2S) \rightarrow \gamma \eta_c(1S)) / \Gamma_{\text{total}}^{\text{total}}$$

$$\Gamma_{41} / \Gamma \times \Gamma_{182}^{\psi(2S)} / \Gamma_{\psi(2S)}$$

VALUE (units 10^{-5})	DOCUMENT ID	TECN	COMMENT
3.0 ± 0.8 OUR FIT	Error includes scale factor of 1.7.		
4.0^{+6.0}_{-2.5}	HIMEL	80B	MRK2 $\psi(2S) \rightarrow \eta_c \gamma$

$$\Gamma(\eta_c(1S) \rightarrow K^+ K^- \pi^+ \pi^-) / \Gamma_{\text{total}} \times \Gamma(h_c(1P) \rightarrow \gamma \eta_c(1S)) / \Gamma_{\text{total}}^{\text{total}}$$

$$\Gamma_{41} / \Gamma \times \Gamma_{25}^{h_c(1P)} / \Gamma_{h_c(1P)}$$

VALUE (units 10^{-3})	EVTS	DOCUMENT ID	TECN	COMMENT
5.0 ± 1.0 OUR FIT	Error includes scale factor of 1.7.			
5.6 ± 1.3 ± 0.4	38	¹ ABLIKIM	12N	BES3 $\psi(2S) \rightarrow \pi^0 \gamma K^+ K^- \pi^+ \pi^-$

¹ABLIKIM 12N reports $[\Gamma(\eta_c(1S) \rightarrow K^+ K^- \pi^+ \pi^-) / \Gamma_{\text{total}} \times \Gamma(h_c(1P) \rightarrow \gamma \eta_c(1S)) / \Gamma_{\text{total}}] \times [B(\psi(2S) \rightarrow h_c(1P) \pi^0)] = (4.16 \pm 0.76 \pm 0.59) \times 10^{-6}$ which we divide by our best value $B(\psi(2S) \rightarrow h_c(1P) \pi^0) = (7.4 \pm 0.5) \times 10^{-4}$. Our first error is their experiment's error and our second error is the systematic error from using our best value.

$$\Gamma(\eta_c(1S) \rightarrow K^0 K^- \pi^+ \pi^- + \text{c.c.}) / \Gamma_{\text{total}} \times \Gamma(h_c(1P) \rightarrow \gamma \eta_c(1S)) / \Gamma_{\text{total}}^{\text{total}}$$

$$\Gamma_{43} / \Gamma \times \Gamma_{25}^{h_c(1P)} / \Gamma_{h_c(1P)}$$

VALUE (units 10^{-2})	DOCUMENT ID	TECN	COMMENT	
3.2 ± 0.8 ± 0.2	1,2	ABLIKIM	12N	BES3 $\psi(2S) \rightarrow \pi^0 \gamma K_S^0 K_{\mp}^{\mp} \pi^{\mp} 2\pi^{\pm}$

¹ABLIKIM 12N quotes $B(\psi(2S) \rightarrow \pi^0 h_c) \cdot B(h_c \rightarrow \gamma \eta_c) \cdot B(\eta_c \rightarrow K_S^0 K^- \pi^+ 2\pi^+) = (12.01 \pm 2.22 \pm 2.04) \times 10^{-6}$ which we multiply by 2 to take c.c. into account.

²ABLIKIM 12N reports $[\Gamma(\eta_c(1S) \rightarrow K^0 K^- \pi^+ \pi^- + \text{c.c.}) / \Gamma_{\text{total}} \times \Gamma(h_c(1P) \rightarrow \gamma \eta_c(1S)) / \Gamma_{\text{total}}] \times [B(\psi(2S) \rightarrow h_c(1P) \pi^0)] = (24.02 \pm 4.44 \pm 4.08) \times 10^{-6}$ which we divide by our best value $B(\psi(2S) \rightarrow h_c(1P) \pi^0) = (7.4 \pm 0.5) \times 10^{-4}$. Our first error is their experiment's error and our second error is the systematic error from using our best value.

$$\Gamma(\eta_c(1S) \rightarrow K^+ K^- 2(\pi^+ \pi^-)) / \Gamma_{\text{total}} \times \Gamma(J/\psi(1S) \rightarrow \gamma \eta_c(1S)) / \Gamma_{\text{total}}^{\text{total}}$$

$$\Gamma_{44} / \Gamma \times \Gamma_{237}^{J/\psi(1S)} / \Gamma_{J/\psi(1S)}$$

VALUE (units 10^{-4})	EVTS	DOCUMENT ID	TECN	COMMENT
1.21 ± 0.32 ± 0.24	100	ABLIKIM	06A	BES2 $J/\psi \rightarrow K^+ K^- 2(\pi^+ \pi^-) \gamma$

$$\Gamma(\eta_c(1S) \rightarrow K^+ K^- 2(\pi^+ \pi^-)) / \Gamma_{\text{total}} \times \Gamma(h_c(1P) \rightarrow \gamma \eta_c(1S)) / \Gamma_{\text{total}}^{\text{total}}$$

$$\Gamma_{44} / \Gamma \times \Gamma_{25}^{h_c(1P)} / \Gamma_{h_c(1P)}$$

VALUE (units 10^{-3})	EVTS	DOCUMENT ID	TECN	COMMENT
4.8 ± 2.5 ± 0.3	10	¹ ABLIKIM	12N	BES3 $\psi(2S) \rightarrow \pi^0 \gamma K^+ K^- 2(\pi^+ \pi^-)$

¹ABLIKIM 12N reports $[\Gamma(\eta_c(1S) \rightarrow K^+ K^- 2(\pi^+ \pi^-)) / \Gamma_{\text{total}} \times \Gamma(h_c(1P) \rightarrow \gamma \eta_c(1S)) / \Gamma_{\text{total}}] \times [B(\psi(2S) \rightarrow h_c(1P) \pi^0)] = (3.60 \pm 1.71 \pm 0.64) \times 10^{-6}$ which we divide by our best value $B(\psi(2S) \rightarrow h_c(1P) \pi^0) = (7.4 \pm 0.5) \times 10^{-4}$. Our first error is their experiment's error and our second error is the systematic error from using our best value.

$$\Gamma(\eta_c(1S) \rightarrow 2(K^+ K^-)) / \Gamma_{\text{total}} \times \Gamma(B^+ \rightarrow \eta_c K^+) / \Gamma_{\text{total}}$$

$$\Gamma_{45} / \Gamma \times \Gamma_{253}^{B^+} / \Gamma_{B^{\pm}}$$

VALUE (units 10^{-6})	EVTS	DOCUMENT ID	TECN	COMMENT
1.6 ± 0.4 OUR FIT	Error includes scale factor of 1.4.			
1.8^{+0.6}_{-0.5}	14.5 ^{+4.6} _{-3.0}	HUANG	03	BELL $B^+ \rightarrow 2(K^+ K^-) K^+$

$$\Gamma(\eta_c(1S) \rightarrow 2(K^+ K^-)) / \Gamma_{\text{total}} \times \Gamma(h_c(1P) \rightarrow \gamma \eta_c(1S)) / \Gamma_{\text{total}}^{\text{total}}$$

$$\Gamma_{45} / \Gamma \times \Gamma_{25}^{h_c(1P)} / \Gamma_{h_c(1P)}$$

VALUE (units 10^{-3})	EVTS	DOCUMENT ID	TECN	COMMENT
0.85 ± 0.24 OUR FIT	Error includes scale factor of 1.3.			
1.3 ± 0.5 ± 0.1	7	¹ ABLIKIM	12N	BES3 $\psi(2S) \rightarrow \pi^0 \gamma 2(K^+ K^-)$

¹ABLIKIM 12N reports $[\Gamma(\eta_c(1S) \rightarrow 2(K^+ K^-)) / \Gamma_{\text{total}} \times \Gamma(h_c(1P) \rightarrow \gamma \eta_c(1S)) / \Gamma_{\text{total}}] \times [B(\psi(2S) \rightarrow h_c(1P) \pi^0)] = (0.94 \pm 0.37 \pm 0.14) \times 10^{-6}$ which we divide by our best value $B(\psi(2S) \rightarrow h_c(1P) \pi^0) = (7.4 \pm 0.5) \times 10^{-4}$. Our first error is their experiment's error and our second error is the systematic error from using our best value.

$$\Gamma(\eta_c(1S) \rightarrow \pi^+ \pi^- \pi^0 \pi^0) / \Gamma_{\text{total}} \times \Gamma(h_c(1P) \rightarrow \gamma \eta_c(1S)) / \Gamma_{\text{total}}^{\text{total}}$$

$$\Gamma_{47} / \Gamma \times \Gamma_{25}^{h_c(1P)} / \Gamma_{h_c(1P)}$$

VALUE (units 10^{-2})	EVTS	DOCUMENT ID	TECN	COMMENT
2.7 ± 0.5 ± 0.2	118	¹ ABLIKIM	12N	BES3 $\psi(2S) \rightarrow \pi^0 \gamma \pi^+ \pi^- 2\pi^0$

¹ABLIKIM 12N reports $[\Gamma(\eta_c(1S) \rightarrow \pi^+ \pi^- \pi^0 \pi^0) / \Gamma_{\text{total}} \times \Gamma(h_c(1P) \rightarrow \gamma \eta_c(1S)) / \Gamma_{\text{total}}] \times [B(\psi(2S) \rightarrow h_c(1P) \pi^0)] = (20.31 \pm 2.20 \pm 3.33) \times 10^{-6}$ which we divide by our best value $B(\psi(2S) \rightarrow h_c(1P) \pi^0) = (7.4 \pm 0.5) \times 10^{-4}$. Our first error is their experiment's error and our second error is the systematic error from using our best value.

$$\Gamma(\eta_c(1S) \rightarrow 2(\pi^+ \pi^-)) / \Gamma_{\text{total}} \times \Gamma(J/\psi(1S) \rightarrow \gamma \eta_c(1S)) / \Gamma_{\text{total}}^{\text{total}}$$

$$\Gamma_{48} / \Gamma \times \Gamma_{237}^{J/\psi(1S)} / \Gamma_{J/\psi(1S)}$$

VALUE (units 10^{-4})	EVTS	DOCUMENT ID	TECN	COMMENT
1.35 ± 0.19 OUR FIT	Error includes scale factor of 1.3.			
1.36 ± 0.23 OUR AVERAGE				
1.3 ± 0.2 ± 0.4	0.5k	BAI	04	BES $J/\psi \rightarrow \gamma 2(\pi^+ \pi^-)$
1.33 ± 0.22 ± 0.20	137	BISELLO	91	DM2 $J/\psi \rightarrow \gamma 2(\pi^+ \pi^-)$
1.6 ± 0.6	25	BALTRUSAIT...86	MRK3	$J/\psi \rightarrow \gamma \eta_c$

$$\Gamma(\eta_c(1S) \rightarrow 2(\pi^+ \pi^-)) / \Gamma_{\text{total}} \times \Gamma(\psi(2S) \rightarrow \gamma \eta_c(1S)) / \Gamma_{\text{total}}^{\text{total}}$$

$$\Gamma_{48} / \Gamma \times \Gamma_{182}^{\psi(2S)} / \Gamma_{\psi(2S)}$$

VALUE (units 10^{-5})	DOCUMENT ID	TECN	COMMENT
3.4 ± 0.7 OUR FIT	Error includes scale factor of 1.3.		
5.7^{+3.9}_{-2.4}	HIMEL	80B	MRK2 $\psi(2S) \rightarrow \eta_c \gamma$

$$\Gamma(\eta_c(1S) \rightarrow 2(\pi^+ \pi^-)) / \Gamma_{\text{total}} \times \Gamma(h_c(1P) \rightarrow \gamma \eta_c(1S)) / \Gamma_{\text{total}}^{\text{total}}$$

$$\Gamma_{48} / \Gamma \times \Gamma_{25}^{h_c(1P)} / \Gamma_{h_c(1P)}$$

VALUE (units 10^{-2})	EVTS	DOCUMENT ID	TECN	COMMENT
0.57 ± 0.09 OUR FIT	Error includes scale factor of 1.3.			
1.01 ± 0.19 ± 0.07	100	¹ ABLIKIM	12N	BES3 $\psi(2S) \rightarrow \pi^0 \gamma 2(\pi^+ \pi^-)$

¹ABLIKIM 12N reports $[\Gamma(\eta_c(1S) \rightarrow 2(\pi^+ \pi^-)) / \Gamma_{\text{total}} \times \Gamma(h_c(1P) \rightarrow \gamma \eta_c(1S)) / \Gamma_{\text{total}}] \times [B(\psi(2S) \rightarrow h_c(1P) \pi^0)] = (7.51 \pm 0.85 \pm 1.11) \times 10^{-6}$ which we divide by our best value $B(\psi(2S) \rightarrow h_c(1P) \pi^0) = (7.4 \pm 0.5) \times 10^{-4}$. Our first error is their experiment's error and our second error is the systematic error from using our best value.

$$\Gamma(\eta_c(1S) \rightarrow 2(\pi^+ \pi^- \pi^0)) / \Gamma_{\text{total}} \times \Gamma(h_c(1P) \rightarrow \gamma \eta_c(1S)) / \Gamma_{\text{total}}^{\text{total}}$$

$$\Gamma_{49} / \Gamma \times \Gamma_{25}^{h_c(1P)} / \Gamma_{h_c(1P)}$$

VALUE (units 10^{-2})	EVTS	DOCUMENT ID	TECN	COMMENT
10.1 ± 1.7 ± 0.7	175	¹ ABLIKIM	12N	BES3 $\psi(2S) \rightarrow \pi^0 \gamma 2(\pi^+ \pi^- \pi^0)$

¹ABLIKIM 12N reports $[\Gamma(\eta_c(1S) \rightarrow 2(\pi^+ \pi^- \pi^0)) / \Gamma_{\text{total}} \times \Gamma(h_c(1P) \rightarrow \gamma \eta_c(1S)) / \Gamma_{\text{total}}] \times [B(\psi(2S) \rightarrow h_c(1P) \pi^0)] = (75.13 \pm 7.42 \pm 9.99) \times 10^{-6}$ which we divide by our best value $B(\psi(2S) \rightarrow h_c(1P) \pi^0) = (7.4 \pm 0.5) \times 10^{-4}$. Our first error is their experiment's error and our second error is the systematic error from using our best value.

$$\Gamma(\eta_c(1S) \rightarrow 3(\pi^+ \pi^-)) / \Gamma_{\text{total}} \times \Gamma(J/\psi(1S) \rightarrow \gamma \eta_c(1S)) / \Gamma_{\text{total}}^{\text{total}}$$

$$\Gamma_{50} / \Gamma \times \Gamma_{237}^{J/\psi(1S)} / \Gamma_{J/\psi(1S)}$$

VALUE (units 10^{-4})	EVTS	DOCUMENT ID	TECN	COMMENT
2.59 ± 0.32 ± 0.47	471	ABLIKIM	06A	BES2 $J/\psi \rightarrow 3(\pi^+ \pi^-) \gamma$

$$\Gamma(\eta_c(1S) \rightarrow 3(\pi^+ \pi^-)) / \Gamma_{\text{total}} \times \Gamma(h_c(1P) \rightarrow \gamma \eta_c(1S)) / \Gamma_{\text{total}}^{\text{total}}$$

$$\Gamma_{50} / \Gamma \times \Gamma_{25}^{h_c(1P)} / \Gamma_{h_c(1P)}$$

VALUE (units 10^{-2})	EVTS	DOCUMENT ID	TECN	COMMENT
1.19 ± 0.30 ± 0.08	51	¹ ABLIKIM	12N	BES3 $\psi(2S) \rightarrow \pi^0 \gamma 3(\pi^+ \pi^-)$

¹ABLIKIM 12N reports $[\Gamma(\eta_c(1S) \rightarrow 3(\pi^+ \pi^-)) / \Gamma_{\text{total}} \times \Gamma(h_c(1P) \rightarrow \gamma \eta_c(1S)) / \Gamma_{\text{total}}] \times [B(\psi(2S) \rightarrow h_c(1P) \pi^0)] = (8.82 \pm 1.57 \pm 1.59) \times 10^{-6}$ which we divide by our best value $B(\psi(2S) \rightarrow h_c(1P) \pi^0) = (7.4 \pm 0.5) \times 10^{-4}$. Our first error is their experiment's error and our second error is the systematic error from using our best value.

$$\Gamma(\eta_c(1S) \rightarrow \rho \bar{\rho}) / \Gamma_{\text{total}} \times \Gamma(J/\psi(1S) \rightarrow \gamma \eta_c(1S)) / \Gamma_{\text{total}}^{\text{total}}$$

$$\Gamma_{51} / \Gamma \times \Gamma_{237}^{J/\psi(1S)} / \Gamma_{J/\psi(1S)}$$

VALUE (units 10^{-5})	EVTS	DOCUMENT ID	TECN	COMMENT
1.88 ± 0.18 OUR FIT	Error includes scale factor of 1.2.			
1.61 ± 0.29 OUR AVERAGE				

1.9 ± 0.3 ± 0.3	213	BAI	04	BES $J/\psi \rightarrow \gamma \rho \bar{\rho}$
1.3 ± 0.4 ± 0.3	18	BISELLO	91	DM2 $J/\psi \rightarrow \gamma \rho \bar{\rho}$
1.4 ± 0.7	23	BALTRUSAIT...86	MRK3	$J/\psi \rightarrow \eta_c \gamma$

$$\Gamma(\eta_c(1S) \rightarrow \rho \bar{\rho}) / \Gamma_{\text{total}} \times \Gamma(h_c(1P) \rightarrow \gamma \eta_c(1S)) / \Gamma_{\text{total}}^{\text{total}}$$

$$\Gamma_{51} / \Gamma \times \Gamma_{25}^{h_c(1P)} / \Gamma_{h_c(1P)}$$

VALUE (units 10^{-4})	EVTS	DOCUMENT ID	TECN	COMMENT
8.0 ± 0.8 OUR FIT				
8.7 ± 2.9 ± 0.6	15	¹ ABLIKIM	12N	BES3 $\psi(2S) \rightarrow \pi^0 \gamma \rho \bar{\rho}$

¹ABLIKIM 12N reports $[\Gamma(\eta_c(1S) \rightarrow \rho \bar{\rho}) / \Gamma_{\text{total}} \times \Gamma(h_c(1P) \rightarrow \gamma \eta_c(1S)) / \Gamma_{\text{total}}] \times [B(\psi(2S) \rightarrow h_c(1P) \pi^0)] = (0.65 \pm 0.19 \pm 0.10) \times 10^{-6}$ which we divide by our best value $B(\psi(2S) \rightarrow h_c(1P) \pi^0) = (7.4 \pm 0.5) \times 10^{-4}$. Our first error is their experiment's error and our second error is the systematic error from using our best value.

$$\Gamma(\eta_c(1S) \rightarrow \rho \bar{\rho}) / \Gamma_{\text{total}} \times \Gamma(\psi(2S) \rightarrow \gamma \eta_c(1S)) / \Gamma_{\text{total}}^{\text{total}}$$

$$\Gamma_{51} / \Gamma \times \Gamma_{182}^{\psi(2S)} / \Gamma_{\psi(2S)}$$

VALUE (units 10^{-6})	DOCUMENT ID	TECN	COMMENT
4.8 ± 0.7 OUR FIT	Error includes scale factor of 1.2.		
8⁺⁸₋₄	HIMEL	80B	MRK2 $\psi(2S) \rightarrow \eta_c \gamma$

See key on page 1171

Meson Particle Listings

$\eta_c(1S), J/\psi(1S)$

$\Gamma(\eta_c(1S) \rightarrow p\bar{p})/\Gamma_{\text{total}} \times \Gamma(B^+ \rightarrow \eta_c K^+)/\Gamma_{\text{total}} \quad \Gamma_{51}/\Gamma \times \Gamma_{25}^{\pm}/\Gamma B^{\pm}$

VALUE (units 10^{-6})	EVTS	DOCUMENT ID	TECN	COMMENT
1.47 ± 0.12 OUR FIT				Error includes scale factor of 1.1.
1.54 ± 0.19 OUR AVERAGE				Error includes scale factor of 1.1.
1.42 ± 0.11 +0.16 -0.20	195	WU	06 BELL	$B^+ \rightarrow p\bar{p}K^+$
1.8 +0.3 -0.2 ± 0.2		AUBERT,B	05L BABR	$e^+e^- \rightarrow \Upsilon(4S)$

$\Gamma(\eta_c(1S) \rightarrow p\bar{p}\pi^0)/\Gamma_{\text{total}} \times \Gamma(h_c(1P) \rightarrow \gamma\eta_c(1S))/\Gamma_{\text{total}} \quad \Gamma_{52}/\Gamma \times \Gamma_{25}^{h_c(1P)}/\Gamma h_c(1P)$

VALUE (units 10^{-3})	DOCUMENT ID	TECN	COMMENT
2.1 ± 0.7 ± 0.1	¹ ABLIKIM 12N BES3		$\psi(2S) \rightarrow \pi^0\gamma p\bar{p}\pi^0$

¹ ABLIKIM 12N reports $[\Gamma(\eta_c(1S) \rightarrow p\bar{p}\pi^0)/\Gamma_{\text{total}} \times \Gamma(h_c(1P) \rightarrow \gamma\eta_c(1S))/\Gamma_{\text{total}}] \times [B(\psi(2S) \rightarrow h_c(1P)\pi^0)] = (1.53 \pm 0.49 \pm 0.23) \times 10^{-6}$ which we divide by our best value $B(\psi(2S) \rightarrow h_c(1P)\pi^0) = (7.4 \pm 0.5) \times 10^{-4}$. Our first error is their experiment's error and our second error is the systematic error from using our best value.

$\Gamma(\eta_c(1S) \rightarrow p\bar{p}\pi^+\pi^-)/\Gamma_{\text{total}} \times \Gamma(h_c(1P) \rightarrow \gamma\eta_c(1S))/\Gamma_{\text{total}} \quad \Gamma_{53}/\Gamma \times \Gamma_{25}^{h_c(1P)}/\Gamma h_c(1P)$

VALUE (units 10^{-3})	EVTS	DOCUMENT ID	TECN	COMMENT
2.19 ± 0.30 OUR FIT				
3.1 ± 1.0 ± 0.2	19	¹ ABLIKIM 12N BES3		$\psi(2S) \rightarrow \pi^0\gamma p\bar{p}\pi^+\pi^-$

¹ ABLIKIM 12N reports $[\Gamma(\eta_c(1S) \rightarrow p\bar{p}\pi^+\pi^-)/\Gamma_{\text{total}} \times \Gamma(h_c(1P) \rightarrow \gamma\eta_c(1S))/\Gamma_{\text{total}}] \times [B(\psi(2S) \rightarrow h_c(1P)\pi^0)] = (2.30 \pm 0.65 \pm 0.36) \times 10^{-6}$ which we divide by our best value $B(\psi(2S) \rightarrow h_c(1P)\pi^0) = (7.4 \pm 0.5) \times 10^{-4}$. Our first error is their experiment's error and our second error is the systematic error from using our best value.

$\Gamma(\eta_c(1S) \rightarrow p\bar{p}\pi^+\pi^-)/\Gamma_{\text{total}} \times \Gamma(B^+ \rightarrow \eta_c K^+)/\Gamma_{\text{total}} \quad \Gamma_{53}/\Gamma \times \Gamma_{25}^{\pm}/\Gamma B^{\pm}$

VALUE (units 10^{-6})	DOCUMENT ID	TECN	COMMENT
4.0 ± 0.4 OUR FIT			
3.94 +0.41 +0.22 -0.39 -0.18	19	CHILIKIN	BELL $e^+e^- \rightarrow \Upsilon(4S)$

$\Gamma(\eta_c(1S) \rightarrow \Lambda\bar{\Lambda})/\Gamma_{\text{total}} \times \Gamma(J/\psi(1S) \rightarrow \gamma\eta_c(1S))/\Gamma_{\text{total}} \quad \Gamma_{54}/\Gamma \times \Gamma_{237}^{J/\psi(1S)}/\Gamma J/\psi(1S)$

VALUE (units 10^{-5})	DOCUMENT ID	TECN	COMMENT
1.5 ± 0.4 OUR FIT			Error includes scale factor of 1.5.
1.98 ± 0.21 ± 0.32		ABLIKIM 12B	BES3 $J/\psi \rightarrow \Lambda\bar{\Lambda}\gamma$

$\Gamma(\eta_c(1S) \rightarrow \Lambda\bar{\Lambda})/\Gamma_{\text{total}} \times \Gamma(B^+ \rightarrow \eta_c K^+)/\Gamma_{\text{total}} \quad \Gamma_{54}/\Gamma \times \Gamma_{25}^{\pm}/\Gamma B^{\pm}$

VALUE (units 10^{-6})	EVTS	DOCUMENT ID	TECN	COMMENT
1.21 ± 0.30 OUR FIT				Error includes scale factor of 1.5.
0.95 +0.25 +0.08 -0.22 -0.11	20	WU	06 BELL	$B^+ \rightarrow \Lambda\bar{\Lambda}K^+$

$\Gamma(\eta_c(1S) \rightarrow \Sigma^+\bar{\Sigma}^-)/\Gamma_{\text{total}} \times \Gamma(J/\psi(1S) \rightarrow \gamma\eta_c(1S))/\Gamma_{\text{total}} \quad \Gamma_{57}/\Gamma \times \Gamma_{237}^{J/\psi(1S)}/\Gamma J/\psi(1S)$

VALUE (units 10^{-5})	EVTS	DOCUMENT ID	TECN	COMMENT
3.60 ± 0.48 ± 0.31	112	ABLIKIM 13C	BES3	$J/\psi \rightarrow \gamma p\bar{p}\pi^0\pi^0$

$\Gamma(\eta_c(1S) \rightarrow \Xi^-\bar{\Xi}^+)/\Gamma_{\text{total}} \times \Gamma(J/\psi(1S) \rightarrow \gamma\eta_c(1S))/\Gamma_{\text{total}} \quad \Gamma_{58}/\Gamma \times \Gamma_{237}^{J/\psi(1S)}/\Gamma J/\psi(1S)$

VALUE (units 10^{-5})	EVTS	DOCUMENT ID	TECN	COMMENT
1.51 ± 0.27 ± 0.14	78	ABLIKIM 13C	BES3	$J/\psi \rightarrow \gamma \Lambda\bar{\Lambda}\pi^+\pi^-$

$\Gamma(\eta_c(1S) \rightarrow \gamma\gamma)/\Gamma_{\text{total}} \times \Gamma(J/\psi(1S) \rightarrow \gamma\eta_c(1S))/\Gamma_{\text{total}} \quad \Gamma_{59}/\Gamma \times \Gamma_{237}^{J/\psi(1S)}/\Gamma J/\psi(1S)$

VALUE (units 10^{-6})	EVTS	DOCUMENT ID	TECN	COMMENT
2.34 ± 0.35 OUR FIT				Error includes scale factor of 1.2.
3.8 +1.3 -1.0 OUR AVERAGE				Error includes scale factor of 1.1.
4.5 ± 1.2 ± 0.6		ABLIKIM 13I	BES3	
1.2 +2.7 -1.1 ± 0.3	1.2 +2.8 -1.1	ADAMS 08	CLEO	$\psi(2S) \rightarrow \pi^+\pi^-J/\psi$

$\Gamma(\eta_c(1S) \rightarrow \gamma\gamma)/\Gamma_{\text{total}} \times \Gamma(B^+ \rightarrow \eta_c K^+)/\Gamma_{\text{total}} \quad \Gamma_{59}/\Gamma \times \Gamma_{25}^{\pm}/\Gamma B^{\pm}$

VALUE (units 10^{-6})	EVTS	DOCUMENT ID	TECN	COMMENT
0.183 ± 0.022 OUR FIT				Error includes scale factor of 1.2.
0.22 +0.09 +0.04 -0.07 -0.02	13	WICHT 08	BELL	$B^{\pm} \rightarrow K^{\pm}\gamma\gamma$

$\eta_c(1S)$ REFERENCES

AAIJ 23AH PR D108 032010	R. Aaij et al.	(LHCb Collab.)
ABLIKIM 21C PR D103 012009	M. Ablikim et al.	(BESIII Collab.)
LEES 21A PR D104 072002	J.P. Lees et al.	(BABAR Collab.)
AAIJ 20H EPJ C80 191	R. Aaij et al.	(LHCb Collab.)
ABLIKIM 19AP PR D100 012003	M. Ablikim et al.	(BESIII Collab.)
ABLIKIM 19AV PR D100 052012	M. Ablikim et al.	(BESIII Collab.)
CHILIKIN 19 PR D100 012001	K. Chilikin et al.	(BELLE Collab.)

LU 19 PR D99 032003	P.-C. Lu et al.	(BELLE Collab.)
XU 18 PR D98 072001	Q.N. Xu et al.	(BELLE Collab.)
AAIJ 17AD PL B769 305	R. Aaij et al.	(LHCb Collab.)
AAIJ 17BB EPJ C77 609	R. Aaij et al.	(LHCb Collab.)
ABLIKIM 17AJ PR D96 112008	M. Ablikim et al.	(BESIII Collab.)
ABLIKIM 17P PR D95 092004	M. Ablikim et al.	(BESIII Collab.)
LEES 16A PR D93 012005	J.P. Lees et al.	(BABAR Collab.)
AAIJ 15BI EPJ C75 311	R. Aaij et al.	(LHCb Collab.)
ANASHIN 14 PL B738 391	V.V. Anashin et al.	(KEDR Collab.)
LEES 14E PR D89 112004	J.P. Lees et al.	(BABAR Collab.)
ABLIKIM 13C PR D87 012003	M. Ablikim et al.	(BESIII Collab.)
ABLIKIM 13I PR D87 032003	M. Ablikim et al.	(BESIII Collab.)
UEHARA 13 PTEP 2013 123C01	S. Uehara et al.	(BELLE Collab.)
ABLIKIM 12B PR D86 032008	M. Ablikim et al.	(BESIII Collab.)
ABLIKIM 12F PRL 108 222002	M. Ablikim et al.	(BESIII Collab.)
ABLIKIM 12N PR D86 092009	M. Ablikim et al.	(BESIII Collab.)
LIU 12B PRL 108 232001	Z.Q. Liu et al.	(BELLE Collab.)
ZHANG 12A PR D86 052002	C.C. Zhang et al.	(BELLE Collab.)
ABLIKIM 11G PR D84 032006	M. Ablikim et al.	(BESIII Collab.)
DEL-AMO-SA... 11M PR D84 012004	P. del Amo Sanchez et al.	(BABAR Collab.)
VINOKUROVA 11 PR B766 139	A. Vinokurova et al.	(BELLE Collab.)
LEES 10 PR D81 052010	J.P. Lees et al.	(BABAR Collab.)
MITCHELL 09 PRL 102 011801	R.E. Mitchell et al.	(CLEO Collab.)
ADAMS 08 PRL 101 101801	G.S. Adams et al.	(CLEO Collab.)
AUBERT 08AB PR D78 012006	B. Aubert et al.	(BABAR Collab.)
UEHARA 08 EPJ C53 1	S. Uehara et al.	(BELLE Collab.)
WICHT 08 PL B662 323	J. Wicht et al.	(BELLE Collab.)
ABE 07 PRL 98 082001	K. Abe et al.	(BELLE Collab.)
ABLIKIM 06A PL B633 19	M. Ablikim et al.	(BES Collab.)
ABLIKIM 06B EPJ C45 337	M. Ablikim et al.	(BES Collab.)
AUBERT 06E PRL 96 052002	B. Aubert et al.	(BABAR Collab.)
PDG 06 PR D83 112003	W.-M. Yao et al.	(PDG Collab.)
WU 06 PRL 97 162003	C.-H. Wu et al.	(BELLE Collab.)
ABLIKIM 05L PR D72 072005	M. Ablikim et al.	(BES Collab.)
AUBERT.B 05 PR D72 051101	B. Aubert et al.	(BABAR Collab.)
KUO 05 PL B621 41	C.C. Kuo et al.	(BELLE Collab.)
ABE 04G PR D70 071102	K. Abe et al.	(BELLE Collab.)
ABLIKIM 04M PR D70 112008	M. Ablikim et al.	(BES Collab.)
ASNER 04 PRL 92 142001	D.M. Asner et al.	(CLEO Collab.)
AUBERT 04D PRL 92 142002	B. Aubert et al.	(BABAR Collab.)
AUBERT.B 04B PR D70 011101	B. Aubert et al.	(BABAR Collab.)
BAI 04 PL B578 16	J.Z. Bai et al.	(BES Collab.)
ABDALLAH 03 EPJ C31 481	J. Abdallah et al.	(DELPHI Collab.)
AMBROGIANI 03 PL B566 45	M. Ambrogiani et al.	(FNAL E835 Collab.)
BAI 03 PL B555 174	J.Z. Bai et al.	(BES Collab.)
FANG 03 PRL 90 071801	F. Fang et al.	(BELLE Collab.)
HUANG 03 PRL 91 241802	H.-C. Huang et al.	(BELLE Collab.)
ABE.K 02 PRL 89 142001	K. Abe et al.	(BELLE Collab.)
BAI 00F PR D62 072001	J.Z. Bai et al.	(BES Collab.)
BRANDENB... 00P PRL 85 3095	G. Brandenburg et al.	(CLEO Collab.)
ACCIARRI 99T PL B461 155	M. Acciarri et al.	(L3 Collab.)
BAI 99B PR D60 072001	J.Z. Bai et al.	(BES Collab.)
ABREU 98O PL B441 479	P. Abreu et al.	(DELPHI Collab.)
SHIRAI 98 PL B424 405	M. Shirai et al.	(AMY Collab.)
ARMSTRONG 95F PR D52 4839	T.A. Armstrong et al.	(FNAL FERR, GENO+)
ALBRECHT 94H PL B338 390	H. Albrecht et al.	(ARGUS Collab.)
ADRIANI 93N PL B318 575	O. Adriani et al.	(L3 Collab.)
BISELLO 91 NP B350 1	D. Bisello et al.	(DM2 Collab.)
BAI 90B PRL 65 1309	Z. Bai et al.	(Mark III Collab.)
CHEN 90B PL B243 169	W.Y. Chen et al.	(CLEO Collab.)
BAGLIN 89 PL B231 557	C. Baglin, S. Baird, G. Bassompierre	(R704 Collab.)
BEHREND 89 ZPHY C42 367	H.J. Behrend et al.	(CELLO Collab.)
BRÄUNSCHE... 89 ZPHY C41 633	W. Braunschweig et al.	(TASSO Collab.)
AIHARA 88D PRL 60 2355	H. Aihara et al.	(TPC Collab.)
BAGLIN 87B PL B187 191	C. Baglin et al.	(R704 Collab.)
BALTRUSAITIS... 86 PR D33 629	R.M. Baltrusaitis et al.	(Mark III Collab.)
BERGER 86 PL 167B 120	C. Berger et al.	(PLUTO Collab.)
GAISER 86 PR D34 711	J. Gaiser et al.	(Crystal Ball Collab.)
ALTHOFF 85B ZPHY C29 189	M. Althoff et al.	(TASSO Collab.)
BALTRUSAITIS... 84 PRL 52 2126	R.M. Baltrusaitis et al.	(CIT, UCS C+JP)
BLOOM 83 ARNS 33 143	E.D. Bloom, C. Peck	(SLAC, CIT)
HIMEL 80B PRL 45 1146	T.M. Himel et al.	(SLAC, LBL, UC)
PARTRIDGE 80B PRL 45 1150	R. Partridge et al.	(CIT, HARV, PRIN+)

J/ψ(1S)

$$I^G(J^{PC}) = 0^-(1^--)$$

J/ψ(1S) MASS

VALUE (MeV)	EVTS	DOCUMENT ID	TECN	COMMENT
3096.900 ± 0.002 OUR AVERAGE				
3096.900 ± 0.002 ± 0.006		¹ ANASHIN 15	KEDR	$e^+e^- \rightarrow$ hadrons
3096.89 ± 0.09	502	² ARTAMONOV 00	OLYA	$e^+e^- \rightarrow$ hadrons
3096.91 ± 0.03 ± 0.01		³ ARMSTRONG 93B	E760	$\bar{p}p \rightarrow e^+e^-$
3096.95 ± 0.1 ± 0.3	193	BAGLIN 87	SPEC	$\bar{p}p \rightarrow e^+e^-X$
• • • We do not use the following data for averages, fits, limits, etc. • • •				
3096.66 ± 0.19 ± 0.02	6.1k	⁴ AAIJ 15BI	LHCb	$pp \rightarrow J/\psi X$
3096.917 ± 0.010 ± 0.007		AULCHENKO 03	KEDR	$e^+e^- \rightarrow$ hadrons
3097.5 ± 0.3		GRIBUSHIN 96	FMP5	$515 \pi^- Be \rightarrow 2\mu X$
3098.4 ± 2.0	38k	LEMOIGNE 82	GOLI	$185 \pi^- Be \rightarrow \gamma\mu^+\mu^- A$
3096.93 ± 0.09	502	⁵ ZHOLENTZ 80	REDE	e^+e^-
3097.0 ± 1		⁶ BRANDELIC 79c	DASP	e^+e^-

¹ Supersedes AULCHENKO 03.
² Reanalysis of ZHOLENTZ 80 using new electron mass (COHEN 87) and radiative corrections (KURAEV 85).
³ Mass central value and systematic error recalculated by us according to Eq. (16) in ARMSTRONG 93b, using the value for the $\psi(2S)$ mass from AULCHENKO 03.
⁴ From a sample of $\eta_c(1S)$ and J/ψ produced in b -hadron decays. Systematic uncertainties not estimated.
⁵ Superseded by ARTAMONOV 00.
⁶ From a simultaneous fit to e^+e^- , $\mu^+\mu^-$ and hadronic channels assuming $\Gamma(e^+e^-) = \Gamma(\mu^+\mu^-)$.

Meson Particle Listings

$J/\psi(1S)$

$J/\psi(1S)$ WIDTH

VALUE (keV)	EVTS	DOCUMENT ID	TECN	COMMENT
92.6 ± 1.7 OUR AVERAGE		Error includes scale factor of 1.1.		
92.45 ± 1.40 ± 1.48		1 ANASHIN	20 KEDR	e^+e^-
96.1 ± 3.2	13k	2 ADAMS	06A CLEO	$e^+e^- \rightarrow \mu^+\mu^-\gamma$
84.4 ± 8.9		BAI	95B BES	e^+e^-
91 ± 11 ± 6		3 ARMSTRONG	93B E760	$\bar{p}p \rightarrow e^+e^-$
85.5 + 6.1 - 5.8		4 HSUEH	92 RVUE	See Υ mini-review
• • • We do not use the following data for averages, fits, limits, etc. • • •				
92.94 ± 1.83		5,6 ANASHIN	18A KEDR	e^+e^-
94.1 ± 2.7		7 ANASHIN	10 KEDR	3.097 $e^+e^- \rightarrow \mu^+\mu^-$
93.7 ± 3.5	7.8k	2 AUBERT	04 BABR	$e^+e^- \rightarrow \mu^+\mu^-\gamma$

1 Based on the same dataset as ANASHIN 18A and correlated to the values reported there
 2 Calculated by us from the reported values of $\Gamma(e^+e^-) \times B(\mu^+\mu^-)$ using $B(e^+e^-) = (5.94 \pm 0.06)\%$ and $B(\mu^+\mu^-) = (5.93 \pm 0.06)\%$.
 3 The initial-state radiation correction reevaluated by ANDREOTTI 07 in its Ref. [4].
 4 Using data from COFFMAN 92, BALDINI-CELIO 75, BOYARSKI 75, ESPOSITO 75B, BRANDELIK 79c.
 5 Using $\Gamma(e^+e^-)$ from ANASHIN 18A and $B(J/\psi(1S) \rightarrow e^+e^-) = (5.971 \pm 0.032)\%$ from PDG 16.
 6 Superseded by ANASHIN 20 that is based on the same dataset.
 7 Assuming $\Gamma(e^+e^-) = \Gamma(\mu^+\mu^-)$ and using $\Gamma(e^+e^-)/\Gamma_{\text{total}} = (5.94 \pm 0.06)\%$.

$J/\psi(1S)$ DECAY MODES

Mode	Fraction (Γ_i/Γ)	Scale factor/ Confidence level
Γ_1 hadrons	(87.7 ± 0.5) %	
Γ_2 virtual $\gamma \rightarrow$ hadrons	(13.46 ± 0.07) %	
Γ_3 ggg	(64.1 ± 1.0) %	
Γ_4 γgg	(8.8 ± 1.1) %	
Γ_5 e^+e^-	(5.971 ± 0.032) %	
Γ_6 $e^+e^-\gamma$	[a] (8.8 ± 1.4) × 10 ⁻³	
Γ_7 $\mu^+\mu^-$	(5.961 ± 0.033) %	
Decays involving hadronic resonances		
Γ_8 $\rho\pi$	(1.88 ± 0.12) %	S=2.6
Γ_9 $\rho^0\pi^0$	(6.2 ± 0.6) × 10 ⁻³	
Γ_{10} $a_2(1320)^0\pi^+\pi^- \rightarrow 2(\pi^+\pi^-)\pi^0$	(2.8 ± 0.6) × 10 ⁻³	
Γ_{11} $a_2(1320)^+\pi^-\pi^0 + c.c. \rightarrow 2(\pi^+\pi^-)\pi^0$	(3.7 ± 0.7) × 10 ⁻³	
Γ_{12} $a_2(1320)\rho$	(1.09 ± 0.22) %	
Γ_{13} $\eta\pi^+\pi^-$	(3.8 ± 0.7) × 10 ⁻⁴	
Γ_{14} $\eta\rho$	(1.93 ± 0.23) × 10 ⁻⁴	
Γ_{15} $\eta\pi^+\pi^-\pi^0$	(1.17 ± 0.20) %	
Γ_{16} $\eta\pi^+\pi^-3\pi^0$	(4.9 ± 1.0) × 10 ⁻³	
Γ_{17} $\eta\phi(2170) \rightarrow \eta\phi f_0(980) \rightarrow \eta\phi\pi^+\pi^-$	(1.2 ± 0.4) × 10 ⁻⁴	
Γ_{18} $\eta\phi(2170) \rightarrow \eta K^*(892)^0 \bar{K}^*(892)^0$	< 2.52 × 10 ⁻⁴	CL=90%
Γ_{19} $\eta K^+ K^-$	(8.6 ± 3.0) × 10 ⁻⁴	
Γ_{20} $\eta K^\pm K_S^0 \pi^\mp$	[b] (2.2 ± 0.4) × 10 ⁻³	
Γ_{21} $\eta K^*(892)^0 \bar{K}^*(892)^0$	(1.15 ± 0.26) × 10 ⁻³	
Γ_{22} $\eta\eta'(958)$	(8.1 ± 0.8) × 10 ⁻⁵	S=1.6
Γ_{23} $\rho^\pm\pi^\mp\pi^+\pi^-2\pi^0$	(2.8 ± 0.8) %	
Γ_{24} $\rho^\pm\rho^-\pi^+\pi^-\pi^0$	(6 ± 4) × 10 ⁻³	
Γ_{25} $\rho^\pm K^+ K^- \pi^- + c.c. \rightarrow K^+ K^- \pi^+ \pi^- \pi^0$	(3.5 ± 0.8) × 10 ⁻³	
Γ_{26} $\rho^\mp K^\pm K_S^0$	(1.9 ± 0.4) × 10 ⁻³	
Γ_{27} $h_1(1415)\eta' \rightarrow \gamma\eta\eta'$	seen	
Γ_{28} $h_1(1595)\eta' \rightarrow \gamma\eta\eta'$	seen	
Γ_{29} $\rho(1450)\pi$	seen	
Γ_{30} $\rho(1450)\pi \rightarrow \pi^+\pi^-\pi^0$	(2.2 ± 1.1) × 10 ⁻⁴	
Γ_{31} $\rho(1450)^\pm\pi^\mp \rightarrow K_S^0 K^\pm\pi^\mp$	(3.3 ± 0.6) × 10 ⁻⁴	
Γ_{32} $\rho(1450)^0\pi^0 \rightarrow K^+K^-\pi^0$	(2.7 ± 0.6) × 10 ⁻⁴	
Γ_{33} $\rho(1450)\eta'(958) \rightarrow \pi^+\pi^-\eta'(958)$	(3.3 ± 0.7) × 10 ⁻⁶	
Γ_{34} $\rho(1700)\pi$	seen	
Γ_{35} $\rho(1700)\pi \rightarrow \pi^+\pi^-\pi^0$	(1.6 ± 1.1) × 10 ⁻⁴	
Γ_{36} $\rho(2150)\pi$	seen	
Γ_{37} $\rho(2150)\pi \rightarrow \pi^+\pi^-\pi^0$	(10 ± 40) × 10 ⁻⁶	
Γ_{38} $\rho_3(1690)\pi \rightarrow \pi^+\pi^-\pi^0$		
Γ_{39} $\omega\pi^0$	(4.5 ± 0.5) × 10 ⁻⁴	S=1.4
Γ_{40} $\omega\pi^0 \rightarrow \pi^+\pi^-\pi^0$	(1.6 ± 0.7) × 10 ⁻⁵	
Γ_{41} $\omega\pi^+\pi^-$	(8.5 ± 1.0) × 10 ⁻³	S=1.3

Γ_{42} $\omega\pi^0\pi^0$	(3.4 ± 0.8) × 10 ⁻³	
Γ_{43} $\omega 3\pi^0$	(1.9 ± 0.6) × 10 ⁻³	
Γ_{44} $\omega f_2(1270)$	(4.3 ± 0.6) × 10 ⁻³	
Γ_{45} $\omega\eta$	(1.74 ± 0.20) × 10 ⁻³	S=1.6
Γ_{46} $\omega\pi^+\pi^-\pi^0$	(4.0 ± 0.7) × 10 ⁻³	
Γ_{47} $\omega\pi^0\eta$	(3.4 ± 1.7) × 10 ⁻⁴	
Γ_{48} $\omega\pi^+\pi^+\pi^-\pi^-$	(8.5 ± 3.4) × 10 ⁻³	
Γ_{49} $\omega\pi^+\pi^-2\pi^0$	(3.3 ± 0.5) %	
Γ_{50} $\omega\eta'\pi^+\pi^-$	(1.12 ± 0.13) × 10 ⁻³	
Γ_{51} $\omega\eta'(958)$	(1.89 ± 0.18) × 10 ⁻⁴	
Γ_{52} $\omega f_0(980)$	(1.4 ± 0.5) × 10 ⁻⁴	
Γ_{53} $\omega f_0(1710) \rightarrow \omega K \bar{K}$	(4.8 ± 1.1) × 10 ⁻⁴	
Γ_{54} $\omega f_1(1420)$	(6.8 ± 2.4) × 10 ⁻⁴	
Γ_{55} $\omega f_2'(1525)$	< 2.2 × 10 ⁻⁴	CL=90%
Γ_{56} $\omega X(1835) \rightarrow \omega p \bar{p}$	< 3.9 × 10 ⁻⁶	CL=95%
Γ_{57} $\omega X(1835), X \rightarrow \eta'\pi^+\pi^-$	< 6.2 × 10 ⁻⁵	
Γ_{58} $\omega K^+ K^-$	(1.52 ± 0.31) × 10 ⁻³	
Γ_{59} $\omega K^\pm K_S^0 \pi^\mp$	[b] (3.4 ± 0.5) × 10 ⁻³	
Γ_{60} $\omega K \bar{K}$	(1.9 ± 0.4) × 10 ⁻³	
Γ_{61} $\omega K^*(892) \bar{K} + c.c.$	(6.1 ± 0.9) × 10 ⁻³	
Γ_{62} $\eta' K^* \pm K^\mp$	(1.48 ± 0.13) × 10 ⁻³	
Γ_{63} $\eta' K^* \pm \bar{K}^0 + c.c.$	(1.66 ± 0.21) × 10 ⁻³	
Γ_{64} $\eta' h_1(1415) \rightarrow \eta' K^* \bar{K} + c.c.$	(2.16 ± 0.31) × 10 ⁻⁴	
Γ_{65} $\eta' h_1(1415) \rightarrow \eta' K^* \pm K^\mp$	(1.51 ± 0.23) × 10 ⁻⁴	
Γ_{66} $\eta' h_1(1415) \rightarrow \gamma\eta'\eta'$	(4.7 ± 1.1 / 2.0) × 10 ⁻⁷	
Γ_{67} $\bar{K} K^*(892) + c.c.$	seen	
Γ_{68} $\bar{K} K^*(892) + c.c. \rightarrow K_S^0 K^\pm \pi^\mp$	(4.8 ± 0.5) × 10 ⁻³	
Γ_{69} $K^+ K^*(892)^- + c.c.$	(6.0 ± 0.8 / 1.0) × 10 ⁻³	S=2.9
Γ_{70} $K^+ K^*(892)^- + c.c. \rightarrow K^+ K^- \pi^0$	(2.69 ± 0.13 / 0.20) × 10 ⁻³	
Γ_{71} $K^+ K^*(892)^- + c.c. \rightarrow K^0 K^\pm \pi^\mp + c.c.$	(3.0 ± 0.4) × 10 ⁻³	
Γ_{72} $K^0 \bar{K}^*(892)^0 + c.c.$	(4.2 ± 0.4) × 10 ⁻³	
Γ_{73} $K^0 \bar{K}^*(892)^0 + c.c. \rightarrow K^0 K^\pm \pi^\mp + c.c.$	(3.2 ± 0.4) × 10 ⁻³	
Γ_{74} $\bar{K}^*(892)^0 K^+ \pi^- + c.c.$	(5.7 ± 0.8) × 10 ⁻³	
Γ_{75} $K^*(892)^\pm K^\mp \pi^0$	(4.1 ± 1.3) × 10 ⁻³	
Γ_{76} $K^*(892)^+ K_S^0 \pi^- + c.c.$	(2.0 ± 0.5) × 10 ⁻³	
Γ_{77} $K^*(892)^+ K_S^0 \pi^- + c.c. \rightarrow K_S^0 K_S^0 \pi^+ \pi^-$	(6.7 ± 2.2) × 10 ⁻⁴	
Γ_{78} $K^*(892)^0 K^- \pi^+ + c.c. \rightarrow K^+ K^- \pi^+ \pi^-$	(3.8 ± 0.5) × 10 ⁻³	
Γ_{79} $K^*(892)^0 K_S^0 \rightarrow \gamma K_S^0 K_S^0$	(6.3 ± 0.6 / 0.5) × 10 ⁻⁶	
Γ_{80} $K^*(892)^0 K_S^0 \pi^0$	(7 ± 4) × 10 ⁻⁴	
Γ_{81} $K^*(892)^\pm K^*(700)^\mp$	(1.1 ± 1.0 / 0.6) × 10 ⁻³	
Γ_{82} $K^*(892)^0 \bar{K}^*(892)^0$	(2.3 ± 0.6) × 10 ⁻⁴	
Γ_{83} $K^*(892)^\pm K^*(892)^\mp$	(1.00 ± 0.22 / 0.40) × 10 ⁻³	
Γ_{84} $K_1(1400)^\pm K^\mp$	(3.8 ± 1.4) × 10 ⁻³	
Γ_{85} $K^*(1410) \bar{K} + c.c.$	seen	
Γ_{86} $K^*(1410) \bar{K} + c.c. \rightarrow K^\pm K^\mp \pi^0$	(7 ± 4) × 10 ⁻⁵	
Γ_{87} $K^*(1410) \bar{K} + c.c. \rightarrow K_S^0 K^\pm \pi^\mp$	(8 ± 5) × 10 ⁻⁵	
Γ_{88} $K_2^*(1430) \bar{K} + c.c.$	seen	
Γ_{89} $K_2^*(1430) \bar{K} + c.c. \rightarrow K^\pm K^\mp \pi^0$	(1.0 ± 0.5) × 10 ⁻⁴	
Γ_{90} $K_2^*(1430) \bar{K} + c.c. \rightarrow K_S^0 K^\pm \pi^\mp$	(3.8 ± 1.0) × 10 ⁻⁴	
Γ_{91} $\bar{K}_2^*(1430) K + c.c.$	< 4.0 × 10 ⁻³	CL=90%
Γ_{92} $K_2^*(1430)^+ K^- + c.c. \rightarrow K^+ K^- \pi^0$	(2.69 ± 0.25 / 0.19) × 10 ⁻⁴	
Γ_{93} $K_2^*(1430)^0 K^- \pi^+ + c.c. \rightarrow K^+ K^- \pi^+ \pi^-$	(2.6 ± 0.9) × 10 ⁻³	
Γ_{94} $K_2^*(1430)^+ K_S^0 \pi^- + c.c.$	(3.6 ± 1.8) × 10 ⁻³	
Γ_{95} $\bar{K}_2^*(1430)^0 K^*(892)^0 + c.c.$	(4.67 ± 0.29) × 10 ⁻³	
Γ_{96} $K_2^*(1430)^- K^*(892)^+ + c.c.$	(3.4 ± 2.9) × 10 ⁻³	
Γ_{97} $K_2^*(1430)^- K^*(892)^+ + c.c. \rightarrow K^*(892)^+ K_S^0 \pi^- + c.c.$	(4 ± 4) × 10 ⁻⁴	
Γ_{98} $K_2^*(1430)^0 \bar{K}_2^*(1430)^0$	< 2.9 × 10 ⁻³	CL=90%

Γ_{99}	$\bar{K}_2^*(1770)^0 K^*(892)^0 + c.c. \rightarrow K^*(892)^0 K^- \pi^+ + c.c.$	$(6.9 \pm 0.9) \times 10^{-4}$		Γ_{166}	$\pi^+ \pi^-$	$(1.47 \pm 0.14) \times 10^{-4}$	
Γ_{100}	$K_2^*(1980)^+ K^- + c.c. \rightarrow K^+ K^- \pi^0$	$(1.10 \pm 0.60) \times 10^{-5}$		Γ_{167}	$2(\pi^+ \pi^-)$	$(3.20 \pm 0.25) \times 10^{-3}$	S=1.2
Γ_{101}	$K_2^*(2045)^+ K^- + c.c. \rightarrow K^+ K^- \pi^0$	$(6.2 \pm 2.9) \times 10^{-6}$		Γ_{168}	$3(\pi^+ \pi^-)$	$(4.3 \pm 0.4) \times 10^{-3}$	
Γ_{102}	$K_1(1270)^\pm K^\mp$	$< 3.0 \times 10^{-3}$	CL=90%	Γ_{169}	$2(\pi^+ \pi^-) 3\pi^0$	$(6.2 \pm 0.9) \%$	
Γ_{103}	$K_1(1270) K_S^0 \rightarrow \gamma K_S^0 K_S^0$	$(8.5 \pm 2.5) \times 10^{-7}$		Γ_{170}	$4(\pi^+ \pi^-) \pi^0$	$(9.0 \pm 3.0) \times 10^{-3}$	
Γ_{104}	$a_2(1320)^\pm \pi^\mp$	$[b] < 4.3 \times 10^{-3}$	CL=90%	Γ_{171}	$2(\pi^+ \pi^-) \eta$	$(2.29 \pm 0.28) \times 10^{-3}$	
Γ_{105}	$\phi \pi^0$	3×10^{-6} or 1×10^{-7}		Γ_{172}	$3(\pi^+ \pi^-) \eta$	$(7.2 \pm 1.5) \times 10^{-4}$	
Γ_{106}	$\phi \pi^+ \pi^-$	$(9.4 \pm 1.5) \times 10^{-4}$	S=1.7	Γ_{173}	$2(\pi^+ \pi^- \pi^0) \eta$	$(1.6 \pm 0.5) \times 10^{-3}$	
Γ_{107}	$\phi \pi^0 \pi^0$	$(5.0 \pm 1.0) \times 10^{-4}$		Γ_{174}	$\pi^+ \pi^- \pi^0 \pi^0 \eta$	$(2.4 \pm 0.5) \times 10^{-3}$	
Γ_{108}	$\phi 2(\pi^+ \pi^-)$	$(1.60 \pm 0.32) \times 10^{-3}$		Γ_{175}	$\rho^\pm \pi^\mp \pi^0 \eta$	$(1.9 \pm 0.8) \times 10^{-3}$	
Γ_{109}	$\phi \eta$	$(7.4 \pm 0.6) \times 10^{-4}$	S=1.2	Γ_{176}	$K^+ K^-$	$(2.86 \pm 0.21) \times 10^{-4}$	
Γ_{110}	$\phi \eta'(958)$	$(4.6 \pm 0.5) \times 10^{-4}$	S=2.2	Γ_{177}	$K_S^0 K_L^0$	$(1.95 \pm 0.11) \times 10^{-4}$	S=2.4
Γ_{111}	$\phi \eta \eta'$	$(2.32 \pm 0.17) \times 10^{-4}$		Γ_{178}	$K_S^0 K_S^0$	$< 1.4 \times 10^{-8}$	CL=95%
Γ_{112}	$\phi f_0(980)$	$(3.2 \pm 0.9) \times 10^{-4}$	S=1.9	Γ_{179}	$K^+ K^- \pi$	$(6.1 \pm 1.0) \times 10^{-3}$	
Γ_{113}	$\phi f_0(980) \rightarrow \phi \pi^+ \pi^-$	$(2.60 \pm 0.34) \times 10^{-4}$		Γ_{180}	$K^+ K^- \pi^0$	$(2.88 \pm 0.12) \times 10^{-3}$	
Γ_{114}	$\phi f_0(980) \rightarrow \phi \pi^0 \pi^0$	$(1.8 \pm 0.5) \times 10^{-4}$		Γ_{181}	$K_S^0 K^\pm \pi^\mp$	$(5.3 \pm 0.5) \times 10^{-3}$	
Γ_{115}	$\phi \pi^0 f_0(980) \rightarrow \phi \pi^0 \pi^+ \pi^-$	$(4.5 \pm 1.0) \times 10^{-6}$		Γ_{182}	$K_S^0 K_L^0 \pi^0$	$(2.06 \pm 0.26) \times 10^{-3}$	
Γ_{116}	$\phi \pi^0 f_0(980) \rightarrow \phi \pi^0 \rho^0 \pi^0$	$(1.7 \pm 0.6) \times 10^{-6}$		Γ_{183}	$K^*(892)^0 \bar{K}^0 + c.c. \rightarrow K_S^0 K_L^0 \pi^0$	$(1.21 \pm 0.18) \times 10^{-3}$	
Γ_{117}	$\phi f_0(980) \eta \rightarrow \eta \phi \pi^+ \pi^-$	$(3.2 \pm 1.0) \times 10^{-4}$		Γ_{184}	$K_2^*(1430)^0 \bar{K}^0 + c.c. \rightarrow K_S^0 K_L^0 \pi^0$	$(4.3 \pm 1.3) \times 10^{-4}$	
Γ_{118}	$\phi a_0(980)^0 \rightarrow \phi \eta \pi^0$	$(4.4 \pm 1.4) \times 10^{-6}$		Γ_{185}	$K^+ K^- \pi^+ \pi^-$	$(7.0 \pm 1.0) \times 10^{-3}$	
Γ_{119}	$\phi f_2(1270)$	$(3.2 \pm 0.6) \times 10^{-4}$		Γ_{186}	$K^+ K^- \pi^0 \pi^0$	$(2.13 \pm 0.22) \times 10^{-3}$	
Γ_{120}	$\phi f_1(1285)$	$(2.6 \pm 0.5) \times 10^{-4}$		Γ_{187}	$K^+ K^- \pi^0 \pi^0 \pi^0$	$(1.61 \pm 0.29) \times 10^{-3}$	
Γ_{121}	$\phi f_1(1285) \rightarrow \phi \pi^0 f_0(980) \rightarrow \phi \pi^0 \pi^+ \pi^-$	$(9.4 \pm 2.8) \times 10^{-7}$		Γ_{188}	$K_S^0 K^\pm \pi^\mp \pi^0 \pi^0$	$(5.3 \pm 0.7) \times 10^{-3}$	
Γ_{122}	$\phi f_1(1285) \rightarrow \phi \pi^0 f_0(980) \rightarrow \phi 3\pi^0$	$(2.1 \pm 2.2) \times 10^{-7}$		Γ_{189}	$K_S^0 K^\pm \pi^\mp \pi^+ \pi^-$	$(6.3 \pm 0.4) \times 10^{-3}$	
Γ_{123}	$\phi \eta(1405) \rightarrow \phi \eta \pi^+ \pi^-$	$(2.0 \pm 1.0) \times 10^{-5}$		Γ_{190}	$K_S^0 K^\pm \rho(770)^\pm \pi^0$	$(2.9 \pm 0.8) \times 10^{-3}$	
Γ_{124}	$\phi f_2'(1525)$	$(8 \pm 4) \times 10^{-4}$	S=2.7	Γ_{191}	$K_S^0 K_L^0 \pi^+ \pi^-$	$(3.8 \pm 0.6) \times 10^{-3}$	
Γ_{125}	$\phi X(1835) \rightarrow \phi p \bar{p}$	$< 2.1 \times 10^{-7}$	CL=90%	Γ_{192}	$K_S^0 K_L^0 \pi^0 \pi^0$	$(1.9 \pm 0.4) \times 10^{-3}$	
Γ_{126}	$\phi X(1835) \rightarrow \phi \eta \pi^+ \pi^-$	$< 2.8 \times 10^{-4}$	CL=90%	Γ_{193}	$K_S^0 K_L^0 \eta$	$(1.45 \pm 0.33) \times 10^{-3}$	
Γ_{127}	$\phi X(1870) \rightarrow \phi \eta \pi^+ \pi^-$	$< 6.13 \times 10^{-5}$	CL=90%	Γ_{194}	$K_S^0 K_L^0 \pi^+ \pi^-$	$(1.68 \pm 0.19) \times 10^{-3}$	
Γ_{128}	$\phi K \bar{K}$	$(1.77 \pm 0.16) \times 10^{-3}$	S=1.3	Γ_{195}	$K^\mp K_S^0 \pi^\pm \pi^0$	$(5.7 \pm 0.5) \times 10^{-3}$	
Γ_{129}	$\phi f_0(1710) \rightarrow \phi K \bar{K}$	$(3.6 \pm 0.6) \times 10^{-4}$		Γ_{196}	$K_S^0 K^\pm \pi^\mp \rho(770)^0$	$(3.1 \pm 0.5) \times 10^{-3}$	
Γ_{130}	$\phi K^+ K^-$	$(8.3 \pm 1.1) \times 10^{-4}$		Γ_{197}	$K^+ K^- 2(\pi^+ \pi^-)$	$(3.1 \pm 1.3) \times 10^{-3}$	
Γ_{131}	$\phi K_S^0 K_S^0$	$(5.9 \pm 1.5) \times 10^{-4}$		Γ_{198}	$K^+ K^- \pi^+ \pi^- \eta$	$(4.7 \pm 0.7) \times 10^{-3}$	
Γ_{132}	$\phi K^\pm K_S^0 \pi^\mp$	$[b] (7.2 \pm 0.8) \times 10^{-4}$		Γ_{199}	$2(K^+ K^-)$	$(7.2 \pm 0.8) \times 10^{-4}$	
Γ_{133}	$\phi K^*(892) \bar{K} + c.c.$	$(2.18 \pm 0.23) \times 10^{-3}$		Γ_{200}	$K^+ K^- K_S^0 K_S^0$	$(4.2 \pm 0.7) \times 10^{-4}$	
Γ_{134}	$b_1(1235)^\pm \pi^\mp$	$[b] (3.0 \pm 0.5) \times 10^{-3}$		Γ_{201}	$K_L^0 K^*(892)^0 \pi^+ \pi^-$	$(1.7 \pm 0.6) \times 10^{-3}$	
Γ_{135}	$b_1(1235)^0 \pi^0$	$(2.3 \pm 0.6) \times 10^{-3}$		Γ_{202}	$K_L^0 K^*(892)^0 \pi^0 \pi^0$	$(1.01 \pm 0.18) \times 10^{-3}$	
Γ_{136}	$f_2'(1525) K^+ K^-$	$(1.04 \pm 0.35) \times 10^{-3}$		Γ_{203}	$K^\mp K^*(892)^\pm \pi^+ \pi^-$	$(3.4 \pm 1.2) \times 10^{-3}$	
Γ_{137}	$\Delta(1232)^+ \bar{p}$	$< 1 \times 10^{-4}$	CL=90%	Γ_{204}	$K^*(892)^\pm K^*(892)^0 \pi^\mp$	$(4.8 \pm 1.0) \times 10^{-3}$	
Γ_{138}	$\Delta(1232)^+ \bar{p} \pi^-$	$(1.6 \pm 0.5) \times 10^{-3}$		Γ_{205}	$K^\mp K^*(892)^\pm \pi^0 \pi^0$	$(1.57 \pm 0.32) \times 10^{-3}$	
Γ_{139}	$\Delta(1232)^+ \bar{\Delta}(1232)^--$	$(1.10 \pm 0.29) \times 10^{-3}$		Γ_{206}	$K^*(892)^+ K^*(892)^- \pi^0$	$(1.12 \pm 0.23) \%$	
Γ_{140}	$\bar{\Sigma}(1385)^0 p K^-$	$(5.1 \pm 3.2) \times 10^{-4}$		Γ_{207}	$p \bar{p}$	$(2.120 \pm 0.029) \times 10^{-3}$	
Γ_{141}	$\Sigma(1385)^0 \bar{\Lambda} + c.c.$	$< 8.2 \times 10^{-6}$	CL=90%	Γ_{208}	$p \bar{p} \pi^0$	$(1.19 \pm 0.08) \times 10^{-3}$	S=1.1
Γ_{142}	$\Sigma(1385)^- \Sigma^+ + c.c.$	$[b] (3.0 \pm 0.7) \times 10^{-4}$		Γ_{209}	$p \bar{p} \pi^+ \pi^-$	$(6.0 \pm 0.5) \times 10^{-3}$	S=1.3
Γ_{143}	$\Sigma(1385)^+ \bar{\Sigma}^- + c.c.$	$(3.3 \pm 0.8) \times 10^{-4}$		Γ_{210}	$p \bar{p} \pi^+ \pi^- \pi^0$	$(2.3 \pm 0.9) \times 10^{-3}$	S=1.9
Γ_{144}	$\Sigma(1385)^- \bar{\Sigma}(1385)^+ + c.c.$	$[b] (1.08 \pm 0.06) \times 10^{-3}$		Γ_{211}	$p \bar{p} \eta$	$(2.00 \pm 0.12) \times 10^{-3}$	
Γ_{145}	$\Sigma(1385)^+ \bar{\Sigma}(1385)^- + c.c.$	$(1.25 \pm 0.07) \times 10^{-3}$		Γ_{212}	$p \bar{p} \rho$	$< 3.1 \times 10^{-4}$	CL=90%
Γ_{146}	$\Sigma(1385)^0 \bar{\Sigma}(1385)^0$	$(1.07 \pm 0.08) \times 10^{-3}$		Γ_{213}	$p \bar{p} \omega$	$(9.8 \pm 1.0) \times 10^{-4}$	S=1.3
Γ_{147}	$\Lambda(1520) \bar{\Lambda} + c.c. \rightarrow \gamma \Lambda \bar{\Lambda}$	$< 4.1 \times 10^{-6}$	CL=90%	Γ_{214}	$p \bar{p} \eta'(958)$	$(1.29 \pm 0.14) \times 10^{-4}$	S=2.0
Γ_{148}	$\bar{\Lambda}(1520) \Lambda + c.c.$	$< 1.80 \times 10^{-3}$	CL=90%	Γ_{215}	$p \bar{p} a_0(980) \rightarrow p \bar{p} \pi^0 \eta$	$(6.8 \pm 1.8) \times 10^{-5}$	
Γ_{149}	$\Xi(1530)^- \Xi^+ + c.c.$	$(1.17 \pm 0.04) \times 10^{-3}$		Γ_{216}	$p \bar{p} \phi$	$(5.19 \pm 0.33) \times 10^{-5}$	
Γ_{150}	$\Xi(1530)^0 \Xi^0$	$(3.18 \pm 0.08) \times 10^{-4}$		Γ_{217}	$p \bar{p} \pi^-$	$(2.12 \pm 0.09) \times 10^{-3}$	
Γ_{151}	$\Xi(1530)^0 \Xi^0$	$(3.2 \pm 1.4) \times 10^{-4}$		Γ_{218}	$n \bar{n}$	$(2.09 \pm 0.16) \times 10^{-3}$	
Γ_{152}	$\Theta(1540) \bar{\Theta}(1540) \rightarrow K_S^0 p K^- \bar{n} + c.c.$	$[c] < 1.1 \times 10^{-5}$	CL=90%	Γ_{219}	$n \bar{n} \pi^+ \pi^-$	$(4 \pm 4) \times 10^{-3}$	
Γ_{153}	$\Theta(1540) K^- \bar{n} \rightarrow K_S^0 p K^- \bar{n}$	$[c] < 2.1 \times 10^{-5}$	CL=90%	Γ_{220}	$n N(1440)$	seen	
Γ_{154}	$\Theta(1540) K_S^0 \bar{p} \rightarrow K_S^0 \bar{p} K^+ n$	$[c] < 1.6 \times 10^{-5}$	CL=90%	Γ_{221}	$n N(1520)$	seen	
Γ_{155}	$\bar{\Theta}(1540) K^+ n \rightarrow K_S^0 \bar{p} K^+ n$	$[c] < 5.6 \times 10^{-5}$	CL=90%	Γ_{222}	$n N(1535)$	seen	
Γ_{156}	$\bar{\Theta}(1540) K_S^0 p \rightarrow K_S^0 p K^- \bar{n}$	$[c] < 1.1 \times 10^{-5}$	CL=90%	Γ_{223}	$\Lambda \bar{\Lambda}$	$(1.88 \pm 0.08) \times 10^{-3}$	S=2.6
Decays into stable hadrons				Γ_{224}	$\Lambda \bar{\Lambda} \pi^0$	$(3.8 \pm 0.4) \times 10^{-5}$	
Γ_{157}	$2(\pi^+ \pi^-) \pi^0$	$(4.2 \pm 0.4) \%$	S=2.1	Γ_{225}	$\Lambda \bar{\Lambda} \pi^+ \pi^-$	$(4.3 \pm 1.0) \times 10^{-3}$	
Γ_{158}	$3(\pi^+ \pi^-) \pi^0$	$(2.9 \pm 0.6) \%$		Γ_{226}	$\Lambda \bar{\Lambda} \eta$	$(1.62 \pm 0.17) \times 10^{-4}$	
Γ_{159}	$\pi^+ \pi^- 3\pi^0$	$(1.9 \pm 0.9) \%$		Γ_{227}	$\Lambda \bar{\Sigma}^- \pi^+ + c.c.$	$[b] (1.26 \pm 0.05) \times 10^{-3}$	S=1.2
Γ_{160}	$\rho^\pm \pi^\mp \pi^0 \pi^0$	$(1.41 \pm 0.22) \%$		Γ_{228}	$\Lambda \bar{\Sigma}^+ \pi^- + c.c.$	$(1.21 \pm 0.07) \times 10^{-3}$	S=1.8
Γ_{161}	$\rho^+ \rho^- \pi^0$	$(6.0 \pm 1.1) \times 10^{-3}$		Γ_{229}	$p K^- \bar{\Lambda} + c.c.$	$(8.6 \pm 1.1) \times 10^{-4}$	
Γ_{162}	$\pi^+ \pi^- 4\pi^0$	$(6.5 \pm 1.3) \times 10^{-3}$		Γ_{230}	$p K^- \bar{\Sigma}^0$	$(2.9 \pm 0.8) \times 10^{-4}$	
Γ_{163}	$\pi^+ \pi^- \pi^0$	$(2.00 \pm 0.07) \%$	S=2.0	Γ_{231}	$\bar{\Lambda} n K_S^0 + c.c.$	$(6.5 \pm 1.1) \times 10^{-4}$	
Γ_{164}	$2(\pi^+ \pi^- \pi^0)$	$(1.61 \pm 0.20) \%$		Γ_{232}	$\Lambda \bar{\Sigma}^+ + c.c.$	$(2.83 \pm 0.23) \times 10^{-5}$	
Γ_{165}	$\pi^+ \pi^- \pi^0 K^+ K^-$	$(1.52 \pm 0.27) \%$	S=1.4	Γ_{233}	$\Sigma^+ \bar{\Sigma}^-$	$(1.07 \pm 0.04) \times 10^{-3}$	
				Γ_{234}	$\Sigma^0 \bar{\Sigma}^0$	$(1.172 \pm 0.032) \times 10^{-3}$	S=1.4
				Γ_{235}	$\Sigma^+ \bar{\Sigma}^- \eta$	$(6.3 \pm 0.4) \times 10^{-5}$	
				Γ_{236}	$\Xi^- \bar{\Xi}^+$	$(9.7 \pm 0.8) \times 10^{-4}$	S=1.4

Meson Particle Listings

 $J/\psi(1S)$

Radiative decays			
$\Gamma_{237} \gamma \eta_c(1S)$	$(1.41 \pm 0.14) \%$	S=1.3	
$\Gamma_{238} \gamma \eta_c(1S) \rightarrow 3\gamma$	seen		
$\Gamma_{239} \gamma \eta_c(1S) \rightarrow \gamma \eta \eta'$	seen		
$\Gamma_{240} 3\gamma$	$(1.16 \pm 0.22) \times 10^{-5}$		
$\Gamma_{241} 4\gamma$	$< 9 \times 10^{-6}$	CL=90%	
$\Gamma_{242} 5\gamma$	$< 1.5 \times 10^{-5}$	CL=90%	
$\Gamma_{243} \gamma \pi^0$	$(3.39 \pm 0.08) \times 10^{-5}$		
$\Gamma_{244} \gamma \pi^0 \pi^0$	$(1.15 \pm 0.05) \times 10^{-3}$		
$\Gamma_{245} \gamma 2\pi^+ 2\pi^-$	$(2.8 \pm 0.5) \times 10^{-3}$	S=1.9	
$\Gamma_{246} \gamma f_2(1270) f_2(1270)$	$(9.5 \pm 1.7) \times 10^{-4}$		
$\Gamma_{247} \gamma f_2(1270) f_2(1270)$ (non resonant)	$(8.2 \pm 1.9) \times 10^{-4}$		
$\Gamma_{248} \gamma \pi^+ \pi^- 2\pi^0$	$(8.3 \pm 3.1) \times 10^{-3}$		
$\Gamma_{249} \gamma K_S^0 K_S^0$	$(8.1 \pm 0.4) \times 10^{-4}$		
$\Gamma_{250} \gamma(K\bar{K}\pi) [J^{PC} = 0^{-+}]$	$(7 \pm 4) \times 10^{-4}$	S=2.1	
$\Gamma_{251} \gamma K^+ K^- \pi^+ \pi^-$	$(2.1 \pm 0.6) \times 10^{-3}$		
$\Gamma_{252} \gamma K^*(892) \bar{K}^*(892)$	$(4.0 \pm 1.3) \times 10^{-3}$		
$\Gamma_{253} \gamma \eta$	$(1.090 \pm 0.013) \times 10^{-3}$		
$\Gamma_{254} \gamma \eta \pi^0$	$(2.14 \pm 0.31) \times 10^{-5}$		
$\Gamma_{255} \gamma f_0(500) \rightarrow \gamma \pi \pi$			
$\Gamma_{256} \gamma f_0(500) \rightarrow \gamma K \bar{K}$			
$\Gamma_{257} \gamma f_0(500) \rightarrow \gamma \eta \eta'$			
$\Gamma_{258} \gamma a_0(980)^0 \rightarrow \gamma \eta \pi^0$	$< 2.5 \times 10^{-6}$	CL=95%	
$\Gamma_{259} \gamma a_2(1320)^0 \rightarrow \gamma \eta \pi^0$	$< 6.6 \times 10^{-6}$	CL=95%	
$\Gamma_{260} \gamma \eta \pi \pi$	$(6.1 \pm 1.0) \times 10^{-3}$		
$\Gamma_{261} \gamma \eta_2(1870) \rightarrow \gamma \eta \pi^+ \pi^-$	$(6.2 \pm 2.4) \times 10^{-4}$		
$\Gamma_{262} \gamma \eta'(958)$	$(5.28 \pm 0.06) \times 10^{-3}$	S=1.3	
$\Gamma_{263} \gamma f_0(980) \rightarrow \gamma \pi \pi$			
$\Gamma_{264} \gamma f_0(980) \rightarrow \gamma K \bar{K}$			
$\Gamma_{265} \gamma \rho \rho$	$(4.5 \pm 0.8) \times 10^{-3}$		
$\Gamma_{266} \gamma \rho \omega$	$< 5.4 \times 10^{-4}$	CL=90%	
$\Gamma_{267} \gamma \rho \phi$	$< 8.8 \times 10^{-5}$	CL=90%	
$\Gamma_{268} \gamma \omega \omega$	$(1.61 \pm 0.33) \times 10^{-3}$		
$\Gamma_{269} \gamma \phi \phi$	$(4.0 \pm 1.2) \times 10^{-4}$	S=2.1	
$\Gamma_{270} \gamma \eta(1405/1475) \rightarrow \gamma K \bar{K} \pi$	$(2.8 \pm 0.6) \times 10^{-3}$	S=1.6	
$\Gamma_{271} \gamma \eta(1405/1475) \rightarrow \gamma \gamma \rho^0$	$(7.8 \pm 2.0) \times 10^{-5}$	S=1.8	
$\Gamma_{272} \gamma \eta(1405/1475) \rightarrow \gamma \eta \pi^+ \pi^-$	$(3.0 \pm 0.5) \times 10^{-4}$		
$\Gamma_{273} \gamma \eta(1405/1475) \rightarrow \gamma \rho^0 \rho^0$	$(1.7 \pm 0.4) \times 10^{-3}$	S=1.3	
$\Gamma_{274} \gamma \eta(1405/1475) \rightarrow \gamma \gamma \phi$	$< 8.2 \times 10^{-5}$	CL=95%	
$\Gamma_{275} \gamma \eta(1405) \rightarrow \gamma \gamma \gamma$	$< 2.63 \times 10^{-6}$	CL=90%	
$\Gamma_{276} \gamma \eta(1475) \rightarrow \gamma \gamma \gamma$	$< 1.86 \times 10^{-6}$	CL=90%	
$\Gamma_{277} \gamma \eta(1760) \rightarrow \gamma \rho^0 \rho^0$	$(1.3 \pm 0.9) \times 10^{-4}$		
$\Gamma_{278} \gamma \eta(1760) \rightarrow \gamma \omega \omega$	$(1.98 \pm 0.33) \times 10^{-3}$		
$\Gamma_{279} \gamma \eta(1760) \rightarrow \gamma \gamma \gamma$	$< 4.80 \times 10^{-6}$	CL=90%	
$\Gamma_{280} \gamma \eta(2225)$	$(3.14 \pm 0.50) \times 10^{-4}$		
$\Gamma_{281} \gamma f_2(1270)$	$(1.63 \pm 0.12) \times 10^{-3}$	S=1.3	
$\Gamma_{282} \gamma f_2(1270) \rightarrow \gamma K_S^0 K_S^0$	$(2.58 \pm 0.60) \times 10^{-5}$		
$\Gamma_{283} \gamma f_1(1285)$	$(6.1 \pm 0.8) \times 10^{-4}$		
$\Gamma_{284} \gamma f_0(1370) \rightarrow \gamma \pi \pi$			
$\Gamma_{285} \gamma f_0(1370) \rightarrow \gamma K \bar{K}$	$(4.2 \pm 1.5) \times 10^{-4}$		
$\Gamma_{286} \gamma f_0(1370) \rightarrow \gamma K_S^0 K_S^0$	$(1.1 \pm 0.4) \times 10^{-5}$		
$\Gamma_{287} \gamma f_0(1370) \rightarrow \gamma \eta \eta'$			
$\Gamma_{288} \gamma f_0(1370) \rightarrow \gamma \eta \eta'$			
$\Gamma_{289} \gamma f_1(1420) \rightarrow \gamma K \bar{K} \pi$	$(7.9 \pm 1.3) \times 10^{-4}$		
$\Gamma_{290} \gamma f_0(1500) \rightarrow \gamma \pi \pi$	$(1.09 \pm 0.24) \times 10^{-4}$		
$\Gamma_{291} \gamma f_0(1500) \rightarrow \gamma \eta \eta'$	$(1.7 \pm 0.6) \times 10^{-5}$		
$\Gamma_{292} \gamma f_0(1500) \rightarrow \gamma K_S^0 K_S^0$	$(1.59 \pm 0.24) \times 10^{-5}$		
$\Gamma_{293} \gamma f_0(1500) \rightarrow \gamma \eta \eta'$			
$\Gamma_{294} \gamma f_1(1510) \rightarrow \gamma \eta \pi^+ \pi^-$	$(4.5 \pm 1.2) \times 10^{-4}$		
$\Gamma_{295} \gamma f_2'(1525)$	$(5.7 \pm 0.8) \times 10^{-4}$	S=1.5	
$\Gamma_{296} \gamma f_2'(1525) \rightarrow \gamma K_S^0 K_S^0$	$(8.0 \pm 0.7) \times 10^{-5}$		
$\Gamma_{297} \gamma f_2'(1525) \rightarrow \gamma \eta \eta'$	$(3.4 \pm 1.4) \times 10^{-5}$		
$\Gamma_{298} \gamma f_2(1565) \rightarrow \gamma \eta \eta'$			
$\Gamma_{299} \gamma f_2(1640) \rightarrow \gamma \omega \omega$	$(2.8 \pm 1.8) \times 10^{-4}$		
$\Gamma_{300} \gamma f_0(1710) \rightarrow \gamma \pi \pi$	$(3.8 \pm 0.5) \times 10^{-4}$		
$\Gamma_{301} \gamma f_0(1710) \rightarrow \gamma K \bar{K}$	$(9.5 \pm 1.0) \times 10^{-4}$	S=1.5	
$\Gamma_{302} \gamma f_0(1710) \rightarrow \gamma \omega \omega$	$(3.1 \pm 1.0) \times 10^{-4}$		
$\Gamma_{303} \gamma f_0(1710) \rightarrow \gamma \eta \eta'$	$(2.4 \pm 1.2) \times 10^{-4}$		
$\Gamma_{304} \gamma f_0(1710) \rightarrow \gamma \eta \eta'$			
$\Gamma_{305} \gamma f_0(1710) \rightarrow \gamma \omega \phi$	$(2.5 \pm 0.6) \times 10^{-4}$		
$\Gamma_{306} \gamma f_0(1770) \rightarrow \gamma K_S^0 K_S^0$	$(1.11 \pm 0.20) \times 10^{-5}$		
$\Gamma_{307} \gamma f_2(1810) \rightarrow \gamma \eta \eta'$	$(5.4 \pm 3.5) \times 10^{-5}$		
$\Gamma_{308} \gamma \eta_1(1855) \rightarrow \gamma \eta \eta'$	$(2.7 \pm 0.4) \times 10^{-6}$		
$\Gamma_{309} \gamma f_0(1770) \rightarrow \gamma \eta \eta'$			
$\Gamma_{310} \gamma f_2(1910) \rightarrow \gamma \omega \omega$	$(2.0 \pm 1.4) \times 10^{-4}$		
$\Gamma_{311} \gamma f_2(1950) \rightarrow \gamma K^*(892) \bar{K}^*(892)$	$(7.0 \pm 2.2) \times 10^{-4}$		
$\Gamma_{312} \gamma f_2(2010) \rightarrow \gamma \eta \eta'$			
$\Gamma_{313} \gamma f_0(2020) \rightarrow \gamma \pi \pi$			
$\Gamma_{314} \gamma f_0(2020) \rightarrow \gamma K \bar{K}$			
$\Gamma_{315} \gamma f_0(2020) \rightarrow \gamma \eta \eta'$			
$\Gamma_{316} \gamma f_0(2020) \rightarrow \gamma \eta' \eta'$	$(2.63 \pm 0.32) \times 10^{-4}$		
$\Gamma_{317} \gamma f_0(2020) \rightarrow \gamma \eta \eta'$			
$\Gamma_{318} \gamma f_4(2050)$	$(2.7 \pm 0.7) \times 10^{-3}$		
$\Gamma_{319} \gamma f_4(2050) \rightarrow \gamma \eta \eta'$			
$\Gamma_{320} \gamma f_0(2100) \rightarrow \gamma \eta \eta'$	$(1.13 \pm 0.60) \times 10^{-4}$		
$\Gamma_{321} \gamma f_0(2100) \rightarrow \gamma K \bar{K}$			
$\Gamma_{322} \gamma f_0(2100) \rightarrow \gamma \pi \pi$	$(6.2 \pm 1.0) \times 10^{-4}$		
$\Gamma_{323} \gamma f_0(2200)$	seen		
$\Gamma_{324} \gamma f_0(2200) \rightarrow \gamma K \bar{K}$	$(5.9 \pm 1.3) \times 10^{-4}$		
$\Gamma_{325} \gamma f_0(2200) \rightarrow \gamma K_S^0 K_S^0$	$(2.72 \pm 0.19) \times 10^{-4}$		
$\Gamma_{326} \gamma f_0(2200) \rightarrow \gamma \pi \pi$			
$\Gamma_{327} \gamma f_0(2200) \rightarrow \gamma \eta \eta'$			
$\Gamma_{328} \gamma f_J(2220)$	seen		
$\Gamma_{329} \gamma f_J(2220) \rightarrow \gamma \pi \pi$	$< 3.9 \times 10^{-5}$	CL=90%	
$\Gamma_{330} \gamma f_J(2220) \rightarrow \gamma K \bar{K}$	$< 4.1 \times 10^{-5}$	CL=90%	
$\Gamma_{331} \gamma f_J(2220) \rightarrow \gamma \rho \bar{\rho}$	$(1.5 \pm 0.8) \times 10^{-5}$		
$\Gamma_{332} \gamma f_0(2330) \rightarrow \gamma K_S^0 K_S^0$	$(4.9 \pm 0.7) \times 10^{-5}$		
$\Gamma_{333} \gamma f_0(2330) \rightarrow \gamma \pi \pi$			
$\Gamma_{334} \gamma f_0(2330) \rightarrow \gamma \eta \eta'$			
$\Gamma_{335} \gamma f_0(2330) \rightarrow \gamma \eta' \eta'$	$(6.1 \pm 4.0) \times 10^{-6}$		
$\Gamma_{336} \gamma f_0(2330) \rightarrow \gamma \eta \eta'$			
$\Gamma_{337} \gamma f_2(2340) \rightarrow \gamma \eta \eta'$	$(5.6 \pm 2.4) \times 10^{-5}$		
$\Gamma_{338} \gamma f_2(2340) \rightarrow \gamma K_S^0 K_S^0$	$(5.5 \pm 4.0) \times 10^{-5}$		
$\Gamma_{339} \gamma f_2(2340) \rightarrow \gamma \eta' \eta'$	$(8.7 \pm 0.9) \times 10^{-6}$		
$\Gamma_{340} \gamma f_0(2470) \rightarrow \gamma \eta' \eta'$	$(8.2 \pm 4.0) \times 10^{-7}$		
$\Gamma_{341} \gamma X(1835) \rightarrow \gamma \pi^+ \pi^- \eta'$	$(2.7 \pm 0.6) \times 10^{-4}$	S=1.6	
$\Gamma_{342} \gamma X(1835) \rightarrow \gamma \rho \bar{\rho}$	$(7.7 \pm 1.5) \times 10^{-5}$		
$\Gamma_{343} \gamma X(1835) \rightarrow \gamma K_S^0 K_S^0 \eta$	$(3.3 \pm 2.0) \times 10^{-5}$		
$\Gamma_{344} \gamma X(1835) \rightarrow \gamma \gamma \phi(1020)$			
$\Gamma_{345} \gamma X(1835) \rightarrow \gamma \gamma \gamma$	$< 3.56 \times 10^{-6}$	CL=90%	
$\Gamma_{346} \gamma X(1835) \rightarrow \gamma 3(\pi^+ \pi^-)$	$(2.4 \pm 0.7) \times 10^{-5}$		
$\Gamma_{347} \gamma X(2370) \rightarrow \gamma K^+ K^- \eta'$	$(1.8 \pm 0.7) \times 10^{-5}$		
$\Gamma_{348} \gamma X(2370) \rightarrow \gamma K_S^0 K_S^0 \eta'$	$(1.2 \pm 0.5) \times 10^{-5}$		
$\Gamma_{349} \gamma X(2370) \rightarrow \gamma \eta \eta \eta'$	$< 9.2 \times 10^{-6}$	CL=90%	
$\Gamma_{350} \gamma \rho \bar{\rho}$	$(3.8 \pm 1.0) \times 10^{-4}$		
$\Gamma_{351} \gamma \rho \bar{\rho} \pi^+ \pi^-$	$< 7.9 \times 10^{-4}$	CL=90%	
$\Gamma_{352} \gamma \Lambda \bar{\Lambda}$	$< 1.3 \times 10^{-4}$	CL=90%	
$\Gamma_{353} \gamma A^0 \rightarrow \gamma$ invisible	$[e] < 1.7 \times 10^{-6}$	CL=90%	
$\Gamma_{354} \gamma A^0 \rightarrow \gamma \mu^+ \mu^-$	$[f] < 7.8 \times 10^{-7}$	CL=90%	
Dalitz decays			
$\Gamma_{355} \pi^0 e^+ e^-$	$(7.6 \pm 1.4) \times 10^{-7}$		
$\Gamma_{356} \eta e^+ e^-$	$(1.42 \pm 0.08) \times 10^{-5}$		
$\Gamma_{357} \eta'(958) e^+ e^-$	$(6.59 \pm 0.18) \times 10^{-5}$		
$\Gamma_{358} X(1835) e^+ e^-, X \rightarrow \pi^+ \pi^- \eta'$	$(3.58 \pm 0.25) \times 10^{-6}$		
$\Gamma_{359} X(2120) e^+ e^-, X \rightarrow \pi^+ \pi^- \eta'$	$(8.2 \pm 1.3) \times 10^{-7}$		
$\Gamma_{360} X(2370) e^+ e^-, X \rightarrow \pi^+ \pi^- \eta'$	$(1.08 \pm 0.17) \times 10^{-6}$		
$\Gamma_{361} \eta U \rightarrow \eta e^+ e^-$	$[g] < 9.11 \times 10^{-7}$	CL=90%	
$\Gamma_{362} \eta'(958) U \rightarrow \eta'(958) e^+ e^-$	$[g] < 2.0 \times 10^{-7}$	CL=90%	
$\Gamma_{363} \phi e^+ e^-$	$< 1.2 \times 10^{-7}$	CL=90%	
Weak decays			
$\Gamma_{364} D^- e^+ \nu_e + c.c.$	$< 7.1 \times 10^{-8}$	CL=90%	
$\Gamma_{365} \bar{D}^0 e^+ e^- + c.c.$	$< 8.5 \times 10^{-8}$	CL=90%	
$\Gamma_{366} D_S^- e^+ \nu_e + c.c.$	$< 1.3 \times 10^{-6}$	CL=90%	

See key on page 1171

Meson Particle Listings

$J/\psi(1S)$

Γ_{367}	$D_s^{*-} e^+ \nu_e + c.c.$	< 1.8	$\times 10^{-6}$	CL=90%
Γ_{368}	$D_s^- \pi^+ + c.c.$	< 7.5	$\times 10^{-5}$	CL=90%
Γ_{369}	$\bar{D}^0 \bar{K}^0 + c.c.$	< 1.7	$\times 10^{-4}$	CL=90%
Γ_{370}	$\bar{D}^0 \bar{K}^{*0} + c.c.$	< 2.5	$\times 10^{-6}$	CL=90%
Γ_{371}	$D_s^- \pi^+ + c.c.$	< 1.3	$\times 10^{-4}$	CL=90%
Γ_{372}	$D_s^- \rho^+ + c.c.$	< 1.3	$\times 10^{-5}$	CL=90%

Charge conjugation (C), Parity (P), Lepton Family number (LF) violating modes

Γ_{373}	$\gamma\gamma$	C	< 2.7	$\times 10^{-7}$	CL=90%
Γ_{374}	$\gamma\phi$	C	< 1.4	$\times 10^{-6}$	CL=90%
Γ_{375}	$e^\pm \mu^\mp$	LF	< 1.6	$\times 10^{-7}$	CL=90%
Γ_{376}	$e^\pm \tau^\mp$	LF	< 7.5	$\times 10^{-8}$	CL=90%
Γ_{377}	$\mu^\pm \tau^\mp$	LF	< 2.0	$\times 10^{-6}$	CL=90%
Γ_{378}	$A_c^\pm e^- + c.c.$		< 6.9	$\times 10^{-8}$	CL=90%

Other decays

Γ_{379}	invisible	< 7	$\times 10^{-4}$	CL=90%
----------------	-----------	-----	------------------	--------

- [a] For $E_\gamma > 100$ MeV.
- [b] The value is for the sum of the charge states or particle/antiparticle states indicated.
- [c] $\Theta(1540)$ is a hypothetical pentaquark state of 1.54 GeV/c² mass and a width of less than 25 MeV/c².
- [d] Includes $p\bar{p}\pi^+\pi^-\gamma$ and excludes $p\bar{p}\eta, p\bar{p}\omega, p\bar{p}\eta'$.
- [e] For a narrow state A with mass less than 960 MeV.
- [f] For a narrow scalar or pseudoscalar A^0 with mass 0.21–3.0 GeV.
- [g] For a dark photon U with mass between 100 and 2100 MeV.

FIT INFORMATION

A multiparticle fit to $\eta_c(1S), J/\psi(1S), \psi(2S), h_c(1P)$, and B^\pm with the total width, 10 combinations of partial widths obtained from integrated cross section, and 38 branching ratios uses 113 measurements to determine 19 parameters. The overall fit has a $\chi^2 = 184.6$ for 94 degrees of freedom.

$J/\psi(1S)$ PARTIAL WIDTHS

$\Gamma(\text{hadrons})$					Γ_1
VALUE (keV)	DOCUMENT ID	TECN	COMMENT		
81.37 ± 1.36 ± 1.30	¹ ANASHIN	20	KEDR	e^+e^-	
••• We do not use the following data for averages, fits, limits, etc. •••					
74.1 ± 8.1	BAI	95B	BES	e^+e^-	
59 ± 24	BALDINI...	75	FRAG	e^+e^-	
59 ± 14	BOYARSKI	75	MRK1	e^+e^-	
50 ± 25	ESPOSITO	75B	FRAM	e^+e^-	

¹ Based on the same dataset as ANASHIN 18A and correlated to the values reported there

$\Gamma(e^+e^-)$					Γ_5
VALUE (keV)	EVTS	DOCUMENT ID	TECN	COMMENT	
5.53 ± 0.10	OUR AVERAGE				
5.550 ± 0.056 ± 0.089		^{1,2} ANASHIN	18A	KEDR	e^+e^-
5.36 ^{+0.29} _{-0.28}		³ HSUEH	92	RVUE	See Υ mini-review
••• We do not use the following data for averages, fits, limits, etc. •••					
5.58 ± 0.05 ± 0.08		⁴ ABLIKIM	16Q	BES3	3.773 $e^+e^- \rightarrow \mu^+\mu^- \gamma$
5.71 ± 0.16	13k	⁵ ADAMS	06A	CLEO	$e^+e^- \rightarrow \mu^+\mu^- \gamma$
5.57 ± 0.19	7.8k	⁵ AUBERT	04	BABR	$e^+e^- \rightarrow \mu^+\mu^- \gamma$
5.14 ± 0.39		BAI	95B	BES	e^+e^-
4.72 ± 0.35		ALEXANDER	89	RVUE	See Υ mini-review
4.4 ± 0.6		³ BRANDELIK	79C	DASP	e^+e^-
4.6 ± 0.8		⁶ BALDINI...	75	FRAG	e^+e^-
4.8 ± 0.6		BOYARSKI	75	MRK1	e^+e^-
4.6 ± 1.0		ESPOSITO	75B	FRAM	e^+e^-

- ¹ From the cross sections of $e^+e^- \rightarrow e^+e^-$ and $e^+e^- \rightarrow \text{hadrons}$ near the $J/\psi(1S)$ peak.
- ² Based on the same dataset as ANASHIN 20 and correlated to the values reported there.
- ³ From a simultaneous fit to $e^+e^-, \mu^+\mu^-$, and hadronic channels assuming $\Gamma(e^+e^-) = \Gamma(\mu^+\mu^-)$.
- ⁴ Using $B(J/\psi \rightarrow \mu^+\mu^-) = (5.973 \pm 0.007 \pm 0.037)\%$ from ABLIKIM 13R.
- ⁵ Calculated by us from the reported values of $\Gamma(e^+e^-) \times B(\mu^+\mu^-)$ using $B(\mu^+\mu^-) = (5.93 \pm 0.06)\%$.
- ⁶ Assuming equal partial widths for e^+e^- and $\mu^+\mu^-$.

$\Gamma(\mu^+\mu^-)$					Γ_7
VALUE (keV)	DOCUMENT ID	TECN	COMMENT		
••• We do not use the following data for averages, fits, limits, etc. •••					
5.13 ± 0.52	BAI	95B	BES	e^+e^-	
4.8 ± 0.6	BOYARSKI	75	MRK1	e^+e^-	
5 ± 1	ESPOSITO	75B	FRAM	e^+e^-	

$\Gamma(\gamma\gamma)$					Γ_{373}
VALUE (eV)	CL%	DOCUMENT ID	TECN	COMMENT	
< 5.4	90	BRANDELIK	79C	DASP	e^+e^-

$J/\psi(1S) \Gamma(I)\Gamma(e^+e^-)/\Gamma(\text{total})$

This combination of a partial width with the partial width into e^+e^- and with the total width is obtained from the integrated cross section in channel(I) in the e^+e^- annihilation.

$\Gamma(\text{hadrons}) \times \Gamma(e^+e^-)/\Gamma_{\text{total}}$					$\Gamma_1\Gamma_5/\Gamma$
VALUE (keV)	DOCUMENT ID	TECN	COMMENT		
••• We do not use the following data for averages, fits, limits, etc. •••					
4.884 ± 0.048 ± 0.078	^{1,2} ANASHIN	18A	KEDR	e^+e^-	
4 ± 0.8	³ BALDINI...	75	FRAG	e^+e^-	
3.9 ± 0.8	³ ESPOSITO	75B	FRAM	e^+e^-	

- ¹ From the cross sections of $e^+e^- \rightarrow e^+e^-$ and $e^+e^- \rightarrow \text{hadrons}$ near the $J/\psi(1S)$ peak.
- ² Based on the same dataset as ANASHIN 20 and correlated to the values reported there.
- ³ Data redundant with branching ratios or partial widths above.

$\Gamma(e^+e^-) \times \Gamma(e^+e^-)/\Gamma_{\text{total}}$					$\Gamma_5\Gamma_5/\Gamma$
VALUE (eV)	DOCUMENT ID	TECN	COMMENT		
••• We do not use the following data for averages, fits, limits, etc. •••					
333.1 ± 6.6 ± 4.0	^{1,2} ANASHIN	18A	KEDR	e^+e^-	
332.3 ± 6.4 ± 4.8	ANASHIN	10	KEDR	3.097 $e^+e^- \rightarrow e^+e^-$	
350 ± 20	BRANDELIK	79C	DASP	e^+e^-	
320 ± 70	³ BALDINI...	75	FRAG	e^+e^-	
340 ± 90	³ ESPOSITO	75B	FRAM	e^+e^-	
360 ± 100	³ FORD	75	SPEC	e^+e^-	

- ¹ From the cross sections of $e^+e^- \rightarrow e^+e^-$ and $e^+e^- \rightarrow \text{hadrons}$ near the $J/\psi(1S)$ peak.
- ² Based on the same dataset as ANASHIN 20 and correlated to the values reported there.
- ³ Data redundant with branching ratios or partial widths above.

$\Gamma(\mu^+\mu^-) \times \Gamma(e^+e^-)/\Gamma_{\text{total}}$					$\Gamma_7\Gamma_5/\Gamma$
VALUE (eV)	EVTS	DOCUMENT ID	TECN	COMMENT	
333 ± 4	OUR AVERAGE				
333.4 ± 2.5 ± 4.4		ABLIKIM	16Q	BES3	3.773 $e^+e^- \rightarrow \mu^+\mu^- \gamma$
331.8 ± 5.2 ± 6.3		ANASHIN	10	KEDR	3.097 $e^+e^- \rightarrow \mu^+\mu^-$
338.4 ± 5.8 ± 7.1	13k	ADAMS	06A	CLEO	$e^+e^- \rightarrow \mu^+\mu^- \gamma$
330.1 ± 7.7 ± 7.3	7.8k	AUBERT	04	BABR	$e^+e^- \rightarrow \mu^+\mu^- \gamma$
••• We do not use the following data for averages, fits, limits, etc. •••					
510 ± 90		DASP	75	DASP	e^+e^-
380 ± 50		¹ ESPOSITO	75B	FRAM	e^+e^-

¹ Data redundant with branching ratios or partial widths above.

$\Gamma(\eta\pi^+\pi^-) \times \Gamma(e^+e^-)/\Gamma_{\text{total}}$					$\Gamma_{13}\Gamma_5/\Gamma$
VALUE (eV)	EVTS	DOCUMENT ID	TECN	COMMENT	
2.3 ± 0.4	OUR AVERAGE				
2.34 ± 0.43 ± 0.16	49	LEES	18	BABR	$e^+e^- \rightarrow \eta\pi^+\pi^- \gamma$
2.22 ± 0.96 ± 0.02	9	¹ AUBERT	07AU	BABR	10.6 $e^+e^- \rightarrow \eta\pi^+\pi^- \gamma$

¹ AUBERT 07AU reports $[\Gamma(J/\psi(1S) \rightarrow \eta\pi^+\pi^-) \times \Gamma(J/\psi(1S) \rightarrow e^+e^-)]/\Gamma_{\text{total}} \times [B(\eta \rightarrow \pi^+\pi^-\pi^0)] = 0.51 \pm 0.22 \pm 0.03$ eV which we divide by our best value $B(\eta \rightarrow \pi^+\pi^-\pi^0) = (23.02 \pm 0.25) \times 10^{-2}$. Our first error is their experiment's error and our second error is the systematic error from using our best value.

$\Gamma(\eta\pi^+\pi^-\pi^0) \times \Gamma(e^+e^-)/\Gamma_{\text{total}}$					$\Gamma_{15}\Gamma_5/\Gamma$
VALUE (eV)	EVTS	DOCUMENT ID	TECN	COMMENT	
64.8 ± 11.1 ± 0.4	200	1 LEES	21C	BABR	$e^+e^- \rightarrow \gamma_{ISR}(\pi^+\pi^-\pi^0)$
••• We do not use the following data for averages, fits, limits, etc. •••					
61. LEES 21C reports $[\Gamma(J/\psi(1S) \rightarrow \eta\pi^+\pi^-\pi^0) \times \Gamma(J/\psi(1S) \rightarrow e^+e^-)]/\Gamma_{\text{total}} \times [B(\eta \rightarrow 3\pi^0)] = 21.1 \pm 1.7 \pm 3.2$ eV which we divide by our best value $B(\eta \rightarrow 3\pi^0) = (32.57 \pm 0.21) \times 10^{-2}$. Our first error is their experiment's error and our second error is the systematic error from using our best value.					

$\Gamma(\eta\pi^+\pi^-3\pi^0) \times \Gamma(e^+e^-)/\Gamma_{\text{total}}$					$\Gamma_{16}\Gamma_5/\Gamma$
VALUE (eV)	EVTS	DOCUMENT ID	TECN	COMMENT	
26.9 ± 5.7 ± 0.1	101	1 LEES	21C	BABR	$e^+e^- \rightarrow \gamma_{ISR}(\pi^+\pi^-3\pi^0) \gamma$
••• We do not use the following data for averages, fits, limits, etc. •••					
61. LEES 21C reports $[\Gamma(J/\psi(1S) \rightarrow \eta\pi^+\pi^-3\pi^0) \times \Gamma(J/\psi(1S) \rightarrow e^+e^-)]/\Gamma_{\text{total}} \times [B(\eta \rightarrow 2\gamma)] = 10.6 \pm 1.6 \pm 1.6$ eV which we divide by our best value $B(\eta \rightarrow 2\gamma) = (39.36 \pm 0.18) \times 10^{-2}$. Our first error is their experiment's error and our second error is the systematic error from using our best value.					

Meson Particle Listings

 $J/\psi(1S)$ $\Gamma(\eta K^+ K^-) \times \Gamma(e^+ e^-)/\Gamma_{\text{total}}$ $\Gamma_{19}\Gamma_5/\Gamma$

VALUE (eV)	DOCUMENT ID	TECN	COMMENT
4.76±1.64±0.03	¹ LEES	23	BABR $e^+ e^- \rightarrow \gamma_{ISR} \text{hadrons}$
¹ LEES 23 reports $[\Gamma(J/\psi(1S) \rightarrow \eta K^+ K^-) \times \Gamma(J/\psi(1S) \rightarrow e^+ e^-)/\Gamma_{\text{total}}] \times [B(\eta \rightarrow 3\pi^0)] = 1.55 \pm 0.51 \pm 0.16$ eV which we divide by our best value $B(\eta \rightarrow 3\pi^0) = (32.57 \pm 0.21) \times 10^{-2}$. Our first error is their experiment's error and our second error is the systematic error from using our best value.			

 $\Gamma(\eta K^\pm K_S^0 \pi^\mp) \times \Gamma(e^+ e^-)/\Gamma_{\text{total}}$ $\Gamma_{20}\Gamma_5/\Gamma$

VALUE (eV)	EVTS	DOCUMENT ID	TECN	COMMENT
7.3±1.4±0.4	44	LEES	17D	BABR $e^+ e^- \rightarrow K_S^0 K^\pm \pi^\mp \pi^0 \gamma$

 $\Gamma(K_S^0 K^\pm \pi^\mp \rho(770)^0) \times \Gamma(e^+ e^-)/\Gamma_{\text{total}}$ $\Gamma_{196}\Gamma_5/\Gamma$

VALUE (eV)	DOCUMENT ID	TECN	COMMENT
17.3±2.1±1.7	LEES	23	BABR $e^+ e^- \rightarrow \gamma_{ISR} \text{hadrons}$

 $\Gamma(\rho^\pm \pi^\mp \pi^+ \pi^- 2\pi^0) \times \Gamma(e^+ e^-)/\Gamma_{\text{total}}$ $\Gamma_{23}\Gamma_5/\Gamma$

VALUE (eV)	EVTS	DOCUMENT ID	TECN	COMMENT
155±26±36	14k	LEES	21	BABR $10.6 e^+ e^- \rightarrow 2(\pi^+ \pi^-) 3\pi^0 \gamma$

 $\Gamma(\rho^\pm \rho^- \pi^+ \pi^- \pi^0) \times \Gamma(e^+ e^-)/\Gamma_{\text{total}}$ $\Gamma_{24}\Gamma_5/\Gamma$

VALUE (eV)	EVTS	DOCUMENT ID	TECN	COMMENT
32±13±15	14k	LEES	21	BABR $10.6 e^+ e^- \rightarrow 2(\pi^+ \pi^-) 3\pi^0 \gamma$

 $\Gamma(\rho^\mp K^\pm K_S^0) \times \Gamma(e^+ e^-)/\Gamma_{\text{total}}$ $\Gamma_{26}\Gamma_5/\Gamma$

VALUE (eV)	EVTS	DOCUMENT ID	TECN	COMMENT
10.4±1.0±1.9	130	LEES	17D	BABR $e^+ e^- \rightarrow K_S^0 K^\pm \pi^\mp \pi^0 \gamma$

 $\Gamma(\omega \pi^+ \pi^-) \times \Gamma(e^+ e^-)/\Gamma_{\text{total}}$ $\Gamma_{41}\Gamma_5/\Gamma$

VALUE (eV)	EVTS	DOCUMENT ID	TECN	COMMENT
53.6±5.0±0.4	788	¹ AUBERT	07AU BABR	$10.6 e^+ e^- \rightarrow \omega \pi^+ \pi^- \gamma$
¹ AUBERT 07AU reports $[\Gamma(J/\psi(1S) \rightarrow \omega \pi^+ \pi^-) \times \Gamma(J/\psi(1S) \rightarrow e^+ e^-)/\Gamma_{\text{total}}] \times [B(\omega(782) \rightarrow \pi^+ \pi^- \pi^0)] = 47.8 \pm 3.1 \pm 3.2$ eV which we divide by our best value $B(\omega(782) \rightarrow \pi^+ \pi^- \pi^0) = (89.2 \pm 0.7) \times 10^{-2}$. Our first error is their experiment's error and our second error is the systematic error from using our best value.				

 $\Gamma(\omega \pi^0 \pi^0) \times \Gamma(e^+ e^-)/\Gamma_{\text{total}}$ $\Gamma_{42}\Gamma_5/\Gamma$

VALUE (eV)	EVTS	DOCUMENT ID	TECN	COMMENT
27.8±3.5±0.2	398	¹ LEES	18E BABR	$10.6 e^+ e^- \rightarrow \pi^+ \pi^- 3\pi^0 \gamma$
¹ LEES 18E reports $[\Gamma(J/\psi(1S) \rightarrow \omega \pi^0 \pi^0) \times \Gamma(J/\psi(1S) \rightarrow e^+ e^-)/\Gamma_{\text{total}}] \times [B(\omega(782) \rightarrow \pi^+ \pi^- \pi^0)] = 24.8 \pm 1.8 \pm 2.5$ eV which we divide by our best value $B(\omega(782) \rightarrow \pi^+ \pi^- \pi^0) = (89.2 \pm 0.7) \times 10^{-2}$. Our first error is their experiment's error and our second error is the systematic error from using our best value.				

 $\Gamma(\omega 3\pi^0) \times \Gamma(e^+ e^-)/\Gamma_{\text{total}}$ $\Gamma_{43}\Gamma_5/\Gamma$

VALUE (eV)	EVTS	DOCUMENT ID	TECN	COMMENT
10.5±3.1±0.1	89	¹ LEES	21C BABR	$e^+ e^- \rightarrow \gamma_{ISR}(\pi^+ \pi^- 4\pi^0)$
¹ LEES 21C reports $[\Gamma(J/\psi(1S) \rightarrow \omega 3\pi^0) \times \Gamma(J/\psi(1S) \rightarrow e^+ e^-)/\Gamma_{\text{total}}] \times [B(\omega(782) \rightarrow \pi^+ \pi^- \pi^0)] = 9.4 \pm 2.3 \pm 1.5$ eV which we divide by our best value $B(\omega(782) \rightarrow \pi^+ \pi^- \pi^0) = (89.2 \pm 0.7) \times 10^{-2}$. Our first error is their experiment's error and our second error is the systematic error from using our best value.				

 $\Gamma(\omega \pi^+ \pi^- \pi^0) \times \Gamma(e^+ e^-)/\Gamma_{\text{total}}$ $\Gamma_{46}\Gamma_5/\Gamma$

VALUE (10 ⁻² keV)	EVTS	DOCUMENT ID	TECN	COMMENT
2.2±0.3±0.2	170	AUBERT	06D BABR	$10.6 e^+ e^- \rightarrow \omega \pi^+ \pi^- \pi^0 \gamma$

 $\Gamma(\omega \eta) \times \Gamma(e^+ e^-)/\Gamma_{\text{total}}$ $\Gamma_{45}\Gamma_5/\Gamma$

VALUE (eV)	DOCUMENT ID	TECN	COMMENT
16.9±7.6±0.2	¹ LEES	21C BABR	$e^+ e^- \rightarrow \gamma_{ISR}(\pi^+ \pi^- 4\pi^0)$
¹ Different final state as in AUBERT 06. LEES 21C reports $[\Gamma(J/\psi(1S) \rightarrow \omega \eta) \times \Gamma(J/\psi(1S) \rightarrow e^+ e^-)/\Gamma_{\text{total}}] \times [B(\eta \rightarrow 3\pi^0)] \times [B(\omega(782) \rightarrow \pi^+ \pi^- \pi^0)] = 4.9 \pm 2.1 \pm 0.7$ eV which we divide by our best values $B(\eta \rightarrow 3\pi^0) = (32.57 \pm 0.21) \times 10^{-2}$, $B(\omega(782) \rightarrow \pi^+ \pi^- \pi^0) = (89.2 \pm 0.7) \times 10^{-2}$. Our first error is their experiment's error and our second error is the systematic error from using our best values.			

 $\Gamma(\omega \pi^0 \eta) \times \Gamma(e^+ e^-)/\Gamma_{\text{total}}$ $\Gamma_{47}\Gamma_5/\Gamma$

VALUE (eV)	EVTS	DOCUMENT ID	TECN	COMMENT
1.90±0.96±0.01	27	¹ LEES	18E BABR	$10.6 e^+ e^- \rightarrow \pi^+ \pi^- \pi^0 \pi^0 \eta \gamma$
¹ LEES 18E reports $[\Gamma(J/\psi(1S) \rightarrow \omega \pi^0 \eta) \times \Gamma(J/\psi(1S) \rightarrow e^+ e^-)/\Gamma_{\text{total}}] \times [B(\omega(782) \rightarrow \pi^+ \pi^- \pi^0)] = 1.7 \pm 0.8 \pm 0.3$ eV which we divide by our best value $B(\omega(782) \rightarrow \pi^+ \pi^- \pi^0) = (89.2 \pm 0.7) \times 10^{-2}$. Our first error is their experiment's error and our second error is the systematic error from using our best value.				

 $\Gamma(\omega \pi^+ \pi^- 2\pi^0) \times \Gamma(e^+ e^-)/\Gamma_{\text{total}}$ $\Gamma_{49}\Gamma_5/\Gamma$

VALUE (eV)	EVTS	DOCUMENT ID	TECN	COMMENT
185±30±1	14k	¹ LEES	21 BABR	$10.6 e^+ e^- \rightarrow 2(\pi^+ \pi^-) 3\pi^0 \gamma$
¹ LEES 21 reports $[\Gamma(J/\psi(1S) \rightarrow \omega \pi^+ \pi^- 2\pi^0) \times \Gamma(J/\psi(1S) \rightarrow e^+ e^-)/\Gamma_{\text{total}}] \times [B(\omega(782) \rightarrow \pi^+ \pi^- \pi^0)] = 165 \pm 9 \pm 25$ eV which we divide by our best value $B(\omega(782) \rightarrow \pi^+ \pi^- \pi^0) = (89.2 \pm 0.7) \times 10^{-2}$. Our first error is their experiment's error and our second error is the systematic error from using our best value.				

 $\Gamma(\omega K^+ K^-) \times \Gamma(e^+ e^-)/\Gamma_{\text{total}}$ $\Gamma_{60}\Gamma_5/\Gamma$

VALUE (eV)	EVTS	DOCUMENT ID	TECN	COMMENT
3.70±1.98±0.03	24	¹ AUBERT	07AU BABR	$10.6 e^+ e^- \rightarrow \omega K^+ K^- \gamma$
¹ AUBERT 07AU reports $[\Gamma(J/\psi(1S) \rightarrow \omega K^+ K^-) \times \Gamma(J/\psi(1S) \rightarrow e^+ e^-)/\Gamma_{\text{total}}] \times [B(\omega(782) \rightarrow \pi^+ \pi^- \pi^0)] = 3.3 \pm 1.3 \pm 1.2$ eV which we divide by our best value $B(\omega(782) \rightarrow \pi^+ \pi^- \pi^0) = (89.2 \pm 0.7) \times 10^{-2}$. Our first error is their experiment's error and our second error is the systematic error from using our best value.				

 $\Gamma(K^+ K^*(892)^- + \text{c.c.}) \times \Gamma(e^+ e^-)/\Gamma_{\text{total}}$ $\Gamma_{69}\Gamma_5/\Gamma$

VALUE (eV)	DOCUMENT ID	TECN	COMMENT
29.0±1.7±1.3	AUBERT	08s BABR	$10.6 e^+ e^- \rightarrow K^+ K^*(892)^- \gamma$

 $\Gamma(K^+ K^*(892)^- + \text{c.c.} \rightarrow K^+ K^- \pi^0) \times \Gamma(e^+ e^-)/\Gamma_{\text{total}}$ $\Gamma_{70}\Gamma_5/\Gamma$

VALUE (eV)	EVTS	DOCUMENT ID	TECN	COMMENT
10.96±0.85±0.70	155	AUBERT	08s BABR	$10.6 e^+ e^- \rightarrow K^+ K^- \pi^0 \gamma$

 $\Gamma(K^+ K^*(892)^- + \text{c.c.} \rightarrow K^0 K^\pm \pi^\mp + \text{c.c.}) \times \Gamma(e^+ e^-)/\Gamma_{\text{total}}$ $\Gamma_{71}\Gamma_5/\Gamma$

VALUE (eV)	EVTS	DOCUMENT ID	TECN	COMMENT
16.76±1.70±1.00	89	AUBERT	08s BABR	$10.6 e^+ e^- \rightarrow K_S^0 K^\pm \pi^\mp \gamma$

 $\Gamma(K^0 \bar{K}^*(892)^0 + \text{c.c.}) \times \Gamma(e^+ e^-)/\Gamma_{\text{total}}$ $\Gamma_{72}\Gamma_5/\Gamma$

VALUE (eV)	DOCUMENT ID	TECN	COMMENT
26.8±2.5±1.5	AUBERT	08s BABR	$10.6 e^+ e^- \rightarrow K^0 \bar{K}^*(892)^0 \gamma$

 $\Gamma(K^0 \bar{K}^*(892)^0 + \text{c.c.} \rightarrow K^0 K^\pm \pi^\mp + \text{c.c.}) \times \Gamma(e^+ e^-)/\Gamma_{\text{total}}$ $\Gamma_{73}\Gamma_5/\Gamma$

VALUE (eV)	EVTS	DOCUMENT ID	TECN	COMMENT
17.70±1.70±1.00	94	AUBERT	08s BABR	$10.6 e^+ e^- \rightarrow K_S^0 K^\pm \pi^\mp \gamma$

 $\Gamma(\bar{K}^*(892)^0 K^+ \pi^- + \text{c.c.}) \times \Gamma(e^+ e^-)/\Gamma_{\text{total}}$ $\Gamma_{74}\Gamma_5/\Gamma$

VALUE (eV)	EVTS	DOCUMENT ID	TECN	COMMENT
42.6±4.8±7.2	99	¹ LEES	17D BABR	$e^+ e^- \rightarrow K_S^0 K^\pm \pi^\mp \pi^0 \gamma$
¹ Dividing by 1/6 to account for $B(K^*(892)^0 \rightarrow K_S^0 \pi^0) = 1/6$.				

 $\Gamma(K^*(892)^\pm K^\mp \pi^0) \times \Gamma(e^+ e^-)/\Gamma_{\text{total}}$ $\Gamma_{75}\Gamma_5/\Gamma$

VALUE (eV)	EVTS	DOCUMENT ID	TECN	COMMENT
22.8±2.8±6.8	80	¹ LEES	17D BABR	$e^+ e^- \rightarrow K_S^0 K^\pm \pi^\mp \pi^0 \gamma$
¹ Dividing by 1/4 to account for $B(K^*(892)^\pm \rightarrow K_S^0 \pi^\pm) = 1/4$.				

 $\Gamma(K^*(892)^+ K_S^0 \pi^- + \text{c.c.}) \times \Gamma(e^+ e^-)/\Gamma_{\text{total}}$ $\Gamma_{76}\Gamma_5/\Gamma$

VALUE (eV)	EVTS	DOCUMENT ID	TECN	COMMENT
11.0±2.8 OUR AVERAGE				
9.2±1.2±3.2	64	¹ LEES	17D BABR	$e^+ e^- \rightarrow K_S^0 K^\pm \pi^\mp \pi^0 \gamma$
14.8±4.8±1.2	53	² LEES	14H BABR	$e^+ e^- \rightarrow \pi^+ \pi^- K_S^0 K_S^0 \gamma$
¹ Dividing by 1/2 to take into account $B(K^*(892)^\pm \rightarrow K^\pm \pi^\mp) = 1/2$.				
² Dividing by 1/4 to take into account $B(K^*(892) \rightarrow K_S^0 \pi) = 1/4$.				

 $\Gamma(K^*(892)^+ K_S^0 \pi^- + \text{c.c.} \rightarrow K_S^0 K_S^0 \pi^+ \pi^-) \times \Gamma(e^+ e^-)/\Gamma_{\text{total}}$ $\Gamma_{77}\Gamma_5/\Gamma$

VALUE (eV)	EVTS	DOCUMENT ID	TECN	COMMENT
3.7±1.2±0.3	53	LEES	14H BABR	$e^+ e^- \rightarrow \pi^+ \pi^- K_S^0 K_S^0 \gamma$
¹ Dividing by 1/2 to take into account $B(K^*(892)^\pm \rightarrow K^\pm \pi^\mp) = 1/2$.				
² Dividing by 1/4 to take into account $B(K^*(892) \rightarrow K_S^0 \pi) = 1/4$.				

 $\Gamma(K^*(892)^0 K_S^0 \pi^0) \times \Gamma(e^+ e^-)/\Gamma_{\text{total}}$ $\Gamma_{80}\Gamma_5/\Gamma$

VALUE (eV)	EVTS	DOCUMENT ID	TECN	COMMENT
3.60±0.75±2.25	34	¹ LEES	17D BABR	$e^+ e^- \rightarrow K_S^0 K^\pm \pi^\mp \pi^0 \gamma$
¹ Dividing by 2/3 to account for $B(K^*(892)^0 \rightarrow K^+ \pi^-) = 2/3$.				

 $\Gamma(K^*(892)^0 \bar{K}^*(892)^0) \times \Gamma(e^+ e^-)/\Gamma_{\text{total}}$ $\Gamma_{82}\Gamma_5/\Gamma$

VALUE (eV)	EVTS	DOCUMENT ID	TECN	COMMENT
1.28±0.34±0.07	47±12	¹ LEES	12F BABR	$10.6 e^+ e^- \rightarrow \pi^+ \pi^- K^+ K^- \gamma$
• • • We do not use the following data for averages, fits, limits, etc. • • •				
1.28±0.40±0.11	25±8	^{1,2} AUBERT	07AK BABR	$10.6 e^+ e^- \rightarrow \pi^+ \pi^- K^+ K^- \gamma$
¹ Dividing by (2/3) ² to take twice into account that $B(K^*0 \rightarrow K^+ \pi^-) = 2/3$ $B(K^*0 \rightarrow K\pi)$.				
² Superseded by LEES 12F.				

 $\Gamma(K^*(892)^\pm K^*(892)^\mp) \times \Gamma(e^+ e^-)/\Gamma_{\text{total}}$ $\Gamma_{83}\Gamma_5/\Gamma$

VALUE (eV)	EVTS	DOCUMENT ID	TECN	COMMENT
0.80±0.48±0.32	1±5	¹ LEES	14H BABR	$e^+ e^- \rightarrow \pi^+ \pi^- K_S^0 K_S^0 \gamma$
¹ Dividing by (1/4) ² to take twice into account $B(K^*(892) \rightarrow K_S^0 \pi) = 1/4$.				

 $\Gamma(K_S^2(1430)^+ K_S^0 \pi^- + \text{c.c.}) \times \Gamma(e^+ e^-)/\Gamma_{\text{total}}$ $\Gamma_{94}\Gamma_5/\Gamma$

VALUE (eV)	EVTS	DOCUMENT ID	TECN	COMMENT
20.1±9.8±0.5	35	^{1,2} LEES	14H BABR	$e^+ e^- \rightarrow \pi^+ \pi^- K_S^0 K_S^0 \gamma$
¹ Dividing by 1/4 to take into account $B(K^*(1430) \rightarrow K_S^0 \pi) = 1/4$ $B(K^*(1430) \rightarrow K\pi)$.				
² LEES 14H reports $[\Gamma(J/\psi(1S) \rightarrow K_S^2(1430)^+ K_S^0 \pi^- + \text{c.c.}) \times \Gamma(J/\psi(1S) \rightarrow e^+ e^-)/\Gamma_{\text{total}}] \times [B(K_S^2(1430) \rightarrow K\pi)] = 10.0 \pm 4.8 \pm 0.8$ eV which we divide by our best value $B(K_S^2(1430) \rightarrow K\pi) = (49.9 \pm 1.2) \times 10^{-2}$. Our first error is their experiment's error and our second error is the systematic error from using our best value.				

See key on page 1171

Meson Particle Listings

 $J/\psi(1S)$

$\Gamma(K_2^*(1430)^0 K^- \pi^+ + c.c. \rightarrow K^+ K^- \pi^+ \pi^-)/\Gamma_{total}$					Γ_{93}/Γ
VALUE (units 10^{-3})	EVTS	DOCUMENT ID	TECN	COMMENT	
2.65 ± 0.80 ± 0.44	1094	ANASHIN	22	KEDR $J/\psi \rightarrow K^+ K^- \pi^+ \pi^-$	

$\Gamma(\overline{K}_2^*(1430)^0 K^*(892)^0 + c.c.) \times \Gamma(e^+ e^-)/\Gamma_{total}$					$\Gamma_{95} \Gamma_5/\Gamma$
VALUE (eV)	EVTS	DOCUMENT ID	TECN	COMMENT	
25.8 ± 1.4 ± 0.6	710	1,2,3 LEES	12F BABR	$10.6 e^+ e^- \rightarrow \pi^+ \pi^- K^+ K^- \gamma$	

• • • We do not use the following data for averages, fits, limits, etc. • • •

33 ± 4 ± 1 317 ^{2,4}AUBERT 07AK BABR $10.6 e^+ e^- \rightarrow \pi^+ \pi^- K^+ K^- \gamma$
¹LEES 12F reports $[\Gamma(J/\psi(1S) \rightarrow \overline{K}_2^*(1430)^0 K^*(892)^0 + c.c.) \times \Gamma(J/\psi(1S) \rightarrow e^+ e^-)/\Gamma_{total}] \times [B(K_2^*(1430) \rightarrow K\pi)] = 12.89 \pm 0.54 \pm 0.41$ eV which we divide by our best value $B(K_2^*(1430) \rightarrow K\pi) = (49.9 \pm 1.2) \times 10^{-2}$. Our first error is their experiment's error and our second error is the systematic error from using our best value.
²Dividing by 2/3 to take into account that $B(K^*0 \rightarrow K^+ \pi^-) = 2/3 B(K^*0 \rightarrow K\pi)$.
³The $K_2^*(1430)$ cannot be distinguished from the $K_0^*(1430)$.

⁴Superseded by LEES 12F. AUBERT 07AK reports $[\Gamma(J/\psi(1S) \rightarrow \overline{K}_2^*(1430)^0 K^*(892)^0 + c.c.) \times \Gamma(J/\psi(1S) \rightarrow e^+ e^-)/\Gamma_{total}] \times [B(K_2^*(1430) \rightarrow K\pi)] = 16.4 \pm 1.1 \pm 1.4$ eV which we divide by our best value $B(K_2^*(1430) \rightarrow K\pi) = (49.9 \pm 1.2) \times 10^{-2}$. Our first error is their experiment's error and our second error is the systematic error from using our best value.

$\Gamma(K_2^*(1430)^0 K^*(892)^+ + c.c.) \times \Gamma(e^+ e^-)/\Gamma_{total}$					$\Gamma_{96} \Gamma_5/\Gamma$
VALUE (eV)	EVTS	DOCUMENT ID	TECN	COMMENT	
18.6 ± 16.1 ± 0.4	8 ± 8	1,2 LEES	14H BABR	$e^+ e^- \rightarrow \pi^+ \pi^- K_S^0 K_S^0 \gamma$	

¹Dividing by $(1/4)^2$ to take into account $B(K^*(892) \rightarrow K_S^0 \pi) = 1/4$ and $B(K^*(1430) \rightarrow K_S^0 \pi) = 1/4 B(K^*(1430) \rightarrow K\pi)$.

²LEES 14H reports $[\Gamma(J/\psi(1S) \rightarrow K_2^*(1430)^0 K^*(892)^+ + c.c.) \times \Gamma(J/\psi(1S) \rightarrow e^+ e^-)/\Gamma_{total}] \times [B(K_2^*(1430) \rightarrow K\pi)] = 9.28 \pm 8.0 \pm 0.32$ eV which we divide by our best value $B(K_2^*(1430) \rightarrow K\pi) = (49.9 \pm 1.2) \times 10^{-2}$. Our first error is their experiment's error and our second error is the systematic error from using our best value.

$\Gamma(K_2^*(1430)^0 K^*(892)^+ + c.c. \rightarrow K^*(892)^+ K_S^0 \pi^- + c.c.) \times \Gamma(e^+ e^-)/\Gamma_{total}$					$\Gamma_{97} \Gamma_5/\Gamma$
VALUE (eV)	EVTS	DOCUMENT ID	TECN	COMMENT	
2.32 ± 2.00 ± 0.08	8 ± 8	¹ LEES	14H BABR	$e^+ e^- \rightarrow \pi^+ \pi^- K_S^0 K_S^0 \gamma$	

¹Dividing by 1/4 to take into account $B(K^*(892) \rightarrow K_S^0 \pi) = 1/4$.

$\Gamma(\overline{K}_2^*(1770)^0 K^*(892)^0 + c.c. \rightarrow K^*(892)^0 K^- \pi^+ + c.c.) \times \Gamma(e^+ e^-)/\Gamma_{total}$					$\Gamma_{99} \Gamma_5/\Gamma$
VALUE (eV)	EVTS	DOCUMENT ID	TECN	COMMENT	
3.8 ± 0.4 ± 0.3	110 ± 14	¹ AUBERT 07AK BABR	$10.6 e^+ e^- \rightarrow \pi^+ \pi^- K^+ K^- \gamma$		

¹Dividing by 2/3 to take into account that $B(K^*0 \rightarrow K^+ \pi^-) = 2/3$.

$\Gamma(\phi \pi^+ \pi^-) \times \Gamma(e^+ e^-)/\Gamma_{total}$					$\Gamma_{106} \Gamma_5/\Gamma$
VALUE (eV)	EVTS	DOCUMENT ID	TECN	COMMENT	
4.48 ± 0.35 OUR AVERAGE					
4.46 ± 0.49 ± 0.05	181	¹ LEES	12F BABR	$10.6 e^+ e^- \rightarrow K^+ K^- \pi^+ \pi^- \gamma$	
4.51 ± 0.48 ± 0.05	254 ± 23	² SHEN	09 BELL	$10.6 e^+ e^- \rightarrow K^+ K^- \pi^+ \pi^- \gamma$	

• • • We do not use the following data for averages, fits, limits, etc. • • •

5.3 ± 0.7 ± 0.1 103 ³AUBERT, BE 06D BABR $10.6 e^+ e^- \rightarrow K^+ K^- \pi^+ \pi^- \gamma$

¹LEES 12F reports $[\Gamma(J/\psi(1S) \rightarrow \phi \pi^+ \pi^-) \times \Gamma(J/\psi(1S) \rightarrow e^+ e^-)/\Gamma_{total}] \times [B(\phi(1020) \rightarrow K^+ K^-)] = 2.19 \pm 0.23 \pm 0.07$ eV which we divide by our best value $B(\phi(1020) \rightarrow K^+ K^-) = (49.1 \pm 0.5) \times 10^{-2}$. Our first error is their experiment's error and our second error is the systematic error from using our best value.

²SHEN 09 reports $4.50 \pm 0.41 \pm 0.26$ eV from a measurement of $[\Gamma(J/\psi(1S) \rightarrow \phi \pi^+ \pi^-) \times \Gamma(J/\psi(1S) \rightarrow e^+ e^-)/\Gamma_{total}] \times [B(\phi(1020) \rightarrow K^+ K^-)]$ assuming $B(\phi(1020) \rightarrow K^+ K^-) = (49.2 \pm 0.6) \times 10^{-2}$, which we rescale to our best value $B(\phi(1020) \rightarrow K^+ K^-) = (49.1 \pm 0.5) \times 10^{-2}$. Our first error is their experiment's error and our second error is the systematic error from using our best value.

³Superseded by LEES 12F. AUBERT, BE 06D reports $[\Gamma(J/\psi(1S) \rightarrow \phi \pi^+ \pi^-) \times \Gamma(J/\psi(1S) \rightarrow e^+ e^-)/\Gamma_{total}] \times [B(\phi(1020) \rightarrow K^+ K^-)] = 2.61 \pm 0.30 \pm 0.18$ eV which we divide by our best value $B(\phi(1020) \rightarrow K^+ K^-) = (49.1 \pm 0.5) \times 10^{-2}$. Our first error is their experiment's error and our second error is the systematic error from using our best value.

$\Gamma(\phi \pi^0 \pi^0) \times \Gamma(e^+ e^-)/\Gamma_{total}$					$\Gamma_{107} \Gamma_5/\Gamma$
VALUE (eV)	EVTS	DOCUMENT ID	TECN	COMMENT	
2.77 ± 0.57 ± 0.03	45	¹ LEES	12F BABR	$10.6 e^+ e^- \rightarrow K^+ K^- \pi^0 \pi^0 \gamma$	

• • • We do not use the following data for averages, fits, limits, etc. • • •

3.13 ± 0.88 ± 0.03 23 ²AUBERT, BE 06D BABR $10.6 e^+ e^- \rightarrow K^+ K^- \pi^0 \pi^0 \gamma$

¹LEES 12F reports $[\Gamma(J/\psi(1S) \rightarrow \phi \pi^0 \pi^0) \times \Gamma(J/\psi(1S) \rightarrow e^+ e^-)/\Gamma_{total}] \times [B(\phi(1020) \rightarrow K^+ K^-)] = 1.36 \pm 0.27 \pm 0.07$ eV which we divide by our best value $B(\phi(1020) \rightarrow K^+ K^-) = (49.1 \pm 0.5) \times 10^{-2}$. Our first error is their experiment's error and our second error is the systematic error from using our best value.

²Superseded by LEES 12F. AUBERT, BE 06D reports $[\Gamma(J/\psi(1S) \rightarrow \phi \pi^0 \pi^0) \times \Gamma(J/\psi(1S) \rightarrow e^+ e^-)/\Gamma_{total}] \times [B(\phi(1020) \rightarrow K^+ K^-)] = 1.54 \pm 0.40 \pm 0.16$ eV which we divide by our best value $B(\phi(1020) \rightarrow K^+ K^-) = (49.1 \pm 0.5) \times 10^{-2}$. Our first error is their experiment's error and our second error is the systematic error from using our best value.

$\Gamma(\phi(2\pi^+ \pi^-)) \times \Gamma(e^+ e^-)/\Gamma_{total}$					$\Gamma_{108} \Gamma_5/\Gamma$
VALUE (10^{-2} keV)	EVTS	DOCUMENT ID	TECN	COMMENT	
0.96 ± 0.19 ± 0.01	35	¹ AUBERT	06D BABR	$10.6 e^+ e^- \rightarrow \phi(2\pi^+ \pi^-) \gamma$	

¹AUBERT 06D reports $[\Gamma(J/\psi(1S) \rightarrow \phi(2\pi^+ \pi^-)) \times \Gamma(J/\psi(1S) \rightarrow e^+ e^-)/\Gamma_{total}] \times [B(\phi(1020) \rightarrow K^+ K^-)] = (0.47 \pm 0.09 \pm 0.03) \times 10^{-2}$ keV which we divide by our best value $B(\phi(1020) \rightarrow K^+ K^-) = (49.1 \pm 0.5) \times 10^{-2}$. Our first error is their experiment's error and our second error is the systematic error from using our best value.

$\Gamma(\phi \eta) \times \Gamma(e^+ e^-)/\Gamma_{total}$					$\Gamma_{109} \Gamma_5/\Gamma$
VALUE (eV)	EVTS	DOCUMENT ID	TECN	COMMENT	
4.6 ± 1.4 OUR AVERAGE					
4.1 ± 1.6 ± 0.4		¹ LEES	23 BABR	$e^+ e^- \rightarrow \gamma ISR$ hadrons	
6.1 ± 2.7 ± 0.4	6	² AUBERT	07AU BABR	$10.6 e^+ e^- \rightarrow \phi \eta \gamma$	

¹LEES 23 quotes $\Gamma_{ee}^{J/\psi} \cdot B(J/\psi \rightarrow \phi \eta) \cdot B(\phi \rightarrow K^+ K^-) \cdot B(\eta \rightarrow 3\pi^0) = 0.64 \pm 0.26 \pm 0.06$ eV.

²AUBERT 07AU quotes $\Gamma_{ee}^{J/\psi} \cdot B(J/\psi \rightarrow \phi \eta) \cdot B(\phi \rightarrow K^+ K^-) \cdot B(\eta \rightarrow 3\pi) = 0.84 \pm 0.37 \pm 0.05$ eV.

$\Gamma(\phi_0(980) \rightarrow \phi \pi^+ \pi^-) \times \Gamma(e^+ e^-)/\Gamma_{total}$					$\Gamma_{113} \Gamma_5/\Gamma$
VALUE (eV)	EVTS	DOCUMENT ID	TECN	COMMENT	
1.44 ± 0.19 OUR AVERAGE					
1.40 ± 0.25 ± 0.01	57 ± 9	¹ LEES	12F BABR	$10.6 e^+ e^- \rightarrow \pi^+ \pi^- K^+ K^- \gamma$	
1.48 ± 0.27 ± 0.09	60 ± 11	² SHEN	09 BELL	$10.6 e^+ e^- \rightarrow K^+ K^- \pi^+ \pi^- \gamma$	

• • • We do not use the following data for averages, fits, limits, etc. • • •

1.02 ± 0.24 ± 0.01 20 ± 5 ³AUBERT 07AK BABR $10.6 e^+ e^- \rightarrow \pi^+ \pi^- K^+ K^- \gamma$

¹LEES 12F reports $[\Gamma(J/\psi(1S) \rightarrow \phi_0(980) \rightarrow \phi \pi^+ \pi^-) \times \Gamma(J/\psi(1S) \rightarrow e^+ e^-)/\Gamma_{total}] \times [B(\phi(1020) \rightarrow K^+ K^-)] = 0.69 \pm 0.11 \pm 0.05$ eV which we divide by our best value $B(\phi(1020) \rightarrow K^+ K^-) = (49.1 \pm 0.5) \times 10^{-2}$. Our first error is their experiment's error and our second error is the systematic error from using our best value.

²Multiplied by 2/3 to take into account the $\phi \pi^+ \pi^-$ mode only. Using $B(\phi \rightarrow K^+ K^-) = (49.2 \pm 0.6)\%$.

³Superseded by LEES 12F. AUBERT 07AK reports $[\Gamma(J/\psi(1S) \rightarrow \phi_0(980) \rightarrow \phi \pi^+ \pi^-) \times \Gamma(J/\psi(1S) \rightarrow e^+ e^-)/\Gamma_{total}] \times [B(\phi(1020) \rightarrow K^+ K^-)] = 0.50 \pm 0.11 \pm 0.04$ eV which we divide by our best value $B(\phi(1020) \rightarrow K^+ K^-) = (49.1 \pm 0.5) \times 10^{-2}$. Our first error is their experiment's error and our second error is the systematic error from using our best value.

$\Gamma(\phi_0(980) \rightarrow \phi \pi^0 \pi^0) \times \Gamma(e^+ e^-)/\Gamma_{total}$					$\Gamma_{114} \Gamma_5/\Gamma$
VALUE (eV)	EVTS	DOCUMENT ID	TECN	COMMENT	
0.98 ± 0.26 ± 0.01	16 ± 4	¹ LEES	12F BABR	$10.6 e^+ e^- \rightarrow \pi^0 \pi^0 K^+ K^- \gamma$	

• • • We do not use the following data for averages, fits, limits, etc. • • •

0.96 ± 0.40 ± 0.01 7.0 ± 2.8 ²AUBERT 07AK BABR $10.6 e^+ e^- \rightarrow \pi^0 \pi^0 K^+ K^- \gamma$

¹LEES 12F reports $[\Gamma(J/\psi(1S) \rightarrow \phi_0(980) \rightarrow \phi \pi^0 \pi^0) \times \Gamma(J/\psi(1S) \rightarrow e^+ e^-)/\Gamma_{total}] \times [B(\phi(1020) \rightarrow K^+ K^-)] = 0.48 \pm 0.12 \pm 0.05$ eV which we divide by our best value $B(\phi(1020) \rightarrow K^+ K^-) = (49.1 \pm 0.5) \times 10^{-2}$. Our first error is their experiment's error and our second error is the systematic error from using our best value.

²Superseded by LEES 12F. AUBERT 07AK reports $[\Gamma(J/\psi(1S) \rightarrow \phi_0(980) \rightarrow \phi \pi^0 \pi^0) \times \Gamma(J/\psi(1S) \rightarrow e^+ e^-)/\Gamma_{total}] \times [B(\phi(1020) \rightarrow K^+ K^-)] = 0.47 \pm 0.19 \pm 0.05$ eV which we divide by our best value $B(\phi(1020) \rightarrow K^+ K^-) = (49.1 \pm 0.5) \times 10^{-2}$. Our first error is their experiment's error and our second error is the systematic error from using our best value.

$\Gamma(\phi_2^*(1270)) \times \Gamma(e^+ e^-)/\Gamma_{total}$					$\Gamma_{119} \Gamma_5/\Gamma$
VALUE (eV)	EVTS	DOCUMENT ID	TECN	COMMENT	
1.79 ± 0.32 ± 0.02	61	1,2,3 LEES	12F BABR	$10.6 e^+ e^- \rightarrow \pi^+ \pi^- K^+ K^- \gamma$	

• • • We do not use the following data for averages, fits, limits, etc. • • •

4.08 ± 0.73 ± 0.05 ± 0.14 44 ^{2,4}AUBERT 07AK BABR $10.6 e^+ e^- \rightarrow \pi^+ \pi^- K^+ K^- \gamma$

¹LEES 12F reports $[\Gamma(J/\psi(1S) \rightarrow \phi_2^*(1270)) \times \Gamma(J/\psi(1S) \rightarrow e^+ e^-)/\Gamma_{total}] \times [B(\phi_2^*(1270) \rightarrow \pi\pi)] = 1.51 \pm 0.25 \pm 0.10$ eV which we divide by our best value $B(\phi_2^*(1270) \rightarrow \pi\pi) = (84.3 \pm 2.8) \times 10^{-2}$. Our first error is their experiment's error and our second error is the systematic error from using our best value.

²Using $B(\phi \rightarrow K^+ K^-) = (48.9 \pm 0.5)\%$.

³Using $\pi^+ \pi^-$ invariant mass between 1.1 and 1.5 GeV. May include other sources such as $f_0(1370)$.

⁴Superseded by LEES 12F. AUBERT 07AK reports $[\Gamma(J/\psi(1S) \rightarrow \phi_2^*(1270)) \times \Gamma(J/\psi(1S) \rightarrow e^+ e^-)/\Gamma_{total}] \times [B(\phi_2^*(1270) \rightarrow \pi\pi)] = 3.44 \pm 0.55 \pm 0.28$ eV which we divide by our best value $B(\phi_2^*(1270) \rightarrow \pi\pi) = (84.3 \pm 2.8) \times 10^{-2}$. Our first error is their experiment's error and our second error is the systematic error from using our best value.

$\Gamma(\phi_2^*(1525)) \times \Gamma(e^+ e^-)/\Gamma_{total}$					$\Gamma_{124} \Gamma_5/\Gamma$
VALUE (eV)	EVTS	DOCUMENT ID	TECN	COMMENT	
8.1 ± 3.2 ± 0.2	11	1,2 LEES	14H BABR	$e^+ e^- \rightarrow K_S^0 K_S^0 K^+ K^- \gamma$	

¹Dividing by 1/4 to take into account $B(f_2^*(1525) \rightarrow K_S^0 K_S^0) = 1/4 B(f_2^*(1525) \rightarrow K\overline{K})$ and using $B(\phi \rightarrow K^+ K^-) = (48.9 \pm 0.5)\%$.

Meson Particle Listings

 $J/\psi(1S)$

² LEES 14H reports $[\Gamma(J/\psi(1S) \rightarrow \phi f_2'(1525)) \times \Gamma(J/\psi(1S) \rightarrow e^+e^-)/\Gamma_{\text{total}}] \times [B(f_2'(1525) \rightarrow K\bar{K})] = 7.2 \pm 2.8 \pm 0.3$ eV which we divide by our best value $B(f_2'(1525) \rightarrow K\bar{K}) = (88.8 \pm 2.2) \times 10^{-2}$. Our first error is their experiment's error and our second error is the systematic error from using our best value.

$\Gamma(\phi K^+ K^-) \times \Gamma(e^+ e^-)/\Gamma_{\text{total}}$ $\Gamma_{130}\Gamma_5/\Gamma$

VALUE (eV)	EVTS	DOCUMENT ID	TECN	COMMENT
4.60 ± 0.62 ± 0.05	163	¹ LEES	12F	BABR 10.6 e ⁺ e ⁻ → K ⁺ K ⁻ K ⁺ K ⁻ γ

¹ LEES 12F reports $[\Gamma(J/\psi(1S) \rightarrow \phi K^+ K^-) \times \Gamma(J/\psi(1S) \rightarrow e^+e^-)/\Gamma_{\text{total}}] \times [B(\phi(1020) \rightarrow K^+ K^-)] = 2.26 \pm 0.26 \pm 0.16$ eV which we divide by our best value $B(\phi(1020) \rightarrow K^+ K^-) = (49.1 \pm 0.5) \times 10^{-2}$. Our first error is their experiment's error and our second error is the systematic error from using our best value.

$\Gamma(\phi K_S^0 K_S^0) \times \Gamma(e^+ e^-)/\Gamma_{\text{total}}$ $\Gamma_{131}\Gamma_5/\Gamma$

VALUE (eV)	EVTS	DOCUMENT ID	TECN	COMMENT
3.26 ± 0.84 ± 0.03	29	¹ LEES	14H	BABR e ⁺ e ⁻ → K _S ⁰ K _S ⁰ K ⁺ K ⁻ γ

¹ LEES 14H reports $[\Gamma(J/\psi(1S) \rightarrow \phi K_S^0 K_S^0) \times \Gamma(J/\psi(1S) \rightarrow e^+e^-)/\Gamma_{\text{total}}] \times [B(\phi(1020) \rightarrow K^+ K^-)] = 1.6 \pm 0.4 \pm 0.1$ eV which we divide by our best value $B(\phi(1020) \rightarrow K^+ K^-) = (49.1 \pm 0.5) \times 10^{-2}$. Our first error is their experiment's error and our second error is the systematic error from using our best value.

$\Gamma(f_2'(1525) K^+ K^-) \times \Gamma(e^+ e^-)/\Gamma_{\text{total}}$ $\Gamma_{136}\Gamma_5/\Gamma$

VALUE (eV)	EVTS	DOCUMENT ID	TECN	COMMENT
5.8 ± 1.9 ± 0.1	16	^{1,2} LEES	14H	BABR e ⁺ e ⁻ → K _S ⁰ K _S ⁰ K ⁺ K ⁻ γ

¹ Dividing by 1/4 to take into account $B(f_2'(1525) \rightarrow K_S^0 K_S^0) = 1/4 B(f_2'(1525) \rightarrow K\bar{K})$.

² LEES 14H reports $[\Gamma(J/\psi(1S) \rightarrow f_2'(1525) K^+ K^-) \times \Gamma(J/\psi(1S) \rightarrow e^+e^-)/\Gamma_{\text{total}}] \times [B(f_2'(1525) \rightarrow K\bar{K})] = 5.12 \pm 1.68 \pm 0.20$ eV which we divide by our best value $B(f_2'(1525) \rightarrow K\bar{K}) = (88.8 \pm 2.2) \times 10^{-2}$. Our first error is their experiment's error and our second error is the systematic error from using our best value.

$\Gamma(2(\pi^+ \pi^- \pi^0)) \times \Gamma(e^+ e^-)/\Gamma_{\text{total}}$ $\Gamma_{157}\Gamma_5/\Gamma$

VALUE (eV)	EVTS	DOCUMENT ID	TECN	COMMENT
303 ± 5 ± 18	4990	AUBERT	07AU	BABR 10.6 e ⁺ e ⁻ → 2(π ⁺ π ⁻)π ⁰ γ

$\Gamma(\pi^+ \pi^- 3\pi^0) \times \Gamma(e^+ e^-)/\Gamma_{\text{total}}$ $\Gamma_{159}\Gamma_5/\Gamma$

VALUE (eV)	EVTS	DOCUMENT ID	TECN	COMMENT
100 ± 50	OUR AVERAGE	Error includes scale factor of 4.3.		
55 ± 16 ± 1	14k	¹ LEES	21	BABR 10.6 e ⁺ e ⁻ → 2(π ⁺ π ⁻)3π ⁰ γ
150.0 ± 4.0 ± 15.0	2.3k	LEES	18E	BABR 10.6 e ⁺ e ⁻ → π ⁺ π ⁻ 3π ⁰ γ

¹ LEES 21 reports $[\Gamma(J/\psi(1S) \rightarrow \pi^+ \pi^- 3\pi^0) \times \Gamma(J/\psi(1S) \rightarrow e^+e^-)/\Gamma_{\text{total}}] \times [\Gamma(\psi(2S) \rightarrow J/\psi(1S) \pi^+ \pi^-)/\Gamma_{\text{total}}] = 19.2 \pm 4.5 \pm 3.2$ eV which we divide by our best value $\Gamma(\psi(2S) \rightarrow J/\psi(1S) \pi^+ \pi^-)/\Gamma_{\text{total}} = 0.3469 \pm 0.0034$. Our first error is their experiment's error and our second error is the systematic error from using our best value.

$\Gamma(\pi^+ \pi^- 4\pi^0) \times \Gamma(e^+ e^-)/\Gamma_{\text{total}}$ $\Gamma_{162}\Gamma_5/\Gamma$

VALUE (eV)	EVTS	DOCUMENT ID	TECN	COMMENT
35.8 ± 4.4 ± 5.4	340	LEES	21C	BABR e ⁺ e ⁻ → γISR(π ⁺ π ⁻ 4π ⁰)

$\Gamma(\rho^\pm \pi^\mp \pi^0 \pi^0) \times \Gamma(e^+ e^-)/\Gamma_{\text{total}}$ $\Gamma_{160}\Gamma_5/\Gamma$

VALUE (eV)	EVTS	DOCUMENT ID	TECN	COMMENT
78.0 ± 9.0 ± 8.0	1.2k	LEES	18E	BABR 10.6 e ⁺ e ⁻ → π ⁺ π ⁻ 3π ⁰ γ

$\Gamma(\rho^+ \rho^- \pi^0) \times \Gamma(e^+ e^-)/\Gamma_{\text{total}}$ $\Gamma_{161}\Gamma_5/\Gamma$

VALUE (eV)	EVTS	DOCUMENT ID	TECN	COMMENT
33.0 ± 5.0 ± 3.3	529	LEES	18E	BABR 10.6 e ⁺ e ⁻ → π ⁺ π ⁻ 3π ⁰ γ

$\Gamma(\pi^+ \pi^- \pi^0) \times \Gamma(e^+ e^-)/\Gamma_{\text{total}}$ $\Gamma_{163}\Gamma_5/\Gamma$

VALUE (keV)	DOCUMENT ID	TECN	COMMENT
0.1248 ± 0.0019 ± 0.0026	LEES	21B	BABR 10.5 e ⁺ e ⁻ → π ⁺ π ⁻ π ⁰ γ
0.122 ± 0.005 ± 0.008	AUBERT,B	04N	BABR 10.6 e ⁺ e ⁻ → π ⁺ π ⁻ π ⁰ γ

• • • We do not use the following data for averages, fits, limits, etc. • • •

$\Gamma(2(\pi^+ \pi^- \pi^0)) \times \Gamma(e^+ e^-)/\Gamma_{\text{total}}$ $\Gamma_{164}\Gamma_5/\Gamma$

VALUE (10 ⁻² keV)	EVTS	DOCUMENT ID	TECN	COMMENT
8.9 ± 0.5 ± 1.0	761	AUBERT	06D	BABR 10.6 e ⁺ e ⁻ → 2(π ⁺ π ⁻)π ⁰ γ

$\Gamma(\pi^+ \pi^- \pi^0 K^+ K^-) \times \Gamma(e^+ e^-)/\Gamma_{\text{total}}$ $\Gamma_{165}\Gamma_5/\Gamma$

VALUE (eV)	EVTS	DOCUMENT ID	TECN	COMMENT
107.0 ± 4.3 ± 6.4	768	AUBERT	07AU	BABR 10.6 e ⁺ e ⁻ → K ⁺ K ⁻ π ⁺ π ⁻ π ⁰ γ

$\Gamma(2(\pi^+ \pi^-)) \times \Gamma(e^+ e^-)/\Gamma_{\text{total}}$ $\Gamma_{167}\Gamma_5/\Gamma$

VALUE (eV)	EVTS	DOCUMENT ID	TECN	COMMENT
20.4 ± 0.9 ± 0.4		LEES	12E	BABR 10.6 e ⁺ e ⁻ → 2π ⁺ 2π ⁻ γ

• • • We do not use the following data for averages, fits, limits, etc. • • •

19.5 ± 1.4 ± 1.3 270 ¹ AUBERT 05D BABR 10.6 e⁺e⁻ → 2(π⁺π⁻)γ

¹ Superseded by LEES 12E.

$\Gamma(3(\pi^+ \pi^-)) \times \Gamma(e^+ e^-)/\Gamma_{\text{total}}$ $\Gamma_{168}\Gamma_5/\Gamma$

VALUE (10 ⁻² keV)	EVTS	DOCUMENT ID	TECN	COMMENT
2.37 ± 0.16 ± 0.14	496	AUBERT	06D	BABR 10.6 e ⁺ e ⁻ → 3(π ⁺ π ⁻)γ

$\Gamma(2(\pi^+ \pi^-) 3\pi^0) \times \Gamma(e^+ e^-)/\Gamma_{\text{total}}$ $\Gamma_{169}\Gamma_5/\Gamma$

VALUE (eV)	EVTS	DOCUMENT ID	TECN	COMMENT
345 ± 10 ± 50	14k	LEES	21	BABR 10.6 e ⁺ e ⁻ → 2(π ⁺ π ⁻)3π ⁰ γ

$\Gamma(2(\pi^+ \pi^-) \eta) \times \Gamma(e^+ e^-)/\Gamma_{\text{total}}$ $\Gamma_{171}\Gamma_5/\Gamma$

VALUE (eV)	EVTS	DOCUMENT ID	TECN	COMMENT
13.1 ± 2.4 ± 0.1	85	¹ AUBERT	07AU	BABR 10.6 e ⁺ e ⁻ → 2(π ⁺ π ⁻)ηγ

¹ AUBERT 07AU reports $[\Gamma(J/\psi(1S) \rightarrow 2(\pi^+ \pi^-) \eta) \times \Gamma(J/\psi(1S) \rightarrow e^+e^-)/\Gamma_{\text{total}}] \times [B(\eta \rightarrow 2\gamma)] = 5.16 \pm 0.85 \pm 0.39$ eV which we divide by our best value $B(\eta \rightarrow 2\gamma) = (39.36 \pm 0.18) \times 10^{-2}$. Our first error is their experiment's error and our second error is the systematic error from using our best value.

$\Gamma(2(\pi^+ \pi^- \pi^0) \eta) \times \Gamma(e^+ e^-)/\Gamma_{\text{total}}$ $\Gamma_{173}\Gamma_5/\Gamma$

VALUE (eV)	EVTS	DOCUMENT ID	TECN	COMMENT
9.1 ± 2.6 ± 1.4	14k	LEES	21	BABR 10.6 e ⁺ e ⁻ → 2(π ⁺ π ⁻)3π ⁰ γ

$\Gamma(\pi^+ \pi^- \pi^0 \pi^0 \eta) \times \Gamma(e^+ e^-)/\Gamma_{\text{total}}$ $\Gamma_{174}\Gamma_5/\Gamma$

VALUE (eV)	EVTS	DOCUMENT ID	TECN	COMMENT
13.1 ± 2.7	OUR AVERAGE			
26.1 ± 17.9 ± 0.3	14k	¹ LEES	21	BABR 10.6 e ⁺ e ⁻ → 2(π ⁺ π ⁻)3π ⁰ γ
12.8 ± 1.8 ± 2.0	203	LEES	18E	BABR 10.6 e ⁺ e ⁻ → π ⁺ π ⁻ π ⁰ π ⁰ ηγ

¹ LEES 21 reports $[\Gamma(J/\psi(1S) \rightarrow \pi^+ \pi^- \pi^0 \pi^0 \eta) \times \Gamma(J/\psi(1S) \rightarrow e^+e^-)/\Gamma_{\text{total}}] \times [B(\eta \rightarrow \pi^+ \pi^- \pi^0)] = 6 \pm 4 \pm 1$ eV which we divide by our best value $B(\eta \rightarrow \pi^+ \pi^- \pi^0) = (23.02 \pm 0.25) \times 10^{-2}$. Our first error is their experiment's error and our second error is the systematic error from using our best value.

$\Gamma(\rho^\pm \pi^\mp \pi^0 \eta) \times \Gamma(e^+ e^-)/\Gamma_{\text{total}}$ $\Gamma_{175}\Gamma_5/\Gamma$

VALUE (eV)	EVTS	DOCUMENT ID	TECN	COMMENT
10.5 ± 4.1 ± 1.6	168	LEES	18E	BABR 10.6 e ⁺ e ⁻ → π ⁺ π ⁻ π ⁰ ηγ

$\Gamma(K^+ K^-) \times \Gamma(e^+ e^-)/\Gamma_{\text{total}}$ $\Gamma_{176}\Gamma_5/\Gamma$

VALUE (eV)	EVTS	DOCUMENT ID	TECN	COMMENT
1.78 ± 0.11 ± 0.05	462	¹ LEES	15J	BABR e ⁺ e ⁻ → K ⁺ K ⁻ γ
1.94 ± 0.11 ± 0.05	462	² LEES	15J	BABR e ⁺ e ⁻ → K ⁺ K ⁻ γ
1.42 ± 0.23 ± 0.08	51	³ LEES	13Q	BABR e ⁺ e ⁻ → K ⁺ K ⁻ γ

• • • We do not use the following data for averages, fits, limits, etc. • • •
¹ sin φ > 0.
² sin φ < 0.
³ Interference with non-resonant K⁺K⁻ production not taken into account.

$\Gamma(K_S^0 K_L^0 \pi^0) \times \Gamma(e^+ e^-)/\Gamma_{\text{total}}$ $\Gamma_{182}\Gamma_5/\Gamma$

VALUE (eV)	EVTS	DOCUMENT ID	TECN	COMMENT
11.4 ± 1.3 ± 0.6	182	LEES	17A	BABR e ⁺ e ⁻ → K _S ⁰ K _L ⁰ π ⁰ γ

$\Gamma(K^*(892)^0 \bar{K}^0 + c.c. \rightarrow K_S^0 K_L^0 \pi^0) \times \Gamma(e^+ e^-)/\Gamma_{\text{total}}$ $\Gamma_{183}\Gamma_5/\Gamma$

VALUE (eV)	EVTS	DOCUMENT ID	TECN	COMMENT
6.7 ± 0.9 ± 0.4	106	LEES	17A	BABR e ⁺ e ⁻ → K _S ⁰ K _L ⁰ π ⁰ γ

$\Gamma(K_S^0(1430)^0 \bar{K}^0 + c.c. \rightarrow K_S^0 K_L^0 \pi^0) \times \Gamma(e^+ e^-)/\Gamma_{\text{total}}$ $\Gamma_{184}\Gamma_5/\Gamma$

VALUE (eV)	EVTS	DOCUMENT ID	TECN	COMMENT
2.4 ± 0.7 ± 0.1	37	LEES	17A	BABR e ⁺ e ⁻ → K _S ⁰ K _L ⁰ π ⁰ γ

$\Gamma(K_S^0 K^*(892)^0 \pi^+ \pi^-) \times \Gamma(e^+ e^-)/\Gamma_{\text{total}}$ $\Gamma_{201}\Gamma_5/\Gamma$

VALUE (eV)	DOCUMENT ID	TECN	COMMENT
9.45 ± 3.15 ± 0.90	LEES	23	BABR e ⁺ e ⁻ → γISR hadrons

$\Gamma(K_S^0 K^*(892)^0 \pi^0 \pi^0) \times \Gamma(e^+ e^-)/\Gamma_{\text{total}}$ $\Gamma_{202}\Gamma_5/\Gamma$

VALUE (eV)	DOCUMENT ID	TECN	COMMENT
5.59 ± 0.79 ± 0.55	LEES	23	BABR e ⁺ e ⁻ → γISR hadrons

$\Gamma(K^\mp K^*(892)^\pm \pi^+ \pi^-) \times \Gamma(e^+ e^-)/\Gamma_{\text{total}}$ $\Gamma_{203}\Gamma_5/\Gamma$

VALUE (eV)	DOCUMENT ID	TECN	COMMENT
18.6 ± 6.3 ± 1.8	LEES	23	BABR e ⁺ e ⁻ → γISR hadrons

$\Gamma(K^\mp K^*(892)^\pm \pi^0 \pi^0) \times \Gamma(e^+ e^-)/\Gamma_{\text{total}}$ $\Gamma_{205}\Gamma_5/\Gamma$

VALUE (eV)	DOCUMENT ID	TECN	COMMENT
8.67 ± 1.56 ± 0.84	LEES	23	BABR e ⁺ e ⁻ → γISR hadrons

$\Gamma(K^*(892)^\pm K^*(892)^0 \pi^\mp) \times \Gamma(e^+ e^-)/\Gamma_{\text{total}}$ $\Gamma_{204}\Gamma_5/\Gamma$

VALUE (eV)	DOCUMENT ID	TECN	COMMENT
26.6 ± 4.5 ± 2.7	LEES	23	BABR e ⁺ e ⁻ → γISR hadrons

$\Gamma(K^*(892)^+ K^*(892)^- \pi^0) \times \Gamma(e^+ e^-)/\Gamma_{\text{total}}$ $\Gamma_{206}\Gamma_5/\Gamma$

VALUE (eV)	DOCUMENT ID	TECN	COMMENT
62.1 ± 10.8 ± 6.30	LEES	23	BABR e ⁺ e ⁻ → γISR hadrons

$\Gamma(K^+ K^- \pi^+ \pi^-) \times \Gamma(e^+ e^-)/\Gamma_{total}$ $\Gamma_{185}\Gamma_5/\Gamma$

VALUE (eV)	EVTS	DOCUMENT ID	TECN	COMMENT
37.94 ± 0.81 ± 1.10	3.1k	LEES	12F	BABR 10.6 $e^+ e^- \rightarrow \pi^+ \pi^- K^+ K^- \gamma$
• • • We do not use the following data for averages, fits, limits, etc. • • •				
36.3 ± 1.3 ± 2.1	1.5k	¹ AUBERT	07AK	BABR 10.6 $e^+ e^- \rightarrow \pi^+ \pi^- K^+ K^- \gamma$
33.6 ± 2.7 ± 2.7	233	² AUBERT	05D	BABR 10.6 $e^+ e^- \rightarrow K^+ K^- \pi^+ \pi^- \gamma$
¹ Superseded by LEES 12F.				
² Superseded by AUBERT 07AK.				

$\Gamma(K^+ K^- \pi^0 \pi^0) \times \Gamma(e^+ e^-)/\Gamma_{total}$ $\Gamma_{186}\Gamma_5/\Gamma$

VALUE (eV)	EVTS	DOCUMENT ID	TECN	COMMENT
11.75 ± 0.81 ± 0.90	388	LEES	12F	BABR 10.6 $e^+ e^- \rightarrow \pi^0 \pi^0 K^+ K^- \gamma$
• • • We do not use the following data for averages, fits, limits, etc. • • •				
13.6 ± 1.1 ± 1.3	203	¹ AUBERT	07AK	BABR 10.6 $e^+ e^- \rightarrow \pi^0 \pi^0 K^+ K^- \gamma$
¹ Superseded by LEES 12F.				

$\Gamma(K^+ K^- \pi^0 \pi^0 \pi^0) \times \Gamma(e^+ e^-)/\Gamma_{total}$ $\Gamma_{187}\Gamma_5/\Gamma$

VALUE (eV)	DOCUMENT ID	TECN	COMMENT
8.9 ± 1.3 ± 0.9	LEES 23	BABR	$e^+ e^- \rightarrow \gamma_{ISR} \text{hadrons}$

$\Gamma(K_S^0 K_L^0 \pi^+ \pi^- \pi^0 \pi^0) \times \Gamma(e^+ e^-)/\Gamma_{total}$ $\Gamma_{188}\Gamma_5/\Gamma$

VALUE (eV)	DOCUMENT ID	TECN	COMMENT
29.3 ± 2.6 ± 2.9	LEES 23	BABR	$e^+ e^- \rightarrow \gamma_{ISR} \text{hadrons}$

$\Gamma(K_S^0 K_L^0 \pi^+ \pi^- \pi^-) \times \Gamma(e^+ e^-)/\Gamma_{total}$ $\Gamma_{189}\Gamma_5/\Gamma$

VALUE (eV)	DOCUMENT ID	TECN	COMMENT
34.6 ± 1.4 ± 1.8	LEES 23	BABR	$e^+ e^- \rightarrow \gamma_{ISR} \text{hadrons}$

$\Gamma(K_S^0 K_L^0 \pi^+ \pi^-) \times \Gamma(e^+ e^-)/\Gamma_{total}$ $\Gamma_{191}\Gamma_5/\Gamma$

VALUE (eV)	EVTS	DOCUMENT ID	TECN	COMMENT
20.8 ± 2.3 ± 2.1	248	LEES	14H	BABR $e^+ e^- \rightarrow \pi^+ \pi^- K_S^0 K_L^0 \gamma$

$\Gamma(K_S^0 K_L^0 \pi^0 \pi^0) \times \Gamma(e^+ e^-)/\Gamma_{total}$ $\Gamma_{192}\Gamma_5/\Gamma$

VALUE (eV)	EVTS	DOCUMENT ID	TECN	COMMENT
10.3 ± 2.3 ± 0.5	47	LEES	17A	BABR $e^+ e^- \rightarrow K_S^0 K_L^0 \pi^0 \pi^0 \gamma$

$\Gamma(K_S^0 K_L^0 \eta) \times \Gamma(e^+ e^-)/\Gamma_{total}$ $\Gamma_{193}\Gamma_5/\Gamma$

VALUE (eV)	EVTS	DOCUMENT ID	TECN	COMMENT
8.0 ± 1.8 ± 0.4	45	LEES	17A	BABR $e^+ e^- \rightarrow K_S^0 K_L^0 \eta \gamma$

$\Gamma(K_S^0 K_S^0 \pi^+ \pi^-) \times \Gamma(e^+ e^-)/\Gamma_{total}$ $\Gamma_{194}\Gamma_5/\Gamma$

VALUE (eV)	EVTS	DOCUMENT ID	TECN	COMMENT
9.3 ± 0.9 ± 0.5	133	LEES	14H	BABR $e^+ e^- \rightarrow \pi^+ \pi^- K_S^0 K_S^0 \gamma$

$\Gamma(K^+ K^- K_S^0 \pi^+ \pi^0) \times \Gamma(e^+ e^-)/\Gamma_{total}$ $\Gamma_{195}\Gamma_5/\Gamma$

VALUE (eV)	EVTS	DOCUMENT ID	TECN	COMMENT
31.7 ± 1.9 ± 1.8	393	LEES	17D	BABR $e^+ e^- \rightarrow K_S^0 K^+ \pi^- \pi^0 \gamma$

$\Gamma(K_S^0 K^\pm \rho(770)^\pm \pi^0) \times \Gamma(e^+ e^-)/\Gamma_{total}$ $\Gamma_{190}\Gamma_5/\Gamma$

VALUE (eV)	DOCUMENT ID	TECN	COMMENT
16.0 ± 4.1 ± 1.6	LEES 23	BABR	$e^+ e^- \rightarrow \gamma_{ISR} \text{hadrons}$

$\Gamma(K^+ K^- 2(\pi^+ \pi^-)) \times \Gamma(e^+ e^-)/\Gamma_{total}$ $\Gamma_{197}\Gamma_5/\Gamma$

VALUE (10 ⁻² eV)	EVTS	DOCUMENT ID	TECN	COMMENT
2.75 ± 0.23 ± 0.17	205	AUBERT	06D	BABR 10.6 $e^+ e^- \rightarrow K^+ K^- 2(\pi^+ \pi^-) \gamma$

$\Gamma(K^+ K^- \pi^+ \pi^- \eta) \times \Gamma(e^+ e^-)/\Gamma_{total}$ $\Gamma_{198}\Gamma_5/\Gamma$

VALUE (eV)	EVTS	DOCUMENT ID	TECN	COMMENT
25.9 ± 3.9 ± 0.1	73	¹ AUBERT	07AU	BABR 10.6 $e^+ e^- \rightarrow K^+ K^- \pi^+ \pi^- \eta \gamma$
¹ AUBERT 07AU reports $[\Gamma(J/\psi(1S) \rightarrow K^+ K^- \pi^+ \pi^- \eta) \times \Gamma(J/\psi(1S) \rightarrow e^+ e^-) / \Gamma_{total}] \times [B(\eta \rightarrow 2\gamma)] = 10.2 \pm 1.3 \pm 0.8$ eV which we divide by our best value $B(\eta \rightarrow 2\gamma) = (39.36 \pm 0.18) \times 10^{-2}$. Our first error is their experiment's error and our second error is the systematic error from using our best value.				

$\Gamma(2(K^+ K^-)) \times \Gamma(e^+ e^-)/\Gamma_{total}$ $\Gamma_{199}\Gamma_5/\Gamma$

VALUE (eV)	EVTS	DOCUMENT ID	TECN	COMMENT
4.00 ± 0.33 ± 0.29	287 ± 24	LEES	12F	BABR 10.6 $e^+ e^- \rightarrow 2(K^+ K^-) \gamma$
• • • We do not use the following data for averages, fits, limits, etc. • • •				
4.11 ± 0.39 ± 0.30	156 ± 15	¹ AUBERT	07AK	BABR 10.6 $e^+ e^- \rightarrow 2(K^+ K^-) \gamma$
4.0 ± 0.7 ± 0.6	38	² AUBERT	05D	BABR 10.6 $e^+ e^- \rightarrow 2(K^+ K^-) \gamma$
¹ Superseded by LEES 12F.				
² Superseded by AUBERT 07AK.				

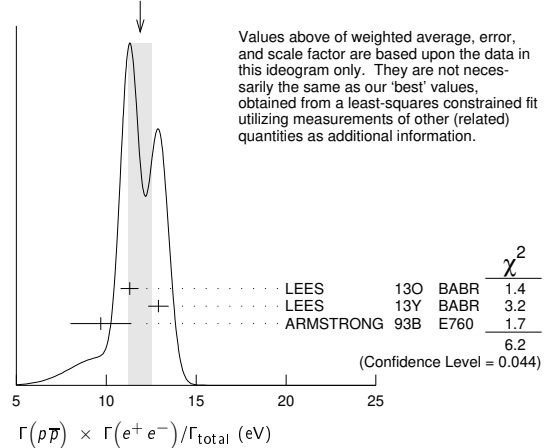
$\Gamma(K^+ K^- K_S^0 K_S^0) \times \Gamma(e^+ e^-)/\Gamma_{total}$ $\Gamma_{200}\Gamma_5/\Gamma$

VALUE (eV)	EVTS	DOCUMENT ID	TECN	COMMENT
2.3 ± 0.4 ± 0.1	29	LEES	14H	BABR $e^+ e^- \rightarrow K_S^0 K_S^0 K^+ K^- \gamma$

$\Gamma(p\bar{p}) \times \Gamma(e^+ e^-)/\Gamma_{total}$ $\Gamma_{207}\Gamma_5/\Gamma$

VALUE (eV)	EVTS	DOCUMENT ID	TECN	COMMENT
11.9 ± 0.6 OUR AVERAGE	Error includes scale factor of 1.8. See the ideogram below.			
11.3 ± 0.4 ± 0.3	821	¹ LEES	13O	BABR $e^+ e^- \rightarrow p\bar{p}\gamma$
12.9 ± 0.4 ± 0.4	918	² LEES	13Y	BABR $e^+ e^- \rightarrow p\bar{p}\gamma$
9.7 ± 1.7		³ ARMSTRONG	93B	E760 $\bar{p}p \rightarrow e^+ e^-$
• • • We do not use the following data for averages, fits, limits, etc. • • •				
12.0 ± 0.6 ± 0.5	438	⁴ AUBERT	06B	BABR $e^+ e^- \rightarrow p\bar{p}\gamma$
¹ ISR photon reconstructed in the detector				
² ISR photon undetected				
³ Using $\Gamma_{total} = 85.5^{+6.1}_{-5.8}$ MeV.				
⁴ Superseded by LEES 13O				

WEIGHTED AVERAGE
11.9±0.6 (Error scaled by 1.8)



$\Gamma(\Lambda\bar{\Lambda}) \times \Gamma(e^+ e^-)/\Gamma_{total}$ $\Gamma_{223}\Gamma_5/\Gamma$

VALUE (eV)	DOCUMENT ID	TECN	COMMENT
10.7 ± 0.9 ± 0.7	AUBERT	07BD	BABR 10.6 $e^+ e^- \rightarrow \Lambda\bar{\Lambda}\gamma$

$\Gamma(\Sigma^+ \bar{\Sigma}^-) \times \Gamma(e^+ e^-)/\Gamma_{total}$ $\Gamma_{233}\Gamma_5/\Gamma$

VALUE (eV)	DOCUMENT ID	TECN	COMMENT
• • • We do not use the following data for averages, fits, limits, etc. • • •			
6.8 ± 1.5 ± 0.8	GONG	23	BELL $e^+ e^- \rightarrow \Sigma^+ \bar{\Sigma}^-$

$\Gamma(\Sigma^0 \bar{\Sigma}^0) \times \Gamma(e^+ e^-)/\Gamma_{total}$ $\Gamma_{234}\Gamma_5/\Gamma$

VALUE (eV)	DOCUMENT ID	TECN	COMMENT
• • • We do not use the following data for averages, fits, limits, etc. • • •			
5.2 ± 1.5 ± 0.6	GONG	23	BELL $e^+ e^- \rightarrow \Sigma^0 \bar{\Sigma}^0$
6.4 ± 1.2 ± 0.6	AUBERT	07BD	BABR 10.6 $e^+ e^- \rightarrow \Sigma^0 \bar{\Sigma}^0 \gamma$

$J/\psi(1S)$ BRANCHING RATIOS

For the first four branching ratios, see also the partial widths, and (partial widths) $\times \Gamma(e^+ e^-)/\Gamma_{total}$ above.

$\Gamma(\text{hadrons})/\Gamma_{total}$ Γ_1/Γ

VALUE	DOCUMENT ID	TECN	COMMENT
0.877 ± 0.005 OUR AVERAGE			
0.878 ± 0.005	BAI	95B	BES $e^+ e^-$
0.86 ± 0.02	BOYARSKI	75	MRK1 $e^+ e^-$

$\Gamma(\text{virtual } \gamma \rightarrow \text{hadrons})/\Gamma_{total}$ Γ_2/Γ

VALUE	DOCUMENT ID	TECN	COMMENT
0.1346 ± 0.0007	¹ LIAO	23	RVUE $e^+ e^-$
• • • We do not use the following data for averages, fits, limits, etc. • • •			
0.135 ± 0.003	^{2,3} SETH	04	RVUE $e^+ e^-$
0.17 ± 0.02	² BOYARSKI	75	MRK1 $e^+ e^-$

¹ Using $B(J/\psi(1S) \rightarrow \ell^+ \ell^-) = (5.967 \pm 0.023)\%$ and $R = 2.26 \pm 0.01$ determined by a fit to data from Mark-I, DM2, BESII, KEDR, and BESIII.

² Included in $\Gamma(\text{hadrons})/\Gamma_{total}$.

³ Using $B(J/\psi \rightarrow \ell^+ \ell^-) = (5.90 \pm 0.09)\%$ from RPP-2002 and $R = 2.28 \pm 0.04$ determined by a fit to data from BAI 00 and BAI 02c. Superseded by LIAO 23.

$\Gamma(g\bar{g})/\Gamma_{total}$ Γ_3/Γ

VALUE (units 10 ⁻²)	EVTS	DOCUMENT ID	TECN	COMMENT
64.1 ± 1.0	6 M	¹ BESSION	08	CLEO $\psi(2S) \rightarrow \pi^+ \pi^- + \text{hadrons}$

¹ Calculated using the value $\Gamma(\gamma g\bar{g})/\Gamma(g\bar{g}) = 0.137 \pm 0.001 \pm 0.016 \pm 0.004$ from BESSION 08 and the PDG 08 values of $B(\ell^+ \ell^-)$, $B(\text{virtual } \gamma \rightarrow \text{hadrons})$, and $B(\gamma \eta_c)$. The statistical error is negligible and the systematic error is partially correlated with that of $\Gamma(\gamma g\bar{g})/\Gamma_{total}$ measurement of BESSION 08.

Meson Particle Listings

$J/\psi(1S)$

$\Gamma(\gamma g g)/\Gamma_{total}$ Γ_4/Γ

VALUE (units 10^{-2})	EVTS	DOCUMENT ID	TECN	COMMENT
8.79 ± 1.05	200 k	¹ BESSON	08	CLEO $\psi(2S) \rightarrow \pi^+ \pi^- \gamma + \text{hadrons}$

¹ Calculated using the value $\Gamma(\gamma g g)/\Gamma(g g g) = 0.137 \pm 0.001 \pm 0.016 \pm 0.004$ from BESSON 08 and the value of $\Gamma(g g g)/\Gamma_{total}$. The statistical error is negligible and the systematic error is partially correlated with that of $\Gamma(g g g)/\Gamma_{total}$ measurement of BESSON 08.

$\Gamma(\gamma g g)/\Gamma(g g g)$ Γ_4/Γ_3

VALUE (units 10^{-2})	EVTS	DOCUMENT ID	TECN	COMMENT
13.7 ± 0.1 ± 0.7	6 M	BESSON	08	CLEO $\psi(2S) \rightarrow \pi^+ \pi^- J/\psi$

$\Gamma(e^+ e^-)/\Gamma_{total}$ Γ_5/Γ

VALUE (units 10^{-2})	EVTS	DOCUMENT ID	TECN	COMMENT
5.971 ± 0.032 OUR AVERAGE				
5.983 ± 0.007 ± 0.037	720k	ABLIKIM	13R	BES3 $\psi(2S) \rightarrow J/\psi \pi^+ \pi^-$
5.945 ± 0.067 ± 0.042	15k	LI	05c	CLEO $\psi(2S) \rightarrow J/\psi \pi^+ \pi^-$
5.90 ± 0.05 ± 0.10		BAI	98D	BES $\psi(2S) \rightarrow J/\psi \pi^+ \pi^-$
6.09 ± 0.33		BAI	95B	BES $e^+ e^-$
5.92 ± 0.15 ± 0.20		COFFMAN	92	MRK3 $\psi(2S) \rightarrow J/\psi \pi^+ \pi^-$
6.9 ± 0.9		BOYARSKI	75	MRK1 $e^+ e^-$

$\Gamma(e^+ e^- \gamma)/\Gamma_{total}$ Γ_6/Γ

VALUE (units 10^{-3})	DOCUMENT ID	TECN	COMMENT
8.8 ± 1.3 ± 0.4	¹ ARMSTRONG	96	E760 $\bar{p} p \rightarrow e^+ e^- \gamma$

¹ For $E_\gamma > 100$ MeV.

$\Gamma(\mu^+ \mu^-)/\Gamma_{total}$ Γ_7/Γ

VALUE (units 10^{-2})	EVTS	DOCUMENT ID	TECN	COMMENT
5.961 ± 0.033 OUR AVERAGE				
5.973 ± 0.007 ± 0.038	770k	ABLIKIM	13R	BES3 $\psi(2S) \rightarrow J/\psi \pi^+ \pi^-$
5.960 ± 0.065 ± 0.050	17k	LI	05c	CLEO $\psi(2S) \rightarrow J/\psi \pi^+ \pi^-$
5.84 ± 0.06 ± 0.10		BAI	98D	BES $\psi(2S) \rightarrow J/\psi \pi^+ \pi^-$
6.08 ± 0.33		BAI	95B	BES $e^+ e^-$
5.90 ± 0.15 ± 0.19		COFFMAN	92	MRK3 $\psi(2S) \rightarrow J/\psi \pi^+ \pi^-$
6.9 ± 0.9		BOYARSKI	75	MRK1 $e^+ e^-$

$\Gamma(e^+ e^-)/\Gamma(\mu^+ \mu^-)$ Γ_5/Γ_7

VALUE	DOCUMENT ID	TECN	COMMENT
1.0016 ± 0.0031 OUR AVERAGE			
1.0022 ± 0.0044 ± 0.0048	¹ AULCHENKO	14	KEDR 3.097 $e^+ e^- \rightarrow e^+ e^- \mu^+ \mu^-$
1.0017 ± 0.0017 ± 0.0033	² ABLIKIM	13R	BES3 $\psi(2S) \rightarrow J/\psi \pi^+ \pi^-$
1.002 ± 0.021 ± 0.013	³ ANASHIN	10	KEDR 3.097 $e^+ e^- \rightarrow e^+ e^- \mu^+ \mu^-$
0.997 ± 0.012 ± 0.006	LI	05c	CLEO $\psi(2S) \rightarrow J/\psi \pi^+ \pi^-$
• • • We do not use the following data for averages, fits, limits, etc. • • •			
1.011 ± 0.013 ± 0.016	BAI	98D	BES $\psi(2S) \rightarrow J/\psi \pi^+ \pi^-$
1.00 ± 0.07	BAI	95B	BES $e^+ e^-$
1.00 ± 0.05	BOYARSKI	75	MRK1 $e^+ e^-$
0.91 ± 0.15	ESPOSITO	75B	FRAM $e^+ e^-$
0.93 ± 0.10	FORD	75	SPEC $e^+ e^-$

¹ From 235.3k $J/\psi \rightarrow e^+ e^-$ and 156.6k $J/\psi \rightarrow \mu^+ \mu^-$ observed events.
² Not independent of the corresponding measurements of $\Gamma(e^+ e^-)/\Gamma_{total}$ and $\Gamma(\mu^+ \mu^-)/\Gamma_{total}$.
³ Not independent of the corresponding measurements of $\Gamma(e^+ e^-) \times \Gamma(e^+ e^-)/\Gamma_{total}$ and $\Gamma(\mu^+ \mu^-) \times \Gamma(e^+ e^-)/\Gamma_{total}$.

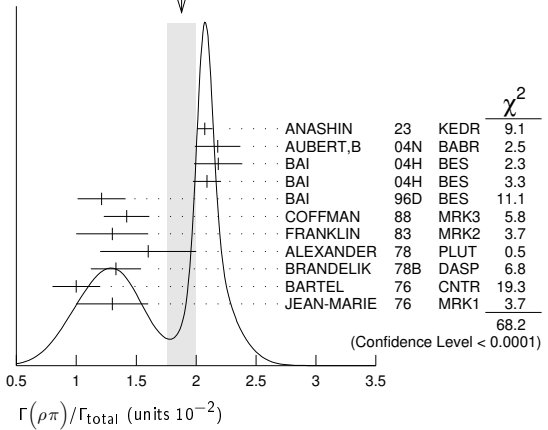
HADRONIC DECAYS

$\Gamma(\rho\pi)/\Gamma_{total}$ Γ_8/Γ

VALUE (units 10^{-2})	EVTS	DOCUMENT ID	TECN	COMMENT
1.88 ± 0.12 OUR AVERAGE				Error includes scale factor of 2.6. See the ideogram below.
2.072 ± 0.017 ± 0.062	19.8k	¹ ANASHIN	23	KEDR $e^+ e^- \rightarrow J/\psi \rightarrow \pi^+ \pi^- \pi^0$
2.18 ± 0.19		^{2,3} AUBERT,B	04N	BABR $10.6 e^+ e^- \rightarrow \pi^+ \pi^- \pi^0 \gamma$
2.184 ± 0.005 ± 0.201	220k	^{3,4} BAI	04H	BES $e^+ e^- \rightarrow J/\psi \rightarrow \pi^+ \pi^- \pi^0$
2.091 ± 0.021 ± 0.116		^{3,5} BAI	04H	BES $\psi(2S) \rightarrow \pi^+ \pi^- J/\psi$
1.21 ± 0.20		BAI	96D	BES $e^+ e^- \rightarrow \rho\pi$
1.42 ± 0.01 ± 0.19		COFFMAN	88	MRK3 $e^+ e^-$
1.3 ± 0.3	150	FRANKLIN	83	MRK2 $e^+ e^-$
1.6 ± 0.4	183	ALEXANDER	78	PLUT $e^+ e^-$
1.33 ± 0.21		BRANDELIK	78B	DASP $e^+ e^-$
1.0 ± 0.2	543	BARTEL	76	CNTR $e^+ e^-$
1.3 ± 0.3	153	JEAN-MARIE	76	MRK1 $e^+ e^-$

¹ By a simultaneous fit of the $\pi\pi$ invariant mass distribution over the decay modes $J/\psi \rightarrow \rho^0 \pi^0, J/\psi \rightarrow \rho^+ \pi^-, J/\psi \rightarrow \rho^- \pi^+$. In the fit only the intermediate states $\rho(770) \pi$ and $\rho(1450) \pi$ are considered.
² From the ratio of $\Gamma(e^+ e^-) B(\pi^+ \pi^- \pi^0)$ and $\Gamma(e^+ e^-) B(\mu^+ \mu^-)$ (AUBERT 04).
³ Not independent of their $B(\pi^+ \pi^- \pi^0)$.
⁴ From $J/\psi \rightarrow \pi^+ \pi^- \pi^0$ events directly.
⁵ Obtained comparing the rates for $\pi^+ \pi^- \pi^0$ and $\mu^+ \mu^-$, using J/ψ events produced via $\psi(2S) \rightarrow \pi^+ \pi^- J/\psi$ and with $B(J/\psi \rightarrow \mu^+ \mu^-) = 5.88 \pm 0.10\%$.

WEIGHTED AVERAGE
1.88 ± 0.12 (Error scaled by 2.6)



$\Gamma(\rho\pi)/\Gamma(\pi^+ \pi^- \pi^0)$ Γ_8/Γ_{163}

VALUE	EVTS	DOCUMENT ID	TECN	COMMENT
1.142 ± 0.011 ± 0.026	20k	¹ LEES	17C	BABR $J/\psi \rightarrow \pi^+ \pi^- \pi^0$
• • • We do not use the following data for averages, fits, limits, etc. • • •				
1.331 ± 0.033	20k	² LEES	17C	BABR $J/\psi \rightarrow \pi^+ \pi^- \pi^0$
¹ From a Dalitz plot analysis in an isobar model. ² From a Dalitz plot analysis in a Veneziano model.				

$\Gamma(\rho^0 \pi^0)/\Gamma(\rho\pi)$ Γ_9/Γ_8

VALUE	DOCUMENT ID	TECN	COMMENT
0.328 ± 0.005 ± 0.027	COFFMAN	88	MRK3 $e^+ e^-$
• • • We do not use the following data for averages, fits, limits, etc. • • •			
0.35 ± 0.08	ALEXANDER	78	PLUT $e^+ e^-$
0.32 ± 0.08	BRANDELIK	78B	DASP $e^+ e^-$
0.39 ± 0.11	BARTEL	76	CNTR $e^+ e^-$
0.37 ± 0.09	JEAN-MARIE	76	MRK1 $e^+ e^-$

$\Gamma(\pi^+ K^+ K^- \pi^- + c.c. \rightarrow K^+ K^- \pi^+ \pi^- \pi^0)/\Gamma_{total}$ Γ_{25}/Γ

VALUE (units 10^{-3})	EVTS	DOCUMENT ID	TECN	COMMENT
3.53 ± 0.16 ± 0.81	485	ANASHIN	22	KEDR $J/\psi \rightarrow K^+ K^- \pi^+ \pi^- \pi^0$

$\Gamma(a_2(1320)^0 \pi^+ \pi^- \rightarrow 2(\pi^+ \pi^- \pi^0))/\Gamma_{total}$ Γ_{10}/Γ

VALUE (units 10^{-3})	EVTS	DOCUMENT ID	TECN	COMMENT
2.84 ± 0.08 ± 0.60	1317	ANASHIN	22	KEDR $J/\psi \rightarrow 2(\pi^+ \pi^- \pi^0)$

$\Gamma(a_2(1320)^+ \pi^- \pi^0 + c.c. \rightarrow 2(\pi^+ \pi^- \pi^0))/\Gamma_{total}$ Γ_{11}/Γ

VALUE (units 10^{-3})	EVTS	DOCUMENT ID	TECN	COMMENT
3.67 ± 0.09 ± 0.73	1628	ANASHIN	22	KEDR $J/\psi \rightarrow 2(\pi^+ \pi^- \pi^0)$

$\Gamma(a_2(1320)\rho)/\Gamma_{total}$ Γ_{12}/Γ

VALUE (units 10^{-3})	EVTS	DOCUMENT ID	TECN	COMMENT
10.9 ± 2.2 OUR AVERAGE				
11.7 ± 0.7 ± 2.5	7584	AUGUSTIN	89	DM2 $J/\psi \rightarrow \rho^0 \rho^\pm \pi^\mp$
8.4 ± 4.5	36	VANNUCCI	77	MRK1 $e^+ e^- \rightarrow 2(\pi^+ \pi^- \pi^0)$

$\Gamma(\eta\pi^+ \pi^-)/\Gamma_{total}$ Γ_{13}/Γ

VALUE (units 10^{-4})	EVTS	DOCUMENT ID	TECN	COMMENT
3.78 ± 0.68	471	¹ ABLIKIM	19Q	BES3 $e^+ e^- \rightarrow J/\psi \rightarrow \eta\pi^+ \pi^-$
¹ From an energy scan of $e^+ e^- \rightarrow J/\psi \rightarrow \eta\pi^+ \pi^-$ assuming PDG 16 values for $\Gamma(e^+ e^-)$, $\Gamma(\mu^+ \mu^-)$, and Γ_{total} .				

$\Gamma(\eta\rho)/\Gamma_{total}$ Γ_{14}/Γ

VALUE (units 10^{-3})	EVTS	DOCUMENT ID	TECN	COMMENT
0.193 ± 0.023 OUR AVERAGE				
0.194 ± 0.017 ± 0.029	299	JOUSSET	90	DM2 $J/\psi \rightarrow \text{hadrons}$
0.193 ± 0.013 ± 0.029		COFFMAN	88	MRK3 $e^+ e^- \rightarrow \pi^+ \pi^- \eta$

$\Gamma(\eta\phi(2170) \rightarrow \eta\phi f_0(980) \rightarrow \eta\phi\pi^+ \pi^-)/\Gamma_{total}$ Γ_{17}/Γ

VALUE (units 10^{-4})	EVTS	DOCUMENT ID	TECN	COMMENT
1.20 ± 0.14 ± 0.37	471	ABLIKIM	15H	BES3 $e^+ e^- \rightarrow J/\psi \rightarrow \phi\eta\pi^+ \pi^-$

$\Gamma(\eta\phi(2170) \rightarrow \eta K^*(892)^0 \bar{K}^*(892)^0)/\Gamma_{total}$ Γ_{18}/Γ

VALUE	CL%	DOCUMENT ID	TECN	COMMENT
< 2.52 × 10⁻⁴	90	ABLIKIM	10c	BES2 $J/\psi \rightarrow \eta K^+ \pi^- K^- \pi^+$

$\Gamma(\eta K^\pm K_S^0 \pi^\mp)/\Gamma_{total}$ Γ_{20}/Γ

VALUE (units 10^{-4})	EVTS	DOCUMENT ID	TECN	COMMENT
21.8 ± 2.2 ± 3.4	232 ± 23	ABLIKIM	08E	BES2 $e^+ e^- \rightarrow J/\psi$

See key on page 1171

Meson Particle Listings

$J/\psi(1S)$

$\Gamma(\eta K^*(892)^0 \bar{K}^*(892)^0)/\Gamma_{total}$ Γ_{21}/Γ

VALUE (units 10^{-3})	EVTS	DOCUMENT ID	TECN	COMMENT
1.15 ± 0.13 ± 0.22	209	ABLIKIM	10c BES2	$J/\psi \rightarrow \eta K^+ \pi^- K^- \pi^+$

$\Gamma(\rho\eta'(958))/\Gamma_{total}$ Γ_{22}/Γ

VALUE (units 10^{-5})	EVTS	DOCUMENT ID	TECN	COMMENT
8.1 ± 0.8 OUR AVERAGE				Error includes scale factor of 1.6.
7.90 ± 0.19 ± 0.49	3476	¹ ABLIKIM	17AK BES3	$J/\psi \rightarrow \pi^+ \pi^- \eta'$
8.3 ± 3.0 ± 1.2	19	JOUSSET	90 DM2	$J/\psi \rightarrow \text{hadrons}$
11.4 ± 1.4 ± 1.6		COFFMAN	88 MRK3	$J/\psi \rightarrow \pi^+ \pi^- \eta'$

¹ From a partial wave analysis of the decay $J/\psi \rightarrow \pi^+ \pi^- \eta'$.

$\Gamma(\rho(1450)\pi \rightarrow \pi^+ \pi^- \pi^0)/\Gamma_{total}$ Γ_{30}/Γ

VALUE (units 10^{-4})	EVTS	DOCUMENT ID	TECN	COMMENT
2.2 ± 0.2 ± 1.1	19.8k	¹ ANASHIN	23 KEDR	$e^+ e^- \rightarrow J/\psi \rightarrow \pi^+ \pi^- \pi^0$

¹ By a simultaneous fit of the $\pi\pi$ invariant mass distribution over the decay modes $J/\psi \rightarrow \rho^0 \pi^0$, $J/\psi \rightarrow \pi^+ \pi^-$, $J/\psi \rightarrow \rho^- \pi^+$. In the fit only the intermediate states $\rho(770)\pi$ and $\rho(1450)\pi$ are considered.

$\Gamma(\rho(1450)\pi \rightarrow \pi^+ \pi^- \pi^0)/\Gamma(\pi^+ \pi^- \pi^0)$ Γ_{30}/Γ_{163}

VALUE (%)	EVTS	DOCUMENT ID	TECN	COMMENT
10.9 ± 1.7 ± 2.7	20k	¹ LEES	17c BABR	$J/\psi \rightarrow \pi^+ \pi^- \pi^0$
0.80 ± 0.27	20k	² LEES	17c BABR	$J/\psi \rightarrow \pi^+ \pi^- \pi^0$

¹ From a Dalitz plot analysis in an isobar model.
² From a Dalitz plot analysis in a Veneziano model.

$\Gamma(\rho(1450)\pi \rightarrow \pi^+ \pi^- \pi^0)/\Gamma(K_S^0 K^\pm \pi^\mp)/\Gamma(K_S^0 K^\pm \pi^\mp)$ Γ_{31}/Γ_{181}

VALUE (%)	EVTS	DOCUMENT ID	TECN	COMMENT
6.3 ± 0.8 ± 0.6	4k	¹ LEES	17c BABR	$J/\psi \rightarrow K_S^0 K^\pm \pi^\mp$

¹ From a Dalitz plot analysis in an isobar model.

$\Gamma(\rho(1450)^0 \pi^0 \rightarrow K^+ K^- \pi^0)/\Gamma(K^+ K^- \pi^0)$ Γ_{32}/Γ_{180}

VALUE (%)	EVTS	DOCUMENT ID	TECN	COMMENT
9.3 ± 2.0 ± 0.6	2k	¹ LEES	17c BABR	$J/\psi \rightarrow K^+ K^- \pi^0$

¹ From a Dalitz plot analysis in an isobar model.

$\Gamma(\rho(1450)\eta'(958) \rightarrow \pi^+ \pi^- \eta'(958))/\Gamma_{total}$ Γ_{33}/Γ

VALUE (units 10^{-6})	EVTS	DOCUMENT ID	TECN	COMMENT
3.28 ± 0.55 ± 0.44	119	¹ ABLIKIM	17AK BES3	$J/\psi \rightarrow \pi^+ \pi^- \eta'$

¹ From a partial wave analysis of the decay $J/\psi \rightarrow \pi^+ \pi^- \eta'$.

$\Gamma(\rho(1700)\pi \rightarrow \pi^+ \pi^- \pi^0)/\Gamma(\pi^+ \pi^- \pi^0)$ Γ_{35}/Γ_{163}

VALUE (units 10^{-3})	EVTS	DOCUMENT ID	TECN	COMMENT
8 ± 2 ± 5	20k	¹ LEES	17c BABR	$J/\psi \rightarrow \pi^+ \pi^- \pi^0$

• • • We do not use the following data for averages, fits, limits, etc. • • •

22 ± 6	20k	² LEES	17c BABR	$J/\psi \rightarrow \pi^+ \pi^- \pi^0$
--------	-----	-------------------	----------	--

¹ From a Dalitz plot analysis in an isobar model.
² From a Dalitz plot analysis in a Veneziano model.

$\Gamma(\rho(2150)\pi \rightarrow \pi^+ \pi^- \pi^0)/\Gamma(\pi^+ \pi^- \pi^0)$ Γ_{37}/Γ_{163}

VALUE (units 10^{-4})	EVTS	DOCUMENT ID	TECN	COMMENT
4 ± 1 ± 20	20k	¹ LEES	17c BABR	$J/\psi \rightarrow \pi^+ \pi^- \pi^0$

• • • We do not use the following data for averages, fits, limits, etc. • • •

60.0 ± 25.0	20k	² LEES	17c BABR	$J/\psi \rightarrow \pi^+ \pi^- \pi^0$
-------------	-----	-------------------	----------	--

¹ From a Dalitz plot analysis in an isobar model.
² From a Dalitz plot analysis in a Veneziano model.

$\Gamma(\rho_3(1690)\pi \rightarrow \pi^+ \pi^- \pi^0)/\Gamma(\pi^+ \pi^- \pi^0)$ Γ_{38}/Γ_{163}

VALUE (units 10^{-3})	EVTS	DOCUMENT ID	TECN	COMMENT
4.0 ± 0.8	20k	¹ LEES	17c BABR	$J/\psi \rightarrow \pi^+ \pi^- \pi^0$

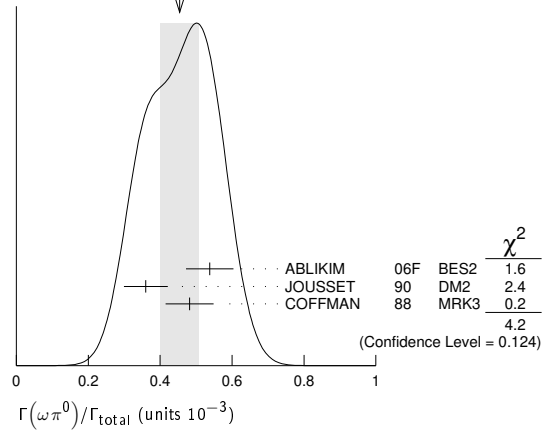
¹ From a Dalitz plot analysis in a Veneziano model.

$\Gamma(\omega\pi^0)/\Gamma_{total}$ Γ_{39}/Γ

VALUE (units 10^{-3})	EVTS	DOCUMENT ID	TECN	COMMENT
0.45 ± 0.05 OUR AVERAGE				Error includes scale factor of 1.4. See the ideogram below.
0.538 ± 0.012 ± 0.065	2090	¹ ABLIKIM	06F BES2	$J/\psi \rightarrow \omega\pi^0$
0.360 ± 0.028 ± 0.054	222	JOUSSET	90 DM2	$J/\psi \rightarrow \text{hadrons}$
0.482 ± 0.019 ± 0.064		COFFMAN	88 MRK3	$e^+ e^- \rightarrow \pi^0 \pi^+ \pi^- \pi^0$

¹ Using $B(\omega \rightarrow \pi^+ \pi^- \pi^0) = (89.1 \pm 0.7)\%$.

WEIGHTED AVERAGE
0.45±0.05 (Error scaled by 1.4)



$\Gamma(\omega\pi^0 \rightarrow \pi^+ \pi^- \pi^0)/\Gamma(\pi^+ \pi^- \pi^0)$ Γ_{40}/Γ_{163}

VALUE (units 10^{-4})	EVTS	DOCUMENT ID	TECN	COMMENT
8 ± 3 ± 2	20k	¹ LEES	17c BABR	$J/\psi \rightarrow \pi^+ \pi^- \pi^0$

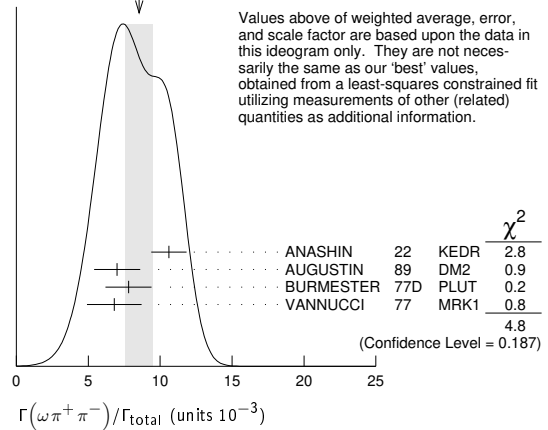
¹ From a Dalitz plot analysis in an isobar model and significance 4.9 σ .

$\Gamma(\omega\pi^+ \pi^-)/\Gamma_{total}$ Γ_{41}/Γ

VALUE (units 10^{-3})	EVTS	DOCUMENT ID	TECN	COMMENT
8.5 ± 1.0 OUR AVERAGE				Error includes scale factor of 1.3. See the ideogram below.
10.6 ± 1.2 ± 0.1	3531	¹ ANASHIN	22 KEDR	$J/\psi \rightarrow 2(\pi^+ \pi^-)\pi^0$
7.0 ± 1.6	18058	AUGUSTIN	89 DM2	$J/\psi \rightarrow 2(\pi^+ \pi^-)\pi^0$
7.8 ± 1.6	215	BURMESTER	77D PLUT	$e^+ e^-$
6.8 ± 1.9	348	VANNUCCI	77 MRK1	$e^+ e^- \rightarrow 2(\pi^+ \pi^-)\pi^0$

¹ ANASHIN 22 reports $[\Gamma(J/\psi(1S) \rightarrow \omega\pi^+ \pi^-)/\Gamma_{total}] \times [B(\omega(782) \rightarrow \pi^+ \pi^- \pi^0)] = (0.946 \pm 0.016 \pm 0.108) \times 10^{-2}$ which we divide by our best value $B(\omega(782) \rightarrow \pi^+ \pi^- \pi^0) = (89.2 \pm 0.7) \times 10^{-2}$. Our first error is their experiment's error and our second error is the systematic error from using our best value.

WEIGHTED AVERAGE
8.5±1.0 (Error scaled by 1.3)



Values above of weighted average, error, and scale factor are based upon the data in this ideogram only. They are not necessarily the same as our 'best' values, obtained from a least-squares constrained fit utilizing measurements of other (related) quantities as additional information.

$\Gamma(\omega\pi^0\pi^0)/\Gamma_{total}$ Γ_{42}/Γ

VALUE (units 10^{-3})	EVTS	DOCUMENT ID	TECN	COMMENT
3.4 ± 0.3 ± 0.7	509	AUGUSTIN	89 DM2	$J/\psi \rightarrow \pi^+ \pi^- 3\pi^0$

$\Gamma(\omega f_2(1270))/\Gamma_{total}$ Γ_{44}/Γ

VALUE (units 10^{-3})	EVTS	DOCUMENT ID	TECN	COMMENT
4.3 ± 0.6 OUR AVERAGE				
4.3 ± 0.2 ± 0.6	5860	AUGUSTIN	89 DM2	$e^+ e^-$
4.0 ± 1.6	70	BURMESTER	77D PLUT	$e^+ e^-$

• • • We do not use the following data for averages, fits, limits, etc. • • •

1.9 ± 0.8	81	VANNUCCI	77 MRK1	$e^+ e^- \rightarrow 2(\pi^+ \pi^-)\pi^0$
-----------	----	----------	---------	---

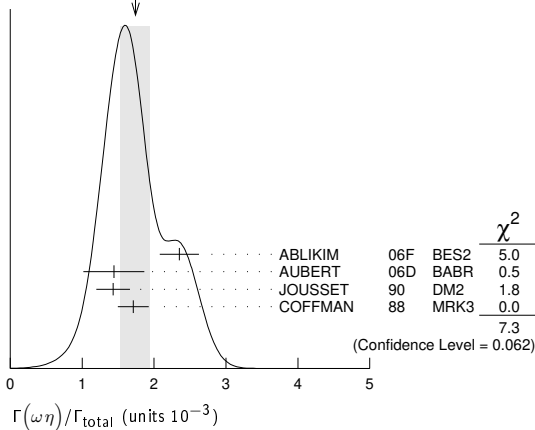
Meson Particle Listings

 $J/\psi(1S)$

$\Gamma(\omega\eta)/\Gamma_{\text{total}}$		Γ_{45}/Γ		
VALUE (units 10^{-3})	EVTS	DOCUMENT ID	TECN	COMMENT
1.74 ± 0.20	OUR AVERAGE	Error	includes scale factor of 1.6.	See the ideogram below.
2.352 ± 0.273	5k	¹ ABLIKIM	06F BES2	$J/\psi \rightarrow \omega\eta$
$1.44 \pm 0.40 \pm 0.14$	13	² AUBERT	06D BABR	$10.6 e^+ e^- \rightarrow \omega\eta\gamma$
$1.43 \pm 0.10 \pm 0.21$	378	JOUSSET	90 DM2	$J/\psi \rightarrow \text{hadrons}$
$1.71 \pm 0.08 \pm 0.20$		COFFMAN	88 MRK3	$e^+ e^- \rightarrow 3\pi\eta$

¹ Using $B(\eta \rightarrow 2\gamma) = (39.43 \pm 0.26)\%$, $B(\eta \rightarrow \pi^+ \pi^- \pi^0) = 22.6 \pm 0.4\%$, $B(\eta \rightarrow \pi^+ \pi^- \gamma) = 4.68 \pm 0.11\%$, and $B(\omega \rightarrow \pi^+ \pi^- \pi^0) = (89.1 \pm 0.7)\%$.
² Using $\Gamma(J/\psi \rightarrow e^+ e^-) = 5.52 \pm 0.14 \pm 0.04$ keV.

WEIGHTED AVERAGE
 1.74 ± 0.20 (Error scaled by 1.6)



$\Gamma(\omega\pi^+\pi^-\pi^-)/\Gamma_{\text{total}}$		Γ_{48}/Γ		
VALUE (units 10^{-4})	EVTS	DOCUMENT ID	TECN	COMMENT
85 ± 34	140	VANNUCCI	77 MRK1	$e^+ e^- \rightarrow 3(\pi^+ \pi^-) \pi^0$

$\Gamma(\omega\eta'\pi^-)/\Gamma_{\text{total}}$		Γ_{50}/Γ		
VALUE (units 10^{-3})	EVTS	DOCUMENT ID	TECN	COMMENT
$1.12 \pm 0.02 \pm 0.13$	14k	¹ ABLIKIM	19AC BES3	$J/\psi \rightarrow \omega\eta'\pi^+ \pi^-$

¹ Using the decays $\omega \rightarrow \pi^+ \pi^- \pi^0$ and $\eta' \rightarrow \eta\pi^+ \pi^-$.

$\Gamma(\omega\eta'(958))/\Gamma_{\text{total}}$		Γ_{51}/Γ		
VALUE (units 10^{-4})	EVTS	DOCUMENT ID	TECN	COMMENT
1.89 ± 0.18	OUR AVERAGE			
$2.08 \pm 0.30 \pm 0.14$	137	¹ ABLIKIM	17AK BES3	$J/\psi \rightarrow \pi^+ \pi^- \eta'$
2.26 ± 0.43	218	² ABLIKIM	06F BES2	$J/\psi \rightarrow \omega\eta'$
$1.8 \pm 1.0 \pm 0.8 \pm 0.3$	6	JOUSSET	90 DM2	$J/\psi \rightarrow \text{hadrons}$
$1.66 \pm 0.17 \pm 0.19$		COFFMAN	88 MRK3	$e^+ e^- \rightarrow 3\pi\eta'$

¹ From a partial wave analysis of the decay $J/\psi \rightarrow \pi^+ \pi^- \eta'$.
² Using $B(\eta' \rightarrow \pi^+ \pi^- \eta) = (44.3 \pm 1.5)\%$, $B(\eta' \rightarrow \pi^+ \pi^- \gamma) = 29.5 \pm 1.0\%$, $B(\eta \rightarrow 2\gamma) = 39.43 \pm 0.26\%$, and $B(\omega \rightarrow \pi^+ \pi^- \pi^0) = (89.1 \pm 0.7)\%$.

$\Gamma(\omega f_0(980))/\Gamma_{\text{total}}$		Γ_{52}/Γ		
VALUE (units 10^{-4})	EVTS	DOCUMENT ID	TECN	COMMENT
$1.41 \pm 0.27 \pm 0.47$		¹ AUGUSTIN	89 DM2	$J/\psi \rightarrow 2(\pi^+ \pi^-) \pi^0$

¹ Assuming $B(f_0(980) \rightarrow \pi\pi) = 0.78$.

$\Gamma(\omega f_0(1710) \rightarrow \omega K\bar{K})/\Gamma_{\text{total}}$		Γ_{53}/Γ		
VALUE (units 10^{-4})	EVTS	DOCUMENT ID	TECN	COMMENT
$4.8 \pm 1.1 \pm 0.3$		^{1,2} FALVARD	88 DM2	$J/\psi \rightarrow \text{hadrons}$

¹ Includes unknown branching fraction $f_0(1710) \rightarrow K\bar{K}$.
² Addition of $f_0(1710) \rightarrow K^+ K^-$ and $f_0(1710) \rightarrow K^0 \bar{K}^0$ branching ratios.

$\Gamma(\omega f_1(1420))/\Gamma_{\text{total}}$		Γ_{54}/Γ		
VALUE (units 10^{-4})	EVTS	DOCUMENT ID	TECN	COMMENT
$6.8 \pm 1.9 \pm 1.6 \pm 1.7$	$111 \pm 31 \pm 26$	BECKER	87 MRK3	$e^+ e^- \rightarrow \text{hadrons}$

$\Gamma(\omega f_2'(1525))/\Gamma_{\text{total}}$		Γ_{55}/Γ		
VALUE	CL%	DOCUMENT ID	TECN	COMMENT
$< 2.2 \times 10^{-4}$	90	¹ VANNUCCI	77 MRK1	$e^+ e^- \rightarrow \pi^+ \pi^- \pi^0 K^+ K^-$
$< 2.8 \times 10^{-4}$	90	¹ FALVARD	88 DM2	$J/\psi \rightarrow \text{hadrons}$

¹ Re-evaluated assuming $B(f_2'(1525) \rightarrow K\bar{K}) = 0.713$.

$\Gamma(\omega X(1835) \rightarrow \omega p\bar{p})/\Gamma_{\text{total}}$		Γ_{56}/Γ		
VALUE	CL%	DOCUMENT ID	TECN	COMMENT
$< 3.9 \times 10^{-6}$	95	ABLIKIM	13P BES3	$J/\psi \rightarrow \gamma\pi^0 p\bar{p}$

$\Gamma(\omega X(1835), X \rightarrow \eta'\pi^+\pi^-)/\Gamma_{\text{total}}$		Γ_{57}/Γ		
VALUE	EVTS	DOCUMENT ID	TECN	COMMENT
$< 6.2 \times 10^{-5}$		¹ ABLIKIM	19AC BES3	$J/\psi \rightarrow \omega\eta'\pi^+\pi^-$

¹ Using the decays $\omega \rightarrow \pi^+ \pi^- \pi^0$ and $\eta' \rightarrow \eta\pi^+ \pi^-$.

$\Gamma(\omega K^+ K^-)/\Gamma_{\text{total}}$		Γ_{58}/Γ		
VALUE (units 10^{-3})	EVTS	DOCUMENT ID	TECN	COMMENT
$1.52 \pm 0.30 \pm 0.01$	276	¹ ANASHIN	22 KEDR	$J/\psi \rightarrow K^+ K^- \pi^+ \pi^- \pi^0$

¹ ANASHIN 22 reports $[\Gamma(J/\psi(1S) \rightarrow \omega K^+ K^-)/\Gamma_{\text{total}}] \times [B(\omega(782) \rightarrow \pi^+ \pi^- \pi^0)] = (0.136 \pm 0.008 \pm 0.026) \times 10^{-2}$ which we divide by our best value $B(\omega(782) \rightarrow \pi^+ \pi^- \pi^0) = (89.2 \pm 0.7) \times 10^{-2}$. Our first error is their experiment's error and our second error is the systematic error from using our best value.

$\Gamma(\omega K^{\pm} K_S^0 \pi^{\mp})/\Gamma_{\text{total}}$		Γ_{59}/Γ		
VALUE (units 10^{-4})	EVTS	DOCUMENT ID	TECN	COMMENT
34 ± 5	OUR AVERAGE			
$37.7 \pm 0.8 \pm 5.8$	1972 ± 41	ABLIKIM	08E BES2	$e^+ e^- \rightarrow J/\psi$
$29.5 \pm 1.4 \pm 7.0$	879 ± 41	BECKER	87 MRK3	$e^+ e^- \rightarrow \text{hadrons}$

$\Gamma(\omega K\bar{K})/\Gamma_{\text{total}}$		Γ_{60}/Γ		
VALUE (units 10^{-4})	EVTS	DOCUMENT ID	TECN	COMMENT
19 ± 4	OUR AVERAGE			
$19.8 \pm 2.1 \pm 3.9$		¹ FALVARD	88 DM2	$J/\psi \rightarrow \text{hadrons}$
16 ± 10	22	FELDMAN	77 MRK1	$e^+ e^-$

¹ Addition of $\omega K^+ K^-$ and $\omega K^0 \bar{K}^0$ branching ratios.

$\Gamma(\omega K^*(892) \bar{K}^0 + \text{c.c.})/\Gamma_{\text{total}}$		Γ_{61}/Γ		
VALUE (units 10^{-4})	EVTS	DOCUMENT ID	TECN	COMMENT
61 ± 9	OUR AVERAGE			
$62.0 \pm 6.8 \pm 10.6$	899 ± 98	ABLIKIM	08E BES2	$J/\psi \rightarrow \omega K_S^0 K^{\pm} \pi^{\mp}$
$65.3 \pm 10.2 \pm 13.5$	176 ± 28	ABLIKIM	08E BES2	$J/\psi \rightarrow \omega K^+ K^- \pi^0$
$53 \pm 14 \pm 14$	530 ± 140	BECKER	87 MRK3	$e^+ e^- \rightarrow \text{hadrons}$

$\Gamma(\eta' K^* \bar{K}^{\mp})/\Gamma_{\text{total}}$		Γ_{62}/Γ		
VALUE (units 10^{-3})	EVTS	DOCUMENT ID	TECN	COMMENT
1.48 ± 0.13	OUR AVERAGE			
$1.50 \pm 0.02 \pm 0.19$		¹ ABLIKIM	18AB BES3	$J/\psi \rightarrow \eta' K^* \bar{K}$
$1.47 \pm 0.03 \pm 0.17$		² ABLIKIM	18AB BES3	$J/\psi \rightarrow \eta' K^* \bar{K}$

¹ From $\eta' K^+ K^- \pi^0$.
² From $\eta' K_S^0 K^{\pm} \pi^{\mp}$.

$\Gamma(\eta' K^* \bar{K}^0 + \text{c.c.})/\Gamma_{\text{total}}$		Γ_{63}/Γ		
VALUE (units 10^{-3})	EVTS	DOCUMENT ID	TECN	COMMENT
$1.66 \pm 0.03 \pm 0.21$		¹ ABLIKIM	18AB BES3	$J/\psi \rightarrow \eta' K^* \bar{K}$

¹ From $\eta' K_S^0 K^{\pm} \pi^{\mp}$.

$\Gamma(\eta' h_1(1415) \rightarrow \eta' K^* \bar{K} + \text{c.c.})/\Gamma_{\text{total}}$		Γ_{64}/Γ		
VALUE (units 10^{-4})	EVTS	DOCUMENT ID	TECN	COMMENT
$2.16 \pm 0.12 \pm 0.29$	1.1k	¹ ABLIKIM	18AB BES3	$J/\psi \rightarrow \eta' h_1 \rightarrow \eta' K^* \bar{K}$

¹ From $\eta' K_S^0 K^{\pm} \pi^{\mp}$.

$\Gamma(\eta' h_1(1415) \rightarrow \eta' K^* \bar{K}^{\mp})/\Gamma_{\text{total}}$		Γ_{65}/Γ		
VALUE (units 10^{-4})	EVTS	DOCUMENT ID	TECN	COMMENT
$1.51 \pm 0.09 \pm 0.21$	1.0k	¹ ABLIKIM	18AB BES3	$J/\psi \rightarrow \eta' h_1 \rightarrow \eta' K^* \bar{K}$

¹ From $\eta' K^+ K^- \pi^0$.

$\Gamma(\eta' h_1(1415) \rightarrow \gamma\eta'\eta')/\Gamma_{\text{total}}$		Γ_{66}/Γ		
VALUE (units 10^{-7})	EVTS	DOCUMENT ID	TECN	COMMENT
$4.69 \pm 0.80 \pm 0.74 \pm 1.82$		¹ ABLIKIM	22c BES3	$J/\psi \rightarrow \gamma\eta'\eta' \rightarrow 4/5\gamma 2(\pi^+ \pi^-)$

¹ From a partial wave analysis of the systems (γX) , with $X \rightarrow \eta'\eta'$, and $(\eta' X)$, with $X \rightarrow \gamma\eta'$ in the decay $J/\psi \rightarrow \gamma\eta'\eta'$. The intermediate resonance X is parametrized by a constant-width, relativistic Breit-Wigner.

$\Gamma(h_1(1415)\eta' \rightarrow \gamma\eta'\eta')/\Gamma_{\text{total}}$		Γ_{27}/Γ		
VALUE (units 10^{-5})	EVTS	DOCUMENT ID	TECN	COMMENT
$0.08 \pm 0.01 \pm 0.01 \pm 0.02$		¹ ABLIKIM	22As BES3	$J/\psi(1S) \rightarrow \gamma\eta'\eta'$

¹ From a Breit-Wigner fit involving 9 resonances and a resonating exotic $\eta_1(1855) \rightarrow \eta\eta'$ P-wave.

$\Gamma(h_1(1595)\eta' \rightarrow \gamma\eta'\eta')/\Gamma_{\text{total}}$		Γ_{28}/Γ		
VALUE (units 10^{-5})	EVTS	DOCUMENT ID	TECN	COMMENT
$0.16 \pm 0.02 \pm 0.03 \pm 0.01$		¹ ABLIKIM	22As BES3	$J/\psi(1S) \rightarrow \gamma\eta'\eta'$

¹ From a Breit-Wigner fit involving 9 resonances and a resonating exotic $\eta_1(1855) \rightarrow \eta\eta'$ P-wave.

See key on page 1171

Meson Particle Listings

$J/\psi(1S)$

$\Gamma(\bar{K}^* K^*(892) + c.c. \rightarrow K_S^0 K^\pm \pi^\mp) / \Gamma(K_S^0 K^\pm \pi^\mp)$					$\Gamma_{68} / \Gamma_{181}$
VALUE (%)	EVTS	DOCUMENT ID	TECN	COMMENT	
90.5 ± 0.9 ± 3.8	4k	¹ LEES	17C BABR	$J/\psi \rightarrow K_S^0 K^\pm \pi^\mp$	

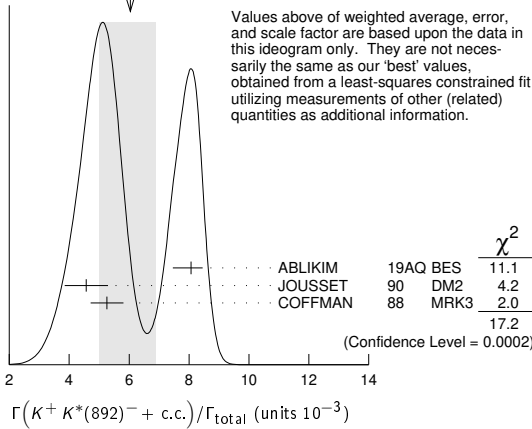
¹ From a Dalitz plot analysis in an isobar model.

$\Gamma(K^+ K^*(892)^- + c.c.) / \Gamma_{total}$					Γ_{69} / Γ
VALUE (units 10 ⁻³)	EVTS	DOCUMENT ID	TECN	COMMENT	
6.0 ^{+0.8} _{-1.0} OUR AVERAGE				Error includes scale factor of 2.9. See the ideogram below.	
8.07 ± 0.04 ^{+0.38} _{-0.61}	183k	ABLIKIM	19AQ BES	$J/\psi \rightarrow K^+ K^- \pi^0$	
4.57 ± 0.17 ± 0.70	2285	JOUSSET	90 DM2	$J/\psi \rightarrow$ hadrons	
5.26 ± 0.13 ± 0.53		COFFMAN	88 MRK3	$J/\psi \rightarrow K^\pm K_S^0 \pi^\mp$, $K^+ K^- \pi^0$	

• • • We do not use the following data for averages, fits, limits, etc. • • •

2.6 ± 0.6	24	FRANKLIN	83 MRK2	$J/\psi \rightarrow K^+ K^- \pi^0$
3.2 ± 0.6	48	VANNUCCI	77 MRK1	$J/\psi \rightarrow K^\pm K_S^0 \pi^\mp$
4.1 ± 1.2	39	BRAUNSCH...	76 DASP	$J/\psi \rightarrow K^\pm X$

WEIGHTED AVERAGE
6.0±0.8-1.0 (Error scaled by 2.9)



$\Gamma(K^+ K^*(892)^- + c.c. \rightarrow K^+ K^- \pi^0) / \Gamma_{total}$					Γ_{70} / Γ
VALUE (units 10 ⁻³)	EVTS	DOCUMENT ID	TECN	COMMENT	
2.69 ± 0.01 ^{+0.13} _{-0.20}	183k	ABLIKIM	19AQ BES	$J/\psi \rightarrow K^+ K^- \pi^0$	

$\Gamma(K^+ K^*(892)^- + c.c. \rightarrow K^+ K^- \pi^0) / \Gamma(K^+ K^- \pi^0)$					$\Gamma_{70} / \Gamma_{180}$
VALUE (%)	EVTS	DOCUMENT ID	TECN	COMMENT	
92.4 ± 1.5 ± 3.4	2k	¹ LEES	17C BABR	$J/\psi \rightarrow K^+ K^- \pi^0$	

¹ From a Dalitz plot analysis in an isobar model.

$\Gamma(K^0 \bar{K}^*(892)^0 + c.c.) / \Gamma_{total}$					Γ_{72} / Γ
VALUE (units 10 ⁻³)	EVTS	DOCUMENT ID	TECN	COMMENT	
4.2 ± 0.4 OUR AVERAGE					
3.96 ± 0.15 ± 0.60	1192	JOUSSET	90 DM2	$J/\psi \rightarrow$ hadrons	
4.33 ± 0.12 ± 0.45		COFFMAN	88 MRK3	$J/\psi \rightarrow K^\pm K_S^0 \pi^\mp$	

• • • We do not use the following data for averages, fits, limits, etc. • • •

2.7 ± 0.6	45	VANNUCCI	77 MRK1	$J/\psi \rightarrow K^\pm K_S^0 \pi^\mp$
-----------	----	----------	---------	--

$\Gamma(\bar{K}^*(892)^0 K^+ \pi^- + c.c.) / \Gamma_{total}$					Γ_{74} / Γ
VALUE (units 10 ⁻³)	EVTS	DOCUMENT ID	TECN	COMMENT	
5.73 ± 0.14 ± 0.82		¹ ANASHIN	22 KEDR	$J/\psi \rightarrow K^+ K^- \pi^+ \pi^-$	

• • • We do not use the following data for averages, fits, limits, etc. • • •

seen		² ABLIKIM	06c BES2	$J/\psi \rightarrow \bar{K}^*(892)^0 K^+ \pi^-$
------	--	----------------------	----------	---

¹ Obtained from $J/\psi \rightarrow K^*(892) K^- \pi^+ + c.c. \rightarrow K^+ K^- \pi^+ \pi^-$ taking the value 2/3 for the probability of the $K^*(892)^0 \rightarrow K^+ \pi^-$ decay.

² A $K_0^*(700)$ is observed by ABLIKIM 06c in the $K^+ \pi^-$ mass spectrum of the $\bar{K}^*(892)^0 K^+ \pi^-$ final state against the $\bar{K}^*(892)$. A corresponding branching fraction of the $J/\psi(1S)$ is not presented.

$\Gamma(K^*(892)^0 K^- \pi^+ + c.c. \rightarrow K^+ K^- \pi^+ \pi^-) / \Gamma_{total}$					Γ_{78} / Γ
VALUE (units 10 ⁻³)	EVTS	DOCUMENT ID	TECN	COMMENT	
3.81 ± 0.10 ± 0.54	1559	ANASHIN	22 KEDR	$J/\psi \rightarrow K^+ K^- \pi^+ \pi^-$	

$\Gamma(K^*(892)^0 K_S^0 \rightarrow \gamma K_S^0 K_S^0) / \Gamma_{total}$					Γ_{79} / Γ
VALUE (units 10 ⁻⁶)	EVTS	DOCUMENT ID	TECN	COMMENT	
6.2 ^{+0.16} _{-0.17} ± 0.59		ABLIKIM	18AA BES3	$J/\psi \rightarrow \gamma K_S^0 K_S^0$	

$\Gamma(K^*(892)^\pm K^*(700)^\mp) / \Gamma_{total}$					Γ_{81} / Γ
VALUE (units 10 ⁻³)	EVTS	DOCUMENT ID	TECN	COMMENT	
1.09 ± 0.18 ^{+0.94} _{-0.54}	655	ABLIKIM	10E BES2	$J/\psi \rightarrow K^\pm K_S^0 \pi^\mp \pi^0$	

$\Gamma(K^*(892)^0 \bar{K}^*(892)^0) / \Gamma_{total}$					Γ_{82} / Γ
VALUE (units 10 ⁻⁴)	CL%	DOCUMENT ID	TECN	COMMENT	
• • • We do not use the following data for averages, fits, limits, etc. • • •					
<5	90	VANNUCCI	77 MRK1	$e^+ e^- \rightarrow \pi^+ \pi^- K^+ K^-$	

$\Gamma(K^*(892)^\pm K^*(892)^\mp) / \Gamma_{total}$					Γ_{83} / Γ
VALUE (units 10 ⁻³)	EVTS	DOCUMENT ID	TECN	COMMENT	
1.00 ± 0.19 ^{+0.11} _{-0.32}	323	ABLIKIM	10E BES2	$J/\psi \rightarrow K^\pm K_S^0 \pi^\mp \pi^0$	

$\Gamma(K_1(1400)^\pm K^\mp) / \Gamma_{total}$					Γ_{84} / Γ
VALUE (units 10 ⁻³)	EVTS	DOCUMENT ID	TECN	COMMENT	
3.8 ± 0.8 ± 1.2		¹ BAI	99c BES	$e^+ e^-$	

¹ Assuming $B(K_1(1400) \rightarrow K^* \pi) = 0.94 \pm 0.06$

$\Gamma(K^*(1410) \bar{K} + c.c. \rightarrow K^\pm K^\mp \pi^0) / \Gamma(K^+ K^- \pi^0)$					$\Gamma_{86} / \Gamma_{180}$
VALUE (%)	EVTS	DOCUMENT ID	TECN	COMMENT	
2.3 ± 1.1 ± 0.7	2k	¹ LEES	17C BABR	$J/\psi \rightarrow K^+ K^- \pi^0$	

¹ From a Dalitz plot analysis in an isobar model.

$\Gamma(K^*(1410) \bar{K} + c.c. \rightarrow K_S^0 K^\pm \pi^\mp) / \Gamma(K_S^0 K^\pm \pi^\mp)$					$\Gamma_{87} / \Gamma_{181}$
VALUE (%)	EVTS	DOCUMENT ID	TECN	COMMENT	
1.5 ± 0.5 ± 0.9	4k	¹ LEES	17C BABR	$J/\psi \rightarrow K_S^0 K^\pm \pi^\mp$	

¹ From a Dalitz plot analysis in an isobar model.

$\Gamma(K_2^*(1430) \bar{K} + c.c. \rightarrow K^\pm K^\mp \pi^0) / \Gamma(K^+ K^- \pi^0)$					$\Gamma_{89} / \Gamma_{180}$
VALUE (%)	EVTS	DOCUMENT ID	TECN	COMMENT	
3.5 ± 1.3 ± 0.9	2k	¹ LEES	17C BABR	$J/\psi \rightarrow K^+ K^- \pi^0$	

¹ From a Dalitz plot analysis in an isobar model.

$\Gamma(K_2^*(1430) \bar{K} + c.c. \rightarrow K_S^0 K^\pm \pi^\mp) / \Gamma(K_S^0 K^\pm \pi^\mp)$					$\Gamma_{90} / \Gamma_{181}$
VALUE (%)	EVTS	DOCUMENT ID	TECN	COMMENT	
7.1 ± 1.3 ± 1.2	4k	¹ LEES	17C BABR	$J/\psi \rightarrow K_S^0 K^\pm \pi^\mp$	

¹ From a Dalitz plot analysis in an isobar model.

$\Gamma(\bar{K}_2^*(1430) K + c.c.) / \Gamma_{total}$					Γ_{91} / Γ
VALUE	CL%	DOCUMENT ID	TECN	COMMENT	
<40 × 10⁻⁴	90	VANNUCCI	77 MRK1	$e^+ e^- \rightarrow K^0 \bar{K}_2^{*0}$	
• • • We do not use the following data for averages, fits, limits, etc. • • •					
<66 × 10 ⁻⁴	90	BRAUNSCH...	76 DASP	$e^+ e^- \rightarrow K^\pm \bar{K}_2^{*\mp}$	

$\Gamma(K_2^*(1430)^+ K^- + c.c. \rightarrow K^+ K^- \pi^0) / \Gamma_{total}$					Γ_{92} / Γ
VALUE (units 10 ⁻⁴)	EVTS	DOCUMENT ID	TECN	COMMENT	
2.69 ± 0.04 ^{+0.25} _{-0.19}	183k	ABLIKIM	19AQ BES	$J/\psi \rightarrow K^+ K^- \pi^0$	

$\Gamma(\bar{K}_2^*(1430)^0 K^*(892)^0 + c.c.) / \Gamma_{total}$					Γ_{95} / Γ
VALUE (units 10 ⁻³)	EVTS	DOCUMENT ID	TECN	COMMENT	
• • • We do not use the following data for averages, fits, limits, etc. • • •					
6.7 ± 2.6	40	VANNUCCI	77 MRK1	$e^+ e^- \rightarrow \pi^+ \pi^- K^+ K^-$	

$\Gamma(K_2^*(1430)^0 \bar{K}_2^*(1430)^0) / \Gamma_{total}$					Γ_{98} / Γ
VALUE	CL%	DOCUMENT ID	TECN	COMMENT	
<29 × 10⁻⁴	90	VANNUCCI	77 MRK1	$e^+ e^- \rightarrow \pi^+ \pi^- K^+ K^-$	

$\Gamma(K_2^*(1980)^+ K^- + c.c. \rightarrow K^+ K^- \pi^0) / \Gamma_{total}$					Γ_{100} / Γ
VALUE (units 10 ⁻⁵)	EVTS	DOCUMENT ID	TECN	COMMENT	
1.1 ± 0.1 ^{+0.6} _{-0.1}	183k	ABLIKIM	19AQ BES	$J/\psi \rightarrow K^+ K^- \pi^0$	

$\Gamma(K_2^*(2045)^+ K^- + c.c. \rightarrow K^+ K^- \pi^0) / \Gamma_{total}$					Γ_{101} / Γ
VALUE (units 10 ⁻⁶)	EVTS	DOCUMENT ID	TECN	COMMENT	
6.2 ± 0.7 ^{+2.8} _{-1.4}	183k	ABLIKIM	19AQ BES	$J/\psi \rightarrow K^+ K^- \pi^0$	

$\Gamma(K_1(1270)^\pm K^\mp) / \Gamma_{total}$					Γ_{102} / Γ
VALUE	CL%	DOCUMENT ID	TECN	COMMENT	
<3.0 × 10⁻³	90	¹ BAI	99c BES	$e^+ e^-$	

¹ Assuming $B(K_1(1270) \rightarrow K \rho) = 0.42 \pm 0.06$

$\Gamma(K_1(1270) K_S^0 \rightarrow \gamma K_S^0 K_S^0) / \Gamma_{total}$					Γ_{103} / Γ
VALUE (units 10 ⁻⁷)	EVTS	DOCUMENT ID	TECN	COMMENT	
8.54 ^{+1.07} _{-1.20} ± 2.35		ABLIKIM	18AA BES3	$J/\psi \rightarrow \gamma K_S^0 K_S^0$	

Meson Particle Listings

 $J/\psi(1S)$

$\Gamma(a_2(1320)^\pm \pi^\mp)/\Gamma_{total}$		Γ_{104}/Γ		
VALUE	CL%	DOCUMENT ID	TECN	COMMENT
$<43 \times 10^{-4}$	90	BRAUNSCH...	76	DASP e^+e^-

$\Gamma(\phi\pi^0)/\Gamma_{total}$		Γ_{105}/Γ		
The two different fit values of ABLIKIM 15k below have the same statistical significance of 6.4σ and cannot be distinguished at this moment.				
VALUE (units 10^{-6})	CL%	EVTS	DOCUMENT ID	TECN COMMENT
$2.94 \pm 0.16 \pm 0.16$		0.8k	¹ ABLIKIM 15k	BES3 $e^+e^- \rightarrow J/\psi \rightarrow K^+K^-\gamma\gamma$
$0.124 \pm 0.033 \pm 0.030$		35 \pm 9	² ABLIKIM 15k	BES3 $e^+e^- \rightarrow J/\psi \rightarrow K^+K^-\gamma\gamma$

<6.4	90	³ ABLIKIM 05B	BES2	$e^+e^- \rightarrow J/\psi \rightarrow \phi\gamma\gamma$
<6.8	90	COFFMAN 88	MRK3	$e^+e^- \rightarrow K^+K^-\pi^0$

• • • We do not use the following data for averages, fits, limits, etc. • • •

¹ Corresponding to one of the two fit solutions with $\delta = (-95.9 \pm 1.5)^\circ$ for the phase angle between the resonant $J/\psi \rightarrow \phi\pi^0$ and non-phi $J/\psi \rightarrow K^+K^-\pi^0$ contributions.
² Corresponding to one of the two fit solutions with $\delta = (-152.1 \pm 7.7)^\circ$ for the phase angle between the resonant $J/\psi \rightarrow \phi\pi^0$ and non-phi $J/\psi \rightarrow K^+K^-\pi^0$ contributions.
³ Superseded by ABLIKIM 15k.

$\Gamma(\phi\pi^+\pi^-)/\Gamma_{total}$		Γ_{106}/Γ		
VALUE (units 10^{-3})	EVTS	DOCUMENT ID	TECN	COMMENT
0.94 ± 0.15 OUR AVERAGE		Error includes scale factor of 1.7.		
$1.09 \pm 0.02 \pm 0.13$		ABLIKIM 05	BES2	$J/\psi \rightarrow \phi\pi^+\pi^-$
$0.78 \pm 0.03 \pm 0.12$		FALVARD 88	DM2	$J/\psi \rightarrow$ hadrons
2.1 ± 0.9	23	FELDMAN 77	MRK1	e^+e^-

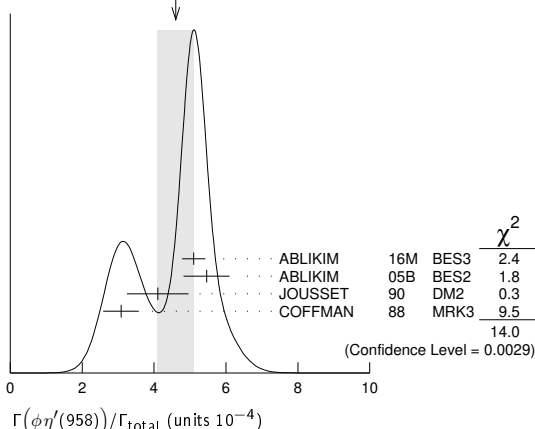
$\Gamma(\phi(2\pi^+\pi^-))/\Gamma_{total}$		Γ_{108}/Γ		
VALUE (units 10^{-4})		DOCUMENT ID	TECN	COMMENT
$16.0 \pm 1.0 \pm 3.0$		FALVARD 88	DM2	$J/\psi \rightarrow$ hadrons

$\Gamma(\phi\eta)/\Gamma_{total}$		Γ_{109}/Γ		
VALUE (units 10^{-3})	EVTS	DOCUMENT ID	TECN	COMMENT
0.74 ± 0.06 OUR AVERAGE		Error includes scale factor of 1.2.		
$0.71 \pm 0.10 \pm 0.05$	99 \pm 14	¹ ZHU 23	BELL	$e^+e^- \rightarrow \Upsilon(nS) \rightarrow \phi\eta\gamma$
$0.898 \pm 0.024 \pm 0.089$		ABLIKIM 05B	BES2	$e^+e^- \rightarrow J/\psi \rightarrow$ hadr
$0.64 \pm 0.04 \pm 0.11$	346	JOUSSET 90	DM2	$J/\psi \rightarrow$ hadrons
$0.661 \pm 0.045 \pm 0.078$		COFFMAN 88	MRK3	$e^+e^- \rightarrow K^+K^-\eta$

¹ From a fit to the combined $\phi\eta$ invariant mass spectrum with a Gaussian function for the J/ψ signals and a second-order polynomial function for the backgrounds.

$\Gamma(\phi\eta'(958))/\Gamma_{total}$		Γ_{110}/Γ		
VALUE (units 10^{-4})	CL%	EVTS	DOCUMENT ID	TECN COMMENT
4.6 ± 0.5 OUR AVERAGE		Error includes scale factor of 2.2. See the ideogram below.		
$5.10 \pm 0.03 \pm 0.32$		31k	ABLIKIM 16M	BES3 $e^+e^- \rightarrow J/\psi \rightarrow$ hadrons
$5.46 \pm 0.31 \pm 0.56$			ABLIKIM 05B	BES2 $e^+e^- \rightarrow J/\psi \rightarrow$ hadrons
$4.1 \pm 0.3 \pm 0.8$		167	JOUSSET 90	DM2 $J/\psi \rightarrow$ hadrons
$3.08 \pm 0.34 \pm 0.36$			COFFMAN 88	MRK3 $e^+e^- \rightarrow K^+K^-\eta'$
<13	90	VANNUCCI 77	MRK1	e^+e^-

WEIGHTED AVERAGE
 4.6 ± 0.5 (Error scaled by 2.2)



$\Gamma(\phi\eta')/\Gamma_{total}$		Γ_{111}/Γ		
VALUE (units 10^{-4})	EVTS	DOCUMENT ID	TECN	COMMENT
$2.32 \pm 0.06 \pm 0.16$	2.2k	¹ ABLIKIM 19AN	BES3	$e^+e^- \rightarrow J/\psi \rightarrow$ hadrons

¹ Including contributions from intermediate resonances. Evidence for an intermediate resonance at $M \approx 2$ GeV and $\Gamma \approx 150$ MeV decaying to $\phi\eta'$ with $J^P = 1^+ \text{ or } J^P = 1^-$, and $B(J/\psi \rightarrow \eta X) \times B(X \rightarrow \phi\eta') \approx 10^{-4}$.

$\Gamma(\phi f_0(980))/\Gamma_{total}$		Γ_{112}/Γ		
VALUE (units 10^{-4})	EVTS	DOCUMENT ID	TECN	COMMENT
3.2 ± 0.9 OUR AVERAGE		Error includes scale factor of 1.9.		
$4.6 \pm 0.4 \pm 0.8$		¹ FALVARD 88	DM2	$J/\psi \rightarrow$ hadrons
2.6 ± 0.6	50	¹ GIDAL 81	MRK2	$J/\psi \rightarrow K^+K^-K^+K^-$

$\Gamma(\phi\pi^0 f_0(980) \rightarrow \phi\pi^0\pi^+\pi^-)/\Gamma_{total}$		Γ_{115}/Γ		
VALUE (units 10^{-6})	EVTS	DOCUMENT ID	TECN	COMMENT
$4.50 \pm 0.80 \pm 0.61$	355	ABLIKIM 15P	BES3	$J/\psi \rightarrow K^+K^-3\pi$

$\Gamma(\phi\pi^0 f_0(980) \rightarrow \phi\pi^0\rho^0\pi^0)/\Gamma_{total}$		Γ_{116}/Γ		
VALUE (units 10^{-6})	EVTS	DOCUMENT ID	TECN	COMMENT
$1.67 \pm 0.50 \pm 0.24$	70	ABLIKIM 15P	BES3	$J/\psi \rightarrow K^+K^-3\pi$

$\Gamma(\phi f_0(980)\eta \rightarrow \eta\phi\pi^+\pi^-)/\Gamma_{total}$		Γ_{117}/Γ		
VALUE (units 10^{-4})	EVTS	DOCUMENT ID	TECN	COMMENT
$3.23 \pm 0.75 \pm 0.73$	52	ABLIKIM 08F	BES	$J/\psi \rightarrow \eta\phi f_0(980)$

$\Gamma(\phi a_0(980)^0 \rightarrow \phi\eta\pi^0)/\Gamma_{total}$		Γ_{118}/Γ		
VALUE (units 10^{-6})		DOCUMENT ID	TECN	COMMENT
4.37 ± 1.35		¹ ABLIKIM 18D	BES3	$J/\psi \rightarrow \phi\eta\pi^0$
$5.0 \pm 2.7 \pm 2.5$		² ABLIKIM 11D	BES3	$J/\psi \rightarrow \phi\eta\pi^0$

• • • We do not use the following data for averages, fits, limits, etc. • • •

¹ Assuming constructive interference between $a_0(980) - f_0(980)$ mixing and electromagnetic decay. Destructive interference gives a value of $(4.93 \pm 1.77) \times 10^{-6}$ for this branching fraction.
² Assuming $a_0(980) - f_0(980)$ mixing and isospin breaking via γ^* and K^*K loops.

$\Gamma(\phi f_2(1270))/\Gamma_{total}$		Γ_{119}/Γ		
VALUE (units 10^{-3})	CL%	DOCUMENT ID	TECN	COMMENT
<0.45	90	FALVARD 88	DM2	$J/\psi \rightarrow$ hadrons
<0.37	90	VANNUCCI 77	MRK1	$e^+e^- \rightarrow \pi^+\pi^-K^+K^-$

$\Gamma(\phi f_1(1285))/\Gamma_{total}$		Γ_{120}/Γ		
VALUE (units 10^{-4})	EVTS	DOCUMENT ID	TECN	COMMENT
2.6 ± 0.5 OUR AVERAGE				
$3.4 \pm 1.8 \pm 1.5$	1.1k	¹ ABLIKIM 15H	BES3	$e^+e^- \rightarrow J/\psi \rightarrow \phi\eta\pi^+\pi^-$
$3.2 \pm 0.6 \pm 0.4$		JOUSSET 90	DM2	$J/\psi \rightarrow \phi(2\pi^+\pi^-)$
$2.1 \pm 0.5 \pm 0.4$	25	² JOUSSET 90	DM2	$J/\psi \rightarrow \phi\eta\pi^+\pi^-$
$0.6 \pm 0.2 \pm 0.1$	16	BECKER 87	MRK3	$J/\psi \rightarrow \phi K\bar{K}\pi$

• • • We do not use the following data for averages, fits, limits, etc. • • •

¹ ABLIKIM 15H reports $[\Gamma(J/\psi(1S) \rightarrow \phi f_1(1285))/\Gamma_{total}] \times [B(f_1(1285) \rightarrow \eta\pi^+\pi^-)] = (1.20 \pm 0.6 \pm 0.14) \times 10^{-4}$ which we divide by our best value $B(f_1(1285) \rightarrow \eta\pi^+\pi^-) = (35 \pm 15) \times 10^{-2}$. Our first error is their experiment's error and our second error is the systematic error from using our best value.
² We attribute to the $f_1(1285)$ the signal observed in the $\pi^+\pi^-\eta$ invariant mass distribution at 1297 MeV.

$\Gamma(\phi f_1(1285) \rightarrow \phi\pi^0 f_0(980) \rightarrow \phi\pi^0\pi^+\pi^-)/\Gamma_{total}$		Γ_{121}/Γ		
VALUE (units 10^{-7})	EVTS	DOCUMENT ID	TECN	COMMENT
$9.36 \pm 2.31 \pm 1.54$	78	ABLIKIM 15P	BES3	$J/\psi \rightarrow K^+K^-3\pi$

$\Gamma(\phi f_1(1285) \rightarrow \phi\pi^0 f_0(980) \rightarrow \phi 3\pi^0)/\Gamma_{total}$		Γ_{122}/Γ		
VALUE (units 10^{-7})	EVTS	DOCUMENT ID	TECN	COMMENT
$2.08 \pm 1.63 \pm 1.47$	9	ABLIKIM 15P	BES3	$J/\psi \rightarrow K^+K^-3\pi$

$\Gamma(\phi\eta(1405) \rightarrow \phi\eta\pi^+\pi^-)/\Gamma_{total}$		Γ_{123}/Γ		
VALUE (units 10^{-5})	CL%	EVTS	DOCUMENT ID	TECN COMMENT
$2.01 \pm 0.58 \pm 0.82$		172	¹ ABLIKIM 15H	BES3 $e^+e^- \rightarrow J/\psi \rightarrow \phi\eta\pi^+\pi^-$

• • • We do not use the following data for averages, fits, limits, etc. • • •

<17 90 ² FALVARD 88 DM2 $J/\psi \rightarrow$ hadrons

¹ With 3.6σ significance.
² Includes unknown branching fraction $\eta(1405) \rightarrow \eta\pi\pi$.

$\Gamma(\phi f_2'(1525))/\Gamma_{total}$		Γ_{124}/Γ		
VALUE (units 10^{-4})	EVTS	DOCUMENT ID	TECN	COMMENT
8 ± 4 OUR AVERAGE		Error includes scale factor of 2.7.		
$12.3 \pm 0.6 \pm 2.0$		^{1,2} FALVARD 88	DM2	$J/\psi \rightarrow$ hadrons
4.8 ± 1.8	46	¹ GIDAL 81	MRK2	$J/\psi \rightarrow K^+K^-K^+K^-$

¹ Re-evaluated using $B(f_2'(1525) \rightarrow K\bar{K}) = 0.713$.
² Including interference with $f_0(1710)$.

$\Gamma(\phi X(1835) \rightarrow \phi\rho\bar{\rho})/\Gamma_{total}$		Γ_{125}/Γ		
VALUE	CL%	DOCUMENT ID	TECN	COMMENT
$<2.1 \times 10^{-7}$	90	¹ ABLIKIM 16K	BES3	$J/\psi \rightarrow \rho\bar{\rho}K_S^0 K_L^0, \rho\bar{\rho}K^+K^-$

¹ Upper limit applies to any $\rho\bar{\rho}$ mass enhancement near threshold.

See key on page 1171

Meson Particle Listings

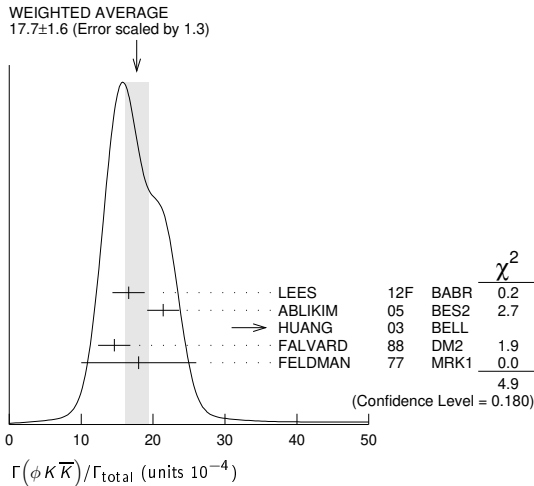
$J/\psi(1S)$

$\Gamma(\phi X(1835) \rightarrow \phi \eta \pi^+ \pi^-) / \Gamma_{\text{total}}$					Γ_{126} / Γ
VALUE	CL%	DOCUMENT ID	TECN	COMMENT	
$< 2.8 \times 10^{-4}$	90	ABLIKIM	15H BES3	$e^+ e^- \rightarrow J/\psi \rightarrow \phi \eta \pi^+ \pi^-$	

$\Gamma(\phi X(1870) \rightarrow \phi \eta \pi^+ \pi^-) / \Gamma_{\text{total}}$					Γ_{127} / Γ
VALUE	CL%	DOCUMENT ID	TECN	COMMENT	
$< 6.13 \times 10^{-5}$	90	ABLIKIM	15H BES3	$e^+ e^- \rightarrow J/\psi \rightarrow \phi \eta \pi^+ \pi^-$	

$\Gamma(\phi K \bar{K}) / \Gamma_{\text{total}}$					Γ_{128} / Γ
VALUE (units 10^{-4})	EVTS	DOCUMENT ID	TECN	COMMENT	
17.7 ± 1.6 OUR AVERAGE	Error includes scale factor of 1.3. See the ideogram below.				
$16.6 \pm 1.9 \pm 1.2$	163 ± 19	LEES	12F BABR	$10.6 e^+ e^- \rightarrow 2(K^+ K^-) \gamma$	
$21.4 \pm 0.4 \pm 2.2$		ABLIKIM	05 BES2	$J/\psi \rightarrow \phi \pi^+ \pi^-$	
$48 \begin{smallmatrix} +20 \\ -16 \end{smallmatrix} \pm 6$	$9.0 \begin{smallmatrix} +3.7 \\ -3.0 \end{smallmatrix}$	1,2 HUANG	03 BELL	$B^+ \rightarrow (\phi K^+ K^-) K^+$	
$14.6 \pm 0.8 \pm 2.1$		3 FALVARD	88 DM2	$J/\psi \rightarrow \text{hadrons}$	
18 ± 8	14	FELDMAN	77 MRK1	$e^+ e^-$	

¹ We have multiplied $K^+ K^-$ measurement by 2 to obtain $K \bar{K}$.
² Using $B(B^+ \rightarrow J/\psi K^+) = (1.01 \pm 0.05) \times 10^{-3}$.
³ Addition of $\phi K^+ K^-$ and $\phi K^0 \bar{K}^0$ branching ratios.



$\Gamma(\phi f_0(1710) \rightarrow \phi K \bar{K}) / \Gamma_{\text{total}}$					Γ_{129} / Γ
VALUE (units 10^{-4})	EVTS	DOCUMENT ID	TECN	COMMENT	
$3.6 \pm 0.2 \pm 0.6$		1,2 FALVARD	88 DM2	$J/\psi \rightarrow \text{hadrons}$	

¹ Including interference with $f_2'(1525)$.
² Includes unknown branching fraction $f_0(1710) \rightarrow K \bar{K}$.

$\Gamma(\phi K^\pm K_S^0 \pi^\mp) / \Gamma_{\text{total}}$					Γ_{132} / Γ
VALUE (units 10^{-4})	EVTS	DOCUMENT ID	TECN	COMMENT	
7.2 ± 0.8 OUR AVERAGE					
$7.4 \pm 0.6 \pm 1.4$	227 ± 19	ABLIKIM	08E BES2	$e^+ e^- \rightarrow J/\psi$	
$7.4 \pm 0.9 \pm 1.1$		FALVARD	88 DM2	$J/\psi \rightarrow \text{hadrons}$	
$7 \pm 0.6 \pm 1.0$	163 ± 15	BECKER	87 MRK3	$e^+ e^- \rightarrow \text{hadrons}$	

$\Gamma(\phi K^*(892) \bar{K} + \text{c.c.}) / \Gamma_{\text{total}}$					Γ_{133} / Γ
VALUE (units 10^{-4})	EVTS	DOCUMENT ID	TECN	COMMENT	
21.8 ± 2.3 OUR AVERAGE					
$20.8 \pm 2.7 \pm 3.9$	195 ± 25	ABLIKIM	08E BES2	$J/\psi \rightarrow \phi K_S^0 K^\pm \pi^\mp$	
$29.6 \pm 3.7 \pm 4.7$	238 ± 30	ABLIKIM	08E BES2	$J/\psi \rightarrow \phi K^+ K^- \pi^0$	
$20.7 \pm 2.4 \pm 3.0$		FALVARD	88 DM2	$J/\psi \rightarrow \text{hadrons}$	
$20 \pm 3 \pm 3$	155 ± 20	BECKER	87 MRK3	$e^+ e^- \rightarrow \text{hadrons}$	

$\Gamma(b_1(1235)^\pm \pi^\mp) / \Gamma_{\text{total}}$					Γ_{134} / Γ
VALUE (units 10^{-4})	EVTS	DOCUMENT ID	TECN	COMMENT	
30 ± 5 OUR AVERAGE					
31 ± 6	4600	AUGUSTIN	89 DM2	$J/\psi \rightarrow 2(\pi^+ \pi^-) \pi^0$	
29 ± 7	87	BURMESTER	77D PLUT	$e^+ e^-$	

$\Gamma(b_1(1235)^0 \pi^0) / \Gamma_{\text{total}}$					Γ_{135} / Γ
VALUE (units 10^{-4})	EVTS	DOCUMENT ID	TECN	COMMENT	
$23 \pm 3 \pm 5$	229	AUGUSTIN	89 DM2	$e^+ e^-$	

$\Gamma(\Delta(1232)^+ \bar{p}) / \Gamma_{\text{total}}$					Γ_{137} / Γ
VALUE	CL%	DOCUMENT ID	TECN	COMMENT	
$< 0.1 \times 10^{-3}$	90	HENRARD	87 DM2	$e^+ e^-$	

$\Gamma(\Delta(1232)^{++} \bar{p} \pi^-) / \Gamma_{\text{total}}$					Γ_{138} / Γ
VALUE (units 10^{-3})	EVTS	DOCUMENT ID	TECN	COMMENT	
$1.58 \pm 0.23 \pm 0.40$	332	EATON	84 MRK2	$e^+ e^-$	

$\Gamma(\Delta(1232)^{++} \bar{\Delta}(1232)^{-}) / \Gamma_{\text{total}}$					Γ_{139} / Γ
VALUE (units 10^{-3})	EVTS	DOCUMENT ID	TECN	COMMENT	
$1.10 \pm 0.09 \pm 0.28$	233	EATON	84 MRK2	$e^+ e^-$	

$\Gamma(\Sigma(1385)^0 \rho K^-) / \Gamma_{\text{total}}$					Γ_{140} / Γ
VALUE (units 10^{-3})	EVTS	DOCUMENT ID	TECN	COMMENT	
$0.51 \pm 0.26 \pm 0.18$	89	EATON	84 MRK2	$e^+ e^-$	

$\Gamma(\Sigma(1385)^0 \bar{\Lambda} + \text{c.c.}) / \Gamma_{\text{total}}$					Γ_{141} / Γ
VALUE	CL%	DOCUMENT ID	TECN	COMMENT	
$< 0.82 \times 10^{-5}$	90	ABLIKIM	13F BES3	$J/\psi \rightarrow \rho \bar{p} \pi^+ \pi^- \gamma \gamma$	
• • • We do not use the following data for averages, fits, limits, etc. • • •					
$< 0.2 \times 10^{-3}$	90	HENRARD	87 DM2	$e^+ e^-$	

$\Gamma(\Sigma(1385)^- \bar{\Sigma}^+ + \text{c.c.}) / \Gamma_{\text{total}}$					Γ_{142} / Γ
VALUE (units 10^{-3})	EVTS	DOCUMENT ID	TECN	COMMENT	
0.30 ± 0.07 OUR AVERAGE					
$0.30 \pm 0.03 \pm 0.08$	74 ± 8	HENRARD	87 DM2	$e^+ e^-$	
$0.29 \pm 0.11 \pm 0.10$	26	EATON	84 MRK2	$e^+ e^-$	

$\Gamma(\Sigma(1385)^+ \bar{\Sigma}^- + \text{c.c.}) / \Gamma_{\text{total}}$					Γ_{143} / Γ
VALUE (units 10^{-3})	EVTS	DOCUMENT ID	TECN	COMMENT	
0.33 ± 0.08 OUR AVERAGE					
$0.34 \pm 0.04 \pm 0.08$	77	HENRARD	87 DM2	$e^+ e^-$	
$0.31 \pm 0.11 \pm 0.11$	28	EATON	84 MRK2	$e^+ e^-$	

$\Gamma(\Sigma(1385)^- \bar{\Sigma}(1385)^+ + \text{c.c.}) / \Gamma_{\text{total}}$					Γ_{144} / Γ
VALUE (units 10^{-3})	EVTS	DOCUMENT ID	TECN	COMMENT	
1.08 ± 0.06 OUR AVERAGE					
$1.096 \pm 0.012 \pm 0.071$	43k	ABLIKIM	16L BES3	$e^+ e^-$	
$1.23 \pm 0.07 \pm 0.30$	0.8k	ABLIKIM	12P BES2	$e^+ e^-$	
$1.00 \pm 0.04 \pm 0.21$	0.6k	HENRARD	87 DM2	$e^+ e^-$	
$0.86 \pm 0.18 \pm 0.22$	56	EATON	84 MRK2	$e^+ e^-$	

$\Gamma(\Sigma(1385)^+ \bar{\Sigma}(1385)^- + \text{c.c.}) / \Gamma_{\text{total}}$					Γ_{145} / Γ
VALUE (units 10^{-3})	EVTS	DOCUMENT ID	TECN	COMMENT	
1.25 ± 0.07 OUR AVERAGE					
$1.258 \pm 0.014 \pm 0.078$	53k	ABLIKIM	16L BES3	$e^+ e^-$	
$1.50 \pm 0.08 \pm 0.38$	1k	ABLIKIM	12P BES2	$e^+ e^-$	
$1.19 \pm 0.04 \pm 0.25$	0.7k	HENRARD	87 DM2	$e^+ e^-$	
$1.03 \pm 0.24 \pm 0.25$	68	EATON	84 MRK2	$e^+ e^-$	

$\Gamma(\Sigma(1385)^0 \Sigma(1385)^0) / \Gamma_{\text{total}}$					Γ_{146} / Γ
VALUE (units 10^{-3})	EVTS	DOCUMENT ID	TECN	COMMENT	
$1.071 \pm 0.009 \pm 0.082$	103k	ABLIKIM	17E BES3	$e^+ e^- \rightarrow J/\psi \rightarrow \text{hadrons}$	

$\Gamma(\Lambda(1520) \bar{\Lambda} + \text{c.c.} \rightarrow \gamma \Lambda \bar{\Lambda}) / \Gamma_{\text{total}}$					Γ_{147} / Γ
VALUE	CL%	DOCUMENT ID	TECN	COMMENT	
$< 4.1 \times 10^{-6}$	90	ABLIKIM	12B BES3	$J/\psi \rightarrow \Lambda \bar{\Lambda} \gamma$	

$\Gamma(\bar{\Lambda}(1520) \Lambda + \text{c.c.}) / \Gamma_{\text{total}}$					Γ_{148} / Γ
VALUE	CL%	DOCUMENT ID	TECN	COMMENT	
$< 1.80 \times 10^{-3}$	90	LU	19 BELL	$B^+ \rightarrow \bar{p} \Lambda K^+ K^+$	

$\Gamma(\Xi^0 \Xi^0) / \Gamma_{\text{total}}$					Γ_{149} / Γ
VALUE (units 10^{-3})	EVTS	DOCUMENT ID	TECN	COMMENT	
1.17 ± 0.04 OUR AVERAGE					
$1.165 \pm 0.004 \pm 0.043$	135k	ABLIKIM	17E BES3	$e^+ e^- \rightarrow J/\psi \rightarrow \text{hadrons}$	
$1.20 \pm 0.12 \pm 0.21$	206	ABLIKIM	08O BES2	$e^+ e^- \rightarrow J/\psi$	

$\Gamma(\Xi(1530)^- \Xi^+ + \text{c.c.}) / \Gamma_{\text{total}}$					Γ_{150} / Γ
VALUE (units 10^{-3})	EVTS	DOCUMENT ID	TECN	COMMENT	
0.318 ± 0.008 OUR AVERAGE					
$0.317 \pm 0.002 \pm 0.008$	70k	ABLIKIM	20 BES3	$e^+ e^- \rightarrow J/\psi$	
$0.59 \pm 0.09 \pm 0.12$	75	HENRARD	87 DM2	$e^+ e^-$	

$\Gamma(\Xi(1530)^0 \Xi^0) / \Gamma_{\text{total}}$					Γ_{151} / Γ
VALUE (units 10^{-3})	EVTS	DOCUMENT ID	TECN	COMMENT	
$0.32 \pm 0.12 \pm 0.07$	24 ± 9	HENRARD	87 DM2	$e^+ e^-$	

$\Gamma(\Theta(1540) \bar{\Theta}(1540) \rightarrow K_S^0 \rho K^- \pi + \text{c.c.}) / \Gamma_{\text{total}}$					Γ_{152} / Γ
VALUE	CL%	DOCUMENT ID	TECN	COMMENT	
$< 1.1 \times 10^{-5}$	90	BAI	04G BES2	$e^+ e^-$	

$\Gamma(\Theta(1540) K^- \pi \rightarrow K_S^0 \rho K^- \pi) / \Gamma_{\text{total}}$					Γ_{153} / Γ
VALUE	CL%	DOCUMENT ID	TECN	COMMENT	
$< 2.1 \times 10^{-5}$	90	BAI	04G BES2	$e^+ e^-$	

$\Gamma(\Theta(1540) K_S^0 \bar{p} \rightarrow K_S^0 \bar{p} K^+ n) / \Gamma_{\text{total}}$					Γ_{154} / Γ
VALUE	CL%	DOCUMENT ID	TECN	COMMENT	
$< 1.6 \times 10^{-5}$	90	BAI	04G BES2	$e^+ e^-$	

Meson Particle Listings

$J/\psi(1S)$

$\Gamma(\bar{\Theta}(1540)K^+n \rightarrow K_S^0 \bar{p}K^+n)/\Gamma_{total}$					Γ_{155}/Γ
VALUE	CL%	DOCUMENT ID	TECN	COMMENT	
$<5.6 \times 10^{-5}$	90	BAI	04G	BES2 e^+e^-	

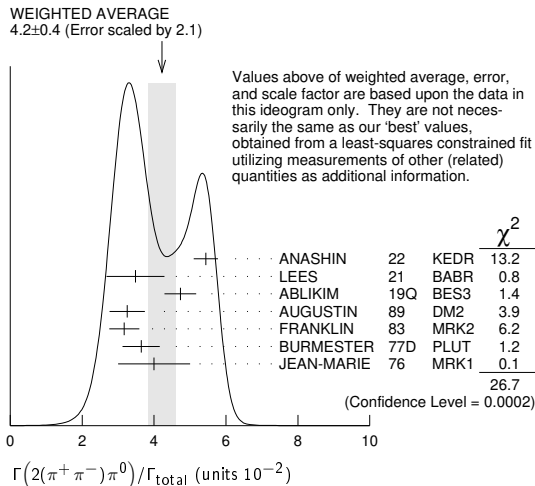
$\Gamma(\bar{\Theta}(1540)K_S^0\rho \rightarrow K_S^0 \rho K^-\pi)/\Gamma_{total}$					Γ_{156}/Γ
VALUE	CL%	DOCUMENT ID	TECN	COMMENT	
$<1.1 \times 10^{-5}$	90	BAI	04G	BES2 e^+e^-	

STABLE HADRONS

$\Gamma(2(\pi^+\pi^-\pi^0))/\Gamma_{total}$					Γ_{157}/Γ
VALUE (units 10^{-2})	EVTS	DOCUMENT ID	TECN	COMMENT	
4.2 ± 0.4 OUR AVERAGE				Error includes scale factor of 2.1. See the ideogram below.	
5.44 ± 0.07 ± 0.33	23K	ANASHIN	22	KEDR $J/\psi \rightarrow 2(\pi^+\pi^-\pi^0)$	
3.5 ± 0.8 ± 0.1	14k	1 LEES	21	BABR 10.6 $e^+e^- \rightarrow 2(\pi^+\pi^-\pi^0)3\pi^0\gamma$	
4.73 ± 0.44	228k	2 ABLIKIM	19Q	BES3 $J/\psi \rightarrow 2(\pi^+\pi^-\pi^0)$	
3.25 ± 0.49	46055	AUGUSTIN	89	DM2 $J/\psi \rightarrow 2(\pi^+\pi^-\pi^0)$	
3.17 ± 0.42	147	FRANKLIN	83	MRK2 $e^+e^- \rightarrow$ hadrons	
3.64 ± 0.52	1500	BURMESTER	77D	PLUT e^+e^-	
4 ± 1	675	JEAN-MARIE	76	MRK1 e^+e^-	

¹ LEES 21 reports $[\Gamma(J/\psi(1S) \rightarrow 2(\pi^+\pi^-\pi^0))/\Gamma_{total}] \times [\Gamma(\psi(2S) \rightarrow e^+e^-)] \times [B(\psi(2S) \rightarrow J/\psi(1S)\pi^0\pi^0)] = (14.8 \pm 2.6 \pm 2.2) \times 10^{-3}$ keV which we divide by our best values $\Gamma(\psi(2S) \rightarrow e^+e^-) = 2.33 \pm 0.04$ keV, $B(\psi(2S) \rightarrow J/\psi(1S)\pi^0\pi^0) = (18.2 \pm 0.5) \times 10^{-2}$. Our first error is their experiment's error and our second error is the systematic error from using our best values.

² From an energy scan of $e^+e^- \rightarrow J/\psi \rightarrow 2(\pi^+\pi^-\pi^0)$, assuming PDG 16 values for $\Gamma(e^+e^-)$, $\Gamma(\mu^+\mu^-)$, and $\Gamma(total)$, and for a phase difference between strong and electromagnetic amplitudes of $(84.9 \pm 3.6)^\circ$. An alternative solution is $(4.85 \pm 0.45)\%$ with a phase of $(-84.7 \pm 3.1)^\circ$.



$\Gamma(3(\pi^+\pi^-\pi^0))/\Gamma_{total}$					Γ_{158}/Γ
VALUE	EVTS	DOCUMENT ID	TECN	COMMENT	
0.029 ± 0.006 OUR AVERAGE					
0.028 ± 0.009	11	FRANKLIN	83	MRK2 $e^+e^- \rightarrow$ hadrons	
0.029 ± 0.007	181	JEAN-MARIE	76	MRK1 e^+e^-	

$\Gamma(\pi^+\pi^-\pi^0)/\Gamma_{total}$					Γ_{163}/Γ
VALUE (units 10^{-3})	EVTS	DOCUMENT ID	TECN	COMMENT	
20.0 ± 0.7 OUR AVERAGE				Error includes scale factor of 2.0. See the ideogram below.	
18.78 ± 0.13 ± 0.51	19.8k	1 ANASHIN	23	KEDR $e^+e^- \rightarrow J/\psi \rightarrow \pi^+\pi^-\pi^0$	
21.37 ± 0.04 ± 0.64 ± 0.62	1.8M	2 ABLIKIM	12H	BES3 $e^+e^- \rightarrow J/\psi \rightarrow \pi^+\pi^-\pi^0$	
23.0 ± 2.0 ± 0.4	256	3 AUBERT	07AU	BABR 10.6 $e^+e^- \rightarrow J/\psi\pi^+\pi^-\gamma$	
21.84 ± 0.05 ± 2.01	220k	4.5 BAI	04H	BES e^+e^-	
20.91 ± 0.21 ± 1.16	5.6	BAI	04H	BES e^+e^-	
15 ± 2	168	FRANKLIN	83	MRK2 e^+e^-	

¹ By a simultaneous fit of the $\pi\pi$ invariant mass distribution over the decay modes $J/\psi \rightarrow \rho^0\pi^0$, $J/\psi \rightarrow \rho^+\pi^-$, $J/\psi \rightarrow \rho^-\pi^+$. In the fit only the intermediate states $\rho(770)\pi$ and $\rho(1450)\pi$ are considered.

² The quoted systematic error includes a contribution of 1.23% (added in quadrature) from the uncertainty on the number of J/ψ events.

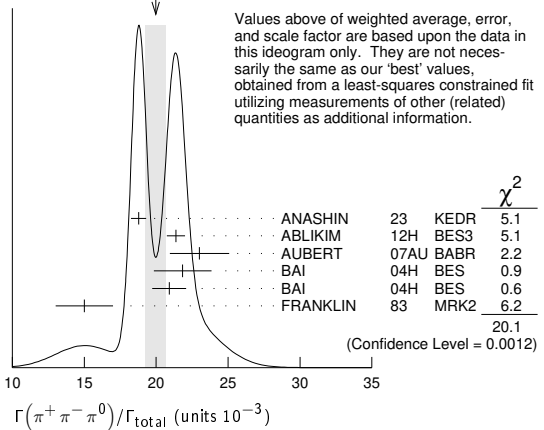
³ AUBERT 07AU reports $[\Gamma(J/\psi(1S) \rightarrow \pi^+\pi^-\pi^0)/\Gamma_{total}] \times [\Gamma(\psi(2S) \rightarrow J/\psi(1S)\pi^+\pi^-) \times \Gamma(\psi(2S) \rightarrow e^+e^-)]/\Gamma_{total} = (18.6 \pm 1.2 \pm 1.1) \times 10^{-3}$ keV which we divide by our best value $\Gamma(\psi(2S) \rightarrow J/\psi(1S)\pi^+\pi^-) \times \Gamma(\psi(2S) \rightarrow e^+e^-)/\Gamma_{total} = 0.808 \pm 0.014$ keV. Our first error is their experiment's error and our second error is the systematic error from using our best value.

⁴ From $J/\psi \rightarrow \pi^+\pi^-\pi^0$ events directly.

⁵ Mostly $\rho\pi$, see also $\rho\pi$ subsection.

⁶ Obtained comparing the rates for $\pi^+\pi^-\pi^0$ and $\mu^+\mu^-$, using J/ψ events produced via $\psi(2S) \rightarrow \pi^+\pi^-J/\psi$ and with $B(J/\psi \rightarrow \mu^+\mu^-) = 5.88 \pm 0.10\%$.

WEIGHTED AVERAGE
20.0 ± 0.7 (Error scaled by 2.0)



$\Gamma(\pi^+\pi^-\pi^0 K^+K^-)/\Gamma_{total}$					Γ_{165}/Γ
VALUE (units 10^{-2})	EVTS	DOCUMENT ID	TECN	COMMENT	
1.52 ± 0.27 OUR AVERAGE				Error includes scale factor of 1.4.	
1.74 ± 0.08 ± 0.24	2616	ANASHIN	22	KEDR $J/\psi \rightarrow K^+K^-\pi^+\pi^-\pi^0$	
1.2 ± 0.3	309	VANNUCCI	77	MRK1 e^+e^-	

$\Gamma(\pi^+\pi^-)/\Gamma_{total}$					Γ_{166}/Γ
VALUE (units 10^{-4})	EVTS	DOCUMENT ID	TECN	COMMENT	
1.47 ± 0.14 OUR AVERAGE					
1.47 ± 0.13 ± 0.13	140	1 METREVELLI	12	$\psi(2S) \rightarrow 2(\pi^+\pi^-)$	
1.58 ± 0.20 ± 0.15	84	BALTRUSAITIS...85D	MRK3	e^+e^-	
1.0 ± 0.5	5	BRANDELIK	78B	DASP e^+e^-	
1.6 ± 1.6	1	VANNUCCI	77	MRK1 e^+e^-	

¹ Obtained by analyzing CLEO-c data but not authored by the CLEO Collaboration.

$\Gamma(2(\pi^+\pi^-))/\Gamma_{total}$					Γ_{167}/Γ
VALUE (units 10^{-3})	EVTS	DOCUMENT ID	TECN	COMMENT	
3.20 ± 0.25 OUR AVERAGE				Error includes scale factor of 1.2.	
2.88 ± 0.14 ± 0.24	2654	ANASHIN	22	KEDR $J/\psi \rightarrow 2(\pi^+\pi^-)$	
3.53 ± 0.12 ± 0.29	1107	1 ABLIKIM	05H	BES2 $e^+e^- \rightarrow \psi(2S) \rightarrow J/\psi\pi^+\pi^-, J/\psi \rightarrow 2(\pi^+\pi^-)$	
4.0 ± 1.0	76	JEAN-MARIE	76	MRK1 e^+e^-	

¹ Computed using $B(J/\psi \rightarrow \mu^+\mu^-) = 0.0588 \pm 0.0010$.

$\Gamma(3(\pi^+\pi^-))/\Gamma_{total}$					Γ_{168}/Γ
VALUE (units 10^{-4})	EVTS	DOCUMENT ID	TECN	COMMENT	
• • • We do not use the following data for averages, fits, limits, etc. • • •					
40 ± 20	32	JEAN-MARIE	76	MRK1 e^+e^-	

$\Gamma(4(\pi^+\pi^-)\pi^0)/\Gamma_{total}$					Γ_{170}/Γ
VALUE (units 10^{-4})	EVTS	DOCUMENT ID	TECN	COMMENT	
90 ± 30					
90 ± 30	13	JEAN-MARIE	76	MRK1 e^+e^-	

$\Gamma(2(\pi^+\pi^-\eta))/\Gamma_{total}$					Γ_{171}/Γ
VALUE (units 10^{-3})	EVTS	DOCUMENT ID	TECN	COMMENT	
2.29 ± 0.28 OUR AVERAGE					
3.1 ± 1.5 ± 0.1	14k	1 LEES	21	BABR 10.6 $e^+e^- \rightarrow 2(\pi^+\pi^-\eta)3\pi^0\gamma$	
2.26 ± 0.08 ± 0.27	4.8k	ABLIKIM	05c	BES2 $e^+e^- \rightarrow 2(\pi^+\pi^-\eta)$	

¹ LEES 21 reports $[\Gamma(J/\psi(1S) \rightarrow 2(\pi^+\pi^-\eta))/\Gamma_{total}] \times [\Gamma(J/\psi(1S) \rightarrow e^+e^-)] \times [B(\eta \rightarrow 3\pi^0)] = (5.6 \pm 2.6 \pm 0.8) \times 10^{-3}$ keV which we divide by our best values $\Gamma(J/\psi(1S) \rightarrow e^+e^-) = 5.53 \pm 0.10$ keV, $B(\eta \rightarrow 3\pi^0) = (32.57 \pm 0.21) \times 10^{-2}$. Our first error is their experiment's error and our second error is the systematic error from using our best values.

$\Gamma(3(\pi^+\pi^-\eta))/\Gamma_{total}$					Γ_{172}/Γ
VALUE (units 10^{-4})	EVTS	DOCUMENT ID	TECN	COMMENT	
7.24 ± 0.96 ± 1.11					
7.24 ± 0.96 ± 1.11	616	ABLIKIM	05c	BES2 $e^+e^- \rightarrow 3(\pi^+\pi^-\eta)$	

$\Gamma(K^+K^-)/\Gamma_{total}$					Γ_{176}/Γ
VALUE (units 10^{-4})	EVTS	DOCUMENT ID	TECN	COMMENT	
2.86 ± 0.09 ± 0.19					
2.86 ± 0.09 ± 0.19	1k	1 METREVELLI	12	$\psi(2S) \rightarrow \pi^+\pi^-K^+K^-$	
• • • We do not use the following data for averages, fits, limits, etc. • • •					
2.39 ± 0.24 ± 0.22	107	2 BALTRUSAITIS...85D	MRK3	e^+e^-	
2.2 ± 0.9	6	2 BRANDELIK	79c	DASP e^+e^-	

¹ Obtained by analyzing CLEO-c data but not authored by the CLEO Collaboration.

² Interference with non-resonant K^+K^- production not taken into account.

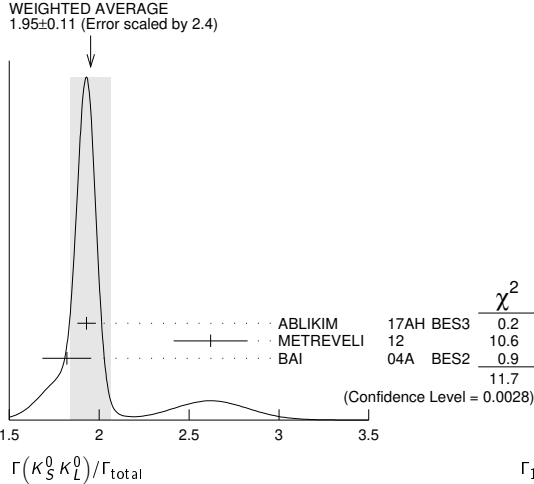
See key on page 1171

Meson Particle Listings

$J/\psi(1S)$

$\Gamma(K_S^0 K_L^0)/\Gamma_{total}$			Γ_{177}/Γ		
VALUE (units 10^{-4})	EVTS	DOCUMENT ID	TECN	COMMENT	
1.95 ± 0.11	OUR AVERAGE	Error includes scale factor of 2.4. See the ideogram below.			
$1.93 \pm 0.01 \pm 0.05$	110k	ABLIKIM	17AH BES3	$J/\psi \rightarrow K_S^0 K_L^0 \rightarrow \pi^+ \pi^- X$	
$2.62 \pm 0.15 \pm 0.14$	0.3k	¹ METREVELI	12	$\psi(2S) \rightarrow \pi^+ \pi^- K_S^0 K_L^0$	
$1.82 \pm 0.04 \pm 0.13$	2.1k	² BAI	04A BES2	$J/\psi \rightarrow K_S^0 K_L^0 \rightarrow \pi^+ \pi^- X$	
• • • We do not use the following data for averages, fits, limits, etc. • • •					
$1.18 \pm 0.12 \pm 0.18$		JOUSSET	90 DM2	$J/\psi \rightarrow$ hadrons	
$1.01 \pm 0.16 \pm 0.09$	74	BALTRUSAIT...	85D MRK3	$e^+ e^-$	

¹ Obtained by analyzing CLEO-c data but not authored by the CLEO Collaboration.
² Using $B(K_S^0 \rightarrow \pi^+ \pi^-) = 0.6868 \pm 0.0027$.



$\Gamma(K_S^0 K_S^0)/\Gamma_{total}$			Γ_{178}/Γ		
VALUE	CL%	DOCUMENT ID	TECN	COMMENT	
$<1.4 \times 10^{-8}$	95	¹ ABLIKIM	17AH BES3	$J/\psi \rightarrow K_S^0 K_S^0 \rightarrow \pi^+ \pi^- \pi^+ \pi^-$	
$<1 \times 10^{-6}$	95	¹ BAI	04D BES	$e^+ e^-$	
$<5.2 \times 10^{-6}$	90	¹ BALTRUSAIT...	85c MRK3	$e^+ e^-$	

• • • We do not use the following data for averages, fits, limits, etc. • • •
¹ Forbidden by CP.

$\Gamma(K \bar{K} \pi)/\Gamma_{total}$			Γ_{179}/Γ		
VALUE (units 10^{-4})	EVTS	DOCUMENT ID	TECN	COMMENT	
61 ± 10	OUR AVERAGE				
55.2 ± 12.0	25	FRANKLIN	83 MRK2	$e^+ e^- \rightarrow K^+ K^- \pi^0$	
78.0 ± 21.0	126	VANNUCCI	77 MRK1	$e^+ e^- \rightarrow K_S^0 K^\pm \pi^\mp$	

$\Gamma(K^+ K^- \pi^0)/\Gamma_{total}$			Γ_{180}/Γ		
VALUE (units 10^{-3})	EVTS	DOCUMENT ID	TECN	COMMENT	
$2.88 \pm 0.01 \pm 0.12$	183k	ABLIKIM	19AQ BES	$J/\psi \rightarrow K^+ K^- \pi^0$	

$\Gamma(K^+ K^- \pi^0)/\Gamma(\pi^+ \pi^- \pi^0)$			$\Gamma_{180}/\Gamma_{163}$		
VALUE (%)	EVTS	DOCUMENT ID	TECN	COMMENT	
$12.0 \pm 0.3 \pm 0.9$	23k	LEES	17c BABR	$J/\psi \rightarrow h^+ h^- \pi^0$	

$\Gamma(K_S^0 K^\pm \pi^\mp)/\Gamma(\pi^+ \pi^- \pi^0)$			$\Gamma_{181}/\Gamma_{163}$		
VALUE (%)	EVTS	DOCUMENT ID	TECN	COMMENT	
$26.5 \pm 0.5 \pm 2.1$	24k	LEES	17c BABR	$J/\psi \rightarrow h^0 h^\pm h^\mp$	

$\Gamma(K^+ K^- \pi^+ \pi^-)/\Gamma_{total}$			Γ_{185}/Γ		
VALUE (units 10^{-3})	EVTS	DOCUMENT ID	TECN	COMMENT	
$7.04 \pm 0.26 \pm 0.92$	2671	ANASHIN	22 KEDR	$J/\psi \rightarrow K^+ K^- \pi^+ \pi^-$	
• • • We do not use the following data for averages, fits, limits, etc. • • •					
7.2 ± 2.3	205	VANNUCCI	77 MRK1	$e^+ e^-$	

$\Gamma(K^+ K^- 2(\pi^+ \pi^-))/\Gamma_{total}$			Γ_{197}/Γ		
VALUE (units 10^{-4})	EVTS	DOCUMENT ID	TECN	COMMENT	
31 ± 13	30	VANNUCCI	77 MRK1	$e^+ e^-$	

$\Gamma(2(K^+ K^-))/\Gamma_{total}$			Γ_{199}/Γ		
VALUE (units 10^{-3})	EVTS	DOCUMENT ID	TECN	COMMENT	
$1.4 \pm 0.5 \pm 0.2$	$11.0 \pm 4.3 \pm 3.5$	¹ HUANG	03 BELL	$B^+ \rightarrow 2(K^+ K^-) K^+$	
0.7 ± 0.3		VANNUCCI	77 MRK1	$e^+ e^-$	

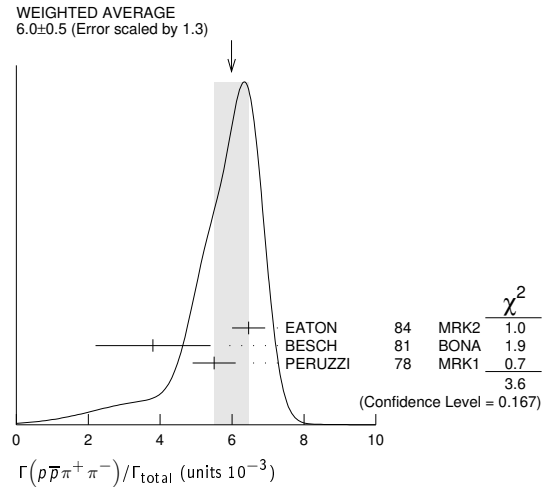
¹ Using $B(B^+ \rightarrow J/\psi K^+) = (1.01 \pm 0.05) \times 10^{-3}$.

$\Gamma(p \bar{p})/\Gamma_{total}$			Γ_{207}/Γ		
VALUE (units 10^{-3})	EVTS	DOCUMENT ID	TECN	COMMENT	
2.120 ± 0.029	OUR AVERAGE	Error includes scale factor of 1.1.			
$2.112 \pm 0.004 \pm 0.031$	314k	ABLIKIM	12c BES3	$e^+ e^-$	
$2.17 \pm 0.16 \pm 0.04$	317	¹ WU	06 BELL	$B^+ \rightarrow p \bar{p} K^+$	
$2.26 \pm 0.01 \pm 0.14$	63316	BAI	04E BES2	$e^+ e^- \rightarrow J/\psi$	
1.97 ± 0.22	99	BALDINI	98 FENI	$e^+ e^-$	
$1.91 \pm 0.04 \pm 0.30$		PALLIN	87 DM2	$e^+ e^-$	
$2.16 \pm 0.07 \pm 0.15$	1420	EATON	84 MRK2	$e^+ e^-$	
2.5 ± 0.4	133	BRANDELIK	79c DASP	$e^+ e^-$	
2.0 ± 0.5		BESCH	78 BONA	$e^+ e^-$	
2.2 ± 0.2	331	² PERUZZI	78 MRK1	$e^+ e^-$	
• • • We do not use the following data for averages, fits, limits, etc. • • •					
2.0 ± 0.3	48	ANTONELLI	93 SPEC	$e^+ e^-$	

¹ WU 06 reports $[\Gamma(J/\psi(1S) \rightarrow p \bar{p})/\Gamma_{total}] \times [B(B^+ \rightarrow J/\psi(1S) K^+)] = (2.21 \pm 0.13 \pm 0.10) \times 10^{-6}$ which we divide by our best value $B(B^+ \rightarrow J/\psi(1S) K^+) = (1.020 \pm 0.019) \times 10^{-3}$. Our first error is their experiment's error and our second error is the systematic error from using our best value.
² Assuming angular distribution $(1 + \cos^2 \theta)$.

$\Gamma(p \bar{p} \pi^0)/\Gamma_{total}$			Γ_{208}/Γ		
VALUE (units 10^{-3})	EVTS	DOCUMENT ID	TECN	COMMENT	
1.19 ± 0.08	OUR AVERAGE	Error includes scale factor of 1.1.			
$1.33 \pm 0.02 \pm 0.11$	11k	ABLIKIM	09B BES2	$e^+ e^-$	
$1.13 \pm 0.09 \pm 0.09$	685	EATON	84 MRK2	$e^+ e^-$	
1.4 ± 0.4		BRANDELIK	79c DASP	$e^+ e^-$	
1.00 ± 0.15	109	PERUZZI	78 MRK1	$e^+ e^-$	

$\Gamma(p \bar{p} \pi^+ \pi^-)/\Gamma_{total}$			Γ_{209}/Γ		
VALUE (units 10^{-3})	EVTS	DOCUMENT ID	TECN	COMMENT	
6.0 ± 0.5	OUR AVERAGE	Error includes scale factor of 1.3. See the ideogram below.			
$6.46 \pm 0.17 \pm 0.43$	1435	EATON	84 MRK2	$e^+ e^-$	
3.8 ± 1.6	48	BESCH	81 BONA	$e^+ e^-$	
5.5 ± 0.6	533	PERUZZI	78 MRK1	$e^+ e^-$	



$\Gamma(p \bar{p} \pi^+ \pi^- \pi^0)/\Gamma_{total}$			Γ_{210}/Γ		
VALUE (units 10^{-3})	EVTS	DOCUMENT ID	TECN	COMMENT	
2.3 ± 0.9	OUR AVERAGE	Including $p \bar{p} \pi^+ \pi^- \pi^0$ and excluding ω, η, η' . Error includes scale factor of 1.9.			
$3.36 \pm 0.65 \pm 0.28$	364	EATON	84 MRK2	$e^+ e^-$	
1.6 ± 0.6	39	PERUZZI	78 MRK1	$e^+ e^-$	

$\Gamma(p \bar{p} \eta)/\Gamma_{total}$			Γ_{211}/Γ		
VALUE (units 10^{-3})	EVTS	DOCUMENT ID	TECN	COMMENT	
2.00 ± 0.12	OUR AVERAGE	Error includes scale factor of 1.3. See the ideogram below.			
$1.91 \pm 0.02 \pm 0.17$	13k	¹ ABLIKIM	09 BES2	$e^+ e^-$	
$2.03 \pm 0.13 \pm 0.15$	826	EATON	84 MRK2	$e^+ e^-$	
2.5 ± 1.2		BRANDELIK	79c DASP	$e^+ e^-$	
2.3 ± 0.4	197	PERUZZI	78 MRK1	$e^+ e^-$	

¹ From the combination of $p \bar{p} \eta \rightarrow p \bar{p} \gamma \gamma$ and $p \bar{p} \eta \rightarrow p \bar{p} \pi^+ \pi^- \pi^0$ channels.

$\Gamma(p \bar{p} \rho)/\Gamma_{total}$			Γ_{212}/Γ		
VALUE	CL%	DOCUMENT ID	TECN	COMMENT	
$<0.31 \times 10^{-3}$	90	EATON	84 MRK2	$e^+ e^- \rightarrow$ hadrons γ	

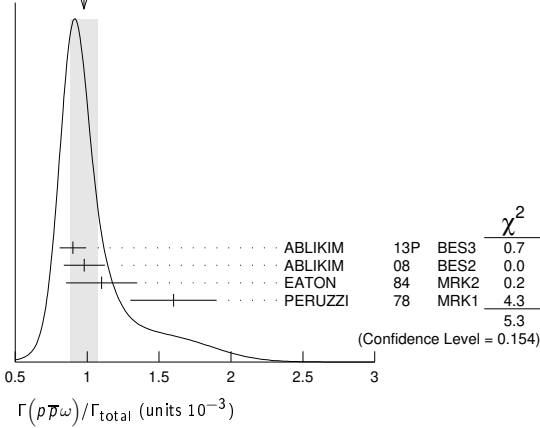
$\Gamma(p \bar{p} \omega)/\Gamma_{total}$			Γ_{213}/Γ		
VALUE (units 10^{-3})	EVTS	DOCUMENT ID	TECN	COMMENT	
0.98 ± 0.10	OUR AVERAGE	Error includes scale factor of 1.3. See the ideogram below.			
$0.90 \pm 0.02 \pm 0.09$	2670	ABLIKIM	13P BES3	$e^+ e^-$	
$0.98 \pm 0.03 \pm 0.14$	2449	ABLIKIM	08 BES2	$e^+ e^-$	

Meson Particle Listings

$J/\psi(1S)$

$1.10 \pm 0.17 \pm 0.18$	486	EATON	84	MRK2	e^+e^-
1.6 ± 0.3	77	PERUZZI	78	MRK1	e^+e^-

WEIGHTED AVERAGE
0.98±0.10 (Error scaled by 1.3)



$\Gamma(p\bar{P}\eta(958))/\Gamma_{total}$ Γ_{214}/Γ

VALUE (units 10^{-3})	EVTS	DOCUMENT ID	TECN	COMMENT
0.129±0.014 OUR AVERAGE		Error includes scale factor of 2.0.		
$0.126 \pm 0.002 \pm 0.007$	16k	¹ ABLIKIM 19N	BES3	e^+e^-
$0.200 \pm 0.023 \pm 0.028$	265 ± 31	² ABLIKIM 09	BES2	e^+e^-
$0.68 \pm 0.23 \pm 0.17$	19	EATON 84	MRK2	e^+e^-
1.8 ± 0.6	19	PERUZZI 78	MRK1	e^+e^-

¹ From the combination of $p\bar{p}\eta' \rightarrow p\bar{p}\pi^+\pi^-\eta$ and $p\bar{p}\eta' \rightarrow p\bar{p}\pi^+\pi^-\gamma$ channels.
² From the combination of $p\bar{p}\eta' \rightarrow p\bar{p}\pi^+\pi^-\eta$ and $p\bar{p}\eta' \rightarrow p\bar{p}\gamma\rho^0$ channels.

$\Gamma(p\bar{P}\eta_0(980) \rightarrow p\bar{P}\pi^0\eta)/\Gamma_{total}$ Γ_{215}/Γ

VALUE (units 10^{-3})	DOCUMENT ID	TECN	COMMENT
6.8±1.2±1.3	ABLIKIM 14N	BES3	$e^+e^- \rightarrow J/\psi$

$\Gamma(p\bar{P}\phi)/\Gamma_{total}$ Γ_{216}/Γ

VALUE (units 10^{-4})	EVTS	DOCUMENT ID	TECN	COMMENT
0.519±0.033 OUR AVERAGE		Error includes scale factor of 2.0.		
$0.523 \pm 0.006 \pm 0.033$	14k	ABLIKIM 16k	BES3	$J/\psi \rightarrow p\bar{p}K_S^0 K_L^0$, $p\bar{p}K^+ K^-$
$0.45 \pm 0.13 \pm 0.07$		FALVARD 88	DM2	$J/\psi \rightarrow$ hadrons

$\Gamma(p\bar{P}\pi^-)/\Gamma_{total}$ Γ_{217}/Γ

VALUE (units 10^{-3})	EVTS	DOCUMENT ID	TECN	COMMENT
2.12±0.09 OUR AVERAGE		Error includes scale factor of 2.0.		
$2.36 \pm 0.02 \pm 0.21$	59k	ABLIKIM 06k	BES2	$J/\psi \rightarrow p\pi^-\bar{\pi}$
$2.47 \pm 0.02 \pm 0.24$	55k	ABLIKIM 06k	BES2	$J/\psi \rightarrow \bar{p}\pi^+n$
$2.02 \pm 0.07 \pm 0.16$	1288	EATON 84	MRK2	$e^+e^- \rightarrow p\pi^-$
$1.93 \pm 0.07 \pm 0.16$	1191	EATON 84	MRK2	$e^+e^- \rightarrow \bar{p}\pi^+$
1.7 ± 0.7	32	BESCH 81	BONA	$e^+e^- \rightarrow p\pi^-$
1.6 ± 1.2	5	BESCH 81	BONA	$e^+e^- \rightarrow \bar{p}\pi^+$
2.16 ± 0.29	194	PERUZZI 78	MRK1	$e^+e^- \rightarrow p\pi^-$
2.04 ± 0.27	204	PERUZZI 78	MRK1	$e^+e^- \rightarrow \bar{p}\pi^+$

$\Gamma(n\bar{n})/\Gamma_{total}$ Γ_{218}/Γ

VALUE (units 10^{-3})	EVTS	DOCUMENT ID	TECN	COMMENT
2.09±0.16 OUR AVERAGE		Error includes scale factor of 2.0.		
$2.07 \pm 0.01 \pm 0.17$	36k	ABLIKIM 12c	BES3	e^+e^-
2.31 ± 0.49	79	BALDINI 98	FENI	e^+e^-
1.8 ± 0.9		BESCH 78	BONA	e^+e^-
• • • We do not use the following data for averages, fits, limits, etc. • • •				
1.90 ± 0.55	40	ANTONELLI 93	SPEC	e^+e^-

$\Gamma(n\bar{n}\pi^+\pi^-)/\Gamma_{total}$ Γ_{219}/Γ

VALUE (units 10^{-3})	EVTS	DOCUMENT ID	TECN	COMMENT
3.8±3.6	5	BESCH 81	BONA	e^+e^-

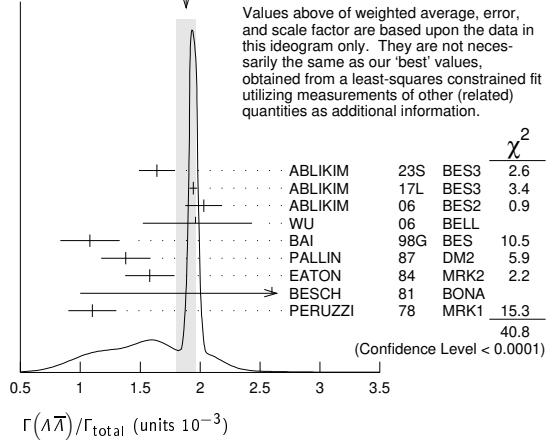
$\Gamma(\Lambda\bar{\Lambda})/\Gamma_{total}$ Γ_{223}/Γ

VALUE (units 10^{-3})	EVTS	DOCUMENT ID	TECN	COMMENT
1.88 ± 0.08 OUR AVERAGE		Error includes scale factor of 2.6. See the ideogram below.		
$1.64 \pm 0.12 \pm 0.09$		ABLIKIM 23s	BES3	$e^+e^- \rightarrow \gamma\Lambda\bar{\Lambda}$
$1.943 \pm 0.003 \pm 0.033$	441k	ABLIKIM 17L	BES3	e^+e^-
$2.03 \pm 0.03 \pm 0.15$	8887	ABLIKIM 06	BES2	$J/\psi \rightarrow \Lambda\bar{\Lambda}$
$1.96 \pm 0.47 \pm 0.04$	46	¹ WU 06	BELL	$B^+ \rightarrow \Lambda\bar{\Lambda}K^+$
$1.08 \pm 0.06 \pm 0.24$	631	BAI 98G	BES	e^+e^-

$1.38 \pm 0.05 \pm 0.20$	1847	PALLIN 87	DM2	e^+e^-
$1.58 \pm 0.08 \pm 0.19$	365	EATON 84	MRK2	e^+e^-
2.6 ± 1.6	5	BESCH 81	BONA	e^+e^-
1.1 ± 0.2	196	PERUZZI 78	MRK1	e^+e^-

¹WU 06 reports $[\Gamma(J/\psi(1S) \rightarrow \Lambda\bar{\Lambda})/\Gamma_{total}] \times [B(B^+ \rightarrow J/\psi(1S)K^+)] = (2.00 \pm 0.34 \pm 0.34) \times 10^{-6}$ which we divide by our best value $B(B^+ \rightarrow J/\psi(1S)K^+) = (1.020 \pm 0.019) \times 10^{-3}$. Our first error is their experiment's error and our second error is the systematic error from using our best value.

WEIGHTED AVERAGE
1.88±0.08 (Error scaled by 2.6)



$\Gamma(\Lambda\bar{\Lambda}\pi^0)/\Gamma_{total}$ Γ_{224}/Γ

VALUE (units 10^{-5})	CL%	EVTS	DOCUMENT ID	TECN	COMMENT
3.78±0.27±0.30		323	¹ ABLIKIM 13F	BES3	$J/\psi \rightarrow p\bar{p}\pi^+\pi^-\gamma\gamma$
• • • We do not use the following data for averages, fits, limits, etc. • • •					
< 6.4		90	² ABLIKIM 07H	BES2	$e^+e^- \rightarrow \psi(2S)$
$23 \pm 7 \pm 8$		11	BAI 98G	BES	e^+e^-
$22 \pm 5 \pm 5$		19	HENRARD 87	DM2	e^+e^-

¹ Using $B(\Lambda \rightarrow \pi^- p) = 63.9\%$ and $B(\pi^0 \rightarrow \gamma\gamma) = 98.8\%$.
² Using $B(\Lambda \rightarrow \pi^- p) = 63.9\%$.

$\Gamma(\Lambda\bar{\Lambda}\pi^+\pi^-)/\Gamma_{total}$ Γ_{225}/Γ

VALUE (units 10^{-3})	EVTS	DOCUMENT ID	TECN	COMMENT
4.30±0.13±0.99	2.4k	ABLIKIM 12P	BES2	J/ψ

$\Gamma(\Lambda\bar{\Lambda}\eta)/\Gamma_{total}$ Γ_{226}/Γ

VALUE (units 10^{-5})	EVTS	DOCUMENT ID	TECN	COMMENT
16.2±1.7 OUR AVERAGE		Error includes scale factor of 1.2.		
$15.7 \pm 0.80 \pm 1.54$	454	¹ ABLIKIM 13F	BES3	$J/\psi \rightarrow p\bar{p}\pi^+\pi^-\gamma\gamma$
$26.2 \pm 6.0 \pm 4.4$	44	² ABLIKIM 07H	BES2	$e^+e^- \rightarrow \psi(2S)$

¹ Using $B(\Lambda \rightarrow \pi^- p) = 63.9\%$ and $B(\eta \rightarrow \gamma\gamma) = 39.31\%$.
² Using $B(\Lambda \rightarrow \pi^- p) = 63.9\%$ and $B(\eta \rightarrow \gamma\gamma) = 39.4\%$.

$\Gamma(\Lambda\bar{\Sigma}^+\pi^- + c.c.)/\Gamma_{total}$ Γ_{227}/Γ

VALUE (units 10^{-3})	EVTS	DOCUMENT ID	TECN	COMMENT
1.26 ± 0.05 OUR AVERAGE		Error includes scale factor of 1.2.		
$1.244 \pm 0.002 \pm 0.045$	2.6M	ABLIKIM 23b	BES3	e^+e^-
$1.52 \pm 0.08 \pm 0.16$	589	¹ ABLIKIM 07H	BES2	e^+e^-
$1.11 \pm 0.06 \pm 0.20$	342 ± 18	HENRARD 87	DM2	e^+e^-
$1.38 \pm 0.21 \pm 0.35$	118	EATON 84	MRK2	e^+e^-

¹ Using $B(\Lambda \rightarrow \pi^- p) = 63.9\%$ and $B(\Sigma^+ \rightarrow \pi^0 p) = 51.6\%$.

$\Gamma(\Lambda\bar{\Sigma}^+\pi^- + c.c.)/\Gamma_{total}$ Γ_{228}/Γ

VALUE (units 10^{-3})	EVTS	DOCUMENT ID	TECN	COMMENT
1.21 ± 0.07 OUR AVERAGE		Error includes scale factor of 1.8.		
$1.221 \pm 0.002 \pm 0.038$	2.7M	ABLIKIM 23B	BES3	e^+e^-
$0.90 \pm 0.06 \pm 0.16$	225	HENRARD 87	DM2	e^+e^-
$1.53 \pm 0.17 \pm 0.38$	135	EATON 84	MRK2	e^+e^-

$\Gamma(pK^-\bar{\Lambda} + c.c.)/\Gamma_{total}$ Γ_{229}/Γ

VALUE (units 10^{-3})	EVTS	DOCUMENT ID	TECN	COMMENT
0.86±0.11 OUR AVERAGE		Error includes scale factor of 1.45.		
$0.84 \pm 0.17 \pm 0.02$	45	¹ LU 19	BELL	$B^+ \rightarrow \bar{p}\Lambda K^+ K^+$
$0.89 \pm 0.07 \pm 0.14$	307	EATON 84	MRK2	e^+e^-

¹ LU 19 reports $(8.32 \pm 1.63 \pm 1.45) \times 10^{-4}$ from a measurement of $[\Gamma(J/\psi(1S) \rightarrow pK^-\bar{\Lambda} + c.c.)/\Gamma_{total}] \times [B(B^+ \rightarrow J/\psi(1S)K^+)]$ assuming $B(B^+ \rightarrow J/\psi(1S)K^+) = (1.026 \pm 0.031) \times 10^{-3}$, which we rescale to our best value $B(B^+ \rightarrow J/\psi(1S)K^+) = (1.020 \pm 0.019) \times 10^{-3}$. Our first error is their experiment's error and our second error is the systematic error from using our best value.

See key on page 1171

Meson Particle Listings

$J/\psi(1S)$

$\Gamma(\rho K^- \bar{\Sigma}^0)/\Gamma_{total}$ Γ_{230}/Γ

VALUE (units 10^{-3})	EVTS	DOCUMENT ID	TECN	COMMENT
0.29 ± 0.06 ± 0.05	90	EATON	84	MRK2 e^+e^-

$\Gamma(\bar{\Lambda} n K_S^0 + c.c.)/\Gamma_{total}$ Γ_{231}/Γ

VALUE (units 10^{-4})	EVTS	DOCUMENT ID	TECN	COMMENT
6.46 ± 0.20 ± 1.07	1058	1 ABLIKIM	08c	BES2 $e^+e^- \rightarrow J/\psi$

¹ Using $B(\bar{\Lambda} \rightarrow \bar{p}\pi^+) = 63.9\%$ and $B(K_S^0 \rightarrow \pi^+\pi^-) = 69.2\%$.

$\Gamma(\bar{\Lambda} \Sigma^+ + c.c.)/\Gamma_{total}$ Γ_{232}/Γ

VALUE (units 10^{-5})	CL%	EVTS	DOCUMENT ID	TECN	COMMENT
2.83 ± 0.23 OUR AVERAGE					
2.74 ± 0.24 ± 0.22		234 ± 21	1 ABLIKIM	12b	BES3 $J/\psi \rightarrow \bar{\Lambda} \Sigma^0$
2.92 ± 0.22 ± 0.24		308 ± 24	2 ABLIKIM	12b	BES3 $J/\psi \rightarrow \bar{\Lambda} \Sigma^0$

• • • We do not use the following data for averages, fits, limits, etc. • • •

<18			2 HENRARD	87	DM2 $J/\psi \rightarrow \bar{\Lambda} \Sigma^0$
<15	90		PERUZZI	78	MRK1 $e^+e^- \rightarrow \Lambda X$

¹ ABLIKIM 12b quotes $B(J/\psi \rightarrow \bar{\Lambda} \Sigma^0)$ which we multiply by 2.
² ABLIKIM 12b and HENRARD 87 quote results for $B(J/\psi \rightarrow \bar{\Lambda} \Sigma^0)$ which we multiply by 2.

$\Gamma(\Sigma^+ \Sigma^-)/\Gamma_{total}$ Γ_{233}/Γ

VALUE (units 10^{-3})	EVTS	DOCUMENT ID	TECN	COMMENT
1.07 ± 0.04 OUR AVERAGE				
1.061 ± 0.004 ± 0.036	87k	ABLIKIM	21AT	BES3 $J/\psi \rightarrow \rho \pi^0 \bar{p} \pi^0$
1.50 ± 0.10 ± 0.22	399	ABLIKIM	08o	BES2 $e^+e^- \rightarrow J/\psi$

$\Gamma(\Sigma^0 \Sigma^0)/\Gamma_{total}$ Γ_{234}/Γ

VALUE (units 10^{-3})	EVTS	DOCUMENT ID	TECN	COMMENT
1.172 ± 0.032 OUR AVERAGE				Error includes scale factor of 1.4.
1.164 ± 0.004 ± 0.023	111k	ABLIKIM	17L	BES3 $J/\psi \rightarrow \Sigma^0 \Sigma^0$
1.33 ± 0.04 ± 0.11	1.7k	ABLIKIM	06	BES2 $J/\psi \rightarrow \Sigma^0 \Sigma^0$
1.06 ± 0.04 ± 0.23	884	PALLIN	87	DM2 $e^+e^- \rightarrow \Sigma^0 \Sigma^0$
1.58 ± 0.16 ± 0.25	90	EATON	84	MRK2 $e^+e^- \rightarrow \Sigma^0 \Sigma^0$
1.3 ± 0.4	52	PERUZZI	78	MRK1 $e^+e^- \rightarrow \Sigma^0 \Sigma^0$

• • • We do not use the following data for averages, fits, limits, etc. • • •

2.4 ± 2.6	3	BESCH	81	BONA $e^+e^- \rightarrow \Sigma^+ \Sigma^-$
-----------	---	-------	----	---

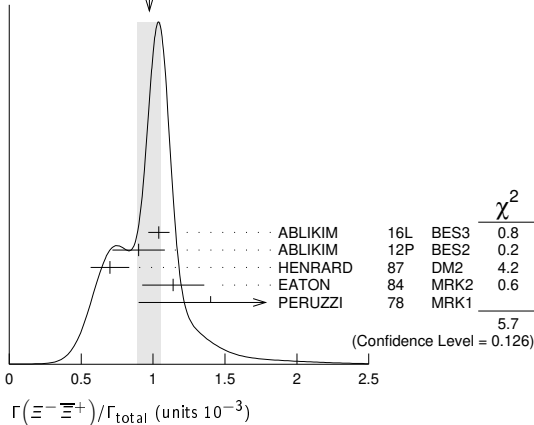
$\Gamma(\Sigma^+ \Sigma^- \eta)/\Gamma_{total}$ Γ_{235}/Γ

VALUE (units 10^{-5})	EVTS	DOCUMENT ID	TECN	COMMENT
6.34 ± 0.21 ± 0.37	1821	ABLIKIM	22AY	BES3 $J/\psi \rightarrow \Sigma^+ \Sigma^- \eta$

$\Gamma(\Xi^- \Xi^+)/\Gamma_{total}$ Γ_{236}/Γ

VALUE (units 10^{-3})	EVTS	DOCUMENT ID	TECN	COMMENT
0.97 ± 0.08 OUR AVERAGE				Error includes scale factor of 1.4. See the ideogram below.
1.040 ± 0.006 ± 0.074	43k	ABLIKIM	16L	BES3 $J/\psi \rightarrow \Xi^- \Xi^+$
0.90 ± 0.03 ± 0.18	961	ABLIKIM	12P	BES2 $J/\psi \rightarrow \Xi^- \Xi^+$
0.70 ± 0.06 ± 0.12	132	HENRARD	87	DM2 $e^+e^- \rightarrow \Xi^- \Xi^+$
1.14 ± 0.08 ± 0.20	194	EATON	84	MRK2 $e^+e^- \rightarrow \Xi^- \Xi^+$
1.4 ± 0.5	51	PERUZZI	78	MRK1 $e^+e^- \rightarrow \Xi^- \Xi^+$

WEIGHTED AVERAGE
0.97±0.08 (Error scaled by 1.4)



RADIATIVE DECAYS

$\Gamma(\gamma \eta_c(1S))/\Gamma_{total}$ Γ_{237}/Γ

VALUE (units 10^{-2})	DOCUMENT ID	TECN	COMMENT
1.41 ± 0.14 OUR FIT			Error includes scale factor of 1.3.
1.7 ± 0.4 OUR AVERAGE			Error includes scale factor of 1.5.
2.00 ± 0.31 ± 0.02	1 MITCHELL	09	CLEO $e^+e^- \rightarrow \gamma X$
1.27 ± 0.36	GAISER	86	CBAL $J/\psi \rightarrow \gamma X$

• • • We do not use the following data for averages, fits, limits, etc. • • •

3.40 ± 0.33	2 ANASHIN	14	KEDR $J/\psi \rightarrow \gamma \eta_c$
-------------	-----------	----	---

¹ MITCHELL 09 reports $(1.98 \pm 0.09 \pm 0.30) \times 10^{-2}$ from a measurement of $[\Gamma(J/\psi(1S) \rightarrow \gamma \eta_c(1S))/\Gamma_{total}] \times [B(\psi(2S) \rightarrow J/\psi(1S)\pi^+\pi^-)]$ assuming $B(\psi(2S) \rightarrow J/\psi(1S)\pi^+\pi^-) = (35.04 \pm 0.07 \pm 0.77) \times 10^{-2}$, which we rescale to our best value $B(\psi(2S) \rightarrow J/\psi(1S)\pi^+\pi^-) = (34.69 \pm 0.34) \times 10^{-2}$. Our first error is their experiment's error and our second error is the systematic error from using our best value.
² Statistical uncertainty only.

$\Gamma(3\gamma)/\Gamma_{total}$ Γ_{240}/Γ

VALUE (units 10^{-6})	CL%	EVTS	DOCUMENT ID	TECN	COMMENT
11.6 ± 2.2 OUR AVERAGE					
11.3 ± 1.8 ± 2.0		113 ± 18	ABLIKIM	13i	BES3 $\psi(2S) \rightarrow \pi^+\pi^- J/\psi$
12 ± 3 ± 2		24.2 ^{+7.2} _{-6.0}	ADAMS	08	CLEO $\psi(2S) \rightarrow \pi^+\pi^- J/\psi$

• • • We do not use the following data for averages, fits, limits, etc. • • •

<55	90		PARTRIDGE	80	CBAL e^+e^-
-----	----	--	-----------	----	---------------

$\Gamma(4\gamma)/\Gamma_{total}$ Γ_{241}/Γ

VALUE	CL%	DOCUMENT ID	TECN	COMMENT
<9 × 10⁻⁶	90	ADAMS	08	CLEO $\psi(2S) \rightarrow \pi^+\pi^- J/\psi$

$\Gamma(5\gamma)/\Gamma_{total}$ Γ_{242}/Γ

VALUE	CL%	DOCUMENT ID	TECN	COMMENT
<15 × 10⁻⁶	90	ADAMS	08	CLEO $\psi(2S) \rightarrow \pi^+\pi^- J/\psi$

$\Gamma(\gamma \pi^0)/\Gamma_{total}$ Γ_{243}/Γ

VALUE (units 10^{-5})	EVTS	DOCUMENT ID	TECN	COMMENT
3.39 ± 0.08 OUR AVERAGE				
3.34 ± 0.02 ± 0.09	176k	ABLIKIM	23BD	BES3 $J/\psi \rightarrow \pi^0 \gamma$
3.59 ± 0.20 ± 0.04	1.6k	1 ABLIKIM	18o	BES3 $\psi(2S) \rightarrow \pi^+\pi^- \gamma \gamma$
3.63 ± 0.36 ± 0.13		PEDLAR	09	CLE3 $J/\psi \rightarrow \pi^0 \gamma$
3.13 ^{+0.65} _{-0.47}	586	ABLIKIM	06E	BES2 $J/\psi \rightarrow \pi^0 \gamma$

• • • We do not use the following data for averages, fits, limits, etc. • • •

3.6 ± 1.1 ± 0.7		BLOOM	83	CBAL e^+e^-
7.3 ± 4.7	10	BRANDELIK	79c	DASP e^+e^-

¹ ABLIKIM 18o reports $[\Gamma(J/\psi(1S) \rightarrow \gamma \pi^0)/\Gamma_{total}] \times [B(\pi^0 \rightarrow 2\gamma)] = (3.57 \pm 0.12 \pm 0.16) \times 10^{-5}$ from a measurement of $[\Gamma(J/\psi(1S) \rightarrow \gamma \pi^0)/\Gamma_{total}] \times [B(\pi^0 \rightarrow 2\gamma)] \times [B(\psi(2S) \rightarrow J/\psi(1S)\pi^+\pi^-)]$ assuming $B(\psi(2S) \rightarrow J/\psi(1S)\pi^+\pi^-) = (34.49 \pm 0.30) \times 10^{-2}$, which we rescale to our best values $B(\pi^0 \rightarrow 2\gamma) = (98.823 \pm 0.034) \times 10^{-2}$, $B(\psi(2S) \rightarrow J/\psi(1S)\pi^+\pi^-) = (34.69 \pm 0.34) \times 10^{-2}$. Our first error is their experiment's error and our second error is the systematic error from using our best values.

$\Gamma(\gamma \pi^0 \pi^0)/\Gamma_{total}$ Γ_{244}/Γ

VALUE (units 10^{-3})	DOCUMENT ID	TECN	COMMENT
1.15 ± 0.05	1 ABLIKIM	15AE	BES3 $J/\psi \rightarrow \gamma \pi^0 \pi^0$

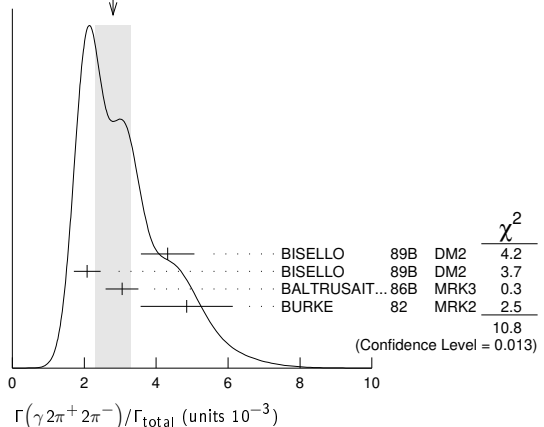
¹ The uncertainty is systematic as statistical is negligible.

$\Gamma(\gamma 2\pi^+ 2\pi^-)/\Gamma_{total}$ Γ_{245}/Γ

VALUE (units 10^{-3})	DOCUMENT ID	TECN	COMMENT
2.8 ± 0.5 OUR AVERAGE			Error includes scale factor of 1.9. See the ideogram below.
4.32 ± 0.14 ± 0.73	1 BISELLO	89B	DM2 $J/\psi \rightarrow 4\pi \gamma$
2.08 ± 0.13 ± 0.35	2 BISELLO	89B	DM2 $J/\psi \rightarrow 4\pi \gamma$
3.05 ± 0.08 ± 0.45	2 BALTRUSAIT...86B	MRK3	$J/\psi \rightarrow 4\pi \gamma$
4.85 ± 0.45 ± 1.20	3 BURKE	82	MRK2 e^+e^-

¹ 4π mass less than 3.0 GeV.
² 4π mass less than 2.0 GeV.
³ 4π mass less than 2.5 GeV.

WEIGHTED AVERAGE
2.8±0.5 (Error scaled by 1.9)



Meson Particle Listings

$J/\psi(1S)$

$\Gamma(\gamma f_2(1270) f_2(1270))/\Gamma_{total}$					Γ_{246}/Γ
VALUE (units 10^{-4})	EVTS	DOCUMENT ID	TECN	COMMENT	
$9.5 \pm 0.7 \pm 1.6$	646 ± 45	ABLIKIM	04M BES	$J/\psi \rightarrow \gamma 2\pi^+ 2\pi^-$	

$\Gamma(\gamma f_2(1270) f_2(1270) \text{ (non resonant)})/\Gamma_{total}$					Γ_{247}/Γ
VALUE (units 10^{-4})	DOCUMENT ID	TECN	COMMENT		
$8.2 \pm 0.8 \pm 1.7$	¹ ABLIKIM	04M BES	$J/\psi \rightarrow \gamma 2\pi^+ 2\pi^-$		
¹ Subtracting contribution from intermediate $\eta_c(1S)$ decays.					

$\Gamma(\gamma \pi^+ \pi^- 2\pi^0)/\Gamma_{total}$					Γ_{248}/Γ
VALUE (units 10^{-3})	DOCUMENT ID	TECN	COMMENT		
$8.3 \pm 0.2 \pm 3.1$	¹ BALTRUSAIT...86B	MRK3	$J/\psi \rightarrow 4\pi\gamma$		
¹ 4π mass less than 2.0 GeV.					

$\Gamma(\gamma K_S^0 K_S^0)/\Gamma_{total}$					Γ_{249}/Γ
VALUE (units 10^{-4})	DOCUMENT ID	TECN	COMMENT		
8.1 ± 0.4	ABLIKIM	18AA BES3	$J/\psi \rightarrow \gamma K_S^0 K_S^0$		

$\Gamma(\gamma(K\bar{K}\pi) [J^{PC} = 0^{-+}])/ \Gamma_{total}$					Γ_{250}/Γ
VALUE (units 10^{-3})	DOCUMENT ID	TECN	COMMENT		
0.7 ± 0.4 OUR AVERAGE	Error includes scale factor of 2.1.				
$0.58 \pm 0.03 \pm 0.20$	¹ BAI	00D BES	$J/\psi \rightarrow \gamma K^\pm K_S^0 \pi^\mp$		
$2.1 \pm 0.1 \pm 0.7$	² BAI	00D BES	$J/\psi \rightarrow \gamma K^\pm K_S^0 \pi^\mp$		
¹ For a broad structure around 1800 MeV.					
² For a broad structure around 2040 MeV.					

$\Gamma(\gamma K^+ K^- \pi^+ \pi^-)/\Gamma_{total}$					Γ_{251}/Γ
VALUE (units 10^{-3})	EVTS	DOCUMENT ID	TECN	COMMENT	
$2.1 \pm 0.1 \pm 0.6$	1516	BAI	00B BES	$J/\psi \rightarrow \gamma K^+ K^0 \pi^+ \pi^-$	

$\Gamma(\gamma K^*(892) \bar{K}^*(892))/\Gamma_{total}$					Γ_{252}/Γ
VALUE (units 10^{-3})	EVTS	DOCUMENT ID	TECN	COMMENT	
$4.0 \pm 0.3 \pm 1.3$	320	¹ BAI	00B BES	$J/\psi \rightarrow \gamma K^+ K^0 \pi^+ \pi^-$	
¹ Summed over all charges.					

$\Gamma(\gamma\eta)/\Gamma_{total}$					Γ_{253}/Γ
VALUE (units 10^{-3})	EVTS	DOCUMENT ID	TECN	COMMENT	
1.090 ± 0.013 OUR AVERAGE					
$1.096 \pm 0.001 \pm 0.019$	2.2M	ABLIKIM	23BD BES3	$J/\psi \rightarrow \eta\gamma$	
$1.067 \pm 0.005 \pm 0.023$	87.9k	ABLIKIM	21AMBES3	$e^+ e^- \rightarrow J/\psi$	
$1.12 \pm 0.05 \pm 0.01$	18.6k	¹ ABLIKIM	18O BES3	$\psi(2S) \rightarrow \pi^+ \pi^- \gamma\gamma\gamma$	
$1.101 \pm 0.029 \pm 0.022$		PEDLAR	09 CLE3	$J/\psi \rightarrow \eta\gamma$	
1.123 ± 0.089	11k	ABLIKIM	06E BES2	$J/\psi \rightarrow \eta\gamma$	
••• We do not use the following data for averages, fits, limits, etc. •••					
$0.88 \pm 0.08 \pm 0.11$		BLOOM	83 CBAL	$e^+ e^-$	
0.82 ± 0.10		BRANDELIK	79C DASP	$e^+ e^-$	
1.3 ± 0.4	21	BARTEL	77 CNTR	$e^+ e^-$	

¹ ABLIKIM 18O reports $[\Gamma(J/\psi(1S) \rightarrow \gamma\eta)/\Gamma_{total}] \times [B(\eta \rightarrow 2\gamma)] = (4.42 \pm 0.04 \pm 0.18) \times 10^{-4}$ from a measurement of $[\Gamma(J/\psi(1S) \rightarrow \gamma\eta)/\Gamma_{total}] \times [B(\eta \rightarrow 2\gamma)] \times [B(\psi(2S) \rightarrow J/\psi(1S)\pi^+\pi^-)]$ assuming $B(\psi(2S) \rightarrow J/\psi(1S)\pi^+\pi^-) = (34.49 \pm 0.30) \times 10^{-2}$, which we rescale to our best values $B(\eta \rightarrow 2\gamma) = (39.36 \pm 0.18) \times 10^{-2}$, $B(\psi(2S) \rightarrow J/\psi(1S)\pi^+\pi^-) = (34.69 \pm 0.34) \times 10^{-2}$. Our first error is their experiment's error and our second error is the systematic error from using our best values.

$\Gamma(\gamma\eta\pi^0)/\Gamma_{total}$					Γ_{254}/Γ
VALUE (units 10^{-6})	EVTS	DOCUMENT ID	TECN	COMMENT	
$21.4 \pm 1.8 \pm 2.5$	596	ABLIKIM	16P BES3	$J/\psi \rightarrow 5\gamma$	

$\Gamma(\gamma a_0(980)^0 \rightarrow \gamma\eta\pi^0)/\Gamma_{total}$					Γ_{258}/Γ
VALUE	CL%	DOCUMENT ID	TECN	COMMENT	
$< 2.5 \times 10^{-6}$	95	ABLIKIM	16P BES3	$J/\psi \rightarrow 5\gamma$	

$\Gamma(\gamma a_2(1320)^0 \rightarrow \gamma\eta\pi^0)/\Gamma_{total}$					Γ_{259}/Γ
VALUE	CL%	DOCUMENT ID	TECN	COMMENT	
$< 6.6 \times 10^{-6}$	95	ABLIKIM	16P BES3	$J/\psi \rightarrow 5\gamma$	

$\Gamma(\gamma\eta\pi\pi)/\Gamma_{total}$					Γ_{260}/Γ
VALUE (units 10^{-3})	DOCUMENT ID	TECN	COMMENT		
6.1 ± 1.0 OUR AVERAGE					
$5.85 \pm 0.3 \pm 1.05$	¹ EDWARDS	83B CBAL	$J/\psi \rightarrow \eta\pi^+\pi^-$		
$7.8 \pm 1.2 \pm 2.4$	¹ EDWARDS	83B CBAL	$J/\psi \rightarrow \eta 2\pi^0$		
¹ Broad enhancement at 1700 MeV.					

$\Gamma(\gamma\eta_2(1870) \rightarrow \gamma\eta\pi^+\pi^-)/\Gamma_{total}$					Γ_{261}/Γ
VALUE (units 10^{-4})	DOCUMENT ID	TECN	COMMENT		
$6.2 \pm 2.2 \pm 0.9$	BAI	99 BES	$J/\psi \rightarrow \gamma\eta\pi^+\pi^-$		

$\Gamma(\gamma\eta'(958))/\Gamma_{total}$					Γ_{262}/Γ
VALUE (units 10^{-3})	EVTS	DOCUMENT ID	TECN	COMMENT	
5.28 ± 0.06 OUR AVERAGE				Error includes scale factor of 1.3. See the ideogram below.	
$5.40 \pm 0.01 \pm 0.11$	638k	ABLIKIM	23BD BES3	$J/\psi \rightarrow \gamma\eta'$	
$5.27 \pm 0.03 \pm 0.05$	36k	ABLIKIM	19T BES	$J/\psi \rightarrow \gamma\eta'$	

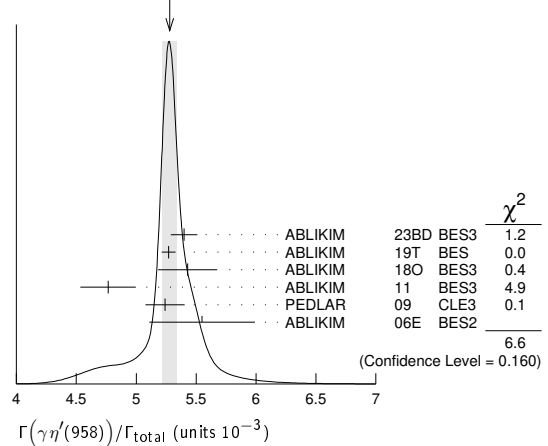
$5.43 \pm 0.23 \pm 0.09$	5.0k	¹ ABLIKIM	18O BES3	$\psi(2S) \rightarrow \pi^+\pi^-\gamma\gamma\gamma$
$4.77 \pm 0.22 \pm 0.06$		² ABLIKIM	11 BES3	$J/\psi \rightarrow \eta'\gamma$
$5.24 \pm 0.12 \pm 0.11$		PEDLAR	09 CLE3	$J/\psi \rightarrow \eta'\gamma$
5.55 ± 0.44	35k	ABLIKIM	06E BES2	$J/\psi \rightarrow \eta'\gamma$

$4.50 \pm 0.14 \pm 0.53$		BOLTON	92B MRK3	$J/\psi \rightarrow \gamma\pi^+\pi^-\eta, \eta \rightarrow \gamma\gamma$
$4.30 \pm 0.31 \pm 0.71$		BOLTON	92B MRK3	$J/\psi \rightarrow \gamma\pi^+\pi^-\eta, \eta \rightarrow \pi^+\pi^-\pi^0$
$4.04 \pm 0.16 \pm 0.85$	622	AUGUSTIN	90 DM2	$J/\psi \rightarrow \gamma\eta\pi^+\pi^-$
$4.39 \pm 0.09 \pm 0.66$	2420	AUGUSTIN	90 DM2	$J/\psi \rightarrow \gamma\eta\pi^+\pi^-$
$4.1 \pm 0.3 \pm 0.6$		BLOOM	83 CBAL	$e^+ e^- \rightarrow 3\gamma + \text{hadrons}$
2.9 ± 1.1	6	BRANDELIK	79C DASP	$e^+ e^- \rightarrow 3\gamma$
2.4 ± 0.7	57	BARTEL	76 CNTR	$e^+ e^- \rightarrow 2\gamma\rho$

¹ ABLIKIM 18O reports $[\Gamma(J/\psi(1S) \rightarrow \gamma\eta'(958))/\Gamma_{total}] \times [B(\eta'(958) \rightarrow \gamma\gamma)] = (1.26 \pm 0.02 \pm 0.05) \times 10^{-4}$ from a measurement of $[\Gamma(J/\psi(1S) \rightarrow \gamma\eta'(958))/\Gamma_{total}] \times [B(\eta'(958) \rightarrow \gamma\gamma)] \times [B(\psi(2S) \rightarrow J/\psi(1S)\pi^+\pi^-)]$ assuming $B(\psi(2S) \rightarrow J/\psi(1S)\pi^+\pi^-) = (34.49 \pm 0.30) \times 10^{-2}$, which we rescale to our best values $B(\eta'(958) \rightarrow \gamma\gamma) = (2.307 \pm 0.033) \times 10^{-2}$, $B(\psi(2S) \rightarrow J/\psi(1S)\pi^+\pi^-) = (34.69 \pm 0.34) \times 10^{-2}$. Our first error is their experiment's error and our second error is the systematic error from using our best values.

² ABLIKIM 11 reports $(4.84 \pm 0.03 \pm 0.24) \times 10^{-3}$ from a measurement of $[\Gamma(J/\psi(1S) \rightarrow \gamma\eta'(958))/\Gamma_{total}] / [B(\eta'(958) \rightarrow \pi^+\pi^-\eta)] / [B(\eta \rightarrow 2\gamma)]$ assuming $B(\eta'(958) \rightarrow \pi^+\pi^-\eta) = (43.2 \pm 0.7) \times 10^{-2}$, $B(\eta \rightarrow 2\gamma) = (39.31 \pm 0.20) \times 10^{-2}$, which we rescale to our best values $B(\eta'(958) \rightarrow \pi^+\pi^-\eta) = (42.5 \pm 0.5) \times 10^{-2}$, $B(\eta \rightarrow 2\gamma) = (39.36 \pm 0.18) \times 10^{-2}$. Our first error is their experiment's error and our second error is the systematic error from using our best values.

WEIGHTED AVERAGE
 5.28 ± 0.06 (Error scaled by 1.3)



$\Gamma(\gamma f_0(500) \rightarrow \gamma\pi\pi)/\Gamma_{total}$					Γ_{255}/Γ
VALUE (units 10^{-4})	DOCUMENT ID	TECN	COMMENT		
10.5 ± 2.0	SARANTSEV	21 RVUE	$J/\psi(1S) \rightarrow \gamma(\pi\pi, K\bar{K}, \eta\eta, \omega\phi)$		

$\Gamma(\gamma f_0(500) \rightarrow \gamma K\bar{K})/\Gamma_{total}$					Γ_{256}/Γ
VALUE (units 10^{-5})	DOCUMENT ID	TECN	COMMENT		
5 ± 5	SARANTSEV	21 RVUE	$J/\psi(1S) \rightarrow \gamma(\pi\pi, K\bar{K}, \eta\eta, \omega\phi)$		

$\Gamma(\gamma f_0(500) \rightarrow \gamma\eta\eta)/\Gamma_{total}$					Γ_{257}/Γ
VALUE (units 10^{-5})	DOCUMENT ID	TECN	COMMENT		
4 ± 3	SARANTSEV	21 RVUE	$J/\psi(1S) \rightarrow \gamma(\pi\pi, K\bar{K}, \eta\eta, \omega\phi)$		

$\Gamma(\gamma f_0(980) \rightarrow \gamma\pi\pi)/\Gamma_{total}$					Γ_{263}/Γ
VALUE (units 10^{-5})	DOCUMENT ID	TECN	COMMENT		
1.3 ± 0.2	SARANTSEV	21 RVUE	$J/\psi(1S) \rightarrow \gamma(\pi\pi, K\bar{K}, \eta\eta, \omega\phi)$		

$\Gamma(\gamma f_0(980) \rightarrow \gamma K\bar{K})/\Gamma_{total}$					Γ_{264}/Γ
VALUE (units 10^{-5})	DOCUMENT ID	TECN	COMMENT		
0.8 ± 0.3	SARANTSEV	21 RVUE	$J/\psi(1S) \rightarrow \gamma(\pi\pi, K\bar{K}, \eta\eta, \omega\phi)$		

$\Gamma(\gamma\rho\rho)/\Gamma_{total}$					Γ_{265}/Γ
VALUE (units 10^{-3})	CL%	DOCUMENT ID	TECN	COMMENT	
4.5 ± 0.8 OUR AVERAGE					
$4.7 \pm 0.3 \pm 0.9$		¹ BALTRUSAIT...86B	MRK3	$J/\psi \rightarrow 4\pi\gamma$	
$3.75 \pm 1.05 \pm 1.20$		² BURKE	82 MRK2	$J/\psi \rightarrow 4\pi\gamma$	

See key on page 1171

Meson Particle Listings

$J/\psi(1S)$

- We do not use the following data for averages, fits, limits, etc. •••
- <0.09 90 ³BISELLO 89B $J/\psi \rightarrow 4\pi\gamma$
- ¹ 4π mass less than 2.0 GeV.
- ² 4π mass less than 2.0 GeV. We have multiplied $2\rho^0$ measurement by 3 to obtain 2ρ .
- ³ 4π mass in the range 2.0–25 GeV.

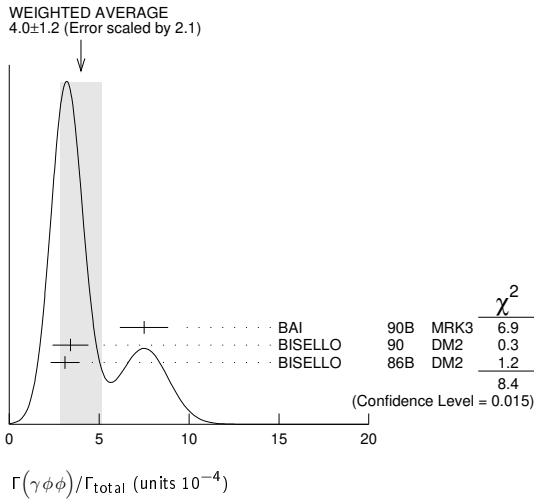
$\Gamma(\gamma\rho\omega)/\Gamma_{\text{total}}$		Γ_{266}/Γ	
VALUE	CL%	DOCUMENT ID	TECN COMMENT
<5.4 × 10⁻⁴	90	ABLIKIM	08A BES2 $e^+e^- \rightarrow J/\psi$

$\Gamma(\gamma\rho\phi)/\Gamma_{\text{total}}$		Γ_{267}/Γ	
VALUE	CL%	DOCUMENT ID	TECN COMMENT
<8.8 × 10⁻⁵	90	ABLIKIM	08A BES2 $e^+e^- \rightarrow J/\psi$

$\Gamma(\gamma\omega)/\Gamma_{\text{total}}$		Γ_{268}/Γ	
VALUE (units 10 ⁻³)	EVTS	DOCUMENT ID	TECN COMMENT
1.61 ± 0.33 OUR AVERAGE			
6.0 ± 4.8 ± 1.8		ABLIKIM	08A BES2 $J/\psi \rightarrow \gamma\omega\pi^+\pi^-$
1.41 ± 0.2 ± 0.42	120 ± 17	BISELLO	87 SPEC e^+e^- , hadrons γ
1.76 ± 0.09 ± 0.45		BALTRUSAIT...85c	MRK3 $e^+e^- \rightarrow$ hadrons γ

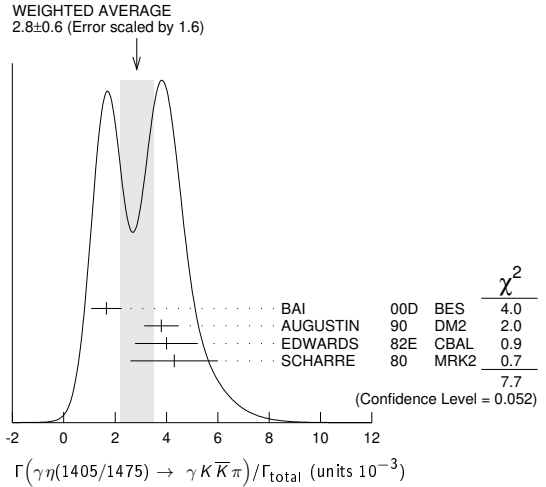
$\Gamma(\gamma\phi)/\Gamma_{\text{total}}$		Γ_{269}/Γ	
VALUE (units 10 ⁻⁴)	EVTS	DOCUMENT ID	TECN COMMENT
4.0 ± 1.2 OUR AVERAGE			Error includes scale factor of 2.1. See the ideogram below.
7.5 ± 0.6 ± 1.2	168	BAI	90B MRK3 $J/\psi \rightarrow \gamma 4K$
3.4 ± 0.8 ± 0.6	33 ± 7	¹ BISELLO	90 DM2 $J/\psi \rightarrow \gamma K^+ K^- K_S^0 K_L^0$
3.1 ± 0.7 ± 0.4		¹ BISELLO	86B DM2 $J/\psi \rightarrow \gamma K^+ K^- K^+ K^-$

¹ ϕ mass less than 2.9 GeV, η_C excluded.



$\Gamma(\gamma\eta(1405/1475) \rightarrow \gamma K\bar{K}\pi)/\Gamma_{\text{total}}$		Γ_{270}/Γ	
VALUE (units 10 ⁻³)	EVTS	DOCUMENT ID	TECN COMMENT
2.8 ± 0.6 OUR AVERAGE			Error includes scale factor of 1.6. See the ideogram below.
1.66 ± 0.1 ± 0.58		^{1,2} BAI	00D BES $J/\psi \rightarrow \gamma K^\pm K_S^0 \pi^\mp$
3.8 ± 0.3 ± 0.6		³ AUGUSTIN	90 DM2 $J/\psi \rightarrow \gamma K\bar{K}\pi$
4.0 ± 0.7 ± 1.0		³ EDWARDS	82E CBAL $J/\psi \rightarrow K^+ K^- \pi^0 \gamma$
4.3 ± 1.7		^{3,4} SCHARRE	80 MRK2 e^+e^-

- We do not use the following data for averages, fits, limits, etc. •••
 - 1.78 ± 0.21 ± 0.33 ^{3,5,6}AUGUSTIN 92 DM2 $J/\psi \rightarrow \gamma K\bar{K}\pi$
 - 0.83 ± 0.13 ± 0.18 ^{3,7,8}AUGUSTIN 92 DM2 $J/\psi \rightarrow \gamma K\bar{K}\pi$
 - 0.66 ± 0.17 ± 0.24 ^{3,6,9}BAI 90c MRK3 $J/\psi \rightarrow \gamma K_S^0 K^\pm \pi^\mp$
 - 0.13 ± 0.16 ± 0.15
 - 1.03 ± 0.21 ± 0.26 ^{3,8,10}BAI 90c MRK3 $J/\psi \rightarrow \gamma K_S^0 K^\pm \pi^\mp$
 - 1.03 ± 0.18 ± 0.19
- ¹ Interference with the $J/\psi(1S)$ radiative transition to the broad $K\bar{K}\pi$ pseudoscalar state around 1800 is $(0.15 \pm 0.01 \pm 0.05) \times 10^{-3}$.
- ² Interference with $J/\psi \rightarrow \gamma f_1(1420)$ is $(-0.03 \pm 0.01 \pm 0.01) \times 10^{-3}$.
- ³ Includes unknown branching fraction $\eta(1405) \rightarrow K\bar{K}\pi$.
- ⁴ Corrected for spin-zero hypothesis for $\eta(1405)$.
- ⁵ From fit to the $a_0(980)\pi 0^-$ partial wave.
- ⁶ $a_0(980)\pi$ mode.
- ⁷ From fit to the $K^*(892)K 0^-$ partial wave.
- ⁸ K^*K mode.
- ⁹ From $a_0(980)\pi$ final state.
- ¹⁰ From $K^*(890)K$ final state.



$\Gamma(\gamma\eta(1405/1475) \rightarrow \gamma\gamma\rho^0)/\Gamma_{\text{total}}$		Γ_{271}/Γ	
VALUE (units 10 ⁻⁴)	EVTS	DOCUMENT ID	TECN COMMENT
0.78 ± 0.20 OUR AVERAGE			Error includes scale factor of 1.8.
1.07 ± 0.17 ± 0.11		¹ BAI	04J BES2 $J/\psi \rightarrow \gamma\gamma\pi^+\pi^-$
0.64 ± 0.12 ± 0.07		¹ COFFMAN	90 MRK3 $J/\psi \rightarrow \gamma\gamma\pi^+\pi^-$

¹ Includes unknown branching fraction $\eta(1405) \rightarrow \gamma\rho^0$.

$\Gamma(\gamma\eta(1405/1475) \rightarrow \gamma\eta\pi^+\pi^-)/\Gamma_{\text{total}}$		Γ_{272}/Γ	
VALUE (units 10 ⁻⁴)	EVTS	DOCUMENT ID	TECN COMMENT
3.0 ± 0.5 OUR AVERAGE			
2.6 ± 0.7 ± 0.4		BAI	99 BES $J/\psi \rightarrow \gamma\eta\pi^+\pi^-$
3.38 ± 0.33 ± 0.64		¹ BOLTON	92B MRK3 $J/\psi \rightarrow \gamma\eta\pi^+\pi^-$

••• We do not use the following data for averages, fits, limits, etc. •••

7.0 ± 0.6 ± 1.1	261	² AUGUSTIN	90 DM2 $J/\psi \rightarrow \gamma\eta\pi^+\pi^-$
-----------------	-----	-----------------------	--

¹ Via $a_0(980)\pi$.

² Includes unknown branching fraction to $\eta\pi^+\pi^-$.

$\Gamma(\gamma\eta(1405/1475) \rightarrow \gamma\rho^0\rho^0)/\Gamma_{\text{total}}$		Γ_{273}/Γ	
VALUE (units 10 ⁻³)	EVTS	DOCUMENT ID	TECN COMMENT
1.7 ± 0.4 OUR AVERAGE			Error includes scale factor of 1.3.
2.1 ± 0.4		BUGG	95 MRK3 $J/\psi \rightarrow \gamma\pi^+\pi^-\pi^+\pi^-$
1.36 ± 0.38		^{1,2} BISELLO	89B DM2 $J/\psi \rightarrow 4\pi\gamma$

¹ Estimated by us from various fits.

² Includes unknown branching fraction to $\rho^0\rho^0$.

$\Gamma(\gamma\eta(1405/1475) \rightarrow \gamma\gamma\phi)/\Gamma_{\text{total}}$		Γ_{274}/Γ	
VALUE (units 10 ⁻⁶)	CL% EVTS	DOCUMENT ID	TECN COMMENT
<82	95	BAI	04J BES2 $J/\psi \rightarrow \gamma\gamma K^+ K^-$

••• We do not use the following data for averages, fits, limits, etc. •••

7.03 ± 0.92 ± 0.91	1.3k	¹ ABLIKIM	18i BES3 $J/\psi \rightarrow \gamma\gamma\phi(1020)$
10.36 ± 1.51 ± 1.54	1.9k	² ABLIKIM	18i BES3 $J/\psi \rightarrow \gamma\gamma\phi(1020)$

¹ Constructive interference between the $X(1835)$ and $\eta(1405)/\eta(1475)$ is assumed in a fit to the $\gamma\phi$ invariant mass.

² Destructive interference between the $X(1835)$ and $\eta(1405)/\eta(1475)$ is assumed in a fit to the $\gamma\phi$ invariant mass.

$\Gamma(\gamma\eta(1405) \rightarrow \gamma\gamma\gamma)/\Gamma_{\text{total}}$		Γ_{275}/Γ	
VALUE	CL%	DOCUMENT ID	TECN COMMENT
<2.63 × 10⁻⁶	90	ABLIKIM	18o BES3 $\psi(2S) \rightarrow \pi^+\pi^-\gamma\gamma\gamma$

$\Gamma(\gamma\eta(1475) \rightarrow \gamma\gamma\gamma)/\Gamma_{\text{total}}$		Γ_{276}/Γ	
VALUE	CL%	DOCUMENT ID	TECN COMMENT
<1.86 × 10⁻⁶	90	ABLIKIM	18o BES3 $\psi(2S) \rightarrow \pi^+\pi^-\gamma\gamma\gamma$

$\Gamma(\gamma\eta(1760) \rightarrow \gamma\rho^0\rho^0)/\Gamma_{\text{total}}$		Γ_{277}/Γ	
VALUE (units 10 ⁻³)	EVTS	DOCUMENT ID	TECN COMMENT
0.13 ± 0.09		^{1,2} BISELLO	89B DM2 $J/\psi \rightarrow 4\pi\gamma$

¹ Estimated by us from various fits.

² Includes unknown branching fraction to $\rho^0\rho^0$.

$\Gamma(\gamma\eta(1760) \rightarrow \gamma\omega)/\Gamma_{\text{total}}$		Γ_{278}/Γ	
VALUE (units 10 ⁻³)	EVTS	DOCUMENT ID	TECN COMMENT
1.98 ± 0.08 ± 0.32	1045	ABLIKIM	06H BES $J/\psi \rightarrow \gamma\omega$

$\Gamma(\gamma\eta(1760) \rightarrow \gamma\gamma\gamma)/\Gamma_{\text{total}}$		Γ_{279}/Γ	
VALUE	CL%	DOCUMENT ID	TECN COMMENT
<4.80 × 10⁻⁶	90	ABLIKIM	18o BES3 $\psi(2S) \rightarrow \pi^+\pi^-\gamma\gamma\gamma$

Meson Particle Listings

$J/\psi(1S)$

$\Gamma(\gamma\eta(2225))/\Gamma_{total}$		Γ_{280}/Γ		
VALUE (units 10^{-4})	EVTS	DOCUMENT ID	TECN	COMMENT

$3.14^{+0.50}_{-0.19}$ OUR AVERAGE

$2.40 \pm 0.10^{+2.47}_{-0.18}$		1,2 ABLIKIM	16N BES3	$J/\psi \rightarrow \gamma K^+ K^- K^+ K^-$
$4.4 \pm 0.4 \pm 0.8$	196	2 ABLIKIM	08I BES	$J/\psi \rightarrow \gamma K^+ K^- K_S^0 K_L^0$
$3.3 \pm 0.8 \pm 0.5$		2 BAI	90b MRK3	$J/\psi \rightarrow \gamma K^+ K^- K^+ K^-$
$2.7 \pm 0.6 \pm 0.6$		2 BAI	90b MRK3	$J/\psi \rightarrow \gamma K^+ K^- K_S^0 K_L^0$
$2.4^{+1.5}_{-1.0}$		3,4 BISELLO	89b DM2	$J/\psi \rightarrow 4\pi\gamma$

¹ From a partial wave analysis of $J/\psi \rightarrow \gamma\phi\phi$ that also finds significant signals for $\eta(2100)$, 0^-+ phase space, $f_0(2100)$, $f_2(2010)$, $f_2(2300)$, $f_2(2340)$, and a previously unseen 0^-+ state $X(2500)$ ($M = 2470^{+15}_{-19} \pm 101^{+64}_{-33}$ MeV, $\Gamma = 230^{+64}_{-35} \pm 56$ MeV).

² Includes unknown branching fraction to $\phi\phi$.

³ Estimated by us from various fits.

⁴ Includes unknown branching fraction to $\rho^0\rho^0$.

$\Gamma(\gamma f_2(1270))/\Gamma_{total}$		Γ_{281}/Γ		
VALUE (units 10^{-3})	EVTS	DOCUMENT ID	TECN	COMMENT

1.63 ± 0.12 OUR AVERAGE Error includes scale factor of 1.3. See the ideogram below.

$2.07 \pm 0.16^{+0.02}_{-0.07}$	2.4k	1,2 DOBBS	15	$J/\psi \rightarrow \gamma\pi\pi$
$1.63 \pm 0.26^{+0.02}_{-0.05}$		3 ABLIKIM	06v BES2	$e^+e^- \rightarrow J/\psi \rightarrow \gamma\pi^+\pi^-$
$1.42 \pm 0.21^{+0.02}_{-0.05}$		4 ABLIKIM	06v BES2	$e^+e^- \rightarrow J/\psi \rightarrow \gamma\pi^0\pi^0$
$1.33 \pm 0.05 \pm 0.20$		5 AUGUSTIN	87 DM2	$J/\psi \rightarrow \gamma\pi^+\pi^-$
$1.36 \pm 0.09 \pm 0.23$		5 BALTRUSAIT..87	MRK3	$J/\psi \rightarrow \gamma\pi^+\pi^-$
$1.48 \pm 0.25 \pm 0.30$	178	EDWARDS	82b CBAL	$e^+e^- \rightarrow 2\pi^0\gamma$
2.0 ± 0.7	35	ALEXANDER	78 PLUT	e^+e^-
1.2 ± 0.6	30	BRANDELIK	78b DASP	$e^+e^- \rightarrow \pi^+\pi^-\gamma$

¹ Using CLEO-c data but not authored by the CLEO Collaboration.

² DOBBS 15 reports $[\Gamma(J/\psi(1S) \rightarrow \gamma f_2(1270))/\Gamma_{total}] \times [B(f_2(1270) \rightarrow \pi\pi)] = (1.744 \pm 0.052 \pm 0.122) \times 10^{-3}$ which we divide by our best value $B(f_2(1270) \rightarrow \pi\pi) = (84.3^{+2.8}_{-1.0}) \times 10^{-2}$. Our first error is their experiment's error and our second error is the systematic error from using our best value.

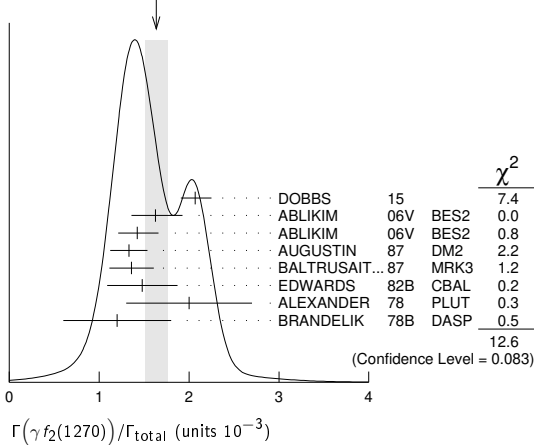
³ ABLIKIM 06v reports $[\Gamma(J/\psi(1S) \rightarrow \gamma f_2(1270))/\Gamma_{total}] \times [B(f_2(1270) \rightarrow \pi\pi)] = (1.371 \pm 0.010 \pm 0.222) \times 10^{-3}$ which we divide by our best value $B(f_2(1270) \rightarrow \pi\pi) = (84.3^{+2.8}_{-1.0}) \times 10^{-2}$. Our first error is their experiment's error and our second error is the systematic error from using our best value.

⁴ ABLIKIM 06v reports $[\Gamma(J/\psi(1S) \rightarrow \gamma f_2(1270))/\Gamma_{total}] \times [B(f_2(1270) \rightarrow \pi\pi)] = (1.200 \pm 0.027 \pm 0.174) \times 10^{-3}$ which we divide by our best value $B(f_2(1270) \rightarrow \pi\pi) = (84.3^{+2.8}_{-1.0}) \times 10^{-2}$. Our first error is their experiment's error and our second error is the systematic error from using our best value.

⁵ Estimated using $B(f_2(1270) \rightarrow \pi\pi) = 0.843 \pm 0.012$. The errors do not contain the uncertainty in the $f_2(1270)$ decay.

⁶ Restated by us to take account of spread of E1, M2, E3 transitions.

WEIGHTED AVERAGE
 1.63 ± 0.12 (Error scaled by 1.3)



$\Gamma(\gamma f_2(1270) \rightarrow \gamma K_S^0 K_S^0)/\Gamma_{total}$		Γ_{282}/Γ		
VALUE (units 10^{-5})	EVTS	DOCUMENT ID	TECN	COMMENT

$2.58^{+0.08+0.59}_{-0.09-0.20}$

		ABLIKIM	18AA BES3	$J/\psi \rightarrow \gamma K_S^0 K_S^0$
--	--	---------	-----------	---

$\Gamma(\gamma f_1(1285))/\Gamma_{total}$		Γ_{283}/Γ		
VALUE (units 10^{-3})	EVTS	DOCUMENT ID	TECN	COMMENT

0.61 ± 0.08 OUR AVERAGE

$0.69 \pm 0.16 \pm 0.20$		1 BAI	04J BES2	$J/\psi \rightarrow \gamma\gamma\rho^0$
$0.61 \pm 0.04 \pm 0.21$		2 BAI	00D BES	$J/\psi \rightarrow \gamma K^\pm K_S^0 \pi^\mp$

$0.45 \pm 0.09 \pm 0.17$		3 BAI	99 BES	$J/\psi \rightarrow \gamma\eta\pi^+\pi^-$
$0.625 \pm 0.063 \pm 0.103$		4 BOLTON	92 MRK3	$J/\psi \rightarrow \gamma f_1(1285)$
$0.70 \pm 0.08 \pm 0.16$		5 BOLTON	92B MRK3	$J/\psi \rightarrow \gamma\eta\pi^+\pi^-$

¹ Assuming $B(f_1(1285) \rightarrow \rho^0\gamma) = 0.055 \pm 0.013$.

² Assuming $\Gamma(f_1(1285) \rightarrow K\bar{K}\pi)/\Gamma_{total} = 0.090 \pm 0.004$.

³ Assuming $\Gamma(f_1(1285) \rightarrow \eta\pi\pi)/\Gamma_{total} = 0.5 \pm 0.18$.

⁴ Obtained summing the sequential decay channels

$B(J/\psi \rightarrow \gamma f_1(1285), f_1(1285) \rightarrow \pi\pi\pi\pi) = (1.44 \pm 0.39 \pm 0.27) \times 10^{-4}$;

$B(J/\psi \rightarrow \gamma f_1(1285), f_1(1285) \rightarrow a_0(980)\pi, a_0(980) \rightarrow \eta\pi) = (3.90 \pm 0.42 \pm 0.87) \times 10^{-4}$;

$B(J/\psi \rightarrow \gamma f_1(1285), f_1(1285) \rightarrow a_0(980)\pi, a_0(980) \rightarrow K\bar{K}) = (0.66 \pm 0.26 \pm 0.29) \times 10^{-4}$;

$B(J/\psi \rightarrow \gamma f_1(1285), f_1(1285) \rightarrow \gamma\rho^0) = (0.25 \pm 0.07 \pm 0.03) \times 10^{-4}$.

⁵ Using $B(f_1(1285) \rightarrow a_0(980)\pi) = 0.37$, and including unknown branching ratio for $a_0(980) \rightarrow \eta\pi$.

$\Gamma(\gamma f_0(1370) \rightarrow \gamma\pi\pi)/\Gamma_{total}$		Γ_{284}/Γ		
VALUE (units 10^{-5})	EVTS	DOCUMENT ID	TECN	COMMENT

• • • We do not use the following data for averages, fits, limits, etc. • • •

38 ± 10		SARANTSEV	21 RVUE	$J/\psi(1S) \rightarrow \gamma(\pi\pi, K\bar{K}, \eta\eta, \omega\phi)$
-------------	--	-----------	---------	---

$\Gamma(\gamma f_0(1370) \rightarrow \gamma K\bar{K})/\Gamma_{total}$		Γ_{285}/Γ		
VALUE (units 10^{-4})	EVTS	DOCUMENT ID	TECN	COMMENT

$4.19 \pm 0.73 \pm 1.34$

• • • We do not use the following data for averages, fits, limits, etc. • • •

1.3 ± 0.4		SARANTSEV	21 RVUE	$J/\psi(1S) \rightarrow \gamma(\pi\pi, K\bar{K}, \eta\eta, \omega\phi)$
---------------	--	-----------	---------	---

¹ Using CLEO-c data but not authored by the CLEO Collaboration.

$\Gamma(\gamma f_0(1370) \rightarrow \gamma K_S^0 K_S^0)/\Gamma_{total}$		Γ_{286}/Γ		
VALUE (units 10^{-5})	EVTS	DOCUMENT ID	TECN	COMMENT

$1.07^{+0.08+0.36}_{-0.07-0.34}$

ABLIKIM 18AA BES3 $J/\psi \rightarrow \gamma K_S^0 K_S^0$

$\Gamma(\gamma f_0(1370) \rightarrow \gamma\eta\eta)/\Gamma_{total}$		Γ_{287}/Γ		
VALUE (units 10^{-5})	EVTS	DOCUMENT ID	TECN	COMMENT

• • • We do not use the following data for averages, fits, limits, etc. • • •

3.5 ± 1.0		SARANTSEV	21 RVUE	$J/\psi(1S) \rightarrow \gamma(\pi\pi, K\bar{K}, \eta\eta, \omega\phi)$
---------------	--	-----------	---------	---

$\Gamma(\gamma f_0(1370) \rightarrow \gamma\eta\eta')/\Gamma_{total}$		Γ_{288}/Γ		
VALUE (units 10^{-5})	EVTS	DOCUMENT ID	TECN	COMMENT

• • • We do not use the following data for averages, fits, limits, etc. • • •

0.9 ± 0.3		SARANTSEV	21 RVUE	$J/\psi(1S) \rightarrow \gamma(\pi\pi, K\bar{K}, \eta\eta, \omega\phi)$
---------------	--	-----------	---------	---

$\Gamma(\gamma f_1(1420) \rightarrow \gamma K\bar{K}\pi)/\Gamma_{total}$		Γ_{289}/Γ		
VALUE (units 10^{-3})	EVTS	DOCUMENT ID	TECN	COMMENT

0.79 ± 0.13 OUR AVERAGE

$0.68 \pm 0.04 \pm 0.24$ BAI 00D BES $J/\psi \rightarrow \gamma K^\pm K_S^0 \pi^\mp$

$0.76 \pm 0.15 \pm 0.21$ 1,2 AUGUSTIN 92 DM2 $J/\psi \rightarrow \gamma K\bar{K}\pi$

$0.87 \pm 0.14^{+0.14}_{-0.11}$ 1 BAI 90c MRK3 $J/\psi \rightarrow \gamma K_S^0 K^\pm \pi^\mp$

¹ Included unknown branching fraction $f_1(1420) \rightarrow K\bar{K}\pi$.

² From fit to the $K^*(892)K1^{++}$ partial wave.

$\Gamma(\gamma f_0(1500) \rightarrow \gamma\pi\pi)/\Gamma_{total}$		Γ_{290}/Γ		
VALUE (units 10^{-4})	EVTS	DOCUMENT ID	TECN	COMMENT

1.09 ± 0.24 OUR AVERAGE

$1.21 \pm 0.29 \pm 0.24$ 174 1 DOBBS 15 $J/\psi \rightarrow \gamma\pi\pi$

$1.00 \pm 0.03 \pm 0.45$ 2 ABLIKIM 06v BES2 $e^+e^- \rightarrow J/\psi \rightarrow \gamma\pi^+\pi^-$

$1.02 \pm 0.09 \pm 0.45$ 2 ABLIKIM 06v BES2 $e^+e^- \rightarrow J/\psi \rightarrow \gamma\pi^0\pi^0$

• • • We do not use the following data for averages, fits, limits, etc. • • •

0.90 ± 0.17 SARANTSEV 21 RVUE $J/\psi(1S) \rightarrow \gamma(\pi\pi, K\bar{K}, \eta\eta, \omega\phi)$

5.7 ± 0.8 3,4 BUGG 95 MRK3 $J/\psi \rightarrow \gamma\pi^+\pi^-\pi^+\pi^-$

¹ Using CLEO-c data but not authored by the CLEO Collaboration.

² Including unknown branching fraction to $\pi\pi$.

³ Including unknown branching ratio for $f_0(1500) \rightarrow \pi^+\pi^-\pi^+\pi^-$.

⁴ Assuming that $f_0(1500)$ decays only to two S-wave dipions.

$\Gamma(\gamma f_0(1500) \rightarrow \gamma\eta\eta)/\Gamma_{total}$		Γ_{291}/Γ		
VALUE (units 10^{-5})	EVTS	DOCUMENT ID	TECN	COMMENT

$1.65^{+0.26+0.51}_{-0.31-1.40}$

5.5k 1 ABLIKIM 13N BES3 $J/\psi \rightarrow \gamma\eta\eta$

• • • We do not use the following data for averages, fits, limits, etc. • • •

1.1 ± 0.4 SARANTSEV 21 RVUE $J/\psi(1S) \rightarrow \gamma(\pi\pi, K\bar{K}, \eta\eta, \omega\phi)$

¹ From partial wave analysis including all possible combinations of 0^{++} , 2^{++} , and 4^{++} resonances.

See key on page 1171

Meson Particle Listings

$J/\psi(1S)$

$\Gamma(\gamma f_0(1500) \rightarrow \gamma K_S^0 K_S^0)/\Gamma_{total}$ Γ_{292}/Γ

VALUE (units 10^{-5})	DOCUMENT ID	TECN	COMMENT
$1.59 \pm 0.16 \pm 0.18$ 0.56	ABLIKIM	18AA BES3	$J/\psi \rightarrow \gamma K_S^0 K_S^0$
• • • We do not use the following data for averages, fits, limits, etc. • • •			
0.7 ± 0.3	SARANTSEV	21 RVUE	$J/\psi(1S) \rightarrow \gamma(\pi\pi, K\bar{K}, \eta\eta, \omega\phi)$

$\Gamma(\gamma f_0(1500) \rightarrow \gamma \eta \eta')/\Gamma_{total}$ Γ_{293}/Γ

VALUE (units 10^{-6})	DOCUMENT ID	TECN	COMMENT
• • • We do not use the following data for averages, fits, limits, etc. • • •			
$18.1 \pm 1.1 \pm 1.9$ -1.3	¹ ABLIKIM	22As BES3	$J/\psi(1S) \rightarrow \gamma \eta \eta'$
12 ± 5	SARANTSEV	21 RVUE	$J/\psi(1S) \rightarrow \gamma(\pi\pi, K\bar{K}, \eta\eta, \omega\phi)$
¹ From a Breit-Wigner fit involving 9 resonances and a resonating exotic $\eta_1(1855) \rightarrow \eta \eta'/P$ -wave.			

$\Gamma(\gamma f_1(1510) \rightarrow \gamma \eta \eta' \pi^\pm \pi^\mp)/\Gamma_{total}$ Γ_{294}/Γ

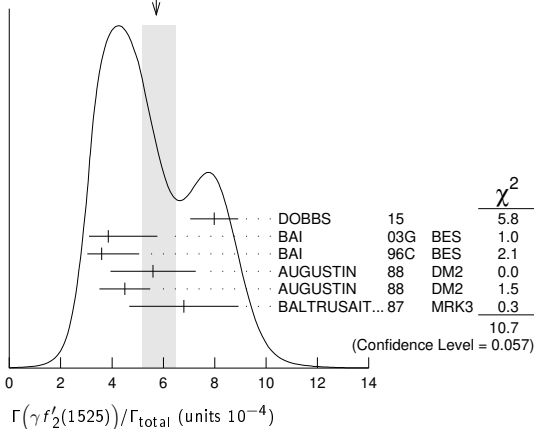
VALUE (units 10^{-4})	DOCUMENT ID	TECN	COMMENT
$4.5 \pm 1.0 \pm 0.7$	BAI	99 BES	$J/\psi \rightarrow \gamma \eta \eta' \pi^\pm \pi^\mp$

$\Gamma(\gamma f_2'(1525))/\Gamma_{total}$ Γ_{295}/Γ

VALUE (units 10^{-4})	CL%	EVTS	DOCUMENT ID	TECN	COMMENT
5.7 ± 0.8 0.5 OUR AVERAGE					Error includes scale factor of 1.5. See the ideogram below.
$8.0 \pm 0.9 \pm 0.2$	75.0	1,2	DOBBS	15	$J/\psi \rightarrow \gamma K\bar{K}$
$3.85 \pm 0.17 \pm 1.91$ -0.73			³ BAI	03G BES	$J/\psi \rightarrow \gamma K\bar{K}$
$3.6 \pm 0.4 \pm 1.4$ -0.4			³ BAI	96c BES	$J/\psi \rightarrow \gamma K^+ K^-$
$5.6 \pm 1.4 \pm 0.9$			³ AUGUSTIN	88 DM2	$J/\psi \rightarrow \gamma K^+ K^-$
$4.5 \pm 0.4 \pm 0.9$			³ AUGUSTIN	88 DM2	$J/\psi \rightarrow \gamma K_S^0 K_S^0$
$6.8 \pm 1.6 \pm 1.4$			³ BALTRUSAIT...87	MRK3	$J/\psi \rightarrow \gamma K^+ K^-$
• • • We do not use the following data for averages, fits, limits, etc. • • •					
<3.4	90	4	⁴ BRANDELIK	79c DASP	$e^+ e^- \rightarrow \pi^+ \pi^- \gamma$
<2.3	90	3	ALEXANDER	78 PLUT	$e^+ e^- \rightarrow K^+ K^- \gamma$

¹ Using CLEO-c data but not authored by the CLEO Collaboration.
² DOBBS 15 reports $[\Gamma(J/\psi(1S) \rightarrow \gamma f_2'(1525))/\Gamma_{total}] \times [B(f_2'(1525) \rightarrow K\bar{K})] = (7.09 \pm 0.46 \pm 0.67) \times 10^{-4}$ which we divide by our best value $B(f_2'(1525) \rightarrow K\bar{K}) = (88.8 \pm 2.2) \times 10^{-2}$. Our first error is their experiment's error and our second error is the systematic error from using our best value.
³ Using $B(f_2'(1525) \rightarrow K\bar{K}) = 0.888$.
⁴ Assuming isotropic production and decay of the $f_2'(1525)$ and isospin.

WEIGHTED AVERAGE
5.7±0.8-0.5 (Error scaled by 1.5)



$\Gamma(\gamma f_2(1565) \rightarrow \gamma \eta \eta')/\Gamma_{total}$ Γ_{298}/Γ

VALUE (units 10^{-5})	DOCUMENT ID	TECN	COMMENT
• • • We do not use the following data for averages, fits, limits, etc. • • •			
$0.32 \pm 0.05 \pm 0.12$ 0.02	¹ ABLIKIM	22As BES3	$J/\psi(1S) \rightarrow \gamma \eta \eta'$
¹ From a Breit-Wigner fit involving 9 resonances and a resonating exotic $\eta_1(1855) \rightarrow \eta \eta'/P$ -wave.			

$\Gamma(\gamma f_2'(1525) \rightarrow \gamma K_S^0 K_S^0)/\Gamma_{total}$ Γ_{296}/Γ

VALUE (units 10^{-5})	DOCUMENT ID	TECN	COMMENT
$7.99 \pm 0.03 \pm 0.69$ $0.04 - 0.50$	ABLIKIM	18AA BES3	$J/\psi \rightarrow \gamma K_S^0 K_S^0$

$\Gamma(\gamma f_2'(1525) \rightarrow \gamma \eta \eta')/\Gamma_{total}$ Γ_{297}/Γ

VALUE (units 10^{-5})	EVTS	DOCUMENT ID	TECN	COMMENT
$3.42 \pm 0.43 \pm 1.37$ $0.51 - 1.30$	5.5k	¹ ABLIKIM	13N BES3	$J/\psi \rightarrow \gamma \eta \eta'$
¹ From partial wave analysis including all possible combinations of $0^{++}, 2^{++}$, and 4^{++} resonances.				

$\Gamma(\gamma f_2(1640) \rightarrow \gamma \omega \omega)/\Gamma_{total}$ Γ_{299}/Γ

VALUE (units 10^{-3})	EVTS	DOCUMENT ID	TECN	COMMENT
$0.28 \pm 0.05 \pm 0.17$	141	ABLIKIM	06H BES	$J/\psi \rightarrow \gamma \omega \omega$

$\Gamma(\gamma f_0(1710) \rightarrow \gamma \pi \pi)/\Gamma_{total}$ Γ_{300}/Γ

VALUE (units 10^{-4})	EVTS	DOCUMENT ID	TECN	COMMENT
3.8 ± 0.5 OUR AVERAGE				
$3.72 \pm 0.30 \pm 0.43$	483	¹ DOBBS	15	$J/\psi \rightarrow \gamma \pi \pi$
$3.96 \pm 0.06 \pm 1.12$		² ABLIKIM	06v BES2	$e^+ e^- \rightarrow J/\psi \rightarrow \gamma \pi^+ \pi^-$
$3.99 \pm 0.15 \pm 2.64$		² ABLIKIM	06v BES2	$e^+ e^- \rightarrow J/\psi \rightarrow \gamma \pi^0 \pi^0$
• • • We do not use the following data for averages, fits, limits, etc. • • •				
0.6 ± 0.2		³ SARANTSEV	21 RVUE	$J/\psi(1S) \rightarrow \gamma(\pi\pi, K\bar{K}, \eta\eta, \omega\phi)$
$2.5 \pm 1.6 \pm 0.8$		BAI	98H BES	$J/\psi \rightarrow \gamma \pi^0 \pi^0$

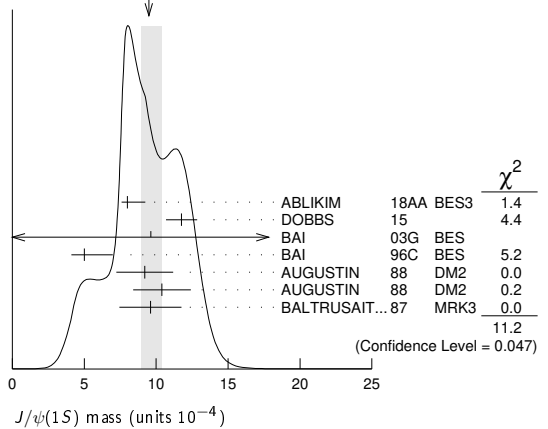
¹ Using CLEO-c data but not authored by the CLEO Collaboration.
² Including unknown branching fraction to $\pi\pi$.
³ There is a further $(2.4 \pm 0.8) \times 10^{-4}$ scalar contribution at 1765 MeV.

$\Gamma(\gamma f_0(1710) \rightarrow \gamma K\bar{K})/\Gamma_{total}$ Γ_{301}/Γ

VALUE (units 10^{-4})	CL%	EVTS	DOCUMENT ID	TECN	COMMENT
9.5 ± 1.0 1.5 OUR AVERAGE					Error includes scale factor of 1.5. See the ideogram below.
$8.00 \pm 0.12 \pm 1.24$ $0.08 - 0.40$			¹ ABLIKIM	18AA BES3	$J/\psi \rightarrow \gamma K_S^0 K_S^0$
$11.76 \pm 0.54 \pm 0.94$		1.2k	² DOBBS	15	$J/\psi \rightarrow \gamma K\bar{K}$
$9.62 \pm 0.29 \pm 3.51$ -1.86			³ BAI	03G BES	$J/\psi \rightarrow \gamma K\bar{K}$
$5.0 \pm 0.8 \pm 1.8$ -0.4			^{1,4} BAI	96c BES	$J/\psi \rightarrow \gamma K^+ K^-$
$9.2 \pm 1.4 \pm 1.4$			¹ AUGUSTIN	88 DM2	$J/\psi \rightarrow \gamma K^+ K^-$
$10.4 \pm 1.2 \pm 1.6$			¹ AUGUSTIN	88 DM2	$J/\psi \rightarrow \gamma K_S^0 K_S^0$
$9.6 \pm 1.2 \pm 1.8$			¹ BALTRUSAIT...87	MRK3	$J/\psi \rightarrow \gamma K^+ K^-$
• • • We do not use the following data for averages, fits, limits, etc. • • •					
2.3 ± 0.8			⁵ SARANTSEV	21 RVUE	$J/\psi(1S) \rightarrow \gamma(\pi\pi, K\bar{K}, \eta\eta, \omega\phi)$
$1.6 \pm 0.2 \pm 0.6$ -0.2			^{1,6} BAI	96c BES	$J/\psi \rightarrow \gamma K^+ K^-$
< 0.8		90	⁷ BISELLO	89B	$J/\psi \rightarrow 4\pi\gamma$
$1.6 \pm 0.4 \pm 0.3$			⁸ BALTRUSAIT...87	MRK3	$J/\psi \rightarrow \gamma \pi^+ \pi^-$
3.8 ± 1.6			⁹ EDWARDS	82D CBAL	$e^+ e^- \rightarrow \eta \eta \gamma$

¹ Includes unknown branching fraction to $K^+ K^-$ or $K_S^0 K_S^0$. We have multiplied $K^+ K^-$ measurement by 2, and $K_S^0 K_S^0$ by 4 to obtain $K\bar{K}$ result.
² Using CLEO-c data but not authored by the CLEO Collaboration.
³ Includes unknown branching ratio to $K^+ K^-$ or $K_S^0 K_S^0$.
⁴ Assuming $J^P = 2^+$ for $f_0(1710)$.
⁵ There is a further $(6 \pm 2) \times 10^{-4}$ scalar contribution at 1765 MeV.
⁶ Assuming $J^P = 0^+$ for $f_0(1710)$.
⁷ Includes unknown branching fraction to $\rho^0 \rho^0$.
⁸ Includes unknown branching fraction to $\pi^+ \pi^-$.
⁹ Includes unknown branching fraction to $\eta \eta$.

WEIGHTED AVERAGE
9.5±1.0-0.5 (Error scaled by 1.5)



Meson Particle Listings

 $J/\psi(1S)$

$\Gamma(\gamma f_0(1710) \rightarrow \gamma \omega) / \Gamma_{\text{total}}$					Γ_{302} / Γ
VALUE (units 10^{-3})	EVTS	DOCUMENT ID	TECN	COMMENT	
$0.31 \pm 0.06 \pm 0.08$	180	ABLIKIM	06H	BES $J/\psi \rightarrow \gamma \omega$	

$\Gamma(\gamma f_0(1710) \rightarrow \gamma \eta \eta) / \Gamma_{\text{total}}$					Γ_{303} / Γ
VALUE (units 10^{-4})	EVTS	DOCUMENT ID	TECN	COMMENT	
$2.35^{+0.13+1.24}_{-0.11-0.74}$	5.5k	¹ ABLIKIM	13N	BES3 $J/\psi \rightarrow \gamma \eta \eta$	
• • • We do not use the following data for averages, fits, limits, etc. • • •					
1.2 ± 0.4		² SARANTSEV	21	RVUE $J/\psi(1S) \rightarrow \gamma(\pi\pi, K\bar{K}, \eta\eta, \omega\phi)$	

¹ From partial wave analysis including all possible combinations of 0^{++} , 2^{++} , and 4^{++} resonances.

² There is a further $(0.7 \pm 0.1) \times 10^{-4}$ scalar contribution at 1765 MeV.

$\Gamma(\gamma f_0(1710) \rightarrow \gamma \eta \eta') / \Gamma_{\text{total}}$					Γ_{304} / Γ
VALUE (units 10^{-5})	DOCUMENT ID	TECN	COMMENT		
6.5 ± 2.5	¹ SARANTSEV	21	RVUE $J/\psi(1S) \rightarrow \gamma(\pi\pi, K\bar{K}, \eta\eta, \omega\phi)$		
• • • We do not use the following data for averages, fits, limits, etc. • • •					
¹ There is a further $(2.5 \pm 1.1) \times 10^{-5}$ scalar contribution at 1765 MeV.					

$\Gamma(\gamma f_0(1710) \rightarrow \gamma \omega \phi) / \Gamma_{\text{total}}$					Γ_{305} / Γ
VALUE (units 10^{-4})	EVTS	DOCUMENT ID	TECN	COMMENT	
2.5 ± 0.6 OUR AVERAGE					
$2.00 \pm 0.08^{+1.38}_{-1.64}$	1.3k	ABLIKIM	13J	BES3 $J/\psi \rightarrow \gamma \omega \phi$	
$2.61 \pm 0.27 \pm 0.65$	95	ABLIKIM	06J	BES2 $J/\psi \rightarrow \gamma \omega \phi$	
• • • We do not use the following data for averages, fits, limits, etc. • • •					
0.1 ± 0.1		¹ SARANTSEV	21	RVUE $J/\psi(1S) \rightarrow \gamma(\pi\pi, K\bar{K}, \eta\eta, \omega\phi)$	

¹ There is a further $(2.2 \pm 0.4) \times 10^{-4}$ scalar contribution at 1765 MeV.

$\Gamma(\gamma f_0(1770) \rightarrow \gamma K_S^0 K_S^0) / \Gamma_{\text{total}}$					Γ_{306} / Γ
VALUE (units 10^{-5})	DOCUMENT ID	TECN	COMMENT		
$1.11 \pm 0.06^{+0.19}_{-0.32}$	ABLIKIM	18AA	BES3	$J/\psi \rightarrow \gamma K_S^0 K_S^0$	

$\Gamma(\gamma f_0(1770) \rightarrow \gamma \eta \eta') / \Gamma_{\text{total}}$					Γ_{309} / Γ
VALUE (units 10^{-5})	DOCUMENT ID	TECN	COMMENT		
$0.11 \pm 0.01^{+0.04}_{-0.03}$	¹ ABLIKIM	22As	BES3	$J/\psi(1S) \rightarrow \gamma \eta \eta'$	

¹ From a Breit-Wigner fit involving 9 resonances and a resonating exotic $\eta_1(1855) \rightarrow \eta \eta' P$ -wave.

$\Gamma(\gamma f_2(1810) \rightarrow \gamma \eta \eta) / \Gamma_{\text{total}}$					Γ_{307} / Γ
VALUE (units 10^{-5})	EVTS	DOCUMENT ID	TECN	COMMENT	
$5.40^{+0.60+3.42}_{-0.67-2.35}$	5.5k	¹ ABLIKIM	13N	$J/\psi \rightarrow \gamma \eta \eta$	

¹ From partial wave analysis including all possible combinations of 0^{++} , 2^{++} , and 4^{++} resonances.

$\Gamma(\gamma \eta_1(1855) \rightarrow \gamma \eta \eta') / \Gamma_{\text{total}}$					Γ_{308} / Γ
VALUE (units 10^{-6})	DOCUMENT ID	TECN	COMMENT		
$2.70 \pm 0.41^{+0.16}_{-0.35}$	¹ ABLIKIM	22Ai	BES3	$J/\psi(1S) \rightarrow \gamma \eta \eta'$	

¹ From a Breit-Wigner fit involving 9 resonances and the resonating exotic $\eta_1(1855) \rightarrow \eta \eta' P$ -wave. For analysis details see ABLIKIM 22As.

$\Gamma(\gamma f_2(1910) \rightarrow \gamma \omega \omega) / \Gamma_{\text{total}}$					Γ_{310} / Γ
VALUE (units 10^{-3})	EVTS	DOCUMENT ID	TECN	COMMENT	
$0.20 \pm 0.04 \pm 0.13$	151	ABLIKIM	06H	BES $J/\psi \rightarrow \gamma \omega \omega$	

$\Gamma(\gamma f_2(1950) \rightarrow \gamma K^*(892) \bar{K}^*(892)) / \Gamma_{\text{total}}$					Γ_{311} / Γ
VALUE (units 10^{-3})	DOCUMENT ID	TECN	COMMENT		
$0.7 \pm 0.1 \pm 0.2$	BAI	00B	BES	$J/\psi \rightarrow \gamma K^+ K^0 \pi^+ \pi^-$	

$\Gamma(\gamma f_2(2010) \rightarrow \gamma \eta \eta') / \Gamma_{\text{total}}$					Γ_{312} / Γ
VALUE (units 10^{-5})	DOCUMENT ID	TECN	COMMENT		
$0.71 \pm 0.06^{+0.10}_{-0.06}$	¹ ABLIKIM	22As	BES3	$J/\psi(1S) \rightarrow \gamma \eta \eta'$	

¹ From a Breit-Wigner fit involving 9 resonances and a resonating exotic $\eta_1(1855) \rightarrow \eta \eta' P$ -wave.

$\Gamma(\gamma f_0(2020) \rightarrow \gamma \pi \pi) / \Gamma_{\text{total}}$					Γ_{313} / Γ
VALUE (units 10^{-5})	DOCUMENT ID	TECN	COMMENT		
42 ± 10	SARANTSEV	21	RVUE $J/\psi(1S) \rightarrow \gamma(\pi\pi, K\bar{K}, \eta\eta, \omega\phi)$		
• • • We do not use the following data for averages, fits, limits, etc. • • •					

$\Gamma(\gamma f_0(2020) \rightarrow \gamma K \bar{K}) / \Gamma_{\text{total}}$					Γ_{314} / Γ
VALUE (units 10^{-5})	DOCUMENT ID	TECN	COMMENT		
55 ± 25	SARANTSEV	21	RVUE $J/\psi(1S) \rightarrow \gamma(\pi\pi, K\bar{K}, \eta\eta, \omega\phi)$		
• • • We do not use the following data for averages, fits, limits, etc. • • •					

$\Gamma(\gamma f_0(2020) \rightarrow \gamma \eta \eta) / \Gamma_{\text{total}}$					Γ_{315} / Γ
VALUE (units 10^{-5})	DOCUMENT ID	TECN	COMMENT		
10 ± 10	SARANTSEV	21	RVUE $J/\psi(1S) \rightarrow \gamma(\pi\pi, K\bar{K}, \eta\eta, \omega\phi)$		
• • • We do not use the following data for averages, fits, limits, etc. • • •					

$\Gamma(\gamma f_0(2020) \rightarrow \gamma \eta' \eta') / \Gamma_{\text{total}}$					Γ_{316} / Γ
VALUE (units 10^{-4})	DOCUMENT ID	TECN	COMMENT		
$2.63 \pm 0.06^{+0.31}_{-0.46}$	¹ ABLIKIM	22c	BES3	$J/\psi \rightarrow \gamma \eta' \eta' \rightarrow 4/5 \gamma 2(\pi^+ \pi^-)$	

¹ From a partial wave analysis of the systems (γX) , with $X \rightarrow \eta' \eta'$, and $(\eta' X)$, with $X \rightarrow \gamma \eta'$ in the decay $J/\psi \rightarrow \gamma \eta' \eta'$. The intermediate resonance X is parametrized by a constant-width, relativistic Breit-Wigner.

$\Gamma(\gamma f_0(2020) \rightarrow \gamma \eta \eta') / \Gamma_{\text{total}}$					Γ_{317} / Γ
VALUE (units 10^{-5})	DOCUMENT ID	TECN	COMMENT		
$2.28 \pm 0.12^{+0.29}_{-0.20}$	¹ ABLIKIM	22As	BES3	$J/\psi(1S) \rightarrow \gamma \eta \eta'$	

¹ From a Breit-Wigner fit involving 9 resonances and a resonating exotic $\eta_1(1855) \rightarrow \eta \eta' P$ -wave.

$\Gamma(\gamma f_4(2050)) / \Gamma_{\text{total}}$					Γ_{318} / Γ
VALUE (units 10^{-3})	DOCUMENT ID	TECN	COMMENT		
$2.7 \pm 0.5 \pm 0.5$	¹ BALTRUSAIT..87	MRK3	$J/\psi \rightarrow \gamma \pi^+ \pi^-$		

¹ Assuming branching fraction $f_4(2050) \rightarrow \pi \pi / \text{total} = 0.167$.

$\Gamma(\gamma f_4(2050) \rightarrow \gamma \eta \eta') / \Gamma_{\text{total}}$					Γ_{319} / Γ
VALUE (units 10^{-5})	DOCUMENT ID	TECN	COMMENT		
$0.06 \pm 0.01^{+0.03}_{-0.01}$	¹ ABLIKIM	22As	BES3	$J/\psi(1S) \rightarrow \gamma \eta \eta'$	

¹ From a Breit-Wigner fit involving 9 resonances and a resonating exotic $\eta_1(1855) \rightarrow \eta \eta' P$ -wave.

$\Gamma(\gamma f_0(2100) \rightarrow \gamma \eta \eta) / \Gamma_{\text{total}}$					Γ_{320} / Γ
VALUE (units 10^{-4})	EVTS	DOCUMENT ID	TECN	COMMENT	
$1.13^{+0.09+0.64}_{-0.10-0.28}$	5.5k	¹ ABLIKIM	13N	BES3 $J/\psi \rightarrow \gamma \eta \eta$	
• • • We do not use the following data for averages, fits, limits, etc. • • •					
1.8 ± 1.5		SARANTSEV	21	RVUE $J/\psi(1S) \rightarrow \gamma(\pi\pi, K\bar{K}, \eta\eta, \omega\phi)$	

¹ From partial wave analysis including all possible combinations of 0^{++} , 2^{++} , and 4^{++} resonances.

$\Gamma(\gamma f_0(2100) \rightarrow \gamma \pi \pi) / \Gamma_{\text{total}}$					Γ_{322} / Γ
VALUE (units 10^{-4})	EVTS	DOCUMENT ID	TECN	COMMENT	
$6.24 \pm 0.48 \pm 0.87$	744	¹ DOBBS	15	$J/\psi \rightarrow \gamma \pi \pi$	
2.0 ± 0.8		SARANTSEV	21	RVUE $J/\psi(1S) \rightarrow \gamma(\pi\pi, K\bar{K}, \eta\eta, \omega\phi)$	

¹ Using CLEO-c data but not authored by the CLEO Collaboration.

$\Gamma(\gamma f_0(2100) \rightarrow \gamma K \bar{K}) / \Gamma_{\text{total}}$					Γ_{321} / Γ
VALUE (units 10^{-5})	DOCUMENT ID	TECN	COMMENT		
32 ± 20	SARANTSEV	21	RVUE $J/\psi(1S) \rightarrow \gamma(\pi\pi, K\bar{K}, \eta\eta, \omega\phi)$		
• • • We do not use the following data for averages, fits, limits, etc. • • •					

$\Gamma(\gamma f_0(2200)) / \Gamma_{\text{total}}$					Γ_{323} / Γ
VALUE (units 10^{-4})	DOCUMENT ID	TECN	COMMENT		
1.5	¹ AUGUSTIN	88	DM2 $J/\psi \rightarrow \gamma K_S^0 K_S^0$		

¹ Includes unknown branching fraction to $K_S^0 K_S^0$.

$\Gamma(\gamma f_0(2200) \rightarrow \gamma \pi \pi) / \Gamma_{\text{total}}$					Γ_{326} / Γ
VALUE (units 10^{-5})	DOCUMENT ID	TECN	COMMENT		
5 ± 2	SARANTSEV	21	RVUE $J/\psi(1S) \rightarrow \gamma(\pi\pi, K\bar{K}, \eta\eta, \omega\phi)$		
• • • We do not use the following data for averages, fits, limits, etc. • • •					

$\Gamma(\gamma f_0(2200) \rightarrow \gamma K \bar{K}) / \Gamma_{\text{total}}$					Γ_{324} / Γ
VALUE (units 10^{-4})	EVTS	DOCUMENT ID	TECN	COMMENT	
$5.86 \pm 0.49 \pm 1.20$	490	¹ DOBBS	15	$J/\psi \rightarrow \gamma K \bar{K}$	
0.5 ± 0.5		SARANTSEV	21	RVUE $J/\psi(1S) \rightarrow \gamma(\pi\pi, K\bar{K}, \eta\eta, \omega\phi)$	

¹ Using CLEO-c data but not authored by the CLEO Collaboration.

$\Gamma(\gamma f_0(2200) \rightarrow \gamma K_S^0 K_S^0)/\Gamma_{\text{total}}$ Γ_{325}/Γ

VALUE (units 10^{-4})	DOCUMENT ID	TECN	COMMENT
$2.72 \pm_{-0.06}^{+0.08} \pm_{-0.47}^{+0.17}$	ABLIKIM	18AA BES3	$J/\psi \rightarrow \gamma K_S^0 K_S^0$

 $\Gamma(\gamma f_0(2200) \rightarrow \gamma \eta \eta)/\Gamma_{\text{total}}$ Γ_{327}/Γ

VALUE (units 10^{-5})	DOCUMENT ID	TECN	COMMENT
0.7 ± 0.4	SARANTSEV 21	RVUE	$J/\psi(1S) \rightarrow \gamma(\pi\pi, K\bar{K}, \eta\eta, \omega\phi)$

 $\Gamma(\gamma f_J(2220))/\Gamma_{\text{total}}$ Γ_{328}/Γ

VALUE (units 10^{-3})	CL%	EVTS	DOCUMENT ID	TECN	COMMENT
>300			¹ BAI	96B BES	$e^+e^- \rightarrow \gamma \bar{p}p, K\bar{K}$
>250	99.9		² HASAN	96 SPEC	$\bar{p}p \rightarrow \pi^+\pi^-$
>2.3	95		³ AUGUSTIN	88 DM2	$J/\psi \rightarrow \gamma K^+K^-$
<1.6	95		³ AUGUSTIN	88 DM2	$J/\psi \rightarrow \gamma K_S^0 K_S^0$
$12.4 \pm_{-5.2}^{+6.4} \pm 2.8$		23	³ BALTRUSAIT...86D	MRK3	$J/\psi \rightarrow \gamma K_S^0 K_S^0$
$8.4 \pm_{-2.8}^{+3.4} \pm 1.6$		93	³ BALTRUSAIT...86D	MRK3	$J/\psi \rightarrow \gamma K^+K^-$

¹Using BARNES 93.²Using BAI 96B.³Includes unknown branching fraction to K^+K^- or $K_S^0 K_S^0$. $\Gamma(\gamma f_J(2220) \rightarrow \gamma \pi\pi)/\Gamma_{\text{total}}$ Γ_{329}/Γ

VALUE (units 10^{-5})	CL%	DOCUMENT ID	TECN	COMMENT
<3.9	90	1,2 DOBBS	15	$J/\psi \rightarrow \gamma \pi\pi$

• • • We do not use the following data for averages, fits, limits, etc. • • •

$14 \pm 8 \pm 4$	BAI	98H BES	$J/\psi \rightarrow \gamma \pi^0 \pi^0$
$8.4 \pm 2.6 \pm 3.0$	BAI	96B BES	$e^+e^- \rightarrow J/\psi \rightarrow \gamma \pi^+\pi^-$

¹Using CLEO-c data but not authored by the CLEO Collaboration.²For $\Gamma = 20/50$ MeV, the 90% CL upper limits for $\pi^+\pi^-$ and $\pi^0\pi^0$ are $2.6/5.2 \times 10^{-5}$ and $1.3/1.9 \times 10^{-5}$, respectively. $\Gamma(\gamma f_J(2220) \rightarrow \gamma K\bar{K})/\Gamma_{\text{total}}$ Γ_{330}/Γ

VALUE (units 10^{-5})	CL%	DOCUMENT ID	TECN	COMMENT
<4.1	90	1,2 DOBBS	15	$J/\psi \rightarrow \gamma K\bar{K}$

• • • We do not use the following data for averages, fits, limits, etc. • • •

<3.6		³ DEL-AMO-SA..10o	BABR	$e^+e^- \rightarrow J/\psi \rightarrow \gamma K^+K^-$
<2.9		³ DEL-AMO-SA..10o	BABR	$e^+e^- \rightarrow J/\psi \rightarrow \gamma K_S^0 K_S^0$
$6.6 \pm 2.9 \pm 2.4$	BAI	96B BES	$e^+e^- \rightarrow J/\psi \rightarrow \gamma K^+K^-$	
$10.8 \pm 4.0 \pm 3.2$	BAI	96B BES	$e^+e^- \rightarrow J/\psi \rightarrow \gamma K_S^0 K_S^0$	

¹Using CLEO-c data but not authored by the CLEO Collaboration.²For $\Gamma = 20/50$ MeV, the 90% CL upper limits for K^+K^- and $K_S^0 K_S^0$ are $1.7/3.1 \times 10^{-5}$ and $1.2/2.0 \times 10^{-5}$, respectively.³For spin 2 and helicity 0; other combinations lead to more stringent upper limits. $\Gamma(\gamma f_J(2220) \rightarrow \gamma \rho\bar{\rho})/\Gamma_{\text{total}}$ Γ_{331}/Γ

VALUE (units 10^{-5})	DOCUMENT ID	TECN	COMMENT
$1.5 \pm 0.6 \pm 0.5$	BAI	96B BES	$e^+e^- \rightarrow J/\psi \rightarrow \gamma \rho\bar{\rho}$

 $\Gamma(\gamma f_0(2330) \rightarrow \gamma K_S^0 K_S^0)/\Gamma_{\text{total}}$ Γ_{332}/Γ

VALUE (units 10^{-5})	DOCUMENT ID	TECN	COMMENT
$4.95 \pm_{-0.72}^{+0.21} \pm_{-0.72}^{+0.66}$	ABLIKIM	18AA BES3	$J/\psi \rightarrow \gamma K_S^0 K_S^0$

• • • We do not use the following data for averages, fits, limits, etc. • • •

0.6 ± 0.1	SARANTSEV 21	RVUE	$J/\psi(1S) \rightarrow \gamma(\pi\pi, K\bar{K}, \eta\eta, \omega\phi)$
---------------	--------------	------	---

 $\Gamma(\gamma f_0(2330) \rightarrow \gamma \pi\pi)/\Gamma_{\text{total}}$ Γ_{333}/Γ

VALUE (units 10^{-5})	DOCUMENT ID	TECN	COMMENT
4 ± 2	SARANTSEV 21	RVUE	$J/\psi(1S) \rightarrow \gamma(\pi\pi, K\bar{K}, \eta\eta, \omega\phi)$

 $\Gamma(\gamma f_0(2330) \rightarrow \gamma \eta \eta)/\Gamma_{\text{total}}$ Γ_{334}/Γ

VALUE (units 10^{-5})	DOCUMENT ID	TECN	COMMENT
1.5 ± 0.4	SARANTSEV 21	RVUE	$J/\psi(1S) \rightarrow \gamma(\pi\pi, K\bar{K}, \eta\eta, \omega\phi)$

 $\Gamma(\gamma f_0(2330) \rightarrow \gamma \eta' \eta')/\Gamma_{\text{total}}$ Γ_{335}/Γ

VALUE (units 10^{-6})	DOCUMENT ID	TECN	COMMENT
$6.09 \pm_{-1.68}^{+0.64} \pm_{-1.68}^{+4.00}$	¹ ABLIKIM	22c BES3	$J/\psi \rightarrow \gamma \eta' \eta' \rightarrow 4/5 \gamma 2(\pi^+\pi^-)$

¹From a partial wave analysis of the systems (γX) , with $X \rightarrow \eta' \eta'$, and $(\eta' X)$, with $X \rightarrow \gamma \eta'$ in the decay $J/\psi \rightarrow \gamma \eta' \eta'$. The intermediate resonance X is parametrized by a constant-width, relativistic Breit-Wigner. $\Gamma(\gamma f_0(2330) \rightarrow \gamma \eta' \eta')/\Gamma_{\text{total}}$ Γ_{336}/Γ

VALUE (units 10^{-5})	DOCUMENT ID	TECN	COMMENT
$0.10 \pm 0.02 \pm_{-0.02}^{+0.01}$	¹ ABLIKIM	22As BES3	$J/\psi(1S) \rightarrow \gamma \eta' \eta'$

¹From a Breit-Wigner fit involving 9 resonances and a resonating exotic $\eta_1(1855) \rightarrow \eta' \eta'$ P-wave. $\Gamma(\gamma f_0(2470) \rightarrow \gamma \eta' \eta')/\Gamma_{\text{total}}$ Γ_{340}/Γ

VALUE (units 10^{-7})	DOCUMENT ID	TECN	COMMENT
$8.18 \pm_{-2.23}^{+1.77} \pm_{-2.23}^{+3.73}$	¹ ABLIKIM	22c BES3	$J/\psi \rightarrow \gamma \eta' \eta' \rightarrow 4/5 \gamma 2(\pi^+\pi^-)$

¹From a partial wave analysis of the systems (γX) , with $X \rightarrow \eta' \eta'$, and $(\eta' X)$, with $X \rightarrow \gamma \eta'$ in the decay $J/\psi \rightarrow \gamma \eta' \eta'$. The intermediate resonance X is parametrized by a constant-width, relativistic Breit-Wigner. $\Gamma(\gamma f_2(2340) \rightarrow \gamma \eta \eta)/\Gamma_{\text{total}}$ Γ_{337}/Γ

VALUE (units 10^{-5})	EVTS	DOCUMENT ID	TECN	COMMENT
$5.60 \pm_{-0.65}^{+0.62} \pm_{-2.07}^{+2.37}$	5.5k	¹ ABLIKIM	13N BES3	$J/\psi \rightarrow \gamma \eta \eta$

¹From partial wave analysis including all possible combinations of 0^{++} , 2^{++} , and 4^{++} resonances. $\Gamma(\gamma f_2(2340) \rightarrow \gamma \eta' \eta')/\Gamma_{\text{total}}$ Γ_{339}/Γ

VALUE (units 10^{-6})	DOCUMENT ID	TECN	COMMENT
$8.67 \pm_{-1.67}^{+0.70} \pm_{-1.67}^{+0.61}$	¹ ABLIKIM	22c BES3	$J/\psi \rightarrow \gamma \eta' \eta' \rightarrow 4/5 \gamma 2(\pi^+\pi^-)$

¹From a partial wave analysis of the systems (γX) , with $X \rightarrow \eta' \eta'$, and $(\eta' X)$, with $X \rightarrow \gamma \eta'$ in the decay $J/\psi \rightarrow \gamma \eta' \eta'$. The intermediate resonance X is parametrized by a constant-width, relativistic Breit-Wigner. $\Gamma(\gamma f_2(2340) \rightarrow \gamma K_S^0 K_S^0)/\Gamma_{\text{total}}$ Γ_{338}/Γ

VALUE (units 10^{-5})	EVTS	DOCUMENT ID	TECN	COMMENT
$5.54 \pm_{-0.40}^{+0.34} \pm_{-1.49}^{+3.82}$		ABLIKIM	18AA BES3	$J/\psi \rightarrow \gamma K_S^0 K_S^0$

 $\Gamma(\gamma X(1835) \rightarrow \gamma \pi^+\pi^-\eta')/\Gamma_{\text{total}}$ Γ_{341}/Γ

VALUE (units 10^{-4})	EVTS	DOCUMENT ID	TECN	COMMENT
$2.7 \pm_{-0.8}^{+0.6}$ OUR AVERAGE				Error includes scale factor of 1.6.
$3.93 \pm 0.38 \pm_{-0.84}^{+0.31}$		¹ ABLIKIM	16j BES3	$J/\psi \rightarrow \gamma \pi^+\pi^-\eta'$
$2.2 \pm 0.4 \pm 0.4$	264	ABLIKIM	05R BES2	$J/\psi \rightarrow \gamma \pi^+\pi^-\eta'$

• • • We do not use the following data for averages, fits, limits, etc. • • •

$2.87 \pm 0.09 \pm_{-0.52}^{+0.49}$	4265	² ABLIKIM	11c BES3	$J/\psi \rightarrow \gamma \pi^+\pi^-\eta'$
-------------------------------------	------	----------------------	----------	---

¹From a fit of the measured $\pi^+\pi^-\eta'$ lineshape that accounts for the abrupt distortion observed at the $p\bar{p}$ threshold with a Flatté formula in addition to known backgrounds and contributors, as well as an *ad hoc* Breit-Wigner ($M \approx 1919$ MeV; $\Gamma \approx 51$ MeV) that is required for a good fit. Another explanation for the distortion provided by ABLIKIM 16j is that a second resonance near 1870 MeV interferes with the $X(1835)$; fits to this possibility yield product branching fraction values compatible with that shown within the respective systematic uncertainties.²From a fit of the $\pi^+\pi^-\eta'$ mass distribution to a combination of $\gamma f_1(1510)$, $\gamma X(1835)$, and two states $\gamma X(2120)$ and $\gamma X(2370)$, for $M(\pi^+\pi^-\eta') < 2.8$ GeV, and accounting for backgrounds from non- η' events and $J/\psi \rightarrow \pi^0\pi^+\pi^-\eta'$. $\Gamma(\gamma X(1835) \rightarrow \gamma \rho\bar{\rho})/\Gamma_{\text{total}}$ Γ_{342}/Γ

VALUE (units 10^{-4})	EVTS	DOCUMENT ID	TECN	COMMENT
$0.77 \pm_{-0.09}^{+0.15}$ OUR AVERAGE				
$0.90 \pm_{-0.11}^{+0.04} \pm_{-0.55}^{+0.27}$		¹ ABLIKIM	12D BES3	$J/\psi \rightarrow \gamma \rho\bar{\rho}$
$1.14 \pm_{-0.30}^{+0.43} \pm_{-0.26}^{+0.42}$	231	² ALEXANDER	10 CLEO	$J/\psi \rightarrow \gamma \rho\bar{\rho}$
$0.70 \pm 0.04 \pm_{-0.08}^{+0.19}$		BAI	03F BES2	$J/\psi \rightarrow \gamma \rho\bar{\rho}$

¹From the fit including final state interaction effects in isospin 0 S-wave according to SIBIRSEV 05A.²From a fit of the $p\bar{p}$ mass distribution to a combination of $\gamma X(1835)$, γR with $M(R) = 2100$ MeV and $\Gamma(R) = 160$ MeV, and $\gamma \rho\bar{\rho}$ phase space, for $M(p\bar{p}) < 2.85$ GeV. $\Gamma(\gamma X(1835) \rightarrow \gamma K_S^0 K_S^0 \eta)/\Gamma_{\text{total}}$ Γ_{343}/Γ

VALUE (units 10^{-5})	DOCUMENT ID	TECN	COMMENT
$3.31 \pm_{-0.30}^{+0.33} \pm_{-1.29}^{+1.96}$	ABLIKIM	15T BES3	$J/\psi \rightarrow \gamma K_S^0 K_S^0 \eta$

 $\Gamma(\gamma X(1835) \rightarrow \gamma \gamma \phi(1020))/\Gamma_{\text{total}}$ Γ_{344}/Γ

VALUE (units 10^{-6})	EVTS	DOCUMENT ID	TECN	COMMENT
$1.77 \pm 0.35 \pm 0.25$	305	¹ ABLIKIM	18i BES3	$J/\psi \rightarrow \gamma \gamma \phi(1020)$
$8.09 \pm 1.99 \pm 1.36$	1.3k	² ABLIKIM	18i BES3	$J/\psi \rightarrow \gamma \gamma \phi(1020)$

¹Constructive interference between the $X(1835)$ and $\eta(1405)/\eta(1475)$ is assumed in a fit to the $\gamma\phi$ invariant mass.²Destructive interference between the $X(1835)$ and $\eta(1405)/\eta(1475)$ is assumed in a fit to the $\gamma\phi$ invariant mass.

Meson Particle Listings

 $J/\psi(1S)$

$\Gamma(\gamma X(1835) \rightarrow \gamma\gamma)/\Gamma_{\text{total}}$					Γ_{345}/Γ
VALUE	CL%	DOCUMENT ID	TECN	COMMENT	
$<3.56 \times 10^{-6}$	90	ABLIKIM	180	BES3	$\psi(2S) \rightarrow \pi^+\pi^-\gamma\gamma$

$\Gamma(\gamma X(1835) \rightarrow \gamma 3(\pi^+\pi^-))/\Gamma_{\text{total}}$					Γ_{346}/Γ
VALUE (units 10^{-5})	EVTS	DOCUMENT ID	TECN	COMMENT	
$2.44 \pm 0.36 \pm 0.60$ 0.74	0.6k	ABLIKIM	13U	BES3	$J/\psi \rightarrow \gamma 3(\pi^+\pi^-)$

$\Gamma(\gamma X(2370) \rightarrow \gamma K^+ K^- \eta)/\Gamma_{\text{total}}$					Γ_{347}/Γ
VALUE (units 10^{-5})	DOCUMENT ID	TECN	COMMENT		
$1.79 \pm 0.23 \pm 0.65$	ABLIKIM	20Q	BES3	$J/\psi \rightarrow \gamma K^+ K^- \eta'$	

$\Gamma(\gamma X(2370) \rightarrow \gamma K_S^0 K_S^0 \eta)/\Gamma_{\text{total}}$					Γ_{348}/Γ
VALUE (units 10^{-5})	DOCUMENT ID	TECN	COMMENT		
$1.18 \pm 0.32 \pm 0.39$	ABLIKIM	20Q	BES3	$J/\psi \rightarrow \gamma K_S^0 K_S^0 \eta'$	

$\Gamma(\gamma X(2370) \rightarrow \gamma \eta \eta \eta)/\Gamma_{\text{total}}$					Γ_{349}/Γ
VALUE	CL%	DOCUMENT ID	TECN	COMMENT	
$<9.2 \times 10^{-6}$	90	ABLIKIM	21C	BES3	$J/\psi(1S) \rightarrow \gamma \eta \eta \eta'$

$\Gamma(\gamma p \bar{p})/\Gamma_{\text{total}}$					Γ_{350}/Γ	
VALUE (units 10^{-3})	CL%	EVTS	DOCUMENT ID	TECN	COMMENT	
$0.38 \pm 0.07 \pm 0.07$		49	EATON	84	MRK2	e^+e^-
<0.11	90		PERUZZI	78	MRK1	e^+e^-

$\Gamma(\gamma p \bar{p} \pi^+ \pi^-)/\Gamma_{\text{total}}$					Γ_{351}/Γ
VALUE	CL%	DOCUMENT ID	TECN	COMMENT	
$<0.79 \times 10^{-3}$	90	EATON	84	MRK2	e^+e^-

$\Gamma(\gamma A^0)/\Gamma_{\text{total}}$					Γ_{352}/Γ
VALUE	CL%	DOCUMENT ID	TECN	COMMENT	
$<0.13 \times 10^{-3}$	90	HENRARD	87	DM2	e^+e^-
$<0.16 \times 10^{-3}$	90	BAI	98G	BES	e^+e^-

$\Gamma(\gamma A^0 \rightarrow \gamma \text{invisible})/\Gamma_{\text{total}}$					Γ_{353}/Γ		
VALUE	CL%	EVTS	DOCUMENT ID	TECN	COMMENT		
$<1.7 \times 10^{-6}$	90	88M	1	ABLIKIM	20K	BES3	$\psi(2S) \rightarrow J/\psi \pi^+ \pi^-$
$<6.3 \times 10^{-6}$	90	3.7M	2	INSLER	10	CLEO	$\psi(2S) \rightarrow J/\psi \pi^+ \pi^-$

¹ For a narrow state, A^0 , with mass $m_{A^0} < 1.2$ GeV. The limit varies with m_{A^0} , reaching its largest value of 1.7×10^{-6} at 1.2 GeV and being 7.0×10^{-7} for $m_{A^0} = 0$.

² The limit varies with mass m_{A^0} of a narrow state A^0 and is 4.3×10^{-6} for $m_{A^0} = 0$, reaches its largest value of 6.3×10^{-6} at $m_{A^0} = 500$ MeV, and is 3.6×10^{-6} at $m_{A^0} = 960$ MeV.

$\Gamma(\gamma A^0 \rightarrow \gamma \mu^+ \mu^-)/\Gamma_{\text{total}}$ (narrow state A^0 with $0.2 \text{ GeV} < m_{A^0} < 3 \text{ GeV}$)					Γ_{354}/Γ	
VALUE	CL%	EVTS	DOCUMENT ID	TECN	COMMENT	
$<7.8 \times 10^{-7}$	90	1	ABLIKIM	22H	BES3	$J/\psi \rightarrow \gamma \mu^+ \mu^-$
$<0.5 \times 10^{-5}$	90	2	ABLIKIM	16E	BES3	$J/\psi \rightarrow \gamma \mu^+ \mu^-$
$<2.1 \times 10^{-5}$	90	3	ABLIKIM	12	BES3	$J/\psi \rightarrow \gamma \mu^+ \mu^-$

¹ For a narrow scalar or pseudoscalar, A^0 , with a mass in the range 0.212–3.0 GeV. The measured 90% CL limit as a function of m_{A^0} is in the range $(1.2\text{--}778.0) \times 10^{-9}$.

² For a narrow scalar or pseudoscalar, A^0 , with a mass in the range 0.212–3 GeV. The measured 90% CL limit as a function of m_{A^0} is in the range $(2.8\text{--}495.3) \times 10^{-8}$.

³ For a narrow scalar or pseudoscalar, A^0 , with a mass in the range 0.21–3.00 GeV. The measured 90% CL limit as a function of m_{A^0} ranges from 4×10^{-7} to 2.1×10^{-5} .

DALITZ DECAYS

$\Gamma(\pi^0 e^+ e^-)/\Gamma_{\text{total}}$					Γ_{355}/Γ
VALUE (units 10^{-7})	EVTS	DOCUMENT ID	TECN	COMMENT	
$7.56 \pm 1.32 \pm 0.50$	39	ABLIKIM	14I	BES3	$J/\psi \rightarrow \pi^0 e^+ e^-$

$\Gamma(\eta e^+ e^-)/\Gamma_{\text{total}}$					Γ_{356}/Γ	
VALUE (units 10^{-5})	EVTS	DOCUMENT ID	TECN	COMMENT		
$1.42 \pm 0.04 \pm 0.07$	2.47k	1,2	ABLIKIM	19A	BES3	$J/\psi \rightarrow \eta e^+ e^-$
$1.16 \pm 0.07 \pm 0.06$	320	1	ABLIKIM	14I	BES3	$J/\psi \rightarrow \eta e^+ e^-$

¹ Using both $\eta \rightarrow \gamma\gamma$ and $\eta \rightarrow \pi^+\pi^-\pi^0$ decays.

² Approximation of the transition form factor squared as an incoherent sum of the ρ -meson and one-pole non-resonant amplitudes gives the pole mass $m(A) = 2.56 \pm 0.04 \pm 0.03$ GeV. Supersedes ABLIKIM 14I.

$\Gamma(\eta'(958) e^+ e^-)/\Gamma_{\text{total}}$					Γ_{357}/Γ	
VALUE (units 10^{-5})	EVTS	DOCUMENT ID	TECN	COMMENT		
$6.59 \pm 0.07 \pm 0.17$	8.9k	1	ABLIKIM	19H	BES3	$J/\psi \rightarrow \eta'(958) e^+ e^-$
$5.81 \pm 0.16 \pm 0.31$	1.4k	1,2	ABLIKIM	14I	BES3	$J/\psi \rightarrow \eta'(958) e^+ e^-$

• • • We do not use the following data for averages, fits, limits, etc. • • •
¹ Using both $\eta' \rightarrow \gamma\pi^+\pi^-$ and $\eta' \rightarrow \pi^+\pi^-\eta$ decays.
² Superseded by ABLIKIM 19H.

$\Gamma(X(1835) e^+ e^-, X \rightarrow \pi^+\pi^-\eta)/\Gamma_{\text{total}}$					Γ_{358}/Γ	
VALUE (units 10^{-6})	EVTS	DOCUMENT ID	TECN	COMMENT		
$3.58 \pm 0.19 \pm 0.16$	1364	1	ABLIKIM	22B	BES3	$J/\psi \rightarrow \pi^+\pi^-\eta' e^+ e^-$

¹ Assuming constructive interference. Destructive interference gives a value of $(4.43 \pm 0.23 \pm 0.19) \times 10^{-6}$ for this branching fraction.

$\Gamma(X(2120) e^+ e^-, X \rightarrow \pi^+\pi^-\eta)/\Gamma_{\text{total}}$					Γ_{359}/Γ
VALUE (units 10^{-6})	EVTS	DOCUMENT ID	TECN	COMMENT	
$0.82 \pm 0.12 \pm 0.06$	310	ABLIKIM	22B	BES3	$J/\psi \rightarrow \pi^+\pi^-\eta' e^+ e^-$

$\Gamma(X(2370) e^+ e^-, X \rightarrow \pi^+\pi^-\eta)/\Gamma_{\text{total}}$					Γ_{360}/Γ
VALUE (units 10^{-6})	EVTS	DOCUMENT ID	TECN	COMMENT	
$1.08 \pm 0.14 \pm 0.10$	397	ABLIKIM	22B	BES3	$J/\psi \rightarrow \pi^+\pi^-\eta' e^+ e^-$

$\Gamma(\eta U \rightarrow \eta e^+ e^-)/\Gamma_{\text{total}}$					Γ_{361}/Γ	
VALUE	CL%	DOCUMENT ID	TECN	COMMENT		
$<9.11 \times 10^{-7}$	90	1	ABLIKIM	19A	BES3	$J/\psi \rightarrow \eta e^+ e^-$

¹ For a dark photon U with mass between 10 and 2400 MeV. Obtained 90% C.L. limits as a function of m_U range from 1.9×10^{-8} to 91.1×10^{-8} .

$\Gamma(\eta'(958) U \rightarrow \eta'(958) e^+ e^-)/\Gamma_{\text{total}}$					Γ_{362}/Γ	
VALUE	CL%	DOCUMENT ID	TECN	COMMENT		
$<2.0 \times 10^{-7}$	90	1	ABLIKIM	19H	BES3	$J/\psi \rightarrow \eta'(958) e^+ e^-$

¹ For a dark photon U with mass between 100 and 2100 MeV. Obtained 90% C.L. limits as a function of m_U range from 1.8×10^{-8} to 2.0×10^{-7} . The corresponding limits on the branching fraction $J/\psi \rightarrow \eta' U$ range from 5.7×10^{-8} to 7.4×10^{-7} .

$\Gamma(\phi e^+ e^-)/\Gamma_{\text{total}}$					Γ_{363}/Γ	
VALUE (units 10^{-7})	CL%	DOCUMENT ID	TECN	COMMENT		
<1.2	90	1	ABLIKIM	19AB	BES3	$J/\psi \rightarrow \phi e^+ e^-$

¹ Using $B(\phi \rightarrow K^+ K^-) = (48.9 \pm 0.5)\%$ and $B(\psi(2S) \rightarrow \pi^+\pi^- J/\psi) = (34.49 \pm 0.30)\%$.

WEAK DECAYS

$\Gamma(D^- e^+ \nu_e + \text{c.c.})/\Gamma_{\text{total}}$					Γ_{364}/Γ
VALUE	CL%	DOCUMENT ID	TECN	COMMENT	
$<7.1 \times 10^{-8}$	90	ABLIKIM	21Q	BES3	$e^+e^- \rightarrow J/\psi$
$<1.2 \times 10^{-5}$	90	ABLIKIM	06M	BES2	$e^+e^- \rightarrow J/\psi$

$\Gamma(D^0 e^+ e^- + \text{c.c.})/\Gamma_{\text{total}}$					Γ_{365}/Γ	
VALUE	CL%	DOCUMENT ID	TECN	COMMENT		
$<8.5 \times 10^{-8}$	90	1	ABLIKIM	17AF	BES3	$e^+e^- \rightarrow J/\psi$
$<1.1 \times 10^{-5}$	90	ABLIKIM	06M	BES2	$e^+e^- \rightarrow J/\psi$	

$\Gamma(D_s^- e^+ \nu_e + \text{c.c.})/\Gamma_{\text{total}}$					Γ_{366}/Γ	
VALUE	CL%	DOCUMENT ID	TECN	COMMENT		
$<1.3 \times 10^{-6}$	90	ABLIKIM	14R	BES3	$e^+e^- \rightarrow J/\psi$	
$<3.6 \times 10^{-5}$	90	1	ABLIKIM	06M	BES2	$e^+e^- \rightarrow J/\psi$

$\Gamma(D_s^{*-} e^+ \nu_e + \text{c.c.})/\Gamma_{\text{total}}$					Γ_{367}/Γ
VALUE	CL%	DOCUMENT ID	TECN	COMMENT	
$<1.8 \times 10^{-6}$	90	ABLIKIM	14R	BES3	$e^+e^- \rightarrow J/\psi$

$\Gamma(D^- \pi^+ + \text{c.c.})/\Gamma_{\text{total}}$					Γ_{368}/Γ
VALUE	CL%	DOCUMENT ID	TECN	COMMENT	
$<7.5 \times 10^{-5}$	90	ABLIKIM	08J	BES2	$e^+e^- \rightarrow J/\psi$

$\Gamma(D^0 \bar{K}^0 + \text{c.c.})/\Gamma_{\text{total}}$					Γ_{369}/Γ
VALUE	CL%	DOCUMENT ID	TECN	COMMENT	
$<1.7 \times 10^{-4}$	90	ABLIKIM	08J	BES2	$e^+e^- \rightarrow J/\psi$

$\Gamma(D^0 \bar{K}^{*0} + \text{c.c.})/\Gamma_{\text{total}}$					Γ_{370}/Γ
VALUE	CL%	DOCUMENT ID	TECN	COMMENT	
$<2.5 \times 10^{-6}$	90	ABLIKIM	14K	BES3	$e^+e^- \rightarrow J/\psi$

Meson Particle Listings

 $J/\psi(1S)$, Branching Ratios of ψ 's and χ 's

AUBERT	06	PR D73 011101	B. Aubert et al.	(BABAR Collab.)
AUBERT	06B	PR D73 012005	B. Aubert et al.	(BABAR Collab.)
AUBERT	06D	PR D73 052003	B. Aubert et al.	(BABAR Collab.)
AUBERT,BE	06D	PR D74 091103	B. Aubert et al.	(BABAR Collab.)
WU	06	PRL 97 162003	C.-H. Wu et al.	(BELLE Collab.)
ABLIKIM	05	PL B607 243	M. Ablikim et al.	(BES Collab.)
ABLIKIM	05B	PR D71 032003	M. Ablikim et al.	(BES Collab.)
ABLIKIM	05C	PL B610 192	M. Ablikim et al.	(BES Collab.)
ABLIKIM	05H	PR D72 012002	M. Ablikim et al.	(BES Collab.)
ABLIKIM	05R	PRL 95 292001	M. Ablikim et al.	(BES Collab.)
AUBERT	05D	PR D71 052001	B. Aubert et al.	(BABAR Collab.)
LI	05C	PR D71 111103	Z. Li et al.	(CLEO Collab.)
SIBIRTSEV	05A	PR D71 054010	A. Sibirtsev, J. Haidenbauer	
ABLIKIM	04	PL B598 172	M. Ablikim et al.	(BES Collab.)
ABLIKIM	04M	PR D70 112008	M. Ablikim et al.	(BES Collab.)
AUBERT	04	PR D69 011103	B. Aubert et al.	(BABAR Collab.)
AUBERT,B	04N	PR D70 072004	B. Aubert et al.	(BABAR Collab.)
BAI	04A	PR D69 012003	J.Z. Bai et al.	(BES Collab.)
BAI	04D	PL B589 7	J.Z. Bai et al.	(BES Collab.)
BAI	04E	PL B591 42	J.Z. Bai et al.	(BES Collab.)
BAI	04G	PR D70 012004	J.Z. Bai et al.	(BES Collab.)
BAI	04H	PR D70 012005	J.Z. Bai et al.	(BES Collab.)
BAI	04J	PL B594 47	J.Z. Bai et al.	(BES Collab.)
SETH	04	PR D69 097503	K.K. Seth	
AULCHENKO	03	PL B573 63	V.M. Aulchenko et al.	(KEDR Collab.)
BAI	03D	PL B561 49	J.Z. Bai et al.	(BES Collab.)
BAI	03F	PRL 91 022001	J.Z. Bai et al.	(BES II Collab.)
BAI	03G	PR D68 052003	J.Z. Bai et al.	(BES Collab.)
HUANG	03	PRL 91 241802	H.-C. Huang et al.	(BELLE Collab.)
BAI	02C	PRL 88 101802	J.Z. Bai et al.	(BES Collab.)
ARTAMONOV	00	PL B474 427	A.S. Artamonov et al.	
BAI	00	PRL 84 594	J.Z. Bai et al.	(BES Collab.)
BAI	00B	PL B472 200	J.Z. Bai et al.	(BES Collab.)
BAI	00D	PL B476 25	J.Z. Bai et al.	(BES Collab.)
BAI	99	PL B446 356	J.Z. Bai et al.	(BES Collab.)
BAI	99C	PRL 83 1918	J.Z. Bai et al.	(BES Collab.)
BAI	98D	PR D58 092006	J.Z. Bai et al.	(BES Collab.)
BAI	98G	PL B424 213	J.Z. Bai et al.	(BES Collab.)
BAI	98H	PRL 81 1179	J.Z. Bai et al.	(BES Collab.)
BALDINI	98	PL B444 111	R. Baldini et al.	(FENICE Collab.)
ARMSTRONG	96	PR D54 7067	T.A. Armstrong et al.	(E760 Collab.)
BAI	96B	PRL 76 3502	J.Z. Bai et al.	(BES Collab.)
BAI	96C	PRL 77 3959	J.Z. Bai et al.	(BES Collab.)
BAI	96D	PR D59 1221	J.Z. Bai et al.	(BES Collab.)
GRIBUSHIN	96	PR D53 4723	J. Gribushin et al.	(E672 and E706 Collab.)
HASAN	96	PL B388 376	A. Hasan, D.V. Bugg	(BRUN, LOQM)
BAI	95B	PL B355 374	J.Z. Bai et al.	(BES Collab.)
BUGG	95	PL B353 378	D.V. Bugg et al.	(LOQM, PNPI, WASH)
ANTONELLI	93	PL B301 317	A. Antonelli et al.	(FENICE Collab.)
ARMSTRONG	93B	PR D47 772	T.A. Armstrong et al.	(FNAL E760 Collab.)
BARNES	93	PL B309 469	P.D. Barnes et al.	(PS185 Collab.)
AUGUSTIN	92	PR D46 1951	J.E. Augustin, G. Cosme	(DM2 Collab.)
BOLTON	92	PL B278 495	T. Bolton et al.	(Mark III Collab.)
BOLTON	92B	PRL 69 3328	T. Bolton et al.	(Mark III Collab.)
COFFMAN	92	PRL 68 282	D.M. Coffman et al.	(Mark III Collab.)
HSHUEH	92	PR D45 2181	S. Hsueh, S. Palestini	(FNAL, TORI)
AUGUSTIN	90	PR D42 10	J.E. Augustin et al.	(DM2 Collab.)
BAI	90B	PRL 65 1309	Z. Bai et al.	(Mark III Collab.)
BAI	90C	PRL 65 2507	Z. Bai et al.	(Mark III Collab.)
BISELLO	90	PL B241 617	D. Bisello et al.	(DM2 Collab.)
COFFMAN	90	PR D41 1410	D.M. Coffman et al.	(Mark III Collab.)
JOUSSET	90	PR D41 1389	J. Jousset et al.	(DM2 Collab.)
ALEXANDER	89	NP B320 45	J.P. Alexander et al.	(LBL, MICH, SLAC)
AUGUSTIN	89	NP B320 1	J.E. Augustin, G. Cosme	(DM2 Collab.)
BISELLO	89B	PR D39 701	J.E. Augustin et al.	(DM2 Collab.)
AUGUSTIN	88	PRL 60 2238	J.E. Augustin et al.	(DM2 Collab.)
COFFMAN	88	PR D38 2695	D.M. Coffman et al.	(Mark III Collab.)
FALVARD	88	PR D38 2706	A. Falvard et al.	(CLER, FRAS, LALO+)
AUGUSTIN	87	ZPHY C36 369	J.E. Augustin et al.	(LALO, CLER, FRAS+)
BAGLIN	87	NP B286 592	C. Baglin et al.	(LAPP, CERN, GENO, LYON+)
BALTRUSAITIS...	87	PR D35 2077	R.M. Baltrusaitis et al.	(Mark III Collab.)
BECKER	87	PRL 59 186	J.J. Becker et al.	(Mark III Collab.)
BISELLO	87	PL B192 239	D. Bisello et al.	(PADO, CLER, FRAS+)
COHEN	87	RMP 59 1121	E.R. Cohen, B.N. Taylor	(RIS C, NBS)
HENRARD	87	NP B292 670	P. Henrard et al.	(CLER, FRAS, LALO+)
FALLIN	87	NP B292 653	D. Fallin et al.	(CLER, FRAS, LALO, PADO)
BALTRUSAITIS...	86B	PR D33 1222	R.M. Baltrusaitis et al.	(Mark III Collab.)
BALTRUSAITIS...	86D	PRL 56 107	R.M. Baltrusaitis et al.	(CIT, UCSC, ILL, SLAC+)
BISELLO	86B	PL B179 294	D. Bisello et al.	(DM2 Collab.)
GAISER	86	PR D34 711	J. Gaiser et al.	(Crystal Ball Collab.)
BALTRUSAITIS...	85C	PRL 55 1723	R.M. Baltrusaitis et al.	(CIT, UCSC+)
BALTRUSAITIS...	85D	PR D32 566	R.M. Baltrusaitis et al.	(CIT, UCSC+)
KURAEV	85	SJNP 41 466	E.A. Kurayev, V.S. Fadin	(NOVO)
Translated from YAF 41 733.				
EATON	84	PR D29 804	M.W. Eaton et al.	(LBL, SLAC)
BLOOM	83	ARNS 33 143	E.D. Bloom, C. Peck	(SLAC, CIT)
EDWARDS	83B	PRL 51 859	C. Edwards et al.	(CIT, HARV, PRIN+)
FRANKLIN	83	PRL 51 963	M.E.B. Franklin et al.	(LBL, SLAC)
BURKE	82	PRL 49 632	D.L. Burke et al.	(LBL, SLAC)
EDWARDS	82B	PR D25 3065	C. Edwards et al.	(CIT, HARV, PRIN+)
EDWARDS	82D	PRL 48 458	C. Edwards et al.	(CIT, HARV, PRIN+)
Also		ARNS 33 143	E.D. Bloom, C. Peck	(SLAC, CIT)
EDWARDS	82E	PRL 49 259	C. Edwards et al.	(CIT, HARV, PRIN+)
LEMOIGNE	82	PL 113B 509	Y. Lemoigne et al.	(SACL, LOIC, SHMP+)
BESCH	81	ZPHY C8 1	H.J. Besch et al.	(BONN, DESY, MAINZ)
GIDAL	81	PL 107B 153	G. Gidal et al.	(SLAC, LBL)
R. PARTRIDGE	80	PRL 44 712	R. Partridge et al.	(CIT, HARV, PRIN+)
SCHARRE	80	PL 97B 329	D.L. Scharre et al.	(SLAC, LBL)
ZHOLENTZ	80	PL 96B 214	A.A. Zholents et al.	(NOVO)
Also		SJNP 34 814	A.A. Zholents et al.	(NOVO)
Translated from YAF 34 1471.				
BRANDELIK	79C	ZPHY C1 233	R. Brandelik et al.	(DASP Collab.)
ALEXANDER	78	PL 72B 493	G. Alexander et al.	(DESY, HAMB, SIEG+)
BESCH	78	PL 78B 347	H.J. Besch et al.	(BONN, DESY, MAINZ)
BRANDELIK	78B	PL 74B 292	R. Brandelik et al.	(DASP Collab.)
PERUZZI	78	PR D17 2901	I. Peruzzi et al.	(SLAC, LBL)
BARTEL	77	PL 66B 489	W. Bartel et al.	(DESY, HEIDP)
BURMESTER	77D	PL 72B 135	J. Burmester et al.	(DESY, HAMB, SIEG+)
FELDMAN	77	PRPL 33C 285	G.J. Feldman, M.L. Perl	(LBL, SLAC)
VANNUCCI	77	PR D15 1814	F. Vannucci et al.	(SLAC, LBL)
BARTEL	76	PL 64B 483	W. Bartel et al.	(DESY, HEIDP)
BRUNSCHEWITZ...	76	PL 63B 487	W. Brunschewitz et al.	(DASP Collab.)
JEAN-MARIE	76	PRL 36 291	B. Jean-Marie et al.	(SLAC, LBL) IG
BALDINI...	75	PL 58B 471	R. Baldini-Celio et al.	(FRAS, ROMA)
BOYARSKI	75	PRL 34 1357	A.M. Boyarski et al.	(SLAC, LBL) JPC
DASP	75	PL 56B 491	W. Brunschewitz et al.	(DASP Collab.)
ESPOSITO	75B	LNC 14 73	B. Esposito et al.	(FRAS, NAPL, PADO+)
FORD	75	PRL 34 604	R.L. Ford et al.	(SLAC, PENN)

BRANCHING RATIOS OF $\psi(2S)$, $\chi_{c0,1,2}$ AND η_c

Updated March 2024 by J.J. Hernández-Rey (IFIC, Valencia), R. Mitchell (Indiana U.), S. Navas (U. of Granada), and C. Patrignani (Bologna Univ., INFN)

Since 2002, the treatment of the branching ratios of the $\psi(2S)$ and $\chi_{c0,1,2}$ has undergone an important restructuring. Since the 2023 online edition, the $\eta_c(1S)$ is now treated in a similar way (see the end of this note).

When measuring a branching ratio experimentally, it is not always possible to normalize the number of events observed in the corresponding decay mode to the total number of particles produced. Therefore, the experimenters sometimes report the number of observed decays with respect to another decay mode of the same or another particle in the relevant decay chain. This is actually equivalent to measuring combinations of branching fractions of several decay modes.

To extract the branching ratio of a given decay mode, the collaborations use some previously reported measurements of the required branching ratios. However, the values are frequently taken from the *Review of Particle Physics* (RPP), which in turn uses the branching ratio reported by the experiment in the following edition, giving rise either to correlations or to plain vicious circles, as discussed in more detail in earlier editions of this review [1,2].

The way to avoid these dependencies and correlations is to extract the branching ratios through a fit that uses the truly measured combinations of branching fractions and partial widths. This fit, in fact, should involve decays from the four concerned particles, $\psi(2S)$, χ_{c0} , χ_{c1} , and χ_{c2} , and occasionally some combinations of branching ratios of more than one of them. This is what is done since the 2002 edition [3].

The PDG policy is to quote the results of the collaborations in a manner as close as possible to what appears in their original publications. However, in order to avoid the problems mentioned above, we had in some cases to work out the values originally measured, using the number of events and detection efficiencies given by the collaborations, or rescaling back the published results. The information was sometimes spread over several articles, and some articles referred to papers still unpublished, which in turn contained the relevant numbers in footnotes.

Even though the experimental collaborations are entitled to extract whatever branching ratios they consider appropriate by using other published results, we would like to encourage them to also quote explicitly in their articles the actual quantities measured, so that they can be used directly in averages and fits of different experimental determinations.

To inform the reader how we computed some of the values used in this edition of RPP, we use footnotes to indicate the branching ratios actually given by the experiments and the quantities they use to derive them from the true combination of branching ratios actually measured.

None of the branching ratios of the $\chi_{c0,1,2}$ are measured independently of the $\psi(2S)$ radiative decays. We tried to identify those branching ratios which can be correlated in a non-trivial

See key on page 1171

Meson Particle Listings

Branching Ratios of ψ 's and χ 's, $\chi_{c0}(1P)$

way, and although we cannot preclude the existence of other cases, we are confident that the most relevant correlations have already been removed. Nevertheless, correlations in the errors of different quantities measured by the same experiment have not been taken into account.

The $\eta_c(1S)$ can be produced in $\gamma\gamma$ collisions, in the radiative decays of vector and axial-vector charmonia (J/ψ , $\psi(2S)$ and $h_c(1P)$) or in B meson decays. As for the $\psi(2S)$ and $\chi_{c0,1,2}$, correlations can be introduced if the derived branching ratios are not properly extracted. We now obtain the corresponding branching ratios using the products of branching ratios originally measured by the experiments, sometimes among different particles (cross-particle branching ratios) and performing an overall fit. In some cases, we were obliged to infer the original product from the information given by the collaborations. However, for recent experiments our policy is not to use anymore extracted branching ratios, so that if the original measured quantity is missing in the relevant publication, the value will not be used in our averages and fits.

1. Fit Information for the $\psi(2S)$ and $\chi_{c0,1,2}$

This is an overall fit to 4 total widths, 1 partial width, 25 combinations of partial widths, 10 branching fractions, and 76 branching ratios or combinations thereof. Of the latter, 58 involve decays of more than one particle.

The overall fit uses 253 measurements to determine 49 parameters and gives a χ^2 of 389.6 for 204 degrees of freedom. We have applied scaling factors in the final errors of the fitted values following the procedure described in section 5.2.3 of our Introduction. After rescaling, the total χ^2 is 149.6.

In the listing we provide the inter-particle correlation coefficients $\langle \delta x_i \delta x_j \rangle / (\delta x_i \cdot \delta x_j)$, in percent, from the fit to the corresponding parameter x_i .

2. Fit Information for the $\eta_c(1S)$

This is an overall fit to 1 total width, 10 combinations of partial widths, 6 branching fractions and 32 branching ratios or combinations thereof. Of the latter, 31 involve decays of more than one particle.

The overall fit uses 113 measurements to determine 19 parameters and has a χ^2 of 184.6 for 94 degrees of freedom. We have applied scaling factors in the final errors of the fitted values following the procedure described in section 5.2.3 of our Introduction. After rescaling, the total χ^2 is 74.1.

In the listing we provide the inter-particle correlation coefficients $\langle \delta x_i \delta x_j \rangle / (\delta x_i \cdot \delta x_j)$, in percent, from the fit to the corresponding parameter x_i .

References

1. Y.F. Gu and X.H. Li, Phys. Lett. **B449**, 361 (1999).
2. C. Patrignani, Phys. Rev. **D64**, 034017 (2001).
3. K. Hagiwara *et al.* (Particle Data Group), Phys. Rev. **D68**, 010001 (2002).

$\chi_{c0}(1P)$

$$I^G(J^{PC}) = 0^+(0^{++})$$

$\chi_{c0}(1P)$ MASS

VALUE (MeV)	EVTs	DOCUMENT ID	TECN	COMMENT
3414.71 ± 0.30 OUR AVERAGE				
3413.0 ± 1.9 ± 0.6	933	¹ AAIJ	17Bb LHCB	$p\bar{p} \rightarrow b\bar{b}X \rightarrow 2(K^+K^-)X$
3414.2 ± 0.5 ± 2.3	5.4k	UEHARA	08 BELL	$\gamma\gamma \rightarrow \chi_{c0} \rightarrow \text{hadrons}$
3406 ± 7 ± 6	230	² ABE	07 BELL	$e^+e^- \rightarrow J/\psi(c\bar{c})$
3414.21 ± 0.39 ± 0.27		ABLIKIM	05c BES2	$\psi(2S) \rightarrow \gamma\chi_{c0}$
3414.7 ± 0.7 ± 0.2		³ ANDREOTTI	03 E835	$\bar{p}p \rightarrow \chi_{c0} \rightarrow \pi^0\pi^0$
3415.5 ± 0.4 ± 0.4	392	⁴ BAGNASCO	02 E835	$\bar{p}p \rightarrow \chi_{c0} \rightarrow J/\psi\gamma$
3417.4 ± 1.8 ± 1.9 ± 0.2		³ AMBROGIANI	99B E835	$\bar{p}p \rightarrow e^+e^-\gamma$
3414.1 ± 0.6 ± 0.8		BAI	99B BES	$\psi(2S) \rightarrow \gamma X$
3417.8 ± 0.4 ± 4		³ GAISER	86 CBAL	$\psi(2S) \rightarrow \gamma X$
3416 ± 3 ± 4		⁵ TANENBAUM	78 MRK1	e^+e^-
••• We do not use the following data for averages, fits, limits, etc. •••				
3414.6 ± 1.1	266	UEHARA	13 BELL	$\gamma\gamma \rightarrow K_S^0 K_S^0$
3416.5 ± 3.0		EISENSTEIN	01 CLE2	$e^+e^- \rightarrow e^+e^-\chi_{c0}$
3422 ± 10		⁵ BARTEL	78B CNTR	$e^+e^- \rightarrow J/\psi 2\gamma$
3415 ± 9		⁵ BIDDICK	77 CNTR	$e^+e^- \rightarrow \gamma X$

¹ From a fit of the $\phi\phi$ invariant mass with the width of $\chi_{c0}(1P)$ fixed to the PDG 16 value.

² From a fit of the J/ψ recoil mass spectrum. Supersedes ABE,K 02 and ABE 04c.

³ Using mass of $\psi(2S) = 3686.0$ MeV.

⁴ Recalculated by ANDREOTTI 05A, using the value of $\psi(2S)$ mass from AULCHENKO 03.

⁵ Mass value shifted by us by amount appropriate for $\psi(2S)$ mass = 3686 MeV and $J/\psi(1S)$ mass = 3097 MeV.

$\chi_{c0}(1P)$ WIDTH

VALUE (MeV)	EVTs	DOCUMENT ID	TECN	COMMENT
10.7 ± 0.6 OUR FIT				Error includes scale factor of 1.1.
10.5 ± 0.8 OUR AVERAGE				Error includes scale factor of 1.1.
10.6 ± 1.9 ± 2.6	5.4k	UEHARA	08 BELL	$\gamma\gamma \rightarrow \chi_{c0} \rightarrow \text{hadrons}$
12.6 ^{+1.5+0.9} _{-1.6-1.1}		ABLIKIM	05c BES2	$\psi(2S) \rightarrow \gamma\chi_{c0}$
8.6 ^{+1.7+0.1} _{-1.3-0.1}		ANDREOTTI	03 E835	$\bar{p}p \rightarrow \chi_{c0} \rightarrow \pi^0\pi^0$
9.7 ± 1.0	392	¹ BAGNASCO	02 E835	$\bar{p}p \rightarrow \chi_{c0} \rightarrow J/\psi\gamma$
16.6 ^{+5.2+0.1} _{-3.7-0.1}		AMBROGIANI	99B E835	$\bar{p}p \rightarrow e^+e^-\gamma$
14.3 ± 2.0 ± 3.0		BAI	98i BES	$\psi(2S) \rightarrow \gamma\pi^+\pi^-$
13.5 ± 3.3 ± 4.2		GAISER	86 CBAL	$\psi(2S) \rightarrow \gamma X, \gamma\pi^0\pi^0$
••• We do not use the following data for averages, fits, limits, etc. •••				
13.2 ± 2.1	266	UEHARA	13 BELL	$\gamma\gamma \rightarrow K_S^0 K_S^0$

¹ Recalculated by ANDREOTTI 05A.

$\chi_{c0}(1P)$ DECAY MODES

Mode	Fraction (Γ_i/Γ)	Scale factor/ Confidence level
Hadronic decays		
Γ_1 $2(\pi^+\pi^-)$	(2.3 ± 0.4) %	S=2.0
Γ_2 $\rho^0\pi^+\pi^-$	(9.1 ± 3.1) × 10 ⁻³	S=1.1
Γ_3 $\rho^0\rho^0$		
Γ_4 $f_0(980)f_0(980)$	(6.7 ± 2.1) × 10 ⁻⁴	
Γ_5 $\pi^+\pi^-\pi^0\pi^0$	(3.3 ± 0.4) %	
Γ_6 $\rho^+\pi^-\pi^0 + \text{c.c.}$	(2.9 ± 0.4) %	
Γ_7 $4\pi^0$	(3.3 ± 0.4) × 10 ⁻³	
Γ_8 $\pi^+\pi^-K^+K^-$	(1.82 ± 0.16) %	S=1.2
Γ_9 $K_0^*(1430)^0 \bar{K}_0^*(1430)^0 \rightarrow \pi^+\pi^-K^+K^-$	(9.9 ^{+4.0} _{-2.8}) × 10 ⁻⁴	
Γ_{10} $K_0^*(1430)^0 \bar{K}_2^*(1430)^0 + \text{c.c.} \rightarrow \pi^+\pi^-K^+K^-$	(8.0 ^{+2.0} _{-2.4}) × 10 ⁻⁴	
Γ_{11} $K_1(1270)^+K^- + \text{c.c.} \rightarrow \pi^+\pi^-K^+K^-$	(6.3 ± 1.9) × 10 ⁻³	
Γ_{12} $K_1(1400)^+K^- + \text{c.c.} \rightarrow \pi^+\pi^-K^+K^-$	< 2.7 × 10 ⁻³	CL=90%
Γ_{13} $f_0(980)f_0(980)$	(1.6 ^{+1.0} _{-0.9}) × 10 ⁻⁴	
Γ_{14} $f_0(980)f_0(2200)$	(7.9 ^{+2.0} _{-2.5}) × 10 ⁻⁴	
Γ_{15} $f_0(1370)f_0(1370)$	< 2.7 × 10 ⁻⁴	CL=90%
Γ_{16} $f_0(1370)f_0(1500)$	< 1.7 × 10 ⁻⁴	CL=90%
Γ_{17} $f_0(1370)f_0(1710)$	(6.7 ^{+3.5} _{-2.3}) × 10 ⁻⁴	
Γ_{18} $f_0(1500)f_0(1370)$	< 1.3 × 10 ⁻⁴	CL=90%
Γ_{19} $f_0(1500)f_0(1500)$	< 5 × 10 ⁻⁵	CL=90%

See key on page 1171

Meson Particle Listings

$\chi_{c0}(1P)$

$\Gamma(\pi\pi) \times \Gamma(\gamma\gamma)/\Gamma_{total}$ $\Gamma_{32}\Gamma_{98}/\Gamma$

VALUE (eV)	EVTS	DOCUMENT ID	TECN	COMMENT
18.7 ± 1.5 OUR FIT				Error includes scale factor of 1.2.
23 ± 5 OUR AVERAGE				
29.7 ^{+17.4} _{-12.0} ± 4.8	103 ⁺⁶⁰ ₋₄₂	¹ UEHARA	09 BELL	10.6 e ⁺ e ⁻ → e ⁺ e ⁻ π ⁰ π ⁰
22.7 ± 3.2 ± 3.5	129 ± 18	² NAKAZAWA	05 BELL	10.6 e ⁺ e ⁻ → e ⁺ e ⁻ π ⁺ π ⁻

¹ We multiplied the measurement by 3 to convert from π⁰π⁰ to ππ. Interference with the continuum included.
² We have multiplied π⁺π⁻ measurement by 3/2 to obtain ππ.

$\Gamma(\eta\eta) \times \Gamma(\gamma\gamma)/\Gamma_{total}$ $\Gamma_{36}\Gamma_{98}/\Gamma$

VALUE (eV)	EVTS	DOCUMENT ID	TECN	COMMENT
9.4 ± 2.3 ± 1.2	22	¹ UEHARA	10A BELL	10.6 e ⁺ e ⁻ → e ⁺ e ⁻ ηη

¹ Interference with the continuum not included.

$\Gamma(\omega\omega) \times \Gamma(\gamma\gamma)/\Gamma_{total}$ $\Gamma_{39}\Gamma_{98}/\Gamma$

VALUE (eV)	CL%	DOCUMENT ID	TECN	COMMENT
• • • We do not use the following data for averages, fits, limits, etc. • • •				
<3.9	90	¹ LIU	12B BELL	γγ → 2(π ⁺ π ⁻ π ⁰)

¹ Using B(ω → π⁺π⁻π⁰) = (89.2 ± 0.7)%.

$\Gamma(\omega\phi) \times \Gamma(\gamma\gamma)/\Gamma_{total}$ $\Gamma_{40}\Gamma_{98}/\Gamma$

VALUE (eV)	CL%	DOCUMENT ID	TECN	COMMENT
• • • We do not use the following data for averages, fits, limits, etc. • • •				
<0.34	90	¹ LIU	12B BELL	γγ → K ⁺ K ⁻ π ⁺ π ⁻ π ⁰

¹ Using B(φ → K⁺K⁻) = (48.9 ± 0.5)% and B(ω → π⁺π⁻π⁰) = (89.2 ± 0.7)%.

$\Gamma(K^+K^-) \times \Gamma(\gamma\gamma)/\Gamma_{total}$ $\Gamma_{42}\Gamma_{98}/\Gamma$

VALUE (eV)	EVTS	DOCUMENT ID	TECN	COMMENT
13.3 ± 1.1 OUR FIT				Error includes scale factor of 1.1.
14.3 ± 1.6 ± 2.3	153 ± 17	NAKAZAWA	05 BELL	10.6 e ⁺ e ⁻ → e ⁺ e ⁻ K ⁺ K ⁻

$\Gamma(K_S^0 K_S^0) \times \Gamma(\gamma\gamma)/\Gamma_{total}$ $\Gamma_{43}\Gamma_{98}/\Gamma$

VALUE (eV)	EVTS	DOCUMENT ID	TECN	COMMENT
7.0 ± 0.6 OUR FIT				Error includes scale factor of 1.2.
8.7 ± 1.7 ± 0.9	266	¹ UEHARA	13 BELL	γγ → K _S ⁰ K _S ⁰
• • • We do not use the following data for averages, fits, limits, etc. • • •				
7.00 ± 0.65 ± 0.71	134 ± 12	CHEN	07B BELL	e ⁺ e ⁻ → e ⁺ e ⁻ χ _{c0}

¹ Supersedes CHEN 07B.

$\Gamma(K^+K^-K^+K^-) \times \Gamma(\gamma\gamma)/\Gamma_{total}$ $\Gamma_{51}\Gamma_{98}/\Gamma$

VALUE (eV)	EVTS	DOCUMENT ID	TECN	COMMENT
6.2 ± 1.0 OUR FIT				Error includes scale factor of 1.5.
7.9 ± 1.3 ± 1.1	215 ± 36	UEHARA	08 BELL	γγ → χ _{c0} → 2(K ⁺ K ⁻)

$\Gamma(\phi\phi) \times \Gamma(\gamma\gamma)/\Gamma_{total}$ $\Gamma_{56}\Gamma_{98}/\Gamma$

VALUE (eV)	EVTS	DOCUMENT ID	TECN	COMMENT
1.86 ± 0.13 OUR FIT				Error includes scale factor of 1.1.
1.72 ± 0.33 ± 0.14	56 ± 11	¹ LIU	12B BELL	γγ → 2(K ⁺ K ⁻)
• • • We do not use the following data for averages, fits, limits, etc. • • •				
2.3 ± 0.9 ± 0.4	23.6 ± 9.6	UEHARA	08 BELL	γγ → χ _{c0} → 2(K ⁺ K ⁻)

¹ Supersedes UEHARA 08. Using B(φ → K⁺K⁻) = (48.9 ± 0.5)%.

$\chi_{c0}(1P)$ BRANCHING RATIOS

HADRONIC DECAYS

$\Gamma(\rho^0\pi^+\pi^-)/\Gamma(2(\pi^+\pi^-))$ Γ_2/Γ_1

VALUE	DOCUMENT ID	TECN	COMMENT
0.39 ± 0.12 OUR FIT			
0.39 ± 0.12	TANENBAUM	78 MRK1	ψ(2S) → γχ _{c0}

$\Gamma(f_0(980)f_0(980))/\Gamma_{total}$ Γ_4/Γ

VALUE (units 10 ⁻⁴)	EVTS	DOCUMENT ID	TECN	COMMENT
6.7 ± 2.1 ± 0.2	36 ± 9	¹ ABLIKIM	04G BES	ψ(2S) → γ2π ⁺ 2π ⁻

¹ ABLIKIM 04G reports [Γ(χ_{c0}(1P) → f₀(980)f₀(980))/Γ_{total}] × [B(ψ(2S) → γχ_{c0}(1P))] = (6.5 ± 1.6 ± 1.3) × 10⁻⁵ which we divide by our best value B(ψ(2S) → γχ_{c0}(1P)) = (9.77 ± 0.23) × 10⁻². Our first error is their experiment's error and our second error is the systematic error from using our best value.

$\Gamma(\pi^+\pi^-\pi^0\pi^0)/\Gamma_{total}$ Γ_5/Γ

VALUE (%)	EVTS	DOCUMENT ID	TECN	COMMENT
3.3 ± 0.4 ± 0.1	1751.4	¹ HE	08B CLEO	e ⁺ e ⁻ → γh ⁺ h ⁻ h ⁰ h ⁰

¹ HE 08B reports 3.54 ± 0.10 ± 0.43 ± 0.18 % from a measurement of [Γ(χ_{c0}(1P) → π⁺π⁻π⁰π⁰)/Γ_{total}] × [B(ψ(2S) → γχ_{c0}(1P))] assuming B(ψ(2S) → γχ_{c0}(1P)) = (9.22 ± 0.11 ± 0.46) × 10⁻², which we rescale to our best value B(ψ(2S) → γχ_{c0}(1P)) = (9.77 ± 0.23) × 10⁻². Our first error is their experiment's error and our second error is the systematic error from using our best value.

$\Gamma(\rho^+\pi^-\pi^0 + c.c.)/\Gamma_{total}$ Γ_6/Γ

VALUE (%)	EVTS	DOCUMENT ID	TECN	COMMENT
2.9 ± 0.4 ± 0.1	1358.5	^{1,2} HE	08B CLEO	e ⁺ e ⁻ → γh ⁺ h ⁻ h ⁰ h ⁰

¹ HE 08B reports 3.04 ± 0.18 ± 0.42 ± 0.16 % from a measurement of [Γ(χ_{c0}(1P) → ρ⁺π⁻π⁰ + c.c.)/Γ_{total}] × [B(ψ(2S) → γχ_{c0}(1P))] assuming B(ψ(2S) → γχ_{c0}(1P)) = (9.22 ± 0.11 ± 0.46) × 10⁻², which we rescale to our best value B(ψ(2S) → γχ_{c0}(1P)) = (9.77 ± 0.23) × 10⁻². Our first error is their experiment's error and our second error is the systematic error from using our best value.
² Calculated by us. We have added the values from HE 08B for ρ⁺π⁻π⁰ and ρ⁻π⁺π⁰ decays assuming uncorrelated statistical and fully correlated systematic uncertainties.

$\Gamma(4\pi^0)/\Gamma_{total}$ Γ_7/Γ

VALUE (units 10 ⁻³)	EVTS	DOCUMENT ID	TECN	COMMENT
3.3 ± 0.4 ± 0.1	3296	¹ ABLIKIM	11A BES3	e ⁺ e ⁻ → ψ(2S) → γχ _{c0}

¹ ABLIKIM 11A reports (3.34 ± 0.06 ± 0.44) × 10⁻³ from a measurement of [Γ(χ_{c0}(1P) → 4π⁰)/Γ_{total}] × [B(ψ(2S) → γχ_{c0}(1P))] assuming B(ψ(2S) → γχ_{c0}(1P)) = (9.62 ± 0.31) × 10⁻², which we rescale to our best value B(ψ(2S) → γχ_{c0}(1P)) = (9.77 ± 0.23) × 10⁻². Our first error is their experiment's error and our second error is the systematic error from using our best value.

$\Gamma(K^+\bar{K}^*(892)^0\pi^- + c.c.)/\Gamma(\pi^+\pi^-K^+K^-)$ Γ_{30}/Γ_8

VALUE	DOCUMENT ID	TECN	COMMENT
0.41 ± 0.09 OUR FIT			
0.41 ± 0.10	TANENBAUM	78 MRK1	ψ(2S) → γχ _{c0}

$\Gamma(K_0^*(1430)^0\bar{K}_0^*(1430)^0 \rightarrow \pi^+\pi^-K^+K^-)/\Gamma_{total}$ Γ_9/Γ

VALUE (units 10 ⁻⁴)	EVTS	DOCUMENT ID	TECN	COMMENT
9.9 ± 3.6 ± 0.2	83	¹ ABLIKIM	05Q BES2	ψ(2S) → γπ ⁺ π ⁻ K ⁺ K ⁻

¹ ABLIKIM 05Q reports (10.44 ± 2.37^{+3.05}_{-1.90}) × 10⁻⁴ from a measurement of [Γ(χ_{c0}(1P) → K₀^{*}(1430)⁰ \bar{K}_0^* (1430)⁰ → π⁺π⁻K⁺K⁻)/Γ_{total}] × [B(ψ(2S) → γχ_{c0}(1P))] assuming B(ψ(2S) → γχ_{c0}(1P)) = (9.22 ± 0.11 ± 0.46) × 10⁻², which we rescale to our best value B(ψ(2S) → γχ_{c0}(1P)) = (9.77 ± 0.23) × 10⁻². Our first error is their experiment's error and our second error is the systematic error from using our best value.

$\Gamma(K_0^*(1430)^0\bar{K}_2^*(1430)^0 + c.c. \rightarrow \pi^+\pi^-K^+K^-)/\Gamma_{total}$ Γ_{10}/Γ

VALUE (units 10 ⁻⁴)	EVTS	DOCUMENT ID	TECN	COMMENT
8.0 ± 2.0 ± 0.2	62	¹ ABLIKIM	05Q BES2	ψ(2S) → γπ ⁺ π ⁻ K ⁺ K ⁻

¹ ABLIKIM 05Q reports (8.49 ± 1.66^{+1.32}_{-1.99}) × 10⁻⁴ from a measurement of [Γ(χ_{c0}(1P) → K₀^{*}(1430)⁰ \bar{K}_2^* (1430)⁰ + c.c. → π⁺π⁻K⁺K⁻)/Γ_{total}] × [B(ψ(2S) → γχ_{c0}(1P))] assuming B(ψ(2S) → γχ_{c0}(1P)) = (9.22 ± 0.11 ± 0.46) × 10⁻², which we rescale to our best value B(ψ(2S) → γχ_{c0}(1P)) = (9.77 ± 0.23) × 10⁻². Our first error is their experiment's error and our second error is the systematic error from using our best value.

$\Gamma(K_1(1270)^+K^- + c.c. \rightarrow \pi^+\pi^-K^+K^-)/\Gamma_{total}$ Γ_{11}/Γ

VALUE (units 10 ⁻³)	EVTS	DOCUMENT ID	TECN	COMMENT
6.3 ± 1.9 ± 0.1	68	¹ ABLIKIM	05Q BES2	ψ(2S) → γπ ⁺ π ⁻ K ⁺ K ⁻

¹ ABLIKIM 05Q reports (6.66 ± 1.31^{+1.60}_{-1.51}) × 10⁻³ from a measurement of [Γ(χ_{c0}(1P) → K₁(1270)⁺K⁻ + c.c. → π⁺π⁻K⁺K⁻)/Γ_{total}] × [B(ψ(2S) → γχ_{c0}(1P))] assuming B(ψ(2S) → γχ_{c0}(1P)) = (9.22 ± 0.11 ± 0.46) × 10⁻², which we rescale to our best value B(ψ(2S) → γχ_{c0}(1P)) = (9.77 ± 0.23) × 10⁻². Our first error is their experiment's error and our second error is the systematic error from using our best value. The measurement assumes B(K₁(1270) → Kρ(770)) = 42 ± 6%.

$\Gamma(K_1(1400)^+K^- + c.c. \rightarrow \pi^+\pi^-K^+K^-)/\Gamma_{total}$ Γ_{12}/Γ

VALUE (units 10 ⁻³)	CL%	DOCUMENT ID	TECN	COMMENT
<2.7	90	¹ ABLIKIM	05Q BES2	ψ(2S) → γπ ⁺ π ⁻ K ⁺ K ⁻

¹ ABLIKIM 05Q reports < 2.85 × 10⁻³ from a measurement of [Γ(χ_{c0}(1P) → K₁(1400)⁺K⁻ + c.c. → π⁺π⁻K⁺K⁻)/Γ_{total}] × [B(ψ(2S) → γχ_{c0}(1P))] assuming B(ψ(2S) → γχ_{c0}(1P)) = (9.22 ± 0.11 ± 0.46) × 10⁻², which we rescale to our best value B(ψ(2S) → γχ_{c0}(1P)) = 9.77 × 10⁻². The measurement assumes B(K₁(1400) → K*(892)π) = 94 ± 6%.

$\Gamma(f_0(980)f_0(980))/\Gamma_{total}$ Γ_{13}/Γ

VALUE (units 10 ⁻⁵)	EVTS	DOCUMENT ID	TECN	COMMENT
16.3 ± 10.5 ± 0.4	28	¹ ABLIKIM	05Q BES2	ψ(2S) → γπ ⁺ π ⁻ K ⁺ K ⁻

¹ ABLIKIM 05Q reports [Γ(χ_{c0}(1P) → f₀(980)f₀(980))/Γ_{total}] × [B(ψ(2S) → γχ_{c0}(1P))] = (1.59 ± 0.50^{+0.89}_{-0.72}) × 10⁻⁵ which we divide by our best value B(ψ(2S) → γχ_{c0}(1P)) = (9.77 ± 0.23) × 10⁻². Our first error is their experiment's error and our second error is the systematic error from using our best value. One of the f₀(980) mesons is identified via decay to π⁺π⁻ while the other via K⁺K⁻ decay.

Meson Particle Listings

 $\chi_{c0}(1P)$

$\Gamma(\bar{f}_0(980)\bar{f}_0(2200))/\Gamma_{\text{total}}$					Γ_{14}/Γ
VALUE (units 10^{-4})	EVTS	DOCUMENT ID	TECN	COMMENT	

$7.9 \pm 2.0_{-2.9} \pm 0.2$ 77 ¹ ABLIKIM 05Q BES2 $\psi(2S) \rightarrow \gamma\pi^+\pi^-K^+K^-$

¹ ABLIKIM 05Q reports $(8.42 \pm 1.42 \pm 1.55_{-2.29}) \times 10^{-4}$ from a measurement of $[\Gamma(\chi_{c0}(1P) \rightarrow \bar{f}_0(980)\bar{f}_0(2200))/\Gamma_{\text{total}}] \times [\text{B}(\psi(2S) \rightarrow \gamma\chi_{c0}(1P))]$ assuming $\text{B}(\psi(2S) \rightarrow \gamma\chi_{c0}(1P)) = (9.22 \pm 0.11 \pm 0.46) \times 10^{-2}$, which we rescale to our best value $\text{B}(\psi(2S) \rightarrow \gamma\chi_{c0}(1P)) = (9.77 \pm 0.23) \times 10^{-2}$. Our first error is their experiment's error and our second error is the systematic error from using our best value. The \bar{f}_0 mesons are identified via $\bar{f}_0(980) \rightarrow \pi^+\pi^-$ and $\bar{f}_0(2200) \rightarrow K^+K^-$ decays.

$\Gamma(\bar{f}_0(1370)\bar{f}_0(1370))/\Gamma_{\text{total}}$					Γ_{15}/Γ
VALUE (units 10^{-4})	CL%	DOCUMENT ID	TECN	COMMENT	

<2.7 90 ¹ ABLIKIM 05Q BES2 $\psi(2S) \rightarrow \gamma\pi^+\pi^-K^+K^-$

¹ ABLIKIM 05Q reports $< 2.9 \times 10^{-4}$ from a measurement of $[\Gamma(\chi_{c0}(1P) \rightarrow \bar{f}_0(1370)\bar{f}_0(1370))/\Gamma_{\text{total}}] \times [\text{B}(\psi(2S) \rightarrow \gamma\chi_{c0}(1P))]$ assuming $\text{B}(\psi(2S) \rightarrow \gamma\chi_{c0}(1P)) = (9.22 \pm 0.11 \pm 0.46) \times 10^{-2}$, which we rescale to our best value $\text{B}(\psi(2S) \rightarrow \gamma\chi_{c0}(1P)) = 9.77 \times 10^{-2}$. One of the $\bar{f}_0(1370)$ mesons is identified via decay to $\pi^+\pi^-$ while the other via K^+K^- decay. Both branching fractions for these \bar{f}_0 decays are implicitly included in the quoted result.

$\Gamma(\bar{f}_0(1370)\bar{f}_0(1500))/\Gamma_{\text{total}}$					Γ_{16}/Γ
VALUE (units 10^{-4})	CL%	DOCUMENT ID	TECN	COMMENT	

<1.7 90 ¹ ABLIKIM 05Q BES2 $\psi(2S) \rightarrow \gamma\pi^+\pi^-K^+K^-$

¹ ABLIKIM 05Q reports $< 1.8 \times 10^{-4}$ from a measurement of $[\Gamma(\chi_{c0}(1P) \rightarrow \bar{f}_0(1370)\bar{f}_0(1500))/\Gamma_{\text{total}}] \times [\text{B}(\psi(2S) \rightarrow \gamma\chi_{c0}(1P))]$ assuming $\text{B}(\psi(2S) \rightarrow \gamma\chi_{c0}(1P)) = (9.22 \pm 0.11 \pm 0.46) \times 10^{-2}$, which we rescale to our best value $\text{B}(\psi(2S) \rightarrow \gamma\chi_{c0}(1P)) = 9.77 \times 10^{-2}$. The \bar{f}_0 mesons are identified via $\bar{f}_0(1370) \rightarrow \pi^+\pi^-$ and $\bar{f}_0(1500) \rightarrow K^+K^-$ decays. Both branching fractions for these \bar{f}_0 decays are implicitly included in the quoted result.

$\Gamma(\bar{f}_0(1370)\bar{f}_0(1710))/\Gamma_{\text{total}}$					Γ_{17}/Γ
VALUE (units 10^{-4})	EVTS	DOCUMENT ID	TECN	COMMENT	

$6.7 \pm 3.3_{-2.5} \pm 0.2$ 61 ¹ ABLIKIM 05Q BES2 $\psi(2S) \rightarrow \gamma\pi^+\pi^-K^+K^-$

¹ ABLIKIM 05Q reports $(7.12 \pm 1.85 \pm 3.28_{-1.68}) \times 10^{-4}$ from a measurement of $[\Gamma(\chi_{c0}(1P) \rightarrow \bar{f}_0(1370)\bar{f}_0(1710))/\Gamma_{\text{total}}] \times [\text{B}(\psi(2S) \rightarrow \gamma\chi_{c0}(1P))]$ assuming $\text{B}(\psi(2S) \rightarrow \gamma\chi_{c0}(1P)) = (9.22 \pm 0.11 \pm 0.46) \times 10^{-2}$, which we rescale to our best value $\text{B}(\psi(2S) \rightarrow \gamma\chi_{c0}(1P)) = (9.77 \pm 0.23) \times 10^{-2}$. Our first error is their experiment's error and our second error is the systematic error from using our best value. The \bar{f}_0 mesons are identified via $\bar{f}_0(1370) \rightarrow \pi^+\pi^-$ and $\bar{f}_0(1710) \rightarrow K^+K^-$ decays. Both branching fractions for these \bar{f}_0 decays are implicitly included in the quoted result.

$\Gamma(\bar{f}_0(1500)\bar{f}_0(1370))/\Gamma_{\text{total}}$					Γ_{18}/Γ
VALUE (units 10^{-4})	CL%	DOCUMENT ID	TECN	COMMENT	

<1.3 90 ¹ ABLIKIM 05Q BES2 $\psi(2S) \rightarrow \gamma\pi^+\pi^-K^+K^-$

¹ ABLIKIM 05Q reports $< 1.4 \times 10^{-4}$ from a measurement of $[\Gamma(\chi_{c0}(1P) \rightarrow \bar{f}_0(1500)\bar{f}_0(1370))/\Gamma_{\text{total}}] \times [\text{B}(\psi(2S) \rightarrow \gamma\chi_{c0}(1P))]$ assuming $\text{B}(\psi(2S) \rightarrow \gamma\chi_{c0}(1P)) = (9.22 \pm 0.11 \pm 0.46) \times 10^{-2}$, which we rescale to our best value $\text{B}(\psi(2S) \rightarrow \gamma\chi_{c0}(1P)) = 9.77 \times 10^{-2}$. The \bar{f}_0 mesons are identified via $\bar{f}_0(1500) \rightarrow \pi^+\pi^-$ and $\bar{f}_0(1370) \rightarrow K^+K^-$ decays. Both branching fractions for these \bar{f}_0 decays are implicitly included in the quoted result.

$\Gamma(\bar{f}_0(1500)\bar{f}_0(1500))/\Gamma_{\text{total}}$					Γ_{19}/Γ
VALUE (units 10^{-4})	CL%	DOCUMENT ID	TECN	COMMENT	

<0.5 90 ¹ ABLIKIM 05Q BES2 $\psi(2S) \rightarrow \gamma\pi^+\pi^-K^+K^-$

¹ ABLIKIM 05Q reports $< 0.55 \times 10^{-4}$ from a measurement of $[\Gamma(\chi_{c0}(1P) \rightarrow \bar{f}_0(1500)\bar{f}_0(1500))/\Gamma_{\text{total}}] \times [\text{B}(\psi(2S) \rightarrow \gamma\chi_{c0}(1P))]$ assuming $\text{B}(\psi(2S) \rightarrow \gamma\chi_{c0}(1P)) = (9.22 \pm 0.11 \pm 0.46) \times 10^{-2}$, which we rescale to our best value $\text{B}(\psi(2S) \rightarrow \gamma\chi_{c0}(1P)) = 9.77 \times 10^{-2}$. One of the $\bar{f}_0(1500)$ is identified via decay to $\pi^+\pi^-$ while the other via K^+K^- decay. Both branching fractions for these \bar{f}_0 decays are implicitly included in the quoted result.

$\Gamma(\bar{f}_0(1500)\bar{f}_0(1710))/\Gamma_{\text{total}}$					Γ_{20}/Γ
VALUE (units 10^{-4})	CL%	DOCUMENT ID	TECN	COMMENT	

<0.7 90 ¹ ABLIKIM 05Q BES2 $\psi(2S) \rightarrow \gamma\pi^+\pi^-K^+K^-$

¹ ABLIKIM 05Q reports $< 0.73 \times 10^{-4}$ from a measurement of $[\Gamma(\chi_{c0}(1P) \rightarrow \bar{f}_0(1500)\bar{f}_0(1710))/\Gamma_{\text{total}}] \times [\text{B}(\psi(2S) \rightarrow \gamma\chi_{c0}(1P))]$ assuming $\text{B}(\psi(2S) \rightarrow \gamma\chi_{c0}(1P)) = (9.22 \pm 0.11 \pm 0.46) \times 10^{-2}$, which we rescale to our best value $\text{B}(\psi(2S) \rightarrow \gamma\chi_{c0}(1P)) = 9.77 \times 10^{-2}$. The \bar{f}_0 mesons are identified via $\bar{f}_0(1500) \rightarrow \pi^+\pi^-$ and $\bar{f}_0(1710) \rightarrow K^+K^-$ decays. Both branching fractions for these \bar{f}_0 decays are implicitly included in the quoted result.

$\Gamma(K^+K^-\pi^+\pi^-)/\Gamma_{\text{total}}$					Γ_{21}/Γ
VALUE (units 10^{-3})	EVTS	DOCUMENT ID	TECN	COMMENT	

$8.61 \pm 0.13 \pm 0.94$ 9.0k ¹ ABLIKIM 13B BES3 $e^+e^- \rightarrow \psi(2S) \rightarrow \gamma\chi_{c0}$

¹ Using 1.06×10^8 $\psi(2S)$ mesons and $\text{B}(\psi(2S) \rightarrow \chi_{c0}\gamma) = (9.68 \pm 0.31)\%$.

$\Gamma(K_S^0 K_S^0 \pi^+\pi^-)/\Gamma_{\text{total}}$					Γ_{22}/Γ
VALUE (units 10^{-3})	EVTS	DOCUMENT ID	TECN	COMMENT	

$4.22 \pm 0.10 \pm 0.43$ 2.7k ¹ ABLIKIM 13B BES3 $e^+e^- \rightarrow \psi(2S) \rightarrow \gamma\chi_{c0}$

¹ Using 1.06×10^8 $\psi(2S)$ mesons and $\text{B}(\psi(2S) \rightarrow \chi_{c0}\gamma) = (9.68 \pm 0.31)\%$.

$\Gamma(K^+K^-\pi^0)/\Gamma_{\text{total}}$					Γ_{23}/Γ
VALUE (%)	EVTS	DOCUMENT ID	TECN	COMMENT	

$0.56 \pm 0.09 \pm 0.01$ 213.5 ¹ HE 08B CLEO $e^+e^- \rightarrow \gamma h^+ h^- h^0 h^0$

¹ HE 08B reports $0.59 \pm 0.05 \pm 0.08 \pm 0.03\%$ from a measurement of $[\Gamma(\chi_{c0}(1P) \rightarrow K^+K^-\pi^0)/\Gamma_{\text{total}}] \times [\text{B}(\psi(2S) \rightarrow \gamma\chi_{c0}(1P))]$ assuming $\text{B}(\psi(2S) \rightarrow \gamma\chi_{c0}(1P)) = (9.22 \pm 0.11 \pm 0.46) \times 10^{-2}$, which we rescale to our best value $\text{B}(\psi(2S) \rightarrow \gamma\chi_{c0}(1P)) = (9.77 \pm 0.23) \times 10^{-2}$. Our first error is their experiment's error and our second error is the systematic error from using our best value.

$\Gamma(K^+\pi^-\bar{K}^0\pi^0 + \text{c.c.})/\Gamma_{\text{total}}$					Γ_{24}/Γ
VALUE (%)	EVTS	DOCUMENT ID	TECN	COMMENT	

$2.49 \pm 0.33 \pm 0.06$ 401.7 ¹ HE 08B CLEO $e^+e^- \rightarrow \gamma h^+ h^- h^0 h^0$

¹ HE 08B reports $2.64 \pm 0.15 \pm 0.31 \pm 0.14\%$ from a measurement of $[\Gamma(\chi_{c0}(1P) \rightarrow K^+\pi^-\bar{K}^0\pi^0 + \text{c.c.})/\Gamma_{\text{total}}] \times [\text{B}(\psi(2S) \rightarrow \gamma\chi_{c0}(1P))]$ assuming $\text{B}(\psi(2S) \rightarrow \gamma\chi_{c0}(1P)) = (9.22 \pm 0.11 \pm 0.46) \times 10^{-2}$, which we rescale to our best value $\text{B}(\psi(2S) \rightarrow \gamma\chi_{c0}(1P)) = (9.77 \pm 0.23) \times 10^{-2}$. Our first error is their experiment's error and our second error is the systematic error from using our best value.

$\Gamma(\rho^+K^-K^0 + \text{c.c.})/\Gamma_{\text{total}}$					Γ_{25}/Γ
VALUE (%)	EVTS	DOCUMENT ID	TECN	COMMENT	

$1.21 \pm 0.21 \pm 0.03$ 179.7 ¹ HE 08B CLEO $e^+e^- \rightarrow \gamma h^+ h^- h^0 h^0$

¹ HE 08B reports $1.28 \pm 0.16 \pm 0.15 \pm 0.07\%$ from a measurement of $[\Gamma(\chi_{c0}(1P) \rightarrow \rho^+K^-K^0 + \text{c.c.})/\Gamma_{\text{total}}] \times [\text{B}(\psi(2S) \rightarrow \gamma\chi_{c0}(1P))]$ assuming $\text{B}(\psi(2S) \rightarrow \gamma\chi_{c0}(1P)) = (9.22 \pm 0.11 \pm 0.46) \times 10^{-2}$, which we rescale to our best value $\text{B}(\psi(2S) \rightarrow \gamma\chi_{c0}(1P)) = (9.77 \pm 0.23) \times 10^{-2}$. Our first error is their experiment's error and our second error is the systematic error from using our best value.

$\Gamma(K^*(892)^-K^+\pi^0 \rightarrow K^+\pi^-\bar{K}^0\pi^0 + \text{c.c.})/\Gamma_{\text{total}}$					Γ_{26}/Γ
VALUE (%)	EVTS	DOCUMENT ID	TECN	COMMENT	

$0.46 \pm 0.12 \pm 0.01$ 64.1 ¹ HE 08B CLEO $e^+e^- \rightarrow \gamma h^+ h^- h^0 h^0$

¹ HE 08B reports $0.49 \pm 0.10 \pm 0.07 \pm 0.03\%$ from a measurement of $[\Gamma(\chi_{c0}(1P) \rightarrow K^*(892)^-K^+\pi^0 \rightarrow K^+\pi^-\bar{K}^0\pi^0 + \text{c.c.})/\Gamma_{\text{total}}] \times [\text{B}(\psi(2S) \rightarrow \gamma\chi_{c0}(1P))]$ assuming $\text{B}(\psi(2S) \rightarrow \gamma\chi_{c0}(1P)) = (9.22 \pm 0.11 \pm 0.46) \times 10^{-2}$, which we rescale to our best value $\text{B}(\psi(2S) \rightarrow \gamma\chi_{c0}(1P)) = (9.77 \pm 0.23) \times 10^{-2}$. Our first error is their experiment's error and our second error is the systematic error from using our best value.

$\Gamma(K_S^0 K_S^0 \pi^+\pi^-)/\Gamma_{\text{total}}$					Γ_{27}/Γ
VALUE (units 10^{-3})	EVTS	DOCUMENT ID	TECN	COMMENT	

$5.7 \pm 1.1 \pm 0.1$ 152 ± 14 ¹ ABLIKIM 05o BES2 $\psi(2S) \rightarrow \gamma\chi_{c0}$

¹ ABLIKIM 05o reports $[\Gamma(\chi_{c0}(1P) \rightarrow K_S^0 K_S^0 \pi^+\pi^-)/\Gamma_{\text{total}}] \times [\text{B}(\psi(2S) \rightarrow \gamma\chi_{c0}(1P))]$ assuming $\text{B}(\psi(2S) \rightarrow \gamma\chi_{c0}(1P)) = (0.558 \pm 0.051 \pm 0.089) \times 10^{-3}$ which we divide by our best value $\text{B}(\psi(2S) \rightarrow \gamma\chi_{c0}(1P)) = (9.77 \pm 0.23) \times 10^{-2}$. Our first error is their experiment's error and our second error is the systematic error from using our best value.

$\Gamma(K^+K^-\eta\pi^0)/\Gamma_{\text{total}}$					Γ_{28}/Γ
VALUE (%)	EVTS	DOCUMENT ID	TECN	COMMENT	

$0.30 \pm 0.07 \pm 0.01$ 56.4 ¹ HE 08B CLEO $e^+e^- \rightarrow \gamma h^+ h^- h^0 h^0$

¹ HE 08B reports $0.32 \pm 0.05 \pm 0.05 \pm 0.02\%$ from a measurement of $[\Gamma(\chi_{c0}(1P) \rightarrow K^+K^-\eta\pi^0)/\Gamma_{\text{total}}] \times [\text{B}(\psi(2S) \rightarrow \gamma\chi_{c0}(1P))]$ assuming $\text{B}(\psi(2S) \rightarrow \gamma\chi_{c0}(1P)) = (9.22 \pm 0.11 \pm 0.46) \times 10^{-2}$, which we rescale to our best value $\text{B}(\psi(2S) \rightarrow \gamma\chi_{c0}(1P)) = (9.77 \pm 0.23) \times 10^{-2}$. Our first error is their experiment's error and our second error is the systematic error from using our best value.

$\Gamma(3(\pi^+\pi^-))/\Gamma_{\text{total}}$					Γ_{29}/Γ
VALUE (units 10^{-3})	EVTS	DOCUMENT ID	TECN	COMMENT	

19.5 ± 2.2 OUR AVERAGE Error includes scale factor of 3.3. See the ideogram below.

20.8 ± 0.5 ± 0.5 145K ¹ ABLIKIM 22Q BES3 $\psi(2S) \rightarrow \gamma 3(\pi^+\pi^-)$

11.7 ± 1.0 ± 1.9 ² BAI 99B BES $\psi(2S) \rightarrow \gamma\chi_{c0}$

12.5 ± 2.9 ± 0.5 ² TANENBAUM 78 MRK1 $\psi(2S) \rightarrow \gamma\chi_{c0}$

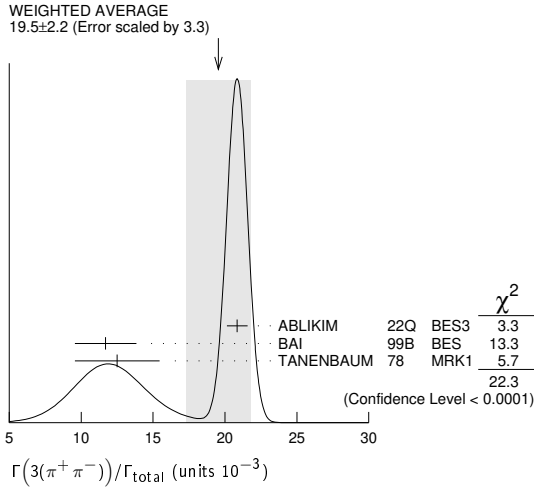
¹ ABLIKIM 22Q reports $(2.080 \pm 0.006 \pm 0.068) \times 10^{-2}$ from a measurement of $[\Gamma(\chi_{c0}(1P) \rightarrow 3(\pi^+\pi^-))/\Gamma_{\text{total}}] \times [\text{B}(\psi(2S) \rightarrow \gamma\chi_{c0}(1P))]$ assuming $\text{B}(\psi(2S) \rightarrow \gamma\chi_{c0}(1P)) = (9.79 \pm 0.2) \times 10^{-2}$, which we rescale to our best value $\text{B}(\psi(2S) \rightarrow \gamma\chi_{c0}(1P)) = (9.77 \pm 0.23) \times 10^{-2}$. Our first error is their experiment's error and our second error is the systematic error from using our best value.

² Rescaled by us using $\text{B}(\psi(2S) \rightarrow \gamma\chi_{c0}) = (9.4 \pm 0.4)\%$ and $\text{B}(\psi(2S) \rightarrow J/\psi(1S)\pi^+\pi^-) = (32.6 \pm 0.5)\%$.

See key on page 1171

Meson Particle Listings

$\chi_{c0}(1P)$



$\Gamma(K^*(892)^0 \bar{K}^*(892)^0) / \Gamma_{total}$ Γ₃₁/Γ

VALUE (units 10 ⁻³)	EVTS	DOCUMENT ID	TECN	COMMENT
1.72 ± 0.60 ± 0.54 ± 0.04	64	¹ ABLIKIM	05Q	BES2 $\psi(2S) \rightarrow \gamma \pi^+ \pi^- K^+ K^-$
• • • We do not use the following data for averages, fits, limits, etc. • • •				
1.57 ± 0.40 ± 0.04	30 ± 6	^{2,3} ABLIKIM	04H	BES Repl. by ABLIKIM 05Q
¹ ABLIKIM 05Q reports $[\Gamma(\chi_{c0}(1P) \rightarrow K^*(892)^0 \bar{K}^*(892)^0) / \Gamma_{total}] \times [B(\psi(2S) \rightarrow \gamma \chi_{c0}(1P))] = (0.168 \pm 0.035 \pm 0.047 \pm 0.040) \times 10^{-3}$ which we divide by our best value $B(\psi(2S) \rightarrow \gamma \chi_{c0}(1P)) = (9.77 \pm 0.23) \times 10^{-2}$. Our first error is their experiment's error and our second error is the systematic error from using our best value.				
² Assumes $B(K^*(892)^0 \rightarrow K^- \pi^+) = 2/3$.				
³ ABLIKIM 04H reports $[\Gamma(\chi_{c0}(1P) \rightarrow K^*(892)^0 \bar{K}^*(892)^0) / \Gamma_{total}] \times [B(\psi(2S) \rightarrow \gamma \chi_{c0}(1P))] = (1.53 \pm 0.29 \pm 0.26) \times 10^{-4}$ which we divide by our best value $B(\psi(2S) \rightarrow \gamma \chi_{c0}(1P)) = (9.77 \pm 0.23) \times 10^{-2}$. Our first error is their experiment's error and our second error is the systematic error from using our best value.				

$\Gamma(\pi^0 \eta_c) / \Gamma_{total}$ Γ₃₅/Γ

VALUE	CL%	DOCUMENT ID	TECN	COMMENT
< 1.6 × 10⁻³	90	¹ ABLIKIM	15N	BES3 $\psi(2S) e^+ e^- \rightarrow \gamma \pi^0 \eta_c$
¹ Using $B(\eta_c \rightarrow K_S^0 K^\pm \pi^\mp) \times B(K_S^0 \rightarrow \pi^+ \pi^-) \times B(\pi^0 \rightarrow \gamma) = (1.66 \pm 0.11) \times 10^{-2}$.				

$\Gamma(\eta \eta') / \Gamma_{total}$ Γ₃₇/Γ

VALUE (units 10 ⁻⁵)	CL%	EVTS	DOCUMENT ID	TECN	COMMENT
9.1 ± 1.1 ± 0.2	85	¹ ABLIKIM	17A	BES3	$\psi(2S) \rightarrow \gamma \eta' \eta$
• • • We do not use the following data for averages, fits, limits, etc. • • •					
< 24	90	35 ± 13	² ASNER	09	CLEO $\psi(2S) \rightarrow \gamma \eta' \eta$
< 50	90		³ ADAMS	07	CLEO $\psi(2S) \rightarrow \gamma \chi_{c0}$
¹ ABLIKIM 17A reports $(8.92 \pm 0.84 \pm 0.65) \times 10^{-5}$ from a measurement of $[\Gamma(\chi_{c0}(1P) \rightarrow \eta \eta') / \Gamma_{total}] \times [B(\psi(2S) \rightarrow \gamma \chi_{c0}(1P))]$ assuming $B(\psi(2S) \rightarrow \gamma \chi_{c0}(1P)) = (9.99 \pm 0.27) \times 10^{-2}$, which we rescale to our best value $B(\psi(2S) \rightarrow \gamma \chi_{c0}(1P)) = (9.77 \pm 0.23) \times 10^{-2}$. Our first error is their experiment's error and our second error is the systematic error from using our best value.					
² ASNER 09 reports $< 0.25 \times 10^{-3}$ from a measurement of $[\Gamma(\chi_{c0}(1P) \rightarrow \eta \eta') / \Gamma_{total}] \times [B(\psi(2S) \rightarrow \gamma \chi_{c0}(1P))]$ assuming $B(\psi(2S) \rightarrow \gamma \chi_{c0}(1P)) = (9.22 \pm 0.11 \pm 0.46) \times 10^{-2}$, which we rescale to our best value $B(\psi(2S) \rightarrow \gamma \chi_{c0}(1P)) = 9.77 \times 10^{-2}$.					
³ Superseded by ASNER 09. ADAMS 07 reports $< 0.5 \times 10^{-3}$ from a measurement of $[\Gamma(\chi_{c0}(1P) \rightarrow \eta \eta') / \Gamma_{total}] \times [B(\psi(2S) \rightarrow \gamma \chi_{c0}(1P))]$ assuming $B(\psi(2S) \rightarrow \gamma \chi_{c0}(1P)) = (9.22 \pm 0.11 \pm 0.46) \times 10^{-2}$, which we rescale to our best value $B(\psi(2S) \rightarrow \gamma \chi_{c0}(1P)) = 9.77 \times 10^{-2}$.					

$\Gamma(\eta' \eta') / \Gamma_{total}$ Γ₃₈/Γ

VALUE (units 10 ⁻³)	EVTS	DOCUMENT ID	TECN	COMMENT
2.17 ± 0.12 OUR AVERAGE				
2.24 ± 0.13 ± 0.05	2.5k	¹ ABLIKIM	17A	BES3 $\psi(2S) \rightarrow \gamma \eta' \eta'$
2.00 ± 0.21 ± 0.05	0.4k	² ASNER	09	CLEO $\psi(2S) \rightarrow \gamma \eta' \eta'$
• • • We do not use the following data for averages, fits, limits, etc. • • •				
1.60 ± 0.41 ± 0.04	23	³ ADAMS	07	CLEO $\psi(2S) \rightarrow \gamma \chi_{c0}$
¹ ABLIKIM 17A reports $(2.19 \pm 0.03 \pm 0.14) \times 10^{-3}$ from a measurement of $[\Gamma(\chi_{c0}(1P) \rightarrow \eta' \eta') / \Gamma_{total}] \times [B(\psi(2S) \rightarrow \gamma \chi_{c0}(1P))]$ assuming $B(\psi(2S) \rightarrow \gamma \chi_{c0}(1P)) = (9.99 \pm 0.27) \times 10^{-2}$, which we rescale to our best value $B(\psi(2S) \rightarrow \gamma \chi_{c0}(1P)) = (9.77 \pm 0.23) \times 10^{-2}$. Our first error is their experiment's error and our second error is the systematic error from using our best value.				
² ASNER 09 reports $(2.12 \pm 0.13 \pm 0.21) \times 10^{-3}$ from a measurement of $[\Gamma(\chi_{c0}(1P) \rightarrow \eta' \eta') / \Gamma_{total}] \times [B(\psi(2S) \rightarrow \gamma \chi_{c0}(1P))]$ assuming $B(\psi(2S) \rightarrow \gamma \chi_{c0}(1P)) = (9.22 \pm 0.11 \pm 0.46) \times 10^{-2}$, which we rescale to our best value $B(\psi(2S) \rightarrow \gamma \chi_{c0}(1P)) = (9.77 \pm 0.23) \times 10^{-2}$. Our first error is their experiment's error and our second error is the systematic error from using our best value.				

³ Superseded by ASNER 09. ADAMS 07 reports $(1.7 \pm 0.4 \pm 0.2) \times 10^{-3}$ from a measurement of $[\Gamma(\chi_{c0}(1P) \rightarrow \eta' \eta') / \Gamma_{total}] \times [B(\psi(2S) \rightarrow \gamma \chi_{c0}(1P))]$ assuming $B(\psi(2S) \rightarrow \gamma \chi_{c0}(1P)) = 0.0922 \pm 0.0011 \pm 0.0046$, which we rescale to our best value $B(\psi(2S) \rightarrow \gamma \chi_{c0}(1P)) = (9.77 \pm 0.23) \times 10^{-2}$. Our first error is their experiment's error and our second error is the systematic error from using our best value.

$\Gamma(\omega \omega) / \Gamma_{total}$ Γ₃₉/Γ

VALUE (units 10 ⁻³)	EVTS	DOCUMENT ID	TECN	COMMENT
0.97 ± 0.11 OUR AVERAGE				
0.94 ± 0.11 ± 0.02	991	¹ ABLIKIM	11K	BES3 $\psi(2S) \rightarrow \gamma$ hadrons
2.2 ± 0.7 ± 0.1	38.1 ± 9.6	² ABLIKIM	05N	BES2 $\psi(2S) \rightarrow \gamma \chi_{c0} \rightarrow \gamma 6\pi$
¹ ABLIKIM 11K reports $(0.95 \pm 0.03 \pm 0.11) \times 10^{-3}$ from a measurement of $[\Gamma(\chi_{c0}(1P) \rightarrow \omega \omega) / \Gamma_{total}] \times [B(\psi(2S) \rightarrow \gamma \chi_{c0}(1P))]$ assuming $B(\psi(2S) \rightarrow \gamma \chi_{c0}(1P)) = (9.62 \pm 0.31) \times 10^{-2}$, which we rescale to our best value $B(\psi(2S) \rightarrow \gamma \chi_{c0}(1P)) = (9.77 \pm 0.23) \times 10^{-2}$. Our first error is their experiment's error and our second error is the systematic error from using our best value.				
² ABLIKIM 05N reports $[\Gamma(\chi_{c0}(1P) \rightarrow \omega \omega) / \Gamma_{total}] \times [B(\psi(2S) \rightarrow \gamma \chi_{c0}(1P))] = (0.212 \pm 0.053 \pm 0.037) \times 10^{-3}$ which we divide by our best value $B(\psi(2S) \rightarrow \gamma \chi_{c0}(1P)) = (9.77 \pm 0.23) \times 10^{-2}$. Our first error is their experiment's error and our second error is the systematic error from using our best value.				

$\Gamma(\omega \phi) / \Gamma_{total}$ Γ₄₀/Γ

VALUE (units 10 ⁻⁴)	EVTS	DOCUMENT ID	TECN	COMMENT
1.42 ± 0.13 ± 0.03	486	¹ ABLIKIM	19J	BES3 $\psi(2S) \rightarrow \gamma$ hadrons
• • • We do not use the following data for averages, fits, limits, etc. • • •				
1.18 ± 0.22 ± 0.03	76	^{2,3} ABLIKIM	11K	BES3 $\psi(2S) \rightarrow \gamma$ hadrons
¹ ABLIKIM 19J reports $[(\chi_{c0}(1P) \rightarrow \omega \phi) / \Gamma_{total}] \times [B(\psi(2S) \rightarrow \gamma \chi_{c0}(1P))] = (13.83 \pm 0.70 \pm 1.01) \times 10^{-6}$ which we divide by our best value $B(\psi(2S) \rightarrow \gamma \chi_{c0}(1P)) = (9.77 \pm 0.23) \times 10^{-2}$. Our first error is their experiment's error and our second error is the systematic error from using our best value.				
² ABLIKIM 11K reports $(1.2 \pm 0.1 \pm 0.2) \times 10^{-4}$ from a measurement of $[\Gamma(\chi_{c0}(1P) \rightarrow \omega \phi) / \Gamma_{total}] \times [B(\psi(2S) \rightarrow \gamma \chi_{c0}(1P))]$ assuming $B(\psi(2S) \rightarrow \gamma \chi_{c0}(1P)) = (9.62 \pm 0.31) \times 10^{-2}$, which we rescale to our best value $B(\psi(2S) \rightarrow \gamma \chi_{c0}(1P)) = (9.77 \pm 0.23) \times 10^{-2}$. Our first error is their experiment's error and our second error is the systematic error from using our best value.				
³ Superseded by ABLIKIM 19J.				

$\Gamma(\omega K^+ K^-) / \Gamma_{total}$ Γ₄₁/Γ

VALUE (units 10 ⁻³)	EVTS	DOCUMENT ID	TECN	COMMENT
1.94 ± 0.06 ± 0.20	1.4k	¹ ABLIKIM	13B	BES3 $e^+ e^- \rightarrow \psi(2S) \rightarrow \gamma \chi_{c0}$
¹ Using 1.06×10^8 $\psi(2S)$ mesons and $B(\psi(2S) \rightarrow \chi_{c0} \gamma) = (9.68 \pm 0.31)\%$.				

$\Gamma(K^+ \pi^- \eta) / \Gamma_{total}$ Γ₄₄/Γ

VALUE (units 10 ⁻³)	CL%	DOCUMENT ID	TECN	COMMENT
< 0.20	90	¹ ATHAR	07	CLEO $\psi(2S) \rightarrow \gamma h^+ h^- h^0$
• • • We do not use the following data for averages, fits, limits, etc. • • •				
< 1.0	90	² ABLIKIM	06R	BES2 $\psi(2S) \rightarrow \gamma \chi_{c0}$
¹ ATHAR 07 reports $< 0.21 \times 10^{-3}$ from a measurement of $[\Gamma(\chi_{c0}(1P) \rightarrow \pi^+ \pi^- \eta) / \Gamma_{total}] \times [B(\psi(2S) \rightarrow \gamma \chi_{c0}(1P))]$ assuming $B(\psi(2S) \rightarrow \gamma \chi_{c0}(1P)) = (9.22 \pm 0.11 \pm 0.46) \times 10^{-2}$, which we rescale to our best value $B(\psi(2S) \rightarrow \gamma \chi_{c0}(1P)) = 9.77 \times 10^{-2}$.				
² ABLIKIM 06R reports $< 1.1 \times 10^{-3}$ from a measurement of $[\Gamma(\chi_{c0}(1P) \rightarrow \pi^+ \pi^- \eta) / \Gamma_{total}] \times [B(\psi(2S) \rightarrow \gamma \chi_{c0}(1P))]$ assuming $B(\psi(2S) \rightarrow \gamma \chi_{c0}(1P)) = (9.2 \pm 0.4) \times 10^{-2}$, which we rescale to our best value $B(\psi(2S) \rightarrow \gamma \chi_{c0}(1P)) = 9.77 \times 10^{-2}$.				

$\Gamma(K^+ \pi^- \eta') / \Gamma_{total}$ Γ₄₅/Γ

VALUE (units 10 ⁻³)	CL%	DOCUMENT ID	TECN	COMMENT
< 0.4	90	¹ ATHAR	07	CLEO $\psi(2S) \rightarrow \gamma h^+ h^- h^0$
¹ ATHAR 07 reports $< 0.38 \times 10^{-3}$ from a measurement of $[\Gamma(\chi_{c0}(1P) \rightarrow \pi^+ \pi^- \eta') / \Gamma_{total}] \times [B(\psi(2S) \rightarrow \gamma \chi_{c0}(1P))]$ assuming $B(\psi(2S) \rightarrow \gamma \chi_{c0}(1P)) = (9.22 \pm 0.11 \pm 0.46) \times 10^{-2}$, which we rescale to our best value $B(\psi(2S) \rightarrow \gamma \chi_{c0}(1P)) = 9.77 \times 10^{-2}$.				

$\Gamma(\bar{K}^0 K^+ \pi^- + c.c.) / \Gamma_{total}$ Γ₄₆/Γ

VALUE (units 10 ⁻³)	CL%	DOCUMENT ID	TECN	COMMENT
< 0.09	90	¹ ATHAR	07	CLEO $\psi(2S) \rightarrow \gamma h^+ h^- h^0$
• • • We do not use the following data for averages, fits, limits, etc. • • •				
< 0.7	90	^{2,3} ABLIKIM	06R	BES2 $\psi(2S) \rightarrow \gamma \chi_{c0}$
< 0.7	90	^{3,4} BAI	99B	BES $\psi(2S) \rightarrow \gamma \chi_{c0}$
¹ ATHAR 07 reports $< 0.10 \times 10^{-3}$ from a measurement of $[\Gamma(\chi_{c0}(1P) \rightarrow \bar{K}^0 K^+ \pi^- + c.c.) / \Gamma_{total}] \times [B(\psi(2S) \rightarrow \gamma \chi_{c0}(1P))]$ assuming $B(\psi(2S) \rightarrow \gamma \chi_{c0}(1P)) = (9.22 \pm 0.11 \pm 0.46) \times 10^{-2}$, which we rescale to our best value $B(\psi(2S) \rightarrow \gamma \chi_{c0}(1P)) = 9.77 \times 10^{-2}$.				
² ABLIKIM 06R reports $< 0.70 \times 10^{-3}$ from a measurement of $[\Gamma(\chi_{c0}(1P) \rightarrow \bar{K}^0 K^+ \pi^- + c.c.) / \Gamma_{total}] \times [B(\psi(2S) \rightarrow \gamma \chi_{c0}(1P))]$ assuming $B(\psi(2S) \rightarrow \gamma \chi_{c0}(1P)) = (9.2 \pm 0.4) \times 10^{-2}$, which we rescale to our best value $B(\psi(2S) \rightarrow \gamma \chi_{c0}(1P)) = 9.77 \times 10^{-2}$.				
³ We have multiplied the $K_S^0 K^+ \pi^-$ measurement by a factor of 2 to convert to $K^0 K^+ \pi^-$.				
⁴ Rescaled by us using $B(\psi(2S) \rightarrow \gamma \chi_{c0}) = (9.4 \pm 0.4)\%$ and $B(\psi(2S) \rightarrow J/\psi(1S) \pi^+ \pi^-) = (32.6 \pm 0.5)\%$.				

Meson Particle Listings

 $\chi_{c0}(1P)$ $\Gamma(K^+ K^- \pi^0)/\Gamma_{\text{total}}$ Γ_{47}/Γ

VALUE (units 10^{-3})	CL%	DOCUMENT ID	TECN	COMMENT
<0.06	90	¹ ATHAR 07	CLEO	$\psi(2S) \rightarrow \gamma h^+ h^- h^0$

¹ ATHAR 07 reports $< 0.06 \times 10^{-3}$ from a measurement of $[\Gamma(\chi_{c0}(1P) \rightarrow K^+ K^- \pi^0)/\Gamma_{\text{total}}] \times [B(\psi(2S) \rightarrow \gamma \chi_{c0}(1P))]$ assuming $B(\psi(2S) \rightarrow \gamma \chi_{c0}(1P)) = (9.22 \pm 0.11 \pm 0.46) \times 10^{-2}$, which we rescale to our best value $B(\psi(2S) \rightarrow \gamma \chi_{c0}(1P)) = 9.77 \times 10^{-2}$.

 $\Gamma(K^+ K^- \eta)/\Gamma_{\text{total}}$ Γ_{48}/Γ

VALUE (units 10^{-3})	CL%	DOCUMENT ID	TECN	COMMENT
<0.23	90	¹ ATHAR 07	CLEO	$\psi(2S) \rightarrow \gamma h^+ h^- h^0$

¹ ATHAR 07 reports $< 0.24 \times 10^{-3}$ from a measurement of $[\Gamma(\chi_{c0}(1P) \rightarrow K^+ K^- \eta)/\Gamma_{\text{total}}] \times [B(\psi(2S) \rightarrow \gamma \chi_{c0}(1P))]$ assuming $B(\psi(2S) \rightarrow \gamma \chi_{c0}(1P)) = (9.22 \pm 0.11 \pm 0.46) \times 10^{-2}$, which we rescale to our best value $B(\psi(2S) \rightarrow \gamma \chi_{c0}(1P)) = 9.77 \times 10^{-2}$.

 $\Gamma(K^+ K^- K_S^0 K_S^0)/\Gamma_{\text{total}}$ Γ_{49}/Γ

VALUE (units 10^{-3})	EVTS	DOCUMENT ID	TECN	COMMENT
1.41 ± 0.47 ± 0.03	16.8 ± 4.8	¹ ABLIKIM 05o	BES2	$\psi(2S) \rightarrow \gamma \chi_{c0}$

¹ ABLIKIM 05o reports $[\Gamma(\chi_{c0}(1P) \rightarrow K^+ K^- K_S^0 K_S^0)/\Gamma_{\text{total}}] \times [B(\psi(2S) \rightarrow \gamma \chi_{c0}(1P))] = (0.138 \pm 0.039 \pm 0.025) \times 10^{-3}$ which we divide by our best value $B(\psi(2S) \rightarrow \gamma \chi_{c0}(1P)) = (9.77 \pm 0.23) \times 10^{-2}$. Our first error is their experiment's error and our second error is the systematic error from using our best value.

 $\Gamma(K_S^0 K_S^0 K_S^0 K_S^0)/\Gamma_{\text{total}}$ Γ_{50}/Γ

VALUE (units 10^{-4})	EVTS	DOCUMENT ID	TECN	COMMENT
5.8 ± 0.5 ± 0.1	319	¹ ABLIKIM 19AA	BES3	$\psi(2S) \rightarrow \gamma 4K_S^0$

¹ Using $B(K_S^0 \rightarrow \pi^+ \pi^-) = (69.20 \pm 0.05)\%$. ABLIKIM 19AA reports $[\Gamma(\chi_{c0}(1P) \rightarrow K_S^0 K_S^0 K_S^0 K_S^0)/\Gamma_{\text{total}}] \times [B(\psi(2S) \rightarrow \gamma \chi_{c0}(1P))] = (5.64 \pm 0.33 \pm 0.37) \times 10^{-5}$ which we divide by our best value $B(\psi(2S) \rightarrow \gamma \chi_{c0}(1P)) = (9.77 \pm 0.23) \times 10^{-2}$. Our first error is their experiment's error and our second error is the systematic error from using our best value.

 $\Gamma(K^+ K^- \phi)/\Gamma_{\text{total}}$ Γ_{52}/Γ

VALUE (units 10^{-3})	EVTS	DOCUMENT ID	TECN	COMMENT
0.97 ± 0.25 ± 0.02	38	¹ ABLIKIM 06T	BES2	$\psi(2S) \rightarrow \gamma 2K^+ 2K^-$

¹ ABLIKIM 06T reports $(1.03 \pm 0.22 \pm 0.15) \times 10^{-3}$ from a measurement of $[\Gamma(\chi_{c0}(1P) \rightarrow K^+ K^- \phi)/\Gamma_{\text{total}}] \times [B(\psi(2S) \rightarrow \gamma \chi_{c0}(1P))]$ assuming $B(\psi(2S) \rightarrow \gamma \chi_{c0}(1P)) = (9.2 \pm 0.4) \times 10^{-2}$, which we rescale to our best value $B(\psi(2S) \rightarrow \gamma \chi_{c0}(1P)) = (9.77 \pm 0.23) \times 10^{-2}$. Our first error is their experiment's error and our second error is the systematic error from using our best value.

 $\Gamma(K^0 K^+ \pi^- \phi + \text{c.c.})/\Gamma_{\text{total}}$ Γ_{53}/Γ

VALUE (units 10^{-3})	DOCUMENT ID	TECN	COMMENT
3.68 ± 0.30 ± 0.50	ABLIKIM 15M	BES3	$\psi(2S) \rightarrow \gamma \chi_{c0}$

 $\Gamma(K^+ K^- \pi^0 \phi)/\Gamma_{\text{total}}$ Γ_{54}/Γ

VALUE (units 10^{-3})	DOCUMENT ID	TECN	COMMENT
1.90 ± 0.14 ± 0.32	ABLIKIM 15M	BES3	$\psi(2S) \rightarrow \gamma \chi_{c0}$

 $\Gamma(\phi \pi^+ \pi^- \pi^0)/\Gamma_{\text{total}}$ Γ_{55}/Γ

VALUE (units 10^{-3})	EVTS	DOCUMENT ID	TECN	COMMENT
1.18 ± 0.07 ± 0.13	538	¹ ABLIKIM 13B	BES3	$e^+ e^- \rightarrow \psi(2S) \rightarrow \gamma \chi_{c0}$

¹ Using 1.06×10^8 $\psi(2S)$ mesons and $B(\psi(2S) \rightarrow \chi_{c0} \gamma) = (9.68 \pm 0.31)\%$.

 $\Gamma(\phi \phi)/\Gamma_{\text{total}}$ Γ_{56}/Γ

VALUE (units 10^{-3})	EVTS	DOCUMENT ID	TECN	COMMENT
0.848 ± 0.031 OUR FIT				
0.859 ± 0.027 ± 0.020	2701	¹ ABLIKIM 23N	BES3	$\psi(2S) \rightarrow \gamma$ hadrons

¹ Measured using $B(\psi(2S) \rightarrow \gamma \chi_{c0}(1P)) = (9.75 \pm 0.24) \times 10^{-2}$ and $B(\phi \rightarrow K^+ K^-) = (49.2 \pm 0.5) \times 10^{-2}$ from PDG 22.

 $\Gamma(\phi \phi \eta)/\Gamma_{\text{total}}$ Γ_{57}/Γ

VALUE (units 10^{-4})	EVTS	DOCUMENT ID	TECN	COMMENT
8.4 ± 1.0 ± 0.2	186.6	¹ ABLIKIM 20b	BES3	$\psi(2S) \rightarrow \gamma \phi \phi \eta$

¹ ABLIKIM 20b reports $(8.41 \pm 0.74 \pm 0.62) \times 10^{-4}$ from a measurement of $[\Gamma(\chi_{c0}(1P) \rightarrow \phi \phi \eta)/\Gamma_{\text{total}}] \times [B(\psi(2S) \rightarrow \gamma \chi_{c0}(1P))]$ assuming $B(\psi(2S) \rightarrow \gamma \chi_{c0}(1P)) = (9.79 \pm 0.20) \times 10^{-2}$, which we rescale to our best value $B(\psi(2S) \rightarrow \gamma \chi_{c0}(1P)) = (9.77 \pm 0.23) \times 10^{-2}$. Our first error is their experiment's error and our second error is the systematic error from using our best value.

 $\Gamma(p\bar{p}\pi^0)/\Gamma_{\text{total}}$ Γ_{59}/Γ

VALUE (units 10^{-3})	DOCUMENT ID	TECN	COMMENT
0.70 ± 0.07 OUR AVERAGE			Error includes scale factor of 1.3.
0.73 ± 0.06 ± 0.02	¹ ONYISI 10	CLE3	$\psi(2S) \rightarrow \gamma p\bar{p}X$
0.56 ± 0.12 ± 0.01	² ATHAR 07	CLEO	$\psi(2S) \rightarrow \gamma h^+ h^- h^0$

¹ ONYISI 10 reports $(7.76 \pm 0.37 \pm 0.51 \pm 0.39) \times 10^{-4}$ from a measurement of $[\Gamma(\chi_{c0}(1P) \rightarrow p\bar{p}\pi^0)/\Gamma_{\text{total}}] \times [B(\psi(2S) \rightarrow \gamma \chi_{c0}(1P))]$ assuming $B(\psi(2S) \rightarrow \gamma \chi_{c0}(1P)) = (9.22 \pm 0.11 \pm 0.46) \times 10^{-2}$, which we rescale to our best value $B(\psi(2S) \rightarrow \gamma \chi_{c0}(1P)) = (9.77 \pm 0.23) \times 10^{-2}$. Our first error is their experiment's error and our second error is the systematic error from using our best value.

² ATHAR 07 reports $(0.59 \pm 0.10 \pm 0.08) \times 10^{-3}$ from a measurement of $[\Gamma(\chi_{c0}(1P) \rightarrow p\bar{p}\pi^0)/\Gamma_{\text{total}}] \times [B(\psi(2S) \rightarrow \gamma \chi_{c0}(1P))]$ assuming $B(\psi(2S) \rightarrow \gamma \chi_{c0}(1P)) = (9.22 \pm 0.11 \pm 0.46) \times 10^{-2}$, which we rescale to our best value $B(\psi(2S) \rightarrow \gamma \chi_{c0}(1P)) = (9.77 \pm 0.23) \times 10^{-2}$. Our first error is their experiment's error and our second error is the systematic error from using our best value.

 $\Gamma(p\bar{p}\eta)/\Gamma_{\text{total}}$ Γ_{60}/Γ

VALUE (units 10^{-3})	DOCUMENT ID	TECN	COMMENT
0.35 ± 0.04 OUR AVERAGE			
0.35 ± 0.04 ± 0.01	¹ ONYISI 10	CLE3	$\psi(2S) \rightarrow \gamma p\bar{p}X$
0.37 ± 0.11 ± 0.01	² ATHAR 07	CLEO	$\psi(2S) \rightarrow \gamma h^+ h^- h^0$

¹ ONYISI 10 reports $(3.73 \pm 0.38 \pm 0.28 \pm 0.19) \times 10^{-4}$ from a measurement of $[\Gamma(\chi_{c0}(1P) \rightarrow p\bar{p}\eta)/\Gamma_{\text{total}}] \times [B(\psi(2S) \rightarrow \gamma \chi_{c0}(1P))]$ assuming $B(\psi(2S) \rightarrow \gamma \chi_{c0}(1P)) = (9.22 \pm 0.11 \pm 0.46) \times 10^{-2}$, which we rescale to our best value $B(\psi(2S) \rightarrow \gamma \chi_{c0}(1P)) = (9.77 \pm 0.23) \times 10^{-2}$. Our first error is their experiment's error and our second error is the systematic error from using our best value.

² ATHAR 07 reports $(0.39 \pm 0.11 \pm 0.04) \times 10^{-3}$ from a measurement of $[\Gamma(\chi_{c0}(1P) \rightarrow p\bar{p}\eta)/\Gamma_{\text{total}}] \times [B(\psi(2S) \rightarrow \gamma \chi_{c0}(1P))]$ assuming $B(\psi(2S) \rightarrow \gamma \chi_{c0}(1P)) = (9.22 \pm 0.11 \pm 0.46) \times 10^{-2}$, which we rescale to our best value $B(\psi(2S) \rightarrow \gamma \chi_{c0}(1P)) = (9.77 \pm 0.23) \times 10^{-2}$. Our first error is their experiment's error and our second error is the systematic error from using our best value.

 $\Gamma(p\bar{p}\omega)/\Gamma_{\text{total}}$ Γ_{61}/Γ

VALUE (units 10^{-3})	DOCUMENT ID	TECN	COMMENT
0.53 ± 0.06 ± 0.01	¹ ONYISI 10	CLE3	$\psi(2S) \rightarrow \gamma p\bar{p}X$

¹ ONYISI 10 reports $(5.57 \pm 0.48 \pm 0.42 \pm 0.14) \times 10^{-4}$ from a measurement of $[\Gamma(\chi_{c0}(1P) \rightarrow p\bar{p}\omega)/\Gamma_{\text{total}}] \times [B(\psi(2S) \rightarrow \gamma \chi_{c0}(1P))]$ assuming $B(\psi(2S) \rightarrow \gamma \chi_{c0}(1P)) = (9.22 \pm 0.11 \pm 0.46) \times 10^{-2}$, which we rescale to our best value $B(\psi(2S) \rightarrow \gamma \chi_{c0}(1P)) = (9.77 \pm 0.23) \times 10^{-2}$. Our first error is their experiment's error and our second error is the systematic error from using our best value.

 $\Gamma(p\bar{p}\phi)/\Gamma_{\text{total}}$ Γ_{62}/Γ

VALUE (units 10^{-3})	EVTS	DOCUMENT ID	TECN	COMMENT
6.0 ± 1.4 ± 0.1	42 ± 8	¹ ABLIKIM 11F	BES3	$\psi(2S) \rightarrow \gamma p\bar{p}K^+ K^-$

¹ ABLIKIM 11F reports $(6.12 \pm 1.18 \pm 0.86) \times 10^{-5}$ from a measurement of $[\Gamma(\chi_{c0}(1P) \rightarrow p\bar{p}\phi)/\Gamma_{\text{total}}] \times [B(\psi(2S) \rightarrow \gamma \chi_{c0}(1P))]$ assuming $B(\psi(2S) \rightarrow \gamma \chi_{c0}(1P)) = (9.62 \pm 0.31) \times 10^{-2}$, which we rescale to our best value $B(\psi(2S) \rightarrow \gamma \chi_{c0}(1P)) = (9.77 \pm 0.23) \times 10^{-2}$. Our first error is their experiment's error and our second error is the systematic error from using our best value.

 $\Gamma(p\bar{p}\pi^+ \pi^-)/\Gamma_{\text{total}}$ Γ_{63}/Γ

VALUE (units 10^{-3})	DOCUMENT ID	TECN	COMMENT
2.1 ± 0.7 OUR EVALUATION			Error includes scale factor of 1.4. Treating systematic error as correlated.
2.1 ± 1.0 OUR AVERAGE			Error includes scale factor of 2.0.
1.57 ± 0.21 ± 0.53	¹ BAI 99B	BES	$\psi(2S) \rightarrow \gamma \chi_{c0}$
4.20 ± 1.15 ± 0.18	¹ TANENBAUM 78	MRK1	$\psi(2S) \rightarrow \gamma \chi_{c0}$

¹ Rescaled by us using $B(\psi(2S) \rightarrow \gamma \chi_{c0}) = (9.4 \pm 0.4)\%$ and $B(\psi(2S) \rightarrow J/\psi(1S) \pi^+ \pi^-) = (32.6 \pm 0.5)\%$.

 $\Gamma(p\bar{p}\pi^0 \pi^0)/\Gamma_{\text{total}}$ Γ_{64}/Γ

VALUE (%)	EVTS	DOCUMENT ID	TECN	COMMENT
0.104 ± 0.028 ± 0.002	39.5	¹ HE 08B	CLEO	$e^+ e^- \rightarrow \gamma h^+ h^- h^0 h^0$

¹ HE 08B reports $0.11 \pm 0.02 \pm 0.02 \pm 0.01$ from a measurement of $[\Gamma(\chi_{c0}(1P) \rightarrow p\bar{p}\pi^0 \pi^0)/\Gamma_{\text{total}}] \times [B(\psi(2S) \rightarrow \gamma \chi_{c0}(1P))]$ assuming $B(\psi(2S) \rightarrow \gamma \chi_{c0}(1P)) = (9.22 \pm 0.11 \pm 0.46) \times 10^{-2}$, which we rescale to our best value $B(\psi(2S) \rightarrow \gamma \chi_{c0}(1P)) = (9.77 \pm 0.23) \times 10^{-2}$. Our first error is their experiment's error and our second error is the systematic error from using our best value.

 $\Gamma(p\bar{p}K^+ K^- (\text{non-resonant}))/\Gamma_{\text{total}}$ Γ_{65}/Γ

VALUE (units 10^{-4})	EVTS	DOCUMENT ID	TECN	COMMENT
1.22 ± 0.26 ± 0.03	48 ± 8	¹ ABLIKIM 11F	BES3	$\psi(2S) \rightarrow \gamma p\bar{p}K^+ K^-$

¹ ABLIKIM 11F reports $(1.24 \pm 0.20 \pm 0.18) \times 10^{-4}$ from a measurement of $[\Gamma(\chi_{c0}(1P) \rightarrow p\bar{p}K^+ K^- (\text{non-resonant}))/\Gamma_{\text{total}}] \times [B(\psi(2S) \rightarrow \gamma \chi_{c0}(1P))]$ assuming $B(\psi(2S) \rightarrow \gamma \chi_{c0}(1P)) = (9.62 \pm 0.31) \times 10^{-2}$, which we rescale to our best value $B(\psi(2S) \rightarrow \gamma \chi_{c0}(1P)) = (9.77 \pm 0.23) \times 10^{-2}$. Our first error is their experiment's error and our second error is the systematic error from using our best value.

 $\Gamma(p\bar{p}K_S^0 K_S^0)/\Gamma_{\text{total}}$ Γ_{66}/Γ

VALUE (units 10^{-4})	CL%	DOCUMENT ID	TECN	COMMENT
<8.8	90	¹ ABLIKIM 06D	BES2	$\psi(2S) \rightarrow \chi_{c0} \gamma$

¹ Using $B(\psi(2S) \rightarrow \chi_{c0} \gamma) = (9.2 \pm 0.5)\%$

See key on page 1171

Meson Particle Listings

$\chi_{c0}(1P)$

$\Gamma(p\bar{p}\pi^-)/\Gamma_{total}$		Γ_{67}/Γ		
VALUE (units 10^{-4})	EVTS	DOCUMENT ID	TECN	COMMENT
12.7±1.1 OUR AVERAGE				
12.9±1.1±0.3	5150	¹ ABLIKIM	12J BES3	$\psi(2S) \rightarrow \gamma p\bar{p}\pi^-$
11.3±3.1±0.3		² ABLIKIM	06i BES2	$\psi(2S) \rightarrow \gamma p\pi^- X$

¹ ABLIKIM 12J reports $[\Gamma(\chi_{c0}(1P) \rightarrow p\bar{p}\pi^-)/\Gamma_{total}] \times [B(\psi(2S) \rightarrow \gamma\chi_{c0}(1P))] = (1.26 \pm 0.02 \pm 0.11) \times 10^{-4}$ which we divide by our best value $B(\psi(2S) \rightarrow \gamma\chi_{c0}(1P)) = (9.77 \pm 0.23) \times 10^{-2}$. Our first error is their experiment's error and our second error is the systematic error from using our best value.

² ABLIKIM 06i reports $[\Gamma(\chi_{c0}(1P) \rightarrow p\bar{p}\pi^-)/\Gamma_{total}] \times [B(\psi(2S) \rightarrow \gamma\chi_{c0}(1P))] = (1.10 \pm 0.24 \pm 0.18) \times 10^{-4}$ which we divide by our best value $B(\psi(2S) \rightarrow \gamma\chi_{c0}(1P)) = (9.77 \pm 0.23) \times 10^{-2}$. Our first error is their experiment's error and our second error is the systematic error from using our best value.

$\Gamma(p\bar{p}n\pi^+)/\Gamma_{total}$		Γ_{68}/Γ		
VALUE (units 10^{-4})	EVTS	DOCUMENT ID	TECN	COMMENT
13.7±1.2±0.3				
	5808	¹ ABLIKIM	12J BES3	$\psi(2S) \rightarrow \gamma p\bar{p}n\pi^+$

¹ ABLIKIM 12J reports $[\Gamma(\chi_{c0}(1P) \rightarrow p\bar{p}n\pi^+)/\Gamma_{total}] \times [B(\psi(2S) \rightarrow \gamma\chi_{c0}(1P))] = (1.34 \pm 0.03 \pm 0.11) \times 10^{-4}$ which we divide by our best value $B(\psi(2S) \rightarrow \gamma\chi_{c0}(1P)) = (9.77 \pm 0.23) \times 10^{-2}$. Our first error is their experiment's error and our second error is the systematic error from using our best value.

$\Gamma(p\bar{p}\pi^-\pi^0)/\Gamma_{total}$		Γ_{69}/Γ		
VALUE (units 10^{-4})	EVTS	DOCUMENT ID	TECN	COMMENT
23.4±2.0±0.5				
	2480	¹ ABLIKIM	12J BES3	$\psi(2S) \rightarrow \gamma p\bar{p}\pi^-\pi^0$

¹ ABLIKIM 12J reports $[\Gamma(\chi_{c0}(1P) \rightarrow p\bar{p}\pi^-\pi^0)/\Gamma_{total}] \times [B(\psi(2S) \rightarrow \gamma\chi_{c0}(1P))] = (2.29 \pm 0.08 \pm 0.18) \times 10^{-4}$ which we divide by our best value $B(\psi(2S) \rightarrow \gamma\chi_{c0}(1P)) = (9.77 \pm 0.23) \times 10^{-2}$. Our first error is their experiment's error and our second error is the systematic error from using our best value.

$\Gamma(p\bar{p}n\pi^+\pi^0)/\Gamma_{total}$		Γ_{70}/Γ		
VALUE (units 10^{-4})	EVTS	DOCUMENT ID	TECN	COMMENT
22.1±1.8±0.5				
	2757	¹ ABLIKIM	12J BES3	$\psi(2S) \rightarrow \gamma p\bar{p}n\pi^+\pi^0$

¹ ABLIKIM 12J reports $[\Gamma(\chi_{c0}(1P) \rightarrow p\bar{p}n\pi^+\pi^0)/\Gamma_{total}] \times [B(\psi(2S) \rightarrow \gamma\chi_{c0}(1P))] = (2.16 \pm 0.07 \pm 0.16) \times 10^{-4}$ which we divide by our best value $B(\psi(2S) \rightarrow \gamma\chi_{c0}(1P)) = (9.77 \pm 0.23) \times 10^{-2}$. Our first error is their experiment's error and our second error is the systematic error from using our best value.

$\Gamma(\Lambda\bar{\Lambda}\pi^+\pi^-)/\Gamma_{total}$		Γ_{72}/Γ			
VALUE (units 10^{-5})	CL%	EVTS	DOCUMENT ID	TECN	COMMENT
118±12±3		426	¹ ABLIKIM	12i BES3	$\psi(2S) \rightarrow \gamma\Lambda\bar{\Lambda}\pi^+\pi^-$

• • • We do not use the following data for averages, fits, limits, etc. • • •

<400 90 ² ABLIKIM 06D BES2 $\psi(2S) \rightarrow \chi_{c0}\gamma$

¹ ABLIKIM 12i reports $(119.0 \pm 6.4 \pm 11.4) \times 10^{-5}$ from a measurement of $[\Gamma(\chi_{c0}(1P) \rightarrow \Lambda\bar{\Lambda}\pi^+\pi^-)/\Gamma_{total}] \times [B(\psi(2S) \rightarrow \gamma\chi_{c0}(1P))] = (9.68 \pm 0.31) \times 10^{-2}$, which we rescale to our best value $B(\psi(2S) \rightarrow \gamma\chi_{c0}(1P)) = (9.77 \pm 0.23) \times 10^{-2}$. Our first error is their experiment's error and our second error is the systematic error from using our best value.

² Using $B(\psi(2S) \rightarrow \chi_{c0}\gamma) = (9.2 \pm 0.5)\%$

$\Gamma(\Lambda\bar{\Lambda}\pi^+\pi^- \text{ (non-resonant)})/\Gamma_{total}$		Γ_{73}/Γ		
VALUE (units 10^{-5})	CL%	DOCUMENT ID	TECN	COMMENT
<50	90	¹ ABLIKIM	12i BES3	$\psi(2S) \rightarrow \gamma\Lambda\bar{\Lambda}\pi^+\pi^-$

¹ ABLIKIM 12i reports $< 54 \times 10^{-5}$ from a measurement of $[\Gamma(\chi_{c0}(1P) \rightarrow \Lambda\bar{\Lambda}\pi^+\pi^- \text{ (non-resonant)})/\Gamma_{total}] \times [B(\psi(2S) \rightarrow \gamma\chi_{c0}(1P))] = (9.68 \pm 0.31) \times 10^{-2}$, which we rescale to our best value $B(\psi(2S) \rightarrow \gamma\chi_{c0}(1P)) = 9.77 \times 10^{-2}$.

$\Gamma(\Sigma(1385)^+\bar{\Lambda}\pi^- + c.c.)/\Gamma_{total}$		Γ_{74}/Γ		
VALUE (units 10^{-5})	CL%	DOCUMENT ID	TECN	COMMENT
<50	90	¹ ABLIKIM	12i BES3	$\psi(2S) \rightarrow \gamma\Sigma(1385)^+\bar{\Lambda}\pi^-$

¹ ABLIKIM 12i reports $< 55 \times 10^{-5}$ from a measurement of $[\Gamma(\chi_{c0}(1P) \rightarrow \Sigma(1385)^+\bar{\Lambda}\pi^- + c.c.)/\Gamma_{total}] \times [B(\psi(2S) \rightarrow \gamma\chi_{c0}(1P))] = (9.68 \pm 0.31) \times 10^{-2}$, which we rescale to our best value $B(\psi(2S) \rightarrow \gamma\chi_{c0}(1P)) = 9.77 \times 10^{-2}$.

$\Gamma(\Sigma(1385)^-\bar{\Lambda}\pi^+ + c.c.)/\Gamma_{total}$		Γ_{75}/Γ		
VALUE (units 10^{-5})	CL%	DOCUMENT ID	TECN	COMMENT
<50	90	¹ ABLIKIM	12i BES3	$\psi(2S) \rightarrow \gamma\Sigma(1385)^-\bar{\Lambda}\pi^+$

¹ ABLIKIM 12i reports $< 50 \times 10^{-5}$ from a measurement of $[\Gamma(\chi_{c0}(1P) \rightarrow \Sigma(1385)^-\bar{\Lambda}\pi^+ + c.c.)/\Gamma_{total}] \times [B(\psi(2S) \rightarrow \gamma\chi_{c0}(1P))] = (9.68 \pm 0.31) \times 10^{-2}$, which we rescale to our best value $B(\psi(2S) \rightarrow \gamma\chi_{c0}(1P)) = 9.77 \times 10^{-2}$.

$\Gamma(K^+\bar{p}\Lambda + c.c.)/\Gamma_{total}$		Γ_{77}/Γ		
VALUE (units 10^{-3})	EVTS	DOCUMENT ID	TECN	COMMENT
1.25±0.12 OUR AVERAGE				
1.31±0.09±0.03	9k	^{1,2} ABLIKIM	13D BES3	$\psi(2S) \rightarrow \gamma\Lambda\bar{p}K^+$
1.01±0.19±0.02		³ ATHAR	07 CLEO	$\psi(2S) \rightarrow \gamma h^+ h^- h^0$

¹ ABLIKIM 13D reports $(1.32 \pm 0.03 \pm 0.10) \times 10^{-3}$ from a measurement of $[\Gamma(\chi_{c0}(1P) \rightarrow K^+\bar{p}\Lambda + c.c.)/\Gamma_{total}] \times [B(\psi(2S) \rightarrow \gamma\chi_{c0}(1P))] = (9.68 \pm 0.31) \times 10^{-2}$, which we rescale to our best value $B(\psi(2S) \rightarrow \gamma\chi_{c0}(1P)) = (9.77 \pm 0.23) \times 10^{-2}$. Our first error is their experiment's error and our second error is the systematic error from using our best value.

² Using $B(\Lambda \rightarrow p\pi^-) = 63.9\%$.

³ ATHAR 07 reports $(1.07 \pm 0.17 \pm 0.12) \times 10^{-3}$ from a measurement of $[\Gamma(\chi_{c0}(1P) \rightarrow K^+\bar{p}\Lambda + c.c.)/\Gamma_{total}] \times [B(\psi(2S) \rightarrow \gamma\chi_{c0}(1P))] = (9.22 \pm 0.11 \pm 0.46) \times 10^{-2}$, which we rescale to our best value $B(\psi(2S) \rightarrow \gamma\chi_{c0}(1P)) = (9.77 \pm 0.23) \times 10^{-2}$. Our first error is their experiment's error and our second error is the systematic error from using our best value.

$\Gamma(K^*(892)^+\bar{p}\Lambda + c.c.)/\Gamma_{total}$		Γ_{79}/Γ		
VALUE (units 10^{-4})	EVTS	DOCUMENT ID	TECN	COMMENT
4.8±0.9±0.1				
	254	¹ ABLIKIM	19Au BES3	$\psi(2S) \rightarrow \gamma K^{*+}\bar{p}\Lambda$

¹ ABLIKIM 19Au reports $[\Gamma(\chi_{c0}(1P) \rightarrow K^*(892)^+\bar{p}\Lambda + c.c.)/\Gamma_{total}] \times [B(\psi(2S) \rightarrow \gamma\chi_{c0}(1P))] = (4.7 \pm 0.7 \pm 0.5) \times 10^{-5}$ which we divide by our best value $B(\psi(2S) \rightarrow \gamma\chi_{c0}(1P)) = (9.77 \pm 0.23) \times 10^{-2}$. Our first error is their experiment's error and our second error is the systematic error from using our best value.

$\Gamma(K^+\bar{p}\Lambda(1520) + c.c.)/\Gamma_{total}$		Γ_{80}/Γ		
VALUE (units 10^{-4})	EVTS	DOCUMENT ID	TECN	COMMENT
3.0±0.7±0.1				
	62 ± 12	¹ ABLIKIM	11F BES3	$\psi(2S) \rightarrow \gamma p\bar{p}K^+K^-$

¹ ABLIKIM 11F reports $(3.00 \pm 0.58 \pm 0.50) \times 10^{-4}$ from a measurement of $[\Gamma(\chi_{c0}(1P) \rightarrow K^+\bar{p}\Lambda(1520) + c.c.)/\Gamma_{total}] \times [B(\psi(2S) \rightarrow \gamma\chi_{c0}(1P))] = (9.62 \pm 0.31) \times 10^{-2}$, which we rescale to our best value $B(\psi(2S) \rightarrow \gamma\chi_{c0}(1P)) = (9.77 \pm 0.23) \times 10^{-2}$. Our first error is their experiment's error and our second error is the systematic error from using our best value.

$\Gamma(nK_S^0\bar{\Lambda} + c.c.)/\Gamma_{total}$		Γ_{78}/Γ		
VALUE (units 10^{-4})	EVTS	DOCUMENT ID	TECN	COMMENT
6.7±0.5±0.2				
	1284	¹ ABLIKIM	21Av BES3	$\psi(2S) \rightarrow \gamma nK_S^0\bar{\Lambda} + c.c.$

¹ ABLIKIM 21Av reports $(6.65 \pm 0.26 \pm 0.41) \times 10^{-4}$ from a measurement of $[\Gamma(\chi_{c0}(1P) \rightarrow nK_S^0\bar{\Lambda} + c.c.)/\Gamma_{total}] \times [B(\psi(2S) \rightarrow \gamma\chi_{c0}(1P))] = 0.0979 \pm 0.0020$, which we rescale to our best value $B(\psi(2S) \rightarrow \gamma\chi_{c0}(1P)) = (9.77 \pm 0.23) \times 10^{-2}$. Our first error is their experiment's error and our second error is the systematic error from using our best value. Also uses $B(\bar{\Lambda} \rightarrow \bar{p}\pi^+) = (63.9 \pm 0.5)\%$ and $B(K_S^0 \rightarrow \pi^+\pi^-) = (69.20 \pm 0.05)\%$.

$\Gamma(\Lambda(1520)\bar{\Lambda}(1520))/\Gamma_{total}$		Γ_{81}/Γ		
VALUE (units 10^{-4})	EVTS	DOCUMENT ID	TECN	COMMENT
3.1±1.2±0.1				
	28 ± 10	¹ ABLIKIM	11F BES3	$\psi(2S) \rightarrow \gamma p\bar{p}K^+K^-$

¹ ABLIKIM 11F reports $(3.18 \pm 1.11 \pm 0.53) \times 10^{-4}$ from a measurement of $[\Gamma(\chi_{c0}(1P) \rightarrow \Lambda(1520)\bar{\Lambda}(1520))/\Gamma_{total}] \times [B(\psi(2S) \rightarrow \gamma\chi_{c0}(1P))] = (9.62 \pm 0.31) \times 10^{-2}$, which we rescale to our best value $B(\psi(2S) \rightarrow \gamma\chi_{c0}(1P)) = (9.77 \pm 0.23) \times 10^{-2}$. Our first error is their experiment's error and our second error is the systematic error from using our best value.

$\Gamma(\Sigma^0\bar{\Sigma}^0)/\Gamma_{total}$		Γ_{82}/Γ		
VALUE (units 10^{-4})	EVTS	DOCUMENT ID	TECN	COMMENT
4.69±0.32 OUR AVERAGE				
4.83±0.34±0.11	1046	¹ ABLIKIM	18v BES3	$\psi(2S) \rightarrow \gamma\Sigma^0\bar{\Sigma}^0$
4.2 ± 0.7 ± 0.1	78 ± 10	² NAIK	08 CLEO	$\psi(2S) \rightarrow \gamma\Sigma^0\bar{\Sigma}^0$

• • • We do not use the following data for averages, fits, limits, etc. • • •

4.7 ± 0.5 ± 0.1 243 ^{3,4} ABLIKIM 13H BES3 $\psi(2S) \rightarrow \gamma\Sigma^0\bar{\Sigma}^0$

¹ ABLIKIM 18v reports $[\Gamma(\chi_{c0}(1P) \rightarrow \Sigma^0\bar{\Sigma}^0)/\Gamma_{total}] \times [B(\psi(2S) \rightarrow \gamma\chi_{c0}(1P))] = (4.72 \pm 0.18 \pm 0.28) \times 10^{-5}$ which we divide by our best value $B(\psi(2S) \rightarrow \gamma\chi_{c0}(1P)) = (9.77 \pm 0.23) \times 10^{-2}$. Our first error is their experiment's error and our second error is the systematic error from using our best value.

² NAIK 08 reports $(4.41 \pm 0.56 \pm 0.47) \times 10^{-4}$ from a measurement of $[\Gamma(\chi_{c0}(1P) \rightarrow \Sigma^0\bar{\Sigma}^0)/\Gamma_{total}] \times [B(\psi(2S) \rightarrow \gamma\chi_{c0}(1P))] = (9.22 \pm 0.11 \pm 0.46) \times 10^{-2}$, which we rescale to our best value $B(\psi(2S) \rightarrow \gamma\chi_{c0}(1P)) = (9.77 \pm 0.23) \times 10^{-2}$. Our first error is their experiment's error and our second error is the systematic error from using our best value.

³ ABLIKIM 13H reports $(4.78 \pm 0.34 \pm 0.39) \times 10^{-4}$ from a measurement of $[\Gamma(\chi_{c0}(1P) \rightarrow \Sigma^0\bar{\Sigma}^0)/\Gamma_{total}] \times [B(\psi(2S) \rightarrow \gamma\chi_{c0}(1P))] = (9.62 \pm 0.31) \times 10^{-2}$, which we rescale to our best value $B(\psi(2S) \rightarrow \gamma\chi_{c0}(1P)) = (9.77 \pm 0.23) \times 10^{-2}$. Our first error is their experiment's error and our second error is the systematic error from using our best value.

⁴ Superseded by ABLIKIM 18v

Meson Particle Listings

 $\chi_{c0}(1P)$ $\Gamma(\Sigma^+ \bar{\Sigma}^-)/\Gamma_{\text{total}}$ Γ_{85}/Γ

VALUE (units 10^{-4})	EVTS	DOCUMENT ID	TECN	COMMENT
4.7 ± 0.8 OUR AVERAGE				Error includes scale factor of 2.6.

5.11 ± 0.35 ± 0.12 747 ¹ ABLIKIM 18v BES3 $\psi(2S) \rightarrow \gamma \Sigma^+ \bar{\Sigma}^-$
 3.1 ± 0.7 ± 0.1 39 ± 7 ² NAIK 08 CLEO $\psi(2S) \rightarrow \gamma \Sigma^+ \bar{\Sigma}^-$

• • • We do not use the following data for averages, fits, limits, etc. • • •

4.5 ± 0.5 ± 0.1 148 ^{3,4} ABLIKIM 13H BES3 $\psi(2S) \rightarrow \gamma \Sigma^+ \bar{\Sigma}^-$

¹ ABLIKIM 18v reports $[\Gamma(\chi_{c0}(1P) \rightarrow \Sigma^+ \bar{\Sigma}^-)/\Gamma_{\text{total}}] \times [B(\psi(2S) \rightarrow \gamma \chi_{c0}(1P))] = (4.99 \pm 0.24 \pm 0.24) \times 10^{-5}$ which we divide by our best value $B(\psi(2S) \rightarrow \gamma \chi_{c0}(1P)) = (9.77 \pm 0.23) \times 10^{-2}$. Our first error is their experiment's error and our second error is the systematic error from using our best value.

² NAIK 08 reports $(3.25 \pm 0.57 \pm 0.43) \times 10^{-4}$ from a measurement of $[\Gamma(\chi_{c0}(1P) \rightarrow \Sigma^+ \bar{\Sigma}^-)/\Gamma_{\text{total}}] \times [B(\psi(2S) \rightarrow \gamma \chi_{c0}(1P))]$ assuming $B(\psi(2S) \rightarrow \gamma \chi_{c0}(1P)) = (9.22 \pm 0.11 \pm 0.46) \times 10^{-2}$, which we rescale to our best value $B(\psi(2S) \rightarrow \gamma \chi_{c0}(1P)) = (9.77 \pm 0.23) \times 10^{-2}$. Our first error is their experiment's error and our second error is the systematic error from using our best value.

³ ABLIKIM 13H reports $(4.54 \pm 0.42 \pm 0.30) \times 10^{-4}$ from a measurement of $[\Gamma(\chi_{c0}(1P) \rightarrow \Sigma^+ \bar{\Sigma}^-)/\Gamma_{\text{total}}] \times [B(\psi(2S) \rightarrow \gamma \chi_{c0}(1P))]$ assuming $B(\psi(2S) \rightarrow \gamma \chi_{c0}(1P)) = (9.62 \pm 0.31) \times 10^{-2}$, which we rescale to our best value $B(\psi(2S) \rightarrow \gamma \chi_{c0}(1P)) = (9.77 \pm 0.23) \times 10^{-2}$. Our first error is their experiment's error and our second error is the systematic error from using our best value.

⁴ Superseded by ABLIKIM 18v

 $\Gamma(\Sigma^- \bar{\Sigma}^+)/\Gamma_{\text{total}}$ Γ_{86}/Γ

VALUE (units 10^{-4})	EVTS	DOCUMENT ID	TECN	COMMENT
5.1 ± 0.5 ± 0.1	2143	¹ ABLIKIM 20i	BES3	$\psi(2S) \rightarrow \gamma \Sigma^- \bar{\Sigma}^+$

¹ ABLIKIM 20i reports $(5.13 \pm 0.24 \pm 0.41) \times 10^{-4}$ from a measurement of $[\Gamma(\chi_{c0}(1P) \rightarrow \Sigma^- \bar{\Sigma}^+)/\Gamma_{\text{total}}] \times [B(\psi(2S) \rightarrow \gamma \chi_{c0}(1P))]$ assuming $B(\psi(2S) \rightarrow \gamma \chi_{c0}(1P)) = (9.79 \pm 0.20) \times 10^{-2}$, which we rescale to our best value $B(\psi(2S) \rightarrow \gamma \chi_{c0}(1P)) = (9.77 \pm 0.23) \times 10^{-2}$. Our first error is their experiment's error and our second error is the systematic error from using our best value.

 $\Gamma(\Sigma(1385)^+ \bar{\Sigma}(1385)^-)/\Gamma_{\text{total}}$ Γ_{87}/Γ

VALUE (units 10^{-5})	EVTS	DOCUMENT ID	TECN	COMMENT
16.3 ± 5.8 ± 0.4	27	¹ ABLIKIM 12i	BES3	$\psi(2S) \rightarrow \gamma \Lambda \bar{\Lambda} \pi^+ \pi^-$

¹ ABLIKIM 12i reports $(16.4 \pm 5.7 \pm 1.6) \times 10^{-5}$ from a measurement of $[\Gamma(\chi_{c0}(1P) \rightarrow \Sigma(1385)^+ \bar{\Sigma}(1385)^-)/\Gamma_{\text{total}}] \times [B(\psi(2S) \rightarrow \gamma \chi_{c0}(1P))]$ assuming $B(\psi(2S) \rightarrow \gamma \chi_{c0}(1P)) = (9.68 \pm 0.31) \times 10^{-2}$, which we rescale to our best value $B(\psi(2S) \rightarrow \gamma \chi_{c0}(1P)) = (9.77 \pm 0.23) \times 10^{-2}$. Our first error is their experiment's error and our second error is the systematic error from using our best value.

 $\Gamma(\Sigma(1385)^- \bar{\Sigma}(1385)^+)/\Gamma_{\text{total}}$ Γ_{88}/Γ

VALUE (units 10^{-5})	EVTS	DOCUMENT ID	TECN	COMMENT
23 ± 7 ± 1	33	¹ ABLIKIM 12i	BES3	$\psi(2S) \rightarrow \gamma \Lambda \bar{\Lambda} \pi^+ \pi^-$

¹ ABLIKIM 12i reports $(23.5 \pm 6.2 \pm 2.3) \times 10^{-5}$ from a measurement of $[\Gamma(\chi_{c0}(1P) \rightarrow \Sigma(1385)^- \bar{\Sigma}(1385)^+)/\Gamma_{\text{total}}] \times [B(\psi(2S) \rightarrow \gamma \chi_{c0}(1P))]$ assuming $B(\psi(2S) \rightarrow \gamma \chi_{c0}(1P)) = (9.68 \pm 0.31) \times 10^{-2}$, which we rescale to our best value $B(\psi(2S) \rightarrow \gamma \chi_{c0}(1P)) = (9.77 \pm 0.23) \times 10^{-2}$. Our first error is their experiment's error and our second error is the systematic error from using our best value.

 $\Gamma(K^- \Lambda \bar{\Sigma}^+ + \text{c.c.})/\Gamma_{\text{total}}$ Γ_{89}/Γ

VALUE (units 10^{-4})	EVTS	DOCUMENT ID	TECN	COMMENT
1.95 ± 0.35 ± 0.05	57	¹ ABLIKIM 15i	BES3	$\psi(2S) \rightarrow \gamma K^- \Lambda \bar{\Sigma}^+ + \text{c.c.}$

¹ ABLIKIM 15i reports $[\Gamma(\chi_{c0}(1P) \rightarrow K^- \Lambda \bar{\Sigma}^+ + \text{c.c.})/\Gamma_{\text{total}}] \times [B(\psi(2S) \rightarrow \gamma \chi_{c0}(1P))] = (1.90 \pm 0.30 \pm 0.16) \times 10^{-5}$ which we divide by our best value $B(\psi(2S) \rightarrow \gamma \chi_{c0}(1P)) = (9.77 \pm 0.23) \times 10^{-2}$. Our first error is their experiment's error and our second error is the systematic error from using our best value.

 $\Gamma(\Xi^0 \Xi^0)/\Gamma_{\text{total}}$ Γ_{90}/Γ

VALUE (units 10^{-4})	EVTS	DOCUMENT ID	TECN	COMMENT
4.5 ± 0.5 OUR AVERAGE				Error includes scale factor of 1.7.

4.68 ± 0.31 ± 0.11 1741 ¹ ABLIKIM 22o BES3 $\psi(2S) \rightarrow \gamma \Xi^0 \Xi^0$
 3.2 ± 0.8 ± 0.1 23.3 ± 4.9 ² NAIK 08 CLEO $\psi(2S) \rightarrow \gamma \Xi^0 \Xi^0$

¹ ABLIKIM 22o reports $(4.67 \pm 0.19 \pm 0.26) \times 10^{-4}$ from a measurement of $[\Gamma(\chi_{c0}(1P) \rightarrow \Xi^0 \Xi^0)/\Gamma_{\text{total}}] \times [B(\psi(2S) \rightarrow \gamma \chi_{c0}(1P))]$ assuming $B(\psi(2S) \rightarrow \gamma \chi_{c0}(1P)) = (9.79 \pm 0.2) \times 10^{-2}$, which we rescale to our best value $B(\psi(2S) \rightarrow \gamma \chi_{c0}(1P)) = (9.77 \pm 0.23) \times 10^{-2}$. Our first error is their experiment's error and our second error is the systematic error from using our best value.

² NAIK 08 reports $(3.34 \pm 0.70 \pm 0.48) \times 10^{-4}$ from a measurement of $[\Gamma(\chi_{c0}(1P) \rightarrow \Xi^0 \Xi^0)/\Gamma_{\text{total}}] \times [B(\psi(2S) \rightarrow \gamma \chi_{c0}(1P))]$ assuming $B(\psi(2S) \rightarrow \gamma \chi_{c0}(1P)) = (9.22 \pm 0.11 \pm 0.46) \times 10^{-2}$, which we rescale to our best value $B(\psi(2S) \rightarrow \gamma \chi_{c0}(1P)) = (9.77 \pm 0.23) \times 10^{-2}$. Our first error is their experiment's error and our second error is the systematic error from using our best value.

 $\Gamma(\Xi^- \bar{\Xi}^+)/\Gamma_{\text{total}}$ Γ_{91}/Γ

VALUE (units 10^{-4})	CL%	EVTS	DOCUMENT ID	TECN	COMMENT
4.47 ± 0.20 OUR AVERAGE					

4.44 ± 0.18 ± 0.10 4932 ¹ ABLIKIM 22o BES3 $\psi(2S) \rightarrow \gamma \Xi^- \bar{\Xi}^+$
 4.9 ± 0.7 ± 0.1 95 ² NAIK 08 CLEO $\psi(2S) \rightarrow \gamma \Xi^- \bar{\Xi}^+$

• • • We do not use the following data for averages, fits, limits, etc. • • •

<10.3 90 ³ ABLIKIM 06D BES2 $\psi(2S) \rightarrow \chi_{c0} \gamma$

¹ ABLIKIM 22o reports $(4.43 \pm 0.08 \pm 0.18) \times 10^{-4}$ from a measurement of $[\Gamma(\chi_{c0}(1P) \rightarrow \Xi^- \bar{\Xi}^+)/\Gamma_{\text{total}}] \times [B(\psi(2S) \rightarrow \gamma \chi_{c0}(1P))]$ assuming $B(\psi(2S) \rightarrow \gamma \chi_{c0}(1P)) = (9.79 \pm 0.2) \times 10^{-2}$, which we rescale to our best value $B(\psi(2S) \rightarrow \gamma \chi_{c0}(1P)) = (9.77 \pm 0.23) \times 10^{-2}$. Our first error is their experiment's error and our second error is the systematic error from using our best value.

² NAIK 08 reports $(5.14 \pm 0.60 \pm 0.47) \times 10^{-4}$ from a measurement of $[\Gamma(\chi_{c0}(1P) \rightarrow \Xi^- \bar{\Xi}^+)/\Gamma_{\text{total}}] \times [B(\psi(2S) \rightarrow \gamma \chi_{c0}(1P))]$ assuming $B(\psi(2S) \rightarrow \gamma \chi_{c0}(1P)) = (9.22 \pm 0.11 \pm 0.46) \times 10^{-2}$, which we rescale to our best value $B(\psi(2S) \rightarrow \gamma \chi_{c0}(1P)) = (9.77 \pm 0.23) \times 10^{-2}$. Our first error is their experiment's error and our second error is the systematic error from using our best value.

³ Using $B(\psi(2S) \rightarrow \chi_{c0} \gamma) = (9.2 \pm 0.5)\%$

 $\Gamma(\Omega^- \bar{\Omega}^+)/\Gamma_{\text{total}}$ Γ_{92}/Γ

VALUE (units 10^{-5})	EVTS	DOCUMENT ID	TECN	COMMENT
3.51 ± 0.54 ± 0.29	284	ABLIKIM 23T	BES3	$\chi_{cJ} \rightarrow \Omega^- \bar{\Omega}^+$

 $\Gamma(\eta_c \pi^+ \pi^-)/\Gamma_{\text{total}}$ Γ_{93}/Γ

VALUE	CL%	DOCUMENT ID	TECN	COMMENT
< 7×10^{-4}		^{1,2} ABLIKIM 13b	BES3	$e^+ e^- \rightarrow \psi(2S) \rightarrow \gamma \chi_{c0}$

• • • We do not use the following data for averages, fits, limits, etc. • • •

< 41×10^{-4} 90 ^{1,3} ABLIKIM 13b BES3 $e^+ e^- \rightarrow \psi(2S) \rightarrow \gamma \chi_{c0}$

¹ Using $1.06 \times 10^8 \psi(2S)$ mesons and $B(\psi(2S) \rightarrow \chi_{c0} \gamma) = (9.68 \pm 0.31)\%$.

² From the $\eta_c \rightarrow K_S^0 K^{\pm} \pi^{\mp}$ decays.

³ From the $\eta_c \rightarrow K^+ K^- \pi^0$ decays.

 $\Gamma(\rho \bar{\rho})/\Gamma_{\text{total}} \times \Gamma(\pi \pi)/\Gamma_{\text{total}}$ $\Gamma_{58}/\Gamma \times \Gamma_{32}/\Gamma$

VALUE (units 10^{-7})	DOCUMENT ID	TECN	COMMENT
18.9 ± 1.5 OUR FIT			Error includes scale factor of 1.5.

15.3 ± 2.4 ± 0.8 ¹ ANDREOTTI 03 E835 $\bar{p} p \rightarrow \chi_{c0} \rightarrow \pi^0 \pi^0$

¹ We have multiplied $B(\rho \bar{\rho}) \cdot B(\pi^0 \pi^0)$ measurement by 3 to obtain $B(\rho \bar{\rho}) \cdot B(\pi \pi)$.

 $\Gamma(\rho \bar{\rho})/\Gamma_{\text{total}} \times \Gamma(\pi^0 \eta)/\Gamma_{\text{total}}$ $\Gamma_{58}/\Gamma \times \Gamma_{33}/\Gamma$

VALUE (units 10^{-7})	DOCUMENT ID	TECN	COMMENT
< 0.4	ANDREOTTI 05c	E835	$\bar{p} p \rightarrow \pi^0 \eta$

 $\Gamma(\rho \bar{\rho})/\Gamma_{\text{total}} \times \Gamma(\pi^0 \eta')/\Gamma_{\text{total}}$ $\Gamma_{58}/\Gamma \times \Gamma_{34}/\Gamma$

VALUE (units 10^{-7})	DOCUMENT ID	TECN	COMMENT
< 2.5	ANDREOTTI 05c	E835	$\bar{p} p \rightarrow \pi^0 \eta$

 $\Gamma(\rho \bar{\rho})/\Gamma_{\text{total}} \times \Gamma(\eta \eta)/\Gamma_{\text{total}}$ $\Gamma_{58}/\Gamma \times \Gamma_{36}/\Gamma$

VALUE (units 10^{-7})	DOCUMENT ID	TECN	COMMENT
6.7 ± 0.7 OUR FIT			Error includes scale factor of 1.4.

4.0 ± 1.2 ± 0.5 ± 0.3 ANDREOTTI 05c E835 $\bar{p} p \rightarrow \eta \eta$

 $\Gamma(\rho \bar{\rho})/\Gamma_{\text{total}} \times \Gamma(\eta \eta')/\Gamma_{\text{total}}$ $\Gamma_{58}/\Gamma \times \Gamma_{37}/\Gamma$

VALUE (units 10^{-6})	DOCUMENT ID	TECN	COMMENT
2.1 ± 2.3 ± 1.5	ANDREOTTI 05c	E835	$\bar{p} p \rightarrow \pi^0 \eta$

• • • We do not use the following data for averages, fits, limits, etc. • • •

RADIATIVE DECAYS

 $\Gamma(\gamma \rho^0)/\Gamma_{\text{total}}$ Γ_{95}/Γ

VALUE (units 10^{-6})	CL%	EVTS	DOCUMENT ID	TECN	COMMENT
< 9		90 1.2 ± 4.5	¹ BENNETT 08A	CLEO	$\psi(2S) \rightarrow \gamma \rho^0$

• • • We do not use the following data for averages, fits, limits, etc. • • •

< 10 90 6 ± 12 ² ABLIKIM 11E BES3 $\psi(2S) \rightarrow \gamma \rho^0$

¹ BENNETT 08A reports $< 9.6 \times 10^{-6}$ from a measurement of $[\Gamma(\chi_{c0}(1P) \rightarrow \gamma \rho^0)/\Gamma_{\text{total}}] \times [B(\psi(2S) \rightarrow \gamma \chi_{c0}(1P))]$ assuming $B(\psi(2S) \rightarrow \gamma \chi_{c0}(1P)) = (9.2 \pm 0.4) \times 10^{-2}$, which we rescale to our best value $B(\psi(2S) \rightarrow \gamma \chi_{c0}(1P)) = 9.77 \times 10^{-2}$.

² ABLIKIM 11E reports $< 10.5 \times 10^{-6}$ from a measurement of $[\Gamma(\chi_{c0}(1P) \rightarrow \gamma \rho^0)/\Gamma_{\text{total}}] \times [B(\psi(2S) \rightarrow \gamma \chi_{c0}(1P))]$ assuming $B(\psi(2S) \rightarrow \gamma \chi_{c0}(1P)) = (9.62 \pm 0.31) \times 10^{-2}$, which we rescale to our best value $B(\psi(2S) \rightarrow \gamma \chi_{c0}(1P)) = 9.77 \times 10^{-2}$.

 $\Gamma(\gamma \omega)/\Gamma_{\text{total}}$ Γ_{96}/Γ

VALUE (units 10^{-6})	CL%	EVTS	DOCUMENT ID	TECN	COMMENT
< 8		90 0.0 ± 2.8	¹ BENNETT 08A	CLEO	$\psi(2S) \rightarrow \gamma \omega$

• • • We do not use the following data for averages, fits, limits, etc. • • •

< 13 90 5 ± 11 ² ABLIKIM 11E BES3 $\psi(2S) \rightarrow \gamma \omega$

¹ BENNETT 08A reports $< 8.8 \times 10^{-6}$ from a measurement of $[\Gamma(\chi_{c0}(1P) \rightarrow \gamma \omega)/\Gamma_{\text{total}}] \times [B(\psi(2S) \rightarrow \gamma \chi_{c0}(1P))]$ assuming $B(\psi(2S) \rightarrow \gamma \chi_{c0}(1P)) = (9.2 \pm 0.4) \times 10^{-2}$, which we rescale to our best value $B(\psi(2S) \rightarrow \gamma \chi_{c0}(1P)) = 9.77 \times 10^{-2}$.

² ABLIKIM 11E reports $< 12.9 \times 10^{-6}$ from a measurement of $[\Gamma(\chi_{c0}(1P) \rightarrow \gamma \omega)/\Gamma_{\text{total}}] \times [B(\psi(2S) \rightarrow \gamma \chi_{c0}(1P))]$ assuming $B(\psi(2S) \rightarrow \gamma \chi_{c0}(1P)) = (9.62 \pm 0.31) \times 10^{-2}$, which we rescale to our best value $B(\psi(2S) \rightarrow \gamma \chi_{c0}(1P)) = 9.77 \times 10^{-2}$.

See key on page 1171

Meson Particle Listings

$\chi_{c0}(1P)$

$\Gamma(\gamma\phi)/\Gamma_{total}$		Γ_{97}/Γ	
VALUE (units 10^{-6})	CL% EVTS	DOCUMENT ID	TECN COMMENT

< 6 90 0.1 ± 1.6 ¹ BENNETT 08A CLEO $\psi(2S) \rightarrow \gamma\phi$
 ••• We do not use the following data for averages, fits, limits, etc. •••
 <16 90 15 ± 7 ² ABLIKIM 11E BES3 $\psi(2S) \rightarrow \gamma\phi$
¹ BENNETT 08A reports $< 6.4 \times 10^{-6}$ from a measurement of $[\Gamma(\chi_{c0}(1P) \rightarrow \gamma\phi)/\Gamma_{total}] \times [B(\psi(2S) \rightarrow \gamma\chi_{c0}(1P))]$ assuming $B(\psi(2S) \rightarrow \gamma\chi_{c0}(1P)) = (9.2 \pm 0.4) \times 10^{-2}$, which we rescale to our best value $B(\psi(2S) \rightarrow \gamma\chi_{c0}(1P)) = 9.77 \times 10^{-2}$.
² ABLIKIM 11E reports $< 16.2 \times 10^{-6}$ from a measurement of $[\Gamma(\chi_{c0}(1P) \rightarrow \gamma\phi)/\Gamma_{total}] \times [B(\psi(2S) \rightarrow \gamma\chi_{c0}(1P))]$ assuming $B(\psi(2S) \rightarrow \gamma\chi_{c0}(1P)) = (9.62 \pm 0.31) \times 10^{-2}$, which we rescale to our best value $B(\psi(2S) \rightarrow \gamma\chi_{c0}(1P)) = 9.77 \times 10^{-2}$.

$\Gamma(e^+e^-J/\psi(1S))/\Gamma_{total}$		Γ_{99}/Γ	
VALUE (units 10^{-4})	EVTS	DOCUMENT ID	TECN COMMENT

••• We do not use the following data for averages, fits, limits, etc. •••
 $1.54 \pm 0.33 \pm 0.04$ 56 ^{1,2} ABLIKIM 17I BES3 $\psi(2S) \rightarrow \gamma e^+e^-J/\psi$
¹ ABLIKIM 17I reports $(1.51 \pm 0.30 \pm 0.13) \times 10^{-4}$ from a measurement of $[\Gamma(\chi_{c0}(1P) \rightarrow e^+e^-J/\psi(1S))/\Gamma_{total}] \times [B(\psi(2S) \rightarrow \gamma\chi_{c0}(1P))]$ assuming $B(\psi(2S) \rightarrow \gamma\chi_{c0}(1P)) = (9.99 \pm 0.27) \times 10^{-2}$, which we rescale to our best value $B(\psi(2S) \rightarrow \gamma\chi_{c0}(1P)) = (9.77 \pm 0.23) \times 10^{-2}$. Our first error is their experiment's error and our second error is the systematic error from using our best value.
² Not independent from other measurements reported by ABLIKIM 17I

$\Gamma(e^+e^-J/\psi(1S))/\Gamma(\gamma J/\psi(1S))$		Γ_{99}/Γ_{94}	
VALUE (units 10^{-3})	EVTS	DOCUMENT ID	TECN COMMENT

$9.5 \pm 1.9 \pm 0.7$ 56 ¹ ABLIKIM 17I BES3 $\psi(2S) \rightarrow e^+e^-J/\psi$
¹ Uses $B(\psi(2S) \rightarrow \gamma\chi_{c0}(1P)) \times B(\chi_{c0}(1P) \rightarrow \gamma J/\psi(1S)) = (15.8 \pm 0.3 \pm 0.6) \times 10^{-4}$ from ABLIKIM 17N and accounts for common systematic errors.

$\Gamma(\mu^+\mu^-J/\psi(1S))/\Gamma(e^+e^-J/\psi(1S))$		Γ_{100}/Γ_{99}	
VALUE	CL% EVTS	DOCUMENT ID	TECN COMMENT

< 0.14 90 <9.5 ABLIKIM 19Z BES3 $\psi(2S) \rightarrow \gamma\chi_c \rightarrow \gamma(\mu^+\mu^-J/\psi)$

$\Gamma(\gamma\gamma)/\Gamma(\gamma J/\psi(1S))$		Γ_{98}/Γ_{94}	
VALUE (units 10^{-2})	DOCUMENT ID	TECN	COMMENT

1.45 ± 0.13 OUR FIT Error includes scale factor of 1.6.
 2.0 ± 0.4 OUR AVERAGE
 $2.2 \pm 0.4 \pm 0.1$ ¹ ANDREOTTI 04 E835 $p\bar{p} \rightarrow \chi_{c0} \rightarrow \gamma\gamma$
 1.45 ± 0.74 ² AMBROGIANI 00B E835 $\bar{p}p \rightarrow \chi_{c2} \rightarrow \gamma\gamma, \gamma J/\psi$
¹ The values of $B(p\bar{p})B(\gamma\gamma)$ and $B(\gamma\gamma)B(\gamma J/\psi)$ measured by ANDREOTTI 04 are not independent. The latter is used in the fit because of smaller systematics.
² Calculated by us using $B(J/\psi(1S) \rightarrow e^+e^-) = 0.0593 \pm 0.0010$.

$\Gamma(p\bar{p})/\Gamma_{total} \times \Gamma(\gamma J/\psi(1S))/\Gamma_{total}$		$\Gamma_{58}/\Gamma \times \Gamma_{94}/\Gamma$	
VALUE (units 10^{-7})	EVTS	DOCUMENT ID	TECN COMMENT

31.1 ± 2.2 OUR FIT Error includes scale factor of 1.4.
 28.2 ± 2.1 OUR AVERAGE
 $28.0 \pm 1.9 \pm 1.3$ 392 ^{1,2,3} BAGNASCO 02 E835 $\bar{p}p \rightarrow \chi_{c0} \rightarrow J/\psi\gamma$
 $29.3 \pm 5.7 \pm 1.5$ 89 ^{1,2} AMBROGIANI 99B $\bar{p}p \rightarrow \chi_{c0} \rightarrow J/\psi\gamma$
¹ Values in $(\Gamma(p\bar{p}) \times \Gamma(\gamma J/\psi(1S))/\Gamma_{total})$ and $(\Gamma(p\bar{p})/\Gamma_{total} \times \Gamma(\gamma J/\psi(1S))/\Gamma_{total})$ are not independent. The latter is used in the fit since it is less correlated to the total width.
² Calculated by us using $B(J/\psi(1S) \rightarrow e^+e^-) = 0.0593 \pm 0.0010$.
³ Recalculated by ANDREOTTI 05A.

$\chi_{c0}(1P)$ CROSS-PARTICLE BRANCHING RATIOS

$\Gamma(\chi_{c0}(1P) \rightarrow p\bar{p})/\Gamma_{total} \times \Gamma(\psi(2S) \rightarrow \gamma\chi_{c0}(1P))/\Gamma_{total}$		$\Gamma_{58}/\Gamma \times \Gamma_{179}^{\psi(2S)}/\Gamma_{\psi(2S)}$	
VALUE (units 10^{-6})	EVTS	DOCUMENT ID	TECN COMMENT

21.6 ± 1.3 OUR FIT Error includes scale factor of 1.5.
 23.7 ± 1.0 OUR AVERAGE
 $23.7 \pm 0.8 \pm 0.9$ 1222 ABLIKIM 13V BES3 $\psi(2S) \rightarrow \gamma p\bar{p}$
 $23.7 \pm 1.4 \pm 1.4$ 383 ± 22 ¹ NAIK 08 CLEO $\psi(2S) \rightarrow \gamma p\bar{p}$
 $23.6 \pm 3.7 \pm 3.4$ 89.5 ± 14 ± 13 BAI 04F BES $\psi(2S) \rightarrow \gamma\chi_{c0}(1P) \rightarrow \gamma p\bar{p}$
¹ Calculated by us. NAIK 08 reports $B(\chi_{c0} \rightarrow p\bar{p}) = (25.7 \pm 1.5 \pm 1.5 \pm 1.3) \times 10^{-5}$ using $B(\psi(2S) \rightarrow \gamma\chi_{c0}) = (9.22 \pm 0.11 \pm 0.46)\%$.

$\Gamma(\chi_{c0}(1P) \rightarrow p\bar{p})/\Gamma_{total} \times \Gamma(\psi(2S) \rightarrow \gamma\chi_{c0}(1P))/\Gamma(\psi(2S) \rightarrow J/\psi(1S)\pi^+\pi^-)$		$\Gamma_{58}/\Gamma \times \Gamma_{179}^{\psi(2S)}/\Gamma_{12}^{\psi(2S)}$	
VALUE (units 10^{-5})	DOCUMENT ID	TECN	COMMENT

6.2 ± 0.4 OUR FIT Error includes scale factor of 1.5.
 4.6 ± 1.9 ¹ BAI 98I BES $\psi(2S) \rightarrow \gamma\chi_{c0} \rightarrow \gamma p\bar{p}$
¹ Calculated by us. The value for $B(\chi_{c0} \rightarrow p\bar{p})$ reported in BAI 98I is derived using $B(\psi(2S) \rightarrow \gamma\chi_{c0}) = (9.3 \pm 0.8)\%$ and $B(\psi(2S) \rightarrow J/\psi(1S)\pi^+\pi^-) = (32.4 \pm 2.6)\%$ [BAI 98C].

$\Gamma(\chi_{c0}(1P) \rightarrow \Lambda\bar{\Lambda})/\Gamma_{total} \times \Gamma(\psi(2S) \rightarrow \gamma\chi_{c0}(1P))/\Gamma_{total}$		$\Gamma_{71}/\Gamma \times \Gamma_{179}^{\psi(2S)}/\Gamma_{\psi(2S)}$	
VALUE (units 10^{-6})	EVTS	DOCUMENT ID	TECN COMMENT

35.2 ± 1.3 OUR FIT
 35.1 ± 1.4 OUR AVERAGE Error includes scale factor of 1.1.
 $35.6 \pm 1.0 \pm 1.0$ 1486 ABLIKIM 21L BES3 $\psi(2S) \rightarrow \gamma p\pi^- \bar{p}\pi^+$
 $31.2 \pm 3.3 \pm 2.0$ 131 ¹ NAIK 08 CLEO $\psi(2S) \rightarrow \gamma\Lambda\bar{\Lambda}$
 ••• We do not use the following data for averages, fits, limits, etc. •••
 $32.0 \pm 1.9 \pm 2.2$ 369 ^{2,3} ABLIKIM 13H BES3 $\psi(2S) \rightarrow \gamma\Lambda\bar{\Lambda}$
¹ Calculated by us. NAIK 08 reports $B(\chi_{c0} \rightarrow \Lambda\bar{\Lambda}) = (33.8 \pm 3.6 \pm 2.2 \pm 1.7) \times 10^{-5}$ using $B(\psi(2S) \rightarrow \gamma\chi_{c0}) = (9.22 \pm 0.11 \pm 0.46)\%$.
² Superseded by ABLIKIM 21L
³ Calculated by us. ABLIKIM 13H reports $B(\chi_{c0} \rightarrow \Lambda\bar{\Lambda}) = (33.3 \pm 2.0 \pm 2.6) \times 10^{-5}$ from a measurement of $B(\chi_{c0} \rightarrow \Lambda\bar{\Lambda}) \times B(\psi(2S) \rightarrow \gamma\chi_{c0})$ assuming $B(\psi(2S) \rightarrow \gamma\chi_{c0}) = (9.62 \pm 0.31)\%$.

$\Gamma(\chi_{c0}(1P) \rightarrow \Lambda\bar{\Lambda})/\Gamma_{total} \times \Gamma(\psi(2S) \rightarrow \gamma\chi_{c0}(1P))/\Gamma(\psi(2S) \rightarrow J/\psi(1S)\pi^+\pi^-)$		$\Gamma_{71}/\Gamma \times \Gamma_{179}^{\psi(2S)}/\Gamma_{12}^{\psi(2S)}$	
VALUE (units 10^{-5})	EVTS	DOCUMENT ID	TECN COMMENT

10.1 ± 0.4 OUR FIT
 **13.0 ± 3.6
 -3.5 ± 2.5** 15.2 ± 4.2
 -4.0 ¹ BAI 03E BES $\psi(2S) \rightarrow \gamma\Lambda\bar{\Lambda}$
¹ BAI 03E reports $[B(\chi_{c0} \rightarrow \Lambda\bar{\Lambda})B(\psi(2S) \rightarrow \gamma\chi_{c0}) / B(\psi(2S) \rightarrow J/\psi\pi^+\pi^-)] \times [B^2(\Lambda \rightarrow \pi^-p) / B(J/\psi \rightarrow p\bar{p})] = (2.45 \pm 0.68 \pm 0.46)\%$. We calculate from this measurement the presented value using $B(\Lambda \rightarrow \pi^-p) = (63.9 \pm 0.5)\%$ and $B(J/\psi \rightarrow p\bar{p}) = (2.17 \pm 0.07) \times 10^{-3}$.

$\Gamma(\chi_{c0}(1P) \rightarrow \Lambda\bar{\Lambda}\eta)/\Gamma_{total} \times \Gamma(\psi(2S) \rightarrow \gamma\chi_{c0}(1P))/\Gamma_{total}$		$\Gamma_{76}/\Gamma \times \Gamma_{179}^{\psi(2S)}/\Gamma_{\psi(2S)}$	
VALUE (units 10^{-5})	EVTS	DOCUMENT ID	TECN COMMENT

$2.26 \pm 0.30 \pm 0.20$ 67 ABLIKIM 22a BES3 $\psi(2S) \rightarrow \gamma p\pi^- \bar{p}\pi^+ \gamma\gamma$

$\Gamma(\chi_{c0}(1P) \rightarrow \gamma J/\psi(1S))/\Gamma_{total} \times \Gamma(\psi(2S) \rightarrow \gamma\chi_{c0}(1P))/\Gamma_{total}$		$\Gamma_{94}/\Gamma \times \Gamma_{179}^{\psi(2S)}/\Gamma_{\psi(2S)}$	
VALUE (units 10^{-2})	EVTS	DOCUMENT ID	TECN COMMENT

0.137 ± 0.009 OUR FIT Error includes scale factor of 1.7.
 0.147 ± 0.029 OUR AVERAGE Error includes scale factor of 4.6.
 $0.158 \pm 0.003 \pm 0.006$ 4.8k ¹ ABLIKIM 17N BES3 $\psi(2S) \rightarrow \gamma\gamma J/\psi$
 $0.024 \pm 0.015 \pm 0.205$ 12k ABLIKIM 17U BES3 $e^+e^- \rightarrow \gamma\chi$
 0.069 ± 0.018 ² OREGLIA 82 CBAL $\psi(2S) \rightarrow \gamma\chi_{c0}$
 0.4 ± 0.3 ³ BRANDELIK 79B DASP $\psi(2S) \rightarrow \gamma\chi_{c0}$
 0.16 ± 0.11 ³ BARTEL 78B CNTR $\psi(2S) \rightarrow \gamma\chi_{c0}$
 3.3 ± 1.7 ⁴ BIDDICK 77 CNTR $e^+e^- \rightarrow \gamma\chi$
 ••• We do not use the following data for averages, fits, limits, etc. •••
 $0.151 \pm 0.003 \pm 0.010$ 4.3k ⁵ ABLIKIM 12a BES3 $\psi(2S) \rightarrow \gamma\chi_{c0}$
 $0.125 \pm 0.007 \pm 0.013$ 5.60 ⁶ MENDEZ 08 CLEO $\psi(2S) \rightarrow \gamma\chi_{c0}$
 $0.18 \pm 0.01 \pm 0.02$ 172 ⁷ ADAM 05A CLEO Repl. by MENDEZ 08
¹ Uses $B(J/\psi \rightarrow e^+e^-) = (5.971 \pm 0.032)\%$ and $B(J/\psi \rightarrow \mu^+\mu^-) = (5.961 \pm 0.033)\%$.
² Recalculated by us using $B(J/\psi(1S) \rightarrow e^+e^-) = 0.1181 \pm 0.0020$.
³ Recalculated by us using $B(J/\psi(1S) \rightarrow \mu^+\mu^-) = 0.0588 \pm 0.0010$.
⁴ Assumes isotropic gamma distribution.
⁵ Superseded by ABLIKIM 17N.
⁶ Not independent from other measurements of MENDEZ 08.
⁷ Not independent from other values reported by ADAM 05A.

$\Gamma(\chi_{c0}(1P) \rightarrow \gamma J/\psi(1S))/\Gamma_{total} \times \Gamma(\psi(2S) \rightarrow \gamma\chi_{c0}(1P))/\Gamma(\psi(2S) \rightarrow J/\psi(1S)\pi^+\pi^-)$		$\Gamma_{94}/\Gamma \times \Gamma_{179}^{\psi(2S)}/\Gamma_{12}^{\psi(2S)}$	
VALUE (units 10^{-2})	EVTS	DOCUMENT ID	TECN COMMENT

0.396 ± 0.025 OUR FIT Error includes scale factor of 1.7.
 $0.358 \pm 0.020 \pm 0.037$ 5.60 MENDEZ 08 CLEO $\psi(2S) \rightarrow \gamma\chi_{c0}$
 ••• We do not use the following data for averages, fits, limits, etc. •••
 $0.55 \pm 0.04 \pm 0.06$ 172 ¹ ADAM 05A CLEO Repl. by MENDEZ 08
¹ Not independent from other values reported by ADAM 05A.

$\Gamma(\chi_{c0}(1P) \rightarrow \gamma\gamma)/\Gamma_{total} \times \Gamma(\psi(2S) \rightarrow \gamma\chi_{c0}(1P))/\Gamma_{total}$		$\Gamma_{98}/\Gamma \times \Gamma_{179}^{\psi(2S)}/\Gamma_{\psi(2S)}$	
VALUE (units 10^{-5})	EVTS	DOCUMENT ID	TECN COMMENT

2.00 ± 0.09 OUR FIT
 1.95 ± 0.09 OUR AVERAGE
 $1.93 \pm 0.08 \pm 0.05$ 3.5k ABLIKIM 17AE BES3 $\psi(2S) \rightarrow \gamma\chi_{c0} \rightarrow 3\gamma$
 $2.17 \pm 0.32 \pm 0.10$ 0.2k ECKLUND 08A CLEO $\psi(2S) \rightarrow \gamma\chi_{c0} \rightarrow 3\gamma$
 $3.7 \pm 1.8 \pm 1.0$ LEE 85 CBAL $\psi(2S) \rightarrow \gamma\chi_{c0}$
 ••• We do not use the following data for averages, fits, limits, etc. •••
 $2.17 \pm 0.17 \pm 0.12$ 0.8k ¹ ABLIKIM 12A BES3 $\psi(2S) \rightarrow \gamma\chi_{c0} \rightarrow 3\gamma$
¹ Superseded by ABLIKIM 17AE.

Meson Particle Listings

 $\chi_{c0}(1P)$

$$\Gamma(\chi_{c0}(1P) \rightarrow \pi\pi)/\Gamma_{\text{total}} \times \Gamma(\psi(2S) \rightarrow \gamma\chi_{c0}(1P))/\Gamma_{\text{total}} \times \Gamma(\psi(2S) \rightarrow \gamma\chi_{c0}(1P))/\Gamma_{\text{total}}$$

VALUE (units 10^{-4})	EVTS	DOCUMENT ID	TECN	COMMENT
8.34 ± 0.34 OUR FIT				Error includes scale factor of 1.2.
8.80 ± 0.34 OUR AVERAGE				

9.11 ± 0.08 ± 0.65	17k	¹ ABLIKIM	10A BES3	$e^+e^- \rightarrow \psi(2S) \rightarrow \gamma\chi_{c0}$
8.81 ± 0.11 ± 0.43	8.9k	² ASNER	09 CLEO	$\psi(2S) \rightarrow \gamma\pi^+\pi^-$
8.13 ± 0.19 ± 0.89	2.8k	³ ASNER	09 CLEO	$\psi(2S) \rightarrow \gamma\pi^0\pi^0$

¹ Calculated by us. ABLIKIM 10A reports $B(\chi_{c0} \rightarrow \pi^0\pi^0) = (3.23 \pm 0.03 \pm 0.23 \pm 0.14) \times 10^{-3}$ using $B(\psi(2S) \rightarrow \gamma\chi_{c0}) = (9.4 \pm 0.4)\%$. We have multiplied the $\pi^0\pi^0$ measurement by 3 to obtain $\pi\pi$.

² Calculated by us. ASNER 09 reports $B(\chi_{c0} \rightarrow \pi^+\pi^-) = (6.37 \pm 0.08 \pm 0.31 \pm 0.32) \times 10^{-3}$ using $B(\psi(2S) \rightarrow \gamma\chi_{c0}) = (9.22 \pm 0.11 \pm 0.46)\%$. We have multiplied the $\pi^+\pi^-$ measurement by 3/2 to obtain $\pi\pi$.

³ Calculated by us. ASNER 09 reports $B(\chi_{c0} \rightarrow \pi^0\pi^0) = (2.94 \pm 0.07 \pm 0.32 \pm 0.15) \times 10^{-3}$ using $B(\psi(2S) \rightarrow \gamma\chi_{c0}) = (9.22 \pm 0.11 \pm 0.46)\%$. We have multiplied the $\pi^0\pi^0$ measurement by 3 to obtain $\pi\pi$.

$$\Gamma(\chi_{c0}(1P) \rightarrow \pi\pi)/\Gamma_{\text{total}} \times \Gamma(\psi(2S) \rightarrow \gamma\chi_{c0}(1P))/\Gamma_{\text{total}} \times \Gamma(\psi(2S) \rightarrow J/\psi(1S)\pi^+\pi^-)$$

VALUE (units 10^{-4})	EVTS	DOCUMENT ID	TECN	COMMENT
24.0 ± 1.0 OUR FIT				Error includes scale factor of 1.2.
20.7 ± 1.7 OUR AVERAGE				

23.9 ± 2.7 ± 4.1	97 ± 11	¹ BAI	03c BES	$\psi(2S) \rightarrow \gamma\chi_{c0} \rightarrow \gamma\pi^0\pi^0$
20.2 ± 1.1 ± 1.5	720 ± 32	² BAI	98i BES	$\psi(2S) \rightarrow \gamma\chi_{c0} \rightarrow \gamma\pi^+\pi^-$

¹ We have multiplied $\pi^0\pi^0$ measurement by 3 to obtain $\pi\pi$.

² Calculated by us. The value for $B(\chi_{c0} \rightarrow \pi^+\pi^-)$ reported in BAI 98i is derived using $B(\psi' \rightarrow \gamma\chi_{c0}) = (9.3 \pm 0.8)\%$ and $B(\psi' \rightarrow J/\psi\pi^+\pi^-) = (32.4 \pm 2.6)\%$ [BAI 98D]. We have multiplied $\pi^+\pi^-$ measurement by 3/2 to obtain $\pi\pi$.

$$\Gamma(\chi_{c0}(1P) \rightarrow \eta\eta)/\Gamma_{\text{total}} \times \Gamma(\psi(2S) \rightarrow \gamma\chi_{c0}(1P))/\Gamma_{\text{total}} \times \Gamma(\psi(2S) \rightarrow \gamma\chi_{c0}(1P))/\Gamma_{\text{total}}$$

VALUE (units 10^{-4})	EVTS	DOCUMENT ID	TECN	COMMENT
2.94 ± 0.22 OUR FIT				Error includes scale factor of 1.2.
3.12 ± 0.19 OUR AVERAGE				

3.23 ± 0.09 ± 0.23	2132	¹ ABLIKIM	10A BES3	$e^+e^- \rightarrow \psi(2S) \rightarrow \gamma\chi_{c0}$
2.93 ± 0.12 ± 0.29	0.9k	² ASNER	09 CLEO	$\psi(2S) \rightarrow \gamma\eta\eta$
2.86 ± 0.46 ± 0.37	48	³ ADAMS	07 CLEO	$\psi(2S) \rightarrow \gamma\chi_{c0}$

¹ Calculated by us. ABLIKIM 10A reports $B(\chi_{c0} \rightarrow \eta\eta) = (3.44 \pm 0.10 \pm 0.24 \pm 0.13) \times 10^{-3}$ using $B(\psi(2S) \rightarrow \gamma\chi_{c0}) = (9.4 \pm 0.4)\%$.

² Calculated by us. ASNER 09 reports $B(\chi_{c0} \rightarrow \eta\eta) = (3.18 \pm 0.13 \pm 0.31 \pm 0.16) \times 10^{-3}$ using $B(\psi(2S) \rightarrow \gamma\chi_{c0}) = (9.22 \pm 0.11 \pm 0.46)\%$.

³ Superseded by ASNER 09. Calculated by us. The value of $B(\chi_{c0}(1P) \rightarrow \eta\eta)$ reported by ADAMS 07 was derived using $B(\psi(2S) \rightarrow \gamma\chi_{c0}(1P)) = (9.22 \pm 0.11 \pm 0.46)\%$ (ATHAR 04).

$$\Gamma(\chi_{c0}(1P) \rightarrow \eta\eta)/\Gamma_{\text{total}} \times \Gamma(\psi(2S) \rightarrow \gamma\chi_{c0}(1P))/\Gamma_{\text{total}} \times \Gamma(\psi(2S) \rightarrow J/\psi(1S)\pi^+\pi^-)$$

VALUE (units 10^{-3})	DOCUMENT ID	TECN	COMMENT
0.85 ± 0.06 OUR FIT			Error includes scale factor of 1.2.
0.578 ± 0.241 ± 0.158	BAI	03c BES	$\psi(2S) \rightarrow \gamma\eta\eta$

$$\Gamma(\chi_{c0}(1P) \rightarrow K^+K^-)/\Gamma_{\text{total}} \times \Gamma(\psi(2S) \rightarrow \gamma\chi_{c0}(1P))/\Gamma_{\text{total}} \times \Gamma(\psi(2S) \rightarrow \gamma\chi_{c0}(1P))/\Gamma_{\text{total}}$$

VALUE (units 10^{-4})	EVTS	DOCUMENT ID	TECN	COMMENT
5.93 ± 0.28 OUR FIT				
5.97 ± 0.07 ± 0.32	8.1k	¹ ASNER	09 CLEO	$\psi(2S) \rightarrow \gamma K^+K^-$

¹ Calculated by us. ASNER 09 reports $B(\chi_{c0} \rightarrow K^+K^-) = (6.47 \pm 0.08 \pm 0.35 \pm 0.32) \times 10^{-3}$ using $B(\psi(2S) \rightarrow \gamma\chi_{c0}) = (9.22 \pm 0.11 \pm 0.46)\%$.

$$\Gamma(\chi_{c0}(1P) \rightarrow K^+K^-)/\Gamma_{\text{total}} \times \Gamma(\psi(2S) \rightarrow \gamma\chi_{c0}(1P))/\Gamma_{\text{total}} \times \Gamma(\psi(2S) \rightarrow J/\psi(1S)\pi^+\pi^-)$$

VALUE (units 10^{-3})	EVTS	DOCUMENT ID	TECN	COMMENT
1.71 ± 0.08 OUR FIT				
1.63 ± 0.10 ± 0.15	774 ± 38	¹ BAI	98i BES	$\psi(2S) \rightarrow \gamma K^+K^-$

¹ Calculated by us. The value for $B(\chi_{c0} \rightarrow K^+K^-)$ reported by BAI 98i is derived using $B(\psi(2S) \rightarrow \gamma\chi_{c0}) = (9.3 \pm 0.8)\%$ and $B(\psi(2S) \rightarrow J/\psi\pi^+\pi^-) = (32.4 \pm 2.6)\%$ [BAI 98D].

$$\Gamma(\chi_{c0}(1P) \rightarrow K_S^0 K_S^0)/\Gamma_{\text{total}} \times \Gamma(\psi(2S) \rightarrow \gamma\chi_{c0}(1P))/\Gamma_{\text{total}} \times \Gamma(\psi(2S) \rightarrow \gamma\chi_{c0}(1P))/\Gamma_{\text{total}}$$

VALUE (units 10^{-4})	EVTS	DOCUMENT ID	TECN	COMMENT
3.10 ± 0.16 OUR FIT				
3.18 ± 0.17 OUR AVERAGE				

3.22 ± 0.07 ± 0.17	2.1k	¹ ASNER	09 CLEO	$\psi(2S) \rightarrow \gamma K_S^0 K_S^0$
3.02 ± 0.19 ± 0.33	322	ABLIKIM	05o BES2	$\psi(2S) \rightarrow \gamma K_S^0 K_S^0$

¹ Calculated by us. ASNER 09 reports $B(\chi_{c0} \rightarrow K_S^0 K_S^0) = (3.49 \pm 0.08 \pm 0.18 \pm 0.17) \times 10^{-3}$ using $B(\psi(2S) \rightarrow \gamma\chi_{c0}) = (9.22 \pm 0.11 \pm 0.46)\%$.

$$\Gamma(\chi_{c0}(1P) \rightarrow K_S^0 K_S^0)/\Gamma_{\text{total}} \times \Gamma(\psi(2S) \rightarrow \gamma\chi_{c0}(1P))/\Gamma_{\text{total}} \times \Gamma(\psi(2S) \rightarrow J/\psi(1S)\pi^+\pi^-)$$

VALUE (units 10^{-4})	DOCUMENT ID	TECN	COMMENT
8.9 ± 0.5 OUR FIT			
5.6 ± 0.8 ± 1.3	¹ BAI	99b BES	$\psi(2S) \rightarrow \gamma K_S^0 K_S^0$

¹ Calculated by us. The value of $B(\chi_{c0} \rightarrow K_S^0 K_S^0)$ reported by BAI 99b was derived using $B(\psi(2S) \rightarrow \gamma\chi_{c0}(1P)) = (9.3 \pm 0.8)\%$ and $B(\psi(2S) \rightarrow J/\psi\pi^+\pi^-) = (32.4 \pm 2.6)\%$ [BAI 98D].

$$\Gamma(\chi_{c0}(1P) \rightarrow 2(\pi^+\pi^-))/\Gamma_{\text{total}} \times \Gamma(\psi(2S) \rightarrow \gamma\chi_{c0}(1P))/\Gamma_{\text{total}} \times \Gamma(\psi(2S) \rightarrow J/\psi(1S)\pi^+\pi^-)$$

VALUE (units 10^{-3})	DOCUMENT ID	TECN	COMMENT
6.6 ± 1.0 OUR FIT			Error includes scale factor of 2.0.
6.9 ± 2.4 OUR AVERAGE			Error includes scale factor of 3.8.

4.4 ± 0.1 ± 0.9	¹ BAI	99b BES	$\psi(2S) \rightarrow \gamma\chi_{c0}$
9.3 ± 0.9	² TANENBAUM	78 MRK1	$\psi(2S) \rightarrow \gamma\chi_{c0}$

¹ Calculated by us. The value for $B(\chi_{c0} \rightarrow 2\pi^+2\pi^-)$ reported in BAI 99b is derived using $B(\psi(2S) \rightarrow \gamma\chi_{c0}) = (9.3 \pm 0.8)\%$ and $B(\psi(2S) \rightarrow J/\psi(1S)\pi^+\pi^-) = (32.4 \pm 2.6)\%$ [BAI 98D].

² The value $B(\psi(1S) \rightarrow \gamma\chi_{c0}) \times B(\chi_{c0} \rightarrow 2\pi^+2\pi^-)$ reported in TANENBAUM 78 is derived using $B(\psi(2S) \rightarrow J/\psi(1S)\pi^+\pi^-) \times B(J/\psi(1S) \rightarrow \ell^+\ell^-) = (4.6 \pm 0.7)\%$. Calculated by us using $B(J/\psi(1S) \rightarrow \ell^+\ell^-) = 0.1181 \pm 0.0020$.

$$\Gamma(\chi_{c0}(1P) \rightarrow \pi^+\pi^-K^+K^-)/\Gamma_{\text{total}} \times \Gamma(\psi(2S) \rightarrow \gamma\chi_{c0}(1P))/\Gamma_{\text{total}} \times \Gamma(\psi(2S) \rightarrow \gamma\chi_{c0}(1P))/\Gamma_{\text{total}}$$

VALUE (units 10^{-3})	DOCUMENT ID	TECN	COMMENT
1.78 ± 0.15 OUR FIT			Error includes scale factor of 1.1.
1.64 ± 0.05 ± 0.2	ABLIKIM	05q BES2	$\psi(2S) \rightarrow \gamma\chi_{c0}$

$$\Gamma(\chi_{c0}(1P) \rightarrow \pi^+\pi^-K^+K^-)/\Gamma_{\text{total}} \times \Gamma(\psi(2S) \rightarrow \gamma\chi_{c0}(1P))/\Gamma_{\text{total}} \times \Gamma(\psi(2S) \rightarrow J/\psi(1S)\pi^+\pi^-)$$

VALUE (units 10^{-3})	DOCUMENT ID	TECN	COMMENT
5.1 ± 0.4 OUR FIT			Error includes scale factor of 1.1.
5.8 ± 1.6 OUR AVERAGE			Error includes scale factor of 2.3.

4.22 ± 0.20 ± 0.97	BAI	99b BES	$\psi(2S) \rightarrow \gamma\chi_{c0}$
7.4 ± 1.0	¹ TANENBAUM	78 MRK1	$\psi(2S) \rightarrow \gamma\chi_{c0}$

¹ The reported value is derived using $B(\psi(2S) \rightarrow \pi^+\pi^-J/\psi) \times B(J/\psi \rightarrow \ell^+\ell^-) = (4.6 \pm 0.7)\%$. Calculated by us using $B(J/\psi \rightarrow \ell^+\ell^-) = 0.1181 \pm 0.0020$.

$$\Gamma(\chi_{c0}(1P) \rightarrow K^+K^-K^+K^-)/\Gamma_{\text{total}} \times \Gamma(\psi(2S) \rightarrow \gamma\chi_{c0}(1P))/\Gamma_{\text{total}} \times \Gamma(\psi(2S) \rightarrow \gamma\chi_{c0}(1P))/\Gamma_{\text{total}}$$

VALUE (units 10^{-4})	EVTS	DOCUMENT ID	TECN	COMMENT
2.8 ± 0.4 OUR FIT				Error includes scale factor of 1.5.
3.20 ± 0.11 ± 0.41	278	¹ ABLIKIM	06t BES2	$\psi(2S) \rightarrow \gamma 2K^+2K^-$

¹ Calculated by us. The value of $B(\chi_{c0} \rightarrow 2K^+2K^-)$ reported by ABLIKIM 06t was derived using $B(\psi(2S) \rightarrow \gamma\chi_{c0}(1P)) = (9.2 \pm 0.4)\%$.

$$\Gamma(\chi_{c0}(1P) \rightarrow K^+K^-K^+K^-)/\Gamma_{\text{total}} \times \Gamma(\psi(2S) \rightarrow \gamma\chi_{c0}(1P))/\Gamma_{\text{total}} \times \Gamma(\psi(2S) \rightarrow J/\psi(1S)\pi^+\pi^-)$$

VALUE (units 10^{-4})	DOCUMENT ID	TECN	COMMENT
8.0 ± 1.2 OUR FIT			Error includes scale factor of 1.5.
6.1 ± 0.8 ± 0.9	¹ BAI	99b BES	$\psi(2S) \rightarrow \gamma 2K^+2K^-$

¹ Calculated by us. The value of $B(\chi_{c0} \rightarrow 2K^+2K^-)$ reported by BAI 99b was derived using $B(\psi(2S) \rightarrow \gamma\chi_{c0}(1P)) = (9.3 \pm 0.8)\%$ and $B(\psi(2S) \rightarrow J/\psi\pi^+\pi^-) = (32.4 \pm 2.6)\%$ [BAI 98D].

$$\Gamma(\chi_{c0}(1P) \rightarrow \phi\phi)/\Gamma_{\text{total}} \times \Gamma(\psi(2S) \rightarrow \gamma\chi_{c0}(1P))/\Gamma_{\text{total}} \times \Gamma(\psi(2S) \rightarrow \gamma\chi_{c0}(1P))/\Gamma_{\text{total}}$$

VALUE (units 10^{-4})	EVTS	DOCUMENT ID	TECN	COMMENT
0.829 ± 0.034 OUR FIT				
0.78 ± 0.08 OUR AVERAGE				

0.77 ± 0.03 ± 0.08	¹ ABLIKIM	11k BES3	$\psi(2S) \rightarrow \gamma$ hadrons
0.86 ± 0.19 ± 0.12	² ABLIKIM	06t BES2	$\psi(2S) \rightarrow \gamma 2K^+2K^-$

¹ Calculated by us. The value of $B(\chi_{c0} \rightarrow \phi\phi)$ reported by ABLIKIM 11k was derived using $B(\psi(2S) \rightarrow \gamma\chi_{c0}(1P)) = (9.62 \pm 0.31)\%$.

² Calculated by us. The value of $B(\chi_{c0} \rightarrow \phi\phi)$ reported by ABLIKIM 06t was derived using $B(\psi(2S) \rightarrow \gamma\chi_{c0}(1P)) = (9.2 \pm 0.4)\%$.

$$\Gamma(\chi_{c0}(1P) \rightarrow \phi\phi)/\Gamma_{\text{total}} \times \Gamma(\psi(2S) \rightarrow \gamma\chi_{c0}(1P))/\Gamma_{\text{total}} \times \Gamma(\psi(2S) \rightarrow J/\psi(1S)\pi^+\pi^-)$$

VALUE (units 10^{-4})	DOCUMENT ID	TECN	COMMENT
2.39 ± 0.10 OUR FIT			
2.6 ± 1.0 ± 1.1	¹ BAI	99b BES	$\psi(2S) \rightarrow \gamma 2K^+2K^-$

¹ Calculated by us. The value of $B(\chi_{c0} \rightarrow \phi\phi)$ reported by BAI 99b was derived using $B(\psi(2S) \rightarrow \gamma\chi_{c0}(1P)) = (9.3 \pm 0.8)\%$ and $B(\psi(2S) \rightarrow J/\psi\pi^+\pi^-) = (32.4 \pm 2.6)\%$ [BAI 98D].

See key on page 1171

Meson Particle Listings

$\chi_{c0}(1P), \chi_{c1}(1P)$

$\Gamma(\chi_{c0}(1P) \rightarrow \Sigma^+ \bar{p} K_S^0 + c.c.) / \Gamma_{total} \times \Gamma(\psi(2S) \rightarrow \gamma \chi_{c0}(1P)) / \Gamma_{total}$
 $\Gamma_{83} / \Gamma \times \Gamma_{179}^{\psi(2S)} / \Gamma_{\psi(2S)}$

Table with columns: VALUE (units 10^-5), EVTS, DOCUMENT ID, TECN, COMMENT. Row 1: 3.45 ± 0.17 ± 0.19, 493, 1 ABLIKIM, 19BB BES3, $\psi(2S) \rightarrow \gamma \Sigma^+ \bar{p} K_S^0 + c.c.$

1 Calculated by us. ABLIKIM 19BB reports $B(\chi_c^0 \rightarrow \Sigma^+ \bar{p} K_S^0 + c.c.) = (3.52 \pm 0.19 \pm 0.21) \times 10^{-4}$ using $B(\psi(2S) \rightarrow \gamma \chi_c^0) = (9.79 \pm 0.20)\%$ and other branching fractions from PDG 18.

$\Gamma(\chi_{c0}(1P) \rightarrow \Sigma^0 \bar{p} K^+ + c.c.) / \Gamma_{total} \times \Gamma(\psi(2S) \rightarrow \gamma \chi_{c0}(1P)) / \Gamma_{total}$
 $\Gamma_{84} / \Gamma \times \Gamma_{179}^{\psi(2S)} / \Gamma_{\psi(2S)}$

Table with columns: VALUE (units 10^-5), EVTS, DOCUMENT ID, TECN, COMMENT. Row 1: 2.97 ± 0.12 ± 0.14, 871, 1 ABLIKIM, 20AE BES3, $\psi(2S) \rightarrow \gamma \Sigma^0 \bar{p} K^+ + c.c.$

1 Calculated by us. ABLIKIM 20AE reports $B(\chi_c^0 \rightarrow \Sigma^0 \bar{p} K^+ + c.c.) = (3.03 \pm 0.12 \pm 0.15) \times 10^{-4}$ using $B(\psi(2S) \rightarrow \gamma \chi_c^0) = (9.79 \pm 0.20)\%$ and other branching fractions from PDG 20.

$\chi_{c0}(1P)$ REFERENCES

Large table of references for $\chi_{c0}(1P)$ with columns: ABLIKIM, TECN, DOCUMENT ID, TECN, COMMENT. Includes entries for JHEP, PR, PTEP, etc.

Table of references for $\chi_{c1}(1P)$ with columns: OREGLIA, BRANDELNIK, BARTEL, TANENBAUM, BIDDICK, EVTS, TECN, COMMENT.

Table of references for $\chi_{c1}(1P)$ with columns: M.J. Oreglia et al., R. Brandelik et al., W. Bartel et al., W.M. Tanenbaum et al., G. Trilling, C.J. Biddick et al., (SLAC, CIT, HARV+), (DASP Collab.), (DESY, HEIDP), (SLAC, LBL), (LBL, UCB), (UCSD, UMD, PAVI+)

$\chi_{c1}(1P)$

$J^{PC} = 0^+(1^{++})$

See the Review on "Branching Ratios of $\psi(2S)$, $\chi_{c0,1,2}$ and $\eta_c(1S)$ " before the $\chi_{c0}(1P)$ Listings.

$\chi_{c1}(1P)$ MASS

Table of $\chi_{c1}(1P)$ mass measurements with columns: VALUE (MeV), EVTS, DOCUMENT ID, TECN, COMMENT. Includes entries for AAIJ, ABLIKIM, ANDREOTTI, BAI, ARMSTRONG, BAGLIN, GAISER, LEMOIGNE, OREGLIA, HIMEL, BRANDELNIK, BARTEL, TANENBAUM, BIDDICK, TANENBAUM.

••• We do not use the following data for averages, fits, limits, etc. •••
1 From a fit of the $\phi\phi$ invariant mass with the width of $\chi_{c1}(1P)$ fixed to the PDG 16 value.
2 AAIJ 17BI reports also $m(\chi_{c2}) - m(\chi_{c1}) = 45.39 \pm 0.07 \pm 0.03$ MeV.
3 Recalculated by ANDREOTTI 05A, using the value of $\psi(2S)$ mass from AULCHENKO 03.
4 Using mass of $\psi(2S) = 3686.0$ MeV.
5 $J/\psi(1S)$ mass constrained to 3097 MeV.
6 Mass value shifted by us by amount appropriate for $\psi(2S)$ mass = 3686 MeV and $J/\psi(1S)$ mass = 3097 MeV.
7 From a simultaneous fit to radiative and hadronic decay channels.

$\chi_{c1}(1P)$ WIDTH

Table of $\chi_{c1}(1P)$ width measurements with columns: VALUE (MeV), CL%, EVTS, DOCUMENT ID, TECN, COMMENT. Includes entries for ABLIKIM, ANDREOTTI, ARMSTRONG, BAGLIN, GAISER.

1 Recalculated by ANDREOTTI 05A.

$\chi_{c1}(1P)$ DECAY MODES

Table of $\chi_{c1}(1P)$ decay modes with columns: Mode, Fraction (Γ_i/Γ), Scale factor/Confidence level. Includes hadronic decays and hadronic decays with branching ratios.

Meson Particle Listings

$\chi_{c1}(1P)$

Γ_{16}	$K^+ K^- \eta \pi^0$	$(1.12 \pm 0.34) \times 10^{-3}$	
Γ_{17}	$\pi^+ \pi^- K_S^0 K_S^0$	$(6.9 \pm 2.9) \times 10^{-4}$	
Γ_{18}	$K^+ K^- \eta$	$(3.2 \pm 1.0) \times 10^{-4}$	
Γ_{19}	$\bar{K}^0 K^+ \pi^- + c.c.$	$(7.0 \pm 0.6) \times 10^{-3}$	S=1.1
Γ_{20}	$K^*(892)^0 \bar{K}^0 + c.c.$	$(1.03 \pm 0.15) \times 10^{-3}$	
Γ_{21}	$K^*(892)^+ K^- + c.c.$	$(1.21 \pm 0.23) \times 10^{-3}$	
Γ_{22}	$K_J^*(1430)^0 \bar{K}^0 + c.c. \rightarrow K_S^0 K^+ \pi^- + c.c.$	$< 8 \times 10^{-4}$	CL=90%
Γ_{23}	$K_J^*(1430)^+ K^- + c.c. \rightarrow K_S^0 K^+ \pi^- + c.c.$	$< 2.1 \times 10^{-3}$	CL=90%
Γ_{24}	$K^+ K^- \pi^0$	$(1.81 \pm 0.24) \times 10^{-3}$	
Γ_{25}	$\eta \pi^+ \pi^-$	$(4.62 \pm 0.24) \times 10^{-3}$	
Γ_{26}	$a_0(980)^+ \pi^- + c.c. \rightarrow \eta \pi^+ \pi^-$	$(3.2 \pm 0.4) \times 10^{-3}$	S=2.1
Γ_{27}	$a_2(1320)^+ \pi^- + c.c. \rightarrow \eta \pi^+ \pi^-$	$(1.76 \pm 0.24) \times 10^{-4}$	
Γ_{28}	$a_2(1700)^+ \pi^- + c.c. \rightarrow \eta \pi^+ \pi^-$	$(4.6 \pm 0.7) \times 10^{-5}$	
Γ_{29}	$f_2(1270) \eta \rightarrow \eta \pi^+ \pi^-$	$(3.5 \pm 0.6) \times 10^{-4}$	
Γ_{30}	$f_4(2050) \eta \rightarrow \eta \pi^+ \pi^-$	$(2.5 \pm 0.9) \times 10^{-5}$	
Γ_{31}	$\pi_1(1400)^+ \pi^- + c.c. \rightarrow \eta \pi^+ \pi^-$	$< 5 \times 10^{-5}$	CL=90%
Γ_{32}	$\pi_1(1600)^+ \pi^- + c.c. \rightarrow \eta \pi^+ \pi^-$	$< 1.5 \times 10^{-5}$	CL=90%
Γ_{33}	$\pi_1(2015)^+ \pi^- + c.c. \rightarrow \eta \pi^+ \pi^-$	$< 8 \times 10^{-6}$	CL=90%
Γ_{34}	$f_2(1270) \eta$	$(6.7 \pm 1.1) \times 10^{-4}$	
Γ_{35}	$\pi^+ \pi^- \eta'$	$(2.2 \pm 0.4) \times 10^{-3}$	
Γ_{36}	$K^+ K^- \eta'(958)$	$(8.8 \pm 0.9) \times 10^{-4}$	
Γ_{37}	$K_0^*(1430)^+ K^- + c.c.$	$(6.4 \pm_{-2.8}^{+2.2}) \times 10^{-4}$	
Γ_{38}	$f_0(980) \eta'(958)$	$(1.6 \pm_{-0.7}^{+1.4}) \times 10^{-4}$	
Γ_{39}	$f_0(1710) \eta'(958)$	$(7 \pm_{-5}^{+7}) \times 10^{-5}$	
Γ_{40}	$f_2'(1525) \eta'(958)$	$(9 \pm 6) \times 10^{-5}$	
Γ_{41}	$K_2^*(1430)^+ K^- + c.c.$	$(1.61 \pm 0.31) \times 10^{-3}$	
Γ_{42}	$K_2^*(1430) \bar{K}^0 + c.c.$	$(1.17 \pm 0.20) \times 10^{-3}$	
Γ_{43}	$\pi^0 f_0(980) \rightarrow \pi^0 \pi^+ \pi^-$	$(3.5 \pm 0.9) \times 10^{-7}$	
Γ_{44}	$K^+ \bar{K}^*(892)^0 \pi^- + c.c.$	$(3.2 \pm 2.1) \times 10^{-3}$	
Γ_{45}	$K^*(892)^0 \bar{K}^*(892)^0$	$(1.4 \pm 0.4) \times 10^{-3}$	
Γ_{46}	$K^+ K^- K_S^0 K_S^0$	$< 4 \times 10^{-4}$	CL=90%
Γ_{47}	$K_S^0 K_S^0 K_S^0 K_S^0$	$(3.5 \pm 1.0) \times 10^{-5}$	
Γ_{48}	$K^+ K^- K^+ K^-$	$(5.4 \pm 1.1) \times 10^{-4}$	
Γ_{49}	$K^+ K^- \phi$	$(4.1 \pm 1.5) \times 10^{-4}$	
Γ_{50}	$\bar{K}^0 K^+ \pi^- \phi + c.c.$	$(3.3 \pm 0.5) \times 10^{-3}$	
Γ_{51}	$K^+ K^- \pi^0 \phi$	$(1.62 \pm 0.30) \times 10^{-3}$	
Γ_{52}	$\phi \pi^+ \pi^- \pi^0$	$(7.5 \pm 1.0) \times 10^{-4}$	
Γ_{53}	$\omega \omega$	$(5.7 \pm 0.7) \times 10^{-4}$	
Γ_{54}	$\omega K^+ K^-$	$(7.8 \pm 0.9) \times 10^{-4}$	
Γ_{55}	$\omega \phi$	$(2.7 \pm 0.4) \times 10^{-5}$	
Γ_{56}	$\phi \phi$	$(4.26 \pm 0.21) \times 10^{-4}$	
Γ_{57}	$\phi \phi \eta$	$(3.0 \pm 0.5) \times 10^{-4}$	
Γ_{58}	$\rho \bar{\rho}$	$(7.6 \pm 0.4) \times 10^{-5}$	S=1.2
Γ_{59}	$\rho \bar{\rho} \pi^0$	$(1.55 \pm 0.18) \times 10^{-4}$	
Γ_{60}	$\rho \bar{\rho} \eta$	$(1.45 \pm 0.25) \times 10^{-4}$	
Γ_{61}	$\rho \bar{\rho} \omega$	$(2.12 \pm 0.31) \times 10^{-4}$	
Γ_{62}	$\rho \bar{\rho} \phi$	$< 1.7 \times 10^{-5}$	CL=90%
Γ_{63}	$\rho \bar{\rho} \pi^+ \pi^-$	$(5.0 \pm 1.9) \times 10^{-4}$	
Γ_{64}	$\rho \bar{\rho} \pi^0 \pi^0$	$< 5 \times 10^{-4}$	CL=90%
Γ_{65}	$\rho \bar{\rho} K^+ K^-$ (non-resonant)	$(1.27 \pm 0.22) \times 10^{-4}$	
Γ_{66}	$\rho \bar{\rho} K_S^0 K_S^0$	$< 4.5 \times 10^{-4}$	CL=90%
Γ_{67}	$\rho \bar{\rho} \pi^-$	$(3.8 \pm 0.5) \times 10^{-4}$	
Γ_{68}	$\rho \bar{\rho} \pi^+$	$(3.9 \pm 0.5) \times 10^{-4}$	
Γ_{69}	$\rho \bar{\rho} \pi^- \pi^0$	$(1.03 \pm 0.12) \times 10^{-3}$	
Γ_{70}	$\rho \bar{\rho} \pi^+ \pi^0$	$(1.01 \pm 0.12) \times 10^{-3}$	
Γ_{71}	$\Lambda \bar{\Lambda}$	$(1.27 \pm 0.09) \times 10^{-4}$	S=1.1
Γ_{72}	$\Lambda \bar{\Lambda} \pi^+ \pi^-$	$(2.9 \pm 0.5) \times 10^{-4}$	
Γ_{73}	$\Lambda \bar{\Lambda} \pi^+ \pi^-$ (non-resonant)	$(2.5 \pm 0.6) \times 10^{-4}$	
Γ_{74}	$\Sigma(1385)^+ \bar{\Lambda} \pi^- + c.c.$	$< 1.3 \times 10^{-4}$	CL=90%
Γ_{75}	$\Sigma(1385)^- \bar{\Lambda} \pi^+ + c.c.$	$< 1.3 \times 10^{-4}$	CL=90%
Γ_{76}	$\Lambda \bar{\Lambda} \eta$	$(5.9 \pm 1.5) \times 10^{-5}$	
Γ_{77}	$K^+ \bar{\rho} \Lambda + c.c.$	$(4.2 \pm 0.4) \times 10^{-4}$	S=1.2
Γ_{78}	$n K_S^0 \bar{\Lambda} + c.c.$	$(1.66 \pm 0.17) \times 10^{-4}$	
Γ_{79}	$K^*(892)^+ \bar{\rho} \Lambda + c.c.$	$(4.9 \pm 0.7) \times 10^{-4}$	
Γ_{80}	$K^+ \bar{\rho} \Lambda(1520) + c.c.$	$(1.7 \pm 0.4) \times 10^{-4}$	
Γ_{81}	$\Lambda(1520) \bar{\Lambda}(1520)$	$< 9 \times 10^{-5}$	CL=90%
Γ_{82}	$\Sigma^0 \bar{\Sigma}^0$	$(4.2 \pm 0.6) \times 10^{-5}$	
Γ_{83}	$\Sigma^+ \bar{\rho} K_S^0 + c.c.$	$(1.53 \pm 0.12) \times 10^{-4}$	
Γ_{84}	$\Sigma^0 \bar{\rho} K^+ + c.c.$	$(1.46 \pm 0.10) \times 10^{-4}$	

Γ_{85}	$\Sigma^+ \bar{\Sigma}^-$	$(3.6 \pm 0.7) \times 10^{-5}$	
Γ_{86}	$\Sigma^- \bar{\Sigma}^+$	$(5.7 \pm 1.5) \times 10^{-5}$	
Γ_{87}	$\Sigma(1385)^+ \bar{\Sigma}(1385)^-$	$< 9 \times 10^{-5}$	CL=90%
Γ_{88}	$\Sigma(1385)^- \bar{\Sigma}(1385)^+$	$< 5 \times 10^{-5}$	CL=90%
Γ_{89}	$K^- \bar{\Lambda} \bar{\Sigma}^+ + c.c.$	$(1.35 \pm 0.24) \times 10^{-4}$	
Γ_{90}	$\Xi^0 \bar{\Xi}^0$	$(7.5 \pm 1.3) \times 10^{-5}$	
Γ_{91}	$\Xi^- \bar{\Xi}^+$	$(6.0 \pm 0.6) \times 10^{-5}$	
Γ_{92}	$\Omega^- \bar{\Omega}^+$	$(1.49 \pm 0.25) \times 10^{-5}$	
Γ_{93}	$\pi^+ \pi^- + K^+ K^-$	$< 2.1 \times 10^{-3}$	
Γ_{94}	$K_S^0 K_S^0$	$< 6 \times 10^{-5}$	CL=90%
Γ_{95}	$\eta_c \pi^+ \pi^-$	$< 3.2 \times 10^{-3}$	CL=90%

Radiative decays

Γ_{96}	$\gamma J/\psi(1S)$	$(34.3 \pm 1.3) \%$	S=1.3
Γ_{97}	$\gamma \rho^0$	$(2.16 \pm 0.17) \times 10^{-4}$	
Γ_{98}	$\gamma \omega$	$(6.8 \pm 0.8) \times 10^{-5}$	
Γ_{99}	$\gamma \phi$	$(2.4 \pm 0.5) \times 10^{-5}$	
Γ_{100}	$\gamma \gamma$	$< 6.3 \times 10^{-6}$	CL=90%
Γ_{101}	$e^+ e^- J/\psi(1S)$	$(3.46 \pm 0.24) \times 10^{-3}$	
Γ_{102}	$\mu^+ \mu^- J/\psi(1S)$	$(2.33 \pm 0.29) \times 10^{-4}$	

CONSTRAINED FIT INFORMATION

A multiparticle fit to $\chi_{c1}(1P)$, $\chi_{c0}(1P)$, $\chi_{c2}(1P)$, and $\psi(2S)$ with 4 total widths, a partial width, 25 combinations of partial widths obtained from integrated cross section, and 86 branching ratios uses 253 measurements to determine 49 parameters. The overall fit has a $\chi^2 = 389.6$ for 204 degrees of freedom.

The following *off-diagonal* array elements are the correlation coefficients $\langle \delta p_i \delta p_j \rangle / (\delta p_i \delta p_j)$, in percent, from the fit to parameters p_i , including the branching fractions, $x_i \equiv \Gamma_i / \Gamma_{\text{total}}$.

x_{48}	4				
x_{58}	-1	0			
x_{71}	12	5	-1		
x_{96}	20	9	-25	23	
Γ	-9	-4	-60	-11	-31
	x_{19}	x_{48}	x_{58}	x_{71}	x_{96}

$\chi_{c1}(1P)$ PARTIAL WIDTHS

$\Gamma(e^+ e^-)$					Γ_2
VALUE (eV)	EVTS	DOCUMENT ID	TECN	COMMENT	
0.12 ± 0.13	250	1 ABLIKIM	22AF BES3	$e^+ e^- \rightarrow \chi_{c1} \rightarrow \gamma J/\psi$	
-0.08					

¹ Assuming $\Gamma(\chi_{c1} \rightarrow \gamma J/\psi) = 0.28$ MeV.

$\chi_{c1}(1P) \Gamma(i) \Gamma(\gamma J/\psi(1S)) / \Gamma(\text{total})$

$\Gamma(\rho \bar{\rho}) \times \Gamma(\gamma J/\psi(1S)) / \Gamma_{\text{total}}$				$\Gamma_{58} \Gamma_{96} / \Gamma$
VALUE (eV)	DOCUMENT ID	TECN	COMMENT	
21.9 ± 0.8 OUR FIT				
21.4 ± 0.9 OUR AVERAGE				
21.5 ± 0.5 ± 0.8	1 ANDREOTTI 05A	E835	$\rho \bar{\rho} \rightarrow e^+ e^- \gamma$	
21.4 ± 1.5 ± 2.2	1,2 ARMSTRONG 92	E760	$\bar{p} p \rightarrow e^+ e^- \gamma$	
19.9 ^{+4.4} _{-4.0}	1 BAGLIN 86B	SPEC	$\bar{p} p \rightarrow e^+ e^- X$	

¹ Calculated by us using $B(J/\psi(1S) \rightarrow e^+ e^-) = 0.0593 \pm 0.0010$.

² Recalculated by ANDREOTTI 05A.

$\chi_{c1}(1P)$ BRANCHING RATIOS

HADRONIC DECAYS

$\Gamma(3(\pi^+ \pi^-)) / \Gamma_{\text{total}}$					Γ_3 / Γ
VALUE (units 10^{-3})	EVTS	DOCUMENT ID	TECN	COMMENT	
10.4 ± 1.6 OUR AVERAGE	Error includes scale factor of 4.6.				
10.92 ± 0.23 ± 0.30	84K	1 ABLIKIM	22Q BES3	$\psi(2S) \rightarrow \gamma 3(\pi^+ \pi^-)$	
5.4 ± 0.7 ± 0.9		2 BAI	99B BES	$\psi(2S) \rightarrow \gamma \chi_{c1}$	
16.0 ± 5.9 ± 0.8		2 TANENBAUM 78	MRK1	$\psi(2S) \rightarrow \gamma \chi_{c1}$	

¹ ABLIKIM 22Q reports $(1.092 \pm 0.004 \pm 0.035) \times 10^{-2}$ from a measurement of $[\Gamma(\chi_{c1}(1P) \rightarrow 3(\pi^+ \pi^-)) / \Gamma_{\text{total}}] \times [B(\psi(2S) \rightarrow \gamma \chi_{c1}(1P))]$ assuming $B(\psi(2S) \rightarrow \gamma \chi_{c1}(1P)) = (9.75 \pm 0.24) \times 10^{-2}$, which we rescale to our best value $B(\psi(2S) \rightarrow \gamma \chi_{c1}(1P)) = (9.75 \pm 0.27) \times 10^{-2}$. Our first error is their experiment's error and our second error is the systematic error from using our best value.

² Rescaled by us using $B(\psi(2S) \rightarrow \gamma \chi_{c1}) = (8.8 \pm 0.4)\%$ and $B(\psi(2S) \rightarrow J/\psi(1S) \pi^+ \pi^-) = (32.6 \pm 0.5)\%$.

$\Gamma(2\pi^+\pi^-)/\Gamma_{\text{total}}$ Γ_4/Γ

VALUE (units 10^{-3})	DOCUMENT ID	TECN	COMMENT
7.6±2.6 OUR EVALUATION	Treating systematic error as correlated.		
8 ±4 OUR AVERAGE	Error includes scale factor of 1.5.		
4.6±2.1±2.6	¹ BAI	99B	BES $\psi(2S) \rightarrow \gamma\chi_{c1}$
12.5±4.2±0.6	¹ TANENBAUM	78	MRK1 $\psi(2S) \rightarrow \gamma\chi_{c1}$
¹ Rescaled by us using $B(\psi(2S) \rightarrow \gamma\chi_{c1}) = (8.8 \pm 0.4)\%$ and $B(\psi(2S) \rightarrow J/\psi(1S)\pi^+\pi^-) = (32.6 \pm 0.5)\%$.			

 $\Gamma(\pi^+\pi^-\pi^0\pi^0)/\Gamma_{\text{total}}$ Γ_5/Γ

VALUE (%)	EVTS	DOCUMENT ID	TECN	COMMENT
1.19±0.15±0.03	604.7	¹ HE	08B	CLEO $e^+e^- \rightarrow \gamma h^+ h^- h^0 h^0$
¹ HE 08B reports $1.28 \pm 0.06 \pm 0.15 \pm 0.08\%$ from a measurement of $[\Gamma(\chi_{c1}(1P) \rightarrow \pi^+\pi^-\pi^0\pi^0)/\Gamma_{\text{total}}] \times [B(\psi(2S) \rightarrow \gamma\chi_{c1}(1P))]$ assuming $B(\psi(2S) \rightarrow \gamma\chi_{c1}(1P)) = (9.07 \pm 0.11 \pm 0.54) \times 10^{-2}$, which we rescale to our best value $B(\psi(2S) \rightarrow \gamma\chi_{c1}(1P)) = (9.75 \pm 0.27) \times 10^{-2}$. Our first error is their experiment's error and our second error is the systematic error from using our best value.				

 $\Gamma(\rho^+\pi^-\pi^0 + c.c.)/\Gamma_{\text{total}}$ Γ_6/Γ

VALUE (%)	EVTS	DOCUMENT ID	TECN	COMMENT
1.45±0.24±0.04	712.3	^{1,2} HE	08B	CLEO $e^+e^- \rightarrow \gamma h^+ h^- h^0 h^0$
¹ HE 08B reports $1.56 \pm 0.13 \pm 0.22 \pm 0.10\%$ from a measurement of $[\Gamma(\chi_{c1}(1P) \rightarrow \rho^+\pi^-\pi^0 + c.c.)/\Gamma_{\text{total}}] \times [B(\psi(2S) \rightarrow \gamma\chi_{c1}(1P))]$ assuming $B(\psi(2S) \rightarrow \gamma\chi_{c1}(1P)) = (9.07 \pm 0.11 \pm 0.54) \times 10^{-2}$, which we rescale to our best value $B(\psi(2S) \rightarrow \gamma\chi_{c1}(1P)) = (9.75 \pm 0.27) \times 10^{-2}$. Our first error is their experiment's error and our second error is the systematic error from using our best value.				
² Calculated by us. We have added the values from HE 08B for $\rho^+\pi^-\pi^0$ and $\rho^-\pi^+\pi^0$ decays assuming uncorrelated statistical and fully correlated systematic uncertainties.				

 $\Gamma(\rho^0\pi^+\pi^-)/\Gamma_{\text{total}}$ Γ_7/Γ

VALUE (units 10^{-3})	DOCUMENT ID	TECN	COMMENT
3.9±3.5	¹ TANENBAUM	78	MRK1 $\psi(2S) \rightarrow \gamma\chi_{c1}$
¹ Estimated using $B(\psi(2S) \rightarrow \gamma\chi_{c1}(1P)) = 0.087$. The errors do not contain the uncertainty in the $\psi(2S)$ decay.			

 $\Gamma(4\pi^0)/\Gamma_{\text{total}}$ Γ_8/Γ

VALUE (units 10^{-4})	EVTS	DOCUMENT ID	TECN	COMMENT
5.4±0.8±0.1	608	¹ ABLIKIM	11A	BES3 $e^+e^- \rightarrow \psi(2S) \rightarrow \gamma\chi_{c1}$
¹ ABLIKIM 11A reports $(0.57 \pm 0.03 \pm 0.08) \times 10^{-3}$ from a measurement of $[\Gamma(\chi_{c1}(1P) \rightarrow 4\pi^0)/\Gamma_{\text{total}}] \times [B(\psi(2S) \rightarrow \gamma\chi_{c1}(1P))]$ assuming $B(\psi(2S) \rightarrow \gamma\chi_{c1}(1P)) = (9.2 \pm 0.4) \times 10^{-2}$, which we rescale to our best value $B(\psi(2S) \rightarrow \gamma\chi_{c1}(1P)) = (9.75 \pm 0.27) \times 10^{-2}$. Our first error is their experiment's error and our second error is the systematic error from using our best value.				

 $\Gamma(\pi^+\pi^-K^+K^-)/\Gamma_{\text{total}}$ Γ_9/Γ

VALUE (units 10^{-3})	DOCUMENT ID	TECN	COMMENT
4.5±1.0 OUR EVALUATION	Treating systematic error as correlated.		
4.5±0.9 OUR AVERAGE			
4.2±0.4±0.9	¹ BAI	99B	BES $\psi(2S) \rightarrow \gamma\chi_{c1}$
7.3±3.0±0.4	¹ TANENBAUM	78	MRK1 $\psi(2S) \rightarrow \gamma\chi_{c1}$
¹ Rescaled by us using $B(\psi(2S) \rightarrow \gamma\chi_{c1}) = (8.8 \pm 0.4)\%$ and $B(\psi(2S) \rightarrow J/\psi(1S)\pi^+\pi^-) = (32.6 \pm 0.5)\%$.			

 $\Gamma(K^+K^-\pi^0\pi^0)/\Gamma_{\text{total}}$ Γ_{10}/Γ

VALUE (units 10^{-3})	EVTS	DOCUMENT ID	TECN	COMMENT
1.12±0.27±0.03	45.1	¹ HE	08B	CLEO $e^+e^- \rightarrow \gamma h^+ h^- h^0 h^0$
¹ HE 08B reports $(0.12 \pm 0.02 \pm 0.02 \pm 0.01) \times 10^{-2}$ from a measurement of $[\Gamma(\chi_{c1}(1P) \rightarrow K^+K^-\pi^0\pi^0)/\Gamma_{\text{total}}] \times [B(\psi(2S) \rightarrow \gamma\chi_{c1}(1P))]$ assuming $B(\psi(2S) \rightarrow \gamma\chi_{c1}(1P)) = (9.07 \pm 0.11 \pm 0.54) \times 10^{-2}$, which we rescale to our best value $B(\psi(2S) \rightarrow \gamma\chi_{c1}(1P)) = (9.75 \pm 0.27) \times 10^{-2}$. Our first error is their experiment's error and our second error is the systematic error from using our best value.				

 $\Gamma(K^+K^-\pi^+\pi^-)/\Gamma_{\text{total}}$ Γ_{11}/Γ

VALUE (units 10^{-3})	EVTS	DOCUMENT ID	TECN	COMMENT
11.46±0.12±1.29	12k	¹ ABLIKIM	13B	BES3 $e^+e^- \rightarrow \psi(2S) \rightarrow \gamma\chi_{c1}$
¹ Using 1.06×10^8 $\psi(2S)$ mesons and $B(\psi(2S) \rightarrow \chi_{c1}\gamma) = (9.2 \pm 0.4)\%$.				

 $\Gamma(K_S^0 K_S^0 \pi^+\pi^-)/\Gamma_{\text{total}}$ Γ_{12}/Γ

VALUE (units 10^{-3})	EVTS	DOCUMENT ID	TECN	COMMENT
7.52±0.11±0.79	5.1k	¹ ABLIKIM	13B	BES3 $e^+e^- \rightarrow \psi(2S) \rightarrow \gamma\chi_{c1}$
¹ Using 1.06×10^8 $\psi(2S)$ mesons and $B(\psi(2S) \rightarrow \chi_{c1}\gamma) = (9.2 \pm 0.4)\%$.				

 $\Gamma(K^+\pi^-\bar{K}^0\pi^0 + c.c.)/\Gamma_{\text{total}}$ Γ_{13}/Γ

VALUE (%)	EVTS	DOCUMENT ID	TECN	COMMENT
0.86±0.13±0.02	141.3	¹ HE	08B	CLEO $e^+e^- \rightarrow \gamma h^+ h^- h^0 h^0$
¹ HE 08B reports $0.92 \pm 0.09 \pm 0.11 \pm 0.06\%$ from a measurement of $[\Gamma(\chi_{c1}(1P) \rightarrow K^+\pi^-\bar{K}^0\pi^0 + c.c.)/\Gamma_{\text{total}}] \times [B(\psi(2S) \rightarrow \gamma\chi_{c1}(1P))]$ assuming $B(\psi(2S) \rightarrow \gamma\chi_{c1}(1P)) = (9.07 \pm 0.11 \pm 0.54) \times 10^{-2}$, which we rescale to our best value $B(\psi(2S) \rightarrow \gamma\chi_{c1}(1P)) = (9.75 \pm 0.27) \times 10^{-2}$. Our first error is their experiment's error and our second error is the systematic error from using our best value.				

 $\Gamma(\rho^-K^+\bar{K}^0 + c.c.)/\Gamma_{\text{total}}$ Γ_{14}/Γ

VALUE (%)	EVTS	DOCUMENT ID	TECN	COMMENT
0.50±0.12±0.01	141.3	¹ HE	08B	CLEO $e^+e^- \rightarrow \gamma h^+ h^- h^0 h^0$
¹ HE 08B reports $0.54 \pm 0.11 \pm 0.07 \pm 0.03\%$ from a measurement of $[\Gamma(\chi_{c1}(1P) \rightarrow \rho^-K^+\bar{K}^0 + c.c.)/\Gamma_{\text{total}}] \times [B(\psi(2S) \rightarrow \gamma\chi_{c1}(1P))]$ assuming $B(\psi(2S) \rightarrow \gamma\chi_{c1}(1P)) = (9.07 \pm 0.11 \pm 0.54) \times 10^{-2}$, which we rescale to our best value $B(\psi(2S) \rightarrow \gamma\chi_{c1}(1P)) = (9.75 \pm 0.27) \times 10^{-2}$. Our first error is their experiment's error and our second error is the systematic error from using our best value.				

 $\Gamma(K^*(892)^0\bar{K}^0\pi^0 \rightarrow K^+\pi^-\bar{K}^0\pi^0 + c.c.)/\Gamma_{\text{total}}$ Γ_{15}/Γ

VALUE (%)	EVTS	DOCUMENT ID	TECN	COMMENT
0.23±0.06±0.01	141.3	¹ HE	08B	CLEO $e^+e^- \rightarrow \gamma h^+ h^- h^0 h^0$
¹ HE 08B reports $0.25 \pm 0.06 \pm 0.03 \pm 0.02\%$ from a measurement of $[\Gamma(\chi_{c1}(1P) \rightarrow K^*(892)^0\bar{K}^0\pi^0 \rightarrow K^+\pi^-\bar{K}^0\pi^0 + c.c.)/\Gamma_{\text{total}}] \times [B(\psi(2S) \rightarrow \gamma\chi_{c1}(1P))]$ assuming $B(\psi(2S) \rightarrow \gamma\chi_{c1}(1P)) = (9.07 \pm 0.11 \pm 0.54) \times 10^{-2}$, which we rescale to our best value $B(\psi(2S) \rightarrow \gamma\chi_{c1}(1P)) = (9.75 \pm 0.27) \times 10^{-2}$. Our first error is their experiment's error and our second error is the systematic error from using our best value.				

 $\Gamma(K^+K^-\eta\pi^0)/\Gamma_{\text{total}}$ Γ_{16}/Γ

VALUE (%)	EVTS	DOCUMENT ID	TECN	COMMENT
0.112±0.034±0.003	141.3	¹ HE	08B	CLEO $e^+e^- \rightarrow \gamma h^+ h^- h^0 h^0$
¹ HE 08B reports $0.12 \pm 0.03 \pm 0.02 \pm 0.01\%$ from a measurement of $[\Gamma(\chi_{c1}(1P) \rightarrow K^+K^-\eta\pi^0)/\Gamma_{\text{total}}] \times [B(\psi(2S) \rightarrow \gamma\chi_{c1}(1P))]$ assuming $B(\psi(2S) \rightarrow \gamma\chi_{c1}(1P)) = (9.07 \pm 0.11 \pm 0.54) \times 10^{-2}$, which we rescale to our best value $B(\psi(2S) \rightarrow \gamma\chi_{c1}(1P)) = (9.75 \pm 0.27) \times 10^{-2}$. Our first error is their experiment's error and our second error is the systematic error from using our best value.				

 $\Gamma(\pi^+\pi^-K_S^0K_S^0)/\Gamma_{\text{total}}$ Γ_{17}/Γ

VALUE (units 10^{-4})	EVTS	DOCUMENT ID	TECN	COMMENT
6.9±2.9±0.2	19.8±7.7	¹ ABLIKIM	05o	BES2 $\psi(2S) \rightarrow \chi_{c1}\gamma$
¹ ABLIKIM 05o reports $[\Gamma(\chi_{c1}(1P) \rightarrow \pi^+\pi^-K_S^0K_S^0)/\Gamma_{\text{total}}] \times [B(\psi(2S) \rightarrow \gamma\chi_{c1}(1P))]$ assuming $B(\psi(2S) \rightarrow \gamma\chi_{c1}(1P)) = (9.75 \pm 0.27) \times 10^{-2}$. Our first error is their experiment's error and our second error is the systematic error from using our best value.				

 $\Gamma(K^+K^-\eta)/\Gamma_{\text{total}}$ Γ_{18}/Γ

VALUE (units 10^{-4})	DOCUMENT ID	TECN	COMMENT
3.2±1.0±0.1	¹ ATHAR	07	CLEO $\psi(2S) \rightarrow \gamma h^+ h^- h^0$
¹ ATHAR 07 reports $(0.34 \pm 0.10 \pm 0.04) \times 10^{-3}$ from a measurement of $[\Gamma(\chi_{c1}(1P) \rightarrow K^+K^-\eta)/\Gamma_{\text{total}}] \times [B(\psi(2S) \rightarrow \gamma\chi_{c1}(1P))]$ assuming $B(\psi(2S) \rightarrow \gamma\chi_{c1}(1P)) = 0.0907 \pm 0.0011 \pm 0.0054$, which we rescale to our best value $B(\psi(2S) \rightarrow \gamma\chi_{c1}(1P)) = (9.75 \pm 0.27) \times 10^{-2}$. Our first error is their experiment's error and our second error is the systematic error from using our best value.			

 $\Gamma(K^*(892)^0\bar{K}^0 + c.c.)/\Gamma_{\text{total}}$ Γ_{20}/Γ

VALUE (units 10^{-3})	EVTS	DOCUMENT ID	TECN	COMMENT
1.03±0.15 OUR AVERAGE				
1.04±0.13±0.10	262	¹ AAIJ	23AH	LHCb $B^+ \rightarrow K^+(K_S^0 K\pi)$
0.98±0.37±0.03	22	² ABLIKIM	06R	BES2 $\psi(2S) \rightarrow \gamma\chi_{c1}$
¹ AAIJ 23AH reports $(1.04 \pm 0.13 \pm 0.04 \pm 0.09) \times 10^{-3}$ from a measurement of $[\Gamma(\chi_{c1}(1P) \rightarrow K^*(892)^0\bar{K}^0 + c.c.)/\Gamma_{\text{total}}] \times [B(\chi_{c1}(1P) \rightarrow \bar{K}^0 K^+\pi^- + c.c.)]$ assuming $B(\chi_{c1}(1P) \rightarrow \bar{K}^0 K^+\pi^- + c.c.) = (7.0 \pm 0.6) \times 10^{-3}$.				
² ABLIKIM 06R reports $(1.1 \pm 0.4 \pm 0.1) \times 10^{-3}$ from a measurement of $[\Gamma(\chi_{c1}(1P) \rightarrow K^*(892)^0\bar{K}^0 + c.c.)/\Gamma_{\text{total}}] \times [B(\psi(2S) \rightarrow \gamma\chi_{c1}(1P))]$ assuming $B(\psi(2S) \rightarrow \gamma\chi_{c1}(1P)) = (8.7 \pm 0.4) \times 10^{-2}$, which we rescale to our best value $B(\psi(2S) \rightarrow \gamma\chi_{c1}(1P)) = (9.75 \pm 0.27) \times 10^{-2}$. Our first error is their experiment's error and our second error is the systematic error from using our best value.				

 $\Gamma(K^*(892)^+K^- + c.c.)/\Gamma_{\text{total}}$ Γ_{21}/Γ

VALUE (units 10^{-3})	EVTS	DOCUMENT ID	TECN	COMMENT
1.21±0.23 OUR AVERAGE				
1.18±0.17±0.17	288	¹ AAIJ	23AH	LHCb $B^+ \rightarrow K^+(K_S^0 K\pi)$
1.43±0.65±0.04	27	² ABLIKIM	06R	BES2 $\psi(2S) \rightarrow \gamma\chi_{c1}$
¹ AAIJ 23AH reports $(1.18 \pm 0.17 \pm 0.14 \pm 0.10) \times 10^{-3}$ from a measurement of $[\Gamma(\chi_{c1}(1P) \rightarrow K^*(892)^+K^- + c.c.)/\Gamma_{\text{total}}] \times [B(\chi_{c1}(1P) \rightarrow \bar{K}^0 K^+\pi^- + c.c.)]$ assuming $B(\chi_{c1}(1P) \rightarrow \bar{K}^0 K^+\pi^- + c.c.) = (7.0 \pm 0.6) \times 10^{-3}$.				
² ABLIKIM 06R reports $(1.6 \pm 0.7 \pm 0.2) \times 10^{-3}$ from a measurement of $[\Gamma(\chi_{c1}(1P) \rightarrow K^*(892)^+K^- + c.c.)/\Gamma_{\text{total}}] \times [B(\psi(2S) \rightarrow \gamma\chi_{c1}(1P))]$ assuming $B(\psi(2S) \rightarrow \gamma\chi_{c1}(1P)) = (8.7 \pm 0.4) \times 10^{-2}$, which we rescale to our best value $B(\psi(2S) \rightarrow \gamma\chi_{c1}(1P)) = (9.75 \pm 0.27) \times 10^{-2}$. Our first error is their experiment's error and our second error is the systematic error from using our best value.				

 $\Gamma(K_S^0(1430)^0\bar{K}^0 + c.c. \rightarrow K_S^0 K^+\pi^- + c.c.)/\Gamma_{\text{total}}$ Γ_{22}/Γ

VALUE	CL%	DOCUMENT ID	TECN	COMMENT
<8 × 10⁻⁴	90	¹ ABLIKIM	06R	BES2 $\psi(2S) \rightarrow \gamma\chi_{c1}$
¹ ABLIKIM 06R reports $< 0.9 \times 10^{-3}$ from a measurement of $[\Gamma(\chi_{c1}(1P) \rightarrow K_S^0(1430)^0\bar{K}^0 + c.c. \rightarrow K_S^0 K^+\pi^- + c.c.)/\Gamma_{\text{total}}] \times [B(\psi(2S) \rightarrow \gamma\chi_{c1}(1P))]$ assuming $B(\psi(2S) \rightarrow \gamma\chi_{c1}(1P)) = (8.7 \pm 0.4) \times 10^{-2}$, which we rescale to our best value $B(\psi(2S) \rightarrow \gamma\chi_{c1}(1P)) = 9.75 \times 10^{-2}$.				

See key on page 1171

Meson Particle Listings

$\chi_{c1}(1P)$

$\Gamma(K_S^0(1430)^+ K^- + c.c.)/\Gamma_{total}$ Γ_{41}/Γ

VALUE (units 10^{-3})	EVTS	DOCUMENT ID	TECN	COMMENT
1.61 ± 0.19 ± 0.24	351	¹ AAIJ	23AH LHCB	$B^+ \rightarrow K^+(K_S^0 K\pi)$

¹AAIJ 23AH reports $(1.61 \pm 0.19 \pm 0.19 \pm 0.14) \times 10^{-3}$ from a measurement of $[\Gamma(\chi_{c1}(1P) \rightarrow K_S^0(1430)^+ K^- + c.c.)/\Gamma_{total}] \times [B(\chi_{c1}(1P) \rightarrow \bar{K}^0 K^+ \pi^- + c.c.)]$ assuming $B(\chi_{c1}(1P) \rightarrow \bar{K}^0 K^+ \pi^- + c.c.) = (7.0 \pm 0.6) \times 10^{-3}$.

$\Gamma(K_S^0(1430)\bar{K}^0 + c.c.)/\Gamma_{total}$ Γ_{42}/Γ

VALUE (units 10^{-3})	EVTS	DOCUMENT ID	TECN	COMMENT
1.17 ± 0.16 ± 0.11	278	¹ AAIJ	23AH LHCB	$B^+ \rightarrow K^+(K_S^0 K\pi)$

¹AAIJ 23AH reports $(1.17 \pm 0.16 \pm 0.05 \pm 0.10) \times 10^{-3}$ from a measurement of $[\Gamma(\chi_{c1}(1P) \rightarrow K_S^0(1430)\bar{K}^0 + c.c.)/\Gamma_{total}] \times [B(\chi_{c1}(1P) \rightarrow \bar{K}^0 K^+ \pi^- + c.c.)]$ assuming $B(\chi_{c1}(1P) \rightarrow \bar{K}^0 K^+ \pi^- + c.c.) = (7.0 \pm 0.6) \times 10^{-3}$.

$\Gamma(K_S^0(1430)^+ K^- + c.c.)/\Gamma_{total}$ Γ_{37}/Γ

VALUE (units 10^{-4})	DOCUMENT ID	TECN	COMMENT
6.41 ± 0.57 + 2.09 - 2.71	¹ ABLIKIM 14J BES3		$\psi(2S) \rightarrow \gamma K^+ K^- \eta'(958)$

¹Normalized to $B(\chi_{c1} \rightarrow K^+ K^- \eta'(958))$ branching fraction.

$\Gamma(f_0(980)\eta'(958))/\Gamma_{total}$ Γ_{38}/Γ

VALUE (units 10^{-4})	DOCUMENT ID	TECN	COMMENT
1.65 ± 0.47 + 1.32 - 0.56	¹ ABLIKIM 14J BES3		$\psi(2S) \rightarrow \gamma K^+ K^- \eta'(958)$

¹Normalized to $B(\chi_{c1} \rightarrow K^+ K^- \eta'(958))$ branching fraction.

$\Gamma(f_0(1710)\eta'(958))/\Gamma_{total}$ Γ_{39}/Γ

VALUE (units 10^{-4})	DOCUMENT ID	TECN	COMMENT
0.71 ± 0.22 + 0.68 - 0.48	¹ ABLIKIM 14J BES3		$\psi(2S) \rightarrow \gamma K^+ K^- \eta'(958)$

¹Normalized to $B(\chi_{c1} \rightarrow K^+ K^- \eta'(958))$ branching fraction.

$\Gamma(f_2'(1525)\eta'(958))/\Gamma_{total}$ Γ_{40}/Γ

VALUE (units 10^{-4})	DOCUMENT ID	TECN	COMMENT
0.92 ± 0.23 + 0.55 - 0.51	¹ ABLIKIM 14J BES3		$\psi(2S) \rightarrow \gamma K^+ K^- \eta'(958)$

¹Normalized to $B(\chi_{c1} \rightarrow K^+ K^- \eta'(958))$ branching fraction.

$\Gamma(\pi^0 f_0(980) \rightarrow \pi^0 \pi^+ \pi^-)/\Gamma_{total}$ Γ_{43}/Γ

VALUE (units 10^{-6})	CL%	DOCUMENT ID	TECN	COMMENT
0.35 ± 0.09		ABLIKIM 18D BES3		$\psi(2S) \rightarrow \gamma \pi^0 \pi^+ \pi^-$
<6	90	¹ ABLIKIM 11D BES3		$\psi(2S) \rightarrow \gamma \pi^0 \pi^+ \pi^-$

¹ABLIKIM 11D reports $[\Gamma(\chi_{c1}(1P) \rightarrow \pi^0 f_0(980) \rightarrow \pi^0 \pi^+ \pi^-)/\Gamma_{total}] \times [B(\psi(2S) \rightarrow \gamma \chi_{c1}(1P))] < 6.0 \times 10^{-7}$ which we divide by our best value $B(\psi(2S) \rightarrow \gamma \chi_{c1}(1P)) = 9.75 \times 10^{-2}$.

$\Gamma(K^+ \bar{K}^*(892)^0 \pi^- + c.c.)/\Gamma_{total}$ Γ_{44}/Γ

VALUE (units 10^{-4})	DOCUMENT ID	TECN	COMMENT
32 ± 21	¹ TANENBAUM 78	MRK1	$\psi(2S) \rightarrow \gamma \chi_{c1}$

¹Estimated using $B(\psi(2S) \rightarrow \gamma \chi_{c1}(1P)) = 0.087$. The errors do not contain the uncertainty in the $\psi(2S)$ decay.

$\Gamma(K^*(892)^0 \bar{K}^*(892)^0)/\Gamma_{total}$ Γ_{45}/Γ

VALUE (units 10^{-3})	EVTS	DOCUMENT ID	TECN	COMMENT
1.44 ± 0.36 ± 0.04	28.4 ± 5.5	^{1,2} ABLIKIM 04H BES		$\psi(2S) \rightarrow \gamma K^+ K^- \pi^+ \pi^-$

¹ABLIKIM 04H reports $[\Gamma(\chi_{c1}(1P) \rightarrow K^*(892)^0 \bar{K}^*(892)^0)/\Gamma_{total}] \times [B(\psi(2S) \rightarrow \gamma \chi_{c1}(1P))] = (1.40 \pm 0.27 \pm 0.22) \times 10^{-4}$ which we divide by our best value $B(\psi(2S) \rightarrow \gamma \chi_{c1}(1P)) = (9.75 \pm 0.27) \times 10^{-2}$. Our first error is their experiment's error and our second error is the systematic error from using our best value.

²Assumes $B(K^*(892)^0 \rightarrow K^- \pi^+) = 2/3$.

$\Gamma(K^+ K^- K_S^0 K_S^0)/\Gamma_{total}$ Γ_{46}/Γ

VALUE	CL%	EVTS	DOCUMENT ID	TECN	COMMENT
<4 × 10⁻⁴	90	3.2 ± 2.4	¹ ABLIKIM 05o BES2		$\psi(2S) \rightarrow \chi_{c1} \gamma$

¹ABLIKIM 05o reports $[\Gamma(\chi_{c1}(1P) \rightarrow K^+ K^- K_S^0 K_S^0)/\Gamma_{total}] \times [B(\psi(2S) \rightarrow \gamma \chi_{c1}(1P))] < 4.2 \times 10^{-5}$ which we divide by our best value $B(\psi(2S) \rightarrow \gamma \chi_{c1}(1P)) = 9.75 \times 10^{-2}$.

$\Gamma(K_S^0 K_S^0 K_S^0 K_S^0)/\Gamma_{total}$ Γ_{47}/Γ

VALUE (units 10^{-4})	EVTS	DOCUMENT ID	TECN	COMMENT
0.35 ± 0.10 ± 0.01	22	¹ ABLIKIM 19AA BES3		$\psi(2S) \rightarrow \gamma 4K_S^0$

¹Using $B(K_S^0 \rightarrow \pi^+ \pi^-) = (69.20 \pm 0.05)\%$. ABLIKIM 19AA reports $[\Gamma(\chi_{c1}(1P) \rightarrow K_S^0 K_S^0 K_S^0 K_S^0)/\Gamma_{total}] \times [B(\psi(2S) \rightarrow \gamma \chi_{c1}(1P))] = (3.4 \pm 0.9 \pm 0.3) \times 10^{-6}$ which we divide by our best value $B(\psi(2S) \rightarrow \gamma \chi_{c1}(1P)) = (9.75 \pm 0.27) \times 10^{-2}$. Our first error is their experiment's error and our second error is the systematic error from using our best value.

$\Gamma(K^+ K^- \phi)/\Gamma_{total}$ Γ_{49}/Γ

VALUE (units 10^{-3})	EVTS	DOCUMENT ID	TECN	COMMENT
0.41 ± 0.15 ± 0.01	17	¹ ABLIKIM 06T BES2		$\psi(2S) \rightarrow \gamma 2K^+ 2K^-$

¹ABLIKIM 06T reports $(0.46 \pm 0.16 \pm 0.06) \times 10^{-3}$ from a measurement of $[\Gamma(\chi_{c1}(1P) \rightarrow K^+ K^- \phi)/\Gamma_{total}] \times [B(\psi(2S) \rightarrow \gamma \chi_{c1}(1P))]$ assuming $B(\psi(2S) \rightarrow \gamma \chi_{c1}(1P)) = (8.7 \pm 0.4) \times 10^{-2}$, which we rescale to our best value $B(\psi(2S) \rightarrow \gamma \chi_{c1}(1P)) = (9.75 \pm 0.27) \times 10^{-2}$. Our first error is their experiment's error and our second error is the systematic error from using our best value.

$\Gamma(\bar{K}^0 K^+ \pi^- \phi + c.c.)/\Gamma_{total}$ Γ_{50}/Γ

VALUE (units 10^{-3})	DOCUMENT ID	TECN	COMMENT
3.27 ± 0.28 ± 0.46	ABLIKIM 15M BES3		$\psi(2S) \rightarrow \gamma \chi_{c1}$

$\Gamma(K^+ K^- \pi^0 \phi)/\Gamma_{total}$ Γ_{51}/Γ

VALUE (units 10^{-3})	DOCUMENT ID	TECN	COMMENT
1.62 ± 0.12 ± 0.28	ABLIKIM 15M BES3		$\psi(2S) \rightarrow \gamma \chi_{c1}$

$\Gamma(\phi \pi^+ \pi^- \pi^0)/\Gamma_{total}$ Γ_{52}/Γ

VALUE (units 10^{-3})	EVTS	DOCUMENT ID	TECN	COMMENT
0.75 ± 0.06 ± 0.08	373	¹ ABLIKIM 13B BES3		$e^+ e^- \rightarrow \psi(2S) \rightarrow \gamma \chi_{c1}$

¹Using $1.06 \times 10^8 \psi(2S)$ mesons and $B(\psi(2S) \rightarrow \chi_{c1} \gamma) = (9.2 \pm 0.4)\%$.

$\Gamma(\omega\omega)/\Gamma_{total}$ Γ_{53}/Γ

VALUE (units 10^{-4})	EVTS	DOCUMENT ID	TECN	COMMENT
5.7 ± 0.7 ± 0.2	597	¹ ABLIKIM 11K BES3		$\psi(2S) \rightarrow \gamma$ hadrons

¹ABLIKIM 11K reports $(6.0 \pm 0.3 \pm 0.7) \times 10^{-4}$ from a measurement of $[\Gamma(\chi_{c1}(1P) \rightarrow \omega\omega)/\Gamma_{total}] \times [B(\psi(2S) \rightarrow \gamma \chi_{c1}(1P))]$ assuming $B(\psi(2S) \rightarrow \gamma \chi_{c1}(1P)) = (9.2 \pm 0.4) \times 10^{-2}$, which we rescale to our best value $B(\psi(2S) \rightarrow \gamma \chi_{c1}(1P)) = (9.75 \pm 0.27) \times 10^{-2}$. Our first error is their experiment's error and our second error is the systematic error from using our best value.

$\Gamma(\omega K^+ K^-)/\Gamma_{total}$ Γ_{54}/Γ

VALUE (units 10^{-3})	EVTS	DOCUMENT ID	TECN	COMMENT
0.78 ± 0.04 ± 0.08	628	¹ ABLIKIM 13B BES3		$e^+ e^- \rightarrow \psi(2S) \rightarrow \gamma \chi_{c1}$

¹Using $1.06 \times 10^8 \psi(2S)$ mesons and $B(\psi(2S) \rightarrow \chi_{c1} \gamma) = (9.2 \pm 0.4)\%$.

$\Gamma(\omega\phi)/\Gamma_{total}$ Γ_{55}/Γ

VALUE (units 10^{-4})	EVTS	DOCUMENT ID	TECN	COMMENT
0.27 ± 0.04 ± 0.01	105	¹ ABLIKIM 19J BES3		$\psi(2S) \rightarrow \gamma$ hadrons

• • • We do not use the following data for averages, fits, limits, etc. • • •

0.21 ± 0.06 ± 0.01	15	^{2,3} ABLIKIM 11K BES3		$\psi(2S) \rightarrow \gamma$ hadrons
--------------------	----	---------------------------------	--	---------------------------------------

¹ABLIKIM 19J reports $[\Gamma(\chi_{c1}(1P) \rightarrow \omega\phi)/\Gamma_{total}] \times [B(\psi(2S) \rightarrow \gamma \chi_{c1}(1P))] = (2.67 \pm 0.31 \pm 0.27) \times 10^{-6}$ which we divide by our best value $B(\psi(2S) \rightarrow \gamma \chi_{c1}(1P)) = (9.75 \pm 0.27) \times 10^{-2}$. Our first error is their experiment's error and our second error is the systematic error from using our best value.

²ABLIKIM 11K reports $(0.22 \pm 0.06 \pm 0.02) \times 10^{-4}$ from a measurement of $[\Gamma(\chi_{c1}(1P) \rightarrow \omega\phi)/\Gamma_{total}] \times [B(\psi(2S) \rightarrow \gamma \chi_{c1}(1P))]$ assuming $B(\psi(2S) \rightarrow \gamma \chi_{c1}(1P)) = (9.2 \pm 0.4) \times 10^{-2}$, which we rescale to our best value $B(\psi(2S) \rightarrow \gamma \chi_{c1}(1P)) = (9.75 \pm 0.27) \times 10^{-2}$. Our first error is their experiment's error and our second error is the systematic error from using our best value.

³Superseded by ABLIKIM 19J.

$\Gamma(\phi\phi)/\Gamma_{total}$ Γ_{56}/Γ

VALUE (units 10^{-4})	EVTS	DOCUMENT ID	TECN	COMMENT
4.26 ± 0.17 ± 0.12	1529	^{1,2} ABLIKIM 23N BES3		$\psi(2S) \rightarrow \gamma$ hadrons

• • • We do not use the following data for averages, fits, limits, etc. • • •

4.2 ± 0.5 ± 0.1	366	³ ABLIKIM 11K BES3		$\psi(2S) \rightarrow \gamma$ hadrons
-----------------	-----	-------------------------------	--	---------------------------------------

¹Using $B(\phi \rightarrow K^+ K^-) = (49.2 \pm 0.5) \times 10^{-2}$ from PDG 22.

²ABLIKIM 23N reports $(4.26 \pm 0.13 \pm 0.15) \times 10^{-4}$ from a measurement of $[\Gamma(\chi_{c1}(1P) \rightarrow \phi\phi)/\Gamma_{total}] \times [B(\psi(2S) \rightarrow \gamma \chi_{c1}(1P))]$ assuming $B(\psi(2S) \rightarrow \gamma \chi_{c1}(1P)) = (9.75 \pm 0.24) \times 10^{-2}$, which we rescale to our best value $B(\psi(2S) \rightarrow \gamma \chi_{c1}(1P)) = (9.75 \pm 0.27) \times 10^{-2}$. Our first error is their experiment's error and our second error is the systematic error from using our best value.

³ABLIKIM 11K reports $(4.4 \pm 0.3 \pm 0.5) \times 10^{-4}$ from a measurement of $[\Gamma(\chi_{c1}(1P) \rightarrow \phi\phi)/\Gamma_{total}] \times [B(\psi(2S) \rightarrow \gamma \chi_{c1}(1P))]$ assuming $B(\psi(2S) \rightarrow \gamma \chi_{c1}(1P)) = (9.2 \pm 0.4) \times 10^{-2}$, which we rescale to our best value $B(\psi(2S) \rightarrow \gamma \chi_{c1}(1P)) = (9.75 \pm 0.27) \times 10^{-2}$. Our first error is their experiment's error and our second error is the systematic error from using our best value.

$\Gamma(\phi\phi\eta)/\Gamma_{total}$ Γ_{57}/Γ

VALUE (units 10^{-4})	EVTS	DOCUMENT ID	TECN	COMMENT
3.0 ± 0.5 ± 0.1	83.6	¹ ABLIKIM 20B BES3		$\psi(2S) \rightarrow \gamma \phi\phi\eta$

¹ABLIKIM 20B reports $(2.96 \pm 0.43 \pm 0.22) \times 10^{-4}$ from a measurement of $[\Gamma(\chi_{c1}(1P) \rightarrow \phi\phi\eta)/\Gamma_{total}] \times [B(\psi(2S) \rightarrow \gamma \chi_{c1}(1P))]$ assuming $B(\psi(2S) \rightarrow \gamma \chi_{c1}(1P)) = (9.75 \pm 0.24) \times 10^{-2}$, which we rescale to our best value $B(\psi(2S) \rightarrow \gamma \chi_{c1}(1P)) = (9.75 \pm 0.27) \times 10^{-2}$. Our first error is their experiment's error and our second error is the systematic error from using our best value.

Meson Particle Listings

 $\chi_{c1}(1P)$ $\Gamma(p\bar{p}\pi^0)/\Gamma_{\text{total}}$ Γ_{59}/Γ

VALUE (units 10^{-3})	DOCUMENT ID	TECN	COMMENT
0.155 ± 0.018 OUR AVERAGE			
0.163 ± 0.019 ± 0.004	¹ ONYISI	10 CLE3	$\psi(2S) \rightarrow \gamma p\bar{p}X$
0.112 ± 0.047 ± 0.003	² ATHAR	07 CLEO	$\psi(2S) \rightarrow \gamma h^+ h^- h^0$
¹ ONYISI 10 reports $(1.75 \pm 0.16 \pm 0.13 \pm 0.11) \times 10^{-4}$ from a measurement of $[\Gamma(\chi_{c1}(1P) \rightarrow p\bar{p}\pi^0)/\Gamma_{\text{total}}] \times [B(\psi(2S) \rightarrow \gamma\chi_{c1}(1P))]$ assuming $B(\psi(2S) \rightarrow \gamma\chi_{c1}(1P)) = (9.07 \pm 0.11 \pm 0.54) \times 10^{-2}$, which we rescale to our best value $B(\psi(2S) \rightarrow \gamma\chi_{c1}(1P)) = (9.75 \pm 0.27) \times 10^{-2}$. Our first error is their experiment's error and our second error is the systematic error from using our best value.			
² ATHAR 07 reports $(1.2 \pm 0.5 \pm 0.1) \times 10^{-4}$ from a measurement of $[\Gamma(\chi_{c1}(1P) \rightarrow p\bar{p}\pi^0)/\Gamma_{\text{total}}] \times [B(\psi(2S) \rightarrow \gamma\chi_{c1}(1P))]$ assuming $B(\psi(2S) \rightarrow \gamma\chi_{c1}(1P)) = (9.07 \pm 0.11 \pm 0.54) \times 10^{-2}$, which we rescale to our best value $B(\psi(2S) \rightarrow \gamma\chi_{c1}(1P)) = (9.75 \pm 0.27) \times 10^{-2}$. Our first error is their experiment's error and our second error is the systematic error from using our best value.			

 $\Gamma(p\bar{p}\eta)/\Gamma_{\text{total}}$ Γ_{60}/Γ

VALUE (units 10^{-3})	CL%	DOCUMENT ID	TECN	COMMENT
0.145 ± 0.024 ± 0.004		¹ ONYISI	10 CLE3	$\psi(2S) \rightarrow \gamma p\bar{p}X$
< 0.15	90	² ATHAR	07 CLEO	$\psi(2S) \rightarrow \gamma h^+ h^- h^0$
¹ ONYISI 10 reports $(1.56 \pm 0.22 \pm 0.14 \pm 0.10) \times 10^{-4}$ from a measurement of $[\Gamma(\chi_{c1}(1P) \rightarrow p\bar{p}\eta)/\Gamma_{\text{total}}] \times [B(\psi(2S) \rightarrow \gamma\chi_{c1}(1P))]$ assuming $B(\psi(2S) \rightarrow \gamma\chi_{c1}(1P)) = (9.07 \pm 0.11 \pm 0.54) \times 10^{-2}$, which we rescale to our best value $B(\psi(2S) \rightarrow \gamma\chi_{c1}(1P)) = (9.75 \pm 0.27) \times 10^{-2}$. Our first error is their experiment's error and our second error is the systematic error from using our best value.				
² ATHAR 07 reports $< 0.16 \times 10^{-3}$ from a measurement of $[\Gamma(\chi_{c1}(1P) \rightarrow p\bar{p}\eta)/\Gamma_{\text{total}}] \times [B(\psi(2S) \rightarrow \gamma\chi_{c1}(1P))]$ assuming $B(\psi(2S) \rightarrow \gamma\chi_{c1}(1P)) = (9.07 \pm 0.11 \pm 0.54) \times 10^{-2}$, which we rescale to our best value $B(\psi(2S) \rightarrow \gamma\chi_{c1}(1P)) = 9.75 \times 10^{-2}$.				

 $\Gamma(p\bar{p}\omega)/\Gamma_{\text{total}}$ Γ_{61}/Γ

VALUE (units 10^{-3})	DOCUMENT ID	TECN	COMMENT
0.212 ± 0.030 ± 0.006	¹ ONYISI	10 CLE3	$\psi(2S) \rightarrow \gamma p\bar{p}X$
¹ ONYISI 10 reports $(2.28 \pm 0.28 \pm 0.16 \pm 0.14) \times 10^{-4}$ from a measurement of $[\Gamma(\chi_{c1}(1P) \rightarrow p\bar{p}\omega)/\Gamma_{\text{total}}] \times [B(\psi(2S) \rightarrow \gamma\chi_{c1}(1P))]$ assuming $B(\psi(2S) \rightarrow \gamma\chi_{c1}(1P)) = (9.07 \pm 0.11 \pm 0.54) \times 10^{-2}$, which we rescale to our best value $B(\psi(2S) \rightarrow \gamma\chi_{c1}(1P)) = (9.75 \pm 0.27) \times 10^{-2}$. Our first error is their experiment's error and our second error is the systematic error from using our best value.			

 $\Gamma(p\bar{p}\phi)/\Gamma_{\text{total}}$ Γ_{62}/Γ

VALUE	CL%	DOCUMENT ID	TECN	COMMENT
< 1.7 × 10⁻⁵	90	¹ ABLIKIM	11F BES3	$\psi(2S) \rightarrow \gamma p\bar{p}K^+ K^-$
¹ ABLIKIM 11F reports $< 1.82 \times 10^{-5}$ from a measurement of $[\Gamma(\chi_{c1}(1P) \rightarrow p\bar{p}\phi)/\Gamma_{\text{total}}] \times [B(\psi(2S) \rightarrow \gamma\chi_{c1}(1P))]$ assuming $B(\psi(2S) \rightarrow \gamma\chi_{c1}(1P)) = (9.2 \pm 0.4) \times 10^{-2}$, which we rescale to our best value $B(\psi(2S) \rightarrow \gamma\chi_{c1}(1P)) = 9.75 \times 10^{-2}$.				

 $\Gamma(p\bar{p}\pi^+ \pi^-)/\Gamma_{\text{total}}$ Γ_{63}/Γ

VALUE (units 10^{-3})	DOCUMENT ID	TECN	COMMENT
0.50 ± 0.19 OUR EVALUATION	Treating systematic error as correlated.		
0.50 ± 0.19 OUR AVERAGE			
0.46 ± 0.12 ± 0.15	¹ BAI	99B BES	$\psi(2S) \rightarrow \gamma\chi_{c1}$
1.08 ± 0.77 ± 0.05	¹ TANENBAUM	78 MRK1	$\psi(2S) \rightarrow \gamma\chi_{c1}$
¹ Rescaled by us using $B(\psi(2S) \rightarrow \gamma\chi_{c1}) = (8.8 \pm 0.4)\%$ and $B(\psi(2S) \rightarrow J/\psi(1S)\pi^+\pi^-) = (32.6 \pm 0.5)\%$.			

 $\Gamma(p\bar{p}\pi^0 \pi^0)/\Gamma_{\text{total}}$ Γ_{64}/Γ

VALUE	CL%	DOCUMENT ID	TECN	COMMENT
< 5 × 10⁻⁴	90	¹ HE	08B CLEO	$e^+e^- \rightarrow \gamma h^+ h^- h^0 h^0$
¹ HE 08B reports $< 0.05 \times 10^{-2}$ from a measurement of $[\Gamma(\chi_{c1}(1P) \rightarrow p\bar{p}\pi^0 \pi^0)/\Gamma_{\text{total}}] \times [B(\psi(2S) \rightarrow \gamma\chi_{c1}(1P))]$ assuming $B(\psi(2S) \rightarrow \gamma\chi_{c1}(1P)) = (9.07 \pm 0.11 \pm 0.54) \times 10^{-2}$, which we rescale to our best value $B(\psi(2S) \rightarrow \gamma\chi_{c1}(1P)) = 9.75 \times 10^{-2}$.				

 $\Gamma(p\bar{p}K^+ K^- \text{ (non-resonant)})/\Gamma_{\text{total}}$ Γ_{65}/Γ

VALUE (units 10^{-4})	EVTS	DOCUMENT ID	TECN	COMMENT
1.27 ± 0.22 ± 0.04	82 ± 9	¹ ABLIKIM	11F BES3	$\psi(2S) \rightarrow \gamma p\bar{p}K^+ K^-$
¹ ABLIKIM 11F reports $(1.35 \pm 0.15 \pm 0.19) \times 10^{-4}$ from a measurement of $[\Gamma(\chi_{c1}(1P) \rightarrow p\bar{p}K^+ K^- \text{ (non-resonant)})/\Gamma_{\text{total}}] \times [B(\psi(2S) \rightarrow \gamma\chi_{c1}(1P))]$ assuming $B(\psi(2S) \rightarrow \gamma\chi_{c1}(1P)) = (9.2 \pm 0.4) \times 10^{-2}$, which we rescale to our best value $B(\psi(2S) \rightarrow \gamma\chi_{c1}(1P)) = (9.75 \pm 0.27) \times 10^{-2}$. Our first error is their experiment's error and our second error is the systematic error from using our best value.				

 $\Gamma(p\bar{p}K_S^0 K_S^0)/\Gamma_{\text{total}}$ Γ_{66}/Γ

VALUE (units 10^{-4})	CL%	DOCUMENT ID	TECN	COMMENT
< 4.5	90	¹ ABLIKIM	06D BES2	$\psi(2S) \rightarrow \gamma\chi_{c1}$
¹ Using $B(\psi(2S) \rightarrow \chi_{c1}\gamma) = (9.1 \pm 0.6)\%$.				

 $\Gamma(p\bar{p}\pi^-)/\Gamma_{\text{total}}$ Γ_{67}/Γ

VALUE (units 10^{-4})	EVTS	DOCUMENT ID	TECN	COMMENT
3.8 ± 0.5 ± 0.1	1412	¹ ABLIKIM	12J BES3	$\psi(2S) \rightarrow \gamma p\bar{p}\pi^-$
¹ ABLIKIM 12J reports $[\Gamma(\chi_{c1}(1P) \rightarrow p\bar{p}\pi^-)/\Gamma_{\text{total}}] \times [B(\psi(2S) \rightarrow \gamma\chi_{c1}(1P))]$ = $(0.37 \pm 0.02 \pm 0.04) \times 10^{-4}$ which we divide by our best value $B(\psi(2S) \rightarrow \gamma\chi_{c1}(1P)) = (9.75 \pm 0.27) \times 10^{-2}$. Our first error is their experiment's error and our second error is the systematic error from using our best value.				

 $\Gamma(p\bar{p}n\pi^+)/\Gamma_{\text{total}}$ Γ_{68}/Γ

VALUE (units 10^{-4})	EVTS	DOCUMENT ID	TECN	COMMENT
3.9 ± 0.5 ± 0.1	1625	¹ ABLIKIM	12J BES3	$\psi(2S) \rightarrow \gamma p\bar{p}n\pi^+$
¹ ABLIKIM 12J reports $[\Gamma(\chi_{c1}(1P) \rightarrow p\bar{p}n\pi^+)/\Gamma_{\text{total}}] \times [B(\psi(2S) \rightarrow \gamma\chi_{c1}(1P))]$ = $(0.38 \pm 0.02 \pm 0.04) \times 10^{-4}$ which we divide by our best value $B(\psi(2S) \rightarrow \gamma\chi_{c1}(1P)) = (9.75 \pm 0.27) \times 10^{-2}$. Our first error is their experiment's error and our second error is the systematic error from using our best value.				

 $\Gamma(p\bar{p}\pi^-\pi^0)/\Gamma_{\text{total}}$ Γ_{69}/Γ

VALUE (units 10^{-4})	EVTS	DOCUMENT ID	TECN	COMMENT
10.3 ± 1.1 ± 0.3	1082	¹ ABLIKIM	12J BES3	$\psi(2S) \rightarrow \gamma p\bar{p}\pi^-\pi^0$
¹ ABLIKIM 12J reports $[\Gamma(\chi_{c1}(1P) \rightarrow p\bar{p}\pi^-\pi^0)/\Gamma_{\text{total}}] \times [B(\psi(2S) \rightarrow \gamma\chi_{c1}(1P))]$ = $(1.00 \pm 0.05 \pm 0.10) \times 10^{-4}$ which we divide by our best value $B(\psi(2S) \rightarrow \gamma\chi_{c1}(1P)) = (9.75 \pm 0.27) \times 10^{-2}$. Our first error is their experiment's error and our second error is the systematic error from using our best value.				

 $\Gamma(p\bar{p}n\pi^+\pi^0)/\Gamma_{\text{total}}$ Γ_{70}/Γ

VALUE (units 10^{-4})	EVTS	DOCUMENT ID	TECN	COMMENT
10.1 ± 1.1 ± 0.3	1261	¹ ABLIKIM	12J BES3	$\psi(2S) \rightarrow \gamma p\bar{p}n\pi^+\pi^0$
¹ ABLIKIM 12J reports $[\Gamma(\chi_{c1}(1P) \rightarrow p\bar{p}n\pi^+\pi^0)/\Gamma_{\text{total}}] \times [B(\psi(2S) \rightarrow \gamma\chi_{c1}(1P))]$ = $(0.98 \pm 0.05 \pm 0.10) \times 10^{-4}$ which we divide by our best value $B(\psi(2S) \rightarrow \gamma\chi_{c1}(1P)) = (9.75 \pm 0.27) \times 10^{-2}$. Our first error is their experiment's error and our second error is the systematic error from using our best value.				

 $\Gamma(\Lambda\bar{\Lambda}\pi^+\pi^-)/\Gamma_{\text{total}}$ Γ_{72}/Γ

VALUE (units 10^{-5})	CL%	EVTS	DOCUMENT ID	TECN	COMMENT
29 ± 5 ± 1		105	¹ ABLIKIM	12J BES3	$\psi(2S) \rightarrow \gamma\Lambda\bar{\Lambda}\pi^+\pi^-$
< 150	90		² ABLIKIM	06D BES2	$\psi(2S) \rightarrow \gamma\chi_{c1}$
¹ ABLIKIM 12J reports $(31.1 \pm 3.4 \pm 3.9) \times 10^{-5}$ from a measurement of $[\Gamma(\chi_{c1}(1P) \rightarrow \Lambda\bar{\Lambda}\pi^+\pi^-)/\Gamma_{\text{total}}] \times [B(\psi(2S) \rightarrow \gamma\chi_{c1}(1P))]$ assuming $B(\psi(2S) \rightarrow \gamma\chi_{c1}(1P)) = (9.2 \pm 0.4) \times 10^{-2}$, which we rescale to our best value $B(\psi(2S) \rightarrow \gamma\chi_{c1}(1P)) = (9.75 \pm 0.27) \times 10^{-2}$. Our first error is their experiment's error and our second error is the systematic error from using our best value.					
² Using $B(\psi(2S) \rightarrow \chi_{c1}\gamma) = (9.1 \pm 0.6)\%$.					

 $\Gamma(\Lambda\bar{\Lambda}\pi^+\pi^- \text{ (non-resonant)})/\Gamma_{\text{total}}$ Γ_{73}/Γ

VALUE (units 10^{-5})	EVTS	DOCUMENT ID	TECN	COMMENT
25 ± 6 ± 1	13	¹ ABLIKIM	12J BES3	$\psi(2S) \rightarrow \gamma\Lambda\bar{\Lambda}\pi^+\pi^-$
¹ ABLIKIM 12J reports $(26.2 \pm 5.5 \pm 3.3) \times 10^{-5}$ from a measurement of $[\Gamma(\chi_{c1}(1P) \rightarrow \Lambda\bar{\Lambda}\pi^+\pi^- \text{ (non-resonant)})/\Gamma_{\text{total}}] \times [B(\psi(2S) \rightarrow \gamma\chi_{c1}(1P))]$ assuming $B(\psi(2S) \rightarrow \gamma\chi_{c1}(1P)) = (9.2 \pm 0.4) \times 10^{-2}$, which we rescale to our best value $B(\psi(2S) \rightarrow \gamma\chi_{c1}(1P)) = (9.75 \pm 0.27) \times 10^{-2}$. Our first error is their experiment's error and our second error is the systematic error from using our best value.				

 $\Gamma(\Sigma(1385)^+\bar{\Lambda}\pi^- + \text{c.c.})/\Gamma_{\text{total}}$ Γ_{74}/Γ

VALUE	CL%	DOCUMENT ID	TECN	COMMENT
< 1.3 × 10⁻⁴	90	¹ ABLIKIM	12J BES3	$\psi(2S) \rightarrow \gamma\Sigma(1385)^+\bar{\Lambda}\pi^-$
¹ ABLIKIM 12J reports $< 14 \times 10^{-5}$ from a measurement of $[\Gamma(\chi_{c1}(1P) \rightarrow \Sigma(1385)^+\bar{\Lambda}\pi^- + \text{c.c.})/\Gamma_{\text{total}}] \times [B(\psi(2S) \rightarrow \gamma\chi_{c1}(1P))]$ assuming $B(\psi(2S) \rightarrow \gamma\chi_{c1}(1P)) = (9.2 \pm 0.4) \times 10^{-2}$, which we rescale to our best value $B(\psi(2S) \rightarrow \gamma\chi_{c1}(1P)) = 9.75 \times 10^{-2}$.				

 $\Gamma(\Sigma(1385)^-\bar{\Lambda}\pi^+ + \text{c.c.})/\Gamma_{\text{total}}$ Γ_{75}/Γ

VALUE (units 10^{-5})	CL%	DOCUMENT ID	TECN	COMMENT
< 13	90	¹ ABLIKIM	12J BES3	$\psi(2S) \rightarrow \gamma\Sigma(1385)^-\bar{\Lambda}\pi^+$
¹ ABLIKIM 12J reports $< 14 \times 10^{-5}$ from a measurement of $[\Gamma(\chi_{c1}(1P) \rightarrow \Sigma(1385)^-\bar{\Lambda}\pi^+ + \text{c.c.})/\Gamma_{\text{total}}] \times [B(\psi(2S) \rightarrow \gamma\chi_{c1}(1P))]$ assuming $B(\psi(2S) \rightarrow \gamma\chi_{c1}(1P)) = (9.2 \pm 0.4) \times 10^{-2}$, which we rescale to our best value $B(\psi(2S) \rightarrow \gamma\chi_{c1}(1P)) = 9.75 \times 10^{-2}$.				

 $\Gamma(K^+\bar{p}\Lambda + \text{c.c.})/\Gamma_{\text{total}}$ Γ_{77}/Γ

VALUE (units 10^{-4})	EVTS	DOCUMENT ID	TECN	COMMENT
4.2 ± 0.4 OUR AVERAGE	Error includes scale factor of 1.2.			
9.2 ± 2.8 ± 0.4	24	¹ LU	19 BELL	$B^+ \rightarrow \bar{p}\Lambda K^+ K^+$
4.2 ± 0.4 ± 0.1	3k	^{2,3} ABLIKIM	13D BES3	$\psi(2S) \rightarrow \gamma\Lambda\bar{p}K^+$
3.1 ± 0.9 ± 0.1		⁴ ATHAR	07 CLEO	$\psi(2S) \rightarrow \gamma h^+ h^- h^0$
¹ LU 19 reports $(9.15 \pm 2.63 \pm 0.86) \times 10^{-4}$ from a measurement of $[\Gamma(\chi_{c1}(1P) \rightarrow K^+\bar{p}\Lambda + \text{c.c.})/\Gamma_{\text{total}}] \times [B(B^+ \rightarrow \chi_{c1}(1P)K^+)]$ assuming $B(B^+ \rightarrow \chi_{c1}(1P)K^+) = (4.79 \pm 0.23) \times 10^{-4}$, which we rescale to our best value $B(B^+ \rightarrow \chi_{c1}(1P)K^+) = (4.74 \pm 0.22) \times 10^{-4}$. Our first error is their experiment's error and our second error is the systematic error from using our best value.				
² ABLIKIM 13D reports $(4.5 \pm 0.2 \pm 0.4) \times 10^{-4}$ from a measurement of $[\Gamma(\chi_{c1}(1P) \rightarrow K^+\bar{p}\Lambda + \text{c.c.})/\Gamma_{\text{total}}] \times [B(\psi(2S) \rightarrow \gamma\chi_{c1}(1P))]$ assuming $B(\psi(2S) \rightarrow \gamma\chi_{c1}(1P)) = (9.2 \pm 0.4) \times 10^{-2}$, which we rescale to our best value $B(\psi(2S) \rightarrow \gamma\chi_{c1}(1P)) = (9.75 \pm 0.27) \times 10^{-2}$. Our first error is their experiment's error and our second error is the systematic error from using our best value.				
³ Using $B(\Lambda \rightarrow p\pi^-) = 63.9\%$.				

See key on page 1171

Meson Particle Listings

$\chi_{c1}(1P)$

⁴ATHAR 07 reports $(3.3 \pm 0.9 \pm 0.4) \times 10^{-4}$ from a measurement of $[\Gamma(\chi_{c1}(1P) \rightarrow K^+ \bar{p} \Lambda + c.c.) / \Gamma_{\text{total}}] \times [B(\psi(2S) \rightarrow \gamma \chi_{c1}(1P))]$ assuming $B(\psi(2S) \rightarrow \gamma \chi_{c1}(1P)) = (9.07 \pm 0.11 \pm 0.54) \times 10^{-2}$, which we rescale to our best value $B(\psi(2S) \rightarrow \gamma \chi_{c1}(1P)) = (9.75 \pm 0.27) \times 10^{-2}$. Our first error is their experiment's error and our second error is the systematic error from using our best value.

$\Gamma(nK_S^0 \bar{\Lambda} + c.c.) / \Gamma_{\text{total}}$		Γ_{78} / Γ		
VALUE (units 10^{-4})	EVTS	DOCUMENT ID	TECN	COMMENT
1.66 ± 0.16 ± 0.05	399	¹ ABLIKIM	21AV BES3	$\psi(2S) \rightarrow \gamma n K_S^0 \bar{\Lambda} + c.c.$

¹ABLIKIM 21AV reports $(1.66 \pm 0.12 \pm 0.12) \times 10^{-4}$ from a measurement of $[\Gamma(\chi_{c1}(1P) \rightarrow n K_S^0 \bar{\Lambda} + c.c.) / \Gamma_{\text{total}}] \times [B(\psi(2S) \rightarrow \gamma \chi_{c1}(1P))]$ assuming $B(\psi(2S) \rightarrow \gamma \chi_{c1}(1P)) = 0.0975 \pm 0.0024$, which we rescale to our best value $B(\psi(2S) \rightarrow \gamma \chi_{c1}(1P)) = (9.75 \pm 0.27) \times 10^{-2}$. Our first error is their experiment's error and our second error is the systematic error from using our best value. Also uses $B(\bar{\Lambda} \rightarrow \bar{p} \pi^+) = (63.9 \pm 0.5)\%$ and $B(K_S^0 \rightarrow \pi^+ \pi^-) = (69.20 \pm 0.05)\%$.

$\Gamma(K^*(892)^+ \bar{p} \Lambda + c.c.) / \Gamma_{\text{total}}$		Γ_{79} / Γ		
VALUE (units 10^{-4})	EVTS	DOCUMENT ID	TECN	COMMENT
4.9 ± 0.7 ± 0.1	328	¹ ABLIKIM	19AU BES3	$\psi(2S) \rightarrow \gamma K^{*+} \bar{p} \Lambda$

¹ABLIKIM 19AU reports $[\Gamma(\chi_{c1}(1P) \rightarrow K^*(892)^+ \bar{p} \Lambda + c.c.) / \Gamma_{\text{total}}] \times [B(\psi(2S) \rightarrow \gamma \chi_{c1}(1P))]$ = $(4.8 \pm 0.5 \pm 0.4) \times 10^{-5}$ which we divide by our best value $B(\psi(2S) \rightarrow \gamma \chi_{c1}(1P)) = (9.75 \pm 0.27) \times 10^{-2}$. Our first error is their experiment's error and our second error is the systematic error from using our best value.

$\Gamma(K^+ \bar{p} \Lambda(1520) + c.c.) / \Gamma_{\text{total}}$		Γ_{80} / Γ		
VALUE (units 10^{-4})	EVTS	DOCUMENT ID	TECN	COMMENT
1.71 ± 0.44 ± 0.05	48 ± 10	¹ ABLIKIM	11F BES3	$\psi(2S) \rightarrow \gamma p \bar{p} K^+ K^-$

¹ABLIKIM 11F reports $(1.81 \pm 0.38 \pm 0.28) \times 10^{-4}$ from a measurement of $[\Gamma(\chi_{c1}(1P) \rightarrow K^+ \bar{p} \Lambda(1520) + c.c.) / \Gamma_{\text{total}}] \times [B(\psi(2S) \rightarrow \gamma \chi_{c1}(1P))]$ assuming $B(\psi(2S) \rightarrow \gamma \chi_{c1}(1P)) = (9.2 \pm 0.4) \times 10^{-2}$, which we rescale to our best value $B(\psi(2S) \rightarrow \gamma \chi_{c1}(1P)) = (9.75 \pm 0.27) \times 10^{-2}$. Our first error is their experiment's error and our second error is the systematic error from using our best value.

$\Gamma(\Lambda(1520) \bar{\Lambda}(1520)) / \Gamma_{\text{total}}$		Γ_{81} / Γ		
VALUE	CL%	DOCUMENT ID	TECN	COMMENT
< 9 × 10⁻⁵	90	¹ ABLIKIM	11F BES3	$\psi(2S) \rightarrow \gamma p \bar{p} K^+ K^-$

¹ABLIKIM 11F reports $< 1.00 \times 10^{-4}$ from a measurement of $[\Gamma(\chi_{c1}(1P) \rightarrow \Lambda(1520) \bar{\Lambda}(1520)) / \Gamma_{\text{total}}] \times [B(\psi(2S) \rightarrow \gamma \chi_{c1}(1P))]$ assuming $B(\psi(2S) \rightarrow \gamma \chi_{c1}(1P)) = (9.2 \pm 0.4) \times 10^{-2}$, which we rescale to our best value $B(\psi(2S) \rightarrow \gamma \chi_{c1}(1P)) = 9.75 \times 10^{-2}$.

$\Gamma(\Sigma^0 \bar{\Sigma}^0) / \Gamma_{\text{total}}$		Γ_{82} / Γ			
VALUE (units 10^{-5})	CL%	EVTS	DOCUMENT ID	TECN	COMMENT
4.2 ± 0.6 ± 0.1		103	¹ ABLIKIM	18V BES3	$\psi(2S) \rightarrow \gamma \Sigma^0 \bar{\Sigma}^0$

• • • We do not use the following data for averages, fits, limits, etc. • • •
 <6 90
 <4 90 3.8 ± 2.5 ²ABLIKIM 13H BES3 $\psi(2S) \rightarrow \gamma \Sigma^0 \bar{\Sigma}^0$
³NAIK 08 CLEO $\psi(2S) \rightarrow \gamma \Sigma^0 \bar{\Sigma}^0$

¹ABLIKIM 18V reports $[\Gamma(\chi_{c1}(1P) \rightarrow \Sigma^0 \bar{\Sigma}^0) / \Gamma_{\text{total}}] \times [B(\psi(2S) \rightarrow \gamma \chi_{c1}(1P))]$ = $(0.41 \pm 0.05 \pm 0.03) \times 10^{-5}$ which we divide by our best value $B(\psi(2S) \rightarrow \gamma \chi_{c1}(1P)) = (9.75 \pm 0.27) \times 10^{-2}$. Our first error is their experiment's error and our second error is the systematic error from using our best value.

²ABLIKIM 13H reports $< 0.62 \times 10^{-4}$ from a measurement of $[\Gamma(\chi_{c1}(1P) \rightarrow \Sigma^0 \bar{\Sigma}^0) / \Gamma_{\text{total}}] \times [B(\psi(2S) \rightarrow \gamma \chi_{c1}(1P))]$ assuming $B(\psi(2S) \rightarrow \gamma \chi_{c1}(1P)) = (9.2 \pm 0.4) \times 10^{-2}$, which we rescale to our best value $B(\psi(2S) \rightarrow \gamma \chi_{c1}(1P)) = 9.75 \times 10^{-2}$.

³NAIK 08 reports $< 0.44 \times 10^{-4}$ from a measurement of $[\Gamma(\chi_{c1}(1P) \rightarrow \Sigma^0 \bar{\Sigma}^0) / \Gamma_{\text{total}}] \times [B(\psi(2S) \rightarrow \gamma \chi_{c1}(1P))]$ assuming $B(\psi(2S) \rightarrow \gamma \chi_{c1}(1P)) = (9.07 \pm 0.11 \pm 0.54) \times 10^{-2}$, which we rescale to our best value $B(\psi(2S) \rightarrow \gamma \chi_{c1}(1P)) = 9.75 \times 10^{-2}$.

$\Gamma(\Sigma^+ \bar{\Sigma}^-) / \Gamma_{\text{total}}$		Γ_{85} / Γ			
VALUE (units 10^{-5})	CL%	EVTS	DOCUMENT ID	TECN	COMMENT
3.6 ± 0.6 ± 0.1		59	¹ ABLIKIM	18V BES3	$\psi(2S) \rightarrow \gamma \Sigma^+ \bar{\Sigma}^-$

• • • We do not use the following data for averages, fits, limits, etc. • • •
 <8 90
 <6 90 4.3 ± 2.3 ²ABLIKIM 13H BES3 $\psi(2S) \rightarrow \gamma \Sigma^+ \bar{\Sigma}^-$
³NAIK 08 CLEO $\psi(2S) \rightarrow \gamma \Sigma^+ \bar{\Sigma}^-$

¹ABLIKIM 18V reports $[\Gamma(\chi_{c1}(1P) \rightarrow \Sigma^+ \bar{\Sigma}^-) / \Gamma_{\text{total}}] \times [B(\psi(2S) \rightarrow \gamma \chi_{c1}(1P))]$ = $(0.35 \pm 0.06 \pm 0.02) \times 10^{-5}$ which we divide by our best value $B(\psi(2S) \rightarrow \gamma \chi_{c1}(1P)) = (9.75 \pm 0.27) \times 10^{-2}$. Our first error is their experiment's error and our second error is the systematic error from using our best value.

²ABLIKIM 13H reports $< 0.87 \times 10^{-4}$ from a measurement of $[\Gamma(\chi_{c1}(1P) \rightarrow \Sigma^+ \bar{\Sigma}^-) / \Gamma_{\text{total}}] \times [B(\psi(2S) \rightarrow \gamma \chi_{c1}(1P))]$ assuming $B(\psi(2S) \rightarrow \gamma \chi_{c1}(1P)) = (9.2 \pm 0.4) \times 10^{-2}$, which we rescale to our best value $B(\psi(2S) \rightarrow \gamma \chi_{c1}(1P)) = 9.75 \times 10^{-2}$.

³NAIK 08 reports $< 0.65 \times 10^{-4}$ from a measurement of $[\Gamma(\chi_{c1}(1P) \rightarrow \Sigma^+ \bar{\Sigma}^-) / \Gamma_{\text{total}}] \times [B(\psi(2S) \rightarrow \gamma \chi_{c1}(1P))]$ assuming $B(\psi(2S) \rightarrow \gamma \chi_{c1}(1P)) = (9.07 \pm 0.11 \pm 0.54) \times 10^{-2}$, which we rescale to our best value $B(\psi(2S) \rightarrow \gamma \chi_{c1}(1P)) = 9.75 \times 10^{-2}$.

$\Gamma(\Sigma^- \bar{\Sigma}^+) / \Gamma_{\text{total}}$		Γ_{86} / Γ		
VALUE (units 10^{-5})	EVTS	DOCUMENT ID	TECN	COMMENT
5.7 ± 1.5 ± 0.2	214	¹ ABLIKIM	20I BES3	$\psi(2S) \rightarrow \gamma \Sigma^- \bar{\Sigma}^+$

¹ABLIKIM 20I reports $(5.7 \pm 1.4 \pm 0.6) \times 10^{-5}$ from a measurement of $[\Gamma(\chi_{c1}(1P) \rightarrow \Sigma^- \bar{\Sigma}^+) / \Gamma_{\text{total}}] \times [B(\psi(2S) \rightarrow \gamma \chi_{c1}(1P))]$ assuming $B(\psi(2S) \rightarrow \gamma \chi_{c1}(1P)) = (9.75 \pm 0.24) \times 10^{-2}$, which we rescale to our best value $B(\psi(2S) \rightarrow \gamma \chi_{c1}(1P)) = (9.75 \pm 0.27) \times 10^{-2}$. Our first error is their experiment's error and our second error is the systematic error from using our best value.

$\Gamma(\Sigma(1385)^- \bar{\Sigma}(1385)^+) / \Gamma_{\text{total}}$		Γ_{87} / Γ		
VALUE	CL%	DOCUMENT ID	TECN	COMMENT
< 9 × 10⁻⁵	90	¹ ABLIKIM	12I BES3	$\psi(2S) \rightarrow \gamma \Lambda^+ \pi^+ \pi^-$

¹ABLIKIM 12I reports $< 10 \times 10^{-5}$ from a measurement of $[\Gamma(\chi_{c1}(1P) \rightarrow \Sigma(1385)^- \bar{\Sigma}(1385)^+) / \Gamma_{\text{total}}] \times [B(\psi(2S) \rightarrow \gamma \chi_{c1}(1P))]$ assuming $B(\psi(2S) \rightarrow \gamma \chi_{c1}(1P)) = (9.2 \pm 0.4) \times 10^{-2}$, which we rescale to our best value $B(\psi(2S) \rightarrow \gamma \chi_{c1}(1P)) = 9.75 \times 10^{-2}$.

$\Gamma(\Sigma(1385)^- \bar{\Sigma}(1385)^+) / \Gamma_{\text{total}}$		Γ_{88} / Γ		
VALUE	CL%	DOCUMENT ID	TECN	COMMENT
< 5 × 10⁻⁵	90	¹ ABLIKIM	12I BES3	$\psi(2S) \rightarrow \gamma \Lambda^+ \pi^+ \pi^-$

¹ABLIKIM 12I reports $< 5.7 \times 10^{-5}$ from a measurement of $[\Gamma(\chi_{c1}(1P) \rightarrow \Sigma(1385)^- \bar{\Sigma}(1385)^+) / \Gamma_{\text{total}}] \times [B(\psi(2S) \rightarrow \gamma \chi_{c1}(1P))]$ assuming $B(\psi(2S) \rightarrow \gamma \chi_{c1}(1P)) = (9.2 \pm 0.4) \times 10^{-2}$, which we rescale to our best value $B(\psi(2S) \rightarrow \gamma \chi_{c1}(1P)) = 9.75 \times 10^{-2}$.

$\Gamma(K^- \bar{\Lambda} \Xi^+ + c.c.) / \Gamma_{\text{total}}$		Γ_{89} / Γ		
VALUE (units 10^{-4})	EVTS	DOCUMENT ID	TECN	COMMENT
1.35 ± 0.24 ± 0.04	49	¹ ABLIKIM	15I BES3	$\psi(2S) \rightarrow \gamma K^- \bar{\Lambda} \Xi^+ + c.c.$

¹ABLIKIM 15I reports $[\Gamma(\chi_{c1}(1P) \rightarrow K^- \bar{\Lambda} \Xi^+ + c.c.) / \Gamma_{\text{total}}] \times [B(\psi(2S) \rightarrow \gamma \chi_{c1}(1P))]$ = $(1.32 \pm 0.20 \pm 0.12) \times 10^{-5}$ which we divide by our best value $B(\psi(2S) \rightarrow \gamma \chi_{c1}(1P)) = (9.75 \pm 0.27) \times 10^{-2}$. Our first error is their experiment's error and our second error is the systematic error from using our best value.

$\Gamma(\Xi^0 \bar{\Xi}^0) / \Gamma_{\text{total}}$		Γ_{90} / Γ			
VALUE (units 10^{-5})	CL%	EVTS	DOCUMENT ID	TECN	COMMENT
7.5 ± 1.2 ± 0.2		325	¹ ABLIKIM	22O BES3	$\psi(2S) \rightarrow \gamma \Xi^0 \bar{\Xi}^0$

• • • We do not use the following data for averages, fits, limits, etc. • • •

<6 90 1.7 ± 2.4 ²NAIK 08 CLEO $\psi(2S) \rightarrow \gamma \Xi^0 \bar{\Xi}^0$
¹ABLIKIM 22O reports $(0.75 \pm 0.11 \pm 0.06) \times 10^{-4}$ from a measurement of $[\Gamma(\chi_{c1}(1P) \rightarrow \Xi^0 \bar{\Xi}^0) / \Gamma_{\text{total}}] \times [B(\psi(2S) \rightarrow \gamma \chi_{c1}(1P))]$ assuming $B(\psi(2S) \rightarrow \gamma \chi_{c1}(1P)) = (9.75 \pm 0.24) \times 10^{-2}$, which we rescale to our best value $B(\psi(2S) \rightarrow \gamma \chi_{c1}(1P)) = (9.75 \pm 0.27) \times 10^{-2}$. Our first error is their experiment's error and our second error is the systematic error from using our best value.

²NAIK 08 reports $< 0.60 \times 10^{-4}$ from a measurement of $[\Gamma(\chi_{c1}(1P) \rightarrow \Xi^0 \bar{\Xi}^0) / \Gamma_{\text{total}}] \times [B(\psi(2S) \rightarrow \gamma \chi_{c1}(1P))]$ assuming $B(\psi(2S) \rightarrow \gamma \chi_{c1}(1P)) = (9.07 \pm 0.11 \pm 0.54) \times 10^{-2}$, which we rescale to our best value $B(\psi(2S) \rightarrow \gamma \chi_{c1}(1P)) = 9.75 \times 10^{-2}$.

$\Gamma(\Xi^- \bar{\Xi}^+) / \Gamma_{\text{total}}$		Γ_{91} / Γ			
VALUE (units 10^{-4})	CL%	EVTS	DOCUMENT ID	TECN	COMMENT
0.60 ± 0.06 OUR AVERAGE		692	¹ ABLIKIM	22O BES3	$\psi(2S) \rightarrow \gamma \Xi^- \bar{\Xi}^+$

0.80 ± 0.21 ± 0.02 16.4 ± 4.3 ²NAIK 08 CLEO $\psi(2S) \rightarrow \gamma \Xi^- \bar{\Xi}^+$

• • • We do not use the following data for averages, fits, limits, etc. • • •

< 3.4 90 ³ABLIKIM 06D BES2 $\psi(2S) \rightarrow \gamma \chi_{c1}$
¹ABLIKIM 22O reports $(0.58 \pm 0.04 \pm 0.05) \times 10^{-4}$ from a measurement of $[\Gamma(\chi_{c1}(1P) \rightarrow \Xi^- \bar{\Xi}^+) / \Gamma_{\text{total}}] \times [B(\psi(2S) \rightarrow \gamma \chi_{c1}(1P))]$ assuming $B(\psi(2S) \rightarrow \gamma \chi_{c1}(1P)) = (9.75 \pm 0.24) \times 10^{-2}$, which we rescale to our best value $B(\psi(2S) \rightarrow \gamma \chi_{c1}(1P)) = (9.75 \pm 0.27) \times 10^{-2}$. Our first error is their experiment's error and our second error is the systematic error from using our best value.

²NAIK 08 reports $(0.86 \pm 0.22 \pm 0.08) \times 10^{-4}$ from a measurement of $[\Gamma(\chi_{c1}(1P) \rightarrow \Xi^- \bar{\Xi}^+) / \Gamma_{\text{total}}] \times [B(\psi(2S) \rightarrow \gamma \chi_{c1}(1P))]$ assuming $B(\psi(2S) \rightarrow \gamma \chi_{c1}(1P)) = (9.07 \pm 0.11 \pm 0.54) \times 10^{-2}$, which we rescale to our best value $B(\psi(2S) \rightarrow \gamma \chi_{c1}(1P)) = (9.75 \pm 0.27) \times 10^{-2}$. Our first error is their experiment's error and our second error is the systematic error from using our best value.

³Using $B(\psi(2S) \rightarrow \chi_{c1} \gamma) = (9.1 \pm 0.6)\%$.

$\Gamma(\Omega^- \bar{\Omega}^+) / \Gamma_{\text{total}}$		Γ_{92} / Γ		
VALUE (units 10^{-5})	EVTS	DOCUMENT ID	TECN	COMMENT
1.49 ± 0.23 ± 0.10	277	ABLIKIM	23T BES3	$\chi_{cJ} \rightarrow \Omega^- \bar{\Omega}^+$

$\Gamma(\pi^+ \pi^-) + \Gamma(K^+ K^-) / \Gamma_{\text{total}}$		Γ_{93} / Γ		
VALUE	CL%	DOCUMENT ID	TECN	COMMENT
< 21 × 10⁻⁴		¹ FELDMAN	77 MRK1	$\psi(2S) \rightarrow \gamma \chi_{c1}$

• • • We do not use the following data for averages, fits, limits, etc. • • •
 < 38 × 10⁻⁴ 90 ¹BRANDELIK 79B DASP $\psi(2S) \rightarrow \gamma \chi_{c1}$

¹Estimated using $B(\psi(2S) \rightarrow \gamma \chi_{c1}(1P)) = 0.087$. The errors do not contain the uncertainty in the $\psi(2S)$ decay.

Meson Particle Listings

$\chi_{c1}(1P)$

$\Gamma(K_S^0 K_S^0)/\Gamma_{total}$		Γ_{94}/Γ	
VALUE	CL%	DOCUMENT ID	TECN COMMENT
$<6 \times 10^{-5}$	90	¹ ABLIKIM 05o	BES2 $\psi(2S) \rightarrow \chi_{c1} \gamma$
¹ ABLIKIM 05o reports $[\Gamma(\chi_{c1}(1P) \rightarrow K_S^0 K_S^0)/\Gamma_{total}] \times [B(\psi(2S) \rightarrow \chi_{c1}(1P))]$ $< 0.6 \times 10^{-5}$ which we divide by our best value $B(\psi(2S) \rightarrow \chi_{c1}(1P)) = 9.75 \times 10^{-2}$.			

$\Gamma(\eta_c \pi^+ \pi^-)/\Gamma_{total}$		Γ_{95}/Γ	
VALUE	CL%	DOCUMENT ID	TECN COMMENT
$<3.2 \times 10^{-3}$	90	^{1,2} ABLIKIM 13b	BES3 $e^+ e^- \rightarrow \psi(2S) \rightarrow \gamma \chi_{c1}$
<ul style="list-style-type: none"> • • • We do not use the following data for averages, fits, limits, etc. • • • 			
$<4.4 \times 10^{-3}$	90	^{1,3} ABLIKIM 13b	BES3 $e^+ e^- \rightarrow \psi(2S) \rightarrow \gamma \chi_{c1}$
¹ Using $1.06 \times 10^8 \psi(2S)$ mesons and $B(\psi(2S) \rightarrow \chi_{c1} \gamma) = (9.2 \pm 0.4)\%$. ² Using the $\eta_c \rightarrow K_S^0 K^\pm \pi^\mp$ decays. ³ Using the $\eta_c \rightarrow K^+ K^- \pi^0$ decays.			

RADIATIVE DECAYS

$\Gamma(\gamma \rho^0)/\Gamma_{total}$		Γ_{97}/Γ	
VALUE (units 10^{-6})	EVTs	DOCUMENT ID	TECN COMMENT
216 ± 17 OUR AVERAGE			
$215 \pm 22 \pm 6$	432 ± 25	¹ ABLIKIM	11E BES3 $\psi(2S) \rightarrow \gamma \gamma \rho^0$
$217 \pm 24 \pm 6$	186 ± 15	² BENNETT	08A CLEO $\psi(2S) \rightarrow \gamma \gamma \rho^0$
¹ ABLIKIM 11E reports $(228 \pm 13 \pm 22) \times 10^{-6}$ from a measurement of $[\Gamma(\chi_{c1}(1P) \rightarrow \gamma \rho^0)/\Gamma_{total}] \times [B(\psi(2S) \rightarrow \gamma \chi_{c1}(1P))]$ assuming $B(\psi(2S) \rightarrow \gamma \chi_{c1}(1P)) = (9.2 \pm 0.4) \times 10^{-2}$, which we rescale to our best value $B(\psi(2S) \rightarrow \gamma \chi_{c1}(1P)) = (9.75 \pm 0.27) \times 10^{-2}$. Our first error is their experiment's error and our second error is the systematic error from using our best value. ² BENNETT 08A reports $(243 \pm 19 \pm 22) \times 10^{-6}$ from a measurement of $[\Gamma(\chi_{c1}(1P) \rightarrow \gamma \rho^0)/\Gamma_{total}] \times [B(\psi(2S) \rightarrow \gamma \chi_{c1}(1P))]$ assuming $B(\psi(2S) \rightarrow \gamma \chi_{c1}(1P)) = (8.7 \pm 0.4) \times 10^{-2}$, which we rescale to our best value $B(\psi(2S) \rightarrow \gamma \chi_{c1}(1P)) = (9.75 \pm 0.27) \times 10^{-2}$. Our first error is their experiment's error and our second error is the systematic error from using our best value.			

$\Gamma(\gamma \omega)/\Gamma_{total}$		Γ_{98}/Γ	
VALUE (units 10^{-6})	EVTs	DOCUMENT ID	TECN COMMENT
68 ± 8 OUR AVERAGE			
$66 \pm 9 \pm 2$	136 ± 14	¹ ABLIKIM	11E BES3 $\psi(2S) \rightarrow \gamma \gamma \omega$
$74 \pm 17 \pm 2$	39 ± 7	² BENNETT	08A CLEO $\psi(2S) \rightarrow \gamma \gamma \omega$
¹ ABLIKIM 11E reports $(69.7 \pm 7.2 \pm 6.6) \times 10^{-6}$ from a measurement of $[\Gamma(\chi_{c1}(1P) \rightarrow \gamma \omega)/\Gamma_{total}] \times [B(\psi(2S) \rightarrow \gamma \chi_{c1}(1P))]$ assuming $B(\psi(2S) \rightarrow \gamma \chi_{c1}(1P)) = (9.2 \pm 0.4) \times 10^{-2}$, which we rescale to our best value $B(\psi(2S) \rightarrow \gamma \chi_{c1}(1P)) = (9.75 \pm 0.27) \times 10^{-2}$. Our first error is their experiment's error and our second error is the systematic error from using our best value. ² BENNETT 08A reports $(83 \pm 15 \pm 12) \times 10^{-6}$ from a measurement of $[\Gamma(\chi_{c1}(1P) \rightarrow \gamma \omega)/\Gamma_{total}] \times [B(\psi(2S) \rightarrow \gamma \chi_{c1}(1P))]$ assuming $B(\psi(2S) \rightarrow \gamma \chi_{c1}(1P)) = (8.7 \pm 0.4) \times 10^{-2}$, which we rescale to our best value $B(\psi(2S) \rightarrow \gamma \chi_{c1}(1P)) = (9.75 \pm 0.27) \times 10^{-2}$. Our first error is their experiment's error and our second error is the systematic error from using our best value.			

$\Gamma(\gamma \phi)/\Gamma_{total}$		Γ_{99}/Γ		
VALUE (units 10^{-6})	CL%	EVTs	DOCUMENT ID	TECN COMMENT
24 ± 5 ± 1		43 ± 9	¹ ABLIKIM	11E BES3 $\psi(2S) \rightarrow \gamma \gamma \phi$
<ul style="list-style-type: none"> • • • We do not use the following data for averages, fits, limits, etc. • • • 				
<23		$90 \ 5.2 \pm 3.1$	² BENNETT	08A CLEO $\psi(2S) \rightarrow \gamma \gamma \phi$
¹ ABLIKIM 11E reports $(25.8 \pm 5.2 \pm 2.3) \times 10^{-6}$ from a measurement of $[\Gamma(\chi_{c1}(1P) \rightarrow \gamma \phi)/\Gamma_{total}] \times [B(\psi(2S) \rightarrow \gamma \chi_{c1}(1P))]$ assuming $B(\psi(2S) \rightarrow \gamma \chi_{c1}(1P)) = (9.2 \pm 0.4) \times 10^{-2}$, which we rescale to our best value $B(\psi(2S) \rightarrow \gamma \chi_{c1}(1P)) = (9.75 \pm 0.27) \times 10^{-2}$. Our first error is their experiment's error and our second error is the systematic error from using our best value. ² BENNETT 08A reports $< 26 \times 10^{-6}$ from a measurement of $[\Gamma(\chi_{c1}(1P) \rightarrow \gamma \phi)/\Gamma_{total}] \times [B(\psi(2S) \rightarrow \gamma \chi_{c1}(1P))]$ assuming $B(\psi(2S) \rightarrow \gamma \chi_{c1}(1P)) = (8.7 \pm 0.4) \times 10^{-2}$, which we rescale to our best value $B(\psi(2S) \rightarrow \gamma \chi_{c1}(1P)) = 9.75 \times 10^{-2}$.				

$\Gamma(\gamma \gamma)/\Gamma_{total}$		Γ_{100}/Γ	
VALUE	CL%	DOCUMENT ID	TECN COMMENT
$< 6.3 \times 10^{-6}$		90	ABLIKIM 17A BES3 $\psi(2S) \rightarrow \gamma \chi_{c1} \rightarrow 3\gamma$
<ul style="list-style-type: none"> • • • We do not use the following data for averages, fits, limits, etc. • • • 			
$< 3.5 \times 10^{-5}$		90	ECKLUND 08A CLEO $\psi(2S) \rightarrow \gamma \chi_{c1} \rightarrow 3\gamma$
$< 150 \times 10^{-5}$		90	¹ YAMADA 77 DASP $e^+ e^- \rightarrow 3\gamma$
¹ Estimated using $B(\psi(2S) \rightarrow \gamma \chi_{c1}(1P)) = 0.087$. The errors do not contain the uncertainty in the $\psi(2S)$ decay.			

$\Gamma(e^+ e^- J/\psi(1S))/\Gamma_{total}$		Γ_{101}/Γ	
VALUE (units 10^{-3})	EVTs	DOCUMENT ID	TECN COMMENT
$3.65 \pm 0.23 \pm 0.10$	1.9k	^{1,2} ABLIKIM 17i	BES3 $\psi(2S) \rightarrow \gamma e^+ e^- J/\psi$
¹ ABLIKIM 17i reports $(3.73 \pm 0.09 \pm 0.25) \times 10^{-3}$ from a measurement of $[\Gamma(\chi_{c1}(1P) \rightarrow e^+ e^- J/\psi(1S))/\Gamma_{total}] \times [B(\psi(2S) \rightarrow \gamma \chi_{c1}(1P))]$ assuming $B(\psi(2S) \rightarrow \gamma \chi_{c1}(1P)) = (9.55 \pm 0.31) \times 10^{-2}$, which we rescale to our best value $B(\psi(2S) \rightarrow \gamma \chi_{c1}(1P)) = (9.75 \pm 0.27) \times 10^{-2}$. Our first error is their experiment's error and our second error is the systematic error from using our best value. ² Not independent from other measurements reported by ABLIKIM 17i			

$\Gamma(e^+ e^- J/\psi(1S))/\Gamma(\gamma J/\psi(1S))$		Γ_{101}/Γ_{96}	
VALUE (units 10^{-3})	EVTs	DOCUMENT ID	TECN COMMENT
10.1 ± 0.3 ± 0.5	1.9k	¹ ABLIKIM 17i	BES3 $\psi(2S) \rightarrow e^+ e^- \gamma J/\psi$
¹ Uses $B(\psi(2S) \rightarrow \gamma \chi_{c1}(1P)) \times B(\chi_{c1}(1P) \rightarrow \gamma J/\psi(1S)) = (351.8 \pm 1.0 \pm 12.0) \times 10^{-4}$ from ABLIKIM 17n and accounts for common systematic errors.			

$\Gamma(\mu^+ \mu^- J/\psi(1S))/\Gamma(e^+ e^- J/\psi(1S))$		$\Gamma_{102}/\Gamma_{101}$	
VALUE (units 10^{-2})	EVTs	DOCUMENT ID	TECN COMMENT
6.73 ± 0.51 ± 0.50	222	ABLIKIM 192	BES3 $\psi(2S) \rightarrow \gamma \chi_c \rightarrow \gamma(\mu^+ \mu^- J/\psi)$

$\chi_{c1}(1P)$ CROSS-PARTICLE BRANCHING RATIOS

$\Gamma(\chi_{c1}(1P) \rightarrow p\bar{p})/\Gamma_{total} \times \Gamma(\psi(2S) \rightarrow \gamma \chi_{c1}(1P))/\Gamma(\psi(2S) \rightarrow J/\psi(1S) \pi^+ \pi^-)$		$\Gamma_{58}/\Gamma \times \Gamma_{180}^{\psi(2S)}/\Gamma_{12}^{\psi(2S)}$	
VALUE (units 10^{-5})	EVTs	DOCUMENT ID	TECN COMMENT
2.13 ± 0.13 OUR FIT			Error includes scale factor of 1.3.
1.1 ± 1.0		¹ BAI 98i	BES $\psi(2S) \rightarrow \gamma \chi_{c1} \rightarrow \gamma \bar{p} p$
¹ Calculated by us. The value for $B(\chi_{c1} \rightarrow p\bar{p})$ reported in BAI 98i is derived using $B(\psi(2S) \rightarrow \gamma \chi_{c1}) = (8.7 \pm 0.8)\%$ and $B(\psi(2S) \rightarrow J/\psi(1S) \pi^+ \pi^-) = (32.4 \pm 2.6)\%$ [BAI 98d].			

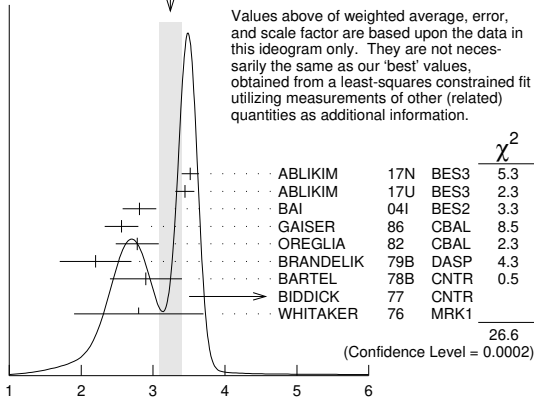
$\Gamma(\chi_{c1}(1P) \rightarrow \Lambda\bar{\Lambda})/\Gamma_{total} \times \Gamma(\psi(2S) \rightarrow \gamma \chi_{c1}(1P))/\Gamma_{total}$		$\Gamma_{71}/\Gamma \times \Gamma_{180}^{\psi(2S)}/\Gamma_{12}^{\psi(2S)}$	
VALUE (units 10^{-6})	EVTs	DOCUMENT ID	TECN COMMENT
12.4 ± 0.9 OUR FIT			Error includes scale factor of 1.1.
12.3 ± 0.9 OUR AVERAGE			Error includes scale factor of 1.2.
$12.8 \pm 0.6 \pm 0.6$	528	ABLIKIM 21L	BES3 $\psi(2S) \rightarrow \gamma p \pi^- \bar{p} \pi^+$
$10.5 \pm 1.6 \pm 0.6$	46	¹ NAIK 08	CLEO $\psi(2S) \rightarrow \gamma \Lambda \bar{\Lambda}$
<ul style="list-style-type: none"> • • • We do not use the following data for averages, fits, limits, etc. • • • 			
$11.2 \pm 1.0 \pm 0.9$	136	^{2,3} ABLIKIM 13H	BES3 $\psi(2S) \rightarrow \gamma \Lambda \bar{\Lambda}$
¹ Calculated by us. NAIK 08 reports $B(\chi_{c1} \rightarrow \Lambda \bar{\Lambda}) = (11.6 \pm 1.8 \pm 0.7 \pm 0.7) \times 10^{-5}$ using $B(\psi(2S) \rightarrow \gamma \chi_{c1}) = (9.07 \pm 0.11 \pm 0.54)\%$. ² Superseded by ABLIKIM 21L. ³ Calculated by us. ABLIKIM 13H reports $B(\chi_{c1} \rightarrow \Lambda \bar{\Lambda}) = (12.2 \pm 1.1 \pm 1.1) \times 10^{-5}$ from a measurement of $B(\chi_{c1} \rightarrow \Lambda \bar{\Lambda}) \times B(\psi(2S) \rightarrow \gamma \chi_{c1})$ assuming $B(\psi(2S) \rightarrow \gamma \chi_{c1}) = (9.2 \pm 0.4)\%$.			

$\Gamma(\chi_{c1}(1P) \rightarrow \Lambda\bar{\Lambda})/\Gamma_{total} \times \Gamma(\psi(2S) \rightarrow \gamma \chi_{c1}(1P))/\Gamma(\psi(2S) \rightarrow J/\psi(1S) \pi^+ \pi^-)$		$\Gamma_{71}/\Gamma \times \Gamma_{180}^{\psi(2S)}/\Gamma_{12}^{\psi(2S)}$	
VALUE (units 10^{-5})	EVTs	DOCUMENT ID	TECN COMMENT
3.58 ± 0.25 OUR FIT			Error includes scale factor of 1.1.
7.1 ± 2.8 ± 1.3	$9.0^{+3.5}_{-3.1}$	¹ BAI 03E	BES $\psi(2S) \rightarrow \gamma \Lambda \bar{\Lambda}$
¹ BAI 03E reports $[B(\chi_{c1} \rightarrow \Lambda \bar{\Lambda}) B(\psi(2S) \rightarrow \gamma \chi_{c1}) / B(\psi(2S) \rightarrow J/\psi \pi^+ \pi^-)] \times [B^2(\Lambda \rightarrow \pi^- p) / B(J/\psi \rightarrow p\bar{p})] = (1.33^{+0.52}_{-0.46} \pm 0.25)\%$. We calculate from this measurement the presented value using $B(\Lambda \rightarrow \pi^- p) = (63.9 \pm 0.5)\%$ and $B(J/\psi \rightarrow p\bar{p}) = (2.17 \pm 0.07) \times 10^{-3}$.			

$\Gamma(\chi_{c1}(1P) \rightarrow \Lambda\bar{\Lambda})/\Gamma_{total} \times \Gamma(\psi(2S) \rightarrow \gamma \chi_{c1}(1P))/\Gamma_{total}$		$\Gamma_{76}/\Gamma \times \Gamma_{180}^{\psi(2S)}/\Gamma_{12}^{\psi(2S)}$	
VALUE (units 10^{-6})	EVTs	DOCUMENT ID	TECN COMMENT
5.72 ± 1.34 ± 0.65	21	ABLIKIM 22a	BES3 $\psi(2S) \rightarrow \gamma p \pi^- \bar{p} \pi^+ \gamma \gamma$

$\Gamma(\chi_{c1}(1P) \rightarrow \gamma J/\psi(1S))/\Gamma_{total} \times \Gamma(\psi(2S) \rightarrow \gamma \chi_{c1}(1P))/\Gamma_{total}$		$\Gamma_{96}/\Gamma \times \Gamma_{180}^{\psi(2S)}/\Gamma_{12}^{\psi(2S)}$	
VALUE (units 10^{-2})	EVTs	DOCUMENT ID	TECN COMMENT
3.34 ± 0.10 OUR FIT			Error includes scale factor of 1.7.
3.24 ± 0.16 OUR AVERAGE			Error includes scale factor of 2.1. See the ideogram below.
$3.518 \pm 0.010 \pm 0.120$	143k	¹ ABLIKIM 17n	BES3 $\psi(2S) \rightarrow \gamma \gamma J/\psi$
$3.442 \pm 0.010 \pm 0.132$	1.9M	ABLIKIM 17u	BES3 $e^+ e^- \rightarrow \gamma X$
$2.81 \pm 0.05 \pm 0.23$	13k	BAI 04i	BES2 $\psi(2S) \rightarrow J/\psi \gamma \gamma$
$2.56 \pm 0.12 \pm 0.20$		GAISER 86	CBAL $\psi(2S) \rightarrow \gamma X$
2.78 ± 0.30		² OREGLIA 82	CBAL $\psi(2S) \rightarrow \gamma \chi_{c1}$
2.2 ± 0.5		³ BRANDELIK 79b	DASP $\psi(2S) \rightarrow \gamma \chi_{c1}$
2.9 ± 0.5		³ BARTEL 78b	CNTR $\psi(2S) \rightarrow \gamma \chi_{c1}$
5.0 ± 1.5		⁴ BIDDICK 77	CNTR $e^+ e^- \rightarrow \gamma X$
2.8 ± 0.9		² WHITAKER 76	MRK1 $e^+ e^-$
<ul style="list-style-type: none"> • • • We do not use the following data for averages, fits, limits, etc. • • • 			
$3.377 \pm 0.009 \pm 0.183$	142k	⁵ ABLIKIM 12o	BES3 $\psi(2S) \rightarrow \gamma \chi_{c1}$
$3.56 \pm 0.03 \pm 0.12$	24.9k	⁶ MENDEZ 08	CLEO $\psi(2S) \rightarrow \gamma \chi_{c1}$
$3.44 \pm 0.06 \pm 0.13$	3.7k	⁷ ADAM 05A	CLEO Repl. by MENDEZ 08
¹ Uses $B(J/\psi \rightarrow e^+ e^-) = (5.971 \pm 0.032)\%$ and $B(J/\psi \rightarrow \mu^+ \mu^-) = (5.961 \pm 0.033)\%$. ² Recalculated by us using $B(J/\psi(1S) \rightarrow \ell^+ \ell^-) = 0.1181 \pm 0.0020$. ³ Recalculated by us using $B(J/\psi(1S) \rightarrow \mu^+ \mu^-) = 0.0588 \pm 0.0010$. ⁴ Assumes isotropic gamma distribution. ⁵ Superseded by ABLIKIM 17n. ⁶ Not independent from other measurements of MENDEZ 08. ⁷ Not independent from other values reported by ADAM 05A.			

WEIGHTED AVERAGE
3.24±0.16 (Error scaled by 2.1)



Values above of weighted average, error, and scale factor are based upon the data in this ideogram only. They are not necessarily the same as our 'best' values, obtained from a least-squares constrained fit utilizing measurements of other (related) quantities as additional information.

$$\Gamma(\chi_{c1}(1P) \rightarrow \gamma J/\psi(1S))/\Gamma_{total} \times \Gamma(\psi(2S) \rightarrow \gamma \chi_{c1}(1P))/\Gamma_{total} \text{ (units } 10^{-2}\text{)}$$

$$\Gamma(\chi_{c1}(1P) \rightarrow \gamma J/\psi(1S))/\Gamma_{total} \times \Gamma(\psi(2S) \rightarrow \gamma \chi_{c1}(1P))/\Gamma(\psi(2S) \rightarrow J/\psi(1S)\pi^+\pi^-) \times \Gamma_{96}/\Gamma \times \Gamma_{180}^{\psi(2S)}/\Gamma_{12}^{\psi(2S)}$$

VALUE (units 10^{-2})	EVTS	DOCUMENT ID	TECN	COMMENT
9.63±0.29 OUR FIT				Error includes scale factor of 1.7.
10.15±0.28 OUR AVERAGE				
10.17±0.07±0.27	24.9k	MENDEZ 08	CLEO	$\psi(2S) \rightarrow \gamma \chi_{c1}$
12.6 ± 0.3 ± 3.8	3k	¹ ABLIKIM 04B	BES	$\psi(2S) \rightarrow J/\psi X$
8.5 ± 2.1		² HIMEL 80	MRK2	$\psi(2S) \rightarrow \gamma \chi_{c1}$
• • • We do not use the following data for averages, fits, limits, etc. • • •				
10.24±0.17±0.23	3.7k	³ ADAM 05A	CLEO	Repl. by MENDEZ 08

¹ From a fit to the J/ψ recoil mass spectra.
² The value for $B(\psi(2S) \rightarrow \gamma \chi_{c1}) \times B(\chi_{c1} \rightarrow \gamma J/\psi(1S))$ quoted in HIMEL 80 is derived using $B(\psi(2S) \rightarrow J/\psi(1S)\pi^+\pi^-) = (33 \pm 3)\%$ and $B(J/\psi(1S) \rightarrow \ell^+\ell^-) = 0.138 \pm 0.018$. Calculated by us using $B(J/\psi(1S) \rightarrow \ell^+\ell^-) = 0.1181 \pm 0.0020$.
³ Not independent from other values reported by ADAM 05A.

$$\Gamma(\chi_{c1}(1P) \rightarrow \bar{K}^0 K^+ \pi^- + c.c.)/\Gamma_{total} \times \Gamma(\psi(2S) \rightarrow \gamma \chi_{c1}(1P))/\Gamma_{total}$$

VALUE (units 10^{-4})	DOCUMENT ID	TECN	COMMENT
6.8±0.6 OUR FIT			Error includes scale factor of 1.1.
7.2±0.6 OUR AVERAGE			
7.3±0.5±0.5	¹ ATHAR 07	CLEO	$\psi(2S) \rightarrow \gamma K_S^0 K^+ \pi^-$
7.0±0.5±0.9	² ABLIKIM 06R	BES2	$\psi(2S) \rightarrow \gamma \chi_{c1}$

¹ Calculated by us. The value of $B(\chi_{c1} \rightarrow K_S^0 K^+ \pi^- + c.c.)$ reported by ATHAR 07 was derived using $B(\psi(2S) \rightarrow \gamma \chi_{c1}(1P)) = (9.07 \pm 0.11 \pm 0.54)\%$.
² Calculated by us. ABLIKIM 06R reports $B(\chi_{c1} \rightarrow K_S^0 K^+ \pi^-) = (4.0 \pm 0.3 \pm 0.5) \times 10^{-3}$. We use $B(\psi(2S) \rightarrow \gamma \chi_{c1}) = (8.7 \pm 0.4) \times 10^{-2}$.

$$\Gamma(\chi_{c1}(1P) \rightarrow \bar{K}^0 K^+ \pi^- + c.c.)/\Gamma_{total} \times \Gamma(\psi(2S) \rightarrow \gamma \chi_{c1}(1P))/\Gamma(\psi(2S) \rightarrow J/\psi(1S)\pi^+\pi^-)$$

VALUE (units 10^{-4})	DOCUMENT ID	TECN	COMMENT
19.6±1.6 OUR FIT			Error includes scale factor of 1.1.
13.2±2.4±3.2	¹ BAI 99B	BES	$\psi(2S) \rightarrow \gamma K_S^0 K^+ \pi^-$

¹ Calculated by us. The value of $B(\chi_{c1} \rightarrow K_S^0 K^+ \pi^-)$ reported by BAI 99B was derived using $B(\psi(2S) \rightarrow \gamma \chi_{c1}(1P)) = (8.7 \pm 0.8)\%$ and $B(\psi(2S) \rightarrow J/\psi\pi^+\pi^-) = (32.4 \pm 2.6)\%$ [BAI 98d].

$$\Gamma(\chi_{c1}(1P) \rightarrow K^+ K^- K^+ K^-)/\Gamma_{total} \times \Gamma(\psi(2S) \rightarrow \gamma \chi_{c1}(1P))/\Gamma_{total}$$

VALUE (units 10^{-4})	EVTS	DOCUMENT ID	TECN	COMMENT
0.53±0.11 OUR FIT				
0.61±0.11±0.08	54	¹ ABLIKIM 06T	BES2	$\psi(2S) \rightarrow \gamma K^+ K^+ K^- K^-$

¹ Calculated by us. The value of $B(\chi_{c1} \rightarrow 2K^+ 2K^-)$ reported by ABLIKIM 06T was derived using $B(\psi(2S) \rightarrow \gamma \chi_{c1}(1P)) = (8.7 \pm 0.8)\%$.

$$\Gamma(\chi_{c1}(1P) \rightarrow K^+ K^- K^+ K^-)/\Gamma_{total} \times \Gamma(\psi(2S) \rightarrow \gamma \chi_{c1}(1P))/\Gamma(\psi(2S) \rightarrow J/\psi(1S)\pi^+\pi^-)$$

VALUE (units 10^{-4})	DOCUMENT ID	TECN	COMMENT
1.52±0.31 OUR FIT			
1.13±0.40±0.29	¹ BAI 99B	BES	$\psi(2S) \rightarrow \gamma K^+ K^+ K^- K^-$

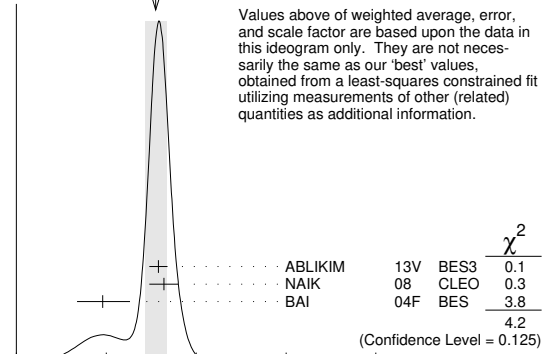
¹ Calculated by us. The value of $B(\chi_{c1} \rightarrow 2K^+ 2K^-)$ reported by BAI 99B was derived using $B(\psi(2S) \rightarrow \gamma \chi_{c1}(1P)) = (8.7 \pm 0.8)\%$ and $B(\psi(2S) \rightarrow J/\psi\pi^+\pi^-) = (32.4 \pm 2.6)\%$ [BAI 98d].

$$\Gamma(\chi_{c1}(1P) \rightarrow p\bar{p})/\Gamma_{total} \times \Gamma(\psi(2S) \rightarrow \gamma \chi_{c1}(1P))/\Gamma_{total}$$

VALUE (units 10^{-6})	EVTS	DOCUMENT ID	TECN	COMMENT
7.4±0.4 OUR FIT				Error includes scale factor of 1.3.
7.8±0.6 OUR AVERAGE				Error includes scale factor of 1.4. See the ideogram below.
7.9±0.4±0.3	453	ABLIKIM 13V	BES3	$\psi(2S) \rightarrow \gamma p\bar{p}$
8.2±0.7±0.4	141 ± 13	¹ NAIK 08	CLEO	$\psi(2S) \rightarrow \gamma p\bar{p}$
4.8 ^{+1.4} _{-1.3} ±0.6	18.2 ^{+5.5} _{-4.9}	BAI 04F	BES	$\psi(2S) \rightarrow \gamma \chi_{c1}(1P) \rightarrow \gamma p\bar{p}$

¹ Calculated by us. NAIK 08 reports $B(\chi_{c1} \rightarrow p\bar{p}) = (9.0 \pm 0.8 \pm 0.4 \pm 0.5) \times 10^{-5}$ using $B(\psi(2S) \rightarrow \gamma \chi_{c1}) = (9.07 \pm 0.11 \pm 0.54)\%$.

WEIGHTED AVERAGE
7.8±0.6 (Error scaled by 1.4)



Values above of weighted average, error, and scale factor are based upon the data in this ideogram only. They are not necessarily the same as our 'best' values, obtained from a least-squares constrained fit utilizing measurements of other (related) quantities as additional information.

$$\Gamma(\chi_{c1}(1P) \rightarrow p\bar{p})/\Gamma_{total} \times \Gamma(\psi(2S) \rightarrow \gamma \chi_{c1}(1P))/\Gamma_{total} \text{ (units } 10^{-6}\text{)}$$

$$\Gamma(\chi_{c1}(1P) \rightarrow \Sigma^+ \bar{p} K_S^0 + c.c.)/\Gamma_{total} \times \Gamma(\psi(2S) \rightarrow \gamma \chi_{c1}(1P))/\Gamma_{total}$$

VALUE (units 10^{-5})	EVTS	DOCUMENT ID	TECN	COMMENT
1.49±0.09±0.07	258	¹ ABLIKIM 19BB	BES3	$\psi(2S) \rightarrow \gamma \Sigma^+ \bar{p} K_S^0 + c.c.$

¹ Calculated by us. ABLIKIM 19BB reports $B(\chi_{c1} \rightarrow \Sigma^+ \bar{p} K_S^0 + c.c.) = (1.53 \pm 0.10 \pm 0.08) \times 10^{-4}$ using $B(\psi(2S) \rightarrow \gamma \chi_{c1}) = (9.75 \pm 0.24)\%$ and other branching fractions from PDG 18.

$$\Gamma(\chi_{c1}(1P) \rightarrow \Sigma^0 \bar{p} K^+ + c.c.)/\Gamma_{total} \times \Gamma(\psi(2S) \rightarrow \gamma \chi_{c1}(1P))/\Gamma_{total}$$

VALUE (units 10^{-5})	EVTS	DOCUMENT ID	TECN	COMMENT
1.42±0.07±0.06	493	¹ ABLIKIM 20AE	BES3	$\psi(2S) \rightarrow \gamma \Sigma^0 \bar{p} K^+ + c.c.$

¹ Calculated by us. ABLIKIM 20AE reports $B(\chi_{c1} \rightarrow \Sigma^0 \bar{p} K^+ + c.c.) = (1.46 \pm 0.07 \pm 0.07) \times 10^{-4}$ using $B(\psi(2S) \rightarrow \gamma \chi_{c1}) = (9.75 \pm 0.24)\%$ and other branching fractions from PDG 20.

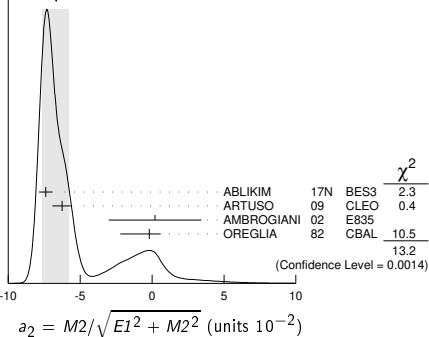
MULTIPOLE AMPLITUDES IN $\chi_{c1}(1P) \rightarrow \gamma J/\psi(1S)$

$$a_2 = M_2/\sqrt{E1^2 + M_2^2} \text{ Magnetic quadrupole fractional transition amplitude}$$

VALUE (units 10^{-2})	EVTS	DOCUMENT ID	TECN	COMMENT
-6.7±0.9 OUR AVERAGE				Error includes scale factor of 2.6. See the ideogram below.
-7.40 ± 0.33 ± 0.34	164k	¹ ABLIKIM 17N	BES3	$\psi(2S) \rightarrow \gamma \gamma \ell^+ \ell^-$
-6.26 ± 0.63 ± 0.24	39k	ARTUSO 09	CLEO	$\psi(2S) \rightarrow \gamma \gamma \ell^+ \ell^-$
0.2 ± 3.2 ± 0.4	2090	AMBROGIANI 02	E835	$p\bar{p} \rightarrow \chi_{c1} \rightarrow J/\psi \gamma$
-0.2 ^{+0.8} _{-2.0}	921	OREGLIA 82	CBAL	$\psi(2S) \rightarrow \chi_{c1} \gamma \rightarrow J/\psi \gamma \gamma$

¹ Correlated with b_2 with correlation coefficient $\rho_{a_2 b_2} = 0.133$.

WEIGHTED AVERAGE
-6.7±0.9 (Error scaled by 2.6)



$$a_2 = M_2/\sqrt{E1^2 + M_2^2} \text{ (units } 10^{-2}\text{)}$$

Meson Particle Listings

$\chi_{c1}(1P), h_c(1P)$

MULTIPOLE AMPLITUDES IN $\psi(2S) \rightarrow \gamma\chi_{c1}(1S)$ RADIATIVE DECAY

$b_2 = M_2/\sqrt{E_1^2 + M^2}$ Magnetic quadrupole fractional transition amplitude

VALUE (units 10^{-2})	EVTS	DOCUMENT ID	TECN	COMMENT
2.5 ± 0.4 OUR AVERAGE				
$2.29 \pm 0.39 \pm 0.27$	164k	¹ ABLIKIM	17N BES3	$\psi(2S) \rightarrow \gamma\gamma\ell^+\ell^-$
$2.76 \pm 0.73 \pm 0.23$	39k	ARTUSO	09 CLEO	$\psi(2S) \rightarrow \gamma\gamma\ell^+\ell^-$
$7.7^{+5.0}_{-4.5}$	921	OREGLIA	82 CBAL	$\psi(2S) \rightarrow \gamma\gamma\ell^+\ell^-$

¹ Correlated with a_2 with correlation coefficient $\rho_{a_2 b_2} = 0.133$.

MULTIPOLE AMPLITUDE RATIOS IN RADIATIVE DECAYS $\psi(2S) \rightarrow \gamma\chi_{c1}(1S)$ and $\chi_{c1} \rightarrow \gamma J/\psi(1S)$

a_2/b_2 Magnetic quadrupole transition amplitude ratio

VALUE	EVTS	DOCUMENT ID	TECN	COMMENT
$-2.27^{+0.57}_{-0.99}$	39k	¹ ARTUSO	09 CLEO	$\psi(2S) \rightarrow \gamma\gamma\ell^+\ell^-$

¹ Statistical and systematic errors combined. Not independent of $a_2(\chi_{c1})$ and $b_2(\chi_{c1})$ values from ARTUSO 09.

$\chi_{c1}(1P)$ REFERENCES

AAU	23AH	PR D108 032010	R. Aaij et al.	(LHCb Collab.)
ABLIKIM	23N	JHEP 2305 069	M. Ablikim et al.	(BESIII Collab.)
ABLIKIM	23T	PR D107 092004	M. Ablikim et al.	(BESIII Collab.)
ABLIKIM	22AF	PRL 129 122001	M. Ablikim et al.	(BESIII Collab.)
ABLIKIM	22AO	PR D106 072004	M. Ablikim et al.	(BESIII Collab.)
ABLIKIM	22O	JHEP 2206 074	M. Ablikim et al.	(BESIII Collab.)
ABLIKIM	22Q	PR D106 032014	M. Ablikim et al.	(BESIII Collab.)
PDG	22	PTEP 2022 083C01	R.L. Workman et al.	(PDG Collab.)
ABLIKIM	21AV	JHEP 2111 217	M. Ablikim et al.	(BESIII Collab.)
ABLIKIM	21L	PR D103 112004	M. Ablikim et al.	(BESIII Collab.)
ABLIKIM	20AE	PR D102 092006	M. Ablikim et al.	(BESIII Collab.)
ABLIKIM	20B	PR D101 012012	M. Ablikim et al.	(BESIII Collab.)
ABLIKIM	20I	PR D101 092002	M. Ablikim et al.	(BESIII Collab.)
PDG	20	PTEP 2020 083C01	P.A. Zyla et al.	(PDG Collab.)
ABLIKIM	19AA	PR D99 052008	M. Ablikim et al.	(BESIII Collab.)
ABLIKIM	19AU	PR D100 052010	M. Ablikim et al.	(BESIII Collab.)
ABLIKIM	19BB	PR D100 092006	M. Ablikim et al.	(BESIII Collab.)
ABLIKIM	19J	PR D99 012015	M. Ablikim et al.	(BESIII Collab.)
ABLIKIM	19Z	PR D99 051101	M. Ablikim et al.	(BESIII Collab.)
LU	19	PR D99 032003	P.-C. Lu et al.	(BELLE Collab.)
ABLIKIM	18D	PRL 121 022001	M. Ablikim et al.	(BESIII Collab.)
ABLIKIM	18V	PR D97 052011	M. Ablikim et al.	(BESIII Collab.)
PDG	18	PR D98 030001	M. Tanabashi et al.	(PDG Collab.)
AAU	17BB	EPJ C77 609	R. Aaij et al.	(LHCb Collab.)
AAU	17BI	PRL 119 221801	R. Aaij et al.	(LHCb Collab.)
ABLIKIM	17AE	PR D96 092007	M. Ablikim et al.	(BESIII Collab.)
ABLIKIM	17I	PRL 118 221802	M. Ablikim et al.	(BESIII Collab.)
ABLIKIM	17K	PR D95 032002	M. Ablikim et al.	(BESIII Collab.)
ABLIKIM	17N	PR D95 072004	M. Ablikim et al.	(BESIII Collab.)
ABLIKIM	17U	PR D96 032001	M. Ablikim et al.	(BESIII Collab.)
PDG	16	CP 100 00001	C. Patrignani et al.	(PDG Collab.)
ABLIKIM	15I	PR D91 092006	M. Ablikim et al.	(BESIII Collab.)
ABLIKIM	15M	PR D91 112008	M. Ablikim et al.	(BESIII Collab.)
ABLIKIM	14J	PR D89 074030	M. Ablikim et al.	(BESIII Collab.)
ABLIKIM	13B	PR D87 012002	M. Ablikim et al.	(BESIII Collab.)
ABLIKIM	13D	PR D87 012007	M. Ablikim et al.	(BESIII Collab.)
ABLIKIM	13H	PR D87 032007	M. Ablikim et al.	(BESIII Collab.)
ABLIKIM	13V	PR D88 112001	M. Ablikim et al.	(BESIII Collab.)
ABLIKIM	12I	PR D86 052004	M. Ablikim et al.	(BESIII Collab.)
ABLIKIM	12J	PR D86 052011	M. Ablikim et al.	(BESIII Collab.)
ABLIKIM	12O	PRL 109 172002	M. Ablikim et al.	(BESIII Collab.)
ABLIKIM	11A	PR D83 012006	M. Ablikim et al.	(BESIII Collab.)
ABLIKIM	11D	PR D83 032003	M. Ablikim et al.	(BESIII Collab.)
ABLIKIM	11E	PR D83 112005	M. Ablikim et al.	(BESIII Collab.)
ABLIKIM	11F	PR D83 112009	M. Ablikim et al.	(BESIII Collab.)
ABLIKIM	11K	PRL 107 092001	M. Ablikim et al.	(BESIII Collab.)
ONYISI	10	PR D82 011103	P.U.E. Onyisi et al.	(CLEO Collab.)
ARTUSO	09	PR D80 112003	M. Artuso et al.	(CLEO Collab.)
BENNETT	08A	PRL 101 151801	J.V. Bennett et al.	(CLEO Collab.)
ECKLUND	08A	PR D78 091501	K.M. Ecklund et al.	(CLEO Collab.)
HE	08B	PR D78 092004	Q. He et al.	(CLEO Collab.)
MENDEZ	08	PR D78 011102	H. Mendez et al.	(CLEO Collab.)
NAIK	08	PR D78 031101	P. Naik et al.	(CLEO Collab.)
ATHAR	07	PR D75 032002	S.B. Athar et al.	(CLEO Collab.)
ABLIKIM	06D	PR D73 052006	M. Ablikim et al.	(BES Collab.)
ABLIKIM	06R	PR D74 072001	M. Ablikim et al.	(BES Collab.)
ABLIKIM	06T	PL B642 197	M. Ablikim et al.	(BES Collab.)
ABLIKIM	05G	PR D71 092002	M. Ablikim et al.	(BES Collab.)
ABLIKIM	05O	PL B630 21	M. Ablikim et al.	(CLEO Collab.)
ADAM	05A	PRL 94 232002	N.E. Adam et al.	(CLEO Collab.)
ANDREOTTI	05A	NP B717 34	M. Andreotti et al.	(FNAL E835 Collab.)
ABLIKIM	04B	PR D70 012003	M. Ablikim et al.	(BES Collab.)
ABLIKIM	04H	PR D70 092003	M. Ablikim et al.	(BES Collab.)
BAI	04F	PR D69 092001	J.Z. Bai et al.	(BES Collab.)
BAI	04I	PR D70 012006	J.Z. Bai et al.	(BES Collab.)
AULCHENKO	03	PL B573 63	V.M. Aulchenko et al.	(KEDR Collab.)
BAI	03E	PR D67 112001	J.Z. Bai et al.	(BES Collab.)
AMBROGIANI	02	PR D65 052002	M. Ambrogiani et al.	(FNAL E835 Collab.)
BAI	99B	PR D60 072001	J.Z. Bai et al.	(BES Collab.)
BAI	98D	PR D58 092006	J.Z. Bai et al.	(BES Collab.)
BAI	98I	PRL 81 3091	J.Z. Bai et al.	(BES Collab.)
ARMSTRONG	92	NP B373 35	T.A. Armstrong et al.	(FNAL, FERR, GENO+)
Also		PRL 68 1468	T.A. Armstrong et al.	(FNAL, FERR, GENO+)
BAGLIN	86B	PL B172 455	C. Baglin	(LAPP, CERN, GENO, LYON, OSLO+)
GAISER	86	PR D34 711	J. Gaiser et al.	(Crystal Ball Collab.)
LEMIGNIE	82	PL 113B 509	Y. Lemignie et al.	(SACL, LOIC, SHMP+)
OREGLIA	82	PR D25 2259	M.J. Oreglia et al.	(SLAC, CIT, HARV+)
Also		Private Comm.	M.J. Oreglia	(EFI)
HIMEL	80	PRL 44 920	T. Himel et al.	(LBL, SLAC)
Also		Private Comm.	G. Trilling	(LBL, UCB)
BRANDELIC	79B	NP B160 426	R. Brandelic et al.	(DASP Collab.)
BARTEL	78B	PL 79B 492	W. Bartel et al.	(DESY, HEIDP)
TANENBAUM	78	PR D17 1731	W.M. Tanenbaum et al.	(SLAC, LBL)
Also		Private Comm.	G. Trilling	(LBL, UCB)
BIDDICK	77	PR 38 1324	C.J. Biddick et al.	(UCSD, UMD, PAVI+)
FELDMAN	77	PRL 33C 285	G.J. Feldman, M.L. Perl	(LBL, SLAC)
YAMADA	77	Hamburg Conf. 69	S. Yamada	(DASP Collab.)
WHITAKER	76	PRL 37 1596	J.S. Whitaker et al.	(SLAC, LBL)
TANENBAUM	75	PRL 35 1323	W.M. Tanenbaum et al.	(LBL, SLAC)

$h_c(1P)$

$$I^G(J^{PC}) = 0^-(1^{+-})$$

Quantum numbers are quark model prediction, $C = -$ established by $\eta_c\gamma$ decay.

$h_c(1P)$ MASS

VALUE (MeV)	EVTS	DOCUMENT ID	TECN	COMMENT
3525.37 ± 0.14 OUR AVERAGE				Error includes scale factor of 1.2.
$3525.32 \pm 0.06 \pm 0.15$	23k	ABLIKIM	22AQ BES3	$\psi(2S) \rightarrow \pi^0$ hadrons; $\pi^0\gamma(\eta_c)$
$3525.20 \pm 0.18 \pm 0.12$	1282	¹ DOBBS	08A CLEO	$\psi(2S) \rightarrow \pi^0\eta_c\gamma$
$3525.8 \pm 0.2 \pm 0.2$	13	ANDREOTTI	05B E835	$\bar{p}p \rightarrow \eta_c\gamma$
••• We do not use the following data for averages, fits, limits, etc. •••				
$3525.31 \pm 0.11 \pm 0.14$	832	^{2,3} ABLIKIM	12N BES3	$\psi(2S) \rightarrow \pi^0\gamma$ hadrons
$3525.40 \pm 0.13 \pm 0.18$	3679	² ABLIKIM	10B BES3	$\psi(2S) \rightarrow \pi^0\gamma\eta_c$
3525.6 ± 0.5	92	ADAMS	09 CLEO	$\psi(2S) \rightarrow 2(\pi^+\pi^-\pi^0)$
$3524.4 \pm 0.6 \pm 0.4$	168	⁴ ROSNER	05 CLEO	$\psi(2S) \rightarrow \pi^0\eta_c\gamma$
3527 ± 0.8	42	ANTONIAZZI	94 E705	$300 \pi^\pm, pLi \rightarrow J/\psi\pi^0 X$
$3525.28 \pm 0.18 \pm 0.19$	59	⁵ ARMSTRONG	92D E760	$\bar{p}p \rightarrow J/\psi\pi^0$
$3525.4 \pm 0.8 \pm 0.4$	5	BAGLIN	86 SPEC	$\bar{p}p \rightarrow J/\psi X$

- ¹ Combination of exclusive and inclusive analyses for the reaction $\psi(2S) \rightarrow \pi^0\eta_c \rightarrow \pi^0\eta_c\gamma$. This result is the average of DOBBS 08A and ROSNER 05.
- ² Superseded by ABLIKIM 22AQ
- ³ With floating width.
- ⁴ Superseded by DOBBS 08A.
- ⁵ Mass central value and systematic error recalculated by us according to Eq. (16) in ARMSTRONG 93B, using the value for the $\psi(2S)$ mass from AULCHENKO 03.

$h_c(1P)$ WIDTH

VALUE (MeV)	CL%	EVTS	DOCUMENT ID	TECN	COMMENT
$0.78^{+0.27}_{-0.24} \pm 0.12$		23k	ABLIKIM	22AQ BES3	$\psi(2S) \rightarrow \pi^0$ hadrons; $\pi^0\gamma(\eta_c)$
••• We do not use the following data for averages, fits, limits, etc. •••					
$0.70 \pm 0.28 \pm 0.22$	832	^{1,2} ABLIKIM	12N BES3	$\psi(2S) \rightarrow \pi^0\gamma$ hadrons	
< 1.44	90	3679	³ ABLIKIM	10B BES3	$\psi(2S) \rightarrow \pi^0\gamma\eta_c$
< 1		13	ANDREOTTI	05B E835	$\bar{p}p \rightarrow \eta_c\gamma$
< 1.1	90	59	ARMSTRONG	92D E760	$\bar{p}p \rightarrow J/\psi\pi^0$

¹ Superseded by ABLIKIM 22AQ
² With floating mass.
³ The central value is $\Gamma = 0.73 \pm 0.45 \pm 0.28$ MeV.

$h_c(1P)$ DECAY MODES

Mode	Fraction (Γ_i/Γ)	Confidence level
Γ_1 $J/\psi(1S)\pi^0$	< 5	$\times 10^{-4}$ 90%
Γ_2 $J/\psi(1S)\pi\pi$	not seen	
Γ_3 $J/\psi(1S)\pi^+\pi^-$	< 2.7	$\times 10^{-3}$ 90%
Γ_4 $p\bar{p}$	< 1.7	$\times 10^{-4}$ 90%
Γ_5 $p\bar{p}\pi^0$	< 8	$\times 10^{-4}$ 90%
Γ_6 $p\bar{p}\pi^+\pi^-$	(3.3 ± 0.6)	$\times 10^{-3}$
Γ_7 $p\bar{p}\pi^0\pi^0$	< 6	$\times 10^{-4}$ 90%
Γ_8 $p\bar{p}\pi^+\pi^-\pi^0$	(4.4 ± 1.3)	$\times 10^{-3}$
Γ_9 $p\bar{p}\eta$	(7.4 ± 2.2)	$\times 10^{-4}$
Γ_{10} $\pi^+\pi^-\pi^0$	(1.9 ± 0.5)	$\times 10^{-3}$
Γ_{11} $\pi^+\pi^-\pi^0\eta$	(8.3 ± 2.4)	$\times 10^{-3}$
Γ_{12} $2\pi^+2\pi^-\pi^0$	(9.4 ± 1.7)	$\times 10^{-3}$
Γ_{13} $3\pi^+3\pi^-\pi^0$	< 1.0	90%
Γ_{14} $K^+K^-\pi^+\pi^-$	< 7	$\times 10^{-4}$ 90%
Γ_{15} $K^+K^-\pi^+\pi^-\pi^0$	(3.8 ± 0.8)	$\times 10^{-3}$
Γ_{16} $K^+K^-\pi^+\pi^-\eta$	< 2.7	$\times 10^{-3}$ 90%
Γ_{17} $K^+K^-\pi^0$	< 6	$\times 10^{-4}$ 90%
Γ_{18} $K^+K^-\pi^0\eta$	< 2.4	$\times 10^{-3}$ 90%
Γ_{19} $K^+K^-\eta$	< 1.0	$\times 10^{-3}$ 90%
Γ_{20} $2K^+2K^-\pi^0$	< 2.8	$\times 10^{-4}$ 90%
Γ_{21} $K_S^0 K^\pm\pi^\mp$	< 6	$\times 10^{-4}$ 90%
Γ_{22} $K_S^0 K^\pm\pi^\mp\pi^\pm\pi^\mp$	(3.2 ± 1.0)	$\times 10^{-3}$

Radiative decays

Γ_{23} $\gamma\eta$	(4.7 ± 2.1)	$\times 10^{-4}$
Γ_{24} $\gamma\eta'(958)$	(1.5 ± 0.4)	$\times 10^{-3}$
Γ_{25} $\gamma\eta_c(1S)$	(60 ± 4)	%

FIT INFORMATION

A multiparticle fit to $\eta_c(1S)$, $J/\psi(1S)$, $\psi(2S)$, $h_c(1P)$, and B^{\pm} with the total width, 10 combinations of partial widths obtained from integrated cross section, and 38 branching ratios uses 113 measurements to determine 19 parameters. The overall fit has a $\chi^2 = 184.6$ for 94 degrees of freedom.

 $h_c(1P)$ PARTIAL WIDTHS $h_c(1P)$ $\Gamma(i\Gamma(\bar{p}p)/\Gamma_{\text{total}})$ $\Gamma(\gamma\eta_c(1S)) \times \Gamma(\bar{p}p)/\Gamma_{\text{total}}$ $\Gamma_{25}\Gamma_4/\Gamma$

VALUE (eV)	EVTS	DOCUMENT ID	TECN	COMMENT
------------	------	-------------	------	---------

• • • We do not use the following data for averages, fits, limits, etc. • • •

12.0 ± 4.5 13 1 ANDREOTTI 05B E835 $\bar{p}p \rightarrow \eta_c \gamma$

1 Assuming $\Gamma = 1$ MeV.

 $h_c(1P)$ BRANCHING RATIOS $\Gamma(J/\psi(1S)\pi^0)/\Gamma(\eta_c(1S))$ Γ_1/Γ_{25}

VALUE	CL%	DOCUMENT ID	TECN	COMMENT
-------	-----	-------------	------	---------

< 9 × 10⁻⁴ 90 1 ABLIKIM 22N BES3 $e^+e^- \rightarrow \pi^+\pi^-h_c$

1 ABLIKIM 22N reports [$\Gamma(h_c(1P) \rightarrow J/\psi(1S)\pi^0)/\Gamma(h_c(1P) \rightarrow \gamma\eta_c(1S))$] / [$B(\eta_c \rightarrow K^+K^-\pi^0)$] < 7.5 × 10⁻² which we multiply by our best value $B(\eta_c \rightarrow K^+K^-\pi^0) = 1/6 B(\eta_c(1S) \rightarrow K\bar{K}\pi) = 1/6 (7.1 \times 10^{-2})$.

 $\Gamma(J/\psi(1S)\pi\pi)/\Gamma(J/\psi(1S)\pi^0)$ Γ_2/Γ_1

VALUE	CL%	DOCUMENT ID	TECN	COMMENT
-------	-----	-------------	------	---------

< 0.18 90 ARMSTRONG 92D E760 $\bar{p}p \rightarrow J/\psi\pi^0$

 $\Gamma(J/\psi(1S)\pi^+\pi^-)/\Gamma_{\text{total}}$ Γ_3/Γ

VALUE	CL%	DOCUMENT ID	TECN	COMMENT
-------	-----	-------------	------	---------

< 2.7 × 10⁻³ 90 1 ABLIKIM 18M BES3 $\psi(2S) \rightarrow \pi^0\pi^+\pi^-J/\psi$

1 ABLIKIM 18M reports [$\Gamma(h_c(1P) \rightarrow J/\psi(1S)\pi^+\pi^-)/\Gamma_{\text{total}}$] × [$B(\psi(2S) \rightarrow h_c(1P)\pi^0)$] < 2.0 × 10⁻⁶ which we divide by our best value $B(\psi(2S) \rightarrow h_c(1P)\pi^0) = 7.4 \times 10^{-4}$.

 $\Gamma(\bar{p}p)/\Gamma_{\text{total}}$ Γ_4/Γ

VALUE	CL%	DOCUMENT ID	TECN	COMMENT
-------	-----	-------------	------	---------

< 1.7 × 10⁻⁴ 90 1 ABLIKIM 13V BES3 $\psi(2S) \rightarrow \gamma\bar{p}p$

1 ABLIKIM 13V reports [$\Gamma(h_c(1P) \rightarrow \bar{p}p)/\Gamma_{\text{total}}$] × [$B(\psi(2S) \rightarrow h_c(1P)\pi^0)$] < 1.3 × 10⁻⁷ which we divide by our best value $B(\psi(2S) \rightarrow h_c(1P)\pi^0) = 7.4 \times 10^{-4}$.

 $\Gamma(\bar{p}p\pi^0)/\Gamma_{\text{total}}$ Γ_5/Γ

VALUE	CL%	DOCUMENT ID	TECN	COMMENT
-------	-----	-------------	------	---------

< 8 × 10⁻⁴ 90 1 ABLIKIM 22M BES3 $\psi(2S) \rightarrow \pi^0h_c(1P)$

1 ABLIKIM 22M reports [$\Gamma(h_c(1P) \rightarrow \bar{p}p\pi^0)/\Gamma_{\text{total}}$] × [$B(\psi(2S) \rightarrow h_c(1P)\pi^0)$] < 5.67 × 10⁻⁷ which we divide by our best value $B(\psi(2S) \rightarrow h_c(1P)\pi^0) = 7.4 \times 10^{-4}$.

 $\Gamma(\bar{p}p\pi^+\pi^-)/\Gamma_{\text{total}}$ Γ_6/Γ

VALUE (units 10 ⁻³)	EVTS	DOCUMENT ID	TECN	COMMENT
---------------------------------	------	-------------	------	---------

3.3 ± 0.5 ± 0.2 230 1 ABLIKIM 19AG BES3 $\psi(2S) \rightarrow \pi^0h_c(1P)$

1 ABLIKIM 19AG reports [$\Gamma(h_c(1P) \rightarrow \bar{p}p\pi^+\pi^-)/\Gamma_{\text{total}}$] × [$B(\psi(2S) \rightarrow h_c(1P)\pi^0)$] = (2.49 ± 0.27 ± 0.28) × 10⁻⁶ which we divide by our best value $B(\psi(2S) \rightarrow h_c(1P)\pi^0) = (7.4 \pm 0.5) \times 10^{-4}$. Our first error is their experiment's error and our second error is the systematic error from using our best value.

 $\Gamma(\bar{p}p\pi^0\pi^0)/\Gamma_{\text{total}}$ Γ_7/Γ

VALUE	CL%	EVTS	DOCUMENT ID	TECN	COMMENT
-------	-----	------	-------------	------	---------

< 6 × 10⁻⁴ 90 12 1 ABLIKIM 20AH BES3 $\psi(2S) \rightarrow \pi^0h_c(1P)$

1 ABLIKIM 20AH reports [$\Gamma(h_c(1P) \rightarrow \bar{p}p\pi^0\pi^0)/\Gamma_{\text{total}}$] × [$B(\psi(2S) \rightarrow h_c(1P)\pi^0)$] < 4.4 × 10⁻⁷ which we divide by our best value $B(\psi(2S) \rightarrow h_c(1P)\pi^0) = 7.4 \times 10^{-4}$.

 $\Gamma(\bar{p}p\pi^+\pi^-\pi^0)/\Gamma_{\text{total}}$ Γ_8/Γ

VALUE (units 10 ⁻³)	EVTS	DOCUMENT ID	TECN	COMMENT
---------------------------------	------	-------------	------	---------

4.4 ± 1.2 ± 0.3 86 1 ABLIKIM 22M BES3 $\psi(2S) \rightarrow \pi^0h_c(1P)$

1 ABLIKIM 22M reports [$\Gamma(h_c(1P) \rightarrow \bar{p}p\pi^+\pi^-\pi^0)/\Gamma_{\text{total}}$] × [$B(\psi(2S) \rightarrow h_c(1P)\pi^0)$] = (3.30 ± 0.71 ± 0.59) × 10⁻⁶ which we divide by our best value $B(\psi(2S) \rightarrow h_c(1P)\pi^0) = (7.4 \pm 0.5) \times 10^{-4}$. Our first error is their experiment's error and our second error is the systematic error from using our best value.

 $\Gamma(\bar{p}p\eta)/\Gamma_{\text{total}}$ Γ_9/Γ

VALUE (units 10 ⁻⁴)	EVTS	DOCUMENT ID	TECN	COMMENT
---------------------------------	------	-------------	------	---------

7.4 ± 2.1 ± 0.5 20 1 ABLIKIM 22M BES3 $\psi(2S) \rightarrow \pi^0h_c(1P)$

1 ABLIKIM 22M reports [$\Gamma(h_c(1P) \rightarrow \bar{p}p\eta)/\Gamma_{\text{total}}$] × [$B(\psi(2S) \rightarrow h_c(1P)\pi^0)$] = (5.51 ± 1.50 ± 0.46) × 10⁻⁷ which we divide by our best value $B(\psi(2S) \rightarrow h_c(1P)\pi^0) = (7.4 \pm 0.5) \times 10^{-4}$. Our first error is their experiment's error and our second error is the systematic error from using our best value.

 $\Gamma(\pi^+\pi^-\pi^0)/\Gamma_{\text{total}}$ Γ_{10}/Γ

VALUE (units 10 ⁻³)	CL%	EVTS	DOCUMENT ID	TECN	COMMENT
---------------------------------	-----	------	-------------	------	---------

1.9 ± 0.5 ± 0.1 101 1 ABLIKIM 19AG BES3 $\psi(2S) \rightarrow \pi^0h_c(1P)$

• • • We do not use the following data for averages, fits, limits, etc. • • •

< 2.6 90 2 ADAMS 09 CLEO $\psi(2S) \rightarrow \pi^0\gamma\eta_c$

1 ABLIKIM 19AG reports [$\Gamma(h_c(1P) \rightarrow \pi^+\pi^-\pi^0)/\Gamma_{\text{total}}$] × [$B(\psi(2S) \rightarrow h_c(1P)\pi^0)$] = (1.38 ± 0.35 ± 0.17) × 10⁻⁶ which we divide by our best value $B(\psi(2S) \rightarrow h_c(1P)\pi^0) = (7.4 \pm 0.5) \times 10^{-4}$. Our first error is their experiment's error and our second error is the systematic error from using our best value.

2 ADAMS 09 reports [$\Gamma(h_c(1P) \rightarrow \pi^+\pi^-\pi^0)/\Gamma_{\text{total}}$] × [$B(\psi(2S) \rightarrow h_c(1P)\pi^0)$] < 0.19 × 10⁻⁵ which we divide by our best value $B(\psi(2S) \rightarrow h_c(1P)\pi^0) = 7.4 \times 10^{-4}$.

 $\Gamma(\pi^+\pi^-\pi^0\eta)/\Gamma_{\text{total}}$ Γ_{11}/Γ

VALUE (units 10 ⁻³)	EVTS	DOCUMENT ID	TECN	COMMENT
---------------------------------	------	-------------	------	---------

8.3 ± 2.3 ± 0.6 35 1 ABLIKIM 20AH BES3 $\psi(2S) \rightarrow \pi^0h_c(1P)$

1 ABLIKIM 20AH reports [$\Gamma(h_c(1P) \rightarrow \pi^+\pi^-\pi^0\eta)/\Gamma_{\text{total}}$] × [$B(\psi(2S) \rightarrow h_c(1P)\pi^0)$] = (6.2 ± 1.6 ± 0.7) × 10⁻⁶ which we divide by our best value $B(\psi(2S) \rightarrow h_c(1P)\pi^0) = (7.4 \pm 0.5) \times 10^{-4}$. Our first error is their experiment's error and our second error is the systematic error from using our best value.

 $\Gamma(2\pi^+2\pi^-\pi^0)/\Gamma_{\text{total}}$ Γ_{12}/Γ

VALUE (units 10 ⁻²)	EVTS	DOCUMENT ID	TECN	COMMENT
---------------------------------	------	-------------	------	---------

0.94 ± 0.17 OUR AVERAGE 254 1 ABLIKIM 19AG BES3 $\psi(2S) \rightarrow \pi^0h_c(1P)$

0.86 ± 0.16 ± 0.06 254 1 ABLIKIM 19AG BES3 $\psi(2S) \rightarrow \pi^0h_c(1P)$

2.5 ± 0.9 ± 0.2 92 2 ADAMS 09 CLEO $\psi(2S) \rightarrow \pi^0\gamma\eta_c$

1 ABLIKIM 19AG reports [$\Gamma(h_c(1P) \rightarrow 2\pi^+2\pi^-\pi^0)/\Gamma_{\text{total}}$] × [$B(\psi(2S) \rightarrow h_c(1P)\pi^0)$] = (6.40 ± 0.81 ± 0.87) × 10⁻⁶ which we divide by our best value $B(\psi(2S) \rightarrow h_c(1P)\pi^0) = (7.4 \pm 0.5) \times 10^{-4}$. Our first error is their experiment's error and our second error is the systematic error from using our best value.

2 ADAMS 09 reports [$\Gamma(h_c(1P) \rightarrow 2\pi^+2\pi^-\pi^0)/\Gamma_{\text{total}}$] × [$B(\psi(2S) \rightarrow h_c(1P)\pi^0)$] = (1.88 ± 0.48 ± 0.47) × 10⁻⁵ which we divide by our best value $B(\psi(2S) \rightarrow h_c(1P)\pi^0) = (7.4 \pm 0.5) \times 10^{-4}$. Our first error is their experiment's error and our second error is the systematic error from using our best value.

 $\Gamma(2\pi^+3\pi^-\pi^0)/\Gamma_{\text{total}}$ Γ_{13}/Γ

VALUE	CL%	DOCUMENT ID	TECN	COMMENT
-------	-----	-------------	------	---------

< 0.010 90 1 ABLIKIM 19AG BES3 $\psi(2S) \rightarrow \pi^0h_c(1P)$

• • • We do not use the following data for averages, fits, limits, etc. • • •

< 0.034 90 2 ADAMS 09 CLEO $\psi(2S) \rightarrow \pi^0\gamma\eta_c$

1 ABLIKIM 19AG reports [$\Gamma(h_c(1P) \rightarrow 2\pi^+3\pi^-\pi^0)/\Gamma_{\text{total}}$] × [$B(\psi(2S) \rightarrow h_c(1P)\pi^0)$] < 7.5 × 10⁻⁶ which we divide by our best value $B(\psi(2S) \rightarrow h_c(1P)\pi^0) = 7.4 \times 10^{-4}$.

2 ADAMS 09 reports [$\Gamma(h_c(1P) \rightarrow 2\pi^+3\pi^-\pi^0)/\Gamma_{\text{total}}$] × [$B(\psi(2S) \rightarrow h_c(1P)\pi^0)$] < 2.5 × 10⁻⁵ which we divide by our best value $B(\psi(2S) \rightarrow h_c(1P)\pi^0) = 7.4 \times 10^{-4}$.

 $\Gamma(K^+K^-\pi^+\pi^-)/\Gamma_{\text{total}}$ Γ_{14}/Γ

VALUE	CL%	DOCUMENT ID	TECN	COMMENT
-------	-----	-------------	------	---------

< 7 × 10⁻⁴ 90 1 ABLIKIM 19AG BES3 $\psi(2S) \rightarrow \pi^0h_c(1P)$

1 ABLIKIM 19AG reports [$\Gamma(h_c(1P) \rightarrow K^+K^-\pi^+\pi^-)/\Gamma_{\text{total}}$] × [$B(\psi(2S) \rightarrow h_c(1P)\pi^0)$] < 0.5 × 10⁻⁶ which we divide by our best value $B(\psi(2S) \rightarrow h_c(1P)\pi^0) = 7.4 \times 10^{-4}$.

 $\Gamma(K^+K^-\pi^+\pi^-\pi^0)/\Gamma_{\text{total}}$ Γ_{15}/Γ

VALUE (units 10 ⁻³)	EVTS	DOCUMENT ID	TECN	COMMENT
---------------------------------	------	-------------	------	---------

3.8 ± 0.8 ± 0.3 80 1 ABLIKIM 20AH BES3 $\psi(2S) \rightarrow \pi^0h_c(1P)$

1 ABLIKIM 20AH reports [$\Gamma(h_c(1P) \rightarrow K^+K^-\pi^+\pi^-\pi^0)/\Gamma_{\text{total}}$] × [$B(\psi(2S) \rightarrow h_c(1P)\pi^0)$] = (2.8 ± 0.5 ± 0.3) × 10⁻⁶ which we divide by our best value $B(\psi(2S) \rightarrow h_c(1P)\pi^0) = (7.4 \pm 0.5) \times 10^{-4}$. Our first error is their experiment's error and our second error is the systematic error from using our best value.

 $\Gamma(K^+K^-\pi^+\pi^-\eta)/\Gamma_{\text{total}}$ Γ_{16}/Γ

VALUE	CL%	EVTS	DOCUMENT ID	TECN	COMMENT
-------	-----	------	-------------	------	---------

< 2.7 × 10⁻³ 90 24 1 ABLIKIM 20AH BES3 $\psi(2S) \rightarrow \pi^0h_c(1P)$

1 ABLIKIM 20AH reports [$\Gamma(h_c(1P) \rightarrow K^+K^-\pi^+\pi^-\eta)/\Gamma_{\text{total}}$] × [$B(\psi(2S) \rightarrow h_c(1P)\pi^0)$] < 2.0 × 10⁻⁶ which we divide by our best value $B(\psi(2S) \rightarrow h_c(1P)\pi^0) = 7.4 \times 10^{-4}$.

 $\Gamma(K^+K^-\pi^0)/\Gamma_{\text{total}}$ Γ_{17}/Γ

VALUE	CL%	EVTS	DOCUMENT ID	TECN	COMMENT
-------	-----	------	-------------	------	---------

< 6 × 10⁻⁴ 90 20 1 ABLIKIM 20AH BES3 $\psi(2S) \rightarrow \pi^0h_c(1P)$

1 ABLIKIM 20AH reports [$\Gamma(h_c(1P) \rightarrow K^+K^-\pi^0)/\Gamma_{\text{total}}$] × [$B(\psi(2S) \rightarrow h_c(1P)\pi^0)$] < 4.8 × 10⁻⁷ which we divide by our best value $B(\psi(2S) \rightarrow h_c(1P)\pi^0) = 7.4 \times 10^{-4}$.

 $\Gamma(K^+K^-\pi^0\eta)/\Gamma_{\text{total}}$ Γ_{18}/Γ

VALUE	CL%	EVTS	DOCUMENT ID	TECN	COMMENT
-------	-----	------	-------------	------	---------

< 2.4 × 10⁻³ 90 20 1 ABLIKIM 20AH BES3 $\psi(2S) \rightarrow \pi^0h_c(1P)$

1 ABLIKIM 20AH reports [$\Gamma(h_c(1P) \rightarrow K^+K^-\pi^0\eta)/\Gamma_{\text{total}}$] × [$B(\psi(2S) \rightarrow h_c(1P)\pi^0)$] < 1.8 × 10⁻⁶ which we divide by our best value $B(\psi(2S) \rightarrow h_c(1P)\pi^0) = 7.4 \times 10^{-4}$.

Meson Particle Listings

$h_c(1P), \chi_{c2}(1P)$

$\Gamma(K^+ K^- \eta)/\Gamma_{total}$			Γ_{19}/Γ		
VALUE	CL%	EVTS	DOCUMENT ID	TECN	COMMENT

$<1.0 \times 10^{-3}$ 90 18 1 ABLIKIM 20AH BES3 $\psi(2S) \rightarrow \pi^0 h_c(1P)$
 1 ABLIKIM 20AH reports $[\Gamma(h_c(1P) \rightarrow K^+ K^- \eta)/\Gamma_{total}] \times [B(\psi(2S) \rightarrow h_c(1P)\pi^0)] < 7.5 \times 10^{-7}$ which we divide by our best value $B(\psi(2S) \rightarrow h_c(1P)\pi^0) = 7.4 \times 10^{-4}$.

$\Gamma(2K^+ 2K^- \pi^0)/\Gamma_{total}$			Γ_{20}/Γ		
VALUE	CL%	EVTS	DOCUMENT ID	TECN	COMMENT

$<2.8 \times 10^{-4}$ 90 11 1 ABLIKIM 20AH BES3 $\psi(2S) \rightarrow \pi^0 h_c(1P)$
 1 ABLIKIM 20AH reports $[\Gamma(h_c(1P) \rightarrow 2K^+ 2K^- \pi^0)/\Gamma_{total}] \times [B(\psi(2S) \rightarrow h_c(1P)\pi^0)] < 2.1 \times 10^{-7}$ which we divide by our best value $B(\psi(2S) \rightarrow h_c(1P)\pi^0) = 7.4 \times 10^{-4}$.

$\Gamma(K_S^0 K^\pm \pi^\mp)/\Gamma_{total}$			Γ_{21}/Γ		
VALUE	CL%	EVTS	DOCUMENT ID	TECN	COMMENT

$<6 \times 10^{-4}$ 90 17 1 ABLIKIM 20AH BES3 $\psi(2S) \rightarrow \pi^0 h_c(1P)$
 1 ABLIKIM 20AH reports $[\Gamma(h_c(1P) \rightarrow K_S^0 K^\pm \pi^\mp)/\Gamma_{total}] \times [B(\psi(2S) \rightarrow h_c(1P)\pi^0)] < 4.8 \times 10^{-7}$ which we divide by our best value $B(\psi(2S) \rightarrow h_c(1P)\pi^0) = 7.4 \times 10^{-4}$.

$\Gamma(K_S^0 K^\pm \pi^\mp \pi^+ \pi^-)/\Gamma_{total}$			Γ_{22}/Γ		
VALUE (units 10^{-3})	EVTS	DOCUMENT ID	TECN	COMMENT	

$3.2 \pm 1.0 \pm 0.2$ 41 1 ABLIKIM 20AH BES3 $\psi(2S) \rightarrow \pi^0 h_c(1P)$
 1 ABLIKIM 20AH reports $[\Gamma(h_c(1P) \rightarrow K_S^0 K^\pm \pi^\mp \pi^+ \pi^-)/\Gamma_{total}] \times [B(\psi(2S) \rightarrow h_c(1P)\pi^0)] = (2.4 \pm 0.7 \pm 0.3) \times 10^{-6}$ which we divide by our best value $B(\psi(2S) \rightarrow h_c(1P)\pi^0) = (7.4 \pm 0.5) \times 10^{-4}$. Our first error is their experiment's error and our second error is the systematic error from using our best value.

RADIATIVE DECAYS

$\Gamma(\gamma\eta)/\Gamma_{total}$			Γ_{23}/Γ		
VALUE (units 10^{-4})	EVTS	DOCUMENT ID	TECN	COMMENT	

$4.7 \pm 1.5 \pm 1.4$ 18 ABLIKIM 16i BES3 $\psi(2S) \rightarrow \pi^0 \gamma \eta$

$\Gamma(\gamma\eta'(958))/\Gamma_{total}$			Γ_{24}/Γ		
VALUE (units 10^{-3})	EVTS	DOCUMENT ID	TECN	COMMENT	

$1.52 \pm 0.27 \pm 0.29$ 44 ABLIKIM 16i BES3 $\psi(2S) \rightarrow \pi^0 \gamma \eta'(958)$

$\Gamma(\gamma\eta_c(1S))/\Gamma_{total}$			Γ_{25}/Γ		
VALUE (units 10^{-2})	EVTS	DOCUMENT ID	TECN	COMMENT	

60 ± 4 OUR FIT
 57 ± 5 OUR AVERAGE

57 ± 4 ± 4 23k 1 ABLIKIM 22AQ BES3 $\psi(2S) \rightarrow \pi^0$ hadrons;
 $\pi^0 \gamma(\eta_c)$

56 ± 6 ± 4 2 DOBBS 08A CLEO $\psi(2S) \rightarrow \pi^0 \eta_c \gamma$

••• We do not use the following data for averages, fits, limits, etc. •••

62 ± 9 ± 4 3679 3,4 ABLIKIM 10B BES3 $\psi(2S) \rightarrow \pi^0 \eta_c \gamma$

56 ± 7 ± 4 1282 5 DOBBS 08A CLEO $\psi(2S) \rightarrow \pi^0 \eta_c \gamma$

54 ± 14 ± 4 168 6 ROSNER 05 CLEO $\psi(2S) \rightarrow \pi^0 \eta_c \gamma$

1 ABLIKIM 22AQ reports $[\Gamma(h_c(1P) \rightarrow \gamma \eta_c(1S))/\Gamma_{total}] \times [B(\psi(2S) \rightarrow h_c(1P)\pi^0)] = (4.22^{+0.27}_{-0.26} \pm 0.19) \times 10^{-4}$ which we divide by our best value $B(\psi(2S) \rightarrow h_c(1P)\pi^0) = (7.4 \pm 0.5) \times 10^{-4}$. Our first error is their experiment's error and our second error is the systematic error from using our best value.

2 Average of DOBBS 08A and ROSNER 05. DOBBS 08A reports $[\Gamma(h_c(1P) \rightarrow \gamma \eta_c(1S))/\Gamma_{total}] \times [B(\psi(2S) \rightarrow h_c(1P)\pi^0)] = (4.16 \pm 0.30 \pm 0.37) \times 10^{-4}$ which we divide by our best value $B(\psi(2S) \rightarrow h_c(1P)\pi^0) = (7.4 \pm 0.5) \times 10^{-4}$. Our first error is their experiment's error and our second error is the systematic error from using our best value.

3 ABLIKIM 10B reports $[\Gamma(h_c(1P) \rightarrow \gamma \eta_c(1S))/\Gamma_{total}] \times [B(\psi(2S) \rightarrow h_c(1P)\pi^0)] = (4.58 \pm 0.40 \pm 0.50) \times 10^{-4}$ which we divide by our best value $B(\psi(2S) \rightarrow h_c(1P)\pi^0) = (7.4 \pm 0.5) \times 10^{-4}$. Our first error is their experiment's error and our second error is the systematic error from using our best value.

4 Superseded by ABLIKIM 22AQ

5 DOBBS 08A reports $[\Gamma(h_c(1P) \rightarrow \gamma \eta_c(1S))/\Gamma_{total}] \times [B(\psi(2S) \rightarrow h_c(1P)\pi^0)] = (4.19 \pm 0.32 \pm 0.45) \times 10^{-4}$ which we divide by our best value $B(\psi(2S) \rightarrow h_c(1P)\pi^0) = (7.4 \pm 0.5) \times 10^{-4}$. Our first error is their experiment's error and our second error is the systematic error from using our best value.

6 ROSNER 05 reports $[\Gamma(h_c(1P) \rightarrow \gamma \eta_c(1S))/\Gamma_{total}] \times [B(\psi(2S) \rightarrow h_c(1P)\pi^0)] = (4.0 \pm 0.8 \pm 0.7) \times 10^{-4}$ which we divide by our best value $B(\psi(2S) \rightarrow h_c(1P)\pi^0) = (7.4 \pm 0.5) \times 10^{-4}$. Our first error is their experiment's error and our second error is the systematic error from using our best value.

$h_c(1P)$ REFERENCES

ABLIKIM 22AQ PR D106 072007	M. Ablikim et al.	(BESIII Collab.)
ABLIKIM 22M JHEP 2205 108	M. Ablikim et al.	(BESIII Collab.)
Also JHEP 2303 022 (errata)	M. Ablikim et al.	(BESIII Collab.)
ABLIKIM 22N JHEP 2205 003	M. Ablikim et al.	(BESIII Collab.)
ABLIKIM 20AH PR D102 112007	M. Ablikim et al.	(BESIII Collab.)
ABLIKIM 19AG PR D99 072008	M. Ablikim et al.	(BESIII Collab.)
ABLIKIM 18M PR D97 052008	M. Ablikim et al.	(BESIII Collab.)
ABLIKIM 16i PRL 116 251802	M. Ablikim et al.	(BESIII Collab.)
ABLIKIM 13V PR D88 112001	M. Ablikim et al.	(BESIII Collab.)
ABLIKIM 12N PR D86 092009	M. Ablikim et al.	(BESIII Collab.)
ABLIKIM 10B PRL 104 132002	M. Ablikim et al.	(BESIII Collab.)

ADAMS 09 PR D80 051106	G.S. Adams et al.	(CLEO Collab.)
DOBBS 08A PRL 101 182003	S. Dobbs et al.	(CLEO Collab.)
ANDREOTTI 05B PR D72 032001	M. Andreotti et al.	(FNAL E835 Collab.)
ROSNER 05 PRL 95 102003	J.L. Rosner et al.	(CLEO Collab.)
AULCHENKO 03 PL B573 63	V.M. Aulchenko et al.	(KEDR Collab.)
ANTONIAZZI 94 PR D50 4258	L. Antoniazzi et al.	(E705 Collab.)
ARMSTRONG 93B PR D47 772	T.A. Armstrong et al.	(FNAL E760 Collab.)
ARMSTRONG 92D PRL 69 2337	T.A. Armstrong et al.	(FNAL, FERR, GENO+)
BAGLIN 86 PL B171 135	C. Baglin et al.	(LAPP, CERN, TORI, STRB+)

$\chi_{c2}(1P)$

$$J^G(J^{PC}) = 0^+(2^+ +)$$

See the Review on "Branching Ratios of $\psi(2S), \chi_{c0,1,2}$ and $\eta_c(1S)$ " before the $\chi_{c0}(1P)$ Listings.

$\chi_{c2}(1P)$ MASS

VALUE (MeV)	EVTS	DOCUMENT ID	TECN	COMMENT
3556.17 ± 0.07 OUR AVERAGE				
3557.3 ± 1.7 ± 0.7	611	1 AAIJ 17Bb LHCB		$p\bar{p} \rightarrow b\bar{b}X \rightarrow 2(K^+ K^-)X$
3556.10 ± 0.06 ± 0.11	4.0k	2 AAIJ 17Bi LHCB		$\chi_{c2} \rightarrow J/\psi \mu^+ \mu^-$
3555.3 ± 0.6 ± 2.2	2.5k	UEHARA 08 BELL		$\gamma\gamma \rightarrow$ hadrons
3555.70 ± 0.59 ± 0.39		ABLIKIM 05G BES2		$\psi(2S) \rightarrow \gamma \chi_{c2}$
3556.173 ± 0.123 ± 0.020		ANDREOTTI 05A E835		$p\bar{p} \rightarrow e^+ e^- \gamma$
3559.9 ± 2.9		EISENSTEIN 01 CLE2		$e^+ e^- \rightarrow e^+ e^- \chi_{c2}$
3556.4 ± 0.7		BAI 99B BES		$\psi(2S) \rightarrow \gamma X$
3556.22 ± 0.131 ± 0.020	585	3 ARMSTRONG 92 E760		$\bar{p}p \rightarrow e^+ e^- \gamma$
3556.9 ± 0.4 ± 0.5	50	BAGLIN 86B SPEC		$\bar{p}p \rightarrow e^+ e^- X$
3557.8 ± 0.2 ± 4		4 GAISER 86 CBAL		$\psi(2S) \rightarrow \gamma X$
3553.4 ± 2.2	66	5 LEMOIGNE 82 GOLI		$185 \pi^- \text{Be} \rightarrow \gamma \mu^+ \mu^- A$
3555.9 ± 0.7		6 OREGLIA 82 CBAL		$e^+ e^- \rightarrow J/\psi 2\gamma$
3557 ± 1.5	69	7 HIMEL 80 MRK2		$e^+ e^- \rightarrow J/\psi 2\gamma$
3551 ± 11	15	BRANDELIC 79B DASP		$e^+ e^- \rightarrow J/\psi 2\gamma$
3553 ± 4		7 BARTEL 78B CNTR		$e^+ e^- \rightarrow J/\psi 2\gamma$
3553 ± 4 ± 4		7,8 TANENBAUM 78 MRK1		$e^+ e^-$
3563 ± 7	360	7 BIDDICK 77 CNTR		$e^+ e^- \rightarrow \gamma X$
••• We do not use the following data for averages, fits, limits, etc. •••				
3555.4 ± 1.3	53	UEHARA 13 BELL		$\gamma\gamma \rightarrow K_S^0 K_S^0$
3543 ± 10	4	WHITAKER 76 MRK1		$e^+ e^- \rightarrow J/\psi 2\gamma$

1 From a fit of the $\phi\phi$ invariant mass with the width of $\chi_{c2}(1P)$ fixed to the PDG 16 value.

2 AAIJ 17Bi reports also $m(\chi_{c2}) - m(\chi_{c1}) = 45.39 \pm 0.07 \pm 0.03$ MeV.

3 Recalculated by ANDREOTTI 05A, using the value of $\psi(2S)$ mass from AULCHENKO 03.

4 Using mass of $\psi(2S) = 3686.0$ MeV.

5 $J/\psi(1S)$ mass constrained to 3097 MeV.

6 Assuming $\psi(2S)$ mass = 3686 MeV and $J/\psi(1S)$ mass = 3097 MeV.

7 Mass value shifted by us by amount appropriate for $\psi(2S)$ mass = 3686 MeV and $J/\psi(1S)$ mass = 3097 MeV.

8 From a simultaneous fit to radiative and hadronic decay channels.

$\chi_{c2}(1P)$ WIDTH

VALUE (MeV)	EVTS	DOCUMENT ID	TECN	COMMENT
1.98 ± 0.09 OUR FIT				Error includes scale factor of 1.1.
2.00 ± 0.11 OUR AVERAGE				
2.10 ± 0.20 ± 0.02	4.0k	AAIJ 17Bi LHCB		$\chi_{c2} \rightarrow J/\psi \mu^+ \mu^-$
1.915 ± 0.188 ± 0.013		ANDREOTTI 05A E835		$p\bar{p} \rightarrow e^+ e^- \gamma$
1.96 ± 0.17 ± 0.07	585	1 ARMSTRONG 92 E760		$\bar{p}p \rightarrow e^+ e^- \gamma$
2.6 $^{+1.4}_{-1.0}$	50	BAGLIN 86B SPEC		$\bar{p}p \rightarrow e^+ e^- X$
2.8 $^{+2.1}_{-2.0}$		2 GAISER 86 CBAL		$\psi(2S) \rightarrow \gamma X$

1 Recalculated by ANDREOTTI 05A.

2 Errors correspond to 90% confidence level; authors give only width range.

$\chi_{c2}(1P)$ DECAY MODES

Mode	Fraction (Γ_i/Γ)	Scale factor/ Confidence level
Hadronic decays		
Γ_1 $2(\pi^+ \pi^-)$	(1.00 ± 0.13) %	S=1.4
Γ_2 $\rho\rho$		
Γ_3 $\pi^+ \pi^- \pi^0 \pi^0$	(1.86 ± 0.24) %	
Γ_4 $\rho^+ \pi^- \pi^0 + c.c.$	(2.22 ± 0.35) %	
Γ_5 $4\pi^0$	(1.13 ± 0.15) × 10 ⁻³	
Γ_6 $K^+ K^- \pi^0 \pi^0$	(2.1 ± 0.4) × 10 ⁻³	
Γ_7 $K^+ \pi^- \bar{K}^0 \pi^0 + c.c.$	(1.41 ± 0.20) %	
Γ_8 $\rho^- K^+ \bar{K}^0 + c.c.$	(4.2 ± 1.3) × 10 ⁻³	
Γ_9 $K^*(892)^0 K^- \pi^+ \rightarrow K^- \pi^+ K^0 \pi^0 + c.c.$	(3.0 ± 0.8) × 10 ⁻³	
Γ_{10} $K^*(892)^0 \bar{K}^0 \pi^0 \rightarrow K^+ \pi^- \bar{K}^0 \pi^0 + c.c.$	(3.9 ± 0.9) × 10 ⁻³	

Meson Particle Listings

$\chi_{c2}(1P)$

139 ± 55 ± 21	2,3 ACCIARRI	99E L3	$e^+e^- \rightarrow e^+e^-\chi_{c2}$
242 ± 65 ± 51	2,4 ACKER...K...	98 OPAL	$e^+e^- \rightarrow e^+e^-\chi_{c2}$
150 ± 42 ± 36	2,5 DOMINICK	94 CLE2	$e^+e^- \rightarrow e^+e^-\chi_{c2}$
470 ± 240 ± 120	2,6 BAUER	93 TPC	$e^+e^- \rightarrow e^+e^-\chi_{c2}$

• • • We do not use the following data for averages, fits, limits, etc. • • •

114 ± 11 ± 9	136	2,7 ABE	02T BELL	$e^+e^- \rightarrow e^+e^-\chi_{c2}$
--------------	-----	---------	----------	--------------------------------------

¹ Calculated from the measured $\Gamma_{\gamma\gamma} \times B(\chi_{c2}(1S) \rightarrow \gamma J/\psi(1S)) \times B(J/\psi(1S) \rightarrow \ell^+\ell^-) = 14.8 \pm 0.3 \pm 0.7$ eV, using $B(J/\psi(1S) \rightarrow \ell^+\ell^-) = 11.93 \pm 0.05\%$.

² Calculated by us using $B(J/\psi \rightarrow \ell^+\ell^-) = 0.1187 \pm 0.0008$.

³ The value for $\Gamma(\chi_{c2} \rightarrow \gamma\gamma)$ reported in ACCIARRI 99E is derived using $B(\chi_{c2} \rightarrow \gamma J/\psi(1S)) \times B(J/\psi(1S) \rightarrow \ell^+\ell^-) = 0.0162 \pm 0.0014$.

⁴ The value for $\Gamma(\chi_{c2} \rightarrow \gamma\gamma)$ reported in ACKERSTAFF, K 98 is derived using $B(\chi_{c2} \rightarrow \gamma J/\psi(1S)) = 0.135 \pm 0.011$ and $B(J/\psi(1S) \rightarrow \ell^+\ell^-) = 0.1203 \pm 0.0038$.

⁵ The value for $\Gamma(\chi_{c2} \rightarrow \gamma\gamma)$ reported in DOMINICK 94 is derived using $B(\chi_{c2} \rightarrow \gamma J/\psi(1S)) = 0.135 \pm 0.011$, $B(J/\psi(1S) \rightarrow e^+e^-) = 0.0627 \pm 0.0020$, and $B(J/\psi(1S) \rightarrow \mu^+\mu^-) = 0.0597 \pm 0.0025$.

⁶ The value for $\Gamma(\chi_{c2} \rightarrow \gamma\gamma)$ reported in BAUER 93 is derived using $B(\chi_{c2} \rightarrow \gamma J/\psi(1S)) = 0.135 \pm 0.011$, $B(J/\psi(1S) \rightarrow e^+e^-) = 0.0627 \pm 0.0020$, and $B(J/\psi(1S) \rightarrow \mu^+\mu^-) = 0.0597 \pm 0.0025$.

⁷ All systematic errors added in quadrature. Superseded by SEINO 23.

$\chi_{c2}(1P) \Gamma(i)\Gamma(\gamma\gamma)/\Gamma(\text{total})$

$\Gamma(2(\pi^+\pi^-)) \times \Gamma(\gamma\gamma)/\Gamma_{\text{total}}$					$\Gamma_1 \Gamma_{98}/\Gamma$
VALUE (eV)	EVTs	DOCUMENT ID	TECN	COMMENT	
5.8 ± 0.7 OUR FIT				Error includes scale factor of 1.4.	
5.2 ± 0.7 OUR AVERAGE					
5.01 ± 0.44 ± 0.55	1597 ± 138	UEHARA	08 BELL	$\gamma\gamma \rightarrow \chi_{c2} \rightarrow 2(\pi^+\pi^-)$	
6.4 ± 1.8 ± 0.8		EISENSTEIN	01 CLE2	$e^+e^- \rightarrow e^+e^-\chi_{c2}$	

$\Gamma(\rho\rho) \times \Gamma(\gamma\gamma)/\Gamma_{\text{total}}$					$\Gamma_2 \Gamma_{98}/\Gamma$
VALUE (eV)	CL%	EVTs	DOCUMENT ID	TECN	COMMENT
• • • We do not use the following data for averages, fits, limits, etc. • • •					
<7.8	90	<598	UEHARA	08 BELL	$\gamma\gamma \rightarrow \chi_{c2} \rightarrow 2(\pi^+\pi^-)$

$\Gamma(K^+K^-\pi^+\pi^-) \times \Gamma(\gamma\gamma)/\Gamma_{\text{total}}$					$\Gamma_{14} \Gamma_{98}/\Gamma$
VALUE (eV)	EVTs	DOCUMENT ID	TECN	COMMENT	
4.8 ± 0.6 OUR FIT				Error includes scale factor of 1.2.	
4.4 ± 0.4 ± 0.53	780 ± 74	UEHARA	08 BELL	$\gamma\gamma \rightarrow \chi_{c2} \rightarrow K^+K^-\pi^+\pi^-$	

$\Gamma(K^+K^-\pi^+\pi^0) \times \Gamma(\gamma\gamma)/\Gamma_{\text{total}}$					$\Gamma_{15} \Gamma_{98}/\Gamma$
VALUE (eV)	EVTs	DOCUMENT ID	TECN	COMMENT	
6.5 ± 0.9 ± 1.5	1250	DEL-AMO-SA...11M	BABR	$\gamma\gamma \rightarrow K^+K^-\pi^+\pi^0$	

$\Gamma(K^*(892)^0\bar{K}^*(892)^0) \times \Gamma(\gamma\gamma)/\Gamma_{\text{total}}$					$\Gamma_{18} \Gamma_{98}/\Gamma$
VALUE (eV)	EVTs	DOCUMENT ID	TECN	COMMENT	
1.3 ± 0.5 OUR FIT				Error includes scale factor of 2.3.	
0.8 ± 0.17 ± 0.27	151 ± 30	UEHARA	08 BELL	$\gamma\gamma \rightarrow \chi_{c2} \rightarrow K^+K^-\pi^+\pi^-$	

$\Gamma(\phi\phi) \times \Gamma(\gamma\gamma)/\Gamma_{\text{total}}$					$\Gamma_{20} \Gamma_{98}/\Gamma$
VALUE (eV)	EVTs	DOCUMENT ID	TECN	COMMENT	
0.71 ± 0.05 OUR FIT				Error includes scale factor of 1.5.	
0.62 ± 0.07 ± 0.05	89 ± 11	¹ LIU	12B BELL	$\gamma\gamma \rightarrow 2(K^+K^-)$	
• • • We do not use the following data for averages, fits, limits, etc. • • •					
0.58 ± 0.18 ± 0.16	26.5 ± 8.1	UEHARA	08 BELL	$\gamma\gamma \rightarrow \chi_{c2} \rightarrow 2(K^+K^-)$	
¹ Supersedes UEHARA 08. Using $B(\phi \rightarrow K^+K^-) = (48.9 \pm 0.5)\%$.					

$\Gamma(\omega\omega) \times \Gamma(\gamma\gamma)/\Gamma_{\text{total}}$					$\Gamma_{22} \Gamma_{98}/\Gamma$
VALUE (eV)	CL%	DOCUMENT ID	TECN	COMMENT	
• • • We do not use the following data for averages, fits, limits, etc. • • •					
<0.64	90	¹ LIU	12B BELL	$\gamma\gamma \rightarrow 2(\pi^+\pi^-\pi^0)$	
¹ Using $B(\omega \rightarrow \pi^+\pi^-\pi^0) = (89.2 \pm 0.7)\%$.					

$\Gamma(\omega\phi) \times \Gamma(\gamma\gamma)/\Gamma_{\text{total}}$					$\Gamma_{24} \Gamma_{98}/\Gamma$
VALUE (eV)	CL%	DOCUMENT ID	TECN	COMMENT	
• • • We do not use the following data for averages, fits, limits, etc. • • •					
<0.04	90	¹ LIU	12B BELL	$\gamma\gamma \rightarrow K^+K^-\pi^+\pi^-\pi^0$	
¹ Using $B(\phi \rightarrow K^+K^-) = (48.9 \pm 0.5)\%$ and $B(\omega \rightarrow \pi^+\pi^-\pi^0) = (89.2 \pm 0.7)\%$.					

$\Gamma(\pi\pi) \times \Gamma(\gamma\gamma)/\Gamma_{\text{total}}$					$\Gamma_{25} \Gamma_{98}/\Gamma$
VALUE (eV)	EVTs	DOCUMENT ID	TECN	COMMENT	
1.31 ± 0.08 OUR FIT				Error includes scale factor of 1.2.	
1.18 ± 0.25 OUR AVERAGE					
1.44 ± 0.54 ± 0.47	34 ± 13	¹ UEHARA	09 BELL	$10.6 e^+e^- \rightarrow e^+e^-\pi^0\pi^0$	
1.14 ± 0.21 ± 0.17	54 ± 10	² NAKAZAWA	05 BELL	$10.6 e^+e^- \rightarrow e^+e^-\pi^+\pi^-$	

¹ We multiplied the measurement by 3 to convert from $\pi^0\pi^0$ to $\pi\pi$. Interference with the continuum included.
² We have multiplied $\pi^+\pi^-$ measurement by 3/2 to obtain $\pi\pi$.

$\Gamma(\rho^0\pi^+\pi^-) \times \Gamma(\gamma\gamma)/\Gamma_{\text{total}}$					$\Gamma_{26} \Gamma_{98}/\Gamma$
VALUE (eV)	EVTs	DOCUMENT ID	TECN	COMMENT	
2.1 ± 0.9 OUR FIT					
3.2 ± 1.9 ± 0.5	986 ± 578	UEHARA	08 BELL	$\gamma\gamma \rightarrow \chi_{c2} \rightarrow 2(\pi^+\pi^-)$	

$\Gamma(\eta\eta) \times \Gamma(\gamma\gamma)/\Gamma_{\text{total}}$					$\Gamma_{31} \Gamma_{98}/\Gamma$
VALUE (eV)	EVTs	DOCUMENT ID	TECN	COMMENT	
0.53 ± 0.22 ± 0.09	8	¹ UEHARA	10A BELL	$10.6 e^+e^- \rightarrow e^+e^-\eta\eta$	
¹ Interference with the continuum not included.					

$\Gamma(K^+K^-) \times \Gamma(\gamma\gamma)/\Gamma_{\text{total}}$					$\Gamma_{32} \Gamma_{98}/\Gamma$
VALUE (eV)	EVTs	DOCUMENT ID	TECN	COMMENT	
0.59 ± 0.09 OUR FIT				Error includes scale factor of 2.1.	
0.44 ± 0.11 ± 0.07	33 ± 8	NAKAZAWA	05 BELL	$10.6 e^+e^- \rightarrow e^+e^-K^+K^-$	

$\Gamma(K_S^0 K_S^0) \times \Gamma(\gamma\gamma)/\Gamma_{\text{total}}$					$\Gamma_{33} \Gamma_{98}/\Gamma$
VALUE (eV)	EVTs	DOCUMENT ID	TECN	COMMENT	
0.307 ± 0.026 OUR FIT				Error includes scale factor of 1.1.	
0.27 ± 0.07 ± 0.03	53	¹ UEHARA	13 BELL	$\gamma\gamma \rightarrow K_S^0 K_S^0$	
• • • We do not use the following data for averages, fits, limits, etc. • • •					
0.31 ± 0.05 ± 0.03	38 ± 7	CHEN	07B BELL	$e^+e^- \rightarrow e^+e^-\chi_{c2}$	
¹ Supersedes CHEN 07B.					

$\Gamma(\bar{K}^0 K^+\pi^- + \text{c.c.}) \times \Gamma(\gamma\gamma)/\Gamma_{\text{total}}$					$\Gamma_{42} \Gamma_{98}/\Gamma$
VALUE (eV)	EVTs	DOCUMENT ID	TECN	COMMENT	
0.75 ± 0.11 OUR FIT					
1.20 ± 0.33 ± 0.13	126	¹ DEL-AMO-SA...11M	BABR	$\gamma\gamma \rightarrow K_S^0 K^\pm \pi^\mp$	
¹ We have multiplied $\bar{K}^0 K^+\pi^-$ by 2/3 to obtain $\bar{K}^0 K^+\pi^- + \text{c.c.}$					

$\Gamma(K^+K^-K^+K^-) \times \Gamma(\gamma\gamma)/\Gamma_{\text{total}}$					$\Gamma_{51} \Gamma_{98}/\Gamma$
VALUE (eV)	EVTs	DOCUMENT ID	TECN	COMMENT	
0.97 ± 0.13 OUR FIT				Error includes scale factor of 1.1.	
1.10 ± 0.21 ± 0.15	126 ± 24	UEHARA	08 BELL	$\gamma\gamma \rightarrow \chi_{c2} \rightarrow 2(K^+K^-)$	

$\Gamma(\eta_c(1S)\pi^+\pi^-) \times \Gamma(\gamma\gamma)/\Gamma_{\text{total}}$					$\Gamma_{93} \Gamma_{98}/\Gamma$
VALUE (eV)	CL%	DOCUMENT ID	TECN	COMMENT	
<15.7	90	LEES	12AE BABR	$e^+e^- \rightarrow e^+e^-\pi^+\pi^-\eta_c$	

$\chi_{c2}(1P)$ BRANCHING RATIOS

HADRONIC DECAYS

$\Gamma(\rho^0\pi^+\pi^-)/\Gamma(2(\pi^+\pi^-))$				Γ_{26}/Γ_1
VALUE	DOCUMENT ID	TECN	COMMENT	
0.36 ± 0.15 OUR FIT				
0.31 ± 0.17	TANENBAUM	78 MRK1	$\psi(2S) \rightarrow \gamma\chi_{c2}$	

$\Gamma(\pi^+\pi^-\pi^0\pi^0)/\Gamma_{\text{total}}$				Γ_3/Γ
VALUE (%)	EVTs	DOCUMENT ID	TECN	COMMENT
1.86 ± 0.23 ± 0.05	903.5	¹ HE	08B CLEO	$e^+e^- \rightarrow \gamma h^+ h^- h^0 h^0$
¹ HE 08B reports $1.87 \pm 0.07 \pm 0.22 \pm 0.13\%$ from a measurement of $[\Gamma(\chi_{c2}(1P) \rightarrow \pi^+\pi^-\pi^0\pi^0)/\Gamma_{\text{total}}] \times [B(\psi(2S) \rightarrow \gamma\chi_{c2}(1P))]$ assuming $B(\psi(2S) \rightarrow \gamma\chi_{c2}(1P)) = (9.33 \pm 0.14 \pm 0.61) \times 10^{-2}$, which we rescale to our best value $B(\psi(2S) \rightarrow \gamma\chi_{c2}(1P)) = (9.36 \pm 0.23) \times 10^{-2}$. Our first error is their experiment's error and our second error is the systematic error from using our best value.				

$\Gamma(\rho^+\pi^-\pi^0 + \text{c.c.})/\Gamma_{\text{total}}$				Γ_4/Γ
VALUE (%)	EVTs	DOCUMENT ID	TECN	COMMENT
2.22 ± 0.34 ± 0.05	1031.9	^{1,2} HE	08B CLEO	$e^+e^- \rightarrow \gamma h^+ h^- h^0 h^0$
¹ HE 08B reports $2.23 \pm 0.11 \pm 0.32 \pm 0.16\%$ from a measurement of $[\Gamma(\chi_{c2}(1P) \rightarrow \rho^+\pi^-\pi^0 + \text{c.c.})/\Gamma_{\text{total}}] \times [B(\psi(2S) \rightarrow \gamma\chi_{c2}(1P))]$ assuming $B(\psi(2S) \rightarrow \gamma\chi_{c2}(1P)) = (9.33 \pm 0.14 \pm 0.61) \times 10^{-2}$, which we rescale to our best value $B(\psi(2S) \rightarrow \gamma\chi_{c2}(1P)) = (9.36 \pm 0.23) \times 10^{-2}$. Our first error is their experiment's error and our second error is the systematic error from using our best value.				
² Calculated by us. We have added the values from HE 08B for $\rho^+\pi^-\pi^0$ and $\rho^-\pi^+\pi^0$ decays assuming uncorrelated statistical and fully correlated systematic uncertainties.				

$\Gamma(4\pi^0)/\Gamma_{\text{total}}$				Γ_5/Γ
VALUE (units 10^{-3})	EVTs	DOCUMENT ID	TECN	COMMENT
1.13 ± 0.15 ± 0.03	1164	¹ ABLIKIM	11A BES3	$e^+e^- \rightarrow \psi(2S) \rightarrow \gamma\chi_{c2}$
¹ ABLIKIM 11A reports $(1.21 \pm 0.05 \pm 0.16) \times 10^{-3}$ from a measurement of $[\Gamma(\chi_{c2}(1P) \rightarrow 4\pi^0)/\Gamma_{\text{total}}] \times [B(\psi(2S) \rightarrow \gamma\chi_{c2}(1P))]$ assuming $B(\psi(2S) \rightarrow \gamma\chi_{c2}(1P)) = (8.74 \pm 0.35) \times 10^{-2}$, which we rescale to our best value $B(\psi(2S) \rightarrow \gamma\chi_{c2}(1P)) = (9.36 \pm 0.23) \times 10^{-2}$. Our first error is their experiment's error and our second error is the systematic error from using our best value.				

See key on page 1171

Meson Particle Listings

$\chi_{c2}(1P)$

$\Gamma(K^+ K^- \pi^0 \pi^0)/\Gamma_{total}$					Γ_6/Γ
VALUE (%)	EVTS	DOCUMENT ID	TECN	COMMENT	

0.21 ± 0.04 ± 0.01 76.9 1 HE 08B CLEO $e^+e^- \rightarrow \gamma h^+ h^- h^0 h^0$
 1 HE 08B reports $0.21 \pm 0.03 \pm 0.03 \pm 0.01$ % from a measurement of $[\Gamma(\chi_{c2}(1P) \rightarrow K^+ K^- \pi^0 \pi^0)/\Gamma_{total}] \times [B(\psi(2S) \rightarrow \gamma \chi_{c2}(1P))]$ assuming $B(\psi(2S) \rightarrow \gamma \chi_{c2}(1P)) = (9.33 \pm 0.14 \pm 0.61) \times 10^{-2}$, which we rescale to our best value $B(\psi(2S) \rightarrow \gamma \chi_{c2}(1P)) = (9.36 \pm 0.23) \times 10^{-2}$. Our first error is their experiment's error and our second error is the systematic error from using our best value.

$\Gamma(K^+ \pi^- \bar{K}^0 \pi^0 + c.c.)/\Gamma_{total}$					Γ_7/Γ
VALUE (%)	EVTS	DOCUMENT ID	TECN	COMMENT	

1.41 ± 0.20 ± 0.03 211.6 1 HE 08B CLEO $e^+e^- \rightarrow \gamma h^+ h^- h^0 h^0$
 1 HE 08B reports $1.41 \pm 0.11 \pm 0.16 \pm 0.10$ % from a measurement of $[\Gamma(\chi_{c2}(1P) \rightarrow K^+ \pi^- \bar{K}^0 \pi^0 + c.c.)/\Gamma_{total}] \times [B(\psi(2S) \rightarrow \gamma \chi_{c2}(1P))]$ assuming $B(\psi(2S) \rightarrow \gamma \chi_{c2}(1P)) = (9.33 \pm 0.14 \pm 0.61) \times 10^{-2}$, which we rescale to our best value $B(\psi(2S) \rightarrow \gamma \chi_{c2}(1P)) = (9.36 \pm 0.23) \times 10^{-2}$. Our first error is their experiment's error and our second error is the systematic error from using our best value.

$\Gamma(\rho^- K^+ \bar{K}^0 + c.c.)/\Gamma_{total}$					Γ_8/Γ
VALUE (%)	EVTS	DOCUMENT ID	TECN	COMMENT	

0.42 ± 0.13 ± 0.01 62.9 1 HE 08B CLEO $e^+e^- \rightarrow \gamma h^+ h^- h^0 h^0$
 1 HE 08B reports $0.42 \pm 0.11 \pm 0.06 \pm 0.03$ % from a measurement of $[\Gamma(\chi_{c2}(1P) \rightarrow \rho^- K^+ \bar{K}^0 + c.c.)/\Gamma_{total}] \times [B(\psi(2S) \rightarrow \gamma \chi_{c2}(1P))]$ assuming $B(\psi(2S) \rightarrow \gamma \chi_{c2}(1P)) = (9.33 \pm 0.14 \pm 0.61) \times 10^{-2}$, which we rescale to our best value $B(\psi(2S) \rightarrow \gamma \chi_{c2}(1P)) = (9.36 \pm 0.23) \times 10^{-2}$. Our first error is their experiment's error and our second error is the systematic error from using our best value.

$\Gamma(K^*(892)^0 K^- \pi^+ \rightarrow K^- \pi^+ K^0 \pi^0 + c.c.)/\Gamma_{total}$					Γ_9/Γ
VALUE (%)	EVTS	DOCUMENT ID	TECN	COMMENT	

0.30 ± 0.08 ± 0.01 38.7 1 HE 08B CLEO $e^+e^- \rightarrow \gamma h^+ h^- h^0 h^0$
 1 HE 08B reports $0.30 \pm 0.07 \pm 0.04 \pm 0.02$ % from a measurement of $[\Gamma(\chi_{c2}(1P) \rightarrow K^*(892)^0 K^- \pi^+ \rightarrow K^- \pi^+ K^0 \pi^0 + c.c.)/\Gamma_{total}] \times [B(\psi(2S) \rightarrow \gamma \chi_{c2}(1P))]$ assuming $B(\psi(2S) \rightarrow \gamma \chi_{c2}(1P)) = (9.33 \pm 0.14 \pm 0.61) \times 10^{-2}$, which we rescale to our best value $B(\psi(2S) \rightarrow \gamma \chi_{c2}(1P)) = (9.36 \pm 0.23) \times 10^{-2}$. Our first error is their experiment's error and our second error is the systematic error from using our best value.

$\Gamma(K^*(892)^0 \bar{K}^0 \pi^0 \rightarrow K^+ \pi^- \bar{K}^0 \pi^0 + c.c.)/\Gamma_{total}$					Γ_{10}/Γ
VALUE (%)	EVTS	DOCUMENT ID	TECN	COMMENT	

0.39 ± 0.09 ± 0.01 63.0 1 HE 08B CLEO $e^+e^- \rightarrow \gamma h^+ h^- h^0 h^0$
 1 HE 08B reports $0.39 \pm 0.07 \pm 0.05 \pm 0.03$ % from a measurement of $[\Gamma(\chi_{c2}(1P) \rightarrow K^*(892)^0 \bar{K}^0 \pi^0 \rightarrow K^+ \pi^- \bar{K}^0 \pi^0 + c.c.)/\Gamma_{total}] \times [B(\psi(2S) \rightarrow \gamma \chi_{c2}(1P))]$ assuming $B(\psi(2S) \rightarrow \gamma \chi_{c2}(1P)) = (9.33 \pm 0.14 \pm 0.61) \times 10^{-2}$, which we rescale to our best value $B(\psi(2S) \rightarrow \gamma \chi_{c2}(1P)) = (9.36 \pm 0.23) \times 10^{-2}$. Our first error is their experiment's error and our second error is the systematic error from using our best value.

$\Gamma(K^*(892)^- K^+ \pi^0 \rightarrow K^+ \pi^- \bar{K}^0 \pi^0 + c.c.)/\Gamma_{total}$					Γ_{11}/Γ
VALUE (%)	EVTS	DOCUMENT ID	TECN	COMMENT	

0.38 ± 0.08 ± 0.01 51.1 1 HE 08B CLEO $e^+e^- \rightarrow \gamma h^+ h^- h^0 h^0$
 1 HE 08B reports $0.38 \pm 0.07 \pm 0.04 \pm 0.03$ % from a measurement of $[\Gamma(\chi_{c2}(1P) \rightarrow K^*(892)^- K^+ \pi^0 \rightarrow K^+ \pi^- \bar{K}^0 \pi^0 + c.c.)/\Gamma_{total}] \times [B(\psi(2S) \rightarrow \gamma \chi_{c2}(1P))]$ assuming $B(\psi(2S) \rightarrow \gamma \chi_{c2}(1P)) = (9.33 \pm 0.14 \pm 0.61) \times 10^{-2}$, which we rescale to our best value $B(\psi(2S) \rightarrow \gamma \chi_{c2}(1P)) = (9.36 \pm 0.23) \times 10^{-2}$. Our first error is their experiment's error and our second error is the systematic error from using our best value.

$\Gamma(K^*(892)^+ \bar{K}^0 \pi^- \rightarrow K^+ \pi^- \bar{K}^0 \pi^0 + c.c.)/\Gamma_{total}$					Γ_{12}/Γ
VALUE (%)	EVTS	DOCUMENT ID	TECN	COMMENT	

0.30 ± 0.08 ± 0.01 39.3 1 HE 08B CLEO $e^+e^- \rightarrow \gamma h^+ h^- h^0 h^0$
 1 HE 08B reports $0.30 \pm 0.07 \pm 0.04 \pm 0.02$ % from a measurement of $[\Gamma(\chi_{c2}(1P) \rightarrow K^*(892)^+ \bar{K}^0 \pi^- \rightarrow K^+ \pi^- \bar{K}^0 \pi^0 + c.c.)/\Gamma_{total}] \times [B(\psi(2S) \rightarrow \gamma \chi_{c2}(1P))]$ assuming $B(\psi(2S) \rightarrow \gamma \chi_{c2}(1P)) = (9.33 \pm 0.14 \pm 0.61) \times 10^{-2}$, which we rescale to our best value $B(\psi(2S) \rightarrow \gamma \chi_{c2}(1P)) = (9.36 \pm 0.23) \times 10^{-2}$. Our first error is their experiment's error and our second error is the systematic error from using our best value.

$\Gamma(K^+ K^- \eta \pi^0)/\Gamma_{total}$					Γ_{13}/Γ
VALUE (%)	EVTS	DOCUMENT ID	TECN	COMMENT	

0.130 ± 0.045 ± 0.003 22.9 1 HE 08B CLEO $e^+e^- \rightarrow \gamma h^+ h^- h^0 h^0$
 1 HE 08B reports $0.13 \pm 0.04 \pm 0.02 \pm 0.01$ % from a measurement of $[\Gamma(\chi_{c2}(1P) \rightarrow K^+ K^- \eta \pi^0)/\Gamma_{total}] \times [B(\psi(2S) \rightarrow \gamma \chi_{c2}(1P))]$ assuming $B(\psi(2S) \rightarrow \gamma \chi_{c2}(1P)) = (9.33 \pm 0.14 \pm 0.61) \times 10^{-2}$, which we rescale to our best value $B(\psi(2S) \rightarrow \gamma \chi_{c2}(1P)) = (9.36 \pm 0.23) \times 10^{-2}$. Our first error is their experiment's error and our second error is the systematic error from using our best value.

$\Gamma(K^+ K^- \pi^+ \pi^- \pi^0)/\Gamma_{total}$					Γ_{15}/Γ
VALUE (units 10^{-3})	EVTS	DOCUMENT ID	TECN	COMMENT	

11.69 ± 0.13 ± 1.31 11k 1 ABLIKIM 13B BES3 $e^+e^- \rightarrow \psi(2S) \rightarrow \gamma \chi_{c2}$
 1 Using 1.06×10^8 $\psi(2S)$ mesons and $B(\psi(2S) \rightarrow \chi_{c2} \gamma) = (8.72 \pm 0.34)$ %.

$\Gamma(K_S^0 K^\pm \pi^\mp \pi^\pm \pi^-)/\Gamma_{total}$					Γ_{16}/Γ
VALUE (units 10^{-3})	EVTS	DOCUMENT ID	TECN	COMMENT	

7.30 ± 0.11 ± 0.75 4.5k 1 ABLIKIM 13B BES3 $e^+e^- \rightarrow \psi(2S) \rightarrow \gamma \chi_{c2}$
 1 Using 1.06×10^8 $\psi(2S)$ mesons and $B(\psi(2S) \rightarrow \chi_{c2} \gamma) = (8.72 \pm 0.34)$ %.

$\Gamma(K^+ \bar{K}^*(892)^0 \pi^- + c.c.)/\Gamma(K^+ K^- \pi^+ \pi^-)$					Γ_{17}/Γ_{14}
VALUE	DOCUMENT ID	TECN	COMMENT		

0.25 ± 0.13 OUR FIT 0.25 ± 0.13 TANENBAUM 78 MRK1 $\psi(2S) \rightarrow \gamma \chi_{c2}$

$\Gamma(3(\pi^+ \pi^-))/\Gamma_{total}$					Γ_{19}/Γ
VALUE (units 10^{-3})	EVTS	DOCUMENT ID	TECN	COMMENT	

15.3 ± 1.9 OUR AVERAGE Error includes scale factor of 3.8.
 15.9 ± 0.4 ± 0.4 112K 1 ABLIKIM 22Q BES3 $\psi(2S) \rightarrow \gamma 3(\pi^+ \pi^-)$
 8.6 ± 0.9 ± 1.6 2 BAI 99B BES $\psi(2S) \rightarrow \gamma \chi_{c2}$
 8.7 ± 5.9 ± 0.4 2 TANENBAUM 78 MRK1 $\psi(2S) \rightarrow \gamma \chi_{c2}$

1 ABLIKIM 22Q reports $(1.565 \pm 0.005 \pm 0.048) \times 10^{-2}$ from a measurement of $[\Gamma(\chi_{c2}(1P) \rightarrow 3(\pi^+ \pi^-))/\Gamma_{total}] \times [B(\psi(2S) \rightarrow \gamma \chi_{c2}(1P))]$ assuming $B(\psi(2S) \rightarrow \gamma \chi_{c2}(1P)) = (9.52 \pm 0.20) \times 10^{-2}$, which we rescale to our best value $B(\psi(2S) \rightarrow \gamma \chi_{c2}(1P)) = (9.36 \pm 0.23) \times 10^{-2}$. Our first error is their experiment's error and our second error is the systematic error from using our best value.
 2 Rescaled by us using $B(\psi(2S) \rightarrow \gamma \chi_{c2}) = (8.3 \pm 0.4)$ % and $B(\psi(2S) \rightarrow J/\psi(1S) \pi^+ \pi^-) = (32.6 \pm 0.5)$ %. Multiplied by a factor of 2 to convert from $K_S^0 K^+ \pi^- \rightarrow K^0 K^+ \pi^-$ decay.

$\Gamma(\phi\phi)/\Gamma_{total}$					Γ_{20}/Γ
VALUE (units 10^{-3})	EVTS	DOCUMENT ID	TECN	COMMENT	

1.23 ± 0.07 OUR FIT Error includes scale factor of 1.9.
1.267 ± 0.028 ± 0.033 4247 1 ABLIKIM 23N BES3 $\psi(2S) \rightarrow \gamma$ hadrons
 1 Measured using $B(\psi(2S) \rightarrow \gamma \chi_{c2}(1P)) = (9.75 \pm 0.24) \times 10^{-2}$ and $B(\phi \rightarrow K^+ K^-) = (49.2 \pm 0.5) \times 10^{-2}$ from PDG 22.

$\Gamma(\phi\phi\eta)/\Gamma_{total}$					Γ_{21}/Γ
VALUE (units 10^{-4})	EVTS	DOCUMENT ID	TECN	COMMENT	

5.4 ± 0.7 ± 0.1 143.6 1 ABLIKIM 20B BES3 $\psi(2S) \rightarrow \gamma\phi\phi\eta$
 1 ABLIKIM 20B reports $(5.33 \pm 0.52 \pm 0.39) \times 10^{-4}$ from a measurement of $[\Gamma(\chi_{c2}(1P) \rightarrow \phi\phi\eta)/\Gamma_{total}] \times [B(\psi(2S) \rightarrow \gamma \chi_{c2}(1P))]$ assuming $B(\psi(2S) \rightarrow \gamma \chi_{c2}(1P)) = (9.52 \pm 0.20) \times 10^{-2}$, which we rescale to our best value $B(\psi(2S) \rightarrow \gamma \chi_{c2}(1P)) = (9.36 \pm 0.23) \times 10^{-2}$. Our first error is their experiment's error and our second error is the systematic error from using our best value.

$\Gamma(\omega\omega)/\Gamma_{total}$					Γ_{22}/Γ
VALUE (units 10^{-3})	EVTS	DOCUMENT ID	TECN	COMMENT	

0.86 ± 0.10 OUR AVERAGE
 0.83 ± 0.10 ± 0.02 762 1 ABLIKIM 11K BES3 $\psi(2S) \rightarrow \gamma$ hadrons
 1.76 ± 0.58 ± 0.04 27.7 ± 7.4 2 ABLIKIM 05N BES2 $\psi(2S) \rightarrow \gamma \chi_{c2} \rightarrow \gamma 6\pi$
 1 ABLIKIM 11K reports $(8.9 \pm 0.3 \pm 1.1) \times 10^{-4}$ from a measurement of $[\Gamma(\chi_{c2}(1P) \rightarrow \omega\omega)/\Gamma_{total}] \times [B(\psi(2S) \rightarrow \gamma \chi_{c2}(1P))]$ assuming $B(\psi(2S) \rightarrow \gamma \chi_{c2}(1P)) = (8.74 \pm 0.35) \times 10^{-2}$, which we rescale to our best value $B(\psi(2S) \rightarrow \gamma \chi_{c2}(1P)) = (9.36 \pm 0.23) \times 10^{-2}$. Our first error is their experiment's error and our second error is the systematic error from using our best value.
 2 ABLIKIM 05N reports $[\Gamma(\chi_{c2}(1P) \rightarrow \omega\omega)/\Gamma_{total}] \times [B(\psi(2S) \rightarrow \gamma \chi_{c2}(1P))]$ = $(0.165 \pm 0.044 \pm 0.032) \times 10^{-3}$ which we divide by our best value $B(\psi(2S) \rightarrow \gamma \chi_{c2}(1P)) = (9.36 \pm 0.23) \times 10^{-2}$. Our first error is their experiment's error and our second error is the systematic error from using our best value.

$\Gamma(\omega K^+ K^-)/\Gamma_{total}$					Γ_{23}/Γ
VALUE (units 10^{-3})	EVTS	DOCUMENT ID	TECN	COMMENT	

0.73 ± 0.04 ± 0.08 512 1 ABLIKIM 13B BES3 $e^+e^- \rightarrow \psi(2S) \rightarrow \gamma \chi_{c2}$
 1 Using 1.06×10^8 $\psi(2S)$ mesons and $B(\psi(2S) \rightarrow \chi_{c2} \gamma) = (8.72 \pm 0.34)$ %.

$\Gamma(\omega\phi)/\Gamma_{total}$					Γ_{24}/Γ
VALUE (units 10^{-6})	CL%	EVTS	DOCUMENT ID	TECN	COMMENT

9.7 ± 2.8 ± 0.2 33 1 ABLIKIM 19J BES3 $\psi(2S) \rightarrow \gamma$ hadrons
 ••• We do not use the following data for averages, fits, limits, etc. •••
 <19 90 2,3 ABLIKIM 11K BES3 $\psi(2S) \rightarrow \gamma$ hadrons
 1 ABLIKIM 19J reports $[\Gamma(\chi_{c2}(1P) \rightarrow \omega\phi)/\Gamma_{total}] \times [B(\psi(2S) \rightarrow \gamma \chi_{c2}(1P))]$ = $(0.91 \pm 0.23 \pm 0.12) \times 10^{-6}$ which we divide by our best value $B(\psi(2S) \rightarrow \gamma \chi_{c2}(1P)) = (9.36 \pm 0.23) \times 10^{-2}$. Our first error is their experiment's error and our second error is the systematic error from using our best value.
 2 ABLIKIM 11K reports $< 2 \times 10^{-5}$ from a measurement of $[\Gamma(\chi_{c2}(1P) \rightarrow \omega\phi)/\Gamma_{total}] \times [B(\psi(2S) \rightarrow \gamma \chi_{c2}(1P))]$ assuming $B(\psi(2S) \rightarrow \gamma \chi_{c2}(1P)) = (8.74 \pm 0.35) \times 10^{-2}$, which we rescale to our best value $B(\psi(2S) \rightarrow \gamma \chi_{c2}(1P)) = 9.36 \times 10^{-2}$.
 3 Superseded by ABLIKIM 19J.

$\Gamma(\pi^+ \pi^- \pi^0 (\text{non-resonant}))/\Gamma_{total}$					Γ_{27}/Γ
VALUE (units 10^{-5})	EVTS	DOCUMENT ID	TECN	COMMENT	

2.0 ± 0.4 ± 0.1 64 1 ABLIKIM 17AG BES3 $\psi(2S) \rightarrow \gamma \pi^+ \pi^- \pi^0$
 1 ABLIKIM 17AG reports $(2.1 \pm 0.4 \pm 0.2) \times 10^{-5}$ from a measurement of $[\Gamma(\chi_{c2}(1P) \rightarrow \pi^+ \pi^- \pi^0 (\text{non-resonant}))/\Gamma_{total}] \times [B(\psi(2S) \rightarrow \gamma \chi_{c2}(1P))]$ assuming $B(\psi(2S) \rightarrow \gamma \chi_{c2}(1P)) = (9.11 \pm 0.31) \times 10^{-2}$, which we rescale to our best value $B(\psi(2S) \rightarrow \gamma \chi_{c2}(1P)) = (9.36 \pm 0.23) \times 10^{-2}$. Our first error is their experiment's error and our second error is the systematic error from using our best value.

See key on page 1171

Meson Particle Listings

$\chi_{c2}(1P)$

$\Gamma(K^+ K^- \eta'(958))/\Gamma_{total}$ Γ_{45}/Γ

VALUE (units 10^{-4})	EVTS	DOCUMENT ID	TECN	COMMENT
1.94 ± 0.34	107	¹ ABLIKIM	14j BES3	$\psi(2S) \rightarrow \gamma K^+ K^- \eta'(958)$

¹ Derived using $B(\psi(2S) \rightarrow \gamma \chi_{c2}) = (8.72 \pm 0.34)\%$. Uncertainty includes both statistical and systematic contributions combined in quadrature.

$\Gamma(\eta\eta')/\Gamma_{total}$ Γ_{46}/Γ

VALUE (units 10^{-5})	CL%	EVTS	DOCUMENT ID	TECN	COMMENT
2.2 ± 0.5 ± 0.1		20	¹ ABLIKIM	17A1 BES3	$\psi(2S) \rightarrow \gamma \eta' \eta$

• • • We do not use the following data for averages, fits, limits, etc. • • •

< 6	90	3.3 ± 8.0	² ASNER	09 CLEO	$\psi(2S) \rightarrow \gamma \eta \eta'$
< 23	90		³ ADAMS	07 CLEO	$\psi(2S) \rightarrow \gamma \chi_{c2}$

¹ ABLIKIM 17A1 reports $(2.27 \pm 0.43 \pm 0.25) \times 10^{-5}$ from a measurement of $[\Gamma(\chi_{c2}(1P) \rightarrow \eta \eta')/\Gamma_{total}] \times [B(\psi(2S) \rightarrow \gamma \chi_{c2}(1P))]$ assuming $B(\psi(2S) \rightarrow \gamma \chi_{c2}(1P)) = (9.11 \pm 0.31) \times 10^{-2}$, which we rescale to our best value $B(\psi(2S) \rightarrow \gamma \chi_{c2}(1P)) = (9.36 \pm 0.23) \times 10^{-2}$. Our first error is their experiment's error and our second error is the systematic error from using our best value.

² ASNER 09 reports $< 0.6 \times 10^{-4}$ from a measurement of $[\Gamma(\chi_{c2}(1P) \rightarrow \eta \eta')/\Gamma_{total}] \times [B(\psi(2S) \rightarrow \gamma \chi_{c2}(1P))]$ assuming $B(\psi(2S) \rightarrow \gamma \chi_{c2}(1P)) = (9.33 \pm 0.14 \pm 0.61) \times 10^{-2}$, which we rescale to our best value $B(\psi(2S) \rightarrow \gamma \chi_{c2}(1P)) = 9.36 \times 10^{-2}$.

³ Superseded by ASNER 09. ADAMS 07 reports $< 2.3 \times 10^{-4}$ from a measurement of $[\Gamma(\chi_{c2}(1P) \rightarrow \eta \eta')/\Gamma_{total}] \times [B(\psi(2S) \rightarrow \gamma \chi_{c2}(1P))]$ assuming $B(\psi(2S) \rightarrow \gamma \chi_{c2}(1P)) = 0.0933 \pm 0.0014 \pm 0.0061$, which we rescale to our best value $B(\psi(2S) \rightarrow \gamma \chi_{c2}(1P)) = 9.36 \times 10^{-2}$.

$\Gamma(\eta' \eta')/\Gamma_{total}$ Γ_{47}/Γ

VALUE (units 10^{-5})	CL%	EVTS	DOCUMENT ID	TECN	COMMENT
4.6 ± 0.6 ± 0.1		60	¹ ABLIKIM	17A1 BES3	$\psi(2S) \rightarrow \gamma \eta' \eta'$

• • • We do not use the following data for averages, fits, limits, etc. • • •

< 10	90	12 ± 7	² ASNER	09 CLEO	$\psi(2S) \rightarrow \gamma \eta' \eta'$
< 31	90		³ ADAMS	07 CLEO	$\psi(2S) \rightarrow \gamma \chi_{c2}$

¹ ABLIKIM 17A1 reports $(4.76 \pm 0.56 \pm 0.38) \times 10^{-5}$ from a measurement of $[\Gamma(\chi_{c2}(1P) \rightarrow \eta' \eta')/\Gamma_{total}] \times [B(\psi(2S) \rightarrow \gamma \chi_{c2}(1P))]$ assuming $B(\psi(2S) \rightarrow \gamma \chi_{c2}(1P)) = (9.11 \pm 0.31) \times 10^{-2}$, which we rescale to our best value $B(\psi(2S) \rightarrow \gamma \chi_{c2}(1P)) = (9.36 \pm 0.23) \times 10^{-2}$. Our first error is their experiment's error and our second error is the systematic error from using our best value.

² ASNER 09 reports $< 1.0 \times 10^{-4}$ from a measurement of $[\Gamma(\chi_{c2}(1P) \rightarrow \eta' \eta')/\Gamma_{total}] \times [B(\psi(2S) \rightarrow \gamma \chi_{c2}(1P))]$ assuming $B(\psi(2S) \rightarrow \gamma \chi_{c2}(1P)) = (9.33 \pm 0.14 \pm 0.61) \times 10^{-2}$, which we rescale to our best value $B(\psi(2S) \rightarrow \gamma \chi_{c2}(1P)) = 9.36 \times 10^{-2}$.

³ Superseded by ASNER 09. ADAMS 07 reports $< 3.1 \times 10^{-4}$ from a measurement of $[\Gamma(\chi_{c2}(1P) \rightarrow \eta' \eta')/\Gamma_{total}] \times [B(\psi(2S) \rightarrow \gamma \chi_{c2}(1P))]$ assuming $B(\psi(2S) \rightarrow \gamma \chi_{c2}(1P)) = 0.0933 \pm 0.0014 \pm 0.0061$, which we rescale to our best value $B(\psi(2S) \rightarrow \gamma \chi_{c2}(1P)) = 9.36 \times 10^{-2}$.

$\Gamma(\pi^+ \pi^- K_S^0 K_S^0)/\Gamma_{total}$ Γ_{48}/Γ

VALUE (units 10^{-3})	EVTS	DOCUMENT ID	TECN	COMMENT
2.2 ± 0.5 ± 0.1	57 ± 11	¹ ABLIKIM	05o BES2	$\psi(2S) \rightarrow \gamma \chi_{c2}$

¹ ABLIKIM 05o reports $[\Gamma(\chi_{c2}(1P) \rightarrow \pi^+ \pi^- K_S^0 K_S^0)/\Gamma_{total}] \times [B(\psi(2S) \rightarrow \gamma \chi_{c2}(1P))] = (0.207 \pm 0.039 \pm 0.033) \times 10^{-3}$ which we divide by our best value $B(\psi(2S) \rightarrow \gamma \chi_{c2}(1P)) = (9.36 \pm 0.23) \times 10^{-2}$. Our first error is their experiment's error and our second error is the systematic error from using our best value.

$\Gamma(K^+ K^- K_S^0 K_S^0)/\Gamma_{total}$ Γ_{49}/Γ

VALUE (units 10^{-4})	CL%	EVTS	DOCUMENT ID	TECN	COMMENT
< 4	90	2.3 ± 2.2	¹ ABLIKIM	05o BES2	$e^+ e^- \rightarrow \chi_{c2} \gamma$

¹ ABLIKIM 05o reports $[\Gamma(\chi_{c2}(1P) \rightarrow K^+ K^- K_S^0 K_S^0)/\Gamma_{total}] \times [B(\psi(2S) \rightarrow \gamma \chi_{c2}(1P))] < 3.5 \times 10^{-5}$ which we divide by our best value $B(\psi(2S) \rightarrow \gamma \chi_{c2}(1P)) = 9.36 \times 10^{-2}$.

$\Gamma(K_S^0 K_S^0 K_S^0 K_S^0)/\Gamma_{total}$ Γ_{50}/Γ

VALUE (units 10^{-4})	EVTS	DOCUMENT ID	TECN	COMMENT
1.15 ± 0.18 ± 0.03	68	¹ ABLIKIM	19AA BES3	$\psi(2S) \rightarrow \gamma K_S^0$

¹ Using $B(K_S^0 \rightarrow \pi^+ \pi^-) = (69.20 \pm 0.05)\%$. ABLIKIM 19AA reports $[\Gamma(\chi_{c2}(1P) \rightarrow K_S^0 K_S^0 K_S^0 K_S^0)/\Gamma_{total}] \times [B(\psi(2S) \rightarrow \gamma \chi_{c2}(1P))] = (10.8 \pm 1.5 \pm 0.8) \times 10^{-6}$ which we divide by our best value $B(\psi(2S) \rightarrow \gamma \chi_{c2}(1P)) = (9.36 \pm 0.23) \times 10^{-2}$. Our first error is their experiment's error and our second error is the systematic error from using our best value..

$\Gamma(K^+ K^- \phi)/\Gamma_{total}$ Γ_{52}/Γ

VALUE (units 10^{-3})	EVTS	DOCUMENT ID	TECN	COMMENT
1.45 ± 0.30 ± 0.04	52	¹ ABLIKIM	06T BES2	$\psi(2S) \rightarrow \gamma 2K^+ 2K^-$

¹ ABLIKIM 06T reports $(1.67 \pm 0.26 \pm 0.24) \times 10^{-3}$ from a measurement of $[\Gamma(\chi_{c2}(1P) \rightarrow K^+ K^- \phi)/\Gamma_{total}] \times [B(\psi(2S) \rightarrow \gamma \chi_{c2}(1P))]$ assuming $B(\psi(2S) \rightarrow \gamma \chi_{c2}(1P)) = (8.1 \pm 0.4) \times 10^{-2}$, which we rescale to our best value $B(\psi(2S) \rightarrow \gamma \chi_{c2}(1P)) = (9.36 \pm 0.23) \times 10^{-2}$. Our first error is their experiment's error and our second error is the systematic error from using our best value.

$\Gamma(K^0 K^+ \pi^- \phi + c.c.)/\Gamma_{total}$ Γ_{53}/Γ

VALUE (units 10^{-3})	DOCUMENT ID	TECN	COMMENT
4.83 ± 0.32 ± 0.66	ABLIKIM	15M BES3	$\psi(2S) \rightarrow \gamma \chi_{c2}$

$\Gamma(K^+ K^- \pi^0 \phi)/\Gamma_{total}$ Γ_{54}/Γ

VALUE (units 10^{-3})	DOCUMENT ID	TECN	COMMENT
2.74 ± 0.16 ± 0.44	ABLIKIM	15M BES3	$\psi(2S) \rightarrow \gamma \chi_{c2}$

$\Gamma(\phi \pi^+ \pi^- \pi^0)/\Gamma_{total}$ Γ_{55}/Γ

VALUE (units 10^{-3})	EVTS	DOCUMENT ID	TECN	COMMENT
0.93 ± 0.06 ± 0.10	408	¹ ABLIKIM	13B BES3	$e^+ e^- \rightarrow \psi(2S) \rightarrow \gamma \chi_{c2}$

¹ Using $1.06 \times 10^8 \psi(2S)$ mesons and $B(\psi(2S) \rightarrow \chi_{c2} \gamma) = (8.72 \pm 0.34)\%$.

$\Gamma(\rho \bar{\rho} \pi^0)/\Gamma_{total}$ Γ_{57}/Γ

VALUE (units 10^{-3})	DOCUMENT ID	TECN	COMMENT
0.47 ± 0.04 OUR AVERAGE			
0.48 ± 0.04 ± 0.01	¹ ONYISI	10 CLE3	$\psi(2S) \rightarrow \gamma \rho \bar{\rho} X$
0.44 ± 0.09 ± 0.01	² ATHAR	07 CLEO	$\psi(2S) \rightarrow \gamma h^+ h^- h^0$

¹ ONYISI 10 reports $(4.83 \pm 0.25 \pm 0.35 \pm 0.31) \times 10^{-4}$ from a measurement of $[\Gamma(\chi_{c2}(1P) \rightarrow \rho \bar{\rho} \pi^0)/\Gamma_{total}] \times [B(\psi(2S) \rightarrow \gamma \chi_{c2}(1P))]$ assuming $B(\psi(2S) \rightarrow \gamma \chi_{c2}(1P)) = (9.33 \pm 0.14 \pm 0.61) \times 10^{-2}$, which we rescale to our best value $B(\psi(2S) \rightarrow \gamma \chi_{c2}(1P)) = (9.36 \pm 0.23) \times 10^{-2}$. Our first error is their experiment's error and our second error is the systematic error from using our best value.

² ATHAR 07 reports $(0.44 \pm 0.08 \pm 0.05) \times 10^{-3}$ from a measurement of $[\Gamma(\chi_{c2}(1P) \rightarrow \rho \bar{\rho} \pi^0)/\Gamma_{total}] \times [B(\psi(2S) \rightarrow \gamma \chi_{c2}(1P))]$ assuming $B(\psi(2S) \rightarrow \gamma \chi_{c2}(1P)) = (9.33 \pm 0.14 \pm 0.61) \times 10^{-2}$, which we rescale to our best value $B(\psi(2S) \rightarrow \gamma \chi_{c2}(1P)) = (9.36 \pm 0.23) \times 10^{-2}$. Our first error is their experiment's error and our second error is the systematic error from using our best value.

$\Gamma(\rho \bar{\rho} \eta)/\Gamma_{total}$ Γ_{58}/Γ

VALUE (units 10^{-3})	DOCUMENT ID	TECN	COMMENT
0.177 ± 0.025 OUR AVERAGE			
0.175 ± 0.027 ± 0.004	¹ ONYISI	10 CLE3	$\psi(2S) \rightarrow \gamma \rho \bar{\rho} X$
0.189 ± 0.071 ± 0.005	² ATHAR	07 CLEO	$\psi(2S) \rightarrow \gamma h^+ h^- h^0$

¹ ONYISI 10 reports $(1.76 \pm 0.23 \pm 0.14 \pm 0.11) \times 10^{-4}$ from a measurement of $[\Gamma(\chi_{c2}(1P) \rightarrow \rho \bar{\rho} \eta)/\Gamma_{total}] \times [B(\psi(2S) \rightarrow \gamma \chi_{c2}(1P))]$ assuming $B(\psi(2S) \rightarrow \gamma \chi_{c2}(1P)) = (9.33 \pm 0.14 \pm 0.61) \times 10^{-2}$, which we rescale to our best value $B(\psi(2S) \rightarrow \gamma \chi_{c2}(1P)) = (9.36 \pm 0.23) \times 10^{-2}$. Our first error is their experiment's error and our second error is the systematic error from using our best value.

² ATHAR 07 reports $(0.19 \pm 0.07 \pm 0.02) \times 10^{-3}$ from a measurement of $[\Gamma(\chi_{c2}(1P) \rightarrow \rho \bar{\rho} \eta)/\Gamma_{total}] \times [B(\psi(2S) \rightarrow \gamma \chi_{c2}(1P))]$ assuming $B(\psi(2S) \rightarrow \gamma \chi_{c2}(1P)) = (9.33 \pm 0.14 \pm 0.61) \times 10^{-2}$, which we rescale to our best value $B(\psi(2S) \rightarrow \gamma \chi_{c2}(1P)) = (9.36 \pm 0.23) \times 10^{-2}$. Our first error is their experiment's error and our second error is the systematic error from using our best value.

$\Gamma(\rho \bar{\rho} \omega)/\Gamma_{total}$ Γ_{59}/Γ

VALUE (units 10^{-3})	DOCUMENT ID	TECN	COMMENT
0.37 ± 0.04 ± 0.01	¹ ONYISI	10 CLE3	$\psi(2S) \rightarrow \gamma \rho \bar{\rho} X$

¹ ONYISI 10 reports $(3.68 \pm 0.35 \pm 0.26 \pm 0.24) \times 10^{-4}$ from a measurement of $[\Gamma(\chi_{c2}(1P) \rightarrow \rho \bar{\rho} \omega)/\Gamma_{total}] \times [B(\psi(2S) \rightarrow \gamma \chi_{c2}(1P))]$ assuming $B(\psi(2S) \rightarrow \gamma \chi_{c2}(1P)) = (9.33 \pm 0.14 \pm 0.61) \times 10^{-2}$, which we rescale to our best value $B(\psi(2S) \rightarrow \gamma \chi_{c2}(1P)) = (9.36 \pm 0.23) \times 10^{-2}$. Our first error is their experiment's error and our second error is the systematic error from using our best value.

$\Gamma(\rho \bar{\rho} \phi)/\Gamma_{total}$ Γ_{60}/Γ

VALUE (units 10^{-5})	EVTS	DOCUMENT ID	TECN	COMMENT
2.8 ± 0.9 ± 0.1	24 ± 7	¹ ABLIKIM	11F BES3	$\psi(2S) \rightarrow \gamma \rho \bar{\rho} K^+ K^-$

¹ ABLIKIM 11F reports $(3.04 \pm 0.85 \pm 0.43) \times 10^{-5}$ from a measurement of $[\Gamma(\chi_{c2}(1P) \rightarrow \rho \bar{\rho} \phi)/\Gamma_{total}] \times [B(\psi(2S) \rightarrow \gamma \chi_{c2}(1P))]$ assuming $B(\psi(2S) \rightarrow \gamma \chi_{c2}(1P)) = (8.74 \pm 0.35) \times 10^{-2}$, which we rescale to our best value $B(\psi(2S) \rightarrow \gamma \chi_{c2}(1P)) = (9.36 \pm 0.23) \times 10^{-2}$. Our first error is their experiment's error and our second error is the systematic error from using our best value.

$\Gamma(\rho \bar{\rho} \pi^+ \pi^-)/\Gamma_{total}$ Γ_{61}/Γ

VALUE (units 10^{-3})	DOCUMENT ID	TECN	COMMENT
1.32 ± 0.34 OUR EVALUATION	Treating systematic error as correlated.		
1.3 ± 0.4 OUR AVERAGE	Error includes scale factor of 1.3.		
1.17 ± 0.19 ± 0.30	¹ BAI	99B BES	$\psi(2S) \rightarrow \gamma \chi_{c2}$
2.64 ± 1.03 ± 0.14	¹ TANENBAUM	78 MRK1	$\psi(2S) \rightarrow \gamma \chi_{c2}$

¹ Rescaled by us using $B(\psi(2S) \rightarrow \gamma \chi_{c2}) = (8.3 \pm 0.4)\%$ and $B(\psi(2S) \rightarrow J/\psi(1S) \pi^+ \pi^-) = (32.6 \pm 0.5)\%$. Multiplied by a factor of 2 to convert from $K_S^0 K^+ \pi^-$ to $K^0 K^+ \pi^-$ decay.

$\Gamma(\rho \bar{\rho} \pi^0 \pi^0)/\Gamma_{total}$ Γ_{62}/Γ

VALUE (%)	EVTS	DOCUMENT ID	TECN	COMMENT
0.080 ± 0.024 ± 0.002	29.2	¹ HE	08B CLEO	$e^+ e^- \rightarrow \gamma h^+ h^- h^0 h^0$

¹ HE 08B reports $0.08 \pm 0.02 \pm 0.01 \pm 0.01\%$ from a measurement of $[\Gamma(\chi_{c2}(1P) \rightarrow \rho \bar{\rho} \pi^0 \pi^0)/\Gamma_{total}] \times [B(\psi(2S) \rightarrow \gamma \chi_{c2}(1P))]$ assuming $B(\psi(2S) \rightarrow \gamma \chi_{c2}(1P)) = (9.33 \pm 0.14 \pm 0.61) \times 10^{-2}$, which we rescale to our best value $B(\psi(2S) \rightarrow \gamma \chi_{c2}(1P)) = (9.36 \pm 0.23) \times 10^{-2}$. Our first error is their experiment's error and our second error is the systematic error from using our best value.

Meson Particle Listings

 $\chi_{c2}(1P)$ $\Gamma(p\bar{p}K^+K^- \text{ (non-resonant)})/\Gamma_{\text{total}}$ Γ_{63}/Γ

VALUE (units 10^{-4})	EVTS	DOCUMENT ID	TECN	COMMENT
1.94 ± 0.32 ± 0.05	131 ± 12	¹ ABLIKIM	11F BES3	$\psi(2S) \rightarrow \gamma p\bar{p}K^+K^-$
¹ ABLIKIM 11F reports $(2.08 \pm 0.19 \pm 0.30) \times 10^{-4}$ from a measurement of $[\Gamma(\chi_{c2}(1P) \rightarrow p\bar{p}K^+K^- \text{ (non-resonant)})/\Gamma_{\text{total}}] \times [B(\psi(2S) \rightarrow \gamma\chi_{c2}(1P))]$ assuming $B(\psi(2S) \rightarrow \gamma\chi_{c2}(1P)) = (8.74 \pm 0.35) \times 10^{-2}$, which we rescale to our best value $B(\psi(2S) \rightarrow \gamma\chi_{c2}(1P)) = (9.36 \pm 0.23) \times 10^{-2}$. Our first error is their experiment's error and our second error is the systematic error from using our best value.				

 $\Gamma(p\bar{p}K_S^0K_S^0)/\Gamma_{\text{total}}$ Γ_{64}/Γ

VALUE (units 10^{-4})	CL%	DOCUMENT ID	TECN	COMMENT
<7.9	90	¹ ABLIKIM	06D BES2	$\psi(2S) \rightarrow \chi_{c2}\gamma$
¹ Using $B(\psi(2S) \rightarrow \chi_{c2}\gamma) = (9.3 \pm 0.6)\%$.				

 $\Gamma(p\bar{p}\pi^-)/\Gamma_{\text{total}}$ Γ_{65}/Γ

VALUE (units 10^{-4})	EVTS	DOCUMENT ID	TECN	COMMENT
8.7 ± 1.0 OUR AVERAGE				
8.5 ± 1.0 ± 0.2	3309	¹ ABLIKIM	12J BES3	$\psi(2S) \rightarrow \gamma p\bar{p}\pi^-$
10.4 ± 3.5 ± 0.3		² ABLIKIM	06I BES2	$\psi(2S) \rightarrow \gamma p\pi^-X$
¹ ABLIKIM 12J reports $[\Gamma(\chi_{c2}(1P) \rightarrow p\bar{p}\pi^-)/\Gamma_{\text{total}}] \times [B(\psi(2S) \rightarrow \gamma\chi_{c2}(1P))] = (0.80 \pm 0.02 \pm 0.09) \times 10^{-4}$ which we divide by our best value $B(\psi(2S) \rightarrow \gamma\chi_{c2}(1P)) = (9.36 \pm 0.23) \times 10^{-2}$. Our first error is their experiment's error and our second error is the systematic error from using our best value.				
² ABLIKIM 06I reports $[\Gamma(\chi_{c2}(1P) \rightarrow p\bar{p}\pi^-)/\Gamma_{\text{total}}] \times [B(\psi(2S) \rightarrow \gamma\chi_{c2}(1P))] = (0.97 \pm 0.20 \pm 0.26) \times 10^{-4}$ which we divide by our best value $B(\psi(2S) \rightarrow \gamma\chi_{c2}(1P)) = (9.36 \pm 0.23) \times 10^{-2}$. Our first error is their experiment's error and our second error is the systematic error from using our best value.				

 $\Gamma(p\bar{p}\pi^+)/\Gamma_{\text{total}}$ Γ_{66}/Γ

VALUE (units 10^{-4})	EVTS	DOCUMENT ID	TECN	COMMENT
9.1 ± 0.8 ± 0.2	3732	¹ ABLIKIM	12J BES3	$\psi(2S) \rightarrow \gamma p\bar{p}\pi^+$
¹ ABLIKIM 12J reports $[\Gamma(\chi_{c2}(1P) \rightarrow p\bar{p}\pi^+)/\Gamma_{\text{total}}] \times [B(\psi(2S) \rightarrow \gamma\chi_{c2}(1P))] = (0.85 \pm 0.02 \pm 0.07) \times 10^{-4}$ which we divide by our best value $B(\psi(2S) \rightarrow \gamma\chi_{c2}(1P)) = (9.36 \pm 0.23) \times 10^{-2}$. Our first error is their experiment's error and our second error is the systematic error from using our best value.				

 $\Gamma(p\bar{p}\pi^-\pi^0)/\Gamma_{\text{total}}$ Γ_{67}/Γ

VALUE (units 10^{-4})	EVTS	DOCUMENT ID	TECN	COMMENT
22.1 ± 1.7 ± 0.5	2128	¹ ABLIKIM	12J BES3	$\psi(2S) \rightarrow \gamma p\bar{p}\pi^-\pi^0$
¹ ABLIKIM 12J reports $[\Gamma(\chi_{c2}(1P) \rightarrow p\bar{p}\pi^-\pi^0)/\Gamma_{\text{total}}] \times [B(\psi(2S) \rightarrow \gamma\chi_{c2}(1P))] = (2.07 \pm 0.06 \pm 0.15) \times 10^{-4}$ which we divide by our best value $B(\psi(2S) \rightarrow \gamma\chi_{c2}(1P)) = (9.36 \pm 0.23) \times 10^{-2}$. Our first error is their experiment's error and our second error is the systematic error from using our best value.				

 $\Gamma(p\bar{p}\pi^+\pi^0)/\Gamma_{\text{total}}$ Γ_{68}/Γ

VALUE (units 10^{-4})	EVTS	DOCUMENT ID	TECN	COMMENT
21.5 ± 1.8 ± 0.5	2352	¹ ABLIKIM	12J BES3	$\psi(2S) \rightarrow \gamma p\bar{p}\pi^+\pi^0$
¹ ABLIKIM 12J reports $[\Gamma(\chi_{c2}(1P) \rightarrow p\bar{p}\pi^+\pi^0)/\Gamma_{\text{total}}] \times [B(\psi(2S) \rightarrow \gamma\chi_{c2}(1P))] = (2.01 \pm 0.06 \pm 0.16) \times 10^{-4}$ which we divide by our best value $B(\psi(2S) \rightarrow \gamma\chi_{c2}(1P)) = (9.36 \pm 0.23) \times 10^{-2}$. Our first error is their experiment's error and our second error is the systematic error from using our best value.				

 $\Gamma(\Lambda\bar{\Lambda}\pi^+\pi^-)/\Gamma_{\text{total}}$ Γ_{70}/Γ

VALUE (units 10^{-5})	CL%	EVTS	DOCUMENT ID	TECN	COMMENT
128 ± 15 ± 3		371	¹ ABLIKIM	12I BES3	$\psi(2S) \rightarrow \gamma\Lambda\bar{\Lambda}\pi^+\pi^-$
••• We do not use the following data for averages, fits, limits, etc. •••					
<35.0	90		² ABLIKIM	06D BES2	$\psi(2S) \rightarrow \chi_{c2}\gamma$
¹ ABLIKIM 12I reports $(137.0 \pm 7.6 \pm 15.7) \times 10^{-5}$ from a measurement of $[\Gamma(\chi_{c2}(1P) \rightarrow \Lambda\bar{\Lambda}\pi^+\pi^-)/\Gamma_{\text{total}}] \times [B(\psi(2S) \rightarrow \gamma\chi_{c2}(1P))]$ assuming $B(\psi(2S) \rightarrow \gamma\chi_{c2}(1P)) = (8.72 \pm 0.34) \times 10^{-2}$, which we rescale to our best value $B(\psi(2S) \rightarrow \gamma\chi_{c2}(1P)) = (9.36 \pm 0.23) \times 10^{-2}$. Our first error is their experiment's error and our second error is the systematic error from using our best value.					
² Using $B(\psi(2S) \rightarrow \chi_{c2}\gamma) = (9.3 \pm 0.6)\%$.					

 $\Gamma(\Lambda\bar{\Lambda}\pi^+\pi^- \text{ (non-resonant)})/\Gamma_{\text{total}}$ Γ_{71}/Γ

VALUE (units 10^{-5})	EVTS	DOCUMENT ID	TECN	COMMENT
67 ± 15 ± 2	36	¹ ABLIKIM	12I BES3	$\psi(2S) \rightarrow \gamma\Lambda\bar{\Lambda}\pi^+\pi^-$
¹ ABLIKIM 12I reports $(71.8 \pm 14.5 \pm 8.2) \times 10^{-5}$ from a measurement of $[\Gamma(\chi_{c2}(1P) \rightarrow \Lambda\bar{\Lambda}\pi^+\pi^- \text{ (non-resonant)})/\Gamma_{\text{total}}] \times [B(\psi(2S) \rightarrow \gamma\chi_{c2}(1P))]$ assuming $B(\psi(2S) \rightarrow \gamma\chi_{c2}(1P)) = (8.72 \pm 0.34) \times 10^{-2}$, which we rescale to our best value $B(\psi(2S) \rightarrow \gamma\chi_{c2}(1P)) = (9.36 \pm 0.23) \times 10^{-2}$. Our first error is their experiment's error and our second error is the systematic error from using our best value.				

 $\Gamma(\Sigma(1385)^+\bar{\Lambda}\pi^- + \text{c.c.})/\Gamma_{\text{total}}$ Γ_{72}/Γ

VALUE (units 10^{-5})	CL%	DOCUMENT ID	TECN	COMMENT
<40	90	¹ ABLIKIM	12I BES3	$\psi(2S) \rightarrow \gamma\Sigma(1385)^+\bar{\Lambda}\pi^-$
¹ ABLIKIM 12I reports $< 42 \times 10^{-5}$ from a measurement of $[\Gamma(\chi_{c2}(1P) \rightarrow \Sigma(1385)^+\bar{\Lambda}\pi^- + \text{c.c.})/\Gamma_{\text{total}}] \times [B(\psi(2S) \rightarrow \gamma\chi_{c2}(1P))]$ assuming $B(\psi(2S) \rightarrow \gamma\chi_{c2}(1P)) = (8.72 \pm 0.34) \times 10^{-2}$, which we rescale to our best value $B(\psi(2S) \rightarrow \gamma\chi_{c2}(1P)) = 9.36 \times 10^{-2}$.				

 $\Gamma(\Sigma(1385)^-\bar{\Lambda}\pi^+ + \text{c.c.})/\Gamma_{\text{total}}$ Γ_{73}/Γ

VALUE (units 10^{-5})	CL%	DOCUMENT ID	TECN	COMMENT
<60	90	¹ ABLIKIM	12I BES3	$\psi(2S) \rightarrow \gamma\Sigma(1385)^-\bar{\Lambda}\pi^+$
¹ ABLIKIM 12I reports $< 61 \times 10^{-5}$ from a measurement of $[\Gamma(\chi_{c2}(1P) \rightarrow \Sigma(1385)^-\bar{\Lambda}\pi^+ + \text{c.c.})/\Gamma_{\text{total}}] \times [B(\psi(2S) \rightarrow \gamma\chi_{c2}(1P))]$ assuming $B(\psi(2S) \rightarrow \gamma\chi_{c2}(1P)) = (8.72 \pm 0.34) \times 10^{-2}$, which we rescale to our best value $B(\psi(2S) \rightarrow \gamma\chi_{c2}(1P)) = 9.36 \times 10^{-2}$.				

 $\Gamma(K^+\bar{p}\Lambda + \text{c.c.})/\Gamma_{\text{total}}$ Γ_{75}/Γ

VALUE (units 10^{-4})	EVTS	DOCUMENT ID	TECN	COMMENT
7.9 ± 0.6 OUR AVERAGE				
7.8 ± 0.5 ± 0.2	5k	^{1,2} ABLIKIM	13D BES3	$\psi(2S) \rightarrow \gamma\Lambda\bar{p}K^+$
8.5 ± 1.6 ± 0.2		³ ATHAR	07 CLEO	$\psi(2S) \rightarrow \gamma h^+h^-h^0$
¹ ABLIKIM 13D reports $(8.4 \pm 0.3 \pm 0.6) \times 10^{-4}$ from a measurement of $[\Gamma(\chi_{c2}(1P) \rightarrow K^+\bar{p}\Lambda + \text{c.c.})/\Gamma_{\text{total}}] \times [B(\psi(2S) \rightarrow \gamma\chi_{c2}(1P))]$ assuming $B(\psi(2S) \rightarrow \gamma\chi_{c2}(1P)) = (8.72 \pm 0.34) \times 10^{-2}$, which we rescale to our best value $B(\psi(2S) \rightarrow \gamma\chi_{c2}(1P)) = (9.36 \pm 0.23) \times 10^{-2}$. Our first error is their experiment's error and our second error is the systematic error from using our best value.				
² Using $B(\Lambda \rightarrow p\pi^-) = 63.9\%$.				
³ ATHAR 07 reports $(8.5 \pm 1.4 \pm 1.0) \times 10^{-4}$ from a measurement of $[\Gamma(\chi_{c2}(1P) \rightarrow K^+\bar{p}\Lambda + \text{c.c.})/\Gamma_{\text{total}}] \times [B(\psi(2S) \rightarrow \gamma\chi_{c2}(1P))]$ assuming $B(\psi(2S) \rightarrow \gamma\chi_{c2}(1P)) = (9.33 \pm 0.14 \pm 0.61) \times 10^{-2}$, which we rescale to our best value $B(\psi(2S) \rightarrow \gamma\chi_{c2}(1P)) = (9.36 \pm 0.23) \times 10^{-2}$. Our first error is their experiment's error and our second error is the systematic error from using our best value.				

 $\Gamma(nK_S^0\bar{\Lambda} + \text{c.c.})/\Gamma_{\text{total}}$ Γ_{76}/Γ

VALUE (units 10^{-4})	EVTS	DOCUMENT ID	TECN	COMMENT
3.64 ± 0.27 ± 0.09	879	¹ ABLIKIM	21AV BES3	$\psi(2S) \rightarrow \gamma nK_S^0\bar{\Lambda} + \text{c.c.}$
¹ ABLIKIM 21AV reports $(3.58 \pm 0.16 \pm 0.23) \times 10^{-4}$ from a measurement of $[\Gamma(\chi_{c2}(1P) \rightarrow nK_S^0\bar{\Lambda} + \text{c.c.})/\Gamma_{\text{total}}] \times [B(\psi(2S) \rightarrow \gamma\chi_{c2}(1P))]$ assuming $B(\psi(2S) \rightarrow \gamma\chi_{c2}(1P)) = 0.0952 \pm 0.0020$, which we rescale to our best value $B(\psi(2S) \rightarrow \gamma\chi_{c2}(1P)) = (9.36 \pm 0.23) \times 10^{-2}$. Our first error is their experiment's error and our second error is the systematic error from using our best value. Also uses $B(\bar{\Lambda} \rightarrow \bar{p}\pi^+) = (63.9 \pm 0.5)\%$ and $B(K_S^0 \rightarrow \pi^+\pi^-) = (69.20 \pm 0.05)\%$.				

 $\Gamma(K^*(892)^+\bar{p}\Lambda + \text{c.c.})/\Gamma_{\text{total}}$ Γ_{77}/Γ

VALUE (units 10^{-4})	EVTS	DOCUMENT ID	TECN	COMMENT
8.3 ± 1.2 ± 0.2	476	¹ ABLIKIM	19AU BES3	$\psi(2S) \rightarrow \gamma K^*\bar{p}\Lambda$
¹ ABLIKIM 19AU reports $[\Gamma(\chi_{c2}(1P) \rightarrow K^*(892)^+\bar{p}\Lambda + \text{c.c.})/\Gamma_{\text{total}}] \times [B(\psi(2S) \rightarrow \gamma\chi_{c2}(1P))] = (7.8 \pm 0.9 \pm 0.6) \times 10^{-5}$ which we divide by our best value $B(\psi(2S) \rightarrow \gamma\chi_{c2}(1P)) = (9.36 \pm 0.23) \times 10^{-2}$. Our first error is their experiment's error and our second error is the systematic error from using our best value.				

 $\Gamma(K^+\bar{p}\Lambda(1520) + \text{c.c.})/\Gamma_{\text{total}}$ Γ_{78}/Γ

VALUE (units 10^{-4})	EVTS	DOCUMENT ID	TECN	COMMENT
2.9 ± 0.7 ± 0.1	79 ± 13	¹ ABLIKIM	11F BES3	$\psi(2S) \rightarrow \gamma p\bar{p}K^+K^-$
¹ ABLIKIM 11F reports $(3.06 \pm 0.50 \pm 0.54) \times 10^{-4}$ from a measurement of $[\Gamma(\chi_{c2}(1P) \rightarrow K^+\bar{p}\Lambda(1520) + \text{c.c.})/\Gamma_{\text{total}}] \times [B(\psi(2S) \rightarrow \gamma\chi_{c2}(1P))]$ assuming $B(\psi(2S) \rightarrow \gamma\chi_{c2}(1P)) = (8.74 \pm 0.35) \times 10^{-2}$, which we rescale to our best value $B(\psi(2S) \rightarrow \gamma\chi_{c2}(1P)) = (9.36 \pm 0.23) \times 10^{-2}$. Our first error is their experiment's error and our second error is the systematic error from using our best value.				

 $\Gamma(\Lambda(1520)\bar{\Lambda}(1520))/\Gamma_{\text{total}}$ Γ_{79}/Γ

VALUE (units 10^{-4})	EVTS	DOCUMENT ID	TECN	COMMENT
4.7 ± 1.5 ± 0.1	29 ± 7	¹ ABLIKIM	11F BES3	$\psi(2S) \rightarrow \gamma p\bar{p}K^+K^-$
¹ ABLIKIM 11F reports $(5.05 \pm 1.29 \pm 0.93) \times 10^{-4}$ from a measurement of $[\Gamma(\chi_{c2}(1P) \rightarrow \Lambda(1520)\bar{\Lambda}(1520))/\Gamma_{\text{total}}] \times [B(\psi(2S) \rightarrow \gamma\chi_{c2}(1P))]$ assuming $B(\psi(2S) \rightarrow \gamma\chi_{c2}(1P)) = (8.74 \pm 0.35) \times 10^{-2}$, which we rescale to our best value $B(\psi(2S) \rightarrow \gamma\chi_{c2}(1P)) = (9.36 \pm 0.23) \times 10^{-2}$. Our first error is their experiment's error and our second error is the systematic error from using our best value.				

 $\Gamma(\Sigma^0\bar{\Sigma}^0)/\Gamma_{\text{total}}$ Γ_{80}/Γ

VALUE (units 10^{-5})	CL%	EVTS	DOCUMENT ID	TECN	COMMENT
3.7 ± 0.6 ± 0.1		91	¹ ABLIKIM	18V BES3	$\psi(2S) \rightarrow \gamma\Sigma^0\bar{\Sigma}^0$
••• We do not use the following data for averages, fits, limits, etc. •••					
<6	90		² ABLIKIM	13H BES3	$\psi(2S) \rightarrow \gamma\Sigma^0\bar{\Sigma}^0$
<7	90	7.5 ± 3.4	³ NAIK	08 CLEO	$\psi(2S) \rightarrow \gamma\Sigma^0\bar{\Sigma}^0$
¹ ABLIKIM 18V reports $[\Gamma(\chi_{c2}(1P) \rightarrow \Sigma^0\bar{\Sigma}^0)/\Gamma_{\text{total}}] \times [B(\psi(2S) \rightarrow \gamma\chi_{c2}(1P))] = (0.35 \pm 0.05 \pm 0.02) \times 10^{-5}$ which we divide by our best value $B(\psi(2S) \rightarrow \gamma\chi_{c2}(1P)) = (9.36 \pm 0.23) \times 10^{-2}$. Our first error is their experiment's error and our second error is the systematic error from using our best value.					
² ABLIKIM 13H reports $< 0.65 \times 10^{-4}$ from a measurement of $[\Gamma(\chi_{c2}(1P) \rightarrow \Sigma^0\bar{\Sigma}^0)/\Gamma_{\text{total}}] \times [B(\psi(2S) \rightarrow \gamma\chi_{c2}(1P))]$ assuming $B(\psi(2S) \rightarrow \gamma\chi_{c2}(1P)) = (8.74 \pm 0.35) \times 10^{-2}$, which we rescale to our best value $B(\psi(2S) \rightarrow \gamma\chi_{c2}(1P)) = 9.36 \times 10^{-2}$.					
³ NAIK 08 reports $< 0.75 \times 10^{-4}$ from a measurement of $[\Gamma(\chi_{c2}(1P) \rightarrow \Sigma^0\bar{\Sigma}^0)/\Gamma_{\text{total}}] \times [B(\psi(2S) \rightarrow \gamma\chi_{c2}(1P))]$ assuming $B(\psi(2S) \rightarrow \gamma\chi_{c2}(1P)) = (9.33 \pm 0.14 \pm 0.61) \times 10^{-2}$, which we rescale to our best value $B(\psi(2S) \rightarrow \gamma\chi_{c2}(1P)) = 9.36 \times 10^{-2}$.					

$\Gamma(\Sigma^+\bar{\Sigma}^-)/\Gamma_{total}$ Γ_{83}/Γ

VALUE (units 10^{-5})	CL%	EVTS	DOCUMENT ID	TECN	COMMENT
3.4 ± 0.7 ± 0.1		55	¹ ABLIKIM	18v BES3	$\psi(2S) \rightarrow \gamma \Sigma^+ \bar{\Sigma}^-$

• • • We do not use the following data for averages, fits, limits, etc. • • •

<8 90 ² ABLIKIM 13h BES3 $\psi(2S) \rightarrow \gamma \Sigma^+ \bar{\Sigma}^-$

<7 90 4.0 ± 3.5 ³ NAIK 08 CLEO $\psi(2S) \rightarrow \gamma \Sigma^+ \bar{\Sigma}^-$

¹ ABLIKIM 18v reports $[\Gamma(\chi_{c2}(1P) \rightarrow \Sigma^+ \bar{\Sigma}^-)/\Gamma_{total}] \times [B(\psi(2S) \rightarrow \chi_{c2}(1P))] = (0.32 \pm 0.06 \pm 0.03) \times 10^{-5}$ which we divide by our best value $B(\psi(2S) \rightarrow \chi_{c2}(1P)) = (9.36 \pm 0.23) \times 10^{-2}$. Our first error is their experiment's error and our second error is the systematic error from using our best value.

² ABLIKIM 13h reports $< 0.88 \times 10^{-4}$ from a measurement of $[\Gamma(\chi_{c2}(1P) \rightarrow \Sigma^+ \bar{\Sigma}^-)/\Gamma_{total}] \times [B(\psi(2S) \rightarrow \chi_{c2}(1P))]$ assuming $B(\psi(2S) \rightarrow \chi_{c2}(1P)) = (8.74 \pm 0.35) \times 10^{-2}$, which we rescale to our best value $B(\psi(2S) \rightarrow \chi_{c2}(1P)) = 9.36 \times 10^{-2}$.

³ NAIK 08 reports $< 0.67 \times 10^{-4}$ from a measurement of $[\Gamma(\chi_{c2}(1P) \rightarrow \Sigma^+ \bar{\Sigma}^-)/\Gamma_{total}] \times [B(\psi(2S) \rightarrow \chi_{c2}(1P))]$ assuming $B(\psi(2S) \rightarrow \chi_{c2}(1P)) = (9.33 \pm 0.14 \pm 0.61) \times 10^{-2}$, which we rescale to our best value $B(\psi(2S) \rightarrow \chi_{c2}(1P)) = 9.36 \times 10^{-2}$.

$\Gamma(\Sigma^-\bar{\Sigma}^+)/\Gamma_{total}$ Γ_{84}/Γ

VALUE (units 10^{-5})	EVTS	DOCUMENT ID	TECN	COMMENT
4.5 ± 1.8 ± 0.1	131	¹ ABLIKIM	20i BES3	$\psi(2S) \rightarrow \gamma \Sigma^- \bar{\Sigma}^+$

¹ ABLIKIM 20i reports $(4.4 \pm 1.7 \pm 0.5) \times 10^{-5}$ from a measurement of $[\Gamma(\chi_{c2}(1P) \rightarrow \Sigma^- \bar{\Sigma}^+)/\Gamma_{total}] \times [B(\psi(2S) \rightarrow \chi_{c2}(1P))]$ assuming $B(\psi(2S) \rightarrow \chi_{c2}(1P)) = (9.52 \pm 0.20) \times 10^{-2}$, which we rescale to our best value $B(\psi(2S) \rightarrow \chi_{c2}(1P)) = (9.36 \pm 0.23) \times 10^{-2}$. Our first error is their experiment's error and our second error is the systematic error from using our best value.

$\Gamma(\Sigma(1385)^+\bar{\Sigma}(1385)^-)/\Gamma_{total}$ Γ_{85}/Γ

VALUE (units 10^{-5})	CL%	DOCUMENT ID	TECN	COMMENT
<16	90	¹ ABLIKIM	12i BES3	$\psi(2S) \rightarrow \gamma \Sigma(1385)^+ \bar{\Sigma}(1385)^-$

¹ ABLIKIM 12i reports $< 17 \times 10^{-5}$ from a measurement of $[\Gamma(\chi_{c2}(1P) \rightarrow \Sigma(1385)^+ \bar{\Sigma}(1385)^-)/\Gamma_{total}] \times [B(\psi(2S) \rightarrow \chi_{c2}(1P))]$ assuming $B(\psi(2S) \rightarrow \chi_{c2}(1P)) = (8.72 \pm 0.34) \times 10^{-2}$, which we rescale to our best value $B(\psi(2S) \rightarrow \chi_{c2}(1P)) = 9.36 \times 10^{-2}$.

$\Gamma(\Sigma(1385)^-\bar{\Sigma}(1385)^+)/\Gamma_{total}$ Γ_{86}/Γ

VALUE (units 10^{-5})	CL%	DOCUMENT ID	TECN	COMMENT
<8	90	¹ ABLIKIM	12i BES3	$\psi(2S) \rightarrow \gamma \Sigma(1385)^- \bar{\Sigma}(1385)^+$

¹ ABLIKIM 12i reports $< 8.5 \times 10^{-5}$ from a measurement of $[\Gamma(\chi_{c2}(1P) \rightarrow \Sigma(1385)^- \bar{\Sigma}(1385)^+)/\Gamma_{total}] \times [B(\psi(2S) \rightarrow \chi_{c2}(1P))]$ assuming $B(\psi(2S) \rightarrow \chi_{c2}(1P)) = (8.72 \pm 0.34) \times 10^{-2}$, which we rescale to our best value $B(\psi(2S) \rightarrow \chi_{c2}(1P)) = 9.36 \times 10^{-2}$.

$\Gamma(K^-\Lambda\bar{\Xi}^+ + c.c.)/\Gamma_{total}$ Γ_{87}/Γ

VALUE (units 10^{-4})	EVTS	DOCUMENT ID	TECN	COMMENT
1.80 ± 0.32 ± 0.04	51	¹ ABLIKIM	15i BES3	$\psi(2S) \rightarrow \gamma K^-\Lambda\bar{\Xi}^+ + c.c.$

¹ ABLIKIM 15i reports $[\Gamma(\chi_{c2}(1P) \rightarrow K^-\Lambda\bar{\Xi}^+ + c.c.)/\Gamma_{total}] \times [B(\psi(2S) \rightarrow \chi_{c2}(1P))] = (1.68 \pm 0.26 \pm 0.15) \times 10^{-5}$ which we divide by our best value $B(\psi(2S) \rightarrow \chi_{c2}(1P)) = (9.36 \pm 0.23) \times 10^{-2}$. Our first error is their experiment's error and our second error is the systematic error from using our best value.

$\Gamma(\Xi^0\bar{\Xi}^0)/\Gamma_{total}$ Γ_{88}/Γ

VALUE (units 10^{-4})	CL%	EVTS	DOCUMENT ID	TECN	COMMENT
1.86 ± 0.22 ± 0.05		804	¹ ABLIKIM	22o BES3	$\psi(2S) \rightarrow \gamma \Xi^0 \bar{\Xi}^0$

• • • We do not use the following data for averages, fits, limits, etc. • • •

<1.1 90 3 ² NAIK 08 CLEO $\psi(2S) \rightarrow \gamma \Xi^0 \bar{\Xi}^0$

¹ ABLIKIM 22o reports $(1.83 \pm 0.15 \pm 0.16) \times 10^{-4}$ from a measurement of $[\Gamma(\chi_{c2}(1P) \rightarrow \Xi^0 \bar{\Xi}^0)/\Gamma_{total}] \times [B(\psi(2S) \rightarrow \chi_{c2}(1P))]$ assuming $B(\psi(2S) \rightarrow \chi_{c2}(1P)) = (9.52 \pm 0.20) \times 10^{-2}$, which we rescale to our best value $B(\psi(2S) \rightarrow \chi_{c2}(1P)) = (9.36 \pm 0.23) \times 10^{-2}$. Our first error is their experiment's error and our second error is the systematic error from using our best value.

² NAIK 08 reports $< 1.06 \times 10^{-4}$ from a measurement of $[\Gamma(\chi_{c2}(1P) \rightarrow \Xi^0 \bar{\Xi}^0)/\Gamma_{total}] \times [B(\psi(2S) \rightarrow \chi_{c2}(1P))]$ assuming $B(\psi(2S) \rightarrow \chi_{c2}(1P)) = (9.33 \pm 0.14 \pm 0.61) \times 10^{-2}$, which we rescale to our best value $B(\psi(2S) \rightarrow \chi_{c2}(1P)) = 9.36 \times 10^{-2}$.

$\Gamma(\Xi^-\bar{\Xi}^+)/\Gamma_{total}$ Γ_{89}/Γ

VALUE (units 10^{-4})	CL%	EVTS	DOCUMENT ID	TECN	COMMENT
1.46 ± 0.12 OUR AVERAGE					
1.47 ± 0.12 ± 0.04		1691	¹ ABLIKIM	22o BES3	$\psi(2S) \rightarrow \gamma \Xi^-\bar{\Xi}^+$
1.45 ± 0.32 ± 0.04		29 ± 5	² NAIK	08 CLEO	$\psi(2S) \rightarrow \gamma \Xi^-\bar{\Xi}^+$

• • • We do not use the following data for averages, fits, limits, etc. • • •

< 3.7 90 ³ ABLIKIM 06d BES2 $\psi(2S) \rightarrow \chi_{c2}\gamma$

¹ ABLIKIM 22o reports $(1.44 \pm 0.06 \pm 0.11) \times 10^{-4}$ from a measurement of $[\Gamma(\chi_{c2}(1P) \rightarrow \Xi^-\bar{\Xi}^+)/\Gamma_{total}] \times [B(\psi(2S) \rightarrow \chi_{c2}(1P))]$ assuming $B(\psi(2S) \rightarrow \chi_{c2}(1P)) = (9.52 \pm 0.20) \times 10^{-2}$, which we rescale to our best value $B(\psi(2S) \rightarrow \chi_{c2}(1P)) = (9.36 \pm 0.23) \times 10^{-2}$. Our first error is their experiment's error and our second error is the systematic error from using our best value.

² NAIK 08 reports $(1.45 \pm 0.30 \pm 0.15) \times 10^{-4}$ from a measurement of $[\Gamma(\chi_{c2}(1P) \rightarrow \Xi^-\bar{\Xi}^+)/\Gamma_{total}] \times [B(\psi(2S) \rightarrow \chi_{c2}(1P))]$ assuming $B(\psi(2S) \rightarrow \chi_{c2}(1P)) =$

$(9.33 \pm 0.14 \pm 0.61) \times 10^{-2}$, which we rescale to our best value $B(\psi(2S) \rightarrow \chi_{c2}(1P)) = (9.36 \pm 0.23) \times 10^{-2}$. Our first error is their experiment's error and our second error is the systematic error from using our best value.

³ Using $B(\psi(2S) \rightarrow \chi_{c2}\gamma) = (9.3 \pm 0.6)\%$.

$\Gamma(\Omega^-\bar{\Omega}^+)/\Gamma_{total}$ Γ_{90}/Γ

VALUE (units 10^{-5})	EVTS	DOCUMENT ID	TECN	COMMENT
4.52 ± 0.24 ± 0.18	1038	ABLIKIM	23t BES3	$\chi_{cJ} \rightarrow \Omega^-\bar{\Omega}^+$

$\Gamma(J/\psi(1S)\pi^+\pi^-\pi^0)/\Gamma_{total}$ Γ_{91}/Γ

VALUE	CL%	DOCUMENT ID	TECN	COMMENT
<0.015	90	BARATE	81 SPEC	190 GeV π^- Be $\rightarrow 2\pi 2\mu$

$\Gamma(\pi^0\eta_c)/\Gamma_{total}$ Γ_{92}/Γ

VALUE	CL%	DOCUMENT ID	TECN	COMMENT
<3.2 × 10⁻³	90	¹ ABLIKIM	15N BES3	$\psi(2S)e^+e^- \rightarrow \gamma\pi^0\eta_c$

¹ Using $B(\eta_c \rightarrow K_S^0 K^\pm \pi^\mp) \times B(K_S^0 \rightarrow \pi^+ \pi^-) \times B(\pi^0 \rightarrow \gamma\gamma) = (1.66 \pm 0.11) \times 10^{-2}$.

$\Gamma(\eta_c(1S)\pi^+\pi^-)/\Gamma_{total}$ Γ_{93}/Γ

VALUE	CL%	DOCUMENT ID	TECN	COMMENT
<0.54 × 10⁻²	90	^{1,2} ABLIKIM	13b BES3	$e^+e^- \rightarrow \psi(2S) \rightarrow \chi_{c2}$

• • • We do not use the following data for averages, fits, limits, etc. • • •

<1.2 × 10⁻² 90 ^{1,3} ABLIKIM 13b BES3 $e^+e^- \rightarrow \psi(2S) \rightarrow \chi_{c2}$

¹ Using $1.06 \times 10^8 \psi(2S)$ mesons and $B(\psi(2S) \rightarrow \chi_{c2}\gamma) = (8.72 \pm 0.34)\%$.

² From the $\eta_c \rightarrow K_S^0 K^\pm \pi^\mp$ decays.

³ From the $\eta_c \rightarrow K^+ K^- \pi^0$ decays.

$\Gamma(\eta_c(1S)\pi^+\pi^-)/\Gamma(K^0 K^+ \pi^- + c.c.)$ Γ_{93}/Γ_{42}

VALUE	CL%	DOCUMENT ID	TECN	COMMENT
<16.4	90	¹ LEES	12AE BABR	$e^+e^- \rightarrow e^+e^-\pi^+\pi^-\eta_c$

¹ We divided the reported limit by 2 to take into account the $K_L^0 K^+ \pi^-$ mode.

———— RADIATIVE DECAYS ————

$\Gamma(\gamma\rho^0)/\Gamma_{total}$ Γ_{95}/Γ

VALUE (units 10^{-6})	CL%	EVTS	DOCUMENT ID	TECN	COMMENT
<19		90 13 ± 11	¹ ABLIKIM	11E BES3	$\psi(2S) \rightarrow \gamma\gamma\rho^0$

• • • We do not use the following data for averages, fits, limits, etc. • • •

<40 90 17.2 ± 6.8 ² BENNETT 08A CLEO $\psi(2S) \rightarrow \gamma\gamma\rho^0$

¹ ABLIKIM 11E reports $< 20.8 \times 10^{-6}$ from a measurement of $[\Gamma(\chi_{c2}(1P) \rightarrow \gamma\rho^0)/\Gamma_{total}] \times [B(\psi(2S) \rightarrow \chi_{c2}(1P))]$ assuming $B(\psi(2S) \rightarrow \chi_{c2}(1P)) = (8.74 \pm 0.35) \times 10^{-2}$, which we rescale to our best value $B(\psi(2S) \rightarrow \chi_{c2}(1P)) = 9.36 \times 10^{-2}$.

² BENNETT 08A reports $< 50 \times 10^{-6}$ from a measurement of $[\Gamma(\chi_{c2}(1P) \rightarrow \gamma\rho^0)/\Gamma_{total}] \times [B(\psi(2S) \rightarrow \chi_{c2}(1P))]$ assuming $B(\psi(2S) \rightarrow \chi_{c2}(1P)) = (8.1 \pm 0.4) \times 10^{-2}$, which we rescale to our best value $B(\psi(2S) \rightarrow \chi_{c2}(1P)) = 9.36 \times 10^{-2}$.

$\Gamma(\gamma\omega)/\Gamma_{total}$ Γ_{96}/Γ

VALUE (units 10^{-6})	CL%	EVTS	DOCUMENT ID	TECN	COMMENT
<6		90 1 ± 6	¹ ABLIKIM	11E BES3	$\psi(2S) \rightarrow \gamma\gamma\omega$

• • • We do not use the following data for averages, fits, limits, etc. • • •

<6 90 0.0 ± 1.8 ² BENNETT 08A CLEO $\psi(2S) \rightarrow \gamma\gamma\omega$

¹ ABLIKIM 11E reports $< 6.1 \times 10^{-6}$ from a measurement of $[\Gamma(\chi_{c2}(1P) \rightarrow \gamma\omega)/\Gamma_{total}] \times [B(\psi(2S) \rightarrow \chi_{c2}(1P))]$ assuming $B(\psi(2S) \rightarrow \chi_{c2}(1P)) = (8.74 \pm 0.35) \times 10^{-2}$, which we rescale to our best value $B(\psi(2S) \rightarrow \chi_{c2}(1P)) = 9.36 \times 10^{-2}$.

² BENNETT 08A reports $< 7.0 \times 10^{-6}$ from a measurement of $[\Gamma(\chi_{c2}(1P) \rightarrow \gamma\omega)/\Gamma_{total}] \times [B(\psi(2S) \rightarrow \chi_{c2}(1P))]$ assuming $B(\psi(2S) \rightarrow \chi_{c2}(1P)) = (8.1 \pm 0.4) \times 10^{-2}$, which we rescale to our best value $B(\psi(2S) \rightarrow \chi_{c2}(1P)) = 9.36 \times 10^{-2}$.

$\Gamma(\gamma\phi)/\Gamma_{total}$ Γ_{97}/Γ

VALUE (units 10^{-6})	CL%	EVTS	DOCUMENT ID	TECN	COMMENT
< 8		90 5 ± 5	¹ ABLIKIM	11E BES3	$\psi(2S) \rightarrow \gamma\gamma\phi$

• • • We do not use the following data for averages, fits, limits, etc. • • •

<11 90 1.3 ± 2.5 ² BENNETT 08A CLEO $\psi(2S) \rightarrow \gamma\gamma\phi$

¹ ABLIKIM 11E reports $< 8.1 \times 10^{-6}$ from a measurement of $[\Gamma(\chi_{c2}(1P) \rightarrow \gamma\phi)/\Gamma_{total}] \times [B(\psi(2S) \rightarrow \chi_{c2}(1P))]$ assuming $B(\psi(2S) \rightarrow \chi_{c2}(1P)) = (8.74 \pm 0.35) \times 10^{-2}$, which we rescale to our best value $B(\psi(2S) \rightarrow \chi_{c2}(1P)) = 9.36 \times 10^{-2}$.

² BENNETT 08A reports $< 13 \times 10^{-6}$ from a measurement of $[\Gamma(\chi_{c2}(1P) \rightarrow \gamma\phi)/\Gamma_{total}] \times [B(\psi(2S) \rightarrow \chi_{c2}(1P))]$ assuming $B(\psi(2S) \rightarrow \chi_{c2}(1P)) = (8.1 \pm 0.4) \times 10^{-2}$, which we rescale to our best value $B(\psi(2S) \rightarrow \chi_{c2}(1P)) = 9.36 \times 10^{-2}$.

$\Gamma(e^+e^-J/\psi(1S))/\Gamma_{total}$ Γ_{99}/Γ

VALUE (units 10^{-3})	EVTS	DOCUMENT ID	TECN	COMMENT
2.41 ± 0.15 ± 0.06	1.3k	^{1,2} ABLIKIM	17i BES3	$\psi(2S) \rightarrow \gamma e^+e^-J/\psi$

• • • We do not use the following data for averages, fits, limits, etc. • • •

¹ ABLIKIM 17i reports $(2.48 \pm 0.08 \pm 0.16) \times 10^{-3}$ from a measurement of $[\Gamma(\chi_{c2}(1P) \rightarrow e^+e^-J/\psi(1S))/\Gamma_{total}] \times [B(\psi(2S) \rightarrow \chi_{c2}(1P))]$ assuming $B(\psi(2S) \rightarrow \chi_{c2}(1P)) = (9.11 \pm 0.31) \times 10^{-2}$, which we rescale to our best value $B(\psi(2S) \rightarrow \chi_{c2}(1P)) = (9.36 \pm 0.23) \times 10^{-2}$. Our first error is their experiment's error and our second error is the systematic error from using our best value.

² Not independent from other measurements reported by ABLIKIM 17i

Meson Particle Listings

 $\chi_{c2}(1P)$ $\Gamma(e^+e^-J/\psi(1S))/\Gamma(\gamma J/\psi(1S))$ Γ_{99}/Γ_{94}

VALUE (units 10^{-3})	EVTS	DOCUMENT ID	TECN	COMMENT
11.3±0.4±0.5	1.3k	¹ ABLIKIM	17i BES3	$\psi(2S) \rightarrow e^+e^- \gamma J/\psi$
¹ Uses $B(\psi(2S) \rightarrow \gamma \chi_{c2}(1P)) \times B(\chi_{c2}(1P) \rightarrow \gamma J/\psi(1S)) = (199.6 \pm 0.8 \pm 7.0) \times 10^{-4}$ from ABLIKIM 17N and accounts for common systematic errors.				

 $\Gamma(\mu^+\mu^-J/\psi(1S))/\Gamma(e^+e^-J/\psi(1S))$ Γ_{100}/Γ_{99}

VALUE (units 10^{-2})	EVTS	DOCUMENT ID	TECN	COMMENT
9.40±0.79±1.15	219	ABLIKIM	19Z BES3	$\psi(2S) \rightarrow \gamma \chi_{c2} \rightarrow \gamma(\mu^+\mu^-J/\psi)$

 $\Gamma(\gamma\gamma)/\Gamma(\gamma J/\psi(1S))$ Γ_{98}/Γ_{94}

VALUE (units 10^{-3})	DOCUMENT ID	TECN	COMMENT
1.50±0.08 OUR FIT	Error includes scale factor of 1.5.		
0.99±0.18	¹ AMBROGIANI 00B	E835	$\bar{p}p \rightarrow \chi_{c2} \rightarrow \gamma\gamma, \gamma J/\psi$
¹ Calculated by us using $B(J/\psi(1S) \rightarrow e^+e^-) = 0.0593 \pm 0.0010$.			

 $\Gamma(\gamma\gamma)/\Gamma_{total} \times \Gamma(\rho\bar{\rho})/\Gamma_{total}$ $\Gamma_{98}/\Gamma \times \Gamma_{56}/\Gamma$

VALUE (units 10^{-8})	DOCUMENT ID	TECN	COMMENT
2.12±0.15 OUR FIT	Error includes scale factor of 1.2.		
1.7 ±0.4 OUR AVERAGE			
1.60±0.42	ARMSTRONG 93	E760	$\bar{p}p \rightarrow \gamma\gamma X$
9.9 ±4.5	BAGLIN	87B SPEC	$\bar{p}p \rightarrow \gamma\gamma X$

 $\chi_{c2}(1P)$ CROSS-PARTICLE BRANCHING RATIOS $\Gamma(\chi_{c2}(1P) \rightarrow K^+K^-\pi^+\pi^-)/\Gamma_{total} \times \Gamma(\psi(2S) \rightarrow \gamma \chi_{c2}(1P))/\Gamma(\psi(2S) \rightarrow J/\psi(1S)\pi^+\pi^-)$ $\Gamma_{14}/\Gamma \times \Gamma_{181}^{\psi(2S)}/\Gamma_{12}^{\psi(2S)}$

VALUE (units 10^{-3})	DOCUMENT ID	TECN	COMMENT
2.24±0.30 OUR FIT	Error includes scale factor of 1.2.		
2.5 ±0.9 OUR AVERAGE	Error includes scale factor of 2.3.		
1.90±0.14±0.44	BAI	99B BES	$\psi(2S) \rightarrow \gamma \chi_{c2}$
3.8 ±0.67	¹ TANENBAUM 78	MRK1	$\psi(2S) \rightarrow \gamma \chi_{c2}$
¹ The reported value is derived using $B(\psi(2S) \rightarrow \pi^+\pi^-J/\psi) \times B(J/\psi \rightarrow \ell^+\ell^-) = (4.6 \pm 0.7)\%$. Calculated by us using $B(J/\psi \rightarrow \ell^+\ell^-) = 0.1181 \pm 0.0020$.			

 $\Gamma(\chi_{c2}(1P) \rightarrow K^*(892)^0\bar{K}^*(892)^0)/\Gamma_{total} \times \Gamma(\psi(2S) \rightarrow \gamma \chi_{c2}(1P))/\Gamma_{total}$ $\Gamma_{18}/\Gamma \times \Gamma_{181}^{\psi(2S)}/\Gamma_{12}^{\psi(2S)}$

VALUE (units 10^{-4})	DOCUMENT ID	TECN	COMMENT
2.1 ±0.9 OUR FIT	Error includes scale factor of 2.3.		
3.11±0.36±0.48	ABLIKIM	04H BES2	$\psi(2S) \rightarrow \gamma \chi_{c2}$

 $\Gamma(\chi_{c2}(1P) \rightarrow \rho\bar{\rho})/\Gamma_{total} \times \Gamma(\psi(2S) \rightarrow \gamma \chi_{c2}(1P))/\Gamma(\psi(2S) \rightarrow J/\psi(1S)\pi^+\pi^-)$ $\Gamma_{56}/\Gamma \times \Gamma_{181}^{\psi(2S)}/\Gamma_{12}^{\psi(2S)}$

VALUE (units 10^{-5})	DOCUMENT ID	TECN	COMMENT
1.96±0.10 OUR FIT	Error includes scale factor of 1.1.		
1.4 ±1.1	¹ BAI	98i BES	$\psi(2S) \rightarrow \gamma \chi_{c2} \rightarrow \gamma \bar{\rho} \rho$

¹ Calculated by us. The value for $B(\chi_{c2} \rightarrow \rho\bar{\rho})$ reported in BAI 98i is derived using $B(\psi(2S) \rightarrow \gamma \chi_{c2}) = (7.8 \pm 0.8)\%$ and $B(\psi(2S) \rightarrow J/\psi(1S)\pi^+\pi^-) = (32.4 \pm 2.6)\%$ [BAI 98D].

 $\Gamma(\chi_{c2}(1P) \rightarrow \rho\bar{\rho})/\Gamma_{total} \times \Gamma(\psi(2S) \rightarrow \gamma \chi_{c2}(1P))/\Gamma_{total}$ $\Gamma_{56}/\Gamma \times \Gamma_{181}^{\psi(2S)}/\Gamma_{12}^{\psi(2S)}$

VALUE (units 10^{-6})	EVTS	DOCUMENT ID	TECN	COMMENT
6.79±0.34 OUR FIT	Error includes scale factor of 1.1.			
7.1 ±0.5 OUR AVERAGE	Error includes scale factor of 1.2.			
7.3 ±0.4 ±0.3	405	ABLIKIM	13v BES3	$\psi(2S) \rightarrow \gamma \rho\bar{\rho}$
7.2 ±0.7 ±0.4	121 ±12	¹ NAIK	08 CLEO	$\psi(2S) \rightarrow \gamma \rho\bar{\rho}$
4.4 +1.6 ±0.6	14.3 +5.2 -4.7	BAI	04F BES	$\psi(2S) \rightarrow \gamma \chi_{c2}(1P) \rightarrow \gamma \bar{\rho} \rho$

¹ Calculated by us. NAIK 08 reports $B(\chi_{c2} \rightarrow \rho\bar{\rho}) = (7.7 \pm 0.8 \pm 0.4 \pm 0.5) \times 10^{-5}$ using $B(\psi(2S) \rightarrow \gamma \chi_{c2}) = (9.33 \pm 0.14 \pm 0.61)\%$.

 $\Gamma(\chi_{c2}(1P) \rightarrow \Lambda\bar{\Lambda})/\Gamma_{total} \times \Gamma(\psi(2S) \rightarrow \gamma \chi_{c2}(1P))/\Gamma_{total}$ $\Gamma_{69}/\Gamma \times \Gamma_{181}^{\psi(2S)}/\Gamma_{12}^{\psi(2S)}$

VALUE (units 10^{-6})	EVTS	DOCUMENT ID	TECN	COMMENT
17.3±1.4 OUR FIT	Error includes scale factor of 2.4.			
17.3±1.5 OUR AVERAGE				
18.2±0.8±1.7	670	ABLIKIM	21L BES3	$\psi(2S) \rightarrow \gamma \rho\pi^-\bar{\rho}\pi^+$
15.9±2.1±1.0	71	¹ NAIK	08 CLEO	$\psi(2S) \rightarrow \gamma \Lambda\bar{\Lambda}$
••• We do not use the following data for averages, fits, limits, etc. •••				
18.2±1.4±0.9	207	^{2,3} ABLIKIM	13H BES3	$\psi(2S) \rightarrow \gamma \Lambda\bar{\Lambda}$

¹ Calculated by us. NAIK 08 reports $B(\chi_{c2} \rightarrow \Lambda\bar{\Lambda}) = (17.0 \pm 2.2 \pm 1.1 \pm 1.1) \times 10^{-5}$ using $B(\psi(2S) \rightarrow \gamma \chi_{c2}) = (9.33 \pm 0.14 \pm 0.61)\%$.

² Superseded by ABLIKIM 21L

³ Calculated by us. ABLIKIM 13H reports $B(\chi_{c2} \rightarrow \Lambda\bar{\Lambda}) = (20.8 \pm 1.6 \pm 2.3) \times 10^{-5}$ from a measurement of $B(\chi_{c2} \rightarrow \Lambda\bar{\Lambda}) \times B(\psi(2S) \rightarrow \gamma \chi_{c2})$ assuming $B(\psi(2S) \rightarrow \gamma \chi_{c2}) = (8.74 \pm 0.35)\%$.

 $\Gamma(\chi_{c2}(1P) \rightarrow \Lambda\bar{\Lambda})/\Gamma_{total} \times \Gamma(\psi(2S) \rightarrow \gamma \chi_{c2}(1P))/\Gamma(\psi(2S) \rightarrow J/\psi(1S)\pi^+\pi^-)$ $\Gamma_{69}/\Gamma \times \Gamma_{181}^{\psi(2S)}/\Gamma_{12}^{\psi(2S)}$

VALUE (units 10^{-5})	EVTS	DOCUMENT ID	TECN	COMMENT
5.0±0.4 OUR FIT				
7.1±3.1 -2.9±1.3	8.3 +3.7 -3.4	¹ BAI	03E BES	$\psi(2S) \rightarrow \gamma \Lambda\bar{\Lambda}$

¹ BAI 03E reports $[B(\chi_{c2} \rightarrow \Lambda\bar{\Lambda}) B(\psi(2S) \rightarrow \gamma \chi_{c2}) / B(\psi(2S) \rightarrow J/\psi\pi^+\pi^-)] \times [B^2(\Lambda \rightarrow \pi^-\rho) / B(J/\psi \rightarrow \rho\bar{\rho})] = (1.33 +0.59 -0.55 \pm 0.25)\%$. We calculate from this measurement the presented value using $B(\Lambda \rightarrow \pi^-\rho) = (63.9 \pm 0.5)\%$ and $B(J/\psi \rightarrow \rho\bar{\rho}) = (2.17 \pm 0.07) \times 10^{-3}$.

 $\Gamma(\chi_{c2}(1P) \rightarrow \Lambda\bar{\Lambda}\eta)/\Gamma_{total} \times \Gamma(\psi(2S) \rightarrow \gamma \chi_{c2}(1P))/\Gamma_{total}$ $\Gamma_{74}/\Gamma \times \Gamma_{181}^{\psi(2S)}/\Gamma_{12}^{\psi(2S)}$

VALUE (units 10^{-5})	EVTS	DOCUMENT ID	TECN	COMMENT
1.00±0.20±0.14	32	ABLIKIM	22A0 BES3	$\psi(2S) \rightarrow \gamma \rho\pi^-\bar{\rho}\pi^+\gamma$

 $\Gamma(\chi_{c2}(1P) \rightarrow \pi\pi)/\Gamma_{total} \times \Gamma(\psi(2S) \rightarrow \gamma \chi_{c2}(1P))/\Gamma_{total}$ $\Gamma_{25}/\Gamma \times \Gamma_{181}^{\psi(2S)}/\Gamma_{12}^{\psi(2S)}$

VALUE (units 10^{-4})	EVTS	DOCUMENT ID	TECN	COMMENT
2.12±0.08 OUR FIT				
2.17±0.09 OUR AVERAGE				
2.19±0.05±0.15	4.5k	¹ ABLIKIM	10A BES3	$e^+e^- \rightarrow \psi(2S) \rightarrow \gamma \chi_{c2}$
2.23±0.06±0.10	2.5k	² ASNER	09 CLEO	$\psi(2S) \rightarrow \gamma \pi^+\pi^-$
1.90±0.08±0.20	0.8k	³ ASNER	09 CLEO	$\psi(2S) \rightarrow \gamma \pi^0\pi^0$

¹ Calculated by us. ABLIKIM 10A reports $B(\chi_{c2} \rightarrow \pi^0\pi^0) = (0.88 \pm 0.02 \pm 0.06 \pm 0.04) \times 10^{-3}$ using $B(\psi(2S) \rightarrow \gamma \chi_{c2}) = (8.3 \pm 0.4)\%$. We have multiplied the $\pi^0\pi^0$ measurement by 3 to obtain $\pi\pi$.

² Calculated by us. ASNER 09 reports $B(\chi_{c2} \rightarrow \pi^+\pi^-) = (1.59 \pm 0.04 \pm 0.07 \pm 0.10) \times 10^{-3}$ using $B(\psi(2S) \rightarrow \gamma \chi_{c2}) = (9.33 \pm 0.14 \pm 0.61)\%$. We have multiplied the $\pi^+\pi^-$ measurement by 3/2 to obtain $\pi\pi$.

³ Calculated by us. ASNER 09 reports $B(\chi_{c2} \rightarrow \pi^0\pi^0) = (0.68 \pm 0.03 \pm 0.07 \pm 0.04) \times 10^{-3}$ using $B(\psi(2S) \rightarrow \gamma \chi_{c2}) = (9.33 \pm 0.14 \pm 0.61)\%$. We have multiplied the $\pi^0\pi^0$ measurement by 3 to obtain $\pi\pi$.

 $\Gamma(\chi_{c2}(1P) \rightarrow \pi\pi)/\Gamma_{total} \times \Gamma(\psi(2S) \rightarrow \gamma \chi_{c2}(1P))/\Gamma(\psi(2S) \rightarrow J/\psi(1S)\pi^+\pi^-)$ $\Gamma_{25}/\Gamma \times \Gamma_{181}^{\psi(2S)}/\Gamma_{12}^{\psi(2S)}$

VALUE (units 10^{-3})	EVTS	DOCUMENT ID	TECN	COMMENT
0.61±0.024 OUR FIT				
0.54 ±0.06 OUR AVERAGE				
0.66 ±0.18 ±0.37	21 ±6	¹ BAI	03C BES	$\psi(2S) \rightarrow \gamma \pi^0\pi^0$
0.54 ±0.05 ±0.04	185 ±16	² BAI	98i BES	$\psi(2S) \rightarrow \gamma \pi^+\pi^-$

¹ We have multiplied $\pi^0\pi^0$ measurement by 3 to obtain $\pi\pi$.

² Calculated by us. The value for $B(\chi_{c2} \rightarrow \pi^+\pi^-)$ reported by BAI 98i is derived using $B(\psi(2S) \rightarrow \gamma \chi_{c2}) = (7.8 \pm 0.8)\%$ and $B(\psi(2S) \rightarrow J/\psi\pi^+\pi^-) = (32.4 \pm 2.6)\%$ [BAI 98D]. We have multiplied $\pi^+\pi^-$ measurement by 3/2 to obtain $\pi\pi$.

 $\Gamma(\chi_{c2}(1P) \rightarrow \eta\eta)/\Gamma_{total} \times \Gamma(\psi(2S) \rightarrow \gamma \chi_{c2}(1P))/\Gamma_{total}$ $\Gamma_{31}/\Gamma \times \Gamma_{181}^{\psi(2S)}/\Gamma_{12}^{\psi(2S)}$

VALUE (units 10^{-4})	CL%	EVTS	DOCUMENT ID	TECN	COMMENT
0.52±0.04 OUR FIT					
0.52±0.04 OUR AVERAGE					
0.54±0.03±0.04		386	¹ ABLIKIM	10A BES3	$e^+e^- \rightarrow \psi(2S) \rightarrow \gamma \chi_{c2}$
0.47±0.05±0.05		156	ASNER	09 CLEO	$\psi(2S) \rightarrow \gamma \eta\eta$
••• We do not use the following data for averages, fits, limits, etc. •••					
< 0.44	90	² ADAMS	07 CLEO	$\psi(2S) \rightarrow \gamma \chi_{c2}$	
< 3	90	BAI	03C BES	$\psi(2S) \rightarrow \gamma \eta\eta \rightarrow 5\gamma$	
0.62±0.31±0.19			LEE	85 CBAL	$\psi(2S) \rightarrow \text{photons}$

¹ Calculated by us. ABLIKIM 10A reports $B(\chi_{c2} \rightarrow \eta\eta) = (0.65 \pm 0.04 \pm 0.05 \pm 0.03) \times 10^{-3}$ using $B(\psi(2S) \rightarrow \gamma \chi_{c2}) = (8.3 \pm 0.4)\%$.

² Superseded by ASNER 09.

 $\Gamma(\chi_{c2}(1P) \rightarrow K^+K^-)/\Gamma_{total} \times \Gamma(\psi(2S) \rightarrow \gamma \chi_{c2}(1P))/\Gamma_{total}$ $\Gamma_{32}/\Gamma \times \Gamma_{181}^{\psi(2S)}/\Gamma_{12}^{\psi(2S)}$

VALUE (units 10^{-5})	EVTS	DOCUMENT ID	TECN	COMMENT
9.5±1.4 OUR FIT	Error includes scale factor of 2.4.			
10.5±0.3±0.6	1.6k	¹ ASNER	09 CLEO	$\psi(2S) \rightarrow \gamma K^+K^-$

¹ Calculated by us. ASNER 09 reports $B(\chi_{c2} \rightarrow K^+K^-) = (1.13 \pm 0.03 \pm 0.06 \pm 0.07) \times 10^{-3}$ using $B(\psi(2S) \rightarrow \gamma \chi_{c2}) = (9.33 \pm 0.14 \pm 0.61)\%$.

 $\Gamma(\chi_{c2}(1P) \rightarrow K^+K^-)/\Gamma_{total} \times \Gamma(\psi(2S) \rightarrow \gamma \chi_{c2}(1P))/\Gamma(\psi(2S) \rightarrow J/\psi(1S)\pi^+\pi^-)$ $\Gamma_{32}/\Gamma \times \Gamma_{181}^{\psi(2S)}/\Gamma_{12}^{\psi(2S)}$

VALUE (units 10^{-3})	EVTS	DOCUMENT ID	TECN	COMMENT
0.27 ±0.04 OUR FIT	Error includes scale factor of 2.4.			
0.190±0.034±0.019	115 ±13	¹ BAI	98i BES	$\psi(2S) \rightarrow \gamma K^+K^-$

¹ Calculated by us. The value for $B(\chi_{c2} \rightarrow K^+K^-)$ reported by BAI 98i is derived using $B(\psi(2S) \rightarrow \gamma \chi_{c2}) = (7.8 \pm 0.8)\%$ and $B(\psi(2S) \rightarrow J/\psi\pi^+\pi^-) = (32.4 \pm 2.6)\%$ [BAI 98D].

See key on page 1171

Meson Particle Listings

$\chi_{c2}(1P)$

$$\Gamma(\chi_{c2}(1P) \rightarrow K_S^0 K_S^0) / \Gamma_{\text{total}} \times \Gamma(\psi(2S) \rightarrow \gamma \chi_{c2}(1P)) / \Gamma_{\text{total}} / \Gamma(\psi(2S) \rightarrow \gamma \chi_{c2}(1P)) / \Gamma_{\text{total}}$$

VALUE (units 10^{-5})	EVTS	DOCUMENT ID	TECN	COMMENT
5.0 ± 0.4 OUR FIT				
5.0 ± 0.4 OUR AVERAGE				
4.9 ± 0.3 ± 0.3	373 ± 20	¹ ASNER 09	CLEO	$\psi(2S) \rightarrow \gamma K_S^0 K_S^0$
5.72 ± 0.76 ± 0.63	65	ABLIKIM 05o	BES2	$\psi(2S) \rightarrow \gamma K_S^0 K_S^0$

¹ Calculated by us. ASNER 09 reports $B(\chi_{c2} \rightarrow K_S^0 K_S^0) = (0.53 \pm 0.03 \pm 0.03 \pm 0.03) \times 10^{-3}$ using $B(\psi(2S) \rightarrow \gamma \chi_{c2}) = (9.33 \pm 0.14 \pm 0.61)\%$.

$$\Gamma(\chi_{c2}(1P) \rightarrow K_S^0 K_S^0) / \Gamma_{\text{total}} \times \Gamma(\psi(2S) \rightarrow \gamma \chi_{c2}(1P)) / \Gamma(\psi(2S) \rightarrow J/\psi(1S) \pi^+ \pi^-)$$

VALUE (units 10^{-5})	DOCUMENT ID	TECN	COMMENT
14.3 ± 1.1 OUR FIT			
14.7 ± 4.1 ± 3.3	¹ BAI 99b	BES	$\psi(2S) \rightarrow \gamma K_S^0 K_S^0$

¹ Calculated by us. The value of $B(\chi_{c2} \rightarrow K_S^0 K_S^0)$ reported by BAI 99b was derived using $B(\psi(2S) \rightarrow \gamma \chi_{c2}(1P)) = (7.8 \pm 0.8)\%$ and $B(\psi(2S) \rightarrow J/\psi \pi^+ \pi^-) = (32.4 \pm 2.6)\%$ [BAI 98d].

$$\Gamma(\chi_{c2}(1P) \rightarrow \bar{K}^0 K^+ \pi^- + \text{c.c.}) / \Gamma_{\text{total}} \times \Gamma(\psi(2S) \rightarrow \gamma \chi_{c2}(1P)) / \Gamma_{\text{total}}$$

VALUE (units 10^{-4})	EVTS	DOCUMENT ID	TECN	COMMENT
1.22 ± 0.17 OUR FIT				
1.15 ± 0.18 OUR AVERAGE				
1.21 ± 0.19 ± 0.09	37	¹ ATHAR 07	CLEO	$\psi(2S) \rightarrow \gamma K^0 K^+ \pi^-$
0.97 ± 0.32 ± 0.13	28	² ABLIKIM 06r	BES2	$\psi(2S) \rightarrow \gamma K_S^0 K^+ \pi^-$

¹ Calculated by us. ATHAR 07 reports $B(\chi_{c2} \rightarrow \bar{K}^0 K^+ \pi^- + \text{c.c.}) = (1.3 \pm 0.2 \pm 0.1 \pm 0.1) \times 10^{-3}$ using $B(\psi(2S) \rightarrow \gamma \chi_{c2}) = (9.33 \pm 0.14 \pm 0.61)\%$.
² Calculated by us. ABLIKIM 06r reports $B(\chi_{c2} \rightarrow K_S^0 K^+ \pi^-) = (0.6 \pm 0.2 \pm 0.1) \times 10^{-3}$ using $B(\psi(2S) \rightarrow \gamma \chi_{c2}) = (8.1 \pm 0.6)\%$. We have multiplied by 2 to obtain $\bar{K}^0 K^+ \pi^- + \text{c.c.}$ from $K_S^0 K^+ \pi^-$.

$$\Gamma(\chi_{c2}(1P) \rightarrow 2(\pi^+ \pi^-)) / \Gamma_{\text{total}} \times \Gamma(\psi(2S) \rightarrow \gamma \chi_{c2}(1P)) / \Gamma(\psi(2S) \rightarrow J/\psi(1S) \pi^+ \pi^-)$$

VALUE (units 10^{-3})	DOCUMENT ID	TECN	COMMENT
2.7 ± 0.4 OUR FIT			Error includes scale factor of 1.4.
3.1 ± 1.0 OUR AVERAGE			Error includes scale factor of 2.5.
2.3 ± 0.1 ± 0.5	¹ BAI 99b	BES	$\psi(2S) \rightarrow \gamma \chi_{c2}$
4.3 ± 0.6	² TANENBAUM 78	MRK1	$\psi(2S) \rightarrow \gamma \chi_{c2}$

¹ Calculated by us. The value for $B(\chi_{c2} \rightarrow 2\pi^+ 2\pi^-)$ reported in BAI 99b is derived using $B(\psi(2S) \rightarrow \gamma \chi_{c2}) = (7.8 \pm 0.8)\%$ and $B(\psi(2S) \rightarrow J/\psi(1S) \pi^+ \pi^-) = (32.4 \pm 2.6)\%$ [BAI 98d].
² The value for $B(\psi(2S) \rightarrow \gamma \chi_{c2}) \times B(\chi_{c2} \rightarrow 2\pi^+ 2\pi^-)$ reported in TANENBAUM 78 is derived using $B(\psi(2S) \rightarrow J/\psi(1S) \pi^+ \pi^-) \times B(J/\psi(1S) \ell^+ \ell^-) = (4.6 \pm 0.7)\%$. Calculated by us using $B(J/\psi(1S) \rightarrow \ell^+ \ell^-) = 0.1181 \pm 0.0020$.

$$\Gamma(\chi_{c2}(1P) \rightarrow K^+ K^- K^+ K^-) / \Gamma_{\text{total}} \times \Gamma(\psi(2S) \rightarrow \gamma \chi_{c2}(1P)) / \Gamma_{\text{total}}$$

VALUE (units 10^{-4})	EVTS	DOCUMENT ID	TECN	COMMENT
1.56 ± 0.21 OUR FIT				Error includes scale factor of 1.1.
1.76 ± 0.16 ± 0.24	160	¹ ABLIKIM 06t	BES2	$\psi(2S) \rightarrow \gamma 2K^+ 2K^-$

¹ Calculated by us. The value of $B(\chi_{c2} \rightarrow 2K^+ 2K^-)$ reported by ABLIKIM 06t was derived using $B(\psi(2S) \rightarrow \gamma \chi_{c2}(1P)) = (8.1 \pm 0.4)\%$.

$$\Gamma(\chi_{c2}(1P) \rightarrow K^+ K^- K^+ K^-) / \Gamma_{\text{total}} \times \Gamma(\psi(2S) \rightarrow \gamma \chi_{c2}(1P)) / \Gamma(\psi(2S) \rightarrow J/\psi(1S) \pi^+ \pi^-)$$

VALUE (units 10^{-4})	DOCUMENT ID	TECN	COMMENT
4.5 ± 0.6 OUR FIT			Error includes scale factor of 1.1.
3.6 ± 0.6 ± 0.6	¹ BAI 99b	BES	$\psi(2S) \rightarrow \gamma 2K^+ 2K^-$

¹ Calculated by us. The value of $B(\chi_{c2} \rightarrow 2K^+ 2K^-)$ reported by BAI 99b was derived using $B(\psi(2S) \rightarrow \gamma \chi_{c2}(1P)) = (7.8 \pm 0.8)\%$ and $B(\psi(2S) \rightarrow J/\psi \pi^+ \pi^-) = (32.4 \pm 2.6)\%$ [BAI 98d].

$$\Gamma(\chi_{c2}(1P) \rightarrow \phi) / \Gamma_{\text{total}} \times \Gamma(\psi(2S) \rightarrow \gamma \chi_{c2}(1P)) / \Gamma_{\text{total}}$$

VALUE (units 10^{-4})	EVTS	DOCUMENT ID	TECN	COMMENT
1.15 ± 0.07 OUR FIT				Error includes scale factor of 1.8.
0.98 ± 0.13 OUR AVERAGE				Error includes scale factor of 1.3.
0.94 ± 0.03 ± 0.10	849	¹ ABLIKIM 11k	BES3	$\psi(2S) \rightarrow \gamma$ hadrons
1.38 ± 0.24 ± 0.23	41	² ABLIKIM 06t	BES2	$\psi(2S) \rightarrow \gamma 2K^+ 2K^-$

¹ Calculated by us. The value of $B(\chi_{c2} \rightarrow \phi)$ reported by ABLIKIM 11k was derived using $B(\psi(2S) \rightarrow \gamma \chi_{c2}(1P)) = (8.74 \pm 0.35)\%$.
² Calculated by us. The value of $B(\chi_{c2} \rightarrow \phi)$ reported by ABLIKIM 06t was derived using $B(\psi(2S) \rightarrow \gamma \chi_{c2}(1P)) = (8.1 \pm 0.4)\%$.

$$\Gamma(\chi_{c2}(1P) \rightarrow \phi) / \Gamma_{\text{total}} \times \Gamma(\psi(2S) \rightarrow \gamma \chi_{c2}(1P)) / \Gamma(\psi(2S) \rightarrow J/\psi(1S) \pi^+ \pi^-)$$

VALUE (units 10^{-4})	DOCUMENT ID	TECN	COMMENT
3.31 ± 0.21 OUR FIT			Error includes scale factor of 1.7.
4.8 ± 1.3 ± 1.3	¹ BAI 99b	BES	$\psi(2S) \rightarrow \gamma 2K^+ 2K^-$

¹ Calculated by us. The value of $B(\chi_{c2} \rightarrow \phi)$ reported by BAI 99b was derived using $B(\psi(2S) \rightarrow \gamma \chi_{c2}(1P)) = (7.8 \pm 0.8)\%$ and $B(\psi(2S) \rightarrow J/\psi \pi^+ \pi^-) = (32.4 \pm 2.6)\%$ [BAI 98d].

$$\Gamma(\chi_{c2}(1P) \rightarrow \Sigma^+ \bar{p} K_S^0 + \text{c.c.}) / \Gamma_{\text{total}} \times \Gamma(\psi(2S) \rightarrow \gamma \chi_{c2}(1P)) / \Gamma_{\text{total}}$$

VALUE (units 10^{-6})	EVTS	DOCUMENT ID	TECN	COMMENT
7.85 ± 0.77 ± 0.44	129	¹ ABLIKIM 19bb	BES3	$\psi(2S) \rightarrow \gamma \Sigma^+ \bar{p} K_S^0 + \text{c.c.}$

¹ Calculated by us. ABLIKIM 19bb reports $B(\chi_{c2} \rightarrow \Sigma^+ \bar{p} K_S^0 + \text{c.c.}) = (8.25 \pm 0.83 \pm 0.49) \times 10^{-5}$ using $B(\psi(2S) \rightarrow \gamma \chi_{c2}) = (9.52 \pm 0.20)\%$ and other branching fractions from PDG 18.

$$\Gamma(\chi_{c2}(1P) \rightarrow \Sigma^0 \bar{p} K^+ + \text{c.c.}) / \Gamma_{\text{total}} \times \Gamma(\psi(2S) \rightarrow \gamma \chi_{c2}(1P)) / \Gamma_{\text{total}}$$

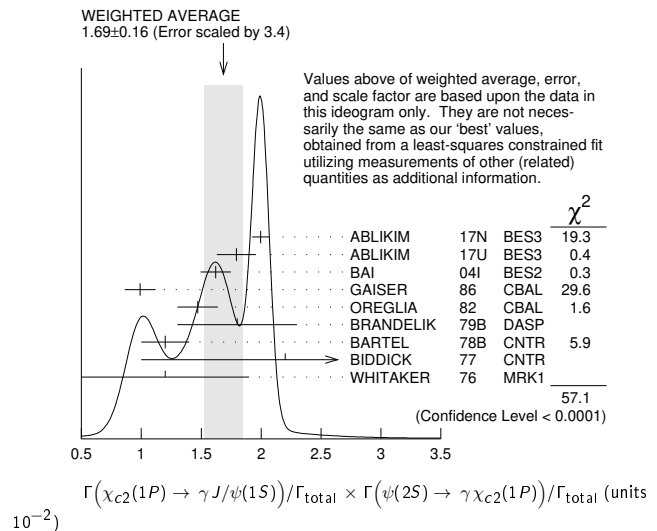
VALUE (units 10^{-5})	EVTS	DOCUMENT ID	TECN	COMMENT
0.87 ± 0.06 ± 0.04	271	¹ ABLIKIM 20AE	BES3	$\psi(2S) \rightarrow \gamma \Sigma^0 \bar{p} K^+ + \text{c.c.}$

¹ Calculated by us. ABLIKIM 20AE reports $B(\chi_{c2} \rightarrow \Sigma^0 \bar{p} K^+ + \text{c.c.}) = (0.91 \pm 0.06 \pm 0.05) \times 10^{-4}$ using $B(\psi(2S) \rightarrow \gamma \chi_{c2}) = (9.52 \pm 0.20)\%$ and other branching fractions from PDG 20.

$$\Gamma(\chi_{c2}(1P) \rightarrow \gamma J/\psi(1S)) / \Gamma_{\text{total}} \times \Gamma(\psi(2S) \rightarrow \gamma \chi_{c2}(1P)) / \Gamma_{\text{total}}$$

VALUE (units 10^{-2})	EVTS	DOCUMENT ID	TECN	COMMENT
1.82 ± 0.07 OUR FIT				Error includes scale factor of 1.9.
1.69 ± 0.16 OUR AVERAGE				Error includes scale factor of 3.4. See the ideogram below.
1.996 ± 0.008 ± 0.070	81k	¹ ABLIKIM 17n	BES3	$\psi(2S) \rightarrow \gamma \gamma J/\psi$
1.793 ± 0.008 ± 0.163	1.0M	ABLIKIM 17u	BES3	$e^+ e^- \rightarrow \gamma X$
1.62 ± 0.04 ± 0.12	5.8k	BAI 04i	BES2	$\psi(2S) \rightarrow J/\psi \gamma \gamma$
0.99 ± 0.10 ± 0.08		GAISER 86	CBAL	$\psi(2S) \rightarrow \gamma X$
1.47 ± 0.17		² OREGLIA 82	CBAL	$\psi(2S) \rightarrow \gamma \chi_{c2}$
1.8 ± 0.5		³ BRANDELIK 79b	DASP	$\psi(2S) \rightarrow \gamma \chi_{c2}$
1.2 ± 0.2		³ BARTEL 78b	CNTR	$\psi(2S) \rightarrow \gamma \chi_{c2}$
2.2 ± 1.2		⁴ BIDDICK 77	CNTR	$e^+ e^- \rightarrow \gamma X$
1.2 ± 0.7		² WHITAKER 76	MRK1	$e^+ e^-$

• • • We do not use the following data for averages, fits, limits, etc. • • •
 1.874 ± 0.007 ± 0.102 76k ⁵ ABLIKIM 12o BES3 $\psi(2S) \rightarrow \gamma \chi_{c2}$
 1.95 ± 0.02 ± 0.07 12.4k ⁶ MENDEZ 08 CLEO $\psi(2S) \rightarrow \gamma \chi_{c2}$
 1.85 ± 0.04 ± 0.07 1.9k ⁷ ADAM 05A CLEO Repl. by MENDEZ 08
¹ Uses $B(J/\psi \rightarrow e^+ e^-) = (5.971 \pm 0.032)\%$ and $B(J/\psi \rightarrow \mu^+ \mu^-) = (5.961 \pm 0.033)\%$.
² Recalculated by us using $B(J/\psi(1S) \rightarrow \ell^+ \ell^-) = 0.1181 \pm 0.0020$.
³ Recalculated by us using $B(J/\psi(1S) \rightarrow \mu^+ \mu^-) = 0.0588 \pm 0.0010$.
⁴ Assumes isotropic gamma distribution.
⁵ Superseded by ABLIKIM 17n.
⁶ Not independent from other measurements of MENDEZ 08.
⁷ Not independent from other values reported by ADAM 05A.



Meson Particle Listings

$\chi_{c2}(1P)$

$$\Gamma(\chi_{c2}(1P) \rightarrow \gamma J/\psi(1S))/\Gamma_{\text{total}} \times \Gamma(\psi(2S) \rightarrow \gamma \chi_{c2}(1P))/\Gamma(\psi(2S) \rightarrow J/\psi(1S)\pi^+\pi^-) / \Gamma_{94}/\Gamma \times \Gamma_{181}^{\psi(2S)}/\Gamma_{12}^{\psi(2S)}$$

VALUE (units 10^{-2})	EVTS	DOCUMENT ID	TECN	COMMENT
5.26±0.19 OUR FIT	Error includes scale factor of 1.8.			
5.53±0.17 OUR AVERAGE				
5.56±0.05±0.16	12.4k	MENDEZ	08	CLEO $\psi(2S) \rightarrow \gamma \chi_{c2}$
6.0 ± 2.8	1.3k	¹ ABLIKIM	04B	BES $\psi(2S) \rightarrow J/\psi X$
3.9 ± 1.2		² HIMEL	80	MRK2 $\psi(2S) \rightarrow \gamma \chi_{c2}$
• • •	We do not use the following data for averages, fits, limits, etc. • • •			
5.52±0.13±0.13	1.9k	³ ADAM	05A	CLEO Repl. by MENDEZ 08

- From a fit to the J/ψ recoil mass spectra.
- The value for $B(\psi(2S) \rightarrow \gamma \chi_{c2}) \times B(\chi_{c2} \rightarrow \gamma J/\psi(1S))$ reported in HIMEL 80 is derived using $B(\psi(2S) \rightarrow J/\psi(1S)\pi^+\pi^-) = (33 \pm 3)\%$ and $B(J/\psi(1S) \rightarrow \ell^+\ell^-) = 0.138 \pm 0.018$. Calculated by us using $B(J/\psi(1S) \rightarrow \ell^+\ell^-) = (0.1181 \pm 0.0020)$.
- Not independent from other values reported by ADAM 05A.

$$\Gamma(\chi_{c2}(1P) \rightarrow \gamma\gamma)/\Gamma_{\text{total}} \times \Gamma(\psi(2S) \rightarrow \gamma \chi_{c2}(1P))/\Gamma_{\text{total}} / \Gamma_{98}/\Gamma \times \Gamma_{181}^{\psi(2S)}/\Gamma_{12}^{\psi(2S)}$$

VALUE (units 10^{-5})	EVTS	DOCUMENT ID	TECN	COMMENT
2.74±0.10 OUR FIT	Error includes scale factor of 1.3.			
2.82±0.10 OUR AVERAGE				
2.83±0.08±0.06	5k	¹ ABLIKIM	17AE	BES3 $\psi(2S) \rightarrow \gamma \chi_{c2} \rightarrow 3\gamma$
2.68±0.28±0.15	0.3k	ECKLUND	08A	CLEO $\psi(2S) \rightarrow \gamma \chi_{c2} \rightarrow 3\gamma$
7.0 ± 2.1 ± 2.0		LEE	85	CBAL $\psi(2S) \rightarrow \gamma \chi_{c2}$
• • •	We do not use the following data for averages, fits, limits, etc. • • •			
2.81±0.17±0.15	1.1k	² ABLIKIM	12A	BES3 $\psi(2S) \rightarrow \gamma \chi_{c2} \rightarrow 3\gamma$

- ABLIKIM 17AE measures the ratio of two-photon partial widths for the helicity $\lambda = 0$ and helicity $\lambda = 2$ components to be $f_{0/2} = \Gamma_{\gamma\gamma}^{\lambda=0} / \Gamma_{\gamma\gamma}^{\lambda=2} = 0.000 \pm 0.006 \pm 0.012$.
- ABLIKIM 12A measures the ratio of two-photon partial widths for the helicity $\lambda = 0$ and helicity $\lambda = 2$ components to be $f_{0/2} = \Gamma_{\gamma\gamma}^{\lambda=0} / \Gamma_{\gamma\gamma}^{\lambda=2} = 0.00 \pm 0.02 \pm 0.02$. Superseded by ABLIKIM 17AE.

$$\Gamma(\chi_{c2}(1P) \rightarrow \gamma\gamma)/\Gamma(\chi_{c0}(1P) \rightarrow \gamma\gamma) / \Gamma_{98}/\Gamma_{98}^{\chi_{c0}(1P)}$$

VALUE	EVTS	DOCUMENT ID	TECN	COMMENT
0.292±0.028 OUR AVERAGE				
0.295±0.014±0.028	8k	¹ ABLIKIM	17AE	BES3 $\psi(2S) \rightarrow \gamma \chi_{cJ} \rightarrow 3\gamma$
0.278±0.050±0.036	0.5k	¹ ECKLUND	08A	CLEO $\psi(2S) \rightarrow \gamma \chi_{cJ} \rightarrow 3\gamma$
• • •	We do not use the following data for averages, fits, limits, etc. • • •			
0.271±0.029±0.030	1.9k	^{1,2} ABLIKIM	12A	BES3 $\psi(2S) \rightarrow \gamma \chi_{cJ} \rightarrow 3\gamma$
¹ Not independent from the values of $\Gamma(\chi_{c0}, \chi_{c2})$ and $B(\psi(2S) \rightarrow \chi_{c0}, \chi_{c2})$.				
² Superseded by ABLIKIM 17AE.				

MULTIPOLE AMPLITUDES IN $\chi_{c2}(1P) \rightarrow \gamma J/\psi(1S)$ RADIATIVE DECAY

$a_2 = M2/\sqrt{E1^2 + M2^2 + E3^2}$ Magnetic quadrupole fractional transition amplitude

VALUE (units 10^{-2})	EVTS	DOCUMENT ID	TECN	COMMENT
-11.0± 1.0 OUR AVERAGE				
-12.0± 1.3±0.4	89k	¹ ABLIKIM	17N	BES3 $\psi(2S) \rightarrow \gamma\gamma\ell^+\ell^-$
- 9.3± 1.6±0.3	19.8k	² ARTUSO	09	CLEO $\psi(2S) \rightarrow \gamma\gamma\ell^+\ell^-$
- 9.3 ^{+3.9} / _{-4.1} ±0.6	5.9k	³ AMBROGIANI	02	E835 $p\bar{p} \rightarrow \chi_{c2} \rightarrow J/\psi\gamma$
-14 ± 6	1.9k	³ ARMSTRONG	93E	E760 $p\bar{p} \rightarrow \chi_{c2} \rightarrow J/\psi\gamma$
-33.3 ^{+11.6} / _{-29.2}	441	³ OREGLIA	82	CBAL $\psi(2S) \rightarrow \chi_{c1}\gamma \rightarrow J/\psi\gamma\gamma$

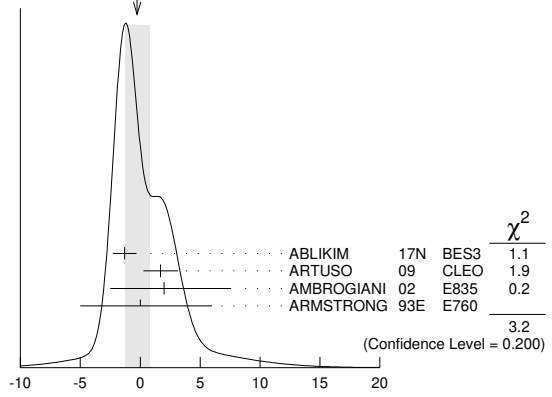
- • • We do not use the following data for averages, fits, limits, etc. • • •
- 7.9± 1.9±0.3 19.8k ⁴ ARTUSO 09 CLEO $\psi(2S) \rightarrow \gamma\gamma\ell^+\ell^-$
- ¹ Correlated with a_3 , b_2 , and b_3 with correlation coefficients $\rho_{a_2 a_3} = 0.733$, $\rho_{a_2 b_2} = -0.605$, and $\rho_{a_2 b_3} = -0.095$.
- ² From a fit with floating $M2$ amplitudes a_2 and b_2 , and fixed $E3$ amplitudes $a_3=b_3=0$.
- ³ Assuming $a_3=0$.
- ⁴ From a fit with floating $M2$ and $E3$ amplitudes a_2 , b_2 , and a_3 , and b_3 .

$a_3 = E3/\sqrt{E1^2 + M2^2 + E3^2}$ Electric octupole fractional transition amplitude

VALUE (units 10^{-2})	EVTS	DOCUMENT ID	TECN	COMMENT
-0.3±1.0 OUR AVERAGE	Error includes scale factor of 1.3. See the ideogram below.			
-1.3±0.9±0.4	89k	¹ ABLIKIM	17N	BES3 $\psi(2S) \rightarrow \gamma\gamma\ell^+\ell^-$
1.7±1.4±0.3	19.8k	² ARTUSO	09	CLEO $\psi(2S) \rightarrow \gamma\gamma\ell^+\ell^-$
2.0 ^{+5.5} / _{-4.4} ±0.9	5908	AMBROGIANI	02	E835 $p\bar{p} \rightarrow \chi_{c2} \rightarrow J/\psi\gamma$
0 ⁺⁶ / ₋₅	1904	ARMSTRONG	93E	E760 $p\bar{p} \rightarrow \chi_{c2} \rightarrow J/\psi\gamma$

- Correlated with a_2 , b_2 , and b_3 with correlation coefficients $\rho_{a_2 a_3} = 0.733$, $\rho_{a_3 b_2} = -0.422$, and $\rho_{a_3 b_3} = -0.024$.
- From a fit with floating $M2$ and $E3$ amplitudes a_2 , b_2 , and a_3 , and b_3 .

WEIGHTED AVERAGE
-0.3±1.0 (Error scaled by 1.3)



$a_3 = E3/\sqrt{E1^2 + M2^2 + E3^2}$ Electric octupole fractional transition amplitude (units 10^{-2})

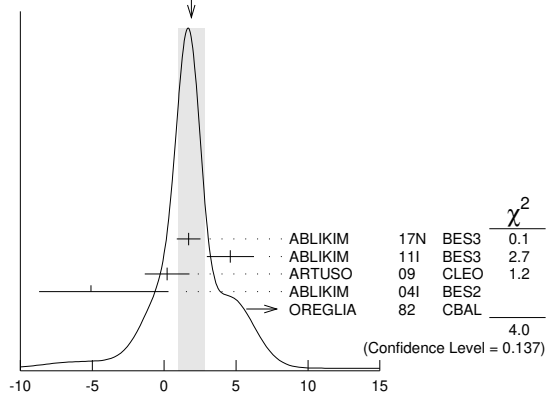
MULTIPOLE AMPLITUDES IN $\psi(2S) \rightarrow \gamma \chi_{c2}(1P)$ RADIATIVE DECAY

$b_2 = M2/\sqrt{E1^2 + M2^2 + E3^2}$ Magnetic quadrupole fractional transition amplitude

VALUE (units 10^{-2})	EVTS	DOCUMENT ID	TECN	COMMENT
1.9±0.9 OUR AVERAGE	Error includes scale factor of 1.4. See the ideogram below.			
1.7±0.8±0.2	89k	¹ ABLIKIM	17N	BES3 $\psi(2S) \rightarrow \gamma\gamma\ell^+\ell^-$
4.6±1.0±1.3	13.8k	² ABLIKIM	11I	BES3 $\psi(2S) \rightarrow \gamma\pi^+\pi^-, \gamma K^+ K^-$
0.2±1.5±0.4	19.8k	³ ARTUSO	09	CLEO $\psi(2S) \rightarrow \gamma\gamma\ell^+\ell^-$
- 5.1 ^{+5.4} / _{-3.6}	721	² ABLIKIM	04I	BES2 $\psi(2S) \rightarrow \gamma\pi^+\pi^-, \gamma K^+ K^-$
13.2 ^{+9.8} / _{-7.5}	441	⁴ OREGLIA	82	CBAL $\psi(2S) \rightarrow \gamma\gamma\ell^+\ell^-$

- • • We do not use the following data for averages, fits, limits, etc. • • •
- 1.0±1.3±0.3 19.8k ⁴ ARTUSO 09 CLEO $\psi(2S) \rightarrow \gamma\gamma\ell^+\ell^-$
- ¹ Correlated with a_2 , a_3 , and b_3 with correlation coefficients $\rho_{a_2 b_2} = -0.605$, $\rho_{a_3 b_2} = -0.422$, and $\rho_{b_2 b_3} = 0.384$.
- ² From a fit with floating $M2$ and $E3$ amplitudes b_2 and b_3 .
- ³ From a fit with floating $M2$ and $E3$ amplitudes a_2 , b_2 , and a_3 , and b_3 .
- ⁴ From a fit with floating $M2$ amplitudes a_2 and b_2 , and fixed $E3$ amplitudes $a_3=b_3=0$.

WEIGHTED AVERAGE
1.9±0.9 (Error scaled by 1.4)



$b_2 = M2/\sqrt{E1^2 + M2^2 + E3^2}$ Magnetic quadrupole fractional transition amplitude (units 10^{-2})

$b_3 = E3/\sqrt{E1^2 + M2^2 + E3^2}$ Electric octupole fractional transition amplitude

VALUE (units 10^{-2})	EVTS	DOCUMENT ID	TECN	COMMENT
-1.0±0.6 OUR AVERAGE				
-1.4±0.7±0.4	89k	¹ ABLIKIM	17N	BES3 $\psi(2S) \rightarrow \gamma\gamma\ell^+\ell^-$
1.5±0.8±1.8	13.8k	² ABLIKIM	11I	BES3 $\psi(2S) \rightarrow \gamma\pi^+\pi^-, \gamma K^+ K^-$
-0.8±1.2±0.2	19.8k	ARTUSO	09	CLEO $\psi(2S) \rightarrow \gamma\gamma\ell^+\ell^-$
-2.7 ^{+4.3} / _{-2.9}	721	² ABLIKIM	04I	BES2 $\psi(2S) \rightarrow \gamma\pi^+\pi^-, \gamma K^+ K^-$

- Correlated with a_2 , a_3 , and b_2 with correlation coefficients $\rho_{a_2 b_3} = -0.095$, $\rho_{a_3 b_3} = -0.024$, and $\rho_{b_2 b_3} = 0.384$.
- From a fit with floating $M2$ and $E3$ amplitudes b_2 and b_3 .

See key on page 1171

Meson Particle Listings

$\chi_{c2}(1P), \eta_c(2S)$

MULTIPOLE AMPLITUDE RATIOS IN RADIATIVE DECAYS
 $\psi(2S) \rightarrow \gamma\chi_{c2}(1P)$ and $\chi_{c2} \rightarrow \gamma J/\psi(1S)$

b_2/a_2 Magnetic quadrupole transition amplitude ratio

Table with columns: VALUE (units 10^-2), EVTS, DOCUMENT ID, TECN, COMMENT. Row: -11+14/-15, 19.8k, 1 ARTUSO 09 CLEO, $\psi(2S) \rightarrow \gamma\gamma\ell^+\ell^-$

1 Statistical and systematic errors combined. From a fit with floating M2 amplitudes a2 and b2, and fixed E3 amplitudes a3=b3=0. Not independent of values for a2(chi_c2(1P)) and b2(chi_c2(1P)) from ARTUSO 09.

Table listing references for chi_c2(1P) decays, including LEMOIGNE, OREGLIA, BARATE, HIMEL, BRANDELIC, BARTEL, TANENBAUM, BIDDICK, WHITAKER.

$\chi_{c2}(1P)$ REFERENCES

Large table of references for chi_c2(1P) decays, listing authors, document IDs, and technical details.

$\eta_c(2S)$

$I^G(J^{PC}) = 0^+(0^{-+})$

Quantum numbers are quark model predictions.

$\eta_c(2S)$ MASS

Table with columns: VALUE (MeV), EVTS, DOCUMENT ID, TECN, COMMENT. Includes 'OUR AVERAGE' and various experimental data points.

••• We do not use the following data for averages, fits, limits, etc. •••
3639 +/- 7 98 9 AUBERT 06E BABR B^+ -> K^+ X c c-bar
3630.8 +/- 3.4 +/- 1.0 112 10 AUBERT 04D BABR gamma -> eta_c(2S) -> K K-bar pi
3654 +/- 6 +/- 8 39 11 CHOI 02 BELL B -> K K_S K^- pi^+
3594 +/- 5 12 EDWARDS 82C CBAL e^+ e^- -> gamma X
1 AAIJ 17AD report m_psi(2S) - m_eta_c(2S) = 52.5 +/- 1.7 +/- 0.6 MeV. We use the current value m_psi(2S) = 3686.097 +/- 0.025 MeV to obtain the quoted mass.
2 From a fit of the phi phi invariant mass with the width of eta_c(2S) fixed to the PDG 16 value.
3 Ignoring possible interference with continuum.
4 With a width fixed to 11.3 MeV.
5 With a width fixed to 11.3 MeV. Using both eta -> gamma gamma and eta -> pi^+ pi^- pi^0 decays.
6 From a simultaneous fit to K_S^0 K^+ pi^- and K^+ K^- pi^0 decay modes.
7 Accounts for interference with non-resonant continuum.
8 From a fit of the J/psi recoil mass spectrum. Supersedes ABE, K 02 and ABE 04g.
9 From the fit of the kaon momentum spectrum. Systematic errors not evaluated.
10 Superseded by DEL-AMO-SANCHEZ 11M.
11 Superseded by VINKUROVA 11.
12 Assuming mass of psi(2S) = 3686 MeV.

$\eta_c(2S)$ WIDTH

Table with columns: VALUE (MeV), CL% EVTS, DOCUMENT ID, TECN, COMMENT. Includes 'OUR AVERAGE' and various experimental data points.

••• We do not use the following data for averages, fits, limits, etc. •••
< 23 22 14 90 98 4 AUBERT 06E BABR B^+ -> K^+ X c c-bar
121 5C AUBERT 05C BABR e^+ e^- -> J/psi c c-bar
17.0 +/- 8.3 +/- 2.5 112 5 AUBERT 04D BABR gamma -> eta_c(2S) -> K K-bar pi
6 CHOI 02 BELL B -> K K_S K^- pi^+
7 EDWARDS 82C CBAL e^+ e^- -> gamma X
1 From a simultaneous fit to K_S^0 K^+ pi^- and K^+ K^- pi^0 decay modes.

Meson Particle Listings

 $\eta_c(2S)$ ² Ignoring possible interference with continuum.³ Accounts for interference with non-resonant continuum.⁴ From the fit of the kaon momentum spectrum. Systematic errors not evaluated.⁵ Superseded by DEL-AMO-SANCHEZ 11M.⁶ For a mass value of 3654 ± 6 MeV. Superseded by VINOKUROVA 11.⁷ For a mass value of 3594 ± 5 MeV $\eta_c(2S)$ DECAY MODES

Mode	Fraction (Γ_i/Γ)	Confidence level
Γ_1 hadrons	seen	
Γ_2 $K\bar{K}\pi$	(1.9 ± 1.2) %	
Γ_3 $K\bar{K}\eta$	(5 ± 4) $\times 10^{-3}$	
Γ_4 $2\pi^+ 2\pi^-$	< 2.1 %	90%
Γ_5 $\rho^0 \rho^0$	< 1.9 $\times 10^{-3}$	90%
Γ_6 $3\pi^+ 3\pi^-$	(1.3 ± 0.9) %	
Γ_7 $K^+ K^- \pi^+ \pi^-$	< 1.4 %	90%
Γ_8 $K^{*0} \bar{K}^{*0}$	< 2.9 $\times 10^{-3}$	90%
Γ_9 $K^+ K^- \pi^+ \pi^- \pi^0$	(1.4 ± 1.0) %	
Γ_{10} $K^+ K^- 2\pi^+ 2\pi^-$	< 1.4 %	90%
Γ_{11} $K_S^0 K^- 2\pi^+ \pi^- + c.c.$	(1.0 ± 0.8) %	
Γ_{12} $2K^+ 2K^-$	< 1.3 $\times 10^{-3}$	90%
Γ_{13} $\phi\phi$	< 1.1 $\times 10^{-3}$	90%
Γ_{14} $\rho\bar{\rho}$	< 2.0 $\times 10^{-3}$	90%
Γ_{15} $\rho\bar{\rho}\pi^+\pi^-$	seen	
Γ_{16} $\gamma\gamma$	(1.8 ± 1.2) $\times 10^{-4}$	
Γ_{17} $\gamma J/\psi(1S)$	< 1.4 %	90%
Γ_{18} $\pi^+ \pi^- \eta$	(4.3 ± 3.2) $\times 10^{-3}$	
Γ_{19} $\pi^+ \pi^- \eta'$	(2.6 ± 1.9) $\times 10^{-3}$	
Γ_{20} $K_S^0(1430) \bar{K} + c.c.$	seen	
Γ_{21} $K_S^0(1950) \bar{K} + c.c.$	seen	
Γ_{22} $a_0(1710)\pi$	seen	
Γ_{23} $a_0(1450)\pi$	seen	
Γ_{24} $a_2(1700)\pi$	seen	
Γ_{25} $K_S^0(2600) \bar{K} + c.c.$	seen	
Γ_{26} $\pi^+ \pi^- \eta_c(1S)$	< 25 %	90%

 $\eta_c(2S)$ PARTIAL WIDTHS

$\Gamma(\gamma\gamma)$	Γ_{16}			
VALUE (keV)	EVTs	DOCUMENT ID	TECN	COMMENT
0.44 ± 0.14	106	¹ XU	18	BELL $e^+e^- \rightarrow e^+e^- \eta' \pi^+ \pi^-$
1.3 ± 0.6		² ASNER	04	CLEO $\gamma\gamma \rightarrow \eta'_c \rightarrow K_S^0 K^\pm \pi^\mp$

¹ Assuming that the branching fraction into $\eta' \pi^+ \pi^-$ is the same as for $\eta_c(1S)$.
² They measure $\Gamma(\eta_c(2S) \rightarrow \eta' \pi^+ \pi^-) / \Gamma(\eta_c(2S) \rightarrow K\bar{K}\pi) = (0.18 \pm 0.05 \pm 0.02) \Gamma(\eta_c(1S) \rightarrow \eta' \pi^+ \pi^-) / \Gamma(\eta_c(1S) \rightarrow K\bar{K}\pi)$. The value for $\Gamma(\eta_c(2S) \rightarrow \gamma\gamma)$ is derived assuming that the branching fractions for $\eta_c(2S)$ and $\eta_c(1S)$ decays to $K_S K\pi$ are equal and using $\Gamma(\eta_c(1S) \rightarrow \gamma\gamma) = 7.4 \pm 0.4 \pm 2.3$ keV.

$\Gamma(\gamma\gamma) \times \Gamma(\pi^+ \pi^- \eta') / \Gamma_{total}$	$\Gamma_{16} \Gamma_{19} / \Gamma$			
VALUE (eV)	EVTs	DOCUMENT ID	TECN	COMMENT
$5.6_{-1.1}^{+1.2} \pm 1.1$	106	XU	18	BELL $e^+e^- \rightarrow e^+e^- \eta' \pi^+ \pi^-$

 $\eta_c(2S) \Gamma(i)\Gamma(\gamma\gamma) / \Gamma_{total}$

$\Gamma(K\bar{K}\pi) \times \Gamma(\gamma\gamma) / \Gamma_{total}$	$\Gamma_{2} \Gamma_{16} / \Gamma$			
VALUE (eV)	EVTs	DOCUMENT ID	TECN	COMMENT
$41 \pm 4 \pm 6$	624	¹ DEL-AMO-SA..11M	BABR	$\gamma\gamma \rightarrow K_S^0 K^\pm \pi^\mp$

¹ Not independent from other measurements reported in DEL-AMO-SANCHEZ 11M.

$\Gamma(2\pi^+ 2\pi^-) \times \Gamma(\gamma\gamma) / \Gamma_{total}$	$\Gamma_{4} \Gamma_{16} / \Gamma$			
VALUE (eV)	CL%	DOCUMENT ID	TECN	COMMENT
< 6.5	90	UEHARA	08	BELL $\gamma\gamma \rightarrow \eta_c(2S) \rightarrow 2(\pi^+ \pi^-)$

$\Gamma(K^+ K^- \pi^+ \pi^-) \times \Gamma(\gamma\gamma) / \Gamma_{total}$	$\Gamma_{7} \Gamma_{16} / \Gamma$			
VALUE (eV)	CL%	DOCUMENT ID	TECN	COMMENT
< 5.0	90	UEHARA	08	BELL $\gamma\gamma \rightarrow \eta_c(2S) \rightarrow K^+ K^- \pi^+ \pi^-$

$\Gamma(K^+ K^- \pi^+ \pi^- \pi^0) \times \Gamma(\gamma\gamma) / \Gamma_{total}$	$\Gamma_{9} \Gamma_{16} / \Gamma$			
VALUE (eV)	EVTs	DOCUMENT ID	TECN	COMMENT
$30 \pm 6 \pm 5$	1201	¹ DEL-AMO-SA..11M	BABR	$\gamma\gamma \rightarrow K^+ K^- \pi^+ \pi^- \pi^0$

¹ Not independent from other measurements reported in DEL-AMO-SANCHEZ 11M.

$\Gamma(2K^+ 2K^-) \times \Gamma(\gamma\gamma) / \Gamma_{total}$	$\Gamma_{12} \Gamma_{16} / \Gamma$			
VALUE (eV)	CL%	DOCUMENT ID	TECN	COMMENT
< 2.9	90	UEHARA	08	BELL $\gamma\gamma \rightarrow \eta_c(2S) \rightarrow 2(K^+ K^-)$

$\Gamma(\pi^+ \pi^- \eta_c(1S)) \times \Gamma(\gamma\gamma) / \Gamma_{total}$	$\Gamma_{26} \Gamma_{16} / \Gamma$			
VALUE (eV)	CL%	DOCUMENT ID	TECN	COMMENT
< 133	90	LEES	12AE BABR	$e^+e^- \rightarrow e^+e^- \pi^+ \pi^- \eta_c$

 $\eta_c(2S) \Gamma(i)\Gamma(\gamma\gamma) / \Gamma^2_{total}$

$\Gamma(\rho\bar{\rho}) / \Gamma_{total} \times \Gamma(\gamma\gamma) / \Gamma_{total}$	$\Gamma_{14} / \Gamma \times \Gamma_{16} / \Gamma$			
VALUE (units 10^{-8})	CL%	DOCUMENT ID	TECN	COMMENT
< 5.6	90	1,2,3 AMBROGIANI	01	E835 $\bar{p}p \rightarrow \gamma\gamma$
• • • We do not use the following data for averages, fits, limits, etc. • • •				
< 8.0	90	1,2,4 AMBROGIANI	01	E835 $\bar{p}p \rightarrow \gamma\gamma$
< 12.0	90	2,4 AMBROGIANI	01	E835 $\bar{p}p \rightarrow \gamma\gamma$

¹ Including the measurements of ARMSTRONG 95F in the AMBROGIANI 01 analysis.² For a total width $\Gamma=5$ MeV.³ For the resonance mass region 3589–3599 MeV/ c^2 .⁴ For the resonance mass region 3575–3660 MeV/ c^2 . $\eta_c(2S)$ BRANCHING RATIOS

$\Gamma(\text{hadrons}) / \Gamma_{total}$	Γ_1 / Γ		
VALUE	DOCUMENT ID	TECN	COMMENT
not seen	ABREU	980	DLPH $e^+e^- \rightarrow e^+e^- + \text{hadrons}$
• • • We do not use the following data for averages, fits, limits, etc. • • •			
seen	¹ EDWARDS	82c	CBAL $e^+e^- \rightarrow \gamma X$

¹ For a mass value of 3594 ± 5 MeV

$\Gamma(K\bar{K}\pi) / \Gamma_{total}$	Γ_2 / Γ			
VALUE (units 10^{-2})	EVTs	DOCUMENT ID	TECN	COMMENT
$1.9 \pm 0.4 \pm 1.1$	59 \pm 12	¹ AUBERT	08AB BABR	$B \rightarrow \eta_c(2S) K \rightarrow K\bar{K}\pi K$
• • • We do not use the following data for averages, fits, limits, etc. • • •				
seen	127 \pm 18	ABLIKIM	12G BES3	$\psi(2S) \rightarrow \gamma K\bar{K}\pi$
seen	39 \pm 11	² CHOI	02 BELL	$B \rightarrow K K_S K^- \pi^+$

¹ Derived from a measurement of $[B(B^+ \rightarrow \eta_c(2S) K^+) \times B(\eta_c(2S) \rightarrow K\bar{K}\pi)] / [B(B^+ \rightarrow \eta_c K^+) \times B(\eta_c \rightarrow K\bar{K}\pi)] = (9.6_{-1.9}^{+2.0} \pm 2.5)\%$ and using $B(B^+ \rightarrow \eta_c(2S) K^+) = (3.4 \pm 1.8) \times 10^{-4}$, and $[B(B^+ \rightarrow \eta_c K^+) \times B(\eta_c \rightarrow K\bar{K}\pi)] = (6.88 \pm 0.77_{-0.66}^{+0.55}) \times 10^{-5}$.² For a mass value of 3654 ± 6 MeV

$\Gamma(K\bar{K}\eta) / \Gamma(K\bar{K}\pi)$	Γ_3 / Γ_2			
VALUE (units 10^{-2})	EVTs	DOCUMENT ID	TECN	COMMENT
$27.3 \pm 7.0 \pm 9.0$	225	¹ LEES	14E BABR	$\gamma\gamma \rightarrow K^+ K^- \gamma\gamma$

¹ LEES 14E reports $B(\eta_c(2S) \rightarrow K^+ K^- \eta) / B(\eta_c(2S) \rightarrow K^+ K^- \pi^0) = 0.82 \pm 0.21 \pm 0.27$, which we divide by 3 to account for isospin symmetry.

$\Gamma(2\pi^+ 2\pi^-) / \Gamma_{total}$	Γ_4 / Γ		
VALUE	DOCUMENT ID	TECN	COMMENT
not seen	UEHARA	08	BELL $\gamma\gamma \rightarrow \eta_c(2S)$

$\Gamma(\rho^0 \rho^0) / \Gamma_{total}$	Γ_5 / Γ		
VALUE	DOCUMENT ID	TECN	COMMENT
not seen	ABLIKIM	11H	BES3 $\psi(2S) \rightarrow \gamma 2\pi^+ 2\pi^-$

$\Gamma(K^+ K^- \pi^+ \pi^-) / \Gamma_{total}$	Γ_7 / Γ		
VALUE	DOCUMENT ID	TECN	COMMENT
not seen	UEHARA	08	BELL $\gamma\gamma \rightarrow \eta_c(2S)$

$\Gamma(K^{*0} \bar{K}^{*0}) / \Gamma_{total}$	Γ_8 / Γ		
VALUE	DOCUMENT ID	TECN	COMMENT
not seen	ABLIKIM	11H	BES3 $\psi(2S) \rightarrow \gamma K^+ K^- \pi^+ \pi^-$

$\Gamma(K^+ K^- \pi^+ \pi^- \pi^0) / \Gamma(K\bar{K}\pi)$	Γ_9 / Γ_2			
VALUE	EVTs	DOCUMENT ID	TECN	COMMENT
$0.73 \pm 0.17 \pm 0.17$	1201	¹ DEL-AMO-SA..11M	BABR	$\gamma\gamma \rightarrow K^+ K^- \pi^+ \pi^- \pi^0$

¹ We have multiplied the value of $\Gamma(K^+ K^- \pi^+ \pi^- \pi^0) / \Gamma(K_S^0 K^\pm \pi^\mp)$ reported in DEL-AMO-SANCHEZ 11M by a factor 1/3 to obtain $\Gamma(K^+ K^- \pi^+ \pi^- \pi^0) / \Gamma(K\bar{K}\pi)$. Not independent from other measurements reported in DEL-AMO-SANCHEZ 11M.

$\Gamma(K_S^0 K^- 2\pi^+ \pi^- + c.c.) / \Gamma_{total}$	Γ_{11} / Γ			
VALUE	EVTs	DOCUMENT ID	TECN	COMMENT
not seen	57 \pm 17	ABLIKIM	13K	BES3 $\psi(2S) \rightarrow \gamma K_S^0 K^\pm \pi^\mp \pi^+ \pi^-$

$\Gamma(2K^+ 2K^-) / \Gamma_{total}$	Γ_{12} / Γ		
VALUE	DOCUMENT ID	TECN	COMMENT
not seen	UEHARA	08	BELL $\gamma\gamma \rightarrow \eta_c(2S)$

$\Gamma(\phi\phi)/\Gamma_{\text{total}}$ Γ_{13}/Γ

VALUE	DOCUMENT ID	TECN	COMMENT
not seen	ABLIKIM	11H BES3	$\psi(2S) \rightarrow \gamma K^+ K^- K^+ K^-$

 $\Gamma(p\bar{p})/\Gamma_{\text{total}}$ Γ_{14}/Γ

VALUE	EVTS	DOCUMENT ID	TECN	COMMENT
seen	106	¹ AAIJ	17AD LHCB	$pp \rightarrow B^+ X \rightarrow p\bar{p}K^+ X$
¹ AAIJ 17AD report a 6.4 standard deviation signal, with $B(B^+ \rightarrow \eta_c(2S)K^+ \rightarrow p\bar{p}K^+)/B(B^+ \rightarrow J/\psi K^+ \rightarrow p\bar{p}K^+) = (1.58 \pm 0.33 \pm 0.09) \times 10^{-2}$.				

 $\Gamma(p\bar{p}\pi^+\pi^-)/\Gamma_{\text{total}}$ Γ_{15}/Γ

VALUE	EVTS	DOCUMENT ID	TECN	COMMENT
seen	110	¹ CHILIKIN	19 BELL	$e^+e^- \rightarrow \Upsilon(4S)$
¹ CHILIKIN 19 reports signals in $B^+ \rightarrow \eta_c(2S)K^+$ and $B^0 \rightarrow \eta_c(2S)K_S^0$ with 12.3 and 5.9 standard deviations, respectively.				

 $\Gamma(\gamma\gamma)/\Gamma_{\text{total}}$ Γ_{16}/Γ

VALUE	CL%	DOCUMENT ID	TECN	COMMENT
$<4 \times 10^{-4}$	90	¹ WICHT	08 BELL	$B^\pm \rightarrow K^\pm \gamma\gamma$
not seen		AMBROGIANI	01 E835	$\bar{p}p \rightarrow \gamma\gamma$
<0.01	90	LEE	85 CBAL	$\psi' \rightarrow \text{photons}$
¹ WICHT 08 reports $[\Gamma(\eta_c(2S) \rightarrow \gamma\gamma)/\Gamma_{\text{total}}] \times [B(B^+ \rightarrow \eta_c(2S)K^+)] < 0.18 \times 10^{-6}$ which we divide by our best value $B(B^+ \rightarrow \eta_c(2S)K^+) = 4.4 \times 10^{-4}$.				

 $\Gamma(\pi^+\pi^-\eta_c(1S))/\Gamma(K\bar{K}\pi)$ Γ_{26}/Γ_2

VALUE	CL%	DOCUMENT ID	TECN	COMMENT
<3.33	90	¹ LEES	12AE BABR	$e^+e^- \rightarrow e^+e^-\pi^+\pi^-\eta_c$

¹We divided the reported limit by 3 to take into account isospin relations.

 $\eta_c(2S)$ CROSS-PARTICLE BRANCHING RATIOS $\Gamma(\eta_c(2S) \rightarrow K\bar{K}\eta)/\Gamma_{\text{total}} \times \Gamma(\psi(2S) \rightarrow \gamma\eta_c(2S))/\Gamma_{\text{total}}$ $\Gamma_3/\Gamma \times \Gamma_{183}^{\psi(2S)}/\Gamma\psi(2S)$

VALUE	CL%	DOCUMENT ID	TECN	COMMENT
$<11.8 \times 10^{-6}$	90	¹ CRONIN-HEN..10	CLEO	$\psi(2S) \rightarrow \gamma K^+ K^- \eta$
¹ CRONIN-HENNESSY 10 reports a limit of $< 5.9 \times 10^{-6}$ for the decay $\eta_c(2S) \rightarrow K^+ K^- \eta$ which we multiply by 2 account for isospin symmetry. It assumes $\Gamma(\eta_c(2S)) = 14$ MeV. It also gives the analytic dependence of limits on width.				

 $\Gamma(\eta_c(2S) \rightarrow 2\pi^+2\pi^-)/\Gamma_{\text{total}} \times \Gamma(\psi(2S) \rightarrow \gamma\eta_c(2S))/\Gamma_{\text{total}}$ $\Gamma_4/\Gamma \times \Gamma_{183}^{\psi(2S)}/\Gamma\psi(2S)$

VALUE	CL%	DOCUMENT ID	TECN	COMMENT
$<14.6 \times 10^{-6}$	90	¹ CRONIN-HEN..10	CLEO	$\psi(2S) \rightarrow \gamma 2\pi^+ 2\pi^-$
¹ Assuming $\Gamma(\eta_c(2S)) = 14$ MeV. CRONIN-HENNESSY 10 gives the analytic dependence of limits on width.				

 $\Gamma(\eta_c(2S) \rightarrow \rho^0\rho^0)/\Gamma_{\text{total}} \times \Gamma(\psi(2S) \rightarrow \gamma\eta_c(2S))/\Gamma_{\text{total}}$ $\Gamma_5/\Gamma \times \Gamma_{183}^{\psi(2S)}/\Gamma\psi(2S)$

VALUE	CL%	DOCUMENT ID	TECN	COMMENT
$<12.7 \times 10^{-7}$	90	ABLIKIM	11H BES3	$\psi(2S) \rightarrow \gamma 2\pi^+ 2\pi^-$

 $\Gamma(\eta_c(2S) \rightarrow 3\pi^+3\pi^-)/\Gamma_{\text{total}} \times \Gamma(\psi(2S) \rightarrow \gamma\eta_c(2S))/\Gamma_{\text{total}}$ $\Gamma_6/\Gamma \times \Gamma_{183}^{\psi(2S)}/\Gamma\psi(2S)$

VALUE (units 10^{-6})	CL%	EVTS	DOCUMENT ID	TECN	COMMENT
$9.2 \pm 1.0 \pm 1.2$		569	ABLIKIM	22Q BES3	$\psi(2S) \rightarrow \gamma 3(\pi^+\pi^-)$
• • • We do not use the following data for averages, fits, limits, etc. • • •					
<13.2	90		¹ CRONIN-HEN..10	CLEO	$\psi(2S) \rightarrow \gamma 3\pi^+ 3\pi^-$
¹ Assuming $\Gamma(\eta_c(2S)) = 14$ MeV. CRONIN-HENNESSY 10 gives the analytic dependence of limits on width.					

 $\Gamma(\eta_c(2S) \rightarrow K^+K^-\pi^+\pi^-)/\Gamma_{\text{total}} \times \Gamma(\psi(2S) \rightarrow \gamma\eta_c(2S))/\Gamma_{\text{total}}$ $\Gamma_7/\Gamma \times \Gamma_{183}^{\psi(2S)}/\Gamma\psi(2S)$

VALUE	CL%	DOCUMENT ID	TECN	COMMENT
$<9.6 \times 10^{-6}$	90	¹ CRONIN-HEN..10	CLEO	$\psi(2S) \rightarrow \gamma K^+ K^- \pi^+ \pi^-$
¹ Assuming $\Gamma(\eta_c(2S)) = 14$ MeV. CRONIN-HENNESSY 10 gives the analytic dependence of limits on width.				

 $\Gamma(\eta_c(2S) \rightarrow K^{*0}\bar{K}^{*0})/\Gamma_{\text{total}} \times \Gamma(\psi(2S) \rightarrow \gamma\eta_c(2S))/\Gamma_{\text{total}}$ $\Gamma_8/\Gamma \times \Gamma_{183}^{\psi(2S)}/\Gamma\psi(2S)$

VALUE	CL%	DOCUMENT ID	TECN	COMMENT
$<19.6 \times 10^{-7}$	90	ABLIKIM	11H BES3	$\psi(2S) \rightarrow \gamma K^+ K^- \pi^+ \pi^-$

 $\Gamma(\eta_c(2S) \rightarrow K^+K^-\pi^+\pi^-)/\Gamma_{\text{total}} \times \Gamma(\psi(2S) \rightarrow \gamma\eta_c(2S))/\Gamma_{\text{total}}$ $\Gamma_9/\Gamma \times \Gamma_{183}^{\psi(2S)}/\Gamma\psi(2S)$

VALUE	CL%	DOCUMENT ID	TECN	COMMENT
$<43.0 \times 10^{-6}$	90	¹ CRONIN-HEN..10	CLEO	$\psi(2S) \rightarrow \gamma K^+ K^- \pi^+ \pi^-$
¹ Assuming $\Gamma(\eta_c(2S)) = 14$ MeV. CRONIN-HENNESSY 10 gives the analytic dependence of limits on width.				

 $\Gamma(\eta_c(2S) \rightarrow K^+K^-2\pi^+2\pi^-)/\Gamma_{\text{total}} \times \Gamma(\psi(2S) \rightarrow \gamma\eta_c(2S))/\Gamma_{\text{total}}$ $\Gamma_{10}/\Gamma \times \Gamma_{183}^{\psi(2S)}/\Gamma\psi(2S)$

VALUE	CL%	DOCUMENT ID	TECN	COMMENT
$<9.7 \times 10^{-6}$	90	¹ CRONIN-HEN..10	CLEO	$\psi(2S) \rightarrow \gamma K^+ K^- 2\pi^+ 2\pi^-$
¹ Assuming $\Gamma(\eta_c(2S)) = 14$ MeV. CRONIN-HENNESSY 10 gives the analytic dependence of limits on width.				

 $\Gamma(\eta_c(2S) \rightarrow K_S^0K^-2\pi^+\pi^- + c.c.)/\Gamma_{\text{total}} \times \Gamma(\psi(2S) \rightarrow \gamma\eta_c(2S))/\Gamma_{\text{total}}$ $\Gamma_{11}/\Gamma \times \Gamma_{183}^{\psi(2S)}/\Gamma\psi(2S)$

VALUE (units 10^{-6})	CL%	EVTS	DOCUMENT ID	TECN	COMMENT
$7.03 \pm 2.10 \pm 0.7$		60	ABLIKIM	13K BES3	$\psi(2S) \rightarrow \gamma K_S^0 K^- 2\pi^+ \pi^- + c.c.$

VALUE	CL%	DOCUMENT ID	TECN	COMMENT
<15.2	90	¹ CRONIN-HEN..10	CLEO	$\psi(2S) \rightarrow \gamma K_S^0 K^- 2\pi^+ \pi^- + c.c.$

¹Assuming $\Gamma(\eta_c(2S)) = 14$ MeV. CRONIN-HENNESSY 10 gives the analytic dependence of limits on width.

 $\Gamma(\eta_c(2S) \rightarrow \phi\phi)/\Gamma_{\text{total}} \times \Gamma(\psi(2S) \rightarrow \gamma\eta_c(2S))/\Gamma_{\text{total}}$ $\Gamma_{13}/\Gamma \times \Gamma_{183}^{\psi(2S)}/\Gamma\psi(2S)$

VALUE	CL%	DOCUMENT ID	TECN	COMMENT
$<7.8 \times 10^{-7}$	90	ABLIKIM	11H BES3	$\psi(2S) \rightarrow \gamma K^+ K^- K^+ K^-$

 $\Gamma(\eta_c(2S) \rightarrow p\bar{p})/\Gamma_{\text{total}} \times \Gamma(\psi(2S) \rightarrow \gamma\eta_c(2S))/\Gamma_{\text{total}}$ $\Gamma_{14}/\Gamma \times \Gamma_{183}^{\psi(2S)}/\Gamma\psi(2S)$

VALUE	CL%	DOCUMENT ID	TECN	COMMENT
$<1.4 \times 10^{-6}$	90	ABLIKIM	13V BES3	$\psi(2S) \rightarrow \gamma p\bar{p}$

 $\Gamma(\eta_c(2S) \rightarrow \gamma J/\psi(1S))/\Gamma_{\text{total}} \times \Gamma(\psi(2S) \rightarrow \gamma\eta_c(2S))/\Gamma_{\text{total}}$ $\Gamma_{17}/\Gamma \times \Gamma_{183}^{\psi(2S)}/\Gamma\psi(2S)$

VALUE	CL%	EVTS	DOCUMENT ID	TECN	COMMENT
$<9.7 \times 10^{-6}$	90	33	¹ ABLIKIM	17N BES3	$\psi(2S) \rightarrow \gamma\gamma J/\psi$
¹ Uses $B(J/\psi \rightarrow e^+e^-) = (5.971 \pm 0.032)\%$ and $B(J/\psi \rightarrow \mu^+\mu^-) = (5.961 \pm 0.033)\%$.					

 $\Gamma(\eta_c(2S) \rightarrow \pi^+\pi^-\eta)/\Gamma_{\text{total}} \times \Gamma(\psi(2S) \rightarrow \gamma\eta_c(2S))/\Gamma_{\text{total}}$ $\Gamma_{18}/\Gamma \times \Gamma_{183}^{\psi(2S)}/\Gamma\psi(2S)$

VALUE (units 10^{-6})	CL%	EVTS	DOCUMENT ID	TECN	COMMENT
$2.97 \pm 0.81 \pm 0.26$		106	ABLIKIM	23Q BES3	$\psi(2S) \rightarrow \gamma\pi^+\pi^-\eta$
• • • We do not use the following data for averages, fits, limits, etc. • • •					
<4.3	90		¹ CRONIN-HEN..10	CLEO	$\psi(2S) \rightarrow \gamma\pi^+\pi^-\eta$
¹ Assuming $\Gamma(\eta_c(2S)) = 14$ MeV. CRONIN-HENNESSY 10 gives the analytic dependence of limits on width.					

 $\Gamma(\eta_c(2S) \rightarrow \pi^+\pi^-\eta')/\Gamma_{\text{total}} \times \Gamma(\psi(2S) \rightarrow \gamma\eta_c(2S))/\Gamma_{\text{total}}$ $\Gamma_{19}/\Gamma \times \Gamma_{183}^{\psi(2S)}/\Gamma\psi(2S)$

VALUE	CL%	DOCUMENT ID	TECN	COMMENT
$<14.2 \times 10^{-6}$	90	¹ CRONIN-HEN..10	CLEO	$\psi(2S) \rightarrow \gamma\pi^+\pi^-\eta'$
¹ Assuming $\Gamma(\eta_c(2S)) = 14$ MeV. CRONIN-HENNESSY 10 gives the analytic dependence of limits on width.				

 $\Gamma(K_S^0(1430)\bar{K} + c.c.)/\Gamma_{\text{total}}$ Γ_{20}/Γ

VALUE	DOCUMENT ID	TECN	COMMENT
seen	¹ AAIJ	23AH LHCB	$B^+ \rightarrow K^+(K_S^0 K\pi)$
¹ From a Dalitz plot analysis of $\eta_c(2S) \rightarrow K_S^0 K^+ \pi^- + c.c.$			

 $\Gamma(a_0(1710)\pi)/\Gamma_{\text{total}}$ Γ_{22}/Γ

VALUE	DOCUMENT ID	TECN	COMMENT
seen	¹ AAIJ	23AH LHCB	$B^+ \rightarrow K^+(K_S^0 K\pi)$
¹ From a Dalitz plot analysis of $\eta_c(2S) \rightarrow K_S^0 K^+ \pi^- + c.c.$			

 $\Gamma(a_0(1450)\pi)/\Gamma_{\text{total}}$ Γ_{23}/Γ

VALUE	DOCUMENT ID	TECN	COMMENT
seen	¹ AAIJ	23AH LHCB	$B^+ \rightarrow K^+(K_S^0 K\pi)$
¹ From a Dalitz plot analysis of $\eta_c(2S) \rightarrow K_S^0 K^+ \pi^- + c.c.$			

Meson Particle Listings

$\eta_c(2S), \psi(2S)$

$\Gamma(\psi(2S) \rightarrow \text{hadrons})/\Gamma_{\text{total}}$		Γ_{25}/Γ	
VALUE	DOCUMENT ID	TECN	COMMENT
seen	¹ AAIJ	23AH LHCB	$B^+ \rightarrow K^+(K_S^0 K \pi)$

¹ From a Dalitz plot analysis of $\eta_c(2S) \rightarrow K_S^0 K^+ \pi^- + \text{c.c.}$.

$\Gamma(K_S^0(2600)\bar{K} + \text{c.c.})/\Gamma_{\text{total}}$		Γ_{25}/Γ	
VALUE	DOCUMENT ID	TECN	COMMENT
seen	¹ AAIJ	23AH LHCB	$B^+ \rightarrow K^+(K_S^0 K \pi)$

¹ From a Dalitz plot analysis of $\eta_c(2S) \rightarrow K_S^0 K^+ \pi^- + \text{c.c.}$.

$\Gamma(K_S^0(1950)\bar{K} + \text{c.c.})/\Gamma_{\text{total}}$		Γ_{21}/Γ	
VALUE	DOCUMENT ID	TECN	COMMENT
seen	¹ AAIJ	23AH LHCB	$B^+ \rightarrow K^+(K_S^0 K \pi)$

¹ From a Dalitz plot analysis of $\eta_c(2S) \rightarrow K_S^0 K^+ \pi^- + \text{c.c.}$.

$\Gamma(\eta_c(2S) \rightarrow \pi^+ \pi^- \eta_c(1S))/\Gamma_{\text{total}} \times \Gamma(\psi(2S) \rightarrow \gamma \eta_c(2S))/\Gamma_{\text{total}}$		$\Gamma_{26}/\Gamma \times \Gamma_{183}^{\psi(2S)}/\Gamma_{\psi(2S)}$	
VALUE	CL%	DOCUMENT ID	TECN COMMENT
$<1.7 \times 10^{-4}$	90	¹ CRONIN-HEN.10	CLEO $\psi(2S) \rightarrow \gamma \pi^+ \pi^- \eta_c(1S)$

¹ Assuming $\Gamma(\eta_c(2S)) = 14$ MeV. CRONIN-HENNESSY 10 gives the analytic dependence of limits on width.

$\eta_c(2S)$ REFERENCES

AAIJ	23AH	PR D108 032010	R. Aaij et al.	(LHCb Collab.)
ABLIKIM	23Q	PR D107 052007	M. Ablikim et al.	(BESIII Collab.)
ABLIKIM	22Q	PR D106 032014	M. Ablikim et al.	(BESIII Collab.)
CHLIKIN	19	PR D100 012001	K. Chilikin et al.	(BELLE Collab.)
XU	18	PR D98 072001	Q.N. Xu et al.	(BELLE Collab.)
AAIJ	17AD	PL B769 305	R. Aaij et al.	(LHCb Collab.)
AAIJ	17BB	EPJ C77 609	R. Aaij et al.	(LHCb Collab.)
ABLIKIM	17N	PR D95 072004	M. Ablikim et al.	(BESIII Collab.)
PDG	16	CP C40 100001	C. Patrignani et al.	(PDG Collab.)
LEES	14E	PR D89 112004	J.P. Lees et al.	(BABAR Collab.)
ABLIKIM	13K	PR D87 052005	M. Ablikim et al.	(BESIII Collab.)
ABLIKIM	13V	PR D88 112001	M. Ablikim et al.	(BESIII Collab.)
ABLIKIM	12G	PRL 109 042003	M. Ablikim et al.	(BESIII Collab.)
LEES	12AE	PR D86 092005	J.P. Lees et al.	(BABAR Collab.)
ABLIKIM	11H	PR D84 091102	M. Ablikim et al.	(BESIII Collab.)
DEL-AMO-SA..	11M	PR D84 012004	P. del Amo Sanchez et al.	(BABAR Collab.)
VINOKUROVA	11	PL B706 139	A. Vinokurova et al.	(BELLE Collab.)
CRONIN-HEN..	10	PR D81 052002	D. Cronin-Hennessey et al.	(CLEO Collab.)
AUBERT	08AB	PR D78 012006	B. Aubert et al.	(BABAR Collab.)
UEHARA	08	EPJ C53 1	S. Uehara et al.	(BELLE Collab.)
WICHT	08	PL B662 323	J. Wicht et al.	(BELLE Collab.)
ABE	07	PRL 98 082001	K. Abe et al.	(BELLE Collab.)
AUBERT	06E	PR 96 052002	B. Aubert et al.	(BABAR Collab.)
AUBERT	05C	PR D72 031101	B. Aubert et al.	(BABAR Collab.)
ABE	04G	PR D70 071102	K. Abe et al.	(BELLE Collab.)
ASNER	04	PRL 92 142001	D.M. Asner et al.	(CLEO Collab.)
AUBERT	04D	PRL 92 142002	B. Aubert et al.	(BABAR Collab.)
ABE,K	02	PRL 89 142001	K. Abe et al.	(BELLE Collab.)
CHOI	02	PRL 89 102001	S.-K. Choi et al.	(BELLE Collab.)
AMBROGIANI	01	PR D64 052003	M. Ambrogiani et al.	(FNAL E835 Collab.)
ABREU	98O	PL B441 479	P. Abreu et al.	(DELPHI Collab.)
ARMSTRONG	95F	PR D52 4839	T.A. Armstrong et al.	(FNAL, FERR, GENO+)
LEE	85	SLAC 282	R.A. Lee	(SLAC)
EDWARDS	82C	PRL 48 70	C. Edwards et al.	(CIT, HARV, PRIN+)

$\psi(2S)$

$$I^G(J^{PC}) = 0^-(1^{--})$$

See the Review on "Branching Ratios of $\psi(2S)$, $\chi_{c0,1,2}$ and $\eta_c(1S)$ " before the $\chi_{c0}(1P)$ Listings.

$\psi(2S)$ MASS

OUR FIT includes measurements of $m_{\psi(2S)}$, $m_{\psi(3770)}$, and $m_{\psi(3770)} - m_{\psi(2S)}$.

VALUE (MeV)	EVTS	DOCUMENT ID	TECN	COMMENT
3686.097 ± 0.011 OUR FIT				Error includes scale factor of 1.1.
3686.097 ± 0.010 OUR AVERAGE				
3686.099 ± 0.004 ± 0.009		¹ ANASHIN 15	KEDR	$e^+e^- \rightarrow \text{hadrons}$
3686.12 ± 0.06 ± 0.10	4k	AAIJ	12H LHCB	$p\bar{p} \rightarrow J/\psi \pi^+ \pi^- X$
3685.95 ± 0.10	413	² ARTAMONOV 00	OLYA	$e^+e^- \rightarrow \text{hadrons}$
3685.98 ± 0.09 ± 0.04		³ ARMSTRONG 93B	E760	$\bar{p}p \rightarrow e^+e^-$
3686.08 ± 0.07	1301	⁴ AAIJ	23AP LHCB	$B_s^0 \rightarrow J/\psi 2(\pi^+ \pi^-)$
3686.114 ± 0.007 ± 0.011 -0.016		⁵ ANASHIN 12	KEDR	$e^+e^- \rightarrow \text{hadrons}$
3686.111 ± 0.025 ± 0.009		AULCHENKO 03	KEDR	$e^+e^- \rightarrow \text{hadrons}$
3686.00 ± 0.10	413	⁶ ZHOLENTZ 80	OLYA	e^+e^-

¹ Supersedes AULCHENKO 03 and ANASHIN 12.
² Reanalysis of ZHOLENTZ 80 using new electron mass (COHEN 87) and radiative corrections (KURAEV 85).
³ Mass central value and systematic error recalculated by us according to Eq. (16) in ARMSTRONG 93B, using the value for the $J/\psi(1S)$ mass from AULCHENKO 03.
⁴ From a fit of a relativistic S-wave Breit-Wigner convolved with the detector resolution. The width of $\psi(2S)$ is constrained to the PDG 22 value. Systematic errors not evaluated.

⁵ From the scans in 2004 and 2006. ANASHIN 12 reports the value $3686.114 \pm 0.007 \pm 0.011 \pm 0.002$ MeV, where the third uncertainty is due to assumptions on the interference between the resonance and hadronic continuum. We combined the two systematic uncertainties.
⁶ Superseded by ARTAMONOV 00.

$m_{\psi(2S)} - m_{J/\psi(1S)}$

VALUE (MeV)	DOCUMENT ID	TECN	COMMENT
589.188 ± 0.028 OUR AVERAGE			
589.194 ± 0.027 ± 0.011	¹ AULCHENKO 03	KEDR	$e^+e^- \rightarrow \text{hadrons}$
589.7 ± 1.2	LEMOIGNE 82	GOLI	$185 \pi^- \text{Be} \rightarrow \gamma \mu^+ \mu^- A$
589.07 ± 0.13	¹ ZHOLENTZ 80	OLYA	e^+e^-
588.7 ± 0.8	LUTH 75	MRK1	
588 ± 1	² BAI	98E	BES e^+e^-

• • • We do not use the following data for averages, fits, limits, etc. • • •
¹ Redundant with data in mass above.
² Systematic errors not evaluated.

$\psi(2S)$ WIDTH

VALUE (keV)	EVTS	DOCUMENT ID	TECN	COMMENT
293 ± 9 OUR FIT				Error includes scale factor of 1.2.
286 ± 16 OUR AVERAGE				
358 ± 88 ± 4		ABLIKIM 08B	BES2	$e^+e^- \rightarrow \text{hadrons}$
290 ± 25 ± 4	2.7k	ANDREOTTI 07	E835	$p\bar{p} \rightarrow e^+e^-, J/\psi X$
331 ± 58 ± 2		ABLIKIM 06L	BES2	$e^+e^- \rightarrow \text{hadrons}$
264 ± 27		¹ BAI 02B	BES2	e^+e^-
287 ± 37 ± 16		² ARMSTRONG 93B	E760	$\bar{p}p \rightarrow e^+e^-$

¹ From a simultaneous fit to the hadronic and $\mu^+ \mu^-$ cross section, assuming $\Gamma = \Gamma_h + \Gamma_e + \Gamma_\mu + \Gamma_\tau$ and lepton universality. Does not include vacuum polarization correction.
² The initial-state radiation correction reevaluated by ANDREOTTI 07 in its Ref. [4].

$\psi(2S)$ DECAY MODES

Mode	Fraction (Γ_i/Γ)	Scale factor/Confidence level
Γ_1 hadrons	(97.85 ± 0.13) %	
Γ_2 virtual $\gamma \rightarrow \text{hadrons}$	(1.79 ± 0.04) %	
Γ_3 $g g g$	(10.6 ± 1.6) %	
Γ_4 $\gamma g g$	(1.03 ± 0.29) %	
Γ_5 light hadrons	(15.4 ± 1.5) %	
Γ_6 K_S^0 anything	(16.0 ± 1.1) %	
Γ_7 e^+e^-	(7.94 ± 0.22) × 10 ⁻³	S=1.3
Γ_8 $\mu^+ \mu^-$	(8.0 ± 0.6) × 10 ⁻³	
Γ_9 $\tau^+ \tau^-$	(3.1 ± 0.4) × 10 ⁻³	
Γ_{10} $J/\psi(1S)$ anything	(61.5 ± 0.7) %	S=1.3
Γ_{11} $J/\psi(1S)$ neutrals	(25.4 ± 0.5) %	S=1.6
Γ_{12} $J/\psi(1S) \pi^+ \pi^-$	(34.69 ± 0.34) %	S=1.1
Γ_{13} $J/\psi(1S) \pi^0 \pi^0$	(18.2 ± 0.5) %	S=1.6
Γ_{14} $J/\psi(1S) \eta$	(3.37 ± 0.06) %	S=1.2
Γ_{15} $J/\psi(1S) \pi^0$	(1.268 ± 0.032) × 10 ⁻³	

Decays into $J/\psi(1S)$ and anything

Hadronic decays

Γ_{16} $\pi^+ \pi^-$	(7.8 ± 2.6) × 10 ⁻⁶	
Γ_{17} $\pi^+ \pi^- \pi^0$	(2.01 ± 0.17) × 10 ⁻⁴	S=1.7
Γ_{18} $\rho(770) \pi \rightarrow \pi^+ \pi^- \pi^0$	(3.2 ± 1.2) × 10 ⁻⁵	S=1.8
Γ_{19} $\rho(2150) \pi \rightarrow \pi^+ \pi^- \pi^0$	(1.9 ± 1.2 -0.4) × 10 ⁻⁴	
Γ_{20} $2(\pi^+ \pi^-)$	(2.4 ± 0.6) × 10 ⁻⁴	S=2.2
Γ_{21} $\rho^0 \pi^+ \pi^-$	(2.2 ± 0.6) × 10 ⁻⁴	S=1.4
Γ_{22} $2(\pi^+ \pi^-) \pi^0$	(2.9 ± 1.0) × 10 ⁻³	S=4.7
Γ_{23} $\rho \partial_2(1320)$	(2.6 ± 0.9) × 10 ⁻⁴	
Γ_{24} $\pi^+ \pi^- \pi^0 \pi^0 \pi^0$	(5.3 ± 1.0) × 10 ⁻³	
Γ_{25} $\rho^\pm \pi^\mp \pi^0 \pi^0$	< 2.7 × 10 ⁻³	CL=90%
Γ_{26} $\pi^+ \pi^- 4\pi^0$	(1.4 ± 1.0) × 10 ⁻³	
Γ_{27} $3(\pi^+ \pi^-)$	(3.5 ± 2.0) × 10 ⁻⁴	S=2.8
Γ_{28} $2(\pi^+ \pi^- \pi^0)$	(4.8 ± 1.5) × 10 ⁻³	
Γ_{29} $3(\pi^+ \pi^-) \pi^0$	(3.5 ± 1.6) × 10 ⁻³	
Γ_{30} $2(\pi^+ \pi^-) 3\pi^0$	(1.42 ± 0.31) %	
Γ_{31} $\eta \pi^+ \pi^-$	< 1.6 × 10 ⁻⁴	CL=90%
Γ_{32} $\eta \pi^+ \pi^- \pi^0$	(9.5 ± 1.7) × 10 ⁻⁴	
Γ_{33} $\eta 2(\pi^+ \pi^-)$	(1.2 ± 0.6) × 10 ⁻³	
Γ_{34} $\eta \pi^+ \pi^- \pi^0 \pi^0$	< 4 × 10 ⁻⁴	CL=90%
Γ_{35} $\eta \pi^+ \pi^- 3\pi^0$	< 2.1 × 10 ⁻³	CL=90%
Γ_{36} $\eta 2(\pi^+ \pi^- \pi^0)$	< 2.1 × 10 ⁻³	CL=90%
Γ_{37} $\rho \eta$	(2.2 ± 0.6) × 10 ⁻⁵	S=1.1
Γ_{38} $\eta' \pi^+ \pi^- \pi^0$	(4.5 ± 2.1) × 10 ⁻⁴	

Γ_{39}	$\eta' \rho$	$(1.9 \pm_{-1.2}^{+1.7}) \times 10^{-5}$		Γ_{109}	$\omega f_1(1285) \rightarrow \omega K_S^0 K^- \pi^+ +$	$(3.0 \pm 1.0) \times 10^{-6}$	
Γ_{40}	$\omega \pi^0$	$(2.1 \pm 0.6) \times 10^{-5}$		Γ_{110}	$\omega f_1(1285) \rightarrow \omega K^+ K^- \pi^0$	$(1.2 \pm 0.7) \times 10^{-6}$	
Γ_{41}	$\omega \pi^+ \pi^-$	$(7.3 \pm 1.2) \times 10^{-4}$	S=2.1	Γ_{111}	$\rho \bar{\rho}$	$(2.94 \pm 0.09) \times 10^{-4}$	S=1.3
Γ_{42}	$\omega \pi^+ \pi^- 2\pi^0$	$(8.7 \pm 2.4) \times 10^{-3}$		Γ_{112}	$n \bar{n}$	$(3.06 \pm 0.15) \times 10^{-4}$	
Γ_{43}	$b_1^\pm \pi^\mp$	$(4.0 \pm 0.6) \times 10^{-4}$	S=1.1	Γ_{113}	$\rho \bar{\rho} \pi^0$	$(1.53 \pm 0.07) \times 10^{-4}$	
Γ_{44}	$\omega f_2(1270)$	$(2.2 \pm 0.4) \times 10^{-4}$		Γ_{114}	$N(940) \bar{p} + \text{c.c.} \rightarrow \rho \bar{\rho} \pi^0$	$(6.4 \pm_{-1.3}^{+1.8}) \times 10^{-5}$	
Γ_{45}	$\omega \pi^0 \pi^0$	$(1.11 \pm 0.35) \times 10^{-3}$		Γ_{115}	$N(1440) \bar{p} + \text{c.c.} \rightarrow \rho \bar{\rho} \pi^0$	$(7.3 \pm_{-1.5}^{+1.7}) \times 10^{-5}$	S=2.5
Γ_{46}	$\omega 3\pi^0$	$< 8 \times 10^{-4}$	CL=90%	Γ_{116}	$N(1520) \bar{p} + \text{c.c.} \rightarrow \rho \bar{\rho} \pi^0$	$(6.4 \pm_{-1.8}^{+2.3}) \times 10^{-6}$	
Γ_{47}	$b_1^0 \pi^0$	$(2.4 \pm 0.6) \times 10^{-4}$		Γ_{117}	$N(1535) \bar{p} + \text{c.c.} \rightarrow \rho \bar{\rho} \pi^0$	$(2.5 \pm 1.0) \times 10^{-5}$	
Γ_{48}	$\omega \eta$	$< 1.1 \times 10^{-5}$	CL=90%	Γ_{118}	$N(1650) \bar{p} + \text{c.c.} \rightarrow \rho \bar{\rho} \pi^0$	$(3.8 \pm_{-1.7}^{+1.4}) \times 10^{-5}$	
Γ_{49}	$\omega \eta'$	$(3.2 \pm_{-2.1}^{+2.5}) \times 10^{-5}$		Γ_{119}	$N(1720) \bar{p} + \text{c.c.} \rightarrow \rho \bar{\rho} \pi^0$	$(1.79 \pm_{-0.70}^{+0.26}) \times 10^{-5}$	
Γ_{50}	$\phi \pi^0$	$< 4 \times 10^{-7}$	CL=90%	Γ_{120}	$N(2300) \bar{p} + \text{c.c.} \rightarrow \rho \bar{\rho} \pi^0$	$(2.6 \pm_{-0.7}^{+1.2}) \times 10^{-5}$	
Γ_{51}	$\phi \pi^+ \pi^-$	$(1.18 \pm 0.26) \times 10^{-4}$	S=1.5	Γ_{121}	$N(2570) \bar{p} + \text{c.c.} \rightarrow \rho \bar{\rho} \pi^0$	$(2.13 \pm_{-0.31}^{+0.40}) \times 10^{-5}$	
Γ_{52}	$\phi f_0(980) \rightarrow \pi^+ \pi^-$	$(7.5 \pm 3.3) \times 10^{-5}$	S=1.6	Γ_{122}	$\rho \bar{\rho} \pi^+ \pi^-$	$(6.0 \pm 0.4) \times 10^{-4}$	
Γ_{53}	$\phi \eta$	$(3.10 \pm 0.31) \times 10^{-5}$		Γ_{123}	$\rho \bar{\rho} K^+ K^-$	$(2.7 \pm 0.7) \times 10^{-5}$	
Γ_{54}	$\eta \phi(2170), \phi(2170) \rightarrow$ $\phi f_0(980), f_0 \rightarrow \pi^+ \pi^-$	$< 2.2 \times 10^{-6}$	CL=90%	Γ_{124}	$\rho \bar{\rho} \eta$	$(6.0 \pm 0.4) \times 10^{-5}$	
Γ_{55}	$\phi \eta'$	$(1.54 \pm 0.20) \times 10^{-5}$		Γ_{125}	$N(1535) \bar{p} + \text{c.c.} \rightarrow \rho \bar{\rho} \eta$	$(4.5 \pm_{-0.6}^{+0.7}) \times 10^{-5}$	
Γ_{56}	$\phi f_1(1285)$	$(3.0 \pm 1.3) \times 10^{-5}$		Γ_{126}	$\rho \bar{\rho} \pi^+ \pi^- \pi^0$	$(7.3 \pm 0.7) \times 10^{-4}$	
Γ_{57}	$\phi \eta(1405) \rightarrow \phi \pi^+ \pi^- \eta$	$(8.5 \pm 1.7) \times 10^{-6}$		Γ_{127}	$\rho \bar{\rho} \rho^0$	$(5.0 \pm 2.2) \times 10^{-5}$	
Γ_{58}	$\phi f_2'(1525)$	$(4.4 \pm 1.6) \times 10^{-5}$		Γ_{128}	$\rho \bar{\rho} \omega$	$(6.9 \pm 2.1) \times 10^{-5}$	
Γ_{59}	$K^+ K^-$	$(7.5 \pm 0.5) \times 10^{-5}$		Γ_{129}	$\rho \bar{\rho} \eta'$	$(1.10 \pm 0.13) \times 10^{-5}$	
Γ_{60}	$K^+ K^- \pi^+ \pi^-$	$(7.3 \pm 0.5) \times 10^{-4}$		Γ_{130}	$\rho \bar{\rho} \phi$	$(6.1 \pm 0.6) \times 10^{-6}$	
Γ_{61}	$K^+ K^- \pi^0$	$(4.07 \pm 0.31) \times 10^{-5}$		Γ_{131}	$\phi X(1835) \rightarrow \rho \bar{\rho} \phi$	$< 1.82 \times 10^{-7}$	CL=90%
Γ_{62}	$K_S^0 K_S^0$	$< 4.6 \times 10^{-6}$		Γ_{132}	$\rho \bar{\rho} \pi^- \text{ or c.c.}$	$(2.48 \pm 0.17) \times 10^{-4}$	
Γ_{63}	$K_S^0 K_L^0$	$(5.34 \pm 0.33) \times 10^{-5}$		Γ_{133}	$\rho \bar{\rho} \pi^- \pi^0$	$(3.2 \pm 0.7) \times 10^{-4}$	
Γ_{64}	$K_S^0 K_L^0 \pi^0$	$< 3.0 \times 10^{-4}$	CL=90%	Γ_{134}	$\Lambda \bar{\Lambda}$	$(3.81 \pm 0.13) \times 10^{-4}$	S=1.4
Γ_{65}	$K^+ K^- \pi^0 \pi^0$	$(2.6 \pm 1.3) \times 10^{-4}$		Γ_{135}	$\Lambda \bar{\Lambda} \pi^0$	$(1.4 \pm 0.7) \times 10^{-6}$	
Γ_{66}	$K^+ K^- \pi^0 \pi^0 \pi^0$	$(6.6 \pm 2.8) \times 10^{-4}$		Γ_{136}	$\Lambda \bar{\Lambda} \eta$	$(2.43 \pm 0.32) \times 10^{-5}$	
Γ_{67}	$K_S^0 K^\pm \pi^\mp \pi^0 \pi^0$	$(1.7 \pm 0.6) \times 10^{-3}$		Γ_{137}	$\Lambda(1670) \bar{\Lambda} \rightarrow \Lambda \bar{\Lambda} \eta$	$(1.3 \pm 0.7) \times 10^{-5}$	
Γ_{68}	$K_S^0 K^\pm \pi^\mp \pi^+ \pi^-$	$(2.2 \pm 0.4) \times 10^{-3}$		Γ_{138}	$\Lambda \bar{\Lambda} \eta'$	$(7.3 \pm 1.0) \times 10^{-6}$	
Γ_{69}	$K^+ K^- \pi^+ \pi^- \pi^0$	$(1.26 \pm 0.09) \times 10^{-3}$		Γ_{139}	$\Lambda \bar{\Lambda} \omega(782)$	$(3.3 \pm 0.4) \times 10^{-5}$	
Γ_{70}	$\omega f_0(1710) \rightarrow \omega K^+ K^-$	$(5.9 \pm 2.2) \times 10^{-5}$		Γ_{140}	$\Lambda \bar{\Lambda} \pi^+ \pi^-$	$(2.8 \pm 0.6) \times 10^{-4}$	
Γ_{71}	$K^*(892)^0 K^- \pi^+ \pi^0 + \text{c.c.}$	$(8.6 \pm 2.2) \times 10^{-4}$		Γ_{141}	$\Lambda \bar{K} K^+$	$(1.00 \pm 0.14) \times 10^{-4}$	
Γ_{72}	$K^*(892)^+ K^- \pi^+ \pi^- + \text{c.c.}$	$(9.6 \pm 2.8) \times 10^{-4}$		Γ_{142}	$\Lambda \bar{K} K^*(892)^+ + \text{c.c.}$	$(6.3 \pm 0.7) \times 10^{-5}$	
Γ_{73}	$K^*(892)^+ K^- \rho^0 + \text{c.c.}$	$(7.3 \pm 2.6) \times 10^{-4}$		Γ_{143}	$\Lambda \bar{K} K^+ \pi^+ \pi^-$	$(1.8 \pm 0.4) \times 10^{-4}$	
Γ_{74}	$K^*(892)^0 K^- \rho^+ + \text{c.c.}$	$(6.1 \pm 1.8) \times 10^{-4}$		Γ_{144}	$\bar{\Lambda} n K_S^0 + \text{c.c.}$	$(8.1 \pm 1.8) \times 10^{-5}$	
Γ_{75}	$K_S^0 K_S^0 \pi^+ \pi^-$	$(2.2 \pm 0.4) \times 10^{-4}$		Γ_{145}	$\Delta^{++} \bar{\Delta}^{--}$	$(1.28 \pm 0.35) \times 10^{-4}$	
Γ_{76}	$K_S^0 K_L^0 \pi^0 \pi^0$	$(1.3 \pm 0.6) \times 10^{-3}$		Γ_{146}	$\Lambda \bar{\Sigma}^+ \pi^- + \text{c.c.}$	$(1.40 \pm 0.13) \times 10^{-4}$	
Γ_{77}	$K_S^0 K^*(892)^0 \pi^0 \pi^0$	$(3.0 \pm 1.3) \times 10^{-4}$		Γ_{147}	$\Lambda \bar{\Sigma}^- \pi^+ + \text{c.c.}$	$(1.54 \pm 0.14) \times 10^{-4}$	
Γ_{78}	$K_S^0 K^\pm \rho(770)^\mp \pi^0$	$< 7 \times 10^{-4}$	CL=90%	Γ_{148}	$\Lambda \bar{\Sigma}^0 + \text{c.c.}$	$(1.6 \pm 0.7) \times 10^{-6}$	
Γ_{79}	$K_S^0 K^\pm \pi^\mp \rho(770)^0$	$< 7 \times 10^{-4}$	CL=90%	Γ_{149}	$\Lambda \bar{\Sigma}^0$		
Γ_{80}	$K^\mp K^*(892)^\pm \pi^0 \pi^0$	$(7.0 \pm 2.9) \times 10^{-4}$		Γ_{150}	$\Sigma^0 \bar{p} K^+ + \text{c.c.}$	$(1.67 \pm 0.18) \times 10^{-5}$	
Γ_{81}	$K^*(892)^+ K^*(892)^- \pi^0$	$(3.6 \pm 1.8) \times 10^{-3}$		Γ_{151}	$\Sigma^+ \bar{\Sigma}^-$	$(2.43 \pm 0.10) \times 10^{-4}$	S=1.4
Γ_{82}	$K_S^0 K_L^0 \eta$	$(1.3 \pm 0.5) \times 10^{-3}$		Γ_{152}	$\Sigma^0 \bar{\Sigma}^0$	$(2.35 \pm 0.09) \times 10^{-4}$	S=1.1
Γ_{83}	$K^+ K^- \rho^0$	$(2.2 \pm 0.4) \times 10^{-4}$		Γ_{153}	$\Sigma^- \bar{\Sigma}^+$	$(2.82 \pm 0.09) \times 10^{-4}$	
Γ_{84}	$K^*(892)^0 \bar{K}_2^*(1430)^0$	$(1.9 \pm 0.5) \times 10^{-4}$		Γ_{154}	$\Sigma^+ \bar{\Sigma}^- \eta$	$(9.6 \pm 2.4) \times 10^{-6}$	
Γ_{85}	$K^+ K^- \pi^+ \pi^- \eta$	$(1.3 \pm 0.7) \times 10^{-3}$		Γ_{155}	$\Sigma^+ \bar{\Sigma}^- \omega$	$(1.89 \pm 0.28) \times 10^{-5}$	
Γ_{86}	$K^+ K^- 2(\pi^+ \pi^-)$	$(1.9 \pm 0.9) \times 10^{-3}$		Γ_{156}	$\Sigma^+ \bar{\Sigma}^- \phi$	$(3.0 \pm 0.7) \times 10^{-6}$	
Γ_{87}	$K^+ K^- 2(\pi^+ \pi^-) \pi^0$	$(1.00 \pm 0.31) \times 10^{-3}$		Γ_{157}	$\Sigma(1385)^+ \bar{\Sigma}(1385)^-$	$(8.5 \pm 0.7) \times 10^{-5}$	
Γ_{88}	$K^+ K^*(892)^- + \text{c.c.}$	$(2.9 \pm 0.4) \times 10^{-5}$	S=1.2	Γ_{158}	$\Sigma(1385)^- \bar{\Sigma}(1385)^+$	$(8.5 \pm 0.8) \times 10^{-5}$	
Γ_{89}	$2(K^+ K^-)$	$(6.3 \pm 1.3) \times 10^{-5}$		Γ_{159}	$\Sigma(1385)^0 \bar{\Sigma}(1385)^0$	$(6.9 \pm 0.7) \times 10^{-5}$	
Γ_{90}	$2(K^+ K^-) \pi^0$	$(1.10 \pm 0.28) \times 10^{-4}$		Γ_{160}	$\Xi^- \bar{\Xi}^+$	$(2.87 \pm 0.11) \times 10^{-4}$	S=1.1
Γ_{91}	$K^+ K^- \phi$	$(7.0 \pm 1.6) \times 10^{-5}$		Γ_{161}	$\Xi^0 \bar{\Xi}^0$	$(2.3 \pm 0.4) \times 10^{-4}$	S=4.2
Γ_{92}	$K_S^0 K_S^0 \phi$	$(3.53 \pm 0.29) \times 10^{-5}$		Γ_{162}	$\Xi(1530)^0 \bar{\Xi}(1530)^0$	$(6.8 \pm 0.4) \times 10^{-5}$	
Γ_{93}	$K_1(1270)^\pm K^\mp$	$(1.00 \pm 0.28) \times 10^{-3}$		Γ_{163}	$\Lambda \bar{\Xi}^+ K^- + \text{c.c.}$	$(3.9 \pm 0.4) \times 10^{-5}$	
Γ_{94}	$K^+ \bar{K}^*(892)^0 \pi^- + \text{c.c.}$	$(6.7 \pm 2.5) \times 10^{-4}$		Γ_{164}	$\Xi(1690)^- \bar{\Xi}^+ \rightarrow K^- \Lambda \bar{\Xi}^+ +$	$(5.2 \pm 1.6) \times 10^{-6}$	
Γ_{95}	$\eta K^+ K^-$, no $\eta \phi$	$(3.49 \pm 0.17) \times 10^{-5}$					
Γ_{96}	$\eta K^+ K^-$	$< 2.6 \times 10^{-4}$	CL=90%				
Γ_{97}	$X(1750) \eta \rightarrow K^+ K^- \eta$	$(4.8 \pm 2.8) \times 10^{-6}$					
Γ_{98}	$K_1(1400)^\pm K^\mp$	$< 3.1 \times 10^{-4}$	CL=90%	Γ_{165}	$\Xi(1820)^- \bar{\Xi}^+ \rightarrow K^- \Lambda \bar{\Xi}^+ +$	$(1.20 \pm 0.32) \times 10^{-5}$	
Γ_{99}	$K_2^*(1430)^\pm K^\mp$	$(7.1 \pm_{-0.9}^{+1.3}) \times 10^{-5}$					
Γ_{100}	$K^*(892)^0 \bar{K}^0 + \text{c.c.}$	$(1.09 \pm 0.20) \times 10^{-4}$		Γ_{166}	$\Xi(1530)^- \bar{\Xi}(1530)^+$	$(1.15 \pm 0.07) \times 10^{-4}$	
Γ_{101}	$\omega K^+ K^-$	$(1.62 \pm 0.11) \times 10^{-4}$	S=1.1	Γ_{167}	$\Xi(1530)^- \bar{\Xi}^+$	$(7.0 \pm 1.2) \times 10^{-6}$	
Γ_{102}	$\omega K_S^0 K_S^0$	$(7.0 \pm 0.5) \times 10^{-5}$		Γ_{168}	$\Xi(1530)^0 \bar{\Xi}^0$	$(5.3 \pm 0.5) \times 10^{-6}$	
Γ_{103}	$\omega K^*(892)^+ K^- + \text{c.c.}$	$(2.07 \pm 0.26) \times 10^{-4}$		Γ_{169}	$\Sigma^0 \bar{\Xi}^+ K^- + \text{c.c.}$	$(3.7 \pm 0.4) \times 10^{-5}$	
Γ_{104}	$\omega K_2^*(1430)^+ K^- + \text{c.c.}$	$(6.1 \pm 1.2) \times 10^{-5}$		Γ_{170}	$\Omega^- \bar{\Omega}^+$	$(5.66 \pm 0.30) \times 10^{-5}$	S=1.3
Γ_{105}	$\omega \bar{K}^*(892)^0 K^0$	$(1.68 \pm 0.30) \times 10^{-4}$		Γ_{171}	$\eta_c \pi^+ \pi^- \pi^0$	$< 1.0 \times 10^{-3}$	CL=90%
Γ_{106}	$\omega \bar{K}_2^*(1430)^0 K^0$	$(5.8 \pm 2.2) \times 10^{-5}$		Γ_{172}	$h_c(1P) \pi^0$	$(7.4 \pm 0.5) \times 10^{-4}$	
Γ_{107}	$\omega X(1440) \rightarrow \omega K_S^0 K^- \pi^+ +$ c.c.	$(1.6 \pm 0.4) \times 10^{-5}$		Γ_{173}	$\Lambda_c^+ \bar{p} e^+ e^- + \text{c.c.}$	$< 1.7 \times 10^{-6}$	CL=90%
Γ_{108}	$\omega X(1440) \rightarrow \omega K^+ K^- \pi^0$	$(1.09 \pm 0.26) \times 10^{-5}$		Γ_{174}	$\Theta(1540) \bar{\Theta}(1540) \rightarrow$ $K_S^0 p K^- \bar{n} + \text{c.c.}$	$[a] < 8.8 \times 10^{-6}$	CL=90%
				Γ_{175}	$\Theta(1540) K^- \bar{n} \rightarrow K_S^0 p K^- \bar{n}$	$[a] < 1.0 \times 10^{-5}$	CL=90%

Meson Particle Listings

$\psi(2S)$

Γ_{176}	$\Theta(1540) K_S^0 \bar{p} \rightarrow K_S^0 \bar{p} K^+ n$	$[a] < 7.0$	$\times 10^{-6}$	CL=90%
Γ_{177}	$\bar{\Theta}(1540) K^+ n \rightarrow K_S^0 \bar{p} K^+ n$	$[a] < 2.6$	$\times 10^{-5}$	CL=90%
Γ_{178}	$\bar{\Theta}(1540) K_S^0 p \rightarrow K_S^0 p K^- \bar{n}$	$[a] < 6.0$	$\times 10^{-6}$	CL=90%

Radiative decays

Γ_{179}	$\gamma \chi_{c0}(1P)$	$(9.77 \pm 0.23) \%$		S=1.1
Γ_{180}	$\gamma \chi_{c1}(1P)$	$(9.75 \pm 0.27) \%$		S=1.1
Γ_{181}	$\gamma \chi_{c2}(1P)$	$(9.36 \pm 0.23) \%$		S=1.2
Γ_{182}	$\gamma \eta_c(1S)$	$(3.6 \pm 0.5) \times 10^{-3}$		S=1.3
Γ_{183}	$\gamma \eta_c(2S)$	$(7 \pm 5) \times 10^{-4}$		
Γ_{184}	$\gamma \pi^0$	$(1.04 \pm 0.22) \times 10^{-6}$		S=1.4
Γ_{185}	$\gamma 2(\pi^+ \pi^-)$	$(4.0 \pm 0.6) \times 10^{-4}$		
Γ_{186}	$\gamma 3(\pi^+ \pi^-)$	< 1.7	$\times 10^{-4}$	CL=90%
Γ_{187}	$\gamma \eta'(958)$	$(1.24 \pm 0.04) \times 10^{-4}$		
Γ_{188}	$\gamma f_2(1270)$	$(2.73 \pm 0.29 \pm 0.25) \times 10^{-4}$		S=1.8
Γ_{189}	$\gamma f_0(1370) \rightarrow \gamma K \bar{K}$	$(3.1 \pm 1.7) \times 10^{-5}$		
Γ_{190}	$\gamma f_0(1500)$	$(9.3 \pm 1.9) \times 10^{-5}$		
Γ_{191}	$\gamma f_2'(1525)$	$(3.3 \pm 0.8) \times 10^{-5}$		
Γ_{192}	$\gamma f_0(1710)$	seen		
Γ_{193}	$\gamma f_0(1710) \rightarrow \gamma \pi \pi$	$(3.5 \pm 0.6) \times 10^{-5}$		
Γ_{194}	$\gamma f_0(1710) \rightarrow \gamma K \bar{K}$	$(6.6 \pm 0.7) \times 10^{-5}$		
Γ_{195}	$\gamma f_0(2100) \rightarrow \gamma \pi \pi$	$(4.8 \pm 1.0) \times 10^{-6}$		
Γ_{196}	$\gamma f_0(2200) \rightarrow \gamma K \bar{K}$	$(3.2 \pm 1.0) \times 10^{-6}$		
Γ_{197}	$\gamma f_J(2220) \rightarrow \gamma \pi \pi$	< 5.8	$\times 10^{-6}$	CL=90%
Γ_{198}	$\gamma f_J(2220) \rightarrow \gamma K \bar{K}$	< 9.5	$\times 10^{-6}$	CL=90%
Γ_{199}	$\gamma \eta$	$(9.2 \pm 1.8) \times 10^{-7}$		
Γ_{200}	$\gamma \eta \pi^+ \pi^-$	$(8.7 \pm 2.1) \times 10^{-4}$		
Γ_{201}	$\gamma \eta(1405)$	seen		
Γ_{202}	$\gamma \eta(1405) \rightarrow \gamma K \bar{K} \pi$	< 9	$\times 10^{-5}$	CL=90%
Γ_{203}	$\gamma \eta(1405) \rightarrow \gamma \eta \pi^+ \pi^-$	$(3.6 \pm 2.5) \times 10^{-5}$		
Γ_{204}	$\gamma \eta(1405) \rightarrow \gamma f_0(980) \pi^0 \rightarrow \gamma \pi^+ \pi^- \pi^0$	< 5.0	$\times 10^{-7}$	CL=90%
Γ_{205}	$\gamma \eta(1475)$	seen		
Γ_{206}	$\gamma \eta(1475) \rightarrow \gamma K \bar{K} \pi$	< 1.4	$\times 10^{-4}$	CL=90%
Γ_{207}	$\gamma \eta(1475) \rightarrow \gamma \eta \pi^+ \pi^-$	< 8.8	$\times 10^{-5}$	CL=90%
Γ_{208}	$\gamma K^{*0} K^+ \pi^- + c.c.$	$(3.7 \pm 0.9) \times 10^{-4}$		
Γ_{209}	$\gamma K^{*0} \bar{K}^{*0}$	$(2.4 \pm 0.7) \times 10^{-4}$		
Γ_{210}	$\gamma K_S^0 K^+ \pi^- + c.c.$	$(2.6 \pm 0.5) \times 10^{-4}$		
Γ_{211}	$\gamma K^+ K^- \pi^+ \pi^-$	$(1.9 \pm 0.5) \times 10^{-4}$		
Γ_{212}	$\gamma K^+ K^- 2(\pi^+ \pi^-)$	< 2.2	$\times 10^{-4}$	CL=90%
Γ_{213}	$\gamma 2(K^+ K^-)$	< 4	$\times 10^{-5}$	CL=90%
Γ_{214}	$\gamma \rho \bar{\rho}$	$(3.9 \pm 0.5) \times 10^{-5}$		S=2.0
Γ_{215}	$\gamma f_2(1950) \rightarrow \gamma \rho \bar{\rho}$	$(1.20 \pm 0.22) \times 10^{-5}$		
Γ_{216}	$\gamma f_2(2150) \rightarrow \gamma \rho \bar{\rho}$	$(7.2 \pm 1.8) \times 10^{-6}$		
Γ_{217}	$\gamma X(1835) \rightarrow \gamma \rho \bar{\rho}$	$(4.6 \pm 1.8 \pm 4.0) \times 10^{-6}$		
Γ_{218}	$\gamma X \rightarrow \gamma \rho \bar{\rho}$	$[b] < 2$	$\times 10^{-6}$	CL=90%
Γ_{219}	$\gamma \rho \bar{\rho} \pi^+ \pi^-$	$(2.8 \pm 1.4) \times 10^{-5}$		
Γ_{220}	$\gamma \gamma$	< 1.5	$\times 10^{-4}$	CL=90%
Γ_{221}	$\gamma \gamma J/\psi$	$(3.1 \pm 1.0 \pm 1.2) \times 10^{-4}$		
Γ_{222}	$e^+ e^- \eta'$	$(1.90 \pm 0.26) \times 10^{-6}$		
Γ_{223}	$e^+ e^- \eta_c(1S)$	$(3.8 \pm 0.4) \times 10^{-5}$		
Γ_{224}	$e^+ e^- \chi_{c0}(1P)$	$(1.06 \pm 0.25) \times 10^{-3}$		
Γ_{225}	$e^+ e^- \chi_{c1}(1P)$	$(8.5 \pm 0.7) \times 10^{-4}$		
Γ_{226}	$e^+ e^- \chi_{c2}(1P)$	$(6.8 \pm 0.8) \times 10^{-4}$		
Weak decays				
Γ_{227}	$D^0 e^+ e^- + c.c.$	< 1.4	$\times 10^{-7}$	CL=90%
Γ_{228}	$L_c^+ \bar{\Sigma}^- + c.c.$	< 1.4	$\times 10^{-5}$	CL=90%
Other decays				
Γ_{229}	invisible	< 1.6	$\%$	CL=90%

[a] $\Theta(1540)$ is a hypothetical pentaquark state of 1.54 GeV/c² mass and a width of less than 25 MeV/c².

[b] For a narrow resonance in the range 2.2 < M(X) < 2.8 GeV.

CONSTRAINED FIT INFORMATION

A multiparticle fit to $\chi_{c1}(1P)$, $\chi_{c0}(1P)$, $\chi_{c2}(1P)$, and $\psi(2S)$ with 4 total widths, a partial width, 25 combinations of partial widths obtained from integrated cross section, and 86 branching ratios uses 253 measurements to determine 49 parameters. The overall fit has a $\chi^2 = 389.6$ for 204 degrees of freedom.

The following *off-diagonal* array elements are the correlation coefficients $\langle \delta p_i \delta p_j \rangle / (\delta p_i \delta p_j)$, in percent, from the fit to parameters p_i , including the branching fractions, $x_i \equiv \Gamma_i / \Gamma_{\text{total}}$.

x_8	3									
x_9	0	0								
x_{12}	21	13	2							
x_{13}	22	5	1	28						
x_{14}	11	6	1	44	11					
x_{111}	0	0	0	3	2	1				
x_{179}	0	0	0	2	1	1	0			
x_{180}	1	0	0	2	0	1	0	0		
x_{181}	1	1	0	4	0	2	0	0	0	
Γ	-85	-4	-1	-29	-31	-15	-4	-1	-1	-2
	x_7	x_8	x_9	x_{12}	x_{13}	x_{14}	x_{111}	x_{179}	x_{180}	x_{181}

FIT INFORMATION

A multiparticle fit to $\eta_c(1S)$, $J/\psi(1S)$, $\psi(2S)$, $h_c(1P)$, and B^\pm with the total width, 10 combinations of partial widths obtained from integrated cross section, and 38 branching ratios uses 113 measurements to determine 19 parameters. The overall fit has a $\chi^2 = 184.6$ for 94 degrees of freedom.

$\psi(2S)$ PARTIAL WIDTHS

$\Gamma(\text{hadrons})$	DOCUMENT ID	TECN	COMMENT	Γ_1
VALUE (keV)				
• • • We do not use the following data for averages, fits, limits, etc. • • •				
258 ± 26	BAI	02B	BES2	$e^+ e^-$
224 ± 56	LUTH	75	MRK1	$e^+ e^-$

$\Gamma(e^+ e^-)$	DOCUMENT ID	TECN	COMMENT	Γ_7
VALUE (keV)				
2.33 ± 0.04 OUR FIT			Error includes scale factor of 1.1.	
2.29 ± 0.06 OUR AVERAGE				
2.23 ± 0.10 ± 0.02	¹ ABLIKIM	15v	BES3	4.0-4.4 $e^+ e^- \rightarrow \pi^+ \pi^- J/\psi$
2.338 ± 0.037 ± 0.096	ABLIKIM	08B	BES2	$e^+ e^- \rightarrow \text{hadrons}$
2.330 ± 0.036 ± 0.110	ABLIKIM	06L	BES2	$e^+ e^- \rightarrow \text{hadrons}$
2.44 ± 0.21	² BAI	02B	BES2	$e^+ e^-$
2.14 ± 0.21	ALEXANDER	89	RVUE	See <i>T</i> mini-review
• • • We do not use the following data for averages, fits, limits, etc. • • •				
2.279 ± 0.015 ± 0.042	³ ANASHIN	18	KEDR	$e^+ e^-$
2.282 ± 0.015 ± 0.042	⁴ ANASHIN	18	KEDR	$e^+ e^-$
2.0 ± 0.3	BRANDELIK	79c	DASP	$e^+ e^-$
2.1 ± 0.3	⁵ LUTH	75	MRK1	$e^+ e^-$

¹ ABLIKIM 15v reports 2.213 ± 0.018 ± 0.099 keV from a measurement of $[\Gamma(\psi(2S) \rightarrow e^+ e^-)] \times [B(\psi(2S) \rightarrow J/\psi(1S) \pi^+ \pi^-)]$ assuming $B(\psi(2S) \rightarrow J/\psi(1S) \pi^+ \pi^-) = (34.95 \pm 0.45) \times 10^{-2}$, which we rescale to our best value $B(\psi(2S) \rightarrow J/\psi(1S) \pi^+ \pi^-) = (34.69 \pm 0.34) \times 10^{-2}$. Our first error is their experiment's error and our second error is the systematic error from using our best value.

² From a simultaneous fit to $e^+ e^-$, $\mu^+ \mu^-$, and hadronic channel, assuming $\Gamma_e = \Gamma_\mu = \Gamma_\tau / 0.38847$.

³ Combining $\Gamma_{e^+ e^-} \cdot B(\mu^+ \mu^-)$ from ANASHIN 18 with $\Gamma_{e^+ e^-} \cdot B(\text{hadrons})$ from ANASHIN 12 and assuming lepton universality.

⁴ From the sum of $\Gamma_{e^+ e^-} \cdot B(\text{hadrons})$ from ANASHIN 12, $\Gamma_{e^+ e^-} \cdot B(e^+ e^-)$ and $\Gamma_{e^+ e^-} \cdot B(\mu^+ \mu^-)$ from ANASHIN 18, and $\Gamma_{e^+ e^-} \cdot B(\tau^+ \tau^-)$ from ANASHIN 07.

⁵ From a simultaneous fit to $e^+ e^-$, $\mu^+ \mu^-$, and hadronic channels assuming $\Gamma(e^+ e^-) = \Gamma(\mu^+ \mu^-)$.

$\Gamma(\gamma\gamma)$	DOCUMENT ID	TECN	COMMENT	Γ_{220}	
VALUE (eV)					
< 43	90	BRANDELIK	79c	DASP	$e^+ e^-$

$\psi(2S) \Gamma(i) \Gamma(e^+ e^-) / \Gamma(\text{total})$

This combination of a partial width with the partial width into $e^+ e^-$ and with the total width is obtained from the integrated cross section into channel(i) in the $e^+ e^-$ annihilation. We list only data that have not been used to determine the partial width $\Gamma(i)$ or the branching ratio $\Gamma(i) / \text{total}$.

$\Gamma(\text{hadrons}) \times \Gamma(e^+ e^-) / \Gamma_{\text{total}}$	DOCUMENT ID	TECN	COMMENT	$\Gamma_1 \Gamma_7 / \Gamma$
VALUE (keV)				
2.233 ± 0.015 ± 0.042	¹ ANASHIN	12	KEDR	$e^+ e^- \rightarrow \text{hadrons}$
• • • We do not use the following data for averages, fits, limits, etc. • • •				
2.2 ± 0.4	ABRAMS	75	MRK1	$e^+ e^-$

¹ ANASHIN 12 reports the value 2.233 ± 0.015 ± 0.037 ± 0.020 keV, where the third uncertainty is due to assumptions on the interference between the resonance and hadronic continuum. We combined the two systematic uncertainties.

See key on page 1171

Meson Particle Listings

$\psi(2S)$

$\Gamma(K_S^0 \text{ anything}) \times \Gamma(e^+ e^-) / \Gamma_{\text{total}}$				$\Gamma_6 \Gamma_7 / \Gamma$
VALUE (keV)	DOCUMENT ID	TECN	COMMENT	
0.3738 ± 0.0067 ± 0.0200	ABLKIM	21s	BES3 $e^+ e^- \rightarrow K_S^0 \text{ anything}$	

$\Gamma(e^+ e^-) \times \Gamma(e^+ e^-) / \Gamma_{\text{total}}$				$\Gamma_7 \Gamma_7 / \Gamma$
VALUE (eV)	DOCUMENT ID	TECN	COMMENT	
21.2 ± 0.7 ± 1.2	¹ ANASHIN	18	KEDR $e^+ e^-$	

¹ From the average of nine scans of the $\psi(2S)$.

$\Gamma(\mu^+ \mu^-) \times \Gamma(e^+ e^-) / \Gamma_{\text{total}}$				$\Gamma_8 \Gamma_7 / \Gamma$
VALUE (eV)	DOCUMENT ID	TECN	COMMENT	
19.3 ± 0.3 ± 0.5	¹ ANASHIN	18	KEDR $\psi(2S) \rightarrow \mu^+ \mu^-$	

¹ From the average of nine scans of the $\psi(2S)$.

$\Gamma(\tau^+ \tau^-) \times \Gamma(e^+ e^-) / \Gamma_{\text{total}}$				$\Gamma_9 \Gamma_7 / \Gamma$
VALUE (eV)	EVTS	DOCUMENT ID	TECN	COMMENT
9.0 ± 2.6	79	¹ ANASHIN	07	KEDR $e^+ e^- \rightarrow \psi(2S) \rightarrow \tau^+ \tau^-$

• • • We do not use the following data for averages, fits, limits, etc. • • •

¹ Using $\psi(2S)$ total width of 337 ± 13 keV. Systematic errors not evaluated.

$\Gamma(J/\psi(1S) \pi^+ \pi^-) \times \Gamma(e^+ e^-) / \Gamma_{\text{total}}$				$\Gamma_{12} \Gamma_7 / \Gamma$
VALUE (keV)	EVTS	DOCUMENT ID	TECN	COMMENT
0.808 ± 0.014 OUR FIT				Error includes scale factor of 1.1.
0.836 ± 0.025 OUR AVERAGE				Error includes scale factor of 1.3. See the ideogram below.
0.78 ± 0.12 ± 0.07		¹ LEES	23	BABR $e^+ e^- \rightarrow \gamma_{ISR} \text{hadrons}$
0.837 ± 0.028 ± 0.005		² LEES	12E	BABR $10.6 e^+ e^- \rightarrow 2\pi^+ 2\pi^- \gamma$
0.852 ± 0.010 ± 0.026	19.5k	ADAM	06	CLEO $3.773 e^+ e^- \rightarrow \gamma \psi(2S)$
0.68 ± 0.09		³ BAI	98E	BES $e^+ e^-$

• • • We do not use the following data for averages, fits, limits, etc. • • •

0.93 ± 0.08 ± 0.03 256 ⁴ AUBERT 07AU BABR 10.6 $e^+ e^- \rightarrow J/\psi \pi^+ \pi^- \gamma$

0.755 ± 0.048 ± 0.004 544 ⁵ AUBERT 05D BABR 10.6 $e^+ e^- \rightarrow \pi^+ \pi^- \mu^+ \mu^- \gamma$

¹ LEES 23 reports $[\Gamma(\psi(2S) \rightarrow J/\psi(1S) \pi^+ \pi^-) \times \Gamma(\psi(2S) \rightarrow e^+ e^-) / \Gamma_{\text{total}}] \times [B(J/\psi(1S) \rightarrow K_S^0 K^\pm \pi^\mp)] = (4.14 \pm 0.55 \pm 0.29) \times 10^{-3}$ keV which we divide by our best value $B(J/\psi(1S) \rightarrow K_S^0 K^\pm \pi^\mp) = (5.3 \pm 0.5) \times 10^{-3}$. Our first error is their experiment's error and our second error is the systematic error from using our best value.

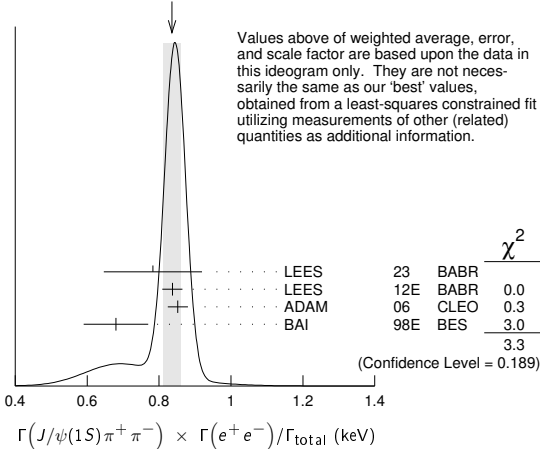
² LEES 12E reports $[\Gamma(\psi(2S) \rightarrow J/\psi(1S) \pi^+ \pi^-) \times \Gamma(\psi(2S) \rightarrow e^+ e^-) / \Gamma_{\text{total}}] \times [B(J/\psi(1S) \rightarrow \mu^+ \mu^-)] = (49.9 \pm 1.3 \pm 1.0) \times 10^{-3}$ keV which we divide by our best value $B(J/\psi(1S) \rightarrow \mu^+ \mu^-) = (5.961 \pm 0.033) \times 10^{-2}$. Our first error is their experiment's error and our second error is the systematic error from using our best value.

³ The value of $\Gamma(e^+ e^-)$ quoted in BAI 98E is derived using $B(\psi(2S) \rightarrow J/\psi(1S) \pi^+ \pi^-) = (32.4 \pm 2.6) \times 10^{-2}$ and $B(J/\psi(1S) \rightarrow \ell^+ \ell^-) = 0.1203 \pm 0.0038$. Recalculated by us using $B(J/\psi(1S) \rightarrow \ell^+ \ell^-) = 0.1181 \pm 0.0020$.

⁴ AUBERT 07AU reports $[\Gamma(\psi(2S) \rightarrow J/\psi(1S) \pi^+ \pi^-) \times \Gamma(\psi(2S) \rightarrow e^+ e^-) / \Gamma_{\text{total}}] \times [B(J/\psi(1S) \rightarrow \pi^+ \pi^- \pi^0)] = 0.0186 \pm 0.0012 \pm 0.0011$ keV which we divide by our best value $B(J/\psi(1S) \rightarrow \pi^+ \pi^- \pi^0) = (2.00 \pm 0.07) \times 10^{-2}$. Our first error is their experiment's error and our second error is the systematic error from using our best value.

⁵ AUBERT 05D reports $[\Gamma(\psi(2S) \rightarrow J/\psi(1S) \pi^+ \pi^-) \times \Gamma(\psi(2S) \rightarrow e^+ e^-) / \Gamma_{\text{total}}] \times [B(J/\psi(1S) \rightarrow \mu^+ \mu^-)] = 0.0450 \pm 0.0018 \pm 0.0022$ keV which we divide by our best value $B(J/\psi(1S) \rightarrow \mu^+ \mu^-) = (5.961 \pm 0.033) \times 10^{-2}$. Our first error is their experiment's error and our second error is the systematic error from using our best value. Superseded by LEES 12E.

WEIGHTED AVERAGE
0.836±0.025 (Error scaled by 1.3)



$\Gamma(J/\psi(1S) \pi^0 \pi^0) \times \Gamma(e^+ e^-) / \Gamma_{\text{total}}$				$\Gamma_{13} \Gamma_7 / \Gamma$
VALUE (keV)	EVTS	DOCUMENT ID	TECN	COMMENT
0.425 ± 0.012 OUR FIT				Error includes scale factor of 1.4.
0.413 ± 0.019 OUR AVERAGE				
0.45 ± 0.13 ± 0.02		¹ LEES	23	BABR $e^+ e^- \rightarrow \gamma_{ISR} \text{hadrons}$
0.45 ± 0.12 ± 0.04		² LEES	23	BABR $e^+ e^- \rightarrow \gamma_{ISR} \text{hadrons}$
0.411 ± 0.008 ± 0.018	3.6k	ADAM	06	CLEO $3.773 e^+ e^- \rightarrow \gamma \psi(2S)$

• • • We do not use the following data for averages, fits, limits, etc. • • •

0.51 ± 0.09 ± 0.02 142 ³ LEES 18E BABR 10.6 $e^+ e^- \rightarrow J/\psi \pi^0 \pi^0 \gamma$

¹ LEES 23 reports $[\Gamma(\psi(2S) \rightarrow J/\psi(1S) \pi^0 \pi^0) \times \Gamma(\psi(2S) \rightarrow e^+ e^-) / \Gamma_{\text{total}}] \times [B(J/\psi(1S) \rightarrow K^+ K^- \pi^0)] = (1.31 \pm 0.35 \pm 0.13) \times 10^{-3}$ keV which we divide by our best value $B(J/\psi(1S) \rightarrow K^+ K^- \pi^0) = (2.88 \pm 0.12) \times 10^{-3}$. Our first error is their experiment's error and our second error is the systematic error from using our best value.

² LEES 23 reports $[\Gamma(\psi(2S) \rightarrow J/\psi(1S) \pi^0 \pi^0) \times \Gamma(\psi(2S) \rightarrow e^+ e^-) / \Gamma_{\text{total}}] \times [B(J/\psi(1S) \rightarrow K_S^0 K^\pm \pi^\mp)] = (2.36 \pm 0.59 \pm 0.24) \times 10^{-3}$ keV which we divide by our best value $B(J/\psi(1S) \rightarrow K_S^0 K^\pm \pi^\mp) = (5.3 \pm 0.5) \times 10^{-3}$. Our first error is their experiment's error and our second error is the systematic error from using our best value.

³ LEES 18E reports $[\Gamma(\psi(2S) \rightarrow J/\psi(1S) \pi^0 \pi^0) \times \Gamma(\psi(2S) \rightarrow e^+ e^-) / \Gamma_{\text{total}}] \times [B(J/\psi(1S) \rightarrow \pi^+ \pi^- \pi^0)] = 0.0101 \pm 0.0015 \pm 0.0011$ keV which we divide by our best value $B(J/\psi(1S) \rightarrow \pi^+ \pi^- \pi^0) = (2.00 \pm 0.07) \times 10^{-2}$. Our first error is their experiment's error and our second error is the systematic error from using our best value.

$\Gamma(J/\psi(1S) \eta) \times \Gamma(e^+ e^-) / \Gamma_{\text{total}}$				$\Gamma_{14} \Gamma_7 / \Gamma$
VALUE (eV)	EVTS	DOCUMENT ID	TECN	COMMENT
78.6 ± 1.8 OUR FIT				Error includes scale factor of 1.1.
87 ± 9 OUR AVERAGE				
83 ± 25 ± 5	14	¹ AUBERT	07AU	BABR $10.6 e^+ e^- \rightarrow J/\psi \pi^+ \pi^- \pi^0 \gamma$

88 ± 6 ± 7 291 ± 24 ADAM 06 CLEO 3.773 $e^+ e^- \rightarrow \gamma \psi(2S)$

¹ AUBERT 07AU quotes $\Gamma_{ee}^{\psi(2S)} \cdot B(\psi(2S) \rightarrow J/\psi \eta) \cdot B(J/\psi \rightarrow \mu^+ \mu^-) \cdot B(\eta \rightarrow \pi^+ \pi^- \pi^0) = 1.11 \pm 0.33 \pm 0.07$ eV.

$\Gamma(J/\psi(1S) \pi^0) \times \Gamma(e^+ e^-) / \Gamma_{\text{total}}$				$\Gamma_{15} \Gamma_7 / \Gamma$	
VALUE (eV)	CL%	EVTS	DOCUMENT ID	TECN	COMMENT
<8	90	<37	ADAM	06	CLEO $3.773 e^+ e^- \rightarrow \gamma \psi(2S)$

$\Gamma(2(\pi^+ \pi^-) \pi^0) \times \Gamma(e^+ e^-) / \Gamma_{\text{total}}$				$\Gamma_{22} \Gamma_7 / \Gamma$
VALUE (eV)	EVTS	DOCUMENT ID	TECN	COMMENT
29.7 ± 2.2 ± 1.8	410	AUBERT	07AU	BABR $10.6 e^+ e^- \rightarrow 2(\pi^+ \pi^-) \pi^0 \gamma$

$\Gamma(\pi^+ \pi^- \pi^0 \pi^0) \times \Gamma(e^+ e^-) / \Gamma_{\text{total}}$				$\Gamma_{24} \Gamma_7 / \Gamma$
VALUE (eV)	EVTS	DOCUMENT ID	TECN	COMMENT
12.4 ± 1.8 ± 1.2	177	LEES	18E	BABR $10.6 e^+ e^- \rightarrow \pi^+ \pi^- 3\pi^0 \gamma$

$\Gamma(\pi^+ \pi^- 4\pi^0) \times \Gamma(e^+ e^-) / \Gamma_{\text{total}}$				$\Gamma_{26} \Gamma_7 / \Gamma$
VALUE (eV)	EVTS	DOCUMENT ID	TECN	COMMENT
3.3 ± 2.3 ± 0.5	18	LEES	21C	BABR $e^+ e^- \rightarrow \gamma_{ISR}(\pi^+ \pi^- 4\pi^0)$

$\Gamma(\rho^\pm \pi^\mp \pi^0 \pi^0) \times \Gamma(e^+ e^-) / \Gamma_{\text{total}}$				$\Gamma_{25} \Gamma_7 / \Gamma$
VALUE (eV)	CL%	DOCUMENT ID	TECN	COMMENT
<6.2	90	LEES	18E	BABR $10.6 e^+ e^- \rightarrow \pi^+ \pi^- 3\pi^0 \gamma$

$\Gamma(2(\pi^+ \pi^- \pi^0)) \times \Gamma(e^+ e^-) / \Gamma_{\text{total}}$				$\Gamma_{28} \Gamma_7 / \Gamma$
VALUE (eV)	EVTS	DOCUMENT ID	TECN	COMMENT
11.2 ± 3.3 ± 1.3	43	AUBERT	06D	BABR $10.6 e^+ e^- \rightarrow 2(\pi^+ \pi^- \pi^0) \gamma$

$\Gamma(2(\pi^+ \pi^-) 3\pi^0) \times \Gamma(e^+ e^-) / \Gamma_{\text{total}}$				$\Gamma_{30} \Gamma_7 / \Gamma$
VALUE (eV)	EVTS	DOCUMENT ID	TECN	COMMENT
33 ± 5 ± 5	14k	LEES	21	BABR $10.6 e^+ e^- \rightarrow 2(\pi^+ \pi^-) 3\pi^0 \gamma$

$\Gamma(\eta 2(\pi^+ \pi^-)) \times \Gamma(e^+ e^-) / \Gamma_{\text{total}}$				$\Gamma_{33} \Gamma_7 / \Gamma$	
VALUE (eV)	CL%	EVTS	DOCUMENT ID	TECN	COMMENT
2.87 ± 1.41 ± 0.01		16	¹ AUBERT	07AU	BABR $10.6 e^+ e^- \rightarrow 2(\pi^+ \pi^-) \eta \gamma$

• • • We do not use the following data for averages, fits, limits, etc. • • •

<7 90 14k ² LEES 21 BABR 10.6 $e^+ e^- \rightarrow 2(\pi^+ \pi^-) 3\pi^0 \gamma$

¹ AUBERT 07AU reports $[\Gamma(\psi(2S) \rightarrow \eta 2(\pi^+ \pi^-)) \times \Gamma(\psi(2S) \rightarrow e^+ e^-) / \Gamma_{\text{total}}] \times [B(\eta \rightarrow 2\gamma)] = 1.13 \pm 0.55 \pm 0.08$ eV which we divide by our best value $B(\eta \rightarrow 2\gamma) = (39.36 \pm 0.18) \times 10^{-2}$. Our first error is their experiment's error and our second error is the systematic error from using our best value.

² LEES 21 reports $[\Gamma(\psi(2S) \rightarrow \eta 2(\pi^+ \pi^-)) \times \Gamma(\psi(2S) \rightarrow e^+ e^-) / \Gamma_{\text{total}}] \times [B(\eta \rightarrow 3\pi^0)] < 2.3$ eV which we divide by our best value $B(\eta \rightarrow 3\pi^0) = 32.57 \times 10^{-2}$.

$\Gamma(\eta \pi^+ \pi^- \pi^0 \pi^0) \times \Gamma(e^+ e^-) / \Gamma_{\text{total}}$				$\Gamma_{34} \Gamma_7 / \Gamma$
VALUE (eV)	CL%	DOCUMENT ID	TECN	COMMENT
<0.85	90	LEES	18E	BABR $10.6 e^+ e^- \rightarrow \pi^+ \pi^- \pi^0 \pi^0 \gamma$

Meson Particle Listings

 $\psi(2S)$ $\Gamma(\eta\pi^+\pi^-3\pi^0) \times \Gamma(e^+e^-)/\Gamma_{total}$ $\Gamma_{35}\Gamma_7/\Gamma$

VALUE (eV)	CL%	DOCUMENT ID	TECN	COMMENT
<5	90	¹ LEES	21c	BABR $e^+e^- \rightarrow \gamma_{ISR}(\pi^+\pi^-3\pi^0\gamma\gamma)$
¹ LEES 21c reports $[\Gamma(\psi(2S) \rightarrow \eta\pi^+\pi^-3\pi^0) \times \Gamma(\psi(2S) \rightarrow e^+e^-)/\Gamma_{total}] \times [B(\eta \rightarrow 2\gamma)] < 1.9$ eV which we divide by our best value $B(\eta \rightarrow 2\gamma) = 39.36 \times 10^{-2}$.				

 $\Gamma(\eta 2(\pi^+\pi^-\pi^0)) \times \Gamma(e^+e^-)/\Gamma_{total}$ $\Gamma_{36}\Gamma_7/\Gamma$

VALUE (eV)	CL%	EVTS	DOCUMENT ID	TECN	COMMENT
<5	90	14k	¹ LEES	21	BABR $10.6 e^+e^- \rightarrow 2(\pi^+\pi^-)3\pi^0\gamma$
¹ LEES 21 reports $[\Gamma(\psi(2S) \rightarrow \eta 2(\pi^+\pi^-\pi^0)) \times \Gamma(\psi(2S) \rightarrow e^+e^-)/\Gamma_{total}] \times [B(\eta \rightarrow 2\gamma)] < 1.9$ eV which we divide by our best value $B(\eta \rightarrow 2\gamma) = 39.36 \times 10^{-2}$.					

 $\Gamma(\omega\pi^+\pi^-) \times \Gamma(e^+e^-)/\Gamma_{total}$ $\Gamma_{41}\Gamma_7/\Gamma$

VALUE (eV)	EVTS	DOCUMENT ID	TECN	COMMENT
3.01 ± 0.84 ± 0.02	37	¹ AUBERT	07AU	BABR $10.6 e^+e^- \rightarrow \omega\pi^+\pi^-$
¹ AUBERT 07AU reports $[\Gamma(\psi(2S) \rightarrow \omega\pi^+\pi^-) \times \Gamma(\psi(2S) \rightarrow e^+e^-)/\Gamma_{total}] \times [B(\omega(782) \rightarrow \pi^+\pi^-\pi^0)] = 2.69 \pm 0.73 \pm 0.16$ eV which we divide by our best value $B(\omega(782) \rightarrow \pi^+\pi^-\pi^0) = (89.2 \pm 0.7) \times 10^{-2}$. Our first error is their experiment's error and our second error is the systematic error from using our best value.				

 $\Gamma(\omega\pi^+\pi^-2\pi^0) \times \Gamma(e^+e^-)/\Gamma_{total}$ $\Gamma_{42}\Gamma_7/\Gamma$

VALUE (eV)	EVTS	DOCUMENT ID	TECN	COMMENT
20.2 ± 5.6 ± 0.1	14k	¹ LEES	21	BABR $10.6 e^+e^- \rightarrow 2(\pi^+\pi^-)3\pi^0\gamma$
¹ LEES 21 reports $[\Gamma(\psi(2S) \rightarrow \omega\pi^+\pi^-2\pi^0) \times \Gamma(\psi(2S) \rightarrow e^+e^-)/\Gamma_{total}] \times [B(\omega(782) \rightarrow \pi^+\pi^-\pi^0)] = 18 \pm 4 \pm 3$ eV which we divide by our best value $B(\omega(782) \rightarrow \pi^+\pi^-\pi^0) = (89.2 \pm 0.7) \times 10^{-2}$. Our first error is their experiment's error and our second error is the systematic error from using our best value.				

 $\Gamma(\omega\pi^0\pi^0) \times \Gamma(e^+e^-)/\Gamma_{total}$ $\Gamma_{45}\Gamma_7/\Gamma$

VALUE (eV)	EVTS	DOCUMENT ID	TECN	COMMENT
2.5 ± 0.82 ± 0.02	33	¹ LEES	18E	BABR $10.6 e^+e^- \rightarrow \pi^+\pi^-\pi^0\gamma$
¹ LEES 18E reports $[\Gamma(\psi(2S) \rightarrow \omega\pi^0\pi^0) \times \Gamma(\psi(2S) \rightarrow e^+e^-)/\Gamma_{total}] \times [B(\omega(782) \rightarrow \pi^+\pi^-\pi^0)] = 2.3 \pm 0.7 \pm 0.2$ eV which we divide by our best value $B(\omega(782) \rightarrow \pi^+\pi^-\pi^0) = (89.2 \pm 0.7) \times 10^{-2}$. Our first error is their experiment's error and our second error is the systematic error from using our best value.				

 $\Gamma(\omega 3\pi^0) \times \Gamma(e^+e^-)/\Gamma_{total}$ $\Gamma_{46}\Gamma_7/\Gamma$

VALUE (eV)	CL%	DOCUMENT ID	TECN	COMMENT
<1.8	90	¹ LEES	21c	BABR $e^+e^- \rightarrow \gamma_{ISR}(\pi^+\pi^-4\pi^0)$
¹ LEES 21c reports $[\Gamma(\psi(2S) \rightarrow \omega 3\pi^0) \times \Gamma(\psi(2S) \rightarrow e^+e^-)/\Gamma_{total}] \times [B(\omega(782) \rightarrow \pi^+\pi^-\pi^0)] < 1.6$ eV which we divide by our best value $B(\omega(782) \rightarrow \pi^+\pi^-\pi^0) = 89.2 \times 10^{-2}$.				

 $\Gamma(\phi\pi^+\pi^-) \times \Gamma(e^+e^-)/\Gamma_{total}$ $\Gamma_{51}\Gamma_7/\Gamma$

VALUE (eV)	EVTS	DOCUMENT ID	TECN	COMMENT
0.55 ± 0.19 ± 0.01	19	¹ LEES	12F	BABR $10.6 e^+e^- \rightarrow K^+K^-\pi^+\pi^-$
• • • We do not use the following data for averages, fits, limits, etc. • • •				
0.57 ± 0.23 ± 0.01	10	² AUBERT, BE 06D	BABR	$10.6 e^+e^- \rightarrow K^+K^-\pi^+\pi^-$
¹ LEES 12F reports $[\Gamma(\psi(2S) \rightarrow \phi\pi^+\pi^-) \times \Gamma(\psi(2S) \rightarrow e^+e^-)/\Gamma_{total}] \times [B(\phi(1020) \rightarrow K^+K^-)] = 0.27 \pm 0.09 \pm 0.02$ eV which we divide by our best value $B(\phi(1020) \rightarrow K^+K^-) = (49.1 \pm 0.5) \times 10^{-2}$. Our first error is their experiment's error and our second error is the systematic error from using our best value.				
² Superseded by LEES 12F. AUBERT, BE 06D reports $[\Gamma(\psi(2S) \rightarrow \phi\pi^+\pi^-) \times \Gamma(\psi(2S) \rightarrow e^+e^-)/\Gamma_{total}] \times [B(\phi(1020) \rightarrow K^+K^-)] = 0.28 \pm 0.11 \pm 0.02$ eV which we divide by our best value $B(\phi(1020) \rightarrow K^+K^-) = (49.1 \pm 0.5) \times 10^{-2}$. Our first error is their experiment's error and our second error is the systematic error from using our best value.				

 $\Gamma(\phi f_0(980) \rightarrow \pi^+\pi^-) \times \Gamma(e^+e^-)/\Gamma_{total}$ $\Gamma_{52}\Gamma_7/\Gamma$

VALUE (eV)	EVTS	DOCUMENT ID	TECN	COMMENT
0.346 ± 0.129 ± 0.004	12	¹ LEES	12F	BABR $10.6 e^+e^- \rightarrow \pi^+\pi^-K^+K^-$
• • • We do not use the following data for averages, fits, limits, etc. • • •				
0.346 ± 0.168 ± 0.004	6 ± 3	² AUBERT	07AK	BABR $10.6 e^+e^- \rightarrow \pi^+\pi^-K^+K^-$
¹ LEES 12F reports $[\Gamma(\psi(2S) \rightarrow \phi f_0(980) \rightarrow \pi^+\pi^-) \times \Gamma(\psi(2S) \rightarrow e^+e^-)/\Gamma_{total}] \times [B(\phi(1020) \rightarrow K^+K^-)] = 0.17 \pm 0.06 \pm 0.02$ eV which we divide by our best value $B(\phi(1020) \rightarrow K^+K^-) = (49.1 \pm 0.5) \times 10^{-2}$. Our first error is their experiment's error and our second error is the systematic error from using our best value.				
² Superseded by LEES 12F. AUBERT 07AK reports $[\Gamma(\psi(2S) \rightarrow \phi f_0(980) \rightarrow \pi^+\pi^-) \times \Gamma(\psi(2S) \rightarrow e^+e^-)/\Gamma_{total}] \times [B(\phi(1020) \rightarrow K^+K^-)] = 0.17 \pm 0.08 \pm 0.02$ eV which we divide by our best value $B(\phi(1020) \rightarrow K^+K^-) = (49.1 \pm 0.5) \times 10^{-2}$. Our first error is their experiment's error and our second error is the systematic error from using our best value.				

 $\Gamma(K^+K^-) \times \Gamma(e^+e^-)/\Gamma_{total}$ $\Gamma_{59}\Gamma_7/\Gamma$

VALUE (eV)	EVTS	DOCUMENT ID	TECN	COMMENT
• • • We do not use the following data for averages, fits, limits, etc. • • •				
0.147 ± 0.035 ± 0.005	66	¹ LEES	15J	BABR $e^+e^- \rightarrow K^+K^-$
0.197 ± 0.035 ± 0.005	66	² LEES	15J	BABR $e^+e^- \rightarrow K^+K^-$
0.35 ± 0.14 ± 0.03	11	³ LEES	13Q	BABR $e^+e^- \rightarrow K^+K^-$
¹ $\sin\phi > 0$.				

² $\sin\phi < 0$.³Interference with non-resonant K^+K^- production not taken into account. $\Gamma(K^+K^-\pi^+\pi^-) \times \Gamma(e^+e^-)/\Gamma_{total}$ $\Gamma_{60}\Gamma_7/\Gamma$

VALUE (eV)	EVTS	DOCUMENT ID	TECN	COMMENT
1.92 ± 0.30 ± 0.06	133	LEES	12F	BABR $10.6 e^+e^- \rightarrow \pi^+\pi^-K^+K^-$
• • • We do not use the following data for averages, fits, limits, etc. • • •				
2.56 ± 0.42 ± 0.16	85	¹ AUBERT	07AK	BABR $10.6 e^+e^- \rightarrow \pi^+\pi^-K^+K^-$
¹ Superseded by LEES 12F.				

 $\Gamma(K_S^0 K_L^0 \pi^0) \times \Gamma(e^+e^-)/\Gamma_{total}$ $\Gamma_{64}\Gamma_7/\Gamma$

VALUE (eV)	CL%	EVTS	DOCUMENT ID	TECN	COMMENT
<0.7	90	8	LEES	17A	BABR $e^+e^- \rightarrow K_S^0 K_L^0 \pi^0\gamma$

 $\Gamma(K^+K^-\pi^0\pi^0) \times \Gamma(e^+e^-)/\Gamma_{total}$ $\Gamma_{65}\Gamma_7/\Gamma$

VALUE (eV)	EVTS	DOCUMENT ID	TECN	COMMENT
0.60 ± 0.31 ± 0.03	17	LEES	12F	BABR $10.6 e^+e^- \rightarrow \pi^0\pi^0 K^+K^-$

 $\Gamma(K^+K^-\pi^0\pi^0) \times \Gamma(e^+e^-)/\Gamma_{total}$ $\Gamma_{66}\Gamma_7/\Gamma$

VALUE (eV)	DOCUMENT ID	TECN	COMMENT
1.54 ± 0.63 ± 0.15	LEES	23	BABR $e^+e^- \rightarrow \gamma_{ISR}$ hadrons

 $\Gamma(K_S^0 K_L^0 \pi^0 \pi^0) \times \Gamma(e^+e^-)/\Gamma_{total}$ $\Gamma_{67}\Gamma_7/\Gamma$

VALUE (eV)	DOCUMENT ID	TECN	COMMENT
4.0 ± 1.4 ± 0.4	LEES	23	BABR $e^+e^- \rightarrow \gamma_{ISR}$ hadrons

 $\Gamma(K_S^0 K_L^0 \pi^+ \pi^-) \times \Gamma(e^+e^-)/\Gamma_{total}$ $\Gamma_{68}\Gamma_7/\Gamma$

VALUE (eV)	DOCUMENT ID	TECN	COMMENT
5.1 ± 0.7 ± 0.4	LEES	23	BABR $e^+e^- \rightarrow \gamma_{ISR}$ hadrons

 $\Gamma(K^+K^-\pi^+\pi^-) \times \Gamma(e^+e^-)/\Gamma_{total}$ $\Gamma_{69}\Gamma_7/\Gamma$

VALUE (eV)	EVTS	DOCUMENT ID	TECN	COMMENT
4.4 ± 1.3 ± 0.3	32	AUBERT	07AU	BABR $10.6 e^+e^- \rightarrow K^+K^-\pi^+\pi^-$

 $\Gamma(K_S^0 K_L^0 \pi^0 \pi^0) \times \Gamma(e^+e^-)/\Gamma_{total}$ $\Gamma_{76}\Gamma_7/\Gamma$

VALUE (eV)	EVTS	DOCUMENT ID	TECN	COMMENT
2.92 ± 1.27 ± 0.15	14	LEES	17A	BABR $e^+e^- \rightarrow K_S^0 K_L^0 \pi^0 \pi^0\gamma$

 $\Gamma(K_S^0 K^*(892)^0 \pi^0 \pi^0) \times \Gamma(e^+e^-)/\Gamma_{total}$ $\Gamma_{77}\Gamma_7/\Gamma$

VALUE (eV)	DOCUMENT ID	TECN	COMMENT
0.71 ± 0.29 ± 0.07	LEES	23	BABR $e^+e^- \rightarrow \gamma_{ISR}$ hadrons

 $\Gamma(K_S^0 K^*(770)^0 \pi^0) \times \Gamma(e^+e^-)/\Gamma_{total}$ $\Gamma_{78}\Gamma_7/\Gamma$

VALUE (eV)	CL%	DOCUMENT ID	TECN	COMMENT
<1.6	90	LEES	23	BABR $e^+e^- \rightarrow \gamma_{ISR}$ hadrons

 $\Gamma(K_S^0 K^*(770)^0) \times \Gamma(e^+e^-)/\Gamma_{total}$ $\Gamma_{79}\Gamma_7/\Gamma$

VALUE (eV)	CL%	DOCUMENT ID	TECN	COMMENT
<1.6	90	LEES	23	BABR $e^+e^- \rightarrow \gamma_{ISR}$ hadrons

 $\Gamma(K^*(892)^+ K^*(892)^- \pi^0) \times \Gamma(e^+e^-)/\Gamma_{total}$ $\Gamma_{81}\Gamma_7/\Gamma$

VALUE (eV)	DOCUMENT ID	TECN	COMMENT
8.46 ± 4.05 ± 0.90	LEES	23	BABR $e^+e^- \rightarrow \gamma_{ISR}$ hadrons

 $\Gamma(K^*(892)^{\pm} \pi^0 \pi^0) \times \Gamma(e^+e^-)/\Gamma_{total}$ $\Gamma_{80}\Gamma_7/\Gamma$

VALUE (eV)	DOCUMENT ID	TECN	COMMENT
1.62 ± 0.66 ± 0.15	LEES	23	BABR $e^+e^- \rightarrow \gamma_{ISR}$ hadrons

 $\Gamma(K_S^0 K_L^0 \eta) \times \Gamma(e^+e^-)/\Gamma_{total}$ $\Gamma_{82}\Gamma_7/\Gamma$

VALUE (eV)	EVTS	DOCUMENT ID	TECN	COMMENT
3.14 ± 1.08 ± 0.16	16	LEES	17A	BABR $e^+e^- \rightarrow K_S^0 K_L^0 \eta\gamma$

 $\Gamma(K^+K^-\pi^+\pi^-\eta) \times \Gamma(e^+e^-)/\Gamma_{total}$ $\Gamma_{85}\Gamma_7/\Gamma$

VALUE (eV)	EVTS	DOCUMENT ID	TECN	COMMENT
3.05 ± 1.80 ± 0.01	7	¹ AUBERT	07AU	BABR $10.6 e^+e^- \rightarrow K^+K^-\pi^+\pi^-\eta$
¹ AUBERT 07AU reports $[\Gamma(\psi(2S) \rightarrow K^+K^-\pi^+\pi^-\eta) \times \Gamma(\psi(2S) \rightarrow e^+e^-)/\Gamma_{total}] \times [B(\eta \rightarrow 2\gamma)] = 1.2 \pm 0.7 \pm 0.1$ eV which we divide by our best value $B(\eta \rightarrow 2\gamma) = (39.36 \pm 0.18) \times 10^{-2}$. Our first error is their experiment's error and our second error is the systematic error from using our best value.				

 $\Gamma(K^+K^-2(\pi^+\pi^-)) \times \Gamma(e^+e^-)/\Gamma_{total}$ $\Gamma_{86}\Gamma_7/\Gamma$

VALUE (eV)	EVTS	DOCUMENT ID	TECN	COMMENT
4.4 ± 2.1 ± 0.3	26	AUBERT	06D	BABR $10.6 e^+e^- \rightarrow K^+K^-2(\pi^+\pi^-)\gamma$

 $\Gamma(2(K^+K^-)) \times \Gamma(e^+e^-)/\Gamma_{total}$ $\Gamma_{89}\Gamma_7/\Gamma$

VALUE (eV)	EVTS	DOCUMENT ID	TECN	COMMENT
0.22 ± 0.10 ± 0.02	13	LEES	12F	BABR $10.6 e^+e^- \rightarrow K^+K^-K^+K^-$

$\Gamma(\rho\bar{\rho}) \times \Gamma(e^+e^-)/\Gamma_{total}$		$\Gamma_{111}\Gamma_7/\Gamma$		
VALUE (eV)	EVTS	DOCUMENT ID	TECN	COMMENT
0.686 ± 0.024 OUR FIT				Error includes scale factor of 1.2.
0.63 ± 0.05 OUR AVERAGE				Error includes scale factor of 1.2.
0.67 ± 0.12 ± 0.02	43	¹ LEES	130 BABR	$e^+e^- \rightarrow \rho\bar{\rho}\gamma$
0.74 ± 0.07 ± 0.04	142	² LEES	13Y BABR	$e^+e^- \rightarrow \rho\bar{\rho}\gamma$
0.579 ± 0.038 ± 0.036	2.7k	ANDREOTTI	07 E835	$\rho\bar{\rho} \rightarrow e^+e^-, J/\psi X$
• • • We do not use the following data for averages, fits, limits, etc. • • •				
0.70 ± 0.17 ± 0.03	22	³ AUBERT	06B BABR	$e^+e^- \rightarrow \rho\bar{\rho}\gamma$
¹ ISR photon reconstructed in the detector				
² ISR photon undetected				
³ Superseded by LEES 130				

$\Gamma(\Lambda\bar{\Lambda}) \times \Gamma(e^+e^-)/\Gamma_{total}$		$\Gamma_{134}\Gamma_7/\Gamma$		
VALUE (eV)	DOCUMENT ID	TECN	COMMENT	
1.5 ± 0.4 ± 0.1	AUBERT	07BD	BABR	10.6 $e^+e^- \rightarrow \Lambda\bar{\Lambda}\gamma$

$\psi(2S)$ BRANCHING RATIOS

$\Gamma(\text{hadrons})/\Gamma_{total}$		Γ_1/Γ		
VALUE	DOCUMENT ID	TECN	COMMENT	
0.9785 ± 0.0013 OUR AVERAGE				
0.9779 ± 0.0015	¹ BAI	02B	BES2	e^+e^-
0.981 ± 0.003	¹ LUTH	75	MRK1	e^+e^-
¹ Includes cascade decay into $J/\psi(1S)$.				

$\Gamma(\text{virtual } \gamma \rightarrow \text{hadrons})/\Gamma_{total}$		Γ_2/Γ		
VALUE	DOCUMENT ID	TECN	COMMENT	
0.0179 ± 0.0004	¹ LIAO	23	RVUE	e^+e^-
• • • We do not use the following data for averages, fits, limits, etc. • • •				
0.0166 ± 0.0010	^{2,3} SETH	04	RVUE	e^+e^-
0.0199 ± 0.0019	² BAI	02B	BES2	e^+e^-
0.029 ± 0.004	² LUTH	75	MRK1	e^+e^-

¹Using $B(\psi(2S) \rightarrow \ell^+\ell^-) = (0.794 \pm 0.017)\%$ and $R = 2.26 \pm 0.01$ determined by a fit to data from Mark-I, DM2, BESII, KEDR, and BESIII.

²Included in $\Gamma(\text{hadrons})/\Gamma_{total}$.

³Using $B(\psi(2S) \rightarrow \ell^+\ell^-) = (0.73 \pm 0.04)\%$ from RPP-2002 and $R = 2.28 \pm 0.04$ determined by a fit to data from BAI 00 and BAI 02c. Superseded by LIAO 23.

$\Gamma(g\bar{g}g)/\Gamma_{total}$		Γ_3/Γ		
VALUE (units 10^{-2})	EVTS	DOCUMENT ID	TECN	COMMENT
10.58 ± 1.62	2.9 M	¹ LIBBY	09	CLEO $\psi(2S) \rightarrow \text{hadrons}$
¹ Calculated using $\Gamma(\gamma g\bar{g})/\Gamma(g\bar{g}g) = 0.097 \pm 0.026 \pm 0.016$ from LIBBY 09, $B(\psi(2S) \rightarrow X J/\psi)$ relative and absolute branching fractions from MENDEZ 08, $B(\psi(2S) \rightarrow \gamma\eta_C)$ from MITCHELL 09, and $B(\psi(2S) \rightarrow \text{virtual } \gamma \rightarrow \text{hadrons})$, $B(\psi(2S) \rightarrow \gamma\chi_{cJ})$, and $B(\psi(2S) \rightarrow \ell^+\ell^-)$ from PDG 08. The statistical error is negligible and the systematic error is largely uncorrelated with that of $\Gamma(\gamma g\bar{g})/\Gamma_{total}$ LIBBY 09 measurement.				

$\Gamma(\gamma\bar{g}g)/\Gamma_{total}$		Γ_4/Γ		
VALUE (units 10^{-2})	EVTS	DOCUMENT ID	TECN	COMMENT
1.025 ± 0.288	200 k	¹ LIBBY	09	CLEO $\psi(2S) \rightarrow \gamma + \text{hadrons}$
¹ Calculated using $\Gamma(\gamma\bar{g}g)/\Gamma(g\bar{g}g) = 0.097 \pm 0.026 \pm 0.016$ from LIBBY 09. The statistical error is negligible and the systematic error is largely uncorrelated with that of $\Gamma(g\bar{g}g)/\Gamma_{total}$ LIBBY 09 measurement.				

$\Gamma(\gamma\bar{g}g)/\Gamma(g\bar{g}g)$		Γ_4/Γ_3		
VALUE (units 10^{-2})	EVTS	DOCUMENT ID	TECN	COMMENT
9.7 ± 2.6 ± 1.6	2.9 M	LIBBY	09	CLEO $\psi(2S) \rightarrow (\gamma +) \text{hadrons}$

$\Gamma(\text{light hadrons})/\Gamma_{total}$		Γ_5/Γ		
VALUE	DOCUMENT ID	TECN	COMMENT	
0.154 ± 0.015	¹ MENDEZ	08	CLEO	$e^+e^- \rightarrow \psi(2S)$
• • • We do not use the following data for averages, fits, limits, etc. • • •				
0.169 ± 0.026	² ADAM	05A	CLEO	$e^+e^- \rightarrow \psi(2S)$
¹ Uses $B(\psi(2S) \rightarrow J/\psi X)$ from MENDEZ 08 and other branching fractions from PDG 07.				
² Uses $B(J/\psi X)$ from ADAM 05A, $B(\chi_{cJ}\gamma)$, $B(\eta_C\gamma)$ from ATHAR 04 and $B(\ell^+\ell^-)$ from PDG 04. Superseded by MENDEZ 08.				

$\Gamma(e^+e^-)/\Gamma_{total}$		Γ_7/Γ		
VALUE (units 10^{-4})	DOCUMENT ID	TECN	COMMENT	
79.4 ± 2.2 OUR FIT				Error includes scale factor of 1.3.
• • • We do not use the following data for averages, fits, limits, etc. • • •				
88 ± 13	¹ FELDMAN	77	RVUE	e^+e^-
¹ From an overall fit assuming equal partial widths for e^+e^- and $\mu^+\mu^-$. For a measurement of the ratio see the entry $\Gamma(\mu^+\mu^-)/\Gamma(e^+e^-)$ below. Includes LUTH 75, HILGER 75, BURMESTER 77.				

$\Gamma(\mu^+\mu^-)/\Gamma_{total}$		Γ_8/Γ		
VALUE (units 10^{-4})	DOCUMENT ID	TECN	COMMENT	
80 ± 6 OUR FIT				

$\Gamma(\mu^+\mu^-)/\Gamma(e^+e^-)$		Γ_8/Γ_7		
VALUE	DOCUMENT ID	TECN	COMMENT	
1.00 ± 0.08 OUR FIT				
• • • We do not use the following data for averages, fits, limits, etc. • • •				
0.89 ± 0.16	BOYARSKI	75c	MRK1	e^+e^-

$\Gamma(\tau^+\tau^-)/\Gamma_{total}$		Γ_9/Γ		
VALUE (units 10^{-4})	DOCUMENT ID	TECN	COMMENT	
31 ± 4 OUR FIT				
30.8 ± 2.1 ± 3.8	¹ ABLIKIM	06W	BES	$e^+e^- \rightarrow \psi(2S)$
¹ Computed using PDG 02 value of $B(\psi(2S) \rightarrow \text{hadrons}) = 0.9810 \pm 0.0030$ to estimate the total number of $\psi(2S)$ events.				

DECAYS INTO $J/\psi(1S)$ AND ANYTHING

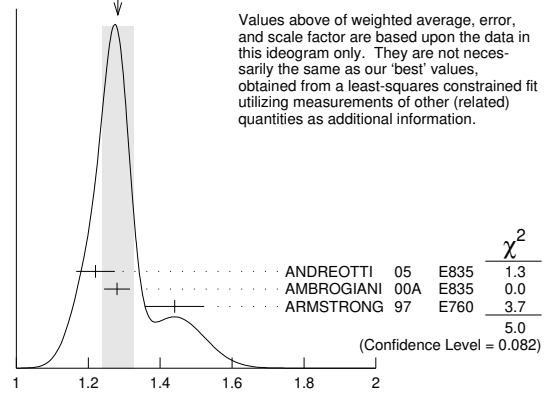
$\Gamma(J/\psi(1S) \text{ anything})/\Gamma_{total}$		$\Gamma_{10}/\Gamma = (\Gamma_{12} + \Gamma_{13} + \Gamma_{14} + 0.343\Gamma_{180} + 0.195\Gamma_{181})/\Gamma$		
VALUE	EVTS	DOCUMENT ID	TECN	COMMENT
0.615 ± 0.007 OUR FIT				Error includes scale factor of 1.3.
0.55 ± 0.07 OUR AVERAGE				
0.51 ± 0.12		BRANDELIK	79c	DASP $e^+e^- \rightarrow \mu^+\mu^-X$
0.57 ± 0.08		ABRAMS	75B	MRK1 $e^+e^- \rightarrow \mu^+\mu^-X$
• • • We do not use the following data for averages, fits, limits, etc. • • •				
0.644 ± 0.006 ± 0.016		¹ ABLIKIM	21z	BES3 $e^+e^- \rightarrow \ell^+\ell^-X$
0.6254 ± 0.0016 ± 0.0155	1.1M	² MENDEZ	08	CLEO $\psi(2S) \rightarrow \ell^+\ell^-X$
0.5950 ± 0.0015 ± 0.0190	151k	ADAM	05A	CLEO Repl. by MENDEZ 08

¹From a fit to the $e^+e^- \rightarrow J/\psi X$ cross section between 3.645 and 3.891 GeV, with $\Gamma(\text{ee})$ and Γ fixed to the PDG 20 values of the cross particle fit which are correlated to "OUR FIT" value for $B(\psi(2S) \rightarrow J/\psi X)$.

²Not independent from other measurements of MENDEZ 08.

$\Gamma(e^+e^-)/\Gamma(J/\psi(1S) \text{ anything})$		Γ_7/Γ_{10}		
VALUE (units 10^{-2})	EVTS	DOCUMENT ID	TECN	COMMENT
1.291 ± 0.035 OUR FIT				Error includes scale factor of 1.3.
1.28 ± 0.04 OUR AVERAGE				Error includes scale factor of 1.6. See the ideogram below.
1.22 ± 0.02 ± 0.05	5097 ± 73	¹ ANDREOTTI	05	E835 $\rho\bar{\rho} \rightarrow \psi(2S) \rightarrow e^+e^-$
1.28 ± 0.03 ± 0.02		¹ AMBROGIANI	00A	E835 $\rho\bar{\rho} \rightarrow \psi(2S)$
1.44 ± 0.08 ± 0.02		¹ ARMSTRONG	97	E760 $\bar{p}p \rightarrow \psi(2S)$
¹ Using $B(J/\psi(1S) \rightarrow e^+e^-) = 0.0593 \pm 0.0010$.				

WEIGHTED AVERAGE
 1.28 ± 0.04 (Error scaled by 1.6)



$\Gamma(\mu^+\mu^-)/\Gamma(J/\psi(1S) \text{ anything})$		Γ_8/Γ_{10}		
VALUE	DOCUMENT ID	TECN	COMMENT	
0.0130 ± 0.0010 OUR FIT				
0.014 ± 0.003	HILGER	75	SPEC	e^+e^-

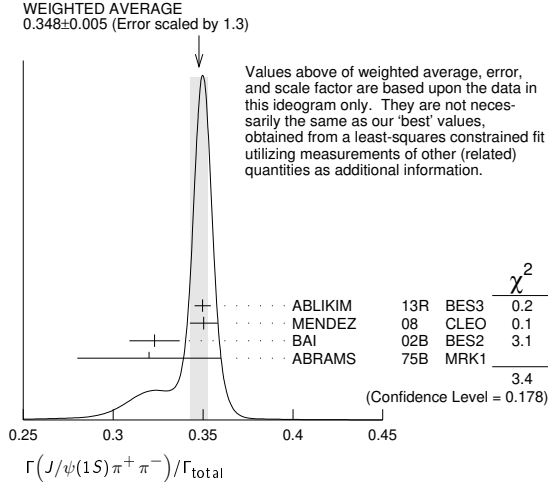
$\Gamma(J/\psi(1S) \text{ neutrals})/\Gamma_{total}$		Γ_{11}/Γ		
VALUE	DOCUMENT ID	TECN	COMMENT	
0.254 ± 0.005 OUR FIT				Error includes scale factor of 1.6.

$\Gamma(J/\psi(1S) \pi^+\pi^-)/\Gamma_{total}$		Γ_{12}/Γ		
VALUE	EVTS	DOCUMENT ID	TECN	COMMENT
0.3469 ± 0.0034 OUR FIT				Error includes scale factor of 1.1.
0.348 ± 0.005 OUR AVERAGE				Error includes scale factor of 1.3. See the ideogram below.
0.3498 ± 0.0002 ± 0.0045	20M	ABLIKIM	13R	BES3 $\psi(2S) \rightarrow J/\psi\pi^+\pi^-$
0.3504 ± 0.0007 ± 0.0077	565k	MENDEZ	08	CLEO $\psi(2S) \rightarrow \ell^+\ell^-\pi^+\pi^-$
0.323 ± 0.014		BAI	02B	BES2 e^+e^-
0.32 ± 0.04		ABRAMS	75B	MRK1 $e^+e^- \rightarrow J/\psi\pi^+\pi^-$

Meson Particle Listings

$\psi(2S)$

• • • We do not use the following data for averages, fits, limits, etc. • • •
 0.3354 ± 0.0014 ± 0.0110 60k ¹ADAM 05A CLEO Repl. by MENDEZ 08
¹ Not independent from other values reported by ADAM 05A.



$\Gamma(e^+e^-)/\Gamma(J/\psi(1S)\pi^+\pi^-)$ Γ_7/Γ_{12}

VALUE	DOCUMENT ID	TECN	COMMENT
0.0229 ± 0.0006 OUR FIT			Error includes scale factor of 1.3.
0.0252 ± 0.0028 ± 0.0011	¹ AUBERT 02B BABR		e^+e^-

¹ Using $B(J/\psi(1S) \rightarrow e^+e^-) = 0.0593 \pm 0.0010$.

$\Gamma(\mu^+\mu^-)/\Gamma(J/\psi(1S)\pi^+\pi^-)$ Γ_8/Γ_{12}

VALUE	DOCUMENT ID	TECN	COMMENT
0.0230 ± 0.0017 OUR FIT			
0.0228 ± 0.0018 OUR AVERAGE			
0.0230 ± 0.0020 ± 0.0012	¹ AAIJ 16V LHCb		$\Lambda_b^0 \rightarrow \psi(2S)X$
0.0216 ± 0.0026 ± 0.0014	² AUBERT 02B BABR		e^+e^-
0.0327 ± 0.0077 ± 0.0072	² GRIBUSHIN 96 FMPS		$515 \pi^- Be \rightarrow 2\mu X$

¹ Using $B(J/\psi(1S) \rightarrow \mu^+\mu^-) = (5.961 \pm 0.033) \times 10^{-2}$.
² Using $B(J/\psi(1S) \rightarrow \mu^+\mu^-) = (5.88 \pm 0.10) \times 10^{-2}$.

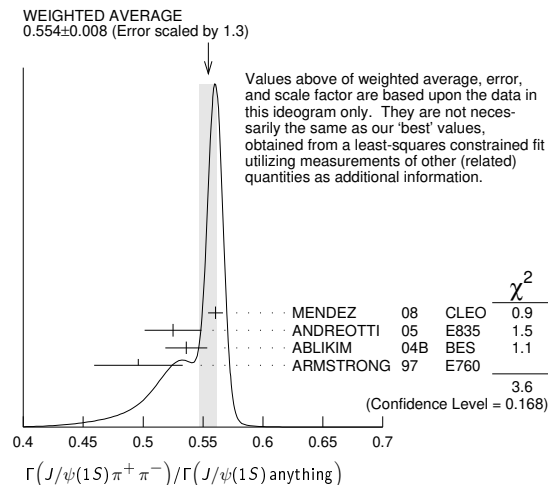
$\Gamma(\tau^+\tau^-)/\Gamma(J/\psi(1S)\pi^+\pi^-)$ Γ_9/Γ_{12}

VALUE (units 10^{-3})	DOCUMENT ID	TECN	COMMENT
8.8 ± 1.1 OUR FIT			
8.73 ± 1.39 ± 1.57	BAI 02 BES		e^+e^-

$\Gamma(J/\psi(1S)\pi^+\pi^-)/\Gamma(J/\psi(1S)\text{anything})$ Γ_{12}/Γ_{10}

VALUE	EVTs	DOCUMENT ID	TECN	COMMENT
0.564 ± 0.004 OUR FIT				Error includes scale factor of 1.7.
0.554 ± 0.008 OUR AVERAGE				Error includes scale factor of 1.3. See the ideogram below.
0.5604 ± 0.0009 ± 0.0062	565k	MENDEZ 08 CLEO		$\psi(2S) \rightarrow \ell^+\ell^-\pi^+\pi^-$
0.525 ± 0.009 ± 0.022	4k	ANDREOTTI 05 E835		$\psi(2S) \rightarrow J/\psi X$
0.536 ± 0.007 ± 0.016	20k	^{1,2} ABLIKIM 04B BES		$\psi(2S) \rightarrow J/\psi X$
0.496 ± 0.037		ARMSTRONG 97 E760		$\bar{p}p \rightarrow \psi(2S)$

• • • We do not use the following data for averages, fits, limits, etc. • • •
 0.5637 ± 0.0027 ± 0.0046 60k ADAM 05A CLEO Repl. by MENDEZ 08
¹ From a fit to the J/ψ recoil mass spectra.
² ABLIKIM 04B quotes $B(\psi(2S) \rightarrow J/\psi X) / B(\psi(2S) \rightarrow J/\psi\pi^+\pi^-)$.



$\Gamma(J/\psi(1S)\text{neutrals})/\Gamma(J/\psi(1S)\pi^+\pi^-)$

$\Gamma_{11}/\Gamma_{12} = (0.9761\Gamma_{13} + 0.719\Gamma_{14} + 0.343\Gamma_{180} + 0.195\Gamma_{181})/\Gamma_{12}$

VALUE	DOCUMENT ID	TECN	COMMENT
0.732 ± 0.013 OUR FIT			Error includes scale factor of 1.7.
0.73 ± 0.09	TANENBAUM 76 MRK1		e^+e^-

$\Gamma(J/\psi(1S)\pi^0\pi^0)/\Gamma(J/\psi(1S)\text{anything})$ Γ_{13}/Γ_{10}

VALUE	EVTs	DOCUMENT ID	TECN	COMMENT
0.297 ± 0.005 OUR FIT				Error includes scale factor of 1.7.
0.320 ± 0.012 OUR AVERAGE				
0.300 ± 0.008 ± 0.022	1655 ± 44	ANDREOTTI 05 E835		$\psi(2S) \rightarrow J/\psi X$
0.328 ± 0.013 ± 0.008		AMBROGIANI 00A E835		$p\bar{p} \rightarrow \psi(2S)$
0.323 ± 0.033		ARMSTRONG 97 E760		$\bar{p}p \rightarrow \psi(2S)$

• • • We do not use the following data for averages, fits, limits, etc. • • •
 0.2829 ± 0.0012 ± 0.0056 61k MENDEZ 08 CLEO $\psi(2S) \rightarrow \ell^+\ell^-2\pi^0$
 0.2776 ± 0.0025 ± 0.0043 13.4k ADAM 05A CLEO Repl. by MENDEZ 08

$\Gamma(J/\psi(1S)\pi^0\pi^0)/\Gamma(J/\psi(1S)\pi^+\pi^-)$ Γ_{13}/Γ_{12}

VALUE	EVTs	DOCUMENT ID	TECN	COMMENT
0.526 ± 0.013 OUR FIT				Error includes scale factor of 1.7.
0.513 ± 0.022 OUR AVERAGE				Error includes scale factor of 2.2.
0.5047 ± 0.0022 ± 0.0102	61k	MENDEZ 08 CLEO		$\psi(2S) \rightarrow \ell^+\ell^-2\pi^0$
0.570 ± 0.009 ± 0.026	14k	¹ ABLIKIM 04B BES		$\psi(2S) \rightarrow J/\psi X$

• • • We do not use the following data for averages, fits, limits, etc. • • •
 0.4924 ± 0.0047 ± 0.0086 73k ^{2,3}ADAM 05A CLEO Repl. by MENDEZ 08
 0.571 ± 0.018 ± 0.044 ⁴ANDREOTTI 05 E835 $\psi(2S) \rightarrow J/\psi X$
 0.53 ± 0.06 TANENBAUM 76 MRK1 e^+e^-
 0.64 ± 0.15 ⁵HILGER 75 SPEC e^+e^-

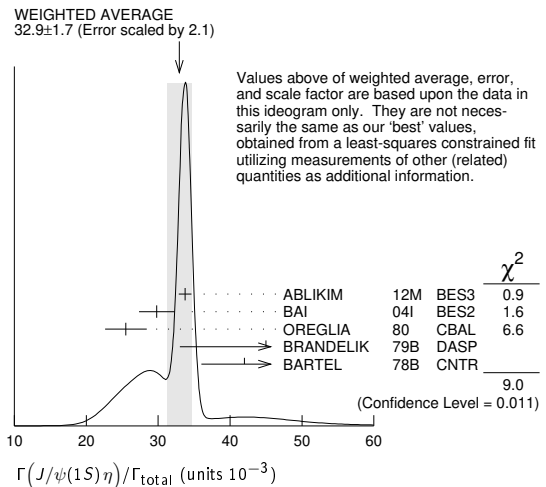
¹ From a fit to the J/ψ recoil mass spectra.
² Not independent from other values reported by ADAM 05A.
³ Using 13,217 $J/\psi\pi^0\pi^0$ and 60,010 $J/\psi\pi^+\pi^-$ events.
⁴ Not independent from other values reported by ANDREOTTI 05.
⁵ Ignoring the $J/\psi(1S)\eta$ and $J/\psi(1S)\gamma\gamma$ decays.

$\Gamma(J/\psi(1S)\eta)/\Gamma_{total}$ Γ_{14}/Γ

VALUE (units 10^{-3})	EVTs	DOCUMENT ID	TECN	COMMENT
33.7 ± 0.6 OUR FIT				Error includes scale factor of 1.2.
32.9 ± 1.7 OUR AVERAGE				Error includes scale factor of 2.1. See the ideogram below.
33.75 ± 0.17 ± 0.86	68.2k	ABLIKIM 12M BES3		$e^+e^- \rightarrow \ell^+\ell^-2\gamma$
29.8 ± 0.9 ± 2.3	5.7k	BAI 04I BES2		$\psi(2S) \rightarrow J/\psi\gamma\gamma$
25.5 ± 2.9	386	¹ OREGLIA 80 CBAL		$e^+e^- \rightarrow J/\psi 2\gamma$
45 ± 12	17	² BRANDELIK 79B DASP		$e^+e^- \rightarrow J/\psi 2\gamma$
42 ± 6	164	² BARTEL 78B CNTR		e^+e^-

• • • We do not use the following data for averages, fits, limits, etc. • • •
 34.3 ± 0.4 ± 0.9 18.4k ³MENDEZ 08 CLEO $\psi(2S) \rightarrow \ell^+\ell^-\eta$
 32.5 ± 0.6 ± 1.1 2.8k ⁴ADAM 05A CLEO Repl. by MENDEZ 08
 43 ± 8 44 TANENBAUM 76 MRK1 e^+e^-

¹ Recalculated by us using $B(J/\psi(1S) \rightarrow \ell^+\ell^-) = 0.1181 \pm 0.0020$.
² Recalculated by us using $B(J/\psi(1S) \rightarrow \mu^+\mu^-) = 0.0588 \pm 0.0010$.
³ Not independent from other measurements of MENDEZ 08.
⁴ Not independent from other values reported by ADAM 05A.



$\Gamma(J/\psi(1S)\eta)/\Gamma(J/\psi(1S)\text{anything})$ Γ_{14}/Γ_{10}

VALUE	EVTs	DOCUMENT ID	TECN	COMMENT
0.0549 ± 0.0009 OUR FIT				Error includes scale factor of 1.2.
0.058 ± 0.007 OUR AVERAGE				Error includes scale factor of 1.4. See the ideogram below.
0.050 ± 0.006 ± 0.003	298 ± 20	ANDREOTTI 05 E835		$\psi(2S) \rightarrow J/\psi X$
0.072 ± 0.009		AMBROGIANI 00A E835		$p\bar{p} \rightarrow \psi(2S)$
0.061 ± 0.015		ARMSTRONG 97 E760		$\bar{p}p \rightarrow \psi(2S)$

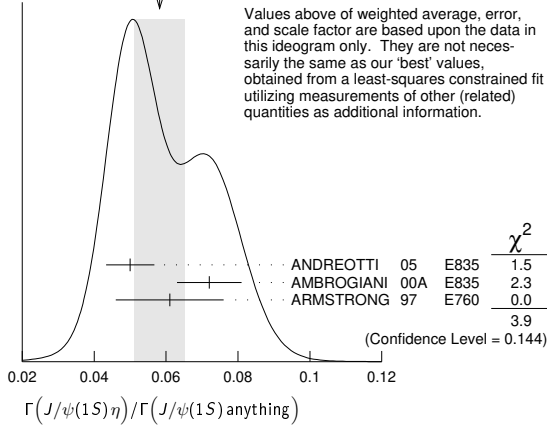
See key on page 1171

Meson Particle Listings

$\psi(2S)$

••• We do not use the following data for averages, fits, limits, etc. •••
 0.0549 ± 0.0006 ± 0.0009 18.4k 1 MENDEZ 08 CLEO $\psi(2S) \rightarrow \ell^+ \ell^- \eta$
 0.0546 ± 0.0010 ± 0.0007 2.8k ADAM 05A CLEO Repl. by MENDEZ 08
 1 Not independent from other measurements of MENDEZ 08.

WEIGHTED AVERAGE
 0.058 ± 0.007 (Error scaled by 1.4)



$\Gamma(J/\psi(1S)\eta)/\Gamma(J/\psi(1S)\pi^+\pi^-)$ Γ_{14}/Γ_{12}
 VALUE EVTS DOCUMENT ID TECN COMMENT
0.0972 ± 0.0016 OUR FIT Error includes scale factor of 1.1.
0.0979 ± 0.0018 OUR AVERAGE
 0.0979 ± 0.0010 ± 0.0015 18.4k MENDEZ 08 CLEO $\psi(2S) \rightarrow \ell^+ \ell^- \eta$
 0.098 ± 0.005 ± 0.010 2k 1 ABLIKIM 04B BES $\psi(2S) \rightarrow J/\psi X$
 0.091 ± 0.021 2 HIMEL 80 MRK2 $e^+e^- \rightarrow \psi(2S)X$
 ••• We do not use the following data for averages, fits, limits, etc. •••
 0.0968 ± 0.0019 ± 0.0013 2.8k 3 ADAM 05A CLEO Repl. by MENDEZ 08
 0.095 ± 0.007 ± 0.007 4 ANDREOTTI 05 E835 $\psi(2S) \rightarrow J/\psi X$
 1 From a fit to the J/ψ recoil mass spectra.
 2 The value for $B(\psi(2S) \rightarrow J/\psi(1S)\eta)$ reported in HIMEL 80 is derived using $B(\psi(2S) \rightarrow J/\psi(1S)\pi^+\pi^-) = (33 \pm 3)\%$ and $B(J/\psi(1S) \rightarrow \ell^+\ell^-) = 0.138 \pm 0.018$. Calculated by us using $B(J/\psi(1S) \rightarrow \ell^+\ell^-) = (0.1181 \pm 0.0020)$.
 3 Not independent from other values reported by ADAM 05A.
 4 Not independent from other values reported by ANDREOTTI 05.

$\Gamma(J/\psi(1S)\pi^0)/\Gamma_{total}$ Γ_{15}/Γ
 VALUE (units 10^{-4}) EVTS DOCUMENT ID TECN COMMENT
12.68 ± 0.32 OUR AVERAGE
 12.6 ± 0.2 ± 0.3 4.1k ABLIKIM 12M BES3 $e^+e^- \rightarrow \ell^+\ell^- 2\gamma$
 13.3 ± 0.8 ± 0.3 530 MENDEZ 08 CLEO $\psi(2S) \rightarrow \ell^+\ell^- 2\gamma$
 14.3 ± 1.4 ± 1.2 280 BAI 04I BES2 $\psi(2S) \rightarrow J/\psi\gamma\gamma$
 14 ± 6 7 HIMEL 80 MRK2 e^+e^-
 9 ± 2 ± 1 23 1 OREGLIA 80 CBAL $\psi(2S) \rightarrow J/\psi 2\gamma$
 ••• We do not use the following data for averages, fits, limits, etc. •••
 13 ± 1 ± 1 88 ADAM 05A CLEO Repl. by MENDEZ 08
 1 Recalculated by us using $B(J/\psi(1S) \rightarrow \ell^+\ell^-) = 0.1181 \pm 0.0020$.

$\Gamma(J/\psi(1S)\pi^0)/\Gamma(J/\psi(1S)anything)$ $\Gamma_{15}/\Gamma_{10} = \Gamma_{15}/(\Gamma_{12} + \Gamma_{13} + \Gamma_{14} + 0.343\Gamma_{180} + 0.195\Gamma_{181})$
 VALUE (units 10^{-2}) EVTS DOCUMENT ID TECN COMMENT
 ••• We do not use the following data for averages, fits, limits, etc. •••
 0.213 ± 0.012 ± 0.003 527 1 MENDEZ 08 CLEO $e^+e^- \rightarrow J/\psi\gamma\gamma$
 0.22 ± 0.02 ± 0.01 2 ADAM 05A CLEO $e^+e^- \rightarrow \psi(2S) \rightarrow J/\psi\gamma\gamma$
 1 Not independent from other values reported by MENDEZ 08. Supersedes ADAM 05A.
 2 Not independent from other values reported by ADAM 05A.

$\Gamma(J/\psi(1S)\pi^0)/\Gamma(J/\psi(1S)\pi^+\pi^-)$ Γ_{15}/Γ_{12}
 VALUE (units 10^{-2}) EVTS DOCUMENT ID TECN COMMENT
 ••• We do not use the following data for averages, fits, limits, etc. •••
 0.380 ± 0.022 ± 0.005 527 1 MENDEZ 08 CLEO $e^+e^- \rightarrow J/\psi\gamma\gamma$
 0.39 ± 0.04 ± 0.01 2 ADAM 05A CLEO $e^+e^- \rightarrow \psi(2S) \rightarrow J/\psi\gamma\gamma$
 1 Not independent from other values reported by MENDEZ 08. Supersedes ADAM 05A.
 2 Not independent from other values reported by ADAM 05A.

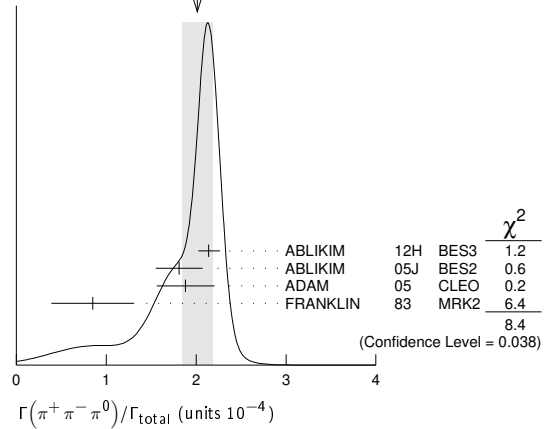
HADRONIC DECAYS

$\Gamma(\pi^+\pi^-)/\Gamma_{total}$ Γ_{16}/Γ
 VALUE (units 10^{-5}) CL% EVTS DOCUMENT ID TECN COMMENT
0.78 ± 0.26 OUR AVERAGE
 0.76 ± 0.25 ± 0.06 30 1 METREVELI 12 $\psi(2S) \rightarrow \pi^+\pi^-$
 8 ± 5 BRANDELIK 79c DASP e^+e^-

••• We do not use the following data for averages, fits, limits, etc. •••
 <2.1 90 DOBBS 06A CLEO $e^+e^- \rightarrow \psi(2S)$
 <5 90 FELDMAN 77 MRK1 e^+e^-
 1 Obtained by analyzing CLEO-c data but not authored by the CLEO Collaboration. Using $\psi(3770) \rightarrow \pi^+\pi^-\pi^0$ for continuum subtraction.

$\Gamma(\pi^+\pi^-\pi^0)/\Gamma_{total}$ Γ_{17}/Γ
 VALUE (units 10^{-4}) EVTS DOCUMENT ID TECN COMMENT
2.01 ± 0.17 OUR AVERAGE Error includes scale factor of 1.7. See the ideogram below.
 2.14 ± 0.03 ± 0.12 7k 1 ABLIKIM 12H BES3 $e^+e^- \rightarrow \psi(2S)$
 1.81 ± 0.18 ± 0.19 260 ± 19 2 ABLIKIM 05J BES2 $e^+e^- \rightarrow \psi(2S)$
 1.88 ± 0.16 ± 0.28 194 ADAM 05 CLEO $e^+e^- \rightarrow \psi(2S)$
 0.85 ± 0.46 4 FRANKLIN 83 MRK2 $e^+e^- \rightarrow$ hadrons
 1 From $\psi(2S) \rightarrow \pi^+\pi^-\pi^0$ events directly. The quoted systematic error includes a contribution of 4% (added in quadrature) from the uncertainty on the number of $\psi(2S)$ events.
 2 From a PW analysis of $\psi(2S) \rightarrow \pi^+\pi^-\pi^0$.

WEIGHTED AVERAGE
 2.01 ± 0.17 (Error scaled by 1.7)



$\Gamma(\rho(770)\pi \rightarrow \pi^+\pi^-\pi^0)/\Gamma_{total}$ Γ_{18}/Γ
 VALUE (units 10^{-4}) CL% EVTS DOCUMENT ID TECN COMMENT
0.32 ± 0.12 OUR AVERAGE Error includes scale factor of 1.8.
 0.51 ± 0.07 ± 0.11 1 ABLIKIM 05J BES2 $\psi(2S) \rightarrow \rho(770)\pi \rightarrow \pi^+\pi^-\pi^0$
 0.24 ± 0.08 ± 0.02 22 ADAM 05 CLEO $e^+e^- \rightarrow \psi(2S)$
 ••• We do not use the following data for averages, fits, limits, etc. •••
 <0.83 90 1 FRANKLIN 83 MRK2 e^+e^-
 <10 90 BARTEL 76 CNTR e^+e^-
 <10 90 2 ABRAMS 75 MRK1 e^+e^-
 1 From a PW analysis of $\psi(2S) \rightarrow \pi^+\pi^-\pi^0$.
 2 Final state $\rho^0\pi^0$.

$\Gamma(\rho(2150)\pi \rightarrow \pi^+\pi^-\pi^0)/\Gamma_{total}$ Γ_{19}/Γ
 VALUE (units 10^{-4}) DOCUMENT ID TECN COMMENT
1.94 ± 0.25 ± 0.15 ± 0.34 1 ABLIKIM 05J BES2 $\psi(2S) \rightarrow \rho(2150)\pi \rightarrow \pi^+\pi^-\pi^0$
 1 From a PW analysis of $\psi(2S) \rightarrow \pi^+\pi^-\pi^0$.

$\Gamma(2(\pi^+\pi^-))/\Gamma_{total}$ Γ_{20}/Γ
 VALUE (units 10^{-4}) EVTS DOCUMENT ID TECN COMMENT
2.4 ± 0.6 OUR AVERAGE Error includes scale factor of 2.2.
 2.2 ± 0.2 ± 0.2 308 BRIERE 05 CLEO $e^+e^- \rightarrow \psi(2S) \rightarrow 2(\pi^+\pi^-)$
 4.5 ± 1.0 TANENBAUM 78 MRK1 e^+e^-

$\Gamma(\rho^0\pi^+\pi^-)/\Gamma_{total}$ Γ_{21}/Γ
 VALUE (units 10^{-4}) EVTS DOCUMENT ID TECN COMMENT
2.2 ± 0.6 OUR AVERAGE Error includes scale factor of 1.4.
 2.0 ± 0.2 ± 0.4 285.5 BRIERE 05 CLEO $e^+e^- \rightarrow \psi(2S) \rightarrow 2(\pi^+\pi^-)$
 4.2 ± 1.5 TANENBAUM 78 MRK1 e^+e^-

$\Gamma(2(\pi^+\pi^-)\pi^0)/\Gamma_{total}$ Γ_{22}/Γ
 VALUE (units 10^{-4}) EVTS DOCUMENT ID TECN COMMENT
29 ± 10 OUR AVERAGE Error includes scale factor of 4.7. See the ideogram below.
 24.9 ± 0.7 ± 3.6 2173 ABLIKIM 07D BES2 $e^+e^- \rightarrow \psi(2S)$
 127 ± 12 ± 2 410 1 AUBERT 07AU BABR 10.6 $e^+e^- \rightarrow 2(\pi^+\pi^-)\pi^0\gamma$
 26.1 ± 0.7 ± 3.0 1703 BRIERE 05 CLEO $e^+e^- \rightarrow \psi(2S) \rightarrow 2(\pi^+\pi^-)\pi^0$

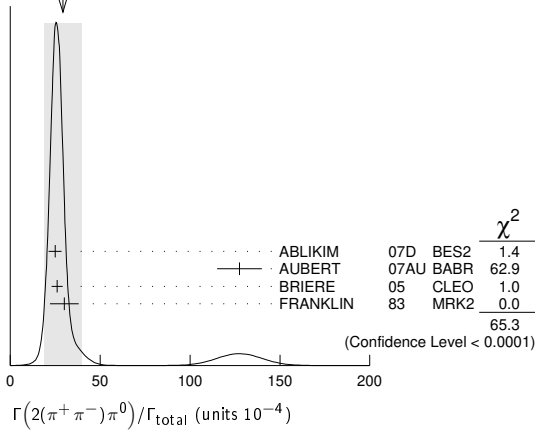
Meson Particle Listings

$\psi(2S)$

30 ± 8 42 FRANKLIN 83 MRK2 e^+e^-

¹AUBERT 07AU reports $[\Gamma(\psi(2S) \rightarrow 2(\pi^+\pi^-\pi^0))/\Gamma_{total}] \times [\Gamma(\psi(2S) \rightarrow e^+e^-)] = (297 \pm 22 \pm 18) \times 10^{-4}$ keV which we divide by our best value $\Gamma(\psi(2S) \rightarrow e^+e^-) = 2.33 \pm 0.04$ keV. Our first error is their experiment's error and our second error is the systematic error from using our best value.

WEIGHTED AVERAGE
29±10 (Error scaled by 4.7)



$\Gamma(\rho_{22}(1320))/\Gamma_{total}$ Γ_{23}/Γ

VALUE (units 10^{-4})	CL%	EVTS	DOCUMENT ID	TECN	COMMENT
2.55 ± 0.73 ± 0.47		112 ± 31	BAI	04c BES2	$\psi(2S) \rightarrow 2(\pi^+\pi^-\pi^0)$
••• We do not use the following data for averages, fits, limits, etc. •••					
<2.3	90		BAI	98J BES	e^+e^-

$\Gamma(3(\pi^+\pi^-))/\Gamma_{total}$ Γ_{27}/Γ

VALUE (units 10^{-4})	EVTS	DOCUMENT ID	TECN	COMMENT
3.5 ± 2.0 OUR AVERAGE		Error includes scale factor of 2.8.		
5.45 ± 0.42 ± 0.87	671	ABLIKIM 05H	BES2	$e^+e^- \rightarrow \psi(2S) \rightarrow 3(\pi^+\pi^-)$
1.5 ± 1.0		¹ TANENBAUM 78	MRK1	e^+e^-
¹ Assuming entirely strong decay.				

$\Gamma(3(\pi^+\pi^-\pi^0))/\Gamma_{total}$ Γ_{29}/Γ

VALUE (units 10^{-4})	EVTS	DOCUMENT ID	TECN	COMMENT
35 ± 16	6	FRANKLIN 83	MRK2	$e^+e^- \rightarrow$ hadrons

$\Gamma(\eta\pi^+\pi^-)/\Gamma_{total}$ Γ_{31}/Γ

VALUE (units 10^{-4})	CL%	DOCUMENT ID	TECN	COMMENT
<1.6	90	BRIERE 05	CLEO	$e^+e^- \rightarrow \psi(2S) \rightarrow 2(\pi^+\pi^-\pi^0)$

$\Gamma(\eta\pi^+\pi^-\pi^0)/\Gamma_{total}$ Γ_{32}/Γ

VALUE (units 10^{-4})	EVTS	DOCUMENT ID	TECN	COMMENT
9.5 ± 0.7 ± 1.5		¹ BRIERE 05	CLEO	$e^+e^- \rightarrow \psi(2S) \rightarrow$ hadr
••• We do not use the following data for averages, fits, limits, etc. •••				
10.3 ± 0.8 ± 1.4	201.7	² BRIERE 05	CLEO	$e^+e^- \rightarrow \psi(2S) \rightarrow \eta 3\pi(\eta \rightarrow \gamma\gamma)$
8.1 ± 1.4 ± 1.6	50.0	² BRIERE 05	CLEO	$e^+e^- \rightarrow \psi(2S) \rightarrow \eta 3\pi(\eta \rightarrow 3\pi)$
¹ Average of $\eta \rightarrow \gamma\gamma$ and $\eta \rightarrow 3\pi$.				
² Not independent from other values reported by BRIERE 05.				

$\Gamma(\rho\eta)/\Gamma_{total}$ Γ_{37}/Γ

VALUE (units 10^{-5})	EVTS	DOCUMENT ID	TECN	COMMENT
2.2 ± 0.6 OUR AVERAGE		Error includes scale factor of 1.1.		
3.0 $^{+1.1}_{-0.9}$ ± 0.2	18	ADAM 05	CLEO	$e^+e^- \rightarrow \psi(2S)$
1.78 $^{+0.67}_{-0.62}$ ± 0.17	13	ABLIKIM 04L	BES	$e^+e^- \rightarrow \psi(2S)$

$\Gamma(\eta'\pi^+\pi^-\pi^0)/\Gamma_{total}$ Γ_{38}/Γ

VALUE (units 10^{-4})	EVTS	DOCUMENT ID	TECN	COMMENT
4.5 ± 1.6 ± 1.3	12.8	BRIERE 05	CLEO	$e^+e^- \rightarrow \psi(2S) \rightarrow$ hadr

$\Gamma(\eta'\rho)/\Gamma_{total}$ Γ_{39}/Γ

VALUE (units 10^{-5})	EVTS	DOCUMENT ID	TECN	COMMENT
1.87 $^{+1.64}_{-1.11}$ ± 0.33	2	ABLIKIM 04L	BES	$e^+e^- \rightarrow \psi(2S)$

••• We do not use the following data for averages, fits, limits, etc. •••

1.02 ± 0.11 ± 0.24	143	¹ ABLIKIM 17AK	BES3	$e^+e^- \rightarrow \psi(2S)$
0.569 ± 0.128 ± 0.236	80	² ABLIKIM 17AK	BES3	$e^+e^- \rightarrow \psi(2S)$

¹ Destructive-interference solution of a partial wave analysis of the decay $\psi(2S) \rightarrow \pi^+\pi^-\eta'$.

² Constructive-interference solution of a partial wave analysis of the decay $\psi(2S) \rightarrow \pi^+\pi^-\eta'$.

$\Gamma(\omega\pi^0)/\Gamma_{total}$ Γ_{40}/Γ

VALUE (units 10^{-5})	EVTS	DOCUMENT ID	TECN	COMMENT
2.1 ± 0.6 OUR AVERAGE				
2.5 $^{+1.2}_{-1.0}$ ± 0.2	14	ADAM 05	CLEO	$e^+e^- \rightarrow \psi(2S)$
1.87 $^{+0.68}_{-0.62}$ ± 0.28	14	ABLIKIM 04L	BES	$e^+e^- \rightarrow \psi(2S)$

$\Gamma(\omega\pi^+\pi^-)/\Gamma_{total}$ Γ_{41}/Γ

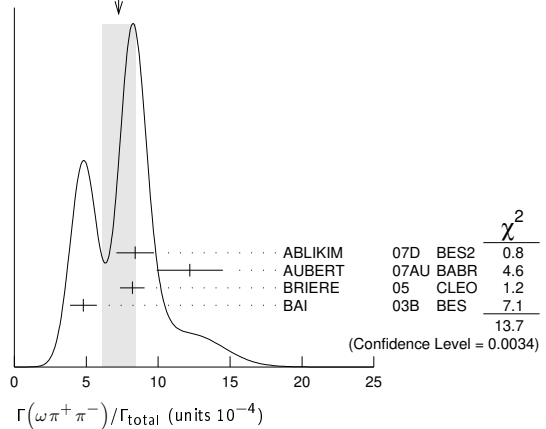
VALUE (units 10^{-4})	EVTS	DOCUMENT ID	TECN	COMMENT
7.3 ± 1.2 OUR AVERAGE		Error includes scale factor of 2.1. See the ideogram below.		
8.4 ± 0.5 ± 1.2	386	ABLIKIM 07D	BES2	$e^+e^- \rightarrow \psi(2S)$
12.2 ± 2.2 ± 0.7	37	¹ AUBERT 07AU	BABR	10.6 $e^+e^- \rightarrow \omega\pi^+\pi^-\gamma$
8.2 ± 0.5 ± 0.7	391	BRIERE 05	CLEO	$e^+e^- \rightarrow \psi(2S) \rightarrow 2(\pi^+\pi^-\pi^0)$

4.8 ± 0.6 ± 0.7 100 ± 22 ²BAI 03B BES $\psi(2S) \rightarrow 2(\pi^+\pi^-\pi^0)$

¹ AUBERT 07AU quotes $\Gamma_{ee}^{\psi(2S)} \cdot B(\psi(2S) \rightarrow \omega\pi^+\pi^-) \cdot B(\omega \rightarrow 3\pi) = 2.69 \pm 0.73 \pm 0.16$ eV.

² Normalized to $B(\psi(2S) \rightarrow J/\psi\pi^+\pi^-) = 0.305 \pm 0.016$.

WEIGHTED AVERAGE
7.3±1.2 (Error scaled by 2.1)



$\Gamma(b_1^\pm\pi^\mp)/\Gamma_{total}$ Γ_{43}/Γ

VALUE (units 10^{-4})	EVTS	DOCUMENT ID	TECN	COMMENT
4.0 ± 0.6 OUR AVERAGE		Error includes scale factor of 1.1.		
5.1 ± 0.6 ± 0.8	202	ABLIKIM 07D	BES2	$e^+e^- \rightarrow \psi(2S)$
4.18 $^{+0.43}_{-0.42}$ ± 0.92	170	ADAM 05	CLEO	$e^+e^- \rightarrow \psi(2S)$
3.2 ± 0.6 ± 0.5	61 ± 11	^{1,2} BAI 03B	BES	$\psi(2S) \rightarrow 2(\pi^+\pi^-\pi^0)$

••• We do not use the following data for averages, fits, limits, etc. •••

¹ Assuming $B(b_1 \rightarrow \omega\pi) = 1$.

² Normalized to $B(\psi(2S) \rightarrow J/\psi\pi^+\pi^-) = 0.305 \pm 0.016$.

$\Gamma(\omega f_2(1270))/\Gamma_{total}$ Γ_{44}/Γ

VALUE (units 10^{-4})	CL%	EVTS	DOCUMENT ID	TECN	COMMENT
2.2 ± 0.4 OUR AVERAGE					
2.3 ± 0.5 ± 0.4		57	ABLIKIM 07D	BES2	$e^+e^- \rightarrow \psi(2S)$
2.05 ± 0.41 ± 0.38		62 ± 12	BAI 04c	BES2	$\psi(2S) \rightarrow 2(\pi^+\pi^-\pi^0)$
••• We do not use the following data for averages, fits, limits, etc. •••					
<1.5	90		¹ BAI 03B	BES	$\psi(2S) \rightarrow 2(\pi^+\pi^-\pi^0)$
<1.7	90		BAI 98J	BES	Repl. by BAI 03B
¹ Normalized to $B(\psi(2S) \rightarrow J/\psi\pi^+\pi^-) = 0.305 \pm 0.016$.					

$\Gamma(b_1^0\pi^0)/\Gamma_{total}$ Γ_{47}/Γ

VALUE (units 10^{-4})	EVTS	DOCUMENT ID	TECN	COMMENT
2.35 $^{+0.47}_{-0.42}$ ± 0.40	45	ADAM 05	CLEO	$e^+e^- \rightarrow \psi(2S)$

$\Gamma(\omega\eta)/\Gamma_{total}$ Γ_{48}/Γ

VALUE (units 10^{-5})	CL%	DOCUMENT ID	TECN	COMMENT
<1.1	90	ADAM 05	CLEO	$e^+e^- \rightarrow \psi(2S)$
••• We do not use the following data for averages, fits, limits, etc. •••				
<3.1	90	ABLIKIM 04K	BES	$e^+e^- \rightarrow \psi(2S)$

$\Gamma(\omega\eta')/\Gamma_{total}$	VALUE (units 10^{-5})	EVTS	DOCUMENT ID	TECN	COMMENT	Γ_{49}/Γ
$3.2 \pm 2.4 \pm 0.7$		4	¹ ABLIKIM	04k	BES $e^+e^- \rightarrow \psi(2S)$	

¹ Calculated combining $\eta' \rightarrow \gamma\rho$ and $\eta\pi^+\pi^-$ channels.

$\Gamma(\phi\pi^0)/\Gamma_{total}$	VALUE (units 10^{-5})	CL%	DOCUMENT ID	TECN	COMMENT	Γ_{50}/Γ
<0.04		90	ABLIKIM	12L	BES3 $e^+e^- \rightarrow \psi(2S)$	
•••	We do not use the following data for averages, fits, limits, etc. •••					
<0.7		90	ADAM	05	CLEO $e^+e^- \rightarrow \psi(2S)$	
<0.4		90	ABLIKIM	04k	BES $e^+e^- \rightarrow \psi(2S)$	

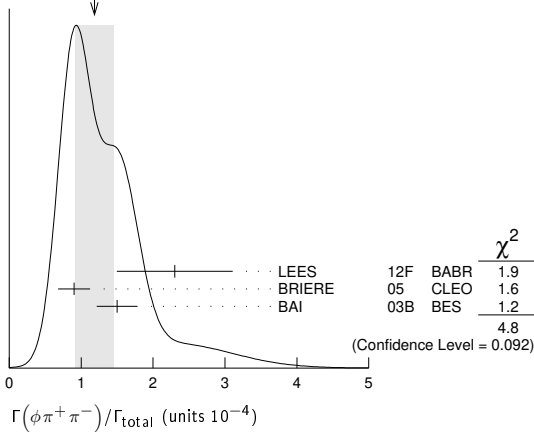
$\Gamma(\phi\pi^+\pi^-)/\Gamma_{total}$	VALUE (units 10^{-4})	EVTS	DOCUMENT ID	TECN	COMMENT	Γ_{51}/Γ
1.18 ± 0.26 OUR AVERAGE		Error	includes scale factor of 1.5. See the ideogram below.			
$2.3 \pm 0.8 \pm 0.1$		19 ± 6	LEES	12F	BABR $10.6 e^+e^- \rightarrow \pi^+\pi^-K^+K^-\gamma$	
$0.9 \pm 0.2 \pm 0.1$		47.6	BRIERE	05	CLEO $e^+e^- \rightarrow \psi(2S) \rightarrow K^+K^-\pi^+\pi^-$	
$1.5 \pm 0.2 \pm 0.2$		51.5 ± 8.3	¹ BAI	03B	BES $\psi(2S) \rightarrow K^+K^-\pi^+\pi^-$	
•••	We do not use the following data for averages, fits, limits, etc. •••					
$2.45 \pm 0.96 \pm 0.04$		10 ± 4	^{2,3} AUBERT	07Ak	BABR $10.6 e^+e^- \rightarrow \pi^+\pi^-K^+K^-\gamma$	

¹ Normalized to $B(\psi(2S) \rightarrow J/\psi\pi^+\pi^-) = 0.305 \pm 0.016$.

² Superseded by LEES 12F. AUBERT 07Ak reports $[\Gamma(\psi(2S) \rightarrow \phi\pi^+\pi^-)/\Gamma_{total}] \times [\Gamma(\psi(2S) \rightarrow e^+e^-)] = (0.57 \pm 0.22 \pm 0.04) \times 10^{-3}$ keV which we divide by our best value $\Gamma(\psi(2S) \rightarrow e^+e^-) = 2.33 \pm 0.04$ keV. Our first error is their experiment's error and our second error is the systematic error from using our best value.

³ Using $B(\phi \rightarrow K^+K^-) = (49.3 \pm 0.6)\%$.

WEIGHTED AVERAGE
 1.18 ± 0.26 (Error scaled by 1.5)



$\Gamma(\phi f_0(980) \rightarrow \pi^+\pi^-)/\Gamma_{total}$	VALUE (units 10^{-4})	EVTS	DOCUMENT ID	TECN	COMMENT	Γ_{52}/Γ
0.75 ± 0.33 OUR AVERAGE		Error	includes scale factor of 1.6.			
$1.5 \pm 0.5 \pm 0.1$		12 ± 4	LEES	12F	BABR $10.6 e^+e^- \rightarrow \pi^+\pi^-K^+K^-\gamma$	
$0.6 \pm 0.2 \pm 0.1$		18.4 ± 6.4	¹ BAI	03B	BES $\psi(2S) \rightarrow K^+K^-\pi^+\pi^-$	
•••	We do not use the following data for averages, fits, limits, etc. •••					
$1.46 \pm 0.71 \pm 0.02$		6 ± 3	^{2,3} AUBERT	07Ak	BABR $10.6 e^+e^- \rightarrow \pi^+\pi^-K^+K^-\gamma$	

¹ Normalized to $B(\psi(2S) \rightarrow J/\psi\pi^+\pi^-) = 0.305 \pm 0.016$.

² Superseded by LEES 12F. AUBERT 07Ak reports $[\Gamma(\psi(2S) \rightarrow \phi f_0(980) \rightarrow \pi^+\pi^-)/\Gamma_{total}] \times [\Gamma(\psi(2S) \rightarrow e^+e^-)] = (0.34 \pm 0.16 \pm 0.04) \times 10^{-3}$ keV which we divide by our best value $\Gamma(\psi(2S) \rightarrow e^+e^-) = 2.33 \pm 0.04$ keV. Our first error is their experiment's error and our second error is the systematic error from using our best value.

³ Using $B(\phi \rightarrow K^+K^-) = (49.3 \pm 0.6)\%$.

$\Gamma(\phi\eta)/\Gamma_{total}$	VALUE (units 10^{-5})	EVTS	DOCUMENT ID	TECN	COMMENT	Γ_{53}/Γ
3.10 ± 0.31 OUR AVERAGE						
$3.14 \pm 0.23 \pm 0.23$		0.2k	ABLIKIM	12L	BES3 $e^+e^- \rightarrow \psi(2S)$	
$2.0 \pm 1.5 \pm 0.4$		6	ADAM	05	CLEO $e^+e^- \rightarrow \psi(2S)$	
$3.3 \pm 1.1 \pm 0.5$		17	ABLIKIM	04k	BES $e^+e^- \rightarrow \psi(2S)$	

$\Gamma(\eta\phi(2170), \phi(2170) \rightarrow \phi f_0(980), f_0 \rightarrow \pi^+\pi^-)/\Gamma_{total}$	VALUE	CL%	DOCUMENT ID	TECN	COMMENT	Γ_{54}/Γ
<2.2 × 10⁻⁶		90	ABLIKIM	19l	BES3 $e^+e^- \rightarrow \eta\phi f_0(980)$	

$\Gamma(\phi\eta')/\Gamma_{total}$	VALUE (units 10^{-5})	EVTS	DOCUMENT ID	TECN	COMMENT	Γ_{55}/Γ
1.54 ± 0.20 OUR AVERAGE						
$1.51 \pm 0.16 \pm 0.12$		201	ABLIKIM	19BA	BES3 $e^+e^- \rightarrow \psi(2S)$	
$3.1 \pm 1.4 \pm 0.7$		8	¹ ABLIKIM	04k	BES $e^+e^- \rightarrow \psi(2S)$	

¹ Calculated combining $\eta' \rightarrow \gamma\rho$ and $\eta\pi^+\pi^-$ channels.

$\Gamma(\phi f_1(1285))/\Gamma_{total}$	VALUE (units 10^{-5})	EVTS	DOCUMENT ID	TECN	COMMENT	Γ_{56}/Γ
$3.0 \pm 0.4 \pm 1.3$		234	¹ ABLIKIM	19BA	BES3 $e^+e^- \rightarrow \psi(2S)$	

¹ ABLIKIM 19BA reports $[\Gamma(\psi(2S) \rightarrow \phi f_1(1285))/\Gamma_{total}] \times [B(f_1(1285) \rightarrow \eta\pi^+\pi^-)] = (1.03 \pm 0.10 \pm 0.09) \times 10^{-5}$ which we divide by our best value $B(f_1(1285) \rightarrow \eta\pi^+\pi^-) = (35 \pm 15) \times 10^{-2}$. Our first error is their experiment's error and our second error is the systematic error from using our best value.

$\Gamma(\phi\eta(1405) \rightarrow \phi\pi^+\pi^-)/\Gamma_{total}$	VALUE (units 10^{-6})	EVTS	DOCUMENT ID	TECN	COMMENT	Γ_{57}/Γ
$8.46 \pm 1.37 \pm 0.92$		195	ABLIKIM	19BA	BES3 $e^+e^- \rightarrow \psi(2S)$	

$\Gamma(\phi f_2'(1525))/\Gamma_{total}$	VALUE (units 10^{-4})	CL%	EVTS	DOCUMENT ID	TECN	COMMENT	Γ_{58}/Γ
$0.44 \pm 0.12 \pm 0.11$			20 ± 6	BAI	04c	$\psi(2S) \rightarrow 2(K^+K^-)$	
•••	We do not use the following data for averages, fits, limits, etc. •••						
<0.45		90		BAI	98J	BES $e^+e^- \rightarrow 2(K^+K^-)$	

$\Gamma(K^+K^-)/\Gamma_{total}$	VALUE (units 10^{-5})	CL%	EVTS	DOCUMENT ID	TECN	COMMENT	Γ_{59}/Γ
$7.48 \pm 0.23 \pm 0.39$			1.3k	¹ METREVELI	12	$\psi(2S) \rightarrow K^+K^-$	
•••	We do not use the following data for averages, fits, limits, etc. •••						
$6.2 \pm 1.5 \pm 0.2$		66	^{2,3}	LEES	15J	BABR $e^+e^- \rightarrow K^+K^-\gamma$	
$8.3 \pm 1.5 \pm 0.2$		66	^{3,4}	LEES	15J	BABR $e^+e^- \rightarrow K^+K^-\gamma$	
$6.3 \pm 0.6 \pm 0.3$				⁵ DOBBS	06A	CLEO e^+e^-	
10 ± 7				⁵ BRANDELIK	79c	DASP e^+e^-	
< 5		90		FELDMAN	77	MRK1 e^+e^-	

¹ Obtained by analyzing CLEO-c data but not authored by the CLEO Collaboration.

² $\sin\phi > 0$.

³ Using $\Gamma(\psi(2S) \rightarrow e^+e^-) = (2.37 \pm 0.04)$ keV.

⁴ $\sin\phi < 0$.

⁵ Interference with non-resonant K^+K^- production not taken into account.

$\Gamma(K^+K^-\pi^+\pi^-)/\Gamma_{total}$	VALUE (units 10^{-4})	EVTS	DOCUMENT ID	TECN	COMMENT	Γ_{60}/Γ
7.3 ± 0.5 OUR AVERAGE						
$8.1 \pm 1.3 \pm 0.3$		133	LEES	12F	BABR $10.6 e^+e^- \rightarrow \pi^+\pi^-K^+K^-\gamma$	
$7.1 \pm 0.3 \pm 0.4$		817.2	BRIERE	05	CLEO $e^+e^- \rightarrow \psi(2S) \rightarrow K^+K^-\pi^+\pi^-$	
16 ± 4			¹ TANENBAUM	78	MRK1 e^+e^-	
•••	We do not use the following data for averages, fits, limits, etc. •••					
$11.0 \pm 1.9 \pm 0.2$		85	² AUBERT	07Ak	BABR $10.6 e^+e^- \rightarrow \pi^+\pi^-K^+K^-\gamma$	

¹ Assuming entirely strong decay.

² Superseded by LEES 12F. AUBERT 07Ak reports $[\Gamma(\psi(2S) \rightarrow K^+K^-\pi^+\pi^-)/\Gamma_{total}] \times [\Gamma(\psi(2S) \rightarrow e^+e^-)] = (2.56 \pm 0.42 \pm 0.16) \times 10^{-3}$ keV which we divide by our best value $\Gamma(\psi(2S) \rightarrow e^+e^-) = 2.33 \pm 0.04$ keV. Our first error is their experiment's error and our second error is the systematic error from using our best value.

$\Gamma(K^+K^-\pi^0)/\Gamma_{total}$	VALUE (units 10^{-5})	CL%	EVTS	DOCUMENT ID	TECN	COMMENT	Γ_{61}/Γ
$4.07 \pm 0.16 \pm 0.26$			0.9k	ABLIKIM	12L	BES3 $e^+e^- \rightarrow \psi(2S)$	
•••	We do not use the following data for averages, fits, limits, etc. •••						
<8.9		90	1	FRANKLIN	83	MRK2 $e^+e^- \rightarrow$ hadrons	

$\Gamma(K_S^0 K_S^0)/\Gamma_{total}$	VALUE (units 10^{-4})	DOCUMENT ID	TECN	COMMENT	Γ_{62}/Γ
<0.046		¹ BAI	04D	BES e^+e^-	

¹ Forbidden by CP.

$\Gamma(K_S^0 K_L^0)/\Gamma_{total}$	VALUE (units 10^{-5})	EVTS	DOCUMENT ID	TECN	COMMENT	Γ_{63}/Γ
5.34 ± 0.33 OUR AVERAGE						
$5.28 \pm 0.25 \pm 0.34$		478 ± 23	¹ METREVELI	12	$\psi(2S) \rightarrow K_S^0 K_L^0$	
$5.8 \pm 0.8 \pm 0.4$			DOBBS	06A	CLEO e^+e^-	
$5.24 \pm 0.47 \pm 0.48$		156 ± 14	² BAI	04B	BES2 $\psi(2S) \rightarrow K_S^0 K_L^0 \rightarrow \pi^+\pi^-X$	

¹ Obtained by analyzing CLEO-c data but not authored by the CLEO Collaboration.

² Using $B(K_S^0 \rightarrow \pi^+\pi^-) = 0.6860 \pm 0.0027$.

Meson Particle Listings

 $\psi(2S)$ $\Gamma(K^+ K^- \pi^+ \pi^- \pi^0)/\Gamma_{total}$ Γ_{69}/Γ

VALUE (units 10^{-4})	EVTS	DOCUMENT ID	TECN	COMMENT
12.6±0.9 OUR AVERAGE				
18.9±5.7±0.3	32	¹ AUBERT	07AU BABR	10.6 $e^+e^- \rightarrow K^+K^-\pi^+\pi^-\pi^0\gamma$
11.7±1.0±1.5	597	ABLIKIM	06G BES2	$\psi(2S) \rightarrow K^+K^-\pi^+\pi^-\pi^0$
12.7±0.5±1.0	711.6	BRIERE	05 CLEO	$e^+e^- \rightarrow \psi(2S) \rightarrow K^+K^-\pi^+\pi^-\pi^0$
¹ AUBERT 07AU reports $[\Gamma(\psi(2S) \rightarrow K^+K^-\pi^+\pi^-\pi^0)/\Gamma_{total}] \times [\Gamma(\psi(2S) \rightarrow e^+e^-)] = (44 \pm 13 \pm 3) \times 10^{-4}$ keV which we divide by our best value $\Gamma(\psi(2S) \rightarrow e^+e^-) = 2.33 \pm 0.04$ keV. Our first error is their experiment's error and our second error is the systematic error from using our best value.				

 $\Gamma(\omega f_0(1710) \rightarrow \omega K^+ K^-)/\Gamma_{total}$ Γ_{70}/Γ

VALUE (units 10^{-5})	EVTS	DOCUMENT ID	TECN	COMMENT
5.9±2.0±0.9	19	ABLIKIM	06G BES2	$\psi(2S) \rightarrow K^+K^-\pi^+\pi^-\pi^0$

 $\Gamma(K^*(892)^0 K^- \pi^+ \pi^0 + c.c.)/\Gamma_{total}$ Γ_{71}/Γ

VALUE (units 10^{-4})	EVTS	DOCUMENT ID	TECN	COMMENT
8.6±1.3±1.8	238	ABLIKIM	06G BES2	$\psi(2S) \rightarrow K^+K^-\pi^+\pi^-\pi^0$

 $\Gamma(K^*(892)^+ K^- \pi^+ \pi^- + c.c.)/\Gamma_{total}$ Γ_{72}/Γ

VALUE (units 10^{-4})	EVTS	DOCUMENT ID	TECN	COMMENT
9.6±2.2±1.7	133	ABLIKIM	06G BES2	$\psi(2S) \rightarrow K^+K^-\pi^+\pi^-\pi^0$

 $\Gamma(K^*(892)^+ K^- \rho^0 + c.c.)/\Gamma_{total}$ Γ_{73}/Γ

VALUE (units 10^{-4})	EVTS	DOCUMENT ID	TECN	COMMENT
7.3±2.2±1.4	78	ABLIKIM	06G BES2	$\psi(2S) \rightarrow K^+K^-\pi^+\pi^-\pi^0$

 $\Gamma(K^*(892)^0 K^- \rho^+ + c.c.)/\Gamma_{total}$ Γ_{74}/Γ

VALUE (units 10^{-4})	EVTS	DOCUMENT ID	TECN	COMMENT
6.1±1.3±1.2	125	ABLIKIM	06G BES2	$\psi(2S) \rightarrow K^+K^-\pi^+\pi^-\pi^0$

 $\Gamma(K_S^0 K_S^0 \pi^+ \pi^-)/\Gamma_{total}$ Γ_{75}/Γ

VALUE (units 10^{-4})	EVTS	DOCUMENT ID	TECN	COMMENT
2.2±0.25±0.37	83 ± 9	ABLIKIM	05o BES2	$e^+e^- \rightarrow \psi(2S)$

 $\Gamma(K^+ K^- \rho^0)/\Gamma_{total}$ Γ_{83}/Γ

VALUE (units 10^{-4})	EVTS	DOCUMENT ID	TECN	COMMENT
2.2±0.2±0.4	223.8	BRIERE	05 CLEO	$e^+e^- \rightarrow \psi(2S) \rightarrow K^+K^-\pi^+\pi^-$

 $\Gamma(K^*(892)^0 K_2^*(1430)^0)/\Gamma_{total}$ Γ_{84}/Γ

VALUE (units 10^{-4})	CL%	EVTS	DOCUMENT ID	TECN	COMMENT
1.86±0.32±0.43		93 ± 16	BAI	04c	$\psi(2S) \rightarrow K^+K^-\pi^+\pi^-$
<1.2		90	BAI	98J BES	e^+e^-
••• We do not use the following data for averages, fits, limits, etc. •••					

 $\Gamma(K^+ K^- \pi^+ \pi^- \eta)/\Gamma_{total}$ Γ_{85}/Γ

VALUE (units 10^{-3})	EVTS	DOCUMENT ID	TECN	COMMENT
1.3±0.7±0.1	7	¹ AUBERT	07AU BABR	10.6 $e^+e^- \rightarrow K^+K^-\pi^+\pi^-\eta\gamma$
¹ AUBERT 07AU quotes $\Gamma_{ee}^{\psi(2S)} \cdot B(\psi(2S) \rightarrow 2(\pi^+\pi^-\eta)) \cdot B(\eta \rightarrow \gamma\gamma) = 1.2 \pm 0.7 \pm 0.1$ eV.				

 $\Gamma(K^+ K^- 2(\pi^+ \pi^-) \pi^0)/\Gamma_{total}$ Γ_{87}/Γ

VALUE (units 10^{-4})	EVTS	DOCUMENT ID	TECN	COMMENT
10.0±2.5±1.8	65	ABLIKIM	07D BES2	$e^+e^- \rightarrow \psi(2S)$

 $\Gamma(K^+ K^*(892)^- + c.c.)/\Gamma_{total}$ Γ_{88}/Γ

VALUE (units 10^{-5})	CL%	EVTS	DOCUMENT ID	TECN	COMMENT
2.9 ± 0.4 OUR AVERAGE					Error includes scale factor of 1.2.
3.18±0.30±0.26		0.2k	ABLIKIM	12L BES3	$e^+e^- \rightarrow \psi(2S)$
2.9 \pm $\frac{+1.3}{-1.7}$ ± 0.4		9.6 ± 4.2	ABLIKIM	05i BES2	$e^+e^- \rightarrow \psi(2S)$
1.3 \pm $\frac{+1.0}{-0.7}$ ± 0.3		7	ADAM	05 CLEO	$e^+e^- \rightarrow \psi(2S)$
••• We do not use the following data for averages, fits, limits, etc. •••					
<5.4		90	FRANKLIN	83 MRK2	$e^+e^- \rightarrow$ hadrons

 $\Gamma(2(K^+ K^-))/\Gamma_{total}$ Γ_{89}/Γ

VALUE (units 10^{-4})	EVTS	DOCUMENT ID	TECN	COMMENT
0.63±0.13 OUR AVERAGE				
0.9 ± 0.4 ± 0.1	13	LEES	12F BABR	10.6 $e^+e^- \rightarrow 2(K^+K^-)\gamma$
0.6 ± 0.1 ± 0.1	59.2	BRIERE	05 CLEO	$e^+e^- \rightarrow \psi(2S) \rightarrow 2(K^+K^-)$

 $\Gamma(2(K^+ K^-) \pi^0)/\Gamma_{total}$ Γ_{90}/Γ

VALUE (units 10^{-4})	EVTS	DOCUMENT ID	TECN	COMMENT
1.1±0.2±0.2	44.7	BRIERE	05 CLEO	$e^+e^- \rightarrow \psi(2S) \rightarrow 2(K^+K^-)\pi^0$

 $\Gamma(K^+ K^- \phi)/\Gamma_{total}$ Γ_{91}/Γ

VALUE (units 10^{-4})	EVTS	DOCUMENT ID	TECN	COMMENT
0.70±0.16 OUR AVERAGE				
0.8 ± 0.2 ± 0.1	36.8	BRIERE	05 CLEO	$e^+e^- \rightarrow \psi(2S) \rightarrow 2(K^+K^-)$
0.6 ± 0.2 ± 0.1	16.1 ± 5.0	¹ BAI	03B BES	$\psi(2S) \rightarrow 2(K^+K^-)$
¹ Normalized to $B(\psi(2S) \rightarrow J/\psi\pi^+\pi^-) = 0.305 \pm 0.016$.				

 $\Gamma(K_S^0 K_S^0 \phi)/\Gamma_{total}$ Γ_{92}/Γ

VALUE (units 10^{-4})	EVTS	DOCUMENT ID	TECN	COMMENT
0.353±0.020±0.021	687	¹ ABLIKIM	23BA BES3	$e^+e^- \rightarrow \psi(2S) \rightarrow K_S^0 K_S^0 K^+ K^-$
¹ Solution with a constructive interference of the signal with the continuum background.				

 $\Gamma(K_1(1270)^\pm K^\mp)/\Gamma_{total}$ Γ_{93}/Γ

VALUE (units 10^{-4})	DOCUMENT ID	TECN	COMMENT
10.0±1.8±2.1	¹ BAI	99c BES	e^+e^-
¹ Assuming $B(K_1(1270) \rightarrow K\rho) = 0.42 \pm 0.06$			

 $\Gamma(K^+ K^*(892)^0 \pi^- + c.c.)/\Gamma_{total}$ Γ_{94}/Γ

VALUE (units 10^{-4})	DOCUMENT ID	TECN	COMMENT
6.7±2.5	TANENBAUM	78 MRK1	e^+e^-

 $\Gamma(\eta K^+ K^- , \text{no } \eta\phi)/\Gamma_{total}$ Γ_{95}/Γ

VALUE (units 10^{-5})	CL%	EVTS	DOCUMENT ID	TECN	COMMENT
3.49±0.09±0.15	1.8k		¹ ABLIKIM	20F BES3	$\psi(2S) \rightarrow K^+K^-\gamma\gamma$
••• We do not use the following data for averages, fits, limits, etc. •••					
3.08±0.29±0.25	0.3k		^{1,2} ABLIKIM	12L BES3	$\psi(2S) \rightarrow K^+K^-\gamma\gamma$
<13	90		BRIERE	05 CLEO	$e^+e^- \rightarrow \psi(2S) \rightarrow K^+K^-\pi^+\pi^-\pi^0$
¹ Excluding $\eta\phi$.					
² Superseded by ABLIKIM 20F.					

 $\Gamma(\eta K^+ K^-) \times \Gamma(e^+ e^-)/\Gamma_{total}$ $\Gamma_{96}\Gamma_7/\Gamma$

VALUE (eV)	CL%	DOCUMENT ID	TECN	COMMENT
<0.6	90	¹ LEES	23 BABR	$e^+e^- \rightarrow \eta SR^h$ hadrons
¹ LEES 23 reports $[\Gamma(\psi(2S) \rightarrow \eta K^+ K^-) \times \Gamma(\psi(2S) \rightarrow e^+ e^-)]/\Gamma_{total} \times B(\eta \rightarrow 3\pi^0) < 0.2$ eV which we divide by our best value $B(\eta \rightarrow 3\pi^0) = 32.57 \times 10^{-2}$.				

 $\Gamma(X(1750)\eta \rightarrow K^+ K^- \eta)/\Gamma_{total}$ Γ_{97}/Γ

VALUE (units 10^{-6})	DOCUMENT ID	TECN	COMMENT
4.8±1.0±2.6	ABLIKIM	20F BES3	$\psi(2S) \rightarrow K^+K^-\eta$

 $\Gamma(K_1(1400)^\pm K^\mp)/\Gamma_{total}$ Γ_{98}/Γ

VALUE (units 10^{-4})	CL%	DOCUMENT ID	TECN	COMMENT
<3.1	90	¹ BAI	99c BES	e^+e^-
¹ Assuming $B(K_1(1400) \rightarrow K^*\pi) = 0.94 \pm 0.06$				

 $\Gamma(K_2^*(1430)^\pm K^\mp)/\Gamma_{total}$ Γ_{99}/Γ

VALUE (units 10^{-5})	EVTS	DOCUMENT ID	TECN	COMMENT
7.12±0.62±$\frac{1.13}{0.61}$	251 ± 22	ABLIKIM	12L BES3	$e^+e^- \rightarrow \psi(2S)$

 $\Gamma(K^*(892)^0 K^0 + c.c.)/\Gamma_{total}$ Γ_{100}/Γ

VALUE (units 10^{-4})	EVTS	DOCUMENT ID	TECN	COMMENT
10.9±2.0 OUR AVERAGE				
13.3 \pm $\frac{+2.4}{-2.8}$ ± 1.7	65.6 ± 9.0	ABLIKIM	05i BES2	$e^+e^- \rightarrow \psi(2S)$
9.2 \pm $\frac{+2.7}{-2.2}$ ± 0.9	25	ADAM	05 CLEO	$e^+e^- \rightarrow \psi(2S)$

 $\Gamma(K^+ K^*(892)^- + c.c.)/\Gamma(K^*(892)^0 K^0 + c.c.)$ Γ_{88}/Γ_{100}

VALUE	DOCUMENT ID	TECN	COMMENT
0.16±0.06 OUR AVERAGE			
0.22 \pm $\frac{+0.10}{-0.14}$	ABLIKIM	05i BES2	$e^+e^- \rightarrow \psi(2S)$
0.14 \pm $\frac{+0.08}{-0.06}$	ADAM	05 CLEO	$e^+e^- \rightarrow \psi(2S)$

 $\Gamma(\omega K^+ K^-)/\Gamma_{total}$ Γ_{101}/Γ

VALUE (units 10^{-4})	EVTS	DOCUMENT ID	TECN	COMMENT
1.62±0.11 OUR AVERAGE				Error includes scale factor of 1.1.
1.56±0.04±0.11	2.8k	ABLIKIM	14G BES3	$\psi(2S) \rightarrow K^+K^-\pi^+\pi^-\pi^0$
2.38±0.37±0.29	78	ABLIKIM	06G BES2	$\psi(2S) \rightarrow K^+K^-\pi^+\pi^-\pi^0$
1.9 ± 0.3 ± 0.3	76.8	BRIERE	05 CLEO	$e^+e^- \rightarrow \psi(2S) \rightarrow K^+K^-\pi^+\pi^-\pi^0$
1.5 ± 0.3 ± 0.2	23	¹ BAI	03B BES	$\psi(2S) \rightarrow K^+K^-\pi^+\pi^-\pi^0$
¹ Normalized to $B(\psi(2S) \rightarrow J/\psi\pi^+\pi^-) = 0.305 \pm 0.016$.				

See key on page 1171

Meson Particle Listings

 $\psi(2S)$

$\Gamma(\omega K_S^0 K_S^0)/\Gamma_{\text{total}}$		Γ_{102}/Γ	
VALUE (units 10^{-5})	EVTS	DOCUMENT ID	TECN COMMENT
$7.04 \pm 0.39 \pm 0.36$	1.5k	ABLIKIM	21AL BES3 $\psi(2S) \rightarrow \pi^+ \pi^- \pi^0 K_S^0 K_S^0$

$\Gamma(\omega K^*(892)^+ K^- + \text{c.c.})/\Gamma_{\text{total}}$		Γ_{103}/Γ	
VALUE (units 10^{-5})	EVTS	DOCUMENT ID	TECN COMMENT
20.7 ± 2.6 OUR AVERAGE			
$18.9 \pm 2.9 \pm 2.2$	396	ABLIKIM	13M BES3 $\psi(2S) \rightarrow \omega K_S^0 K^- \pi^+$
$22.6 \pm 3.0 \pm 2.4$	535	ABLIKIM	13M BES3 $\psi(2S) \rightarrow \omega K^+ K^- \pi^0$

$\Gamma(\omega K_2^*(1430)^+ K^- + \text{c.c.})/\Gamma_{\text{total}}$		Γ_{104}/Γ	
VALUE (units 10^{-5})	EVTS	DOCUMENT ID	TECN COMMENT
6.1 ± 1.2 OUR AVERAGE			
$6.39 \pm 1.50 \pm 0.78$	128	ABLIKIM	13M BES3 $\psi(2S) \rightarrow \omega K_S^0 K^- \pi^+$
$5.86 \pm 1.61 \pm 0.83$	143	ABLIKIM	13M BES3 $\psi(2S) \rightarrow \omega K^+ K^- \pi^0$

$\Gamma(\omega \bar{K}^*(892)^0 K^0)/\Gamma_{\text{total}}$		Γ_{105}/Γ	
VALUE (units 10^{-5})	EVTS	DOCUMENT ID	TECN COMMENT
$16.8 \pm 2.5 \pm 1.6$	356	ABLIKIM	13M BES3 $\psi(2S) \rightarrow \omega K_S^0 K^- \pi^+$

$\Gamma(\omega \bar{K}_2^*(1430)^0 K^0)/\Gamma_{\text{total}}$		Γ_{106}/Γ	
VALUE (units 10^{-5})	EVTS	DOCUMENT ID	TECN COMMENT
$5.82 \pm 2.08 \pm 0.72$	116	ABLIKIM	13M BES3 $\psi(2S) \rightarrow \omega K_S^0 K^- \pi^+$

$\Gamma(\omega X(1440) \rightarrow \omega K_S^0 K^- \pi^+ + \text{c.c.})/\Gamma_{\text{total}}$		Γ_{107}/Γ	
VALUE (units 10^{-5})	EVTS	DOCUMENT ID	TECN COMMENT
$1.60 \pm 0.27 \pm 0.24$	109	¹ ABLIKIM	13M BES3 $\psi(2S) \rightarrow \omega K_S^0 K^- \pi^+$

¹ X(1440) compatible with $\eta(1405)$ and $\eta(1475)$. A $f_1(1420)$ is also possible.

$\Gamma(\omega X(1440) \rightarrow \omega K^+ K^- \pi^0)/\Gamma_{\text{total}}$		Γ_{108}/Γ	
VALUE (units 10^{-5})	EVTS	DOCUMENT ID	TECN COMMENT
$1.09 \pm 0.20 \pm 0.16$	82	¹ ABLIKIM	13M BES3 $\psi(2S) \rightarrow \omega K^+ K^- \pi^0$

¹ X(1440) compatible with $\eta(1405)$ and $\eta(1475)$. A $f_1(1420)$ is also possible.

$\Gamma(\omega f_1(1285) \rightarrow \omega K_S^0 K^- \pi^+ + \text{c.c.})/\Gamma_{\text{total}}$		Γ_{109}/Γ	
VALUE (units 10^{-5})	EVTS	DOCUMENT ID	TECN COMMENT
$0.302 \pm 0.098 \pm 0.027$	22	¹ ABLIKIM	13M BES3 $\psi(2S) \rightarrow \omega K_S^0 K^- \pi^+$

¹ Statistical significance 4.5 σ . This measurement is equivalent to a limit of $< 0.478 \times 10^{-5}$ at 90% C.L.

$\Gamma(\omega f_1(1285) \rightarrow \omega K^+ K^- \pi^0)/\Gamma_{\text{total}}$		Γ_{110}/Γ	
VALUE (units 10^{-5})	EVTS	DOCUMENT ID	TECN COMMENT
$0.125 \pm 0.070 \pm 0.013$	10	¹ ABLIKIM	13M BES3 $\psi(2S) \rightarrow \omega K^+ K^- \pi^0$

¹ Statistical significance 3.2 σ . This measurement is equivalent to a limit of $< 0.221 \times 10^{-5}$ at 90% C.L.

$\Gamma(p\bar{p})/\Gamma_{\text{total}}$		Γ_{111}/Γ	
VALUE (units 10^{-4})	EVTS	DOCUMENT ID	TECN COMMENT
2.94 ± 0.09 OUR FIT			Error includes scale factor of 1.3.
3.02 ± 0.08 OUR AVERAGE			
$3.05 \pm 0.02 \pm 0.12$	19k	ABLIKIM	18T BES3 $e^+ e^- \rightarrow \psi(2S) \rightarrow p\bar{p}$
$3.08 \pm 0.05 \pm 0.18$	4.5k	¹ DOBBS	14 $e^+ e^- \rightarrow \psi(2S) \rightarrow p\bar{p}$
$3.36 \pm 0.09 \pm 0.25$	1.6k	ABLIKIM	07C BES $e^+ e^- \rightarrow \psi(2S) \rightarrow p\bar{p}$
$2.87 \pm 0.12 \pm 0.15$	557	PEDLAR	05 CLEO $e^+ e^- \rightarrow \psi(2S) \rightarrow p\bar{p}$
1.4 ± 0.8	4	BRANDELIC	79C DASP $e^+ e^- \rightarrow \psi(2S) \rightarrow p\bar{p}$
2.3 ± 0.7		FELDMAN	77 MRK1 $e^+ e^- \rightarrow \psi(2S) \rightarrow p\bar{p}$

¹ Using CLEO-c data but not authored by the CLEO Collaboration.

$\Gamma(p\bar{p})/\Gamma(J/\psi(1S)\pi^+\pi^-)$		Γ_{111}/Γ_{12}	
VALUE (units 10^{-4})	EVTS	DOCUMENT ID	TECN COMMENT
8.49 ± 0.28 OUR FIT			Error includes scale factor of 1.3.
$6.98 \pm 0.49 \pm 0.97$		BAI	01 BES $e^+ e^- \rightarrow \psi(2S) \rightarrow p\bar{p}$

$\Gamma(n\bar{n})/\Gamma_{\text{total}}$		Γ_{112}/Γ	
VALUE (units 10^{-4})	EVTS	DOCUMENT ID	TECN COMMENT
$3.06 \pm 0.06 \pm 0.14$	6k	ABLIKIM	18T BES3 $e^+ e^- \rightarrow \psi(2S) \rightarrow n\bar{n}$

$\Gamma(p\bar{p}\pi^0)/\Gamma_{\text{total}}$		Γ_{113}/Γ	
VALUE (units 10^{-4})	EVTS	DOCUMENT ID	TECN COMMENT
1.53 ± 0.07 OUR AVERAGE			
$1.65 \pm 0.03 \pm 0.15$	4.5k	ABLIKIM	13A BES3 $\psi(2S) \rightarrow p\bar{p}\pi^0$
$1.54 \pm 0.06 \pm 0.06$	948	ALEXANDER	10 CLEO $\psi(2S) \rightarrow \pi^0 p\bar{p}$
$1.32 \pm 0.10 \pm 0.15$	256	¹ ABLIKIM	05E BES2 $e^+ e^- \rightarrow \psi(2S) \rightarrow p\bar{p}\gamma\gamma$
1.4 ± 0.5	9	FRANKLIN	83 MRK2 $e^+ e^-$

¹ Computed using $B(\pi^0 \rightarrow \gamma\gamma) = (98.80 \pm 0.03)\%$.

$\Gamma(N(940)\bar{p} + \text{c.c.} \rightarrow p\bar{p}\pi^0)/\Gamma_{\text{total}}$		Γ_{114}/Γ	
VALUE (units 10^{-5})	EVTS	DOCUMENT ID	TECN COMMENT
$6.42 \pm 0.20 \pm 1.78$	1.9k	¹ ABLIKIM	13A BES3 $\psi(2S) \rightarrow p\bar{p}\pi^0$

¹ From a fit of $\pi^0 p\bar{p}$ data to eight distinct intermediate $N\bar{p}$ resonant states.

$\Gamma(N(1440)\bar{p} + \text{c.c.} \rightarrow p\bar{p}\pi^0)/\Gamma_{\text{total}}$		Γ_{115}/Γ	
VALUE (units 10^{-5})	EVTS	DOCUMENT ID	TECN COMMENT
7.3 ± 1.7			OUR AVERAGE Error includes scale factor of 2.5.

$3.58 \pm 0.25 \pm 1.59$	1.1k	¹ ABLIKIM	13A BES3 $\psi(2S) \rightarrow p\bar{p}\pi^0$
$8.1 \pm 0.7 \pm 0.3$	474	² ALEXANDER	10 CLEO $\psi(2S) \rightarrow \pi^0 p\bar{p}$

¹ From a fit of $\pi^0 p\bar{p}$ data to eight distinct intermediate $N\bar{p}$ resonant states.

² From a fit of the $p\bar{p}$ and $p\pi^0$ mass distributions to a combination of $N(1440)\bar{p}$, a broad $p\bar{p}$ enhancement around 2100 MeV, and two other broad, unestablished resonances.

$\Gamma(N(1520)\bar{p} + \text{c.c.} \rightarrow p\bar{p}\pi^0)/\Gamma_{\text{total}}$		Γ_{116}/Γ	
VALUE (units 10^{-5})	EVTS	DOCUMENT ID	TECN COMMENT
$0.64 \pm 0.05 \pm 0.22$	0.2k	¹ ABLIKIM	13A BES3 $\psi(2S) \rightarrow p\bar{p}\pi^0$

¹ From a fit of $\pi^0 p\bar{p}$ data to eight distinct intermediate $N\bar{p}$ resonant states.

$\Gamma(N(1535)\bar{p} + \text{c.c.} \rightarrow p\bar{p}\pi^0)/\Gamma_{\text{total}}$		Γ_{117}/Γ	
VALUE (units 10^{-5})	EVTS	DOCUMENT ID	TECN COMMENT
$2.47 \pm 0.28 \pm 0.99$	0.7k	¹ ABLIKIM	13A BES3 $\psi(2S) \rightarrow p\bar{p}\pi^0$

¹ From a fit of $\pi^0 p\bar{p}$ data to eight distinct intermediate $N\bar{p}$ resonant states.

$\Gamma(N(1650)\bar{p} + \text{c.c.} \rightarrow p\bar{p}\pi^0)/\Gamma_{\text{total}}$		Γ_{118}/Γ	
VALUE (units 10^{-5})	EVTS	DOCUMENT ID	TECN COMMENT
$3.76 \pm 0.28 \pm 1.37$	1.1k	¹ ABLIKIM	13A BES3 $\psi(2S) \rightarrow p\bar{p}\pi^0$

¹ From a fit of $\pi^0 p\bar{p}$ data to eight distinct intermediate $N\bar{p}$ resonant states.

$\Gamma(N(1720)\bar{p} + \text{c.c.} \rightarrow p\bar{p}\pi^0)/\Gamma_{\text{total}}$		Γ_{119}/Γ	
VALUE (units 10^{-5})	EVTS	DOCUMENT ID	TECN COMMENT
$1.79 \pm 0.10 \pm 0.24$	0.5k	¹ ABLIKIM	13A BES3 $\psi(2S) \rightarrow p\bar{p}\pi^0$

¹ From a fit of $\pi^0 p\bar{p}$ data to eight distinct intermediate $N\bar{p}$ resonant states.

$\Gamma(N(2300)\bar{p} + \text{c.c.} \rightarrow p\bar{p}\pi^0)/\Gamma_{\text{total}}$		Γ_{120}/Γ	
VALUE (units 10^{-5})	EVTS	DOCUMENT ID	TECN COMMENT
$2.62 \pm 0.28 \pm 1.12$	0.9k	¹ ABLIKIM	13A BES3 $\psi(2S) \rightarrow p\bar{p}\pi^0$

¹ From a fit of $\pi^0 p\bar{p}$ data to eight distinct intermediate $N\bar{p}$ resonant states.

$\Gamma(N(2570)\bar{p} + \text{c.c.} \rightarrow p\bar{p}\pi^0)/\Gamma_{\text{total}}$		Γ_{121}/Γ	
VALUE (units 10^{-5})	EVTS	DOCUMENT ID	TECN COMMENT
$2.13 \pm 0.08 \pm 0.40$	0.8k	¹ ABLIKIM	13A BES3 $\psi(2S) \rightarrow p\bar{p}\pi^0$

¹ From a fit of $\pi^0 p\bar{p}$ data to eight distinct intermediate $N\bar{p}$ resonant states.

$\Gamma(p\bar{p}\pi^+\pi^-)/\Gamma_{\text{total}}$		Γ_{122}/Γ	
VALUE (units 10^{-4})	EVTS	DOCUMENT ID	TECN COMMENT
6.0 ± 0.4 OUR AVERAGE			
$5.9 \pm 0.2 \pm 0.4$	904.5	BRIERE	05 CLEO $e^+ e^- \rightarrow \psi(2S) \rightarrow p\bar{p}\pi^+\pi^-$
8 ± 2		¹ TANENBAUM	78 MRK1 $e^+ e^-$

¹ Assuming entirely strong decay.

$\Gamma(p\bar{p}K^+K^-)/\Gamma_{\text{total}}$		Γ_{123}/Γ	
VALUE (units 10^{-5})	EVTS	DOCUMENT ID	TECN COMMENT
$2.7 \pm 0.6 \pm 0.4$	30.1	BRIERE	05 CLEO $e^+ e^- \rightarrow \psi(2S) \rightarrow p\bar{p}K^+K^-$

$\Gamma(p\bar{p}\eta)/\Gamma_{\text{total}}$		Γ_{124}/Γ	
VALUE (units 10^{-5})	EVTS	DOCUMENT ID	TECN COMMENT
6.0 ± 0.4 OUR AVERAGE			
$6.4 \pm 0.2 \pm 0.6$	679	¹ ABLIKIM	13s BES3 $\psi(2S) \rightarrow \eta p\bar{p}$
$5.6 \pm 0.6 \pm 0.3$	154	¹ ALEXANDER	10 CLEO $\psi(2S) \rightarrow \eta p\bar{p}$
$5.8 \pm 1.1 \pm 0.7$	44.8 \pm 8.5	² ABLIKIM	05E BES2 $e^+ e^- \rightarrow \psi(2S) \rightarrow p\bar{p}\gamma\gamma$
$8 \pm 3 \pm 3$	9.8	BRIERE	05 CLEO $e^+ e^- \rightarrow \psi(2S) \rightarrow p\bar{p}\pi^+\pi^- \pi^0$

¹ With $N(1535)$ decaying to $p\eta$.

² Computed using $B(\eta \rightarrow \gamma\gamma) = (39.43 \pm 0.26)\%$.

$\Gamma(N(1535)\bar{p} + \text{c.c.} \rightarrow p\bar{p}\eta)/\Gamma_{\text{total}}$		Γ_{125}/Γ	
VALUE (units 10^{-5})	EVTS	DOCUMENT ID	TECN COMMENT
4.5 ± 0.7			OUR AVERAGE

$5.2 \pm 0.3 \pm 3.2$	527	¹ ABLIKIM	13s BES3 $\psi(2S) \rightarrow \eta p\bar{p}$
$4.4 \pm 0.6 \pm 0.3$	123	² ALEXANDER	10 CLEO $\psi(2S) \rightarrow \eta p\bar{p}$

¹ With $N(1535)$ decaying to $p\eta$.

² From a fit of the $p\bar{p}$ and $p\eta$ distributions to a combination of $N^*(1535)\bar{p}$ and a broad $p\bar{p}$ enhancement around 2100 MeV.

Meson Particle Listings

$\psi(2S)$

$\Gamma(p\bar{p}\pi^+\pi^-\pi^0)/\Gamma_{total}$				Γ_{126}/Γ
VALUE (units 10^{-4})	EVTs	DOCUMENT ID	TECN	COMMENT
$7.3 \pm 0.4 \pm 0.6$	434.9	BRIERE	05	CLEO $e^+e^- \rightarrow \psi(2S) \rightarrow p\bar{p}\pi^+\pi^-\pi^0$

$\Gamma(p\bar{p}\rho^0)/\Gamma_{total}$				Γ_{127}/Γ
VALUE (units 10^{-4})	EVTs	DOCUMENT ID	TECN	COMMENT
$0.5 \pm 0.1 \pm 0.2$	61.1	BRIERE	05	CLEO $e^+e^- \rightarrow \psi(2S) \rightarrow p\bar{p}\pi^+\pi^-$

$\Gamma(p\bar{p}\omega)/\Gamma_{total}$				Γ_{128}/Γ
VALUE (units 10^{-4})	EVTs	DOCUMENT ID	TECN	COMMENT
0.69 ± 0.21 OUR AVERAGE				
$0.6 \pm 0.2 \pm 0.2$	21.2	BRIERE	05	CLEO $e^+e^- \rightarrow \psi(2S) \rightarrow p\bar{p}\pi^+\pi^-\pi^0$
$0.8 \pm 0.3 \pm 0.1$	14.9 ± 0.1	¹ BAI	03B	BES $\psi(2S) \rightarrow p\bar{p}\pi^+\pi^-\pi^0$
¹ Normalized to $B(\psi(2S) \rightarrow J/\psi\pi^+\pi^-) = 0.305 \pm 0.016$.				

$\Gamma(p\bar{p}\eta')/\Gamma_{total}$				Γ_{129}/Γ
VALUE (units 10^{-5})	EVTs	DOCUMENT ID	TECN	COMMENT
$1.10 \pm 0.10 \pm 0.08$	491	¹ ABLIKIM	19N	BES3 $\psi(2S) \rightarrow \eta' p\bar{p}$
¹ From the combination of $p\bar{p}\eta' \rightarrow p\bar{p}\pi^+\pi^-\eta$ and $p\bar{p}\eta' \rightarrow p\bar{p}\pi^+\pi^-\gamma$ channels.				

$\Gamma(p\bar{p}\phi)/\Gamma_{total}$				Γ_{130}/Γ	
VALUE (units 10^{-6})	CL%	EVTs	DOCUMENT ID	TECN	COMMENT
$6.06 \pm 0.38 \pm 0.48$		753	ABLIKIM	19A0	BES3 $e^+e^- \rightarrow \psi(2S) \rightarrow p\bar{p}K^+K^-$

• • • We do not use the following data for averages, fits, limits, etc. • • •

<24	90	BRIERE	05	CLEO $e^+e^- \rightarrow \psi(2S) \rightarrow p\bar{p}K^+K^-$
<26	90	¹ BAI	03B	BES $\psi(2S) \rightarrow K^+K^-p\bar{p}$

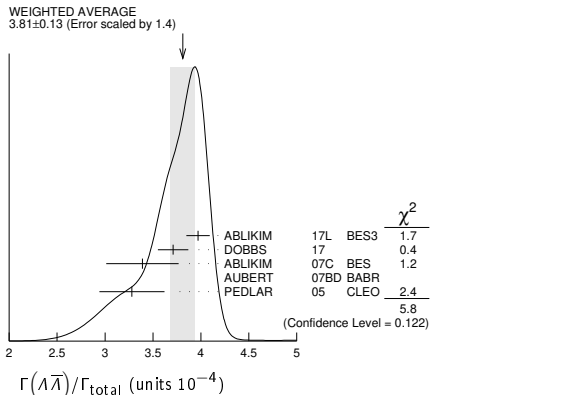
¹Normalized to $B(\psi(2S) \rightarrow J/\psi\pi^+\pi^-) = 0.305 \pm 0.016$.

$\Gamma(\phi X(1835) \rightarrow p\bar{p}\phi)/\Gamma_{total}$				Γ_{131}/Γ
VALUE	CL%	DOCUMENT ID	TECN	COMMENT
$<1.82 \times 10^{-7}$	90	ABLIKIM	19A0	BES3 $e^+e^- \rightarrow \psi(2S) \rightarrow p\bar{p}K^+K^-$

$\Gamma(p\bar{p}\pi^- \text{ or c.c.})/\Gamma_{total}$				Γ_{132}/Γ
VALUE (units 10^{-4})	EVTs	DOCUMENT ID	TECN	COMMENT
2.48 ± 0.17 OUR AVERAGE				
$2.45 \pm 0.11 \pm 0.21$	851	ABLIKIM	06i	BES2 $e^+e^- \rightarrow p\pi^-X$
$2.52 \pm 0.12 \pm 0.22$	849	ABLIKIM	06i	BES2 $e^+e^- \rightarrow \bar{p}\pi^+X$

$\Gamma(p\bar{p}\pi^-\pi^0)/\Gamma_{total}$				Γ_{133}/Γ
VALUE (units 10^{-4})	EVTs	DOCUMENT ID	TECN	COMMENT
$3.18 \pm 0.50 \pm 0.50$	135 ± 21	ABLIKIM	06i	BES2 $e^+e^- \rightarrow p\pi^-\pi^0X$

$\Gamma(\Lambda\bar{\Lambda})/\Gamma_{total}$				Γ_{134}/Γ	
VALUE (units 10^{-4})	CL%	EVTs	DOCUMENT ID	TECN	COMMENT
3.81 ± 0.13 OUR AVERAGE					Error includes scale factor of 1.4. See the ideogram below.
$3.97 \pm 0.02 \pm 0.12$		31k	ABLIKIM	17L	BES3 $e^+e^- \rightarrow \Lambda\bar{\Lambda}$
$3.71 \pm 0.05 \pm 0.15$	6.5k	¹ DOBBS	17		$e^+e^- \rightarrow \Lambda\bar{\Lambda}$
$3.39 \pm 0.20 \pm 0.32$	337	ABLIKIM	07C	BES	$e^+e^- \rightarrow \psi(2S) \rightarrow \text{hadrons}$
$6.4 \pm 1.8 \pm 0.1$		² AUBERT	07BD	BABR	$10.6 e^+e^- \rightarrow \Lambda\bar{\Lambda}\gamma$
$3.28 \pm 0.23 \pm 0.25$	208	PEDLAR	05	CLEO	$e^+e^- \rightarrow \psi(2S) \rightarrow \text{hadrons}$
• • • We do not use the following data for averages, fits, limits, etc. • • •					
$3.75 \pm 0.09 \pm 0.23$	1.9k	^{1,3} DOBBS	14		$e^+e^- \rightarrow \Lambda\bar{\Lambda}$
$1.81 \pm 0.20 \pm 0.27$	80	⁴ BAI	01	BES	$e^+e^- \rightarrow \psi(2S) \rightarrow \text{hadrons}$
< 4	90	FELDMAN	77	MRK1	$e^+e^- \rightarrow \psi(2S) \rightarrow \text{hadrons}$



¹Using CLEO-c data but not authored by the CLEO Collaboration.

²AUBERT 07BD reports $[\Gamma(\psi(2S) \rightarrow \Lambda\bar{\Lambda})/\Gamma_{total}] \times [\Gamma(\psi(2S) \rightarrow e^+e^-)] = (15 \pm 4 \pm 1) \times 10^{-4}$ keV which we divide by our best value $\Gamma(\psi(2S) \rightarrow e^+e^-) = 2.33 \pm 0.04$ keV. Our first error is their experiment's error and our second error is the systematic error from using our best value.

³Superseded by DOBBS 17.

⁴Estimated using $B(\psi(2S) \rightarrow J/\psi\pi^+\pi^-) = 0.310 \pm 0.028$.

$\Gamma(\Lambda\bar{\Lambda}\pi^0)/\Gamma_{total}$				Γ_{135}/Γ	
VALUE (units 10^{-6})	CL%	EVTs	DOCUMENT ID	TECN	COMMENT
$1.42 \pm 0.39 \pm 0.59$		23	¹ ABLIKIM	22AP	BES3 $\psi(2S) \rightarrow p\bar{p}\pi^+\pi^-\gamma\gamma$
• • • We do not use the following data for averages, fits, limits, etc. • • •					
< 2.9	90		² ABLIKIM	13F	BES3 $\psi(2S) \rightarrow p\bar{p}\pi^+\pi^-\gamma\gamma$
<120	90		³ ABLIKIM	07H	BES2 $e^+e^- \rightarrow \psi(2S)$

¹With a significance of 3.7 σ . The corresponding 90% CL upper limit is 2.47×10^{-6} .

²Using $B(\Lambda \rightarrow \pi^-p) = 63.9\%$ and $B(\pi^0 \rightarrow \gamma\gamma) = 98.8\%$.

³Using $B(\Lambda \rightarrow \pi^-p) = 63.9\%$ and $B(\eta \rightarrow \gamma\gamma) = 39.4\%$.

$\Gamma(\Lambda\bar{\Lambda}\eta)/\Gamma_{total}$				Γ_{136}/Γ	
VALUE (units 10^{-5})	CL%	EVTs	DOCUMENT ID	TECN	COMMENT
2.43 ± 0.32 OUR AVERAGE					
$2.34 \pm 0.18 \pm 0.52$		218	ABLIKIM	22AP	BES3 $\psi(2S) \rightarrow p\bar{p}\pi^+\pi^-\gamma\gamma$
$2.48 \pm 0.34 \pm 0.19$		60	¹ ABLIKIM	13F	BES3 $\psi(2S) \rightarrow p\bar{p}\pi^+\pi^-\gamma\gamma$
• • • We do not use the following data for averages, fits, limits, etc. • • •					
<4.9	90		² ABLIKIM	07H	BES2 $e^+e^- \rightarrow \psi(2S)$

¹Using $B(\Lambda \rightarrow \pi^-p) = 63.9\%$ and $B(\eta \rightarrow \gamma\gamma) = 39.31\%$.

²Using $B(\Lambda \rightarrow \pi^-p) = 63.9\%$.

$\Gamma(\Lambda\bar{\Lambda}\eta\gamma)/\Gamma_{total}$				Γ_{138}/Γ
VALUE (units 10^{-6})	EVTs	DOCUMENT ID	TECN	COMMENT
$7.34 \pm 0.94 \pm 0.43$	218	ABLIKIM	23Bv	BES3 $\psi(2S) \rightarrow p\bar{p}2(\pi^+\pi^-)\gamma(\gamma)$

$\Gamma(\Lambda\bar{\Lambda}\omega(782))/\Gamma_{total}$				Γ_{139}/Γ
VALUE (units 10^{-5})	EVTs	DOCUMENT ID	TECN	COMMENT
$3.30 \pm 0.34 \pm 0.29$	207	¹ ABLIKIM	22Az	BES3 $e^+e^- \rightarrow \psi(2S)$
¹ Using $B(\Lambda \rightarrow \pi^-p) = 0.639$ and $B(\omega \rightarrow \pi^+\pi^-\pi^0) = 0.893$.				

$\Gamma(\Lambda(1670)\bar{\Lambda} \rightarrow \Lambda\bar{\Lambda}\eta)/\Gamma_{total}$				Γ_{137}/Γ
VALUE (units 10^{-5})	EVTs	DOCUMENT ID	TECN	COMMENT
$1.29 \pm 0.31 \pm 0.62$	116	¹ ABLIKIM	22AP	BES3 $\psi(2S) \rightarrow p\bar{p}\pi^+\pi^-\gamma\gamma$
¹ From a partial wave analysis of the $\Lambda\eta$ system.				

$\Gamma(\Lambda\bar{\Lambda}\pi^+\pi^-)/\Gamma_{total}$				Γ_{140}/Γ
VALUE (units 10^{-4})	EVTs	DOCUMENT ID	TECN	COMMENT
$2.8 \pm 0.4 \pm 0.5$	73.4	BRIERE	05	CLEO $e^+e^- \rightarrow \psi(2S) \rightarrow p\bar{p}2(\pi^+\pi^-)$

$\Gamma(\Lambda\bar{p}K^+)/\Gamma_{total}$				Γ_{141}/Γ
VALUE (units 10^{-4})	EVTs	DOCUMENT ID	TECN	COMMENT
$1.0 \pm 0.1 \pm 0.1$	74.0	BRIERE	05	CLEO $e^+e^- \rightarrow \psi(2S) \rightarrow p\bar{p}K^+\pi^-$

$\Gamma(\Lambda\bar{p}K^*(892)^+ + \text{c.c.})/\Gamma_{total}$				Γ_{142}/Γ
VALUE (units 10^{-5})	EVTs	DOCUMENT ID	TECN	COMMENT
$6.3 \pm 0.5 \pm 0.5$	1011	ABLIKIM	19Au	BES3 $e^+e^- \rightarrow \psi(2S)$

$\Gamma(\Lambda\bar{p}K^+\pi^+\pi^-)/\Gamma_{total}$				Γ_{143}/Γ
VALUE (units 10^{-4})	EVTs	DOCUMENT ID	TECN	COMMENT
$1.8 \pm 0.3 \pm 0.3$	45.8	BRIERE	05	CLEO $e^+e^- \rightarrow \psi(2S) \rightarrow p\bar{p}K^+\pi^+\pi^-$

$\Gamma(\bar{\Lambda}nK_S^0 + \text{c.c.})/\Gamma_{total}$				Γ_{144}/Γ
VALUE (units 10^{-4})	EVTs	DOCUMENT ID	TECN	COMMENT
$0.81 \pm 0.11 \pm 0.14$	50	¹ ABLIKIM	08c	BES2 $e^+e^- \rightarrow J/\psi$
¹ Using $B(\bar{\Lambda} \rightarrow \bar{p}\pi^+) = 63.9\%$ and $B(K_S^0 \rightarrow \pi^+\pi^-) = 69.2\%$.				

$\Gamma(\Delta^+\bar{\Delta}^-)/\Gamma_{total}$				Γ_{145}/Γ
VALUE (units 10^{-5})	EVTs	DOCUMENT ID	TECN	COMMENT
$12.8 \pm 1.0 \pm 3.4$	157	¹ BAI	01	BES $e^+e^- \rightarrow \psi(2S) \rightarrow \text{hadrons}$
¹ Estimated using $B(\psi(2S) \rightarrow J/\psi\pi^+\pi^-) = 0.310 \pm 0.028$.				

$\Gamma(\Lambda\Sigma^+\pi^- + \text{c.c.})/\Gamma_{total}$				Γ_{146}/Γ
VALUE (units 10^{-4})	EVTs	DOCUMENT ID	TECN	COMMENT
$1.40 \pm 0.03 \pm 0.13$	2.8k	ABLIKIM	13w	BES3 $\psi(2S) \rightarrow \text{hadrons}$

$\Gamma(\Lambda\Sigma^-\pi^+ + \text{c.c.})/\Gamma_{total}$				Γ_{147}/Γ
VALUE (units 10^{-4})	EVTs	DOCUMENT ID	TECN	COMMENT
$1.54 \pm 0.04 \pm 0.13$	2.8k	ABLIKIM	13w	BES3 $\psi(2S) \rightarrow \text{hadrons}$

See key on page 1171

Meson Particle Listings

$\psi(2S)$

$\Gamma(\Lambda\bar{\Sigma}^0 + c.c.)/\Gamma_{\text{total}}$					Γ_{148}/Γ
VALUE (units 10^{-5})	EVTS	DOCUMENT ID	TECN	COMMENT	
$1.60 \pm 0.31 \pm 0.59$	60	ABLIKIM	21L BES3	$e^+e^- \rightarrow \psi(2S) \rightarrow$ hadrons	

$\Gamma(\Lambda\bar{\Sigma}^0)/\Gamma_{\text{total}}$					Γ_{149}/Γ
VALUE (units 10^{-5})	EVTS	DOCUMENT ID	TECN	COMMENT	
$1.23 \pm 0.23 \pm 0.08$	30	¹ DOBBS	17	$e^+e^- \rightarrow \psi(2S) \rightarrow$ hadrons	
¹ Using CLEO-c data but not authored by the CLEO Collaboration.					

$\Gamma(\Sigma^0 \bar{p} K^+ + c.c.)/\Gamma_{\text{total}}$					Γ_{150}/Γ
VALUE (units 10^{-5})	EVTS	DOCUMENT ID	TECN	COMMENT	
$1.67 \pm 0.13 \pm 0.12$	276	¹ ABLIKIM	13D BES3	$\psi(2S) \rightarrow \gamma \Lambda \bar{p} K^+$	
¹ Using $B(\Lambda \rightarrow p \pi^-) = 63.9\%$, and $B(\Sigma^0 \rightarrow \Lambda \gamma) = 100\%$.					

$\Gamma(\Sigma^+ \bar{\Sigma}^-)/\Gamma_{\text{total}}$					Γ_{151}/Γ
VALUE (units 10^{-4})	EVTS	DOCUMENT ID	TECN	COMMENT	
2.43 ± 0.10 OUR AVERAGE		Error includes scale factor of 1.4.			
$2.52 \pm 0.04 \pm 0.09$	5.4k	ABLIKIM	21AT BES3	$\psi(2S) \rightarrow p \pi^0 \bar{p} \pi^0$	
$2.31 \pm 0.06 \pm 0.10$	1.9k	¹ DOBBS	17	$e^+e^- \rightarrow \psi(2S) \rightarrow$ hadrons	
$2.57 \pm 0.44 \pm 0.68$	35	PEDLAR	05 CLEO	$e^+e^- \rightarrow \psi(2S) \rightarrow$ hadrons	
••• We do not use the following data for averages, fits, limits, etc. •••					
$2.51 \pm 0.15 \pm 0.16$	281	^{1,2} DOBBS	14	$e^+e^- \rightarrow \psi(2S) \rightarrow$ hadrons	
¹ Using CLEO-c data but not authored by the CLEO Collaboration.					
² Superseded by DOBBS 17.					

$\Gamma(\Sigma^0 \bar{\Sigma}^0)/\Gamma_{\text{total}}$					Γ_{152}/Γ
VALUE (units 10^{-4})	EVTS	DOCUMENT ID	TECN	COMMENT	
2.35 ± 0.09 OUR AVERAGE		Error includes scale factor of 1.1.			
$2.44 \pm 0.03 \pm 0.11$	7k	ABLIKIM	17L BES3	$e^+e^- \rightarrow \psi(2S) \rightarrow$ hadrons	
$2.22 \pm 0.05 \pm 0.11$	2.6k	¹ DOBBS	17	$e^+e^- \rightarrow \psi(2S) \rightarrow$ hadrons	
$2.35 \pm 0.36 \pm 0.32$	59	ABLIKIM	07c BES	$e^+e^- \rightarrow \psi(2S) \rightarrow$ hadrons	
$2.63 \pm 0.35 \pm 0.21$	58	PEDLAR	05 CLEO	$e^+e^- \rightarrow \psi(2S) \rightarrow$ hadrons	
••• We do not use the following data for averages, fits, limits, etc. •••					
$2.25 \pm 0.11 \pm 0.16$	439	^{1,2} DOBBS	14	$e^+e^- \rightarrow \psi(2S) \rightarrow$ hadrons	
$1.2 \pm 0.4 \pm 0.4$	8	³ BAI	01 BES	$e^+e^- \rightarrow \psi(2S) \rightarrow$ hadrons	
¹ Using CLEO-c data but not authored by the CLEO Collaboration.					
² Superseded by DOBBS 17.					
³ Estimated using $B(\psi(2S) \rightarrow J/\psi \pi^+ \pi^-) = 0.310 \pm 0.028$.					

$\Gamma(\Sigma^- \bar{\Sigma}^+)/\Gamma_{\text{total}}$					Γ_{153}/Γ
VALUE (units 10^{-4})	EVTS	DOCUMENT ID	TECN	COMMENT	
$2.82 \pm 0.04 \pm 0.08$	6.6k	ABLIKIM	22AV BES3	$\psi(2S) \rightarrow n \pi^- \bar{n} \pi^+$	

$\Gamma(\Sigma^+ \bar{\Sigma}^- \eta)/\Gamma_{\text{total}}$					Γ_{154}/Γ
VALUE (units 10^{-6})	EVTS	DOCUMENT ID	TECN	COMMENT	
$9.59 \pm 2.37 \pm 0.61$	21	ABLIKIM	22AY BES3	$\psi(2S) \rightarrow \Sigma^+ \bar{\Sigma}^- \eta$	

$\Gamma(\Sigma^+ \bar{\Sigma}^- \omega)/\Gamma_{\text{total}}$					Γ_{155}/Γ
VALUE (units 10^{-5})	EVTS	DOCUMENT ID	TECN	COMMENT	
$1.89 \pm 0.18 \pm 0.21$	199	ABLIKIM	23BE BES3	$e^+e^- \rightarrow \psi(2S) \rightarrow$ hadrons	

$\Gamma(\Sigma^+ \bar{\Sigma}^- \phi)/\Gamma_{\text{total}}$					Γ_{156}/Γ
VALUE (units 10^{-6})	EVTS	DOCUMENT ID	TECN	COMMENT	
$2.96 \pm 0.54 \pm 0.41$	55	ABLIKIM	23BE BES3	$e^+e^- \rightarrow \psi(2S) \rightarrow$ hadrons	

$\Gamma(\Sigma(1385)^+ \bar{\Sigma}(1385)^-)/\Gamma_{\text{total}}$					Γ_{157}/Γ
VALUE (units 10^{-5})	EVTS	DOCUMENT ID	TECN	COMMENT	
8.5 ± 0.7 OUR AVERAGE					
$8.4 \pm 0.5 \pm 0.5$	1.5k	ABLIKIM	16L BES3	$\psi(2S) \rightarrow \Sigma(1385)^+ \bar{\Sigma}(1385)^-$	
$11 \pm 3 \pm 3$	14	¹ BAI	01 BES	$e^+e^- \rightarrow \psi(2S) \rightarrow$ hadrons	
¹ Estimated using $B(\psi(2S) \rightarrow J/\psi \pi^+ \pi^-) = 0.310 \pm 0.028$.					

$\Gamma(\Sigma(1385)^- \bar{\Sigma}(1385)^+)/\Gamma_{\text{total}}$					Γ_{158}/Γ
VALUE (units 10^{-5})	EVTS	DOCUMENT ID	TECN	COMMENT	
$8.5 \pm 0.6 \pm 0.6$	1.4k	ABLIKIM	16L BES3	$\psi(2S) \rightarrow \Sigma(1385)^- \bar{\Sigma}(1385)^+$	

$\Gamma(\Sigma(1385)^0 \bar{\Sigma}(1385)^0)/\Gamma_{\text{total}}$					Γ_{159}/Γ
VALUE (units 10^{-4})	EVTS	DOCUMENT ID	TECN	COMMENT	
$0.69 \pm 0.05 \pm 0.05$	2.2k	ABLIKIM	17E BES3	$e^+e^- \rightarrow \psi(2S) \rightarrow$ hadrons	

$\Gamma(\Xi^- \bar{\Xi}^+)/\Gamma_{\text{total}}$					Γ_{160}/Γ
VALUE (units 10^{-4})	CL% EVTS	DOCUMENT ID	TECN	COMMENT	
2.87 ± 0.11 OUR AVERAGE		Error includes scale factor of 1.1.			
$3.03 \pm 0.05 \pm 0.14$	3.6k	¹ DOBBS	17	$e^+e^- \rightarrow \psi(2S) \rightarrow$ hadrons	
$2.78 \pm 0.05 \pm 0.14$	5k	ABLIKIM	16L BES3	$\psi(2S) \rightarrow \Xi^- \bar{\Xi}^+$	
$3.03 \pm 0.40 \pm 0.32$	67	ABLIKIM	07c BES	$e^+e^- \rightarrow \psi(2S) \rightarrow$ hadrons	
$2.38 \pm 0.30 \pm 0.21$	63	PEDLAR	05 CLEO	$e^+e^- \rightarrow \psi(2S) \rightarrow$ hadrons	

$\Gamma(\Xi^0 \bar{\Xi}^0)/\Gamma_{\text{total}}$					Γ_{161}/Γ
VALUE (units 10^{-4})	CL% EVTS	DOCUMENT ID	TECN	COMMENT	
2.3 ± 0.4 OUR AVERAGE		Error includes scale factor of 4.2.			
$2.73 \pm 0.03 \pm 0.13$	11k	ABLIKIM	17E BES3	$e^+e^- \rightarrow \psi(2S) \rightarrow$ hadrons	
$1.97 \pm 0.06 \pm 0.11$	1.2k	¹ DOBBS	17	$e^+e^- \rightarrow \psi(2S) \rightarrow$ hadrons	
$2.75 \pm 0.64 \pm 0.61$	19	PEDLAR	05 CLEO	$e^+e^- \rightarrow \psi(2S) \rightarrow$ hadrons	
••• We do not use the following data for averages, fits, limits, etc. •••					
$2.02 \pm 0.19 \pm 0.15$	112	^{1,2} DOBBS	14	$e^+e^- \rightarrow \psi(2S) \rightarrow$ hadrons	
¹ Using CLEO-c data but not authored by the CLEO Collaboration.					
² Superseded by DOBBS 17.					
³ Estimated using $B(\psi(2S) \rightarrow J/\psi \pi^+ \pi^-) = 0.310 \pm 0.028$.					

¹ Using CLEO-c data but not authored by the CLEO Collaboration.
² Superseded by DOBBS 17.
³ Estimated using $B(\psi(2S) \rightarrow J/\psi \pi^+ \pi^-) = 0.310 \pm 0.028$.

$\Gamma(\Xi(1530)^0 \bar{\Xi}(1530)^0)/\Gamma_{\text{total}}$					Γ_{162}/Γ
VALUE (units 10^{-5})	CL% EVTS	DOCUMENT ID	TECN	COMMENT	
$6.77 \pm 0.14 \pm 0.39$	2951	ABLIKIM	21A0 BES3	$e^+e^- \rightarrow \psi(2S) \rightarrow$ hadrons	
••• We do not use the following data for averages, fits, limits, etc. •••					
< 32	90	PEDLAR	05 CLEO	$e^+e^- \rightarrow \psi(2S) \rightarrow$ hadrons	
< 8.1	90	¹ BAI	01 BES	$e^+e^- \rightarrow \psi(2S) \rightarrow$ hadrons	
¹ Estimated using $B(\psi(2S) \rightarrow J/\psi \pi^+ \pi^-) = 0.310 \pm 0.028$.					

$\Gamma(\Lambda \bar{\Xi}^+ K^- + c.c.)/\Gamma_{\text{total}}$					Γ_{163}/Γ
VALUE (units 10^{-5})	EVTS	DOCUMENT ID	TECN	COMMENT	
$3.86 \pm 0.27 \pm 0.32$	236	ABLIKIM	15I BES3	$e^+e^- \rightarrow \psi(2S) \rightarrow$ $K^- \Lambda \bar{\Xi}^+ + c.c.$	

$\Gamma(\Xi(1530)^- \bar{\Xi}(1530)^+)/\Gamma_{\text{total}}$					Γ_{166}/Γ
VALUE (units 10^{-5})	EVTS	DOCUMENT ID	TECN	COMMENT	
$11.45 \pm 0.40 \pm 0.59$	5k	ABLIKIM	19AT BES3	$e^+e^- \rightarrow \psi(2S) \rightarrow$ hadrons	

$\Gamma(\Xi(1530)^0 \bar{\Xi}^+)/\Gamma_{\text{total}}$					Γ_{167}/Γ
VALUE (units 10^{-6})	EVTS	DOCUMENT ID	TECN	COMMENT	
$7.0 \pm 1.1 \pm 0.4$	399	ABLIKIM	19AT BES3	$e^+e^- \rightarrow \psi(2S) \rightarrow$ hadrons	

$\Gamma(\Xi(1530)^0 \bar{\Xi}^0)/\Gamma_{\text{total}}$					Γ_{168}/Γ
VALUE (units 10^{-5})	EVTS	DOCUMENT ID	TECN	COMMENT	
$0.53 \pm 0.04 \pm 0.03$	278	ABLIKIM	21A0 BES3	$e^+e^- \rightarrow \psi(2S) \rightarrow$ hadrons	

$\Gamma(\Xi(1690)^- \bar{\Xi}^+ \rightarrow K^- \Lambda \bar{\Xi}^+ + c.c.)/\Gamma_{\text{total}}$					Γ_{164}/Γ
VALUE (units 10^{-6})	EVTS	DOCUMENT ID	TECN	COMMENT	
$5.21 \pm 1.48 \pm 0.57$	74	ABLIKIM	15I BES3	$e^+e^- \rightarrow \psi(2S) \rightarrow$ $K^- \Lambda \bar{\Xi}^+ + c.c.$	

$\Gamma(\Xi(1820)^- \bar{\Xi}^+ \rightarrow K^- \Lambda \bar{\Xi}^+ + c.c.)/\Gamma_{\text{total}}$					Γ_{165}/Γ
VALUE (units 10^{-6})	EVTS	DOCUMENT ID	TECN	COMMENT	
$12.03 \pm 2.94 \pm 1.22$	136	ABLIKIM	15I BES3	$e^+e^- \rightarrow \psi(2S) \rightarrow$ $K^- \Lambda \bar{\Xi}^+ + c.c.$	

$\Gamma(\Sigma^0 \bar{\Xi}^+ K^- + c.c.)/\Gamma_{\text{total}}$					Γ_{169}/Γ
VALUE (units 10^{-5})	EVTS	DOCUMENT ID	TECN	COMMENT	
$3.67 \pm 0.33 \pm 0.28$	142	ABLIKIM	15I BES3	$e^+e^- \rightarrow \psi(2S) \rightarrow$ $K^- \Sigma^0 \bar{\Xi}^+ + c.c.$	

$\Gamma(\Omega^- \bar{\Omega}^+)/\Gamma_{\text{total}}$					Γ_{170}/Γ
VALUE (units 10^{-5})	CL% EVTS	DOCUMENT ID	TECN	COMMENT	
5.66 ± 0.30 OUR AVERAGE		Error includes scale factor of 1.3.			
$5.85 \pm 0.12 \pm 0.25$	4k	¹ ABLIKIM	21E BES3	$\psi(2S) \rightarrow \Omega^- \bar{\Omega}^+ \rightarrow$ $\Lambda K^- \bar{\Lambda} K^+$	
$5.2 \pm 0.3 \pm 0.3$	326	^{1,2} DOBBS	17	$e^+e^- \rightarrow \psi(2S) \rightarrow$ hadrons	

••• We do not use the following data for averages, fits, limits, etc. •••					
$4.7 \pm 0.9 \pm 0.5$	27	^{1,2,3} DOBBS	14	$e^+e^- \rightarrow \psi(2S) \rightarrow$ hadrons	
< 15	90	ABLIKIM	12Q BES2	$e^+e^- \rightarrow \psi(2S) \rightarrow$ hadrons	
< 16	90	PEDLAR	05 CLEO	$e^+e^- \rightarrow \psi(2S) \rightarrow$ hadrons	
< 7.3	90	⁴ BAI	01 BES	$e^+e^- \rightarrow \psi(2S) \rightarrow$ hadrons	

¹ Using $B(\Omega^- \rightarrow \Lambda K^-) = (67.8 \pm 0.7)\%$ and $B(\Lambda \rightarrow p \pi^-) = (63.9 \pm 0.5)\%$.
² Using CLEO-c data but not authored by the CLEO Collaboration.
³ Superseded by DOBBS 17.
⁴ Estimated using $B(\psi(2S) \rightarrow J/\psi \pi^+ \pi^-) = 0.310 \pm 0.028$.

Meson Particle Listings

$\psi(2S)$

$\Gamma(\eta_c \pi^+ \pi^- \pi^0)/\Gamma_{\text{total}}$				Γ_{171}/Γ
VALUE (units 10^{-3})	CL%	DOCUMENT ID	TECN	COMMENT
<1.0	90	PEDLAR	07	CLEO $e^+ e^- \rightarrow \psi(2S)$

$\Gamma(h_c(1P) \pi^0)/\Gamma_{\text{total}}$				Γ_{172}/Γ
VALUE (units 10^{-4})	EVTS	DOCUMENT ID	TECN	COMMENT
7.4 ± 0.5 OUR AVERAGE				
7.32 ± 0.34 ± 0.41	46k	ABLIKIM	22Aq	BES3 $\psi(2S) \rightarrow \pi^0$ hadrons
9.0 ± 1.5 ± 1.3	3k	¹ GE	11	CLEO $\psi(2S) \rightarrow \pi^0$ anything
8.4 ± 1.3 ± 1.0	11k	² ABLIKIM	10b	BES3 $\psi(2S) \rightarrow \pi^0 h_c$
seen	92 ⁺²³ ₋₂₂	ADAMS	09	CLEO $\psi(2S) \rightarrow 2\pi^+ 2\pi^- 2\pi^0$
seen	1282	DOBBS	08A	CLEO $\psi(2S) \rightarrow \pi^0 \eta_c \gamma$
seen	168 ± 40	ROSNER	05	CLEO $\psi(2S) \rightarrow \pi^0 \eta_c \gamma$

¹ Assuming a width $\Gamma(h_c(1P)) = 0.86 \text{ MeV} \equiv \Gamma_0$, a measured dependence of the central value of $B = (7.6 + 1.4 \times \Gamma(h_c(1P))/\Gamma_0) \times 10^{-4}$, and with a systematic error that accounts for the width variation range 0.43–1.29 MeV.

² Superseded by ABLIKIM 22Aq

$\Gamma(A_c^+ \bar{p} e^+ e^- + \text{c.c.})/\Gamma_{\text{total}}$				Γ_{173}/Γ	
VALUE	CL%	EVTS	DOCUMENT ID	TECN	COMMENT
<1.7 × 10⁻⁶	90	450M	ABLIKIM	18q	BES3 $e^+ e^- \rightarrow \psi(2S)$

$\Gamma(\Theta(1540) \bar{\Theta}(1540) \rightarrow K_S^0 p K^- \bar{n} + \text{c.c.})/\Gamma_{\text{total}}$				Γ_{174}/Γ
VALUE (units 10^{-5})	CL%	DOCUMENT ID	TECN	COMMENT
<0.88	90	BAI	04G	BES2 $e^+ e^-$

$\Gamma(\Theta(1540) K^- \bar{n} \rightarrow K_S^0 p K^- \bar{n})/\Gamma_{\text{total}}$				Γ_{175}/Γ
VALUE (units 10^{-5})	CL%	DOCUMENT ID	TECN	COMMENT
<1.0	90	BAI	04G	BES2 $e^+ e^-$

$\Gamma(\Theta(1540) K_S^0 \bar{p} \rightarrow K_S^0 \bar{p} K^+ n)/\Gamma_{\text{total}}$				Γ_{176}/Γ
VALUE (units 10^{-5})	CL%	DOCUMENT ID	TECN	COMMENT
<0.70	90	BAI	04G	BES2 $e^+ e^-$

$\Gamma(\bar{\Theta}(1540) K^+ n \rightarrow K_S^0 \bar{p} K^+ n)/\Gamma_{\text{total}}$				Γ_{177}/Γ
VALUE (units 10^{-5})	CL%	DOCUMENT ID	TECN	COMMENT
<2.6	90	BAI	04G	BES2 $e^+ e^-$

$\Gamma(\bar{\Theta}(1540) K_S^0 \bar{p} \rightarrow K_S^0 \bar{p} K^- \bar{n})/\Gamma_{\text{total}}$				Γ_{178}/Γ
VALUE (units 10^{-5})	CL%	DOCUMENT ID	TECN	COMMENT
<0.60	90	BAI	04G	BES2 $e^+ e^-$

RADIATIVE DECAYS

$\Gamma(\gamma \chi_{c0}(1P))/\Gamma_{\text{total}}$				Γ_{179}/Γ
VALUE (units 10^{-2})	EVTS	DOCUMENT ID	TECN	COMMENT
9.77 ± 0.23 OUR FIT				Error includes scale factor of 1.1.
9.33 ± 0.26 OUR AVERAGE				
9.389 ± 0.014 ± 0.332	4.7M	ABLIKIM	17u	BES3 $e^+ e^- \rightarrow \gamma X$
9.22 ± 0.11 ± 0.46	72k	ATHAR	04	CLEO $e^+ e^- \rightarrow \gamma X$
9.9 ± 0.5 ± 0.8		¹ GAISER	86	CBAL $e^+ e^- \rightarrow \gamma X$
7.2 ± 2.3		¹ BIDDICK	77	CNTR $e^+ e^- \rightarrow \gamma X$
7.5 ± 2.6		¹ WHITAKER	76	MRK1 $e^+ e^-$

¹ Angular distribution $(1 + \cos^2 \theta)$ assumed.

$\Gamma(\gamma \chi_{c1}(1P))/\Gamma_{\text{total}}$				Γ_{180}/Γ
VALUE (units 10^{-2})	EVTS	DOCUMENT ID	TECN	COMMENT
9.75 ± 0.27 OUR FIT				Error includes scale factor of 1.1.
9.54 ± 0.29 OUR AVERAGE				
9.905 ± 0.011 ± 0.353	5.0M	ABLIKIM	17u	BES3 $e^+ e^- \rightarrow \gamma X$
9.07 ± 0.11 ± 0.54	76k	ATHAR	04	CLEO $e^+ e^- \rightarrow \gamma X$
9.0 ± 0.5 ± 0.7		¹ GAISER	86	CBAL $e^+ e^- \rightarrow \gamma X$
7.1 ± 1.9		² BIDDICK	77	CNTR $e^+ e^- \rightarrow \gamma X$

¹ Angular distribution $(1 - 0.189 \cos^2 \theta)$ assumed.

² Valid for isotropic distribution of the photon.

$\Gamma(\gamma \chi_{c0}(1P))/\Gamma(\gamma \chi_{c1}(1P))$				$\Gamma_{179}/\Gamma_{180}$
VALUE	DOCUMENT ID	TECN	COMMENT	
1.02 ± 0.01 ± 0.07	¹ ATHAR	04	CLEO $e^+ e^- \rightarrow \gamma X$	

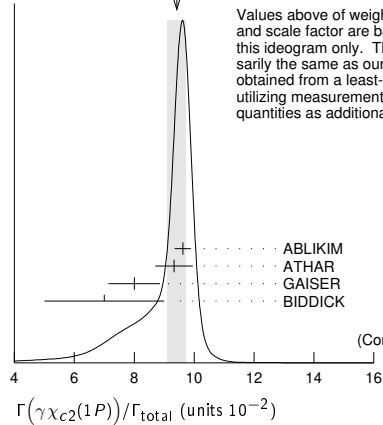
¹ Not independent from ATHAR 04 measurements of $B(\gamma \chi_{cJ})$.

$\Gamma(\gamma \chi_{c2}(1P))/\Gamma_{\text{total}}$				Γ_{181}/Γ
VALUE (units 10^{-2})	EVTS	DOCUMENT ID	TECN	COMMENT
9.36 ± 0.23 OUR FIT				Error includes scale factor of 1.2.
9.42 ± 0.31 OUR AVERAGE				Error includes scale factor of 1.3. See the ideogram below.
9.621 ± 0.013 ± 0.272	4.2M	ABLIKIM	17u	BES3 $e^+ e^- \rightarrow \gamma X$
9.33 ± 0.14 ± 0.61	79k	ATHAR	04	CLEO $e^+ e^- \rightarrow \gamma X$
8.0 ± 0.5 ± 0.7		¹ GAISER	86	CBAL $e^+ e^- \rightarrow \gamma X$
7.0 ± 2.0		² BIDDICK	77	CNTR $e^+ e^- \rightarrow \gamma X$

¹ Angular distribution $(1 - 0.052 \cos^2 \theta)$ assumed.

² Valid for isotropic distribution of the photon.

WEIGHTED AVERAGE
9.42 ± 0.31 (Error scaled by 1.3)



Values above of weighted average, error, and scale factor are based upon the data in this ideogram only. They are not necessarily the same as our 'best' values, obtained from a least-squares constrained fit utilizing measurements of other (related) quantities as additional information.

VALUE	DOCUMENT ID	TECN	COMMENT	χ^2
17u	BES3	0.6		
04	CLEO	0.0		
86	CBAL	2.7		
77	CNTR			
				3.3

(Confidence Level = 0.193)

$[\Gamma(\gamma \chi_{c0}(1P)) + \Gamma(\gamma \chi_{c1}(1P)) + \Gamma(\gamma \chi_{c2}(1P))]/\Gamma_{\text{total}}$				$(\Gamma_{179} + \Gamma_{180} + \Gamma_{181})/\Gamma$
VALUE	DOCUMENT ID	TECN	COMMENT	

• • • We do not use the following data for averages, fits, limits, etc. • • •

27.6 ± 0.3 ± 2.0 ¹ATHAR 04 CLEO $e^+ e^- \rightarrow \gamma X$

¹ Not independent from ATHAR 04 measurements of $B(\gamma \chi_{cJ})$.

$\Gamma(\gamma \chi_{c0}(1P))/\Gamma(\gamma \chi_{c2}(1P))$				$\Gamma_{179}/\Gamma_{181}$
VALUE	DOCUMENT ID	TECN	COMMENT	

• • • We do not use the following data for averages, fits, limits, etc. • • •

0.99 ± 0.02 ± 0.08 ¹ATHAR 04 CLEO $e^+ e^- \rightarrow \gamma X$

¹ Not independent from ATHAR 04 measurements of $B(\gamma \chi_{cJ})$.

$\Gamma(\gamma \chi_{c2}(1P))/\Gamma(\gamma \chi_{c1}(1P))$				$\Gamma_{181}/\Gamma_{180}$
VALUE	DOCUMENT ID	TECN	COMMENT	

• • • We do not use the following data for averages, fits, limits, etc. • • •

1.03 ± 0.02 ± 0.03 ¹ATHAR 04 CLEO $e^+ e^- \rightarrow \gamma X$

¹ Not independent from ATHAR 04 measurements of $B(\gamma \chi_{cJ})$.

$\Gamma(\gamma \eta_c(1S))/\Gamma_{\text{total}}$				Γ_{182}/Γ
VALUE (units 10^{-2})	EVTS	DOCUMENT ID	TECN	COMMENT

0.36 ± 0.05 OUR FIT Error includes scale factor of 1.3.

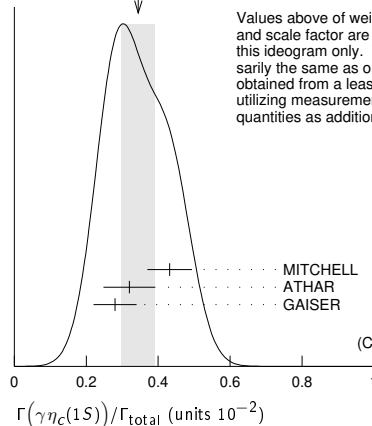
0.34 ± 0.05 OUR AVERAGE Error includes scale factor of 1.3. See the ideogram below.

0.432 ± 0.016 ± 0.060		MITCHELL	09	CLEO $e^+ e^- \rightarrow \gamma X$
0.32 ± 0.04 ± 0.06	2.5k	¹ ATHAR	04	CLEO $e^+ e^- \rightarrow \gamma X$
0.28 ± 0.06		² GAISER	86	CBAL $e^+ e^- \rightarrow \gamma X$

¹ ATHAR 04 used $\Gamma_{\eta_c(1S)} = 24.8 \pm 4.9 \text{ MeV}$ to obtain this result.

² GAISER 86 used $\Gamma_{\eta_c(1S)} = 11.5 \pm 4.5 \text{ MeV}$ to obtain this result.

WEIGHTED AVERAGE
0.34 ± 0.05 (Error scaled by 1.3)



Values above of weighted average, error, and scale factor are based upon the data in this ideogram only. They are not necessarily the same as our 'best' values, obtained from a least-squares constrained fit utilizing measurements of other (related) quantities as additional information.

VALUE	DOCUMENT ID	TECN	COMMENT	χ^2
09	CLEO	2.0		
04	CLEO	0.1		
86	CBAL	1.2		
				3.3

(Confidence Level = 0.196)

$\Gamma(\gamma \eta_c(2S))/\Gamma_{\text{total}}$				Γ_{183}/Γ
VALUE (units 10^{-4})	CL%	DOCUMENT ID	TECN	COMMENT

7 ± 2 ± 4 ¹ABLIKIM 12g BES3 $\psi(2S) \rightarrow \gamma K^0 K \pi, K K \pi^0$

••• We do not use the following data for averages, fits, limits, etc. •••

< 8	90	² CRONIN-HENL.10	CLEO	$\psi(2S) \rightarrow \gamma K \bar{K} \pi$
<20	90	ATHAR 04	CLEO	$e^+ e^- \rightarrow \gamma X$
20-130	95	EDWARDS 82c	CBAL	$e^+ e^- \rightarrow \gamma X$

¹ ABLIKIM 12G reports $[\Gamma(\psi(2S) \rightarrow \gamma \eta_c(2S))/\Gamma_{\text{total}}] \times [B(\eta_c(2S) \rightarrow K \bar{K} \pi)] = (1.30 \pm 0.20 \pm 0.30) \times 10^{-5}$ which we divide by our best value $B(\eta_c(2S) \rightarrow K \bar{K} \pi) = (1.9 \pm 1.2) \times 10^{-2}$. Our first error is their experiment's error and our second error is the systematic error from using our best value.

² CRONIN-HENNESSY 10 reports $[\Gamma(\psi(2S) \rightarrow \gamma \eta_c(2S))/\Gamma_{\text{total}}] \times [B(\eta_c(2S) \rightarrow K \bar{K} \pi)] < 14.5 \times 10^{-6}$ which we divide by our best value $B(\eta_c(2S) \rightarrow K \bar{K} \pi) = 1.9 \times 10^{-2}$. This measurement assumes $\Gamma(\eta_c(2S)) = 14$ MeV. CRONIN-HENNESSY 10 gives the analytic dependence of limits on width.

$\Gamma(\gamma \pi^0)/\Gamma_{\text{total}}$ Γ_{184}/Γ

VALUE (units 10^{-6})	CL%	EVTS	DOCUMENT ID	TECN	COMMENT
1.04 ± 0.22 OUR AVERAGE					Error includes scale factor of 1.4.
< 5	90	423	ABLIKIM 17X	BES3	$\psi(2S) \rightarrow \gamma \pi^0$
1.58 ± 0.40 ± 0.13	37		ABLIKIM 10F	BES3	$\psi(2S) \rightarrow \gamma \pi^0$

••• We do not use the following data for averages, fits, limits, etc. •••

< 5	90	PEDLAR 09	CLE3	$\psi(2S) \rightarrow \gamma X$
<5400	95	¹ LIBERMAN 75	SPEC	$e^+ e^-$
< 1×10^4	90	WIJK 75	DASP	$e^+ e^-$

¹ Restated by us using $B(\psi(2S) \rightarrow \mu^+ \mu^-) = 0.0077$.

$\Gamma(\gamma 2(\pi^+ \pi^-))/\Gamma_{\text{total}}$ Γ_{185}/Γ

VALUE (units 10^{-5})	EVTS	DOCUMENT ID	TECN	COMMENT
39.6 ± 2.8 ± 5.0	583	ABLIKIM 07D	BES2	$e^+ e^- \rightarrow \psi(2S)$

$\Gamma(\gamma 3(\pi^+ \pi^-))/\Gamma_{\text{total}}$ Γ_{186}/Γ

VALUE (units 10^{-5})	CL%	DOCUMENT ID	TECN	COMMENT
<17	90	ABLIKIM 07D	BES2	$e^+ e^- \rightarrow \psi(2S)$

$\Gamma(\gamma \eta'(958))/\Gamma_{\text{total}}$ Γ_{187}/Γ

VALUE (units 10^{-4})	CL%	EVTS	DOCUMENT ID	TECN	COMMENT
1.24 ± 0.04 OUR AVERAGE					
1.251 ± 0.022 ± 0.062	56k		ABLIKIM 17X	BES3	$\psi(2S) \rightarrow \gamma \pi^+ \pi^- \eta$, $\gamma \pi^0 \pi^0 \eta$
1.26 ± 0.03 ± 0.08	2226	¹ ABLIKIM 10F	BES3	$\psi(2S) \rightarrow 3\gamma \pi^+ \pi^-$, $2\gamma \pi^+ \pi^-$	
1.19 ± 0.08 ± 0.03		PEDLAR 09	CLE3	$\psi(2S) \rightarrow \gamma X$	
1.24 ± 0.27 ± 0.15	23	ABLIKIM 06R	BES2	$e^+ e^- \rightarrow \psi(2S)$	
1.54 ± 0.31 ± 0.20	~ 43	BAI 98F	BES	$\psi(2S) \rightarrow \pi^+ \pi^- 2\gamma$, $\pi^+ \pi^- 3\gamma$	

••• We do not use the following data for averages, fits, limits, etc. •••

< 60	90	² BRAUNSCH... 77	DASP	$e^+ e^-$
< 11	90	³ BARTEL 76	CNTR	$e^+ e^-$

¹ Combining the results from $\eta' \rightarrow \pi^+ \pi^- \eta$ and $\eta' \rightarrow \pi^+ \pi^- \gamma$ decay modes.

² Restated by us using total decay width 228 keV.

³ The value is normalized to the branching ratio for $\Gamma(J/\psi(1S) \eta)/\Gamma_{\text{total}}$.

$\Gamma(\gamma f_2(1270))/\Gamma_{\text{total}}$ Γ_{188}/Γ

VALUE (units 10^{-4})	EVTS	DOCUMENT ID	TECN	COMMENT
2.73 ± 0.29 ± 0.25 OUR AVERAGE				Error includes scale factor of 1.8.
2.84 ± 0.15 ± 0.03	1.9k	^{1,2} DOBBS 15		$\psi(2S) \rightarrow \gamma \pi \pi$
2.12 ± 0.19 ± 0.32		^{3,4} BAI 03c	BES	$\psi(2S) \rightarrow \gamma \pi \pi$

••• We do not use the following data for averages, fits, limits, etc. •••

2.08 ± 0.19 ± 0.33	200.6 ± 18.8	³ BAI 03c	BES	$\psi(2S) \rightarrow \gamma \pi^+ \pi^-$
2.90 ± 1.08 ± 1.07	29.9 ± 11.1	³ BAI 03c	BES	$\psi(2S) \rightarrow \gamma \pi^0 \pi^0$

¹ Using CLEO-c data but not authored by the CLEO Collaboration.

² DOBBS 15 reports $[\Gamma(\psi(2S) \rightarrow \gamma f_2(1270))/\Gamma_{\text{total}}] \times [B(f_2(1270) \rightarrow \pi \pi)] = (2.39 \pm 0.09 \pm 0.09) \times 10^{-4}$ which we divide by our best value $B(f_2(1270) \rightarrow \pi \pi) = (84.3^{+2.8}_{-1.0}) \times 10^{-2}$. Our first error is their experiment's error and our second error is the systematic error from using our best value.

³ Normalized to $B(\psi(2S) \rightarrow J/\psi \pi^+ \pi^-) = 0.305 \pm 0.016$.

⁴ Combining the results from $\pi^+ \pi^-$ and $\pi^0 \pi^0$ decay modes.

$\Gamma(\gamma f_0(1370) \rightarrow \gamma K \bar{K})/\Gamma_{\text{total}}$ Γ_{189}/Γ

VALUE (units 10^{-5})	EVTS	DOCUMENT ID	TECN	COMMENT
3.1 ± 1.0 ± 1.4	175	¹ DOBBS 15		$\psi(2S) \rightarrow \gamma K \bar{K}$

¹ Using CLEO-c data but not authored by the CLEO Collaboration.

$\Gamma(\gamma f_0(1500))/\Gamma_{\text{total}}$ Γ_{190}/Γ

VALUE (units 10^{-5})	EVTS	DOCUMENT ID	TECN	COMMENT
9.3 ± 1.8 ± 0.6	274	^{1,2} DOBBS 15		$\psi(2S) \rightarrow \gamma \pi \pi$

¹ DOBBS 15 reports $[\Gamma(\psi(2S) \rightarrow \gamma f_0(1500))/\Gamma_{\text{total}}] \times [B(f_0(1500) \rightarrow \pi \pi)] = (3.2 \pm 0.6 \pm 0.2) \times 10^{-5}$ which we divide by our best value $B(f_0(1500) \rightarrow \pi \pi) = (34.5 \pm 2.2) \times 10^{-2}$. Our first error is their experiment's error and our second error is the systematic error from using our best value.

² Using CLEO-c data but not authored by the CLEO Collaboration.

$\Gamma(\gamma f_2'(1525))/\Gamma_{\text{total}}$ Γ_{191}/Γ

VALUE (units 10^{-5})	EVTS	DOCUMENT ID	TECN	COMMENT
3.3 ± 0.8 ± 0.1	136	^{1,2} DOBBS 15		$\psi(2S) \rightarrow \gamma K \bar{K}$

¹ DOBBS 15 reports $[\Gamma(\psi(2S) \rightarrow \gamma f_2'(1525))/\Gamma_{\text{total}}] \times [B(f_2'(1525) \rightarrow K \bar{K})] = (2.9 \pm 0.6 \pm 0.3) \times 10^{-5}$ which we divide by our best value $B(f_2'(1525) \rightarrow K \bar{K}) = (88.8 \pm 2.2) \times 10^{-2}$. Our first error is their experiment's error and our second error is the systematic error from using our best value.

² Using CLEO-c data but not authored by the CLEO Collaboration.

$\Gamma(\gamma f_0(1710) \rightarrow \gamma \pi \pi)/\Gamma_{\text{total}}$ Γ_{193}/Γ

VALUE (units 10^{-5})	EVTS	DOCUMENT ID	TECN	COMMENT
3.5 ± 0.6 OUR AVERAGE				
3.6 ± 0.4 ± 0.5	290	¹ DOBBS 15		$\psi(2S) \rightarrow \gamma \pi \pi$
3.01 ± 0.41 ± 1.24	35.6 ± 4.8	² BAI 03c	BES	$\psi(2S) \rightarrow \gamma \pi^+ \pi^-$

¹ Using CLEO-c data but not authored by the CLEO Collaboration.

² Normalized to $B(\psi(2S) \rightarrow J/\psi \pi^+ \pi^-) = 0.305 \pm 0.016$.

$\Gamma(\gamma f_0(1710) \rightarrow \gamma K \bar{K})/\Gamma_{\text{total}}$ Γ_{194}/Γ

VALUE (units 10^{-5})	CL%	EVTS	DOCUMENT ID	TECN	COMMENT
6.6 ± 0.7 OUR AVERAGE					
6.7 ± 0.6 ± 0.6		375	¹ DOBBS 15		$\psi(2S) \rightarrow \gamma K \bar{K}$
6.04 ± 0.90 ± 1.32		39.6 ± 5.9	^{2,3} BAI 03c	BES	$\psi(2S) \rightarrow \gamma K^+ K^-$

••• We do not use the following data for averages, fits, limits, etc. •••

< 15.6	90	6.8 ± 3.1	^{2,3} BAI 03c	BES	$\psi(2S) \rightarrow \gamma K_S^0 K_S^0$
--------	----	-----------	------------------------	-----	---

¹ Using CLEO-c data but not authored by the CLEO Collaboration.

² Includes unknown branching fractions to $K^+ K^-$ or $K_S^0 K_S^0$. We have multiplied the $K^+ K^-$ result by a factor of 2 and the $K_S^0 K_S^0$ result by a factor of 4 to obtain the $K \bar{K}$ result.

³ Normalized to $B(\psi(2S) \rightarrow J/\psi \pi^+ \pi^-) = 0.305 \pm 0.016$.

$\Gamma(\gamma f_0(2100) \rightarrow \gamma \pi \pi)/\Gamma_{\text{total}}$ Γ_{195}/Γ

VALUE (units 10^{-6})	EVTS	DOCUMENT ID	TECN	COMMENT
4.8 ± 0.5 ± 0.9	373	¹ DOBBS 15		$\psi(2S) \rightarrow \gamma \pi \pi$

¹ Using CLEO-c data but not authored by the CLEO Collaboration.

$\Gamma(\gamma f_0(2200) \rightarrow \gamma K \bar{K})/\Gamma_{\text{total}}$ Γ_{196}/Γ

VALUE (units 10^{-6})	EVTS	DOCUMENT ID	TECN	COMMENT
3.2 ± 0.6 ± 0.8	207	¹ DOBBS 15		$\psi(2S) \rightarrow \gamma K \bar{K}$

¹ Using CLEO-c data but not authored by the CLEO Collaboration.

$\Gamma(\gamma f_J(2220) \rightarrow \gamma \pi \pi)/\Gamma_{\text{total}}$ Γ_{197}/Γ

VALUE	CL%	DOCUMENT ID	TECN	COMMENT
< 5.8 × 10⁻⁶	90	^{1,2} DOBBS 15		$\psi(2S) \rightarrow \gamma \pi \pi$

¹ Using CLEO-c data but not authored by the CLEO Collaboration.

² For $\Gamma = 20/50$ MeV, the 90% CL upper limits for $\pi^+ \pi^-$ and $\pi^0 \pi^0$ are $3.2/4.3 \times 10^{-6}$ and $2.6/4.0 \times 10^{-6}$, respectively.

$\Gamma(\gamma f_J(2220) \rightarrow \gamma K \bar{K})/\Gamma_{\text{total}}$ Γ_{198}/Γ

VALUE	CL%	DOCUMENT ID	TECN	COMMENT
< 9.5 × 10⁻⁶	90	^{1,2} DOBBS 15		$\psi(2S) \rightarrow \gamma K \bar{K}$

¹ Using CLEO-c data but not authored by the CLEO Collaboration.

² For $\Gamma = 20/50$ MeV, the 90% CL upper limits for $K^+ K^-$ and $K_S^0 K_S^0$ are $2.1/4.3 \times 10^{-6}$ and $3.7/5.5 \times 10^{-6}$, respectively.

$\Gamma(\gamma \eta)/\Gamma_{\text{total}}$ Γ_{199}/Γ

VALUE (units 10^{-6})	CL%	EVTS	DOCUMENT ID	TECN	COMMENT
0.92 ± 0.18 OUR AVERAGE					
0.85 ± 0.18 ± 0.04		382	¹ ABLIKIM 17X	BES3	$\psi(2S) \rightarrow \gamma \pi^+ \pi^- \pi^0$, $\gamma 3\pi^0$
1.38 ± 0.48 ± 0.09		13	¹ ABLIKIM 10F	BES3	$\psi(2S) \rightarrow \gamma \pi^+ \pi^- \pi^0$, $\gamma 3\pi^0$

••• We do not use the following data for averages, fits, limits, etc. •••

< 2	90	PEDLAR 09	CLE3	$\psi(2S) \rightarrow \gamma X$
< 90	90	BAI 98F	BES	$\psi(2S) \rightarrow \pi^+ \pi^- 3\gamma$
<200	90	YAMADA 77	DASP	$e^+ e^- \rightarrow 3\gamma$

¹ Combining the results from $\eta \rightarrow \pi^+ \pi^- \pi^0$ and $\eta \rightarrow 3\pi^0$ decay modes.

$\Gamma(\gamma \eta \pi^+ \pi^-)/\Gamma_{\text{total}}$ Γ_{200}/Γ

VALUE (units 10^{-4})	EVTS	DOCUMENT ID	TECN	COMMENT
8.71 ± 1.25 ± 1.64	418	ABLIKIM 06R	BES2	$\psi(2S) \rightarrow \gamma \eta \pi^+ \pi^-$

$\Gamma(\gamma \eta(1405) \rightarrow \gamma K \bar{K} \pi)/\Gamma_{\text{total}}$ Γ_{202}/Γ

VALUE (units 10^{-4})	CL%	DOCUMENT ID	TECN	COMMENT
<0.9	90	ABLIKIM 06R	BES2	$\psi(2S) \rightarrow \gamma K_S^0 K^+ \pi^- + \text{c.c.}$

••• We do not use the following data for averages, fits, limits, etc. •••

<1.3	90	ABLIKIM 06R	BES2	$\psi(2S) \rightarrow \gamma K^+ K^- \pi^0$
<1.2	90	¹ SCHARRE 80	MRK1	$e^+ e^-$

¹ Includes unknown branching fraction $\eta(1405) \rightarrow K \bar{K} \pi$.

Meson Particle Listings

 $\psi(2S)$ $\Gamma(\gamma\eta(1405) \rightarrow \gamma\eta\pi^+\pi^-)/\Gamma_{\text{total}}$ Γ_{203}/Γ

VALUE (units 10^{-4})	EVTS	DOCUMENT ID	TECN	COMMENT
$0.36 \pm 0.25 \pm 0.05$	10	ABLIKIM	06R BES2	$\psi(2S) \rightarrow \gamma\eta\pi^+\pi^-$

 $\Gamma(\gamma\eta(1405) \rightarrow \gamma f_0(980)\pi^0 \rightarrow \gamma\pi^+\pi^-\pi^0)/\Gamma_{\text{total}}$ Γ_{204}/Γ

VALUE	CL%	DOCUMENT ID	TECN	COMMENT
$<5.0 \times 10^{-7}$	90	ABLIKIM	17AJ BES3	$\psi(2S) \rightarrow \gamma\pi^+\pi^-\pi^0$

 $\Gamma(\gamma\eta(1475) \rightarrow \gamma K\bar{K}\pi)/\Gamma_{\text{total}}$ Γ_{206}/Γ

VALUE (units 10^{-4})	CL%	DOCUMENT ID	TECN	COMMENT
<1.4	90	ABLIKIM	06R BES2	$\psi(2S) \rightarrow \gamma K^+ K^- \pi^0$

••• We do not use the following data for averages, fits, limits, etc. •••

<1.5	90	ABLIKIM	06R BES2	$\psi(2S) \rightarrow \gamma K_S^0 K^+ \pi^- + \text{c.c.}$
--------	----	---------	----------	---

 $\Gamma(\gamma\eta(1475) \rightarrow \gamma\eta\pi^+\pi^-)/\Gamma_{\text{total}}$ Γ_{207}/Γ

VALUE (units 10^{-4})	CL%	DOCUMENT ID	TECN	COMMENT
<0.88	90	ABLIKIM	06R BES2	$\psi(2S) \rightarrow \gamma\eta\pi^+\pi^-$

 $\Gamma(\gamma K^*0 K^+ \pi^- + \text{c.c.})/\Gamma_{\text{total}}$ Γ_{208}/Γ

VALUE (units 10^{-5})	EVTS	DOCUMENT ID	TECN	COMMENT
$37.0 \pm 6.1 \pm 7.2$	237	ABLIKIM	07D BES2	$e^+e^- \rightarrow \psi(2S)$

 $\Gamma(\gamma K^*0 \bar{K}^*0)/\Gamma_{\text{total}}$ Γ_{209}/Γ

VALUE (units 10^{-5})	EVTS	DOCUMENT ID	TECN	COMMENT
$24.0 \pm 4.5 \pm 5.0$	41	ABLIKIM	07D BES2	$e^+e^- \rightarrow \psi(2S)$

 $\Gamma(\gamma K_S^0 K^+ \pi^- + \text{c.c.})/\Gamma_{\text{total}}$ Γ_{210}/Γ

VALUE (units 10^{-5})	EVTS	DOCUMENT ID	TECN	COMMENT
$25.6 \pm 3.6 \pm 3.6$	115	ABLIKIM	07D BES2	$e^+e^- \rightarrow \psi(2S)$

 $\Gamma(\gamma K^+ K^- \pi^+ \pi^-)/\Gamma_{\text{total}}$ Γ_{211}/Γ

VALUE (units 10^{-5})	EVTS	DOCUMENT ID	TECN	COMMENT
$19.1 \pm 2.7 \pm 4.3$	132	ABLIKIM	07D BES2	$e^+e^- \rightarrow \psi(2S)$

 $\Gamma(\gamma K^+ K^- 2(\pi^+ \pi^-))/\Gamma_{\text{total}}$ Γ_{212}/Γ

VALUE (units 10^{-5})	CL%	DOCUMENT ID	TECN	COMMENT
<22	90	ABLIKIM	07D BES2	$e^+e^- \rightarrow \psi(2S)$

 $\Gamma(\gamma 2(K^+ K^-))/\Gamma_{\text{total}}$ Γ_{213}/Γ

VALUE (units 10^{-5})	CL%	DOCUMENT ID	TECN	COMMENT
<4	90	ABLIKIM	07D BES2	$e^+e^- \rightarrow \psi(2S)$

 $\Gamma(\gamma p\bar{p})/\Gamma_{\text{total}}$ Γ_{214}/Γ

VALUE (units 10^{-5})	EVTS	DOCUMENT ID	TECN	COMMENT
3.9 ± 0.5 OUR AVERAGE	Error includes scale factor of 2.0.			
$4.18 \pm 0.26 \pm 0.18$	348	¹ ALEXANDER	10 CLEO	$\psi(2S) \rightarrow \gamma p\bar{p}$
$2.9 \pm 0.4 \pm 0.4$	142	ABLIKIM	07D BES2	$e^+e^- \rightarrow \psi(2S)$

¹ From a fit of the $p\bar{p}$ mass distribution to a combination of $\gamma f_2(1950)$, $\gamma f_2(2150)$, and $\gamma p\bar{p}$ phase space, for $M(p\bar{p}) < 2.85$ GeV, and accounting for backgrounds from $\psi(2S) \rightarrow \pi^0 p\bar{p}$ and continuum.

 $\Gamma(\gamma f_2(1950) \rightarrow \gamma p\bar{p})/\Gamma_{\text{total}}$ Γ_{215}/Γ

VALUE (units 10^{-5})	EVTS	DOCUMENT ID	TECN	COMMENT
$1.2 \pm 0.2 \pm 0.1$	111	¹ ALEXANDER	10 CLEO	$\psi(2S) \rightarrow \gamma p\bar{p}$

¹ From a fit of the $p\bar{p}$ mass distribution to a combination of $\gamma f_2(1950)$, $\gamma f_2(2150)$, and $\gamma p\bar{p}$ phase space, for $M(p\bar{p}) < 2.85$ GeV, and accounting for backgrounds from $\psi(2S) \rightarrow \pi^0 p\bar{p}$ and continuum.

 $\Gamma(\gamma f_2(2150) \rightarrow \gamma p\bar{p})/\Gamma_{\text{total}}$ Γ_{216}/Γ

VALUE (units 10^{-5})	EVTS	DOCUMENT ID	TECN	COMMENT
$0.72 \pm 0.18 \pm 0.03$	73	¹ ALEXANDER	10 CLEO	$\psi(2S) \rightarrow \gamma p\bar{p}$

¹ From a fit of the $p\bar{p}$ mass distribution to a combination of $\gamma f_2(1950)$, $\gamma f_2(2150)$, and $\gamma p\bar{p}$ phase space, for $M(p\bar{p}) < 2.85$ GeV, and accounting for backgrounds from $\psi(2S) \rightarrow \pi^0 p\bar{p}$ and continuum.

 $\Gamma(\gamma X(1835) \rightarrow \gamma p\bar{p})/\Gamma_{\text{total}}$ Γ_{217}/Γ

VALUE (units 10^{-6})	CL%	DOCUMENT ID	TECN	COMMENT
$4.57 \pm 0.36 \pm 1.77$ 4.26		ABLIKIM	12D BES3	$J/\psi \rightarrow \gamma p\bar{p}$

••• We do not use the following data for averages, fits, limits, etc. •••

<1.6	90	ALEXANDER	10 CLEO	$\psi(2S) \rightarrow \gamma p\bar{p}$
--------	----	-----------	---------	--

<5.4	90	ABLIKIM	07D BES	$\psi(2S) \rightarrow \gamma p\bar{p}$
--------	----	---------	---------	--

 $\Gamma(\gamma X \rightarrow \gamma p\bar{p})/\Gamma_{\text{total}}$ Γ_{218}/Γ

For a narrow resonance in the range $2.2 < M(X) < 2.8$ GeV.

VALUE (units 10^{-6})	CL%	DOCUMENT ID	TECN	COMMENT
<2	90	ALEXANDER	10 CLEO	$\psi(2S) \rightarrow \gamma p\bar{p}$

 $\Gamma(\gamma p\bar{p}\pi^+\pi^-)/\Gamma_{\text{total}}$ Γ_{219}/Γ

VALUE (units 10^{-5})	EVTS	DOCUMENT ID	TECN	COMMENT
$2.8 \pm 1.2 \pm 0.7$	17	ABLIKIM	07D BES2	$e^+e^- \rightarrow \psi(2S)$

 $\Gamma(\gamma J/\psi)/\Gamma_{\text{total}}$ Γ_{221}/Γ

VALUE (units 10^{-4})	EVTS	DOCUMENT ID	TECN	COMMENT
$3.1 \pm 0.6 \pm 0.8$ 1.0	1.1k	ABLIKIM	12O BES3	$e^+e^- \rightarrow \psi(2S)$

••• We do not use the following data for averages, fits, limits, etc. •••

3.2 ± 0.6	1.1k	¹ ABLIKIM	17N BES3	$\psi(2S) \rightarrow \gamma J/\psi$
---------------	------	----------------------	----------	--------------------------------------

¹ Uses $B(J/\psi \rightarrow e^+e^-) = (5.971 \pm 0.032)\%$ and $B(J/\psi \rightarrow \mu^+\mu^-) = (5.961 \pm 0.033)\%$. No systematic error estimation.

 $\Gamma(e^+e^-\eta')/\Gamma_{\text{total}}$ Γ_{222}/Γ

VALUE (units 10^{-6})	EVTS	DOCUMENT ID	TECN	COMMENT
1.90 ± 0.26 OUR AVERAGE				
$1.99 \pm 0.33 \pm 0.12$	57	ABLIKIM	18Z BES3	$\psi(2S) \rightarrow \eta' e^+e^-$, $\eta' \rightarrow \gamma\pi^+\pi^-$

$1.79 \pm 0.38 \pm 0.11$	20	ABLIKIM	18Z BES3	$\psi(2S) \rightarrow \eta' e^+e^-$, $\eta' \rightarrow \eta\pi^+\pi^-$
--------------------------	----	---------	----------	---

 $\Gamma(e^+e^-\eta_c(1S))/\Gamma_{\text{total}}$ Γ_{223}/Γ

VALUE (units 10^{-5})	EVTS	DOCUMENT ID	TECN	COMMENT
$3.77 \pm 0.40 \pm 0.18$	3k	¹ ABLIKIM	22AX BES3	$e^+e^- \rightarrow \psi(2S)$

¹ From a fit to the recoil mass distribution of e^+e^- with inclusive $\eta_c(1S)$ decays.

 $\Gamma(e^+e^-\chi_{c0}(1P))/\Gamma_{\text{total}}$ Γ_{224}/Γ

VALUE (units 10^{-6})	EVTS	DOCUMENT ID	TECN	COMMENT
$10.6 \pm 2.4 \pm 0.7$	48	¹ ABLIKIM	17I BES3	$\psi(2S) \rightarrow e^+e^-\gamma J/\psi$

¹ ABLIKIM 17I reports $(11.7 \pm 2.5 \pm 1.0) \times 10^{-4}$ from a measurement of $[\Gamma(\psi(2S) \rightarrow e^+e^-\chi_{c0}(1P))/\Gamma_{\text{total}}] \times [B(\chi_{c0}(1P) \rightarrow \gamma J/\psi(1S))]$ assuming $B(\chi_{c0}(1P) \rightarrow \gamma J/\psi(1S)) = (1.27 \pm 0.06) \times 10^{-2}$, which we rescale to our best value $B(\chi_{c0}(1P) \rightarrow \gamma J/\psi(1S)) = (1.41 \pm 0.09) \times 10^{-2}$. Our first error is their experiment's error and our second error is the systematic error from using our best value.

 $\Gamma(e^+e^-\chi_{c0}(1P))/\Gamma(\gamma\chi_{c0}(1P))$ $\Gamma_{224}/\Gamma_{179}$

VALUE (units 10^{-3})	EVTS	DOCUMENT ID	TECN	COMMENT
$9.4 \pm 1.9 \pm 0.6$	48	¹ ABLIKIM	17I BES3	$\psi(2S) \rightarrow e^+e^-\gamma J/\psi$

¹ Uses $B(\psi(2S) \rightarrow \gamma\chi_{c0}(1P)) \times B(\chi_{c0}(1P) \rightarrow \gamma J/\psi(1S)) = (15.8 \pm 0.3 \pm 0.6) \times 10^{-4}$ from ABLIKIM 17N and accounts for common systematic errors.

 $\Gamma(e^+e^-\chi_{c1}(1P))/\Gamma_{\text{total}}$ Γ_{225}/Γ

VALUE (units 10^{-4})	EVTS	DOCUMENT ID	TECN	COMMENT
$8.5 \pm 0.6 \pm 0.3$	873	¹ ABLIKIM	17I BES3	$\psi(2S) \rightarrow e^+e^-\gamma J/\psi$

¹ ABLIKIM 17I reports $(8.6 \pm 0.3 \pm 0.6) \times 10^{-4}$ from a measurement of $[\Gamma(\psi(2S) \rightarrow e^+e^-\chi_{c1}(1P))/\Gamma_{\text{total}}] \times [B(\chi_{c1}(1P) \rightarrow \gamma J/\psi(1S))]$ assuming $B(\chi_{c1}(1P) \rightarrow \gamma J/\psi(1S)) = (33.9 \pm 1.2) \times 10^{-2}$, which we rescale to our best value $B(\chi_{c1}(1P) \rightarrow \gamma J/\psi(1S)) = (34.3 \pm 1.3) \times 10^{-2}$. Our first error is their experiment's error and our second error is the systematic error from using our best value.

 $\Gamma(e^+e^-\chi_{c1}(1P))/\Gamma(\gamma\chi_{c1}(1P))$ $\Gamma_{225}/\Gamma_{180}$

VALUE (units 10^{-3})	EVTS	DOCUMENT ID	TECN	COMMENT
$8.3 \pm 0.3 \pm 0.4$	873	¹ ABLIKIM	17I BES3	$\psi(2S) \rightarrow e^+e^-\gamma J/\psi$

¹ Uses $B(\psi(2S) \rightarrow \gamma\chi_{c1}(1P)) \times B(\chi_{c1}(1P) \rightarrow \gamma J/\psi(1S)) = (351.8 \pm 1.0 \pm 12.0) \times 10^{-4}$ from ABLIKIM 17N and accounts for common systematic errors.

 $\Gamma(e^+e^-\chi_{c2}(1P))/\Gamma_{\text{total}}$ Γ_{226}/Γ

VALUE (units 10^{-4})	EVTS	DOCUMENT ID	TECN	COMMENT
$6.8 \pm 0.7 \pm 0.3$	227	¹ ABLIKIM	17I BES3	$\psi(2S) \rightarrow e^+e^-\gamma J/\psi$

¹ ABLIKIM 17I reports $(6.9 \pm 0.5 \pm 0.6) \times 10^{-4}$ from a measurement of $[\Gamma(\psi(2S) \rightarrow e^+e^-\chi_{c2}(1P))/\Gamma_{\text{total}}] \times [B(\chi_{c2}(1P) \rightarrow \gamma J/\psi(1S))]$ assuming $B(\chi_{c2}(1P) \rightarrow \gamma J/\psi(1S)) = (19.2 \pm 0.7) \times 10^{-2}$, which we rescale to our best value $B(\chi_{c2}(1P) \rightarrow \gamma J/\psi(1S)) = (19.5 \pm 0.8) \times 10^{-2}$. Our first error is their experiment's error and our second error is the systematic error from using our best value.

 $\Gamma(e^+e^-\chi_{c2}(1P))/\Gamma(\gamma\chi_{c2}(1P))$ $\Gamma_{226}/\Gamma_{181}$

VALUE (units 10^{-3})	EVTS	DOCUMENT ID	TECN	COMMENT
$6.6 \pm 0.5 \pm 0.4$	227	¹ ABLIKIM	17I BES3	$\psi(2S) \rightarrow e^+e^-\gamma J/\psi$

¹ Uses $B(\psi(2S) \rightarrow \gamma\chi_{c2}(1P)) \times B(\chi_{c2}(1P) \rightarrow \gamma J/\psi(1S)) = (199.6 \pm 0.8 \pm 7.0) \times 10^{-4}$ from ABLIKIM 17N and accounts for common systematic errors.

WEAK DECAYS

 $\Gamma(D^0 e^+e^- + \text{c.c.})/\Gamma_{\text{total}}$ Γ_{227}/Γ

VALUE	CL%	DOCUMENT ID	TECN	COMMENT
$<1.4 \times 10^{-7}$	90	¹ ABLIKIM	17AF BES3	$e^+e^- \rightarrow \psi(2S)$

¹ Using D^0 decays to $K^-\pi^+$, $K^-\pi^+\pi^0$, and $K^-\pi^+\pi^+\pi^-$.

 $\Gamma(\Lambda_c^+ \Sigma^- + \text{c.c.})/\Gamma_{\text{total}}$ Γ_{228}/Γ

VALUE	CL%	DOCUMENT ID	TECN	COMMENT
$<1.4 \times 10^{-5}$	90	¹ ABLIKIM	23 BES3	$e^+e^- \rightarrow \psi(2S)$

¹ Using $\Lambda_c^+ \rightarrow p K^- \pi^+$ and $\Sigma^- \rightarrow \bar{p} \pi^0$.

See key on page 1171

Meson Particle Listings

$\psi(2S)$

OTHER DECAYS

Table with 5 columns: VALUE, CL%, DOCUMENT ID, TECN, COMMENT. Row 1: <2.0, 90, LEES, 131, BABR B -> K(*) psi(2S)

psi(2S) CROSS-PARTICLE BRANCHING RATIOS

For measurements involving B(psi(2S) -> gamma chi_c J(1P)) x B(chi_c J(1P) -> X) see the corresponding entries in the chi_c J(1P) sections.

MULTIPOLE AMPLITUDE RATIOS IN RADIATIVE DECAYS psi(2S) -> gamma chi_c J(1P) and chi_c J -> gamma J/psi(1S)

Table with 5 columns: VALUE (units 10^-2), EVTS, DOCUMENT ID, TECN, COMMENT. Section: a2(chi_c1)/a2(chi_c2) Magnetic quadrupole transition amplitude ratio. Row 1: 63 +/- 7 OUR AVERAGE, 253k, 1 ABLIKIM, 17N, BES3, psi(2S) -> gamma gamma l+ l-

Table with 5 columns: VALUE (units 10^-2), EVTS, DOCUMENT ID, TECN, COMMENT. Section: b2(chi_c2)/b2(chi_c1) Magnetic quadrupole transition amplitude ratio. Row 1: 60 +/- 31 OUR AVERAGE, 59k, 2 ARTUSO, 09, CLEO, psi(2S) -> gamma gamma l+ l-

psi(2S) REFERENCES

Extensive list of references for psi(2S) decays, including authors (e.g., AAIJ, ABLIKIM, LEES), journals (e.g., JHEP, PRL, EPJ), and collaboration names (e.g., BABAR, BESIII, CLEO).

Meson Particle Listings

$\psi(2S), \psi(3770)$

HILGER	75	PRL 35 625	E. Hilger et al.	(STAN, PENN)
LIBERMAN	75	Stanford Symp. 55	A.D. Liberman	(STAN)
LUTH	75	PRL 35 1124	V. Luth et al.	(SLAC, LBL)JPC
WIIK	75	Stanford Symp. 69	B.H. Wiik	(DESY)

$\psi(3770)$

$$I^G(J^{PC}) = 0^-(1^{--})$$

$\psi(3770)$ MASS (MeV)

OUR FIT includes measurements of $m_{\psi(2S)}$, $m_{\psi(3770)}$, and $m_{\psi(3770)} - m_{\psi(2S)}$.

VALUE (MeV)	EVTS	DOCUMENT ID	TECN	COMMENT
3773.7 ± 0.7 OUR FIT	Error includes scale factor of 2.3.			
3778.1 ± 0.7 OUR AVERAGE				
3778.1 ± 0.7 ± 0.6	1	AAIJ	19M	LHCb $pp \rightarrow D\bar{D} + \text{anything}$
3779.2 ^{+1.8+0.6} _{-1.7-0.8}	2	ANASHIN	12A	KEDR $e^+e^- \rightarrow D\bar{D}$
3775.5 ± 2.4 ± 0.5	57	AUBERT	08b	BABR $B \rightarrow D\bar{D}K$
3776 ± 5 ± 4	68	BRODZICKA	08	BELL $B^+ \rightarrow D^0\bar{D}^0K^+$
3778.8 ± 1.9 ± 0.9		AUBERT	07bE	BABR $e^+e^- \rightarrow D\bar{D}\gamma$
••• We do not use the following data for averages, fits, limits, etc. •••				
3779.8 ± 0.6	3	SHAMOV	17	RVUE $e^+e^- \rightarrow D\bar{D}, \text{hadrons}$
3772.0 ± 1.9	4,5	ABLIKIM	08b	BES2 $e^+e^- \rightarrow \text{hadrons}$
3778.4 ± 3.0 ± 1.3	34	CHISTOV	04	BELL Sup. by BRODZICKA 08

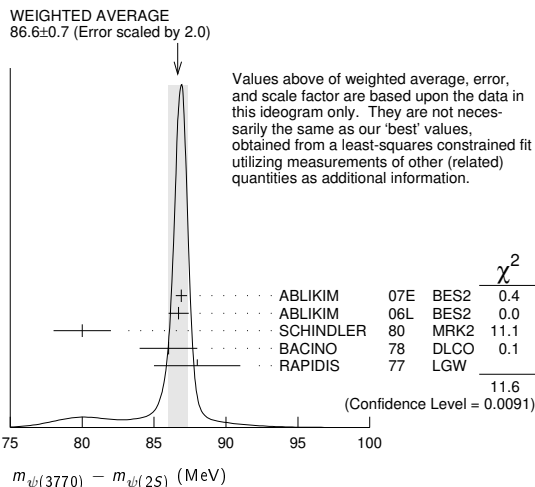
- Measured in prompt hadroproduction.
- Taking into account interference between the resonant and non-resonant $D\bar{D}$ production.
- From the joint analysis of the data on the $D\bar{D}$ and inclusive hadronic cross sections in the $\psi(3770)$ region from BaBar, Belle, BES-II, CLEO and KEDR.
- Reanalysis of data presented in BAI 02c. From a global fit over the center-of-mass energy region 3.7–5.0 GeV covering the $\psi(3770)$, $\psi(4040)$, $\psi(4160)$, and $\psi(4415)$ resonances. Phase angle fixed in the fit to $\delta = 0^\circ$.
- Interference between the resonant and non-resonant $D\bar{D}$ production not taken into account.

$m_{\psi(3770)} - m_{\psi(2S)}$

OUR FIT includes measurements of $m_{\psi(2S)}$, $m_{\psi(3770)}$, and $m_{\psi(3770)} - m_{\psi(2S)}$.

VALUE (MeV)	DOCUMENT ID	TECN	COMMENT
87.6 ± 0.7 OUR FIT	Error includes scale factor of 2.3.		
86.6 ± 0.7 OUR AVERAGE	Error includes scale factor of 2.0. See the ideogram below.		
86.9 ± 0.4	1	ABLIKIM	07E BES2 $e^+e^- \rightarrow \text{hadrons}$
86.7 ± 0.7		ABLIKIM	06L BES2 $e^+e^- \rightarrow \text{hadrons}$
80 ± 2		SCHINDLER	80 MRK2 e^+e^-
86 ± 2	2	BACINO	78 DLCO e^+e^-
88 ± 3		RAPIDIS	77 LGW e^+e^-

- BES-II $\psi(2S)$ mass subtracted (see ABLIKIM 06L).
- SPEAR $\psi(2S)$ mass subtracted (see SCHINDLER 80).



$\psi(3770)$ WIDTH

VALUE (MeV)	EVTS	DOCUMENT ID	TECN	COMMENT
27.2 ± 1.0 OUR FIT				
27.5 ± 0.9 OUR AVERAGE				
24.9 ^{+4.6+0.5} _{-4.0-1.1}	1	ANASHIN	12A	KEDR $e^+e^- \rightarrow D\bar{D}$
30.4 ± 8.5	2,3	ABLIKIM	08b	BES2 $e^+e^- \rightarrow \text{hadrons}$
27 ± 10 ± 5	68	BRODZICKA	08	BELL $B^+ \rightarrow D^0\bar{D}^0K^+$
28.5 ± 1.2 ± 0.2	3	ABLIKIM	07E	BES2 $e^+e^- \rightarrow \text{hadrons}$

23.5 ± 3.7 ± 0.9	AUBERT	07bE	BABR	$e^+e^- \rightarrow D\bar{D}\gamma$
26.9 ± 2.4 ± 0.3	3	ABLIKIM	06L	BES2 $e^+e^- \rightarrow \text{hadrons}$
24 ± 5	3	SCHINDLER	80	MRK2 e^+e^-
24 ± 5	3	BACINO	78	DLCO e^+e^-
28 ± 5	3	RAPIDIS	77	LGW e^+e^-

••• We do not use the following data for averages, fits, limits, etc. •••

25.8 ± 1.3 4 SHAMOV 17 RVUE $e^+e^- \rightarrow D\bar{D}, \text{hadrons}$

- Taking into account interference between the resonant and non-resonant $D\bar{D}$ production.
- Reanalysis of data presented in BAI 02c. From a global fit over the center-of-mass energy region 3.7–5.0 GeV covering the $\psi(3770)$, $\psi(4040)$, $\psi(4160)$, and $\psi(4415)$ resonances. Phase angle fixed in the fit to $\delta = 0^\circ$.
- Interference between the resonant and non-resonant $D\bar{D}$ production not taken into account.
- From the joint analysis of the data on the $D\bar{D}$ and inclusive hadronic cross sections in the $\psi(3770)$ region from BaBar, Belle, BES-II, CLEO and KEDR.

$\psi(3770)$ DECAY MODES

Mode	Fraction (Γ_i/Γ)	Scale factor / Confidence level
$\Gamma_1 D\bar{D}$	(93 ⁺⁸ ₋₅) %	S=2.0
$\Gamma_2 D^0\bar{D}^0$	(52 ⁺⁴ ₋₅) %	S=2.0
$\Gamma_3 D^+D^-$	(41 ± 4) %	S=2.0
$\Gamma_4 J/\psi X$	(5.0 ± 2.2) × 10 ⁻³	
$\Gamma_5 J/\psi \pi^+\pi^-$	(1.93 ± 0.28) × 10 ⁻³	
$\Gamma_6 J/\psi \pi^0\pi^0$	(8.0 ± 3.0) × 10 ⁻⁴	
$\Gamma_7 J/\psi \eta$	(8.7 ± 1.2) × 10 ⁻⁴	
$\Gamma_8 J/\psi \pi^0$	< 2.8 × 10 ⁻⁴	CL=90%
$\Gamma_9 e^+e^-$	(9.6 ± 0.7) × 10 ⁻⁶	S=1.3

Decays to light hadrons

$\Gamma_{10} b_1(1235)\pi$	< 1.4	× 10 ⁻⁵	CL=90%
$\Gamma_{11} \phi\eta'$	< 2.3	× 10 ⁻⁵	CL=90%
$\Gamma_{12} \omega\eta'$	< 4	× 10 ⁻⁴	CL=90%
$\Gamma_{13} \rho^0\eta'$	< 6	× 10 ⁻⁴	CL=90%
$\Gamma_{14} \phi\eta$	(3.1 ± 0.7) × 10 ⁻⁴		
$\Gamma_{15} \omega\eta$	< 1.4	× 10 ⁻⁵	CL=90%
$\Gamma_{16} \rho^0\eta$	< 5	× 10 ⁻⁴	CL=90%
$\Gamma_{17} \phi\pi^0$	< 3	× 10 ⁻⁵	CL=90%
$\Gamma_{18} \omega\pi^0$	< 6	× 10 ⁻⁴	CL=90%
$\Gamma_{19} \pi^+\pi^-\pi^0$	< 5	× 10 ⁻⁶	CL=90%
$\Gamma_{20} \rho\pi$	< 5	× 10 ⁻⁶	CL=90%
$\Gamma_{21} K^+K^-$	not seen		
$\Gamma_{22} K^*(892)^+K^- + \text{c.c.}$	< 1.4	× 10 ⁻⁵	CL=90%
$\Gamma_{23} K^*(892)^0\bar{K}^0 + \text{c.c.}$	< 1.2	× 10 ⁻³	CL=90%
$\Gamma_{24} K_S^0 K_L^0$	< 1.2	× 10 ⁻⁵	CL=90%
$\Gamma_{25} 2(\pi^+\pi^-)$	< 1.12	× 10 ⁻³	CL=90%
$\Gamma_{26} 2(\pi^+\pi^-)\pi^0$	< 1.06	× 10 ⁻³	CL=90%
$\Gamma_{27} 2(\pi^+\pi^-\pi^0)$	< 5.85	%	CL=90%
$\Gamma_{28} \omega\pi^+\pi^-$	< 6.0	× 10 ⁻⁴	CL=90%
$\Gamma_{29} 3(\pi^+\pi^-)$	< 9.1	× 10 ⁻³	CL=90%
$\Gamma_{30} 3(\pi^+\pi^-)\pi^0$	< 1.37	%	CL=90%
$\Gamma_{31} 3(\pi^+\pi^-)2\pi^0$	< 11.74	%	CL=90%
$\Gamma_{32} \eta\pi^+\pi^-$	< 1.24	× 10 ⁻³	CL=90%
$\Gamma_{33} \pi^+\pi^-2\pi^0$	< 8.9	× 10 ⁻³	CL=90%
$\Gamma_{34} \rho^0\pi^+\pi^-$	< 6.9	× 10 ⁻³	CL=90%
$\Gamma_{35} \eta 3\pi$	< 1.34	× 10 ⁻³	CL=90%
$\Gamma_{36} \eta 2(\pi^+\pi^-)$	< 2.43	%	CL=90%
$\Gamma_{37} \eta\rho^0\pi^+\pi^-$	< 1.45	%	CL=90%
$\Gamma_{38} \eta' 3\pi$	< 2.44	× 10 ⁻³	CL=90%
$\Gamma_{39} K^+K^-\pi^+\pi^-$	< 9.0	× 10 ⁻⁴	CL=90%
$\Gamma_{40} \phi\pi^+\pi^-$	< 4.1	× 10 ⁻⁴	CL=90%
$\Gamma_{41} K^+K^-2\pi^0$	< 4.2	× 10 ⁻³	CL=90%
$\Gamma_{42} 4(\pi^+\pi^-)$	< 1.67	%	CL=90%
$\Gamma_{43} 4(\pi^+\pi^-)\pi^0$	< 3.06	%	CL=90%
$\Gamma_{44} \phi f_0(980)$	< 4.5	× 10 ⁻⁴	CL=90%
$\Gamma_{45} K^+K^-\pi^+\pi^-\pi^0$	< 2.36	× 10 ⁻³	CL=90%
$\Gamma_{46} K^+K^-\rho^0\pi^0$	< 8	× 10 ⁻⁴	CL=90%
$\Gamma_{47} K^+K^-\rho^+\pi^-$	< 1.46	%	CL=90%
$\Gamma_{48} \omega K^+K^-$	< 3.4	× 10 ⁻⁴	CL=90%
$\Gamma_{49} \phi\pi^+\pi^-\pi^0$	< 3.8	× 10 ⁻³	CL=90%
$\Gamma_{50} K^{*0}K^-\pi^+\pi^0 + \text{c.c.}$	< 1.62	%	CL=90%
$\Gamma_{51} K^{*+}K^-\pi^+\pi^- + \text{c.c.}$	< 3.23	%	CL=90%
$\Gamma_{52} K^+K^-\pi^+\pi^-2\pi^0$	< 2.67	%	CL=90%
$\Gamma_{53} K^+K^-2(\pi^+\pi^-)$	< 1.03	%	CL=90%
$\Gamma_{54} K^+K^-2(\pi^+\pi^-)\pi^0$	< 3.60	%	CL=90%
$\Gamma_{55} \eta K^+K^-$	< 4.1	× 10 ⁻⁴	CL=90%

Γ_{56}	$\eta K^+ K^- \pi^+ \pi^-$	< 1.24	%	CL=90%
Γ_{57}	$\rho^0 K^+ K^-$	< 5.0	$\times 10^{-3}$	CL=90%
Γ_{58}	$2(K^+ K^-)$	< 6.0	$\times 10^{-4}$	CL=90%
Γ_{59}	$\phi K^+ K^-$	< 7.5	$\times 10^{-4}$	CL=90%
Γ_{60}	$2(K^+ K^-)\pi^0$	< 2.9	$\times 10^{-4}$	CL=90%
Γ_{61}	$2(K^+ K^-)\pi^+ \pi^-$	< 3.2	$\times 10^{-3}$	CL=90%
Γ_{62}	$K_S^0 K^- \pi^+$	< 3.2	$\times 10^{-3}$	CL=90%
Γ_{63}	$K_S^0 K^- \pi^+ \pi^0$	< 1.33	%	CL=90%
Γ_{64}	$K_S^0 K^- \rho^+$	< 6.6	$\times 10^{-3}$	CL=90%
Γ_{65}	$K_S^0 K^- 2\pi^+ \pi^-$	< 8.7	$\times 10^{-3}$	CL=90%
Γ_{66}	$K_S^0 K^- \pi^+ \rho^0$	< 1.6	%	CL=90%
Γ_{67}	$K_S^0 K^- \pi^+ \eta$	< 1.3	%	CL=90%
Γ_{68}	$K_S^0 K^- 2\pi^+ \pi^- \pi^0$	< 4.18	%	CL=90%
Γ_{69}	$K_S^0 K^- 2\pi^+ \pi^- \eta$	< 4.8	%	CL=90%
Γ_{70}	$K_S^0 K^- \pi^+ 2(\pi^+ \pi^-)$	< 1.22	%	CL=90%
Γ_{71}	$K_S^0 K^- \pi^+ 2\pi^0$	< 2.65	%	CL=90%
Γ_{72}	$K_S^0 K^- K^+ K^- \pi^+$	< 4.9	$\times 10^{-3}$	CL=90%
Γ_{73}	$K_S^0 K^- K^+ K^- \pi^+ \pi^0$	< 3.0	%	CL=90%
Γ_{74}	$K_S^0 K^- K^+ K^- \pi^+ \eta$	< 2.2	%	CL=90%
Γ_{75}	$K^{*0} K^- \pi^+ + c.c.$	< 9.7	$\times 10^{-3}$	CL=90%
Γ_{76}	$\rho \bar{\rho}$	not seen		
Γ_{77}	$\rho \bar{\rho} \pi^0$	< 4	$\times 10^{-5}$	CL=90%
Γ_{78}	$\rho \bar{\rho} \pi^+ \pi^-$	< 5.8	$\times 10^{-4}$	CL=90%
Γ_{79}	$\Lambda \bar{\Lambda}$	< 1.2	$\times 10^{-4}$	CL=90%
Γ_{80}	$\rho \bar{\rho} \pi^+ \pi^- \pi^0$	< 1.85	$\times 10^{-3}$	CL=90%
Γ_{81}	$\omega \rho \bar{\rho}$	< 2.9	$\times 10^{-4}$	CL=90%
Γ_{82}	$\Lambda \bar{\Lambda} \pi^0$	< 7	$\times 10^{-5}$	CL=90%
Γ_{83}	$\rho \bar{\rho} 2(\pi^+ \pi^-)$	< 2.6	$\times 10^{-3}$	CL=90%
Γ_{84}	$\eta \rho \bar{\rho}$	< 5.4	$\times 10^{-4}$	CL=90%
Γ_{85}	$\eta \rho \bar{\rho} \pi^+ \pi^-$	< 3.3	$\times 10^{-3}$	CL=90%
Γ_{86}	$\rho^0 \rho \bar{\rho}$	< 1.7	$\times 10^{-3}$	CL=90%
Γ_{87}	$\rho \bar{\rho} K^+ K^-$	< 3.2	$\times 10^{-4}$	CL=90%
Γ_{88}	$\eta \rho \bar{\rho} K^+ K^-$	< 6.9	$\times 10^{-3}$	CL=90%
Γ_{89}	$\pi^0 \rho \bar{\rho} K^+ K^-$	< 1.2	$\times 10^{-3}$	CL=90%
Γ_{90}	$\phi \rho \bar{\rho}$	< 1.3	$\times 10^{-4}$	CL=90%
Γ_{91}	$\Lambda \bar{\Lambda} \pi^+ \pi^-$	< 2.5	$\times 10^{-4}$	CL=90%
Γ_{92}	$\Lambda \bar{\rho} K^+$	< 2.8	$\times 10^{-4}$	CL=90%
Γ_{93}	$\Lambda \bar{\rho} K^+ \pi^+ \pi^-$	< 6.3	$\times 10^{-4}$	CL=90%
Γ_{94}	$\Lambda \bar{\Lambda} \eta$	< 1.9	$\times 10^{-4}$	CL=90%
Γ_{95}	$\Sigma^+ \Sigma^-$	< 1.0	$\times 10^{-4}$	CL=90%
Γ_{96}	$\Sigma^0 \Sigma^0$	< 4	$\times 10^{-5}$	CL=90%
Γ_{97}	$\Xi^+ \Xi^-$	< 1.5	$\times 10^{-4}$	CL=90%
Γ_{98}	$\Xi^0 \Xi^0$	< 1.4	$\times 10^{-4}$	CL=90%
Γ_{99}	$\Xi^- \Xi^+$	(1.4 \pm 0.4)	$\times 10^{-4}$	

Radiative decays

Γ_{100}	$\gamma \chi_{c2}$	< 6.4	$\times 10^{-4}$	CL=90%
Γ_{101}	$\gamma \chi_{c1}$	(2.49 \pm 0.23)	$\times 10^{-3}$	
Γ_{102}	$\gamma \chi_{c0}$	(6.9 \pm 0.6)	$\times 10^{-3}$	
Γ_{103}	$\gamma \eta_c$	< 7	$\times 10^{-4}$	CL=90%
Γ_{104}	$\gamma \eta_c(2S)$	< 9	$\times 10^{-4}$	CL=90%
Γ_{105}	$\gamma \eta'$	< 1.8	$\times 10^{-4}$	CL=90%
Γ_{106}	$\gamma \eta$	< 1.5	$\times 10^{-4}$	CL=90%
Γ_{107}	$\gamma \pi^0$	< 2	$\times 10^{-4}$	CL=90%

CONSTRAINED FIT INFORMATION

An overall fit to the total width, a partial width, and 3 branching ratios uses 23 measurements and one constraint to determine 5 parameters. The overall fit has a $\chi^2 = 20.1$ for 19 degrees of freedom.

The following *off-diagonal* array elements are the correlation coefficients $\langle \delta p_i \delta p_j \rangle / (\delta p_i \delta p_j)$, in percent, from the fit to parameters p_i , including the branching fractions, $x_i \equiv \Gamma_i / \Gamma_{\text{total}}$. The fit constrains the x_i whose labels appear in this array to sum to one.

x_3	99		
x_9	0	0	
Γ	0	0	-44
	x_2	x_3	x_9

Mode	Rate (MeV)	Scale factor	
Γ_2	$D^0 \bar{D}^0$	14.0 \pm 1.4	1.8
Γ_3	$D^+ D^-$	11.2 \pm 1.1	1.7
Γ_9	$e^+ e^-$	(2.62 \pm 0.18) $\times 10^{-4}$	1.4

$\psi(3770)$ PARTIAL WIDTHS

$\Gamma(e^+ e^-)$		Γ_9		
VALUE (keV)	EVTs	DOCUMENT ID	TECN	COMMENT
0.262 \pm 0.018 OUR FIT Error includes scale factor of 1.4.				
0.256 \pm 0.016 OUR AVERAGE Error includes scale factor of 1.2.				
0.154 \pm 0.079 \pm 0.021 -0.058 -0.027		1,2 ANASHIN	12A KEDR	$e^+ e^- \rightarrow D \bar{D}$
0.22 \pm 0.05		3,4 ABLIKIM	08D BES2	$e^+ e^- \rightarrow$ hadrons
0.277 \pm 0.011 \pm 0.013		4 ABLIKIM	07E BES2	$e^+ e^- \rightarrow$ hadrons
0.203 \pm 0.003 \pm 0.041 -0.027	1.4M	4,5 BESSON	06 CLEO	$e^+ e^- \rightarrow$ hadrons
0.276 \pm 0.050		4 SCHINDLER	80 MRK2	$e^+ e^-$
0.18 \pm 0.06		4 BACINO	78 DLCO	$e^+ e^-$
• • • We do not use the following data for averages, fits, limits, etc. • • •				
0.196 \pm 0.018		6 SHAMOV	17 RVUE	$e^+ e^- \rightarrow D \bar{D}$, hadrons
0.414 \pm 0.072 \pm 0.093 -0.080 -0.028		2,7 ANASHIN	12A KEDR	$e^+ e^- \rightarrow D \bar{D}$
0.37 \pm 0.09		8 RAPIDIS	77 LGW	$e^+ e^-$

$\psi(3770) \Gamma(i) \times \Gamma(e^+ e^-) / \Gamma(\text{total})$		$\Gamma_{99} \Gamma_9 / \Gamma$		
VALUE (10^{-2} eV)	EVTs	DOCUMENT ID	TECN	COMMENT
3.55 \pm 0.92				
		1 ABLIKIM	23Bk BES3	$e^+ e^- \rightarrow \psi(3770)$
1 From a fit to $e^+ e^- \rightarrow \Xi^- \bar{\Xi}^+$ cross sections. Signal significance is 4.5 σ .				

$\psi(3770)$ BRANCHING RATIOS

$\Gamma(D \bar{D}) / \Gamma_{\text{total}}$		$\Gamma_1 / \Gamma = (\Gamma_2 + \Gamma_3) / \Gamma$		
VALUE	EVTs	DOCUMENT ID	TECN	COMMENT
0.93 \pm 0.08 OUR FIT Error includes scale factor of 2.0.				
0.93 \pm 0.08 OUR AVERAGE Error includes scale factor of 2.1.				
0.849 \pm 0.056 \pm 0.018		1 ABLIKIM	08B BES2	$e^+ e^- \rightarrow$ non- $D \bar{D}$
1.033 \pm 0.014 \pm 0.048 0.066	1.427M	2 BESSON	06 CLEO	$e^+ e^- \rightarrow$ hadrons
• • • We do not use the following data for averages, fits, limits, etc. • • •				
0.836 \pm 0.049		3 SHAMOV	17 RVUE	$e^+ e^- \rightarrow D \bar{D}$, hadrons
0.866 \pm 0.050 \pm 0.036		4,5 ABLIKIM	07k BES2	$e^+ e^- \rightarrow$ non- $D \bar{D}$
0.836 \pm 0.073 \pm 0.042		5 ABLIKIM	06L BES2	$e^+ e^- \rightarrow D \bar{D}$
0.855 \pm 0.017 \pm 0.058		5,6 ABLIKIM	06N BES2	$e^+ e^- \rightarrow D \bar{D}$

1 Neglecting interference.
 2 Obtained by comparing a measurement of the total cross section (corrected in BESSON 10) with that of $D \bar{D}$ reported by CLEO in DOBBS 07.
 3 From the joint analysis of the data on the $D \bar{D}$ and inclusive hadronic cross sections in the $\psi(3770)$ region from BaBar, Belle, BES-II, CLEO and KEDR.
 4 Using $\sigma^{\text{obs}} = 7.07 \pm 0.58$ nb and neglecting interference.
 5 Not independent of ABLIKIM 08B.
 6 From a measurement of $\sigma(e^+ e^- \rightarrow D \bar{D})$ at $\sqrt{s} = 3773$ MeV, using the $\psi(3770)$ resonance parameters measured by ABLIKIM 06L.

$\Gamma(D^0 \bar{D}^0) / \Gamma_{\text{total}}$		Γ_2 / Γ		
VALUE	EVTs	DOCUMENT ID	TECN	COMMENT
0.52 \pm 0.04 OUR FIT Error includes scale factor of 2.0.				
• • • We do not use the following data for averages, fits, limits, etc. • • •				
0.467 \pm 0.047 \pm 0.023		ABLIKIM	06L BES2	$e^+ e^- \rightarrow D^0 \bar{D}^0$
0.499 \pm 0.013 \pm 0.038		1 ABLIKIM	06N BES2	$e^+ e^- \rightarrow D^0 \bar{D}^0$
1 From a measurement of $\sigma(e^+ e^- \rightarrow D \bar{D})$ at $\sqrt{s} = 3773$ MeV, using the $\psi(3770)$ resonance parameters measured by ABLIKIM 06L.				

$\Gamma(D^+ D^-) / \Gamma_{\text{total}}$		Γ_3 / Γ		
VALUE	EVTs	DOCUMENT ID	TECN	COMMENT
0.41 \pm 0.04 OUR FIT Error includes scale factor of 2.0.				
• • • We do not use the following data for averages, fits, limits, etc. • • •				
0.369 \pm 0.037 \pm 0.028		ABLIKIM	06L BES2	$e^+ e^- \rightarrow D^+ D^-$
0.357 \pm 0.011 \pm 0.034		1 ABLIKIM	06N BES2	$e^+ e^- \rightarrow D^+ D^-$
1 From a measurement of $\sigma(e^+ e^- \rightarrow D \bar{D})$ at $\sqrt{s} = 3773$ MeV, using the $\psi(3770)$ resonance parameters measured by ABLIKIM 06L.				

Meson Particle Listings

 $\psi(3770)$ $\Gamma(D^0\bar{D}^0)/\Gamma(D^+D^-)$

VALUE	EVTS	DOCUMENT ID	TECN	COMMENT	Γ_2/Γ_3
1.253±0.016 OUR FIT					
1.253±0.016 OUR AVERAGE					
1.252±0.009±0.013	5.3M	BONVICINI	14	CLEO $e^+e^- \rightarrow D\bar{D}$	
1.39 ± 0.31 ± 0.12		PAKHLOVA	08	BELL $10.6 e^+e^- \rightarrow D\bar{D}\gamma$	
1.78 ± 0.33 ± 0.24		AUBERT	07B	BABR $e^+e^- \rightarrow D\bar{D}\gamma$	
1.27 ± 0.12 ± 0.08		ABLIKIM	06L	BES2 $e^+e^- \rightarrow D\bar{D}$	
2.43 ± 1.50 ± 0.43	34	1 CHISTOV	04	BELL $B^+ \rightarrow \psi(3770) K^+$	
1.258±0.016±0.014		2 DOBBS	07	CLEO $e^+e^- \rightarrow D\bar{D}$	

• • • We do not use the following data for averages, fits, limits, etc. • • •

¹ See ADLER 88c for older measurements of this quantity.
² Superseded by BONVICINI 14.

 $\Gamma(J/\psi X)/\Gamma_{\text{total}}$

VALUE (%)	DOCUMENT ID	TECN	COMMENT	Γ_4/Γ
0.5±0.2±0.1	1 ABLIKIM	21Z	BES3 $e^+e^- \rightarrow \ell^+\ell^-X$	

¹ From a fit to the $e^+e^- \rightarrow J/\psi X$ cross section between 3.645 and 3.891 GeV, with $\psi(2S)$ and $\psi(3770)$ masses, total widths and leptonic widths fixed to the values from the PDG 20. An alternative fit with an improved χ^2 , corresponding to a significance of 5.3 σ , uses an additional resonance with a mass of $3766.2 \pm 3.8 \pm 0.4$ MeV/ c^2 , a total width of $22.2 \pm 5.9 \pm 1.4$ MeV, and $\Gamma(e^-e^-B(J/\psi X)) = 79.4 \pm 85.5 \pm 11.7$ eV, possibly compatible with the results of ABLIKIM 08H.

 $\Gamma(J/\psi\pi^+\pi^-)/\Gamma_{\text{total}}$

VALUE (units 10^{-3})	EVTS	DOCUMENT ID	TECN	COMMENT	Γ_5/Γ
1.93±0.28 OUR AVERAGE					
1.89±0.20±0.20	231 ± 33	ADAM	06	CLEO $e^+e^- \rightarrow \psi(3770)$	
3.4 ± 1.4 ± 0.9	17.8 ± 4.8	BAI	05	BES2 $e^+e^- \rightarrow \psi(3770)$	

 $\Gamma(J/\psi\pi^0\pi^0)/\Gamma_{\text{total}}$

VALUE (units 10^{-2})	EVTS	DOCUMENT ID	TECN	COMMENT	Γ_6/Γ
0.080±0.025±0.016	39 ± 14	ADAM	06	CLEO $e^+e^- \rightarrow \psi(3770)$	

 $\Gamma(J/\psi\eta)/\Gamma_{\text{total}}$

VALUE (units 10^{-4})	EVTS	DOCUMENT ID	TECN	COMMENT	Γ_7/Γ
8.7±1.2 OUR AVERAGE					
8.7±1.0±0.8	232 ± 23	1 ABLIKIM	23V	BES3 $e^+e^- \rightarrow \psi(3770)$	
8.7±3.3±2.2	22 ± 10	ADAM	06	CLEO $e^+e^- \rightarrow \psi(3770)$	

¹ Incoherent fit. Alternate fits that include interference with background yield results between $(11.2 \pm 5.8 \pm 1.1) \times 10^{-4}$ and $(11.6 \pm 6.0 \pm 1.1) \times 10^{-4}$.

 $\Gamma(J/\psi\pi^0)/\Gamma_{\text{total}}$

VALUE (units 10^{-5})	CL%	EVTS	DOCUMENT ID	TECN	COMMENT	Γ_8/Γ
<28	90	<10	ADAM	06	CLEO $e^+e^- \rightarrow \psi(3770)$	

 $\Gamma(e^+e^-)/\Gamma_{\text{total}}$

VALUE (units 10^{-5})	DOCUMENT ID	TECN	COMMENT	Γ_9/Γ
0.96±0.07 OUR FIT	Error includes scale factor of 1.3.			
1.3 ± 0.2	RAPIDIS	77	LGW e^+e^-	

DECAYS TO LIGHT HADRONS

 $\Gamma(b_1(1235)\pi)/\Gamma_{\text{total}}$

VALUE (units 10^{-5})	CL%	DOCUMENT ID	TECN	COMMENT	Γ_{10}/Γ
<1.4	90	1 ADAMS	06	CLEO $e^+e^- \rightarrow \psi(3770)$	

¹ Comparing cross sections at $\sqrt{s} = 3.773$ GeV and $\sqrt{s} = 3.671$ GeV, neglecting interference, and using $\sigma(\psi(3770) \rightarrow D\bar{D}) = 6.39 \pm 0.20$ nb.

 $\Gamma(\phi\eta)/\Gamma_{\text{total}}$

VALUE	CL%	DOCUMENT ID	TECN	COMMENT	Γ_{11}/Γ
<2.3 × 10⁻⁵	90	1 ABLIKIM	23B	BES3 $e^+e^- \rightarrow \psi(3770)$	

• • • We do not use the following data for averages, fits, limits, etc. • • •

<7 × 10⁻⁴ 90 2 ADAMS 06 CLEO $e^+e^- \rightarrow \psi(3770)$

¹ ABLIKIM 23Bc fit to $e^+e^- \rightarrow \phi\eta'$ cross sections between 3.508 and 4.951 GeV considering interference between continuum and $\psi(3770)$ amplitudes.
² ADAMS 06 compare cross sections at $\sqrt{s} = 3.773$ GeV and $\sqrt{s} = 3.671$ GeV, neglecting interference, and using $\sigma(\psi(3770) \rightarrow D\bar{D}) = 6.39 \pm 0.20$ nb.

 $\Gamma(\omega\eta)/\Gamma_{\text{total}}$

VALUE (units 10^{-4})	CL%	DOCUMENT ID	TECN	COMMENT	Γ_{12}/Γ
<4	90	1 ADAMS	06	CLEO $e^+e^- \rightarrow \psi(3770)$	

¹ Comparing cross sections at $\sqrt{s} = 3.773$ GeV and $\sqrt{s} = 3.671$ GeV, neglecting interference, and using $\sigma(\psi(3770) \rightarrow D\bar{D}) = 6.39 \pm 0.20$ nb.

 $\Gamma(\rho^0\eta)/\Gamma_{\text{total}}$

VALUE (units 10^{-4})	CL%	DOCUMENT ID	TECN	COMMENT	Γ_{13}/Γ
<6	90	1 ADAMS	06	CLEO $e^+e^- \rightarrow \psi(3770)$	

¹ Comparing cross sections at $\sqrt{s} = 3.773$ GeV and $\sqrt{s} = 3.671$ GeV, neglecting interference, and using $\sigma(\psi(3770) \rightarrow D\bar{D}) = 6.39 \pm 0.20$ nb.

 $\Gamma(\phi\eta)/\Gamma_{\text{total}}$

VALUE (units 10^{-4})	CL%	DOCUMENT ID	TECN	COMMENT	Γ_{14}/Γ
3.1±0.6±0.3		1 ADAMS	06	CLEO $3.773 e^+e^- \rightarrow \phi\eta$	

• • • We do not use the following data for averages, fits, limits, etc. • • •

<19 90 2 ABLIKIM 07B BES2 $e^+e^- \rightarrow \psi(3770)$

¹ Comparing cross sections at $\sqrt{s} = 3.773$ GeV and $\sqrt{s} = 3.671$ GeV, neglecting interference, and using $\sigma(\psi(3770) \rightarrow D\bar{D}) = 6.39 \pm 0.20$ nb.
² Assuming that interference effects between resonance and continuum can be neglected and using $\sigma^{\text{obs}}(e^+e^- \rightarrow \psi(3770)) = 7.15 \pm 0.38$ nb.

 $\Gamma(\omega\eta)/\Gamma_{\text{total}}$

VALUE (units 10^{-5})	CL%	DOCUMENT ID	TECN	COMMENT	Γ_{15}/Γ
<1.4	90	1 ADAMS	06	CLEO $e^+e^- \rightarrow \psi(3770)$	

¹ Comparing cross sections at $\sqrt{s} = 3.773$ GeV and $\sqrt{s} = 3.671$ GeV, neglecting interference, and using $\sigma(\psi(3770) \rightarrow D\bar{D}) = 6.39 \pm 0.20$ nb.

 $\Gamma(\rho^0\eta)/\Gamma_{\text{total}}$

VALUE (units 10^{-4})	CL%	DOCUMENT ID	TECN	COMMENT	Γ_{16}/Γ
<5	90	1 ADAMS	06	CLEO $e^+e^- \rightarrow \psi(3770)$	

¹ Comparing cross sections at $\sqrt{s} = 3.773$ GeV and $\sqrt{s} = 3.671$ GeV, neglecting interference, and using $\sigma(\psi(3770) \rightarrow D\bar{D}) = 6.39 \pm 0.20$ nb.

 $\Gamma(\phi\pi^0)/\Gamma_{\text{total}}$

VALUE (units 10^{-5})	CL%	DOCUMENT ID	TECN	COMMENT	Γ_{17}/Γ
<3	90	1 ADAMS	06	CLEO $e^+e^- \rightarrow \psi(3770)$	

• • • We do not use the following data for averages, fits, limits, etc. • • •

<50 90 2 ABLIKIM 07B BES2 $e^+e^- \rightarrow \psi(3770)$

¹ Comparing cross sections at $\sqrt{s} = 3.773$ GeV and $\sqrt{s} = 3.671$ GeV, neglecting interference, and using $\sigma(\psi(3770) \rightarrow D\bar{D}) = 6.39 \pm 0.20$ nb.
² Assuming that interference effects between resonance and continuum can be neglected and using $\sigma^{\text{obs}}(e^+e^- \rightarrow \psi(3770)) = 7.15 \pm 0.38$ nb.

 $\Gamma(\omega\pi^0)/\Gamma_{\text{total}}$

VALUE (units 10^{-4})	CL%	DOCUMENT ID	TECN	COMMENT	Γ_{18}/Γ
<6	90	1 ADAMS	06	CLEO $e^+e^- \rightarrow \psi(3770)$	

¹ Comparing cross sections at $\sqrt{s} = 3.773$ GeV and $\sqrt{s} = 3.671$ GeV, neglecting interference, and using $\sigma(\psi(3770) \rightarrow D\bar{D}) = 6.39 \pm 0.20$ nb.

 $\Gamma(\pi^+\pi^-\pi^0)/\Gamma_{\text{total}}$

VALUE (units 10^{-6})	CL%	DOCUMENT ID	TECN	COMMENT	Γ_{19}/Γ
<5	90	1,2 ADAMS	06	CLEO $e^+e^- \rightarrow \psi(3770)$	

¹ Data suggest possible destructive interference with continuum.
² Comparing cross sections at $\sqrt{s} = 3.773$ GeV and $\sqrt{s} = 3.671$ GeV, neglecting interference, and using $\sigma(\psi(3770) \rightarrow D\bar{D}) = 6.39 \pm 0.20$ nb.

 $\Gamma(\rho\pi)/\Gamma_{\text{total}}$

VALUE (units 10^{-6})	CL%	DOCUMENT ID	TECN	COMMENT	Γ_{20}/Γ
<5	90	1,2 ADAMS	06	CLEO $e^+e^- \rightarrow \psi(3770)$	

¹ Comparing cross sections at $\sqrt{s} = 3.773$ GeV and $\sqrt{s} = 3.671$ GeV, neglecting interference, and using $\sigma(\psi(3770) \rightarrow D\bar{D}) = 6.39 \pm 0.20$ nb.
² Data suggest possible destructive interference with continuum.

 $\Gamma(K^+K^-)/\Gamma_{\text{total}}$

VALUE	DOCUMENT ID	TECN	COMMENT	Γ_{21}/Γ
$\sim 10^{-5}$	1 DRUZHININ	15	RVUE $e^+e^- \rightarrow \psi(3770)$	

• • • We do not use the following data for averages, fits, limits, etc. • • •

¹ DRUZHININ 15 uses BABAR and CLEO data taking into account interference of the processes $e^+e^- \rightarrow K^+K^-$ and $e^+e^- \rightarrow K_S^0 K_L^0$.

 $\Gamma(K^*(892)^+K^- + \text{c.c.})/\Gamma_{\text{total}}$

VALUE (units 10^{-5})	CL%	DOCUMENT ID	TECN	COMMENT	Γ_{22}/Γ
<1.4	90	1 ADAMS	06	CLEO $e^+e^- \rightarrow \psi(3770)$	

¹ Comparing cross sections at $\sqrt{s} = 3.773$ GeV and $\sqrt{s} = 3.671$ GeV, neglecting interference, and using $\sigma(\psi(3770) \rightarrow D\bar{D}) = 6.39 \pm 0.20$ nb.

 $\Gamma(K^*(892)^0\bar{K}^0 + \text{c.c.})/\Gamma_{\text{total}}$

VALUE (units 10^{-3})	CL%	DOCUMENT ID	TECN	COMMENT	Γ_{23}/Γ
<1.2	90	1 ADAMS	06	CLEO $e^+e^- \rightarrow \psi(3770)$	

¹ Comparing cross sections at $\sqrt{s} = 3.773$ GeV and $\sqrt{s} = 3.671$ GeV, neglecting interference, and using $\sigma(\psi(3770) \rightarrow D\bar{D}) = 6.39 \pm 0.20$ nb.

 $\Gamma(K_S^0 K_L^0)/\Gamma_{\text{total}}$

VALUE (units 10^{-5})	CL%	DOCUMENT ID	TECN	COMMENT	Γ_{24}/Γ
<1.2	90	1 CRONIN-HEN.	.06	CLEO $e^+e^- \rightarrow \psi(3770)$	

• • • We do not use the following data for averages, fits, limits, etc. • • •

<21 90 2 ABLIKIM 04F BES $e^+e^- \rightarrow \psi(3770)$

¹ Using $\sigma(e^+e^- \rightarrow \psi(3770) \rightarrow \text{hadrons}) = (6.38 \pm 0.08^{+0.41}_{-0.30})$ nb from BESSON 06 and $B(K_S^0 \rightarrow \pi^+\pi^-) = 0.6895 \pm 0.0014$.
² Using $B(K_S^0 \rightarrow \pi^+\pi^-) = 0.6860 \pm 0.0027$.

Meson Particle Listings

 $\psi(3770)$

$\Gamma(\phi\pi^+\pi^-\pi^0)/\Gamma_{\text{total}}$				Γ_{49}/Γ
VALUE (units 10^{-4})	CL%	DOCUMENT ID	TECN	COMMENT

<38 90 ¹ ABLIKIM 07i BES2 3.77 e^+e^-
¹ Assuming that interference effects between resonance and continuum can be neglected and using $\sigma^{\text{obs}}(e^+e^- \rightarrow \psi(3770)) = 7.15 \pm 0.38$ nb.

$\Gamma(K^{*0}K^-\pi^+\pi^0 + \text{c.c.})/\Gamma_{\text{total}}$				Γ_{50}/Γ
VALUE (units 10^{-4})	CL%	DOCUMENT ID	TECN	COMMENT

<162 90 ¹ ABLIKIM 07i BES2 3.77 e^+e^-
¹ Assuming that interference effects between resonance and continuum can be neglected and using $\sigma^{\text{obs}}(e^+e^- \rightarrow \psi(3770)) = 7.15 \pm 0.38$ nb.

$\Gamma(K^{*+}K^-\pi^+\pi^- + \text{c.c.})/\Gamma_{\text{total}}$				Γ_{51}/Γ
VALUE (units 10^{-4})	CL%	DOCUMENT ID	TECN	COMMENT

<323 90 ¹ ABLIKIM 07i BES2 3.77 e^+e^-
¹ Assuming that interference effects between resonance and continuum can be neglected and using $\sigma^{\text{obs}}(e^+e^- \rightarrow \psi(3770)) = 7.15 \pm 0.38$ nb.

$\Gamma(K^+K^-\pi^+\pi^-2\pi^0)/\Gamma_{\text{total}}$				Γ_{52}/Γ	
VALUE (units 10^{-3})	CL%	EVTS	DOCUMENT ID	TECN	COMMENT

<26.7 90 24 ABLIKIM 08N BES2 $e^+e^- \rightarrow \psi(3770)$

$\Gamma(K^+K^-2(\pi^+\pi^-))/\Gamma_{\text{total}}$				Γ_{53}/Γ
VALUE (units 10^{-3})	CL%	DOCUMENT ID	TECN	COMMENT

<10.3 90 ¹ ABLIKIM 07F BES2 $e^+e^- \rightarrow \psi(3770)$
¹ Assuming that interference effects between resonance and continuum can be neglected and using $\sigma^{\text{obs}}(e^+e^- \rightarrow \psi(3770)) = 7.15 \pm 0.38$ nb.

$\Gamma(K^+K^-2(\pi^+\pi^-)\pi^0)/\Gamma_{\text{total}}$				Γ_{54}/Γ
VALUE (units 10^{-3})	CL%	DOCUMENT ID	TECN	COMMENT

<36.0 90 ¹ ABLIKIM 07F BES2 $e^+e^- \rightarrow \psi(3770)$
¹ Assuming that interference effects between resonance and continuum can be neglected and using $\sigma^{\text{obs}}(e^+e^- \rightarrow \psi(3770)) = 7.15 \pm 0.38$ nb.

$\Gamma(\eta K^+K^-)/\Gamma_{\text{total}}$				Γ_{55}/Γ
VALUE (units 10^{-4})	CL%	DOCUMENT ID	TECN	COMMENT

< 4.1 90 ¹ HUANG 06A CLEO $e^+e^- \rightarrow \psi(3770)$
 • • • We do not use the following data for averages, fits, limits, etc. • • •
 <31 90 ² ABLIKIM 10D BES2 $e^+e^- \rightarrow \psi(3770)$

¹ Using $\sigma_{\text{tot}}(e^+e^- \rightarrow \psi(3770)) = 7.9 \pm 0.6$ nb at the resonance.
² Assuming that interference effects between resonance and continuum can be neglected and using $\sigma^{\text{obs}}(e^+e^- \rightarrow \psi(3770)) = 7.15 \pm 0.38$ nb.

$\Gamma(\eta K^+K^-\pi^+\pi^-)/\Gamma_{\text{total}}$				Γ_{56}/Γ
VALUE (units 10^{-2})	CL%	DOCUMENT ID	TECN	COMMENT

<1.24 90 ¹ ABLIKIM 10D BES2 $e^+e^- \rightarrow \psi(3770)$
¹ Assuming that interference effects between resonance and continuum can be neglected and using $\sigma^{\text{obs}}(e^+e^- \rightarrow \psi(3770)) = 7.15 \pm 0.38$ nb.

$\Gamma(\rho^0 K^+K^-)/\Gamma_{\text{total}}$				Γ_{57}/Γ
VALUE (units 10^{-3})	CL%	DOCUMENT ID	TECN	COMMENT

<5.0 90 ¹ ABLIKIM 07F BES2 $e^+e^- \rightarrow \psi(3770)$
¹ Assuming that interference effects between resonance and continuum can be neglected and using $\sigma^{\text{obs}}(e^+e^- \rightarrow \psi(3770)) = 7.15 \pm 0.38$ nb.

$\Gamma(2(K^+K^-))/\Gamma_{\text{total}}$				Γ_{58}/Γ
VALUE (units 10^{-4})	CL%	DOCUMENT ID	TECN	COMMENT

< 6.0 90 ¹ HUANG 06A CLEO $e^+e^- \rightarrow \psi(3770)$
 • • • We do not use the following data for averages, fits, limits, etc. • • •
 <17 90 ² ABLIKIM 07B BES2 $e^+e^- \rightarrow \psi(3770)$

¹ Using $\sigma_{\text{tot}}(e^+e^- \rightarrow \psi(3770)) = 7.9 \pm 0.6$ nb at the resonance.
² Assuming that interference effects between resonance and continuum can be neglected and using $\sigma^{\text{obs}}(e^+e^- \rightarrow \psi(3770)) = 7.15 \pm 0.38$ nb.

$\Gamma(\phi K^+K^-)/\Gamma_{\text{total}}$				Γ_{59}/Γ
VALUE (units 10^{-4})	CL%	DOCUMENT ID	TECN	COMMENT

< 7.5 90 ¹ HUANG 06A CLEO $e^+e^- \rightarrow \psi(3770)$
 • • • We do not use the following data for averages, fits, limits, etc. • • •
 <24 90 ² ABLIKIM 07B BES2 $e^+e^- \rightarrow \psi(3770)$

¹ Using $\sigma_{\text{tot}}(e^+e^- \rightarrow \psi(3770)) = 7.9 \pm 0.6$ nb at the resonance.
² Assuming that interference effects between resonance and continuum can be neglected and using $\sigma^{\text{obs}}(e^+e^- \rightarrow \psi(3770)) = 7.15 \pm 0.38$ nb.

$\Gamma(2(K^+K^-)\pi^0)/\Gamma_{\text{total}}$				Γ_{60}/Γ
VALUE (units 10^{-4})	CL%	DOCUMENT ID	TECN	COMMENT

< 2.9 90 ¹ HUANG 06A CLEO $e^+e^- \rightarrow \psi(3770)$

• • • We do not use the following data for averages, fits, limits, etc. • • •

<46 90 ² ABLIKIM 07B BES2 $e^+e^- \rightarrow \psi(3770)$

¹ Using $\sigma_{\text{tot}}(e^+e^- \rightarrow \psi(3770)) = 7.9 \pm 0.6$ nb at the resonance.

² Assuming that interference effects between resonance and continuum can be neglected and using $\sigma^{\text{obs}}(e^+e^- \rightarrow \psi(3770)) = 7.15 \pm 0.38$ nb.

$\Gamma(2(K^+K^-)\pi^+\pi^-)/\Gamma_{\text{total}}$				Γ_{61}/Γ
VALUE (units 10^{-3})	CL%	DOCUMENT ID	TECN	COMMENT

<3.2 90 ¹ ABLIKIM 07F BES2 $e^+e^- \rightarrow \psi(3770)$
¹ Assuming that interference effects between resonance and continuum can be neglected and using $\sigma^{\text{obs}}(e^+e^- \rightarrow \psi(3770)) = 7.15 \pm 0.38$ nb.

$\Gamma(K_S^0 K^-\pi^+)/\Gamma_{\text{total}}$				Γ_{62}/Γ	
VALUE (units 10^{-3})	CL%	EVTS	DOCUMENT ID	TECN	COMMENT

<3.2 90 18 ABLIKIM 08M BES2 $e^+e^- \rightarrow \psi(3770)$

$\Gamma(K_S^0 K^-\pi^+\pi^0)/\Gamma_{\text{total}}$				Γ_{63}/Γ	
VALUE (units 10^{-3})	CL%	EVTS	DOCUMENT ID	TECN	COMMENT

<13.3 90 40 ABLIKIM 08M BES2 $e^+e^- \rightarrow \psi(3770)$

$\Gamma(K_S^0 K^-\rho^+)/\Gamma_{\text{total}}$				Γ_{64}/Γ
VALUE (units 10^{-3})	CL%	DOCUMENT ID	TECN	COMMENT

<6.6 90 ABLIKIM 09C BES2 $e^+e^- \rightarrow \psi(3770)$

$\Gamma(K_S^0 K^-2\pi^+\pi^-)/\Gamma_{\text{total}}$				Γ_{65}/Γ	
VALUE (units 10^{-3})	CL%	EVTS	DOCUMENT ID	TECN	COMMENT

<8.7 90 39 ABLIKIM 08M BES2 $e^+e^- \rightarrow \psi(3770)$

$\Gamma(K_S^0 K^-\pi^+\rho^0)/\Gamma_{\text{total}}$				Γ_{66}/Γ
VALUE (units 10^{-2})	CL%	DOCUMENT ID	TECN	COMMENT

<1.6 90 ABLIKIM 09C BES2 $e^+e^- \rightarrow \psi(3770)$

$\Gamma(K_S^0 K^-\pi^+\eta)/\Gamma_{\text{total}}$				Γ_{67}/Γ
VALUE (units 10^{-2})	CL%	DOCUMENT ID	TECN	COMMENT

<1.3 90 ABLIKIM 09C BES2 $e^+e^- \rightarrow \psi(3770)$

$\Gamma(K_S^0 K^-2\pi^+\pi^-\pi^0)/\Gamma_{\text{total}}$				Γ_{68}/Γ	
VALUE (units 10^{-3})	CL%	EVTS	DOCUMENT ID	TECN	COMMENT

<41.8 90 23 ABLIKIM 08M BES2 $e^+e^- \rightarrow \psi(3770)$

$\Gamma(K_S^0 K^-2\pi^+\pi^-\eta)/\Gamma_{\text{total}}$				Γ_{69}/Γ
VALUE (units 10^{-2})	CL%	DOCUMENT ID	TECN	COMMENT

<4.8 90 ABLIKIM 09C BES2 $e^+e^- \rightarrow \psi(3770)$

$\Gamma(K_S^0 K^-\pi^+2(\pi^+\pi^-))/\Gamma_{\text{total}}$				Γ_{70}/Γ	
VALUE (units 10^{-3})	CL%	EVTS	DOCUMENT ID	TECN	COMMENT

<12.2 90 4 ABLIKIM 08M BES2 $e^+e^- \rightarrow \psi(3770)$

$\Gamma(K_S^0 K^-\pi^+2\pi^0)/\Gamma_{\text{total}}$				Γ_{71}/Γ	
VALUE (units 10^{-3})	CL%	EVTS	DOCUMENT ID	TECN	COMMENT

<26.5 90 17 ABLIKIM 08M BES2 $e^+e^- \rightarrow \psi(3770)$

$\Gamma(K_S^0 K^-K^+K^-\pi^+)/\Gamma_{\text{total}}$				Γ_{72}/Γ
VALUE (units 10^{-3})	CL%	DOCUMENT ID	TECN	COMMENT

<4.9 90 ABLIKIM 09C BES2 $e^+e^- \rightarrow \psi(3770)$

$\Gamma(K_S^0 K^-K^+K^-\pi^+\pi^0)/\Gamma_{\text{total}}$				Γ_{73}/Γ
VALUE (units 10^{-2})	CL%	DOCUMENT ID	TECN	COMMENT

<3.0 90 ABLIKIM 09C BES2 $e^+e^- \rightarrow \psi(3770)$

$\Gamma(K_S^0 K^-K^+K^-\pi^+\eta)/\Gamma_{\text{total}}$				Γ_{74}/Γ
VALUE (units 10^{-2})	CL%	DOCUMENT ID	TECN	COMMENT

<2.2 90 ABLIKIM 09C BES2 $e^+e^- \rightarrow \psi(3770)$

$\Gamma(K^{*0}K^-\pi^+ + \text{c.c.})/\Gamma_{\text{total}}$				Γ_{75}/Γ
VALUE (units 10^{-3})	CL%	DOCUMENT ID	TECN	COMMENT

<9.7 90 ¹ ABLIKIM 07F BES2 $e^+e^- \rightarrow \psi(3770)$
¹ Assuming that interference effects between resonance and continuum can be neglected and using $\sigma^{\text{obs}}(e^+e^- \rightarrow \psi(3770)) = 7.15 \pm 0.38$ nb.

$\Gamma(\rho\bar{\rho})/\Gamma_{\text{total}}$				Γ_{76}/Γ
VALUE (units 10^{-6})	EVTS	DOCUMENT ID	TECN	COMMENT

• • • We do not use the following data for averages, fits, limits, etc. • • •
 not seen ¹ AAIJ 17AD LHCB $pp \rightarrow B^+X \rightarrow p\bar{p}K^+X$

$7.1^{+8.6}_{-2.9}$ 684 ² ABLIKIM 14L BES3 $e^+e^- \rightarrow \psi(3770)$

310 ± 30 684 ³ ABLIKIM 14L BES3 $e^+e^- \rightarrow \psi(3770)$

¹ AAIJ 17AD reports $B(B^+ \rightarrow \psi(3770)K^+ \rightarrow p\bar{p}K^+)/B(B^+ \rightarrow J/\psi K^+ \rightarrow p\bar{p}K^+) < 0.09$ (0.10) at 90% (95%) CL.

² Solution I of two equivalent solutions in a fit with a resonance interfering with continuum.

³ Solution II of two equivalent solutions in a fit with a resonance interfering with continuum.

$\Gamma(\rho\bar{\rho}\pi^0)/\Gamma_{\text{total}}$ Γ_{77}/Γ

VALUE (units 10^{-4})	CL%	DOCUMENT ID	TECN	COMMENT
< 0.4	90	1,2 ABLIKIM	14o BES3	$e^+e^- \rightarrow \psi(3770)$
• • • We do not use the following data for averages, fits, limits, etc. • • •				
59 \pm $\frac{3}{2}$ \pm 5		1,3 ABLIKIM	14o BES3	$e^+e^- \rightarrow \psi(3770)$
<12	90	4 ABLIKIM	07B BES2	$e^+e^- \rightarrow \psi(3770)$

- ¹ Calculated by the authors using $\sigma(e^+e^- \rightarrow \psi(3770) \rightarrow \text{hadrons}) = 6.36 \pm 0.08^{+0.41}_{-0.30}$ nb from BESSON 10.
² Solution I of two equivalent solutions in a fit with a resonance interfering with continuum.
³ Solution II of two equivalent solutions in a fit with a resonance interfering with continuum.
⁴ Assuming that interference effects between resonance and continuum can be neglected and using $\sigma^{\text{obs}}(e^+e^- \rightarrow \psi(3770)) = 7.15 \pm 0.38$ nb.

 $\Gamma(\rho\bar{\rho}\pi^+\pi^-)/\Gamma_{\text{total}}$ Γ_{78}/Γ

VALUE (units 10^{-4})	CL%	DOCUMENT ID	TECN	COMMENT
< 5.8	90	1 HUANG	06A CLEO	$e^+e^- \rightarrow \psi(3770)$
• • • We do not use the following data for averages, fits, limits, etc. • • •				
<16	90	2 ABLIKIM	07B BES2	$e^+e^- \rightarrow \psi(3770)$

- ¹ Using $\sigma_{\text{tot}}(e^+e^- \rightarrow \psi(3770)) = 7.9 \pm 0.6$ nb at the resonance.
² Assuming that interference effects between resonance and continuum can be neglected and using $\sigma^{\text{obs}}(e^+e^- \rightarrow \psi(3770)) = 7.15 \pm 0.38$ nb.

 $\Gamma(\Lambda\bar{\Lambda})/\Gamma_{\text{total}}$ Γ_{79}/Γ

VALUE	CL%	DOCUMENT ID	TECN	COMMENT
< 1.2×10^{-4}	90	1 HUANG	06A CLEO	$e^+e^- \rightarrow \psi(3770)$
• • • We do not use the following data for averages, fits, limits, etc. • • •				
< 1.8×10^{-4}	90	2 ABLIKIM	21As BES3	$e^+e^- \rightarrow \psi(3770)$
< 4×10^{-4}	90	3 ABLIKIM	07F BES2	$e^+e^- \rightarrow \psi(3770)$

- ¹ Using $\sigma_{\text{tot}}(e^+e^- \rightarrow \psi(3770)) = 7.9 \pm 0.6$ nb at the resonance.
² From a measurement of the $e^+e^- \rightarrow \Lambda\bar{\Lambda}$ cross section between 3.5 and 4.6 GeV. At a 90% CL the lower bound is $> 2.4 \times 10^{-6}$.
³ Assuming that interference effects between resonance and continuum can be neglected and using $\sigma^{\text{obs}}(e^+e^- \rightarrow \psi(3770)) = 7.15 \pm 0.38$ nb.

 $\Gamma(\rho\bar{\rho}\pi^+\pi^-\pi^0)/\Gamma_{\text{total}}$ Γ_{80}/Γ

VALUE (units 10^{-4})	CL%	DOCUMENT ID	TECN	COMMENT
<18.5	90	1 HUANG	06A CLEO	$e^+e^- \rightarrow \psi(3770)$
• • • We do not use the following data for averages, fits, limits, etc. • • •				
<73	90	2 ABLIKIM	07B BES2	$e^+e^- \rightarrow \psi(3770)$

- ¹ Using $\sigma_{\text{tot}}(e^+e^- \rightarrow \psi(3770)) = 7.9 \pm 0.6$ nb at the resonance.
² Assuming that interference effects between resonance and continuum can be neglected and using $\sigma^{\text{obs}}(e^+e^- \rightarrow \psi(3770)) = 7.15 \pm 0.38$ nb.

 $\Gamma(\omega\rho\bar{\rho})/\Gamma_{\text{total}}$ Γ_{81}/Γ

VALUE (units 10^{-4})	CL%	DOCUMENT ID	TECN	COMMENT
< 2.9	90	1 HUANG	06A CLEO	$e^+e^- \rightarrow \psi(3770)$
• • • We do not use the following data for averages, fits, limits, etc. • • •				
<30	90	2 ABLIKIM	07i BES2	$3.77 e^+e^-$

- ¹ Using $\sigma_{\text{tot}}(e^+e^- \rightarrow \psi(3770)) = 7.9 \pm 0.6$ nb at the resonance.
² Using $\sigma^{\text{obs}} = 7.15 \pm 0.27 \pm 0.27$ nb and neglecting interference.

 $\Gamma(\Lambda\bar{\Lambda}\pi^0)/\Gamma_{\text{total}}$ Γ_{82}/Γ

VALUE (units 10^{-4})	CL%	DOCUMENT ID	TECN	COMMENT
< 0.7	90	1 ABLIKIM	13q BES3	$e^+e^- \rightarrow \psi(3770)$
• • • We do not use the following data for averages, fits, limits, etc. • • •				
<12	90	2 ABLIKIM	07i BES2	$3.77 e^+e^-$

- ¹ Assuming that interference effects between resonance and continuum can be neglected.
² Assuming that interference effects between resonance and continuum can be neglected and using $\sigma^{\text{obs}}(e^+e^- \rightarrow \psi(3770)) = 7.15 \pm 0.38$ nb.

 $\Gamma(\rho\bar{\rho}2(\pi^+\pi^-))/\Gamma_{\text{total}}$ Γ_{83}/Γ

VALUE (units 10^{-3})	CL%	DOCUMENT ID	TECN	COMMENT
<2.6	90	1 ABLIKIM	07F BES2	$e^+e^- \rightarrow \psi(3770)$

- ¹ Assuming that interference effects between resonance and continuum can be neglected and using $\sigma^{\text{obs}}(e^+e^- \rightarrow \psi(3770)) = 7.15 \pm 0.38$ nb.

 $\Gamma(\eta\rho\bar{\rho})/\Gamma_{\text{total}}$ Γ_{84}/Γ

VALUE (units 10^{-4})	CL%	DOCUMENT ID	TECN	COMMENT
< 5.4	90	1 HUANG	06A CLEO	$e^+e^- \rightarrow \psi(3770)$
• • • We do not use the following data for averages, fits, limits, etc. • • •				
<11	90	2 ABLIKIM	10D BES2	$e^+e^- \rightarrow \psi(3770)$

- ¹ Using $\sigma_{\text{tot}}(e^+e^- \rightarrow \psi(3770)) = 7.9 \pm 0.6$ nb at the resonance.
² Assuming that interference effects between resonance and continuum can be neglected and using $\sigma^{\text{obs}}(e^+e^- \rightarrow \psi(3770)) = 7.15 \pm 0.38$ nb.

 $\Gamma(\eta\rho\bar{\rho}\pi^+\pi^-)/\Gamma_{\text{total}}$ Γ_{85}/Γ

VALUE (units 10^{-3})	CL%	DOCUMENT ID	TECN	COMMENT
<3.3	90	1 ABLIKIM	10D BES2	$e^+e^- \rightarrow \psi(3770)$

- ¹ Assuming that interference effects between resonance and continuum can be neglected and using $\sigma^{\text{obs}}(e^+e^- \rightarrow \psi(3770)) = 7.15 \pm 0.38$ nb.

 $\Gamma(\rho^0\rho\bar{\rho})/\Gamma_{\text{total}}$ Γ_{86}/Γ

VALUE (units 10^{-3})	CL%	DOCUMENT ID	TECN	COMMENT
<1.7	90	1 ABLIKIM	07F BES2	$e^+e^- \rightarrow \psi(3770)$

- ¹ Assuming that interference effects between resonance and continuum can be neglected and using $\sigma^{\text{obs}}(e^+e^- \rightarrow \psi(3770)) = 7.15 \pm 0.38$ nb.

 $\Gamma(\rho\bar{\rho}K^+K^-)/\Gamma_{\text{total}}$ Γ_{87}/Γ

VALUE (units 10^{-4})	CL%	DOCUMENT ID	TECN	COMMENT
< 3.2	90	1 HUANG	06A CLEO	$e^+e^- \rightarrow \psi(3770)$
• • • We do not use the following data for averages, fits, limits, etc. • • •				
<11	90	2 ABLIKIM	07B BES2	$e^+e^- \rightarrow \psi(3770)$

- ¹ Using $\sigma_{\text{tot}}(e^+e^- \rightarrow \psi(3770)) = 7.9 \pm 0.6$ nb at the resonance.
² Assuming that interference effects between resonance and continuum can be neglected and using $\sigma^{\text{obs}}(e^+e^- \rightarrow \psi(3770)) = 7.15 \pm 0.38$ nb.

 $\Gamma(\eta\rho\bar{\rho}K^+K^-)/\Gamma_{\text{total}}$ Γ_{88}/Γ

VALUE (units 10^{-3})	CL%	DOCUMENT ID	TECN	COMMENT
<6.9	90	1 ABLIKIM	10D BES2	$e^+e^- \rightarrow \psi(3770)$

- ¹ Assuming that interference effects between resonance and continuum can be neglected and using $\sigma^{\text{obs}}(e^+e^- \rightarrow \psi(3770)) = 7.15 \pm 0.38$ nb.

 $\Gamma(\pi^0\rho\bar{\rho}K^+K^-)/\Gamma_{\text{total}}$ Γ_{89}/Γ

VALUE (units 10^{-3})	CL%	DOCUMENT ID	TECN	COMMENT
<1.2	90	1 ABLIKIM	10D BES2	$e^+e^- \rightarrow \psi(3770)$

- ¹ Assuming that interference effects between resonance and continuum can be neglected and using $\sigma^{\text{obs}}(e^+e^- \rightarrow \psi(3770)) = 7.15 \pm 0.38$ nb.

 $\Gamma(\phi\rho\bar{\rho})/\Gamma_{\text{total}}$ Γ_{90}/Γ

VALUE (units 10^{-4})	CL%	DOCUMENT ID	TECN	COMMENT
<1.3	90	1 HUANG	06A CLEO	$e^+e^- \rightarrow \psi(3770)$
• • • We do not use the following data for averages, fits, limits, etc. • • •				
<9	90	2 ABLIKIM	07B BES2	$e^+e^- \rightarrow \psi(3770)$

- ¹ Using $\sigma_{\text{tot}}(e^+e^- \rightarrow \psi(3770)) = 7.9 \pm 0.6$ nb at the resonance.
² Assuming that interference effects between resonance and continuum can be neglected and using $\sigma^{\text{obs}}(e^+e^- \rightarrow \psi(3770)) = 7.15 \pm 0.38$ nb.

 $\Gamma(\Lambda\bar{\Lambda}\pi^+\pi^-)/\Gamma_{\text{total}}$ Γ_{91}/Γ

VALUE (units 10^{-4})	CL%	DOCUMENT ID	TECN	COMMENT
< 2.5	90	1 HUANG	06A CLEO	$e^+e^- \rightarrow \psi(3770)$
• • • We do not use the following data for averages, fits, limits, etc. • • •				
< 4.7	90	2 ABLIKIM	13q BES3	$e^+e^- \rightarrow \psi(3770)$
<39	90	3 ABLIKIM	07F BES2	$e^+e^- \rightarrow \psi(3770)$

- ¹ Using $\sigma_{\text{tot}}(e^+e^- \rightarrow \psi(3770)) = 7.9 \pm 0.6$ nb at the resonance.
² Assuming that interference effects between resonance and continuum can be neglected.
³ Assuming that interference effects between resonance and continuum can be neglected and using $\sigma^{\text{obs}}(e^+e^- \rightarrow \psi(3770)) = 7.15 \pm 0.38$ nb.

 $\Gamma(\Lambda\bar{\Lambda}K^+)/\Gamma_{\text{total}}$ Γ_{92}/Γ

VALUE (units 10^{-4})	CL%	DOCUMENT ID	TECN	COMMENT
<2.8	90	1 HUANG	06A CLEO	$e^+e^- \rightarrow \psi(3770)$

- ¹ Using $\sigma_{\text{tot}}(e^+e^- \rightarrow \psi(3770)) = 7.9 \pm 0.6$ nb at the resonance.

 $\Gamma(\Lambda\bar{\Lambda}K^+\pi^+\pi^-)/\Gamma_{\text{total}}$ Γ_{93}/Γ

VALUE (units 10^{-4})	CL%	DOCUMENT ID	TECN	COMMENT
<6.3	90	1 HUANG	06A CLEO	$e^+e^- \rightarrow \psi(3770)$

- ¹ Using $\sigma_{\text{tot}}(e^+e^- \rightarrow \psi(3770)) = 7.9 \pm 0.6$ nb at the resonance.

 $\Gamma(\Lambda\bar{\Lambda}\eta)/\Gamma_{\text{total}}$ Γ_{94}/Γ

VALUE (units 10^{-4})	CL%	DOCUMENT ID	TECN	COMMENT
<1.9	90	1 ABLIKIM	13q BES3	$e^+e^- \rightarrow \psi(3770)$

- ¹ Assuming that interference effects between resonance and continuum can be neglected.

 $\Gamma(\Sigma^+\bar{\Sigma}^-)/\Gamma_{\text{total}}$ Γ_{95}/Γ

VALUE (units 10^{-4})	CL%	DOCUMENT ID	TECN	COMMENT
<1.0	90	1 ABLIKIM	13q BES3	$e^+e^- \rightarrow \psi(3770)$

- ¹ Assuming that interference effects between resonance and continuum can be neglected.

 $\Gamma(\Sigma^0\bar{\Sigma}^0)/\Gamma_{\text{total}}$ Γ_{96}/Γ

VALUE (units 10^{-4})	CL%	DOCUMENT ID	TECN	COMMENT
<0.4	90	1 ABLIKIM	13q BES3	$e^+e^- \rightarrow \psi(3770)$

- ¹ Assuming that interference effects between resonance and continuum can be neglected.

 $\Gamma(\Xi^+\bar{\Xi}^-)/\Gamma_{\text{total}}$ Γ_{97}/Γ

VALUE (units 10^{-4})	CL%	DOCUMENT ID	TECN	COMMENT
<1.5	90	1 ABLIKIM	13q BES3	$e^+e^- \rightarrow \psi(3770)$

- ¹ Assuming that interference effects between resonance and continuum can be neglected.

Meson Particle Listings

$\psi(3770)$

$\Gamma(\Xi^0 \Xi^0)/\Gamma_{total}$		Γ_{98}/Γ	
VALUE (units 10^{-4})	CL%	DOCUMENT ID	TECN COMMENT
<1.4	90	¹ ABLIKIM	13Q BES3 $e^+e^- \rightarrow \psi(3770)$

¹ Assuming that interference effects between resonance and continuum can be neglected.

RADIATIVE DECAYS

$\Gamma(\gamma\chi_{c2})/\Gamma_{total}$		Γ_{100}/Γ	
VALUE (units 10^{-3})	CL%	DOCUMENT ID	TECN COMMENT
<0.64	90	¹ ABLIKIM	15J BES3 $e^+e^- \rightarrow \psi(3770) \rightarrow \gamma\gamma J/\psi$
••• We do not use the following data for averages, fits, limits, etc. •••			
<2.0	90	² BRIERE	06 CLEO $e^+e^- \rightarrow \psi(3770) \rightarrow \gamma + \text{hadrons}$
<0.9	90	³ COAN	06A CLEO $e^+e^- \rightarrow \psi(3770) \rightarrow \gamma\gamma J/\psi$

¹ This limit is equivalent to $(0.25 \pm 0.21 \pm 0.18) \times 10^{-3}$ branching fraction value.
² Uses $B(\psi(2S) \rightarrow \gamma\chi_{c2}) = 9.22 \pm 0.11 \pm 0.46\%$ from ATHAR 04, $\psi(2S)$ mass and width from PDG 04, and $\Gamma_{ee}(\psi(2S)) = 2.54 \pm 0.03 \pm 0.11$ keV from ADAM 06.
³ Using $\Gamma_{ee}(\psi(2S)) = (2.54 \pm 0.03 \pm 0.11)$ keV from ADAM 06 and taking $\sigma(e^+e^- \rightarrow D\bar{D})$ from HE 05 for $\sigma(e^+e^- \rightarrow \psi(3770))$.

$\Gamma(\gamma\chi_{c1})/\Gamma_{total}$		Γ_{101}/Γ	
VALUE (units 10^{-3})	EVTS	DOCUMENT ID	TECN COMMENT
2.49 ± 0.23 OUR AVERAGE			
2.0 ± 0.8 ± 0.1	202	¹ ABLIKIM	16B BES3 $e^+e^- \rightarrow \psi(3770) \rightarrow \gamma + \text{hadrons}$
2.48 ± 0.15 ± 0.23	0.6k	ABLIKIM	15J BES3 $e^+e^- \rightarrow \psi(3770) \rightarrow \gamma\gamma J/\psi$
2.4 ± 0.8 ± 0.2		² ABLIKIM	14H BES3 $e^+e^- \rightarrow \psi(3770) \rightarrow K_S^0 K^\pm \pi^\mp$
2.9 ± 0.5 ± 0.4		³ BRIERE	06 CLEO $e^+e^- \rightarrow \psi(3770) \rightarrow \gamma + \text{hadrons}, \gamma\gamma J/\psi$
••• We do not use the following data for averages, fits, limits, etc. •••			
3.9 ± 1.4 ± 0.6	54	⁴ BRIERE	06 CLEO $e^+e^- \rightarrow \psi(3770) \rightarrow \gamma + \text{hadrons}$
2.8 ± 0.5 ± 0.4	53	⁵ COAN	06A CLEO $e^+e^- \rightarrow \psi(3770) \rightarrow \gamma\gamma J/\psi$

¹ ABLIKIM 16B reports $(1.94 \pm 0.42 \pm 0.64) \times 10^{-3}$ from a measurement of $[\Gamma(\psi(3770) \rightarrow \gamma\chi_{c1})/\Gamma_{total}] / [B(\psi(2S) \rightarrow \gamma\chi_{c1}(1P))]$ assuming $B(\psi(2S) \rightarrow \gamma\chi_{c1}(1P)) = (9.55 \pm 0.31) \times 10^{-2}$, which we rescale to our best value $B(\psi(2S) \rightarrow \gamma\chi_{c1}(1P)) = (9.75 \pm 0.27) \times 10^{-2}$. Our first error is their experiment's error and our second error is the systematic error from using our best value.
² ABLIKIM 14H reports $[\Gamma(\psi(3770) \rightarrow \gamma\chi_{c1})/\Gamma_{total}] \times [B(\chi_{c1}(1P) \rightarrow K_S^0 K^\pm \pi^\mp)] = (8.51 \pm 2.39 \pm 1.42) \times 10^{-6}$ which we divide by our best value $B(\chi_{c1}(1P) \rightarrow K_S^0 K^\pm \pi^\mp) = 0.00349 \pm 0.00031$. Our first error is their experiment's error and our second error is the systematic error from using our best value. We have calculated the best value of $B(\chi_{c1}(1P) \rightarrow K_S^0 K^\pm \pi^\mp)$ as $1/2$ of $B(\chi_{c1}(1P) \rightarrow K^0 K^\pm \pi^\mp + c.c.) = (7.0 \pm 0.6) \times 10^{-3}$.
³ Averages the two measurements from COAN 06A and BRIERE 06.
⁴ Uses $B(\psi(2S) \rightarrow \gamma\chi_{c1}) = 9.07 \pm 0.11 \pm 0.54\%$ from ATHAR 04, $\psi(2S)$ mass and width from PDG 04, and $\Gamma_{ee}(\psi(2S)) = 2.54 \pm 0.03 \pm 0.11$ keV from ADAM 06.
⁵ Using $\Gamma_{ee}(\psi(2S)) = (2.54 \pm 0.03 \pm 0.11)$ keV from ADAM 06 and taking $\sigma(e^+e^- \rightarrow D\bar{D})$ from HE 05 for $\sigma(e^+e^- \rightarrow \psi(3770))$.

$\Gamma(\gamma\chi_{c1})/\Gamma(J/\psi\pi^+\pi^-)$		Γ_{101}/Γ_5	
VALUE	EVTS	DOCUMENT ID	TECN COMMENT
1.49 ± 0.31 ± 0.26	53 ± 10	¹ COAN	06A CLEO $e^+e^- \rightarrow \psi(3770) \rightarrow \gamma\gamma J/\psi$

¹ Using $B(\psi(3770) \rightarrow J/\psi\pi^+\pi^-) = (1.89 \pm 0.20 \pm 0.20) \times 10^{-3}$ from ADAM 06.

$\Gamma(\gamma\chi_{c0})/\Gamma_{total}$		Γ_{102}/Γ	
VALUE (units 10^{-3})	CL% EVTS	DOCUMENT ID	TECN COMMENT
6.9 ± 0.6 OUR AVERAGE			
6.7 ± 0.7 ± 0.2	2.2k	¹ ABLIKIM	16B BES3 $e^+e^- \rightarrow \psi(3770) \rightarrow \gamma + \text{hadrons}$
7.3 ± 0.7 ± 0.6	274	BRIERE	06 CLEO $e^+e^- \rightarrow \psi(3770) \rightarrow \gamma + \text{hadrons}$

••• We do not use the following data for averages, fits, limits, etc. •••

< 44 90 ² COAN 06A CLEO $e^+e^- \rightarrow \psi(3770) \rightarrow \gamma\gamma J/\psi$

¹ ABLIKIM 16B reports $(6.88 \pm 0.28 \pm 0.67) \times 10^{-3}$ from a measurement of $[\Gamma(\psi(3770) \rightarrow \gamma\chi_{c0})/\Gamma_{total}] / [B(\psi(2S) \rightarrow \gamma\chi_{c0}(1P))]$ assuming $B(\psi(2S) \rightarrow \gamma\chi_{c0}(1P)) = (9.99 \pm 0.27) \times 10^{-2}$, which we rescale to our best value $B(\psi(2S) \rightarrow \gamma\chi_{c0}(1P)) = (9.77 \pm 0.23) \times 10^{-2}$. Our first error is their experiment's error and our second error is the systematic error from using our best value.
² Using $\Gamma_{ee}(\psi(2S)) = (2.54 \pm 0.03 \pm 0.11)$ keV from ADAM 06 and taking $\sigma(e^+e^- \rightarrow D\bar{D})$ from HE 05 for $\sigma(e^+e^- \rightarrow \psi(3770))$.

$\Gamma(\gamma\chi_{c0})/\Gamma(\gamma\chi_{c2})$		$\Gamma_{102}/\Gamma_{100}$	
VALUE	CL%	DOCUMENT ID	TECN COMMENT
>8	90	¹ BRIERE	06 CLEO $e^+e^- \rightarrow \psi(3770)$

¹ Not independent of other results in BRIERE 06.

$\Gamma(\gamma\chi_{c0})/\Gamma(\gamma\chi_{c1})$		$\Gamma_{102}/\Gamma_{101}$	
VALUE	CL%	DOCUMENT ID	TECN COMMENT
2.5 ± 0.6		¹ BRIERE	06 CLEO $e^+e^- \rightarrow \psi(3770)$

••• We do not use the following data for averages, fits, limits, etc. •••

¹ Not independent of other results in BRIERE 06.

$\Gamma(\gamma\eta_c)/\Gamma_{total}$		Γ_{103}/Γ	
VALUE	CL%	DOCUMENT ID	TECN COMMENT
<7 × 10 ⁻⁴	90	¹ ABLIKIM	14H BES3

¹ ABLIKIM 14H reports $[\Gamma(\psi(3770) \rightarrow \gamma\eta_c)/\Gamma_{total}] \times [B(\eta_c(1S) \rightarrow K_S^0 K^\pm \pi^\mp)] < 16 \times 10^{-6}$ which we divide by our best value $B(\eta_c(1S) \rightarrow K_S^0 K^\pm \pi^\mp) = 2.38 \times 10^{-2}$. We have calculated the best value of $B(\eta_c(1S) \rightarrow K_S^0 K^\pm \pi^\mp)$ as $1/3$ of $B(\eta_c(1S) \rightarrow K\bar{K}\pi) = 7.1 \times 10^{-2}$.

$\Gamma(\gamma\eta_c(2S))/\Gamma_{total}$		Γ_{104}/Γ	
VALUE	CL%	DOCUMENT ID	TECN COMMENT
<9 × 10 ⁻⁴	90	¹ ABLIKIM	14H BES3

¹ ABLIKIM 14H reports $[\Gamma(\psi(3770) \rightarrow \gamma\eta_c(2S))/\Gamma_{total}] \times [B(\eta_c(2S) \rightarrow K_S^0 K^\pm \pi^\mp)] < 5.6 \times 10^{-6}$ which we divide by our best value $B(\eta_c(2S) \rightarrow K_S^0 K^\pm \pi^\mp) = 6 \times 10^{-3}$. We have calculated the best value of $B(\eta_c(2S) \rightarrow K_S^0 K^\pm \pi^\mp)$ as $1/3$ of $B(\eta_c(2S) \rightarrow K\bar{K}\pi) = 1.9 \times 10^{-2}$.

$\Gamma(\gamma\eta)/\Gamma_{total}$		Γ_{105}/Γ	
VALUE (units 10^{-4})	CL%	DOCUMENT ID	TECN COMMENT
<1.8	90	¹ PEDLAR	09 CLE3 $\psi(2S) \rightarrow \gamma X$

¹ Assuming maximal destructive interference between $\psi(3770)$ and continuum sources.

$\Gamma(\gamma\eta)/\Gamma_{total}$		Γ_{106}/Γ	
VALUE (units 10^{-4})	CL%	DOCUMENT ID	TECN COMMENT
<1.5	90	¹ PEDLAR	09 CLE3 $\psi(2S) \rightarrow \gamma X$

¹ Assuming maximal destructive interference between $\psi(3770)$ and continuum sources.

$\Gamma(\gamma\pi^0)/\Gamma_{total}$		Γ_{107}/Γ	
VALUE (units 10^{-4})	CL%	DOCUMENT ID	TECN COMMENT
<2	90	PEDLAR	09 CLE3 $\psi(2S) \rightarrow \gamma X$

$\psi(3770)$ REFERENCES

ABLIKIM	23BC	PR D108 052015	M. Ablikim et al.	(BESIII Collab.)
ABLIKIM	23BK	JHEP 2311 228	M. Ablikim et al.	(BESIII Collab.)
ABLIKIM	23V	PR D107 L091101	M. Ablikim et al.	(BESIII Collab.)
ABLIKIM	21A5	PR D104 L091104	M. Ablikim et al.	(BESIII Collab.)
ABLIKIM	21Z	PRL 127 082002	M. Ablikim et al.	(BESIII Collab.)
PDG	20	PTEP 2020 083C01	P.A. Zyla et al.	(PDG Collab.)
AALIJ	19M	JHEP 1907 035	R. Aaij et al.	(LHCb Collab.)
AALIJ	17AD	PL B769 305	R. Aaij et al.	(LHCb Collab.)
SHAMOV	17	PL B769 187	A.G. Shamov, K.Yu. Todyshv	
ABLIKIM	16B	PL B753 103	M. Ablikim et al.	(BESIII Collab.)
ABLIKIM	15J	PR D91 092009	M. Ablikim et al.	(BESIII Collab.)
DRUZHININ	15	PR D92 054024	V.P. Druzhinin	(NOVO)
ABLIKIM	14H	PR D89 112005	M. Ablikim et al.	(BESIII Collab.)
ABLIKIM	14L	PL B735 101	M. Ablikim et al.	(BESIII Collab.)
ABLIKIM	14O	PR D90 032007	M. Ablikim et al.	(BESIII Collab.)
BONVICINI	14	PR D89 072002	G. Bonvicini et al.	(CLEO Collab.)
ABLIKIM	13Q	PR D87 112011	M. Ablikim et al.	(BESIII Collab.)
ANASHIN	12A	PL B711 292	V.V. Anashin et al.	(NEDR Collab.)
ABLIKIM	10D	EPJ C66 11	M. Ablikim et al.	(BES II Collab.)
BESSON	10	PRL 104 159901 (err.)	D. Besson et al.	(CLEO Collab.)
ABLIKIM	09C	EPJ C64 243	M. Ablikim et al.	(BES Collab.)
PEDLAR	09	PR D79 111101	T.K. Pedlar et al.	(CLEO Collab.)
ABLIKIM	08B	PL B659 74	M. Ablikim et al.	(BES Collab.)
ABLIKIM	08D	PL B660 315	M. Ablikim et al.	(BES Collab.)
ABLIKIM	08H	PRL 101 102004	M. Ablikim et al.	(BES Collab.)
ABLIKIM	08M	PL B670 179	M. Ablikim et al.	(BES Collab.)
ABLIKIM	08N	PL B670 184	M. Ablikim et al.	(BES Collab.)
AUBERT	08B	PR D77 011102	B. Aubert et al.	(BABAR Collab.)
BRODZICKA	08	PRL 100 092001	J. Brodzicka et al.	(BELLE Collab.)
PAKHOVA	08	PR D77 011103	G. Pakhlova et al.	(BELLE Collab.)
ABLIKIM	07B	PL B650 111	M. Ablikim et al.	(BES Collab.)
ABLIKIM	07E	PL B652 238	M. Ablikim et al.	(BES Collab.)
ABLIKIM	07F	PL B656 30	M. Ablikim et al.	(BES Collab.)
ABLIKIM	07I	EPJ C52 805	M. Ablikim et al.	(BES Collab.)
ABLIKIM	07K	PR D76 122002	M. Ablikim et al.	(BES Collab.)
AUBERT	07B	PR D76 111105	B. Aubert et al.	(BABAR Collab.)
DOBBS	07	PR D76 112001	S. Dobbs et al.	(CLEO Collab.)
ABLIKIM	06L	PRL 97 121801	M. Ablikim et al.	(BES Collab.)
ABLIKIM	06N	PL B641 145	M. Ablikim et al.	(BES Collab.)
ADAM	06	PRL 96 082004	N.E. Adam et al.	(CLEO Collab.)
ADAMS	06	PR D73 012002	G.S. Adams et al.	(CLEO Collab.)
BESSON	06	PRL 96 092002	D. Besson et al.	(CLEO Collab.)
Also		PRL 104 159901 (err.)	D. Besson et al.	(CLEO Collab.)
BRIERE	06	PR D74 031106	R.A. Briere et al.	(CLEO Collab.)
COAN	06A	PRL 96 182002	T.E. Coan et al.	(CLEO Collab.)
CRONIN-HENNESSY	06	PR D74 012005	D. Cronin-Hennessy et al.	(CLEO Collab.)
HUANG	06A	PRL 96 032003	G.S. Huang et al.	(CLEO Collab.)
BAI	05	PL B605 63	J.Z. Bai et al.	(BES Collab.)
HE	05	PRL 95 121801	Q. He et al.	(CLEO Collab.)
Also		PRL 96 199903 (err.)	Q. He et al.	(CLEO Collab.)
ABLIKIM	04F	PR D70 077101	M. Ablikim et al.	(BES Collab.)
ATHAR	04	PR D70 112002	S.B. Athar et al.	(CLEO Collab.)
CHRISTOV	04	PRL 93 051803	R. Christov et al.	(BELLE Collab.)
PDG	04	PL B592 1	S. Eidelman et al.	(PDG Collab.)
BAI	02C	PRL 88 101802	J.Z. Bai et al.	(BES Collab.)
ADLER	88C	PRL 60 89	J. Adler et al.	(Mark III Collab.)
SCHINDLER	80	PR D21 2716	R.H. Schindler et al.	(Mark II Collab.)
BACINO	78	PRL 40 671	W.J. Bacino et al.	(SLAC, UCLA, UC)
RAPIDIS	77	PRL 39 526	P.A. Rapidis et al.	(LWJ Collab.)

$\psi_2(3823)$

$I^G(J^{PC}) = 0^-(2^{--})$
I, J, P need confirmation.

was $\psi(3823)$, $X(3823)$

Seen by BHARDWAJ 13 in $B \rightarrow \chi_{c1} \gamma K$ and ABLIKIM 15S in $e^+e^- \rightarrow \pi^+\pi^-\gamma\chi_{c1}$ decays as a narrow peak in the invariant mass distribution of the $\chi_{c1} \gamma$ system. Properties consistent with the $\psi_2(1^3D_2)$ $c\bar{c}$ state.

$\psi_2(3823)$ MASS

VALUE (MeV)	EVTs	DOCUMENT ID	TECN	COMMENT
3823.51 ± 0.34 OUR AVERAGE				
3824.5 ± 2.4 ± 1.0	30	¹ ABLIKIM	23J BES3	$e^+e^- \rightarrow \pi^0\pi^0\chi_{c1}\gamma$
3823.12 ± 0.43 ± 0.13	120	ABLIKIM	22R BES3	$e^+e^- \rightarrow \pi^+\pi^-\chi_{c1}\gamma$
3824.08 ± 0.53 ± 0.14	137	² AAIJ	20s LHCB	$B^+ \rightarrow J/\psi\pi^+\pi^-K^+$
3823.1 ± 1.8 ± 0.7	33 ± 10	³ BHARDWAJ	13 BELL	$B^\pm \rightarrow \chi_{c1}\gamma K^\pm$
• • • We do not use the following data for averages, fits, limits, etc. • • •				
3821.7 ± 1.3 ± 0.7	19 ± 5	⁴ ABLIKIM	15s BES3	$e^+e^- \rightarrow \pi^+\pi^-\chi_{c1}\gamma$

- ¹ Using the measured $m_{\psi_2(3823)} - m_{\psi(2S)}$ and assuming $m_{\psi(2S)} = 3686.097$ MeV from PDG 22.
- ² Using the measured $m_{\psi_2(3823)} - m_{\psi(2S)} = 137.98 \pm 0.53 \pm 0.14$ MeV.
- ³ From a simultaneous fit to $B^\pm \rightarrow (\chi_{c1}\gamma)K^\pm$ and $B^0 \rightarrow (\chi_{c1}\gamma)K_S^0$ with significance 4.0 σ including systematics. Corrected for the measured $\psi(2S)$ mass using $B \rightarrow \psi(2S)K \rightarrow (\gamma\chi_{c1})K$ decays.
- ⁴ From a simultaneous unbinned maximum likelihood fit of $e^+e^- \rightarrow \pi^+\pi^-\chi_{c1}\gamma$ data (the $\pi^+\pi^-$ recoil mass) taken at \sqrt{s} values of 4.23, 4.26, 4.36, 4.42, and 4.60 GeV to simulated events including both $\psi(2S) \rightarrow \chi_{c1}\gamma$ and $\psi_2(3823) \rightarrow \chi_{c1}\gamma$ together, with floating mass scale offset for $\psi(2S)$, floating $\psi_2(3823)$ mass, and zero $\psi_2(3823)$ width, resulting in a significance of 5.9 σ when including systematic uncertainties. Superseded by ABLIKIM 22R.

$m_{\psi_2(3823)} - m_{\psi(2S)}$

VALUE (MeV)	EVTs	DOCUMENT ID	TECN	COMMENT
137.98 ± 0.53 ± 0.14	137	¹ AAIJ	20s LHCB	$B^+ \rightarrow J/\psi\pi^+\pi^-K^+$
• • • We do not use the following data for averages, fits, limits, etc. • • •				
¹ AAIJ 20s also reports $m_{\chi_{c1}(3872)} - m_{\psi_2(3823)} = 47.50 \pm 0.53 \pm 0.13$ MeV.				

$\psi_2(3823)$ WIDTH

VALUE (MeV)	CL%	EVTs	DOCUMENT ID	TECN	COMMENT
< 2.9	90	120	ABLIKIM	22R BES3	$e^+e^- \rightarrow \pi^+\pi^-\chi_{c1}\gamma$
• • • We do not use the following data for averages, fits, limits, etc. • • •					
<18.8	90	30	¹ ABLIKIM	23J BES3	$e^+e^- \rightarrow \pi^0\pi^0\chi_{c1}\gamma$
< 5.2	90		² AAIJ	20s LHCB	$B^+ \rightarrow J/\psi\pi^+\pi^-K^+$
<16	90		³ ABLIKIM	15s BES3	$e^+e^- \rightarrow \pi^+\pi^-\chi_{c1}\gamma$
<24	90		⁴ BHARDWAJ	13 BELL	$B^\pm \rightarrow \chi_{c1}\gamma K^\pm$

- ¹ From a fit of $e^+e^- \rightarrow \pi^0\pi^0\chi_{c1}\gamma$ data at \sqrt{s} values from 4.23 to 4.70 GeV to a Breit-Wigner function with floating width, using the Bayesian approach.
- ² AAIJ 20s also provides a limit of < 6.6 MeV with 95% CL.
- ³ From a fit of $e^+e^- \rightarrow \pi^+\pi^-\chi_{c1}\gamma$ data (the $\pi^+\pi^-$ recoil mass) taken at \sqrt{s} values of 4.23, 4.26, 4.36, 4.42, and 4.60 GeV to a Breit-Wigner function with the mass fixed from the likelihood fit above, Gaussian resolution smearing, and floating width.
- ⁴ From a simultaneous fit to $B^\pm \rightarrow (\chi_{c1}\gamma)K^\pm$ and $B^0 \rightarrow (\chi_{c1}\gamma)K_S^0$ with significance 4.0 σ including systematics.

$\psi_2(3823)$ DECAY MODES

Branching fractions are given relative to the one DEFINED AS 1.

Mode	Fraction (Γ_i/Γ)	Confidence level
Γ_1 $J/\psi(1S)\pi^+\pi^-$	<0.06	90%
Γ_2 $J/\psi(1S)\pi^0\pi^0$	<0.11	90%
Γ_3 $J/\psi(1S)\pi^0$	<0.030	90%
Γ_4 $J/\psi(1S)\eta$	<0.14	90%
Γ_5 $\chi_{c0}\gamma$	<0.24	90%
Γ_6 $\chi_{c1}\gamma$	DEFINED AS 1	
Γ_7 $\chi_{c2}\gamma$	0.28 $^{+0.14}_{-0.11}$	

$\psi_2(3823)$ BRANCHING RATIOS

$\Gamma(J/\psi(1S)\pi^+\pi^-)/\Gamma_{total}$	Γ_1/Γ			
VALUE	EVTs	DOCUMENT ID	TECN	COMMENT
• • • We do not use the following data for averages, fits, limits, etc. • • •				
not seen		¹ ABLIKIM	21o BES3	$e^+e^- \rightarrow \pi^+\pi^-X$
seen	137 ± 26	AAIJ	20s LHCB	$B^+ \rightarrow J/\psi\pi^+\pi^-K^+$

- ¹ From a simultaneous unbinned maximum likelihood fit of the $\pi^+\pi^-$ recoil mass distributions of seven decay channels in the process $e^+e^- \rightarrow \pi^+\pi^-X$.

$\Gamma(J/\psi(1S)\pi^+\pi^-)/\Gamma(\chi_{c1}\gamma)$	Γ_1/Γ_6			
VALUE	CL%	DOCUMENT ID	TECN	COMMENT
<0.06	90	¹ ABLIKIM	21o BES3	$e^+e^- \rightarrow \pi^+\pi^-X$

- ¹ From a simultaneous unbinned maximum likelihood fit of the $\pi^+\pi^-$ recoil mass distributions of seven decay channels in the process $e^+e^- \rightarrow \pi^+\pi^-X$.

$\Gamma(J/\psi(1S)\pi^0\pi^0)/\Gamma(\chi_{c1}\gamma)$	Γ_2/Γ_6			
VALUE	CL%	DOCUMENT ID	TECN	COMMENT
<0.11	90	¹ ABLIKIM	21o BES3	$e^+e^- \rightarrow \pi^+\pi^-X$

- ¹ From a simultaneous unbinned maximum likelihood fit of the $\pi^+\pi^-$ recoil mass distributions of seven decay channels in the process $e^+e^- \rightarrow \pi^+\pi^-X$.

$\Gamma(J/\psi(1S)\pi^0)/\Gamma(\chi_{c1}\gamma)$	Γ_3/Γ_6			
VALUE	CL%	DOCUMENT ID	TECN	COMMENT
<0.03	90	¹ ABLIKIM	21o BES3	$e^+e^- \rightarrow \pi^+\pi^-X$

- ¹ From a simultaneous unbinned maximum likelihood fit of the $\pi^+\pi^-$ recoil mass distributions of seven decay channels in the process $e^+e^- \rightarrow \pi^+\pi^-X$.

$\Gamma(J/\psi(1S)\eta)/\Gamma(\chi_{c1}\gamma)$	Γ_4/Γ_6			
VALUE	CL%	DOCUMENT ID	TECN	COMMENT
<0.14	90	¹ ABLIKIM	21o BES3	$e^+e^- \rightarrow \pi^+\pi^-X$

- ¹ From a simultaneous unbinned maximum likelihood fit of the $\pi^+\pi^-$ recoil mass distributions of seven decay channels in the process $e^+e^- \rightarrow \pi^+\pi^-X$.

$\Gamma(J/\psi(1S)\eta)/\Gamma(J/\psi(1S)\pi^+\pi^-)$	Γ_4/Γ_1		
VALUE	DOCUMENT ID	TECN	COMMENT
4.4 + $^{2.5}_{-1.3}$ ± 0.9	¹ AAIJ	22D LHCB	$B^+ \rightarrow J/\psi(1S)\eta K^+$

- ¹ Using the branching ratio for $B^+ \rightarrow \psi_2(3823)K^+$ with $\psi_2(3823) \rightarrow J/\psi(1S)\pi^+\pi^-$ from AAIJ 20s.

$\Gamma(\chi_{c0}\gamma)/\Gamma_{total}$	Γ_5/Γ		
VALUE	DOCUMENT ID	TECN	COMMENT
• • • We do not use the following data for averages, fits, limits, etc. • • •			
not seen	¹ ABLIKIM	21o BES3	$e^+e^- \rightarrow \pi^+\pi^-X$

- ¹ From a simultaneous unbinned maximum likelihood fit of the $\pi^+\pi^-$ recoil mass distributions of seven decay channels in the process $e^+e^- \rightarrow \pi^+\pi^-X$.

$\Gamma(\chi_{c1}\gamma)/\Gamma_{total}$	Γ_6/Γ			
VALUE	EVTs	DOCUMENT ID	TECN	COMMENT
• • • We do not use the following data for averages, fits, limits, etc. • • •				
seen	120	¹ ABLIKIM	22R BES3	$e^+e^- \rightarrow \pi^+\pi^-\chi_{c1}\gamma$
seen	63 ± 9	² ABLIKIM	21o BES3	$e^+e^- \rightarrow \pi^+\pi^-X$
seen	16 ± 5	³ ABLIKIM	21o BES3	$e^+e^- \rightarrow \pi^0\pi^0X$
seen	33 ± 10	⁴ BHARDWAJ	13 BELL	$B^\pm \rightarrow \chi_{c1}\gamma K^\pm$

- ¹ From a fit to the $e^+e^- \rightarrow \pi^+\pi^-\psi(3823)$ cross section between 4.23 and 4.70 GeV with two coherent Breit-Wigner resonances. The data is also consistent with a single peak R with mass $4417.5 \pm 26.2 \pm 3.5$ MeV and width $245 \pm 48 \pm 13$ MeV, which leads to $\Gamma(e^+e^-)B(R \rightarrow \pi^+\pi^-\psi_2(3823))B(\psi_2(3823) \rightarrow \chi_{c1}\gamma) = 0.57 \pm 0.08$ eV.
- ² From a simultaneous unbinned maximum likelihood fit of the $\pi^+\pi^-$ recoil mass distributions of seven decay channels in the process $e^+e^- \rightarrow \pi^+\pi^-X$. Signal has a 11.8 σ significance.
- ³ From a fit of the invariant $\pi^0\pi^0$ recoil-mass distribution. Signal has a 4.3 σ significance.
- ⁴ BHARDWAJ 13 reports $B(B^\pm \rightarrow \psi_2(3823)K^\pm) \times B(\psi_2(3823) \rightarrow \gamma\chi_{c1}) = (9.7 \pm 2.8 \pm 1.1) \times 10^{-6}$ with statistical significance 3.8 σ .

$\Gamma(\chi_{c0}\gamma)/\Gamma(\chi_{c1}\gamma)$	Γ_5/Γ_6			
VALUE	CL%	DOCUMENT ID	TECN	COMMENT
<0.24	90	¹ ABLIKIM	21o BES3	$e^+e^- \rightarrow \pi^+\pi^-X$

- ¹ From a simultaneous unbinned maximum likelihood fit of the $\pi^+\pi^-$ recoil mass distributions of seven decay channels in the process $e^+e^- \rightarrow \pi^+\pi^-X$.

$\Gamma(\chi_{c2}\gamma)/\Gamma_{total}$	Γ_7/Γ		
VALUE	DOCUMENT ID	TECN	COMMENT
• • • We do not use the following data for averages, fits, limits, etc. • • •			
seen	¹ ABLIKIM	21o BES3	$e^+e^- \rightarrow \pi^+\pi^-X$
not seen	² ABLIKIM	15s BES3	$e^+e^- \rightarrow \pi^+\pi^-\chi_{c2}\gamma$
not seen	³ BHARDWAJ	13 BELL	$B^\pm \rightarrow \chi_{c2}\gamma K^\pm$

- ¹ From a simultaneous unbinned maximum likelihood fit of the $\pi^+\pi^-$ recoil mass distributions of seven decay channels in the process $e^+e^- \rightarrow \pi^+\pi^-X$. Signal has a 3.2 σ significance.
- ² From a simultaneous unbinned maximum likelihood fit of $e^+e^- \rightarrow \pi^+\pi^-\chi_{c2}\gamma$ data (the $\pi^+\pi^-$ recoil mass) taken at \sqrt{s} values of 4.23, 4.26, 4.36, 4.42, and 4.60 GeV to simulated events including both $\psi(2S) \rightarrow \chi_{c2}\gamma$ and $\psi_2(3823) \rightarrow \chi_{c2}\gamma$ together, with floating mass scale offset for $\psi(2S)$, $\psi_2(3823)$ mass floating (fixed to that above), and zero $\psi_2(3823)$ width.
- ³ BHARDWAJ 13 reports $B(B^\pm \rightarrow \psi_2(3823)K^\pm) \times B(\psi_2(3823) \rightarrow \gamma\chi_{c2}) < 3.6 \times 10^{-6}$ at 90% CL.

$\Gamma(\chi_{c2}\gamma)/\Gamma(\chi_{c1}\gamma)$	Γ_7/Γ_6				
VALUE	CL%	EVTs	DOCUMENT ID	TECN	COMMENT
0.28 + $^{0.14}_{-0.11}$ ± 0.02	9 ± 4		¹ ABLIKIM	21o BES3	$e^+e^- \rightarrow \pi^+\pi^-\chi_{c2}\gamma$

Meson Particle Listings

$\psi_2(3823)$, $\psi_3(3842)$, $\chi_{c0}(3860)$, $\chi_{c1}(3872)$

• • • We do not use the following data for averages, fits, limits, etc. • • •

<0.42	90	2	ABLIKIM	15s	BES3	$e^+e^- \rightarrow \pi^+\pi^-\chi_{c2}\gamma$
<0.41	90		BHARDWAJ	13	BELL	$B^\pm \rightarrow \chi_{c1}/c_2\gamma K^\pm$

¹ From a simultaneous unbinned maximum likelihood fit of the $\pi^+\pi^-$ recoil mass distributions of seven decay channels in the process $e^+e^- \rightarrow \pi^+\pi^-X$.

² From a simultaneous unbinned maximum likelihood fit of $e^+e^- \rightarrow \pi^+\pi^-\chi_{c1(2)}\gamma$ data (the $\pi^+\pi^-$ recoil mass) taken at \sqrt{s} values of 4.23, 4.26, 4.36, 4.42, and 4.60 GeV to simulated events including both $\psi(2S) \rightarrow \chi_{c1(2)}\gamma$ and $\psi_2(3823) \rightarrow \chi_{c1(2)}\gamma$ together, with floating mass scale offset for $\psi(2S)$, $\psi_2(3823)$ mass floating (fixed to that above), and zero $\psi_2(3823)$ width.

$\psi_2(3823)$ REFERENCES

ABLIKIM	23J	JHEP 2302 171	M. Ablikim et al.	(BESIII Collab.)
AAIJ	22D	JHEP 2204 046	R. Aaij et al.	(LHCb Collab.)
ABLIKIM	22R	PRL 129 102003	M. Ablikim et al.	(BESIII Collab.)
PDG	22	PTEP 2022 083C01	R.L. Workman et al.	(PDG Collab.)
ABLIKIM	21O	PR D103 L091102	M. Ablikim et al.	(BESIII Collab.)
AAIJ	20S	JHEP 2008 123	R. Aaij et al.	(LHCb Collab.)
ABLIKIM	15S	PRL 115 011803	M. Ablikim et al.	(BESIII Collab.)
BHARDWAJ	13	PRL 111 032001	V. Bhardwaj et al.	(BELLE Collab.)

$\psi_3(3842)$

$$J^{G(J^{PC})} = 0^-(3^{--})$$

J, P need confirmation.

J^P has not been measured, 3^- is the quark model prediction.

$\psi_3(3842)$ MASS

VALUE (MeV)	DOCUMENT ID	TECN	COMMENT
3842.71 ± 0.16 ± 0.12	AAIJ	19M	LHCb $pp \rightarrow D\bar{D} + \text{anything}$

$\psi_3(3842)$ WIDTH

VALUE (MeV)	DOCUMENT ID	TECN	COMMENT
2.79 ± 0.51 ± 0.35	AAIJ	19M	LHCb $pp \rightarrow D\bar{D} + \text{anything}$

$\psi_3(3842)$ DECAY MODES

Mode	Fraction (Γ_i/Γ)
Γ_1 D^+D^-	seen
Γ_2 $D^0\bar{D}^0$	seen

$\psi_3(3842)$ BRANCHING RATIOS

$\Gamma(D^+D^-)/\Gamma_{\text{total}}$	DOCUMENT ID	TECN	COMMENT	Γ_1/Γ
seen	AAIJ	19M	LHCb $pp \rightarrow D\bar{D} + \text{anything}$	

• • • We do not use the following data for averages, fits, limits, etc. • • •

possibly seen ¹ ABLIKIM 22AL BES3 $e^+e^- \rightarrow \pi^+\pi^-D^+D^-$

¹ From a fit to the $\pi^+\pi^-$ recoil mass for $e^+e^- \rightarrow D^+D^-\pi^+\pi^-$.

$\Gamma(D^0\bar{D}^0)/\Gamma_{\text{total}}$	DOCUMENT ID	TECN	COMMENT	Γ_2/Γ
seen	AAIJ	19M	LHCb $pp \rightarrow D\bar{D} + \text{anything}$	

$\psi_3(3842)$ REFERENCES

ABLIKIM	22AL	PR D106 052012	M. Ablikim et al.	(BESIII Collab.)
AAIJ	19M	JHEP 1907 035	R. Aaij et al.	(LHCb Collab.)

$\chi_{c0}(3860)$

$$J^{G(J^{PC})} = 0^+(0^{++})$$

OMITTED FROM SUMMARY TABLE

The assignment $J^P = 0^+$ is preferred over 2^+ by 2.5 sigma.

Observed by CHILIKIN 17 using full amplitude analysis of the process $e^+e^- \rightarrow J/\psi D\bar{D}$, where $D = D^0, D^+$. Not seen by AAIJ 20A1 in the decay $B^+ \rightarrow D^+D^-K^+$.

$\chi_{c0}(3860)$ MASS

VALUE (MeV)	DOCUMENT ID	TECN	COMMENT
3862 ± 26 +40 -32 -13	CHILIKIN	17	BELL $e^+e^- \rightarrow J/\psi D\bar{D}$

$\chi_{c0}(3860)$ WIDTH

VALUE (MeV)	DOCUMENT ID	TECN	COMMENT
201 ± 154 +88 -67 -82	CHILIKIN	17	BELL $e^+e^- \rightarrow J/\psi D\bar{D}$

$\chi_{c0}(3860)$ DECAY MODES

Mode	Fraction (Γ_i/Γ)
Γ_1 $D^0\bar{D}^0$	seen
Γ_2 D^+D^-	seen

$\chi_{c0}(3860)$ BRANCHING RATIOS

$\Gamma(D^0\bar{D}^0)/\Gamma_{\text{total}}$	DOCUMENT ID	TECN	COMMENT	Γ_1/Γ
seen	CHILIKIN	17	BELL $e^+e^- \rightarrow J/\psi D^0\bar{D}^0$	

$\Gamma(D^+D^-)/\Gamma_{\text{total}}$	DOCUMENT ID	TECN	COMMENT	Γ_2/Γ
seen	CHILIKIN	17	BELL $e^+e^- \rightarrow J/\psi D^+D^-$	

$\chi_{c0}(3860)$ REFERENCES

AAIJ	20A1	PR D102 112003	R. Aaij et al.	(LHCb Collab.)
CHILIKIN	17	PR D95 112003	K. Chilikin et al.	(BELLE Collab.) JPC

$\chi_{c1}(3872)$

$$J^{G(J^{PC})} = 0^+(1^{++})$$

also known as X(3872)

This state shows properties different from a conventional $q\bar{q}$ state. A candidate for an exotic structure. See the review on non- $q\bar{q}$ states.

First observed by CHOI 03 in $B \rightarrow K\pi^+\pi^-J/\psi(1S)$ decays as a narrow peak in the invariant mass distribution of the $\pi^+\pi^-J/\psi(1S)$ final state. Isovector hypothesis excluded by AUBERT 05B and CHOI 11.

AAIJ 13Q perform a full five-dimensional amplitude analysis of the angular correlations between the decay products in $B^+ \rightarrow \chi_{c1}(3872)K^+$ decays, where $\chi_{c1}(3872) \rightarrow J/\psi\pi^+\pi^-$ and $J/\psi \rightarrow \mu^+\mu^-$, which unambiguously gives the $J^{PC} = 1^{++}$ assignment under the assumption that the $\pi^+\pi^-$ and J/ψ are in an S-wave. AAIJ 15AO extend this analysis with more data to limit D-wave contributions to < 4% at 95% CL.

See the review on "Spectroscopy of Mesons Containing Two Heavy Quarks."

$\chi_{c1}(3872)$ MASS FROM $J/\psi X$ MODE

VALUE (MeV)	EVTS	DOCUMENT ID	TECN	COMMENT
3871.64 ± 0.06 OUR AVERAGE				
3870.2 ± 0.7 ± 0.3	24.6	ABLIKIM	23W	BES3 $e^+e^- \rightarrow J/\psi(1S)\pi^+\pi^-\omega$
3871.64 ± 0.06 ± 0.01	19.8k	¹ AAIJ	20S	LHCb $B^+ \rightarrow J/\psi\pi^+\pi^-K^+$
3871.9 ± 0.7 ± 0.2	20	ABLIKIM	14	BES3 $e^+e^- \rightarrow J/\psi\pi^+\pi^-\gamma$
3871.95 ± 0.48 ± 0.12	0.6k	AAIJ	12H	LHCb $pp \rightarrow J/\psi\pi^+\pi^-X$
3871.85 ± 0.27 ± 0.19	170	² CHOI	11	BELL $B \rightarrow K\pi^+\pi^-J/\psi$
3873 ± 1.8 -1.6 ± 1.3	27	³ DEL-AMO-SA...	10B	BABR $B \rightarrow \omega J/\psi K$
3871.61 ± 0.16 ± 0.19	6k	^{3,4} AALTONEN	09AU	CDF2 $p\bar{p} \rightarrow J/\psi\pi^+\pi^-X$
3871.4 ± 0.6 ± 0.1	93.4	AUBERT	08Y	BABR $B^+ \rightarrow K^+J/\psi\pi^+\pi^-$
3868.7 ± 1.5 ± 0.4	9.4	AUBERT	08Y	BABR $B^0 \rightarrow K_S^0 J/\psi\pi^+\pi^-$
3871.8 ± 3.1 ± 3.0	522	^{3,5} ABAZOV	04F	D0 $p\bar{p} \rightarrow J/\psi\pi^+\pi^-X$
3871.57 ± 0.09	155	⁶ AAIJ	23AP	LHCb $B_S^0 \rightarrow J/\psi 2(\pi^+\pi^-)$
3871.695 ± 0.067 ± 0.068	15.6k	⁷ AAIJ	20AD	LHCb $pp \rightarrow J/\psi\pi^+\pi^-X$
3871.59 ± 0.06 ± 0.03	4.2k	⁸ AAIJ	20S	LHCb $B^+ \rightarrow J/\psi\pi^+\pi^-K^+$
3873.3 ± 1.1 ± 1.0	45	⁹ ABLIKIM	19V	BES $e^+e^- \rightarrow \gamma\omega J/\psi$
3860.0 ± 10.4	13.6	^{3,10} AGHASYAN	18A	COMP $\gamma^*N \rightarrow X\pi^\pm N'$
3868.6 ± 1.2 ± 0.2	8	¹¹ AUBERT	06	BABR $B^0 \rightarrow K_S^0 J/\psi\pi^+\pi^-$

• • • We do not use the following data for averages, fits, limits, etc. • • •

See key on page 1171

Meson Particle Listings

$\chi_{c1}(3872)$

MASS (MeV)	CL%	EVTS	DOCUMENT ID	TECN	COMMENT
3871.3 ± 0.6 ± 0.1	61	11	AUBERT	06	BABR $B^- \rightarrow K^- J/\psi \pi^+ \pi^-$
3873.4 ± 1.4	25	12	AUBERT	05R	BABR $B^+ \rightarrow K^+ J/\psi \pi^+ \pi^-$
3871.3 ± 0.7 ± 0.4	730	3,13	ACOSTA	04	CDF2 $p\bar{p} \rightarrow J/\psi \pi^+ \pi^- X$
3872.0 ± 0.6 ± 0.5	36	14	CHOI	03	BELL $B \rightarrow K \pi^+ \pi^- J/\psi$
3836 ± 13	58	3,15	ANTONIAZZI	94	E705 $300 \pi^\pm L_i \rightarrow J/\psi \pi^+ \pi^- X$

- 1 Calculated from $m_{\chi_{c1}(3872)} - m_{\psi(2S)} = 185.54 \pm 0.06$ MeV obtained by combining the data with $\chi_{c1}(3872)$ produced in B^+ decays from AAIJ 20s and inclusive b -hadron decays from AAIJ 20AD and using $m_{\psi(2S)} = 3686.097$ MeV. Breit-Wigner parametrization.
- 2 The mass difference for the $\chi_{c1}(3872)$ produced in B^+ and B^0 decays is $(-0.71 \pm 0.96 \pm 0.19)$ MeV.
- 3 Width consistent with detector resolution.
- 4 A possible equal mixture of two states with a mass difference greater than 3.6 MeV/ c^2 is excluded at 95% CL.
- 5 Calculated from the corresponding $m_{\chi_{c1}(3872)} - m_{J/\psi}$ using $m_{J/\psi} = 3096.916$ MeV.
- 6 From a fit of a relativistic S -wave Breit-Wigner convolved with the detector resolution. The width of $\chi_{c1}(3872)$ is constrained to the PDG 22 value. Systematic errors not evaluated.
- 7 Using $\chi_{c1}(3872)$ produced in inclusive b -hadron decays and $m_{\psi(2S)} = 3686.097 \pm 0.010$ MeV. Breit-Wigner parametrization. Superseded by the combined value in AAIJ 20s.
- 8 Using Breit-Wigner parametrization. Superseded by the combined value in AAIJ 20s.
- 9 Fit with fixed width and including two resonances, $\chi_{c0}(3915)$ and $X(3960)$.
- 10 Could be a different state.
- 11 Calculated from the corresponding $m_{\chi_{c1}(3872)} - m_{\psi(2S)}$ using $m_{\psi(2S)} = 3686.093$ MeV. Superseded by AUBERT 08y.
- 12 Calculated from the corresponding $m_{\chi_{c1}(3872)} - m_{\psi(2S)}$ using $m_{\psi(2S)} = 3685.96$ MeV. Superseded by AUBERT 06.
- 13 Superseded by AALTONEN 09Au.
- 14 Superseded by CHOI 11.
- 15 A lower mass value can be due to an incorrect momentum scale for soft pions.

$\chi_{c1}(3872)$ MASS FROM $\bar{D}^{*0} D^0$ MODE

VALUE (MeV)	CL%	EVTS	DOCUMENT ID	TECN	COMMENT	
3873.71 ± 0.56 ± 0.13		1	HIRATA	23	BELL $B^0 \rightarrow D^0 \bar{D}^{*0} K^0, B^+ \rightarrow D^0 \bar{D}^{*0} K^+$	
3872.9 ± 0.6 ± 0.4		50	2,3	AUSHEV	10	BELL $B \rightarrow \bar{D}^{*0} D^0 K$
3875.1 ± 0.7 ± 0.5		33 ± 6	3	AUBERT	08B	BABR $B \rightarrow \bar{D}^{*0} D^0 K$
3875.2 ± 0.7 ± 0.9		24 ± 6	3,4	GOKHROO	06	BELL $B \rightarrow D^0 \bar{D}^0 \pi^0 K$

- 1 From a fit of a Breit-Wigner function with energy dependent width.
- 2 Calculated from the measured $m_{\chi_{c1}(3872)} - m_{D^{*0}} - m_{D^0} = 1.1^{+0.6+0.1}_{-0.4-0.3}$ MeV.
- 3 Experiments report $D^{*0} \bar{D}^0$ invariant mass above $D^{*0} \bar{D}^0$ threshold because D^{*0} decay products are kinematically constrained to the D^{*0} mass, even though the D^{*0} may decay off-shell.
- 4 Superseded by AUSHEV 10.

$m_{\chi_{c1}(3872)} - m_{J/\psi}$

VALUE (MeV)	CL%	EVTS	DOCUMENT ID	TECN	COMMENT
774.9 ± 3.1 ± 3.0		522	ABAZOV	04F	D0 $p\bar{p} \rightarrow J/\psi \pi^+ \pi^- X$

$m_{\chi_{c1}(3872)} - m_{\psi(2S)}$

VALUE (MeV)	CL%	EVTS	DOCUMENT ID	TECN	COMMENT
185.598 ± 0.067 ± 0.068	15.6k	1	AAIJ	20AD	LHCB $pp \rightarrow J/\psi \pi^+ \pi^- X$
185.54 ± 0.06	19.8k	2	AAIJ	20s	LHCB $pp \rightarrow J/\psi \pi^+ \pi^- X$
187.4 ± 1.4	25	3	AUBERT	05R	BABR $B^+ \rightarrow K^+ J/\psi \pi^+ \pi^-$

- 1 Using $\chi_{c1}(3872)$ produced in inclusive b -hadron decays. Breit-Wigner parametrization. Superseded by the combined value in AAIJ 20s.
- 2 Combining $m_{\chi_{c1}(3872)} - m_{\psi(2S)} = 185.49 \pm 0.06 \pm 0.03$ MeV from AAIJ 20s and the measured mass difference from AAIJ 20AD. Breit-Wigner parametrization.
- 3 Superseded by AUBERT 06.

$\chi_{c1}(3872)$ WIDTH

VALUE (MeV)	CL%	EVTS	DOCUMENT ID	TECN	COMMENT
1.19 ± 0.21 OUR AVERAGE					Error includes scale factor of 1.1.
1.39 ± 0.24 ± 0.10	15.6k	1	AAIJ	20AD	LHCB $pp \rightarrow J/\psi \pi^+ \pi^- X$
0.96 ± 0.19 ± 0.21	4.2k	2	AAIJ	20s	LHCB $B^+ \rightarrow J/\psi \pi^+ \pi^- K^+$

VALUE (MeV)	CL%	EVTS	DOCUMENT ID	TECN	COMMENT	
< 2.4	90		ABLIKIM	14	BES3 $e^+ e^- \rightarrow J/\psi \pi^+ \pi^- \gamma$	
< 1.2	90		CHOI	11	BELL $B \rightarrow K \pi^+ \pi^- J/\psi$	
< 3.3	90		AUBERT	08Y	BABR $B^+ \rightarrow K^+ J/\psi \pi^+ \pi^-$	
< 4.1	90	69	AUBERT	06	BABR $B \rightarrow K \pi^+ \pi^- J/\psi$	
< 2.3	90	36	3	CHOI	03	BELL $B \rightarrow K \pi^+ \pi^- J/\psi$

- 1 Using $\chi_{c1}(3872)$ produced in inclusive b -hadron decays. Breit-Wigner parametrization.
- 2 Using Breit-Wigner parametrization. Partially overlapping dataset with that of AAIJ 20AD.
- 3 Superseded by CHOI 11.

$\chi_{c1}(3872)$ WIDTH FROM $\bar{D}^{*0} D^0$ MODE

VALUE (MeV)	CL%	EVTS	DOCUMENT ID	TECN	COMMENT	
5.2 ± 2.2 ± 0.4			1	HIRATA	23	BELL $B^0 \rightarrow D^0 \bar{D}^{*0} K^0, B^+ \rightarrow D^0 \bar{D}^{*0} K^+$
3.9 ± 2.8 ± 0.2		50	2	AUSHEV	10	BELL $B \rightarrow \bar{D}^{*0} D^0 K$
3.0 ± 1.9 ± 0.9		33 ± 6		AUBERT	08B	BABR $B \rightarrow \bar{D}^{*0} D^0 K$

- 1 From a fit of a Breit-Wigner function with energy dependent width.
- 2 With a measured value of $B(B \rightarrow \chi_{c1}(3872) K) \times B(\chi_{c1}(3872) \rightarrow D^{*0} \bar{D}^0) = (0.80 \pm 0.20 \pm 0.10) \times 10^{-4}$, assumed to be equal for both charged and neutral modes.

$\chi_{c1}(3872)$ DECAY MODES

Mode	Fraction (Γ_i/Γ)	Confidence level
Γ_1 $e^+ e^-$	< 2.7	$\times 10^{-7}$ 90%
Γ_2 $\pi^+ \pi^- \pi^0$	< 8	$\times 10^{-3}$ 90%
Γ_3 $\pi^+ \pi^- J/\psi(1S)$	(3.5 ± 0.9) %	
Γ_4 $\pi^+ \pi^- \pi^0 J/\psi(1S)$	not seen	
Γ_5 $\omega \eta_c(1S)$	< 30	% 90%
Γ_6 $\rho(770)^0 J/\psi(1S)$	(2.8 ± 0.7) %	
Γ_7 $\omega J/\psi(1S)$	(4.1 ± 1.4) %	
Γ_8 $\phi \phi$	not seen	
Γ_9 $D^0 \bar{D}^0 \pi^0$	(45 ± 21) %	
Γ_{10} $\bar{D}^{*0} D^0$	(34 ± 12) %	
Γ_{11} $\gamma \gamma$	< 10	% 90%
Γ_{12} $D^0 \bar{D}^0$	< 26	% 90%
Γ_{13} $D^+ D^-$	< 17	% 90%
Γ_{14} $\pi^0 \chi_{c2}$	< 4	% 90%
Γ_{15} $\pi^0 \chi_{c1}$	(3.1 ± 1.5) %	
Γ_{16} $\pi^0 \chi_{c0}$	< 13	% 90%
Γ_{17} $\pi^+ \pi^- \eta_c(1S)$	< 13	% 90%
Γ_{18} $\pi^0 \pi^0 \chi_{c0}$	< 6	% 90%
Γ_{19} $\pi^+ \pi^- \chi_{c0}$	< 2.0	% 90%
Γ_{20} $\pi^+ \pi^- \chi_{c1}$	< 7	$\times 10^{-3}$ 90%
Γ_{21} $p\bar{p}$	< 2.2	$\times 10^{-5}$ 95%
Radiative decays		
Γ_{22} $\gamma D^+ D^-$	< 3.5	% 90%
Γ_{23} $\gamma \bar{D}^0 D^0$	< 6	% 90%
Γ_{24} $\gamma J/\psi$	(7.8 ± 2.9) $\times 10^{-3}$	
Γ_{25} $\gamma \chi_{c1}$	< 8	$\times 10^{-3}$ 90%
Γ_{26} $\gamma \chi_{c2}$	< 2.9	% 90%
Γ_{27} $\gamma \psi(2S)$	possibly seen	
C-violating decays		
Γ_{28} $\eta J/\psi$	< 1.7	% 90%

$\chi_{c1}(3872)$ PARTIAL WIDTHS

$\Gamma(e^+ e^-)$	VALUE (eV)	CL%	DOCUMENT ID	TECN	COMMENT
< 0.32	90	1	ABLIKIM	23o	BES3 $e^+ e^- \rightarrow \pi^+ \pi^- J/\psi$
< 4.3	90	2	ABLIKIM	15v	BES3 $4.0-4.4 e^+ e^- \rightarrow \pi^+ \pi^- J/\psi$
< 280	90	3	YUAN	04	RVUE $e^+ e^- \rightarrow \pi^+ \pi^- J/\psi$

$\Gamma(\pi^+ \pi^- J/\psi(1S)) \times \Gamma(e^+ e^-)/\Gamma_{total}$

VALUE (eV)	CL%	DOCUMENT ID	TECN	COMMENT	
< 7.5 $\times 10^{-3}$	90	1	ABLIKIM	23o	BES3 $e^+ e^- \rightarrow \pi^+ \pi^- J/\psi$
< 0.13	90		ABLIKIM	15v	BES3 $4.0-4.4 e^+ e^- \rightarrow \pi^+ \pi^- J/\psi$
< 6.2	90	2,3	AUBERT	05D	BABR $10.6 e^+ e^- \rightarrow \pi^+ \pi^- J/\psi$
< 8.3	90	3	DOBBS	05	CLE3 $10.6 e^+ e^- \rightarrow \pi^+ \pi^- J/\psi$
< 10	90	4	YUAN	04	RVUE $e^+ e^- \rightarrow \pi^+ \pi^- J/\psi$

$\chi_{c1}(3872)$ $\Gamma(I)\Gamma(e^+ e^-)/\Gamma_{total}$

$\Gamma(\pi^+ \pi^- J/\psi(1S)) \times \Gamma(e^+ e^-)/\Gamma_{total}$	VALUE (eV)	CL%	DOCUMENT ID	TECN	COMMENT
< 7.5 $\times 10^{-3}$	90	1	ABLIKIM	23o	BES3 $e^+ e^- \rightarrow \pi^+ \pi^- J/\psi$
< 0.13	90		ABLIKIM	15v	BES3 $4.0-4.4 e^+ e^- \rightarrow \pi^+ \pi^- J/\psi$
< 6.2	90	2,3	AUBERT	05D	BABR $10.6 e^+ e^- \rightarrow \pi^+ \pi^- J/\psi$
< 8.3	90	3	DOBBS	05	CLE3 $10.6 e^+ e^- \rightarrow \pi^+ \pi^- J/\psi$
< 10	90	4	YUAN	04	RVUE $e^+ e^- \rightarrow \pi^+ \pi^- J/\psi$

$\Gamma_3 \Gamma_1 / \Gamma$

- 1 Fit to cross section using a total width value of 1.19 ± 0.21 MeV and $B(\chi_{c1}(3872) \rightarrow \pi^+ \pi^- J/\psi(1S)) = (3.8 \pm 1.2)\%$ from PDG 20.
- 2 ABLIKIM 15v reports this limit from the measurement of $\Gamma(\chi_{c1}(3872) \rightarrow \pi^+ \pi^- J/\psi(1S)) \times \Gamma(\chi_{c1}(3872) \rightarrow e^+ e^-)/\Gamma < 0.13$ eV using $\Gamma(\chi_{c1}(3872) \rightarrow \pi^+ \pi^- J/\psi(1S))/\Gamma = 3\%$.
- 3 Using BAI 98E data on $e^+ e^- \rightarrow \pi^+ \pi^- \ell^+ \ell^-$. Assuming that $\Gamma(\pi^+ \pi^- J/\psi)$ of $\chi_{c1}(3872)$ is the same as that of $\psi(2S)$ (85.4 keV).

Meson Particle Listings

 $\chi_{c1}(3872)$

² Using $B(\chi_{c1}(3872) \rightarrow J/\psi \pi^+ \pi^-) \cdot B(J/\psi \rightarrow \mu^+ \mu^-) \cdot \Gamma(\chi_{c1}(3872) \rightarrow e^+ e^-) < 0.37$ eV from AUBERT 05D and $B(J/\psi \rightarrow \mu^+ \mu^-) = 0.0588 \pm 0.0010$ from the PDG 04.
³ Assuming $\chi_{c1}(3872)$ has $J^{PC} = 1^{--}$.
⁴ Using BAI 98E data on $e^+ e^- \rightarrow \pi^+ \pi^- \ell^+ \ell^-$. From theoretical calculation of the production cross section and using $B(J/\psi \rightarrow \mu^+ \mu^-) = (5.88 \pm 0.10)\%$.

 $\chi_{c1}(3872) \Gamma(i)\Gamma(\gamma\gamma)/\Gamma(\text{total})$ $\Gamma(\pi^+ \pi^- J/\psi(1S)) \times \Gamma(\gamma\gamma)/\Gamma(\text{total})$ $\Gamma_3/\Gamma_{11}/\Gamma$

VALUE (eV)	CL%	EVTS	DOCUMENT ID	TECN	COMMENT
$5.5^{+4.1}_{-3.8} \pm 0.7$		3	¹ TERAMOTO 21	BELL	$e^+ e^- \rightarrow \gamma^* \gamma$ at $\mathcal{T}(nS)$
< 12.9	90		² DOBBS 05	CLE3	$e^+ e^- \rightarrow \pi^+ \pi^- J/\psi \gamma$

• • • We do not use the following data for averages, fits, limits, etc. • • •

¹ Measured in single-tag two-photon production assuming Q^2 dependence of a $c\bar{c}$ meson model. Here, $\Gamma(\chi_{c1}(3872) \rightarrow \gamma\gamma)$ is the reduced two-photon decay width, $\Gamma_{\gamma\gamma}$.

² Assuming $\chi_{c1}(3872)$ has positive C parity and spin 0.

 $\Gamma(\omega J/\psi(1S)) \times \Gamma(\gamma\gamma)/\Gamma(\text{total})$ $\Gamma_7/\Gamma_{11}/\Gamma$

VALUE (eV)	CL%	DOCUMENT ID	TECN	COMMENT
< 1.7	90	¹ LEES 12AD	BABR	$e^+ e^- \rightarrow e^+ e^- \omega J/\psi$

• • • We do not use the following data for averages, fits, limits, etc. • • •

¹ Assuming $\chi_{c1}(3872)$ has spin 2.

 $\Gamma(\pi^+ \pi^- \eta_c(1S)) \times \Gamma(\gamma\gamma)/\Gamma(\text{total})$ $\Gamma_{17}/\Gamma_{11}/\Gamma$

VALUE (eV)	CL%	DOCUMENT ID	TECN	COMMENT
< 11.1	90	LEES 12AE	BABR	$e^+ e^- \rightarrow e^+ e^- \pi^+ \pi^- \eta_c$

• • • We do not use the following data for averages, fits, limits, etc. • • •

 $\chi_{c1}(3872)$ BRANCHING RATIOS $\Gamma(\pi^+ \pi^- \pi^0)/\Gamma(\text{total})$ Γ_2/Γ

VALUE (%)	CL%	DOCUMENT ID	TECN	COMMENT
< 0.8	90	^{1,2} YIN 23	BELL	$B^+ \rightarrow \chi_{c1}(3872) K^+$

• • • We do not use the following data for averages, fits, limits, etc. • • •

VALUE (%)	CL%	DOCUMENT ID	TECN	COMMENT
< 1.1	90	^{2,3} YIN 23	BELL	$B^0 \rightarrow \chi_{c1}(3872) K^0$

¹ YIN 23 reports $[\Gamma(\chi_{c1}(3872) \rightarrow \pi^+ \pi^- \pi^0)/\Gamma(\text{total})] \times [B(B^+ \rightarrow \chi_{c1}(3872) K^+)] < 1.9 \times 10^{-6}$ which we divide by our best value $B(B^+ \rightarrow \chi_{c1}(3872) K^+) = 2.3 \times 10^{-4}$.
² Assuming the decay products, $\pi^+ \pi^- \pi^0$, are uniformly distributed in phase space. The limit is the 90% "credible" upper limit (i.e. Bayesian).
³ YIN 23 reports $[\Gamma(\chi_{c1}(3872) \rightarrow \pi^+ \pi^- \pi^0)/\Gamma(\text{total})] \times [B(B^0 \rightarrow \chi_{c1}(3872) K^0)] < 1.5 \times 10^{-6}$ which we divide by our best value $B(B^0 \rightarrow \chi_{c1}(3872) K^0) = 1.4 \times 10^{-4}$.

• • • We do not use the following data for averages, fits, limits, etc. • • •

 $\Gamma(\pi^+ \pi^- J/\psi(1S))/\Gamma(\text{total})$ Γ_3/Γ

VALUE	EVTS	DOCUMENT ID	TECN	COMMENT
$0.035 \pm 0.002 \pm 0.009$		¹ AAIJ 20s	LHCB	$B^+ \rightarrow J/\psi \pi^+ \pi^- K^+$
$0.038 \pm 0.004 \pm 0.010$		² CHOI 11	BELL	$B^+ \rightarrow \pi^+ \pi^- J/\psi K^+$
$0.037 \pm 0.007 \pm 0.009$	93	^{3,4} AUBERT 08Y	BABR	$B \rightarrow \chi_{c1}(3872) K$

• • • We do not use the following data for averages, fits, limits, etc. • • •

VALUE	EVTS	DOCUMENT ID	TECN	COMMENT
seen	151	⁵ BALA 15	BELL	$B \rightarrow \chi_{c1}(3872) K \pi$
$0.056 \pm 0.018 \pm 0.014$	30	⁶ AUBERT 05R	BABR	$B^+ \rightarrow K^+ \pi^+ \pi^- J/\psi$
$0.060 \pm 0.013 \pm 0.016$	36	⁷ CHOI 03	BELL	$B^+ \rightarrow K^+ \pi^+ \pi^- J/\psi$

¹ AAIJ 20s reports $[\Gamma(\chi_{c1}(3872) \rightarrow \pi^+ \pi^- J/\psi(1S))/\Gamma(\text{total})] \times [B(B^+ \rightarrow \chi_{c1}(3872) K^+)] = (7.95 \pm 0.15 \pm 0.33) \times 10^{-6}$ which we divide by our best value $B(B^+ \rightarrow \chi_{c1}(3872) K^+) = (2.3 \pm 0.6) \times 10^{-4}$. Our first error is their experiment's error and our second error is the systematic error from using our best value.
² CHOI 11 reports $[\Gamma(\chi_{c1}(3872) \rightarrow \pi^+ \pi^- J/\psi(1S))/\Gamma(\text{total})] \times [B(B^+ \rightarrow \chi_{c1}(3872) K^+)] = (8.63 \pm 0.82 \pm 0.52) \times 10^{-6}$ which we divide by our best value $B(B^+ \rightarrow \chi_{c1}(3872) K^+) = (2.3 \pm 0.6) \times 10^{-4}$. Our first error is their experiment's error and our second error is the systematic error from using our best value.
³ AUBERT 08Y reports $[\Gamma(\chi_{c1}(3872) \rightarrow \pi^+ \pi^- J/\psi(1S))/\Gamma(\text{total})] \times [B(B^+ \rightarrow \chi_{c1}(3872) K^+)] = (8.4 \pm 1.5 \pm 0.7) \times 10^{-6}$ which we divide by our best value $B(B^+ \rightarrow \chi_{c1}(3872) K^+) = (2.3 \pm 0.6) \times 10^{-4}$. Our first error is their experiment's error and our second error is the systematic error from using our best value.
⁴ superseded by LEES 20c
⁵ BALA 15 reports $B(\chi_{c1}(3872) \rightarrow \pi^+ \pi^- J/\psi) \times B(B^0 \rightarrow \chi_{c1}(3872) K^+ \pi^-) = (7.9 \pm 1.3 \pm 0.4) \times 10^{-6}$ and $B(\chi_{c1}(3872) \rightarrow \pi^+ \pi^- J/\psi) \times B(B^+ \rightarrow \chi_{c1}(3872) K^0 \pi^+) = (10.6 \pm 3.0 \pm 0.9) \times 10^{-6}$.
⁶ Superseded by AUBERT 08Y. AUBERT 05R reports $[\Gamma(\chi_{c1}(3872) \rightarrow \pi^+ \pi^- J/\psi(1S))/\Gamma(\text{total})] \times [B(B^+ \rightarrow \chi_{c1}(3872) K^+)] = (1.28 \pm 0.41) \times 10^{-5}$ which we divide by our best value $B(B^+ \rightarrow \chi_{c1}(3872) K^+) = (2.3 \pm 0.6) \times 10^{-4}$. Our first error is their experiment's error and our second error is the systematic error from using our best value.
⁷ CHOI 03 reports $[\Gamma(\chi_{c1}(3872) \rightarrow \pi^+ \pi^- J/\psi(1S))/\Gamma(\text{total})] \times [B(B^+ \rightarrow \chi_{c1}(3872) K^+)] / [B(B^+ \rightarrow \psi(2S) K^+)] / [B(\psi(2S) \rightarrow J/\psi(1S) \pi^+ \pi^-)] = 0.063 \pm 0.012 \pm 0.007$ which we multiply or divide by our best values $B(B^+ \rightarrow \chi_{c1}(3872) K^+) = (2.3 \pm 0.6) \times 10^{-4}$, $B(B^+ \rightarrow \psi(2S) K^+) = (6.24 \pm 0.21) \times 10^{-4}$, $B(\psi(2S) \rightarrow J/\psi(1S) \pi^+ \pi^-) = (34.69 \pm 0.34) \times 10^{-2}$. Our first error is their experiment's error and our second error is the systematic error from using our best values.

 $\Gamma(\pi^+ \pi^- \pi^0 J/\psi(1S))/\Gamma(\text{total})$ Γ_4/Γ

VALUE	DOCUMENT ID	TECN	COMMENT
not seen	¹ WANG 11B	BELL	$\mathcal{T}(2S) \rightarrow \gamma X$
not seen	² SHEN 10A	BELL	$\mathcal{T}(1S) \rightarrow \gamma X$

¹ WANG 11B reports $B(\mathcal{T}(2S) \rightarrow \gamma \chi_{c1}(3872)) \times B(\chi_{c1} \rightarrow \pi^+ \pi^- \pi^0 J/\psi) < 2.4 \times 10^{-6}$ at 95% CL.
² SHEN 10A reports $B(\mathcal{T}(1S) \rightarrow \gamma \chi_{c1}(3872)) \times B(\chi_{c1} \rightarrow \pi^+ \pi^- \pi^0 J/\psi) < 2.8 \times 10^{-6}$ at 95% CL.

 $\Gamma(\omega \eta_c(1S))/\Gamma(\text{total})$ Γ_5/Γ

VALUE	CL%	DOCUMENT ID	TECN	COMMENT
< 0.30	90	¹ VINOKUROVA 15	BELL	$B^+ \rightarrow \omega \eta_c K^+$

¹ VINOKUROVA 15 reports $[\Gamma(\chi_{c1}(3872) \rightarrow \omega \eta_c(1S))/\Gamma(\text{total})] \times [B(B^+ \rightarrow \chi_{c1}(3872) K^+)] < 6.9 \times 10^{-5}$ which we divide by our best value $B(B^+ \rightarrow \chi_{c1}(3872) K^+) = 2.3 \times 10^{-4}$.

 $\Gamma(\rho(770)^0 J/\psi(1S))/\Gamma(\pi^+ \pi^- J/\psi(1S))$ Γ_6/Γ_3

VALUE (%)	DOCUMENT ID	TECN	COMMENT
$78.6 \pm 2.3 \pm 2.0$	¹ AAIJ 23s	LHCB	$B^+ \rightarrow K^+ J/\psi \pi^+ \pi^-$

¹ Assuming pure ρ contribution only, i.e. excluding the contribution from ρ - ω interference. Using $B(\rho^0 \rightarrow \pi^+ \pi^-) = 100\%$.

 $\Gamma(\omega J/\psi(1S))/\Gamma(\text{total})$ Γ_7/Γ

VALUE	EVTS	DOCUMENT ID	TECN	COMMENT
$0.026 \pm 0.010 \pm 0.007$	21 \pm 7	¹ DEL-AMO-SA...10B	BABR	$B^+ \rightarrow \omega J/\psi K^+$

• • • We do not use the following data for averages, fits, limits, etc. • • •

¹ DEL-AMO-SANCHEZ 10B reports $[\Gamma(\chi_{c1}(3872) \rightarrow \omega J/\psi(1S))/\Gamma(\text{total})] \times [B(B^+ \rightarrow \chi_{c1}(3872) K^+)] = (6 \pm 2 \pm 1) \times 10^{-6}$ which we divide by our best value $B(B^+ \rightarrow \chi_{c1}(3872) K^+) = (2.3 \pm 0.6) \times 10^{-4}$. Our first error is their experiment's error and our second error is the systematic error from using our best value. DEL-AMO-SANCHEZ 10B also reports $B(B^0 \rightarrow \chi_{c1}(3872) K^0) \times B(\chi_{c1}(3872) \rightarrow J/\psi \omega) = (6 \pm 3 \pm 1) \times 10^{-6}$.

 $\Gamma(\omega J/\psi(1S))/\Gamma(\pi^+ \pi^- J/\psi(1S))$ Γ_7/Γ_3

VALUE	DOCUMENT ID	TECN	COMMENT
1.16 ± 0.24 OUR AVERAGE	Error includes scale factor of 1.2.		
$1.24 \pm 0.33 \pm 0.10$	^{1,2} AAIJ 23s	LHCB	$B^+ \rightarrow K^+ J/\psi \pi^+ \pi^-$
$1.6^{+0.4}_{-0.3} \pm 0.2$	³ ABLIKIM 19v	BES	$e^+ e^- \rightarrow \gamma \omega J/\psi$
0.8 ± 0.3	⁴ DEL-AMO-SA...10B	BABR	$B \rightarrow \omega J/\psi K$

¹ AAIJ 23s reports $[\Gamma(\chi_{c1}(3872) \rightarrow \omega J/\psi(1S))/\Gamma(\chi_{c1}(3872) \rightarrow \pi^+ \pi^- J/\psi(1S))] \times [B(\omega(782) \rightarrow \pi^+ \pi^-)] = (1.9 \pm 0.4 \pm 0.3) \times 10^{-2}$ which we divide by our best value $B(\omega(782) \rightarrow \pi^+ \pi^-) = (1.53 \pm 0.12) \times 10^{-2}$. Our first error is their experiment's error and our second error is the systematic error from using our best value.
² Excluding ρ - ω interference effects.
³ Fit with fixed width and including two resonances, $\chi_{c0}(3915)$ and $X(3960)$.
⁴ Statistical and systematic errors added in quadrature. Uses the values of $B(B \rightarrow \chi_{c1}(3872) K) \times B(\chi_{c1}(3872) \rightarrow J/\psi \pi^+ \pi^-)$ reported in AUBERT 08Y, taking into account the common systematics.

• • • We do not use the following data for averages, fits, limits, etc. • • •

 $\Gamma(\pi^+ \pi^- J/\psi(1S))/\Gamma(\text{total})$ Γ_8/Γ

VALUE	DOCUMENT ID	TECN	COMMENT
not seen	¹ AAIJ 17BB	LHCB	pp at 7, 8 TeV

¹ AAIJ 17BB reports $B(b \rightarrow \chi_{c1}(3872) \text{ anything}) \times B(\chi_{c1}(3872) \rightarrow \phi \phi) < 4.5 \times 10^{-7}$ at 95% CL.

 $\Gamma(D^0 \bar{D}^0 \pi^0)/\Gamma(\text{total})$ Γ_9/Γ

VALUE	CL%	EVTS	DOCUMENT ID	TECN	COMMENT
$0.45 \pm 0.16 \pm 0.11$		17	¹ GOKHROO 06	BELL	$B^+ \rightarrow D^0 \bar{D}^0 \pi^0 K^+$
-0.19 ± 0.12					

• • • We do not use the following data for averages, fits, limits, etc. • • •

VALUE	CL%	DOCUMENT ID	TECN	COMMENT
< 0.26	90	² CHISTOV 04	BELL	Sup. by GOKHROO 06

¹ GOKHROO 06 reports $[\Gamma(\chi_{c1}(3872) \rightarrow D^0 \bar{D}^0 \pi^0)/\Gamma(\text{total})] \times [B(B^+ \rightarrow \chi_{c1}(3872) K^+)] = (1.02 \pm 0.31 \pm 0.21) \times 10^{-4}$ which we divide by our best value $B(B^+ \rightarrow \chi_{c1}(3872) K^+) = (2.3 \pm 0.6) \times 10^{-4}$. Our first error is their experiment's error and our second error is the systematic error from using our best value.
² CHISTOV 04 reports $[\Gamma(\chi_{c1}(3872) \rightarrow D^0 \bar{D}^0 \pi^0)/\Gamma(\text{total})] \times [B(B^+ \rightarrow \chi_{c1}(3872) K^+)] < 0.6 \times 10^{-4}$ which we divide by our best value $B(B^+ \rightarrow \chi_{c1}(3872) K^+) = 2.3 \times 10^{-4}$.

 $\Gamma(D^0 \bar{D}^0 \pi^0)/\Gamma(\pi^+ \pi^- J/\psi(1S))$ Γ_9/Γ_3

VALUE	CL%	DOCUMENT ID	TECN	COMMENT
< 1.16	90	ABLIKIM 20w	BES3	$e^+ e^- \rightarrow \gamma \chi_{c1}(3872)$

• • • We do not use the following data for averages, fits, limits, etc. • • •

 $\Gamma(\bar{D}^{*0} D^0)/\Gamma(\text{total})$ Γ_{10}/Γ

VALUE	EVTS	DOCUMENT ID	TECN	COMMENT
$0.34 \pm 0.08 \pm 0.09$	41^{+9}_{-8}	¹ AUSHEV 10	BELL	$B^+ \rightarrow D^{*0} \bar{D}^0 K^+$

• • • We do not use the following data for averages, fits, limits, etc. • • •

VALUE	EVTS	DOCUMENT ID	TECN	COMMENT
$0.73 \pm 0.26 \pm 0.19$	27 \pm 6	² AUBERT 08B	BABR	$B^+ \rightarrow \bar{D}^{*0} D^0 K^+$

¹ AUSHEV 10 reports $[\Gamma(\chi_{c1}(3872) \rightarrow \bar{D}^{*0} D^0)/\Gamma(\text{total})] \times [B(B^+ \rightarrow \chi_{c1}(3872) K^+)] = (0.77 \pm 0.16 \pm 0.10) \times 10^{-4}$ which we divide by our best value $B(B^+ \rightarrow \chi_{c1}(3872) K^+) = (2.3 \pm 0.6) \times 10^{-4}$. Our first error is their experiment's error and our second error is the systematic error from using our best value.

²AUBERT 08b reports $[\Gamma(\chi_{c1}(3872) \rightarrow \bar{D}^*0 D^0)/\Gamma_{total}] \times [B(B^+ \rightarrow \chi_{c1}(3872) K^+)] = (1.67 \pm 0.36 \pm 0.47) \times 10^{-4}$ which we divide by our best value $B(B^+ \rightarrow \chi_{c1}(3872) K^+) = (2.3 \pm 0.6) \times 10^{-4}$. Our first error is their experiment's error and our second error is the systematic error from using our best value.

$\Gamma(\bar{D}^*0 D^0)/\Gamma(\pi^+ \pi^- J/\psi(1S))$		Γ_{10}/Γ_3	
VALUE	EVTS	DOCUMENT ID	TECN COMMENT
11.77±3.09	50	ABLIKIM	20w BES3 $e^+e^- \rightarrow \gamma\chi_{c1}(3872)$

$\Gamma(\gamma\gamma)/\Gamma_{total}$		Γ_{11}/Γ	
VALUE	CL%	DOCUMENT ID	TECN COMMENT
<0.10	90	¹ WICHT 08	BELL $e^+e^- \rightarrow \Upsilon(4S)$

¹WICHT 08 reports $[\Gamma(\chi_{c1}(3872) \rightarrow \gamma\gamma)/\Gamma_{total}] \times [B(B^+ \rightarrow \chi_{c1}(3872) K^+)] < 2.4 \times 10^{-5}$ which we divide by our best value $B(B^+ \rightarrow \chi_{c1}(3872) K^+) = 2.3 \times 10^{-4}$.

$\Gamma(D^0 \bar{D}^0)/\Gamma_{total}$		Γ_{12}/Γ	
VALUE	CL%	DOCUMENT ID	TECN COMMENT
<0.26	90	¹ CHISTOV 04	BELL $B \rightarrow K D^0 \bar{D}^0$

¹CHISTOV 04 reports $[\Gamma(\chi_{c1}(3872) \rightarrow D^0 \bar{D}^0)/\Gamma_{total}] \times [B(B^+ \rightarrow \chi_{c1}(3872) K^+)] < 6 \times 10^{-5}$ which we divide by our best value $B(B^+ \rightarrow \chi_{c1}(3872) K^+) = 2.3 \times 10^{-4}$.

$\Gamma(D^+ D^-)/\Gamma_{total}$		Γ_{13}/Γ	
VALUE	CL%	DOCUMENT ID	TECN COMMENT
<0.17	90	¹ CHISTOV 04	BELL $B \rightarrow K D^+ D^-$

¹CHISTOV 04 reports $[\Gamma(\chi_{c1}(3872) \rightarrow D^+ D^-)/\Gamma_{total}] \times [B(B^+ \rightarrow \chi_{c1}(3872) K^+)] < 4 \times 10^{-5}$ which we divide by our best value $B(B^+ \rightarrow \chi_{c1}(3872) K^+) = 2.3 \times 10^{-4}$.

$\Gamma(\pi^0 \chi_{c2})/\Gamma(\pi^+ \pi^- J/\psi(1S))$		Γ_{14}/Γ_3	
VALUE	CL%	DOCUMENT ID	TECN COMMENT
<1.1	90	ABLIKIM	19u BES3 $e^+e^- \rightarrow \gamma\chi_{c1}(3872)$

$\Gamma(\pi^0 \chi_{c1})/\Gamma_{total}$		Γ_{15}/Γ	
VALUE	CL%	DOCUMENT ID	TECN COMMENT
<0.035	90	¹ BHARDWAJ 19	BELL $B^\pm \rightarrow \pi^0 \chi_{c1} K^\pm$

¹BHARDWAJ 19 reports $[\Gamma(\chi_{c1}(3872) \rightarrow \pi^0 \chi_{c1})/\Gamma_{total}] \times [B(B^+ \rightarrow \chi_{c1}(3872) K^+)] < 8.1 \times 10^{-6}$ which we divide by our best value $B(B^+ \rightarrow \chi_{c1}(3872) K^+) = 2.3 \times 10^{-4}$.

$\Gamma(\pi^0 \chi_{c1})/\Gamma(\pi^+ \pi^- J/\psi(1S))$		Γ_{15}/Γ_3	
VALUE (units 10^{-2})	EVTS	DOCUMENT ID	TECN COMMENT
88⁺³³₋₂₇±10	10.8	ABLIKIM	19u BES3 $e^+e^- \rightarrow \gamma\chi_{c1}(3872)$

$\Gamma(\pi^0 \chi_{c0})/\Gamma(\pi^+ \pi^- J/\psi(1S))$		Γ_{16}/Γ_3	
VALUE	CL%	DOCUMENT ID	TECN COMMENT
< 3.6	90	ABLIKIM	22d BES3 $e^+e^- \rightarrow \gamma\chi_{c1}(3872)$

••• We do not use the following data for averages, fits, limits, etc. **••••**

$\Gamma(\pi^+ \pi^- \eta_c(1S))/\Gamma_{total}$		Γ_{17}/Γ	
VALUE	CL%	DOCUMENT ID	TECN COMMENT
<0.13	90	¹ VINOKUROVA 15	BELL $B^+ \rightarrow \pi^+ \pi^- \eta_c K^+$

¹VINOKUROVA 15 reports $[\Gamma(\chi_{c1}(3872) \rightarrow \pi^+ \pi^- \eta_c(1S))/\Gamma_{total}] \times [B(B^+ \rightarrow \chi_{c1}(3872) K^+)] < 3.0 \times 10^{-5}$ which we divide by our best value $B(B^+ \rightarrow \chi_{c1}(3872) K^+) = 2.3 \times 10^{-4}$.

$\Gamma(\pi^0 \pi^0 \chi_{c0})/\Gamma(\pi^+ \pi^- J/\psi(1S))$		Γ_{18}/Γ_3	
VALUE	CL%	DOCUMENT ID	TECN COMMENT
<1.7	90	ABLIKIM	22d BES3 $e^+e^- \rightarrow \gamma\chi_{c1}(3872)$

$\Gamma(\pi^+ \pi^- \chi_{c0})/\Gamma(\pi^+ \pi^- J/\psi(1S))$		Γ_{19}/Γ_3	
VALUE	CL%	DOCUMENT ID	TECN COMMENT
<0.56	90	ABLIKIM	22d BES3 $e^+e^- \rightarrow \gamma\chi_{c1}(3872)$

$\Gamma(\pi^+ \pi^- \chi_{c1})/\Gamma_{total}$		Γ_{20}/Γ	
VALUE	CL%	DOCUMENT ID	TECN COMMENT
<7 × 10⁻³	90	¹ BHARDWAJ 16	BELL $B^+ \rightarrow \pi^+ \pi^- \chi_{c1} K^+$

¹BHARDWAJ 16 reports $[\Gamma(\chi_{c1}(3872) \rightarrow \pi^+ \pi^- \chi_{c1})/\Gamma_{total}] \times [B(B^+ \rightarrow \chi_{c1}(3872) K^+)] < 1.5 \times 10^{-6}$ which we divide by our best value $B(B^+ \rightarrow \chi_{c1}(3872) K^+) = 2.3 \times 10^{-4}$.

$\Gamma(p\bar{p})/\Gamma_{total}$		Γ_{21}/Γ	
VALUE	CL%	DOCUMENT ID	TECN COMMENT
<2.2 × 10⁻⁵	95	¹ AAIJ	17AD LHCB $B^+ \rightarrow p\bar{p}K^+$

••• We do not use the following data for averages, fits, limits, etc. **••••**

¹AAIJ 17AD reports $[\Gamma(\chi_{c1}(3872) \rightarrow p\bar{p})/\Gamma_{total}] \times [B(B^+ \rightarrow \chi_{c1}(3872) K^+)] < 0.5 \times 10^{-8}$ which we divide by our best value $B(B^+ \rightarrow \chi_{c1}(3872) K^+) = 2.3 \times 10^{-4}$.

²AAIJ 13s reports $[\Gamma(\chi_{c1}(3872) \rightarrow p\bar{p})/\Gamma_{total}] \times [B(B^+ \rightarrow \chi_{c1}(3872) K^+)] < 1.7 \times 10^{-8}$ which we divide by our best value $B(B^+ \rightarrow \chi_{c1}(3872) K^+) = 2.3 \times 10^{-4}$.

Radiative decays

$\Gamma(\gamma D^+ D^-)/\Gamma(\pi^+ \pi^- J/\psi(1S))$		Γ_{22}/Γ_3	
VALUE	CL%	DOCUMENT ID	TECN COMMENT
<0.99	90	ABLIKIM	20w BES3 $e^+e^- \rightarrow \gamma\chi_{c1}(3872)$

$\Gamma(\gamma \bar{D}^0 D^0)/\Gamma(\pi^+ \pi^- J/\psi(1S))$		Γ_{23}/Γ_3	
VALUE	CL%	DOCUMENT ID	TECN COMMENT
<1.58	90	ABLIKIM	20w BES3 $e^+e^- \rightarrow \gamma\chi_{c1}(3872)$

$\Gamma(\gamma J/\psi)/\Gamma_{total}$		Γ_{24}/Γ	
VALUE (units 10^{-3})	EVTS	DOCUMENT ID	TECN COMMENT
7.8^{+2.2}_{-2.0}±2.0		¹ BHARDWAJ 11	BELL $B^\pm \rightarrow \gamma J/\psi K^\pm$

••• We do not use the following data for averages, fits, limits, etc. **••••**

12.2±3.5±3.2 20 ²AUBERT 09b BABR $B^+ \rightarrow \gamma J/\psi K^+$

14 ±5 ±4 19 ³AUBERT, BE 06M BABR $B^+ \rightarrow \gamma J/\psi K^+$

¹BHARDWAJ 11 reports $[\Gamma(\chi_{c1}(3872) \rightarrow \gamma J/\psi)/\Gamma_{total}] \times [B(B^+ \rightarrow \chi_{c1}(3872) K^+)] = (1.78 \pm 0.48 \pm 0.12) \times 10^{-6}$ which we divide by our best value $B(B^+ \rightarrow \chi_{c1}(3872) K^+) = (2.3 \pm 0.6) \times 10^{-4}$. Our first error is their experiment's error and our second error is the systematic error from using our best value.

²AUBERT 09b reports $[\Gamma(\chi_{c1}(3872) \rightarrow \gamma J/\psi)/\Gamma_{total}] \times [B(B^+ \rightarrow \chi_{c1}(3872) K^+)] = (2.8 \pm 0.8 \pm 0.1) \times 10^{-6}$ which we divide by our best value $B(B^+ \rightarrow \chi_{c1}(3872) K^+) = (2.3 \pm 0.6) \times 10^{-4}$. Our first error is their experiment's error and our second error is the systematic error from using our best value.

³Superseded by AUBERT 09b. AUBERT, BE 06M reports $[\Gamma(\chi_{c1}(3872) \rightarrow \gamma J/\psi)/\Gamma_{total}] \times [B(B^+ \rightarrow \chi_{c1}(3872) K^+)] = (3.3 \pm 1.0 \pm 0.3) \times 10^{-6}$ which we divide by our best value $B(B^+ \rightarrow \chi_{c1}(3872) K^+) = (2.3 \pm 0.6) \times 10^{-4}$. Our first error is their experiment's error and our second error is the systematic error from using our best value.

$\Gamma(\gamma J/\psi)/\Gamma(\pi^+ \pi^- J/\psi(1S))$		Γ_{24}/Γ_3	
VALUE	CL%	DOCUMENT ID	TECN COMMENT
0.79±0.28		ABLIKIM	20w BES3 $e^+e^- \rightarrow \gamma\chi_{c1}(3872)$

$\Gamma(\gamma\chi_{c1})/\Gamma_{total}$		Γ_{25}/Γ	
VALUE	CL%	DOCUMENT ID	TECN COMMENT
<8 × 10⁻³	90	¹ BHARDWAJ 13	BELL $B^\pm \rightarrow \chi_{c1} \gamma K^\pm$

¹BHARDWAJ 13 reports $[\Gamma(\chi_{c1}(3872) \rightarrow \gamma\chi_{c1})/\Gamma_{total}] \times [B(B^+ \rightarrow \chi_{c1}(3872) K^+)] < 1.9 \times 10^{-6}$ which we divide by our best value $B(B^+ \rightarrow \chi_{c1}(3872) K^+) = 2.3 \times 10^{-4}$.

$\Gamma(\gamma\chi_{c1})/\Gamma(\pi^+ \pi^- J/\psi(1S))$		Γ_{25}/Γ_3	
VALUE	CL%	DOCUMENT ID	TECN COMMENT
<0.89	90	CHOI	03 BELL $B \rightarrow K \pi^+ \pi^- J/\psi$

$\Gamma(\gamma\chi_{c2})/\Gamma_{total}$		Γ_{26}/Γ	
VALUE	CL%	DOCUMENT ID	TECN COMMENT
<0.029	90	¹ BHARDWAJ 13	BELL $B^\pm \rightarrow \chi_{c2} \gamma K^\pm$

¹BHARDWAJ 13 reports $[\Gamma(\chi_{c1}(3872) \rightarrow \gamma\chi_{c2})/\Gamma_{total}] \times [B(B^+ \rightarrow \chi_{c1}(3872) K^+)] < 6.7 \times 10^{-6}$ which we divide by our best value $B(B^+ \rightarrow \chi_{c1}(3872) K^+) = 2.3 \times 10^{-4}$.

$\Gamma(\gamma\psi(2S))/\Gamma_{total}$		Γ_{27}/Γ	
VALUE	EVTS	DOCUMENT ID	TECN COMMENT
possibly seen	36 ± 9	¹ AAIJ	14AH LHCB $B^+ \rightarrow \gamma\psi(2S) K^+$

••• We do not use the following data for averages, fits, limits, etc. **••••**

not seen ²BHARDWAJ 11 BELL $B^+ \rightarrow \gamma\psi(2S) K^+$

0.042±0.012±0.011 25 ± 7 ³AUBERT 09b BABR $B^+ \rightarrow \gamma\psi(2S) K^+$

¹From 36.4 ± 9.0 events of $\chi_{c1}(3872) \rightarrow J/\psi\gamma$ decays with a statistical significance of 4.4σ.

²BHARDWAJ 11 reports $B(B^+ \rightarrow K^+ \chi_{c1}(3872)) \times B(\chi_{c1} \rightarrow \gamma\psi(2S)) < 3.45 \times 10^{-6}$ at 90% CL.

³AUBERT 09b reports $[\Gamma(\chi_{c1}(3872) \rightarrow \gamma\psi(2S))/\Gamma_{total}] \times [B(B^+ \rightarrow \chi_{c1}(3872) K^+)] = (9.5 \pm 2.7 \pm 0.6) \times 10^{-6}$ which we divide by our best value $B(B^+ \rightarrow \chi_{c1}(3872) K^+) = (2.3 \pm 0.6) \times 10^{-4}$. Our first error is their experiment's error and our second error is the systematic error from using our best value.

$\Gamma(\gamma\psi(2S))/\Gamma(\pi^+ \pi^- J/\psi(1S))$		Γ_{27}/Γ_3	
VALUE	CL%	DOCUMENT ID	TECN COMMENT
<0.42	90	ABLIKIM	20w BES3 $e^+e^- \rightarrow \gamma\chi_{c1}(3872)$

$\Gamma(\gamma\psi(2S))/\Gamma(\gamma J/\psi)$		Γ_{27}/Γ_{24}		
VALUE	CL%	EVTS	DOCUMENT ID	TECN COMMENT
<0.59	90		ABLIKIM	20w BES3 $e^+e^- \rightarrow \gamma\chi_{c1}(3872)$

••• We do not use the following data for averages, fits, limits, etc. **••••**

2.46±0.64±0.29 36 ± 9 ¹AAIJ 14AH LHCB $B^+ \rightarrow \gamma\psi(2S) K^+$

<2.1 90 BHARDWAJ 11 BELL $B^+ \rightarrow \gamma\psi(2S) K^+$

3.4 ± 1.4 AUBERT 09b BABR $B^+ \rightarrow \gamma c\bar{c} K'$

¹From 36.4 ± 9.0 events of $\chi_{c1}(3872) \rightarrow J/\psi\gamma$ decays with a statistical significance of 4.4σ.

Meson Particle Listings

$\chi_{c1}(3872), \chi_{c0}(3915)$

C-violating decays

$\Gamma(\eta J/\psi)/\Gamma_{total}$	CL%	DOCUMENT ID	TECN	COMMENT	Γ_{28}/Γ
<0.017	90	1,2 IWASHITA	14 BELL	$B \rightarrow K \eta J/\psi$	
<0.034	90	3 AUBERT	04Y BABR	$B \rightarrow K \eta J/\psi$	

• • • We do not use the following data for averages, fits, limits, etc. • • •

¹ IWASHITA 14 reports $[\Gamma(\chi_{c1}(3872) \rightarrow \eta J/\psi)/\Gamma_{total}] \times [B(B^+ \rightarrow \chi_{c1}(3872) K^+)] < 3.8 \times 10^{-6}$ which we divide by our best value $B(B^+ \rightarrow \chi_{c1}(3872) K^+) = 2.3 \times 10^{-4}$.

² IWASHITA 14 also scans the $\eta J/\psi$ mass range 3.8–4.75 GeV and sets upper limits for $B(B^\pm \rightarrow \chi_{c1}(3872) K^\pm) \times B(\chi_{c1}(3872) \rightarrow \eta J/\psi)$ in 5 MeV intervals.

³ AUBERT 04Y reports $[\Gamma(\chi_{c1}(3872) \rightarrow \eta J/\psi)/\Gamma_{total}] \times [B(B^+ \rightarrow \chi_{c1}(3872) K^+)] < 7.7 \times 10^{-6}$ which we divide by our best value $B(B^+ \rightarrow \chi_{c1}(3872) K^+) = 2.3 \times 10^{-4}$.

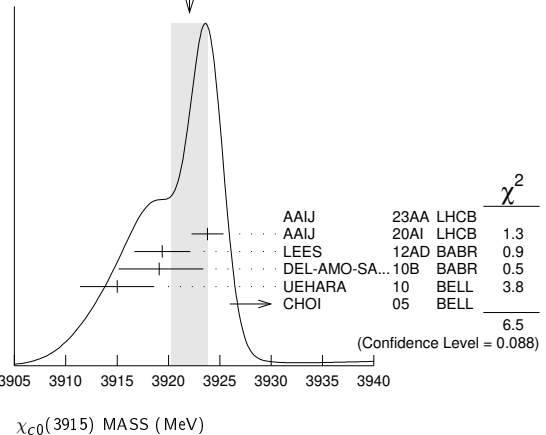
$\chi_{c1}(3872)$ REFERENCES

AAIJ	23AP	JHEP 2307 084	R. Aaij et al.	(LHCb Collab.)
AAIJ	235	PR D108 1011103	R. Aaij et al.	(LHCb Collab.)
ABLIKIM	23O	PR D107 032007	M. Ablikim et al.	(BESIII Collab.)
ABLIKIM	23W	PRL 130 151904	M. Ablikim et al.	(BESIII Collab.)
HIRATA	23	PR D107 112011	H. Hirata et al.	(BELLE Collab.)
YIN	23	PR D107 052004	J.H. Yin et al.	(BELLE Collab.)
ABLIKIM	22D	PR D105 072009	M. Ablikim et al.	(BESIII Collab.)
PDG	22	PTEP 2022 083C01	R.L. Workman et al.	(PDG Collab.)
TERAMOTO	21	PRL 126 122001	Y. Teramoto et al.	(BELLE Collab.)
AAIJ	20AD	PR D102 092005	R. Aaij et al.	(LHCb Collab.)
AAIJ	20S	JHEP 2008 123	R. Aaij et al.	(LHCb Collab.)
ABLIKIM	20W	PRL 124 242001	M. Ablikim et al.	(BESIII Collab.)
LEES	20C	PR 124 152001	J.P. Lees et al.	(BABAR Collab.)
PDG	20	PTEP 2020 083C01	P.A. Zyla et al.	(PDG Collab.)
ABLIKIM	19U	PRL 122 202001	M. Ablikim et al.	(BESIII Collab.)
ABLIKIM	19V	PRL 122 232002	M. Ablikim et al.	(BESIII Collab.)
BHARDWAJ	19	PR D99 111101	V. Bhardwaj et al.	(BELLE Collab.)
AGHASYAN	18A	PL B783 334	M. Aghasyan et al.	(COMPASS Collab.)
AAIJ	17AD	PL B769 305	R. Aaij et al.	(LHCb Collab.)
AAIJ	17BB	EPJ C77 609	R. Aaij et al.	(LHCb Collab.)
BHARDWAJ	16	PR D93 052016	V. Bhardwaj et al.	(BELLE Collab.)
AAIJ	15AO	PR D92 011102	R. Aaij et al.	(LHCb Collab.)
ABLIKIM	15V	PL B749 414	M. Ablikim et al.	(BESIII Collab.)
BALA	15	PR D91 051101	A. Bala et al.	(BELLE Collab.)
VINOKUROVA	15	JHEP 1506 132	A. Vinokurova et al.	(BELLE Collab.)
Also		JHEP 1702 088 (err.)	A. Vinokurava et al.	(BELLE Collab.)
AAIJ	14AH	NP B886 665	R. Aaij et al.	(LHCb Collab.)
ABLIKIM	14	PRL 112 092001	M. Ablikim et al.	(BESIII Collab.)
IWASHITA	14	PTEP 2014 043C01	T. Iwashita et al.	(BELLE Collab.)
AAIJ	13Q	PRL 110 222001	R. Aaij et al.	(LHCb Collab.) JP
AAIJ	13S	EPJ C73 2462	R. Aaij et al.	(LHCb Collab.)
BHARDWAJ	13	PRL 111 032001	V. Bhardwaj et al.	(BELLE Collab.)
AAIJ	12H	EPJ C72 1972	R. Aaij et al.	(LHCb Collab.)
LEES	12AD	PR D86 072002	J.P. Lees et al.	(BABAR Collab.)
LEES	12AE	PR D86 092005	J.P. Lees et al.	(BABAR Collab.)
BHARDWAJ	11	PRL 107 091803	V. Bhardwaj et al.	(BELLE Collab.)
CHOI	11	PR D84 052004	S.-K. Choi et al.	(BELLE Collab.)
WANG	11B	PR D84 071107	X.L. Wang et al.	(BELLE Collab.)
AUSHEV	10	PR D81 031103	T. Aushev et al.	(BELLE Collab.)
DEL-AMO-SA...	10B	PR D82 011101	P. del Amo Sanchez et al.	(BABAR Collab.)
SHEN	10A	PR D82 051504	C.P. Shen et al.	(BELLE Collab.)
AALTONEN	09AU	PRL 103 152001	T. Aaltonen et al.	(CDF Collab.)
AUBERT	09B	PRL 102 132001	B. Aubert et al.	(BABAR Collab.)
AUBERT	08B	PR D77 011102	B. Aubert et al.	(BABAR Collab.)
AUBERT	08Y	PR D77 111101	B. Aubert et al.	(BABAR Collab.)
WICHT	08	PL B662 323	J. Wicht et al.	(BELLE Collab.)
AUBERT	06	PR D73 011101	B. Aubert et al.	(BABAR Collab.)
AUBERT,BE	06M	PR D74 071101	B. Aubert et al.	(BABAR Collab.)
GOKHROO	06	PRL 97 162002	G. Gokhroo et al.	(BELLE Collab.)
AUBERT	05B	PR D71 031501	B. Aubert et al.	(BABAR Collab.)
AUBERT	05D	PR D71 052001	B. Aubert et al.	(BABAR Collab.)
AUBERT	05R	PR D71 071103	B. Aubert et al.	(BABAR Collab.)
DOBBS	05	PRL 94 032004	S. Dobbs et al.	(CLEO Collab.)
ABAZOV	04F	PRL 93 162002	V.M. Abazov et al.	(DO Collab.)
ACOSTA	04	PRL 93 072001	D. Acosta et al.	(CDF Collab.)
AUBERT	04Y	PRL 93 041801	B. Aubert et al.	(BABAR Collab.)
CHRISTOV	04	PRL 93 051803	R. Christov et al.	(BELLE Collab.)
PDG	04	PL B592 1	S. Eidelman et al.	(PDG Collab.)
YUAN	04	PL B579 74	C.Z. Yuan et al.	(BELLE Collab.)
CHOI	03	PRL 91 262001	S.-K. Choi et al.	(BELLE Collab.)
BAI	95E	PR D57 3854	J.Z. Bai et al.	(BES Collab.)
ANTONIAZZI	94	PR D50 4258	L. Antoniazzi et al.	(E705 Collab.)

3919.4 ± 2.2 ± 1.6	59 ± 10	LEES	12AD BABR	$e^+e^- \rightarrow e^+e^-\omega J/\psi$
3919.1 ± 3.8 ± 3.4	± 2.0	DEL-AMO-SA...	10B BABR	$B \rightarrow \omega J/\psi K$
3915 ± 3 ± 2	49 ± 15	UEHARA	10 BELL	10.6 $e^+e^- \rightarrow e^+e^-\omega J/\psi$
3943 ± 11 ± 13	58 ± 11	³ CHOI	05 BELL	$B \rightarrow \omega J/\psi K$
3922.4 ± 6.5 ± 2.0		⁴ WANG	22A BELL	$\gamma\gamma \rightarrow \gamma\psi(2S)$
3926.4 ± 2.2 ± 1.2		⁵ ABLIKIM	19V BES	$e^+e^- \rightarrow \gamma\omega J/\psi$
3914.6 ± 3.8 ± 2.0		³ AUBERT	08W BABR	Superseded by DEL-AMO-SANCHEZ 10B

- ¹ $D_s^+ D_s^-$ near-threshold enhancement parameterized with a Flatte-like function .
- ² Obtained from the full amplitude analysis. Parameterized with the relativistic Breit-Wigner line shape.
- ³ $\omega J/\psi$ threshold enhancement fitted as an S-wave Breit-Wigner resonance.
- ⁴ Not distinguished from the $\chi_{c2}(3930)$.
- ⁵ Could also be $X(3940)$. Significance 3.1 σ . Fit with additional resonance at 3963.7 ± 5.7 MeV, significance 3.4 σ .

WEIGHTED AVERAGE
3922.1 ± 1.8 (Error scaled by 1.5)



$\chi_{c0}(3915)$ WIDTH

VALUE (MeV)	EVTS	DOCUMENT ID	TECN	COMMENT
20 ± 4 OUR AVERAGE		Error includes scale factor of 1.1.		
43 ± 13 ± 8	360	¹ AAIJ	23AA LHCb	$B^+ \rightarrow D_s^+ D_s^- K^+$
17.4 ± 5.1 ± 0.8	1.2k	² AAIJ	20AI LHCb	$B^+ \rightarrow D^+ D^- K^+$
13 ± 6 ± 3	59	LEES	12AD BABR	$e^+e^- \rightarrow e^+e^-\omega J/\psi$
31 ± 10 ± 8	± 5	DEL-AMO-SA...	10B BABR	$B \rightarrow \omega J/\psi K$
17 ± 10 ± 3	49	UEHARA	10 BELL	10.6 $e^+e^- \rightarrow e^+e^-\omega J/\psi$
87 ± 22 ± 26	58	³ CHOI	05 BELL	$B \rightarrow \omega J/\psi K$
22 ± 17 ± 4		⁴ WANG	22A BELL	$\gamma\gamma \rightarrow \gamma\psi(2S)$
3.8 ± 7.5 ± 2.6		⁵ ABLIKIM	19V BES	$e^+e^- \rightarrow \gamma\omega J/\psi$
34 ± 12 ± 8	± 5	³ AUBERT	08W BABR	Superseded by DEL-AMO-SANCHEZ 10B

- ¹ $D_s^+ D_s^-$ near-threshold enhancement parameterized with a Flatte-like function .
- ² Obtained from the full amplitude analysis. Parameterized with the relativistic Breit-Wigner line shape.
- ³ $\omega J/\psi$ threshold enhancement fitted as an S-wave Breit-Wigner resonance.
- ⁴ Not distinguished from the $\chi_{c2}(3930)$.
- ⁵ Could also be $X(3940)$. Significance 3.1 σ . Fit with additional resonance at 3963.7 ± 5.7 MeV, significance 3.4 σ .

$\chi_{c0}(3915)$ DECAY MODES

Mode	Fraction (Γ_i/Γ)
Γ_1 $\omega J/\psi$	seen
Γ_2 $\overline{D}^{*0} D^0$	not seen
Γ_3 $D^+ D^-$	seen
Γ_4 $D_s^+ D_s^-$	seen
Γ_5 $\pi^+ \pi^- \eta_c(1S)$	not seen
Γ_6 $\eta_c \eta$	not seen
Γ_7 $\eta_c \pi^0$	not seen
Γ_8 $K \overline{K}$	not seen
Γ_9 $\gamma\gamma$	seen
Γ_{10} $\gamma\psi(2S)$	not seen
Γ_{11} $\pi^0 \chi_{c1}$	not seen

$\chi_{c0}(3915)$

$$I^G(J^{PC}) = 0^+(0^{++})$$

was $X(3915)$

The $\chi_{c0}(3915)$ was originally seen by BELLE in its $\omega J/\psi$ decay mode and was produced in both B decays in CHOI 05 and $\gamma\gamma$ collisions in UEHARA 10. The J^{PC} was determined to be 0^{++} by BABAR in LEES 12AD but this assignment was questioned by ZHOU 15C. In AAIJ 20AI LHCb found the $D^+ D^-$ decay mode of the $\chi_{c0}(3915)$ using B decays and determined its J^{PC} to be 0^{++} . Based on their compatible mass, width, and J^{PC} , we assume the state decaying to $\omega J/\psi$ and the state decaying to $D^+ D^-$ are both the $\chi_{c0}(3915)$. See also the $\chi_{c2}(3930)$.

$\chi_{c0}(3915)$ MASS

VALUE (MeV)	EVTS	DOCUMENT ID	TECN	COMMENT
3922.1 ± 1.8 OUR AVERAGE		Error includes scale factor of 1.5. See the ideogram below.		
3956 ± 5 ± 10	360	¹ AAIJ	23AA LHCb	$B^+ \rightarrow D_s^+ D_s^- K^+$
3923.8 ± 1.5 ± 0.4	1.2k	² AAIJ	20AI LHCb	$B^+ \rightarrow D^+ D^- K^+$

See key on page 1171

Meson Particle Listings

$\chi_{c0}(3915), \chi_{c2}(3930)$

$\chi_{c0}(3915) \Gamma(i)\Gamma(\gamma\gamma)/\Gamma(\text{total})$

$\Gamma(\omega J/\psi) \times \Gamma(\gamma\gamma)/\Gamma_{\text{total}}$	$\Gamma_1\Gamma_9/\Gamma$			
VALUE (eV)	EVTs	DOCUMENT ID	TECN	COMMENT
54 ± 9 OUR AVERAGE				
52 ± 10 ± 3	59 ± 10	¹ LEES	12AD BABR	$e^+e^- \rightarrow e^+e^-\omega J/\psi$
61 ± 17 ± 8	49 ± 15	¹ UEHARA	10 BELL	10.6 $e^+e^- \rightarrow e^+e^-\omega J/\psi$
• • • We do not use the following data for averages, fits, limits, etc. • • •				
18 ± 5 ± 2	49 ± 15	² UEHARA	10 BELL	10.6 $e^+e^- \rightarrow e^+e^-\omega J/\psi$
¹ For $J^P = 0^+$.				
² For $J^P = 2^+$, helicity-2.				

$\Gamma(\gamma\psi(2S)) \times \Gamma(\gamma\gamma)/\Gamma_{\text{total}}$	$\Gamma_{10}\Gamma_9/\Gamma$		
VALUE (eV)	DOCUMENT ID	TECN	COMMENT
9.8 ± 3.6 ± 1.3	¹ WANG	22A BELL	$\gamma\gamma \rightarrow \gamma\psi(2S)$
¹ Not distinguished from the $\chi_{c2}(3930)$.			

$\Gamma(\pi^+\pi^-\eta_c(1S)) \times \Gamma(\gamma\gamma)/\Gamma_{\text{total}}$	$\Gamma_5\Gamma_9/\Gamma$			
VALUE (eV)	CL%	DOCUMENT ID	TECN	COMMENT
<16	90	LEES	12AE BABR	$e^+e^- \rightarrow e^+e^-\pi^+\pi^-\eta_c$

$\Gamma(K\bar{K}) \times \Gamma(\gamma\gamma)/\Gamma_{\text{total}}$	$\Gamma_8\Gamma_9/\Gamma$			
VALUE (eV)	CL%	DOCUMENT ID	TECN	COMMENT
<1.96	90	UEHARA	13 BELL	$\gamma\gamma \rightarrow K_S^0 K_S^0$

$\chi_{c0}(3915)$ BRANCHING RATIOS

$\Gamma(\omega J/\psi)/\Gamma_{\text{total}}$	Γ_1/Γ		
VALUE	DOCUMENT ID	TECN	COMMENT
seen	¹ DEL-AMO-SA...10B	BABR	$B \rightarrow \omega J/\psi K$
seen	² CHOI	05 BELL	$B \rightarrow \omega J/\psi K$
¹ DEL-AMO-SANCHEZ 10B reports $B(B^\pm \rightarrow \chi_{c0}(3915) K^\pm) \times B(\chi_{c0}(3915) \rightarrow J/\psi\omega) = (3.0_{-0.6}^{+0.7+0.5}) \times 10^{-5}$ and $B(B^0 \rightarrow \chi_{c0}(3915) K^0) \times B(\chi_{c0}(3915) \rightarrow J/\psi\omega) = (2.1 \pm 0.9 \pm 0.3) \times 10^{-5}$.			
² CHOI 05 reports $B(B \rightarrow \chi_{c0}(3915) K) \times B(\chi_{c0}(3915) \rightarrow J/\psi\omega) = (7.1 \pm 1.3 \pm 3.1) \times 10^{-5}$.			

$\Gamma(\omega J/\psi)/\Gamma(D^{*0}D^0)$	Γ_1/Γ_2			
VALUE	CL%	DOCUMENT ID	TECN	COMMENT
>0.71	90	¹ AUSHEV	10 BELL	$B \rightarrow D^{*0}D^0 K$
¹ By combining the upper limit $B(B \rightarrow \chi_{c0}(3915) K) \times B(\chi_{c0}(3915) \rightarrow D^{*0}D^0) < 0.67 \times 10^{-4}$ from AUSHEV 10 with the average of CHOI 05 and AUBERT 08w measurements $B(B \rightarrow \chi_{c0}(3915) K) \times B(\chi_{c0}(3915) \rightarrow \omega J/\psi) = (0.51 \pm 0.11) \times 10^{-4}$.				

$\Gamma(D^+D^-)/\Gamma_{\text{total}}$	Γ_3/Γ		
VALUE	DOCUMENT ID	TECN	COMMENT
seen	AAIJ	20A1 LHCB	$B^+ \rightarrow D^+D^-K^+$

$\Gamma(D^+D^-)/\Gamma(D_s^+D_s^-)$	Γ_3/Γ_4		
VALUE	DOCUMENT ID	TECN	COMMENT
0.29 ± 0.09 ± 0.10 ± 0.08	¹ AAIJ	23AA LHCB	$B^+ \rightarrow D_s^+D_s^-K^+$
¹ Assuming that AAIJ 20A1 reporting on $B^+ \rightarrow D^+D^-K^+$ also refers to $\chi_{c0}(3915)$. The last uncertainty is due to the values of $B(D^+ \rightarrow K^-\pi^+\pi^+)$ and $B(D_s^+ \rightarrow K^-K^+\pi^+)$ from PDG 22.			

$\Gamma(\eta_c\eta)/\Gamma_{\text{total}}$	Γ_6/Γ			
VALUE	CL%	DOCUMENT ID	TECN	COMMENT
not seen	90	¹ VINOKUROVA	15 BELL	$B^+ \rightarrow K^+\eta_c\eta$
¹ VINOKUROVA 15 reports $B(B^+ \rightarrow K^+\chi_{c0}(3915)) \times B(\chi_{c0}(3915) \rightarrow \eta_c\eta) < 4.7 \times 10^{-5}$ at 90% CL.				

$\Gamma(\eta_c\pi^0)/\Gamma_{\text{total}}$	Γ_7/Γ			
VALUE	CL%	DOCUMENT ID	TECN	COMMENT
not seen	90	¹ VINOKUROVA	15 BELL	$B^+ \rightarrow K^+\eta_c\pi^0$
¹ VINOKUROVA 15 reports $B(B^+ \rightarrow K^+\chi_{c0}(3915)^0) \times B(\chi_{c0}(3915) \rightarrow \eta_c\pi^0) < 1.7 \times 10^{-5}$ at 90% CL.				

$\Gamma(\gamma\gamma)/\Gamma_{\text{total}}$	Γ_9/Γ			
VALUE	EVTs	DOCUMENT ID	TECN	COMMENT
seen	59 ± 10	LEES	12AD BABR	$e^+e^- \rightarrow e^+e^-\omega J/\psi$
seen		UEHARA	10 BELL	10.6 $e^+e^- \rightarrow e^+e^-\omega J/\psi$

$\Gamma(\pi^0\chi_{c1})/\Gamma_{\text{total}}$	Γ_{11}/Γ			
VALUE	EVTs	DOCUMENT ID	TECN	COMMENT
not seen	42 ± 14	¹ BHARDWAJ	19 BELL	$B^\pm \rightarrow \chi_{c1}\pi^0 K^\pm$
¹ BHARDWAJ 19 reports $B(B^+ \rightarrow K^+\chi_{c0}(3915)) \times B(\chi_{c0}(3915) \rightarrow \chi_{c1}\pi^0) < 3.8 \times 10^{-5}$ at 90% CL. A signal significance 2.3 standard deviations.				

$\chi_{c0}(3915)$ REFERENCES

AAIJ	23AA	PRL 131 071901	R. Aaij et al.	(LHCb Collab.)
PDG	22	PTEP 2022 083C01	R.L. Workman et al.	(PDG Collab.)
WANG	22A	PR D105 112011	X.L. Wang et al.	(BELLE Collab.)
AAIJ	20A1	PR D102 112003	R. Aaij et al.	(LHCb Collab.) JPC
ABLIKIM	19V	PRL 122 232002	M. Ablikim et al.	(BESIII Collab.)
BHARDWAJ	19	PR D99 111101	V. Bhardwaj et al.	(BELLE Collab.)
VINOKUROVA	15	JHEP 1506 132	A. Vinokurova et al.	(BELLE Collab.)
	Also	JHEP 1702 088 (err.)	A. Vinokurava et al.	(BELLE Collab.)
ZHOU	15C	PRL 115 022001	Z.-Y. Zhou, Z. Xiao, H.-Q. Zhou	(BEIJT, NANJ)
UEHARA	13	PTEP 2013 123C01	S. Uehara et al.	(BELLE Collab.)
LEES	12AD	PR D86 072002	J.P. Lees et al.	(BABAR Collab.)
LEES	12AE	PR D86 092005	J.P. Lees et al.	(BABAR Collab.)
AUSHEV	10	PR D81 031103	T. Aushev et al.	(BELLE Collab.)
DEL-AMO-SA...	10B	PR D82 011101	P. del Amo Sanchez et al.	(BABAR Collab.)
UEHARA	10	PRL 104 092001	S. Uehara et al.	(BELLE Collab.)
AUBERT	08W	PRL 101 082001	B. Aubert et al.	(BABAR Collab.)
CHOI	05	PRL 94 182002	S.-K. Choi et al.	(BELLE Collab.)

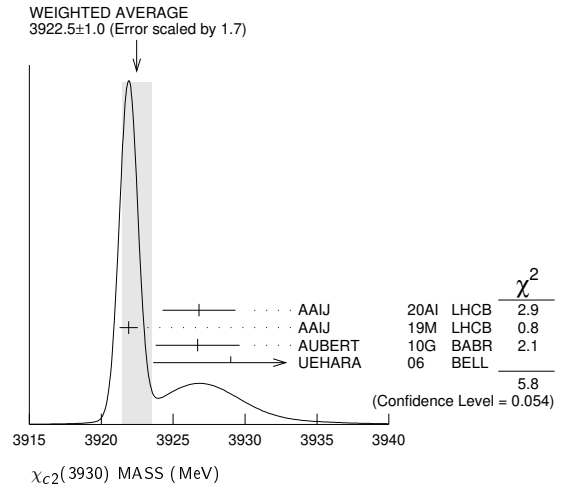
$\chi_{c2}(3930)$

$$J^G(J^{PC}) = 0^+(2^{++})$$

$\chi_{c2}(3930)$ MASS

VALUE (MeV)	EVTs	DOCUMENT ID	TECN	COMMENT
3922.5 ± 1.0 OUR AVERAGE				Error includes scale factor of 1.7. See the ideogram below.
3926.8 ± 2.4 ± 0.8	1.2k	¹ AAIJ	20A1 LHCB	$B^+ \rightarrow D^+D^-K^+$
3921.9 ± 0.6 ± 0.2		² AAIJ	19M LHCB	$pp \rightarrow D\bar{D} + \text{anything}$
3926.7 ± 2.7 ± 1.1	76 ± 17	AUBERT	10G BABR	10.6 $e^+e^- \rightarrow e^+e^-D\bar{D}$
3929 ± 5 ± 2	64	UEHARA	06 BELL	10.6 $e^+e^- \rightarrow e^+e^-D\bar{D}$

¹ Obtained from the full amplitude analysis. Parameterized with the relativistic Breit-Wigner line shape. Previous measurements assumed a single state in this region. This analysis revealed the presence of $\chi_{c0}(3930)$ with the same mass.
² Measured in prompt hadroproduction.



$\chi_{c2}(3930)$ WIDTH

VALUE (MeV)	EVTs	DOCUMENT ID	TECN	COMMENT
35.2 ± 2.2 OUR AVERAGE				Error includes scale factor of 1.2.
34.2 ± 6.6 ± 1.1	1.2k	¹ AAIJ	20A1 LHCB	$B^+ \rightarrow D^+D^-K^+$
36.6 ± 1.9 ± 0.9		² AAIJ	19M LHCB	$pp \rightarrow D\bar{D} + \text{anything}$
21.3 ± 6.8 ± 3.6	76 ± 17	AUBERT	10G BABR	10.6 $e^+e^- \rightarrow e^+e^-D\bar{D}$
29 ± 10 ± 2	64	UEHARA	06 BELL	10.6 $e^+e^- \rightarrow e^+e^-D\bar{D}$

¹ Obtained from the full amplitude analysis. Parameterized with the relativistic Breit-Wigner line shape. Previous measurements assumed a single state in this region. This analysis revealed the presence of $\chi_{c0}(3930)$ with the same mass.
² Measured in prompt hadroproduction.

$\chi_{c2}(3930)$ DECAY MODES

Mode	Fraction (Γ_i/Γ)
Γ_1 $\gamma\gamma$	seen
Γ_2 $K\bar{K}\pi$	not seen
Γ_3 $K^+K^-\pi^+\pi^-\pi^0$	not seen
Γ_4 $D\bar{D}$	seen
Γ_5 D^+D^-	seen
Γ_6 $D^0\bar{D}^0$	seen
Γ_7 $\pi^+\pi^-\eta_c(1S)$	not seen
Γ_8 $K\bar{K}$	not seen

Meson Particle Listings

$\chi_{c2}(3930)$, $X(3940)$, $\psi(4040)$

$\chi_{c2}(3930)$ PARTIAL WIDTHS

$\chi_{c2}(3930) \Gamma(i)\Gamma(\gamma\gamma)/\Gamma(\text{total})$

$\Gamma(K\bar{K}\pi) \times \Gamma(\gamma\gamma)/\Gamma_{\text{total}}$	Γ_2/Γ
VALUE (eV) CL% DOCUMENT ID TECN COMMENT	
<2.1 90 DEL-AMO-SA...11M BABR $\gamma\gamma \rightarrow K_S^0 K^\pm \pi^\mp$	

$\Gamma(K^+ K^- \pi^+ \pi^- \pi^0) \times \Gamma(\gamma\gamma)/\Gamma_{\text{total}}$	Γ_3/Γ
VALUE (eV) CL% DOCUMENT ID TECN COMMENT	
<3.4 90 DEL-AMO-SA...11M BABR $\gamma\gamma \rightarrow K^+ K^- \pi^+ \pi^- \pi^0$	

$\Gamma(D\bar{D}) \times \Gamma(\gamma\gamma)/\Gamma_{\text{total}}$	Γ_4/Γ
VALUE (keV) EVTS DOCUMENT ID TECN COMMENT	
0.21 ± 0.04 OUR AVERAGE	
$0.24 \pm 0.05 \pm 0.04$ 76 \pm 17 AUBERT 10G BABR $10.6 e^+ e^- \rightarrow e^+ e^- D\bar{D}$	
$0.18 \pm 0.05 \pm 0.03$ 64 1 UEHARA 06 BELL $10.6 e^+ e^- \rightarrow e^+ e^- D\bar{D}$	
1 Assuming $B(D^+ D^-) = 0.89 B(D^0 \bar{D}^0)$.	

$\Gamma(\pi^+ \pi^- \eta_c(1S)) \times \Gamma(\gamma\gamma)/\Gamma_{\text{total}}$	Γ_7/Γ
VALUE (eV) CL% DOCUMENT ID TECN COMMENT	
<18 90 LEES 12AE BABR $e^+ e^- \rightarrow e^+ e^- \pi^+ \pi^- \eta_c$	

$\Gamma(K\bar{K}) \times \Gamma(\gamma\gamma)/\Gamma_{\text{total}}$	Γ_8/Γ
VALUE (eV) CL% DOCUMENT ID TECN COMMENT	
<0.256 90 UEHARA 13 BELL $\gamma\gamma \rightarrow K_S^0 K_S^0$	

$\chi_{c2}(3930)$ BRANCHING RATIOS

$\Gamma(D^+ D^-)/\Gamma(D^0 \bar{D}^0)$	Γ_5/Γ_6
VALUE EVTS DOCUMENT ID TECN COMMENT	
$0.74 \pm 0.43 \pm 0.16$ 64 UEHARA 06 BELL $10.6 e^+ e^- \rightarrow e^+ e^- D\bar{D}$	

$\chi_{c2}(3930)$ REFERENCES

AAJ 20AI PR D102 112003 R. Aaij et al. (LHCb Collab.)
AAJ 19M JHEP 1907 035 R. Aaij et al. (LHCb Collab.)
UEHARA 13 PTEP 2013 123C01 S. Uehara et al. (BELLE Collab.)
LEES 12AE PR D86 092005 J.P. Lees et al. (BABAR Collab.)
DEL-AMO-SA...11M PR D84 012004 P. del Amo Sanchez et al. (BABAR Collab.)
AUBERT 10G PR D81 092003 B. Aubert et al. (BABAR Collab.)
UEHARA 06 PRL 96 082003 S. Uehara et al. (BELLE Collab.)

$X(3940)$

$$I^G(J^{PC}) = ?(???)$$

OMITTED FROM SUMMARY TABLE
Reported by ABE 07, observed in $e^+ e^- \rightarrow J/\psi X$.

$X(3940)$ MASS

VALUE (MeV) EVTS DOCUMENT ID TECN COMMENT
$3942 \pm \frac{7}{6} \pm 6$ 52 PAKHLOV 08 BELL $e^+ e^- \rightarrow J/\psi X$
$3943 \pm 6 \pm 6$ 25 1 ABE 07 BELL $e^+ e^- \rightarrow J/\psi X$
3936 ± 14 266 2 ABE 07 BELL $e^+ e^- \rightarrow J/\psi(c\bar{c})$

- • • We do not use the following data for averages, fits, limits, etc. • • •
- 1 From a fit to $D^{*+} D^-$ and $D^{*0} \bar{D}^0$ events.
- 2 From the inclusive fit. Not independent of the exclusive measurement by ABE 07.

$X(3940)$ WIDTH

VALUE (MeV) CL% EVTS DOCUMENT ID TECN COMMENT
$37 \pm \frac{26}{15} \pm 8$ 52 PAKHLOV 08 BELL $e^+ e^- \rightarrow J/\psi X$
<52 90 25 ABE 07 BELL $e^+ e^- \rightarrow J/\psi X$

$X(3940)$ DECAY MODES

Mode	Fraction (Γ_i/Γ)
Γ_1 $D\bar{D}^* + c.c.$	seen
Γ_2 $D\bar{D}$	not seen
Γ_3 $J/\psi\omega$	not seen

$X(3940)$ BRANCHING RATIOS

$\Gamma(D\bar{D}^* + c.c.)/\Gamma_{\text{total}}$	Γ_1/Γ
VALUE CL% EVTS DOCUMENT ID TECN COMMENT	
>0.45 90 25 1,2 ABE 07 BELL $e^+ e^- \rightarrow J/\psi X$	
1 For $X(3940)$ decaying to final states with more than two tracks.	
2 PAKHLOV 08 finds that the inclusive peak near 3940 MeV/ c^2 may consist of several states.	

$\Gamma(D\bar{D})/\Gamma_{\text{total}}$

VALUE CL% DOCUMENT ID TECN COMMENT
<0.41 90 1,2 ABE 07 BELL $e^+ e^- \rightarrow J/\psi X$

- • • We do not use the following data for averages, fits, limits, etc. • • •
- 1 For $X(3940)$ decaying to final states with more than two tracks.
- 2 PAKHLOV 08 finds that the inclusive peak near 3940 MeV/ c^2 may consist of several states.

$\Gamma(J/\psi\omega)/\Gamma_{\text{total}}$

VALUE CL% DOCUMENT ID TECN COMMENT
<0.26 90 1,2 ABE 07 BELL $e^+ e^- \rightarrow J/\psi X$

- • • We do not use the following data for averages, fits, limits, etc. • • •
- 1 For $X(3940)$ decaying to final states with more than two tracks.
- 2 PAKHLOV 08 finds that the inclusive peak near 3940 MeV/ c^2 may consist of several states.

$X(3940)$ REFERENCES

PAKHLOV 08 PRL 100 202001 P. Pakhlov et al. (BELLE Collab.)
ABE 07 PRL 98 082001 K. Abe et al. (BELLE Collab.)

$\psi(4040)$

$$I^G(J^{PC}) = 0^-(1^{--})$$

$\psi(4040)$ MASS

VALUE (MeV) DOCUMENT ID TECN COMMENT
4039.6 ± 4.3 1 ABLIKIM 08d BES2 $e^+ e^- \rightarrow$ hadrons
4034 ± 6 2 MO 10 RVUE $e^+ e^- \rightarrow$ hadrons
4037 ± 2 3 SETH 05A RVUE $e^+ e^- \rightarrow$ hadrons
4040 ± 1 4 SETH 05A RVUE $e^+ e^- \rightarrow$ hadrons
4040 ± 10 BRANDELIK 78c DASP $e^+ e^-$

- 1 Reanalysis of data presented in BAI 02c. From a global fit over the center-of-mass energy region 3.7–5.0 GeV covering the $\psi(3770)$, $\psi(4040)$, $\psi(4160)$, and $\psi(4415)$ resonances. Phase angle fixed in the fit to $\delta = (130 \pm 46)^\circ$.
- 2 Reanalysis of data presented in BAI 00 and BAI 02c. From a global fit over the center-of-mass energy 3.8–4.8 GeV covering the $\psi(4040)$, $\psi(4160)$ and $\psi(4415)$ resonances and including interference effects.
- 3 From a fit to Crystal Ball (OSTERHELD 86) data.
- 4 From a fit to BES (BAI 02c) data.

$\psi(4040)$ WIDTH

VALUE (MeV) DOCUMENT ID TECN COMMENT
84.5 ± 12.3 5 ABLIKIM 08d BES2 $e^+ e^- \rightarrow$ hadrons
87 ± 11 6 MO 10 RVUE $e^+ e^- \rightarrow$ hadrons
85 ± 10 7 SETH 05A RVUE $e^+ e^- \rightarrow$ hadrons
89 ± 6 8 SETH 05A RVUE $e^+ e^- \rightarrow$ hadrons
52 ± 10 BRANDELIK 78c DASP $e^+ e^-$

- 5 Reanalysis of data presented in BAI 02c. From a global fit over the center-of-mass energy region 3.7–5.0 GeV covering the $\psi(3770)$, $\psi(4040)$, $\psi(4160)$, and $\psi(4415)$ resonances. Phase angle fixed in the fit to $\delta = (130 \pm 46)^\circ$.
- 6 Reanalysis of data presented in BAI 00 and BAI 02c. From a global fit over the center-of-mass energy 3.8–4.8 GeV covering the $\psi(4040)$, $\psi(4160)$ and $\psi(4415)$ resonances and including interference effects.
- 7 From a fit to Crystal Ball (OSTERHELD 86) data.
- 8 From a fit to BES (BAI 02c) data.

$\psi(4040)$ DECAY MODES

Due to the complexity of the $c\bar{c}$ threshold region, in this listing, “seen” (“not seen”) means that a cross section for the mode in question has been measured at effective \sqrt{s} near this particle’s central mass value, more (less) than 2σ above zero, without regard to any peaking behavior in \sqrt{s} or absence thereof. See mode listing(s) for details and references.

Mode	Fraction (Γ_i/Γ)	Confidence level
Γ_1 $e^+ e^-$	$(1.02 \pm 0.17) \times 10^{-5}$	
Γ_2 $D\bar{D}$	seen	
Γ_3 $D^0 \bar{D}^0$	seen	
Γ_4 $D^+ D^-$	seen	
Γ_5 $D^* \bar{D} + c.c.$	seen	
Γ_6 $D^*(2007)^0 \bar{D}^0 + c.c.$	seen	
Γ_7 $D^*(2010)^+ D^- + c.c.$	seen	
Γ_8 $D^* \bar{D}^*$	seen	
Γ_9 $D^*(2007)^0 \bar{D}^*(2007)^0$	seen	
Γ_{10} $D^*(2010)^+ D^*(2010)^-$	seen	
Γ_{11} $D\bar{D}\pi$ (excl. $D^* \bar{D}$)	not seen	
Γ_{12} $D^0 D^- \pi^+ + c.c.$ (excl. $D^*(2010)^+ D^- + c.c.$)	not seen	

Γ_{13}	$D\bar{D}^*\pi$ (excl. $D^*\bar{D}^*$)	not seen		
Γ_{14}	$D^0\bar{D}^{*+}\pi^+ + c.c.$ (excl. $D^*(2010)^+\bar{D}^*(2010)^-$)	seen		
Γ_{15}	$D_s^+D_s^-$	seen		
Γ_{16}	$\pi^+\pi^+\pi^-\pi^-\pi^0$	seen		
Γ_{17}	$J/\psi(1S)$ hadrons	seen		
Γ_{18}	$J/\psi\pi^+\pi^-$	< 4	$\times 10^{-3}$	90%
Γ_{19}	$J/\psi\pi^0\pi^0$	< 2	$\times 10^{-3}$	90%
Γ_{20}	$J/\psi\eta$	(5.2 ± 0.7)	$\times 10^{-3}$	
Γ_{21}	$J/\psi\pi^0$	< 2.8	$\times 10^{-4}$	90%
Γ_{22}	$J/\psi\pi^+\pi^-\pi^0$	< 2	$\times 10^{-3}$	90%
Γ_{23}	$\chi_{c1}\gamma$	< 3.4	$\times 10^{-3}$	90%
Γ_{24}	$\chi_{c2}\gamma$	< 5	$\times 10^{-3}$	90%
Γ_{25}	$\chi_{c1}\pi^+\pi^-\pi^0$	< 1.1	%	90%
Γ_{26}	$\chi_{c2}\pi^+\pi^-\pi^0$	< 3.2	%	90%
Γ_{27}	$h_c(1P)\pi^+\pi^-$	< 3	$\times 10^{-3}$	90%
Γ_{28}	$\phi\pi^+\pi^-$	< 3	$\times 10^{-3}$	90%
Γ_{29}	$\Lambda\bar{\Lambda}\pi^+\pi^-$	< 2.9	$\times 10^{-4}$	90%
Γ_{30}	$\Lambda\bar{\Lambda}\pi^0$	< 9	$\times 10^{-5}$	90%
Γ_{31}	$\Lambda\bar{\Lambda}\eta$	< 3.0	$\times 10^{-4}$	90%
Γ_{32}	$\Lambda\bar{\Lambda}$	< 6	$\times 10^{-6}$	90%
Γ_{33}	$\Sigma^+\Sigma^-$	< 1.3	$\times 10^{-4}$	90%
Γ_{34}	$\Sigma^0\Sigma^0$	< 7	$\times 10^{-5}$	90%
Γ_{35}	$\Xi^+\Xi^-$	< 1.6	$\times 10^{-4}$	90%
Γ_{36}	$\Xi^0\Xi^0$	< 1.8	$\times 10^{-4}$	90%
Γ_{37}	$\Xi^-\Xi^+$	< 6	$\times 10^{-5}$	90%
Γ_{38}	$\mu^+\mu^-$	(9 ± 6)	$\times 10^{-6}$	

$\psi(4040)$ PARTIAL WIDTHS

$\Gamma(e^+e^-)$	Γ_1
VALUE (keV)	DOCUMENT ID TECN COMMENT
0.86 ± 0.07 OUR ESTIMATE	
0.83 ± 0.20	⁹ ABLIKIM 08d BES2 $e^+e^- \rightarrow$ hadrons
••• We do not use the following data for averages, fits, limits, etc. •••	
0.6 to 1.4	¹⁰ MO 10 RVUE $e^+e^- \rightarrow$ hadrons
0.88±0.11	¹¹ SETH 05A RVUE $e^+e^- \rightarrow$ hadrons
0.91±0.13	¹² SETH 05A RVUE $e^+e^- \rightarrow$ hadrons
0.75±0.15	BRANDELIK 78c DASP e^+e^-

⁹ Reanalysis of data presented in BAI 02c. From a global fit over the center-of-mass energy region 3.7–5.0 GeV covering the $\psi(3770)$, $\psi(4040)$, $\psi(4160)$, and $\psi(4415)$ resonances. Phase angle fixed in the fit to $\delta = (130 \pm 46)^\circ$.

¹⁰ Reanalysis of data presented in BAI 00 and BAI 02c. From a global fit over the center-of-mass energy 3.8–4.8 GeV covering the $\psi(4040)$, $\psi(4160)$ and $\psi(4415)$ resonances and including interference effects. Four sets of solutions are obtained with the same fit quality, mass and total width, but with different e^+e^- partial widths. We quote only the range of values.

¹¹ From a fit to Crystal Ball (OSTERHELD 86) data.

¹² From a fit to BES (BAI 02c) data.

$\Gamma(\mu^+\mu^-)$	Γ_{38}
VALUE (keV)	DOCUMENT ID TECN COMMENT
$0.73 \pm 0.48 \pm 0.12$	^{13,14} ABLIKIM 20Ag BES3 $e^+e^- \rightarrow \mu^+\mu^-$

¹³ From a fit to the $e^+e^- \rightarrow \mu^+\mu^-$ cross section between 3.8 and 4.6 GeV to the coherent sum of four resonant amplitudes assuming $\Gamma(\mu^+\mu^-) = \Gamma(e^+e^-)$.

¹⁴ From solution 1 of 8 with equal fit quality. Other solutions range from $0.58 \pm 0.52 \pm 0.10$ to $0.80 \pm 0.48 \pm 0.13$ keV.

$\psi(4040)$ $\Gamma(i) \times \Gamma(e^+e^-)/\Gamma(\text{total})$

$\Gamma(J/\psi\eta) \times \Gamma(e^+e^-)/\Gamma_{\text{total}}$	$\Gamma_{20}\Gamma_1/\Gamma$
VALUE (eV)	DOCUMENT ID TECN COMMENT
••• We do not use the following data for averages, fits, limits, etc. •••	
1.5±0.3	¹⁵ ABLIKIM 20o BES3 $e^+e^- \rightarrow \eta J/\psi$
1.4±0.3	¹⁶ ABLIKIM 20o BES3 $e^+e^- \rightarrow \eta J/\psi$
7.0±0.6	¹⁷ ABLIKIM 20o BES3 $e^+e^- \rightarrow \eta J/\psi$

¹⁵ Solution 1 of three equivalent fit solutions using three resonant structures.

¹⁶ Solution 2 of three equivalent fit solutions using three resonant structures.

¹⁷ Solution 3 of three equivalent fit solutions using three resonant structures.

$\Gamma(\chi_{c1}\gamma) \times \Gamma(e^+e^-)/\Gamma_{\text{total}}$	$\Gamma_{23}\Gamma_1/\Gamma$
VALUE (eV)	CL% DOCUMENT ID TECN COMMENT
< 2.9	90 ¹⁸ HAN 15 BELL $10.58 e^+e^- \rightarrow \chi_{c1}\gamma$

¹⁸ Using $B(\eta \rightarrow \gamma\gamma) = (39.41 \pm 0.21)\%$.

$\Gamma(\chi_{c2}\gamma) \times \Gamma(e^+e^-)/\Gamma_{\text{total}}$	$\Gamma_{24}\Gamma_1/\Gamma$
VALUE (eV)	CL% DOCUMENT ID TECN COMMENT
< 4.6	90 ¹⁹ HAN 15 BELL $10.58 e^+e^- \rightarrow \chi_{c2}\gamma$

¹⁹ Using $B(\eta \rightarrow \gamma\gamma) = (39.41 \pm 0.21)\%$.

$\Gamma(\Lambda\bar{\Lambda}) \times \Gamma(e^+e^-)/\Gamma_{\text{total}}$	$\Gamma_{32}\Gamma_1/\Gamma$
VALUE (eV)	CL% DOCUMENT ID TECN COMMENT
$< 5.5 \times 10^{-3}$	90 ²⁰ ABLIKIM 21As BES3 $e^+e^- \rightarrow \psi(4040)$

²⁰ From a measurement of the $e^+e^- \rightarrow \Lambda\bar{\Lambda}$ cross section between 3.5 and 4.6 GeV.

$\Gamma(\Xi^-\Xi^+) \times \Gamma(e^+e^-)/\Gamma_{\text{total}}$	$\Gamma_{37}\Gamma_1/\Gamma$
VALUE (eV)	CL% DOCUMENT ID TECN COMMENT
< 0.0519	90 ²¹ ABLIKIM 23Bk BES3 $e^+e^- \rightarrow \psi(4040)$

²¹ From a fit to $e^+e^- \rightarrow \Xi^-\Xi^+$ cross sections.

$\psi(4040)$ $\Gamma(i) \times \Gamma(e^+e^-)/\Gamma^2(\text{total})$

$\Gamma(J/\psi\eta)/\Gamma_{\text{total}} \times \Gamma(e^+e^-)/\Gamma_{\text{total}}$	$\Gamma_{20}/\Gamma \times \Gamma_1/\Gamma$
VALUE (units 10^{-8})	DOCUMENT ID TECN COMMENT
••• We do not use the following data for averages, fits, limits, etc. •••	
$5.1 \pm 1.4 \pm 1.5$	²² WANG 13B BELL $e^+e^- \rightarrow J/\psi\eta\gamma$
$12.8 \pm 2.1 \pm 1.9$	²³ WANG 13B BELL $e^+e^- \rightarrow J/\psi\eta\gamma$

²² Solution I of two equivalent solutions in a fit using two interfering resonances. Mass and width fixed at 4039 MeV and 80 MeV, respectively.

²³ Solution II of two equivalent solutions in a fit using two interfering resonances. Mass and width fixed at 4039 MeV and 80 MeV, respectively.

$\psi(4040)$ BRANCHING RATIOS

$\Gamma(e^+e^-)/\Gamma_{\text{total}}$	Γ_1/Γ
VALUE (units 10^{-5})	DOCUMENT ID TECN COMMENT
••• We do not use the following data for averages, fits, limits, etc. •••	
~ 1.0	FELDMAN 77 MRK1 e^+e^-

$\Gamma(D^0\bar{D}^0)/\Gamma_{\text{total}}$	Γ_3/Γ
VALUE	DOCUMENT ID TECN COMMENT
seen	AUBERT 09M BABR $e^+e^- \rightarrow D^0\bar{D}^0\gamma$
seen	CRONIN-HEN..09 CLEO $e^+e^- \rightarrow D^0\bar{D}^0$
seen	PAKHOVA 08 BELL $e^+e^- \rightarrow D^0\bar{D}^0\gamma$

$\Gamma(D^+D^-)/\Gamma_{\text{total}}$	Γ_4/Γ
VALUE	DOCUMENT ID TECN COMMENT
seen	AUBERT 09M BABR $e^+e^- \rightarrow D^+D^-\gamma$
seen	CRONIN-HEN..09 CLEO $e^+e^- \rightarrow D^+D^-$
seen	PAKHOVA 08 BELL $e^+e^- \rightarrow D^+D^-\gamma$

$\Gamma(D\bar{D})/\Gamma(D^*\bar{D} + c.c.)$	Γ_2/Γ_5
VALUE	DOCUMENT ID TECN COMMENT
$0.24 \pm 0.05 \pm 0.12$	AUBERT 09M BABR $e^+e^- \rightarrow \gamma D^*(*)\bar{D}$

$\Gamma(D^0\bar{D}^0)/\Gamma(D^*(2007)^0\bar{D}^0 + c.c.)$	Γ_3/Γ_6
VALUE	DOCUMENT ID TECN COMMENT
0.05 ± 0.03	²⁴ GOLDHABER 77 MRK1 e^+e^-

²⁴ Phase-space factor (p^3) explicitly removed.

$\Gamma(D^*(2007)^0\bar{D}^0 + c.c.)/\Gamma_{\text{total}}$	Γ_6/Γ
VALUE	DOCUMENT ID TECN COMMENT
seen	AUBERT 09M BABR $e^+e^- \rightarrow D^{*0}\bar{D}^0\gamma$
seen	CRONIN-HEN..09 CLEO $e^+e^- \rightarrow D^{*0}\bar{D}^0$

$\Gamma(D^*(2010)^+D^- + c.c.)/\Gamma_{\text{total}}$	Γ_7/Γ
VALUE	DOCUMENT ID TECN COMMENT
seen	²⁵ ZHUKOVA 18 BELL $e^+e^- \rightarrow D^{*+}D^-\gamma$
seen	AUBERT 09M BABR $e^+e^- \rightarrow D^{*+}D^-\gamma$
seen	CRONIN-HEN..09 CLEO $e^+e^- \rightarrow D^{*+}D^-$

••• We do not use the following data for averages, fits, limits, etc. •••

seen PAKHOVA 07 BELL $e^+e^- \rightarrow D^{*+}D^-\gamma$

²⁵ Supersedes PAKHOVA 07.

$\Gamma(D^*(2010)^+D^- + c.c.)/\Gamma(D^*(2007)^0\bar{D}^0 + c.c.)$	Γ_7/Γ_6
VALUE	DOCUMENT ID TECN COMMENT
$0.95 \pm 0.09 \pm 0.10$	AUBERT 09M BABR $e^+e^- \rightarrow \gamma D^*\bar{D}$

$\Gamma(D^*\bar{D}^*)/\Gamma(D^*\bar{D} + c.c.)$	Γ_8/Γ_5
VALUE	DOCUMENT ID TECN COMMENT
$0.18 \pm 0.14 \pm 0.03$	AUBERT 09M BABR $e^+e^- \rightarrow \gamma D^*(*)\bar{D}^*(*)$

$\Gamma(D^*(2007)^0\bar{D}^*(2007)^0)/\Gamma_{\text{total}}$	Γ_9/Γ
VALUE	DOCUMENT ID TECN COMMENT
seen	AUBERT 09M BABR $e^+e^- \rightarrow D^{*0}\bar{D}^{*0}\gamma$
seen	CRONIN-HEN..09 CLEO $e^+e^- \rightarrow D^{*0}\bar{D}^{*0}$

Meson Particle Listings

 $\psi(4040)$ $\Gamma(D^*(2007)^0 \bar{D}^*(2007)^0) / \Gamma(D^*(2007)^0 \bar{D}^0 + c.c.)$ Γ_9 / Γ_6

VALUE	DOCUMENT ID	TECN	COMMENT
32.0 ± 12.0	26 GOLDHABER 77	MRK1	e^+e^-

²⁶Phase-space factor (p^3) explicitly removed.

 $\Gamma(D^*(2010)^+ D^*(2010)^-) / \Gamma_{\text{total}}$ Γ_{10} / Γ

VALUE	DOCUMENT ID	TECN	COMMENT
seen	27 ZHUKOVA 18	BELL	$e^+e^- \rightarrow D^{*+} D^{*-} \gamma$
seen	AUBERT 09M	BABR	$e^+e^- \rightarrow D^{*+} D^{*-} \gamma$
seen	CRONIN-HEN..09	CLEO	$e^+e^- \rightarrow D^{*+} D^{*-}$

• • • We do not use the following data for averages, fits, limits, etc. • • •

seen PAKHLOVA 07 BELL $e^+e^- \rightarrow D^{*+} D^{*-} \gamma$

²⁷Supersedes PAKHLOVA 07.

 $\Gamma(D^0 D^- \pi^+ + c.c. \text{ (excl. } D^*(2010)^+ D^- + c.c.)) / \Gamma_{\text{total}}$ Γ_{12} / Γ

VALUE	DOCUMENT ID	TECN	COMMENT
not seen	PAKHLOVA 08A	BELL	$e^+e^- \rightarrow D^0 D^- \pi^+ \gamma$

 $\Gamma(D \bar{D}^* \pi \text{ (excl. } D^* \bar{D}^*)) / \Gamma_{\text{total}}$ Γ_{13} / Γ

VALUE	DOCUMENT ID	TECN	COMMENT
not seen	CRONIN-HEN..09	CLEO	$e^+e^- \rightarrow D \bar{D}^* \pi$

 $\Gamma(D^0 \bar{D}^{*-} \pi^+ + c.c. \text{ (excl. } D^*(2010)^+ D^*(2010)^-) / \Gamma_{\text{total}}$ Γ_{14} / Γ

VALUE	DOCUMENT ID	TECN	COMMENT
seen	PAKHLOVA 09	BELL	$e^+e^- \rightarrow D^0 D^{*-} \pi^+ \gamma$

 $\Gamma(D_s^+ D_s^-) / \Gamma_{\text{total}}$ Γ_{15} / Γ

VALUE	DOCUMENT ID	TECN	COMMENT
seen	PAKHLOVA 11	BELL	$e^+e^- \rightarrow D_s^+ D_s^- \gamma$
seen	DEL-AMO-SA..10N	BABR	$e^+e^- \rightarrow D_s^+ D_s^- \gamma$
seen	CRONIN-HEN..09	CLEO	$e^+e^- \rightarrow D_s^+ D_s^-$

 $\Gamma(\pi^+ \pi^+ \pi^- \pi^- \pi^0) / \Gamma_{\text{total}}$ Γ_{16} / Γ

VALUE	DOCUMENT ID	TECN	COMMENT
• • •			We do not use the following data for averages, fits, limits, etc. • • •
$(3.51 \pm 1.89 \pm 1.24) \times 10^{-5}$	28 ABLIKIM 21AW	BES3	$e^+e^- \rightarrow 2\pi^+ 2\pi^- \pi^0$
$(2.41 \pm 0.05 \pm 0.79) \times 10^{-2}$	29 ABLIKIM 21AW	BES3	$e^+e^- \rightarrow 2\pi^+ 2\pi^- \pi^0$

²⁸Solution 1 of two solutions with equal fit quality. The significance of the $\psi(4040)$ signal is 3.6 σ .

²⁹Solution 2 of two solutions with equal fit quality. The significance of the $\psi(4040)$ signal is 3.6 σ .

 $\Gamma(J/\psi \pi^+ \pi^-) / \Gamma_{\text{total}}$ Γ_{18} / Γ

VALUE (units 10^{-3})	CL%	DOCUMENT ID	TECN	COMMENT
<4	90	COAN 06	CLEO	$3.97-4.06 e^+e^- \rightarrow \text{hadrons}$

 $\Gamma(J/\psi \pi^0 \pi^0) / \Gamma_{\text{total}}$ Γ_{19} / Γ

VALUE (units 10^{-3})	CL%	DOCUMENT ID	TECN	COMMENT
<2	90	COAN 06	CLEO	$3.97-4.06 e^+e^- \rightarrow \text{hadrons}$

 $\Gamma(J/\psi \eta) / \Gamma_{\text{total}}$ Γ_{20} / Γ

VALUE (units 10^{-3})	CL%	DOCUMENT ID	TECN	COMMENT
5.2 ± 0.5 ± 0.5		30 ABLIKIM 12K	BES3	$e^+e^- \rightarrow \ell^+ \ell^- 2\gamma$

• • • We do not use the following data for averages, fits, limits, etc. • • •

<7 90 COAN 06 CLEO $3.97-4.06 e^+e^- \rightarrow \text{hadrons}$

³⁰ABLIKIM 12K measure $\sigma(e^+e^- \rightarrow J/\psi \eta) = 32.1 \pm 2.8 \pm 1.3$ pb. They assume the $\eta/J/\psi$ fully originates from $\psi(4040)$ decays.

 $\Gamma(J/\psi \pi^0) / \Gamma_{\text{total}}$ Γ_{21} / Γ

VALUE (units 10^{-3})	CL%	DOCUMENT ID	TECN	COMMENT
<0.28	90	31 ABLIKIM 12K	BES3	$e^+e^- \rightarrow \ell^+ \ell^- 2\gamma$

• • • We do not use the following data for averages, fits, limits, etc. • • •

<2 90 COAN 06 CLEO $3.97-4.06 e^+e^- \rightarrow \text{hadrons}$

³¹ABLIKIM 12K measure $\sigma(e^+e^- \rightarrow J/\psi \pi^0) < 1.6$ pb. They assume the $\eta/J/\psi$ fully originates from $\psi(4040)$ decays.

 $\Gamma(J/\psi \pi^+ \pi^- \pi^0) / \Gamma_{\text{total}}$ Γ_{22} / Γ

VALUE (units 10^{-3})	CL%	DOCUMENT ID	TECN	COMMENT
<2	90	COAN 06	CLEO	$3.97-4.06 e^+e^- \rightarrow \text{hadrons}$

 $\Gamma(\chi_{c1} \gamma) / \Gamma_{\text{total}}$ Γ_{23} / Γ

VALUE (units 10^{-3})	CL%	DOCUMENT ID	TECN	COMMENT
• • •				We do not use the following data for averages, fits, limits, etc. • • •
<11	90	COAN 06	CLEO	$3.97-4.06 e^+e^- \rightarrow \text{hadrons}$

 $\Gamma(\chi_{c2} \gamma) / \Gamma_{\text{total}}$ Γ_{24} / Γ

VALUE (units 10^{-3})	CL%	DOCUMENT ID	TECN	COMMENT
• • •				We do not use the following data for averages, fits, limits, etc. • • •
<17	90	COAN 06	CLEO	$3.97-4.06 e^+e^- \rightarrow \text{hadrons}$

 $\Gamma(\chi_{c1} \pi^+ \pi^- \pi^0) / \Gamma_{\text{total}}$ Γ_{25} / Γ

VALUE (units 10^{-3})	CL%	DOCUMENT ID	TECN	COMMENT
<11	90	COAN 06	CLEO	$3.97-4.06 e^+e^- \rightarrow \text{hadrons}$

 $\Gamma(\chi_{c2} \pi^+ \pi^- \pi^0) / \Gamma_{\text{total}}$ Γ_{26} / Γ

VALUE (units 10^{-3})	CL%	DOCUMENT ID	TECN	COMMENT
<32	90	COAN 06	CLEO	$3.97-4.06 e^+e^- \rightarrow \text{hadrons}$

 $\Gamma(h_c(1P) \pi^+ \pi^-) / \Gamma_{\text{total}}$ Γ_{27} / Γ

VALUE (units 10^{-3})	CL%	DOCUMENT ID	TECN	COMMENT
<3	90	32 PEDLAR 11	CLEO	$e^+e^- \rightarrow h_c(1P) \pi^+ \pi^-$

³²From several values of \sqrt{s} near the peak of the $\psi(4040)$, PEDLAR 11 measures $\sigma(e^+e^- \rightarrow h_c(1P) \pi^+ \pi^-) = 1.0 \pm 8.0 \pm 5.4 \pm 0.2$ pb, where the errors are statistical, systematic, and due to uncertainty in $B(\psi(2S) \rightarrow \pi^0 h_c(1P))$, respectively.

 $\Gamma(\phi \pi^+ \pi^-) / \Gamma_{\text{total}}$ Γ_{28} / Γ

VALUE (units 10^{-3})	CL%	DOCUMENT ID	TECN	COMMENT
<3	90	COAN 06	CLEO	$3.97-4.06 e^+e^- \rightarrow \text{hadrons}$

 $\Gamma(\Lambda \bar{\Lambda} \pi^+ \pi^-) / \Gamma_{\text{total}}$ Γ_{29} / Γ

VALUE (units 10^{-4})	CL%	DOCUMENT ID	TECN	COMMENT
<2.9	90	33 ABLIKIM 13Q	BES3	$e^+e^- \rightarrow \psi(4040)$

³³Assuming that interference effects between resonance and continuum can be neglected.

 $\Gamma(\Lambda \bar{\Lambda} \pi^0) / \Gamma_{\text{total}}$ Γ_{30} / Γ

VALUE (units 10^{-4})	CL%	DOCUMENT ID	TECN	COMMENT
<0.9	90	34 ABLIKIM 13Q	BES3	$e^+e^- \rightarrow \psi(4040)$

³⁴Assuming that interference effects between resonance and continuum can be neglected.

 $\Gamma(\Lambda \bar{\Lambda} \eta) / \Gamma_{\text{total}}$ Γ_{31} / Γ

VALUE (units 10^{-4})	CL%	DOCUMENT ID	TECN	COMMENT
<3.0	90	35 ABLIKIM 13Q	BES3	$e^+e^- \rightarrow \psi(4040)$

³⁵Assuming that interference effects between resonance and continuum can be neglected.

 $\Gamma(\Sigma^+ \bar{\Sigma}^-) / \Gamma_{\text{total}}$ Γ_{33} / Γ

VALUE (units 10^{-4})	CL%	DOCUMENT ID	TECN	COMMENT
<1.3	90	36 ABLIKIM 13Q	BES3	$e^+e^- \rightarrow \psi(4040)$

³⁶Assuming that interference effects between resonance and continuum can be neglected.

 $\Gamma(\Sigma^0 \bar{\Sigma}^0) / \Gamma_{\text{total}}$ Γ_{34} / Γ

VALUE (units 10^{-4})	CL%	DOCUMENT ID	TECN	COMMENT
<0.7	90	37 ABLIKIM 13Q	BES3	$e^+e^- \rightarrow \psi(4040)$

³⁷Assuming that interference effects between resonance and continuum can be neglected.

 $\Gamma(\Xi^+ \bar{\Xi}^-) / \Gamma_{\text{total}}$ Γ_{35} / Γ

VALUE (units 10^{-4})	CL%	DOCUMENT ID	TECN	COMMENT
<1.6	90	38 ABLIKIM 13Q	BES3	$e^+e^- \rightarrow \psi(4040)$

³⁸Assuming that interference effects between resonance and continuum can be neglected.

 $\Gamma(\Xi^0 \bar{\Xi}^0) / \Gamma_{\text{total}}$ Γ_{36} / Γ

VALUE (units 10^{-4})	CL%	DOCUMENT ID	TECN	COMMENT
<1.8	90	39 ABLIKIM 13Q	BES3	$e^+e^- \rightarrow \psi(4040)$

³⁹Assuming that interference effects between resonance and continuum can be neglected.

 $\psi(4040)$ REFERENCES

ABLIKIM 23BK	JHEP 2311 228	M. Ablikim et al.	(BESIII Collab.)
ABLIKIM 21A5	PR D104 L091104	M. Ablikim et al.	(BESIII Collab.)
ABLIKIM 21AW	PR D104 112009	M. Ablikim et al.	(BESIII Collab.)
ABLIKIM 20AG	PR D102 112009	M. Ablikim et al.	(BESIII Collab.)
ABLIKIM 20P	PR D102 031101	M. Ablikim et al.	(BESIII Collab.)
ZHUKOVA 18	PR D97 012002	V. Zhukova et al.	(BELLE Collab.)
HAN 15	PR D92 012011	Y.L. Han et al.	(BELLE Collab.)
ABLIKIM 13Q	PR D87 112011	M. Ablikim et al.	(BESIII Collab.)
WANG 13B	PR D87 051101	X.L. Wang et al.	(BELLE Collab.)
ABLIKIM 12K	PR D86 071101	M. Ablikim et al.	(BESIII Collab.)
PAKHLOVA 11	PR D83 011101	G. Pakhlova et al.	(BELLE Collab.)
PEDLAR 11	PRL 107 041803	T. Pedlar et al.	(CLEO Collab.)
DEL-AMO-SA...10N	PR D82 052004	P. del Amo Sanchez et al.	(BABAR Collab.)
MO 10	PR D82 077501	X.H. Mo, C.Z. Yuan, P. Wang	(BHEP)
AUBERT 09M	PR D79 092001	B. Aubert et al.	(BABAR Collab.)
CRONIN-HEN...09	PR D80 072001	D. Cronin-Hennessy et al.	(CLEO Collab.)
PAKHLOVA 09	PR D80 091101	G. Pakhlova et al.	(BELLE Collab.)
ABLIKIM 08D	PL B660 315	M. Ablikim et al.	(BES Collab.)
PAKHLOVA 08	PR D77 011103	G. Pakhlova et al.	(BELLE Collab.)
PAKHLOVA 08A	PRL 100 062001	G. Pakhlova et al.	(BELLE Collab.)
PAKHLOVA 07	PRL 98 092001	G. Pakhlova et al.	(BELLE Collab.)
COAN 06	PRL 96 162003	T.E. Coan et al.	(CLEO Collab.)
SETH 05A	PR D72 017501	K.K. Seth	
BAI 02C	PRL 88 101802	J.Z. Bai et al.	(BES Collab.)
BAI 00	PRL 84 594	J.Z. Bai et al.	(BES Collab.)
OSTERHELD 86	SLAC-PUB-4160	A. Osterheld et al.	(SLAC Crystal Ball Collab.)
BRANDELIK 78C	PL 76B 361	R. Brandelik et al.	(DASP Collab.)
Also	ZPHY C1 233	R. Brandelik et al.	(DASP Collab.)
FELDMAN 77	PRPL 33C 285	G.J. Feldman, M.L. Perl	(LBL, SLAC)
GOLDHABER 77	PL 69B 503	G. Goldhaber et al.	(Mark I Collab.)

See key on page 1171

Meson Particle Listings

$\chi_{c1}(4140), \psi(4160)$

$\chi_{c1}(4140)$

$$I^G(J^{PC}) = 0^+(1^{++})$$

was $X(4140)$

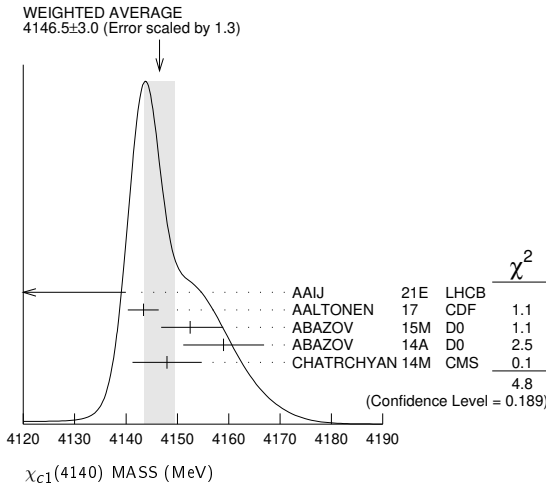
This state shows properties different from a conventional $q\bar{q}$ state. A candidate for an exotic structure. See the review on non- $q\bar{q}$ states.

Seen by AALTONEN 09AH, ABAZOV 14A, CHATRCHYAN 14M, AAIJ 17C in $B^+ \rightarrow \chi_{c1} K^+$, $\chi_{c1} \rightarrow J/\psi\phi$, and by ABAZOV 15M separately in both prompt (4.7 σ) and non-prompt (5.6 σ) production in $p\bar{p} \rightarrow J/\psi\phi + \text{anything}$. Not seen by SHEN 10 in $\gamma\gamma \rightarrow J/\psi\phi$ and ABLIKIM 15 in $e^+e^- \rightarrow \gamma J/\psi\phi$ at $\sqrt{s} = 4.23, 4.26, 4.36$ GeV.

$\chi_{c1}(4140)$ MASS

VALUE (MeV)	EVTS	DOCUMENT ID	TECN	COMMENT
4146.5 ± 3.0 OUR AVERAGE		Error includes scale factor of 1.3. See the ideogram below.		
4118 ± 11 ⁺¹⁹ ₋₃₆	24k	¹ AAIJ	21E LHCb	$B^+ \rightarrow J/\psi\phi K^+$
4143.4 ^{+2.9} _{-3.0} ± 0.6	19	² AALTONEN	17 CDF	$B^+ \rightarrow J/\psi\phi K^+$
4152.5 ± 1.7 ^{+6.2} _{-5.4}	616	³ ABAZOV	15M D0	$p\bar{p} \rightarrow J/\psi\phi + \text{anything}$
4159.0 ± 4.3 ± 6.6	52	⁴ ABAZOV	14A D0	$B^+ \rightarrow J/\psi\phi K^+$
4148.0 ± 2.4 ± 6.3	0.3k	⁵ CHATRCHYAN 14M	CMS	$B^+ \rightarrow J/\psi\phi K^+$
••• We do not use the following data for averages, fits, limits, etc. •••				
4146.5 ± 4.5 ^{+4.6} _{-2.8}	4289	^{6,7} AAIJ	17c LHCb	$B^+ \rightarrow J/\psi\phi K^+$
4143.0 ± 2.9 ± 1.2	14	^{8,9} AALTONEN	09AH CDF	$B^+ \rightarrow J/\psi\phi K^+$

- From an amplitude analysis of the decay $B^+ \rightarrow J/\psi\phi K^+$ with a significance of 13 σ .
- Statistical significance of more than 5 σ .
- Statistical significance of more than 6 σ .
- Statistical significance of 3.1 σ .
- From a fit assuming an S-wave relativistic Breit-Wigner shape above a three-body phase-space non-resonant component with statistical significance of more than 5 σ .
- From an amplitude analysis of the decay $B^+ \rightarrow J/\psi\phi K^+$ with a significance of 8.4 σ .
- Superseded by AAIJ 21E.
- Statistical significance of 3.8 σ .
- Superseded by AALTONEN 17.



$\chi_{c1}(4140)$ WIDTH

VALUE (MeV)	EVTS	DOCUMENT ID	TECN	COMMENT
19⁺⁷₋₅ OUR AVERAGE				
162 ± 21 ⁺²⁴ ₋₄₉	24k	¹ AAIJ	21E LHCb	$B^+ \rightarrow J/\psi\phi K^+$
15.3 ^{+10.4} _{-6.1} ± 2.5	19	² AALTONEN	17 CDF	$B^+ \rightarrow J/\psi\phi K^+$
16.3 ± 5.6 ± 11.4	616	³ ABAZOV	15M D0	$p\bar{p} \rightarrow J/\psi\phi + \text{anything}$
20 ± 13 ⁺³ ₋₈	52	⁴ ABAZOV	14A D0	$B^+ \rightarrow J/\psi\phi K^+$
28 ⁺¹⁵ ₋₁₁ ± 19	0.3k	⁵ CHATRCHYAN 14M	CMS	$B^+ \rightarrow J/\psi\phi K^+$
••• We do not use the following data for averages, fits, limits, etc. •••				
83 ± 21 ⁺²¹ ₋₁₄	4289	^{6,7} AAIJ	17c LHCb	$B^+ \rightarrow J/\psi\phi K^+$
11.7 ^{+8.3} _{-5.0} ± 3.7	14	^{8,9} AALTONEN	09AH CDF	$B^+ \rightarrow J/\psi\phi K^+$

- From an amplitude analysis of the decay $B^+ \rightarrow J/\psi\phi K^+$ with a significance of 13 σ .
- Statistical significance of more than 5 σ .
- Statistical significance of more than 6 σ .
- Statistical significance of 3.1 σ .

- From a fit assuming an S-wave relativistic Breit-Wigner shape above a three-body phase-space non-resonant component with statistical significance of more than 5 σ .
- From an amplitude analysis of the decay $B^+ \rightarrow J/\psi\phi K^+$ with a significance of 8.4 σ .
- Superseded by AAIJ 21E.
- Statistical significance of 3.8 σ .
- Superseded by AALTONEN 17.

$\chi_{c1}(4140)$ DECAY MODES

Mode	Fraction (Γ_i/Γ)
Γ_1 $J/\psi\phi$	seen
Γ_2 $\gamma\gamma$	not seen

$\chi_{c1}(4140)$ $\Gamma(i)\Gamma(\gamma\gamma)/\Gamma(\text{total})$

$\Gamma(\gamma\gamma) \times \Gamma(J/\psi\phi)/\Gamma_{\text{total}}$	VALUE (eV)	CL%	DOCUMENT ID	TECN	COMMENT	$\Gamma_2\Gamma_1/\Gamma$
<41	90		¹ SHEN	10 BELL	10.6 $e^+e^- \rightarrow e^+e^- J/\psi\phi$	
••• We do not use the following data for averages, fits, limits, etc. •••						
< 6	90		² SHEN	10 BELL	10.6 $e^+e^- \rightarrow e^+e^- J/\psi\phi$	
¹ For $J^P = 0^+$.						
² For $J^P = 2^+$.						

$\chi_{c1}(4140)$ BRANCHING RATIOS

$\Gamma(J/\psi\phi)/\Gamma_{\text{total}}$	VALUE	EVTS	DOCUMENT ID	TECN	COMMENT	Γ_1/Γ
seen	24k		¹ AAIJ	21E LHCb	$B^+ \rightarrow J/\psi\phi K^+$	
seen	616		² ABAZOV	15M D0	$p\bar{p} \rightarrow J/\psi\phi + \text{anything}$	
seen	52		³ ABAZOV	14A D0	$B^+ \rightarrow J/\psi\phi K^+$	
seen	0.3k		⁴ CHATRCHYAN 14M	CMS	$B^+ \rightarrow J/\psi\phi K^+$	
seen	14		⁵ AALTONEN	09AH CDF	$B^+ \rightarrow J/\psi\phi K^+$	
••• We do not use the following data for averages, fits, limits, etc. •••						
seen	4289		^{6,7} AAIJ	17c LHCb	$B^+ \rightarrow J/\psi\phi K^+$	
not seen			⁸ ABLIKIM	15 BES3	$e^+e^- \rightarrow \gamma\phi J/\psi$	
not seen			⁹ AAIJ	12AA LHCb	$p\bar{p} \rightarrow B^+ X$ at 7 TeV	

- From an amplitude analysis of the decay $B^+ \rightarrow J/\psi\phi K^+$ with a significance of 13 σ .
- Statistical significance of more than 6 σ .
- ABAZOV 14A reports $B(B^+ \rightarrow \chi_{c1}(4140) K^+ \rightarrow J/\psi\phi K^+)/B(B^+ \rightarrow J/\psi\phi K^+) = (19 \pm 7 \pm 4)\%$ with 3.1 σ significance.
- From a fit assuming an S-wave relativistic Breit-Wigner shape above a three-body phase-space non-resonant component with statistical significance of more than 5 σ .
- Statistical significance of 3.8 σ .
- From an amplitude analysis of the decay $B^+ \rightarrow J/\psi\phi K^+$ with a significance of 8.4 σ .
- Superseded by AAIJ 21E.
- Reported $\sigma(e^+e^- \rightarrow \gamma\chi_{c1}(4140)) \cdot B(\chi_{c1}(4140) \rightarrow J/\psi\phi) < 0.35, 0.28, \text{ and } 0.33$ pb at 4.23, 4.26, and 4.36 GeV, respectively, at 90% CL.
- Reported $B(B^+ \rightarrow \chi_{c1}(4140) K^+) \cdot B(\chi_{c1}(4140) \rightarrow J/\psi\phi)/B(B^+ \rightarrow J/\psi\phi K^+) < 0.07$ at 90% CL.

$\Gamma(\gamma\gamma)/\Gamma_{\text{total}}$	VALUE	DOCUMENT ID	TECN	COMMENT	Γ_2/Γ
not seen		SHEN	10 BELL	10.6 $e^+e^- \rightarrow e^+e^- J/\psi\phi$	

$\chi_{c1}(4140)$ REFERENCES

AAIJ 21E PRL 127 082001 R. Aaij *et al.* (LHCb Collab.)
 AAIJ 17C PRL 118 022003 R. Aaij *et al.* (LHCb Collab.) JP
 Also PR D95 012002 R. Aaij *et al.* (LHCb Collab.)
 AALTONEN 17 MPL A32 1750139 T. Aaltonen *et al.* (CDF Collab.)
 ABAZOV 15M PRL 115 232001 V.M. Abazov *et al.* (D0 Collab.)
 ABLIKIM 15 PR D91 032002 M. Ablikim *et al.* (BESIII Collab.)
 ABAZOV 14A PR D89 012004 V.M. Abazov *et al.* (D0 Collab.)
 CHATRCHYAN 14M PL B734 261 S. Chatrchyan *et al.* (CMS Collab.)
 AAIJ 12AA PR D85 091103 R. Aaij *et al.* (LHCb Collab.)
 SHEN 10 PRL 104 112004 C.P. Shen *et al.* (BELLE Collab.)
 AALTONEN 09AH PRL 102 242002 T. Aaltonen *et al.* (CDF Collab.)

$\psi(4160)$

$$I^G(J^{PC}) = 0^-(1^{--})$$

$\psi(4160)$ MASS

VALUE (MeV)	DOCUMENT ID	TECN	COMMENT
4191 ± 5 OUR AVERAGE			
4186.8 ± 8.7 ± 30	¹ ABLIKIM	23BH BES3	$e^+e^- \rightarrow D_s^* + D_s^{*-}$
4191 ⁺⁹ ₋₈	AAIJ	13Bc LHCb	$B^+ \rightarrow K^+ \mu^+ \mu^-$
4191.7 ± 6.5	² ABLIKIM	08D BES2	$e^+e^- \rightarrow \text{hadrons}$

Meson Particle Listings

 $\psi(4160)$

••• We do not use the following data for averages, fits, limits, etc. •••

4193 \pm 7	³ MO	10	RVUE	$e^+e^- \rightarrow$ hadrons
4151 \pm 4	⁴ SETH	05A	RVUE	$e^+e^- \rightarrow$ hadrons
4155 \pm 5	⁵ SETH	05A	RVUE	$e^+e^- \rightarrow$ hadrons
4159 \pm 20	BRANDELIK	78C	DASP	e^+e^-

¹ Could also be the $\psi(4230)$.

² Reanalysis of data presented in BAI 02c. From a global fit over the center-of-mass energy region 3.7–5.0 GeV covering the $\psi(3770)$, $\psi(4040)$, $\psi(4160)$, and $\psi(4415)$ resonances. Phase angle fixed in the fit to $\delta = (293 \pm 57)^\circ$.

³ Reanalysis of data presented in BAI 00 and BAI 02c. From a global fit over the center-of-mass energy 3.8–4.8 GeV covering the $\psi(4040)$, $\psi(4160)$ and $\psi(4415)$ resonances and including interference effects.

⁴ From a fit to Crystal Ball (OSTERHELD 86) data.

⁵ From a fit to BES (BAI 02c) data.

 $\psi(4160)$ WIDTH

VALUE (MeV)	DOCUMENT ID	TECN	COMMENT
69 \pm 10 OUR AVERAGE			
55 \pm 15 \pm 53	¹ ABLIKIM	23BH BES3	$e^+e^- \rightarrow D_s^{*+} D_s^{*-}$
65 $\begin{smallmatrix} +22 \\ -16 \end{smallmatrix}$	AAIJ	13Bc LHCb	$B^+ \rightarrow K^+ \mu^+ \mu^-$
71.8 \pm 12.3	² ABLIKIM	08D BES2	$e^+e^- \rightarrow$ hadrons
79 \pm 14	³ MO	10	RVUE $e^+e^- \rightarrow$ hadrons
107 \pm 10	⁴ SETH	05A	RVUE $e^+e^- \rightarrow$ hadrons
107 \pm 16	⁵ SETH	05A	RVUE $e^+e^- \rightarrow$ hadrons
78 \pm 20	BRANDELIK	78C	DASP e^+e^-

¹ Could also be the $\psi(4230)$.

² Reanalysis of data presented in BAI 02c. From a global fit over the center-of-mass energy region 3.7–5.0 GeV covering the $\psi(3770)$, $\psi(4040)$, $\psi(4160)$, and $\psi(4415)$ resonances. Phase angle fixed in the fit to $\delta = (293 \pm 57)^\circ$.

³ Reanalysis of data presented in BAI 00 and BAI 02c. From a global fit over the center-of-mass energy 3.8–4.8 GeV covering the $\psi(4040)$, $\psi(4160)$ and $\psi(4415)$ resonances and including interference effects.

⁴ From a fit to Crystal Ball (OSTERHELD 86) data.

⁵ From a fit to BES (BAI 02c) data.

 $\psi(4160)$ DECAY MODES

Due to the complexity of the $c\bar{c}$ threshold region, in this listing, “seen” (“not seen”) means that a cross section for the mode in question has been measured at effective \sqrt{s} near this particle’s central mass value, more (less) than 2σ above zero, without regard to any peaking behavior in \sqrt{s} or absence thereof. See mode listing(s) for details and references.

Mode	Fraction (Γ_i/Γ)	Confidence level
Γ_1 e^+e^-	(6.9 \pm 3.3) $\times 10^{-6}$	
Γ_2 $\mu^+\mu^-$	seen	
Γ_3 $D\bar{D}$	seen	
Γ_4 $D^0\bar{D}^0$	seen	
Γ_5 D^+D^-	seen	
Γ_6 $D^*\bar{D} + c.c.$	seen	
Γ_7 $D^*(2007)^0\bar{D}^0 + c.c.$	seen	
Γ_8 $D^*(2010)^+D^- + c.c.$	seen	
Γ_9 $D^*\bar{D}^*$	seen	
Γ_{10} $D^*(2007)^0\bar{D}^*(2007)^0$	seen	
Γ_{11} $D^*(2010)^+D^*(2010)^-$	seen	
Γ_{12} $D^0D^-\pi^+ + c.c. (excl. D^*(2010)^+D^- + c.c.)$	not seen	
Γ_{13} $D\bar{D}^*\pi + c.c. (excl. D^*\bar{D}^*)$	seen	
Γ_{14} $D^0D^*\pi^+ + c.c. (excl. D^*(2010)^+D^*(2010)^-)$	not seen	
Γ_{15} $D_s^+D_s^-$	not seen	
Γ_{16} $D_s^{*+}D_s^{*-} + c.c.$	seen	
Γ_{17} $J/\psi\pi^+\pi^-$	$< 3 \times 10^{-3}$	90%
Γ_{18} $J/\psi\pi^0\pi^0$	$< 3 \times 10^{-3}$	90%
Γ_{19} $J/\psi K^+K^-$	$< 2 \times 10^{-3}$	90%
Γ_{20} $J/\psi\eta$	$< 8 \times 10^{-3}$	90%
Γ_{21} $J/\psi\pi^0$	$< 1 \times 10^{-3}$	90%
Γ_{22} $J/\psi\eta'$	$< 5 \times 10^{-3}$	90%
Γ_{23} $J/\psi\pi^+\pi^-\pi^0$	$< 1 \times 10^{-3}$	90%
Γ_{24} $\psi(2S)\pi^+\pi^-$	$< 4 \times 10^{-3}$	90%
Γ_{25} $\chi_{c1}\gamma$	$< 5 \times 10^{-3}$	90%
Γ_{26} $\chi_{c2}\gamma$	< 1.3 %	90%
Γ_{27} $\chi_{c1}\pi^+\pi^-\pi^0$	$< 2 \times 10^{-3}$	90%
Γ_{28} $\chi_{c2}\pi^+\pi^-\pi^0$	$< 8 \times 10^{-3}$	90%
Γ_{29} $h_c(1P)\pi^+\pi^-$	$< 5 \times 10^{-3}$	90%
Γ_{30} $h_c(1P)\pi^0\pi^0$	$< 2 \times 10^{-3}$	90%

Γ_{31} $h_c(1P)\eta$	< 2	$\times 10^{-3}$	90%
Γ_{32} $h_c(1P)\pi^0$	< 4	$\times 10^{-4}$	90%
Γ_{33} $\omega\pi^+\pi^-$	seen		
Γ_{34} $\phi\pi^+\pi^-$	< 2	$\times 10^{-3}$	90%
Γ_{35} $\gamma\chi_{c1}(3872)$	< 1.9	$\times 10^{-3}$	90%
Γ_{36} $\gamma\chi_{c0}(3915) \rightarrow \gamma J/\psi\pi^+\pi^-$	< 1.36	$\times 10^{-4}$	90%
Γ_{37} $\gamma X(3930) \rightarrow \gamma J/\psi\pi^+\pi^-$	< 1.18	$\times 10^{-4}$	90%
Γ_{38} $\gamma X(3940) \rightarrow \gamma J/\psi\pi^+\pi^-$	< 1.47	$\times 10^{-4}$	90%
Γ_{39} $\gamma\chi_{c0}(3915) \rightarrow \gamma\gamma J/\psi$	< 1.26	$\times 10^{-4}$	90%
Γ_{40} $\gamma X(3930) \rightarrow \gamma\gamma J/\psi$	< 8.8	$\times 10^{-5}$	90%
Γ_{41} $\gamma X(3940) \rightarrow \gamma\gamma J/\psi$	< 1.79	$\times 10^{-4}$	90%
Γ_{42} $\omega\pi^0$	not seen		
Γ_{43} $\omega\eta$	not seen		
Γ_{44} K^+K^-	not seen		
Γ_{45} $K_S^0 K^\pm\pi^\mp$	seen		
Γ_{46} $\rho^+\rho^-\rho^0$	not seen		
Γ_{47} $\Lambda\bar{\Lambda}$	< 1.5	$\times 10^{-6}$	90%
Γ_{48} $\Xi^-\Xi^+$	< 8	$\times 10^{-5}$	90%
Γ_{49} $\rho K^-\bar{\Lambda} + c.c.$	< 6	$\times 10^{-6}$	90%

 $\psi(4160)$ PARTIAL WIDTHS

VALUE (keV)	DOCUMENT ID	TECN	COMMENT	Γ_1
0.48 \pm 0.22	¹ ABLIKIM	08D BES2	$e^+e^- \rightarrow$ hadrons	
0.4 to 1.1	² MO	10	RVUE $e^+e^- \rightarrow$ hadrons	
0.83 \pm 0.08	³ SETH	05A	RVUE $e^+e^- \rightarrow$ hadrons	
0.84 \pm 0.13	⁴ SETH	05A	RVUE $e^+e^- \rightarrow$ hadrons	
0.77 \pm 0.23	BRANDELIK	78C	DASP e^+e^-	

¹ Reanalysis of data presented in BAI 02c. From a global fit over the center-of-mass energy region 3.7–5.0 GeV covering the $\psi(3770)$, $\psi(4040)$, $\psi(4160)$, and $\psi(4415)$ resonances. Phase angle fixed in the fit to $\delta = (293 \pm 57)^\circ$.

² Reanalysis of data presented in BAI 00 and BAI 02c. From a global fit over the center-of-mass energy 3.8–4.8 GeV covering the $\psi(4040)$, $\psi(4160)$ and $\psi(4415)$ resonances and including interference effects. Four sets of solutions are obtained with the same fit quality, mass and total width, but with different e^+e^- partial widths. We quote only the range of values.

³ From a fit to Crystal Ball (OSTERHELD 86) data.

⁴ From a fit to BES (BAI 02c) data.

VALUE (keV)	DOCUMENT ID	TECN	COMMENT	Γ_2
2.45 \pm 1.24 \pm 0.94	^{1,2} ABLIKIM	20A BES3	$e^+e^- \rightarrow \mu^+\mu^-$	
0.4 to 1.1	¹ From a fit to the $e^+e^- \rightarrow \mu^+\mu^-$ cross section between 3.8 and 4.6 GeV to the coherent sum of four resonant amplitudes assuming $\Gamma(\mu^+\mu^-) = \Gamma(e^+e^-)$.			
0.83 \pm 0.08	² From solution I of 8 with equal fit quality. Other solutions range from $2.08 \pm 0.99 \pm 0.80$ to $2.45 \pm 1.24 \pm 0.94$ keV.			

 $\psi(4160)$ $\Gamma(i) \times \Gamma(e^+e^-)/\Gamma(\text{total})$

VALUE (eV)	EVTS	DOCUMENT ID	TECN	COMMENT	$\Gamma_{22}\Gamma_1/\Gamma$
0.17 \pm 0.04	86	^{1,2} ABLIKIM	20A BES3	$e^+e^- \rightarrow \eta' J/\psi$	
1.07 \pm 0.09	86	^{1,3} ABLIKIM	20A BES3	$e^+e^- \rightarrow \eta' J/\psi$	
		¹ Based on a fit to $\sigma(e^+e^- \rightarrow \eta' J/\psi)$ from $\sqrt{s} = 4.18$ to 4.60 GeV assuming interfering $\psi(4160)$ and $\psi(4260)$ contributions. At $\sqrt{s} = 4.18$ GeV, $\sigma(e^+e^- \rightarrow \eta' J/\psi) = 2.4 \pm 0.3 \pm 0.2$ pb.			
		² Solution I of the fit, corresponding to a phase of -0.03 ± 0.44 rad.			
		³ Solution II of the fit, corresponding to a phase of 2.54 ± 0.04 rad.			

VALUE (eV)	CL%	DOCUMENT ID	TECN	COMMENT	$\Gamma_{25}\Gamma_1/\Gamma$
< 2.2	90	¹ HAN	15	BELL 10.58 $e^+e^- \rightarrow \chi_{c1}\gamma$	
		¹ Using $B(\eta \rightarrow \gamma\gamma) = (39.41 \pm 0.21)\%$.			

VALUE (eV)	CL%	DOCUMENT ID	TECN	COMMENT	$\Gamma_{26}\Gamma_1/\Gamma$
< 6.1	90	¹ HAN	15	BELL 10.58 $e^+e^- \rightarrow \chi_{c2}\gamma$	
		¹ Using $B(\eta \rightarrow \gamma\gamma) = (39.41 \pm 0.21)\%$.			

VALUE (eV)	DOCUMENT ID	TECN	COMMENT	$\Gamma_{33}\Gamma_1/\Gamma$
0.0011 \pm 0.0008 \pm 0.0001	^{1,2} ABLIKIM	23AQ BES3	fit to cross sections	
0.651 \pm 0.012 \pm 0.040	^{2,3} ABLIKIM	23AQ BES3	fit to cross sections	

¹ Solution I of the fit.

² From a fit to $e^+e^- \rightarrow \omega\pi^+\pi^-$ cross sections between 4 and 4.6 GeV. Recalculated from 12 $\pi\Gamma(e^+e^-)B(\psi(4230) \rightarrow \omega\pi^+\pi^-)$. First uncertainty is from statistical and uncommon systematic uncertainties, and the second is a 6.2% common systematic uncertainty quoted in the paper.

³ Solution II of the fit.

$\Gamma(K_S^0 K^\pm \pi^\mp) \times \Gamma(e^+ e^-)/\Gamma_{total}$ $\Gamma_{45} \Gamma_1/\Gamma$

VALUE (eV)	DOCUMENT ID	TECN	COMMENT
• • • We do not use the following data for averages, fits, limits, etc. • • •			
2.71 ± 0.13 ± 0.12	¹ ABLIKIM	19AE BES3	$e^+ e^- \rightarrow K_S^0 K^\pm \pi^\mp$
0.0095 ± 0.0088 ± 0.0004	² ABLIKIM	19AE BES3	$e^+ e^- \rightarrow K_S^0 K^\pm \pi^\mp$

¹ Solution I of the fit including the $\psi(4160)$ with mass 4191 ± 5 MeV and width 70 ± 10 MeV from PDG 16 and the $\psi(4230)$ with mass $4219.6 \pm 3.3 \pm 5.1$ MeV and width $56.0 \pm 3.6 \pm 6.9$ MeV from GAO 17.
² Solution II of the fit including the $\psi(4160)$ with mass 4191 ± 5 MeV and width 70 ± 10 MeV from PDG 16 and the $\psi(4230)$ with mass $4219.6 \pm 3.3 \pm 5.1$ MeV and width $56.0 \pm 3.6 \pm 6.9$ MeV from GAO 17.

$\Gamma(\Lambda\bar{\Lambda}) \times \Gamma(e^+ e^-)/\Gamma_{total}$ $\Gamma_{47} \Gamma_1/\Gamma$

VALUE (eV)	CL%	DOCUMENT ID	TECN	COMMENT
$< 0.7 \times 10^{-3}$	90	¹ ABLIKIM	21AS BES3	$e^+ e^- \rightarrow \psi(4160)$

¹ From a measurement of the $e^+ e^- \rightarrow \Lambda\bar{\Lambda}$ cross section between 3.5 and 4.6 GeV.

$\Gamma(\Xi-\bar{\Xi}) \times \Gamma(e^+ e^-)/\Gamma_{total}$ $\Gamma_{48} \Gamma_1/\Gamma$

VALUE (eV)	CL%	DOCUMENT ID	TECN	COMMENT
$< 3.72 \times 10^{-2}$	90	¹ ABLIKIM	23BK BES3	$e^+ e^- \rightarrow \psi(4160)$

¹ From a fit to $e^+ e^- \rightarrow \Xi-\bar{\Xi}$ cross sections.

$\Gamma(pK-\bar{p}K + c.c.) \times \Gamma(e^+ e^-)/\Gamma_{total}$ $\Gamma_{49} \Gamma_1/\Gamma$

VALUE (eV)	CL%	DOCUMENT ID	TECN	COMMENT
$< 3.0 \times 10^{-3}$	90	¹ ABLIKIM	23BL BES3	$e^+ e^- \rightarrow \psi(4160)$

¹ From a fit to $e^+ e^- \rightarrow pK-\bar{p}K + c.c.$ cross sections.

$\psi(4160) \Gamma(i) \times \Gamma(e^+ e^-)/\Gamma^2(total)$

$\Gamma(J/\psi\eta)/\Gamma_{total} \times \Gamma(e^+ e^-)/\Gamma_{total}$ $\Gamma_{20}/\Gamma \times \Gamma_1/\Gamma$

VALUE (units 10^{-8})	DOCUMENT ID	TECN	COMMENT
• • • We do not use the following data for averages, fits, limits, etc. • • •			
2.8 ± 0.9 ± 0.9	¹ WANG	13B BELL	$e^+ e^- \rightarrow J/\psi\eta\gamma$
12.8 ± 1.7 ± 2.0	² WANG	13B BELL	$e^+ e^- \rightarrow J/\psi\eta\gamma$

¹ Solution I of two equivalent solutions in a fit using two interfering resonances. Mass and width fixed at 4153 MeV and 103 MeV, respectively.
² Solution II of two equivalent solutions in a fit using two interfering resonances. Mass and width fixed at 4153 MeV and 103 MeV, respectively.

$\psi(4160)$ BRANCHING RATIOS

$\Gamma(\mu^+ \mu^-)/\Gamma_{total}$ Γ_2/Γ

VALUE	DOCUMENT ID	TECN	COMMENT
seen	¹ AAIJ	13BC LHCB	$B^+ \rightarrow K^+ \mu^+ \mu^-$

¹ AAIJ 13bc report $B(B^+ \rightarrow K^+ \psi(4160)) B(\psi(4160) \rightarrow \mu^+ \mu^-) = (3.5^{+0.9}_{-0.8}) \times 10^{-9}$.

$\Gamma(D\bar{D})/\Gamma(D^* \bar{D}^*)$ Γ_3/Γ_9

VALUE	DOCUMENT ID	TECN	COMMENT
0.02 ± 0.03 ± 0.02	AUBERT	09M BABR	$e^+ e^- \rightarrow \gamma D^{(*)} \bar{D}^{(*)}$

$\Gamma(D^0 \bar{D}^0)/\Gamma_{total}$ Γ_4/Γ

VALUE	DOCUMENT ID	TECN	COMMENT
seen	CRONIN-HEN..09	CLEO	$e^+ e^- \rightarrow D^0 \bar{D}^0$
seen	PAKHLOVA	08 BELL	$e^+ e^- \rightarrow D^0 \bar{D}^0 \gamma$
• • • We do not use the following data for averages, fits, limits, etc. • • •			
not seen	AUBERT	09M BABR	$e^+ e^- \rightarrow D^0 \bar{D}^0 \gamma$

$\Gamma(D^+ D^-)/\Gamma_{total}$ Γ_5/Γ

VALUE	DOCUMENT ID	TECN	COMMENT
seen	CRONIN-HEN..09	CLEO	$e^+ e^- \rightarrow D^+ D^-$
seen	PAKHLOVA	08 BELL	$e^+ e^- \rightarrow D^+ D^- \gamma$
• • • We do not use the following data for averages, fits, limits, etc. • • •			
not seen	AUBERT	09M BABR	$e^+ e^- \rightarrow D^+ D^- \gamma$

$\Gamma(D^*(2007)^0 \bar{D}^0 + c.c.)/\Gamma_{total}$ Γ_7/Γ

VALUE	DOCUMENT ID	TECN	COMMENT
seen	AUBERT	09M BABR	$e^+ e^- \rightarrow D^{*0} \bar{D}^0 \gamma$
seen	CRONIN-HEN..09	CLEO	$e^+ e^- \rightarrow D^{*0} \bar{D}^0$

$\Gamma(D^*(2010)^+ D^- + c.c.)/\Gamma_{total}$ Γ_8/Γ

VALUE	DOCUMENT ID	TECN	COMMENT
seen	¹ ZHUKOVA	18 BELL	$e^+ e^- \rightarrow D^{*+} D^- \gamma$
seen	AUBERT	09M BABR	$e^+ e^- \rightarrow D^{*+} D^- \gamma$
seen	CRONIN-HEN..09	CLEO	$e^+ e^- \rightarrow D^{*+} D^-$
• • • We do not use the following data for averages, fits, limits, etc. • • •			
seen	PAKHLOVA	07 BELL	$e^+ e^- \rightarrow D^{*+} D^- \gamma$

¹ Supersedes PAKHLOVA 07.

$\Gamma(D^* \bar{D}^+ + c.c.)/\Gamma(D^* \bar{D}^*)$ Γ_6/Γ_9

VALUE	DOCUMENT ID	TECN	COMMENT
0.34 ± 0.14 ± 0.05	AUBERT	09M BABR	$e^+ e^- \rightarrow \gamma D^{(*)} \bar{D}^{(*)}$

$\Gamma(D^*(2007)^0 \bar{D}^*(2007)^0)/\Gamma_{total}$ Γ_{10}/Γ

VALUE	DOCUMENT ID	TECN	COMMENT
seen	AUBERT	09M BABR	$e^+ e^- \rightarrow D^{*0} \bar{D}^{*0} \gamma$
seen	CRONIN-HEN..09	CLEO	$e^+ e^- \rightarrow D^{*0} \bar{D}^{*0}$

$\Gamma(D^*(2010)^+ D^*(2010)^-)/\Gamma_{total}$ Γ_{11}/Γ

VALUE	DOCUMENT ID	TECN	COMMENT
seen	¹ ZHUKOVA	18 BELL	$e^+ e^- \rightarrow D^{*+} D^{*-} \gamma$
seen	AUBERT	09M BABR	$e^+ e^- \rightarrow D^{*+} D^{*-} \gamma$
seen	CRONIN-HEN..09	CLEO	$e^+ e^- \rightarrow D^{*+} D^{*-}$
• • • We do not use the following data for averages, fits, limits, etc. • • •			
seen	PAKHLOVA	07 BELL	$e^+ e^- \rightarrow D^{*+} D^{*-} \gamma$

¹ Supersedes PAKHLOVA 07.

$\Gamma(D^0 D^- \pi^+ + c.c. (excl. D^*(2010)^+ D^- + c.c.))/\Gamma_{total}$ Γ_{12}/Γ

VALUE	DOCUMENT ID	TECN	COMMENT
not seen	PAKHLOVA	08A BELL	$e^+ e^- \rightarrow D^0 D^- \pi^+ \gamma$

$\Gamma(D \bar{D}^* \pi + c.c. (excl. D^* \bar{D}^*))/\Gamma_{total}$ Γ_{13}/Γ

VALUE	DOCUMENT ID	TECN	COMMENT
seen	CRONIN-HEN..09	CLEO	$e^+ e^- \rightarrow D \bar{D}^* \pi$

$\Gamma(D^0 D^{*-} \pi^+ + c.c. (excl. D^*(2010)^+ D^*(2010)^-))/\Gamma_{total}$ Γ_{14}/Γ

VALUE	DOCUMENT ID	TECN	COMMENT
not seen	PAKHLOVA	09 BELL	$e^+ e^- \rightarrow D^0 D^{*-} \pi^+ \gamma$

$\Gamma(D_S^+ D_S^-)/\Gamma_{total}$ Γ_{15}/Γ

VALUE	DOCUMENT ID	TECN	COMMENT
not seen	PAKHLOVA	11 BELL	$e^+ e^- \rightarrow D_S^+ D_S^- \gamma$
not seen	DEL-AMO-SA..10N	BABR	$e^+ e^- \rightarrow D_S^+ D_S^- \gamma$
not seen	CRONIN-HEN..09	CLEO	$e^+ e^- \rightarrow D_S^+ D_S^-$

$\Gamma(D_S^{*+} D_S^- + c.c.)/\Gamma_{total}$ Γ_{16}/Γ

VALUE	DOCUMENT ID	TECN	COMMENT
seen	PAKHLOVA	11 BELL	$e^+ e^- \rightarrow D_S^{*+} D_S^- \gamma$
seen	DEL-AMO-SA..10N	BABR	$e^+ e^- \rightarrow D_S^{*+} D_S^- \gamma$
seen	CRONIN-HEN..09	CLEO	$e^+ e^- \rightarrow D_S^{*+} D_S^-$

$\Gamma(J/\psi \pi^+ \pi^-)/\Gamma_{total}$ Γ_{17}/Γ

VALUE (units 10^{-3})	CL%	DOCUMENT ID	TECN	COMMENT
< 3	90	COAN	06 CLEO	4.12-4.2 $e^+ e^- \rightarrow$ hadrons

$\Gamma(J/\psi \pi^0 \pi^0)/\Gamma_{total}$ Γ_{18}/Γ

VALUE (units 10^{-3})	CL%	DOCUMENT ID	TECN	COMMENT
< 3	90	COAN	06 CLEO	4.12-4.2 $e^+ e^- \rightarrow$ hadrons

$\Gamma(J/\psi K^+ K^-)/\Gamma_{total}$ Γ_{19}/Γ

VALUE (units 10^{-3})	CL%	DOCUMENT ID	TECN	COMMENT
< 2	90	COAN	06 CLEO	4.12-4.2 $e^+ e^- \rightarrow$ hadrons

$\Gamma(J/\psi\eta)/\Gamma_{total}$ Γ_{20}/Γ

VALUE (units 10^{-3})	CL%	DOCUMENT ID	TECN	COMMENT
< 8	90	COAN	06 CLEO	4.12-4.2 $e^+ e^- \rightarrow$ hadrons

• • • We do not use the following data for averages, fits, limits, etc. • • •
 possibly seen ¹ ABLIKIM 15L BES3 $e^+ e^- \rightarrow J/\psi\eta$
 seen WANG 13B BELL $e^+ e^- \rightarrow J/\psi\eta\gamma$

¹ An enhancement around 4.2 GeV is observed.

$\Gamma(J/\psi \pi^0)/\Gamma_{total}$ Γ_{21}/Γ

VALUE (units 10^{-3})	CL%	DOCUMENT ID	TECN	COMMENT
< 1	90	COAN	06 CLEO	4.12-4.2 $e^+ e^- \rightarrow$ hadrons

$\Gamma(J/\psi\eta')/\Gamma_{total}$ Γ_{22}/Γ

VALUE (units 10^{-3})	CL%	DOCUMENT ID	TECN	COMMENT
< 5	90	COAN	06 CLEO	4.12-4.2 $e^+ e^- \rightarrow$ hadrons

$\Gamma(J/\psi \pi^+ \pi^- \pi^0)/\Gamma_{total}$ Γ_{23}/Γ

VALUE (units 10^{-3})	CL%	DOCUMENT ID	TECN	COMMENT
< 1	90	COAN	06 CLEO	4.12-4.2 $e^+ e^- \rightarrow$ hadrons

$\Gamma(\psi(2S) \pi^+ \pi^-)/\Gamma_{total}$ Γ_{24}/Γ

VALUE (units 10^{-3})	CL%	DOCUMENT ID	TECN	COMMENT
< 4	90	COAN	06 CLEO	4.12-4.2 $e^+ e^- \rightarrow$ hadrons

$\Gamma(\chi_{c1} \gamma)/\Gamma_{total}$ Γ_{25}/Γ

VALUE (units 10^{-3})	CL%	DOCUMENT ID	TECN	COMMENT
< 7	90	COAN	06 CLEO	4.12-4.2 $e^+ e^- \rightarrow$ hadrons

• • • We do not use the following data for averages, fits, limits, etc. • • •

Meson Particle Listings

 $\psi(4160)$, $X(4160)$

$\Gamma(\chi_{c2}\gamma)/\Gamma_{\text{total}}$					Γ_{26}/Γ
VALUE (units 10^{-3})	CL%	DOCUMENT ID	TECN	COMMENT	
<13	90	COAN	06	CLEO	4.12–4.2 $e^+e^- \rightarrow$ hadrons

$\Gamma(\chi_{c1}\pi^+\pi^-\pi^0)/\Gamma_{\text{total}}$					Γ_{27}/Γ
VALUE (units 10^{-3})	CL%	DOCUMENT ID	TECN	COMMENT	
<2	90	COAN	06	CLEO	4.12–4.2 $e^+e^- \rightarrow$ hadrons

$\Gamma(\chi_{c2}\pi^+\pi^-\pi^0)/\Gamma_{\text{total}}$					Γ_{28}/Γ
VALUE (units 10^{-3})	CL%	DOCUMENT ID	TECN	COMMENT	
<8	90	COAN	06	CLEO	4.12–4.2 $e^+e^- \rightarrow$ hadrons

$\Gamma(h_c(1P)\pi^+\pi^-)/\Gamma_{\text{total}}$					Γ_{29}/Γ
VALUE (units 10^{-3})	CL%	DOCUMENT ID	TECN	COMMENT	
<5	90	¹ PEDLAR	11	CLEO	$e^+e^- \rightarrow h_c(1P)\pi^+\pi^-$

¹ At $\sqrt{s} = 4170$ MeV, PEDLAR 11 measures $\sigma(e^+e^- \rightarrow h_c(1P)\pi^+\pi^-) = 15.6 \pm 2.3 \pm 1.9 \pm 3.0$ pb, where the errors are statistical, systematic, and due to uncertainty in $B(\psi(2S) \rightarrow \pi^0 h_c(1P))$, respectively.

$\Gamma(h_c(1P)\pi^0\pi^0)/\Gamma_{\text{total}}$					Γ_{30}/Γ
VALUE (units 10^{-3})	CL%	DOCUMENT ID	TECN	COMMENT	
<2	90	¹ PEDLAR	11	CLEO	$e^+e^- \rightarrow h_c(1P)\pi^0\pi^0$

¹ At $\sqrt{s} = 4170$ MeV, PEDLAR 11 measures $\sigma(e^+e^- \rightarrow h_c(1P)\pi^0\pi^0) = 3.0 \pm 3.3 \pm 1.1 \pm 0.6$ pb, where the errors are statistical, systematic, and due to uncertainty in $B(\psi(2S) \rightarrow \pi^0 h_c(1P))$, respectively.

$\Gamma(h_c(1P)\eta)/\Gamma_{\text{total}}$					Γ_{31}/Γ
VALUE (units 10^{-3})	CL%	DOCUMENT ID	TECN	COMMENT	
<2	90	¹ PEDLAR	11	CLEO	$e^+e^- \rightarrow h_c(1P)\eta$

• • • We do not use the following data for averages, fits, limits, etc. • • •

possibly seen 41 ² ABLIKIM 17R BES3 $e^+e^- \rightarrow h_c(1P)\eta$

¹ At $\sqrt{s} = 4170$ MeV, PEDLAR 11 measures $\sigma(e^+e^- \rightarrow h_c(1P)\eta) = 4.7 \pm 1.7 \pm 1.0 \pm 0.9$ pb, where the errors are statistical, systematic, and due to uncertainty in $B(\psi(2S) \rightarrow \pi^0 h_c(1P))$, respectively.

² An enhancement around 4.2 GeV is observed.

$\Gamma(h_c(1P)\pi^0)/\Gamma_{\text{total}}$					Γ_{32}/Γ
VALUE (units 10^{-3})	CL%	DOCUMENT ID	TECN	COMMENT	
<0.4	90	¹ PEDLAR	11	CLEO	$e^+e^- \rightarrow h_c(1P)\pi^0$

¹ At $\sqrt{s} = 4170$ MeV, PEDLAR 11 measures $\sigma(e^+e^- \rightarrow h_c(1P)\pi^0) = -0.7 \pm 1.8 \pm 0.7 \pm 0.1$ pb, where the errors are statistical, systematic, and due to uncertainty in $B(\psi(2S) \rightarrow \pi^0 h_c(1P))$, respectively.

$\Gamma(\phi\pi^+\pi^-)/\Gamma_{\text{total}}$					Γ_{34}/Γ
VALUE (units 10^{-3})	CL%	DOCUMENT ID	TECN	COMMENT	
<2	90	COAN	06	CLEO	4.12–4.2 $e^+e^- \rightarrow$ hadrons

$\Gamma(\gamma\chi_{c1}(3872))/\Gamma_{\text{total}}$					Γ_{35}/Γ
VALUE	CL%	DOCUMENT ID	TECN	COMMENT	
<1.9 $\times 10^{-3}$	90	^{1,2} XIAO	13	$\psi(4160) \rightarrow \gamma J/\psi\pi^+\pi^-$	

• • • We do not use the following data for averages, fits, limits, etc. • • •

<0.013 90 ^{1,3} XIAO 13 $\psi(4160) \rightarrow \gamma J/\psi\pi^+\pi^-$

¹ Obtained by analyzing CLEO data but not authored by the CLEO Collaboration.

² XIAO 13 reports $[\Gamma(\psi(4160) \rightarrow \gamma\chi_{c1}(3872))/\Gamma_{\text{total}}] \times [B(\chi_{c1}(3872) \rightarrow \pi^+\pi^- J/\psi(1S))] < 0.68 \times 10^{-4}$ which we divide by our best value $B(\chi_{c1}(3872) \rightarrow \pi^+\pi^- J/\psi(1S)) = 3.5 \times 10^{-2}$.

³ XIAO 13 reports $[\Gamma(\psi(4160) \rightarrow \gamma\chi_{c1}(3872))/\Gamma_{\text{total}}] \times [B(\chi_{c1}(3872) \rightarrow \gamma J/\psi)] < 1.05 \times 10^{-4}$ which we divide by our best value $B(\chi_{c1}(3872) \rightarrow \gamma J/\psi) = 7.8 \times 10^{-3}$.

$\Gamma(\gamma\chi_{c0}(3915) \rightarrow \gamma J/\psi\pi^+\pi^-)/\Gamma_{\text{total}}$					Γ_{36}/Γ
VALUE	CL%	DOCUMENT ID	TECN	COMMENT	
<1.36 $\times 10^{-4}$	90	¹ XIAO	13	$\psi(4160) \rightarrow \gamma J/\psi\pi^+\pi^-$	

¹ Obtained by analyzing CLEO data but not authored by the CLEO Collaboration.

$\Gamma(\gamma X(3930) \rightarrow \gamma J/\psi\pi^+\pi^-)/\Gamma_{\text{total}}$					Γ_{37}/Γ
VALUE	CL%	DOCUMENT ID	TECN	COMMENT	
<1.18 $\times 10^{-4}$	90	¹ XIAO	13	$\psi(4160) \rightarrow \gamma J/\psi\pi^+\pi^-$	

¹ Obtained by analyzing CLEO data but not authored by the CLEO Collaboration.

$\Gamma(\gamma X(3940) \rightarrow \gamma J/\psi\pi^+\pi^-)/\Gamma_{\text{total}}$					Γ_{38}/Γ
VALUE	CL%	DOCUMENT ID	TECN	COMMENT	
<1.47 $\times 10^{-4}$	90	¹ XIAO	13	$\psi(4160) \rightarrow \gamma J/\psi\pi^+\pi^-$	

¹ Obtained by analyzing CLEO data but not authored by the CLEO Collaboration.

$\Gamma(\gamma\chi_{c0}(3915) \rightarrow \gamma\gamma J/\psi)/\Gamma_{\text{total}}$					Γ_{39}/Γ
VALUE	CL%	DOCUMENT ID	TECN	COMMENT	
<1.26 $\times 10^{-4}$	90	¹ XIAO	13	$\psi(4160) \rightarrow \gamma\gamma J/\psi$	

¹ Obtained by analyzing CLEO data but not authored by the CLEO Collaboration.

$\Gamma(\gamma X(3930) \rightarrow \gamma\gamma J/\psi)/\Gamma_{\text{total}}$					Γ_{40}/Γ
VALUE	CL%	DOCUMENT ID	TECN	COMMENT	
<0.88 $\times 10^{-4}$	90	¹ XIAO	13	$\psi(4160) \rightarrow \gamma\gamma J/\psi$	

¹ Obtained by analyzing CLEO data but not authored by the CLEO Collaboration.

$\Gamma(\gamma X(3940) \rightarrow \gamma\gamma J/\psi)/\Gamma_{\text{total}}$					Γ_{41}/Γ
VALUE	CL%	DOCUMENT ID	TECN	COMMENT	
<1.79 $\times 10^{-4}$	90	¹ XIAO	13	$\psi(4160) \rightarrow \gamma\gamma J/\psi$	

¹ Obtained by analyzing CLEO data but not authored by the CLEO Collaboration.

$\Gamma(\omega\pi^0)/\Gamma_{\text{total}}$					Γ_{42}/Γ
VALUE	CL%	DOCUMENT ID	TECN	COMMENT	
not seen		ABLIKIM	22k	BES3	$e^+e^- \rightarrow \omega\pi^0$

$\Gamma(\omega\eta)/\Gamma_{\text{total}}$					Γ_{43}/Γ
VALUE	CL%	DOCUMENT ID	TECN	COMMENT	
not seen		ABLIKIM	22k	BES3	$e^+e^- \rightarrow \omega\eta$

$\Gamma(K^+K^-)/\Gamma_{\text{total}}$					Γ_{44}/Γ
VALUE	CL%	DOCUMENT ID	TECN	COMMENT	
<2 $\times 10^{-5}$	90	¹ DRUZHININ	15	RVUE	$e^+e^- \rightarrow \psi(3770)$

• • • We do not use the following data for averages, fits, limits, etc. • • •

¹ DRUZHININ 15 uses BABAR and CLEO data taking into account interference of the processes $e^+e^- \rightarrow K^+K^-$ and $e^+e^- \rightarrow K_S^0 K_L^0$.

$\Gamma(\rho\bar{\rho}\rho\bar{\rho})/\Gamma_{\text{total}}$					Γ_{46}/Γ
VALUE	CL%	DOCUMENT ID	TECN	COMMENT	
not seen		ABLIKIM	21d	BES3	4.0–4.6 $e^+e^- \rightarrow \rho\bar{\rho}\rho\bar{\rho}$

 $\psi(4160)$ REFERENCES

ABLIKIM	23AQ	JHEP	2308	159	M. Ablikim et al.	(BESIII Collab.)
ABLIKIM	23BH	PRL	131	151903	M. Ablikim et al.	(BESIII Collab.)
ABLIKIM	23BK	JHEP	2311	228	M. Ablikim et al.	(BESIII Collab.)
ABLIKIM	23BL	JHEP	2312	027	M. Ablikim et al.	(BESIII Collab.)
ABLIKIM	22K	JHEP	2207	064	M. Ablikim et al.	(BESIII Collab.)
ABLIKIM	21AS	PR	D104	L091104	M. Ablikim et al.	(BESIII Collab.)
ABLIKIM	21D	PR	D103	052003	M. Ablikim et al.	(BESIII Collab.)
ABLIKIM	20A	PR	D101	012008	M. Ablikim et al.	(BESIII Collab.)
ABLIKIM	20AG	PR	D102	112009	M. Ablikim et al.	(BESIII Collab.)
ABLIKIM	19AE	PR	D99	072005	M. Ablikim et al.	(BESIII Collab.)
ZHUKOVA	18	PR	D97	012002	V. Zhukova et al.	(BELLE Collab.)
ABLIKIM	17R	PR	D96	012001	M. Ablikim et al.	(BESIII Collab.)
GAO	17	PR	D95	092007	X.Y. Gao, C.P. Shen, C.Z. Yuan	(PDG Collab.)
PDG	16	CP	C40	100001	C. Patrignani et al.	(PDG Collab.)
ABLIKIM	15L	PR	D91	112005	M. Ablikim et al.	(BESIII Collab.)
DRUZHININ	15	PR	D92	054024	V.P. Druzhinin	(NOVO)
HAN	15	PR	D92	012011	Y.L. Han et al.	(BELLE Collab.)
AAIJ	13BC	PRL	111	112003	R. Aaij et al.	(LHCb Collab.)
WANG	13B	PR	D87	051101	X.L. Wang et al.	(BELLE Collab.)
XIAO	13	PR	D87	057501	T. Xiao et al.	(NWES, WAWN)
PAKHLOVA	11	PR	D83	011101	G. Pakhlova et al.	(BELLE Collab.)
PEDLAR	11	PRL	107	041803	T. Pedlar et al.	(CLEO Collab.)
DEL-AMO-SA...	10N	PR	D82	052004	P. del Amo Sanchez et al.	(BABAR Collab.)
MO	10	PR	D82	077501	X.H. Mo, C.Z. Yuan, P. Wang	(BHEP)
AUBERT	09M	PR	D79	092001	B. Aubert et al.	(BABAR Collab.)
CRONIN-HEN...	09	PR	D80	072001	D. Cronin-Hennessy et al.	(CLEO Collab.)
PAKHLOVA	09	PR	D80	091101	G. Pakhlova et al.	(BELLE Collab.)
ABLIKIM	08D	PL	B660	315	M. Ablikim et al.	(BES Collab.)
PAKHLOVA	08	PR	D77	011103	G. Pakhlova et al.	(BELLE Collab.)
PAKHLOVA	08A	PRL	100	062001	G. Pakhlova et al.	(BELLE Collab.)
PAKHLOVA	07	PRL	98	092001	G. Pakhlova et al.	(BELLE Collab.)
COAN	06	PRL	96	162003	T.E. Coan et al.	(CLEO Collab.)
SETH	05A	PR	D72	017501	K.K. Seth	(CLEO Collab.)
BAI	02C	PRL	88	101802	J.Z. Bai et al.	(BES Collab.)
BAI	00	PRL	84	594	J.Z. Bai et al.	(BES Collab.)
OSTERHELD	86	SLAC-PUB-4160			A. Osterheld et al.	(SLAC Crystal Ball Collab.)
BRANDELIC	78C	PL	B6B	361	R. Brandelik et al.	(DASP Collab.)

 $X(4160)$

$$I^G(J^{PC}) = ?(???)$$

OMITTED FROM SUMMARY TABLE

Seen by PAKHLOV 08 in $e^+e^- \rightarrow J/\psi X$, $X \rightarrow D^* \bar{D}^*$

A state with consistent mass and width is seen by AAIJ 21E in $B^+ \rightarrow X(4160)K^+$ with $X(4160) \rightarrow J/\psi\phi$ using an amplitude analysis of $B^+ \rightarrow J/\psi\phi K^+$ with a significance (accounting for systematic uncertainties) of 4.8 σ . The $J^{PC} = 2^{-+}$ assignment is favored over other assignments with a significance of more than 4 σ .

 $X(4160)$ MASS

VALUE (MeV)	EVTS	DOCUMENT ID	TECN	COMMENT
4153 \pm 23	OUR AVERAGE			
4146 \pm 18 \pm 33	24k	¹ AAIJ	21E	LHCB $B^+ \rightarrow J/\psi\phi K^+$
4156 \pm 25 \pm 15	24	PAKHLOV	08	BELL $e^+e^- \rightarrow J/\psi X$

¹ From an amplitude analysis of the decay $B^+ \rightarrow J/\psi\phi K^+$ with a significance of 4.8 σ .

Meson Particle Listings

X(4160), $\psi(4230)$

X(4160) WIDTH

VALUE (MeV)	EVTS	DOCUMENT ID	TECN	COMMENT
136 ± 60	35	OUR AVERAGE		
135 ± 28 ± 59	24k	1 AAIJ	21E LHCB	$B^+ \rightarrow J/\psi \phi K^+$
139 ± 111	24	PAKHLOV	08 BELL	$e^+ e^- \rightarrow J/\psi X$

¹ From an amplitude analysis of the decay $B^+ \rightarrow J/\psi \phi K^+$ with a significance of 4.8 σ .

X(4160) DECAY MODES

Mode	Fraction (Γ_i/Γ)
Γ_1 $D\bar{D}$	not seen
Γ_2 $D^* \bar{D} + c.c.$	not seen
Γ_3 $D^* \bar{D}^*$	seen
Γ_4 $J/\psi \phi$	seen

X(4160) BRANCHING RATIOS

$\Gamma(D\bar{D})/\Gamma(D^*\bar{D}^*)$					Γ_1/Γ_3
VALUE	CL%	DOCUMENT ID	TECN	COMMENT	
<0.09	90	PAKHLOV	08 BELL	$e^+ e^- \rightarrow J/\psi X$	
$\Gamma(D^*\bar{D} + c.c.)/\Gamma(D^*\bar{D}^*)$					Γ_2/Γ_3
VALUE	CL%	DOCUMENT ID	TECN	COMMENT	
<0.22	90	PAKHLOV	08 BELL	$e^+ e^- \rightarrow J/\psi X$	
$\Gamma(J/\psi \phi)/\Gamma_{total}$					Γ_4/Γ
VALUE	EVTS	DOCUMENT ID	TECN	COMMENT	
seen	24k	1 AAIJ	21E LHCB	$B^+ \rightarrow J/\psi \phi K^+$	

¹ From an amplitude analysis of the decay $B^+ \rightarrow J/\psi \phi K^+$ with a significance of 4.8 σ .

X(4160) REFERENCES

AAIJ	21E	PRL 127 082001	R. Aaij et al.	(LHCb Collab.)
PAKHLOV	08	PRL 100 202001	P. Pakhlov et al.	(BELLE Collab.)

4230 ± 8 ± 6	180	14 ABLIKIM	15c BES3	$e^+ e^- \rightarrow \omega \chi_{c0}$
4258.6 ± 8.3 ± 12.1		15 LIU	13B BELL	$e^+ e^- \rightarrow \gamma \pi^+ \pi^- J/\psi$
4245 ± 5 ± 4		16 LEES	12Ac BABR	10.58 $e^+ e^- \rightarrow \gamma \pi^+ \pi^- J/\psi$
4247 ± 12 ± 17		15,17 YUAN	07 BELL	10.58 $e^+ e^- \rightarrow \gamma \pi^+ \pi^- J/\psi$
4284 ± 17		HE	06B CLEO	9.4–10.6 $e^+ e^- \rightarrow \gamma \pi^+ \pi^- J/\psi$
4259 ± 8 ± 6	125	18 AUBERT,B	05i BABR	10.58 $e^+ e^- \rightarrow \gamma \pi^+ \pi^- J/\psi$

- From a three-resonance fit to the dressed cross section in the range $\sqrt{s} = 4.128\text{--}4.950$ GeV.
- From a cross-section measurement of $e^+ e^- \rightarrow D^* \bar{D}^* \pi^+$ between 4.189 and 4.951 GeV, assuming a coherent sum of 3 Breit-Wigner resonances plus a continuum amplitude. The two other resonances have masses (widths) 4675.3 ± 29.7 (218.3 ± 73.5) MeV and 4469.1 ± 26.4 (246.3 ± 37.9) MeV.
- From a three-resonance fit to the Born cross section in the range $\sqrt{s} = 3.7730\text{--}4.7008$ GeV.
- From a two-resonance fit to the dressed cross section in the range $\sqrt{s} = 4.127\text{--}4.600$ GeV. The second resonance has a mass of $4484.7 \pm 13.3 \pm 24.1$ MeV and a total width of $111.1 \pm 30.1 \pm 15.2$ MeV.
- From a three-resonance fit to the Born cross section in the range $\sqrt{s} = 4.008\text{--}4.698$ GeV.
- Solution 1 of 8 with equal fit quality to the $e^+ e^- \rightarrow \mu^+ \mu^-$ cross section between 3.8 and 4.6 GeV to the coherent sum of four resonant amplitudes. Other solutions range from $4212.8 \pm 7.2 \pm 4.0$ to $4219.4 \pm 11.2 \pm 4.1$ MeV.
- From a fit of the measured cross section in the range $\sqrt{s} = 3.808\text{--}4.600$ GeV.
- From a fit of the measured cross section from $\sqrt{s} = 4.178\text{--}4.278$ GeV. Supersedes ABLIKIM 15c.
- Simultaneous fit to $\chi_{c1} \rightarrow \omega J/\psi$ and $\chi_{c1} \rightarrow \pi^+ \pi^- J/\psi$.
- From a three-resonance fit. Superseded by ABLIKIM 22Am.
- From a fit to the cross section for $e^+ e^- \rightarrow \pi^+ \pi^- \psi(2S) \rightarrow 2(\pi^+ \pi^-) \ell^+ \ell^-$ obtained from 16 center-of-mass energies between 4.008 and 4.600 GeV and comprising 5.1 fb⁻¹. Superseded by ABLIKIM 21Aj.
- From a three-resonance fit.
- From a combined fit of BELLE, BABAR and BES3 $e^+ e^- \rightarrow \pi^+ \pi^- J/\psi$ and $e^+ e^- \rightarrow \pi^+ \pi^- \psi(2S)$ data.
- From a 3-parameter fit of measured cross sections from $\sqrt{s} = 4.21\text{--}4.42$ GeV to a phase-space modified Breit-Wigner function, using the decays $\chi_{c0} \rightarrow \pi^+ \pi^-$, $\chi_{c0} \rightarrow K^+ K^-$, and $\omega \rightarrow \pi^+ \pi^- \pi^0$.
- From a two-resonance fit.
- From a single-resonance fit. Supersedes AUBERT,B 05i.
- Superseded by LIU 13B.
- From a single-resonance fit. Two interfering resonances are not excluded. Superseded by LEES 12Ac.

$\psi(4230)$

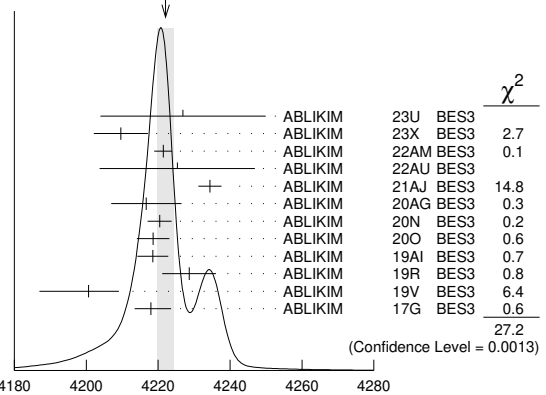
$$J^G(J^{PC}) = 0^-(1^{--})$$

also known as Y(4230); was $\psi(4260)$

The original $\psi(4260)$ (also known as Y(4260)) was observed by AUBERT,B 05i as a peak in the energy dependence of the $e^+ e^- \rightarrow \pi^+ \pi^- J/\psi$ cross section and was confirmed by HE 06B, YUAN 07, LEES 12Ac, and LIU 13B in the same process. A higher-statistics analysis by ABLIKIM 17B revealed an asymmetry in the cross section and resulted in a shift of the peak position to a lower mass. The $\psi(4260)$ was therefore renamed $\psi(4230)$. The energy-dependent cross sections for $e^+ e^-$ to other channels also exhibit peaks in the same mass region. The parameters corresponding to those peaks are also listed here, but the number of states in this region remains to be determined.

For details see the review on "Spectroscopy of mesons containing two heavy quarks."

WEIGHTED AVERAGE
4222.1±2.3 (Error scaled by 1.7)



$\psi(4230)$ MASS

VALUE (MeV)	EVTS	DOCUMENT ID	TECN	COMMENT
4222.1 ± 2.3	OUR AVERAGE	Error includes scale factor of 1.7. See the ideogram below.		
4226.9 ± 6.6 ± 22.0		1 ABLIKIM	23U BES3	$e^+ e^- \rightarrow K_S^0 K_S^0 J/\psi$
4209.6 ± 4.7 ± 5.9		2 ABLIKIM	23X BES3	$e^+ e^- \rightarrow D^{*0} D^{*-} \pi^+$
4221.4 ± 1.5 ± 2.0		3 ABLIKIM	22AM BES3	$e^+ e^- \rightarrow \pi^+ \pi^- J/\psi$
4225.3 ± 2.3 ± 21.5		4 ABLIKIM	22AU BES3	$e^+ e^- \rightarrow K^+ K^- J/\psi$
4234.4 ± 3.2 ± 0.2		5 ABLIKIM	21AJ BES3	$e^+ e^- \rightarrow \pi^+ \pi^- \psi(2S)$
4216.7 ± 8.9 ± 4.1		6 ABLIKIM	20AG BES3	$e^+ e^- \rightarrow \mu^+ \mu^-$
4220.4 ± 2.4 ± 2.3		7 ABLIKIM	20N BES3	$e^+ e^- \rightarrow \pi^0 \pi^0 J/\psi$
4218.6 ± 3.8 ± 2.5		7 ABLIKIM	20O BES3	$e^+ e^- \rightarrow \eta J/\psi$
4218.5 ± 1.6 ± 4.0		8 ABLIKIM	19AI BES3	$e^+ e^- \rightarrow \omega \chi_{c0}$
4228.6 ± 4.1 ± 6.3		8 ABLIKIM	19R BES3	$e^+ e^- \rightarrow \pi^+ D^0 D^{*-} + c.c.$
4200.6 ± 7.9		9 ABLIKIM	19V BES3	$e^+ e^- \rightarrow \gamma \chi_{c1}(3872)$
4218 ± 5.9 ± 0.9		ABLIKIM	17G BES3	$e^+ e^- \rightarrow \pi^+ \pi^- h_c$
• • • We do not use the following data for averages, fits, limits, etc. • • •				
4231.9 ± 5.3 ± 4.9		ABLIKIM	20N BES3	$e^+ e^- \rightarrow \pi^0 J_{c\bar{c}1}(3900)^0$, $J_{c\bar{c}1}^0 \rightarrow \pi^0 J/\psi$
4222.0 ± 3.1 ± 1.4		10 ABLIKIM	17B BES3	$e^+ e^- \rightarrow \pi^+ \pi^- J/\psi$
4209.5 ± 7.4 ± 1.4		11 ABLIKIM	17V BES3	$e^+ e^- \rightarrow \pi^+ \pi^- \psi(2S)$
4209.1 ± 6.8 ± 7.0		12 ZHANG	17B RVUE	$e^+ e^- \rightarrow \pi^+ \pi^- \psi(2S)$
4223.3 ± 1.6 ± 2.5		13 ZHANG	17C RVUE	$e^+ e^- \rightarrow \pi^+ \pi^- J/\psi$ or $\psi(2S)$

$\psi(4230)$ WIDTH

VALUE (MeV)	EVTS	DOCUMENT ID	TECN	COMMENT
49 ± 7	OUR AVERAGE	Error includes scale factor of 3.4. See the ideogram below.		
71.7 ± 16.2 ± 32.8		1 ABLIKIM	23U BES3	$e^+ e^- \rightarrow K_S^0 K_S^0 J/\psi$
81.6 ± 17.8 ± 9.0		2 ABLIKIM	23X BES3	$e^+ e^- \rightarrow D^{*0} D^{*-} \pi^+$
41.8 ± 2.9 ± 2.7		3 ABLIKIM	22AM BES3	$e^+ e^- \rightarrow \pi^+ \pi^- J/\psi$
72.9 ± 6.1 ± 30.8		4 ABLIKIM	22AU BES3	$e^+ e^- \rightarrow K^+ K^- J/\psi$
17.6 ± 18.1 ± 0.9		5 ABLIKIM	21AJ BES3	$e^+ e^- \rightarrow \pi^+ \pi^- \psi(2S)$
47.2 ± 22.8 ± 10.5		6 ABLIKIM	20AG BES3	$e^+ e^- \rightarrow \mu^+ \mu^-$
46.2 ± 4.7 ± 2.1		7 ABLIKIM	20N BES3	$e^+ e^- \rightarrow \pi^0 \pi^0 J/\psi$
82.0 ± 5.7 ± 0.4		7 ABLIKIM	20O BES3	$e^+ e^- \rightarrow \eta J/\psi$
28.2 ± 3.9 ± 1.6		8 ABLIKIM	19AI BES3	$e^+ e^- \rightarrow \omega \chi_{c0}$
77.0 ± 6.8 ± 6.3		ABLIKIM	19R BES3	$e^+ e^- \rightarrow \pi^+ D^0 D^{*-} + c.c.$
115 ± 38		9 ABLIKIM	19V BES3	$e^+ e^- \rightarrow \gamma \chi_{c1}(3872)$
66.0 ± 12.3		ABLIKIM	17G BES3	$e^+ e^- \rightarrow \pi^+ \pi^- h_c$
8.3 ± 0.4				

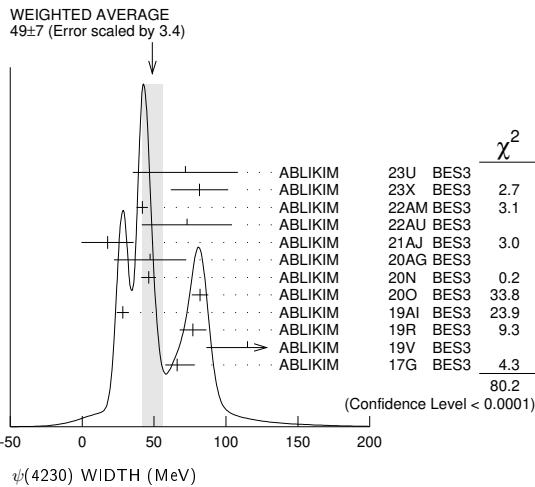
Meson Particle Listings

$\psi(4230)$

••• We do not use the following data for averages, fits, limits, etc. •••

41.2±16.0±16.4	ABLIKIM	20N	BES3	$e^+e^- \rightarrow \pi^0 T_{cc1}(3900)^0,$ $T_{cc1}^0 \rightarrow \pi^0 J/\psi$
44.1± 4.3± 2.0	10 ABLIKIM	17B	BES3	$e^+e^- \rightarrow \pi^+\pi^- J/\psi$
80.1±24.6± 2.9	11 ABLIKIM	17V	BES3	$e^+e^- \rightarrow \pi^+\pi^- \psi(2S)$
76.6±14.2± 2.4	12 ZHANG	17B	RVUE	$e^+e^- \rightarrow \pi^+\pi^- \psi(2S)$
54.2± 2.6± 1.0	13 ZHANG	17C	RVUE	$e^+e^- \rightarrow \pi^+\pi^- J/\psi$ or $\psi(2S)$
38 ±12 ± 2 180	14 ABLIKIM	15C	BES3	$e^+e^- \rightarrow \omega \chi_{c0}$
134.1±16.4± 5.5	15 LIU	13B	BELL	$e^+e^- \rightarrow \gamma \pi^+\pi^- J/\psi$
114 $\frac{+16}{-15}$ ± 7	16 LEES	12AC	BABR	10.58 $e^+e^- \rightarrow \gamma \pi^+\pi^- J/\psi$
108 ±19 ±10	15,17 YUAN	07	BELL	10.58 $e^+e^- \rightarrow \gamma \pi^+\pi^- J/\psi$
73 $\frac{+39}{-25}$ ± 5 13.6	HE	06B	CLEO	9.4-10.6 $e^+e^- \rightarrow \gamma \pi^+\pi^- J/\psi$
88 ±23 $\frac{+6}{-4}$ 125	18 AUBERT,B	05i	BABR	10.58 $e^+e^- \rightarrow \gamma \pi^+\pi^- J/\psi$

- 1 From a three-resonance fit to the dressed cross section in the range $\sqrt{s} = 4.128-4.950$ GeV.
- 2 From a cross-section measurement of $e^+e^- \rightarrow D^{*0}D^{*-}\pi^+$ between 4.189 and 4.951 GeV, assuming a coherent sum of 3 Breit-Wigner resonances plus a continuum amplitude. The two other resonances have masses (widths) 4675.3 ± 29.7 (218.3 ± 73.5) MeV and 4469.1 ± 26.4 (246.3 ± 37.9) MeV.
- 3 From a three-resonance fit to the Born cross section in the range $\sqrt{s} = 3.7730-4.7008$ GeV.
- 4 From a two-resonance fit to the dressed cross section in the range $\sqrt{s} = 4.127-4.600$ GeV. The second resonance has a mass of 4484.7 ± 13.3 ± 24.1 MeV and a total width of 111.1 ± 30.1 ± 15.2 MeV.
- 5 From a three-resonance fit to the Born cross section in the range $\sqrt{s} = 4.008-4.698$ GeV.
- 6 Solution 1 of 8 with equal fit quality to the $e^+e^- \rightarrow \mu^+\mu^-$ cross section between 3.8 and 4.6 GeV to the coherent sum of four resonant amplitudes. Other solutions range from 36.4 ± 16.8 ± 8.1 to 49.6 ± 22.6 ± 11.0 MeV.
- 7 From a fit of the measured cross section in the range $\sqrt{s} = 3.808-4.600$ GeV.
- 8 From a fit of the measured cross section from $\sqrt{s} = 4.178-4.278$ GeV. Supersedes ABLIKIM 15C.
- 9 Simultaneous fit to $\chi_{c1} \rightarrow \omega J/\psi$ and $\chi_{c1} \rightarrow \pi^+\pi^- J/\psi$.
- 10 From a three-resonance fit. Superseded by ABLIKIM 22AM.
- 11 From a fit to the cross section for $e^+e^- \rightarrow \pi^+\pi^- \psi(2S) \rightarrow 2(\pi^+\pi^-)\ell^+\ell^-$ obtained from 16 center-of-mass energies between 4.008 and 4.600 GeV and comprising 5.1 fb⁻¹. Superseded by ABLIKIM 21AJ.
- 12 From a three-resonance fit.
- 13 From a combined fit of BELLE, BABAR and BES3 $e^+e^- \rightarrow \pi^+\pi^- J/\psi$ and $e^+e^- \rightarrow \pi^+\pi^- \psi(2S)$ data.
- 14 From a 3-parameter fit of measured cross sections from $\sqrt{s} = 4.21-4.42$ GeV to a phase-space modified Breit-Wigner function, using the decays $\chi_{c0} \rightarrow \pi^+\pi^-, \chi_{c0} \rightarrow K^+K^-,$ and $\omega \rightarrow \pi^+\pi^-\pi^0$.
- 15 From a two-resonance fit.
- 16 From a single-resonance fit. Supersedes AUBERT,B 05i.
- 17 Superseded by LIU 13B.
- 18 From a single-resonance fit. Two interfering resonances are not excluded. Superseded by LEES 12AC.



$\psi(4230)$ DECAY MODES

Mode	Fraction (Γ_i/Γ)
Γ_1 e^+e^-	
Γ_2 $\mu^+\mu^-$	$(3.1 \pm 2.8) \times 10^{-5}$
Γ_3 $\eta_c(1S)\pi^+\pi^-$	not seen
Γ_4 $\eta_c(1S)\pi^+\pi^-\pi^0$	seen
Γ_5 $J/\psi\pi^+\pi^-$	seen
Γ_6 $J/\psi f_0(980), f_0(980) \rightarrow \pi^+\pi^-$	seen

Γ_7 $T_{cc1}(3900)^\pm \pi^\mp, T_{cc1}^\pm \rightarrow J/\psi \pi^\pm$	seen
Γ_8 $J/\psi \pi^0 \pi^0$	seen
Γ_9 $J/\psi K^+K^-$	seen
Γ_{10} $J/\psi K_S^0 K_S^0$	not seen
Γ_{11} $J/\psi \eta$	seen
Γ_{12} $J/\psi \pi^0$	not seen
Γ_{13} $J/\psi \eta'$	seen
Γ_{14} $J/\psi \pi^+\pi^-\pi^0$	not seen
Γ_{15} $J/\psi \eta \pi^0$	not seen
Γ_{16} $J/\psi \eta \eta$	not seen
Γ_{17} $\psi(2S)\pi^+\pi^-$	seen
Γ_{18} $\psi(2S)\eta$	not seen
Γ_{19} $\chi_{c0}\omega$	seen
Γ_{20} $\chi_{c1}\pi^+\pi^-\pi^0$	not seen
Γ_{21} $\chi_{c2}\pi^+\pi^-\pi^0$	not seen
Γ_{22} $h_c(1P)\pi^+\pi^-$	seen
Γ_{23} $\phi\pi^+\pi^-$	not seen
Γ_{24} $\phi f_0(980) \rightarrow \phi\pi^+\pi^-$	not seen
Γ_{25} ϕK^+K^-	not seen
Γ_{26} $\phi K_S^0 K_S^0$	not seen
Γ_{27} $\phi \eta$	not seen
Γ_{28} $\phi \eta'$	not seen
Γ_{29} $D\bar{D}$	not seen
Γ_{30} $D^0\bar{D}^0$	not seen
Γ_{31} D^+D^-	not seen
Γ_{32} $D^*\bar{D} + c.c.$	not seen
Γ_{33} $D^*(2007)^0\bar{D}^0 + c.c.$	not seen
Γ_{34} $D^*(2010)^+D^- + c.c.$	not seen
Γ_{35} $D^*\bar{D}^*$	not seen
Γ_{36} $D^*(2007)^0\bar{D}^*(2007)^0$	not seen
Γ_{37} $D^*(2010)^+D^*(2010)^-$	not seen
Γ_{38} $D\bar{D}\pi + c.c.$	not seen
Γ_{39} $D^0D^-\pi^+ + c.c. (excl. D^*(2007)^0\bar{D}^{*0} + c.c., D^*(2010)^+D^- + c.c.)$	not seen
Γ_{40} $D\bar{D}^*\pi + c.c. (excl. D^*\bar{D}^*)$	not seen
Γ_{41} $D^0D^*(2010)^-\pi^+ + c.c.$	seen
Γ_{42} $D_1(2420)\bar{D} + c.c.$	not seen
Γ_{43} $D^*\bar{D}^*\pi$	seen
Γ_{44} $D^{*0}D^{*-}\pi^+$	seen
Γ_{45} $D_s^\pm D_s^\mp$	not seen
Γ_{46} $D_s^{*+}D_s^{*-} + c.c.$	not seen
Γ_{47} $D_s^{*+}D_s^{*-}$	not seen
Γ_{48} $p\bar{p}$	not seen
Γ_{49} $p\bar{p}\pi^0$	not seen
Γ_{50} $p\bar{p}\eta$	not seen
Γ_{51} $\omega\pi^+\pi^-$	seen
Γ_{52} $p\bar{p}\omega$	not seen
Γ_{53} $\Xi^-\Xi^+$	not seen
Γ_{54} $\pi^+\pi^+\pi^-\pi^-$	not seen
Γ_{55} $\pi^+\pi^+\pi^-\pi^-\pi^0$	not seen
Γ_{56} $\omega\pi^0$	not seen
Γ_{57} $\omega\eta$	not seen
Γ_{58} $K_S^0 K^\pm \pi^\mp$	not seen
Γ_{59} $K_S^0 K^\pm \pi^\mp \pi^0$	not seen
Γ_{60} $K_S^0 K^\pm \pi^\mp \eta$	not seen
Γ_{61} $K^+K^-\pi^0$	not seen
Γ_{62} $K^+K^-\pi^+\pi^-$	not seen
Γ_{63} $K^+K^-\pi^+\pi^-\pi^0$	not seen
Γ_{64} $K^+K^+K^-K^-$	not seen
Γ_{65} $K^+K^+K^-K^-\pi^0$	not seen
Γ_{66} $p\bar{p}\pi^+\pi^-$	not seen
Γ_{67} $p\bar{p}\pi^+\pi^-\pi^0$	not seen
Γ_{68} $p\bar{p}p\bar{p}$	not seen
Γ_{69} $\Lambda\bar{\Lambda}$	not seen
Γ_{70} $\rho K^-\bar{\Lambda} + c.c.$	

Radiative decays

Γ_{71} $\eta_c(1S)\gamma$	possibly seen
Γ_{72} $\eta_c(1S)\pi^0\gamma$	not seen
Γ_{73} $\chi_{c1}\gamma$	not seen
Γ_{74} $\chi_{c2}\gamma$	not seen
Γ_{75} $\chi_{c1}(3872)\gamma$	seen

$\psi(4230)$ PARTIAL WIDTHS

$\Gamma(\mu^+\mu^-)$				Γ_2
VALUE (keV)	DOCUMENT ID	TECN	COMMENT	
1.53 ± 1.26 ± 0.54	1,2 ABLIKIM	20A BES3	$e^+e^- \rightarrow \mu^+\mu^-$	

¹ From a fit to the $e^+e^- \rightarrow \mu^+\mu^-$ cross section between 3.8 and 4.6 GeV to the coherent sum of four resonant amplitudes assuming $\Gamma(\mu^+\mu^-) = \Gamma(e^+e^-)$.
² From solution 1 of 8 with equal fit quality. Other solutions range from 1.09 ± 0.84 ± 0.39 to 1.53 ± 1.26 ± 0.54 keV.

$\psi(4230) \Gamma(i) \times \Gamma(e^+e^-)/\Gamma(\text{total})$

$\Gamma(J/\psi\pi^+\pi^-) \times \Gamma(e^+e^-)/\Gamma(\text{total})$				$\Gamma_5\Gamma_1/\Gamma$
VALUE (eV)	EVTS	DOCUMENT ID	TECN	COMMENT
9.2 ± 1.0 OUR AVERAGE				
9.2 ± 0.8 ± 0.7		¹ LEES	12AC BABR	10.58 $e^+e^- \rightarrow \gamma\pi^+\pi^- J/\psi$
8.9 ^{+3.9} _{-3.1} ± 1.8	8.1	HE	06B CLEO	9.4-10.6 $e^+e^- \rightarrow \gamma\pi^+\pi^- J/\psi$

• • • We do not use the following data for averages, fits, limits, etc. • • •

6.4 ± 0.8 ± 0.6		² LIU	13B BELL	$e^+e^- \rightarrow \gamma\pi^+\pi^- J/\psi$
20.5 ± 1.4 ± 2.0		³ LIU	13B BELL	$e^+e^- \rightarrow \gamma\pi^+\pi^- J/\psi$
6.0 ± 1.2 ^{+4.7} _{-0.5}		^{2,4} YUAN	07 BELL	10.58 $e^+e^- \rightarrow \gamma\pi^+\pi^- J/\psi$
20.6 ± 2.3 ^{+9.1} _{-1.7}		^{3,4} YUAN	07 BELL	10.58 $e^+e^- \rightarrow \gamma\pi^+\pi^- J/\psi$
5.5 ± 1.0 ^{+9.8} _{-0.7}	125	⁵ AUBERT,B	05i BABR	10.58 $e^+e^- \rightarrow \gamma\pi^+\pi^- J/\psi$

¹ From a single-resonance fit. Supersedes AUBERT,B 05i.
² Solution I of two equivalent solutions in a fit using two interfering resonances.
³ Solution II of two equivalent solutions in a fit using two interfering resonances.
⁴ Superseded by LIU 13B.
⁵ From a single-resonance fit. Two interfering resonances are not excluded. Superseded by LEES 12AC.

$\Gamma(J/\psi K^+K^-) \times \Gamma(e^+e^-)/\Gamma(\text{total})$				$\Gamma_9\Gamma_1/\Gamma$
VALUE (eV)	CL%	DOCUMENT ID	TECN	COMMENT
• • • We do not use the following data for averages, fits, limits, etc. • • •				
0.42 ± 0.04 ± 0.15		¹ ABLIKIM	22AU BES3	$e^+e^- \rightarrow K^+K^- J/\psi$
0.29 ± 0.02 ± 0.10		² ABLIKIM	22AU BES3	$e^+e^- \rightarrow K^+K^- J/\psi$
<1.7	90	³ SHEN	14 BELL	9.4-10.9 $e^+e^- \rightarrow \gamma K^+K^- J/\psi$
<1.2	90	⁴ YUAN	08 BELL	$e^+e^- \rightarrow \gamma K^+K^- J/\psi$

¹ Solution I from a two-resonance fit to the dressed cross section in the range $\sqrt{s} = 4.127-4.600$ GeV. The second resonance has a mass of 4484.7 ± 13.3 ± 24.1 MeV, a total width of 111.1 ± 30.1 ± 15.2 MeV, and $\Gamma_{ee^-B} = 1.35 \pm 0.14 \pm 0.07$ eV. The phase difference is 1.72 ± 0.09 ± 0.52 rad.
² Solution II from a two-resonance fit to the dressed cross section in the range $\sqrt{s} = 4.127-4.600$ GeV. The second resonance has a mass of 4484.7 ± 13.3 ± 24.1 MeV, a total width of 111.1 ± 30.1 ± 15.2 MeV, and $\Gamma_{ee^-B} = 0.41 \pm 0.08 \pm 0.13$ eV. The phase difference is 5.49 ± 0.35 ± 0.58 rad.
³ From a fit of the broad $K^+K^- J/\psi$ enhancement including a coherent $\psi(4260)$ amplitude with mass and width from LIU 13B. Supersedes YUAN 08. The shape of the cross section observed by ABLIKIM 18N between 4.2 and 4.3 GeV is incompatible with that of $e^+e^- \rightarrow \pi^+\pi^- J/\psi$ in ABLIKIM 13T and ABLIKIM 17B. They also observe a broad enhancement around 4.5 GeV.
⁴ From a fit of the broad $K^+K^- J/\psi$ enhancement including a coherent $\psi(4260)$ amplitude with mass and width from YUAN 07.

$\Gamma(J/\psi K_S^0 K_S^0) \times \Gamma(e^+e^-)/\Gamma(\text{total})$				$\Gamma_{10}\Gamma_1/\Gamma$
VALUE (eV)	CL%	DOCUMENT ID	TECN	COMMENT
<0.85	90	¹ SHEN	14 BELL	9.4-10.9 $e^+e^- \rightarrow \gamma K_S^0 K_S^0 J/\psi$

• • • We do not use the following data for averages, fits, limits, etc. • • •

0.13 ± 0.02 ± 0.05		^{2,3} ABLIKIM	23U BES3	$e^+e^- \rightarrow K_S K_S J/\psi$
0.14 ± 0.03 ± 0.06		^{2,4} ABLIKIM	23U BES3	$e^+e^- \rightarrow K_S K_S J/\psi$
0.18 ± 0.05 ± 0.07		^{2,5} ABLIKIM	23U BES3	$e^+e^- \rightarrow K_S K_S J/\psi$
0.20 ± 0.04 ± 0.07		^{2,6} ABLIKIM	23U BES3	$e^+e^- \rightarrow K_S K_S J/\psi$

¹ From a fit of the $K_S^0 K_S^0 J/\psi$ mass range from 4.4 to 5.5 GeV including a coherent $\psi(4260)$ amplitude with mass and width from LIU 13B.
² A three-resonance fit to the dressed cross section in the range $\sqrt{s} = 4.128-4.950$ GeV.
³ Solution I.
⁴ Solution II.
⁵ Solution III.
⁶ Solution IV.

$\Gamma(J/\psi\eta) \times \Gamma(e^+e^-)/\Gamma(\text{total})$				$\Gamma_{11}\Gamma_1/\Gamma$
VALUE (eV)	CL%	DOCUMENT ID	TECN	COMMENT
• • • We do not use the following data for averages, fits, limits, etc. • • •				
8.0 ± 1.7		¹ ABLIKIM	20u BES3	$e^+e^- \rightarrow \eta J/\psi$
4.8 ± 1.0		² ABLIKIM	20u BES3	$e^+e^- \rightarrow \eta J/\psi$
7.0 ± 1.5		³ ABLIKIM	20u BES3	$e^+e^- \rightarrow \eta J/\psi$
<14.2	90	WANG	13B BELL	$e^+e^- \rightarrow J/\psi\eta\gamma$

¹ Solution 1 of three equivalent fit solutions using three resonant structures.
² Solution 2 of three equivalent fit solutions using three resonant structures.
³ Solution 3 of three equivalent fit solutions using three resonant structures.

$\Gamma(J/\psi\eta') \times \Gamma(e^+e^-)/\Gamma(\text{total})$				$\Gamma_{13}\Gamma_1/\Gamma$
VALUE (eV)	EVTS	DOCUMENT ID	TECN	COMMENT
• • • We do not use the following data for averages, fits, limits, etc. • • •				
0.06 ± 0.03	46	^{1,2} ABLIKIM	20A BES3	$e^+e^- \rightarrow \eta' J/\psi$
1.38 ± 0.11	46	^{1,3} ABLIKIM	20A BES3	$e^+e^- \rightarrow \eta' J/\psi$

¹ Based on a fit to $\sigma(e^+e^- \rightarrow \eta' J/\psi)$ from $\sqrt{s} = 4.18$ to 4.60 GeV assuming interfering $\psi(4160)$ and $\psi(4260)$ contributions. At $\sqrt{s} = 4.23$ GeV, $\sigma(e^+e^- \rightarrow \eta' J/\psi) = 3.6 \pm 0.6 \pm 0.3$ pb.
² Solution I of the fit, corresponding to a phase of -0.03 ± 0.44 rad.
³ Solution II of the fit, corresponding to a phase of 2.54 ± 0.04 rad.

$\Gamma(\psi(2S)\pi^+\pi^-) \times \Gamma(e^+e^-)/\Gamma(\text{total})$				$\Gamma_{17}\Gamma_1/\Gamma$
VALUE (eV)	CL%	DOCUMENT ID	TECN	COMMENT
• • • We do not use the following data for averages, fits, limits, etc. • • •				
1.59 ± 0.75		¹ ABLIKIM	21AJ BES3	$e^+e^- \rightarrow \pi^+\pi^-\psi(2S)$
1.63 ± 0.78		² ABLIKIM	21AJ BES3	$e^+e^- \rightarrow \pi^+\pi^-\psi(2S)$
0.02 ± 0.01		³ ABLIKIM	21AJ BES3	$e^+e^- \rightarrow \pi^+\pi^-\psi(2S)$
1.6 ± 1.3		⁴ ABLIKIM	19K BES3	$e^+e^- \rightarrow \pi^+\pi^-\psi(2S)$
1.8 ± 1.4		⁵ ABLIKIM	19K BES3	$e^+e^- \rightarrow \pi^+\pi^-\psi(2S)$
<4.3	90	⁶ LIU	08H RVUE	10.58 $e^+e^- \rightarrow \psi(2S)\pi^+\pi^-\gamma$
7.4 ^{+2.1} _{-1.7}		⁷ LIU	08H RVUE	10.58 $e^+e^- \rightarrow \psi(2S)\pi^+\pi^-\gamma$

¹ Solution I of four equivalent solutions in a fit using three interfering resonances.
² Solution II of four equivalent solutions in a fit using three interfering resonances.
³ Solutions III and IV of four equivalent solutions in a fit using three interfering resonances.
⁴ Solution I of two equivalent solutions in a fit using two interfering resonances.
⁵ Solution II of two equivalent solutions in a fit using two interfering resonances.
⁶ For constructive interference with the $\psi(4360)$ in a combined fit of AUBERT 07s and WANG 07b data with three resonances.
⁷ For destructive interference with the $\psi(4360)$ in a combined fit of AUBERT 07s and WANG 07b data with three resonances.

$\Gamma(\chi_{c0}\omega) \times \Gamma(e^+e^-)/\Gamma(\text{total})$				$\Gamma_{19}\Gamma_1/\Gamma$
VALUE (eV)	EVTS	DOCUMENT ID	TECN	COMMENT
• • • We do not use the following data for averages, fits, limits, etc. • • •				
2.5 ± 0.2 ± 0.3		¹ ABLIKIM	19AI BES3	$e^+e^- \rightarrow \omega\chi_{c0}$
2.7 ± 0.5 ± 0.4	180	² ABLIKIM	15c BES3	$e^+e^- \rightarrow \omega\chi_{c0}$

¹ From a fit of the measured cross section from $\sqrt{s} = 4.178-4.278$ GeV. Supersedes ABLIKIM 15c.
² From a 3-parameter fit of measured cross sections from $\sqrt{s} = 4.21-4.42$ GeV to a phase-space modified Breit-Wigner function, using the decays $\chi_{c0} \rightarrow \pi^+\pi^-$, $\chi_{c0} \rightarrow K^+K^-$, and $\omega \rightarrow \pi^+\pi^-\pi^0$.

$\Gamma(h_c(1P)\pi^+\pi^-) \times \Gamma(e^+e^-)/\Gamma(\text{total})$				$\Gamma_{22}\Gamma_1/\Gamma$
VALUE (eV)	CL%	DOCUMENT ID	TECN	COMMENT
4.6 ± 2.9^{+1.4}_{-0.8}		ABLIKIM	17G BES3	$e^+e^- \rightarrow \pi^+\pi^-h_c$

$\Gamma(\phi\pi^+\pi^-) \times \Gamma(e^+e^-)/\Gamma(\text{total})$				$\Gamma_{23}\Gamma_1/\Gamma$
VALUE (eV)	CL%	DOCUMENT ID	TECN	COMMENT
<0.4	90	AUBERT,BE	06D BABR	10.6 $e^+e^- \rightarrow K^+K^-\pi^+\pi^-\gamma$

$\Gamma(\phi_0(980) \rightarrow \phi\pi^+\pi^-) \times \Gamma(e^+e^-)/\Gamma(\text{total})$				$\Gamma_{24}\Gamma_1/\Gamma$
VALUE (eV)	CL%	DOCUMENT ID	TECN	COMMENT
<0.28	90	¹ AUBERT	07AK BABR	10.6 $e^+e^- \rightarrow \pi^+\pi^-K^+K^-\gamma$

¹ AUBERT 07AK reports $[\Gamma(\psi(4230) \rightarrow \phi_0(980) \rightarrow \phi\pi^+\pi^-) \times \Gamma(\psi(4230) \rightarrow e^+e^-)]/\Gamma(\text{total}) \times [B(\phi(1020) \rightarrow K^+K^-)] < 0.14$ eV which we divide by our best value $B(\phi(1020) \rightarrow K^+K^-) = 49.1 \times 10^{-2}$.

$\Gamma(\phi K^+K^-) \times \Gamma(e^+e^-)/\Gamma(\text{total})$				$\Gamma_{25}\Gamma_1/\Gamma$
VALUE (eV)	CL%	DOCUMENT ID	TECN	COMMENT
<1.75	90	ABLIKIM	23AE BES3	$e^+e^- \rightarrow \phi K^+K^-$

$\Gamma(\phi K_S^0 K_S^0) \times \Gamma(e^+e^-)/\Gamma(\text{total})$				$\Gamma_{26}\Gamma_1/\Gamma$
VALUE (eV)	CL%	DOCUMENT ID	TECN	COMMENT
<0.47	90	ABLIKIM	23AE BES3	$e^+e^- \rightarrow \phi K_S^0 K_S^0$

$\Gamma(\phi\eta') \times \Gamma(e^+e^-)/\Gamma(\text{total})$				$\Gamma_{28}\Gamma_1/\Gamma$
VALUE (eV)	CL%	DOCUMENT ID	TECN	COMMENT
<0.53	90	ABLIKIM	23R BES3	$e^+e^- \rightarrow \phi\eta'$

$\Gamma(D^{*0}D^{*-}\pi^+) \times \Gamma(e^+e^-)/\Gamma(\text{total})$				$\Gamma_{44}\Gamma_1/\Gamma$
VALUE (eV)	CL%	DOCUMENT ID	TECN	COMMENT
• • • We do not use the following data for averages, fits, limits, etc. • • •				
5 to 22		¹ ABLIKIM	23X BES3	$e^+e^- \rightarrow D^{*0}D^{*-}\pi^+$

¹ From a cross-section measurement of $e^+e^- \rightarrow D^{*0}D^{*-}\pi^+$ between 4.189 and 4.951 GeV, assuming a coherent sum of 3 Breit-Wigner resonances plus a continuum amplitude. Depending on solutions I - VIII with the same fit qualities.

Meson Particle Listings

 $\psi(4230)$ $\Gamma(\omega\pi^+\pi^-) \times \Gamma(e^+e^-)/\Gamma_{\text{total}}$ $\Gamma_{51}\Gamma/\Gamma$

VALUE (eV)	CL%	DOCUMENT ID	TECN	COMMENT
<0.0251	90	^{1,2} ABLIKIM	23AQ BES3	fit to cross sections
$0.487 \pm 0.008 \pm 0.030$		^{2,3} ABLIKIM	23AQ BES3	fit to cross sections

• • • We do not use the following data for averages, fits, limits, etc. • • •
¹ Solution I of the fit.
² From a fit to $e^+e^- \rightarrow \omega\pi^+\pi^-$ cross sections between 4 and 4.6 GeV. Recalculated from 12 $\pi\pi\pi$ $B(\psi(4230) \rightarrow \omega\pi^+\pi^-)$. First uncertainty is from statistical and uncommon systematic uncertainties, and the second is a 6.2% common systematic uncertainty quoted in the paper.
³ Solution II of the fit.

 $\Gamma(\Xi^-\Xi^+) \times \Gamma(e^+e^-)/\Gamma_{\text{total}}$ $\Gamma_{53}\Gamma/\Gamma$

VALUE (eV)	CL%	DOCUMENT ID	TECN	COMMENT
<0.0251	90	¹ ABLIKIM	23BK BES3	$e^+e^- \rightarrow \psi(4230)$
$<2.7 \times 10^{-4}$	90	² ABLIKIM	20c BES3	$e^+e^- \rightarrow \Xi^-\Xi^+$

• • • We do not use the following data for averages, fits, limits, etc. • • •
¹ From a fit to $e^+e^- \rightarrow \Xi^-\Xi^+$ cross sections.
² Superseded by ABLIKIM 23Bk.

 $\Gamma(\pi^+\pi^+\pi^-\pi^-) \times \Gamma(e^+e^-)/\Gamma_{\text{total}}$ $\Gamma_{54}\Gamma/\Gamma$

VALUE (eV)	CL%	DOCUMENT ID	TECN	COMMENT
<32	90	ABLIKIM	21AW BES3	$e^+e^- \rightarrow 2\pi^+2\pi^-$

 $\Gamma(\pi^+\pi^+\pi^-\pi^0) \times \Gamma(e^+e^-)/\Gamma_{\text{total}}$ $\Gamma_{55}\Gamma/\Gamma$

VALUE (eV)	CL%	DOCUMENT ID	TECN	COMMENT
<16	90	ABLIKIM	21AW BES3	$e^+e^- \rightarrow 2\pi^+2\pi^-\pi^0$

 $\Gamma(K_S^0 K^\pm \pi^\mp) \times \Gamma(e^+e^-)/\Gamma_{\text{total}}$ $\Gamma_{58}\Gamma/\Gamma$

VALUE (eV)	CL%	DOCUMENT ID	TECN	COMMENT
$2.04 \pm 0.19 \pm 0.09$		¹ ABLIKIM	19AE BES3	$e^+e^- \rightarrow K_S^0 K^\pm \pi^\mp$
$0.0027 \pm 0.0023 \pm 0.0001$		² ABLIKIM	19AE BES3	$e^+e^- \rightarrow K_S^0 K^\pm \pi^\mp$
< 0.5 at 90% CL		AUBERT	08s BABR	$10.6 e^+e^- \rightarrow K_S^0 K^\pm \pi^\mp$

• • • We do not use the following data for averages, fits, limits, etc. • • •
¹ Solution I of the fit including the $\psi(4160)$ with mass 4191 ± 5 MeV and width 70 ± 10 MeV from PDG 16 and the $\psi(4230)$ with mass $4219.6 \pm 3.3 \pm 5.1$ MeV and width $56.0 \pm 3.6 \pm 6.9$ MeV from GAO 17.
² Solution II of the fit including the $\psi(4160)$ with mass 4191 ± 5 MeV and width 70 ± 10 MeV from PDG 16 and the $\psi(4230)$ with mass $4219.6 \pm 3.3 \pm 5.1$ MeV and width $56.0 \pm 3.6 \pm 6.9$ MeV from GAO 17.

 $\Gamma(K_S^0 K^\pm \pi^\mp \pi^0) \times \Gamma(e^+e^-)/\Gamma_{\text{total}}$ $\Gamma_{59}\Gamma/\Gamma$

VALUE (eV)	CL%	DOCUMENT ID	TECN	COMMENT
<0.05	90	ABLIKIM	19 BES3	$e^+e^- \rightarrow K_S^0 K^\pm \pi^\mp \pi^0$

 $\Gamma(K_S^0 K^\pm \pi^\mp \eta) \times \Gamma(e^+e^-)/\Gamma_{\text{total}}$ $\Gamma_{60}\Gamma/\Gamma$

VALUE (eV)	CL%	DOCUMENT ID	TECN	COMMENT
<0.19	90	ABLIKIM	19 BES3	$e^+e^- \rightarrow K_S^0 K^\pm \pi^\mp \eta$

 $\Gamma(K^+K^-\pi^0) \times \Gamma(e^+e^-)/\Gamma_{\text{total}}$ $\Gamma_{61}\Gamma/\Gamma$

VALUE (eV)	CL%	DOCUMENT ID	TECN	COMMENT
<0.6	90	AUBERT	08s BABR	$10.6 e^+e^- \rightarrow K^+K^-\pi^0\gamma$

 $\Gamma(K^+K^-\pi^+\pi^-) \times \Gamma(e^+e^-)/\Gamma_{\text{total}}$ $\Gamma_{62}\Gamma/\Gamma$

VALUE (eV)	CL%	DOCUMENT ID	TECN	COMMENT
<20	90	ABLIKIM	21AW BES3	$e^+e^- \rightarrow K^+K^-\pi^+\pi^-$

 $\Gamma(K^+K^-\pi^+\pi^0) \times \Gamma(e^+e^-)/\Gamma_{\text{total}}$ $\Gamma_{63}\Gamma/\Gamma$

VALUE (eV)	CL%	DOCUMENT ID	TECN	COMMENT
<43	90	ABLIKIM	21AW BES3	$e^+e^- \rightarrow K^+K^-\pi^+\pi^0$

 $\Gamma(K^+K^+K^-K^-) \times \Gamma(e^+e^-)/\Gamma_{\text{total}}$ $\Gamma_{64}\Gamma/\Gamma$

VALUE (eV)	CL%	DOCUMENT ID	TECN	COMMENT
<3.8	90	ABLIKIM	21AW BES3	$e^+e^- \rightarrow 2K^+2K^-$

 $\Gamma(K^+K^+K^-K^-\pi^0) \times \Gamma(e^+e^-)/\Gamma_{\text{total}}$ $\Gamma_{65}\Gamma/\Gamma$

VALUE (eV)	CL%	DOCUMENT ID	TECN	COMMENT
<2.1	90	ABLIKIM	21AW BES3	$e^+e^- \rightarrow 2K^+2K^-\pi^0$

 $\Gamma(p\bar{p}\pi^+\pi^-) \times \Gamma(e^+e^-)/\Gamma_{\text{total}}$ $\Gamma_{66}\Gamma/\Gamma$

VALUE (eV)	CL%	DOCUMENT ID	TECN	COMMENT
<7.2	90	ABLIKIM	21AW BES3	$e^+e^- \rightarrow p\bar{p}\pi^+\pi^-$

 $\Gamma(p\bar{p}\pi^+\pi^0) \times \Gamma(e^+e^-)/\Gamma_{\text{total}}$ $\Gamma_{67}\Gamma/\Gamma$

VALUE (eV)	CL%	DOCUMENT ID	TECN	COMMENT
<15	90	ABLIKIM	21AW BES3	$e^+e^- \rightarrow p\bar{p}\pi^+\pi^0$

 $\Gamma(\Lambda\bar{\Lambda}) \times \Gamma(e^+e^-)/\Gamma_{\text{total}}$ $\Gamma_{69}\Gamma/\Gamma$

VALUE (eV)	CL%	DOCUMENT ID	TECN	COMMENT
$<0.8 \times 10^{-3}$	90	¹ ABLIKIM	21As BES3	$e^+e^- \rightarrow \psi(4260)$

¹ From a measurement of the $e^+e^- \rightarrow \Lambda\bar{\Lambda}$ cross section between 3.5 and 4.6 GeV.

 $\Gamma(pK^-\bar{\Lambda} + \text{c.c.}) \times \Gamma(e^+e^-)/\Gamma_{\text{total}}$ $\Gamma_{70}\Gamma/\Gamma$

VALUE (eV)	CL%	DOCUMENT ID	TECN	COMMENT
$<1.3 \times 10^{-3}$	90	¹ ABLIKIM	23BL BES3	$e^+e^- \rightarrow \psi(4230)$

¹ From a fit to $e^+e^- \rightarrow pK^-\bar{\Lambda} + \text{c.c.}$ cross sections.

 $\Gamma(\chi_{c1}\gamma) \times \Gamma(e^+e^-)/\Gamma_{\text{total}}$ $\Gamma_{73}\Gamma/\Gamma$

VALUE (eV)	CL%	DOCUMENT ID	TECN	COMMENT
<1.4	90	¹ HAN	15 BELL	$10.58 e^+e^- \rightarrow \chi_{c1}\gamma$

¹ Using $B(\eta \rightarrow \gamma\gamma) = (39.41 \pm 0.21)\%$.

 $\Gamma(\chi_{c2}\gamma) \times \Gamma(e^+e^-)/\Gamma_{\text{total}}$ $\Gamma_{74}\Gamma/\Gamma$

VALUE (eV)	CL%	DOCUMENT ID	TECN	COMMENT
<4.0	90	¹ HAN	15 BELL	$10.58 e^+e^- \rightarrow \chi_{c2}\gamma$

¹ Using $B(\eta \rightarrow \gamma\gamma) = (39.41 \pm 0.21)\%$.

 $\psi(4230) \Gamma(i) \times \Gamma(e^+e^-)/\Gamma^2(\text{total})$ $\Gamma(D^0 D^{*+}(2010)^- \pi^+ + \text{c.c.})/\Gamma_{\text{total}} \times \Gamma(e^+e^-)/\Gamma_{\text{total}}$ $\Gamma_{41}/\Gamma \times \Gamma_1/\Gamma$

VALUE (eV)	CL%	DOCUMENT ID	TECN	COMMENT
$<0.42 \times 10^{-6}$	90	¹ PAKHLOVA	09 BELL	$e^+e^- \rightarrow D^0 D^{*+} \pi^+$

¹ Using 4263_{-9}^{+8} MeV for the mass of $\psi(4260)$.

 $\psi(4230)$ BRANCHING RATIOS $\Gamma(\eta_c(1S)\pi^+\pi^-)/\Gamma_{\text{total}}$ Γ_3/Γ

VALUE	DOCUMENT ID	TECN	COMMENT
not seen	¹ ABLIKIM	21B BES3	$e^+e^- \rightarrow \pi^+\pi^-\eta_c$

¹ Not seen in $e^+e^- \rightarrow \pi^+\pi^-\eta_c$ at $\sqrt{s} = 4.226$ GeV with a 90% C.L. upper limit on the cross section of 16.8 pb.

 $\Gamma(\eta_c(1S)\pi^+\pi^-\pi^0)/\Gamma_{\text{total}}$ Γ_4/Γ

VALUE	DOCUMENT ID	TECN	COMMENT
seen	¹ ABLIKIM	21B BES3	$e^+e^- \rightarrow \pi^+\pi^-\pi^0\eta_c$

¹ Seen as a peak in the $e^+e^- \rightarrow \pi^+\pi^-\pi^0\eta_c$ cross section with a peak value of $46.1_{-9.4}^{+9.5} \pm 6.6$ pb at $\sqrt{s} = 4.226$ GeV.

 $\Gamma(J/\psi\pi^+\pi^-)/\Gamma_{\text{total}}$ Γ_5/Γ

VALUE	DOCUMENT ID	TECN	COMMENT
seen	¹ ABLIKIM	22AMB BES3	$e^+e^- \rightarrow \pi^+\pi^-J/\psi$

• • • We do not use the following data for averages, fits, limits, etc. • • •
¹ From a three-resonance fit to the Born cross section in the range $\sqrt{s} = 3.7730\text{--}4.7008$ GeV.
² From a three-resonance fit. Superseded by ABLIKIM 22AM.

 $\Gamma(J/\psi\pi^+\pi^-\pi^0)/\Gamma_{\text{total}}$ Γ_6/Γ_5

VALUE	DOCUMENT ID	TECN	COMMENT
seen	¹ ABLIKIM	22AMB BES3	$e^+e^- \rightarrow \pi^+\pi^-\pi^0J/\psi$

• • • We do not use the following data for averages, fits, limits, etc. • • •
¹ From a three-resonance fit to the Born cross section in the range $\sqrt{s} = 3.7730\text{--}4.7008$ GeV.
² From a three-resonance fit. Superseded by ABLIKIM 22AM.

 $\Gamma(J/\psi f_0(980), f_0(980) \rightarrow \pi^+\pi^-)/\Gamma(J/\psi\pi^+\pi^-)$ Γ_6/Γ_5

VALUE	DOCUMENT ID	TECN	COMMENT
0.17 ± 0.13	¹ LEES	12AC BABR	$10.58 e^+e^- \rightarrow \gamma\pi^+\pi^-J/\psi$

¹ Systematic uncertainties not estimated.

 $\Gamma(T_{c\bar{c}1}(3900)^\pm \pi^\mp, T_{c\bar{c}1}^\pm \rightarrow J/\psi\pi^\pm)/\Gamma(J/\psi\pi^+\pi^-)$ Γ_7/Γ_5

VALUE	DOCUMENT ID	TECN	COMMENT
$0.215 \pm 0.033 \pm 0.075$	¹ ABLIKIM	13T BES3	$e^+e^- \rightarrow \pi^+\pi^-J/\psi$

• • • We do not use the following data for averages, fits, limits, etc. • • •
¹ Assuming that the cross section of $e^+e^- \rightarrow \pi^+\pi^-J/\psi$ is fully due to the $\psi(4260)$.
² Systematic error not evaluated.

 $\Gamma(J/\psi\pi^0\pi^0)/\Gamma_{\text{total}}$ Γ_8/Γ

VALUE	DOCUMENT ID	TECN	COMMENT
seen	¹ ABLIKIM	20N BES3	$e^+e^- \rightarrow \pi^0\pi^0J/\psi$

¹ From a fit to the cross section $e^+e^- \rightarrow \pi^0\pi^0J/\psi$ at center-of-mass energies between 3.808 and 4.600 GeV.

 $\Gamma(J/\psi K_S^0 K_S^0)/\Gamma_{\text{total}}$ Γ_{10}/Γ

VALUE	DOCUMENT ID	TECN	COMMENT
not seen	SHEN	14 BELL	$9.4\text{--}10.9 e^+e^- \rightarrow \gamma K_S^0 K_S^0 J/\psi$

 $\Gamma(J/\psi\eta)/\Gamma_{\text{total}}$ Γ_{11}/Γ

VALUE	DOCUMENT ID	TECN	COMMENT
seen	ABLIKIM	20o BES3	$e^+e^- \rightarrow \eta J/\psi$

 $\Gamma(J/\psi\eta\pi^0)/\Gamma_{\text{total}}$ Γ_{15}/Γ

VALUE	DOCUMENT ID	TECN	COMMENT
not seen	ABLIKIM	15q BES3	$4.0\text{--}4.6 e^+e^- \rightarrow J/\psi\eta\pi^0$

$\Gamma(\psi(2S)\pi^+\pi^-)/\Gamma_{total}$	DOCUMENT ID	TECN	COMMENT	Γ_{17}/Γ
seen	1 ABLIKIM	17v	BES3 $e^+e^- \rightarrow \pi^+\pi^-\psi(2S)$	
¹ From a fit to the cross section for $e^+e^- \rightarrow \pi^+\pi^-\psi(2S) \rightarrow 2(\pi^+\pi^-)\ell^+\ell^-$ obtained from 16 center-of-mass energies between 4.008 and 4.600 GeV and comprising 5.1 fb^{-1} .				

$\Gamma(\psi(2S)\pi^+\pi^-)/\Gamma(J/\psi\pi^+\pi^-)$	DOCUMENT ID	TECN	COMMENT	Γ_{17}/Γ_5
••• We do not use the following data for averages, fits, limits, etc. •••				
$(0.11 \pm 0.03 \pm 0.03)$ to $(0.55 \pm 0.18 \pm 0.19)$	1 ZHANG	17c	RVUE $e^+e^- \rightarrow \pi^+\pi^-J/\psi$ or $\psi(2S)$	
¹ From a combined fit of BELLE, BABAR and BES3 $e^+e^- \rightarrow \pi^+\pi^-J/\psi$ and $e^+e^- \rightarrow \pi^+\pi^-\psi(2S)$ data.				

$\Gamma(\chi_{c0}\omega)/\Gamma_{total}$	DOCUMENT ID	TECN	COMMENT	Γ_{19}/Γ
seen	1 ABLIKIM	15c	BES3 $e^+e^- \rightarrow \omega\chi_{c0}$	
¹ From a 3-parameter fit of measured cross sections from $\sqrt{s} = 4.21\text{--}4.42 \text{ GeV}$ to a phase-space modified Breit-Wigner function, using the decays $\chi_{c0} \rightarrow \pi^+\pi^-$, $\chi_{c0} \rightarrow K^+K^-$, and $\omega \rightarrow \pi^+\pi^-\pi^0$.				

$\Gamma(h_c(1P)\pi^+\pi^-)/\Gamma_{total}$	DOCUMENT ID	TECN	COMMENT	Γ_{22}/Γ
seen	ABLIKIM	17g	BES3 $e^+e^- \rightarrow \pi^+\pi^-h_c$	

$\Gamma(h_c(1P)\pi^+\pi^-)/\Gamma(J/\psi\pi^+\pi^-)$	DOCUMENT ID	TECN	COMMENT	Γ_{22}/Γ_5
seen	1 PEDLAR	11	CLEO $e^+e^- \rightarrow h_c(1P)\pi^+\pi^-$	
¹ At $\sqrt{s} = 4260 \text{ MeV}$, PEDLAR 11 measures $\sigma(e^+e^- \rightarrow h_c(1P)\pi^+\pi^-) = 32 \pm 17 \pm 6 \pm 6 \text{ pb}$, where the errors are statistical, systematic, and due to uncertainty in $B(\psi(2S) \rightarrow \pi^0 h_c(1P))$, respectively.				

$\Gamma(\phi\eta)/\Gamma_{total}$	DOCUMENT ID	TECN	COMMENT	Γ_{27}/Γ
not seen	ABLIKIM	23BT	BES3 $e^+e^- \rightarrow \phi\eta$	

$\Gamma(D\bar{D})/\Gamma(J/\psi\pi^+\pi^-)$	DOCUMENT ID	TECN	COMMENT	Γ_{29}/Γ_5
seen	1 AUBERT	07BE	BABR $e^+e^- \rightarrow D\bar{D}\gamma$	
••• We do not use the following data for averages, fits, limits, etc. •••				
<4.0	90	CRONIN-HEN..09	CLEO e^+e^-	
¹ Using $4259 \pm 10 \text{ MeV}$ for the mass and $88 \pm 24 \text{ MeV}$ for the width of $\psi(4260)$.				

$\Gamma(D^0\bar{D}^0)/\Gamma_{total}$	DOCUMENT ID	TECN	COMMENT	Γ_{30}/Γ
not seen	CRONIN-HEN..09	CLEO	$e^+e^- \rightarrow D^0\bar{D}^0$	
••• We do not use the following data for averages, fits, limits, etc. •••				
not seen	AUBERT	09M	BABR $e^+e^- \rightarrow D^0\bar{D}^0\gamma$	
not seen	PAKHLOVA	08	BELL $e^+e^- \rightarrow D^0\bar{D}^0\gamma$	

$\Gamma(D^+D^-)/\Gamma_{total}$	DOCUMENT ID	TECN	COMMENT	Γ_{31}/Γ
not seen	CRONIN-HEN..09	CLEO	$e^+e^- \rightarrow D^+D^-$	
••• We do not use the following data for averages, fits, limits, etc. •••				
not seen	AUBERT	09M	BABR $e^+e^- \rightarrow D^+D^-\gamma$	
not seen	PAKHLOVA	08	BELL $e^+e^- \rightarrow D^+D^-\gamma$	

$\Gamma(D^*\bar{D}^+c.c.)/\Gamma(J/\psi\pi^+\pi^-)$	DOCUMENT ID	TECN	COMMENT	Γ_{32}/Γ_5
seen	90	AUBERT	09M	BABR $e^+e^- \rightarrow \gamma D^*\bar{D}$
••• We do not use the following data for averages, fits, limits, etc. •••				
<45	90	CRONIN-HEN..09	CLEO e^+e^-	

$\Gamma(D^*(2007)^0\bar{D}^0+c.c.)/\Gamma_{total}$	DOCUMENT ID	TECN	COMMENT	Γ_{33}/Γ
not seen	CRONIN-HEN..09	CLEO	$e^+e^- \rightarrow D^{*0}\bar{D}^0$	
••• We do not use the following data for averages, fits, limits, etc. •••				
not seen	AUBERT	09M	BABR $e^+e^- \rightarrow D^{*0}\bar{D}^0\gamma$	

$\Gamma(D^*(2010)^+D^-+c.c.)/\Gamma_{total}$	DOCUMENT ID	TECN	COMMENT	Γ_{34}/Γ
not seen	CRONIN-HEN..09	CLEO	$e^+e^- \rightarrow D^{*+}D^-$	
not seen	PAKHLOVA	07	BELL $e^+e^- \rightarrow D^{*+}D^-\gamma$	
••• We do not use the following data for averages, fits, limits, etc. •••				
not seen	AUBERT	09M	BABR $e^+e^- \rightarrow D^{*+}D^-\gamma$	

$\Gamma(D^*\bar{D}^*)/\Gamma(J/\psi\pi^+\pi^-)$	DOCUMENT ID	TECN	COMMENT	Γ_{35}/Γ_5
seen	90	CRONIN-HEN..09	CLEO e^+e^-	
••• We do not use the following data for averages, fits, limits, etc. •••				
<40	90	AUBERT	09M	BABR $e^+e^- \rightarrow \gamma D^*\bar{D}^*$

$\Gamma(D^*(2007)^0\bar{D}^*(2007)^0)/\Gamma_{total}$	DOCUMENT ID	TECN	COMMENT	Γ_{36}/Γ
not seen	CRONIN-HEN..09	CLEO	$e^+e^- \rightarrow D^{*0}\bar{D}^{*0}$	
••• We do not use the following data for averages, fits, limits, etc. •••				
not seen	AUBERT	09M	BABR $e^+e^- \rightarrow D^{*0}\bar{D}^{*0}\gamma$	

$\Gamma(D^*(2010)^+D^*(2010)^-)/\Gamma_{total}$	DOCUMENT ID	TECN	COMMENT	Γ_{37}/Γ
not seen	CRONIN-HEN..09	CLEO	$e^+e^- \rightarrow D^{*+}D^{*-}$	
not seen	PAKHLOVA	07	BELL $e^+e^- \rightarrow D^{*+}D^{*-}\gamma$	
••• We do not use the following data for averages, fits, limits, etc. •••				
not seen	AUBERT	09M	BABR $e^+e^- \rightarrow D^{*+}D^{*-}\gamma$	

$\Gamma(D^0D^-\pi^++c.c. \text{ (excl. } D^*(2007)^0\bar{D}^{*0}+c.c., D^*(2010)^+D^-+c.c.)/\Gamma_{total}$	DOCUMENT ID	TECN	COMMENT	Γ_{39}/Γ
not seen	PAKHLOVA	08A	BELL $10.6 e^+e^- \rightarrow D^0D^-\pi^+\gamma$	

$\Gamma(D\bar{D}^*\pi+c.c. \text{ (excl. } D^*\bar{D}^*)/\Gamma_{total}$	DOCUMENT ID	TECN	COMMENT	Γ_{40}/Γ
not seen	CRONIN-HEN..09	CLEO	$e^+e^- \rightarrow D^*\bar{D}\pi$	

$\Gamma(D\bar{D}^*\pi+c.c. \text{ (excl. } D^*\bar{D}^*)/\Gamma(J/\psi\pi^+\pi^-)$	DOCUMENT ID	TECN	COMMENT	Γ_{40}/Γ_5
seen	90	CRONIN-HEN..09	CLEO e^+e^-	

$\Gamma(D^0D^*(2010)^-\pi^++c.c.)/\Gamma_{total}$	DOCUMENT ID	TECN	COMMENT	Γ_{41}/Γ
seen	ABLIKIM	19R	BES3 $e^+e^- \rightarrow \pi^+D^0D^{*-}+c.c.$	
••• We do not use the following data for averages, fits, limits, etc. •••				
not seen	PAKHLOVA	09	BELL $e^+e^- \rightarrow D^0D^{*-}\pi^+\gamma$	

$\Gamma(D^0D^*(2010)^-\pi^++c.c.)/\Gamma(J/\psi\pi^+\pi^-)$	DOCUMENT ID	TECN	COMMENT	Γ_{41}/Γ_5
seen	90	PAKHLOVA	09	BELL $e^+e^- \rightarrow D^0D^{*-}\pi^+$

$\Gamma(D_1(2420)\bar{D}^+c.c.)/\Gamma_{total}$	DOCUMENT ID	TECN	COMMENT	Γ_{42}/Γ
not seen	1 ABLIKIM	19AR	BES3 $e^+e^- \rightarrow \pi^+\pi^-D\bar{D}$	
¹ Results from a measurement of $\sigma(e^+e^- \rightarrow D_1(2420)\bar{D}^+c.c.)$ between $\sqrt{s} = 4.3$ and 4.6 GeV .				

$\Gamma(D^*\bar{D}^*\pi)/\Gamma_{total}$	DOCUMENT ID	TECN	COMMENT	Γ_{43}/Γ
seen	CRONIN-HEN..09	CLEO	$e^+e^- \rightarrow D^*\bar{D}^*\pi$	

$\Gamma(D^*\bar{D}^*\pi)/\Gamma(J/\psi\pi^+\pi^-)$	DOCUMENT ID	TECN	COMMENT	Γ_{43}/Γ_5
seen	90	CRONIN-HEN..09	CLEO e^+e^-	

$\Gamma(D_s^+D_s^-)/\Gamma_{total}$	DOCUMENT ID	TECN	COMMENT	Γ_{45}/Γ
not seen	DEL-AMO-SA..10N	BABR	$e^+e^- \rightarrow D_s^+D_s^-\gamma$	
not seen	CRONIN-HEN..09	CLEO	$e^+e^- \rightarrow D_s^+D_s^-$	
••• We do not use the following data for averages, fits, limits, etc. •••				
not seen	PAKHLOVA	11	BELL $e^+e^- \rightarrow D_s^+D_s^-\gamma$	

$\Gamma(D_s^+D_s^-)/\Gamma(J/\psi\pi^+\pi^-)$	DOCUMENT ID	TECN	COMMENT	Γ_{45}/Γ_5
seen	95	DEL-AMO-SA..10N	BABR $10.6 e^+e^-$	
••• We do not use the following data for averages, fits, limits, etc. •••				
<1.3	90	CRONIN-HEN..09	CLEO e^+e^-	

$\Gamma(D_s^{*+}D_s^-+c.c.)/\Gamma_{total}$	DOCUMENT ID	TECN	COMMENT	Γ_{46}/Γ
not seen	DEL-AMO-SA..10N	BABR	$e^+e^- \rightarrow D_s^{*+}D_s^-\gamma$	
not seen	CRONIN-HEN..09	CLEO	$e^+e^- \rightarrow D_s^{*+}D_s^-$	
••• We do not use the following data for averages, fits, limits, etc. •••				
not seen	PAKHLOVA	11	BELL $e^+e^- \rightarrow D_s^{*+}D_s^-\gamma$	

$\Gamma(D_s^{*+}D_s^-+c.c.)/\Gamma(J/\psi\pi^+\pi^-)$	DOCUMENT ID	TECN	COMMENT	Γ_{46}/Γ_5
seen	90	CRONIN-HEN..09	CLEO e^+e^-	
••• We do not use the following data for averages, fits, limits, etc. •••				
<44	95	DEL-AMO-SA..10N	BABR $10.6 e^+e^-$	

$\Gamma(D_s^{*+}D_s^{*-})/\Gamma_{total}$	DOCUMENT ID	TECN	COMMENT	Γ_{47}/Γ
not seen	CRONIN-HEN..09	CLEO	$e^+e^- \rightarrow D_s^{*+}D_s^{*-}$	
••• We do not use the following data for averages, fits, limits, etc. •••				
not seen	PAKHLOVA	11	BELL $e^+e^- \rightarrow D_s^{*+}D_s^{*-}\gamma$	
not seen	DEL-AMO-SA..10N	BABR	$e^+e^- \rightarrow D_s^{*+}D_s^{*-}\gamma$	

Meson Particle Listings

$\psi(4230)$, $\chi_{c1}(4274)$

$\Gamma(D_s^{*+} D_s^{*-})/\Gamma(J/\psi\pi^+\pi^-)$ Γ_{47}/Γ_5

VALUE	CL%	DOCUMENT ID	TECN	COMMENT
< 9.5	90	CRONIN-HEN..09	CLEO	e^+e^-
••• We do not use the following data for averages, fits, limits, etc. •••				
< 30	95	DEL-AMO-SA...10N	BABR	$10.6 e^+e^-$

$\Gamma(p\bar{p})/\Gamma(J/\psi\pi^+\pi^-)$ Γ_{48}/Γ_5

VALUE	CL%	DOCUMENT ID	TECN	COMMENT
< 0.13	90	¹ AUBERT	06B BABR	$e^+e^- \rightarrow p\bar{p}\gamma$
¹ Using 4259 ± 10 MeV for the mass and 88 ± 24 MeV for the width of $\psi(4260)$.				

$\Gamma(p\bar{p}\pi^0)/\Gamma(J/\psi\pi^+\pi^-)$ Γ_{49}/Γ_5

VALUE	CL%	DOCUMENT ID	TECN	COMMENT
< 2 × 10 ⁻⁴	90	ABLIKIM	17F BES3	$e^+e^- \rightarrow \psi(4260) \rightarrow$ hadrons

$\Gamma(p\bar{p}\eta)/\Gamma_{total}$ Γ_{50}/Γ

VALUE	DOCUMENT ID	TECN	COMMENT
not seen	ABLIKIM	21AN BES3	$e^+e^- \rightarrow p\bar{p}\eta$

$\Gamma(p\bar{p}\omega)/\Gamma_{total}$ Γ_{52}/Γ

VALUE	DOCUMENT ID	TECN	COMMENT
not seen	ABLIKIM	21AN BES3	$e^+e^- \rightarrow p\bar{p}\omega$

$\Gamma(\omega\pi^0)/\Gamma_{total}$ Γ_{56}/Γ

VALUE	DOCUMENT ID	TECN	COMMENT
not seen	ABLIKIM	22K BES3	$e^+e^- \rightarrow \omega\pi^0$

$\Gamma(\omega\eta)/\Gamma_{total}$ Γ_{57}/Γ

VALUE	DOCUMENT ID	TECN	COMMENT
not seen	ABLIKIM	22K BES3	$e^+e^- \rightarrow \omega\eta$

$\Gamma(p\bar{p}p\bar{p})/\Gamma_{total}$ Γ_{68}/Γ

VALUE	DOCUMENT ID	TECN	COMMENT
not seen	ABLIKIM	21D BES3	$4.0-4.6 e^+e^- \rightarrow p\bar{p}p\bar{p}$

Radiative decays

$\Gamma(\eta_c(1S)\gamma)/\Gamma_{total}$ Γ_{71}/Γ

VALUE	DOCUMENT ID	COMMENT
possibly seen	¹ ABLIKIM	17W $e^+e^- \rightarrow \gamma\eta_c(1S)$
¹ Significance ranges from 4.2 σ to as low as 1.5 σ for a flat component plus $\psi(4260)$ spectrum. Needs confirmation.		

$\Gamma(\eta_c(1S)\pi^0\gamma)/\Gamma_{total}$ Γ_{72}/Γ

VALUE	DOCUMENT ID	TECN	COMMENT
not seen	¹ ABLIKIM	21B BES3	$e^+e^- \rightarrow \gamma\pi^0\eta_c$
¹ Not seen in $e^+e^- \rightarrow \gamma\pi^0\eta_c$ at $\sqrt{s} = 4.226$ GeV with a 90% C.L. upper limit on the cross section of 11.2 pb.			

$\Gamma(\chi_{c1}(3872)\gamma)/\Gamma_{total}$ Γ_{75}/Γ

VALUE	DOCUMENT ID	TECN	COMMENT
seen	ABLIKIM	19v BES3	$e^+e^- \rightarrow \gamma\chi_{c1}(3872)$
seen	20 ± 5	ABLIKIM	14 BES3 $e^+e^- \rightarrow J/\psi\pi^+\pi^-\gamma$

$\psi(4230)$ REFERENCES

ABLIKIM	23AE	PR D108 032004	M. Ablikim et al.	(BESIII Collab.)
ABLIKIM	23AQ	JHEP 2308 159	M. Ablikim et al.	(BESIII Collab.)
ABLIKIM	23BK	JHEP 2311 228	M. Ablikim et al.	(BESIII Collab.)
ABLIKIM	23BL	JHEP 2312 027	M. Ablikim et al.	(BESIII Collab.)
ABLIKIM	23BT	PR D108 112011	M. Ablikim et al.	(BESIII Collab.)
ABLIKIM	23R	PR D107 072003	M. Ablikim et al.	(BESIII Collab.)
ABLIKIM	23U	PR D107 092005	M. Ablikim et al.	(BESIII Collab.)
ABLIKIM	23X	PRL 130 121901	M. Ablikim et al.	(BESIII Collab.)
ABLIKIM	22AM	PR D106 072001	M. Ablikim et al.	(BESIII Collab.)
ABLIKIM	22AU	CP C45 111002	M. Ablikim et al.	(BESIII Collab.)
ABLIKIM	22K	JHEP 2207 064	M. Ablikim et al.	(BESIII Collab.)
ABLIKIM	21AJ	PR D104 052012	M. Ablikim et al.	(BESIII Collab.)
ABLIKIM	21AN	PR D104 092008	M. Ablikim et al.	(BESIII Collab.)
ABLIKIM	21AS	PR D104 L091104	M. Ablikim et al.	(BESIII Collab.)
ABLIKIM	21AW	PR D104 112009	M. Ablikim et al.	(BESIII Collab.)
ABLIKIM	21B	PR D103 032006	M. Ablikim et al.	(BESIII Collab.)
ABLIKIM	21D	PR D103 052003	M. Ablikim et al.	(BESIII Collab.)
ABLIKIM	20A	PR D101 012008	M. Ablikim et al.	(BESIII Collab.)
ABLIKIM	20AG	PR D102 112009	M. Ablikim et al.	(BESIII Collab.)
ABLIKIM	20C	PRL 124 032002	M. Ablikim et al.	(BESIII Collab.)
ABLIKIM	20N	PR D102 012009	M. Ablikim et al.	(BESIII Collab.)
ABLIKIM	20O	PR D102 031101	M. Ablikim et al.	(BESIII Collab.)
ABLIKIM	19	PR D99 012003	M. Ablikim et al.	(BESIII Collab.)
ABLIKIM	19AE	PR D99 072005	M. Ablikim et al.	(BESIII Collab.)
ABLIKIM	19AI	PR D99 091103	M. Ablikim et al.	(BESIII Collab.)
ABLIKIM	19AR	PR D100 032005	M. Ablikim et al.	(BESIII Collab.)
ABLIKIM	19K	PR D99 019903 (err.)	M. Ablikim et al.	(BESIII Collab.)
ABLIKIM	19R	PRL 122 102002	M. Ablikim et al.	(BESIII Collab.)
ABLIKIM	19V	PRL 122 232002	M. Ablikim et al.	(BESIII Collab.)
ABLIKIM	18N	PR D97 071101	M. Ablikim et al.	(BESIII Collab.)
ABLIKIM	17B	PRL 118 092001	M. Ablikim et al.	(BESIII Collab.)
ABLIKIM	17F	PL B771 45	M. Ablikim et al.	(BESIII Collab.)
ABLIKIM	17G	PRL 118 092002	M. Ablikim et al.	(BESIII Collab.)
ABLIKIM	17V	PR D96 032004	M. Ablikim et al.	(BESIII Collab.)
Also		PR D99 019903 (err.)	M. Ablikim et al.	(BESIII Collab.)
ABLIKIM	17W	PR D96 051101	M. Ablikim et al.	(BESIII Collab.)
GAO	17	PR D95 092007	X.Y. Gao, C.P. Shen, C.Z. Yuan	

ZHANG	17B	PR D96 054008	J. Zhang, J. Zhang	
ZHANG	17C	EPJ C77 727	J. Zhang, L. Yuan	
PDG	16	CP C40 100001	C. Patrignani et al.	(PDG Collab.)
ABLIKIM	15C	PRL 114 092003	M. Ablikim et al.	(BESIII Collab.)
ABLIKIM	15Q	PR D92 012008	M. Ablikim et al.	(BESIII Collab.)
HAN	15	PR D92 012011	Y.L. Han et al.	(BELLE Collab.)
ABLIKIM	14	PRL 112 092001	M. Ablikim et al.	(BESIII Collab.)
SHEN	14	PR D89 072015	C.P. Shen et al.	(BELLE Collab.)
ABLIKIM	13T	PRL 110 252001	M. Ablikim et al.	(BESIII Collab.)
LIU	13B	PRL 110 252002	Z.Q. Liu et al.	(BELLE Collab.)
WANG	13B	PR D87 051101	X.L. Wang et al.	(BELLE Collab.)
LEES	12AC	PR D86 051102	J.P. Lees et al.	(BABAR Collab.)
PAKHOVA	11	PR D83 011101	G. Pakhlova et al.	(BELLE Collab.)
PEDLAR	11	PRL 107 041803	T. Pedlar et al.	(CLEO Collab.)
DEL-AMO-SA...	10N	PR D82 052004	P. del Amo Sanchez et al.	(BABAR Collab.)
AUBERT	09M	PR D79 092001	B. Aubert et al.	(BABAR Collab.)
CRONIN-HEN...	09	PR D80 072001	D. Cronin-Hennessy et al.	(CLEO Collab.)
PAKHOVA	09	PR D80 091101	G. Pakhlova et al.	(BELLE Collab.)
AUBERT	08S	PR D77 092002	B. Aubert et al.	(BABAR Collab.)
LIU	08H	PR D78 014032	Z.Q. Liu, X.S. Qin, C.Z. Yuan	(BELLE Collab.)
PAKHOVA	08	PR D77 011103	G. Pakhlova et al.	(BELLE Collab.)
PAKHOVA	08A	PRL 100 062001	G. Pakhlova et al.	(BELLE Collab.)
YUAN	08	PR D77 011105	C.Z. Yuan et al.	(BELLE Collab.)
AUBERT	07AK	PR D76 012008	B. Aubert et al.	(BABAR Collab.)
AUBERT	07BE	PR D76 111105	B. Aubert et al.	(BABAR Collab.)
AUBERT	07S	PRL 98 212001	B. Aubert et al.	(BABAR Collab.)
PAKHOVA	07	PRL 98 092001	G. Pakhlova et al.	(BELLE Collab.)
WANG	07D	PRL 99 142002	X.L. Wang et al.	(BELLE Collab.)
YUAN	07	PRL 99 182004	C.Z. Yuan et al.	(BELLE Collab.)
AUBERT	06B	PR D73 012005	B. Aubert et al.	(BABAR Collab.)
AUBERT, BE	06D	PR D74 091103	B. Aubert et al.	(BABAR Collab.)
HE	06B	PR D74 091104	Q. He et al.	(CLEO Collab.)
AUBERT, B	05I	PRL 95 142001	B. Aubert et al.	(BABAR Collab.)

$\chi_{c1}(4274)$

$$J^G(J^{PC}) = 0^+(1^{++})$$

was X(4274)

This state shows properties different from a conventional $q\bar{q}$ state. A candidate for an exotic structure. See the review on non- $q\bar{q}$ states.

Seen by AAIJ 17C in $B^+ \rightarrow \chi_{c1} K^+$, $\chi_{c1} \rightarrow J/\psi\phi$ using an amplitude analysis of $B^+ \rightarrow J/\psi\phi K^+$ with a significance (accounting for systematic uncertainties) of 6.0 σ .

$\chi_{c1}(4274)$ MASS

VALUE (MeV)	EVTS	DOCUMENT ID	TECN	COMMENT
4286 ± 8	OUR AVERAGE	Error includes scale factor of 1.7.		
4294 ± 4	± 3	24k	¹ AAIJ	21E LHCB $B^+ \rightarrow J/\psi\phi K^+$
4274.4 ± 8.4	± 1.9	22	² AALTONEN	17 CDF $B^+ \rightarrow J/\psi\phi K^+$
••• We do not use the following data for averages, fits, limits, etc. •••				
4273.3 ± 8.3	± 17.2	4289	^{3,4} AAIJ	17C LHCB $B^+ \rightarrow J/\psi\phi K^+$

- From an amplitude analysis of the decay $B^+ \rightarrow J/\psi\phi K^+$ with a significance of 18 σ .
- From a fit to the invariant mass spectrum with a significance of 3.1 σ .
- From an amplitude analysis of the decay $B^+ \rightarrow J/\psi\phi K^+$ with a significance of 6.0 σ .
- Superseded by AAIJ 21E.

$\chi_{c1}(4274)$ WIDTH

VALUE (MeV)	EVTS	DOCUMENT ID	TECN	COMMENT
51 ± 7	OUR AVERAGE			
53 ± 5	5	24k	¹ AAIJ	21E LHCB $B^+ \rightarrow J/\psi\phi K^+$
32.3 ± 21.9	± 7.6	22	² AALTONEN	17 CDF $B^+ \rightarrow J/\psi\phi K^+$
••• We do not use the following data for averages, fits, limits, etc. •••				
56 ± 11	± 8	4289	^{3,4} AAIJ	17C LHCB $B^+ \rightarrow J/\psi\phi K^+$

- From an amplitude analysis of the decay $B^+ \rightarrow J/\psi\phi K^+$ with a significance of 18 σ .
- From a fit to the invariant mass spectrum with a significance of 3.1 σ .
- From an amplitude analysis of the decay $B^+ \rightarrow J/\psi\phi K^+$ with a significance of 6.0 σ .
- Superseded by AAIJ 21E.

$\chi_{c1}(4274)$ DECAY MODES

Mode	Fraction (Γ_i/Γ)
Γ_1 $J/\psi\phi$	seen

$\chi_{c1}(4274)$ BRANCHING RATIOS

$\Gamma(J/\psi\phi)/\Gamma_{total}$	VALUE	EVTS	DOCUMENT ID	TECN	COMMENT
seen	24k	¹ AAIJ	21E LHCB	$B^+ \rightarrow J/\psi\phi K^+$	
••• We do not use the following data for averages, fits, limits, etc. •••					
seen	4289	^{2,3} AAIJ	17C LHCB	$B^+ \rightarrow J/\psi\phi K^+$	
¹ From an amplitude analysis of the decay $B^+ \rightarrow J/\psi\phi K^+$ with a significance of 18 σ .					
² From an amplitude analysis of the decay $B^+ \rightarrow J/\psi\phi K^+$ with a significance of 6.0 σ .					
³ Superseded by AAIJ 21E.					

$\chi_{c1}(4274)$ REFERENCES

AAU	21E	PRL 127 092001	R. Aaij et al.	(LHCb Collab.)
AAU	17C	PRL 118 022003	R. Aaij et al.	(LHCb Collab.) JP
Also		PR D95 012002	R. Aaij et al.	(LHCb Collab.)
AALTONEN	17	MPL A32 1750139	T. Altonen et al.	(CDF Collab.)

$X(4350) \quad I^G(J^{PC}) = 0^+(?^{?+})$

OMITTED FROM SUMMARY TABLE
Seen by SHEN 10 in the $\gamma\gamma \rightarrow J/\psi\phi$. Needs confirmation.

$X(4350)$ MASS

VALUE (MeV)	EVTS	DOCUMENT ID	TECN	COMMENT
$4350.6^{+4.6}_{-5.1} \pm 0.7$	$8.8^{+4.2}_{-3.2}$	¹ SHEN	10	BELL $10.6 e^+e^- \rightarrow e^+e^- J/\psi\phi$

¹ Statistical significance of 3.2 σ .

$X(4350)$ WIDTH

VALUE (MeV)	EVTS	DOCUMENT ID	TECN	COMMENT
$13^{+18}_{-9} \pm 4$	$8.8^{+4.2}_{-3.2}$	¹ SHEN	10	BELL $10.6 e^+e^- \rightarrow e^+e^- J/\psi\phi$

¹ Statistical significance of 3.2 σ .

$X(4350)$ DECAY MODES

Mode	Fraction (Γ_i/Γ)
$\Gamma_1 \quad J/\psi\phi$	seen
$\Gamma_2 \quad \gamma\gamma$	seen

$X(4350) \Gamma(i)\Gamma(\gamma\gamma)/\Gamma(\text{total})$

$\Gamma(\gamma\gamma) \times \Gamma(J/\psi\phi)/\Gamma_{\text{total}}$	EVTS	DOCUMENT ID	TECN	COMMENT	$\Gamma_2\Gamma_1/\Gamma$
$6.7^{+3.2}_{-2.4} \pm 1.1$	$8.8^{+4.2}_{-3.2}$	¹ SHEN	10	BELL $10.6 e^+e^- \rightarrow e^+e^- J/\psi\phi$	

• • • We do not use the following data for averages, fits, limits, etc. • • •

$1.5^{+0.7}_{-0.6} \pm 0.3$	$8.8^{+4.2}_{-3.2}$	² SHEN	10	BELL $10.6 e^+e^- \rightarrow e^+e^- J/\psi\phi$	
-----------------------------	---------------------	-------------------	----	--	--

¹ For $J^P = 0^+$. Statistical significance of 3.2 σ .
² For $J^P = 2^+$. Statistical significance of 3.2 σ .

$X(4350)$ BRANCHING RATIOS

$\Gamma(J/\psi\phi)/\Gamma_{\text{total}}$	DOCUMENT ID	TECN	COMMENT	Γ_1/Γ
seen	¹ SHEN	10	BELL $10.6 e^+e^- \rightarrow e^+e^- J/\psi\phi$	

¹ Statistical significance of 3.2 σ .

$\Gamma(\gamma\gamma)/\Gamma_{\text{total}}$	DOCUMENT ID	TECN	COMMENT	Γ_2/Γ
seen	¹ SHEN	10	BELL $10.6 e^+e^- \rightarrow e^+e^- J/\psi\phi$	

¹ Statistical significance of 3.2 σ .

$X(4350)$ REFERENCES

SHEN	10	PRL 104 112004	C.P. Shen et al.	(BELLE Collab.)
------	----	----------------	------------------	-----------------

$\psi(4360) \quad I^G(J^{PC}) = 0^-(1^{--})$

also known as $Y(4360)$; was $X(4360)$
This state shows properties different from a conventional $q\bar{q}$ state. A candidate for an exotic structure. See the review on non- $q\bar{q}$ states.

Seen in radiative return from e^+e^- collisions at $\sqrt{s} = 9.54\text{--}10.58$ GeV by AUBERT 07s, WANG 07D, and LEES 14F. See also the review on "Spectroscopy of mesons containing two heavy quarks."

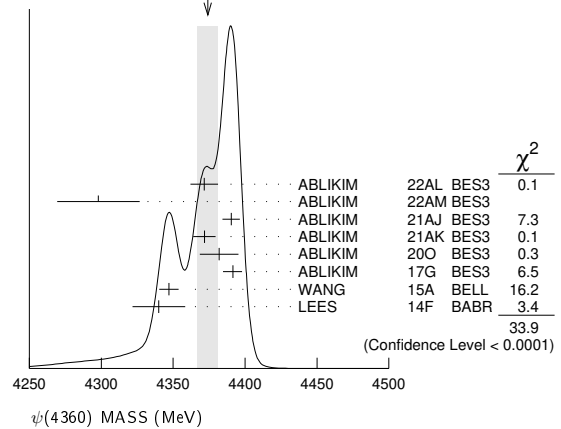
$\psi(4360)$ MASS

VALUE (MeV)	EVTS	DOCUMENT ID	TECN	COMMENT
4374 ± 7 OUR AVERAGE				Error includes scale factor of 2.4. See the ideogram below.
$4371.6 \pm 2.5 \pm 9.2$		¹ ABLIKIM	22AL BES3	$e^+e^- \rightarrow \pi^+\pi^- D^+D^-$
$4298 \pm 12 \pm 26$		² ABLIKIM	22AMBES3	$e^+e^- \rightarrow \pi^+\pi^- J/\psi$

$4390.3 \pm 6.0 \pm 0.7$		³ ABLIKIM	21AJ BES3	$e^+e^- \rightarrow \pi^+\pi^- \psi(2S)$
$4371.7 \pm 7.5 \pm 1.8$		⁴ ABLIKIM	21AK BES3	$e^+e^- \rightarrow \gamma\chi_{c2} \rightarrow \gamma\gamma J/\psi$
$4382.0 \pm 13.3 \pm 1.7$		⁵ ABLIKIM	200 BES3	$e^+e^- \rightarrow \eta J/\psi$
$4391.5^{+6.3}_{-6.8} \pm 1.0$		ABLIKIM	17G BES3	$e^+e^- \rightarrow \pi^+\pi^- h_c$
$4347 \pm 6 \pm 3$	279	⁶ WANG	15A BELL	$10.58 e^+e^- \rightarrow \gamma\pi^+\pi^-\psi(2S)$
$4340 \pm 16 \pm 9$	37	⁷ LEES	14F BABR	$10.58 e^+e^- \rightarrow \gamma\pi^+\pi^-\psi(2S)$
• • • We do not use the following data for averages, fits, limits, etc. • • •				
$4406.9 \pm 17.2 \pm 4.5$		⁸ ABLIKIM	22R BES3	$e^+e^- \rightarrow \pi^+\pi^- \chi_{c1}\gamma$
$4320.0 \pm 10.4 \pm 7.0$		⁹ ABLIKIM	17B BES3	$e^+e^- \rightarrow \pi^+\pi^- J/\psi$
$4383.8 \pm 4.2 \pm 0.8$		¹⁰ ABLIKIM	17V BES3	$e^+e^- \rightarrow \pi^+\pi^- \psi(2S)$
$4383.7 \pm 2.9 \pm 6.2$		¹¹ ZHANG	17B RVUE	$e^+e^- \rightarrow \pi^+\pi^- \psi(2S)$
$4386.4 \pm 2.1 \pm 6.4$		¹² ZHANG	17C RVUE	$e^+e^- \rightarrow \pi^+\pi^- J/\psi$ or $\psi(2S)$
$4355^{+9}_{-10} \pm 9$	74	¹³ LIU	08H RVUE	$10.58 e^+e^- \rightarrow \gamma\pi^+\pi^-\psi(2S)$
4324 ± 24		¹⁴ AUBERT	07s BABR	$10.58 e^+e^- \rightarrow \gamma\pi^+\pi^-\psi(2S)$
$4361 \pm 9 \pm 9$	47	⁷ WANG	07D BELL	$10.58 e^+e^- \rightarrow \gamma\pi^+\pi^-\psi(2S)$

- ¹ From a fit to the cross section for $e^+e^- \rightarrow D^+D^-\pi^+\pi^-$ in the range $\sqrt{s} = 4.190\text{--}4.946$ GeV.
- ² From a three-resonance fit to the Born cross section in the range $\sqrt{s} = 3.7730\text{--}4.7008$ GeV. Parameters depend on the existence or non-existence of a state near 4.5 GeV.
- ³ From a three-resonance fit to the Born cross section in the range $\sqrt{s} = 4.008\text{--}4.698$ GeV.
- ⁴ From a five-resonance fit to the cross section for $e^+e^- \rightarrow \gamma\gamma J/\psi \rightarrow \gamma\gamma \ell^+\ell^-$.
- ⁵ From a fit of the measured cross section in the range $\sqrt{s} = 3.808\text{--}4.600$ GeV.
- ⁶ From a two-resonance fit. Supersedes WANG 07D.
- ⁷ From a two-resonance fit.
- ⁸ From a fit to the $e^+e^- \rightarrow \pi^+\pi^-\psi(3823)$ cross section between 4.23 and 4.70 GeV with two coherent Breit-Wigner resonances. The data is also consistent with a single peak with mass $4417.5 \pm 26.2 \pm 3.5$ MeV and width $245 \pm 48 \pm 13$ MeV.
- ⁹ From a three-resonance fit. Superseded by ABLIKIM 22AM.
- ¹⁰ From a fit to the cross section for $e^+e^- \rightarrow \pi^+\pi^-\psi(2S) \rightarrow 2(\pi^+\pi^-\ell^+\ell^-)$ obtained from 16 center-of-mass energies between 4.008 and 4.600 GeV and comprising 5.1 fb^{-1} . Superseded by ABLIKIM 21AJ.
- ¹¹ From a three-resonance fit.
- ¹² From a combined fit of BELLE, BABAR and BES3 $e^+e^- \rightarrow \pi^+\pi^- J/\psi$ and $e^+e^- \rightarrow \pi^+\pi^-\psi(2S)$ data.
- ¹³ From a combined fit of AUBERT 07s and WANG 07D data with two resonances.
- ¹⁴ From a single-resonance fit. Systematic errors not estimated.

WEIGHTED AVERAGE
 4374 ± 7 (Error scaled by 2.4)



$\psi(4360)$ WIDTH

VALUE (MeV)	EVTS	DOCUMENT ID	TECN	COMMENT
118 ± 12 OUR AVERAGE				Error includes scale factor of 2.1. See the ideogram below.
$167 \pm 4 \pm 29$		¹ ABLIKIM	22AL BES3	$e^+e^- \rightarrow \pi^+\pi^- D^+D^-$
$127 \pm 17 \pm 10$		² ABLIKIM	22AMBES3	$e^+e^- \rightarrow \pi^+\pi^- J/\psi$
$143.3 \pm 10.0 \pm 0.5$		³ ABLIKIM	21AJ BES3	$e^+e^- \rightarrow \pi^+\pi^- \psi(2S)$
$51.1 \pm 17.6 \pm 1.9$		⁴ ABLIKIM	21AK BES3	$e^+e^- \rightarrow \gamma\chi_{c2} \rightarrow \gamma\gamma J/\psi$
$135.8 \pm 60.8 \pm 22.5$		⁵ ABLIKIM	200 BES3	$e^+e^- \rightarrow \eta J/\psi$
$139.5^{+16.2}_{-20.6} \pm 0.6$		ABLIKIM	17G BES3	$e^+e^- \rightarrow \pi^+\pi^- h_c$
$103 \pm 9 \pm 5$	279	⁶ WANG	15A BELL	$10.58 e^+e^- \rightarrow \gamma\pi^+\pi^-\psi(2S)$
$94 \pm 32 \pm 13$	37	⁷ LEES	14F BABR	$10.58 e^+e^- \rightarrow \gamma\pi^+\pi^-\psi(2S)$
• • • We do not use the following data for averages, fits, limits, etc. • • •				
$128.1 \pm 37.2 \pm 2.3$		⁸ ABLIKIM	22R BES3	$e^+e^- \rightarrow \pi^+\pi^- \chi_{c1}\gamma$
$101.4^{+25.3}_{-19.7} \pm 10.2$		⁹ ABLIKIM	17B BES3	$e^+e^- \rightarrow \pi^+\pi^- J/\psi$
$84.2 \pm 12.5 \pm 2.1$		¹⁰ ABLIKIM	17V BES3	$e^+e^- \rightarrow \pi^+\pi^- \psi(2S)$

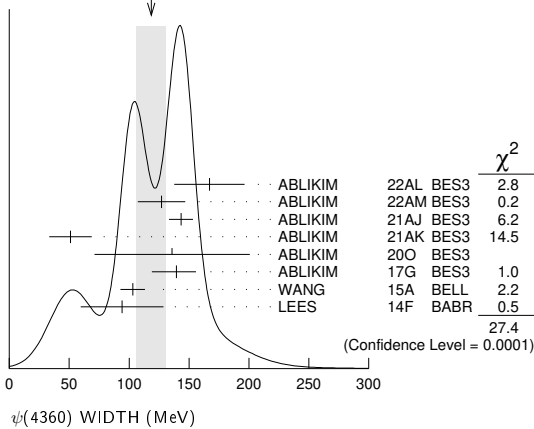
Meson Particle Listings

$\psi(4360)$

$94.2 \pm 7.3 \pm 2.0$	11	ZHANG	17B	RVUE	$e^+e^- \rightarrow \pi^+\pi^-\psi(2S)$	
$96.0 \pm 6.7 \pm 2.7$	12	ZHANG	17c	RVUE	$e^+e^- \rightarrow \pi^+\pi^- J/\psi$ or $\psi(2S)$	
$103^{+17}_{-15} \pm 11$	74	13	LIU	08H	RVUE	$10.58 e^+e^- \rightarrow \gamma\pi^+\pi^-\psi(2S)$
172 ± 33	14	AUBERT	07s	BABR	$10.58 e^+e^- \rightarrow \gamma\pi^+\pi^-\psi(2S)$	
$74 \pm 15 \pm 10$	47	7	WANG	07D	BELL	$10.58 e^+e^- \rightarrow \gamma\pi^+\pi^-\psi(2S)$

- ¹ From a fit to the cross section for $e^+e^- \rightarrow D^+D^-\pi^+\pi^-$ in the range $\sqrt{s} = 4.190\text{--}4.946$ GeV.
- ² From a three-resonance fit to the Born cross section in the range $\sqrt{s} = 3.7730\text{--}4.7008$ GeV. Parameters depend on the existence or non-existence of a state near 4.5 GeV.
- ³ From a three-resonance fit to the Born cross section in the range $\sqrt{s} = 4.008\text{--}4.698$ GeV.
- ⁴ From a five-resonance fit to the cross section for $e^+e^- \rightarrow \gamma\gamma J/\psi \rightarrow \gamma\gamma\ell^+\ell^-$.
- ⁵ From a fit of the measured cross section in the range $\sqrt{s} = 3.808\text{--}4.600$ GeV.
- ⁶ From a two-resonance fit. Supersedes WANG 07D.
- ⁷ From a two-resonance fit.
- ⁸ From a fit to the $e^+e^- \rightarrow \pi^+\pi^-\psi(3823)$ cross section between 4.23 and 4.70 GeV with two coherent Breit-Wigner resonances. The data is also consistent with a single peak with mass $4417.5 \pm 26.2 \pm 3.5$ MeV and width $245 \pm 48 \pm 13$ MeV.
- ⁹ From a three-resonance fit. Superseded by ABLIKIM 22AM.
- ¹⁰ From a fit to the cross section for $e^+e^- \rightarrow \pi^+\pi^-\psi(2S) \rightarrow 2(\pi^+\pi^-\ell^+\ell^-)$ obtained from 16 center-of-mass energies between 4.008 and 4.600 GeV and comprising 5.1 fb^{-1} . Superseded by ABLIKIM 21AJ.
- ¹¹ From a three-resonance fit.
- ¹² From a combined fit of BELLE, BABAR and BES3 $e^+e^- \rightarrow \pi^+\pi^- J/\psi$ and $e^+e^- \rightarrow \pi^+\pi^-\psi(2S)$ data.
- ¹³ From a combined fit of AUBERT 07s and WANG 07D data with two resonances.
- ¹⁴ From a single-resonance fit. Systematic errors not estimated.

WEIGHTED AVERAGE
118±12 (Error scaled by 2.1)



$\psi(4360)$ DECAY MODES

Mode	Fraction (Γ_i/Γ)
Γ_1 e^+e^-	seen
Γ_2 $h_c\pi^+\pi^-$	seen
Γ_3 $J/\psi\pi^+\pi^-$	seen
Γ_4 $\psi(2S)\pi^+\pi^-$	seen
Γ_5 $\psi(3770)\pi^+\pi^-$	possibly seen
Γ_6 $\psi_2(3823)\pi^+\pi^-$	seen
Γ_7 $J/\psi\eta$	seen
Γ_8 $D^0D^{*-}\pi^+$	not seen
Γ_9 $D^+D^-\pi^+\pi^-$	seen
Γ_{10} $D_1(2420)\bar{D}^+$ c.c.	possibly seen
Γ_{11} $\phi\eta$	not seen
Γ_{12} $\omega\pi^0$	not seen
Γ_{13} $\omega\eta$	not seen
Γ_{14} $p\bar{p}\eta$	not seen
Γ_{15} $p\bar{p}\omega$	not seen
Γ_{16} $\chi_{c1}\gamma$	not seen
Γ_{17} $\chi_{c2}\gamma$	not seen
Γ_{18} $\Xi^-\Xi^+$	not seen
Γ_{19} $pK^-\bar{\Lambda}$ c.c.	not seen

$\psi(4360) \Gamma(i) \times \Gamma(e^+e^-)/\Gamma(\text{total})$

VALUE (eV)	DOCUMENT ID	TECN	COMMENT	Γ_2/Γ
$11.6^{+5.0}_{-4.4} \pm 1.9$	ABLIKIM	17G	BES3	$e^+e^- \rightarrow \pi^+\pi^-h_c$

$\Gamma(\psi(2S)\pi^+\pi^-) \times \Gamma(e^+e^-)/\Gamma_{\text{total}}$

VALUE (eV)	EVTS	DOCUMENT ID	TECN	COMMENT	Γ_4/Γ
10.7 ± 4.1		¹ ABLIKIM	21AJ	BES3	$e^+e^- \rightarrow \pi^+\pi^-\psi(2S)$
20.7 ± 2.5		² ABLIKIM	21AJ	BES3	$e^+e^- \rightarrow \pi^+\pi^-\psi(2S)$
9.9 ± 4.1		³ ABLIKIM	21AJ	BES3	$e^+e^- \rightarrow \pi^+\pi^-\psi(2S)$
19.4 ± 2.0		⁴ ABLIKIM	21AJ	BES3	$e^+e^- \rightarrow \pi^+\pi^-\psi(2S)$
7.3 ± 2.8		⁵ ABLIKIM	19K	BES3	$e^+e^- \rightarrow \pi^+\pi^-\psi(2S)$
11.0 ± 3.8		⁶ ABLIKIM	19K	BES3	$e^+e^- \rightarrow \pi^+\pi^-\psi(2S)$
$9.2 \pm 0.6 \pm 0.6$	279	⁷ WANG	15A	BELL	$10.58 e^+e^- \rightarrow \gamma\pi^+\pi^-\psi(2S)$
$10.9 \pm 0.6 \pm 0.7$	279	⁸ WANG	15A	BELL	$10.58 e^+e^- \rightarrow \gamma\pi^+\pi^-\psi(2S)$
$6.0 \pm 1.0 \pm 0.5$	37	⁵ LEES	14F	BABR	$10.58 e^+e^- \rightarrow \gamma\pi^+\pi^-\psi(2S)$
$7.2 \pm 1.0 \pm 0.6$	37	⁶ LEES	14F	BABR	$10.58 e^+e^- \rightarrow \gamma\pi^+\pi^-\psi(2S)$
$11.1^{+1.3}_{-1.2}$	74	⁹ LIU	08H	RVUE	$10.58 e^+e^- \rightarrow \gamma\pi^+\pi^-\psi(2S)$
12.3 ± 1.2	74	¹⁰ LIU	08H	RVUE	$10.58 e^+e^- \rightarrow \gamma\pi^+\pi^-\psi(2S)$
$10.4 \pm 1.7 \pm 1.5$	47	⁵ WANG	07D	BELL	$10.58 e^+e^- \rightarrow \gamma\pi^+\pi^-\psi(2S)$
$11.8 \pm 1.8 \pm 1.4$	47	⁶ WANG	07D	BELL	$10.58 e^+e^- \rightarrow \gamma\pi^+\pi^-\psi(2S)$

- • • We do not use the following data for averages, fits, limits, etc. • • •
- ¹ Solution I of four equivalent solutions in a fit using three interfering resonances. Supersedes ABLIKIM 19K.
- ² Solution II of four equivalent solutions in a fit using three interfering resonances. Supersedes ABLIKIM 19K.
- ³ Solution III of four equivalent solutions in a fit using three interfering resonances. Supersedes ABLIKIM 19K.
- ⁴ Solution IV of four equivalent solutions in a fit using three interfering resonances. Supersedes ABLIKIM 19K.
- ⁵ Solution I of two equivalent solutions in a fit using two interfering resonances.
- ⁶ Solution II of two equivalent solutions in a fit using two interfering resonances.
- ⁷ Solution I of two equivalent solutions from a fit using two interfering resonances. Supersedes WANG 07D.
- ⁸ Solution II of two equivalent solutions from a fit using two interfering resonances. Supersedes WANG 07D.
- ⁹ Solution I in a combined fit of AUBERT 07s and WANG 07D data with two resonances.
- ¹⁰ Solution II in a combined fit of AUBERT 07s and WANG 07D data with two resonances.

$\Gamma(J/\psi\eta) \times \Gamma(e^+e^-)/\Gamma_{\text{total}}$

VALUE (eV)	CL%	DOCUMENT ID	TECN	COMMENT	Γ_7/Γ
3.4 ± 2.2		¹ ABLIKIM	20O	BES3	$e^+e^- \rightarrow \eta J/\psi$
1.5 ± 1.0		² ABLIKIM	20O	BES3	$e^+e^- \rightarrow \eta J/\psi$
1.7 ± 1.1		³ ABLIKIM	20O	BES3	$e^+e^- \rightarrow \eta J/\psi$
<6.8	90	WANG	13B	BELL	$e^+e^- \rightarrow J/\psi\eta\gamma$

- • • We do not use the following data for averages, fits, limits, etc. • • •
- ¹ Solution 1 of three equivalent fit solutions using three resonant structures.
- ² Solution 2 of three equivalent fit solutions using three resonant structures.
- ³ Solution 3 of three equivalent fit solutions using three resonant structures.

$\Gamma(\chi_{c1}\gamma) \times \Gamma(e^+e^-)/\Gamma_{\text{total}}$

VALUE (eV)	CL%	DOCUMENT ID	TECN	COMMENT	Γ_{16}/Γ
<0.57	90	¹ HAN	15	BELL	$10.58 e^+e^- \rightarrow \chi_{c1}\gamma$

- ¹ Using $B(\eta \rightarrow \gamma\gamma) = (39.41 \pm 0.21)\%$.

$\Gamma(\chi_{c2}\gamma) \times \Gamma(e^+e^-)/\Gamma_{\text{total}}$

VALUE (eV)	CL%	DOCUMENT ID	TECN	COMMENT	Γ_{17}/Γ
<1.9	90	¹ HAN	15	BELL	$10.58 e^+e^- \rightarrow \chi_{c2}\gamma$

- ¹ Using $B(\eta \rightarrow \gamma\gamma) = (39.41 \pm 0.21)\%$.

$\Gamma(\Xi^-\Xi^+) \times \Gamma(e^+e^-)/\Gamma_{\text{total}}$

VALUE (eV)	CL%	DOCUMENT ID	TECN	COMMENT	Γ_{18}/Γ
<0.0448	90	¹ ABLIKIM	23Bk	BES3	$e^+e^- \rightarrow \psi(4360)$

- ¹ From a fit to $e^+e^- \rightarrow \Xi^-\Xi^+$ cross sections.

$\Gamma(pK^-\bar{\Lambda} + \text{c.c.}) \times \Gamma(e^+e^-)/\Gamma_{\text{total}}$

VALUE (eV)	CL%	DOCUMENT ID	TECN	COMMENT	Γ_{19}/Γ
$<4.7 \times 10^{-3}$	90	¹ ABLIKIM	23Bl	BES3	$e^+e^- \rightarrow \psi(4360)$

- ¹ From a fit to $e^+e^- \rightarrow pK^-\bar{\Lambda} + \text{c.c.}$ cross sections.

$\psi(4360)$ BRANCHING RATIOS

$\Gamma(h_c\pi^+\pi^-)/\Gamma_{\text{total}}$	DOCUMENT ID	TECN	COMMENT	Γ_2/Γ
seen	ABLIKIM	17G	BES3	$e^+e^- \rightarrow \pi^+\pi^-h_c$

$\Gamma(\psi(2S)\pi^+\pi^-)/\Gamma_{\text{total}}$	DOCUMENT ID	TECN	COMMENT	Γ_4/Γ
seen	¹ ABLIKIM	17V	BES3	$e^+e^- \rightarrow \pi^+\pi^-\psi(2S)$

- ¹ From a fit to the cross section for $e^+e^- \rightarrow \pi^+\pi^-\psi(2S) \rightarrow 2(\pi^+\pi^-\ell^+\ell^-)$ obtained from 16 center-of-mass energies between 4.008 and 4.600 GeV and comprising 5.1 fb^{-1} .

See key on page 1171

Meson Particle Listings

$\psi(4360), \psi(4415)$

$\Gamma(\psi(2S)\pi^+\pi^-)/\Gamma(J/\psi\pi^+\pi^-)$ Γ_4/Γ_3

VALUE	DOCUMENT ID	TECN	COMMENT
• • • We do not use the following data for averages, fits, limits, etc. • • •			
$(0.81 \pm 0.12 \pm 0.13)$ to $(42 \pm 15 \pm 15)$	¹ ZHANG	17c RVUE	$e^+e^- \rightarrow \pi^+\pi^- J/\psi$ or $\psi(2S)$
¹ From a combined fit of BELLE, BABAR and BES3 $e^+e^- \rightarrow \pi^+\pi^- J/\psi$ and $e^+e^- \rightarrow \pi^+\pi^-\psi(2S)$ data.			

$\Gamma(\psi(3770)\pi^+\pi^-)/\Gamma_{total}$ Γ_5/Γ

VALUE	DOCUMENT ID	TECN	COMMENT
possibly seen	¹ ABLIKIM	19AR BES3	$e^+e^- \rightarrow \pi^+\pi^- D\bar{D}$
¹ Observe $e^+e^- \rightarrow \pi^+\pi^-\psi(3770)$ at $\sqrt{s} = 4.26, 4.36,$ and 4.42 GeV but cannot establish if continuum or resonant.			

$\Gamma(\psi_2(3823)\pi^+\pi^-)/\Gamma_{total}$ Γ_6/Γ

VALUE	DOCUMENT ID	TECN	COMMENT
seen	¹ ABLIKIM	22R BES3	$e^+e^- \rightarrow \pi^+\pi^- \chi_{c1} \gamma$
• • • We do not use the following data for averages, fits, limits, etc. • • •			
possibly seen	19	² ABLIKIM	15s BES3 $e^+e^- \rightarrow \pi^+\pi^- \chi_{c1} \gamma$
¹ From a fit to the $e^+e^- \rightarrow \pi^+\pi^-\psi(3823)$ cross section between 4.23 and 4.70 GeV with two coherent Breit-Wigner resonances.			
² From a fit of $e^+e^- \rightarrow \pi^+\pi^-\psi_2(3823), \psi_2(3823) \rightarrow \chi_{c1} \gamma$ cross sections taken at \sqrt{s} values of 4.23, 4.26, 4.36, 4.42, and 4.60 GeV to the $\psi(4360)$ line shape.			

$\Gamma(J/\psi\eta)/\Gamma_{total}$ Γ_7/Γ

VALUE	DOCUMENT ID	TECN	COMMENT
seen	¹ ABLIKIM	20o BES3	$e^+e^- \rightarrow \eta J/\psi$
¹ With a significance of 6.0 σ .			

$\Gamma(D^0 D^{*-} \pi^+)/\Gamma_{total} \times \Gamma(e^+e^-)/\Gamma_{total}$ $\Gamma_8/\Gamma \times \Gamma_1/\Gamma$

VALUE	CL%	DOCUMENT ID	TECN	COMMENT
$<0.72 \times 10^{-6}$	90	¹ PAKHLOVA	09 BELL	$e^+e^- \rightarrow \psi(4360) \rightarrow D^0 D^{*-} \pi^+$
¹ Using $4355^{+9}_{-10} \pm 9$ MeV for the mass of $\psi(4360)$.				

$\Gamma(D^0 D^{*-} \pi^+)/\Gamma(\psi(2S)\pi^+\pi^-)$ Γ_8/Γ_4

VALUE	CL%	DOCUMENT ID	TECN	COMMENT
<8	90	PAKHLOVA	09 BELL	$e^+e^- \rightarrow \psi(4360) \rightarrow D^0 D^{*-} \pi^+$

$\Gamma(D^+ D^- \pi^+ \pi^-)/\Gamma_{total}$ Γ_9/Γ

VALUE	DOCUMENT ID	TECN	COMMENT
seen	¹ ABLIKIM	22AL BES3	$e^+e^- \rightarrow \pi^+\pi^- D^+ D^-$
¹ From a fit to the cross section for $e^+e^- \rightarrow D^+ D^- \pi^+ \pi^-$ in the range $\sqrt{s} = 4.190$ - 4.946 GeV.			

$\Gamma(D_1(2420)\bar{D} + c.c.)/\Gamma_{total}$ Γ_{10}/Γ

VALUE	DOCUMENT ID	TECN	COMMENT
possibly seen	¹ ABLIKIM	19AR BES3	$e^+e^- \rightarrow \pi^+\pi^- D\bar{D}$
¹ Evidence for $e^+e^- \rightarrow D_1(2420)\bar{D} + c.c.$ between $\sqrt{s} = 4.3$ and 4.6 GeV, not necessarily resonant.			

$\Gamma(\phi\eta)/\Gamma_{total}$ Γ_{11}/Γ

VALUE	DOCUMENT ID	TECN	COMMENT
not seen	ABLIKIM	23BT BES3	$e^+e^- \rightarrow \phi\eta$

$\Gamma(\omega\pi^0)/\Gamma_{total}$ Γ_{12}/Γ

VALUE	DOCUMENT ID	TECN	COMMENT
not seen	ABLIKIM	22K BES3	$e^+e^- \rightarrow \omega\pi^0$

$\Gamma(\omega\eta)/\Gamma_{total}$ Γ_{13}/Γ

VALUE	DOCUMENT ID	TECN	COMMENT
not seen	ABLIKIM	22K BES3	$e^+e^- \rightarrow \omega\eta$

$\Gamma(p\bar{p}\eta)/\Gamma_{total}$ Γ_{14}/Γ

VALUE	DOCUMENT ID	TECN	COMMENT
not seen	ABLIKIM	21AN BES3	$e^+e^- \rightarrow p\bar{p}\eta$

$\Gamma(p\bar{p}\omega)/\Gamma_{total}$ Γ_{15}/Γ

VALUE	DOCUMENT ID	TECN	COMMENT
not seen	ABLIKIM	21AN BES3	$e^+e^- \rightarrow p\bar{p}\omega$

$\psi(4360)$ REFERENCES

ABLIKIM	23BK	JHEP 2311 228	M. Ablikim et al.	(BESIII Collab.)
ABLIKIM	23BL	JHEP 2312 027	M. Ablikim et al.	(BESIII Collab.)
ABLIKIM	23BT	PR D108 112011	M. Ablikim et al.	(BESIII Collab.)
ABLIKIM	22AL	PR D106 052012	M. Ablikim et al.	(BESIII Collab.)
ABLIKIM	22AM	PR D106 072001	M. Ablikim et al.	(BESIII Collab.)
ABLIKIM	22K	JHEP 2207 064	M. Ablikim et al.	(BESIII Collab.)
ABLIKIM	22R	PRL 129 102003	M. Ablikim et al.	(BESIII Collab.)
ABLIKIM	21AJ	PR D104 052012	M. Ablikim et al.	(BESIII Collab.)
ABLIKIM	21AK	PR D104 092001	M. Ablikim et al.	(BESIII Collab.)
ABLIKIM	21AN	PR D104 092008	M. Ablikim et al.	(BESIII Collab.)
ABLIKIM	20O	PR D102 031101	M. Ablikim et al.	(BESIII Collab.)
ABLIKIM	19AR	PR D100 032005	M. Ablikim et al.	(BESIII Collab.)
ABLIKIM	19K	PR D99 019903 (errata.)	M. Ablikim et al.	(BESIII Collab.)

ABLIKIM	17B	PRL 118 092001	M. Ablikim et al.	(BESIII Collab.)
ABLIKIM	17G	PRL 118 092002	M. Ablikim et al.	(BESIII Collab.)
ABLIKIM	17V	PR D96 032004	M. Ablikim et al.	(BESIII Collab.)
Also		PR D99 019903 (errata.)	M. Ablikim et al.	(BESIII Collab.)
ZHANG	17B	PR D96 054008	J. Zhang, J. Zhang	
ZHANG	17C	EPJ C77 727	J. Zhang, L. Yuan	
ABLIKIM	15S	PRL 115 011803	M. Ablikim et al.	(BESIII Collab.)
HAN	15	PR D92 012011	Y.L. Han et al.	(BELLE Collab.)
WANG	15A	PR D91 112007	X.L. Wang et al.	(BELLE Collab.)
LEES	14F	PR D89 111103	J.P. Lees et al.	(BABAR Collab.)
WANG	13B	PR D87 051101	X.L. Wang et al.	(BELLE Collab.)
PAKHLOVA	09	PR D80 091101	G. Pakhlova et al.	(BELLE Collab.)
LIU	08H	PR D78 014032	Z.Q. Liu, X.S. Qin, C.Z. Yuan	
AUBERT	07S	PRL 98 212001	B. Aubert et al.	(BABAR Collab.)
WANG	07D	PRL 99 142002	X.L. Wang et al.	(BELLE Collab.)

$\psi(4415)$

$$J^{PC} = 0^-(1^--)$$

$\psi(4415)$ MASS

VALUE (MeV)	DOCUMENT ID	TECN	COMMENT
4415 ± 5 OUR AVERAGE			
$4414.6 \pm 3.4 \pm 6.1$	ABLIKIM	23BH BES3	$e^+e^- \rightarrow D_s^{*+} D_s^{*-}$
4415.1 ± 7.9	¹ ABLIKIM	08D BES2	$e^+e^- \rightarrow$ hadrons
• • • We do not use the following data for averages, fits, limits, etc. • • •			
4412 ± 15	² MO	10 RVUE	$e^+e^- \rightarrow$ hadrons
4411 ± 7	³ PAKHLOVA	08A BELL	$10.6 e^+e^- \rightarrow D^0 D^- \pi^+ \gamma$
4425 ± 6	⁴ SETH	05A RVUE	$e^+e^- \rightarrow$ hadrons
4429 ± 9	⁵ SETH	05A RVUE	$e^+e^- \rightarrow$ hadrons
4417 ± 10	BRA NDELIK	78C DASP	e^+e^-
4414 ± 7	SIEGRIST	76 MRK1	e^+e^-
¹ Reanalysis of data presented in BAI 02c. From a global fit over the center-of-mass energy region 3.7-5.0 GeV covering the $\psi(3770), \psi(4040), \psi(4160),$ and $\psi(4415)$ resonances. Phase angle fixed in the fit to $\delta = (234 \pm 88)^\circ$.			
² Reanalysis of data presented in BAI 00 and BAI 02c. From a global fit over the center-of-mass energy 3.8-4.8 GeV covering the $\psi(4040), \psi(4160)$ and $\psi(4415)$ resonances and including interference effects.			
³ Systematic uncertainties not estimated.			
⁴ From a fit to Crystal Ball (OSTERHELD 86) data.			
⁵ From a fit to BES (BAI 02c) data.			

$\psi(4415)$ WIDTH

VALUE (MeV)	DOCUMENT ID	TECN	COMMENT
110 ± 22 OUR AVERAGE			Error includes scale factor of 2.3.
$122.5 \pm 7.5 \pm 8.1$	ABLIKIM	23BH BES3	$e^+e^- \rightarrow D_s^{*+} D_s^{*-}$
71.5 ± 19.0	⁶ ABLIKIM	08D BES2	$e^+e^- \rightarrow$ hadrons
• • • We do not use the following data for averages, fits, limits, etc. • • •			
118 ± 32	⁷ MO	10 RVUE	$e^+e^- \rightarrow$ hadrons
77 ± 20	⁸ PAKHLOVA	08A BELL	$10.6 e^+e^- \rightarrow D^0 D^- \pi^+ \gamma$
119 ± 16	⁹ SETH	05A RVUE	$e^+e^- \rightarrow$ hadrons
118 ± 35	¹⁰ SETH	05A RVUE	$e^+e^- \rightarrow$ hadrons
66 ± 15	BRA NDELIK	78C DASP	e^+e^-
33 ± 10	SIEGRIST	76 MRK1	e^+e^-
⁶ Reanalysis of data presented in BAI 02c. From a global fit over the center-of-mass energy region 3.7-5.0 GeV covering the $\psi(3770), \psi(4040), \psi(4160),$ and $\psi(4415)$ resonances. Phase angle fixed in the fit to $\delta = (234 \pm 88)^\circ$.			
⁷ Reanalysis of data presented in BAI 00 and BAI 02c. From a global fit over the center-of-mass energy 3.8-4.8 GeV covering the $\psi(4040), \psi(4160)$ and $\psi(4415)$ resonances and including interference effects.			
⁸ Systematic uncertainties not estimated.			
⁹ From a fit to Crystal Ball (OSTERHELD 86) data.			
¹⁰ From a fit to BES (BAI 02c) data.			

$\psi(4415)$ DECAY MODES

Due to the complexity of the $c\bar{c}$ threshold region, in this listing, "seen" ("not seen") means that a cross section for the mode in question has been measured at effective \sqrt{s} near this particle's central mass value, more (less) than 2σ above zero, without regard to any peaking behavior in \sqrt{s} or absence thereof. See mode listing(s) for details and references.

Mode	Fraction (Γ_i/Γ)	Confidence level
Γ_1	$D\bar{D}$	seen
Γ_2	$D^0\bar{D}^0$	seen
Γ_3	D^+D^-	seen
Γ_4	$D^*\bar{D} + c.c.$	seen
Γ_5	$D^*(2007)^0\bar{D}^0 + c.c.$	seen
Γ_6	$D^*(2010)^+D^- + c.c.$	seen
Γ_7	$D^*\bar{D}^*$	seen
Γ_8	$D^*(2007)^0\bar{D}^*(2007)^0 + c.c.$	seen
Γ_9	$D^*(2010)^+D^*(2010)^- + c.c.$	seen
Γ_{10}	$D^0D^-\pi^+$ (excl. $D^*(2010)^+D^- + c.c.$)	< 2.3 %
Γ_{11}	$D\bar{D}_2^*(2460) \rightarrow D^0D^-\pi^+ + c.c.$	(10 ± 4) %

Meson Particle Listings

$\psi(4415)$

Γ_{12}	$D^0 D^{*-} \pi^+ + c.c.$	< 19	%	90%
Γ_{13}	$D_1(2420) \bar{D}^+ + c.c.$		possibly seen	
Γ_{14}	$D_s^+ D_s^-$		not seen	
Γ_{15}	$\omega \chi_{c2}$		possibly seen	
Γ_{16}	$D_s^{*+} D_s^- + c.c.$		seen	
Γ_{17}	$D_s^{*+} D_s^{*-}$		seen	
Γ_{18}	$\psi_2(3823) \pi^+ \pi^-$		possibly seen	
Γ_{19}	$\psi(3770) \pi^+ \pi^-$		possibly seen	
Γ_{20}	$J/\psi \eta$	< 6	$\times 10^{-3}$	90%
Γ_{21}	$\chi_{c1} \gamma$	< 8	$\times 10^{-4}$	90%
Γ_{22}	$\chi_{c2} \gamma$	< 4	$\times 10^{-3}$	90%
Γ_{23}	$\Lambda \bar{\Lambda}$	< 3.1	$\times 10^{-6}$	90%
Γ_{24}	$\Xi^- \Xi^+$	< 4	$\times 10^{-5}$	90%
Γ_{25}	$p K^- \bar{\Lambda} + c.c.$	< 6	$\times 10^{-6}$	90%
Γ_{26}	$\omega \pi^0$		not seen	
Γ_{27}	$\omega \eta$		not seen	
Γ_{28}	$e^+ e^-$	(5.3 ± 1.2)	$\times 10^{-6}$	
Γ_{29}	$\mu^+ \mu^-$	(1.1 ± 0.5)	$\times 10^{-5}$	

$\psi(4415)$ PARTIAL WIDTHS

$\Gamma(e^+ e^-)$	DOCUMENT ID	TECN	COMMENT	Γ_{28}
VALUE (keV)				
0.58 ± 0.07 OUR ESTIMATE				
0.35 ± 0.12	11 ABLIKIM	08D BES2	$e^+ e^- \rightarrow$ hadrons	
• • • We do not use the following data for averages, fits, limits, etc. • • •				
0.4 to 0.8	12 MO	10 RVUE	$e^+ e^- \rightarrow$ hadrons	
0.72 ± 0.11	13 SETH	05A RVUE	$e^+ e^- \rightarrow$ hadrons	
0.64 ± 0.23	14 SETH	05A RVUE	$e^+ e^- \rightarrow$ hadrons	
0.49 ± 0.13	BRANDELIK	78c DASP	$e^+ e^-$	
0.44 ± 0.14	SIEGRIST	76 MRK1	$e^+ e^-$	

¹¹ Reanalysis of data presented in BAI 02c. From a global fit over the center-of-mass energy region 3.7–5.0 GeV covering the $\psi(3770)$, $\psi(4040)$, $\psi(4160)$, and $\psi(4415)$ resonances. Phase angle fixed in the fit to $\delta = (234 \pm 88)^\circ$.

¹² Reanalysis of data presented in BAI 00 and BAI 02c. From a global fit over the center-of-mass energy 3.8–4.8 GeV covering the $\psi(4040)$, $\psi(4160)$ and $\psi(4415)$ resonances and including interference effects. Four sets of solutions are obtained with the same fit quality, mass and total width, but with different $e^+ e^-$ partial widths. We quote only the range of values.

¹³ From a fit to Crystal Ball (OSTERHELD 86) data.

¹⁴ From a fit to BES (BAI 02c) data.

$\Gamma(\mu^+ \mu^-)$	DOCUMENT ID	TECN	COMMENT	Γ_{29}
VALUE (keV)				
1.25 ± 0.28 ± 0.35	15,16 ABLIKIM	20Ag BES3	$e^+ e^- \rightarrow \mu^+ \mu^-$	
¹⁵ From a fit to the $e^+ e^- \rightarrow \mu^+ \mu^-$ cross section between 3.8 and 4.6 GeV to the coherent sum of four resonant amplitudes assuming $\Gamma(\mu^+ \mu^-) = \Gamma(e^+ e^-)$.				
¹⁶ From solution 1 of 8 with equal fit quality. Other solutions range from 1.24 ± 0.28 ± 0.35 to 1.27 ± 0.41 ± 0.36 keV.				

$\psi(4415) \Gamma(i) \times \Gamma(e^+ e^-) / \Gamma(\text{total})$

$\Gamma(J/\psi \eta) \times \Gamma(e^+ e^-) / \Gamma_{\text{total}}$	CL%	DOCUMENT ID	TECN	COMMENT	$\Gamma_{20} \Gamma_{28} / \Gamma$
VALUE (eV)					
< 3.6	90	WANG	13B BELL	$e^+ e^- \rightarrow J/\psi \eta \gamma$	

$\Gamma(\chi_{c1} \gamma) \times \Gamma(e^+ e^-) / \Gamma_{\text{total}}$	CL%	DOCUMENT ID	TECN	COMMENT	$\Gamma_{21} \Gamma_{28} / \Gamma$
VALUE (eV)					
< 0.47	90	17 HAN	15 BELL	$10.58 e^+ e^- \rightarrow \chi_{c1} \gamma$	
¹⁷ Using $B(\eta \rightarrow \gamma \gamma) = (39.41 \pm 0.21)\%$.					

$\Gamma(\chi_{c2} \gamma) \times \Gamma(e^+ e^-) / \Gamma_{\text{total}}$	CL%	DOCUMENT ID	TECN	COMMENT	$\Gamma_{22} \Gamma_{28} / \Gamma$
VALUE (eV)					
< 2.3	90	18 HAN	15 BELL	$10.58 e^+ e^- \rightarrow \chi_{c2} \gamma$	
¹⁸ Using $B(\eta \rightarrow \gamma \gamma) = (39.41 \pm 0.21)\%$.					

$\Gamma(\Lambda \bar{\Lambda}) \times \Gamma(e^+ e^-) / \Gamma_{\text{total}}$	CL%	DOCUMENT ID	TECN	COMMENT	$\Gamma_{23} \Gamma_{28} / \Gamma$
VALUE (eV)					
< 1.8 × 10⁻³	90	19 ABLIKIM	21As BES3	$e^+ e^- \rightarrow \psi(4415)$	
¹⁹ From a measurement of the $e^+ e^- \rightarrow \Lambda \bar{\Lambda}$ cross section between 3.5 and 4.6 GeV.					

$\Gamma(\Xi^- \Xi^+) \times \Gamma(e^+ e^-) / \Gamma_{\text{total}}$	CL%	DOCUMENT ID	TECN	COMMENT	$\Gamma_{24} \Gamma_{28} / \Gamma$
VALUE (eV)					
< 0.0217	90	20 ABLIKIM	23Bk BES3	$e^+ e^- \rightarrow \psi(4415)$	
²⁰ From a fit to $e^+ e^- \rightarrow \Xi^- \Xi^+$ cross sections.					

$\Gamma(p K^- \bar{\Lambda} + c.c.) \times \Gamma(e^+ e^-) / \Gamma_{\text{total}}$	CL%	DOCUMENT ID	TECN	COMMENT	$\Gamma_{25} \Gamma_{28} / \Gamma$
VALUE (eV)					
< 3.4 × 10⁻³	90	21 ABLIKIM	23Bl BES3	$e^+ e^- \rightarrow \psi(4415)$	
²¹ From a fit to $e^+ e^- \rightarrow p K^- \bar{\Lambda} + c.c.$ cross sections.					

$\psi(4415) \Gamma(i) \times \Gamma(e^+ e^-) / \Gamma^2(\text{total})$

VALUE	CL%	DOCUMENT ID	TECN	COMMENT	$\Gamma_{12} / \Gamma \times \Gamma_{28} / \Gamma$
< 0.99 × 10⁻⁶	90	22 PAKHLOVA	09 BELL	$e^+ e^- \rightarrow D^0 D^{*-} \pi^+$	
²² Using 4421 ± 4 MeV for the mass of $\psi(4415)$.					

$\psi(4415)$ BRANCHING RATIOS

$\Gamma(D^0 \bar{D}^0) / \Gamma_{\text{total}}$	DOCUMENT ID	TECN	COMMENT	Γ_2 / Γ
VALUE				
seen	PAKHLOVA	08 BELL	$e^+ e^- \rightarrow D^0 \bar{D}^0 \gamma$	
• • • We do not use the following data for averages, fits, limits, etc. • • •				
not seen	AUBERT	09M BABR	$e^+ e^- \rightarrow D^0 \bar{D}^0 \gamma$	

$\Gamma(D^+ D^-) / \Gamma_{\text{total}}$	DOCUMENT ID	TECN	COMMENT	Γ_3 / Γ
VALUE				
seen	PAKHLOVA	08 BELL	$e^+ e^- \rightarrow D^+ D^- \gamma$	
• • • We do not use the following data for averages, fits, limits, etc. • • •				
not seen	AUBERT	09M BABR	$e^+ e^- \rightarrow D^+ D^- \gamma$	

$\Gamma(D^*(2007)^0 \bar{D}^0 + c.c.) / \Gamma_{\text{total}}$	DOCUMENT ID	TECN	COMMENT	Γ_5 / Γ
VALUE				
seen	AUBERT	09M BABR	$e^+ e^- \rightarrow D^{*0} \bar{D}^0 \gamma$	

$\Gamma(D^*(2010)^+ D^- + c.c.) / \Gamma_{\text{total}}$	DOCUMENT ID	TECN	COMMENT	Γ_6 / Γ
VALUE				
seen	23 ZHUKOVA	18 BELL	$e^+ e^- \rightarrow D^{*+} D^- \gamma$	
seen	AUBERT	09M BABR	$e^+ e^- \rightarrow D^{*+} D^- \gamma$	
• • • We do not use the following data for averages, fits, limits, etc. • • •				
not seen	PAKHLOVA	07 BELL	$e^+ e^- \rightarrow D^{*+} D^- \gamma$	
²³ Supersedes PAKHLOVA 07.				

$\Gamma(D \bar{D}) / \Gamma(D^* \bar{D}^*)$	DOCUMENT ID	TECN	COMMENT	Γ_1 / Γ_7
VALUE				
0.14 ± 0.12 ± 0.03	AUBERT	09M BABR	$e^+ e^- \rightarrow \gamma D^{(*)} \bar{D}^{(*)}$	

$\Gamma(D^* \bar{D}^* + c.c.) / \Gamma(D^* \bar{D}^*)$	DOCUMENT ID	TECN	COMMENT	Γ_4 / Γ_7
VALUE				
0.17 ± 0.25 ± 0.03	AUBERT	09M BABR	$e^+ e^- \rightarrow \gamma D^{(*)} \bar{D}^{(*)}$	

$\Gamma(D^*(2007)^0 \bar{D}^*(2007)^0 + c.c.) / \Gamma_{\text{total}}$	DOCUMENT ID	TECN	COMMENT	Γ_8 / Γ
VALUE				
seen	AUBERT	09M BABR	$e^+ e^- \rightarrow D^{*0} \bar{D}^{*0} \gamma$	

$\Gamma(D^*(2010)^+ D^*(2010)^- + c.c.) / \Gamma_{\text{total}}$	DOCUMENT ID	TECN	COMMENT	Γ_9 / Γ
VALUE				
seen	24 ZHUKOVA	18 BELL	$e^+ e^- \rightarrow D^{*+} D^{*-} \gamma$	
seen	AUBERT	09M BABR	$e^+ e^- \rightarrow D^{*+} D^{*-} \gamma$	
• • • We do not use the following data for averages, fits, limits, etc. • • •				
not seen	PAKHLOVA	07 BELL	$e^+ e^- \rightarrow D^{*+} D^{*-} \gamma$	
²⁴ Supersedes PAKHLOVA 07.				

$\Gamma(D \bar{D}_2^*(2460) \rightarrow D^0 D^- \pi^+ + c.c.) / \Gamma_{\text{total}}$	DOCUMENT ID	TECN	COMMENT	Γ_{11} / Γ
VALUE (units 10 ⁻²)				
10.5 ± 2.4 ± 3.8	25 PAKHLOVA	08A BELL	$10.6 e^+ e^- \rightarrow D^0 D^- \pi^+ \gamma$	
²⁵ Using 4421 ± 4 MeV for the mass and 62 ± 20 MeV for the width of $\psi(4415)$.				

$\Gamma(D^0 D^- \pi^+ (\text{excl. } D^*(2010)^+ D^- + c.c.) / \Gamma(D \bar{D}_2^*(2460) \rightarrow D^0 D^- \pi^+ + c.c.)$	CL%	DOCUMENT ID	TECN	COMMENT	$\Gamma_{10} / \Gamma_{11}$
VALUE					
< 0.22	90	26 PAKHLOVA	08A BELL	$10.6 e^+ e^- \rightarrow D^0 D^- \pi^+ \gamma$	
²⁶ Using 4421 ± 4 MeV for the mass and 62 ± 20 MeV for the width of $\psi(4415)$.					

$\Gamma(D_1(2420) \bar{D}^+ + c.c.) / \Gamma_{\text{total}}$	DOCUMENT ID	TECN	COMMENT	Γ_{13} / Γ
VALUE				
possibly seen	27 ABLIKIM	19AR BES3	$e^+ e^- \rightarrow \pi^+ \pi^- D \bar{D}$	
²⁷ Evidence for $e^+ e^- \rightarrow D_1(2420) \bar{D}^+ + c.c.$ between $\sqrt{s} = 4.3$ and 4.6 GeV, not necessarily resonant.				

$\Gamma(D_s^+ D_s^-) / \Gamma_{\text{total}}$	DOCUMENT ID	TECN	COMMENT	Γ_{14} / Γ
VALUE				
not seen	PAKHLOVA	11 BELL	$e^+ e^- \rightarrow D_s^+ D_s^- \gamma$	
not seen	DEL-AMO-SA...10N	BABR	$e^+ e^- \rightarrow D_s^+ D_s^- \gamma$	

$\Gamma(\omega \chi_{c2}) / \Gamma_{\text{total}}$	DOCUMENT ID	TECN	COMMENT	Γ_{15} / Γ
VALUE				
possibly seen	ABLIKIM	16A BES3	$e^+ e^- \rightarrow \gamma \pi^+ \pi^- \pi^0 \ell^+ \ell^-$	

See key on page 1171

Meson Particle Listings

$\psi(4415)$, $\chi_{c0}(4500)$, $X(4630)$

$\Gamma(D_s^{*+} D_s^- + c.c.) / \Gamma_{total}$ Γ_{16} / Γ

VALUE	DOCUMENT ID	TECN	COMMENT
seen	PAKHLOVA 11	BELL	$e^+ e^- \rightarrow D_s^{*+} D_s^- \gamma$
seen	DEL-AMO-SA...10N	BABR	$e^+ e^- \rightarrow D_s^{*+} D_s^- \gamma$

$\Gamma(D_s^{*+} D_s^{*-}) / \Gamma_{total}$ Γ_{17} / Γ

VALUE	DOCUMENT ID	TECN	COMMENT
seen	ABLIKIM 23BH	BES3	$e^+ e^- \rightarrow D_s^{*+} D_s^{*-}$
• • • We do not use the following data for averages, fits, limits, etc. • • •			
not seen	PAKHLOVA 11	BELL	$e^+ e^- \rightarrow D_s^{*+} D_s^{*-} \gamma$
not seen	DEL-AMO-SA...10N	BABR	$e^+ e^- \rightarrow D_s^{*+} D_s^{*-} \gamma$

$\Gamma(\psi_2(3823) \pi^+ \pi^-) / \Gamma_{total}$ Γ_{18} / Γ

VALUE	EVTS	DOCUMENT ID	TECN	COMMENT
possibly seen	19	28 ABLIKIM	15s	BES3 $e^+ e^- \rightarrow \pi^+ \pi^- \chi_{c1} \gamma$
²⁸ From a fit of $e^+ e^- \rightarrow \pi^+ \pi^- \psi_2(3823)$, $\psi_2(3823) \rightarrow \chi_{c1} \gamma$ cross sections taken at \sqrt{s} values of 4.23, 4.26, 4.36, 4.42, and 4.60 GeV to the $\psi(4415)$ line shape.				

$\Gamma(\psi(3770) \pi^+ \pi^-) / \Gamma_{total}$ Γ_{19} / Γ

VALUE	DOCUMENT ID	TECN	COMMENT	
possibly seen	29 ABLIKIM	19AR	BES3 $e^+ e^- \rightarrow \pi^+ \pi^- D \bar{D}$	
²⁹ Observe $e^+ e^- \rightarrow \pi^+ \pi^- \psi(3770)$ at $\sqrt{s} = 4.26, 4.36, \text{ and } 4.42$ GeV but cannot establish if continuum or resonant.				

$\Gamma(\omega \pi^0) / \Gamma_{total}$ Γ_{26} / Γ

VALUE	DOCUMENT ID	TECN	COMMENT
not seen	ABLIKIM 22K	BES3	$e^+ e^- \rightarrow \omega \pi^0$

$\Gamma(\omega \eta) / \Gamma_{total}$ Γ_{27} / Γ

VALUE	DOCUMENT ID	TECN	COMMENT
not seen	ABLIKIM 22K	BES3	$e^+ e^- \rightarrow \omega \eta$

$\psi(4415)$ REFERENCES

ABLIKIM 23BH	PRL 131 151903	M. Ablikim et al.	(BESIII Collab.)
ABLIKIM 23BK	JHEP 2311 228	M. Ablikim et al.	(BESIII Collab.)
ABLIKIM 23BL	JHEP 2312 027	M. Ablikim et al.	(BESIII Collab.)
ABLIKIM 22K	JHEP 2207 064	M. Ablikim et al.	(BESIII Collab.)
ABLIKIM 21AS	PR D104 L091104	M. Ablikim et al.	(BESIII Collab.)
ABLIKIM 20AG	PR D102 112009	M. Ablikim et al.	(BESIII Collab.)
ABLIKIM 19AR	PR D100 032005	M. Ablikim et al.	(BESIII Collab.)
ZHUKOVA 18	PR D97 012002	V. Zhukova et al.	(BELLE Collab.)
ABLIKIM 16A	PR D93 011102	M. Ablikim et al.	(BESIII Collab.)
ABLIKIM 15S	PRL 115 011803	M. Ablikim et al.	(BESIII Collab.)
HAN 15	PR D92 012011	Y.L. Han et al.	(BELLE Collab.)
WANG 13B	PR D87 051101	X.L. Wang et al.	(BELLE Collab.)
PAKHLOVA 11	PR D83 011101	G. Pakhlova et al.	(BELLE Collab.)
DEL-AMO-SA... 10N	PR D82 052004	P. del Amo Sanchez et al.	(BABAR Collab.)
MO 10	PR D82 077501	X.H. Mo, C.Z. Yuan, P. Wang	(BHEP)
AUBERT 09M	PR D79 092001	B. Aubert et al.	(BABAR Collab.)
PAKHLOVA 09	PR D80 091101	G. Pakhlova et al.	(BELLE Collab.)
ABLIKIM 05D	PL B660 315	M. Ablikim et al.	(BES Collab.)
PAKHLOVA 08	PR D77 011103	G. Pakhlova et al.	(BELLE Collab.)
PAKHLOVA 08A	PRL 100 062001	G. Pakhlova et al.	(BELLE Collab.)
PAKHLOVA 07	PRL 98 092001	G. Pakhlova et al.	(BELLE Collab.)
SETH 05A	PR D72 017501	K.K. Seth	(BES Collab.)
BAI 02C	PRL 88 101802	J.Z. Bai et al.	(BES Collab.)
BAI 00	PRL 84 594	J.Z. Bai et al.	(BES Collab.)
OSTERHELD 86	SLAC-PUB-4160	A. Osterheld et al.	(SLAC Crystal Ball Collab.)
BRANDELIK 78C	PL 76B 361	R. Brandelik et al.	(DASP Collab.)
SIEGRIST 76	PRL 36 700	J.L. Siegrist et al.	(LBL, SLAC)

$\chi_{c0}(4500)$

$$I^G(J^{PC}) = 0^+(0^{++})$$

OMITTED FROM SUMMARY TABLE was $X(4500)$

This state shows properties different from a conventional $q\bar{q}$ state. A candidate for an exotic structure. See the review on non- $q\bar{q}$ states.

Seen by AAIJ 17C in $B^+ \rightarrow \chi_{c0} K^+$, $\chi_{c0} \rightarrow J/\psi \phi$ using an amplitude analysis of $B^+ \rightarrow J/\psi \phi K^+$ with a significance (accounting for systematic uncertainties) of 6.1 σ .

$\chi_{c0}(4500)$ MASS

VALUE (MeV)	EVTS	DOCUMENT ID	TECN	COMMENT
$4474 \pm 3 \pm 3$	24k	¹ AAIJ	21E	LHCB $B^+ \rightarrow J/\psi \phi K^+$
• • • We do not use the following data for averages, fits, limits, etc. • • •				
$4506 \pm 11 \pm 15$	4289	^{2,3} AAIJ	17C	LHCB $B^+ \rightarrow J/\psi \phi K^+$

¹ From an amplitude analysis of the decay $B^+ \rightarrow J/\psi \phi K^+$ with a significance of 20 σ .
² From an amplitude analysis of the decay $B^+ \rightarrow J/\psi \phi K^+$ with a significance of 6.1 σ .
³ Superseded by AAIJ 21E.

$\chi_{c0}(4500)$ WIDTH

VALUE (MeV)	EVTS	DOCUMENT ID	TECN	COMMENT
$77 \pm 6 \pm 10 \pm 8$	24k	¹ AAIJ	21E	LHCB $B^+ \rightarrow J/\psi \phi K^+$
• • • We do not use the following data for averages, fits, limits, etc. • • •				
$92 \pm 21 \pm 21 \pm 20$	4289	^{2,3} AAIJ	17C	LHCB $B^+ \rightarrow J/\psi \phi K^+$

¹ From an amplitude analysis of the decay $B^+ \rightarrow J/\psi \phi K^+$ with a significance of 20 σ .
² From an amplitude analysis of the decay $B^+ \rightarrow J/\psi \phi K^+$ with a significance of 6.1 σ .
³ Superseded by AAIJ 21E.

$\chi_{c0}(4500)$ DECAY MODES

Mode	Fraction (Γ_i / Γ)
Γ_1 $J/\psi \phi$	seen

$\chi_{c0}(4500)$ BRANCHING RATIOS

$\Gamma(J/\psi \phi) / \Gamma_{total}$	Γ_1 / Γ			
seen	24k	¹ AAIJ	21E	LHCB $B^+ \rightarrow J/\psi \phi K^+$
• • • We do not use the following data for averages, fits, limits, etc. • • •				
seen	4289	^{2,3} AAIJ	17C	LHCB $B^+ \rightarrow J/\psi \phi K^+$

¹ From an amplitude analysis of the decay $B^+ \rightarrow J/\psi \phi K^+$ with a significance of 20 σ .
² From an amplitude analysis of the decay $B^+ \rightarrow J/\psi \phi K^+$ with a significance of 6.1 σ .
³ Superseded by AAIJ 21E.

$\chi_{c0}(4500)$ REFERENCES

AAIJ 21E	PRL 127 082001	R. Aaij et al.	(LHCb Collab.)
AAIJ 17C	PRL 118 022003	R. Aaij et al.	(LHCb Collab.)
Also	PR D95 012002	R. Aaij et al.	(LHCb Collab.)

$X(4630)$

$$I^G(J^{PC}) = 0^+(?^{?+})$$

OMITTED FROM SUMMARY TABLE

This state shows properties different from a conventional $q\bar{q}$ state. A candidate for an exotic structure. See the review on "Heavy Non- $q\bar{q}$ Mesons."

Seen by AAIJ 21E in $B^+ \rightarrow X(4630) K^+$ with $X(4630) \rightarrow J/\psi \phi$ using an amplitude analysis of $B^+ \rightarrow J/\psi \phi K^+$ with a significance (accounting for systematic uncertainties) of 5.5 σ . The $J^P = 1^-$ assignment is favored over 2^- with a significance of 3 σ and other assignments are disfavored by more than 5 σ .

$X(4630)$ MASS

VALUE (MeV)	EVTS	DOCUMENT ID	TECN	COMMENT
$4626 \pm 16 \pm 18 \pm 110$	24k	¹ AAIJ	21E	LHCB $B^+ \rightarrow J/\psi \phi K^+$

¹ From an amplitude analysis of the decay $B^+ \rightarrow J/\psi \phi K^+$ with a significance of 5.5 σ .

$X(4630)$ WIDTH

VALUE (MeV)	EVTS	DOCUMENT ID	TECN	COMMENT
$174 \pm 27 \pm 134 \pm 73$	24k	¹ AAIJ	21E	LHCB $B^+ \rightarrow J/\psi \phi K^+$

¹ From an amplitude analysis of the decay $B^+ \rightarrow J/\psi \phi K^+$ with a significance of 5.5 σ .

$X(4630)$ DECAY MODES

Mode	Fraction (Γ_i / Γ)
Γ_1 $J/\psi \phi$	seen

$\Gamma(J/\psi \phi) / \Gamma_{total}$	Γ_1 / Γ			
seen	24k	¹ AAIJ	21E	LHCB $B^+ \rightarrow J/\psi \phi K^+$

¹ From an amplitude analysis of the decay $B^+ \rightarrow J/\psi \phi K^+$ with a significance of 5.5 σ .

$X(4630)$ REFERENCES

AAIJ 21E	PRL 127 082001	R. Aaij et al.	(LHCb Collab.)
----------	----------------	----------------	----------------

Meson Particle Listings

$\psi(4660)$

$\psi(4660)$

$$I^G(J^{PC}) = 0^-(1^{--})$$

also known as $Y(4660)$; was $X(4660)$

This state shows properties different from a conventional $q\bar{q}$ state. A candidate for an exotic structure. See the review on non- $q\bar{q}$ states.

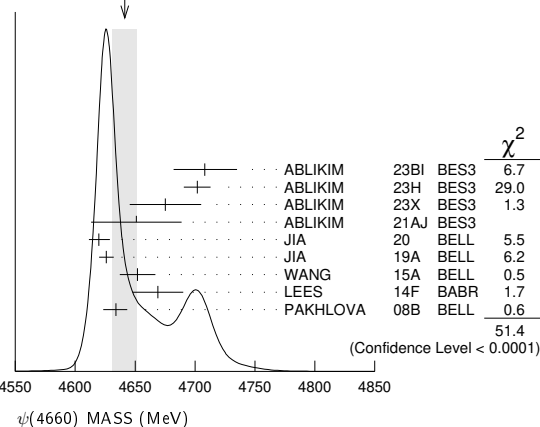
Seen in radiative return from e^+e^- collisions at $\sqrt{s} = 9.54\text{--}10.58$ GeV by WANG 07D. Also obtained in a combined fit of WANG 07D, AUBERT 07s, and LEES 14F. See also the review on "Spectroscopy of mesons containing two heavy quarks."

$\psi(4660)$ MASS

VALUE (MeV)	EVTs	DOCUMENT ID	TECN	COMMENT
4641 ± 10	OUR AVERAGE	Error includes scale factor of 2.7. See the ideogram below.		
4708 $^{+17}_{-15}$ ± 21	1	ABLIKIM 23BI	BES3	$e^+e^- \rightarrow K^+K^-J/\psi$
4701.8 ± 10.9 ± 2.7	2	ABLIKIM 23H	BES3	$e^+e^- \rightarrow \phi\chi_{C2}$
4675.3 ± 29.5 ± 3.5	3	ABLIKIM 23X	BES3	$e^+e^- \rightarrow D^{*0}D^{*-}\pi^+$
4651.0 ± 37.8 ± 2.1	4	ABLIKIM 21AJ	BES3	$e^+e^- \rightarrow \pi^+\pi^-\psi(2S)$
4619.8 $^{+8.9}_{-8.0}$ ± 2.3	66	5	JIA	20 BELL $e^+e^- \rightarrow \gamma D_s^+ D_s^{*2-}(2573)^-$
4625.9 $^{+6.2}_{-6.0}$ ± 0.4	89	6	JIA	19A BELL $e^+e^- \rightarrow \gamma D_s^+ D_{s1}(2536)^-$
4652 ± 10 ± 11	279	7	WANG	15A BELL 10.58 $e^+e^- \rightarrow \gamma\pi^+\pi^-\psi(2S)$
4669 ± 21 ± 3	37	8	LEES	14F BABR 10.58 $e^+e^- \rightarrow \gamma\pi^+\pi^-\psi(2S)$
4634 $^{+8}_{-7}$ $^{+5}_{-8}$	142	9	PAKHOVA	08B BELL $e^+e^- \rightarrow \Lambda_C^+ \Lambda_C^-$
• • • We do not use the following data for averages, fits, limits, etc. • • •				
4647.9 ± 8.6 ± 0.8	10	ABLIKIM 22R	BES3	$e^+e^- \rightarrow \pi^+\pi^-\chi_{C1}\gamma$
4652.5 ± 3.4 ± 1.1	11	DAI	17 RVUE	$e^+e^- \rightarrow \Lambda_C^+ \Lambda_C^-$
4645.2 ± 9.5 ± 6.0	12	ZHANG	17B RVUE	$e^+e^- \rightarrow \pi^+\pi^-\psi(2S)$
4646.4 ± 9.7 ± 4.8	13	ZHANG	17C RVUE	$e^+e^- \rightarrow \pi^+\pi^-J/\psi$ or $\psi(2S)$
4661 $^{+9}_{-8}$ ± 6	44	14	LIU	08H RVUE 10.58 $e^+e^- \rightarrow \gamma\pi^+\pi^-\psi(2S)$
4664 ± 11 ± 5	44	WANG	07D BELL	10.58 $e^+e^- \rightarrow \gamma\pi^+\pi^-\psi(2S)$

- Seen as a peak in the c.m. energy dependence of the $e^+e^- \rightarrow K^+K^-J/\psi$ cross section using 5.85 fb^{-1} of data at c.m. energies 4.61–4.95 GeV. Statistical significance is over 5σ .
- Fit model parameterized as the coherent sum of a Breit-Wigner resonance and a continuum amplitude term.
- From a cross-section measurement of $e^+e^- \rightarrow D^{*0}D^{*-}\pi^+$ between 4.189 and 4.951 GeV, assuming a coherent sum of 3 Breit-Wigner resonances plus a continuum amplitude. The two other resonances have masses (widths) 4209.6 ± 7.5 (81.6 ± 19.9) MeV and 4469.1 ± 26.4 (246.3 ± 37.9) MeV.
- From a three-resonance fit to the Born cross section in the range $\sqrt{s} = 4.008\text{--}4.698$ GeV.
- Using $D_s^{*2-}(2573)^- \rightarrow \bar{D}^0 K^-$ decays.
- From a fit of a Breit-Wigner convolved with a Gaussian.
- From a two-resonance fit. Supersedes WANG 07D.
- From a two-resonance fit.
- The $\pi^+\pi^-\psi(2S)$ and $\Lambda_C^+\Lambda_C^-$ states are not necessarily the same.
- From a fit to the $e^+e^- \rightarrow \pi^+\pi^-\psi(3823)$ cross section between 4.23 and 4.70 GeV with two coherent Breit-Wigner resonances. The data is also consistent with a single peak with mass $4417.5 \pm 26.2 \pm 3.5$ MeV and width $245 \pm 48 \pm 13$ MeV.
- The pole parameters are extracted from the speed plot.
- From a three-resonance fit.
- From a combined fit of BELLE, BABAR and BES3 $e^+e^- \rightarrow \pi^+\pi^-J/\psi$ and $e^+e^- \rightarrow \pi^+\pi^-\psi(2S)$ data.
- From a combined fit of AUBERT 07s and WANG 07D data with two resonances.

WEIGHTED AVERAGE
4641±10 (Error scaled by 2.7)

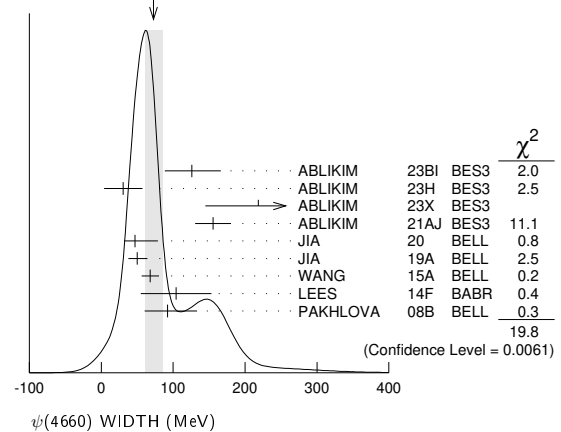


$\psi(4660)$ WIDTH

VALUE (MeV)	EVTs	DOCUMENT ID	TECN	COMMENT
73 $^{+13}_{-11}$	OUR AVERAGE	Error includes scale factor of 1.7. See the ideogram below.		
126 $^{+27}_{-23}$ ± 30	1	ABLIKIM 23BI	BES3	$e^+e^- \rightarrow K^+K^-J/\psi$
30.5 ± 22.3 ± 14.6	2	ABLIKIM 23H	BES3	$e^+e^- \rightarrow \phi\chi_{C2}$
218.3 ± 72.9 ± 9.3	3	ABLIKIM 23X	BES3	$e^+e^- \rightarrow D^{*0}D^{*-}\pi^+$
155.4 ± 24.8 ± 0.8	4	ABLIKIM 21AJ	BES3	$e^+e^- \rightarrow \pi^+\pi^-\psi(2S)$
47.0 $^{+31.3}_{-14.8}$ ± 4.6	66	5	JIA	20 BELL $e^+e^- \rightarrow \gamma D_s^+ D_s^{*2-}(2573)^-$
49.8 $^{+13.9}_{-11.5}$ ± 4.0	89	6	JIA	19A BELL $e^+e^- \rightarrow \gamma D_s^+ D_{s1}(2536)^-$
68 ± 11 ± 5	279	7	WANG	15A BELL 10.58 $e^+e^- \rightarrow \gamma\pi^+\pi^-\psi(2S)$
104 ± 48 ± 10	37	8	LEES	14F BABR 10.58 $e^+e^- \rightarrow \gamma\pi^+\pi^-\psi(2S)$
92 $^{+40}_{-24}$ $^{+10}_{-21}$	142	9	PAKHOVA	08B BELL $e^+e^- \rightarrow \Lambda_C^+ \Lambda_C^-$
• • • We do not use the following data for averages, fits, limits, etc. • • •				
33.1 ± 18.6 ± 4.1	10	ABLIKIM 22R	BES3	$e^+e^- \rightarrow \pi^+\pi^-\chi_{C1}\gamma$
62.6 ± 5.6 ± 4.3	11	DAI	17 RVUE	$e^+e^- \rightarrow \Lambda_C^+ \Lambda_C^-$
113.8 ± 18.1 ± 3.4	12	ZHANG	17B RVUE	$e^+e^- \rightarrow \pi^+\pi^-\psi(2S)$
103.5 ± 15.6 ± 4.0	13	ZHANG	17C RVUE	$e^+e^- \rightarrow \pi^+\pi^-J/\psi$ or $\psi(2S)$
42 $^{+17}_{-12}$ ± 6	44	14	LIU	08H RVUE 10.58 $e^+e^- \rightarrow \gamma\pi^+\pi^-\psi(2S)$
48 ± 15 ± 3	44	WANG	07D BELL	10.58 $e^+e^- \rightarrow \gamma\pi^+\pi^-\psi(2S)$

- Seen as a peak in the c.m. energy dependence of the $e^+e^- \rightarrow K^+K^-J/\psi$ cross section using 5.85 fb^{-1} of data at c.m. energies 4.61–4.95 GeV. Statistical significance is over 5σ .
- Fit model parameterized as the coherent sum of a Breit-Wigner resonance and a continuum amplitude term.
- From a cross-section measurement of $e^+e^- \rightarrow D^{*0}D^{*-}\pi^+$ between 4.189 and 4.951 GeV, assuming a coherent sum of 3 Breit-Wigner resonances plus a continuum amplitude. The two other resonances have masses (widths) 4209.6 ± 7.5 (81.6 ± 19.9) MeV and 4469.1 ± 26.4 (246.3 ± 37.9) MeV.
- From a three-resonance fit to the Born cross section in the range $\sqrt{s} = 4.008\text{--}4.698$ GeV.
- Using $D_s^{*2-}(2573)^- \rightarrow \bar{D}^0 K^-$ decays.
- From a fit of a Breit-Wigner convolved with a Gaussian.
- From a two-resonance fit. Supersedes WANG 07D.
- From a two-resonance fit.
- The $\pi^+\pi^-\psi(2S)$ and $\Lambda_C^+\Lambda_C^-$ states are not necessarily the same.
- From a fit to the $e^+e^- \rightarrow \pi^+\pi^-\psi(3823)$ cross section between 4.23 and 4.70 GeV with two coherent Breit-Wigner resonances. The data is also consistent with a single peak with mass $4417.5 \pm 26.2 \pm 3.5$ MeV and width $245 \pm 48 \pm 13$ MeV.
- The pole parameters are extracted from the speed plot.
- From a three-resonance fit.
- From a combined fit of BELLE, BABAR and BES3 $e^+e^- \rightarrow \pi^+\pi^-J/\psi$ and $e^+e^- \rightarrow \pi^+\pi^-\psi(2S)$ data.
- From a combined fit of AUBERT 07s and WANG 07D data with two resonances.

WEIGHTED AVERAGE
73+13-11 (Error scaled by 1.7)



$\psi(4660)$ DECAY MODES

Mode	Fraction (Γ_i/Γ)	
Γ_1	e^+e^-	not seen
Γ_2	$\psi(2S)\pi^+\pi^-$	seen
Γ_3	$J/\psi\eta$	not seen
Γ_4	$D^0D^{*-}\pi^+$	not seen
Γ_5	$D^{*0}D^{*-}\pi^+$	seen

See key on page 1171

Meson Particle Listings

$\psi(4660)$

Γ_6	$\psi_2(3823)\pi^+\pi^-$	seen
Γ_7	$\chi_{c1}\gamma$	not seen
Γ_8	$\chi_{c1}\phi$	not seen
Γ_9	$\chi_{c2}\gamma$	not seen
Γ_{10}	$\chi_{c2}\phi$	not seen
Γ_{11}	$\Lambda_c^+\Lambda_c^-$	seen
Γ_{12}	$D_s^+D_{s1}(2536)^-$	seen
Γ_{13}	$D_s^+D_{s2}^*(2573)^-$	seen
Γ_{14}	$\omega\pi^0$	not seen
Γ_{15}	$\omega\eta$	not seen
Γ_{16}	$\Xi^-\Xi^+$	not seen
Γ_{17}	$pK^-\bar{\Lambda} + c.c.$	not seen

$\psi(4660)\Gamma(i) \times \Gamma(e^+e^-)/\Gamma(\text{total})$

$\Gamma(\psi(2S)\pi^+\pi^-) \times \Gamma(e^+e^-)/\Gamma(\text{total})$	$\Gamma_2\Gamma_1/\Gamma$			
VALUE (eV)	EVTS	DOCUMENT ID	TECN	COMMENT

• • • We do not use the following data for averages, fits, limits, etc. • • •

4.7±3.8	1	ABLIKIM	21AJ	BES3	$e^+e^- \rightarrow \pi^+\pi^-\psi(2S)$
11.2±3.2	2	ABLIKIM	21AJ	BES3	$e^+e^- \rightarrow \pi^+\pi^-\psi(2S)$
4.7±4.2	3	ABLIKIM	21AJ	BES3	$e^+e^- \rightarrow \pi^+\pi^-\psi(2S)$
11.3±3.3	4	ABLIKIM	21AJ	BES3	$e^+e^- \rightarrow \pi^+\pi^-\psi(2S)$
2.0±0.3±0.2	279	5	WANG	15A	BELL 10.58 $e^+e^- \rightarrow \gamma\pi^+\pi^-\psi(2S)$
8.1±1.1±1.0	279	6	WANG	15A	BELL 10.58 $e^+e^- \rightarrow \gamma\pi^+\pi^-\psi(2S)$
2.7±1.3±0.5	37	7	LEES	14F	BABR 10.58 $e^+e^- \rightarrow \gamma\pi^+\pi^-\psi(2S)$
7.5±1.7±0.7	37	8	LEES	14F	BABR 10.58 $e^+e^- \rightarrow \gamma\pi^+\pi^-\psi(2S)$
2.2 ^{+0.7} _{-0.6}	44	9	LIU	08H	RVUE 10.58 $e^+e^- \rightarrow \gamma\pi^+\pi^-\psi(2S)$
5.9±1.6	44	10	LIU	08H	RVUE 10.58 $e^+e^- \rightarrow \gamma\pi^+\pi^-\psi(2S)$
3.0±0.9±0.3	44	7	WANG	07D	BELL 10.58 $e^+e^- \rightarrow \gamma\pi^+\pi^-\psi(2S)$
7.6±1.8±0.8	44	8	WANG	07D	BELL 10.58 $e^+e^- \rightarrow \gamma\pi^+\pi^-\psi(2S)$

- Solution I of four equivalent solutions in a fit using three interfering resonances.
- Solution II of four equivalent solutions in a fit using three interfering resonances.
- Solution III of four equivalent solutions in a fit using three interfering resonances.
- Solution IV of four equivalent solutions in a fit using three interfering resonances.
- Solution I of two equivalent solutions from a fit using two interfering resonances. Supercedes WANG 07D.
- Solution II of two equivalent solutions from a fit using two interfering resonances. Supercedes WANG 07D.
- Solution I of two equivalent solutions in a fit using two interfering resonances.
- Solution II of two equivalent solutions in a fit using two interfering resonances.
- Solution I in a combined fit of AUBERT 07s and WANG 07D data with two resonances.
- Solution II in a combined fit of AUBERT 07s and WANG 07D data with two resonances.

$\Gamma(J/\psi\eta) \times \Gamma(e^+e^-)/\Gamma(\text{total})$	$\Gamma_3\Gamma_1/\Gamma$			
VALUE (eV)	CL%	DOCUMENT ID	TECN	COMMENT

• • • We do not use the following data for averages, fits, limits, etc. • • •

<0.94	90	WANG	13B	BELL $e^+e^- \rightarrow J/\psi\eta\gamma$
-------	----	------	-----	--

$\Gamma(D^{*0}D^{*-}\pi^+) \times \Gamma(e^+e^-)/\Gamma(\text{total})$	$\Gamma_5\Gamma_1/\Gamma$			
VALUE (eV)	CL%	DOCUMENT ID	TECN	COMMENT

• • • We do not use the following data for averages, fits, limits, etc. • • •

19 to 2005	1	ABLIKIM	23X	BES3 $e^+e^- \rightarrow D^{*0}D^{*-}\pi^+$
------------	---	---------	-----	---

1 From a cross-section measurement of $e^+e^- \rightarrow D^{*0}D^{*-}\pi^+$ between 4.189 and 4.951 GeV, assuming a coherent sum of 3 Breit-Wigner resonances plus a continuum amplitude. Depending on solutions I – VIII with same fit qualities.

$\Gamma(\chi_{c1}\gamma) \times \Gamma(e^+e^-)/\Gamma(\text{total})$	$\Gamma_7\Gamma_1/\Gamma$			
VALUE (eV)	CL%	DOCUMENT ID	TECN	COMMENT

<0.45 90 1 HAN 15 BELL 10.58 $e^+e^- \rightarrow \chi_{c1}\gamma$

1 Using $B(\eta \rightarrow \gamma\gamma) = (39.41 \pm 0.21)\%$.

$\Gamma(\chi_{c1}\phi) \times \Gamma(e^+e^-)/\Gamma(\text{total})$	$\Gamma_8\Gamma_1/\Gamma$			
VALUE (eV)	CL%	DOCUMENT ID	TECN	COMMENT

• • • We do not use the following data for averages, fits, limits, etc. • • •

<0.04	90	1	ABLIKIM	23H	BES3 $e^+e^- \rightarrow \phi\chi_{c1}$
-------	----	---	---------	-----	---

1 Fit model parameterized as the coherent sum of a Breit-Wigner resonance and a continuum amplitude term.

$\Gamma(\chi_{c2}\gamma) \times \Gamma(e^+e^-)/\Gamma(\text{total})$	$\Gamma_9\Gamma_1/\Gamma$			
VALUE (eV)	CL%	DOCUMENT ID	TECN	COMMENT

<2.1 90 1 HAN 15 BELL 10.58 $e^+e^- \rightarrow \chi_{c2}\gamma$

1 Using $B(\eta \rightarrow \gamma\gamma) = (39.41 \pm 0.21)\%$.

$\Gamma(\chi_{c2}\phi) \times \Gamma(e^+e^-)/\Gamma(\text{total})$ $\Gamma_{10}\Gamma_1/\Gamma$

VALUE (eV)	CL%	DOCUMENT ID	TECN	COMMENT
------------	-----	-------------	------	---------

• • • We do not use the following data for averages, fits, limits, etc. • • •

0.13±0.13 1 ABLIKIM 23H BES3 $e^+e^- \rightarrow \phi\chi_{c2}$

1 Fit model parameterized as the coherent sum of a Breit-Wigner resonance and a continuum amplitude term. Constructive solution of the interference. Destructive solution gives 0.66 ± 0.41 eV.

$\Gamma(D_s^+D_{s1}(2536)^-) \times \Gamma(e^+e^-)/\Gamma(\text{total})$	$\Gamma_{12}\Gamma_1/\Gamma$			
VALUE (eV)	EVTS	DOCUMENT ID	TECN	COMMENT

14.3^{+2.8}_{-2.6}±1.5 89 1 JIA 19A BELL $e^+e^- \rightarrow \gamma D_s^+D_{s1}(2536)^-$

1 Assuming $B(D_{s1}(2536)^- \rightarrow \bar{D}^{*0}K^-) = 1$.

$\Gamma(D_s^+D_{s2}^*(2573)^-) \times \Gamma(e^+e^-)/\Gamma(\text{total})$	$\Gamma_{13}\Gamma_1/\Gamma$			
VALUE (eV)	EVTS	DOCUMENT ID	TECN	COMMENT

14.7^{+5.9}_{-4.5}±3.6 66 1 JIA 20 BELL $e^+e^- \rightarrow \gamma D_s^+D_{s2}^*(2573)^-$

1 Assuming $B(D_{s2}^*(2573)^- \rightarrow \bar{D}^0K^-) = 1$.

$\Gamma(\Xi^-\Xi^+) \times \Gamma(e^+e^-)/\Gamma(\text{total})$	$\Gamma_{16}\Gamma_1/\Gamma$			
VALUE (eV)	CL%	DOCUMENT ID	TECN	COMMENT

<0.0199 90 1 ABLIKIM 23BK BES3 $e^+e^- \rightarrow \psi(4660)$

1 From a fit to $e^+e^- \rightarrow \Xi^-\Xi^+$ cross sections.

$\Gamma(pK^-\bar{\Lambda} + c.c.) \times \Gamma(e^+e^-)/\Gamma(\text{total})$	$\Gamma_{17}\Gamma_1/\Gamma$			
VALUE (eV)	CL%	DOCUMENT ID	TECN	COMMENT

<2.8 × 10⁻³ 90 1 ABLIKIM 23BL BES3 $e^+e^- \rightarrow \psi(4660)$

1 From a fit to $e^+e^- \rightarrow pK^-\bar{\Lambda} + c.c.$ cross sections.

$\psi(4660)\Gamma(i) \times \Gamma(e^+e^-)/\Gamma^2(\text{total})$

$\Gamma(D^0D^{*-}\pi^+)/\Gamma(\text{total}) \times \Gamma(e^+e^-)/\Gamma(\text{total})$	$\Gamma_4/\Gamma \times \Gamma_1/\Gamma$			
VALUE	CL%	DOCUMENT ID	TECN	COMMENT

<0.37 × 10⁻⁶ 90 1 PAKHLOVA 09 BELL $e^+e^- \rightarrow D^0D^{*-}\pi^+$

1 Using $4664 \pm 11 \pm 5$ MeV for the mass of $\psi(4660)$.

$\Gamma(\Lambda_c^+\Lambda_c^-)/\Gamma(\text{total}) \times \Gamma(e^+e^-)/\Gamma(\text{total})$	$\Gamma_{11}/\Gamma \times \Gamma_1/\Gamma$			
VALUE (units 10 ⁻⁶)	EVTS	DOCUMENT ID	TECN	COMMENT

0.68^{+0.16+0.29}_{-0.15-0.30} 142 1 PAKHLOVA 08B BELL $e^+e^- \rightarrow \Lambda_c^+\Lambda_c^-$

1 The $\pi^+\pi^-\psi(2S)$ and $\Lambda_c^+\Lambda_c^-$ states are not necessarily the same.

$\psi(4660)$ BRANCHING RATIOS

$\Gamma(D^0D^{*-}\pi^+)/\Gamma(\psi(2S)\pi^+\pi^-)$	Γ_4/Γ_2			
VALUE	CL%	DOCUMENT ID	TECN	COMMENT

<10 90 PAKHLOVA 09 BELL $e^+e^- \rightarrow D^0D^{*-}\pi^+$

$\Gamma(\psi_2(3823)\pi^+\pi^-)/\Gamma(\text{total})$	Γ_6/Γ		
VALUE	DOCUMENT ID	TECN	COMMENT

seen 1 ABLIKIM 22R BES3 $e^+e^- \rightarrow \pi^+\pi^-\chi_{c1}\gamma$

1 From a fit to the $e^+e^- \rightarrow \pi^+\pi^-\psi(3823)$ cross section between 4.23 and 4.70 GeV with two coherent Breit-Wigner resonances.

$\Gamma(\omega\pi^0)/\Gamma(\text{total})$	Γ_{14}/Γ		
VALUE	DOCUMENT ID	TECN	COMMENT

not seen ABLIKIM 22K BES3 $e^+e^- \rightarrow \omega\pi^0$

$\Gamma(\omega\eta)/\Gamma(\text{total})$	Γ_{15}/Γ		
VALUE	DOCUMENT ID	TECN	COMMENT

not seen ABLIKIM 22K BES3 $e^+e^- \rightarrow \omega\eta$

$\psi(4660)$ REFERENCES

ABLIKIM 23BI PRL 131 211902	M. Ablikim <i>et al.</i>	(BESIII Collab.)
ABLIKIM 23BK JHEP 2311 228	M. Ablikim <i>et al.</i>	(BESIII Collab.)
ABLIKIM 23BL JHEP 2312 027	M. Ablikim <i>et al.</i>	(BESIII Collab.)
ABLIKIM 23H JHEP 2301 132	M. Ablikim <i>et al.</i>	(BESIII Collab.)
ABLIKIM 23X PRL 130 121901	M. Ablikim <i>et al.</i>	(BESIII Collab.)
ABLIKIM 22K JHEP 2207 064	M. Ablikim <i>et al.</i>	(BESIII Collab.)
ABLIKIM 22R PRL 129 102003	M. Ablikim <i>et al.</i>	(BESIII Collab.)
ABLIKIM 21AJ PR D104 052012	M. Ablikim <i>et al.</i>	(BESIII Collab.)
JIA 20 PR D101 091101	S. Jia <i>et al.</i>	(BELLE Collab.)
JIA 19A PR D100 111103	S. Jia <i>et al.</i>	(BELLE Collab.)
DAI 17 PR D96 116001	L.-Y. Dai, J. Haidenbauer, U.-G. Meissner	(JULI-1)
ZHANG 17B PR D96 054008	J. Zhang, J. Zhang	
ZHANG 17C EPJ C77 727	J. Zhang, L. Yuan	
HAN 15 PR D92 012011	Y.L. Han <i>et al.</i>	(BELLE Collab.)
WANG 15A PR D91 112007	X.L. Wang <i>et al.</i>	(BELLE Collab.)
LEES 14F PR D89 111103	J.P. Lees <i>et al.</i>	(BABAR Collab.)
WANG 13B PR D87 051101	X.L. Wang <i>et al.</i>	(BELLE Collab.)
PAKHLOVA 09 PR D80 091101	G. Pakhlova <i>et al.</i>	(BELLE Collab.)
LIU 08H PR D78 014032	Z.Q. Liu, X.S. Qin, C.Z. Yuan	(BELLE Collab.)
PAKHLOVA 08B PRL 101 172001	C. Pakhlova <i>et al.</i>	(BELLE Collab.)
AUBERT 07S PRL 98 212001	B. Aubert <i>et al.</i>	(BABAR Collab.)
WANG 07D PRL 99 142002	X.L. Wang <i>et al.</i>	(BELLE Collab.)

Meson Particle Listings

 $\chi_{c1}(4685)$, $\chi_{c0}(4700)$ **$\chi_{c1}(4685)$**

$$I^G(J^{PC}) = 0^+(1^{++})$$

OMITTED FROM SUMMARY TABLE

This state shows properties different from a conventional $q\bar{q}$ state. A candidate for an exotic structure. See the review on "Heavy Non- $q\bar{q}$ Mesons."

Seen by AAIJ 21E in $B^+ \rightarrow \chi_{c1}(4685)K^+$ with $\chi_{c1}(4685) \rightarrow J/\psi\phi$ using an amplitude analysis of $B^+ \rightarrow J/\psi\phi K^+$ with a significance (accounting for systematic uncertainties) of 15σ . The $J^P = 1^+$ assignment is favored with high significance.

 $\chi_{c1}(4685)$ MASS

VALUE (MeV)	EVTS	DOCUMENT ID	TECN	COMMENT
$4684 \pm 7^{+13}_{-16}$	24k	¹ AAIJ	21E LHCb	$B^+ \rightarrow J/\psi\phi K^+$

¹ From an amplitude analysis of the decay $B^+ \rightarrow J/\psi\phi K^+$ with a significance of 15σ .

 $\chi_{c1}(4685)$ WIDTH

VALUE (MeV)	EVTS	DOCUMENT ID	TECN	COMMENT
$126 \pm 15^{+37}_{-41}$	24k	¹ AAIJ	21E LHCb	$B^+ \rightarrow J/\psi\phi K^+$

¹ From an amplitude analysis of the decay $B^+ \rightarrow J/\psi\phi K^+$ with a significance of 15σ .

 $\chi_{c1}(4685)$ DECAY MODES

Mode	Fraction (Γ_i/Γ)
Γ_1 $J/\psi\phi$	seen

$\Gamma(J/\psi\phi)/\Gamma_{\text{total}}$ Γ_1/Γ

VALUE	EVTS	DOCUMENT ID	TECN	COMMENT
seen	24k	¹ AAIJ	21E LHCb	$B^+ \rightarrow J/\psi\phi K^+$

¹ From an amplitude analysis of the decay $B^+ \rightarrow J/\psi\phi K^+$ with a significance of 15σ .

 $\chi_{c1}(4685)$ REFERENCES

AAIJ 21E PRL 127 082001 R. Aaij *et al.* (LHCb Collab.) JP

 $\chi_{c0}(4700)$

$$I^G(J^{PC}) = 0^+(0^{++})$$

OMITTED FROM SUMMARY TABLE

was X(4700)

This state shows properties different from a conventional $q\bar{q}$ state. A candidate for an exotic structure. See the review on non- $q\bar{q}$ states.

Seen by AAIJ 17C in $B^+ \rightarrow \chi_{c0}K^+$, $\chi_{c0} \rightarrow J/\psi\phi$ using an amplitude analysis of $B^+ \rightarrow J/\psi\phi K^+$ with a significance (accounting for systematic uncertainties) of 5.6σ .

 $\chi_{c0}(4700)$ MASS

VALUE (MeV)	EVTS	DOCUMENT ID	TECN	COMMENT
$4694 \pm 4^{+16}_{-3}$	24k	¹ AAIJ	21E LHCb	$B^+ \rightarrow J/\psi\phi K^+$
$4741 \pm 6 \pm 6$	175	² AAIJ	21c LHCb	$B_S^0 \rightarrow J/\psi\phi\pi^+\pi^-$
$4704 \pm 10^{+14}_{-24}$	4289	^{3,4} AAIJ	17c LHCb	$B^+ \rightarrow J/\psi\phi K^+$

¹ From an amplitude analysis of the decay $B^+ \rightarrow J/\psi\phi K^+$ with a significance of 17σ .

² From a 1D fit to the $J/\psi\phi$ mass distribution with a significance of 5.3σ . The identification of this structure as the $\chi_{c0}(4700)$ needs confirmation.

³ From an amplitude analysis of the decay $B^+ \rightarrow J/\psi\phi K^+$ with a significance of 5.6σ .

⁴ Superseded by AAIJ 21E.

 $\chi_{c0}(4700)$ WIDTH

VALUE (MeV)	EVTS	DOCUMENT ID	TECN	COMMENT
$87 \pm 8^{+16}_{-6}$	24k	¹ AAIJ	21E LHCb	$B^+ \rightarrow J/\psi\phi K^+$
$53 \pm 15 \pm 11$	175	² AAIJ	21c LHCb	$B_S^0 \rightarrow J/\psi\phi\pi^+\pi^-$
$120 \pm 31^{+42}_{-33}$	4289	^{3,4} AAIJ	17c LHCb	$B^+ \rightarrow J/\psi\phi K^+$

¹ From an amplitude analysis of the decay $B^+ \rightarrow J/\psi\phi K^+$ with a significance of 17σ .

² From a 1D fit to the $J/\psi\phi$ mass distribution with a significance of 5.3σ . The identification of this structure as the $\chi_{c0}(4700)$ needs confirmation.

³ From an amplitude analysis of the decay $B^+ \rightarrow J/\psi\phi K^+$ with a significance of 5.6σ .

⁴ Superseded by AAIJ 21E.

 $\chi_{c0}(4700)$ DECAY MODES

Mode	Fraction (Γ_i/Γ)
Γ_1 $J/\psi\phi$	seen

 $\chi_{c0}(4700)$ BRANCHING RATIOS

$\Gamma(J/\psi\phi)/\Gamma_{\text{total}}$ Γ_1/Γ

VALUE	EVTS	DOCUMENT ID	TECN	COMMENT
seen	24k	¹ AAIJ	21E LHCb	$B^+ \rightarrow J/\psi\phi K^+$
seen	175	² AAIJ	21c LHCb	$B_S^0 \rightarrow J/\psi\phi\pi^+\pi^-$
seen	4289	^{3,4} AAIJ	17c LHCb	$B^+ \rightarrow J/\psi\phi K^+$

¹ From an amplitude analysis of the decay $B^+ \rightarrow J/\psi\phi K^+$ with a significance of 17σ .

² From a 1D fit to the $J/\psi\phi$ mass distribution with a significance of 5.3σ . The identification of this structure as the $\chi_{c0}(4700)$ needs confirmation.

³ From an amplitude analysis of the decay $B^+ \rightarrow J/\psi\phi K^+$ with a significance of 5.6σ .

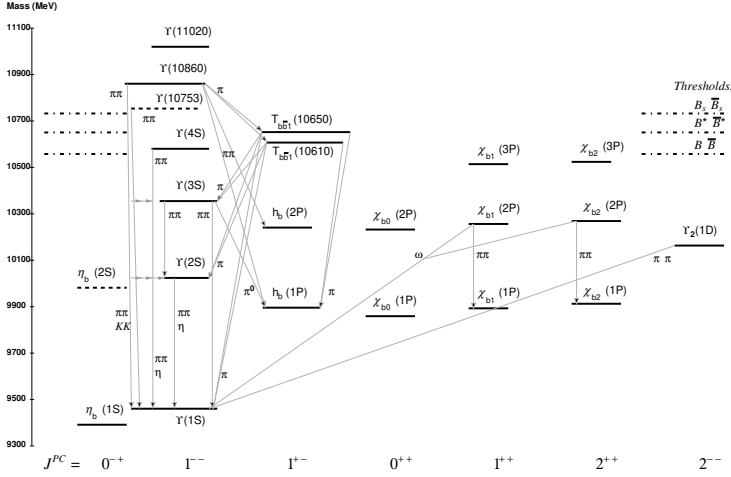
⁴ Superseded by AAIJ 21E.

 $\chi_{c0}(4700)$ REFERENCES

AAIJ 21C JHEP 2102 024 R. Aaij *et al.* (LHCb Collab.)
 AAIJ 21E PRL 127 082001 R. Aaij *et al.* (LHCb Collab.)
 AAIJ 17C PRL 118 022003 R. Aaij *et al.* (LHCb Collab.) JP
 Also PR D95 012002 R. Aaij *et al.* (LHCb Collab.)

$b\bar{b}$ MESONS (including possibly non- $q\bar{q}$ states)

Updated March 2024.



The level scheme of meson states containing a minimal quark content of $b\bar{b}$ and having $S = C = B = 0$. The name of a state is determined by its quantum numbers $I^G J^{PC}$ (see the review “Naming Scheme for Hadrons”). States included in the Summary Tables are shown with solid lines; those requiring confirmation are shown with dotted lines. The arrows indicate the most dominant hadronic transitions. Single photon transitions, including $\Upsilon(nS) \rightarrow \gamma\eta_b(mS)$, $\Upsilon(nS) \rightarrow \gamma\chi_{bJ}(mP)$, and $\chi_{bJ}(nP) \rightarrow \gamma\Upsilon(mS)$, are omitted for clarity. For orientation, the location of the thresholds related to a pair of ground state open bottom mesons is indicated in the figure. Decays to open flavour final states are not shown in the figure. The transitions $\Upsilon(10753) \rightarrow \omega\chi_{b1}(1P)$, $\omega\chi_{b2}(1P)$ have also been reported.

WIDTH DETERMINATIONS OF THE Υ STATES

As is the case for the $J/\psi(1S)$ and $\psi(2S)$, the full widths of the $b\bar{b}$ states $\Upsilon(1S)$, $\Upsilon(2S)$, and $\Upsilon(3S)$ are not directly measurable, since they are much narrower than the energy resolution of the e^+e^- storage rings where these states are produced. The common indirect method to determine Γ starts from

$$\Gamma = \Gamma_{\ell\ell}/B_{\ell\ell}, \quad (1)$$

where $\Gamma_{\ell\ell}$ is one leptonic partial width and $B_{\ell\ell}$ is the corresponding branching fraction ($\ell = e, \mu, \text{ or } \tau$). One then assumes $e\text{-}\mu\text{-}\tau$ universality and uses

$$\begin{aligned} \Gamma_{\ell\ell} &= \Gamma_{ee} \\ B_{\ell\ell} &= \text{average of } B_{ee}, B_{\mu\mu}, \text{ and } B_{\tau\tau}. \end{aligned} \quad (2)$$

The electronic partial width Γ_{ee} is also not directly measurable at e^+e^- storage rings, only in the combination $\Gamma_{ee}\Gamma_{\text{had}}/\Gamma$, where Γ_{had} is the hadronic partial width and

$$\Gamma_{\text{had}} + 3\Gamma_{ee} = \Gamma. \quad (3)$$

This combination is obtained experimentally from the energy-integrated hadronic cross section

$$\begin{aligned} &\int_{\text{resonance}} \sigma(e^+e^- \rightarrow \Upsilon \rightarrow \text{hadrons})dE \\ &= \frac{6\pi^2 \Gamma_{ee}\Gamma_{\text{had}}}{M^2 \Gamma} C_r = \frac{6\pi^2 \Gamma_{ee}^{(0)}\Gamma_{\text{had}}}{M^2 \Gamma} C_r^{(0)}, \end{aligned} \quad (4)$$

where M is the Υ mass, and C_r and $C_r^{(0)}$ are radiative correction factors. C_r is used for obtaining Γ_{ee} as defined in Eq. (1), and contains corrections from all orders of QED for describing $(b\bar{b}) \rightarrow e^+e^-$. The lowest order QED value $\Gamma_{ee}^{(0)}$, relevant for comparison with potential-model calculations, is defined by the lowest order QED graph (Born term) alone, and is about 7% lower than Γ_{ee} .

The Listings give experimental results on B_{ee} , $B_{\mu\mu}$, $B_{\tau\tau}$, and $\Gamma_{ee}\Gamma_{\text{had}}/\Gamma$. The entries of the last quantity have been re-evaluated consistently using the correction procedure of KURAEV 85 [1]. The partial width Γ_{ee} is obtained from the average values for $\Gamma_{ee}\Gamma_{\text{had}}/\Gamma$ and $B_{\ell\ell}$ using

$$\Gamma_{ee} = \frac{\Gamma_{ee}\Gamma_{\text{had}}}{\Gamma(1 - 3B_{\ell\ell})}. \quad (5)$$

The total width Γ is then obtained from Eq. (1). We do not list Γ_{ee} and Γ values of individual experiments. The Γ_{ee} values in the Meson Summary Table are also those defined in Eq. (1).

References

1. E.A. Kuraev, V.S. Fadin, Sov. J. Nucl. Phys. **41**, 466 (1985).

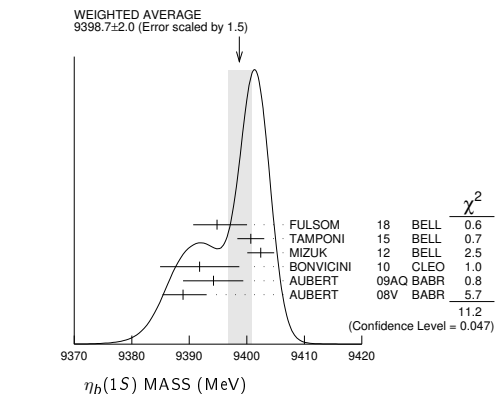
$\eta_b(1S)$

$$I^G(J^{PC}) = 0^+(0^{-+})$$

Quantum numbers shown are quark-model predictions. Observed in radiative decay of the $\Upsilon(3S)$, therefore $C = +$.

$\eta_b(1S)$ MASS

VALUE (MeV)	EVTS	DOCUMENT ID	TECN	COMMENT
9398.7 ± 2.0 OUR AVERAGE		Error includes scale factor of 1.5. See the ideogram below.		
9394.8 ^{+2.7+4.5} _{-3.1-2.7}	29k	FULSOM	18 BELL	$\Upsilon(2S) \rightarrow \gamma X$
9400.7 ± 1.7 ± 1.6	33.1k	TAMPONI	15 BELL	$e^+e^- \rightarrow \gamma\eta + \text{hadrons}$
9402.4 ± 1.5 ± 1.8	34k	1 MIZUK	12 BELL	$e^+e^- \rightarrow \gamma\pi^+\pi^- + \text{hadrons}$
9391.8 ± 6.6 ± 2.0	2.3k	2 BONVICINI	10 CLEO	$\Upsilon(3S) \rightarrow \gamma X$
9394.2 ^{+4.8+2.0} _{-4.9}	13k	2 AUBERT	09AQ BABR	$\Upsilon(2S) \rightarrow \gamma X$
9388.9 ^{+3.1+2.7} _{-2.3}	19k	2 AUBERT	08V BABR	$\Upsilon(3S) \rightarrow \gamma X$
9393.2 ± 3.4 ± 2.3	10	2,3 DOBBS	12	$\Upsilon(2S) \rightarrow \gamma \text{hadrons}$
9300 ± 20 ± 20		HEISTER	02D ALEP	181-209 e^+e^-



¹With floating width. Not independent of the corresponding mass difference measurement.

Meson Particle Listings

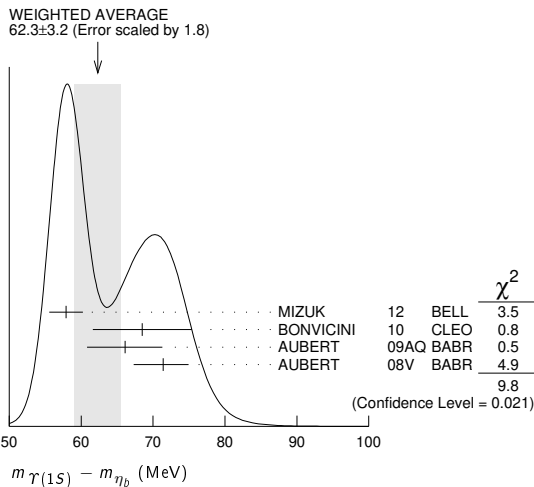
$\eta_b(1S), \Upsilon(1S)$

² Assuming $\Gamma_{\eta_b(1S)} = 10$ MeV. Not independent of the corresponding γ energy or mass difference measurements.
³ Obtained by analyzing CLEO III data but not authored by the CLEO Collaboration.

$m_{\Upsilon(1S)} - m_{\eta_b}$

VALUE (MeV)	EVTS	DOCUMENT ID	TECN	COMMENT
62.3 ± 3.2 OUR AVERAGE	34k			Error includes scale factor of 1.8. See the ideogram below.
57.9 ± 1.5 ± 1.8		¹ MIZUK	12 BELL	$e^+e^- \rightarrow \gamma\pi^+\pi^-$ + hadrons
68.5 ± 6.6 ± 2.0	2.3 ± 0.5k	² BONVICINI	10 CLEO	$\Upsilon(3S) \rightarrow \gamma X$
66.1 ^{+4.8} _{-4.9} ± 2.0	13 ± 5k	² AUBERT	09AQ BABR	$\Upsilon(2S) \rightarrow \gamma X$
71.4 ^{+2.3} _{-3.1} ± 2.7	19 ± 3k	² AUBERT	08V BABR	$\Upsilon(3S) \rightarrow \gamma X$
67.1 ± 3.4 ± 2.3	10 ⁺⁵ ₋₄	^{2,3} DOBBS	12	$\Upsilon(2S) \rightarrow \gamma$ hadrons

• • • We do not use the following data for averages, fits, limits, etc. • • •
¹ With floating width. Not independent of the corresponding mass measurement.
² Assuming $\Gamma_{\eta_b(1S)} = 10$ MeV. Not independent of the corresponding γ energy or mass measurements.
³ Obtained by analyzing CLEO III data but not authored by the CLEO Collaboration.



γ ENERGY IN $\Upsilon(3S)$ DECAY

VALUE (MeV)	EVTS	DOCUMENT ID	TECN	COMMENT
920.6^{+2.8}_{-3.2} OUR AVERAGE				
918.6 ± 6.0 ± 1.9	2.3 ± 0.5k	¹ BONVICINI	10 CLEO	$\Upsilon(3S) \rightarrow \gamma X$
921.2 ^{+2.1} _{-2.8} ± 2.4	19 ± 3k	¹ AUBERT	08V BABR	$\Upsilon(3S) \rightarrow \gamma X$

¹ Assuming $\Gamma_{\eta_b(1S)} = 10$ MeV. Not independent of the corresponding mass or mass difference measurements.

γ ENERGY IN $\Upsilon(2S)$ DECAY

VALUE (MeV)	EVTS	DOCUMENT ID	TECN	COMMENT
609.3^{+4.6}_{-4.5} ± 1.9	13 ± 5k	¹ AUBERT	09AQ BABR	$\Upsilon(2S) \rightarrow \gamma X$

¹ Assuming $\Gamma_{\eta_b(1S)} = 10$ MeV. Not independent of the corresponding mass or mass difference measurements.

$\eta_b(1S)$ WIDTH

VALUE (MeV)	EVTS	DOCUMENT ID	TECN	COMMENT
10⁺⁵₋₄ OUR AVERAGE				
8 ⁺⁶ ₋₅ ± 5	33.1k	¹ TAMPONI	15 BELL	$e^+e^- \rightarrow \gamma\eta$ + hadrons
10.8 ^{+4.0} _{-3.7} ± 4.5	34k	¹ MIZUK	12 BELL	$e^+e^- \rightarrow \gamma\pi^+\pi^-$ + hadrons

¹ With floating mass.

$\eta_b(1S)$ DECAY MODES

Mode	Fraction (Γ_i/Γ)	Confidence level
Γ_1 hadrons	seen	
Γ_2 $3h^+3h^-$	not seen	
Γ_3 $2h^+2h^-$	not seen	
Γ_4 $4h^+4h^-$	not seen	
Γ_5 $\gamma\gamma$	not seen	
Γ_6 $\mu^+\mu^-$	$< 9 \times 10^{-3}$	90%
Γ_7 $\tau^+\tau^-$	$< 8\%$	90%

$\eta_b(1S) \Gamma(i)\Gamma(\gamma\gamma)/\Gamma(\text{total})$

VALUE (eV)	CL%	DOCUMENT ID	TECN	COMMENT
$\Gamma(3h^+3h^-) \times \Gamma(\gamma\gamma)/\Gamma_{\text{total}}$				
< 470	95	ABDALLAH	06 DLPH	161-209 e^+e^-
< 132	95	HEISTER	02D ALEP	181-209 e^+e^-

• • • We do not use the following data for averages, fits, limits, etc. • • •

VALUE (eV)	CL%	DOCUMENT ID	TECN	COMMENT
$\Gamma(2h^+2h^-) \times \Gamma(\gamma\gamma)/\Gamma_{\text{total}}$				
< 190	95	ABDALLAH	06 DLPH	161-209 e^+e^-
< 48	95	HEISTER	02D ALEP	181-209 e^+e^-

• • • We do not use the following data for averages, fits, limits, etc. • • •

VALUE (eV)	CL%	DOCUMENT ID	TECN	COMMENT
$\Gamma(4h^+4h^-) \times \Gamma(\gamma\gamma)/\Gamma_{\text{total}}$				
< 660	95	ABDALLAH	06 DLPH	161-209 e^+e^-

• • • We do not use the following data for averages, fits, limits, etc. • • •

$\eta_b(1S)$ BRANCHING RATIOS

$\Gamma(\text{hadrons})/\Gamma_{\text{total}}$	VALUE	EVTS	DOCUMENT ID	TECN	COMMENT
seen	34k		MIZUK	12 BELL	$e^+e^- \rightarrow \gamma\pi^+\pi^-$ + hadrons

$\Gamma(\mu^+\mu^-)/\Gamma_{\text{total}}$	VALUE	CL%	DOCUMENT ID	TECN	COMMENT
$< 9 \times 10^{-3}$	90		¹ AUBERT	09Z BABR	$e^+e^- \rightarrow \Upsilon(2S, 3S) \rightarrow \gamma\eta_b$

¹ Obtained using $B(\Upsilon(2S) \rightarrow \gamma\eta_b) = (4.2^{+1.1}_{-1.0} \pm 0.9) \times 10^{-4}$ and $B(\Upsilon(3S) \rightarrow \gamma\eta_b) = (4.8 \pm 0.5 \pm 0.6) \times 10^{-4}$. This limit is equivalent to $B(\eta_b \rightarrow \mu^+\mu^-) = (-0.25 \pm 0.51 \pm 0.33)\%$ measurement.

$\Gamma(\tau^+\tau^-)/\Gamma_{\text{total}}$	VALUE	CL%	DOCUMENT ID	TECN	COMMENT
$< 8 \times 10^{-2}$	90		AUBERT	09P BABR	$e^+e^- \rightarrow \gamma\tau^+\tau^-$

$\eta_b(1S)$ REFERENCES

FULSOM	18	PRL 121 232001	B. G. Fulsom <i>et al.</i>	(BELLE Collab.)
TAMPONI	15	PRL 115 142001	U. Tamponi <i>et al.</i>	(BELLE Collab.)
DOBBS	12	PRL 109 082001	S. Dobbs <i>et al.</i>	
MIZUK	12	PRL 109 232002	R. Mizuk <i>et al.</i>	(BELLE Collab.)
BONVICINI	10	PR D81 031104	G. Bonvicini <i>et al.</i>	(CLEO Collab.)
AUBERT	09AQ	PRL 103 161801	B. Aubert <i>et al.</i>	(BABAR Collab.)
AUBERT	09P	PRL 103 181801	B. Aubert <i>et al.</i>	(BABAR Collab.)
AUBERT	09Z	PRL 103 081803	B. Aubert <i>et al.</i>	(BABAR Collab.)
AUBERT	08V	PRL 101 071801	B. Aubert <i>et al.</i>	(BABAR Collab.)
ABDALLAH	06	PL B634 340	J. M. Abdallah <i>et al.</i>	(DELPHI Collab.)
HEISTER	02D	PL B530 56	A. Heister <i>et al.</i>	(ALEPH Collab.)

$\Upsilon(1S)$

$$J^{PC} = 0^{-}(1^{-}-)$$

$\Upsilon(1S)$ MASS

VALUE (MeV)	DOCUMENT ID	TECN	COMMENT
9460.40 ± 0.09 ± 0.04	¹ SHAMOV	23 RVUE	$e^+e^- \rightarrow$ hadrons
9460.11 ± 0.11 ± 0.07	² SHAMOV	23 RVUE	$e^+e^- \rightarrow$ hadrons
9460.51 ± 0.09 ± 0.05	^{3,4} ARTAMONOV	00 MD1	$e^+e^- \rightarrow$ hadrons
9460.60 ± 0.09 ± 0.05	^{5,6} BARU	92B MD1	$e^+e^- \rightarrow$ hadrons
9460.59 ± 0.12	BARU	86 MD1	$e^+e^- \rightarrow$ hadrons
9460.6 ± 0.4	^{6,7} ARTAMONOV	84 MD1	$e^+e^- \rightarrow$ hadrons
9459.97 ± 0.11 ± 0.07	⁸ MACKAY	84 CUSB	$e^+e^- \rightarrow$ hadrons

¹ Reanalysis of MD1 data using the electron mass from COHEN 87, the radiative corrections from KURAEV 85 and interference effects.
² Obtained by reanalysing CUSB data (MACKAY 84), but not authored by the CUSB collaboration.
³ Reanalysis of BARU 92B and ARTAMONOV 84 using new electron mass (COHEN 87).
⁴ Superseded by SHAMOV 23.
⁵ Supersedes BARU 86.
⁶ Superseded by ARTAMONOV 00.
⁷ Value includes data of ARTAMONOV 82.
⁸ Reanalysed by SHAMOV 23.

$\Upsilon(1S)$ WIDTH

VALUE (keV)	DOCUMENT ID	COMMENT
54.02 ± 1.25 OUR EVALUATION		See the Note on "Width Determinations of the Υ States"

$\Upsilon(1S)$ DECAY MODES

Mode	Fraction (Γ_i/Γ)	Scale factor/ Confidence level
Γ_1 $\tau^+ \tau^-$	(2.60 ± 0.10) %	
Γ_2 $e^+ e^-$	(2.39 ± 0.08) %	
Γ_3 $\mu^+ \mu^-$	(2.48 ± 0.04) %	
Hadronic decays		
Γ_4 ggg	(81.7 ± 0.7) %	
Γ_5 γgg	(2.2 ± 0.6) %	
Γ_6 $\eta'(958)$ anything	(2.94 ± 0.24) %	
Γ_7 $J/\psi(1S)$ anything	(5.4 ± 0.4) × 10 ⁻⁴	S=1.4
Γ_8 $J/\psi(1S)\eta_c$	< 2.2	× 10 ⁻⁶ CL=90%
Γ_9 $J/\psi(1S)\chi_{c0}$	< 3.4	× 10 ⁻⁶ CL=90%
Γ_{10} $J/\psi(1S)\chi_{c1}$	(3.9 ± 1.2) × 10 ⁻⁶	
Γ_{11} $J/\psi(1S)\chi_{c2}$	< 1.4	× 10 ⁻⁶ CL=90%
Γ_{12} $J/\psi(1S)\eta_c(2S)$	< 2.2	× 10 ⁻⁶ CL=90%
Γ_{13} $J/\psi(1S)X(3940)$	< 5.4	× 10 ⁻⁶ CL=90%
Γ_{14} $J/\psi(1S)X(4160)$	< 5.4	× 10 ⁻⁶ CL=90%
Γ_{15} $X(4350)$ anything, $X \rightarrow J/\psi(1S)\phi$	< 8.1	× 10 ⁻⁶ CL=90%
Γ_{16} $T_{c\bar{c}1}(3900)^\pm$ anything, $T_{c\bar{c}1} \rightarrow J/\psi(1S)\pi^\pm$	< 1.3	× 10 ⁻⁵ CL=90%
Γ_{17} $T_{c\bar{c}1}(4200)^\pm$ anything, $Z_c \rightarrow J/\psi(1S)\pi^\pm$	< 6.0	× 10 ⁻⁵ CL=90%
Γ_{18} $T_{c\bar{c}1}(4430)^\pm$ anything, $T_{c\bar{c}1} \rightarrow J/\psi(1S)\pi^\pm$	< 4.9	× 10 ⁻⁵ CL=90%
Γ_{19} X_{cs}^\pm anything, $X \rightarrow J/\psi K^\pm$	< 5.7	× 10 ⁻⁶ CL=90%
Γ_{20} $\psi(4230)$ anything, $\psi \rightarrow J/\psi(1S)\pi^+\pi^-$	< 3.8	× 10 ⁻⁵ CL=90%
Γ_{21} $\psi(4230)$ anything, $\psi \rightarrow J/\psi(1S)K^+K^-$	< 7.5	× 10 ⁻⁶ CL=90%
Γ_{22} $\chi_{c1}(4140)$ anything, $\chi_{c1} \rightarrow J/\psi(1S)\phi$	< 5.2	× 10 ⁻⁶ CL=90%
Γ_{23} χ_{c0} anything	< 4	× 10 ⁻³ CL=90%
Γ_{24} χ_{c1} anything	(1.90 ± 0.35) × 10 ⁻⁴	
Γ_{25} $\chi_{c1}(1P)X_{tetra}$	< 3.78	× 10 ⁻⁵ CL=90%
Γ_{26} χ_{c2} anything	(2.8 ± 0.8) × 10 ⁻⁴	
Γ_{27} $\psi(2S)$ anything	(1.23 ± 0.20) × 10 ⁻⁴	
Γ_{28} $\psi(2S)\eta_c$	< 3.6	× 10 ⁻⁶ CL=90%
Γ_{29} $\psi(2S)\chi_{c0}$	< 6.5	× 10 ⁻⁶ CL=90%
Γ_{30} $\psi(2S)\chi_{c1}$	< 4.5	× 10 ⁻⁶ CL=90%
Γ_{31} $\psi(2S)\chi_{c2}$	< 2.1	× 10 ⁻⁶ CL=90%
Γ_{32} $\psi(2S)\eta_c(2S)$	< 3.2	× 10 ⁻⁶ CL=90%
Γ_{33} $\psi(2S)X(3940)$	< 2.9	× 10 ⁻⁶ CL=90%
Γ_{34} $\psi(2S)X(4160)$	< 2.9	× 10 ⁻⁶ CL=90%
Γ_{35} $\psi(4230)$ anything, $\psi \rightarrow \psi(2S)\pi^+\pi^-$	< 7.9	× 10 ⁻⁵ CL=90%
Γ_{36} $\psi(4360)$ anything, $\psi \rightarrow \psi(2S)\pi^+\pi^-$	< 5.2	× 10 ⁻⁵ CL=90%
Γ_{37} $\psi(4660)$ anything, $\psi \rightarrow \psi(2S)\pi^+\pi^-$	< 2.2	× 10 ⁻⁵ CL=90%
Γ_{38} $T_{c\bar{c}1}(4050)^\pm$ anything, $X \rightarrow \psi(2S)\pi^\pm$	< 8.8	× 10 ⁻⁵ CL=90%
Γ_{39} $T_{c\bar{c}1}(4430)^\pm$ anything, $T_{c\bar{c}1} \rightarrow \psi(2S)\pi^\pm$	< 6.7	× 10 ⁻⁵ CL=90%
Γ_{40} $\chi_{c1}(3872)$ anything	< 2.7	× 10 ⁻⁴ CL=90%
Γ_{41} $T_{c\bar{c}1}(4200)^+ T_{c\bar{c}1}(4200)^-$	< 2.23	× 10 ⁻⁵ CL=90%
Γ_{42} $T_{c\bar{c}1}(3900)^\pm T_{c\bar{c}1}(4200)^\mp$	< 8.1	× 10 ⁻⁶ CL=90%
Γ_{43} $T_{c\bar{c}1}(3900)^+ T_{c\bar{c}1}(3900)^-$	< 1.8	× 10 ⁻⁶ CL=90%
Γ_{44} $T_{c\bar{c}1}(4050)^+ T_{c\bar{c}1}(4050)^-$	< 1.58	× 10 ⁻⁵ CL=90%
Γ_{45} $T_{c\bar{c}1}(4250)^+ T_{c\bar{c}1}(4250)^-$	< 2.66	× 10 ⁻⁵ CL=90%
Γ_{46} $T_{c\bar{c}1}(4050)^\pm T_{c\bar{c}1}(4250)^\mp$	< 4.42	× 10 ⁻⁵ CL=90%
Γ_{47} $T_{c\bar{c}1}(4430)^+ T_{c\bar{c}1}(4430)^-$	< 2.03	× 10 ⁻⁵ CL=90%
Γ_{48} $T_{c\bar{c}1}(4055)^\pm T_{c\bar{c}1}(4055)^\mp$	< 2.33	× 10 ⁻⁵ CL=90%
Γ_{49} $T_{c\bar{c}1}(4055)^\pm T_{c\bar{c}1}(4430)^\mp$	< 4.55	× 10 ⁻⁵ CL=90%
Γ_{50} $\rho\pi$	< 3.68	× 10 ⁻⁶ CL=90%
Γ_{51} $\omega\pi^0$	< 3.90	× 10 ⁻⁶ CL=90%
Γ_{52} $\pi^+ \pi^-$	< 5	× 10 ⁻⁴ CL=90%
Γ_{53} $K^+ K^-$	< 5	× 10 ⁻⁴ CL=90%
Γ_{54} $p\bar{p}$	< 5	× 10 ⁻⁴ CL=90%
Γ_{55} $\pi^+ \pi^- \pi^0$	(2.1 ± 0.8) × 10 ⁻⁶	
Γ_{56} $\phi K^+ K^-$	(2.4 ± 0.5) × 10 ⁻⁶	
Γ_{57} $\omega\pi^+\pi^-$	(4.5 ± 1.0) × 10 ⁻⁶	
Γ_{58} $K^*(892)^0 K^- \pi^+ + c.c.$	(4.4 ± 0.8) × 10 ⁻⁶	

Γ_{59} $\phi f_2'(1525)$	< 1.63	× 10 ⁻⁶ CL=90%
Γ_{60} $\omega f_2'(1270)$	< 1.79	× 10 ⁻⁶ CL=90%
Γ_{61} $\rho(770) a_2(1320)$	< 2.24	× 10 ⁻⁶ CL=90%
Γ_{62} $K^*(892)^0 \bar{K}_2^0(1430)^0 + c.c.$	(3.0 ± 0.8) × 10 ⁻⁶	
Γ_{63} $K_1(1270)^\pm K^\mp$	< 2.41	× 10 ⁻⁶ CL=90%
Γ_{64} $K_1(1400)^\pm K^\mp$	(1.0 ± 0.4) × 10 ⁻⁶	
Γ_{65} $b_1(1235)^\pm \pi^\mp$	< 1.25	× 10 ⁻⁶ CL=90%
Γ_{66} $\pi^+ \pi^- \pi^0 \pi^0$	(1.28 ± 0.30) × 10 ⁻⁵	
Γ_{67} $K_S^0 K^+ \pi^- + c.c.$	(1.6 ± 0.4) × 10 ⁻⁶	
Γ_{68} $K^*(892)^0 \bar{K}^0 + c.c.$	(2.9 ± 0.9) × 10 ⁻⁶	
Γ_{69} $K^*(892)^- K^+ + c.c.$	< 1.11	× 10 ⁻⁶ CL=90%
Γ_{70} $f_1(1285)$ anything	(4.6 ± 3.1) × 10 ⁻³	
Γ_{71} $D^*(2010)^\pm$ anything	(2.52 ± 0.20) %	
Γ_{72} $f_1(1285)X_{tetra}$	< 6.24	× 10 ⁻⁵ CL=90%
Γ_{73} 2H anything	(2.85 ± 0.25) × 10 ⁻⁵	
Γ_{74} Sum of 100 exclusive modes	(1.200 ± 0.017) %	
Radiative decays		
Γ_{75} $\gamma\pi^+\pi^-$	(6.3 ± 1.8) × 10 ⁻⁵	
Γ_{76} $\gamma\pi^0\pi^0$	(1.7 ± 0.7) × 10 ⁻⁵	
Γ_{77} $\gamma\pi\pi$ (S-wave)	(4.6 ± 0.7) × 10 ⁻⁵	
Γ_{78} $\gamma\pi^0\eta$	< 2.4	× 10 ⁻⁶ CL=90%
Γ_{79} $\gamma K^+ K^-$	[a] (1.14 ± 0.13) × 10 ⁻⁵	
Γ_{80} $\gamma p\bar{p}$	[b] < 6	× 10 ⁻⁶ CL=90%
Γ_{81} $\gamma 2h^+ 2h^-$	(7.0 ± 1.5) × 10 ⁻⁴	
Γ_{82} $\gamma 3h^+ 3h^-$	(5.4 ± 2.0) × 10 ⁻⁴	
Γ_{83} $\gamma 4h^+ 4h^-$	(7.4 ± 3.5) × 10 ⁻⁴	
Γ_{84} $\gamma\pi^+\pi^- K^+ K^-$	(2.9 ± 0.9) × 10 ⁻⁴	
Γ_{85} $\gamma 2\pi^+ 2\pi^-$	(2.5 ± 0.9) × 10 ⁻⁴	
Γ_{86} $\gamma 3\pi^+ 3\pi^-$	(2.5 ± 1.2) × 10 ⁻⁴	
Γ_{87} $\gamma 2\pi^+ 2\pi^- K^+ K^-$	(2.4 ± 1.2) × 10 ⁻⁴	
Γ_{88} $\gamma\pi^+\pi^- p\bar{p}$	(1.5 ± 0.6) × 10 ⁻⁴	
Γ_{89} $\gamma 2\pi^+ 2\pi^- p\bar{p}$	(4 ± 6) × 10 ⁻⁵	
Γ_{90} $\gamma 2K^+ 2K^-$	(2.0 ± 2.0) × 10 ⁻⁵	
Γ_{91} $\gamma\eta'(958)$	< 1.9	× 10 ⁻⁶ CL=90%
Γ_{92} $\gamma\eta$	< 1.0	× 10 ⁻⁶ CL=90%
Γ_{93} $\gamma f_0(980)$	< 3	× 10 ⁻⁵ CL=90%
Γ_{94} $\gamma f_2'(1525)$	(2.9 ± 0.6) × 10 ⁻⁵	
Γ_{95} $\gamma f_2(1270)$	(1.01 ± 0.06) × 10 ⁻⁴	
Γ_{96} $\gamma\eta(1405)$	< 8.2	× 10 ⁻⁵ CL=90%
Γ_{97} $\gamma f_0(1500)$	< 1.5	× 10 ⁻⁵ CL=90%
Γ_{98} $\gamma f_0(1500) \rightarrow \gamma K^+ K^-$	(1.0 ± 0.4) × 10 ⁻⁵	
Γ_{99} $\gamma f_0(1710)$	< 2.6	× 10 ⁻⁴ CL=90%
Γ_{100} $\gamma f_0(1710) \rightarrow \gamma K^+ K^-$	(1.01 ± 0.32) × 10 ⁻⁵	
Γ_{101} $\gamma f_0(1710) \rightarrow \gamma\pi^+\pi^-$	(5.3 ± 2.0) × 10 ⁻⁶	
Γ_{102} $\gamma f_0(1710) \rightarrow \gamma\pi^0\pi^0$	< 1.4	× 10 ⁻⁶ CL=90%
Γ_{103} $\gamma f_0(1710) \rightarrow \gamma\eta\eta$	< 1.8	× 10 ⁻⁶ CL=90%
Γ_{104} $\gamma f_4(2050)$	< 5.3	× 10 ⁻⁵ CL=90%
Γ_{105} $\gamma f_6(2200) \rightarrow \gamma K^+ K^-$	< 2	× 10 ⁻⁴ CL=90%
Γ_{106} $\gamma f_J(2220) \rightarrow \gamma K^+ K^-$	< 8	× 10 ⁻⁷ CL=90%
Γ_{107} $\gamma f_J(2220) \rightarrow \gamma\pi^+\pi^-$	< 6	× 10 ⁻⁷ CL=90%
Γ_{108} $\gamma f_J(2220) \rightarrow \gamma p\bar{p}$	< 1.1	× 10 ⁻⁶ CL=90%
Γ_{109} $\gamma\eta(2225) \rightarrow \gamma\phi\phi$	< 3	× 10 ⁻³ CL=90%
Γ_{110} $\gamma\eta_c(1S)$	< 2.9	× 10 ⁻⁵ CL=90%
Γ_{111} $\gamma\eta_c(2S)$	< 4	× 10 ⁻⁴ CL=90%
Γ_{112} $\gamma\chi_{c0}$	< 6.6	× 10 ⁻⁵ CL=90%
Γ_{113} $\gamma\chi_{c1}$	(4.7 ^{+2.4} _{-1.9}) × 10 ⁻⁵	
Γ_{114} $\gamma\chi_{c2}$	< 7.6	× 10 ⁻⁶ CL=90%
Γ_{115} $\gamma\chi_{c1}(3872)$	< 5	× 10 ⁻⁵ CL=90%
Γ_{116} $\gamma\chi_{c1}(3872), \chi_{c1} \rightarrow \pi^+\pi^-\pi^0 J/\psi$	< 2.8	× 10 ⁻⁶ CL=90%
Γ_{117} $\gamma\chi_{c0}(3915) \rightarrow \omega J/\psi$	< 3.0	× 10 ⁻⁶ CL=90%
Γ_{118} $\gamma\chi_{c1}(4140) \rightarrow \phi J/\psi$	< 2.2	× 10 ⁻⁶ CL=90%
Γ_{119} $\gamma X\bar{X} (m_X < 3.1 \text{ GeV})$	[c] < 1	× 10 ⁻³ CL=90%
Γ_{120} $\gamma X\bar{X} (m_X < 4.5 \text{ GeV})$	[d] < 2.4	× 10 ⁻⁴ CL=90%
Γ_{121} $\gamma X \rightarrow \gamma + \geq 4 \text{ prongs}$	[e] < 1.78	× 10 ⁻⁴ CL=95%
Γ_{122} γA^0	[f]	
Γ_{123} $\gamma A^0 \rightarrow \gamma\mu^+\mu^-$	[g] < 9	× 10 ⁻⁶ CL=90%
Γ_{124} $\gamma A^0 \rightarrow \gamma\tau^+\tau^-$	[a] < 1.30	× 10 ⁻⁴ CL=90%
Γ_{125} $\gamma A^0 \rightarrow \gamma gg$	[h] < 1	% CL=90%
Γ_{126} $\gamma A^0 \rightarrow \gamma s\bar{s}$	[h] < 1	× 10 ⁻³ CL=90%
Lepton Family number (LF) violating modes		
Γ_{127} $e^\pm \mu^\mp$	LF < 3.9	× 10 ⁻⁷ CL=90%
Γ_{128} $\mu^\pm \tau^\mp$	LF < 2.7	× 10 ⁻⁶ CL=90%

Meson Particle Listings

 $\Upsilon(1S)$

Γ_{129}	$e^{\pm}\tau^{\mp}$	LF	< 2.7	$\times 10^{-6}$	CL=90%				
Γ_{130}	$\gamma e^{\pm}\mu^{\mp}$	LF	< 4.2	$\times 10^{-7}$	CL=90%				
Γ_{131}	$\gamma\mu^{\pm}\tau^{\mp}$	LF	< 6.1	$\times 10^{-6}$	CL=90%				
Γ_{132}	$\gamma e^{\pm}\tau^{\mp}$	LF	< 6.5	$\times 10^{-6}$	CL=90%				

Other decays

Γ_{133}	invisible		< 3.0	$\times 10^{-4}$	CL=90%				
Γ_{134}	hadrons		(96 \pm 4)	%					

[a] $2m_{\tau} < M(\tau^{+}\tau^{-}) < 9.2$ GeV

[b] 2 GeV $< m_{K^{+}K^{-}} < 3$ GeV

[c] $X\bar{X}$ = vectors with $m < 3.1$ GeV

[d] X and \bar{X} = zero spin with $m < 4.5$ GeV

[e] 1.5 GeV $< m_{X} < 5.0$ GeV

[f] A^0 = scalar with $m < 8.0$ GeV

[g] 201 MeV $< M(\mu^{+}\mu^{-}) < 3565$ MeV

[h] 0.5 GeV $< m_{X} < 9.0$ GeV, where m_{X} is the invariant mass of the hadronic final state.

 $\Upsilon(1S) \Gamma(i)\Gamma(e^{+}e^{-})/\Gamma(\text{total})$

$\Gamma(\mu^{+}\mu^{-}) \times \Gamma(e^{+}e^{-})/\Gamma(\text{total})$	Γ_{32}/Γ		
VALUE (eV)	DOCUMENT ID	TECN	COMMENT
31.2\pm1.6\pm1.7	KOBEL	92	CBAL $e^{+}e^{-} \rightarrow \mu^{+}\mu^{-}$

$\Gamma(\text{hadrons}) \times \Gamma(e^{+}e^{-})/\Gamma(\text{total})$	Γ_{1342}/Γ		
VALUE (keV)	DOCUMENT ID	TECN	COMMENT
1.240\pm0.016 OUR AVERAGE			
1.252 \pm 0.004 \pm 0.019	¹ ROSNER	06	CLEO 9.5 $e^{+}e^{-} \rightarrow$ hadrons
1.187 \pm 0.023 \pm 0.031	¹ BARU	92B	MD1 $e^{+}e^{-} \rightarrow$ hadrons
1.23 \pm 0.02 \pm 0.05	¹ JAKUBOWSKI	88	CBAL $e^{+}e^{-} \rightarrow$ hadrons
1.37 \pm 0.06 \pm 0.09	² GILES	84B	CLEO $e^{+}e^{-} \rightarrow$ hadrons
1.23 \pm 0.08 \pm 0.04	² ALBRECHT	82	DASP $e^{+}e^{-} \rightarrow$ hadrons
1.13 \pm 0.07 \pm 0.11	² NICZYPORUK	82	LENA $e^{+}e^{-} \rightarrow$ hadrons
1.09 \pm 0.25	² BOCK	80	CNTR $e^{+}e^{-} \rightarrow$ hadrons
1.35 \pm 0.14	³ BERGER	79	PLUT $e^{+}e^{-} \rightarrow$ hadrons

¹ Radiative corrections evaluated following KURAEV 85.² Radiative corrections reevaluated by BUCHMUELLER 88 following KURAEV 85.³ Radiative corrections reevaluated by ALEXANDER 89 using $B(\mu\mu) = 0.026$. $\Upsilon(1S)$ PARTIAL WIDTHS

$\Gamma(e^{+}e^{-})$	Γ_2
VALUE (keV)	DOCUMENT ID
1.340\pm0.018 OUR EVALUATION	

 $\Upsilon(1S)$ BRANCHING RATIOS

$\Gamma(\tau^{+}\tau^{-})/\Gamma(\text{total})$	Γ_1/Γ			
VALUE (units 10^{-2})	EVTS	DOCUMENT ID	TECN	COMMENT
2.60\pm0.10 OUR AVERAGE				
2.53 \pm 0.13 \pm 0.04	60k	¹ BESSON	07	CLEO $e^{+}e^{-} \rightarrow \Upsilon(1S) \rightarrow \tau^{+}\tau^{-}$
2.61 \pm 0.12 \pm 0.09	25k	CINABRO	94B	CLE2 $e^{+}e^{-} \rightarrow \tau^{+}\tau^{-}$
2.7 \pm 0.4 \pm 0.2		² ALBRECHT	85c	ARG $\Upsilon(2S) \rightarrow \pi^{+}\pi^{-}\tau^{+}\tau^{-}$
3.4 \pm 0.4 \pm 0.4		GILES	83	CLEO $e^{+}e^{-} \rightarrow \tau^{+}\tau^{-}$

¹ BESSON 07 reports $[\Gamma(\Upsilon(1S) \rightarrow \tau^{+}\tau^{-})/\Gamma(\text{total})] / [B(\Upsilon(1S) \rightarrow \mu^{+}\mu^{-})] = 1.02 \pm 0.02 \pm 0.05$ which we multiply by our best value $B(\Upsilon(1S) \rightarrow \mu^{+}\mu^{-}) = (2.48 \pm 0.04) \times 10^{-2}$. Our first error is their experiment's error and our second error is the systematic error from using our best value.² Using $B(\Upsilon(1S) \rightarrow ee) = B(\Upsilon(1S) \rightarrow \mu\mu) = 0.0256$; not used for width evaluations.

$\Gamma(e^{+}e^{-})/\Gamma(\text{total})$	Γ_2/Γ			
VALUE (units 10^{-2})	EVTS	DOCUMENT ID	TECN	COMMENT
2.39\pm0.08 OUR AVERAGE				
2.40 \pm 0.01 \pm 0.12	191k	PATRA	22	BELL $\Upsilon(2S) \rightarrow \pi^{+}\pi^{-}e^{+}e^{-}$
2.29 \pm 0.08 \pm 0.11		ALEXANDER	98	CLE2 $\Upsilon(2S) \rightarrow \pi^{+}\pi^{-}e^{+}e^{-}$
2.42 \pm 0.14 \pm 0.14	307	ALBRECHT	87	ARG $\Upsilon(2S) \rightarrow \pi^{+}\pi^{-}e^{+}e^{-}$
2.8 \pm 0.3 \pm 0.2	826	BESSON	84	CLEO $\Upsilon(2S) \rightarrow \pi^{+}\pi^{-}e^{+}e^{-}$
5.1 \pm 3.0		BERGER	80c	PLUT $e^{+}e^{-} \rightarrow e^{+}e^{-}$

$\Gamma(\mu^{+}\mu^{-})/\Gamma(\text{total})$	Γ_3/Γ			
VALUE (units 10^{-2})	EVTS	DOCUMENT ID	TECN	COMMENT
2.48\pm0.04 OUR AVERAGE				
2.46 \pm 0.01 \pm 0.11	246k	PATRA	22	BELL $\Upsilon(2S) \rightarrow \pi^{+}\pi^{-}\mu^{+}\mu^{-}$
2.49 \pm 0.02 \pm 0.07	345k	ADAMS	05	CLEO $e^{+}e^{-} \rightarrow \mu^{+}\mu^{-}$
2.49 \pm 0.08 \pm 0.13		ALEXANDER	98	CLE2 $\Upsilon(2S) \rightarrow \pi^{+}\pi^{-}\mu^{+}\mu^{-}$
2.12 \pm 0.20 \pm 0.10		¹ BARU	92	MD1 $e^{+}e^{-} \rightarrow \mu^{+}\mu^{-}$
2.31 \pm 0.12 \pm 0.10		¹ KOBEL	92	CBAL $e^{+}e^{-} \rightarrow \mu^{+}\mu^{-}$

2.52 \pm 0.07 \pm 0.07		CHEN	89b	CLEO $e^{+}e^{-} \rightarrow \mu^{+}\mu^{-}$
2.61 \pm 0.09 \pm 0.11		KAARSBERG	89	CSB2 $e^{+}e^{-} \rightarrow \mu^{+}\mu^{-}$
2.30 \pm 0.25 \pm 0.13	86	ALBRECHT	87	ARG $\Upsilon(2S) \rightarrow \pi^{+}\pi^{-}\mu^{+}\mu^{-}$
2.9 \pm 0.3 \pm 0.2	864	BESSON	84	CLEO $\Upsilon(2S) \rightarrow \pi^{+}\pi^{-}\mu^{+}\mu^{-}$
2.7 \pm 0.3 \pm 0.3		ANDREWS	83	CLEO $e^{+}e^{-} \rightarrow \mu^{+}\mu^{-}$
3.2 \pm 1.3 \pm 0.3		ALBRECHT	82	DASP $e^{+}e^{-} \rightarrow \mu^{+}\mu^{-}$
3.8 \pm 1.5 \pm 0.2		NICZYPORUK	82	LENA $e^{+}e^{-} \rightarrow \mu^{+}\mu^{-}$
1.4 \pm 3.4		BOCK	80	CNTR $e^{+}e^{-} \rightarrow \mu^{+}\mu^{-}$
2.2 \pm 2.0		BERGER	79	PLUT $e^{+}e^{-} \rightarrow \mu^{+}\mu^{-}$

¹ Taking into account interference between the resonance and continuum.

$\Gamma(\tau^{+}\tau^{-})/\Gamma(\mu^{+}\mu^{-})$	Γ_1/Γ_3			
VALUE	EVTS	DOCUMENT ID	TECN	COMMENT
1.008\pm0.023 OUR AVERAGE				
1.005 \pm 0.013 \pm 0.022	0.7M	¹ DEL-AMO-SA...	10c	BABR $\Upsilon(3S) \rightarrow \pi^{+}\pi^{-}\Upsilon(1S)$
1.02 \pm 0.02 \pm 0.05	60k	BESSON	07	CLEO $e^{+}e^{-} \rightarrow \Upsilon(1S)$

¹ Allows any number of extra photons with total energy < 500 MeV.

$\Gamma(ggg)/\Gamma(\text{total})$	Γ_4/Γ			
VALUE (units 10^{-2})	EVTS	DOCUMENT ID	TECN	COMMENT
81.7\pm0.7	20M	¹ BESSON	06A	CLEO $\Upsilon(1S) \rightarrow$ hadrons

¹ Calculated using the value $\Gamma(\gamma gg)/\Gamma(ggg) = (2.70 \pm 0.01 \pm 0.13 \pm 0.24)\%$ from BESSON 06A and PDG 08 values of $B(\mu^{+}\mu^{-}) = (2.48 \pm 0.05)\%$ and $R_{\text{hadrons}} = 3.51$. The statistical error is negligible and the systematic error is partially correlated with that of $\Gamma(\gamma gg)/\Gamma(\text{total})$ measurement of BESSON 06A.

$\Gamma(\gamma gg)/\Gamma(\text{total})$	Γ_5/Γ			
VALUE (units 10^{-2})	EVTS	DOCUMENT ID	TECN	COMMENT
2.20\pm0.60	400k	¹ BESSON	06A	CLEO $\Upsilon(1S) \rightarrow \gamma +$ hadrons

¹ Calculated using BESSON 06A values of $\Gamma(\gamma gg)/\Gamma(ggg) = (2.70 \pm 0.01 \pm 0.13 \pm 0.24)\%$ and $\Gamma(ggg)/\Gamma(\text{total})$. The statistical error is negligible and the systematic error is partially correlated with that of $\Gamma(ggg)/\Gamma(\text{total})$ measurement of BESSON 06A.

$\Gamma(\gamma gg)/\Gamma(ggg)$	Γ_5/Γ_4			
VALUE (units 10^{-2})	EVTS	DOCUMENT ID	TECN	COMMENT
2.70\pm0.01\pm0.27	20M	BESSON	06A	CLEO $\Upsilon(1S) \rightarrow (\gamma +)$ hadrons

$\Gamma(\eta'(958) \text{ anything})/\Gamma(\text{total})$	Γ_6/Γ		
VALUE	DOCUMENT ID	TECN	COMMENT
0.0294\pm0.0024 OUR AVERAGE			
0.030 \pm 0.002 \pm 0.002	AQUINES	06A	CLE3 $\Upsilon(1S) \rightarrow \eta'/\text{anything}$
0.028 \pm 0.004 \pm 0.002	ARTUSO	03	CLE2 $\Upsilon(1S) \rightarrow \eta'/\text{anything}$

$\Gamma(J/\psi(1S) \text{ anything})/\Gamma(\text{total})$	Γ_7/Γ			
VALUE (units 10^{-4})	CL% EVTS	DOCUMENT ID	TECN	COMMENT
5.4 \pm 0.4 OUR FIT				Error includes scale factor of 1.4.
5.4 \pm 0.4 OUR AVERAGE				Error includes scale factor of 1.5.
5.25 \pm 0.13 \pm 0.25	3k	SHEN	16	BELL $e^{+}e^{-} \rightarrow J/\psi X$
6.4 \pm 0.4 \pm 0.6	730	BRIERE	04	CLEO $e^{+}e^{-} \rightarrow J/\psi X$
11 \pm 4 \pm 2		¹ FULTON	89	CLEO $e^{+}e^{-} \rightarrow \mu^{+}\mu^{-} X$

••• We do not use the following data for averages, fits, limits, etc. •••

<6.8	90	ALBRECHT	92j	ARG $e^{+}e^{-} \rightarrow e^{+}e^{-} X, \mu^{+}\mu^{-} X$
<17	90	MASCHMANN	90	CBAL $e^{+}e^{-} \rightarrow$ hadrons
<200	90	NICZYPORUK	83	LENA

¹ Using $B((J/\psi) \rightarrow \mu^{+}\mu^{-}) = (6.9 \pm 0.9)\%$.

$\Gamma(J/\psi(1S)\eta_c)/\Gamma(\text{total})$	Γ_8/Γ			
VALUE	CL%	DOCUMENT ID	TECN	COMMENT
<2.2 $\times 10^{-6}$	90	YANG	14	BELL $e^{+}e^{-} \rightarrow J/\psi X$

$\Gamma(J/\psi(1S)\chi_{c0})/\Gamma(\text{total})$	Γ_9/Γ			
VALUE	CL%	DOCUMENT ID	TECN	COMMENT
<3.4 $\times 10^{-6}$	90	YANG	14	BELL $e^{+}e^{-} \rightarrow J/\psi X$

$\Gamma(J/\psi(1S)\chi_{c1})/\Gamma(\text{total})$	Γ_{10}/Γ			
VALUE (units 10^{-6})	EVTS	DOCUMENT ID	TECN	COMMENT
3.90\pm1.21\pm0.23	20	YANG	14	BELL $e^{+}e^{-} \rightarrow J/\psi X$

$\Gamma(J/\psi(1S)\chi_{c2})/\Gamma(\text{total})$	Γ_{11}/Γ			
VALUE	CL%	DOCUMENT ID	TECN	COMMENT
<1.4 $\times 10^{-6}$	90	YANG	14	BELL $e^{+}e^{-} \rightarrow J/\psi X$

$\Gamma(J/\psi(1S)\eta_c(2S))/\Gamma(\text{total})$	Γ_{12}/Γ			
VALUE	CL%	DOCUMENT ID	TECN	COMMENT
<2.2 $\times 10^{-6}$	90	YANG	14	BELL $e^{+}e^{-} \rightarrow J/\psi X$

$\Gamma(J/\psi(1S)X(3940))/\Gamma(\text{total})$	Γ_{13}/Γ			
VALUE	CL%	DOCUMENT ID	TECN	COMMENT
<5.4 $\times 10^{-6}$	90	YANG	14	BELL $e^{+}e^{-} \rightarrow J/\psi X$

See key on page 1171

Meson Particle Listings
 $\Upsilon(1S)$

$\Gamma(J/\psi(1S)X(4160))/\Gamma_{\text{total}}$					Γ_{14}/Γ
VALUE	CL%	DOCUMENT ID	TECN	COMMENT	
$<5.4 \times 10^{-6}$	90	YANG	14	BELL	$e^+e^- \rightarrow J/\psi X$

$\Gamma(X(4350) \text{ anything}, X \rightarrow J/\psi(1S)\phi)/\Gamma_{\text{total}}$					Γ_{15}/Γ
VALUE	CL%	DOCUMENT ID	TECN	COMMENT	
$<8.1 \times 10^{-6}$	90	SHEN	16	BELL	$\Upsilon(1S) \rightarrow J/\psi K^+ K^- X$

$\Gamma(T_{c\bar{c}1}(3900)^\pm \text{ anything}, T_{c\bar{c}1} \rightarrow J/\psi(1S)\pi^\pm)/\Gamma_{\text{total}}$					Γ_{16}/Γ
VALUE	CL%	DOCUMENT ID	TECN	COMMENT	
$<1.3 \times 10^{-5}$	90	SHEN	16	BELL	$\Upsilon(1S) \rightarrow J/\psi \pi^\pm X$

$\Gamma(T_{c\bar{c}1}(4200)^\pm \text{ anything}, Z_c \rightarrow J/\psi(1S)\pi^\pm)/\Gamma_{\text{total}}$					Γ_{17}/Γ
VALUE	CL%	DOCUMENT ID	TECN	COMMENT	
$<6.0 \times 10^{-5}$	90	SHEN	16	BELL	$\Upsilon(1S) \rightarrow J/\psi \pi^\pm X$

$\Gamma(T_{c\bar{c}1}(4430)^\pm \text{ anything}, T_{c\bar{c}1} \rightarrow J/\psi(1S)\pi^\pm)/\Gamma_{\text{total}}$					Γ_{18}/Γ
VALUE	CL%	DOCUMENT ID	TECN	COMMENT	
$<4.9 \times 10^{-5}$	90	SHEN	16	BELL	$\Upsilon(1S) \rightarrow J/\psi \pi^\pm X$

$\Gamma(X_{cb}^\pm \text{ anything}, X \rightarrow J/\psi K^\pm)/\Gamma_{\text{total}}$					Γ_{19}/Γ
VALUE	CL%	DOCUMENT ID	TECN	COMMENT	
$<5.7 \times 10^{-6}$	90	SHEN	16	BELL	$\Upsilon(1S) \rightarrow J/\psi K^- X$

$\Gamma(\psi(4230) \text{ anything}, \psi \rightarrow J/\psi(1S)\pi^+\pi^-)/\Gamma_{\text{total}}$					Γ_{20}/Γ
VALUE	CL%	DOCUMENT ID	TECN	COMMENT	
$<3.8 \times 10^{-5}$	90	SHEN	16	BELL	$\Upsilon(1S) \rightarrow J/\psi \pi^+ \pi^- X$

$\Gamma(\psi(4230) \text{ anything}, \psi \rightarrow J/\psi(1S)K^+K^-)/\Gamma_{\text{total}}$					Γ_{21}/Γ
VALUE	CL%	DOCUMENT ID	TECN	COMMENT	
$<7.5 \times 10^{-6}$	90	SHEN	16	BELL	$\Upsilon(1S) \rightarrow J/\psi K^+ K^- X$

$\Gamma(\chi_{c1}(4140) \text{ anything}, \chi_{c1} \rightarrow J/\psi(1S)\phi)/\Gamma_{\text{total}}$					Γ_{22}/Γ
VALUE	CL%	DOCUMENT ID	TECN	COMMENT	
$<5.2 \times 10^{-6}$	90	SHEN	16	BELL	$\Upsilon(1S) \rightarrow J/\psi K^+ K^- X$

$\Gamma(\chi_{c0} \text{ anything})/\Gamma(J/\psi(1S) \text{ anything})$					Γ_{23}/Γ_7
VALUE	CL%	DOCUMENT ID	TECN	COMMENT	
<7.4	90	BRIERE	04	CLEO	$e^+e^- \rightarrow J/\psi X$

$\Gamma(\chi_{c1} \text{ anything})/\Gamma_{\text{total}}$					Γ_{24}/Γ
VALUE (units 10^{-4})	EVTS	DOCUMENT ID	TECN	COMMENT	
1.90 ± 0.35	OUR FIT				
$1.90 \pm 0.43 \pm 0.14$	215	JIA	17	BELL	$\Upsilon(1S) \rightarrow \gamma J/\psi(1S)$

$\Gamma(\chi_{c1} \text{ anything})/\Gamma(J/\psi(1S) \text{ anything})$					Γ_{24}/Γ_7
VALUE	EVTS	DOCUMENT ID	TECN	COMMENT	
0.35 ± 0.07	OUR FIT				
$0.35 \pm 0.08 \pm 0.06$	52 ± 12	BRIERE	04	CLEO	$e^+e^- \rightarrow J/\psi X$

$\Gamma(\chi_{c1}(1P)X_{tetra})/\Gamma_{\text{total}}$					Γ_{25}/Γ
VALUE	CL%	DOCUMENT ID	TECN	COMMENT	
$<37.8 \times 10^{-6}$	90	¹ JIA	17A	BELL	$e^+e^- \rightarrow \text{hadrons}$

¹ For a tetraquark state X_{tetra} , with mass in the range 1.16–2.46 GeV and width in the range 0–0.3 GeV. Measured 90% CL limits as a function of X_{tetra} mass and width range from 4.4×10^{-6} to 37.8×10^{-6} .

$\Gamma(\chi_{c2} \text{ anything})/\Gamma(J/\psi(1S) \text{ anything})$					Γ_{26}/Γ_7
VALUE	EVTS	DOCUMENT ID	TECN	COMMENT	
$0.52 \pm 0.12 \pm 0.09$	47 ± 11	BRIERE	04	CLEO	$e^+e^- \rightarrow J/\psi X$

$\Gamma(\psi(2S) \text{ anything})/\Gamma_{\text{total}}$					Γ_{27}/Γ
VALUE (units 10^{-4})	EVTS	DOCUMENT ID	TECN	COMMENT	
$1.23 \pm 0.17 \pm 0.11$	215	SHEN	16	BELL	$e^+e^- \rightarrow \psi(2S) X$

$\Gamma(\psi(2S) \text{ anything})/\Gamma(J/\psi(1S) \text{ anything})$					Γ_{27}/Γ_7
VALUE	EVTS	DOCUMENT ID	TECN	COMMENT	
$0.41 \pm 0.11 \pm 0.08$	42 ± 11	BRIERE	04	CLEO	$e^+e^- \rightarrow J/\psi \pi^+ \pi^- X$

$\Gamma(\psi(2S)\eta_c)/\Gamma_{\text{total}}$					Γ_{28}/Γ
VALUE	CL%	DOCUMENT ID	TECN	COMMENT	
$<3.6 \times 10^{-6}$	90	YANG	14	BELL	$e^+e^- \rightarrow \psi(2S) X$

$\Gamma(\psi(2S)\chi_{c0})/\Gamma_{\text{total}}$					Γ_{29}/Γ
VALUE	CL%	DOCUMENT ID	TECN	COMMENT	
$<6.5 \times 10^{-6}$	90	YANG	14	BELL	$e^+e^- \rightarrow \psi(2S) X$

$\Gamma(\psi(2S)\chi_{c1})/\Gamma_{\text{total}}$					Γ_{30}/Γ
VALUE	CL%	DOCUMENT ID	TECN	COMMENT	
$<4.5 \times 10^{-6}$	90	YANG	14	BELL	$e^+e^- \rightarrow \psi(2S) X$

$\Gamma(\psi(2S)\chi_{c2})/\Gamma_{\text{total}}$					Γ_{31}/Γ
VALUE	CL%	DOCUMENT ID	TECN	COMMENT	
$<2.1 \times 10^{-6}$	90	YANG	14	BELL	$e^+e^- \rightarrow \psi(2S) X$

$\Gamma(\psi(2S)\eta_c(2S))/\Gamma_{\text{total}}$					Γ_{32}/Γ
VALUE	CL%	DOCUMENT ID	TECN	COMMENT	
$<3.2 \times 10^{-6}$	90	YANG	14	BELL	$e^+e^- \rightarrow \psi(2S) X$

$\Gamma(\psi(2S)X(3940))/\Gamma_{\text{total}}$					Γ_{33}/Γ
VALUE	CL%	DOCUMENT ID	TECN	COMMENT	
$<2.9 \times 10^{-6}$	90	YANG	14	BELL	$e^+e^- \rightarrow \psi(2S) X$

$\Gamma(\psi(2S)X(4160))/\Gamma_{\text{total}}$					Γ_{34}/Γ
VALUE	CL%	DOCUMENT ID	TECN	COMMENT	
$<2.9 \times 10^{-6}$	90	YANG	14	BELL	$e^+e^- \rightarrow \psi(2S) X$

$\Gamma(\psi(4230) \text{ anything}, \psi \rightarrow \psi(2S)\pi^+\pi^-)/\Gamma_{\text{total}}$					Γ_{35}/Γ
VALUE	CL%	DOCUMENT ID	TECN	COMMENT	
$<7.9 \times 10^{-5}$	90	SHEN	16	BELL	$\Upsilon(1S) \rightarrow \psi(2S)\pi^+\pi^- X$

$\Gamma(\psi(4360) \text{ anything}, \psi \rightarrow \psi(2S)\pi^+\pi^-)/\Gamma_{\text{total}}$					Γ_{36}/Γ
VALUE	CL%	DOCUMENT ID	TECN	COMMENT	
$<5.2 \times 10^{-5}$	90	SHEN	16	BELL	$\Upsilon(1S) \rightarrow \psi(2S)\pi^+\pi^- X$

$\Gamma(\psi(4660) \text{ anything}, \psi \rightarrow \psi(2S)\pi^+\pi^-)/\Gamma_{\text{total}}$					Γ_{37}/Γ
VALUE	CL%	DOCUMENT ID	TECN	COMMENT	
$<2.2 \times 10^{-5}$	90	SHEN	16	BELL	$\Upsilon(1S) \rightarrow \psi(2S)\pi^+\pi^- X$

$\Gamma(T_{c\bar{c}1}(4050)^\pm \text{ anything}, X \rightarrow \psi(2S)\pi^\pm)/\Gamma_{\text{total}}$					Γ_{38}/Γ
VALUE	CL%	DOCUMENT ID	TECN	COMMENT	
$<8.8 \times 10^{-5}$	90	SHEN	16	BELL	$\Upsilon(1S) \rightarrow \psi(2S)\pi^\pm X$

$\Gamma(T_{c\bar{c}1}(4430)^\pm \text{ anything}, T_{c\bar{c}1} \rightarrow \psi(2S)\pi^\pm)/\Gamma_{\text{total}}$					Γ_{39}/Γ
VALUE	CL%	DOCUMENT ID	TECN	COMMENT	
$<6.7 \times 10^{-5}$	90	SHEN	16	BELL	$\Upsilon(1S) \rightarrow \psi(2S)\pi^\pm X$

$\Gamma(\chi_{c1}(3872) \text{ anything})/\Gamma_{\text{total}}$					Γ_{40}/Γ
VALUE	CL%	DOCUMENT ID	TECN	COMMENT	
$<2.7 \times 10^{-4}$	90	¹ SHEN	16	BELL	$\Upsilon(1S) \rightarrow J/\psi \pi^+ \pi^- X$

¹ SHEN 16 reports $[\Gamma(\Upsilon(1S) \rightarrow \chi_{c1}(3872) \text{ anything})/\Gamma_{\text{total}}] \times [B(\chi_{c1}(3872) \rightarrow \pi^+\pi^- J/\psi(1S))] < 9.5 \times 10^{-6}$ which we divide by our best value $B(\chi_{c1}(3872) \rightarrow \pi^+\pi^- J/\psi(1S)) = 3.5 \times 10^{-2}$.

$\Gamma(T_{c\bar{c}1}(4200)^+ T_{c\bar{c}1}(4200)^-)/\Gamma_{\text{total}}$					Γ_{41}/Γ
VALUE	CL%	DOCUMENT ID	TECN	COMMENT	
$<22.3 \times 10^{-6}$	90	¹ JIA	18	BELL	$\Upsilon(1S) \rightarrow J/\psi \pi^\pm X$

¹ Assuming $B(T_{c\bar{c}1}(4200)^\pm \rightarrow J/\psi \pi^\pm) = 1$.

$\Gamma(T_{c\bar{c}1}(3900)^\pm T_{c\bar{c}1}(4200)^\mp)/\Gamma_{\text{total}}$					Γ_{42}/Γ
VALUE	CL%	DOCUMENT ID	TECN	COMMENT	
$<8.1 \times 10^{-6}$	90	¹ JIA	18	BELL	$\Upsilon(1S) \rightarrow J/\psi \pi^\pm X$

¹ Assuming $B(T_{c\bar{c}1}(4200)^\pm \rightarrow J/\psi \pi^\pm) = 1 = B(T_{c\bar{c}1}(3900)^\pm \rightarrow J/\psi \pi^\pm)$.

$\Gamma(T_{c\bar{c}1}(3900)^+ T_{c\bar{c}1}(3900)^-)/\Gamma_{\text{total}}$					Γ_{43}/Γ
VALUE	CL%	DOCUMENT ID	TECN	COMMENT	
$<1.8 \times 10^{-6}$	90	¹ JIA	18	BELL	$\Upsilon(1S) \rightarrow J/\psi \pi^\pm X$

¹ Assuming $B(T_{c\bar{c}1}(3900)^\pm \rightarrow J/\psi \pi^\pm) = 1$

$\Gamma(T_{c\bar{c}1}(4050)^+ T_{c\bar{c}1}(4050)^-)/\Gamma_{\text{total}}$					Γ_{44}/Γ
VALUE	CL%	DOCUMENT ID	TECN	COMMENT	
$<15.8 \times 10^{-6}$	90	¹ JIA	18	BELL	$\Upsilon(1S) \rightarrow \chi_{c1}(1P)\pi^\pm X$

¹ Assuming $B(T_{c\bar{c}1}(4050)^\pm \rightarrow \chi_{c1}(1P)\pi^\pm) = 1$

$\Gamma(T_{c\bar{c}1}(4250)^+ T_{c\bar{c}1}(4250)^-)/\Gamma_{\text{total}}$					Γ_{45}/Γ
VALUE	CL%	DOCUMENT ID	TECN	COMMENT	
$<26.6 \times 10^{-6}$	90	¹ JIA	18	BELL	$\Upsilon(1S) \rightarrow \chi_{c1}(1P)\pi^\pm X$

¹ Assuming $B(T_{c\bar{c}1}(4250)^\pm \rightarrow \chi_{c1}(1P)\pi^\pm) = 1$

$\Gamma(T_{c\bar{c}1}(4050)^\pm T_{c\bar{c}1}(4250)^\mp)/\Gamma_{\text{total}}$					Γ_{46}/Γ
VALUE	CL%	DOCUMENT ID	TECN	COMMENT	
$<44.2 \times 10^{-6}$	90	¹ JIA	18	BELL	$\Upsilon(1S) \rightarrow \chi_{c1}(1P)\pi^\pm X$

¹ Assuming $B(T_{c\bar{c}1}(4050)^\pm \rightarrow \chi_{c1}(1P)\pi^\pm) = 1 = B(T_{c\bar{c}1}(4250)^\pm \rightarrow \chi_{c1}(1P)\pi^\pm)$

$\Gamma(T_{c\bar{c}1}(4430)^+ T_{c\bar{c}1}(4430)^-)/\Gamma_{\text{total}}$					Γ_{47}/Γ
VALUE	CL%	DOCUMENT ID	TECN	COMMENT	
$<20.3 \times 10^{-6}$	90	¹ JIA	18	BELL	$\Upsilon(2S) \rightarrow \psi(2S)\pi^\pm X$

¹ Assuming $B(T_{c\bar{c}1}(4430)^\pm \rightarrow \psi(2S)\pi^\pm) = 1$

Meson Particle Listings

 $\Upsilon(1S)$

$\Gamma(T_{c\bar{c}}(4055)^\pm T_{c\bar{c}}(4055)^\mp)/\Gamma_{\text{total}}$					Γ_{48}/Γ
VALUE	CL%	DOCUMENT ID	TECN	COMMENT	
$<23.3 \times 10^{-6}$	90	¹ JIA	18	BELL $\Upsilon(1S) \rightarrow \psi(2S)\pi^\pm X$	
¹ Assuming $B(T_{c\bar{c}}(4055)^\pm \rightarrow \psi(2S)\pi^\pm) = 1$					

$\Gamma(T_{c\bar{c}}(4055)^\pm T_{c\bar{c}}(4430)^\mp)/\Gamma_{\text{total}}$					Γ_{49}/Γ
VALUE	CL%	DOCUMENT ID	TECN	COMMENT	
$<45.5 \times 10^{-6}$	90	¹ JIA	18	BELL $\Upsilon(1S) \rightarrow \psi(2S)\pi^\pm X$	
¹ Assuming $B(T_{c\bar{c}}(4055)^\pm \rightarrow \psi(2S)\pi^\pm) = 1 = B(T_{c\bar{c}}(4430)^\pm \rightarrow \psi(2S)\pi^\pm)$					

$\Gamma(\rho\pi)/\Gamma_{\text{total}}$					Γ_{50}/Γ
VALUE (units 10^{-6})	CL%	DOCUMENT ID	TECN	COMMENT	
<3.68	90	SHEN	13	BELL $\Upsilon(1S) \rightarrow \pi^+\pi^-\pi^0$	
••• We do not use the following data for averages, fits, limits, etc. •••					
$<1 \times 10^3$	90	BLINOV	90	MD1 $\Upsilon(1S) \rightarrow \rho^0\pi^0$	
$<2 \times 10^2$	90	FULTON	90B	$\Upsilon(1S) \rightarrow \rho^0\pi^0$	
$<2.1 \times 10^3$	90	NICZYPORUK	83	LENA $\Upsilon(1S) \rightarrow \rho^0\pi^0$	

$\Gamma(\omega\pi^0)/\Gamma_{\text{total}}$					Γ_{51}/Γ
VALUE (units 10^{-6})	CL%	DOCUMENT ID	TECN	COMMENT	
<3.90	90	SHEN	13	BELL $\Upsilon(1S) \rightarrow \pi^+\pi^-\pi^0\pi^0$	

$\Gamma(\pi^+\pi^-)/\Gamma_{\text{total}}$					Γ_{52}/Γ
VALUE (units 10^{-4})	CL%	DOCUMENT ID	TECN	COMMENT	
<5	90	BARU	92	MD1 $\Upsilon(1S) \rightarrow \pi^+\pi^-$	

$\Gamma(K^+K^-)/\Gamma_{\text{total}}$					Γ_{53}/Γ
VALUE (units 10^{-4})	CL%	DOCUMENT ID	TECN	COMMENT	
<5	90	BARU	92	MD1 $\Upsilon(1S) \rightarrow K^+K^-$	

$\Gamma(p\bar{p})/\Gamma_{\text{total}}$					Γ_{54}/Γ
VALUE (units 10^{-4})	CL%	DOCUMENT ID	TECN	COMMENT	
<5	90	¹ BARU	96	MD1 $\Upsilon(1S) \rightarrow p\bar{p}$	
¹ Supersedes BARU 92 in this node.					

$\Gamma(\pi^+\pi^-\pi^0)/\Gamma_{\text{total}}$					Γ_{55}/Γ
VALUE (units 10^{-6})	CL%	EVTS	DOCUMENT ID	TECN	COMMENT
$2.14 \pm 0.72 \pm 0.34$		26 ± 9	SHEN	13	BELL $\Upsilon(1S) \rightarrow \pi^+\pi^-\pi^0$
••• We do not use the following data for averages, fits, limits, etc. •••					
<18.4	90		ANASTASSOV	99	CLE2 $e^+e^- \rightarrow \text{hadrons}$

$\Gamma(\phi K^+K^-)/\Gamma_{\text{total}}$					Γ_{56}/Γ
VALUE (units 10^{-6})	EVTS	DOCUMENT ID	TECN	COMMENT	
$2.36 \pm 0.37 \pm 0.29$	56	SHEN	12A	BELL $\Upsilon(1S) \rightarrow 2(K^+K^-)$	

$\Gamma(\omega\pi^+\pi^-)/\Gamma_{\text{total}}$					Γ_{57}/Γ
VALUE (units 10^{-6})	EVTS	DOCUMENT ID	TECN	COMMENT	
$4.46 \pm 0.67 \pm 0.72$	64	SHEN	12A	BELL $\Upsilon(1S) \rightarrow 2(\pi^+\pi^-)\pi^0$	

$\Gamma(K^*(892)^0 K^- \pi^+ + \text{c.c.})/\Gamma_{\text{total}}$					Γ_{58}/Γ
VALUE (units 10^{-6})	EVTS	DOCUMENT ID	TECN	COMMENT	
$4.42 \pm 0.50 \pm 0.58$	173	SHEN	12A	BELL $\Upsilon(1S) \rightarrow K^+K^-\pi^+\pi^-$	

$\Gamma(\phi f_2(1525))/\Gamma_{\text{total}}$					Γ_{59}/Γ
VALUE (units 10^{-6})	CL%	DOCUMENT ID	TECN	COMMENT	
<1.63	90	SHEN	12A	BELL $\Upsilon(1S) \rightarrow 2(K^+K^-)$	

$\Gamma(\omega f_2(1270))/\Gamma_{\text{total}}$					Γ_{60}/Γ
VALUE (units 10^{-6})	CL%	DOCUMENT ID	TECN	COMMENT	
<1.79	90	SHEN	12A	BELL $\Upsilon(1S) \rightarrow 2(\pi^+\pi^-)\pi^0$	

$\Gamma(\rho(770)\rho_2(1320))/\Gamma_{\text{total}}$					Γ_{61}/Γ
VALUE (units 10^{-6})	CL%	DOCUMENT ID	TECN	COMMENT	
<2.24	90	SHEN	12A	BELL $\Upsilon(1S) \rightarrow 2(\pi^+\pi^-)\pi^0$	

$\Gamma(K^*(892)^0 \bar{K}_2^0(1430)^0 + \text{c.c.})/\Gamma_{\text{total}}$					Γ_{62}/Γ
VALUE (units 10^{-6})	EVTS	DOCUMENT ID	TECN	COMMENT	
$3.02 \pm 0.68 \pm 0.34$	42	SHEN	12A	BELL $\Upsilon(1S) \rightarrow K^+K^-\pi^+\pi^-$	

$\Gamma(K_1(1270)^\pm K^\mp)/\Gamma_{\text{total}}$					Γ_{63}/Γ
VALUE (units 10^{-6})	CL%	DOCUMENT ID	TECN	COMMENT	
<2.41	90	SHEN	12A	BELL $\Upsilon(1S) \rightarrow K^+K^-\pi^+\pi^-$	

$\Gamma(K_1(1400)^\pm K^\mp)/\Gamma_{\text{total}}$					Γ_{64}/Γ
VALUE (units 10^{-6})	EVTS	DOCUMENT ID	TECN	COMMENT	
$1.02 \pm 0.35 \pm 0.22$	24	SHEN	12A	BELL $\Upsilon(1S) \rightarrow K^+K^-\pi^+\pi^-$	

$\Gamma(b_1(1235)^\pm \pi^\mp)/\Gamma_{\text{total}}$					Γ_{65}/Γ
VALUE (units 10^{-6})	CL%	DOCUMENT ID	TECN	COMMENT	
<1.25	90	SHEN	12A	BELL $\Upsilon(1S) \rightarrow 2(\pi^+\pi^-)\pi^0$	

$\Gamma(\pi^+\pi^-\pi^0)/\Gamma_{\text{total}}$					Γ_{66}/Γ
VALUE (units 10^{-6})	EVTS	DOCUMENT ID	TECN	COMMENT	
$12.8 \pm 2.0 \pm 2.3$	143 ± 22	SHEN	13	BELL $\Upsilon(1S) \rightarrow \pi^+\pi^-\pi^0\pi^0$	

$\Gamma(K_S^0 K^+ \pi^- + \text{c.c.})/\Gamma_{\text{total}}$					Γ_{67}/Γ
VALUE (units 10^{-6})	CL%	EVTS	DOCUMENT ID	TECN	COMMENT
$1.59 \pm 0.33 \pm 0.18$		37 ± 8	SHEN	13	BELL $\Upsilon(1S) \rightarrow K_S^0 K^-\pi^+$
••• We do not use the following data for averages, fits, limits, etc. •••					
<3.4	90		¹ DOBBS	12A	$\Upsilon(1S) \rightarrow K_S^0 K^-\pi^+$
¹ Obtained by analyzing CLEO III data but not authored by the CLEO Collaboration.					

$\Gamma(K^*(892)^0 \bar{K}^0 + \text{c.c.})/\Gamma_{\text{total}}$					Γ_{68}/Γ
VALUE (units 10^{-6})	EVTS	DOCUMENT ID	TECN	COMMENT	
$2.92 \pm 0.85 \pm 0.37$	16 ± 5	SHEN	13	BELL $\Upsilon(1S) \rightarrow K_S^0 K^-\pi^+$	

$\Gamma(K^*(892)^- K^+ + \text{c.c.})/\Gamma_{\text{total}}$					Γ_{69}/Γ
VALUE (units 10^{-6})	CL%	DOCUMENT ID	TECN	COMMENT	
<1.11	90	SHEN	13	BELL $\Upsilon(1S) \rightarrow K_S^0 K^-\pi^+$	

$\Gamma(f_1(1285) \text{ anything})/\Gamma_{\text{total}}$					Γ_{70}/Γ
VALUE (units 10^{-3})	EVTS	DOCUMENT ID	TECN	COMMENT	
$4.6 \pm 2.8 \pm 1.3$	3.1k	JIA	17A	BELL $e^+e^- \rightarrow \text{hadrons}$	

$\Gamma(D^*(2010)^\pm \text{ anything})/\Gamma_{\text{total}}$					Γ_{71}/Γ
VALUE (units 10^{-3})	CL%	EVTS	DOCUMENT ID	TECN	COMMENT
$25.2 \pm 1.3 \pm 1.5$		$\approx 2k$	¹ AUBERT	10c	BABR $\Upsilon(2S) \rightarrow \pi^+\pi^-\Upsilon(1S)$
••• We do not use the following data for averages, fits, limits, etc. •••					
<19	90		² ALBRECHT	92J	ARG $e^+e^- \rightarrow D^0\pi^\pm X$
¹ For $x_p > 0.1$.					
² For $x_p > 0.2$.					

$\Gamma(f_1(1285) X_{tetra})/\Gamma_{\text{total}}$					Γ_{72}/Γ
VALUE	CL%	DOCUMENT ID	TECN	COMMENT	
$<62.4 \times 10^{-6}$	90	¹ JIA	17A	BELL $e^+e^- \rightarrow \text{hadrons}$	
¹ For a tetraquark state X_{tetra} , with mass in the range 1.16–2.46 GeV and width in the range 0–0.3 GeV. Measured 90% CL limits as a function of X_{tetra} mass and width range from 4.6×10^{-6} to 62.4×10^{-6} .					

$\Gamma(2H \text{ anything})/\Gamma_{\text{total}}$					Γ_{73}/Γ
VALUE (units 10^{-5})	EVTS	DOCUMENT ID	TECN	COMMENT	
2.85 ± 0.25	OUR AVERAGE				
$2.81 \pm 0.49 \pm 0.20$		LEES	14G	BABR $e^+e^- \rightarrow 2H X$	
$2.86 \pm 0.19 \pm 0.21$	455	ASNER	07	CLEO $e^+e^- \rightarrow 2H X$	

$\Gamma(\text{Sum of 100 exclusive modes})/\Gamma_{\text{total}}$					Γ_{74}/Γ
VALUE (units 10^{-2})	DOCUMENT ID	TECN	COMMENT		
1.200 ± 0.017	^{1,2} DOBBS	12A	$\Upsilon(1S) \rightarrow \text{hadrons}$		
¹ DOBBS 12A presents individual exclusive branching fractions or upper limits for 100 modes of four to ten pions, kaons, or protons.					
² Obtained by analyzing CLEO III data but not authored by the CLEO Collaboration.					

$\Gamma(ggg, \gamma g g \rightarrow \bar{d} \text{ anything})/\Gamma(ggg, \gamma g g \rightarrow \text{anything})$					Γ_{75}/Γ
VALUE (units 10^{-5})	EVTS	DOCUMENT ID	TECN	COMMENT	
$3.36 \pm 0.23 \pm 0.25$	455	ASNER	07	CLEO $e^+e^- \rightarrow \bar{d} X$	

$\Gamma(\gamma\pi^+\pi^-)/\Gamma_{\text{total}}$					Γ_{76}/Γ
VALUE (units 10^{-5})	DOCUMENT ID	TECN	COMMENT		
$6.3 \pm 1.2 \pm 1.3$	¹ ANASTASSOV	99	CLE2	$e^+e^- \rightarrow \text{hadrons}$	
¹ For $m_{\pi\pi} > 1$ GeV.					

$\Gamma(\gamma\pi^0\pi^0)/\Gamma_{\text{total}}$					Γ_{76}/Γ
VALUE (units 10^{-5})	DOCUMENT ID	TECN	COMMENT		
$1.7 \pm 0.6 \pm 0.3$	¹ ANASTASSOV	99	CLE2	$e^+e^- \rightarrow \text{hadrons}$	
¹ For $m_{\pi\pi} > 1$ GeV.					

$\Gamma(\gamma\pi\pi(\text{S-wave}))/\Gamma_{\text{total}}$					Γ_{77}/Γ
VALUE (units 10^{-5})	DOCUMENT ID	TECN	COMMENT		
$4.63 \pm 0.56 \pm 0.48$	LEES	18A	BABR	$\Upsilon(1S) \rightarrow \gamma\pi^+\pi^-$	

$\Gamma(\gamma\pi^0\eta)/\Gamma_{\text{total}}$					Γ_{78}/Γ
VALUE (units 10^{-6})	CL%	DOCUMENT ID	TECN	COMMENT	
<2.4	90	¹ BESSON	07A	CLEO $e^+e^- \rightarrow \Upsilon(1S)$	
¹ BESSON 07A obtained this limit for $0.7 < m_{\pi^0\eta} < 3$ GeV.					

Meson Particle Listings

$\Upsilon(1S)$

$\Gamma(\gamma K^+ K^-)/\Gamma_{total}$ ($2 < m_{K^+ K^-} < 3 \text{ GeV}$) Γ_{79}/Γ

VALUE (units 10^{-5})	CL%	DOCUMENT ID	TECN	COMMENT
1.14 ± 0.08 ± 0.10	90	ATHAR	06 CLE3	$\Upsilon(1S) \rightarrow \gamma K^+ K^-$

$\Gamma(\gamma p \bar{p})/\Gamma_{total}$ ($2 < m_{p \bar{p}} < 3 \text{ GeV}$) Γ_{80}/Γ

VALUE (units 10^{-5})	CL%	DOCUMENT ID	TECN	COMMENT
< 0.6	90	ATHAR	06 CLE3	$\Upsilon(1S) \rightarrow \gamma p \bar{p}$

$\Gamma(\gamma 2h + 2h^-)/\Gamma_{total}$ Γ_{81}/Γ

VALUE (units 10^{-4})	EVTS	DOCUMENT ID	TECN	COMMENT
7.0 ± 1.1 ± 1.0	80 ± 12	FULTON	90B CLEO	$e^+ e^- \rightarrow \text{hadrons}$

$\Gamma(\gamma 3h + 3h^-)/\Gamma_{total}$ Γ_{82}/Γ

VALUE (units 10^{-4})	EVTS	DOCUMENT ID	TECN	COMMENT
5.4 ± 1.5 ± 1.3	39 ± 11	FULTON	90B CLEO	$e^+ e^- \rightarrow \text{hadrons}$

$\Gamma(\gamma 4h + 4h^-)/\Gamma_{total}$ Γ_{83}/Γ

VALUE (units 10^{-4})	EVTS	DOCUMENT ID	TECN	COMMENT
7.4 ± 2.5 ± 2.5	36 ± 12	FULTON	90B CLEO	$e^+ e^- \rightarrow \text{hadrons}$

$\Gamma(\gamma \pi^+ \pi^- K^+ K^-)/\Gamma_{total}$ Γ_{84}/Γ

VALUE (units 10^{-4})	EVTS	DOCUMENT ID	TECN	COMMENT
2.9 ± 0.7 ± 0.6	29 ± 8	FULTON	90B CLEO	$e^+ e^- \rightarrow \text{hadrons}$

$\Gamma(\gamma 2\pi^+ 2\pi^-)/\Gamma_{total}$ Γ_{85}/Γ

VALUE (units 10^{-4})	EVTS	DOCUMENT ID	TECN	COMMENT
2.5 ± 0.7 ± 0.5	26 ± 7	FULTON	90B CLEO	$e^+ e^- \rightarrow \text{hadrons}$

$\Gamma(\gamma 3\pi^+ 3\pi^-)/\Gamma_{total}$ Γ_{86}/Γ

VALUE (units 10^{-4})	EVTS	DOCUMENT ID	TECN	COMMENT
2.5 ± 0.9 ± 0.8	17 ± 5	FULTON	90B CLEO	$e^+ e^- \rightarrow \text{hadrons}$

$\Gamma(\gamma 2\pi^+ 2\pi^- K^+ K^-)/\Gamma_{total}$ Γ_{87}/Γ

VALUE (units 10^{-4})	EVTS	DOCUMENT ID	TECN	COMMENT
2.4 ± 0.9 ± 0.8	18 ± 7	FULTON	90B CLEO	$e^+ e^- \rightarrow \text{hadrons}$

$\Gamma(\gamma \pi^+ \pi^- p \bar{p})/\Gamma_{total}$ Γ_{88}/Γ

VALUE (units 10^{-4})	EVTS	DOCUMENT ID	TECN	COMMENT
1.5 ± 0.5 ± 0.3	22 ± 6	FULTON	90B CLEO	$e^+ e^- \rightarrow \text{hadrons}$

$\Gamma(\gamma 2\pi^+ 2\pi^- p \bar{p})/\Gamma_{total}$ Γ_{89}/Γ

VALUE (units 10^{-4})	EVTS	DOCUMENT ID	TECN	COMMENT
0.4 ± 0.4 ± 0.4	7 ± 6	FULTON	90B CLEO	$e^+ e^- \rightarrow \text{hadrons}$

$\Gamma(\gamma 2K^+ 2K^-)/\Gamma_{total}$ Γ_{90}/Γ

VALUE (units 10^{-4})	EVTS	DOCUMENT ID	TECN	COMMENT
0.2 ± 0.2	2 ± 2	FULTON	90B CLEO	$e^+ e^- \rightarrow \text{hadrons}$

$\Gamma(\gamma \eta(958))/\Gamma_{total}$ Γ_{91}/Γ

VALUE (units 10^{-6})	CL%	DOCUMENT ID	TECN	COMMENT
< 1.9	90	ATHAR	07A CLEO	$\Upsilon(1S) \rightarrow \gamma \eta' \rightarrow \gamma \pi^+ \pi^- \eta, \gamma p$
<16	90	RICHICHI	01B CLE2	$\Upsilon(1S) \rightarrow \gamma \eta' \rightarrow \gamma \eta \pi^+ \pi^-$

$\Gamma(\gamma \eta)/\Gamma_{total}$ Γ_{92}/Γ

VALUE (units 10^{-6})	CL%	DOCUMENT ID	TECN	COMMENT
< 1.0	90	ATHAR	07A CLEO	$\Upsilon(1S) \rightarrow \gamma \eta \rightarrow \gamma \gamma \gamma, \gamma \pi^+ \pi^- \pi^0, \gamma 3\pi^0$

$\Gamma(\gamma f_0(980))/\Gamma_{total}$ Γ_{93}/Γ

VALUE (units 10^{-5})	CL%	DOCUMENT ID	TECN	COMMENT
< 3	90	ATHAR	06 CLE3	$\Upsilon(1S) \rightarrow \gamma \pi^+ \pi^-$

$\Gamma(\gamma f'_2(1525))/\Gamma_{total}$ Γ_{94}/Γ

VALUE (units 10^{-5})	CL%	EVTS	DOCUMENT ID	TECN	COMMENT
2.9 ± 0.6 OUR AVERAGE					
2.13 ± 0.28 ± 0.72			1 LEES	18A BABR	$\Upsilon(1S) \rightarrow \gamma K^+ K^-$
4.0 ± 1.4 ± 0.1	17		2 BESSON	11 CLEO	$\Upsilon(1S) \rightarrow K_S^0 K_S^0$
3.7 ± 0.9 ± 0.8			ATHAR	06 CLE3	$\Upsilon(1S) \rightarrow \gamma K^+ K^-$

• • • We do not use the following data for averages, fits, limits, etc. • • •

VALUE (units 10^{-5})	CL%	DOCUMENT ID	TECN	COMMENT
<14	90	3 FULTON	90B CLEO	$\Upsilon(1S) \rightarrow \gamma K^+ K^-$
<19.4	90	3 ALBRECHT	89 ARG	$\Upsilon(1S) \rightarrow \gamma K^+ K^-$

¹ Using $B(f'_2(1525) \rightarrow K \bar{K}) = 0.887 \pm 0.022$ and $B(K^0 \bar{K}^0) = 1/2 B(K \bar{K})$.

² BESSON 11 reports $(4.0 \pm 1.3 \pm 0.6) \times 10^{-5}$ from a measurement of $[\Gamma(\Upsilon(1S) \rightarrow \gamma f'_2(1525))/\Gamma_{total}] \times [B(f'_2(1525) \rightarrow K \bar{K})]$ assuming $B(f'_2(1525) \rightarrow K \bar{K}) = (88.8 \pm 3.1) \times 10^{-2}$, which we rescale to our best value $B(f'_2(1525) \rightarrow K \bar{K}) = (88.8 \pm 2.2) \times 10^{-2}$. Our first error is their experiment's error and our second error is the systematic error from using our best value. The result also assumes $B(K_S^0 \rightarrow \pi^+ \pi^-) = (69.20 \pm 0.05)\%$ and $B(f'_2(1525) \rightarrow K \bar{K}) = 4 B(f'_2(1525) \rightarrow K_S^0 K_S^0)$.

³ Assuming $B(f'_2(1525) \rightarrow K \bar{K}) = 0.71$.

$\Gamma(\gamma f_2(1270))/\Gamma_{total}$ Γ_{95}/Γ

VALUE (units 10^{-5})	CL%	DOCUMENT ID	TECN	COMMENT
10.1 ± 0.6 OUR AVERAGE				
10.15 ± 0.59 ± 0.43		1 LEES	18A BABR	$\Upsilon(1S) \rightarrow \gamma \pi^+ \pi^-$
10.5 ± 1.6 ± 1.8		2 BESSON	07A CLE3	$\Upsilon(1S) \rightarrow \gamma \pi^0 \pi^0$
10.2 ± 0.8 ± 0.7		ATHAR	06 CLE3	$\Upsilon(1S) \rightarrow \gamma \pi^+ \pi^-$
8.1 ± 2.3 ± 2.9 ± 2.7		3 ANASTASSOV	99 CLE2	$e^+ e^- \rightarrow \text{hadrons}$

• • • We do not use the following data for averages, fits, limits, etc. • • •

VALUE (units 10^{-5})	CL%	DOCUMENT ID	TECN	COMMENT
<21	90	3 FULTON	90B CLEO	$\Upsilon(1S) \rightarrow \gamma \pi^+ \pi^-$
<13	90	3 ALBRECHT	89 ARG	$\Upsilon(1S) \rightarrow \gamma \pi^+ \pi^-$
<81	90	SCHMITT	88 CBAL	$\Upsilon(1S) \rightarrow \gamma X$

¹ Using $B(f_2(1270) \rightarrow \pi^0 \pi^0) = 1/3 B(f_2(1270) \rightarrow \pi \pi)$ and $B(f_2(1270) \rightarrow \pi \pi) = (84.2 \pm 2.9 \pm 0.9)\%$.

² Using $B(f_2(1270) \rightarrow \pi^0 \pi^0) = B(f_2(1270) \rightarrow \pi \pi)/3$ and $B(f_2(1270) \rightarrow \pi \pi) = (84.7 \pm 2.5 \pm 1.2)\%$.

³ Using $B(f_2(1270) \rightarrow \pi \pi) = 0.84$.

$\Gamma(\gamma \eta(1405))/\Gamma_{total}$ Γ_{96}/Γ

VALUE (units 10^{-5})	CL%	DOCUMENT ID	TECN	COMMENT
< 8.2	90	1 FULTON	90B CLEO	$\Upsilon(1S) \rightarrow \gamma K^\pm \pi^\mp K_S^0$

¹ Includes unknown branching ratio of $\eta(1405) \rightarrow K^\pm \pi^\mp K_S^0$.

$\Gamma(\gamma f_0(1500))/\Gamma_{total}$ Γ_{97}/Γ

VALUE (units 10^{-5})	CL%	DOCUMENT ID	TECN	COMMENT
< 1.5	90	1 BESSON	07A CLEO	$e^+ e^- \rightarrow \Upsilon(1S) \rightarrow \gamma \pi^0 \pi^0$
<6.1	90	2 BESSON	07A CLEO	$e^+ e^- \rightarrow \Upsilon(1S) \rightarrow \gamma \eta \eta$

• • • We do not use the following data for averages, fits, limits, etc. • • •

¹ Using $B(f_0(1500) \rightarrow \pi^0 \pi^0) = B(f_0(1500) \rightarrow \pi \pi)/3$ and $B(f_0(1500) \rightarrow \pi \pi) = (0.349 \pm 0.023)\%$.

² Calculated by us using $B(f_0(1500) \rightarrow \eta \eta) = (5.1 \pm 0.9)\%$.

$\Gamma(\gamma f_0(1500) \rightarrow \gamma K^+ K^-)/\Gamma_{total}$ Γ_{98}/Γ

VALUE (units 10^{-5})	DOCUMENT ID	TECN	COMMENT
1.04 ± 0.14 ± 0.33	1 LEES	18A BABR	$e^+ e^- \rightarrow \Upsilon(1S) \rightarrow \gamma K^+ K^-$

¹ LEES 18A quotes $B(\Upsilon(1S) \rightarrow \gamma f_0(1500) \rightarrow \gamma K \bar{K}) = (2.08 \pm 0.27 \pm 0.65) \times 10^{-5}$ assuming $B(K^0 \bar{K}^0) = 1/2 B(K \bar{K})$.

$\Gamma(\gamma f_0(1710))/\Gamma_{total}$ Γ_{99}/Γ

VALUE (units 10^{-4})	CL%	DOCUMENT ID	TECN	COMMENT
< 2.6	90	1 ALBRECHT	89 ARG	$\Upsilon(1S) \rightarrow \gamma K^+ K^-$
< 6.3	90	1 FULTON	90B CLEO	$\Upsilon(1S) \rightarrow \gamma K^+ K^-$
< 19	90	1 FULTON	90B CLEO	$\Upsilon(1S) \rightarrow \gamma K_S^0 K_S^0$
< 8	90	2 ALBRECHT	89 ARG	$\Upsilon(1S) \rightarrow \gamma \pi^+ \pi^-$
< 24	90	3 SCHMITT	88 CBAL	$\Upsilon(1S) \rightarrow \gamma X$

¹ Assuming $B(f_0(1710) \rightarrow K \bar{K}) = 0.38$.

² Assuming $B(f_0(1710) \rightarrow \pi \pi) = 0.04$.

³ Assuming $B(f_0(1710) \rightarrow \eta \eta) = 0.18$.

$\Gamma(\gamma f_0(1710) \rightarrow \gamma K^+ K^-)/\Gamma_{total}$ Γ_{100}/Γ

VALUE (units 10^{-5})	CL%	DOCUMENT ID	TECN	COMMENT
1.01 ± 0.26 ± 0.18		1 LEES	18A BABR	$e^+ e^- \rightarrow \Upsilon(1S) \rightarrow \gamma K^+ K^-$

• • • We do not use the following data for averages, fits, limits, etc. • • •

VALUE (units 10^{-5})	CL%	DOCUMENT ID	TECN	COMMENT
< 0.7	90	ATHAR	06 CLEO	$e^+ e^- \rightarrow \Upsilon(1S) \rightarrow \gamma K^+ K^-$

¹ LEES 18A quotes $B(\Upsilon(1S) \rightarrow \gamma f_0(1710) \rightarrow \gamma K \bar{K}) = (2.02 \pm 0.51 \pm 0.35) \times 10^{-5}$ assuming $B(K^0 \bar{K}^0) = 1/2 B(K \bar{K})$.

$\Gamma(\gamma f_0(1710) \rightarrow \gamma \pi^+ \pi^-)/\Gamma_{total}$ Γ_{101}/Γ

VALUE (units 10^{-5})	DOCUMENT ID	TECN	COMMENT
0.53 ± 0.17 ± 0.11	1 LEES	18A BABR	$\Upsilon(1S) \rightarrow \gamma \pi^+ \pi^-$

¹ LEES 18A quotes $B(\Upsilon(1S) \rightarrow \gamma f_0(1710) \rightarrow \gamma \pi \pi) = (0.79 \pm 0.26 \pm 0.17) \times 10^{-5}$ assuming $B(\pi^0 \pi^0) = 1/3 B(\pi \pi)$.

$\Gamma(\gamma f_0(1710) \rightarrow \gamma \pi^0 \pi^0)/\Gamma_{total}$ Γ_{102}/Γ

VALUE (units 10^{-6})	CL%	DOCUMENT ID	TECN	COMMENT
< 1.4	90	BESSON	07A CLEO	$e^+ e^- \rightarrow \Upsilon(1S) \rightarrow \gamma \pi^0 \pi^0$

Meson Particle Listings

 $\Upsilon(1S)$

$\Gamma(\gamma f_0(1710) \rightarrow \gamma \eta \eta)/\Gamma_{\text{total}}$					Γ_{103}/Γ
VALUE (units 10^{-6})	CL%	DOCUMENT ID	TECN	COMMENT	
<1.8	90	BESSON	07A	CLEO $e^+e^- \rightarrow \Upsilon(1S) \rightarrow \gamma \eta \eta$	

$\Gamma(\gamma f_4(2050))/\Gamma_{\text{total}}$					Γ_{104}/Γ
VALUE (units 10^{-5})	CL%	DOCUMENT ID	TECN	COMMENT	
<5.3	90	¹ ATHAR	06	CLE3 $\Upsilon(1S) \rightarrow \gamma \pi^+ \pi^-$	
¹ Assuming $B(f_4(2050) \rightarrow \pi \pi) = 0.17$.					

$\Gamma(\gamma f_0(2200) \rightarrow \gamma K^+ K^-)/\Gamma_{\text{total}}$					Γ_{105}/Γ
VALUE	CL%	DOCUMENT ID	TECN	COMMENT	
<0.0002	90	BARU	89	MD1 $\Upsilon(1S) \rightarrow \gamma K^+ K^-$	

$\Gamma(\gamma f_J(2220) \rightarrow \gamma K^+ K^-)/\Gamma_{\text{total}}$					Γ_{106}/Γ
VALUE (units 10^{-7})	CL%	DOCUMENT ID	TECN	COMMENT	
< 8	90	ATHAR	06	CLE3 $\Upsilon(1S) \rightarrow \gamma K^+ K^-$	
••• We do not use the following data for averages, fits, limits, etc. •••					
< 160	90	MASEK	02	CLEO $\Upsilon(1S) \rightarrow \gamma K^+ K^-$	
< 150	90	FULTON	90B	CLEO $\Upsilon(1S) \rightarrow \gamma K^+ K^-$	
< 290	90	ALBRECHT	89	ARG $\Upsilon(1S) \rightarrow \gamma K^+ K^-$	
<2000	90	BARU	89	MD1 $\Upsilon(1S) \rightarrow \gamma K^+ K^-$	

$\Gamma(\gamma f_J(2220) \rightarrow \gamma \pi^+ \pi^-)/\Gamma_{\text{total}}$					Γ_{107}/Γ
VALUE (units 10^{-7})	CL%	DOCUMENT ID	TECN	COMMENT	
< 6	90	ATHAR	06	CLE3 $\Upsilon(1S) \rightarrow \gamma \pi^+ \pi^-$	
••• We do not use the following data for averages, fits, limits, etc. •••					
<120	90	MASEK	02	CLEO $\Upsilon(1S) \rightarrow \gamma \pi^+ \pi^-$	

$\Gamma(\gamma f_J(2220) \rightarrow \gamma \rho \bar{\rho})/\Gamma_{\text{total}}$					Γ_{108}/Γ
VALUE (units 10^{-7})	CL%	DOCUMENT ID	TECN	COMMENT	
< 11	90	ATHAR	06	CLE3 $\Upsilon(1S) \rightarrow \gamma \rho \bar{\rho}$	
••• We do not use the following data for averages, fits, limits, etc. •••					
<160	90	MASEK	02	CLEO $\Upsilon(1S) \rightarrow \gamma \rho \bar{\rho}$	

$\Gamma(\gamma \eta(2225) \rightarrow \gamma \phi \phi)/\Gamma_{\text{total}}$					Γ_{109}/Γ
VALUE	CL%	DOCUMENT ID	TECN	COMMENT	
<0.003	90	BARU	89	MD1 $\Upsilon(1S) \rightarrow \gamma K^+ K^- K^+ K^-$	

$\Gamma(\gamma \eta_c(1S))/\Gamma_{\text{total}}$					Γ_{110}/Γ
VALUE	CL%	DOCUMENT ID	TECN	COMMENT	
<2.9 $\times 10^{-5}$	90	¹ KATRENKO	20	BELL $e^+e^- \rightarrow \gamma + \text{hadrons}$	
••• We do not use the following data for averages, fits, limits, etc. •••					
<5.7 $\times 10^{-5}$	90	SHEN	10A	BELL $\Upsilon(1S) \rightarrow \gamma X$	
¹ Using $\Upsilon(2S) \rightarrow \Upsilon(1S) \pi^+ \pi^-$ decays.					

$\Gamma(\gamma \eta_c(2S))/\Gamma_{\text{total}}$					Γ_{111}/Γ
VALUE	CL%	DOCUMENT ID	TECN	COMMENT	
<4 $\times 10^{-4}$	90	¹ KATRENKO	20	BELL $e^+e^- \rightarrow \gamma + \text{hadrons}$	
¹ Using $\Upsilon(2S) \rightarrow \Upsilon(1S) \pi^+ \pi^-$ decays.					

$\Gamma(\gamma \chi_{c0})/\Gamma_{\text{total}}$					Γ_{112}/Γ
VALUE	CL%	DOCUMENT ID	TECN	COMMENT	
<6.6 $\times 10^{-5}$	90	¹ KATRENKO	20	BELL $\Upsilon(1S) \rightarrow \gamma + \text{hadrons}$	
••• We do not use the following data for averages, fits, limits, etc. •••					
<6.5 $\times 10^{-4}$	90	SHEN	10A	BELL $\Upsilon(1S) \rightarrow \gamma X$	
¹ Using $\Upsilon(2S) \rightarrow \Upsilon(1S) \pi^+ \pi^-$ decays.					

$\Gamma(\gamma \chi_{c1})/\Gamma_{\text{total}}$					Γ_{113}/Γ
VALUE (units 10^{-5})	CL%	EVTS	DOCUMENT ID	TECN	COMMENT
4.7 \pm 2.4 \pm 0.4 -1.8 -0.5		5	¹ KATRENKO	20	BELL $\Upsilon(1S) \rightarrow \gamma + \text{hadrons}$
••• We do not use the following data for averages, fits, limits, etc. •••					
<2.3	90		SHEN	10A	BELL $\Upsilon(1S) \rightarrow \gamma X$
¹ Using $\Upsilon(2S) \rightarrow \Upsilon(1S) \pi^+ \pi^-$ decays.					

$\Gamma(\gamma \chi_{c2})/\Gamma_{\text{total}}$					Γ_{114}/Γ
VALUE	CL%	DOCUMENT ID	TECN	COMMENT	
<7.6 $\times 10^{-6}$	90	SHEN	10A	BELL $\Upsilon(1S) \rightarrow \gamma X$	
••• We do not use the following data for averages, fits, limits, etc. •••					
<3.3 $\times 10^{-5}$	90	¹ KATRENKO	20	BELL $\Upsilon(1S) \rightarrow \gamma + \text{hadrons}$	
¹ Using $\Upsilon(2S) \rightarrow \Upsilon(1S) \pi^+ \pi^-$ decays.					

$\Gamma(\gamma \chi_{c1}(3872))/\Gamma_{\text{total}}$					Γ_{115}/Γ
VALUE	CL%	DOCUMENT ID	TECN	COMMENT	
<5 $\times 10^{-5}$	90	¹ SHEN	10A	BELL $\Upsilon(1S) \rightarrow \gamma X$	
¹ SHEN 10A reports $[\Gamma(\Upsilon(1S) \rightarrow \gamma \chi_{c1}(3872))/\Gamma_{\text{total}}] \times [B(\chi_{c1}(3872) \rightarrow \pi^+ \pi^- J/\psi(1S))] < 1.6 \times 10^{-6}$ which we divide by our best value $B(\chi_{c1}(3872) \rightarrow \pi^+ \pi^- J/\psi(1S)) = 3.5 \times 10^{-2}$.					

$\Gamma(\gamma \chi_{c1}(3872), \chi_{c1} \rightarrow \pi^+ \pi^- \pi^0 J/\psi)/\Gamma_{\text{total}}$					Γ_{116}/Γ
VALUE	CL%	DOCUMENT ID	TECN	COMMENT	
<2.8 $\times 10^{-6}$	90	SHEN	10A	BELL $\Upsilon(1S) \rightarrow \gamma X$	

$\Gamma(\gamma \chi_{c0}(3915) \rightarrow \omega J/\psi)/\Gamma_{\text{total}}$					Γ_{117}/Γ
VALUE (units 10^{-6})	CL%	DOCUMENT ID	TECN	COMMENT	
<3.0	90	SHEN	10A	BELL $\Upsilon(1S) \rightarrow \gamma X$	

$\Gamma(\gamma \chi_{c1}(4140) \rightarrow \phi J/\psi)/\Gamma_{\text{total}}$					Γ_{118}/Γ
VALUE (units 10^{-6})	CL%	DOCUMENT ID	TECN	COMMENT	
<2.2	90	SHEN	10A	BELL $\Upsilon(1S) \rightarrow \gamma X$	

$\Gamma(\gamma X \bar{X}(m_X < 3.1 \text{ GeV}))/\Gamma_{\text{total}}$					Γ_{119}/Γ
$(X \bar{X} = \text{vectors with } m < 3.1 \text{ GeV})$					
VALUE (units 10^{-3})	CL%	DOCUMENT ID	TECN	COMMENT	
<1	90	¹ BALEST	95	CLEO $e^+e^- \rightarrow \gamma + X \bar{X}$	
¹ For a noninteracting vector X with mass < 3.1 GeV.					

$\Gamma(\gamma X \bar{X}(m_X < 4.5 \text{ GeV}))/\Gamma_{\text{total}}$					Γ_{120}/Γ
$X \text{ and } \bar{X} = \text{zero spin with } m < 4.5 \text{ GeV}$					
VALUE (units 10^{-3})	CL%	DOCUMENT ID	TECN	COMMENT	
<24	90	¹ DEL-AMO-SA...111	BABR	$e^+e^- \rightarrow \gamma + X \bar{X}$	
¹ For a noninteracting scalar X with mass < 4.5 GeV.					

$\Gamma(\gamma X \rightarrow \gamma + \geq 4 \text{ prongs})/\Gamma_{\text{total}}$					Γ_{121}/Γ
$(1.5 \text{ GeV} < m_X < 5.0 \text{ GeV})$					
VALUE (units 10^{-4})	CL%	DOCUMENT ID	TECN	COMMENT	
<1.78	95	ROSNER	07A	CLEO $e^+e^- \rightarrow \gamma X$	

$\Gamma(\gamma A^0)/\Gamma_{\text{total}}$					Γ_{122}/Γ
$(A^0 = \text{scalar with } m < 8.0 \text{ GeV})$					
VALUE	CL%	DOCUMENT ID	TECN	COMMENT	
••• We do not use the following data for averages, fits, limits, etc. •••					
<4.5 $\times 10^{-6}$	90	¹ DEL-AMO-SA...111	BABR	$e^+e^- \rightarrow \gamma + X$	
<3 $\times 10^{-5}$	90	² BALEST	95	CLEO $e^+e^- \rightarrow \gamma + X$	
<5.6 $\times 10^{-5}$	90	² ANTREASAN	90C	CBAL $e^+e^- \rightarrow \gamma + X$	
¹ For a non-interacting scalar or pseudoscalar, A^0 , with mass $m_{A^0} < 8.0 \text{ GeV}$. 90% CL upper limits range from 1.9×10^{-6} to 4.5×10^{-6} .					
² For any non-interacting long-lived particle with mass < 7.2 GeV.					

$\Gamma(\gamma A^0 \rightarrow \gamma \mu^+ \mu^-)/\Gamma_{\text{total}}$					Γ_{123}/Γ
$(201 < M(\mu^+ \mu^-) < 3565 \text{ MeV})$					
VALUE (units 10^{-6})	CL%	DOCUMENT ID	TECN	COMMENT	
< 9	90	¹ LOVE	08	CLEO $e^+e^- \rightarrow \gamma A^0 \rightarrow \gamma \mu^+ \mu^-$	
••• We do not use the following data for averages, fits, limits, etc. •••					
<16	90	² JIA	22	BELL $\Upsilon(2S) \rightarrow \gamma \mu^+ \mu^- \pi^+ \pi^-$	
< 9.7	90	³ LEES	13c	BABR $e^+e^- \rightarrow \gamma A^0 \rightarrow \gamma \mu^+ \mu^-$	
¹ For a narrow scalar or pseudoscalar, A^0 , with $201 < M(\mu^+ \mu^-) < 3565 \text{ MeV}$, excluding J/ψ . Measured 90% CL limits as a function of $M(\mu^+ \mu^-)$ range from $1-9 \times 10^{-6}$.					
² For a narrow scalar or pseudoscalar, A^0 , with $0.22 < M(A^0) < 9.2 \text{ GeV}$, resulting in 90% CL upper limits ranging from 3.1×10^{-7} at $M(A^0) = 0.22 \text{ GeV}$ to 1.6×10^{-5} at $M(A^0) = 9.2 \text{ GeV}$.					
³ For a narrow scalar or pseudoscalar, A^0 , with mass in the range $0.212-9.2 \text{ GeV}$, excluding J/ψ and $\psi(2S)$. Measured 90% CL limits as a function of m_{A^0} are in the range $0.28-9.7 \times 10^{-6}$.					

$\Gamma(\gamma A^0 \rightarrow \gamma \tau^+ \tau^-)/\Gamma_{\text{total}}$					Γ_{124}/Γ
$(2m_\tau < M(\tau^+ \tau^-) < 9.2 \text{ GeV})$					
VALUE (units 10^{-6})	CL%	DOCUMENT ID	TECN	COMMENT	
<130	90	¹ LEES	13R	BABR $\Upsilon(2S) \rightarrow \gamma \tau^+ \tau^- \pi^+ \pi^-$	
••• We do not use the following data for averages, fits, limits, etc. •••					
<150	90	² JIA	22	BELL $\Upsilon(2S) \rightarrow \gamma \tau^+ \tau^- \pi^+ \pi^-$	
< 50	90	³ LOVE	08	CLEO $e^+e^- \rightarrow \gamma A^0 \rightarrow \gamma \tau^+ \tau^-$	
¹ For a narrow scalar or pseudoscalar, A^0 , with $2m_\tau < M(A^0) < 9.2 \text{ GeV}$, resulting in 90% CL upper limits of 0.9×10^{-5} at $M(A^0) = 2m_\tau$, $\approx 1.5 \times 10^{-5}$ at $M(A^0) = 7.5 \text{ GeV}$, and 13×10^{-5} at $M(A^0) = 9.2 \text{ GeV}$.					
² For a narrow scalar or pseudoscalar, A^0 , with $2m_\tau < M(A^0) < 9.2 \text{ GeV}$, resulting in 90% CL upper limits ranging from 3.8×10^{-6} at $M(A^0) = 2m_\tau$ to 1.5×10^{-4} at $M(A^0) = 9.2 \text{ GeV}$.					
³ For a narrow scalar or pseudoscalar, A^0 , with $2m_\tau < M(A^0) < 7.5 \text{ GeV}$, resulting in 90% CL limits ranging from 1×10^{-5} at $M(A^0) = 2m_\tau$ to 5×10^{-5} at $M(A^0) = 7.5 \text{ GeV}$.					

$\Gamma(\gamma A^0 \rightarrow \gamma g g)/\Gamma_{\text{total}}$					Γ_{125}/Γ
$(0.5 \text{ GeV} < m < 9.0 \text{ GeV})$					
VALUE	CL%	DOCUMENT ID	TECN	COMMENT	
<1 $\times 10^{-2}$	90	¹ LEES	13L	BABR $\Upsilon(1S) \rightarrow \gamma X$	
¹ For a narrow, CP-odd pseudoscalar, A^0 , searched for in 26 hadronic decay modes with invariant mass $0.5 \text{ GeV} < m_{A^0} < 9.0 \text{ GeV}$. Measured 90% CL limits as a function of m_{A^0} range from 10^{-6} to 10^{-2} .					

$\Gamma(\gamma A^0 \rightarrow \gamma S^3)/\Gamma_{total}$
(0.5 GeV < m < 9.0 GeV) Γ_{126}/Γ

Table with columns: VALUE, CL%, DOCUMENT ID, TECN, COMMENT. Includes entry for LEES 13L BABR $\Upsilon(1S) \rightarrow \gamma X$. Includes footnote 1: For a narrow, CP-odd pseudoscalar, A0, searched for in 14 hadronic decay modes with invariant mass 1.5 GeV < m_A0 < 9.0 GeV.

LEPTON FAMILY NUMBER (LF) VIOLATING MODES

$\Gamma(e^\pm \mu^\mp)/\Gamma_{total}$ Γ_{127}/Γ

Table with columns: VALUE (units 10^-7), CL%, DOCUMENT ID, TECN, COMMENT. Includes entry for PATRA 22 BELL $\Upsilon(2S) \rightarrow \pi^+ \pi^- e^\pm \mu^\mp$.

$\Gamma(\mu^\pm \tau^\mp)/\Gamma_{total}$ Γ_{128}/Γ

Table with columns: VALUE, CL%, DOCUMENT ID, TECN, COMMENT. Includes entry for PATRA 22 BELL $\Upsilon(2S) \rightarrow \pi^+ \pi^- \mu^\pm \tau^\mp$. Includes footnote: We do not use the following data for averages, fits, limits, etc.

$\Gamma(e^\pm \tau^\mp)/\Gamma_{total}$ Γ_{129}/Γ

Table with columns: VALUE (units 10^-6), CL%, DOCUMENT ID, TECN, COMMENT. Includes entry for PATRA 22 BELL $\Upsilon(2S) \rightarrow \pi^+ \pi^- e^\pm \tau^\mp$.

$\Gamma(\gamma e^\pm \mu^\mp)/\Gamma_{total}$ Γ_{130}/Γ

Table with columns: VALUE (units 10^-7), CL%, DOCUMENT ID, TECN, COMMENT. Includes entry for PATRA 22 BELL $\Upsilon(2S) \rightarrow \pi^+ \pi^- \gamma e^\pm \mu^\mp$.

$\Gamma(\gamma \mu^\pm \tau^\mp)/\Gamma_{total}$ Γ_{131}/Γ

Table with columns: VALUE (units 10^-6), CL%, DOCUMENT ID, TECN, COMMENT. Includes entry for PATRA 22 BELL $\Upsilon(2S) \rightarrow \pi^+ \pi^- \gamma \mu^\pm \tau^\mp$.

$\Gamma(\gamma e^\pm \tau^\mp)/\Gamma_{total}$ Γ_{132}/Γ

Table with columns: VALUE (units 10^-6), CL%, DOCUMENT ID, TECN, COMMENT. Includes entry for PATRA 22 BELL $\Upsilon(2S) \rightarrow \pi^+ \pi^- \gamma e^\pm \tau^\mp$.

OTHER DECAYS

$\Gamma(\text{invisible})/\Gamma_{total}$ Γ_{133}/Γ

Table with columns: VALUE (units 10^-4), CL%, DOCUMENT ID, TECN, COMMENT. Includes entries for AUBERT 09AX BABR $\Upsilon(3S) \rightarrow \pi^+ \pi^- \Upsilon(1S)$, RUBIN 07 CLEO $\Upsilon(2S) \rightarrow \pi^+ \pi^- \Upsilon(1S)$, and TA JIMA 07 BELL $\Upsilon(3S) \rightarrow \pi^+ \pi^- \Upsilon(1S)$.

$\Upsilon(1S)$ REFERENCES

Large reference table listing authors (e.g., SHAMOV, JIA, PATRA), document IDs, and publication details for $\Upsilon(1S)$ studies.

Large table listing authors (e.g., ALBRECHT, BARU, KOBEL), document IDs, and publication details for various meson decays.

$\chi_{b0}(1P)$

$J^G(J^{PC}) = 0^+(0^+ +)$
J needs confirmation.

Observed in radiative decay of the $\Upsilon(2S)$, therefore C = +. Branching ratio requires E1 transition, M1 is strongly disfavored, therefore P = +.

$\chi_{b0}(1P)$ MASS

Table with columns: VALUE (MeV), DOCUMENT ID. Includes entry: 9859.44 ± 0.42 ± 0.31 OUR EVALUATION From average γ energy below, using $\Upsilon(2S)$ mass = 10023.26 ± 0.31 MeV.

$m_{\chi_{b1}(1P)} - m_{\chi_{b0}(1P)}$

Table with columns: VALUE (MeV), DOCUMENT ID, TECN, COMMENT. Includes entry: LEES 14M BABR $\Upsilon(2S) \rightarrow \gamma \gamma \mu^+ \mu^-$.

γ ENERGY IN $\Upsilon(2S)$ DECAY

Table with columns: VALUE (MeV), DOCUMENT ID, TECN, COMMENT. Includes entry: 162.5 ± 0.4 OUR AVERAGE. Includes entry: EDWARDS 99 CLE2 $\Upsilon(2S) \rightarrow \gamma \chi(1P)$.

$\chi_{b0}(1P)$ DECAY MODES

Table with columns: Mode, Fraction (Γ_i/Γ), Confidence level. Lists decay modes like $\Upsilon(1S)$, $D^0 X$, $\pi^+ \pi^- K^+ K^- \pi^0$, etc., with their respective fractions and confidence levels.

Meson Particle Listings

 $\chi_{b0}(1P)$ $\chi_{b0}(1P)$ BRANCHING RATIOS

$\Gamma(\gamma \Upsilon(1S))/\Gamma_{\text{total}}$ Γ_1/Γ

VALUE (%)	CL%	EVTS	DOCUMENT ID	TECN	COMMENT
1.94 ± 0.27 OUR AVERAGE					
2.07 ± 0.24 ± 0.21			1,2 LEES	14M BABR	$\Upsilon(2S) \rightarrow \gamma\gamma\mu^+\mu^-$
1.76 ± 0.30 ± 0.18	87		3,4 KORNICER	11 CLEO	$e^+e^- \rightarrow \gamma\gamma\ell^+\ell^-$

• • • We do not use the following data for averages, fits, limits, etc. • • •

< 4.6	90		5 LEES	11J BABR	$\Upsilon(2S) \rightarrow X\gamma$
< 6	90		WALK	86 CBAL	$\Upsilon(2S) \rightarrow \gamma\gamma\ell^+\ell^-$
< 11	90		PAUSS	83 CUSB	$\Upsilon(2S) \rightarrow \gamma\gamma\ell^+\ell^-$

1 LEES 14M quotes $\Gamma(\chi_{b0}(1P) \rightarrow \gamma\Upsilon(1S))/\Gamma_{\text{total}} \times \Gamma(\Upsilon(2S) \rightarrow \gamma\chi_{b0}(1P))/\Gamma_{\text{total}} = (7.75 \pm 0.91) \times 10^{-4}$ combining the results from samples of $\Upsilon(2S) \rightarrow \gamma\gamma\mu^+\mu^-$ with and without converted photons. Assumes $B(\Upsilon(1S) \rightarrow \mu^+\mu^-) = (2.48 \pm 0.05)\%$.

2 LEES 14M reports $[\Gamma(\chi_{b0}(1P) \rightarrow \gamma\Upsilon(1S))/\Gamma_{\text{total}}] \times [B(\Upsilon(2S) \rightarrow \gamma\chi_{b0}(1P))] = (7.75 \pm 0.91) \times 10^{-4}$ which we divide by our best value $B(\Upsilon(2S) \rightarrow \gamma\chi_{b0}(1P)) = (3.8 \pm 0.4) \times 10^{-2}$. Our first error is their experiment's error and our second error is the systematic error from using our best value.

3 Assuming $B(\Upsilon(1S) \rightarrow \ell^+\ell^-) = (2.48 \pm 0.05)\%$.

4 KORNICER 11 reports $[\Gamma(\chi_{b0}(1P) \rightarrow \gamma\Upsilon(1S))/\Gamma_{\text{total}}] \times [B(\Upsilon(2S) \rightarrow \gamma\chi_{b0}(1P))] = (6.59 \pm 0.96 \pm 0.60) \times 10^{-4}$ which we divide by our best value $B(\Upsilon(2S) \rightarrow \gamma\chi_{b0}(1P)) = (3.8 \pm 0.4) \times 10^{-2}$. Our first error is their experiment's error and our second error is the systematic error from using our best value.

5 LEES 11J quotes a central value of $\Gamma(\chi_{b0}(1P) \rightarrow \gamma\Upsilon(1S))/\Gamma_{\text{total}} \times \Gamma(\Upsilon(2S) \rightarrow \gamma\chi_{b0}(1P))/\Gamma_{\text{total}} = (8.3 \pm 5.6^{+3.7}_{-2.6}) \times 10^{-4}$.

$\Gamma(D^0 X)/\Gamma_{\text{total}}$ Γ_2/Γ

VALUE	CL%	DOCUMENT ID	TECN	COMMENT
< 10.4 × 10⁻²	90	6,7 BRIERE	08 CLEO	$\Upsilon(2S) \rightarrow \gamma D^0 X$

6 For $p_{D^0} > 2.5$ GeV/c.

7 The authors also present their result as $(5.6 \pm 3.6 \pm 0.5) \times 10^{-2}$.

$\Gamma(\pi^+\pi^-K^+K^-\pi^0)/\Gamma_{\text{total}}$ Γ_3/Γ

VALUE (units 10 ⁻⁴)	CL%	DOCUMENT ID	TECN	COMMENT
< 1.6	90	8 ASNER	08A CLEO	$\Upsilon(2S) \rightarrow \gamma\pi^+\pi^-K^+K^-\pi^0$

8 ASNER 08A reports $[\Gamma(\chi_{b0}(1P) \rightarrow \pi^+\pi^-K^+K^-\pi^0)/\Gamma_{\text{total}}] \times [B(\Upsilon(2S) \rightarrow \gamma\chi_{b0}(1P))] < 6 \times 10^{-6}$ which we divide by our best value $B(\Upsilon(2S) \rightarrow \gamma\chi_{b0}(1P)) = 3.8 \times 10^{-2}$.

$\Gamma(2\pi^+\pi^-K^-K_S^0)/\Gamma_{\text{total}}$ Γ_4/Γ

VALUE (units 10 ⁻⁴)	CL%	DOCUMENT ID	TECN	COMMENT
< 0.5	90	9 ASNER	08A CLEO	$\Upsilon(2S) \rightarrow \gamma 2\pi^+\pi^-K^-K_S^0$

9 ASNER 08A reports $[\Gamma(\chi_{b0}(1P) \rightarrow 2\pi^+\pi^-K^-K_S^0)/\Gamma_{\text{total}}] \times [B(\Upsilon(2S) \rightarrow \gamma\chi_{b0}(1P))] < 2 \times 10^{-6}$ which we divide by our best value $B(\Upsilon(2S) \rightarrow \gamma\chi_{b0}(1P)) = 3.8 \times 10^{-2}$.

$\Gamma(2\pi^+\pi^-K^-K_S^0 2\pi^0)/\Gamma_{\text{total}}$ Γ_5/Γ

VALUE (units 10 ⁻⁴)	CL%	DOCUMENT ID	TECN	COMMENT
< 5	90	10 ASNER	08A CLEO	$\Upsilon(2S) \rightarrow \gamma 2\pi^+\pi^-K^-2\pi^0$

10 ASNER 08A reports $[\Gamma(\chi_{b0}(1P) \rightarrow 2\pi^+\pi^-K^-K_S^0 2\pi^0)/\Gamma_{\text{total}}] \times [B(\Upsilon(2S) \rightarrow \gamma\chi_{b0}(1P))] < 18 \times 10^{-6}$ which we divide by our best value $B(\Upsilon(2S) \rightarrow \gamma\chi_{b0}(1P)) = 3.8 \times 10^{-2}$.

$\Gamma(2\pi^+2\pi^-2\pi^0)/\Gamma_{\text{total}}$ Γ_6/Γ

VALUE (units 10 ⁻⁴)	CL%	DOCUMENT ID	TECN	COMMENT
< 2.1	90	11 ASNER	08A CLEO	$\Upsilon(2S) \rightarrow \gamma 2\pi^+2\pi^-2\pi^0$

11 ASNER 08A reports $[\Gamma(\chi_{b0}(1P) \rightarrow 2\pi^+2\pi^-2\pi^0)/\Gamma_{\text{total}}] \times [B(\Upsilon(2S) \rightarrow \gamma\chi_{b0}(1P))] < 8 \times 10^{-6}$ which we divide by our best value $B(\Upsilon(2S) \rightarrow \gamma\chi_{b0}(1P)) = 3.8 \times 10^{-2}$.

$\Gamma(2\pi^+2\pi^-K^+K^-)/\Gamma_{\text{total}}$ Γ_7/Γ

VALUE (units 10 ⁻⁴)	EVTS	DOCUMENT ID	TECN	COMMENT
1.1 ± 0.6 ± 0.1	7	12 ASNER	08A CLEO	$\Upsilon(2S) \rightarrow \gamma 2\pi^+2\pi^-K^+K^-$

12 ASNER 08A reports $[\Gamma(\chi_{b0}(1P) \rightarrow 2\pi^+2\pi^-K^+K^-)/\Gamma_{\text{total}}] \times [B(\Upsilon(2S) \rightarrow \gamma\chi_{b0}(1P))] = (4 \pm 2 \pm 1) \times 10^{-6}$ which we divide by our best value $B(\Upsilon(2S) \rightarrow \gamma\chi_{b0}(1P)) = (3.8 \pm 0.4) \times 10^{-2}$. Our first error is their experiment's error and our second error is the systematic error from using our best value.

$\Gamma(2\pi^+2\pi^-K^+K^-\pi^0)/\Gamma_{\text{total}}$ Γ_8/Γ

VALUE (units 10 ⁻⁴)	CL%	DOCUMENT ID	TECN	COMMENT
< 2.7	90	13 ASNER	08A CLEO	$\Upsilon(2S) \rightarrow \gamma 2\pi^+2\pi^-K^+K^-\pi^0$

13 ASNER 08A reports $[\Gamma(\chi_{b0}(1P) \rightarrow 2\pi^+2\pi^-K^+K^-\pi^0)/\Gamma_{\text{total}}] \times [B(\Upsilon(2S) \rightarrow \gamma\chi_{b0}(1P))] < 10 \times 10^{-6}$ which we divide by our best value $B(\Upsilon(2S) \rightarrow \gamma\chi_{b0}(1P)) = 3.8 \times 10^{-2}$.

$\Gamma(2\pi^+2\pi^-K^+K^-2\pi^0)/\Gamma_{\text{total}}$ Γ_9/Γ

VALUE (units 10 ⁻⁴)	CL%	DOCUMENT ID	TECN	COMMENT
< 5	90	14 ASNER	08A CLEO	$\Upsilon(2S) \rightarrow \gamma 2\pi^+2\pi^-K^+K^-2\pi^0$

14 ASNER 08A reports $[\Gamma(\chi_{b0}(1P) \rightarrow 2\pi^+2\pi^-K^+K^-2\pi^0)/\Gamma_{\text{total}}] \times [B(\Upsilon(2S) \rightarrow \gamma\chi_{b0}(1P))] < 20 \times 10^{-6}$ which we divide by our best value $B(\Upsilon(2S) \rightarrow \gamma\chi_{b0}(1P)) = 3.8 \times 10^{-2}$.

$\Gamma(3\pi^+2\pi^-K^-K_S^0\pi^0)/\Gamma_{\text{total}}$ Γ_{10}/Γ

VALUE (units 10 ⁻⁴)	CL%	DOCUMENT ID	TECN	COMMENT
< 1.6	90	15 ASNER	08A CLEO	$\Upsilon(2S) \rightarrow \gamma 3\pi^+2\pi^-K^-K_S^0\pi^0$

15 ASNER 08A reports $[\Gamma(\chi_{b0}(1P) \rightarrow 3\pi^+2\pi^-K^-K_S^0\pi^0)/\Gamma_{\text{total}}] \times [B(\Upsilon(2S) \rightarrow \gamma\chi_{b0}(1P))] < 6 \times 10^{-6}$ which we divide by our best value $B(\Upsilon(2S) \rightarrow \gamma\chi_{b0}(1P)) = 3.8 \times 10^{-2}$.

$\Gamma(3\pi^+3\pi^-)/\Gamma_{\text{total}}$ Γ_{11}/Γ

VALUE (units 10 ⁻⁴)	CL%	DOCUMENT ID	TECN	COMMENT
< 0.8	90	16 ASNER	08A CLEO	$\Upsilon(2S) \rightarrow \gamma 3\pi^+3\pi^-$

16 ASNER 08A reports $[\Gamma(\chi_{b0}(1P) \rightarrow 3\pi^+3\pi^-)/\Gamma_{\text{total}}] \times [B(\Upsilon(2S) \rightarrow \gamma\chi_{b0}(1P))] < 3 \times 10^{-6}$ which we divide by our best value $B(\Upsilon(2S) \rightarrow \gamma\chi_{b0}(1P)) = 3.8 \times 10^{-2}$.

$\Gamma(3\pi^+3\pi^-2\pi^0)/\Gamma_{\text{total}}$ Γ_{12}/Γ

VALUE (units 10 ⁻⁴)	CL%	DOCUMENT ID	TECN	COMMENT
< 6	90	17 ASNER	08A CLEO	$\Upsilon(2S) \rightarrow \gamma 3\pi^+3\pi^-2\pi^0$

17 ASNER 08A reports $[\Gamma(\chi_{b0}(1P) \rightarrow 3\pi^+3\pi^-2\pi^0)/\Gamma_{\text{total}}] \times [B(\Upsilon(2S) \rightarrow \gamma\chi_{b0}(1P))] < 22 \times 10^{-6}$ which we divide by our best value $B(\Upsilon(2S) \rightarrow \gamma\chi_{b0}(1P)) = 3.8 \times 10^{-2}$.

$\Gamma(3\pi^+3\pi^-K^+K^-)/\Gamma_{\text{total}}$ Γ_{13}/Γ

VALUE (units 10 ⁻⁴)	EVTS	DOCUMENT ID	TECN	COMMENT
2.4 ± 1.2 ± 0.2	9	18 ASNER	08A CLEO	$\Upsilon(2S) \rightarrow \gamma 3\pi^+3\pi^-K^+K^-$

18 ASNER 08A reports $[\Gamma(\chi_{b0}(1P) \rightarrow 3\pi^+3\pi^-K^+K^-)/\Gamma_{\text{total}}] \times [B(\Upsilon(2S) \rightarrow \gamma\chi_{b0}(1P))] = (9 \pm 4 \pm 2) \times 10^{-6}$ which we divide by our best value $B(\Upsilon(2S) \rightarrow \gamma\chi_{b0}(1P)) = (3.8 \pm 0.4) \times 10^{-2}$. Our first error is their experiment's error and our second error is the systematic error from using our best value.

$\Gamma(3\pi^+3\pi^-K^+K^-\pi^0)/\Gamma_{\text{total}}$ Γ_{14}/Γ

VALUE (units 10 ⁻⁴)	CL%	DOCUMENT ID	TECN	COMMENT
< 10	90	19 ASNER	08A CLEO	$\Upsilon(2S) \rightarrow \gamma 3\pi^+3\pi^-K^+K^-\pi^0$

19 ASNER 08A reports $[\Gamma(\chi_{b0}(1P) \rightarrow 3\pi^+3\pi^-K^+K^-\pi^0)/\Gamma_{\text{total}}] \times [B(\Upsilon(2S) \rightarrow \gamma\chi_{b0}(1P))] < 37 \times 10^{-6}$ which we divide by our best value $B(\Upsilon(2S) \rightarrow \gamma\chi_{b0}(1P)) = 3.8 \times 10^{-2}$.

$\Gamma(4\pi^+4\pi^-)/\Gamma_{\text{total}}$ Γ_{15}/Γ

VALUE (units 10 ⁻⁴)	CL%	DOCUMENT ID	TECN	COMMENT
< 0.8	90	20 ASNER	08A CLEO	$\Upsilon(2S) \rightarrow \gamma 4\pi^+4\pi^-$

20 ASNER 08A reports $[\Gamma(\chi_{b0}(1P) \rightarrow 4\pi^+4\pi^-)/\Gamma_{\text{total}}] \times [B(\Upsilon(2S) \rightarrow \gamma\chi_{b0}(1P))] < 3 \times 10^{-6}$ which we divide by our best value $B(\Upsilon(2S) \rightarrow \gamma\chi_{b0}(1P)) = 3.8 \times 10^{-2}$.

$\Gamma(4\pi^+4\pi^-2\pi^0)/\Gamma_{\text{total}}$ Γ_{16}/Γ

VALUE (units 10 ⁻⁴)	CL%	DOCUMENT ID	TECN	COMMENT
< 21	90	21 ASNER	08A CLEO	$\Upsilon(2S) \rightarrow \gamma 4\pi^+4\pi^-2\pi^0$

21 ASNER 08A reports $[\Gamma(\chi_{b0}(1P) \rightarrow 4\pi^+4\pi^-2\pi^0)/\Gamma_{\text{total}}] \times [B(\Upsilon(2S) \rightarrow \gamma\chi_{b0}(1P))] < 77 \times 10^{-6}$ which we divide by our best value $B(\Upsilon(2S) \rightarrow \gamma\chi_{b0}(1P)) = 3.8 \times 10^{-2}$.

$\Gamma(J/\psi J/\psi)/\Gamma_{\text{total}}$ Γ_{17}/Γ

VALUE (units 10 ⁻⁵)	CL%	DOCUMENT ID	TECN	COMMENT
< 7	90	22 SHEN	12 BELL	$\Upsilon(2S) \rightarrow \gamma\psi X$

22 SHEN 12 reports $< 7.1 \times 10^{-5}$ from a measurement of $[\Gamma(\chi_{b0}(1P) \rightarrow J/\psi J/\psi)/\Gamma_{\text{total}}] \times [B(\Upsilon(2S) \rightarrow \gamma\chi_{b0}(1P))] \text{ assuming } B(\Upsilon(2S) \rightarrow \gamma\chi_{b0}(1P)) = (3.8 \pm 0.4) \times 10^{-2}$.

$\Gamma(J/\psi\psi(2S))/\Gamma_{\text{total}}$ Γ_{18}/Γ

VALUE (units 10 ⁻⁵)	CL%	DOCUMENT ID	TECN	COMMENT
< 12	90	23 SHEN	12 BELL	$\Upsilon(2S) \rightarrow \gamma\psi X$

23 SHEN 12 reports $< 12 \times 10^{-5}$ from a measurement of $[\Gamma(\chi_{b0}(1P) \rightarrow J/\psi\psi(2S))/\Gamma_{\text{total}}] \times [B(\Upsilon(2S) \rightarrow \gamma\chi_{b0}(1P))] \text{ assuming } B(\Upsilon(2S) \rightarrow \gamma\chi_{b0}(1P)) = (3.8 \pm 0.4) \times 10^{-2}$.

$\Gamma(\psi(2S)\psi(2S))/\Gamma_{\text{total}}$ Γ_{19}/Γ

VALUE (units 10 ⁻⁵)	CL%	DOCUMENT ID	TECN	COMMENT
< 3.1	90	24 SHEN	12 BELL	$\Upsilon(2S) \rightarrow \gamma\psi X$

24 SHEN 12 reports $< 3.1 \times 10^{-5}$ from a measurement of $[\Gamma(\chi_{b0}(1P) \rightarrow \psi(2S)\psi(2S))/\Gamma_{\text{total}}] \times [B(\Upsilon(2S) \rightarrow \gamma\chi_{b0}(1P))] \text{ assuming } B(\Upsilon(2S) \rightarrow \gamma\chi_{b0}(1P)) = (3.8 \pm 0.4) \times 10^{-2}$.

$\Gamma(J/\psi(1S) \text{ anything})/\Gamma_{\text{total}}$ Γ_{20}/Γ

VALUE	CL%	DOCUMENT ID	TECN	COMMENT
< 2.3 × 10⁻³	90	JIA	17A BELL	$e^+e^- \rightarrow \text{hadrons}$

 $\chi_{b0}(1P)$ CROSS-PARTICLE BRANCHING RATIOS

$\Gamma(\chi_{b0}(1P) \rightarrow \gamma\Upsilon(1S))/\Gamma_{\text{total}} \times \Gamma(\Upsilon(2S) \rightarrow \gamma\chi_{b0}(1P))/\Gamma_{\text{total}}$ $\Gamma_1/\Gamma \times \Gamma_{25}/\Gamma_{73}$

VALUE	CL%	DOCUMENT ID	TECN	COMMENT
< 1.7 × 10⁻³	90	25 LEES	11J BABR	$\Upsilon(2S) \rightarrow X\gamma$

25 LEES 11J quotes a central value of $\Gamma(\chi_{b0}(1P) \rightarrow \gamma\Upsilon(1S))/\Gamma_{\text{total}} \times \Gamma(\Upsilon(2S) \rightarrow \gamma\chi_{b0}(1P))/\Gamma_{\text{total}} = (8.3 \pm 5.6^{+3.7}_{-2.6}) \times 10^{-4}$ and derives a 90% CL upper limit of $\Gamma(\gamma\Upsilon(1S))/\Gamma_{\text{total}} < 4.6\%$ using $B(\Upsilon(2S) \rightarrow \gamma\chi_{b0}(1P)) = (3.8 \pm 0.4)\%$.

See key on page 1171

Meson Particle Listings

$\chi_{b0}(1P), \chi_{b1}(1P)$

$B(\chi_{b0}(1P) \rightarrow \gamma T(1S)) \times B(T(2S) \rightarrow \gamma \chi_{b0}(1P)) \times B(T(1S) \rightarrow \ell^+ \ell^-)$

VALUE (units 10^{-5})	EVTS	DOCUMENT ID	TECN	COMMENT
1.67 ± 0.28 OUR AVERAGE				

2.9	$\frac{+1.7}{-1.4} \frac{+0.1}{-0.8}$	²⁶ LEES	14M BABR	$T(2S) \rightarrow \gamma \gamma \mu^+ \mu^-$
1.63 ± 0.24 ± 0.15	87	KORNICER	11 CLEO	$e^+ e^- \rightarrow \gamma \gamma \ell^+ \ell^-$

²⁶ From a sample of $T(2S) \rightarrow \gamma \gamma \mu^+ \mu^-$ with one converted photon.

$[B(\chi_{b0}(1P) \rightarrow \gamma T(1S)) \times B(T(2S) \rightarrow \gamma \chi_{b0}(1P))] / [B(\chi_{b1}(1P) \rightarrow \gamma T(1S)) \times B(T(2S) \rightarrow \gamma \chi_{b1}(1P))]$

VALUE (%)	DOCUMENT ID	TECN	COMMENT
3.28 ± 0.37	²⁷ LEES	14M BABR	$T(2S) \rightarrow \gamma \gamma \mu^+ \mu^-$

²⁷ From a sample of $T(2S) \rightarrow \gamma \gamma \mu^+ \mu^-$ without converted photons.

$\chi_{b0}(1P)$ REFERENCES

JIA	17A	PR D96 112002	S. Jia et al.	(BELLE Collab.)
LEES	14M	PR D90 112010	J.P. Lees et al.	(BABAR Collab.)
SHEN	12	PR D85 071102	C.P. Shen et al.	(BELLE Collab.)
KORNICER	11	PR D83 054003	M. Kornicer et al.	(CLEO Collab.)
LEES	11J	PR D84 072002	J.P. Lees et al.	(BABAR Collab.)
ASNER	08A	PR D78 091103	D.M. Asner et al.	(CLEO Collab.)
BRIERE	08	PR D78 092007	R.A. Briere et al.	(CLEO Collab.)
ARTUSO	05	PRL 94 032001	M. Artuso et al.	(CLEO Collab.)
EDWARDS	99	PR D59 032003	K.W. Edwards et al.	(CLEO Collab.)
WALK	86	PR D34 2611	W.S. Walk et al.	(Crystal Ball Collab.)
ALBRECHT	85E	PL 160B 331	H. Albrecht et al.	(ARGUS Collab.)
NERNST	85	PRL 54 2195	R. Nernst et al.	(Crystal Ball Collab.)
HAAS	84	PRL 52 799	J. Haas et al.	(CLEO Collab.)
KLOPFEN...	83	PRL 51 160	C. Klopfenstein et al.	(CUSB Collab.)
PAUSS	83	PL 130B 439	F. Pauss et al.	(MPIM, COLU, CORN, LSU+)

$\chi_{b1}(1P)$

$J^{G(JPC)} = 0^+(1^{++})$
 J needs confirmation.

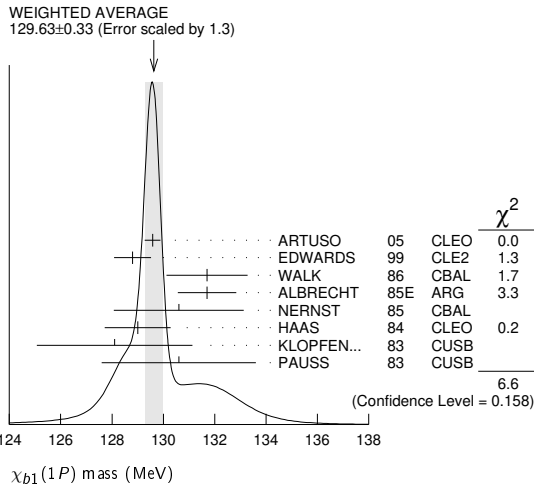
Observed in radiative decay of the $T(2S)$, therefore $C = +$. Branching ratio requires E1 transition, M1 is strongly disfavored, therefore $P = +$. $J = 1$ from SKWARNICKI 87.

$\chi_{b1}(1P)$ MASS

VALUE (MeV)	DOCUMENT ID
9892.78 ± 0.26 ± 0.31 OUR EVALUATION	From average γ energy below, using $T(2S)$ mass = 10023.26 ± 0.31 MeV

γ ENERGY IN $T(2S)$ DECAY

VALUE (MeV)	DOCUMENT ID	TECN	COMMENT
129.63 ± 0.33 OUR AVERAGE	Error includes scale factor of 1.3. See the ideogram below.		
129.58 ± 0.09 ± 0.29	ARTUSO 05	CLEO	$T(2S) \rightarrow \gamma X$
128.8 ± 0.4 ± 0.6	EDWARDS 99	CLE2	$T(2S) \rightarrow \gamma \chi(1P)$
131.7 ± 0.9 ± 1.3	WALK 86	CBAL	$T(2S) \rightarrow \gamma \gamma \ell^+ \ell^-$
131.7 ± 0.3 ± 1.1	ALBRECHT 85E	ARG	$T(2S) \rightarrow \text{conv.} \gamma X$
130.6 ± 0.8 ± 2.4	NERNST 85	CBAL	$T(2S) \rightarrow \gamma X$
129 ± 0.8 ± 1	HAAS 84	CLEO	$T(2S) \rightarrow \text{conv.} \gamma X$
128.1 ± 0.4 ± 3.0	KLOPFEN... 83	CUSB	$T(2S) \rightarrow \gamma X$
130.6 ± 3.0	PAUSS 83	CUSB	$T(2S) \rightarrow \gamma \gamma \ell^+ \ell^-$



$\chi_{b1}(1P)$ DECAY MODES

Mode	Fraction (Γ_i/Γ)	Confidence level
$\Gamma_1 \gamma T(1S)$	(35.2 ± 2.0) %	
$\Gamma_2 D^0 X$	(12.6 ± 2.2) %	
$\Gamma_3 \pi^+ \pi^- K^+ K^- \pi^0$	(2.0 ± 0.6) × 10 ⁻⁴	
$\Gamma_4 2\pi^+ \pi^- K^- K_S^0$	(1.3 ± 0.5) × 10 ⁻⁴	
$\Gamma_5 2\pi^+ \pi^- K^- K_S^0 2\pi^0$	< 6 × 10 ⁻⁴	90%
$\Gamma_6 2\pi^+ 2\pi^- 2\pi^0$	(8.0 ± 2.5) × 10 ⁻⁴	
$\Gamma_7 2\pi^+ 2\pi^- K^+ K^-$	(1.5 ± 0.5) × 10 ⁻⁴	
$\Gamma_8 2\pi^+ 2\pi^- K^+ K^- \pi^0$	(3.5 ± 1.2) × 10 ⁻⁴	
$\Gamma_9 2\pi^+ 2\pi^- K^+ K^- 2\pi^0$	(8.6 ± 3.2) × 10 ⁻⁴	
$\Gamma_{10} 3\pi^+ 2\pi^- K^- K_S^0 \pi^0$	(9.3 ± 3.3) × 10 ⁻⁴	
$\Gamma_{11} 3\pi^+ 3\pi^-$	(1.9 ± 0.6) × 10 ⁻⁴	
$\Gamma_{12} 3\pi^+ 3\pi^- 2\pi^0$	(1.7 ± 0.5) × 10 ⁻³	
$\Gamma_{13} 3\pi^+ 3\pi^- K^+ K^-$	(2.6 ± 0.8) × 10 ⁻⁴	
$\Gamma_{14} 3\pi^+ 3\pi^- K^+ K^- \pi^0$	(7.5 ± 2.6) × 10 ⁻⁴	
$\Gamma_{15} 4\pi^+ 4\pi^-$	(2.6 ± 0.9) × 10 ⁻⁴	
$\Gamma_{16} 4\pi^+ 4\pi^- 2\pi^0$	(1.4 ± 0.6) × 10 ⁻³	
$\Gamma_{17} \omega \text{ anything}$	(4.9 ± 1.4) %	
$\Gamma_{18} \omega X_{tetra}$	< 4.4 × 10 ⁻⁴	90%
$\Gamma_{19} J/\psi J/\psi$	< 2.7 × 10 ⁻⁵	90%
$\Gamma_{20} J/\psi \psi(2S)$	< 1.7 × 10 ⁻⁵	90%
$\Gamma_{21} \psi(2S) \psi(2S)$	< 6 × 10 ⁻⁵	90%
$\Gamma_{22} J/\psi(1S) \text{ anything}$	< 1.1 × 10 ⁻³	90%
$\Gamma_{23} J/\psi(1S) X_{tetra}$	< 2.27 × 10 ⁻⁴	90%

$\chi_{b1}(1P)$ BRANCHING RATIOS

VALUE	EVTS	DOCUMENT ID	TECN	COMMENT	Γ_1/Γ
0.352 ± 0.020 OUR AVERAGE					

0.356 ^{+0.016} _{-0.022} ± 0.019	964k	¹ FULSOM	18 BELL	$T(2S) \rightarrow \gamma X$	
0.364 ± 0.017 ± 0.019		^{2,3,4} LEES	14M BABR	$T(2S) \rightarrow \gamma \gamma \mu^+ \mu^-$	
0.331 ± 0.018 ± 0.017	3222	^{4,5} KORNICER	11 CLEO	$e^+ e^- \rightarrow \gamma \gamma \ell^+ \ell^-$	
0.350 ± 0.023 ± 0.018	13k	⁶ LEES	11J BABR	$T(2S) \rightarrow X \gamma$	
0.34 ± 0.07 ± 0.02	53	^{4,7,8} WALK	86 CBAL	$T(2S) \rightarrow \gamma \gamma \ell^+ \ell^-$	
0.47 ± 0.18		KLOPFEN...	83 CUSB	$T(2S) \rightarrow \gamma \gamma \ell^+ \ell^-$	

- FULSOM 18 reports $[\Gamma(\chi_{b1}(1P) \rightarrow \gamma T(1S))/\Gamma_{total}] \times [B(T(2S) \rightarrow \gamma \chi_{b1}(1P))]$ = $(2.45 \pm 0.02 \pm \frac{0.11}{0.15}) \times 10^{-2}$ which we divide by our best value $B(T(2S) \rightarrow \gamma \chi_{b1}(1P))$ = $(6.9 \pm 0.4) \times 10^{-2}$. Our first error is their experiment's error and our second error is the systematic error from using our best value.
- LEES 14M quotes $\Gamma(\chi_{b1}(1P) \rightarrow \gamma T(1S))/\Gamma_{total} \times \Gamma(T(2S) \rightarrow \gamma \chi_{b1}(1P))/\Gamma_{total}$ = $(2.51 \pm 0.12) \%$ combining the results from samples of $T(2S) \rightarrow \gamma \gamma \mu^+ \mu^-$ with and without converted photons.
- LEES 14M reports $[\Gamma(\chi_{b1}(1P) \rightarrow \gamma T(1S))/\Gamma_{total}] \times [B(T(2S) \rightarrow \gamma \chi_{b1}(1P))]$ = $(2.51 \pm 0.12) \times 10^{-2}$ which we divide by our best value $B(T(2S) \rightarrow \gamma \chi_{b1}(1P))$ = $(6.9 \pm 0.4) \times 10^{-2}$. Our first error is their experiment's error and our second error is the systematic error from using our best value.
- Assuming $B(T(1S) \rightarrow \mu^+ \mu^-) = (2.48 \pm 0.05) \%$.
- KORNICER 11 reports $[\Gamma(\chi_{b1}(1P) \rightarrow \gamma T(1S))/\Gamma_{total}] \times [B(T(2S) \rightarrow \gamma \chi_{b1}(1P))]$ = $(22.8 \pm 0.4 \pm 1.2) \times 10^{-3}$ which we divide by our best value $B(T(2S) \rightarrow \gamma \chi_{b1}(1P))$ = $(6.9 \pm 0.4) \times 10^{-2}$. Our first error is their experiment's error and our second error is the systematic error from using our best value.
- LEES 11J reports $[\Gamma(\chi_{b1}(1P) \rightarrow \gamma T(1S))/\Gamma_{total}] \times [B(T(2S) \rightarrow \gamma \chi_{b1}(1P))]$ = $(24.1 \pm 0.6 \pm 1.5) \times 10^{-3}$ which we divide by our best value $B(T(2S) \rightarrow \gamma \chi_{b1}(1P))$ = $(6.9 \pm 0.4) \times 10^{-2}$. Our first error is their experiment's error and our second error is the systematic error from using our best value.
- WALK 86 quotes $B(T(2S) \rightarrow \gamma \chi_{b1}(1P)) \times B(\chi_{b1}(1P) \rightarrow \gamma T(1S)) \times B(T(1S) \rightarrow \ell^+ \ell^-)$ = $(5.8 \pm 0.9 \pm 0.7) \%$.
- WALK 86 reports $[\Gamma(\chi_{b1}(1P) \rightarrow \gamma T(1S))/\Gamma_{total}] \times [B(T(2S) \rightarrow \gamma \chi_{b1}(1P))]$ = $(23.4 \pm 3.63 \pm 2.82) \times 10^{-3}$ which we divide by our best value $B(T(2S) \rightarrow \gamma \chi_{b1}(1P))$ = $(6.9 \pm 0.4) \times 10^{-2}$. Our first error is their experiment's error and our second error is the systematic error from using our best value.

$\Gamma(D^0 X)/\Gamma_{total}$

VALUE (units 10^{-2})	EVTS	DOCUMENT ID	TECN	COMMENT	Γ_2/Γ
12.6 ± 1.9 ± 1.1	2310	¹ BRIERE	08 CLEO	$T(2S) \rightarrow \gamma D^0 X$	

¹ For $p_{D^0} > 2.5$ GeV/c.

$\Gamma(\pi^+ \pi^- K^+ K^- \pi^0)/\Gamma_{total}$

VALUE (units 10^{-4})	EVTS	DOCUMENT ID	TECN	COMMENT	Γ_3/Γ
2.0 ± 0.6 ± 0.1	18	¹ ASNER	08A CLEO	$T(2S) \rightarrow \gamma \pi^+ \pi^- K^+ K^- \pi^0$	

¹ ASNER 08A reports $[\Gamma(\chi_{b1}(1P) \rightarrow \pi^+ \pi^- K^+ K^- \pi^0)/\Gamma_{total}] \times [B(T(2S) \rightarrow \gamma \chi_{b1}(1P))]$ = $(14 \pm 3 \pm 3) \times 10^{-6}$ which we divide by our best value $B(T(2S) \rightarrow \gamma \chi_{b1}(1P))$ = $(6.9 \pm 0.4) \times 10^{-2}$. Our first error is their experiment's error and our second error is the systematic error from using our best value.

Meson Particle Listings

 $\chi_{b1}(1P)$ $\Gamma(2\pi^+\pi^-K^-K_S^0)/\Gamma_{\text{total}}$ Γ_4/Γ

VALUE (units 10^{-4})	EVTS	DOCUMENT ID	TECN	COMMENT
1.3 ± 0.5 ± 0.1	11	¹ ASNER	08A CLEO	$\Upsilon(2S) \rightarrow \gamma 2\pi^+\pi^-K^-K_S^0$

¹ ASNER 08A reports $[\Gamma(\chi_{b1}(1P) \rightarrow 2\pi^+\pi^-K^-K_S^0)/\Gamma_{\text{total}}] \times [B(\Upsilon(2S) \rightarrow \gamma\chi_{b1}(1P))]$ = $(9 \pm 3 \pm 2) \times 10^{-6}$ which we divide by our best value $B(\Upsilon(2S) \rightarrow \gamma\chi_{b1}(1P)) = (6.9 \pm 0.4) \times 10^{-2}$. Our first error is their experiment's error and our second error is the systematic error from using our best value.

 $\Gamma(2\pi^+\pi^-K^-K_S^0 2\pi^0)/\Gamma_{\text{total}}$ Γ_5/Γ

VALUE (units 10^{-4})	CL%	DOCUMENT ID	TECN	COMMENT
<6	90	¹ ASNER	08A CLEO	$\Upsilon(2S) \rightarrow \gamma 2\pi^+\pi^-K^-2\pi^0$

¹ ASNER 08A reports $[\Gamma(\chi_{b1}(1P) \rightarrow 2\pi^+\pi^-K^-K_S^0 2\pi^0)/\Gamma_{\text{total}}] \times [B(\Upsilon(2S) \rightarrow \gamma\chi_{b1}(1P))]$ < 42×10^{-6} which we divide by our best value $B(\Upsilon(2S) \rightarrow \gamma\chi_{b1}(1P)) = 6.9 \times 10^{-2}$.

 $\Gamma(2\pi^+2\pi^-2\pi^0)/\Gamma_{\text{total}}$ Γ_6/Γ

VALUE (units 10^{-4})	EVTS	DOCUMENT ID	TECN	COMMENT
8.0 ± 2.4 ± 0.4	46	¹ ASNER	08A CLEO	$\Upsilon(2S) \rightarrow \gamma 2\pi^+2\pi^-2\pi^0$

¹ ASNER 08A reports $[\Gamma(\chi_{b1}(1P) \rightarrow 2\pi^+2\pi^-2\pi^0)/\Gamma_{\text{total}}] \times [B(\Upsilon(2S) \rightarrow \gamma\chi_{b1}(1P))]$ = $(55 \pm 9 \pm 14) \times 10^{-6}$ which we divide by our best value $B(\Upsilon(2S) \rightarrow \gamma\chi_{b1}(1P)) = (6.9 \pm 0.4) \times 10^{-2}$. Our first error is their experiment's error and our second error is the systematic error from using our best value.

 $\Gamma(2\pi^+2\pi^-K^+K^-)/\Gamma_{\text{total}}$ Γ_7/Γ

VALUE (units 10^{-4})	EVTS	DOCUMENT ID	TECN	COMMENT
1.5 ± 0.5 ± 0.1	18	¹ ASNER	08A CLEO	$\Upsilon(2S) \rightarrow \gamma 2\pi^+2\pi^-K^+K^-$

¹ ASNER 08A reports $[\Gamma(\chi_{b1}(1P) \rightarrow 2\pi^+2\pi^-K^+K^-)/\Gamma_{\text{total}}] \times [B(\Upsilon(2S) \rightarrow \gamma\chi_{b1}(1P))]$ = $(10 \pm 3 \pm 2) \times 10^{-6}$ which we divide by our best value $B(\Upsilon(2S) \rightarrow \gamma\chi_{b1}(1P)) = (6.9 \pm 0.4) \times 10^{-2}$. Our first error is their experiment's error and our second error is the systematic error from using our best value.

 $\Gamma(2\pi^+2\pi^-K^+K^- \pi^0)/\Gamma_{\text{total}}$ Γ_8/Γ

VALUE (units 10^{-4})	EVTS	DOCUMENT ID	TECN	COMMENT
3.5 ± 1.2 ± 0.2	22	¹ ASNER	08A CLEO	$\Upsilon(2S) \rightarrow \gamma 2\pi^+2\pi^-K^+K^- \pi^0$

¹ ASNER 08A reports $[\Gamma(\chi_{b1}(1P) \rightarrow 2\pi^+2\pi^-K^+K^- \pi^0)/\Gamma_{\text{total}}] \times [B(\Upsilon(2S) \rightarrow \gamma\chi_{b1}(1P))]$ = $(24 \pm 6 \pm 6) \times 10^{-6}$ which we divide by our best value $B(\Upsilon(2S) \rightarrow \gamma\chi_{b1}(1P)) = (6.9 \pm 0.4) \times 10^{-2}$. Our first error is their experiment's error and our second error is the systematic error from using our best value.

 $\Gamma(2\pi^+2\pi^-K^+K^- 2\pi^0)/\Gamma_{\text{total}}$ Γ_9/Γ

VALUE (units 10^{-4})	EVTS	DOCUMENT ID	TECN	COMMENT
8.6 ± 3.2 ± 0.4	26	¹ ASNER	08A CLEO	$\Upsilon(2S) \rightarrow \gamma 2\pi^+2\pi^-K^+K^- 2\pi^0$

¹ ASNER 08A reports $[\Gamma(\chi_{b1}(1P) \rightarrow 2\pi^+2\pi^-K^+K^- 2\pi^0)/\Gamma_{\text{total}}] \times [B(\Upsilon(2S) \rightarrow \gamma\chi_{b1}(1P))]$ = $(59 \pm 14 \pm 17) \times 10^{-6}$ which we divide by our best value $B(\Upsilon(2S) \rightarrow \gamma\chi_{b1}(1P)) = (6.9 \pm 0.4) \times 10^{-2}$. Our first error is their experiment's error and our second error is the systematic error from using our best value.

 $\Gamma(3\pi^+2\pi^-K^-K_S^0 \pi^0)/\Gamma_{\text{total}}$ Γ_{10}/Γ

VALUE (units 10^{-4})	EVTS	DOCUMENT ID	TECN	COMMENT
9.3 ± 3.3 ± 0.5	21	¹ ASNER	08A CLEO	$\Upsilon(2S) \rightarrow \gamma 3\pi^+2\pi^-K^-K_S^0 \pi^0$

¹ ASNER 08A reports $[\Gamma(\chi_{b1}(1P) \rightarrow 3\pi^+2\pi^-K^-K_S^0 \pi^0)/\Gamma_{\text{total}}] \times [B(\Upsilon(2S) \rightarrow \gamma\chi_{b1}(1P))]$ = $(64 \pm 16 \pm 16) \times 10^{-6}$ which we divide by our best value $B(\Upsilon(2S) \rightarrow \gamma\chi_{b1}(1P)) = (6.9 \pm 0.4) \times 10^{-2}$. Our first error is their experiment's error and our second error is the systematic error from using our best value.

 $\Gamma(3\pi^+3\pi^-)/\Gamma_{\text{total}}$ Γ_{11}/Γ

VALUE (units 10^{-4})	EVTS	DOCUMENT ID	TECN	COMMENT
1.9 ± 0.6 ± 0.1	25	¹ ASNER	08A CLEO	$\Upsilon(2S) \rightarrow \gamma 3\pi^+3\pi^-$

¹ ASNER 08A reports $[\Gamma(\chi_{b1}(1P) \rightarrow 3\pi^+3\pi^-)/\Gamma_{\text{total}}] \times [B(\Upsilon(2S) \rightarrow \gamma\chi_{b1}(1P))]$ = $(13 \pm 3 \pm 3) \times 10^{-6}$ which we divide by our best value $B(\Upsilon(2S) \rightarrow \gamma\chi_{b1}(1P)) = (6.9 \pm 0.4) \times 10^{-2}$. Our first error is their experiment's error and our second error is the systematic error from using our best value.

 $\Gamma(3\pi^+3\pi^- 2\pi^0)/\Gamma_{\text{total}}$ Γ_{12}/Γ

VALUE (units 10^{-4})	EVTS	DOCUMENT ID	TECN	COMMENT
17 ± 5 ± 1	56	¹ ASNER	08A CLEO	$\Upsilon(2S) \rightarrow \gamma 3\pi^+3\pi^- 2\pi^0$

¹ ASNER 08A reports $[\Gamma(\chi_{b1}(1P) \rightarrow 3\pi^+3\pi^- 2\pi^0)/\Gamma_{\text{total}}] \times [B(\Upsilon(2S) \rightarrow \gamma\chi_{b1}(1P))]$ = $(119 \pm 18 \pm 32) \times 10^{-6}$ which we divide by our best value $B(\Upsilon(2S) \rightarrow \gamma\chi_{b1}(1P)) = (6.9 \pm 0.4) \times 10^{-2}$. Our first error is their experiment's error and our second error is the systematic error from using our best value.

 $\Gamma(3\pi^+3\pi^-K^+K^-)/\Gamma_{\text{total}}$ Γ_{13}/Γ

VALUE (units 10^{-4})	EVTS	DOCUMENT ID	TECN	COMMENT
2.6 ± 0.8 ± 0.1	21	¹ ASNER	08A CLEO	$\Upsilon(2S) \rightarrow \gamma 3\pi^+3\pi^-K^+K^-$

¹ ASNER 08A reports $[\Gamma(\chi_{b1}(1P) \rightarrow 3\pi^+3\pi^-K^+K^-)/\Gamma_{\text{total}}] \times [B(\Upsilon(2S) \rightarrow \gamma\chi_{b1}(1P))]$ = $(18 \pm 4 \pm 4) \times 10^{-6}$ which we divide by our best value $B(\Upsilon(2S) \rightarrow \gamma\chi_{b1}(1P)) = (6.9 \pm 0.4) \times 10^{-2}$. Our first error is their experiment's error and our second error is the systematic error from using our best value.

 $\Gamma(3\pi^+3\pi^-K^+K^- \pi^0)/\Gamma_{\text{total}}$ Γ_{14}/Γ

VALUE (units 10^{-4})	EVTS	DOCUMENT ID	TECN	COMMENT
7.5 ± 2.6 ± 0.4	28	¹ ASNER	08A CLEO	$\Upsilon(2S) \rightarrow \gamma 3\pi^+3\pi^-K^+K^- \pi^0$

¹ ASNER 08A reports $[\Gamma(\chi_{b1}(1P) \rightarrow 3\pi^+3\pi^-K^+K^- \pi^0)/\Gamma_{\text{total}}] \times [B(\Upsilon(2S) \rightarrow \gamma\chi_{b1}(1P))]$ = $(52 \pm 11 \pm 14) \times 10^{-6}$ which we divide by our best value $B(\Upsilon(2S) \rightarrow \gamma\chi_{b1}(1P)) = (6.9 \pm 0.4) \times 10^{-2}$. Our first error is their experiment's error and our second error is the systematic error from using our best value.

 $\Gamma(4\pi^+4\pi^-)/\Gamma_{\text{total}}$ Γ_{15}/Γ

VALUE (units 10^{-4})	EVTS	DOCUMENT ID	TECN	COMMENT
2.6 ± 0.9 ± 0.1	24	¹ ASNER	08A CLEO	$\Upsilon(2S) \rightarrow \gamma 4\pi^+4\pi^-$

¹ ASNER 08A reports $[\Gamma(\chi_{b1}(1P) \rightarrow 4\pi^+4\pi^-)/\Gamma_{\text{total}}] \times [B(\Upsilon(2S) \rightarrow \gamma\chi_{b1}(1P))]$ = $(18 \pm 4 \pm 5) \times 10^{-6}$ which we divide by our best value $B(\Upsilon(2S) \rightarrow \gamma\chi_{b1}(1P)) = (6.9 \pm 0.4) \times 10^{-2}$. Our first error is their experiment's error and our second error is the systematic error from using our best value.

 $\Gamma(4\pi^+4\pi^- 2\pi^0)/\Gamma_{\text{total}}$ Γ_{16}/Γ

VALUE (units 10^{-4})	EVTS	DOCUMENT ID	TECN	COMMENT
14 ± 5 ± 1	26	¹ ASNER	08A CLEO	$\Upsilon(2S) \rightarrow \gamma 4\pi^+4\pi^- 2\pi^0$

¹ ASNER 08A reports $[\Gamma(\chi_{b1}(1P) \rightarrow 4\pi^+4\pi^- 2\pi^0)/\Gamma_{\text{total}}] \times [B(\Upsilon(2S) \rightarrow \gamma\chi_{b1}(1P))]$ = $(96 \pm 24 \pm 29) \times 10^{-6}$ which we divide by our best value $B(\Upsilon(2S) \rightarrow \gamma\chi_{b1}(1P)) = (6.9 \pm 0.4) \times 10^{-2}$. Our first error is their experiment's error and our second error is the systematic error from using our best value.

 $\Gamma(\omega \text{ anything})/\Gamma_{\text{total}}$ Γ_{17}/Γ

VALUE (units 10^{-2})	EVTS	DOCUMENT ID	TECN	COMMENT
4.9 ± 1.3 ± 0.6	51k	JIA	17A BELL	$e^+e^- \rightarrow \text{hadrons}$

 $\Gamma(\omega X_{tetra})/\Gamma_{\text{total}}$ Γ_{18}/Γ

VALUE	CL%	DOCUMENT ID	TECN	COMMENT
<44.4 × 10⁻⁵	90	¹ JIA	17A BELL	$e^+e^- \rightarrow \text{hadrons}$

¹ For a tetraquark state X_{tetra} , with mass in the range 1.16–2.46 GeV and width in the range 0–0.3 GeV. Measured 90% CL limits as a function of X_{tetra} mass and width range from 3.3×10^{-5} to 44.4×10^{-5} .

 $\Gamma(J/\psi J/\psi)/\Gamma_{\text{total}}$ Γ_{19}/Γ

VALUE (units 10^{-5})	CL%	DOCUMENT ID	TECN	COMMENT
<2.7	90	¹ SHEN	12 BELL	$\Upsilon(2S) \rightarrow \gamma\psi X$

¹ SHEN 12 reports $< 2.7 \times 10^{-5}$ from a measurement of $[\Gamma(\chi_{b1}(1P) \rightarrow J/\psi J/\psi)/\Gamma_{\text{total}}] \times [B(\Upsilon(2S) \rightarrow \gamma\chi_{b1}(1P))]$ assuming $B(\Upsilon(2S) \rightarrow \gamma\chi_{b1}(1P)) = (6.9 \pm 0.4) \times 10^{-2}$.

 $\Gamma(J/\psi\psi(2S))/\Gamma_{\text{total}}$ Γ_{20}/Γ

VALUE (units 10^{-5})	CL%	DOCUMENT ID	TECN	COMMENT
<1.7	90	¹ SHEN	12 BELL	$\Upsilon(2S) \rightarrow \gamma\psi X$

¹ SHEN 12 reports $< 1.7 \times 10^{-5}$ from a measurement of $[\Gamma(\chi_{b1}(1P) \rightarrow J/\psi\psi(2S))/\Gamma_{\text{total}}] \times [B(\Upsilon(2S) \rightarrow \gamma\chi_{b1}(1P))]$ assuming $B(\Upsilon(2S) \rightarrow \gamma\chi_{b1}(1P)) = (6.9 \pm 0.4) \times 10^{-2}$.

 $\Gamma(\psi(2S)\psi(2S))/\Gamma_{\text{total}}$ Γ_{21}/Γ

VALUE (units 10^{-5})	CL%	DOCUMENT ID	TECN	COMMENT
<6	90	¹ SHEN	12 BELL	$\Upsilon(2S) \rightarrow \gamma\psi X$

¹ SHEN 12 reports $< 6.2 \times 10^{-5}$ from a measurement of $[\Gamma(\chi_{b1}(1P) \rightarrow \psi(2S)\psi(2S))/\Gamma_{\text{total}}] \times [B(\Upsilon(2S) \rightarrow \gamma\chi_{b1}(1P))]$ assuming $B(\Upsilon(2S) \rightarrow \gamma\chi_{b1}(1P)) = (6.9 \pm 0.4) \times 10^{-2}$.

 $\Gamma(J/\psi(1S) \text{ anything})/\Gamma_{\text{total}}$ Γ_{22}/Γ

VALUE	CL%	DOCUMENT ID	TECN	COMMENT
<1.1 × 10⁻³	90	JIA	17A BELL	$e^+e^- \rightarrow \text{hadrons}$

 $\Gamma(J/\psi(1S) X_{tetra})/\Gamma_{\text{total}}$ Γ_{23}/Γ

VALUE	CL%	DOCUMENT ID	TECN	COMMENT
<22.7 × 10⁻⁵	90	¹ JIA	17A BELL	$e^+e^- \rightarrow \text{hadrons}$

¹ For a tetraquark state X_{tetra} , with mass in the range 1.16–2.46 GeV and width in the range 0–0.3 GeV. Measured 90% CL limits as a function of X_{tetra} mass and width range from 1.8×10^{-5} to 22.7×10^{-5} .

 $\chi_{b1}(1P)$ Cross-Particle Branching Ratios $\Gamma(\chi_{b1}(1P) \rightarrow \gamma \Upsilon(1S))/\Gamma_{\text{total}} \times \Gamma(\Upsilon(2S) \rightarrow \gamma\chi_{b1}(1P))/\Gamma_{\text{total}}$
 $\Gamma_1/\Gamma \times \Gamma_{\Upsilon(2S)}^{\Upsilon(1S)}/\Gamma_{\Upsilon(2S)}$

VALUE (units 10^{-3})	EVTS	DOCUMENT ID	TECN	COMMENT
24.1 ± 0.6 ± 1.5	13k	LEES	11J BABR	$\Upsilon(2S) \rightarrow X \gamma$

 $B(\chi_{b1}(1P) \rightarrow \gamma \Upsilon(1S)) \times B(\Upsilon(2S) \rightarrow \gamma\chi_{b1}(1P)) \times B(\Upsilon(1S) \rightarrow \ell^+\ell^-)$

VALUE (units 10^{-4})	EVTS	DOCUMENT ID	TECN	COMMENT
5.90 ± 0.34 OUR AVERAGE		Error includes scale factor of 1.3. See the ideogram below.		

6.86 ^{+0.47} _{-0.45} ± 0.35		¹ LEES	14M BABR	$\Upsilon(2S) \rightarrow \gamma\gamma\mu^+\mu^-$
5.65 ± 0.11 ± 0.27	3222	KORNICER	11 CLEO	$e^+e^- \rightarrow \gamma\gamma\ell^+\ell^-$
5.8 ± 0.9 ± 0.7	53	WALK	86 CBAL	$\Upsilon(2S) \rightarrow \gamma\gamma\ell^+\ell^-$

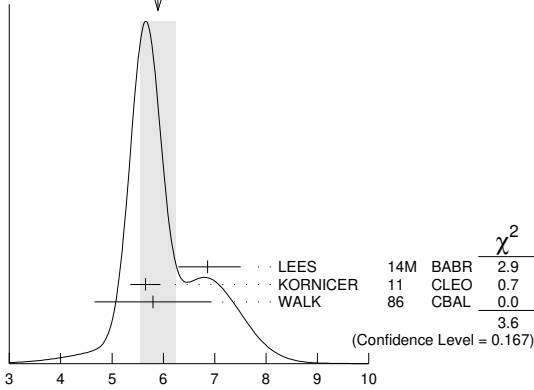
¹ From a sample of $\Upsilon(2S) \rightarrow \gamma\gamma\mu^+\mu^-$ with one converted photon.

See key on page 1171

Meson Particle Listings

$\chi_{b1}(1P), h_b(1P), \chi_{b2}(1P)$

WEIGHTED AVERAGE
5.90±0.34 (Error scaled by 1.3)



$$B(\chi_{b1}(1P) \rightarrow \gamma \Upsilon(1S)) \times B(\Upsilon(2S) \rightarrow \gamma \chi_{b1}(1P)) \times B(\Upsilon(1S) \rightarrow \ell^+ \ell^-)$$

(units 10^{-4})

$$B(\chi_{b1}(1P) \rightarrow \gamma \Upsilon(1S)) \times B(\Upsilon(3S) \rightarrow \gamma \chi_{b1}(1P)) \times B(\Upsilon(1S) \rightarrow \ell^+ \ell^-)$$

VALUE (units 10^{-5})	EVTS	DOCUMENT ID	TECN	COMMENT
1.30±0.34 OUR AVERAGE				

1.16 ^{+0.78+0.14} _{-0.67-0.16}		¹ LEES	14M BABR	$\Upsilon(3S) \rightarrow \gamma \mu^+ \mu^-$
--	--	-------------------	----------	---

1.33±0.30±0.23	50	KORNICER	11 CLEO	$e^+ e^- \rightarrow \gamma \gamma \ell^+ \ell^-$
----------------	----	----------	---------	---

¹ From a sample of $\Upsilon(3S) \rightarrow \gamma \mu^+ \mu^-$ with converted photons.

$$B(\chi_{b2}(1P) \rightarrow \rho X + \bar{\rho} X) / B(\chi_{b1}(1P) \rightarrow \rho X + \bar{\rho} X)$$

VALUE	DOCUMENT ID	TECN	COMMENT
1.068±0.010±0.040	BRIERE 07	CLEO	$\Upsilon(2S) \rightarrow \gamma \chi_{bJ}(1P)$

$$B(\chi_{b0}(1P) \rightarrow \rho X + \bar{\rho} X) / B(\chi_{b1}(1P) \rightarrow \rho X + \bar{\rho} X)$$

VALUE	DOCUMENT ID	TECN	COMMENT
1.11±0.15±0.20	BRIERE 07	CLEO	$\Upsilon(2S) \rightarrow \gamma \chi_{bJ}(1P)$

$\chi_{b1}(1P)$ REFERENCES

NAME	YEAR	DOCUMENT ID	TECN	COMMENT
FULSOM	18	PRL 121 232001		B. G. Fulsom et al. (BELLE Collab.)
JIA	17A	PR D96 112002		S. Jia et al. (BELLE Collab.)
LEES	14M	PR D90 112010		J.P. Lees et al. (BABAR Collab.)
SHEN	12	PR D85 071102		C.P. Shen et al. (BELLE Collab.)
KORNICER	11	PR D83 054003		M. Kornicer et al. (CLEO Collab.)
LEES	11J	PR D84 072002		J.P. Lees et al. (BABAR Collab.)
ASNER	08A	PR D78 091103		D.M. Asner et al. (CLEO Collab.)
BRIERE	08B	PR D78 092007		R.A. Briere et al. (CLEO Collab.)
BRIERE	07	PR D76 012005		R.A. Briere et al. (CLEO Collab.)
ARTUSO	05	PRL 94 032001		M. Artuso et al. (CLEO Collab.)
EDWARDS	99	PR D59 032003		K.W. Edwards et al. (CLEO Collab.)
SKWARNICKI	87	PRL 58 972		T. Skwarnicki et al. (Crystal Ball Collab.) ^J
WALK	86	PR D34 2611		W.S. Walk et al. (Crystal Ball Collab.)
ALBRECHT	85E	PL 160B 331		H. Albrecht et al. (ARGUS Collab.)
NERNST	85	PRL 54 2195		R. Nernst et al. (Crystal Ball Collab.)
HAAS	84	PRL 52 739		J. Haas et al. (CLEO Collab.)
KLOPFEN...	83	PRL 51 160		C. Klopffenstein et al. (CUSB Collab.)
PAUSS	83	PL 130B 439		F. Pauss et al. (MPIM, COLU, CORN, LSU+)

$h_b(1P)$

$$I^G(J^{PC}) = 0^-(1^{+-})$$

Quantum numbers are quark model predictions, $C = -$ established by $\eta_b \gamma$ decay.

$h_b(1P)$ MASS

VALUE (MeV)	EVTS	DOCUMENT ID	TECN	COMMENT
9899.3±0.8 OUR AVERAGE				

9899.3±0.4±1.0	112k	TAMPONI	15 BELL	$e^+ e^- \rightarrow \gamma \eta + \text{hadrons}$
----------------	------	---------	---------	--

9899.1±0.4±1.0	70k	MIZUK	12 BELL	$e^+ e^- \rightarrow \pi^+ \pi^- \text{hadrons}$
----------------	-----	-------	---------	--

9902 ±4 ±2	10.8k	LEES	11K BABR	$\Upsilon(3S) \rightarrow \eta_b \gamma \pi^0$
------------	-------	------	----------	--

••• We do not use the following data for averages, fits, limits, etc. •••

9898.2 ^{+1.1+1.0} _{-1.0-1.1}	50.0k	¹ ADACHI	12 BELL	10.86 $e^+ e^- \rightarrow \pi^+ \pi^- \text{MM}$
--	-------	---------------------	---------	---

¹ Superseded by MIZUK 12.

$h_b(1P)$ DECAY MODES

Mode	Fraction (Γ_i/Γ)
Γ_1 $\eta_b(1S) \gamma$	(52 ⁺⁶ ₋₅) %

$h_b(1P)$ BRANCHING RATIOS

$\Gamma(\eta_b(1S)\gamma)/\Gamma_{\text{total}}$	VALUE (units 10^{-2})	EVTS	DOCUMENT ID	TECN	COMMENT	Γ_i/Γ
--	--------------------------	------	-------------	------	---------	-------------------

52⁺⁶₋₅ OUR AVERAGE

56 ±8 ±4	33.1k	¹ TAMPONI	15 BELL	$e^+ e^- \rightarrow \gamma \eta + \text{hadrons}$
----------	-------	----------------------	---------	--

49.2±5.7 ^{+5.6} _{-3.3}	24k	MIZUK	12 BELL	$e^+ e^- \rightarrow (\gamma) \pi^+ \pi^- \text{hadrons}$
--	-----	-------	---------	---

••• We do not use the following data for averages, fits, limits, etc. •••

seen	10.8k	LEES	11K BABR	$\Upsilon(3S) \rightarrow \eta_b \gamma \pi^0$
------	-------	------	----------	--

¹ Using $B(\eta \rightarrow 2\gamma) = (39.41 \pm 0.20)\%$.

$h_b(1P)$ REFERENCES

NAME	YEAR	DOCUMENT ID	TECN	COMMENT
TAMPONI	15	PRL 115 142001		U. Tamponi et al. (BELLE Collab.)
ADACHI	12	PRL 108 032001		I. Adachi et al. (BELLE Collab.)
MIZUK	12	PRL 109 232002		R. Mizuk et al. (BELLE Collab.)
LEES	11K	PR D84 091101		J.P. Lees et al. (BABAR Collab.)

$\chi_{b2}(1P)$

$$I^G(J^{PC}) = 0^+(2^{++})$$

J needs confirmation.

Observed in radiative decay of the $\Upsilon(2S)$, therefore $C = +$. Branching ratio requires E1 transition, M1 is strongly disfavored, therefore $P = +$. $J = 2$ from SKWARNICKI 87.

$\chi_{b2}(1P)$ MASS

VALUE (MeV)	DOCUMENT ID
9912.21±0.26±0.31 OUR EVALUATION	From average γ energy below, using $\Upsilon(2S)$ mass = 10023.26 ± 0.31 MeV

$m_{\chi_{b2}(1P)} - m_{\chi_{b1}(1P)}$

VALUE (MeV)	DOCUMENT ID	TECN	COMMENT
19.10±0.25 OUR AVERAGE	Error includes scale factor of 1.1.		

19.81±0.65±0.20	¹ AAIJ	14B6 LHCB	$pp \rightarrow \gamma \mu^+ \mu^- X$
-----------------	-------------------	-----------	---------------------------------------

19.01±0.24	LEES	14M BABR	$\Upsilon(2S) \rightarrow \gamma \gamma \mu^+ \mu^-$
------------	------	----------	--

¹ From the $\chi_{bJ}(1P) \rightarrow \Upsilon(1S) \gamma$ transition.

γ ENERGY IN $\Upsilon(2S)$ DECAY

VALUE (MeV)	DOCUMENT ID	TECN	COMMENT
110.44±0.29 OUR AVERAGE	Error includes scale factor of 1.1.		

110.58±0.08±0.30	ARTUSO	05 CLEO	$\Upsilon(2S) \rightarrow \gamma X$
------------------	--------	---------	-------------------------------------

110.8 ±0.3 ±0.6	EDWARDS	99 CLE2	$\Upsilon(2S) \rightarrow \gamma \chi(1P)$
-----------------	---------	---------	--

107.0 ±1.1 ±1.3	WALK	86 CBAL	$\Upsilon(2S) \rightarrow \gamma \gamma \ell^+ \ell^-$
-----------------	------	---------	--

110.6 ±0.3 ±0.9	ALBRECHT	85E ARG	$\Upsilon(2S) \rightarrow \text{conv. } \gamma X$
-----------------	----------	---------	---

110.4 ±0.8 ±2.2	NERNST	85 CBAL	$\Upsilon(2S) \rightarrow \gamma X$
-----------------	--------	---------	-------------------------------------

109.5 ±0.7 ±1.0	HAAS	84 CLEO	$\Upsilon(2S) \rightarrow \text{conv. } \gamma X$
-----------------	------	---------	---

108.2 ±0.3 ±2.0	KLOPFEN...	83 CUSB	$\Upsilon(2S) \rightarrow \gamma X$
-----------------	------------	---------	-------------------------------------

108.8 ±4.0	PAUSS	83 CUSB	$\Upsilon(2S) \rightarrow \gamma \gamma \ell^+ \ell^-$
------------	-------	---------	--

$\chi_{b2}(1P)$ DECAY MODES

Mode	Fraction (Γ_i/Γ)	Confidence level
Γ_1 $\gamma \Upsilon(1S)$	(18.0±1.0) %	
Γ_2 $D^0 X$	< 7.9 %	90%
Γ_3 $\pi^+ \pi^- K^+ K^- \pi^0$	(8 ±5) × 10 ⁻⁵	
Γ_4 $2\pi^+ \pi^- K^- K_S^0$	< 1.0 × 10 ⁻⁴	90%
Γ_5 $2\pi^+ \pi^- K^- K_S^0 2\pi^0$	(5.3±2.4) × 10 ⁻⁴	
Γ_6 $2\pi^+ 2\pi^- 2\pi^0$	(3.5±1.4) × 10 ⁻⁴	
Γ_7 $2\pi^+ 2\pi^- K^+ K^-$	(1.1±0.4) × 10 ⁻⁴	
Γ_8 $2\pi^+ 2\pi^- K^+ K^- \pi^0$	(2.1±0.9) × 10 ⁻⁴	
Γ_9 $2\pi^+ 2\pi^- K^+ K^- 2\pi^0$	(3.9±1.8) × 10 ⁻⁴	
Γ_{10} $3\pi^+ 2\pi^- K^- K_S^0 \pi^0$	< 5 × 10 ⁻⁴	90%
Γ_{11} $3\pi^+ 3\pi^-$	(7.0±3.1) × 10 ⁻⁵	
Γ_{12} $3\pi^+ 3\pi^- 2\pi^0$	(1.0±0.4) × 10 ⁻³	
Γ_{13} $3\pi^+ 3\pi^- K^+ K^-$	< 8 × 10 ⁻⁵	90%
Γ_{14} $3\pi^+ 3\pi^- K^+ K^- \pi^0$	(3.6±1.5) × 10 ⁻⁴	
Γ_{15} $4\pi^+ 4\pi^-$	(8 ±4) × 10 ⁻⁵	
Γ_{16} $4\pi^+ 4\pi^- 2\pi^0$	(1.8±0.7) × 10 ⁻³	
Γ_{17} $J/\psi J/\psi$	< 4 × 10 ⁻⁵	90%
Γ_{18} $J/\psi \psi(2S)$	< 5 × 10 ⁻⁵	90%
Γ_{19} $\psi(2S) \psi(2S)$	< 1.6 × 10 ⁻⁵	90%
Γ_{20} $J/\psi(1S) \text{anything}$	(1.5±0.4) × 10 ⁻³	

Meson Particle Listings

 $\chi_{b2}(1P)$ $\chi_{b2}(1P)$ BRANCHING RATIOS

$\Gamma(\gamma \mathcal{T}(1S))/\Gamma_{\text{total}}$					Γ_1/Γ
VALUE	EVTS	DOCUMENT ID	TECN	COMMENT	
0.180 ± 0.010 OUR AVERAGE					
0.164 ± 0.009 -0.016 ± 0.008	503k	¹ FULSOM	18 BELL	$\mathcal{T}(2S) \rightarrow \gamma X$	
0.185 ± 0.008 ± 0.009	2,3,4	LEES	14M BABR	$\mathcal{T}(2S) \rightarrow \gamma \gamma \mu^+ \mu^-$	
0.186 ± 0.011 ± 0.009	1770	^{4,5} KORNICER	11 CLEO	$e^+ e^- \rightarrow \gamma \gamma \ell^+ \ell^-$	
0.194 ± 0.014 -0.017 ± 0.009	8k	⁶ LEES	11J BABR	$\mathcal{T}(2S) \rightarrow X \gamma$	
0.25 ± 0.06 ± 0.01	35	^{4,7,8} WALK	86 CBAL	$\mathcal{T}(2S) \rightarrow \gamma \gamma \ell^+ \ell^-$	
0.20 ± 0.05		KLOPFEN...	83 CUSB	$\mathcal{T}(2S) \rightarrow \gamma \gamma \ell^+ \ell^-$	

¹ FULSOM 18 reports $[\Gamma(\chi_{b2}(1P) \rightarrow \gamma \mathcal{T}(1S))/\Gamma_{\text{total}}] \times [B(\mathcal{T}(2S) \rightarrow \gamma \chi_{b2}(1P))] = (1.17 \pm 0.01 \pm 0.09 \pm 0.07) \times 10^{-2}$ which we divide by our best value $B(\mathcal{T}(2S) \rightarrow \gamma \chi_{b2}(1P)) = (7.15 \pm 0.35) \times 10^{-2}$. Our first error is their experiment's error and our second error is the systematic error from using our best value.

² LEES 14M quotes $\Gamma(\chi_{b2}(1P) \rightarrow \gamma \mathcal{T}(1S))/\Gamma_{\text{total}} \times \Gamma(\mathcal{T}(2S) \rightarrow \gamma \chi_{b2}(1P))/\Gamma_{\text{total}} = (1.32 \pm 0.06)\%$ combining the results from samples of $\mathcal{T}(2S) \rightarrow \gamma \gamma \mu^+ \mu^-$ with and without converted photons.

³ LEES 14M reports $[\Gamma(\chi_{b2}(1P) \rightarrow \gamma \mathcal{T}(1S))/\Gamma_{\text{total}}] \times [B(\mathcal{T}(2S) \rightarrow \gamma \chi_{b2}(1P))] = (1.32 \pm 0.06) \times 10^{-2}$ which we divide by our best value $B(\mathcal{T}(2S) \rightarrow \gamma \chi_{b2}(1P)) = (7.15 \pm 0.35) \times 10^{-2}$. Our first error is their experiment's error and our second error is the systematic error from using our best value.

⁴ Assuming $B(\mathcal{T}(1S) \rightarrow \mu^+ \mu^-) = (2.48 \pm 0.05)\%$.

⁵ KORNICER 11 reports $[\Gamma(\chi_{b2}(1P) \rightarrow \gamma \mathcal{T}(1S))/\Gamma_{\text{total}}] \times [B(\mathcal{T}(2S) \rightarrow \gamma \chi_{b2}(1P))] = (1.33 \pm 0.04 \pm 0.07) \times 10^{-2}$ which we divide by our best value $B(\mathcal{T}(2S) \rightarrow \gamma \chi_{b2}(1P)) = (7.15 \pm 0.35) \times 10^{-2}$. Our first error is their experiment's error and our second error is the systematic error from using our best value.

⁶ LEES 11J reports $[\Gamma(\chi_{b2}(1P) \rightarrow \gamma \mathcal{T}(1S))/\Gamma_{\text{total}}] \times [B(\mathcal{T}(2S) \rightarrow \gamma \chi_{b2}(1P))] = (13.9 \pm 0.5 \pm 0.9 \pm 1.1) \times 10^{-3}$ which we divide by our best value $B(\mathcal{T}(2S) \rightarrow \gamma \chi_{b2}(1P)) = (7.15 \pm 0.35) \times 10^{-2}$. Our first error is their experiment's error and our second error is the systematic error from using our best value.

⁷ WALK 86 quotes $B(\mathcal{T}(2S) \rightarrow \gamma \chi_{b2}(1P)) \times B(\chi_{b2}(1P) \rightarrow \gamma \mathcal{T}(1S)) \times B(\mathcal{T}(1S) \rightarrow \ell^+ \ell^-) = (4.4 \pm 0.9 \pm 0.5)\%$.

⁸ WALK 86 reports $[\Gamma(\chi_{b2}(1P) \rightarrow \gamma \mathcal{T}(1S))/\Gamma_{\text{total}}] \times [B(\mathcal{T}(2S) \rightarrow \gamma \chi_{b2}(1P))] = (17.7 \pm 3.6 \pm 2.0) \times 10^{-3}$ which we divide by our best value $B(\mathcal{T}(2S) \rightarrow \gamma \chi_{b2}(1P)) = (7.15 \pm 0.35) \times 10^{-2}$. Our first error is their experiment's error and our second error is the systematic error from using our best value.

$\Gamma(D^0 X)/\Gamma_{\text{total}}$					Γ_2/Γ
VALUE	CL%	DOCUMENT ID	TECN	COMMENT	
< 7.9 × 10⁻²	90	^{1,2} BRIERE	08 CLEO	$\mathcal{T}(2S) \rightarrow \gamma D^0 X$	

¹ For $p_{D^0} > 2.5$ GeV/c.

² The authors also present their result as $(5.4 \pm 1.9 \pm 0.5) \times 10^{-2}$.

$\Gamma(\pi^+ \pi^- K^+ K^- \pi^0)/\Gamma_{\text{total}}$					Γ_3/Γ
VALUE (units 10 ⁻⁴)	EVTS	DOCUMENT ID	TECN	COMMENT	
0.84 ± 0.50 ± 0.04	8	¹ ASNER	08A CLEO	$\mathcal{T}(2S) \rightarrow \gamma \pi^+ \pi^- K^+ K^- \pi^0$	

¹ ASNER 08A reports $[\Gamma(\chi_{b2}(1P) \rightarrow \pi^+ \pi^- K^+ K^- \pi^0)/\Gamma_{\text{total}}] \times [B(\mathcal{T}(2S) \rightarrow \gamma \chi_{b2}(1P))] = (6 \pm 3 \pm 2) \times 10^{-6}$ which we divide by our best value $B(\mathcal{T}(2S) \rightarrow \gamma \chi_{b2}(1P)) = (7.15 \pm 0.35) \times 10^{-2}$. Our first error is their experiment's error and our second error is the systematic error from using our best value.

$\Gamma(2\pi^+ \pi^- K^- K_S^0)/\Gamma_{\text{total}}$					Γ_4/Γ
VALUE (units 10 ⁻⁴)	CL%	DOCUMENT ID	TECN	COMMENT	
< 1.0	90	¹ ASNER	08A CLEO	$\mathcal{T}(2S) \rightarrow \gamma 2\pi^+ \pi^- K^- K_S^0$	

¹ ASNER 08A reports $[\Gamma(\chi_{b2}(1P) \rightarrow 2\pi^+ \pi^- K^- K_S^0)/\Gamma_{\text{total}}] \times [B(\mathcal{T}(2S) \rightarrow \gamma \chi_{b2}(1P))] < 7 \times 10^{-6}$ which we divide by our best value $B(\mathcal{T}(2S) \rightarrow \gamma \chi_{b2}(1P)) = 7.15 \times 10^{-2}$.

$\Gamma(2\pi^+ \pi^- K^- K_S^0 2\pi^0)/\Gamma_{\text{total}}$					Γ_5/Γ
VALUE (units 10 ⁻⁴)	EVTS	DOCUMENT ID	TECN	COMMENT	
5.3 ± 2.4 ± 0.3	11	¹ ASNER	08A CLEO	$\mathcal{T}(2S) \rightarrow \gamma 2\pi^+ \pi^- K^- 2\pi^0$	

¹ ASNER 08A reports $[\Gamma(\chi_{b2}(1P) \rightarrow 2\pi^+ \pi^- K^- K_S^0 2\pi^0)/\Gamma_{\text{total}}] \times [B(\mathcal{T}(2S) \rightarrow \gamma \chi_{b2}(1P))] = (38 \pm 14 \pm 10) \times 10^{-6}$ which we divide by our best value $B(\mathcal{T}(2S) \rightarrow \gamma \chi_{b2}(1P)) = (7.15 \pm 0.35) \times 10^{-2}$. Our first error is their experiment's error and our second error is the systematic error from using our best value.

$\Gamma(2\pi^+ 2\pi^- 2\pi^0)/\Gamma_{\text{total}}$					Γ_6/Γ
VALUE (units 10 ⁻⁴)	EVTS	DOCUMENT ID	TECN	COMMENT	
3.5 ± 1.4 ± 0.2	19	¹ ASNER	08A CLEO	$\mathcal{T}(2S) \rightarrow \gamma 2\pi^+ 2\pi^- 2\pi^0$	

¹ ASNER 08A reports $[\Gamma(\chi_{b2}(1P) \rightarrow 2\pi^+ 2\pi^- 2\pi^0)/\Gamma_{\text{total}}] \times [B(\mathcal{T}(2S) \rightarrow \gamma \chi_{b2}(1P))] = (25 \pm 8 \pm 6) \times 10^{-6}$ which we divide by our best value $B(\mathcal{T}(2S) \rightarrow \gamma \chi_{b2}(1P)) = (7.15 \pm 0.35) \times 10^{-2}$. Our first error is their experiment's error and our second error is the systematic error from using our best value.

 $\Gamma(2\pi^+ 2\pi^- K^+ K^-)/\Gamma_{\text{total}}$ Γ_7/Γ

VALUE (units 10 ⁻⁴)	EVTS	DOCUMENT ID	TECN	COMMENT	
1.1 ± 0.4 ± 0.1	14	¹ ASNER	08A CLEO	$\mathcal{T}(2S) \rightarrow \gamma 2\pi^+ 2\pi^- K^+ K^-$	

¹ ASNER 08A reports $[\Gamma(\chi_{b2}(1P) \rightarrow 2\pi^+ 2\pi^- K^+ K^-)/\Gamma_{\text{total}}] \times [B(\mathcal{T}(2S) \rightarrow \gamma \chi_{b2}(1P))] = (8 \pm 2 \pm 2) \times 10^{-6}$ which we divide by our best value $B(\mathcal{T}(2S) \rightarrow \gamma \chi_{b2}(1P)) = (7.15 \pm 0.35) \times 10^{-2}$. Our first error is their experiment's error and our second error is the systematic error from using our best value.

 $\Gamma(2\pi^+ 2\pi^- K^+ K^- \pi^0)/\Gamma_{\text{total}}$ Γ_8/Γ

VALUE (units 10 ⁻⁴)	EVTS	DOCUMENT ID	TECN	COMMENT	
2.1 ± 0.9 ± 0.1	13	¹ ASNER	08A CLEO	$\mathcal{T}(2S) \rightarrow \gamma 2\pi^+ 2\pi^- K^+ K^- \pi^0$	

¹ ASNER 08A reports $[\Gamma(\chi_{b2}(1P) \rightarrow 2\pi^+ 2\pi^- K^+ K^- \pi^0)/\Gamma_{\text{total}}] \times [B(\mathcal{T}(2S) \rightarrow \gamma \chi_{b2}(1P))] = (15 \pm 5 \pm 4) \times 10^{-6}$ which we divide by our best value $B(\mathcal{T}(2S) \rightarrow \gamma \chi_{b2}(1P)) = (7.15 \pm 0.35) \times 10^{-2}$. Our first error is their experiment's error and our second error is the systematic error from using our best value.

 $\Gamma(2\pi^+ 2\pi^- K^+ K^- 2\pi^0)/\Gamma_{\text{total}}$ Γ_9/Γ

VALUE (units 10 ⁻⁴)	EVTS	DOCUMENT ID	TECN	COMMENT	
3.9 ± 1.8 ± 0.2	11	¹ ASNER	08A CLEO	$\mathcal{T}(2S) \rightarrow \gamma 2\pi^+ 2\pi^- K^+ K^- 2\pi^0$	

¹ ASNER 08A reports $[\Gamma(\chi_{b2}(1P) \rightarrow 2\pi^+ 2\pi^- K^+ K^- 2\pi^0)/\Gamma_{\text{total}}] \times [B(\mathcal{T}(2S) \rightarrow \gamma \chi_{b2}(1P))] = (28 \pm 11 \pm 7) \times 10^{-6}$ which we divide by our best value $B(\mathcal{T}(2S) \rightarrow \gamma \chi_{b2}(1P)) = (7.15 \pm 0.35) \times 10^{-2}$. Our first error is their experiment's error and our second error is the systematic error from using our best value.

 $\Gamma(3\pi^+ 2\pi^- K^- K_S^0 \pi^0)/\Gamma_{\text{total}}$ Γ_{10}/Γ

VALUE (units 10 ⁻⁴)	CL%	DOCUMENT ID	TECN	COMMENT	
< 5	90	¹ ASNER	08A CLEO	$\mathcal{T}(2S) \rightarrow \gamma 3\pi^+ 2\pi^- K^- K_S^0 \pi^0$	

¹ ASNER 08A reports $[\Gamma(\chi_{b2}(1P) \rightarrow 3\pi^+ 2\pi^- K^- K_S^0 \pi^0)/\Gamma_{\text{total}}] \times [B(\mathcal{T}(2S) \rightarrow \gamma \chi_{b2}(1P))] < 36 \times 10^{-6}$ which we divide by our best value $B(\mathcal{T}(2S) \rightarrow \gamma \chi_{b2}(1P)) = 7.15 \times 10^{-2}$.

 $\Gamma(3\pi^+ 3\pi^-)/\Gamma_{\text{total}}$ Γ_{11}/Γ

VALUE (units 10 ⁻⁴)	EVTS	DOCUMENT ID	TECN	COMMENT	
0.70 ± 0.31 ± 0.03	9	¹ ASNER	08A CLEO	$\mathcal{T}(2S) \rightarrow \gamma 3\pi^+ 3\pi^-$	

¹ ASNER 08A reports $[\Gamma(\chi_{b2}(1P) \rightarrow 3\pi^+ 3\pi^-)/\Gamma_{\text{total}}] \times [B(\mathcal{T}(2S) \rightarrow \gamma \chi_{b2}(1P))] = (5 \pm 2 \pm 1) \times 10^{-6}$ which we divide by our best value $B(\mathcal{T}(2S) \rightarrow \gamma \chi_{b2}(1P)) = (7.15 \pm 0.35) \times 10^{-2}$. Our first error is their experiment's error and our second error is the systematic error from using our best value.

 $\Gamma(3\pi^+ 3\pi^- 2\pi^0)/\Gamma_{\text{total}}$ Γ_{12}/Γ

VALUE (units 10 ⁻⁴)	EVTS	DOCUMENT ID	TECN	COMMENT	
10.2 ± 3.6 ± 0.5	34	¹ ASNER	08A CLEO	$\mathcal{T}(2S) \rightarrow \gamma 3\pi^+ 3\pi^- 2\pi^0$	

¹ ASNER 08A reports $[\Gamma(\chi_{b2}(1P) \rightarrow 3\pi^+ 3\pi^- 2\pi^0)/\Gamma_{\text{total}}] \times [B(\mathcal{T}(2S) \rightarrow \gamma \chi_{b2}(1P))] = (73 \pm 16 \pm 20) \times 10^{-6}$ which we divide by our best value $B(\mathcal{T}(2S) \rightarrow \gamma \chi_{b2}(1P)) = (7.15 \pm 0.35) \times 10^{-2}$. Our first error is their experiment's error and our second error is the systematic error from using our best value.

 $\Gamma(3\pi^+ 3\pi^- K^+ K^-)/\Gamma_{\text{total}}$ Γ_{13}/Γ

VALUE (units 10 ⁻⁴)	CL%	DOCUMENT ID	TECN	COMMENT	
< 0.8	90	¹ ASNER	08A CLEO	$\mathcal{T}(2S) \rightarrow \gamma 3\pi^+ 3\pi^- K^+ K^-$	

¹ ASNER 08A reports $[\Gamma(\chi_{b2}(1P) \rightarrow 3\pi^+ 3\pi^- K^+ K^-)/\Gamma_{\text{total}}] \times [B(\mathcal{T}(2S) \rightarrow \gamma \chi_{b2}(1P))] < 6 \times 10^{-6}$ which we divide by our best value $B(\mathcal{T}(2S) \rightarrow \gamma \chi_{b2}(1P)) = 7.15 \times 10^{-2}$.

 $\Gamma(3\pi^+ 3\pi^- K^+ K^- \pi^0)/\Gamma_{\text{total}}$ Γ_{14}/Γ

VALUE (units 10 ⁻⁴)	EVTS	DOCUMENT ID	TECN	COMMENT	
3.6 ± 1.5 ± 0.2	14	¹ ASNER	08A CLEO	$\mathcal{T}(2S) \rightarrow \gamma 3\pi^+ 3\pi^- K^+ K^- \pi^0$	

¹ ASNER 08A reports $[\Gamma(\chi_{b2}(1P) \rightarrow 3\pi^+ 3\pi^- K^+ K^- \pi^0)/\Gamma_{\text{total}}] \times [B(\mathcal{T}(2S) \rightarrow \gamma \chi_{b2}(1P))] = (26 \pm 8 \pm 7) \times 10^{-6}$ which we divide by our best value $B(\mathcal{T}(2S) \rightarrow \gamma \chi_{b2}(1P)) = (7.15 \pm 0.35) \times 10^{-2}$. Our first error is their experiment's error and our second error is the systematic error from using our best value.

 $\Gamma(4\pi^+ 4\pi^-)/\Gamma_{\text{total}}$ Γ_{15}/Γ

VALUE (units 10 ⁻⁴)	EVTS	DOCUMENT ID	TECN	COMMENT	
0.84 ± 0.40 ± 0.04	7	¹ ASNER	08A CLEO	$\mathcal{T}(2S) \rightarrow \gamma 4\pi^+ 4\pi^-$	

¹ ASNER 08A reports $[\Gamma(\chi_{b2}(1P) \rightarrow 4\pi^+ 4\pi^-)/\Gamma_{\text{total}}] \times [B(\mathcal{T}(2S) \rightarrow \gamma \chi_{b2}(1P))] = (6 \pm 2 \pm 2) \times 10^{-6}$ which we divide by our best value $B(\mathcal{T}(2S) \rightarrow \gamma \chi_{b2}(1P)) = (7.15 \pm 0.35) \times 10^{-2}$. Our first error is their experiment's error and our second error is the systematic error from using our best value.

 $\Gamma(4\pi^+ 4\pi^- 2\pi^0)/\Gamma_{\text{total}}$ Γ_{16}/Γ

VALUE (units 10 ⁻⁴)	EVTS	DOCUMENT ID	TECN	COMMENT	
18 ± 7 ± 1	29	¹ ASNER	08A CLEO	$\mathcal{T}(2S) \rightarrow \gamma 4\pi^+ 4\pi^- 2\pi^0$	

¹ ASNER 08A reports $[\Gamma(\chi_{b2}(1P) \rightarrow 4\pi^+ 4\pi^- 2\pi^0)/\Gamma_{\text{total}}] \times [B(\mathcal{T}(2S) \rightarrow \gamma \chi_{b2}(1P))] = (132 \pm 31 \pm 40) \times 10^{-6}$ which we divide by our best value $B(\mathcal{T}(2S) \rightarrow \gamma \chi_{b2}(1P)) = (7.15 \pm 0.35) \times 10^{-2}$. Our first error is their experiment's error and our second error is the systematic error from using our best value.

See key on page 1171

Meson Particle Listings

$\chi_{b2}(1P), \eta_b(2S), \Upsilon(2S)$

$\Gamma(J/\psi J/\psi)/\Gamma_{total}$		Γ_{17}/Γ	
VALUE (units 10^{-5})	CL%	DOCUMENT ID	TECN COMMENT

<5 90 1 SHEN 12 BELL $\Upsilon(2S) \rightarrow \gamma\psi X$
 1 SHEN 12 reports $< 4.5 \times 10^{-5}$ from a measurement of $[\Gamma(\chi_{b2}(1P) \rightarrow J/\psi J/\psi)/\Gamma_{total}] \times [B(\Upsilon(2S) \rightarrow \gamma\chi_{b2}(1P))]$ assuming $B(\Upsilon(2S) \rightarrow \gamma\chi_{b2}(1P)) = (7.15 \pm 0.35) \times 10^{-2}$.

$\Gamma(J/\psi\psi(2S))/\Gamma_{total}$		Γ_{18}/Γ	
VALUE (units 10^{-5})	CL%	DOCUMENT ID	TECN COMMENT

<5 90 1 SHEN 12 BELL $\Upsilon(2S) \rightarrow \gamma\psi X$
 1 SHEN 12 reports $< 4.9 \times 10^{-5}$ from a measurement of $[\Gamma(\chi_{b2}(1P) \rightarrow J/\psi\psi(2S))/\Gamma_{total}] \times [B(\Upsilon(2S) \rightarrow \gamma\chi_{b2}(1P))]$ assuming $B(\Upsilon(2S) \rightarrow \gamma\chi_{b2}(1P)) = (7.15 \pm 0.35) \times 10^{-2}$.

$\Gamma(\psi(2S)\psi(2S))/\Gamma_{total}$		Γ_{19}/Γ	
VALUE (units 10^{-5})	CL%	DOCUMENT ID	TECN COMMENT

<1.6 90 1 SHEN 12 BELL $\Upsilon(2S) \rightarrow \gamma\psi X$
 1 SHEN 12 reports $< 1.6 \times 10^{-5}$ from a measurement of $[\Gamma(\chi_{b2}(1P) \rightarrow \psi(2S)\psi(2S))/\Gamma_{total}] \times [B(\Upsilon(2S) \rightarrow \gamma\chi_{b2}(1P))]$ assuming $B(\Upsilon(2S) \rightarrow \gamma\chi_{b2}(1P)) = (7.15 \pm 0.35) \times 10^{-2}$.

$\Gamma(J/\psi(1S) \text{ anything})/\Gamma_{total}$		Γ_{20}/Γ	
VALUE (units 10^{-3})	EVTS	DOCUMENT ID	TECN COMMENT

1.50 ± 0.34 ± 0.22 462 JIA 17A BELL $e^+e^- \rightarrow \text{hadrons}$

$\chi_{b2}(1P)$ Cross-Particle Branching Ratios

$\Gamma(\chi_{b2}(1P) \rightarrow \gamma\Upsilon(1S))/\Gamma_{total} \times \Gamma(\Upsilon(2S) \rightarrow \gamma\chi_{b2}(1P))/\Gamma_{total}$		$\Gamma_1/\Gamma \times \Gamma_{72}^{T(2S)}/\Gamma_{T(2S)}$	
VALUE (units 10^{-3})	EVTS	DOCUMENT ID	TECN COMMENT

13.9 ± 0.5 ± 0.9 8k LEES 11J BABR $\Upsilon(2S) \rightarrow X\gamma$

$B(\chi_{b2}(1P) \rightarrow \gamma\Upsilon(1S)) \times B(\Upsilon(2S) \rightarrow \gamma\chi_{b2}(1P)) \times B(\Upsilon(1S) \rightarrow \ell^+\ell^-)$

VALUE (units 10^{-4})	EVTS	DOCUMENT ID	TECN COMMENT
--------------------------	------	-------------	--------------

3.38 ± 0.16 OUR AVERAGE
 3.63^{+0.36+0.18}_{-0.34-0.19} 1 LEES 14M BABR $\Upsilon(2S) \rightarrow \gamma\gamma\mu^+\mu^-$
 3.29 ± 0.09 ± 0.16 1770 KORNICER 11 CLEO $e^+e^- \rightarrow \gamma\gamma\ell^+\ell^-$
 4.4 ± 0.9 ± 0.5 35 WALK 86 CBAL $\Upsilon(2S) \rightarrow \gamma\gamma\ell^+\ell^-$

1 From a sample of $\Upsilon(2S) \rightarrow \gamma\gamma\mu^+\mu^-$ with converted photons.

$[B(\chi_{b2}(1P) \rightarrow \gamma\Upsilon(1S)) \times B(\Upsilon(2S) \rightarrow \gamma\chi_{b2}(1P))] / [B(\chi_{b1}(1P) \rightarrow \gamma\Upsilon(1S)) \times B(\Upsilon(2S) \rightarrow \gamma\chi_{b1}(1P))]$

VALUE (%)	DOCUMENT ID	TECN COMMENT
-----------	-------------	--------------

55.6 ± 1.6 1 LEES 14M BABR $\Upsilon(2S) \rightarrow \gamma\gamma\mu^+\mu^-$

1 From a sample of $\Upsilon(2S) \rightarrow \gamma\gamma\mu^+\mu^-$ events without converted photons.

$B(\chi_{b2}(1P) \rightarrow \gamma\Upsilon(1S)) \times B(\Upsilon(3S) \rightarrow \gamma\chi_{b2}(1P)) \times B(\Upsilon(1S) \rightarrow \ell^+\ell^-)$

VALUE (units 10^{-5})	EVTS	DOCUMENT ID	TECN COMMENT
--------------------------	------	-------------	--------------

3.8 ± 0.5 OUR AVERAGE
 4.68^{+0.99}_{-0.92} ± 0.37 1 LEES 14M BABR $\Upsilon(3S) \rightarrow \gamma\gamma\mu^+\mu^-$
 3.56 ± 0.40 ± 0.41 126 KORNICER 11 CLEO $e^+e^- \rightarrow \gamma\gamma\ell^+\ell^-$

1 From a sample of $\Upsilon(3S) \rightarrow \gamma\gamma\mu^+\mu^-$ with converted photons.

$\chi_{b2}(1P)$ REFERENCES

FULSOM 18 PRL 121 232001 B.G. Fulsom et al. (BELLE Collab.)	JIA 17A PR D96 112002 S. Jia et al. (BELLE Collab.)
AJAJ 14BG JHEP 1410 088 R. Ajaj et al. (LHCb Collab.)	LEES 14M PR D90 112010 J.P. Lees et al. (BABAR Collab.)
SHEN 12 PR D85 071102 C.P. Shen et al. (BELLE Collab.)	KORNICER 11 PR D83 054003 M. Kornicer et al. (CLEO Collab.)
LEES 11J PR D84 072002 J.P. Lees et al. (BABAR Collab.)	ASNER 08A PR D78 091103 D.M. Asner et al. (CLEO Collab.)
BRIERE 08 PR D78 092007 R.A. Briere et al. (CLEO Collab.)	ARTUSO 05 PR 94 032001 M. Artuso et al. (CLEO Collab.)
EDWARDS 99 PR D59 032003 K.W. Edwards et al. (CLEO Collab.)	SKWARNICI 87 PRL 58 972 T. Skwarnicki et al. (Crystal Ball Collab.)
WALK 86 PR D34 2611 W.S. Walk et al. (Crystal Ball Collab.)	ALBRECHT 85E PL 160B 331 H. Albrecht et al. (ARGUS Collab.)
NERNST 85 PR 54 2195 R. Nernst et al. (Crystal Ball Collab.)	HAAS 84 PRL 52 799 J. Haas et al. (CLEO Collab.)
KLOPFEN... 83 PRL 51 160 C. Klopffenstein et al. (CUSB Collab.)	PAUSS 83 PL 130B 439 F. Pauss et al. (MPIM, COLU, CORN, LSU+)

$\eta_b(2S)$

$$J^{PC} = 0^+(0^-)$$

OMITTED FROM SUMMARY TABLE
 Quantum numbers shown are quark-model predictions.

$\eta_b(2S)$ MASS

VALUE (MeV)	EVTS	DOCUMENT ID	TECN COMMENT
-------------	------	-------------	--------------

9999.0 ± 3.5 ± 1.9 26k 1 MIZUK 12 BELL $e^+e^- \rightarrow \gamma\pi^+\pi^- + \text{hadrons}$

••• We do not use the following data for averages, fits, limits, etc. •••
 9974.6 ± 2.3 ± 2.1 11 ± 4^{2,3,4} DOBBS 12 $\Upsilon(2S) \rightarrow \gamma \text{ hadrons}$

- Assuming $\Gamma_{\eta_b(2S)} = 4.9$ MeV. Not independent of the corresponding mass difference measurement.
- SANDILYA 13 (Belle Collab.) search for such a state reconstructed in the same 26 exclusive hadronic final states as DOBBS 12 using a sample of $(157.8 \pm 3.6) \times 10^6$ $\Upsilon(2S)$ decays or about 17 times larger and find no evidence for a signal. Their 90% C.L. upper limit on the branching fraction $B(\Upsilon(2S) \rightarrow \eta_b(2S)\gamma) \times \sum_i B(\eta_b(2S) \rightarrow X_i) < 4.9 \times 10^{-6}$, summed over the exclusive hadronic final states X_i , is an order of magnitude smaller than that reported by DOBBS 12.
- Obtained by analyzing CLEO III data but not authored by the CLEO Collaboration.
- Assuming $\Gamma_{\eta_b(2S)} = 5$ MeV. Not independent of the corresponding mass difference measurement.

$m_{\Upsilon(2S)} - m_{\eta_b(2S)}$

VALUE (MeV)	EVTS	DOCUMENT ID	TECN COMMENT
-------------	------	-------------	--------------

24.3 ± 3.5 ± 2.8 26k 5 MIZUK 12 BELL $e^+e^- \rightarrow \gamma\pi^+\pi^- + \text{hadrons}$

- We do not use the following data for averages, fits, limits, etc. •••
 48.7 ± 2.3 ± 2.1 11 ± 4^{6,7,8} DOBBS 12 $\Upsilon(2S) \rightarrow \gamma \text{ hadrons}$
- Assuming $\Gamma_{\eta_b(2S)} = 4.9$ MeV. Not independent of the corresponding mass measurement.
 - SANDILYA 13 (Belle Collab.) search for such a state reconstructed in the same 26 exclusive hadronic final states as DOBBS 12 using a sample of $(157.8 \pm 3.6) \times 10^6$ $\Upsilon(2S)$ decays or about 17 times larger and find no evidence for a signal. Their 90% C.L. upper limit on the branching fraction $B(\Upsilon(2S) \rightarrow \eta_b(2S)\gamma) \times \sum_i B(\eta_b(2S) \rightarrow X_i) < 4.9 \times 10^{-6}$, summed over the exclusive hadronic final states X_i , is an order of magnitude smaller than that reported by DOBBS 12.
 - Obtained by analyzing CLEO III data but not authored by the CLEO Collaboration.
 - Assuming $\Gamma_{\eta_b(2S)} = 5$ MeV. Not independent of the corresponding mass measurement.

$\eta_b(2S)$ WIDTH

VALUE (MeV)	CL%	DOCUMENT ID	TECN COMMENT
-------------	-----	-------------	--------------

<24 90 MIZUK 12 BELL $e^+e^- \rightarrow \gamma\pi^+\pi^- \text{ hadrons}$

$\eta_b(2S)$ DECAY MODES

Mode	Fraction (Γ_i/Γ)
------	--------------------------------

Γ_1 hadrons seen

$\eta_b(2S)$ BRANCHING RATIOS

$\Gamma(\text{hadrons})/\Gamma_{total}$		Γ_1/Γ	
VALUE	EVTS	DOCUMENT ID	TECN COMMENT

seen 26k MIZUK 12 BELL $e^+e^- \rightarrow \gamma\pi^+\pi^- \text{ hadrons}$
 ••• We do not use the following data for averages, fits, limits, etc. •••
 9,10 DOBBS 12 $\Upsilon(2S) \rightarrow \gamma \text{ hadrons}$

- SANDILYA 13 (Belle Collab.) search for such a state reconstructed in the same 26 exclusive hadronic final states as DOBBS 12 using a sample of $(157.8 \pm 3.6) \times 10^6$ $\Upsilon(2S)$ decays or about 17 times larger and find no evidence for a signal. Their 90% C.L. upper limit on the branching fraction $B(\Upsilon(2S) \rightarrow \eta_b(2S)\gamma) \times \sum_i B(\eta_b(2S) \rightarrow X_i) < 4.9 \times 10^{-6}$, summed over the exclusive hadronic final states X_i , is an order of magnitude smaller than that reported by DOBBS 12.
- Obtained by analyzing CLEO III data but not authored by the CLEO Collaboration.

$\eta_b(2S)$ REFERENCES

SANDILYA 13 PRL 111 112001 S. Sandilya et al. (BELLE Collab.)	DOBBS 12 PRL 109 082001 S. Dobbs et al.	MIZUK 12 PRL 109 232002 R. Mizuk et al. (BELLE Collab.)
---	---	---

$\Upsilon(2S)$

$$J^{PC} = 0^-(1^-)$$

$\Upsilon(2S)$ MASS

VALUE (MeV)	DOCUMENT ID	TECN COMMENT
-------------	-------------	--------------

10023.4 ± 0.5 1 SHAMOV 23 RVUE $e^+e^- \rightarrow \text{hadrons}$
 ••• We do not use the following data for averages, fits, limits, etc. •••
 10022.7 ± 0.4 2 SHAMOV 23 RVUE $e^+e^- \rightarrow \text{hadrons}$
 10023.5 ± 0.5 3,4 ARTA MONOV 00 MD1 $e^+e^- \rightarrow \text{hadrons}$
 10023.6 ± 0.5 5,6 BARU 86B MD1 $e^+e^- \rightarrow \text{hadrons}$
 10023.1 ± 0.4 7 BARBER 84 ARG $e^+e^- \rightarrow \text{hadrons}$

- Reanalysis of MD1 data using the electron mass from COHEN 87, the radiative corrections from KURAEV 85 and interference effects.
- Obtained by reanalysing ARGUS and Crystal Ball data (BARBER 84), but not authored by the ARGUS and Crystal Ball collaboration.
- Reanalysis of BARU 86B using new electron mass (COHEN 87).
- Superseded by SHAMOV 23.
- Reanalysis of ARTA MONOV 84.
- Superseded by ARTA MONOV 00.
- Reanalysed by SHAMOV 23.

Meson Particle Listings

 $\Upsilon(2S)$ $m\Upsilon(3S) - m\Upsilon(2S)$

VALUE (MeV)	DOCUMENT ID	TECN	COMMENT
331.50 ± 0.02 ± 0.13	LEES	11c	BABR $e^+e^- \rightarrow \pi^+\pi^-X$

 $\Upsilon(2S)$ WIDTH

VALUE (keV)	DOCUMENT ID	COMMENT
31.98 ± 2.63 OUR EVALUATION	See the Note on "Width Determinations of the Υ States"	

 $\Upsilon(2S)$ DECAY MODES

Mode	Fraction (Γ_i/Γ)	Scale factor/ Confidence level
Γ_1 $\Upsilon(1S)\pi^+\pi^-$	(17.85 ± 0.26) %	
Γ_2 $\Upsilon(1S)\pi^0\pi^0$	(8.6 ± 0.4) %	
Γ_3 $\tau^+\tau^-$	(2.00 ± 0.21) %	
Γ_4 $\mu^+\mu^-$	(1.93 ± 0.17) %	S=2.2
Γ_5 e^+e^-	(1.91 ± 0.16) %	
Γ_6 $\Upsilon(1S)\pi^0$	< 4 $\times 10^{-5}$	CL=90%
Γ_7 $\Upsilon(1S)\eta$	(2.9 ± 0.4) $\times 10^{-4}$	S=2.0
Γ_8 $J/\psi(1S)$ anything	< 6 $\times 10^{-3}$	CL=90%
Γ_9 $J/\psi(1S)\eta_c$	< 5.4 $\times 10^{-6}$	CL=90%
Γ_{10} $J/\psi(1S)\chi_{c0}$	< 3.4 $\times 10^{-6}$	CL=90%
Γ_{11} $J/\psi(1S)\chi_{c1}$	< 1.2 $\times 10^{-6}$	CL=90%
Γ_{12} $J/\psi(1S)\chi_{c2}$	< 2.0 $\times 10^{-6}$	CL=90%
Γ_{13} $J/\psi(1S)\eta_c(2S)$	< 2.5 $\times 10^{-6}$	CL=90%
Γ_{14} $J/\psi(1S)X(3940)$	< 2.0 $\times 10^{-6}$	CL=90%
Γ_{15} $J/\psi(1S)X(4160)$	< 2.0 $\times 10^{-6}$	CL=90%
Γ_{16} χ_{c1} anything	(2.2 ± 0.5) $\times 10^{-4}$	
Γ_{17} $\chi_{c1}(1P)^0 X_{tetra}$	< 3.67 $\times 10^{-5}$	CL=90%
Γ_{18} χ_{c2} anything	(2.3 ± 0.8) $\times 10^{-4}$	
Γ_{19} $\psi(2S)\eta_c$	< 5.1 $\times 10^{-6}$	CL=90%
Γ_{20} $\psi(2S)\chi_{c0}$	< 4.7 $\times 10^{-6}$	CL=90%
Γ_{21} $\psi(2S)\chi_{c1}$	< 2.5 $\times 10^{-6}$	CL=90%
Γ_{22} $\psi(2S)\chi_{c2}$	< 1.9 $\times 10^{-6}$	CL=90%
Γ_{23} $\psi(2S)\eta_c(2S)$	< 3.3 $\times 10^{-6}$	CL=90%
Γ_{24} $\psi(2S)X(3940)$	< 3.9 $\times 10^{-6}$	CL=90%
Γ_{25} $\psi(2S)X(4160)$	< 3.9 $\times 10^{-6}$	CL=90%
Γ_{26} $T_{c\bar{c}1}(3900)^+ T_{c\bar{c}1}(3900)^-$	< 1.0 $\times 10^{-6}$	CL=90%
Γ_{27} $T_{c\bar{c}1}(4200)^+ T_{c\bar{c}1}(4200)^-$	< 1.67 $\times 10^{-5}$	CL=90%
Γ_{28} $T_{c\bar{c}1}(3900)^\pm T_{c\bar{c}1}(4200)^\mp$	< 7.3 $\times 10^{-6}$	CL=90%
Γ_{29} $T_{c\bar{c}2}(4050)^+ T_{c\bar{c}2}(4050)^-$	< 1.35 $\times 10^{-5}$	CL=90%
Γ_{30} $T_{c\bar{c}2}(4250)^+ T_{c\bar{c}2}(4250)^-$	< 2.67 $\times 10^{-5}$	CL=90%
Γ_{31} $T_{c\bar{c}2}(4050)^\pm T_{c\bar{c}2}(4250)^\mp$	< 2.72 $\times 10^{-5}$	CL=90%
Γ_{32} $T_{c\bar{c}1}(4430)^+ T_{c\bar{c}1}(4430)^-$	< 2.03 $\times 10^{-5}$	CL=90%
Γ_{33} $T_{c\bar{c}2}(4055)^\pm T_{c\bar{c}2}(4055)^\mp$	< 1.11 $\times 10^{-5}$	CL=90%
Γ_{34} $T_{c\bar{c}2}(4055)^\pm T_{c\bar{c}1}(4430)^\mp$	< 2.11 $\times 10^{-5}$	CL=90%
Γ_{35} 2H anything	(2.78 $^{+0.30}_{-0.26}$) $\times 10^{-5}$	S=1.2
Γ_{36} hadrons	(94 ± 11) %	
Γ_{37} ggg	(58.8 ± 1.2) %	
Γ_{38} γgg	(1.87 ± 0.28) %	
Γ_{39} $\phi K^+ K^-$	(1.6 ± 0.4) $\times 10^{-6}$	
Γ_{40} $\omega\pi^+\pi^-$	< 2.58 $\times 10^{-6}$	CL=90%
Γ_{41} $K^*(892)^0 K^- \pi^+ + c.c.$	(2.3 ± 0.7) $\times 10^{-6}$	
Γ_{42} $\phi f_2'(1525)$	< 1.33 $\times 10^{-6}$	CL=90%
Γ_{43} $\omega f_2'(1270)$	< 5.7 $\times 10^{-7}$	CL=90%
Γ_{44} $\rho(770) a_2(1320)$	< 8.8 $\times 10^{-7}$	CL=90%
Γ_{45} $K^*(892)^0 \bar{K}_2^0(1430)^0 + c.c.$	(1.5 ± 0.6) $\times 10^{-6}$	
Γ_{46} $K_1(1270)^\pm K^\mp$	< 3.22 $\times 10^{-6}$	CL=90%
Γ_{47} $K_1(1400)^\pm K^\mp$	< 8.3 $\times 10^{-7}$	CL=90%
Γ_{48} $b_1(1235)^\pm \pi^\mp$	< 4.0 $\times 10^{-7}$	CL=90%
Γ_{49} $\rho\pi$	< 1.16 $\times 10^{-6}$	CL=90%
Γ_{50} $\pi^+\pi^-\pi^0$	< 8.0 $\times 10^{-7}$	CL=90%
Γ_{51} $\omega\pi^0$	< 1.63 $\times 10^{-6}$	CL=90%
Γ_{52} $\pi^+\pi^-\pi^0\pi^0$	(1.30 ± 0.28) $\times 10^{-5}$	
Γ_{53} $K_S^0 K^+ \pi^- + c.c.$	(1.14 ± 0.33) $\times 10^{-6}$	
Γ_{54} $K^*(892)^0 \bar{K}^0 + c.c.$	< 4.22 $\times 10^{-6}$	CL=90%
Γ_{55} $K^*(892)^- K^+ + c.c.$	< 1.45 $\times 10^{-6}$	CL=90%
Γ_{56} $f_1(1285)$ anything	(2.2 ± 1.6) $\times 10^{-3}$	
Γ_{57} $f_1(1285) X_{tetra}$	< 6.47 $\times 10^{-5}$	CL=90%
Γ_{58} $D_s^+ D_{s1}(2536)^-$		
Γ_{59} $D_s^+ D_{s1}(2536)^-, D_{s1}^- \rightarrow K^- D^*(2007)^0$	(1.6 ± 0.4) $\times 10^{-5}$	

$$\Gamma_{60} D_s^+ D_{s1}(2536)^-, D_{s1}^- \rightarrow K_S^0 D^*(2010)^- \quad (8.4 \pm 2.3) \times 10^{-6}$$

$$\Gamma_{61} D_s^{*+} D_{s1}(2536)^- \quad (1.4 \pm 0.4) \times 10^{-5}$$

$$\Gamma_{62} D_s^{*+} D_{s1}(2536)^-, D_{s1}^- \rightarrow K^- D^*(2007)^0 \quad (8.2 \pm 3.1) \times 10^{-6}$$

$$\Gamma_{63} D_s^{*+} D_{s1}(2536)^-, D_{s1}^- \rightarrow K_S^0 D^*(2010)^- \quad (1.4 \pm 0.4) \times 10^{-5}$$

$$\Gamma_{64} D_s^+ D_{s2}^*(2573)^- \quad (6.9 \pm 3.0) \times 10^{-6}$$

$$\Gamma_{65} D_s^+ D_{s2}^*(2573)^-, D_{s2}^{*-} \rightarrow K^- D^0 \quad (9 \pm 5) \times 10^{-6}$$

$$\Gamma_{66} D_s^+ D_{s2}^*(2573)^-, D_{s2}^{*-} \rightarrow K_S^0 D^- \quad (5 \pm 6) \times 10^{-6}$$

$$\Gamma_{67} D_s^{*+} D_{s2}^*(2573)^- \quad (2.90 \pm 0.30) \times 10^{-3}$$

$$\Gamma_{68} D_s^{*+} D_{s2}^*(2573)^-, D_{s2}^{*-} \rightarrow K^- D^0 \quad (2.90 \pm 0.30) \times 10^{-3}$$

$$\Gamma_{69} D_s^{*+} D_{s2}^*(2573)^-, D_{s2}^{*-} \rightarrow K_S^0 D^- \quad (2.90 \pm 0.30) \times 10^{-3}$$

$$\Gamma_{70} \text{Sum of 100 exclusive modes} \quad (2.90 \pm 0.30) \times 10^{-3}$$

Radiative decays

$$\Gamma_{71} \gamma \chi_{b1}(1P) \quad (6.9 \pm 0.4) \%$$

$$\Gamma_{72} \gamma \chi_{b2}(1P) \quad (7.15 \pm 0.35) \%$$

$$\Gamma_{73} \gamma \chi_{b0}(1P) \quad (3.8 \pm 0.4) \%$$

$$\Gamma_{74} \gamma f_0(1710) \quad < 5.9 \times 10^{-4} \quad \text{CL=90\%}$$

$$\Gamma_{75} \gamma f_2'(1525) \quad < 5.3 \times 10^{-4} \quad \text{CL=90\%}$$

$$\Gamma_{76} \gamma f_2'(1270) \quad < 2.41 \times 10^{-4} \quad \text{CL=90\%}$$

$$\Gamma_{77} \gamma f_J(2220) \quad < 2.7 \times 10^{-5} \quad \text{CL=90\%}$$

$$\Gamma_{78} \gamma \eta_c(1S) \quad < 1.0 \times 10^{-4} \quad \text{CL=90\%}$$

$$\Gamma_{79} \gamma \chi_{c0} \quad < 3.6 \times 10^{-6} \quad \text{CL=90\%}$$

$$\Gamma_{80} \gamma \chi_{c1} \quad < 1.5 \times 10^{-5} \quad \text{CL=90\%}$$

$$\Gamma_{81} \gamma \chi_{c2} \quad < 2.3 \times 10^{-5} \quad \text{CL=90\%}$$

$$\Gamma_{82} \gamma \chi_{c1}(3872) \quad < 2.4 \times 10^{-6} \quad \text{CL=90\%}$$

$$\Gamma_{83} \gamma \chi_{c1}(3872), \chi_{c1} \rightarrow \pi^+ \pi^- \pi^0 J/\psi \quad < 2.8 \times 10^{-6} \quad \text{CL=90\%}$$

$$\Gamma_{84} \gamma \chi_{c0}(3915) \rightarrow \omega J/\psi \quad < 1.2 \times 10^{-6} \quad \text{CL=90\%}$$

$$\Gamma_{85} \gamma \chi_{c1}(4140) \rightarrow \phi J/\psi \quad < 1.3 \times 10^{-6} \quad \text{CL=90\%}$$

$$\Gamma_{86} \gamma X(4350) \rightarrow \phi J/\psi \quad < 1.3 \times 10^{-6} \quad \text{CL=90\%}$$

$$\Gamma_{87} \gamma \eta_b(1S) \quad (5.5 \pm 0.9) \times 10^{-4} \quad \text{S=1.2}$$

$$\Gamma_{88} \gamma \eta_b(1S) \rightarrow \gamma \text{Sum of 26 exclusive modes} \quad < 3.7 \times 10^{-6} \quad \text{CL=90\%}$$

$$\Gamma_{89} \gamma X_{b\bar{b}} \rightarrow \gamma \text{Sum of 26 exclusive modes} \quad < 4.9 \times 10^{-6} \quad \text{CL=90\%}$$

$$\Gamma_{90} \gamma X \rightarrow \gamma + \geq 4 \text{ prongs} \quad [a] < 1.95 \times 10^{-4} \quad \text{CL=95\%}$$

$$\Gamma_{91} \gamma A^0 \rightarrow \gamma \text{hadrons} \quad < 8 \times 10^{-5} \quad \text{CL=90\%}$$

$$\Gamma_{92} \gamma A^0 \rightarrow \gamma \mu^+ \mu^- \quad < 8.3 \times 10^{-6} \quad \text{CL=90\%}$$

Lepton Family number (LF) violating modes

$$\Gamma_{93} e^\pm \tau^\mp \quad LF \quad < 3.2 \times 10^{-6} \quad \text{CL=90\%}$$

$$\Gamma_{94} \mu^\pm \tau^\mp \quad LF \quad < 3.3 \times 10^{-6} \quad \text{CL=90\%}$$

$$[a] 1.5 \text{ GeV} < m_X < 5.0 \text{ GeV}$$

FIT INFORMATION

An overall fit to 3 branching ratios uses 13 measurements to determine 2 parameters. The overall fit has a $\chi^2 = 11.8$ for 11 degrees of freedom.

The following *off-diagonal* array elements are the correlation coefficients $\langle \delta x_i \delta x_j \rangle / (\delta x_i \delta x_j)$, in percent, from the fit to the branching fractions, $x_i \equiv \Gamma_i/\Gamma_{\text{total}}$.

$$x_7 \begin{matrix} \text{---} 2 \\ \text{---} x_1 \end{matrix}$$

 $\Upsilon(2S) \Gamma(i)\Gamma(e^+e^-)/\Gamma(\text{total})$

$\Gamma(\mu^+\mu^-) \times \Gamma(e^+e^-)/\Gamma_{\text{total}}$	$\Gamma_4\Gamma_5/\Gamma$		
VALUE (eV)	DOCUMENT ID	TECN	COMMENT
6.5 ± 1.5 ± 1.0	KOBEL	92	CBAL $e^+e^- \rightarrow \mu^+\mu^-$

$\Gamma(\Upsilon(1S)\pi^+\pi^-) \times \Gamma(e^+e^-)/\Gamma_{\text{total}}$	$\Gamma_1\Gamma_5/\Gamma$			
VALUE (eV)	EVTS	DOCUMENT ID	TECN	COMMENT
105.4 ± 1.0 ± 4.2	11.8k	¹ AUBERT	08BP	BABR 10.58 $e^+e^- \rightarrow \gamma\pi^+\pi^-\ell^+\ell^-$

¹Using B($\Upsilon(1S) \rightarrow e^+e^-$) = (2.38 ± 0.11)% and B($\Upsilon(1S) \rightarrow \mu^+\mu^-$) = (2.48 ± 0.05)%.

See key on page 1171

Meson Particle Listings

$\Upsilon(2S)$

$\Gamma(\text{hadrons}) \times \Gamma(e^+e^-)/\Gamma_{\text{total}}$		$\Gamma_{36}\Gamma_5/\Gamma$	
VALUE (keV)	DOCUMENT ID	TECN	COMMENT
0.577±0.009 OUR AVERAGE			
0.581±0.004±0.009	¹ ROSNER 06	CLEO	10.0 $e^+e^- \rightarrow \text{hadrons}$
0.552±0.031±0.017	¹ BARU 96	MD1	$e^+e^- \rightarrow \text{hadrons}$
0.54 ±0.04 ±0.02	¹ JAKUBOWSKI 88	CBAL	$e^+e^- \rightarrow \text{hadrons}$
0.58 ±0.03 ±0.04	² GILES 84B	CLEO	$e^+e^- \rightarrow \text{hadrons}$
0.60 ±0.12 ±0.07	² ALBRECHT 82	DASP	$e^+e^- \rightarrow \text{hadrons}$
0.54 ±0.07 ^{+0.09} / _{-0.05}	² NICZYPORUK 81c	LENA	$e^+e^- \rightarrow \text{hadrons}$
0.41 ±0.18	² BOCK 80	CNTR	$e^+e^- \rightarrow \text{hadrons}$

¹Radiative corrections evaluated following KURAEV 85.
²Radiative corrections reevaluated by BUCHMUELLER 88 following KURAEV 85.

$\Upsilon(2S)$ PARTIAL WIDTHS

$\Gamma(e^+e^-)$		Γ_5
VALUE (keV)	DOCUMENT ID	
0.612±0.011 OUR EVALUATION		

$\Upsilon(2S)$ BRANCHING RATIOS

$\Gamma(\Upsilon(1S)\pi^+\pi^-)/\Gamma_{\text{total}}$		Γ_1/Γ		
VALUE (units 10^{-2})	EVTS	DOCUMENT ID	TECN	COMMENT
17.85±0.26 OUR FIT				
17.92±0.26 OUR AVERAGE				
16.8 ±1.1 ±1.3	906k	¹ LEES 11c	BABR	$e^+e^- \rightarrow \pi^+\pi^- X$
17.80±0.05±0.37	170k	² LEES 11L	BABR	$\Upsilon(2S) \rightarrow \pi^+\pi^-\mu^+\mu^-$
18.02±0.02±0.61	851k	³ BHARI 09	CLEO	$e^+e^- \rightarrow \pi^+\pi^- MM$
17.22±0.17±0.75	11.8k	⁴ AUBERT 08BP	BABR	$e^+e^- \rightarrow \gamma\pi^+\pi^-\ell^+\ell^-$
19.2 ±0.2 ±1.0	52.6k	⁵ ALEXANDER 98	CLE2	$\pi^+\pi^-\ell^+\ell^-, \pi^+\pi^- MM$
18.1 ±0.5 ±1.0	11.6k	ALBRECHT 87	ARG	$e^+e^- \rightarrow \pi^+\pi^- MM$
16.9 ±4.0		GELPHMAN 85	CBAL	$e^+e^- \rightarrow e^+e^-\pi^+\pi^-$
19.1 ±1.2 ±0.6		BESSION 84	CLEO	$\pi^+\pi^- MM$
18.9 ±2.6		FONSECA 84	CUSB	$e^+e^- \rightarrow \ell^+\ell^-\pi^+\pi^-$
21 ±7	7	NICZYPORUK 81B	LENA	$e^+e^- \rightarrow \ell^+\ell^-\pi^+\pi^-$

¹ LEES 11c reports $[\Gamma(\Upsilon(2S) \rightarrow \Upsilon(1S)\pi^+\pi^-)/\Gamma_{\text{total}}] \times [B(\Upsilon(3S) \rightarrow \Upsilon(2S)\text{anything}) = (1.78 \pm 0.02 \pm 0.11) \times 10^{-2}$ which we divide by our best value $B(\Upsilon(3S) \rightarrow \Upsilon(2S)\text{anything}) = (10.6 \pm 0.8) \times 10^{-2}$. Our first error is their experiment's error and our second error is the systematic error from using our best value.

² Using $B(\Upsilon(1S) \rightarrow \mu^+\mu^-) = (2.48 \pm 0.05)\%$.

³ A weighted average of the inclusive and exclusive results.

⁴ Using $B(\Upsilon(2S) \rightarrow e^+e^-) = (1.91 \pm 0.16)\%$, $B(\Upsilon(2S) \rightarrow \mu^+\mu^-) = (1.93 \pm 0.17)\%$ and, $\Gamma_{ee}(\Upsilon(2S)) = 0.612 \pm 0.011$ keV.

⁵ Using $B(\Upsilon(1S) \rightarrow e^+e^-) = (2.52 \pm 0.17)\%$ and $B(\Upsilon(1S) \rightarrow \mu^+\mu^-) = (2.48 \pm 0.07)\%$.

$\Gamma(\Upsilon(1S)\pi^0\pi^0)/\Gamma_{\text{total}}$		Γ_2/Γ		
VALUE (units 10^{-2})	EVTS	DOCUMENT ID	TECN	COMMENT
8.6 ±0.4 OUR AVERAGE				
8.43±0.16±0.42	38k	¹ BHARI 09	CLEO	$e^+e^- \rightarrow \pi^0\pi^0\ell^+\ell^-$
9.2 ±0.6 ±0.8	275	² ALEXANDER 98	CLE2	$e^+e^- \rightarrow \pi^0\pi^0\ell^+\ell^-$
9.5 ±1.9 ±1.9	25	ALBRECHT 87	ARG	$e^+e^- \rightarrow \pi^0\pi^0\ell^+\ell^-$
8.0 ±1.5		GELPHMAN 85	CBAL	$e^+e^- \rightarrow \pi^0\pi^0\ell^+\ell^-$
10.3 ±2.3		FONSECA 84	CUSB	$e^+e^- \rightarrow \pi^0\pi^0\ell^+\ell^-$

¹ Authors assume $B(\Upsilon(1S) \rightarrow e^+e^-) + B(\Upsilon(1S) \rightarrow \mu^+\mu^-) = 4.96\%$.

² Using $B(\Upsilon(1S) \rightarrow e^+e^-) = (2.52 \pm 0.17)\%$ and $B(\Upsilon(1S) \rightarrow \mu^+\mu^-) = (2.48 \pm 0.07)\%$.

$\Gamma(\Upsilon(1S)\pi^0\pi^0)/\Gamma(\Upsilon(1S)\pi^+\pi^-)$		Γ_2/Γ_1	
VALUE	DOCUMENT ID	TECN	COMMENT
0.462±0.037	¹ BHARI 09	CLEO	$e^+e^- \rightarrow \Upsilon(2S)$

¹ Not independent of other values reported by BHARI 09.

$\Gamma(\tau^+\tau^-)/\Gamma_{\text{total}}$		Γ_3/Γ		
VALUE (units 10^{-2})	EVTS	DOCUMENT ID	TECN	COMMENT
2.00±0.21 OUR AVERAGE				
2.00±0.12±0.18	22k	¹ BESSION 07	CLEO	$e^+e^- \rightarrow \Upsilon(2S) \rightarrow \tau^+\tau^-$
1.7 ±1.5 ±0.6		HAAS 84B	CLEO	$e^+e^- \rightarrow \tau^+\tau^-$

¹ BESSION 07 reports $[\Gamma(\Upsilon(2S) \rightarrow \tau^+\tau^-)/\Gamma_{\text{total}}] / [B(\Upsilon(2S) \rightarrow \mu^+\mu^-)] = 1.04 \pm 0.04 \pm 0.05$ which we multiply by our best value $B(\Upsilon(2S) \rightarrow \mu^+\mu^-) = (1.93 \pm 0.17) \times 10^{-2}$. Our first error is their experiment's error and our second error is the systematic error from using our best value.

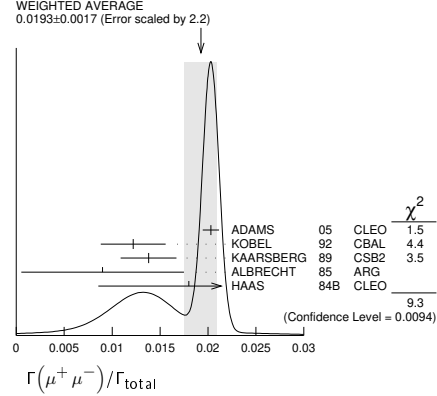
$\Gamma(\mu^+\mu^-)/\Gamma_{\text{total}}$		Γ_4/Γ		
VALUE	CL% EVTS	DOCUMENT ID	TECN	COMMENT
0.0193±0.0017 OUR AVERAGE				
0.0203±0.0003±0.0008	120k	ADAMS 05	CLEO	$e^+e^- \rightarrow \mu^+\mu^-$
0.0122±0.0028±0.0019		¹ KOBEL 92	CBAL	$e^+e^- \rightarrow \mu^+\mu^-$
0.0138±0.0025±0.0015		KAARSBERG 89	CSB2	$e^+e^- \rightarrow \mu^+\mu^-$
0.009 ±0.006 ±0.006		² ALBRECHT 85	ARG	$e^+e^- \rightarrow \mu^+\mu^-$
0.018 ±0.008 ±0.005		HAAS 84B	CLEO	$e^+e^- \rightarrow \mu^+\mu^-$

Error includes scale factor of 2.2. See the ideogram below.

••• We do not use the following data for averages, fits, limits, etc. •••

VALUE	DOCUMENT ID	TECN	COMMENT
<0.038	90	NICZYPORUK 81c	LENA $e^+e^- \rightarrow \mu^+\mu^-$

¹ Taking into account interference between the resonance and continuum.
² Re-evaluated using $B(\Upsilon(1S) \rightarrow \mu^+\mu^-) = 0.026$.



$\Gamma(\tau^+\tau^-)/\Gamma(\mu^+\mu^-)$		Γ_3/Γ_4		
VALUE	EVTS	DOCUMENT ID	TECN	COMMENT
1.04±0.04±0.05	22k	BESSION 07	CLEO	$e^+e^- \rightarrow \Upsilon(2S)$

$\Gamma(\Upsilon(1S)\pi^0)/\Gamma_{\text{total}}$		Γ_6/Γ		
VALUE (units 10^{-5})	CL%	DOCUMENT ID	TECN	COMMENT
< 4	90	¹ TAMPONI 13	BELL	$e^+e^- \rightarrow \Upsilon(1S)\pi^0$
< 18	90	² HE 08A	CLEO	$e^+e^- \rightarrow \ell^+\ell^-\gamma\gamma$
<110	90	ALEXANDER 98	CLE2	$e^+e^- \rightarrow \ell^+\ell^-\gamma\gamma$
<800	90	LURZ 87	CBAL	$e^+e^- \rightarrow \ell^+\ell^-\gamma\gamma$

¹ TAMPONI 13 reports $[\Gamma(\Upsilon(2S) \rightarrow \Upsilon(1S)\pi^0)/\Gamma_{\text{total}}] / [B(\Upsilon(2S) \rightarrow \Upsilon(1S)\pi^+\pi^-)] < 2.3 \times 10^{-4}$ which we multiply by our best value $B(\Upsilon(2S) \rightarrow \Upsilon(1S)\pi^+\pi^-) = 17.85 \times 10^{-2}$.

² Authors assume $B(\Upsilon(1S) \rightarrow e^+e^-) + B(\Upsilon(1S) \rightarrow \mu^+\mu^-) = 4.96\%$.

$\Gamma(\Upsilon(1S)\pi^0)/\Gamma(\Upsilon(1S)\pi^+\pi^-)$		Γ_6/Γ_1		
VALUE (units 10^{-4})	CL%	DOCUMENT ID	TECN	COMMENT
<2.3	90	TAMPONI 13	BELL	$e^+e^- \rightarrow \Upsilon(1S)\pi^0$

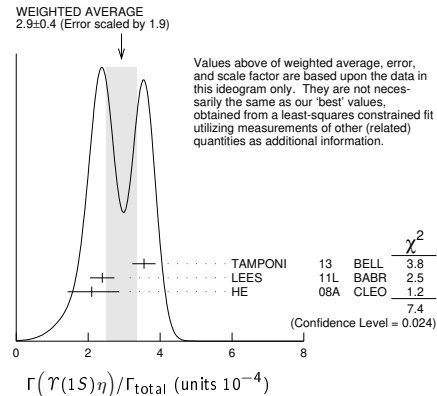
$\Gamma(\Upsilon(1S)\eta)/\Gamma_{\text{total}}$		Γ_7/Γ		
VALUE (units 10^{-4})	CL% EVTS	DOCUMENT ID	TECN	COMMENT
2.9 ±0.4 OUR FIT				Error includes scale factor of 2.0.
2.9 ±0.4 OUR AVERAGE				Error includes scale factor of 1.9. See the ideogram below.
2.39±0.31±0.14	112	¹ LEES 11L	BABR	$\Upsilon(2S) \rightarrow \ell^+\ell^-\eta$
2.1 ^{+0.7} / _{-0.6} ±0.3	14	² HE 08A	CLEO	$e^+e^- \rightarrow \ell^+\ell^-\eta$

••• We use the following data for averages but not for fits. •••

VALUE	EVTS	DOCUMENT ID	TECN	COMMENT
3.55±0.32±0.05	241	³ TAMPONI 13	BELL	$e^+e^- \rightarrow \Upsilon(1S)\eta$

••• We do not use the following data for averages, fits, limits, etc. •••

VALUE	DOCUMENT ID	TECN	COMMENT
< 9	90	^{1,4} AUBERT 08BP	BABR $e^+e^- \rightarrow \gamma\pi^+\pi^-\pi^0\ell^+\ell^-$
< 28	90	ALEXANDER 98	CLE2 $e^+e^- \rightarrow \ell^+\ell^-\eta$
< 50	90	ALBRECHT 87	ARG $e^+e^- \rightarrow \pi^+\pi^-\ell^+\ell^- MM$
< 70	90	LURZ 87	CBAL $e^+e^- \rightarrow \ell^+\ell^-(\gamma\gamma, 3\pi^0)$
< 100	90	BESSION 84	CLEO $e^+e^- \rightarrow \pi^+\pi^-\ell^+\ell^- \pi^0$
< 20	90	FONSECA 84	CUSB $e^+e^- \rightarrow \ell^+\ell^-(\gamma\gamma, \pi^+\pi^-\pi^0)$



¹ Using $B(\Upsilon(1S) \rightarrow e^+e^-) = (2.38 \pm 0.11)\%$ and $B(\Upsilon(1S) \rightarrow \mu^+\mu^-) = (2.48 \pm 0.05)\%$.

Meson Particle Listings

 $\Upsilon(2S)$

² Authors assume $B(\Upsilon(1S) \rightarrow e^+e^-) + B(\Upsilon(1S) \rightarrow \mu^+\mu^-) = 4.96\%$.
³ TAMPONI 13 reports $[\Gamma(\Upsilon(2S) \rightarrow \Upsilon(1S)\eta)/\Gamma_{\text{total}}] / [B(\Upsilon(2S) \rightarrow \Upsilon(1S)\pi^+\pi^-)] = (1.99 \pm 0.14 \pm 0.11) \times 10^{-3}$ which we multiply by our best value $B(\Upsilon(2S) \rightarrow \Upsilon(1S)\pi^+\pi^-) = (17.85 \pm 0.26) \times 10^{-2}$. Our first error is their experiment's error and our second error is the systematic error from using our best value.
⁴ Using $\Gamma_{ee}(\Upsilon(2S)) = 0.612 \pm 0.011$ keV.

 $\Gamma(\Upsilon(1S)\eta)/\Gamma(\Upsilon(1S)\pi^+\pi^-)$ Γ_7/Γ_1

VALUE (units 10^{-3})	CL% EVTS	DOCUMENT ID	TECN	COMMENT
1.64 ± 0.25 OUR FIT				Error includes scale factor of 2.0.
1.99 ± 0.14 ± 0.11	241	TAMPONI 13	BELL	$e^+e^- \rightarrow \Upsilon(1S)\eta$
• • • We do not use the following data for averages, fits, limits, etc. • • •				
1.35 ± 0.17 ± 0.08		¹ LEES 11L	BABR	$\Upsilon(2S) \rightarrow (\pi^+\pi^-)(\gamma\gamma)\mu^+\mu^-$
< 5.2	90	² AUBERT 08BP	BABR	$e^+e^- \rightarrow \gamma\pi^+\pi^-(\pi^0)\ell^+\ell^-$
¹ Not independent of other values reported by LEES 11L.				
² Not independent of other values reported by AUBERT 08BP.				

 $\Gamma(\Upsilon(1S)\pi^0)/\Gamma(\Upsilon(1S)\eta)$ Γ_6/Γ_7

VALUE	CL%	DOCUMENT ID	TECN	COMMENT
< 0.13	90	TAMPONI 13	BELL	$e^+e^- \rightarrow \Upsilon(1S)\pi^0$

 $\Gamma(J/\psi(1S) \text{ anything})/\Gamma_{\text{total}}$ Γ_8/Γ

VALUE	CL%	DOCUMENT ID	TECN	COMMENT
< 0.006	90	MASCHMANN 90	CBAL	$e^+e^- \rightarrow$ hadrons

 $\Gamma(J/\psi(1S)\eta_c)/\Gamma_{\text{total}}$ Γ_9/Γ

VALUE	CL%	DOCUMENT ID	TECN	COMMENT
< 5.4 × 10⁻⁶	90	YANG 14	BELL	$e^+e^- \rightarrow J/\psi X$

 $\Gamma(J/\psi(1S)\chi_{c0})/\Gamma_{\text{total}}$ Γ_{10}/Γ

VALUE	CL%	DOCUMENT ID	TECN	COMMENT
< 3.4 × 10⁻⁶	90	YANG 14	BELL	$e^+e^- \rightarrow J/\psi X$

 $\Gamma(J/\psi(1S)\chi_{c1})/\Gamma_{\text{total}}$ Γ_{11}/Γ

VALUE	CL%	DOCUMENT ID	TECN	COMMENT
< 1.2 × 10⁻⁶	90	YANG 14	BELL	$e^+e^- \rightarrow J/\psi X$

 $\Gamma(J/\psi(1S)\chi_{c2})/\Gamma_{\text{total}}$ Γ_{12}/Γ

VALUE	CL%	DOCUMENT ID	TECN	COMMENT
< 2.0 × 10⁻⁶	90	YANG 14	BELL	$e^+e^- \rightarrow J/\psi X$

 $\Gamma(J/\psi(1S)\eta_c(2S))/\Gamma_{\text{total}}$ Γ_{13}/Γ

VALUE	CL%	DOCUMENT ID	TECN	COMMENT
< 2.5 × 10⁻⁶	90	YANG 14	BELL	$e^+e^- \rightarrow J/\psi X$

 $\Gamma(J/\psi(1S)X(3940))/\Gamma_{\text{total}}$ Γ_{14}/Γ

VALUE	CL%	DOCUMENT ID	TECN	COMMENT
< 2.0 × 10⁻⁶	90	YANG 14	BELL	$e^+e^- \rightarrow J/\psi X$

 $\Gamma(J/\psi(1S)X(4160))/\Gamma_{\text{total}}$ Γ_{15}/Γ

VALUE	CL%	DOCUMENT ID	TECN	COMMENT
< 2.0 × 10⁻⁶	90	YANG 14	BELL	$e^+e^- \rightarrow J/\psi X$

 $\Gamma(\chi_{c1} \text{ anything})/\Gamma_{\text{total}}$ Γ_{16}/Γ

VALUE (units 10^{-4})	EVTS	DOCUMENT ID	TECN	COMMENT
2.24 ± 0.44 ± 0.20	376	JIA 17	BELL	$\Upsilon(2S) \rightarrow \gamma J/\psi(1S)$

 $\Gamma(\chi_{c1}(1P)^0 X_{tetra})/\Gamma_{\text{total}}$ Γ_{17}/Γ

VALUE	CL%	DOCUMENT ID	TECN	COMMENT
< 36.7 × 10⁻⁶	90	¹ JIA 17A	BELL	$e^+e^- \rightarrow$ hadrons

¹ For a tetraquark state X_{tetra} , with mass in the range 1.16–2.46 GeV and width in the range 0–0.3 GeV. Measured 90% CL limits as a function of X_{tetra} mass and width range from 4.4×10^{-6} to 36.7×10^{-6} .

 $\Gamma(\chi_{c2} \text{ anything})/\Gamma_{\text{total}}$ Γ_{18}/Γ

VALUE (units 10^{-4})	DOCUMENT ID	TECN	COMMENT
2.28 ± 0.73 ± 0.34	JIA 17	BELL	$\Upsilon(2S) \rightarrow \gamma J/\psi(1S)$

 $\Gamma(\psi(2S)\eta_c)/\Gamma_{\text{total}}$ Γ_{19}/Γ

VALUE	CL%	DOCUMENT ID	TECN	COMMENT
< 5.1 × 10⁻⁶	90	YANG 14	BELL	$e^+e^- \rightarrow \psi(2S) X$

 $\Gamma(\psi(2S)\chi_{c0})/\Gamma_{\text{total}}$ Γ_{20}/Γ

VALUE	CL%	DOCUMENT ID	TECN	COMMENT
< 4.7 × 10⁻⁶	90	YANG 14	BELL	$e^+e^- \rightarrow \psi(2S) X$

 $\Gamma(\psi(2S)\chi_{c1})/\Gamma_{\text{total}}$ Γ_{21}/Γ

VALUE	CL%	DOCUMENT ID	TECN	COMMENT
< 2.5 × 10⁻⁶	90	YANG 14	BELL	$e^+e^- \rightarrow \psi(2S) X$

 $\Gamma(\psi(2S)\chi_{c2})/\Gamma_{\text{total}}$ Γ_{22}/Γ

VALUE	CL%	DOCUMENT ID	TECN	COMMENT
< 1.9 × 10⁻⁶	90	YANG 14	BELL	$e^+e^- \rightarrow \psi(2S) X$

 $\Gamma(\psi(2S)\eta_c(2S))/\Gamma_{\text{total}}$ Γ_{23}/Γ

VALUE	CL%	DOCUMENT ID	TECN	COMMENT
< 3.3 × 10⁻⁶	90	YANG 14	BELL	$e^+e^- \rightarrow \psi(2S) X$

 $\Gamma(\psi(2S)X(3940))/\Gamma_{\text{total}}$ Γ_{24}/Γ

VALUE	CL%	DOCUMENT ID	TECN	COMMENT
< 3.9 × 10⁻⁶	90	YANG 14	BELL	$e^+e^- \rightarrow \psi(2S) X$

 $\Gamma(\psi(2S)X(4160))/\Gamma_{\text{total}}$ Γ_{25}/Γ

VALUE	CL%	DOCUMENT ID	TECN	COMMENT
< 3.9 × 10⁻⁶	90	YANG 14	BELL	$e^+e^- \rightarrow \psi(2S) X$

 $\Gamma(T_{c\bar{c}1}(3900)^+ T_{c\bar{c}1}(3900)^-)/\Gamma_{\text{total}}$ Γ_{26}/Γ

VALUE	CL%	DOCUMENT ID	TECN	COMMENT
< 1.0 × 10⁻⁶	90	¹ JIA 18	BELL	$\Upsilon(2S) \rightarrow J/\psi\pi^\pm X$

¹ Assuming $B(T_{c\bar{c}1}(3900)^\pm \rightarrow J/\psi\pi^\pm) = 1$.

 $\Gamma(T_{c\bar{c}1}(4200)^+ T_{c\bar{c}1}(4200)^-)/\Gamma_{\text{total}}$ Γ_{27}/Γ

VALUE	CL%	DOCUMENT ID	TECN	COMMENT
< 16.7 × 10⁻⁶	90	¹ JIA 18	BELL	$\Upsilon(1S) \rightarrow J/\psi\pi^\pm X$

¹ Assuming $B(T_{c\bar{c}1}(4200)^\pm \rightarrow J/\psi\pi^\pm) = 1$

 $\Gamma(T_{c\bar{c}1}(3900)^\pm T_{c\bar{c}1}(4200)^\mp)/\Gamma_{\text{total}}$ Γ_{28}/Γ

VALUE	CL%	DOCUMENT ID	TECN	COMMENT
< 7.3 × 10⁻⁶	90	¹ JIA 18	BELL	$\Upsilon(2S) \rightarrow J/\psi\pi^\pm X$

¹ Assuming $B(T_{c\bar{c}1}(4200)^\pm \rightarrow J/\psi\pi^\pm) = 1 = B(T_{c\bar{c}1}(3900)^\pm \rightarrow J/\psi\pi^\pm)$.

 $\Gamma(T_{c\bar{c}1}(4050)^+ T_{c\bar{c}1}(4050)^-)/\Gamma_{\text{total}}$ Γ_{29}/Γ

VALUE	CL%	DOCUMENT ID	TECN	COMMENT
< 13.5 × 10⁻⁶	90	¹ JIA 18	BELL	$\Upsilon(2S) \rightarrow \chi_{c1}(1P)\pi^\pm X$

¹ Assuming $B(T_{c\bar{c}1}(4050)^\pm \rightarrow \chi_{c1}(1P)\pi^\pm)$

 $\Gamma(T_{c\bar{c}1}(4250)^+ T_{c\bar{c}1}(4250)^-)/\Gamma_{\text{total}}$ Γ_{30}/Γ

VALUE	CL%	DOCUMENT ID	TECN	COMMENT
< 26.7 × 10⁻⁶	90	¹ JIA 18	BELL	$\Upsilon(2S) \rightarrow \chi_{c1}(1P)\pi^\pm X$

¹ Assuming $B(T_{c\bar{c}1}(4250)^\pm \rightarrow \chi_{c1}(1P)\pi^\pm) = 1$

 $\Gamma(T_{c\bar{c}1}(4050)^\pm T_{c\bar{c}1}(4250)^\mp)/\Gamma_{\text{total}}$ Γ_{31}/Γ

VALUE	CL%	DOCUMENT ID	TECN	COMMENT
< 27.2 × 10⁻⁶	90	¹ JIA 18	BELL	$\Upsilon(2S) \rightarrow \chi_{c1}(1P)\pi^\pm X$

¹ Assuming $B(T_{c\bar{c}1}(4050)^\pm \rightarrow \chi_{c1}(1P)\pi^\pm) = 1 = B(T_{c\bar{c}1}(4250)^\pm \rightarrow \chi_{c1}(1P)\pi^\pm)$

 $\Gamma(T_{c\bar{c}1}(4430)^+ T_{c\bar{c}1}(4430)^-)/\Gamma_{\text{total}}$ Γ_{32}/Γ

VALUE	CL%	DOCUMENT ID	TECN	COMMENT
< 20.3 × 10⁻⁶	90	¹ JIA 18	BELL	$\Upsilon(2S) \rightarrow \psi(2S)\pi^\pm X$

¹ Assuming $B(T_{c\bar{c}1}(4430)^\pm \rightarrow \psi(2P)\pi^\pm) = 1$

 $\Gamma(T_{c\bar{c}1}(4055)^\pm T_{c\bar{c}1}(4055)^\mp)/\Gamma_{\text{total}}$ Γ_{33}/Γ

VALUE	CL%	DOCUMENT ID	TECN	COMMENT
< 11.1 × 10⁻⁶	90	¹ JIA 18	BELL	$\Upsilon(2S) \rightarrow \psi(2S)\pi^\pm X$

¹ Assuming $B(T_{c\bar{c}1}(4055)^\pm \rightarrow \psi(2S)\pi^\pm) = 1$

 $\Gamma(T_{c\bar{c}1}(4055)^\pm T_{c\bar{c}1}(4430)^\mp)/\Gamma_{\text{total}}$ Γ_{34}/Γ

VALUE	CL%	DOCUMENT ID	TECN	COMMENT
< 21.1 × 10⁻⁶	90	¹ JIA 18	BELL	$\Upsilon(2S) \rightarrow \psi(2S)\pi^\pm X$

¹ Assuming $B(T_{c\bar{c}1}(4055)^\pm \rightarrow \psi(2S)\pi^\pm) = 1 = B(T_{c\bar{c}1}(4430)^\pm \rightarrow \psi(2S)\pi^\pm)$

 $\Gamma(\overline{2}H \text{ anything})/\Gamma_{\text{total}}$ Γ_{35}/Γ

VALUE (units 10^{-5})	EVTS	DOCUMENT ID	TECN	COMMENT
2.78^{+0.30}_{-0.26} OUR AVERAGE				Error includes scale factor of 1.2.

2.64 ± 0.11 ^{+0.26} _{-0.21}		LEES 14G	BABR	$e^+e^- \rightarrow \overline{2}H X$
3.37 ± 0.50 ± 0.25	58	ASNER 07	CLEO	$e^+e^- \rightarrow \overline{2}H X$

 $\Gamma(ggg)/\Gamma_{\text{total}}$ Γ_{37}/Γ

VALUE (units 10^{-2})	EVTS	DOCUMENT ID	TECN	COMMENT
58.8 ± 1.2	6M	¹ BESSON 06A	CLEO	$\Upsilon(2S) \rightarrow$ hadrons

¹ Calculated using the value $\Gamma(\gamma gg)/\Gamma(ggg) = (3.18 \pm 0.04 \pm 0.22 \pm 0.41)\%$ from BESSON 06A and PDG 08 values of $B(\pi^+\pi^-\Upsilon(1S)) = (18.1 \pm 0.4)\%$, $B(\pi^0\pi^0\Upsilon(1S)) = (8.6 \pm 0.4)\%$, $B(\mu^+\mu^-\Upsilon(1S)) = (1.93 \pm 0.17)\%$, and $R_{\text{hadrons}} = 3.51$. The statistical error is negligible and the systematic error is partially correlated with that of $\Gamma(\gamma gg)/\Gamma_{\text{total}}$ measurement of BESSON 06A.

 $\Gamma(\gamma gg)/\Gamma(ggg)$ Γ_{38}/Γ_{37}

VALUE (units 10^{-2})	EVTS	DOCUMENT ID	TECN	COMMENT
3.18 ± 0.04 ± 0.47	6M	BESSON 06A	CLEO	$\Upsilon(2S) \rightarrow (\gamma +) \text{ hadrons}$

$\Gamma(\phi K^+ K^-)/\Gamma_{\text{total}}$		Γ_{39}/Γ	
VALUE (units 10^{-6})	EVTS	DOCUMENT ID	TECN COMMENT
1.58 ± 0.33 ± 0.18	58	SHEN	12A BELL $\Upsilon(1S) \rightarrow 2(K^+ K^-)$

$\Gamma(\omega \pi^+ \pi^-)/\Gamma_{\text{total}}$		Γ_{40}/Γ	
VALUE (units 10^{-6})	CL%	DOCUMENT ID	TECN COMMENT
<2.58	90	SHEN	12A BELL $\Upsilon(1S) \rightarrow 2(\pi^+ \pi^-) \pi^0$

$\Gamma(K^*(892)^0 K^- \pi^+ + \text{c.c.})/\Gamma_{\text{total}}$		Γ_{41}/Γ	
VALUE (units 10^{-6})	EVTS	DOCUMENT ID	TECN COMMENT
2.32 ± 0.40 ± 0.54	135	SHEN	12A BELL $\Upsilon(1S) \rightarrow K^+ K^- \pi^+ \pi^-$

$\Gamma(\phi f_2'(1525))/\Gamma_{\text{total}}$		Γ_{42}/Γ	
VALUE (units 10^{-6})	CL%	DOCUMENT ID	TECN COMMENT
<1.33	90	SHEN	12A BELL $\Upsilon(1S) \rightarrow 2(K^+ K^-)$

$\Gamma(\omega f_2(1270))/\Gamma_{\text{total}}$		Γ_{43}/Γ	
VALUE (units 10^{-6})	CL%	DOCUMENT ID	TECN COMMENT
<0.57	90	SHEN	12A BELL $\Upsilon(1S) \rightarrow 2(\pi^+ \pi^-) \pi^0$

$\Gamma(\rho(770) a_2(1320))/\Gamma_{\text{total}}$		Γ_{44}/Γ	
VALUE (units 10^{-6})	CL%	DOCUMENT ID	TECN COMMENT
<0.88	90	SHEN	12A BELL $\Upsilon(1S) \rightarrow 2(\pi^+ \pi^-) \pi^0$

$\Gamma(K^*(892)^0 K_2^*(1430)^0 + \text{c.c.})/\Gamma_{\text{total}}$		Γ_{45}/Γ	
VALUE (units 10^{-6})	EVTS	DOCUMENT ID	TECN COMMENT
1.53 ± 0.52 ± 0.19	32	SHEN	12A BELL $\Upsilon(1S) \rightarrow K^+ K^- \pi^+ \pi^-$

$\Gamma(K_1(1270)^\pm K^\mp)/\Gamma_{\text{total}}$		Γ_{46}/Γ	
VALUE (units 10^{-6})	CL%	DOCUMENT ID	TECN COMMENT
<3.22	90	SHEN	12A BELL $\Upsilon(1S) \rightarrow K^+ K^- \pi^+ \pi^-$

$\Gamma(K_1(1400)^\pm K^\mp)/\Gamma_{\text{total}}$		Γ_{47}/Γ	
VALUE (units 10^{-6})	CL%	DOCUMENT ID	TECN COMMENT
<0.83	90	SHEN	12A BELL $\Upsilon(1S) \rightarrow K^+ K^- \pi^+ \pi^-$

$\Gamma(b_1(1235)^\pm \pi^\mp)/\Gamma_{\text{total}}$		Γ_{48}/Γ	
VALUE (units 10^{-6})	CL%	DOCUMENT ID	TECN COMMENT
<0.40	90	SHEN	12A BELL $\Upsilon(1S) \rightarrow 2(\pi^+ \pi^-) \pi^0$

$\Gamma(\rho\pi)/\Gamma_{\text{total}}$		Γ_{49}/Γ	
VALUE (units 10^{-6})	CL%	DOCUMENT ID	TECN COMMENT
<1.16	90	SHEN	13 BELL $\Upsilon(2S) \rightarrow \pi^+ \pi^- \pi^0$

$\Gamma(\pi^+ \pi^- \pi^0)/\Gamma_{\text{total}}$		Γ_{50}/Γ	
VALUE (units 10^{-6})	CL%	DOCUMENT ID	TECN COMMENT
<0.80	90	SHEN	13 BELL $\Upsilon(2S) \rightarrow \pi^+ \pi^- \pi^0$

$\Gamma(\omega \pi^0)/\Gamma_{\text{total}}$		Γ_{51}/Γ	
VALUE (units 10^{-6})	CL%	DOCUMENT ID	TECN COMMENT
<1.63	90	SHEN	13 BELL $\Upsilon(2S) \rightarrow \pi^+ \pi^- \pi^0 \pi^0$

$\Gamma(\pi^+ \pi^- \pi^0 \pi^0)/\Gamma_{\text{total}}$		Γ_{52}/Γ	
VALUE (units 10^{-6})	EVTS	DOCUMENT ID	TECN COMMENT
13.0 ± 1.9 ± 2.1	261 ± 37	SHEN	13 BELL $\Upsilon(2S) \rightarrow \pi^+ \pi^- \pi^0 \pi^0$

$\Gamma(K_S^0 K^+ \pi^- + \text{c.c.})/\Gamma_{\text{total}}$		Γ_{53}/Γ		
VALUE (units 10^{-6})	CL%	EVTS	DOCUMENT ID	TECN COMMENT
1.14 ± 0.30 ± 0.13		40 ± 10	SHEN	13 BELL $\Upsilon(2S) \rightarrow K_S^0 K^- \pi^+$

• • • We do not use the following data for averages, fits, limits, etc. • • •
 <3.2 90 ¹ DOBBS 12A $\Upsilon(2S) \rightarrow K_S^0 K^- \pi^+$
¹ Obtained by analyzing CLEO III data but not authored by the CLEO Collaboration.

$\Gamma(K^*(892)^0 \bar{K}^0 + \text{c.c.})/\Gamma_{\text{total}}$		Γ_{54}/Γ	
VALUE (units 10^{-6})	CL%	DOCUMENT ID	TECN COMMENT
<4.22	90	SHEN	13 BELL $\Upsilon(2S) \rightarrow K_S^0 K^- \pi^+$

$\Gamma(K^*(892)^- K^+ + \text{c.c.})/\Gamma_{\text{total}}$		Γ_{55}/Γ	
VALUE (units 10^{-6})	CL%	DOCUMENT ID	TECN COMMENT
<1.45	90	SHEN	13 BELL $\Upsilon(2S) \rightarrow K_S^0 K^- \pi^+$

$\Gamma(f_1(1285) \text{ anything})/\Gamma_{\text{total}}$		Γ_{56}/Γ	
VALUE (units 10^{-3})	EVTS	DOCUMENT ID	TECN COMMENT
2.20 ± 1.50 ± 0.63	2.9k	JIA	17A BELL $e^+ e^- \rightarrow \text{hadrons}$

$\Gamma(f_1(1285) X_{tetra})/\Gamma_{\text{total}}$		Γ_{57}/Γ	
VALUE	CL%	DOCUMENT ID	TECN COMMENT
<64.7 × 10⁻⁶	90	¹ JIA	17A BELL $e^+ e^- \rightarrow \text{hadrons}$

¹ For a tetraquark state X_{tetra} , with mass in the range 1.16–2.46 GeV and width in the range 0–0.3 GeV. Measured 90% CL limits as a function of X_{tetra} mass and width range from 7.8×10^{-6} to 64.7×10^{-6} .

$\Gamma(D_s^+ D_{s1}(2536)^-, D_{s1}^- \rightarrow K^- D^*(2007)^0)/\Gamma_{\text{total}}$		Γ_{59}/Γ	
VALUE (units 10^{-5})	DOCUMENT ID	TECN	COMMENT
1.6 ± 0.3 ± 0.2	GAO	23	BELL $e^+ e^-$ at 10.52 GeV

$\Gamma(D_s^+ D_{s1}(2536)^-, D_{s1}^- \rightarrow K_S^0 D^*(2010)^-)/\Gamma_{\text{total}}$		Γ_{60}/Γ	
VALUE (units 10^{-5})	DOCUMENT ID	TECN	COMMENT
0.84 ± 0.18 ± 0.15	GAO	23	BELL $e^+ e^-$ at 10.52 GeV

$\Gamma(D_s^{*+} D_{s1}(2536)^-, D_{s1}^- \rightarrow K^- D^*(2007)^0)/\Gamma_{\text{total}}$		Γ_{62}/Γ	
VALUE (units 10^{-5})	DOCUMENT ID	TECN	COMMENT
1.4 ± 0.4 ± 0.2	GAO	23	BELL $e^+ e^-$ at 10.52 GeV

$\Gamma(D_s^{*+} D_{s1}(2536)^-, D_{s1}^- \rightarrow K_S^0 D^*(2010)^-)/\Gamma_{\text{total}}$		Γ_{63}/Γ	
VALUE (units 10^{-5})	DOCUMENT ID	TECN	COMMENT
0.82 ± 0.25 ± 0.19	GAO	23	BELL $e^+ e^-$ at 10.52 GeV

$\Gamma(D_s^+ D_{s2}^*(2573)^-, D_{s2}^{*-} \rightarrow K^- D^0)/\Gamma_{\text{total}}$		Γ_{65}/Γ	
VALUE (units 10^{-5})	DOCUMENT ID	TECN	COMMENT
1.4 ± 0.4 ± 0.2	GAO	23	BELL $e^+ e^-$ at 10.52 GeV

$\Gamma(D_s^+ D_{s2}^*(2573)^-, D_{s2}^{*-} \rightarrow K_S^0 D^-)/\Gamma_{\text{total}}$		Γ_{66}/Γ	
VALUE (units 10^{-5})	DOCUMENT ID	TECN	COMMENT
0.69 ± 0.20 ± 0.22	GAO	23	BELL $e^+ e^-$ at 10.52 GeV

$\Gamma(D_s^{*+} D_{s2}^*(2573)^-, D_{s2}^{*-} \rightarrow K^- D^0)/\Gamma_{\text{total}}$		Γ_{68}/Γ	
VALUE (units 10^{-5})	DOCUMENT ID	TECN	COMMENT
0.9 ± 0.5 ± 0.2	GAO	23	BELL $e^+ e^-$ at 10.52 GeV

$\Gamma(D_s^{*+} D_{s2}^*(2573)^-, D_{s2}^{*-} \rightarrow K_S^0 D^-)/\Gamma_{\text{total}}$		Γ_{69}/Γ	
VALUE (units 10^{-5})	DOCUMENT ID	TECN	COMMENT
0.54 ± 0.31 ± 0.47	GAO	23	BELL $e^+ e^-$ at 10.52 GeV

$\Gamma(\text{Sum of 100 exclusive modes})/\Gamma_{\text{total}}$		Γ_{70}/Γ	
VALUE (units 10^{-2})	DOCUMENT ID	TECN	COMMENT
0.29 ± 0.03	^{1,2} DOBBS	12A	$\Upsilon(2S) \rightarrow \text{hadrons}$

¹ DOBBS 12A presents individual exclusive branching fractions or upper limits for 100 modes of four to ten pions, kaons, or protons.
² Obtained by analyzing CLEO III data but not authored by the CLEO Collaboration.

$\Gamma(\gamma \chi_{b1}(1P))/\Gamma_{\text{total}}$		Γ_{71}/Γ	
VALUE	EVTS	DOCUMENT ID	TECN COMMENT
0.069 ± 0.004 OUR AVERAGE	407k		

0.0693 ± 0.0012 ± 0.0041	ARTUSO	05	CLEO $e^+ e^- \rightarrow \gamma X$
0.069 ± 0.005 ± 0.009	EDWARDS	99	CLE2 $\Upsilon(2S) \rightarrow \gamma \chi(1P)$
0.091 ± 0.018 ± 0.022	ALBRECHT	85E	ARG $e^+ e^- \rightarrow \gamma \text{conv. } X$
0.065 ± 0.007 ± 0.012	NERNST	85	CBAL $e^+ e^- \rightarrow \gamma X$
0.080 ± 0.017 ± 0.016	HAAS	84	CLEO $e^+ e^- \rightarrow \gamma \text{conv. } X$
0.059 ± 0.014	KLOPFEN...	83	CUSB $e^+ e^- \rightarrow \gamma X$

$\Gamma(\gamma \chi_{b2}(1P))/\Gamma_{\text{total}}$		Γ_{72}/Γ	
VALUE	EVTS	DOCUMENT ID	TECN COMMENT
0.0715 ± 0.0035 OUR AVERAGE	410k		

0.0724 ± 0.0011 ± 0.0040	ARTUSO	05	CLEO $e^+ e^- \rightarrow \gamma X$
0.074 ± 0.005 ± 0.008	EDWARDS	99	CLE2 $\Upsilon(2S) \rightarrow \gamma \chi(1P)$
0.098 ± 0.021 ± 0.024	ALBRECHT	85E	ARG $e^+ e^- \rightarrow \gamma \text{conv. } X$
0.058 ± 0.007 ± 0.010	NERNST	85	CBAL $e^+ e^- \rightarrow \gamma X$
0.102 ± 0.018 ± 0.021	HAAS	84	CLEO $e^+ e^- \rightarrow \gamma \text{conv. } X$
0.061 ± 0.014	KLOPFEN...	83	CUSB $e^+ e^- \rightarrow \gamma X$

$\Gamma(\gamma \chi_{b0}(1P))/\Gamma_{\text{total}}$		Γ_{73}/Γ	
VALUE	EVTS	DOCUMENT ID	TECN COMMENT
0.038 ± 0.004 OUR AVERAGE	198k		

0.0375 ± 0.0012 ± 0.0047	ARTUSO	05	CLEO $e^+ e^- \rightarrow \gamma X$
0.034 ± 0.005 ± 0.006	EDWARDS	99	CLE2 $\Upsilon(2S) \rightarrow \gamma \chi(1P)$
0.064 ± 0.014 ± 0.016	ALBRECHT	85E	ARG $e^+ e^- \rightarrow \gamma \text{conv. } X$
0.036 ± 0.008 ± 0.009	NERNST	85	CBAL $e^+ e^- \rightarrow \gamma X$
0.044 ± 0.023 ± 0.009	HAAS	84	CLEO $e^+ e^- \rightarrow \gamma \text{conv. } X$
0.035 ± 0.014	KLOPFEN...	83	CUSB $e^+ e^- \rightarrow \gamma X$

• • • We do not use the following data for averages, fits, limits, etc. • • •

Meson Particle Listings

$\Upsilon(2S)$

$\Gamma(\gamma f_0(1710))/\Gamma_{total}$ Γ_{74}/Γ

VALUE (units 10^{-5})	CL%	DOCUMENT ID	TECN	COMMENT
<5.9	90	¹ ALBRECHT 89	ARG	$\Upsilon(2S) \rightarrow \gamma K^+ K^-$
• • • We do not use the following data for averages, fits, limits, etc. • • •				
< 5.9	90	² ALBRECHT 89	ARG	$\Upsilon(2S) \rightarrow \gamma \pi^+ \pi^-$
¹ Re-evaluated assuming $B(f_0(1710) \rightarrow K^+ K^-) = 0.19$.				
² Includes unknown branching ratio of $f_0(1710) \rightarrow \pi^+ \pi^-$.				

$\Gamma(\gamma f_2'(1525))/\Gamma_{total}$ Γ_{75}/Γ

VALUE (units 10^{-5})	CL%	DOCUMENT ID	TECN	COMMENT
<5.3	90	¹ ALBRECHT 89	ARG	$\Upsilon(2S) \rightarrow \gamma K^+ K^-$
¹ Re-evaluated assuming $B(f_2'(1525) \rightarrow K \bar{K}) = 0.71$.				

$\Gamma(\gamma f_2(1270))/\Gamma_{total}$ Γ_{76}/Γ

VALUE (units 10^{-5})	CL%	DOCUMENT ID	TECN	COMMENT
<24.1	90	¹ ALBRECHT 89	ARG	$\Upsilon(2S) \rightarrow \gamma \pi^+ \pi^-$
¹ Using $B(f_2(1270) \rightarrow \pi \pi) = 0.84$.				

$\Gamma(\gamma f_3(2220))/\Gamma_{total}$ Γ_{77}/Γ

VALUE (units 10^{-5})	CL%	DOCUMENT ID	TECN	COMMENT
<6.8	90	¹ ALBRECHT 89	ARG	$\Upsilon(2S) \rightarrow \gamma K^+ K^-$
• • • We do not use the following data for averages, fits, limits, etc. • • •				
¹ Includes unknown branching ratio of $f_3(2220) \rightarrow K^+ K^-$.				

$\Gamma(\gamma \eta_c(1S))/\Gamma_{total}$ Γ_{78}/Γ

VALUE	CL%	DOCUMENT ID	TECN	COMMENT
<2.7 × 10 ⁻⁵	90	WANG 11b	BELL	$\Upsilon(2S) \rightarrow \gamma X$

$\Gamma(\gamma \chi_{c0})/\Gamma_{total}$ Γ_{79}/Γ

VALUE	CL%	DOCUMENT ID	TECN	COMMENT
<1.0 × 10 ⁻⁴	90	WANG 11b	BELL	$\Upsilon(2S) \rightarrow \gamma X$

$\Gamma(\gamma \chi_{c1})/\Gamma_{total}$ Γ_{80}/Γ

VALUE	CL%	DOCUMENT ID	TECN	COMMENT
<3.6 × 10 ⁻⁶	90	WANG 11b	BELL	$\Upsilon(2S) \rightarrow \gamma X$

$\Gamma(\gamma \chi_{c2})/\Gamma_{total}$ Γ_{81}/Γ

VALUE	CL%	DOCUMENT ID	TECN	COMMENT
<1.5 × 10 ⁻⁵	90	WANG 11b	BELL	$\Upsilon(2S) \rightarrow \gamma X$

$\Gamma(\gamma \chi_{c1}(3872))/\Gamma_{total}$ Γ_{82}/Γ

VALUE	CL%	DOCUMENT ID	TECN	COMMENT
<2.3 × 10 ⁻⁵	90	¹ WANG 11b	BELL	$\Upsilon(2S) \rightarrow \gamma X$
¹ WANG 11b reports $[\Gamma(\Upsilon(2S) \rightarrow \gamma \chi_{c1}(3872))/\Gamma_{total}] \times [B(\chi_{c1}(3872) \rightarrow \pi^+ \pi^- J/\psi(1S))] < 0.8 \times 10^{-6}$ which we divide by our best value $B(\chi_{c1}(3872) \rightarrow \pi^+ \pi^- J/\psi(1S)) = 3.5 \times 10^{-2}$.				

$\Gamma(\gamma \chi_{c1}(3872), \chi_{c1} \rightarrow \pi^+ \pi^- \pi^0 J/\psi)/\Gamma_{total}$ Γ_{83}/Γ

VALUE	CL%	DOCUMENT ID	TECN	COMMENT
<2.4 × 10 ⁻⁶	90	WANG 11b	BELL	$\Upsilon(2S) \rightarrow \gamma X$

$\Gamma(\gamma \chi_{c0}(3915) \rightarrow \omega J/\psi)/\Gamma_{total}$ Γ_{84}/Γ

VALUE	CL%	DOCUMENT ID	TECN	COMMENT
<2.8 × 10 ⁻⁶	90	WANG 11b	BELL	$\Upsilon(2S) \rightarrow \gamma X$

$\Gamma(\gamma \chi_{c1}(4140) \rightarrow \phi J/\psi)/\Gamma_{total}$ Γ_{85}/Γ

VALUE	CL%	DOCUMENT ID	TECN	COMMENT
<1.2 × 10 ⁻⁶	90	WANG 11b	BELL	$\Upsilon(2S) \rightarrow \gamma X$

$\Gamma(\gamma X(4350) \rightarrow \phi J/\psi)/\Gamma_{total}$ Γ_{86}/Γ

VALUE	CL%	DOCUMENT ID	TECN	COMMENT
<1.3 × 10 ⁻⁶	90	WANG 11b	BELL	$\Upsilon(2S) \rightarrow \gamma X$

$\Gamma(\gamma \eta_b(1S))/\Gamma_{total}$ Γ_{87}/Γ

VALUE (units 10^{-4})	CL%	EVTS	DOCUMENT ID	TECN	COMMENT
5.5 ± 0.9 OUR AVERAGE					Error includes scale factor of 1.2.
6.1 ± 0.6 + 0.9 - 0.7		29k	FULSOM 18	BELL	$\Upsilon(2S) \rightarrow \gamma X$
3.9 ± 1.1 ± 1.1 - 0.9		13 ± 5k	¹ AUBERT 09aQ	BABR	$\Upsilon(2S) \rightarrow \gamma X$
• • • We do not use the following data for averages, fits, limits, etc. • • •					
<21	90		LEES 11j	BABR	$\Upsilon(2S) \rightarrow X \gamma$
< 8.4	90		¹ BONVICINI 10	CLEO	$\Upsilon(2S) \rightarrow \gamma X$
< 5.1	90		² ARTUSO 05	CLEO	$e^+ e^- \rightarrow \gamma X$
¹ Assuming $\Gamma_{\eta_b(1S)} = 10$ MeV.					
² Superseded by BONVICINI 10.					

$\Gamma(\gamma \eta_b(1S) \rightarrow \gamma \text{Sum of 26 exclusive modes})/\Gamma_{total}$ Γ_{88}/Γ

VALUE	CL%	DOCUMENT ID	TECN	COMMENT
<3.7 × 10 ⁻⁶	90	SANDILYA 13	BELL	$\Upsilon(2S) \rightarrow \gamma$ hadrons

$\Gamma(\gamma X_{b\bar{b}} \rightarrow \gamma \text{Sum of 26 exclusive modes})/\Gamma_{total}$ Γ_{89}/Γ

VALUE (units 10^{-6})	CL%	EVTS	DOCUMENT ID	TECN	COMMENT
< 4.9	90		SANDILYA 13	BELL	$\Upsilon(2S) \rightarrow \gamma$ hadrons
• • • We do not use the following data for averages, fits, limits, etc. • • •					
46.2 ± 29.7 - 14.2 ± 10.6		10	¹ DOBBS 12		$\Upsilon(2S) \rightarrow \gamma$ hadrons
¹ Obtained by analyzing CLEO III data but not authored by the CLEO Collaboration.					

$\Gamma(\gamma X \rightarrow \gamma + \geq 4 \text{ prongs})/\Gamma_{total}$ Γ_{90}/Γ

(1.5 GeV < m_X < 5.0 GeV)

VALUE (units 10^{-4})	CL%	DOCUMENT ID	TECN	COMMENT
<1.95	95	ROSNER 07a	CLEO	$e^+ e^- \rightarrow \gamma X$

$\Gamma(\gamma A^0 \rightarrow \gamma \text{hadrons})/\Gamma_{total}$ Γ_{91}/Γ

(0.3 GeV < m_{A^0} < 7 GeV)

VALUE	CL%	DOCUMENT ID	TECN	COMMENT
<8 × 10 ⁻⁵	90	¹ LEES 11h	BABR	$\Upsilon(2S) \rightarrow \gamma$ hadrons
¹ For a narrow scalar or pseudoscalar, A^0 , excluding known resonances, with mass in the range 0.3–7 GeV. Measured 90% CL limits as a function of m_{A^0} range from 1×10^{-6} to 8×10^{-5} .				

$\Gamma(\gamma A^0 \rightarrow \gamma \mu^+ \mu^-)/\Gamma_{total}$ Γ_{92}/Γ

VALUE (units 10^{-6})	CL%	DOCUMENT ID	TECN	COMMENT
<8.3	90	¹ AUBERT 09z	BABR	$e^+ e^- \rightarrow A^0 \rightarrow \gamma \mu^+ \mu^-$
¹ For a narrow scalar or pseudoscalar, A^0 , with mass in the range 212–9300 MeV, excluding J/ψ and $\psi(2S)$. Measured 90% CL limits as a function of m_{A^0} range from 0.26–8.3 × 10 ⁻⁶ .				

LEPTON FAMILY NUMBER (LF) VIOLATING MODES

$\Gamma(e^\pm \tau^\mp)/\Gamma_{total}$ Γ_{93}/Γ

VALUE (units 10^{-6})	CL%	DOCUMENT ID	TECN	COMMENT
<3.2	90	LEES 10b	BABR	$e^+ e^- \rightarrow e^\pm \tau^\mp$

$\Gamma(\mu^\pm \tau^\mp)/\Gamma_{total}$ Γ_{94}/Γ

VALUE (units 10^{-6})	CL%	DOCUMENT ID	TECN	COMMENT
< 3.3	90	LEES 10b	BABR	$e^+ e^- \rightarrow \mu^\pm \tau^\mp$
• • • We do not use the following data for averages, fits, limits, etc. • • •				
<14.4	95	LOVE 08a	CLEO	$e^+ e^- \rightarrow \mu^\pm \tau^\mp$

$\Upsilon(2S)$ Cross-Particle Branching Ratios

$B(\Upsilon(2S) \rightarrow \pi^+ \pi^-) \times B(\Upsilon(3S) \rightarrow \Upsilon(2S) X)$

VALUE (units 10^{-2})	EVTS	DOCUMENT ID	TECN	COMMENT
1.78 ± 0.02 ± 0.11	906k	LEES 11c	BABR	$e^+ e^- \rightarrow \pi^+ \pi^- X$

$\Upsilon(2S)$ REFERENCES

GAO	23	PR D108 112015	B.S. Gao <i>et al.</i>	(BELLE Collab.)
SHAMOV	23	PL B839 137766	A.G. Shamov, O.L. Rezanova	(NOVO, NOVOU)
FULSOM	18	PRL 121 232001	B.G. Fulsom <i>et al.</i>	(BELLE Collab.)
JIA	18	PR D97 112004	S. Jia <i>et al.</i>	(BELLE Collab.)
JIA	17	PR D95 012001	S. Jia <i>et al.</i>	(BELLE Collab.)
JIA	17A	PR D96 112002	S. Jia <i>et al.</i>	(BELLE Collab.)
LEES	14G	PR D89 111102	J.P. Lees <i>et al.</i>	(BABAR Collab.)
YANG	14	PR D90 112008	S.D. Yang <i>et al.</i>	(BELLE Collab.)
SANDILYA	13	PRL 111 112001	S. Sandilya <i>et al.</i>	(BELLE Collab.)
SHEN	13	PR D88 011102	C.P. Shen <i>et al.</i>	(BELLE Collab.)
TAMPONI	13	PR D87 011104	U. Tamponi <i>et al.</i>	(BELLE Collab.)
DOBBS	12	PRL 109 082001	S. Dobbs <i>et al.</i>	(BELLE Collab.)
DOBBS	12A	PR D86 052003	S. Dobbs <i>et al.</i>	(BELLE Collab.)
SHEN	12A	PR D86 031102	C.P. Shen <i>et al.</i>	(BABAR Collab.)
LEES	11C	PR D84 011104	J.P. Lees <i>et al.</i>	(BABAR Collab.)
LEES	11H	PRL 107 221803	J.P. Lees <i>et al.</i>	(BABAR Collab.)
LEES	11J	PR D84 072002	J.P. Lees <i>et al.</i>	(BABAR Collab.)
LEES	11B	PR D84 092003	J.P. Lees <i>et al.</i>	(BABAR Collab.)
WANG	11L	PR D84 071107	X.L. Wang <i>et al.</i>	(BELLE Collab.)
BONVICINI	10	PR D81 031104	G. Bonvicini <i>et al.</i>	(CLEO Collab.)
LEES	10B	PRL 104 151802	J.P. Lees <i>et al.</i>	(BABAR Collab.)
AUBERT	09Aq	PRL 103 161801	B. Aubert <i>et al.</i>	(BABAR Collab.)
AUBERT	09Z	PRL 103 081803	B. Aubert <i>et al.</i>	(BABAR Collab.)
BHARI	09	PR D79 011103	S.R. Bhari <i>et al.</i>	(CLEO Collab.)
AUBERT	08BP	PR D78 112002	B. Aubert <i>et al.</i>	(BABAR Collab.)
HE	08A	PRL 101 192001	Q. He <i>et al.</i>	(CLEO Collab.)
LOVE	08A	PRL 101 201601	W. Love <i>et al.</i>	(CLEO Collab.)
PDG	08	PL B667 1	C. Amsler <i>et al.</i>	(PDG Collab.)
ASNER	07	PR D75 012009	D.M. Asner <i>et al.</i>	(CLEO Collab.)
BESSION	07	PRL 98 052002	D. Besson <i>et al.</i>	(CLEO Collab.)
ROSNER	07A	PR D76 117102	J.L. Rosner <i>et al.</i>	(CLEO Collab.)
BESSION	06A	PR D74 012003	D. Besson <i>et al.</i>	(CLEO Collab.)
ROSNER	06	PRL 96 092003	J.L. Rosner <i>et al.</i>	(CLEO Collab.)
ADAMS	05	PRL 94 012001	G.S. Adams <i>et al.</i>	(CLEO Collab.)
ARTUSO	05	PRL 94 032001	M. Artuso <i>et al.</i>	(CLEO Collab.)
ARTAMONOV	00	PL B474 427	A.S. Artamonov <i>et al.</i>	(CLEO Collab.)
EDWARDS	99	PR D59 032003	K.W. Edwards <i>et al.</i>	(CLEO Collab.)
ALEXANDER	98	PR D58 052004	J.P. Alexander <i>et al.</i>	(CLEO Collab.)
BARU	96	PRPL 267 71	S.E. Baru <i>et al.</i>	(NOVO)
KOBEL	92	ZPHY C53 193	M. Kobel <i>et al.</i>	(Crystal Ball Collab.)
MASCHMANN	90	ZPHY C46 555	W.S. Maschmann <i>et al.</i>	(Crystal Ball Collab.)
ALBRECHT	89	ZPHY C42 349	H. Albrecht <i>et al.</i>	(ARGUS Collab.)
KAARSBERG	89	PRL 62 2077	T.M. Kaarsberg <i>et al.</i>	(CUSB Collab.)
BUCHMUELLER	88	HE $e^+ e^-$ Physics 412	W. Buchmueller, S. Cooper	(HANN, DESY, MIT)
Editors: A. Ali and P. Soeding, World Scientific, Singapore				
JAKUBOWSKI	88	ZPHY C40 49	Z. Jakubowski <i>et al.</i>	(Crystal Ball Collab.) IJGPG

See key on page 1171

Meson Particle Listings

$\Upsilon(2S)$, $\Upsilon_2(1D)$, $\chi_{b0}(2P)$

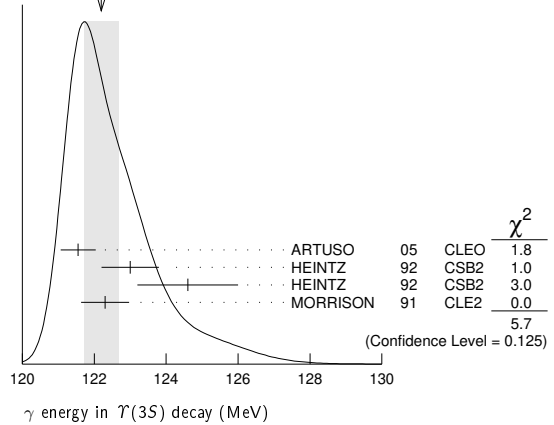
NAME	EVTS	DOCUMENT ID	TECN	COMMENT
ALBRECHT	87	ZPHY C35 283		H. Albrecht et al. (ARGUS Collab.)
COHEN	87	RMP 59 1121		E.R. Cohen, B.N. Taylor (RIS C, NBS)
LURZ	87	ZPHY C36 383		B. Lurz et al. (Crystal Ball Collab.)
BARU	86B	ZPHY C32 622 (errata.)		S.E. Baru et al. (NOVO)
ALBRECHT	85	ZPHY C28 45		H. Albrecht et al. (ARGUS Collab.)
ALBRECHT	85E	PL 160B 331		H. Albrecht et al. (ARGUS Collab.)
GELPHMAN	85	PR D32 2893		D. Gelpman et al. (Crystal Ball Collab.)
KURAEV	85	SJNP 41 466		E.A. Kuraev, V.S. Fadin (NOVO)
		Translated from YAF 41 73.		
NERNST	85	PRL 54 2195		R. Nernst et al. (Crystal Ball Collab.)
ARTAMONOV	84	PL 137B 272		A.S. Artamonov et al. (NOVO)
BARBER	84	PL 135B 498		D.P. Barber et al.
BESSON	84	PR D30 1433		D. Besson et al. (CLEO Collab.)
FONSECA	84	NP B242 31		V. Fonseca et al. (CLEO Collab.)
GILES	84B	PR D29 1285		R. Giles et al. (CLEO Collab.)
HAAS	84	PRL 52 799		J. Haas et al. (CLEO Collab.)
HAAS	84B	PR D30 1996		J. Haas et al. (CLEO Collab.)
KLOPFEN...	83	PRL 51 160		C. Klopfenstein et al. (CLEO Collab.)
ALBRECHT	82	PL 116B 383		H. Albrecht et al. (DESY, DORT, HEIDH+)
NICZYPORUK	81B	PL 100B 95		B. Niczyporuk et al. (LENA Collab.)
NICZYPORUK	81C	PL 99B 169		B. Niczyporuk et al. (LENA Collab.)
BOCK	80	ZPHY C6 125		P. Bock et al. (HEIDP, MPIM, DESY, HAMB)

γ ENERGY IN $\Upsilon(3S)$ DECAY

VALUE (MeV)	EVTS	DOCUMENT ID	TECN	COMMENT
121.9 ± 0.4 OUR EVALUATION				Treating systematic errors as correlated
122.2 ± 0.5 OUR AVERAGE				Error includes scale factor of 1.4. See the ideogram below.
121.55 ± 0.16 ± 0.46		ARTUSO	05	CLEO $\Upsilon(3S) \rightarrow \gamma X$
123.0 ± 0.8	4959	¹ HEINTZ	92	CSB2 $e^+e^- \rightarrow \gamma X$
124.6 ± 1.4	17	² HEINTZ	92	CSB2 $e^+e^- \rightarrow \ell^+\ell^-\gamma\gamma$
122.3 ± 0.3 ± 0.6	9903	MORRISON	91	CLE2 $e^+e^- \rightarrow \gamma X$

¹ A systematic uncertainty on the energy scale of 0.9% not included. Supersedes NARAIN 91.
² A systematic uncertainty on the energy scale of 0.9% not included. Supersedes HEINTZ 91.

WEIGHTED AVERAGE
122.2±0.5 (Error scaled by 1.4)



$\Upsilon_2(1D)$ $I^G(J^{PC}) = 0^-(2^{--})$

was $\Upsilon(1D)$
 First observed by BONVICINI 04 in the decay to $\gamma\gamma \Upsilon(1S)$ and confirmed by DEL-AMO-SANCHEZ 10R in the decay to $\pi^+\pi^- \Upsilon(1S)$.
 Data consistent with $J^P = 2^-$. The states with $J = 1$ and 3 also possibly seen, but need confirmation.

$\Upsilon_2(1D)$ MASS

VALUE (MeV)	EVTS	DOCUMENT ID	TECN	COMMENT
10163.7 ± 1.4 OUR AVERAGE				Error includes scale factor of 1.7.
10164.5 ± 0.8 ± 0.5		DEL-AMO-SA...10R	BABR	$\Upsilon(3S) \rightarrow \gamma\gamma\pi^+\pi^-\ell^+\ell^-$
10161.1 ± 0.6 ± 1.6	38	BONVICINI 04	CLE3	$\Upsilon(3S) \rightarrow 4\gamma\ell^+\ell^-$

$\Upsilon_2(1D)$ DECAY MODES

Mode	Fraction (Γ_i/Γ)
Γ_1 $\gamma\gamma \Upsilon(1S)$	seen
Γ_2 $\gamma\chi_{bJ}(1P)$	seen
Γ_3 $\eta \Upsilon(1S)$	not seen
Γ_4 $\pi^+\pi^- \Upsilon(1S)$	$(6.6 \pm 1.6) \times 10^{-3}$

$\Upsilon_2(1D)$ BRANCHING RATIOS

$\Gamma(\eta \Upsilon(1S))/\Gamma(\gamma\gamma \Upsilon(1S))$	CL%	DOCUMENT ID	TECN	COMMENT	Γ_3/Γ_1
<0.25	90	BONVICINI 04	CLE3	$\Upsilon(3S) \rightarrow 4\gamma\ell^+\ell^-$	

$\Gamma(\pi^+\pi^- \Upsilon(1S))/\Gamma_{total}$	DOCUMENT ID	TECN	COMMENT	Γ_4/Γ
0.66 ± 0.15 0.14 ± 0.06	¹ DEL-AMO-SA...10R	BABR	$\Upsilon(3S) \rightarrow \gamma\gamma\pi^+\pi^-\ell^+\ell^-$	

¹ Using theoretical predictions for $B(\chi_{bJ}(2P) \rightarrow \gamma \Upsilon_2(1D))$.

$\Gamma(\pi^+\pi^- \Upsilon(1S))/\Gamma(\gamma\gamma \Upsilon(1S))$	CL%	DOCUMENT ID	TECN	COMMENT	Γ_4/Γ_1
<1.2	90	² BONVICINI 04	CLE3	$\Upsilon(3S) \rightarrow 4\gamma\ell^+\ell^-$	

² Assuming $J = 2$.

$\Upsilon_2(1D)$ REFERENCES

DEL-AMO-SA...10R	PR D82 111102	P. del Amo Sanchez et al. (BABAR Collab.)
BONVICINI 04	PR D70 032001	G. Bonvicini et al. (CLEO Collab.)

$\chi_{b0}(2P)$ $I^G(J^{PC}) = 0^+(0^{++})$
 J needs confirmation.

Observed in radiative decay of the $\Upsilon(3S)$, therefore $C = +$. Branching ratio requires E1 transition, M1 is strongly disfavored, therefore $P = +$.

$\chi_{b0}(2P)$ MASS

VALUE (MeV)	DOCUMENT ID
10232.5 ± 0.4 ± 0.5 OUR EVALUATION	From γ energy below, using $\Upsilon(3S)$ mass = 10355.2 ± 0.5 MeV

$m_{\chi_{b1}(2P)} - m_{\chi_{b0}(2P)}$	DOCUMENT ID	TECN	COMMENT
23.8 ± 1.7	LEES	14M	BABR $\Upsilon(3S) \rightarrow \gamma\gamma\mu^+\mu^-$

$\chi_{b0}(2P)$ DECAY MODES

Mode	Fraction (Γ_i/Γ)	Confidence level
Γ_1 $\gamma \Upsilon(2S)$	$(1.38 \pm 0.30) \%$	
Γ_2 $\gamma \Upsilon(1S)$	$(3.8 \pm 1.7) \times 10^{-3}$	
Γ_3 $D^0 X$	< 8.2 %	90%
Γ_4 $\pi^+\pi^- K^+ K^- \pi^0$	< 3.4 $\times 10^{-5}$	90%
Γ_5 $2\pi^+\pi^- K^- K_S^0$	< 5 $\times 10^{-5}$	90%
Γ_6 $2\pi^+\pi^- K^- K_S^0 2\pi^0$	< 2.2 $\times 10^{-4}$	90%
Γ_7 $2\pi^+ 2\pi^- 2\pi^0$	< 2.4 $\times 10^{-4}$	90%
Γ_8 $2\pi^+ 2\pi^- K^+ K^-$	< 1.5 $\times 10^{-4}$	90%
Γ_9 $2\pi^+ 2\pi^- K^+ K^- \pi^0$	< 2.2 $\times 10^{-4}$	90%
Γ_{10} $2\pi^+ 2\pi^- K^+ K^- 2\pi^0$	< 1.1 $\times 10^{-3}$	90%
Γ_{11} $3\pi^+ 2\pi^- K^- K_S^0 \pi^0$	< 7 $\times 10^{-4}$	90%
Γ_{12} $3\pi^+ 3\pi^-$	< 7 $\times 10^{-5}$	90%
Γ_{13} $3\pi^+ 3\pi^- 2\pi^0$	< 1.2 $\times 10^{-3}$	90%
Γ_{14} $3\pi^+ 3\pi^- K^+ K^-$	< 1.5 $\times 10^{-4}$	90%
Γ_{15} $3\pi^+ 3\pi^- K^+ K^- \pi^0$	< 7 $\times 10^{-4}$	90%
Γ_{16} $4\pi^+ 4\pi^-$	< 1.7 $\times 10^{-4}$	90%
Γ_{17} $4\pi^+ 4\pi^- 2\pi^0$	< 6 $\times 10^{-4}$	90%

$\chi_{b0}(2P)$ BRANCHING RATIOS

$\Gamma(\gamma \Upsilon(2S))/\Gamma_{total}$	CL%	DOCUMENT ID	TECN	COMMENT	Γ_1/Γ
1.38 ± 0.30 OUR AVERAGE					
1.31 ± 0.27 ± 0.13 -0.12		^{3,4} LEES	14M	BABR $\Upsilon(3S) \rightarrow \gamma\gamma\mu^+\mu^-$	
3.6 ± 1.6 ± 0.3		^{3,5} HEINTZ	92	CSB2 $e^+e^- \rightarrow \ell^+\ell^-\gamma\gamma$	
<2.8	90	⁶ LEES	11J	BABR $\Upsilon(3S) \rightarrow X\gamma$	
<8.9	90	⁷ CRAWFORD	92B	CLE2 $e^+e^- \rightarrow \ell^+\ell^-\gamma\gamma$	

³ Assuming $B(\Upsilon(2S) \rightarrow \mu^+\mu^-) = (1.93 \pm 0.17)\%$.
⁴ LEES 14M reports $[\Gamma(\chi_{b0}(2P) \rightarrow \gamma \Upsilon(2S))/\Gamma_{total}] \times [B(\Upsilon(3S) \rightarrow \gamma \chi_{b0}(2P))] = (7.7 \pm 1.6) \times 10^{-4}$ which we divide by our best value $B(\Upsilon(3S) \rightarrow \gamma \chi_{b0}(2P)) = (5.9 \pm 0.6) \times 10^{-2}$. Our first error is their experiment's error and our second error is the systematic error from using our best value.
⁵ Recalculated by us. HEINTZ 92 quotes $B(\Upsilon(3S) \rightarrow \gamma \chi_{b0}(2P)) \times B(\chi_{b0}(2P) \rightarrow \gamma \Upsilon(2S)) = (0.28 \pm 0.12 \pm 0.03)\%$ using $B(\Upsilon(2S) \rightarrow \mu^+\mu^-) = (1.44 \pm 0.10)\%$. Supersedes HEINTZ 91.
⁶ LEES 11J quotes a central value of $\Gamma(\chi_{b0}(2P) \rightarrow \gamma \Upsilon(2S))/\Gamma_{total} \times \Gamma(\Upsilon(3S) \rightarrow \gamma \chi_{b0}(2P)) = (-0.3 \pm 0.2_{-0.4}^{+0.5})\%$.
⁷ Using $B(\Upsilon(2S) \rightarrow \mu^+\mu^-) = (1.37 \pm 0.26)\%$, $B(\Upsilon(3S) \rightarrow \gamma \Upsilon(2S)) \times 2B(\Upsilon(2S) \rightarrow \mu^+\mu^-) < 1.19 \times 10^{-4}$, and $B(\Upsilon(3S) \rightarrow \chi_{b0}(2P)\gamma) = 0.049$.

Meson Particle Listings

 $\chi_{b0}(2P)$ $\Gamma(\gamma T(1S))/\Gamma_{\text{total}}$ Γ_2/Γ

VALUE (%)	CL%	DOCUMENT ID	TECN	COMMENT
0.38 ± 0.17 OUR AVERAGE				
0.36 ± 0.17 ± 0.03		8,9,10 LEES	14M BABR	$T(3S) \rightarrow \gamma\gamma\mu^+\mu^-$
0.9 ± 0.7 ± 0.1		9,11 HEINTZ	92 CSB2	$e^+e^- \rightarrow \ell^+\ell^-\gamma\gamma$

• • • We do not use the following data for averages, fits, limits, etc. • • •

<1.2	90	12 LEES	11J BABR	$T(3S) \rightarrow X\gamma$
<2.5	90	13 CRAWFORD	92B CLE2	$e^+e^- \rightarrow \ell^+\ell^-\gamma\gamma$

8 LEES 14M quotes $\Gamma(\chi_{b0}(2P) \rightarrow \gamma T(1S))/\Gamma_{\text{total}} \times \Gamma(T(3S) \rightarrow \gamma\chi_{b0}(2P))/\Gamma_{\text{total}} = (2.1 \pm 1.0) \times 10^{-4}$ combining the results from $T(3S) \rightarrow \gamma\gamma\mu^+\mu^-$ samples with and without photon conversions.

9 Assuming $B(T(1S) \rightarrow \mu^+\mu^-) = (2.48 \pm 0.05)\%$.

10 LEES 14M reports $[\Gamma(\chi_{b0}(2P) \rightarrow \gamma T(1S))/\Gamma_{\text{total}}] \times [B(T(3S) \rightarrow \gamma\chi_{b0}(2P))] = (2.1 \pm 1.0) \times 10^{-4}$ which we divide by our best value $B(T(3S) \rightarrow \gamma\chi_{b0}(2P)) = (5.9 \pm 0.6) \times 10^{-2}$. Our first error is their experiment's error and our second error is the systematic error from using our best value.

11 Recalculated by us. HEINTZ 92 quotes $B(T(3S) \rightarrow \gamma\chi_{b0}(2P)) \times B(\chi_{b0}(2P) \rightarrow \gamma T(1S)) = (0.05 \pm 0.04 \pm 0.01)\%$ using $B(T(1S) \rightarrow \mu^+\mu^-) = (2.57 \pm 0.05)\%$. Supersedes HEINTZ 91.

12 LEES 11J quotes a central value of $\Gamma(\chi_{b0}(2P) \rightarrow \gamma T(1S))/\Gamma_{\text{total}} \times \Gamma(T(3S) \rightarrow \gamma\chi_{b0}(2P))/\Gamma_{\text{total}} = (3.9 \pm 2.2^{+1.0}_{-0.6}) \times 10^{-4}$.

13 Using $B(T(1S) \rightarrow \mu^+\mu^-) = (2.57 \pm 0.07)\%$, $B(T(3S) \rightarrow \gamma\gamma T(1S)) \times 2 B(T(1S) \rightarrow \mu^+\mu^-) < 0.63 \times 10^{-4}$, and $B(T(3S) \rightarrow \chi_{b0}(2P)\gamma) = 0.049$.

 $\Gamma(D^0 X)/\Gamma_{\text{total}}$ Γ_3/Γ

VALUE	CL%	DOCUMENT ID	TECN	COMMENT
<8.2 × 10⁻²	90	14,15 BRIERE	08 CLEO	$T(3S) \rightarrow \gamma D^0 X$

14 For $p_{D^0} > 2.5$ GeV/c.

15 The authors also present their result as $(4.1 \pm 3.0 \pm 0.4) \times 10^{-2}$.

 $\Gamma(\pi^+\pi^-K^+K^-\pi^0)/\Gamma_{\text{total}}$ Γ_4/Γ

VALUE (units 10 ⁻⁴)	CL%	DOCUMENT ID	TECN	COMMENT
<0.34	90	16 ASNER	08A CLEO	$T(3S) \rightarrow \gamma\pi^+\pi^-K^+K^-\pi^0$

16 ASNER 08A reports $[\Gamma(\chi_{b0}(2P) \rightarrow \pi^+\pi^-K^+K^-\pi^0)/\Gamma_{\text{total}}] \times [B(T(3S) \rightarrow \gamma\chi_{b0}(2P))] < 2 \times 10^{-6}$ which we divide by our best value $B(T(3S) \rightarrow \gamma\chi_{b0}(2P)) = 5.9 \times 10^{-2}$.

 $\Gamma(2\pi^+\pi^-K^-K_S^0)/\Gamma_{\text{total}}$ Γ_5/Γ

VALUE (units 10 ⁻⁴)	CL%	DOCUMENT ID	TECN	COMMENT
<0.5	90	17 ASNER	08A CLEO	$T(3S) \rightarrow \gamma 2\pi^+\pi^-K^-K_S^0$

17 ASNER 08A reports $[\Gamma(\chi_{b0}(2P) \rightarrow 2\pi^+\pi^-K^-K_S^0)/\Gamma_{\text{total}}] \times [B(T(3S) \rightarrow \gamma\chi_{b0}(2P))] < 3 \times 10^{-6}$ which we divide by our best value $B(T(3S) \rightarrow \gamma\chi_{b0}(2P)) = 5.9 \times 10^{-2}$.

 $\Gamma(2\pi^+\pi^-K^-K_S^0 2\pi^0)/\Gamma_{\text{total}}$ Γ_6/Γ

VALUE (units 10 ⁻⁴)	CL%	DOCUMENT ID	TECN	COMMENT
<2.2	90	18 ASNER	08A CLEO	$T(3S) \rightarrow \gamma 2\pi^+\pi^-K^-2\pi^0$

18 ASNER 08A reports $[\Gamma(\chi_{b0}(2P) \rightarrow 2\pi^+\pi^-K^-K_S^0 2\pi^0)/\Gamma_{\text{total}}] \times [B(T(3S) \rightarrow \gamma\chi_{b0}(2P))] < 13 \times 10^{-6}$ which we divide by our best value $B(T(3S) \rightarrow \gamma\chi_{b0}(2P)) = 5.9 \times 10^{-2}$.

 $\Gamma(2\pi^+2\pi^-2\pi^0)/\Gamma_{\text{total}}$ Γ_7/Γ

VALUE (units 10 ⁻⁴)	CL%	DOCUMENT ID	TECN	COMMENT
<2.4	90	19 ASNER	08A CLEO	$T(3S) \rightarrow \gamma 2\pi^+2\pi^-2\pi^0$

19 ASNER 08A reports $[\Gamma(\chi_{b0}(2P) \rightarrow 2\pi^+2\pi^-2\pi^0)/\Gamma_{\text{total}}] \times [B(T(3S) \rightarrow \gamma\chi_{b0}(2P))] < 14 \times 10^{-6}$ which we divide by our best value $B(T(3S) \rightarrow \gamma\chi_{b0}(2P)) = 5.9 \times 10^{-2}$.

 $\Gamma(2\pi^+2\pi^-K^+K^-)/\Gamma_{\text{total}}$ Γ_8/Γ

VALUE (units 10 ⁻⁴)	CL%	DOCUMENT ID	TECN	COMMENT
<1.5	90	20 ASNER	08A CLEO	$T(3S) \rightarrow \gamma 2\pi^+2\pi^-K^+K^-$

20 ASNER 08A reports $[\Gamma(\chi_{b0}(2P) \rightarrow 2\pi^+2\pi^-K^+K^-)/\Gamma_{\text{total}}] \times [B(T(3S) \rightarrow \gamma\chi_{b0}(2P))] < 9 \times 10^{-6}$ which we divide by our best value $B(T(3S) \rightarrow \gamma\chi_{b0}(2P)) = 5.9 \times 10^{-2}$.

 $\Gamma(2\pi^+2\pi^-K^+K^-\pi^0)/\Gamma_{\text{total}}$ Γ_9/Γ

VALUE (units 10 ⁻⁴)	CL%	DOCUMENT ID	TECN	COMMENT
<2.2	90	21 ASNER	08A CLEO	$T(3S) \rightarrow \gamma 2\pi^+2\pi^-K^+K^-\pi^0$

21 ASNER 08A reports $[\Gamma(\chi_{b0}(2P) \rightarrow 2\pi^+2\pi^-K^+K^-\pi^0)/\Gamma_{\text{total}}] \times [B(T(3S) \rightarrow \gamma\chi_{b0}(2P))] < 13 \times 10^{-6}$ which we divide by our best value $B(T(3S) \rightarrow \gamma\chi_{b0}(2P)) = 5.9 \times 10^{-2}$.

 $\Gamma(2\pi^+2\pi^-K^+K^-2\pi^0)/\Gamma_{\text{total}}$ Γ_{10}/Γ

VALUE (units 10 ⁻⁴)	CL%	DOCUMENT ID	TECN	COMMENT
<11	90	22 ASNER	08A CLEO	$T(3S) \rightarrow \gamma 2\pi^+2\pi^-K^+K^-2\pi^0$

22 ASNER 08A reports $[\Gamma(\chi_{b0}(2P) \rightarrow 2\pi^+2\pi^-K^+K^-2\pi^0)/\Gamma_{\text{total}}] \times [B(T(3S) \rightarrow \gamma\chi_{b0}(2P))] < 63 \times 10^{-6}$ which we divide by our best value $B(T(3S) \rightarrow \gamma\chi_{b0}(2P)) = 5.9 \times 10^{-2}$.

 $\Gamma(3\pi^+2\pi^-K^-K_S^0\pi^0)/\Gamma_{\text{total}}$ Γ_{11}/Γ

VALUE (units 10 ⁻⁴)	CL%	DOCUMENT ID	TECN	COMMENT
<7	90	23 ASNER	08A CLEO	$T(3S) \rightarrow \gamma 3\pi^+2\pi^-K^-K_S^0\pi^0$

23 ASNER 08A reports $[\Gamma(\chi_{b0}(2P) \rightarrow 3\pi^+2\pi^-K^-K_S^0\pi^0)/\Gamma_{\text{total}}] \times [B(T(3S) \rightarrow \gamma\chi_{b0}(2P))] < 39 \times 10^{-6}$ which we divide by our best value $B(T(3S) \rightarrow \gamma\chi_{b0}(2P)) = 5.9 \times 10^{-2}$.

 $\Gamma(3\pi^+3\pi^-)/\Gamma_{\text{total}}$ Γ_{12}/Γ

VALUE (units 10 ⁻⁴)	CL%	DOCUMENT ID	TECN	COMMENT
<0.7	90	24 ASNER	08A CLEO	$T(3S) \rightarrow \gamma 3\pi^+3\pi^-$

24 ASNER 08A reports $[\Gamma(\chi_{b0}(2P) \rightarrow 3\pi^+3\pi^-)/\Gamma_{\text{total}}] \times [B(T(3S) \rightarrow \gamma\chi_{b0}(2P))] < 4 \times 10^{-6}$ which we divide by our best value $B(T(3S) \rightarrow \gamma\chi_{b0}(2P)) = 5.9 \times 10^{-2}$.

 $\Gamma(3\pi^+3\pi^-2\pi^0)/\Gamma_{\text{total}}$ Γ_{13}/Γ

VALUE (units 10 ⁻⁴)	CL%	DOCUMENT ID	TECN	COMMENT
<12	90	25 ASNER	08A CLEO	$T(3S) \rightarrow \gamma 3\pi^+3\pi^-2\pi^0$

25 ASNER 08A reports $[\Gamma(\chi_{b0}(2P) \rightarrow 3\pi^+3\pi^-2\pi^0)/\Gamma_{\text{total}}] \times [B(T(3S) \rightarrow \gamma\chi_{b0}(2P))] < 72 \times 10^{-6}$ which we divide by our best value $B(T(3S) \rightarrow \gamma\chi_{b0}(2P)) = 5.9 \times 10^{-2}$.

 $\Gamma(3\pi^+3\pi^-K^+K^-)/\Gamma_{\text{total}}$ Γ_{14}/Γ

VALUE (units 10 ⁻⁴)	CL%	DOCUMENT ID	TECN	COMMENT
<1.5	90	26 ASNER	08A CLEO	$T(3S) \rightarrow \gamma 3\pi^+3\pi^-K^+K^-$

26 ASNER 08A reports $[\Gamma(\chi_{b0}(2P) \rightarrow 3\pi^+3\pi^-K^+K^-)/\Gamma_{\text{total}}] \times [B(T(3S) \rightarrow \gamma\chi_{b0}(2P))] < 9 \times 10^{-6}$ which we divide by our best value $B(T(3S) \rightarrow \gamma\chi_{b0}(2P)) = 5.9 \times 10^{-2}$.

 $\Gamma(3\pi^+3\pi^-K^+K^-\pi^0)/\Gamma_{\text{total}}$ Γ_{15}/Γ

VALUE (units 10 ⁻⁴)	CL%	DOCUMENT ID	TECN	COMMENT
<7	90	27 ASNER	08A CLEO	$T(3S) \rightarrow \gamma 3\pi^+3\pi^-K^+K^-\pi^0$

27 ASNER 08A reports $[\Gamma(\chi_{b0}(2P) \rightarrow 3\pi^+3\pi^-K^+K^-\pi^0)/\Gamma_{\text{total}}] \times [B(T(3S) \rightarrow \gamma\chi_{b0}(2P))] < 43 \times 10^{-6}$ which we divide by our best value $B(T(3S) \rightarrow \gamma\chi_{b0}(2P)) = 5.9 \times 10^{-2}$.

 $\Gamma(4\pi^+4\pi^-)/\Gamma_{\text{total}}$ Γ_{16}/Γ

VALUE (units 10 ⁻⁴)	CL%	DOCUMENT ID	TECN	COMMENT
<1.7	90	28 ASNER	08A CLEO	$T(3S) \rightarrow \gamma 4\pi^+4\pi^-$

28 ASNER 08A reports $[\Gamma(\chi_{b0}(2P) \rightarrow 4\pi^+4\pi^-)/\Gamma_{\text{total}}] \times [B(T(3S) \rightarrow \gamma\chi_{b0}(2P))] < 10 \times 10^{-6}$ which we divide by our best value $B(T(3S) \rightarrow \gamma\chi_{b0}(2P)) = 5.9 \times 10^{-2}$.

 $\Gamma(4\pi^+4\pi^-2\pi^0)/\Gamma_{\text{total}}$ Γ_{17}/Γ

VALUE (units 10 ⁻⁴)	CL%	DOCUMENT ID	TECN	COMMENT
<6	90	29 ASNER	08A CLEO	$T(3S) \rightarrow \gamma 4\pi^+4\pi^-2\pi^0$

29 ASNER 08A reports $[\Gamma(\chi_{b0}(2P) \rightarrow 4\pi^+4\pi^-2\pi^0)/\Gamma_{\text{total}}] \times [B(T(3S) \rightarrow \gamma\chi_{b0}(2P))] < 38 \times 10^{-6}$ which we divide by our best value $B(T(3S) \rightarrow \gamma\chi_{b0}(2P)) = 5.9 \times 10^{-2}$.

 $\Gamma(\chi_{b0}(2P) \rightarrow \gamma T(1S))/\Gamma_{\text{total}} \times \Gamma(T(3S) \rightarrow \gamma\chi_{b0}(2P))/\Gamma_{\text{total}}$ $\Gamma_2/\Gamma \times \Gamma_{22}^{(3S)}/\Gamma T(3S)$

VALUE (units 10 ⁻⁴)	CL%	DOCUMENT ID	TECN	COMMENT
<8.2	90	30 LEES	11J BABR	$T(3S) \rightarrow X\gamma$

30 LEES 11J quotes a central value of $\Gamma(\chi_{b0}(2P) \rightarrow \gamma T(1S))/\Gamma_{\text{total}} \times \Gamma(T(3S) \rightarrow \gamma\chi_{b0}(2P))/\Gamma_{\text{total}} = (3.9 \pm 2.2^{+1.2}_{-0.6}) \times 10^{-4}$ and derives a 90% CL upper limit of $B(\chi_{b0}(2P) \rightarrow \gamma T(1S)) < 1.2\%$ using $B(T(3S) \rightarrow \gamma\chi_{b0}(2P)) = (5.9 \pm 0.6)\%$.

 $B(\chi_{b0}(2P) \rightarrow \gamma T(1S)) \times B(T(3S) \rightarrow \gamma\chi_{b0}(2P)) \times B(T(1S) \rightarrow \ell^+\ell^-)$

VALUE (units 10 ⁻⁹)	DOCUMENT ID	TECN	COMMENT
1.4 ± 0.9 OUR AVERAGE			

1.7 ^{+1.5} _{-1.4} ± 0.1	31 LEES	14M BABR	$T(3S) \rightarrow \gamma\gamma\mu^+\mu^-$
1.3 ± 1.0 ± 0.3	32 HEINTZ	92 CSB2	$T(3S) \rightarrow \gamma\gamma\ell^+\ell^-$

31 From a sample of $T(3S) \rightarrow \gamma\gamma\mu^+\mu^-$ with one converted photon.

32 Calculated by us. HEINTZ 92 quotes $B(T(3S) \rightarrow \gamma\chi_{b0}(2P)) \times B(\chi_{b0}(2P) \rightarrow \gamma T(1S)) = (0.05 \pm 0.04 \pm 0.01)\%$ using $B(T(1S) \rightarrow \mu^+\mu^-) = (2.57 \pm 0.05)\%$.

 $[B(\chi_{b0}(2P) \rightarrow \gamma T(1S)) \times B(T(3S) \rightarrow \gamma\chi_{b0}(2P))] / [B(\chi_{b1}(2P) \rightarrow \gamma T(1S)) \times B(T(3S) \rightarrow \gamma\chi_{b1}(2P))]$

VALUE (%)	DOCUMENT ID	TECN	COMMENT
1.71 ± 0.80	33 LEES	14M BABR	$T(3S) \rightarrow \gamma\gamma\mu^+\mu^-$

33 From a sample of $T(3S) \rightarrow \gamma\gamma\mu^+\mu^-$ without converted photons.

 $\Gamma(\chi_{b0}(2P) \rightarrow \gamma T(2S))/\Gamma_{\text{total}} \times \Gamma(T(3S) \rightarrow \gamma\chi_{b0}(2P))/\Gamma_{\text{total}}$ $\Gamma_1/\Gamma \times \Gamma_{22}^{(3S)}/\Gamma T(3S)$

VALUE (units 10 ⁻³)	CL%	DOCUMENT ID	TECN	COMMENT
<1.6	90	34 LEES	11J BABR	$T(3S) \rightarrow X\gamma$

34 LEES 11J quotes a central value of $\Gamma(\chi_{b0}(2P) \rightarrow \gamma T(2S))/\Gamma_{\text{total}} \times \Gamma(T(3S) \rightarrow \gamma\chi_{b0}(2P))/\Gamma_{\text{total}} = (-0.3 \pm 0.2^{+0.5}_{-0.4})\%$ and derives a 90% CL upper limit of $B(\chi_{b0}(2P) \rightarrow \gamma T(2S)) < 2.8\%$ using $B(T(3S) \rightarrow \gamma\chi_{b0}(2P)) = (5.9 \pm 0.6)\%$.

See key on page 1171

Meson Particle Listings

$\chi_{b0}(2P), \chi_{b1}(2P)$

$B(\chi_{b0}(2P) \rightarrow \gamma T(2S)) \times B(T(3S) \rightarrow \gamma \chi_{b0}(2P)) \times B(T(2S) \rightarrow \ell^+ \ell^-)$

VALUE (units 10^{-5})	DOCUMENT ID	TECN	COMMENT
4.4 ± 1.6 OUR AVERAGE			

6.6 ^{+4.9+2.0} _{-4.0-0.3}	³⁵ LEES	14M BABR	$T(3S) \rightarrow \gamma \gamma \mu^+ \mu^-$
4.0 ± 1.7 ± 0.3	³⁶ HEINTZ	92 CSB2	$T(3S) \rightarrow \gamma \gamma \ell^+ \ell^-$

³⁵ From a sample of $T(3S) \rightarrow \gamma \gamma \mu^+ \mu^-$ with one converted photon.
³⁶ Calculated by us. HEINTZ 92 quotes $B(T(3S) \rightarrow \gamma \chi_{b0}(2P)) \times B(\chi_{b0}(2P) \rightarrow \gamma T(2S)) = (0.28 \pm 0.12 \pm 0.03)\%$ using $B(T(2S) \rightarrow \mu^+ \mu^-) = (1.44 \pm 0.10)\%$.

$[B(\chi_{b0}(2P) \rightarrow \gamma T(2S)) \times B(T(3S) \rightarrow \gamma \chi_{b0}(2P))] / [B(\chi_{b1}(2P) \rightarrow \gamma T(2S)) \times B(T(3S) \rightarrow \gamma \chi_{b1}(2P))]$

VALUE (%)	DOCUMENT ID	TECN	COMMENT
3.31 ± 0.56	³⁷ LEES	14M BABR	$T(3S) \rightarrow \gamma \gamma \mu^+ \mu^-$

³⁷ From a sample of $T(3S) \rightarrow \gamma \gamma \mu^+ \mu^-$ without converted photons.

$\chi_{b0}(2P)$ REFERENCES

LEES	14M	PR D90 112010	J.P. Lees et al.	(BABAR Collab.)
LEES	11J	PR D84 072002	J.P. Lees et al.	(BABAR Collab.)
ASNER	08A	PR D78 091103	D.M. Asner et al.	(CLEO Collab.)
BRIERE	08	PR D78 092007	R.A. Briere et al.	(CLEO Collab.)
ARTUSO	05	PRL 94 032001	M. Artuso et al.	(CLEO Collab.)
CRAWFORD	92B	PL B294 139	G. Crawford et al.	(CLEO Collab.)
HEINTZ	92	PR D46 1928	U. Heintz et al.	(CUSB II Collab.)
HEINTZ	91	PRL 66 1563	U. Heintz et al.	(CUSB Collab.)
MORRISON	91	PRL 67 1696	R.J. Morrison et al.	(CLEO Collab.)
NARAIN	91	PRL 66 3113	M. Narain et al.	(CUSB Collab.)

$\chi_{b1}(2P)$ $J^G(J^{PC}) = 0^+(1^{++})$
 J needs confirmation.

Observed in radiative decay of the $T(3S)$, therefore $C = +$. Branching ratio requires E1 transition, M1 is strongly disfavored, therefore $P = +$.

$\chi_{b1}(2P)$ MASS

VALUE (MeV)	DOCUMENT ID
10295.46 ± 0.22 ± 0.50 OUR EVALUATION	From γ energy below, using $T(3S)$ mass = 10395.2 ± 0.5 MeV

$m_{\chi_{b1}(2P)} - m_{\chi_{b0}(2P)}$

VALUE (MeV)	DOCUMENT ID	TECN	COMMENT
23.5 ± 0.7 ± 0.7	¹ HEINTZ	92 CSB2	$e^+ e^- \rightarrow \gamma X, \ell^+ \ell^- \gamma \gamma$

¹ From the average photon energy for inclusive and exclusive events. Supersedes NARAIN 91.

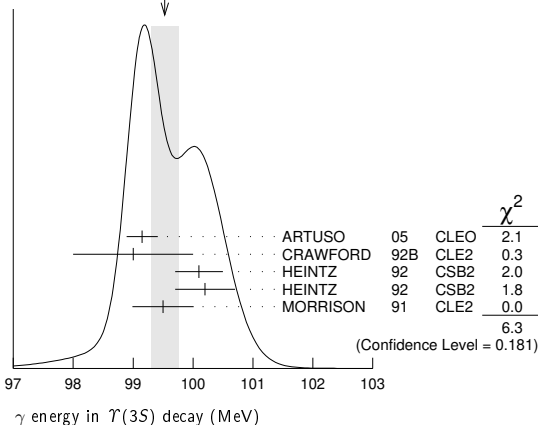
γ ENERGY IN $T(3S)$ DECAY

VALUE (MeV)	EVTS	DOCUMENT ID	TECN	COMMENT
99.26 ± 0.22 OUR EVALUATION				Treating systematic errors as correlated
99.53 ± 0.23 OUR AVERAGE				Error includes scale factor of 1.3. See the ideogram below.
99.15 ± 0.07 ± 0.25		ARTUSO 05	CLEO	$T(3S) \rightarrow \gamma X$
99 ± 1	169	CRAWFORD 92B	CLE2	$e^+ e^- \rightarrow \ell^+ \ell^- \gamma \gamma$
100.1 ± 0.4	11147	² HEINTZ 92	CSB2	$e^+ e^- \rightarrow \gamma X$
100.2 ± 0.5	223	³ HEINTZ 92	CSB2	$e^+ e^- \rightarrow \ell^+ \ell^- \gamma \gamma$
99.5 ± 0.1 ± 0.5	25759	MORRISON 91	CLE2	$e^+ e^- \rightarrow \gamma X$

² A systematic uncertainty on the energy scale of 0.9% not included. Supersedes NARAIN 91.

³ A systematic uncertainty on the energy scale of 0.9% not included. Supersedes HEINTZ 91.

WEIGHTED AVERAGE
 99.53 ± 0.23 (Error scaled by 1.3)



$\chi_{b1}(2P)$ DECAY MODES

Mode	Fraction (Γ_i/Γ)
Γ_1 $\omega T(1S)$	(1.63 ^{+0.40} _{-0.34}) %
Γ_2 $\gamma T(2S)$	(18.1 ± 1.9) %
Γ_3 $\gamma T(1S)$	(9.9 ± 1.0) %
Γ_4 $\pi \pi \chi_{b1}(1P)$	(9.1 ± 1.3) × 10 ⁻³
Γ_5 $D^0 X$	(8.8 ± 1.7) %
Γ_6 $\pi^+ \pi^- K^+ K^- \pi^0$	(3.1 ± 1.0) × 10 ⁻⁴
Γ_7 $2\pi^+ \pi^- K^- K_S^0$	(1.1 ± 0.5) × 10 ⁻⁴
Γ_8 $2\pi^+ \pi^- K^- K_S^0 2\pi^0$	(7.7 ± 3.2) × 10 ⁻⁴
Γ_9 $2\pi^+ 2\pi^- 2\pi^0$	(5.9 ± 2.0) × 10 ⁻⁴
Γ_{10} $2\pi^+ 2\pi^- K^+ K^-$	(10 ± 4) × 10 ⁻⁵
Γ_{11} $2\pi^+ 2\pi^- K^+ K^- \pi^0$	(5.5 ± 0.5) × 10 ⁻⁴
Γ_{12} $2\pi^+ 2\pi^- K^+ K^- 2\pi^0$	(10 ± 4) × 10 ⁻⁴
Γ_{13} $3\pi^+ 2\pi^- K^- K_S^0 \pi^0$	(6.7 ± 2.6) × 10 ⁻⁴
Γ_{14} $3\pi^+ 3\pi^-$	(1.2 ± 0.4) × 10 ⁻⁴
Γ_{15} $3\pi^+ 3\pi^- 2\pi^0$	(1.2 ± 0.4) × 10 ⁻³
Γ_{16} $3\pi^+ 3\pi^- K^+ K^-$	(2.0 ± 0.8) × 10 ⁻⁴
Γ_{17} $3\pi^+ 3\pi^- K^+ K^- \pi^0$	(6.1 ± 2.2) × 10 ⁻⁴
Γ_{18} $4\pi^+ 4\pi^-$	(1.7 ± 0.6) × 10 ⁻⁴
Γ_{19} $4\pi^+ 4\pi^- 2\pi^0$	(1.9 ± 0.7) × 10 ⁻³

$\chi_{b1}(2P)$ BRANCHING RATIOS

$\Gamma(\omega T(1S))/\Gamma_{total}$	Γ_1/Γ
---------------------------------------	-------------------

VALUE (units 10^{-2})	EVTS	DOCUMENT ID	TECN	COMMENT
1.63 ± 0.35 ± 0.16	32.6 ^{+6.9} _{-6.1}	⁴ CRONIN-HEN..04	CLE3	$T(3S) \rightarrow \gamma \omega T(1S)$

⁴ Using $B(T(3S) \rightarrow \gamma \chi_{b1}(2P)) = (11.3 \pm 0.6)\%$ and $B(T(1S) \rightarrow \ell^+ \ell^-) = 2 B(T(1S) \rightarrow \mu^+ \mu^-) = 2(2.48 \pm 0.06)\%$.

$\Gamma(\gamma T(2S))/\Gamma_{total}$	Γ_2/Γ
---------------------------------------	-------------------

VALUE	EVTS	DOCUMENT ID	TECN	COMMENT
0.181 ± 0.019 OUR AVERAGE				

0.211 ± 0.017 ± 0.019	5,6,7	LEES	14M BABR	$T(3S) \rightarrow \gamma \gamma \mu^+ \mu^-$
0.190 ± 0.018 ± 0.017	4,3k	⁸ LEES	11J BABR	$T(3S) \rightarrow X \gamma$
0.206 ± 0.035 ± 0.019	5,9	CRAWFORD 92B	CLE2	$e^+ e^- \rightarrow \ell^+ \ell^- \gamma \gamma$
0.132 ± 0.018 ± 0.012	5,10	HEINTZ	92 CSB2	$e^+ e^- \rightarrow \ell^+ \ell^- \gamma \gamma$

⁵ Assuming $B(T(2S) \rightarrow \mu^+ \mu^-) = (1.93 \pm 0.17)\%$.

⁶ LEES 14M quotes $\Gamma(\chi_{b1}(2P) \rightarrow \gamma T(2S))/\Gamma_{total} \times \Gamma(T(3S) \rightarrow \gamma \chi_{b1}(2P))/\Gamma_{total} = (2.66 \pm 0.22)\%$ combining the results from $T(3S) \rightarrow \gamma \gamma \mu^+ \mu^-$ samples with and without photon conversions.

⁷ LEES 14M reports $[\Gamma(\chi_{b1}(2P) \rightarrow \gamma T(2S))/\Gamma_{total}] \times [B(T(3S) \rightarrow \gamma \chi_{b1}(2P))]/\Gamma_{total} = (2.66 \pm 0.22) \times 10^{-2}$ which we divide by our best value $B(T(3S) \rightarrow \gamma \chi_{b1}(2P)) = (12.6 \pm 1.2) \times 10^{-2}$. Our first error is their experiment's error and our second error is the systematic error from using our best value.

⁸ LEES 11J reports $[\Gamma(\chi_{b1}(2P) \rightarrow \gamma T(2S))/\Gamma_{total}] \times [B(T(3S) \rightarrow \gamma \chi_{b1}(2P))]/\Gamma_{total} = (2.4 \pm 0.1 \pm 0.2) \times 10^{-2}$ which we divide by our best value $B(T(3S) \rightarrow \gamma \chi_{b1}(2P)) = (12.6 \pm 1.2) \times 10^{-2}$. Our first error is their experiment's error and our second error is the systematic error from using our best value.

⁹ CRAWFORD 92B quotes $B(T(3S) \rightarrow \gamma \chi_{b1}(2P)) \times B(\chi_{b1}(2P) \rightarrow \gamma T(2S)) \times 2 B(T(2S) \rightarrow \ell^+ \ell^-) = (10.23 \pm 1.20 \pm 1.26) 10^{-4}$.

¹⁰ Recalculated by us. HEINTZ 92 quotes $B(T(3S) \rightarrow \gamma \chi_{b1}(2P)) \times B(\chi_{b1}(2P) \rightarrow \gamma T(2S)) = (2.29 \pm 0.23 \pm 0.21) \%$ using $B(T(2S) \rightarrow \mu^+ \mu^-) = (1.44 \pm 0.10)\%$. Supersedes HEINTZ 91.

$\Gamma(\gamma T(1S))/\Gamma_{total}$	Γ_3/Γ
---------------------------------------	-------------------

VALUE	EVTS	DOCUMENT ID	TECN	COMMENT
0.099 ± 0.010 OUR AVERAGE				

0.107 ± 0.006 ± 0.010	11,12,13	LEES	14M BABR	$T(3S) \rightarrow \gamma \gamma \mu^+ \mu^-$
0.098 ± 0.005 ± 0.009	15k	¹⁴ LEES	11J BABR	$T(3S) \rightarrow X \gamma$
0.103 ± 0.023 ± 0.009	11,15	CRAWFORD 92B	CLE2	$e^+ e^- \rightarrow \ell^+ \ell^- \gamma \gamma$
0.075 ± 0.010 ± 0.007	11,16	HEINTZ	92 CSB2	$e^+ e^- \rightarrow \ell^+ \ell^- \gamma \gamma$

¹¹ Assuming $B(T(1S) \rightarrow \mu^+ \mu^-) = (2.48 \pm 0.05)\%$.

¹² LEES 14M quotes $\Gamma(\chi_{b1}(2P) \rightarrow \gamma T(1S))/\Gamma_{total} \times \Gamma(T(3S) \rightarrow \gamma \chi_{b1}(2P))/\Gamma_{total} = (13.48 \pm 0.72) \times 10^{-3}$ combining the results from samples of $T(3S) \rightarrow \gamma \gamma \mu^+ \mu^-$ with and without converted photons.

¹³ LEES 14M reports $[\Gamma(\chi_{b1}(2P) \rightarrow \gamma T(1S))/\Gamma_{total}] \times [B(T(3S) \rightarrow \gamma \chi_{b1}(2P))]/\Gamma_{total} = (13.48 \pm 0.72) \times 10^{-3}$ which we divide by our best value $B(T(3S) \rightarrow \gamma \chi_{b1}(2P)) = (12.6 \pm 1.2) \times 10^{-2}$. Our first error is their experiment's error and our second error is the systematic error from using our best value.

¹⁴ LEES 11J reports $[\Gamma(\chi_{b1}(2P) \rightarrow \gamma T(1S))/\Gamma_{total}] \times [B(T(3S) \rightarrow \gamma \chi_{b1}(2P))]/\Gamma_{total} = (12.4 \pm 0.3 \pm 0.6) \times 10^{-3}$ which we divide by our best value $B(T(3S) \rightarrow \gamma \chi_{b1}(2P)) = (12.6 \pm 1.2) \times 10^{-2}$. Our first error is their experiment's error and our second error is the systematic error from using our best value.

¹⁵ CRAWFORD 92B quotes $B(T(3S) \rightarrow \gamma \chi_{b1}(2P)) \times B(\chi_{b1}(2P) \rightarrow \gamma T(1S)) \times 2 B(T(1S) \rightarrow \ell^+ \ell^-) = (6.47 \pm 1.12 \pm 0.82) 10^{-4}$.

¹⁶ Recalculated by us. HEINTZ 92 quotes $B(T(3S) \rightarrow \gamma \chi_{b1}(2P)) \times B(\chi_{b1}(2P) \rightarrow \gamma T(1S)) = (0.91 \pm 0.11 \pm 0.06)\%$ using $B(T(1S) \rightarrow \mu^+ \mu^-) = (2.57 \pm 0.05)\%$. Supersedes HEINTZ 91.

Meson Particle Listings

 $\chi_{b1}(2P)$

$\Gamma(\pi\pi\chi_{b1}(1P))/\Gamma_{\text{total}}$		Γ_4/Γ	
VALUE (units 10^{-3})	EVTS	DOCUMENT ID	TECN COMMENT

9.1 ± 1.3 OUR AVERAGE

9.2 ± 1.1 ± 0.8	31k	17 LEES	11c BABR $e^+e^- \rightarrow \pi^+\pi^-X$
8.6 ± 2.3 ± 2.1		18 CAWFIELD	06 CLE3 $\Upsilon(3S) \rightarrow 2(\gamma\pi\ell)$
17 LEES 11c measures $B(\Upsilon(3S) \rightarrow \chi_{b1}(2P)X) \times B(\chi_{b1}(2P) \rightarrow \chi_{b1}(1P)\pi^+\pi^-) = (1.16 \pm 0.07 \pm 0.12) \times 10^{-3}$. We derive the value assuming $B(\Upsilon(3S) \rightarrow \chi_{b1}(2P)X) = B(\Upsilon(3S) \rightarrow \chi_{b1}(2P)\gamma) = (12.6 \pm 1.2) \times 10^{-2}$.			
18 CAWFIELD 06 quote $\Gamma(\chi_{b1}(2P) \rightarrow \pi\pi\chi_{b1}(1P)) = 0.83 \pm 0.22 \pm 0.08 \pm 0.19$ keV assuming 1-spin conservation, no D-wave contribution, $\Gamma(\chi_{b1}(2P)) = 96 \pm 16$ keV, and $\Gamma(\chi_{b2}(2P)) = 138 \pm 19$ keV.			

$\Gamma(D^0X)/\Gamma_{\text{total}}$		Γ_5/Γ	
VALUE (units 10^{-2})	EVTS	DOCUMENT ID	TECN COMMENT

8.8 ± 1.5 ± 0.8

8.8 ± 1.5 ± 0.8	2243	19 BRIERE	08 CLEO $\Upsilon(3S) \rightarrow \gamma D^0X$
19 For $p_{D^0} > 2.5$ GeV/c.			

$\Gamma(\pi^+\pi^-K^+K^-\pi^0)/\Gamma_{\text{total}}$		Γ_6/Γ	
VALUE (units 10^{-4})	EVTS	DOCUMENT ID	TECN COMMENT

3.1 ± 1.0 ± 0.3

3.1 ± 1.0 ± 0.3	30	20 ASNER	08a CLEO $\Upsilon(3S) \rightarrow \gamma\pi^+\pi^-K^+K^-\pi^0$
20 ASNER 08a reports $[\Gamma(\chi_{b1}(2P) \rightarrow \pi^+\pi^-K^+K^-\pi^0)/\Gamma_{\text{total}}] \times [B(\Upsilon(3S) \rightarrow \gamma\chi_{b1}(2P))] = (39 \pm 8 \pm 9) \times 10^{-6}$ which we divide by our best value $B(\Upsilon(3S) \rightarrow \gamma\chi_{b1}(2P)) = (12.6 \pm 1.2) \times 10^{-2}$. Our first error is their experiment's error and our second error is the systematic error from using our best value.			

$\Gamma(2\pi^+\pi^-K^-K_S^0)/\Gamma_{\text{total}}$		Γ_7/Γ	
VALUE (units 10^{-4})	EVTS	DOCUMENT ID	TECN COMMENT

1.1 ± 0.5 ± 0.1

1.1 ± 0.5 ± 0.1	10	21 ASNER	08a CLEO $\Upsilon(3S) \rightarrow \gamma 2\pi^+\pi^-K^-K_S^0$
21 ASNER 08a reports $[\Gamma(\chi_{b1}(2P) \rightarrow 2\pi^+\pi^-K^-K_S^0)/\Gamma_{\text{total}}] \times [B(\Upsilon(3S) \rightarrow \gamma\chi_{b1}(2P))] = (14 \pm 5 \pm 3) \times 10^{-6}$ which we divide by our best value $B(\Upsilon(3S) \rightarrow \gamma\chi_{b1}(2P)) = (12.6 \pm 1.2) \times 10^{-2}$. Our first error is their experiment's error and our second error is the systematic error from using our best value.			

$\Gamma(2\pi^+\pi^-K^-K_S^0 2\pi^0)/\Gamma_{\text{total}}$		Γ_8/Γ	
VALUE (units 10^{-4})	EVTS	DOCUMENT ID	TECN COMMENT

7.7 ± 3.1 ± 0.7

7.7 ± 3.1 ± 0.7	15	22 ASNER	08a CLEO $\Upsilon(3S) \rightarrow \gamma 2\pi^+\pi^-K^-2\pi^0$
22 ASNER 08a reports $[\Gamma(\chi_{b1}(2P) \rightarrow 2\pi^+\pi^-K^-K_S^0 2\pi^0)/\Gamma_{\text{total}}] \times [B(\Upsilon(3S) \rightarrow \gamma\chi_{b1}(2P))] = (97 \pm 30 \pm 26) \times 10^{-6}$ which we divide by our best value $B(\Upsilon(3S) \rightarrow \gamma\chi_{b1}(2P)) = (12.6 \pm 1.2) \times 10^{-2}$. Our first error is their experiment's error and our second error is the systematic error from using our best value.			

$\Gamma(2\pi^+2\pi^-2\pi^0)/\Gamma_{\text{total}}$		Γ_9/Γ	
VALUE (units 10^{-4})	EVTS	DOCUMENT ID	TECN COMMENT

5.9 ± 2.0 ± 0.5

5.9 ± 2.0 ± 0.5	36	23 ASNER	08a CLEO $\Upsilon(3S) \rightarrow \gamma 2\pi^+2\pi^-2\pi^0$
23 ASNER 08a reports $[\Gamma(\chi_{b1}(2P) \rightarrow 2\pi^+2\pi^-2\pi^0)/\Gamma_{\text{total}}] \times [B(\Upsilon(3S) \rightarrow \gamma\chi_{b1}(2P))] = (74 \pm 16 \pm 19) \times 10^{-6}$ which we divide by our best value $B(\Upsilon(3S) \rightarrow \gamma\chi_{b1}(2P)) = (12.6 \pm 1.2) \times 10^{-2}$. Our first error is their experiment's error and our second error is the systematic error from using our best value.			

$\Gamma(2\pi^+2\pi^-K^+K^-)/\Gamma_{\text{total}}$		Γ_{10}/Γ	
VALUE (units 10^{-4})	EVTS	DOCUMENT ID	TECN COMMENT

1.0 ± 0.4 ± 0.1

1.0 ± 0.4 ± 0.1	12	24 ASNER	08a CLEO $\Upsilon(3S) \rightarrow \gamma 2\pi^+2\pi^-K^+K^-$
24 ASNER 08a reports $[\Gamma(\chi_{b1}(2P) \rightarrow 2\pi^+2\pi^-K^+K^-)/\Gamma_{\text{total}}] \times [B(\Upsilon(3S) \rightarrow \gamma\chi_{b1}(2P))] = (12 \pm 4 \pm 3) \times 10^{-6}$ which we divide by our best value $B(\Upsilon(3S) \rightarrow \gamma\chi_{b1}(2P)) = (12.6 \pm 1.2) \times 10^{-2}$. Our first error is their experiment's error and our second error is the systematic error from using our best value.			

$\Gamma(2\pi^+2\pi^-K^+K^-\pi^0)/\Gamma_{\text{total}}$		Γ_{11}/Γ	
VALUE (units 10^{-4})	EVTS	DOCUMENT ID	TECN COMMENT

5.5 ± 1.7 ± 0.5

5.5 ± 1.7 ± 0.5	38	25 ASNER	08a CLEO $\Upsilon(3S) \rightarrow \gamma 2\pi^+2\pi^-K^+K^-\pi^0$
25 ASNER 08a reports $[\Gamma(\chi_{b1}(2P) \rightarrow 2\pi^+2\pi^-K^+K^-\pi^0)/\Gamma_{\text{total}}] \times [B(\Upsilon(3S) \rightarrow \gamma\chi_{b1}(2P))] = (69 \pm 13 \pm 17) \times 10^{-6}$ which we divide by our best value $B(\Upsilon(3S) \rightarrow \gamma\chi_{b1}(2P)) = (12.6 \pm 1.2) \times 10^{-2}$. Our first error is their experiment's error and our second error is the systematic error from using our best value.			

$\Gamma(2\pi^+2\pi^-K^+K^-2\pi^0)/\Gamma_{\text{total}}$		Γ_{12}/Γ	
VALUE (units 10^{-4})	EVTS	DOCUMENT ID	TECN COMMENT

9.6 ± 3.5 ± 0.9

9.6 ± 3.5 ± 0.9	27	26 ASNER	08a CLEO $\Upsilon(3S) \rightarrow \gamma 2\pi^+2\pi^-K^+K^-2\pi^0$
26 ASNER 08a reports $[\Gamma(\chi_{b1}(2P) \rightarrow 2\pi^+2\pi^-K^+K^-2\pi^0)/\Gamma_{\text{total}}] \times [B(\Upsilon(3S) \rightarrow \gamma\chi_{b1}(2P))] = (121 \pm 29 \pm 33) \times 10^{-6}$ which we divide by our best value $B(\Upsilon(3S) \rightarrow \gamma\chi_{b1}(2P)) = (12.6 \pm 1.2) \times 10^{-2}$. Our first error is their experiment's error and our second error is the systematic error from using our best value.			

$\Gamma(3\pi^+2\pi^-K^-K_S^0\pi^0)/\Gamma_{\text{total}}$		Γ_{13}/Γ	
VALUE (units 10^{-4})	EVTS	DOCUMENT ID	TECN COMMENT

6.7 ± 2.5 ± 0.6

6.7 ± 2.5 ± 0.6	17	27 ASNER	08a CLEO $\Upsilon(3S) \rightarrow \gamma 3\pi^+2\pi^-K^-K_S^0\pi^0$
27 ASNER 08a reports $[\Gamma(\chi_{b1}(2P) \rightarrow 3\pi^+2\pi^-K^-K_S^0\pi^0)/\Gamma_{\text{total}}] \times [B(\Upsilon(3S) \rightarrow \gamma\chi_{b1}(2P))] = (85 \pm 23 \pm 22) \times 10^{-6}$ which we divide by our best value $B(\Upsilon(3S) \rightarrow \gamma\chi_{b1}(2P)) = (12.6 \pm 1.2) \times 10^{-2}$. Our first error is their experiment's error and our second error is the systematic error from using our best value.			

$\Gamma(3\pi^+3\pi^-)/\Gamma_{\text{total}}$		Γ_{14}/Γ	
VALUE (units 10^{-4})	EVTS	DOCUMENT ID	TECN COMMENT

1.2 ± 0.4 ± 0.1

1.2 ± 0.4 ± 0.1	18	28 ASNER	08a CLEO $\Upsilon(3S) \rightarrow \gamma 3\pi^+3\pi^-$
28 ASNER 08a reports $[\Gamma(\chi_{b1}(2P) \rightarrow 3\pi^+3\pi^-)/\Gamma_{\text{total}}] \times [B(\Upsilon(3S) \rightarrow \gamma\chi_{b1}(2P))] = (15 \pm 4 \pm 3) \times 10^{-6}$ which we divide by our best value $B(\Upsilon(3S) \rightarrow \gamma\chi_{b1}(2P)) = (12.6 \pm 1.2) \times 10^{-2}$. Our first error is their experiment's error and our second error is the systematic error from using our best value.			

$\Gamma(3\pi^+3\pi^-2\pi^0)/\Gamma_{\text{total}}$		Γ_{15}/Γ	
VALUE (units 10^{-4})	EVTS	DOCUMENT ID	TECN COMMENT

12 ± 4 ± 1

12 ± 4 ± 1	44	29 ASNER	08a CLEO $\Upsilon(3S) \rightarrow \gamma 3\pi^+3\pi^-2\pi^0$
29 ASNER 08a reports $[\Gamma(\chi_{b1}(2P) \rightarrow 3\pi^+3\pi^-2\pi^0)/\Gamma_{\text{total}}] \times [B(\Upsilon(3S) \rightarrow \gamma\chi_{b1}(2P))] = (150 \pm 30 \pm 40) \times 10^{-6}$ which we divide by our best value $B(\Upsilon(3S) \rightarrow \gamma\chi_{b1}(2P)) = (12.6 \pm 1.2) \times 10^{-2}$. Our first error is their experiment's error and our second error is the systematic error from using our best value.			

$\Gamma(3\pi^+3\pi^-K^+K^-)/\Gamma_{\text{total}}$		Γ_{16}/Γ	
VALUE (units 10^{-4})	EVTS	DOCUMENT ID	TECN COMMENT

2.0 ± 0.7 ± 0.2

2.0 ± 0.7 ± 0.2	16	30 ASNER	08a CLEO $\Upsilon(3S) \rightarrow \gamma 3\pi^+3\pi^-K^+K^-$
30 ASNER 08a reports $[\Gamma(\chi_{b1}(2P) \rightarrow 3\pi^+3\pi^-K^+K^-)/\Gamma_{\text{total}}] \times [B(\Upsilon(3S) \rightarrow \gamma\chi_{b1}(2P))] = (25 \pm 7 \pm 6) \times 10^{-6}$ which we divide by our best value $B(\Upsilon(3S) \rightarrow \gamma\chi_{b1}(2P)) = (12.6 \pm 1.2) \times 10^{-2}$. Our first error is their experiment's error and our second error is the systematic error from using our best value.			

$\Gamma(3\pi^+3\pi^-K^+K^-2\pi^0)/\Gamma_{\text{total}}$		Γ_{17}/Γ	
VALUE (units 10^{-4})	EVTS	DOCUMENT ID	TECN COMMENT

6.1 ± 2.1 ± 0.6

6.1 ± 2.1 ± 0.6	25	31 ASNER	08a CLEO $\Upsilon(3S) \rightarrow \gamma 3\pi^+3\pi^-K^+K^-2\pi^0$
31 ASNER 08a reports $[\Gamma(\chi_{b1}(2P) \rightarrow 3\pi^+3\pi^-K^+K^-2\pi^0)/\Gamma_{\text{total}}] \times [B(\Upsilon(3S) \rightarrow \gamma\chi_{b1}(2P))] = (77 \pm 17 \pm 21) \times 10^{-6}$ which we divide by our best value $B(\Upsilon(3S) \rightarrow \gamma\chi_{b1}(2P)) = (12.6 \pm 1.2) \times 10^{-2}$. Our first error is their experiment's error and our second error is the systematic error from using our best value.			

$\Gamma(4\pi^+4\pi^-)/\Gamma_{\text{total}}$		Γ_{18}/Γ	
VALUE (units 10^{-4})	EVTS	DOCUMENT ID	TECN COMMENT

1.7 ± 0.6 ± 0.2

1.7 ± 0.6 ± 0.2	16	32 ASNER	08a CLEO $\Upsilon(3S) \rightarrow \gamma 4\pi^+4\pi^-$
32 ASNER 08a reports $[\Gamma(\chi_{b1}(2P) \rightarrow 4\pi^+4\pi^-)/\Gamma_{\text{total}}] \times [B(\Upsilon(3S) \rightarrow \gamma\chi_{b1}(2P))] = (22 \pm 6 \pm 5) \times 10^{-6}$ which we divide by our best value $B(\Upsilon(3S) \rightarrow \gamma\chi_{b1}(2P)) = (12.6 \pm 1.2) \times 10^{-2}$. Our first error is their experiment's error and our second error is the systematic error from using our best value.			

$\Gamma(4\pi^+4\pi^-2\pi^0)/\Gamma_{\text{total}}$		Γ_{19}/Γ	
VALUE (units 10^{-4})	EVTS	DOCUMENT ID	TECN COMMENT

19 ± 7 ± 2

19 ± 7 ± 2	41	33 ASNER	08a CLEO $\Upsilon(3S) \rightarrow \gamma 4\pi^+4\pi^-2\pi^0$
33 ASNER 08a reports $[\Gamma(\chi_{b1}(2P) \rightarrow 4\pi^+4\pi^-2\pi^0)/\Gamma_{\text{total}}] \times [B(\Upsilon(3S) \rightarrow \gamma\chi_{b1}(2P))] = (241 \pm 47 \pm 72) \times 10^{-6}$ which we divide by our best value $B(\Upsilon(3S) \rightarrow \gamma\chi_{b1}(2P)) = (12.6 \pm 1.2) \times 10^{-2}$. Our first error is their experiment's error and our second error is the systematic error from using our best value.			

 $\chi_{b1}(2P)$ Cross-Particle Branching Ratios

$\Gamma(\chi_{b1}(2P) \rightarrow \gamma\Upsilon(1S))/\Gamma_{\text{total}} \times \Gamma(\Upsilon(3S) \rightarrow \gamma\chi_{b1}(2P))/\Gamma_{\text{total}}$		$\Gamma_3/\Gamma \times \Gamma_{21}^{(3S)}/\Gamma\Upsilon(3S)$	
VALUE (units 10^{-3})	EVTS	DOCUMENT ID	TECN COMMENT

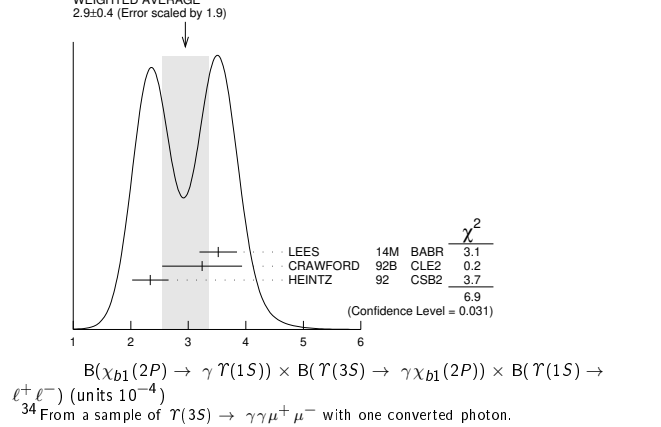
12.4 ± 0.3 ± 0.6

12.4 ± 0.3 ± 0.6	15k	LEES	11j BABR $\Upsilon(3S) \rightarrow X\gamma$
------------------	-----	------	---

$B(\chi_{b1}(2P) \rightarrow \gamma\Upsilon(1S)) \times B(\Upsilon(3S) \rightarrow \gamma\chi_{b1}(2P)) \times B(\Upsilon(1S) \rightarrow \ell^+\ell^-)$		$\Gamma_{21}^{(3S)}/\Gamma\Upsilon(3S)$	
VALUE (units 10^{-4})	EVTS	DOCUMENT ID	TECN COMMENT

2.9 ± 0.4 OUR AVERAGE

3.52 ± 0.28 ± 0.17		34 LEES	14M BABR $\Upsilon(3S) \rightarrow \gamma\gamma\mu^+\mu^-$
0.27 - 0.18			
3.24 ± 0.56 ± 0.41	58	35 CRAWFORD	92B CLE2 $\Upsilon(3S) \rightarrow \gamma\gamma\ell^+\ell^-$
2.34 ± 0.28 ± 0.15		36 HEINTZ	92 CSB2 $\Upsilon(3S) \rightarrow \gamma\gamma\ell^+\ell^-$



See key on page 1171

Meson Particle Listings

$\chi_{b1}(2P)$, $h_b(2P)$, $\chi_{b2}(2P)$

³⁵ CRAWFORD 92b quotes $2 \times B(\Upsilon(3S) \rightarrow \gamma \chi_{bJ}(2P)) B(\chi_{bJ}(2P) \rightarrow \gamma \Upsilon(nS))$
 $B(\Upsilon(nS) \rightarrow \ell^+ \ell^-)$.

³⁶ Calculated by us. HEINTZ 92 quotes $B(\Upsilon(3S) \rightarrow \gamma \chi_{b1}(2P)) \times B(\chi_{b1}(2P) \rightarrow \gamma \Upsilon(1S)) = (0.91 \pm 0.11 \pm 0.06)\%$ using $B(\Upsilon(1S) \rightarrow \mu^+ \mu^-) = (2.57 \pm 0.05)\%$.

$$\Gamma(\chi_{b1}(2P) \rightarrow \gamma \Upsilon(2S))/\Gamma_{\text{total}} \times \Gamma(\Upsilon(3S) \rightarrow \gamma \chi_{b1}(2P))/\Gamma_{\text{total}} = \Gamma_2/\Gamma \times \Gamma_{21}^{\Upsilon(3S)}/\Gamma \Upsilon(3S)$$

VALUE (units 10^{-2})	EVTS	DOCUMENT ID	TECN	COMMENT
2.4 ± 0.1 ± 0.2	4.3k	LEES	11j	BABR $\Upsilon(3S) \rightarrow X \gamma$

$$B(\chi_{b1}(2P) \rightarrow \gamma \Upsilon(2S)) \times B(\Upsilon(3S) \rightarrow \gamma \chi_{b1}(2P)) \times B(\Upsilon(2S) \rightarrow \ell^+ \ell^-)$$

VALUE (units 10^{-4})	EVTS	DOCUMENT ID	TECN	COMMENT
3.8 ± 0.6 OUR AVERAGE				Error includes scale factor of 1.8. See the ideogram below.

4.95 ^{+0.75} _{-0.70} ± 0.24		37 LEES	14M	BABR $\Upsilon(3S) \rightarrow \gamma \gamma \mu^+ \mu^-$
5.12 ± 0.60 ± 0.63	111	38 CRAWFORD	92B	CLE2 $\Upsilon(3S) \rightarrow \gamma \gamma \ell^+ \ell^-$
3.30 ± 0.33 ± 0.20		39 HEINTZ	92	CSB2 $\Upsilon(3S) \rightarrow \gamma \gamma \ell^+ \ell^-$

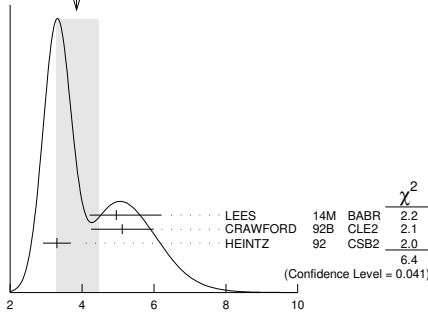
³⁷ From a sample of $\Upsilon(3S) \rightarrow \gamma \gamma \mu^+ \mu^-$ with one converted photon.

³⁸ CRAWFORD 92b quotes $2 \times B(\Upsilon(3S) \rightarrow \gamma \chi_{bJ}(2P)) B(\chi_{bJ}(2P) \rightarrow \gamma \Upsilon(nS))$

$B(\Upsilon(nS) \rightarrow \ell^+ \ell^-)$.

³⁹ Calculated by us. HEINTZ 92 quotes $B(\Upsilon(3S) \rightarrow \gamma \chi_{b1}(2P)) \times B(\chi_{b1}(2P) \rightarrow \gamma \Upsilon(2S)) = (2.29 \pm 0.23 \pm 0.21)\%$ using $B(\Upsilon(2S) \rightarrow \mu^+ \mu^-) = (1.44 \pm 0.10)\%$.

WEIGHTED AVERAGE
3.8 ± 0.6 (Error scaled by 1.8)



$$B(\chi_{b1}(2P) \rightarrow \gamma \Upsilon(2S)) \times B(\Upsilon(3S) \rightarrow \gamma \chi_{b1}(2P)) \times B(\Upsilon(2S) \rightarrow \ell^+ \ell^-)$$

(units 10^{-4})

$$B(\chi_{b1}(2P) \rightarrow \chi_{b1}(1P) \pi^+ \pi^-) \times B(\Upsilon(3S) \rightarrow \chi_{b1}(2P) X)$$

VALUE (units 10^{-3})	EVTS	DOCUMENT ID	TECN	COMMENT
1.16 ± 0.07 ± 0.12	31k	LEES	11c	BABR $e^+ e^- \rightarrow \pi^+ \pi^- X$

$$B(\chi_{b2}(2P) \rightarrow \rho X + \bar{\rho} X)/B(\chi_{b1}(2P) \rightarrow \rho X + \bar{\rho} X)$$

VALUE	DOCUMENT ID	TECN	COMMENT
1.109 ± 0.007 ± 0.040	BRIERE	07	CLEO $\Upsilon(3S) \rightarrow \gamma \chi_{bJ}(2P)$

$$B(\chi_{b0}(2P) \rightarrow \rho X + \bar{\rho} X)/B(\chi_{b1}(2P) \rightarrow \rho X + \bar{\rho} X)$$

VALUE	DOCUMENT ID	TECN	COMMENT
1.082 ± 0.025 ± 0.060	BRIERE	07	CLEO $\Upsilon(3S) \rightarrow \gamma \chi_{bJ}(2P)$

$\chi_{b1}(2P)$ REFERENCES

LEES	14M	PR D90 112010	J.P. Lees et al.	(BABAR Collab.)
LEES	11C	PR D84 011104	J.P. Lees et al.	(BABAR Collab.)
LEES	11J	PR D84 072002	J.P. Lees et al.	(BABAR Collab.)
ASNER	08A	PR D78 091103	D.M. Asner et al.	(CLEO Collab.)
BRIERE	08	PR D78 092007	R.A. Briere et al.	(CLEO Collab.)
BRIERE	07	PR D76 012005	R.A. Briere et al.	(CLEO Collab.)
CAWLFIELD	06	PR D73 012003	C. Cawfield et al.	(CLEO Collab.)
ARTUSO	05	PRL 94 032001	M. Artuso et al.	(CLEO Collab.)
CRONIN-HENNESSY	04	PRL 92 222002	D. Cronin-Hennessy et al.	(CLEO Collab.)
CRAWFORD	92B	PL B294 139	G. Crawford et al.	(CLEO Collab.)
HEINTZ	92	PR D46 1928	U. Heintz et al.	(CUSP II Collab.)
HEINTZ	91	PRL 66 1563	U. Heintz et al.	(CUSB Collab.)
MORRISON	91	PRL 67 1696	R.J. Morrison et al.	(CLEO Collab.)
NARAIN	91	PRL 66 3113	M. Narain et al.	(CUSB Collab.)

$h_b(2P)$

$$J^{G(J^{PC})} = 0^-(1^{+-})$$

Quantum numbers are quark model predictions. $C = -$ established by $\eta_b \gamma$ decay.

$h_b(2P)$ MASS

VALUE (MeV)	EVTS	DOCUMENT ID	TECN	COMMENT
10259.8 ± 0.5 ± 1.1	90k	1 MIZUK	12	BELL $e^+ e^- \rightarrow \pi^+ \pi^-$ hadrons

••• We do not use the following data for averages, fits, limits, etc. •••

10259.8 ± 0.6 ^{+1.4} _{-1.0}	83.9k	2 ADACHI	12	BELL 10.86 $e^+ e^- \rightarrow \pi^+ \pi^-$ MM
---	-------	----------	----	---

¹ Observed with 9 standard deviations significance.
² Superseded by MIZUK 12.

$h_b(2P)$ DECAY MODES

Mode	Fraction (Γ_i/Γ)
Γ_1 hadrons	not seen
Γ_2 $\eta_b(1S) \gamma$	(22 ± 5) %
Γ_3 $\eta_b(2S) \gamma$	(48 ± 13) %

$h_b(2P)$ BRANCHING RATIOS

$\Gamma(\text{hadrons})/\Gamma_{\text{total}}$	DOCUMENT ID	TECN	COMMENT	Γ_1/Γ
not seen	83.9k	ADACHI	12	BELL 10.86 $e^+ e^- \rightarrow \pi^+ \pi^-$ MM

$\Gamma(\eta_b(1S) \gamma)/\Gamma_{\text{total}}$	DOCUMENT ID	TECN	COMMENT	Γ_2/Γ
22.3 ± 3.8^{+3.1}_{-3.3}	10k	MIZUK	12	BELL $e^+ e^- \rightarrow (\gamma) \pi^+ \pi^-$ hadrons

$\Gamma(\eta_b(2S) \gamma)/\Gamma_{\text{total}}$	DOCUMENT ID	TECN	COMMENT	Γ_3/Γ
47.5 ± 10.5^{+6.8}_{-7.7}	26k	MIZUK	12	BELL $e^+ e^- \rightarrow (\gamma) \pi^+ \pi^-$ hadrons

$h_b(2P)$ REFERENCES

ADACHI	12	PRL 108 032001	I. Adachi et al.	(BELLE Collab.)
MIZUK	12	PRL 109 232002	R. Mizuk et al.	(BELLE Collab.)

$\chi_{b2}(2P)$

$$J^{G(J^{PC})} = 0^+(2^{+-})$$

J needs confirmation.

Observed in radiative decay of the $\Upsilon(3S)$, therefore $C = +$. Branching ratio requires E1 transition, M1 is strongly disfavored, therefore $P = +$.

$\chi_{b2}(2P)$ MASS

VALUE (MeV)	DOCUMENT ID
10268.65 ± 0.22 ± 0.50 OUR EVALUATION	
10355.2 ± 0.5 MeV	From γ energy below, using $\Upsilon(3S)$ mass =

$m_{\chi_{b2}(2P)} - m_{\chi_{b1}(2P)}$

VALUE (MeV)	DOCUMENT ID	TECN	COMMENT
13.10 ± 0.24 OUR AVERAGE			
12.3 ± 2.6 ± 0.6	¹ AAIJ	14Bg	LHCB $p p \rightarrow \gamma \mu^+ \mu^- X$
13.04 ± 0.26	LEES	14M	BABR $\Upsilon(3S) \rightarrow \gamma \gamma \mu^+ \mu^-$
13.5 ± 0.4 ± 0.5	² HEINTZ	92	CSB2 $e^+ e^- \rightarrow \gamma X, \ell^+ \ell^- \gamma \gamma$

¹ From the $\chi_{bJ}(2P) \rightarrow \Upsilon(1S) \gamma$ transition.

² From the average photon energy for inclusive and exclusive events. Supersedes NARAIN 91.

γ ENERGY IN $\Upsilon(3S)$ DECAY

VALUE (MeV)	EVTS	DOCUMENT ID	TECN	COMMENT
86.19 ± 0.22 OUR EVALUATION				Treating systematic errors as correlated
86.40 ± 0.18 OUR AVERAGE				

86.04 ± 0.06 ± 0.27		ARTUSO	05	CLEO $\Upsilon(3S) \rightarrow \gamma X$
86 ± 1	101	CRAWFORD	92B	CLE2 $e^+ e^- \rightarrow \ell^+ \ell^- \gamma \gamma$
86.7 ± 0.4	10319	³ HEINTZ	92	CSB2 $e^+ e^- \rightarrow \gamma X$
86.9 ± 0.4	157	⁴ HEINTZ	92	CSB2 $e^+ e^- \rightarrow \ell^+ \ell^- \gamma \gamma$
86.4 ± 0.1 ± 0.4	30741	MORRISON	91	CLE2 $e^+ e^- \rightarrow \gamma X$

³ A systematic uncertainty on the energy scale of 0.9% not included. Supersedes NARAIN 91.

⁴ A systematic uncertainty on the energy scale of 0.9% not included. Supersedes HEINTZ 91.

$\chi_{b2}(2P)$ DECAY MODES

Mode	Fraction (Γ_i/Γ)	Confidence level
Γ_1 $\omega \Upsilon(1S)$	(1.10 ^{+0.34} _{-0.30}) %	
Γ_2 $\gamma \Upsilon(2S)$	(8.9 ± 1.2) %	
Γ_3 $\gamma \Upsilon(1S)$	(6.6 ± 0.8) %	
Γ_4 $\pi \pi \chi_{b2}(1P)$	(5.1 ± 0.9) × 10 ⁻³	
Γ_5 $D^0 X$	< 2.4 %	90%
Γ_6 $\pi^+ \pi^- K^+ K^- \pi^0$	< 1.1 × 10 ⁻⁴	90%
Γ_7 $2\pi^+ \pi^- K^- K_S^0$	< 9 × 10 ⁻⁵	90%
Γ_8 $2\pi^+ \pi^- K^- K_S^0 2\pi^0$	< 7 × 10 ⁻⁴	90%
Γ_9 $2\pi^+ 2\pi^- 2\pi^0$	(3.9 ± 1.6) × 10 ⁻⁴	

Meson Particle Listings

 $\chi_{b2}(2P)$

Γ_{10}	$2\pi^+ 2\pi^- K^+ K^-$	$(9 \pm 4) \times 10^{-5}$		
Γ_{11}	$2\pi^+ 2\pi^- K^+ K^- \pi^0$	$(2.4 \pm 1.1) \times 10^{-4}$		
Γ_{12}	$2\pi^+ 2\pi^- K^+ K^- 2\pi^0$	$(4.7 \pm 2.3) \times 10^{-4}$		
Γ_{13}	$3\pi^+ 2\pi^- K^- K_S^0 \pi^0$	$< 4 \times 10^{-4}$	90%	
Γ_{14}	$3\pi^+ 3\pi^-$	$(9 \pm 4) \times 10^{-5}$		
Γ_{15}	$3\pi^+ 3\pi^- 2\pi^0$	$(1.2 \pm 0.4) \times 10^{-3}$		
Γ_{16}	$3\pi^+ 3\pi^- K^+ K^-$	$(1.4 \pm 0.7) \times 10^{-4}$		
Γ_{17}	$3\pi^+ 3\pi^- K^+ K^- \pi^0$	$(4.2 \pm 1.7) \times 10^{-4}$		
Γ_{18}	$4\pi^+ 4\pi^-$	$(9 \pm 5) \times 10^{-5}$		
Γ_{19}	$4\pi^+ 4\pi^- 2\pi^0$	$(1.3 \pm 0.5) \times 10^{-3}$		

 $\chi_{b2}(2P)$ BRANCHING RATIOS

$\Gamma(\omega \mathcal{T}(1S))/\Gamma_{\text{total}}$					Γ_1/Γ
VALUE (units 10^{-2})	EVTS	DOCUMENT ID	TECN	COMMENT	
$1.10 \pm 0.32 \pm 0.11$ $-0.28 - 0.10$	20.1 ^{+5.8} _{-5.1}	5 CRONIN-HEN..04	CLE3	$\mathcal{T}(3S) \rightarrow \gamma \omega \mathcal{T}(1S)$	
				⁵ Using $B(\mathcal{T}(3S) \rightarrow \gamma \chi_{b2}(2P)) = (11.4 \pm 0.8)\%$ and $B(\mathcal{T}(1S) \rightarrow \ell^+ \ell^-) = 2 B(\mathcal{T}(1S) \rightarrow \mu^+ \mu^-) = 2(2.48 \pm 0.06)\%$.	

$\Gamma(\gamma \mathcal{T}(2S))/\Gamma_{\text{total}}$					Γ_2/Γ
VALUE	EVTS	DOCUMENT ID	TECN	COMMENT	
0.089 ± 0.012 OUR AVERAGE					
$0.085 \pm 0.010 \pm 0.010$	6,7,8	LEES	14M	BABR $\mathcal{T}(3S) \rightarrow \gamma \gamma \mu^+ \mu^-$	
$0.084 \pm 0.011 \pm 0.010$	2.5k	9 LEES	11J	BABR $\mathcal{T}(3S) \rightarrow X \gamma$	
$0.096 \pm 0.022 \pm 0.012$	7,10	CRAWFORD	92B	CLE2 $e^+ e^- \rightarrow \ell^+ \ell^- \gamma \gamma$	
$0.102 \pm 0.016 \pm 0.013$	7,11	HEINTZ	92	CSB2 $e^+ e^- \rightarrow \ell^+ \ell^- \gamma \gamma$	
				⁶ LEES 14M quotes $\Gamma(\chi_{b2}(2P) \rightarrow \gamma \mathcal{T}(2S))/\Gamma_{\text{total}} \times \Gamma(\mathcal{T}(3S) \rightarrow \gamma \chi_{b2}(2P))/\Gamma_{\text{total}} = (1.12 \pm 0.13)\%$ combining the results from samples of $\mathcal{T}(3S) \rightarrow \gamma \gamma \mu^+ \mu^-$ with and without converted photons.	
				⁷ Assuming $B(\mathcal{T}(2S) \rightarrow \mu^+ \mu^-) = (1.93 \pm 0.17)\%$.	
				⁸ LEES 14M reports $[\Gamma(\chi_{b2}(2P) \rightarrow \gamma \mathcal{T}(2S))/\Gamma_{\text{total}}] \times [B(\mathcal{T}(3S) \rightarrow \gamma \chi_{b2}(2P))] = (1.12 \pm 0.13) \times 10^{-2}$ which we divide by our best value $B(\mathcal{T}(3S) \rightarrow \gamma \chi_{b2}(2P)) = (13.1 \pm 1.6) \times 10^{-2}$. Our first error is their experiment's error and our second error is the systematic error from using our best value.	
				⁹ LEES 11J reports $[\Gamma(\chi_{b2}(2P) \rightarrow \gamma \mathcal{T}(2S))/\Gamma_{\text{total}}] \times [B(\mathcal{T}(3S) \rightarrow \gamma \chi_{b2}(2P))] = (1.1 \pm 0.1 \pm 0.1) \times 10^{-2}$ which we divide by our best value $B(\mathcal{T}(3S) \rightarrow \gamma \chi_{b2}(2P)) = (13.1 \pm 1.6) \times 10^{-2}$. Our first error is their experiment's error and our second error is the systematic error from using our best value.	
				¹⁰ CRAWFORD 92B quotes $B(\mathcal{T}(3S) \rightarrow \gamma \chi_{b1}(2P)) \times B(\chi_{b2}(2P) \rightarrow \gamma \mathcal{T}(2S)) \times 2 B(\mathcal{T}(2S) \rightarrow \ell^+ \ell^-) = (4.98 \pm 0.94 \pm 0.62) 10^{-4}$.	
				¹¹ Recalculated by us. HEINTZ 92 quotes $B(\mathcal{T}(3S) \rightarrow \gamma \chi_{b2}(2P)) \times B(\chi_{b2}(2P) \rightarrow \gamma \mathcal{T}(2S)) = (1.90 \pm 0.23 \pm 0.18) \%$ using $B(\mathcal{T}(2S) \rightarrow \mu^+ \mu^-) = (1.44 \pm 0.10)\%$. Supersedes HEINTZ 91.	

$\Gamma(\gamma \mathcal{T}(1S))/\Gamma_{\text{total}}$					Γ_3/Γ
VALUE	EVTS	DOCUMENT ID	TECN	COMMENT	
0.066 ± 0.008 OUR AVERAGE					
$0.061 \pm 0.004 \pm 0.007$	12,13,14	LEES	14M	BABR $\mathcal{T}(3S) \rightarrow \gamma \gamma \mu^+ \mu^-$	
$0.070 \pm 0.004 \pm 0.008$	11k	15 LEES	11J	BABR $\mathcal{T}(3S) \rightarrow X \gamma$	
$0.077 \pm 0.018 \pm 0.009$	13,16	CRAWFORD	92B	CLE2 $e^+ e^- \rightarrow \ell^+ \ell^- \gamma \gamma$	
$0.061 \pm 0.009 \pm 0.007$	13,17	HEINTZ	92	CSB2 $e^+ e^- \rightarrow \ell^+ \ell^- \gamma \gamma$	
				¹² LEES 14M quotes $\Gamma(\chi_{b2}(2P) \rightarrow \gamma \mathcal{T}(1S))/\Gamma_{\text{total}} \times \Gamma(\mathcal{T}(3S) \rightarrow \gamma \chi_{b2}(2P))/\Gamma_{\text{total}} = (8.03 \pm 0.50) \times 10^{-3}$ combining the results from samples of $\mathcal{T}(3S) \rightarrow \gamma \gamma \mu^+ \mu^-$ with and without converted photons.	
				¹³ Assuming $B(\mathcal{T}(1S) \rightarrow \mu^+ \mu^-) = (2.48 \pm 0.05)\%$.	
				¹⁴ LEES 14M reports $[\Gamma(\chi_{b2}(2P) \rightarrow \gamma \mathcal{T}(1S))/\Gamma_{\text{total}}] \times [B(\mathcal{T}(3S) \rightarrow \gamma \chi_{b2}(2P))] = (8.03 \pm 0.50) \times 10^{-3}$ which we divide by our best value $B(\mathcal{T}(3S) \rightarrow \gamma \chi_{b2}(2P)) = (13.1 \pm 1.6) \times 10^{-2}$. Our first error is their experiment's error and our second error is the systematic error from using our best value.	
				¹⁵ LEES 11J reports $[\Gamma(\chi_{b2}(2P) \rightarrow \gamma \mathcal{T}(1S))/\Gamma_{\text{total}}] \times [B(\mathcal{T}(3S) \rightarrow \gamma \chi_{b2}(2P))] = (9.2 \pm 0.3 \pm 0.4) \times 10^{-3}$ which we divide by our best value $B(\mathcal{T}(3S) \rightarrow \gamma \chi_{b2}(2P)) = (13.1 \pm 1.6) \times 10^{-2}$. Our first error is their experiment's error and our second error is the systematic error from using our best value.	
				¹⁶ CRAWFORD 92B quotes $B(\mathcal{T}(3S) \rightarrow \gamma \chi_{b2}(2P)) \times B(\chi_{b2}(2P) \rightarrow \gamma \mathcal{T}(1S)) \times 2 B(\mathcal{T}(1S) \rightarrow \ell^+ \ell^-) = (5.03 \pm 0.94 \pm 0.63) 10^{-4}$.	
				¹⁷ Recalculated by us. HEINTZ 92 quotes $B(\mathcal{T}(3S) \rightarrow \gamma \chi_{b2}(2P)) \times B(\chi_{b2}(2P) \rightarrow \gamma \mathcal{T}(1S)) = (0.77 \pm 0.11 \pm 0.05)\%$ using $B(\mathcal{T}(1S) \rightarrow \mu^+ \mu^-) = (2.57 \pm 0.05)\%$. Supersedes HEINTZ 91.	

$\Gamma(\pi \pi \chi_{b2}(1P))/\Gamma_{\text{total}}$					Γ_4/Γ
VALUE (units 10^{-3})	EVTS	DOCUMENT ID	TECN	COMMENT	
5.1 ± 0.9 OUR AVERAGE					
$4.9 \pm 0.7 \pm 0.6$	17k	18 LEES	11c	BABR $e^+ e^- \rightarrow \pi^+ \pi^- X$	
$6.0 \pm 1.6 \pm 1.4$		19 CAWLFIELD	06	CLE3 $\mathcal{T}(3S) \rightarrow 2(\gamma \pi \ell)$	
				¹⁸ $(0.64 \pm 0.05 \pm 0.08) \times 10^{-3}$. We derive the value assuming $B(\mathcal{T}(3S) \rightarrow \chi_{b2}(2P) X) = B(\mathcal{T}(3S) \rightarrow \chi_{b2}(2P) \gamma) = (13.1 \pm 1.6) \times 10^{-2}$.	
				¹⁹ CAWLFIELD 06 quote $\Gamma(\chi_{b2}(2P) \rightarrow \pi \pi \chi_{b1}(1P)) = 0.83 \pm 0.22 \pm 0.08 \pm 0.19$ keV assuming l-spin conservation, no D-wave contribution, $\Gamma(\chi_{b1}(2P)) = 96 \pm 16$ keV, and $\Gamma(\chi_{b2}(2P)) = 138 \pm 19$ keV.	

$\Gamma(D^0 X)/\Gamma_{\text{total}}$					Γ_5/Γ
VALUE	CL%	DOCUMENT ID	TECN	COMMENT	
$< 2.4 \times 10^{-2}$	90	20,21 BRIERE	08	CLEO $\mathcal{T}(3S) \rightarrow \gamma D^0 X$	
				²⁰ For $p_{D^0} > 2.5$ GeV/c.	
				²¹ The authors also present their result as $(0.2 \pm 1.4 \pm 0.1) \times 10^{-2}$.	

$\Gamma(\pi^+ \pi^- K^+ K^- \pi^0)/\Gamma_{\text{total}}$					Γ_6/Γ
VALUE (units 10^{-4})	CL%	DOCUMENT ID	TECN	COMMENT	
< 1.1	90	22 ASNER	08A	CLEO $\mathcal{T}(3S) \rightarrow \gamma \pi^+ \pi^- K^+ K^- \pi^0$	
				²² ASNER 08A reports $[\Gamma(\chi_{b2}(2P) \rightarrow \pi^+ \pi^- K^+ K^- \pi^0)/\Gamma_{\text{total}}] \times [B(\mathcal{T}(3S) \rightarrow \gamma \chi_{b2}(2P))] < 14 \times 10^{-6}$ which we divide by our best value $B(\mathcal{T}(3S) \rightarrow \gamma \chi_{b2}(2P)) = 13.1 \times 10^{-2}$.	

$\Gamma(2\pi^+ \pi^- K^- K_S^0)/\Gamma_{\text{total}}$					Γ_7/Γ
VALUE (units 10^{-4})	CL%	DOCUMENT ID	TECN	COMMENT	
< 0.9	90	23 ASNER	08A	CLEO $\mathcal{T}(3S) \rightarrow \gamma 2\pi^+ \pi^- K^- K_S^0$	
				²³ ASNER 08A reports $[\Gamma(\chi_{b2}(2P) \rightarrow 2\pi^+ \pi^- K^- K_S^0)/\Gamma_{\text{total}}] \times [B(\mathcal{T}(3S) \rightarrow \gamma \chi_{b2}(2P))] < 12 \times 10^{-6}$ which we divide by our best value $B(\mathcal{T}(3S) \rightarrow \gamma \chi_{b2}(2P)) = 13.1 \times 10^{-2}$.	

$\Gamma(2\pi^+ \pi^- K^- K_S^0 2\pi^0)/\Gamma_{\text{total}}$					Γ_8/Γ
VALUE (units 10^{-4})	CL%	DOCUMENT ID	TECN	COMMENT	
< 7	90	24 ASNER	08A	CLEO $\mathcal{T}(3S) \rightarrow \gamma 2\pi^+ \pi^- K^- 2\pi^0$	
				²⁴ ASNER 08A reports $[\Gamma(\chi_{b2}(2P) \rightarrow 2\pi^+ \pi^- K^- K_S^0 2\pi^0)/\Gamma_{\text{total}}] \times [B(\mathcal{T}(3S) \rightarrow \gamma \chi_{b2}(2P))] < 87 \times 10^{-6}$ which we divide by our best value $B(\mathcal{T}(3S) \rightarrow \gamma \chi_{b2}(2P)) = 13.1 \times 10^{-2}$.	

$\Gamma(2\pi^+ 2\pi^- 2\pi^0)/\Gamma_{\text{total}}$					Γ_9/Γ
VALUE (units 10^{-4})	EVTS	DOCUMENT ID	TECN	COMMENT	
$3.9 \pm 1.6 \pm 0.5$	23	25 ASNER	08A	CLEO $\mathcal{T}(3S) \rightarrow \gamma 2\pi^+ 2\pi^- 2\pi^0$	
				²⁵ ASNER 08A reports $[\Gamma(\chi_{b2}(2P) \rightarrow 2\pi^+ 2\pi^- 2\pi^0)/\Gamma_{\text{total}}] \times [B(\mathcal{T}(3S) \rightarrow \gamma \chi_{b2}(2P))] = (51 \pm 16 \pm 13) \times 10^{-6}$ which we divide by our best value $B(\mathcal{T}(3S) \rightarrow \gamma \chi_{b2}(2P)) = (13.1 \pm 1.6) \times 10^{-2}$. Our first error is their experiment's error and our second error is the systematic error from using our best value.	

$\Gamma(2\pi^+ 2\pi^- K^+ K^-)/\Gamma_{\text{total}}$					Γ_{10}/Γ
VALUE (units 10^{-4})	EVTS	DOCUMENT ID	TECN	COMMENT	
$0.9 \pm 0.4 \pm 0.1$	11	26 ASNER	08A	CLEO $\mathcal{T}(3S) \rightarrow \gamma 2\pi^+ 2\pi^- K^+ K^-$	
				²⁶ ASNER 08A reports $[\Gamma(\chi_{b2}(2P) \rightarrow 2\pi^+ 2\pi^- K^+ K^-)/\Gamma_{\text{total}}] \times [B(\mathcal{T}(3S) \rightarrow \gamma \chi_{b2}(2P))] = (12 \pm 4 \pm 3) \times 10^{-6}$ which we divide by our best value $B(\mathcal{T}(3S) \rightarrow \gamma \chi_{b2}(2P)) = (13.1 \pm 1.6) \times 10^{-2}$. Our first error is their experiment's error and our second error is the systematic error from using our best value.	

$\Gamma(2\pi^+ 2\pi^- K^+ K^- \pi^0)/\Gamma_{\text{total}}$					Γ_{11}/Γ
VALUE (units 10^{-4})	EVTS	DOCUMENT ID	TECN	COMMENT	
$2.4 \pm 1.0 \pm 0.3$	16	27 ASNER	08A	CLEO $\mathcal{T}(3S) \rightarrow \gamma 2\pi^+ 2\pi^- K^+ K^- \pi^0$	
				²⁷ ASNER 08A reports $[\Gamma(\chi_{b2}(2P) \rightarrow 2\pi^+ 2\pi^- K^+ K^- \pi^0)/\Gamma_{\text{total}}] \times [B(\mathcal{T}(3S) \rightarrow \gamma \chi_{b2}(2P))] = (32 \pm 11 \pm 8) \times 10^{-6}$ which we divide by our best value $B(\mathcal{T}(3S) \rightarrow \gamma \chi_{b2}(2P)) = (13.1 \pm 1.6) \times 10^{-2}$. Our first error is their experiment's error and our second error is the systematic error from using our best value.	

$\Gamma(2\pi^+ 2\pi^- K^+ K^- 2\pi^0)/\Gamma_{\text{total}}$					Γ_{12}/Γ
VALUE (units 10^{-4})	EVTS	DOCUMENT ID	TECN	COMMENT	
$4.7 \pm 2.2 \pm 0.6$	14	28 ASNER	08A	CLEO $\mathcal{T}(3S) \rightarrow \gamma 2\pi^+ 2\pi^- K^+ K^- 2\pi^0$	
				²⁸ ASNER 08A reports $[\Gamma(\chi_{b2}(2P) \rightarrow 2\pi^+ 2\pi^- K^+ K^- 2\pi^0)/\Gamma_{\text{total}}] \times [B(\mathcal{T}(3S) \rightarrow \gamma \chi_{b2}(2P))] = (62 \pm 23 \pm 17) \times 10^{-6}$ which we divide by our best value $B(\mathcal{T}(3S) \rightarrow \gamma \chi_{b2}(2P)) = (13.1 \pm 1.6) \times 10^{-2}$. Our first error is their experiment's error and our second error is the systematic error from using our best value.	

$\Gamma(3\pi^+ 2\pi^- K^- K_S^0 \pi^0)/\Gamma_{\text{total}}$					Γ_{13}/Γ
VALUE (units 10^{-4})	CL%	DOCUMENT ID	TECN	COMMENT	
< 4	90	29 ASNER	08A	CLEO $\mathcal{T}(3S) \rightarrow \gamma 3\pi^+ 2\pi^- K^- K_S^0 \pi^0$	
				²⁹ ASNER 08A reports $[\Gamma(\chi_{b2}(2P) \rightarrow 3\pi^+ 2\pi^- K^- K_S^0 \pi^0)/\Gamma_{\text{total}}] \times [B(\mathcal{T}(3S) \rightarrow \gamma \chi_{b2}(2P))] < 58 \times 10^{-6}$ which we divide by our best value $B(\mathcal{T}(3S) \rightarrow \gamma \chi_{b2}(2P)) = 13.1 \times 10^{-2}$.	

$\Gamma(3\pi^+ 3\pi^-)/\Gamma_{\text{total}}$					Γ_{14}/Γ
VALUE (units 10^{-4})	EVTS	DOCUMENT ID	TECN	COMMENT	
$0.9 \pm 0.4 \pm 0.1$	14	30 ASNER	08A	CLEO $\mathcal{T}(3S) \rightarrow \gamma 3\pi^+ 3\pi^-$	
				³⁰ ASNER 08A reports $[\Gamma(\chi_{b2}(2P) \rightarrow 3\pi^+ 3\pi^-)/\Gamma_{\text{total}}] \times [B(\mathcal{T}(3S) \rightarrow \gamma \chi_{b2}(2P))] = (12 \pm 4 \pm 3) \times 10^{-6}$ which we divide by our best value $B(\mathcal{T}(3S) \rightarrow \gamma \chi_{b2}(2P)) = (13.1 \pm 1.6) \times 10^{-2}$. Our first error is their experiment's error and our second error is the systematic error from using our best value.	

$\chi_{b2}(2P), \Upsilon(3S)$

$\Gamma(3\pi^+3\pi^-2\pi^0)/\Gamma_{total}$ Γ_{15}/Γ

VALUE (units 10 ⁻⁴)	EVTS	DOCUMENT ID	TECN	COMMENT
12±4±1	45	31 ASNER	08A CLEO	$\Upsilon(3S) \rightarrow \gamma 3\pi^+ 3\pi^- 2\pi^0$

³¹ ASNER 08A reports $[\Gamma(\chi_{b2}(2P) \rightarrow 3\pi^+ 3\pi^- 2\pi^0)/\Gamma_{total}] \times [B(\Upsilon(3S) \rightarrow \gamma \chi_{b2}(2P))]$ = $(159 \pm 33 \pm 43) \times 10^{-6}$ which we divide by our best value $B(\Upsilon(3S) \rightarrow \gamma \chi_{b2}(2P))$ = $(13.1 \pm 1.6) \times 10^{-2}$. Our first error is their experiment's error and our second error is the systematic error from using our best value.

$\Gamma(3\pi^+3\pi^-K^+K^-)/\Gamma_{total}$ Γ_{16}/Γ

VALUE (units 10 ⁻⁴)	EVTS	DOCUMENT ID	TECN	COMMENT
1.4±0.7±0.2	12	32 ASNER	08A CLEO	$\Upsilon(3S) \rightarrow \gamma 3\pi^+ 3\pi^- K^+ K^-$

³² ASNER 08A reports $[\Gamma(\chi_{b2}(2P) \rightarrow 3\pi^+ 3\pi^- K^+ K^-)/\Gamma_{total}] \times [B(\Upsilon(3S) \rightarrow \gamma \chi_{b2}(2P))]$ = $(19 \pm 7 \pm 5) \times 10^{-6}$ which we divide by our best value $B(\Upsilon(3S) \rightarrow \gamma \chi_{b2}(2P))$ = $(13.1 \pm 1.6) \times 10^{-2}$. Our first error is their experiment's error and our second error is the systematic error from using our best value.

$\Gamma(3\pi^+3\pi^-K^+K^-\pi^0)/\Gamma_{total}$ Γ_{17}/Γ

VALUE (units 10 ⁻⁴)	EVTS	DOCUMENT ID	TECN	COMMENT
4.2±1.7±0.5	16	33 ASNER	08A CLEO	$\Upsilon(3S) \rightarrow \gamma 3\pi^+ 3\pi^- K^+ K^-\pi^0$

³³ ASNER 08A reports $[\Gamma(\chi_{b2}(2P) \rightarrow 3\pi^+ 3\pi^- K^+ K^-\pi^0)/\Gamma_{total}] \times [B(\Upsilon(3S) \rightarrow \gamma \chi_{b2}(2P))]$ = $(55 \pm 16 \pm 15) \times 10^{-6}$ which we divide by our best value $B(\Upsilon(3S) \rightarrow \gamma \chi_{b2}(2P))$ = $(13.1 \pm 1.6) \times 10^{-2}$. Our first error is their experiment's error and our second error is the systematic error from using our best value.

$\Gamma(4\pi^+4\pi^-)/\Gamma_{total}$ Γ_{18}/Γ

VALUE (units 10 ⁻⁴)	EVTS	DOCUMENT ID	TECN	COMMENT
0.9±0.4±0.1	9	34 ASNER	08A CLEO	$\Upsilon(3S) \rightarrow \gamma 4\pi^+ 4\pi^-$

³⁴ ASNER 08A reports $[\Gamma(\chi_{b2}(2P) \rightarrow 4\pi^+ 4\pi^-)/\Gamma_{total}] \times [B(\Upsilon(3S) \rightarrow \gamma \chi_{b2}(2P))]$ = $(12 \pm 5 \pm 3) \times 10^{-6}$ which we divide by our best value $B(\Upsilon(3S) \rightarrow \gamma \chi_{b2}(2P))$ = $(13.1 \pm 1.6) \times 10^{-2}$. Our first error is their experiment's error and our second error is the systematic error from using our best value.

$\Gamma(4\pi^+4\pi^-2\pi^0)/\Gamma_{total}$ Γ_{19}/Γ

VALUE (units 10 ⁻⁴)	EVTS	DOCUMENT ID	TECN	COMMENT
13±5±2	27	35 ASNER	08A CLEO	$\Upsilon(3S) \rightarrow \gamma 4\pi^+ 4\pi^- 2\pi^0$

³⁵ ASNER 08A reports $[\Gamma(\chi_{b2}(2P) \rightarrow 4\pi^+ 4\pi^- 2\pi^0)/\Gamma_{total}] \times [B(\Upsilon(3S) \rightarrow \gamma \chi_{b2}(2P))]$ = $(165 \pm 46 \pm 50) \times 10^{-6}$ which we divide by our best value $B(\Upsilon(3S) \rightarrow \gamma \chi_{b2}(2P))$ = $(13.1 \pm 1.6) \times 10^{-2}$. Our first error is their experiment's error and our second error is the systematic error from using our best value.

$\chi_{b2}(2P)$ Cross-Particle Branching Ratios

$\Gamma(\chi_{b2}(2P) \rightarrow \gamma \Upsilon(1S))/\Gamma_{total} \times \Gamma(\Upsilon(3S) \rightarrow \gamma \chi_{b2}(2P))/\Gamma_{total}$ $\Gamma_3/\Gamma \times \Gamma_{20}^{\Upsilon(3S)}/\Gamma \Upsilon(3S)$

VALUE (units 10 ⁻³)	EVTS	DOCUMENT ID	TECN	COMMENT
9.2±0.3±0.4	11k	LEES	11j BABR	$\Upsilon(3S) \rightarrow X \gamma$

$\Gamma(\chi_{b2}(2P) \rightarrow \gamma \Upsilon(2S))/\Gamma_{total} \times \Gamma(\Upsilon(3S) \rightarrow \gamma \chi_{b2}(2P))/\Gamma_{total}$ $\Gamma_2/\Gamma \times \Gamma_{20}^{\Upsilon(3S)}/\Gamma \Upsilon(3S)$

VALUE (units 10 ⁻²)	EVTS	DOCUMENT ID	TECN	COMMENT
1.1±0.1±0.1	2.5k	LEES	11j BABR	$\Upsilon(3S) \rightarrow X \gamma$

$B(\chi_{b2}(2P) \rightarrow \chi_{b2}(1P)\pi^+\pi^-) \times B(\Upsilon(3S) \rightarrow \chi_{b2}(2P)X)$

VALUE (units 10 ⁻³)	EVTS	DOCUMENT ID	TECN	COMMENT
0.64±0.05±0.08	17k	LEES	11c BABR	$e^+e^- \rightarrow \pi^+\pi^-X$

$B(\chi_{b2}(2P) \rightarrow \gamma \Upsilon(1S)) \times B(\Upsilon(3S) \rightarrow \gamma \chi_{b2}(2P)) \times B(\Upsilon(1S) \rightarrow \ell^+\ell^-)$

VALUE (units 10 ⁻⁴)	EVTS	DOCUMENT ID	TECN	COMMENT
2.02±0.18 OUR AVERAGE				
1.95 ^{+0.22+0.10} _{-0.21-0.16}		36 LEES	14M BABR	$\Upsilon(3S) \rightarrow \gamma \gamma \mu^+ \mu^-$
2.52±0.47±0.32	48	37 CRAWFORD	92B CLE2	$\Upsilon(3S) \rightarrow \gamma \gamma \ell^+ \ell^-$
1.98±0.28±0.12		38 HEINTZ	92 CSB2	$\Upsilon(3S) \rightarrow \gamma \gamma \ell^+ \ell^-$

³⁶ From a sample of $\Upsilon(3S) \rightarrow \gamma \gamma \mu^+ \mu^-$ with converted photons.
³⁷ CRAWFORD 92B quotes $2 \times B(\Upsilon(3S) \rightarrow \gamma \chi_{b,j}(2P)) B(\chi_{b,j}(2P) \rightarrow \gamma \Upsilon(nS)) B(\Upsilon(nS) \rightarrow \ell^+ \ell^-)$.
³⁸ Calculated by us. HEINTZ 92 quotes $B(\Upsilon(3S) \rightarrow \gamma \chi_{b2}(2P)) \times B(\chi_{b2}(2P) \rightarrow \gamma \Upsilon(1S)) = (0.77 \pm 0.11 \pm 0.05)\%$ using $B(\Upsilon(1S) \rightarrow \mu^+ \mu^-) = (2.57 \pm 0.05)\%$.

$[B(\chi_{b2}(2P) \rightarrow \gamma \Upsilon(1S)) \times B(\Upsilon(3S) \rightarrow \gamma \chi_{b2}(2P))] / [B(\chi_{b1}(2P) \rightarrow \gamma \Upsilon(1S)) \times B(\Upsilon(3S) \rightarrow \gamma \chi_{b1}(2P))]$

VALUE (%)	DOCUMENT ID	TECN	COMMENT
66.6±3.0	39 LEES	14M BABR	$\Upsilon(3S) \rightarrow \gamma \gamma \mu^+ \mu^-$

³⁹ From a sample of $\Upsilon(3S) \rightarrow \gamma \gamma \mu^+ \mu^-$ events without converted photons.

$B(\chi_{b2}(2P) \rightarrow \gamma \Upsilon(2S)) \times B(\Upsilon(3S) \rightarrow \gamma \chi_{b2}(2P)) \times B(\Upsilon(2S) \rightarrow \ell^+\ell^-)$

VALUE (units 10 ⁻⁴)	EVTS	DOCUMENT ID	TECN	COMMENT
2.74±0.29 OUR AVERAGE				
3.22 ^{+0.58+0.16} _{-0.53-0.71}		40 LEES	14M BABR	$\Upsilon(3S) \rightarrow \gamma \gamma \mu^+ \mu^-$

2.49±0.47±0.31	53	41 CRAWFORD	92B CLE2	$\Upsilon(3S) \rightarrow \gamma \gamma \ell^+ \ell^-$
2.74±0.33±0.18		42 HEINTZ	92 CSB2	$\Upsilon(3S) \rightarrow \gamma \gamma \ell^+ \ell^-$

⁴⁰ From a sample of $\Upsilon(3S) \rightarrow \gamma \gamma \mu^+ \mu^-$ with converted photons.
⁴¹ CRAWFORD 92B quotes $2 \times B(\Upsilon(3S) \rightarrow \gamma \chi_{b,j}(2P)) B(\chi_{b,j}(2P) \rightarrow \gamma \Upsilon(nS)) B(\Upsilon(nS) \rightarrow \ell^+ \ell^-)$.
⁴² Calculated by us. HEINTZ 92 quotes $B(\Upsilon(3S) \rightarrow \gamma \chi_{b2}(2P)) \times B(\chi_{b2}(2P) \rightarrow \gamma \Upsilon(2S)) = (1.90 \pm 0.23 \pm 0.18)\%$ using $B(\Upsilon(2S) \rightarrow \mu^+ \mu^-) = (1.44 \pm 0.10)\%$.

$[B(\chi_{b2}(2P) \rightarrow \gamma \Upsilon(2S)) \times B(\Upsilon(3S) \rightarrow \gamma \chi_{b2}(2P))] / [B(\chi_{b1}(2P) \rightarrow \gamma \Upsilon(2S)) \times B(\Upsilon(3S) \rightarrow \gamma \chi_{b1}(2P))]$

VALUE (%)	DOCUMENT ID	TECN	COMMENT
46.9±2.0	43 LEES	14M BABR	$\Upsilon(3S) \rightarrow \gamma \gamma \mu^+ \mu^-$

⁴³ From a sample of $\Upsilon(3S) \rightarrow \gamma \gamma \mu^+ \mu^-$ without converted photons.

$\chi_{b2}(2P)$ REFERENCES

AALI	14B JHEP	1410 088	R. Aaij et al.	(LHCb Collab.)
LEES	14M PR	D90 112010	J.P. Lees et al.	(BABAR Collab.)
LEES	11C PR	D84 011104	J.P. Lees et al.	(BABAR Collab.)
LEES	11J PR	D84 072002	J.P. Lees et al.	(BABAR Collab.)
ASNER	08A PR	D78 091103	D.M. Asner et al.	(CLEO Collab.)
BRIERE	08 PR	D78 092007	R.A. Briere et al.	(CLEO Collab.)
CRAWFIELD	06 PR	D73 012003	C. Cawfield et al.	(CLEO Collab.)
ARTUSO	05 PRL	94 032001	M. Artuso et al.	(CLEO Collab.)
CRONIN-HENNESSY	04 PRL	92 222002	D. Cronin-Hennessy et al.	(CLEO Collab.)
CRAWFORD	92B PL	B294 139	G. Crawford et al.	(CLEO Collab.)
HEINTZ	92 PR	D46 1928	U. Heintz et al.	(CUSP II Collab.)
HEINTZ	91 PRL	66 1563	U. Heintz et al.	(CUSP Collab.)
MORRISON	91 PRL	67 1696	R.J. Morrison et al.	(CLEO Collab.)
NARAIN	91 PRL	66 3113	M. Narain et al.	(CUSB Collab.)

$\Upsilon(3S)$

$J^{PC} = 0^{-}(1^{-}-)$

$\Upsilon(3S)$ MASS

VALUE (MeV)	DOCUMENT ID	TECN	COMMENT
10355.1±0.5	1 SHAMOV	23 RVUE	$e^+e^- \rightarrow$ hadrons
••• We do not use the following data for averages, fits, limits, etc. •••			
10355.2±0.5	2,3 ARTAMONOV	00 MD1	$e^+e^- \rightarrow$ hadrons
10355.3±0.5	4,5 BARU	86B MD1	$e^+e^- \rightarrow$ hadrons

¹ Reanalysis of MD1 data using the electron mass from COHEN 87, the radiative corrections from KURAEV 85 and interference effects.
² Reanalysis of BARU 86B using new electron mass (COHEN 87).
³ Superseded by SHAMOV 23.
⁴ Reanalysis of ARTAMONOV 84.
⁵ Superseded by ARTAMONOV 00.

$m_{\Upsilon(3S)} - m_{\Upsilon(2S)}$

VALUE (MeV)	DOCUMENT ID	TECN	COMMENT
331.50±0.02±0.13	LEES	11c BABR	$e^+e^- \rightarrow \pi^+\pi^-X$

$\Upsilon(3S)$ WIDTH

VALUE (keV)	DOCUMENT ID
20.32±1.85 OUR EVALUATION	See the Note on "Width Determinations of the Υ States"

$\Upsilon(3S)$ DECAY MODES

Mode	Fraction (Γ_i/Γ)	Scale factor/ Confidence level
Γ_1 $\Upsilon(2S)$ anything	(10.6 ± 0.8) %	
Γ_2 $\Upsilon(2S)\pi^+\pi^-$	(2.82± 0.18) %	S=1.6
Γ_3 $\Upsilon(2S)\pi^0\pi^0$	(1.85± 0.14) %	
Γ_4 $\Upsilon(2S)\gamma\gamma$	(5.0 ± 0.7) %	
Γ_5 $\Upsilon(2S)\pi^0$	< 5.1	× 10 ⁻⁴ CL=90%
Γ_6 $\Upsilon(1S)\pi^+\pi^-$	(4.37± 0.08) %	
Γ_7 $\Upsilon(1S)\pi^0\pi^0$	(2.20± 0.13) %	
Γ_8 $\Upsilon(1S)\eta$	< 1	× 10 ⁻⁴ CL=90%
Γ_9 $\Upsilon(1S)\pi^0$	< 7	× 10 ⁻⁵ CL=90%
Γ_{10} $h_b(1P)\pi^0$	< 1.2	× 10 ⁻³ CL=90%
Γ_{11} $h_b(1P)\pi^0 \rightarrow \gamma h_b(1S)\pi^0$	(4.3 ± 1.4) × 10 ⁻⁴	
Γ_{12} $h_b(1P)\pi^+\pi^-$	< 1.2	× 10 ⁻⁴ CL=90%
Γ_{13} $\tau^+\tau^-$	(2.29± 0.30) %	
Γ_{14} $\mu^+\mu^-$	(2.18± 0.21) %	S=2.1
Γ_{15} e^+e^-	(2.18± 0.20) %	
Γ_{16} hadrons	(93 ± 12) %	
Γ_{17} ggg	(35.7 ± 2.6) %	
Γ_{18} γgg	(9.7 ± 1.8) × 10 ⁻³	
Γ_{19} 2H anything	(2.33± 0.33) × 10 ⁻⁵	

Meson Particle Listings

$\Upsilon(3S)$

Radiative decays

Γ_{20}	$\gamma \chi_{b2}(2P)$	$(13.1 \pm 1.6) \%$	$S=3.4$
Γ_{21}	$\gamma \chi_{b1}(2P)$	$(12.6 \pm 1.2) \%$	$S=2.4$
Γ_{22}	$\gamma \chi_{b0}(2P)$	$(5.9 \pm 0.6) \%$	$S=1.4$
Γ_{23}	$\gamma \chi_{b2}(1P)$	$(10.0 \pm 1.0) \times 10^{-3}$	$S=1.7$
Γ_{24}	$\gamma \chi_{b1}(1P)$	$(9 \pm 5) \times 10^{-4}$	$S=1.8$
Γ_{25}	$\gamma \chi_{b0}(1P)$	$(2.7 \pm 0.4) \times 10^{-3}$	
Γ_{26}	$\gamma \eta_b(2S)$	$< 6.2 \times 10^{-4}$	$CL=90\%$
Γ_{27}	$\gamma \eta_b(1S)$	$(5.1 \pm 0.7) \times 10^{-4}$	
Γ_{28}	$\gamma A^0 \rightarrow \gamma \text{hadrons}$	$< 8 \times 10^{-5}$	$CL=90\%$
Γ_{29}	$\gamma X \rightarrow \gamma + \geq 4 \text{ prongs}$	$[a] < 2.2 \times 10^{-4}$	$CL=95\%$
Γ_{30}	$\gamma A^0 \rightarrow \gamma \mu^+ \mu^-$	$< 5.5 \times 10^{-6}$	$CL=90\%$
Γ_{31}	$\gamma A^0 \rightarrow \gamma \tau^+ \tau^-$	$[b] < 1.6 \times 10^{-4}$	$CL=90\%$

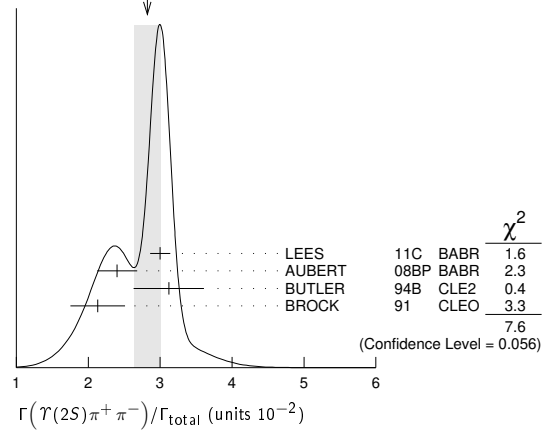
Lepton Family number (LF) violating modes

Γ_{32}	$e^\pm \tau^\mp$	LF	$< 4.2 \times 10^{-6}$	$CL=90\%$
Γ_{33}	$e^\pm \mu^\mp$	LF	$< 3.6 \times 10^{-7}$	$CL=90\%$
Γ_{34}	$\mu^\pm \tau^\mp$	LF	$< 3.1 \times 10^{-6}$	$CL=90\%$

[a] $1.5 \text{ GeV} < m_X < 5.0 \text{ GeV}$

[b] For $m_{\tau^+\tau^-}$ in the ranges 4.03–9.52 and 9.61–10.10 GeV.

WEIGHTED AVERAGE
2.82±0.18 (Error scaled by 1.6)



$\Upsilon(3S) \Gamma(i)\Gamma(e^+e^-)/\Gamma(\text{total})$

$\Gamma(\text{hadrons}) \times \Gamma(e^+e^-)/\Gamma_{\text{total}}$				$\Gamma_{16}\Gamma_{15}/\Gamma$
VALUE (keV)	DOCUMENT ID	TECN	COMMENT	
0.414±0.007 OUR AVERAGE				
0.413±0.004±0.006	ROSNER	06	CLEO	10.4 $e^+e^- \rightarrow \text{hadrons}$
0.45 ± 0.03 ± 0.03	6 GILES	84B	CLEO	$e^+e^- \rightarrow \text{hadrons}$

⁶Radiative corrections reevaluated by BUCHMUELLER 88 following KURAEV 85.

$\Gamma(\Upsilon(1S)\pi^+\pi^-) \times \Gamma(e^+e^-)/\Gamma_{\text{total}}$				$\Gamma_6\Gamma_{15}/\Gamma$
VALUE (eV)	EVTS	DOCUMENT ID	TECN	COMMENT
18.46±0.27±0.77	6.4k	7 AUBERT	08BP	BABR $e^+e^- \rightarrow \gamma\pi^+\pi^-\ell^+\ell^-$

⁷Using $B(\Upsilon(1S) \rightarrow e^+e^-) = (2.38 \pm 0.11)\%$ and $B(\Upsilon(1S) \rightarrow \mu^+\mu^-) = (2.48 \pm 0.05)\%$.

$\Upsilon(3S)$ PARTIAL WIDTHS

$\Gamma(e^+e^-)$	Γ_{15}
VALUE (keV)	DOCUMENT ID
0.443±0.008 OUR EVALUATION	

$\Upsilon(3S)$ BRANCHING RATIOS

$\Gamma(\Upsilon(2S)\text{anything})/\Gamma_{\text{total}}$				Γ_1/Γ
VALUE	EVTS	DOCUMENT ID	TECN	COMMENT
0.106 ± 0.008 OUR AVERAGE				
0.1023±0.0105	4625	8,9,10 BUTLER	94B	CLE2 $e^+e^- \rightarrow \ell^+\ell^-X$
0.111 ± 0.012	4891	9,10,11 BROCK	91	CLEO $e^+e^- \rightarrow \pi^+\pi^-X$, $\pi^+\pi^-\ell^+\ell^-$

⁸Using $B(\Upsilon(2S) \rightarrow \Upsilon(1S)\gamma\gamma) = (0.038 \pm 0.007)\%$, and $B(\Upsilon(2S) \rightarrow \Upsilon(1S)\pi^0\pi^0) = (1/2)B(\Upsilon(2S) \rightarrow \Upsilon(1S)\pi^+\pi^-)$.

⁹Using $B(\Upsilon(1S) \rightarrow \mu^+\mu^-) = (2.48 \pm 0.06)\%$. With the assumption of $e\mu$ universality.

¹⁰Using $B(\Upsilon(2S) \rightarrow \Upsilon(1S)\pi^+\pi^-) = (18.5 \pm 0.8)\%$.

¹¹Using $B(\Upsilon(2S) \rightarrow \mu^+\mu^-) = (1.31 \pm 0.21)\%$, $B(\Upsilon(2S) \rightarrow \Upsilon(1S)\gamma\gamma) \times 2B(\Upsilon(1S) \rightarrow \mu^+\mu^-) = (0.188 \pm 0.035)\%$, and $B(\Upsilon(2S) \rightarrow \Upsilon(1S)\pi^0\pi^0) \times 2B(\Upsilon(1S) \rightarrow \mu^+\mu^-) = (0.436 \pm 0.056)\%$. With the assumption of $e\mu$ universality.

$\Gamma(\Upsilon(2S)\pi^+\pi^-)/\Gamma_{\text{total}}$				Γ_2/Γ
VALUE (units 10^{-2})	EVTS	DOCUMENT ID	TECN	COMMENT
2.82±0.18 OUR AVERAGE				Error includes scale factor of 1.6. See the ideogram below.
3.00±0.02±0.14	543k	LEES	11C	BABR $e^+e^- \rightarrow \pi^+\pi^-X$
2.40±0.10±0.26	800	12 AUBERT	08BP	BABR $e^+e^- \rightarrow \gamma\pi^+\pi^-e^+e^-$
3.12±0.49	980	13,14 BUTLER	94B	CLE2 $e^+e^- \rightarrow \pi^+\pi^-\ell^+\ell^-$
2.13±0.38	974	15 BROCK	91	CLEO $e^+e^- \rightarrow \pi^+\pi^-X$, $\pi^+\pi^-\ell^+\ell^-$

••• We do not use the following data for averages, fits, limits, etc. •••

4.82±0.65±0.53	138	15 WU	93	CUSB $\Upsilon(3S) \rightarrow \pi^+\pi^-\ell^+\ell^-$
3.1 ± 2.0	5	MAGERAS	82	CUSB $\Upsilon(3S) \rightarrow \pi^+\pi^-\ell^+\ell^-$

¹²Using $B(\Upsilon(1S) \rightarrow e^+e^-) = (2.38 \pm 0.11)\%$, $B(\Upsilon(1S) \rightarrow \mu^+\mu^-) = (2.48 \pm 0.05)\%$, and $\Gamma_{ee}(\Upsilon(3S)) = 0.443 \pm 0.008 \text{ keV}$.

¹³From the exclusive mode.

¹⁴Using $B(\Upsilon(2S) \rightarrow \Upsilon(1S)\gamma\gamma) = (0.038 \pm 0.007)\%$, and $B(\Upsilon(2S) \rightarrow \Upsilon(1S)\pi^0\pi^0) = (1/2)B(\Upsilon(2S) \rightarrow \Upsilon(1S)\pi^+\pi^-)$.

¹⁵Using $B(\Upsilon(2S) \rightarrow \mu^+\mu^-) = (1.31 \pm 0.21)\%$, $B(\Upsilon(2S) \rightarrow \Upsilon(1S)\gamma\gamma) \times 2B(\Upsilon(1S) \rightarrow \mu^+\mu^-) = (0.188 \pm 0.035)\%$, and $B(\Upsilon(2S) \rightarrow \Upsilon(1S)\pi^0\pi^0) \times 2B(\Upsilon(1S) \rightarrow \mu^+\mu^-) = (0.436 \pm 0.056)\%$. With the assumption of $e\mu$ universality.

$\Gamma(\Upsilon(2S)\pi^0\pi^0)/\Gamma_{\text{total}}$

VALUE (units 10^{-2})	EVTS	DOCUMENT ID	TECN	COMMENT
1.85±0.14 OUR AVERAGE				
1.82±0.09±0.12	4391	16 BHARI	09	CLEO $e^+e^- \rightarrow \pi^0\pi^0\ell^+\ell^-$
2.16±0.39		17,18 BUTLER	94B	CLE2 $e^+e^- \rightarrow \pi^0\pi^0\ell^+\ell^-$
1.7 ± 0.5 ± 0.2	10	19 HEINTZ	92	CSB2 $e^+e^- \rightarrow \pi^0\pi^0\ell^+\ell^-$

¹⁶Authors assume $B(\Upsilon(1S) \rightarrow e^+e^-) + B(\Upsilon(1S) \rightarrow \mu^+\mu^-) = 4.06\%$.

¹⁷ $B(\Upsilon(2S) \rightarrow \mu^+\mu^-) = (1.31 \pm 0.21)\%$ and assuming $e\mu$ universality.

¹⁸From the exclusive mode.

¹⁹ $B(\Upsilon(2S) \rightarrow \mu^+\mu^-) = (1.44 \pm 0.10)\%$ and assuming $e\mu$ universality. Supersedes HEINTZ 91.

$\Gamma(\Upsilon(2S)\gamma\gamma)/\Gamma_{\text{total}}$

VALUE	DOCUMENT ID	TECN	COMMENT
0.0502±0.0069	20 BUTLER	94B	CLE2 $e^+e^- \rightarrow \ell^+\ell^-2\gamma$

²⁰From the exclusive mode.

$\Gamma(\Upsilon(2S)\pi^0)/\Gamma_{\text{total}}$

VALUE (units 10^{-3})	CL%	DOCUMENT ID	TECN	COMMENT
<0.51	90	21 HE	08A	CLEO $e^+e^- \rightarrow \ell^+\ell^-\gamma\gamma$

²¹Authors assume $B(\Upsilon(2S) \rightarrow e^+e^-) + B(\Upsilon(1S) \rightarrow \mu^+\mu^-) = 4.06\%$.

$\Gamma(\Upsilon(1S)\pi^+\pi^-)/\Gamma_{\text{total}}$

Abbreviation MM in the COMMENT field below stands for missing mass.

VALUE (units 10^{-2})	EVTS	DOCUMENT ID	TECN	COMMENT
4.37±0.08 OUR AVERAGE				
4.32±0.07±0.13	90k	22 LEES	11L	BABR $\Upsilon(3S) \rightarrow \pi^+\pi^-\ell^+\ell^-$
4.46±0.01±0.13	190k	23 BHARI	09	CLEO $e^+e^- \rightarrow \pi^+\pi^-MM$
4.17±0.06±0.19	6.4k	24 AUBERT	08BP	BABR 10.58 $e^+e^- \rightarrow \gamma\pi^+\pi^-\ell^+\ell^-$
4.52±0.35	11830	25 BUTLER	94B	CLE2 $e^+e^- \rightarrow \pi^+\pi^-X$, $\pi^+\pi^-\ell^+\ell^-$
4.46±0.34±0.50	451	25 WU	93	CUSB $\Upsilon(3S) \rightarrow \pi^+\pi^-\ell^+\ell^-$
4.46±0.30	11221	25 BROCK	91	CLEO $e^+e^- \rightarrow \pi^+\pi^-X$, $\pi^+\pi^-\ell^+\ell^-$

••• We do not use the following data for averages, fits, limits, etc. •••

4.9 ± 1.0
 22 | GREEN | 82 | CLEO $\Upsilon(3S) \rightarrow \pi^+\pi^-\ell^+\ell^-$ |

3.9 ± 1.3
 26 | MAGERAS | 82 | CUSB $\Upsilon(3S) \rightarrow \pi^+\pi^-\ell^+\ell^-$ |

²²Using $B(\Upsilon(1S) \rightarrow e^+e^-) = (2.38 \pm 0.11)\%$ and $B(\Upsilon(1S) \rightarrow \mu^+\mu^-) = (2.48 \pm 0.05)\%$.

²³A weighted average of the inclusive and exclusive results.

²⁴Using $B(\Upsilon(2S) \rightarrow e^+e^-) = (1.91 \pm 0.16)\%$, $B(\Upsilon(2S) \rightarrow \mu^+\mu^-) = (1.93 \pm 0.17)\%$, and $\Gamma_{ee}(\Upsilon(3S)) = 0.443 \pm 0.008 \text{ keV}$.

²⁵Using $B(\Upsilon(1S) \rightarrow \mu^+\mu^-) = (2.48 \pm 0.06)\%$. With the assumption of $e\mu$ universality.

$\Gamma(\Upsilon(2S)\pi^+\pi^-)/\Gamma(\Upsilon(1S)\pi^+\pi^-)$

VALUE	EVTS	DOCUMENT ID	TECN	COMMENT
0.577±0.026±0.060	800	26 AUBERT	08BP	BABR $e^+e^- \rightarrow \gamma\pi^+\pi^-\ell^+\ell^-$

••• We do not use the following data for averages, fits, limits, etc. •••

²⁶Using $B(\Upsilon(1S) \rightarrow e^+e^-) = (2.38 \pm 0.11)\%$, $B(\Upsilon(1S) \rightarrow \mu^+\mu^-) = (2.48 \pm 0.05)\%$, $B(\Upsilon(2S) \rightarrow e^+e^-) = (1.91 \pm 0.16)\%$, and $B(\Upsilon(2S) \rightarrow \mu^+\mu^-) = (1.93 \pm 0.17)\%$. Not independent of other values reported by AUBERT 08BP.

$\Gamma(\Upsilon(1S)\pi^0\pi^0)/\Gamma_{\text{total}}$

VALUE (units 10^{-2})	EVTS	DOCUMENT ID	TECN	COMMENT
2.20±0.13 OUR AVERAGE				
2.24±0.09±0.11	6584	27 BHARI	09	CLEO $e^+e^- \rightarrow \pi^0\pi^0\ell^+\ell^-$
1.99±0.34	56	28 BUTLER	94B	CLE2 $e^+e^- \rightarrow \pi^0\pi^0\ell^+\ell^-$
2.2 ± 0.4 ± 0.3	33	29 HEINTZ	92	CSB2 $e^+e^- \rightarrow \pi^0\pi^0\ell^+\ell^-$

²⁷Authors assume $B(\Upsilon(1S) \rightarrow e^+e^-) + B(\Upsilon(1S) \rightarrow \mu^+\mu^-) = 4.96\%$.

²⁸Using $B(\Upsilon(1S) \rightarrow \mu^+\mu^-) = (2.48 \pm 0.06)\%$ and assuming $e\mu$ universality.

²⁹Using $B(\Upsilon(1S) \rightarrow \mu^+\mu^-) = (2.57 \pm 0.07)\%$ and assuming $e\mu$ universality. Supersedes HEINTZ 91.

$\Gamma(\Upsilon(1S)\pi^0\pi^0)/\Gamma(\Upsilon(1S)\pi^+\pi^-)$ Γ_7/Γ_6

VALUE	DOCUMENT ID	TECN	COMMENT
0.501 ± 0.043	30 BHARI	09	CLEO $e^+e^- \rightarrow \Upsilon(3S)$

• • • We do not use the following data for averages, fits, limits, etc. • • •
 30 Not independent of other values reported by BHARI 09.

$\Gamma(\Upsilon(1S)\eta)/\Gamma_{total}$ Γ_8/Γ

VALUE (units 10^{-3})	CL%	DOCUMENT ID	TECN	COMMENT
<0.1	90	31 LEES	11L BABR	$\Upsilon(3S) \rightarrow (\pi^+\pi^-\gamma)\ell^+\ell^-$
<0.8	90	31,32 AUBERT	08BP BABR	$e^+e^- \rightarrow \gamma\pi^+\pi^-\pi^0\ell^+\ell^-$
<0.18	90	33 HE	08A CLEO	$e^+e^- \rightarrow \ell^+\ell^-\eta$
<2.2	90	BROCK	91 CLEO	$e^+e^- \rightarrow \ell^+\ell^-\eta$

31 Using $B(\Upsilon(1S) \rightarrow e^+e^-) = (2.38 \pm 0.11)\%$, $B(\Upsilon(1S) \rightarrow \mu^+\mu^-) = (2.48 \pm 0.05)\%$.
 32 Using $\Gamma_{ee}(\Upsilon(3S)) = 0.443 \pm 0.008$ keV.
 33 Authors assume $B(\Upsilon(1S) \rightarrow e^+e^-) + B(\Upsilon(1S) \rightarrow \mu^+\mu^-) = 4.96\%$.

$\Gamma(\Upsilon(1S)\eta)/\Gamma(\Upsilon(1S)\pi^+\pi^-)$ Γ_8/Γ_6

VALUE (units 10^{-2})	CL%	DOCUMENT ID	TECN	COMMENT
<0.23	90	34 LEES	11L BABR	$\Upsilon(3S) \rightarrow (\pi^+\pi^-\gamma)\ell^+\ell^-$
<1.9	90	35 AUBERT	08BP BABR	$e^+e^- \rightarrow \gamma\pi^+\pi^-(\pi^0)\ell^+\ell^-$

34 Not independent of other values reported by LEES 11L.
 35 Not independent of other values reported by AUBERT 08BP.

$\Gamma(\Upsilon(1S)\pi^0)/\Gamma_{total}$ Γ_9/Γ

VALUE (units 10^{-3})	CL%	DOCUMENT ID	TECN	COMMENT
<0.07	90	36 HE	08A CLEO	$e^+e^- \rightarrow \ell^+\ell^-\gamma\gamma$

36 Authors assume $B(\Upsilon(1S) \rightarrow e^+e^-) + B(\Upsilon(1S) \rightarrow \mu^+\mu^-) = 4.96\%$.

$\Gamma(h_b(1P)\pi^0)/\Gamma_{total}$ Γ_{10}/Γ

VALUE	CL%	DOCUMENT ID	TECN	COMMENT
<1.2 × 10 ⁻³	90	37 GE	11 CLEO	$\Upsilon(3S) \rightarrow \pi^0$ anything

37 Assuming $M(h_b(1P)) = 9900$ MeV and $\Gamma(h_b(1P)) = 0$ MeV, and allowing $B(h_b(1P) \rightarrow \gamma\eta_b(1S))$ to vary from 0–100%.

$\Gamma(h_b(1P)\pi^0 \rightarrow \gamma\eta_b(1S)\pi^0)/\Gamma_{total}$ Γ_{11}/Γ

VALUE (units 10^{-4})	DOCUMENT ID	TECN	COMMENT
4.3 ± 1.1 ± 0.9	LEES	11k BABR	$\Upsilon(3S) \rightarrow \eta_b\gamma\pi^0$

$\Gamma(h_b(1P)\pi^+\pi^-)/\Gamma_{total}$ Γ_{12}/Γ

VALUE (units 10^{-4})	CL%	DOCUMENT ID	TECN	COMMENT
< 1.2	90	38 LEES	11c BABR	$e^+e^- \rightarrow \pi^+\pi^-X$
<18		38 BUTLER	94B CLE2	$e^+e^- \rightarrow \pi^+\pi^-X$
<15		38 BROCK	91 CLEO	$e^+e^- \rightarrow \pi^+\pi^-X$

38 For $M(h_b(1P)) = 9900$ MeV.

$\Gamma(\tau^+\tau^-)/\Gamma_{total}$ Γ_{13}/Γ

VALUE (units 10^{-2})	EVTS	DOCUMENT ID	TECN	COMMENT
2.29 ± 0.21 ± 0.22	15k	39 BESSON	07 CLEO	$e^+e^- \rightarrow \Upsilon(3S) \rightarrow \tau^+\tau^-$

39 BESSON 07 reports $[\Gamma(\Upsilon(3S) \rightarrow \tau^+\tau^-)/\Gamma_{total}] / [B(\Upsilon(3S) \rightarrow \mu^+\mu^-)] = 1.05 \pm 0.08 \pm 0.05$ which we multiply by our best value $B(\Upsilon(3S) \rightarrow \mu^+\mu^-) = (2.18 \pm 0.21) \times 10^{-2}$. Our first error is their experiment's error and our second error is the systematic error from using our best value.

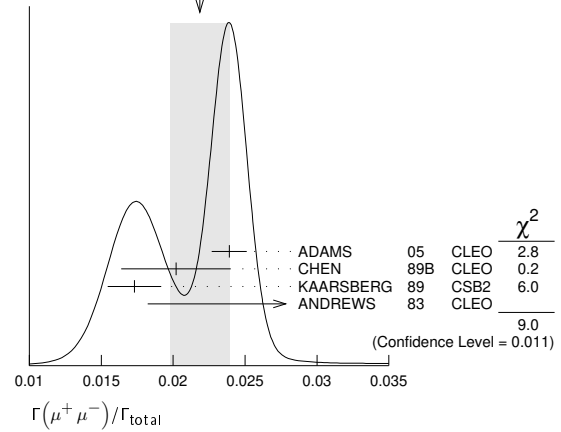
$\Gamma(\tau^+\tau^-)/\Gamma(\mu^+\mu^-)$ Γ_{13}/Γ_{14}

VALUE	EVTS	DOCUMENT ID	TECN	COMMENT
0.968 ± 0.016 OUR AVERAGE				
0.966 ± 0.008 ± 0.014	2.2M	LEES	20E BABR	$e^+e^- \rightarrow \Upsilon(3S)$
1.05 ± 0.08 ± 0.05	15k	BESSON	07 CLEO	$e^+e^- \rightarrow \Upsilon(3S)$

$\Gamma(\mu^+\mu^-)/\Gamma_{total}$ Γ_{14}/Γ

VALUE	EVTS	DOCUMENT ID	TECN	COMMENT
0.0218 ± 0.0021 OUR AVERAGE				Error includes scale factor of 2.1. See the ideogram below.
0.0239 ± 0.0007 ± 0.0010	81k	ADAMS	05 CLEO	$e^+e^- \rightarrow \mu^+\mu^-$
0.0202 ± 0.0019 ± 0.0033		CHEN	89B CLEO	$e^+e^- \rightarrow \mu^+\mu^-$
0.0173 ± 0.0015 ± 0.0011		KAARSBERG	89 CSB2	$e^+e^- \rightarrow \mu^+\mu^-$
0.033 ± 0.013 ± 0.007	1096	ANDREWS	83 CLEO	$e^+e^- \rightarrow \mu^+\mu^-$

WEIGHTED AVERAGE
0.0218±0.0021 (Error scaled by 2.1)



$\Gamma(ggg)/\Gamma_{total}$ Γ_{17}/Γ

VALUE (units 10^{-2})	EVTS	DOCUMENT ID	TECN	COMMENT
35.7 ± 2.6	3M	40 BESSON	06A CLEO	$\Upsilon(3S) \rightarrow$ hadrons

40 Calculated using BESSON 06A value of $\Gamma(\gamma gg)/\Gamma(ggg) = (2.72 \pm 0.06 \pm 0.32 \pm 0.37)\%$ and the PDG 08 values of $B(\Upsilon(2S) + \text{anything}) = (10.6 \pm 0.8)\%$, $B(\pi^+\pi^-\Upsilon(1S)) = (4.40 \pm 0.10)\%$, $B(\pi^0\pi^0\Upsilon(1S)) = (2.20 \pm 0.13)\%$, $B(\gamma\chi_{b2}(2P)) = (13.1 \pm 1.6)\%$, $B(\gamma\chi_{b1}(2P)) = (12.6 \pm 1.2)\%$, $B(\gamma\chi_{b0}(2P)) = (5.9 \pm 0.6)\%$, $B(\gamma\chi_{b0}(1P)) = (0.30 \pm 0.11)\%$, $B(\mu^+\mu^-) = (2.18 \pm 0.21)\%$, and $R_{\text{hadrons}} = 3.51$. The statistical error is negligible and the systematic error is partially correlated with $\Gamma(\gamma gg)/\Gamma_{total}$ BESSON 06A value.

$\Gamma(\gamma gg)/\Gamma_{total}$ Γ_{18}/Γ

VALUE (units 10^{-2})	EVTS	DOCUMENT ID	TECN	COMMENT
0.97 ± 0.18	60k	41 BESSON	06A CLEO	$\Upsilon(3S) \rightarrow \gamma +$ hadrons

41 Calculated using BESSON 06A values of $\Gamma(\gamma gg)/\Gamma(ggg) = (2.72 \pm 0.06 \pm 0.32 \pm 0.37)\%$ and $\Gamma(ggg)/\Gamma_{total}$. The statistical error is negligible and the systematic error is partially correlated with $\Gamma(ggg)/\Gamma_{total}$ BESSON 06A value.

$\Gamma(\gamma gg)/\Gamma(ggg)$ Γ_{18}/Γ_{17}

VALUE (units 10^{-2})	EVTS	DOCUMENT ID	TECN	COMMENT
2.72 ± 0.06 ± 0.49	3M	BESSON	06A CLEO	$\Upsilon(3S) \rightarrow (\gamma +)$ hadrons

$\Gamma(2H \text{ anything})/\Gamma_{total}$ Γ_{19}/Γ

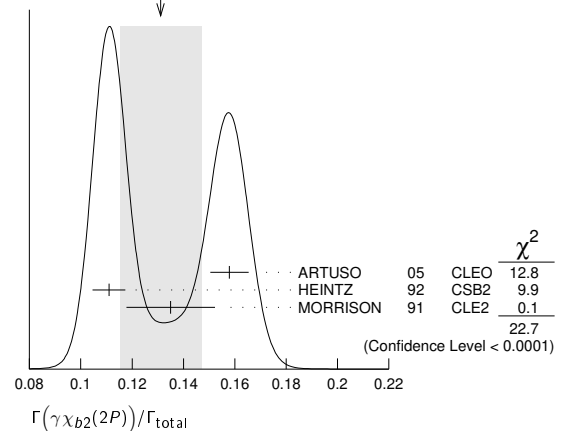
VALUE (units 10^{-3})	DOCUMENT ID	TECN	COMMENT
2.33 ± 0.15 ± 0.31 -0.28	LEES	14G BABR	$e^+e^- \rightarrow 2H X$

$\Gamma(\gamma\chi_{b2}(2P))/\Gamma_{total}$ Γ_{20}/Γ

VALUE	EVTS	DOCUMENT ID	TECN	COMMENT
0.131 ± 0.016 OUR AVERAGE				Error includes scale factor of 3.4. See the ideogram below.
0.1579 ± 0.0017 ± 0.0073	568k	ARTUSO	05 CLEO	$e^+e^- \rightarrow \gamma X$
0.111 ± 0.005 ± 0.004	10319	42 HEINTZ	92 CSB2	$e^+e^- \rightarrow \gamma X$
0.135 ± 0.003 ± 0.017	30741	MORRISON	91 CLE2	$e^+e^- \rightarrow \gamma X$

42 Supersedes NARAIN 91.

WEIGHTED AVERAGE
0.131±0.016 (Error scaled by 3.4)

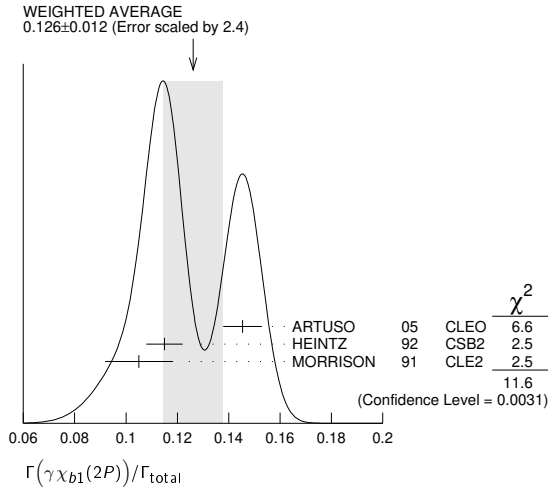


Meson Particle Listings

 $\Upsilon(3S)$ $\Gamma(\gamma\chi_{b1}(2P))/\Gamma_{\text{total}}$

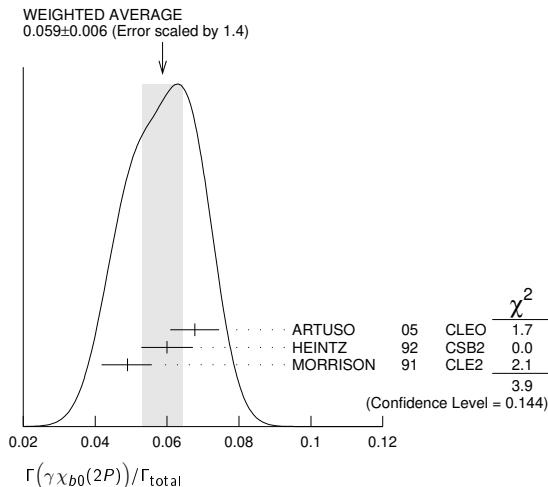
VALUE	CL%	EVTS	DOCUMENT ID	TECN	COMMENT
0.126 ± 0.012	OUR AVERAGE				Error includes scale factor of 2.4. See the ideogram below.
0.1454 ± 0.0018 ± 0.0073		537k	ARTUSO	05	CLEO $e^+e^- \rightarrow \gamma X$
0.115 ± 0.005 ± 0.005		11147	⁴³ HEINTZ	92	CSB2 $e^+e^- \rightarrow \gamma X$
0.105 $^{+0.003}_{-0.002}$ ± 0.013		25759	MORRISON	91	CLE2 $e^+e^- \rightarrow \gamma X$

⁴³ Supersedes NARAIN 91.

 $\Gamma(\gamma\chi_{b0}(2P))/\Gamma_{\text{total}}$

VALUE	CL%	EVTS	DOCUMENT ID	TECN	COMMENT
0.059 ± 0.006	OUR AVERAGE				Error includes scale factor of 1.4. See the ideogram below.
0.0677 ± 0.0020 ± 0.0065		225k	ARTUSO	05	CLEO $e^+e^- \rightarrow \gamma X$
0.060 ± 0.004 ± 0.006		4959	⁴⁴ HEINTZ	92	CSB2 $e^+e^- \rightarrow \gamma X$
0.049 $^{+0.003}_{-0.004}$ ± 0.006		9903	MORRISON	91	CLE2 $e^+e^- \rightarrow \gamma X$

⁴⁴ Supersedes NARAIN 91.

 $\Gamma(\gamma\chi_{b2}(1P))/\Gamma_{\text{total}}$

VALUE (units 10^{-3})	CL%	EVTS	DOCUMENT ID	TECN	COMMENT
10.0 ± 1.0	OUR AVERAGE				Error includes scale factor of 1.7.
8.0 ± 1.3 ± 0.4		126	^{45,46} KORNICER	11	CLEO $e^+e^- \rightarrow \gamma\gamma\ell^+\ell^-$
10.5 ± 0.3 $^{+0.7}_{-0.6}$		9.7k	LEES	11J	BABR $\Upsilon(3S) \rightarrow X\gamma$

• • • We do not use the following data for averages, fits, limits, etc. • • •

<19	90	⁴⁷ ASNER	08A	CLEO	$\Upsilon(3S) \rightarrow \gamma + \text{hadrons}$ seen
		⁴⁸ HEINTZ	92	CSB2	$e^+e^- \rightarrow \gamma\gamma\ell^+\ell^-$

⁴⁵ Assuming $B(\Upsilon(1S) \rightarrow \ell^+\ell^-) = (2.48 \pm 0.05)\%$.

⁴⁶ KORNICER 11 reports $[\Gamma(\Upsilon(3S) \rightarrow \gamma\chi_{b2}(1P))/\Gamma_{\text{total}}] \times [B(\chi_{b2}(1P) \rightarrow \gamma\Upsilon(1S))] = (1.435 \pm 0.162 \pm 0.169) \times 10^{-3}$ which we divide by our best value $B(\chi_{b2}(1P) \rightarrow \gamma\Upsilon(1S)) = (18.0 \pm 1.0) \times 10^{-2}$. Our first error is their experiment's error and our second error is the systematic error from using our best value.

⁴⁷ ASNER 08A reports $[\Gamma(\Upsilon(3S) \rightarrow \gamma\chi_{b2}(1P))/\Gamma_{\text{total}}] / [B(\Upsilon(2S) \rightarrow \gamma\chi_{b2}(1P))] < 27.1 \times 10^{-2}$ which we multiply by our best value $B(\Upsilon(2S) \rightarrow \gamma\chi_{b2}(1P)) = 7.15 \times 10^{-2}$.

⁴⁸ HEINTZ 92, while unable to distinguish between different J states, measures $\sum_J B(\Upsilon(3S) \rightarrow \gamma\chi_{bJ}) \times B(\chi_{bJ} \rightarrow \gamma\Upsilon(1S)) = (1.7 \pm 0.4 \pm 0.6) \times 10^{-3}$ for $J = 0, 1, 2$ using inclusive $\Upsilon(1S)$ decays and $(1.2^{+0.4}_{-0.3} \pm 0.09) \times 10^{-3}$ for $J = 1, 2$ using $\Upsilon(1S) \rightarrow \ell^+\ell^-$.

 $\Gamma(\gamma\chi_{b1}(1P))/\Gamma_{\text{total}}$

VALUE (units 10^{-3})	CL%	EVTS	DOCUMENT ID	TECN	COMMENT
0.9 ± 0.5	OUR AVERAGE				Error includes scale factor of 1.8.
1.5 ± 0.4 ± 0.1		50	^{49,50} KORNICER	11	CLEO $e^+e^- \rightarrow \gamma\gamma\ell^+\ell^-$
0.5 ± 0.3 $^{+0.2}_{-0.1}$			LEES	11J	BABR $\Upsilon(3S) \rightarrow X\gamma$

• • • We do not use the following data for averages, fits, limits, etc. • • •

<1.7	90	⁵¹ ASNER	08A	CLEO	$\Upsilon(3S) \rightarrow \gamma + \text{hadrons}$ seen
		⁵² HEINTZ	92	CSB2	$e^+e^- \rightarrow \gamma\gamma\ell^+\ell^-$

⁴⁹ Assuming $B(\Upsilon(1S) \rightarrow \ell^+\ell^-) = (2.48 \pm 0.05)\%$.

⁵⁰ KORNICER 11 reports $[\Gamma(\Upsilon(3S) \rightarrow \gamma\chi_{b1}(1P))/\Gamma_{\text{total}}] \times [B(\chi_{b1}(1P) \rightarrow \gamma\Upsilon(1S))] = (5.38 \pm 1.20 \pm 0.95) \times 10^{-4}$ which we divide by our best value $B(\chi_{b1}(1P) \rightarrow \gamma\Upsilon(1S)) = (35.2 \pm 2.0) \times 10^{-2}$. Our first error is their experiment's error and our second error is the systematic error from using our best value.

⁵¹ ASNER 08A reports $[\Gamma(\Upsilon(3S) \rightarrow \gamma\chi_{b1}(1P))/\Gamma_{\text{total}}] / [B(\Upsilon(2S) \rightarrow \gamma\chi_{b1}(1P))] < 2.5 \times 10^{-2}$ which we multiply by our best value $B(\Upsilon(2S) \rightarrow \gamma\chi_{b1}(1P)) = 6.9 \times 10^{-2}$.

⁵² HEINTZ 92, while unable to distinguish between different J states, measures $\sum_J B(\Upsilon(3S) \rightarrow \gamma\chi_{bJ}) \times B(\chi_{bJ} \rightarrow \gamma\Upsilon(1S)) = (1.7 \pm 0.4 \pm 0.6) \times 10^{-3}$ for $J = 0, 1, 2$ using inclusive $\Upsilon(1S)$ decays and $(1.2^{+0.4}_{-0.3} \pm 0.09) \times 10^{-3}$ for $J = 1, 2$ using $\Upsilon(1S) \rightarrow \ell^+\ell^-$.

 $\Gamma(\gamma\chi_{b0}(1P))/\Gamma_{\text{total}}$

VALUE (units 10^{-2})	CL%	EVTS	DOCUMENT ID	TECN	COMMENT
0.27 ± 0.04	OUR AVERAGE				
0.27 ± 0.04 ± 0.02		2.3k	LEES	11J	BABR $\Upsilon(3S) \rightarrow X\gamma$
0.30 ± 0.04 ± 0.10		8.7k	ARTUSO	05	CLEO $e^+e^- \rightarrow \gamma X$

• • • We do not use the following data for averages, fits, limits, etc. • • •

<0.8	90	⁵³ ASNER	08A	CLEO	$\Upsilon(3S) \rightarrow \gamma + \text{hadrons}$
------	----	---------------------	-----	------	--

⁵³ ASNER 08A reports $[\Gamma(\Upsilon(3S) \rightarrow \gamma\chi_{b0}(1P))/\Gamma_{\text{total}}] / [B(\Upsilon(2S) \rightarrow \gamma\chi_{b0}(1P))] < 21.9 \times 10^{-2}$ which we multiply by our best value $B(\Upsilon(2S) \rightarrow \gamma\chi_{b0}(1P)) = 3.8 \times 10^{-2}$.

 $\Gamma(\gamma\eta_b(2S))/\Gamma_{\text{total}}$

VALUE (units 10^{-4})	CL%	DOCUMENT ID	TECN	COMMENT	
< 6.2		90	ARTUSO	05	CLEO $e^+e^- \rightarrow \gamma X$
• • •					We do not use the following data for averages, fits, limits, etc. • • •
<19		90	LEES	11J	BABR $\Upsilon(3S) \rightarrow X\gamma$

 $\Gamma(\gamma\eta_b(1S))/\Gamma_{\text{total}}$

VALUE (units 10^{-4})	CL%	EVTS	DOCUMENT ID	TECN	COMMENT
5.1 ± 0.7	OUR AVERAGE				
7.1 ± 1.8 ± 1.3		2.3 ± 0.5k	⁵⁴ BONVICINI	10	CLEO $\Upsilon(3S) \rightarrow \gamma X$
4.8 ± 0.5 ± 0.6		19 ± 3k	⁵⁴ AUBERT	09AQ	BABR $\Upsilon(3S) \rightarrow \gamma X$
• • •					We do not use the following data for averages, fits, limits, etc. • • •
<8.5		90	LEES	11J	BABR $\Upsilon(3S) \rightarrow X\gamma$
4.8 ± 0.5 ± 1.2		19 ± 3k	^{54,55} AUBERT	08V	BABR $\Upsilon(3S) \rightarrow \gamma X$
<4.3		90	⁵⁶ ARTUSO	05	CLEO $e^+e^- \rightarrow \gamma X$

⁵⁴ Assuming $\Gamma_{\eta_b(1S)} = 10$ MeV.

⁵⁵ Systematic error re-evaluated by AUBERT 09AQ.

⁵⁶ Superseded by BONVICINI 10.

 $\Gamma(\gamma A^0 \rightarrow \gamma + \text{hadrons})/\Gamma_{\text{total}}$

VALUE	CL%	DOCUMENT ID	TECN	COMMENT	
< 8 × 10⁻⁵		90	⁵⁷ LEES	11H	BABR $\Upsilon(3S) \rightarrow \gamma + \text{hadrons}$

⁵⁷ For a narrow scalar or pseudoscalar, A^0 , excluding known resonances, with mass in the range 0.3–7 GeV. Measured 90% CL limits as a function of m_{A^0} range from 1×10^{-6} to 8×10^{-5} .

 $\Gamma(\gamma X \rightarrow \gamma + \geq 4 \text{ prongs})/\Gamma_{\text{total}}$

VALUE (units 10^{-4})	CL%	DOCUMENT ID	TECN	COMMENT	
< 2.2		95	ROSNER	07A	CLEO $e^+e^- \rightarrow \gamma X$

 $\Gamma(\gamma A^0 \rightarrow \gamma\mu^+\mu^-)/\Gamma_{\text{total}}$

VALUE (units 10^{-6})	CL%	DOCUMENT ID	TECN	COMMENT	
< 5.5		90	⁵⁸ AUBERT	09Z	BABR $e^+e^- \rightarrow \gamma A^0 \rightarrow \gamma\mu^+\mu^-$

⁵⁸ For a narrow scalar or pseudoscalar, A^0 , with mass in the range 212–9300 MeV, excluding J/ψ and $\psi(2S)$. Measured 90% CL limits as a function of m_{A^0} range from 0.27–5.5 × 10⁻⁶.

 $\Gamma(\gamma A^0 \rightarrow \gamma\tau^+\tau^-)/\Gamma_{\text{total}}$

VALUE	CL%	DOCUMENT ID	TECN	COMMENT	
< 1.6 × 10⁻⁴		90	⁵⁹ AUBERT	09P	BABR $e^+e^- \rightarrow \gamma A^0 \rightarrow \gamma\tau^+\tau^-$

⁵⁹ For a narrow scalar or pseudoscalar, A^0 , with $M(\tau^+\tau^-)$ in the ranges 4.03–9.52 and 9.61–10.10 GeV. Measured 90% CL limits as a function of $M(\tau^+\tau^-)$ range from 1.5–16 × 10⁻⁵.

See key on page 1171

Meson Particle Listings

$\Upsilon(3S), \chi_{b1}(3P), \chi_{b2}(3P)$

LEPTON FAMILY NUMBER (LF) VIOLATING MODES

$\Gamma(e^\pm \tau^\mp)/\Gamma_{\text{total}}$					Γ_{32}/Γ
VALUE (units 10^{-6})	CL%	DOCUMENT ID	TECN	COMMENT	
<4.2	90	LEES	10B	BABR $e^+ e^- \rightarrow e^\pm \tau^\mp$	

$\Gamma(e^\pm \mu^\mp)/\Gamma_{\text{total}}$					Γ_{33}/Γ
VALUE	CL%	DOCUMENT ID	TECN	COMMENT	
<3.6 $\times 10^{-7}$	90	LEES	22A	BABR $e^+ e^- \rightarrow e^\pm \mu^\mp$	

$\Gamma(\mu^\pm \tau^\mp)/\Gamma_{\text{total}}$					Γ_{34}/Γ
VALUE (units 10^{-6})	CL%	DOCUMENT ID	TECN	COMMENT	
< 3.1	90	LEES	10B	BABR $e^+ e^- \rightarrow \mu^\pm \tau^\mp$	
• • • We do not use the following data for averages, fits, limits, etc. • • •					
<20.3	95	LOVE	08A	CLEO $e^+ e^- \rightarrow \mu^\pm \tau^\mp$	

$\Upsilon(3S)$ REFERENCES

SHAMOV	23	PL B839 137766	A.G. Shamov, O.L. Rezanova	(NOVO, NOVOU)
LEES	22A	PRL 128 091804	J.P. Lees et al.	(BABAR Collab.)
LEES	20E	PRL 125 241801	J.P. Lees et al.	(BABAR Collab.)
LEES	14G	PR D89 111102	J.P. Lees et al.	(BABAR Collab.)
GE	11	PR D84 032008	J.Y. Ge et al.	(CLEO Collab.)
KORNICER	11	PR D83 054003	M. Kornicer et al.	(CLEO Collab.)
LEES	11C	PR D84 011104	J.P. Lees et al.	(BABAR Collab.)
LEES	11H	PRL 107 221803	J.P. Lees et al.	(BABAR Collab.)
LEES	11J	PR D84 072002	J.P. Lees et al.	(BABAR Collab.)
LEES	11K	PR D84 091101	J.P. Lees et al.	(BABAR Collab.)
LEES	11L	PR D84 092003	J.P. Lees et al.	(BABAR Collab.)
BONVICINI	10	PR D81 031104	G. Bonvicini et al.	(CLEO Collab.)
LEES	10B	PRL 104 151802	J.P. Lees et al.	(BABAR Collab.)
AUBERT	09AQ	PRL 103 161801	B. Aubert et al.	(BABAR Collab.)
AUBERT	09P	PRL 103 181801	B. Aubert et al.	(BABAR Collab.)
AUBERT	09Z	PRL 103 081803	B. Aubert et al.	(BABAR Collab.)
BHARI	09	PR D79 011103	S.R. Bhari et al.	(CLEO Collab.)
ASNER	08A	PR D78 091103	D.M. Asner et al.	(CLEO Collab.)
AUBERT	08BP	PR D78 112002	B. Aubert et al.	(BABAR Collab.)
AUBERT	08V	PRL 101 071801	B. Aubert et al.	(BABAR Collab.)
HE	08A	PRL 101 192001	Q. He et al.	(CLEO Collab.)
LOVE	08A	PRL 101 201601	W. Love et al.	(CLEO Collab.)
PDG	08	PL B667 1	C. Amstutz et al.	(PDG Collab.)
BESSON	07	PRL 98 052002	D. Besson et al.	(CLEO Collab.)
ROSNER	07A	PR D76 117102	J.L. Rosner et al.	(CLEO Collab.)
BESSON	06A	PR D74 012003	D. Besson et al.	(CLEO Collab.)
ROSNER	06	PRL 96 092003	J.L. Rosner et al.	(CLEO Collab.)
ADAMS	05	PRL 94 012001	G.S. Adams et al.	(CLEO Collab.)
ARTUSO	05	PRL 94 032001	M. Artuso et al.	(CLEO Collab.)
ARTAMONOV	00	PL B474 427	A.S. Artamonov et al.	(CLEO Collab.)
BUTLER	94B	PR D49 40	F. Butler et al.	(CLEO Collab.)
WU	92	PL B301 307	Q.W. Wu et al.	(CUSB Collab.)
HEINTZ	92	PR D46 1928	U. Heintz et al.	(CUSB Collab.)
BROCK	91	PR D43 1448	I.C. Brock et al.	(CLEO Collab.)
HEINTZ	91	PRL 66 1563	U. Heintz et al.	(CUSB Collab.)
MORRISON	91	PRL 67 1696	R.J. Morrison et al.	(CLEO Collab.)
NARAIN	91	PRL 66 3113	M. Narain et al.	(CUSB Collab.)
CHEN	89B	PR D39 3528	W.Y. Chen et al.	(CLEO Collab.)
KAARSBERG	89	PRL 62 2077	T.M. Kaarsberg et al.	(CUSB Collab.)
BUCHMUELLER	88	HE $e^+ e^-$ Physics 412	W. Buchmueller, S. Cooper	(HANN, DESY, MIT)
Editors: A. Ali and P. Soeding, World Scientific, Singapore				
COHEN	87	RMP 59 1121	E.R. Cohen, B.N. Taylor	(RISC, NBS)
BARU	86B	ZPHY C32 622 (errata)	E.E. Baru et al.	(NOVO)
KURAEV	85	SJNP 41 466	E.A. Kurayev, V.S. Fadin	(NOVO)
Translated from YAF 41 723				
ARTAMONOV	84	PL 137B 272	A.S. Artamonov et al.	(NOVO)
GILES	84B	PR D29 1285	R. Giles et al.	(CLEO Collab.)
ANDREWS	83	PRL 50 807	D.E. Andrews et al.	(CLEO Collab.)
GREEN	82	PRL 49 617	J. Green et al.	(CLEO Collab.)
MAGERAS	82	PL 118B 453	G. Mageras et al.	(COLU, CORN, LSU+)

⁵ The mass barycenter of the merged lineshapes from the $J = 1$ and 2 states.

$\chi_{b1}(3P)$ DECAY MODES

Mode	Fraction (Γ_i/Γ)
Γ_1 $\Upsilon(1S)\gamma$	seen
Γ_2 $\Upsilon(2S)\gamma$	seen
Γ_3 $\Upsilon(3S)\gamma$	seen

$\chi_{b1}(3P)$ BRANCHING RATIOS

$\Gamma(\Upsilon(1S)\gamma)/\Gamma_{\text{total}}$					Γ_1/Γ
VALUE	EVTS	DOCUMENT ID	TECN	COMMENT	
seen	169	¹ AAIJ	14Bg LHCb	$pp \rightarrow \gamma \mu^+ \mu^- X$	
• • • We do not use the following data for averages, fits, limits, etc. • • •					
seen	AAD	12A	ATLS	$pp \rightarrow \gamma \mu^+ \mu^- X$	
seen	ABAZOV	12Q	D0	$p\bar{p} \rightarrow \gamma \mu^+ \mu^- X$	

¹ From $\chi_{b1}(3P) \rightarrow \Upsilon(1S, 2S)\gamma$ transitions assuming $m_{\chi_{b2}(3P)} - m_{\chi_{b1}(3P)} = 10.5 \pm 1.5$ MeV and allowing for $\pm 30\%$ variation in the $\chi_{b2}(3P)$ production rate relative to that of $\chi_{b1}(3P)$.

$\Gamma(\Upsilon(2S)\gamma)/\Gamma_{\text{total}}$					Γ_2/Γ
VALUE	EVTS	DOCUMENT ID	TECN	COMMENT	
seen	169	¹ AAIJ	14Bg LHCb	$pp \rightarrow \gamma \mu^+ \mu^- X$	
• • • We do not use the following data for averages, fits, limits, etc. • • •					
seen	AAD	12A	ATLS	$pp \rightarrow \gamma \mu^+ \mu^- X$	

¹ From $\chi_{b1}(3P) \rightarrow \Upsilon(1S, 2S)\gamma$ transitions assuming $m_{\chi_{b2}(3P)} - m_{\chi_{b1}(3P)} = 10.5 \pm 1.5$ MeV and allowing for $\pm 30\%$ variation in the $\chi_{b2}(3P)$ production rate relative to that of $\chi_{b1}(3P)$.

$\Gamma(\Upsilon(3S)\gamma)/\Gamma_{\text{total}}$					Γ_3/Γ
VALUE	EVTS	DOCUMENT ID	TECN	COMMENT	
seen		SIRUNYAN	18N	CMS	$pp \rightarrow \gamma \mu^+ \mu^- X$
seen	182	AAIJ	14B1	LHCb	$pp \rightarrow \gamma \mu^+ \mu^- X$

$\chi_{b1}(3P)$ REFERENCES

SIRUNYAN	18N	PRL 121 092002	A.M. Sirunyan et al.	(CMS Collab.)
AAIJ	14Bg	JHEP 1410 088	R. Aaij et al.	(LHCb Collab.)
AAIJ	14B1	EPL C74 3092	R. Aaij et al.	(LHCb Collab.)
AAD	12A	PRL 108 152001	G. Aad et al.	(ATLAS Collab.)
ABAZOV	12Q	PR D86 031103	V.M. Abazov et al.	(D0 Collab.)

$\chi_{b2}(3P)$

$$I^G(J^{PC}) = 0^+(2^{++})$$

Observed in the radiative decay to $\Upsilon(3S)$, therefore $C = +$. J needs confirmation.

$\chi_{b1}(3P)$

$$I^G(J^{PC}) = 0^+(1^{++})$$

Observed in the radiative decay to $\Upsilon(1S, 2S, 3S)$, therefore $C = +$. J needs confirmation.

$\chi_{b1}(3P)$ MASS

VALUE (MeV)	EVTS	DOCUMENT ID	TECN	COMMENT
10513.42 \pm 0.41 \pm 0.53		¹ SIRUNYAN	18N	CMS $pp \rightarrow \gamma \mu^+ \mu^- X$
• • • We do not use the following data for averages, fits, limits, etc. • • •				
10515.7 \pm 2.2 \pm 1.5	169	² AAIJ	14Bg	LHCb $pp \rightarrow \gamma \mu^+ \mu^- X$
- 3.9 \pm 2.1				
10512.1 \pm 2.1 \pm 0.9	351	³ AAIJ	14Bg	LHCb $pp \rightarrow \gamma \mu^+ \mu^- X$
10511.3 \pm 1.7 \pm 2.5	182	⁴ AAIJ	14B1	LHCb $pp \rightarrow \gamma \mu^+ \mu^- X$
10530 \pm 5 \pm 9		⁵ AAD	12A	ATLS $pp \rightarrow \gamma \mu^+ \mu^- X$
10551 \pm 14 \pm 17		⁵ ABAZOV	12Q	D0 $p\bar{p} \rightarrow \gamma \mu^+ \mu^- X$

¹ Systematic error includes an additional 0.5 MeV for the uncertainty on the $\Upsilon(3S)$ mass. Also measures $m_{\chi_{b2}(3P)} - m_{\chi_{b1}(3P)} = 10.60 \pm 0.64 \pm 0.17$ MeV. A total of 372 $\chi_{b1}(3P)$ and $\chi_{b2}(3P)$ events was observed.

² From $\chi_{b1}(3P) \rightarrow \Upsilon(1S, 2S)\gamma$ transitions assuming $m_{\chi_{b2}(3P)} - m_{\chi_{b1}(3P)} = 10.5 \pm 1.5$ MeV and allowing for $\pm 30\%$ variation in the $\chi_{b2}(3P)$ production rate relative to that of $\chi_{b1}(3P)$.

³ The mass of the $\chi_{b1}(3P)$ state obtained by combining the results of AAIJ 14Bg with that of AAIJ 14B1. The first uncertainty is experimental and the second attributable to the unknown mass splitting, assumed to be $m_{\chi_{b2}(3P)} - m_{\chi_{b1}(3P)} = 10.5 \pm 1.5$ MeV.

⁴ From $\chi_{b1}(3P) \rightarrow \Upsilon(3S)\gamma$ transition assuming $m_{\chi_{b2}(3P)} - m_{\chi_{b1}(3P)} = 10.5 \pm 1.5$ MeV.

$\chi_{b2}(3P)$ MASS

VALUE (MeV)	DOCUMENT ID	TECN	COMMENT
10524.02 \pm 0.57 \pm 0.53	¹ SIRUNYAN	18N	CMS $pp \rightarrow \gamma \mu^+ \mu^- X$
• • • We do not use the following data for averages, fits, limits, etc. • • •			
10530 \pm 5 \pm 9	² AAD	12A	ATLS $pp \rightarrow \gamma \mu^+ \mu^- X$

¹ Systematic error includes an additional 0.5 MeV for the uncertainty on the $\Upsilon(3S)$ mass. Also measures $m_{\chi_{b2}(3P)} - m_{\chi_{b1}(3P)} = 10.60 \pm 0.64 \pm 0.17$ MeV. A total of 372 $\chi_{b1}(3P)$ and $\chi_{b2}(3P)$ events was observed.

² The mass barycenter of the merged lineshapes from the $J = 1$ and 2 states.

$\chi_{b2}(3P)$ DECAY MODES

Mode	Fraction (Γ_i/Γ)
Γ_1 $\Upsilon(3S)\gamma$	seen

$\chi_{b2}(3P)$ BRANCHING RATIOS

$\Gamma(\Upsilon(3S)\gamma)/\Gamma_{\text{total}}$					Γ_1/Γ
VALUE	EVTS	DOCUMENT ID	TECN	COMMENT	
seen		SIRUNYAN	18N	CMS	$pp \rightarrow \gamma \mu^+ \mu^- X$

Meson Particle Listings

$\chi_{b2}(3P), \Upsilon(4S)$

$\chi_{b2}(3P)$ REFERENCES

SIRUNYAN AAD	18N 12A	PRL 121 092002 PRL 108 152001	A.M. Sirunyan et al. G. Aad et al.	(CMS Collab.) (ATLAS Collab.)
-----------------	------------	----------------------------------	---------------------------------------	----------------------------------

$\Upsilon(4S)$

$$I^G(J^{PC}) = 0^-(1^{--})$$

also known as $\Upsilon(10580)$

$\Upsilon(4S)$ MASS

VALUE (MeV)	DOCUMENT ID	TECN	COMMENT
10579.4 ± 1.2 OUR AVERAGE			
10579.3 ± 0.4 ± 1.2	AUBERT	05Q	BABR $e^+e^- \rightarrow$ hadrons
10580.0 ± 3.5	¹ BEBEK	87	CLEO $e^+e^- \rightarrow$ hadrons
••• We do not use the following data for averages, fits, limits, etc. •••			
10577.4 ± 1.0	² LOVELOCK	85	CUSB $e^+e^- \rightarrow$ hadrons
¹ Reanalysis of BESSON 85.			
² No systematic error given.			

$\Upsilon(4S)$ WIDTH

VALUE (MeV)	DOCUMENT ID	TECN	COMMENT
20.5 ± 2.5 OUR AVERAGE			
20.7 ± 1.6 ± 2.5	AUBERT	05Q	BABR $e^+e^- \rightarrow$ hadrons
20 ± 2 ± 4	BESSON	85	CLEO $e^+e^- \rightarrow$ hadrons
••• We do not use the following data for averages, fits, limits, etc. •••			
25 ± 2.5	LOVELOCK	85	CUSB $e^+e^- \rightarrow$ hadrons

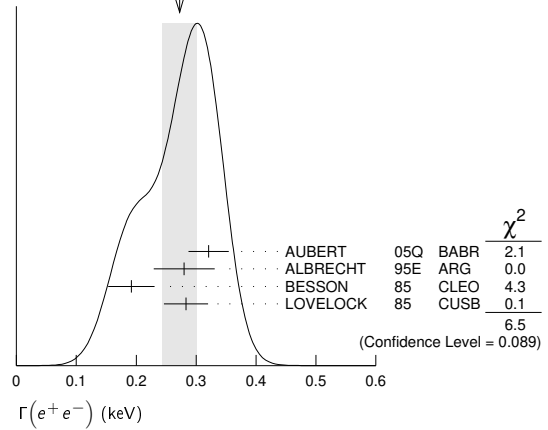
$\Upsilon(4S)$ DECAY MODES

Mode	Fraction (Γ_i/Γ)	Confidence level
Γ_1 $B\bar{B}$	> 96 %	95%
Γ_2 B^+B^-	(51.4 ± 0.6) %	
Γ_3 D_s^+ anything + c.c.	(17.8 ± 2.6) %	
Γ_4 $B^0\bar{B}^0$	(48.6 ± 0.6) %	
Γ_5 $J/\psi K_S^0 + (J/\psi, \eta_c) K_S^0$	< 4 × 10 ⁻⁷	90%
Γ_6 non- $B\bar{B}$	< 4 %	95%
Γ_7 e^+e^-	(1.57 ± 0.08) × 10 ⁻⁵	
Γ_8 $\rho^+\rho^-$	< 5.7 × 10 ⁻⁶	90%
Γ_9 $K^*(892)^0\bar{K}^0$	< 2.0 × 10 ⁻⁶	90%
Γ_{10} $J/\psi(1S)$ anything	< 1.9 × 10 ⁻⁴	95%
Γ_{11} D^{*+} anything + c.c.	< 7.4 %	90%
Γ_{12} ϕ anything	(7.1 ± 0.6) %	
Γ_{13} $\phi\eta$	< 1.8 × 10 ⁻⁶	90%
Γ_{14} $\phi\eta'$	< 4.3 × 10 ⁻⁶	90%
Γ_{15} $\rho\eta$	< 1.3 × 10 ⁻⁶	90%
Γ_{16} $\rho\eta'$	< 2.5 × 10 ⁻⁶	90%
Γ_{17} $\Upsilon(1S)$ anything	< 4 × 10 ⁻³	90%
Γ_{18} $\Upsilon(1S)\pi^+\pi^-$	(8.2 ± 0.4) × 10 ⁻⁵	
Γ_{19} $\Upsilon(1S)\eta$	(1.81 ± 0.18) × 10 ⁻⁴	
Γ_{20} $\Upsilon(1S)\eta'$	(3.4 ± 0.9) × 10 ⁻⁵	
Γ_{21} $\Upsilon(2S)\pi^+\pi^-$	(8.2 ± 0.8) × 10 ⁻⁵	
Γ_{22} $h_b(1P)\pi^+\pi^-$	not seen	
Γ_{23} $h_b(1P)\eta$	(2.18 ± 0.21) × 10 ⁻³	
Γ_{24} $\eta_b(1S)\omega$	< 1.8 × 10 ⁻⁴	90%
Γ_{25} 2H anything	< 1.3 × 10 ⁻⁵	90%
Double Radiative Decays		
Γ_{26} $\gamma\gamma \Upsilon(D) \rightarrow \gamma\gamma\eta \Upsilon(1S)$	< 2.3 × 10 ⁻⁵	90%

$\Upsilon(4S)$ PARTIAL WIDTHS

$\Gamma(e^+e^-)$	DOCUMENT ID	TECN	COMMENT
0.272 ± 0.029 OUR AVERAGE			Error includes scale factor of 1.5. See the ideogram below.
0.321 ± 0.017 ± 0.029	AUBERT	05Q	BABR $e^+e^- \rightarrow$ hadrons
0.28 ± 0.05 ± 0.01	¹ ALBRECHT	95E	ARG $e^+e^- \rightarrow$ hadrons
0.192 ± 0.007 ± 0.038	BESSON	85	CLEO $e^+e^- \rightarrow$ hadrons
0.283 ± 0.037	LOVELOCK	85	CUSB $e^+e^- \rightarrow$ hadrons
¹ Using LEYAOUANC 77 parametrization of $\Gamma(s)$.			

WEIGHTED AVERAGE
0.272 ± 0.029 (Error scaled by 1.5)



$\Upsilon(4S)$ BRANCHING RATIOS

$B\bar{B}$ DECAYS

The ratio of branching fraction to charged and neutral B mesons is often derived assuming isospin invariance in the decays, and relies on the knowledge of the B^+/B^0 lifetime ratio. "OUR EVALUATION" is obtained based on averages of rescaled data listed below. The average and rescaling were performed by the Heavy Flavor Averaging Group (HFLAV) and are described at <https://hflav.web.cern.ch/>. The averaging/rescaling procedure takes into account the common dependence of the measurement on the value of the lifetime ratio.

$\Gamma(B^+B^-)/\Gamma_{total}$	DOCUMENT ID	TECN	COMMENT
0.514 ± 0.006 OUR EVALUATION			(Produced by HFLAV) Assuming $B(\Upsilon(4S) \rightarrow B\bar{B}) = 1$

$\Gamma(D_s^+ \text{ anything + c.c.})/\Gamma_{total}$	DOCUMENT ID	TECN	COMMENT
0.178 ± 0.021 ± 0.016	¹ ARTUSO	05B	CLE3 $e^+e^- \rightarrow D_X X$
¹ ARTUSO 05B reports $[\Gamma(\Upsilon(4S) \rightarrow D_s^+ \text{ anything + c.c.})/\Gamma_{total}] \times [B(D_s^+ \rightarrow \phi\pi^+)] = (8.0 \pm 0.2 \pm 0.9) \times 10^{-3}$ which we divide by our best value $B(D_s^+ \rightarrow \phi\pi^+) = (4.5 \pm 0.4) \times 10^{-2}$. Our first error is their experiment's error and our second error is the systematic error from using our best value.			

$\Gamma(B^0\bar{B}^0)/\Gamma_{total}$	DOCUMENT ID	TECN	COMMENT
0.486 ± 0.006 OUR EVALUATION			Assuming $B(\Upsilon(4S) \rightarrow B\bar{B}) = 1$
••• We do not use the following data for averages, fits, limits, etc. •••			
0.487 ± 0.010 ± 0.008	¹ AUBERT, B	05H	BABR $\Upsilon(4S) \rightarrow \bar{B}B \rightarrow D^* \ell \nu_\ell$
¹ Direct measurement. This value is averaged with the value extracted from the $\Gamma(B^+B^-) / \Gamma(B^0\bar{B}^0)$ measurements.			

$\Gamma(B^+B^-)/\Gamma(B^0\bar{B}^0)$	DOCUMENT ID	TECN	COMMENT
1.058 ± 0.024 OUR EVALUATION			
1.065 ± 0.012 ± 0.051	¹ CHOUDHURY	23	BELL $\Upsilon(4S) \rightarrow B\bar{B} \rightarrow J/\psi K$
1.006 ± 0.036 ± 0.031	² AUBERT	04F	BABR $\Upsilon(4S) \rightarrow B\bar{B} \rightarrow J/\psi K$
1.01 ± 0.03 ± 0.09	² HASTINGS	03	BELL $\Upsilon(4S) \rightarrow B\bar{B} \rightarrow$ dileptons
1.058 ± 0.084 ± 0.136	³ ATHAR	02	CLEO $\Upsilon(4S) \rightarrow B\bar{B} \rightarrow D^* \ell \nu$
1.10 ± 0.06 ± 0.05	⁴ AUBERT	02	BABR $\Upsilon(4S) \rightarrow B\bar{B} \rightarrow (c\bar{c}) K^*$
1.04 ± 0.07 ± 0.04	⁵ ALEXANDER	01	CLEO $\Upsilon(4S) \rightarrow B\bar{B} \rightarrow J/\psi K^*$
¹ CHOUDHURY 23 includes uncertainty due to the isospin symmetry assumption in $B \rightarrow J/\psi K$ decays.			
² HASTINGS 03 and AUBERT 04F assume $\tau(B^+) / \tau(B^0) = 1.083 \pm 0.017$.			
³ ATHAR 02 assumes $\tau(B^+) / \tau(B^0) = 1.074 \pm 0.028$. Supersedes BARISH 95.			
⁴ AUBERT 02 assumes $\tau(B^+) / \tau(B^0) = 1.062 \pm 0.029$.			
⁵ ALEXANDER 01 assumes $\tau(B^+) / \tau(B^0) = 1.066 \pm 0.024$.			

$[\Gamma(J/\psi K_S^0) + \Gamma((J/\psi, \eta_c) K_S^0)]/\Gamma_{total}$	DOCUMENT ID	TECN	COMMENT
< 4			Forbidden by CP invariance.
< 4	¹ TAJIMA	07A	BELL $\Upsilon(4S) \rightarrow B^0\bar{B}^0$
¹ $\Upsilon(4S)$ with CP = +1 decays to the final state with CP = -1.			

non- $B\bar{B}$ DECAYS

$\Gamma(\text{non-}B\bar{B})/\Gamma_{total}$	DOCUMENT ID	TECN	COMMENT
< 0.04			
< 0.04		95	BARISH 96B CLEO e^+e^-

Meson Particle Listings

$\Upsilon(4S)$

$\Gamma(e^+e^-)/\Gamma_{\text{total}}$ Γ_7/Γ

VALUE (units 10^{-9})	CL%	DOCUMENT ID	TECN	COMMENT
1.57 ± 0.08 OUR AVERAGE				
$1.55 \pm 0.04 \pm 0.07$		AUBERT	05Q BABR	$e^+e^- \rightarrow$ hadrons
$2.77 \pm 0.50 \pm 0.49$		¹ ALBRECHT	95E ARG	$e^+e^- \rightarrow$ hadrons

¹ Using LEYAOUANC 77 parametrization of $\Gamma(s)$.

$\Gamma(\rho^+\rho^-)/\Gamma_{\text{total}}$ Γ_8/Γ

VALUE	CL%	DOCUMENT ID	TECN	COMMENT
$<5.7 \times 10^{-6}$	90	AUBERT	08B0 BABR	$e^+e^- \rightarrow \pi^+\pi^-2\pi^0$

$\Gamma(K^*(892)^0\bar{K}^0)/\Gamma_{\text{total}}$ Γ_9/Γ

VALUE	CL%	DOCUMENT ID	TECN	COMMENT
$<2.0 \times 10^{-6}$	90	SHEN	13A BELL	$e^+e^- \rightarrow K^*(892)^0\bar{K}^0$

$\Gamma(J/\psi(1S) \text{ anything})/\Gamma_{\text{total}}$ Γ_{10}/Γ

VALUE (units 10^{-4})	CL%	DOCUMENT ID	TECN	COMMENT
<1.9	95	¹ ABE	02D BELL	$e^+e^- \rightarrow J/\psi X \rightarrow \ell^+\ell^-X$
<4.7	90	¹ AUBERT	01c BABR	$e^+e^- \rightarrow J/\psi X \rightarrow \ell^+\ell^-X$

¹ Uses $B(J/\psi \rightarrow e^+e^-) = 0.0593 \pm 0.0010$ and $B(J/\psi \rightarrow \mu^+\mu^-) = 0.0588 \pm 0.0010$.

$\Gamma(D^{*+} \text{ anything} + c.c.)/\Gamma_{\text{total}}$ Γ_{11}/Γ

VALUE	CL%	DOCUMENT ID	TECN	COMMENT
<0.074	90	¹ ALEXANDER	90c CLEO	e^+e^-

¹ For $x > 0.473$.

$\Gamma(\phi \text{ anything})/\Gamma_{\text{total}}$ Γ_{12}/Γ

VALUE (units 10^{-2})	CL%	DOCUMENT ID	TECN	COMMENT
$7.1 \pm 0.1 \pm 0.6$		HUANG	07 CLEO	$\Upsilon(4S) \rightarrow \phi X$
<0.23	90	¹ ALEXANDER	90c CLEO	e^+e^-

¹ For $x > 0.52$.

$\Gamma(\phi\eta)/\Gamma_{\text{total}}$ Γ_{13}/Γ

VALUE (units 10^{-6})	CL%	DOCUMENT ID	TECN	COMMENT
<1.8	90	¹ BELOUS	09 BELL	$e^+e^- \rightarrow \phi\eta$
<2.5	90	AUBERT, BE	06F BABR	$e^+e^- \rightarrow \phi\eta$

¹ Using all intermedite branching fraction values from PDG 08.

$\Gamma(\phi\eta')/\Gamma_{\text{total}}$ Γ_{14}/Γ

VALUE (units 10^{-6})	CL%	DOCUMENT ID	TECN	COMMENT
<4.3	90	¹ BELOUS	09 BELL	$e^+e^- \rightarrow \phi\eta'$

¹ Using all intermedite branching fraction values from PDG 08.

$\Gamma(\rho\eta)/\Gamma_{\text{total}}$ Γ_{15}/Γ

VALUE (units 10^{-6})	CL%	DOCUMENT ID	TECN	COMMENT
<1.3	90	¹ BELOUS	09 BELL	$e^+e^- \rightarrow \rho\eta$

¹ Using all intermedite branching fraction values from PDG 08.

$\Gamma(\rho\eta')/\Gamma_{\text{total}}$ Γ_{16}/Γ

VALUE (units 10^{-6})	CL%	DOCUMENT ID	TECN	COMMENT
<2.5	90	¹ BELOUS	09 BELL	$e^+e^- \rightarrow \rho\eta'$

¹ Using all intermedite branching fraction values from PDG 08.

$\Gamma(\Upsilon(1S) \text{ anything})/\Gamma_{\text{total}}$ Γ_{17}/Γ

VALUE	CL%	DOCUMENT ID	TECN	COMMENT
<0.004	90	ALEXANDER	90c CLEO	e^+e^-

$\Gamma(\Upsilon(1S)\pi^+\pi^-)/\Gamma_{\text{total}}$ Γ_{18}/Γ

VALUE (units 10^{-5})	CL%	EVTS	DOCUMENT ID	TECN	COMMENT
8.2 ± 0.4 OUR AVERAGE					
$8.2 \pm 0.5 \pm 0.4$		515	GUIDO	17 BELL	$\Upsilon(4S) \rightarrow \pi^+\pi^-\mu^+\mu^-$
$8.5 \pm 1.3 \pm 0.1$		113 ± 16	¹ SOKOLOV	09 BELL	$e^+e^- \rightarrow \pi^+\pi^-\mu^+\mu^-$
$8.00 \pm 0.64 \pm 0.27$		430	² AUBERT	08BP BABR	$\Upsilon(4S) \rightarrow \pi^+\pi^-\ell^+\ell^-$
$17.8 \pm 4.0 \pm 0.3$			^{3,4} SOKOLOV	07 BELL	$e^+e^- \rightarrow \pi^+\pi^-\mu^+\mu^-$
$9.0 \pm 1.5 \pm 0.2$		167 ± 19	⁵ AUBERT	06R BABR	$e^+e^- \rightarrow \pi^+\pi^-\mu^+\mu^-$
<12	90		GLENN	99 CLE2	e^+e^-

¹ SOKOLOV 09 reports $[\Gamma(\Upsilon(4S) \rightarrow \Upsilon(1S)\pi^+\pi^-)/\Gamma_{\text{total}}] \times [B(\Upsilon(1S) \rightarrow \mu^+\mu^-)] = (0.211 \pm 0.030 \pm 0.014) \times 10^{-5}$ which we divide by our best value $B(\Upsilon(1S) \rightarrow \mu^+\mu^-) = (2.48 \pm 0.04) \times 10^{-2}$. Our first error is their experiment's error and our second error is the systematic error from using our best value.

² Using $B(\Upsilon(1S) \rightarrow e^+e^-) = (2.38 \pm 0.11)\%$ and $B(\Upsilon(1S) \rightarrow \mu^+\mu^-) = (2.48 \pm 0.05)\%$.

³ SOKOLOV 07 reports $[\Gamma(\Upsilon(4S) \rightarrow \Upsilon(1S)\pi^+\pi^-)/\Gamma_{\text{total}}] \times [B(\Upsilon(1S) \rightarrow \mu^+\mu^-)] = (4.42 \pm 0.81 \pm 0.56) \times 10^{-6}$ which we divide by our best value $B(\Upsilon(1S) \rightarrow \mu^+\mu^-) = (2.48 \pm 0.04) \times 10^{-2}$. Our first error is their experiment's error and our second error is the systematic error from using our best value.

⁴ According to the authors, systematic errors were underestimated.

⁵ Superseded by AUBERT 08BP. AUBERT 06R reports $[\Gamma(\Upsilon(4S) \rightarrow \Upsilon(1S)\pi^+\pi^-)/\Gamma_{\text{total}}] \times [B(\Upsilon(1S) \rightarrow \mu^+\mu^-)] = (2.23 \pm 0.25 \pm 0.27) \times 10^{-6}$ which we divide by our best value $B(\Upsilon(1S) \rightarrow \mu^+\mu^-) = (2.48 \pm 0.04) \times 10^{-2}$. Our first error is their experiment's error and our second error is the systematic error from using our best value.

$\Gamma(\Upsilon(1S)\eta)/\Gamma_{\text{total}}$ Γ_{19}/Γ

VALUE (units 10^{-4})	CL%	EVTS	DOCUMENT ID	TECN	COMMENT
1.81 ± 0.18 OUR AVERAGE					
$1.70 \pm 0.23 \pm 0.08$		49	GUIDO	17 BELL	$\Upsilon(4S) \rightarrow \pi^+\pi^-\pi^0\mu^+\mu^-$
$1.96 \pm 0.26 \pm 0.09$		56	¹ AUBERT	08BP BABR	$\Upsilon(4S) \rightarrow \pi^+\pi^-\pi^0\ell^+\ell^-$

• • • We do not use the following data for averages, fits, limits, etc. • • •

¹ Using $B(\Upsilon(1S) \rightarrow e^+e^-) = (2.38 \pm 0.11)\%$ and $B(\Upsilon(1S) \rightarrow \mu^+\mu^-) = (2.48 \pm 0.05)\%$.

² Using $B(\eta \rightarrow 2\gamma) = (39.41 \pm 0.20)\%$.

$\Gamma(\Upsilon(1S)\eta')/\Gamma_{\text{total}}$ Γ_{20}/Γ

VALUE (units 10^{-5})	EVTS	DOCUMENT ID	TECN	COMMENT
$3.43 \pm 0.88 \pm 0.21$	27	GUIDO	18 BELL	$\Upsilon(4S) \rightarrow (\rho^0\gamma, \pi^+\pi^-\eta)\mu^+\mu^-$

$\Gamma(\Upsilon(1S)\eta)/\Gamma(\Upsilon(1S)\pi^+\pi^-)$ Γ_{19}/Γ_{18}

VALUE	EVTS	DOCUMENT ID	TECN	COMMENT
$2.41 \pm 0.40 \pm 0.12$	56	¹ AUBERT	08BP BABR	$\Upsilon(4S) \rightarrow \pi^+\pi^-(\pi^0)\ell^+\ell^-$

¹ Not independent of other values reported by AUBERT 08BP.

$\Gamma(\Upsilon(2S)\pi^+\pi^-)/\Gamma_{\text{total}}$ Γ_{21}/Γ

VALUE (units 10^{-5})	CL%	EVTS	DOCUMENT ID	TECN	COMMENT
8.2 ± 0.8 OUR AVERAGE					
$7.9 \pm 1.0 \pm 0.4$		181	GUIDO	17 BELL	$\Upsilon(4S) \rightarrow \pi^+\pi^-\mu^+\mu^-$
$8.6 \pm 1.1 \pm 0.7$		220	¹ AUBERT	08BP BABR	$\Upsilon(4S) \rightarrow \pi^+\pi^-\ell^+\ell^-$
$8.8 \pm 1.7 \pm 0.8$		97 ± 15	² AUBERT	06R BABR	$e^+e^- \rightarrow \pi^+\pi^-\mu^+\mu^-$
<3.9	90		GLENN	99 CLE2	e^+e^-

¹ Using $B(\Upsilon(2S) \rightarrow e^+e^-) = (1.91 \pm 0.16)\%$ and $B(\Upsilon(2S) \rightarrow \mu^+\mu^-) = (1.93 \pm 0.17)\%$.

² Superseded by AUBERT 08BP. AUBERT 06R reports $[\Gamma(\Upsilon(4S) \rightarrow \Upsilon(2S)\pi^+\pi^-)/\Gamma_{\text{total}}] \times [B(\Upsilon(2S) \rightarrow \mu^+\mu^-)] = (1.69 \pm 0.26 \pm 0.20) \times 10^{-6}$ which we divide by our best value $B(\Upsilon(2S) \rightarrow \mu^+\mu^-) = (1.93 \pm 0.17) \times 10^{-2}$. Our first error is their experiment's error and our second error is the systematic error from using our best value.

$\Gamma(\Upsilon(2S)\pi^+\pi^-)/\Gamma(\Upsilon(1S)\pi^+\pi^-)$ Γ_{21}/Γ_{18}

VALUE	EVTS	DOCUMENT ID	TECN	COMMENT
$1.16 \pm 0.16 \pm 0.14$	220	¹ AUBERT	08BP BABR	$\Upsilon(4S) \rightarrow \pi^+\pi^-\ell^+\ell^-$

¹ Using $B(\Upsilon(1S) \rightarrow e^+e^-) = (2.38 \pm 0.11)\%$, $B(\Upsilon(1S) \rightarrow \mu^+\mu^-) = (2.48 \pm 0.05)\%$, $B(\Upsilon(2S) \rightarrow e^+e^-) = (1.91 \pm 0.16)\%$, and $B(\Upsilon(2S) \rightarrow \mu^+\mu^-) = (1.93 \pm 0.17)\%$. Not independent of other values reported by AUBERT 08BP.

$\Gamma(h_b(1P)\pi^+\pi^-)/\Gamma_{\text{total}}$ Γ_{22}/Γ

VALUE	EVTS	DOCUMENT ID	TECN	COMMENT
not seen	$(35 \pm 32)k$	¹ ADACHI	12 BELL	$10.58 e^+e^- \rightarrow h_b(1P)\pi^+\pi^-$

¹ From the upper limit on the ratio of $\sigma(e^+e^- \rightarrow h_b(1P)\pi^+\pi^-)$ at the $\Upsilon(4S)$ to that at the $\Upsilon(5S)$ of 0.27.

$\Gamma(h_b(1P)\eta)/\Gamma_{\text{total}}$ Γ_{23}/Γ

VALUE (units 10^{-3})	EVTS	DOCUMENT ID	TECN	COMMENT
$2.18 \pm 0.11 \pm 0.18$	112k	¹ TAMPONI	15 BELL	$e^+e^- \rightarrow h_b(1P)\eta$

¹ Using $B(\eta \rightarrow 2\gamma) = (39.41 \pm 0.20)\%$.

$\Gamma(h_b(1S)\omega)/\Gamma_{\text{total}}$ Γ_{24}/Γ

VALUE	CL%	DOCUMENT ID	TECN	COMMENT
$<1.8 \times 10^{-4}$	90	OSKIN	20 BELL	$e^+e^- \rightarrow \omega X$

$\Gamma(h_b(1S)\omega)/\Gamma(h_b(1P)\eta)$ Γ_{24}/Γ_{23}

VALUE	CL%	DOCUMENT ID	TECN	COMMENT
$<8.4 \times 10^{-2}$	90	¹ OSKIN	20 BELL	$e^+e^- \rightarrow \omega X$

¹ Using $B(\Upsilon(4S) \rightarrow h_b(1P)\eta) = (2.18 \pm 0.11 \pm 0.18) \times 10^{-3}$ from TAMPONI 15.

$\Gamma(\bar{2}H \text{ anything})/\Gamma_{\text{total}}$ Γ_{25}/Γ

VALUE (units 10^{-5})	CL%	DOCUMENT ID	TECN	COMMENT
<1.3	90	ASNER	07 CLEO	$e^+e^- \rightarrow \bar{D}X$

Double Radiative Decays

$\Gamma(\gamma\gamma\Upsilon(D) \rightarrow \gamma\gamma\Upsilon(1S))/\Gamma_{\text{total}}$ Γ_{26}/Γ

VALUE	CL%	DOCUMENT ID	TECN	COMMENT
$<2.3 \times 10^{-5}$	90	GUIDO	17 BELL	$\Upsilon(4S) \rightarrow \gamma\gamma\pi^+\pi^-\pi^0\mu^+\mu^-$

Meson Particle Listings

 $\Upsilon(4S)$, $\Upsilon(10753)$, $\Upsilon(10860)$ $\Upsilon(4S)$ REFERENCES

NAME	PR	YEAR	DOC ID	TECN	COMMENT	COLLAB
CHOUDHURY	23	PR	D107 1031102			(BELLE Collab.)
OSKIN	20	PR	D102 092011			(BELLE Collab.)
GUIDO	18	PRL	121 062001			(BELLE Collab.)
GUIDO	17	PR	D96 052005			(BELLE Collab.)
TAMPONI	15	PRL	115 142001			(BELLE Collab.)
SHEN	13A	PR	D88 052019			(BELLE Collab.)
ADACHI	12	PRL	108 032001			(BELLE Collab.)
BELOUS	09	PL	B681 400			(BELLE Collab.)
SOKOLOV	09	PR	D79 051103			(BELLE Collab.)
AUBERT	08B0	PR	D78 071103			(BABAR Collab.)
AUBERT	08BP	PR	D78 112002			(BABAR Collab.)
PDG	08	PL	B667 1			(PDG Collab.)
ASNER	07	PR	D75 012009			(CLEO Collab.)
HUANG	07	PR	D75 012002			(CLEO Collab.)
SOKOLOV	07	PR	D75 071103			(BELLE Collab.)
TAJIMA	07A	PRL	99 211601			(BELLE Collab.)
AUBERT	06R	PRL	96 232001			(BABAR Collab.)
AUBERT, BE	06F	PR	D74 111103			(BABAR Collab.)
ARTUSO	05B	PRL	95 261801			(CLEO Collab.)
AUBERT	05Q	PR	D72 032005			(BABAR Collab.)
AUBERT, B	05H	PRL	95 042001			(BABAR Collab.)
AUBERT	04F	PR	D69 071101			(BABAR Collab.)
HASTINGS	03	PR	D67 052004			(BELLE Collab.)
ABE	02D	PR	88 052001			(CLEO Collab.)
ATHAR	02	PR	D66 052003			(CLEO Collab.)
AUBERT	02	PR	D65 032001			(BABAR Collab.)
ALEXANDER	01	PRL	86 2737			(CLEO Collab.)
AUBERT	01C	PRL	87 162002			(BABAR Collab.)
GLENN	99	PR	D59 052003			(CLEO Collab.)
BARISH	96B	PRL	76 1570			(CLEO Collab.)
ALBRECHT	95E	ZPHY	C65 619			(ARGUS Collab.)
BARISH	95	PR	D51 1014			(CLEO Collab.)
ALEXANDER	90C	PRL	64 2226			(CLEO Collab.)
BEBEK	87	PR	D36 1289			(CLEO Collab.)
BESSION	85	PRL	54 381			(CLEO Collab.)
LOVELOCK	85	PRL	54 377			(CUSB Collab.)
LEYAOUANC	77	PL	B71 397			(ORSAY)

 $\Upsilon(10753)$

$$I^G(J^{PC}) = ?^?(1^{--})$$

OMITTED FROM SUMMARY TABLE

A candidate for $\Upsilon(3D)$ state or an exotic structure.Seen by MIZUK 19 in $e^+e^- \rightarrow \Upsilon(nS)\pi^+\pi^-$ ($n=1,2,3$) with a significance of 5.2 σ . $\Upsilon(10753)$ MASS

VALUE (MeV)	DOCUMENT ID	TECN	COMMENT
10752.7 \pm 5.9 \pm 0.7 \pm 1.1	¹ MIZUK	19	BELL $e^+e^- \rightarrow \Upsilon(nS)\pi^+\pi^-$
10761 \pm 2	² DONG	20A	$e^+e^- \rightarrow b\bar{b}$

- • • We do not use the following data for averages, fits, limits, etc. • • •
- ¹ From a simultaneous fit to the $\Upsilon(nS)\pi^+\pi^-$, $n = 1, 2, 3$, cross sections at 28 energy points within $\sqrt{s} = 10.63$ –11.02 GeV, including the initial-state radiation at $\Upsilon(10860)$.
- ² From a fit to the dressed cross sections of AUBERT 09E by BaBar and SANTEL 16 by Belle above 10.68 GeV with a coherent sum of a continuum amplitude and three Breit-Wigner functions with constant widths.

 $\Upsilon(10753)$ WIDTH

VALUE (MeV)	DOCUMENT ID	TECN	COMMENT
35.5 \pm 17.6 \pm 3.9 \pm 11.3 \pm 3.3	¹ MIZUK	19	BELL $e^+e^- \rightarrow \Upsilon(nS)\pi^+\pi^-$
48.5 \pm 3.0	² DONG	20A	$e^+e^- \rightarrow b\bar{b}$

- • • We do not use the following data for averages, fits, limits, etc. • • •
- ¹ From a simultaneous fit to the $\Upsilon(nS)\pi^+\pi^-$, $n = 1, 2, 3$, cross sections at 28 energy points within $\sqrt{s} = 10.63$ –11.02 GeV, including the initial-state radiation at $\Upsilon(10860)$.
- ² From a fit to the dressed cross sections of AUBERT 09E by BaBar and SANTEL 16 by Belle above 10.68 GeV with a coherent sum of a continuum amplitude and three Breit-Wigner functions with constant widths.

 $\Upsilon(10753)$ DECAY MODES

Mode	Γ
$\Upsilon(1S)\pi^+\pi^-$	Γ_1
$\Upsilon(2S)\pi^+\pi^-$	Γ_2
$\Upsilon(3S)\pi^+\pi^-$	Γ_3
$\omega\chi_{b1}(1P)$	Γ_4
$\omega\chi_{b2}(1P)$	Γ_5
e^+e^-	Γ_6

 $\Upsilon(10753)$ $\Gamma(i)\Gamma(e^+e^-)/\Gamma(\text{total})$

VALUE (eV)	DOCUMENT ID	TECN	COMMENT	$\Gamma_1\Gamma_6/\Gamma$
0.295 \pm 0.175	^{1,2} MIZUK	19	BELL $e^+e^- \rightarrow \Upsilon(nS)\pi^+\pi^-$	

- • • We do not use the following data for averages, fits, limits, etc. • • •
- ¹ From a simultaneous fit to the $\Upsilon(nS)\pi^+\pi^-$, $n = 1, 2, 3$, cross sections at 28 energy points within $\sqrt{s} = 10.63$ –11.02 GeV, including the initial-state radiation at $\Upsilon(10860)$.
- ² Reported as the range 0.12–0.47 eV obtained from multiple solutions of an amplitude fit within a model composed as a sum of Breit-Wigner functions.

 $\Upsilon(2S)\pi^+\pi^- \times \Gamma(e^+e^-)/\Gamma(\text{total})$

VALUE (eV)	DOCUMENT ID	TECN	COMMENT	$\Gamma_2\Gamma_6/\Gamma$
0.875 \pm 0.345	^{1,2} MIZUK	19	BELL $e^+e^- \rightarrow \Upsilon(nS)\pi^+\pi^-$	

- • • We do not use the following data for averages, fits, limits, etc. • • •
- ¹ From a simultaneous fit to the $\Upsilon(nS)\pi^+\pi^-$, $n = 1, 2, 3$, cross sections at 28 energy points within $\sqrt{s} = 10.63$ –11.02 GeV, including the initial-state radiation at $\Upsilon(10860)$.
- ² Reported as the range 0.53–1.22 eV obtained from multiple solutions of an amplitude fit within a model composed as a sum of Breit-Wigner functions.

 $\Upsilon(3S)\pi^+\pi^- \times \Gamma(e^+e^-)/\Gamma(\text{total})$

VALUE (eV)	DOCUMENT ID	TECN	COMMENT	$\Gamma_3\Gamma_6/\Gamma$
0.235 \pm 0.025	^{1,2} MIZUK	19	BELL $e^+e^- \rightarrow \Upsilon(nS)\pi^+\pi^-$	

- • • We do not use the following data for averages, fits, limits, etc. • • •
- ¹ From a simultaneous fit to the $\Upsilon(nS)\pi^+\pi^-$, $n = 1, 2, 3$, cross sections at 28 energy points within $\sqrt{s} = 10.63$ –11.02 GeV, including the initial-state radiation at $\Upsilon(10860)$.
- ² Reported as the range 0.21–0.26 eV obtained from multiple solutions of an amplitude fit within a model composed as a sum of Breit-Wigner functions.

 $\Upsilon(\omega\chi_{b1}(1P)) \times \Gamma(e^+e^-)/\Gamma(\text{total})$

VALUE (eV)	CL%	DOCUMENT ID	TECN	COMMENT	$\Gamma_4\Gamma_6/\Gamma$
0.63 \pm 0.39 \pm 0.20	68	¹ ADACHI	23	BELL $e^+e^- \rightarrow \pi^+\pi^-\pi^0\gamma\Upsilon(1S)$	

- ¹ A fit solution with constructive interference. The other solution corresponding to destructive interference gives a value of $2.01 \pm 0.38 \pm 0.76$ eV.

 $\Upsilon(\omega\chi_{b2}(1P)) \times \Gamma(e^+e^-)/\Gamma(\text{total})$

VALUE (eV)	CL%	DOCUMENT ID	TECN	COMMENT	$\Gamma_5\Gamma_6/\Gamma$
0.53 \pm 0.46 \pm 0.15	68	¹ ADACHI	23	BELL $e^+e^- \rightarrow \pi^+\pi^-\pi^0\gamma\Upsilon(1S)$	

- ¹ A fit solution with constructive interference. The other solution corresponding to destructive interference gives a value of $1.32 \pm 0.44 \pm 0.55$ eV.

 $\Upsilon(10753)$ REFERENCES

ADACHI	23	PRL	130 091902	I. Adachi et al.	(BELLE II Collab.)
DONG	20A	CP	C44 083001	X.-K. Dong et al.	
MIZUK	19	JHEP	1910 220	R. Mizuk et al.	(BELLE Collab.)
SANTEL	16	PR	D93 011101	D. Santel et al.	(BELLE Collab.)
AUBERT	09E	PRL	102 012001	B. Aubert et al.	(BABAR Collab.)

 $\Upsilon(10860)$

$$I^G(J^{PC}) = 0^-(1^{--})$$

 $\Upsilon(10860)$ MASS

VALUE (MeV)	DOCUMENT ID	TECN	COMMENT
10885.2 \pm 2.6 \pm 1.6	OUR AVERAGE		

10885.3 \pm 1.5 \pm 2.2 \pm 0.9	¹ MIZUK	19	BELL $e^+e^- \rightarrow \Upsilon(nS)\pi^+\pi^-$
10884.7 \pm 3.6 \pm 8.9 \pm 3.4 \pm 1.0	² MIZUK	16	BELL $e^+e^- \rightarrow h_b(1P, 2P)\pi^+\pi^-$

- • • We do not use the following data for averages, fits, limits, etc. • • •
- 10882 \pm 1
- 10881.8 \pm 1.0 \pm 1.2
- 10891.1 \pm 3.2 \pm 1.2 \pm 2.0
- 10879 \pm 3
- 10888.4 \pm 2.7 \pm 2.6 \pm 1.2
- 10876 \pm 2
- 10869 \pm 2
- 10868 \pm 6 \pm 5
- 10845 \pm 20
- ³ DONG 20A $e^+e^- \rightarrow b\bar{b}$
- ^{4,5} SANTEL 16 BELL $e^+e^- \rightarrow \text{hadrons}$
- ^{6,7} SANTEL 16 BELL $e^+e^- \rightarrow \Upsilon(1S, 2S, 3S)\pi^+\pi^-$
- ^{8,9} CHEN 10 BELL $e^+e^- \rightarrow \text{hadrons}$
- ¹⁰ CHEN 10 BELL $e^+e^- \rightarrow \Upsilon(1S, 2S, 3S)\pi^+\pi^-$
- ¹¹ AUBERT 09E BABR $e^+e^- \rightarrow \text{hadrons}$
- ¹² BESSION 85 CLEO $e^+e^- \rightarrow \text{hadrons}$
- ¹³ LOVELOCK 85 CUSB $e^+e^- \rightarrow \text{hadrons}$

- ¹ From a simultaneous fit to the $\Upsilon(nS)\pi^+\pi^-$, $n = 1, 2, 3$, cross sections at 28 energy points within $\sqrt{s} = 10.6$ –11.05 GeV, including the initial-state radiation at $\Upsilon(10860)$.
- ² From a simultaneous fit to the $h_b(nP)\pi^+\pi^-$, $n = 1, 2$ cross sections at 22 energy points within $\sqrt{s} = 10.77$ –11.02 GeV to a pair of interfering Breit-Wigner amplitudes modified by phase space factors, with eight resonance parameters (a mass and width for each of $\Upsilon(10860)$ and $\Upsilon(11020)$, a single relative phase, a single relative amplitude, and two overall normalization factors, one for each n). The systematic error estimate is dominated by possible interference with a small nonresonant continuum amplitude.
- ³ From a fit to the dressed cross sections of AUBERT 09E by BaBar and SANTEL 16 by Belle above 10.68 GeV with a coherent sum of a continuum amplitude and three Breit-Wigner functions with constant widths.
- ⁴ From a fit to the total hadronic cross sections measured at 60 energy points within $\sqrt{s} = 10.82$ –11.05 GeV to a pair of interfering Breit-Wigner amplitudes and two floating continuum amplitudes with $1/\sqrt{s}$ dependence, one coherent with the resonances and one incoherent, with six resonance parameters (a mass, width, and an amplitude for each of $\Upsilon(10860)$ and $\Upsilon(11020)$, one relative phase, and one decoherence coefficient).
- ⁵ Not including uncertain and potentially large systematic errors due to assumed continuum amplitude $1/\sqrt{s}$ dependence and related interference contributions.
- ⁶ From a simultaneous fit to the $\Upsilon(nS)\pi^+\pi^-$, $n = 1, 2, 3$, cross sections at 25 energy points within $\sqrt{s} = 10.6$ –11.05 GeV to a pair of interfering Breit-Wigner amplitudes modified by phase space factors, with fourteen resonance parameters (a mass, width, and three amplitudes for each of $\Upsilon(10860)$ and $\Upsilon(11020)$, a single universal relative phase, and three decoherence coefficients, one for each n). Continuum contributions were measured (and therefore fixed) to be zero.

- ⁷ Superseded by MIZUK 19.
⁸ In a model where a flat non-resonant $b\bar{b}$ -continuum is incoherently added to a second flat component interfering with two Breit-Wigner resonances. Systematic uncertainties not estimated.
⁹ The parameters of the $\Upsilon(11020)$ are fixed to those in AUBERT 09E.
¹⁰ In a model where a flat nonresonant $\Upsilon(1S, 2S, 3S)\pi^+\pi^-$ continuum interferes with a single Breit-Wigner resonance.
¹¹ In a model where a non-resonant $b\bar{b}$ -continuum represented by a threshold function at $\sqrt{s}=2m_B$ is incoherently added to a flat component interfering with two Breit-Wigner resonances. Not independent of other AUBERT 09E results. Systematic uncertainties not estimated.
¹² Assuming four Gaussians with radiative tails and a single step in R .
¹³ In a coupled-channel model with three resonances and a smooth step in R .

$\Upsilon(10860)$ WIDTH

VALUE (MeV)	DOCUMENT ID	TECN	COMMENT
37 ± 4 OUR AVERAGE			
$36.6^{+4.5+0.5}_{-3.9-1.1}$	¹ MIZUK	19	BELL $e^+e^- \rightarrow \Upsilon(nS)\pi^+\pi^-$
$40.6^{+12.7+1.1}_{-8.0-19.1}$	² MIZUK	16	BELL $e^+e^- \rightarrow h_b(1P, 2P)\pi^+\pi^-$
• • • We do not use the following data for averages, fits, limits, etc. • • •			
49.5 ± 1.5	³ DONG	20A	$e^+e^- \rightarrow b\bar{b}$
$48.5^{+1.9+2.0}_{-1.8-2.8}$	^{4,5} SANTEL	16	BELL $e^+e^- \rightarrow$ hadrons
$53.7^{+7.1+1.3}_{-5.6-5.4}$	^{6,7} SANTEL	16	BELL $e^+e^- \rightarrow \Upsilon(1S, 2S, 3S)\pi^+\pi^-$
$46 \pm \frac{9}{7}$	^{8,9} CHEN	10	BELL $e^+e^- \rightarrow$ hadrons
$30.7^{+8.3}_{-7.0} \pm 3.1$	¹⁰ CHEN	10	BELL $e^+e^- \rightarrow \Upsilon(1S, 2S, 3S)\pi^+\pi^-$
43 ± 4	⁸ AUBERT	09E	BABR $e^+e^- \rightarrow$ hadrons
74 ± 4	¹¹ AUBERT	09E	BABR $e^+e^- \rightarrow$ hadrons
$112 \pm 17 \pm 23$	¹² BESSON	85	CLEO $e^+e^- \rightarrow$ hadrons
110 ± 15	¹³ LOVELOCK	85	CUSB $e^+e^- \rightarrow$ hadrons

- ¹ From a simultaneous fit to the $\Upsilon(nS)\pi^+\pi^-$, $n = 1, 2, 3$, cross sections at 28 energy points within $\sqrt{s} = 10.6\text{--}11.05$ GeV, including the initial-state radiation at $\Upsilon(10860)$.
² From a simultaneous fit to the $h_b(nP)\pi^+\pi^-$, $n = 1, 2$ cross sections at 22 energy points within $\sqrt{s} = 10.77\text{--}11.02$ GeV to a pair of interfering Breit-Wigner amplitudes modified by phase space factors, with eight resonance parameters (a mass and width for each of $\Upsilon(10860)$ and $\Upsilon(11020)$, a single relative phase, a single relative amplitude, and two overall normalization factors, one for each n). The systematic error estimate is dominated by possible interference with a small nonresonant continuum amplitude.
³ From a fit to the dressed cross sections of AUBERT 09E by BaBar and SANTEL 16 by Belle above 10.68 GeV with a coherent sum of a continuum amplitude and three Breit-Wigner functions with constant widths.
⁴ From a fit to the total hadronic cross sections measured at 60 energy points within $\sqrt{s} = 10.82\text{--}11.05$ GeV to a pair of interfering Breit-Wigner amplitudes and two floating continuum amplitudes with $1/\sqrt{s}$ dependence, one coherent with the resonances and one incoherent, with six resonance parameters (a mass, width, and an amplitude for each of $\Upsilon(10860)$ and $\Upsilon(11020)$, one relative phase, and one decoherence coefficient).
⁵ Not including uncertain and potentially large systematic errors due to assumed continuum amplitude $1/\sqrt{s}$ dependence and related interference contributions.
⁶ From a simultaneous fit to the $\Upsilon(nS)\pi^+\pi^-$, $n = 1, 2, 3$, cross sections at 25 energy points within $\sqrt{s} = 10.6\text{--}11.05$ GeV to a pair of interfering Breit-Wigner amplitudes modified by phase space factors, with fourteen resonance parameters (a mass, width, and three amplitudes for each of $\Upsilon(10860)$ and $\Upsilon(11020)$, a single universal relative phase, and three decoherence coefficients, one for each n). Continuum contributions were measured (and therefore fixed) to be zero.
⁷ Superseded by MIZUK 19.
⁸ In a model where a flat non-resonant $b\bar{b}$ -continuum is incoherently added to a second flat component interfering with two Breit-Wigner resonances. Systematic uncertainties not estimated.
⁹ The parameters of the $\Upsilon(11020)$ are fixed to those in AUBERT 09E.
¹⁰ In a model where a flat nonresonant $\Upsilon(1S, 2S, 3S)\pi^+\pi^-$ continuum interferes with a single Breit-Wigner resonance.
¹¹ In a model where a non-resonant $b\bar{b}$ -continuum represented by a threshold function at $\sqrt{s}=2m_B$ is incoherently added to a flat component interfering with two Breit-Wigner resonances. Not independent of other AUBERT 09E results. Systematic uncertainties not estimated.
¹² Assuming four Gaussians with radiative tails and a single step in R .
¹³ In a coupled-channel model with three resonances and a smooth step in R .

$\Upsilon(10860)$ DECAY MODES

Mode	Fraction (Γ_i/Γ)	Confidence level
Γ_1 $B\bar{B}X$	$(76.2^{+2.7}_{-4.0})\%$	
Γ_2 $B\bar{B}$	$(5.5 \pm 1.0)\%$	
Γ_3 $B\bar{B}^* + \text{c.c.}$	$(13.7 \pm 1.6)\%$	
Γ_4 $B^*\bar{B}^*$	$(38.1 \pm 3.4)\%$	
Γ_5 $B\bar{B}^{(*)}\pi$	$< 19.7\%$	90%
Γ_6 $B\bar{B}\pi$	$(0.0 \pm 1.2)\%$	
Γ_7 $B^*\bar{B}\pi + B\bar{B}^*\pi$	$(7.3 \pm 2.3)\%$	
Γ_8 $B^*\bar{B}^*\pi$	$(1.0 \pm 1.4)\%$	
Γ_9 $B\bar{B}\pi\pi$	$< 8.9\%$	90%
Γ_{10} $B_s^{(*)}\bar{B}_s^{(*)}$	$(20.1 \pm 3.1)\%$	
Γ_{11} $B_s\bar{B}_s$	$(5 \pm 5) \times 10^{-3}$	

Γ_{12} $B_s\bar{B}_s^* + \text{c.c.}$	$(1.35 \pm 0.32)\%$	
Γ_{13} $B_s^*\bar{B}_s$	$(17.6 \pm 2.7)\%$	
Γ_{14} no open-bottom	$(3.8^{+5.0}_{-0.5})\%$	
Γ_{15} e^+e^-	$(8.3 \pm 2.1) \times 10^{-6}$	
Γ_{16} $K^*(892)^0\bar{K}^0$	$< 1.0 \times 10^{-5}$	90%
Γ_{17} $\Upsilon(1S)\pi^+\pi^-$	$(5.3 \pm 0.6) \times 10^{-3}$	
Γ_{18} $\Upsilon(1S)\eta$	$(8.5 \pm 1.7) \times 10^{-4}$	
Γ_{19} $\Upsilon(1S)\eta'$	$< 6.9 \times 10^{-5}$	90%
Γ_{20} $\Upsilon(2S)\pi^+\pi^-$	$(7.8 \pm 1.3) \times 10^{-3}$	
Γ_{21} $\Upsilon(2S)\eta$	$(4.1 \pm 0.6) \times 10^{-3}$	
Γ_{22} $\Upsilon(3S)\pi^+\pi^-$	$(4.8^{+1.9}_{-1.7}) \times 10^{-3}$	
Γ_{23} $\Upsilon(1S)K^+K^-$	$(6.1 \pm 1.8) \times 10^{-4}$	
Γ_{24} $\eta\Upsilon(1D)$	$(4.8 \pm 1.1) \times 10^{-3}$	
Γ_{25} $h_b(1P)\pi^+\pi^-$	$(3.5^{+1.0}_{-1.3}) \times 10^{-3}$	
Γ_{26} $h_b(2P)\pi^+\pi^-$	$(5.7^{+1.7}_{-2.1}) \times 10^{-3}$	
Γ_{27} $\chi_{bJ}(1P)\pi^+\pi^-\pi^0$	$(2.5 \pm 2.3) \times 10^{-3}$	
Γ_{28} $\chi_{b0}(1P)\pi^+\pi^-\pi^0$	$< 6.3 \times 10^{-3}$	90%
Γ_{29} $\chi_{b0}(1P)\omega$	$< 3.9 \times 10^{-3}$	90%
Γ_{30} $\chi_{b0}(1P)(\pi^+\pi^-\pi^0)_{\text{non-}\omega}$	$< 4.8 \times 10^{-3}$	90%
Γ_{31} $\chi_{b1}(1P)\pi^+\pi^-\pi^0$	$(1.85 \pm 0.33) \times 10^{-3}$	
Γ_{32} $\chi_{b1}(1P)\omega$	$(1.57 \pm 0.30) \times 10^{-3}$	
Γ_{33} $\chi_{b1}(1P)(\pi^+\pi^-\pi^0)_{\text{non-}\omega}$	$(5.2 \pm 1.9) \times 10^{-4}$	
Γ_{34} $\chi_{b2}(1P)\pi^+\pi^-\pi^0$	$(1.17 \pm 0.30) \times 10^{-3}$	
Γ_{35} $\chi_{b2}(1P)\omega$	$(6.0 \pm 2.7) \times 10^{-4}$	
Γ_{36} $\chi_{b2}(1P)(\pi^+\pi^-\pi^0)_{\text{non-}\omega}$	$(6 \pm 4) \times 10^{-4}$	
Γ_{37} $\gamma\chi_b \rightarrow \gamma\Upsilon(1S)\omega$	$< 3.8 \times 10^{-5}$	90%
Γ_{38} $\eta_b(1S)\omega$	$< 1.3 \times 10^{-3}$	90%
Γ_{39} $\eta_b(2S)\omega$	$< 5.6 \times 10^{-3}$	90%

Inclusive Decays.

These decay modes are submodes of one or more of the decay modes above.

Γ_{40} ϕ anything	$(13.8^{+2.4}_{-1.7})\%$
Γ_{41} D^0 anything + c.c.	$(112 \pm 6)\%$
Γ_{42} D_s anything + c.c.	$(44.7 \pm 2.6)\%$
Γ_{43} J/ψ anything	$(2.06 \pm 0.21)\%$
Γ_{44} B^0 anything + c.c.	$(77 \pm 8)\%$
Γ_{45} B^+ anything + c.c.	$(72 \pm 6)\%$

$\Upsilon(10860)$ PARTIAL WIDTHS

VALUE (keV)	DOCUMENT ID	TECN	COMMENT	Γ_{15}
0.31 ± 0.07 OUR AVERAGE Error includes scale factor of 1.3.				
$0.22 \pm 0.05 \pm 0.07$	BESSON	85	CLEO $e^+e^- \rightarrow$ hadrons	
0.365 ± 0.070	LOVELOCK	85	CUSB $e^+e^- \rightarrow$ hadrons	

VALUE (eV)	DOCUMENT ID	TECN	COMMENT	$\Gamma_{15}\Gamma_{17}/\Gamma$
• • • We do not use the following data for averages, fits, limits, etc. • • •				
1.09 ± 0.34	^{1,2} MIZUK	19	BELL $e^+e^- \rightarrow \Upsilon(nS)\pi^+\pi^-$	

- ¹ From a simultaneous fit to the $\Upsilon(nS)\pi^+\pi^-$, $n = 1, 2, 3$, cross sections at 28 energy points within $\sqrt{s} = 10.6\text{--}11.05$ GeV, including the initial-state radiation at $\Upsilon(10860)$.
² Reported as the range 0.75–1.43 eV obtained from multiple solutions of an amplitude fit within a model composed as a sum of Breit-Wigner functions.

VALUE (eV)	DOCUMENT ID	TECN	COMMENT	$\Gamma_{15}\Gamma_{20}/\Gamma$
• • • We do not use the following data for averages, fits, limits, etc. • • •				
2.58 ± 1.22	^{1,2} MIZUK	19	BELL $e^+e^- \rightarrow \Upsilon(nS)\pi^+\pi^-$	

- ¹ From a simultaneous fit to the $\Upsilon(nS)\pi^+\pi^-$, $n = 1, 2, 3$, cross sections at 28 energy points within $\sqrt{s} = 10.6\text{--}11.05$ GeV, including the initial-state radiation at $\Upsilon(10860)$.
² Reported as the range 1.35–3.80 eV obtained from multiple solutions of an amplitude fit within a model composed as a sum of Breit-Wigner functions.

VALUE (eV)	DOCUMENT ID	TECN	COMMENT	$\Gamma_{15}\Gamma_{22}/\Gamma$
• • • We do not use the following data for averages, fits, limits, etc. • • •				
0.73 ± 0.30	^{1,2} MIZUK	19	BELL $e^+e^- \rightarrow \Upsilon(nS)\pi^+\pi^-$	

- ¹ From a simultaneous fit to the $\Upsilon(nS)\pi^+\pi^-$, $n = 1, 2, 3$, cross sections at 28 energy points within $\sqrt{s} = 10.6\text{--}11.05$ GeV, including the initial-state radiation at $\Upsilon(10860)$.
² Reported as the range 0.43–1.03 eV obtained from multiple solutions of an amplitude fit within a model composed as a sum of Breit-Wigner functions.

Meson Particle Listings

 $\Upsilon(10860)$ $\Upsilon(10860)$ BRANCHING RATIOS

"OUR EVALUATION" is obtained based on averages of rescaled data listed below. The averages and rescaling were performed by the Heavy Flavor Averaging Group (HFLAV) and are described at <https://hflav.web.cern.ch/>.

 $\Gamma(B\bar{B}X)/\Gamma_{\text{total}}$

VALUE	EVTS	DOCUMENT ID	TECN	COMMENT
$0.762^{+0.027}_{-0.043}$ OUR EVALUATION				(Produced by HFLAV)
0.71 ± 0.06 OUR AVERAGE				
$0.737 \pm 0.032 \pm 0.051$	1063	¹ DRUTSKOY	10 BELL	$\Upsilon(5S) \rightarrow B^+X, B^0X$
$0.589 \pm 0.100 \pm 0.092$		² HUANG	07 CLEO	$\Upsilon(5S) \rightarrow \text{hadrons}$

¹ Not independent of DRUTSKOY 10 values for $\Upsilon(5S) \rightarrow B^{\pm,0}$ anything.
² Using measurements or limits from AQUINES 06.

 $\Gamma(B\bar{B}^*)/\Gamma_{\text{total}}$

VALUE (units 10^{-2})	CL%	DOCUMENT ID	TECN	COMMENT
$5.5^{+1.0}_{-0.9} \pm 0.4$		¹ DRUTSKOY	10 BELL	$\Upsilon(5S) \rightarrow B^+X, B^0X$
<13.8	90	² HUANG	07 CLEO	$\Upsilon(5S) \rightarrow \text{hadrons}$

• • • We do not use the following data for averages, fits, limits, etc. • • •
¹ Assuming isospin conservation.
² Using measurements or limits from AQUINES 06.

 $\Gamma(B\bar{B}^*)/\Gamma(B\bar{B}X)$

VALUE	CL%	DOCUMENT ID	TECN	COMMENT
<0.22	90	AQUINES	06 CLE3	$\Upsilon(5S) \rightarrow \text{hadrons}$

 $\Gamma(B\bar{B}^* + \text{c.c.})/\Gamma_{\text{total}}$

VALUE	DOCUMENT ID	TECN	COMMENT
0.137 ± 0.016 OUR AVERAGE			
$0.137 \pm 0.013 \pm 0.011$	¹ DRUTSKOY	10 BELL	$\Upsilon(5S) \rightarrow B^+X, B^0X$
$0.143 \pm 0.053 \pm 0.027$	² HUANG	07 CLEO	$\Upsilon(5S) \rightarrow \text{hadrons}$

¹ Assuming isospin conservation.
² Using measurements or limits from AQUINES 06.

 $\Gamma(B\bar{B}^* + \text{c.c.})/\Gamma(B\bar{B}X)$

VALUE	EVTS	DOCUMENT ID	TECN	COMMENT
$0.24 \pm 0.09 \pm 0.03$	10	AQUINES	06 CLE3	$\Upsilon(5S) \rightarrow \text{hadrons}$

 $\Gamma(B^*\bar{B}^*)/\Gamma_{\text{total}}$

VALUE	DOCUMENT ID	TECN	COMMENT
0.381 ± 0.034 OUR AVERAGE			
$0.375^{+0.023}_{-0.019} \pm 0.030$	¹ DRUTSKOY	10 BELL	$\Upsilon(5S) \rightarrow B^+X, B^0X$
$0.436 \pm 0.083 \pm 0.072$	² HUANG	07 CLEO	$\Upsilon(5S) \rightarrow \text{hadrons}$

¹ Assuming isospin conservation.
² Using measurements or limits from AQUINES 06.

 $\Gamma(B^*\bar{B}^*)/\Gamma(B\bar{B}X)$

VALUE	EVTS	DOCUMENT ID	TECN	COMMENT
$0.74 \pm 0.15 \pm 0.08$	31	AQUINES	06 CLE3	$\Upsilon(5S) \rightarrow \text{hadrons}$

 $\Gamma(B\bar{B}^*(\pi))/\Gamma_{\text{total}}$

VALUE	CL%	DOCUMENT ID	TECN	COMMENT
<0.197	90	¹ HUANG	07 CLEO	$\Upsilon(5S) \rightarrow \text{hadrons}$

¹ Using measurements or limits from AQUINES 06.

 $\Gamma(B\bar{B}^*(\pi))/\Gamma(B\bar{B}X)$

VALUE	CL%	DOCUMENT ID	TECN	COMMENT
<0.32	90	AQUINES	06 CLE3	$\Upsilon(5S) \rightarrow \text{hadrons}$

 $\Gamma(B\bar{B}\pi)/\Gamma_{\text{total}}$

VALUE (units 10^{-2})	EVTS	DOCUMENT ID	TECN	COMMENT
$0.0 \pm 1.2 \pm 0.3$	0	¹ DRUTSKOY	10 BELL	$\Upsilon(5S) \rightarrow B^+,0\pi^-X$

¹ Assuming isospin conservation.

 $[\Gamma(B^*\bar{B}\pi) + \Gamma(B\bar{B}^*\pi)]/\Gamma_{\text{total}}$

VALUE (units 10^{-2})	EVTS	DOCUMENT ID	TECN	COMMENT
$7.3^{+2.3}_{-2.1} \pm 0.8$	38	¹ DRUTSKOY	10 BELL	$\Upsilon(5S) \rightarrow B^+,0\pi^-X$

¹ Assuming isospin conservation.

 $\Gamma(B^*\bar{B}^*\pi)/\Gamma_{\text{total}}$

VALUE (units 10^{-2})	EVTS	DOCUMENT ID	TECN	COMMENT
$1.0^{+1.4}_{-1.3} \pm 0.4$	5	¹ DRUTSKOY	10 BELL	$\Upsilon(5S) \rightarrow B^+,0\pi^-X$

¹ Assuming isospin conservation.

 $\Gamma(B\bar{B}\pi\pi)/\Gamma_{\text{total}}$

VALUE	CL%	DOCUMENT ID	TECN	COMMENT
<0.089	90	¹ HUANG	07 CLEO	$\Upsilon(5S) \rightarrow \text{hadrons}$

¹ Using measurements or limits from AQUINES 06.

 $\Gamma(B\bar{B}\pi\pi)/\Gamma(B\bar{B}X)$

VALUE	CL%	DOCUMENT ID	TECN	COMMENT
<0.14	90	AQUINES	06 CLE3	$\Upsilon(5S) \rightarrow \text{hadrons}$

 $\Gamma(B_s^{(*)}\bar{B}_s^{(*)})/\Gamma_{\text{total}}$

VALUE	DOCUMENT ID	TECN	COMMENT
$0.201^{+0.030}_{-0.031}$ OUR EVALUATION			
$0.189^{+0.027}_{-0.021}$ OUR AVERAGE			
0.172 ± 0.030	¹ ESEN	13 BELL	$\Upsilon(5S) \rightarrow D^0X, D_sX$
$0.21^{+0.06}_{-0.03}$	² HUANG	07 CLEO	$\Upsilon(5S) \rightarrow D_sX$

• • • We do not use the following data for averages, fits, limits, etc. • • •

$0.180 \pm 0.013 \pm 0.032$	³ DRUTSKOY	07 BELL	$\Upsilon(5S) \rightarrow D^0X, D_sX$
$0.160 \pm 0.026 \pm 0.058$	⁴ ARTUSO	05B CLEO	$e^+e^- \rightarrow D_sX$

¹ Supersedes DRUTSKOY 07.
² Supersedes ARTUSO 05B. Combining inclusive $\phi, D_s,$ and B measurements. Using $B(D_s^+ \rightarrow \phi\pi^+) = 4.4 \pm 0.6\%$ from PDG 06.

³ Using $B(D_s^+ \rightarrow \phi\pi^+) = (4.4 \pm 0.6)\%$ from PDG 06.
⁴ Uses a model-dependent estimate $B(D_s \rightarrow D_sX) = (92 \pm 11)\%$.

¹ Supersedes DRUTSKOY 07.
² Supersedes ARTUSO 05B. Combining inclusive $\phi, D_s,$ and B measurements. Using $B(D_s^+ \rightarrow \phi\pi^+) = 4.4 \pm 0.6\%$ from PDG 06.

³ Using $B(D_s^+ \rightarrow \phi\pi^+) = (4.4 \pm 0.6)\%$ from PDG 06.
⁴ Uses a model-dependent estimate $B(D_s \rightarrow D_sX) = (92 \pm 11)\%$.

 $\Gamma(B_s^{(*)}\bar{B}_s^{(*)})/\Gamma(B\bar{B}X)$

VALUE	DOCUMENT ID
$0.264^{+0.052}_{-0.045}$ OUR EVALUATION	

 $\Gamma(B_s^{(*)}\bar{B}_s^{(*)})/\Gamma(B_s^{(*)}\bar{B}_s^{(*)})$

VALUE (units 10^{-2})	EVTS	DOCUMENT ID	TECN	COMMENT
87.8 ± 1.5 OUR AVERAGE				
87.0 ± 1.7	^{1,2} ESEN	13 BELL	$B_s^0 \rightarrow D_s^- \pi^+$	
$90.5 \pm 3.2 \pm 0.1$	227	^{2,3} LI	12 BELL	$B_s^0 \rightarrow J/\psi\eta'(\prime)$

• • • We do not use the following data for averages, fits, limits, etc. • • •

$90.1^{+3.8}_{-4.0} \pm 0.2$	⁴ LOUVOT	09 BELL	$10.86 e^+e^- \rightarrow B_s^{(*)}\bar{B}_s^{(*)}$
$93^{+7}_{-9} \pm 1$	⁴ DRUTSKOY	07A BELL	Superseded by LOUVOT 09

¹ Supersedes LOUVOT 09.
² With $N(B_s^{(*)}\bar{B}_s^{(*)}) = (7.11 \pm 1.30) \times 10^6$.

³ The ratios $N(B_s^{(*)}\bar{B}_s^{(*)})/N(B_s^{(*)}\bar{B}_s^{(*)})$ and $N(B_s^{(*)}\bar{B}_s^{(*)})/N(B_s^{(*)}\bar{B}_s^{(*)})$ are measured with a correlation coefficient of -0.72 .

⁴ From a measurement of $\sigma(e^+e^- \rightarrow B_s^*\bar{B}_s^*)/\sigma(e^+e^- \rightarrow B_s^{(*)}\bar{B}_s^{(*)})$ at $\sqrt{s} = 10.86$ GeV.

 $\Gamma(B_s\bar{B}_s)/\Gamma(B_s^{(*)}\bar{B}_s^{(*)})$

VALUE (units 10^{-2})	DOCUMENT ID	TECN	COMMENT
$2.6^{+2.6}_{-2.5}$	LOUVOT	09 BELL	$10.86 e^+e^- \rightarrow B_s^{(*)}\bar{B}_s^{(*)}$

¹ Supersedes LOUVOT 09.
² With $N(B_s^{(*)}\bar{B}_s^{(*)}) = (7.11 \pm 1.30) \times 10^6$.

³ The ratios $N(B_s\bar{B}_s)/N(B_s^{(*)}\bar{B}_s^{(*)})$ and $N(B_s\bar{B}_s)/N(B_s^{(*)}\bar{B}_s^{(*)})$ are measured with a correlation coefficient of -0.72 .

⁴ From a measurement of $\sigma(e^+e^- \rightarrow B_s^*\bar{B}_s^*)/\sigma(e^+e^- \rightarrow B_s^{(*)}\bar{B}_s^{(*)})$ at $\sqrt{s} = 10.86$ GeV.

 $\Gamma(B_s\bar{B}_s)/\Gamma(B_s^{(*)}\bar{B}_s^{(*)})$

VALUE	CL%	DOCUMENT ID	TECN	COMMENT
<0.16	90	BONVICINI	06 CLE3	e^+e^-

 $\Gamma(B_s\bar{B}_s^* + \text{c.c.})/\Gamma(B_s^{(*)}\bar{B}_s^{(*)})$

VALUE (units 10^{-2})	EVTS	DOCUMENT ID	TECN	COMMENT
6.7 ± 1.2 OUR AVERAGE				
7.3 ± 1.4	^{1,2} ESEN	13 BELL	$B_s^0 \rightarrow D_s^- \pi^+$	
$4.9 \pm 2.5 \pm 0.0$	227	^{2,3} LI	12 BELL	$B_s^0 \rightarrow J/\psi\eta'(\prime)$

• • • We do not use the following data for averages, fits, limits, etc. • • •

$7.3^{+3.3}_{-3.0} \pm 0.1$	LOUVOT	09 BELL	$10.86 e^+e^- \rightarrow B_s^{(*)}\bar{B}_s^{(*)}$
-----------------------------	--------	---------	---

¹ Supersedes LOUVOT 09.
² With $N(B_s^{(*)}\bar{B}_s^{(*)}) = (7.11 \pm 1.30) \times 10^6$.

³ The ratios $N(B_s\bar{B}_s^*)/N(B_s^{(*)}\bar{B}_s^{(*)})$ and $N(B_s\bar{B}_s^*)/N(B_s^{(*)}\bar{B}_s^{(*)})$ are measured with a correlation coefficient of -0.72 .

 $\Gamma(B_s\bar{B}_s^* + \text{c.c.})/\Gamma(B_s^{(*)}\bar{B}_s^{(*)})$

VALUE	CL%	DOCUMENT ID	TECN	COMMENT
<0.16	90	BONVICINI	06 CLE3	e^+e^-

 $\Gamma(\text{no open-bottom})/\Gamma_{\text{total}}$

VALUE	DOCUMENT ID
$0.038^{+0.051}_{-0.005}$ OUR EVALUATION	

 $\Gamma(K^*(892)^0\bar{K}^0)/\Gamma_{\text{total}}$

VALUE	CL%	DOCUMENT ID	TECN	COMMENT
$<1.0 \times 10^{-5}$	90	SHEN	13A BELL	$e^+e^- \rightarrow K^*(892)^0\bar{K}^0$

$\Gamma(\eta T_J(1D))/\Gamma_{\text{total}}$					Γ_{24}/Γ
VALUE (units 10^{-3})	DOCUMENT ID	TECN	COMMENT		
$4.82 \pm 0.92 \pm 0.67$	¹ TAMPONI	18	BELL	$e^+e^- \rightarrow \Upsilon(5S) \rightarrow \eta X$	
¹ Mainly $J = 2$, assumes no continuum contribution under $\Upsilon(5S)$.					

$\Gamma(\Upsilon(1S)\pi^+\pi^-)/\Gamma_{\text{total}}$					Γ_{17}/Γ
VALUE (units 10^{-3})	EVTS	DOCUMENT ID	TECN	COMMENT	
$5.3 \pm 0.3 \pm 0.5$	325	¹ CHEN	08	BELL	$10.87 e^+e^- \rightarrow \Upsilon(1S)\pi^+\pi^-$
¹ Assuming that the observed events are solely due to the $\Upsilon(5S)$ resonance.					

$\Gamma(\Upsilon(1S)\eta)/\Gamma_{\text{total}}$					Γ_{18}/Γ
VALUE (units 10^{-3})	DOCUMENT ID	TECN	COMMENT		
$0.85 \pm 0.15 \pm 0.08$	^{1,2} KOVALENKO	21	BELL	$e^+e^- \rightarrow \Upsilon(5S)$	
¹ Assuming that the observed events are solely due to the $\Upsilon(5S)$ resonance.					
² Using a data sample of 118.3 fb^{-1} of e^+e^- collisions at $\sqrt{s} = 10.866 \text{ GeV}$.					

$\Gamma(\Upsilon(1S)\eta')/\Gamma_{\text{total}}$					Γ_{19}/Γ
VALUE	CL%	DOCUMENT ID	TECN	COMMENT	
$<6.9 \times 10^{-5}$	90	^{1,2} KOVALENKO	21	BELL	$e^+e^- \rightarrow \Upsilon(5S)$
¹ Assuming that the observed events are solely due to the $\Upsilon(5S)$ resonance.					
² Using a data sample of 118.3 fb^{-1} of e^+e^- collisions at $\sqrt{s} = 10.866 \text{ GeV}$.					

$\Gamma(\Upsilon(2S)\pi^+\pi^-)/\Gamma_{\text{total}}$					Γ_{20}/Γ
VALUE (units 10^{-3})	EVTS	DOCUMENT ID	TECN	COMMENT	
$7.8 \pm 0.6 \pm 1.1$	186	¹ CHEN	08	BELL	$10.87 e^+e^- \rightarrow \Upsilon(2S)\pi^+\pi^-$
¹ Assuming that the observed events are solely due to the $\Upsilon(5S)$ resonance.					

$\Gamma(\Upsilon(2S)\eta)/\Gamma_{\text{total}}$					Γ_{21}/Γ
VALUE (units 10^{-3})	DOCUMENT ID	TECN	COMMENT		
$4.13 \pm 0.41 \pm 0.37$	^{1,2} KOVALENKO	21	BELL	$e^+e^- \rightarrow \Upsilon(5S)$	
¹ Assuming that the observed events are solely due to the $\Upsilon(5S)$ resonance.					
² Using a data sample of 118.3 fb^{-1} of e^+e^- collisions at $\sqrt{s} = 10.866 \text{ GeV}$.					

$\Gamma(\Upsilon(3S)\pi^+\pi^-)/\Gamma_{\text{total}}$					Γ_{22}/Γ
VALUE (units 10^{-3})	EVTS	DOCUMENT ID	TECN	COMMENT	
$4.8 \pm 1.8 \pm 0.7$	10	¹ CHEN	08	BELL	$10.87 e^+e^- \rightarrow \Upsilon(3S)\pi^+\pi^-$
¹ Assuming that the observed events are solely due to the $\Upsilon(5S)$ resonance.					

$\Gamma(\Upsilon(1S)K^+K^-)/\Gamma_{\text{total}}$					Γ_{23}/Γ
VALUE (units 10^{-4})	EVTS	DOCUMENT ID	TECN	COMMENT	
$6.1 \pm 1.6 \pm 1.0$	20	¹ CHEN	08	BELL	$10.87 e^+e^- \rightarrow \Upsilon(1S)K^+K^-$
¹ Assuming that the observed events are solely due to the $\Upsilon(5S)$ resonance.					

$\Gamma(h_b(1P)\pi^+\pi^-)/\Gamma(\Upsilon(2S)\pi^+\pi^-)$					Γ_{25}/Γ_{20}
VALUE	DOCUMENT ID	TECN	COMMENT		
$0.45 \pm 0.08 \pm 0.07$ -0.12	ADACHI	12	BELL	$10.86 e^+e^- \rightarrow \text{hadrons}$	

$\Gamma(h_b(2P)\pi^+\pi^-)/\Gamma(\Upsilon(2S)\pi^+\pi^-)$					Γ_{26}/Γ_{20}
VALUE	DOCUMENT ID	TECN	COMMENT		
$0.77 \pm 0.08 \pm 0.22$ -0.17	ADACHI	12	BELL	$10.86 e^+e^- \rightarrow \text{hadrons}$	

$\Gamma(h_b(1P)\pi^+\pi^-)/\Gamma(h_b(2P)\pi^+\pi^-)$					Γ_{25}/Γ_{26}
VALUE	DOCUMENT ID	TECN	COMMENT		
$0.616 \pm 0.052 \pm 0.017$	MIZUK	16	BELL	$e^+e^- \rightarrow h_b(1P, 2P)\pi^+\pi^-$	

$\Gamma(\chi_{bJ}(1P)\pi^+\pi^-\pi^0)/\Gamma_{\text{total}}$					Γ_{27}/Γ
VALUE (units 10^{-3})	DOCUMENT ID	TECN	COMMENT		
$2.5 \pm 0.6 \pm 2.2$	YIN	18	BELL	$e^+e^- \rightarrow \text{hadrons}$	

$\Gamma(\chi_{b0}(1P)\pi^+\pi^-\pi^0)/\Gamma_{\text{total}}$					Γ_{28}/Γ
VALUE	CL%	DOCUMENT ID	TECN	COMMENT	
$<3.9 \times 10^{-3}$	90	¹ HE	14	BELL	$\Upsilon(5S) \rightarrow \pi^+\pi^-\pi^0\gamma\Upsilon(1S)$
¹ Assuming that all the $b\bar{b}$ events are from $\Upsilon(5S)$ resonance decays and using $\sigma(e^+e^- \rightarrow b\bar{b}) = 0.340 \pm 0.016 \text{ nb}$ from ESEN 13. Correlated with other results from HE 14.					

$\Gamma(\chi_{b0}(1P)\omega)/\Gamma_{\text{total}}$					Γ_{29}/Γ
VALUE	CL%	DOCUMENT ID	TECN	COMMENT	
$<3.9 \times 10^{-3}$	90	¹ HE	14	BELL	$\Upsilon(5S) \rightarrow \pi^+\pi^-\pi^0\gamma\Upsilon(1S)$
¹ Assuming that all the $b\bar{b}$ events are from $\Upsilon(5S)$ resonance decays and using $\sigma(e^+e^- \rightarrow b\bar{b}) = 0.340 \pm 0.016 \text{ nb}$ from ESEN 13. Correlated with other results from HE 14.					

$\Gamma(\chi_{b0}(1P)(\pi^+\pi^-\pi^0)_{\text{non-}\omega})/\Gamma_{\text{total}}$					Γ_{30}/Γ
VALUE	CL%	DOCUMENT ID	TECN	COMMENT	
$<4.8 \times 10^{-3}$	90	¹ HE	14	BELL	$\Upsilon(5S) \rightarrow \pi^+\pi^-\pi^0\gamma\Upsilon(1S)$
¹ Assuming that all the $b\bar{b}$ events are from $\Upsilon(5S)$ resonance decays and using $\sigma(e^+e^- \rightarrow b\bar{b}) = 0.340 \pm 0.016 \text{ nb}$ from ESEN 13. Correlated with other results from HE 14.					

$\Gamma(\chi_{b1}(1P)\pi^+\pi^-\pi^0)/\Gamma_{\text{total}}$					Γ_{31}/Γ
VALUE (units 10^{-3})	EVTS	DOCUMENT ID	TECN	COMMENT	
$1.85 \pm 0.23 \pm 0.23$	80	¹ HE	14	BELL	$\Upsilon(5S) \rightarrow \pi^+\pi^-\pi^0\gamma\Upsilon(1S)$
¹ Assuming that all the $b\bar{b}$ events are from $\Upsilon(5S)$ resonance decays and using $\sigma(e^+e^- \rightarrow b\bar{b}) = 0.340 \pm 0.016 \text{ nb}$ from ESEN 13. Correlated with other results from HE 14.					

$\Gamma(\chi_{b1}(1P)\omega)/\Gamma_{\text{total}}$					Γ_{32}/Γ
VALUE (units 10^{-3})	EVTS	DOCUMENT ID	TECN	COMMENT	
$1.57 \pm 0.22 \pm 0.21$	60	¹ HE	14	BELL	$\Upsilon(5S) \rightarrow \pi^+\pi^-\pi^0\gamma\Upsilon(1S)$
¹ Assuming that all the $b\bar{b}$ events are from $\Upsilon(5S)$ resonance decays and using $\sigma(e^+e^- \rightarrow b\bar{b}) = 0.340 \pm 0.016 \text{ nb}$ from ESEN 13. Correlated with other results from HE 14.					

$\Gamma(\chi_{b1}(1P)(\pi^+\pi^-\pi^0)_{\text{non-}\omega})/\Gamma_{\text{total}}$					Γ_{33}/Γ
VALUE (units 10^{-3})	EVTS	DOCUMENT ID	TECN	COMMENT	
$0.52 \pm 0.15 \pm 0.11$	24	¹ HE	14	BELL	$\Upsilon(5S) \rightarrow \pi^+\pi^-\pi^0\gamma\Upsilon(1S)$
¹ Assuming that all the $b\bar{b}$ events are from $\Upsilon(5S)$ resonance decays and using $\sigma(e^+e^- \rightarrow b\bar{b}) = 0.340 \pm 0.016 \text{ nb}$ from ESEN 13. Correlated with other results from HE 14.					

$\Gamma(\chi_{b2}(1P)\pi^+\pi^-\pi^0)/\Gamma_{\text{total}}$					Γ_{34}/Γ
VALUE (units 10^{-3})	EVTS	DOCUMENT ID	TECN	COMMENT	
$1.17 \pm 0.27 \pm 0.14$	29	¹ HE	14	BELL	$\Upsilon(5S) \rightarrow \pi^+\pi^-\pi^0\gamma\Upsilon(1S)$
¹ Assuming that all the $b\bar{b}$ events are from $\Upsilon(5S)$ resonance decays and using $\sigma(e^+e^- \rightarrow b\bar{b}) = 0.340 \pm 0.016 \text{ nb}$ from ESEN 13. Correlated with other results from HE 14.					

$\Gamma(\chi_{b2}(1P)\omega)/\Gamma_{\text{total}}$					Γ_{35}/Γ
VALUE (units 10^{-3})	EVTS	DOCUMENT ID	TECN	COMMENT	
$0.60 \pm 0.23 \pm 0.15$	13	¹ HE	14	BELL	$\Upsilon(5S) \rightarrow \pi^+\pi^-\pi^0\gamma\Upsilon(1S)$
¹ Assuming that all the $b\bar{b}$ events are from $\Upsilon(5S)$ resonance decays and using $\sigma(e^+e^- \rightarrow b\bar{b}) = 0.340 \pm 0.016 \text{ nb}$ from ESEN 13. Correlated with other results from HE 14.					

$\Gamma(\chi_{b2}(1P)\omega)/\Gamma(\chi_{b1}(1P)\omega)$					Γ_{35}/Γ_{32}
VALUE	DOCUMENT ID	TECN	COMMENT		
$0.38 \pm 0.16 \pm 0.09$	¹ HE	14	BELL	$\Upsilon(5S) \rightarrow \pi^+\pi^-\pi^0\gamma\Upsilon(1S)$	
¹ Accounting for correlated systematics.					

$\Gamma(\chi_{b2}(1P)(\pi^+\pi^-\pi^0)_{\text{non-}\omega})/\Gamma_{\text{total}}$					Γ_{36}/Γ
VALUE (units 10^{-3})	EVTS	DOCUMENT ID	TECN	COMMENT	
$0.61 \pm 0.22 \pm 0.28$	16	¹ HE	14	BELL	$\Upsilon(5S) \rightarrow \pi^+\pi^-\pi^0\gamma\Upsilon(1S)$
¹ Assuming that all the $b\bar{b}$ events are from $\Upsilon(5S)$ resonance decays and using $\sigma(e^+e^- \rightarrow b\bar{b}) = 0.340 \pm 0.016 \text{ nb}$ from ESEN 13. Correlated with other results from HE 14.					

$\Gamma(\chi_{b2}(1P)(\pi^+\pi^-\pi^0)_{\text{non-}\omega})/\Gamma(\chi_{b1}(1P)(\pi^+\pi^-\pi^0)_{\text{non-}\omega})$					Γ_{36}/Γ_{33}
VALUE	DOCUMENT ID	TECN	COMMENT		
$1.20 \pm 0.55 \pm 0.65$	¹ HE	14	BELL	$\Upsilon(5S) \rightarrow \pi^+\pi^-\pi^0\gamma\Upsilon(1S)$	
¹ Accounting for correlated systematics.					

$\Gamma(\eta_b(1S)\omega)/\Gamma_{\text{total}}$					Γ_{38}/Γ
VALUE	CL%	DOCUMENT ID	TECN	COMMENT	
$<1.3 \times 10^{-3}$	90	¹ OSKIN	20	BELL	$e^+e^- \rightarrow \omega X$
¹ Using $\sigma_{b\bar{b}} = 0.340 \pm 0.016 \text{ nb}$ from TAMPONI 15.					

$\Gamma(\eta_b(2S)\omega)/\Gamma_{\text{total}}$					Γ_{39}/Γ
VALUE	CL%	DOCUMENT ID	TECN	COMMENT	
$<5.6 \times 10^{-3}$	90	¹ OSKIN	20	BELL	$e^+e^- \rightarrow \omega X$
¹ Using $\sigma_{b\bar{b}} = 0.340 \pm 0.016 \text{ nb}$ from TAMPONI 15.					

$\Gamma(\gamma X_b \rightarrow \gamma \Upsilon(1S)\omega)/\Gamma_{\text{total}}$					Γ_{37}/Γ
VALUE	CL%	DOCUMENT ID	TECN	COMMENT	
$<3.8 \times 10^{-5}$	90	¹ HE	14	BELL	$\Upsilon(5S) \rightarrow \pi^+\pi^-\pi^0\gamma\Upsilon(1S)$
¹ Assuming that all the $b\bar{b}$ events are from $\Upsilon(5S)$ resonance decays and using $\sigma(e^+e^- \rightarrow b\bar{b}) = 0.340 \pm 0.016 \text{ nb}$ from ESEN 13. Correlated with other results from HE 14. For a state X_b with mass between $10.55 \text{ GeV}/c^2$ and $10.65 \text{ GeV}/c^2$, the obtained 90% upper limit as a function of m_{X_b} varies from 2.6×10^{-5} to 3.8×10^{-5} .					

$\Gamma(\phi \text{ anything})/\Gamma_{\text{total}}$					Γ_{40}/Γ
VALUE	DOCUMENT ID	TECN	COMMENT		
$0.138 \pm 0.007 \pm 0.023$ -0.015	HUANG	07	CLEO	$\Upsilon(5S) \rightarrow \phi X$	

$\Gamma(D^0 \text{ anything} + \text{c.c.})/\Gamma_{\text{total}}$					Γ_{41}/Γ
VALUE	DOCUMENT ID	TECN	COMMENT		
$1.117 \pm 0.005 \pm 0.060$	¹ ZHUKOVA	23	BELL	$\Upsilon(5S) \rightarrow D^0 X, \bar{D}^0 X$	
¹ We do not use the following data for averages, fits, limits, etc. • • •					
$1.076 \pm 0.040 \pm 0.068$	DRUTSKOY	07	BELL	$\Upsilon(5S) \rightarrow D^0 X, \bar{D}^0 X$	
¹ Supersedes DRUTSKOY 07.					

Meson Particle Listings

 $\Upsilon(10860)$, $\Upsilon(11020)$ $\Gamma(D_s \text{ anything} + \text{c.c.})/\Gamma_{\text{total}}$ Γ_{42}/Γ

VALUE	DOCUMENT ID	TECN	COMMENT
0.447 ± 0.026 OUR AVERAGE			
0.447 ± 0.003 ± 0.027	¹ ZHUKOVA 23	BELL	$\Upsilon(5S) \rightarrow D_s^\pm X$
0.44 ± 0.09 ± 0.04	² ARTUSO 05B	CLE3	$\Upsilon(5S) \rightarrow D_s^\pm X$
0.472 ± 0.024 ± 0.072	³ DRUTSKOY 07	BELL	$\Upsilon(5S) \rightarrow D_s^\pm X$

• • • We do not use the following data for averages, fits, limits, etc. • • •

¹ Supersedes DRUTSKOY 07.
² ARTUSO 05B reports $[\Gamma(\Upsilon(10860) \rightarrow D_s \text{ anything} + \text{c.c.})/\Gamma_{\text{total}}] \times [B(D_s^\pm \rightarrow \phi\pi^\pm)] = 0.0198 \pm 0.0019 \pm 0.0038$ which we divide by our best value $B(D_s^\pm \rightarrow \phi\pi^\pm) = (4.5 \pm 0.4) \times 10^{-2}$. Our first error is their experiment's error and our second error is the systematic error from using our best value.
³ Using $B(D_s^\pm \rightarrow \phi\pi^\pm) = (4.4 \pm 0.6)\%$ from PDG 06.

 $\Gamma(J/\psi \text{ anything})/\Gamma_{\text{total}}$ Γ_{43}/Γ

VALUE (units 10^{-2})	DOCUMENT ID	TECN	COMMENT
2.060 ± 0.160 ± 0.134	DRUTSKOY 07	BELL	$\Upsilon(5S) \rightarrow J/\psi X$

 $\Gamma(B^0 \text{ anything} + \text{c.c.})/\Gamma_{\text{total}}$ Γ_{44}/Γ

VALUE	EVTS	DOCUMENT ID	TECN	COMMENT
0.770 $^{+0.058}_{-0.056}$ ± 0.061	352	DRUTSKOY 10	BELL	$\Upsilon(5S) \rightarrow B^0 X$

 $\Gamma(B^+ \text{ anything} + \text{c.c.})/\Gamma_{\text{total}}$ Γ_{45}/Γ

VALUE	EVTS	DOCUMENT ID	TECN	COMMENT
0.721 $^{+0.039}_{-0.038}$ ± 0.050	711	DRUTSKOY 10	BELL	$\Upsilon(5S) \rightarrow B^+ X$

 $\Upsilon(10860)$ REFERENCES

ZHUKOVA 23	JHEP 2308 131	V. Zhukova et al.	(BELLE Collab.)
KOVALENKO 21	PR D104 112006	E. Kovalenko et al.	(BELLE Collab.)
DONG 20A	CP C44 083001	X.-K. Dong et al.	(BELLE Collab.)
OSKIN 20	PR D102 092011	P. Oskin et al.	(BELLE Collab.)
MIZUK 19	JHEP 1910 220	R. Mizuk et al.	(BELLE Collab.)
TAMPONI 18	EPL C78 633	U. Tamponi et al.	(BELLE Collab.)
YIN 18	PR D98 091102	J.H. Yin et al.	(BELLE Collab.)
MIZUK 16	PRL 117 142001	R. Mizuk et al.	(BELLE Collab.)
SANTEL 16	PR D93 011101	D. Santel et al.	(BELLE Collab.)
TAMPONI 15	PRL 115 142001	U. Tamponi et al.	(BELLE Collab.)
HE 14	PRL 113 142001	X.H. He et al.	(BELLE Collab.)
ESEN 13	PR D87 031101	S. Esen et al.	(BELLE Collab.)
SHEN 13A	PR D88 052019	C.P. Shen et al.	(BELLE Collab.)
ADACHI 12	PRL 108 032001	I. Adachi et al.	(BELLE Collab.)
LI 12	PRL 108 181008	J. Li et al.	(BELLE Collab.)
CHEN 10	PR D82 091106	K.-F. Chen et al.	(BELLE Collab.)
DRUTSKOY 10	PR D81 112003	A. Drutskoy et al.	(BELLE Collab.)
AUBERT 09E	PRL 102 012001	B. Aubert et al.	(BABAR Collab.)
LOUVOT 09	PRL 102 021801	R. Louvot et al.	(BELLE Collab.)
CHEN 08	PRL 100 112001	K.-F. Chen et al.	(BELLE Collab.)
DRUTSKOY 07	PRL 98 052001	A. Drutskoy et al.	(BELLE Collab.)
DRUTSKOY 07A	PR D76 012002	A. Drutskoy et al.	(BELLE Collab.)
HUANG 07	PR D75 012002	G.S. Huang et al.	(CLEO Collab.)
AQUINES 06	PRL 96 152001	O. Aquines et al.	(CLEO Collab.)
BONVICINI 06	PRL 96 022002	G. Bonvicini et al.	(CLEO Collab.)
PDC 06	JP 633 1	W.-M. Yao et al.	(PDG Collab.)
ARTUSO 05B	PR 95 261801	M. Artuso et al.	(CLEO Collab.)
BESSON 08	PRL 94 3811	D. Besson et al.	(CLEO Collab.)
LOVELOCK 85	PRL 54 377	D.M.J. Lovelock et al.	(CUSB Collab.)

 $\Upsilon(11020)$

$$I^G(J^{PC}) = 0^-(1^{--})$$

 $\Upsilon(11020)$ MASS

VALUE (MeV)	DOCUMENT ID	TECN	COMMENT
11000 ± 4 OUR AVERAGE			
11000.0 $^{+4.0}_{-4.5}$ ± 1.0	¹ MIZUK 19	BELL	$e^+e^- \rightarrow \Upsilon(1S, 2S, 3S)\pi^+\pi^-$
10999.0 $^{+7.3}_{-7.8}$ ± 1.6	² MIZUK 16	BELL	$e^+e^- \rightarrow h_b(1P, 2P)\pi^+\pi^-$
11001 ± 1	³ DONG 20A		$e^+e^- \rightarrow b\bar{b}$
11003.0 ± 1.1 ± 0.9	^{4,5} SANTEL 16	BELL	$e^+e^- \rightarrow \text{hadrons}$
10987.5 $^{+6.4}_{-2.5}$ ± 9.1	^{6,7} SANTEL 16	BELL	$e^+e^- \rightarrow \Upsilon(1S, 2S, 3S)\pi^+\pi^-$
10996 ± 2	⁸ AUBERT 09E	BABR	$e^+e^- \rightarrow \text{hadrons}$
11019 ± 5 ± 7	BESSON 85	CLEO	$e^+e^- \rightarrow \text{hadrons}$
11020 ± 30	LOVELOCK 85	CUSB	$e^+e^- \rightarrow \text{hadrons}$

• • • We do not use the following data for averages, fits, limits, etc. • • •

¹ From a simultaneous fit to the $\Upsilon(nS)\pi^+\pi^-$, $n=1, 2, 3$, cross sections at 28 energy points within $\sqrt{s} = 10.6\text{--}11.05$ GeV, including the initial-state radiation at $\Upsilon(10860)$.
² From a simultaneous fit to the $h_b(nP)\pi^+\pi^-$, $n=1, 2$ cross sections at 22 energy points within $\sqrt{s} = 10.77\text{--}11.02$ GeV to a pair of interfering Breit-Wigner amplitudes modified by phase space factors, with eight resonance parameters (a mass and width for each of $\Upsilon(10860)$ and $\Upsilon(11020)$, a single relative phase, a single relative amplitude, and two overall normalization factors, one for each n). The systematic error estimate is dominated by possible interference with a small nonresonant continuum amplitude.
³ From a fit to the dressed cross sections of AUBERT 09E by BaBar and SANTEL 16 by Belle above 10.68 GeV with a coherent sum of a continuum amplitude and three Breit-Wigner functions with constant widths.

- ⁴ From a fit to the total hadronic cross sections measured at 60 energy points within $\sqrt{s} = 10.82\text{--}11.05$ GeV to a pair of interfering Breit-Wigner amplitudes and two floating continuum amplitudes with $1/\sqrt{s}$ dependence, one coherent with the resonances and one incoherent, with six resonance parameters (a mass, width, and an amplitude for each of $\Upsilon(10860)$ and $\Upsilon(11020)$, one relative phase, and one decoherence coefficient).
⁵ Not including uncertain and potentially large systematic errors due to assumed continuum amplitude $1/\sqrt{s}$ dependence and related interference contributions.
⁶ From a simultaneous fit to the $\Upsilon(nS)\pi^+\pi^-$, $n=1, 2, 3$, cross sections at 25 energy points within $\sqrt{s} = 10.6\text{--}11.05$ GeV to a pair of interfering Breit-Wigner amplitudes modified by phase space factors, with fourteen resonance parameters (a mass, width, and three amplitudes for each of $\Upsilon(10860)$ and $\Upsilon(11020)$, a single universal relative phase, and three decoherence coefficients, one for each n). Continuum contributions were measured (and therefore fixed) to be zero.
⁷ Superseded by MIZUK 19.
⁸ In a model where a flat non-resonant $b\bar{b}$ -continuum is incoherently added to a second flat component interfering with two Breit-Wigner resonances. Systematic uncertainties not estimated.

 $\Upsilon(11020)$ WIDTH

VALUE (MeV)	DOCUMENT ID	TECN	COMMENT
24 $^{+8}_{-6}$ OUR AVERAGE			
23.8 $^{+8.0}_{-6.8}$ ± 0.7	¹ MIZUK 19	BELL	$e^+e^- \rightarrow \Upsilon(nS)\pi^+\pi^-$
27 $^{+27}_{-11}$ ± 5	² MIZUK 16	BELL	$e^+e^- \rightarrow h_b(1P, 2P)\pi^+\pi^-$
35.1 ± 1.2	³ DONG 20A		$e^+e^- \rightarrow b\bar{b}$
39.3 $^{+1.7}_{-1.6}$ ± 1.3	^{4,5} SANTEL 16	BELL	$e^+e^- \rightarrow \text{hadrons}$
61 $^{+9}_{-19}$ ± 2	^{6,7} SANTEL 16	BELL	$e^+e^- \rightarrow \Upsilon(1S, 2S, 3S)\pi^+\pi^-$
37 ± 3	⁸ AUBERT 09E	BABR	$e^+e^- \rightarrow \text{hadrons}$
61 ± 13 ± 22	BESSON 85	CLEO	$e^+e^- \rightarrow \text{hadrons}$
90 ± 20	LOVELOCK 85	CUSB	$e^+e^- \rightarrow \text{hadrons}$

• • • We do not use the following data for averages, fits, limits, etc. • • •

¹ From a simultaneous fit to the $\Upsilon(nS)\pi^+\pi^-$, $n=1, 2, 3$, cross sections at 28 energy points within $\sqrt{s} = 10.6\text{--}11.05$ GeV, including the initial-state radiation at $\Upsilon(10860)$.
² From a simultaneous fit to the $h_b(nP)\pi^+\pi^-$, $n=1, 2$ cross sections at 22 energy points within $\sqrt{s} = 10.77\text{--}11.02$ GeV to a pair of interfering Breit-Wigner amplitudes modified by phase space factors, with eight resonance parameters (a mass and width for each of $\Upsilon(10860)$ and $\Upsilon(11020)$, a single relative phase, a single relative amplitude, and two overall normalization factors, one for each n). The systematic error estimate is dominated by possible interference with a small nonresonant continuum amplitude.
³ From a fit to the dressed cross sections of AUBERT 09E by BaBar and SANTEL 16 by Belle above 10.68 GeV with a coherent sum of a continuum amplitude and three Breit-Wigner functions with constant widths.
⁴ From a fit to the total hadronic cross sections measured at 60 energy points within $\sqrt{s} = 10.82\text{--}11.05$ GeV to a pair of interfering Breit-Wigner amplitudes and two floating continuum amplitudes with $1/\sqrt{s}$ dependence, one coherent with the resonances and one incoherent, with six resonance parameters (a mass, width, and an amplitude for each of $\Upsilon(10860)$ and $\Upsilon(11020)$, one relative phase, and one decoherence coefficient).
⁵ Not including uncertain and potentially large systematic errors due to assumed continuum amplitude $1/\sqrt{s}$ dependence and related interference contributions.
⁶ From a simultaneous fit to the $\Upsilon(nS)\pi^+\pi^-$, $n=1, 2, 3$, cross sections at 25 energy points within $\sqrt{s} = 10.6\text{--}11.05$ GeV to a pair of interfering Breit-Wigner amplitudes modified by phase space factors, with fourteen resonance parameters (a mass, width, and three amplitudes for each of $\Upsilon(10860)$ and $\Upsilon(11020)$, a single universal relative phase, and three decoherence coefficients, one for each n). Continuum contributions were measured (and therefore fixed) to be zero.
⁷ Superseded by MIZUK 19.
⁸ In a model where a flat non-resonant $b\bar{b}$ -continuum is incoherently added to a second flat component interfering with two Breit-Wigner resonances. Systematic uncertainties not estimated.

 $\Upsilon(11020)$ DECAY MODES

Mode	Fraction (Γ_i/Γ)
Γ_1 e^+e^-	$(5.4 ^{+1.9}_{-2.1}) \times 10^{-6}$
Γ_2 $\Upsilon(1S)\pi^+\pi^-$	
Γ_3 $\Upsilon(2S)\pi^+\pi^-$	
Γ_4 $\Upsilon(3S)\pi^+\pi^-$	
Γ_5 $\chi_{bJ}(1P)\pi^+\pi^-\pi^0$	$(9 ^{+9}_{-8}) \times 10^{-3}$
Γ_6 $\chi_{b1}(1P)\pi^+\pi^-\pi^0$	seen
Γ_7 $\chi_{b2}(1P)\pi^+\pi^-\pi^0$	seen

 $\Upsilon(11020)$ PARTIAL WIDTHS

$\Gamma(e^+e^-)$	DOCUMENT ID	TECN	COMMENT
0.130 ± 0.030 OUR AVERAGE			
0.095 ± 0.03 ± 0.035	BESSON 85	CLEO	$e^+e^- \rightarrow \text{hadrons}$
0.156 ± 0.040	LOVELOCK 85	CUSB	$e^+e^- \rightarrow \text{hadrons}$

See key on page 1171

Meson Particle Listings
 $\Upsilon(11020)$

$\Gamma(e^+e^-) \times \Gamma(\Upsilon(1S)\pi^+\pi^-)/\Gamma_{\text{total}}$	$\Gamma_1\Gamma_2/\Gamma$
VALUE (eV)	DOCUMENT ID TECN COMMENT

• • • We do not use the following data for averages, fits, limits, etc. • • •

0.46±0.08	1,2 MIZUK 19 BELL $e^+e^- \rightarrow \Upsilon(nS)\pi^+\pi^-$
-----------	---

¹ From a simultaneous fit to the $\Upsilon(nS)\pi^+\pi^-$, $n = 1, 2, 3$, cross sections at 28 energy points within $\sqrt{s} = 10.6\text{--}11.05$ GeV, including the initial-state radiation at $\Upsilon(10860)$.
² Reported as the range 0.38–0.54 eV obtained from multiple solutions of an amplitude fit within a model composed as a sum of Breit-Wigner functions.

$\Gamma(e^+e^-) \times \Gamma(\Upsilon(2S)\pi^+\pi^-)/\Gamma_{\text{total}}$	$\Gamma_1\Gamma_3/\Gamma$
VALUE (eV)	DOCUMENT ID TECN COMMENT

• • • We do not use the following data for averages, fits, limits, etc. • • •

0.65±0.52	1,2 MIZUK 19 BELL $e^+e^- \rightarrow \Upsilon(nS)\pi^+\pi^-$
-----------	---

¹ From a simultaneous fit to the $\Upsilon(nS)\pi^+\pi^-$, $n = 1, 2, 3$, cross sections at 28 energy points within $\sqrt{s} = 10.6\text{--}11.05$ GeV, including the initial-state radiation at $\Upsilon(10860)$.
² Reported as the range 0.13–1.16 eV obtained from multiple solutions of an amplitude fit within a model composed as a sum of Breit-Wigner functions.

$\Gamma(e^+e^-) \times \Gamma(\Upsilon(3S)\pi^+\pi^-)/\Gamma_{\text{total}}$	$\Gamma_1\Gamma_4/\Gamma$
VALUE (eV)	DOCUMENT ID TECN COMMENT

• • • We do not use the following data for averages, fits, limits, etc. • • •

0.33±0.16	1,2 MIZUK 19 BELL $e^+e^- \rightarrow \Upsilon(nS)\pi^+\pi^-$
-----------	---

¹ From a simultaneous fit to the $\Upsilon(nS)\pi^+\pi^-$, $n = 1, 2, 3$, cross sections at 28 energy points within $\sqrt{s} = 10.6\text{--}11.05$ GeV, including the initial-state radiation at $\Upsilon(10860)$.
² Reported as the range 0.17–0.49 eV obtained from multiple solutions of an amplitude fit within a model composed as a sum of Breit-Wigner functions.

$\Gamma(\chi_{bJ}(1P)\pi^+\pi^-\pi^0)/\Gamma_{\text{total}}$	Γ_5/Γ
VALUE (units 10^{-3})	DOCUMENT ID TECN COMMENT

$8.7 \pm 4.3^{+7.6}_{-6.6}$	YIN 18 BELL $e^+e^- \rightarrow \text{hadrons}$
-----------------------------	---

$\Gamma(\chi_{b1}(1P)\pi^+\pi^-\pi^0)/\Gamma_{\text{total}}$	Γ_6/Γ
VALUE	DOCUMENT ID TECN COMMENT

seen	YIN 18 BELL $e^+e^- \rightarrow \text{hadrons}$
------	---

$\Gamma(\chi_{b2}(1P)\pi^+\pi^-\pi^0)/\Gamma_{\text{total}}$	Γ_7/Γ
VALUE	DOCUMENT ID TECN COMMENT

seen	YIN 18 BELL $e^+e^- \rightarrow \text{hadrons}$
------	---

$\Gamma(\chi_{b2}(1P)\pi^+\pi^-\pi^0)/\Gamma(\chi_{b1}(1P)\pi^+\pi^-\pi^0)$	Γ_7/Γ_6
VALUE	DOCUMENT ID TECN COMMENT

0.4 ± 0.2	YIN 18 BELL $e^+e^- \rightarrow \text{hadrons}$
---------------	---

 $\Upsilon(11020)$ REFERENCES

DONG	20A	CP C44 083001	X.-K. Dong <i>et al.</i>	
MIZUK	19	JHEP 1910 220	R. Mizuk <i>et al.</i>	(BELLE Collab.)
YIN	18	PR D98 091102	J.H. Yin <i>et al.</i>	(BELLE Collab.)
MIZUK	16	PRL 117 142001	R. Mizuk <i>et al.</i>	(BELLE Collab.)
SANTEL	16	PR D93 011101	D. Santel <i>et al.</i>	(BELLE Collab.)
AUBERT	09E	PRL 102 012001	B. Aubert <i>et al.</i>	(BABAR Collab.)
BESSON	85	PRL 54 381	D. Besson <i>et al.</i>	(CLEO Collab.)
LOVELOCK	85	PRL 54 377	D.M.J. Lovelock <i>et al.</i>	(CUSP Collab.)

Meson Particle Listings

Other Mesons, $T_{cs0}^*(2870)^0$, $T_{cs1}^*(2900)^0$, $T_{c\bar{s}0}^*(2900)$, $T_{cc}(3875)^+$ **OTHER MESONS** **$T_{cs0}^*(2870)^0$**

$$I(J^P) = ?(0^+)$$

OMITTED FROM SUMMARY TABLE
was $X_0(2900)$ An exotic state with minimal quark content $\bar{c}d\bar{s}u$. Observed by AAIJ 20A1 using full amplitude analysis of $B^+ \rightarrow D^+ D^- K^+$ decays. **$T_{cs0}^*(2870)^0$ MASS**

VALUE (MeV)	EVTS	DOCUMENT ID	TECN	COMMENT
2866 ± 7 ± 2	1.2k	¹ AAIJ	20A1 LHCb	$B^+ \rightarrow D^+ D^- K^+$

¹ Obtained from the full amplitude analysis. Parameterized with the relativistic Breit-Wigner line shape. Also confirmed by the model-independent analysis of AAIJ 20Af. **$T_{cs0}^*(2870)^0$ WIDTH**

VALUE (MeV)	EVTS	DOCUMENT ID	TECN	COMMENT
57 ± 12 ± 4	1.2k	¹ AAIJ	20A1 LHCb	$B^+ \rightarrow D^+ D^- K^+$

¹ Obtained from the full amplitude analysis. Parameterized with the relativistic Breit-Wigner line shape. Also confirmed by the model-independent analysis of AAIJ 20Af. **$T_{cs0}^*(2870)^0$ DECAY MODES**

Mode	Fraction (Γ_i/Γ)
Γ_1 $D^- K^+$	seen

 $T_{cs0}^*(2870)^0$ BRANCHING RATIOS

$\Gamma(D^- K^+)/\Gamma_{\text{total}}$	Γ_1/Γ
seen	seen

 $T_{cs0}^*(2870)^0$ REFERENCES

AAIJ	20AF	PRL 125 242001	R. Aaij et al.	(LHCb Collab.)
AAIJ	20A1	PR D102 112003	R. Aaij et al.	(LHCb Collab.)

 $T_{cs1}^*(2900)^0$

$$I(J^P) = ?(1^-)$$

OMITTED FROM SUMMARY TABLE
was $X_1(2900)$ An exotic state with minimal quark content $\bar{c}d\bar{s}u$. Observed by AAIJ 20A1 using full amplitude analysis of $B^+ \rightarrow D^+ D^- K^+$ decays. **$T_{cs1}^*(2900)^0$ MASS**

VALUE (MeV)	EVTS	DOCUMENT ID	TECN	COMMENT
2904 ± 5 ± 1	1.2k	¹ AAIJ	20A1 LHCb	$B^+ \rightarrow D^+ D^- K^+$

¹ Obtained from the full amplitude analysis. Parameterized with the relativistic Breit-Wigner line shape. Also confirmed by the model-independent analysis of AAIJ 20Af. **$T_{cs1}^*(2900)^0$ WIDTH**

VALUE (MeV)	EVTS	DOCUMENT ID	TECN	COMMENT
110 ± 11 ± 4	1.2k	¹ AAIJ	20A1 LHCb	$B^+ \rightarrow D^+ D^- K^+$

¹ Obtained from the full amplitude analysis. Parameterized with the relativistic Breit-Wigner line shape. Also confirmed by the model-independent analysis of AAIJ 20Af. **$T_{cs1}^*(2900)^0$ DECAY MODES**

Mode	Fraction (Γ_i/Γ)
Γ_1 $D^- K^+$	seen

 $T_{cs1}^*(2900)^0$ BRANCHING RATIOS

$\Gamma(D^- K^+)/\Gamma_{\text{total}}$	Γ_1/Γ
seen	seen

 $T_{cs1}^*(2900)^0$ REFERENCES

AAIJ	20AF	PRL 125 242001	R. Aaij et al.	(LHCb Collab.)
AAIJ	20A1	PR D102 112003	R. Aaij et al.	(LHCb Collab.)

 $T_{c\bar{s}0}^*(2900)$

$$I(J^P) = 1(0^+)$$

OMITTED FROM SUMMARY TABLE

Observed by LHCb in AAIJ 23B using a simultaneous amplitude analysis of $B^0 \rightarrow \bar{D}^0 D_s^+ \pi^-$ and $B^+ \rightarrow D^- D_s^+ \pi^+$. The $T_{c\bar{s}0}^*(2900)^0 \rightarrow D_s^+ \pi^-$ and $T_{c\bar{s}0}^*(2900)^{++} \rightarrow D_s^+ \pi^+$ decays are observed with 8.0 and 6.5 σ significance, respectively. **$T_{c\bar{s}0}^*(2900)^0$ MASS**

VALUE (MeV)	DOCUMENT ID	TECN	COMMENT
2892 ± 14 ± 15	¹ AAIJ	23c LHCb	$B^0 \rightarrow \bar{D}^0 D_s^+ \pi^-$

¹ From an amplitude analysis of $B^0 \rightarrow \bar{D}^0 D_s^+ \pi^-$. A simultaneous fit to $B^0 \rightarrow \bar{D}^0 D_s^+ \pi^-$ and $B^- \rightarrow D^- D_s^+ \pi^+$ assuming isospin symmetry yields a mass of $2908 \pm 11 \pm 20$ MeV. **$T_{c\bar{s}0}^*(2900)^{++}$ MASS**

VALUE (MeV)	DOCUMENT ID	TECN	COMMENT
2921 ± 17 ± 20	² AAIJ	23c LHCb	$B^- \rightarrow D^- D_s^+ \pi^+$

² From an amplitude analysis of $B^- \rightarrow D^- D_s^+ \pi^+$. A simultaneous fit to $B^0 \rightarrow \bar{D}^0 D_s^+ \pi^-$ and $B^- \rightarrow D^- D_s^+ \pi^+$ assuming isospin symmetry yields a mass of $2908 \pm 11 \pm 20$ MeV. **$T_{c\bar{s}0}^*(2900)^0$ WIDTH**

VALUE (MeV)	DOCUMENT ID	TECN	COMMENT
119 ± 26 ± 13	³ AAIJ	23c LHCb	$B^0 \rightarrow \bar{D}^0 D_s^+ \pi^-$

³ From an amplitude analysis of $B^0 \rightarrow \bar{D}^0 D_s^+ \pi^-$. A simultaneous fit to $B^0 \rightarrow \bar{D}^0 D_s^+ \pi^-$ and $B^- \rightarrow D^- D_s^+ \pi^+$ assuming isospin symmetry yields a width of $136 \pm 23 \pm 13$ MeV. **$T_{c\bar{s}0}^*(2900)^{++}$ WIDTH**

VALUE (MeV)	DOCUMENT ID	TECN	COMMENT
137 ± 32 ± 17	⁴ AAIJ	23c LHCb	$B^- \rightarrow D^- D_s^+ \pi^+$

⁴ From an amplitude analysis of $B^- \rightarrow D^- D_s^+ \pi^+$. A simultaneous fit to $B^0 \rightarrow \bar{D}^0 D_s^+ \pi^-$ and $B^- \rightarrow D^- D_s^+ \pi^+$ assuming isospin symmetry yields a width of $136 \pm 23 \pm 13$ MeV. **$T_{c\bar{s}0}^*(2900)$ DECAY MODES**

Mode	Fraction (Γ_i/Γ)
Γ_1 $D_s^+ \pi^-$	seen
Γ_2 $D_s^+ \pi^+$	seen

 $T_{c\bar{s}0}^*(2900)$ BRANCHING RATIOS

$\Gamma(D_s^+ \pi^-)/\Gamma_{\text{total}}$	Γ_1/Γ
seen	seen

$\Gamma(D_s^+ \pi^+)/\Gamma_{\text{total}}$	Γ_2/Γ
seen	seen

 $T_{c\bar{s}0}^*(2900)$ REFERENCES

AAIJ	23B	PR D108 012017	R. Aaij et al.	(LHCb Collab.)
AAIJ	23C	PRL 131 041902	R. Aaij et al.	(LHCb Collab.)

 $T_{cc}(3875)^+$

$$I(J^P) = ?(?^?)$$

OMITTED FROM SUMMARY TABLE

Observed with large significance by AAIJ 22E in the doubly-charmed ($C = 2$) decay mode $D^0 D^0 \pi^+$ using inclusive pp collisions at 7, 8, and 13 TeV. **$T_{cc}(3875)^+$ MASS**OUR FIT value comes from the measurement of $m_{T_{cc}^+} - (m_{D^{*++}} + m_{D^0})$ below and $m_{D^{*++}} + m_{D^0}$ values.

VALUE (MeV)	DOCUMENT ID
3874.83 ± 0.11 OUR FIT	

See key on page 1171

Meson Particle Listings

$T_{cc}(3875)^+$, $T_{c\bar{c}1}(3900)$

$m_{T_{cc}^+} - (m_{D^{*+}} + m_{D^0})$

VALUE (MeV)	EVTS	DOCUMENT ID	TECN	COMMENT
-0.27 ± 0.06 OUR FIT				
-0.273 ± 0.061^{+0.012}_{-0.015}	117	1 AAIJ	22E LHCb	$pp \rightarrow D^0 D^0 \pi^+ X$

¹ The fit assumes a relativistic P -wave Breit Wigner function modified by Blatt-Weisskopf form factor with radius 3.5 GeV⁻¹. The significance for $m_{T_{cc}^+} - (m_{D^{*+}} + m_{D^0}) < 0$ is 4.3 σ .

$T_{cc}(3875)^+$ WIDTH

VALUE (MeV)	EVTS	DOCUMENT ID	TECN	COMMENT
0.410 ± 0.165^{+0.047}_{-0.057}	117	1 AAIJ	22E LHCb	$pp \rightarrow D^0 D^0 \pi^+ X$

¹ The fit assumes a relativistic P -wave Breit Wigner function modified by Blatt-Weisskopf form factor with radius 3.5 GeV⁻¹.

$T_{cc}(3875)^+$ DECAY MODES

Mode	Fraction (Γ_i/Γ)
Γ_1 $D^0 D^0 \pi^+$	seen

$T_{cc}(3875)^+$ BRANCHING RATIOS

$\Gamma(D^0 D^0 \pi^+)/\Gamma_{total}$	VALUE	EVTS	DOCUMENT ID	TECN	COMMENT	Γ_i/Γ
seen		117	AAIJ	22E LHCb	$pp \rightarrow D^0 D^0 \pi^+ X$	

$T_{cc}(3875)^+$ REFERENCES

AAJ	22E	NATP 18 751	R. Aaij et al.	(LHCb Collab.)
-----	-----	-------------	----------------	----------------

$T_{c\bar{c}1}(3900)$

$I^G(J^{PC}) = 1^+(1^{+-})$

was $Z_c(3900)$, $X(3900)$

Properties incompatible with a $q\bar{q}$ structure (exotic state). See the review on non- $q\bar{q}$ states.

Charged $T_{c\bar{c}1}(3900)^\pm$ seen as a peak in the invariant mass distribution of the $J/\psi \pi^\pm$ system by BES III (ABLIKIM 13T) in $e^+ e^- \rightarrow \pi^+ \pi^- J/\psi$ at c.m. energy of 4.26 GeV and by radiative return from $e^+ e^-$ collisions at \sqrt{s} from 9.46 to 10.86 GeV at Belle (LIU 13B). Partial wave analysis of ABLIKIM 17J determines $J^P = 1^+$ with more than 7 σ significance. Neutral $T_{c\bar{c}1}(3900)^0$ seen in the $J/\psi \pi^0$ invariant mass distribution in $e^+ e^- \rightarrow \pi^0 \pi^0 J/\psi$ at c.m. energies of 4.23, 4.26, and 4.36 GeV by BES III (ABLIKIM 15U) and at 4.17 GeV by XIAO 13A. Peaks in $(D\bar{D}^*)_{0,1}^\pm$ reported by BES III (ABLIKIM 14A, ABLIKIM 15AB) are assumed to be related.

$T_{c\bar{c}1}(3900)$ MASS

VALUE (MeV)	EVTS	DOCUMENT ID	TECN	CHG	COMMENT
3887.1 ± 2.6 OUR AVERAGE					Error includes scale factor of 1.7. See the ideogram below.
3893.1 ± 2.2 ± 3.0		1 ABLIKIM	20N BES3	0	$e^+ e^- \rightarrow \pi^0 \pi^0 J/\psi$
3902.6 ^{+5.2} _{-5.0} ± 3.3		2,3 ABAZOV	19 D0	±	1.96 TeV $p\bar{p} \rightarrow J/\psi \pi^+ \pi^- X$
3881.2 ± 4.2 ± 52.7	6k	4 ABLIKIM	17J BES3	±	$e^+ e^- \rightarrow \pi^+ \pi^- J/\psi$
3885.7 ^{+4.3} _{-5.7} ± 8.4		2,4 ABLIKIM	15AB BES3	0	$e^+ e^- \rightarrow \pi^0 (D\bar{D}^*)^0$
3881.7 ± 1.6 ± 1.6	1.2k	2,4 ABLIKIM	15AC BES3	±	$e^+ e^- \rightarrow \pi^\pm (D\bar{D}^*)^\mp$
3883.9 ± 1.5 ± 4.2	1.2k	2,4 ABLIKIM	14A BES3	±	$e^+ e^- \rightarrow \pi^\pm (D\bar{D}^*)^\mp$
3894.5 ± 6.6 ± 4.5	159	2 LIU	13B BELL	±	$e^+ e^- \rightarrow \gamma \pi^+ \pi^- J/\psi$
3886 ± 4 ± 2	81	2,5 XIAO	13A	±	4.17 $e^+ e^- \rightarrow \pi^+ \pi^- J/\psi$
3904 ± 9 ± 5	25	2,5 XIAO	13A	0	4.17 $e^+ e^- \rightarrow \pi^0 \pi^0 J/\psi$

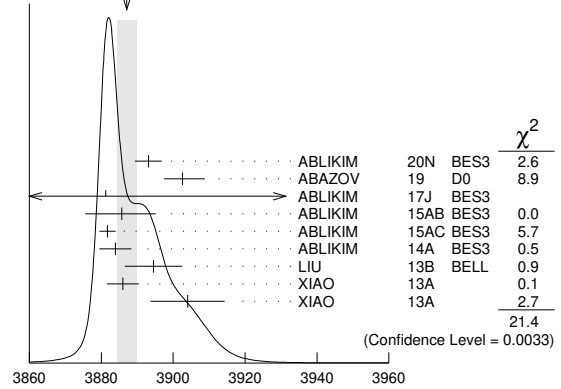
• • • We do not use the following data for averages, fits, limits, etc. • • •

3895.0 ± 5.2 ^{+4.0} _{-2.7}	502	2,6 ABAZOV	18B D0	±	1.96 TeV $p\bar{p} \rightarrow J/\psi \pi^+ \pi^- X$
3894.8 ± 2.3 ± 3.2	356	2,7 ABLIKIM	15U BES3	0	$e^+ e^- \rightarrow \pi^0 \pi^0 J/\psi$
3899.0 ± 3.6 ± 4.9	307	2,8 ABLIKIM	13T BES3	±	$e^+ e^- \rightarrow \pi^+ \pi^- J/\psi$

¹ Pole mass obtained from a fit to a relativistic Breit-Wigner.
² Neglecting interference between the $T_{c\bar{c}1}(3900)$ and other processes.
³ Measured in weak decays of b -flavored hadrons (nonprompt).
⁴ Pole mass obtained from a fit to a Flatte-like formula.
⁵ For $M^2(\pi^+ \pi^-) < 0.65$ GeV². Obtained by analyzing CLEO-c data but not authored by the CLEO Collaboration.

⁶ The signal of the $T_{c\bar{c}1}(3900)$ is correlated with a parent $J/\psi \pi^+ \pi^-$ system in the invariant mass range 4.2–4.7 GeV. Superseded by ABAZOV 19.
⁷ Superseded by ABLIKIM 20N.
⁸ Superseded by ABLIKIM 17J.

WEIGHTED AVERAGE
3887.1 ± 2.6 (Error scaled by 1.7)



$T_{c\bar{c}1}(3900)$ MASS

$T_{c\bar{c}1}(3900)$ WIDTH

VALUE (MeV)	EVTS	DOCUMENT ID	TECN	CHG	COMMENT
28.4 ± 2.6 OUR AVERAGE					
44.4 ± 5.2 ± 14.0		1 ABLIKIM	20N BES3	0	$e^+ e^- \rightarrow \pi^0 \pi^0 J/\psi$
32 ⁺²⁸ ₋₂₁ ± 26		2,3 ABAZOV	19 D0	±	1.96 TeV $p\bar{p} \rightarrow \pi^+ \pi^- J/\psi X$ (non-prompt)
51.8 ± 4.6 ± 36.0	6k	4 ABLIKIM	17J BES3	±	$e^+ e^- \rightarrow \pi^+ \pi^- J/\psi$
35 ⁺¹¹ ₋₁₂ ± 15		2,4 ABLIKIM	15AB BES3	0	$e^+ e^- \rightarrow \pi^0 (D\bar{D}^*)^0$
26.6 ± 2.0 ± 2.1	1248	2,4 ABLIKIM	15AC BES3	±	$e^+ e^- \rightarrow \pi^\pm (D\bar{D}^*)^\mp$
24.8 ± 3.3 ± 11.0	1212	2,4 ABLIKIM	14A BES3	±	$e^+ e^- \rightarrow \pi^\pm (D\bar{D}^*)^\mp$
63 ± 24 ± 26	159	2 LIU	13B BELL	±	$e^+ e^- \rightarrow \gamma \pi^+ \pi^- J/\psi$
37 ± 4 ± 8	81	2,5 XIAO	13A	±	4.17 $e^+ e^- \rightarrow \pi^+ \pi^- J/\psi$
29.6 ± 8.2 ± 8.2	356	2,6 ABLIKIM	15U BES3	0	$e^+ e^- \rightarrow \pi^0 \pi^0 J/\psi$
46 ± 10 ± 20	307	2,7 ABLIKIM	13T BES3	±	$e^+ e^- \rightarrow \pi^+ \pi^- J/\psi$

• • • We do not use the following data for averages, fits, limits, etc. • • •

¹ Pole width obtained from a fit to a relativistic Breit-Wigner.
² Neglecting interference between the $T_{c\bar{c}1}(3900)$ and other processes.
³ Measured in weak decays of b -flavored hadrons (nonprompt).
⁴ Pole width obtained from a fit to a Flatte-like formula.
⁵ For $M^2(\pi^+ \pi^-) < 0.65$ GeV². Obtained by analyzing CLEO-c data but not authored by the CLEO Collaboration.
⁶ Superseded by ABLIKIM 20N.
⁷ Superseded by ABLIKIM 17J.

$T_{c\bar{c}1}(3900)$ DECAY MODES

Mode	Fraction (Γ_i/Γ)
Γ_1 $J/\psi \pi$	seen
Γ_2 $h_c \pi^\pm$	not seen
Γ_3 $\eta_c \pi^+ \pi^-$	not seen
Γ_4 $\eta_c(1S) \rho(770)^\pm$	seen
Γ_5 $(D\bar{D}^*)^\pm$	seen
Γ_6 $D^0 D^{*-} + c.c.$	seen
Γ_7 $D^- D^{*0} + c.c.$	seen
Γ_8 $\omega \pi^\pm$	not seen
Γ_9 $J/\psi \eta$	not seen
Γ_{10} $D^+ D^{*-} + c.c.$	seen
Γ_{11} $D^0 \bar{D}^{*0} + c.c.$	seen

$T_{c\bar{c}1}(3900)$ BRANCHING RATIOS

$\Gamma(J/\psi \pi)/\Gamma_{total}$	VALUE	EVTS	DOCUMENT ID	TECN	CHG	COMMENT	Γ_i/Γ
seen			ABLIKIM	20N BES3	0	$e^+ e^- \rightarrow \pi^0 \pi^0 J/\psi$	
seen			1 ABAZOV	19 D0	±	1.96 TeV $p\bar{p} \rightarrow \pi^+ \pi^- J/\psi X$ (prompt)	
seen			ABLIKIM	17J BES3	±	$e^+ e^- \rightarrow \pi^+ \pi^- J/\psi$	
seen		356	ABLIKIM	15U BES3	0	$e^+ e^- \rightarrow \pi^0 \pi^0 J/\psi$	

Meson Particle Listings

 $T_{c\bar{c}1}(3900)$, $T_{c\bar{c}1}(4000)$

not seen		² ADOLPH	15D	COMP	±	$\gamma N \rightarrow J/\psi \pi^\pm N$
seen	307	ABLIKIM	13T	BES3	±	$e^+e^- \rightarrow \pi^+\pi^- J/\psi$
seen	25	XIAO	13A	0		$4.17 e^+e^- \rightarrow \pi^0 \pi^0 J/\psi$

¹ But not seen in the "prompt" sample (no b-hadron enhancement).

² ADOLPH 15D measure $B(T_{c\bar{c}1}(3900)^\pm \rightarrow J/\psi \pi^\pm) \sigma(\gamma N \rightarrow T_{c\bar{c}1}(3900)^\pm N)/\sigma(\gamma N \rightarrow J/\psi \pi^\pm) < 3.7 \times 10^{-3}$ at 90% CL.

³ Obtained by analyzing CLEO-c data but not authored by the CLEO Collaboration.

$\Gamma(h_c \pi^\pm)/\Gamma_{\text{total}}$	DOCUMENT ID	TECN	CHG	COMMENT	Γ_2/Γ
not seen	ABLIKIM	13X	BES3	±	$e^+e^- \rightarrow h_c \pi^+ \pi^-$

$\Gamma(\eta_c \pi^+ \pi^-)/\Gamma_{\text{total}}$	DOCUMENT ID	TECN	CHG	COMMENT	Γ_3/Γ
not seen	¹ VINOKUROVA	15	BELL	0	$B^+ \rightarrow K^+ \eta_c \pi^+ \pi^-$

¹ VINOKUROVA 15 reports $B(B^+ \rightarrow K^+ Z_c(3900)^0) \times B(X \rightarrow \eta_c \pi^+ \pi^-) < 4.7 \times 10^{-5}$ at 90% CL.

$\Gamma(\eta_c(1S)\rho(770)^\pm)/\Gamma(J/\psi\pi)$	EVTS	DOCUMENT ID	TECN	COMMENT	Γ_4/Γ_1
2.3 ± 0.8	332	¹ ABLIKIM	19Bc	BES3	$e^+e^- \rightarrow \pi^+\pi^-\pi^0 \eta_c(1S)$

¹ Using $e^+e^- \rightarrow \pi^\mp(T_{c\bar{c}1}(3900)^\pm \rightarrow J/\psi \pi^\pm)$ cross section at 4.23 and 4.26 GeV from ABLIKIM 17i.

$\Gamma((D\bar{D}^*)^\pm)/\Gamma(J/\psi\pi)$	DOCUMENT ID	TECN	CHG	COMMENT	Γ_5/Γ_1
$6.2 \pm 1.1 \pm 2.7$	¹ ABLIKIM	14A	BES3	±	$e^+e^- \rightarrow \pi^\pm(D\bar{D}^*)^\mp$

¹ Assuming the same origin of the $(D\bar{D}^*)^\pm$ and $\pi^\pm J/\psi$ decay modes.

$\Gamma(D^0 D^{*-} + \text{c.c.})/\Gamma_{\text{total}}$	DOCUMENT ID	TECN	CHG	COMMENT	Γ_6/Γ
seen	ABLIKIM	15Ac	BES3	±	$e^+e^- \rightarrow \pi^+ D^0 D^{*-} + \text{c.c.}$
seen	ABLIKIM	14A	BES3	±	$e^+e^- \rightarrow \pi^+ D^0 D^{*-} + \text{c.c.}$

$\Gamma(D^- D^{*0} + \text{c.c.})/\Gamma_{\text{total}}$	DOCUMENT ID	TECN	CHG	COMMENT	Γ_7/Γ
seen	ABLIKIM	15Ac	BES3	±	$e^+e^- \rightarrow \pi^+ D^- D^{*0} + \text{c.c.}$
seen	ABLIKIM	14A	BES3	±	$e^+e^- \rightarrow \pi^+ D^- D^{*0} + \text{c.c.}$

$\Gamma(\omega \pi^\pm)/\Gamma_{\text{total}}$	DOCUMENT ID	TECN	CHG	COMMENT	Γ_8/Γ
not seen	ABLIKIM	15R	BES3	±	$e^+e^- \rightarrow \omega \pi^+ \pi^-$

$\Gamma(J/\psi\eta)/\Gamma_{\text{total}}$	DOCUMENT ID	TECN	CHG	COMMENT	Γ_9/Γ
not seen	ABLIKIM	15Q	BES3	0	$4.0\text{--}4.6 e^+e^- \rightarrow J/\psi \eta \pi^0$

$\Gamma(J/\psi\eta)/\Gamma(J/\psi\pi)$	DOCUMENT ID	TECN	CHG	COMMENT	Γ_9/Γ_1	
<0.15	90	ABLIKIM	15Q	BES3	0	$4.226 e^+e^- \rightarrow J/\psi \eta \pi^0$

• • • We do not use the following data for averages, fits, limits, etc. • • •

<0.65	90	ABLIKIM	15Q	BES3	0	$4.257 e^+e^- \rightarrow J/\psi \eta \pi^0$
-------	----	---------	-----	------	---	--

$\Gamma(D^+ D^{*-} + \text{c.c.})/\Gamma_{\text{total}}$	DOCUMENT ID	TECN	CHG	COMMENT	Γ_{10}/Γ
seen	ABLIKIM	15Ab	BES3	0	$e^+e^- \rightarrow \pi^0(D\bar{D}^*)^0$

$\Gamma(D^0 \bar{D}^{*0} + \text{c.c.})/\Gamma_{\text{total}}$	DOCUMENT ID	TECN	CHG	COMMENT	Γ_{11}/Γ
seen	ABLIKIM	15Ab	BES3	0	$e^+e^- \rightarrow \pi^0(D\bar{D}^*)^0$

$\Gamma(D^+ D^{*-} + \text{c.c.})/\Gamma(D^0 \bar{D}^{*0} + \text{c.c.})$	DOCUMENT ID	TECN	CHG	COMMENT	Γ_{10}/Γ_{11}
$0.96 \pm 0.18 \pm 0.12$	ABLIKIM	15Ab	BES3	0	$e^+e^- \rightarrow \pi^0(D\bar{D}^*)^0$

 $T_{c\bar{c}1}(3900)$ REFERENCES

ABLIKIM	20N	PR D102 012009	M. Ablikim et al.	(BESIII Collab.) JP
ABAZOV	19	PR D100 012005	V.M. Abazov et al.	(DO Collab.)
ABLIKIM	19Bc	PR D100 111102	M. Ablikim et al.	(BESIII Collab.)
ABAZOV	18B	PR D98 052010	V.M. Abazov et al.	(DO Collab.)
ABLIKIM	17J	PRL 119 072001	M. Ablikim et al.	(BESIII Collab.) JP
ABLIKIM	15Ab	PRL 115 222002	M. Ablikim et al.	(BESIII Collab.)
ABLIKIM	15Ac	PR D92 092006	M. Ablikim et al.	(BESIII Collab.) JP
ABLIKIM	15Q	PR D92 012008	M. Ablikim et al.	(BESIII Collab.)
ABLIKIM	15R	PR D92 032009	M. Ablikim et al.	(BESIII Collab.)

ABLIKIM	15U	PRL 115 112003	M. Ablikim et al.	(BESIII Collab.)
ADOLPH	15D	PL B742 330	C. Adolph et al.	(COMPASS Collab.)
VINOKUROVA	15	JHEP 1506 132	A. Vinokurova et al.	(BELLE Collab.)
	Also	JHEP 1702 088 (err.)	A. Vinokurova et al.	(BELLE Collab.)
ABLIKIM	14A	PRL 112 022001	M. Ablikim et al.	(BESIII Collab.) JP
ABLIKIM	13T	PRL 110 252001	M. Ablikim et al.	(BESIII Collab.)
ABLIKIM	13X	PRL 111 242001	M. Ablikim et al.	(BESIII Collab.)
LIU	13B	PRL 110 252002	Z.Q. Liu et al.	(BELLE Collab.)
XIAO	13A	PL B727 366	T. Xiao et al.	(NWES)

 $T_{c\bar{c}1}(4000)$

$$J(J^P) = \frac{1}{2}(1^+)$$

OMITTED FROM SUMMARY TABLE

was $Z_{cs}(4000)$

Properties incompatible with a $q\bar{q}$ structure (exotic state). See the review on "Heavy Non- $q\bar{q}$ Mesons."

Seen by AAIJ 21E in $B^+ \rightarrow T_{c\bar{c}1}(4000)^+ \phi$ with $T_{c\bar{c}1}(4000)^+ \rightarrow J/\psi K^+$ using an amplitude analysis of $B^+ \rightarrow J/\psi \phi K^+$ with a significance (accounting for systematic uncertainties) of 15σ . The $J^P = 1^+$ assignment is favored with high significance. ABLIKIM 21G also reports a $J^P = 1^+ Z_{cs}$ state in this mass region using $e^+e^- \rightarrow K^+(D_s^- D^{*0} + D_s^{*-} D^0)$ with a significance of 5.3σ . The incompatible values for the widths reported by AAIJ 21E and ABLIKIM 21G could either indicate the existence of two separate states or possibly be explained in a coupled channel model (see ORTEGA 21).

 $T_{c\bar{c}1}(4000)$ MASS

VALUE (MeV)	EVTS	DOCUMENT ID	TECN	COMMENT
3980–4010 OUR EVALUATION				
3988 ± 5 OUR AVERAGE Error includes scale factor of 2.7.				
3991	$+12_{-10}^{+9}_{-17}$	¹ AAIJ	23Aq	LHCB $B^0 \rightarrow J/\psi \phi K_S^0$
3992.2 ± 1.7 ± 1.6		² ABLIKIM	22Ae	BES3 $e^+e^- \rightarrow K_S^0(D_s^- D^{*+} + D_s^{*-} D^+)$
4003 ± 6	$+4_{-14}$	24k	³ AAIJ	21E LHCB $B^+ \rightarrow J/\psi \phi K^+$
3982.5 ± 1.8 ± 2.1		⁴ ABLIKIM	21G	BES3 $e^+e^- \rightarrow K^+(D_s^- D^{*0} + D_s^{*-} D^0)$

¹ From an amplitude analysis of the decay $B^0 \rightarrow J/\psi \phi K_S^0$ with a significance of 4.0σ . The mass difference with respect to the charged partner in AAIJ 21E is $-12_{-10}^{+11} + 6_{-4}$ MeV.

² Pole mass for a mass-, width-dependent Breit-Wigner fit to the mass spectrum recoiling against K_S^0 at center of mass energies between 4.628 and 4.699 GeV, with a significance of 4.6σ .

³ From an amplitude analysis of the decay $B^+ \rightarrow J/\psi \phi K^+$ with a significance of 15σ .

⁴ Pole mass for a mass-dependent Breit-Wigner fit to the mass spectrum recoiling against K^+ at center of mass energies between 4.628 and 4.698 GeV, with a significance of 5.3σ .

 $T_{c\bar{c}1}(4000)$ WIDTH

VALUE (MeV)	EVTS	DOCUMENT ID	TECN	COMMENT
5–150 OUR EVALUATION				
14 ± 4 OUR AVERAGE Error includes scale factor of 1.1.				
105	$+29_{-25}^{+17}_{-23}$	¹ AAIJ	23Aq	LHCB $B^0 \rightarrow J/\psi \phi K_S^0$
$7.7_{-4.1}^{+4.1} \pm 4.3$		² ABLIKIM	22Ae	BES3 $e^+e^- \rightarrow K_S^0(D_s^- D^{*+} + D_s^{*-} D^+)$
131 ± 15 ± 26	24k	³ AAIJ	21E	LHCB $B^+ \rightarrow J/\psi \phi K^+$
$12.8_{-4.4}^{+5.3} \pm 3.0$		⁴ ABLIKIM	21G	BES3 $e^+e^- \rightarrow K^+(D_s^- D^{*0} + D_s^{*-} D^0)$

¹ From an amplitude analysis of the decay $B^0 \rightarrow J/\psi \phi K_S^0$ with a significance of 4.0σ .

² Pole width for a mass-, width-dependent Breit-Wigner fit to the mass spectrum recoiling against K_S^0 at center of mass energies between 4.628 and 4.699 GeV, with a significance of 4.6σ .

³ From an amplitude analysis of the decay $B^+ \rightarrow J/\psi \phi K^+$ with a significance of 15σ .

⁴ Pole width for a mass-dependent Breit-Wigner fit to the mass spectrum recoiling against K^+ at center of mass energies between 4.628 and 4.698 GeV, with a significance of 5.3σ .

Mode	Fraction (Γ_i/Γ)
Γ_1 $J/\psi K^+$	seen
Γ_2 $J/\psi K_S^0$	seen
Γ_3 $D_s^+ \bar{D}^{*0}$ or $D_s^{*+} \bar{D}^0$	seen
Γ_4 $D_s^+ D^{*-}$ or $D_s^{*+} D^-$	seen

See key on page 1171

Meson Particle Listings

$T_{c\bar{c}1}(4000)$, $T_{c\bar{c}}(4020)$

$T_{c\bar{c}1}(4000)$ DECAY MODES

$\Gamma(J/\psi K^+)/\Gamma_{total}$					Γ_1/Γ
VALUE	EVTs	DOCUMENT ID	TECN	COMMENT	
seen	24k	¹ AAIJ	21E LHCb	$B^+ \rightarrow J/\psi \phi K^+$	
¹ From an amplitude analysis of the decay $B^+ \rightarrow J/\psi \phi K^+$ with a significance of 15 σ .					

$\Gamma(J/\psi K_S^0)/\Gamma_{total}$					Γ_2/Γ
VALUE	EVTs	DOCUMENT ID	TECN	COMMENT	
seen		¹ AAIJ	23AQ LHCB	$B^0 \rightarrow J/\psi \phi K_S^0$	
¹ From an amplitude analysis of the decay $B^0 \rightarrow J/\psi \phi K_S^0$ with a significance of 4.0 σ .					

$\Gamma(D_s^+ \bar{D}^{*0} \text{ or } D_s^{*+} \bar{D}^0)/\Gamma_{total}$					Γ_3/Γ
VALUE	EVTs	DOCUMENT ID	TECN	COMMENT	
seen		¹ ABLIKIM	21G BES3	$e^+ e^- \rightarrow K^+(D_s^- D^{*0} + D_s^{*-} D^0)$	
¹ Seen in the spectrum recoiling against K^+ in $e^+ e^- \rightarrow K^+(D_s^- D^{*0} + D_s^{*-} D^0)$ collisions at center of mass energies between 4.628 and 4.698 GeV, with a significance of 5.3 σ .					

$\Gamma(J/\psi K^+)/\Gamma(D_s^+ \bar{D}^{*0} \text{ or } D_s^{*+} \bar{D}^0)$					Γ_1/Γ_3
VALUE	CL%	DOCUMENT ID	TECN	COMMENT	
<0.03	90	ABLIKIM	23BI BES3	$e^+ e^- \rightarrow K^+ K^- J/\psi$	

$\Gamma(D_s^+ D^{*-} \text{ or } D_s^{*+} D^-)/\Gamma_{total}$					Γ_4/Γ
VALUE	EVTs	DOCUMENT ID	TECN	COMMENT	
seen		¹ ABLIKIM	22AE BES3	$e^+ e^- \rightarrow K_S^0(D_s^- D^{*+} + D_s^{*-} D^+)$	
¹ Seen in the mass spectrum recoiling against K_S^0 at center of mass energies between 4.628 and 4.699 GeV, with a significance of 4.6 σ .					

$T_{c\bar{c}1}(4000)$ REFERENCES

AAIJ	23AQ	PRL 131 131901	R. Aaij <i>et al.</i>	(LHCb Collab.)
ABLIKIM	23BI	PRL 131 211902	M. Ablikim <i>et al.</i>	(BESIII Collab.)
ABLIKIM	22AE	PRL 129 112003	M. Ablikim <i>et al.</i>	(BESIII Collab.)
AAIJ	21E	PRL 127 082001	R. Aaij <i>et al.</i>	(LHCb Collab.)
ABLIKIM	21G	PRL 126 102001	M. Ablikim <i>et al.</i>	(BESIII Collab.)
ORTEGA	21	PL B818 136382	P.G. Ortega, D.R. Entem, F. Fernandez	

$T_{c\bar{c}}(4020)$

$I^G(J^{PC}) = 1^+(?^-)$

was $X(4020)$

Properties incompatible with a $q\bar{q}$ structure (exotic state). See the review on non- $q\bar{q}$ states.

Charged $T_{c\bar{c}}(4020)$ seen by ABLIKIM 13X from $e^+ e^- \rightarrow \pi^+ \pi^- h_c(1P)$ at c.m. energy from 3.90 to 4.42 GeV as a peak in the invariant mass distribution of the $\pi^\pm h_c(1P)$ system, and by ABLIKIM 14B from $e^+ e^- \rightarrow (D^* \bar{D}^*)^\pm \pi^\mp$ events in $(D^* \bar{D}^*)^\pm$ mass. A neutral $T_{c\bar{c}}(4020)$ seen by ABLIKIM 14P at three c.m. energies in the same range in $e^+ e^- \rightarrow \pi^0 \pi^0 h_c(1P)$ as a peak in the larger of the two masses recoiling against a π^0 . ABLIKIM 15AA observes a 5.9 σ signal in $(D^* \bar{D}^*)^0$ in $e^+ e^- \rightarrow (D^* \bar{D}^*)^0 \pi^0$ events using collisions at two c.m. energies. Production rates and mass values support grouping neutral and charged $T_{c\bar{c}}(4020)$ together as manifestations of a single $I = 1$ particle.

$T_{c\bar{c}}(4020)$ MASS

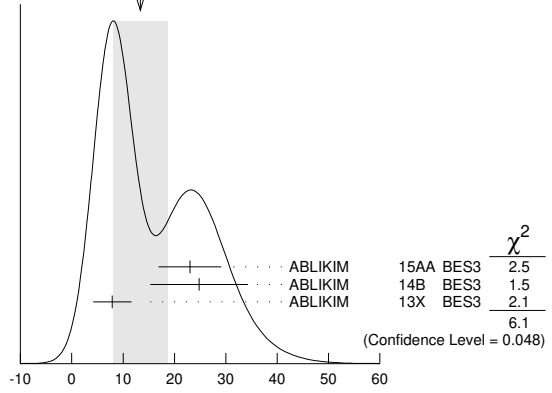
VALUE (MeV)	EVTs	DOCUMENT ID	TECN	CHG	COMMENT
4024.1 ± 1.9 OUR AVERAGE					
4025.5 ^{+2.0} _{-4.7} ± 3.1	116	¹ ABLIKIM	15AA BES3	0	$e^+ e^- \rightarrow (D^* \bar{D}^*)^0 \pi^0$
4026.3 ± 2.6 ± 3.7	401	¹ ABLIKIM	14B BES3	±	$e^+ e^- \rightarrow (D^* \bar{D}^*)^\pm \pi^\mp$
4023.9 ± 2.2 ± 3.8	61	^{1,2} ABLIKIM	14P BES3	0	$e^+ e^- \rightarrow \pi^0 \pi^0 h_c$
4022.9 ± 0.8 ± 2.7	253	¹ ABLIKIM	13X BES3	±	$e^+ e^- \rightarrow \pi^+ \pi^- h_c$

¹ Neglecting interference between the $T_{c\bar{c}}(4020)$ and non-resonant continuum.
² Assuming $J^P = 1^+$ and width of 7.9 ± 2.6 MeV.

$T_{c\bar{c}}(4020)$ WIDTH

VALUE (MeV)	EVTs	DOCUMENT ID	TECN	CHG	COMMENT
13 ± 5 OUR AVERAGE					Error includes scale factor of 1.7. See the ideogram below.
23.0 ± 6.0 ± 1.0	116	¹ ABLIKIM	15AA BES3	0	$e^+ e^- \rightarrow (D^* \bar{D}^*)^0 \pi^0$
24.8 ± 5.6 ± 7.7	401	¹ ABLIKIM	14B BES3	±	$e^+ e^- \rightarrow (D^* \bar{D}^*)^\pm \pi^\mp$
7.9 ± 2.7 ± 2.6	253	¹ ABLIKIM	13X BES3	±	$e^+ e^- \rightarrow \pi^+ \pi^- h_c$

WEIGHTED AVERAGE
13±5 (Error scaled by 1.7)



¹ Neglecting interference between the $T_{c\bar{c}}(4020)$ and non-resonant continuum.

$T_{c\bar{c}}(4020)$ DECAY MODES

Mode	Fraction (Γ_i/Γ)
Γ_1 $h_c(1P)\pi$	seen
Γ_2 $D^* \bar{D}^*$	seen
Γ_3 $D \bar{D}^* + c.c.$	not seen
Γ_4 $\eta_c \pi^+ \pi^-$	not seen
Γ_5 $\eta_c(1S)\rho(770)^\pm$	
Γ_6 $J/\psi(1S)\pi^\pm$	not seen

$T_{c\bar{c}}(4020)$ BRANCHING RATIOS

$\Gamma(h_c(1P)\pi)/\Gamma_{total}$					Γ_1/Γ
VALUE	EVTs	DOCUMENT ID	TECN	CHG	COMMENT
seen	61	ABLIKIM	14P BES3	0	$e^+ e^- \rightarrow \pi^0 \pi^0 h_c$
seen	253	ABLIKIM	13X BES3	±	$e^+ e^- \rightarrow \pi^+ \pi^- h_c$

$\Gamma(D^* \bar{D}^*)/\Gamma_{total}$					Γ_2/Γ
VALUE	EVTs	DOCUMENT ID	TECN	CHG	COMMENT
seen	116	¹ ABLIKIM	15AA BES3	0	$e^+ e^- \rightarrow (D^* \bar{D}^*)^0 \pi^0$
seen	401	¹ ABLIKIM	14B BES3	±	$e^+ e^- \rightarrow (D^* \bar{D}^*)^\pm \pi^\mp$

¹ Neglecting interference between the $T_{c\bar{c}}(4020)$ and non-resonant continuum.

$\Gamma(D \bar{D}^* + c.c.)/\Gamma_{total}$					Γ_3/Γ
VALUE	EVTs	DOCUMENT ID	TECN	CHG	COMMENT
not seen		ABLIKIM	15AC BES3	±	$e^+ e^- \rightarrow \pi^\pm (D \bar{D}^*)^\mp$

$\Gamma(\eta_c \pi^+ \pi^-)/\Gamma_{total}$					Γ_4/Γ
VALUE	EVTs	DOCUMENT ID	TECN	COMMENT	
not seen		¹ VINOKUROVA 15	BELLE	$B^+ \rightarrow K^+ \eta_c \pi^+ \pi^-$	
¹ VINOKUROVA 15 reports $B(B^+ \rightarrow K^+ T_{c\bar{c}}(4020)^0) \times B(T_{c\bar{c}} \rightarrow \eta_c \pi^+ \pi^-) < 1.6 \times 10^{-5}$ at 90% CL.					

$\Gamma(\eta_c(1S)\rho(770)^\pm)/\Gamma(h_c(1P)\pi)$					Γ_5/Γ_1
VALUE	CL%	DOCUMENT ID	TECN	COMMENT	
<1.2	90	¹ ABLIKIM	19Bc BES3	$e^+ e^- \rightarrow \pi^+ \pi^- \pi^0 \eta_c(1S)$	
¹ Using $e^+ e^- \rightarrow \pi^\mp(Z_c(4020)^\pm \rightarrow h_c(1P)\pi^\pm)$ cross section at 4.23, 4.26 and 4.36 GeV from ABLIKIM 13X.					

$\Gamma(J/\psi(1S)\pi^\pm)/\Gamma_{total}$					Γ_6/Γ
VALUE	EVTs	DOCUMENT ID	TECN	COMMENT	
not seen		¹ ABLIKIM	17J BES3	$e^+ e^- \rightarrow \pi^+ \pi^- J/\psi$	
¹ From Partial Wave Analysis assuming $J^P = 1^+$.					

$T_{c\bar{c}}(4020)$ REFERENCES

ABLIKIM	19Bc	PR D100 111102	M. Ablikim <i>et al.</i>	(BESIII Collab.)
ABLIKIM	17J	PRL 119 072001	M. Ablikim <i>et al.</i>	(BESIII Collab.)
ABLIKIM	15AA	PRL 115 182002	M. Ablikim <i>et al.</i>	(BESIII Collab.)
ABLIKIM	15AC	PR D92 092006	M. Ablikim <i>et al.</i>	(BESIII Collab.)
VINOKUROVA	15	JHEP 1506 132	A. Vinokurova <i>et al.</i>	(BELLE Collab.)
Also	JHEP	1702 088 (err.)	A. Vinokurova <i>et al.</i>	(BELLE Collab.)
ABLIKIM	14B	PRL 112 132001	M. Ablikim <i>et al.</i>	(BESIII Collab.)
ABLIKIM	14P	PRL 113 212002	M. Ablikim <i>et al.</i>	(BESIII Collab.)
ABLIKIM	13X	PRL 111 242001	M. Ablikim <i>et al.</i>	(BESIII Collab.)

Meson Particle Listings

 $T_{c\bar{c}}(4050)^+$, $T_{c\bar{c}}(4055)^+$ $T_{c\bar{c}}(4050)^+$

$I^G(J^{PC}) = 1^-(?^{?+})$
I, G, C need confirmation.

OMITTED FROM SUMMARY TABLE
was X(4050)

Properties incompatible with a $q\bar{q}$ structure (exotic state). See the review on non- $q\bar{q}$ states.

Observed by MIZUK 08 in the $\pi^+\chi_{c1}(1P)$ invariant mass distribution in $\bar{B}^0 \rightarrow K^-\pi^+\chi_{c1}(1P)$ decays. Not seen by LEES 12B in this same mode after accounting for $K\pi$ resonant mass and angular structure.

 $T_{c\bar{c}}(4050)^+$ MASS

VALUE (MeV)	DOCUMENT ID	TECN	COMMENT
$4051 \pm 14^{+20}_{-41}$	¹ MIZUK	08	BELL $\bar{B}^0 \rightarrow K^-\pi^+\chi_{c1}(1P)$

¹ From a Dalitz plot analysis with two Breit-Wigner amplitudes.

 $T_{c\bar{c}}(4050)^+$ WIDTH

VALUE (MeV)	DOCUMENT ID	TECN	COMMENT
82^{+21+47}_{-17-22}	¹ MIZUK	08	BELL $\bar{B}^0 \rightarrow K^-\pi^+\chi_{c1}(1P)$

¹ From a Dalitz plot analysis with two Breit-Wigner amplitudes.

 $T_{c\bar{c}}(4050)^+$ DECAY MODES

Mode	Fraction (Γ_i/Γ)
Γ_1 $\pi^+\chi_{c1}(1P)$	seen
Γ_2 $\pi^+\psi(3770)$	not seen
Γ_3 $\pi^+\chi_{c0}(1P)$	not seen
Γ_4 $\pi^+\chi_{c2}(1P)$	not seen

 $T_{c\bar{c}}(4050)^+$ BRANCHING RATIOS

$\Gamma(\pi^+\chi_{c1}(1P))/\Gamma_{\text{total}}$	VALUE	EVTS	DOCUMENT ID	TECN	COMMENT	Γ_1/Γ
seen		18	¹ MIZUK	08	BELL $\bar{B}^0 \rightarrow K^-\pi^+\chi_{c1}(1P)$	

• • • We do not use the following data for averages, fits, limits, etc. • • •

not seen	16	² ABLIKIM	21W	BES3	$e^+e^- \rightarrow \chi_{cJ}\pi^+\pi^+$
not seen		³ LEES	12B	BABR	$B \rightarrow K\pi\chi_{c1}(1P)$

¹ With a product branching fraction measurement of $B(\bar{B}^0 \rightarrow K^-T_{c\bar{c}}(4050)^+) \times B(T_{c\bar{c}}(4050)^+ \rightarrow \pi^+\chi_{c1}(1P)) = (3.0^{+1.5+3.7}_{-0.8-1.6}) \times 10^{-5}$.

² ABLIKIM 21W measurement is limited by statistics.

³ With a product branching fraction limit of $B(\bar{B}^0 \rightarrow T_{c\bar{c}}(4050)^+K^-) \times B(T_{c\bar{c}}(4050)^+ \rightarrow \chi_{c1}\pi^+) < 1.8 \times 10^{-5}$ at 90% CL.

$\Gamma(\pi^+\chi_{c0}(1P))/\Gamma_{\text{total}}$	VALUE	EVTS	DOCUMENT ID	TECN	COMMENT	Γ_3/Γ
not seen	18		¹ ABLIKIM	21W	BES3	$e^+e^- \rightarrow \chi_{cJ}\pi^+\pi^+$

¹ ABLIKIM 21W measurement is limited by statistics.

$\Gamma(\pi^+\chi_{c2}(1P))/\Gamma_{\text{total}}$	VALUE	EVTS	DOCUMENT ID	TECN	COMMENT	Γ_4/Γ
not seen	14		¹ ABLIKIM	21W	BES3	$e^+e^- \rightarrow \chi_{cJ}\pi^+\pi^+$

¹ ABLIKIM 21W measurement is limited by statistics.

$\Gamma(\pi^+\psi(3770))/\Gamma_{\text{total}}$	VALUE	DOCUMENT ID	TECN	COMMENT	Γ_2/Γ
not seen		¹ ABLIKIM	19AR	BES3	$e^+e^- \rightarrow \pi^+\pi^-D\bar{D}$

¹ From a measurement of $\sigma(e^+e^- \rightarrow \pi^+\pi^-D\bar{D})$ between $\sqrt{s} = 4.08$ and 4.6 GeV.

 $T_{c\bar{c}}(4050)^+$ REFERENCES

ABLIKIM	21W	PR D103 052010	M. Ablikim et al.	(BESIII Collab.)
ABLIKIM	19AR	PR D100 032005	M. Ablikim et al.	(BESIII Collab.)
LEES	12B	PR D85 052003	J.P. Lees et al.	(BABAR Collab.)
MIZUK	08	PR D78 072004	R. Mizuk et al.	(BELLE Collab.)

 $T_{c\bar{c}}(4055)^+$

$I^G(J^{PC}) = 1^+(?^{?-})$
I, G, C need confirmation.

OMITTED FROM SUMMARY TABLE
was X(4055)[±]

Properties incompatible with a $q\bar{q}$ structure (exotic state). See the review on non- $q\bar{q}$ states.

Needs confirmation. Seen by WANG 15A in the $\psi(2S)\pi^+$ invariant mass distribution in $\psi(4360) \rightarrow \psi(2S)\pi^+\pi^-$ decay.

 $T_{c\bar{c}}(4055)^+$ MASS

VALUE (MeV)	DOCUMENT ID	TECN	COMMENT
$4054 \pm 3 \pm 1$	¹ WANG	15A	BELL $10.58 e^+e^- \rightarrow \gamma\pi^+\pi^-\psi(2S)$

• • • We do not use the following data for averages, fits, limits, etc. • • •

4039.3 ± 6.0	² ABLIKIM	18K	BES3 $e^+e^- \rightarrow \pi^0\pi^0\psi(2S)$
4032.1 ± 2.4	³ ABLIKIM	17V	BES3 $e^+e^- \rightarrow \pi^+\pi^-\psi(2S)$

¹ Statistical significance of 3.5 σ .

² Statistical error only, with significance of 5.9 σ (from a fit with a 19% CL). Identified as the same structure observed in ABLIKIM 17V in $e^+e^- \rightarrow \pi^+\pi^-\psi(2S)$ decays.

³ Statistical error only, with significance of 9.2 σ . From an unbinned maximum likelihood fit of the $\pi^+\pi^-\psi(2S)$ Dalitz plot from data collected at $\sqrt{s} = 4.416$ GeV for a $J^C = 1^+$ state. The fit does not match the detailed structure of the data, having a C.L. of only 8%.

 $T_{c\bar{c}}(4055)^+$ WIDTH

VALUE (MeV)	DOCUMENT ID	TECN	COMMENT
$45 \pm 11 \pm 6$	¹ WANG	15A	BELL $10.58 e^+e^- \rightarrow \gamma\pi^+\pi^-\psi(2S)$

• • • We do not use the following data for averages, fits, limits, etc. • • •

31.9 ± 14.8	² ABLIKIM	18K	BES3 $e^+e^- \rightarrow \pi^0\pi^0\psi(2S)$
26.1 ± 5.3	³ ABLIKIM	17V	BES3 $e^+e^- \rightarrow \pi^+\pi^-\psi(2S)$

¹ Statistical significance of 3.5 σ .

² Statistical error only, with significance of 5.9 σ (from a fit with a 19% CL). Identified as the same structure observed in ABLIKIM 17V in $e^+e^- \rightarrow \pi^+\pi^-\psi(2S)$ decays.

³ Statistical error only, with significance of 9.2 σ . From an unbinned maximum likelihood fit of the $\pi^+\pi^-\psi(2S)$ Dalitz plot from data collected at $\sqrt{s} = 4.416$ GeV for a $J^C = 1^+$ state. The fit does not match the detailed structure of the data, having a C.L. of only 8%.

 $T_{c\bar{c}}(4055)^+$ DECAY MODES

Mode	Fraction (Γ_i/Γ)
Γ_1 $\pi^+\psi(2S)$	seen
Γ_2 $\pi^+\psi(3770)$	not seen

 $T_{c\bar{c}}(4055)^+$ BRANCHING RATIOS

$\Gamma(\pi^+\psi(2S))/\Gamma_{\text{total}}$	VALUE	DOCUMENT ID	TECN	COMMENT	Γ_1/Γ
seen		¹ WANG	15A	BELL $10.58 e^+e^- \rightarrow \gamma\pi^+\pi^-\psi(2S)$	

¹ Statistical significance of 3.5 σ .

$\Gamma(\pi^+\psi(3770))/\Gamma_{\text{total}}$	VALUE	DOCUMENT ID	TECN	COMMENT	Γ_2/Γ
not seen		¹ ABLIKIM	19AR	BES3 $e^+e^- \rightarrow \pi^+\pi^-D\bar{D}$	

¹ From a measurement of $\sigma(e^+e^- \rightarrow \pi^+\pi^-D\bar{D})$ between $\sqrt{s} = 4.08$ and 4.6 GeV.

 $T_{c\bar{c}}(4055)^+$ REFERENCES

ABLIKIM	19AR	PR D100 032005	M. Ablikim et al.	(BESIII Collab.)
ABLIKIM	18K	PR D97 052001	M. Ablikim et al.	(BESIII Collab.)
ABLIKIM	17V	PR D96 032004	M. Ablikim et al.	(BESIII Collab.)
Also		PR D99 019903 (errata.)	M. Ablikim et al.	(BESIII Collab.)
WANG	15A	PR D91 112007	X.L. Wang et al.	(BELLE Collab.)

See key on page 1171

Meson Particle Listings

 $T_{c\bar{c}}(4100)^+$, $T_{c\bar{c}1}(4200)^+$, $T_{c\bar{c}31}(4220)^+$, $T_{c\bar{c}0}(4240)^+$ $T_{c\bar{c}}(4100)^+$

$$J^G(J^{PC}) = 1^-(?^?+)$$

OMITTED FROM SUMMARY TABLE
was $X(4100)^\pm$ Properties incompatible with a $q\bar{q}$ structure (exotic state). See the review on non- $q\bar{q}$ states.Reported by AAIJ 18AN in the $\eta_c(1S)\pi^-$ invariant mass distribution in $B^0 \rightarrow \eta_c(1S)K^+\pi^-$ decays with a significance of 3.4σ . $J^P = 0^+$ or 1^- assignment consistent with data. $T_{c\bar{c}}(4100)^+$ MASS

VALUE (MeV)	DOCUMENT ID	TECN	COMMENT
$4096 \pm 20^{+18}_{-22}$	AAIJ	18AN LHCb	$B^0 \rightarrow \eta_c(1S)K^+\pi^-$

 $T_{c\bar{c}}(4100)^+$ WIDTH

VALUE (MeV)	DOCUMENT ID	TECN	COMMENT
$152 \pm 58^{+60}_{-35}$	AAIJ	18AN LHCb	$B^0 \rightarrow \eta_c(1S)K^+\pi^-$

 $T_{c\bar{c}}(4100)^+$ DECAY MODES

Mode	Fraction (Γ_i/Γ)
Γ_1 $\eta_c(1S)\pi^-$	seen
Γ_2 $\pi^\pm\psi(3770)$	not seen

 $T_{c\bar{c}}(4100)^+$ BRANCHING RATIOS

$\Gamma(\eta_c(1S)\pi^-)/\Gamma_{\text{total}}$	Γ_1/Γ		
VALUE	DOCUMENT ID	TECN	COMMENT
seen	¹ AAIJ	18AN LHCb	$B^0 \rightarrow \eta_c(1S)K^+\pi^-$
¹ AAIJ 18AN quotes a fit fraction for $B^0 \rightarrow T_{c\bar{c}}(4100)^+K^+ \rightarrow \eta_c(1S)\pi^-K^+$ of $(3.3 \pm 1.1^{+1.2}_{-1.1})\%$ from an amplitude analysis.			

$\Gamma(\pi^\pm\psi(3770))/\Gamma_{\text{total}}$	Γ_2/Γ		
VALUE	DOCUMENT ID	TECN	COMMENT
not seen	¹ ABLIKIM	19AR BES3	$e^+e^- \rightarrow \pi^+\pi^-D\bar{D}$
¹ From a measurement of $\sigma(e^+e^- \rightarrow \pi^+\pi^-D\bar{D})$ between $\sqrt{s} = 4.08$ and 4.6 GeV.			

 $T_{c\bar{c}}(4100)^+$ REFERENCES

ABLIKIM	19AR PR D100 032005	M. Ablikim et al.	(BESIII Collab.)
AAIJ	18AN EPJ C78 1019	R. Aaij et al.	(LHCb Collab.)

 $T_{c\bar{c}1}(4200)^+$

$$J^G(J^{PC}) = 1^+(1^{+-})$$

 I, G, C need confirmation.

OMITTED FROM SUMMARY TABLE
was $Z_c(4200)^\pm$, $X(4200)^\pm$ This state shows properties different from a conventional $q\bar{q}$ state. A candidate for an exotic structure. See the review on non- $q\bar{q}$ states.Reported by CHILIKIN 14 in $J/\psi\pi^+$ at a significance of 6.2σ . Assignments of 0^- , 1^- , 2^- , and 2^+ excluded at 6.1σ , 7.4σ , 4.4σ , and 7.0σ level, respectively. Needs confirmation. $T_{c\bar{c}1}(4200)^+$ MASS

VALUE (MeV)	DOCUMENT ID	TECN	COMMENT
$4196 \pm 31^{+17}_{-29-13}$	CHILIKIN	14 BELL	$\bar{B}^0 \rightarrow J/\psi K^- \pi^+$

 $T_{c\bar{c}1}(4200)^+$ WIDTH

VALUE (MeV)	DOCUMENT ID	TECN	COMMENT
$370 \pm 70^{+70}_{-132}$	CHILIKIN	14 BELL	$\bar{B}^0 \rightarrow J/\psi K^- \pi^+$

 $T_{c\bar{c}1}(4200)^+$ DECAY MODES

Mode	Fraction (Γ_i/Γ)
Γ_1 $J/\psi\pi^+$	seen

 $T_{c\bar{c}1}(4200)^+$ BRANCHING RATIOS

$\Gamma(J/\psi\pi^+)/\Gamma_{\text{total}}$	Γ_1/Γ		
VALUE	DOCUMENT ID	TECN	COMMENT
seen	CHILIKIN	14 BELL	$\bar{B}^0 \rightarrow J/\psi K^- \pi^+$
••• We do not use the following data for averages, fits, limits, etc. •••			
possibly seen	¹ AAIJ	19R LHCb	$B^0 \rightarrow K^+\pi^-J/\psi + c.c.$
¹ From a model-independent analysis.			

 $T_{c\bar{c}1}(4200)^+$ REFERENCES

AAIJ	19R PRL 122 152002	R. Aaij et al.	(LHCb Collab.)
CHILIKIN	14 PR D90 112009	K. Chilikin et al.	(BELLE Collab.)

 $T_{c\bar{c}31}(4220)^+$

$$I(J^P) = \frac{1}{2}(1^+)$$

OMITTED FROM SUMMARY TABLE
was $Z_{cs}(4220)^+$ Properties incompatible with a $q\bar{q}$ structure (exotic state). See the review on "Heavy Non- $q\bar{q}$ Mesons."Seen by AAIJ 21E in $B^+ \rightarrow T_{c\bar{c}31}(4220)^+\phi$ with $T_{c\bar{c}31}(4220)^+ \rightarrow J/\psi K^+$ using an amplitude analysis of $B^+ \rightarrow J/\psi\phi K^+$ with a significance (accounting for systematic uncertainties) of 5.9σ . The $J^P = 1^+$ assignment is favored over 1^- with a significance of 2σ and other assignments are disfavored by 4.9σ . $T_{c\bar{c}31}(4220)^+$ MASS

VALUE (MeV)	EVTS	DOCUMENT ID	TECN	COMMENT
$4216 \pm 24^{+43}_{-30}$	24k	¹ AAIJ	21E LHCb	$B^+ \rightarrow J/\psi\phi K^+$

¹ From an amplitude analysis of the decay $B^+ \rightarrow J/\psi\phi K^+$ with a significance of 5.9σ . $T_{c\bar{c}31}(4220)^+$ WIDTH

VALUE (MeV)	EVTS	DOCUMENT ID	TECN	COMMENT
$233 \pm 52^{+97}_{-75}$	24k	¹ AAIJ	21E LHCb	$B^+ \rightarrow J/\psi\phi K^+$

¹ From an amplitude analysis of the decay $B^+ \rightarrow J/\psi\phi K^+$ with a significance of 5.9σ . $T_{c\bar{c}31}(4220)^+$ DECAY MODES

Mode	Fraction (Γ_i/Γ)
Γ_1 $J/\psi K^+$	seen

 $\Gamma(J/\psi K^+)/\Gamma_{\text{total}}$ Γ_1/Γ

VALUE	EVTS	DOCUMENT ID	TECN	COMMENT
seen	24k	¹ AAIJ	21E LHCb	$B^+ \rightarrow J/\psi\phi K^+$

¹ From an amplitude analysis of the decay $B^+ \rightarrow J/\psi\phi K^+$ with a significance of 5.9σ . $T_{c\bar{c}31}(4220)^+$ REFERENCES

AAIJ	21E PRL 127 082001	R. Aaij et al.	(LHCb Collab.)JP
------	--------------------	----------------	------------------

 $T_{c\bar{c}0}(4240)^+$

$$J^G(J^{PC}) = 1^+(0^{--})$$

 I, G, C need confirmation.

OMITTED FROM SUMMARY TABLE
was $R_{c0}(4240)$, $X(4240)^\pm$ Properties incompatible with a $q\bar{q}$ structure (exotic state). See the review on non- $q\bar{q}$ states.Spin and parity assignment $J^P = 0^-$ is favored over 1^- , 2^- , and 2^+ by 8σ and over 1^+ by 1σ , according to the four-dimensional amplitude analysis of AAIJ 14AG. $T_{c\bar{c}0}(4240)^+$ MASS

VALUE (MeV)	DOCUMENT ID	TECN	COMMENT
$4239 \pm 18^{+45}_{-10}$	¹ AAIJ	14AG LHCb	$B^0 \rightarrow K^+\pi^-\psi(2S)$

¹ From a 4-dimensional analysis when a second, lower mass resonance is allowed in the $T_{c\bar{c}1}(4430)$ fit, with significance 6σ including systematic variations.

Meson Particle Listings

 $T_{c\bar{c}0}(4240)^+$, $T_{c\bar{c}}(4250)^+$, $T_{c\bar{c}1}(4430)^+$ $T_{c\bar{c}0}(4240)^+$ WIDTH

VALUE (MeV)	DOCUMENT ID	TECN	COMMENT
$220 \pm 47^{+108}_{-74}$	¹ AAIJ	14AG LHCb	$B^0 \rightarrow K^+ \pi^- \psi(2S)$

¹ From a 4-dimensional analysis when a second, lower mass resonance is allowed in the $T_{c\bar{c}1}(4430)$ fit, with significance 6 σ including systematic variations.

 $T_{c\bar{c}0}(4240)^+$ DECAY MODES

Mode	Fraction (Γ_i/Γ)
Γ_1 $\pi^- \psi(2S)$	seen

 $T_{c\bar{c}0}(4240)^+$ BRANCHING RATIOS

$\Gamma(\pi^- \psi(2S))/\Gamma_{\text{total}}$	DOCUMENT ID	TECN	COMMENT	Γ_1/Γ
seen	¹ AAIJ	14AG LHCb	$B^0 \rightarrow K^+ \pi^- \psi(2S)$	

¹ From a 4-dimensional analysis when a second, lower mass resonance is allowed in the $T_{c\bar{c}1}(4430)$ fit. No partial branching fraction quoted.

 $T_{c\bar{c}0}(4240)^+$ REFERENCES

AAIJ 14AG PRL 112 222002 R. Aaij *et al.* (LHCb Collab.)

 $T_{c\bar{c}}(4250)^+$

$I^G(J^{PC}) = 1^-(?^{2+})$
I, G, C need confirmation.

OMITTED FROM SUMMARY TABLE

was $X(4250)^\pm$

Properties incompatible with a $q\bar{q}$ structure (exotic state). See the review on non- $q\bar{q}$ states.

Observed by MIZUK 08 in the $\pi^+ \chi_{c1}(1P)$ invariant mass distribution in $\bar{B}^0 \rightarrow K^- \pi^+ \chi_{c1}(1P)$ decays. Not seen by LEES 12B in this same mode after accounting for $K\pi$ resonant mass and angular structure.

 $T_{c\bar{c}}(4250)^+$ MASS

VALUE (MeV)	DOCUMENT ID	TECN	COMMENT
$4248 \pm 44^{+180}_{-35}$	¹ MIZUK	08 BELL	$\bar{B}^0 \rightarrow K^- \pi^+ \chi_{c1}(1P)$

¹ From a Dalitz plot analysis with two Breit-Wigner amplitudes.

 $T_{c\bar{c}}(4250)^+$ WIDTH

VALUE (MeV)	DOCUMENT ID	TECN	COMMENT
$177 \pm 54^{+316}_{-61}$	¹ MIZUK	08 BELL	$\bar{B}^0 \rightarrow K^- \pi^+ \chi_{c1}(1P)$

¹ From a Dalitz plot analysis with two Breit-Wigner amplitudes.

 $T_{c\bar{c}}(4250)^+$ DECAY MODES

Mode	Fraction (Γ_i/Γ)
Γ_1 $\pi^+ \chi_{c1}(1P)$	seen

 $T_{c\bar{c}}(4250)^+$ BRANCHING RATIOS

$\Gamma(\pi^+ \chi_{c1}(1P))/\Gamma_{\text{total}}$	DOCUMENT ID	TECN	COMMENT	Γ_1/Γ
seen	¹ MIZUK	08 BELL	$\bar{B}^0 \rightarrow K^- \pi^+ \chi_{c1}(1P)$	
not seen	² LEES	12b BABR	$B \rightarrow K\pi \chi_{c1}(1P)$	

• • • We do not use the following data for averages, fits, limits, etc. • • •

¹ With a product branching fraction measurement of $B(\bar{B}^0 \rightarrow K^- T_{c\bar{c}}(4250)^+) \times B(T_{c\bar{c}}(4250)^+ \rightarrow \pi^+ \chi_{c1}(1P)) = (4.0^{+2.3+19.7}_{-0.9-0.5}) \times 10^{-5}$.

² With a product branching fraction limit of $B(\bar{B}^0 \rightarrow T_{c\bar{c}}(4250)^+ K^-) \times B(T_{c\bar{c}}(4250)^+ \rightarrow \chi_{c1} \pi^+) < 4.0 \times 10^{-5}$ at 90% CL.

 $T_{c\bar{c}}(4250)^+$ REFERENCES

LEES 12B PR D85 052003 J.P. Lees *et al.* (BABAR Collab.)
MIZUK 08 PR D78 072004 R. Mizuk *et al.* (BELLE Collab.)

 $T_{c\bar{c}1}(4430)^+$

$I^G(J^{PC}) = 1^+(1^+ -)$
G, C need confirmation.

was $Z_c(4430)$, $X(4430)^\pm$

Properties incompatible with a $q\bar{q}$ structure (exotic state). See the review on non- $q\bar{q}$ states.

First seen by CHOI 08 in $B \rightarrow K\pi^+ \psi(2S)$ decays, confirmed by AAIJ 14AG, and confirmed in a model-independent way by AAIJ 15BH. Also seen by CHILIKIN 14 in $B \rightarrow K^+ \pi^- J/\psi$ decays. J^P was determined by CHILIKIN 13 and AAIJ 14AG.

 $T_{c\bar{c}1}(4430)^+$ MASS

VALUE (MeV)	DOCUMENT ID	TECN	COMMENT
$4478 \pm 15^{+15}_{-18}$	OUR AVERAGE		

$4475 \pm 7^{+15}_{-25}$	¹ AAIJ	14AG LHCb	$B^0 \rightarrow K^+ \pi^- \psi(2S)$
--------------------------	-------------------	-----------	--------------------------------------

$4485 \pm 22^{+28}_{-11}$	¹ CHILIKIN	13 BELL	$B^0 \rightarrow K^+ \pi^- \psi(2S)$
---------------------------	-----------------------	---------	--------------------------------------

• • • We do not use the following data for averages, fits, limits, etc. • • •

$4443 \pm 15^{+19}_{-12-13}$	² MIZUK	09 BELL	$B \rightarrow K\pi^+ \psi(2S)$
------------------------------	--------------------	---------	---------------------------------

$4433 \pm 4 \pm 2$	³ CHOI	08 BELL	$B \rightarrow K\pi^+ \psi(2S)$
--------------------	-------------------	---------	---------------------------------

¹ From a four-dimensional amplitude analysis.

² From a Dalitz plot analysis. Superseded by CHILIKIN 13.

³ Superseded by MIZUK 09 and CHILIKIN 13.

 $T_{c\bar{c}1}(4430)^+$ WIDTH

VALUE (MeV)	DOCUMENT ID	TECN	COMMENT
181 ± 31	OUR AVERAGE		

$172 \pm 13^{+37}_{-34}$	¹ AAIJ	14AG LHCb	$B^0 \rightarrow K^+ \pi^- \psi(2S)$
--------------------------	-------------------	-----------	--------------------------------------

$200 \pm 41^{+26}_{-46-35}$	¹ CHILIKIN	13 BELL	$B^0 \rightarrow K^+ \pi^- \psi(2S)$
-----------------------------	-----------------------	---------	--------------------------------------

• • • We do not use the following data for averages, fits, limits, etc. • • •

$107 \pm 86^{+74}_{-43-56}$	² MIZUK	09 BELL	$B \rightarrow K\pi^+ \psi(2S)$
-----------------------------	--------------------	---------	---------------------------------

$45 \pm 18^{+30}_{-13-13}$	³ CHOI	08 BELL	$B \rightarrow K\pi^+ \psi(2S)$
----------------------------	-------------------	---------	---------------------------------

¹ From a four-dimensional amplitude analysis.

² From a Dalitz plot analysis. Superseded by CHILIKIN 13.

³ Superseded by MIZUK 09 and CHILIKIN 13.

 $T_{c\bar{c}1}(4430)^+$ DECAY MODES

Mode	Fraction (Γ_i/Γ)
Γ_1 $\pi^+ \psi(2S)$	seen
Γ_2 $\pi^+ J/\psi$	seen

 $T_{c\bar{c}1}(4430)^+$ BRANCHING RATIOS

$\Gamma(\pi^+ \psi(2S))/\Gamma_{\text{total}}$	DOCUMENT ID	TECN	COMMENT	Γ_1/Γ
--	-------------	------	---------	-------------------

seen	¹ AAIJ	14AG LHCb	$B^0 \rightarrow K^+ \pi^- \psi(2S)$	
-------------	-------------------	-----------	--------------------------------------	--

seen	² CHILIKIN	13 BELL	$B^0 \rightarrow K^+ \pi^- \psi(2S)$	
-------------	-----------------------	---------	--------------------------------------	--

• • • We do not use the following data for averages, fits, limits, etc. • • •

not seen	³ AUBERT	09AA BABR	$B \rightarrow K\pi^+ \psi(2S)$	
----------	---------------------	-----------	---------------------------------	--

seen	⁴ MIZUK	09 BELL	$B \rightarrow K\pi^+ \psi(2S)$	
-------------	--------------------	---------	---------------------------------	--

¹ From a four-dimensional amplitude analysis. No product of branching fractions quoted.

² From a four-dimensional amplitude analysis. Measured a product of branching fractions

$B(\bar{B}^0 \rightarrow T_{c\bar{c}1}(4430)^+ K^-) \times B(T_{c\bar{c}1}(4430)^+ \rightarrow \psi(2S) \pi^-) = (6.0^{+1.7+2.5}_{-2.0-1.4}) \times 10^{-5}$

³ AUBERT 09AA quotes $B(B^+ \rightarrow \bar{K}^0 T_{c\bar{c}1}(4430)^+) \times B(T_{c\bar{c}1}(4430)^+ \rightarrow \pi^+ \psi(2S)) < 4.7 \times 10^{-5}$ and $B(\bar{B}^0 \rightarrow K^- T_{c\bar{c}1}(4430)^+) \times B(T_{c\bar{c}1}(4430)^+ \rightarrow \pi^+ \psi(2S)) < 3.1 \times 10^{-5}$ at 95% CL.

⁴ Measured a product of branching fractions $B(\bar{B}^0 \rightarrow K^- T_{c\bar{c}1}(4430)^+) \times B(T_{c\bar{c}1}(4430)^+ \rightarrow \pi^+ \psi(2S)) = (3.2^{+1.8+5.3}_{-0.9-1.6}) \times 10^{-5}$. Superseded by CHILIKIN 13.

$\Gamma(\pi^+ J/\psi)/\Gamma_{\text{total}}$	DOCUMENT ID	TECN	COMMENT	Γ_2/Γ
--	-------------	------	---------	-------------------

seen	^{1,2} CHILIKIN	14 BELL	$\bar{B}^0 \rightarrow K^- \pi^+ J/\psi$	
-------------	-------------------------	---------	--	--

• • • We do not use the following data for averages, fits, limits, etc. • • •

not seen	³ AUBERT	09AA BABR	$B \rightarrow K\pi^+ J/\psi$	
----------	---------------------	-----------	-------------------------------	--

¹ CHILIKIN 14 reports $B(\bar{B}^0 \rightarrow T_{c\bar{c}1}(4430)^+ K^-) \times B(T_{c\bar{c}1}(4430)^+ \rightarrow J/\psi \pi^+) = (5.4^{+4.0+1.1}_{-1.0-0.9}) \times 10^{-6}$.

² A broad enhancement seen by AAIJ 19R in the decays $B^0 \rightarrow J/\psi \pi^+ K^-$ at 4600 MeV can be due to an interplay of $T_{c\bar{c}1}(4430)$, $T_{c\bar{c}1}(4200)$ and the fitting polynomials.

³ AUBERT 09AA quotes $B(B^+ \rightarrow \bar{K}^0 T_{c\bar{c}1}(4430)^+) \times B(T_{c\bar{c}1}(4430)^+ \rightarrow \pi^+ J/\psi) < 1.5 \times 10^{-5}$ and $B(\bar{B}^0 \rightarrow K^- T_{c\bar{c}1}(4430)^+) \times B(T_{c\bar{c}1}(4430)^+ \rightarrow \pi^+ J/\psi) < 0.4 \times 10^{-5}$ at 95% CL.

$T_{c\bar{c}1}(4430)^+$, $T_{b\bar{s}}(5568)^+$, $T_{cc\bar{c}c}(6900)^0$, $T_{b\bar{b}1}(10610)$ $T_{c\bar{c}1}(4430)^+$ REFERENCES

AAJ	19R	PRL 122 152002	R. Aaij et al.	(LHCb Collab.)
AAJ	15BH	PR D92 112009	R. Aaij et al.	(LHCb Collab.)
AAJ	14AG	PRL 112 222002	R. Aaij et al.	(LHCb Collab.)
CHILIKIN	14	PR D90 112009	K. Chilikin et al.	(BELLE Collab.)
CHILIKIN	13	PR D88 074026	K. Chilikin et al.	(BELLE Collab.)
AUBERT	09AA	PR D79 112001	B. Aubert et al.	(BABAR Collab.)
MIZUK	09	PR D80 031104	R. Mizuk et al.	(BELLE Collab.)
CHOI	08	PRL 100 142001	S.-K. Choi et al.	(BELLE Collab.)

 $T_{b\bar{s}}(5568)^+$ REFERENCES

ABOUD	18L	PRL 120 202007	M. Aboud et al.	(ATLAS Collab.)
AALTONEN	18A	PRL 120 202006	T. Aaltonen et al.	(CDF Collab.)
ABAZOV	18A	PR D97 092004	V.M. Abazov et al.	(DO Collab.)
SIRUNYAN	18J	PRL 120 202005	A.M. Sirunyan et al.	(CMS Collab.)
AAJ	16AI	PRL 117 152003	R. Aaij et al.	(LHCb Collab.)
ABAZOV	16E	PRL 117 022003	V.M. Abazov et al.	(DO Collab.)

 $T_{b\bar{s}}(5568)^+$

$I(J^P) = 1(?^?)$

OMITTED FROM SUMMARY TABLE
was $X(5568)^\pm$

Seen as a peak in the $B_s \pi^\pm$ mass spectrum with a significance of more than 3σ by ABAZOV 16E and ABAZOV 18A in inclusive $p\bar{p}$ collisions at 1.96 TeV. Not seen by AAJ 16AI, ABOUD 18L, AALTONEN 18A, and SIRUNYAN 18J. Needs confirmation.

 $T_{b\bar{s}}(5568)^+$ MASS

VALUE (MeV)	EVTS	DOCUMENT ID	TECN	COMMENT
$5566.9^{+3.2+0.6}_{-3.1-1.2}$	278	¹ ABAZOV	18A D0	$p\bar{p} \rightarrow B_s^0 \pi^\pm X$
• • • We do not use the following data for averages, fits, limits, etc. • • •				
$5567.8 \pm 2.9^{+0.9}_{-1.9}$	133	² ABAZOV	16E D0	$p\bar{p} \rightarrow B_s^0 \pi^\pm X$

¹ From the combined analysis of $B_s^0 \rightarrow J/\psi \phi$ and $B_s^0 \rightarrow D_s^\pm \mu^\mp X$ decays.² Assumes $T_{b\bar{s}}(5568)^\pm \rightarrow B_s \pi^\pm$ decay. If $T_{b\bar{s}}(5568)^\pm \rightarrow B_s^* \pi^\pm$ decay is assumed, the mass shifts upward by 49 MeV. $T_{b\bar{s}}(5568)^+$ WIDTH

VALUE (MeV)	EVTS	DOCUMENT ID	TECN	COMMENT
$18.6^{+7.9+3.5}_{-6.1-3.8}$	278	¹ ABAZOV	18A D0	$p\bar{p} \rightarrow B_s \pi^\pm X$
• • • We do not use the following data for averages, fits, limits, etc. • • •				
$21.9 \pm 6.4^{+5.0}_{-2.5}$	133	ABAZOV	16E D0	$p\bar{p} \rightarrow B_s \pi^\pm X$

¹ From the combined analysis of $B_s^0 \rightarrow J/\psi \phi$ and $B_s^0 \rightarrow D_s^\pm \mu^\mp X$ decays. $T_{b\bar{s}}(5568)^+$ DECAY MODES

Mode	Fraction (Γ_i/Γ)
Γ_1 $B_s \pi^\pm$	seen

 $T_{b\bar{s}}(5568)^+$ BRANCHING RATIOS

$\Gamma(B_s \pi^\pm)/\Gamma_{\text{total}}$	EVTS	DOCUMENT ID	TECN	COMMENT	Γ_1/Γ
seen	145	¹ ABAZOV	18A D0	$p\bar{p} \rightarrow B_s^0 \pi^\pm X$	
seen	133	² ABAZOV	16E D0	$p\bar{p} \rightarrow B_s^0 \pi^\pm X$	
• • • We do not use the following data for averages, fits, limits, etc. • • •					
not seen		³ ABOUD	18L ATLS	$p\bar{p} \rightarrow B_s^0 \pi^\pm X$	
not seen		⁴ AALTONEN	18A CDF	$p\bar{p} \rightarrow B_s^0 \pi^\pm X$	
not seen		⁵ SIRUNYAN	18J CMS	$p\bar{p} \rightarrow B_s^0 \pi^\pm X$	
not seen		⁶ AAJ	16AI LHCB	$p\bar{p} \rightarrow B_s^0 \pi^\pm X$	

¹ With B_s mesons reconstructed in decays to $D_s^\pm \mu^\mp X$.² Seen in $p\bar{p}$ collisions at 1.96 TeV at a rate of $(8.6 \pm 1.9 \pm 1.4)\%$ relative to inclusive B_s production in the kinematic region $10 < p_{\mathcal{T}}(B_s) < 30$ GeV/c, with B_s mesons reconstructed in decays to $J/\psi \phi$. An alternative possibility, $T_{b\bar{s}}(5568)^\pm \rightarrow B_s^* \pi^\pm$ with a missing γ , could not be ruled out.³ Not seen in 24.4 fb^{-1} of $p\bar{p}$ collision data at $\sqrt{s} = 7$ and 8 TeV with B_s mesons reconstructed in decays to $J/\psi \phi$. An upper limit on the production rate times branching fraction for $T_{b\bar{s}}(5568)^\pm \rightarrow B_s \pi^\pm$ relative to inclusive B_s production is less than 1.5% at $p_{\mathcal{T}}(B_s) > 10$ GeV/c and less than 1.6% at $p_{\mathcal{T}}(B_s) > 15$ GeV/c at 95% CL.⁴ Not seen in 9.6 fb^{-1} of $p\bar{p}$ collision data at $\sqrt{s} = 1.96$ TeV with B_s mesons reconstructed in decays to $J/\psi \phi$. An upper limit on the production rate times branching fraction for $T_{b\bar{s}}(5568)^\pm \rightarrow B_s \pi^\pm$ relative to inclusive B_s production is less than 6.7% at 95% CL.⁵ Not seen in 19.7 fb^{-1} of $p\bar{p}$ collisions data at $\sqrt{s} = 8$ TeV with B_s mesons reconstructed in decays to $J/\psi \phi$. An upper limit on the production rate times branching fraction for $T_{b\bar{s}}(5568)^\pm \rightarrow B_s \pi^\pm$ relative to inclusive B_s production is less than 1.1% at $p_{\mathcal{T}}(B_s) > 10$ GeV/c and less than 1.0% at $p_{\mathcal{T}}(B_s) > 15$ GeV/c at 95% CL.⁶ Not seen in 3 fb^{-1} of $p\bar{p}$ collision data at $\sqrt{s} = 7$ and 8 TeV in a scan over the $T_{b\bar{s}}(5568)$ mass and width, with B_s mesons reconstructed in decays to $D_s^\pm \pi^\pm$ or $J/\psi \phi$. An upper limit on the production rate times branching fraction for $T_{b\bar{s}}(5568)^\pm \rightarrow B_s \pi^\pm$ relative to inclusive B_s production is less than 2.1% at $p_{\mathcal{T}}(B_s) > 10$ GeV/c at 90% CL. $T_{cc\bar{c}c}(6900)^0$

$I^G(J^{PC}) = 0^+(?^?+)$

OMITTED FROM SUMMARY TABLE
was $X(6900)$

State incompatible with a $q\bar{q}$ structure. See the review on "Heavy Non- $q\bar{q}$ Mesons."

 $T_{cc\bar{c}c}(6900)^0$ MASS

VALUE (MeV)	DOCUMENT ID	TECN	COMMENT
6899 ± 12 OUR AVERAGE	Error includes scale factor of 1.1.		
$6910 \pm 10 \pm 10$	¹ AAD	23BL ATLS	$p\bar{p} \rightarrow J/\psi J/\psi X$
$6886 \pm 11 \pm 11$	² AAJ	20AY LHCB	$p\bar{p} \rightarrow J/\psi J/\psi X$
• • • We do not use the following data for averages, fits, limits, etc. • • •			
$6960 \pm 50 \pm 30$	³ AAD	23BL ATLS	$p\bar{p} \rightarrow J/\psi \psi(2S) X$

¹ In a model with two resonances, one describing the broad structure above threshold (mass $6650 \pm 20^{+30}_{-20}$ MeV, width $440 \pm 50^{+60}_{-50}$ MeV) interfering with single parton scattering, and a non-interfering $T_{cc\bar{c}c}(6900)$.² In a model where the broad structure above threshold interferes with non-resonant single parton scattering. Without interference the mass is $6905 \pm 11 \pm 7$ MeV.³ Assuming a single resonance (could be another state). A 3σ signal is observed for an additional resonance with mass $7220 \pm 30^{+10}_{-40}$ MeV and width $90 \pm 60^{+60}_{-50}$ MeV. $T_{cc\bar{c}c}(6900)^0$ WIDTH

VALUE (MeV)	DOCUMENT ID	TECN	COMMENT
153 ± 29 OUR AVERAGE			
$150 \pm 30 \pm 10$	¹ AAD	23BL ATLS	$p\bar{p} \rightarrow J/\psi J/\psi X$
$168 \pm 33 \pm 69$	² AAJ	20AY LHCB	$p\bar{p} \rightarrow J/\psi J/\psi X$
• • • We do not use the following data for averages, fits, limits, etc. • • •			
$510 \pm 170^{+110}_{-100}$	³ AAD	23BL ATLS	$p\bar{p} \rightarrow J/\psi \psi(2S) X$

¹ In a model with two resonances, one describing the broad structure above threshold (mass $6650 \pm 20^{+30}_{-20}$ MeV, width $440 \pm 50^{+60}_{-50}$ MeV) interfering with single parton scattering, and a non-interfering $T_{cc\bar{c}c}(6900)$.² In a model where the broad structure above threshold interferes with non-resonant single parton scattering. Without interference the width is 80 ± 38 MeV.³ Assuming a single resonance (could be another state). A 3σ signal is observed for an additional resonance with mass $7220 \pm 30^{+10}_{-40}$ MeV and width $90 \pm 60^{+60}_{-50}$ MeV. $T_{cc\bar{c}c}(6900)^0$ DECAY MODES

Mode	Fraction (Γ_i/Γ)
Γ_1 $J/\psi J/\psi$	seen

$\Gamma(J/\psi J/\psi)/\Gamma_{\text{total}}$	DOCUMENT ID	TECN	COMMENT	Γ_1/Γ
seen	AAD	23BL ATLS	$p\bar{p} \rightarrow J/\psi J/\psi X$	
seen	AAJ	20AY LHCB	$p\bar{p} \rightarrow J/\psi J/\psi X$	

 $T_{cc\bar{c}c}(6900)^0$ REFERENCES

AAD	23BL	PRL 131 151902	G. Aad et al.	(ATLAS)
AAJ	20AY	SCIB 65 1983	R. Aaij et al.	(LHCb Collab.)

 $T_{b\bar{b}1}(10610)$

$I^G(J^{PC}) = 1^+(1^+ -)$

was $Z_b(10610)$, $X(10610)$

Properties incompatible with a $q\bar{q}$ structure (exotic state). See the review on non- $q\bar{q}$ states.

Observed by BONDAR 12 in $\Upsilon(5S)$ decays to $\Upsilon(nS)\pi^+\pi^-$ ($n = 1, 2, 3$) and $h_b(mP)\pi^+\pi^-$ ($m = 1, 2$). $J^P = 1^+$ is favored from angular analyses.

Meson Particle Listings

 $T_{b\bar{b}1}(10610)$ $T_{b\bar{b}1}(10610)^\pm$ MASS

VALUE (MeV)	DOCUMENT ID	TECN	COMMENT
10607.2 ± 2.0	¹ BONDAR 12	BELL	$e^+e^- \rightarrow$ hadrons
• • • We do not use the following data for averages, fits, limits, etc. • • •			
10608.5 ± 3.4 ^{+3.7} _{-1.4}	² GARMASH 15	BELL	$e^+e^- \rightarrow \Upsilon(1S)\pi^+\pi^-$
10608.1 ± 1.2 ^{+1.5} _{-0.2}	² GARMASH 15	BELL	$e^+e^- \rightarrow \Upsilon(2S)\pi^+\pi^-$
10607.4 ± 1.5 ^{+0.8} _{-0.2}	² GARMASH 15	BELL	$e^+e^- \rightarrow \Upsilon(3S)\pi^+\pi^-$
10611 ± 4 ± 3	³ BONDAR 12	BELL	$e^+e^- \rightarrow \Upsilon(1S)\pi^+\pi^-$
10609 ± 2 ± 3	³ BONDAR 12	BELL	$e^+e^- \rightarrow \Upsilon(2S)\pi^+\pi^-$
10608 ± 2 ± 3	³ BONDAR 12	BELL	$e^+e^- \rightarrow \Upsilon(3S)\pi^+\pi^-$
10605 ± 2 ⁺³ ₋₁	³ BONDAR 12	BELL	$e^+e^- \rightarrow h_b(1P)\pi^+\pi^-$
10599 ⁺⁶ ₋₃ ± 5 ⁺⁵ ₋₄	³ BONDAR 12	BELL	$e^+e^- \rightarrow h_b(2P)\pi^+\pi^-$

¹ Average of the BONDAR 12 measurements in separate channels.² Correlated with the corresponding result from BONDAR 12.³ Superseded by the average measurement of BONDAR 12. $T_{b\bar{b}1}(10610)^0$ MASS

VALUE (MeV)	DOCUMENT ID	TECN	COMMENT
10609 ± 4 ± 4	¹ KROKOVNY 13	BELL	$e^+e^- \rightarrow \Upsilon(2S)/\Upsilon(3S)\pi^0\pi^0$
¹ From a simultaneous fit to the KROKOVNY 13 Dalitz analysis of $e^+e^- \rightarrow \Upsilon(2S)/\Upsilon(3S)\pi^0\pi^0$ decays with fixed width $\Gamma(T_{b\bar{b}1}(10610)^0) = 18.4$ MeV.			

 $T_{b\bar{b}1}(10610)^\pm$ WIDTH

VALUE (MeV)	DOCUMENT ID	TECN	COMMENT
18.4 ± 2.4	¹ BONDAR 12	BELL	$e^+e^- \rightarrow$ hadrons
• • • We do not use the following data for averages, fits, limits, etc. • • •			
18.5 ± 5.3 ^{+6.1} _{-2.3}	² GARMASH 15	BELL	$e^+e^- \rightarrow \Upsilon(1S)\pi^+\pi^-$
20.8 ± 2.5 ^{+0.3} _{-2.1}	² GARMASH 15	BELL	$e^+e^- \rightarrow \Upsilon(2S)\pi^+\pi^-$
18.7 ± 3.4 ^{+2.5} _{-1.3}	² GARMASH 15	BELL	$e^+e^- \rightarrow \Upsilon(3S)\pi^+\pi^-$
22.3 ± 7.7 ^{+3.0} _{-4.0}	³ BONDAR 12	BELL	$e^+e^- \rightarrow \Upsilon(1S)\pi^+\pi^-$
24.2 ± 3.1 ^{+2.0} _{-3.0}	³ BONDAR 12	BELL	$e^+e^- \rightarrow \Upsilon(2S)\pi^+\pi^-$
17.6 ± 3.0 ± 3.0	³ BONDAR 12	BELL	$e^+e^- \rightarrow \Upsilon(3S)\pi^+\pi^-$
11.4 ^{+4.5} _{-3.9} ± 2.1 ^{+2.1} _{-1.2}	³ BONDAR 12	BELL	$e^+e^- \rightarrow h_b(1P)\pi^+\pi^-$
13 ⁺¹⁰ ₋₈ ± 9 ⁺⁹ ₋₇	³ BONDAR 12	BELL	$e^+e^- \rightarrow h_b(2P)\pi^+\pi^-$

¹ Average of the BONDAR 12 measurements in separate channels.² Correlated with the corresponding result from BONDAR 12.³ Superseded by the average measurement of BONDAR 12. $T_{b\bar{b}1}(10610)$ DECAY MODES

Mode	Fraction (Γ_i/Γ)
Γ_1 $\Upsilon(1S)\pi^+$	(5.4 ^{+1.9} _{-1.5}) × 10 ⁻³
Γ_2 $\Upsilon(1S)\pi^0$	not seen
Γ_3 $\Upsilon(2S)\pi^+$	(3.6 ^{+1.1} _{-0.8}) %
Γ_4 $\Upsilon(2S)\pi^0$	seen
Γ_5 $\Upsilon(3S)\pi^+$	(2.1 ^{+0.8} _{-0.6}) %
Γ_6 $\Upsilon(3S)\pi^0$	seen
Γ_7 $h_b(1P)\pi^+$	(3.5 ^{+1.2} _{-0.9}) %
Γ_8 $h_b(2P)\pi^+$	(4.7 ^{+1.7} _{-1.3}) %
Γ_9 $B^+\bar{B}^0$	not seen
Γ_{10} $B^+\bar{B}^{*0} + B^{*+}\bar{B}^0$	(85.6 ^{+2.1} _{-2.9}) %

 $T_{b\bar{b}1}(10610)$ BRANCHING RATIOS

$\Gamma(\Upsilon(1S)\pi^+)/\Gamma_{\text{total}}$	Γ_1/Γ		
VALUE (units 10 ⁻³)	DOCUMENT ID	TECN	COMMENT
5.4^{+1.5}_{-1.3} ± 1.1^{+0.8}_{-0.8}	¹ GARMASH 16	BELL	$e^+e^- \rightarrow \pi^-B^+\bar{B}^{*0}, \pi^-\bar{B}^0B^{*+}$
• • • We do not use the following data for averages, fits, limits, etc. • • •			
seen	GARMASH 15	BELL	$e^+e^- \rightarrow \Upsilon(1S)\pi^+\pi^-$
seen	BONDAR 12	BELL	$e^+e^- \rightarrow \Upsilon(1S)\pi^+\pi^-$

¹ Assuming the $T_{b\bar{b}1}(10610)$ decay width is saturated by the channels $\pi^+\Upsilon(1S, 2S, 3S), \pi^+h_b(1P, 2P)$, and $B^+\bar{B}^{*0} + \bar{B}^0B^{*+}$, and using the results from BONDAR 12 and MIZUK 16. $\Gamma(\Upsilon(1S)\pi^0)/\Gamma_{\text{total}}$

VALUE	DOCUMENT ID	TECN	COMMENT	Γ_2/Γ
not seen	KROKOVNY 13	BELL	$e^+e^- \rightarrow \Upsilon(1S)\pi^0\pi^0$	

 $\Gamma(\Upsilon(2S)\pi^+)/\Gamma_{\text{total}}$

VALUE (units 10 ⁻²)	DOCUMENT ID	TECN	COMMENT	Γ_3/Γ
3.62^{+0.76}_{-0.59} ± 0.79^{+0.79}_{-0.53}	¹ GARMASH 16	BELL	$e^+e^- \rightarrow \pi^-B^+\bar{B}^{*0}, \pi^-\bar{B}^0B^{*+}$	
• • • We do not use the following data for averages, fits, limits, etc. • • •				
seen	GARMASH 15	BELL	$e^+e^- \rightarrow \Upsilon(2S)\pi^+\pi^-$	
seen	BONDAR 12	BELL	$e^+e^- \rightarrow \Upsilon(2S)\pi^+\pi^-$	

¹ Assuming the $T_{b\bar{b}1}(10610)$ decay width is saturated by the channels $\pi^+\Upsilon(1S, 2S, 3S), \pi^+h_b(1P, 2P)$, and $B^+\bar{B}^{*0} + \bar{B}^0B^{*+}$, and using the results from BONDAR 12 and MIZUK 16. $\Gamma(\Upsilon(2S)\pi^0)/\Gamma_{\text{total}}$

VALUE	DOCUMENT ID	TECN	COMMENT	Γ_4/Γ
seen	¹ KROKOVNY 13	BELL	$e^+e^- \rightarrow \Upsilon(2S)\pi^0\pi^0$	
¹ Combined significance in $e^+e^- \rightarrow \Upsilon(2S)/\Upsilon(3S)\pi^0\pi^0$, including systematics, of 6.5 σ .				

 $\Gamma(\Upsilon(3S)\pi^+)/\Gamma_{\text{total}}$

VALUE (units 10 ⁻²)	DOCUMENT ID	TECN	COMMENT	Γ_5/Γ
2.15^{+0.55}_{-0.42} ± 0.60^{+0.60}_{-0.43}	¹ GARMASH 16	BELL	$e^+e^- \rightarrow \pi^-B^+\bar{B}^{*0}, \pi^-\bar{B}^0B^{*+}$	
• • • We do not use the following data for averages, fits, limits, etc. • • •				
seen	GARMASH 15	BELL	$e^+e^- \rightarrow \Upsilon(3S)\pi^+\pi^-$	
seen	BONDAR 12	BELL	$e^+e^- \rightarrow \Upsilon(3S)\pi^+\pi^-$	

¹ Assuming the $T_{b\bar{b}1}(10610)$ decay width is saturated by the channels $\pi^+\Upsilon(1S, 2S, 3S), \pi^+h_b(1P, 2P)$, and $B^+\bar{B}^{*0} + \bar{B}^0B^{*+}$, and using the results from BONDAR 12 and MIZUK 16. $\Gamma(\Upsilon(3S)\pi^0)/\Gamma_{\text{total}}$

VALUE	DOCUMENT ID	TECN	COMMENT	Γ_6/Γ
seen	¹ KROKOVNY 13	BELL	$e^+e^- \rightarrow \Upsilon(3S)\pi^0\pi^0$	
¹ Combined significance in $e^+e^- \rightarrow \Upsilon(2S)/\Upsilon(3S)\pi^0\pi^0$, including systematics, of 6.5 σ .				

 $\Gamma(h_b(1P)\pi^+)/\Gamma_{\text{total}}$

VALUE (units 10 ⁻²)	DOCUMENT ID	TECN	COMMENT	Γ_7/Γ
3.45^{+0.87}_{-0.71} ± 0.86^{+0.86}_{-0.63}	¹ GARMASH 16	BELL	$e^+e^- \rightarrow \pi^-B^+\bar{B}^{*0}, \pi^-\bar{B}^0B^{*+}$	
• • • We do not use the following data for averages, fits, limits, etc. • • •				
possibly seen	² MIZUK 16	BELL	$e^+e^- \rightarrow h_b(1P)\pi^+\pi^-$	
seen	³ BONDAR 12	BELL	$e^+e^- \rightarrow h_b(1P)\pi^+\pi^-$	

¹ Assuming the $T_{b\bar{b}1}(10610)$ decay width is saturated by the channels $\pi^+\Upsilon(1S, 2S, 3S), \pi^+h_b(1P, 2P)$, and $B^+\bar{B}^{*0} + \bar{B}^0B^{*+}$, and using the results from BONDAR 12 and MIZUK 16.² Using e^+e^- energies near the $\Upsilon(11020)$.³ Using e^+e^- energies near the $\Upsilon(10860)$. $\Gamma(h_b(2P)\pi^+)/\Gamma_{\text{total}}$

VALUE (units 10 ⁻²)	DOCUMENT ID	TECN	COMMENT	Γ_8/Γ
4.67^{+1.24}_{-1.00} ± 1.18^{+1.18}_{-0.89}	¹ GARMASH 16	BELL	$e^+e^- \rightarrow \pi^-B^+\bar{B}^{*0}, \pi^-\bar{B}^0B^{*+}$	
• • • We do not use the following data for averages, fits, limits, etc. • • •				
possibly seen	² MIZUK 16	BELL	$e^+e^- \rightarrow h_b(2P)\pi^+\pi^-$	
seen	³ BONDAR 12	BELL	$e^+e^- \rightarrow h_b(2P)\pi^+\pi^-$	

¹ Assuming the $T_{b\bar{b}1}(10610)$ decay width is saturated by the channels $\pi^+\Upsilon(1S, 2S, 3S), \pi^+h_b(1P, 2P)$, and $B^+\bar{B}^{*0} + \bar{B}^0B^{*+}$, and using the results from BONDAR 12 and MIZUK 16.² Using e^+e^- energies near the $\Upsilon(11020)$.³ Using e^+e^- energies near the $\Upsilon(10860)$. $\Gamma(B^+\bar{B}^0)/\Gamma_{\text{total}}$

VALUE	DOCUMENT ID	TECN	COMMENT	Γ_9/Γ
not seen	GARMASH 16	BELL	$e^+e^- \rightarrow \pi^-B^+\bar{B}^0$	

 $[\Gamma(B^+\bar{B}^{*0}) + \Gamma(B^{*+}\bar{B}^0)]/\Gamma_{\text{total}}$

VALUE (units 10 ⁻²)	EVTS	DOCUMENT ID	TECN	COMMENT	Γ_{10}/Γ
85.6^{+1.5}_{-2.0} ± 1.5^{+1.5}_{-2.1}	357	¹ GARMASH 16	BELL	$e^+e^- \rightarrow \pi^-B^+\bar{B}^{*0}, \pi^-B^{*+}\bar{B}^0$	

¹ Assuming the $T_{b\bar{b}1}(10610)$ decay width is saturated by the channels $\pi^+\Upsilon(1S, 2S, 3S), \pi^+h_b(1P, 2P)$, and $B^+\bar{B}^{*0} + B^{*+}\bar{B}^0$, and using the results from BONDAR 12 and MIZUK 16. Using the mass and width of the $T_{b\bar{b}1}(10610)$ from BONDAR 12.

See key on page 1171

Meson Particle Listings

 $T_{b\bar{b}1}(10610), T_{b\bar{b}1}(10650)^+$

$$\frac{[\Gamma(B^+\bar{B}^0) + \Gamma(B^{*+}\bar{B}^0)] / [\Gamma(\Upsilon(1S)\pi^+) + \Gamma(\Upsilon(2S)\pi^+) + \Gamma(\Upsilon(3S)\pi^+) + \Gamma(h_b(1P)\pi^+) + \Gamma(h_b(2P)\pi^+)]}{\Gamma_{10}/(\Gamma_1 + \Gamma_3 + \Gamma_5 + \Gamma_7 + \Gamma_8)}$$

VALUE (units 10^{-2})	EVTS	DOCUMENT ID	TECN	COMMENT
$5.93^{+0.99+1.01}_{-0.69-0.73}$	357	¹ GARMASH	16 BELL	$e^+e^- \rightarrow \pi^- B^+ \bar{B}^0,$ $\pi^- \bar{B}^0 B^{*+}$

¹ Combined with the results of BONDAR 12 and MIZUK 16. Not independent from $T_{b\bar{b}1}(10610)$ branching fractions to $\pi^+ \Upsilon(1S, 2S, 3S), \pi^+ h_b(1P, 2P)$, and $B^+ \bar{B}^0 + \bar{B}^0 B^{*+}$.

 $T_{b\bar{b}1}(10610)$ REFERENCES

GARMASH 16	PRL 116 212001	A. Garmash et al.	(BELLE Collab.)
MIZUK 16	PRL 117 142001	R. Mizuk et al.	(BELLE Collab.)
GARMASH 15	PR D91 072003	A. Garmash et al.	(BELLE Collab.)
KROKOVNY 13	PR D88 052016	P. Krokovny et al.	(BELLE Collab.)
BONDAR 12	PRL 108 122001	A. Bondar et al.	(BELLE Collab.)

 $T_{b\bar{b}1}(10650)^+$

$$J^G(J^{PC}) = 1^+(1^+ -)$$

I, G, C need confirmation.

was $Z_b(10650), X(10650)^+$ Properties incompatible with a $q\bar{q}$ structure (exotic state). See the review on non- $q\bar{q}$ states.Observed by BONDAR 12 in $\Upsilon(5S)$ decays to $\Upsilon(nS)\pi^+\pi^-$ ($n = 1, 2, 3$) and $h_b(mP)\pi^+\pi^-$ ($m = 1, 2$). $J^P = 1^+$ is favored from angular analyses. $T_{b\bar{b}1}(10650)^+$ MASS

VALUE (MeV)	DOCUMENT ID	TECN	COMMENT
10652.2 ± 1.5	¹ BONDAR 12	BELL	$e^+e^- \rightarrow$ hadrons
$10656.7 \pm 5.0^{+1.1}_{-3.1}$	² GARMASH 15	BELL	$e^+e^- \rightarrow \Upsilon(1S)\pi^+\pi^-$
$10650.7 \pm 1.5^{+0.5}_{-0.2}$	² GARMASH 15	BELL	$e^+e^- \rightarrow \Upsilon(2S)\pi^+\pi^-$
$10651.2 \pm 1.0^{+0.4}_{-0.3}$	² GARMASH 15	BELL	$e^+e^- \rightarrow \Upsilon(3S)\pi^+\pi^-$
$10657 \pm 6 \pm 3$	³ BONDAR 12	BELL	$e^+e^- \rightarrow \Upsilon(1S)\pi^+\pi^-$
$10651 \pm 2 \pm 3$	³ BONDAR 12	BELL	$e^+e^- \rightarrow \Upsilon(2S)\pi^+\pi^-$
$10652 \pm 1 \pm 2$	³ BONDAR 12	BELL	$e^+e^- \rightarrow \Upsilon(3S)\pi^+\pi^-$
$10654 \pm 3^{+1}_{-2}$	³ BONDAR 12	BELL	$e^+e^- \rightarrow h_b(1P)\pi^+\pi^-$
$10651^{+2}_{-3} \pm 3^{+3}_{-2}$	³ BONDAR 12	BELL	$e^+e^- \rightarrow h_b(2P)\pi^+\pi^-$

¹ Average of the BONDAR 12 measurements in separate channels.² Correlated with the corresponding result from BONDAR 12.³ Superseded by the average measurement of BONDAR 12. $T_{b\bar{b}1}(10650)^+$ WIDTH

VALUE (MeV)	DOCUMENT ID	TECN	COMMENT
11.5 ± 2.2	¹ BONDAR 12	BELL	$e^+e^- \rightarrow$ hadrons
$12.1^{+11.3+2.7}_{-4.8-0.6}$	² GARMASH 15	BELL	$e^+e^- \rightarrow \Upsilon(1S)\pi^+\pi^-$
$14.2 \pm 3.7^{+0.9}_{-0.4}$	² GARMASH 15	BELL	$e^+e^- \rightarrow \Upsilon(2S)\pi^+\pi^-$
$9.3 \pm 2.2^{+0.3}_{-0.5}$	² GARMASH 15	BELL	$e^+e^- \rightarrow \Upsilon(3S)\pi^+\pi^-$
$16.3 \pm 9.8^{+6.0}_{-2.0}$	³ BONDAR 12	BELL	$e^+e^- \rightarrow \Upsilon(1S)\pi^+\pi^-$
$13.3 \pm 3.3^{+4.0}_{-3.0}$	³ BONDAR 12	BELL	$e^+e^- \rightarrow \Upsilon(2S)\pi^+\pi^-$
$8.4 \pm 2.0 \pm 2.0$	³ BONDAR 12	BELL	$e^+e^- \rightarrow \Upsilon(3S)\pi^+\pi^-$
$20.9^{+5.4+2.1}_{-4.7-5.7}$	³ BONDAR 12	BELL	$e^+e^- \rightarrow h_b(1P)\pi^+\pi^-$
$19 \pm 7^{+11}_{-7}$	³ BONDAR 12	BELL	$e^+e^- \rightarrow h_b(2P)\pi^+\pi^-$

¹ Average of the BONDAR 12 measurements in separate channels.² Correlated with the corresponding result from BONDAR 12.³ Superseded by the average measurement of BONDAR 12. $T_{b\bar{b}1}(10650)^+$ DECAY MODES $T_{b\bar{b}1}(10650)^-$ decay modes are charge conjugates of the modes below.

Mode	Fraction (Γ_i/Γ)
$\Gamma_1 \quad \Upsilon(1S)\pi^+$	$(1.7^{+0.8}_{-0.6}) \times 10^{-3}$
$\Gamma_2 \quad \Upsilon(2S)\pi^+$	$(1.4^{+0.6}_{-0.4})\%$
$\Gamma_3 \quad \Upsilon(3S)\pi^+$	$(1.6^{+0.7}_{-0.5})\%$

$\Gamma_4 \quad h_b(1P)\pi^+$	$(8.4^{+2.9}_{-2.4})\%$
$\Gamma_5 \quad h_b(2P)\pi^+$	$(15 \pm 4)\%$
$\Gamma_6 \quad B^+ \bar{B}^0$	not seen
$\Gamma_7 \quad B^+ \bar{B}^0 + B^{*+} \bar{B}^0$	not seen
$\Gamma_8 \quad B^{*+} \bar{B}^0$	$(74^{+4}_{-6})\%$

 $T_{b\bar{b}1}(10650)^+$ BRANCHING RATIOS

$\Gamma(\Upsilon(1S)\pi^+)/\Gamma_{\text{total}}$	DOCUMENT ID	TECN	COMMENT	Γ_1/Γ
$1.7^{+0.7+0.3}_{-0.6-0.2}$	¹ GARMASH 16	BELL	$e^+e^- \rightarrow \pi^- B^{*+} \bar{B}^0$	

• • • We do not use the following data for averages, fits, limits, etc. • • •

seen	GARMASH 15	BELL	$e^+e^- \rightarrow \Upsilon(1S)\pi^+\pi^-$
seen	BONDAR 12	BELL	$e^+e^- \rightarrow \Upsilon(1S)\pi^+\pi^-$

¹ Assuming the $T_{b\bar{b}1}(10650)$ decay width is saturated by the channels $\pi^+ \Upsilon(1S, 2S, 3S), \pi^+ h_b(1P, 2P)$, and $B^{*+} \bar{B}^0$, and using the results from BONDAR 12 and MIZUK 16.

$\Gamma(\Upsilon(2S)\pi^+)/\Gamma_{\text{total}}$	DOCUMENT ID	TECN	COMMENT	Γ_2/Γ
$1.39^{+0.48+0.34}_{-0.38-0.23}$	¹ GARMASH 16		$e^+e^- \rightarrow \pi^- B^{*+} \bar{B}^0$	

• • • We do not use the following data for averages, fits, limits, etc. • • •

seen	GARMASH 15	BELL	$e^+e^- \rightarrow \Upsilon(2S)\pi^+\pi^-$
seen	BONDAR 12	BELL	$e^+e^- \rightarrow \Upsilon(2S)\pi^+\pi^-$

¹ Assuming the $T_{b\bar{b}1}(10650)$ decay width is saturated by the channels $\pi^+ \Upsilon(1S, 2S, 3S), \pi^+ h_b(1P, 2P)$, and $B^{*+} \bar{B}^0$, and using the results from BONDAR 12 and MIZUK 16.

$\Gamma(\Upsilon(3S)\pi^+)/\Gamma_{\text{total}}$	DOCUMENT ID	TECN	COMMENT	Γ_3/Γ
$1.63^{+0.53+0.39}_{-0.42-0.28}$	¹ GARMASH 16	BELL	$e^+e^- \rightarrow \pi^- B^{*+} \bar{B}^0$	

• • • We do not use the following data for averages, fits, limits, etc. • • •

seen	GARMASH 15	BELL	$e^+e^- \rightarrow \Upsilon(3S)\pi^+\pi^-$
seen	BONDAR 12	BELL	$e^+e^- \rightarrow \Upsilon(3S)\pi^+\pi^-$

¹ Assuming the $T_{b\bar{b}1}(10650)$ decay width is saturated by the channels $\pi^+ \Upsilon(1S, 2S, 3S), \pi^+ h_b(1P, 2P)$, and $B^{*+} \bar{B}^0$, and using the results from BONDAR 12 and MIZUK 16.

$\Gamma(h_b(1P)\pi^+)/\Gamma_{\text{total}}$	DOCUMENT ID	TECN	COMMENT	Γ_4/Γ
$8.41^{+2.43+1.49}_{-2.12-1.06}$	¹ GARMASH 16	BELL	$e^+e^- \rightarrow \pi^- B^{*+} \bar{B}^0$	

• • • We do not use the following data for averages, fits, limits, etc. • • •

seen	² MIZUK 16	BELL	$e^+e^- \rightarrow h_b(1P)\pi^+\pi^-$
seen	³ BONDAR 12	BELL	$e^+e^- \rightarrow h_b(1P)\pi^+\pi^-$

¹ Assuming the $T_{b\bar{b}1}(10650)$ decay width is saturated by the channels $\pi^+ \Upsilon(1S, 2S, 3S), \pi^+ h_b(1P, 2P)$, and $B^{*+} \bar{B}^0$, and using the results from BONDAR 12 and MIZUK 16.² Using e^+e^- energies near the $\Upsilon(11020)$.³ Using e^+e^- energies near the $\Upsilon(10860)$.

$\Gamma(h_b(2P)\pi^+)/\Gamma_{\text{total}}$	DOCUMENT ID	TECN	COMMENT	Γ_5/Γ
$14.7^{+3.2+2.8}_{-2.8-2.8}$	¹ GARMASH 16	BELL	$e^+e^- \rightarrow \pi^- B^{*+} \bar{B}^0$	

• • • We do not use the following data for averages, fits, limits, etc. • • •

possibly seen	² MIZUK 16	BELL	$e^+e^- \rightarrow h_b(2P)\pi^+\pi^-$
seen	³ BONDAR 12	BELL	$e^+e^- \rightarrow h_b(2P)\pi^+\pi^-$

¹ Assuming the $T_{b\bar{b}1}(10650)$ decay width is saturated by the channels $\pi^+ \Upsilon(1S, 2S, 3S), \pi^+ h_b(1P, 2P)$, and $B^{*+} \bar{B}^0$, and using the results from BONDAR 12 and MIZUK 16.² Using e^+e^- energies near the $\Upsilon(11020)$.³ Using e^+e^- energies near the $\Upsilon(10860)$.

$\Gamma(B^+ \bar{B}^0)/\Gamma_{\text{total}}$	DOCUMENT ID	TECN	COMMENT	Γ_6/Γ
not seen	GARMASH 16	BELL	$e^+e^- \rightarrow \pi^- B^+ \bar{B}^0$	

$[\Gamma(B^+ \bar{B}^0) + \Gamma(B^{*+} \bar{B}^0)]/\Gamma_{\text{total}}$	DOCUMENT ID	TECN	COMMENT	Γ_7/Γ
not seen	GARMASH 16	BELL	$e^+e^- \rightarrow \pi^- B^+ \bar{B}^0,$ $\pi^- \bar{B}^0 B^{*+}$	

$\Gamma(B^{*+} \bar{B}^0)/\Gamma_{\text{total}}$	EVTS	DOCUMENT ID	TECN	COMMENT	Γ_8/Γ
$73.7^{+3.4+2.7}_{-4.4-3.5}$	161	¹ GARMASH 16	BELL	$e^+e^- \rightarrow \pi^- B^{*+} \bar{B}^0$	

¹ Assuming the $T_{b\bar{b}1}(10650)$ decay width is saturated by the channels $\pi^+ \Upsilon(1S, 2S, 3S), \pi^+ h_b(1P, 2P)$, and $B^{*+} \bar{B}^0$, and using the results from BONDAR 12 and MIZUK 16. Using the mass and width of the $T_{b\bar{b}1}(10650)$ from BONDAR 12.

Meson Particle Listings

 $T_{b\bar{b}1}(10650)^+$, Further States

$$\Gamma(B^{*+}\bar{B}^{*0}) / [\Gamma(\Upsilon(1S)\pi^+) + \Gamma(\Upsilon(2S)\pi^+) + \Gamma(\Upsilon(3S)\pi^+) + \Gamma(h_b(1P)\pi^+) + \Gamma(h_b(2P)\pi^+)] \quad \Gamma_8 / (\Gamma_1 + \Gamma_2 + \Gamma_3 + \Gamma_4 + \Gamma_5)$$

VALUE (units 10^{-2})	EVTS	DOCUMENT ID	TECN	COMMENT
--------------------------	------	-------------	------	---------

• • • We do not use the following data for averages, fits, limits, etc. • • •

$2.80^{+0.69+0.54}_{-0.40-0.36}$	161	¹ GARMASH	16	BELL $e^+e^- \rightarrow \pi^- B^{*+} \bar{B}^{*0}$
----------------------------------	-----	----------------------	----	---

¹ Combined with the results of BONDAR 12 and MIZUK 16. Not independent from $T_{b\bar{b}1}(10650)$ branching fractions to $\pi^+ \Upsilon(1S, 2S, 3S)$, $\pi^+ h_b(1P, 2P)$, and $B^{*+} \bar{B}^{*0}$.

 $T_{b\bar{b}1}(10650)^+$ REFERENCES

GARMASH	16	PRL 116 212001	A. Garmash et al.	(BELLE Collab.)
MIZUK	16	PRL 117 142001	R. Mizuk et al.	(BELLE Collab.)
GARMASH	15	PR D91 072003	A. Garmash et al.	(BELLE Collab.)
BONDAR	12	PRL 108 122001	A. Bondar et al.	(BELLE Collab.)

Further States

OMITTED FROM SUMMARY TABLE

This section contains states observed by a single group or states poorly established that thus need confirmation.

QUANTUM NUMBERS, MASSES, WIDTHS, AND BRANCHING RATIOS

$$X(360) \quad I^G(J^{PC}) = ?(??^+)$$

MASS (MeV)	WIDTH (MeV)	EVTS	DOCUMENT ID	TECN	COMMENT
------------	-------------	------	-------------	------	---------

$360 \pm 7 \pm 9$	64 ± 18	2.3k	¹ ABRAAMYAN 09	CNTR	$2.75 dC \rightarrow \gamma\gamma X$
-------------------	-------------	------	---------------------------	------	--------------------------------------

¹ Not seen in $pC \rightarrow \gamma\gamma X$ at 5.5 GeV/c.

$$X(1070) \quad I^G(J^{PC}) = ??(0^{++})$$

MASS (MeV)	WIDTH (MeV)	DOCUMENT ID	COMMENT
------------	-------------	-------------	---------

1072 ± 1	3.5 ± 0.5	¹ VLADIMIRSK...08	$40 \pi^- p \rightarrow K_S^0 K_S^0 n + m\pi^0$
--------------	---------------	------------------------------	---

¹ Supersedes GRIGOR'EV 05.

$$X(1110) \quad I^G(J^{PC}) = 0^+(\text{even}^{++})$$

MASS (MeV)	WIDTH (MeV)	DOCUMENT ID	TECN	COMMENT
------------	-------------	-------------	------	---------

1107 ± 4	$111 \pm 8 \pm 15$	DAFTARI 87	DBC	$0. \bar{p}n \rightarrow \rho^- \pi^+ \pi^-$
--------------	--------------------	------------	-----	--

$$f_0(1200-1600) \quad I^G(J^{PC}) = 0^+(0^{++})$$

MASS (MeV)	WIDTH (MeV)	DOCUMENT ID	TECN	COMMENT
------------	-------------	-------------	------	---------

1323 ± 8	237 ± 20	VLADIMIRSK...06	SPEC	$40 \pi^- p \rightarrow K_S^0 K_S^0 n$
--------------	--------------	-----------------	------	--

1480^{+100}_{-150}	1030^{+80}_{-170}	¹ ANISOVICH 03	SPEC	
----------------------	---------------------	---------------------------	------	--

1530^{+90}_{-250}	560 ± 40	² ANISOVICH 03	SPEC	
---------------------	--------------	---------------------------	------	--

¹ K-matrix pole from combined analysis of $\pi^- p \rightarrow \pi^0 \pi^0 n$, $\pi^- p \rightarrow K \bar{K} n$, $\pi^+ \pi^- \rightarrow \pi^+ \pi^-$, $\bar{p}p \rightarrow \pi^0 \pi^0 \pi^0$, $\pi^0 \eta \eta$, $\pi^0 \pi^0 \eta$, $\pi^+ \pi^- \pi^0$, $K^+ K^- \pi^0$, $K_S^0 K_S^0 \pi^0$, $K^+ K_S^0 \pi^-$ at rest, $\bar{p}n \rightarrow \pi^- \pi^- \pi^+$, $K_S^0 K^- \pi^0$, $K_S^0 K_S^0 \pi^-$ at rest.

² K-matrix pole from combined analysis of $\pi^- p \rightarrow \pi^0 \pi^0 n$, $\pi^- p \rightarrow K \bar{K} n$, $\bar{p}p \rightarrow \pi^0 \pi^0 \pi^0$, $\pi^0 \eta \eta$, $\pi^0 \pi^0 \eta$ at rest.

$$X(1420) \quad I^G(J^{PC}) = 2^+(0^{++})$$

MASS (MeV)	WIDTH (MeV)	DOCUMENT ID	TECN	COMMENT
------------	-------------	-------------	------	---------

1420 ± 20	160 ± 10	FILIPPI 00	OBLX	$0 \bar{p}p \rightarrow \pi^+ \pi^+ \pi^-$
---------------	--------------	------------	------	--

$$X(1545) \quad I^G(J^{PC}) = ?(??^{++})$$

MASS (MeV)	WIDTH (MeV)	DOCUMENT ID	COMMENT
------------	-------------	-------------	---------

1545 ± 3	6.0 ± 2.5	¹ VLADIMIRSK...08	$40 \pi^- p \rightarrow K_S^0 K_S^0 n + m\pi^0$
--------------	---------------	------------------------------	---

¹ Supersedes VLADIMIRSKII 00.

$$X(1575) \quad I^G(J^{PC}) = ?(1^{--})$$

MASS (MeV)	WIDTH (MeV)	DOCUMENT ID	TECN	COMMENT
------------	-------------	-------------	------	---------

1576^{+49+98}_{-55-91}	$818^{+22+64}_{-23-133}$	¹ ABLKIM 06s	BES	$J/\psi \rightarrow K^+ K^- \pi^0$
--------------------------	--------------------------	-------------------------	-----	------------------------------------

¹ A broad peak observed at $K^+ K^-$ invariant mass. Mass and width above are its pole position. The observed branching ratio is $B(J/\psi \rightarrow X \pi^0) B(X \rightarrow K^+ K^-) = (8.5 \pm 0.6^{+2.7}_{-3.6}) \times 10^{-4}$.

$$X(1600) \quad I^G(J^{PC}) = 2^+(2^{++})$$

MASS (MeV)	WIDTH (MeV)	DOCUMENT ID	TECN	COMMENT
------------	-------------	-------------	------	---------

1600 ± 100	400 ± 200	¹ ALBRECHT 91F	ARG	$10.2 e^+ e^- \rightarrow e^+ e^- 2(\pi^+ \pi^-)$
----------------	---------------	---------------------------	-----	---

¹ Our estimate.

$$X(1650) \quad I^G(J^{PC}) = 0^-(??^-)$$

MASS (MeV)	WIDTH (MeV)	EVTS	DOCUMENT ID	TECN	COMMENT
------------	-------------	------	-------------	------	---------

1652 ± 7	<50	100	PROKOSHKIN 96	GAM2	$32,38 \pi p \rightarrow \omega \eta n$
--------------	-------	-----	---------------	------	---

$$X(1730) \quad I^G(J^{PC}) = ?(??^+)$$

MASS (MeV)	WIDTH (MeV)	EVTS	DOCUMENT ID	TECN	COMMENT
------------	-------------	------	-------------	------	---------

$1731.0 \pm 1.2 \pm 2.0$	$3.2 \pm 0.8 \pm 1.3$	58	VLADIMIRSK...07	SPEC	$40 \pi^- p \rightarrow K_S^0 K_S^0 X$
--------------------------	-----------------------	----	-----------------	------	--

$$f_2(1750) \quad I^G(J^{PC}) = 0^+(2^{++})$$

MASS (MeV)	WIDTH (MeV)	EVTS	DOCUMENT ID	TECN	COMMENT
------------	-------------	------	-------------	------	---------

1755 ± 10	67 ± 12	870	¹ SCHEGELSKY 06A	RVUE	$\gamma\gamma \rightarrow K_S^0 K_S^0$
---------------	-------------	-----	-----------------------------	------	--

$$\Gamma(K\bar{K})$$

VALUE (MeV)	EVTS	DOCUMENT ID	TECN	COMMENT
-------------	------	-------------	------	---------

17 ± 5	870	² SCHEGELSKY 06A	RVUE	$\gamma\gamma \rightarrow K_S^0 K_S^0$
------------	-----	-----------------------------	------	--

$$\Gamma(\gamma\gamma)$$

VALUE (keV)	EVTS	DOCUMENT ID	TECN	COMMENT
-------------	------	-------------	------	---------

0.13 ± 0.04	870	² SCHEGELSKY 06A	RVUE	$\gamma\gamma \rightarrow K_S^0 K_S^0$
-----------------	-----	-----------------------------	------	--

$$\Gamma(\pi\pi)$$

VALUE (MeV)	EVTS	DOCUMENT ID	TECN	COMMENT
-------------	------	-------------	------	---------

1.3 ± 1.0	870	² SCHEGELSKY 06A	RVUE	$\gamma\gamma \rightarrow K_S^0 K_S^0$
---------------	-----	-----------------------------	------	--

$$\Gamma(\eta\eta)$$

VALUE (MeV)	EVTS	DOCUMENT ID	TECN	COMMENT
-------------	------	-------------	------	---------

2.0 ± 0.5	870	² SCHEGELSKY 06A	RVUE	$\gamma\gamma \rightarrow K_S^0 K_S^0$
---------------	-----	-----------------------------	------	--

¹ From analysis of L3 data at 91 and 183-209 GeV.

² From analysis of L3 data at 91 and 183-209 GeV and using SU(3) relations.

$$X(1775) \quad I^G(J^{PC}) = 1^-(??^-)$$

MASS (MeV)	WIDTH (MeV)	DOCUMENT ID	TECN	COMMENT
------------	-------------	-------------	------	---------

1763 ± 20	192 ± 60	CONDO 91	SHF	$\gamma p \rightarrow (p\pi^+) (\pi^+ \pi^- \pi^-)$
---------------	--------------	----------	-----	---

1787 ± 18	118 ± 60	CONDO 91	SHF	$\gamma p \rightarrow n\pi^+ \pi^+ \pi^-$
---------------	--------------	----------	-----	---

$$X(1850 - 3100) \quad I^G(J^{PC}) = ?(1^{--})$$

$\Gamma(e^+e^-)B(X \rightarrow \text{hadrons})$ (eV)	CL%	DOCUMENT ID	TECN	COMMENT
--	-----	-------------	------	---------

<120	90	¹ ANASHIN 11	KEDR	$e^+ e^- \rightarrow \text{hadrons}$
--------	----	-------------------------	------	--------------------------------------

¹ This limit is center-of-mass energy dependent. We quote the most stringent one.

$$X(1855) \quad I^G(J^{PC}) = ?(??^?)$$

MASS (MeV)	WIDTH (MeV)	DOCUMENT ID	TECN	COMMENT
------------	-------------	-------------	------	---------

1856.6 ± 5	20 ± 5	BRIDGES 86D	SPEC	$0. \bar{p}d \rightarrow \pi\pi N$
----------------	------------	-------------	------	------------------------------------

$$X(1870) \quad I^G(J^{PC}) = ?(2^{??})$$

MASS (MeV)	WIDTH (MeV)	DOCUMENT ID	TECN	COMMENT
------------	-------------	-------------	------	---------

1870 ± 40	250 ± 30	ALDE 86D	GAM4	$100 \pi^- p \rightarrow 2\eta X$
---------------	--------------	----------	------	-----------------------------------

$$a_3(1875) \quad I^G(J^{PC}) = 1^-(3^{++})$$

MASS (MeV)	WIDTH (MeV)	DOCUMENT ID	TECN	COMMENT
------------	-------------	-------------	------	---------

$1874 \pm 43 \pm 96$	$385 \pm 121 \pm 114$	CHUNG 02	B852	$18.3 \pi^- p \rightarrow \pi^+ \pi^- \pi^- p$
----------------------	-----------------------	----------	------	--

$$B(a_3(1875) \rightarrow f_2(1270)\pi) / B(a_3(1875) \rightarrow \rho\pi)$$

VALUE	DOCUMENT ID	TECN	COMMENT
-------	-------------	------	---------

0.8 ± 0.2	¹ CHUNG 02	B852	$18.3 \pi^- p \rightarrow \pi^+ \pi^- \pi^- p$
---------------	-----------------------	------	--

¹ Using the observable fractions of 50.0% $\rho\pi$, 56.5% $f_2\pi$, and 11.8% $\rho_3\pi$.

$$B(a_3(1875) \rightarrow \rho_3(1690)\pi) / B(a_3(1875) \rightarrow \rho\pi)$$

VALUE	DOCUMENT ID	TECN	COMMENT
-------	-------------	------	---------

0.9 ± 0.3	¹ CHUNG 02	B852	$18.3 \pi^- p \rightarrow \pi^+ \pi^- \pi^- p$
---------------	-----------------------	------	--

¹ Using the observable fractions of 50.0% $\rho\pi$, 56.5% $f_2\pi$, and 11.8% $\rho_3\pi$.

$$a_1(1930) \quad I^G(J^{PC}) = 1^-(1^{++})$$

MASS (MeV)	WIDTH (MeV)	DOCUMENT ID	TECN	COMMENT
------------	-------------	-------------	------	---------

1930^{+30}_{-70}	155 ± 45	ANISOVICH 01F	SPEC	$2.0 \bar{p}p \rightarrow 3\pi^0, \pi^0 \eta, \pi^0 \eta'$
--------------------	--------------	---------------	------	--

$$X(1935) \quad I^G(J^{PC}) = 1^+(1^{--})$$

MASS (MeV)	WIDTH (MeV)	DOCUMENT ID	TECN	COMMENT
------------	-------------	-------------	------	---------

1935 ± 20	215 ± 30	EVANGELIS... 79	OMEG	$10,16 \pi^- p \rightarrow \bar{p}pn$
---------------	--------------	-----------------	------	---------------------------------------

$\rho_2(1940)$ $I^G(J^{PC}) = 1^+(2^{--})$

MASS (MeV)	WIDTH (MeV)	DOCUMENT ID	TECN	COMMENT
1940 ± 40	155 ± 40	¹ ANISOVICH	02	SPEC 0.6-1.9 $p\bar{p} \rightarrow \omega\pi^0, \omega\eta\pi^0, \pi^+\pi^-$

¹ From the combined analysis of ANISOVICH 00J, ANISOVICH 01D, ANISOVICH 01E, and ANISOVICH 02.

$\omega_3(1945)$ $I^G(J^{PC}) = 0^-(3^{--})$

MASS (MeV)	WIDTH (MeV)	DOCUMENT ID	TECN	COMMENT
1945 ± 20	115 ± 22	¹ ANISOVICH	02B	SPEC 0.6-1.9 $p\bar{p} \rightarrow \omega\eta, \omega\pi^0\pi^0$

¹ From the combined analysis of ANISOVICH 00D, ANISOVICH 01C, and ANISOVICH 02B.

$a_2(1950)$ $I^G(J^{PC}) = 1^-(2^{++})$

MASS (MeV)	WIDTH (MeV)	DOCUMENT ID	TECN	COMMENT
1950 ⁺³⁰ ₋₇₀	180 ⁺³⁰ ₋₇₀	¹ ANISOVICH	01F	SPEC 1.96-2.41 $p\bar{p}$

¹ From the combined analysis of ANISOVICH 99C, ANISOVICH 99E, and ANISOVICH 01F.

$\omega(1960)$ $I^G(J^{PC}) = 0^-(1^{--})$

MASS (MeV)	WIDTH (MeV)	DOCUMENT ID	TECN	COMMENT
1960 ± 25	195 ± 60	¹ ANISOVICH	02B	SPEC 0.6-1.9 $p\bar{p} \rightarrow \omega\eta, \omega\pi^0\pi^0$

¹ From the combined analysis of ANISOVICH 00D, ANISOVICH 01C, and ANISOVICH 02B.

$b_1(1960)$ $I^G(J^{PC}) = 1^+(1^{+-})$

MASS (MeV)	WIDTH (MeV)	DOCUMENT ID	TECN	COMMENT
1960 ± 35	230 ± 50	¹ ANISOVICH	02	SPEC 0.6-1.9 $p\bar{p} \rightarrow \omega\pi^0, \omega\eta\pi^0, \pi^+\pi^-$

¹ From the combined analysis of ANISOVICH 00J, ANISOVICH 01D, ANISOVICH 01E, and ANISOVICH 02.

$h_1(1965)$ $I^G(J^{PC}) = 0^-(1^{+-})$

MASS (MeV)	WIDTH (MeV)	DOCUMENT ID	TECN	COMMENT
1965 ± 45	345 ± 75	¹ ANISOVICH	02B	SPEC 0.6-1.9 $p\bar{p} \rightarrow \omega\eta, \omega\pi^0\pi^0$

¹ From the combined analysis of ANISOVICH 00D, ANISOVICH 01C, and ANISOVICH 02B.

$f_1(1970)$ $I^G(J^{PC}) = 0^+(1^{++})$

MASS (MeV)	WIDTH (MeV)	DOCUMENT ID	TECN	COMMENT
1971 ± 15	240 ± 45	ANISOVICH	00J	SPEC

$X(1970)$ $I^G(J^{PC}) = ?^?(?^{??})$

MASS (MeV)	WIDTH (MeV)	DOCUMENT ID	TECN	COMMENT
1970 ± 10	40 ± 20	CHLIAPNIK...	80	HBC 32 $K^+\rho \rightarrow 2K_S^0 2\pi X$

$X(1975)$ $I^G(J^{PC}) = ?^?(?^{??})$

MASS (MeV)	WIDTH (MeV)	EVTs	DOCUMENT ID	TECN	COMMENT
1973 ± 15	80	30	CASO	70	HBC 11.2 $\pi^-\rho \rightarrow \rho 2\pi$

$\omega_2(1975)$ $I^G(J^{PC}) = 0^-(2^{--})$

MASS (MeV)	WIDTH (MeV)	DOCUMENT ID	TECN	COMMENT
1975 ± 20	175 ± 25	¹ ANISOVICH	02B	SPEC 0.6-1.9 $p\bar{p} \rightarrow \omega\eta, \omega\pi^0\pi^0$

¹ From the combined analysis of ANISOVICH 00D, ANISOVICH 01C, and ANISOVICH 02B.

$a_2(1990)$ $I^G(J^{PC}) = 1^-(2^{++})$

MASS (MeV)	WIDTH (MeV)	EVTs	DOCUMENT ID	TECN	COMMENT
2050 ± 10 ± 40	190 ± 22 ± 100	18k	¹ SCHEGELSKY	06	RVUE $\gamma\gamma \rightarrow \pi^+\pi^-\pi^0$
2003 ± 10 ± 19	249 ± 23 ± 32		LU	05	B852 18 $\pi^-\rho \rightarrow \omega\pi^-\pi^0\rho$

¹ From analysis of L3 data at 183-209 GeV.

$\Gamma(\gamma\gamma) \Gamma(\pi^+\pi^-\pi^0) / \Gamma(\text{total})$

VALUE (keV)	EVTs	DOCUMENT ID	TECN	COMMENT
0.11 ± 0.04 ± 0.05	18k	¹ SCHEGELSKY	06	RVUE $\gamma\gamma \rightarrow \pi^+\pi^-\pi^0$

¹ From analysis of L3 data at 183-209 GeV.

$\rho(2000)$ $I^G(J^{PC}) = 1^+(1^{--})$

MASS (MeV)	WIDTH (MeV)	DOCUMENT ID	TECN	COMMENT
2000 ± 30	260 ± 45	¹ BUGG	04c	RVUE Compilation
~ 1988	~ 244	HASAN	94	RVUE $p\bar{p} \rightarrow \pi\pi$

¹ From the combined analysis of ANISOVICH 00J, ANISOVICH 01D, ANISOVICH 01E, and ANISOVICH 02.

$f_2(2000)$ $I^G(J^{PC}) = 0^+(2^{++})$

MASS (MeV)	WIDTH (MeV)	DOCUMENT ID	TECN	COMMENT
2001 ± 10	312 ± 32	ANISOVICH	00J	SPEC
~ 1996	~ 134	HASAN	94	RVUE $p\bar{p} \rightarrow \pi\pi$

$X(2000)$ $I^G(J^{PC}) = 1^-(?^{?+})$

MASS (MeV)	WIDTH (MeV)	DOCUMENT ID	TECN	CHG	COMMENT
1964 ± 35	225 ± 50	¹ ARMSTRONG	93D	E760	$p\bar{p} \rightarrow 3\pi^0 \rightarrow 6\gamma$
~ 2100	~ 500	¹ ANTIPOV	77	CIBS -	25 $\pi^-\rho \rightarrow \rho\pi^-\rho_3$
2214 ± 15	355 ± 21	² BALTAY	77	HBC 0	15 $\pi^-\rho \rightarrow \Delta^{++} 3\pi$
2080 ± 40	340 ± 80	KALELKAR	75	HBC +	15 $\pi^+\rho \rightarrow \rho\pi^+\rho_3$

¹ Cannot determine spin to be 3.
² BALTAY 77 favors $J^P = ,3^+$.

$X(2000)$ $I^G(J^{PC}) = ?^?(4^{++})$

MASS (MeV)	WIDTH (MeV)	DOCUMENT ID	TECN	COMMENT
1998 ± 3 ± 5	<15	VLADIMIRSK..03		SPEC $\pi^-\rho \rightarrow K_S^0 K_S^0 M M$

$\eta(2010)$ $I^G(J^{PC}) = 0^+(0^{-+})$

MASS (MeV)	WIDTH (MeV)	DOCUMENT ID	TECN	COMMENT
2010 ⁺³⁵ ₋₆₀	270 ± 60	ANISOVICH	00J	SPEC

$\pi_1(2015)$ $I^G(J^{PC}) = 1^-(1^{-+})$

MASS (MeV)	WIDTH (MeV)	EVTs	DOCUMENT ID	TECN	COMMENT
2014 ± 20 ± 16	230 ± 32 ± 73	145k	LU	05	B852 18 $\pi^-\rho \rightarrow \omega\pi^-\pi^0\rho$
2001 ± 30 ± 92	333 ± 52 ± 49	69k	KUHN	04	B852 18 $\pi^-\rho \rightarrow \eta\pi^+\pi^-\pi^-\rho$

$a_0(2020)$ $I^G(J^{PC}) = 1^-(0^{++})$

MASS (MeV)	WIDTH (MeV)	DOCUMENT ID	TECN	COMMENT
2025 ± 30	330 ± 75	ANISOVICH	99C	SPEC

$X(2020)$ $I^G(J^{PC}) = ?^?(?^{??})$

MASS (MeV)	WIDTH (MeV)	DOCUMENT ID	TECN	COMMENT
2015 ± 3	10 ± 4	FERRER	99	RVUE $\pi\rho \rightarrow \rho p\bar{p}\pi(\pi)$

$h_3(2025)$ $I^G(J^{PC}) = 0^-(3^{+-})$

MASS (MeV)	WIDTH (MeV)	DOCUMENT ID	TECN	COMMENT
2025 ± 20	145 ± 30	¹ ANISOVICH	02B	SPEC 0.6-1.9 $p\bar{p} \rightarrow \omega\eta, \omega\pi^0\pi^0$

¹ From the combined analysis of ANISOVICH 00D, ANISOVICH 01C, and ANISOVICH 02B.

$b_3(2030)$ $I^G(J^{PC}) = 1^+(3^{+-})$

MASS (MeV)	WIDTH (MeV)	DOCUMENT ID	TECN	COMMENT
2032 ± 12	117 ± 11	¹ ANISOVICH	02	SPEC 0.6-1.9 $p\bar{p} \rightarrow \omega\pi^0, \omega\eta\pi^0, \pi^+\pi^-$

¹ From the combined analysis of ANISOVICH 00J, ANISOVICH 01D, ANISOVICH 01E, and ANISOVICH 02.

$a_2(2030)$ $I^G(J^{PC}) = 1^-(2^{++})$

MASS (MeV)	WIDTH (MeV)	DOCUMENT ID	TECN	COMMENT
2030 ± 20	205 ± 30	¹ ANISOVICH	01F	SPEC 1.96-2.41 $p\bar{p}$

¹ From the combined analysis of ANISOVICH 99C, ANISOVICH 99E, and ANISOVICH 01F.

$a_3(2030)$ $I^G(J^{PC}) = 1^-(3^{++})$

MASS (MeV)	WIDTH (MeV)	DOCUMENT ID	TECN	COMMENT
2031 ± 12	150 ± 18	¹ ANISOVICH	01F	SPEC 1.96-2.41 $p\bar{p}$

¹ From the combined analysis of ANISOVICH 99C, ANISOVICH 99E, and ANISOVICH 01F.

$\eta_2(2030)$ $I^G(J^{PC}) = 0^+(2^{-+})$

MASS (MeV)	WIDTH (MeV)	DOCUMENT ID	TECN	COMMENT
2030 ± 5 ± 15	205 ± 10 ± 15	ANISOVICH	00E	SPEC

$B(a_2\pi)_L=0/B(a_2\pi)_L=2$

VALUE	DOCUMENT ID	TECN	COMMENT
0.05 ± 0.03	¹ ANISOVICH	11	SPEC 0.9-1.94 $p\bar{p}$

¹ Reanalysis of ADOMEIT 96 and ANISOVICH 00E.

$B(a_0\pi)/B(a_2\pi)_L=2$

VALUE	DOCUMENT ID	TECN	COMMENT
0.10 ± 0.08	¹ ANISOVICH	11	SPEC 0.9-1.94 $p\bar{p}$

¹ Reanalysis of ADOMEIT 96 and ANISOVICH 00E.

Meson Particle Listings

Further States

B($f_2\eta$)/B($a_2\pi$)$L=2$					
VALUE	DOCUMENT ID	TECN	COMMENT		
0.13±0.06	¹ ANISOVICH	11	SPEC	0.9-1.94 $p\bar{p}$	
¹ Reanalysis of ADOMEIT 96 and ANISOVICH 00E.					

$f_3(2050)$ $I^G(J^{PC}) = 0^+(3^{++})$					
MASS (MeV)	WIDTH (MeV)	DOCUMENT ID	TECN	COMMENT	
2048±8	213±34	ANISOVICH	00J	SPEC	2.0 $p\bar{p} \rightarrow \eta\pi^0\pi^0$

$f_0(2060)$ $I^G(J^{PC}) = 0^+(0^{++})$					
MASS (MeV)	WIDTH (MeV)	DOCUMENT ID	TECN	COMMENT	
~2050	~120	¹ OAKDEN	94	RVUE	0.36-1.55 $p\bar{p} \rightarrow \pi\pi$
~2060	~50	¹ OAKDEN	94	RVUE	0.36-1.55 $p\bar{p} \rightarrow \pi\pi$
¹ See SEMENOV 99 and KLOET 96.					

$\pi(2070)$ $I^G(J^{PC}) = 1^-(0^{-+})$					
MASS (MeV)	WIDTH (MeV)	DOCUMENT ID	TECN	COMMENT	
2070±35	310 ⁺¹⁰⁰ ₋₅₀	ANISOVICH	01F	SPEC	2.0 $p\bar{p} \rightarrow 3\pi^0, \pi^0\eta, \pi^0\eta'$

X(2075) $I^G(J^{PC}) = ?^?(1^{++})$					
MASS (MeV)	WIDTH (MeV)	DOCUMENT ID	TECN	COMMENT	
2084 ⁺⁴ ₋₂ ±9	58 ⁺⁴ ₋₃ ±25	^{1,2} ABLIKIM	238G	BES3	$e^+e^- \rightarrow pK^-\bar{A}$
2075±12±5	90±35±9	³ ABLIKIM	04J	BES2	$J/\psi \rightarrow K^-\rho\bar{A}$

- ¹ The reported mass and width are the pole positions in the complex (M, Γ) plane.
² Signal observed with a statistical significance $>20\sigma$ comes from 3883 candidate events. Spin parity determined to be $J^P = 1^+$ with a statistical significance $>5\sigma$ over $0^-, 1^-, 2^+$ hypotheses, and in the range within 3.1-7.5 σ with respect to 2^- .
³ From a fit in the region $M_{p\bar{A}} - M_{p-A} < 150$ MeV. S-wave in the $p\bar{A}$ system preferred.

A similar near-threshold enhancement in the $p\bar{A}$ system is observed in $B^+ \rightarrow p\bar{A}D^0$ by CHEN 11f.

X(2080) $I^G(J^{PC}) = ?^?(2^{++})$					
MASS (MeV)	WIDTH (MeV)	DOCUMENT ID	TECN	COMMENT	
2080±10	110±20	KREYMER	80	STRC	13 $\pi^-d \rightarrow p\bar{p}n(n_S)$

X(2080) $I^G(J^{PC}) = ?^?(3^{--})$					
MASS (MeV)	WIDTH (MeV)	DOCUMENT ID	TECN	COMMENT	
2080±10	190±15	ROZANSKA	80	SPRK	18 $\pi^-p \rightarrow p\bar{p}n$

$a_1(2095)$ $I^G(J^{PC}) = 1^-(1^{+-})$					
MASS (MeV)	WIDTH (MeV)	EVTS	DOCUMENT ID	TECN	COMMENT
2096±17±121	451±41±81	69k	KUHN	04	B852 18 $\pi^-p \rightarrow \eta\pi^+\pi^-\pi^-p$

B($a_1(2095) \rightarrow f_1(1285)\pi$) / B($a_1(2095) \rightarrow a_1(1260)$)					
VALUE	EVTS	DOCUMENT ID	TECN	COMMENT	
3.18±0.64	69k	KUHN	04	B852	18 $\pi^-p \rightarrow \eta\pi^+\pi^-\pi^-p$

$\eta(2100)$ $I^G(J^{PC}) = 0^+(0^{-+})$					
MASS (MeV)	WIDTH (MeV)	EVTS	DOCUMENT ID	TECN	COMMENT
2050 ⁺³⁰⁺⁷⁵ ₋₂₄₋₂₆	250 ⁺³⁶⁺¹⁸¹ ₋₃₀₋₁₆₄		¹ ABLIKIM	16N	BES3 $J/\psi \rightarrow \gamma K^+$
2103±50	187±75	586	² BISELLO	89B	DM2 $J/\psi \rightarrow 4\pi\gamma$

- ¹ From a partial wave analysis of $J/\psi \rightarrow \gamma\phi\phi$, for which the primary signal is $\eta(2225) \rightarrow \phi\phi$, and that also finds significant signals for for 0^-+ phase space, $f_0(2100)$, $f_2(2010)$, $f_2(2300)$, $f_2(2340)$, and a previously unseen 0^-+ state X(2500) (M = 2470⁺¹⁵⁺¹⁰¹₋₁₉₋₂₃ MeV, $\Gamma = 230$ ⁺⁶⁴⁺⁵⁶₋₃₅₋₃₃ MeV).
² ASTON 81B sees no peak, has 850 events in Ajinenko+Barth bins. ARESTOV 80 sees no peak.

X(2100) $I^G(J^{PC}) = ?^?(0^{??})$					
MASS (MeV)	WIDTH (MeV)	DOCUMENT ID	TECN	COMMENT	
2100±40	250±40	ALDE	86D	GAM4	100 $\pi^-p \rightarrow 2\eta X$

X(2110) $I^G(J^{PC}) = 1^+(3^{-?})$					
MASS (MeV)	WIDTH (MeV)	DOCUMENT ID	TECN	COMMENT	
2110±10	330±20	EVANGELIS...	79	OMEG	10,16 $\pi^-p \rightarrow \bar{p}pn$

X(2120) $I^G(J^{PC}) = ?^?(0^{??})$					
MASS (MeV)	WIDTH (MeV)	EVTS	DOCUMENT ID	TECN	COMMENT
2122.4±6.7 ^{+4.7} _{-2.7}	83±16 ⁺³¹ ₋₁₁	647	ABLIKIM	11c	BES3 $J/\psi \rightarrow \gamma\pi^+\pi^-\eta'$

$f_2(2140)$ $I^G(J^{PC}) = 0^+(2^{++})$					
MASS (MeV)	WIDTH (MeV)	EVTS	DOCUMENT ID	TECN	COMMENT
2141±12	49±28	389	GREEN	86	MPSF 400 $pA \rightarrow 4KX$

X(2150) $I^G(J^{PC}) = ?^?(2^{+?})$					
MASS (MeV)	WIDTH (MeV)	DOCUMENT ID	TECN	COMMENT	
2150±10	260±10	ROZANSKA	80	SPRK	18 $\pi^-p \rightarrow p\bar{p}n$

$a_2(2175)$ $I^G(J^{PC}) = 1^-(2^{+-})$					
MASS (MeV)	WIDTH (MeV)	DOCUMENT ID	TECN	COMMENT	
2175±40	310 ⁺⁹⁰ ₋₄₅	ANISOVICH	01F	SPEC	2.0 $p\bar{p} \rightarrow 3\pi^0, \pi^0\eta, \pi^0\eta'$

$\eta(2190)$ $I^G(J^{PC}) = 0^+(0^{-+})$					
MASS (MeV)	WIDTH (MeV)	DOCUMENT ID	TECN	COMMENT	
2190±50	850±100	BUGG	99	BES	

$\omega_2(2195)$ $I^G(J^{PC}) = 0^-(2^{--})$					
MASS (MeV)	WIDTH (MeV)	DOCUMENT ID	TECN	COMMENT	
2195±30	225±40	¹ ANISOVICH	02B	SPEC	0.6-1.9 $p\bar{p} \rightarrow \omega\eta, \omega\pi^0\pi^0$
¹ From the combined analysis of ANISOVICH 00D, ANISOVICH 01c, and ANISOVICH 02B.					

X(2210) $I^G(J^{PC}) = ?^?(2^{+?})$					
MASS (MeV)	WIDTH (MeV)	DOCUMENT ID	TECN	COMMENT	
2210 ⁺⁷⁹ ₋₂₁	203 ⁺⁴³⁷ ₋₈₇	EVANGELIS...	79B	OMEG	10 $\pi^-p \rightarrow K^+K^-n$
2207±22	130	CASO	70	HBC	11.2 π^-p

X₂(2210) $I^G(J^{PC}) = 0^+(2^{++})$					
MASS (MeV)	WIDTH (MeV)	DOCUMENT ID	TECN	COMMENT	
2210±60	360±120	¹ KLEMPF	22	RVUE	$J/\psi \rightarrow \gamma\pi^0\pi^0, \gamma K_S^0 K_S^0$

- ¹ Fit of the tensor partial waves from BES3 in the multipole basis. Might be a cluster of $J^P = 2^{++}$ resonances. The ratio of decay widths $K^+K^-/\pi\pi$ is 0.23±0.05.

$h_1(2215)$ $I^G(J^{PC}) = 0^-(1^{+-})$					
MASS (MeV)	WIDTH (MeV)	DOCUMENT ID	TECN	COMMENT	
2215±40	325±55	¹ ANISOVICH	02B	SPEC	0.6-1.9 $p\bar{p} \rightarrow \omega\eta, \omega\pi^0\pi^0$
¹ From the combined analysis of ANISOVICH 00D, ANISOVICH 01c, and ANISOVICH 02B.					

$\rho_2(2225)$ $I^G(J^{PC}) = 1^+(2^{--})$					
MASS (MeV)	WIDTH (MeV)	DOCUMENT ID	TECN	COMMENT	
2225±35	335 ⁺¹⁰⁰ ₋₅₀	¹ ANISOVICH	02	SPEC	0.6-1.9 $p\bar{p} \rightarrow \omega\pi^0, \omega\eta\pi^0, \pi^+\pi^-$

- ¹ From the combined analysis of ANISOVICH 00J, ANISOVICH 01D, ANISOVICH 01E, and ANISOVICH 02.

$\rho_4(2230)$ $I^G(J^{PC}) = 1^+(4^{--})$					
MASS (MeV)	WIDTH (MeV)	DOCUMENT ID	TECN	COMMENT	
2230±25	210±30	¹ ANISOVICH	02	SPEC	0.6-1.9 $p\bar{p} \rightarrow \omega\pi^0, \omega\eta\pi^0, \pi^+\pi^-$

- ¹ From the combined analysis of ANISOVICH 00J, ANISOVICH 01D, ANISOVICH 01E, and ANISOVICH 02.

$b_1(2240)$ $I^G(J^{PC}) = 1^+(1^{+-})$					
MASS (MeV)	WIDTH (MeV)	DOCUMENT ID	TECN	COMMENT	
2240±35	320±85	¹ ANISOVICH	02	SPEC	0.6-1.9 $p\bar{p} \rightarrow \omega\pi^0, \omega\eta\pi^0, \pi^+\pi^-$

- ¹ From the combined analysis of ANISOVICH 00J, ANISOVICH 01D, ANISOVICH 01E, and ANISOVICH 02.

$f_2(2240)$ $I^G(J^{PC}) = 0^+(2^{++})$					
MASS (MeV)	WIDTH (MeV)	DOCUMENT ID	TECN	COMMENT	
2240±15	241±30	¹ ANISOVICH	00J	SPEC	1.92-2.41 $p\bar{p}$
••• We do not use the following data for averages, fits, limits, etc. •••					
~2226	~226	HASAN	94	RVUE	$p\bar{p} \rightarrow \pi\pi$

- ¹ From the combined analysis of ANISOVICH 99C, ANISOVICH 99F, ANISOVICH 99J, ANISOVICH 99K, and ANISOVICH 00B. See also ANISOVICH 12.

$b_3(2245)$ $I^G(J^{PC}) = 1^+(3^+ -)$					
MASS (MeV)	WIDTH (MeV)	DOCUMENT ID	TECN	COMMENT	
2245 ± 50	320 ± 70	¹ BUGG	04c	RVUE	

¹ From the combined analysis of ANISOVICH 00J, ANISOVICH 01D, ANISOVICH 01E, and ANISOVICH 02.

$\eta_2(2250)$ $I^G(J^{PC}) = 0^+(2^- +)$					
MASS (MeV)	WIDTH (MeV)	DOCUMENT ID	TECN	COMMENT	
2248 ± 20	280 ± 20	ANISOVICH	00I	SPEC	
2267 ± 14	290 ± 50	ANISOVICH	00J	SPEC	

$\pi_4(2250)$ $I^G(J^{PC}) = 1^-(4^- +)$					
MASS (MeV)	WIDTH (MeV)	DOCUMENT ID	TECN	COMMENT	
2250 ± 15	215 ± 25	ANISOVICH	01F	SPEC	2.0 $\bar{p}p \rightarrow 3\pi^0, \pi^0\eta, \pi^0\eta'$

$\omega_4(2250)$ $I^G(J^{PC}) = 0^-(4^- -)$					
MASS (MeV)	WIDTH (MeV)	DOCUMENT ID	TECN	COMMENT	
2250 ± 30	150 ± 50	¹ ANISOVICH	02B	SPEC	0.6-1.9 $p\bar{p} \rightarrow \omega\eta, \omega\pi^0\pi^0$

¹ From the combined analysis of ANISOVICH 00D, ANISOVICH 01c, and ANISOVICH 02B.

$\omega_5(2250)$ $I^G(J^{PC}) = 0^-(5^- -)$					
MASS (MeV)	WIDTH (MeV)	DOCUMENT ID	TECN	COMMENT	
2250 ± 70	320 ± 95	¹ BUGG	04	RVUE	

¹ From the combined analysis of ANISOVICH 00D, ANISOVICH 01c, and ANISOVICH 02B.

$\omega_3(2255)$ $I^G(J^{PC}) = 0^-(3^- -)$					
MASS (MeV)	WIDTH (MeV)	DOCUMENT ID	TECN	COMMENT	
2255 ± 15	175 ± 30	¹ ANISOVICH	02B	SPEC	0.6-1.9 $p\bar{p} \rightarrow \omega\eta, \omega\pi^0\pi^0$

¹ From the combined analysis of ANISOVICH 00D, ANISOVICH 01c, and ANISOVICH 02B.

$a_4(2255)$ $I^G(J^{PC}) = 1^-(4^+ +)$					
MASS (MeV)	WIDTH (MeV)	DOCUMENT ID	TECN	COMMENT	
2237 ± 5	291 ± 12	UMAN	06	E835	5.2 $\bar{p}p \rightarrow \eta\eta\pi^0$
2255 ± 40	330 ⁺¹¹⁰ ₋₅₀	¹ ANISOVICH	01F	SPEC	1.96-2.41 $\bar{p}p$

¹ From the combined analysis of ANISOVICH 99c, ANISOVICH 99E, and ANISOVICH 01F.

$a_2(2255)$ $I^G(J^{PC}) = 1^-(2^+ +)$					
MASS (MeV)	WIDTH (MeV)	DOCUMENT ID	TECN	COMMENT	
2255 ± 20	230 ± 15	¹ ANISOVICH	01G	SPEC	1.96-2.41 $\bar{p}p$

¹ From the combined analysis of ANISOVICH 99c, ANISOVICH 99E, ANISOVICH 01F, and ANISOVICH 01G.

$X(2260)$ $I^G(J^{PC}) = 0^+(4^+?)$					
MASS (MeV)	WIDTH (MeV)	DOCUMENT ID	TECN	COMMENT	
2260 ± 20	400 ± 100	EVANGELIS...	79	OMEG	10,16 $\pi^- p \rightarrow \bar{p}pn$

$\rho(2270)$ $I^G(J^{PC}) = 1^+(1^- -)$					
MASS (MeV)	WIDTH (MeV)	DOCUMENT ID	TECN	COMMENT	
2265 ± 40	325 ± 80	¹ ANISOVICH	02	SPEC	0.6-1.9 $p\bar{p} \rightarrow \omega\pi^0, \omega\eta\pi^0, \pi^+\pi^-$
2280 ± 50	440 ± 110	ATKINSON	85	OMEG	20-70 $\gamma p \rightarrow p\omega\pi^+\pi^-\pi^0$

¹ From the combined analysis of ANISOVICH 00J, ANISOVICH 01D, ANISOVICH 01E, and ANISOVICH 02.

$a_1(2270)$ $I^G(J^{PC}) = 1^-(1^+ +)$					
MASS (MeV)	WIDTH (MeV)	DOCUMENT ID	TECN	COMMENT	
2270 ⁺⁵⁵ ₋₄₀	305 ⁺⁷⁰ ₋₄₀	ANISOVICH	01F	SPEC	2.0 $\bar{p}p \rightarrow 3\pi^0, \pi^0\eta, \pi^0\eta'$

$h_3(2275)$ $I^G(J^{PC}) = 0^-(3^+ -)$					
MASS (MeV)	WIDTH (MeV)	DOCUMENT ID	TECN	COMMENT	
2275 ± 25	190 ± 45	¹ ANISOVICH	02B	SPEC	0.6-1.9 $p\bar{p} \rightarrow \omega\eta, \omega\pi^0\pi^0$

¹ From the combined analysis of ANISOVICH 00D, ANISOVICH 01c, and ANISOVICH 02B.

$a_3(2275)$ $I^G(J^{PC}) = 1^-(3^+ +)$					
MASS (MeV)	WIDTH (MeV)	DOCUMENT ID	TECN	COMMENT	
2275 ± 35	350 ⁺¹⁰⁰ ₋₅₀	¹ ANISOVICH	01G	SPEC	1.96-2.41 $\bar{p}p$

¹ From the combined analysis of ANISOVICH 99c, ANISOVICH 99E, ANISOVICH 01F, and ANISOVICH 01G.

$\pi_2(2285)$ $I^G(J^{PC}) = 1^-(2^- +)$					
MASS (MeV)	WIDTH (MeV)	DOCUMENT ID	TECN	COMMENT	
2285 ± 20 ± 25	250 ± 20 ± 25	¹ ANISOVICH	11	SPEC	0.9-1.94 $p\bar{p}$

¹ Reanalysis of ADOMEIT 96 and ANISOVICH 00E.

$\omega_3(2285)$ $I^G(J^{PC}) = 0^-(3^- -)$					
MASS (MeV)	WIDTH (MeV)	DOCUMENT ID	TECN	COMMENT	
2278 ± 28	224 ± 50	¹ BUGG	04A	RVUE	
2285 ± 60	230 ± 40	² ANISOVICH	02B	SPEC	0.6-1.9 $p\bar{p} \rightarrow \omega\eta, \omega\pi^0\pi^0$

¹ Partial wave analysis of the data on $p\bar{p} \rightarrow \bar{\Lambda}\Lambda$ from BARNES 00.
² From the combined analysis of ANISOVICH 00D, ANISOVICH 01c, and ANISOVICH 02B.

$\omega(2290)$ $I^G(J^{PC}) = 0^-(1^- -)$					
MASS (MeV)	WIDTH (MeV)	DOCUMENT ID	TECN	COMMENT	
2290 ± 20	275 ± 35	¹ BUGG	04A	RVUE	

¹ Partial wave analysis of the data on $p\bar{p} \rightarrow \bar{\Lambda}\Lambda$ from BARNES 00.

$f_2(2295)$ $I^G(J^{PC}) = 0^+(2^+ +)$					
MASS (MeV)	WIDTH (MeV)	DOCUMENT ID	TECN	COMMENT	
2293 ± 13	216 ± 37	¹ ANISOVICH	00J	SPEC	1.92-2.41 $p\bar{p}$

¹ From the combined analysis of ANISOVICH 99c, ANISOVICH 99F, ANISOVICH 99J, ANISOVICH 99K, and ANISOVICH 00B. See also ANISOVICH 12.

$f_3(2300)$ $I^G(J^{PC}) = 0^+(3^+ +)$					
MASS (MeV)	WIDTH (MeV)	DOCUMENT ID	TECN	COMMENT	
2334 ± 25	200 ± 20	¹ BUGG	04A	RVUE	

¹ Partial wave analysis of the data on $p\bar{p} \rightarrow \bar{\Lambda}\Lambda$ from BARNES 00.

$f_1(2310)$ $I^G(J^{PC}) = 0^+(1^+ +)$					
MASS (MeV)	WIDTH (MeV)	DOCUMENT ID	TECN	COMMENT	
2310 ± 60	255 ± 70	ANISOVICH	00J	SPEC	

$\eta(2320)$ $I^G(J^{PC}) = 0^+(0^- +)$					
MASS (MeV)	WIDTH (MeV)	DOCUMENT ID	TECN	COMMENT	
2320 ± 15	230 ± 35	¹ ANISOVICH	00M	SPEC	

¹ From the combined analysis of $\bar{p}p \rightarrow \eta\eta\eta$ from ANISOVICH 00M and $\bar{p}p \rightarrow \eta\pi^0\pi^0$ from ANISOVICH 00J.

$\eta_4(2330)$ $I^G(J^{PC}) = 0^+(4^- +)$					
MASS (MeV)	WIDTH (MeV)	DOCUMENT ID	TECN	COMMENT	
2328 ± 38	240 ± 90	ANISOVICH	00J	SPEC	2.0 $p\bar{p} \rightarrow \eta\pi^0\pi^0$

$\omega(2330)$ $I^G(J^{PC}) = 0^-(1^- -)$					
MASS (MeV)	WIDTH (MeV)	DOCUMENT ID	TECN	COMMENT	
2330 ± 30	435 ± 75	ATKINSON	88	OMEG	25-50 $\gamma p \rightarrow \rho^\pm\rho^0\pi^\mp$

$X(2340)$ $I^G(J^{PC}) = ?^?(?^?)$					
MASS (MeV)	WIDTH (MeV)	EVTS	DOCUMENT ID	TECN	COMMENT
2340 ± 20	180 ± 60	126	¹ BALTAY	75	HBC 15 $\pi^+ p \rightarrow p5\pi$

¹ Dominant decay into $\rho^0\rho^0\pi^+$. BALTAY 78 finds confirmation in $2\pi^+\pi^-\pi^0$ events which contain $\rho^+\rho^0\pi^0$ and $2\rho^+\pi^-$.

$\pi(2360)$ $I^G(J^{PC}) = 1^-(0^- +)$					
MASS (MeV)	WIDTH (MeV)	DOCUMENT ID	TECN	COMMENT	
2360 ± 25	300 ⁺¹⁰⁰ ₋₅₀	ANISOVICH	01F	SPEC	2.0 $\bar{p}p \rightarrow 3\pi^0, \pi^0\eta, \pi^0\eta'$

$X(2360)$ $I^G(J^{PC}) = ?^?(4^+?)$					
MASS (MeV)	WIDTH (MeV)	DOCUMENT ID	TECN	COMMENT	
2360 ± 10	430 ± 30	ROZANSKA	80	SPRK	18 $\pi^- p \rightarrow p\bar{p}n$
••• We do not use the following data for averages, fits, limits, etc. •••					
2356 ± 7 ± 15	304 ± 28 ± 54	¹ ABLIKIM	23AY	BES3	$e^+e^- \rightarrow (\Lambda\bar{\Lambda})\eta$

¹ Assuming $J^{PC} = 1^- -$.

$X(2440)$ $I^G(J^{PC}) = ?^?(5^-?)$					
MASS (MeV)	WIDTH (MeV)	DOCUMENT ID	TECN	COMMENT	
2440 ± 10	310 ± 20	ROZANSKA	80	SPRK	18 $\pi^- p \rightarrow p\bar{p}n$

Meson Particle Listings

Further States

$a_6(2450)$ $J^G(J^{PC}) = 1^-(6^{++})$

MASS (MeV)	WIDTH (MeV)	DOCUMENT ID	TECN	COMMENT
2450 ± 130	400 ± 250	CLELAND	82B	SPEC $50 \pi p \rightarrow K_S^0 K^\pm p$

$X(2540)$ $J^G(J^{PC}) = 0^+(0^{++})$

MASS (MeV)	WIDTH (MeV)	DOCUMENT ID	TECN	COMMENT
2539 ± 14 +38 -14	274 +77 +126 -61 -163	UEHARA	13	BELL $\gamma\gamma \rightarrow K_S^0 K_S^0$

$\Gamma(\gamma\gamma) \times B(K\bar{K})$

VALUE (eV)	DOCUMENT ID	TECN	COMMENT
40 +9 +17 -7 -40	UEHARA	13	BELL $\gamma\gamma \rightarrow K_S^0 K_S^0$

$X(2600)$ $J^G(J^{PC}) = ?^?(?^{??})$

MASS (MeV)	WIDTH (MeV)	DOCUMENT ID	TECN	COMMENT
2618.3 ± 2.0 +16.3 -1.4	195 ± 5 +26 -17	ABLİKİM	22G	BES3 $J/\psi \rightarrow \gamma\pi^+\pi^-\eta'$

$B(J/\psi \rightarrow \gamma X(2600)) \times B(X(2600) \rightarrow f_0(1500)\eta') \times B(f_0(1500) \rightarrow \pi^+\pi^-)$

VALUE (units 10^{-5})	DOCUMENT ID	TECN	COMMENT
3.09 ± 0.21 +1.14 -0.77	1 ABLİKİM	22G	BES3 $J/\psi \rightarrow \gamma\pi^+\pi^-\eta'$

¹ The $\pi^+\pi^-$ mass spectrum is described by a coherent sum of two Breit-Wigner resonances, $f_0(1500)$ and a new $X(1540)$ with mass $1540.2 \pm 7.0 +36.3$
-6.1 MeV and width $157 \pm 19 +11$
-77 MeV.

$B(J/\psi \rightarrow \gamma X(2600)) \times B(X(2600) \rightarrow X(1540)\eta') \times B(X(1540) \rightarrow \pi^+\pi^-)$

VALUE (units 10^{-5})	DOCUMENT ID	TECN	COMMENT
2.69 ± 0.19 +0.38 -1.21	1 ABLİKİM	22G	BES3 $J/\psi \rightarrow \gamma\pi^+\pi^-\eta'$

¹ The $\pi^+\pi^-$ mass spectrum is described by a coherent sum of two Breit-Wigner resonances, $f_0(1500)$ and a new $X(1540)$ with mass $1540.2 \pm 7.0 +36.3$
-6.1 MeV and width $157 \pm 19 +11$
-77 MeV.

$K_0^*(2600)$ $J^G(J^{PC}) = 1(2(0^+))$

MASS (MeV)	WIDTH (MeV)	DOCUMENT ID	TECN	COMMENT
2662 ± 59 ± 201	480 ± 47 ± 72	1 AAJ	23AH	LHCb $B^+ \rightarrow K^+(K_S^0 K\pi)$

¹ From Dalitz plot analyses of $\eta_c(1S, 2S) \rightarrow K_S^0 K^+\pi^- + c.c.$

$X(2632)$ $J^G(J^{PC}) = ?^?(?^{??})$

MASS (MeV)	WIDTH (MeV)	DOCUMENT ID	TECN	COMMENT
2635.2 ± 3.3		1 EVĐOKIMOV	04	SELX $X(2632) \rightarrow D_2^+\eta$
2631.6 ± 2.1	< 17	2 EVĐOKIMOV	04	SELX $X(2632) \rightarrow D_0^+K^+$

¹ From a mass difference to D_2^+ of 666.9 ± 3.3 MeV.

² From a mass difference to D_0^+ of 767.0 ± 2.0 MeV.

$B(X(2632) \rightarrow D_0^+K^+)/B(X(2632) \rightarrow D_2^+\eta)$

VALUE	DOCUMENT ID	TECN	COMMENT
0.14 ± 0.06	1 EVĐOKIMOV	04	SELX

¹ Possible interpretation of this decay pattern is discussed by YASUI 07.

$X(2680)$ $J^G(J^{PC}) = ?^?(?^{??})$

MASS (MeV)	WIDTH (MeV)	DOCUMENT ID	TECN	COMMENT
2676 ± 27	150	CASO	70	HBC $11.2 \pi^- p \rightarrow \rho^- \pi^+\pi^- p$

$X(2710)$ $J^G(J^{PC}) = ?^?(6^{+?})$

MASS (MeV)	WIDTH (MeV)	DOCUMENT ID	TECN	COMMENT
2710 ± 20	170 ± 40	ROZANSKA	80	SPRK $18 \pi^- p \rightarrow \rho \bar{p} n$

$X(2750)$ $J^G(J^{PC}) = ?^?(7^{-?})$

MASS (MeV)	WIDTH (MeV)	DOCUMENT ID	TECN	COMMENT
2747 ± 32	195 ± 75	DENNEY	83	LASS $10 \pi^+ p \rightarrow K^+ K^- \pi^+ p$

$f_6(3100)$ $J^G(J^{PC}) = 0^+(6^{++})$

MASS (MeV)	WIDTH (MeV)	DOCUMENT ID	TECN	COMMENT
3100 ± 100	700 ± 130	BINON	05	GAMS $33 \pi^- p \rightarrow \eta\eta n$

$X(3250)$ $J^G(J^{PC}) = ?^?(?^{??})$ 3-Body Decays

MASS (MeV)	WIDTH (MeV)	DOCUMENT ID	TECN	COMMENT
3250 ± 8 ± 20	45 ± 18	ALEEV	93	BIS2 $X(3250) \rightarrow \Lambda \bar{p} K^+$
3265 ± 7 ± 20	40 ± 18	ALEEV	93	BIS2 $X(3250) \rightarrow \bar{\Lambda} p K^-$

$X(3250)$ $J^G(J^{PC}) = ?^?(?^{??})$ 4-Body Decays

MASS (MeV)	WIDTH (MeV)	DOCUMENT ID	TECN	COMMENT
3245 ± 8 ± 20	25 ± 11	ALEEV	93	BIS2 $X(3250) \rightarrow \Lambda \bar{p} K^+ \pi^\pm$
3250 ± 9 ± 20	50 ± 20	ALEEV	93	BIS2 $X(3250) \rightarrow \bar{\Lambda} p K^- \pi^\mp$
3270 ± 8 ± 20	25 ± 11	ALEEV	93	BIS2 $X(3250) \rightarrow K_S^0 \rho \bar{p} K^\pm$

$X(3350)$ $J^G(J^{PC}) = ?^?(?^{??})$

MASS (MeV)	WIDTH (MeV)	EVTS	DOCUMENT ID	TECN	COMMENT
3350 +10 -20 ± 20	70 +40 -30 ± 40	50 ± 10	1 GABYSHEV	06A	BELL $B^- \rightarrow \Lambda_c^+ \bar{p} \pi^-$

¹ A similar enhancement in the $\Lambda_c^+ \bar{p}$ final state is also reported by BABAR collaboration in AUBERT 10H.

$\psi(4500)$ $J^G(J^{PC}) = 0^-(1^{--})$

MASS (MeV)	WIDTH (MeV)	DOCUMENT ID	TECN	COMMENT
4469.1 ± 26.2 ± 3.6	246.3 ± 36.7 ± 9.4	1 ABLİKİM	23X	BES3 $e^+ e^- \rightarrow D^{*0} D^{*-} \pi^+$
4484.7 ± 13.3 ± 24.1	111.1 ± 30 ± 15.2	2 ABLİKİM	22AU	BES3 $e^+ e^- \rightarrow \bar{\Lambda} p K^- J/\psi$

¹ From a cross-section measurement of $e^+ e^- \rightarrow D^{*0} D^{*-} \pi^+$ between 4.189 and 4.951 GeV, assuming a coherent sum of 3 Breit-Wigner resonances plus a continuum amplitude. $\Gamma(e^+ e^-) B(D^{*0} D^{*-} \pi^+) = 107-1744$ eV depending on solutions I - VIII with the same fit qualities. The two other resonances have masses (widths) 4209.6 ± 7.5 (81.6 ± 19.9) MeV and 4675.3 ± 29.7 (218.3 ± 73.5) MeV.

² ABLİKİM 22AU cross sections analysis of the process $e^+ e^- \rightarrow K^+ K^- J/\psi$ at c.m. energies 4.127-4.600 GeV from 15.6 fb⁻¹ of data.

REFERENCES for Further States

AAJ	23AH	PR D108 032010	R. Aaij et al.	(LHCb Collab.)
ABLİKİM	23AY	PR D107 112001	M. Ablikim et al.	(BESIII Collab.)
ABLİKİM	23BG	PRL 131 151901	M. Ablikim et al.	(BESIII Collab.)
ABLİKİM	23X	PRL 130 121901	M. Ablikim et al.	(BESIII Collab.)
ABLİKİM	22AU	CP C46 111002	M. Ablikim et al.	(BESIII Collab.)
ABLİKİM	22G	PRL 129 042001	M. Ablikim et al.	(BESIII Collab.)
KLEMP T	22	PL B830 137171	E. Klemp t et al.	(BO N N)
ABLİKİM	16N	PR D93 112011	M. Ablikim	(BESIII Collab.)
UEHARA	13	PTEP 2013 123C01	S. Uehara et al.	(BELLE Collab.)
ANISOVICH	12	PR D85 014001	A.V. Anisovich et al.	
ABLİKİM	11C	PRL 106 072002	M. Ablikim et al.	(BESIII Collab.)
ANASHIN	11	PL B703 543	V.V. Anashin et al.	(KEDR Collab.)
ANISOVICH	11	EPJ C71 1511	A.V. Anisovich et al.	(LOQM, RAL, FNPI)
CHEN	11F	PR D84 071501	P. Chen et al.	(BELLE Collab.)
AUBERT	10H	PR D82 031102	B. Aubert et al.	(BABAR Collab.)
ABRAAMYAN	09	PR C80 034001	Kh.U. Abraamyan et al.	
VLADIMIRSK...	08	PAN 71 2129	V.V. Vladimirovsky et al.	(ITEP)
VLADIMIRSK...	07	Translated from YAF 71 2166.	V.V. Vladimirovsky et al.	
		Translated from YAF 70 1751.		
YASUI	07	PR D76 034009	S. Yasui, M. Oka	
ABLİKİM	06S	PRL 97 142002	M. Ablikim et al.	(BES Collab.)
GABYSHEV	06A	PRL 97 242001	N. Gabyshev et al.	(BELLE Collab.)
SCHEGELSKY	06	EPJ A27 199	V.A. Schegelsky et al.	
SCHEGELSKY	06A	EPJ A27 207	V.A. Schegelsky et al.	
UMAN	06	PR D73 052009	I. Uman et al.	(FNAL E835)
VLADIMIRSK...	06	PAN 69 493	V.V. Vladimirovsky et al.	(ITEP, Moscow)
BINON	05	Translated from YAF 69 515.	B. Binon et al.	
		PAN 68 960		
GRIGOR'EV	05	Translated from YAF 68 998.	V.K. Grigor'ev et al.	(ITEP)
		PAN 68 1271		
		Translated from YAF 68 1324.		
LU	05	PRL 94 032002	M. Lu et al.	(BNL E852 Collab.)
ABLİKİM	04J	PRL 93 112002	M. Ablikim et al.	(BES Collab.)
BUGG	04	PL B595 556 (errat.)	D.V. Bugg	
BUGG	04A	EPJ C36 161	D.V. Bugg	
BUGG	04C	PRPL 397 257	D.V. Bugg	
EVĐOKIMOV	04	PRL 93 242001	A.V. Evdokimov et al.	(SELEX Collab.)
KUHN	04	PL B595 109	J. Kuhn et al.	(BNL E852 Collab.)
ANISOVICH	03	EPJ A16 229	V.V. Anisovich et al.	
VLADIMIRSK...	03	PAN 66 700	V.V. Vladimirovsky et al.	
		Translated from YAF 66 729.		
ANISOVICH	02	PL B542 8	A.V. Anisovich et al.	
ANISOVICH	02B	PL B542 19	A.V. Anisovich et al.	
CHUNG	02	PR D65 072001	S.U. Chung et al.	(BNL E852 Collab.)
ANISOVICH	01C	PL B507 23	A.V. Anisovich et al.	
ANISOVICH	01D	PL B508 6	A.V. Anisovich et al.	
ANISOVICH	01E	PL B513 281	A.V. Anisovich et al.	
ANISOVICH	01F	PL B517 261	A.V. Anisovich et al.	
ANISOVICH	01G	PL B517 273	A.V. Anisovich et al.	
ANISOVICH	00B	NP A662 319	A.V. Anisovich et al.	
ANISOVICH	00D	PL B476 15	A.V. Anisovich et al.	
ANISOVICH	00E	PL B477 19	A.V. Anisovich et al.	
ANISOVICH	00I	PL B491 40	A.V. Anisovich et al.	
ANISOVICH	00J	PL B491 47	A.V. Anisovich et al.	(RAL, LOQM, FNPI+)
ANISOVICH	00M	PL B496 145	A.V. Anisovich et al.	
BARNES	00	PR C62 055203	P.D. Barnes et al.	
FILIPPI	00	PL B495 284	A. Filippi et al.	(OBELIX Experiment)
VLADIMIRSKII	00	JETPL 72 486	V.V. Vladimirovsky et al.	
		Translated from ZETFP 72 698.		
ANISOVICH	99C	PL B452 173	A.V. Anisovich et al.	
ANISOVICH	99E	PL B452 187	A.V. Anisovich et al.	
ANISOVICH	99F	NP A651 253	A.V. Anisovich et al.	
ANISOVICH	99J	PL B471 271	A.V. Anisovich et al.	
ANISOVICH	99K	PL B468 309	A.V. Anisovich et al.	
BUGG	99	PL B458 511	D.V. Bugg et al.	
FERRER	99	EPJ C10 249	A. Ferrer et al.	
SEMENOV	99	SPU 42 847	S.V. Semenov	
		Translated from UFN 42 937.		
ADOMEIT	96	ZPHY C71 227	J. Adomeit et al.	(Crystal Barrel Collab.)
KLOET	96	PR D53 6120	W.M. Kloet, F. Myhrer	(RUTG, NORD)
PROKOSHNIK	96	PL 41 24 7	V.D. Prokoshkin, V.D. Samoilenko	(SERP)
		Translated from DANS 348 461.		
HASAN	94	PL B334 215	A. Hasan, D.V. Bugg	(LOQM)
OAKDEN	94	NP A574 731	M.N. Oakden, M.R. Pennington	(DURH)
ALEEV	93	PAN 56 1358	A.N. Aleev et al.	(BIS-2 Collab.)
		Translated from YAF 56 100.		
ARMSTRONG	93D	PL B307 319	T.A. Armstrong et al.	(FNAL, FERR, GENO+)
ALBRECHT	91F	ZPHY C50 1	H. Albrecht et al.	(ARGUS Collab.)
CONDO	91	PR D43 2787	G.T. Condo et al.	(SLAC Hybrid Collab.)
BISELLO	89B	PR D39 701	G. Busetto et al.	(DM2 Collab.)

See key on page 1171

Meson Particle Listings
Further States

ATKINSON	88	ZPHY C38 535	M. Atkinson <i>et al.</i>	(BONN, CERN, GLAS+)	KREYMER	80	PR D22 36	A.E. Krejmer <i>et al.</i>	(IND, PURD, SLAC+)
DAFTARI	87	PRL 58 859	I.K. Daftari <i>et al.</i>	(SYRA)	ROZANSKA	80	NP B162 505	M. Rozanska <i>et al.</i>	(MPIM, CERN)
ALDE	86D	NP B269 485	D.M. Alde <i>et al.</i>	(BELG, LAPP, SERP, CERN+)	EVANGELIS...	79	NP B153 253	C. Evangelista <i>et al.</i>	(BARI, BONN, CERN+)
BRIDGES	86D	PL B180 313	D.L. Bridges <i>et al.</i>	(SYRA, BNL, CASE+)	EVANGELIS...	79B	NP B154 381	C. Evangelista <i>et al.</i>	(BARI, BONN, CERN+)
GREEN	86	PRL 56 1639	D.R. Green <i>et al.</i>	(FNAL, ARIZ, FSU+)	BALTAY	78	PR D17 52	C. Baltay <i>et al.</i>	(COLU, BING)
ATKINSON	85	ZPHY C29 333	M. Atkinson <i>et al.</i>	(BONN, CERN, GLAS+)	ANTIPOV	77	NP B119 45	Y.M. Antipov <i>et al.</i>	(SERP, GEVA)
DENNEY	83	PR D28 2726	D.L. Denney <i>et al.</i>	(IOWA, MICH)	BALTAY	77	PRL 39 591	C. Baltay, C.V. Cautis, M. Kalelkar	(COLU)
CLELAND	82B	NP B206 228	W.E. Cleland <i>et al.</i>	(DURH, GEVA, LAUS+)	BALTAY	75	PRL 35 891	C. Baltay <i>et al.</i>	(COLU, BING)
ASTON	81B	NP B189 205	D. Aston <i>et al.</i>	(BONN, CERN, EPOL, GLAS+)	KALELKAR	75	Thesis Nevis 207	M.S. Kalelkar	(COLU)
ARESTOV	80	IHEP 80-165	Y.I. Arestov <i>et al.</i>	(SERP)	CASO	70	LNC 3 707	C. Caso <i>et al.</i>	(GENO, HAMB, MILA, SACL)
CHLIAPNIK...	80	ZPHY C3 285	P.V. Chliapnikov <i>et al.</i>	(SERP, BRUX, MONS)					



N BARYONS ($S = 0, I = 1/2$)	
p	2081
n	2091
N resonances	2096

Δ BARYONS ($S = 0, I = 3/2$)	
Δ resonances	2137

Λ BARYONS ($S = -1, I = 0$)	
Λ	2161
Λ resonances	2164

Σ BARYONS ($S = -1, I = 1$)	
Σ^+	2187
Σ^0	2189
Σ^-	2190
Σ resonances	2192

Ξ BARYONS ($S = -2, I = 1/2$)	
Ξ^0	2218
Ξ^-	2221
Ξ resonances	2224

Ω BARYONS ($S = -3, I = 0$)	
Ω^-	2231
Ω resonances	2233

CHARMED BARYONS ($C = +1$)	
Λ_c^+	2234
$\Lambda_c(2595)^+$	2243
$\Lambda_c(2625)^+$	2244
$\Lambda_c(2765)^+$ aka $\Sigma_c(2765)$	2245
$\Lambda_c(2860)^+$	2245
$\Lambda_c(2880)^+$	2245
$\Lambda_c(2910)^+$	2246
$\Lambda_c(2940)^+$	2246
$\Sigma_c(2455)$	2246
$\Sigma_c(2520)$	2247
$\Sigma_c(2800)$	2248
Ξ_c^+	2249
Ξ_c^0	2250
$\Xi_c'^+$	2252
$\Xi_c'^0$	2253
$\Xi_c(2645)$	2253
$\Xi_c(2790)$	2253
$\Xi_c(2815)$	2254
$\Xi_c(2882)$	2255
$\Xi_c(2923)$	2255
$\Xi_c(2930)$	2255
$\Xi_c(2970)$ was $\Xi_c(2980)$	2256
$\Xi_c(3055)$	2257
$\Xi_c(3080)$	2257
$\Xi_c(3123)$	2257
Ω_c^0	2258
$\Omega_c(2770)^0$	2259
$\Omega_c(3000)^0$	2259
$\Omega_c(3050)^0$	2260
$\Omega_c(3065)^0$	2260
$\Omega_c(3090)^0$	2260

$\Omega_c(3120)^0$	2261
$\Omega_c(3185)^0$	2261
$\Omega_c(3327)^0$	2261
Ξ_{cc}^+	2262
Ξ_{cc}^{++}	2262

BOTTOM (BEAUTY) BARYONS ($B = -1$)	
Λ_b^0	2263
$\Lambda_b(5912)^0$	2271
$\Lambda_b(5920)^0$	2272
$\Lambda_b(6070)^0$	2272
$\Lambda_b(6146)^0$	2272
$\Lambda_b(6152)^0$	2273
Σ_b	2273
Σ_b^*	2273
$\Sigma_b(6097)^+$	2274
$\Sigma_b(6097)^-$	2274
Ξ_b^-	2275
Ξ_b^0	2277
$\Xi_b'(5935)^-$	2278
$\Xi_b(5945)^0$	2278
$\Xi_b(5955)^-$	2279
$\Xi_b(6087)^0$	2279
$\Xi_b(6095)^0$	2279
$\Xi_b(6100)^-$	2279
$\Xi_b(6227)^-$	2280
$\Xi_b(6227)^0$	2280
$\Xi_b(6327)^0$	2280
$\Xi_b(6333)^0$	2281
Ξ_{bc}^0	2281
Ω_b^-	2281
$\Omega_b(6316)^-$	2282
$\Omega_b(6330)^-$	2282
$\Omega_b(6340)^-$	2282
$\Omega_b(6350)^-$	2283
b -baryon ADMIXTURE ($\Lambda_b, \Xi_b, \Omega_b$)	2283

EXOTIC BARYONS	
$P_{c\bar{c}}(4312)^+$	2285
$P_{c\bar{c}s}(4338)^0$	2285
$P_{c\bar{c}}(4380)^+$	2285
$P_{c\bar{c}}(4440)^+$	2285
$P_{c\bar{c}}(4457)^+$ was $P_c(4450)$	2286
$P_{c\bar{c}s}(4459)^0$	2286

Notes in the Listings	
Radiative hyperon decays	2219
Ξ resonances (rev.)	2223

Related Reviews in Volume 1	
80. Baryon decay parameters	1001
81. N and Δ resonances	1002
82. Λ and Σ resonances	1007
83. Pole structure of the $\Lambda(1405)$ region	1010
84. Pentaquarks (rev.)	1012



N BARYONS

(S = 0, I = 1/2)

$p, N^+ = uud; \quad n, N^0 = udd$



$$I(J^P) = \frac{1}{2}(\frac{1}{2}^+) \text{ Status: } ***$$

p MASS (atomic mass units u)

The mass is known more precisely in u (atomic mass units) than in MeV. See the next data block.

VALUE (u)	DOCUMENT ID	TECN	COMMENT
1.007276466621 ± 0.00000000053	OUR EVALUATION	2018 CODATA	
1.007276466574 ± 0.00000000010	¹ FINK 21	SPEC	Penning trap
1.007276466621 ± 0.00000000053	² TIESINGA 21	RVUE	2018 CODATA value
• • • We do not use the following data for averages, fits, limits, etc. • • •			
1.007276466598 ± 0.00000000033	³ HEISSE 19	SPEC	Penning Trap
1.007276466583 ± 0.00000000032	⁴ HEISSE 17	SPEC	See HEISSE 19
1.007276466879 ± 0.00000000091	MOHR 16	RVUE	2014 CODATA value
1.007276466812 ± 0.00000000090	MOHR 12	RVUE	2010 CODATA value
1.00727646677 ± 0.00000000010	MOHR 08	RVUE	2006 CODATA value
1.00727646688 ± 0.00000000013	MOHR 05	RVUE	2002 CODATA value
1.00727646688 ± 0.00000000013	MOHR 99	RVUE	1998 CODATA value
1.007276470 ± 0.000000012	COHEN 87	RVUE	1986 CODATA value

- ¹FINK 21 simultaneously measure the cyclotron frequencies of an H_2^+ ion and a deuteron in a coupled magnetron orbit. The proton mass is extracted using the precise deuteron mass value.
- The 2018 CODATA combination in TIESINGA 21 includes data from HEISSE 17, but does not include updates in HEISSE 19, which superseded HEISSE 17. Consequently, we do not average HEISSE 19 and TIESINGA 21. Updating the 2018 CODATA combination to use HEISSE 19 would shift the central value for the proton mass upwards by less than half a standard deviation. Therefore, we take the 2018 CODATA result in TIESINGA 21 as the recommended value for the proton mass.
- The value is an update of HEISSE 17; the result is shifted by 1.5×10^{-11} u, corresponding to 0.45 σ due to the corrected motional temperatures of the particles. The statistical and total systematic uncertainties are given as 16 and 29 in the last two digits.
- The statistical and systematic errors are 15 and 29 in the last two places of the value. Superseded by HEISSE 19.

p MASS (MeV)

The mass is known more precisely in u (atomic mass units) than in MeV. The conversion is: 1 u = 931.494 102 42(28) MeV/c² (2018 CODATA value, TIESINGA 21).

VALUE (MeV)	DOCUMENT ID	TECN	COMMENT
938.27208816 ± 0.00000029	OUR EVALUATION	2018 CODATA	
938.27208812 ± 0.00000029	¹ FINK 21	SPEC	Penning trap
938.27208816 ± 0.00000029	TIESINGA 21	RVUE	2018 CODATA value
• • • We do not use the following data for averages, fits, limits, etc. • • •			
938.2720813 ± 0.0000058	MOHR 16	RVUE	2014 CODATA value
938.272046 ± 0.000021	MOHR 12	RVUE	2010 CODATA value
938.272013 ± 0.000023	MOHR 08	RVUE	2006 CODATA value
938.272029 ± 0.000080	MOHR 05	RVUE	2002 CODATA value
938.271998 ± 0.000038	MOHR 99	RVUE	1998 CODATA value
938.27231 ± 0.00028	COHEN 87	RVUE	1986 CODATA value
938.2796 ± 0.0027	COHEN 73	RVUE	1973 CODATA value

- ¹FINK 21 quote the more precise mass in atomic mass units.

$$|m_p - m_{\bar{p}}|/m_p$$

A test of CPT invariance. Note that the comparison of the \bar{p} and p charge-to-mass ratio, given in the next data block, is much better determined.

VALUE	CL%	DOCUMENT ID	TECN	COMMENT
<7 × 10⁻¹⁰	90	¹ HORI 11	SPEC	$\bar{p}e^-$ He atom
• • • We do not use the following data for averages, fits, limits, etc. • • •				
<2 × 10 ⁻⁹	90	¹ HORI 06	SPEC	$\bar{p}e^-$ He atom
<1.0 × 10 ⁻⁸	90	¹ HORI 03	SPEC	$\bar{p}e^-$ ⁴ He, $\bar{p}e^-$ ³ He
<6 × 10 ⁻⁸	90	¹ HORI 01	SPEC	$\bar{p}e^-$ He atom
<5 × 10 ⁻⁷		² TORII 99	SPEC	$\bar{p}e^-$ He atom

- ¹HORI 01, HORI 03, HORI 06, and HORI 11 use the more-precisely-known constraint on the \bar{p} charge-to-mass ratio of GABRIELSE 99 (see below) to get their results. Their results are not independent of the HORI 01, HORI 03, HORI 06, and HORI 11 values for $|q_p + q_{\bar{p}}|/e$, below.

²TORII 99 uses the more-precisely-known constraint on the \bar{p} charge-to-mass ratio of GABRIELSE 95 (see below) to get this result. This is not independent of the TORII 99 value for $|q_p + q_{\bar{p}}|/e$, below.

$$\bar{p}/p \text{ CHARGE-TO-MASS RATIO, } \left| \frac{q_{\bar{p}}}{m_{\bar{p}}} \right| / \left(\frac{q_p}{m_p} \right)$$

A test of CPT invariance. Listed here are measurements involving the inertial masses. For a discussion of what may be inferred about the ratio of \bar{p} and p gravitational masses, see ERICSON 90; they obtain an upper bound of 10^{-6} – 10^{-7} for violation of the equivalence principle for \bar{p} 's.

VALUE	DOCUMENT ID	TECN	COMMENT
1.000000000003 ± 0.00000000016	OUR AVERAGE		
1.000000000003 ± 0.00000000016	BORCHERT 22	TRAP	Penning trap
1.000000000001 ± 0.00000000069	ULMER 15	TRAP	Penning trap
• • • We do not use the following data for averages, fits, limits, etc. • • •			
0.99999999991 ± 0.00000000009	GABRIELSE 99	TRAP	Penning trap
1.0000000015 ± 0.0000000011	¹ GABRIELSE 95	TRAP	Penning trap
1.0000000023 ± 0.0000000042	² GABRIELSE 90	TRAP	Penning trap

¹Equation (2) of GABRIELSE 95 should read $M(\bar{p})/M(p) = 0.999\,999\,9985$ (11) (G. Gabrielse, private communication).

²GABRIELSE 90 also measures $m_{\bar{p}}/m_{e^-} = 1836.152660 \pm 0.000083$ and $m_p/m_{e^-} = 1836.152680 \pm 0.000088$. Both are completely consistent with the 1986 CODATA (COHEN 87) value for m_p/m_{e^-} of 1836.152701 ± 0.000037 .

$$\left(\left| \frac{q_{\bar{p}}}{m_{\bar{p}}} \right| - \frac{q_p}{m_p} \right) / \frac{q_p}{m_p}$$

A test of CPT invariance. Taken from the \bar{p}/p charge-to-mass ratio, above.

VALUE	DOCUMENT ID
(0.3 ± 1.6) × 10⁻¹¹	OUR EVALUATION

$$|q_p + q_{\bar{p}}|/e$$

A test of CPT invariance. Note that the comparison of the \bar{p} and p charge-to-mass ratios given above is much better determined. See also a similar test involving the electron.

VALUE	CL%	DOCUMENT ID	TECN	COMMENT
<7 × 10⁻¹⁰	90	¹ HORI 11	SPEC	$\bar{p}e^-$ He atom
• • • We do not use the following data for averages, fits, limits, etc. • • •				
<2 × 10 ⁻⁹	90	¹ HORI 06	SPEC	$\bar{p}e^-$ He atom
<1.0 × 10 ⁻⁸	90	¹ HORI 03	SPEC	$\bar{p}e^-$ ⁴ He, $\bar{p}e^-$ ³ He
<6 × 10 ⁻⁸	90	¹ HORI 01	SPEC	$\bar{p}e^-$ He atom
<5 × 10 ⁻⁷		² TORII 99	SPEC	$\bar{p}e^-$ He atom
<2 × 10 ⁻⁵		³ HUGHES 92	RVUE	

¹HORI 01, HORI 03, HORI 06, and HORI 11 use the more-precisely-known constraint on the \bar{p} charge-to-mass ratio of GABRIELSE 99 (see above) to get their results. Their results are not independent of the HORI 01, HORI 03, HORI 06, and HORI 11 values for $|m_p - m_{\bar{p}}|/m_p$, above.

²TORII 99 uses the more-precisely-known constraint on the \bar{p} charge-to-mass ratio of GABRIELSE 95 (see above) to get this result. This is not independent of the TORII 99 value for $|m_p - m_{\bar{p}}|/m_p$, above.

³HUGHES 92 uses recent measurements of Rydberg-energy and cyclotron-frequency ratios.

$$|q_p + q_e|/e$$

See BRESSI 11 for a summary of experiments on the neutrality of matter. See also "n CHARGE" in the neutron Listings.

VALUE	DOCUMENT ID	COMMENT
<1 × 10⁻²¹	¹ BRESSI 11	Neutrality of SF ₆
• • • We do not use the following data for averages, fits, limits, etc. • • •		
<3.2 × 10 ⁻²⁰	² SENGUPTA 00	binary pulsar
<0.8 × 10 ⁻²¹	MARINELLI 84	Magnetic levitation
<1.0 × 10 ⁻²¹	¹ DYLLA 73	Neutrality of SF ₆

¹BRESSI 11 uses the method of DYLLA 73 but finds serious errors in that experiment that greatly reduce its accuracy. The BRESSI 11 limit assumes that $n \rightarrow p e^- \nu_e$ conserves charge. Thus the limit applies equally to the charge of the neutron.

²SENGUPTA 00 uses the difference between the observed rate of rotational energy loss by the binary pulsar PSR B1913+16 and the rate predicted by general relativity to set this limit. See the paper for assumptions.

p MAGNETIC MOMENT

See the "Quark Model" review.

VALUE (μ_N)	DOCUMENT ID	TECN	COMMENT
2.79284734463 ± 0.0000000082	TIESINGA 21	RVUE	2018 CODATA value

Baryon Particle Listings

 p

• • • We do not use the following data for averages, fits, limits, etc. • • •

2.79284734462 ± 0.0000000082	SCHNEIDER	17	TRAP	Double Penning trap
2.7928473508 ± 0.0000000085	MOHR	16	RVUE	2014 CODATA value
2.792847356 ± 0.0000000023	MOHR	12	RVUE	2010 CODATA value
2.792847356 ± 0.0000000023	MOHR	08	RVUE	2006 CODATA value
2.792847351 ± 0.0000000028	MOHR	05	RVUE	2002 CODATA value
2.792847337 ± 0.0000000029	MOHR	99	RVUE	1998 CODATA value
2.792847386 ± 0.0000000063	COHEN	87	RVUE	1986 CODATA value

 \bar{p} MAGNETIC MOMENT

A few early results have been omitted.

VALUE (μ_N)	DOCUMENT ID	TECN	COMMENT
-2.7928473441 ± 0.0000000042	SMORRA	17	TRAP Hot/cold \bar{p} frequencies, Penning traps

• • • We do not use the following data for averages, fits, limits, etc. • • •

-2.7928465 ± 0.0000023	NAGAHAMA	17	TRAP	Single \bar{p} , Penning trap
-2.792845 ± 0.000012	DISCIACCA	13	TRAP	Single \bar{p} , Penning trap
-2.7862 ± 0.0083	PASK	09	CNTR	\bar{p} He ⁺ hyperfine structure
-2.8005 ± 0.0090	KREISSL	88	CNTR	\bar{p} ²⁰⁸ Pb 11 → 10 X-ray
-2.817 ± 0.048	ROBERTS	78	CNTR	
-2.791 ± 0.021	HU	75	CNTR	Exotic atoms

$$(\mu_p + \mu_{\bar{p}}) / \mu_p$$

A test of *CPT* invariance.

VALUE (units 10^{-6})	DOCUMENT ID	TECN	COMMENT
0.002 ± 0.004	SMORRA	17	TRAP Hot/cold \bar{p} frequencies, Penning traps

• • • We do not use the following data for averages, fits, limits, etc. • • •

0.3 ± 0.8	NAGAHAMA	17	TRAP	Single \bar{p} , Penning trap
0 ± 5	DISCIACCA	13	TRAP	Single \bar{p} , Penning trap

 p ELECTRIC DIPOLE MOMENT

A nonzero value is forbidden by both *T* invariance and *P* invariance.

VALUE (10^{-23} e cm)	DOCUMENT ID	TECN	COMMENT
< 0.021	1 SAHOO	17	Theory plus ¹⁹⁹ Hg atom EDM
• • • We do not use the following data for averages, fits, limits, etc. • • •			
< 0.54	1 DMITRIEV	03	Theory plus ¹⁹⁹ Hg atom EDM
- 3.7 ± 6.3	CHO	89	NMR TI F molecules
< 400	DZUBA	85	THEO Uses ¹²⁹ Xe moment
130 ± 200	2 WILKENING	84	
900 ± 1400	3 WILKENING	84	
700 ± 900	HARRISON	69	MBR Molecular beam

¹ SAHOO 17 and DMITRIEV 03 are not direct measurements of the proton electric dipole moment. They use theory to calculate this limit from the limit on the electric dipole moment of the ¹⁹⁹Hg atom.

² This WILKENING 84 value includes a finite-size effect and a magnetic effect.

³ This WILKENING 84 value is more cautious than the other and excludes the finite-size effect, which relies on uncertain nuclear integrals.

 p ELECTRIC POLARIZABILITY α_p

For a very complete review of the "polarizability of the nucleon and Compton scattering," see SCHUMACHER 05, updated in SCHUMACHER 19.

See LI 22d and therein for measurements of the mean square proton electric polarizability radius.

VALUE (10^{-4} fm ³)	DOCUMENT ID	TECN	COMMENT
11.2 ± 0.4 OUR AVERAGE			
10.65 ± 0.35 ± 0.36	MCGOVERN	13	RVUE χ EFT + Compton scattering
12.1 ± 1.1 ± 0.5	1 BEANE	03	EFT + γp
11.82 ± 0.98 ± 0.52 -0.98	2 BLANPIED	01	LEGS $p(\vec{\gamma}, \gamma), p(\vec{\gamma}, \pi^0), p(\vec{\gamma}, \pi^+)$
11.9 ± 0.5 ± 1.3	3 OLMOSDEL...	01	CNTR γp Compton scattering
12.1 ± 0.8 ± 0.5	4 MACGIBBON	95	RVUE global average
• • • We do not use the following data for averages, fits, limits, etc. • • •			
12.03 ± 0.48 -0.54	5 PASQUINI	19	fit of RCS data sets
11.7 ± 0.8 ± 0.7	6 BARANOV	01	RVUE Global average
12.5 ± 0.6 ± 0.9	MACGIBBON	95	CNTR γp Compton scattering
9.8 ± 0.4 ± 1.1	HALLIN	93	CNTR γp Compton scattering
10.62 ± 1.25 ± 1.07 -1.19 - 1.03	ZIEGER	92	CNTR γp Compton scattering
10.9 ± 2.2 ± 1.3	7 FEDERSPIEL	91	CNTR γp Compton scattering

¹ BEANE 03 uses effective field theory and low-energy γp and γd Compton-scattering data. It also gets for the isoscalar polarizabilities (see the erratum) $\alpha_N = (13.0 \pm 1.9 + 3.9) \times 10^{-4}$ fm³ and $\beta_N = (-1.8 \pm 1.9 + 2.1) \times 10^{-4}$ fm³.

² BLANPIED 01 gives $\alpha_p + \beta_p$ and $\alpha_p - \beta_p$. The separate α_p and β_p are provided to us by A. Sandorfi. The first error above is statistics plus systematics; the second is from the model.

³ This OLMOSDELEON 01 result uses the TAPS data alone, and does not use the (re-evaluated) sum-rule constraint that $\alpha + \beta = (13.8 \pm 0.4) \times 10^{-4}$ fm³. See the paper for a discussion.

⁴ MACGIBBON 95 combine the results of ZIEGER 92, FEDERSPIEL 91, and their own experiment to get a "global average" in which model errors and systematic errors are treated in a consistent way. See MACGIBBON 95 for a discussion.

⁵ PASQUINI 19 fit data sets for the unpolarized proton RCS cross section, using fixed-t subtracted dispersion relations and a bootstrap-based fitting technique.

⁶ BARANOV 01 combines the results of 10 experiments from 1958 through 1995 to get a global average that takes into account both systematic and model errors and does not use the theoretical constraint on the sum $\alpha_p + \beta_p$.

⁷ FEDERSPIEL 91 obtains for the (static) electric polarizability α_p , defined in terms of the induced electric dipole moment by $\mathbf{D} = 4\pi\epsilon_0\alpha_p\mathbf{E}$, the value $(7.0 \pm 2.2 \pm 1.3) \times 10^{-4}$ fm³.

 p MAGNETIC POLARIZABILITY β_p

The electric and magnetic polarizabilities are subject to a dispersion sum-rule constraint $\bar{\alpha} + \bar{\beta} = (14.2 \pm 0.5) \times 10^{-4}$ fm³. Errors here are anticorrelated with those on $\bar{\alpha}_p$ due to this constraint.

See LI 22d and therein for measurements of the mean square proton magnetic polarizability radius.

VALUE (10^{-4} fm ³)	DOCUMENT ID	TECN	COMMENT
2.5 ± 0.4 OUR AVERAGE			Error includes scale factor of 1.2.
3.15 ± 0.35 ± 0.36	MCGOVERN	13	RVUE χ EFT + Compton scattering
3.4 ± 1.1 ± 0.1	1 BEANE	03	EFT + γp
1.43 ± 0.98 ± 0.52 -0.98	2 BLANPIED	01	LEGS $p(\vec{\gamma}, \gamma), p(\vec{\gamma}, \pi^0), p(\vec{\gamma}, \pi^+)$
1.2 ± 0.7 ± 0.5	3 OLMOSDEL...	01	CNTR γp Compton scattering
2.1 ± 0.8 ± 0.5	4 MACGIBBON	95	RVUE global average
• • • We do not use the following data for averages, fits, limits, etc. • • •			
1.77 ± 0.52 -0.54	5 PASQUINI	19	fit of RCS data sets
2.3 ± 0.9 ± 0.7	6 BARANOV	01	RVUE Global average
1.7 ± 0.6 ± 0.9	MACGIBBON	95	CNTR γp Compton scattering
4.4 ± 0.4 ± 1.1	HALLIN	93	CNTR γp Compton scattering
3.58 ± 1.19 ± 1.03 -1.25 - 1.07	ZIEGER	92	CNTR γp Compton scattering
3.3 ± 2.2 ± 1.3	FEDERSPIEL	91	CNTR γp Compton scattering

¹ BEANE 03 uses effective field theory and low-energy γp and γd Compton-scattering data. It also gets for the isoscalar polarizabilities (see the erratum) $\alpha_N = (13.0 \pm 1.9 + 3.9) \times 10^{-4}$ fm³ and $\beta_N = (-1.8 \pm 1.9 + 2.1) \times 10^{-4}$ fm³.

² BLANPIED 01 gives $\alpha_p + \beta_p$ and $\alpha_p - \beta_p$. The separate α_p and β_p are provided to us by A. Sandorfi. The first error above is statistics plus systematics; the second is from the model.

³ This OLMOSDELEON 01 result uses the TAPS data alone, and does not use the (re-evaluated) sum-rule constraint that $\alpha + \beta = (13.8 \pm 0.4) \times 10^{-4}$ fm³. See the paper for a discussion.

⁴ MACGIBBON 95 combine the results of ZIEGER 92, FEDERSPIEL 91, and their own experiment to get a "global average" in which model errors and systematic errors are treated in a consistent way. See MACGIBBON 95 for a discussion.

⁵ PASQUINI 19 fit data sets for the unpolarized proton RCS cross section, using fixed-t subtracted dispersion relations and a bootstrap-based fitting technique.

⁶ BARANOV 01 combines the results of 10 experiments from 1958 through 1995 to get a global average that takes into account both systematic and model errors and does not use the theoretical constraint on the sum $\alpha_p + \beta_p$.

 p CHARGE RADIUS

This is the rms electric charge radius, $\sqrt{\langle r_E^2 \rangle}$.

There are three kinds of measurements of the proton radius: via transitions in atomic hydrogen; via electron scattering off hydrogen; and via muonic hydrogen Lamb shift. Most measurements of the radius of the proton involve electron-proton interactions, the most recent of which is the electron scattering measurement $r_p = 0.831(14)$ fm (XIONG 19), and the atomic-hydrogen value, $r_p = 0.833(10)$ fm (BEZGINOV 19). These agree well with another recent atomic-hydrogen value $r_p = 0.8335(95)$ fm (BEYER 17), and with the best measurement using muonic hydrogen $r_p = 0.84087(39)$ fm (ANTOGNINI 13), that is far more precise.

The MOHR 16 value (2014 CODATA), obtained from the electronic results available at the time, was 0.8751(61) fm. This differs by 5.6 standard deviations from the muonic hydrogen value, leading to the so-called proton charge radius puzzle. See our 2018 edition (Physical Review **D98** 030001 (2018)) for a further discussion of interpretations of this puzzle. However, reflecting the new electronic measurements, the 2018 CODATA, TIESINGA 21, recommended value is 0.8414(19) fm, and the puzzle appears to be resolved.

See our 2014 edition (Chinese Physics **C38** 070001 (2014)) for values published before 2003.

VALUE (fm)	DOCUMENT ID	TECN	COMMENT
0.8409 ± 0.0014 OUR AVERAGE			
0.833 ± 0.010	1 BEZGINOV	19	LASR 2S-2P transition in H
0.831 ± 0.007 ± 0.012	2 XIONG	19	SPEC $e p \rightarrow e p$ form factor
0.84087 ± 0.00026 ± 0.00029	ANTOGNINI	13	LASR μp -atom Lamb shift

• • • We do not use the following data for averages, fits, limits, etc. • • •

0.847 ± 0.008	³ CUI	21	FIT	use existing <i>ep</i> data
0.878 ± 0.011 ± 0.031	⁴ MIHOVLOVIC	21	ISR <i>ep</i> → <i>ep</i>	reanalysis
0.877 ± 0.013	⁵ FLEURBAEY	18	LASR	1S-3S transition in H
0.8335 ± 0.0095	⁶ BEYER	17	LASR	2S-4P transition in H
0.8751 ± 0.0061	MOHR	16	RVUE	2014 CODATA value
0.895 ± 0.014 ± 0.014	⁷ LEE	15	SPEC	Just 2010 Mainz data
0.916 ± 0.024	LEE	15	SPEC	World data, no Mainz
0.8775 ± 0.0051	MOHR	12	RVUE	2010 CODATA, <i>ep</i> data
0.875 ± 0.008 ± 0.006	ZHAN	11	SPEC	Recoil polarimetry
0.879 ± 0.005 ± 0.006	BERNAUER	10	SPEC	<i>ep</i> → <i>ep</i> form factor
0.912 ± 0.009 ± 0.007	BORISYUK	10		reanalyzes old <i>ep</i> data
0.871 ± 0.009 ± 0.003	HILL	10		z-expansion reanalysis
0.84184 ± 0.00036 ± 0.00056	POHL	10	LASR	See ANTOGNINI 13
0.8768 ± 0.0069	MOHR	08	RVUE	2006 CODATA value
0.844 ± 0.008 ± 0.004	BELUSHKIN	07		Dispersion analysis
0.897 ± 0.018	BLUNDEN	05		SICK 03 + 2γ correction
0.8750 ± 0.0068	MOHR	05	RVUE	2002 CODATA value
0.895 ± 0.010 ± 0.013	SICK	03		<i>ep</i> → <i>ep</i> reanalysis

- BEZGINOV 19 measures the $2S_{1/2}$ to $2P_{1/2}$ transition frequency in atomic hydrogen using the frequency-offset separated oscillatory field (FOSOF) technique. The result agrees well with the muonic hydrogen Lamb shift value.
- The XIONG 19 value from *ep* → *ep* scattering and supports the muonic hydrogen Lamb shift value.
- CUI 21 employ a new mathematical procedure (statistical SPM, Schlessinger point method) based on form-unbiased interpolations of existing *ep* scattering data.
- MIHOVLOVIC 21 reports a value of $0.878 \pm 0.011 \pm 0.031 \pm 0.002$ fm where the last uncertainty comes from the dependence on the model form factor function.
- FLEURBAEY 18 measures the 1S-3S transition frequency in hydrogen and in combination with the 1S-2S transition frequency deduces the proton radius and the Rydberg constant.
- The BEYER 17 result is 3.3 combined standard deviations below the MOHR 16 (2014 CODATA) value. The experiment measures the 2S-4P transition in hydrogen and gets the proton radius and the Rydberg constant.
- Authors also provide values for combinations of all available data.

p MAGNETIC RADIUS

This is the rms magnetic radius, $\sqrt{\langle r_M^2 \rangle}$.

VALUE (fm)	DOCUMENT ID	TECN	COMMENT
0.851 ± 0.026	¹ LEE	15	Combination of world and Mainz data

• • • We do not use the following data for averages, fits, limits, etc. • • •

0.817 ± 0.027	² CUI	21B	FIT use existing <i>ep</i> data
0.87 ± 0.02	EPSTEIN	14	Using <i>ep</i> , <i>en</i> , $\pi\pi$ data
0.867 ± 0.009 ± 0.018	ZHAN	11	SPEC Recoil polarimetry
0.777 ± 0.013 ± 0.010	BERNAUER	10	SPEC <i>ep</i> → <i>ep</i> form factor
0.876 ± 0.010 ± 0.016	BORISYUK	10	Reanalyzes old <i>ep</i> → <i>ep</i> data
0.854 ± 0.005	BELUSHKIN	07	Dispersion analysis

- In a consistent reanalysis LEE 2015 extract values separately for the Mainz 2010 data only (0.776±0.034±0.017) fm and for the world data without Mainz data (0.914±0.035) fm. The quoted value is a simple combination of the two, which ignores possible discrepancies and unknown correlations and should be considered with caution.
- CUI 21B employ a new mathematical procedure (statistical SPM, Schlessinger point method) based on form-unbiased interpolations of existing *ep* scattering data.

p MEAN LIFE

A test of baryon conservation. See the “p Partial Mean Lives” section below for limits for identified final states. The limits here are to “anything” or are for “disappearance” modes of a bound proton (*p*) or (*n*). See also the 3ν modes in the “Partial Mean Lives” section. Table 1 of BACK 03 is a nice summary.

LIMIT (years)	PARTICLE	CL%	DOCUMENT ID	TECN	COMMENT
>0.96 × 10³⁰	p	90	¹ ALLEGA	22	SNO+ <i>p</i> → invisible
>0.9 × 10³⁰	n	90	² ALLEGA	22	SNO+ <i>n</i> → invisible

• • • We do not use the following data for averages, fits, limits, etc. • • •

>3.6 × 10 ²⁹	<i>p</i>	90	³ ANDERSON	19A	SNO+ <i>p</i> → invisible
>2.5 × 10 ²⁹	<i>n</i>	90	³ ANDERSON	19A	SNO+ <i>n</i> → invisible
>5.8 × 10 ²⁹	<i>n</i>	90	⁴ ARAKI	06	KLND <i>n</i> → invisible
>2.1 × 10 ²⁹	<i>p</i>	90	³ AHMED	04	SNO <i>p</i> → invisible
>1.9 × 10 ²⁹	<i>n</i>	90	³ AHMED	04	SNO <i>n</i> → invisible
>1.8 × 10 ²⁵	<i>n</i>	90	⁵ BACK	03	BORX
>1.1 × 10 ²⁶	<i>p</i>	90	⁵ BACK	03	BORX
>3.5 × 10 ²⁸	<i>p</i>	90	⁶ ZDESENKO	03	<i>p</i> → invisible
>1 × 10 ²⁸	<i>p</i>	90	⁷ AHMAD	02	SNO <i>p</i> → invisible
>4 × 10 ²³	<i>p</i>	95	TRETYAK	01	<i>d</i> → <i>n</i> + ?
>1.9 × 10 ²⁴	<i>p</i>	90	⁸ BERNABEI	00B	DAMA
>1.6 × 10 ²⁵	<i>p, n</i>		^{9,10} EVANS	77	
>3 × 10 ²³	<i>p</i>		¹⁰ DIX	70	CNTR
>3 × 10 ²³	<i>p, n</i>		^{10,11} FLEROV	58	

- ALLEGA 22 look for γ rays from the de-excitation of a residual $^{15}\text{O}^*$ following the disappearance of *p* in ^{16}O .
- ALLEGA 22 look for γ rays from the de-excitation of a residual $^{15}\text{O}^*$ following the disappearance of *n* in ^{16}O .

- AHMED 04 and ANDERSON 19A look for γ rays from the de-excitation of a residual $^{15}\text{O}^*$ or $^{15}\text{N}^*$ following the disappearance of a neutron or proton in ^{16}O .
- ARAKI 06 looks for signs of de-excitation of the residual nucleus after disappearance of a neutron from the s shell of ^{12}C .
- BACK 03 looks for decays of unstable nuclides left after *N* decays of parent ^{12}C , ^{13}C , ^{16}O nuclei. These are “invisible channel” limits.
- ZDESENKO 03 gets this limit on proton disappearance in deuterium by analyzing SNO data in AHMAD 02.
- AHMAD 02 (see its footnote 7) looks for neutrons left behind after the disappearance of the proton in deuterons.
- BERNABEI 00B looks for the decay of a $^{128}_{53}\text{Xe}$ nucleus following the disappearance of a proton in the otherwise-stable ^{129}Xe nucleus.
- EVANS 77 looks for the daughter nuclide ^{129}Xe from possible ^{130}Te decays in ancient Te ore samples.
- This mean-life limit has been obtained from a half-life limit by dividing the latter by $\ln(2) = 0.693$.
- FLEROV 58 looks for the spontaneous fission of a ^{232}Th nucleus after the disappearance of one of its nucleons.

\bar{p} MEAN LIFE

Of the two astrophysical limits here, that of GEER 00D involves considerably more refinements in its modeling. The other limits come from direct observations of stored antiprotons. See also “ \bar{p} Partial Mean Lives” after “p Partial Mean Lives,” below, for exclusive-mode limits. The best (lifetime/branching fraction) limit there is 7×10^5 years, for $\bar{p} \rightarrow e^- \gamma$. We advance only the exclusive-mode limits to our Summary Tables.

LIMIT (years)	CL%	EVTS	DOCUMENT ID	TECN	COMMENT
>5.0	90		SELLNER	17	TRAP Penning trap
>8 × 10 ⁵	90		¹ GEER	00D	\bar{p}/p ratio, cosmic rays
>0.28			GABRIELSE	90	TRAP Penning trap
>0.08	90	1	BELL	79	CNTR Storage ring
>1 × 10 ⁷			GOLDEN	79	SPEC \bar{p}/p ratio, cosmic rays
>3.7 × 10 ⁻³			BREGMAN	78	CNTR Storage ring

- GEER 00D uses agreement between a model of galactic \bar{p} production and propagation and the observed \bar{p}/p cosmic-ray spectrum to set this limit.

p DECAY MODES

See the “Note on Nucleon Decay” in our 1994 edition (Phys. Rev. **D50**, 1173) for a short review.

The “partial mean life” limits tabulated here are the limits on τ/B_j , where τ is the total mean life and B_j is the branching fraction for the mode in question. For *N* decays, *p* and *n* indicate proton and neutron partial lifetimes.

Mode	Partial mean life (10 ³⁰ years)	Confidence level
Antilepton + meson		
τ_1 <i>N</i> → <i>e</i> ⁺ π	> 5300 (<i>n</i>), > 24000 (<i>p</i>)	90%
τ_2 <i>N</i> → μ^+ π	> 3500 (<i>n</i>), > 16000 (<i>p</i>)	90%
τ_3 <i>N</i> → $\nu\pi$	> 1100 (<i>n</i>), > 390 (<i>p</i>)	90%
τ_4 <i>p</i> → <i>e</i> ⁺ η	> 10000	90%
τ_5 <i>p</i> → $\mu^+\eta$	> 4700	90%
τ_6 <i>n</i> → $\nu\eta$	> 158	90%
τ_7 <i>N</i> → <i>e</i> ⁺ ρ	> 217 (<i>n</i>), > 720 (<i>p</i>)	90%
τ_8 <i>N</i> → $\mu^+\rho$	> 228 (<i>n</i>), > 570 (<i>p</i>)	90%
τ_9 <i>N</i> → $\nu\rho$	> 19 (<i>n</i>), > 162 (<i>p</i>)	90%
τ_{10} <i>p</i> → <i>e</i> ⁺ ω	> 1600	90%
τ_{11} <i>p</i> → $\mu^+\omega$	> 2800	90%
τ_{12} <i>n</i> → $\nu\omega$	> 108	90%
τ_{13} <i>N</i> → <i>e</i> ⁺ K	> 17 (<i>n</i>), > 1000 (<i>p</i>)	90%
τ_{14} <i>p</i> → <i>e</i> ⁺ K_S^0		
τ_{15} <i>p</i> → <i>e</i> ⁺ K_L^0		
τ_{16} <i>N</i> → μ^+K	> 26 (<i>n</i>), > 4500 (<i>p</i>)	90%
τ_{17} <i>p</i> → $\mu^+K_S^0$		
τ_{18} <i>p</i> → $\mu^+K_L^0$		
τ_{19} <i>N</i> → νK	> 86 (<i>n</i>), > 5900 (<i>p</i>)	90%
τ_{20} <i>n</i> → νK_S^0	> 260	90%
τ_{21} <i>p</i> → <i>e</i> ⁺ $K^*(892)^0$	> 84	90%
τ_{22} <i>N</i> → $\nu K^*(892)$	> 78 (<i>n</i>), > 51 (<i>p</i>)	90%
Antilepton + mesons		
τ_{23} <i>p</i> → <i>e</i> ⁺ $\pi^+\pi^-$	> 82	90%
τ_{24} <i>p</i> → <i>e</i> ⁺ $\pi^0\pi^0$	> 147	90%
τ_{25} <i>n</i> → <i>e</i> ⁺ $\pi^-\pi^0$	> 52	90%
τ_{26} <i>p</i> → $\mu^+\pi^+\pi^-$	> 133	90%
τ_{27} <i>p</i> → $\mu^+\pi^0\pi^0$	> 101	90%
τ_{28} <i>n</i> → $\mu^+\pi^-\pi^0$	> 74	90%
τ_{29} <i>n</i> → <i>e</i> ⁺ $K^0\pi^-$	> 18	90%

Baryon Particle Listings

ρ

Lepton + meson			
τ_{30}	$n \rightarrow e^- \pi^+$	> 65	90%
τ_{31}	$n \rightarrow \mu^- \pi^+$	> 49	90%
τ_{32}	$n \rightarrow e^- \rho^+$	> 62	90%
τ_{33}	$n \rightarrow \mu^- \rho^+$	> 7	90%
τ_{34}	$n \rightarrow e^- K^+$	> 32	90%
τ_{35}	$n \rightarrow \mu^- K^+$	> 57	90%

Lepton + mesons			
τ_{36}	$p \rightarrow e^- \pi^+ \pi^+$	> 30	90%
τ_{37}	$n \rightarrow e^- \pi^+ \pi^0$	> 29	90%
τ_{38}	$p \rightarrow \mu^- \pi^+ \pi^+$	> 17	90%
τ_{39}	$n \rightarrow \mu^- \pi^+ \pi^0$	> 34	90%
τ_{40}	$p \rightarrow e^- \pi^+ K^+$	> 75	90%
τ_{41}	$p \rightarrow \mu^- \pi^+ K^+$	> 245	90%

Antilepton + photon(s)			
τ_{42}	$p \rightarrow e^+ \gamma$	> 670	90%
τ_{43}	$p \rightarrow \mu^+ \gamma$	> 478	90%
τ_{44}	$n \rightarrow \nu \gamma$	> 550	90%
τ_{45}	$p \rightarrow e^+ \gamma \gamma$	> 100	90%
τ_{46}	$n \rightarrow \nu \gamma \gamma$	> 219	90%

Antilepton + single massless			
τ_{47}	$p \rightarrow e^+ X$	> 790	90%
τ_{48}	$p \rightarrow \mu^+ X$	> 410	90%

Three (or more) leptons			
τ_{49}	$p \rightarrow e^+ e^+ e^-$	> 34000	90%
τ_{50}	$p \rightarrow e^+ \mu^+ \mu^-$	> 9200	90%
τ_{51}	$p \rightarrow e^+ \nu \nu$	> 170	90%
τ_{52}	$n \rightarrow e^+ e^- \nu$	> 257	90%
τ_{53}	$n \rightarrow \mu^+ e^- \nu$	> 83	90%
τ_{54}	$n \rightarrow \mu^+ \mu^- \nu$	> 79	90%
τ_{55}	$p \rightarrow \mu^+ e^+ e^-$	> 23000	90%
τ_{56}	$p \rightarrow \mu^- e^+ e^+$	> 19000	90%
τ_{57}	$p \rightarrow \mu^+ \mu^+ \mu^-$	> 10000	90%
τ_{58}	$p \rightarrow \mu^+ \nu \nu$	> 220	90%
τ_{59}	$p \rightarrow e^- \mu^+ \mu^+$	> 11000	90%
τ_{60}	$n \rightarrow 3\nu$	> 5×10^{-4}	90%
τ_{61}	$n \rightarrow 5\nu$		

Inclusive modes			
τ_{62}	$N \rightarrow e^+$ anything	> 0.6 (n, p)	90%
τ_{63}	$N \rightarrow \mu^+$ anything	> 12 (n, p)	90%
τ_{64}	$N \rightarrow \nu$ anything		
τ_{65}	$N \rightarrow e^+ \pi^0$ anything	> 0.6 (n, p)	90%
τ_{66}	$N \rightarrow 2$ bodies, ν -free		

$\Delta B = 2$ dinucleon modes

The following are lifetime limits per iron nucleus.

τ_{67}	$p p \rightarrow \pi^+ \pi^+$	> 72.2	90%
τ_{68}	$p n \rightarrow \pi^+ \pi^0$	> 170	90%
τ_{69}	$n n \rightarrow \pi^+ \pi^-$	> 0.7	90%
τ_{70}	$n n \rightarrow \pi^0 \pi^0$	> 404	90%
τ_{71}	$p p \rightarrow K^+ K^+$	> 170	90%
τ_{72}	$p p \rightarrow e^+ e^+$	> 5.8	90%
τ_{73}	$p p \rightarrow e^+ \mu^+$	> 3.6	90%
τ_{74}	$p p \rightarrow \mu^+ \mu^+$	> 1.7	90%
τ_{75}	$p n \rightarrow e^+ \bar{\nu}$	> 260	90%
τ_{76}	$p n \rightarrow \mu^+ \bar{\nu}$	> 200	90%
τ_{77}	$p n \rightarrow \tau^+ \bar{\nu}_\tau$	> 29	90%
τ_{78}	$n n \rightarrow$ invisible	> 1.4	90%
τ_{79}	$n n \rightarrow \nu_e \bar{\nu}_e$	> 1.4	90%
τ_{80}	$n n \rightarrow \nu_\mu \bar{\nu}_\mu$	> 1.4	90%
τ_{81}	$p n \rightarrow$ invisible	> 0.06	90%
τ_{82}	$p p \rightarrow$ invisible	> 0.11	90%

\bar{p} DECAY MODES

Mode	Partial mean life (years)	Confidence level	
τ_{83}	$\bar{p} \rightarrow e^- \gamma$	> 7×10^5	90%
τ_{84}	$\bar{p} \rightarrow \mu^- \gamma$	> 5×10^4	90%
τ_{85}	$\bar{p} \rightarrow e^- \pi^0$	> 4×10^5	90%
τ_{86}	$\bar{p} \rightarrow \mu^- \pi^0$	> 5×10^4	90%
τ_{87}	$\bar{p} \rightarrow e^- \eta$	> 2×10^4	90%
τ_{88}	$\bar{p} \rightarrow \mu^- \eta$	> 8×10^3	90%

τ_{89}	$\bar{p} \rightarrow e^- K_S^0$	> 900	90%
τ_{90}	$\bar{p} \rightarrow \mu^- K_S^0$	> 4×10^3	90%
τ_{91}	$\bar{p} \rightarrow e^- K_L^0$	> 9×10^3	90%
τ_{92}	$\bar{p} \rightarrow \mu^- K_L^0$	> 7×10^3	90%
τ_{93}	$\bar{p} \rightarrow e^- \gamma \gamma$	> 2×10^4	90%
τ_{94}	$\bar{p} \rightarrow \mu^- \gamma \gamma$	> 2×10^4	90%
τ_{95}	$\bar{p} \rightarrow e^- \omega$	> 200	90%

ρ PARTIAL MEAN LIVES

The "partial mean life" limits tabulated here are the limits on τ/B_i , where τ is the total mean life for the proton and B_i is the branching fraction for the mode in question.

Decaying particle: p = proton, n = bound neutron. The same event may appear under more than one partial decay mode. Background estimates may be accurate to a factor of two.

Antilepton + meson

$\tau(N \rightarrow e^+ \pi)$				τ_1	
LIMIT (10 ²⁰ years)	PARTICLE	CL%	EVT/S BKGD EST	DOCUMENT ID	TECN
> 24000	p	90	0 0.59	¹ TAKENAKA	20 SKAM
> 5300	n	90	0 0.41	ABE	17D SKAM
••• We do not use the following data for averages, fits, limits, etc. •••					
> 16000	p	90	0 0.61	ABE	17 SKAM
> 2000	n	90	0 0.27	NISHINO	12 SKAM
> 8200	p	90	0 0.3	NISHINO	09 SKAM
> 540	p	90	0 0.2	MCGREW	99 IMB3
> 158	n	90	3 5	MCGREW	99 IMB3
> 1600	p	90	0 0.1	SHIOZAWA	98 SKAM
> 70	p	90	0 0.5	BERGER	91 FREJ
> 70	n	90	0 < 0.1	BERGER	91 FREJ
> 550	p	90	0 0.7	² BECKER-SZ...	90 IMB3
> 260	p	90	0 < 0.04	HIRATA	89c KAMI
> 130	n	90	0 < 0.2	HIRATA	89c KAMI
> 310	p	90	0 0.6	SEIDEL	88 IMB
> 100	n	90	0 1.6	SEIDEL	88 IMB
> 1.3	p	90	0	BARTELT	87 SOUD
> 1.3	n	90	0	BARTELT	87 SOUD
> 250	p	90	0 0.3	HAINES	86 IMB
> 31	n	90	8 9	HAINES	86 IMB
> 64	p	90	0 < 0.4	ARISAKA	85 KAMI
> 26	n	90	0 < 0.7	ARISAKA	85 KAMI
> 82	p (free)	90	0 0.2	BLEWITT	85 IMB
> 250	p	90	0 0.2	BLEWITT	85 IMB
> 25	n	90	4 4	PARK	85 IMB
> 15	p, n	90	0	BATTISTONI	84 NUSX
> 0.5	p	90	1 0.3	³ BARTELT	83 SOUD
> 0.5	n	90	1 0.3	³ BARTELT	83 SOUD
> 5.8	p	90	2	⁴ KRISHNA...	82 KOLR
> 5.8	n	90	2	⁴ KRISHNA...	82 KOLR
> 0.1	n	90	0	⁵ GURR	67 CNTR

¹ TAKENAKA 20 includes data of ABE 17, and thus supersedes ABE 17.

² This BECKER-SZENDY 90 result includes data from SEIDEL 88.

³ Limit based on zero events.

⁴ We have calculated 90% CL limit from 1 confined event.

⁵ We have converted half-life to 90% CL mean life.

$\tau(N \rightarrow \mu^+ \pi)$				τ_2	
LIMIT (10 ²⁰ years)	PARTICLE	CL%	EVT/S BKGD EST	DOCUMENT ID	TECN
> 16000	p	90	1 0.94	¹ TAKENAKA	20 SKAM
> 3500	n	90	1 0.77	ABE	17D SKAM
••• We do not use the following data for averages, fits, limits, etc. •••					
> 7700	p	90	2 0.87	ABE	17 SKAM
> 1000	n	90	1 0.43	NISHINO	12 SKAM
> 6600	p	90	0 0.3	NISHINO	09 SKAM
> 473	p	90	0 0.6	MCGREW	99 IMB3
> 90	n	90	1 1.9	MCGREW	99 IMB3
> 81	p	90	0 0.2	BERGER	91 FREJ
> 35	n	90	1 1.0	BERGER	91 FREJ
> 230	p	90	0 < 0.07	HIRATA	89c KAMI
> 100	n	90	0 < 0.2	HIRATA	89c KAMI
> 270	p	90	0 0.5	SEIDEL	88 IMB
> 63	n	90	0 0.5	SEIDEL	88 IMB
> 76	p	90	2 1	HAINES	86 IMB
> 23	n	90	8 7	HAINES	86 IMB
> 46	p	90	0 < 0.7	ARISAKA	85 KAMI
> 20	n	90	0 < 0.4	ARISAKA	85 KAMI
> 59	p (free)	90	0 0.2	BLEWITT	85 IMB
> 100	p	90	1 0.4	BLEWITT	85 IMB
> 38	n	90	1 4	PARK	85 IMB
> 10	p, n	90	0	BATTISTONI	84 NUSX
> 1.3	p, n	90	0	ALEKSEEV	81 BAKS

¹ TAKENAKA 20 includes the data of ABE 17 and thus supersedes ABE 17.

$\tau(N \rightarrow \nu\pi)$

73

LIMIT (10 ³⁰ years)	PARTICLE	CL%	EVTs	BKGD EST	DOCUMENT ID	TECN
> 390	p	90	52.8		ABE 14E	SKAM
>1100	n	90	19.1		ABE 14E	SKAM
••• We do not use the following data for averages, fits, limits, etc. •••						
> 16	p	90	6 6.7		WALL 00B	SOU2
> 39	n	90	4 3.8		WALL 00B	SOU2
> 10	p	90	15 20.3		MCGREW 99	IMB3
> 112	n	90	6 6.6		MCGREW 99	IMB3
> 13	n	90	1 1.2		BERGER 89	FREJ
> 10	p	90	11 14		BERGER 89	FREJ
> 25	p	90	32 32.8		¹ HIRATA 89c	KAMI
> 100	n	90	1 3		HIRATA 89c	KAMI
> 6	n	90	73 60		HAINES 86	IMB
> 2	p	90	16 13		KAJITA 86	KAMI
> 40	n	90	0 1		KAJITA 86	KAMI
> 7	n	90	28 19		PARK 85	IMB
> 7	n	90	0		BATTISTONI 84	NUSX
> 2	p	90	≤ 3		BATTISTONI 84	NUSX
> 5.8	p	90	1		² KRISHNA... 82	KOLR
> 0.3	p	90	2		³ CHERRY 81	HOME
> 0.1	p	90			⁴ GURR 67	CNTR

¹ In estimating the background, this HIRATA 89c limit (as opposed to the later limits of WALL 00B and MCGREW 99) does not take into account present understanding that the flux of ν_μ originating in the upper atmosphere is depleted. Doing so would reduce the background and thus also would reduce the limit here.
² We have calculated 90% CL limit from 1 confined event.
³ We have converted 2 possible events to 90% CL limit.
⁴ We have converted half-life to 90% CL mean life.

••• We do not use the following data for averages, fits, limits, etc. •••

> 30	n	90	4 0.87		ABE	17D SKAM
>710	p	90	0 0.35		NISHINO	12 SKAM
> 70	n	90	1 0.38		NISHINO	12 SKAM
> 29	p	90	0 2.2		BERGER	91 FREJ
> 41	n	90	0 1.4		BERGER	91 FREJ
> 75	p	90	2 2.7		HIRATA	89c KAMI
> 58	n	90	0 1.9		HIRATA	89c KAMI
> 38	n	90	2 4.1		SEIDEL	88 IMB
> 1.2	p	90	0		BARTELT	87 SOUD
> 1.5	n	90	0		BARTELT	87 SOUD
> 17	p	90	7 7		HAINES	86 IMB
> 14	n	90	9 4		HAINES	86 IMB
> 12	p	90	0 <1.2		ARISAKA	85 KAMI
> 6	n	90	2 <1		ARISAKA	85 KAMI
> 6.7	p (free)	90	6 6		BLEWITT	85 IMB
> 17	p	90	7 7		BLEWITT	85 IMB
> 12	n	90	4 2		PARK	85 IMB
> 0.6	n	90	1 0.3		¹ BARTELT	83 SOUD
> 0.5	p	90	1 0.3		¹ BARTELT	83 SOUD
> 9.8	p	90	1		² KRISHNA...	82 KOLR
> 0.8	p	90	2		³ CHERRY	81 HOME

¹ Limit based on zero events.
² We have calculated 90% CL limit from 0 confined events.
³ We have converted 2 possible events to 90% CL limit.

$\tau(N \rightarrow \mu^+\rho)$

78

LIMIT (10 ³⁰ years)	PARTICLE	CL%	EVTs	BKGD EST	DOCUMENT ID	TECN
>570	p	90	1 1.30		ABE	17D SKAM
>228	n	90	3 9.5		MCGREW 99	IMB3

••• We do not use the following data for averages, fits, limits, etc. •••

> 60	n	90	1 0.96		ABE	17D SKAM
>160	p	90	1 0.42		NISHINO	12 SKAM
> 36	n	90	0 0.29		NISHINO	12 SKAM
> 12	p	90	0 0.5		BERGER	91 FREJ
> 22	n	90	0 1.1		BERGER	91 FREJ
>110	p	90	0 1.7		HIRATA	89c KAMI
> 23	n	90	1 1.8		HIRATA	89c KAMI
> 4.3	p	90	0 0.7		PHILLIPS	89 HPW
> 30	p	90	0 0.5		SEIDEL	88 IMB
> 11	n	90	1 1.1		SEIDEL	88 IMB
> 16	p	90	4 4.5		HAINES	86 IMB
> 7	n	90	6 5		HAINES	86 IMB
> 12	p	90	0 <0.7		ARISAKA	85 KAMI
> 5	n	90	1 <1.2		ARISAKA	85 KAMI
> 5.5	p (free)	90	4 5		BLEWITT	85 IMB
> 16	p	90	4 5		BLEWITT	85 IMB
> 9	n	90	1 2		PARK	85 IMB

$\tau(N \rightarrow \nu\rho)$

79

LIMIT (10 ³⁰ years)	PARTICLE	CL%	EVTs	BKGD EST	DOCUMENT ID	TECN
>162	p	90	18 21.7		MCGREW 99	IMB3
> 19	n	90	0 0.5		SEIDEL	88 IMB

••• We do not use the following data for averages, fits, limits, etc. •••

> 9	n	90	4 2.4		BERGER	89 FREJ
> 24	p	90	0 0.9		BERGER	89 FREJ
> 27	p	90	5 1.5		HIRATA	89c KAMI
> 13	n	90	4 3.6		HIRATA	89c KAMI
> 13	p	90	1 1.1		SEIDEL	88 IMB
> 8	p	90	6 5		HAINES	86 IMB
> 2	n	90	15 10		HAINES	86 IMB
> 11	p	90	2 1		KAJITA	86 KAMI
> 4	n	90	2 2		KAJITA	86 KAMI
> 4.1	p (free)	90	6 7		BLEWITT	85 IMB
> 8.4	p	90	6 5		BLEWITT	85 IMB
> 2	n	90	7 3		PARK	85 IMB
> 0.9	p	90	2		¹ CHERRY	81 HOME
> 0.6	n	90	2		¹ CHERRY	81 HOME

¹ We have converted 2 possible events to 90% CL limit.

$\tau(p \rightarrow e^+\omega)$

710

LIMIT (10 ³⁰ years)	PARTICLE	CL%	EVTs	BKGD EST	DOCUMENT ID	TECN
>1600	p	90	1 1.35		ABE	17D SKAM

••• We do not use the following data for averages, fits, limits, etc. •••

> 320	p	90	1 0.53		NISHINO	12 SKAM
> 107	p	90	7 10.8		MCGREW 99	IMB3
> 17	p	90	0 1.1		BERGER	91 FREJ
> 45	p	90	2 1.45		HIRATA	89c KAMI
> 26	p	90	1 1.0		SEIDEL	88 IMB
> 1.5	p	90	0		BARTELT	87 SOUD
> 37	p	90	6 5.3		HAINES	86 IMB
> 25	p	90	1 <1.4		ARISAKA	85 KAMI
> 12	p (free)	90	6 7.5		BLEWITT	85 IMB

$\tau(p \rightarrow e^+\eta)$

74

LIMIT (10 ³⁰ years)	PARTICLE	CL%	EVTs	BKGD EST	DOCUMENT ID	TECN
>10000	p	90	0 0.78		ABE	17D SKAM
••• We do not use the following data for averages, fits, limits, etc. •••						
> 4200	p	90	0 0.44		NISHINO	12 SKAM
> 81	p	90	1 1.7		WALL 00B	SOU2
> 313	p	90	0 0.2		MCGREW 99	IMB3
> 44	p	90	0 0.1		BERGER 91	FREJ
> 140	p	90	0 <0.04		HIRATA 89c	KAMI
> 100	p	90	0 0.6		SEIDEL	88 IMB
> 200	p	90	5 3.3		HAINES	86 IMB
> 64	p	90	0 <0.8		ARISAKA	85 KAMI
> 64	p (free)	90	5 6.5		BLEWITT	85 IMB
> 200	p	90	5 4.7		BLEWITT	85 IMB
> 1.2	p	90	2		¹ CHERRY	81 HOME

¹ We have converted 2 possible events to 90% CL limit.

$\tau(p \rightarrow \mu^+\eta)$

75

LIMIT (10 ³⁰ years)	PARTICLE	CL%	EVTs	BKGD EST	DOCUMENT ID	TECN
>4700	p	90	2 0.85		ABE	17D SKAM
••• We do not use the following data for averages, fits, limits, etc. •••						
>1300	p	90	2 0.49		NISHINO	12 SKAM
> 89	p	90	0 1.6		WALL 00B	SOU2
> 126	p	90	3 2.8		MCGREW 99	IMB3
> 26	p	90	1 0.8		BERGER 91	FREJ
> 69	p	90	1 <0.08		HIRATA 89c	KAMI
> 1.3	p	90	0 0.7		PHILLIPS	89 HPW
> 34	p	90	1 1.5		SEIDEL	88 IMB
> 46	p	90	7 6		HAINES	86 IMB
> 26	p	90	1 <0.8		ARISAKA	85 KAMI
> 17	p (free)	90	6 6		BLEWITT	85 IMB
> 46	p	90	7 8		BLEWITT	85 IMB

$\tau(n \rightarrow \nu\eta)$

76

LIMIT (10 ³⁰ years)	PARTICLE	CL%	EVTs	BKGD EST	DOCUMENT ID	TECN
>158	n	90	0 1.2		MCGREW 99	IMB3
••• We do not use the following data for averages, fits, limits, etc. •••						
> 71	n	90	2 3.7		WALL 00B	SOU2
> 29	n	90	0 0.9		BERGER 89	FREJ
> 54	n	90	2 0.9		HIRATA 89c	KAMI
> 16	n	90	3 2.1		SEIDEL	88 IMB
> 25	n	90	7 6		HAINES	86 IMB
> 30	n	90	0 0.4		KAJITA	86 KAMI
> 18	n	90	4 3		PARK	85 IMB
> 0.6	n	90	2		¹ CHERRY	81 HOME

¹ We have converted 2 possible events to 90% CL limit.

$\tau(N \rightarrow e^+\rho)$

77

LIMIT (10 ³⁰ years)	PARTICLE	CL%	EVTs	BKGD EST	DOCUMENT ID	TECN
>720	p	90	2 0.64		ABE	17D SKAM
>217	n	90	4 4.8		MCGREW 99	IMB3

Baryon Particle Listings

p

> 37	p	90	6	5.7	BLEWITT	85	IMB
> 0.6	p	90	1	0.3	¹ BARTELT	83	SOUND
> 9.8	p	90	1		² KRISHNA...	82	KOLR
> 2.8	p	90	2		³ CHERRY	81	HOME

¹ Limit based on zero events.
² We have calculated 90% CL limit from 0 confined events.
³ We have converted 2 possible events to 90% CL limit.

$\tau(p \rightarrow \mu^+ \omega)$ 711

LIMIT (10 ³⁰ years)	PARTICLE	CL%	EVTs	BKGD EST	DOCUMENT ID	TECN
>2800	p	90	0	1.09	ABE	17d SKAM
•••	We do not use the following data for averages, fits, limits, etc. •••					
> 780	p	90	0	0.48	NISHINO	12 SKAM
> 117	p	90	11	12.1	MCGREW	99 IMB3
> 11	p	90	0	1.0	BERGER	91 FREJ
> 57	p	90	2	1.9	HIRATA	89c KAMI
> 4.4	p	90	0	0.7	PHILLIPS	89 HPW
> 10	p	90	2	1.3	SEIDEL	88 IMB
> 23	p	90	2	1	HAINES	86 IMB
> 6.5	p (free)	90	9	8.7	BLEWITT	85 IMB
> 23	p	90	8	7	BLEWITT	85 IMB

$\tau(n \rightarrow \nu \omega)$ 712

LIMIT (10 ³⁰ years)	PARTICLE	CL%	EVTs	BKGD EST	DOCUMENT ID	TECN
>108	n	90	12	22.5	MCGREW	99 IMB3
•••	We do not use the following data for averages, fits, limits, etc. •••					
> 17	n	90	1	0.7	BERGER	89 FREJ
> 43	n	90	3	2.7	HIRATA	89c KAMI
> 6	n	90	2	1.3	SEIDEL	88 IMB
> 12	n	90	6	6	HAINES	86 IMB
> 18	n	90	2	2	KAJITA	86 KAMI
> 16	n	90	1	2	PARK	85 IMB
> 2.0	n	90	2		¹ CHERRY	81 HOME

¹ We have converted 2 possible events to 90% CL limit.

$\tau(N \rightarrow e^+ K)$ 713

LIMIT (10 ³⁰ years)	PARTICLE	CL%	EVTs	BKGD EST	DOCUMENT ID	TECN
>1000	p	90	6	4.7	KOBAYASHI	05 SKAM
> 17	n	90	35	29.4	MCGREW	99 IMB3
•••	We do not use the following data for averages, fits, limits, etc. •••					
> 85	p	90	3	4.9	WALL	00 SOU2
> 31	p	90	23	25.2	MCGREW	99 IMB3
> 60	p	90	0		BERGER	91 FREJ
> 150	p	90	0	<0.27	HIRATA	89c KAMI
> 70	p	90	0	1.8	SEIDEL	88 IMB
> 77	p	90	5	4.5	HAINES	86 IMB
> 38	p	90	0	<0.8	ARISAKA	85 KAMI
> 24	p (free)	90	7	8.5	BLEWITT	85 IMB
> 77	p	90	5	4	BLEWITT	85 IMB
> 1.3	p	90	0		ALEKSEEV	81 BAKS
> 1.3	n	90	0		ALEKSEEV	81 BAKS

$\tau(p \rightarrow e^+ K_S^0)$ 714

LIMIT (10 ³⁰ years)	PARTICLE	CL%	EVTs	BKGD EST	DOCUMENT ID	TECN
>120	p	90	1	1.3	WALL	00 SOU2
> 76	p	90	0	0.5	BERGER	91 FREJ

$\tau(p \rightarrow e^+ K_L^0)$ 715

LIMIT (10 ³⁰ years)	PARTICLE	CL%	EVTs	BKGD EST	DOCUMENT ID	TECN
>51	p	90	2	3.5	WALL	00 SOU2
>44	p	90	0	≤ 0.1	BERGER	91 FREJ

$\tau(N \rightarrow \mu^+ K)$ 716

LIMIT (10 ³⁰ years)	PARTICLE	CL%	EVTs	BKGD EST	DOCUMENT ID	TECN
>4500	p	90	1	3.08	¹ MATSUMOTO 22	SKAM
> 26	n	90	20	28.4	MCGREW	99 IMB3
•••	We do not use the following data for averages, fits, limits, etc. •••					
>3600	p	90	14	16.3	² MATSUMOTO 22	SKAM
>1600	p	90	13	13.2	REGIS	12 SKAM
>1300	p	90	3	3.9	KOBAYASHI	05 SKAM
> 120	p	90	0	<1.2	WALL	00 SOU2
> 120	p	90	4	7.2	MCGREW	99 IMB3
> 54	p	90	0		BERGER	91 FREJ
> 120	p	90	1	0.4	HIRATA	89c KAMI
> 3.0	p	90	0	0.7	PHILLIPS	89 HPW
> 19	p	90	3	2.5	SEIDEL	88 IMB
> 1.5	p	90	0		³ BARTELT	87 SOUND
> 1.1	n	90	0		BARTELT	87 SOUND

> 40	p	90	7	6	HAINES	86 IMB
> 19	p	90	1	<1.1	ARISAKA	85 KAMI
> 6.7	p (free)	90	11	13	BLEWITT	85 IMB
> 40	p	90	7	8	BLEWITT	85 IMB
> 6	p	90	1		BATTISTONI	84 NUSX
> 0.6	p	90	0		⁴ BARTELT	83 SOUND
> 0.4	n	90	0		⁴ BARTELT	83 SOUND
> 5.8	p	90	2		⁵ KRISHNA...	82 KOLR
> 2.0	p	90	0		CHERRY	81 HOME
> 0.2	n	90			⁶ GURR	67 CNTR

¹ MATSUMOTO 22 limit > 4500 × 10³⁰ is derived from the latest dataset SKA IV phase (from 2008 to 2018) with 0.20 Mton-years of exposure.

² MATSUMOTO 22 limit > 3600 × 10³⁰ is derived from a combination of all datasets SKA I, II, III and IV phase (from 1996 to 2018) with a total of 0.37 Mton-years of exposure. Note, the limit from only SKA IV is stronger, because there were some events observed in SKA II.

³ BARTELT 87 limit applies to $p \rightarrow \mu^+ K_S^0$.

⁴ Limit based on zero events.
⁵ We have calculated 90% CL limit from 1 confined event.
⁶ We have converted half-life to 90% CL mean life.

$\tau(p \rightarrow \mu^+ K_S^0)$ 717

LIMIT (10 ³⁰ years)	PARTICLE	CL%	EVTs	BKGD EST	DOCUMENT ID	TECN
>150	p	90	0	<0.8	WALL	00 SOU2
> 64	p	90	0	1.2	BERGER	91 FREJ

$\tau(p \rightarrow \mu^+ K_L^0)$ 718

LIMIT (10 ³⁰ years)	PARTICLE	CL%	EVTs	BKGD EST	DOCUMENT ID	TECN
>83	p	90	0	0.4	WALL	00 SOU2
>44	p	90	0	≤ 0.1	BERGER	91 FREJ

$\tau(N \rightarrow \nu K)$ 719

LIMIT (10 ³⁰ years)	PARTICLE	CL%	EVTs	BKGD EST	DOCUMENT ID	TECN
>5900	p	90	0	1.0	ABE	14g SKAM
> 86	n	90	0	2.4	HIRATA	89c KAMI
•••	We do not use the following data for averages, fits, limits, etc. •••					
> 540	p	90	0	0.9	ASAKURA	15 KLND
>2300	p	90	0	1.3	KOBAYASHI	05 SKAM
> 26	n	90	16	9.1	WALL	00 SOU2
> 670	p	90			HAYATO	99 SKAM
> 151	p	90	15	21.4	MCGREW	99 IMB3
> 30	n	90	34	34.1	MCGREW	99 IMB3
> 43	p	90	1	1.54	¹ ALLISON	98 SOU2
> 15	n	90	1	1.8	BERGER	89 FREJ
> 15	p	90	1	1.8	BERGER	89 FREJ
> 100	p	90	9	7.3	HIRATA	89c KAMI
> 0.28	p	90	0	0.7	PHILLIPS	89 HPW
> 0.3	p	90	0		BARTELT	87 SOUND
> 0.75	n	90	0		² BARTELT	87 SOUND
> 10	p	90	6	5	HAINES	86 IMB
> 15	n	90	3	5	HAINES	86 IMB
> 28	p	90	3	3	KAJITA	86 KAMI
> 32	n	90	0	1.4	KAJITA	86 KAMI
> 1.8	p (free)	90	6	11	BLEWITT	85 IMB
> 9.6	p	90	6	5	BLEWITT	85 IMB
> 10	n	90	2	2	PARK	85 IMB
> 5	n	90	0		BATTISTONI	84 NUSX
> 2	p	90	0		BATTISTONI	84 NUSX
> 0.3	n	90	0		³ BARTELT	83 SOUND
> 0.1	p	90	0		³ BARTELT	83 SOUND
> 5.8	p	90	1		⁴ KRISHNA...	82 KOLR
> 0.3	n	90	2		⁵ CHERRY	81 HOME

¹ This ALLISON 98 limit is with no background subtraction; with subtraction the limit becomes > 46 × 10³⁰ years.

² BARTELT 87 limit applies to $n \rightarrow \nu K_S^0$.

³ Limit based on zero events.
⁴ We have calculated 90% CL limit from 1 confined event.
⁵ We have converted 2 possible events to 90% CL limit.

$\tau(n \rightarrow \nu K_S^0)$ 720

LIMIT (10 ³⁰ years)	PARTICLE	CL%	EVTs	BKGD EST	DOCUMENT ID	TECN
>260	n	90	34	30	¹ KOBAYASHI	05 SKAM
•••	We do not use the following data for averages, fits, limits, etc. •••					
> 51	n	90	16	9.1	WALL	00 SOU2

¹ We have doubled the $n \rightarrow \nu K^0$ limit given in KOBAYASHI 05 to obtain this $n \rightarrow \nu K_S^0$ limit.

$\tau(p \rightarrow e^+ K^*(892)^0)$ 721

LIMIT (10 ³⁰ years)	PARTICLE	CL%	EVTs	BKGD EST	DOCUMENT ID	TECN
>84	p	90	38	52.0	MCGREW	99 IMB3

• • • We do not use the following data for averages, fits, limits, etc. • • •

>	p	90	0	0.8	BERGER	91	FREJ
>52	p	90	2	1.55	HIRATA	89c	KAMI
>10	p	90	1	<1	ARISAKA	85	KAMI

$\tau(N \rightarrow \nu K^*(892))$ 722

LIMIT (10 ³⁰ years)	PARTICLE	CL%	EVTs	BKGD EST	DOCUMENT ID	TECN
>51	p	90	7	9.1	MCGREW	99 IMB3
>78	n	90	40	50	MCGREW	99 IMB3

• • • We do not use the following data for averages, fits, limits, etc. • • •

>22	n	90	0	2.1	BERGER	89	FREJ
>17	p	90	0	2.4	BERGER	89	FREJ
>20	p	90	5	2.1	HIRATA	89c	KAMI
>21	n	90	4	2.4	HIRATA	89c	KAMI
>10	p	90	7	6	HAINES	86	IMB
>5	n	90	8	7	HAINES	86	IMB
>8	p	90	3	2	KAJITA	86	KAMI
>6	n	90	2	1.6	KAJITA	86	KAMI
>5.8	p (free)	90	10	16	BLEWITT	85	IMB
>9.6	p	90	7	6	BLEWITT	85	IMB
>7	n	90	1	4	PARK	85	IMB
>2.1	p	90	1		1 BATTISTONI	82	NUSX

¹ We have converted 1 possible event to 90% CL limit.

Antilepton + mesons

$\tau(p \rightarrow e^+ \pi^+ \pi^-)$ 723

LIMIT (10 ³⁰ years)	PARTICLE	CL%	EVTs	BKGD EST	DOCUMENT ID	TECN
>82	p	90	16	23.1	MCGREW	99 IMB3

• • • We do not use the following data for averages, fits, limits, etc. • • •

>21	p	90	0	2.2	BERGER	91	FREJ
-----	---	----	---	-----	--------	----	------

$\tau(p \rightarrow e^+ \pi^0 \pi^0)$ 724

LIMIT (10 ³⁰ years)	PARTICLE	CL%	EVTs	BKGD EST	DOCUMENT ID	TECN
>147	p	90	2	0.8	MCGREW	99 IMB3

• • • We do not use the following data for averages, fits, limits, etc. • • •

>38	p	90	1	0.5	BERGER	91	FREJ
-----	---	----	---	-----	--------	----	------

$\tau(n \rightarrow e^+ \pi^- \pi^0)$ 725

LIMIT (10 ³⁰ years)	PARTICLE	CL%	EVTs	BKGD EST	DOCUMENT ID	TECN
>52	n	90	38	34.2	MCGREW	99 IMB3

• • • We do not use the following data for averages, fits, limits, etc. • • •

>32	n	90	1	0.8	BERGER	91	FREJ
-----	---	----	---	-----	--------	----	------

$\tau(p \rightarrow \mu^+ \pi^+ \pi^-)$ 726

LIMIT (10 ³⁰ years)	PARTICLE	CL%	EVTs	BKGD EST	DOCUMENT ID	TECN
>133	p	90	25	38.0	MCGREW	99 IMB3

• • • We do not use the following data for averages, fits, limits, etc. • • •

>17	p	90	1	2.6	BERGER	91	FREJ
>3.3	p	90	0	0.7	PHILLIPS	89	HPW

$\tau(p \rightarrow \mu^+ \pi^0 \pi^0)$ 727

LIMIT (10 ³⁰ years)	PARTICLE	CL%	EVTs	BKGD EST	DOCUMENT ID	TECN
>101	p	90	3	1.6	MCGREW	99 IMB3

• • • We do not use the following data for averages, fits, limits, etc. • • •

>33	p	90	1	0.9	BERGER	91	FREJ
-----	---	----	---	-----	--------	----	------

$\tau(n \rightarrow \mu^+ \pi^- \pi^0)$ 728

LIMIT (10 ³⁰ years)	PARTICLE	CL%	EVTs	BKGD EST	DOCUMENT ID	TECN
>74	n	90	17	20.8	MCGREW	99 IMB3

• • • We do not use the following data for averages, fits, limits, etc. • • •

>33	n	90	0	1.1	BERGER	91	FREJ
-----	---	----	---	-----	--------	----	------

$\tau(n \rightarrow e^+ K^0 \pi^-)$ 729

LIMIT (10 ³⁰ years)	PARTICLE	CL%	EVTs	BKGD EST	DOCUMENT ID	TECN	
>18	n	90	1	0.2	BERGER	91	FREJ

Lepton + meson

$\tau(n \rightarrow e^- \pi^+)$ 730

LIMIT (10 ³⁰ years)	PARTICLE	CL%	EVTs	BKGD EST	DOCUMENT ID	TECN	
>65	n	90	0	1.6	SEIDEL	88	IMB

• • • We do not use the following data for averages, fits, limits, etc. • • •

>55	n	90	0	1.09	BERGER	91B	FREJ
>16	n	90	9	7	HAINES	86	IMB
>25	n	90	2	4	PARK	85	IMB

$\tau(n \rightarrow \mu^- \pi^+)$ 731

LIMIT (10 ³⁰ years)	PARTICLE	CL%	EVTs	BKGD EST	DOCUMENT ID	TECN	
>49	n	90	0	0.5	SEIDEL	88	IMB

• • • We do not use the following data for averages, fits, limits, etc. • • •

>33	n	90	0	1.40	BERGER	91B	FREJ
>2.7	n	90	0	0.7	PHILLIPS	89	HPW
>25	n	90	7	6	HAINES	86	IMB
>27	n	90	2	3	PARK	85	IMB

$\tau(n \rightarrow e^- \rho^+)$ 732

LIMIT (10 ³⁰ years)	PARTICLE	CL%	EVTs	BKGD EST	DOCUMENT ID	TECN	
>62	n	90	2	4.1	SEIDEL	88	IMB

• • • We do not use the following data for averages, fits, limits, etc. • • •

>12	n	90	13	6	HAINES	86	IMB
>12	n	90	5	3	PARK	85	IMB

$\tau(n \rightarrow \mu^- \rho^+)$ 733

LIMIT (10 ³⁰ years)	PARTICLE	CL%	EVTs	BKGD EST	DOCUMENT ID	TECN	
>7	n	90	1	1.1	SEIDEL	88	IMB

• • • We do not use the following data for averages, fits, limits, etc. • • •

>2.6	n	90	0	0.7	PHILLIPS	89	HPW
>9	n	90	7	5	HAINES	86	IMB
>9	n	90	2	2	PARK	85	IMB

$\tau(n \rightarrow e^- K^+)$ 734

LIMIT (10 ³⁰ years)	PARTICLE	CL%	EVTs	BKGD EST	DOCUMENT ID	TECN	
>32	n	90	3	2.96	BERGER	91B	FREJ

• • • We do not use the following data for averages, fits, limits, etc. • • •

>0.23	n	90	0	0.7	PHILLIPS	89	HPW
-------	---	----	---	-----	----------	----	-----

$\tau(n \rightarrow \mu^- K^+)$ 735

LIMIT (10 ³⁰ years)	PARTICLE	CL%	EVTs	BKGD EST	DOCUMENT ID	TECN	
>57	n	90	0	2.18	BERGER	91B	FREJ

• • • We do not use the following data for averages, fits, limits, etc. • • •

>4.7	n	90	0	0.7	PHILLIPS	89	HPW
------	---	----	---	-----	----------	----	-----

Lepton + mesons

$\tau(p \rightarrow e^- \pi^+ \pi^+)$ 736

LIMIT (10 ³⁰ years)	PARTICLE	CL%	EVTs	BKGD EST	DOCUMENT ID	TECN	
>30	p	90	1	2.50	BERGER	91B	FREJ

• • • We do not use the following data for averages, fits, limits, etc. • • •

>2.0	p	90	0	0.7	PHILLIPS	89	HPW
------	---	----	---	-----	----------	----	-----

$\tau(n \rightarrow e^- \pi^+ \pi^0)$ 737

LIMIT (10 ³⁰ years)	PARTICLE	CL%	EVTs	BKGD EST	DOCUMENT ID	TECN	
>29	n	90	1	0.78	BERGER	91B	FREJ

$\tau(p \rightarrow \mu^- \pi^+ \pi^+)$ 738

LIMIT (10 ³⁰ years)	PARTICLE	CL%	EVTs	BKGD EST	DOCUMENT ID	TECN	
>17	p	90	1	1.72	BERGER	91B	FREJ

• • • We do not use the following data for averages, fits, limits, etc. • • •

>7.8	p	90	0	0.7	PHILLIPS	89	HPW
------	---	----	---	-----	----------	----	-----

$\tau(n \rightarrow \mu^- \pi^+ \pi^0)$ 739

LIMIT (10 ³⁰ years)	PARTICLE	CL%	EVTs	BKGD EST	DOCUMENT ID	TECN	
>34	n	90	0	0.78	BERGER	91B	FREJ

$\tau(p \rightarrow e^- \pi^+ K^+)$ 740

LIMIT (10 ³⁰ years)	PARTICLE	CL%	EVTs	BKGD EST	DOCUMENT ID	TECN
>75	p	90	81	127.2	MCGREW	99 IMB3

• • • We do not use the following data for averages, fits, limits, etc. • • •

>20	p	90	3	2.50	BERGER	91B	FREJ
-----	---	----	---	------	--------	-----	------

$\tau(p \rightarrow \mu^- \pi^+ K^+)$ 741

LIMIT (10 ³⁰ years)	PARTICLE	CL%	EVTs	BKGD EST	DOCUMENT ID	TECN
>245	p	90	3	4.0	MCGREW	99 IMB3

• • • We do not use the following data for averages, fits, limits, etc. • • •

>5	p	90	2	0.78	BERGER	91B	FREJ
----	---	----	---	------	--------	-----	------

Antilepton + photon(s)

$\tau(p \rightarrow e^+ \gamma)$ 742

LIMIT (10 ³⁰ years)	PARTICLE	CL%	EVTs	BKGD EST	DOCUMENT ID	TECN
>670	p	90	0	0.1	MCGREW	99 IMB3

Baryon Particle Listings

 p

••• We do not use the following data for averages, fits, limits, etc. •••

>133	p	90	0	0.3	BERGER	91	FREJ
>460	p	90	0	0.6	SEIDEL	88	IMB
>360	p	90	0	0.3	HAINES	86	IMB
> 87	p (free)	90	0	0.2	BLEWITT	85	IMB
>360	p	90	0	0.2	BLEWITT	85	IMB
> 0.1	p	90			¹ GURR	67	CNTR

¹ We have converted half-life to 90% CL mean life.

$\tau(p \rightarrow \mu^+ \gamma)$ 743

LIMIT (10^{30} years)	PARTICLE	CL%	EVTs	BKGD EST	DOCUMENT ID	TECN
>478	p	90	0	0.1	MCGREW	99 IMB3

••• We do not use the following data for averages, fits, limits, etc. •••

>155	p	90	0	0.1	BERGER	91	FREJ
>380	p	90	0	0.5	SEIDEL	88	IMB
> 97	p	90	3	2	HAINES	86	IMB
> 61	p (free)	90	0	0.2	BLEWITT	85	IMB
>280	p	90	0	0.6	BLEWITT	85	IMB
> 0.3	p	90			¹ GURR	67	CNTR

¹ We have converted half-life to 90% CL mean life.

$\tau(n \rightarrow \nu \gamma)$ 744

LIMIT (10^{30} years)	PARTICLE	CL%	EVTs	BKGD EST	DOCUMENT ID	TECN
>550	n	90			TAKHISTOV	15 SKAM

••• We do not use the following data for averages, fits, limits, etc. •••

> 28	n	90	163	144.7	MCGREW	99	IMB3
> 24	n	90	10	6.86	BERGER	91B	FREJ
> 9	n	90	73	60	HAINES	86	IMB
> 11	n	90	28	19	PARK	85	IMB

$\tau(p \rightarrow e^+ \gamma \gamma)$ 745

LIMIT (10^{30} years)	PARTICLE	CL%	EVTs	BKGD EST	DOCUMENT ID	TECN	
>100	p	90	1	0.8	BERGER	91	FREJ

$\tau(n \rightarrow \nu \gamma \gamma)$ 746

LIMIT (10^{30} years)	PARTICLE	CL%	EVTs	BKGD EST	DOCUMENT ID	TECN	
>219	n	90	5	7.5	MCGREW	99	IMB3

Antilepton + single massless

$\tau(p \rightarrow e^+ X)$ 747

VALUE (10^{30} years)	CL%	DOCUMENT ID	TECN
>790	90	TAKHISTOV 15	SKAM

$\tau(p \rightarrow \mu^+ X)$ 748

VALUE (10^{30} years)	CL%	DOCUMENT ID	TECN
>410	90	TAKHISTOV 15	SKAM

Three (or more) leptons

$\tau(p \rightarrow e^+ e^+ e^-)$ 749

LIMIT (10^{30} years)	PARTICLE	CL%	EVTs	BKGD EST	DOCUMENT ID	TECN	
>34000	p	90	0	0.58	TANAKA	20	SKAM

••• We do not use the following data for averages, fits, limits, etc. •••

> 793	p	90	0	0.5	MCGREW	99	IMB3
> 147	p	90	0	0.1	BERGER	91	FREJ
> 510	p	90	0	0.3	HAINES	86	IMB
> 89	p (free)	90	0	0.5	BLEWITT	85	IMB
> 510	p	90	0	0.7	BLEWITT	85	IMB

$\tau(p \rightarrow e^+ \mu^+ \mu^-)$ 750

LIMIT (10^{30} years)	PARTICLE	CL%	EVTs	BKGD EST	DOCUMENT ID	TECN	
>9200	p	90	1	0.27	TANAKA	20	SKAM

••• We do not use the following data for averages, fits, limits, etc. •••

> 359	p	90	1	0.9	MCGREW	99	IMB3
> 81	p	90	0	0.16	BERGER	91	FREJ
> 5.0	p	90	0	0.7	PHILLIPS	89	HPW

$\tau(p \rightarrow e^+ \nu \nu)$ 751

LIMIT (10^{30} years)	PARTICLE	CL%	EVTs	BKGD EST	DOCUMENT ID	TECN	
>170	p	90			¹ TAKHISTOV	14	SKAM

••• We do not use the following data for averages, fits, limits, etc. •••

> 17	p	90	152	153.7	MCGREW	99	IMB3
> 11	p	90	11	6.08	BERGER	91B	FREJ

¹ Allowed events at 90% CL are 459.

$\tau(n \rightarrow e^+ e^- \nu)$ 752

LIMIT (10^{30} years)	PARTICLE	CL%	EVTs	BKGD EST	DOCUMENT ID	TECN	
>257	n	90	5	7.5	MCGREW	99	IMB3

••• We do not use the following data for averages, fits, limits, etc. •••

> 74	n	90	0	< 0.1	BERGER	91B	FREJ
> 45	n	90	5	5	HAINES	86	IMB
> 26	n	90	4	3	PARK	85	IMB

$\tau(n \rightarrow \mu^+ e^- \nu)$ 753

LIMIT (10^{30} years)	PARTICLE	CL%	EVTs	BKGD EST	DOCUMENT ID	TECN	
>83	n	90	25	29.4	MCGREW	99	IMB3

••• We do not use the following data for averages, fits, limits, etc. •••

>47	n	90	0	< 0.1	BERGER	91B	FREJ
-----	-----	----	---	-------	--------	-----	------

$\tau(n \rightarrow \mu^+ \mu^- \nu)$ 754

LIMIT (10^{30} years)	PARTICLE	CL%	EVTs	BKGD EST	DOCUMENT ID	TECN	
>79	n	90	100	145	MCGREW	99	IMB3

••• We do not use the following data for averages, fits, limits, etc. •••

>42	n	90	0	1.4	BERGER	91B	FREJ
> 5.1	n	90	0	0.7	PHILLIPS	89	HPW
>16	n	90	14	7	HAINES	86	IMB
>19	n	90	4	7	PARK	85	IMB

$\tau(p \rightarrow \mu^+ e^+ e^-)$ 755

LIMIT (10^{30} years)	PARTICLE	CL%	EVTs	BKGD EST	DOCUMENT ID	TECN	
>23000	p	90	0	0.5	TANAKA	20	SKAM

••• We do not use the following data for averages, fits, limits, etc. •••

> 529	p	90	0	1.0	MCGREW	99	IMB3
> 91	p	90	0	≤ 0.1	BERGER	91	FREJ

$\tau(p \rightarrow \mu^- e^+ e^+)$ 756

LIMIT (10^{30} years)	PARTICLE	CL%	EVTs	BKGD EST	DOCUMENT ID	TECN	
>19000	p	90	0	0.5	TANAKA	20	SKAM

$\tau(p \rightarrow \mu^+ \mu^+ \mu^-)$ 757

LIMIT (10^{30} years)	PARTICLE	CL%	EVTs	BKGD EST	DOCUMENT ID	TECN	
>10000	p	90	1	0.4	TANAKA	20	SKAM

••• We do not use the following data for averages, fits, limits, etc. •••

> 675	p	90	0	0.3	MCGREW	99	IMB3
> 119	p	90	0	0.2	BERGER	91	FREJ
> 10.5	p	90	0	0.7	PHILLIPS	89	HPW
> 190	p	90	1	0.1	HAINES	86	IMB
> 44	p (free)	90	1	0.7	BLEWITT	85	IMB
> 190	p	90	1	0.9	BLEWITT	85	IMB
> 2.1	p	90	1		¹ BATTISTONI	82	NUSX

¹ We have converted 1 possible event to 90% CL limit.

$\tau(p \rightarrow \mu^+ \nu \nu)$ 758

LIMIT (10^{30} years)	PARTICLE	CL%	EVTs	BKGD EST	DOCUMENT ID	TECN	
>220	p	90			¹ TAKHISTOV	14	SKAM

••• We do not use the following data for averages, fits, limits, etc. •••

> 21	p	90	7	11.23	BERGER	91B	FREJ
------	-----	----	---	-------	--------	-----	------

¹ Allowed events at 90% CL are 286.

$\tau(p \rightarrow e^- \mu^+ \mu^+)$ 759

LIMIT (10^{30} years)	PARTICLE	CL%	EVTs	BKGD EST	DOCUMENT ID	TECN	
>11000	p	90	1	0.27	TANAKA	20	SKAM

••• We do not use the following data for averages, fits, limits, etc. •••

> 6.0	p	90	0	0.7	PHILLIPS	89	HPW
-------	-----	----	---	-----	----------	----	-----

$\tau(n \rightarrow 3\nu)$ 760

See also the "to anything" and "disappearance" limits for bound nucleons in the "p Mean Life" data block just in front of the list of possible p decay modes. Such modes could of course be to three (or five) neutrinos, and the limits are stronger, but we do not repeat them here.

LIMIT (10^{30} years)	PARTICLE	CL%	EVTs	BKGD EST	DOCUMENT ID	TECN	
>0.00049	n	90	2	2	¹ SUZUKI	93B	KAMI

••• We do not use the following data for averages, fits, limits, etc. •••

>0.0023	n	90			2	GLICENSTEIN	97	KAMI
>0.00003	n	90	11	6.1	3	BERGER	91B	FREJ
>0.00012	n	90	7	11.2	3	BERGER	91B	FREJ
>0.0005	n	90	0			LEARNED	79	RVUE

¹ The SUZUKI 93B limit applies to any of $\nu_e \nu_e \bar{\nu}_e$, $\nu_\mu \nu_\mu \bar{\nu}_\mu$, or $\nu_\tau \nu_\tau \bar{\nu}_\tau$.

² GLICENSTEIN 97 uses Kamioka data and the idea that the disappearance of the neutron's magnetic moment should produce radiation.

³ The first BERGER 91B limit is for $n \rightarrow \nu_e \nu_e \bar{\nu}_e$, the second is for $n \rightarrow \nu_\mu \nu_\mu \bar{\nu}_\mu$.

$\tau(n \rightarrow 5\nu)$ 761

See the note on $\tau(n \rightarrow 3\nu)$ on the previous data block.

LIMIT (10^{30} years)	PARTICLE	CL%	EVTs	BKGD EST	DOCUMENT ID	TECN	
>0.0017	n	90			¹ GLICENSTEIN	97	KAMI

••• We do not use the following data for averages, fits, limits, etc. •••

¹ GLICENSTEIN 97 uses Kamioka data and the idea that the disappearance of the neutron's magnetic moment should produce radiation.

Inclusive modes

$\tau(N \rightarrow e^+$ anything) 762

LIMIT (10 ³⁰ years)	PARTICLE	CL%	EVTs	BKGD EST	DOCUMENT ID	TECN	COMMENT
>0.6	p, n	90			1 LEARNED 79	RVUE	

¹ The electron may be primary or secondary.

$\tau(N \rightarrow \mu^+$ anything) 763

LIMIT (10 ³⁰ years)	PARTICLE	CL%	EVTs	BKGD EST	DOCUMENT ID	TECN	COMMENT
>12	p, n	90	2		1,2 CHERRY 81	HOME	
> 1.8	p, n	90			2 COWSIK 80	CNTR	
> 6	p, n	90			2 LEARNED 79	RVUE	

¹ We have converted 2 possible events to 90% CL limit.

² The muon may be primary or secondary.

$\tau(N \rightarrow \nu$ anything) 764

Anything = π, ρ, K, \dots

LIMIT (10 ³⁰ years)	PARTICLE	CL%	EVTs	BKGD EST	DOCUMENT ID	TECN	COMMENT
>0.0002	p, n	90	0		LEARNED 79	RVUE	

$\tau(N \rightarrow e^+ \pi^0$ anything) 765

LIMIT (10 ³⁰ years)	PARTICLE	CL%	EVTs	BKGD EST	DOCUMENT ID	TECN	COMMENT
>0.6	p, n	90	0		LEARNED 79	RVUE	

$\tau(N \rightarrow 2$ bodies, ν -free) 766

LIMIT (10 ³⁰ years)	PARTICLE	CL%	EVTs	BKGD EST	DOCUMENT ID	TECN	COMMENT
>1.3	p, n	90	0		ALEKSEEV 81	BAKS	

$\Delta B = 2$ dinucleon modes

$\tau(pp \rightarrow \pi^+ \pi^+)$ 767

LIMIT (10 ³⁰ years)	CL%	EVTs	BKGD EST	DOCUMENT ID	TECN	COMMENT
>72.2	90	2	4.45	GUSTAFSON 15	SKAM	per oxygen nucleus
> 0.7	90	4	2.34	BERGER 91B	FREJ	per iron nucleus

$\tau(pn \rightarrow \pi^+ \pi^0)$ 768

LIMIT (10 ³⁰ years)	CL%	EVTs	BKGD EST	DOCUMENT ID	TECN	COMMENT
>170	90			GUSTAFSON 15	SKAM	per oxygen nucleus
> 2.0	90	0	0.31	BERGER 91B	FREJ	per iron nucleus

$\tau(nn \rightarrow \pi^+ \pi^-)$ 769

LIMIT (10 ³⁰ years)	CL%	EVTs	BKGD EST	DOCUMENT ID	TECN	COMMENT
>0.7	90	4	2.18	BERGER 91B	FREJ	τ per iron nucleus

$\tau(nn \rightarrow \pi^0 \pi^0)$ 770

LIMIT (10 ³⁰ years)	CL%	EVTs	BKGD EST	DOCUMENT ID	TECN	COMMENT
>404	90			GUSTAFSON 15	SKAM	per oxygen nucleus
> 3.4	90	0	0.78	BERGER 91B	FREJ	per iron nucleus

$\tau(pp \rightarrow K^+ K^+)$ 771

LIMIT (10 ³⁰ years)	CL%	EVTs	BKGD EST	DOCUMENT ID	TECN	COMMENT
>170	90	0	0.28	LITOS 14	SKAM	τ per oxygen nucleus

$\tau(pp \rightarrow e^+ e^+)$ 772

LIMIT (10 ³⁰ years)	CL%	EVTs	BKGD EST	DOCUMENT ID	TECN	COMMENT
>5.8	90	0	<0.1	BERGER 91B	FREJ	τ per iron nucleus

$\tau(pp \rightarrow e^+ \mu^+)$ 773

LIMIT (10 ³⁰ years)	CL%	EVTs	BKGD EST	DOCUMENT ID	TECN	COMMENT
>3.6	90	0	<0.1	BERGER 91B	FREJ	τ per iron nucleus

$\tau(pp \rightarrow \mu^+ \mu^+)$ 774

LIMIT (10 ³⁰ years)	CL%	EVTs	BKGD EST	DOCUMENT ID	TECN	COMMENT
>1.7	90	0	0.62	BERGER 91B	FREJ	τ per iron nucleus

$\tau(pn \rightarrow e^+ \bar{\nu})$ 775

LIMIT (10 ³⁰ years)	CL%	EVTs	BKGD EST	DOCUMENT ID	TECN	COMMENT
>260	90			TAKHISTOV 15	SKAM	
> 2.8	90	5	9.67	BERGER 91B	FREJ	τ per iron nucleus

$\tau(pn \rightarrow \mu^+ \bar{\nu})$ 776

LIMIT (10 ³⁰ years)	CL%	EVTs	BKGD EST	DOCUMENT ID	TECN	COMMENT
>200	90			TAKHISTOV 15	SKAM	
> 1.6	90	4	4.37	BERGER 91B	FREJ	τ per iron nucleus

$\tau(pn \rightarrow \tau^+ \bar{\nu}_\tau)$ 777

LIMIT (10 ³⁰ years)	CL%	EVTs	BKGD EST	DOCUMENT ID	TECN	COMMENT
>29	90			TAKHISTOV 15	SKAM	
> 1	90			1 BRYMAN 14	CHER	

¹ BRYMAN 14 uses a MCGREW 99 limit on the $p \rightarrow e^+ \nu \nu$ lifetime to extract this value.

$\tau(nn \rightarrow \text{invisible})$ 778

LIMIT (10 ³⁰ years)	CL%	EVTs	BKGD EST	DOCUMENT ID	TECN	COMMENT
>1.4	90			1 ARAKI 06	KLND	$nn \rightarrow$ invisible
>0.015	90			2,3 ALLEGA 22	SNO+	$nn \rightarrow$ invisible
>0.013	90			2 ANDERSON 19A	SNO+	$nn \rightarrow$ invisible
>0.000042	90			4 TRETAK 04	CNTR	$nn \rightarrow$ invisible
>0.000049	90			5 BACK 03	BORX	$nn \rightarrow$ invisible
>0.000012	90			6 BERNABEI 00B	DAMA	$nn \rightarrow$ invisible

¹ ARAKI 06 looks for signs of de-excitation of the residual nucleus after disappearance of two neutrons from the s shell of ¹²C.

² ALLEGA 22 and ANDERSON 19A look for γ rays from the de-excitation of a residual ¹⁴O* following the disappearance of nn in ¹⁶O.

³ ALLEGA 22 replaces the previous SNO+ value of ANDERSON 19A.

⁴ TRETAK 04 uses data from an old Homestake-mine radiochemical experiment on limits for invisible decays of ³⁹K to ³⁷Ar.

⁵ BACK 03 looks for decays of unstable nuclides left after NN decays of parent ¹²C, ¹³C, ¹⁶O nuclei. These are "invisible channel" limits.

⁶ BERNABEI 00B looks for the decay of a ¹²⁷Xe nucleus following the disappearance of an nn pair in the otherwise-stable ¹²⁹Xe nucleus. The limit here applies as well to $nn \rightarrow \nu_\mu \bar{\nu}_\mu, nn \rightarrow \nu_\tau \bar{\nu}_\tau$, or any "disappearance" mode.

$\tau(nn \rightarrow \nu_e \bar{\nu}_e)$ 779

LIMIT (10 ³⁰ years)	CL%	EVTs	BKGD EST	DOCUMENT ID	TECN	COMMENT
>0.000012	90	5	9.7	BERGER 91B	FREJ	τ per iron nucleus

$\tau(nn \rightarrow \nu_\mu \bar{\nu}_\mu)$ 780

See the preceding data block. "Invisible modes" would include any multi-neutrino mode.

$\tau(nn \rightarrow \nu_\mu \bar{\nu}_\mu)$ 780

LIMIT (10 ³⁰ years)	CL%	EVTs	BKGD EST	DOCUMENT ID	TECN	COMMENT
> 1.4 (CL=90%)	OUR LIMIT					
>0.000006	90	4	4.4	BERGER 91B	FREJ	τ per iron nucleus

$\tau(pn \rightarrow \text{invisible})$ 781

This violates charge conservation as well as baryon number conservation.

VALUE (10 ³⁰ years)	CL%	DOCUMENT ID	TECN
>0.06	90	1,2 ALLEGA 22	SNO+
>0.026	90	1 ANDERSON 19A	SNO+
>0.000021	90	3 TRETAK 04	CNTR

¹ ALLEGA 22 and ANDERSON 19A look for γ rays from the de-excitation of a residual ¹⁴N* following the disappearance of pn in ¹⁶O.

² ALLEGA 22 replaces the previous SNO+ value of ANDERSON 19A.

³ TRETAK 04 uses data from an old Homestake-mine radiochemical experiment on limits for invisible decays of ³⁹K to ³⁷Ar.

$\tau(pp \rightarrow \text{invisible})$ 782

This violates charge conservation as well as baryon number conservation.

VALUE (10 ³⁰ years)	CL%	DOCUMENT ID	TECN
>0.11	90	1 ALLEGA 22	SNO+
>0.047	90	1 ANDERSON 19A	SNO+
>0.00005	90	2 BACK 03	BORX
>0.00000055	90	3 BERNABEI 00B	DAMA

¹ ALLEGA 22 look for γ rays from the de-excitation of a residual ¹⁴C* following the disappearance of pp in ¹⁶O. Supersedes ANDERSON 19A result.

² BACK 03 looks for decays of unstable nuclides left after NN decays of parent ¹²C, ¹³C, ¹⁶O nuclei. These are "invisible channel" limits.

³ BERNABEI 00B looks for the decay of a ¹²⁷Xe nucleus following the disappearance of a pp pair in the otherwise-stable ¹²⁹Xe nucleus.

Baryon Particle Listings

\bar{p}

$\Delta B = 1$

\bar{p} PARTIAL MEAN LIVES

The "partial mean life" limits tabulated here are the limits on $\bar{\tau}/B_j$, where $\bar{\tau}$ is the total mean life for the antiproton and B_j is the branching fraction for the mode in question.

$\tau(\bar{p} \rightarrow e^- \gamma)$ 783

VALUE (years)	CL%	DOCUMENT ID	TECN	COMMENT
$> 7 \times 10^5$	90	GEER 00	APEX	8.9 GeV/c \bar{p} beam
••• We do not use the following data for averages, fits, limits, etc. •••				
> 1848	95	GEER 94	CALO	8.9 GeV/c \bar{p} beam

$\tau(\bar{p} \rightarrow \mu^- \gamma)$ 784

VALUE (years)	CL%	DOCUMENT ID	TECN	COMMENT
$> 5 \times 10^4$	90	GEER 00	APEX	8.9 GeV/c \bar{p} beam
••• We do not use the following data for averages, fits, limits, etc. •••				
$> 5.0 \times 10^4$	90	HU 98B	APEX	8.9 GeV/c \bar{p} beam

$\tau(\bar{p} \rightarrow e^- \pi^0)$ 785

VALUE (years)	CL%	DOCUMENT ID	TECN	COMMENT
$> 4 \times 10^5$	90	GEER 00	APEX	8.9 GeV/c \bar{p} beam
••• We do not use the following data for averages, fits, limits, etc. •••				
> 554	95	GEER 94	CALO	8.9 GeV/c \bar{p} beam

$\tau(\bar{p} \rightarrow \mu^- \pi^0)$ 786

VALUE (years)	CL%	DOCUMENT ID	TECN	COMMENT
$> 5 \times 10^4$	90	GEER 00	APEX	8.9 GeV/c \bar{p} beam
••• We do not use the following data for averages, fits, limits, etc. •••				
$> 4.8 \times 10^4$	90	HU 98B	APEX	8.9 GeV/c \bar{p} beam

$\tau(\bar{p} \rightarrow e^- \eta)$ 787

VALUE (years)	CL%	DOCUMENT ID	TECN	COMMENT
$> 2 \times 10^4$	90	GEER 00	APEX	8.9 GeV/c \bar{p} beam
••• We do not use the following data for averages, fits, limits, etc. •••				
> 171	95	GEER 94	CALO	8.9 GeV/c \bar{p} beam

$\tau(\bar{p} \rightarrow \mu^- \eta)$ 788

VALUE (years)	CL%	DOCUMENT ID	TECN	COMMENT
$> 8 \times 10^3$	90	GEER 00	APEX	8.9 GeV/c \bar{p} beam
••• We do not use the following data for averages, fits, limits, etc. •••				
$> 7.9 \times 10^3$	90	HU 98B	APEX	8.9 GeV/c \bar{p} beam

$\tau(\bar{p} \rightarrow e^- K_S^0)$ 789

VALUE (years)	CL%	DOCUMENT ID	TECN	COMMENT
> 900	90	GEER 00	APEX	8.9 GeV/c \bar{p} beam
••• We do not use the following data for averages, fits, limits, etc. •••				
> 29	95	GEER 94	CALO	8.9 GeV/c \bar{p} beam

$\tau(\bar{p} \rightarrow \mu^- K_S^0)$ 790

VALUE (years)	CL%	DOCUMENT ID	TECN	COMMENT
$> 4 \times 10^3$	90	GEER 00	APEX	8.9 GeV/c \bar{p} beam
••• We do not use the following data for averages, fits, limits, etc. •••				
$> 4.3 \times 10^3$	90	HU 98B	APEX	8.9 GeV/c \bar{p} beam

$\tau(\bar{p} \rightarrow e^- K_L^0)$ 791

VALUE (years)	CL%	DOCUMENT ID	TECN	COMMENT
$> 9 \times 10^3$	90	GEER 00	APEX	8.9 GeV/c \bar{p} beam
••• We do not use the following data for averages, fits, limits, etc. •••				
> 9	95	GEER 94	CALO	8.9 GeV/c \bar{p} beam

$\tau(\bar{p} \rightarrow \mu^- K_L^0)$ 792

VALUE (years)	CL%	DOCUMENT ID	TECN	COMMENT
$> 7 \times 10^3$	90	GEER 00	APEX	8.9 GeV/c \bar{p} beam
••• We do not use the following data for averages, fits, limits, etc. •••				
$> 6.5 \times 10^3$	90	HU 98B	APEX	8.9 GeV/c \bar{p} beam

$\tau(\bar{p} \rightarrow e^- \gamma \gamma)$ 793

VALUE (years)	CL%	DOCUMENT ID	TECN	COMMENT
$> 2 \times 10^4$	90	GEER 00	APEX	8.9 GeV/c \bar{p} beam

$\tau(\bar{p} \rightarrow \mu^- \gamma \gamma)$ 794

VALUE (years)	CL%	DOCUMENT ID	TECN	COMMENT
$> 2 \times 10^4$	90	GEER 00	APEX	8.9 GeV/c \bar{p} beam
••• We do not use the following data for averages, fits, limits, etc. •••				
$> 2.3 \times 10^4$	90	HU 98B	APEX	8.9 GeV/c \bar{p} beam

$\tau(\bar{p} \rightarrow e^- \omega)$ 795

VALUE (years)	CL%	DOCUMENT ID	TECN	COMMENT
> 200	90	GEER 00	APEX	8.9 GeV/c \bar{p} beam

\bar{p} REFERENCES

ALLEGA 22 PR D105 112012 (SNO+ Collab.)
 BORCHERT 22 NAT 601 53 (BASE Collab.)
 LI 22D NAT 611 265
 MATSUMOTO 22 PR D106 072003
 CUI 21 PRL 127 092001 (Super-Kamiokande Collab.)
 CUI 21B CPL 38 121401 (NJU, ECT, HZDR)
 FINK 21 PRL 127 243001
 MIHOVILOVIC 21 EPJ A57 107 (FSU)
 TIESINGA 21 RMP 93 025010 (LJUB, MAINZ, MIT+)
 TAKENAKA 20 PR D102 112011 (NIST)
 TANAKA 20 PR D101 052011 A. Takenaka et al. (Super-Kamiokande Collab.)
 ANDERSON 19A PR D99 032008 M. Anderson et al. (Super-Kamiokande Collab.)
 BEZGINOV 19 SCI 365 1007 (SNO+ Collab.)
 HEISSE 19 PR A100 022518 N. Bezginov et al. (YORKC, TNT0)
 PASQUINI 19 JP G46 104001 F. Heisse et al. (MPIK, GSI, MAINZ)
 SCHUMACHER 19 LHEP 4 4 B. Pasquini, P. Pedroni, S. Sconfietti (PAVI)
 XIONG 19 NAT 575 147 W. Xiong et al. (GOET)
 FLEURBAEY 18 PRL 120 183001 H. Fleurbaey et al. (PRad Collab.)
 PDG 18 PR D98 030001 M. Tanabashi et al. (PDG Collab.)
 ABE 17 PR D95 012004 K. Abe et al. (Super-Kamiokande Collab.)
 BEYER 17D PR D96 012003 A. Beyer et al. (Super-Kamiokande Collab.)
 HEISSE 17 PRL 119 033001 F. Heisse et al. (MPIK, GSI, MAINZ, RIKEN)
 NAGAHAMA 17 NAT C 8 14084 H. Nagahama et al. (RIKEN, TOKY, CERN+)
 SAHOO 17 PR D95 013002 B.K. Sahoo (AHMEB)
 SCHNEIDER 17 SCI 358 1081 G. Schneider et al. (MAINZ, RIKEN, +)
 SELLNER 17 NJP 19 083023 S. Sellner et al. (RIKEN, MPIK, +)
 SMORRA 17 NAT 550 371 C. Smorra et al. (RIKEN, CERN, +)
 MOHR 16 RMP 88 035009 P.J. Mohr, D.B. Newell, B.N. Taylor (NIST)
 ASAKURA 15 PR D92 052006 K. Asakura et al. (KamLAND Collab.)
 GUSTAFSON 15 PR D91 072009 J. Gustafson et al. (Super-Kamiokande Collab.)
 LEE 15 PR D92 013013 G. Lee, J.R. Arrington, R.J. Hill (ANL, EFT+)
 TAKHISTOV 15 PRL 115 121803 V. Takhistov et al. (Super-Kamiokande Collab.)
 ULMER 15 NAT 524 196 S. Ulmer et al. (RIKEN, CERN, MPIK, +)
 ABE 14E PRL 113 121802 K. Abe et al. (Super-Kamiokande Collab.)
 ABE 14G PR D90 072005 K. Abe et al. (Super-Kamiokande Collab.)
 BRYMAN 14 PL B733 190 D. Bryman (BRCO)
 EPSTEIN 14 PR D90 074027 Z. Epstein, G. Paz, J. Roy (UMD, WAYN)
 LITOS 14 PRL 112 131803 M. Litos et al. (Super-Kamiokande Collab.)
 PDG 14 CP C38 070001 K. Olive et al. (PDG Collab.)
 TAKHISTOV 14 PRL 113 101801 V. Takhistov et al. (Super-Kamiokande Collab.)
 ANTOGNINI 13 SCI 339 417 A. Antognini et al. (MPIM, ETH, UPM+)
 DISCIACCA 13 PRL 110 130801 J. Disciacca et al. (ATRAP Collab.)
 MCGOVERN 13 EPJ D49 12 P.J. McGovern, D.R. Phillips, H.W. Griggsammer (NIST)
 MOHR 12 RMP 84 1527 P.J. Mohr, B.N. Taylor, D.B. Newell (NIST)
 NISHINO 12 PR D85 112001 H. Nishino et al. (Super-Kamiokande Collab.)
 REGIS 12 PR D86 012006 C. Regis et al. (Super-Kamiokande Collab.)
 BRESSI 11 PR A83 052101 G. Bressi et al. (LEGN, PAVII, PADO, TRST+)
 HORI 11 NAT 475 484 M. Hori et al. (MPIG, TOKY, BUDA, +)
 ZHAN 11 PL B705 59 X. Zhan et al. (JLAB-Hall A Collab.)
 BERNAUER 10 PRL 105 242001 J.C. Bernauer et al. (MAMI A1 Collab.)
 Also PR C90 015206 J.C. Bernauer et al. (MAMI A1 Collab.)
 BORISYUK 10 NP A843 59 D. Borisjuk (KIEV)
 HILL 10 PR D82 113005 R.J. Hill, G. Paz (CHIC)
 POHL 10 NAT 466 213 R. Pohl et al. (MPIK, ENSP, COLM, +)
 NISHINO 09 PRL 102 141801 H. Nishino et al. (Super-Kamiokande Collab.)
 PASK 09 PL B678 55 T. Pask et al. (Stefan Meyer Inst., Vienna, TOKY+)
 MOHR 08 RMP 80 633 P.J. Mohr, B.N. Taylor, D.B. Newell (NIST)
 BELUSHKIN 07 PR C75 035202 M.A. Belushkin, H.W. Hammer, U.-G. Meißner (BONN+)
 ARAKI 06 PRL 96 101802 T. Araki et al. (KamLAND Collab.)
 HORI 06 PRL 96 243401 M. Hori et al. (CERN, TOKYO+)
 BLUNDEN 05 PR C72 057601 P.G. Blunden, I. Sick (MANI, BASL)
 KOBAYASHI 05 PR D72 052007 K. Kobayashi et al. (Super-Kamiokande Collab.)
 MOHR 05 RMP 77 1 P.J. Mohr, B.N. Taylor (NIST)
 SCHUMACHER 05 PNP 55 567 M. Schumacher (GOET)
 AHMED 04 PRL 92 102004 S.N. Ahmed et al. (SNO Collab.)
 TRETAYAK 04 JETPL 79 106 V.I. Tretyak, V.Yu. Denisov, Yu.G. Zdesenko (KIEV)
 Also translated from ZETFP 79 136.
 BACK 03 PL B563 23 H.O. Back et al. (Borexino Collab.)
 BEANE 03 PL B567 200 S.R. Beane et al.
 Also PL B607 320 (errat.) S.R. Beane et al.
 DMITRIEV 03 PRL 91 212303 V.F. Dmitriev, R.A. Senkov (NOVO)
 HORI 03 PRL 91 123401 M. Hori et al. (CERN ASACUSA Collab.)
 SICK 03 PL B576 62 I. Sick (BASL)
 ZDESENKO 03 PL B553 135 Yu.G. Zdesenko, V.I. Tretyak (KIEV)
 AHMAD 02 PR D89 011301 Q.R. Ahmad et al. (SNO Collab.)
 BARANOV 01 PPN 32 376 P.S. Baranov et al.
 Also translated from FECAY 32 699.
 BLANPIED 01 PR C64 025203 G. Blanpied et al. (BNL LEGS Collab.)
 HORI 01 PRL 87 093401 M. Hori et al. (CERN ASACUSA Collab.)
 OLMOSDEL... 01 EPJ A10 207 V. Olmos de Leon et al. (MAMI TAPS Collab.)
 TRETAYAK 01 PL B505 59 V.I. Tretyak, Yu.G. Zdesenko (KIEV)
 BERNABEI 00B PL B493 12 R. Bernabei et al. (Gran Sasso DAMA Collab.)
 GEER 00 PRL 84 590 S. Geer et al. (FNAL APEX Collab.)
 Also PR D92 052004 S. Geer et al. (FNAL APEX Collab.)
 Also PRL 85 3546 (errat.) S. Geer et al.
 GEER 00D APJ 532 648 S.H. Geer, D.C. Kennedy (FNAL APEX Collab.)
 SENGUPTA 00 PL B484 275 S. Sengupta
 WALL 00 PR D61 072004 D. Wall et al. (Soudan-2 Collab.)
 WALL 00B PR D62 092003 D. Wall et al. (Soudan-2 Collab.)
 GABRIELSE 09 PRL 82 3198 G. Gabrielse et al.
 HAYATO 99 PRL 83 1529 Y. Hayato et al. (Super-Kamiokande Collab.)
 MCGREW 99 PR D59 052004 C. McGrew et al. (IMB-3 Collab.)
 MOHR 99 JPICRD 28 1713 P.J. Mohr, B.N. Taylor (NIST)
 Also RMP 72 351 P.J. Mohr, B.N. Taylor (NIST)
 TORII 99 PR A59 223 H.A. Torii et al. (CERN PS-205 Collab.)
 ALLISON 98 PL B427 217 W.W.M. Allison et al. (Soudan-2 Collab.)
 HU 98B PR D58 111101 M. Hu et al. (FNAL APEX Collab.)
 SHIOZAWA 98 PRL 81 3319 M. Shiozawa et al. (Super-Kamiokande Collab.)
 GLICENSTEIN 97 PL B411 326 J.F. Glacienstein (SACL)
 GABRIELSE 95 PRL 74 3544 G. Gabrielse et al. (HARV, MAINZ, SEOUL)
 MACGIBBON 95 PR C52 2097 B.E. MacGibbon et al. (ILL, SASK, INRM)
 GEER 94 PRL 72 1596 S. Geer et al. (FNAL, UCLA, PSU)
 HALLIN 93 PR C48 1497 E.L. Hallin et al. (SASK, BOST, ILL)
 SUZUKI 93B PL B311 357 Y. Suzuki et al. (Kamiokande Collab.)
 HUGHES 92 PRL 69 578 R.J. Hughes, B.I. Deutch (LANL, AARH)
 ZIEGER 92 PL B297 34 A. Zieger et al. (MPCM)
 Also PL B281 417 (errat.) A. Zieger et al. (MPCM)
 BERGER 91 ZPHY C50 385 C. Berger et al. (FREJUS Collab.)
 BERGER 91B PL B269 227 C. Berger et al. (FREJUS Collab.)
 FEDERSPIEL 91 PRL 67 1511 F.J. Federspiel et al. (ILL)
 BECKER-SZ... 90 PR D42 2974 R.A. Becker-Szendy et al. (IMB-3 Collab.)
 ERICSON 90 PRL 61 295 T.E.O. Ericson, A. Richter (CERN, DARM)
 GABRIELSE 90 PRL 65 1317 G. Gabrielse et al. (HARV, MAINZ, WASH+)
 BERGER 89 NP B313 509 C. Berger et al. (FREJUS Collab.)
 CHO 89 PRL 63 2559 D. Cho, K. Sangster, E.A. Hinds (YALE)
 HIRATA 89C PL B220 308 K.S. Hirata et al. (Kamiokande Collab.)
 PHILLIPS 89 PL B224 348 T.J. Phillips et al. (MPCM)
 KREISSL 88 ZPHY C37 557 A. Kneissl et al. (CERN PS176 Collab.)
 SEIDEL 88 PRL 61 2522 S. Seidel et al. (IMB Collab.)

See key on page 1171

Baryon Particle Listings

p, n

BARTELT	87	PR D36 1990	J.E. Bartelt et al.	(Soudan Collab.)
Also		PR D40 1701 (errat.)	J.E. Bartelt et al.	(Soudan Collab.)
COHEN	87	RMP 59 1121	E.R. Cohen, B.N. Taylor	(RIS C, NBS)
HAINES	86	PRL 57 1986	T.J. Haines et al.	(IMB Collab.)
KAJITA	86	JPS J 55 711	T. Kajita et al.	(Kamiokande Collab.)
ARISAKA	85	JPS J 54 3213	K. Arisaka et al.	(Kamiokande Collab.)
BLEWITT	85	PRL 55 2114	G.B. Blewitt et al.	(IMB Collab.)
DZUBA	85	PL 154B 93	V.A. Dzuba, V.V. Flambaum, P.G. Silvestrov	(NOVO)
PARK	85	PRL 54 22	H.S. Park et al.	(IMB Collab.)
BATTISTONI	84	PL 133B 454	G. Battistoni et al.	(NUSEX Collab.)
MARINELLI	84	PL 137B 439	M. Marinelli, G. Morpurgo	(GENO)
WILKENING	84	PR A29 425	D.A. Wilkening, N.F. Ramsey, D.J. Larson	(HARV+)
BARTELT	83	PRL 50 651	J.E. Bartelt et al.	(MINN, ANL)
BATTISTONI	82	PL 118B 461	G. Battistoni et al.	(NUSEX Collab.)
KRISHNA...	82	PL 115B 349	M.R. Krishnaswamy et al.	(TATA, OSKC+)
ALEKSEEV	81	JETPL 33 651	E.N. Alekseev et al.	(PNPI)
CHERRY	81	PRL 47 1507	M.L. Cherry et al.	(PENN, BNL)
COWSIK	80	PR D22 2204	R. Cowsik, V.S. Narasimham	(TATA)
BELL	79	PL 86B 215	M. Bell et al.	(CERN)
GOLDEN	79	PRL 43 1196	R.L. Golden et al.	(NASA, PSSL)
LEARNED	79	PL 43 907	J.G. Learned, F. Reines, A. Soni	(UCI)
BREGMAN	78	PL 78B 174	M. Bregman et al.	(CERN)
ROBERTS	78	PR D17 358	B.L. Roberts	(WILL, RHEL)
EVANS	77	SCI 197 989	J.C. Evans Jr., R.I. Steinberg	(BNL, PENN)
HU	75	NP A254 403	E. Hu et al.	(COLU, YALE)
COHEN	73	JPCRD 2 664	E.R. Cohen, B.N. Taylor	(RIS C, NBS)
DYLLA	73	PR A7 1224	H.F. Dylla, J.G. King	(MIT)
DIX	70	Thesis Case	F.W. Dix	(CASE)
HARRISON	69	PRL 22 1263	G.E. Harrison, P.G.H. Sanders, S.J. Wright	(OXF)
GURR	67	PR 158 1321	H.S. Gurr et al.	(CASE, WITW)
FLEROV	58	DOKL 3 79	G.N. Flerov et al.	(ASCI)

$$(m_n - m_{\bar{n}}) / m_n$$

A test of CPT invariance. Calculated from the n and \bar{n} masses, above.

VALUE DOCUMENT ID
(9±5) × 10⁻⁵ OUR EVALUATION

VALUE (MeV)	DOCUMENT ID	TECN	COMMENT
1.2933236 ± 0.0000046	1 TIESINGA	21	RVUE 2018 CODATA value
• • • We do not use the following data for averages, fits, limits, etc. • • •			
1.2933205 ± 0.00000051	2 MOHR	16	RVUE 2014 CODATA value
1.2933217 ± 0.00000042	3 MOHR	12	RVUE 2010 CODATA value
1.2933214 ± 0.00000043	4 MOHR	08	RVUE 2006 CODATA value
1.2933317 ± 0.00000005	5 MOHR	05	RVUE 2002 CODATA value
1.2933318 ± 0.00000005	6 MOHR	99	RVUE 1998 CODATA value
1.293318 ± 0.0000009	7 COHEN	87	RVUE 1986 CODATA value
1.2933328 ± 0.0000072	GREENE	86	SPEC $n\bar{p} \rightarrow d\gamma$
1.293429 ± 0.0000036	COHEN	73	RVUE 1973 CODATA value

- The 2018 CODATA mass difference in u is $m_n - m_p = 1.38844933(49) \times 10^{-3} u$.
- The 2014 CODATA mass difference in u is $m_n - m_p = 1.38844900(51) \times 10^{-3} u$.
- The 2010 CODATA mass difference in u is $m_n - m_p = 1.38844919(45) \times 10^{-3} u$.
- Calculated by us from the MOHR 08 ratio $m_n/m_p = 1.00137841918(46)$. In u , $m_n - m_p = 1.38844920(46) \times 10^{-3} u$.
- Calculated by us from the MOHR 05 ratio $m_n/m_p = 1.00137841870 \pm 0.0000000058$. In u , $m_n - m_p = (1.3884487 \pm 0.00000006) \times 10^{-3} u$.
- Calculated by us from the MOHR 99 ratio $m_n/m_p = 1.00137841887 \pm 0.0000000058$. In u , $m_n - m_p = (1.3884489 \pm 0.00000006) \times 10^{-3} u$.
- Calculated by us from the COHEN 87 ratio $m_n/m_p = 1.001378404 \pm 0.00000009$. In u , $m_n - m_p = 0.001388434 \pm 0.000000009 u$.

n

$$I(J^P) = \frac{1}{2}(\frac{1}{2}^+) \text{ Status: } ***$$

We have omitted some results that have been superseded by later experiments. See our earlier editions.

Anyone interested in the neutron should look at these two review articles: D. Dubbers and M.G. Schmidt, "The neutron and its role in cosmology and particle physics," *Reviews of Modern Physics* **83** 1111 (2011); and F.E. Wietfeldt and G.L. Greene, "The neutron lifetime," *Reviews of Modern Physics* **83** 1173 (2011).

n MASS (atomic mass units u)

The mass is known much more precisely in u (atomic mass units) than in MeV. See the next data block.

VALUE (u)	DOCUMENT ID	TECN	COMMENT
1.00866491595 ± 0.0000000049	TIESINGA	21	RVUE 2018 CODATA value
• • • We do not use the following data for averages, fits, limits, etc. • • •			
1.00866491588 ± 0.0000000049	MOHR	16	RVUE 2014 CODATA value
1.00866491600 ± 0.0000000043	MOHR	12	RVUE 2010 CODATA value
1.00866491597 ± 0.0000000043	MOHR	08	RVUE 2006 CODATA value
1.00866491560 ± 0.0000000055	MOHR	05	RVUE 2002 CODATA value
1.00866491578 ± 0.0000000055	MOHR	99	RVUE 1998 CODATA value
1.008665904 ± 0.000000014	COHEN	87	RVUE 1986 CODATA value

n MASS (MeV)

The mass is known more precisely in u (atomic mass units) than in MeV. The conversion is: $1 u = 931.494 102 42(28) \text{ MeV}/c^2$ (2018 CODATA value, TIESINGA 21).

VALUE (MeV)	DOCUMENT ID	TECN	COMMENT
939.56542052 ± 0.00000054	TIESINGA	21	RVUE 2018 CODATA value
• • • We do not use the following data for averages, fits, limits, etc. • • •			
939.5654133 ± 0.0000058	MOHR	16	RVUE 2014 CODATA value
939.565379 ± 0.000021	MOHR	12	RVUE 2010 CODATA value
939.565346 ± 0.000023	MOHR	08	RVUE 2006 CODATA value
939.565360 ± 0.000081	MOHR	05	RVUE 2002 CODATA value
939.565331 ± 0.000037	1 KESSLER	99	SPEC $n\bar{p} \rightarrow d\gamma$
939.565330 ± 0.000038	MOHR	99	RVUE 1998 CODATA value
939.56565 ± 0.00028	2,3 DIFILIPPO	94	TRAP Penning trap
939.56563 ± 0.00028	COHEN	87	RVUE 1986 CODATA value
939.56564 ± 0.00028	3,4 GREENE	86	SPEC $n\bar{p} \rightarrow d\gamma$
939.5731 ± 0.0027	3 COHEN	73	RVUE 1973 CODATA value

- We use the 1998 CODATA u -to-MeV conversion factor (see the heading above) to get this mass in MeV from the much more precisely measured KESSLER 99 value of $1.00866491637 \pm 0.0000000082 u$.
- The mass is known much more precisely in u : $m = 1.0086649235 \pm 0.0000000023 u$. We use the 1986 CODATA conversion factor to get the mass in MeV.
- These determinations are not independent of the $m_n - m_p$ measurements below.
- The mass is known much more precisely in u : $m = 1.008664919 \pm 0.000000014 u$.

\bar{n} MASS

VALUE (MeV)	EVTS	DOCUMENT ID	TECN	COMMENT
939.485 ± 0.051	59	1 CRESTI	86	HBC $\bar{p}p \rightarrow \bar{\pi}n$

- This is a corrected result (see the erratum). The error is statistical. The maximum systematic error is 0.029 MeV.

n MEAN LIFE

Limits on lifetimes for *bound* neutrons are given in the section "p PARTIAL MEAN LIVES."

We average eight of the best nine measurements, those made with ultracold neutrons (UCN's). If we include the one in-beam measurement with a comparable error (YUE 13), we get 878.6 ± 0.6 s, where the scale factor is now 2.2.

For a recent discussion of the long-standing disagreement between in-beam and UCN results, see CZARNECKI 18 (*Physical Review Letters* **120** 202002 (2018)). For a full review of all matters concerning the neutron lifetime until about 2010, see WIETFELDT 11, F.E. Wietfeldt and G.L. Greene, "The neutron lifetime," *Reviews of Modern Physics* **83** 1173 (2011).

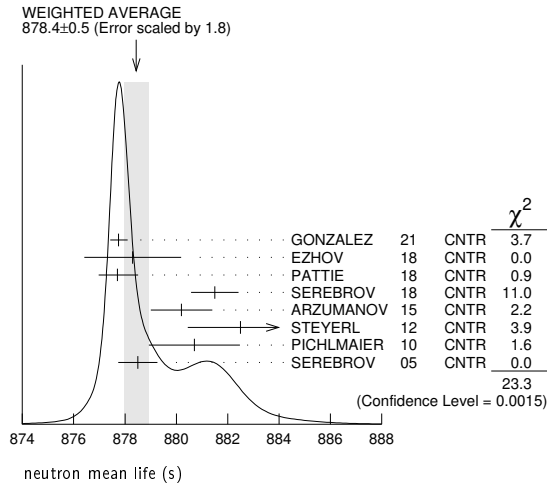
VALUE (s)	DOCUMENT ID	TECN	COMMENT
878.4 ± 0.5 OUR AVERAGE			Error includes scale factor of 1.8. See the ideogram below.
877.75 ± 0.28 + 0.22 - 0.16	GONZALEZ	21	CNTR UCN asym. magnetic trap
878.3 ± 1.6 ± 1.0	EZHOV	18	CNTR UCN magneto-gravit. trap
877.7 ± 0.7 ± 0.4 - 0.2	1 PATTIE	18	CNTR UCN asym. magnetic trap
881.5 ± 0.7 ± 0.6	SEREBROV	18	CNTR UCN gravitational trap
880.2 ± 1.2	2 ARZUMANOV	15	CNTR UCN double bottle
882.5 ± 1.4 ± 1.5	3 STEYERL	12	CNTR UCN material bottle
880.7 ± 1.3 ± 1.2	PICHLMAIER	10	CNTR UCN material bottle
878.5 ± 0.7 ± 0.3	SEREBROV	05	CNTR UCN gravitational trap
• • • We do not use the following data for averages, fits, limits, etc. • • •			
887 ± 14 + 7 - 3	4 WILSON	21	CNTR space-based n rate
887.7 ± 1.2 ± 1.9	5 YUE	13	CNTR In-beam n , trapped p
881.6 ± 0.8 ± 1.9	6 ARZUMANOV	12	CNTR See ARZUMANOV 15
886.3 ± 1.2 ± 3.2	NICO	05	CNTR See YUE 13
886.8 ± 1.2 ± 3.2	DEWEY	03	CNTR See NICO 05
885.4 ± 0.9 ± 0.4	ARZUMANOV	00	CNTR See ARZUMANOV 12
889.2 ± 3.0 ± 3.8	BYRNE	96	CNTR Penning trap
882.6 ± 2.7	7 MAMPE	93	CNTR UCN material bottle
888.4 ± 3.1 ± 1.1	8 NESVIZHEV...	92	CNTR UCN material bottle
888.4 ± 2.9	ALFIMENKOV	90	CNTR See NESVIZHEVSKI 92
893.6 ± 3.8 ± 3.7	BYRNE	90	CNTR See BYRNE 96
878 ± 27 ± 14	KOSSAKOW...	89	TPC Pulsed beam
887.6 ± 3.0	MAMPE	89	CNTR See STEYERL 12
877 ± 10	PAUL	89	CNTR Magnetic storage ring
876 ± 10 ± 19	LAST	88	SPEC Pulsed beam
891 ± 9	SPIVAK	88	CNTR Beam
903 ± 13	KOSVINTSEV	86	CNTR UCN material bottle
937 ± 18	9 BYRNE	80	CNTR
875 ± 95	KOSVINTSEV	80	CNTR
881 ± 8	BONDAREN...	78	CNTR See SPIVAK 88
918 ± 14	CHRISTENSEN72		CNTR

- PATTIE 18 uses a new technique, with a semi-toroidal magneto-gravitational asymmetric trap and a novel in situ n -detector.

Baryon Particle Listings

n

- ² ARZUMANOV 15 is a reanalysis of their 2008–2010 dataset, with improved systematic corrections of ARZUMANOV 00 and ARZUMANOV 12.
- ³ STEYERL 12 is a detailed reanalysis of neutron storage loss corrections to the raw data of MAMPE 89, and it replaces that value.
- ⁴ WILSON 21 extract the value from the flux of *n* escaping the moon using data from the Lunar Prospector Neutron Spectrometer.
- ⁵ YUE 13 differs from NICO 05 in that a different and better method was used to measure the neutron density in the fiducial volume. This shifted the lifetime by +1.4 seconds and reduced the previously largest source of systematic uncertainty by a factor of five.
- ⁶ ARZUMANOV 12 reanalyzes its systematic corrections in ARZUMANOV 00 and obtains this corrected value.
- ⁷ IGNATOVICH 95 calls into question some of the corrections and averaging procedures used by MAMPE 93. The response, BONDARENKO 96, denies the validity of the criticisms.
- ⁸ The NESVIZHEVSKII 92 measurement has been withdrawn by A. Serebrov.
- ⁹ The BYRNE 80 measurement has been withdrawn (J. Byrne, private communication, 1990).



n MAGNETIC MOMENT

See the "Quark Model" review.

VALUE (μ_N)	DOCUMENT ID	TECN	COMMENT
-1.91304273 ± 0.00000045	TIESINGA 21	RVUE	2018 CODATA value
• • • We do not use the following data for averages, fits, limits, etc. • • •			
-1.91304273 ± 0.00000045	MOHR 16	RVUE	2014 CODATA value
-1.91304272 ± 0.00000045	MOHR 12	RVUE	2010 CODATA value
-1.91304273 ± 0.00000045	MOHR 08	RVUE	2006 CODATA value
-1.91304273 ± 0.00000045	MOHR 05	RVUE	2002 CODATA value
-1.91304272 ± 0.00000045	MOHR 99	RVUE	1998 CODATA value
-1.91304275 ± 0.00000045	COHEN 87	RVUE	1986 CODATA value
-1.91304277 ± 0.00000048	¹ GREENE 82	MRS	

¹ GREENE 82 measures the moment to be $(1.04187564 \pm 0.00000026) \times 10^{-3}$ Bohr magnetons. The value above is obtained by multiplying this by $m_p/m_e = 1836.152701 \pm 0.000037$ (the 1986 CODATA value from COHEN 87).

n ELECTRIC DIPOLE MOMENT

A nonzero value is forbidden by both *T* invariance and *P* invariance. A number of early results have been omitted. See RAMSEY 90, GOLUB 94, and LAMOREAUX 09 for reviews.

The results are upper limits on $|d_n|$.

VALUE (10^{-25} e cm)	CL %	DOCUMENT ID	TECN	COMMENT
< 0.18	90	¹ ABEL 20	MRS	UCN
• • • We do not use the following data for averages, fits, limits, etc. • • •				
< 0.22	95	² SAHOO 17		¹⁹⁹ Hg atom EDM + theory
< 0.16	95	GRANER 16	MRS	¹⁹⁹ Hg atom EDM + theory
< 0.30	90	³ PENDLEBURY 15	MRS	Supersedes BAKER 06
< 0.55	90	SEREBROV 15	MRS	UCN's, $h\nu = 2\mu_n B \pm 2d_n E$
< 0.55	90	⁴ SEREBROV 14	MRS	See SEREBROV 15
< 0.29	90	⁵ BAKER 06	MRS	See PENDLEBURY 15
< 0.63	90	⁶ HARRIS 99	MRS	$d = (-0.1 \pm 0.36) \times 10^{-25}$
< 0.97	90	ALTAREV 96	MRS	See SEREBROV 14
< 1.1	95	ALTAREV 92	MRS	See ALTAREV 96
< 1.2	95	SMITH 90	MRS	See HARRIS 99
< 2.6	95	ALTAREV 86	MRS	$d = (-1.4 \pm 0.6) \times 10^{-25}$
0.3 ± 4.8		PENDLEBURY 84	MRS	Ultracold neutrons
< 6	90	ALTAREV 81	MRS	$d = (2.1 \pm 2.4) \times 10^{-25}$
< 16	90	ALTAREV 79	MRS	$d = (4.0 \pm 7.5) \times 10^{-25}$

¹ ABEL 20 reports $d = (0.0 \pm 1.1 \pm 0.2) \times 10^{-26}$ e cm value corresponding to the listed limit.

- ² SAHOO 17 develops theory to calculate this limit from the measured limit by GRANER 16 of the ¹⁹⁹Hg atom EDM.
- ³ PENDLEBURY 15 reports $d = (-0.21 \pm 1.82) \times 10^{-26}$ e cm value corresponding to the listed limit.
- ⁴ SEREBROV 14 includes the data of ALTAREV 96.
- ⁵ LAMOREAUX 07 faults BAKER 06 for not including in the estimate of systematic error an effect due to the Earth's rotation. BAKER 07 replies (1) that the effect was included implicitly in the analysis and (2) that further analysis confirms that the BAKER 06 limit is correct as is. See also SILENKO 07.
- ⁶ This HARRIS 99 result includes the result of SMITH 90. However, the averaging of the results of these two experiments has been criticized by LAMOREAUX 00.

n MEAN-SQUARE CHARGE RADIUS

The mean-square charge radius of the neutron, $\langle r_n^2 \rangle$, is related to the neutron-electron scattering length b_{ne} by $\langle r_n^2 \rangle = 3(m_e a_0 / m_n) b_{ne}$, where m_e and m_n are the masses of the electron and neutron, and a_0 is the Bohr radius. Numerically, $\langle r_n^2 \rangle = 86.34 b_{ne}$, if we use a_0 for a nucleus with infinite mass.

VALUE (fm ²)	DOCUMENT ID	COMMENT
-0.1155 ± 0.0017 OUR AVERAGE		
-0.115 ± 0.002 ± 0.003	KOPECKY 97	<i>ne</i> scattering (Pb)
-0.124 ± 0.003 ± 0.005	KOPECKY 97	<i>ne</i> scattering (Bi)
-0.114 ± 0.003	KOESTER 95	<i>ne</i> scattering (Ne, Bi)
-0.115 ± 0.003	¹ KROHN 73	<i>ne</i> scattering (Ne, Ar, Kr, Xe)
• • • We do not use the following data for averages, fits, limits, etc. • • •		
-0.1101 ± 0.0089	² HEACOCK 21	<i>n</i> interferometry
-0.106 +0.007 -0.005	³ FILIN 20	chiral EFT analysis
-0.117 +0.007 -0.011	BELUSHKIN 07	Dispersion analysis
-0.113 ± 0.003 ± 0.004	KOPECKY 95	<i>ne</i> scattering (Pb)
-0.134 ± 0.009	ALEKSANDR... 86	<i>ne</i> scattering (Bi)
-0.114 ± 0.003	KOESTER 86	<i>ne</i> scattering (Pb, Bi)
-0.118 ± 0.002	KOESTER 76	<i>ne</i> scattering (Pb)
-0.120 ± 0.002	KOESTER 76	<i>ne</i> scattering (Bi)
-0.116 ± 0.003	KROHN 66	<i>ne</i> scattering (Ne, Ar, Kr, Xe)

- ¹ KROHN 73 measured -0.112 ± 0.003 fm². This value is as corrected by KOESTER 76.
- ² HEACOCK 21 extract the value from Pendeloesung interferometry to measure the neutron structure factors of silicon. This value is strongly anti-correlated with the mean-square thermal atomic displacement.
- ³ FILIN 20 extract the value based on their chiral-EFT calculation of the deuteron structure radius and use as input the atomic data for the difference of the deuteron and proton charge radii.

n MAGNETIC RADIUS

This is the rms magnetic radius, $\sqrt{\langle r_M^2 \rangle}$.

VALUE (fm)	DOCUMENT ID	COMMENT
0.864 +0.009 -0.008 OUR AVERAGE		
0.89 ± 0.03	EPSTEIN 14	Using <i>ep</i> , <i>en</i> , $\pi\pi$ data
0.862 +0.009 -0.008	BELUSHKIN 07	Dispersion analysis

n ELECTRIC POLARIZABILITY α_n

Following is the electric polarizability α_n defined in terms of the induced electric dipole moment by $\mathbf{D} = 4\pi\epsilon_0\alpha_n\mathbf{E}$. For a review, see SCHMIED-MAYER 89.

For a very complete reviews of the polarizability of the nucleon and Compton scattering, see SCHUMACHER 05, updated in SCHUMACHER 19, and GRIESSHAMMER 12.

VALUE (10^{-4} fm ³)	DOCUMENT ID	TECN	COMMENT
11.8 ± 1.1 OUR AVERAGE			
11.55 ± 1.25 ± 0.8	MYERS 14	CNTR	$\gamma d \rightarrow \gamma d$
12.5 ± 1.8 +1.6 -1.3	¹ KOSSERT 03	CNTR	$\gamma d \rightarrow \gamma p n$
12.0 ± 1.5 ± 2.0	SCHMIEDM... 91	CNTR	<i>n</i> Pb transmission
10.7 + 3.3 -10.7	ROSE 90B	CNTR	$\gamma d \rightarrow \gamma n p$
• • • We do not use the following data for averages, fits, limits, etc. • • •			
8.8 ± 2.4 ± 3.0	² LUNDIN 03	CNTR	$\gamma d \rightarrow \gamma d$
13.6	³ KOLB 00	CNTR	$\gamma d \rightarrow \gamma n p$
0.0 ± 5.0	⁴ KOESTER 95	CNTR	<i>n</i> Pb, <i>n</i> Bi transmission
11.7 + 4.3 -11.7	ROSE 90	CNTR	See ROSE 90B
8 ± 10	KOESTER 88	CNTR	<i>n</i> Pb, <i>n</i> Bi transmission
12 ± 10	SCHMIEDM... 88	CNTR	<i>n</i> Pb, <i>n</i> C transmission

- ¹ KOSSERT 03 gets $\alpha_n - \beta_n = (9.8 \pm 3.6 +2.1 -1.1 \pm 2.2) \times 10^{-4}$ fm³, and uses $\alpha_n + \beta_n = (15.2 \pm 0.5) \times 10^{-4}$ fm³ from LEVCHUK 00. Thus the errors on α_n and β_n are anti-correlated.
- ² LUNDIN 03 measures $\alpha_N - \beta_N = (6.4 \pm 2.4) \times 10^{-4}$ fm³ and uses accurate values for α_p and α_p and a precise sum-rule result for $\alpha_n + \beta_n$. The second error is a model

uncertainty, and errors on α_n and β_n are anticorrelated. The data from this paper are included in the analysis of MYERS 14.

³ KOLB 00 obtains this value with a lower limit of $7.6 \times 10^{-4} \text{ fm}^3$ but no upper limit from this experiment alone. Combined with results of ROSE 90, the $1-\sigma$ range is $(7.6\text{--}14.0) \times 10^{-4} \text{ fm}^3$.

⁴ KOESTER 95 uses natural Pb and the isotopes 208, 207, and 206. See this paper for a discussion of methods used by various groups to extract α_n from data.

***n* MAGNETIC POLARIZABILITY β_n**

VALUE (10^{-4} fm^3)	DOCUMENT ID	TECN	COMMENT
3.7 ± 1.2 OUR AVERAGE			
$3.65 \pm 1.25 \pm 0.8$	MYERS	14 CNTR	$\gamma d \rightarrow \gamma d$
$2.7 \pm 1.8 \begin{smallmatrix} +1.3 \\ -1.6 \end{smallmatrix}$	¹ KOSSERT	03 CNTR	$\gamma d \rightarrow \gamma p n$
$6.5 \pm 2.4 \pm 3.0$	² LUNDIN	03 CNTR	$\gamma d \rightarrow \gamma d$
1.6	³ KOLB	00 CNTR	$\gamma d \rightarrow \gamma n p$

• • • We do not use the following data for averages, fits, limits, etc. • • •

¹ KOSSERT 03 gets $\alpha_n - \beta_n = (9.8 \pm 3.6 \pm 2.1 \pm 2.2) \times 10^{-4} \text{ fm}^3$, and uses $\alpha_n + \beta_n = (15.2 \pm 0.5) \times 10^{-4} \text{ fm}^3$ from LEVCHUK 00. Thus the errors on α_n and β_n are anti-correlated.

² LUNDIN 03 measures $\alpha_n - \beta_n = (6.4 \pm 2.4) \times 10^{-4} \text{ fm}^3$ and uses accurate values for α_p and α_d and a precise sum-rule result for $\alpha_n + \beta_n$. The second error is a model uncertainty, and errors on α_n and β_n are anticorrelated.

³ KOLB 00 obtains this value with an upper limit of $7.6 \times 10^{-4} \text{ fm}^3$ but no lower limit from this experiment alone. Combined with results of ROSE 90, the $1-\sigma$ range is $(1.2\text{--}7.6) \times 10^{-4} \text{ fm}^3$.

***n* CHARGE**

See also " $|q_p + q_e|/e$ " in the proton Listings.

VALUE ($10^{-21} e$)	DOCUMENT ID	TECN	COMMENT
-0.2 ± 0.8 OUR AVERAGE			
-0.1 ± 1.1	¹ BRESSI	11	Neutrality of SF ₆
-0.4 ± 1.1	² BAUMANN	88	Cold <i>n</i> deflection
-15 ± 22	³ GAEHLER	82 CNTR	Cold <i>n</i> deflection

• • • We do not use the following data for averages, fits, limits, etc. • • •

¹ As a limit, this BRESSI 11 value is $< 1 \times 10^{-21} e$.

² The BAUMANN 88 error ± 1.1 gives the 68% CL limits about the the value -0.4 .

³ The GAEHLER 82 error ± 22 gives the 90% CL limits about the the value -15 .

LIMIT ON $n\bar{n}$ OSCILLATIONS

Mean Time for $n\bar{n}$ Transition

A test of $\Delta B=2$ baryon number nonconservation. MOHAPATRA 80 and MOHAPATRA 89 discuss the theoretical motivations for looking for $n\bar{n}$ oscillations. DOVER 83 and DOVER 85 give phenomenological analyses. The best limits come from looking for the decay of neutrons bound in nuclei. However, these analyses require model-dependent corrections for nuclear effects. See KABIR 83, DOVER 89, ALBERICO 91, and GAL 00 for discussions. Direct searches for $n \rightarrow \bar{n}$ transitions using reactor neutrons are cleaner but give somewhat poorer limits. We include limits for both free and bound neutrons in the Summary Table. See MOHAPATRA 09 and PHILLIPS 16 for recent reviews.

VALUE (s)	CL%	DOCUMENT ID	TECN	COMMENT
$> 4.7 \times 10^8$	90	¹ ABE	21 CNTR	<i>n</i> bound in oxygen
$> 8.6 \times 10^7$	90	BALDO...	94 CNTR	Reactor (free) neutrons
• • • We do not use the following data for averages, fits, limits, etc. • • •				
$> 1.37 \times 10^8$	90	² AHARMIM	17 SNO	<i>n</i> bound in deuterium
$> 2.7 \times 10^8$	90	ABE	15c CNTR	<i>n</i> bound in oxygen
$> 1.3 \times 10^8$	90	CHUNG	02b SOU2	<i>n</i> bound in iron
$> 1 \times 10^7$	90	BALDO...	90 CNTR	See BALDO-CEOLIN 94
$> 1.2 \times 10^8$	90	BERGER	90 FREJ	<i>n</i> bound in iron
$> 4.9 \times 10^5$	90	BRESSI	90 CNTR	Reactor neutrons
$> 4.7 \times 10^5$	90	BRESSI	89 CNTR	See BRESSI 90
$> 1.2 \times 10^8$	90	TAKITA	86 CNTR	<i>n</i> bound in oxygen
$> 1 \times 10^6$	90	FIDECARO	85 CNTR	Reactor neutrons
$> 8.8 \times 10^7$	90	PARK	85b CNTR	
$> 3 \times 10^7$		BATTISTONI	84 NUSX	
$> 0.27\text{--}1.1 \times 10^8$		JONES	84 CNTR	
$> 2 \times 10^7$		CHERRY	83 CNTR	

¹ ABE 21 supersedes ABE 15c.

² The AHARMIM 17 value is an unbounded limit (it does not assume a positive lifetime). The bounded limit is 1.23×10^8 sec.

LIMIT ON nn' OSCILLATIONS

Lee and Yang (LEE 56) proposed the existence of mirror world in an attempt to restore global parity symmetry. A possible candidate for dark matter. Limits depend on assumptions about fields *B* and *B'*. See the papers for details. See BEREZHIANI 18 for a recent discussion.

VALUE (s)	CL%	DOCUMENT ID	TECN	COMMENT
> 448	90	SEREBROV	09a CNTR	Assumes $B' < 100 \text{ nT}$

• • • We do not use the following data for averages, fits, limits, etc. • • •

> 1	95	¹ BAN	23 CNTR	UCN, scan of <i>B</i> field
		² ALMAZAN	22 CNTR	STEREO, hidden neutron search $ m_n - m_{n'} \geq 0$.
> 9	95	³ ABEL	21 CNTR	UCN, scan of <i>B</i> field
> 17	95	⁴ BEREZHIANI	18 CNTR	UCN, scan of <i>B</i> field
> 12	95	⁵ ALTAREV	09a CNTR	UCN, scan $0 \leq B \leq 12.5 \mu\text{T}$
> 414	90	SEREBROV	08 CNTR	UCN, <i>B</i> field on & off
> 103	95	BAN	07 CNTR	UCN, <i>B</i> field on & off

¹ BAN 23 determine limits on the oscillation time for the $|\delta m(nn')|$ range of 2–59 peV. The quoted value is $\tau_{nn'}/\sqrt{\cos(\beta)} > 1$ sec. for *B* in 30–1143 μT , for the case $\beta = 0$.

² ALMAZAN 22 reports an experimental constraint on the probability for neutron conversion into a hidden neutron, $p < 3.1 \times 10^{-11}$ at 95% CL, which may be used to set a limit on the nn' oscillation time.

³ ABEL 21 determine several limits on the oscillation time as a function of the mirror magnetic field *B'*, and of the fixed angle, β , between the applied magnetic field and *B'*. The latter is assumed to be bound to Earth. Two values are quoted from two analysis methods: (i) $\tau_{nn'}/\sqrt{\cos(\beta)} > 9$ sec for *B'* in 5–25.4 μT , and (ii) for any angle β , $\tau_{nn'} > 6$ sec for *B'* in 0.4–25.7 μT . The authors also quote a limit of 352 sec for the case $B' = 0$ T.

⁴ The *B* field was set to (0.09, 0.12, 0.21) G. Limits on oscillation time are valid for any mirror field *B'* in (0.08–0.17) G, and for aligned fields *B* and *B'*. For larger values of *B'*, the limits are significantly reduced.

⁵ Losses of neutrons due to oscillations to mirror neutrons would be maximal when the magnetic fields *B* and *B'* in the two worlds were equal. Hence the scan over *B* by ALTAREV 09a: the limit applies for any *B'* over the given range. At $B' = 0$, the limit is 141 s (95% CL).

***n* DECAY MODES**

Mode	Fraction (Γ_i/Γ)	Confidence level
Γ_1 $p e^- \bar{\nu}_e$	100 %	
Γ_2 $p e^- \bar{\nu}_e \gamma$	[a] $(9.2 \pm 0.7) \times 10^{-3}$	
Γ_3 hydrogen-atom $\bar{\nu}_e$	$< 2.7 \times 10^{-3}$	95%

Charge conservation (*Q*) violating mode

Γ_4 $p \nu_e \bar{\nu}_e$	$Q < 8 \times 10^{-27}$	68%
----------------------------------	-------------------------	-----

Baryon number violating decay

Γ_5 $e^+ e^-$ invisible		
--------------------------------	--	--

[a] This limit is for γ energies between 0.4 and 782 keV.

***n* BRANCHING RATIOS**

$\Gamma(p e^- \bar{\nu}_e \gamma)/\Gamma_{\text{total}}$	Γ_2/Γ			
VALUE (units 10^{-3})	CL%	DOCUMENT ID	TECN	COMMENT
$9.17 \pm 0.24 \pm 0.64$		¹ BALES	16 RDK2	Two different set-ups
$3.09 \pm 0.11 \pm 0.30$		² COOPER	10 CNTR	See BALES 16
$3.13 \pm 0.11 \pm 0.33$		NICO	06 CNTR	See COOPER 10
< 6.9	90	³ BECK	02 CNTR	γ, p, e^- coincidence

¹ BALES 16 gets a branching fraction of $(5.82 \pm 0.23 \pm 0.62) \times 10^{-3}$ for a photon energy range 0.4 to 14.0 keV, and with a different detector array, $(3.35 \pm 0.05 \pm 0.15) \times 10^{-3}$ for 14.1 to 782 keV. Our result above is the sum; the error on the sum is completely dominated by the error on the lower range.

² This COOPER 10 result is for γ energies between 15 and 340 keV.

³ This BECK 02 limit is for γ energies between 35 and 100 keV.

$\Gamma(\text{hydrogen-atom } \bar{\nu}_e)/\Gamma_{\text{total}}$

VALUE	CL%	DOCUMENT ID	TECN	COMMENT
$< 0.27 \times 10^{-2}$		¹ CZARNECKI	18	Lifetime analysis
$< 3 \times 10^{-2}$	95	² GREEN	90 RVUE	

• • • We do not use the following data for averages, fits, limits, etc. • • •

¹ CZARNECKI 18 limit from an analysis of experimental discrepancies on the neutron lifetime and axial coupling applies as well to other possible exotic neutron decays.

² GREEN 90 infers that $\tau(\text{hydrogen-atom } \bar{\nu}_e) > 3 \times 10^4$ s by comparing neutron lifetime measurements made in storage experiments with those made in β -decay experiments. However, the result depends sensitively on the lifetime measurements, and does not of course take into account more recent measurements of same.

$\Gamma(p \nu_e \bar{\nu}_e)/\Gamma_{\text{total}}$

Forbidden by charge conservation.

VALUE	CL%	DOCUMENT ID	TECN	COMMENT
$< 8 \times 10^{-27}$	68	¹ NORMAN	96 RVUE	$^{71}\text{Ga} \rightarrow ^{71}\text{Ge}$ neutrals
• • • We do not use the following data for averages, fits, limits, etc. • • •				
$< 9.7 \times 10^{-18}$	90	ROY	83 CNTR	$^{113}\text{Cd} \rightarrow ^{113m}\text{In}$ neut.
$< 7.9 \times 10^{-21}$		VAIDYA	83 CNTR	$^{87}\text{Rb} \rightarrow ^{87m}\text{Sr}$ neut.
$< 9 \times 10^{-24}$	90	BARABANOV	80 CNTR	$^{71}\text{Ga} \rightarrow ^{71}\text{GeX}$
$< 3 \times 10^{-19}$		NORMAN	79 CNTR	$^{87}\text{Rb} \rightarrow ^{87m}\text{Sr}$ neut.

¹ NORMAN 96 gets this limit by attributing SAGE and GALLEX counting rates to the charge-nonconserving transition $^{71}\text{Ga} \rightarrow ^{71}\text{Ge} + \text{neutrals}$ rather than to solar-neutrino reactions.

Baryon Particle Listings

n

$\Gamma(e^+ e^- \text{invisible})/\Gamma_{\text{total}}$ Γ_S/Γ
 Baryon number violating decay

VALUE	CL%	DOCUMENT ID	TECN	COMMENT
<0.01	90	1 KLOPF	19 CNTR	re-interpretation of MUND 13
<1 × 10 ⁻⁴	90	2 SUN	18 SPEC	Ultracold <i>n</i> , polarized

1 KLOPF 19 value is for baryon number violating decay of neutron to electrons plus an invisible state, χ . The limit is valid for KE($e^+ e^-$) range between 32 keV and 664 keV, strengthening to few × 10⁻⁴ above approximately 100 keV.
 2 SUN 18 value is for baryon number violating decay of neutron to electrons plus an invisible state, χ . The limit is valid for 644 keV > KE($e^+ e^-$) > 100 keV. Assuming this decay $\chi e e$ is the only allowed χ decay channel, a 0.01 BR is ruled out for 644 keV > E($e^+ e^-$) > 100 keV at over 5 σ .

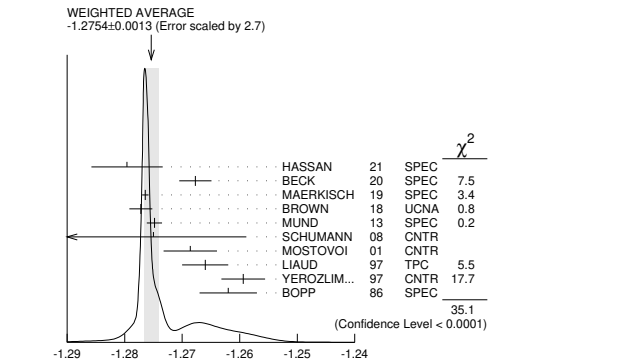
See the related review(s):
 Baryon Decay Parameters

n → *p* *e*⁻ $\bar{\nu}_e$ DECAY PARAMETERS

See the above "Note on Baryon Decay Parameters." For discussions of recent results, see the references cited at the beginning of the section on the neutron mean life. For discussions of the values of the weak coupling constants g_A and g_V obtained using the neutron lifetime and asymmetry parameter *A*, comparisons with other methods of obtaining these constants, and implications for particle physics and for astrophysics, see DUBBERS 91 and WOOLCOCK 91. For tests of the *V*-*A* theory of neutron decay, see EROZOLIMSKII 91B, MOSTOVOI 96, NICO 05, SEVERIJS 06, and ABELE 08.

$\lambda \equiv g_A / g_V$

VALUE	DOCUMENT ID	TECN	COMMENT
-1.2754 ± 0.0013 OUR AVERAGE	Error includes scale factor of 2.7. See the ideogram below.		
-1.2796 ± 0.0062	1 HASSAN	21 SPEC	Proton recoil spectrum
-1.2677 ± 0.0028	2 BECK	20 SPEC	Proton recoil spectrum
-1.27641 ± 0.00045 ± 0.00033	3 MAERKISCH	19 SPEC	pulsed cold <i>n</i> , polarized
-1.2772 ± 0.0020	4 BROWN	18 UCNA	Ultracold <i>n</i> , polarized
-1.2748 ± 0.0008 ± 0.0010 -0.0011	5 MUND	13 SPEC	Cold <i>n</i> , polarized
-1.275 ± 0.006 ± 0.015	6 SCHUMANN	08 CNTR	Cold <i>n</i> , polarized
-1.2686 ± 0.0046 ± 0.0007	6 MOSTOVOI	01 CNTR	A and B × polarizations
-1.266 ± 0.004	LIAUD	97 TPC	Cold <i>n</i> , polarized, A
-1.2594 ± 0.0038	7 YEROZLIM...	97 CNTR	Cold <i>n</i> , polarized, A
-1.262 ± 0.005	BOPP	86 SPEC	Cold <i>n</i> , polarized, A
• • • We do not use the following data for averages, fits, limits, etc. • • •			
-1.27607 ± 0.00068	8 SAUL	20 SPEC	Cold <i>n</i> , polarized, A
-1.284 ± 0.014	9 DARIUS	17 SPEC	Cold <i>n</i> , unpolarized
-1.2755 ± 0.0030	10 MENDENHALL13	UCNA	See BROWN 18
-1.27590 ± 0.00239 ± 0.00331 -0.00377	11 PLASTER	12 UCNA	See MENDENHALL 13
-1.27590 ± 0.00409 -0.00445	LIU	10 UCNA	See PLASTER 12
-1.2739 ± 0.0019	12 ABELE	02 SPEC	See MUND 13
-1.274 ± 0.003	ABELE	97D SPEC	Cold <i>n</i> , polarized, A
-1.266 ± 0.004	SCHRECK...	95 TPC	See LIAUD 97
-1.2544 ± 0.0036	EROZOLIM...	91 CNTR	See YEROZOLIM-SKY 97
-1.226 ± 0.042	MOSTOVOY	83 RVUE	
-1.261 ± 0.012	EROZOLIM...	79 CNTR	Cold <i>n</i> , polarized, A
-1.259 ± 0.017	13 STRATOWA	78 CNTR	<i>p</i> recoil spectrum, <i>a</i>
-1.263 ± 0.015	EROZOLIM...	77 CNTR	See EROZOLIMSKII 79
-1.250 ± 0.036	13 DOBROZE...	75 CNTR	See STRATOWA 78
-1.258 ± 0.015	14 KROHN	75 CNTR	Cold <i>n</i> , polarized, A
-1.263 ± 0.016	15 KROPF	74 RVUE	<i>n</i> decay alone
-1.250 ± 0.009	15 KROPF	74 RVUE	<i>n</i> decay + nuclear ft



$\lambda \equiv g_A / g_V$

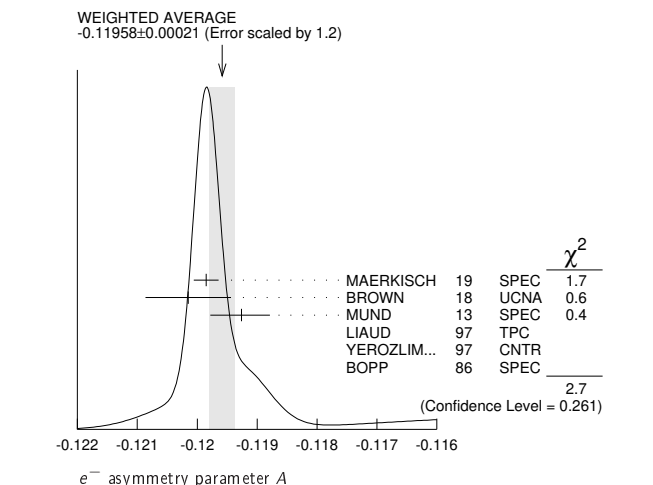
1 HASSAN 21 include earlier data of DARIUS 17. The value is extracted from the angular correlation coefficient *a*.

2 BECK 20 calculates this value from the measurement of the β -decay $e-\bar{\nu}_e$ angular correlation coefficient *a*.
 3 MAERKISCH 19 gets $A = -0.11985 \pm 0.00017 \pm 0.00012$.
 4 BROWN 18 gets $A = -0.12054 \pm 0.00044 \pm 0.00068$ and $\lambda = -1.2783 \pm 0.0022$. We quote the combined values that include the earlier UCNA measurements (MENDENHALL 13).
 5 This MUND 13 value includes earlier PERKEO II measurements (ABELE 02 and ABELE 97D).
 6 MOSTOVOI 01 measures the two *P*-odd correlations *A* and *B*, or rather *SA* and *SB*, where *S* is the *n* polarization, in free neutron decay.
 7 YEROZOLIMSKY 97 makes a correction to the EROZOLIMSKII 91 value.
 8 SAUL 20 quote this value of λ under the SM assumption of the Fierz term *b* = 0. In a combined fit authors extract a value of $\lambda = -1.2792 \pm 0.0060$.
 9 DARIUS 17 calculates this value from the measurement of the *a* parameter (see below). Data is included in HASSAN 21.
 10 MENDENHALL 13 gets $A = -0.11954 \pm 0.00055 \pm 0.00098$ and $\lambda = -1.2756 \pm 0.0030$. We quote the nearly identical values that include the earlier UCNA measurement (PLASTER 12), with a correction to that result.
 11 This PLASTER 12 value is identical with that given in LIU 10, but the experiment is now described in detail.
 12 This is the combined result of ABELE 02 and ABELE 97D.
 13 These experiments measure the absolute value of g_A/g_V only.
 14 KROHN 75 includes events of CHRISTENSEN 70.
 15 KROPF 74 reviews all data through 1972.

e⁻ ASYMMETRY PARAMETER *A*

This is the neutron-spin electron-momentum correlation coefficient. Unless otherwise noted, the values are corrected for radiative effects and weak magnetism. In the Standard Model, *A* is related to $\lambda \equiv g_A/g_V$ by $A = -2 \lambda (\lambda + 1) / (1 + 3\lambda^2)$; this assumes that g_A and g_V are real.

VALUE	DOCUMENT ID	TECN	COMMENT
-0.11958 ± 0.00021 OUR AVERAGE	Error includes scale factor of 1.2. See the ideogram below.		
-0.11985 ± 0.00017 ± 0.00012	1 MAERKISCH	19 SPEC	pulsed cold <i>n</i> , polarized
-0.12015 ± 0.00034 ± 0.00063	2 BROWN	18 UCNA	Ultracold <i>n</i> , polarized
-0.11926 ± 0.00031 ± 0.00036 -0.00042	3 MUND	13 SPEC	Cold <i>n</i> , polarized
-0.1160 ± 0.0009 ± 0.0012	LIAUD	97 TPC	Cold <i>n</i> , polarized
-0.1135 ± 0.0014	4 YEROZLIM...	97 CNTR	Cold <i>n</i> , polarized
-0.1146 ± 0.0019	BOPP	86 SPEC	Cold <i>n</i> , polarized
• • • We do not use the following data for averages, fits, limits, etc. • • •			
-0.11972 ± 0.00025	5 SAUL	20 SPEC	Cold <i>n</i> , polarized
-0.11952 ± 0.00110	6 MENDENHALL13	UCNA	See BROWN 18
-0.11966 ± 0.00089 ± 0.00123 -0.00140	7 PLASTER	12 UCNA	See MENDENHALL 13
-0.11966 ± 0.00089 ± 0.00123 -0.00140	LIU	10 UCNA	See PLASTER 12
-0.1138 ± 0.0046 ± 0.0021	PATTIE	09 SPEC	Ultracold <i>n</i> , polarized
-0.1189 ± 0.0007	8 ABELE	02 SPEC	See MUND 13
-0.1168 ± 0.0017	9 MOSTOVOI	01 CNTR	Inferred
-0.1189 ± 0.0012	ABELE	97D SPEC	Cold <i>n</i> , polarized
-0.1160 ± 0.0009 ± 0.0011	SCHRECK...	95 TPC	See LIAUD 97
-0.1116 ± 0.0014	EROZOLIM...	91 CNTR	See YEROZOLIM-SKY 97
-0.114 ± 0.005	10 EROZOLIM...	79 CNTR	Cold <i>n</i> , polarized
-0.113 ± 0.006	10 KROHN	75 CNTR	Cold <i>n</i> , polarized



1 MAERKISCH 19 further derive a value for the CKM-element $|V_{ud}| = 0.97351 \pm 0.00060$, using $\tau_n = 879.7(8)$ sec and the relation from CZARNECKI 18.
 2 BROWN 18 gets $A = -0.12054 \pm 0.00044 \pm 0.00068$ and $\lambda = -1.2783 \pm 0.0022$. We quote the combined values that include the earlier UCNA measurements (MENDENHALL 13).
 3 This MUND 13 value includes earlier PERKEO II measurements (ABELE 02 and ABELE 97D), with a correction to those results.
 4 YEROZOLIMSKY 97 makes a correction to the EROZOLIMSKII 91 value.
 5 Under the SM assumption that the Fierz term *b* = 0, SAUL 20 obtain the quoted asymmetry parameter *A* and $\lambda = -1.27607 \pm 0.00068$. In a combined fit authors extract the values $A = -0.1209 \pm 0.0015$, $\lambda = -1.2792 \pm 0.0060$, and $b = 0.017 \pm 0.021$.

See key on page 1171

Baryon Particle Listings

n

⁶ MENDENHALL 13 gets $A = -0.11954 \pm 0.00055 \pm 0.00098$ and $\lambda = -1.2756 \pm 0.0030$. We quote the nearly identical values that include the earlier UCNA measurement (PLASTER 12), with a correction to that result.

⁷ This PLASTER 12 value is identical with that given in LIU 10, but the experiment is now described in detail.

⁸ This is the combined result of ABELE 02 and ABELE 97d.

⁹ MOSTOVOI 01 calculates this from its measurement of $\lambda = g_A/g_V$ above.

¹⁰ These results are not corrected for radiative effects and weak magnetism, but the corrections are small compared to the errors.

 $\bar{\nu}_e$ ASYMMETRY PARAMETER B

This is the neutron-spin antineutrino-momentum correlation coefficient. In the Standard Model, B is related to $\lambda \equiv g_A/g_V$ by $B = 2\lambda(\lambda - 1) / (1 + 3\lambda^2)$; this assumes that g_A and g_V are real.

VALUE	DOCUMENT ID	TECN	COMMENT
-0.9807 ± 0.0030 OUR AVERAGE			
$0.9802 \pm 0.0034 \pm 0.0036$	SCHUMANN 07	CNTR	Cold n , polarized
$0.967 \pm 0.006 \pm 0.010$	KREUZ 05	CNTR	Cold n , polarized
0.9801 ± 0.0046	SEREBROV 98	CNTR	Cold n , polarized
0.9894 ± 0.0083	KUZNETSOV 95	CNTR	Cold n , polarized
1.00 ± 0.05	CHRISTENSEN70	CNTR	Cold n , polarized
0.995 ± 0.034	EROZOLIM... 70c	CNTR	Cold n , polarized
••• We do not use the following data for averages, fits, limits, etc. •••			
0.9876 ± 0.0004	¹ MOSTOVOI 01	CNTR	Inferred

¹ MOSTOVOI 01 calculates this from its measurement of $\lambda = g_A/g_V$ above.

PROTON ASYMMETRY PARAMETER C

Describes the correlation between the neutron spin and the proton momentum. In the Standard Model, C is related to $\lambda \equiv g_A/g_V$ by $C = -x_c(A + B) = x_c 4\lambda/(1 + 3\lambda^2)$, where $x_c = 0.27484$ is a kinematic factor; this assumes that g_A and g_V are real.

VALUE	DOCUMENT ID	TECN	COMMENT
$-0.2377 \pm 0.0010 \pm 0.0024$	SCHUMANN 08	CNTR	Cold n , polarized

 $e\bar{\nu}_e$ ANGULAR CORRELATION COEFFICIENT a

For a review of past experiments and plans for future measurements of the a parameter, see WIETFELDT 05. In the Standard Model, a is related to $\lambda \equiv g_A/g_V$ by $a = (1 - \lambda^2) / (1 + 3\lambda^2)$; this assumes that g_A and g_V are real.

VALUE	DOCUMENT ID	TECN	COMMENT
-0.1049 ± 0.0013 OUR AVERAGE			Error includes scale factor of 1.8.
$-0.10782 \pm 0.00124 \pm 0.00133$	¹ HASSAN 21	SPEC	Proton recoil spectrum
-0.10430 ± 0.00084	BECK 20	SPEC	Proton recoil spectrum
-0.1054 ± 0.0055	BYRNE 02	SPEC	Proton recoil spectrum
-0.1017 ± 0.0051	STRATOWA 78	CNTR	Proton recoil spectrum
-0.091 ± 0.039	GRIGOREV 68	SPEC	Proton recoil spectrum
••• We do not use the following data for averages, fits, limits, etc. •••			
$-0.1090 \pm 0.0030 \pm 0.0028$	² DARIUS 17	SPEC	Cold n , unpolarized
-0.1045 ± 0.0014	³ MOSTOVOI 01	CNTR	Inferred

¹ The result of HASSAN 21 includes the data of DARIUS 17, and thus supersedes those entries. HASSAN 21 uses the asymmetry in time-of-flight between the beta electron and recoil proton in delayed coincidence.

² DARIUS 17 exploits a "wishbone" correlation, where the p time of flight is correlated with the momentum of the electron in delayed coincidence. Data is included in HASSAN 21.

³ MOSTOVOI 01 calculates this from its measurement of $\lambda = g_A/g_V$ above.

 ϕ_{AV} , PHASE OF g_A RELATIVE TO g_V

Time reversal invariance requires this to be 0 or 180°. This is related to D given in the next data block and $\lambda \equiv g_A/g_V$ by $\sin(\phi_{AV}) \equiv D(1+3\lambda^2)/2|\lambda|$; this assumes that g_A and g_V are real.

VALUE (°)	CL%	DOCUMENT ID	TECN	COMMENT
180.017 ± 0.026 OUR AVERAGE				
180.012 ± 0.028	68	CHUPP 12	CNTR	Cold n , polarized > 91%
180.04 ± 0.09		SOLDNER 04	CNTR	Cold n , polarized
180.08 ± 0.13		LISING 00	CNTR	Polarized > 93%
••• We do not use the following data for averages, fits, limits, etc. •••				
180.013 ± 0.028		MUMM 11	CNTR	See CHUPP 12
179.71 ± 0.39		EROZOLIM... 78	CNTR	Cold n , polarized
180.35 ± 0.43		EROZOLIM... 74	CNTR	Cold n , polarized
181.1 ± 1.3		¹ KROPP 74	RVUE	n decay
180.14 ± 0.22		STEINBERG 74	CNTR	Cold n , polarized

¹ KROPP 74 reviews all data through 1972.

TRIPLE CORRELATION COEFFICIENT D

These are measurements of the component of n spin perpendicular to the decay plane in β decay. Should be zero if T invariance is not violated.

VALUE (units 10^{-4})	DOCUMENT ID	TECN	COMMENT
-1.2 ± 2.0 OUR AVERAGE			
$-0.94 \pm 1.89 \pm 0.97$	CHUPP 12	CNTR	Cold n , polarized > 91%
$-2.8 \pm 6.4 \pm 3.0$	SOLDNER 04	CNTR	Cold n , polarized
$-6 \pm 12 \pm 5$	LISING 00	CNTR	Polarized > 93%
••• We do not use the following data for averages, fits, limits, etc. •••			
$-0.96 \pm 1.89 \pm 1.01$	MUMM 11	CNTR	See CHUPP 12
$+27 \pm 30$	EROZOLIM... 78	CNTR	Cold n , polarized
-27 ± 50	¹ EROZOLIM... 74	CNTR	Cold n , polarized
-11 ± 17	STEINBERG 74	CNTR	Cold n , polarized

¹ EROZOLIMSKII 78 says asymmetric proton losses and nonuniform beam polarization may give a systematic error up to 30×10^{-4} , thus increasing the EROZOLIMSKII 74 error to 50×10^{-4} . STEINBERG 74 and STEINBERG 76 estimate these systematic errors to be insignificant in their experiment.

TRIPLE CORRELATION COEFFICIENT R

Another test of time-reversal invariance. R measures the polarization of the electron in the direction perpendicular to the plane defined by the neutron spin and the electron momentum. $R = 0$ for T invariance.

VALUE	DOCUMENT ID	TECN	COMMENT
$+0.004 \pm 0.012 \pm 0.005$	¹ KOZELA 12	CNTR	Mott polarimeter
••• We do not use the following data for averages, fits, limits, etc. •••			
$+0.008 \pm 0.015 \pm 0.005$	KOZELA 09	CNTR	See KOZELA 12

¹ KOZELA 12 also measures the polarization of the electron along the direction of the neutron spin. This is nonzero in the Standard Model; the correlation coefficient is $N = +0.067 \pm 0.011 \pm 0.004$.

FIERZ INTERFERENCE TERM b

The coefficient of the Fierz interference term, b , probes additional contributions to the differential decay rate of the neutron from scalar or tensor current interactions, beyond the Standard Model.

VALUE	DOCUMENT ID	TECN	COMMENT
$0.017 \pm 0.020 \pm 0.003$	¹ SAUL 20	SPEC	Cold n , polarized

¹ In a combined fit SAUL 20 extract this best fit value of the Fierz interference term b and the values $A = -0.1209 \pm 0.0015$ and $\lambda = -1.2792 \pm 0.0060$. For b it translates into a 90% CL region of $-0.018 \leq b \leq 0.052$ as a function of A .

n REFERENCES

We have omitted some papers that have been superseded by later experiments. See our earlier editions.

BAN 23	PRL 131 191801	G. Ban et al.	(CAEN, ZURI, ISNG, SOB+)
ALMAZAN 22	PRL 128 061801	H. Almazan et al.	(STEREO Collab.)
ABE 21	PR D103 012008	K. Abe et al.	(Super-Kamiokande Collab.)
ABEL 21	PL B617 135993	C. Abel et al.	(nEDM Collab.)
GONZALEZ 21	PRL 127 162501	F.M. Gonzalez et al.	(UCNtau Collab.)
HASSAN 21	PR C103 045502	M.T. Hassan et al.	(aCONR Collab.)
HEACOCK 21	SCI 373 1239	B. Heacock et al.	(NIST, RIKEN, NAGO+)
TIESINGA 21	RMP 93 025010	E. Tiesinga et al.	(NIST)
WILSON 21	PR C104 045501	J.T. Wilson et al.	(JHU, DURH)
ABEL 20	PRL 124 081803	C. Abel et al.	(nEDM Collab.)
BECK 20	PR C101 055506	M. Beck et al.	(aSPECT Collab.)
FLIN 20	PRL 124 082501	A.A. Flin et al.	
SAUL 20	PRL 125 112501	H. Saul et al.	(PERKEO III Collab.)
KLOPP 19	PRL 122 222503	M. Klopp et al.	(PERKEO II Collab.)
MAERKISCH 19	PRL 122 242501	B. Maerksch et al.	(TUM, ILL+)
SCHUMACHER 19	LEP 4 4	M. Schumacher	(GOET)
BEREZHIANI 18	EPJ C78 717	Z. Berezhiani et al.	(AQU, INFN, ILLG+)
BROWN 18	PR C97 035505	M.A.-P. Brown et al.	(UCNA Collab.)
CZARNECKI 18	PRL 120 202002	A. Czarnecki, W.J. Marciano, A. Sirlin	(ALBE+)
EZHOV 18	JETPL 107 671	V.F. Ezhov et al.	(PNPI, LENSU, CAEN+)
PATTIE 18	SCI 360 627	R.W. Pattie Jr. et al.	(LASL, IND, NCSU+)
SEREBROV 18	PR C97 055503	A.P. Serebrov et al.	(PNPI, ILLG, RAL)
Also	JETPL 106 623	A.P. Serebrov et al.	(PNPI, ILLG, RAL)
SUN 18	PR C97 082501	X. Sun et al.	(UCNA Collab.)
AHARIMIM 17	PR D96 092005	B. Aharim in et al.	(SN O Collab.)
DARIUS 17	PRL 119 042502	G. Darius et al.	(aCONR at NIST)
SAHOO 17	PR D95 013002	B.K. Sahoo	(AHMEB)
BALES 16	PRL 116 242501	M.J. Bales et al.	(RDK II Collab.)
GRANER 16	PRL 116 161601	B. Graner et al.	(WASH)
Also	PRL 119 119901 (err.)	B. Graner et al.	(WASH)
MOHR 16	RMP 88 035009	P.J. Mohr, D.B. Newell, B.N. Taylor	(NIST)
PHILLIPS 16	PRPL 612 1	D.G. Phillips II et al.	
ABE 15C	PR D91 072006	K. Abe et al.	(Super-Kamiokande Collab.)
ARZUMANOV 15	PL B745 79	S. Arzumanov et al.	(ILLG, KIAE)
PENDELBURY 15	PR D92 092003	J.M. Pendlebury et al.	(ETHZ, PSI, SUSS)
SEREBROV 15	PR C92 085501	A.P. Serebrov et al.	(PNPI, ILLG, IOFF)
EPSTEIN 14	PR D90 074027	Z. Epstein, G. Paz, J. Roy	(UMD, WYAN)
MYERS 14	PRL 113 262506	L.S. Myers et al.	(COMPTON/MAX-lab Collab.)
SEREBROV 14	JETPL 99 4	A.P. Serebrov et al.	(PNPI, ILL, IOFF)
MENDENHALL 13	PR C87 032501	M.P. Mendenhall et al.	(UCNA Collab.)
MUND 13	PRL 110 172502	D. Mund et al.	(HEID, ILLG)
YUE 13	PRL 111 222501	A.T. Yue et al.	(UMD, NIST, TENN, ORNL+)
ARZUMANOV 12	JETPL 95 224	S.S. Arzumanov et al.	(KIAE)
Translated from ZETFP 95 248.			
CHUPP 12	PR C86 035505	T.E. Chupp et al.	(MICH, UCB, WASH+)
GRSSHAM... 12	PNPI 97 841	H.V. Gresshammer et al.	(GWU, MCHS+)
KOZELA 12	PR C85 045501	A. Kozela et al.	(nTRV Collab.)
MOHR 12	RMP 84 1527	P.J. Mohr, B.N. Taylor, D.B. Newell	(NIST)
PLASTER 12	PR C86 055501	B. Plaster et al.	(UCNA Collab.)
STEYERL 12	PR C85 065503	A. Steyerl et al.	(URI, SUSS)
BRESSI 11	PR A83 052101	G. Bressi et al.	(LEGN, PAVI, PADO, TRST+)
DUBBERS 11	RMP 83 1111	D. Dubbers, M.G. Schmidt	(HEID)
MUMM 11	PRL 107 102301	H.P. Mumm et al.	(NIST, WASH, MICH, LBL+)
WIETFELDT 11	RMP 83 1173	F.E. Wietfeldt, G.L. Greene	(TULA, TENN)
COOPER 10	PR C81 035503	R.L. Cooper et al.	(MICH, NIST, TULA+)
LIU 10	PRL 105 181803	J. Liu et al.	(UCNA Collab.)
Also	PRL 105 219903 (err.)	J. Liu et al.	(UCNA Collab.)
PICHLMAIER 10	PL B693 221	A. Pichlmaier et al.	(TUM, PNPI, ILLG)
ALTAREV 09A	PR D80 032003	I. Altarev et al.	(TUM, RAL, CAEN+)
KOZELA 09	PRL 102 172301	A. Kozela et al.	(JAGL, CRAC, PSI, CAEN+)
LAMOREAUX 09	JP G36 104002	S.K. Lamoreaux, R. Golub	(YALE, NCSU)
MOHAPATRA 09	JP G36 104006	R.N. Mohapatra	(UMD)
PATTIE 09	PRL 102 012301	R.W. Pattie Jr. et al.	(Los Alamos UCNA Collab.)
SEREBROV 09A	NIM A611 137	A.P. Serebrov et al.	(PNPI, IOFF, ILLG+)
ABELE 08	PNP 60 1	H. Abele	(HEID)
MOHR 08	RMP 80 633	P.J. Mohr, B.N. Taylor, D.B. Newell	(NIST)
SCHUMANN 08	PRL 100 151801	M. Schumann et al.	(HEID, ILLG, KARL+)
SEREBROV 08	PL B663 181	A.P. Serebrov et al.	(PNPI, IOFF, ILLG+)
BAKER 07	PRL 98 149102	C.A. Baker et al.	(RAL, SUSS, ILLG)
BAN 07	PRL 99 161603	G. Ban et al.	(CAEN, JAGL, PSI, JINR+)
BELUSHKIN 07	PR C75 035202	M.A. Belushkin, H.W. Hammer, U.-G. Meissner	(BONN+)
LAMOREAUX 07	PRL 98 149101	S.K. Lamoreaux, R. Golub	(YALE, NCSU)
SCHUMANN 07	PRL 99 191803	M. Schumann et al.	(HEID, ILLG, KARL+)
SILENKO 07	PNPL 4 4 68	A.Ya. Silenko	(Belarussian U.)
Translated from PFECAY 6 784.			
BAKER 06	PRL 97 131801	C.A. Baker et al.	(RAL, SUSS, ILLG)
NICO 06	NAT 444 3059	J.S. Nico et al.	(NIST, TULN, MICH, UMD+)
SEVERIJNS 06	RMP 78 991	N. Severijns, M. Beck, O. Naviliat-Cuncic	(UCNA Collab.)
KREUZ 05	PL B619 263	M. Kreuz et al.	(HEID, ILLG, MAINZ, KARL+)
MOHR 05	RMP 77 1	P.J. Mohr, B.N. Taylor	(NIST)
NICO 05	PR C71 055502	J.S. Nico et al.	(NIST, TULN, IND, TENN+)
SCHUMACHER 05	PNP 55 567	M. Schumacher	(GOET)
SEREBROV 05	PL B605 72	A.P. Serebrov et al.	(PNPI, JINR, ILLG)
Also	SPU 48 8 67	A.P. Serebrov et al.	(PPNI, JINR, ILLG)
Translated from UFN 175 905.			

Baryon Particle Listings

n , N 's and Δ 's, $N(1440)$

WIETFFELDT	05	MPL A20 1783	F.E. Wietfeldt	(TULN)
SOLDNER	04	PL B581 49	T. Soldner et al.	(ILLG, TUM)
DEWEY	03	PRL 91 192302	M.S. Dewey et al.	(NIST, TULN, INO+)
KOSSERT	03	EPJ A16 259	K. Kossert et al.	(Mainz MAMI Collab.)
Also				
LUNDIN	03	PRL 88 162301	M. Lundin et al.	(Mainz MAMI Collab.)
ABELE	02	PRL 88 211801	H. Abele et al.	(PERKEO-II Collab.)
BECK	02	JETPL 76 332	M. Beck et al.	(LEUV, SUSS, KIAE, PNPI)
Also				
BYRNE	02	JP G28 1325	J. Byrne et al.	
CHUNG	02B	PR D66 032004	J. Chung et al.	(SOUDAN-2 Collab.)
MOSTOVOI	01	PAN 64 1955	Yu.A. Mostovoi et al.	
Also				
ARZUMANOV	00	PL B483 15	S. Arzumanov et al.	
GAL	00	PR C61 028201	A. Gal	
KOLB	00	PRL 85 1388	N.R. Kolb et al.	
LAMOREAUX	00	PR D61 051301	S.K. Lamoreaux, R. Golub	
LEVCHUK	00	NP A674 1401	M. Levchuk, A.I. L'vov	(BELA, LEBD)
LISING	00	PR C62 055501	L.J. Lising et al.	(NIST emIT Collab.)
HARRIS	99	PRL 82 904	P.G. Harris et al.	
KESSLER	99	PL A255 221	E.G. Kessler Jr et al.	
MOHR	99	JPCRD 28 1713	P.J. Mohr, B.N. Taylor	(NIST)
Also				
SEREBROV	98	RMP 72 351	P.J. Mohr, B.N. Taylor	(NIST)
Also				
JETP 86 1074			A.P. Serebrov et al.	
Also				
Translated from ZETFP 113 1963.				
ABELE	97D	PL B407 212	H. Abele et al.	(HEIDP, ILLG)
KOPECKY	97	PR C56 2229	S. Kopecky et al.	
LIAUD	97	NP A612 53	P. Liaud et al.	(ILLG, LAPP)
YERAZLIM...	97	PL B412 240	B.G. Eroozolimsky et al.	(HARV, PNPI, KIAE)
ALTAREV	96	PAN 59 1152	I.S. Altarev et al.	(PNPI)
Also				
Translated from YAF 59 1204.				
BONDAREN...	96	JETPL 64 416	L.N. Bondarenko et al.	(KIAE)
Also				
Translated from ZETFP 64 382.				
BYRNE	96	EPL 33 187	J. Byrne et al.	(SUSS, ILLG)
MOSTOVOI	96	PAN 59 968	Yu.A. Mostovoi	(KIAE)
Also				
Translated from YAF 59 1013.				
NORMAN	96	PR D53 4086	E.B. Norman, J.N. Bahcall, M. Goldhaber	(LBL+)
IGNATOVICH	95	JETPL 62 1	V.K. Ignatovich	(JINR)
Also				
Translated from ZETFP 62 3.				
KOESTER	95	PR C51 3363	L. Koester et al.	(TUM, JINR, LATV)
KOPECKY	95	PRL 74 2427	S. Kopecky et al.	
KUZNETSOV	95	PRL 75 794	I.A. Kuznetsov et al.	(PNPI, KIAE, HARV+)
SCHRECK...	95	PL B349 427	K. Schreckenbach et al.	(TUM, ILLG, LAPP)
BALDO...	94	ZPHY C63 409	M. Baldo-Ceolin et al.	(HEID, ILLG, PADO+)
DIFILIPPO	94	PRL 73 1481	F. Difilippo et al.	(MIT)
Also				
PRL 71 1998			V. Natarajan et al.	(MIT)
GOLUB	94	PRPL 237C 1	R. Golub, K. Lamoreaux	(HAHN, WASH)
MAMPE	93	JETPL 57 82	B. Mampe et al.	(KIAE)
Also				
Translated from ZETFP 57 77.				
ALTAREV	92	PL B276 242	I.S. Altarev et al.	(PNPI)
NESVIZHEV...	92	JETP 75 405	V.V. Nesvizhevsky et al.	(PNPI, JINR)
Also				
Translated from ZETFP 102 740.				
ALBERICO	91	NP A523 488	W.M. Alberico, A. de Pace, M. Pignone	(TORI)
DUBBERS	91	NP A527 239c	D. Dubbers	(ILLG)
Also				
EPL 11 195			D. Dubbers, W. Mampe, J. Dohner	(ILLG, HEID)
ERZOZOLIM...	91	PL B263 33	B.G. Eroozolimsky et al.	(PNPI, KIAE)
Also				
SJNP 52 999			B.G. Eroozolimsky et al.	(PNPI, KIAE)
Also				
Translated from YAF 52 1563.				
ERZOZOLIM...	91B	SJNP 53 260	B.G. Eroozolimsky, Y.A. Mostovoi	(KIAE)
Also				
Translated from YAF 53 418.				
SCHMIEDM...	91	PRL 66 1015	J. Schmiedmayer et al.	(TUW, ORNL)
WOOLCOCK	91	MPL A6 2579	W.S. Woolcock	(CANB)
ALFIMENKOV	90	JETPL 52 373	V.P. Alfimenkov et al.	(PNPI, JINR)
Also				
Translated from ZETFP 52 984.				
BALDO...	90	PL B236 95	M. Baldo-Ceolin et al.	(PADO, PAVI, HEIDP+)
BERGER	90	PRL B240 237	G. Berger et al.	(FRESUS Collab.)
BRESSI	90	NC 103A 731	G. Bressi et al.	(PAVI, ROMA, MILA)
BYRNE	90	PRL 65 289	J. Byrne et al.	(SUSS, NBS, SCOT, CBMN)
GREEN	90	JP G16 L75	K. Green, D. Thompson	(RAL)
RAMSEY	90	ARNPS 40 1	N.F. Ramsey	(HARV)
ROSE	90	PL B234 460	K.W. Rose et al.	(GOET, MPCM, MAINZ)
ROSE	90B	NP A514 621	K.W. Rose et al.	(GOET, MPCM)
SMITH	90	PL B234 191	K.F. Smith et al.	(SUSS, RAL, HARV+)
BRESSI	89	ZPHY C43 175	G. Bressi et al.	(INFN, MILA, PAVI, ROMA)
DOVER	89	NIM A284 13	C.B. Dover, A. Gal, J.M. Richard	(BNL, HEBR+)
KOSSAKOW...	89	NP A503 473	R. Kossakowski et al.	(LAPP, SAVO, ISNG+)
MAIPE	89	PRL 63 838	W. Mampe et al.	(ILLG, RISL, SUSS, URI)
MOHAPATRA	89	NIM A284 1	R.N. Mohapatra	(UMD)
PAUL	89	ZPHY C45 25	W. Paul et al.	(BONN, WUPP, MPIK, ILLG)
SCHMIEDM...	89	NIM A284 137	J. Schmiedmayer, H. Rauch, P. Rihs	(WIEN)
BAUMANN	88	PR D37 3107	J. Baumann et al.	(BAYR, MUNI, ILLG)
KOESTER	88	ZPHY A329 229	L. Koester, W. Waschkowski, J. Meier	(MUNI, TUM)
LAST	88	PRL 60 995	I. Last et al.	(HEIDP, ILLG, ANL)
SCHMIEDM...	88	PRL 61 1065	J. Schmiedmayer, H. Rauch, P. Rihs	(TUW)
Also			J. Schmiedmayer, H. Rauch, P. Rihs	(TUW)
PRL 61 2509 (errat.)				
SPIVAK	88	JETP 67 1735	P.E. Spivak	(KIAE)
Also				
Translated from ZETFP 94 1				
COHEN	87	RMP 59 1121	E.R. Cohen, B.N. Taylor	(RISC, NBS)
ALEKSANDR...	86	SJNP 44 900	Yu.A. Aleksandrov et al.	
Also				
Translated from YAF 44 1384.				
ALTAREV	86	JETPL 44 460	I.S. Altarev et al.	(PNPI)
Also				
Translated from ZETFP 44 360.				
BOPP	86	PRL 56 919	P. Bopp et al.	(HEIDP, ANL, ILLG)
Also				
ZPHY C37 179			E. Klempf et al.	(HEIDP, ANL, ILLG)
CRESTI	86	PL B177 206	M. Cresti et al.	(PADO)
Also				
PL B200 587 (errat.)			M. Cresti et al.	(PADO)
GREENE	86	PRL 56 819	G.L. Greene et al.	(NBS, ILLG)
KOESTER	86	Physica B137 282	L. Koester et al.	
KOSVINTSEV	86	JETPL 44 571	Y.Y. Kosvintsev, V.I. Morozov, G.I. Terekhov	(KIAE)
Also				
Translated from ZETFP 44 444.				
TAKITA	86	PR D34 902	M. Takita et al.	(KEK, TOKY+)
DOVER	85	PR C31 1423	C.B. Dover, A. Gal, J.M. Richard	(BNL)
FIDEGARO	85	PL B50B 122	G. Fidigarò et al.	(CERN, ILLG, PADO+)
PARK	85B	NP B252 261	H.S. Park et al.	(IMB Collab.)
BATTISTONI	84	PL B133B 454	G. Battistoni et al.	(NUSX Collab.)
JONES	84	PRL 52 720	T.W. Jones et al.	(IMB Collab.)
PENDELBURY	84	PL B136B 327	J.M. Pendlebury et al.	(SUSS, HARV, RAL+)
CHERRY	83	PRL 50 1354	M.L. Cherry et al.	(PENN, BNL)
DOVER	83	PR D27 1090	C.B. Dover, A. Gal, J.M. Richard	(BNL)
KABIR	83	PRL 51 231	P.K. Kabir	(HARV)
MOSTOVOY	83	JETPL 37 196	Yu.A. Mostovoi	(KIAE)
Also				
Translated from ZETFP 37 162.				
ROY	83	PR D28 1770	A. Roy et al.	(TATA)
VAIDYA	83	PR D27 486	S.C. Vaidya et al.	(TATA)
GAELER	82	PR D25 2887	R. Gahler, J. Kalus, W. Mampe	(BAYR, ILLG)
GREENE	82	Metrologia 18 93	G.L. Greene et al.	(YALE, HARV, ILLG+)
ALTAREV	81	PL 102B 13	I.S. Altarev et al.	(PNPI)
BARABANOV	80	JETPL 32 359	I.R. Barabanov et al.	(PNPI)
Also				
Translated from ZETFP 32 384.				
BYRNE	80	PL 92B 274	J. Byrne et al.	(SUSS, RL)
KOSVINTSEV	80	JETPL 31 236	Y.Y. Kosvintsev et al.	(JINR)
Also				
Translated from ZETFP 31 257.				
MOHAPATRA	80	PRL 44 1316	R.N. Mohapatra, R.E. Marshak	(CUNY, VPI)
ALTAREV	79	JETPL 29 730	I.S. Altarev et al.	(PNPI)
Also				
Translated from ZETFP 29 794.				

ERZOZOLIM...	79	SJNP 30 356	B.G. Eroozolimsky et al.	(KIAE)
Also				
Translated from YAF 30 692.				
NORMAN	79	PRL 43 1226	E.B. Norman, A.G. Seamster	(WASH)
BONDAREN...	78	JETPL 28 303	L.N. Bondarenko et al.	(KIAE)
Also				
Translated from ZETFP 28 328.				
SMOLENICE CONF.				
ERZOZOLIM...	78	SJNP 28 48	P.G. Bondarenko	(KIAE)
Also				
Translated from YAF 28 98.				
STRATOWA	78	PR D18 3970	C. Stratowa, R. Dobrozemsky, P. Weinzierl	(SEIB)
ERZOZOLIM...	77	JETPL 23 663	B.G. Eroozolimsky et al.	(KIAE)
Also				
Translated from ZETFP 23 720.				
KOESTER	76	PRL 36 1021	L. Koester et al.	
STEINBERG	76	PR D13 2469	R.I. Steinberg et al.	(YALE, ISNG)
DOBROZE...	75	PR D11 510	R. Dobrozemsky et al.	(SEIB)
KROHN	75	PL 65B 175	V.E. Krohn, G.R. Ringo	(ANL)
ERZOZOLIM...	74	JETPL 20 345	B.G. Eroozolimsky et al.	
Also				
Translated from ZETFP 20 745.				
KROPF	74	ZPHY 267 129	H. Kropf, E. Paul	(LINZ)
Also				
NP A154 160			H. Paul	(WIEN)
STEINBERG	74	PRL 33 441	R.I. Steinberg et al.	(YALE, ISNG)
COHEN	73	JPCRD 2 664	E.R. Cohen, B.N. Taylor	(RISC, NBS)
KROHN	73	PR D8 1305	V.E. Krohn, G.R. Ringo	
CHRISTENSEN	72	PR D5 1628	C.J. Christensen et al.	(RIS O)
CHRISTENSEN	70	PR C1 1693	C.J. Christensen, V.E. Krohn, G.R. Ringo	(ANL)
ERZOZOLIM...	70C	PL 33B 351	B.G. Eroozolimsky et al.	(KIAE)
GRIGOREV	68	SJNP 6 239	V.K. Grigoriev et al.	(ITEP)
Also				
Translated from YAF 6 329.				
KROHN	66	PR 148 1303	V.E. Krohn, G.R. Ringo	
LEE	56	PR 104 254	T.D. Lee, C.N. Yang	(COLU, BNL)

See the related review(s):

N and Δ Resonances

$N(1440) 1/2^+$

$I(J^P) = \frac{1}{2}(\frac{1}{2}^+)$ Status: * * * *

Older and obsolete values are listed and referenced in the 2014 edition, Chinese Physics C38 070001 (2014).

$N(1440)$ POLE POSITION

REAL PART

VALUE (MeV)	DOCUMENT ID	TECN	COMMENT
1360 to 1380 (\approx 1370) OUR ESTIMATE			
1353 \pm 1	ROENCHEN	22	DPWA Multichannel
1369 \pm 3	SOKHOYAN	15A	DPWA Multichannel
1363 \pm 2 \pm 2	SVARC	14	L+P $\pi N \rightarrow \pi N$
1375 \pm 30	CUTKOSKY	80	IPWA $\pi N \rightarrow \pi N$
• • • We do not use the following data for averages, fits, limits, etc. • • •			
1360	HUNT	19	DPWA Multichannel
1355	ROENCHEN	15A	DPWA Multichannel
1386	SHKLYAR	13	DPWA Multichannel
1370 \pm 4	ANISOVICH	12A	DPWA Multichannel
1363 \pm 11	BATINIC	10	DPWA $\pi N \rightarrow N\pi, N\eta$
1359	ARNDT	06	DPWA $\pi N \rightarrow \pi N, \eta N$
1383	VRANA	00	DPWA Multichannel
1385	HOEHLER	93	SPED $\pi N \rightarrow \pi N$
¹ Fit to the amplitudes of HOEHLER 79.			

−2xIMAGINARY PART

VALUE (MeV)	DOCUMENT ID	TECN	COMMENT
180 to 205 (\approx 190) OUR ESTIMATE			
203 \pm 2	ROENCHEN	22	DPWA Multichannel
189 \pm 5	SOKHOYAN	15A	DPWA Multichannel
180 \pm 4 \pm 5	SVARC	14	L+P $\pi N \rightarrow \pi N$
180 \pm 40	CUTKOSKY	80	IPWA $\pi N \rightarrow \pi N$
• • • We do not use the following data for averages, fits, limits, etc. • • •			
186	HUNT	19	DPWA Multichannel
215	ROENCHEN	15A	DPWA Multichannel
277	SHKLYAR	13	DPWA Multichannel
190 \pm 7	ANISOVICH	12A	DPWA Multichannel
151 \pm 13	BATINIC	10	DPWA $\pi N \rightarrow N\pi, N\eta$
162	ARNDT	06	DPWA $\pi N \rightarrow \pi N, \eta N$
316	VRANA	00	DPWA Multichannel
164	HOEHLER	93	SPED $\pi N \rightarrow \pi N$
¹ Fit to the amplitudes of HOEHLER 79.			

$N(1440)$ ELASTIC POLE RESIDUE

MODULUS $|r|$

VALUE (MeV)	DOCUMENT ID	TECN	COMMENT
50 to 60 (\approx 55) OUR ESTIMATE			
59 \pm 1	ROENCHEN	22	DPWA Multichannel
49 \pm 3	SOKHOYAN	15A	DPWA Multichannel
50 \pm 1 \pm 2	SVARC	14	L+P $\pi N \rightarrow \pi N$
52 \pm 5	CUTKOSKY	80	IPWA $\pi N \rightarrow \pi N$
• • • We do not use the following data for averages, fits, limits, etc. • • •			
62	ROENCHEN	15A	DPWA Multichannel
126	SHKLYAR	13	DPWA Multichannel
48 \pm 3	ANISOVICH	12A	DPWA Multichannel
44	BATINIC	10	DPWA $\pi N \rightarrow N\pi, N\eta$
38	ARNDT	06	DPWA $\pi N \rightarrow \pi N, \eta N$
40	HOEHLER	93	SPED $\pi N \rightarrow \pi N$
¹ Fit to the amplitudes of HOEHLER 79.			

PHASE θ

VALUE (°)	DOCUMENT ID	TECN	COMMENT
-100 to -80 (≈ -90) OUR ESTIMATE			
-104 ± 2	ROENCHEN 22	DPWA	Multichannel
-82 ± 5	SOKHOYAN 15A	DPWA	Multichannel
-88 ± 1 ± 2	¹ SVARC 14	L+P	$\pi N \rightarrow \pi N$
-100 ± 35	CUTKOSKY 80	IPWA	$\pi N \rightarrow \pi N$
••• We do not use the following data for averages, fits, limits, etc. •••			
-98	ROENCHEN 15A	DPWA	Multichannel
-60	SHKLYAR 13	DPWA	Multichannel
-78 ± 4	ANISOVICH 12A	DPWA	Multichannel
-88	BATINIC 10	DPWA	$\pi N \rightarrow N\pi, N\eta$
-98	ARNDT 06	DPWA	$\pi N \rightarrow \pi N, \eta N$
¹ Fit to the amplitudes of HOEHLER 79.			

N(1440) INELASTIC POLE RESIDUE

The "normalized residue" is the residue divided by $\Gamma_{pole}/2$.

Normalized residue in $N\pi \rightarrow N(1440) \rightarrow N\eta$

MODULUS	PHASE (°)	DOCUMENT ID	TECN	COMMENT
0.084 ± 0.002	-28 ± 2	ROENCHEN 22	DPWA	Multichannel
••• We do not use the following data for averages, fits, limits, etc. •••				
0.078	-27	ROENCHEN 15A	DPWA	Multichannel

Normalized residue in $N\pi \rightarrow N(1440) \rightarrow \Delta\pi, P$ -wave

MODULUS	PHASE (°)	DOCUMENT ID	TECN	COMMENT
0.27 ± 0.02	38 ± 5	SOKHOYAN 15A	DPWA	Multichannel
••• We do not use the following data for averages, fits, limits, etc. •••				
0.27 ± 0.02	40 ± 5	ANISOVICH 12A	DPWA	Multichannel

Normalized residue in $N\pi \rightarrow N(1440) \rightarrow \Lambda K$

MODULUS	PHASE (°)	DOCUMENT ID	TECN	COMMENT
0.025 ± 0.005	-92 ± 43	ROENCHEN 22	DPWA	Multichannel
••• We do not use the following data for averages, fits, limits, etc. •••				
0.016	145	ROENCHEN 15A	DPWA	Multichannel

Normalized residue in $N\pi \rightarrow N(1440) \rightarrow \Sigma K$

MODULUS	PHASE (°)	DOCUMENT ID	TECN	COMMENT
0.002 ± 0.003	-32 ± 77	ROENCHEN 22	DPWA	Multichannel
••• We do not use the following data for averages, fits, limits, etc. •••				
0.027	113	ROENCHEN 15A	DPWA	Multichannel

Normalized residue in $N\pi \rightarrow N(1440) \rightarrow N(\pi\pi)_{S=0}^{I=0}$

MODULUS	PHASE (°)	DOCUMENT ID	TECN	COMMENT
0.21 ± 0.04	-136 ± 4	SOKHOYAN 15A	DPWA	Multichannel
••• We do not use the following data for averages, fits, limits, etc. •••				
0.21 ± 0.05	-135 ± 7	ANISOVICH 12A	DPWA	Multichannel

N(1440) BREIT-WIGNER MASS

VALUE (MeV)	DOCUMENT ID	TECN	COMMENT
1410 to 1470 (≈ 1440) OUR ESTIMATE			
1417 ± 4	¹ HUNT 19	DPWA	Multichannel
1430 ± 10	SOKHOYAN 15A	DPWA	Multichannel
1515 ± 15	¹ SHKLYAR 13	DPWA	Multichannel
1485.0 ± 1.2	¹ ARNDT 06	DPWA	$\pi N \rightarrow \pi N, \eta N$
1440 ± 30	CUTKOSKY 80	IPWA	$\pi N \rightarrow \pi N$
1410 ± 12	HOEHLER 79	IPWA	$\pi N \rightarrow \pi N$
••• We do not use the following data for averages, fits, limits, etc. •••			
1430 ± 8	ANISOVICH 12A	DPWA	Multichannel
1412 ± 2	¹ SHRESTHA 12A	DPWA	Multichannel
1439 ± 19	BATINIC 10	DPWA	$\pi N \rightarrow N\pi, N\eta$
1518 ± 5	PENNER 02C	DPWA	Multichannel
1479 ± 80	VRANA 00	DPWA	Multichannel
¹ Statistical error only.			

N(1440) BREIT-WIGNER WIDTH

VALUE (MeV)	DOCUMENT ID	TECN	COMMENT
250 to 410 (≈ 350) OUR ESTIMATE			
257 ± 11	¹ HUNT 19	DPWA	Multichannel
360 ± 30	SOKHOYAN 15A	DPWA	Multichannel
605 ± 90	¹ SHKLYAR 13	DPWA	Multichannel
284 ± 18	¹ ARNDT 06	DPWA	$\pi N \rightarrow \pi N, \eta N$
340 ± 70	CUTKOSKY 80	IPWA	$\pi N \rightarrow \pi N$
135 ± 10	HOEHLER 79	IPWA	$\pi N \rightarrow \pi N$
••• We do not use the following data for averages, fits, limits, etc. •••			
365 ± 35	ANISOVICH 12A	DPWA	Multichannel
248 ± 5	¹ SHRESTHA 12A	DPWA	Multichannel
437 ± 141	BATINIC 10	DPWA	$\pi N \rightarrow N\pi, N\eta$
668 ± 41	PENNER 02C	DPWA	Multichannel
490 ± 120	VRANA 00	DPWA	Multichannel
¹ Statistical error only.			

N(1440) DECAY MODES

The following branching fractions are our estimates, not fits or averages.

Mode	Fraction (Γ_i/Γ)
Γ_1 $N\pi$	55-75 %
Γ_2 $N\eta$	<1 %
Γ_3 $N\pi\pi$	17-50 %
Γ_4 $\Delta(1232)\pi, P$ -wave	6-27 %
Γ_5 $N\sigma$	11-23 %
Γ_6 $p\gamma, \text{helicity}=1/2$	0.035-0.048 %
Γ_7 $n\gamma, \text{helicity}=1/2$	0.02-0.04 %

N(1440) BRANCHING RATIOS

$\Gamma(N\pi)/\Gamma_{total}$	VALUE (%)	DOCUMENT ID	TECN	COMMENT	Γ_1/Γ
-------------------------------	-----------	-------------	------	---------	-------------------

55 to 75 (≈ 65) OUR ESTIMATE

59 ± 2	¹ HUNT 19	DPWA	Multichannel		
63 ± 2	SOKHOYAN 15A	DPWA	Multichannel		
56 ± 2	¹ SHKLYAR 13	DPWA	Multichannel		
78.7 ± 1.6	¹ ARNDT 06	DPWA	$\pi N \rightarrow \pi N, \eta N$		
68 ± 4	CUTKOSKY 80	IPWA	$\pi N \rightarrow \pi N$		
51 ± 5	HOEHLER 79	IPWA	$\pi N \rightarrow \pi N$		
••• We do not use the following data for averages, fits, limits, etc. •••					
62 ± 3	ANISOVICH 12A	DPWA	Multichannel		
64.8 ± 0.9	¹ SHRESTHA 12A	DPWA	Multichannel		
62 ± 4	BATINIC 10	DPWA	$\pi N \rightarrow N\pi, N\eta$		
57 ± 1	PENNER 02C	DPWA	Multichannel		
72 ± 5	VRANA 00	DPWA	Multichannel		
¹ Statistical error only.					

$\Gamma(N\eta)/\Gamma_{total}$	VALUE (%)	DOCUMENT ID	TECN	COMMENT	Γ_2/Γ
--------------------------------	-----------	-------------	------	---------	-------------------

0 ± 1	VRANA 00	DPWA	Multichannel		
••• We do not use the following data for averages, fits, limits, etc. •••					

$\Gamma(\Delta(1232)\pi, P\text{-wave})/\Gamma_{total}$	VALUE (%)	DOCUMENT ID	TECN	COMMENT	Γ_4/Γ
---	-----------	-------------	------	---------	-------------------

6 to 27 (≈ 15) OUR ESTIMATE

22 ± 4	¹ HUNT 19	DPWA	Multichannel		
12 ⁺⁵ ₋₃	SHKLYAR 16	DPWA	Multichannel		
20 ± 7	SOKHOYAN 15A	DPWA	Multichannel		
••• We do not use the following data for averages, fits, limits, etc. •••					
21 ± 8	ANISOVICH 12A	DPWA	Multichannel		
6.5 ± 0.8	¹ SHRESTHA 12A	DPWA	Multichannel		
16 ± 1	VRANA 00	DPWA	Multichannel		
¹ Statistical error only.					

$\Gamma(N\sigma)/\Gamma_{total}$	VALUE (%)	DOCUMENT ID	TECN	COMMENT	Γ_5/Γ
----------------------------------	-----------	-------------	------	---------	-------------------

16 ± 3	¹ HUNT 19	DPWA	Multichannel		
27 ⁺⁴ ₋₉	SHKLYAR 16	DPWA	Multichannel		
17 ± 6	SOKHOYAN 15A	DPWA	Multichannel		
••• We do not use the following data for averages, fits, limits, etc. •••					
17 ± 7	ANISOVICH 12A	DPWA	Multichannel		
27 ± 1	¹ SHRESTHA 12A	DPWA	Multichannel		
12 ± 1	VRANA 00	DPWA	Multichannel		
¹ Statistical error only.					

N(1440) PHOTON DECAY AMPLITUDES AT THE POLE

N(1440) → p γ , helicity-1/2 amplitude $A_{1/2}$

MODULUS (GeV ^{-1/2})	PHASE (°)	DOCUMENT ID	TECN	COMMENT
-0.090 ± 0.007	-30 ± 3	ROENCHEN 22	DPWA	Multichannel
-0.044 ± 0.005	-40 ± 8	SOKHOYAN 15A	DPWA	Multichannel
••• We do not use the following data for averages, fits, limits, etc. •••				
-0.060	-23	ROENCHEN 15A	DPWA	Multichannel

N(1440) → n γ , helicity-1/2 amplitude $A_{1/2}$

MODULUS (GeV ^{-1/2})	PHASE (°)	DOCUMENT ID	TECN	COMMENT
0.041 ± 0.005	23 ± 10	ANISOVICH 17E	DPWA	Multichannel

N(1440) BREIT-WIGNER PHOTON DECAY AMPLITUDES

N(1440) → p γ , helicity-1/2 amplitude $A_{1/2}$

VALUE (GeV ^{-1/2})	DOCUMENT ID	TECN	COMMENT
-0.080 to -0.050 (≈ -0.065) OUR ESTIMATE			
-0.091 ± 0.007	¹ HUNT 19	DPWA	Multichannel

Baryon Particle Listings

$N(1440), N(1520)$

-0.061 ± 0.006	SOKHOYAN	15A	DPWA	Multichannel
-0.085 ± 0.003	¹ SHKLYAR	13	DPWA	Multichannel
-0.056 ± 0.001	¹ WORKMAN	12A	DPWA	$\gamma N \rightarrow N\pi$
-0.051 ± 0.002	¹ DUGGER	07	DPWA	$\gamma N \rightarrow \pi N$
••• We do not use the following data for averages, fits, limits, etc. •••				
-0.061 ± 0.008	ANISOVICH	12A	DPWA	Multichannel
-0.084 ± 0.003	¹ SHRESTHA	12A	DPWA	Multichannel
-0.061	DRECHSEL	07	DPWA	$\gamma N \rightarrow \pi N$
-0.087	PENNER	02D	DPWA	Multichannel

¹ Statistical error only.

$N(1440) \rightarrow n\gamma$, helicity-1/2 amplitude $A_{1/2}$

VALUE (GeV ^{-1/2})	DOCUMENT ID	TECN	COMMENT	
0.035 to 0.055 (≈ 0.045) OUR ESTIMATE				
0.013 ± 0.012	¹ HUNT	19	DPWA Multichannel	
0.053 ± 0.007	ANISOVICH	17E	DPWA Multichannel	
0.048 ± 0.004	¹ CHEN	12A	DPWA $\gamma N \rightarrow \pi N$	
••• We do not use the following data for averages, fits, limits, etc. •••				
0.043 ± 0.012	ANISOVICH	13B	DPWA Multichannel	
0.040 ± 0.005	¹ SHRESTHA	12A	DPWA Multichannel	
0.054	DRECHSEL	07	DPWA $\gamma N \rightarrow \pi N$	
0.121	PENNER	02D	DPWA Multichannel	

¹ Statistical error only.

$N(1440)$ REFERENCES

For early references, see Physics Letters **111B** 1 (1982).

ROENCHEN	22	EPJ A58 229	D. Roenchen et al.	(JULI, GWU, BONN+)
HUNT	19	PR C99 055205	B. C. Hunt, D.M. Manley	
ANISOVICH	17E	PR C96 055202	A.V. Anisovich et al.	(BONN, PNPI, JLAB+)
SHKLYAR	16	PR C93 045206	V. Shklyar, H. Lenseke, U. Mosel	(GIES)
ROENCHEN	15A	EPJ A51 70	D. Roenchen et al.	
SOKHOYAN	15A	EPJ A51 95	V. Sokhoyan et al.	(CBELSA/TAPS Collab.)
PDG	14	CP C38 070001	K. Olive et al.	(PDG Collab.)
SVARC	14	PR C89 045205	A. Svarc et al.	(RBI Zagreb, UNI Tuzla)
ANISOVICH	13B	EPJ A49 67	A.V. Anisovich et al.	
SHKLYAR	13	PR C87 015201	V. Shklyar, H. Lenseke, U. Mosel	(GIES)
ANISOVICH	12A	EPJ A48 15	A.V. Anisovich et al.	(BONN, PNPI)
CHEN	12A	PR C86 015206	W. Chen et al.	(DUKE, GWU, MSST, ITEP+)
SHRESTHA	12A	PR C86 055203	M. Shrestha, D.M. Manley	(KSU)
WORKMAN	12A	PR C86 015202	R. Workman et al.	(GWU)
BATINIC	10	PR C82 038203	M. Batinic et al.	(ZAGR)
DRECHSEL	07	EPJ A34 69	D. Drechsel, S.S. Kamalov, L. Tiator	(MAINZ, JINR)
DUGGER	07	PR C76 025211	M. Dugger et al.	(JLab CLAS Collab.)
ARNDT	06	PR C74 045205	R.A. Arndt et al.	(GWU)
PENNER	02C	PR C66 055211	G. Penner, U. Mosel	(GIES)
PENNER	02D	PR C66 055212	G. Penner, U. Mosel	(GIES)
VRANA	00	PRPL 326 181	T.P. Vrana, S.A. Dytman, T.-S.H. Lee	(PITT, ANL)
HOEHLER	93	πN Newsletter 9 1	G. Hoehler	(KARL)
CUTKOSKY	80	Toronto Conf. 19	R.E. Cutkosky et al.	(CMU, LBL) IJP
		Also PR D20 2839	R.E. Cutkosky et al.	(CMU, LBL) IJP
HOEHLER	79	PDAT 12-1	G. Hoehler et al.	(KARLT) IJP
		Also Toronto Conf. 3	R. Koch	(KARLT) IJP

$N(1520) 3/2^-$

$$J(J^P) = \frac{1}{2}(3/2^-) \text{ Status: } ***$$

Older and obsolete values are listed and referenced in the 2014 edition, Chinese Physics **C38** 070001 (2014).

$N(1520)$ POLE POSITION

REAL PART	VALUE (MeV)	DOCUMENT ID	TECN	COMMENT
1505 to 1515 (≈ 1510) OUR ESTIMATE				
1482 ± 3	ROENCHEN	22	DPWA	Multichannel
1507 ± 2	SOKHOYAN	15A	DPWA	Multichannel
1506 ± 1 ± 1	¹ SVARC	14	L+P	$\pi N \rightarrow \pi N$
1510 ± 5	CUTKOSKY	80	IPWA	$\pi N \rightarrow \pi N$
••• We do not use the following data for averages, fits, limits, etc. •••				
1500	HUNT	19	DPWA	Multichannel
1512	ROENCHEN	15A	DPWA	Multichannel
1492	SHKLYAR	13	DPWA	Multichannel
1507 ± 3	ANISOVICH	12A	DPWA	Multichannel
1506 ± 9	BATINIC	10	DPWA	$\pi N \rightarrow N\pi, N\eta$
1515	ARNDT	06	DPWA	$\pi N \rightarrow \pi N, \eta N$
1504	VRANA	00	DPWA	Multichannel
1510	HOEHLER	93	ARGD	$\pi N \rightarrow \pi N$

¹ Fit to the amplitudes of HOEHLER 79.

-2xIMAGINARY PART

VALUE (MeV)	DOCUMENT ID	TECN	COMMENT	
105 to 120 (≈ 110) OUR ESTIMATE				
126 ± 9	ROENCHEN	22	DPWA Multichannel	
111 ± 3	SOKHOYAN	15A	DPWA Multichannel	
115 ± 2 ± 1	¹ SVARC	14	L+P $\pi N \rightarrow \pi N$	
114 ± 10	CUTKOSKY	80	IPWA $\pi N \rightarrow \pi N$	
••• We do not use the following data for averages, fits, limits, etc. •••				
117	HUNT	19	DPWA Multichannel	
89	ROENCHEN	15A	DPWA Multichannel	

94	SHKLYAR	13	DPWA	Multichannel
111 ± 5	ANISOVICH	12A	DPWA	Multichannel
122 ± 9	BATINIC	10	DPWA	$\pi N \rightarrow N\pi, N\eta$
113	ARNDT	06	DPWA	$\pi N \rightarrow \pi N, \eta N$
112	VRANA	00	DPWA	Multichannel
120	HOEHLER	93	ARGD	$\pi N \rightarrow \pi N$

¹ Fit to the amplitudes of HOEHLER 79.

$N(1520)$ ELASTIC POLE RESIDUE

MODULUS $|r|$

VALUE (MeV)	DOCUMENT ID	TECN	COMMENT	
32 to 38 (≈ 35) OUR ESTIMATE				
27 ± 11	ROENCHEN	22	DPWA Multichannel	
36 ± 2	SOKHOYAN	15A	DPWA Multichannel	
33 ± 1 ± 1	¹ SVARC	14	L+P $\pi N \rightarrow \pi N$	
35 ± 2	CUTKOSKY	80	IPWA $\pi N \rightarrow \pi N$	
••• We do not use the following data for averages, fits, limits, etc. •••				
37	ROENCHEN	15A	DPWA Multichannel	
27	SHKLYAR	13	DPWA Multichannel	
36 ± 3	ANISOVICH	12A	DPWA Multichannel	
35	BATINIC	10	DPWA $\pi N \rightarrow N\pi, N\eta$	
38	ARNDT	06	DPWA $\pi N \rightarrow \pi N, \eta N$	
32	HOEHLER	93	ARGD $\pi N \rightarrow \pi N$	

¹ Fit to the amplitudes of HOEHLER 79.

PHASE θ

VALUE (°)	DOCUMENT ID	TECN	COMMENT	
-15 to -5 (≈ -10) OUR ESTIMATE				
-36 ± 24	ROENCHEN	22	DPWA Multichannel	
-14 ± 3	SOKHOYAN	15A	DPWA Multichannel	
-15 ± 1 ± 1	¹ SVARC	14	L+P $\pi N \rightarrow \pi N$	
-12 ± 5	CUTKOSKY	80	IPWA $\pi N \rightarrow \pi N$	
••• We do not use the following data for averages, fits, limits, etc. •••				
-6	ROENCHEN	15A	DPWA Multichannel	
-35	SHKLYAR	13	DPWA Multichannel	
-14 ± 3	ANISOVICH	12A	DPWA Multichannel	
-7	BATINIC	10	DPWA $\pi N \rightarrow N\pi, N\eta$	
-5	ARNDT	06	DPWA $\pi N \rightarrow \pi N, \eta N$	
-8	HOEHLER	93	ARGD $\pi N \rightarrow \pi N$	

¹ Fit to the amplitudes of HOEHLER 79.

$N(1520)$ INELASTIC POLE RESIDUE

The "normalized residue" is the residue divided by $\Gamma_{pole}/2$.

Normalized residue in $N\pi \rightarrow N(1520) \rightarrow \Delta\pi, S\text{-wave}$

MODULUS	PHASE (°)	DOCUMENT ID	TECN	COMMENT
0.33 ± 0.04	155 ± 15	SOKHOYAN	15A	DPWA Multichannel
••• We do not use the following data for averages, fits, limits, etc. •••				
0.33 ± 0.05	150 ± 20	ANISOVICH	12A	DPWA Multichannel

Normalized residue in $N\pi \rightarrow N(1520) \rightarrow \Delta\pi, D\text{-wave}$

MODULUS	PHASE (°)	DOCUMENT ID	TECN	COMMENT
0.25 ± 0.03	105 ± 18	SOKHOYAN	15A	DPWA Multichannel
••• We do not use the following data for averages, fits, limits, etc. •••				
0.25 ± 0.03	100 ± 20	ANISOVICH	12A	DPWA Multichannel

Normalized residue in $N\pi \rightarrow N(1520) \rightarrow N\eta$

MODULUS	PHASE (°)	DOCUMENT ID	TECN	COMMENT
0.021 ± 0.009	34 ± 27	ROENCHEN	22	DPWA Multichannel
••• We do not use the following data for averages, fits, limits, etc. •••				
0.026	95	ROENCHEN	15A	DPWA Multichannel

Normalized residue in $N\pi \rightarrow N(1520) \rightarrow \Lambda K$

MODULUS	PHASE (°)	DOCUMENT ID	TECN	COMMENT
0.026 ± 0.010	127 ± 24	ROENCHEN	22	DPWA Multichannel
••• We do not use the following data for averages, fits, limits, etc. •••				
0.069	158	ROENCHEN	15A	DPWA Multichannel

Normalized residue in $N\pi \rightarrow N(1520) \rightarrow \Sigma K$

MODULUS	PHASE (°)	DOCUMENT ID	TECN	COMMENT
0.010 ± 0.006	94 ± 34	ROENCHEN	22	DPWA Multichannel
••• We do not use the following data for averages, fits, limits, etc. •••				
0.049	-41	ROENCHEN	15A	DPWA Multichannel

Normalized residue in $N\pi \rightarrow N(1520) \rightarrow N\sigma$

MODULUS	PHASE (°)	DOCUMENT ID	TECN	COMMENT
0.08 ± 0.03	-45 ± 25	SOKHOYAN	15A	DPWA Multichannel

N(1520) BREIT-WIGNER MASS

VALUE (MeV)	DOCUMENT ID	TECN	COMMENT
1510 to 1520 (\approx 1515) OUR ESTIMATE			
1512.0 \pm 1.5	¹ HUNT	19	DPWA Multichannel
1516 \pm 2	SOKHOYAN	15A	DPWA Multichannel
1505 \pm 4	¹ SHKLYAR	13	DPWA Multichannel
1514.5 \pm 0.2	¹ ARNDT	06	DPWA $\pi N \rightarrow \pi N, \eta N$
1525 \pm 10	CUTKOSKY	80	IPWA $\pi N \rightarrow \pi N$
1519 \pm 4	HOEHLER	79	IPWA $\pi N \rightarrow \pi N$
• • • We do not use the following data for averages, fits, limits, etc. • • •			
1517 \pm 3	ANISOVICH	12A	DPWA Multichannel
1512.6 \pm 0.5	¹ SHRESTHA	12A	DPWA Multichannel
1522 \pm 8	BATINIC	10	DPWA $\pi N \rightarrow N\pi, N\eta$
1509 \pm 1	PENNER	02C	DPWA Multichannel
1518 \pm 3	VRANA	00	DPWA Multichannel

¹ Statistical error only.

N(1520) BREIT-WIGNER WIDTH

VALUE (MeV)	DOCUMENT ID	TECN	COMMENT
100 to 120 (\approx 110) OUR ESTIMATE			
121 \pm 3	¹ HUNT	19	DPWA Multichannel
113 \pm 4	SOKHOYAN	15A	DPWA Multichannel
100 \pm 2	¹ SHKLYAR	13	DPWA Multichannel
103.6 \pm 0.4	¹ ARNDT	06	DPWA $\pi N \rightarrow \pi N, \eta N$
120 \pm 15	CUTKOSKY	80	IPWA $\pi N \rightarrow \pi N$
114 \pm 7	HOEHLER	79	IPWA $\pi N \rightarrow \pi N$
• • • We do not use the following data for averages, fits, limits, etc. • • •			
114 \pm 5	ANISOVICH	12A	DPWA Multichannel
117 \pm 1	¹ SHRESTHA	12A	DPWA Multichannel
132 \pm 11	BATINIC	10	DPWA $\pi N \rightarrow N\pi, N\eta$
100 \pm 2	PENNER	02C	DPWA Multichannel
124 \pm 4	VRANA	00	DPWA Multichannel

¹ Statistical error only.

N(1520) DECAY MODES

The following branching fractions are our estimates, not fits or averages.

Mode	Fraction (Γ_i/Γ)
Γ_1 $N\pi$	55–65 %
Γ_2 $N\eta$	0.07–0.09 %
Γ_3 $N\pi\pi$	25–35 %
Γ_4 $\Delta(1232)\pi$	22–34 %
Γ_5 $\Delta(1232)\pi, S\text{-wave}$	15–23 %
Γ_6 $\Delta(1232)\pi, D\text{-wave}$	7–11 %
Γ_7 $N\rho$	10–16 %
Γ_8 $N\rho, S=3/2, S\text{-wave}$	10–16 %
Γ_9 $N\rho, S=1/2, D\text{-wave}$	0.2–0.4 %
Γ_{10} $N\sigma$	<10 %
Γ_{11} $p\gamma$	0.31–0.52 %
Γ_{12} $p\gamma, \text{helicity}=1/2$	0.01–0.02 %
Γ_{13} $p\gamma, \text{helicity}=3/2$	0.30–0.50 %
Γ_{14} $n\gamma$	0.30–0.53 %
Γ_{15} $n\gamma, \text{helicity}=1/2$	0.04–0.10 %
Γ_{16} $n\gamma, \text{helicity}=3/2$	0.25–0.45 %

N(1520) BRANCHING RATIOS

$\Gamma(N\pi)/\Gamma_{\text{total}}$	DOCUMENT ID	TECN	COMMENT	Γ_1/Γ
55 to 65 (\approx 60) OUR ESTIMATE				
58.3 \pm 1.5	¹ HUNT	19	DPWA Multichannel	
61 \pm 2	SOKHOYAN	15A	DPWA Multichannel	
57 \pm 2	¹ SHKLYAR	13	DPWA Multichannel	
63.2 \pm 0.1	¹ ARNDT	06	DPWA $\pi N \rightarrow \pi N, \eta N$	
58 \pm 3	CUTKOSKY	80	IPWA $\pi N \rightarrow \pi N$	
54 \pm 3	HOEHLER	79	IPWA $\pi N \rightarrow \pi N$	
• • • We do not use the following data for averages, fits, limits, etc. • • •				
62 \pm 3	ANISOVICH	12A	DPWA Multichannel	
62.7 \pm 0.5	¹ SHRESTHA	12A	DPWA Multichannel	
55 \pm 5	BATINIC	10	DPWA $\pi N \rightarrow N\pi, N\eta$	
56 \pm 1	PENNER	02C	DPWA Multichannel	
63 \pm 2	VRANA	00	DPWA Multichannel	

¹ Statistical error only.

$\Gamma(N\eta)/\Gamma_{\text{total}}$	DOCUMENT ID	TECN	COMMENT	Γ_2/Γ
VALUE (%)				
<0.1	MUELLER	20	DPWA Multichannel	
0.03 \pm 0.01	¹ HUNT	19	DPWA Multichannel	
0.08 \pm 0.01	TIATOR	99	DPWA $\gamma p \rightarrow p\eta$	
• • • We do not use the following data for averages, fits, limits, etc. • • •				
<1	SHKLYAR	13	DPWA Multichannel	
0.1 \pm 0.1	BATINIC	10	DPWA $\pi N \rightarrow N\pi, N\eta$	
0.2 \pm 0.1	THOMA	08	DPWA Multichannel	
0.08 to 0.12	ARNDT	05	DPWA Multichannel	
0.23 \pm 0.04	PENNER	02C	DPWA Multichannel	
0 \pm 1	VRANA	00	DPWA Multichannel	

¹ Statistical error only.

$\Gamma(\Delta(1232)\pi, S\text{-wave})/\Gamma_{\text{total}}$	DOCUMENT ID	TECN	COMMENT	Γ_5/Γ
VALUE (%)				
12.1 \pm 2.1	ADAMCZEW...	20	DPWA Multichannel	
21 \pm 2	¹ HUNT	19	DPWA Multichannel	
19 \pm 4	SOKHOYAN	15A	DPWA Multichannel	
• • • We do not use the following data for averages, fits, limits, etc. • • •				
19 \pm 4	ANISOVICH	12A	DPWA Multichannel	
9.3 \pm 0.7	¹ SHRESTHA	12A	DPWA Multichannel	
15 \pm 2	VRANA	00	DPWA Multichannel	

¹ Statistical error only.

$\Gamma(\Delta(1232)\pi, D\text{-wave})/\Gamma_{\text{total}}$	DOCUMENT ID	TECN	COMMENT	Γ_6/Γ
VALUE (%)				
6 \pm 2	ADAMCZEW...	20	DPWA Multichannel	
6 \pm 1	¹ HUNT	19	DPWA Multichannel	
9 \pm 2	SOKHOYAN	15A	DPWA Multichannel	
• • • We do not use the following data for averages, fits, limits, etc. • • •				
9 \pm 2	ANISOVICH	12A	DPWA Multichannel	
6.3 \pm 0.5	¹ SHRESTHA	12A	DPWA Multichannel	
11 \pm 2	VRANA	00	DPWA Multichannel	

¹ Statistical error only.

$\Gamma(N\rho, S=3/2, S\text{-wave})/\Gamma_{\text{total}}$	DOCUMENT ID	TECN	COMMENT	Γ_8/Γ
VALUE (%)				
10–16 % OUR EVALUATION				
11.8 \pm 1.9	ADAMCZEW...	20	DPWA Multichannel	
14.1 \pm 1.5	¹ HUNT	19	DPWA Multichannel	

¹ Statistical error only.

$\Gamma(N\rho, S=1/2, D\text{-wave})/\Gamma_{\text{total}}$	DOCUMENT ID	TECN	COMMENT	Γ_9/Γ
VALUE (%)				
0.2–0.4 % OUR EVALUATION				
0.4 \pm 0.2	ADAMCZEW...	20	DPWA Multichannel	

$\Gamma(N\sigma)/\Gamma_{\text{total}}$	DOCUMENT ID	TECN	COMMENT	Γ_{10}/Γ
VALUE (%)				
<10 % OUR ESTIMATE				
7 \pm 3	ADAMCZEW...	20	DPWA Multichannel	
<0.7	¹ HUNT	19	DPWA Multichannel	
<2	SOKHOYAN	15A	DPWA Multichannel	
• • • We do not use the following data for averages, fits, limits, etc. • • •				
<1	¹ SHRESTHA	12A	DPWA Multichannel	
<4	THOMA	08	DPWA Multichannel	
1 \pm 1	VRANA	00	DPWA Multichannel	

¹ Statistical error only.

N(1520) PHOTON DECAY AMPLITUDES AT THE POLE

N(1520) $\rightarrow p\gamma, \text{helicity}=1/2$ amplitude $A_{1/2}$			
MODULUS ($\text{GeV}^{-1/2}$)	PHASE ($^\circ$)	DOCUMENT ID	TECN COMMENT
-0.043 \pm 0.013	-47 \pm 10	ROENCHEN	22 DPWA Multichannel
-0.023 \pm 0.004	-6 \pm 5	SOKHOYAN	15A DPWA Multichannel
• • • We do not use the following data for averages, fits, limits, etc. • • •			
-0.031	-17	ROENCHEN	15A DPWA Multichannel
N(1520) $\rightarrow p\gamma, \text{helicity}=3/2$ amplitude $A_{3/2}$			
MODULUS ($\text{GeV}^{-1/2}$)	PHASE ($^\circ$)	DOCUMENT ID	TECN COMMENT
0.112 \pm 0.032	1.8 \pm 19	ROENCHEN	22 DPWA Multichannel
0.131 \pm 0.006	4 \pm 4	SOKHOYAN	15A DPWA Multichannel
• • • We do not use the following data for averages, fits, limits, etc. • • •			
0.075	1.7	ROENCHEN	15A DPWA Multichannel
N(1520) $\rightarrow n\gamma, \text{helicity}=1/2$ amplitude $A_{1/2}$			
MODULUS ($\text{GeV}^{-1/2}$)	PHASE ($^\circ$)	DOCUMENT ID	TECN COMMENT
-0.045 \pm 0.005	-5 \pm 4	ANISOVICH	17E DPWA Multichannel

Baryon Particle Listings

 $N(1520)$, $N(1535)$ $N(1520) \rightarrow n\gamma$, helicity-3/2 amplitude $A_{3/2}$

MODULUS ($\text{GeV}^{-1/2}$)	PHASE ($^\circ$)	DOCUMENT ID	TECN	COMMENT
-0.119 ± 0.005	5 ± 4	ANISOVICH	17E	DPWA Multichannel

 $N(1520)$ BREIT-WIGNER PHOTON DECAY AMPLITUDES $N(1520) \rightarrow p\gamma$, helicity-1/2 amplitude $A_{1/2}$

VALUE ($\text{GeV}^{-1/2}$)	DOCUMENT ID	TECN	COMMENT
-0.030 to -0.015 (≈ -0.025) OUR ESTIMATE			
-0.034 ± 0.003	¹ HUNT	19	DPWA Multichannel
-0.024 ± 0.004	SOKHOYAN	15A	DPWA Multichannel
-0.015 ± 0.001	¹ SHKLYAR	13	DPWA Multichannel
-0.019 ± 0.002	¹ WORKMAN	12A	DPWA $\gamma N \rightarrow N\pi$
-0.028 ± 0.002	¹ DUGGER	07	DPWA $\gamma N \rightarrow \pi N$
-0.038 ± 0.003	¹ AHRENS	02	DPWA $\gamma N \rightarrow \pi N$
• • • We do not use the following data for averages, fits, limits, etc. • • •			
-0.022 ± 0.004	ANISOVICH	12A	DPWA Multichannel
-0.034 ± 0.001	¹ SHRESTHA	12A	DPWA Multichannel
-0.027	DRECHSEL	07	DPWA $\gamma N \rightarrow \pi N$
-0.003	PENNER	02D	DPWA Multichannel
$-0.052 \pm 0.010 \pm 0.007$	¹ MUKHOPAD...	98	$\gamma\rho \rightarrow \eta\rho$
¹ Statistical error only.			

 $N(1520) \rightarrow p\gamma$, helicity-3/2 amplitude $A_{3/2}$

VALUE ($\text{GeV}^{-1/2}$)	DOCUMENT ID	TECN	COMMENT
0.135 to 0.145 (≈ 0.140) OUR ESTIMATE			
0.142 ± 0.003	¹ HUNT	19	DPWA Multichannel
0.130 ± 0.006	SOKHOYAN	15A	DPWA Multichannel
0.146 ± 0.001	¹ SHKLYAR	13	DPWA Multichannel
0.141 ± 0.002	¹ WORKMAN	12A	DPWA $\gamma N \rightarrow N\pi$
0.143 ± 0.002	¹ DUGGER	07	DPWA $\gamma N \rightarrow \pi N$
0.147 ± 0.010	¹ AHRENS	02	DPWA $\gamma N \rightarrow \pi N$
• • • We do not use the following data for averages, fits, limits, etc. • • •			
0.131 ± 0.010	ANISOVICH	12A	DPWA Multichannel
0.127 ± 0.003	¹ SHRESTHA	12A	DPWA Multichannel
0.161	DRECHSEL	07	DPWA $\gamma N \rightarrow \pi N$
0.151	PENNER	02D	DPWA Multichannel
$0.130 \pm 0.020 \pm 0.015$	¹ MUKHOPAD...	98	$\gamma\rho \rightarrow \eta\rho$
¹ Statistical error only.			

 $N(1520) \rightarrow n\gamma$, helicity-1/2 amplitude $A_{1/2}$

VALUE ($\text{GeV}^{-1/2}$)	DOCUMENT ID	TECN	COMMENT
-0.055 to -0.040 (≈ -0.050) OUR ESTIMATE			
-0.072 ± 0.003	¹ HUNT	19	DPWA Multichannel
-0.046 ± 0.005	ANISOVICH	17E	DPWA Multichannel
-0.046 ± 0.006	¹ CHEN	12A	DPWA $\gamma N \rightarrow \pi N$
• • • We do not use the following data for averages, fits, limits, etc. • • •			
-0.049 ± 0.008	ANISOVICH	13B	DPWA Multichannel
-0.038 ± 0.003	¹ SHRESTHA	12A	DPWA Multichannel
-0.077	DRECHSEL	07	DPWA $\gamma N \rightarrow \pi N$
-0.084	PENNER	02D	DPWA Multichannel
¹ Statistical error only.			

 $N(1520) \rightarrow n\gamma$, helicity-3/2 amplitude $A_{3/2}$

VALUE ($\text{GeV}^{-1/2}$)	DOCUMENT ID	TECN	COMMENT
-0.120 to -0.100 (≈ -0.115) OUR ESTIMATE			
-0.123 ± 0.006	¹ HUNT	19	DPWA Multichannel
-0.118 ± 0.005	ANISOVICH	17E	DPWA Multichannel
-0.115 ± 0.005	¹ CHEN	12A	DPWA $\gamma N \rightarrow \pi N$
• • • We do not use the following data for averages, fits, limits, etc. • • •			
-0.113 ± 0.012	ANISOVICH	13B	DPWA Multichannel
-0.101 ± 0.004	¹ SHRESTHA	12A	DPWA Multichannel
-0.154	DRECHSEL	07	DPWA $\gamma N \rightarrow \pi N$
-0.159	PENNER	02D	DPWA Multichannel
¹ Statistical error only.			

 $N(1520)$ REFERENCES

For early references, see Physics Letters **111B** 1 (1982). For very early references, see Reviews of Modern Physics **37** 633 (1965).

ROENCHEN	22	EPJ A58 229	D. Roenchen et al.	(JULI, GWU, BONN+)
ADAMCZEW...	20	PR C102 024001	J. Adamczewski-Musch et al.	(HADES Collab.)
MUELLER	20	PL B803 135323	J. Mueller et al.	(CBELSA/TAPS Collab.)
HUNT	19	PR C99 055205	B. C. Hunt, D. M. Manley	
ANISOVICH	17E	PR C96 055202	A. V. Anisovich et al.	(BONN, PNPI, JLAB+)
ROENCHEN	15A	EPJ A51 70	D. Roenchen et al.	
SOKHOYAN	15A	EPJ A51 95	V. Sokhoyan et al.	(CBELSA/TAPS Collab.)
PDG	14	CP C38 070001	K. Olive et al.	(PDG Collab.)
SVARC	14	PR C89 045205	A. Svarc et al.	(RBI Zagreb, UNI Tuzla)
ANISOVICH	13B	EPJ A49 67	A. V. Anisovich et al.	
SHKLYAR	13	PR C87 015201	V. Shklyar, H. Lense, U. Mosel	(GIES)
ANISOVICH	12A	EPJ A48 15	A. V. Anisovich et al.	(BONN, PNPI)
CHEN	12A	PR C86 015206	W. Chen et al.	(DUKE, GWU, MSST, ITEP+)
SHRESTHA	12A	PR C86 055203	M. Shrestha, D. M. Manley	(KSU)
WORKMAN	12A	PR C86 015202	R. Workman et al.	(GWU)

BATINIC	10	PR C82 038203	M. Batinic et al.	(ZAGR)
THOMA	08	PL B659 87	U. Thoma et al.	(CB-ELSA Collab.)
DRECHSEL	07	EPJ A34 69	D. Drechsel, S.S. Kamalov, L. Tiator	(MAINZ, JINR)
DUGGER	07	PR C76 025211	M. Dugger et al.	(JLab CLAS Collab.)
ARNDT	06	PR C74 045205	R.A. Arndt et al.	(GWU)
ARNDT	05	PR C72 045202	R.A. Arndt et al.	(GWU, PNPI)
AHRENS	02	PR L88 232002	J. Ahrens et al.	(Mainz MAMI GDH/A2 Collab.)
PENNER	02C	PR C66 055211	G. Penner, U. Mosel	(GIES)
PENNER	02D	PR C66 055212	G. Penner, U. Mosel	(GIES)
VRANA	00	PRPL 329 181	T.P. Vrana, S.A. Dytman, T.-S.H. Lee	(PITT, ANL)
TIATOR	99	PR C60 035210	L. Tiator et al.	
MUKHOPAD...	98	PL B444 7	N. C. Mukhopadhyay, N. Mathur	
HOEHLER	93	πN Newsletter 9 1	G. Hoehler	(KARL)
CUTKOSKY	80	Toronto Conf. 19	R.E. Cutkosky et al.	(CMU, LBL) IJP
Also		PR D20 2839	R.E. Cutkosky et al.	(CMU, LBL) IJP
HOEHLER	79	PDAT 12-1	G. Hoehler et al.	(KARLT) IJP
Also		Toronto Conf. 3	R. Koch	(KARLT) IJP

 $N(1535) 1/2^-$

$$I(J^P) = \frac{1}{2}(\frac{1}{2}^-) \text{ Status: } ***$$

Older and obsolete values are listed and referenced in the 2014 edition, Chinese Physics **C38** 070001 (2014).

 $N(1535)$ POLE POSITION

REAL PART

VALUE (MeV)	DOCUMENT ID	TECN	COMMENT
1500 to 1520 (≈ 1510) OUR ESTIMATE			
1504 ± 0	ROENCHEN	22	DPWA Multichannel
1496 ± 4	AFZAL	20	DPWA Multichannel
1500 ± 4	SOKHOYAN	15A	DPWA Multichannel
$1509 \pm 4 \pm 2$	¹ SVARC	14	L+P $\pi N \rightarrow \pi N$
1510 ± 50	CUTKOSKY	80	IPWA $\pi N \rightarrow \pi N$
• • • We do not use the following data for averages, fits, limits, etc. • • •			
1496	HUNT	19	DPWA Multichannel
1499	ROENCHEN	15A	DPWA Multichannel
1490	SHKLYAR	13	DPWA Multichannel
1501 ± 4	ANISOVICH	12A	DPWA Multichannel
1521 ± 14	BATINIC	10	DPWA $\pi N \rightarrow N\pi, N\eta$
1502	ARNDT	06	DPWA $\pi N \rightarrow \pi N, \eta N$
1525	VRANA	00	DPWA Multichannel
1487	HOEHLER	93	SPED $\pi N \rightarrow \pi N$
¹ Fit to the amplitudes of HOEHLER 79.			

-2xIMAGINARY PART

VALUE (MeV)	DOCUMENT ID	TECN	COMMENT
80 to 130 (≈ 110) OUR ESTIMATE			
74 ± 1	ROENCHEN	22	DPWA Multichannel
125 ± 6	AFZAL	20	DPWA Multichannel
128 ± 9	SOKHOYAN	15A	DPWA Multichannel
$118 \pm 9 \pm 2$	² SVARC	14	L+P $\pi N \rightarrow \pi N$
260 ± 80	CUTKOSKY	80	IPWA $\pi N \rightarrow \pi N$
• • • We do not use the following data for averages, fits, limits, etc. • • •			
119	HUNT	19	DPWA Multichannel
104	ROENCHEN	15A	DPWA Multichannel
100	SHKLYAR	13	DPWA Multichannel
134 ± 11	ANISOVICH	12A	DPWA Multichannel
190 ± 28	BATINIC	10	DPWA $\pi N \rightarrow N\pi, N\eta$
95	ARNDT	06	DPWA $\pi N \rightarrow \pi N, \eta N$
102	VRANA	00	DPWA Multichannel
² Fit to the amplitudes of HOEHLER 79.			

 $N(1535)$ ELASTIC POLE RESIDUEMODULUS $|r|$

VALUE (MeV)	DOCUMENT ID	TECN	COMMENT
15 to 35 (≈ 25) OUR ESTIMATE			
18 ± 1	ROENCHEN	22	DPWA Multichannel
29 ± 4	SOKHOYAN	15A	DPWA Multichannel
$22 \pm 2 \pm 0.4$	³ SVARC	14	L+P $\pi N \rightarrow \pi N$
120 ± 40	CUTKOSKY	80	IPWA $\pi N \rightarrow \pi N$
• • • We do not use the following data for averages, fits, limits, etc. • • •			
22	ROENCHEN	15A	DPWA Multichannel
15	SHKLYAR	13	DPWA Multichannel
31 ± 4	ANISOVICH	12A	DPWA Multichannel
68	BATINIC	10	DPWA $\pi N \rightarrow N\pi, N\eta$
16	ARNDT	06	DPWA $\pi N \rightarrow \pi N, \eta N$
³ Fit to the amplitudes of HOEHLER 79.			

PHASE θ

VALUE ($^\circ$)	DOCUMENT ID	TECN	COMMENT
-40 to 0 (≈ -20) OUR ESTIMATE			
-37 ± 2	ROENCHEN	22	DPWA Multichannel
-20 ± 10	SOKHOYAN	15A	DPWA Multichannel
$-5 \pm 5 \pm 3$	⁴ SVARC	14	L+P $\pi N \rightarrow \pi N$
$+15 \pm 45$	CUTKOSKY	80	IPWA $\pi N \rightarrow \pi N$

••• We do not use the following data for averages, fits, limits, etc. •••

-46	ROENCHEN	15A	DPWA	Multichannel
-51	SHKLYAR	13	DPWA	Multichannel
-29 ± 5	ANISOVICH	12A	DPWA	Multichannel
12	BATINIC	10	DPWA	$\pi N \rightarrow N\pi, N\eta$
-16	ARNDT	06	DPWA	$\pi N \rightarrow \pi N, \eta N$

⁴ Fit to the amplitudes of HOEHLER 79.

N(1535) INELASTIC POLE RESIDUEThe "normalized residue" is the residue divided by $\Gamma_{pole}/2$.**Normalized residue in $N\pi \rightarrow N(1535) \rightarrow N\eta$**

MODULUS	PHASE (°)	DOCUMENT ID	TECN	COMMENT
0.50 ± 0.02	118 ± 1	ROENCHEN 22	DPWA	Multichannel
0.43 ± 0.03	-76 ± 5	ANISOVICH 12A	DPWA	Multichannel
0.51	112	ROENCHEN 15A	DPWA	Multichannel

••• We do not use the following data for averages, fits, limits, etc. •••

Normalized residue in $N\pi \rightarrow N(1535) \rightarrow \Lambda K$

MODULUS	PHASE (°)	DOCUMENT ID	TECN	COMMENT
0.26 ± 0.01	-67 ± 2	ROENCHEN 22	DPWA	Multichannel
0.05	32	ROENCHEN 15A	DPWA	Multichannel

••• We do not use the following data for averages, fits, limits, etc. •••

Normalized residue in $N\pi \rightarrow N(1535) \rightarrow \Sigma K$

MODULUS	PHASE (°)	DOCUMENT ID	TECN	COMMENT
0.28 ± 0.01	92 ± 2	ROENCHEN 22	DPWA	Multichannel
0.05	-69	ROENCHEN 15A	DPWA	Multichannel

••• We do not use the following data for averages, fits, limits, etc. •••

Normalized residue in $N\pi \rightarrow N(1535) \rightarrow \Delta\pi, D\text{-wave}$

MODULUS	PHASE (°)	DOCUMENT ID	TECN	COMMENT
0.11 ± 0.02	160 ± 20	SOKHOYAN 15A	DPWA	Multichannel
0.12 ± 0.03	145 ± 17	ANISOVICH 12A	DPWA	Multichannel

••• We do not use the following data for averages, fits, limits, etc. •••

Normalized residue in $N\pi \rightarrow N(1535) \rightarrow N\sigma$

MODULUS	PHASE (°)	DOCUMENT ID	TECN	COMMENT
0.16 ± 0.07	25 ± 40	SOKHOYAN 15A	DPWA	Multichannel

Normalized residue in $N\pi \rightarrow N(1535) \rightarrow N(1440)\pi$

MODULUS	PHASE (°)	DOCUMENT ID	TECN	COMMENT
0.21 ± 0.14	-45 ± 50	SOKHOYAN 15A	DPWA	Multichannel

N(1535) BREIT-WIGNER MASS

VALUE (MeV)	DOCUMENT ID	TECN	COMMENT
1515 to 1545 (≈ 1530) OUR ESTIMATE			
1525 ± 2	⁵ HUNT 19	DPWA	Multichannel
1528 ± 6	KASHEVAROV 17	DPWA	$\gamma p \rightarrow \eta p, \eta' p$
1517 ± 4	SOKHOYAN 15A	DPWA	Multichannel
1526 ± 2	⁵ SHKLYAR 13	DPWA	Multichannel
1547.0 ± 0.7	⁵ ARNDT 06	DPWA	$\pi N \rightarrow \pi N, \eta N$
1550 ± 40	CUTKOSKY 80	IPWA	$\pi N \rightarrow \pi N$
1526 ± 7	HOEHLER 79	IPWA	$\pi N \rightarrow \pi N$
••• We do not use the following data for averages, fits, limits, etc. •••			
1519 ± 5	ANISOVICH 12A	DPWA	Multichannel
1538 ± 1	⁵ SHRESTHA 12A	DPWA	Multichannel
1553 ± 8	BATINIC 10	DPWA	$\pi N \rightarrow N\pi, N\eta$
1546.7 ± 2.2	ARNDT 04	DPWA	$\pi N \rightarrow \pi N, \eta N$
1526 ± 2	PENNER 02c	DPWA	Multichannel
1530 ± 10	BAI 01b	BES	$J/\psi \rightarrow p\bar{p}\eta$
1522 ± 11	THOMPSON 01	CLAS	$\gamma^* p \rightarrow p\eta$
1542 ± 3	VRANA 00	DPWA	Multichannel
1532 ± 5	ARMSTRONG 99b	DPWA	$\gamma^* p \rightarrow p\eta$

⁵ Statistical error only.

N(1535) BREIT-WIGNER WIDTH

VALUE (MeV)	DOCUMENT ID	TECN	COMMENT
125 to 175 (≈ 150) OUR ESTIMATE			
147 ± 5	⁶ HUNT 19	DPWA	Multichannel
163 ± 25	KASHEVAROV 17	DPWA	$\gamma p \rightarrow \eta p, \eta' p$
120 ± 10	SOKHOYAN 15A	DPWA	Multichannel
131 ± 12	⁶ SHKLYAR 13	DPWA	Multichannel
188.4 ± 3.8	⁶ ARNDT 06	DPWA	$\pi N \rightarrow \pi N, \eta N$
240 ± 80	CUTKOSKY 80	IPWA	$\pi N \rightarrow \pi N$
120 ± 20	HOEHLER 79	IPWA	$\pi N \rightarrow \pi N$
••• We do not use the following data for averages, fits, limits, etc. •••			
128 ± 14	ANISOVICH 12A	DPWA	Multichannel
141 ± 4	⁶ SHRESTHA 12A	DPWA	Multichannel
182 ± 25	BATINIC 10	DPWA	$\pi N \rightarrow N\pi, N\eta$

129 ± 8	PENNER 02c	DPWA	Multichannel
95 ± 25	BAI 01b	BES	$J/\psi \rightarrow p\bar{p}\eta$
143 ± 18	THOMPSON 01	CLAS	$\gamma^* p \rightarrow p\eta$
112 ± 19	VRANA 00	DPWA	Multichannel
154 ± 20	ARMSTRONG 99b	DPWA	$\gamma^* p \rightarrow p\eta$

⁶ Statistical error only.**N(1535) DECAY MODES**

The following branching fractions are our estimates, not fits or averages.

Mode	Fraction (Γ_i/Γ)
Γ_1 $N\pi$	32–52 %
Γ_2 $N\eta$	30–55 %
Γ_3 $N\pi\pi$	4–31 %
Γ_4 $\Delta(1232)\pi, D\text{-wave}$	1–4 %
Γ_5 $N\rho$	2–17 %
Γ_6 $N\rho, S=1/2, S\text{-wave}$	2–16 %
Γ_7 $N\rho, S=3/2, D\text{-wave}$	<1 %
Γ_8 $N\sigma$	2–10 %
Γ_9 $N(1440)\pi$	5–12 %
Γ_{10} $p\gamma, \text{helicity}=1/2$	0.15–0.30 %
Γ_{11} $n\gamma, \text{helicity}=1/2$	0.01–0.25 %

N(1535) BRANCHING RATIOS

$\Gamma(N\pi)/\Gamma_{total}$	VALUE (%)	DOCUMENT ID	TECN	COMMENT	Γ_1/Γ
32–52 % OUR ESTIMATE					
42 ± 2	⁷ HUNT 19	DPWA	Multichannel		
52 ± 5	SOKHOYAN 15A	DPWA	Multichannel		
35 ± 3	⁷ SHKLYAR 13	DPWA	Multichannel		
35.5 ± 0.2	⁷ ARNDT 06	DPWA	$\pi N \rightarrow \pi N, \eta N$		
50 ± 10	CUTKOSKY 80	IPWA	$\pi N \rightarrow \pi N$		
38 ± 4	HOEHLER 79	IPWA	$\pi N \rightarrow \pi N$		
••• We do not use the following data for averages, fits, limits, etc. •••					
54 ± 5	ANISOVICH 12A	DPWA	Multichannel		
37 ± 1	⁷ SHRESTHA 12A	DPWA	Multichannel		
46 ± 7	BATINIC 10	DPWA	$\pi N \rightarrow N\pi, N\eta$		
36 ± 1	PENNER 02c	DPWA	Multichannel		
35 ± 8	VRANA 00	DPWA	Multichannel		

⁷ Statistical error only.

$\Gamma(N\eta)/\Gamma_{total}$	VALUE (%)	DOCUMENT ID	TECN	COMMENT	Γ_2/Γ
30–55 % OUR ESTIMATE					
41 ± 4	MUELLER 20	DPWA	Multichannel		
43 ± 3	⁸ HUNT 19	DPWA	Multichannel		
41 ± 4	⁹ KASHEVAROV 17	DPWA	$\gamma p \rightarrow \eta p, \eta' p$		
58 ± 4	⁸ SHKLYAR 13	DPWA	Multichannel		
33 ± 5	ANISOVICH 12A	DPWA	Multichannel		
53 ± 1	PENNER 02c	DPWA	Multichannel		
51 ± 5	VRANA 00	DPWA	Multichannel		
••• We do not use the following data for averages, fits, limits, etc. •••					
41 ± 2	⁸ SHRESTHA 12A	DPWA	Multichannel		
50 ± 7	BATINIC 10	DPWA	$\pi N \rightarrow N\pi, N\eta$		

⁸ Statistical error only.
⁹ Assuming $A_{1/2} = 0.115 \text{ GeV}^{-1/2}$.

$\Gamma(N\eta)/\Gamma(N\pi)$	VALUE	DOCUMENT ID	TECN	COMMENT	Γ_2/Γ_1
••• We do not use the following data for averages, fits, limits, etc. •••					
0.95 ± 0.03	AZNAURYAN 09	CLAS	π, η electroproduction		

$\Gamma(\Delta(1232)\pi, D\text{-wave})/\Gamma_{total}$	VALUE (%)	DOCUMENT ID	TECN	COMMENT	Γ_4/Γ
1–4 % OUR ESTIMATE					
3 ± 1	ADAMCZEW... 20	DPWA	Multichannel		
<1.1	¹⁰ HUNT 19	DPWA	Multichannel		
2.5 ± 1.5	SOKHOYAN 15A	DPWA	Multichannel		
••• We do not use the following data for averages, fits, limits, etc. •••					
2.5 ± 1.5	ANISOVICH 12A	DPWA	Multichannel		
1.8 ± 0.8	¹⁰ SHRESTHA 12A	DPWA	Multichannel		
1 ± 1	VRANA 00	DPWA	Multichannel		

¹⁰ Statistical error only.

$\Gamma(N\rho, S=1/2, S\text{-wave})/\Gamma_{total}$	VALUE (%)	DOCUMENT ID	TECN	COMMENT	Γ_6/Γ
2–16 % OUR ESTIMATE					
2.7 ± 0.6	ADAMCZEW... 20	DPWA	Multichannel		
14 ± 2	¹¹ HUNT 19	DPWA	Multichannel		

¹¹ Statistical error only.

Baryon Particle Listings

 $N(1535)$, $N(1650)$ $\Gamma(N\rho, S=3/2, D\text{-wave})/\Gamma_{\text{total}}$

VALUE (%)	DOCUMENT ID	TECN	COMMENT
<1 % OUR ESTIMATE			
0.5 ± 0.5	ADAMCZEW...20	DPWA	Multichannel
<0.3	12 HUNT	19 DPWA	Multichannel
12 Statistical error only.			

 $\Gamma(N\sigma)/\Gamma_{\text{total}}$

VALUE (%)	DOCUMENT ID	TECN	COMMENT
2-10 % OUR ESTIMATE			
<1	13 HUNT	19 DPWA	Multichannel
6 ± 4	SOKHOYAN	15A DPWA	Multichannel
••• We do not use the following data for averages, fits, limits, etc. •••			
1.5 ± 0.5	13 SHRESTHA	12A DPWA	Multichannel
2 ± 1	VRANA	00 DPWA	Multichannel
13 Statistical error only.			

 $\Gamma(N(1440)\pi)/\Gamma_{\text{total}}$

VALUE (%)	DOCUMENT ID	TECN	COMMENT
5-12 % OUR ESTIMATE			
<0.01	14 HUNT	19 DPWA	Multichannel
12 ± 8	SOKHOYAN	15A DPWA	Multichannel
8 ± 2	14 STAROSTIN	03	$\pi^- p \rightarrow n3\pi^0$
••• We do not use the following data for averages, fits, limits, etc. •••			
<1	14 SHRESTHA	12A DPWA	Multichannel
10 ± 9	VRANA	00 DPWA	Multichannel
14 This value is an estimate made using simplest assumptions.			

 $N(1535)$ PHOTON DECAY AMPLITUDES AT THE POLE $N(1535) \rightarrow \rho\gamma$, helicity-1/2 amplitude $A_{1/2}$

MODULUS ($\text{GeV}^{-1/2}$)	PHASE ($^\circ$)	DOCUMENT ID	TECN	COMMENT
0.084 ± 0.002	-12 ± 2	ROENCHEN	22 DPWA	Multichannel
0.093 ± 0.009	8 ± 4	ANISOVICH	17D DPWA	Multichannel
••• We do not use the following data for averages, fits, limits, etc. •••				
0.114 ± 0.008	10 ± 5	ANISOVICH	15A DPWA	Multichannel
0.106	5.2	ROENCHEN	15A DPWA	Multichannel
0.114 ± 0.008	10 ± 5	SOKHOYAN	15A DPWA	Multichannel

 $N(1535) \rightarrow n\gamma$, helicity-1/2 amplitude $A_{1/2}$

MODULUS ($\text{GeV}^{-1/2}$)	PHASE ($^\circ$)	DOCUMENT ID	TECN	COMMENT
-0.088 ± 0.004	5 ± 4	ANISOVICH	17D DPWA	Multichannel
••• We do not use the following data for averages, fits, limits, etc. •••				
-0.095 ± 0.006	8 ± 5	ANISOVICH	15A DPWA	Multichannel

 $N(1535)$ BREIT-WIGNER PHOTON DECAY AMPLITUDES $N(1535) \rightarrow \rho\gamma$, helicity-1/2 amplitude $A_{1/2}$

VALUE ($\text{GeV}^{-1/2}$)	DOCUMENT ID	TECN	COMMENT
0.090 to 0.120 (≈ 0.105) OUR ESTIMATE			
0.107 ± 0.003	15 HUNT	19 DPWA	Multichannel
0.101 ± 0.007	SOKHOYAN	15A DPWA	Multichannel
0.091 ± 0.004	15 SHKLYAR	13 DPWA	Multichannel
0.128 ± 0.004	15 WORKMAN	12A DPWA	$\gamma N \rightarrow \pi N$
0.091 ± 0.002	15 DUGGER	07 DPWA	$\gamma N \rightarrow \pi N$
••• We do not use the following data for averages, fits, limits, etc. •••			
0.105 ± 0.010	ANISOVICH	12A DPWA	Multichannel
0.059 ± 0.003	15 SHRESTHA	12A DPWA	Multichannel
0.066	DRECHSEL	07 DPWA	$\gamma N \rightarrow \pi N$
0.090	PENNER	02D DPWA	Multichannel
15 Statistical error only.			

 $N(1535) \rightarrow n\gamma$, helicity-1/2 amplitude $A_{1/2}$

VALUE ($\text{GeV}^{-1/2}$)	DOCUMENT ID	TECN	COMMENT
-0.095 to -0.055 (≈ -0.075) OUR ESTIMATE			
-0.055 ± 0.006	16 HUNT	19 DPWA	Multichannel
-0.081 ± 0.006	ANISOVICH	17E DPWA	Multichannel
-0.058 ± 0.006	16 CHEN	12A DPWA	$\gamma N \rightarrow \pi N$
••• We do not use the following data for averages, fits, limits, etc. •••			
-0.093 ± 0.011	ANISOVICH	13B DPWA	Multichannel
-0.049 ± 0.003	16 SHRESTHA	12A DPWA	Multichannel
-0.051	DRECHSEL	07 DPWA	$\gamma N \rightarrow \pi N$
-0.024	PENNER	02D DPWA	Multichannel
16 Statistical error only.			

 $N(1535) \rightarrow N\gamma$, ratio $A_{1/2}^0/A_{1/2}^+$

VALUE ($\text{GeV}^{-1/2}$)	DOCUMENT ID	TECN	COMMENT
••• We do not use the following data for averages, fits, limits, etc. •••			
-0.84 ± 0.15	MUKHOPAD... 95B	IPWA	

 $N(1535)$ REFERENCESFor early references, see Physics Letters **111B** 1 (1982).

ROENCHEN	22	EPJ A58 229	D. Roenchen <i>et al.</i>	(JULI, GWU, BONN+)
ADAMCZEW...	20	PR C102 024001	J. Adamczewski-Musch <i>et al.</i>	(HADES Collab.)
AFZAL	20	PRL 125 152002	F. Afzal <i>et al.</i>	(CBELSA/TAPS Collab.)
MUELLER	20	PL B803 135323	J. Mueller <i>et al.</i>	(CBELSA/TAPS Collab.)
HUNT	19	PR C99 055205	B.C. Hunt, D.M. Manley	
ANISOVICH	17D	PR C95 035211	A.V. Anisovich <i>et al.</i>	
ANISOVICH	17E	PR C96 055202	A.V. Anisovich <i>et al.</i>	(BONN, PNPI, JLAB+)
KASHEVAROV	17	PRL 118 212001	V.L. Kashevarov <i>et al.</i>	(A2/MAMI Collab.)
ANISOVICH	15A	EPJ A51 72	A.V. Anisovich <i>et al.</i>	
ROENCHEN	15A	EPJ A51 70	D. Roenchen <i>et al.</i>	
SOKHOYAN	15A	EPJ A51 95	V. Sokhoyan <i>et al.</i>	(CBELSA/TAPS Collab.)
PDG	14	CP C38 070001	K. Olive <i>et al.</i>	(PDG Collab.)
SVARC	14	PR C89 045205	A. Svarc <i>et al.</i>	(RBI Zagreb, UNI Tuzla)
ANISOVICH	13B	EPJ A49 67	A.V. Anisovich <i>et al.</i>	
SHKLYAR	13	PR C87 015201	V. Shklyar, H. Lenske, U. Mosel	(GIES)
ANISOVICH	12A	EPJ A48 15	A.V. Anisovich <i>et al.</i>	(BONN, PNPI)
CHEN	12A	PR C86 015206	W. Chen <i>et al.</i>	(DUKE, GWU, MSST, ITEP+)
SHRESTHA	12A	PR C86 055203	M. Shrestha, D.M. Manley	(KSU)
WORKMAN	12A	PR C86 015202	R. Workman <i>et al.</i>	(GWU)
BATINIC	10	PR C82 038203	M. Batinic <i>et al.</i>	(ZAGR)
AZNAURYAN	09	PR C80 055203	I.G. Aznauryan <i>et al.</i>	(JLab CLAS Collab.)
DRECHSEL	07	EPJ A34 69	D. Drechsel, S.S. Kamalov, L. Tiator	(PDG Collab.)
DUGGER	07	PR C74 025211	M. Dugger <i>et al.</i>	(JLab CLAS Collab.)
ARNDT	06	PR C74 045205	R.A. Arndt <i>et al.</i>	(GWU)
ARNDT	04	PR C69 035213	R.A. Arndt <i>et al.</i>	(GWU, TRIU)
STAROSTIN	03	PR C67 068201	A. Starostin <i>et al.</i>	(BNL Crystal Ball Collab.)
PENNER	02C	PR C66 085211	G. Penner, U. Mosel	(GIES)
PENNER	02D	PR C66 055212	G. Penner, U. Mosel	(GIES)
BAI	01B	PL B510 75	J.Z. Bai <i>et al.</i>	(BES Collab.)
THOMPSON	01	PRL 86 1702	R. Thompson <i>et al.</i>	(JLab CLAS Collab.)
VRANA	00	PRPL 328 181	T.P. Vrana, S.A. Dytman, T.-S.H. Lee	(PITT, ANL)
ARMSTRONG	99B	PR D60 052004	C.S. Armstrong <i>et al.</i>	
MUKHOPAD...	95B	PL B364 1	N.C. Mukhopadhyay, J.F. Zhang, M. Benmerrouche	
HOEHLER	93	πN Newsletter 9 1	G. Hoehler	(KARL)
CUTKOSKY	80	Toronto Conf. 19	R.E. Cutkosky <i>et al.</i>	(CMU, LBL) IJP
Also		PR D20 2839	R.E. Cutkosky <i>et al.</i>	(CMU, LBL) IJP
HOEHLER	79	PDAT 12-1	G. Hoehler <i>et al.</i>	(KARL) IJP
Also		Toronto Conf. 3	R. Koch	(KARL) IJP

 $N(1650) 1/2^-$

$$I(J^P) = \frac{1}{2}(\frac{1}{2}^-) \text{ Status: } ***$$

Older and obsolete values are listed and referenced in the 2014 edition, Chinese Physics **C38** 070001 (2014). **$N(1650)$ POLE POSITION****REAL PART**

VALUE (MeV)	DOCUMENT ID	TECN	COMMENT
1650 to 1680 (≈ 1665) OUR ESTIMATE			
1678 ± 2	ROENCHEN	22 DPWA	Multichannel
1664 ± 4	AFZAL	20 DPWA	Multichannel
1658 ± 10	ANISOVICH	17A DPWA	Multichannel
1660 ± 5	1 ANISOVICH	17A L+P	$\gamma p, \pi^- p \rightarrow K\Lambda$
$1660 \pm 3.5 \pm 1$	2 SVARC	14 L+P	$\pi N \rightarrow \pi N$
1640 ± 20	CUTKOSKY	80 IPWA	$\pi N \rightarrow \pi N$
••• We do not use the following data for averages, fits, limits, etc. •••			
1656	HUNT	19 DPWA	Multichannel
1672	ROENCHEN	15A DPWA	Multichannel
1652 ± 7	SOKHOYAN	15A DPWA	Multichannel
1650	SHKLYAR	13 DPWA	Multichannel
1647 ± 6	ANISOVICH	12A DPWA	Multichannel
1646 ± 8	BATINIC	10 DPWA	$\pi N \rightarrow N\pi, N\eta$
1648	ARNDT	06 DPWA	$\pi N \rightarrow \pi N, \eta N$
1663	VRANA	00 DPWA	Multichannel
1670	HOEHLER	93 ARGD	$\pi N \rightarrow \pi N$

1 Statistical error only.

2 Fit to the amplitudes of HOEHLER 79.

-2xIMAGINARY PART

VALUE (MeV)	DOCUMENT ID	TECN	COMMENT
100 to 170 (≈ 135) OUR ESTIMATE			
127 ± 2	ROENCHEN	22 DPWA	Multichannel
98 ± 6	AFZAL	20 DPWA	Multichannel
102 ± 8	ANISOVICH	17A DPWA	Multichannel
59 ± 16	1 ANISOVICH	17A L+P	$\gamma p, \pi^- p \rightarrow K\Lambda$
$167 \pm 8 \pm 2$	2 SVARC	14 L+P	$\pi N \rightarrow \pi N$
150 ± 30	CUTKOSKY	80 IPWA	$\pi N \rightarrow \pi N$
••• We do not use the following data for averages, fits, limits, etc. •••			
130	HUNT	19 DPWA	Multichannel
137	ROENCHEN	15A DPWA	Multichannel
102 ± 8	SOKHOYAN	15A DPWA	Multichannel
89	SHKLYAR	13 DPWA	Multichannel
103 ± 8	ANISOVICH	12A DPWA	Multichannel
204 ± 17	BATINIC	10 DPWA	$\pi N \rightarrow N\pi, N\eta$
80	ARNDT	06 DPWA	$\pi N \rightarrow \pi N, \eta N$
240	VRANA	00 DPWA	Multichannel
163	HOEHLER	93 ARGD	$\pi N \rightarrow \pi N$

1 Statistical error only.

2 Fit to the amplitudes of HOEHLER 79.

N(1650) ELASTIC POLE RESIDUE

MODULUS $|r|$

VALUE (MeV)	DOCUMENT ID	TECN	COMMENT
25 to 55 (≈ 45) OUR ESTIMATE			
59 ± 11	ROENCHEN 22	DPWA	Multichannel
27 ± 6	SOKHOYAN 15A	DPWA	Multichannel
47 ± 3 ± 1	¹ SVARC 14	L+P	$\pi N \rightarrow \pi N$
60 ± 10	CUTKOSKY 80	IPWA	$\pi N \rightarrow \pi N$
• • • We do not use the following data for averages, fits, limits, etc. • • •			
37	ROENCHEN 15A	DPWA	Multichannel
19	SHKLYAR 13	DPWA	Multichannel
24 ± 3	ANISOVICH 12A	DPWA	Multichannel
100	BATINIC 10	DPWA	$\pi N \rightarrow N\pi, N\eta$
14	ARNDT 06	DPWA	$\pi N \rightarrow \pi N, \eta N$
39	HOEHLER 93	ARGD	$\pi N \rightarrow \pi N$

¹ Fit to the amplitudes of HOEHLER 79.PHASE θ

VALUE (°)	DOCUMENT ID	TECN	COMMENT
-80 to -50 (≈ -70) OUR ESTIMATE			
-18 ± 23	ROENCHEN 22	DPWA	Multichannel
-60 ± 20	SOKHOYAN 15A	DPWA	Multichannel
-47 ± 3 ± 1	¹ SVARC 14	L+P	$\pi N \rightarrow \pi N$
-75 ± 25	CUTKOSKY 80	IPWA	$\pi N \rightarrow \pi N$
• • • We do not use the following data for averages, fits, limits, etc. • • •			
-59	ROENCHEN 15A	DPWA	Multichannel
-46	SHKLYAR 13	DPWA	Multichannel
-75 ± 12	ANISOVICH 12A	DPWA	Multichannel
-65	BATINIC 10	DPWA	$\pi N \rightarrow N\pi, N\eta$
-69	ARNDT 06	DPWA	$\pi N \rightarrow \pi N, \eta N$
-37	HOEHLER 93	ARGD	$\pi N \rightarrow \pi N$

¹ Fit to the amplitudes of HOEHLER 79.

N(1650) INELASTIC POLE RESIDUE

The "normalized residue" is the residue divided by $\Gamma_{pole}/2$.Normalized residue in $N\pi \rightarrow N(1650) \rightarrow N\eta$

MODULUS	PHASE (°)	DOCUMENT ID	TECN	COMMENT
0.34 ± 0.06	71 ± 23	ROENCHEN 22	DPWA	Multichannel
0.29 ± 0.03	134 ± 10	ANISOVICH 12A	DPWA	Multichannel
• • • We do not use the following data for averages, fits, limits, etc. • • •				
0.21	48	ROENCHEN 15A	DPWA	Multichannel

Normalized residue in $N\pi \rightarrow N(1650) \rightarrow \Lambda K$

MODULUS	PHASE (°)	DOCUMENT ID	TECN	COMMENT
0.26 ± 0.05	-40 ± 23	ROENCHEN 22	DPWA	Multichannel
0.26 ± 0.10	110 ± 20	ANISOVICH 17A	DPWA	Multichannel
0.10 ± 0.10	95 ± 33	¹ ANISOVICH 17A	L+P	$\gamma p, \pi^- p \rightarrow K\Lambda$
• • • We do not use the following data for averages, fits, limits, etc. • • •				
0.20	-54	ROENCHEN 15A	DPWA	Multichannel
0.23 ± 0.09	85 ± 9	ANISOVICH 12A	DPWA	Multichannel

¹ Statistical error only.Normalized residue in $N\pi \rightarrow N(1650) \rightarrow \Sigma K$

MODULUS	PHASE (°)	DOCUMENT ID	TECN	COMMENT
0.41 ± 0.07	-21 ± 24	ROENCHEN 22	DPWA	Multichannel
• • • We do not use the following data for averages, fits, limits, etc. • • •				
0.026	-74	ROENCHEN 15A	DPWA	Multichannel

Normalized residue in $N\pi \rightarrow N(1650) \rightarrow \Delta\pi, D\text{-wave}$

MODULUS	PHASE (°)	DOCUMENT ID	TECN	COMMENT
0.19 ± 0.06	-30 ± 20	SOKHOYAN 15A	DPWA	Multichannel
• • • We do not use the following data for averages, fits, limits, etc. • • •				
0.23 ± 0.04	-30 ± 20	ANISOVICH 12A	DPWA	Multichannel

Normalized residue in $N\pi \rightarrow N(1650) \rightarrow N\sigma$

MODULUS	PHASE (°)	DOCUMENT ID	TECN	COMMENT
0.20 ± 0.15	undefined	SOKHOYAN 15A	DPWA	Multichannel

Normalized residue in $N\pi \rightarrow N(1650) \rightarrow N(1440)\pi$

MODULUS	PHASE (°)	DOCUMENT ID	TECN	COMMENT
0.30 ± 0.17	undefined	SOKHOYAN 15A	DPWA	Multichannel

N(1650) BREIT-WIGNER MASS

VALUE (MeV)	DOCUMENT ID	TECN	COMMENT
1635 to 1665 (≈ 1650) OUR ESTIMATE			
1657 ± 6	GOLOVATCH 19	DPWA	$\gamma p \rightarrow \pi^+ \pi^- p$
1666 ± 3	¹ HUNT 19	DPWA	Multichannel
1634 ± 5	KASHEVAROV 17	DPWA	$\gamma p \rightarrow \eta p, \eta' p$
1654 ± 6	SOKHOYAN 15A	DPWA	Multichannel
1665 ± 2	¹ SHKLYAR 13	DPWA	Multichannel
1634.7 ± 1.1	¹ ARNDT 06	DPWA	$\pi N \rightarrow \pi N, \eta N$
1650 ± 30	CUTKOSKY 80	IPWA	$\pi N \rightarrow \pi N$
1670 ± 8	HOEHLER 79	IPWA	$\pi N \rightarrow \pi N$

• • • We do not use the following data for averages, fits, limits, etc. • • •

1651 ± 6	ANISOVICH 12A	DPWA	Multichannel
1664 ± 2	¹ SHRESTHA 12A	DPWA	Multichannel
1652 ± 9	BATINIC 10	DPWA	$\pi N \rightarrow N\pi, N\eta$
1665 ± 2	PENNER 02c	DPWA	Multichannel
1647 ± 20	BAI 01B	BES	$J/\psi \rightarrow p\bar{p}\eta$
1689 ± 12	VRANA 00	DPWA	Multichannel

¹ Statistical error only.

N(1650) BREIT-WIGNER WIDTH

VALUE (MeV)	DOCUMENT ID	TECN	COMMENT
100 to 150 (≈ 125) OUR ESTIMATE			
154 ± 28	GOLOVATCH 19	DPWA	$\gamma p \rightarrow \pi^+ \pi^- p$
133 ± 7	¹ HUNT 19	DPWA	Multichannel
128 ± 16	KASHEVAROV 17	DPWA	$\gamma p \rightarrow \eta p, \eta' p$
102 ± 8	SOKHOYAN 15A	DPWA	Multichannel
147 ± 14	¹ SHKLYAR 13	DPWA	Multichannel
115.4 ± 2.8	¹ ARNDT 06	DPWA	$\pi N \rightarrow \pi N, \eta N$
150 ± 40	CUTKOSKY 80	IPWA	$\pi N \rightarrow \pi N$
180 ± 20	HOEHLER 79	IPWA	$\pi N \rightarrow \pi N$

• • • We do not use the following data for averages, fits, limits, etc. • • •

104 ± 10	ANISOVICH 12A	DPWA	Multichannel
126 ± 3	¹ SHRESTHA 12A	DPWA	Multichannel
202 ± 16	BATINIC 10	DPWA	$\pi N \rightarrow N\pi, N\eta$
138 ± 7	PENNER 02c	DPWA	Multichannel
145 +80 -45	BAI 01B	BES	$J/\psi \rightarrow p\bar{p}\eta$
202 ± 40	VRANA 00	DPWA	Multichannel

¹ Statistical error only.

N(1650) DECAY MODES

The following branching fractions are our estimates, not fits or averages.

Mode	Fraction (Γ_i/Γ)
Γ_1 $N\pi$	50-70 %
Γ_2 $N\eta$	15-35 %
Γ_3 ΛK	5-15 %
Γ_4 $N\pi\pi$	20-58 %
Γ_5 $\Delta(1232)\pi, D\text{-wave}$	6-18 %
Γ_6 $N\rho$	12-22 %
Γ_7 $N\rho, S=1/2, S\text{-wave}$	<4 %
Γ_8 $N\rho, S=3/2, D\text{-wave}$	12-18 %
Γ_9 $N\sigma$	2-18 %
Γ_{10} $N(1440)\pi$	6-26 %
Γ_{11} $\rho\gamma, \text{ helicity}=1/2$	0.04-0.20 %
Γ_{12} $\eta\gamma, \text{ helicity}=1/2$	0.003-0.17 %

N(1650) BRANCHING RATIOS

$\Gamma(N\pi)/\Gamma_{total}$	DOCUMENT ID	TECN	COMMENT	Γ_1/Γ
50 to 70 (≈ 60) OUR ESTIMATE				
64 ± 4	¹ HUNT 19	DPWA	Multichannel	
51 ± 4	SOKHOYAN 15A	DPWA	Multichannel	
74 ± 3	¹ SHKLYAR 13	DPWA	Multichannel	
65 ± 10	CUTKOSKY 80	IPWA	$\pi N \rightarrow \pi N$	
61 ± 4	HOEHLER 79	IPWA	$\pi N \rightarrow \pi N$	
• • • We do not use the following data for averages, fits, limits, etc. • • •				
51 ± 4	ANISOVICH 12A	DPWA	Multichannel	
57 ± 2	¹ SHRESTHA 12A	DPWA	Multichannel	
79 ± 6	BATINIC 10	DPWA	$\pi N \rightarrow N\pi, N\eta$	
100	ARNDT 06	DPWA	$\pi N \rightarrow \pi N, \eta N$	
65 ± 4	PENNER 02c	DPWA	Multichannel	
74 ± 2	VRANA 00	DPWA	Multichannel	

¹ Statistical error only.

$\Gamma(N\eta)/\Gamma_{total}$	DOCUMENT ID	TECN	COMMENT	Γ_2/Γ
15 to 35 (≈ 25) OUR ESTIMATE				
33 ± 4	MUELLER 20	DPWA	Multichannel	
0.8 ± 0.6	¹ HUNT 19	DPWA	Multichannel	
28 ± 11	² KASHEVAROV 17	DPWA	$\gamma p \rightarrow \eta p, \eta' p$	
< 3	SHKLYAR 13	DPWA	Multichannel	
18 ± 4	ANISOVICH 12A	DPWA	Multichannel	
• • • We do not use the following data for averages, fits, limits, etc. • • •				
21 ± 2	¹ SHRESTHA 12A	DPWA	Multichannel	
13 ± 5	BATINIC 10	DPWA	$\pi N \rightarrow N\pi, N\eta$	
1.0 ± 0.6	PENNER 02c	DPWA	Multichannel	
6 ± 1	VRANA 00	DPWA	Multichannel	

¹ Statistical error only.² Assuming $A_{1/2} = 0.045 \text{ GeV}^{-1/2}$.

Baryon Particle Listings

 $N(1650)$, $N(1675)$ $\Gamma(\Lambda K)/\Gamma_{\text{total}}$

VALUE (%)	DOCUMENT ID	TECN	COMMENT	Γ_3/Γ
5 to 15 (≈ 10) OUR ESTIMATE				
3.5 ± 0.2	¹ HUNT 19	DPWA	Multichannel	
10 ± 5	ANISOVICH 12A	DPWA	Multichannel	
4 ± 1	¹ SHKLYAR 05	DPWA	Multichannel	
••• We do not use the following data for averages, fits, limits, etc. •••				
8 ± 1	¹ SHRESTHA 12A	DPWA	Multichannel	
2.7 ± 0.4	PENNER 02C	DPWA	Multichannel	
¹ Statistical error only.				

 $\Gamma(N\pi\pi)/\Gamma_{\text{total}}$

VALUE	DOCUMENT ID	TECN	COMMENT	Γ_4/Γ
0.12 \pm 0.02	GOLOVATCH 19	DPWA	$\gamma p \rightarrow \pi^+ \pi^- p$	

 $\Gamma(\Delta(1232)\pi, D\text{-wave})/\Gamma_{\text{total}}$

VALUE (%)	DOCUMENT ID	TECN	COMMENT	Γ_5/Γ
< 0.2	¹ HUNT 19	DPWA	Multichannel	
12 ± 6	SOKHOYAN 15A	DPWA	Multichannel	
••• We do not use the following data for averages, fits, limits, etc. •••				
19 ± 9	ANISOVICH 12A	DPWA	Multichannel	
7 ± 2	¹ SHRESTHA 12A	DPWA	Multichannel	
2 ± 1	VRANA 00	DPWA	Multichannel	
¹ Statistical error only.				

 $\Gamma(N\rho, S=1/2, S\text{-wave})/\Gamma_{\text{total}}$

VALUE (%)	DOCUMENT ID	TECN	COMMENT	Γ_7/Γ
1.8 ± 1.7	¹ HUNT 19	DPWA	Multichannel	
¹ Statistical error only.				

 $\Gamma(N\rho, S=3/2, D\text{-wave})/\Gamma_{\text{total}}$

VALUE (%)	DOCUMENT ID	TECN	COMMENT	Γ_8/Γ
15 ± 3	¹ HUNT 19	DPWA	Multichannel	
¹ Statistical error only.				

 $\Gamma(N\sigma)/\Gamma_{\text{total}}$

VALUE (%)	DOCUMENT ID	TECN	COMMENT	Γ_9/Γ
12 ± 4	¹ HUNT 19	DPWA	Multichannel	
10 ± 8	SOKHOYAN 15A	DPWA	Multichannel	
••• We do not use the following data for averages, fits, limits, etc. •••				
< 1	¹ SHRESTHA 12A	DPWA	Multichannel	
1 ± 1	VRANA 00	DPWA	Multichannel	
¹ Statistical error only.				

 $\Gamma(N(1440)\pi)/\Gamma_{\text{total}}$

VALUE (%)	DOCUMENT ID	TECN	COMMENT	Γ_{10}/Γ
2 ± 1	¹ HUNT 19	DPWA	Multichannel	
16 ± 10	SOKHOYAN 15A	DPWA	Multichannel	
••• We do not use the following data for averages, fits, limits, etc. •••				
< 1	¹ SHRESTHA 12A	DPWA	Multichannel	
3 ± 1	VRANA 00	DPWA	Multichannel	
¹ Statistical error only.				

 $N(1650)$ PHOTON DECAY AMPLITUDES AT THE POLE $N(1650) \rightarrow p\gamma$, helicity-1/2 amplitude $A_{1/2}$

MODULUS ($\text{GeV}^{-1/2}$)	PHASE ($^\circ$)	DOCUMENT ID	TECN	COMMENT
0.039 ± 0.005	-0.2 ± 14	ROENCHEN 22	DPWA	Multichannel
0.032 ± 0.006	7 ± 7	ANISOVICH 17D	DPWA	Multichannel
••• We do not use the following data for averages, fits, limits, etc. •••				
0.032 ± 0.007	-2 ± 11	ANISOVICH 15A	DPWA	Multichannel
0.059	-14	ROENCHEN 15A	DPWA	Multichannel
0.032 ± 0.006	-2 ± 11	SOKHOYAN 15A	DPWA	Multichannel

 $N(1650) \rightarrow n\gamma$, helicity-1/2 amplitude $A_{1/2}$

MODULUS ($\text{GeV}^{-1/2}$)	PHASE ($^\circ$)	DOCUMENT ID	TECN	COMMENT
0.016 ± 0.004	-28 ± 10	ANISOVICH 17D	DPWA	Multichannel
••• We do not use the following data for averages, fits, limits, etc. •••				
0.019 ± 0.006	0 ± 15	ANISOVICH 15A	DPWA	Multichannel

 $N(1650)$ BREIT-WIGNER PHOTON DECAY AMPLITUDES $N(1650) \rightarrow p\gamma$, helicity-1/2 amplitude $A_{1/2}$

VALUE ($\text{GeV}^{-1/2}$)	DOCUMENT ID	TECN	COMMENT
0.035 to 0.055 (≈ 0.045) OUR ESTIMATE			
0.0605 ± 0.0077	GOLOVATCH 19	DPWA	$\gamma p \rightarrow \pi^+ \pi^- p$
0.048 ± 0.003	¹ HUNT 19	DPWA	Multichannel
0.032 ± 0.006	SOKHOYAN 15A	DPWA	Multichannel
0.063 ± 0.006	¹ SHKLYAR 13	DPWA	Multichannel
0.055 ± 0.030	¹ WORKMAN 12A	DPWA	$\gamma N \rightarrow N\pi$
0.022 ± 0.007	¹ DUGGER 07	DPWA	$\gamma N \rightarrow \pi N$

••• We do not use the following data for averages, fits, limits, etc. •••

0.033 ± 0.007	ANISOVICH 12A	DPWA	Multichannel
0.030 ± 0.003	¹ SHRESTHA 12A	DPWA	Multichannel
0.033	DRECHSEL 07	DPWA	$\gamma N \rightarrow \pi N$
0.049	PENNER 02D	DPWA	Multichannel

¹ Statistical error only. **$N(1650) \rightarrow n\gamma$, helicity-1/2 amplitude $A_{1/2}$**

VALUE ($\text{GeV}^{-1/2}$)	DOCUMENT ID	TECN	COMMENT
-0.040 to 0.030 (≈ -0.010) OUR ESTIMATE			
0.001 ± 0.006	¹ HUNT 19	DPWA	Multichannel
-0.016 ± 0.005	ANISOVICH 17E	DPWA	Multichannel
-0.040 ± 0.010	¹ CHEN 12A	DPWA	$\gamma N \rightarrow \pi N$
••• We do not use the following data for averages, fits, limits, etc. •••			
0.025 ± 0.020	ANISOVICH 13B	DPWA	Multichannel
0.011 ± 0.002	¹ SHRESTHA 12A	DPWA	Multichannel
0.009	DRECHSEL 07	DPWA	$\gamma N \rightarrow \pi N$
-0.011	PENNER 02D	DPWA	Multichannel

¹ Statistical error only. **$N(1650)$ REFERENCES**For early references, see Physics Letters **111B** 1 (1982).

ROENCHEN 22	EPJ A58 229	D. Roenchen et al.	(JULI, GWU, BONN+)
AFZAL 20	PRL 125 152002	F. Afzal et al.	(CBELSA/TAPS Collab.)
MUELLER 20	PL B803 135323	J. Mueller et al.	(CBELSA/TAPS Collab.)
GOLOVATCH 19	PL B788 371	E. Golovatch et al.	(CLAS Collab.)
HUNT 19	PR C99 055205	B.C. Hunt, D.M. Manley	
ANISOVICH 17A	PRL 119 062004	A.V. Anisovich et al.	
ANISOVICH 17D	PR C95 035211	A.V. Anisovich et al.	
ANISOVICH 17E	PR C96 055202	A.V. Anisovich et al.	(BONN, PNPI, JLAB+)
KASHEVAROV 17	PRL 118 212001	V.L. Kashevarov et al.	(A2/MAMI Collab.)
ANISOVICH 15A	EPJ A51 72	A.V. Anisovich et al.	
ROENCHEN 15A	EPJ A51 70	D. Roenchen et al.	
SOKHOYAN 15A	EPJ A51 95	V. Sokhoyan et al.	(CBELSA/TAPS Collab.)
PDG 14	CP C38 070001	K. Olive et al.	(PDG Collab.)
SVARC 14	PR C89 045205	A. Svarc et al.	(RBI Zagreb, UNI Tuzla)
ANISOVICH 13B	EPJ A49 67	A.V. Anisovich et al.	
SHKLYAR 13	PR C87 015201	V. Shklyar, H. Lenske, U. Mosel	(GIES)
ANISOVICH 12A	EPJ A48 15	A.V. Anisovich et al.	(BONN, PNPI)
CHEN 12A	PR C86 015206	W. Chen et al.	(DUKE, GWU, MSST, ITEP+)
SHRESTHA 12A	PR C86 055203	M. Shrestha, D.M. Manley	(KSU)
WORKMAN 12A	PR C86 015202	R. Workman et al.	(GWU)
BATINIC 10	PR C82 038203	M. Batinic et al.	(ZAGR)
DRECHSEL 07	EPJ A34 69	D. Drechsel, S.S. Kamalov, L. Tiator	(MAINZ, JINR)
DUGGER 07	PR C74 025211	M. Dugger et al.	(JLab CLAS Collab.)
ARNDT 06	PR C74 045205	R.A. Arndt et al.	(GWU)
SHKLYAR 05	PR C72 015210	V. Shklyar, H. Lenske, U. Mosel	(GIES)
PENNER 02C	PR C66 055211	G. Penner, U. Mosel	(GIES)
PENNER 02D	PR C66 055212	G. Penner, U. Mosel	(GIES)
BAI 01B	PL B510 75	J.Z. Bai et al.	(BES Collab.)
VRANA 00	PRPL 328 181	T.P. Vrana, S.A. Dytman, T.-S.H. Lee	(PITT, ANL)
HOEHLER 93	πN Newsletter 9 1	G. Hoehler	(KARL)
CUTKOSKY 80	Toronto Conf. 19	R.E. Cutkosky et al.	(CMU, LBL) IJP
Also	PR D20 2839	R.E. Cutkosky et al.	(CMU, LBL) IJP
HOEHLER 79	PDAT 12-1	G. Hoehler et al.	(KARL) IJP
Also	Toronto Conf. 3	R. Koch	(KARL) IJP

 $N(1675) 5/2^-$

$$I(J^P) = \frac{1}{2}(\frac{5}{2}^-) \text{ Status: } ***$$

Older and obsolete values are listed and referenced in the 2014 edition, Chinese Physics **C38** 070001 (2014). **$N(1675)$ POLE POSITION****REAL PART**

VALUE (MeV)	DOCUMENT ID	TECN	COMMENT
1650 to 1660 (≈ 1655) OUR ESTIMATE			
1652 ± 2	ROENCHEN 22	DPWA	Multichannel
1655 ± 4	SOKHOYAN 15A	DPWA	Multichannel
1654 ± 2	¹ SVARC 14	L+P	$\pi N \rightarrow \pi N$
1660 ± 10	CUTKOSKY 80	IPWA	$\pi N \rightarrow \pi N$
••• We do not use the following data for averages, fits, limits, etc. •••			
1646	HUNT 19	DPWA	Multichannel
1646	ROENCHEN 15A	DPWA	Multichannel
1640	SHKLYAR 13	DPWA	Multichannel
1654 ± 4	ANISOVICH 12A	DPWA	Multichannel
1658 ± 9	BATINIC 10	DPWA	$\pi N \rightarrow N\pi, N\eta$
1657	ARNDT 06	DPWA	$\pi N \rightarrow \pi N, \eta N$
1674	VRANA 00	DPWA	Multichannel
1656	HOEHLER 93	ARGD	$\pi N \rightarrow \pi N$

¹ Fit to the amplitudes of HOEHLER 79.**-2xIMAGINARY PART**

VALUE (MeV)	DOCUMENT ID	TECN	COMMENT
120 to 150 (≈ 135) OUR ESTIMATE			
119 ± 1	ROENCHEN 22	DPWA	Multichannel
147 ± 5	SOKHOYAN 15A	DPWA	Multichannel
$125 \pm 3 \pm 1$	¹ SVARC 14	L+P	$\pi N \rightarrow \pi N$
140 ± 10	CUTKOSKY 80	IPWA	$\pi N \rightarrow \pi N$

••• We do not use the following data for averages, fits, limits, etc. •••

146	HUNT	19	DPWA	Multichannel
125	ROENCHEN	15A	DPWA	Multichannel
108	SHKLYAR	13	DPWA	Multichannel
151 ± 5	ANISOVICH	12A	DPWA	Multichannel
137 ± 7	BATINIC	10	DPWA	$\pi N \rightarrow N\pi, N\eta$
139	ARNDT	06	DPWA	$\pi N \rightarrow \pi N, \eta N$
120	VRANA	00	DPWA	Multichannel
126	HOEHLER	93	ARGD	$\pi N \rightarrow \pi N$

¹ Fit to the amplitudes of HOEHLER 79.

N(1675) ELASTIC POLE RESIDUE

MODULUS |r|

VALUE (MeV)	DOCUMENT ID	TECN	COMMENT
22 to 32 (≈ 26) OUR ESTIMATE			
22 ± 1	ROENCHEN	22	DPWA Multichannel
28 ± 1	SOKHOYAN	15A	DPWA Multichannel
23 ± 1	¹ SVARC	14	L+P $\pi N \rightarrow \pi N$
31 ± 5	CUTKOSKY	80	IPWA $\pi N \rightarrow \pi N$

••• We do not use the following data for averages, fits, limits, etc. •••

24	ROENCHEN	15A	DPWA Multichannel
20	SHKLYAR	13	DPWA Multichannel
28 ± 1	ANISOVICH	12A	DPWA Multichannel
25	BATINIC	10	DPWA $\pi N \rightarrow N\pi, N\eta$
27	ARNDT	06	DPWA $\pi N \rightarrow \pi N, \eta N$
23	HOEHLER	93	ARGD $\pi N \rightarrow \pi N$

¹ Fit to the amplitudes of HOEHLER 79.

PHASE θ

VALUE (°)	DOCUMENT ID	TECN	COMMENT
-27 to -17 (≈ -22) OUR ESTIMATE			
-17 ± 1	ROENCHEN	22	DPWA Multichannel
-24 ± 4	SOKHOYAN	15A	DPWA Multichannel
-25 ± 2	¹ SVARC	14	L+P $\pi N \rightarrow \pi N$
-30 ± 10	CUTKOSKY	80	IPWA $\pi N \rightarrow \pi N$

••• We do not use the following data for averages, fits, limits, etc. •••

-22	ROENCHEN	15A	DPWA Multichannel
-49	SHKLYAR	13	DPWA Multichannel
-26 ± 4	ANISOVICH	12A	DPWA Multichannel
-16	BATINIC	10	DPWA $\pi N \rightarrow N\pi, N\eta$
-21	ARNDT	06	DPWA $\pi N \rightarrow \pi N, \eta N$
-22	HOEHLER	93	ARGD $\pi N \rightarrow \pi N$

¹ Fit to the amplitudes of HOEHLER 79.

N(1675) INELASTIC POLE RESIDUE

The "normalized residue" is the residue divided by $\Gamma_{pole}/2$.

Normalized residue in $N\pi \rightarrow N(1675) \rightarrow \Delta\pi, D\text{-wave}$

MODULUS	PHASE (°)	DOCUMENT ID	TECN	COMMENT
0.33 ± 0.04	90 ± 15	SOKHOYAN	15A	DPWA Multichannel
0.33 ± 0.05	82 ± 10	ANISOVICH	12A	DPWA Multichannel

Normalized residue in $N\pi \rightarrow N(1675) \rightarrow N\eta$

MODULUS	PHASE (°)	DOCUMENT ID	TECN	COMMENT
0.063 ± 0.005	-39 ± 1	ROENCHEN	22	DPWA Multichannel
0.044	-43	ROENCHEN	15A	DPWA Multichannel

Normalized residue in $N\pi \rightarrow N(1675) \rightarrow \Lambda K$

MODULUS	PHASE (°)	DOCUMENT ID	TECN	COMMENT
0.001 ± 0.001	174 ± 80	ROENCHEN	22	DPWA Multichannel
0.001	100	ROENCHEN	15A	DPWA Multichannel

Normalized residue in $N\pi \rightarrow N(1675) \rightarrow \Sigma K$

MODULUS	PHASE (°)	DOCUMENT ID	TECN	COMMENT
0.024 ± 0.001	-166 ± 3	ROENCHEN	22	DPWA Multichannel
0.031	-175	ROENCHEN	15A	DPWA Multichannel

Normalized residue in $N\pi \rightarrow N(1675) \rightarrow N\sigma$

MODULUS	PHASE (°)	DOCUMENT ID	TECN	COMMENT
0.13 ± 0.03	125 ± 20	SOKHOYAN	15A	DPWA Multichannel
0.15 ± 0.04	132 ± 18	ANISOVICH	12A	DPWA Multichannel

N(1675) BREIT-WIGNER MASS

VALUE (MeV)	DOCUMENT ID	TECN	COMMENT
1665 to 1680 (≈ 1675) OUR ESTIMATE			
1669 ± 2	¹ HUNT	19	DPWA Multichannel
1663 ± 4	SOKHOYAN	15A	DPWA Multichannel
1666 ± 2	¹ SHKLYAR	13	DPWA Multichannel
1674.1 ± 0.2	¹ ARNDT	06	DPWA $\pi N \rightarrow \pi N, \eta N$
1675 ± 10	CUTKOSKY	80	IPWA $\pi N \rightarrow \pi N$
1679 ± 8	HOEHLER	79	IPWA $\pi N \rightarrow \pi N$
1664 ± 5	ANISOVICH	12A	DPWA Multichannel
1679 ± 1	¹ SHRESTHA	12A	DPWA Multichannel
1679 ± 9	BATINIC	10	DPWA $\pi N \rightarrow N\pi, N\eta$
1685 ± 4	VRANA	00	DPWA Multichannel

¹ Statistical error only.

N(1675) BREIT-WIGNER WIDTH

VALUE (MeV)	DOCUMENT ID	TECN	COMMENT
130 to 160 (≈ 145) OUR ESTIMATE			
161 ± 8	¹ HUNT	19	DPWA Multichannel
146 ± 6	SOKHOYAN	15A	DPWA Multichannel
148 ± 1	¹ SHKLYAR	13	DPWA Multichannel
146.5 ± 1.0	¹ ARNDT	06	DPWA $\pi N \rightarrow \pi N, \eta N$
160 ± 20	CUTKOSKY	80	IPWA $\pi N \rightarrow \pi N$
120 ± 15	HOEHLER	79	IPWA $\pi N \rightarrow \pi N$
152 ± 7	ANISOVICH	12A	DPWA Multichannel
145 ± 4	¹ SHRESTHA	12A	DPWA Multichannel
152 ± 8	BATINIC	10	DPWA $\pi N \rightarrow N\pi, N\eta$
131 ± 10	VRANA	00	DPWA Multichannel

¹ Statistical error only.

N(1675) DECAY MODES

The following branching fractions are our estimates, not fits or averages.

Mode	Fraction (Γ_i/Γ)
Γ_1 $N\pi$	38-42 %
Γ_2 $N\eta$	< 1 %
Γ_3 ΛK	< 0.04 %
Γ_4 $N\pi\pi$	25-45 %
Γ_5 $\Delta(1232)\pi, D\text{-wave}$	23-37 %
Γ_6 $N\rho$	0.1-0.9 %
Γ_7 $N\rho, S=1/2$	< 0.2 %
Γ_8 $N\rho, S=3/2, D\text{-wave}$	0.1-0.7 %
Γ_9 $N\sigma$	3-7 %
Γ_{10} $p\gamma$	0-0.02 %
Γ_{11} $p\gamma, \text{helicity}=1/2$	0-0.01 %
Γ_{12} $p\gamma, \text{helicity}=3/2$	0-0.01 %
Γ_{13} $n\gamma$	0-0.15 %
Γ_{14} $n\gamma, \text{helicity}=1/2$	0-0.05 %
Γ_{15} $n\gamma, \text{helicity}=3/2$	0-0.10 %

N(1675) BRANCHING RATIOS

$\Gamma(N\pi)/\Gamma_{total}$	VALUE (%)	DOCUMENT ID	TECN	COMMENT	Γ_1/Γ
38 to 42 (≈ 40) OUR ESTIMATE					
	33 ± 1	¹ HUNT	19	DPWA Multichannel	
	41 ± 2	SOKHOYAN	15A	DPWA Multichannel	
	41 ± 1	¹ SHKLYAR	13	DPWA Multichannel	
	39.3 ± 0.1	¹ ARNDT	06	DPWA $\pi N \rightarrow \pi N, \eta N$	
	38 ± 5	CUTKOSKY	80	IPWA $\pi N \rightarrow \pi N$	
	38 ± 3	HOEHLER	79	IPWA $\pi N \rightarrow \pi N$	
	40 ± 3	ANISOVICH	12A	DPWA Multichannel	
	38.6 ± 0.6	¹ SHRESTHA	12A	DPWA Multichannel	
	35 ± 4	BATINIC	10	DPWA $\pi N \rightarrow N\pi, N\eta$	
	35 ± 1	VRANA	00	DPWA Multichannel	

¹ Statistical error only.

$\Gamma(N\eta)/\Gamma_{total}$	VALUE (%)	DOCUMENT ID	TECN	COMMENT	Γ_2/Γ
	0.5 ± 0.5	MUELLER	20	DPWA Multichannel	
	2.0 ± 0.3	¹ HUNT	19	DPWA Multichannel	
	< 1	SHKLYAR	13	DPWA Multichannel	

Baryon Particle Listings

 $N(1675)$

• • • We do not use the following data for averages, fits, limits, etc. • • •

VALUE (%)	DOCUMENT ID	TECN	COMMENT
<1	¹ SHRESTHA 12A	DPWA	Multichannel
0.1 ± 0.1	BATINIC 10	DPWA	$\pi N \rightarrow N\pi, N\eta$
3 ± 3	THOMA 08	DPWA	Multichannel
0 ± 1	VRANA 00	DPWA	Multichannel

¹ Statistical error only.

 $\Gamma(\Lambda K)/\Gamma_{\text{total}}$ Γ_3/Γ

VALUE (%)	DOCUMENT ID	TECN	COMMENT
<0.04 % OUR ESTIMATE			
<0.04	¹ HUNT 19	DPWA	Multichannel

¹ Statistical error only.

 $\Gamma(\Delta(1232)\pi, D\text{-wave})/\Gamma_{\text{total}}$ Γ_5/Γ

VALUE (%)	DOCUMENT ID	TECN	COMMENT
58.3 ± 0.2	¹ HUNT 19	DPWA	Multichannel
30 ± 7	SOKHOYAN 15A	DPWA	Multichannel

• • • We do not use the following data for averages, fits, limits, etc. • • •

33 ± 8	ANISOVICH 12A	DPWA	Multichannel
46 ± 1	¹ SHRESTHA 12A	DPWA	Multichannel
63 ± 2	VRANA 00	DPWA	Multichannel

¹ Statistical error only.

 $\Gamma(N\rho, S=1/2)/\Gamma_{\text{total}}$ Γ_7/Γ

VALUE (%)	DOCUMENT ID	TECN	COMMENT
<0.2 % OUR ESTIMATE			
<0.2	¹ HUNT 19	DPWA	Multichannel

¹ Statistical error only.

 $\Gamma(N\rho, S=3/2, D\text{-wave})/\Gamma_{\text{total}}$ Γ_8/Γ

VALUE (%)	DOCUMENT ID	TECN	COMMENT
0.1–0.7 % OUR ESTIMATE			
0.4 ± 0.3	¹ HUNT 19	DPWA	Multichannel

¹ Statistical error only.

 $\Gamma(N\sigma)/\Gamma_{\text{total}}$ Γ_9/Γ

VALUE (%)	DOCUMENT ID	TECN	COMMENT
5 ± 2	SOKHOYAN 15A	DPWA	Multichannel

• • • We do not use the following data for averages, fits, limits, etc. • • •

7 ± 3	ANISOVICH 12A	DPWA	Multichannel
-------	---------------	------	--------------

 $N(1675)$ PHOTON DECAY AMPLITUDES AT THE POLE $N(1675) \rightarrow p\gamma, \text{ helicity-1/2 amplitude } A_{1/2}$

MODULUS ($\text{GeV}^{-1/2}$)	PHASE ($^\circ$)	DOCUMENT ID	TECN	COMMENT
0.025 ± 0.002	-1.2 ± 3.9	ROENCHEN 22	DPWA	Multichannel
0.022 ± 0.003	-12 ± 7	SOKHOYAN 15A	DPWA	Multichannel

• • • We do not use the following data for averages, fits, limits, etc. • • •

0.032	36	ROENCHEN 15A	DPWA	Multichannel
-------	----	--------------	------	--------------

 $N(1675) \rightarrow p\gamma, \text{ helicity-3/2 amplitude } A_{3/2}$

MODULUS ($\text{GeV}^{-1/2}$)	PHASE ($^\circ$)	DOCUMENT ID	TECN	COMMENT
0.051 ± 0.002	-1.0 ± 1.9	ROENCHEN 22	DPWA	Multichannel
0.028 ± 0.006	-17 ± 6	SOKHOYAN 15A	DPWA	Multichannel

• • • We do not use the following data for averages, fits, limits, etc. • • •

0.051	-9.3	ROENCHEN 15A	DPWA	Multichannel
-------	------	--------------	------	--------------

 $N(1675) \rightarrow n\gamma, \text{ helicity-1/2 amplitude } A_{1/2}$

MODULUS ($\text{GeV}^{-1/2}$)	PHASE ($^\circ$)	DOCUMENT ID	TECN	COMMENT
-0.053 ± 0.004	-3 ± 5	ANISOVICH 17E	DPWA	Multichannel

 $N(1675) \rightarrow n\gamma, \text{ helicity-3/2 amplitude } A_{3/2}$

MODULUS ($\text{GeV}^{-1/2}$)	PHASE ($^\circ$)	DOCUMENT ID	TECN	COMMENT
-0.073 ± 0.005	-12 ± 5	ANISOVICH 17E	DPWA	Multichannel

 $N(1675)$ BREIT-WIGNER PHOTON DECAY AMPLITUDES $N(1675) \rightarrow p\gamma, \text{ helicity-1/2 amplitude } A_{1/2}$

VALUE ($\text{GeV}^{-1/2}$)	DOCUMENT ID	TECN	COMMENT
0.010 to 0.025 (≈ 0.018) OUR ESTIMATE			
0.026 ± 0.002	¹ HUNT 19	DPWA	Multichannel
0.022 ± 0.003	SOKHOYAN 15A	DPWA	Multichannel
0.009 ± 0.001	¹ SHKLYAR 13	DPWA	Multichannel
0.013 ± 0.001	¹ WORKMAN 12A	DPWA	$\gamma N \rightarrow N\pi$
0.018 ± 0.002	¹ DUGGER 07	DPWA	$\gamma N \rightarrow \pi N$

• • • We do not use the following data for averages, fits, limits, etc. • • •

0.024 ± 0.003	ANISOVICH 12A	DPWA	Multichannel
0.011 ± 0.001	¹ SHRESTHA 12A	DPWA	Multichannel
0.015	DRECHSEL 07	DPWA	$\gamma N \rightarrow \pi N$

¹ Statistical error only.

 $N(1675) \rightarrow p\gamma, \text{ helicity-3/2 amplitude } A_{3/2}$

VALUE ($\text{GeV}^{-1/2}$)	DOCUMENT ID	TECN	COMMENT
0.015 to 0.030 (≈ 0.022) OUR ESTIMATE			
0.005 ± 0.002	¹ HUNT 19	DPWA	Multichannel
0.027 ± 0.006	SOKHOYAN 15A	DPWA	Multichannel
0.021 ± 0.001	¹ SHKLYAR 13	DPWA	Multichannel
0.016 ± 0.001	¹ WORKMAN 12A	DPWA	$\gamma N \rightarrow N\pi$
0.021 ± 0.001	¹ DUGGER 07	DPWA	$\gamma N \rightarrow \pi N$

• • • We do not use the following data for averages, fits, limits, etc. • • •

0.025 ± 0.007	ANISOVICH 12A	DPWA	Multichannel
0.020 ± 0.001	¹ SHRESTHA 12A	DPWA	Multichannel
0.022	DRECHSEL 07	DPWA	$\gamma N \rightarrow \pi N$

¹ Statistical error only.

• • • We do not use the following data for averages, fits, limits, etc. • • •

0.025 ± 0.007	ANISOVICH 12A	DPWA	Multichannel
0.020 ± 0.001	¹ SHRESTHA 12A	DPWA	Multichannel
0.022	DRECHSEL 07	DPWA	$\gamma N \rightarrow \pi N$

¹ Statistical error only.

 $N(1675) \rightarrow n\gamma, \text{ helicity-1/2 amplitude } A_{1/2}$

VALUE ($\text{GeV}^{-1/2}$)	DOCUMENT ID	TECN	COMMENT
-0.065 to -0.055 (≈ -0.060) OUR ESTIMATE			
-0.069 ± 0.005	¹ HUNT 19	DPWA	Multichannel
-0.053 ± 0.004	ANISOVICH 17E	DPWA	Multichannel
-0.058 ± 0.002	¹ CHEN 12A	DPWA	$\gamma N \rightarrow \pi N$

• • • We do not use the following data for averages, fits, limits, etc. • • •

-0.060 ± 0.007	ANISOVICH 13B	DPWA	Multichannel
-0.040 ± 0.004	¹ SHRESTHA 12A	DPWA	Multichannel
-0.062	DRECHSEL 07	DPWA	$\gamma N \rightarrow \pi N$

¹ Statistical error only.

• • • We do not use the following data for averages, fits, limits, etc. • • •

-0.060 ± 0.007	ANISOVICH 13B	DPWA	Multichannel
-0.040 ± 0.004	¹ SHRESTHA 12A	DPWA	Multichannel
-0.062	DRECHSEL 07	DPWA	$\gamma N \rightarrow \pi N$

¹ Statistical error only.

 $N(1675) \rightarrow n\gamma, \text{ helicity-3/2 amplitude } A_{3/2}$

VALUE ($\text{GeV}^{-1/2}$)	DOCUMENT ID	TECN	COMMENT
-0.095 to -0.075 (≈ -0.085) OUR ESTIMATE			
-0.031 ± 0.005	¹ HUNT 19	DPWA	Multichannel
-0.072 ± 0.005	ANISOVICH 17E	DPWA	Multichannel
-0.080 ± 0.005	¹ CHEN 12A	DPWA	$\gamma N \rightarrow \pi N$

• • • We do not use the following data for averages, fits, limits, etc. • • •

-0.088 ± 0.010	ANISOVICH 13B	DPWA	Multichannel
-0.068 ± 0.004	¹ SHRESTHA 12A	DPWA	Multichannel
-0.084	DRECHSEL 07	DPWA	$\gamma N \rightarrow \pi N$

¹ Statistical error only.

 $N(1675)$ REFERENCES

For early references, see Physics Letters **111B** 1 (1982).

ROENCHEN 22	EPJ A58 229	D. Roenchen et al.	(JULI, GWU, BONN+)
MUELLER 20	PL B803 135323	J. Mueller et al.	(CBELSA/TAPS Collab.)
HUNT 19	PR C99 055205	B. C. Hunt, D. M. Manley	
ANISOVICH 17E	PR C96 055202	A.V. Anisovich et al.	(BONN, PNPI, JLAB+)
ROENCHEN 15A	EPJ A51 70	D. Roenchen et al.	
SOKHOYAN 15A	EPJ A51 95	V. Sokhoyan et al.	(CBELSA/TAPS Collab.)
PDG 14	CP C38 070001	K. Olive et al.	(PDG Collab.)
SVARC 14	PR C89 045205	A. Svarc et al.	(RBI Zagreb, UNI Tuzla)
ANISOVICH 13B	EPJ A49 67	A.V. Anisovich et al.	
SHKLYAR 13	PR C87 015201	V. Shklyar, H. Lenske, U. Mosel	(GIES)
ANISOVICH 12A	EPJ A48 15	A.V. Anisovich et al.	(BONN, PNPI)
CHEN 12A	PR C86 015206	W. Chen et al.	(DUKE, GWU, MSST, ITEP+)
SHRESTHA 12A	PR C86 055203	M. Shrestha, D.M. Manley	(KSU)
WORKMAN 12A	PR C86 015202	R. Workman et al.	(GWU)
BATINIC 10	PR C82 038203	M. Batinic et al.	(ZAGR)
THOMA 08	PL B659 87	U. Thoma et al.	(CB-ELSA Collab.)
DRECHSEL 07	EPJ A34 69	D. Drechsel, S.S. Kamalov, L. Tiator	(MAINZ, JINR)
DUGGER 07	PR C76 025211	M. Dugger et al.	(JLab CLAS Collab.)
ARNDT 06	PR C74 045205	R.A. Arndt et al.	(GWU)
VRANA 00	PRPL 328 181	T.P. Vrana, S.A. Dytman, T.-S.H. Lee	(PITT, ANL)
HOEHLER 93	πN Newsletter 9 1	G. Hohlner	(KARL)
CUTKOSKY 80	Toronto Conf. 19	R.E. Cutkosky et al.	(CMU, LBL) IJP
Also	PR D20 2839	R.E. Cutkosky et al.	(CMU, LBL) IJP
HOEHLER 79	PDAT 12-1	G. Hohlner et al.	(KARL) IJP
Also	Toronto Conf. 3	R. Koch	(KARL) IJP

N(1680) 5/2⁺

$I(J^P) = \frac{1}{2}(\frac{5}{2}^+)$ Status: ****

Older and obsolete values are listed and referenced in the 2014 edition, Chinese Physics C38 070001 (2014).

N(1680) POLE POSITION

REAL PART

VALUE (MeV)	DOCUMENT ID	TECN	COMMENT
1660 to 1680 (≈ 1670) OUR ESTIMATE			
1657 ± 2	ROENCHEN 22	DPWA	Multichannel
1678 ± 5	SOKHOYAN 15A	DPWA	Multichannel
1674 ± 2 ± 1	¹ SVARC 14	L+P	$\pi N \rightarrow \pi N$
1667 ± 5	CUTKOSKY 80	IPWA	$\pi N \rightarrow \pi N$
••• We do not use the following data for averages, fits, limits, etc. •••			
1668	HUNT 19	DPWA	Multichannel
1669	ROENCHEN 15A	DPWA	Multichannel
1660	SHKLYAR 13	DPWA	Multichannel
1676 ± 6	ANISOVICH 12A	DPWA	Multichannel
1666 ± 8	BATINIC 10	DPWA	$\pi N \rightarrow N\pi, N\eta$
1674	ARNDT 06	DPWA	$\pi N \rightarrow \pi N, \eta N$
1667	VRANA 00	DPWA	Multichannel
1673	HOEHLER 93	ARGD	$\pi N \rightarrow \pi N$

¹ Fit to the amplitudes of HOEHLER 79.

-2xIMAGINARY PART

VALUE (MeV)	DOCUMENT ID	TECN	COMMENT
110 to 135 (≈ 120) OUR ESTIMATE			
120 ± 1	ROENCHEN 22	DPWA	Multichannel
113 ± 4	SOKHOYAN 15A	DPWA	Multichannel
129 ± 3 ± 1	¹ SVARC 14	L+P	$\pi N \rightarrow \pi N$
110 ± 10	CUTKOSKY 80	IPWA	$\pi N \rightarrow \pi N$
••• We do not use the following data for averages, fits, limits, etc. •••			
118	HUNT 19	DPWA	Multichannel
100	ROENCHEN 15A	DPWA	Multichannel
98	SHKLYAR 13	DPWA	Multichannel
113 ± 4	ANISOVICH 12A	DPWA	Multichannel
135 ± 6	BATINIC 10	DPWA	$\pi N \rightarrow N\pi, N\eta$
115	ARNDT 06	DPWA	$\pi N \rightarrow \pi N, \eta N$
122	VRANA 00	DPWA	Multichannel
135	HOEHLER 93	ARGD	$\pi N \rightarrow \pi N$

¹ Fit to the amplitudes of HOEHLER 79.

N(1680) ELASTIC POLE RESIDUE

MODULUS |r|

VALUE (MeV)	DOCUMENT ID	TECN	COMMENT
35 to 45 (≈ 40) OUR ESTIMATE			
36 ± 1	ROENCHEN 22	DPWA	Multichannel
45 ± 4	SOKHOYAN 15A	DPWA	Multichannel
44 ± 1 ± 1	¹ SVARC 14	L+P	$\pi N \rightarrow \pi N$
34 ± 2	CUTKOSKY 80	IPWA	$\pi N \rightarrow \pi N$
••• We do not use the following data for averages, fits, limits, etc. •••			
34	ROENCHEN 15A	DPWA	Multichannel
33	SHKLYAR 13	DPWA	Multichannel
43 ± 4	ANISOVICH 12A	DPWA	Multichannel
44	BATINIC 10	DPWA	$\pi N \rightarrow N\pi, N\eta$
42	ARNDT 06	DPWA	$\pi N \rightarrow \pi N, \eta N$
44	HOEHLER 93	ARGD	$\pi N \rightarrow \pi N$

¹ Fit to the amplitudes of HOEHLER 79.

PHASE θ

VALUE (°)	DOCUMENT ID	TECN	COMMENT
-30 to -10 (≈ -20) OUR ESTIMATE			
-31 ± 1	ROENCHEN 22	DPWA	Multichannel
5 ± 10	SOKHOYAN 15A	DPWA	Multichannel
-16 ± 1 ± 1	¹ SVARC 14	L+P	$\pi N \rightarrow \pi N$
-25 ± 5	CUTKOSKY 80	IPWA	$\pi N \rightarrow \pi N$
••• We do not use the following data for averages, fits, limits, etc. •••			
-19	ROENCHEN 15A	DPWA	Multichannel
-32	SHKLYAR 13	DPWA	Multichannel
-2 ± 10	ANISOVICH 12A	DPWA	Multichannel
-19	BATINIC 10	DPWA	$\pi N \rightarrow N\pi, N\eta$
-4	ARNDT 06	DPWA	$\pi N \rightarrow \pi N, \eta N$
-17	HOEHLER 93	ARGD	$\pi N \rightarrow \pi N$

¹ Fit to the amplitudes of HOEHLER 79.

N(1680) INELASTIC POLE RESIDUE

The "normalized residue" is the residue divided by $\Gamma_{pole}/2$.

Normalized residue in $N\pi \rightarrow N(1680) \rightarrow \Delta\pi, P$ -wave

MODULUS	PHASE (°)	DOCUMENT ID	TECN	COMMENT
0.15 ± 0.03	-60 ± 30	SOKHOYAN 15A	DPWA	Multichannel
••• We do not use the following data for averages, fits, limits, etc. •••				
0.15 ± 0.03	-70 ± 45	ANISOVICH 12A	DPWA	Multichannel

Normalized residue in $N\pi \rightarrow N(1680) \rightarrow \Delta\pi, F$ -wave

MODULUS	PHASE (°)	DOCUMENT ID	TECN	COMMENT
0.23 ± 0.04	90 ± 12	SOKHOYAN 15A	DPWA	Multichannel
••• We do not use the following data for averages, fits, limits, etc. •••				
0.23 ± 0.04	85 ± 15	ANISOVICH 12A	DPWA	Multichannel

Normalized residue in $N\pi \rightarrow N(1680) \rightarrow N\eta$

MODULUS	PHASE (°)	DOCUMENT ID	TECN	COMMENT
0.006 ± 0.004	118 ± 1	ROENCHEN 22	DPWA	Multichannel
••• We do not use the following data for averages, fits, limits, etc. •••				
0.027	136	ROENCHEN 15A	DPWA	Multichannel

Normalized residue in $N\pi \rightarrow N(1680) \rightarrow \Lambda K$

MODULUS	PHASE (°)	DOCUMENT ID	TECN	COMMENT
0.006 ± 0.001	-119 ± 2	ROENCHEN 22	DPWA	Multichannel
••• We do not use the following data for averages, fits, limits, etc. •••				
0.001	90	ROENCHEN 15A	DPWA	Multichannel

Normalized residue in $N\pi \rightarrow N(1680) \rightarrow \Sigma K$

MODULUS	PHASE (°)	DOCUMENT ID	TECN	COMMENT
0.001 ± 0.001	-46 ± 15	ROENCHEN 22	DPWA	Multichannel
••• We do not use the following data for averages, fits, limits, etc. •••				
0.004	148	ROENCHEN 15A	DPWA	Multichannel

Normalized residue in $N\pi \rightarrow N(1680) \rightarrow N(\pi\pi)_{S=0}^{I=0}$

MODULUS	PHASE (°)	DOCUMENT ID	TECN	COMMENT
0.29 ± 0.06	-45 ± 15	SOKHOYAN 15A	DPWA	Multichannel
••• We do not use the following data for averages, fits, limits, etc. •••				
0.26 ± 0.04	-56 ± 15	ANISOVICH 12A	DPWA	Multichannel

N(1680) BREIT-WIGNER MASS

VALUE (MeV)	DOCUMENT ID	TECN	COMMENT
1680 to 1690 (≈ 1685) OUR ESTIMATE			
1686 ± 5	GOLOVATCH 19	DPWA	$\gamma p \rightarrow \pi^+ \pi^- p$
1681.0 ± 0.1	¹ HUNT 19	DPWA	Multichannel
1690 ± 5	SOKHOYAN 15A	DPWA	Multichannel
1676 ± 2	¹ SHKLYAR 13	DPWA	Multichannel
1680.1 ± 0.2	¹ ARNDT 06	DPWA	$\pi N \rightarrow \pi N, \eta N$
1680 ± 10	CUTKOSKY 80	IPWA	$\pi N \rightarrow \pi N$
1684 ± 3	HOEHLER 79	IPWA	$\pi N \rightarrow \pi N$
••• We do not use the following data for averages, fits, limits, etc. •••			
1689 ± 6	ANISOVICH 12A	DPWA	Multichannel
1682.7 ± 0.5	¹ SHRESTHA 12A	DPWA	Multichannel
1680 ± 7	BATINIC 10	DPWA	$\pi N \rightarrow N\pi, N\eta$
1679 ± 3	VRANA 00	DPWA	Multichannel

¹ Statistical error only.

N(1680) BREIT-WIGNER WIDTH

VALUE (MeV)	DOCUMENT ID	TECN	COMMENT
115 to 130 (≈ 120) OUR ESTIMATE			
118 ± 20	GOLOVATCH 19	DPWA	$\gamma p \rightarrow \pi^+ \pi^- p$
123 ± 3	¹ HUNT 19	DPWA	Multichannel
119 ± 4	SOKHOYAN 15A	DPWA	Multichannel
115 ± 1	¹ SHKLYAR 13	DPWA	Multichannel
128.0 ± 1.1	¹ ARNDT 06	DPWA	$\pi N \rightarrow \pi N, \eta N$
120 ± 10	CUTKOSKY 80	IPWA	$\pi N \rightarrow \pi N$
128 ± 8	HOEHLER 79	IPWA	$\pi N \rightarrow \pi N$
••• We do not use the following data for averages, fits, limits, etc. •••			
118 ± 6	ANISOVICH 12A	DPWA	Multichannel
126 ± 1	¹ SHRESTHA 12A	DPWA	Multichannel
142 ± 7	BATINIC 10	DPWA	$\pi N \rightarrow N\pi, N\eta$
128 ± 9	VRANA 00	DPWA	Multichannel

¹ Statistical error only.

Baryon Particle Listings

 $N(1680)$ $N(1680)$ DECAY MODES

The following branching fractions are our estimates, not fits or averages.

Mode	Fraction (Γ_i/Γ)
Γ_1 $N\pi$	60–70 %
Γ_2 $N\eta$	<1 %
Γ_3 $N\pi\pi$	28–53 %
Γ_4 $\Delta(1232)\pi$	11–23 %
Γ_5 $\Delta(1232)\pi$, P -wave	4–10 %
Γ_6 $\Delta(1232)\pi$, F -wave	1–13 %
Γ_7 $N\rho$	8–11 %
Γ_8 $N\rho$, $S=3/2$, P -wave	6–8 %
Γ_9 $N\rho$, $S=3/2$, F -wave	2–3 %
Γ_{10} $N\sigma$	9–19 %
Γ_{11} $p\gamma$	0.21–0.32 %
Γ_{12} $p\gamma$, helicity=1/2	0.001–0.011 %
Γ_{13} $p\gamma$, helicity=3/2	0.20–0.32 %
Γ_{14} $n\gamma$	0.021–0.046 %
Γ_{15} $n\gamma$, helicity=1/2	0.004–0.029 %
Γ_{16} $n\gamma$, helicity=3/2	0.01–0.024 %

 $N(1680)$ BRANCHING RATIOS

$\Gamma(N\pi)/\Gamma_{\text{total}}$	Γ_1/Γ		
VALUE (%)	DOCUMENT ID	TECN	COMMENT
60 to 70 (≈ 65) OUR ESTIMATE			
68.0 \pm 0.1	¹ HUNT	19	DPWA Multichannel
62 \pm 4	SOKHOYAN	15A	DPWA Multichannel
68 \pm 1	¹ SHKLYAR	13	DPWA Multichannel
70.1 \pm 0.1	¹ ARNDT	06	DPWA $\pi N \rightarrow \pi N, \eta N$
62 \pm 5	CUTKOSKY	80	IPWA $\pi N \rightarrow \pi N$
65 \pm 2	HOEHLER	79	IPWA $\pi N \rightarrow \pi N$
••• We do not use the following data for averages, fits, limits, etc. •••			
64 \pm 5	ANISOVICH	12A	DPWA Multichannel
68.0 \pm 0.5	¹ SHRESTHA	12A	DPWA Multichannel
67 \pm 3	BATINIC	10	DPWA $\pi N \rightarrow N\pi, N\eta$
69 \pm 2	VRANA	00	DPWA Multichannel

¹ Statistical error only.

$\Gamma(N\eta)/\Gamma_{\text{total}}$	Γ_2/Γ		
VALUE (%)	DOCUMENT ID	TECN	COMMENT
0.2 \pm 0.1	MUELLER	20	DPWA Multichannel
0.09 \pm 0.02	¹ HUNT	19	DPWA Multichannel
<1	SHKLYAR	13	DPWA Multichannel
0.15 \pm _{-0.10} ^{+0.35}	TIATOR	99	DPWA $\gamma p \rightarrow p\eta$
••• We do not use the following data for averages, fits, limits, etc. •••			
1.0 \pm 0.3	¹ SHRESTHA	12A	DPWA Multichannel
0.4 \pm 0.2	BATINIC	10	DPWA $\pi N \rightarrow N\pi, N\eta$
<1	THOMA	08	DPWA Multichannel
0 \pm 1	VRANA	00	DPWA Multichannel

¹ Statistical error only.

$\Gamma(N\pi\pi)/\Gamma_{\text{total}}$	Γ_3/Γ		
VALUE (%)	DOCUMENT ID	TECN	COMMENT
28–53 % OUR ESTIMATE			
24 \pm 4	GOLOVATCH	19	DPWA $\gamma p \rightarrow \pi^+\pi^-\rho$

$\Gamma(\Delta(1232)\pi, P\text{-wave})/\Gamma_{\text{total}}$	Γ_5/Γ		
VALUE (%)	DOCUMENT ID	TECN	COMMENT
13 \pm 1	¹ HUNT	19	DPWA Multichannel
7 \pm 3	SOKHOYAN	15A	DPWA Multichannel
••• We do not use the following data for averages, fits, limits, etc. •••			
5 \pm 3	ANISOVICH	12A	DPWA Multichannel
10.5 \pm 0.9	¹ SHRESTHA	12A	DPWA Multichannel
14 \pm 3	VRANA	00	DPWA Multichannel

¹ Statistical error only.

$\Gamma(\Delta(1232)\pi, F\text{-wave})/\Gamma_{\text{total}}$	Γ_6/Γ		
VALUE (%)	DOCUMENT ID	TECN	COMMENT
< 0.3	¹ HUNT	19	DPWA Multichannel
10 \pm 3	SOKHOYAN	15A	DPWA Multichannel
••• We do not use the following data for averages, fits, limits, etc. •••			
10 \pm 3	ANISOVICH	12A	DPWA Multichannel
1.0 \pm 0.1	¹ SHRESTHA	12A	DPWA Multichannel
1 \pm 1	VRANA	00	DPWA Multichannel

¹ Statistical error only.

 $\Gamma(N\rho, S=3/2, P\text{-wave})/\Gamma_{\text{total}}$ Γ_8/Γ

VALUE (%)	DOCUMENT ID	TECN	COMMENT
6–8 % OUR ESTIMATE			
7 \pm 1	¹ HUNT	19	DPWA Multichannel

¹ Statistical error only.

 $\Gamma(N\rho, S=3/2, F\text{-wave})/\Gamma_{\text{total}}$ Γ_9/Γ

VALUE (%)	DOCUMENT ID	TECN	COMMENT
2–3 % OUR ESTIMATE			
2.4 \pm 0.4	¹ HUNT	19	DPWA Multichannel

¹ Statistical error only.

 $\Gamma(N\sigma)/\Gamma_{\text{total}}$ Γ_{10}/Γ

VALUE (%)	DOCUMENT ID	TECN	COMMENT
8.7 \pm 1.5	¹ HUNT	19	DPWA Multichannel
14 \pm 5	SOKHOYAN	15A	DPWA Multichannel
••• We do not use the following data for averages, fits, limits, etc. •••			
14 \pm 7	ANISOVICH	12A	DPWA Multichannel
9.4 \pm 0.8	¹ SHRESTHA	12A	DPWA Multichannel
9 \pm 1	VRANA	00	DPWA Multichannel

¹ Statistical error only.

 $N(1680)$ PHOTON DECAY AMPLITUDES AT THE POLE $N(1680) \rightarrow p\gamma$, helicity-1/2 amplitude $A_{1/2}$

MODULUS ($\text{GeV}^{-1/2}$)	PHASE ($^\circ$)	DOCUMENT ID	TECN	COMMENT
-0.017 \pm 0.003	70 \pm 7	ROENCHEN	22	DPWA Multichannel
-0.013 \pm 0.003	-20 \pm 17	SOKHOYAN	15A	DPWA Multichannel
••• We do not use the following data for averages, fits, limits, etc. •••				
-0.022	-28	ROENCHEN	15A	DPWA Multichannel

 $N(1680) \rightarrow p\gamma$, helicity-3/2 amplitude $A_{3/2}$

MODULUS ($\text{GeV}^{-1/2}$)	PHASE ($^\circ$)	DOCUMENT ID	TECN	COMMENT
0.095 \pm 0.003	-57 \pm 4	ROENCHEN	22	DPWA Multichannel
0.135 \pm 0.005	1 \pm 3	SOKHOYAN	15A	DPWA Multichannel
••• We do not use the following data for averages, fits, limits, etc. •••				
0.102	-11	ROENCHEN	15A	DPWA Multichannel

 $N(1680) \rightarrow n\gamma$, helicity-1/2 amplitude $A_{1/2}$

MODULUS ($\text{GeV}^{-1/2}$)	PHASE ($^\circ$)	DOCUMENT ID	TECN	COMMENT
0.032 \pm 0.003	-7 \pm 5	ANISOVICH	17E	DPWA Multichannel

 $N(1680) \rightarrow n\gamma$, helicity-3/2 amplitude $A_{3/2}$

MODULUS ($\text{GeV}^{-1/2}$)	PHASE ($^\circ$)	DOCUMENT ID	TECN	COMMENT
-0.063 \pm 0.004	-10 \pm 5	ANISOVICH	17E	DPWA Multichannel

 $N(1680)$ BREIT-WIGNER PHOTON DECAY AMPLITUDES $N(1680) \rightarrow p\gamma$, helicity-1/2 amplitude $A_{1/2}$

VALUE ($\text{GeV}^{-1/2}$)	DOCUMENT ID	TECN	COMMENT
-0.018 to -0.005 (≈ -0.010) OUR ESTIMATE			
-0.0278 \pm 0.0036	GOLOVATCH	19	DPWA $\gamma p \rightarrow \pi^+\pi^-\rho$
-0.026 \pm 0.004	¹ HUNT	19	DPWA Multichannel
-0.015 \pm 0.002	SOKHOYAN	15A	DPWA Multichannel
0.003 \pm 0.001	¹ SHKLYAR	13	DPWA Multichannel
-0.007 \pm 0.002	¹ WORKMAN	12A	DPWA $\gamma N \rightarrow N\pi$
-0.017 \pm 0.001	¹ DUGGER	07	DPWA $\gamma N \rightarrow \pi N$
••• We do not use the following data for averages, fits, limits, etc. •••			
-0.013 \pm 0.003	ANISOVICH	12A	DPWA Multichannel
-0.017 \pm 0.001	¹ SHRESTHA	12A	DPWA Multichannel
-0.025	DRECHSEL	07	DPWA $\gamma N \rightarrow \pi N$

¹ Statistical error only.

 $N(1680) \rightarrow p\gamma$, helicity-3/2 amplitude $A_{3/2}$

VALUE ($\text{GeV}^{-1/2}$)	DOCUMENT ID	TECN	COMMENT
0.130 to 0.140 (≈ 0.135) OUR ESTIMATE			
0.128 \pm 0.011	GOLOVATCH	19	DPWA $\gamma p \rightarrow \pi^+\pi^-\rho$
0.112 \pm 0.005	¹ HUNT	19	DPWA Multichannel
0.136 \pm 0.005	SOKHOYAN	15A	DPWA Multichannel
0.116 \pm 0.001	¹ SHKLYAR	13	DPWA Multichannel
0.140 \pm 0.002	¹ WORKMAN	12A	DPWA $\gamma N \rightarrow N\pi$
0.134 \pm 0.002	¹ DUGGER	07	DPWA $\gamma N \rightarrow \pi N$
••• We do not use the following data for averages, fits, limits, etc. •••			
0.135 \pm 0.006	ANISOVICH	12A	DPWA Multichannel
0.136 \pm 0.001	¹ SHRESTHA	12A	DPWA Multichannel
0.134	DRECHSEL	07	DPWA $\gamma N \rightarrow \pi N$

¹ Statistical error only.

See key on page 1171

Baryon Particle Listings

$N(1680)$, $N(1700)$

$N(1680) \rightarrow n\gamma$, helicity-1/2 amplitude $A_{1/2}$

VALUE (GeV ^{-1/2})	DOCUMENT ID	TECN	COMMENT
0.020 to 0.040 (≈ 0.030) OUR ESTIMATE			
0.005 ± 0.004	¹ HUNT	19	DPWA Multichannel
0.033 ± 0.003	ANISOVICH	17E	DPWA Multichannel
0.026 ± 0.004	¹ CHEN	12A	DPWA $\gamma N \rightarrow \pi N$
••• We do not use the following data for averages, fits, limits, etc. •••			
0.034 ± 0.006	ANISOVICH	13B	DPWA Multichannel
0.029 ± 0.002	¹ SHRESTHA	12A	DPWA Multichannel
0.028	DRECHSEL	07	DPWA $\gamma N \rightarrow \pi N$

¹ Statistical error only.

$N(1680) \rightarrow n\gamma$, helicity-3/2 amplitude $A_{3/2}$

VALUE (GeV ^{-1/2})	DOCUMENT ID	TECN	COMMENT
-0.050 to -0.025 (≈ -0.035) OUR ESTIMATE			
-0.061 ± 0.004	¹ HUNT	19	DPWA Multichannel
-0.063 ± 0.004	ANISOVICH	17E	DPWA Multichannel
-0.029 ± 0.002	¹ CHEN	12A	DPWA $\gamma N \rightarrow \pi N$
••• We do not use the following data for averages, fits, limits, etc. •••			
-0.044 ± 0.009	ANISOVICH	13B	DPWA Multichannel
-0.059 ± 0.002	¹ SHRESTHA	12A	DPWA Multichannel
-0.038	DRECHSEL	07	DPWA $\gamma N \rightarrow \pi N$

¹ Statistical error only.

$N(1680)$ REFERENCES

For early references, see Physics Letters **111B** 1 (1982). For very early references, see Reviews of Modern Physics **37** 633 (1965).

ROENCHEN 22	EPJ A58 229	D. Roenchen et al.	(JULI, GWU, BONN+)
MUELLER 20	PL B803 135233	J. Mueller et al.	(CBELSA/TAPS Collab.)
GOLOVATCH 19	PL B788 371	E. Golovatch et al.	(CLAS Collab.)
HUNT 19	PR C99 055205	B. C. Hunt, D.M. Manley	
ANISOVICH 17E	PR C96 055202	A.V. Anisovich et al.	(BONN, PNPI, JLAB+)
ROENCHEN 15A	EPJ A51 70	D. Roenchen et al.	
SOKHOYAN 15A	EPJ A51 95	V. Sokhoyan et al.	(CBELSA/TAPS Collab.)
PDG 14	CP C38 070001	K. Olive et al.	(PDG Collab.)
SVARC 14	PR C89 045205	A. Svarc et al.	(RBI Zagreb, UNI Tuzla)
ANISOVICH 13B	EPJ A49 67	A.V. Anisovich et al.	
SHKLYAR 13	PR C87 015201	V. Shklyar, H. Lenske, U. Mosel	(GIES)
ANISOVICH 12A	EPJ A48 15	A.V. Anisovich et al.	(BONN, PNPI)
CHEN 12A	PR C86 015206	W. Chen et al.	(DUKE, GWU, MSST, ITEP+)
SHRESTHA 12A	PR C86 055203	M. Shrestha, D.M. Manley	(KSU)
WORKMAN 12A	PR C86 015202	R. Workman et al.	(GWU)
BATINIC 10	PR C82 038203	M. Batinic et al.	(ZAGR)
THOMA 08	PL B659 87	U. Thoma et al.	(CB-ELSA Collab.)
DRECHSEL 07	EPJ A34 69	D. Drechsel, S.S. Kamalov, L. Tiator	(MAINZ, JINR)
DUGGER 07	PR C76 025211	M. Dugger et al.	(JLab CLAS Collab.)
ARMDT 06	PR C74 045205	R.A. Arndt et al.	(GWU)
VRANA 00	PRPL 328 181	T.P. Vrana, S.A. Dytman, T.-S.H. Lee	(PITT, ANL)
TIATOR 99	PR C60 035210	L. Tiator et al.	
HOEHLER 93	πN Newsletter 9 1	G. Hohlner	(KARL)
CUTKOSKY 80	Toronto Conf. 19	R.E. Cutkosky et al.	(CMU, LBL) IJP
Also	PR D20 2839	R.E. Cutkosky et al.	(CMU, LBL) IJP
HOEHLER 79	PDAT 12-1	G. Hohlner et al.	(KARLT) IJP
Also	Toronto Conf. 3	R. Koch	(KARLT) IJP

$N(1700) 3/2^-$

$$I(J^P) = \frac{1}{2}(\frac{3}{2}^-) \text{ Status: } **$$

Older and obsolete values are listed and referenced in the 2014 edition, Chinese Physics **C38** 070001 (2014).

$N(1700)$ POLE POSITION

REAL PART

VALUE (MeV)	DOCUMENT ID	TECN	COMMENT
1650 to 1750 (≈ 1700) OUR ESTIMATE			
1780 ± 35	SOKHOYAN	15A	DPWA Multichannel
1757 ± 4 ± 1	¹ SVARC	14	L+P $\pi N \rightarrow \pi N$
1660 ± 30	CUTKOSKY	80	IPWA $\pi N \rightarrow \pi N$
••• We do not use the following data for averages, fits, limits, etc. •••			
1647	HUNT	19	DPWA Multichannel
1770 ± 40	ANISOVICH	12A	DPWA Multichannel
1806 ± 23	BATINIC	10	DPWA $\pi N \rightarrow N\pi, N\eta$
1704	VRANA	00	DPWA Multichannel
1700	HOEHLER	93	SPED $\pi N \rightarrow \pi N$

¹ Fit to the amplitudes of HOEHLER 79.

-2xIMAGINARY PART

VALUE (MeV)	DOCUMENT ID	TECN	COMMENT
100 to 300 (≈ 200) OUR ESTIMATE			
420 ± 140	SOKHOYAN	15A	DPWA Multichannel
136 ± 7 ± 4	¹ SVARC	14	L+P $\pi N \rightarrow \pi N$
90 ± 40	CUTKOSKY	80	IPWA $\pi N \rightarrow \pi N$
••• We do not use the following data for averages, fits, limits, etc. •••			
79	HUNT	19	DPWA Multichannel
420 ± 180	ANISOVICH	12A	DPWA Multichannel
129 ± 33	BATINIC	10	DPWA $\pi N \rightarrow N\pi, N\eta$
156	VRANA	00	DPWA Multichannel
120	HOEHLER	93	SPED $\pi N \rightarrow \pi N$

¹ Fit to the amplitudes of HOEHLER 79.

$N(1700)$ ELASTIC POLE RESIDUE

MODULUS $|r|$

VALUE (MeV)	DOCUMENT ID	TECN	COMMENT
5 to 50 (≈ 10) OUR ESTIMATE			
60 ± 30	SOKHOYAN	15A	DPWA Multichannel
7 ± 1 ± 1	¹ SVARC	14	L+P $\pi N \rightarrow \pi N$
6 ± 3	CUTKOSKY	80	IPWA $\pi N \rightarrow \pi N$
••• We do not use the following data for averages, fits, limits, etc. •••			
50 ± 40	ANISOVICH	12A	DPWA Multichannel
7	BATINIC	10	DPWA $\pi N \rightarrow N\pi, N\eta$
5	HOEHLER	93	SPED $\pi N \rightarrow \pi N$

¹ Fit to the amplitudes of HOEHLER 79.

PHASE θ

VALUE (°)	DOCUMENT ID	TECN	COMMENT
-120 to 0 (≈ -90) OUR ESTIMATE			
-115 ± 30	SOKHOYAN	15A	DPWA Multichannel
-113 ± 4 ± 2	¹ SVARC	14	L+P $\pi N \rightarrow \pi N$
0 ± 50	CUTKOSKY	80	IPWA $\pi N \rightarrow \pi N$
••• We do not use the following data for averages, fits, limits, etc. •••			
-100 ± 40	ANISOVICH	12A	DPWA Multichannel
-34	BATINIC	10	DPWA $\pi N \rightarrow N\pi, N\eta$

¹ Fit to the amplitudes of HOEHLER 79.

$N(1700)$ INELASTIC POLE RESIDUE

The "normalized residue" is the residue divided by $\Gamma_{pole}/2$.

Normalized residue in $N\pi \rightarrow N(1700) \rightarrow \Delta\pi, S\text{-wave}$

MODULUS	PHASE (°)	DOCUMENT ID	TECN	COMMENT
0.33 ± 0.10	-70 ± 25	SOKHOYAN	15A	DPWA Multichannel
••• We do not use the following data for averages, fits, limits, etc. •••				
0.34 ± 0.21	-60 ± 40	ANISOVICH	12A	DPWA Multichannel

Normalized residue in $N\pi \rightarrow N(1700) \rightarrow \Delta\pi, D\text{-wave}$

MODULUS	PHASE (°)	DOCUMENT ID	TECN	COMMENT
0.10 ± 0.06	75 ± 30	SOKHOYAN	15A	DPWA Multichannel
••• We do not use the following data for averages, fits, limits, etc. •••				
0.08 ± 0.06	90 ± 35	ANISOVICH	12A	DPWA Multichannel

Normalized residue in $N\pi \rightarrow N(1700) \rightarrow N\sigma$

MODULUS	PHASE (°)	DOCUMENT ID	TECN	COMMENT
0.13 ± 0.08	-100 ± 35	SOKHOYAN	15A	DPWA Multichannel

Normalized residue in $N\pi \rightarrow N(1700) \rightarrow N(1440)\pi$

MODULUS	PHASE (°)	DOCUMENT ID	TECN	COMMENT
0.13 ± 0.05	40 ± 35	SOKHOYAN	15A	DPWA Multichannel

Normalized residue in $N\pi \rightarrow N(1700) \rightarrow N(1520)\pi, P\text{-wave}$

MODULUS	PHASE (°)	DOCUMENT ID	TECN	COMMENT
0.07 ± 0.03	160 ± 45	SOKHOYAN	15A	DPWA Multichannel

$N(1700)$ BREIT-WIGNER MASS

VALUE (MeV)	DOCUMENT ID	TECN	COMMENT
1650 to 1800 (≈ 1720) OUR ESTIMATE			
1653 ± 5	¹ HUNT	19	DPWA Multichannel
1800 ± 35	SOKHOYAN	15A	DPWA Multichannel
1675 ± 25	CUTKOSKY	80	IPWA $\pi N \rightarrow \pi N$
1731 ± 15	HOEHLER	79	IPWA $\pi N \rightarrow \pi N$
••• We do not use the following data for averages, fits, limits, etc. •••			
1790 ± 40	ANISOVICH	12A	DPWA Multichannel
1665 ± 3	¹ SHRESTHA	12A	DPWA Multichannel
1817 ± 22	BATINIC	10	DPWA $\pi N \rightarrow N\pi, N\eta$
1736 ± 33	VRANA	00	DPWA Multichannel

¹ Statistical error only.

$N(1700)$ BREIT-WIGNER WIDTH

VALUE (MeV)	DOCUMENT ID	TECN	COMMENT
100 to 300 (≈ 200) OUR ESTIMATE			
81 ± 13	¹ HUNT	19	DPWA Multichannel
400 ± 100	SOKHOYAN	15A	DPWA Multichannel
90 ± 40	CUTKOSKY	80	IPWA $\pi N \rightarrow \pi N$
110 ± 30	HOEHLER	79	IPWA $\pi N \rightarrow \pi N$
••• We do not use the following data for averages, fits, limits, etc. •••			
390 ± 140	ANISOVICH	12A	DPWA Multichannel
56 ± 8	¹ SHRESTHA	12A	DPWA Multichannel
134 ± 37	BATINIC	10	DPWA $\pi N \rightarrow N\pi, N\eta$
175 ± 133	VRANA	00	DPWA Multichannel

¹ Statistical error only.

Baryon Particle Listings

 $N(1700)$ $N(1700)$ DECAY MODES

The following branching fractions are our estimates, not fits or averages.

Mode	Fraction (Γ_i/Γ)
Γ_1 $N\pi$	7–17 %
Γ_2 $N\eta$	1–2 %
Γ_3 $N\omega$	10–34 %
Γ_4 ΛK	1–2 %
Γ_5 $N\pi\pi$	>89 %
Γ_6 $\Delta(1232)\pi$	55–85 %
Γ_7 $\Delta(1232)\pi, S\text{-wave}$	50–80 %
Γ_8 $\Delta(1232)\pi, D\text{-wave}$	4–14 %
Γ_9 $N\rho, S=3/2, S\text{-wave}$	32–44 %
Γ_{10} $N\sigma$	2–14 %
Γ_{11} $N(1440)\pi$	3–11 %
Γ_{12} $N(1520)\pi$	<4 %
Γ_{13} $p\gamma$	0.01–0.05 %
Γ_{14} $p\gamma, \text{helicity}=1/2$	0.0–0.024 %
Γ_{15} $p\gamma, \text{helicity}=3/2$	0.002–0.026 %
Γ_{16} $n\gamma$	0.01–0.13 %
Γ_{17} $n\gamma, \text{helicity}=1/2$	0.0–0.09 %
Γ_{18} $n\gamma, \text{helicity}=3/2$	0.01–0.05 %

 $N(1700)$ BRANCHING RATIOS

$\Gamma(N\pi)/\Gamma_{\text{total}}$	VALUE (%)	DOCUMENT ID	TECN	COMMENT	Γ_1/Γ
7 to 17 (≈ 12) OUR ESTIMATE					
3.7 ± 0.1		¹ HUNT	19	DPWA Multichannel	
15 ± 6		SOKHOYAN	15A	DPWA Multichannel	
11 ± 5		CUTKOSKY	80	IPWA $\pi N \rightarrow \pi N$	
8 ± 3		HOEHLER	79	IPWA $\pi N \rightarrow \pi N$	
••• We do not use the following data for averages, fits, limits, etc. •••					
12 ± 5		ANISOVICH	12A	DPWA Multichannel	
2.8 ± 0.5		¹ SHRESTHA	12A	DPWA Multichannel	
9 ± 6		BATINIC	10	DPWA $\pi N \rightarrow N\pi, N\eta$	
4 ± 2		VRANA	00	DPWA Multichannel	
¹ Statistical error only.					

$\Gamma(N\eta)/\Gamma_{\text{total}}$	VALUE (%)	DOCUMENT ID	TECN	COMMENT	Γ_2/Γ
1–2 % OUR ESTIMATE					
1 ± 1		MUELLER	20	DPWA Multichannel	
1.1 ± 0.6		¹ HUNT	19	DPWA Multichannel	
••• We do not use the following data for averages, fits, limits, etc. •••					
14 ± 5		BATINIC	10	DPWA $\pi N \rightarrow N\pi, N\eta$	
10 ± 5		THOMA	08	DPWA Multichannel	
0 ± 1		VRANA	00	DPWA Multichannel	
¹ Statistical error only.					

$\Gamma(N\omega)/\Gamma_{\text{total}}$	VALUE (%)	DOCUMENT ID	TECN	COMMENT	Γ_3/Γ
22 ± 12		DENISENKO	16	DPWA Multichannel	

$\Gamma(\Lambda K)/\Gamma_{\text{total}}$	VALUE (%)	DOCUMENT ID	TECN	COMMENT	Γ_4/Γ
1–2 % OUR ESTIMATE					
1.3 ± 0.7		¹ HUNT	19	DPWA Multichannel	
¹ Statistical error only.					

$\Gamma(\Delta(1232)\pi, S\text{-wave})/\Gamma_{\text{total}}$	VALUE (%)	DOCUMENT ID	TECN	COMMENT	Γ_7/Γ
11 ± 8		¹ HUNT	19	DPWA Multichannel	
65 ± 15		SOKHOYAN	15A	DPWA Multichannel	
••• We do not use the following data for averages, fits, limits, etc. •••					
72 ± 23		ANISOVICH	12A	DPWA Multichannel	
31 ± 9		¹ SHRESTHA	12A	DPWA Multichannel	
11 ± 1		VRANA	00	DPWA Multichannel	
¹ Statistical error only.					

$\Gamma(\Delta(1232)\pi, D\text{-wave})/\Gamma_{\text{total}}$	VALUE (%)	DOCUMENT ID	TECN	COMMENT	Γ_8/Γ
13 ± 5		¹ HUNT	19	DPWA Multichannel	
9 ± 5		SOKHOYAN	15A	DPWA Multichannel	
••• We do not use the following data for averages, fits, limits, etc. •••					
<10		ANISOVICH	12A	DPWA Multichannel	
3 ± 2		¹ SHRESTHA	12A	DPWA Multichannel	
79 ± 56		VRANA	00	DPWA Multichannel	
¹ Statistical error only.					

 $\Gamma(N\rho, S=3/2, S\text{-wave})/\Gamma_{\text{total}}$

VALUE (%)	DOCUMENT ID	TECN	COMMENT	Γ_9/Γ
7.5 ± 3.6	¹ HUNT	19	DPWA Multichannel	
••• We do not use the following data for averages, fits, limits, etc. •••				
38 ± 6	¹ SHRESTHA	12A	DPWA Multichannel	
7 ± 1	VRANA	00	DPWA Multichannel	
¹ Statistical error only.				

 $\Gamma(N\sigma)/\Gamma_{\text{total}}$

VALUE (%)	DOCUMENT ID	TECN	COMMENT	Γ_{10}/Γ
62 ± 9	¹ HUNT	19	DPWA Multichannel	
8 ± 6	SOKHOYAN	15A	DPWA Multichannel	
••• We do not use the following data for averages, fits, limits, etc. •••				
24 ± 6	¹ SHRESTHA	12A	DPWA Multichannel	
18 ± 12	THOMA	08	DPWA Multichannel	
0 ± 1	VRANA	00	DPWA Multichannel	
¹ Statistical error only.				

 $\Gamma(N(1440)\pi)/\Gamma_{\text{total}}$

VALUE (%)	DOCUMENT ID	TECN	COMMENT	Γ_{11}/Γ
7 ± 4	SOKHOYAN	15A	DPWA Multichannel	

 $\Gamma(N(1520)\pi)/\Gamma_{\text{total}}$

VALUE (%)	DOCUMENT ID	TECN	COMMENT	Γ_{12}/Γ
<4	SOKHOYAN	15A	DPWA Multichannel	

 $N(1700)$ PHOTON DECAY AMPLITUDES AT THE POLE $N(1700) \rightarrow p\gamma, \text{helicity-1/2 amplitude } A_{1/2}$

MODULUS ($\text{GeV}^{-1/2}$)	PHASE ($^\circ$)	DOCUMENT ID	TECN	COMMENT
0.047 ± 0.016	75 ± 30	SOKHOYAN	15A	DPWA Multichannel

 $N(1700) \rightarrow p\gamma, \text{helicity-3/2 amplitude } A_{3/2}$

MODULUS ($\text{GeV}^{-1/2}$)	PHASE ($^\circ$)	DOCUMENT ID	TECN	COMMENT
-0.041 ± 0.014	0 ± 20	SOKHOYAN	15A	DPWA Multichannel

 $N(1700)$ BREIT-WIGNER PHOTON DECAY AMPLITUDES $N(1700) \rightarrow p\gamma, \text{helicity-1/2 amplitude } A_{1/2}$

VALUE ($\text{GeV}^{-1/2}$)	DOCUMENT ID	TECN	COMMENT
0.032 ± 0.005	¹ HUNT	19	DPWA Multichannel
0.041 ± 0.017	ANISOVICH	12A	DPWA Multichannel
••• We do not use the following data for averages, fits, limits, etc. •••			
0.021 ± 0.005	¹ SHRESTHA	12A	DPWA Multichannel
¹ Statistical error only.			

 $N(1700) \rightarrow p\gamma, \text{helicity-3/2 amplitude } A_{3/2}$

VALUE ($\text{GeV}^{-1/2}$)	DOCUMENT ID	TECN	COMMENT
0.034 ± 0.006	¹ HUNT	19	DPWA Multichannel
-0.037 ± 0.014	SOKHOYAN	15A	DPWA Multichannel
••• We do not use the following data for averages, fits, limits, etc. •••			
-0.034 ± 0.013	ANISOVICH	12A	DPWA Multichannel
0.050 ± 0.009	¹ SHRESTHA	12A	DPWA Multichannel
¹ Statistical error only.			

 $N(1700) \rightarrow n\gamma, \text{helicity-1/2 amplitude } A_{1/2}$

VALUE ($\text{GeV}^{-1/2}$)	DOCUMENT ID	TECN	COMMENT
0.005 ± 0.011	¹ HUNT	19	DPWA Multichannel
0.025 ± 0.010	ANISOVICH	13B	DPWA Multichannel
••• We do not use the following data for averages, fits, limits, etc. •••			
-0.049 ± 0.008	¹ SHRESTHA	12A	DPWA Multichannel
¹ Statistical error only.			

 $N(1700) \rightarrow n\gamma, \text{helicity-3/2 amplitude } A_{3/2}$

VALUE ($\text{GeV}^{-1/2}$)	DOCUMENT ID	TECN	COMMENT
-0.094 ± 0.017	¹ HUNT	19	DPWA Multichannel
-0.032 ± 0.018	ANISOVICH	13B	DPWA Multichannel
••• We do not use the following data for averages, fits, limits, etc. •••			
-0.092 ± 0.014	¹ SHRESTHA	12A	DPWA Multichannel
¹ Statistical error only.			

 $N(1700)$ REFERENCES

For early references, see Physics Letters **111B** 1 (1982).

MUELLER	20	PL B803 135323	J. Mueller et al.	(CBELSA/TAPS Collab.)
HUNT	19	PR C99 055205	B.C. Hunt, D.M. Manley	
DENISENKO	16	PL B755 97	I. Denisenko et al.	
SOKHOYAN	15A	EPJ A51 95	V. Sokhoyan et al.	(CBELSA/TAPS Collab.)
PDG	14	CP C38 070001	K. Olive et al.	(PDG Collab.)
SVARC	14	PR C89 045205	A. Svarc et al.	(RBI Zagreb, UNI Tuzla)
ANISOVICH	13B	EPJ A49 67	A.V. Anisovich et al.	

See key on page 1171

Baryon Particle Listings

$N(1700)$, $N(1710)$

ANISOVICH	12A	EPJ A48 15	A.V. Anisovich <i>et al.</i>	(BONN, PNPI)
SHRESTHA	12A	PR C86 055203	M. Shrestha, D.M. Manley	(KSU)
BATINIC	10	PR C82 038203	M. Batinic <i>et al.</i>	(ZAGR)
THOMA	08	PL B659 87	U. Thoma <i>et al.</i>	(CB-ELSA Collab.)
VRANA	00	PRPL 328 181	T.P. Vrana, S.A. Dytman, T.-S.H. Lee	(PITT, ANL)
HOEHLER	93	πN Newsletter 9 1	G. H\"ohler	(KARL)
CUTKOSKY	80	Toronto Conf. 19	R.E. Cutkosky <i>et al.</i>	(CMU, LBL) IJP
Also		PR D20 2839	R.E. Cutkosky <i>et al.</i>	(CMU, LBL) IJP
HOEHLER	79	PDAT 12-1	G. H\"ohler <i>et al.</i>	(KARLT) IJP
Also		Toronto Conf. 3	R. Koch	(KARLT) IJP

$N(1710) 1/2^+$

$$I(J^P) = \frac{1}{2}(1/2^+) \text{ Status: } ****$$

Older and obsolete values are listed and referenced in the 2014 edition, Chinese Physics C38 070001 (2014).

$N(1710)$ POLE POSITION

REAL PART

VALUE (MeV)	DOCUMENT ID	TECN	COMMENT
1650 to 1750 (≈ 1700) OUR ESTIMATE			
1605 \pm 7	ROENCHEN 22	DPWA	Multichannel
1690 \pm 15	ANISOVICH 17A	DPWA	Multichannel
1697 \pm 23	¹ ANISOVICH 17A	L+P	$\gamma p, \pi^- p \rightarrow K\Lambda$
1770 \pm 5 \pm 2	2 SVARC 14	L+P	$\pi N \rightarrow \pi N$
1690 \pm 20	CUTKOSKY 80	IPWA	$\pi N \rightarrow \pi N$
••• We do not use the following data for averages, fits, limits, etc. •••			
1615	HUNT 19	DPWA	Multichannel
1651	ROENCHEN 15A	DPWA	Multichannel
1690 \pm 15	SOKHOYAN 15A	DPWA	Multichannel
1690 \pm 15	GUTZ 14	DPWA	Multichannel
1670	SHKLYAR 13	DPWA	Multichannel
1687 \pm 17	ANISOVICH 12A	DPWA	Multichannel
1711 \pm 15	³ BATINIC 10	DPWA	$\pi N \rightarrow N\pi, N\eta$
1679	VRANA 00	DPWA	Multichannel
1690	HOEHLER 93	SPED	$\pi N \rightarrow \pi N$
1698	CUTKOSKY 90	IPWA	$\pi N \rightarrow \pi N$

¹ Statistical error only.

² Fit to the amplitudes of HOEHLER 79.

³ BATINIC 10 finds evidence for a second P_{11} state with all parameters except for the phase of the pole residue very similar to the parameters we give here.

$-2\times$ IMAGINARY PART

VALUE (MeV)	DOCUMENT ID	TECN	COMMENT
80 to 160 (≈ 120) OUR ESTIMATE			
115 \pm 5	ROENCHEN 22	DPWA	Multichannel
155 \pm 25	ANISOVICH 17A	DPWA	Multichannel
84 \pm 34	¹ ANISOVICH 17A	L+P	$\gamma p, \pi^- p \rightarrow K\Lambda$
98 \pm 8 \pm 5	² SVARC 14	L+P	$\pi N \rightarrow \pi N$
80 \pm 20	CUTKOSKY 80	IPWA	$\pi N \rightarrow \pi N$
••• We do not use the following data for averages, fits, limits, etc. •••			
169	HUNT 19	DPWA	Multichannel
121	ROENCHEN 15A	DPWA	Multichannel
170 \pm 20	SOKHOYAN 15A	DPWA	Multichannel
170 \pm 20	GUTZ 14	DPWA	Multichannel
159	SHKLYAR 13	DPWA	Multichannel
200 \pm 25	ANISOVICH 12A	DPWA	Multichannel
174 \pm 16	³ BATINIC 10	DPWA	$\pi N \rightarrow N\pi, N\eta$
132	VRANA 00	DPWA	Multichannel
200	HOEHLER 93	SPED	$\pi N \rightarrow \pi N$
88	CUTKOSKY 90	IPWA	$\pi N \rightarrow \pi N$

¹ Statistical error only.

² Fit to the amplitudes of HOEHLER 79.

³ BATINIC 10 finds evidence for a second P_{11} state with all parameters except for the phase of the pole residue very similar to the parameters we give here.

$N(1710)$ ELASTIC POLE RESIDUE

MODULUS $|r|$

VALUE (MeV)	DOCUMENT ID	TECN	COMMENT
4 to 10 (≈ 7) OUR ESTIMATE			
5.5 \pm 2.4	ROENCHEN 22	DPWA	Multichannel
6 \pm 3	SOKHOYAN 15A	DPWA	Multichannel
5 \pm 1 \pm 1	¹ SVARC 14	L+P	$\pi N \rightarrow \pi N$
8 \pm 2	CUTKOSKY 80	IPWA	$\pi N \rightarrow \pi N$
••• We do not use the following data for averages, fits, limits, etc. •••			
3.2	ROENCHEN 15A	DPWA	Multichannel
6 \pm 3	GUTZ 14	DPWA	Multichannel
11	SHKLYAR 13	DPWA	Multichannel
6 \pm 4	ANISOVICH 12A	DPWA	Multichannel
24	² BATINIC 10	DPWA	$\pi N \rightarrow N\pi, N\eta$
15	HOEHLER 93	SPED	$\pi N \rightarrow \pi N$
9	CUTKOSKY 90	IPWA	$\pi N \rightarrow \pi N$

¹ Fit to the amplitudes of HOEHLER 79.

² BATINIC 10 finds evidence for a second P_{11} state with all parameters except for the phase of the pole residue very similar to the parameters we give here.

PHASE θ

VALUE ($^\circ$)	DOCUMENT ID	TECN	COMMENT
120 to 270 (≈ 190) OUR ESTIMATE			
-114 \pm 29	ROENCHEN 22	DPWA	Multichannel
130 \pm 35	SOKHOYAN 15A	DPWA	Multichannel
-104 \pm 7 \pm 3	¹ SVARC 14	L+P	$\pi N \rightarrow \pi N$
175 \pm 35	CUTKOSKY 80	IPWA	$\pi N \rightarrow \pi N$
••• We do not use the following data for averages, fits, limits, etc. •••			
55	ROENCHEN 15A	DPWA	Multichannel
120 \pm 45	GUTZ 14	DPWA	Multichannel
9	SHKLYAR 13	DPWA	Multichannel
120 \pm 70	ANISOVICH 12A	DPWA	Multichannel
20	² BATINIC 10	DPWA	$\pi N \rightarrow N\pi, N\eta$
-167	CUTKOSKY 90	IPWA	$\pi N \rightarrow \pi N$

¹ Fit to the amplitudes of HOEHLER 79.

² BATINIC 10 finds evidence for a second P_{11} state with all parameters except for the phase of the pole residue very similar to the parameters we give here.

$N(1710)$ INELASTIC POLE RESIDUE

The "normalized residue" is the residue divided by $\Gamma_{pole}/2$.

Normalized residue in $N\pi \rightarrow N(1710) \rightarrow N\eta$

MODULUS	PHASE ($^\circ$)	DOCUMENT ID	TECN	COMMENT
0.28 \pm 0.13	91 \pm 32	ROENCHEN 22	DPWA	Multichannel
0.12 \pm 0.04	0 \pm 45	ANISOVICH 12A	DPWA	Multichannel
••• We do not use the following data for averages, fits, limits, etc. •••				
0.16	-180	ROENCHEN 15A	DPWA	Multichannel

Normalized residue in $N\pi \rightarrow N(1710) \rightarrow \Lambda K$

MODULUS	PHASE ($^\circ$)	DOCUMENT ID	TECN	COMMENT
0.20 \pm 0.10	-144 \pm 39	ROENCHEN 22	DPWA	Multichannel
0.16 \pm 0.05	-160 \pm 25	ANISOVICH 17A	DPWA	Multichannel
0.12 \pm 0.24	-119 \pm 83	¹ ANISOVICH 17A	L+P	$\gamma p, \pi^- p \rightarrow K\Lambda$
-0.12				
••• We do not use the following data for averages, fits, limits, etc. •••				
0.12	-32	ROENCHEN 15A	DPWA	Multichannel
0.17 \pm 0.06	-110 \pm 20	ANISOVICH 12A	DPWA	Multichannel

¹ Statistical error only.

Normalized residue in $N\pi \rightarrow N(1710) \rightarrow \Sigma K$

MODULUS	PHASE ($^\circ$)	DOCUMENT ID	TECN	COMMENT
0.055 \pm 0.024	162 \pm 153	ROENCHEN 22	DPWA	Multichannel
••• We do not use the following data for averages, fits, limits, etc. •••				
0.004	-43	ROENCHEN 15A	DPWA	Multichannel

Normalized residue in $N\pi \rightarrow N(1710) \rightarrow N(1535)\pi$

MODULUS	PHASE ($^\circ$)	DOCUMENT ID	TECN	COMMENT
0.10 \pm 0.04	140 \pm 40	GUTZ 14	DPWA	Multichannel

$N(1710)$ BREIT-WIGNER MASS

VALUE (MeV)	DOCUMENT ID	TECN	COMMENT
1680 to 1740 (≈ 1710) OUR ESTIMATE			
1648 \pm 16	¹ HUNT 19	DPWA	Multichannel
1715 \pm 20	SOKHOYAN 15A	DPWA	Multichannel
1737 \pm 17	¹ SHKLYAR 13	DPWA	Multichannel
1700 \pm 50	CUTKOSKY 80	IPWA	$\pi N \rightarrow \pi N$
1723 \pm 9	HOEHLER 79	IPWA	$\pi N \rightarrow \pi N$
••• We do not use the following data for averages, fits, limits, etc. •••			
1715 \pm 20	GUTZ 14	DPWA	Multichannel
1710 \pm 20	ANISOVICH 12A	DPWA	Multichannel
1662 \pm 7	¹ SHRESTHA 12A	DPWA	Multichannel
1729 \pm 16	² BATINIC 10	DPWA	$\pi N \rightarrow N\pi, N\eta$
1752 \pm 3	PENNER 02c	DPWA	Multichannel
1699 \pm 65	VRANA 00	DPWA	Multichannel

¹ Statistical error only.

² BATINIC 10 finds evidence for a second P_{11} state with all parameters except for the phase of the pole residue very similar to the parameters we give here.

$N(1710)$ BREIT-WIGNER WIDTH

VALUE (MeV)	DOCUMENT ID	TECN	COMMENT
80 to 200 (≈ 140) OUR ESTIMATE			
195 \pm 46	¹ HUNT 19	DPWA	Multichannel
175 \pm 15	SOKHOYAN 15A	DPWA	Multichannel
368 \pm 120	¹ SHKLYAR 13	DPWA	Multichannel
93 \pm 30	CUTKOSKY 90	IPWA	$\pi N \rightarrow \pi N$
90 \pm 30	CUTKOSKY 80	IPWA	$\pi N \rightarrow \pi N$
120 \pm 15	HOEHLER 79	IPWA	$\pi N \rightarrow \pi N$
••• We do not use the following data for averages, fits, limits, etc. •••			
175 \pm 15	GUTZ 14	DPWA	Multichannel
200 \pm 18	ANISOVICH 12A	DPWA	Multichannel
116 \pm 17	¹ SHRESTHA 12A	DPWA	Multichannel
180 \pm 17	² BATINIC 10	DPWA	$\pi N \rightarrow N\pi, N\eta$

Baryon Particle Listings

 $N(1710)$

386 ± 59	PENNER	02c	DPWA	Multichannel
143 ± 100	VRANA	00	DPWA	Multichannel

¹ Statistical error only.

² BATINIC 10 finds evidence for a second P_{11} state with all parameters except for the phase of the pole residue very similar to the parameters we give here.

 $N(1710)$ DECAY MODES

The following branching fractions are our estimates, not fits or averages.

Mode	Fraction (Γ_i/Γ)
Γ_1 $N\pi$	5–20 %
Γ_2 $N\eta$	10–50 %
Γ_3 $N\omega$	1–5 %
Γ_4 ΛK	5–25 %
Γ_5 ΣK	seen
Γ_6 $N\pi\pi$	14–48 %
Γ_7 $\Delta(1232)\pi$, P -wave	3–9 %
Γ_8 $N\rho$, $S=1/2$, P -wave	11–23 %
Γ_9 $N\sigma$	<16 %
Γ_{10} $N(1535)\pi$	9–21 %
Γ_{11} $p\gamma$, helicity=1/2	0.002–0.08 %
Γ_{12} $n\gamma$, helicity=1/2	0.0–0.02 %

 $N(1710)$ BRANCHING RATIOS

$\Gamma(N\pi)/\Gamma_{\text{total}}$	DOCUMENT ID	TECN	COMMENT	Γ_1/Γ
5 to 20 (≈ 10) OUR ESTIMATE				
12 ± 6	¹ HUNT	19	DPWA	Multichannel
5 ± 3	SOKHOYAN	15A	DPWA	Multichannel
2 ± 2	¹ SHKLYAR	13	PWA	Multichannel
20 ± 4	CUTKOSKY	80	IPWA	$\pi N \rightarrow \pi N$
12 ± 4	HOEHLER	79	IPWA	$\pi N \rightarrow \pi N$
••• We do not use the following data for averages, fits, limits, etc. •••				
5 ± 3	GUTZ	14	DPWA	Multichannel
5 ± 4	ANISOVICH	12A	DPWA	Multichannel
15 ± 4	¹ SHRESTHA	12A	DPWA	Multichannel
22 ± 24	² BATINIC	10	DPWA	$\pi N \rightarrow N\pi$, $N\eta$
14 ± 8	PENNER	02c	DPWA	Multichannel
27 ± 13	VRANA	00	DPWA	Multichannel

¹ Statistical error only.

² BATINIC 10 finds evidence for a second P_{11} state with all parameters except for the phase of the pole residue very similar to the parameters we give here.

$\Gamma(N\eta)/\Gamma_{\text{total}}$	DOCUMENT ID	TECN	COMMENT	Γ_2/Γ
10 to 50 (≈ 30) OUR ESTIMATE				
18 ± 10	MUELLER	20	DPWA	Multichannel
17 ± 8	¹ HUNT	19	DPWA	Multichannel
45 ± 4	¹ SHKLYAR	13	DPWA	Multichannel
17 ± 10	ANISOVICH	12A	DPWA	Multichannel
••• We do not use the following data for averages, fits, limits, etc. •••				
11 ± 7	¹ SHRESTHA	12A	DPWA	Multichannel
6 ± 8	² BATINIC	10	DPWA	$\pi N \rightarrow N\pi$, $N\eta$
36 ± 11	PENNER	02c	DPWA	Multichannel
6 ± 1	VRANA	00	DPWA	Multichannel

¹ Statistical error only.

² BATINIC 10 finds evidence for a second P_{11} state with all parameters except for the phase of the pole residue very similar to the parameters we give here.

$\Gamma(N\omega)/\Gamma_{\text{total}}$	DOCUMENT ID	TECN	COMMENT	Γ_3/Γ
1 to 5 (≈ 3) OUR ESTIMATE				
2 ± 2	DENISENKO	16	DPWA	Multichannel
3 ± 2	¹ SHKLYAR	13	DPWA	Multichannel
••• We do not use the following data for averages, fits, limits, etc. •••				
13 ± 2	PENNER	02c	DPWA	Multichannel

¹ Statistical error only.

$\Gamma(\Lambda K)/\Gamma_{\text{total}}$	DOCUMENT ID	TECN	COMMENT	Γ_4/Γ
5 to 25 (≈ 15) OUR ESTIMATE				
1.8 ± 1.5	¹ HUNT	19	DPWA	Multichannel
23 ± 7	ANISOVICH	12A	DPWA	Multichannel
5 ± 3	SHKLYAR	05	DPWA	Multichannel
••• We do not use the following data for averages, fits, limits, etc. •••				
8 ± 4	¹ SHRESTHA	12A	DPWA	Multichannel
5 ± 2	PENNER	02c	DPWA	Multichannel
10 ± 10	VRANA	00	DPWA	Multichannel

¹ Statistical error only.

$\Gamma(\Sigma K)/\Gamma_{\text{total}}$	DOCUMENT ID	TECN	COMMENT	Γ_5/Γ
3–9 % OUR ESTIMATE				
28 ± 9	¹ HUNT	19	DPWA	Multichannel
••• We do not use the following data for averages, fits, limits, etc. •••				
6 ± 3	¹ SHRESTHA	12A	DPWA	Multichannel
39 ± 8	VRANA	00	DPWA	Multichannel

¹ Statistical error only.

$\Gamma(\Delta(1232)\pi, P\text{-wave})/\Gamma_{\text{total}}$	DOCUMENT ID	TECN	COMMENT	Γ_7/Γ
11–23 % OUR ESTIMATE				
17 ± 9	¹ HUNT	19	DPWA	Multichannel
••• We do not use the following data for averages, fits, limits, etc. •••				
17 ± 6	¹ SHRESTHA	12A	DPWA	Multichannel
17 ± 1	VRANA	00	DPWA	Multichannel

¹ Statistical error only.

$\Gamma(N\rho, S=1/2, P\text{-wave})/\Gamma_{\text{total}}$	DOCUMENT ID	TECN	COMMENT	Γ_8/Γ
11–23 % OUR ESTIMATE				
17 ± 9	¹ HUNT	19	DPWA	Multichannel
••• We do not use the following data for averages, fits, limits, etc. •••				
17 ± 6	¹ SHRESTHA	12A	DPWA	Multichannel
17 ± 1	VRANA	00	DPWA	Multichannel

¹ Statistical error only.

$\Gamma(N\sigma)/\Gamma_{\text{total}}$	DOCUMENT ID	TECN	COMMENT	Γ_9/Γ
<16 % OUR ESTIMATE				
<16	¹ HUNT	19	DPWA	Multichannel

¹ Statistical error only.

$\Gamma(N(1535)\pi)/\Gamma_{\text{total}}$	DOCUMENT ID	TECN	COMMENT	Γ_{10}/Γ
15 ± 6	GUTZ	14	DPWA	Multichannel

 $N(1710)$ PHOTON DECAY AMPLITUDES AT THE POLE **$N(1710) \rightarrow p\gamma$, helicity-1/2 amplitude $A_{1/2}$**

MODULUS ($\text{GeV}^{-1/2}$)	PHASE ($^\circ$)	DOCUMENT ID	TECN	COMMENT
-0.018 ± 0.010	40 ± 55	ROENCHEN	22	DPWA
••• We do not use the following data for averages, fits, limits, etc. •••				
0.020	–83	ROENCHEN	15A	DPWA

 $N(1710) \rightarrow n\gamma$, helicity-1/2 amplitude $A_{1/2}$

MODULUS ($\text{GeV}^{-1/2}$)	PHASE ($^\circ$)	DOCUMENT ID	TECN	COMMENT
0.029 ± 0.007	80 ± 20	ANISOVICH	17E	DPWA

 $N(1710)$ BREIT-WIGNER PHOTON DECAY AMPLITUDES **$N(1710) \rightarrow p\gamma$, helicity-1/2 amplitude $A_{1/2}$**

VALUE ($\text{GeV}^{-1/2}$)	DOCUMENT ID	TECN	COMMENT
0.014 ± 0.008	¹ HUNT	19	DPWA
0.050 ± 0.010	SOKHOYAN	15A	DPWA
-0.050 ± 0.001	¹ SHKLYAR	13	DPWA
••• We do not use the following data for averages, fits, limits, etc. •••			
0.05 ± 0.01	GUTZ	14	DPWA
0.052 ± 0.015	ANISOVICH	12A	DPWA
-0.008 ± 0.003	¹ SHRESTHA	12A	DPWA
0.044	PENNER	02D	DPWA

¹ Statistical error only.

 $N(1710) \rightarrow n\gamma$, helicity-1/2 amplitude $A_{1/2}$

VALUE ($\text{GeV}^{-1/2}$)	DOCUMENT ID	TECN	COMMENT
0.0053 ± 0.0003	¹ HUNT	19	DPWA
-0.040 ± 0.020	ANISOVICH	13B	DPWA
••• We do not use the following data for averages, fits, limits, etc. •••			
0.017 ± 0.003	¹ SHRESTHA	12A	DPWA
–0.024	PENNER	02D	DPWA

¹ Statistical error only.

 $N(1710)$ REFERENCES

For early references, see Physics Letters **111B** 1 (1982).

ROENCHEN	22	EPJ A58 229	D. Roenchen <i>et al.</i>	(JULI, GWU, BONN+)
MUELLER	20	PL B803 135323	J. Mueller <i>et al.</i>	(CBELSA/TAPS Collab.)
HUNT	19	PR C99 055205	B.C. Hunt, D.M. Manley	
ANISOVICH	17A	PRL 119 062004	A.V. Anisovich <i>et al.</i>	
ANISOVICH	17E	PR C96 055202	A.V. Anisovich <i>et al.</i>	(BONN, PNPI, JLAB+)
DENISENKO	16	PL B755 97	I. Denisenko <i>et al.</i>	
ROENCHEN	15A	EPJ A51 70	D. Roenchen <i>et al.</i>	
SOKHOYAN	15A	EPJ A51 95	V. Sokhoyan <i>et al.</i>	(CBELSA/TAPS Collab.)
GUTZ	14	EPJ A50 74	E. Gutz <i>et al.</i>	(CBELSA/TAPS Collab.)
PDG	14	CP C38 070001	K. Olive <i>et al.</i>	(PDG Collab.)
SVARC	14	PR C89 045205	A. Svarc <i>et al.</i>	(RBI Zagreb, UNI Tuzla)
ANISOVICH	13B	EPJ A49 67	A.V. Anisovich <i>et al.</i>	

Baryon Particle Listings

$N(1710)$, $N(1720)$

SHKLYAR	13	PR C87 015201	V. Shklyar, H. Lense, U. Mosel	(GIES)
ANISOVICH	12A	EPJ A48 15	A.V. Anisovich et al.	(BONN, PNPI)
SHRESTHA	12A	PR C86 055203	M. Shrestha, D.M. Manley	(KSU)
BATINIC	10	PR C82 038203	M. Batinic et al.	(ZAGR)
SHKLYAR	05	PR C72 015210	V. Shklyar, H. Lense, U. Mosel	(GIES)
PENNER	02C	PR C66 055211	G. Penner, U. Mosel	(GIES)
PENNER	02D	PR C66 055212	G. Penner, U. Mosel	(GIES)
VRANA	00	PRPL 328 181	T.P. Vrana, S.A. Dyfman, T.-S.H. Lee	(PITT, ANL)
HOEHLER	93	πN Newsletter 9 1	G. Höhler	(KARL)
CUTKOSKY	90	PR D42 235	R.E. Cutkosky, S. Wang	(CMU)
CUTKOSKY	80	Toronto Conf. 19	R.E. Cutkosky et al.	(CMU, LBL) JUP
Also		PR D20 2839	R.E. Cutkosky et al.	(CMU, LBL) JUP
HOEHLER	79	PDAT 12-1	G. Höhler et al.	(KARLT) JUP
Also		Toronto Conf. 3	R. Koch	(KARLT) JUP

– 45	SHKLYAR	13	DPWA	Multichannel
–115 ± 30	ANISOVICH	12A	DPWA	Multichannel
–109	BATINIC	10	DPWA	$\pi N \rightarrow N\pi, N\eta$
– 94	ARNDT	06	DPWA	$\pi N \rightarrow \pi N, \eta N$

¹ Fit to the amplitudes of HOEHLER 79.

$N(1720)$ INELASTIC POLE RESIDUE

The “normalized residue” is the residue divided by $\Gamma_{pole}/2$.

Normalized residue in $N\pi \rightarrow N(1720) \rightarrow N\eta$

MODULUS	PHASE (°)	DOCUMENT ID	TECN	COMMENT
0.049 ± 0.005	64 ± 5	ROENCHEN 22	DPWA	Multichannel
0.03 ± 0.02		ANISOVICH 12A	DPWA	Multichannel
•••		We do not use the following data for averages, fits, limits, etc. •••		
0.007	106	ROENCHEN 15A	DPWA	Multichannel

Normalized residue in $N\pi \rightarrow N(1720) \rightarrow \Lambda K$

MODULUS	PHASE (°)	DOCUMENT ID	TECN	COMMENT
0.034 ± 0.002	–101 ± 4	ROENCHEN 22	DPWA	Multichannel
0.06 ± 0.04	–150 ± 45	ANISOVICH 12A	DPWA	Multichannel
•••		We do not use the following data for averages, fits, limits, etc. •••		
0.011	–70	ROENCHEN 15A	DPWA	Multichannel

Normalized residue in $N\pi \rightarrow N(1720) \rightarrow \Sigma K$

MODULUS	PHASE (°)	DOCUMENT ID	TECN	COMMENT
0.059 ± 0.005	82 ± 3	ROENCHEN 22	DPWA	Multichannel
•••		We do not use the following data for averages, fits, limits, etc. •••		
0.002	79	ROENCHEN 15A	DPWA	Multichannel

Normalized residue in $N\pi \rightarrow N(1720) \rightarrow \Delta\pi, P$ -wave

MODULUS	PHASE (°)	DOCUMENT ID	TECN	COMMENT
0.28 ± 0.09	95 ± 30	SOKHOYAN 15A	DPWA	Multichannel
•••		We do not use the following data for averages, fits, limits, etc. •••		
0.29 ± 0.08	80 ± 40	ANISOVICH 12A	DPWA	Multichannel

Normalized residue in $N\pi \rightarrow N(1720) \rightarrow \Delta\pi, F$ -wave

MODULUS	PHASE (°)	DOCUMENT ID	TECN	COMMENT
0.07 ± 0.05		SOKHOYAN 15A	DPWA	Multichannel
•••		We do not use the following data for averages, fits, limits, etc. •••		
0.03 ± 0.03		ANISOVICH 12A	DPWA	Multichannel

Normalized residue in $N\pi \rightarrow N(1720) \rightarrow N\sigma$

MODULUS	PHASE (°)	DOCUMENT ID	TECN	COMMENT
0.08 ± 0.04	–110 ± 35	SOKHOYAN 15A	DPWA	Multichannel

Normalized residue in $N\pi \rightarrow N(1720) \rightarrow N(1520)\pi, S$ -wave

MODULUS	PHASE (°)	DOCUMENT ID	TECN	COMMENT
0.05 ± 0.04	undefined	SOKHOYAN 15A	DPWA	Multichannel

$N(1720)$ BREIT-WIGNER MASS

VALUE (MeV)	DOCUMENT ID	TECN	COMMENT
1680 to 1750 (≈ 1720) OUR ESTIMATE			
1745 ± 6	GOLOVATCH 19	DPWA	$\gamma p \rightarrow \pi^+ \pi^- p$
1711 ± 4	¹ HUNT 19	DPWA	Multichannel
1690 ± 30	SOKHOYAN 15A	DPWA	Multichannel
1700 ± 10	¹ SHKLYAR 13	DPWA	Multichannel
1763.8 ± 4.6	ARNDT 06	DPWA	$\pi N \rightarrow \pi N, \eta N$
1700 ± 50	CUTKOSKY 80	IPWA	$\pi N \rightarrow \pi N$
1710 ± 20	HOEHLER 79	IPWA	$\pi N \rightarrow \pi N$
•••	We do not use the following data for averages, fits, limits, etc. •••		
1748 ± 5	² MOKEEV 20	DPWA	$\gamma p \rightarrow \pi^+ \pi^- p$
1725 ± 10	³ MOKEEV 20	DPWA	$\gamma p \rightarrow \pi^+ \pi^- p$
1690 ± 70	ANISOVICH 12A	DPWA	Multichannel
1720 ± 5	¹ SHRESTHA 12A	DPWA	Multichannel
1720 ± 18	BATINIC 10	DPWA	$\pi N \rightarrow N\pi, N\eta$
1705 ± 10	PENNER 02C	DPWA	Multichannel
1716 ± 112	VRANA 00	DPWA	Multichannel

¹ Statistical error only.

² State a) of two states seen by the CLAS collaboration.

³ State b) of two states seen by the CLAS collaboration.

$N(1720)$ BREIT-WIGNER WIDTH

VALUE (MeV)	DOCUMENT ID	TECN	COMMENT
150 to 400 (≈ 250) OUR ESTIMATE			
116 ± 27	GOLOVATCH 19	DPWA	$\gamma p \rightarrow \pi^+ \pi^- p$
229 ± 22	¹ HUNT 19	DPWA	Multichannel
420 ± 80	SOKHOYAN 15A	DPWA	Multichannel
152 ± 2	¹ SHKLYAR 13	DPWA	Multichannel
210 ± 22	ARNDT 06	DPWA	$\pi N \rightarrow \pi N, \eta N$
125 ± 70	CUTKOSKY 80	IPWA	$\pi N \rightarrow \pi N$
190 ± 30	HOEHLER 79	IPWA	$\pi N \rightarrow \pi N$

$N(1720) 3/2^+$

$$I(J^P) = \frac{1}{2}(\frac{3}{2}^+) \text{ Status: } ***$$

Older and obsolete values are listed and referenced in the 2014 edition, Chinese Physics C38 070001 (2014).

$N(1720)$ POLE POSITION

REAL PART

VALUE (MeV)	DOCUMENT ID	TECN	COMMENT
1660 to 1710 (≈ 1680) OUR ESTIMATE			
1726 ± 4	ROENCHEN 22	DPWA	Multichannel
1670 ± 25	SOKHOYAN 15A	DPWA	Multichannel
1677 ± 4 ± 1	¹ SVARC 14	L+P	$\pi N \rightarrow \pi N$
1680 ± 30	CUTKOSKY 80	IPWA	$\pi N \rightarrow \pi N$
•••	We do not use the following data for averages, fits, limits, etc. •••		
1654	HUNT 19	DPWA	Multichannel
1710	ROENCHEN 15A	DPWA	Multichannel
1670	SHKLYAR 13	DPWA	Multichannel
1660 ± 30	ANISOVICH 12A	DPWA	Multichannel
1691 ± 23	BATINIC 10	DPWA	$\pi N \rightarrow N\pi, N\eta$
1666	ARNDT 06	DPWA	$\pi N \rightarrow \pi N, \eta N$
1692	VRANA 00	DPWA	Multichannel
1686	HOEHLER 93	SPED	$\pi N \rightarrow \pi N$

¹ Fit to the amplitudes of HOEHLER 79.

–2×IMAGINARY PART

VALUE (MeV)	DOCUMENT ID	TECN	COMMENT
150 to 300 (≈ 200) OUR ESTIMATE			
185 ± 6	ROENCHEN 22	DPWA	Multichannel
430 ± 100	SOKHOYAN 15A	DPWA	Multichannel
184 ± 8 ± 1	¹ SVARC 14	L+P	$\pi N \rightarrow \pi N$
120 ± 40	CUTKOSKY 80	IPWA	$\pi N \rightarrow \pi N$
•••	We do not use the following data for averages, fits, limits, etc. •••		
100	HUNT 19	DPWA	Multichannel
219	ROENCHEN 15A	DPWA	Multichannel
118	SHKLYAR 13	DPWA	Multichannel
450 ± 100	ANISOVICH 12A	DPWA	Multichannel
233 ± 23	BATINIC 10	DPWA	$\pi N \rightarrow N\pi, N\eta$
355	ARNDT 06	DPWA	$\pi N \rightarrow \pi N, \eta N$
94	VRANA 00	DPWA	Multichannel
187	HOEHLER 93	SPED	$\pi N \rightarrow \pi N$

¹ Fit to the amplitudes of HOEHLER 79.

$N(1720)$ ELASTIC POLE RESIDUE

MODULUS $|r|$

VALUE (MeV)	DOCUMENT ID	TECN	COMMENT
10 to 25 (≈ 15) OUR ESTIMATE			
15 ± 1	ROENCHEN 22	DPWA	Multichannel
26 ± 10	SOKHOYAN 15A	DPWA	Multichannel
13 ± 1	¹ SVARC 14	L+P	$\pi N \rightarrow \pi N$
8 ± 2	CUTKOSKY 80	IPWA	$\pi N \rightarrow \pi N$
•••	We do not use the following data for averages, fits, limits, etc. •••		
4.2	ROENCHEN 15A	DPWA	Multichannel
12	SHKLYAR 13	DPWA	Multichannel
22 ± 8	ANISOVICH 12A	DPWA	Multichannel
20	BATINIC 10	DPWA	$\pi N \rightarrow N\pi, N\eta$
25	ARNDT 06	DPWA	$\pi N \rightarrow \pi N, \eta N$
15	HOEHLER 93	SPED	$\pi N \rightarrow \pi N$

¹ Fit to the amplitudes of HOEHLER 79.

PHASE θ

VALUE (°)	DOCUMENT ID	TECN	COMMENT
–160 to –60 (≈ –110) OUR ESTIMATE			
– 60 ± 3	ROENCHEN 22	DPWA	Multichannel
–100 ± 25	SOKHOYAN 15A	DPWA	Multichannel
–115 ± 3 ± 2	¹ SVARC 14	L+P	$\pi N \rightarrow \pi N$
–160 ± 30	CUTKOSKY 80	IPWA	$\pi N \rightarrow \pi N$
•••	We do not use the following data for averages, fits, limits, etc. •••		
– 47	ROENCHEN 15A	DPWA	Multichannel

Baryon Particle Listings

 $N(1720)$

••• We do not use the following data for averages, fits, limits, etc. •••

114 ± 6		2	MOKEEV	20	DPWA	$\gamma p \rightarrow \pi^+ \pi^- p$
120 ± 6		3	MOKEEV	20	DPWA	$\gamma p \rightarrow \pi^+ \pi^- p$
420 ± 100			ANISOVICH	12A	DPWA	Multichannel
200 ± 20		1	SHRESTHA	12A	DPWA	Multichannel
244 ± 28			BATINIC	10	DPWA	$\pi N \rightarrow N\pi, N\eta$
237 ± 73			PENNER	02c	DPWA	Multichannel
121 ± 39			VRANA	00	DPWA	Multichannel

¹ Statistical error only.

² State a) of two states seen by the CLAS collaboration.

³ State b) of two states seen by the CLAS collaboration.

 $N(1720)$ DECAY MODES

The following branching fractions are our estimates, not fits or averages.

Mode	Fraction (Γ_i/Γ)
Γ_1 $N\pi$	8–14 %
Γ_2 $N\eta$	1–5 %
Γ_3 $N\omega$	12–40 %
Γ_4 ΛK	4–19 %
Γ_5 $N\pi\pi$	>50 %
Γ_6 $\Delta(1232)\pi$	47–89 %
Γ_7 $\Delta(1232)\pi, P$ -wave	47–77 %
Γ_8 $\Delta(1232)\pi, F$ -wave	<12 %
Γ_9 $N\rho$	
Γ_{10} $N\rho, S=1/2, P$ -wave	1–2 %
Γ_{11} $N\sigma$	2–14 %
Γ_{12} $N(1440)\pi$	<2 %
Γ_{13} $N(1520)\pi, S$ -wave	1–5 %
Γ_{14} $p\gamma$	0.05–0.25 %
Γ_{15} $p\gamma, \text{helicity}=1/2$	0.05–0.15 %
Γ_{16} $p\gamma, \text{helicity}=3/2$	0.002–0.16 %
Γ_{17} $n\gamma$	0.0–0.016 %
Γ_{18} $n\gamma, \text{helicity}=1/2$	0.0–0.01 %
Γ_{19} $n\gamma, \text{helicity}=3/2$	0.0–0.015 %

 $N(1720)$ BRANCHING RATIOS

$\Gamma(N\pi)/\Gamma_{\text{total}}$	DOCUMENT ID	TECN	COMMENT	Γ_1/Γ
8 to 14 (≈ 11) OUR ESTIMATE				
18 ± 2	1 HUNT	19	DPWA Multichannel	
11 ± 4	SOKHOYAN	15A	DPWA Multichannel	
17 ± 2	1 SHKLYAR	13	DPWA Multichannel	
9.4 ± 0.5	ARNDT	06	DPWA $\pi N \rightarrow \pi N, \eta N$	
10 ± 4	CUTKOSKY	80	IPWA $\pi N \rightarrow \pi N$	
14 ± 3	HOEHLER	79	IPWA $\pi N \rightarrow \pi N$	
••• We do not use the following data for averages, fits, limits, etc. •••				
10 ± 5	ANISOVICH	12A	DPWA Multichannel	
13.6 ± 0.6	1 SHRESTHA	12A	DPWA Multichannel	
18 ± 3	BATINIC	10	DPWA $\pi N \rightarrow N\pi, N\eta$	
17 ± 2	PENNER	02c	DPWA Multichannel	
5 ± 5	VRANA	00	DPWA Multichannel	

¹ Statistical error only.

$\Gamma(N\eta)/\Gamma_{\text{total}}$	DOCUMENT ID	TECN	COMMENT	Γ_2/Γ
1 to 5 (≈ 3) OUR ESTIMATE				
3 ± 2	MUELLER	20	DPWA Multichannel	
3.8 ± 0.5	1 HUNT	19	DPWA Multichannel	
< 1	SHKLYAR	13	DPWA Multichannel	
3 ± 2	ANISOVICH	12A	DPWA Multichannel	
••• We do not use the following data for averages, fits, limits, etc. •••				
< 1	1 SHRESTHA	12A	DPWA Multichannel	
0 ± 1	BATINIC	10	DPWA $\pi N \rightarrow N\pi, N\eta$	
10 ± 7	THOMA	08	DPWA Multichannel	
0.2 ± 0.2	PENNER	02c	DPWA Multichannel	
4 ± 1	VRANA	00	DPWA Multichannel	

¹ Statistical error only.

$\Gamma(N\omega)/\Gamma_{\text{total}}$	DOCUMENT ID	TECN	COMMENT	Γ_3/Γ
26 ± 14	DENISENKO	16	DPWA Multichannel	

$\Gamma(\Lambda K)/\Gamma_{\text{total}}$	DOCUMENT ID	TECN	COMMENT	Γ_4/Γ
4–19 % OUR ESTIMATE				
16 ± 3	1 HUNT	19	DPWA Multichannel	
4.3 ± 0.4	SHKLYAR	05	DPWA Multichannel	

••• We do not use the following data for averages, fits, limits, etc. •••

2.8 ± 0.4		1	SHRESTHA	12A	DPWA	Multichannel
12 ± 9			THOMA	08	DPWA	Multichannel
9 ± 3			PENNER	02c	DPWA	Multichannel

¹ Statistical error only.

$\Gamma(N\pi\pi)/\Gamma_{\text{total}}$	DOCUMENT ID	TECN	COMMENT	Γ_5/Γ
>50 % OUR ESTIMATE				
84 ± 16	GOLOVATCH	19	DPWA $\gamma p \rightarrow \pi^+ \pi^- p$	

$\Gamma(\Delta(1232)\pi)/\Gamma_{\text{total}}$	DOCUMENT ID	TECN	COMMENT	Γ_6/Γ
---	-------------	------	---------	-------------------

••• We do not use the following data for averages, fits, limits, etc. •••

45 ± 8		1	MOKEEV	20	DPWA	$\gamma p \rightarrow \pi^+ \pi^- p$
54 ± 8		2	MOKEEV	20	DPWA	$\gamma p \rightarrow \pi^+ \pi^- p$

¹ State a) of two states seen by the CLAS collaboration.

² State b) of two states seen by the CLAS collaboration.

$\Gamma(\Delta(1232)\pi, P\text{-wave})/\Gamma_{\text{total}}$	DOCUMENT ID	TECN	COMMENT	Γ_7/Γ
--	-------------	------	---------	-------------------

••• We do not use the following data for averages, fits, limits, etc. •••

62 ± 15			SOKHOYAN	15A	DPWA	Multichannel
75 ± 15			ANISOVICH	12A	DPWA	Multichannel

$\Gamma(\Delta(1232)\pi, F\text{-wave})/\Gamma_{\text{total}}$	DOCUMENT ID	TECN	COMMENT	Γ_8/Γ
--	-------------	------	---------	-------------------

••• We do not use the following data for averages, fits, limits, etc. •••

6 ± 6			SOKHOYAN	15A	DPWA	Multichannel
-------	--	--	----------	-----	------	--------------

$\Gamma(N\rho)/\Gamma_{\text{total}}$	DOCUMENT ID	TECN	COMMENT	Γ_9/Γ
---------------------------------------	-------------	------	---------	-------------------

••• We do not use the following data for averages, fits, limits, etc. •••

38 ± 8		1	MOKEEV	20	DPWA	$\gamma p \rightarrow \pi^+ \pi^- p$
7 ± 3		2	MOKEEV	20	DPWA	$\gamma p \rightarrow \pi^+ \pi^- p$

¹ State a) of two states seen by the CLAS collaboration.

² State b) of two states seen by the CLAS collaboration.

$\Gamma(N\rho, S=1/2, P\text{-wave})/\Gamma_{\text{total}}$	DOCUMENT ID	TECN	COMMENT	Γ_{10}/Γ
---	-------------	------	---------	----------------------

••• We do not use the following data for averages, fits, limits, etc. •••

1.4 ± 0.5		1	SHRESTHA	12A	DPWA	Multichannel
91 ± 1			VRANA	00	DPWA	Multichannel

¹ Statistical error only.

$\Gamma(N\sigma)/\Gamma_{\text{total}}$	DOCUMENT ID	TECN	COMMENT	Γ_{11}/Γ
---	-------------	------	---------	----------------------

••• We do not use the following data for averages, fits, limits, etc. •••

8 ± 6			SOKHOYAN	15A	DPWA	Multichannel
-------	--	--	----------	-----	------	--------------

$\Gamma(N(1440)\pi)/\Gamma_{\text{total}}$	DOCUMENT ID	TECN	COMMENT	Γ_{12}/Γ
--	-------------	------	---------	----------------------

••• We do not use the following data for averages, fits, limits, etc. •••

< 2			SOKHOYAN	15A	DPWA	Multichannel
-----	--	--	----------	-----	------	--------------

$\Gamma(N(1520)\pi, S\text{-wave})/\Gamma_{\text{total}}$	DOCUMENT ID	TECN	COMMENT	Γ_{13}/Γ
---	-------------	------	---------	----------------------

••• We do not use the following data for averages, fits, limits, etc. •••

3 ± 2			SOKHOYAN	15A	DPWA	Multichannel
-------	--	--	----------	-----	------	--------------

 $N(1720)$ PHOTON DECAY AMPLITUDES AT THE POLE **$N(1720) \rightarrow p\gamma, \text{helicity-1/2 amplitude } A_{1/2}$**

MODULUS ($\text{GeV}^{-1/2}$)	PHASE ($^\circ$)	DOCUMENT ID	TECN	COMMENT
0.039 ± 0.004	60 ± 5	ROENCHEN	22	DPWA Multichannel
0.115 ± 0.045	0 ± 35	SOKHOYAN	15A	DPWA Multichannel

••• We do not use the following data for averages, fits, limits, etc. •••

0.039	5.3	ROENCHEN	15A	DPWA Multichannel
-------	-----	----------	-----	-------------------

 $N(1720) \rightarrow p\gamma, \text{helicity-3/2 amplitude } A_{3/2}$

MODULUS ($\text{GeV}^{-1/2}$)	PHASE ($^\circ$)	DOCUMENT ID	TECN	COMMENT
−0.025 ± 0.004	−5.7 ± 7	ROENCHEN	22	DPWA Multichannel
0.140 ± 0.040	65 ± 35	SOKHOYAN	15A	DPWA Multichannel

••• We do not use the following data for averages, fits, limits, etc. •••

0.032	66	ROENCHEN	15A	DPWA Multichannel
-------	----	----------	-----	-------------------

 $N(1720) \rightarrow n\gamma, \text{helicity-1/2 amplitude } A_{1/2}$

MODULUS ($\text{GeV}^{-1/2}$)	PHASE ($^\circ$)	DOCUMENT ID	TECN	COMMENT
−0.025 ± 0.015	−75 ± 35	ANISOVICH	17E	DPWA Multichannel
0.040 ± 0.040				

 $N(1720) \rightarrow n\gamma, \text{helicity-3/2 amplitude } A_{3/2}$

MODULUS ($\text{GeV}^{-1/2}$)	PHASE ($^\circ$)	DOCUMENT ID	TECN	COMMENT
0.100 ± 0.035	−80 ± 35	ANISOVICH	17E	DPWA Multichannel

$N(1720)$ BREIT-WIGNER PHOTON DECAY AMPLITUDES

$N(1720) \rightarrow \rho\gamma$, helicity-1/2 amplitude $A_{1/2}$

VALUE (GeV ^{-1/2})	DOCUMENT ID	TECN	COMMENT
0.080 to 0.120 (≈ 0.100) OUR ESTIMATE			
0.0809 ± 0.0115	GOLOVATCH	19	DPWA $\gamma\rho \rightarrow \pi^+\pi^-\rho$
0.068 ± 0.004	¹ HUNT	19	DPWA Multichannel
0.115 ± 0.045	SOKHOYAN	15A	DPWA Multichannel
-0.065 ± 0.002	¹ SHKLYAR	13	DPWA Multichannel
0.095 ± 0.002	WORKMAN	12A	DPWA $\gamma N \rightarrow \pi N$
••• We do not use the following data for averages, fits, limits, etc. •••			
0.110 ± 0.045	ANISOVICH	12A	DPWA Multichannel
0.057 ± 0.003	¹ SHRESTHA	12A	DPWA Multichannel
0.073	DRECHSEL	07	DPWA $\gamma N \rightarrow \pi N$
0.097 ± 0.003	DUGGER	07	DPWA $\gamma N \rightarrow \pi N$
-0.053	PENNER	02D	DPWA Multichannel

¹ Statistical error only.

$N(1720) \rightarrow \rho\gamma$, helicity-3/2 amplitude $A_{3/2}$

VALUE (GeV ^{-1/2})	DOCUMENT ID	TECN	COMMENT
-0.034 ± 0.0076	GOLOVATCH	19	DPWA $\gamma\rho \rightarrow \pi^+\pi^-\rho$
0.028 ± 0.003	¹ HUNT	19	DPWA Multichannel
0.135 ± 0.040	SOKHOYAN	15A	DPWA Multichannel
0.035 ± 0.002	¹ SHKLYAR	13	DPWA Multichannel
-0.048 ± 0.002	WORKMAN	12A	DPWA $\gamma N \rightarrow \pi N$
••• We do not use the following data for averages, fits, limits, etc. •••			
0.150 ± 0.030	ANISOVICH	12A	DPWA Multichannel
-0.019 ± 0.002	¹ SHRESTHA	12A	DPWA Multichannel
-0.011	DRECHSEL	07	DPWA $\gamma N \rightarrow \pi N$
-0.039 ± 0.003	DUGGER	07	DPWA $\gamma N \rightarrow \pi N$
0.027	PENNER	02D	DPWA Multichannel

¹ Statistical error only.

$N(1720) \rightarrow n\gamma$, helicity-1/2 amplitude $A_{1/2}$

VALUE (GeV ^{-1/2})	DOCUMENT ID	TECN	COMMENT
-0.064 ± 0.006	¹ HUNT	19	DPWA Multichannel
-0.028 ± 0.015 -0.040	ANISOVICH	17E	DPWA Multichannel
••• We do not use the following data for averages, fits, limits, etc. •••			
-0.080 ± 0.050	ANISOVICH	13B	DPWA Multichannel
-0.002 ± 0.001	¹ SHRESTHA	12A	DPWA Multichannel
-0.003	DRECHSEL	07	DPWA $\gamma N \rightarrow \pi N$
-0.004	PENNER	02D	DPWA Multichannel

¹ Statistical error only.

$N(1720) \rightarrow n\gamma$, helicity-3/2 amplitude $A_{3/2}$

VALUE (GeV ^{-1/2})	DOCUMENT ID	TECN	COMMENT
-0.004 ± 0.006	¹ HUNT	19	DPWA Multichannel
-0.140 ± 0.065	ANISOVICH	13B	DPWA Multichannel
••• We do not use the following data for averages, fits, limits, etc. •••			
-0.001 ± 0.002	¹ SHRESTHA	12A	DPWA Multichannel
-0.031	DRECHSEL	07	DPWA $\gamma N \rightarrow \pi N$
0.003	PENNER	02D	DPWA Multichannel

¹ Statistical error only.

$N(1720)$ REFERENCES

For early references, see Physics Letters **111B** 1 (1982).

ROENCHEN	22	EPJ A58 229	D. Roenchen <i>et al.</i>	(JULI, GWU, BONN+)
MOKEEV	20	PL B805 135457	V.I. Mokeev <i>et al.</i>	(CLAS Collab.)
MUELLER	20	PL B803 135323	J. Mueller <i>et al.</i>	(CBELSA/TAPS Collab.)
GOLOVATCH	19	PL B788 371	E. Golovatch <i>et al.</i>	(CLAS Collab.)
HUNT	19	PR C99 055205	B. C. Hunt, D.M. Manley	
ANISOVICH	17E	PR C96 055202	A.V. Anisovich <i>et al.</i>	(BONN, PNPI, JLAB+)
DENISENKO	16	PL B755 97	I. Denisenko <i>et al.</i>	
ROENCHEN	15A	EPJ A51 70	D. Roenchen <i>et al.</i>	
SOKHOYAN	15A	EPJ A51 95	V. Sokhoyan <i>et al.</i>	(CBELSA/TAPS Collab.)
PDG	14	CP C38 070001	K. Olive <i>et al.</i>	(PDG Collab.)
SVARC	14	PR C89 045205	A. Svarc <i>et al.</i>	(RBI Zagreb, UNI Tuzla)
ANISOVICH	13B	EPJ A49 67	A.V. Anisovich <i>et al.</i>	
SHKLYAR	13	PR C87 015201	V. Shklyar, H. Lense, U. Mosel	(GIES)
ANISOVICH	12A	EPJ A48 15	A.V. Anisovich <i>et al.</i>	(BONN, PNPI)
SHRESTHA	12A	PR C86 055203	M. Shrestha, D.M. Manley	(KSU)
WORKMAN	12A	PR C86 015202	R. Workman <i>et al.</i>	(GWU)
BATINIC	10	PR C82 038203	M. Batinic <i>et al.</i>	(ZAGR)
THOMA	08	PL B659 87	U. Thoma <i>et al.</i>	(CB-ELSA Collab.)
DRECHSEL	07	EPJ A34 69	D. Drechsel, S.S. Kamalov, L. Tiator	(MAINZ, JINR)
DUGGER	07	PR C76 025211	M. Dugger <i>et al.</i>	(JLab CLAS Collab.)
ARNDT	06	PR C74 045205	R.A. Arndt <i>et al.</i>	(GWU)
SHKLYAR	05C	PR C72 015210	V. Shklyar, H. Lense, U. Mosel	(GIES)
PENNER	02C	PR C66 055211	G. Penner, U. Mosel	(GIES)
PENNER	02D	PR C66 055212	G. Penner, U. Mosel	(GIES)
VRANA	00	PRPL 328 181	T.P. Vrana, S.A. Dytman, T.-S.H. Lee	(PITT, ANL)
HOEHLER	93	πN Newsletter 9 1	G. Hohler	(KARL)
CUTKOSKY	80	Toronto Conf. 19	R.E. Cutkosky <i>et al.</i>	(CMU, LBL) IJP
Also		PR D20 2839	R.E. Cutkosky <i>et al.</i>	(CMU, LBL) IJP
HOEHLER	79	PDAT 12-1	G. Hohler <i>et al.</i>	(KARL) IJP
Also		Toronto Conf. 3	R. Koch	(KARL) IJP

$N(1860) 5/2^+$

$I(J^P) = \frac{1}{2}(\frac{5}{2}^+)$ Status: **

OMITTED FROM SUMMARY TABLE

Before the 2012 Review, all the evidence for a $J^P = 5/2^+$ state with a mass above 1800 MeV was filed under a two-star $N(2000)$. There is now some evidence from ANISOVICH 12A for two $5/2^+$ states in this region, so we have split the older data (according to mass) between two two-star $5/2^+$ states, an $N(1860)$ and an $N(2000)$.

$N(1860)$ POLE POSITION

REAL PART

VALUE (MeV)	DOCUMENT ID	TECN	COMMENT
1834 ± 19 ± 6	¹ SVARC	14	L+P $\pi N \rightarrow \pi N$
1830 ⁺¹²⁰ ₋₆₀	ANISOVICH	12A	DPWA Multichannel
••• We do not use the following data for averages, fits, limits, etc. •••			
1871	HUNT	19	DPWA Multichannel
1807	ARNDT	06	DPWA $\pi N \rightarrow \pi N, \eta N$

¹ Fit to the amplitudes of HOEHLER 79.

-2×IMAGINARY PART

VALUE (MeV)	DOCUMENT ID	TECN	COMMENT
122 ± 34 ± 7	² SVARC	14	L+P $\pi N \rightarrow \pi N$
250 ⁺¹⁵⁰ ₋₅₀	ANISOVICH	12A	DPWA Multichannel
••• We do not use the following data for averages, fits, limits, etc. •••			
337	HUNT	19	DPWA Multichannel
109	ARNDT	06	DPWA $\pi N \rightarrow \pi N, \eta N$

² Fit to the amplitudes of HOEHLER 79.

$N(1860)$ ELASTIC POLE RESIDUE

MODULUS $|r|$

VALUE (MeV)	DOCUMENT ID	TECN	COMMENT
4 ± 1 ± 1	³ SVARC	14	L+P $\pi N \rightarrow \pi N$
50 ± 20	ANISOVICH	12A	DPWA Multichannel
••• We do not use the following data for averages, fits, limits, etc. •••			
60	ARNDT	06	DPWA $\pi N \rightarrow \pi N, \eta N$

³ Fit to the amplitudes of HOEHLER 79.

PHASE θ

VALUE (°)	DOCUMENT ID	TECN	COMMENT
-39 ± 18 ± 9	⁴ SVARC	14	L+P $\pi N \rightarrow \pi N$
-80 ± 40	ANISOVICH	12A	DPWA Multichannel
••• We do not use the following data for averages, fits, limits, etc. •••			
-67	ARNDT	06	DPWA $\pi N \rightarrow \pi N, \eta N$

⁴ Fit to the amplitudes of HOEHLER 79.

$N(1860)$ BREIT-WIGNER MASS

VALUE (MeV)	DOCUMENT ID	TECN	COMMENT
1928 ± 21	⁵ HUNT	19	DPWA Multichannel
1860 ± 120 -60	ANISOVICH	12A	DPWA Multichannel
1882 ± 10	HOEHLER	79	IPWA $\pi N \rightarrow \pi N$
••• We do not use the following data for averages, fits, limits, etc. •••			
1900 ± 7	⁵ SHRESTHA	12A	DPWA Multichannel
1817.7	ARNDT	06	DPWA $\pi N \rightarrow \pi N, \eta N$

⁵ Statistical error only.

$N(1860)$ BREIT-WIGNER WIDTH

VALUE (MeV)	DOCUMENT ID	TECN	COMMENT
376 ± 58	⁶ HUNT	19	DPWA Multichannel
270 ± 140 -50	ANISOVICH	12A	DPWA Multichannel
95 ± 20	HOEHLER	79	IPWA $\pi N \rightarrow \pi N$
••• We do not use the following data for averages, fits, limits, etc. •••			
219 ± 23	⁶ SHRESTHA	12A	DPWA Multichannel
117.6	ARNDT	06	DPWA $\pi N \rightarrow \pi N, \eta N$

⁶ Statistical error only.

$N(1860)$ DECAY MODES

Mode	Fraction (Γ_i/Γ)
$\Gamma_1 N\pi$	4-20 %
$\Gamma_2 N\eta$	0-6 %
$\Gamma_3 \Lambda K$	<0.01 %
$\Gamma_4 N\pi\pi$	>61 %
$\Gamma_5 \Delta\pi$	20-54 %
$\Gamma_6 \Delta\pi, P$ -wave	4-16 %

Baryon Particle Listings

 $N(1860)$, $N(1875)$

Γ_7	$\Delta\pi$, F -wave	16–38 %
Γ_8	$N\rho$	<8.6 %
Γ_9	$N\rho$, $S=3/2$, P -wave	<8.5 %
Γ_{10}	$N\rho$, $S=3/2$, F -wave	<0.1 %
Γ_{11}	$N\sigma$	41–61 %
Γ_{12}	$p\gamma$	
Γ_{13}	$p\gamma$, helicity=1/2	seen
Γ_{14}	$p\gamma$, helicity=3/2	seen
Γ_{15}	$n\gamma$	0.0017–0.062 %
Γ_{16}	$n\gamma$, helicity=1/2	0.0003–0.019 %
Γ_{17}	$n\gamma$, helicity=3/2	0.0014–0.043 %

 $N(1860)$ BRANCHING RATIOS

$\Gamma(N\pi)/\Gamma_{\text{total}}$	DOCUMENT ID	TECN	COMMENT	Γ_1/Γ
4–20 % OUR ESTIMATE				
8.0±0.1	7 HUNT	19	DPWA Multichannel	
20 ±6	ANISOVICH	12A	DPWA Multichannel	
4 ±2	HOEHLER	79	IPWA $\pi N \rightarrow \pi N$	
••• We do not use the following data for averages, fits, limits, etc. •••				
17 ±1	7 SHRESTHA	12A	DPWA Multichannel	
12.7	ARNDT	06	DPWA $\pi N \rightarrow \pi N, \eta N$	
⁷ Statistical error only.				

$\Gamma(N\eta)/\Gamma_{\text{total}}$	DOCUMENT ID	TECN	COMMENT	Γ_2/Γ
0–6 % OUR ESTIMATE				
0.11±0.09	8 HUNT	19	DPWA Multichannel	
••• We do not use the following data for averages, fits, limits, etc. •••				
4 ±2	8 SHRESTHA	12A	DPWA Multichannel	
⁸ Statistical error only.				

$\Gamma(KK)/\Gamma_{\text{total}}$	DOCUMENT ID	TECN	COMMENT	Γ_3/Γ
<0.01 % OUR ESTIMATE				
<0.01	9 HUNT	19	DPWA Multichannel	
⁹ Statistical error only.				

$\Gamma(\Delta\pi, P\text{-wave})/\Gamma_{\text{total}}$	DOCUMENT ID	TECN	COMMENT	Γ_6/Γ
4–16 % OUR ESTIMATE				
10±6	10 HUNT	19	DPWA Multichannel	
¹⁰ Statistical error only.				

$\Gamma(\Delta\pi, F\text{-wave})/\Gamma_{\text{total}}$	DOCUMENT ID	TECN	COMMENT	Γ_7/Γ
16–38 % OUR ESTIMATE				
27±11	11 HUNT	19	DPWA Multichannel	
¹¹ Statistical error only.				

$\Gamma(N\rho, S=3/2, P\text{-wave})/\Gamma_{\text{total}}$	DOCUMENT ID	TECN	COMMENT	Γ_9/Γ
<8.5 % OUR ESTIMATE				
<8.5	12 HUNT	19	DPWA Multichannel	
¹² Statistical error only.				

$\Gamma(N\rho, S=3/2, F\text{-wave})/\Gamma_{\text{total}}$	DOCUMENT ID	TECN	COMMENT	Γ_{10}/Γ
<0.1 % OUR ESTIMATE				
<0.1	13 HUNT	19	DPWA Multichannel	
¹³ Statistical error only.				

$\Gamma(N\sigma)/\Gamma_{\text{total}}$	DOCUMENT ID	TECN	COMMENT	Γ_{11}/Γ
41–61 % OUR ESTIMATE				
51±10	14 HUNT	19	DPWA Multichannel	
••• We do not use the following data for averages, fits, limits, etc. •••				
41±6	14 SHRESTHA	12A	DPWA Multichannel	
¹⁴ Statistical error only.				

 $N(1860)$ BREIT-WIGNER PHOTON DECAY AMPLITUDES

$N(1860) \rightarrow p\gamma$, helicity-1/2 amplitude $A_{1/2}$	DOCUMENT ID	TECN	COMMENT
VALUE (GeV ^{-1/2})			
–0.022±0.020	15 HUNT	19	DPWA Multichannel
••• We do not use the following data for averages, fits, limits, etc. •••			
–0.017±0.003	15 SHRESTHA	12A	DPWA Multichannel
¹⁵ Statistical error only.			

 $N(1860) \rightarrow p\gamma$, helicity-3/2 amplitude $A_{3/2}$

VALUE	DOCUMENT ID	TECN	COMMENT
–0.032±0.034	16 HUNT	19	DPWA Multichannel
••• We do not use the following data for averages, fits, limits, etc. •••			
0.029±0.004	16 SHRESTHA	12A	DPWA Multichannel
¹⁶ Statistical error only.			

 $N(1860) \rightarrow n\gamma$, helicity-1/2 amplitude $A_{1/2}$

VALUE (GeV ^{-1/2})	DOCUMENT ID	TECN	COMMENT
0.021±0.029	17 HUNT	19	DPWA Multichannel
0.021±0.013	ANISOVICH	13B	DPWA Multichannel
••• We do not use the following data for averages, fits, limits, etc. •••			
0.010±0.005	17 SHRESTHA	12A	DPWA Multichannel
¹⁷ Statistical error only.			

 $N(1860) \rightarrow n\gamma$, helicity-3/2 amplitude $A_{3/2}$

VALUE (GeV ^{-1/2})	DOCUMENT ID	TECN	COMMENT
0.070±0.035	18 HUNT	19	DPWA Multichannel
0.034±0.017	ANISOVICH	13B	DPWA Multichannel
••• We do not use the following data for averages, fits, limits, etc. •••			
–0.009±0.005	18 SHRESTHA	12A	DPWA Multichannel
¹⁸ Statistical error only.			

 $N(1860)$ REFERENCES

HUNT	19	PR C99 055205	B.C. Hunt, D.M. Manley	
SVARC	14	PR C89 045205	A. Svarc et al.	(RBI Zagreb, UNI Tuzla)
ANISOVICH	13B	EPJ A49 67	A.V. Anisovich et al.	
ANISOVICH	12A	EPJ A48 15	A.V. Anisovich et al.	(BONN, PNPI)
SHRESTHA	12A	PR C86 055203	M. Shrestha, D.M. Manley	(KSU)
ARNDT	06	PR C74 045205	R.A. Arndt et al.	(GWU)
HOEHLER	79	PDAT 12-1	G. Hohler et al.	(KARLT)

$N(1875) 3/2^-$ $I(J^P) = \frac{1}{2}(3/2^-)$ Status: ***
was $N(2080)$

Before the 2012 Review, all the evidence for a $J^P = 3/2^-$ state with a mass above 1800 MeV was filed under a two-star $N(2080)$. There is now evidence from ANISOVICH 12A for two $3/2^-$ states in this region, so we have split the older data (according to mass) between a three-star $N(1875)$ and a two-star $N(2120)$.

 $N(1875)$ POLE POSITION

REAL PART

VALUE (MeV)	DOCUMENT ID	TECN	COMMENT
1850 to 1950 (≈ 1900) OUR ESTIMATE			
1870±20	SOKHOYAN	15A	DPWA Multichannel
1880±100	CUTKOSKY	80	IPWA $\pi N \rightarrow \pi N$ (lower m)
••• We do not use the following data for averages, fits, limits, etc. •••			
1993	HUNT	19	DPWA Multichannel
1810	SHKLYAR	13	DPWA Multichannel
1860±25	ANISOVICH	12A	DPWA Multichannel
1957±49	BATINIC	10	DPWA $\pi N \rightarrow N\pi, N\eta$
1824	VRANA	00	DPWA Multichannel

–2xIMAGINARY PART

VALUE (MeV)	DOCUMENT ID	TECN	COMMENT
100 to 220 (≈ 160) OUR ESTIMATE			
200±15	SOKHOYAN	15A	DPWA Multichannel
160±80	CUTKOSKY	80	IPWA $\pi N \rightarrow \pi N$ (lower m)
••• We do not use the following data for averages, fits, limits, etc. •••			
319	HUNT	19	DPWA Multichannel
98	SHKLYAR	13	DPWA Multichannel
200±20	ANISOVICH	12A	DPWA Multichannel
467±106	BATINIC	10	DPWA $\pi N \rightarrow N\pi, N\eta$
614	VRANA	00	DPWA Multichannel

 $N(1875)$ ELASTIC POLE RESIDUEMODULUS $|r|$

VALUE (MeV)	DOCUMENT ID	TECN	COMMENT
3 to 15 (≈ 10) OUR ESTIMATE			
3 ±1.5	SOKHOYAN	15A	DPWA Multichannel
10 ±5	CUTKOSKY	80	IPWA $\pi N \rightarrow \pi N$ (lower m)
••• We do not use the following data for averages, fits, limits, etc. •••			
3	SHKLYAR	13	DPWA Multichannel
2.5±1.0	ANISOVICH	12A	DPWA Multichannel
53	BATINIC	10	DPWA $\pi N \rightarrow N\pi, N\eta$

See key on page 1171

Baryon Particle Listings
N(1875)

PHASE θ

VALUE (°)	DOCUMENT ID	TECN	COMMENT
50 to 200 (≈ 100) OUR ESTIMATE			
160±50	SOKHOYAN 15A	DPWA	Multichannel
100±80	CUTKOSKY 80	IPWA	$\pi N \rightarrow \pi N$ (lower m)
• • • We do not use the following data for averages, fits, limits, etc. • • •			
- 76	SHKLYAR 13	DPWA	Multichannel
- 65	BATINIC 10	DPWA	$\pi N \rightarrow N\pi, N\eta$

N(1875) INELASTIC POLE RESIDUE

The "normalized residue" is the residue divided by $\Gamma_{pole}/2$.

Normalized residue in $N\pi \rightarrow N(1875) \rightarrow \Lambda K$

MODULUS	PHASE (°)	DOCUMENT ID	TECN	COMMENT
0.015±0.005		ANISOVICH 12A	DPWA	Multichannel

Normalized residue in $N\pi \rightarrow N(1875) \rightarrow \Sigma K$

MODULUS	PHASE (°)	DOCUMENT ID	TECN	COMMENT
0.04±0.02		ANISOVICH 12A	DPWA	Multichannel

Normalized residue in $N\pi \rightarrow N(1875) \rightarrow N\sigma$

MODULUS	PHASE (°)	DOCUMENT ID	TECN	COMMENT
0.09±0.03	-175 ± 45	SOKHOYAN 15A	DPWA	Multichannel
• • • We do not use the following data for averages, fits, limits, etc. • • •				
0.08±0.03	-170 ± 65	ANISOVICH 12A	DPWA	Multichannel

Normalized residue in $N\pi \rightarrow N(1875) \rightarrow \Delta(1232)\pi, S\text{-wave}$

MODULUS	PHASE (°)	DOCUMENT ID	TECN	COMMENT
0.05±0.03	undefined	SOKHOYAN 15A	DPWA	Multichannel

Normalized residue in $N\pi \rightarrow N(1875) \rightarrow \Delta(1232)\pi, D\text{-wave}$

MODULUS	PHASE (°)	DOCUMENT ID	TECN	COMMENT
0.04±0.02	undefined	SOKHOYAN 15A	DPWA	Multichannel

Normalized residue in $N\pi \rightarrow N(1875) \rightarrow N(1440)\pi$

MODULUS	PHASE (°)	DOCUMENT ID	TECN	COMMENT
0.03±0.02	undefined	SOKHOYAN 15A	DPWA	Multichannel

N(1875) BREIT-WIGNER MASS

VALUE (MeV)	DOCUMENT ID	TECN	COMMENT
1850 to 1920 (≈ 1875) OUR ESTIMATE			
2005 ± 12	¹ HUNT 19	DPWA	Multichannel
1875 ± 20	SOKHOYAN 15A	DPWA	Multichannel
1934 ± 10	¹ SHKLYAR 13	DPWA	Multichannel
1880 ± 100	CUTKOSKY 80	IPWA	$\pi N \rightarrow \pi N$
• • • We do not use the following data for averages, fits, limits, etc. • • •			
1880 ± 20	ANISOVICH 12A	DPWA	Multichannel
1951 ± 27	¹ SHRESTHA 12A	DPWA	Multichannel
2048 ± 65	BATINIC 10	DPWA	$\pi N \rightarrow N\pi, N\eta$
1946 ± 1	PENNER 02c	DPWA	Multichannel
1895	MART 00	DPWA	$\gamma p \rightarrow \Lambda K^+$
2003 ± 18	VRANA 00	DPWA	Multichannel
¹ Statistical error only.			

N(1875) BREIT-WIGNER WIDTH

VALUE (MeV)	DOCUMENT ID	TECN	COMMENT
120 to 250 (≈ 200) OUR ESTIMATE			
321 ± 21	¹ HUNT 19	DPWA	Multichannel
200 ± 25	SOKHOYAN 15A	DPWA	Multichannel
857 ± 100	¹ SHKLYAR 13	DPWA	Multichannel
180 ± 60	CUTKOSKY 80	IPWA	$\pi N \rightarrow \pi N$ (lower m)
• • • We do not use the following data for averages, fits, limits, etc. • • •			
200 ± 25	ANISOVICH 12A	DPWA	Multichannel
500 ± 45	¹ SHRESTHA 12A	DPWA	Multichannel
529 ± 128	BATINIC 10	DPWA	$\pi N \rightarrow N\pi, N\eta$
859 ± 7	PENNER 02c	DPWA	Multichannel
372	MART 00	DPWA	$\gamma p \rightarrow \Lambda K^+$
1070 ± 858	VRANA 00	DPWA	Multichannel
¹ Statistical error only.			

N(1875) DECAY MODES

Mode	Fraction (Γ_i/Γ)
Γ_1 $N\pi$	3-11 %
Γ_2 $N\eta$	3-16 %
Γ_3 $N\omega$	15-25 %
Γ_4 ΛK	1-2 %
Γ_5 ΣK	0.3-1.1 %
Γ_6 $N\pi\pi$	>56 %
Γ_7 $\Delta(1232)\pi$	4-44 %

Γ_8	$\Delta(1232)\pi, S\text{-wave}$	2-21 %
Γ_9	$\Delta(1232)\pi, D\text{-wave}$	2-23 %
Γ_{10}	$N\rho, S=3/2, S\text{-wave}$	36-56 %
Γ_{11}	$N\sigma$	16-60 %
Γ_{12}	$N(1440)\pi$	2-8 %
Γ_{13}	$N(1520)\pi$	<2 %
Γ_{14}	$\Lambda K^*(892)$	<0.2 %
Γ_{15}	$p\gamma$	0.001-0.025 %
Γ_{16}	$p\gamma, \text{helicity}=1/2$	0.001-0.021 %
Γ_{17}	$p\gamma, \text{helicity}=3/2$	<0.003 %
Γ_{18}	$n\gamma$	<0.040 %
Γ_{19}	$n\gamma, \text{helicity}=1/2$	<0.007 %
Γ_{20}	$n\gamma, \text{helicity}=3/2$	<0.033 %

N(1875) BRANCHING RATIOS

$\Gamma(N\pi)/\Gamma_{total}$

VALUE (%)	DOCUMENT ID	TECN	COMMENT	Γ_1/Γ
3 to 11 (≈ 7) OUR ESTIMATE				
7.5±0.1	¹ HUNT 19	DPWA	Multichannel	
4 ± 2	SOKHOYAN 15A	DPWA	Multichannel	
11 ± 1	¹ SHKLYAR 13	DPWA	Multichannel	
10 ± 4	CUTKOSKY 80	IPWA	$\pi N \rightarrow \pi N$ (lower m)	
• • • We do not use the following data for averages, fits, limits, etc. • • •				
3 ± 2	ANISOVICH 12A	DPWA	Multichannel	
7 ± 2	¹ SHRESTHA 12A	DPWA	Multichannel	
17 ± 7	BATINIC 10	DPWA	$\pi N \rightarrow N\pi, N\eta$	
12 ± 2	PENNER 02c	DPWA	Multichannel	
13 ± 3	VRANA 00	DPWA	Multichannel	
¹ Statistical error only.				

$\Gamma(N\eta)/\Gamma_{total}$

VALUE (%)	DOCUMENT ID	TECN	COMMENT	Γ_2/Γ
3-16 % OUR ESTIMATE				
10 ± 6	MUELLER 20	DPWA	Multichannel	
3.3±0.8	¹ HUNT 19	DPWA	Multichannel	
< 1	SHKLYAR 13	DPWA	Multichannel	
• • • We do not use the following data for averages, fits, limits, etc. • • •				
8 ± 3	BATINIC 10	DPWA	$\pi N \rightarrow N\pi, N\eta$	
7 ± 2	PENNER 02c	DPWA	Multichannel	
0 ± 2	VRANA 00	DPWA	Multichannel	
¹ Statistical error only.				

$\Gamma(N\omega)/\Gamma_{total}$

VALUE (%)	DOCUMENT ID	TECN	COMMENT	Γ_3/Γ
13±7	DENISENKO 16	DPWA	Multichannel	
20±5	¹ SHKLYAR 13	DPWA	Multichannel	
• • • We do not use the following data for averages, fits, limits, etc. • • •				
21±7	PENNER 02c	DPWA	Multichannel	
¹ Statistical error only.				

$\Gamma(\Lambda K)/\Gamma_{total}$

VALUE (%)	DOCUMENT ID	TECN	COMMENT	Γ_4/Γ
1-2 % OUR ESTIMATE				
1.1±0.4	¹ HUNT 19	DPWA	Multichannel	
• • • We do not use the following data for averages, fits, limits, etc. • • •				
0.2±0.2	PENNER 02c	DPWA	Multichannel	
¹ Statistical error only.				

$\Gamma(\Sigma K)/\Gamma_{total}$

VALUE (%)	DOCUMENT ID	TECN	COMMENT	Γ_5/Γ
0.3-1.1 % OUR ESTIMATE				
0.7±0.4	PENNER 02c	DPWA	Multichannel	

$\Gamma(\Delta(1232)\pi, S\text{-wave})/\Gamma_{total}$

VALUE (%)	DOCUMENT ID	TECN	COMMENT	Γ_6/Γ
2-21 % OUR ESTIMATE				
< 2	¹ HUNT 19	DPWA	Multichannel	
14 ± 7	SOKHOYAN 15A	DPWA	Multichannel	
• • • We do not use the following data for averages, fits, limits, etc. • • •				
87 ± 3	¹ SHRESTHA 12A	DPWA	Multichannel	
40 ± 10	VRANA 00	DPWA	Multichannel	
¹ Statistical error only.				

$\Gamma(\Delta(1232)\pi, D\text{-wave})/\Gamma_{total}$

VALUE (%)	DOCUMENT ID	TECN	COMMENT	Γ_7/Γ
2-23 % OUR ESTIMATE				
17 ± 6	¹ HUNT 19	DPWA	Multichannel	
7 ± 5	SOKHOYAN 15A	DPWA	Multichannel	
• • • We do not use the following data for averages, fits, limits, etc. • • •				
< 6	¹ SHRESTHA 12A	DPWA	Multichannel	
17 ± 10	VRANA 00	DPWA	Multichannel	
¹ Statistical error only.				

Baryon Particle Listings

 $N(1875)$, $N(1880)$ $\Gamma(N\rho, S=3/2, S\text{-wave})/\Gamma_{\text{total}}$

VALUE (%)	DOCUMENT ID	TECN	COMMENT	Γ_{10}/Γ
36-56 % OUR ESTIMATE				
46 ± 10	¹ HUNT	19	DPWA Multichannel	
• • • We do not use the following data for averages, fits, limits, etc. • • •				
< 5	¹ SHRESTHA	12A	DPWA Multichannel	
6 ± 6	VRANA	00	DPWA Multichannel	
¹ Statistical error only.				

 $\Gamma(N\sigma)/\Gamma_{\text{total}}$

VALUE (%)	DOCUMENT ID	TECN	COMMENT	Γ_{11}/Γ
16-60 % OUR ESTIMATE				
24.3 ± 8.6	¹ HUNT	19	DPWA Multichannel	
45 ± 15	SOKHOYAN	15A	DPWA Multichannel	
• • • We do not use the following data for averages, fits, limits, etc. • • •				
< 4	¹ SHRESTHA	12A	DPWA Multichannel	
24 ± 24	VRANA	00	DPWA Multichannel	
¹ Statistical error only.				

 $\Gamma(N(1440)\pi)/\Gamma_{\text{total}}$

VALUE (%)	DOCUMENT ID	TECN	COMMENT	Γ_{12}/Γ
5 ± 3	SOKHOYAN	15A	DPWA Multichannel	

 $\Gamma(N(1520)\pi)/\Gamma_{\text{total}}$

VALUE (%)	DOCUMENT ID	TECN	COMMENT	Γ_{13}/Γ
< 2	SOKHOYAN	15A	DPWA Multichannel	

 $\Gamma(\Lambda K^*(892))/\Gamma_{\text{total}}$

VALUE (%)	DOCUMENT ID	TECN	COMMENT	Γ_{14}/Γ
< 0.2 % OUR ESTIMATE				
< 0.2	ANISOVICH	17B	DPWA Multichannel	

 $N(1875)$ PHOTON DECAY AMPLITUDES AT THE POLE $N(1875) \rightarrow p\gamma$, helicity-1/2 amplitude $A_{1/2}$

MODULUS ($\text{GeV}^{-1/2}$)	PHASE ($^\circ$)	DOCUMENT ID	TECN	COMMENT
0.017 ± 0.009	-110 ± 40	SOKHOYAN	15A	DPWA Multichannel

 $N(1875) \rightarrow p\gamma$, helicity-3/2 amplitude $A_{3/2}$

MODULUS ($\text{GeV}^{-1/2}$)	PHASE ($^\circ$)	DOCUMENT ID	TECN	COMMENT
0.008 ± 0.004	180 ± 40	SOKHOYAN	15A	DPWA Multichannel

 $N(1875) \rightarrow n\gamma$, helicity-1/2 amplitude $A_{1/2}$

MODULUS ($\text{GeV}^{-1/2}$)	PHASE ($^\circ$)	DOCUMENT ID	TECN	COMMENT
0.004 ± 0.003	-85 ± 35	ANISOVICH	17E	DPWA Multichannel

 $N(1875) \rightarrow n\gamma$, helicity-3/2 amplitude $A_{3/2}$

MODULUS ($\text{GeV}^{-1/2}$)	PHASE ($^\circ$)	DOCUMENT ID	TECN	COMMENT
-0.006 ± 0.004	-85 ± 45	ANISOVICH	17E	DPWA Multichannel

 $N(1875)$ BREIT-WIGNER PHOTON DECAY AMPLITUDES $N(1875) \rightarrow p\gamma$, helicity-1/2 amplitude $A_{1/2}$

VALUE ($\text{GeV}^{-1/2}$)	DOCUMENT ID	TECN	COMMENT
0.010 to 0.025 (≈ 0.015) OUR ESTIMATE			
-0.013 ± 0.008	¹ HUNT	19	DPWA Multichannel
0.011 ± 0.001	¹ SHKLYAR	13	DPWA Multichannel
0.018 ± 0.010	ANISOVICH	12A	DPWA Multichannel
• • • We do not use the following data for averages, fits, limits, etc. • • •			
0.007 ± 0.008	¹ SHRESTHA	12A	DPWA Multichannel
0.012	PENNER	02D	DPWA Multichannel
¹ Statistical error only.			

 $N(1875) \rightarrow p\gamma$, helicity-3/2 amplitude $A_{3/2}$

VALUE ($\text{GeV}^{-1/2}$)	DOCUMENT ID	TECN	COMMENT
-0.010 to 0.025 (≈ -0.005) OUR ESTIMATE			
-0.093 ± 0.009	¹ HUNT	19	DPWA Multichannel
-0.007 ± 0.004	SOKHOYAN	15A	DPWA Multichannel
0.026 ± 0.001	¹ SHKLYAR	13	DPWA Multichannel
• • • We do not use the following data for averages, fits, limits, etc. • • •			
-0.009 ± 0.005	ANISOVICH	12A	DPWA Multichannel
0.043 ± 0.022	¹ SHRESTHA	12A	DPWA Multichannel
-0.010	PENNER	02D	DPWA Multichannel
¹ Statistical error only.			

 $N(1875) \rightarrow n\gamma$, helicity-1/2 amplitude $A_{1/2}$

VALUE ($\text{GeV}^{-1/2}$)	DOCUMENT ID	TECN	COMMENT
0.050 ± 0.009	¹ HUNT	19	DPWA Multichannel
0.010 ± 0.006	ANISOVICH	13B	DPWA Multichannel

• • • We do not use the following data for averages, fits, limits, etc. • • •

0.055 ± 0.021	¹ SHRESTHA	12A	DPWA Multichannel
0.023	PENNER	02D	DPWA Multichannel
¹ Statistical error only.			

 $N(1875) \rightarrow n\gamma$, helicity-3/2 amplitude $A_{3/2}$

VALUE ($\text{GeV}^{-1/2}$)	DOCUMENT ID	TECN	COMMENT
0.141 ± 0.022	¹ HUNT	19	DPWA Multichannel
-0.020 ± 0.015	ANISOVICH	13B	DPWA Multichannel
• • • We do not use the following data for averages, fits, limits, etc. • • •			
-0.085 ± 0.031	¹ SHRESTHA	12A	DPWA Multichannel
-0.009	PENNER	02D	DPWA Multichannel
¹ Statistical error only.			

 $N(1875)$ REFERENCESFor early references, see Physics Letters **111B** 1 (1982).

MUELLER	20	PL B803 135323	J. Mueller <i>et al.</i>	(CBELSA/TAPS Collab.)
HUNT	19	PR C99 055205	B.C. Hunt, D.M. Manley	
ANISOVICH	17B	PL B771 142	A.V. Anisovich <i>et al.</i>	
ANISOVICH	17E	PR C96 055202	A.V. Anisovich <i>et al.</i>	(BONN, PNPI, JLAB+)
DENISENKO	16	PL B755 97	I. Denisenko <i>et al.</i>	
SOKHOYAN	15A	EPJ A51 95	V. Sokhoyan <i>et al.</i>	(CBELSA/TAPS Collab.)
ANISOVICH	13B	EPJ A49 67	A.V. Anisovich <i>et al.</i>	
SHKLYAR	13	PR C87 015201	V. Shklyar, H. Lenske, U. Mosel	(GIES)
ANISOVICH	12A	EPJ A49 15	A.V. Anisovich <i>et al.</i>	(BONN, PNPI)
SHRESTHA	12A	PR C86 055203	M. Shrestha, D.M. Manley	(KSU)
BATINIC	10	PR C82 038203	M. Batinic <i>et al.</i>	(ZAGR)
PENNER	02C	PR C66 055211	G. Penner, U. Mosel	(GIES)
PENNER	02D	PR C66 055212	G. Penner, U. Mosel	(GIES)
MART	00	PR C61 012201	T. Mart, C. Bennhold	
VRANA	00	PRPL 328 181	T.P. Vrana, S.A. Dytman, T.-S.H. Lee	(PITT, ANL)
CUTKOSKY	80	Toronto Conf. 19	R.E. Cutkosky <i>et al.</i>	(CMU, LBL) IJP
Also		PR D20 2839	R.E. Cutkosky <i>et al.</i>	(CMU, LBL) IJP

 $N(1880) 1/2^+$

$$I(J^P) = \frac{1}{2}(\frac{1}{2}^+) \text{ Status: } ** *$$

 $N(1880)$ POLE POSITION**REAL PART**

VALUE (MeV)	DOCUMENT ID	TECN	COMMENT
1820 to 1900 (≈ 1860) OUR ESTIMATE			
1860 ± 40	ANISOVICH	17A	DPWA Multichannel
• • • We do not use the following data for averages, fits, limits, etc. • • •			
1880	HUNT	19	DPWA Multichannel
1875 ± 11	¹ ANISOVICH	17A	L+P $\gamma p, \pi^- p \rightarrow K\Lambda$
1870 ± 40	SOKHOYAN	15A	DPWA Multichannel
1870 ± 40	GUTZ	14	DPWA Multichannel
1860 ± 35	ANISOVICH	12A	DPWA Multichannel
¹ Statistical error only.			

-2xIMAGINARY PART

VALUE (MeV)	DOCUMENT ID	TECN	COMMENT
180 to 280 (≈ 230) OUR ESTIMATE			
230 ± 50	ANISOVICH	17A	DPWA Multichannel
• • • We do not use the following data for averages, fits, limits, etc. • • •			
429	HUNT	19	DPWA Multichannel
33 ± 9	² ANISOVICH	17A	L+P $\gamma p, \pi^- p \rightarrow K\Lambda$
220 ± 50	SOKHOYAN	15A	DPWA Multichannel
220 ± 50	GUTZ	14	DPWA Multichannel
250 ± 70	ANISOVICH	12A	DPWA Multichannel
² Statistical error only.			

 $N(1880)$ ELASTIC POLE RESIDUE**MODULUS $|r|$**

VALUE (MeV)	DOCUMENT ID	TECN	COMMENT
6 ± 4	SOKHOYAN	15A	DPWA Multichannel
• • • We do not use the following data for averages, fits, limits, etc. • • •			
6 ± 4	GUTZ	14	DPWA Multichannel
6 ± 4	ANISOVICH	12A	DPWA Multichannel

PHASE θ

VALUE ($^\circ$)	DOCUMENT ID	TECN	COMMENT
70 ± 60	SOKHOYAN	15A	DPWA Multichannel
• • • We do not use the following data for averages, fits, limits, etc. • • •			
70 ± 60	GUTZ	14	DPWA Multichannel
80 ± 65	ANISOVICH	12A	DPWA Multichannel

N(1880) INELASTIC POLE RESIDUE

The "normalized residue" is the residue divided by $\Gamma_{pole}/2$.

Normalized residue in $N\pi \rightarrow N(1880) \rightarrow N\eta$

MODULUS	PHASE (°)	DOCUMENT ID	TECN	COMMENT
0.11±0.07	-75 ± 55	ANISOVICH 12A	DPWA	Multichannel

Normalized residue in $N\pi \rightarrow N(1880) \rightarrow \Lambda K$

MODULUS	PHASE (°)	DOCUMENT ID	TECN	COMMENT
0.05±0.02	27 ± 30	ANISOVICH 17A	DPWA	$\gamma p, \pi^- p \rightarrow K\Lambda$

••• We do not use the following data for averages, fits, limits, etc. •••

MODULUS	PHASE (°)	DOCUMENT ID	TECN	COMMENT
0.3 ± 0.1	82 ± 9	³ ANISOVICH 17A	L+P	$\gamma p, \pi^- p \rightarrow K\Lambda$
0.03±0.02	40 ± 40	ANISOVICH 12A	DPWA	Multichannel

³ Statistical error only.

Normalized residue in $N\pi \rightarrow N(1880) \rightarrow \Sigma K$

MODULUS	PHASE (°)	DOCUMENT ID	TECN	COMMENT
0.11±0.06	95 ± 40	ANISOVICH 12A	DPWA	Multichannel

••• We do not use the following data for averages, fits, limits, etc. •••

Normalized residue in $N\pi \rightarrow N(1880) \rightarrow \Delta\pi, P\text{-wave}$

MODULUS	PHASE (°)	DOCUMENT ID	TECN	COMMENT
0.14±0.08	-150 ± 55	SOKHOYAN 15A	DPWA	Multichannel

••• We do not use the following data for averages, fits, limits, etc. •••

MODULUS	PHASE (°)	DOCUMENT ID	TECN	COMMENT
0.20±0.08	-150 ± 50	ANISOVICH 12A	DPWA	Multichannel

Normalized residue in $N\pi \rightarrow N(1880) \rightarrow N(1535)\pi$

MODULUS	PHASE (°)	DOCUMENT ID	TECN	COMMENT
0.09±0.05	130 ± 60	GUTZ 14	DPWA	Multichannel

Normalized residue in $N\pi \rightarrow N(1880) \rightarrow N\omega(980)$

MODULUS	PHASE (°)	DOCUMENT ID	TECN	COMMENT
0.04±0.03	40 ± 65	GUTZ 14	DPWA	Multichannel

Normalized residue in $N\pi \rightarrow N(1880) \rightarrow N\sigma$

MODULUS	PHASE (°)	DOCUMENT ID	TECN	COMMENT
0.10±0.05	-140 ± 55	SOKHOYAN 15A	DPWA	Multichannel

N(1880) BREIT-WIGNER MASS

VALUE (MeV)	DOCUMENT ID	TECN	COMMENT
1830 to 1930 (≈ 1880) OUR ESTIMATE			
1967 ± 20	⁴ HUNT 19	DPWA	Multichannel
1875 ± 40	SOKHOYAN 15A	DPWA	Multichannel

••• We do not use the following data for averages, fits, limits, etc. •••

VALUE (MeV)	DOCUMENT ID	TECN	COMMENT
1875 ± 40	GUTZ 14	DPWA	Multichannel
1870 ± 35	ANISOVICH 12A	DPWA	Multichannel
1900 ± 36	⁴ SHRESTHA 12A	DPWA	Multichannel

⁴ Statistical error only.

N(1880) BREIT-WIGNER WIDTH

VALUE (MeV)	DOCUMENT ID	TECN	COMMENT
200 to 400 (≈ 300) OUR ESTIMATE			
500 ± 77	HUNT 19	DPWA	Multichannel
230 ± 50	SOKHOYAN 15A	DPWA	Multichannel

••• We do not use the following data for averages, fits, limits, etc. •••

VALUE (MeV)	DOCUMENT ID	TECN	COMMENT
230 ± 50	GUTZ 14	DPWA	Multichannel
235 ± 65	ANISOVICH 12A	DPWA	Multichannel
485 ± 142	⁵ SHRESTHA 12A	DPWA	Multichannel

⁵ Statistical error only.

N(1880) DECAY MODES

Mode	Fraction (Γ_i/Γ)
Γ_1 $N\pi$	3-31 %
Γ_2 $N\eta$	1-55 %
Γ_3 $N\omega$	12-28 %
Γ_4 ΛK	1-3 %
Γ_5 ΣK	10-24 %
Γ_6 $N\pi\pi$	>32 %
Γ_7 $\Delta(1232)\pi$	5-42 %
Γ_8 $N\rho, S=1/2, P\text{-wave}$	19-45 %
Γ_9 $N\sigma$	8-40 %
Γ_{10} $N(1535)\pi$	4-12 %
Γ_{11} $N\omega(980)$	1-5 %
Γ_{12} $\Lambda K^*(892)$	0.5-1.1 %
Γ_{13} $p\gamma, \text{ helicity}=1/2$	seen
Γ_{14} $n\gamma, \text{ helicity}=1/2$	0.002-0.63 %

N(1880) BRANCHING RATIOS

$\Gamma(N\pi)/\Gamma_{total}$ Γ_1/Γ

VALUE (%)	DOCUMENT ID	TECN	COMMENT
-----------	-------------	------	---------

3-31 % OUR ESTIMATE

25 ± 6	⁶ HUNT 19	DPWA	Multichannel
6 ± 3	SOKHOYAN 15A	DPWA	Multichannel

••• We do not use the following data for averages, fits, limits, etc. •••

6 ± 3	GUTZ 14	DPWA	Multichannel
5 ± 3	ANISOVICH 12A	DPWA	Multichannel
15 ± 5	⁶ SHRESTHA 12A	DPWA	Multichannel

⁶ Statistical error only.

$\Gamma(N\eta)/\Gamma_{total}$ Γ_2/Γ

VALUE (%)	DOCUMENT ID	TECN	COMMENT
-----------	-------------	------	---------

1-55 % OUR ESTIMATE

18 ± 8	MUELLER 20	DPWA	Multichannel
2 ± 1	⁷ HUNT 19	DPWA	Multichannel
25 ± 30	ANISOVICH 12A	DPWA	Multichannel

••• We do not use the following data for averages, fits, limits, etc. •••

16 ± 7	⁷ SHRESTHA 12A	DPWA	Multichannel
--------	---------------------------	------	--------------

⁷ Statistical error only.

$\Gamma(N\omega)/\Gamma_{total}$ Γ_3/Γ

VALUE (%)	DOCUMENT ID	TECN	COMMENT
-----------	-------------	------	---------

12-28 % OUR ESTIMATE

20 ± 8	DENISENKO 16	DPWA	Multichannel
--------	--------------	------	--------------

$\Gamma(\Lambda K)/\Gamma_{total}$ Γ_4/Γ

VALUE (%)	DOCUMENT ID	TECN	COMMENT
-----------	-------------	------	---------

1-3 % OUR ESTIMATE

2 ± 1	⁸ HUNT 19	DPWA	Multichannel
2 ± 1	ANISOVICH 12A	DPWA	Multichannel

••• We do not use the following data for averages, fits, limits, etc. •••

32 ± 10	⁸ SHRESTHA 12A	DPWA	Multichannel
---------	---------------------------	------	--------------

⁸ Statistical error only.

$\Gamma(\Delta(1232)\pi)/\Gamma_{total}$ Γ_7/Γ

VALUE (%)	DOCUMENT ID	TECN	COMMENT
-----------	-------------	------	---------

5-42 % OUR ESTIMATE

11 ± 6	⁹ HUNT 19	DPWA	Multichannel
30 ± 12	SOKHOYAN 15A	DPWA	Multichannel

••• We do not use the following data for averages, fits, limits, etc. •••

29 ± 12	ANISOVICH 12A	DPWA	Multichannel
< 2	⁹ SHRESTHA 12A	DPWA	Multichannel

⁹ Statistical error only.

$\Gamma(N\rho, S=1/2, P\text{-wave})/\Gamma_{total}$ Γ_8/Γ

VALUE (%)	DOCUMENT ID	TECN	COMMENT
-----------	-------------	------	---------

19-45 % OUR ESTIMATE

32 ± 13	¹⁰ HUNT 19	DPWA	Multichannel
---------	-----------------------	------	--------------

¹⁰ Statistical error only.

$\Gamma(N\sigma)/\Gamma_{total}$ Γ_9/Γ

VALUE (%)	DOCUMENT ID	TECN	COMMENT
-----------	-------------	------	---------

8-40 % OUR ESTIMATE

< 9	¹¹ HUNT 19	DPWA	Multichannel
25 ± 15	SOKHOYAN 15A	DPWA	Multichannel

••• We do not use the following data for averages, fits, limits, etc. •••

8 ± 5	¹¹ SHRESTHA 12A	DPWA	Multichannel
-------	----------------------------	------	--------------

¹¹ Statistical error only.

$\Gamma(N(1535)\pi)/\Gamma_{total}$ Γ_{10}/Γ

VALUE (%)	DOCUMENT ID	TECN	COMMENT
-----------	-------------	------	---------

4-12 % OUR ESTIMATE

8 ± 4	GUTZ 14	DPWA	Multichannel
-------	---------	------	--------------

$\Gamma(N\omega(980))/\Gamma_{total}$ Γ_{11}/Γ

VALUE (%)	DOCUMENT ID	TECN	COMMENT
-----------	-------------	------	---------

1-5 % OUR ESTIMATE

3 ± 2	GUTZ 14	DPWA	Multichannel
-------	---------	------	--------------

$\Gamma(\Lambda K^*(892))/\Gamma_{total}$ Γ_{12}/Γ

VALUE (%)	DOCUMENT ID	TECN	COMMENT
-----------	-------------	------	---------

0.5-1.1 % OUR ESTIMATE

0.8 ± 0.3	ANISOVICH 17B	DPWA	Multichannel
-----------	---------------	------	--------------

Baryon Particle Listings

 $N(1880)$, $N(1895)$ $N(1880)$ PHOTON DECAY AMPLITUDES AT THE POLE $N(1880) \rightarrow n\gamma$, helicity-1/2 amplitude $A_{1/2}$

MODULUS (GeV ^{-1/2})	PHASE (°)	DOCUMENT ID	TECN	COMMENT
0.072±0.024	-30 ± 30	ANISOVICH	17E	DPWA Multichannel

 $N(1880)$ BREIT-WIGNER PHOTON DECAY AMPLITUDES $N(1880) \rightarrow p\gamma$, helicity-1/2 amplitude $A_{1/2}$

VALUE (GeV ^{-1/2})	DOCUMENT ID	TECN	COMMENT
0.119±0.015	¹² HUNT	19	DPWA Multichannel
0.021±0.006	¹² SHRESTHA	12A	DPWA Multichannel

¹² Statistical error only. $N(1880) \rightarrow n\gamma$, helicity-1/2 amplitude $A_{1/2}$

VALUE (GeV ^{-1/2})	DOCUMENT ID	TECN	COMMENT
0.016±0.010	¹³ HUNT	19	DPWA Multichannel
0.070±0.022	ANISOVICH	17E	DPWA Multichannel
-0.060±0.050	ANISOVICH	13B	DPWA Multichannel
0.014±0.007	¹³ SHRESTHA	12A	DPWA Multichannel

¹³ Statistical error only. $N(1880)$ REFERENCES

MUELLER	20	PL B803 135323	J. Mueller et al.	(CBELSA/TAPS Collab.)
HUNT	19	PR C99 055205	B.C. Hunt, D.M. Manley	
ANISOVICH	17A	PRL 119 062004	A.V. Anisovich et al.	
ANISOVICH	17B	PL B771 142	A.V. Anisovich et al.	
ANISOVICH	17E	PR C96 055202	A.V. Anisovich et al.	(BONN, PNPI, JLAB+)
DENISENKO	16	PL B795 97	L. Denisenko et al.	
SOKHOYAN	15A	EPJ A51 95	V. Sokhoyan et al.	(CBELSA/TAPS Collab.)
GUTZ	14	EPJ A50 74	E. Gutz et al.	(CBELSA/TAPS Collab.)
ANISOVICH	13B	EPJ A49 67	A.V. Anisovich et al.	
ANISOVICH	12A	EPJ A48 15	A.V. Anisovich et al.	(BONN, PNPI)
SHRESTHA	12A	PR C86 055203	M. Shrestha, D.M. Manley	(KSU)

 $N(1895) 1/2^-$

$$I(J^P) = \frac{1}{2}(1/2^-) \text{ Status: } ***$$

was $N(2090)$

Before our 2012 Review, this state appeared in our Listings as the $N(2090)$. Any structure in the S_{11} wave above 1800 MeV is listed here. A few early results that are now obsolete have been omitted.

 $N(1895)$ POLE POSITION

REAL PART

VALUE (MeV)	DOCUMENT ID	TECN	COMMENT
1890 to 1930 (≈ 1910) OUR ESTIMATE			
1907 ± 10	AFZAL	20	DPWA Multichannel
1895 ± 15	ANISOVICH	17A	DPWA Multichannel
1906 ± 17	¹ ANISOVICH	17A	L+P $\gamma p, \pi^- p \rightarrow K\Lambda$
1917 ± 19 ± 1	² SVARC	14	L+P $\pi N \rightarrow \pi N$
1956	HUNT	19	DPWA Multichannel
1907 ± 10	ANISOVICH	17C	DPWA Multichannel
1907 ± 10	SOKHOYAN	15A	DPWA Multichannel
1900 ± 15	ANISOVICH	12A	DPWA Multichannel
1797 ± 26	BATINIC	10	DPWA $\pi N \rightarrow N\pi, N\eta$
1795	VRANA	00	DPWA Multichannel
2150 ± 70	CUTKOSKY	80	IPWA $\pi N \rightarrow \pi N$

¹ Statistical error only.² Fit to the amplitudes of HOEHLER 79.

-2xIMAGINARY PART

VALUE (MeV)	DOCUMENT ID	TECN	COMMENT
80 to 140 (≈ 110) OUR ESTIMATE			
100 ± $\begin{smallmatrix} 40 \\ -10 \end{smallmatrix}$	AFZAL	20	DPWA Multichannel
132 ± 30	ANISOVICH	17A	DPWA Multichannel
100 ± 10	¹ ANISOVICH	17A	L+P $\gamma p, \pi^- p \rightarrow K\Lambda$
101 ± 36 ± 1	^{1,2} SVARC	14	L+P $\pi N \rightarrow \pi N$
449	HUNT	19	DPWA Multichannel
100 ± $\begin{smallmatrix} 40 \\ -10 \end{smallmatrix}$	ANISOVICH	17C	DPWA Multichannel
100 ± $\begin{smallmatrix} 40 \\ -15 \end{smallmatrix}$	SOKHOYAN	15A	DPWA Multichannel
90 ± $\begin{smallmatrix} 30 \\ -15 \end{smallmatrix}$	ANISOVICH	12A	DPWA Multichannel
420 ± 45	BATINIC	10	DPWA $\pi N \rightarrow N\pi, N\eta$
220	VRANA	00	DPWA Multichannel
350 ± 100	CUTKOSKY	80	IPWA $\pi N \rightarrow \pi N$

¹ Statistical error only.² Fit to the amplitudes of HOEHLER 79. $N(1895)$ ELASTIC POLE RESIDUEMODULUS $|r|$

VALUE (MeV)	DOCUMENT ID	TECN	COMMENT
1 to 5 (≈ 3) OUR ESTIMATE			
3 ± 2	SOKHOYAN	15A	DPWA Multichannel
3.1 ± 1.4	¹ SVARC	14	L+P $\pi N \rightarrow \pi N$
1 ± 1	ANISOVICH	12A	DPWA Multichannel
60	BATINIC	10	DPWA $\pi N \rightarrow N\pi, N\eta$
40 ± 20	CUTKOSKY	80	IPWA $\pi N \rightarrow \pi N$

¹ Fit to the amplitudes of HOEHLER 79.PHASE θ

VALUE (°)	DOCUMENT ID	TECN	COMMENT
125 ± 45	SOKHOYAN	15A	DPWA Multichannel
-107 ± 23 ± 2	¹ SVARC	14	L+P $\pi N \rightarrow \pi N$
0 ± 90	CUTKOSKY	80	IPWA $\pi N \rightarrow \pi N$
-164	BATINIC	10	DPWA $\pi N \rightarrow N\pi, N\eta$

¹ Fit to the amplitudes of HOEHLER 79. $N(1895)$ INELASTIC POLE RESIDUEThe "normalized residue" is the residue divided by $\Gamma_{pole}/2$.Normalized residue in $N\pi \rightarrow N(1895) \rightarrow \Lambda K$

MODULUS	PHASE (°)	DOCUMENT ID	TECN	COMMENT
0.09 ± 0.03	8 ± 30	ANISOVICH	17A	DPWA Multichannel
0.06 ± 0.02	87 ± 27	¹ ANISOVICH	17A	L+P $\gamma p, \pi^- p \rightarrow K\Lambda$
0.05 ± 0.02	-90 ± 30	ANISOVICH	12A	DPWA Multichannel

¹ Statistical error only.Normalized residue in $N\pi \rightarrow N(1895) \rightarrow \Sigma K$

MODULUS	PHASE (°)	DOCUMENT ID	TECN	COMMENT
0.06 ± 0.02	40 ± 30	ANISOVICH	12A	DPWA Multichannel

Normalized residue in $N\pi \rightarrow N(1895) \rightarrow \Delta(1232)\pi$

MODULUS	PHASE (°)	DOCUMENT ID	TECN	COMMENT
0.05 ± 0.025	-100 ± 45	SOKHOYAN	15A	DPWA Multichannel

Normalized residue in $N\pi \rightarrow N(1895) \rightarrow N(1440)\pi$

MODULUS	PHASE (°)	DOCUMENT ID	TECN	COMMENT
0.05 ± 0.025	-100 ± 45	SOKHOYAN	15A	DPWA Multichannel

 $N(1895)$ BREIT-WIGNER MASS

VALUE (MeV)	DOCUMENT ID	TECN	COMMENT
1870 to 1920 (≈ 1895) OUR ESTIMATE			
2000 ± 29	¹ HUNT	19	DPWA Multichannel
1890 ± $\begin{smallmatrix} 9 \\ -23 \end{smallmatrix}$	KASHEVAROV	17	DPWA $\gamma p \rightarrow \eta p, \eta' p$
1905 ± 12	SOKHOYAN	15A	DPWA Multichannel
1880 ± 20	HOEHLER	79	IPWA $\pi N \rightarrow \pi N$
1895 ± 15	ANISOVICH	12A	DPWA Multichannel
1910 ± 15	¹ SHRESTHA	12A	DPWA Multichannel
1812 ± 25	BATINIC	10	DPWA $\pi N \rightarrow N\pi, N\eta$
1822 ± 43	VRANA	00	DPWA Multichannel
2180 ± 80	CUTKOSKY	80	IPWA $\pi N \rightarrow \pi N$

¹ Statistical error only. $N(1895)$ BREIT-WIGNER WIDTH

VALUE (MeV)	DOCUMENT ID	TECN	COMMENT
80 to 200 (≈ 120) OUR ESTIMATE			
466 ± 72	¹ HUNT	19	DPWA Multichannel
150 ± 57	KASHEVAROV	17	DPWA $\gamma p \rightarrow \eta p, \eta' p$
100 ± $\begin{smallmatrix} 30 \\ -10 \end{smallmatrix}$	SOKHOYAN	15A	DPWA Multichannel
95 ± 30	HOEHLER	79	IPWA $\pi N \rightarrow \pi N$
90 ± $\begin{smallmatrix} 30 \\ -15 \end{smallmatrix}$	ANISOVICH	12A	DPWA Multichannel
502 ± 47	¹ SHRESTHA	12A	DPWA Multichannel
405 ± 40	BATINIC	10	DPWA $\pi N \rightarrow N\pi, N\eta$
248 ± 185	VRANA	00	DPWA Multichannel
350 ± 100	CUTKOSKY	80	IPWA $\pi N \rightarrow \pi N$

¹ Statistical error only.

N(1895) DECAY MODES

Mode	Fraction (Γ_i/Γ)
Γ_1 $N\pi$	2-18 %
Γ_2 $N\eta$	15-45 %
Γ_3 $N\eta'$	10-40 %
Γ_4 $N\omega$	16-40 %
Γ_5 ΛK	3-23 %
Γ_6 ΣK	6-20 %
Γ_7 $N\pi\pi$	17-74 %
Γ_8 $\Delta(1232)\pi, D\text{-wave}$	3-11 %
Γ_9 $N\rho$	14-50 %
Γ_{10} $N\rho, S=1/2, S\text{-wave}$	<18 %
Γ_{11} $N\rho, S=3/2, D\text{-wave}$	14-32 %
Γ_{12} $N\sigma$	<13 %
Γ_{13} $N(1440)\pi$	2-12 %
Γ_{14} $\Lambda K^*(892)$	4-9 %
Γ_{15} $p\gamma, \text{helicity}=1/2$	0.01-0.06 %
Γ_{16} $n\gamma, \text{helicity}=1/2$	0.003-0.05 %

N(1895) BRANCHING RATIOS

$\Gamma(N\pi)/\Gamma_{\text{total}}$	Γ_1/Γ
VALUE (%)	DOCUMENT ID TECN COMMENT
2-18 % OUR ESTIMATE	
8 \pm 4	¹ HUNT 19 DPWA Multichannel
2.5 \pm 1.5	SOKHOYAN 15A DPWA Multichannel
9 \pm 5	HOEHLER 79 IPWA $\pi N \rightarrow \pi N$
••• We do not use the following data for averages, fits, limits, etc. •••	
2 \pm 1	ANISOVICH 12A DPWA Multichannel
17 \pm 2	¹ SHRESTHA 12A DPWA Multichannel
32 \pm 6	BATINIC 10 DPWA $\pi N \rightarrow N\pi, N\eta$
17 \pm 3	VRANA 00 DPWA Multichannel
18 \pm 8	CUTKOSKY 80 IPWA $\pi N \rightarrow \pi N$
¹ Statistical error only.	

$\Gamma(N\eta)/\Gamma_{\text{total}}$	Γ_2/Γ
VALUE (%)	DOCUMENT ID TECN COMMENT
15-45 % OUR ESTIMATE	
10 \pm 5	MUELLER 20 DPWA Multichannel
37 \pm 9	¹ HUNT 19 DPWA Multichannel
10 \pm 5	ANISOVICH 17C DPWA Multichannel
20 \pm 6	² KASHEVAROV 17 DPWA $\gamma p \rightarrow \eta p, \eta' p$
••• We do not use the following data for averages, fits, limits, etc. •••	
21 \pm 6	ANISOVICH 12A DPWA Multichannel
40 \pm 4	¹ SHRESTHA 12A DPWA Multichannel
22 \pm 10	BATINIC 10 DPWA $\pi N \rightarrow N\pi, N\eta$
41 \pm 4	VRANA 00 DPWA Multichannel
¹ Statistical error only.	
² Assuming $A_{1/2} = -0.030 \text{ GeV}^{-1/2}$.	

$\Gamma(N\eta')/\Gamma_{\text{total}}$	Γ_3/Γ
VALUE (%)	DOCUMENT ID TECN COMMENT
10-40 % OUR ESTIMATE	
13 \pm 5	ANISOVICH 17C DPWA Multichannel
38 \pm 20	¹ KASHEVAROV 17 DPWA $\gamma p \rightarrow \eta p, \eta' p$
¹ Assuming $A_{1/2} = -0.030 \text{ GeV}^{-1/2}$.	

$\Gamma(N\omega)/\Gamma_{\text{total}}$	Γ_4/Γ
VALUE (%)	DOCUMENT ID TECN COMMENT
16-40 % OUR ESTIMATE	
28 \pm 12	DENISENKO 16 DPWA Multichannel

$\Gamma(\Lambda K)/\Gamma_{\text{total}}$	Γ_5/Γ
VALUE (%)	DOCUMENT ID TECN COMMENT
3-23 % OUR ESTIMATE	
7 \pm 4	¹ HUNT 19 DPWA Multichannel
18 \pm 5	ANISOVICH 12A DPWA Multichannel
••• We do not use the following data for averages, fits, limits, etc. •••	
1.8 \pm 0.8	¹ SHRESTHA 12A DPWA Multichannel
¹ Statistical error only.	

$\Gamma(\Sigma K)/\Gamma_{\text{total}}$	Γ_6/Γ
VALUE (%)	DOCUMENT ID TECN COMMENT
6-20 % OUR ESTIMATE	
13 \pm 7	ANISOVICH 12A DPWA Multichannel

$\Gamma(\Delta(1232)\pi, D\text{-wave})/\Gamma_{\text{total}}$	Γ_8/Γ
VALUE (%)	DOCUMENT ID TECN COMMENT
3-11 % OUR ESTIMATE	
<10	¹ HUNT 19 DPWA Multichannel
7 \pm 4	SOKHOYAN 15A DPWA Multichannel

••• We do not use the following data for averages, fits, limits, etc. •••

VALUE (%)	DOCUMENT ID	TECN	COMMENT
7 \pm 3	¹ SHRESTHA 12A	DPWA	Multichannel
1 \pm 1	VRANA 00	DPWA	Multichannel

¹ Statistical error only.

$\Gamma(N\rho, S=1/2, S\text{-wave})/\Gamma_{\text{total}}$	Γ_{10}/Γ
VALUE (%)	DOCUMENT ID TECN COMMENT
<18 % OUR ESTIMATE	
<18	¹ HUNT 19 DPWA Multichannel
••• We do not use the following data for averages, fits, limits, etc. •••	
< 2	¹ SHRESTHA 12A DPWA Multichannel
36 \pm 1	VRANA 00 DPWA Multichannel
¹ Statistical error only.	

$\Gamma(N\rho, S=3/2, D\text{-wave})/\Gamma_{\text{total}}$	Γ_{11}/Γ
VALUE (%)	DOCUMENT ID TECN COMMENT
14-32 % OUR ESTIMATE	
23 \pm 9	¹ HUNT 19 DPWA Multichannel
••• We do not use the following data for averages, fits, limits, etc. •••	
9 \pm 3	¹ SHRESTHA 12A DPWA Multichannel
1 \pm 1	VRANA 00 DPWA Multichannel
¹ Statistical error only.	

$\Gamma(N\sigma)/\Gamma_{\text{total}}$	Γ_{12}/Γ
VALUE (%)	DOCUMENT ID TECN COMMENT
<13 % OUR ESTIMATE	
<13	¹ HUNT 19 DPWA Multichannel
••• We do not use the following data for averages, fits, limits, etc. •••	
< 2	¹ SHRESTHA 12A DPWA Multichannel
2 \pm 1	VRANA 00 DPWA Multichannel
¹ Statistical error only.	

$\Gamma(N(1440)\pi)/\Gamma_{\text{total}}$	Γ_{13}/Γ
VALUE (%)	DOCUMENT ID TECN COMMENT
2-12 % OUR ESTIMATE	
7 \pm 5	¹ HUNT 19 DPWA Multichannel
2.5 \pm 1.5	SOKHOYAN 15A DPWA Multichannel
••• We do not use the following data for averages, fits, limits, etc. •••	
24 \pm 4	¹ SHRESTHA 12A DPWA Multichannel
2 \pm 1	VRANA 00 DPWA Multichannel
¹ Statistical error only.	

$\Gamma(\Lambda K^*(892))/\Gamma_{\text{total}}$	Γ_{14}/Γ
VALUE (%)	DOCUMENT ID TECN COMMENT
4-9 % OUR ESTIMATE	
6.3 \pm 2.5	ANISOVICH 17B DPWA Multichannel

N(1895) PHOTON DECAY AMPLITUDES AT THE POLE

N(1895) $\rightarrow p\gamma, \text{helicity-1/2}$ amplitude $A_{1/2}$

MODULUS ($\text{GeV}^{-1/2}$)	PHASE ($^\circ$)	DOCUMENT ID	TECN	COMMENT
-0.015 \pm 0.006	-35 \pm 35	ANISOVICH 17C	DPWA	Multichannel
••• We do not use the following data for averages, fits, limits, etc. •••				
0.015 \pm 0.006	145 \pm 35	SOKHOYAN 15A	DPWA	Multichannel

N(1895) $\rightarrow n\gamma, \text{helicity-1/2}$ amplitude $A_{1/2}$

MODULUS ($\text{GeV}^{-1/2}$)	PHASE ($^\circ$)	DOCUMENT ID	TECN	COMMENT
-0.015 \pm 0.010	60 \pm 25	ANISOVICH 17E	DPWA	Multichannel

N(1895) BREIT-WIGNER PHOTON DECAY AMPLITUDES

N(1895) $\rightarrow p\gamma, \text{helicity-1/2}$ amplitude $A_{1/2}$

VALUE ($\text{GeV}^{-1/2}$)	DOCUMENT ID	TECN	COMMENT
0.017 \pm 0.005	¹ HUNT 19	DPWA	Multichannel
-0.016 \pm 0.006	SOKHOYAN 15A	DPWA	Multichannel
••• We do not use the following data for averages, fits, limits, etc. •••			
0.012 \pm 0.006	¹ SHRESTHA 12A	DPWA	Multichannel
¹ Statistical error only.			

N(1895) $\rightarrow n\gamma, \text{helicity-1/2}$ amplitude $A_{1/2}$

VALUE ($\text{GeV}^{-1/2}$)	DOCUMENT ID	TECN	COMMENT
0.002 \pm 0.013	¹ HUNT 19	DPWA	Multichannel
-0.014 \pm 0.010	ANISOVICH 17E	DPWA	Multichannel
••• We do not use the following data for averages, fits, limits, etc. •••			
0.013 \pm 0.006	ANISOVICH 13B	DPWA	Multichannel
0.003 \pm 0.007	¹ SHRESTHA 12A	DPWA	Multichannel
¹ Statistical error only.			

Baryon Particle Listings

 $N(1895)$, $N(1900)$ $N(1895)$ REFERENCES

AFZAL	20	PRL 125 152002	F. Afzal <i>et al.</i>	(CBELSA/TAPS Collab.)
MUELLER	20	PL B803 135323	J. Mueller <i>et al.</i>	(CBELSA/TAPS Collab.)
HUNT	19	PR C99 055205	B. C. Hunt, D.M. Manley	
ANISOVICH	17A	PRL 119 062004	A.V. Anisovich <i>et al.</i>	
ANISOVICH	17B	PL B771 142	A.V. Anisovich <i>et al.</i>	
ANISOVICH	17C	PL B772 247	A.V. Anisovich <i>et al.</i>	
ANISOVICH	17E	PR C96 055202	A.V. Anisovich <i>et al.</i>	(BONN, PNPI, JLAB+)
KASHEVAROV	17	PRL 118 212001	V.L. Kashevarov <i>et al.</i>	(A2/MAMI Collab.)
DENISENKO	16	PL B755 97	I. Denisenko <i>et al.</i>	
SOKHOYAN	15A	EPJ A51 95	V. Sokhoyan <i>et al.</i>	(CBELSA/TAPS Collab.)
SVARC	14	PR C89 045205	A. Svarc <i>et al.</i>	(RBI Zagreb, UNI Tuzla)
ANISOVICH	13B	EPJ A49 67	A.V. Anisovich <i>et al.</i>	
ANISOVICH	12A	EPJ A48 15	A.V. Anisovich <i>et al.</i>	(BONN, PNPI)
SHRESTHA	12A	PR C86 055203	M. Shrestha, D.M. Manley	(KSU)
BATINIC	10	PR C82 038203	M. Batinic <i>et al.</i>	(ZAGR)
VRANA	00	PRPL 328 181	T.P. Vrana, S.A. Dytman, T.-S.H. Lee	(PITT, ANL)
CUTKOSKY	80	Toronto Conf. 19	R.E. Cutkosky <i>et al.</i>	(CMU, LBL)JJP
Also		PR D20 2839	R.E. Cutkosky <i>et al.</i>	(CMU, LBL)
HOEHLER	79	PDAT 12-1	G. Hoehler <i>et al.</i>	(KARLT)JJP
Also		Toronto Conf. 3	R. Koch	(KARLT)JJP

 $N(1900) 3/2^+$

$$I(J^P) = \frac{1}{2}(3/2^+) \text{ Status: } ***$$

 $N(1900)$ POLE POSITION

REAL PART

VALUE (MeV)	DOCUMENT ID	TECN	COMMENT
1900 to 1940 (≈ 1920) OUR ESTIMATE			
1905 \pm 2	ROENCHEN 22	DPWA	Multichannel
1945 \pm 35	ANISOVICH 17A	DPWA	Multichannel
1928 \pm 18 \pm 2	¹ SVARC 14	L+P	$\pi N \rightarrow \pi N$
••• We do not use the following data for averages, fits, limits, etc. •••			
1856	HUNT 19	DPWA	Multichannel
1912 \pm 30	² ANISOVICH 17A	L+P	$\gamma p, \pi^- p \rightarrow K \Lambda$
1910 \pm 30	SOKHOYAN 15A	DPWA	Multichannel
1910 \pm 30	GUTZ 14	DPWA	Multichannel
1910	SHKLYAR 13	DPWA	Multichannel
1900 \pm 30	ANISOVICH 12A	DPWA	Multichannel

¹ Fit to the amplitudes of HOEHLER 79.² Statistical error only.

-2xIMAGINARY PART

VALUE (MeV)	DOCUMENT ID	TECN	COMMENT
90 to 160 (≈ 130) OUR ESTIMATE			
93 \pm 2	ROENCHEN 22	DPWA	Multichannel
135 \pm 70	ANISOVICH 17A	DPWA	Multichannel
152 \pm 40 \pm 9	¹ SVARC 14	L+P	$\pi N \rightarrow \pi N$
••• We do not use the following data for averages, fits, limits, etc. •••			
241	HUNT 19	DPWA	Multichannel
166 \pm 30	² ANISOVICH 17A	L+P	$\gamma p, \pi^- p \rightarrow K \Lambda$
280 \pm 50	SOKHOYAN 15A	DPWA	Multichannel
280 \pm 50	GUTZ 14	DPWA	Multichannel
173	SHKLYAR 13	DPWA	Multichannel
200 \pm 100	ANISOVICH 12A	DPWA	Multichannel

¹ Fit to the amplitudes of HOEHLER 79.² Statistical error only. $N(1900)$ ELASTIC POLE RESIDUEMODULUS $|r|$

VALUE (MeV)	DOCUMENT ID	TECN	COMMENT
2 to 6 (≈ 4) OUR ESTIMATE			
1.6 \pm 0.2	ROENCHEN 22	DPWA	Multichannel
4 \pm 2	SOKHOYAN 15A	DPWA	Multichannel
4 \pm 1 \pm 1	¹ SVARC 14	L+P	$\pi N \rightarrow \pi N$
••• We do not use the following data for averages, fits, limits, etc. •••			
4 \pm 2	GUTZ 14	DPWA	Multichannel
10	SHKLYAR 13	DPWA	Multichannel
3 \pm 2	ANISOVICH 12A	DPWA	Multichannel

¹ Fit to the amplitudes of HOEHLER 79.PHASE θ

VALUE ($^\circ$)	DOCUMENT ID	TECN	COMMENT
-40 to 20 (≈ -10) OUR ESTIMATE			
44 \pm 11	ROENCHEN 22	DPWA	Multichannel
-10 \pm 40	SOKHOYAN 15A	DPWA	Multichannel
-29 \pm 15 \pm 2	¹ SVARC 14	L+P	$\pi N \rightarrow \pi N$
••• We do not use the following data for averages, fits, limits, etc. •••			
-10 \pm 40	GUTZ 14	DPWA	Multichannel
-64	SHKLYAR 13	DPWA	Multichannel
10 \pm 35	ANISOVICH 12A	DPWA	Multichannel

¹ Fit to the amplitudes of HOEHLER 79. $N(1900)$ INELASTIC POLE RESIDUEThe "normalized residue" is the residue divided by $\Gamma_{pole}/2$.Normalized residue in $N\pi \rightarrow N(1900) \rightarrow N\eta$

MODULUS	PHASE ($^\circ$)	DOCUMENT ID	TECN	COMMENT
0.010 \pm 0.002	55 \pm 15	ROENCHEN 22	DPWA	Multichannel
0.05 \pm 0.02	70 \pm 60	ANISOVICH 12A	DPWA	Multichannel

Normalized residue in $N\pi \rightarrow N(1900) \rightarrow \Lambda K$

MODULUS	PHASE ($^\circ$)	DOCUMENT ID	TECN	COMMENT
0.029 \pm 0.003	5.4 \pm 9.3	ROENCHEN 22	DPWA	Multichannel
0.03 \pm 0.02	90 \pm 40	ANISOVICH 17A	DPWA	Multichannel
••• We do not use the following data for averages, fits, limits, etc. •••				
0.07 \pm 0.03	135 \pm 25	ANISOVICH 12A	DPWA	Multichannel

Normalized residue in $N\pi \rightarrow N(1900) \rightarrow \Sigma K$

MODULUS	PHASE ($^\circ$)	DOCUMENT ID	TECN	COMMENT
0.013 \pm 0.002	-40 \pm 9	ROENCHEN 22	DPWA	Multichannel
0.04 \pm 0.02	110 \pm 30	ANISOVICH 12A	DPWA	Multichannel

Normalized residue in $N\pi \rightarrow N(1900) \rightarrow N(1535)\pi$

MODULUS	PHASE ($^\circ$)	DOCUMENT ID	TECN	COMMENT
0.04 \pm 0.01	170 \pm 30	GUTZ 14	DPWA	Multichannel

Normalized residue in $N\pi \rightarrow N(1900) \rightarrow \Delta(1232)\pi, P\text{-wave}$

MODULUS	PHASE ($^\circ$)	DOCUMENT ID	TECN	COMMENT
0.07 \pm 0.04	-65 \pm 30	SOKHOYAN 15A	DPWA	Multichannel

Normalized residue in $N\pi \rightarrow N(1900) \rightarrow \Delta(1232)\pi, F\text{-wave}$

MODULUS	PHASE ($^\circ$)	DOCUMENT ID	TECN	COMMENT
0.10 \pm 0.05	80 \pm 30	SOKHOYAN 15A	DPWA	Multichannel

Normalized residue in $N\pi \rightarrow N(1900) \rightarrow N(1520)\pi$

MODULUS	PHASE ($^\circ$)	DOCUMENT ID	TECN	COMMENT
0.07 \pm 0.04	-105 \pm 35	SOKHOYAN 15A	DPWA	Multichannel

Normalized residue in $N\pi \rightarrow N(1900) \rightarrow N\sigma$

MODULUS	PHASE ($^\circ$)	DOCUMENT ID	TECN	COMMENT
0.03 \pm 0.02	-110 \pm 35	SOKHOYAN 15A	DPWA	Multichannel

 $N(1900)$ BREIT-WIGNER MASS

VALUE (MeV)	DOCUMENT ID	TECN	COMMENT
1890 to 1950 (≈ 1920) OUR ESTIMATE			
1911 \pm 6	¹ HUNT 19	DPWA	Multichannel
1910 \pm 30	SOKHOYAN 15A	DPWA	Multichannel
1998 \pm 3	¹ SHKLYAR 13	DPWA	Multichannel
••• We do not use the following data for averages, fits, limits, etc. •••			
1910 \pm 30	GUTZ 14	DPWA	Multichannel
1905 \pm 30	ANISOVICH 12A	DPWA	Multichannel
1900 \pm 8	¹ SHRESTHA 12A	DPWA	Multichannel
1951 \pm 53	PENNER 02C	DPWA	Multichannel

¹ Statistical error only. $N(1900)$ BREIT-WIGNER WIDTH

VALUE (MeV)	DOCUMENT ID	TECN	COMMENT
100 to 320 (≈ 200) OUR ESTIMATE			
292 \pm 16	¹ HUNT 19	DPWA	Multichannel
270 \pm 50	SOKHOYAN 15A	DPWA	Multichannel
359 \pm 10	¹ SHKLYAR 13	DPWA	Multichannel
••• We do not use the following data for averages, fits, limits, etc. •••			
270 \pm 50	GUTZ 14	DPWA	Multichannel
250 \pm 120	ANISOVICH 12A	DPWA	Multichannel
101 \pm 15	¹ SHRESTHA 12A	DPWA	Multichannel
622 \pm 42	PENNER 02C	DPWA	Multichannel

¹ Statistical error only. $N(1900)$ DECAY MODES

Mode	Fraction (Γ_i/Γ)
Γ_1 $N\pi$	1-20 %
Γ_2 $N\eta$	2-14 %
Γ_3 $N\eta'$	4-8 %
Γ_4 $N\omega$	7-13 %
Γ_5 ΛK	2-20 %
Γ_6 ΣK	3-7 %
Γ_7 $N\pi\pi$	>56 %
Γ_8 $\Delta(1232)\pi$	30-70 %
Γ_9 $\Delta(1232)\pi, P\text{-wave}$	9-25 %
Γ_{10} $\Delta(1232)\pi, F\text{-wave}$	21-45 %

See key on page 1171

Baryon Particle Listings
N(1900)

Γ_{11}	$N\rho, S=1/2$	25-40 %
Γ_{12}	$N\sigma$	1-7 %
Γ_{13}	$N(1520)\pi$	7-23 %
Γ_{14}	$N(1535)\pi$	4-10 %
Γ_{15}	$\Lambda K^*(892)$	< 0.2 %
Γ_{16}	$p\gamma$	0.001-0.025 %
Γ_{17}	$p\gamma, \text{ helicity}=1/2$	0.001-0.021 %
Γ_{18}	$p\gamma, \text{ helicity}=3/2$	<0.003 %
Γ_{19}	$n\gamma$	<0.040 %
Γ_{20}	$n\gamma, \text{ helicity}=1/2$	<0.007 %
Γ_{21}	$n\gamma, \text{ helicity}=3/2$	<0.033 %

N(1900) BRANCHING RATIOS

$\Gamma(N\pi)/\Gamma_{\text{total}}$	DOCUMENT ID	TECN	COMMENT	Γ_1/Γ
VALUE (%)				

1-20 % OUR ESTIMATE

1.9±0.1	¹ HUNT	19	DPWA	Multichannel
3 ±2	SOKHOYAN	15A	DPWA	Multichannel
25 ±1	¹ SHKLYAR	13	DPWA	Multichannel
••• We do not use the following data for averages, fits, limits, etc. •••				
3 ±2	GUTZ	14	DPWA	Multichannel
3 ±2	ANISOVICH	12A	DPWA	Multichannel
7 ±4	¹ SHRESTHA	12A	DPWA	Multichannel
16 ±2	PENNER	02C	DPWA	Multichannel

¹ Statistical error only.

$\Gamma(N\eta)/\Gamma_{\text{total}}$	DOCUMENT ID	TECN	COMMENT	Γ_2/Γ
VALUE (%)				

2 ±2	MUELLER	20	DPWA	Multichannel
1.3±0.5	¹ HUNT	19	DPWA	Multichannel
2 ±2	¹ SHKLYAR	13	DPWA	Multichannel
10 ±4	ANISOVICH	12A	DPWA	Multichannel
••• We do not use the following data for averages, fits, limits, etc. •••				
< 1	¹ SHRESTHA	12A	DPWA	Multichannel
14 ±5	PENNER	02C	DPWA	Multichannel

¹ Statistical error only.

$\Gamma(N\eta')/\Gamma_{\text{total}}$	DOCUMENT ID	TECN	COMMENT	Γ_3/Γ
VALUE (%)				

4-8 % OUR ESTIMATE

6±2	ANISOVICH	17C	DPWA	Multichannel
-----	-----------	-----	------	--------------

$\Gamma(N\omega)/\Gamma_{\text{total}}$	DOCUMENT ID	TECN	COMMENT	Γ_4/Γ
VALUE (%)				

15±8	DENISENKO	16	DPWA	Multichannel
10±3	¹ SHKLYAR	13	DPWA	Multichannel
••• We do not use the following data for averages, fits, limits, etc. •••				
39±9	PENNER	02C	DPWA	Multichannel

¹ Statistical error only.

$\Gamma(\Lambda K)/\Gamma_{\text{total}}$	DOCUMENT ID	TECN	COMMENT	Γ_5/Γ
VALUE (%)				

13.7±0.3	¹ HUNT	19	DPWA	Multichannel
16 ±5	ANISOVICH	12A	DPWA	Multichannel
2.4±0.3	¹ SHKLYAR	05	DPWA	Multichannel
••• We do not use the following data for averages, fits, limits, etc. •••				
14 ±5	¹ SHRESTHA	12A	DPWA	Multichannel
5 to 15	NIKONOV	08	DPWA	Multichannel
0.1±0.1	PENNER	02C	DPWA	Multichannel

¹ Statistical error only.

$\Gamma(\Sigma K)/\Gamma_{\text{total}}$	DOCUMENT ID	TECN	COMMENT	Γ_6/Γ
VALUE (%)				

5±2	ANISOVICH	12A	DPWA	Multichannel
••• We do not use the following data for averages, fits, limits, etc. •••				
1±1	PENNER	02C	DPWA	Multichannel

$\Gamma(\Delta(1232)\pi, P\text{-wave})/\Gamma_{\text{total}}$	DOCUMENT ID	TECN	COMMENT	Γ_9/Γ
VALUE (%)				

17±8	SOKHOYAN	15A	DPWA	Multichannel
------	----------	-----	------	--------------

$\Gamma(\Delta(1232)\pi, F\text{-wave})/\Gamma_{\text{total}}$	DOCUMENT ID	TECN	COMMENT	Γ_{10}/Γ
VALUE (%)				

33±12	SOKHOYAN	15A	DPWA	Multichannel
-------	----------	-----	------	--------------

$\Gamma(N\rho, S=1/2)/\Gamma_{\text{total}}$	DOCUMENT ID	TECN	COMMENT	Γ_{11}/Γ
VALUE (%)				

25-40 % OUR ESTIMATE

32±7	¹ HUNT	19	DPWA	Multichannel
------	-------------------	----	------	--------------

¹ Statistical error only.

$\Gamma(N\sigma)/\Gamma_{\text{total}}$	DOCUMENT ID	TECN	COMMENT	Γ_{12}/Γ
VALUE (%)				

4±3	SOKHOYAN	15A	DPWA	Multichannel
-----	----------	-----	------	--------------

$\Gamma(N(1520)\pi)/\Gamma_{\text{total}}$	DOCUMENT ID	TECN	COMMENT	Γ_{13}/Γ
VALUE (%)				

15±8	SOKHOYAN	15A	DPWA	Multichannel
------	----------	-----	------	--------------

$\Gamma(N(1535)\pi)/\Gamma_{\text{total}}$	DOCUMENT ID	TECN	COMMENT	Γ_{14}/Γ
VALUE (%)				

7±3	GUTZ	14	DPWA	Multichannel
-----	------	----	------	--------------

$\Gamma(\Lambda K^*(892))/\Gamma_{\text{total}}$	DOCUMENT ID	TECN	COMMENT	Γ_{15}/Γ
VALUE (%)				

< 0.2 % OUR ESTIMATE

<0.2	ANISOVICH	17B	DPWA	Multichannel
------	-----------	-----	------	--------------

N(1900) PHOTON DECAY AMPLITUDES AT THE POLE

N(1900) → pγ, helicity-1/2 amplitude A_{1/2}

MODULUS (GeV ^{-1/2})	PHASE (°)	DOCUMENT ID	TECN	COMMENT
0.0091±0.0014	80 ± 12	ROENCHEN	22	DPWA Multichannel
0.026 ±0.014	60 ± 35	SOKHOYAN	15A	DPWA Multichannel

N(1900) → pγ, helicity-3/2 amplitude A_{3/2}

MODULUS (GeV ^{-1/2})	PHASE (°)	DOCUMENT ID	TECN	COMMENT
-0.0077±0.0017	-42 ± 12	ROENCHEN	22	DPWA Multichannel
-0.070 ±0.030	70 ± 50	SOKHOYAN	15A	DPWA Multichannel

N(1900) → nγ, helicity-1/2 amplitude A_{1/2}

MODULUS (GeV ^{-1/2})	PHASE (°)	DOCUMENT ID	TECN	COMMENT
-0.098±0.020	-13 ± 20	ANISOVICH	17E	DPWA Multichannel

N(1900) → nγ, helicity-3/2 amplitude A_{3/2}

MODULUS (GeV ^{-1/2})	PHASE (°)	DOCUMENT ID	TECN	COMMENT
0.074±0.015	5 ± 15	ANISOVICH	17E	DPWA Multichannel

N(1900) BREIT-WIGNER PHOTON DECAY AMPLITUDES

N(1900) → pγ, helicity-1/2 amplitude A_{1/2}

VALUE (GeV ^{-1/2})	DOCUMENT ID	TECN	COMMENT
0.040±0.004	¹ HUNT	19	DPWA Multichannel
0.024±0.014	SOKHOYAN	15A	DPWA Multichannel
-0.008±0.001	¹ SHKLYAR	13	DPWA Multichannel

••• We do not use the following data for averages, fits, limits, etc. •••			
0.024±0.014	GUTZ	14	DPWA Multichannel
0.026±0.015	ANISOVICH	12A	DPWA Multichannel
0.041±0.008	¹ SHRESTHA	12A	DPWA Multichannel
-0.017	PENNER	02D	DPWA Multichannel

¹ Statistical error only.N(1900) → pγ, helicity-3/2 amplitude A_{3/2}

VALUE (GeV ^{-1/2})	DOCUMENT ID	TECN	COMMENT
-0.094±0.007	¹ HUNT	19	DPWA Multichannel
-0.067±0.030	SOKHOYAN	15A	DPWA Multichannel
< 0.001	SHKLYAR	13	DPWA Multichannel

••• We do not use the following data for averages, fits, limits, etc. •••			
-0.067±0.030	GUTZ	14	DPWA Multichannel
-0.065±0.030	ANISOVICH	12A	DPWA Multichannel
-0.004±0.006	¹ SHRESTHA	12A	DPWA Multichannel
0.031	PENNER	02D	DPWA Multichannel

¹ Statistical error only.N(1900) → nγ, helicity-1/2 amplitude A_{1/2}

VALUE (GeV ^{-1/2})	DOCUMENT ID	TECN	COMMENT
0.007±0.014	¹ HUNT	19	DPWA Multichannel
-0.102±0.020	ANISOVICH	17E	DPWA Multichannel

••• We do not use the following data for averages, fits, limits, etc. •••			
0.000±0.030	ANISOVICH	13B	DPWA Multichannel
-0.010±0.004	¹ SHRESTHA	12A	DPWA Multichannel
-0.016	PENNER	02D	DPWA Multichannel

¹ Statistical error only.N(1900) → nγ, helicity-3/2 amplitude A_{3/2}

VALUE (GeV ^{-1/2})	DOCUMENT ID	TECN	COMMENT
0.007±0.011	¹ HUNT	19	DPWA Multichannel
0.073±0.015	ANISOVICH	17E	DPWA Multichannel

••• We do not use the following data for averages, fits, limits, etc. •••			
-0.060±0.045	ANISOVICH	13B	DPWA Multichannel
-0.011±0.007	¹ SHRESTHA	12A	DPWA Multichannel
-0.002	PENNER	02D	DPWA Multichannel

Baryon Particle Listings

 $N(1900)$, $N(1990)$ ¹ Statistical error only. $N(1900)$ REFERENCES

ROENCHEN	22	EPJ A58 229	D. Roenchen et al.	(JULI, GWU, BONN+)
MUELLER	20	PL B803 135323	J. Mueller et al.	(CBELSA/TAPS Collab.)
HUNT	19	PR C99 055205	B.C. Hunt, D.M. Manley	
ANISOVICH	17A	PRL 119 062004	A.V. Anisovich et al.	
ANISOVICH	17B	PL B771 142	A.V. Anisovich et al.	
ANISOVICH	17C	PL B772 247	A.V. Anisovich et al.	
ANISOVICH	17E	PR C96 055202	A.V. Anisovich et al.	(BONN, PNPI, JLAB+)
DENISENKO	16	PL B755 97	I. Denisenko et al.	
SOKHOYAN	15A	EPJ A51 95	V. Sokhoyan et al.	(CBELSA/TAPS Collab.)
GUTZ	14	EPJ A50 74	E. Gutz et al.	(CBELSA/TAPS Collab.)
SVARC	14	PR C89 045205	A. Svarc et al.	(RBI Zagreb, UNI Tuzla)
ANISOVICH	13B	EPJ A49 67	A.V. Anisovich et al.	
SHKLYAR	13	PR C87 015201	V. Shklyar, H. Lenske, U. Mosel	(GIES)
ANISOVICH	12A	EPJ A48 15	A.V. Anisovich et al.	(BONN, PNPI)
SHRESTHA	12A	PR C86 055203	M. Shrestha, D.M. Manley	(KSU)
NIKONOV	08	PL B662 245	V.A. Nikonov et al.	(Bonn, Gatchina)
SHKLYAR	05	PR C72 015210	V. Shklyar, H. Lenske, U. Mosel	(GIES)
PENNER	02C	PR C66 055211	G. Penner, U. Mosel	(GIES)
PENNER	02D	PR C66 055212	G. Penner, U. Mosel	(GIES)
HOEHLER	79	PDAT 12-1	G. Hoehler et al.	(KARLT)

 $N(1990) 7/2^+$

$$I(J^P) = \frac{1}{2}(\frac{7}{2}^+) \text{ Status: } **$$

OMITTED FROM SUMMARY TABLE

Older and obsolete values are listed and referenced in the 2014 edition, Chinese Physics C38 070001 (2014).

 $N(1990)$ POLE POSITION

REAL PART

VALUE (MeV)	DOCUMENT ID	TECN	COMMENT
1861 ± 5	ROENCHEN 22	DPWA	Multichannel
2030 ± 65	ANISOVICH 12A	DPWA	Multichannel
1900 ± 30	CUTKOSKY 80	IPWA	$\pi N \rightarrow \pi N$

••• We do not use the following data for averages, fits, limits, etc. •••

1913	HUNT 19	DPWA	Multichannel
1738	ROENCHEN 15A	DPWA	Multichannel
2301	VRANA 00	DPWA	Multichannel

-2xIMAGINARY PART

VALUE (MeV)	DOCUMENT ID	TECN	COMMENT
72 ± 3	ROENCHEN 22	DPWA	Multichannel
240 ± 60	ANISOVICH 12A	DPWA	Multichannel
260 ± 60	CUTKOSKY 80	IPWA	$\pi N \rightarrow \pi N$

••• We do not use the following data for averages, fits, limits, etc. •••

163	HUNT 19	DPWA	Multichannel
188	ROENCHEN 15A	DPWA	Multichannel
202	VRANA 00	DPWA	Multichannel

 $N(1990)$ ELASTIC POLE RESIDUEMODULUS $|r|$

VALUE (MeV)	DOCUMENT ID	TECN	COMMENT
0.16 ± 0.01	ROENCHEN 22	DPWA	Multichannel
2 ± 1	ANISOVICH 12A	DPWA	Multichannel
9 ± 3	CUTKOSKY 80	IPWA	$\pi N \rightarrow \pi N$

••• We do not use the following data for averages, fits, limits, etc. •••

4.3	ROENCHEN 15A	DPWA	Multichannel
-----	--------------	------	--------------

PHASE θ

VALUE (°)	DOCUMENT ID	TECN	COMMENT
-119 ± 2	ROENCHEN 22	DPWA	Multichannel
125 ± 65	ANISOVICH 12A	DPWA	Multichannel
-60 ± 30	CUTKOSKY 80	IPWA	$\pi N \rightarrow \pi N$

••• We do not use the following data for averages, fits, limits, etc. •••

-70	ROENCHEN 15A	DPWA	Multichannel
-----	--------------	------	--------------

 $\Delta(1990)$ INELASTIC POLE RESIDUEThe "normalized residue" is the residue divided by $\Gamma_{pole}/2$.Normalized residue in $N\pi \rightarrow N(1990) \rightarrow N\eta$

MODULUS	PHASE (°)	DOCUMENT ID	TECN	COMMENT
0.048 ± 0.001	-43 ± 2	ROENCHEN 22	DPWA	Multichannel

••• We do not use the following data for averages, fits, limits, etc. •••

0.013	-82	ROENCHEN 15A	DPWA	Multichannel
-------	-----	--------------	------	--------------

Normalized residue in $N\pi \rightarrow N(1990) \rightarrow \Lambda K$

MODULUS	PHASE (°)	DOCUMENT ID	TECN	COMMENT
0.004 ± 0.001	133 ± 2	ROENCHEN 22	DPWA	Multichannel

••• We do not use the following data for averages, fits, limits, etc. •••

0.022	-111	ROENCHEN 15A	DPWA	Multichannel
-------	------	--------------	------	--------------

Normalized residue in $N\pi \rightarrow N(1990) \rightarrow \Sigma K$

MODULUS	PHASE (°)	DOCUMENT ID	TECN	COMMENT
0.010 ± 0.002	-54 ± 2	ROENCHEN 22	DPWA	Multichannel

••• We do not use the following data for averages, fits, limits, etc. •••

0.005	24	ROENCHEN 15A	DPWA	Multichannel
-------	----	--------------	------	--------------

 $N(1990)$ BREIT-WIGNER MASS

VALUE (MeV)	DOCUMENT ID	TECN	COMMENT
1950 to 2100 (≈ 2020) OUR ESTIMATE			
2028 ± 19	¹ HUNT 19	DPWA	Multichannel
2060 ± 65	ANISOVICH 12A	DPWA	Multichannel
1970 ± 50	CUTKOSKY 80	IPWA	$\pi N \rightarrow \pi N$
2005 ± 150	HOEHLER 79	IPWA	$\pi N \rightarrow \pi N$

••• We do not use the following data for averages, fits, limits, etc. •••

1990 ± 45	¹ SHRESTHA 12A	DPWA	Multichannel
2311 ± 16	VRANA 00	DPWA	Multichannel

••• We do not use the following data for averages, fits, limits, etc. •••

1990 ± 45	¹ SHRESTHA 12A	DPWA	Multichannel
2311 ± 16	VRANA 00	DPWA	Multichannel

••• We do not use the following data for averages, fits, limits, etc. •••

1990 ± 45	¹ SHRESTHA 12A	DPWA	Multichannel
2311 ± 16	VRANA 00	DPWA	Multichannel

••• We do not use the following data for averages, fits, limits, etc. •••

1990 ± 45	¹ SHRESTHA 12A	DPWA	Multichannel
2311 ± 16	VRANA 00	DPWA	Multichannel

••• We do not use the following data for averages, fits, limits, etc. •••

1990 ± 45	¹ SHRESTHA 12A	DPWA	Multichannel
2311 ± 16	VRANA 00	DPWA	Multichannel

••• We do not use the following data for averages, fits, limits, etc. •••

1990 ± 45	¹ SHRESTHA 12A	DPWA	Multichannel
2311 ± 16	VRANA 00	DPWA	Multichannel

••• We do not use the following data for averages, fits, limits, etc. •••

1990 ± 45	¹ SHRESTHA 12A	DPWA	Multichannel
2311 ± 16	VRANA 00	DPWA	Multichannel

••• We do not use the following data for averages, fits, limits, etc. •••

1990 ± 45	¹ SHRESTHA 12A	DPWA	Multichannel
2311 ± 16	VRANA 00	DPWA	Multichannel

••• We do not use the following data for averages, fits, limits, etc. •••

1990 ± 45	¹ SHRESTHA 12A	DPWA	Multichannel
2311 ± 16	VRANA 00	DPWA	Multichannel

••• We do not use the following data for averages, fits, limits, etc. •••

1990 ± 45	¹ SHRESTHA 12A	DPWA	Multichannel
2311 ± 16	VRANA 00	DPWA	Multichannel

••• We do not use the following data for averages, fits, limits, etc. •••

1990 ± 45	¹ SHRESTHA 12A	DPWA	Multichannel
2311 ± 16	VRANA 00	DPWA	Multichannel

••• We do not use the following data for averages, fits, limits, etc. •••

1990 ± 45	¹ SHRESTHA 12A	DPWA	Multichannel
2311 ± 16	VRANA 00	DPWA	Multichannel

••• We do not use the following data for averages, fits, limits, etc. •••

1990 ± 45	¹ SHRESTHA 12A	DPWA	Multichannel
2311 ± 16	VRANA 00	DPWA	Multichannel

••• We do not use the following data for averages, fits, limits, etc. •••

1990 ± 45	¹ SHRESTHA 12A	DPWA	Multichannel
2311 ± 16	VRANA 00	DPWA	Multichannel

••• We do not use the following data for averages, fits, limits, etc. •••

1990 ± 45	¹ SHRESTHA 12A	DPWA	Multichannel
2311 ± 16	VRANA 00	DPWA	Multichannel

••• We do not use the following data for averages, fits, limits, etc. •••

1990 ± 45	¹ SHRESTHA 12A	DPWA	Multichannel
2311 ± 16	VRANA 00	DPWA	Multichannel

••• We do not use the following data for averages, fits, limits, etc. •••

1990 ± 45	¹ SHRESTHA 12A	DPWA	Multichannel
2311 ± 16	VRANA 00	DPWA	Multichannel

••• We do not use the following data for averages, fits, limits, etc. •••

1990 ± 45	¹ SHRESTHA 12A	DPWA	Multichannel
2311 ± 16	VRANA 00	DPWA	Multichannel

••• We do not use the following data for averages, fits, limits, etc. •••

1990 ± 45	¹ SHRESTHA 12A	DPWA	Multichannel
2311 ± 16	VRANA 00	DPWA	Multichannel

••• We do not use the following data for averages, fits, limits, etc. •••

1990 ± 45	¹ SHRESTHA 12A	DPWA	Multichannel
2311 ± 16	VRANA 00	DPWA	Multichannel

••• We do not use the following data for averages, fits, limits, etc. •••

1990 ± 45	¹ SHRESTHA 12A	DPWA	Multichannel
2311 ± 16	VRANA 00	DPWA	Multichannel

••• We do not use the following data for averages, fits, limits, etc. •••

1990 ± 45	¹ SHRESTHA 12A	DPWA	Multichannel
2311 ± 16	VRANA 00	DPWA	Multichannel

••• We do not use the following data for averages, fits, limits, etc. •••

1990 ± 45	¹ SHRESTHA 12A	DPWA	Multichannel
2311 ± 16	VRANA 00	DPWA	Multichannel

••• We do not use the following data for averages, fits, limits, etc. •••

1990 ± 45	¹ SHRESTHA 12A	DPWA	Multichannel
2311 ± 16	VRANA 00	DPWA	Multichannel

••• We do not use the following data for averages, fits, limits, etc. •••

1990 ± 45	¹ SHRESTHA 12A	DPWA	Multichannel
2311 ± 16	VRANA 00	DPWA	Multichannel

••• We do not use the following data for averages, fits, limits, etc. •••

1990 ± 45	¹ SHRESTHA 12A	DPWA	Multichannel
2311 ± 16	VRANA 00	DPWA	Multichannel

••• We do not use the following data for averages, fits, limits, etc. •••

1990 ± 45	¹ SHRESTHA 12A	DPWA	Multichannel
2311 ± 16	VRANA 00	DPWA	Multichannel

••• We do not use the following data for averages, fits, limits, etc. •••

1990 ± 45	¹ SHRESTHA 12A	DPWA	Multichannel
2311 ± 16	VRANA 00	DPWA	Multichannel

••• We do not use the following data for averages, fits, limits, etc. •••

1990 ± 45	¹ SHRESTHA 12A	DPWA	Multichannel
2311 ± 16	VRANA 00	DPWA	Multichannel

••• We do not use the following data for averages, fits, limits, etc. •••

1990 ± 45	¹ SHRESTHA 12A	DPWA	Multichannel
2311 ± 16	VRANA 00	DPWA	Multichannel

••• We do not use the following data for averages, fits, limits, etc. •••

1990 ± 45	¹ SHRESTHA 12A	DPWA	Multichannel
2311 ± 16	VRANA 00	DPWA	Multichannel

••• We do not use the following data for averages, fits, limits, etc. •••

1990 ± 45	¹ SHRESTHA 12A	DPWA	Multichannel
2311 ± 16	VRANA 00	DPWA	Multichannel

 $N(1990)$ PHOTON DECAY AMPLITUDES AT THE POLE $N(1990) \rightarrow p\gamma$, helicity-1/2 amplitude $A_{1/2}$

MODULUS (GeV ^{-1/2})	PHASE (°)	DOCUMENT ID	TECN	COMMENT
-0.030 ± 0.008	-135 ± 13	ROENCHEN 22	DPWA	Multichannel

••• We do not use the following data for averages, fits, limits, etc. •••

0.029	67	ROENCHEN 15A	DPWA	Multichannel
-------	----	--------------	------	--------------

See key on page 1171

Baryon Particle Listings
N(1990), N(2000)

N(1990) → pγ, helicity-3/2 amplitude A_{3/2}

MODULUS (GeV ^{-1/2})	PHASE (°)	DOCUMENT ID	TECN	COMMENT
-0.018 ± 0.006	53 ± 16	ROENCHEN 22	DPWA	Multichannel
••• We do not use the following data for averages, fits, limits, etc. •••				
0.033	39	ROENCHEN 15A	DPWA	Multichannel

N(1990) → nγ, helicity-1/2 amplitude A_{1/2}

MODULUS (GeV ^{-1/2})	PHASE (°)	DOCUMENT ID	TECN	COMMENT
-0.032 ± 0.015	5 ± 20	ANISOVICH 17E	DPWA	Multichannel

N(1990) → nγ, helicity-3/2 amplitude A_{3/2}

MODULUS (GeV ^{-1/2})	PHASE (°)	DOCUMENT ID	TECN	COMMENT
-0.070 ± 0.025	0 ± 20	ANISOVICH 17E	DPWA	Multichannel

N(1990) BREIT-WIGNER PHOTON DECAY AMPLITUDES

N(1990) → pγ, helicity-1/2 amplitude A_{1/2}

VALUE (GeV ^{-1/2})	DOCUMENT ID	TECN	COMMENT
0.006 ± 0.003	¹ HUNT 19	DPWA	Multichannel
0.040 ± 0.012	ANISOVICH 12A	DPWA	Multichannel

¹ Statistical error only.

N(1990) → pγ, helicity-3/2 amplitude A_{3/2}

VALUE (GeV ^{-1/2})	DOCUMENT ID	TECN	COMMENT
-0.055 ± 0.008	¹ HUNT 19	DPWA	Multichannel
0.057 ± 0.012	ANISOVICH 12A	DPWA	Multichannel

¹ Statistical error only.

N(1990) → nγ, helicity-1/2 amplitude A_{1/2}

VALUE (GeV ^{-1/2})	DOCUMENT ID	TECN	COMMENT
-0.027 ± 0.024	¹ HUNT 19	DPWA	Multichannel
-0.032 ± 0.015	ANISOVICH 17E	DPWA	Multichannel
••• We do not use the following data for averages, fits, limits, etc. •••			
-0.045 ± 0.020	ANISOVICH 13B	DPWA	Multichannel

¹ Statistical error only.

N(1990) → nγ, helicity-3/2 amplitude A_{3/2}

VALUE (GeV ^{-1/2})	DOCUMENT ID	TECN	COMMENT
0.051 ± 0.020	¹ HUNT 19	DPWA	Multichannel
-0.072 ± 0.025	ANISOVICH 17E	DPWA	Multichannel
••• We do not use the following data for averages, fits, limits, etc. •••			
-0.052 ± 0.027	ANISOVICH 13B	DPWA	Multichannel

¹ Statistical error only.

N(1990) REFERENCES

For early references, see Physics Letters **111B 1** (1982).

ROENCHEN 22	EPJ A58 229	D. Roenchen et al.	(JULI, GWU, BONN+)
MUELLER 20	PL B803 135323	J. Mueller et al.	(CBELSA/TAPS Collab.)
HUNT 19	PR C9 055205	B. C. Hunt, D.M. Manley	
ANISOVICH 17E	PR C9 055202	A.V. Anisovich et al.	(BONN, PNPI, JLAB+)
ROENCHEN 15A	EPJ A51 70	D. Roenchen et al.	
PDG 14	CP C38 070001	K. Olive et al.	(PDG Collab.)
ANISOVICH 13B	EPJ A49 67	A.V. Anisovich et al.	
ANISOVICH 12A	EPJ A48 15	A.V. Anisovich et al.	(BONN, PNPI)
SHRESTHA 12A	PR C86 055203	M. Shrestha, D.M. Manley	(KSU)
VRANA 00	PRPL 328 161	T.P. Vrana, S.A. Dytman, T.-S.H. Lee	(PIT. ANL)
CUTKOSKY 80	Toronto Conf. 19	R.E. Cutkosky et al.	(CMU, LBL) JUP
Also	PR D20 2839	R.E. Cutkosky et al.	(CMU, LBL) JUP
HOEHLER 79	PDAT 12-1	G. Hoehler et al.	(KARLT) JUP
Also	Toronto Conf. 3	R. Koch	(KARLT) JUP

N(2000) 5/2⁺

$I(J^P) = \frac{1}{2}(\frac{5}{2}^+)$ Status: **

OMITTED FROM SUMMARY TABLE was N(1900)

Before the 2012 Review, all the evidence for a $J^P = 5/2^+$ state with a mass above 1800 MeV was filed under a two-star N(2000). There is now some evidence from ANISOVICH 12A for two 5/2⁺ states in this region, so we have split the older data (according to mass) between two two-star 5/2⁺ states, an N(1860) and an N(2000).

N(2000) POLE POSITION

REAL PART

VALUE (MeV)	DOCUMENT ID	TECN	COMMENT
2030 ± 40	SOKHOYAN 15A	DPWA	Multichannel
••• We do not use the following data for averages, fits, limits, etc. •••			
1900	SHKLYAR 13	DPWA	Multichannel
2030 ± 110	ANISOVICH 12A	DPWA	Multichannel

-2xIMAGINARY PART

VALUE (MeV)	DOCUMENT ID	TECN	COMMENT
380 ± 60	SOKHOYAN 15A	DPWA	Multichannel
••• We do not use the following data for averages, fits, limits, etc. •••			
123	SHKLYAR 13	DPWA	Multichannel
480 ± 100	ANISOVICH 12A	DPWA	Multichannel

N(2000) ELASTIC POLE RESIDUE

MODULUS |r|

VALUE (MeV)	DOCUMENT ID	TECN	COMMENT
18 ± 8	SOKHOYAN 15A	DPWA	Multichannel
••• We do not use the following data for averages, fits, limits, etc. •••			
11	SHKLYAR 13	DPWA	Multichannel
35 ⁺⁸⁰ ₋₁₅	ANISOVICH 12A	DPWA	Multichannel

PHASE θ

VALUE (°)	DOCUMENT ID	TECN	COMMENT
-150 ± 40	SOKHOYAN 15A	DPWA	Multichannel
••• We do not use the following data for averages, fits, limits, etc. •••			
-6	SHKLYAR 13	DPWA	Multichannel
-100 ± 40	ANISOVICH 12A	DPWA	Multichannel

N(2000) INELASTIC POLE RESIDUE

The "normalized residue" is the residue divided by $\Gamma_{pole}/2$.

Normalized residue in Nπ → N(2000) → Δ(1232)π, P-wave

MODULUS	PHASE (°)	DOCUMENT ID	TECN	COMMENT
0.16 ± 0.06	100 ± 50	SOKHOYAN 15A	DPWA	Multichannel

Normalized residue in Nπ → N(2000) → Δ(1232)π, F-wave

MODULUS	PHASE (°)	DOCUMENT ID	TECN	COMMENT
0.20 ± 0.10	-20 ± 45	SOKHOYAN 15A	DPWA	Multichannel

Normalized residue in Nπ → N(2000) → Nσ

MODULUS	PHASE (°)	DOCUMENT ID	TECN	COMMENT
0.12 ± 0.06	80 ± 40	SOKHOYAN 15A	DPWA	Multichannel

Normalized residue in Nπ → N(2000) → N(1520)π, D-wave

MODULUS	PHASE (°)	DOCUMENT ID	TECN	COMMENT
0.17 ± 0.09	-60 ± 35	SOKHOYAN 15A	DPWA	Multichannel

N(2000) BREIT-WIGNER MASS

VALUE (MeV)	DOCUMENT ID	TECN	COMMENT
2060 ± 30	SOKHOYAN 15A	DPWA	Multichannel
1946 ± 4	¹ SHKLYAR 13	DPWA	Multichannel
••• We do not use the following data for averages, fits, limits, etc. •••			
2090 ± 120	ANISOVICH 12A	DPWA	Multichannel

¹ Statistical error only.

N(2000) BREIT-WIGNER WIDTH

VALUE (MeV)	DOCUMENT ID	TECN	COMMENT
390 ± 55	SOKHOYAN 15A	DPWA	Multichannel
198 ± 2	² SHKLYAR 13	DPWA	Multichannel
••• We do not use the following data for averages, fits, limits, etc. •••			
460 ± 100	ANISOVICH 12A	DPWA	Multichannel

² Statistical error only.

N(2000) DECAY MODES

Mode	Fraction (Γ _i /Γ)
Γ ₁ Nπ	6-10 %
Γ ₂ Nη	<4 %
Γ ₃ Nω	<2 %
Γ ₄ Nππ	35-90 %
Γ ₅ Δ(1232)π	30-80 %
Γ ₆ Δ(1232)π, P-wave	12-32 %
Γ ₇ Δ(1232)π, F-wave	19-49 %
Γ ₈ Nσ	5-15 %
Γ ₉ N(1520)π, D-wave	11-31 %
Γ ₁₀ N(1680)π, P-wave	17-25 %
Γ ₁₁ ΛK*(892)	1-3 %
Γ ₁₂ pγ	0.01-0.08 %
Γ ₁₃ pγ, helicity=1/2	0.003-0.031 %
Γ ₁₄ pγ, helicity=3/2	0.008-0.048 %
Γ ₁₅ nγ	0.002-0.07 %
Γ ₁₆ nγ, helicity=1/2	<0.017 %
Γ ₁₇ nγ, helicity=3/2	0.001-0.056 %

Baryon Particle Listings

 $N(2000)$, $N(2040)$, $N(2060)$ $N(2000)$ BRANCHING RATIOS

$\Gamma(N\pi)/\Gamma_{\text{total}}$	DOCUMENT ID	TECN	COMMENT	Γ_1/Γ
VALUE (%)				

6 to 10 (≈ 8) OUR ESTIMATE

8 \pm 4	SOKHOYAN	15A	DPWA	Multichannel
10 \pm 1	³ SHKLYAR	13	DPWA	Multichannel
9 \pm 4	ANISOVICH	12A	DPWA	Multichannel

• • • We do not use the following data for averages, fits, limits, etc. • • •

³ Statistical error only.

$\Gamma(N\eta)/\Gamma_{\text{total}}$	DOCUMENT ID	TECN	COMMENT	Γ_2/Γ
VALUE (%)				

2 \pm 2	MUELLER	20	DPWA	Multichannel
2 \pm 2	⁴ SHKLYAR	13	DPWA	Multichannel

⁴ Statistical error only.

$\Gamma(N\omega)/\Gamma_{\text{total}}$	DOCUMENT ID	TECN	COMMENT	Γ_3/Γ
VALUE (%)				

18 \pm 8	DENISENKO	16	DPWA	Multichannel
1 \pm 1	⁵ SHKLYAR	13	DPWA	Multichannel

⁵ Statistical error only.

$\Gamma(\Delta(1232)\pi, P\text{-wave})/\Gamma_{\text{total}}$	DOCUMENT ID	TECN	COMMENT	Γ_6/Γ
VALUE (%)				

22 \pm 10	SOKHOYAN	15A	DPWA	Multichannel
-------------	----------	-----	------	--------------

$\Gamma(\Delta(1232)\pi, F\text{-wave})/\Gamma_{\text{total}}$	DOCUMENT ID	TECN	COMMENT	Γ_7/Γ
VALUE (%)				

34 \pm 15	SOKHOYAN	15A	DPWA	Multichannel
-------------	----------	-----	------	--------------

$\Gamma(N\sigma)/\Gamma_{\text{total}}$	DOCUMENT ID	TECN	COMMENT	Γ_8/Γ
VALUE (%)				

10 \pm 5	SOKHOYAN	15A	DPWA	Multichannel
------------	----------	-----	------	--------------

$\Gamma(N(1520)\pi, D\text{-wave})/\Gamma_{\text{total}}$	DOCUMENT ID	TECN	COMMENT	Γ_9/Γ
VALUE (%)				

21 \pm 10	SOKHOYAN	15A	DPWA	Multichannel
-------------	----------	-----	------	--------------

$\Gamma(N(1680)\pi, P\text{-wave})/\Gamma_{\text{total}}$	DOCUMENT ID	TECN	COMMENT	Γ_{10}/Γ
VALUE (%)				

16 \pm 9	SOKHOYAN	15A	DPWA	Multichannel
------------	----------	-----	------	--------------

$\Gamma(\Lambda K^*(892))/\Gamma_{\text{total}}$	DOCUMENT ID	TECN	COMMENT	Γ_{11}/Γ
VALUE (%)				

1-3 % OUR EVALUATION	ANISOVICH	17B	DPWA	Multichannel
2.2 \pm 1.0				

 $N(2000)$ PHOTON DECAY AMPLITUDES AT THE POLE $N(2000) \rightarrow p\gamma$, helicity-1/2 amplitude $A_{1/2}$

MODULUS ($\text{GeV}^{-1/2}$)	PHASE ($^\circ$)	DOCUMENT ID	TECN	COMMENT
0.033 \pm 0.010	15 \pm 25	SOKHOYAN	15A	DPWA Multichannel

 $N(2000) \rightarrow p\gamma$, helicity-3/2 amplitude $A_{3/2}$

MODULUS ($\text{GeV}^{-1/2}$)	PHASE ($^\circ$)	DOCUMENT ID	TECN	COMMENT
0.045 \pm 0.008	-140 \pm 25	SOKHOYAN	15A	DPWA Multichannel

 $N(2000) \rightarrow n\gamma$, helicity-1/2 amplitude $A_{1/2}$

MODULUS ($\text{GeV}^{-1/2}$)	PHASE ($^\circ$)	DOCUMENT ID	TECN	COMMENT
0.019 \pm 0.010	-80 \pm 40	ANISOVICH	17E	DPWA Multichannel

 $N(2000) \rightarrow n\gamma$, helicity-3/2 amplitude $A_{3/2}$

MODULUS ($\text{GeV}^{-1/2}$)	PHASE ($^\circ$)	DOCUMENT ID	TECN	COMMENT
0.011 \pm 0.005	82 \pm 30	ANISOVICH	17E	DPWA Multichannel

 $N(2000)$ BREIT-WIGNER PHOTON DECAY AMPLITUDES $N(2000) \rightarrow p\gamma$, helicity-1/2 amplitude $A_{1/2}$

VALUE ($\text{GeV}^{-1/2}$)	DOCUMENT ID	TECN	COMMENT
0.031 \pm 0.010	SOKHOYAN	15A	DPWA Multichannel
0.011 \pm 0.001	⁶ SHKLYAR	13	DPWA Multichannel

⁶ Statistical error only.

 $N(2000) \rightarrow p\gamma$, helicity-3/2 amplitude $A_{3/2}$

VALUE ($\text{GeV}^{-1/2}$)	DOCUMENT ID	TECN	COMMENT
-0.043 \pm 0.008	SOKHOYAN	15A	DPWA Multichannel
0.025 \pm 0.001	⁷ SHKLYAR	13	DPWA Multichannel

⁷ Statistical error only.

 $N(2000) \rightarrow n\gamma$, helicity-1/2 amplitude $A_{1/2}$

VALUE ($\text{GeV}^{-1/2}$)	DOCUMENT ID	TECN	COMMENT
-0.018 \pm 0.012	ANISOVICH	13B	DPWA Multichannel

 $N(2000) \rightarrow n\gamma$, helicity-3/2 amplitude $A_{3/2}$

VALUE ($\text{GeV}^{-1/2}$)	DOCUMENT ID	TECN	COMMENT
-0.035 \pm 0.020	ANISOVICH	13B	DPWA Multichannel

 $N(2000)$ REFERENCES

MUELLER	20	PL B803 135323	J. Mueller <i>et al.</i>	(CBELSA/TAPS Collab.)
ANISOVICH	17B	PL B771 142	A.V. Anisovich <i>et al.</i>	
ANISOVICH	17E	PR C96 055202	A.V. Anisovich <i>et al.</i>	(BONN, PNPI, JLAB+)
DENISENKO	16	PL B755 97	I. Denisenko <i>et al.</i>	
SOKHOYAN	15A	EPJ A51 95	V. Sokhoyan <i>et al.</i>	(CBELSA/TAPS Collab.)
ANISOVICH	13B	EPJ A49 67	A.V. Anisovich <i>et al.</i>	
SHKLYAR	13	PR C87 015201	V. Shklyar, H. Lenske, U. Mosele	(GIES)
ANISOVICH	12A	EPJ A48 15	A.V. Anisovich <i>et al.</i>	(BONN, PNPI)

 $N(2040) 3/2^+$

$J^P = \frac{3}{2}^+$

Status: *

OMITTED FROM SUMMARY TABLE

 $N(2040)$ MASS

VALUE (MeV)	DOCUMENT ID	TECN	COMMENT
2040 $^{+4}_{-4}$ \pm 25	ABLIKIM	09B	BES2 $J/\psi \rightarrow p\bar{p}\pi^0$

2068 \pm 3 $^{+15}_{-40}$	ABLIKIM	06K	BES2 $J/\psi \rightarrow p\bar{p}\pi^-, n\bar{p}\pi^+$
-----------------------------	---------	-----	--

• • • We do not use the following data for averages, fits, limits, etc. • • •

2244 \pm 30	^{1,2} HUNT	19	DPWA Multichannel
---------------	---------------------	----	-------------------

¹ Statistical error only.

² We list here candidates for high-mass $3/2^+$ states.

 $N(2040)$ WIDTH

VALUE (MeV)	DOCUMENT ID	TECN	COMMENT
230 \pm 8 \pm 52	ABLIKIM	09B	BES2 $J/\psi \rightarrow p\bar{p}\pi^0$
165 \pm 14 \pm 40	ABLIKIM	06K	BES2 $J/\psi \rightarrow p\bar{p}\pi^-, n\bar{p}\pi^+$

• • • We do not use the following data for averages, fits, limits, etc. • • •

530 \pm 89	^{3,4} HUNT	19	DPWA Multichannel
--------------	---------------------	----	-------------------

³ Statistical error only.

⁴ We list here candidates for high-mass $3/2^+$ states.

 $N(2040)$ REFERENCES

HUNT	19	PR C99 055205	B.C. Hunt, D.M. Manley	
ABLIKIM	09B	PR D80 052004	M. Ablikim <i>et al.</i>	(BES II Collab.)
ABLIKIM	06K	PRL 97 062001	M. Ablikim <i>et al.</i>	(BES II Collab.)

 $N(2060) 5/2^-$

$I(J^P) = \frac{1}{2}(\frac{5}{2}^-)$

Status: ***

was $N(2200)$

Before our 2012 *Review*, this state appeared in our Listings as the $N(2200)$.

 $N(2060)$ POLE POSITION

REAL PART

VALUE (MeV)	DOCUMENT ID	TECN	COMMENT
2020 to 2130 (≈ 2070) OUR ESTIMATE			

2030 \pm 15	SOKHOYAN	15A	DPWA Multichannel
---------------	----------	-----	-------------------

2119 \pm 11 \pm 1	¹ SVARC	14	L+P $\pi N \rightarrow \pi N$
-----------------------	--------------------	----	-------------------------------

2100 \pm 60	CUTKOSKY	80	IPWA $\pi N \rightarrow \pi N$
---------------	----------	----	--------------------------------

• • • We do not use the following data for averages, fits, limits, etc. • • •

2010	HUNT	19	DPWA Multichannel
------	------	----	-------------------

2040 \pm 15	ANISOVICH	12A	DPWA Multichannel
---------------	-----------	-----	-------------------

2144 \pm 31	BATINIC	10	DPWA $\pi N \rightarrow N\pi, N\eta$
---------------	---------	----	--------------------------------------

¹ Fit to the amplitudes of HOEHLER 79.

-2xIMAGINARY PART

VALUE (MeV)	DOCUMENT ID	TECN	COMMENT
350 to 430 (≈ 400) OUR ESTIMATE			

400 \pm 35	SOKHOYAN	15A	DPWA Multichannel
--------------	----------	-----	-------------------

370 \pm 20 \pm 5	¹ SVARC	14	L+P $\pi N \rightarrow \pi N$
----------------------	--------------------	----	-------------------------------

360 \pm 80	CUTKOSKY	80	IPWA $\pi N \rightarrow \pi N$
--------------	----------	----	--------------------------------

• • • We do not use the following data for averages, fits, limits, etc. • • •

395	HUNT	19	DPWA Multichannel
-----	------	----	-------------------

390 \pm 25	ANISOVICH	12A	DPWA Multichannel
--------------	-----------	-----	-------------------

438 \pm 13	BATINIC	10	DPWA $\pi N \rightarrow N\pi, N\eta$
--------------	---------	----	--------------------------------------

¹ Fit to the amplitudes of HOEHLER 79.

N(2060) ELASTIC POLE RESIDUE

MODULUS $|r|$

VALUE (MeV)	DOCUMENT ID	TECN	COMMENT
15 to 30 (≈ 20) OUR ESTIMATE			
25 \pm 8	SOKHOYAN	15A	DPWA Multichannel
19 \pm 1 \pm 1	¹ SVARC	14	L+P $\pi N \rightarrow \pi N$
20 \pm 10	CUTKOSKY	80	IPWA $\pi N \rightarrow \pi N$
• • • We do not use the following data for averages, fits, limits, etc. • • •			
19 \pm 5	ANISOVICH	12A	DPWA Multichannel
26	BATINIC	10	DPWA $\pi N \rightarrow N\pi, N\eta$
¹ Fit to the amplitudes of HOEHLER 79.			

PHASE θ

VALUE ($^\circ$)	DOCUMENT ID	TECN	COMMENT
-130 to -90 (≈ -110) OUR ESTIMATE			
-130 \pm 20	SOKHOYAN	15A	DPWA Multichannel
-94 \pm 5 \pm 1	¹ SVARC	14	L+P $\pi N \rightarrow \pi N$
-90 \pm 50	CUTKOSKY	80	IPWA $\pi N \rightarrow \pi N$
• • • We do not use the following data for averages, fits, limits, etc. • • •			
-125 \pm 20	ANISOVICH	12A	DPWA Multichannel
-71	BATINIC	10	DPWA $\pi N \rightarrow N\pi, N\eta$
¹ Fit to the amplitudes of HOEHLER 79.			

N(2060) INELASTIC POLE RESIDUE

The "normalized residue" is the residue divided by $\Gamma_{pole}/2$.

Normalized residue in $N\pi \rightarrow N(2060) \rightarrow N\eta$

MODULUS	PHASE ($^\circ$)	DOCUMENT ID	TECN	COMMENT
0.05 \pm 0.03	40 \pm 25	ANISOVICH	12A	DPWA Multichannel

Normalized residue in $N\pi \rightarrow N(2060) \rightarrow \Lambda K$

MODULUS	PHASE ($^\circ$)	DOCUMENT ID	TECN	COMMENT
0.01 \pm 0.005		ANISOVICH	12A	DPWA Multichannel

Normalized residue in $N\pi \rightarrow N(2060) \rightarrow \Sigma K$

MODULUS	PHASE ($^\circ$)	DOCUMENT ID	TECN	COMMENT
0.04 \pm 0.02	-70 \pm 30	ANISOVICH	12A	DPWA Multichannel

Normalized residue in $N\pi \rightarrow N(2060) \rightarrow \Delta(1232)\pi, D\text{-wave}$

MODULUS	PHASE ($^\circ$)	DOCUMENT ID	TECN	COMMENT
0.06 \pm 0.03	-90 \pm 40	SOKHOYAN	15A	DPWA Multichannel

Normalized residue in $N\pi \rightarrow N(2060) \rightarrow N\sigma$

MODULUS	PHASE ($^\circ$)	DOCUMENT ID	TECN	COMMENT
0.12 \pm 0.06	80 \pm 40	SOKHOYAN	15A	DPWA Multichannel

Normalized residue in $N\pi \rightarrow N(2060) \rightarrow N(1440)\pi$

MODULUS	PHASE ($^\circ$)	DOCUMENT ID	TECN	COMMENT
0.17 \pm 0.09	-60 \pm 35	SOKHOYAN	15A	DPWA Multichannel

Normalized residue in $N\pi \rightarrow N(2060) \rightarrow N(1520)\pi, P\text{-wave}$

MODULUS	PHASE ($^\circ$)	DOCUMENT ID	TECN	COMMENT
0.14 \pm 0.06	-45 \pm 15	SOKHOYAN	15A	DPWA Multichannel

N(2060) BREIT-WIGNER MASS

VALUE (MeV)	DOCUMENT ID	TECN	COMMENT
2030 to 2200 (≈ 2100) OUR ESTIMATE			
2111 \pm 17	¹ HUNT	19	DPWA Multichannel
2045 \pm 15	SOKHOYAN	15A	DPWA Multichannel
2180 \pm 80	CUTKOSKY	80	IPWA $\pi N \rightarrow \pi N$
2228 \pm 30	HOEHLER	79	IPWA $\pi N \rightarrow \pi N$
• • • We do not use the following data for averages, fits, limits, etc. • • •			
2060 \pm 15	ANISOVICH	12A	DPWA Multichannel
2116 \pm 21	¹ SHRESTHA	12A	DPWA Multichannel
2217 \pm 27	BATINIC	10	DPWA $\pi N \rightarrow N\pi, N\eta$
¹ Statistical error only.			

N(2060) BREIT-WIGNER WIDTH

VALUE (MeV)	DOCUMENT ID	TECN	COMMENT
300 to 450 (≈ 400) OUR ESTIMATE			
499 \pm 70	¹ HUNT	19	DPWA Multichannel
420 \pm 30	SOKHOYAN	15A	DPWA Multichannel
400 \pm 100	CUTKOSKY	80	IPWA $\pi N \rightarrow \pi N$
310 \pm 50	HOEHLER	79	IPWA $\pi N \rightarrow \pi N$
• • • We do not use the following data for averages, fits, limits, etc. • • •			
375 \pm 25	ANISOVICH	12A	DPWA Multichannel
307 \pm 112	¹ SHRESTHA	12A	DPWA Multichannel
481 \pm 17	BATINIC	10	DPWA $\pi N \rightarrow N\pi, N\eta$
¹ Statistical error only.			

N(2060) DECAY MODES

Mode	Fraction (Γ_i/Γ)
Γ_1 $N\pi$	7-12 %
Γ_2 $N\eta$	2-38 %
Γ_3 $N\omega$	1-7 %
Γ_4 ΛK	10-20 %
Γ_5 ΣK	1-5 %
Γ_6 $N\pi\pi$	12-52 %
Γ_7 $\Delta(1232)\pi, D\text{-wave}$	4-10 %
Γ_8 $N\rho$	5-33 %
Γ_9 $N\rho, S=1/2, P\text{-wave}$	<10 %
Γ_{10} $N\rho, S=3/2, D\text{-wave}$	5-23 %
Γ_{11} $N\sigma$	3-9 %
Γ_{12} $N(1440)\pi$	4-14 %
Γ_{13} $N(1520)\pi, P\text{-wave}$	9-21 %
Γ_{14} $N(1680)\pi, S\text{-wave}$	8-22 %
Γ_{15} $\Lambda K^*(892)$	0.3-1.3 %
Γ_{16} $p\gamma$	0.03-0.19 %
Γ_{17} $p\gamma, \text{helicity}=1/2$	0.02-0.08 %
Γ_{18} $p\gamma, \text{helicity}=3/2$	0.01-0.10 %
Γ_{19} $n\gamma$	0.003-0.07 %
Γ_{20} $n\gamma, \text{helicity}=1/2$	0.001-0.02 %
Γ_{21} $n\gamma, \text{helicity}=3/2$	0.002-0.05 %

N(2060) BRANCHING RATIOS

$\Gamma(N\pi)/\Gamma_{total}$	DOCUMENT ID	TECN	COMMENT	Γ_1/Γ
7 to 12 (≈ 10) OUR ESTIMATE				
5.3 \pm 1.4	¹ HUNT	19	DPWA Multichannel	
11 \pm 2	SOKHOYAN	15A	DPWA Multichannel	
10 \pm 3	CUTKOSKY	80	IPWA $\pi N \rightarrow \pi N$	
7 \pm 2	HOEHLER	79	IPWA $\pi N \rightarrow \pi N$	
• • • We do not use the following data for averages, fits, limits, etc. • • •				
8 \pm 2	ANISOVICH	12A	DPWA Multichannel	
9 \pm 2	¹ SHRESTHA	12A	DPWA Multichannel	
13 \pm 4	BATINIC	10	DPWA $\pi N \rightarrow N\pi, N\eta$	
¹ Statistical error only.				

$\Gamma(N\eta)/\Gamma_{total}$	DOCUMENT ID	TECN	COMMENT	Γ_2/Γ
2-38 % OUR ESTIMATE				
6 \pm 2	MUELLER	20	DPWA Multichannel	
30 \pm 8	¹ HUNT	19	DPWA Multichannel	
4 \pm 2	ANISOVICH	12A	DPWA Multichannel	
• • • We do not use the following data for averages, fits, limits, etc. • • •				
< 1	¹ SHRESTHA	12A	DPWA Multichannel	
0.2 \pm 1.0	BATINIC	10	DPWA $\pi N \rightarrow N\pi, N\eta$	
¹ Statistical error only.				

$\Gamma(N\omega)/\Gamma_{total}$	DOCUMENT ID	TECN	COMMENT	Γ_3/Γ
4 \pm 3				
4 \pm 3	DENISENKO	16	DPWA Multichannel	

$\Gamma(\Lambda K)/\Gamma_{total}$	DOCUMENT ID	TECN	COMMENT	Γ_4/Γ
10-20 % OUR ESTIMATE				
15 \pm 5	¹ HUNT	19	DPWA Multichannel	
¹ Statistical error only.				

$\Gamma(\Sigma K)/\Gamma_{total}$	DOCUMENT ID	TECN	COMMENT	Γ_5/Γ
3 \pm 2				
3 \pm 2	ANISOVICH	12A	DPWA Multichannel	

$\Gamma(\Delta(1232)\pi, D\text{-wave})/\Gamma_{total}$	DOCUMENT ID	TECN	COMMENT	Γ_7/Γ
4-10 % OUR ESTIMATE				
15 \pm 6	¹ HUNT	19	DPWA Multichannel	
7 \pm 3	SOKHOYAN	15A	DPWA Multichannel	
• • • We do not use the following data for averages, fits, limits, etc. • • •				
40 \pm 13	¹ SHRESTHA	12A	DPWA Multichannel	
¹ Statistical error only.				

$\Gamma(N\rho, S=1/2, P\text{-wave})/\Gamma_{total}$	DOCUMENT ID	TECN	COMMENT	Γ_9/Γ
<10 % OUR ESTIMATE				
<10	¹ HUNT	19	DPWA Multichannel	
• • • We do not use the following data for averages, fits, limits, etc. • • •				
21 \pm 15	¹ SHRESTHA	12A	DPWA Multichannel	
¹ Statistical error only.				

Baryon Particle Listings

 $N(2060)$, $N(2100)$ $\Gamma(N\rho, S=3/2, D\text{-wave})/\Gamma_{\text{total}}$ Γ_{10}/Γ

VALUE (%)	DOCUMENT ID	TECN	COMMENT
5-23 % OUR ESTIMATE			
14 ± 9	¹ HUNT 19	DPWA	Multichannel

¹ Statistical error only. $\Gamma(N\sigma)/\Gamma_{\text{total}}$ Γ_{11}/Γ

VALUE (%)	DOCUMENT ID	TECN	COMMENT
6 ± 3	SOKHOYAN 15A	DPWA	Multichannel

 $\Gamma(N(1440)\pi)/\Gamma_{\text{total}}$ Γ_{12}/Γ

VALUE (%)	DOCUMENT ID	TECN	COMMENT
9 ± 5	SOKHOYAN 15A	DPWA	Multichannel

 $\Gamma(N(1520)\pi, P\text{-wave})/\Gamma_{\text{total}}$ Γ_{13}/Γ

VALUE (%)	DOCUMENT ID	TECN	COMMENT
15 ± 6	SOKHOYAN 15A	DPWA	Multichannel

 $\Gamma(N(1680)\pi, S\text{-wave})/\Gamma_{\text{total}}$ Γ_{14}/Γ

VALUE (%)	DOCUMENT ID	TECN	COMMENT
15 ± 7	SOKHOYAN 15A	DPWA	Multichannel

 $\Gamma(\Lambda K^*(892))/\Gamma_{\text{total}}$ Γ_{15}/Γ

VALUE (%)	DOCUMENT ID	TECN	COMMENT
0.3-1.3 % OUR ESTIMATE			
0.8 ± 0.5	ANISOVICH 17B	DPWA	Multichannel

N(2060) PHOTON DECAY AMPLITUDES AT THE POLE

 $N(2060) \rightarrow \rho\gamma$, helicity-1/2 amplitude $A_{1/2}$

MODULUS ($\text{GeV}^{-1/2}$)	PHASE ($^\circ$)	DOCUMENT ID	TECN	COMMENT
0.064 ± 0.010	12 ± 8	SOKHOYAN 15A	DPWA	Multichannel

 $N(2060) \rightarrow \rho\gamma$, helicity-3/2 amplitude $A_{3/2}$

MODULUS ($\text{GeV}^{-1/2}$)	PHASE ($^\circ$)	DOCUMENT ID	TECN	COMMENT
0.060 ± 0.020	13 ± 10	SOKHOYAN 15A	DPWA	Multichannel

 $N(2060) \rightarrow n\gamma$, helicity-1/2 amplitude $A_{1/2}$

MODULUS ($\text{GeV}^{-1/2}$)	PHASE ($^\circ$)	DOCUMENT ID	TECN	COMMENT
0.052 ± 0.025	-5 ± 20	ANISOVICH 17E	DPWA	Multichannel

 $N(2060) \rightarrow n\gamma$, helicity-3/2 amplitude $A_{3/2}$

MODULUS ($\text{GeV}^{-1/2}$)	PHASE ($^\circ$)	DOCUMENT ID	TECN	COMMENT
0.012 ± 0.007	-40 ± 35	ANISOVICH 17E	DPWA	Multichannel

N(2060) BREIT-WIGNER PHOTON DECAY AMPLITUDES

 $N(2060) \rightarrow \rho\gamma$, helicity-1/2 amplitude $A_{1/2}$

VALUE ($\text{GeV}^{-1/2}$)	DOCUMENT ID	TECN	COMMENT
-0.019 ± 0.005	¹ HUNT 19	DPWA	Multichannel
0.062 ± 0.010	SOKHOYAN 15A	DPWA	Multichannel
••• We do not use the following data for averages, fits, limits, etc. •••			
0.018 ± 0.004	¹ SHRESTHA 12A	DPWA	Multichannel

¹ Statistical error only. $N(2060) \rightarrow \rho\gamma$, helicity-3/2 amplitude $A_{3/2}$

VALUE ($\text{GeV}^{-1/2}$)	DOCUMENT ID	TECN	COMMENT
0.039 ± 0.005	¹ HUNT 19	DPWA	Multichannel
0.062 ± 0.020	SOKHOYAN 15A	DPWA	Multichannel
••• We do not use the following data for averages, fits, limits, etc. •••			
0.010 ± 0.004	¹ SHRESTHA 12A	DPWA	Multichannel

¹ Statistical error only. $N(2060) \rightarrow n\gamma$, helicity-1/2 amplitude $A_{1/2}$

VALUE ($\text{GeV}^{-1/2}$)	DOCUMENT ID	TECN	COMMENT
0.069 ± 0.017	¹ HUNT 19	DPWA	Multichannel
0.052 ± 0.024	ANISOVICH 17E	DPWA	Multichannel
••• We do not use the following data for averages, fits, limits, etc. •••			
0.025 ± 0.011	ANISOVICH 13B	DPWA	Multichannel
-0.012 ± 0.017	¹ SHRESTHA 12A	DPWA	Multichannel

¹ Statistical error only. $N(2060) \rightarrow n\gamma$, helicity-3/2 amplitude $A_{3/2}$

VALUE ($\text{GeV}^{-1/2}$)	DOCUMENT ID	TECN	COMMENT
-0.023 ± 0.020	¹ HUNT 19	DPWA	Multichannel
0.012 ± 0.007	ANISOVICH 17E	DPWA	Multichannel
••• We do not use the following data for averages, fits, limits, etc. •••			
-0.037 ± 0.017	ANISOVICH 13B	DPWA	Multichannel
-0.023 ± 0.023	¹ SHRESTHA 12A	DPWA	Multichannel

¹ Statistical error only.

N(2060) REFERENCES

MUELLER 20	PL B803 135323	J. Mueller et al.	(CBELSA/TAPS Collab.)
HUNT 19	PR C99 055205	B.C. Hunt, D.M. Manley	
ANISOVICH 17B	PL B771 142	A.V. Anisovich et al.	
ANISOVICH 17E	PR C96 055202	A.V. Anisovich et al.	(BONN, PNPI, JLAB+)
DENISENKO 16	PL B755 97	I. Denisenko et al.	
SOKHOYAN 15A	EPJ A51 95	V. Sokhoyan et al.	(CBELSA/TAPS Collab.)
SVARC 14	PR C89 045205	A. Svarc et al.	(RBI Zagreb, UNI Tuzla)
ANISOVICH 13B	EPJ A49 67	A.V. Anisovich et al.	(BONN, PNPI)
ANISOVICH 12A	EPJ A48 15	A.V. Anisovich et al.	(ZAGR)
SHRESTHA 12A	PR C86 055203	M. Shrestha, D.M. Manley	(KSU)
BATINIC 10	PR C82 038203	M. Batinic et al.	(ZAGR)
CUTKOSKY 80	Toronto Conf. 19	R.E. Cutkosky et al.	(CMU, LBL) IJP
Also	PR D20 2839	R.E. Cutkosky et al.	(CMU, LBL)
HOEHLER 79	PDAT 12-1	G. Hoehler et al.	(KARLT) IJP
Also	Toronto Conf. 3	R. Koch	(KARLT) IJP

 $N(2100) 1/2^+$

$$I(J^P) = \frac{1}{2}(\frac{1}{2}^+) \text{ Status: } ***$$

N(2100) POLE POSITION

REAL PART

VALUE (MeV)	DOCUMENT ID	TECN	COMMENT
-------------	-------------	------	---------

2050 to 2150 (≈ 2100) OUR ESTIMATE

2120 ± 25	SOKHOYAN 15A	DPWA	Multichannel
2052 ± 6 ± 3	¹ SVARC 14	L+P	$\pi N \rightarrow \pi N$
2120 ± 40	CUTKOSKY 80	IPWA	$\pi N \rightarrow \pi N$

••• We do not use the following data for averages, fits, limits, etc. •••

2217	HUNT 19	DPWA	Multichannel
2120 ± 47	BATINIC 10	DPWA	$\pi N \rightarrow N\pi, N\eta$
1810	VRANA 00	DPWA	Multichannel

¹ Fit to the amplitudes of HOEHLER 79.

-2xIMAGINARY PART

VALUE (MeV)	DOCUMENT ID	TECN	COMMENT
-------------	-------------	------	---------

240 to 340 (≈ 300) OUR ESTIMATE

290 ± 30	SOKHOYAN 15A	DPWA	Multichannel
337 ± 10 ± 4	¹ SVARC 14	L+P	$\pi N \rightarrow \pi N$
240 ± 80	CUTKOSKY 80	IPWA	$\pi N \rightarrow \pi N$

••• We do not use the following data for averages, fits, limits, etc. •••

545	HUNT 19	DPWA	Multichannel
346 ± 80	BATINIC 10	DPWA	$\pi N \rightarrow N\pi, N\eta$
622	VRANA 00	DPWA	Multichannel

¹ Fit to the amplitudes of HOEHLER 79.

N(2100) ELASTIC POLE RESIDUE

MODULUS $|r|$

VALUE (MeV)	DOCUMENT ID	TECN	COMMENT
-------------	-------------	------	---------

15 to 30 (≈ 20) OUR ESTIMATE

23 ± 5	SOKHOYAN 15A	DPWA	Multichannel
30 ± 1 ± 1	¹ SVARC 14	L+P	$\pi N \rightarrow \pi N$
14 ± 7	CUTKOSKY 80	IPWA	$\pi N \rightarrow \pi N$

••• We do not use the following data for averages, fits, limits, etc. •••

33	BATINIC 10	DPWA	$\pi N \rightarrow N\pi, N\eta$
----	------------	------	---------------------------------

¹ Fit to the amplitudes of HOEHLER 79.PHASE θ

VALUE ($^\circ$)	DOCUMENT ID	TECN	COMMENT
--------------------	-------------	------	---------

-100 to -60 (≈ -80) OUR ESTIMATE

-70 ± 25	SOKHOYAN 15A	DPWA	Multichannel
-92 ± 3 ± 2	¹ SVARC 14	L+P	$\pi N \rightarrow \pi N$
35 ± 25	CUTKOSKY 80	IPWA	$\pi N \rightarrow \pi N$

••• We do not use the following data for averages, fits, limits, etc. •••

-59	BATINIC 10	DPWA	$\pi N \rightarrow N\pi, N\eta$
-----	------------	------	---------------------------------

¹ Fit to the amplitudes of HOEHLER 79.

N(2100) INELASTIC POLE RESIDUE

Normalized residue in $N\pi \rightarrow N(2100) \rightarrow \Delta(1232)\pi$

MODULUS	PHASE ($^\circ$)	DOCUMENT ID	TECN	COMMENT
0.11 ± 0.05	20 ± 60	SOKHOYAN 15A	DPWA	Multichannel

Normalized residue in $N\pi \rightarrow N(2100) \rightarrow N\sigma$

MODULUS	PHASE ($^\circ$)	DOCUMENT ID	TECN	COMMENT
0.18 ± 0.06	125 ± 25	SOKHOYAN 15A	DPWA	Multichannel

Normalized residue in $N\pi \rightarrow N(2100) \rightarrow N(1535)\pi$

MODULUS	PHASE ($^\circ$)	DOCUMENT ID	TECN	COMMENT
0.22 ± 0.06	-40 ± 25	SOKHOYAN 15A	DPWA	Multichannel

N(2100) BREIT-WIGNER MASS

VALUE (MeV)	DOCUMENT ID	TECN	COMMENT
2050 to 2150 (\approx 2100) OUR ESTIMATE			
2221 \pm 92	¹ HUNT	19	DPWA Multichannel
2115 \pm 20	SOKHOYAN	15A	DPWA Multichannel
2125 \pm 75	CUTKOSKY	80	IPWA $\pi N \rightarrow \pi N$
2050 \pm 20	HOEHLER	79	IPWA $\pi N \rightarrow \pi N$
• • • We do not use the following data for averages, fits, limits, etc. • • •			
2157 \pm 42	BATINIC	10	DPWA $\pi N \rightarrow N\pi, N\eta$
2068 \pm 3 ⁺¹⁵ ₋₄₀	ABLIKIM	06K	BES2 $J/\psi \rightarrow (p\pi^-)\bar{n}$
2084 \pm 93	VRANA	00	DPWA Multichannel
¹ Statistical error only.			

N(2100) BREIT-WIGNER WIDTH

VALUE (MeV)	DOCUMENT ID	TECN	COMMENT
200 to 320 (\approx 260) OUR ESTIMATE			
545 \pm 170	¹ HUNT	19	DPWA Multichannel
290 \pm 20	SOKHOYAN	15A	DPWA Multichannel
260 \pm 100	CUTKOSKY	80	IPWA $\pi N \rightarrow \pi N$
200 \pm 30	HOEHLER	79	IPWA $\pi N \rightarrow \pi N$
• • • We do not use the following data for averages, fits, limits, etc. • • •			
355 \pm 88	BATINIC	10	DPWA $\pi N \rightarrow N\pi, N\eta$
165 \pm 14 \pm 40	ABLIKIM	06K	BES2 $J/\psi \rightarrow (p\pi^-)\bar{n}$
1077 \pm 643	VRANA	00	DPWA Multichannel
¹ Statistical error only.			

N(2100) DECAY MODES

Mode	Fraction (Γ_i/Γ)
Γ_1 $N\pi$	8–32 %
Γ_2 $N\eta$	5–45 %
Γ_3 $N\eta'$	5–11 %
Γ_4 $N\omega$	10–25 %
Γ_5 ΛK	<1.0 %
Γ_6 $N\pi\pi$	>55 %
Γ_7 $\Delta(1232)\pi, P$ -wave	6–14 %
Γ_8 $N\rho, S=1/2, P$ -wave	35–70 %
Γ_9 $N\sigma$	14–35 %
Γ_{10} $N(1535)\pi$	26–34 %
Γ_{11} $\Lambda K^*(892)$	3–11 %
Γ_{12} $p\gamma, \text{helicity}=1/2$	0.001–0.13 %
Γ_{13} $n\gamma, \text{helicity}=1/2$	0.004–0.09 %

N(2100) BRANCHING RATIOS

$\Gamma(N\pi)/\Gamma_{\text{total}}$	DOCUMENT ID	TECN	COMMENT	Γ_1/Γ
8–32 % OUR ESTIMATE				
21 \pm 11	¹ HUNT	19	DPWA Multichannel	
16 \pm 5	SOKHOYAN	15A	DPWA Multichannel	
12 \pm 3	CUTKOSKY	80	IPWA $\pi N \rightarrow \pi N$	
10 \pm 4	HOEHLER	79	IPWA $\pi N \rightarrow \pi N$	
• • • We do not use the following data for averages, fits, limits, etc. • • •				
16 \pm 5	BATINIC	10	DPWA $\pi N \rightarrow N\pi, N\eta$	
2 \pm 5	VRANA	00	DPWA Multichannel	
¹ Statistical error only.				

$\Gamma(N\eta)/\Gamma_{\text{total}}$	DOCUMENT ID	TECN	COMMENT	Γ_2/Γ
5–45 % OUR ESTIMATE				
30 \pm 15	MUELLER	20	DPWA Multichannel	
< 4.7	¹ HUNT	19	DPWA Multichannel	
• • • We do not use the following data for averages, fits, limits, etc. • • •				
83 \pm 5	BATINIC	10	DPWA $\pi N \rightarrow N\pi, N\eta$	
61 \pm 61	VRANA	00	DPWA Multichannel	
¹ Statistical error only.				

$\Gamma(N\eta')/\Gamma_{\text{total}}$	DOCUMENT ID	TECN	COMMENT	Γ_3/Γ
5–11 % OUR ESTIMATE				
8 \pm 3	ANISOVICH	17C	DPWA Multichannel	

$\Gamma(N\omega)/\Gamma_{\text{total}}$	DOCUMENT ID	TECN	COMMENT	Γ_4/Γ
10–25 % OUR ESTIMATE				
15 \pm 10	DENISENKO	16	DPWA Multichannel	

$\Gamma(\Lambda K)/\Gamma_{\text{total}}$	DOCUMENT ID	TECN	COMMENT	Γ_5/Γ
<1.0 % OUR ESTIMATE				
< 1.0	¹ HUNT	19	DPWA Multichannel	
• • • We do not use the following data for averages, fits, limits, etc. • • •				
21 \pm 20	VRANA	00	DPWA Multichannel	
¹ Statistical error only.				

$\Gamma(\Delta(1232)\pi, P$ -wave)/ Γ_{total}	DOCUMENT ID	TECN	COMMENT	Γ_7/Γ
6–14 % OUR ESTIMATE				
< 7.5	¹ HUNT	19	DPWA Multichannel	
10 \pm 4	SOKHOYAN	15A	DPWA Multichannel	
• • • We do not use the following data for averages, fits, limits, etc. • • •				
2 \pm 1	VRANA	00	DPWA Multichannel	
¹ Statistical error only.				

$\Gamma(N\rho, S=1/2, P$ -wave)/ Γ_{total}	DOCUMENT ID	TECN	COMMENT	Γ_8/Γ
35–70 % OUR ESTIMATE				
52 \pm 19	¹ HUNT	19	DPWA Multichannel	
• • • We do not use the following data for averages, fits, limits, etc. • • •				
4 \pm 1	VRANA	00	DPWA Multichannel	
¹ Statistical error only.				

$\Gamma(\Lambda K^*(892))/\Gamma_{\text{total}}$	DOCUMENT ID	TECN	COMMENT	Γ_{11}/Γ
3–11 % OUR ESTIMATE				
7 \pm 4	ANISOVICH	17B	DPWA Multichannel	

$\Gamma(N\sigma)/\Gamma_{\text{total}}$	DOCUMENT ID	TECN	COMMENT	Γ_9/Γ
14–35 % OUR ESTIMATE				
< 35	¹ HUNT	19	DPWA Multichannel	
20 \pm 6	SOKHOYAN	15A	DPWA Multichannel	
• • • We do not use the following data for averages, fits, limits, etc. • • •				
10 \pm 1	VRANA	00	DPWA Multichannel	
¹ Statistical error only.				

$\Gamma(N(1535)\pi)/\Gamma_{\text{total}}$	DOCUMENT ID	TECN	COMMENT	Γ_{10}/Γ
26–34 % OUR ESTIMATE				
30 \pm 4	SOKHOYAN	15A	DPWA Multichannel	

N(2100) PHOTON DECAY AMPLITUDES AT THE POLE

N(2100) $\rightarrow p\gamma, \text{helicity-1/2}$ amplitude $A_{1/2}$

MODULUS ($\text{GeV}^{-1/2}$)	PHASE ($^\circ$)	DOCUMENT ID	TECN	COMMENT
0.011 \pm 0.004	65 \pm 30	SOKHOYAN	15A	DPWA Multichannel

N(2100) $\rightarrow n\gamma, \text{helicity-1/2}$ amplitude $A_{1/2}$

MODULUS	PHASE ($^\circ$)	DOCUMENT ID	TECN	COMMENT
0.029 \pm 0.009	35 \pm 20	ANISOVICH	17E	DPWA Multichannel

N(2100) BREIT-WIGNER PHOTON DECAY AMPLITUDES

N(2100) $\rightarrow p\gamma, \text{helicity-1/2}$ amplitude $A_{1/2}$

VALUE ($\text{GeV}^{-1/2}$)	DOCUMENT ID	TECN	COMMENT
0.032 \pm 0.014	¹ HUNT	19	DPWA Multichannel
0.010 \pm 0.004	SOKHOYAN	15A	DPWA Multichannel
¹ Statistical error only.			

N(2100) $\rightarrow n\gamma, \text{helicity-1/2}$ amplitude $A_{1/2}$

VALUE ($\text{GeV}^{-1/2}$)	DOCUMENT ID	TECN	COMMENT
0.026 \pm 0.013	¹ HUNT	19	DPWA Multichannel
0.029 \pm 0.010	ANISOVICH	17E	DPWA Multichannel
¹ Statistical error only.			

N(2100) REFERENCES

MUELLER	20	PL B803 135323	J. Mueller et al.	(CBELSA/TAPS Collab.)
HUNT	19	PR C99 055205	B. C. Hunt, D.M. Manley	
ANISOVICH	17B	PL B771 142	A.V. Anisovich et al.	
ANISOVICH	17C	PL B772 247	A.V. Anisovich et al.	
ANISOVICH	17E	PR C96 055202	A.V. Anisovich et al.	(BONN, PNPI, JLAB+)
DENISENKO	16	PL B755 97	I. Denisenko et al.	
SOKHOYAN	15A	EPJ A51 95	V. Sokhoyan et al.	(CBELSA/TAPS Collab.)
SVARC	14	PR C89 045205	A. Svarc et al.	(RBI Zagreb, UNI Tuzla)
BATINIC	10	PR C82 038203	M. Batinic et al.	(ZAGR)
ABLIKIM	06K	PRL 97 062001	M. Alikim et al.	(BES-II Collab.)
VRANA	00	PRPL 328 181	T.P. Vrana, S.A. Dytman, T.-S.H. Lee	(PITT, ANL)
CUTKOSKY	80	Toronto Conf. 19	R.E. Cutkosky et al.	(CMU, LBL) IUP
		Abo	R.E. Cutkosky et al.	(CMU, LBL)
HOEHLER	79	PDAT 12-1	G. Hoehler et al.	(KARLT) IUP
		Abo	R. Koch	(KARLT) IUP
		Toronto Conf. 3		

Baryon Particle Listings

 $N(2120)$ $N(2120) 3/2^-$

$$I(J^P) = \frac{1}{2}(\frac{3}{2}^-) \text{ Status: } ***$$

Before the 2012 *Review*, all the evidence for a $J^P = 3/2^-$ state with a mass above 1800 MeV was filed under a two-star $N(2080)$.

There is now evidence from ANISOVICH 12A for two $3/2^-$ states in this region, so we have split the older data (according to mass) between a three-star $N(1875)$ and a two-star $N(2120)$.

 $N(2120)$ POLE POSITION

REAL PART

VALUE (MeV)	DOCUMENT ID	TECN	COMMENT
2050 to 2150 (≈ 2100) OUR ESTIMATE			
2115 \pm 40	SOKHOYAN 15A	DPWA	Multichannel
2094 \pm 7 \pm 11	SVARC 14	L+P	$\pi N \rightarrow \pi N$
2050 \pm 70	CUTKOSKY 80	IPWA	$\pi N \rightarrow \pi N$ (higher m)
• • • We do not use the following data for averages, fits, limits, etc. • • •			
2357	HUNT 19	DPWA	Multichannel
2115 \pm 40	GUTZ 14	DPWA	Multichannel
2110 \pm 50	ANISOVICH 12A	DPWA	Multichannel

-2 \times IMAGINARY PART

VALUE (MeV)	DOCUMENT ID	TECN	COMMENT
200 to 360 (≈ 280) OUR ESTIMATE			
345 \pm 35	SOKHOYAN 15A	DPWA	Multichannel
296 \pm 15 \pm 4	SVARC 14	L+P	$\pi N \rightarrow \pi N$
200 \pm 80	CUTKOSKY 80	IPWA	$\pi N \rightarrow \pi N$ (higher m)
• • • We do not use the following data for averages, fits, limits, etc. • • •			
503	HUNT 19	DPWA	Multichannel
345 \pm 35	GUTZ 14	DPWA	Multichannel
340 \pm 45	ANISOVICH 12A	DPWA	Multichannel

 $N(2120)$ ELASTIC POLE RESIDUEMODULUS $|r|$

VALUE (MeV)	DOCUMENT ID	TECN	COMMENT
10 to 30 (≈ 20) OUR ESTIMATE			
11 \pm 6	SOKHOYAN 15A	DPWA	Multichannel
13 \pm 1 \pm 1	SVARC 14	L+P	$\pi N \rightarrow \pi N$
30 \pm 20	CUTKOSKY 80	IPWA	$\pi N \rightarrow \pi N$ (higher m)
• • • We do not use the following data for averages, fits, limits, etc. • • •			
11 \pm 6	GUTZ 14	DPWA	Multichannel
13 \pm 3	ANISOVICH 12A	DPWA	Multichannel

PHASE θ

VALUE ($^\circ$)	DOCUMENT ID	TECN	COMMENT
-40 to 20 (≈ -10) OUR ESTIMATE			
-30 \pm 20	SOKHOYAN 15A	DPWA	Multichannel
-2 \pm 4 \pm 9	SVARC 14	L+P	$\pi N \rightarrow \pi N$
0 \pm 100	CUTKOSKY 80	IPWA	$\pi N \rightarrow \pi N$ (higher m)
• • • We do not use the following data for averages, fits, limits, etc. • • •			
-30 \pm 20	GUTZ 14	DPWA	Multichannel
-20 \pm 10	ANISOVICH 12A	DPWA	Multichannel

 $N(2120)$ INELASTIC POLE RESIDUE

The "normalized residue" is the residue divided by $\Gamma_{\text{pole}}/2$.

Normalized residue in $N\pi \rightarrow N(2120) \rightarrow \Lambda K$

MODULUS	PHASE ($^\circ$)	DOCUMENT ID	TECN	COMMENT
0.03 \pm 0.01	100 \pm 30	ANISOVICH 12A	DPWA	Multichannel

Normalized residue in $N\pi \rightarrow N(2120) \rightarrow \Sigma K$

MODULUS	PHASE ($^\circ$)	DOCUMENT ID	TECN	COMMENT
0.02 \pm 0.015	-50 \pm 40	ANISOVICH 12A	DPWA	Multichannel

Normalized residue in $N\pi \rightarrow N(2120) \rightarrow N(1535)\pi$

MODULUS	PHASE ($^\circ$)	DOCUMENT ID	TECN	COMMENT
0.15 \pm 0.08	-90 \pm 40	GUTZ 14	DPWA	Multichannel

Normalized residue in $N\pi \rightarrow N(2120) \rightarrow \Delta(1232)\pi, S\text{-wave}$

MODULUS	PHASE ($^\circ$)	DOCUMENT ID	TECN	COMMENT
0.25 \pm 0.10	undefined	SOKHOYAN 15A	DPWA	Multichannel

Normalized residue in $N\pi \rightarrow N(2120) \rightarrow \Delta(1232)\pi, D\text{-wave}$

MODULUS	PHASE ($^\circ$)	DOCUMENT ID	TECN	COMMENT
0.15 \pm 0.06	-35 \pm 30	SOKHOYAN 15A	DPWA	Multichannel

Normalized residue in $N\pi \rightarrow N(2120) \rightarrow N\sigma$

MODULUS	PHASE ($^\circ$)	DOCUMENT ID	TECN	COMMENT
0.09 \pm 0.05	-80 \pm 50	SOKHOYAN 15A	DPWA	Multichannel

 $N(2120)$ BREIT-WIGNER MASS

VALUE (MeV)	DOCUMENT ID	TECN	COMMENT
2060 to 2160 (≈ 2120) OUR ESTIMATE			
2353 \pm 29	¹ HUNT 19	DPWA	Multichannel
2120 \pm 45	SOKHOYAN 15A	DPWA	Multichannel
2060 \pm 80	CUTKOSKY 80	IPWA	$\pi N \rightarrow \pi N$
2081 \pm 20	HOEHLER 79	IPWA	$\pi N \rightarrow \pi N$
• • • We do not use the following data for averages, fits, limits, etc. • • •			
2120 \pm 35	GUTZ 14	DPWA	Multichannel
2150 \pm 60	ANISOVICH 12A	DPWA	Multichannel

¹ Statistical error only.

 $N(2120)$ BREIT-WIGNER WIDTH

VALUE (MeV)	DOCUMENT ID	TECN	COMMENT
260 to 360 (≈ 300) OUR ESTIMATE			
503 \pm 62	¹ HUNT 19	DPWA	Multichannel
340 \pm 35	SOKHOYAN 15A	DPWA	Multichannel
300 \pm 100	CUTKOSKY 80	IPWA	$\pi N \rightarrow \pi N$ (higher m)
265 \pm 40	HOEHLER 79	IPWA	$\pi N \rightarrow \pi N$
• • • We do not use the following data for averages, fits, limits, etc. • • •			
340 \pm 35	GUTZ 14	DPWA	Multichannel
330 \pm 45	ANISOVICH 12A	DPWA	Multichannel

¹ Statistical error only.

 $N(2120)$ DECAY MODES

Mode	Fraction (Γ_i/Γ)
Γ_1 $N\pi$	5-15 %
Γ_2 $N\eta$	1-5 %
Γ_3 $N\eta'$	2-6 %
Γ_4 $N\omega$	4-20 %
Γ_5 ΛK	6-11 %
Γ_6 $N\pi\pi$	>27 %
Γ_7 $\Delta(1232)\pi$	>23 %
Γ_8 $\Delta(1232)\pi, S\text{-wave}$	15-70 %
Γ_9 $\Delta(1232)\pi, D\text{-wave}$	8-45 %
Γ_{10} $N\rho, S=3/2, S\text{-wave}$	< 3 %
Γ_{11} $N\sigma$	4-15 %
Γ_{12} $N(1535)\pi$	7-23 %
Γ_{13} $\Lambda K^*(892)$	< 0.2 %
Γ_{14} $p\gamma$	0.16-2.1 %
Γ_{15} $p\gamma, \text{helicity}=1/2$	0.07-0.80 %
Γ_{16} $p\gamma, \text{helicity}=3/2$	0.09-1.3 %
Γ_{17} $n\gamma$	0.04-0.72 %
Γ_{18} $n\gamma, \text{helicity}=1/2$	0.04-0.60 %
Γ_{19} $n\gamma, \text{helicity}=3/2$	0.001-0.12 %

 $N(2120)$ BRANCHING RATIOS

$\Gamma(N\pi)/\Gamma_{\text{total}}$	VALUE (%)	DOCUMENT ID	TECN	COMMENT	Γ_1/Γ
5-15 % OUR ESTIMATE					
19 \pm 2		¹ HUNT 19	DPWA	Multichannel	
5 \pm 3		SOKHOYAN 15A	DPWA	Multichannel	
14 \pm 7		CUTKOSKY 80	IPWA	$\pi N \rightarrow \pi N$ (higher m)	
6 \pm 2		HOEHLER 79	IPWA	$\pi N \rightarrow \pi N$	
• • • We do not use the following data for averages, fits, limits, etc. • • •					
5 \pm 3		GUTZ 14	DPWA	Multichannel	
6 \pm 2		ANISOVICH 12A	DPWA	Multichannel	
¹ Statistical error only.					

$\Gamma(N\eta)/\Gamma_{\text{total}}$	VALUE (%)	DOCUMENT ID	TECN	COMMENT	Γ_2/Γ
1-5 % OUR ESTIMATE					
<1		MUELLER 20	DPWA	Multichannel	
3.1 \pm 2.4		¹ HUNT 19	DPWA	Multichannel	
¹ Statistical error only.					

$\Gamma(N\eta')/\Gamma_{\text{total}}$	VALUE (%)	DOCUMENT ID	TECN	COMMENT	Γ_3/Γ
2-6 % OUR ESTIMATE					
4 \pm 2		ANISOVICH 17C	DPWA	Multichannel	

$\Gamma(N\omega)/\Gamma_{\text{total}}$	VALUE (%)	DOCUMENT ID	TECN	COMMENT	Γ_4/Γ
4-20 % OUR ESTIMATE					
12 \pm 8		DENISENKO 16	DPWA	Multichannel	

See key on page 1171

Baryon Particle Listings
 $N(2120)$, $N(2190)$ $\Gamma(\Lambda K)/\Gamma_{\text{total}}$ Γ_5/Γ

VALUE (%)	DOCUMENT ID	TECN	COMMENT
6-11 % OUR ESTIMATE			
8.5 ± 2.5	¹ HUNT	19	DPWA Multichannel

¹ Statistical error only. $\Gamma(\Delta(1232)\pi, S\text{-wave})/\Gamma_{\text{total}}$ Γ_8/Γ

VALUE (%)	DOCUMENT ID	TECN	COMMENT
15-70 % OUR ESTIMATE			
25 ± 11	¹ HUNT	19	DPWA Multichannel
50 ± 20	SOKHOYAN	15A	DPWA Multichannel

¹ Statistical error only. $\Gamma(\Delta(1232)\pi, D\text{-wave})/\Gamma_{\text{total}}$ Γ_9/Γ

VALUE (%)	DOCUMENT ID	TECN	COMMENT
8-45 % OUR ESTIMATE			
34 ± 11	¹ HUNT	19	DPWA Multichannel
20 ± 12	SOKHOYAN	15A	DPWA Multichannel

¹ Statistical error only. $\Gamma(N\rho, S=3/2, S\text{-wave})/\Gamma_{\text{total}}$ Γ_{10}/Γ

VALUE (%)	DOCUMENT ID	TECN	COMMENT
< 3 % OUR ESTIMATE			
< 3	¹ HUNT	19	DPWA Multichannel

¹ Statistical error only. $\Gamma(N\sigma)/\Gamma_{\text{total}}$ Γ_{11}/Γ

VALUE (%)	DOCUMENT ID	TECN	COMMENT
4-15 % OUR ESTIMATE			
9 ± 5	¹ HUNT	19	DPWA Multichannel
11 ± 4	SOKHOYAN	15A	DPWA Multichannel

¹ Statistical error only. $\Gamma(N(1535)\pi)/\Gamma_{\text{total}}$ Γ_{12}/Γ

VALUE (%)	DOCUMENT ID	TECN	COMMENT
7-23 % OUR ESTIMATE			
15 ± 8	GUTZ	14	DPWA Multichannel

 $\Gamma(\Lambda K^*(892))/\Gamma_{\text{total}}$ Γ_{13}/Γ

VALUE (%)	DOCUMENT ID	TECN	COMMENT
< 0.2 % OUR ESTIMATE			
< 0.2	ANISOVICH	17B	DPWA Multichannel

 $N(2120)$ PHOTON DECAY AMPLITUDES AT THE POLE $N(2120) \rightarrow p\gamma$, helicity-1/2 amplitude $A_{1/2}$

MODULUS ($\text{GeV}^{-1/2}$)	PHASE ($^\circ$)	DOCUMENT ID	TECN	COMMENT
0.130 ± 0.045	-40 ± 25	SOKHOYAN	15A	DPWA Multichannel

 $N(2120) \rightarrow p\gamma$, helicity-3/2 amplitude $A_{3/2}$

MODULUS ($\text{GeV}^{-1/2}$)	PHASE ($^\circ$)	DOCUMENT ID	TECN	COMMENT
0.160 ± 0.060	-30 ± 15	SOKHOYAN	15A	DPWA Multichannel

 $N(2120) \rightarrow n\gamma$, helicity-1/2 amplitude $A_{1/2}$

MODULUS ($\text{GeV}^{-1/2}$)	PHASE ($^\circ$)	DOCUMENT ID	TECN	COMMENT
0.080 ± 0.030	15 ± 25	ANISOVICH	17E	DPWA Multichannel

 $N(2120) \rightarrow n\gamma$, helicity-3/2 amplitude $A_{3/2}$

MODULUS ($\text{GeV}^{-1/2}$)	PHASE ($^\circ$)	DOCUMENT ID	TECN	COMMENT
-0.033 ± 0.020	-60 ± 35	ANISOVICH	17E	DPWA Multichannel

 $N(2120)$ BREIT-WIGNER PHOTON DECAY AMPLITUDES $N(2120) \rightarrow p\gamma$, helicity-1/2 amplitude $A_{1/2}$

VALUE ($\text{GeV}^{-1/2}$)	DOCUMENT ID	TECN	COMMENT
0.047 ± 0.009	¹ HUNT	19	DPWA Multichannel
0.130 ± 0.050	SOKHOYAN	15A	DPWA Multichannel
• • • We do not use the following data for averages, fits, limits, etc. • • •			
0.130 ± 0.050	GUTZ	14	DPWA Multichannel

¹ Statistical error only. $N(2120) \rightarrow p\gamma$, helicity-3/2 amplitude $A_{3/2}$

VALUE ($\text{GeV}^{-1/2}$)	DOCUMENT ID	TECN	COMMENT
0.001 ± 0.007	¹ HUNT	19	DPWA Multichannel
0.160 ± 0.065	SOKHOYAN	15A	DPWA Multichannel
• • • We do not use the following data for averages, fits, limits, etc. • • •			
0.160 ± 0.065	GUTZ	14	DPWA Multichannel

¹ Statistical error only. $N(2120) \rightarrow n\gamma$, helicity-1/2 amplitude $A_{1/2}$

VALUE ($\text{GeV}^{-1/2}$)	DOCUMENT ID	TECN	COMMENT
-0.020 ± 0.013	¹ HUNT	19	DPWA Multichannel
0.081 ± 0.030	ANISOVICH	17E	DPWA Multichannel
• • • We do not use the following data for averages, fits, limits, etc. • • •			
0.110 ± 0.045	ANISOVICH	13B	DPWA Multichannel

¹ Statistical error only. $N(2120) \rightarrow n\gamma$, helicity-3/2 amplitude $A_{3/2}$

VALUE ($\text{GeV}^{-1/2}$)	DOCUMENT ID	TECN	COMMENT
-0.00 ± 0.02	¹ HUNT	19	DPWA Multichannel
-0.032 ± 0.020	ANISOVICH	17E	DPWA Multichannel
• • • We do not use the following data for averages, fits, limits, etc. • • •			
0.040 ± 0.030	ANISOVICH	13B	DPWA Multichannel

¹ Statistical error only. **$N(2120)$ REFERENCES**

MUELLER	20	PL B803 135323	J. Mueller <i>et al.</i>	(CBELSA/TAPS Collab.)
HUNT	19	PR C99 055205	B.C. Hunt, D.M. Manley	
ANISOVICH	17B	PL B771 142	A.V. Anisovich <i>et al.</i>	
ANISOVICH	17C	PL B772 247	A.V. Anisovich <i>et al.</i>	
ANISOVICH	17E	PR C96 055202	A.V. Anisovich <i>et al.</i>	(BONN, PNPI, JLAB+)
DENISENKO	16	PL B755 97	I. Denisenko <i>et al.</i>	
SOKHOYAN	15A	EPJ A51 95	V. Sokhoyan <i>et al.</i>	(CBELSA/TAPS Collab.)
GUTZ	14	EPJ A50 74	E. Gutz <i>et al.</i>	(CBELSA/TAPS Collab.)
SVARC	14	PR C89 045205	A. Svarc <i>et al.</i>	(RBI Zagreb, UNI Tuzla)
ANISOVICH	13B	EPJ A49 67	A.V. Anisovich <i>et al.</i>	
ANISOVICH	12A	EPJ A48 15	A.V. Anisovich <i>et al.</i>	(BONN, PNPI)
CUTKOSKY	80	Toronto Conf. 19	R.E. Cutkosky <i>et al.</i>	(CMU, LBL)
HOEHLER	79	PDAT 12-1	G. Hoehler <i>et al.</i>	(KARLT)

 $N(2190) 7/2^-$

$$I(J^P) = \frac{1}{2}(\frac{7}{2}^-) \text{ Status: } ***$$

Older and obsolete values are listed and referenced in the 2014 edition, Chinese Physics **C38** 070001 (2014). **$N(2190)$ POLE POSITION****REAL PART**

VALUE (MeV)	DOCUMENT ID	TECN	COMMENT
1950 to 2150 (≈ 2050) OUR ESTIMATE			
1965 ± 6	ROENCHEN	22	DPWA Multichannel
2140 ± 20	AFZAL	20	DPWA Multichannel
2150 ± 25	SOKHOYAN	15A	DPWA Multichannel
2079 ± 4 ± 9	¹ SVARC	14	L+P $\pi N \rightarrow \pi N$
2100 ± 50	CUTKOSKY	80	IPWA $\pi N \rightarrow \pi N$
• • • We do not use the following data for averages, fits, limits, etc. • • •			
2162	HUNT	19	DPWA Multichannel
2074	ROENCHEN	15A	DPWA Multichannel
2150 ± 25	ANISOVICH	12A	DPWA Multichannel
2063 ± 32	BATINIC	10	DPWA $\pi N \rightarrow N\pi, N\eta$
2070	ARNDT	06	DPWA $\pi N \rightarrow \pi N, \eta N$
2107	VRANA	00	DPWA Multichannel
2042	HOEHLER	93	SPED $\pi N \rightarrow \pi N$

¹ Fit to the amplitudes of HOEHLER 79.**-2xIMAGINARY PART**

VALUE (MeV)	DOCUMENT ID	TECN	COMMENT
300 to 500 (≈ 400) OUR ESTIMATE			
287 ± 33	ROENCHEN	22	DPWA Multichannel
420 +120 - 40	AFZAL	20	DPWA Multichannel
325 ± 25	SOKHOYAN	15A	DPWA Multichannel
509 ± 7 ± 16	¹ SVARC	14	L+P $\pi N \rightarrow \pi N$
400 ± 160	CUTKOSKY	80	IPWA $\pi N \rightarrow \pi N$
• • • We do not use the following data for averages, fits, limits, etc. • • •			
407	HUNT	19	DPWA Multichannel
327	ROENCHEN	15A	DPWA Multichannel
330 ± 30	ANISOVICH	12A	DPWA Multichannel
330 ± 101	BATINIC	10	DPWA $\pi N \rightarrow N\pi, N\eta$
520	ARNDT	06	DPWA $\pi N \rightarrow \pi N, \eta N$
380	VRANA	00	DPWA Multichannel
482	HOEHLER	93	SPED $\pi N \rightarrow \pi N$

¹ Fit to the amplitudes of HOEHLER 79. **$N(2190)$ ELASTIC POLE RESIDUE****MODULUS $|r|$**

VALUE (MeV)	DOCUMENT ID	TECN	COMMENT
20 to 60 (≈ 40) OUR ESTIMATE			
18 ± 4	ROENCHEN	22	DPWA Multichannel
30 ± 4	SOKHOYAN	15A	DPWA Multichannel
54 ± 1 ± 3	¹ SVARC	14	L+P $\pi N \rightarrow \pi N$
25 ± 10	CUTKOSKY	80	IPWA $\pi N \rightarrow \pi N$

Baryon Particle Listings

 $N(2190)$

••• We do not use the following data for averages, fits, limits, etc. •••

35	ROENCHEN	15A	DPWA	Multichannel
30 ± 5	ANISOVICH	12A	DPWA	Multichannel
34	BATINIC	10	DPWA	$\pi N \rightarrow N\pi, N\eta$
72	ARNDT	06	DPWA	$\pi N \rightarrow \pi N, \eta N$
45	HOEHLER	93	SPED	$\pi N \rightarrow \pi N$

¹ Fit to the amplitudes of HOEHLER 79.

PHASE θ

VALUE (°)	DOCUMENT ID	TECN	COMMENT
-30 to 30 (≈ 0) OUR ESTIMATE			
-45 ± 14	ROENCHEN	22	DPWA Multichannel
28 ± 10	SOKHOYAN	15A	DPWA Multichannel
-18 ± 1 ± 3	¹ SVARC	14	L+P $\pi N \rightarrow \pi N$
-30 ± 50	CUTKOSKY	80	IPWA $\pi N \rightarrow \pi N$
••• We do not use the following data for averages, fits, limits, etc. •••			
-40	ROENCHEN	15A	DPWA Multichannel
30 ± 10	ANISOVICH	12A	DPWA Multichannel
-19	BATINIC	10	DPWA $\pi N \rightarrow N\pi, N\eta$
-32	ARNDT	06	DPWA $\pi N \rightarrow \pi N, \eta N$

¹ Fit to the amplitudes of HOEHLER 79.

 $N(2190)$ INELASTIC POLE RESIDUE

The "normalized residue" is the residue divided by $\Gamma_{pole}/2$.

Normalized residue in $N\pi \rightarrow N(2190) \rightarrow \Lambda K$

MODULUS	PHASE (°)	DOCUMENT ID	TECN	COMMENT
0.026 ± 0.007	-78 ± 15	ROENCHEN	22	DPWA Multichannel
0.03 ± 0.01	20 ± 15	ANISOVICH	12A	DPWA Multichannel
••• We do not use the following data for averages, fits, limits, etc. •••				
0.005	-51	ROENCHEN	15A	DPWA Multichannel

Normalized residue in $N\pi \rightarrow N(2190) \rightarrow \Sigma K$

MODULUS	PHASE (°)	DOCUMENT ID	TECN	COMMENT
0.005 ± 0.001	-92 ± 16	ROENCHEN	22	DPWA Multichannel
••• We do not use the following data for averages, fits, limits, etc. •••				
0.013	-69	ROENCHEN	15A	DPWA Multichannel

Normalized residue in $N\pi \rightarrow N(2190) \rightarrow N\eta$

MODULUS	PHASE (°)	DOCUMENT ID	TECN	COMMENT
0.021 ± 0.005	-65 ± 15	ROENCHEN	22	DPWA Multichannel
••• We do not use the following data for averages, fits, limits, etc. •••				
0.016	129	ROENCHEN	15A	DPWA Multichannel

Normalized residue in $N\pi \rightarrow N(2190) \rightarrow \Delta(1232)\pi, D\text{-wave}$

MODULUS	PHASE (°)	DOCUMENT ID	TECN	COMMENT
0.27 ± 0.04	-165 ± 20	SOKHOYAN	15A	DPWA Multichannel

Normalized residue in $N\pi \rightarrow N(2190) \rightarrow N\sigma$

MODULUS	PHASE (°)	DOCUMENT ID	TECN	COMMENT
0.13 ± 0.05	50 ± 15	SOKHOYAN	15A	DPWA Multichannel

 $N(2190)$ BREIT-WIGNER MASS

VALUE (MeV)	DOCUMENT ID	TECN	COMMENT
2140 to 2220 (≈ 2180) OUR ESTIMATE			
2222 ± 15	¹ HUNT	19	DPWA Multichannel
2205 ± 18	SOKHOYAN	15A	DPWA Multichannel
2152.4 ± 1.4	¹ ARNDT	06	DPWA $\pi N \rightarrow \pi N, \eta N$
2200 ± 70	CUTKOSKY	80	IPWA $\pi N \rightarrow \pi N$
2140 ± 12	HOEHLER	79	IPWA $\pi N \rightarrow \pi N$
••• We do not use the following data for averages, fits, limits, etc. •••			
2180 ± 20	ANISOVICH	12A	DPWA Multichannel
2150 ± 26	¹ SHRESTHA	12A	DPWA Multichannel
2125 ± 61	BATINIC	10	DPWA $\pi N \rightarrow N\pi, N\eta$
2168 ± 18	VRANA	00	DPWA Multichannel

¹ Statistical error only.

 $N(2190)$ BREIT-WIGNER WIDTH

VALUE (MeV)	DOCUMENT ID	TECN	COMMENT
300 to 500 (≈ 400) OUR ESTIMATE			
442 ± 40	¹ HUNT	19	DPWA Multichannel
355 ± 30	SOKHOYAN	15A	DPWA Multichannel
484 ± 13	¹ ARNDT	06	DPWA $\pi N \rightarrow \pi N, \eta N$
500 ± 150	CUTKOSKY	80	IPWA $\pi N \rightarrow \pi N$
390 ± 30	HOEHLER	79	IPWA $\pi N \rightarrow \pi N$
••• We do not use the following data for averages, fits, limits, etc. •••			
335 ± 40	ANISOVICH	12A	DPWA Multichannel
500 ± 74	¹ SHRESTHA	12A	DPWA Multichannel
381 ± 160	BATINIC	10	DPWA $\pi N \rightarrow N\pi, N\eta$
453 ± 101	VRANA	00	DPWA Multichannel

¹ Statistical error only.

 $N(2190)$ DECAY MODES

The following branching fractions are our estimates, not fits or averages.

Mode	Fraction (Γ_i/Γ)
Γ_1 $N\pi$	10–20 %
Γ_2 $N\eta$	1–5 %
Γ_3 $N\omega$	8–20 %
Γ_4 ΛK	0.2–0.8 %
Γ_5 $N\pi\pi$	22–51 %
Γ_6 $\Delta(1232)\pi, D\text{-wave}$	19–31 %
Γ_7 $N\rho, S=3/2, D\text{-wave}$	<11 %
Γ_8 $N\sigma$	3–9 %
Γ_9 $\Lambda K^*(892)$	0.2–0.8 %
Γ_{10} $p\gamma$	<0.08 %
Γ_{11} $p\gamma, \text{helicity}=1/2$	<0.06 %
Γ_{12} $p\gamma, \text{helicity}=3/2$	<0.02 %
Γ_{13} $n\gamma$	<0.04 %
Γ_{14} $n\gamma, \text{helicity}=1/2$	<0.01 %
Γ_{15} $n\gamma, \text{helicity}=3/2$	<0.03 %

 $N(2190)$ BRANCHING RATIOS

$\Gamma(N\pi)/\Gamma_{\text{total}}$	DOCUMENT ID	TECN	COMMENT	Γ_1/Γ
10–20 % OUR ESTIMATE				
22.9 ± 0.6	¹ HUNT	19	DPWA Multichannel	
16 ± 2	SOKHOYAN	15A	DPWA Multichannel	
23.8 ± 0.1	¹ ARNDT	06	DPWA $\pi N \rightarrow \pi N, \eta N$	
12 ± 6	CUTKOSKY	80	IPWA $\pi N \rightarrow \pi N$	
14 ± 2	HOEHLER	79	IPWA $\pi N \rightarrow \pi N$	
••• We do not use the following data for averages, fits, limits, etc. •••				
16 ± 2	ANISOVICH	12A	DPWA Multichannel	
20 ± 1	¹ SHRESTHA	12A	DPWA Multichannel	
18 ± 12	BATINIC	10	DPWA $\pi N \rightarrow N\pi, N\eta$	
20 ± 4	VRANA	00	DPWA Multichannel	

¹ Statistical error only.

$\Gamma(N\eta)/\Gamma_{\text{total}}$	DOCUMENT ID	TECN	COMMENT	Γ_2/Γ
1–5 % OUR ESTIMATE				
4 ± 2	MUELLER	20	DPWA Multichannel	
2.7 ± 2.2	¹ HUNT	19	DPWA Multichannel	
••• We do not use the following data for averages, fits, limits, etc. •••				
2 ± 1	¹ SHRESTHA	12A	DPWA Multichannel	
0.1 ± 0.3	BATINIC	10	DPWA $\pi N \rightarrow \pi N, N\eta$	
0 ± 1	VRANA	00	DPWA Multichannel	

¹ Statistical error only.

$\Gamma(N\omega)/\Gamma_{\text{total}}$	DOCUMENT ID	TECN	COMMENT	Γ_3/Γ
8–20 % OUR ESTIMATE				
14 ± 6	DENISENKO	16	DPWA Multichannel	
••• We do not use the following data for averages, fits, limits, etc. •••				
seen	WILLIAMS	09	IPWA $\gamma p \rightarrow p\omega$	

$\Gamma(\Lambda K)/\Gamma_{\text{total}}$	DOCUMENT ID	TECN	COMMENT	Γ_4/Γ
0.2–0.8 % OUR ESTIMATE				
0.6 ± 0.1	¹ HUNT	19	DPWA Multichannel	
0.5 ± 0.3	ANISOVICH	12A	DPWA Multichannel	
••• We do not use the following data for averages, fits, limits, etc. •••				
<1	¹ SHRESTHA	12A	DPWA Multichannel	

¹ Statistical error only.

$\Gamma(\Delta(1232)\pi, D\text{-wave})/\Gamma_{\text{total}}$	DOCUMENT ID	TECN	COMMENT	Γ_6/Γ
19–31 % OUR ESTIMATE				
25 ± 6	SOKHOYAN	15A	DPWA Multichannel	

$\Gamma(N\rho, S=3/2, D\text{-wave})/\Gamma_{\text{total}}$	DOCUMENT ID	TECN	COMMENT	Γ_7/Γ
<11 % OUR ESTIMATE				
<11	¹ HUNT	19	DPWA Multichannel	
••• We do not use the following data for averages, fits, limits, etc. •••				
29 ± 28	VRANA	00	DPWA Multichannel	

¹ Statistical error only.

$\Gamma(N\sigma)/\Gamma_{\text{total}}$	DOCUMENT ID	TECN	COMMENT	Γ_8/Γ
3–9 % OUR ESTIMATE				
6 ± 3	SOKHOYAN	15A	DPWA Multichannel	

$\Gamma(\Lambda K^*(892))/\Gamma_{\text{total}}$	Γ_9/Γ		
VALUE (%)	DOCUMENT ID	TECN	COMMENT
0.2-0.8 % OUR ESTIMATE			
0.5 ± 0.3	ANISOVICH	17B	DPWA Multichannel

 $N(2190)$ PHOTON DECAY AMPLITUDES AT THE POLE **$N(2190) \rightarrow p\gamma$, helicity-1/2 amplitude $A_{1/2}$**

MODULUS ($\text{GeV}^{-1/2}$)	PHASE ($^\circ$)	DOCUMENT ID	TECN	COMMENT
-0.015 ± 0.004	111 ± 9	ROENCHEN	22	DPWA Multichannel
0.068 ± 0.005	-170 ± 12	SOKHOYAN	15A	DPWA Multichannel
• • • We do not use the following data for averages, fits, limits, etc. • • •				
-0.041	-21	ROENCHEN	15A	DPWA Multichannel

 $N(2190) \rightarrow p\gamma$, helicity-3/2 amplitude $A_{3/2}$

MODULUS ($\text{GeV}^{-1/2}$)	PHASE ($^\circ$)	DOCUMENT ID	TECN	COMMENT
0.062 ± 0.011	179 ± 13	ROENCHEN	22	DPWA Multichannel
0.025 ± 0.010	22 ± 10	SOKHOYAN	15A	DPWA Multichannel
• • • We do not use the following data for averages, fits, limits, etc. • • •				
0.085	-22	ROENCHEN	15A	DPWA Multichannel

 $N(2190) \rightarrow n\gamma$, helicity-1/2 amplitude $A_{1/2}$

MODULUS ($\text{GeV}^{-1/2}$)	PHASE ($^\circ$)	DOCUMENT ID	TECN	COMMENT
0.030 ± 0.007	5 ± 15	ANISOVICH	17E	DPWA Multichannel

 $N(2190) \rightarrow n\gamma$, helicity-3/2 amplitude $A_{3/2}$

MODULUS ($\text{GeV}^{-1/2}$)	PHASE ($^\circ$)	DOCUMENT ID	TECN	COMMENT
-0.023 ± 0.008	13 ± 20	ANISOVICH	17E	DPWA Multichannel

 $N(2190)$ BREIT-WIGNER PHOTON DECAY AMPLITUDES **$N(2190) \rightarrow p\gamma$, helicity-1/2 amplitude $A_{1/2}$**

VALUE ($\text{GeV}^{-1/2}$)	DOCUMENT ID	TECN	COMMENT
0.001 ± 0.002	¹ HUNT	19	DPWA Multichannel
-0.071 ± 0.006	SOKHOYAN	15A	DPWA Multichannel
• • • We do not use the following data for averages, fits, limits, etc. • • •			
-0.065 ± 0.008	ANISOVICH	12A	DPWA Multichannel

¹ Statistical error only. **$N(2190) \rightarrow p\gamma$, helicity-3/2 amplitude $A_{3/2}$**

VALUE ($\text{GeV}^{-1/2}$)	DOCUMENT ID	TECN	COMMENT
0.015 ± 0.003	¹ HUNT	19	DPWA Multichannel
0.027 ± 0.010	SOKHOYAN	15A	DPWA Multichannel
• • • We do not use the following data for averages, fits, limits, etc. • • •			
0.035 ± 0.017	ANISOVICH	12A	DPWA Multichannel

¹ Statistical error only. **$N(2190) \rightarrow p\gamma$, ratio of helicity amplitudes $A_{3/2}/A_{1/2}$**

VALUE	DOCUMENT ID	TECN	COMMENT
• • • We do not use the following data for averages, fits, limits, etc. • • •			
-0.17 ± 0.15	WILLIAMS	09	IPWA $\gamma p \rightarrow p\omega$

 $N(2190) \rightarrow n\gamma$, helicity-1/2 amplitude $A_{1/2}$

VALUE ($\text{GeV}^{-1/2}$)	DOCUMENT ID	TECN	COMMENT
-0.01 ± 0.02	¹ HUNT	19	DPWA Multichannel
0.030 ± 0.007	ANISOVICH	17E	DPWA Multichannel
• • • We do not use the following data for averages, fits, limits, etc. • • •			
-0.015 ± 0.013	ANISOVICH	13B	DPWA Multichannel

¹ Statistical error only. **$N(2190) \rightarrow n\gamma$, helicity-3/2 amplitude $A_{3/2}$**

VALUE ($\text{GeV}^{-1/2}$)	DOCUMENT ID	TECN	COMMENT
-0.023 ± 0.022	¹ HUNT	19	DPWA Multichannel
-0.023 ± 0.008	ANISOVICH	17E	DPWA Multichannel
• • • We do not use the following data for averages, fits, limits, etc. • • •			
-0.034 ± 0.022	ANISOVICH	13B	DPWA Multichannel

¹ Statistical error only. **$N(2190)$ REFERENCES**For early references, see Physics Letters **111B** 1 (1982).

ROENCHEN	22	EPJ A58 229	D. Roenchen et al.	(JULI, GWU, BONN+)
AFZAL	20	PRL 125 152002	F. Afzal et al.	(CBELSA/TAPS Collab.)
MUELLER	20	PL B603 135323	J. Mueller et al.	(CBELSA/TAPS Collab.)
HUNT	19	PR C9 055205	B. C. Hunt, D. M. Manley	
ANISOVICH	17B	PL B771 142	A.V. Anisovich et al.	
ANISOVICH	17E	PR C96 055202	A.V. Anisovich et al.	(BONN, PNPI, JLAB+)
DENISENKO	16	PL B755 97	I. Denisenko et al.	
ROENCHEN	15A	EPJ A51 70	D. Roenchen et al.	
SOKHOYAN	15A	EPJ A51 95	V. Sokhoyan et al.	(CBELSA/TAPS Collab.)
PDG	14	CP C38 070001	K. Olive et al.	(PDG Collab.)

SVARC	14	PR C89 045205	A. Svarc et al.	(RBI Zagreb, UNI Tuzla)
ANISOVICH	13B	EPJ A49 67	A.V. Anisovich et al.	
ANISOVICH	12A	EPJ A48 15	A.V. Anisovich et al.	(BONN, PNPI)
SHRESTHA	12A	PR C86 055203	M. Shrestha, D.M. Manley	(KSU)
BATINIC	10	PR C82 038203	M. Batinic et al.	(ZAGR)
WILLIAMS	09	PR C80 065209	M. Williams et al.	(JLab CLAS Collab.)
ARNDT	06	PR C74 045205	R.A. Arndt et al.	(GWU)
VRANA	00	PRPL 328 181	T.P. Vrana, S.A. Dytman, T.-S.H. Lee	(PITT, ANL)
HOEHLER	93	πN Newsletter 9 1	G. Hoehler	(KARL)
CUTKOSKY	80	Toronto Conf. 19	R.E. Cutkosky et al.	(CMU, LBL) IUP
Also		PR D20 2839	R.E. Cutkosky et al.	(CMU, LBL) IUP
HOEHLER	79	PDAT 12-1	G. Hoehler et al.	(KARLT) IUP
Also		Toronto Conf. 3	R. Koch	(KARLT) IUP

 $N(2220) 9/2^+$

$$I(J^P) = \frac{1}{2}(\frac{9}{2}^+) \text{ Status: } ***$$

Older and obsolete values are listed and referenced in the 2014 edition, Chinese Physics **C38** 070001 (2014). **$N(2220)$ POLE POSITION****REAL PART**

VALUE (MeV)	DOCUMENT ID	TECN	COMMENT
2130 to 2200 (≈ 2150) OUR ESTIMATE			
2131 ± 6	ROENCHEN	22	DPWA Multichannel
2127 ± 3 ± 24	¹ SVARC	14	L+P $\pi N \rightarrow \pi N$
2150 ± 35	ANISOVICH	12A	DPWA Multichannel
2160 ± 80	CUTKOSKY	80	IPWA $\pi N \rightarrow \pi N$
• • • We do not use the following data for averages, fits, limits, etc. • • •			
2171	ROENCHEN	15A	DPWA Multichannel
2199	ARNDT	06	DPWA $\pi N \rightarrow \pi N, \eta N$
2135	HOEHLER	93	ARGD $\pi N \rightarrow \pi N$

¹ Fit to the amplitudes of HOEHLER 79.**-2xIMAGINARY PART**

VALUE (MeV)	DOCUMENT ID	TECN	COMMENT
360 to 480 (≈ 400) OUR ESTIMATE			
388 ± 6	ROENCHEN	22	DPWA Multichannel
380 ± 7 ± 22	¹ SVARC	14	L+P $\pi N \rightarrow \pi N$
440 ± 40	ANISOVICH	12A	DPWA Multichannel
480 ± 100	CUTKOSKY	80	IPWA $\pi N \rightarrow \pi N$
• • • We do not use the following data for averages, fits, limits, etc. • • •			
593	ROENCHEN	15A	DPWA Multichannel
372	ARNDT	06	DPWA $\pi N \rightarrow \pi N, \eta N$
400	HOEHLER	93	ARGD $\pi N \rightarrow \pi N$

¹ Fit to the amplitudes of HOEHLER 79. **$N(2220)$ ELASTIC POLE RESIDUE****MODULUS $|r|$**

VALUE (MeV)	DOCUMENT ID	TECN	COMMENT
35 to 60 (≈ 45) OUR ESTIMATE			
48 ± 5	ROENCHEN	22	DPWA Multichannel
38 ± 1 ± 5	¹ SVARC	14	L+P $\pi N \rightarrow \pi N$
60 ± 12	ANISOVICH	12A	DPWA Multichannel
45 ± 20	CUTKOSKY	80	IPWA $\pi N \rightarrow \pi N$
• • • We do not use the following data for averages, fits, limits, etc. • • •			
62	ROENCHEN	15A	DPWA Multichannel
33	ARNDT	06	DPWA $\pi N \rightarrow \pi N, \eta N$
40	HOEHLER	93	ARGD $\pi N \rightarrow \pi N$

¹ Fit to the amplitudes of HOEHLER 79.**PHASE θ**

VALUE ($^\circ$)	DOCUMENT ID	TECN	COMMENT
-60 to -10 (≈ -40) OUR ESTIMATE			
-13 ± 2	ROENCHEN	22	DPWA Multichannel
-52 ± 1 ± 14	¹ SVARC	14	L+P $\pi N \rightarrow \pi N$
-58 ± 12	ANISOVICH	12A	DPWA Multichannel
-45 ± 25	CUTKOSKY	80	IPWA $\pi N \rightarrow \pi N$
• • • We do not use the following data for averages, fits, limits, etc. • • •			
-59	ROENCHEN	15A	DPWA Multichannel
-33	ARNDT	06	DPWA $\pi N \rightarrow \pi N, \eta N$
-50	HOEHLER	93	ARGD $\pi N \rightarrow \pi N$

¹ Fit to the amplitudes of HOEHLER 79. **$N(2220)$ INELASTIC POLE RESIDUE**The "normalized residue" is the residue divided by $\Gamma_{\text{pole}}/2$.**Normalized residue in $N\pi \rightarrow N(2220) \rightarrow N\eta$**

MODULUS	PHASE ($^\circ$)	DOCUMENT ID	TECN	COMMENT
0.042 ± 0.006	-48 ± 2	ROENCHEN	22	DPWA Multichannel
• • • We do not use the following data for averages, fits, limits, etc. • • •				
0.004	-101	ROENCHEN	15A	DPWA Multichannel

Baryon Particle Listings

 $N(2220)$, $N(2250)$ Normalized residue in $N\pi \rightarrow N(2220) \rightarrow \Lambda K$

MODULUS	PHASE (°)	DOCUMENT ID	TECN	COMMENT
0.020 ± 0.003	-60 ± 2	ROENCHEN 22	DPWA	Multichannel
••• We do not use the following data for averages, fits, limits, etc. •••				
0.007	62	ROENCHEN 15A	DPWA	Multichannel

Normalized residue in $N\pi \rightarrow N(2220) \rightarrow \Sigma K$

MODULUS	PHASE (°)	DOCUMENT ID	TECN	COMMENT
0.003 ± 0.008	-70 ± 2	ROENCHEN 22	DPWA	Multichannel
••• We do not use the following data for averages, fits, limits, etc. •••				
0.009	-128	ROENCHEN 15A	DPWA	Multichannel

 $N(2220)$ BREIT-WIGNER MASS

VALUE (MeV)	DOCUMENT ID	TECN	COMMENT
2200 to 2300 (≈ 2250) OUR ESTIMATE			
2316.3 ± 2.9	¹ ARNDT 06	DPWA	$\pi N \rightarrow \pi N, \eta N$
2230 ± 80	CUTKOSKY 80	IPWA	$\pi N \rightarrow \pi N$
2205 ± 10	HOEHLER 79	IPWA	$\pi N \rightarrow \pi N$

¹ Statistical error only. $N(2220)$ BREIT-WIGNER WIDTH

VALUE (MeV)	DOCUMENT ID	TECN	COMMENT
350 to 500 (≈ 400) OUR ESTIMATE			
633 ± 17	¹ ARNDT 06	DPWA	$\pi N \rightarrow \pi N, \eta N$
500 ± 150	CUTKOSKY 80	IPWA	$\pi N \rightarrow \pi N$
365 ± 30	HOEHLER 79	IPWA	$\pi N \rightarrow \pi N$

¹ Statistical error only. $N(2220)$ DECAY MODES

The following branching fractions are our estimates, not fits or averages.

Mode	Fraction (Γ_i/Γ)
Γ_1 $N\pi$	15–30 %

 $N(2220)$ BRANCHING RATIOS

$\Gamma(N\pi)/\Gamma_{\text{total}}$	DOCUMENT ID	TECN	COMMENT	Γ_1/Γ
15 to 30 (≈ 25) OUR ESTIMATE				
24 ± 5	ANISOVICH 12A	DPWA	Multichannel	
24.6 ± 0.1	¹ ARNDT 06	DPWA	$\pi N \rightarrow \pi N, \eta N$	
15 ± 3	CUTKOSKY 80	IPWA	$\pi N \rightarrow \pi N$	
18.0 ± 1.5	HOEHLER 79	IPWA	$\pi N \rightarrow \pi N$	

¹ Statistical error only. $N(2220)$ PHOTON DECAY AMPLITUDES AT THE POLE $N(2220) \rightarrow p\gamma$, helicity-1/2 amplitude $A_{1/2}$

MODULUS (GeV ^{-1/2})	PHASE (°)	DOCUMENT ID	TECN	COMMENT
0.357 ± 0.020	-91 ± 4	ROENCHEN 22	DPWA	Multichannel
••• We do not use the following data for averages, fits, limits, etc. •••				
0.135	114	ROENCHEN 15A	DPWA	Multichannel

 $N(2220) \rightarrow p\gamma$, helicity-3/2 amplitude $A_{3/2}$

MODULUS (GeV ^{-1/2})	PHASE (°)	DOCUMENT ID	TECN	COMMENT
-0.273 ± 0.025	-102 ± 3	ROENCHEN 22	DPWA	Multichannel
••• We do not use the following data for averages, fits, limits, etc. •••				
0.082	-41	ROENCHEN 15A	DPWA	Multichannel

 $N(2220)$ REFERENCESFor early references, see Physics Letters **111B** 1 (1982).

ROENCHEN 22	EPJ A58 229	D. Roenchen et al.	(JULI, GWU, BONN+)
ROENCHEN 15A	EPJ A51 70	D. Roenchen et al.	
PDG 14	CP C38 070001	K. Olive et al.	(PDG Collab.)
SVARC 14	PR C69 045205	A. Svare et al.	(RBI Zagreb, UNI Tuzla)
ANISOVICH 12A	EPJ A48 15	A.V. Anisovich et al.	(BONN, PNPI)
ARNDT 06	PR C74 045205	R.A. Arndt et al.	(GWU)
HOEHLER 93	πN Newsletter 9 1	G. Höhler	(KARL)
CUTKOSKY 80	Toronto Conf. 19	R.E. Cutkosky et al.	(CMU, LBL) IJP
Also	PR D20 2839	R.E. Cutkosky et al.	(CMU, LBL) IJP
HOEHLER 79	PDAT 12-1	G. Höhler et al.	(KARLT) IJP
Also	Toronto Conf. 3	R. Koch	(KARLT) IJP

 $N(2250) 9/2^-$

$$I(J^P) = \frac{1}{2} \left(\frac{9}{2}^-\right) \text{ Status: } ***$$

Older and obsolete values are listed and referenced in the 2014 edition, Chinese Physics **C38** 070001 (2014). $N(2250)$ POLE POSITION

REAL PART

VALUE (MeV)	DOCUMENT ID	TECN	COMMENT
2100 to 2200 (≈ 2150) OUR ESTIMATE			
2095 ± 10	ROENCHEN 22	DPWA	Multichannel
2195 ± 45	AFZAL 20	DPWA	Multichannel
$2157 \pm 3 \pm 14$	¹ SVARC 14	L+P	$\pi N \rightarrow \pi N$
2195 ± 45	ANISOVICH 12A	DPWA	Multichannel
2150 ± 50	CUTKOSKY 80	IPWA	$\pi N \rightarrow \pi N$
••• We do not use the following data for averages, fits, limits, etc. •••			
2127	HUNT 19	DPWA	Multichannel
2062	ROENCHEN 15A	DPWA	Multichannel
2217	ARNDT 06	DPWA	$\pi N \rightarrow \pi N, \eta N$
2187	HOEHLER 93	SPED	$\pi N \rightarrow \pi N$

¹ Fit to the amplitudes of HOEHLER 79.

-2×IMAGINARY PART

VALUE (MeV)	DOCUMENT ID	TECN	COMMENT
350 to 500 (≈ 420) OUR ESTIMATE			
422 ± 13	ROENCHEN 22	DPWA	Multichannel
470 ± 50	AFZAL 20	DPWA	Multichannel
$412 \pm 7 \pm 44$	¹ SVARC 14	L+P	$\pi N \rightarrow \pi N$
470 ± 50	ANISOVICH 12A	DPWA	Multichannel
360 ± 100	CUTKOSKY 80	IPWA	$\pi N \rightarrow \pi N$
••• We do not use the following data for averages, fits, limits, etc. •••			
262	HUNT 19	DPWA	Multichannel
403	ROENCHEN 15A	DPWA	Multichannel
431	ARNDT 06	DPWA	$\pi N \rightarrow \pi N, \eta N$
388	HOEHLER 93	SPED	$\pi N \rightarrow \pi N$

¹ Fit to the amplitudes of HOEHLER 79. $N(2250)$ ELASTIC POLE RESIDUEMODULUS $|r|$

VALUE (MeV)	DOCUMENT ID	TECN	COMMENT
15 to 30 (≈ 25) OUR ESTIMATE			
14 ± 1	ROENCHEN 22	DPWA	Multichannel
$24 \pm 1 \pm 5$	¹ SVARC 14	L+P	$\pi N \rightarrow \pi N$
26 ± 5	ANISOVICH 12A	DPWA	Multichannel
20 ± 6	CUTKOSKY 80	IPWA	$\pi N \rightarrow \pi N$
••• We do not use the following data for averages, fits, limits, etc. •••			
8.2	ROENCHEN 15A	DPWA	Multichannel
21	ARNDT 06	DPWA	$\pi N \rightarrow \pi N, \eta N$
21	HOEHLER 93	SPED	$\pi N \rightarrow \pi N$

¹ Fit to the amplitudes of HOEHLER 79.PHASE θ

VALUE (°)	DOCUMENT ID	TECN	COMMENT
-60 to -20 (≈ -40) OUR ESTIMATE			
-67 ± 9	ROENCHEN 22	DPWA	Multichannel
$-62 \pm 1 \pm 11$	¹ SVARC 14	L+P	$\pi N \rightarrow \pi N$
-38 ± 25	ANISOVICH 12A	DPWA	Multichannel
-50 ± 20	CUTKOSKY 80	IPWA	$\pi N \rightarrow \pi N$
••• We do not use the following data for averages, fits, limits, etc. •••			
-64	ROENCHEN 15A	DPWA	Multichannel
-20	ARNDT 06	DPWA	$\pi N \rightarrow \pi N, \eta N$

¹ Fit to the amplitudes of HOEHLER 79. $N(2250)$ INELASTIC POLE RESIDUEThe "normalized residue" is the residue divided by $\Gamma_{\text{pole}}/2$.Normalized residue in $N\pi \rightarrow N(2250) \rightarrow N\eta$

MODULUS	PHASE (°)	DOCUMENT ID	TECN	COMMENT
0.018 ± 0.001	-89 ± 5	ROENCHEN 22	DPWA	Multichannel
••• We do not use the following data for averages, fits, limits, etc. •••				
0.017	-89	ROENCHEN 15A	DPWA	Multichannel

Normalized residue in $N\pi \rightarrow N(2250) \rightarrow \Lambda K$

MODULUS	PHASE (°)	DOCUMENT ID	TECN	COMMENT
0.003 ± 0.001	80 ± 5	ROENCHEN 22	DPWA	Multichannel
••• We do not use the following data for averages, fits, limits, etc. •••				
0.006	-101	ROENCHEN 15A	DPWA	Multichannel

See key on page 1171

Baryon Particle Listings

$N(2250)$, $N(2300)$, $N(2570)$, $N(2600)$

Normalized residue in $N\pi \rightarrow N(2250) \rightarrow \Sigma K$

MODULUS	PHASE (°)	DOCUMENT ID	TECN	COMMENT
0.004 ± 0.002	-111 ± 5	ROENCHEN 22	DPWA	Multichannel
••• We do not use the following data for averages, fits, limits, etc. •••				
0.002	70	ROENCHEN 15A	DPWA	Multichannel

 $N(2250)$ BREIT-WIGNER MASS

VALUE (MeV)	DOCUMENT ID	TECN	COMMENT
2250 to 2320 (≈ 2280) OUR ESTIMATE			
2200 ± 10	¹ HUNT 19	DPWA	Multichannel
2280 ± 40	ANISOVICH 12A	DPWA	Multichannel
2302 ± 6	¹ ARNDT 06	DPWA	$\pi N \rightarrow \pi N, \eta N$
2250 ± 80	CUTKOSKY 80	IPWA	$\pi N \rightarrow \pi N$
2268 ± 15	HOEHLER 79	IPWA	$\pi N \rightarrow \pi N$
¹ Statistical error only.			

 $N(2250)$ BREIT-WIGNER WIDTH

VALUE (MeV)	DOCUMENT ID	TECN	COMMENT
300 to 600 (≈ 500) OUR ESTIMATE			
343 ± 51	¹ HUNT 19	DPWA	Multichannel
520 ± 50	ANISOVICH 12A	DPWA	Multichannel
628 ± 28	¹ ARNDT 06	DPWA	$\pi N \rightarrow \pi N, \eta N$
480 ± 120	CUTKOSKY 80	IPWA	$\pi N \rightarrow \pi N$
300 ± 40	HOEHLER 79	IPWA	$\pi N \rightarrow \pi N$
¹ Statistical error only.			

 $N(2250)$ DECAY MODES

The following branching fractions are our estimates, not fits or averages.

Mode	Fraction (Γ_i/Γ)
Γ_1 $N\pi$	5–15 %
Γ_2 $N\eta$	<5 %
Γ_3 ΛK	1–3 %

 $N(2250)$ BRANCHING RATIOS

$\Gamma(N\pi)/\Gamma_{\text{total}}$	DOCUMENT ID	TECN	COMMENT	Γ_1/Γ
5–15 % OUR ESTIMATE				
8.5 ± 0.4	¹ HUNT 19	DPWA	Multichannel	
12 ± 4	ANISOVICH 12A	DPWA	Multichannel	
8.9 ± 0.1	¹ ARNDT 06	DPWA	$\pi N \rightarrow \pi N, \eta N$	
10 ± 2	CUTKOSKY 80	IPWA	$\pi N \rightarrow \pi N$	
10 ± 2	HOEHLER 79	IPWA	$\pi N \rightarrow \pi N$	
¹ Statistical error only.				

$\Gamma(N\eta)/\Gamma_{\text{total}}$	DOCUMENT ID	TECN	COMMENT	Γ_2/Γ
<5 % OUR ESTIMATE				
<5	¹ HUNT 19	DPWA	Multichannel	
¹ Statistical error only.				

$\Gamma(\Lambda K)/\Gamma_{\text{total}}$	DOCUMENT ID	TECN	COMMENT	Γ_3/Γ
1–3 % OUR ESTIMATE				
2.0 ± 0.6	¹ HUNT 19	DPWA	Multichannel	
¹ Statistical error only.				

 $N(2250)$ PHOTON DECAY AMPLITUDES AT THE POLE **$N(2250) \rightarrow p\gamma$, helicity-1/2 amplitude $A_{1/2}$**

MODULUS ($\text{GeV}^{-1/2}$)	PHASE (°)	DOCUMENT ID	TECN	COMMENT
-0.108 ± 0.007	112 ± 4	ROENCHEN 22	DPWA	Multichannel
••• We do not use the following data for averages, fits, limits, etc. •••				
0.026	-26	ROENCHEN 15A	DPWA	Multichannel

 $N(2250) \rightarrow p\gamma$, helicity-3/2 amplitude $A_{3/2}$

MODULUS ($\text{GeV}^{-1/2}$)	PHASE (°)	DOCUMENT ID	TECN	COMMENT
0.050 ± 0.011	69 ± 8	ROENCHEN 22	DPWA	Multichannel
••• We do not use the following data for averages, fits, limits, etc. •••				
0.119	-42	ROENCHEN 15A	DPWA	Multichannel

 $N(2250)$ BREIT-WIGNER PHOTON DECAY AMPLITUDES **$N(2250) \rightarrow p\gamma$, helicity-1/2 amplitude $A_{1/2}$**

VALUE ($\text{GeV}^{-1/2}$)	DOCUMENT ID	TECN	COMMENT
0.0006 ± 0.0037	¹ HUNT 19	DPWA	Multichannel
¹ Statistical error only.			

 $N(2250) \rightarrow p\gamma$, helicity-3/2 amplitude $A_{3/2}$

VALUE ($\text{GeV}^{-1/2}$)	DOCUMENT ID	TECN	COMMENT
0.013 ± 0.004	¹ HUNT 19	DPWA	Multichannel
¹ Statistical error only.			

 $N(2250)$ REFERENCES

ROENCHEN 22	EPJ A58 229	D. Roenchen et al.	(JULI, GWU, BONN+)
AFZAL 20	PRL 125 152002	F. Afzal et al.	(CBELSA/TAPS Collab.)
HUNT 19	PR C99 055205	B.C. Hunt, D.M. Manley	
ROENCHEN 15A	EPJ A51 70	D. Roenchen et al.	
PDG 14	CP C38 070001	K. Olive et al.	(PDG Collab.)
SVARC 14	PR C89 045205	A. Svarc et al.	(RBI Zagreb, UNI Tuzla)
ANISOVICH 12A	EPJ A48 15	A.V. Anisovich et al.	(BONN, PMP)
ARNDT 06	PR C74 045205	R.A. Arndt et al.	(GWU)
HOEHLER 93	πN Newsletter 9 1	G. Hohlner	(KARL)
CUTKOSKY 80	Toronto Conf. 19	R.E. Cutkosky et al.	(CMU, LBL) IJP
Also	PR D20 2839	R.E. Cutkosky et al.	(CMU, LBL) IJP
HOEHLER 79	PDAT 12-1	G. Hohlner et al.	(KARL) IJP
Also	Toronto Conf. 3	R. Koch	(KARL) IJP

 $N(2300) 1/2^+$ $I(J^P) = \frac{1}{2}(\frac{1}{2}^+)$ Status: **

OMITTED FROM SUMMARY TABLE

 $N(2300)$ MASS

VALUE (MeV)	DOCUMENT ID	TECN	COMMENT
$2300^{+40+109}_{-30-0}$	ABLIKIM 13A	BES3	$\psi(2S) \rightarrow p\bar{p}\pi^0$

 $N(2300)$ WIDTH

VALUE (MeV)	DOCUMENT ID	TECN	COMMENT
$340 \pm 30^{+110}_{-58}$	ABLIKIM 13A	BES3	$\psi(2S) \rightarrow p\bar{p}\pi^0$

 $N(2300)$ REFERENCES

ABLIKIM 13A	PRL 110 022001	M. Ablikim et al.	(BESIII Collab.)
-------------	----------------	-------------------	------------------

 $N(2570) 5/2^-$ $I(J^P) = \frac{1}{2}(\frac{5}{2}^-)$ Status: **

OMITTED FROM SUMMARY TABLE

 $N(2570)$ MASS

VALUE (MeV)	DOCUMENT ID	TECN	COMMENT
2570^{+19+34}_{-10-10}	ABLIKIM 13A	BES3	$\psi(2S) \rightarrow p\bar{p}\pi^0$

 $N(2570)$ WIDTH

VALUE (MeV)	DOCUMENT ID	TECN	COMMENT
250^{+14+69}_{-24-21}	ABLIKIM 13A	BES3	$\psi(2S) \rightarrow p\bar{p}\pi^0$

 $N(2570)$ REFERENCES

ABLIKIM 13A	PRL 110 022001	M. Ablikim et al.	(BESIII Collab.)
-------------	----------------	-------------------	------------------

 $N(2600) 11/2^-$ $I(J^P) = \frac{1}{2}(\frac{11}{2}^-)$ Status: ** **$N(2600)$ BREIT-WIGNER MASS**

VALUE (MeV)	DOCUMENT ID	TECN	COMMENT
2550 to 2750 (≈ 2600) OUR ESTIMATE			
2623 ± 197	ARNDT 06	DPWA	$\pi N \rightarrow \pi N, \eta N$
2577 ± 50	HOEHLER 79	IPWA	$\pi N \rightarrow \pi N$

Baryon Particle Listings

 $N(2600)$, $N(2700)$, $N(\sim 3000)$ $N(2600)$ BREIT-WIGNER WIDTH

VALUE (MeV)	DOCUMENT ID	TECN	COMMENT
500 to 800 (≈ 650) OUR ESTIMATE			
1311 \pm 996	ARNDT	06	DPWA $\pi N \rightarrow \pi N, \eta N$
400 \pm 100	HOEHLER	79	IPWA $\pi N \rightarrow \pi N$

 $N(2600)$ DECAY MODES

Mode	Fraction (Γ_i/Γ)
Γ_1 $N\pi$	3-8 %

 $N(2600)$ BRANCHING RATIOS

$\Gamma(N\pi)/\Gamma_{\text{total}}$	DOCUMENT ID	TECN	COMMENT	Γ_1/Γ
3 to 8 (≈ 5) OUR ESTIMATE				
5.0 \pm 1.8	ARNDT	06	DPWA $\pi N \rightarrow \pi N, \eta N$	
5 \pm 1	HOEHLER	79	IPWA $\pi N \rightarrow \pi N$	

 $N(2600)$ REFERENCES

ARNDT	06	PR C74 045205	R.A. Arndt et al.	(GWU)
HOEHLER	79	PDAT 12-1	G. Hohler et al.	(KARLT) IJP
Also		Toronto Conf. 3	R. Koch	(KARLT) IJP

 $N(2700) 13/2^+$

$$I(J^P) = \frac{1}{2}(13^+) \text{ Status: } **$$

OMITTED FROM SUMMARY TABLE

 $N(2700)$ BREIT-WIGNER MASS

VALUE (MeV)	DOCUMENT ID	TECN	COMMENT
2612 \pm 45	HOEHLER	79	IPWA $\pi N \rightarrow \pi N$

 $N(2700)$ BREIT-WIGNER WIDTH

VALUE (MeV)	DOCUMENT ID	TECN	COMMENT
350 \pm 50	HOEHLER	79	IPWA $\pi N \rightarrow \pi N$

 $N(2700)$ DECAY MODES

Mode	Fraction (Γ_i/Γ)
Γ_1 $N\pi$	3-5 %

 $N(2700)$ BRANCHING RATIOS

$\Gamma(N\pi)/\Gamma_{\text{total}}$	DOCUMENT ID	TECN	COMMENT	Γ_1/Γ
4 \pm 1	HOEHLER	79	IPWA $\pi N \rightarrow \pi N$	

 $N(2700)$ REFERENCES

HOEHLER	79	PDAT 12-1	G. Hohler et al.	(KARLT) IJP
Also		Toronto Conf. 3	R. Koch	(KARLT) IJP

 $N(\sim 3000)$ Region
Partial-Wave Analyses

OMITTED FROM SUMMARY TABLE

We list here miscellaneous high-mass candidates for isospin-1/2 resonances found in partial-wave analyses.

Our 1982 edition had an $N(3245)$, an $N(3690)$, and an $N(3755)$, each a narrow peak seen in a production experiment. Since nothing has been heard from them since the 1960's, we declare them to be dead. There was also an $N(3030)$, deduced from total cross-section and 180° elastic cross-section measurements; it is the KOCH 80 $L_{1,15}$ state below.

 $N(\sim 3000)$ BREIT-WIGNER MASS

VALUE (MeV)	DOCUMENT ID	TECN	COMMENT
≈ 3000 OUR ESTIMATE			
2600	KOCH	80	IPWA $\pi N \rightarrow \pi N D_{13}$
3100	KOCH	80	IPWA $\pi N \rightarrow \pi N L_{1,15}$ wave
3500	KOCH	80	IPWA $\pi N \rightarrow \pi N M_{1,17}$ wave
3500 to 4000	KOCH	80	IPWA $\pi N \rightarrow \pi N N_{1,19}$ wave
3500 \pm 200	HENDRY	78	MPWA $\pi N \rightarrow \pi N L_{1,15}$ wave
3800 \pm 200	HENDRY	78	MPWA $\pi N \rightarrow \pi N M_{1,17}$ wave
4100 \pm 200	HENDRY	78	MPWA $\pi N \rightarrow \pi N N_{1,19}$ wave

 $N(\sim 3000)$ BREIT-WIGNER WIDTH

VALUE (MeV)	DOCUMENT ID	TECN	COMMENT
1300 \pm 200	HENDRY	78	MPWA $\pi N \rightarrow \pi N L_{1,15}$ wave
1600 \pm 200	HENDRY	78	MPWA $\pi N \rightarrow \pi N M_{1,17}$ wave
1900 \pm 300	HENDRY	78	MPWA $\pi N \rightarrow \pi N N_{1,19}$ wave

 $N(\sim 3000)$ DECAY MODES

Mode	Fraction (Γ_i/Γ)
Γ_1 $N\pi$	2-8 %

 $N(\sim 3000)$ BRANCHING RATIOS

$\Gamma(N\pi)/\Gamma_{\text{total}}$	DOCUMENT ID	TECN	COMMENT	Γ_1/Γ
2-8 % OUR ESTIMATE				
6 \pm 2	HENDRY	78	MPWA $\pi N \rightarrow \pi N L_{1,15}$ wave	
4.0 \pm 1.5	HENDRY	78	MPWA $\pi N \rightarrow \pi N M_{1,17}$ wave	
3.0 \pm 1.5	HENDRY	78	MPWA $\pi N \rightarrow \pi N N_{1,19}$ wave	

 $N(\sim 3000)$ REFERENCES

KOCH	80	Toronto Conf. 3	R. Koch	(KARLT) IJP
HENDRY	78	PRL 41 222	A.W. Hendry	(IND, LBL) IJP
Also		ANP 136 1	A.W. Hendry	(IND) IJP

See key on page 1171

Baryon Particle Listings

 $\Delta(1232)$ Δ BARYONS
($S = 0, I = 3/2$)

$$\Delta^{++} = uuu, \Delta^+ = uud, \Delta^0 = udd, \Delta^- = ddd$$

 $\Delta(1232) 3/2^+$

$$I(J^P) = \frac{3}{2}(\frac{3}{2}^+) \text{ Status: } ****$$

Older and obsolete values are listed and referenced in the 2014 edition, Chinese Physics C38 070001 (2014).

 $\Delta(1232)$ POLE POSITIONS

REAL PART, MIXED CHARGES

VALUE (MeV)	DOCUMENT ID	TECN	COMMENT
1209 to 1211 (≈ 1210) OUR ESTIMATE			
1211 $\pm 1 \pm 1$	¹ SVARC 14	L+P	$\pi N \rightarrow \pi N$
1210.5 ± 1.0	ANISOVICH 12A	DPWA	Multichannel
1210 ± 1	CUTKOSKY 80	IPWA	$\pi N \rightarrow \pi N$
••• We do not use the following data for averages, fits, limits, etc. •••			
1215 ± 1	ROENCHEN 22	DPWA	Multichannel
1212.4	HUNT 19	DPWA	Multichannel
1218	ROENCHEN 15A	DPWA	Multichannel
1211 ± 1	ANISOVICH 10	DPWA	Multichannel
1211	ARNDT 06	DPWA	$\pi N \rightarrow \pi N, \eta N$
1210	ARNDT 04	DPWA	$\pi N \rightarrow \pi N, \eta N$
1209	² HOEHLER 93	ARGD	$\pi N \rightarrow \pi N$

¹ Fit to the amplitudes of HOEHLER 79.² See HOEHLER 93 for a detailed discussion of the evidence for and the pole parameters of N and Δ resonances as determined from Argand diagrams of πN elastic partial-wave amplitudes and from plots of the speeds with which the amplitudes traverse the diagrams. $-2\times$ IMAGINARY PART, MIXED CHARGES

VALUE (MeV)	DOCUMENT ID	TECN	COMMENT
98 to 102 (≈ 100) OUR ESTIMATE			
93 ± 1	ROENCHEN 22	DPWA	Multichannel
98 $\pm 2 \pm 1$	¹ SVARC 14	L+P	$\pi N \rightarrow \pi N$
99 ± 2	ANISOVICH 12A	DPWA	Multichannel
100 ± 2	CUTKOSKY 80	IPWA	$\pi N \rightarrow \pi N$
••• We do not use the following data for averages, fits, limits, etc. •••			
96.8	HUNT 19	DPWA	Multichannel
92	ROENCHEN 15A	DPWA	Multichannel
100 ± 2	ANISOVICH 10	DPWA	Multichannel
99	ARNDT 06	DPWA	$\pi N \rightarrow \pi N, \eta N$
100	ARNDT 04	DPWA	$\pi N \rightarrow \pi N, \eta N$
100	² HOEHLER 93	ARGD	$\pi N \rightarrow \pi N$

¹ Fit to the amplitudes of HOEHLER 79.² See HOEHLER 93 for a detailed discussion of the evidence for and the pole parameters of N and Δ resonances as determined from Argand diagrams of πN elastic partial-wave amplitudes and from plots of the speeds with which the amplitudes traverse the diagrams.REAL PART, $\Delta(1232)^{++}$

VALUE (MeV)	DOCUMENT ID	COMMENT
••• We do not use the following data for averages, fits, limits, etc. •••		
1212.50 ± 0.24	BERNICA 96	Fit to PEDRONI 78

 $-2\times$ IMAGINARY PART, $\Delta(1232)^{++}$

VALUE (MeV)	DOCUMENT ID	COMMENT
••• We do not use the following data for averages, fits, limits, etc. •••		
97.37 ± 0.42	BERNICA 96	Fit to PEDRONI 78

REAL PART, $\Delta(1232)^+$

VALUE (MeV)	DOCUMENT ID	TECN	COMMENT
••• We do not use the following data for averages, fits, limits, etc. •••			
1211 ± 1 to 1212 ± 1	HANSTEIN 96	DPWA	$\gamma N \rightarrow \pi N$
1206.9 ± 0.9 to 1210.5 ± 1.8	MIROSHNIC... 79		Fit photoproduction

 $-2\times$ IMAGINARY PART, $\Delta(1232)^+$

VALUE (MeV)	DOCUMENT ID	TECN	COMMENT
••• We do not use the following data for averages, fits, limits, etc. •••			
102 ± 2 to 99 ± 2	¹ HANSTEIN 96	DPWA	$\gamma N \rightarrow \pi N$
111.2 ± 2.0 to 116.6 ± 2.2	MIROSHNIC... 79		Fit photoproduction

¹ The second (lower) value of HANSTEIN 96 here goes with the second (higher) value of the real part in the preceding data block.REAL PART, $\Delta(1232)^0$

VALUE (MeV)	DOCUMENT ID	COMMENT
••• We do not use the following data for averages, fits, limits, etc. •••		
1213.20 ± 0.66	BERNICA 96	Fit to PEDRONI 78

 $-2\times$ IMAGINARY PART, $\Delta(1232)^0$

VALUE (MeV)	DOCUMENT ID	COMMENT
••• We do not use the following data for averages, fits, limits, etc. •••		
104.10 ± 1.01	BERNICA 96	Fit to PEDRONI 78

 $\Delta(1232)$ ELASTIC POLE RESIDUES

ABSOLUTE VALUE, MIXED CHARGES

VALUE (MeV)	DOCUMENT ID	TECN	COMMENT
49 to 52 (≈ 50) OUR ESTIMATE			
50 ± 1	ROENCHEN 22	DPWA	Multichannel
50 $\pm 1 \pm 1$	¹ SVARC 14	L+P	$\pi N \rightarrow \pi N$
51.6 ± 0.6	ANISOVICH 12A	DPWA	Multichannel
53 ± 2	CUTKOSKY 80	IPWA	$\pi N \rightarrow \pi N$
••• We do not use the following data for averages, fits, limits, etc. •••			
46	ROENCHEN 15A	DPWA	Multichannel
52	ARNDT 06	DPWA	$\pi N \rightarrow \pi N, \eta N$
53	ARNDT 04	DPWA	$\pi N \rightarrow \pi N, \eta N$
50	HOEHLER 93	ARGD	$\pi N \rightarrow \pi N$

PHASE, MIXED CHARGES

VALUE ($^\circ$)	DOCUMENT ID	TECN	COMMENT
-48 to -45 (≈ -46) OUR ESTIMATE			
-39 ± 1	ROENCHEN 22	DPWA	Multichannel
-46 $\pm 1 \pm 1$	¹ SVARC 14	L+P	$\pi N \rightarrow \pi N$
-46 ± 1	ANISOVICH 12A	DPWA	Multichannel
-47 ± 1	CUTKOSKY 80	IPWA	$\pi N \rightarrow \pi N$
••• We do not use the following data for averages, fits, limits, etc. •••			
-36	ROENCHEN 15A	DPWA	Multichannel
-47	ARNDT 06	DPWA	$\pi N \rightarrow \pi N, \eta N$
-47	ARNDT 04	DPWA	$\pi N \rightarrow \pi N, \eta N$
-48	HOEHLER 93	ARGD	$\pi N \rightarrow \pi N$

¹ Fit to the amplitudes of HOEHLER 79. $\Delta(1232)$ BREIT-WIGNER MASSES

MIXED CHARGES

VALUE (MeV)	DOCUMENT ID	TECN	COMMENT
1230 to 1234 (≈ 1232) OUR ESTIMATE			
1230.8 ± 0.4	¹ HUNT 19	DPWA	Multichannel
1228 ± 2	ANISOVICH 12A	DPWA	Multichannel
1233.4 ± 0.4	¹ ARNDT 06	DPWA	$\pi N \rightarrow \pi N, \eta N$
1232 ± 3	CUTKOSKY 80	IPWA	$\pi N \rightarrow \pi N$
1233 ± 2	HOEHLER 79	IPWA	$\pi N \rightarrow \pi N$
••• We do not use the following data for averages, fits, limits, etc. •••			
1231.1 ± 0.2	¹ SHRESTHA 12A	DPWA	Multichannel
1230 ± 2	ANISOVICH 10	DPWA	Multichannel
1232.9 ± 1.2	ARNDT 04	DPWA	$\pi N \rightarrow \pi N, \eta N$
1228 ± 1	PENNER 02c	DPWA	Multichannel

¹ Statistical error only. $\Delta(1232)^{++}$ MASS

VALUE (MeV)	DOCUMENT ID	TECN	COMMENT
••• We do not use the following data for averages, fits, limits, etc. •••			
1230.55 ± 0.20	GRIDNEV 06	DPWA	$\pi N \rightarrow \pi N$
1231.88 ± 0.29	BERNICA 96		Fit to PEDRONI 78
1230.5 ± 0.2	ABAEV 95	IPWA	$\pi N \rightarrow \pi N$
1230.9 ± 0.3	KOCH 80b	IPWA	$\pi N \rightarrow \pi N$
1231.1 ± 0.2	PEDRONI 78		$\pi N \rightarrow \pi N$ 70-370 MeV

 $\Delta(1232)^+$ MASS

VALUE (MeV)	DOCUMENT ID	COMMENT
••• We do not use the following data for averages, fits, limits, etc. •••		
1234.9 ± 1.4	MIROSHNIC... 79	Fit photoproduction

 $\Delta(1232)^0$ MASS

VALUE (MeV)	DOCUMENT ID	TECN	COMMENT
••• We do not use the following data for averages, fits, limits, etc. •••			
1231.3 ± 0.6	BREITSCHOP... 06	CNTR	Using new CHEX data
1233.40 ± 0.22	GRIDNEV 06	DPWA	$\pi N \rightarrow \pi N$
1234.35 ± 0.75	BERNICA 96		Fit to PEDRONI 78
1233.1 ± 0.3	ABAEV 95	IPWA	$\pi N \rightarrow \pi N$
1233.6 ± 0.5	KOCH 80b	IPWA	$\pi N \rightarrow \pi N$
1233.8 ± 0.2	PEDRONI 78		$\pi N \rightarrow \pi N$ 70-370 MeV

 $m_{\Delta^0} - m_{\Delta^+}$

VALUE (MeV)	DOCUMENT ID	TECN	COMMENT
••• We do not use the following data for averages, fits, limits, etc. •••			
2.86 ± 0.30	GRIDNEV 06	DPWA	$\pi N \rightarrow \pi N$
2.25 ± 0.68	BERNICA 96		Fit to PEDRONI 78
2.6 ± 0.4	ABAEV 95	IPWA	$\pi N \rightarrow \pi N$
2.7 ± 0.3	¹ PEDRONI 78		See the masses

¹ Using $\pi^\pm d$ as well, PEDRONI 78 determine $(M^- - M^{++}) + (M^0 - M^+)/3 = 4.6 \pm 0.2$ MeV.

Baryon Particle Listings

 $\Delta(1232)$ $\Delta(1232)$ BREIT-WIGNER WIDTHS

MIXED CHARGES

VALUE (MeV)	DOCUMENT ID	TECN	COMMENT
114 to 120 (≈ 117) OUR ESTIMATE			
110.9 \pm 0.8	¹ HUNT	19	DPWA Multichannel
110 \pm 3	ANISOVICH	12A	DPWA Multichannel
118.7 \pm 0.6	¹ ARNDT	06	DPWA $\pi N \rightarrow \pi N, \eta N$
120 \pm 5	CUTKOSKY	80	IPWA $\pi N \rightarrow \pi N$
116 \pm 5	HOEHLER	79	IPWA $\pi N \rightarrow \pi N$
• • • We do not use the following data for averages, fits, limits, etc. • • •			
113.0 \pm 0.5	¹ SHRESTHA	12A	DPWA Multichannel
112 \pm 4	ANISOVICH	10	DPWA Multichannel
118.0 \pm 2.2	ARNDT	04	DPWA $\pi N \rightarrow \pi N, \eta N$
106 \pm 1	PENNER	02C	DPWA Multichannel

¹ Statistical error only. $\Delta(1232)^{++}$ WIDTH

VALUE (MeV)	DOCUMENT ID	TECN	COMMENT
• • • We do not use the following data for averages, fits, limits, etc. • • •			
112.2 \pm 0.7	GRIDNEV	06	DPWA $\pi N \rightarrow \pi N$
109.07 \pm 0.48	BERNICHIA	96	Fit to PEDRONI 78
111.0 \pm 1.0	KOCH	80B	IPWA $\pi N \rightarrow \pi N$
111.3 \pm 0.5	PEDRONI	78	$\pi N \rightarrow \pi N$ 70–370 MeV

 $\Delta(1232)^+$ WIDTH

VALUE (MeV)	DOCUMENT ID	COMMENT
• • • We do not use the following data for averages, fits, limits, etc. • • •		
131.1 \pm 2.4	MIROSHNIC...	79 Fit photoproduction

 $\Delta(1232)^0$ WIDTH

VALUE (MeV)	DOCUMENT ID	TECN	COMMENT
• • • We do not use the following data for averages, fits, limits, etc. • • •			
112.5 \pm 1.9	BREITSCHEP..06	CNTR	Using new CHEX data
116.9 \pm 0.7	GRIDNEV	06	DPWA $\pi N \rightarrow \pi N$
117.58 \pm 1.16	BERNICHIA	96	Fit to PEDRONI 78
113.0 \pm 1.5	KOCH	80B	IPWA $\pi N \rightarrow \pi N$
117.9 \pm 0.9	PEDRONI	78	$\pi N \rightarrow \pi N$ 70–370 MeV

 Δ^0 - Δ^{++} WIDTH DIFFERENCE

VALUE (MeV)	DOCUMENT ID	TECN	COMMENT
• • • We do not use the following data for averages, fits, limits, etc. • • •			
4.66 \pm 1.0	GRIDNEV	06	DPWA $\pi N \rightarrow \pi N$
8.45 \pm 1.11	BERNICHIA	96	Fit to PEDRONI 78
5.1 \pm 1.0	ABAEV	95	IPWA $\pi N \rightarrow \pi N$
6.6 \pm 1.0	PEDRONI	78	See the widths

 $\Delta(1232)$ DECAY MODES

The following branching fractions are our estimates, not fits or averages.

Mode	Fraction (Γ_j/Γ)
Γ_1 $N\pi$	99.4 %
Γ_2 $N\gamma$	0.55–0.65 %
Γ_3 $N\gamma$, helicity=1/2	0.11–0.13 %
Γ_4 $N\gamma$, helicity=3/2	0.44–0.52 %
Γ_5 $p e^+ e^-$	(4.2 \pm 0.7) $\times 10^{-5}$

 $\Delta(1232)$ BRANCHING RATIOS

$\Gamma(N\pi)/\Gamma_{\text{total}}$	DOCUMENT ID	TECN	COMMENT	Γ_1/Γ
0.994 OUR ESTIMATE				
0.9939 \pm 0.0001	¹ HUNT	19	DPWA Multichannel	
1.00	ARNDT	06	DPWA $\pi N \rightarrow \pi N, \eta N$	
1.0	CUTKOSKY	80	IPWA $\pi N \rightarrow \pi N$	
1.0	HOEHLER	79	IPWA $\pi N \rightarrow \pi N$	
• • • We do not use the following data for averages, fits, limits, etc. • • •				
0.994	SHRESTHA	12A	DPWA Multichannel	
1.0	ANISOVICH	10	DPWA Multichannel	
1.000	ARNDT	04	DPWA $\pi N \rightarrow \pi N, \eta N$	
1.00	PENNER	02C	DPWA Multichannel	

¹ Statistical error only.

$\Gamma(p e^+ e^-)/\Gamma_{\text{total}}$	DOCUMENT ID	COMMENT	Γ_5/Γ
4.19\pm0.34\pm0.62	¹ ADAMCZEW...17		

¹ The systematic uncertainty includes the model dependence. $\Delta(1232)$ PHOTON DECAY AMPLITUDES AT THE POLE $\Delta(1232) \rightarrow N\gamma$, helicity-1/2 amplitude $A_{1/2}$

MODULUS ($\text{GeV}^{-1/2}$)	PHASE ($^\circ$)	DOCUMENT ID	TECN	COMMENT
-0.126 \pm 0.002	-18 \pm 2	ROENCHEN	22	DPWA Multichannel
• • • We do not use the following data for averages, fits, limits, etc. • • •				
-0.117	-6.6	ROENCHEN	15A	DPWA Multichannel

 $\Delta(1232) \rightarrow N\gamma$, helicity-3/2 amplitude $A_{3/2}$

MODULUS ($\text{GeV}^{-1/2}$)	PHASE ($^\circ$)	DOCUMENT ID	TECN	COMMENT
-0.245 \pm 0.004	-0.7 \pm 0.9	ROENCHEN	22	DPWA Multichannel
• • • We do not use the following data for averages, fits, limits, etc. • • •				
-0.226	2.8	ROENCHEN	15A	DPWA Multichannel

 $\Delta(1232)$ BREIT-WIGNER PHOTON DECAY AMPLITUDESPapers on γN amplitudes predating 1981 may be found in our 2006 edition, Journal of Physics **G33** 1 (2006). $\Delta(1232) \rightarrow N\gamma$, helicity-1/2 amplitude $A_{1/2}$

VALUE ($\text{GeV}^{-1/2}$)	DOCUMENT ID	TECN	COMMENT
-0.142 to -0.129 (≈ -0.135) OUR ESTIMATE			
-0.146 \pm 0.002	¹ HUNT	19	DPWA Multichannel
-0.131 \pm 0.004	ANISOVICH	12A	DPWA Multichannel
-0.139 \pm 0.002	¹ WORKMAN	12A	DPWA $\gamma N \rightarrow N\pi$
-0.139 \pm 0.004	¹ DUGGER	07	DPWA $\gamma N \rightarrow \pi N$
-0.137 \pm 0.005	AHRENS	04A	DPWA $\tilde{\gamma}\tilde{p} \rightarrow N\pi$
-0.1357 \pm 0.0013 \pm 0.0037	BLANPIED	01	LEGS $\gamma p \rightarrow p\gamma, p\pi^0, n\pi^+$
-0.131 \pm 0.001	¹ BECK	00	IPWA $\tilde{\gamma}p \rightarrow p\pi^0, n\pi^+$
-0.140 \pm 0.005	KAMALOV	99	DPWA $\gamma N \rightarrow \pi N$
-0.1294 \pm 0.0013	HANSTEIN	98	IPWA $\gamma N \rightarrow \pi N$
-0.1278 \pm 0.0012	DAVIDSON	97	DPWA $\gamma N \rightarrow \pi N$
• • • We do not use the following data for averages, fits, limits, etc. • • •			
-0.137 \pm 0.001	¹ SHRESTHA	12A	DPWA Multichannel
-0.136 \pm 0.005	ANISOVICH	10	DPWA Multichannel
-0.140	DRECHSEL	07	DPWA $\gamma N \rightarrow \pi N$
-0.129 \pm 0.001	ARNDT	02	DPWA $\gamma p \rightarrow N\pi$
-0.128	PENNER	02D	DPWA Multichannel
-0.1312	HANSTEIN	98	DPWA $\gamma N \rightarrow \pi N$

¹ Statistical error only. $\Delta(1232) \rightarrow N\gamma$, helicity-3/2 amplitude $A_{3/2}$

VALUE ($\text{GeV}^{-1/2}$)	DOCUMENT ID	TECN	COMMENT
-0.262 to -0.248 (≈ -0.255) OUR ESTIMATE			
-0.250 \pm 0.002	¹ HUNT	19	DPWA Multichannel
-0.254 \pm 0.005	ANISOVICH	12A	DPWA Multichannel
-0.262 \pm 0.003	WORKMAN	12A	DPWA $\gamma N \rightarrow N\pi$
-0.258 \pm 0.005	DUGGER	07	DPWA $\gamma N \rightarrow \pi N$
-0.256 \pm 0.003	AHRENS	04A	DPWA $\tilde{\gamma}\tilde{p} \rightarrow N\pi$
-0.2669 \pm 0.0016 \pm 0.0078	BLANPIED	01	LEGS $\gamma p \rightarrow p\gamma, p\pi^0, n\pi^+$
-0.251 \pm 0.001	BECK	00	IPWA $\tilde{\gamma}p \rightarrow p\pi^0, n\pi^+$
-0.258 \pm 0.006	KAMALOV	99	DPWA $\gamma N \rightarrow \pi N$
-0.2466 \pm 0.0013	HANSTEIN	98	IPWA $\gamma N \rightarrow \pi N$
-0.2524 \pm 0.0013	DAVIDSON	97	DPWA $\gamma N \rightarrow \pi N$
• • • We do not use the following data for averages, fits, limits, etc. • • •			
-0.251 \pm 0.001	¹ SHRESTHA	12A	DPWA Multichannel
-0.267 \pm 0.008	ANISOVICH	10	DPWA Multichannel
-0.265	DRECHSEL	07	DPWA $\gamma N \rightarrow \pi N$
-0.243 \pm 0.001	ARNDT	02	DPWA $\gamma p \rightarrow N\pi$
-0.247	PENNER	02D	DPWA Multichannel
-0.2522	HANSTEIN	98	DPWA $\gamma N \rightarrow \pi N$

¹ Statistical error only. $\Delta(1232) \rightarrow N\gamma$, E_2/M_1 ratio

VALUE	DOCUMENT ID	TECN	COMMENT
-0.030 to -0.020 (≈ -0.025) OUR ESTIMATE			
-0.0274 \pm 0.0003 \pm 0.0030	AHRENS	04A	DPWA $\tilde{\gamma}\tilde{p} \rightarrow N\pi$
-0.020 \pm 0.002	ARNDT	02	DPWA $\gamma p \rightarrow N\pi$
-0.0307 \pm 0.0026 \pm 0.0024	BLANPIED	01	LEGS $\gamma p \rightarrow p\gamma, p\pi^0, n\pi^+$
-0.016 \pm 0.004 \pm 0.002	GALLER	01	DPWA $\gamma p \rightarrow \gamma p$
-0.025 \pm 0.001 \pm 0.002	BECK	00	IPWA $\tilde{\gamma}p \rightarrow p\pi^0, n\pi^+$
-0.0233 \pm 0.0017	HANSTEIN	98	IPWA $\gamma N \rightarrow \pi N$
-0.015 \pm 0.005	¹ ARNDT	97	IPWA $\gamma N \rightarrow \pi N$
-0.0319 \pm 0.0024	DAVIDSON	97	DPWA $\gamma N \rightarrow \pi N$
• • • We do not use the following data for averages, fits, limits, etc. • • •			
-0.022	DRECHSEL	07	DPWA $\gamma N \rightarrow \pi N$
-0.026	PENNER	02D	DPWA Multichannel
-0.0254 \pm 0.0010	HANSTEIN	98	DPWA $\gamma N \rightarrow \pi N$
-0.025 \pm 0.002 \pm 0.002	BECK	97	IPWA $\gamma N \rightarrow \pi N$
-0.030 \pm 0.003 \pm 0.002	BLANPIED	97	DPWA $\gamma N \rightarrow \pi N, \gamma N$

¹ This ARNDT 97 value is very sensitive to the database being fitted. The result is from a fit to the full pion photoproduction database, apart from the BLANPIED 97 cross-section measurements.

See key on page 1171

Baryon Particle Listings

$\Delta(1232), \Delta(1600)$

$\Delta(1232) \rightarrow N\gamma$, absolute value of E_2/M_1 ratio at pole

VALUE	DOCUMENT ID	TECN	COMMENT
••• We do not use the following data for averages, fits, limits, etc. •••			
0.065 ± 0.007	ARNDT 97	DPWA	$\gamma N \rightarrow \pi N$
0.058	HANSTEIN 96	DPWA	$\gamma N \rightarrow \pi N$

$\Delta(1232) \rightarrow N\gamma$, phase of E_2/M_1 ratio at pole

VALUE	DOCUMENT ID	TECN	COMMENT
••• We do not use the following data for averages, fits, limits, etc. •••			
-122 ± 5	ARNDT 97	DPWA	$\gamma N \rightarrow \pi N$
-127.2	HANSTEIN 96	DPWA	$\gamma N \rightarrow \pi N$

$\Delta(1232)$ MAGNETIC MOMENTS

$\Delta(1232)^{++}$ MAGNETIC MOMENT

The values are extracted from UCLA and SIN data on $\pi^+ p$ bremsstrahlung using a variety of different theoretical approximations and methods. Our estimate is *only* a rough guess of the range we expect the moment to lie within.

VALUE (μ_N)	DOCUMENT ID	TECN	COMMENT
••• We do not use the following data for averages, fits, limits, etc. •••			
6.14 ± 0.51	LOPEZCAST... 01	DPWA	$\pi^+ p \rightarrow \pi^+ p \gamma$
4.52 ± 0.50 ± 0.45	BOSSHARD 91		$\pi^+ p \rightarrow \pi^+ p \gamma$ (SIN data)
3.7 to 4.2	LIN 91B		$\pi^+ p \rightarrow \pi^+ p \gamma$ (from UCLA data)
4.6 to 4.9	LIN 91B		$\pi^+ p \rightarrow \pi^+ p \gamma$ (from SIN data)
5.6 to 7.5	WITTMAN 88		$\pi^+ p \rightarrow \pi^+ p \gamma$ (from UCLA data)
6.9 to 9.8	HELLER 87		$\pi^+ p \rightarrow \pi^+ p \gamma$ (from UCLA data)
4.7 to 6.7	NEFKENS 78		$\pi^+ p \rightarrow \pi^+ p \gamma$ (UCLA data)

$\Delta(1232)^+$ MAGNETIC MOMENT

VALUE (μ_N)	DOCUMENT ID	TECN	COMMENT
••• We do not use the following data for averages, fits, limits, etc. •••			
2.7 +1.0 -1.3 ± 1.5 ± 3	¹ KOTULLA 02		$\gamma p \rightarrow p \pi^0 \gamma$

¹ The second error is systematic, the third is an estimate of theoretical uncertainties.

$\Delta(1232)$ REFERENCES

For early references, see Physics Letters **111B** 1 (1982).

ROENCHEN 22	EPJ A58 229	D. Roenchen <i>et al.</i>	(JULI, GWU, BONN+)
HUNT 19	PR C99 055205	B. C. Hunt, D.M. Manley	
ADAMCZEW... 17	PR C95 065205	J. Adamczewski-Musch <i>et al.</i>	(HADES Collab.)
ROENCHEN 15A	EPJ A51 70	D. Roenchen <i>et al.</i>	
PDG 14	CP C38 070001	K. Olive <i>et al.</i>	(PDG Collab.)
SVARC 14	PR C89 045205	A. Svarc <i>et al.</i>	(RBI Zagreb, UNI Tuzla)
ANISOVICH 12A	EPJ A48 15	A.V. Anisovich <i>et al.</i>	(BONN, PNPI)
SHRESTHA 12A	PR C86 055203	M. Shrestha, D.M. Manley	(KSU)
WORKMAN 12A	PR C86 015202	R. Workman <i>et al.</i>	(GWU)
ANISOVICH 10	EPJ A44 203	A.V. Anisovich <i>et al.</i>	(BONN, PNPI)
DRECHSEL 07	EPJ A34 69	D. Drechsel, S.S. Kamalov, L. Tiator	(MAINZ, JINR)
DUGGER 07	PR C76 025211	M. Dugger <i>et al.</i>	(JLab CLAS Collab.)
ARNDT 06	PR C74 045205	R.A. Arndt <i>et al.</i>	(GWU)
BREITSCHOP... 06	PL B639 424	J. Breitschopf <i>et al.</i>	(TUBIN, HEBR, CSUS)
GRIDNEV 06	PAN 69 1542	A.B. Gridnev <i>et al.</i>	(PNPI, BONN, GWU)
PDG 06	JP G33 1	W.-M. Yao <i>et al.</i>	(PDG Collab.)
AHRENS 04A	EPJ A21 323	J. Ahrens <i>et al.</i>	(A2 Collab.)
ARNDT 04	PR C69 035213	R.A. Arndt <i>et al.</i>	(GWU, TRIU)
ARNDT 02	PR C66 055213	R.A. Arndt <i>et al.</i>	(GWU)
KOTULLA 02	PR L89 272001	M. Kotulla <i>et al.</i>	(MAMI TAPS Collab.)
PENNER 02C	PR C66 055211	G. Penner, U. Mosel	(GIES)
PENNER 02D	PR C66 055212	G. Penner, U. Mosel	(GIES)
BLANPIED 01	PR C64 025203	G. Blanpied <i>et al.</i>	(BNL LEGS Collab.)
GALLER 01	PL B503 245	G. Galler <i>et al.</i>	(Mainz LARA Collab.)
LOPEZCAST... 01	PL B517 339	G. Lopez Castro, A. Mariano	
Also	NP A697 440	G. Lopez Castro, A. Mariano	
BECK 00	PR C61 035204	R. Beck <i>et al.</i>	(Mainz Microtron DAPHNE Col.)
KAMALOV 99	PR L83 4494	S.S. Kamalov, S.N. Yang	(Taiwan U.)
HANSTEIN 98	NP A632 561	O. Hanstein, D. Drechsel, L. Tiator	
ARNDT 97	PR C56 577	R.A. Arndt, I.I. Strakovsky, R.L. Workman	(VPI)
BECK 97	PR L78 606	R. Beck <i>et al.</i>	(MAINZ, SACL, PAVI, GLAS)
Also	PR L79 4510	R.L. Beck, H.P. Krahn	(MAINZ)
Also	PR L79 4512	R.L. Beck, H.P. Krahn	(MAINZ)
Also	PR L79 4515 (err.)	R.L. Beck <i>et al.</i>	(MAINZ, SACL, PAVI, GLAS)
BLANPIED 97	PR L79 4337	G.S. Blanpied <i>et al.</i>	(LEGS Collab.)
DAVIDSON 97	PR L79 4509	R.M. Davidson, N.C.A. Mukhopadhyay	(RPI)
BERNICHIA 96	NP A597 623	A. Bernichia, G. Lopez Castro, J. Pestieau	(LOUV+)
HANSTEIN 96	PL B385 45	O. Hanstein, D. Drechsel, L. Tiator	(MAINZ)
ABAEV 95	ZPHY A352 85	V.V. Abaev, S.P. Kruglov	(PNPI)
HOEHLER 93	πN Newsletter 9 1	G. Hoehler	(KARL)
BOSSHARD 91	PR D44 1942	A. Bosshard <i>et al.</i>	(ZURI, LBL, VILL+)
Also	PR L64 2619	A. Bosshard <i>et al.</i>	(CATH, LAUS, LBL+)
LIN 91B	PR C44 1819	D.H. Lin, M.K. Liou, Z.M. Ding	(CUNY, CSOK)
Also	PR C43 R930	D. Lin, M.K. Liou	(CUNY)
WITTMAN 88	PR C37 2075	R. Wittman	(TRIU)
HELLER 87	PR C35 718	L. Heller <i>et al.</i>	(LANL, MIT, ILL)
CUTKOSKY 80	Toronto Conf. 19	R.E. Cutkosky <i>et al.</i>	(CMU, LBL) IJP
Also	PR D20 2839	R.E. Cutkosky <i>et al.</i>	(CMU, LBL)
KOCH 80B	NP A336 331	R. Koch, E. Pietarinen	(KARLT) IJP
HOEHLER 79	PDAT 12-1	G. Hoehler <i>et al.</i>	(KARLT) IJP
Also	Toronto Conf. 3	R. Koch	(KARLT) IJP
MIROSHNIC... 79	SJNP 29 94	I.I. Miroshnichenko <i>et al.</i>	(KFTI) IJP
Also	Translated from YAF 29 188		
NEFKENS 78	PR D18 3911	B.M.K. Nefkens <i>et al.</i>	(UCLA, CATH) IJP
PEDRONI 78	NP A300 321	E. Pedroni <i>et al.</i>	(SIN, ISNG, KARLE+) IJP

$\Delta(1600) 3/2^+$

$$I(J^P) = \frac{3}{2}(\frac{3}{2}^+) \text{ Status: } ***$$

Older and obsolete values are listed and referenced in the 2014 edition, Chinese Physics **C38** 070001 (2014).

$\Delta(1600)$ POLE POSITION

REAL PART

VALUE (MeV)	DOCUMENT ID	TECN	COMMENT
1470 to 1590 (≈ 1520) OUR ESTIMATE			
1590 ± 1	ROENCHEN 22	DPWA	Multichannel
1515 ± 20	SOKHOYAN 15A	DPWA	Multichannel
1469 ± 10 ± 5	¹ SVARC 14	L+P	$\pi N \rightarrow \pi N$
1550 ± 40	CUTKOSKY 80	IPWA	$\pi N \rightarrow \pi N$
••• We do not use the following data for averages, fits, limits, etc. •••			
1619	HUNT 19	DPWA	Multichannel
1552	ROENCHEN 15A	DPWA	Multichannel
1498 ± 25	ANISOVICH 12A	DPWA	Multichannel
1457	ARNDT 06	DPWA	$\pi N \rightarrow \pi N, \eta N$
1599	VRANA 00	DPWA	Multichannel
1550	HOEHLER 93	SPED	$\pi N \rightarrow \pi N$

¹ Fit to the amplitudes of HOEHLER 79.

-2xIMAGINARY PART

VALUE (MeV)	DOCUMENT ID	TECN	COMMENT
150 to 320 (≈ 280) OUR ESTIMATE			
136 ± 1	ROENCHEN 22	DPWA	Multichannel
250 ± 30	SOKHOYAN 15A	DPWA	Multichannel
314 ± 18 ± 8	¹ SVARC 14	L+P	$\pi N \rightarrow \pi N$
200 ± 60	CUTKOSKY 80	IPWA	$\pi N \rightarrow \pi N$
••• We do not use the following data for averages, fits, limits, etc. •••			
295	HUNT 19	DPWA	Multichannel
350	ROENCHEN 15A	DPWA	Multichannel
230 ± 50	ANISOVICH 12A	DPWA	Multichannel
400	ARNDT 06	DPWA	$\pi N \rightarrow \pi N, \eta N$
312	VRANA 00	DPWA	Multichannel

¹ Fit to the amplitudes of HOEHLER 79.

$\Delta(1600)$ ELASTIC POLE RESIDUE

MODULUS $|r|$

VALUE (MeV)	DOCUMENT ID	TECN	COMMENT
110 to 40 (≈ 25) OUR ESTIMATE			
11 ± 1	ROENCHEN 22	DPWA	Multichannel
13 ± 3	SOKHOYAN 15A	DPWA	Multichannel
38 ± 2 ± 2	¹ SVARC 14	L+P	$\pi N \rightarrow \pi N$
17 ± 4	CUTKOSKY 80	IPWA	$\pi N \rightarrow \pi N$
••• We do not use the following data for averages, fits, limits, etc. •••			
24	ROENCHEN 15A	DPWA	Multichannel
11 ± 6	ANISOVICH 12A	DPWA	Multichannel
44	ARNDT 06	DPWA	$\pi N \rightarrow \pi N, \eta N$

¹ Fit to the amplitudes of HOEHLER 79.

PHASE θ

VALUE (°)	DOCUMENT ID	TECN	COMMENT
180 to 250 (≈ 210) OUR ESTIMATE			
-106 ± 1	ROENCHEN 22	DPWA	Multichannel
-155 ± 20	SOKHOYAN 15A	DPWA	Multichannel
173 ± 5 ± 5	¹ SVARC 14	L+P	$\pi N \rightarrow \pi N$
-150 ± 30	CUTKOSKY 80	IPWA	$\pi N \rightarrow \pi N$
••• We do not use the following data for averages, fits, limits, etc. •••			
-155	ROENCHEN 15A	DPWA	Multichannel
-160 ± 33	ANISOVICH 12A	DPWA	Multichannel
+147	ARNDT 06	DPWA	$\pi N \rightarrow \pi N, \eta N$

¹ Fit to the amplitudes of HOEHLER 79.

$\Delta(1600)$ INELASTIC POLE RESIDUE

The "normalized residue" is the residue divided by $\Gamma_{pole}/2$.

Normalized residue in $N\pi \rightarrow \Delta(1600) \rightarrow \Delta\pi, P$ -wave

MODULUS	PHASE (°)	DOCUMENT ID	TECN	COMMENT
0.30 ± 0.02	87 ± 2	ROENCHEN 22	DPWA	Multichannel
0.15 ± 0.04	30 ± 35	SOKHOYAN 15A	DPWA	Multichannel
••• We do not use the following data for averages, fits, limits, etc. •••				
0.31	31	ROENCHEN 15A	DPWA	Multichannel
0.14 ± 0.10	154 ± 40	ANISOVICH 12A	DPWA	Multichannel

Baryon Particle Listings

 $\Delta(1600)$ Normalized residue in $N\pi \rightarrow \Delta(1600) \rightarrow \Delta\pi, F\text{-wave}$

MODULUS	PHASE ($^\circ$)	DOCUMENT ID	TECN	COMMENT
0.004 ± 0.0002	-62 ± 5	ROENCHEN 22	DPWA	Multichannel
0.010 ± 0.005		SOKHOYAN 15A	DPWA	Multichannel
••• We do not use the following data for averages, fits, limits, etc. •••				
0.013	29	ROENCHEN 15A	DPWA	Multichannel
0.010 ± 0.005		ANISOVICH 12A	DPWA	Multichannel

Normalized residue in $N\pi \rightarrow \Delta(1600) \rightarrow \Sigma K$

MODULUS	PHASE ($^\circ$)	DOCUMENT ID	TECN	COMMENT
0.14 ± 0.01	14 ± 1	ROENCHEN 22	DPWA	Multichannel
••• We do not use the following data for averages, fits, limits, etc. •••				
0.13	-5.6	ROENCHEN 15A	DPWA	Multichannel

 $\Delta(1600)$ BREIT-WIGNER MASS

VALUE (MeV)	DOCUMENT ID	TECN	COMMENT
1500 to 1640 (≈ 1570) OUR ESTIMATE			
1664 ± 16	¹ HUNT 19	DPWA	Multichannel
1520 ± 20	SOKHOYAN 15A	DPWA	Multichannel
1600 ± 50	CUTKOSKY 80	IPWA	$\pi N \rightarrow \pi N$
1522 ± 13	HOEHLER 79	IPWA	$\pi N \rightarrow \pi N$
••• We do not use the following data for averages, fits, limits, etc. •••			
1510 ± 20	ANISOVICH 12A	DPWA	Multichannel
1626 ± 8	¹ SHRESTHA 12A	DPWA	Multichannel
1667 ± 1	PENNER 02C	DPWA	Multichannel
1687 ± 44	VRANA 00	DPWA	Multichannel
¹ Statistical error only.			

 $\Delta(1600)$ BREIT-WIGNER WIDTH

VALUE (MeV)	DOCUMENT ID	TECN	COMMENT
200 to 300 (≈ 250) OUR ESTIMATE			
322 ± 46	¹ HUNT 19	DPWA	Multichannel
235 ± 30	SOKHOYAN 15A	DPWA	Multichannel
300 ± 100	CUTKOSKY 80	IPWA	$\pi N \rightarrow \pi N$
220 ± 40	HOEHLER 79	IPWA	$\pi N \rightarrow \pi N$
••• We do not use the following data for averages, fits, limits, etc. •••			
220 ± 45	ANISOVICH 12A	DPWA	Multichannel
225 ± 18	¹ SHRESTHA 12A	DPWA	Multichannel
397 ± 10	PENNER 02C	DPWA	Multichannel
493 ± 75	VRANA 00	DPWA	Multichannel
¹ Statistical error only.			

 $\Delta(1600)$ DECAY MODES

The following branching fractions are our estimates, not fits or averages.

Mode	Fraction (Γ_i/Γ)
Γ_1 $N\pi$	8-24%
Γ_2 $N\pi\pi$	58-84%
Γ_3 $\Delta(1232)\pi$	58-82%
Γ_4 $\Delta(1232)\pi, P\text{-wave}$	72-82%
Γ_5 $\Delta(1232)\pi, F\text{-wave}$	<2%
Γ_6 $N(1440)\pi$	17-27%
Γ_7 $N\gamma$	0.001-0.035%
Γ_8 $N\gamma, \text{helicity}=1/2$	0.0-0.02%
Γ_9 $N\gamma, \text{helicity}=3/2$	0.001-0.015%

 $\Delta(1600)$ BRANCHING RATIOS

$\Gamma(N\pi)/\Gamma_{\text{total}}$	DOCUMENT ID	TECN	COMMENT	Γ_1/Γ
8-24% OUR ESTIMATE				
10.7 ± 1.9	¹ HUNT 19	DPWA	Multichannel	
14 ± 4	SOKHOYAN 15A	DPWA	Multichannel	
18 ± 4	CUTKOSKY 80	IPWA	$\pi N \rightarrow \pi N$	
21 ± 6	HOEHLER 79	IPWA	$\pi N \rightarrow \pi N$	
••• We do not use the following data for averages, fits, limits, etc. •••				
12 ± 5	ANISOVICH 12A	DPWA	Multichannel	
8 ± 2	¹ SHRESTHA 12A	DPWA	Multichannel	
13 ± 1	PENNER 02C	DPWA	Multichannel	
28 ± 5	VRANA 00	DPWA	Multichannel	
¹ Statistical error only.				

$\Gamma(\Delta(1232)\pi, P\text{-wave})/\Gamma_{\text{total}}$	DOCUMENT ID	TECN	COMMENT	Γ_4/Γ
72-82% OUR ESTIMATE				
64 ± 6	¹ HUNT 19	DPWA	Multichannel	
77 ± 5	SOKHOYAN 15A	DPWA	Multichannel	

78 ± 6	ANISOVICH 12A	DPWA	Multichannel
70 ± 3	¹ SHRESTHA 12A	DPWA	Multichannel
59 ± 10	VRANA 00	DPWA	Multichannel
¹ Statistical error only.			

$\Gamma(\Delta(1232)\pi, F\text{-wave})/\Gamma_{\text{total}}$	DOCUMENT ID	TECN	COMMENT	Γ_5/Γ
<2% OUR ESTIMATE				
<2	SOKHOYAN 15A	DPWA	Multichannel	

$\Gamma(N(1440)\pi)/\Gamma_{\text{total}}$	DOCUMENT ID	TECN	COMMENT	Γ_6/Γ
17-27% OUR ESTIMATE				
22 ± 5	¹ HUNT 19	DPWA	Multichannel	
••• We do not use the following data for averages, fits, limits, etc. •••				
22 ± 3	¹ SHRESTHA 12A	DPWA	Multichannel	
13 ± 4	VRANA 00	DPWA	Multichannel	
¹ Statistical error only.				

 $\Delta(1600)$ PHOTON DECAY AMPLITUDES AT THE POLE $\Delta(1600) \rightarrow N\gamma, \text{helicity-1/2 amplitude } A_{1/2}$

MODULUS ($\text{GeV}^{-1/2}$)	PHASE ($^\circ$)	DOCUMENT ID	TECN	COMMENT
0.025 ± 0.005	0.5 ± 3.0	ROENCHEN 22	DPWA	Multichannel
0.053 ± 0.010	130 ± 15	SOKHOYAN 15A	DPWA	Multichannel
••• We do not use the following data for averages, fits, limits, etc. •••				
-0.230	-42	ROENCHEN 15A	DPWA	Multichannel

 $\Delta(1600) \rightarrow N\gamma, \text{helicity-3/2 amplitude } A_{3/2}$

MODULUS ($\text{GeV}^{-1/2}$)	PHASE ($^\circ$)	DOCUMENT ID	TECN	COMMENT
-0.006 ± 0.0013	62 ± 32	ROENCHEN 22	DPWA	Multichannel
0.055 ± 0.010	152 ± 15	SOKHOYAN 15A	DPWA	Multichannel
••• We do not use the following data for averages, fits, limits, etc. •••				
0.332	-71	ROENCHEN 15A	DPWA	Multichannel

 $\Delta(1600)$ BREIT-WIGNER PHOTON DECAY AMPLITUDES $\Delta(1600) \rightarrow N\gamma, \text{helicity-1/2 amplitude } A_{1/2}$

VALUE ($\text{GeV}^{-1/2}$)	DOCUMENT ID	TECN	COMMENT
-0.060 to -0.030 (≈ -0.045) OUR ESTIMATE			
0.0082 ± 0.0014	¹ HUNT 19	DPWA	Multichannel
-0.051 ± 0.010	SOKHOYAN 15A	DPWA	Multichannel
-0.018 ± 0.015	¹ ARNDT 96	IPWA	$\gamma N \rightarrow \pi N$
••• We do not use the following data for averages, fits, limits, etc. •••			
-0.050 ± 0.009	ANISOVICH 12A	DPWA	Multichannel
0.006 ± 0.005	¹ SHRESTHA 12A	DPWA	Multichannel
0.0	PENNER 02D	DPWA	Multichannel
¹ Statistical error only.			

 $\Delta(1600) \rightarrow N\gamma, \text{helicity-3/2 amplitude } A_{3/2}$

VALUE ($\text{GeV}^{-1/2}$)	DOCUMENT ID	TECN	COMMENT
-0.050 to -0.020 (≈ -0.035) OUR ESTIMATE			
0.048 ± 0.014	¹ HUNT 19	DPWA	Multichannel
-0.055 ± 0.010	SOKHOYAN 15A	DPWA	Multichannel
-0.025 ± 0.015	¹ ARNDT 96	IPWA	$\gamma N \rightarrow \pi N$
••• We do not use the following data for averages, fits, limits, etc. •••			
-0.040 ± 0.012	ANISOVICH 12A	DPWA	Multichannel
0.052 ± 0.008	¹ SHRESTHA 12A	DPWA	Multichannel
-0.024	PENNER 02D	DPWA	Multichannel
¹ Statistical error only.			

 $\Delta(1600)$ REFERENCES

For early references, see Physics Letters **111B** 1 (1982).

ROENCHEN 22	EPJ A58 229	D. Roenchen <i>et al.</i>	(JULI, GWU, BONN+)
HUNT 19	PR C93 055205	B.C. Hunt, D.M. Manley	
ROENCHEN 15A	EPJ A51 70	D. Roenchen <i>et al.</i>	
SOKHOYAN 15A	EPJ A51 95	V. Sokhoyan <i>et al.</i>	(CBELSA/TAPS Collab.)
PDG 14	CP C38 070001	K. Olive <i>et al.</i>	(PDG Collab.)
SVARC 14	PR C89 045205	A. Svarc <i>et al.</i>	(RBI Zagreb, UNI Tuzla)
ANISOVICH 12A	EPJ A48 15	A.V. Anisovich <i>et al.</i>	(BONN, PNPI)
SHRESTHA 12A	PR C86 055203	M. Shrestha, D.M. Manley	(KSU)
ARNDT 06	PR C74 045205	R.A. Arndt <i>et al.</i>	(GWU)
PENNER 02C	PR C66 055211	G. Penner, U. Mosel	(GIES)
PENNER 02D	PR C66 055212	G. Penner, U. Mosel	(GIES)
VRANA 00	PRPL 328 181	T.P. Vrana, S.A. Dytman, T.-S.H. Lee	(PITT, ANL)
ARNDT 96	PR C53 430	R.A. Arndt, I.I. Strakovsky, R.L. Workman	(VPI)
HOEHLER 93	πN Newsletter 9 1	G. Hoehler	(KARL)
CUTKOSKY 80	Toronto Conf. 19	R.E. Cutkosky <i>et al.</i>	(CMU, LBL) IUP
Also	PR D20 2839	R.E. Cutkosky <i>et al.</i>	(CMU, LBL) IUP
HOEHLER 79	PDAT 12-1	G. Hoehler <i>et al.</i>	(KARL) IUP
Also	Toronto Conf. 3	R. Koch	(KARL) IUP

See key on page 1171

Baryon Particle Listings

$\Delta(1620)$

$\Delta(1620) 1/2^-$

$I(J^P) = \frac{3}{2}(\frac{1}{2}^-)$ Status: ****

Older and obsolete values are listed and referenced in the 2014 edition, Chinese Physics C38 070001 (2014).

$\Delta(1620)$ POLE POSITION

REAL PART

VALUE (MeV)	DOCUMENT ID	TECN	COMMENT
1590 to 1610 (≈ 1600) OUR ESTIMATE			
1607 \pm 2	ROENCHEN 22	DPWA	Multichannel
1597 \pm 5	SOKHOYAN 15A	DPWA	Multichannel
1603 \pm 7 \pm 2	¹ SVARC 14	L+P	$\pi N \rightarrow \pi N$
1600 \pm 15	CUTKOSKY 80	IPWA	$\pi N \rightarrow \pi N$
● ● ● We do not use the following data for averages, fits, limits, etc. ● ● ●			
1577	HUNT 19	DPWA	Multichannel
1600	ROENCHEN 15A	DPWA	Multichannel
1597 \pm 4	ANISOVICH 12A	DPWA	Multichannel
1595	ARNDT 06	DPWA	$\pi N \rightarrow \pi N, \eta N$
1607	VRANA 00	DPWA	Multichannel
1608	HOEHLER 93	SPED	$\pi N \rightarrow \pi N$

¹ Fit to the amplitudes of HOEHLER 79.

-2xIMAGINARY PART

VALUE (MeV)	DOCUMENT ID	TECN	COMMENT
80 to 140 (≈ 110) OUR ESTIMATE			
85 \pm 3	ROENCHEN 22	DPWA	Multichannel
134 \pm 8	SOKHOYAN 15A	DPWA	Multichannel
114 \pm 12 \pm 4	¹ SVARC 14	L+P	$\pi N \rightarrow \pi N$
120 \pm 20	CUTKOSKY 80	IPWA	$\pi N \rightarrow \pi N$
● ● ● We do not use the following data for averages, fits, limits, etc. ● ● ●			
101	HUNT 19	DPWA	Multichannel
65	ROENCHEN 15A	DPWA	Multichannel
130 \pm 9	ANISOVICH 12A	DPWA	Multichannel
135	ARNDT 06	DPWA	$\pi N \rightarrow \pi N, \eta N$
148	VRANA 00	DPWA	Multichannel
116	HOEHLER 93	SPED	$\pi N \rightarrow \pi N$

¹ Fit to the amplitudes of HOEHLER 79.

$\Delta(1620)$ ELASTIC POLE RESIDUE

MODULUS $|r|$

VALUE (MeV)	DOCUMENT ID	TECN	COMMENT
10 to 20 (≈ 15) OUR ESTIMATE			
12 \pm 1	ROENCHEN 22	DPWA	Multichannel
20 \pm 3	SOKHOYAN 15A	DPWA	Multichannel
17 \pm 2 \pm 1	¹ SVARC 14	L+P	$\pi N \rightarrow \pi N$
15 \pm 2	CUTKOSKY 80	IPWA	$\pi N \rightarrow \pi N$
● ● ● We do not use the following data for averages, fits, limits, etc. ● ● ●			
16	ROENCHEN 15A	DPWA	Multichannel
18 \pm 2	ANISOVICH 12A	DPWA	Multichannel
15	ARNDT 06	DPWA	$\pi N \rightarrow \pi N, \eta N$
19	HOEHLER 93	SPED	$\pi N \rightarrow \pi N$

¹ Fit to the amplitudes of HOEHLER 79.

PHASE θ

VALUE (°)	DOCUMENT ID	TECN	COMMENT
-120 to -80 (≈ -100) OUR ESTIMATE			
126 \pm 2	ROENCHEN 22	DPWA	Multichannel
-90 \pm 15	SOKHOYAN 15A	DPWA	Multichannel
-106 \pm 10 \pm 4	¹ SVARC 14	L+P	$\pi N \rightarrow \pi N$
-110 \pm 20	CUTKOSKY 80	IPWA	$\pi N \rightarrow \pi N$
● ● ● We do not use the following data for averages, fits, limits, etc. ● ● ●			
-104	ROENCHEN 15A	DPWA	Multichannel
-100 \pm 5	ANISOVICH 12A	DPWA	Multichannel
-92	ARNDT 06	DPWA	$\pi N \rightarrow \pi N, \eta N$
-95	HOEHLER 93	SPED	$\pi N \rightarrow \pi N$

¹ Fit to the amplitudes of HOEHLER 79.

$\Delta(1620)$ INELASTIC POLE RESIDUE

The "normalized residue" is the residue divided by $\Gamma_{pole}/2$.

Normalized residue in $N\pi \rightarrow \Delta(1620) \rightarrow \Delta\pi, D\text{-wave}$

MODULUS	PHASE (°)	DOCUMENT ID	TECN	COMMENT
0.32 \pm 0.01	81 \pm 1	ROENCHEN 22	DPWA	Multichannel
0.42 \pm 0.06	-90 \pm 20	SOKHOYAN 15A	DPWA	Multichannel
● ● ● We do not use the following data for averages, fits, limits, etc. ● ● ●				
0.57	105	ROENCHEN 15A	DPWA	Multichannel
0.38 \pm 0.09	-85 \pm 30	ANISOVICH 12A	DPWA	Multichannel

Normalized residue in $N\pi \rightarrow \Delta(1620) \rightarrow \Sigma K$

MODULUS	PHASE (°)	DOCUMENT ID	TECN	COMMENT
0.11 \pm 0.01	-120 \pm 3	ROENCHEN 22	DPWA	Multichannel
● ● ● We do not use the following data for averages, fits, limits, etc. ● ● ●				
0.22	-105	ROENCHEN 15A	DPWA	Multichannel

Normalized residue in $N\pi \rightarrow \Delta(1620) \rightarrow N(1440)\pi$

MODULUS	PHASE (°)	DOCUMENT ID	TECN	COMMENT
0.10 \pm 0.06	-65 \pm 30	SOKHOYAN 15A	DPWA	Multichannel

$\Delta(1620)$ BREIT-WIGNER MASS

VALUE (MeV)	DOCUMENT ID	TECN	COMMENT
1590 to 1630 (≈ 1610) OUR ESTIMATE			
1635 \pm 8	GOLOVATCH 19	DPWA	$\gamma p \rightarrow \pi^+ \pi^- p$
1589 \pm 3	¹ HUNT 19	DPWA	Multichannel
1595 \pm 8	SOKHOYAN 15A	DPWA	Multichannel
1615.2 \pm 0.4	¹ ARNDT 06	DPWA	$\pi N \rightarrow \pi N, \eta N$
1620 \pm 20	CUTKOSKY 80	IPWA	$\pi N \rightarrow \pi N$
1610 \pm 7	HOEHLER 79	IPWA	$\pi N \rightarrow \pi N$
● ● ● We do not use the following data for averages, fits, limits, etc. ● ● ●			
1600 \pm 8	ANISOVICH 12A	DPWA	Multichannel
1600 \pm 1	¹ SHRESTHA 12A	DPWA	Multichannel
1612 \pm 2	PENNER 02C	DPWA	Multichannel
1617 \pm 15	VRANA 00	DPWA	Multichannel

¹ Statistical error only.

$\Delta(1620)$ BREIT-WIGNER WIDTH

VALUE (MeV)	DOCUMENT ID	TECN	COMMENT
110 to 150 (≈ 130) OUR ESTIMATE			
144 \pm 16	GOLOVATCH 19	DPWA	$\gamma p \rightarrow \pi^+ \pi^- p$
107 \pm 7	¹ HUNT 19	DPWA	Multichannel
135 \pm 9	SOKHOYAN 15A	DPWA	Multichannel
146.9 \pm 1.9	¹ ARNDT 06	DPWA	$\pi N \rightarrow \pi N, \eta N$
140 \pm 20	CUTKOSKY 80	IPWA	$\pi N \rightarrow \pi N$
139 \pm 18	HOEHLER 79	IPWA	$\pi N \rightarrow \pi N$
● ● ● We do not use the following data for averages, fits, limits, etc. ● ● ●			
130 \pm 11	ANISOVICH 12A	DPWA	Multichannel
112 \pm 2	¹ SHRESTHA 12A	DPWA	Multichannel
202 \pm 7	PENNER 02C	DPWA	Multichannel
143 \pm 42	VRANA 00	DPWA	Multichannel

¹ Statistical error only.

$\Delta(1620)$ DECAY MODES

The following branching fractions are our estimates, not fits or averages.

Mode	Fraction (Γ_i/Γ)
Γ_1 $N\pi$	25-35 %
Γ_2 $N\pi\pi$	>67 %
Γ_3 $\Delta(1232)\pi, D\text{-wave}$	44-72 %
Γ_4 $N\rho$	23-32%
Γ_5 $N\rho, S=1/2, S\text{-wave}$	23-32%
Γ_6 $N\rho, S=3/2, D\text{-wave}$	<0.04%
Γ_7 $N(1440)\pi$	<9 %
Γ_8 $N\gamma, \text{helicity}=1/2$	0.03-0.10 %

$\Delta(1620)$ BRANCHING RATIOS

$\Gamma(N\pi)/\Gamma_{total}$	DOCUMENT ID	TECN	COMMENT	Γ_1/Γ
25 to 35 (≈ 30) OUR ESTIMATE				
24 \pm 2	¹ HUNT 19	DPWA	Multichannel	
28 \pm 3	SOKHOYAN 15A	DPWA	Multichannel	
31.5 \pm 0.1	¹ ARNDT 06	DPWA	$\pi N \rightarrow \pi N, \eta N$	
25 \pm 3	CUTKOSKY 80	IPWA	$\pi N \rightarrow \pi N$	
35 \pm 6	HOEHLER 79	IPWA	$\pi N \rightarrow \pi N$	
● ● ● We do not use the following data for averages, fits, limits, etc. ● ● ●				
28 \pm 3	ANISOVICH 12A	DPWA	Multichannel	
33 \pm 2	¹ SHRESTHA 12A	DPWA	Multichannel	
34 \pm 1	PENNER 02C	DPWA	Multichannel	
45 \pm 5	VRANA 00	DPWA	Multichannel	

¹ Statistical error only.

$\Gamma(N\pi\pi)/\Gamma_{total}$	DOCUMENT ID	TECN	COMMENT	Γ_2/Γ
0.90 \pm 0.10	GOLOVATCH 19	DPWA	$\gamma p \rightarrow \pi^+ \pi^- p$	

Baryon Particle Listings

 $\Delta(1620)$, $\Delta(1700)$ $\Gamma(\Delta(1232)\pi, D\text{-wave})/\Gamma_{\text{total}}$

VALUE (%)	DOCUMENT ID	TECN	COMMENT	Γ_3/Γ
48 ± 4	1 HUNT	19	DPWA Multichannel	
62 ± 10	SOKHOYAN	15A	DPWA Multichannel	
• • • We do not use the following data for averages, fits, limits, etc. • • •				
60 ± 17	ANISOVICH	12A	DPWA Multichannel	
32 ± 2	1 SHRESTHA	12A	DPWA Multichannel	
39 ± 2	VRANA	00	DPWA Multichannel	

¹ Statistical error only.

 $\Gamma(N\rho, S=1/2, S\text{-wave})/\Gamma_{\text{total}}$

VALUE (%)	DOCUMENT ID	TECN	COMMENT	Γ_5/Γ
27 ± 4	1 HUNT	19	DPWA Multichannel	
• • • We do not use the following data for averages, fits, limits, etc. • • •				
26 ± 2	1 SHRESTHA	12A	DPWA Multichannel	
14 ± 3	VRANA	00	DPWA Multichannel	

¹ Statistical error only.

 $\Gamma(N\rho, S=3/2, D\text{-wave})/\Gamma_{\text{total}}$

VALUE (%)	DOCUMENT ID	TECN	COMMENT	Γ_6/Γ
<0.04	1 HUNT	19	DPWA Multichannel	
• • • We do not use the following data for averages, fits, limits, etc. • • •				
2 ± 1	VRANA	00	DPWA Multichannel	

¹ Statistical error only.

 $\Gamma(N(1440)\pi)/\Gamma_{\text{total}}$

VALUE (%)	DOCUMENT ID	TECN	COMMENT	Γ_7/Γ
<0.02	1 HUNT	19	DPWA Multichannel	
6 ± 3	SOKHOYAN	15A	DPWA Multichannel	
• • • We do not use the following data for averages, fits, limits, etc. • • •				
9 ± 1	1 SHRESTHA	12A	DPWA Multichannel	
0 ± 1	VRANA	00	DPWA Multichannel	

¹ Statistical error only.

 $\Delta(1620)$ PHOTON DECAY AMPLITUDES AT THE POLE $\Delta(1620) \rightarrow N\gamma$, helicity-1/2 amplitude $A_{1/2}$

MODULUS ($\text{GeV}^{-1/2}$)	PHASE ($^\circ$)	DOCUMENT ID	TECN	COMMENT
0.011 ± 0.002	57 ± 12	ROENCHEN	22	DPWA Multichannel
0.054 ± 0.007	-6 ± 7	SOKHOYAN	15A	DPWA Multichannel
• • • We do not use the following data for averages, fits, limits, etc. • • •				
0.014	26	ROENCHEN	15A	DPWA Multichannel

 $\Delta(1620)$ BREIT-WIGNER PHOTON DECAY AMPLITUDES $\Delta(1620) \rightarrow N\gamma$, helicity-1/2 amplitude $A_{1/2}$

VALUE ($\text{GeV}^{-1/2}$)	DOCUMENT ID	TECN	COMMENT
0.030 to 0.060 (≈ 0.050) OUR ESTIMATE			
0.029 ± 0.0062	GOLOVATCH	19	DPWA $\gamma\rho \rightarrow \pi^+\pi^-\rho$
0.0124 ± 0.0007	1 HUNT	19	DPWA Multichannel
0.055 ± 0.007	SOKHOYAN	15A	DPWA Multichannel
0.029 ± 0.003	1 WORKMAN	12A	DPWA $\gamma N \rightarrow N\pi$
0.050 ± 0.002	1 DUGGER	07	DPWA $\gamma N \rightarrow \pi N$
• • • We do not use the following data for averages, fits, limits, etc. • • •			
0.052 ± 0.005	ANISOVICH	12A	DPWA Multichannel
-0.003 ± 0.003	1 SHRESTHA	12A	DPWA Multichannel
0.066	DRECHSEL	07	DPWA $\gamma N \rightarrow \pi N$
-0.050	PENNER	02D	DPWA Multichannel

¹ Statistical error only.

 $\Delta(1620)$ REFERENCES

For early references, see Physics Letters **111B** 1 (1982).

ROENCHEN	22	EPJ A58 229	D. Roenchen <i>et al.</i>	(JULI, GWU, BONN+)
GOLOVATCH	19	PL B788 371	E. Golovatch <i>et al.</i>	(CLAS Collab.)
HUNT	19	PR C99 055205	B. C. Hunt, D.M. Manley	
ROENCHEN	15A	EPJ A51 70	D. Roenchen <i>et al.</i>	
SOKHOYAN	15A	EPJ A51 95	V. Sokhoyan <i>et al.</i>	(CBELSA/TAPS Collab.)
PDG	14	CP C38 070001	K. Olive <i>et al.</i>	(PDG Collab.)
SVARC	14	PR C89 045205	A. Svarc <i>et al.</i>	(RBI Zagreb, UNI Tuzla)
ANISOVICH	12A	EPJ A48 15	A.V. Anisovich <i>et al.</i>	(BONN, PNPI)
SHRESTHA	12A	PR C86 055203	M. Shrestha, D.M. Manley	(KSU)
WORKMAN	12A	PR C86 015202	R. Workman <i>et al.</i>	(GWU)
DRECHSEL	07	EPJ A34 69	D. Drechsel, S.S. Kamalov, L. Tiator	(MAINZ, JINR)
DUGGER	07	PR C76 025211	M. Dugger <i>et al.</i>	(JLab CLAS Collab.)
ARNDT	06	PR C74 045205	R.A. Arndt <i>et al.</i>	(GWU)
PENNER	02C	PR C66 055211	G. Penner, U. Mosel	(GIES)
PENNER	02D	PR C66 055212	G. Penner, U. Mosel	(GIES)
VRANA	00	PRPL 328 181	T.P. Vrana, S.A. Dytman, T.-S.H. Lee	(PITT, ANL)
HOEHLER	93	πN Newsletter 9 1	G. Hohlner	(KARL)
CUTKOSKY	80	Toronto Conf. 19	R.E. Cutkosky <i>et al.</i>	(CMU, LBL) IUP
Also		PR D20 2839	R.E. Cutkosky <i>et al.</i>	(CMU, LBL) IUP
HOEHLER	79	PDAT 12-1	G. Hohlner <i>et al.</i>	(KARL) IUP
Also		Toronto Conf. 3	R. Koch	(KARL) IUP

 $\Delta(1700) 3/2^-$

$$I(J^P) = \frac{3}{2}(\frac{3}{2}^-) \text{ Status: } ***$$

Older and obsolete values are listed and referenced in the 2014 edition, Chinese Physics **C38** 070001 (2014).

 $\Delta(1700)$ POLE POSITION

REAL PART

VALUE (MeV)	DOCUMENT ID	TECN	COMMENT
1640 to 1690 (≈ 1665) OUR ESTIMATE			
1637 ± 32	ROENCHEN	22	DPWA Multichannel
1685 ± 10	SOKHOYAN	15A	DPWA Multichannel
1643 ± 6 ± 3	1 SVARC	14	L+P $\pi N \rightarrow \pi N$
1675 ± 25	CUTKOSKY	80	IPWA $\pi N \rightarrow \pi N$
• • • We do not use the following data for averages, fits, limits, etc. • • •			
1693	HUNT	19	DPWA Multichannel
1677	ROENCHEN	15A	DPWA Multichannel
1685 ± 10	GUTZ	14	DPWA Multichannel
1680 ± 10	ANISOVICH	12A	DPWA Multichannel
1632	ARNDT	06	DPWA $\pi N \rightarrow \pi N, \eta N$
1726	VRANA	00	DPWA Multichannel
1651	HOEHLER	93	SPED $\pi N \rightarrow \pi N$

¹ Fit to the amplitudes of HOEHLER 79.

-2xIMAGINARY PART

VALUE (MeV)	DOCUMENT ID	TECN	COMMENT
200 to 300 (≈ 250) OUR ESTIMATE			
295 ± 29	ROENCHEN	22	DPWA Multichannel
300 ± 15	SOKHOYAN	15A	DPWA Multichannel
217 ± 10 ± 8	1 SVARC	14	L+P $\pi N \rightarrow \pi N$
220 ± 40	CUTKOSKY	80	IPWA $\pi N \rightarrow \pi N$
• • • We do not use the following data for averages, fits, limits, etc. • • •			
213	HUNT	19	DPWA Multichannel
305	ROENCHEN	15A	DPWA Multichannel
300 ± 15	GUTZ	14	DPWA Multichannel
305 ± 15	ANISOVICH	12A	DPWA Multichannel
253	ARNDT	06	DPWA $\pi N \rightarrow \pi N, \eta N$
118	VRANA	00	DPWA Multichannel
159	HOEHLER	93	SPED $\pi N \rightarrow \pi N$

¹ Fit to the amplitudes of HOEHLER 79.

 $\Delta(1700)$ ELASTIC POLE RESIDUEMODULUS $|r|$

VALUE (MeV)	DOCUMENT ID	TECN	COMMENT
10 to 40 (≈ 25) OUR ESTIMATE			
15 ± 12	ROENCHEN	22	DPWA Multichannel
40 ± 6	SOKHOYAN	15A	DPWA Multichannel
13 ± 1 ± 1	1 SVARC	14	L+P $\pi N \rightarrow \pi N$
13 ± 3	CUTKOSKY	80	IPWA $\pi N \rightarrow \pi N$
• • • We do not use the following data for averages, fits, limits, etc. • • •			
24	ROENCHEN	15A	DPWA Multichannel
40 ± 6	GUTZ	14	DPWA Multichannel
42 ± 7	ANISOVICH	12A	DPWA Multichannel
18	ARNDT	06	DPWA $\pi N \rightarrow \pi N, \eta N$
10	HOEHLER	93	SPED $\pi N \rightarrow \pi N$

¹ Fit to the amplitudes of HOEHLER 79.

PHASE θ

VALUE ($^\circ$)	DOCUMENT ID	TECN	COMMENT
-40 to 0 (≈ -20) OUR ESTIMATE			
-13 ± 74	ROENCHEN	22	DPWA Multichannel
-1 ± 10	SOKHOYAN	15A	DPWA Multichannel
-30 ± 4 ± 3	1 SVARC	14	L+P $\pi N \rightarrow \pi N$
-40	ARNDT	06	DPWA $\pi N \rightarrow \pi N, \eta N$
-20 ± 25	CUTKOSKY	80	IPWA $\pi N \rightarrow \pi N$
• • • We do not use the following data for averages, fits, limits, etc. • • •			
-7.3	ROENCHEN	15A	DPWA Multichannel
-1 ± 10	GUTZ	14	DPWA Multichannel
-3 ± 15	ANISOVICH	12A	DPWA Multichannel

¹ Fit to the amplitudes of HOEHLER 79.

 $\Delta(1700)$ INELASTIC POLE RESIDUE

The "normalized residue" is the residue divided by $\Gamma_{\text{pole}}/2$.

Normalized residue in $N\pi \rightarrow \Delta(1700) \rightarrow \Delta\eta$

MODULUS	PHASE ($^\circ$)	DOCUMENT ID	TECN	COMMENT
0.12 ± 0.02	-60 ± 12	GUTZ	14	DPWA Multichannel
• • • We do not use the following data for averages, fits, limits, etc. • • •				
0.12 ± 0.03	-60 ± 15	ANISOVICH	12A	DPWA Multichannel

Normalized residue in $N\pi \rightarrow \Delta(1700) \rightarrow \Sigma K$

MODULUS	PHASE (°)	DOCUMENT ID	TECN	COMMENT
0.007 ± 0.008	-176 ± 160	ROENCHEN 22	DPWA	Multichannel
••• We do not use the following data for averages, fits, limits, etc. •••				
0.011	-147	ROENCHEN 15A	DPWA	Multichannel

Normalized residue in $N\pi \rightarrow \Delta(1700) \rightarrow N(1535)\pi$

MODULUS	PHASE (°)	DOCUMENT ID	TECN	COMMENT
0.035 ± 0.015	-75 ± 30	GUTZ 14	DPWA	Multichannel

Normalized residue in $N\pi \rightarrow \Delta(1700) \rightarrow \Delta(1232)\pi, S\text{-wave}$

MODULUS	PHASE (°)	DOCUMENT ID	TECN	COMMENT
0.20 ± 0.15	146 ± 133	ROENCHEN 22	DPWA	Multichannel
0.25 ± 0.12	135 ± 45	SOKHOYAN 15A	DPWA	Multichannel
••• We do not use the following data for averages, fits, limits, etc. •••				
0.39	151	ROENCHEN 15A	DPWA	Multichannel

Normalized residue in $N\pi \rightarrow \Delta(1700) \rightarrow \Delta(1232)\pi, D\text{-wave}$

MODULUS	PHASE (°)	DOCUMENT ID	TECN	COMMENT
0.038 ± 0.039	127 ± 127	ROENCHEN 22	DPWA	Multichannel
0.12 ± 0.06	-160 ± 30	SOKHOYAN 15A	DPWA	Multichannel
••• We do not use the following data for averages, fits, limits, etc. •••				
0.054	166	ROENCHEN 15A	DPWA	Multichannel

Normalized residue in $N\pi \rightarrow \Delta(1700) \rightarrow N(1520)\pi, P\text{-wave}$

MODULUS	PHASE (°)	DOCUMENT ID	TECN	COMMENT
0.10 ± 0.03	-10 ± 20	SOKHOYAN 15A	DPWA	Multichannel

 $\Delta(1700)$ BREIT-WIGNER MASS

VALUE (MeV)	DOCUMENT ID	TECN	COMMENT
1690 to 1730 (≈ 1710) OUR ESTIMATE			
1704 ± 8	GOLOVATCH 19	DPWA	$\gamma p \rightarrow \pi^+ \pi^- p$
1720 ± 5	¹ HUNT 19	DPWA	Multichannel
1715 ± 20	SOKHOYAN 15A	DPWA	Multichannel
1695.0 ± 1.3	¹ ARNDT 06	DPWA	$\pi N \rightarrow \pi N, \eta N$
1710 ± 30	CUTKOSKY 80	IPWA	$\pi N \rightarrow \pi N$
1680 ± 70	HOEHLER 79	IPWA	$\pi N \rightarrow \pi N$
••• We do not use the following data for averages, fits, limits, etc. •••			
1715 ± 20	GUTZ 14	DPWA	Multichannel
1715 ± 30	ANISOVICH 12A	DPWA	Multichannel
1691 ± 4	¹ SHRESTHA 12A	DPWA	Multichannel
1678 ± 1	PENNER 02C	DPWA	Multichannel
1732 ± 23	VRANA 00	DPWA	Multichannel

¹ Statistical error only. $\Delta(1700)$ BREIT-WIGNER WIDTH

VALUE (MeV)	DOCUMENT ID	TECN	COMMENT
220 to 380 (≈ 300) OUR ESTIMATE			
295 ± 35	GOLOVATCH 19	DPWA	$\gamma p \rightarrow \pi^+ \pi^- p$
226 ± 14	¹ HUNT 19	DPWA	Multichannel
300 ± 25	SOKHOYAN 15A	DPWA	Multichannel
375.5 ± 7.0	¹ ARNDT 06	DPWA	$\pi N \rightarrow \pi N, \eta N$
280 ± 80	CUTKOSKY 80	IPWA	$\pi N \rightarrow \pi N$
230 ± 80	HOEHLER 79	IPWA	$\pi N \rightarrow \pi N$
••• We do not use the following data for averages, fits, limits, etc. •••			
300 ± 25	GUTZ 14	DPWA	Multichannel
310 ± 40	ANISOVICH 12A	DPWA	Multichannel
248 ± 9	¹ SHRESTHA 12A	DPWA	Multichannel
606 ± 15	PENNER 02C	DPWA	Multichannel
119 ± 70	VRANA 00	DPWA	Multichannel

¹ Statistical error only. $\Delta(1700)$ DECAY MODES

The following branching fractions are our estimates, not fits or averages.

Mode	Fraction (Γ_j/Γ)
Γ_1 $N\pi$	10–20 %
Γ_2 $N\pi\pi$	>31 %
Γ_3 $\Delta(1232)\pi$	9–70 %
Γ_4 $\Delta(1232)\pi, S\text{-wave}$	5–54 %
Γ_5 $\Delta(1232)\pi, D\text{-wave}$	4–16 %
Γ_6 $N\rho, S=3/2, S\text{-wave}$	22–32 %
Γ_7 $N(1520)\pi, P\text{-wave}$	1–5 %
Γ_8 $N(1535)\pi$	0.5–1.5 %
Γ_9 $\Delta(1232)\eta$	3–7 %
Γ_{10} $N\gamma$	0.22–0.60 %
Γ_{11} $N\gamma, \text{helicity}=1/2$	0.12–0.30 %
Γ_{12} $N\gamma, \text{helicity}=3/2$	0.10–0.30 %

 $\Delta(1700)$ BRANCHING RATIOS $\Gamma(N\pi)/\Gamma_{\text{total}}$

VALUE (%)	DOCUMENT ID	TECN	COMMENT	Γ_1/Γ
10 to 20 OUR ESTIMATE				
15 ± 2	¹ HUNT 19	DPWA	Multichannel	
22 ± 4	SOKHOYAN 15A	DPWA	Multichannel	
15.6 ± 0.1	¹ ARNDT 06	DPWA	$\pi N \rightarrow \pi N, \eta N$	
12 ± 3	CUTKOSKY 80	IPWA	$\pi N \rightarrow \pi N$	
20 ± 3	HOEHLER 79	IPWA	$\pi N \rightarrow \pi N$	
••• We do not use the following data for averages, fits, limits, etc. •••				
22 ± 4	GUTZ 14	DPWA	Multichannel	
22 ± 4	ANISOVICH 12A	DPWA	Multichannel	
14 ± 1	¹ SHRESTHA 12A	DPWA	Multichannel	
14 ± 1	PENNER 02C	DPWA	Multichannel	
5 ± 1	VRANA 00	DPWA	Multichannel	

¹ Statistical error only. $\Gamma(N\pi\pi)/\Gamma_{\text{total}}$

VALUE (%)	DOCUMENT ID	TECN	COMMENT	Γ_2/Γ
0.89 ± 0.11	GOLOVATCH 19	DPWA	$\gamma p \rightarrow \pi^+ \pi^- p$	

 $\Gamma(\Delta(1232)\pi, S\text{-wave})/\Gamma_{\text{total}}$

VALUE (%)	DOCUMENT ID	TECN	COMMENT	Γ_4/Γ
49 ± 5	¹ HUNT 19	DPWA	Multichannel	
20 ± 15	SOKHOYAN 15A	DPWA	Multichannel	
••• We do not use the following data for averages, fits, limits, etc. •••				
20 ± 25	ANISOVICH 12A	DPWA	Multichannel	
-13				
54 ± 3	¹ SHRESTHA 12A	DPWA	Multichannel	
90 ± 2	VRANA 00	DPWA	Multichannel	

¹ Statistical error only. $\Gamma(\Delta(1232)\pi, D\text{-wave})/\Gamma_{\text{total}}$

VALUE (%)	DOCUMENT ID	TECN	COMMENT	Γ_5/Γ
7.6 ± 0.3	¹ HUNT 19	DPWA	Multichannel	
10 ± 6	SOKHOYAN 15A	DPWA	Multichannel	
••• We do not use the following data for averages, fits, limits, etc. •••				
12 ± 14	ANISOVICH 12A	DPWA	Multichannel	
-7				
1 ± 1	¹ SHRESTHA 12A	DPWA	Multichannel	
4 ± 1	VRANA 00	DPWA	Multichannel	

¹ Statistical error only. $\Gamma(N\rho, S=3/2, S\text{-wave})/\Gamma_{\text{total}}$

VALUE (%)	DOCUMENT ID	TECN	COMMENT	Γ_6/Γ
27 ± 5	¹ HUNT 19	DPWA	Multichannel	
••• We do not use the following data for averages, fits, limits, etc. •••				
30 ± 3	¹ SHRESTHA 12A	DPWA	Multichannel	
1 ± 1	VRANA 00	DPWA	Multichannel	

¹ Statistical error only. $\Gamma(N(1520)\pi, P\text{-wave})/\Gamma_{\text{total}}$

VALUE (%)	DOCUMENT ID	TECN	COMMENT	Γ_7/Γ
3 ± 2	SOKHOYAN 15A	DPWA	Multichannel	

 $\Gamma(N(1535)\pi)/\Gamma_{\text{total}}$

VALUE (%)	DOCUMENT ID	TECN	COMMENT	Γ_8/Γ
1.0 ± 0.5	GUTZ 14	DPWA	Multichannel	
••• We do not use the following data for averages, fits, limits, etc. •••				
4 ± 2	HORN 08A	DPWA	Multichannel	

 $\Gamma(\Delta(1232)\eta)/\Gamma_{\text{total}}$

VALUE (%)	DOCUMENT ID	TECN	COMMENT	Γ_9/Γ
5 ± 2	GUTZ 14	DPWA	Multichannel	
••• We do not use the following data for averages, fits, limits, etc. •••				
5 ± 2	ANISOVICH 12A	DPWA	Multichannel	

 $\Gamma(N(1535)\pi)/\Gamma(\Delta(1232)\eta)$

VALUE (%)	DOCUMENT ID	TECN	COMMENT	Γ_8/Γ_9
••• We do not use the following data for averages, fits, limits, etc. •••				
0.67	KASHEVAROV 09	CBAL	$\gamma p \rightarrow p\pi^0\eta$	

 $\Delta(1700)$ PHOTON DECAY AMPLITUDES AT THE POLE $\Delta(1700) \rightarrow N\gamma, \text{helicity-1/2 amplitude } A_{1/2}$

MODULUS ($\text{GeV}^{-1/2}$)	PHASE (°)	DOCUMENT ID	TECN	COMMENT
0.163 ± 0.060	-4.4 ± 39	ROENCHEN 22	DPWA	Multichannel
0.175 ± 0.020	50 ± 10	SOKHOYAN 15A	DPWA	Multichannel
••• We do not use the following data for averages, fits, limits, etc. •••				
0.123	1.1	ROENCHEN 15A	DPWA	Multichannel

Baryon Particle Listings

 $\Delta(1700)$, $\Delta(1750)$ $\Delta(1700) \rightarrow N\gamma$, helicity-3/2 amplitude $A_{3/2}$

MODULUS ($\text{GeV}^{-1/2}$)	PHASE ($^\circ$)	DOCUMENT ID	TECN	COMMENT
0.221 ± 0.093	-12 ± 40	ROENCHEN	22	DPWA Multichannel
0.180 ± 0.020	45 ± 10	SOKHOYAN	15A	DPWA Multichannel
• • • We do not use the following data for averages, fits, limits, etc. • • •				
0.124	22	ROENCHEN	15A	DPWA Multichannel

 $\Delta(1700)$ BREIT-WIGNER PHOTON DECAY AMPLITUDES $\Delta(1700) \rightarrow N\gamma$, helicity-1/2 amplitude $A_{1/2}$

VALUE ($\text{GeV}^{-1/2}$)	DOCUMENT ID	TECN	COMMENT
0.100 to 0.160 (≈ 0.130) OUR ESTIMATE			
0.0872 ± 0.0189	GOLOVATCH 19	DPWA	$\gamma p \rightarrow \pi^+ \pi^- p$
0.156 ± 0.017	¹ HUNT 19	DPWA	Multichannel
0.165 ± 0.020	SOKHOYAN 15A	DPWA	Multichannel
0.132 ± 0.005	¹ DUGGER 13	DPWA	$\gamma N \rightarrow \pi N$
0.105 ± 0.005	¹ WORKMAN 12A	DPWA	$\gamma N \rightarrow \pi N$
• • • We do not use the following data for averages, fits, limits, etc. • • •			
0.165 ± 0.020	GUTZ 14	DPWA	Multichannel
0.160 ± 0.020	ANISOVICH 12A	DPWA	Multichannel
0.058 ± 0.010	¹ SHRESTHA 12A	DPWA	Multichannel
0.226	DRECHSEL 07	DPWA	$\gamma N \rightarrow \pi N$
0.125 ± 0.003	DUGGER 07	DPWA	$\gamma N \rightarrow \pi N$
0.096	PENNER 02D	DPWA	Multichannel

¹ Statistical error only. $\Delta(1700) \rightarrow N\gamma$, helicity-3/2 amplitude $A_{3/2}$

VALUE ($\text{GeV}^{-1/2}$)	DOCUMENT ID	TECN	COMMENT
0.090 to 0.170 (≈ 0.130) OUR ESTIMATE			
0.0872 ± 0.0164	GOLOVATCH 19	DPWA	$\gamma p \rightarrow \pi^+ \pi^- p$
0.0125 ± 0.0016	¹ HUNT 19	DPWA	Multichannel
0.170 ± 0.025	SOKHOYAN 15A	DPWA	Multichannel
0.108 ± 0.005	¹ DUGGER 13	DPWA	$\gamma N \rightarrow \pi N$
0.092 ± 0.004	¹ WORKMAN 12A	DPWA	$\gamma N \rightarrow \pi N$
• • • We do not use the following data for averages, fits, limits, etc. • • •			
0.170 ± 0.025	GUTZ 14	DPWA	Multichannel
0.165 ± 0.025	ANISOVICH 12A	DPWA	Multichannel
0.097 ± 0.008	¹ SHRESTHA 12A	DPWA	Multichannel
0.210	DRECHSEL 07	DPWA	$\gamma N \rightarrow \pi N$
0.105 ± 0.003	DUGGER 07	DPWA	$\gamma N \rightarrow \pi N$
0.154	PENNER 02D	DPWA	Multichannel

¹ Statistical error only. $\Delta(1700)$ REFERENCESFor early references, see Physics Letters **111B** 1 (1982).

ROENCHEN 22	EPJ A58 229	D. Roenchen <i>et al.</i>	(JULI, GWU, BONN+)
GOLOVATCH 19	PL B788 371	E. Golovatch <i>et al.</i>	(CLAS Collab.)
HUNT 19	PR C99 055205	B. C. Hunt, D.M. Manley	
ROENCHEN 15A	EPJ A51 70	D. Roenchen <i>et al.</i>	
SOKHOYAN 15A	EPJ A51 95	V. Sokhoyan <i>et al.</i>	(CBELSA/TAPS Collab.)
GUTZ 14	EPJ A50 74	E. Gutz <i>et al.</i>	(CBELSA/TAPS Collab.)
PDG 14	CP C38 070001	K. Olive <i>et al.</i>	(PDG Collab.)
SVARC 14	PR C89 043205	A. Svare <i>et al.</i>	(RBI Zagreb, UNI Tuzla)
DUGGER 13	PR C88 065203	M. Dugger <i>et al.</i>	(JLab CLAS Collab.)
ANISOVICH 12A	EPJ A48 15	A.V. Anisovich <i>et al.</i>	(BONN, PNPI)
SHRESTHA 12A	PR C86 055203	M. Shrestha, D.M. Manley	(KSU)
WORKMAN 12A	PR C86 015202	R. Workman <i>et al.</i>	(GWU)
KASHEVAROV 09	EPJ A42 141	V.L. Kashevarov <i>et al.</i>	(MAMI Crystal Ball/TAPS)
HORN 08A	EPJ A38 173	I. Horn <i>et al.</i>	(CB-ELSA Collab.)
Also	PR L101 202002	I. Horn <i>et al.</i>	(CB-ELSA Collab.)
DRECHSEL 07	EPJ A34 69	D. Drechsel, S.S. Kamalov, L. Tiator	(MAINZ, JINR)
DUGGER 07	PR C76 025211	M. Dugger <i>et al.</i>	(JLab CLAS Collab.)
ARNDT 06	PR C74 045205	R.A. Arndt <i>et al.</i>	(GWU)
PENNER 02C	PR C66 055211	G. Penner, U. Mosel	(GIES)
PENNER 02D	PR C66 055212	G. Penner, U. Mosel	(GIES)
VRANA 00	PRPL 328 181	T.P. Vrana, S.A. Dytman, T.-S.H. Lee	(PITT, ANL)
HOEHLER 93	πN Newsletter 9 1	G. Hohlner	(KARL)
CUTKOSKY 80	Toronto Conf. 19	R.E. Cutkosky <i>et al.</i>	(CMU, LBL) IJP
Also	PR D20 2839	R.E. Cutkosky <i>et al.</i>	(CMU, LBL) IJP
HOEHLER 79	PDAT 12-1	G. Hohlner <i>et al.</i>	(KARL) IJP
Also	Toronto Conf. 3	R. Koch	(KARL) IJP

 $\Delta(1750) 1/2^+$

$$I(J^P) = \frac{3}{2}(1/2^+) \text{ Status: } *$$

OMITTED FROM SUMMARY TABLE

 $\Delta(1750)$ POLE POSITION

REAL PART

VALUE (MeV)	DOCUMENT ID	TECN	COMMENT
• • • We do not use the following data for averages, fits, limits, etc. • • •			
1748	ARNDT 04	DPWA	$\pi N \rightarrow \pi N, \eta N$
1714	VRANA 00	DPWA	Multichannel

 $-2 \times \text{IMAGINARY PART}$

VALUE (MeV)	DOCUMENT ID	TECN	COMMENT
• • • We do not use the following data for averages, fits, limits, etc. • • •			
524	ARNDT 04	DPWA	$\pi N \rightarrow \pi N, \eta N$
68	VRANA 00	DPWA	Multichannel

 $\Delta(1750)$ ELASTIC POLE RESIDUEMODULUS $|r|$

VALUE (MeV)	DOCUMENT ID	TECN	COMMENT
• • • We do not use the following data for averages, fits, limits, etc. • • •			
48	ARNDT 04	DPWA	$\pi N \rightarrow \pi N, \eta N$

PHASE θ

VALUE ($^\circ$)	DOCUMENT ID	TECN	COMMENT
• • • We do not use the following data for averages, fits, limits, etc. • • •			
158	ARNDT 04	DPWA	$\pi N \rightarrow \pi N, \eta N$

 $\Delta(1750)$ BREIT-WIGNER MASS

VALUE (MeV)	DOCUMENT ID	TECN	COMMENT
• • • We do not use the following data for averages, fits, limits, etc. • • •			
1712 ± 1	PENNER 02C	DPWA	Multichannel
1721 ± 61	VRANA 00	DPWA	Multichannel

 $\Delta(1750)$ BREIT-WIGNER WIDTH

VALUE (MeV)	DOCUMENT ID	TECN	COMMENT
• • • We do not use the following data for averages, fits, limits, etc. • • •			
643 ± 17	PENNER 02C	DPWA	Multichannel
70 ± 50	VRANA 00	DPWA	Multichannel

 $\Delta(1750)$ DECAY MODES

Mode	Fraction (Γ_i/Γ)
Γ_1 $N\pi$	seen
Γ_2 $N(1440)\pi$	seen
Γ_3 ΣK	seen

 $\Delta(1750)$ BRANCHING RATIOS

$\Gamma(N\pi)/\Gamma_{\text{total}}$	DOCUMENT ID	TECN	COMMENT	Γ_1/Γ
• • • We do not use the following data for averages, fits, limits, etc. • • •				
1 ± 1	PENNER 02C	DPWA	Multichannel	
6 ± 9	VRANA 00	DPWA	Multichannel	

$\Gamma(N(1440)\pi)/\Gamma_{\text{total}}$	DOCUMENT ID	TECN	COMMENT	Γ_2/Γ
• • • We do not use the following data for averages, fits, limits, etc. • • •				
83 ± 1	VRANA 00	DPWA	Multichannel	

$\Gamma(\Sigma K)/\Gamma_{\text{total}}$	DOCUMENT ID	TECN	COMMENT	Γ_3/Γ
• • • We do not use the following data for averages, fits, limits, etc. • • •				
0.1 ± 0.1	PENNER 02C	DPWA	Multichannel	

 $\Delta(1750)$ BREIT-WIGNER PHOTON DECAY AMPLITUDESPapers on γN amplitudes predating 1981 may be found in our 2006 edition, Journal of Physics **G33** 1 (2006). $\Delta(1750) \rightarrow N\gamma$, helicity-1/2 amplitude $A_{1/2}$

VALUE ($\text{GeV}^{-1/2}$)	DOCUMENT ID	TECN	COMMENT
• • • We do not use the following data for averages, fits, limits, etc. • • •			
0.053	PENNER 02D	DPWA	Multichannel

 $\Delta(1750)$ REFERENCES

PDG 06	JP G33 1	W.-M. Yao <i>et al.</i>	(PDG Collab.)
ARNDT 04	PR C69 035213	R.A. Arndt <i>et al.</i>	(GWU, TRIU)
PENNER 02C	PR C66 055211	G. Penner, U. Mosel	(GIES)
PENNER 02D	PR C66 055212	G. Penner, U. Mosel	(GIES)
VRANA 00	PRPL 328 181	T.P. Vrana, S.A. Dytman, T.-S.H. Lee	(PITT, ANL)

See key on page 1171

Baryon Particle Listings
 $\Delta(1900)$

$\Delta(1900) 1/2^-$

$I(J^P) = \frac{3}{2}(\frac{1}{2}^-)$ Status: ***

Older and obsolete values are listed and referenced in the 2014 edition, Chinese Physics C38 070001 (2014).

$\Delta(1900)$ POLE POSITION

REAL PART

VALUE (MeV)	DOCUMENT ID	TECN	COMMENT
1830 to 1900 (≈ 1865) OUR ESTIMATE			
1845 \pm 20	SOKHOYAN 15A	DPWA	Multichannel
1865 \pm 35 \pm 19	¹ SVARC 14	L+P	$\pi N \rightarrow \pi N$
1870 \pm 40	CUTKOSKY 80	IPWA	$\pi N \rightarrow \pi N$
• • • We do not use the following data for averages, fits, limits, etc. • • •			
1957	HUNT 19	DPWA	Multichannel
1845 \pm 20	GUTZ 14	DPWA	Multichannel
1845 \pm 25	ANISOVICH 12A	DPWA	Multichannel
1795	VRANA 00	DPWA	Multichannel
1780	HOEHLER 93	SPED	$\pi N \rightarrow \pi N$

¹ Fit to the amplitudes of HOEHLER 79.

-2xIMAGINARY PART

VALUE (MeV)	DOCUMENT ID	TECN	COMMENT
180 to 300 (≈ 240) OUR ESTIMATE			
295 \pm 35	SOKHOYAN 15A	DPWA	Multichannel
187 \pm 50 \pm 19	¹ SVARC 14	L+P	$\pi N \rightarrow \pi N$
180 \pm 50	CUTKOSKY 80	IPWA	$\pi N \rightarrow \pi N$
• • • We do not use the following data for averages, fits, limits, etc. • • •			
447	HUNT 19	DPWA	Multichannel
295 \pm 35	GUTZ 14	DPWA	Multichannel
300 \pm 45	ANISOVICH 12A	DPWA	Multichannel
58	VRANA 00	DPWA	Multichannel

¹ Fit to the amplitudes of HOEHLER 79.

$\Delta(1900)$ ELASTIC POLE RESIDUE

MODULUS |r|

VALUE (MeV)	DOCUMENT ID	TECN	COMMENT
8 to 14 (≈ 11) OUR ESTIMATE			
11 \pm 2	SOKHOYAN 15A	DPWA	Multichannel
11 \pm 4 \pm 2	¹ SVARC 14	L+P	$\pi N \rightarrow \pi N$
10 \pm 3	CUTKOSKY 80	IPWA	$\pi N \rightarrow \pi N$
• • • We do not use the following data for averages, fits, limits, etc. • • •			
11 \pm 2	GUTZ 14	DPWA	Multichannel
10 \pm 3	ANISOVICH 12A	DPWA	Multichannel

¹ Fit to the amplitudes of HOEHLER 79.

PHASE θ

VALUE ($^\circ$)	DOCUMENT ID	TECN	COMMENT
-115 \pm 20	SOKHOYAN 15A	DPWA	Multichannel
20 \pm 27 \pm 19	¹ SVARC 14	L+P	$\pi N \rightarrow \pi N$
+ 20 \pm 40	CUTKOSKY 80	IPWA	$\pi N \rightarrow \pi N$
• • • We do not use the following data for averages, fits, limits, etc. • • •			
-115 \pm 20	GUTZ 14	DPWA	Multichannel
-125 \pm 20	ANISOVICH 12A	DPWA	Multichannel

¹ Fit to the amplitudes of HOEHLER 79.

$\Delta(1900)$ INELASTIC POLE RESIDUE

The "normalized residue" is the residue divided by $\Gamma_{pole}/2$.

Normalized residue in $N\pi \rightarrow \Delta(1900) \rightarrow \Sigma K$

MODULUS	PHASE ($^\circ$)	DOCUMENT ID	TECN	COMMENT
0.07 \pm 0.02	-50 \pm 30	ANISOVICH 12A	DPWA	Multichannel

Normalized residue in $N\pi \rightarrow \Delta(1900) \rightarrow \Delta\pi, D\text{-wave}$

MODULUS	PHASE ($^\circ$)	DOCUMENT ID	TECN	COMMENT
0.18 \pm 0.10	105 \pm 25	SOKHOYAN 15A	DPWA	Multichannel
• • • We do not use the following data for averages, fits, limits, etc. • • •				
0.12 $^{+0.08}_{-0.05}$	110 \pm 20	ANISOVICH 12A	DPWA	Multichannel

Normalized residue in $N\pi \rightarrow \Delta(1900) \rightarrow \Delta(1232)\eta$

MODULUS	PHASE ($^\circ$)	DOCUMENT ID	TECN	COMMENT
0.013 \pm 0.006	undefined	GUTZ 14	DPWA	Multichannel

Normalized residue in $N\pi \rightarrow \Delta(1900) \rightarrow N(1440)\pi$

MODULUS	PHASE ($^\circ$)	DOCUMENT ID	TECN	COMMENT
0.11 \pm 0.06	115 \pm 30	SOKHOYAN 15A	DPWA	Multichannel

Normalized residue in $N\pi \rightarrow \Delta(1900) \rightarrow N(1520)\pi$

MODULUS	PHASE ($^\circ$)	DOCUMENT ID	TECN	COMMENT
0.06 \pm 0.03	undefined	SOKHOYAN 15A	DPWA	Multichannel

$\Delta(1900)$ BREIT-WIGNER MASS

VALUE (MeV)	DOCUMENT ID	TECN	COMMENT
1840 to 1920 (≈ 1860) OUR ESTIMATE			
1989 \pm 22	¹ HUNT 19	DPWA	Multichannel
1840 \pm 20	SOKHOYAN 15A	DPWA	Multichannel
1890 \pm 50	CUTKOSKY 80	IPWA	$\pi N \rightarrow \pi N$
1908 \pm 30	HOEHLER 79	IPWA	$\pi N \rightarrow \pi N$
• • • We do not use the following data for averages, fits, limits, etc. • • •			
1840 \pm 20	GUTZ 14	DPWA	Multichannel
1840 \pm 30	ANISOVICH 12A	DPWA	Multichannel
1868 \pm 12	¹ SHRESTHA 12A	DPWA	Multichannel
1802 \pm 87	VRANA 00	DPWA	Multichannel

¹ Statistical error only.

$\Delta(1900)$ BREIT-WIGNER WIDTH

VALUE (MeV)	DOCUMENT ID	TECN	COMMENT
180 to 320 (≈ 250) OUR ESTIMATE			
457 \pm 60	¹ HUNT 19	DPWA	Multichannel
295 \pm 30	SOKHOYAN 15A	DPWA	Multichannel
170 \pm 50	CUTKOSKY 80	IPWA	$\pi N \rightarrow \pi N$
140 \pm 40	HOEHLER 79	IPWA	$\pi N \rightarrow \pi N$
• • • We do not use the following data for averages, fits, limits, etc. • • •			
295 \pm 30	GUTZ 14	DPWA	Multichannel
300 \pm 45	ANISOVICH 12A	DPWA	Multichannel
234 \pm 27	¹ SHRESTHA 12A	DPWA	Multichannel
48 \pm 45	VRANA 00	DPWA	Multichannel

¹ Statistical error only.

$\Delta(1900)$ DECAY MODES

The following branching fractions are our estimates, not fits or averages.

Mode	Fraction (Γ_i/Γ)
$\Gamma_1 N\pi$	4-12%
$\Gamma_2 \Sigma K$	seen
$\Gamma_3 N\pi\pi$	> 52%
$\Gamma_4 \Delta(1232)\pi, D\text{-wave}$	30-70%
$\Gamma_5 N\rho$	22-60%
$\Gamma_6 N\rho, S=1/2, S\text{-wave}$	11-35%
$\Gamma_7 N\rho, S=3/2, D\text{-wave}$	11-25%
$\Gamma_8 N(1440)\pi$	3-32%
$\Gamma_9 N(1520)\pi$	2-10%
$\Gamma_{10} \Delta(1232)\eta$	< 2%
$\Gamma_{11} N\gamma, \text{ helicity}=1/2$	0.06-0.43%

$\Delta(1900)$ BRANCHING RATIOS

$\Gamma(N\pi)/\Gamma_{total}$	DOCUMENT ID	TECN	COMMENT	Γ_1/Γ
4-12% OUR ESTIMATE				
3.7 \pm 0.8	¹ HUNT 19	DPWA	Multichannel	
7 \pm 2	SOKHOYAN 15A	DPWA	Multichannel	
10 \pm 3	CUTKOSKY 80	IPWA	$\pi N \rightarrow \pi N$	
8 \pm 4	HOEHLER 79	IPWA	$\pi N \rightarrow \pi N$	
• • • We do not use the following data for averages, fits, limits, etc. • • •				
7 \pm 2	GUTZ 14	DPWA	Multichannel	
7 \pm 3	ANISOVICH 12A	DPWA	Multichannel	
8 \pm 1	¹ SHRESTHA 12A	DPWA	Multichannel	
33 \pm 10	VRANA 00	DPWA	Multichannel	

¹ Statistical error only.

$\Gamma(\Delta(1232)\pi, D\text{-wave})/\Gamma_{total}$	DOCUMENT ID	TECN	COMMENT	Γ_4/Γ
30-70% OUR ESTIMATE				
42 \pm 8	¹ HUNT 19	DPWA	Multichannel	
50 \pm 20	SOKHOYAN 15A	DPWA	Multichannel	
• • • We do not use the following data for averages, fits, limits, etc. • • •				
15 $^{+50}_{-10}$	ANISOVICH 12A	DPWA	Multichannel	
56 \pm 6	¹ SHRESTHA 12A	DPWA	Multichannel	
28 \pm 1	VRANA 00	DPWA	Multichannel	

¹ Statistical error only.

Baryon Particle Listings

 $\Delta(1900)$, $\Delta(1905)$ $\Gamma(N\rho, S=1/2, S\text{-wave})/\Gamma_{\text{total}}$ Γ_6/Γ

VALUE (%)	DOCUMENT ID	TECN	COMMENT
11-35% OUR ESTIMATE			
23±12	¹ HUNT	19	DPWA Multichannel
••• We do not use the following data for averages, fits, limits, etc. •••			
12±4	¹ SHRESTHA	12A	DPWA Multichannel
30±2	VRANA	00	DPWA Multichannel
¹ Statistical error only.			

 $\Gamma(N\rho, S=3/2, D\text{-wave})/\Gamma_{\text{total}}$ Γ_7/Γ

VALUE (%)	DOCUMENT ID	TECN	COMMENT
11-25% OUR ESTIMATE			
18±7	¹ HUNT	19	DPWA Multichannel
••• We do not use the following data for averages, fits, limits, etc. •••			
23±5	¹ SHRESTHA	12A	DPWA Multichannel
5±1	VRANA	00	DPWA Multichannel
¹ Statistical error only.			

 $\Gamma(N(1440)\pi)/\Gamma_{\text{total}}$ Γ_8/Γ

VALUE (%)	DOCUMENT ID	TECN	COMMENT
3-32% OUR ESTIMATE			
12±9	¹ HUNT	19	DPWA Multichannel
20±12	SOKHOYAN	15A	DPWA Multichannel
••• We do not use the following data for averages, fits, limits, etc. •••			
<1	¹ SHRESTHA	12A	DPWA Multichannel
4±1	VRANA	00	DPWA Multichannel
¹ Statistical error only.			

 $\Gamma(N(1520)\pi)/\Gamma_{\text{total}}$ Γ_9/Γ

VALUE (%)	DOCUMENT ID	TECN	COMMENT
2-10% OUR ESTIMATE			
6±4	SOKHOYAN	15A	DPWA Multichannel

 $\Gamma(\Delta(1232)\eta)/\Gamma_{\text{total}}$ Γ_{10}/Γ

VALUE (%)	DOCUMENT ID	TECN	COMMENT
<2% OUR ESTIMATE			
1±1	GUTZ	14	DPWA Multichannel

 $\Delta(1900)$ PHOTON DECAY AMPLITUDES AT THE POLE $\Delta(1900) \rightarrow N\gamma$, helicity-1/2 amplitude $A_{1/2}$

MODULUS ($\text{GeV}^{-1/2}$)	PHASE ($^\circ$)	DOCUMENT ID	TECN	COMMENT
0.064±0.015	60±20	SOKHOYAN	15A	DPWA Multichannel

 $\Delta(1900)$ BREIT-WIGNER PHOTON DECAY AMPLITUDES $\Delta(1900) \rightarrow N\gamma$, helicity-1/2 amplitude $A_{1/2}$

VALUE ($\text{GeV}^{-1/2}$)	DOCUMENT ID	TECN	COMMENT
0.212±0.029	¹ HUNT	19	DPWA Multichannel
0.065±0.015	SOKHOYAN	15A	DPWA Multichannel
••• We do not use the following data for averages, fits, limits, etc. •••			
0.057±0.014	GUTZ	14	DPWA Multichannel
-0.082±0.009	¹ SHRESTHA	12A	DPWA Multichannel
¹ Statistical error only.			

 $\Delta(1900)$ REFERENCES

For early references, see Physics Letters **111B** 1 (1982).

HUNT	19	PR C99 055205	B.C. Hunt, D.M. Manley	
SOKHOYAN	15A	EPJ A51 95	V. Sokhoyan et al.	(CBELSA/TAPS Collab.)
GUTZ	14	EPJ A50 74	E. Gutz et al.	(CBELSA/TAPS Collab.)
PDG	14	CP C38 070001	K. Olive et al.	(PDG Collab.)
SVARC	14	PR C89 045205	A. Svarc et al.	(RBI Zagreb, UNI Tuzla)
ANISOVICH	12A	EPJ A48 15	A.V. Anisovich et al.	(BONN, PNPI)
SHRESTHA	12A	PR C86 055203	M. Shrestha, D.M. Manley	(KSU)
VRANA	00	PRPL 329 161	T.P. Vrana, S.A. Dytman, T.-S.H. Lee	(PITT, ANL)
HOEHLER	93	πN Newsletter 9 1	G. Hoehler	(KARL)
CUTKOSKY	80	Toronto Conf. 19	R.E. Cutkosky et al.	(CMU, LBL)JUP
		Also PR D20 2839	R.E. Cutkosky et al.	(CMU, LBL)JUP
HOEHLER	79	PDAT 12-1	G. Hoehler et al.	(KARLT)JUP
		Also Toronto Conf. 3	R. Koch	(KARLT)JUP

 $\Delta(1905) 5/2^+$

$$I(J^P) = \frac{3}{2}(\frac{5}{2}^+) \text{ Status: } ***$$

Older and obsolete values are listed and referenced in the 2014 edition, Chinese Physics **C38** 070001 (2014).

 $\Delta(1905)$ POLE POSITION

REAL PART	DOCUMENT ID	TECN	COMMENT
1750 to 1800 (≈ 1770) OUR ESTIMATE			
1707±1	ROENCHEN	22	DPWA Multichannel
1800±6	SOKHOYAN	15A	DPWA Multichannel
1752±3±2	¹ SVARC	14	L+P $\pi N \rightarrow \pi N$
1830±40	CUTKOSKY	80	IPWA $\pi N \rightarrow \pi N$

••• We do not use the following data for averages, fits, limits, etc. •••

1819	HUNT	19	DPWA Multichannel
1795	ROENCHEN	15A	DPWA Multichannel
1800±6	GUTZ	14	DPWA Multichannel
1805±10	ANISOVICH	12A	DPWA Multichannel
1819	ARNDT	06	DPWA $\pi N \rightarrow \pi N, \eta N$
1793	VRANA	00	DPWA Multichannel
1829	HOEHLER	93	SPED $\pi N \rightarrow \pi N$
¹ Fit to the amplitudes of HOEHLER 79.			

 $-2 \times \text{IMAGINARY PART}$

VALUE (MeV)	DOCUMENT ID	TECN	COMMENT
260 to 340 (≈ 300) OUR ESTIMATE			
127±4	ROENCHEN	22	DPWA Multichannel
290±15	SOKHOYAN	15A	DPWA Multichannel
346±6±2	¹ SVARC	14	L+P $\pi N \rightarrow \pi N$
280±60	CUTKOSKY	80	IPWA $\pi N \rightarrow \pi N$
••• We do not use the following data for averages, fits, limits, etc. •••			
253	HUNT	19	DPWA Multichannel
247	ROENCHEN	15A	DPWA Multichannel
290±15	GUTZ	14	DPWA Multichannel
300±15	ANISOVICH	12A	DPWA Multichannel
247	ARNDT	06	DPWA $\pi N \rightarrow \pi N, \eta N$
302	VRANA	00	DPWA Multichannel
303	HOEHLER	93	SPED $\pi N \rightarrow \pi N$
¹ Fit to the amplitudes of HOEHLER 79.			

 $\Delta(1905)$ ELASTIC POLE RESIDUEMODULUS $|r|$

VALUE (MeV)	DOCUMENT ID	TECN	COMMENT
15 to 25 (≈ 20) OUR ESTIMATE			
3.7±1.0	ROENCHEN	22	DPWA Multichannel
19±2	SOKHOYAN	15A	DPWA Multichannel
24±1±1	¹ SVARC	14	L+P $\pi N \rightarrow \pi N$
25±8	CUTKOSKY	80	IPWA $\pi N \rightarrow \pi N$
••• We do not use the following data for averages, fits, limits, etc. •••			
5.3	ROENCHEN	15A	DPWA Multichannel
19±2	GUTZ	14	DPWA Multichannel
20±2	ANISOVICH	12A	DPWA Multichannel
15	ARNDT	06	DPWA $\pi N \rightarrow \pi N, \eta N$
25	HOEHLER	93	SPED $\pi N \rightarrow \pi N$
¹ Fit to the amplitudes of HOEHLER 79.			

PHASE θ

VALUE ($^\circ$)	DOCUMENT ID	TECN	COMMENT
-120 to -30 (≈ -45) OUR ESTIMATE			
-92±6	ROENCHEN	22	DPWA Multichannel
-45±4	SOKHOYAN	15A	DPWA Multichannel
-114±1±2	¹ SVARC	14	L+P $\pi N \rightarrow \pi N$
-50±20	CUTKOSKY	80	IPWA $\pi N \rightarrow \pi N$
••• We do not use the following data for averages, fits, limits, etc. •••			
-89	ROENCHEN	15A	DPWA Multichannel
-45±4	GUTZ	14	DPWA Multichannel
-44±5	ANISOVICH	12A	DPWA Multichannel
-30	ARNDT	06	DPWA $\pi N \rightarrow \pi N, \eta N$
¹ Fit to the amplitudes of HOEHLER 79.			

 $\Delta(1905)$ INELASTIC POLE RESIDUE

The "normalized residue" is the residue divided by $\Gamma_{\text{pole}}/2$.

Normalized residue in $N\pi \rightarrow \Delta(1905) \rightarrow \Delta\pi, P\text{-wave}$

MODULUS	PHASE ($^\circ$)	DOCUMENT ID	TECN	COMMENT
0.10±0.01	-109±7	ROENCHEN	22	DPWA Multichannel
0.19±0.07	10±30	SOKHOYAN	15A	DPWA Multichannel
••• We do not use the following data for averages, fits, limits, etc. •••				
0.0870	72	ROENCHEN	15A	DPWA Multichannel
0.25±0.06	0±15	ANISOVICH	12A	DPWA Multichannel

Normalized residue in $N\pi \rightarrow \Delta(1905) \rightarrow \Delta\pi, F\text{-wave}$

MODULUS	PHASE ($^\circ$)	DOCUMENT ID	TECN	COMMENT
0.017±0.002	18±8	ROENCHEN	22	DPWA Multichannel
••• We do not use the following data for averages, fits, limits, etc. •••				
0.009	64	ROENCHEN	15A	DPWA Multichannel

Normalized residue in $N\pi \rightarrow \Delta(1905) \rightarrow \Sigma K$

MODULUS	PHASE ($^\circ$)	DOCUMENT ID	TECN	COMMENT
0.0020±0.0002	154±6	ROENCHEN	22	DPWA Multichannel
••• We do not use the following data for averages, fits, limits, etc. •••				
0.001	-155	ROENCHEN	15A	DPWA Multichannel

Normalized residue in $N\pi \rightarrow \Delta(1905) \rightarrow N(1535)\pi$

MODULUS	PHASE ($^\circ$)	DOCUMENT ID	TECN	COMMENT
0.025±0.010	130±35	GUTZ	14	DPWA Multichannel

See key on page 1171

Baryon Particle Listings
 $\Delta(1905)$ Normalized residue in $N\pi \rightarrow \Delta(1905) \rightarrow \Delta(1232)\eta$

MODULUS	PHASE (°)	DOCUMENT ID	TECN	COMMENT
0.07±0.02	40 ± 20	GUTZ	14	DPWA Multichannel

 $\Delta(1905)$ BREIT-WIGNER MASS

VALUE (MeV)	DOCUMENT ID	TECN	COMMENT
1855 to 1910 (≈ 1880) OUR ESTIMATE			
1883 ± 19	GOLOVATCH 19	DPWA	$\gamma p \rightarrow \pi^+ \pi^- p$
1866 ± 9	¹ HUNT 19	DPWA	Multichannel
1856 ± 6	SOKHOYAN 15A	DPWA	Multichannel
1857.8 ± 1.6	¹ ARNDT 06	DPWA	$\pi N \rightarrow \pi N, \eta N$
1910 ± 30	CUTKOSKY 80	IPWA	$\pi N \rightarrow \pi N$
1905 ± 20	HOEHLER 79	IPWA	$\pi N \rightarrow \pi N$
• • • We do not use the following data for averages, fits, limits, etc. • • •			
1856 ± 6	GUTZ 14	DPWA	Multichannel
1861 ± 6	ANISOVICH 12A	DPWA	Multichannel
1818 ± 8	¹ SHRESTHA 12A	DPWA	Multichannel
1873 ± 77	VRANA 00	DPWA	Multichannel

¹ Statistical error only. $\Delta(1905)$ BREIT-WIGNER WIDTH

VALUE (MeV)	DOCUMENT ID	TECN	COMMENT
270 to 400 (≈ 330) OUR ESTIMATE			
327 ± 69	GOLOVATCH 19	DPWA	$\gamma p \rightarrow \pi^+ \pi^- p$
289 ± 20	¹ HUNT 19	DPWA	Multichannel
325 ± 15	SOKHOYAN 15A	DPWA	Multichannel
320.6 ± 8.6	¹ ARNDT 06	DPWA	$\pi N \rightarrow \pi N, \eta N$
400 ± 100	CUTKOSKY 80	IPWA	$\pi N \rightarrow \pi N$
260 ± 20	HOEHLER 79	IPWA	$\pi N \rightarrow \pi N$
• • • We do not use the following data for averages, fits, limits, etc. • • •			
325 ± 15	GUTZ 14	DPWA	Multichannel
335 ± 18	ANISOVICH 12A	DPWA	Multichannel
278 ± 18	¹ SHRESTHA 12A	DPWA	Multichannel
461 ± 111	VRANA 00	DPWA	Multichannel

¹ Statistical error only. $\Delta(1905)$ DECAY MODES

The following branching fractions are our estimates, not fits or averages.

Mode	Fraction (Γ_i/Γ)
Γ_1 $N\pi$	9–15%
Γ_2 $N\pi\pi$	>65%
Γ_3 $\Delta(1232)\pi$	>48%
Γ_4 $\Delta(1232)\pi, P$ -wave	8–43%
Γ_5 $\Delta(1232)\pi, F$ -wave	40–58%
Γ_6 $N\rho, S=3/2, P$ -wave	17–35%
Γ_7 $N(1535)\pi$	< 1%
Γ_8 $N(1680)\pi, P$ -wave	5–15%
Γ_9 $\Delta(1232)\eta$	2–6%
Γ_{10} $N\gamma$	0.012–0.036 %
Γ_{11} $N\gamma, \text{helicity}=1/2$	0.002–0.006 %
Γ_{12} $N\gamma, \text{helicity}=3/2$	0.01–0.03 %

 $\Delta(1905)$ BRANCHING RATIOS

$\Gamma(N\pi)/\Gamma_{\text{total}}$	DOCUMENT ID	TECN	COMMENT	Γ_1/Γ
9–15% OUR ESTIMATE				
17 ± 1	¹ HUNT 19	DPWA	Multichannel	
13 ± 2	SOKHOYAN 15A	DPWA	Multichannel	
12.2 ± 0.1	¹ ARNDT 06	DPWA	$\pi N \rightarrow \pi N, \eta N$	
8 ± 3	CUTKOSKY 80	IPWA	$\pi N \rightarrow \pi N$	
15 ± 2	HOEHLER 79	IPWA	$\pi N \rightarrow \pi N$	
• • • We do not use the following data for averages, fits, limits, etc. • • •				
13 ± 2	GUTZ 14	DPWA	Multichannel	
13 ± 2	ANISOVICH 12A	DPWA	Multichannel	
6 ± 1	¹ SHRESTHA 12A	DPWA	Multichannel	
9 ± 1	VRANA 00	DPWA	Multichannel	

¹ Statistical error only.

$\Gamma(N\pi\pi)/\Gamma_{\text{total}}$	DOCUMENT ID	TECN	COMMENT	Γ_2/Γ
>65% OUR ESTIMATE				
0.85 ± 0.15	GOLOVATCH 19	DPWA	$\gamma p \rightarrow \pi^+ \pi^- p$	

$\Gamma(\Delta(1232)\pi, P\text{-wave})/\Gamma_{\text{total}}$	DOCUMENT ID	TECN	COMMENT	Γ_4/Γ
8–43% OUR ESTIMATE				
8.4 ± 0.5	¹ HUNT 19	DPWA	Multichannel	
33 ± 10	SOKHOYAN 15A	DPWA	Multichannel	

• • • We do not use the following data for averages, fits, limits, etc. • • •

45 ± 14	ANISOVICH 12A	DPWA	Multichannel
28 ± 7	¹ SHRESTHA 12A	DPWA	Multichannel
23 ± 1	VRANA 00	DPWA	Multichannel

¹ Statistical error only.

$\Gamma(\Delta(1232)\pi, F\text{-wave})/\Gamma_{\text{total}}$	DOCUMENT ID	TECN	COMMENT	Γ_5/Γ
40–58% OUR ESTIMATE				
49 ± 9	¹ HUNT 19	DPWA	Multichannel	

• • • We do not use the following data for averages, fits, limits, etc. • • •

64 ± 8	¹ SHRESTHA 12A	DPWA	Multichannel
44 ± 1	VRANA 00	DPWA	Multichannel

¹ Statistical error only.

$\Gamma(N\rho, S=3/2, P\text{-wave})/\Gamma_{\text{total}}$	DOCUMENT ID	TECN	COMMENT	Γ_6/Γ
17–35% OUR ESTIMATE				
26 ± 9	¹ HUNT 19	DPWA	Multichannel	

• • • We do not use the following data for averages, fits, limits, etc. • • •

< 6	¹ SHRESTHA 12A	DPWA	Multichannel
24 ± 1	VRANA 00	DPWA	Multichannel

¹ Statistical error only.

$\Gamma(N(1535)\pi)/\Gamma_{\text{total}}$	DOCUMENT ID	TECN	COMMENT	Γ_7/Γ
< 1% OUR ESTIMATE				
< 1	GUTZ 14	DPWA	Multichannel	

$\Gamma(N(1680)\pi, P\text{-wave})/\Gamma_{\text{total}}$	DOCUMENT ID	TECN	COMMENT	Γ_8/Γ
5–15% OUR ESTIMATE				
10 ± 5	SOKHOYAN 15A	DPWA	Multichannel	

$\Gamma(\Delta(1232)\eta)/\Gamma_{\text{total}}$	DOCUMENT ID	TECN	COMMENT	Γ_9/Γ
2–6% OUR ESTIMATE				
4 ± 2	GUTZ 14	DPWA	Multichannel	

 $\Delta(1905)$ PHOTON DECAY AMPLITUDES AT THE POLE $\Delta(1905) \rightarrow N\gamma, \text{helicity-1/2 amplitude } A_{1/2}$

MODULUS ($\text{GeV}^{-1/2}$)	PHASE (°)	DOCUMENT ID	TECN	COMMENT
0.055 ± 0.004	–159 ± 2	ROENCHEN 22	DPWA	Multichannel
0.025 ± 0.005	–28 ± 12	SOKHOYAN 15A	DPWA	Multichannel
• • • We do not use the following data for averages, fits, limits, etc. • • •				
0.053	89	ROENCHEN 15A	DPWA	Multichannel

 $\Delta(1905) \rightarrow N\gamma, \text{helicity-3/2 amplitude } A_{3/2}$

MODULUS ($\text{GeV}^{-1/2}$)	PHASE (°)	DOCUMENT ID	TECN	COMMENT
–0.168 ± 0.020	172 ± 0.9	ROENCHEN 22	DPWA	Multichannel
–0.050 ± 0.004	5 ± 10	SOKHOYAN 15A	DPWA	Multichannel
• • • We do not use the following data for averages, fits, limits, etc. • • •				
–0.030	80	ROENCHEN 15A	DPWA	Multichannel

 $\Delta(1905)$ BREIT-WIGNER PHOTON DECAY AMPLITUDES $\Delta(1905) \rightarrow N\gamma, \text{helicity-1/2 amplitude } A_{1/2}$

VALUE ($\text{GeV}^{-1/2}$)	DOCUMENT ID	TECN	COMMENT
0.017 to 0.027 (≈ 0.022) OUR ESTIMATE			
0.019 ± 0.0076	GOLOVATCH 19	DPWA	$\gamma p \rightarrow \pi^+ \pi^- p$
0.077 ± 0.010	¹ HUNT 19	DPWA	Multichannel
0.025 ± 0.005	SOKHOYAN 15A	DPWA	Multichannel
0.020 ± 0.002	¹ DUGGER 13	DPWA	$\gamma N \rightarrow \pi N$
0.019 ± 0.002	¹ WORKMAN 12A	DPWA	$\gamma N \rightarrow \pi N$
• • • We do not use the following data for averages, fits, limits, etc. • • •			
0.025 ± 0.005	GUTZ 14	DPWA	Multichannel
0.025 ± 0.004	ANISOVICH 12A	DPWA	Multichannel
0.066 ± 0.018	¹ SHRESTHA 12A	DPWA	Multichannel
0.018	DRECHSEL 07	DPWA	$\gamma N \rightarrow \pi N$

¹ Statistical error only. $\Delta(1905) \rightarrow N\gamma, \text{helicity-3/2 amplitude } A_{3/2}$

VALUE ($\text{GeV}^{-1/2}$)	DOCUMENT ID	TECN	COMMENT
–0.055 to –0.035 (≈ –0.045) OUR ESTIMATE			
–0.0432 ± 0.0173	GOLOVATCH 19	DPWA	$\gamma p \rightarrow \pi^+ \pi^- p$
–0.053 ± 0.029	¹ HUNT 19	DPWA	Multichannel
–0.050 ± 0.005	SOKHOYAN 15A	DPWA	Multichannel
–0.049 ± 0.005	¹ DUGGER 13	DPWA	$\gamma N \rightarrow \pi N$
–0.038 ± 0.004	WORKMAN 12A	DPWA	$\gamma N \rightarrow \pi N$

Baryon Particle Listings

 $\Delta(1905)$, $\Delta(1910)$

••• We do not use the following data for averages, fits, limits, etc. •••

-0.050 ± 0.005	GUTZ	14	DPWA	Multichannel
-0.049 ± 0.004	ANISOVICH	12A	DPWA	Multichannel
-0.223 ± 0.029	¹ SHRESTHA	12A	DPWA	Multichannel
-0.028	DRECHSEL	07	DPWA	$\gamma N \rightarrow \pi N$

¹ Statistical error only.

 $\Delta(1905)$ REFERENCES

For early references, see Physics Letters **111B** 1 (1982).

ROENCHEN	22	EPJ A58 229	D. Roenchen <i>et al.</i>	(JULI, GWU, BONN+)
GOLOVATICH	19	PL B788 371	E. Golovatch <i>et al.</i>	(CLAS Collab.)
HUNT	19	PR C99 055205	B. C. Hunt, D.M. Manley	
ROENCHEN	15A	EPJ A51 70	D. Roenchen <i>et al.</i>	
SOKHOYAN	15A	EPJ A51 95	V. Sokhoyan <i>et al.</i>	(CBELSA/TAPS Collab.)
GUTZ	14	EPJ A50 74	E. Gutz <i>et al.</i>	(CBELSA/TAPS Collab.)
PDG	14	CP C38 070001	K. Olive <i>et al.</i>	(PDG Collab.)
SVARC	14	PR C89 045205	A. Svarc <i>et al.</i>	(RBI Zagreb, UNI Tuzla)
DUGGER	13	PR C88 065203	M. Dugger <i>et al.</i>	(JLab CLAS Collab.)
ANISOVICH	12A	EPJ A48 15	A.V. Anisovich <i>et al.</i>	(BONN, PNPI)
SHRESTHA	12A	PR C86 055203	M. Shrestha, D.M. Manley	(KSU)
WORKMAN	12A	PR C86 015202	R. Workman <i>et al.</i>	(GWU)
DRECHSEL	07	EPJ A34 69	D. Drechsel, S.S. Kamalov, L. Tiator	(MAINZ, JINR)
ARNDT	06	PR C74 045205	R.A. Arndt <i>et al.</i>	(GWU)
VRANA	00	PRPL 328 181	T.P. Vrana, S.A. Dytman, T.-S.H. Lee	(PITT, ANL)
HOEHLER	93	πN Newsletter 9 1	G. Hohler <i>et al.</i>	(KARL)
CUTKOSKY	80	Toronto Conf. 19	R.E. Cutkosky <i>et al.</i>	(CMU, LBL) IUP
Also		PR D20 2839	R.E. Cutkosky <i>et al.</i>	(CMU, LBL) IUP
HOEHLER	79	PDAT 12-1	G. Hohler <i>et al.</i>	(KARLT) IUP
Also		Toronto Conf. 3	R. Koch	(KARLT) IUP

$$\Delta(1910) 1/2^+$$

$$I(J^P) = \frac{3}{2}(\frac{1}{2}^+) \text{ Status: } ***$$

Older and obsolete values are listed and referenced in the 2014 edition, Chinese Physics **C38** 070001 (2014).

 $\Delta(1910)$ POLE POSITION

REAL PART

VALUE (MeV)	DOCUMENT ID	TECN	COMMENT
1800 to 1900 (≈ 1850) OUR ESTIMATE			
1802 ± 6	ROENCHEN	22	DPWA Multichannel
1840 ± 40	SOKHOYAN	15A	DPWA Multichannel
1896 ± 11	¹ SVARC	14	L+P $\pi N \rightarrow \pi N$
1880 ± 30	CUTKOSKY	80	IPWA $\pi N \rightarrow \pi N$
••• We do not use the following data for averages, fits, limits, etc. •••			
1801	HUNT	19	DPWA Multichannel
1799	ROENCHEN	15A	DPWA Multichannel
1840 ± 40	GUTZ	14	DPWA Multichannel
1850 ± 40	ANISOVICH	12A	DPWA Multichannel
1771	ARNDT	06	DPWA $\pi N \rightarrow \pi N, \eta N$
1880	VRANA	00	DPWA Multichannel
1874	HOEHLER	93	SPED $\pi N \rightarrow \pi N$

¹ Fit to the amplitudes of HOEHLER 79.

 $-2 \times$ IMAGINARY PART

VALUE (MeV)	DOCUMENT ID	TECN	COMMENT
200 to 500 (≈ 350) OUR ESTIMATE			
550 ± 11	ROENCHEN	22	DPWA Multichannel
370 ± 60	SOKHOYAN	15A	DPWA Multichannel
302 ± 22	¹ SVARC	14	L+P $\pi N \rightarrow \pi N$
200 ± 40	CUTKOSKY	80	IPWA $\pi N \rightarrow \pi N$
••• We do not use the following data for averages, fits, limits, etc. •••			
224	HUNT	19	DPWA Multichannel
648	ROENCHEN	15A	DPWA Multichannel
370 ± 60	GUTZ	14	DPWA Multichannel
350 ± 45	ANISOVICH	12A	DPWA Multichannel
479	ARNDT	06	DPWA $\pi N \rightarrow \pi N, \eta N$
496	VRANA	00	DPWA Multichannel
283	HOEHLER	93	SPED $\pi N \rightarrow \pi N$

¹ Fit to the amplitudes of HOEHLER 79.

 $\Delta(1910)$ ELASTIC POLE RESIDUEMODULUS $|r|$

VALUE (MeV)	DOCUMENT ID	TECN	COMMENT
20 to 30 (≈ 25) OUR ESTIMATE			
35 ± 13	ROENCHEN	22	DPWA Multichannel
25 ± 6	SOKHOYAN	15A	DPWA Multichannel
29 ± 2	¹ SVARC	14	L+P $\pi N \rightarrow \pi N$
20 ± 4	CUTKOSKY	80	IPWA $\pi N \rightarrow \pi N$
••• We do not use the following data for averages, fits, limits, etc. •••			
90	ROENCHEN	15A	DPWA Multichannel
25 ± 6	GUTZ	14	DPWA Multichannel
24 ± 6	ANISOVICH	12A	DPWA Multichannel
45	ARNDT	06	DPWA $\pi N \rightarrow \pi N, \eta N$
38	HOEHLER	93	SPED $\pi N \rightarrow \pi N$

¹ Fit to the amplitudes of HOEHLER 79.

PHASE θ

VALUE ($^\circ$)	DOCUMENT ID	TECN	COMMENT
-180 to 90 (≈ -90) OUR ESTIMATE			
93 ± 7	ROENCHEN	22	DPWA Multichannel
-155 ± 30	SOKHOYAN	15A	DPWA Multichannel
$-83 \pm 4 \pm 1$	¹ SVARC	14	L+P $\pi N \rightarrow \pi N$
-90 ± 30	CUTKOSKY	80	IPWA $\pi N \rightarrow \pi N$
••• We do not use the following data for averages, fits, limits, etc. •••			
-83	ROENCHEN	15A	DPWA Multichannel
-155 ± 30	GUTZ	14	DPWA Multichannel
-145 ± 30	ANISOVICH	12A	DPWA Multichannel
$+172$	ARNDT	06	DPWA $\pi N \rightarrow \pi N, \eta N$

¹ Fit to the amplitudes of HOEHLER 79.

 $\Delta(1910)$ INELASTIC POLE RESIDUE

The "normalized residue" is the residue divided by $\Gamma_{pole}/2$.

Normalized residue in $N\pi \rightarrow \Delta(1910) \rightarrow \Sigma K$

MODULUS	PHASE ($^\circ$)	DOCUMENT ID	TECN	COMMENT
0.002 ± 0.002	138 ± 10	ROENCHEN	22	DPWA Multichannel
0.07 ± 0.02	-110 ± 30	ANISOVICH	12A	DPWA Multichannel
••• We do not use the following data for averages, fits, limits, etc. •••				
0.019	-123	ROENCHEN	15A	DPWA Multichannel

Normalized residue in $N\pi \rightarrow \Delta(1910) \rightarrow \Delta\pi, P$ -wave

MODULUS	PHASE ($^\circ$)	DOCUMENT ID	TECN	COMMENT
0.24 ± 0.09	-42 ± 7	ROENCHEN	22	DPWA Multichannel
0.24 ± 0.10	85 ± 35	SOKHOYAN	15A	DPWA Multichannel
••• We do not use the following data for averages, fits, limits, etc. •••				
0.58	131	ROENCHEN	15A	DPWA Multichannel
0.16 ± 0.09	95 ± 40	ANISOVICH	12A	DPWA Multichannel

Normalized residue in $N\pi \rightarrow \Delta(1910) \rightarrow \Delta(1232)\eta$

MODULUS	PHASE ($^\circ$)	DOCUMENT ID	TECN	COMMENT
0.11 ± 0.04	-150 ± 50	GUTZ	14	DPWA Multichannel

Normalized residue in $N\pi \rightarrow \Delta(1910) \rightarrow N(1440)\pi$

MODULUS	PHASE ($^\circ$)	DOCUMENT ID	TECN	COMMENT
0.06 ± 0.03	170 ± 45	SOKHOYAN	15A	DPWA Multichannel

 $\Delta(1910)$ BREIT-WIGNER MASS

VALUE (MeV)	DOCUMENT ID	TECN	COMMENT
1850 to 1950 (≈ 1900) OUR ESTIMATE			
1846 ± 18	¹ HUNT	19	DPWA Multichannel
1845 ± 40	SOKHOYAN	15A	DPWA Multichannel
2067.9 ± 1.7	¹ ARNDT	06	DPWA $\pi N \rightarrow \pi N, \eta N$
1910 ± 40	CUTKOSKY	80	IPWA $\pi N \rightarrow \pi N$
1888 ± 20	HOEHLER	79	IPWA $\pi N \rightarrow \pi N$
••• We do not use the following data for averages, fits, limits, etc. •••			
1845 ± 40	GUTZ	14	DPWA Multichannel
1860 ± 40	ANISOVICH	12A	DPWA Multichannel
1934 ± 5	¹ SHRESTHA	12A	DPWA Multichannel
1995 ± 12	VRANA	00	DPWA Multichannel

¹ Statistical error only.

 $\Delta(1910)$ BREIT-WIGNER WIDTH

VALUE (MeV)	DOCUMENT ID	TECN	COMMENT
200 to 400 (≈ 300) OUR ESTIMATE			
260 ± 57	¹ HUNT	19	DPWA Multichannel
360 ± 60	SOKHOYAN	15A	DPWA Multichannel
543 ± 10	¹ ARNDT	06	DPWA $\pi N \rightarrow \pi N, \eta N$
225 ± 50	CUTKOSKY	80	IPWA $\pi N \rightarrow \pi N$
280 ± 50	HOEHLER	79	IPWA $\pi N \rightarrow \pi N$
••• We do not use the following data for averages, fits, limits, etc. •••			
360 ± 60	GUTZ	14	DPWA Multichannel
350 ± 55	ANISOVICH	12A	DPWA Multichannel
211 ± 11	¹ SHRESTHA	12A	DPWA Multichannel
713 ± 465	VRANA	00	DPWA Multichannel

¹ Statistical error only.

 $\Delta(1910)$ DECAY MODES

The following branching fractions are our estimates, not fits or averages.

Mode	Fraction (Γ_i/Γ)
Γ_1 $N\pi$	10–30%
Γ_2 ΣK	4–14%
Γ_3 $\Delta(1232)\pi$	34–66%
Γ_4 $N(1440)\pi$	3–45%
Γ_5 $\Delta(1232)\eta$	5–13%
Γ_6 $N\gamma$, helicity=1/2	0.0–0.02%

$\Delta(1910)$ BRANCHING RATIOS

$\Gamma(N\pi)/\Gamma_{total}$	DOCUMENT ID	TECN	COMMENT	Γ_1/Γ
10-30% OUR ESTIMATE				
13 ± 3	¹ HUNT	19	DPWA Multichannel	
12 ± 3	SOKHOYAN	15A	DPWA Multichannel	
23.9 ± 0.1	¹ ARNDT	06	DPWA $\pi N \rightarrow \pi N, \eta N$	
19 ± 3	CUTKOSKY	80	IPWA $\pi N \rightarrow \pi N$	
24 ± 6	HOEHLER	79	IPWA $\pi N \rightarrow \pi N$	
• • • We do not use the following data for averages, fits, limits, etc. • • •				
12 ± 3	GUTZ	14	DPWA Multichannel	
12 ± 3	ANISOVICH	12A	DPWA Multichannel	
17 ± 1	¹ SHRESTHA	12A	DPWA Multichannel	
29 ± 21	VRANA	00	DPWA Multichannel	

¹ Statistical error only.

$\Gamma(\Sigma K)/\Gamma_{total}$	DOCUMENT ID	TECN	COMMENT	Γ_2/Γ
4-14% OUR ESTIMATE				
9 ± 5	ANISOVICH	12A	DPWA Multichannel	

$\Gamma(\Delta(1232)\pi)/\Gamma_{total}$	DOCUMENT ID	TECN	COMMENT	Γ_3/Γ
34-66% OUR ESTIMATE				
50 ± 16	SOKHOYAN	15A	DPWA Multichannel	
• • • We do not use the following data for averages, fits, limits, etc. • • •				
60 ± 28	ANISOVICH	12A	DPWA Multichannel	

$\Gamma(N(1440)\pi)/\Gamma_{total}$	DOCUMENT ID	TECN	COMMENT	Γ_4/Γ
3-45% OUR ESTIMATE				
33 ± 12	¹ HUNT	19	DPWA Multichannel	
6 ± 3	SOKHOYAN	15A	DPWA Multichannel	
• • • We do not use the following data for averages, fits, limits, etc. • • •				
47 ± 6	¹ SHRESTHA	12A	DPWA Multichannel	
56 ± 7	VRANA	00	DPWA Multichannel	

¹ Statistical error only.

$\Gamma(\Delta(1232)\eta)/\Gamma_{total}$	DOCUMENT ID	TECN	COMMENT	Γ_5/Γ
5-13% OUR ESTIMATE				
9 ± 4	GUTZ	14	DPWA Multichannel	

$\Delta(1910)$ PHOTON DECAY AMPLITUDES AT THE POLE

$\Delta(1910) \rightarrow N\gamma$, helicity-1/2 amplitude $A_{1/2}$	MODULUS (GeV ^{-1/2})	PHASE (°)	DOCUMENT ID	TECN	COMMENT
	-0.446 ± 0.036	-70 ± 11	ROENCHEN	22	DPWA Multichannel
	0.027 ± 0.009	-30 ± 60	SOKHOYAN	15A	DPWA Multichannel
• • • We do not use the following data for averages, fits, limits, etc. • • •					
	0.321	39	ROENCHEN	15A	DPWA Multichannel

$\Delta(1910)$ BREIT-WIGNER PHOTON DECAY AMPLITUDES

$\Delta(1910) \rightarrow N\gamma$, helicity-1/2 amplitude $A_{1/2}$	VALUE (GeV ^{-1/2})	DOCUMENT ID	TECN	COMMENT
0.010 to 0.030 (≈ 0.020) OUR ESTIMATE				
	0.203 ± 0.056	¹ HUNT	19	DPWA Multichannel
	0.026 ± 0.008	SOKHOYAN	15A	DPWA Multichannel
	-0.002 ± 0.008	¹ ARNDT	96	IPWA $\gamma N \rightarrow \pi N$
• • • We do not use the following data for averages, fits, limits, etc. • • •				
	0.026 ± 0.008	GUTZ	14	DPWA Multichannel
	0.022 ± 0.009	ANISOVICH	12A	DPWA Multichannel
	0.030 ± 0.002	¹ SHRESTHA	12A	DPWA Multichannel

¹ Statistical error only.

$\Delta(1910)$ REFERENCES

For early references, see Physics Letters **111B** 1 (1982).

ROENCHEN 22	EPJ A58 229	D. Roenchen et al.	(JULI, GWU, BONN+)
HUNT 19	PR C9 055205	B.C. Hunt, D.M. Manley	
ROENCHEN 15A	EPJ A51 70	D. Roenchen et al.	
SOKHOYAN 15A	EPJ A51 95	V. Sokhoyan et al.	(CBELSA/TAPS Collab.)
GUTZ 14	EPJ A50 74	E. Gutz et al.	(CBELSA/TAPS Collab.)
PDG 14	CP C38 070001	K. Olive et al.	(PDG Collab.)
SVARC 14	PR C89 045205	A. Svarc et al.	(RBI Zagreb, UNI Tuzla)
ANISOVICH 12A	EPJ A48 15	A.V. Anisovich et al.	(BONN, PNPI)
SHRESTHA 12A	PR C86 055203	M. Shrestha, D.M. Manley	(KSU)
ARNDT 06	PR C74 045205	R.A. Arndt et al.	(GWU)
VRANA 00	PRPL 328 181	T.P. Vrana, S.A. Dytman, T.-S.H. Lee	(PITT, ANL)
ARNDT 96	PR C53 430	R.A. Arndt, I.I. Strakovsky, R.L. Workman	(VPI)
HOEHLER 93	πN Newsletter 9 1	G. Hoehler	(KARL)
CUTKOSKY 80	Toronto Conf. 19	R.E. Cutkosky et al.	(CMU, LBL) JUP
Also	PR D20 2839	R.E. Cutkosky et al.	(CMU, LBL) JUP
HOEHLER 79	PDAT 12-1	G. Hoehler et al.	(KARLT) JUP
Also	Toronto Conf. 3	R. Koch	(KARLT) JUP

$\Delta(1920) 3/2^+$

$I(J^P) = \frac{3}{2}(\frac{3}{2}^+)$ Status: ***

Older and obsolete values are listed and referenced in the 2014 edition, Chinese Physics **C38** 070001 (2014).

$\Delta(1920)$ POLE POSITION

REAL PART	DOCUMENT ID	TECN	COMMENT
1850 to 1950 (≈ 1900) OUR ESTIMATE			
1883 ± 2	ROENCHEN	22	DPWA Multichannel
1875 ± 30	SOKHOYAN	15A	DPWA Multichannel
1906 ± 10 ± 2	¹ SVARC	14	L+P $\pi N \rightarrow \pi N$
1900 ± 80	CUTKOSKY	80	IPWA $\pi N \rightarrow \pi N$
• • • We do not use the following data for averages, fits, limits, etc. • • •			
1910	HUNT	19	DPWA Multichannel
1715	ROENCHEN	15A	DPWA Multichannel
1875 ± 30	GUTZ	14	DPWA Multichannel
1890 ± 30	ANISOVICH	12A	DPWA Multichannel
1880	VRANA	00	DPWA Multichannel
1900	HOEHLER	93	SPED $\pi N \rightarrow \pi N$

¹ Fit to the amplitudes of HOEHLER 79.

-2xIMAGINARY PART

VALUE (MeV)	DOCUMENT ID	TECN	COMMENT
200 to 400 (≈ 300) OUR ESTIMATE			
844 ± 5	ROENCHEN	22	DPWA Multichannel
300 ± 40	SOKHOYAN	15A	DPWA Multichannel
310 ± 20 ± 11	¹ SVARC	14	L+P $\pi N \rightarrow \pi N$
300 ± 100	CUTKOSKY	80	IPWA $\pi N \rightarrow \pi N$
• • • We do not use the following data for averages, fits, limits, etc. • • •			
472	HUNT	19	DPWA Multichannel
882	ROENCHEN	15A	DPWA Multichannel
300 ± 40	GUTZ	14	DPWA Multichannel
300 ± 60	ANISOVICH	12A	DPWA Multichannel
120	VRANA	00	DPWA Multichannel

¹ Fit to the amplitudes of HOEHLER 79.

$\Delta(1920)$ ELASTIC POLE RESIDUE

MODULUS r	DOCUMENT ID	TECN	COMMENT
15 to 35 (≈ 25) OUR ESTIMATE			
41 ± 3	ROENCHEN	22	DPWA Multichannel
16 ± 6	SOKHOYAN	15A	DPWA Multichannel
26 ± 3 ± 2	¹ SVARC	14	L+P $\pi N \rightarrow \pi N$
24 ± 4	CUTKOSKY	80	IPWA $\pi N \rightarrow \pi N$
• • • We do not use the following data for averages, fits, limits, etc. • • •			
38	ROENCHEN	15A	DPWA Multichannel
16 ± 6	GUTZ	14	DPWA Multichannel
17 ± 8	ANISOVICH	12A	DPWA Multichannel

¹ Fit to the amplitudes of HOEHLER 79.

PHASE θ

VALUE (°)	DOCUMENT ID	TECN	COMMENT
-150 to -50 (≈ -100) OUR ESTIMATE			
11 ± 4	ROENCHEN	22	DPWA Multichannel
-50 ± 25	SOKHOYAN	15A	DPWA Multichannel
-130 ± 5 ± 3	¹ SVARC	14	L+P $\pi N \rightarrow \pi N$
-150 ± 30	CUTKOSKY	80	IPWA $\pi N \rightarrow \pi N$
• • • We do not use the following data for averages, fits, limits, etc. • • •			
146	ROENCHEN	15A	DPWA Multichannel
-50 ± 25	GUTZ	14	DPWA Multichannel
-40 ± 20	ANISOVICH	12A	DPWA Multichannel

¹ Fit to the amplitudes of HOEHLER 79.

$\Delta(1920)$ INELASTIC POLE RESIDUE

The "normalized residue" is the residue divided by $\Gamma_{pole}/2$.

Normalized residue in $N\pi \rightarrow \Delta(1920) \rightarrow \Delta\eta$	MODULUS	PHASE (°)	DOCUMENT ID	TECN	COMMENT
	0.15 ± 0.04	70 ± 20	GUTZ	14	DPWA Multichannel
• • • We do not use the following data for averages, fits, limits, etc. • • •					
	0.17 ± 0.08	70 ± 20	ANISOVICH	12A	DPWA Multichannel

Normalized residue in $N\pi \rightarrow \Delta(1920) \rightarrow \Sigma K$	MODULUS	PHASE (°)	DOCUMENT ID	TECN	COMMENT
	0.20 ± 0.01	104 ± 2	ROENCHEN	22	DPWA Multichannel
	0.09 ± 0.03	80 ± 40	ANISOVICH	12A	DPWA Multichannel
• • • We do not use the following data for averages, fits, limits, etc. • • •					
	0.17	-35	ROENCHEN	15A	DPWA Multichannel

Baryon Particle Listings

 $\Delta(1920)$ Normalized residue in $N\pi \rightarrow \Delta(1920) \rightarrow \Delta\pi, P\text{-wave}$

MODULUS	PHASE (°)	DOCUMENT ID	TECN	COMMENT
0.057±0.003	-48 ± 3	ROENCHEN 22	DPWA	Multichannel
0.20 ± 0.08	-105 ± 25	SOKHOYAN 15A	DPWA	Multichannel
••• We do not use the following data for averages, fits, limits, etc. •••				
0.069	131	ROENCHEN 15A	DPWA	Multichannel
0.20 ± 0.12	-120 ± 30	ANISOVICH 12A	DPWA	Multichannel

Normalized residue in $N\pi \rightarrow \Delta(1920) \rightarrow \Delta\pi, F\text{-wave}$

MODULUS	PHASE (°)	DOCUMENT ID	TECN	COMMENT
0.020±0.002	147 ± 4	ROENCHEN 22	DPWA	Multichannel
0.37 ± 0.10	-90 ± 20	SOKHOYAN 15A	DPWA	Multichannel
••• We do not use the following data for averages, fits, limits, etc. •••				
0.013	-115	ROENCHEN 15A	DPWA	Multichannel
0.28 ± 0.07	-95 ± 35	ANISOVICH 12A	DPWA	Multichannel

Normalized residue in $N\pi \rightarrow \Delta(1920) \rightarrow N(1535)\pi$

MODULUS	PHASE (°)	DOCUMENT ID	TECN	COMMENT
0.03±0.02	35 ± 45	GUTZ 14	DPWA	Multichannel

Normalized residue in $N\pi \rightarrow \Delta(1920) \rightarrow N_{a_0}(980)$

MODULUS	PHASE (°)	DOCUMENT ID	TECN	COMMENT
0.03±0.02	-85 ± 45	GUTZ 14	DPWA	Multichannel

Normalized residue in $N\pi \rightarrow \Delta(1920) \rightarrow N(1440)\pi$

MODULUS	PHASE (°)	DOCUMENT ID	TECN	COMMENT
0.04±0.03	undefined	SOKHOYAN 15A	DPWA	Multichannel

Normalized residue in $N\pi \rightarrow \Delta(1920) \rightarrow N(1520)\pi, S\text{-wave}$

MODULUS	PHASE (°)	DOCUMENT ID	TECN	COMMENT
0.05±0.05	undefined	SOKHOYAN 15A	DPWA	Multichannel

 $\Delta(1920)$ BREIT-WIGNER MASS

VALUE (MeV)	DOCUMENT ID	TECN	COMMENT
1870 to 1970 (≈ 1920) OUR ESTIMATE			
1976 ± 49	HUNT 19	DPWA	Multichannel
1880 ± 30	SOKHOYAN 15A	DPWA	Multichannel
2146 ± 32	¹ SHRESTHA 12A	DPWA	Multichannel
1920 ± 80	CUTKOSKY 80	IPWA	$\pi N \rightarrow \pi N$
1868 ± 10	HOEHLER 79	IPWA	$\pi N \rightarrow \pi N$
••• We do not use the following data for averages, fits, limits, etc. •••			
1880 ± 30	GUTZ 14	DPWA	Multichannel
1900 ± 30	ANISOVICH 12A	DPWA	Multichannel
2057 ± 1	PENNER 02c	DPWA	Multichannel
1889 ± 100	VRANA 00	DPWA	Multichannel

¹ Statistical error only. $\Delta(1920)$ BREIT-WIGNER WIDTH

VALUE (MeV)	DOCUMENT ID	TECN	COMMENT
240 to 360 (≈ 300) OUR ESTIMATE			
509 ± 170	HUNT 19	DPWA	Multichannel
300 ± 40	SOKHOYAN 15A	DPWA	Multichannel
400 ± 80	¹ SHRESTHA 12A	DPWA	Multichannel
300 ± 100	CUTKOSKY 80	IPWA	$\pi N \rightarrow \pi N$
220 ± 80	HOEHLER 79	IPWA	$\pi N \rightarrow \pi N$
••• We do not use the following data for averages, fits, limits, etc. •••			
300 ± 40	GUTZ 14	DPWA	Multichannel
310 ± 60	ANISOVICH 12A	DPWA	Multichannel
525 ± 32	PENNER 02c	DPWA	Multichannel
123 ± 53	VRANA 00	DPWA	Multichannel

¹ Statistical error only. $\Delta(1920)$ DECAY MODES

The following branching fractions are our estimates, not fits or averages.

Mode	Fraction (Γ_j/Γ)
Γ_1 $N\pi$	5–20 %
Γ_2 ΣK	2–6 %
Γ_3 $N\pi\pi$	>46 %
Γ_4 $\Delta(1232)\pi$	>46 %
Γ_5 $\Delta(1232)\pi, P\text{-wave}$	2–28 %
Γ_6 $\Delta(1232)\pi, F\text{-wave}$	44–72 %
Γ_7 $N(1440)\pi, P\text{-wave}$	4–86 %
Γ_8 $N(1520)\pi, S\text{-wave}$	<5 %
Γ_9 $N(1535)\pi$	<2 %
Γ_{10} $N_{a_0}(980)$	seen
Γ_{11} $\Delta(1232)\eta$	5–17 %
Γ_{12} $N\gamma$	0.01–0.84 %
Γ_{13} $N\gamma, \text{helicity}=1/2$	0.0–0.42 %
Γ_{14} $N\gamma, \text{helicity}=3/2$	0.01–0.42 %

 $\Delta(1920)$ BRANCHING RATIOS

$\Gamma(N\pi)/\Gamma_{\text{total}}$	DOCUMENT ID	TECN	COMMENT	Γ_1/Γ
5–20 % OUR ESTIMATE				
10.5 ± 3.0	¹ HUNT 19	DPWA	Multichannel	
8 ± 4	SOKHOYAN 15A	DPWA	Multichannel	
20 ± 5	CUTKOSKY 80	IPWA	$\pi N \rightarrow \pi N$	
14 ± 4	HOEHLER 79	IPWA	$\pi N \rightarrow \pi N$	
••• We do not use the following data for averages, fits, limits, etc. •••				
8 ± 4	GUTZ 14	DPWA	Multichannel	
8 ± 4	ANISOVICH 12A	DPWA	Multichannel	
16 ± 4	¹ SHRESTHA 12A	DPWA	Multichannel	
15 ± 1	PENNER 02c	DPWA	Multichannel	
5 ± 4	VRANA 00	DPWA	Multichannel	

¹ Statistical error only.

$\Gamma(\Sigma K)/\Gamma_{\text{total}}$	DOCUMENT ID	TECN	COMMENT	Γ_2/Γ
2–6 % OUR ESTIMATE				
4 ± 2	ANISOVICH 12A	DPWA	Multichannel	
••• We do not use the following data for averages, fits, limits, etc. •••				
2.1 ± 0.3	PENNER 02c	DPWA	Multichannel	

$\Gamma(\Delta(1232)\pi, P\text{-wave})/\Gamma_{\text{total}}$	DOCUMENT ID	TECN	COMMENT	Γ_5/Γ
2–28 % OUR ESTIMATE				
< 1.6	¹ HUNT 19	DPWA	Multichannel	
18 ± 10	SOKHOYAN 15A	DPWA	Multichannel	
••• We do not use the following data for averages, fits, limits, etc. •••				
22 ± 12	ANISOVICH 12A	DPWA	Multichannel	
7 ± 5	¹ SHRESTHA 12A	DPWA	Multichannel	
41 ± 3	VRANA 00	DPWA	Multichannel	

¹ Statistical error only.

$\Gamma(\Delta(1232)\pi, F\text{-wave})/\Gamma_{\text{total}}$	DOCUMENT ID	TECN	COMMENT	Γ_6/Γ
44–72 % OUR ESTIMATE				
58 ± 14	SOKHOYAN 15A	DPWA	Multichannel	
••• We do not use the following data for averages, fits, limits, etc. •••				
45 ± 20	ANISOVICH 12A	DPWA	Multichannel	

$\Gamma(N(1440)\pi, P\text{-wave})/\Gamma_{\text{total}}$	DOCUMENT ID	TECN	COMMENT	Γ_7/Γ
4–86 % OUR ESTIMATE				
77 ± 9	¹ HUNT 19	DPWA	Multichannel	
< 4	SOKHOYAN 15A	DPWA	Multichannel	
••• We do not use the following data for averages, fits, limits, etc. •••				
< 20	¹ SHRESTHA 12A	DPWA	Multichannel	
53 ± 8	VRANA 00	DPWA	Multichannel	

¹ Statistical error only.

$\Gamma(N(1520)\pi, S\text{-wave})/\Gamma_{\text{total}}$	DOCUMENT ID	TECN	COMMENT	Γ_8/Γ
< 5 % OUR ESTIMATE				
< 5	SOKHOYAN 15A	DPWA	Multichannel	

$\Gamma(N(1535)\pi)/\Gamma_{\text{total}}$	DOCUMENT ID	TECN	COMMENT	Γ_9/Γ
< 2 % OUR ESTIMATE				
< 2	GUTZ 14	DPWA	Multichannel	

$\Gamma(N_{a_0}(980))/\Gamma_{\text{total}}$	DOCUMENT ID	TECN	COMMENT	Γ_{10}/Γ
seen OUR ESTIMATE				
••• We do not use the following data for averages, fits, limits, etc. •••				
4 ± 2	HORN 08A	DPWA	Multichannel	

$\Gamma(\Delta(1232)\eta)/\Gamma_{\text{total}}$	DOCUMENT ID	TECN	COMMENT	Γ_{11}/Γ
5–17 % OUR ESTIMATE				
11 ± 6	GUTZ 14	DPWA	Multichannel	
••• We do not use the following data for averages, fits, limits, etc. •••				
15 ± 8	ANISOVICH 12A	DPWA	Multichannel	

 $\Delta(1920)$ PHOTON DECAY AMPLITUDES AT THE POLE $\Delta(1920) \rightarrow N\gamma, \text{helicity}=1/2$ amplitude $A_{1/2}$

MODULUS ($\text{GeV}^{-1/2}$)	PHASE (°)	DOCUMENT ID	TECN	COMMENT
0.138 ± 0.006	-8.9 ± 2.0	ROENCHEN 22	DPWA	Multichannel
0.110 ± 0.030	-5.0 ± 2.0	SOKHOYAN 15A	DPWA	Multichannel
••• We do not use the following data for averages, fits, limits, etc. •••				
-0.192	46	ROENCHEN 15A	DPWA	Multichannel

See key on page 1171

Baryon Particle Listings

$\Delta(1920), \Delta(1930)$

$\Delta(1920) \rightarrow N\gamma$, helicity-3/2 amplitude $A_{3/2}$

MODULUS (GeV ^{-1/2})	PHASE (°)	DOCUMENT ID	TECN	COMMENT
0.252 ± 0.007	14 ± 2	ROENCHEN	22	DPWA Multichannel
-0.100 ± 0.040	0 ± 20	SOKHOYAN	15A	DPWA Multichannel
• • • We do not use the following data for averages, fits, limits, etc. • • •				
0.522	67	ROENCHEN	15A	DPWA Multichannel

$\Delta(1920)$ BREIT-WIGNER PHOTON DECAY AMPLITUDES

$\Delta(1920) \rightarrow N\gamma$, helicity-1/2 amplitude $A_{1/2}$

VALUE (GeV ^{-1/2})	DOCUMENT ID	TECN	COMMENT
-0.028 ± 0.010	¹ HUNT	19	DPWA Multichannel
0.110 ± 0.030	SOKHOYAN	15A	DPWA Multichannel
• • • We do not use the following data for averages, fits, limits, etc. • • •			
0.110 ± 0.030	GUTZ	14	DPWA Multichannel
0.130 ± 0.030 -0.060	ANISOVICH	12A	DPWA Multichannel
0.051 ± 0.010	¹ SHRESTHA	12A	DPWA Multichannel
-0.007	PENNER	02D	DPWA Multichannel
¹ Statistical error only.			

$\Delta(1920) \rightarrow N\gamma$, helicity-3/2 amplitude $A_{3/2}$

VALUE (GeV ^{-1/2})	DOCUMENT ID	TECN	COMMENT
-0.043 ± 0.014	¹ HUNT	19	DPWA Multichannel
-0.105 ± 0.035	SOKHOYAN	15A	DPWA Multichannel
• • • We do not use the following data for averages, fits, limits, etc. • • •			
-0.105 ± 0.035	GUTZ	14	DPWA Multichannel
-0.115 ± 0.025 -0.050	ANISOVICH	12A	DPWA Multichannel
0.017 ± 0.015	¹ SHRESTHA	12A	DPWA Multichannel
-0.001	PENNER	02D	DPWA Multichannel
¹ Statistical error only.			

$\Delta(1920)$ REFERENCES

For early references, see Physics Letters **111B** 1 (1982).

ROENCHEN	22	EPJ A58 229	D. Roenchen et al.	(JULI, GWU, BONN+)
HUNT	19	PR C9 055205	B. C. Hunt, D.M. Manley	
ROENCHEN	15A	EPJ A51 70	D. Roenchen et al.	
SOKHOYAN	15A	EPJ A51 95	V. Sokhoyan et al.	(CBELSA/TAPS Collab.)
GUTZ	14	EPJ A50 74	E. Gutz et al.	(CBELSA/TAPS Collab.)
PDG	14	CP C38 070001	K. Olive et al.	(PDG Collab.)
SVARC	14	PR C89 045205	A. Svarc et al.	(RBI Zagreb, UNI Tuzla)
ANISOVICH	12A	EPJ A48 15	A.V. Anisovich et al.	(BONN, PNPI)
SHRESTHA	12A	PR C86 055203	M. Shrestha, D.M. Manley	(KSU)
HORN	08A	EPJ A38 173	I. Horn et al.	(CB-ELSA Collab.)
Also		PRL 101 202002	I. Horn et al.	(CB-ELSA Collab.)
PENNER	02C	PR C66 055211	G. Penner, U. Mosel	(GIES)
PENNER	02D	PR C66 055212	G. Penner, U. Mosel	(GIES)
VRANA	00	PRPL 328 181	T. P. Vrana, S.A. Dytman,	(PITT, ANL)
HOEHLER	93	πN Newsletter 9 1	G. Hoehler	(KARL)
CUTKOSKY	80	Toronto Conf. 19	R.E. Cutkosky et al.	(CMU, LBL) IJP
Also		PR D20 2839	R.E. Cutkosky et al.	(CMU, LBL) IJP
HOEHLER	79	PDAT 12-1	G. Hoehler et al.	(KARLT) IJP
Also		Toronto Conf. 3	R. Koch	(KARLT) IJP

$\Delta(1930) 5/2^-$

$$I(J^P) = \frac{3}{2}(\frac{5}{2}^-) \text{ Status: } ***$$

Older and obsolete values are listed and referenced in the 2014 edition, Chinese Physics **C38** 070001 (2014).

$\Delta(1930)$ POLE POSITION

REAL PART

VALUE (MeV)	DOCUMENT ID	TECN	COMMENT
1820 to 1880 (≈ 1850) OUR ESTIMATE			
1821 ± 2	ROENCHEN	22	DPWA Multichannel
1848 ± 9 ± 19	¹ SVARC	14	L+P $\pi N \rightarrow \pi N$
1890 ± 50	CUTKOSKY	80	IPWA $\pi N \rightarrow \pi N$
• • • We do not use the following data for averages, fits, limits, etc. • • •			
1863	HUNT	19	DPWA Multichannel
1836	ROENCHEN	15A	DPWA Multichannel
2001	ARNDT	06	DPWA $\pi N \rightarrow \pi N, \eta N$
1883	VRANA	00	DPWA Multichannel
1850	HOEHLER	93	SPED $\pi N \rightarrow \pi N$
¹ Fit to the amplitudes of HOEHLER 79.			
-2xIMAGINARY PART			
VALUE (MeV)	DOCUMENT ID	TECN	COMMENT
300 to 450 (≈ 320) OUR ESTIMATE			
447 ± 7	ROENCHEN	22	DPWA Multichannel
321 ± 17 ± 7	¹ SVARC	14	L+P $\pi N \rightarrow \pi N$
260 ± 60	CUTKOSKY	80	IPWA $\pi N \rightarrow \pi N$

• • • We do not use the following data for averages, fits, limits, etc. • • •

260	HUNT	19	DPWA Multichannel
724	ROENCHEN	15A	DPWA Multichannel
387	ARNDT	06	DPWA $\pi N \rightarrow \pi N, \eta N$
250	VRANA	00	DPWA Multichannel
180	HOEHLER	93	SPED $\pi N \rightarrow \pi N$

¹ Fit to the amplitudes of HOEHLER 79.

$\Delta(1930)$ ELASTIC POLE RESIDUE

MODULUS $|r|$

VALUE (MeV)	DOCUMENT ID	TECN	COMMENT
8 to 20 (≈ 14) OUR ESTIMATE			
15 ± 2	ROENCHEN	22	DPWA Multichannel
9 ± 1 ± 1	¹ SVARC	14	L+P $\pi N \rightarrow \pi N$
18 ± 6	CUTKOSKY	80	IPWA $\pi N \rightarrow \pi N$
• • • We do not use the following data for averages, fits, limits, etc. • • •			
34	ROENCHEN	15A	DPWA Multichannel
7	ARNDT	06	DPWA $\pi N \rightarrow \pi N, \eta N$
20	HOEHLER	93	SPED $\pi N \rightarrow \pi N$

¹ Fit to the amplitudes of HOEHLER 79.

PHASE θ

VALUE (°)	DOCUMENT ID	TECN	COMMENT
-100 to -10 (≈ -50) OUR ESTIMATE			
-108 ± 5	ROENCHEN	22	DPWA Multichannel
-37 ± 3 ± 7	¹ SVARC	14	L+P $\pi N \rightarrow \pi N$
-20 ± 40	CUTKOSKY	80	IPWA $\pi N \rightarrow \pi N$
• • • We do not use the following data for averages, fits, limits, etc. • • •			
-155	ROENCHEN	15A	DPWA Multichannel
-12	ARNDT	06	DPWA $\pi N \rightarrow \pi N, \eta N$

¹ Fit to the amplitudes of HOEHLER 79.

$\Delta(1930)$ INELASTIC POLE RESIDUE

The "normalized residue" is the residue divided by $\Gamma_{pole}/2$.

Normalized residue in $N\pi \rightarrow \Delta(1930) \rightarrow \Sigma K$

MODULUS	PHASE (°)	DOCUMENT ID	TECN	COMMENT
0.010 ± 0.001	49 ± 5	ROENCHEN	22	DPWA Multichannel
• • • We do not use the following data for averages, fits, limits, etc. • • •				
0.043	-0.5	ROENCHEN	15A	DPWA Multichannel

Normalized residue in $N\pi \rightarrow \Delta(1930) \rightarrow \Delta\pi, D$ -wave

MODULUS	PHASE (°)	DOCUMENT ID	TECN	COMMENT
0.12 ± 0.02	64 ± 4	ROENCHEN	22	DPWA Multichannel
• • • We do not use the following data for averages, fits, limits, etc. • • •				
0.15	30	ROENCHEN	15A	DPWA Multichannel

Normalized residue in $N\pi \rightarrow \Delta(1930) \rightarrow \Delta\pi, G$ -wave

MODULUS	PHASE (°)	DOCUMENT ID	TECN	COMMENT
0.008 ± 0.001	148 ± 2	ROENCHEN	22	DPWA Multichannel
• • • We do not use the following data for averages, fits, limits, etc. • • •				
0.009	121	ROENCHEN	15A	DPWA Multichannel

$\Delta(1930)$ BREIT-WIGNER MASS

VALUE (MeV)	DOCUMENT ID	TECN	COMMENT
1900 to 2000 (≈ 1950) OUR ESTIMATE			
1988 ± 32	¹ HUNT	19	DPWA Multichannel
2233 ± 53	¹ ARNDT	06	DPWA $\pi N \rightarrow \pi N, \eta N$
1940 ± 30	CUTKOSKY	80	IPWA $\pi N \rightarrow \pi N$
1901 ± 15	HOEHLER	79	IPWA $\pi N \rightarrow \pi N$
• • • We do not use the following data for averages, fits, limits, etc. • • •			
1930 ± 12	¹ SHRESTHA	12A	DPWA Multichannel
1932 ± 100	VRANA	00	DPWA Multichannel
¹ Statistical error only.			

$\Delta(1930)$ BREIT-WIGNER WIDTH

VALUE (MeV)	DOCUMENT ID	TECN	COMMENT
200 to 400 (≈ 300) OUR ESTIMATE			
500 ± 160	¹ HUNT	19	DPWA Multichannel
773 ± 187	ARNDT	06	DPWA $\pi N \rightarrow \pi N, \eta N$
320 ± 60	CUTKOSKY	80	IPWA $\pi N \rightarrow \pi N$
195 ± 60	HOEHLER	79	IPWA $\pi N \rightarrow \pi N$
• • • We do not use the following data for averages, fits, limits, etc. • • •			
235 ± 39	¹ SHRESTHA	12A	DPWA Multichannel
316 ± 237	VRANA	00	DPWA Multichannel
¹ Statistical error only.			

Baryon Particle Listings

 $\Delta(1930)$, $\Delta(1940)$ $\Delta(1930)$ DECAY MODES

The following branching fractions are our estimates, not fits or averages.

Mode	Fraction (Γ_i/Γ)
Γ_1 $N\pi$	5–15 %
Γ_2 $N\gamma$	0.0–0.01 %
Γ_3 $N\gamma$, helicity=1/2	0.0–0.005 %
Γ_4 $N\gamma$, helicity=3/2	0.0–0.004 %

 $\Delta(1930)$ BRANCHING RATIOS

$\Gamma(N\pi)/\Gamma_{\text{total}}$	VALUE (%)	DOCUMENT ID	TECN	COMMENT	Γ_1/Γ
5 to 15 (≈ 10) OUR ESTIMATE					
9.5 \pm 0.1		¹ HUNT	19	DPWA	Multichannel
8.1 \pm 1.2		¹ ARNDT	06	DPWA	$\pi N \rightarrow \pi N, \eta N$
14 \pm 4		CUTKOSKY	80	IPWA	$\pi N \rightarrow \pi N$
4 \pm 3		HOEHLER	79	IPWA	$\pi N \rightarrow \pi N$
••• We do not use the following data for averages, fits, limits, etc. •••					
7.9 \pm 0.4		¹ SHRESTHA	12A	DPWA	Multichannel
9 \pm 8		VRANA	00	DPWA	Multichannel
¹ Statistical error only.					

 $\Delta(1930)$ PHOTON DECAY AMPLITUDES AT THE POLE $\Delta(1930) \rightarrow N\gamma$, helicity-1/2 amplitude $A_{1/2}$

MODULUS ($\text{GeV}^{-1/2}$)	PHASE ($^\circ$)	DOCUMENT ID	TECN	COMMENT
0.104 \pm 0.009	129 \pm 8	ROENCHEN	22	DPWA Multichannel
••• We do not use the following data for averages, fits, limits, etc. •••				
–0.270	33	ROENCHEN	15A	DPWA Multichannel

 $\Delta(1930) \rightarrow N\gamma$, helicity-3/2 amplitude $A_{3/2}$

MODULUS ($\text{GeV}^{-1/2}$)	PHASE ($^\circ$)	DOCUMENT ID	TECN	COMMENT
0.322 \pm 0.022	142 \pm 4	ROENCHEN	22	DPWA Multichannel
••• We do not use the following data for averages, fits, limits, etc. •••				
0.153	81	ROENCHEN	15A	DPWA Multichannel

 $\Delta(1930)$ BREIT-WIGNER PHOTON DECAY AMPLITUDES $\Delta(1930) \rightarrow N\gamma$, helicity-1/2 amplitude $A_{1/2}$

VALUE ($\text{GeV}^{-1/2}$)	DOCUMENT ID	TECN	COMMENT
–0.043 \pm 0.008	¹ HUNT	19	DPWA Multichannel
–0.007 \pm 0.010	¹ ARNDT	96	IPWA $\gamma N \rightarrow \pi N$
••• We do not use the following data for averages, fits, limits, etc. •••			
0.011 \pm 0.003	¹ SHRESTHA	12A	DPWA Multichannel
¹ Statistical error only.			

 $\Delta(1930) \rightarrow N\gamma$, helicity-3/2 amplitude $A_{3/2}$

VALUE ($\text{GeV}^{-1/2}$)	DOCUMENT ID	TECN	COMMENT
–0.020 \pm 0.017	¹ HUNT	19	DPWA Multichannel
0.005 \pm 0.010	¹ ARNDT	96	IPWA $\gamma N \rightarrow \pi N$
••• We do not use the following data for averages, fits, limits, etc. •••			
0.002 \pm 0.002	¹ SHRESTHA	12A	DPWA Multichannel
¹ Statistical error only.			

 $\Delta(1930)$ REFERENCES

For early references, see Physics Letters **111B** 1 (1982).

ROENCHEN	22	EPJ A58 229	D. Roenchen et al.	(JULI, GWU, BONN+)
HUNT	19	PR C99 055205	B. C. Hunt, D.M. Manley	
ROENCHEN	15A	EPJ A51 70	D. Roenchen et al.	
PDG	14	CP C38 070001	K. Olive et al.	(PDG Collab.)
SVARC	14	PR C89 045205	A. Svarc et al.	(RBI Zagreb, UNI Tuzla)
SHRESTHA	12A	PR C86 055203	M. Shrestha, D.M. Manley	(KSU)
ARNDT	06	PR C74 045205	R.A. Arndt et al.	(GWU)
VRANA	00	PRPL 328 181	T.P. Vrana, S.A. Dytman, T.-S.H. Lee	(PITT, ANL)
ARNDT	96	PR C53 430	R.A. Arndt, I.I. Strakovsky, R.L. Workman	(VPI)
HOEHLER	93	πN Newsletter 9 1	G. Hohlner	(KARL)
CUTKOSKY	80	Toronto Conf. 19	R.E. Cutkosky et al.	(CMU, LBL)JUP
Also		PR D20 2839	R.E. Cutkosky et al.	(CMU, LBL)JUP
HOEHLER	79	PDAT 12-1	G. Hohlner et al.	(KARLT)JUP
Also		Toronto Conf. 3	R. Koch	(KARLT)JUP

 $\Delta(1940) 3/2^-$

$$I(J^P) = \frac{3}{2}(\frac{3}{2}^-) \text{ Status: } * *$$

OMITTED FROM SUMMARY TABLE

 $\Delta(1940)$ POLE POSITION

REAL PART	VALUE (MeV)	DOCUMENT ID	TECN	COMMENT
1850 to 2050 (≈ 1950) OUR ESTIMATE				
2040 \pm 50		SOKHOYAN	15A	DPWA Multichannel
1878 \pm 11 \pm 5.5		¹ SVARC	14	L+P $\pi N \rightarrow \pi N$
1900 \pm 100		CUTKOSKY	80	IPWA $\pi N \rightarrow \pi N$

••• We do not use the following data for averages, fits, limits, etc. •••

2139	HUNT	19	DPWA	Multichannel
2040 \pm 50	GUTZ	14	DPWA	Multichannel
1990 \pm 100	ANISOVICH	12A	DPWA	Multichannel

¹ Fit to the amplitudes of HOEHLER 79.

–2xIMAGINARY PART

VALUE (MeV)	DOCUMENT ID	TECN	COMMENT
200 to 500 (≈ 350) OUR ESTIMATE			

450 \pm 90	SOKHOYAN	15A	DPWA	Multichannel
212 \pm 21 \pm 6	¹ SVARC	14	L+P	$\pi N \rightarrow \pi N$
200 \pm 60	CUTKOSKY	80	IPWA	$\pi N \rightarrow \pi N$

••• We do not use the following data for averages, fits, limits, etc. •••

400	HUNT	19	DPWA	Multichannel
450 \pm 90	GUTZ	14	DPWA	Multichannel
450 \pm 90	ANISOVICH	12A	DPWA	Multichannel

¹ Fit to the amplitudes of HOEHLER 79.

 $\Delta(1940)$ ELASTIC POLE RESIDUE

MODULUS $ r $	VALUE (MeV)	DOCUMENT ID	TECN	COMMENT
4 to 10 (≈ 7) OUR ESTIMATE				

6 \pm 3	SOKHOYAN	15A	DPWA	Multichannel
9 \pm 1 \pm 1	¹ SVARC	14	L+P	$\pi N \rightarrow \pi N$
8 \pm 3	CUTKOSKY	80	IPWA	$\pi N \rightarrow \pi N$

••• We do not use the following data for averages, fits, limits, etc. •••

4 \pm 3	GUTZ	14	DPWA	Multichannel
4 \pm 4	ANISOVICH	12A	DPWA	Multichannel

¹ Fit to the amplitudes of HOEHLER 79.

PHASE θ

VALUE ($^\circ$)	DOCUMENT ID	TECN	COMMENT
150 to 250 (≈ 200) OUR ESTIMATE			

– 90 \pm 35	SOKHOYAN	15A	DPWA	Multichannel
140 \pm 7 \pm 7	¹ SVARC	14	L+P	$\pi N \rightarrow \pi N$
135 \pm 45	CUTKOSKY	80	IPWA	$\pi N \rightarrow \pi N$

••• We do not use the following data for averages, fits, limits, etc. •••

– 50 \pm 35	GUTZ	14	DPWA	Multichannel
---------------	------	----	------	--------------

¹ Fit to the amplitudes of HOEHLER 79.

 $\Delta(1940)$ INELASTIC POLE RESIDUE

The “normalized residue” is the residue divided by $\Gamma_{\text{pole}}/2$.

Normalized residue in $N\pi \rightarrow \Delta(1940) \rightarrow \Delta(1232)\eta$

MODULUS	PHASE ($^\circ$)	DOCUMENT ID	TECN	COMMENT
<0.01	undefined	GUTZ	14	DPWA Multichannel

Normalized residue in $N\pi \rightarrow \Delta(1940) \rightarrow N(1535)\pi$

MODULUS	PHASE ($^\circ$)	DOCUMENT ID	TECN	COMMENT
<0.03	undefined	GUTZ	14	DPWA Multichannel

Normalized residue in $N\pi \rightarrow \Delta(1940) \rightarrow \Delta(1232)\pi$, S-wave

MODULUS	PHASE ($^\circ$)	DOCUMENT ID	TECN	COMMENT
0.12 \pm 0.06	120 \pm 45	SOKHOYAN	15A	DPWA Multichannel

Normalized residue in $N\pi \rightarrow \Delta(1940) \rightarrow \Delta(1232)\pi$, D-wave

MODULUS	PHASE ($^\circ$)	DOCUMENT ID	TECN	COMMENT
0.06 \pm 0.04	– 80 \pm 35	SOKHOYAN	15A	DPWA Multichannel

 $\Delta(1940)$ BREIT-WIGNER MASS

VALUE (MeV)	DOCUMENT ID	TECN	COMMENT
1940 to 2060 (≈ 2000) OUR ESTIMATE			

2137 \pm 13	¹ HUNT	19	DPWA	Multichannel
2050 \pm 40	SOKHOYAN	15A	DPWA	Multichannel
1940 \pm 100	CUTKOSKY	80	IPWA	$\pi N \rightarrow \pi N$

••• We do not use the following data for averages, fits, limits, etc. •••

2050 \pm 40	GUTZ	14	DPWA	Multichannel
1995 \pm 105	ANISOVICH	12A	DPWA	Multichannel

¹ Statistical error only.

 $\Delta(1940)$ BREIT-WIGNER WIDTH

VALUE (MeV)	DOCUMENT ID	TECN	COMMENT
300 to 500 (≈ 400) OUR ESTIMATE			

400 \pm 43	¹ HUNT	19	DPWA	Multichannel
450 \pm 70	SOKHOYAN	15A	DPWA	Multichannel
200 \pm 100	CUTKOSKY	80	IPWA	$\pi N \rightarrow \pi N$

••• We do not use the following data for averages, fits, limits, etc. •••

450 \pm 70	GUTZ	14	DPWA	Multichannel
450 \pm 100	ANISOVICH	12A	DPWA	Multichannel

¹ Statistical error only.

See key on page 1171

Baryon Particle Listings
 $\Delta(1940), \Delta(1950)$

$\Delta(1940)$ DECAY MODES

Mode	Fraction (Γ_i/Γ)
Γ_1 $N\pi$	1-20 %
Γ_2 $N\pi\pi$	>81 %
Γ_3 $\Delta(1232)\pi$	6-85 %
Γ_4 $\Delta(1232)\pi, S$ -wave	1-65 %
Γ_5 $\Delta(1232)\pi, D$ -wave	5-20 %
Γ_6 $N\rho, S=3/2, S$ -wave	75-85 %
Γ_7 $N(1535)\pi$	2-14 %
Γ_8 $N a_0(980)$	seen
Γ_9 $\Delta(1232)\eta$	4-16 %
Γ_{10} $N\gamma$	0.06-2.53 %
Γ_{11} $N\gamma, \text{helicity}=1/2$	0.06-1.51 %
Γ_{12} $N\gamma, \text{helicity}=3/2$	0-1.02 %

$\Delta(1940)$ BRANCHING RATIOS

$\Gamma(N\pi)/\Gamma_{\text{total}}$	DOCUMENT ID	TECN	COMMENT	Γ_1/Γ
1-20 % OUR ESTIMATE				
16±4	1 HUNT	19 DPWA	Multichannel	
2±1	SOKHOYAN	15A DPWA	Multichannel	
5±2	CUTKOSKY	80 IPWA	$\pi N \rightarrow \pi N$	
••• We do not use the following data for averages, fits, limits, etc. •••				
2±1	GUTZ	14 DPWA	Multichannel	
¹ Statistical error only.				

$\Gamma(\Delta(1232)\pi, S\text{-wave})/\Gamma_{\text{total}}$	DOCUMENT ID	TECN	COMMENT	Γ_4/Γ
1-65 % OUR ESTIMATE				
< 0.9	1 HUNT	19 DPWA	Multichannel	
46 ±20	SOKHOYAN	15A DPWA	Multichannel	
¹ Statistical error only.				

$\Gamma(\Delta(1232)\pi, D\text{-wave})/\Gamma_{\text{total}}$	DOCUMENT ID	TECN	COMMENT	Γ_5/Γ
5-20 % OUR ESTIMATE				
< 6.3	1 HUNT	19 DPWA	Multichannel	
12 ±7	SOKHOYAN	15A DPWA	Multichannel	
¹ Statistical error only.				

$\Gamma(N\rho, S=3/2, S\text{-wave})/\Gamma_{\text{total}}$	DOCUMENT ID	TECN	COMMENT	Γ_6/Γ
75-85 % OUR ESTIMATE				
80±5	1 HUNT	19 DPWA	Multichannel	
¹ Statistical error only.				

$\Gamma(N(1535)\pi)/\Gamma_{\text{total}}$	DOCUMENT ID	TECN	COMMENT	Γ_7/Γ
2-14 % OUR ESTIMATE				
8±6	GUTZ	14 DPWA	Multichannel	
••• We do not use the following data for averages, fits, limits, etc. •••				
2±1	HORN	08A DPWA	Multichannel	

$\Gamma(N a_0(980))/\Gamma_{\text{total}}$	DOCUMENT ID	TECN	COMMENT	Γ_8/Γ
seen OUR ESTIMATE				
••• We do not use the following data for averages, fits, limits, etc. •••				
2±1	HORN	08A DPWA	Multichannel	

$\Gamma(\Delta(1232)\eta)/\Gamma_{\text{total}}$	DOCUMENT ID	TECN	COMMENT	Γ_9/Γ
4-16 % OUR ESTIMATE				
10±6	GUTZ	14 DPWA	Multichannel	
••• We do not use the following data for averages, fits, limits, etc. •••				
4±2	HORN	08A DPWA	Multichannel	

$\Delta(1940)$ PHOTON DECAY AMPLITUDES AT THE POLE

$\Delta(1940) \rightarrow N\gamma, \text{helicity-1/2 amplitude } A_{1/2}$

MODULUS ($\text{GeV}^{-1/2}$)	PHASE ($^\circ$)	DOCUMENT ID	TECN	COMMENT
0.170 ^{+0.120} _{-0.100}	-10 ± 30	SOKHOYAN	15A DPWA	Multichannel

$\Delta(1940) \rightarrow N\gamma, \text{helicity-3/2 amplitude } A_{3/2}$

MODULUS ($\text{GeV}^{-1/2}$)	PHASE ($^\circ$)	DOCUMENT ID	TECN	COMMENT
0.150±0.080	-10 ± 30	SOKHOYAN	15A DPWA	Multichannel

$\Delta(1940)$ BREIT-WIGNER PHOTON DECAY AMPLITUDES

$\Delta(1940) \rightarrow N\gamma, \text{helicity-1/2 amplitude } A_{1/2}$

VALUE ($\text{GeV}^{-1/2}$)	DOCUMENT ID	TECN	COMMENT
0.1614±0.0031	1 HUNT	19 DPWA	Multichannel
0.170 ^{+0.110} _{-0.080}	SOKHOYAN	15A DPWA	Multichannel
••• We do not use the following data for averages, fits, limits, etc. •••			
0.170 ^{+0.110} _{-0.080}	GUTZ	14 DPWA	Multichannel
¹ Statistical error only.			

$\Delta(1940) \rightarrow N\gamma, \text{helicity-3/2 amplitude } A_{3/2}$

VALUE ($\text{GeV}^{-1/2}$)	DOCUMENT ID	TECN	COMMENT
-0.209±0.023	1 HUNT	19 DPWA	Multichannel
0.150±0.080	SOKHOYAN	15A DPWA	Multichannel
••• We do not use the following data for averages, fits, limits, etc. •••			
0.150±0.080	GUTZ	14 DPWA	Multichannel
¹ Statistical error only.			

$\Delta(1940)$ REFERENCES

HUNT	19	PR C99 055205	B.C. Hunt, D.M. Manley	
SOKHOYAN	15A	EPJ A51 95	V. Sokhoyan <i>et al.</i>	(CBELSA/TAPS Collab.)
GUTZ	14	EPJ A50 74	E. Gutz <i>et al.</i>	(CBELSA/TAPS Collab.)
SVARC	14	PR C89 045205	A. Svarc <i>et al.</i>	(RBI Zagreb, UNI Tuzla)
ANISOVICH	12A	EPJ A48 15	A.V. Anisovich <i>et al.</i>	(BONN, PNPI)
HORN	08A	EPJ A38 173	I. Horn <i>et al.</i>	(CB-ELSA Collab.)
		PRL 101 202002	I. Horn <i>et al.</i>	(CB-ELSA Collab.)
CUTKOSKY	80	Toronto Conf. 19	R.E. Cutkosky <i>et al.</i>	(CMU, LBL) IJP
		PR D20 2839	R.E. Cutkosky <i>et al.</i>	(CMU, LBL)
HOEHLER	79	PDAT 12-1	G. Hoehler <i>et al.</i>	(KARLT)

$\Delta(1950) 7/2^+$

$I(J^P) = \frac{3}{2}(\frac{7}{2}^+)$ Status: ***

Older and obsolete values are listed and referenced in the 2014 edition, Chinese Physics C38 070001 (2014).

$\Delta(1950)$ POLE POSITION

REAL PART

VALUE (MeV)	DOCUMENT ID	TECN	COMMENT
1870 to 1890 (≈ 1880) OUR ESTIMATE			
1875 ± 1	ROENCHEN	22 DPWA	Multichannel
1888 ± 4	SOKHOYAN	15A DPWA	Multichannel
1877 ± 2±1	1 SVARC	14 L+P	$\pi N \rightarrow \pi N$
1890±15	CUTKOSKY	80 IPWA	$\pi N \rightarrow \pi N$
••• We do not use the following data for averages, fits, limits, etc. •••			
1871	HUNT	19 DPWA	Multichannel
1874	ROENCHEN	15A DPWA	Multichannel
1888 ± 4	GUTZ	14 DPWA	Multichannel
1890 ± 4	ANISOVICH	12A DPWA	Multichannel
1876	ARNDT	06 DPWA	$\pi N \rightarrow \pi N, \eta N$
1910	VRANA	00 DPWA	Multichannel
1878	HOEHLER	93 ARGD	$\pi N \rightarrow \pi N$
¹ Fit to the amplitudes of HOEHLER 79.			

-2xIMAGINARY PART

VALUE (MeV)	DOCUMENT ID	TECN	COMMENT
220 to 260 (≈ 240) OUR ESTIMATE			
166 ± 2	ROENCHEN	22 DPWA	Multichannel
245 ± 8	SOKHOYAN	15A DPWA	Multichannel
223 ± 4±1	1 SVARC	14 L+P	$\pi N \rightarrow \pi N$
260±40	CUTKOSKY	80 IPWA	$\pi N \rightarrow \pi N$
••• We do not use the following data for averages, fits, limits, etc. •••			
206	HUNT	19 DPWA	Multichannel
239	ROENCHEN	15A DPWA	Multichannel
245 ± 8	GUTZ	14 DPWA	Multichannel
243 ± 8	ANISOVICH	12A DPWA	Multichannel
227	ARNDT	06 DPWA	$\pi N \rightarrow \pi N, \eta N$
230	VRANA	00 DPWA	Multichannel
230	HOEHLER	93 ARGD	$\pi N \rightarrow \pi N$
¹ Fit to the amplitudes of HOEHLER 79.			

$\Delta(1950)$ ELASTIC POLE RESIDUE

MODULUS $|r|$

VALUE (MeV)	DOCUMENT ID	TECN	COMMENT
44 to 60 (≈ 52) OUR ESTIMATE			
27 ± 1	ROENCHEN	22 DPWA	Multichannel
58 ± 2	SOKHOYAN	15A DPWA	Multichannel
44 ± 1	1 SVARC	14 L+P	$\pi N \rightarrow \pi N$
50 ± 7	CUTKOSKY	80 IPWA	$\pi N \rightarrow \pi N$

Baryon Particle Listings

 $\Delta(1950)$

••• We do not use the following data for averages, fits, limits, etc. •••

56	ROENCHEN	15A	DPWA	Multichannel
58±2	GUTZ	14	DPWA	Multichannel
58±2	ANISOVICH	12A	DPWA	Multichannel
53	ARNDT	06	DPWA	$\pi N \rightarrow \pi N, \eta N$
47	HOEHLER	93	ARGD	$\pi N \rightarrow \pi N$

¹ Fit to the amplitudes of HOEHLER 79.

PHASE θ

VALUE (°)	DOCUMENT ID	TECN	COMMENT
-40 to -24 (≈ -32) OUR ESTIMATE			
1.1±1.0	ROENCHEN	22	DPWA Multichannel
-24 ±3	SOKHOYAN	15A	DPWA Multichannel
-39 ±1 ±1	¹ SVARC	14	L+P $\pi N \rightarrow \pi N$
-33 ±8	CUTKOSKY	80	IPWA $\pi N \rightarrow \pi N$
••• We do not use the following data for averages, fits, limits, etc. •••			
-33	ROENCHEN	15A	DPWA Multichannel
-24 ±3	GUTZ	14	DPWA Multichannel
-24 ±3	ANISOVICH	12A	DPWA Multichannel
-31	ARNDT	06	DPWA $\pi N \rightarrow \pi N, \eta N$
-32	HOEHLER	93	ARGD $\pi N \rightarrow \pi N$

¹ Fit to the amplitudes of HOEHLER 79.

 $\Delta(1950)$ INELASTIC POLE RESIDUE

The "normalized residue" is the residue divided by $\Gamma_{pole}/2$.

Normalized residue in $N\pi \rightarrow \Delta(1950) \rightarrow \Sigma K$

MODULUS	PHASE (°)	DOCUMENT ID	TECN	COMMENT
0.020±0.002	-40 ±4	ROENCHEN	22	DPWA Multichannel
0.05 ±0.01	-65 ±25	ANISOVICH	12A	DPWA Multichannel
••• We do not use the following data for averages, fits, limits, etc. •••				
0.031	-87	ROENCHEN	15A	DPWA Multichannel

Normalized residue in $N\pi \rightarrow \Delta(1950) \rightarrow \Delta\pi, F\text{-wave}$

MODULUS	PHASE (°)	DOCUMENT ID	TECN	COMMENT
0.30±0.27	166 ±1	ROENCHEN	22	DPWA Multichannel
0.12±0.04	undefined	SOKHOYAN	15A	DPWA Multichannel
••• We do not use the following data for averages, fits, limits, etc. •••				
0.54	131	ROENCHEN	15A	DPWA Multichannel
0.12±0.04	12 ±10	ANISOVICH	12A	DPWA Multichannel

Normalized residue in $N\pi \rightarrow \Delta(1950) \rightarrow \Delta\pi, H\text{-wave}$

MODULUS	PHASE (°)	DOCUMENT ID	TECN	COMMENT
0.051±0.004	-11 ±1	ROENCHEN	22	DPWA Multichannel
••• We do not use the following data for averages, fits, limits, etc. •••				
0.033	-97	ROENCHEN	15A	DPWA Multichannel

Normalized residue in $N\pi \rightarrow \Delta(1950) \rightarrow \Delta(1232)\eta$

MODULUS	PHASE (°)	DOCUMENT ID	TECN	COMMENT
0.035±0.005	90 ±25	GUTZ	14	DPWA Multichannel

 $\Delta(1950)$ BREIT-WIGNER MASS

VALUE (MeV)	DOCUMENT ID	TECN	COMMENT
1915 to 1950 (≈ 1930) OUR ESTIMATE			
1943 ±18	GOLOVATCH	19	DPWA $\gamma p \rightarrow \pi^+ \pi^- p$
1913 ±4	¹ HUNT	19	DPWA Multichannel
1917 ±4	ANISOVICH	17	DPWA Multichannel
1921.3±0.2	¹ ARNDT	06	DPWA $\pi N \rightarrow \pi N, \eta N$
1950 ±15	CUTKOSKY	80	IPWA $\pi N \rightarrow \pi N$
1913 ±8	HOEHLER	79	IPWA $\pi N \rightarrow \pi N$
••• We do not use the following data for averages, fits, limits, etc. •••			
1917 ±4	SOKHOYAN	15A	DPWA Multichannel
1917 ±4	GUTZ	14	DPWA Multichannel
1915 ±6	ANISOVICH	12A	DPWA Multichannel
1918 ±1	¹ SHRESTHA	12A	DPWA Multichannel
1936 ±5	VRANA	00	DPWA Multichannel

¹ Statistical error only.

 $\Delta(1950)$ BREIT-WIGNER WIDTH

VALUE (MeV)	DOCUMENT ID	TECN	COMMENT
235 to 335 (≈ 285) OUR ESTIMATE			
230 ±88	GOLOVATCH	19	DPWA $\gamma p \rightarrow \pi^+ \pi^- p$
241 ±10	¹ HUNT	19	DPWA Multichannel
251 ±8	ANISOVICH	17	DPWA Multichannel
271.1±1.1	¹ ARNDT	06	DPWA $\pi N \rightarrow \pi N, \eta N$
340 ±5.0	CUTKOSKY	80	IPWA $\pi N \rightarrow \pi N$
224 ±10	HOEHLER	79	IPWA $\pi N \rightarrow \pi N$

••• We do not use the following data for averages, fits, limits, etc. •••

251 ±8	SOKHOYAN	15A	DPWA Multichannel
251 ±8	GUTZ	14	DPWA Multichannel
246 ±10	ANISOVICH	12A	DPWA Multichannel
259 ±4	¹ SHRESTHA	12A	DPWA Multichannel
245 ±12	VRANA	00	DPWA Multichannel

¹ Statistical error only.

 $\Delta(1950)$ DECAY MODES

The following branching fractions are our estimates, not fits or averages.

Mode	Fraction (Γ_i/Γ)
Γ_1 $N\pi$	35–45 %
Γ_2 ΣK	0.3–0.5 %
Γ_3 $N\pi\pi$	37–77 %
Γ_4 $\Delta(1232)\pi, F\text{-wave}$	1–9 %
Γ_5 $N(1680)\pi, P\text{-wave}$	3–9 %
Γ_6 $\Delta(1232)\eta$	< 0.6 %
Γ_7 $N\gamma$	0.06–0.14 %
Γ_8 $N\gamma, \text{helicity}=1/2$	0.03–0.05 %
Γ_9 $N\gamma, \text{helicity}=3/2$	0.04–0.09 %

 $\Delta(1950)$ BRANCHING RATIOS

$\Gamma(N\pi)/\Gamma_{\text{total}}$	VALUE (%)	DOCUMENT ID	TECN	COMMENT	Γ_1/Γ
35–45 % OUR ESTIMATE					
38 ±2		¹ HUNT	19	DPWA Multichannel	
46 ±2		ANISOVICH	17	DPWA Multichannel	
47.1 ±0.1		¹ ARNDT	06	DPWA $\pi N \rightarrow \pi N, \eta N$	
39 ±4		CUTKOSKY	80	IPWA $\pi N \rightarrow \pi N$	
38 ±2		HOEHLER	79	IPWA $\pi N \rightarrow \pi N$	
••• We do not use the following data for averages, fits, limits, etc. •••					
0.046±0.002		SOKHOYAN	15A	DPWA Multichannel	
46 ±2		GUTZ	14	DPWA Multichannel	
45 ±2		ANISOVICH	12A	DPWA Multichannel	
45.6 ±0.4		¹ SHRESTHA	12A	DPWA Multichannel	
44 ±1		VRANA	00	DPWA Multichannel	

¹ Statistical error only.

$\Gamma(N\pi\pi)/\Gamma_{\text{total}}$	VALUE (%)	DOCUMENT ID	TECN	COMMENT	Γ_3/Γ
57±20		GOLOVATCH	19	DPWA $\gamma p \rightarrow \pi^+ \pi^- p$	

$\Gamma(\Sigma K)/\Gamma_{\text{total}}$	VALUE (%)	DOCUMENT ID	TECN	COMMENT	Γ_2/Γ
0.6±0.2		ANISOVICH	17	DPWA Multichannel	
••• We do not use the following data for averages, fits, limits, etc. •••					
0.4±0.1		ANISOVICH	12A	DPWA Multichannel	

$\Gamma(\Delta(1232)\pi, F\text{-wave})/\Gamma_{\text{total}}$	VALUE (%)	DOCUMENT ID	TECN	COMMENT	Γ_4/Γ
5 ±3		ANISOVICH	17	DPWA Multichannel	
8 ±1		¹ SHRESTHA	12A	DPWA Multichannel	
••• We do not use the following data for averages, fits, limits, etc. •••					
5 ±4		SOKHOYAN	15A	DPWA Multichannel	
2.8±1.4		ANISOVICH	12A	DPWA Multichannel	
36 ±1		VRANA	00	DPWA Multichannel	

¹ Statistical error only.

$\Gamma(N(1680)\pi, P\text{-wave})/\Gamma_{\text{total}}$	VALUE (%)	DOCUMENT ID	TECN	COMMENT	Γ_5/Γ
6±3		SOKHOYAN	15A	DPWA Multichannel	

$\Gamma(\Delta(1232)\eta)/\Gamma_{\text{total}}$	VALUE (%)	DOCUMENT ID	TECN	COMMENT	Γ_6/Γ
0.3±0.3		ANISOVICH	17	DPWA Multichannel	
••• We do not use the following data for averages, fits, limits, etc. •••					
<1		GUTZ	14	DPWA Multichannel	

 $\Delta(1950)$ PHOTON DECAY AMPLITUDES AT THE POLE $\Delta(1950) \rightarrow N\gamma, \text{helicity}=1/2$ amplitude $A_{1/2}$

MODULUS ($\text{GeV}^{-1/2}$)	PHASE (°)	DOCUMENT ID	TECN	COMMENT
-0.031±0.002	-81 ±4	ROENCHEN	22	DPWA Multichannel
-0.067±0.004	-10 ±5	SOKHOYAN	15A	DPWA Multichannel
••• We do not use the following data for averages, fits, limits, etc. •••				
-0.068	-19	ROENCHEN	15A	DPWA Multichannel

$\Delta(1950) \rightarrow N\gamma$, helicity-3/2 amplitude $A_{3/2}$

MODULUS (GeV ^{-1/2})	PHASE (°)	DOCUMENT ID	TECN	COMMENT
-0.045 ± 0.002	-89 ± 2	ROENCHEN 22	DPWA	Multichannel
-0.095 ± 0.004	-10 ± 5	SOKHOYAN 15A	DPWA	Multichannel
• • • We do not use the following data for averages, fits, limits, etc. • • •				
-0.084	-19	ROENCHEN 15A	DPWA	Multichannel

 $\Delta(1950)$ BREIT-WIGNER PHOTON DECAY AMPLITUDES $\Delta(1950) \rightarrow N\gamma$, helicity-1/2 amplitude $A_{1/2}$

VALUE (GeV ^{-1/2})	DOCUMENT ID	TECN	COMMENT
-0.075 to -0.065 (≈ -0.070) OUR ESTIMATE			
-0.0698 ± 0.0141	GOLOVATCH 19	DPWA	$\gamma p \rightarrow \pi^+ \pi^- p$
-0.047 ± 0.002	¹ HUNT 19	DPWA	Multichannel
-0.067 ± 0.005	ANISOVICH 17	DPWA	Multichannel
-0.083 ± 0.004	WORKMAN 12A	DPWA	$\gamma N \rightarrow N\pi$
• • • We do not use the following data for averages, fits, limits, etc. • • •			
-0.067 ± 0.005	SOKHOYAN 15A	DPWA	Multichannel
-0.067 ± 0.005	GUTZ 14	DPWA	Multichannel
-0.071 ± 0.004	ANISOVICH 12A	DPWA	Multichannel
-0.065 ± 0.001	¹ SHRESTHA 12A	DPWA	Multichannel
-0.094	DRECHSEL 07	DPWA	$\gamma N \rightarrow \pi N$

¹ Statistical error only. $\Delta(1950) \rightarrow N\gamma$, helicity-3/2 amplitude $A_{3/2}$

VALUE (GeV ^{-1/2})	DOCUMENT ID	TECN	COMMENT
-0.100 to -0.080 (≈ -0.090) OUR ESTIMATE			
-0.1181 ± 0.0193	GOLOVATCH 19	DPWA	$\gamma p \rightarrow \pi^+ \pi^- p$
-0.074 ± 0.002	¹ HUNT 19	DPWA	Multichannel
-0.094 ± 0.004	ANISOVICH 17	DPWA	Multichannel
-0.096 ± 0.004	WORKMAN 12A	DPWA	$\gamma N \rightarrow N\pi$
• • • We do not use the following data for averages, fits, limits, etc. • • •			
-0.094 ± 0.004	SOKHOYAN 15A	DPWA	Multichannel
-0.094 ± 0.004	GUTZ 14	DPWA	Multichannel
-0.094 ± 0.005	ANISOVICH 12A	DPWA	Multichannel
-0.083 ± 0.001	¹ SHRESTHA 12A	DPWA	Multichannel
-0.121	DRECHSEL 07	DPWA	$\gamma N \rightarrow \pi N$

¹ Statistical error only. $\Delta(1950)$ REFERENCES

ROENCHEN 22	EPJ A58 229	D. Roenchen et al.	(JULI, GWU, BONN+)
GOLOVATCH 19	PL B788 371	E. Golovatch et al.	(CLAS Collab.)
HUNT 19	PR C39 055205	B. C. Hunt, D.M. Manley	
ANISOVICH 17	PL B766 357	A.V. Anisovich et al.	
ROENCHEN 15A	EPJ A51 70	D. Roenchen et al.	
SOKHOYAN 15A	EPJ A51 95	V. Sokhoyan et al.	(CBELSA/TAPS Collab.)
GUTZ 14	EPJ A50 74	E. Gutz et al.	(CBELSA/TAPS Collab.)
PDG 14	CP C38 070001	K. Olive et al.	(PDG Collab.)
SVARC 14	PR C89 045205	A. Svarc et al.	(RBI Zagreb, UNI Tuzla)
ANISOVICH 12A	EPJ A48 15	A.V. Anisovich et al.	(BONN, PNPI)
SHRESTHA 12A	PR C86 055203	M. Shrestha, D.M. Manley	(KSU)
WORKMAN 12A	PR C86 015202	R. Workman et al.	(GWU)
DRECHSEL 07	EPJ A34 69	D. Drechsel, S.S. Kamalov, L. Tiator	(MAINZ, JINR)
ARNDT 06	PR C74 045205	R.A. Arndt et al.	(GWU)
VRANA 00	PRPL 328 181	T.P. Vrana, S.A. Dylman, T.-S.H. Lee	(PITT, ANL)
HOEHLER 93	πN Newsletter 9 1	G. Hoehler	(KARL)
CUTKOSKY 80	Toronto Conf. 19	R.E. Cutkosky et al.	(CMU, LBL)UP
Also	PR D20 2839	R.E. Cutkosky et al.	(CMU, LBL)UP
HOEHLER 79	PDAT 12-1	G. Hoehler et al.	(KARLT)UP
Also	Toronto Conf. 3	R. Koch	(KARLT)UP

 $\Delta(2000) 5/2^+$

$$I(J^P) = \frac{3}{2}(\frac{5}{2}^+) \text{ Status: } **$$

OMITTED FROM SUMMARY TABLE

 $\Delta(2000)$ POLE POSITION

REAL PART

VALUE (MeV)	DOCUMENT ID	TECN	COMMENT
1998 ± 4 ± 4	¹ SVARC 14	L+P	$\pi N \rightarrow \pi N$
1976	SHRESTHA 12A	DPWA	Multichannel
2150 ± 100	CUTKOSKY 80	IPWA	$\pi N \rightarrow \pi N$
• • • We do not use the following data for averages, fits, limits, etc. • • •			
1697	VRANA 00	DPWA	Multichannel

¹ Fit to the amplitudes of HOEHLER 79.

-2xIMAGINARY PART

VALUE (MeV)	DOCUMENT ID	TECN	COMMENT
404 ± 10 ± 4	¹ SVARC 14	L+P	$\pi N \rightarrow \pi N$
350 ± 100	CUTKOSKY 80	IPWA	$\pi N \rightarrow \pi N$
• • • We do not use the following data for averages, fits, limits, etc. • • •			
488	SHRESTHA 12A	DPWA	Multichannel
112	VRANA 00	DPWA	Multichannel

¹ Fit to the amplitudes of HOEHLER 79. $\Delta(2000)$ ELASTIC POLE RESIDUEMODULUS $|r|$

VALUE (MeV)	DOCUMENT ID	TECN	COMMENT
34 ± 1 ± 1	¹ SVARC 14	L+P	$\pi N \rightarrow \pi N$
16 ± 5	CUTKOSKY 80	IPWA	$\pi N \rightarrow \pi N$

¹ Fit to the amplitudes of HOEHLER 79.PHASE θ

VALUE (°)	DOCUMENT ID	TECN	COMMENT
110 ± 1 ± 3	¹ SVARC 14	L+P	$\pi N \rightarrow \pi N$
150 ± 90	CUTKOSKY 80	IPWA	$\pi N \rightarrow \pi N$

¹ Fit to the amplitudes of HOEHLER 79. $\Delta(2000)$ BREIT-WIGNER MASS

VALUE (MeV)	DOCUMENT ID	TECN	COMMENT
2015 ± 24	¹ SHRESTHA 12A	DPWA	Multichannel
2200 ± 125	CUTKOSKY 80	IPWA	$\pi N \rightarrow \pi N$
• • • We do not use the following data for averages, fits, limits, etc. • • •			
1724 ± 61	VRANA 00	DPWA	Multichannel
1752 ± 32	MANLEY 92	IPWA	$\pi N \rightarrow \pi N$ & $N\pi\pi$

¹ Statistical error only. $\Delta(2000)$ BREIT-WIGNER WIDTH

VALUE (MeV)	DOCUMENT ID	TECN	COMMENT
500 ± 52	¹ SHRESTHA 12A	DPWA	Multichannel
400 ± 125	CUTKOSKY 80	IPWA	$\pi N \rightarrow \pi N$
• • • We do not use the following data for averages, fits, limits, etc. • • •			
138 ± 68	VRANA 00	DPWA	Multichannel
251 ± 93	MANLEY 92	IPWA	$\pi N \rightarrow \pi N$ & $N\pi\pi$

¹ Statistical error only. $\Delta(2000)$ DECAY MODES

Mode	Fraction (Γ_i/Γ)
Γ_1 $N\pi$	3-11 %
Γ_2 $N\pi\pi$	>87 %
Γ_3 $\Delta(1232)\pi$	<9 %
Γ_4 $\Delta(1232)\pi$, P-wave	<6 %
Γ_5 $\Delta(1232)\pi$, F-wave	<3 %
Γ_6 $N\rho$, S=3/2, P-wave	seen
Γ_7 $N\gamma$	seen
Γ_8 $N\gamma$, helicity=1/2	seen
Γ_9 $N\gamma$, helicity=3/2	seen

 $\Delta(2000)$ BRANCHING RATIOS

$\Gamma(N\pi)/\Gamma_{\text{total}}$	DOCUMENT ID	TECN	COMMENT	Γ_i/Γ
7 ± 1	¹ SHRESTHA 12A	DPWA	Multichannel	
7 ± 4	CUTKOSKY 80	IPWA	$\pi N \rightarrow \pi N$	
• • • We do not use the following data for averages, fits, limits, etc. • • •				
0 ± 1	VRANA 00	DPWA	Multichannel	
2 ± 1	MANLEY 92	IPWA	$\pi N \rightarrow \pi N$ & $N\pi\pi$	

¹ Statistical error only. $\Gamma(\Delta(1232)\pi, P\text{-wave})/\Gamma_{\text{total}}$

VALUE (%)	DOCUMENT ID	TECN	COMMENT	Γ_4/Γ
3 ± 3	¹ SHRESTHA 12A	DPWA	Multichannel	
• • • We do not use the following data for averages, fits, limits, etc. • • •				
0 ± 1	VRANA 00	DPWA	Multichannel	

¹ Statistical error only. $\Gamma(\Delta(1232)\pi, F\text{-wave})/\Gamma_{\text{total}}$

VALUE (%)	DOCUMENT ID	TECN	COMMENT	Γ_5/Γ
< 3	SHRESTHA 12A	DPWA	Multichannel	
• • • We do not use the following data for averages, fits, limits, etc. • • •				
40 ± 1	VRANA 00	DPWA	Multichannel	

 $\Gamma(N\rho, S=3/2, P\text{-wave})/\Gamma_{\text{total}}$

VALUE (%)	DOCUMENT ID	TECN	COMMENT	Γ_6/Γ
90 ± 3	¹ SHRESTHA 12A	DPWA	Multichannel	
• • • We do not use the following data for averages, fits, limits, etc. • • •				
60 ± 60	VRANA 00	DPWA	Multichannel	

¹ Statistical error only.

Baryon Particle Listings

$\Delta(2000)$, $\Delta(2150)$, $\Delta(2200)$

$\Delta(2000)$ BREIT-WIGNER PHOTON DECAY AMPLITUDES

$\Delta(2000) \rightarrow p\gamma$, helicity-1/2 amplitude $A_{1/2}$

VALUE (GeV ^{-1/2})	DOCUMENT ID	TECN	COMMENT
-0.061 ± 0.018	¹ SHRESTHA 12A	DPWA	Multichannel
¹ Statistical error only.			

$\Delta(2000) \rightarrow p\gamma$, helicity-3/2 amplitude $A_{3/2}$

VALUE (GeV ^{-1/2})	DOCUMENT ID	TECN	COMMENT
0.158 ± 0.032	¹ SHRESTHA 12A	DPWA	Multichannel
¹ Statistical error only.			

$\Delta(2000)$ REFERENCES

SVARC 14	PR C89 045205	A. Svarc et al.	(RBI Zagreb, UNI Tuzla)
SHRESTHA 12A	PR C86 055203	M. Shrestha, D.M. Manley	(KSU)
VRANA 00	PRPL 328 181	T.P. Vrana, S.A. Dytman, T.-S.H. Lee	(PITT, ANL)
MANLEY 92	PR D45 4002	D.M. Manley, E.M. Saleski	(KSA) IJP
Also	PR D30 904	D.M. Manley et al.	(VPI)
CUTKOSKY 80	Toronto Conf. 19	R.E. Cutkosky et al.	(CMU, LBL)
Also	PR D20 2839	R.E. Cutkosky et al.	(CMU, LBL)
HOEHLER 79	PDAT 12-1	G. Hoehler et al.	(KARLT)

$\Delta(2150)$ 1/2⁻

$$I(J^P) = \frac{3}{2}(\frac{1}{2}^-) \text{ Status: } *$$

OMITTED FROM SUMMARY TABLE

$\Delta(2150)$ POLE POSITION

REAL PART

VALUE (MeV)	DOCUMENT ID	TECN	COMMENT
2140 ± 80	CUTKOSKY 80	IPWA	$\pi N \rightarrow \pi N$

-2xIMAGINARY PART

VALUE (MeV)	DOCUMENT ID	TECN	COMMENT
200 ± 80	CUTKOSKY 80	IPWA	$\pi N \rightarrow \pi N$

$\Delta(2150)$ ELASTIC POLE RESIDUE

MODULUS |r|

VALUE (MeV)	DOCUMENT ID	TECN	COMMENT
7 ± 2	CUTKOSKY 80	IPWA	$\pi N \rightarrow \pi N$

PHASE θ

VALUE (°)	DOCUMENT ID	TECN	COMMENT
-60 ± 90	CUTKOSKY 80	IPWA	$\pi N \rightarrow \pi N$

$\Delta(2150)$ BREIT-WIGNER MASS

VALUE (MeV)	DOCUMENT ID	TECN	COMMENT
2150 ± 100	CUTKOSKY 80	IPWA	$\pi N \rightarrow \pi N$

$\Delta(2150)$ BREIT-WIGNER WIDTH

VALUE (MeV)	DOCUMENT ID	TECN	COMMENT
200 ± 100	CUTKOSKY 80	IPWA	$\pi N \rightarrow \pi N$

$\Delta(2150)$ DECAY MODES

Mode	Fraction (Γ_i/Γ)
Γ_1 $N\pi$	6-10 %

$\Delta(2150)$ BRANCHING RATIOS

$\Gamma(N\pi)/\Gamma_{\text{total}}$	DOCUMENT ID	TECN	COMMENT	Γ_1/Γ
8 ± 2	CUTKOSKY 80	IPWA	$\pi N \rightarrow \pi N$	

$\Delta(2150)$ REFERENCES

CUTKOSKY 80	Toronto Conf. 19	R.E. Cutkosky et al.	(CMU, LBL) IJP
Also	PR D20 2839	R.E. Cutkosky et al.	(CMU, LBL)

$\Delta(2200)$ 7/2⁻

$$I(J^P) = \frac{3}{2}(\frac{7}{2}^-) \text{ Status: } ***$$

$\Delta(2200)$ POLE POSITION

REAL PART

VALUE (MeV)	DOCUMENT ID	TECN	COMMENT
2050 to 2150 (≈ 2100) OUR ESTIMATE			
1963 ± 1	ROENCHEN 22	DPWA	Multichannel
2100 ± 50	CUTKOSKY 80	IPWA	$\pi N \rightarrow \pi N$
• • • We do not use the following data for averages, fits, limits, etc. • • •			
2142	ROENCHEN 15A	DPWA	Multichannel

-2xIMAGINARY PART

VALUE (MeV)	DOCUMENT ID	TECN	COMMENT
260 to 420 (≈ 340) OUR ESTIMATE			
328 ± 2	ROENCHEN 22	DPWA	Multichannel
340 ± 80	CUTKOSKY 80	IPWA	$\pi N \rightarrow \pi N$
• • • We do not use the following data for averages, fits, limits, etc. • • •			
486	ROENCHEN 15A	DPWA	Multichannel

$\Delta(2200)$ ELASTIC POLE RESIDUE

MODULUS |r|

VALUE (MeV)	DOCUMENT ID	TECN	COMMENT
6.8 ± 0.3	ROENCHEN 22	DPWA	Multichannel
8 ± 3	CUTKOSKY 80	IPWA	$\pi N \rightarrow \pi N$
• • • We do not use the following data for averages, fits, limits, etc. • • •			
17	ROENCHEN 15A	DPWA	Multichannel

PHASE θ

VALUE (°)	DOCUMENT ID	TECN	COMMENT
-80 ± 1	ROENCHEN 22	DPWA	Multichannel
-70 ± 40	CUTKOSKY 80	IPWA	$\pi N \rightarrow \pi N$
• • • We do not use the following data for averages, fits, limits, etc. • • •			
-56	ROENCHEN 15A	DPWA	Multichannel

$\Delta(2200)$ INELASTIC POLE RESIDUE

The "normalized residue" is the residue divided by $\Gamma_{\text{pole}}/2$.

Normalized residue in $N\pi \rightarrow \Delta(2200) \rightarrow \Sigma K$

MODULUS	PHASE (°)	DOCUMENT ID	TECN	COMMENT
0.001 ± 0.002	-123 ± 1	ROENCHEN 22	DPWA	Multichannel
• • • We do not use the following data for averages, fits, limits, etc. • • •				
0.005	-103	ROENCHEN 15A	DPWA	Multichannel

Normalized residue in $N\pi \rightarrow \Delta(2200) \rightarrow \Delta\pi$, D-wave

MODULUS	PHASE (°)	DOCUMENT ID	TECN	COMMENT
0.16 ± 0.01	100 ± 1	ROENCHEN 22	DPWA	Multichannel
• • • We do not use the following data for averages, fits, limits, etc. • • •				
0.23	107	ROENCHEN 15A	DPWA	Multichannel

Normalized residue in $N\pi \rightarrow \Delta(2200) \rightarrow \Delta\pi$, G-wave

MODULUS	PHASE (°)	DOCUMENT ID	TECN	COMMENT
0.003 ± 0.001	152 ± 3	ROENCHEN 22	DPWA	Multichannel
• • • We do not use the following data for averages, fits, limits, etc. • • •				
0.022	-151	ROENCHEN 15A	DPWA	Multichannel

$\Delta(2200)$ BREIT-WIGNER MASS

VALUE (MeV)	DOCUMENT ID	TECN	COMMENT
2150 to 2250 (≈ 2200) OUR ESTIMATE			
2176 ± 40	ANISOVICH 17	DPWA	Multichannel
2200 ± 80	CUTKOSKY 80	IPWA	$\pi N \rightarrow \pi N$
2215 ± 60	HOEHLER 79	IPWA	$\pi N \rightarrow \pi N$

$\Delta(2200)$ BREIT-WIGNER WIDTH

VALUE (MeV)	DOCUMENT ID	TECN	COMMENT
200 to 500 (≈ 350) OUR ESTIMATE			
210 ± 70	ANISOVICH 17	DPWA	Multichannel
450 ± 100	CUTKOSKY 80	IPWA	$\pi N \rightarrow \pi N$
400 ± 100	HOEHLER 79	IPWA	$\pi N \rightarrow \pi N$

See key on page 1171

Baryon Particle Listings
 $\Delta(2200)$, $\Delta(2300)$, $\Delta(2350)$

$\Delta(2200)$ DECAY MODES

Mode	Fraction (Γ_i/Γ)
Γ_1 $N\pi$	2-8 %
Γ_2 ΣK	1-7 %
Γ_3 $N\pi\pi$	>45 %
Γ_4 $\Delta\pi$	>45 %
Γ_5 $\Delta\pi, D$ -wave	>40 %
Γ_6 $\Delta\pi, G$ -wave	5-25 %
Γ_7 $\Delta\eta$	
Γ_8 $\Delta\eta, D$ -wave	seen

$\Delta(2200)$ BRANCHING RATIOS

$\Gamma(N\pi)/\Gamma_{total}$	DOCUMENT ID	TECN	COMMENT	Γ_1/Γ
VALUE (%)				
2-8 % OUR ESTIMATE				
3.5 ± 1.5	ANISOVICH 17	DPWA	Multichannel	
6 ± 2	CUTKOSKY 80	IPWA	$\pi N \rightarrow \pi N$	
5 ± 2	HOEHLER 79	IPWA	$\pi N \rightarrow \pi N$	
$\Gamma(\Sigma K)/\Gamma_{total}$				Γ_2/Γ
VALUE	DOCUMENT ID	TECN	COMMENT	
0.04 ± 0.03	ANISOVICH 17	DPWA	Multichannel	
$\Gamma(\Delta\pi, D$ -wave)/ Γ_{total}				Γ_5/Γ
VALUE	DOCUMENT ID	TECN	COMMENT	
>40 % OUR ESTIMATE				
0.70 ± 0.30	ANISOVICH 17	DPWA	Multichannel	
$\Gamma(\Delta\pi, G$ -wave)/ Γ_{total}				Γ_6/Γ
VALUE	DOCUMENT ID	TECN	COMMENT	
0.15 ± 0.10	ANISOVICH 17	DPWA	Multichannel	
$\Gamma(\Delta\eta, D$ -wave)/ Γ_{total}				Γ_8/Γ
VALUE	DOCUMENT ID	TECN	COMMENT	
~ 0.01	ANISOVICH 17	DPWA	Multichannel	

$\Delta(2200)$ PHOTON DECAY AMPLITUDES AT THE POLE

$\Delta(2200) \rightarrow N\gamma$, helicity-1/2 amplitude $A_{1/2}$				
MODULUS ($\text{GeV}^{-1/2}$)	PHASE ($^\circ$)	DOCUMENT ID	TECN	COMMENT
0.104 ± 0.011	-139 ± 2	ROENCHEN 22	DPWA	Multichannel
••• We do not use the following data for averages, fits, limits, etc. •••				
0.106	-23	ROENCHEN 15A	DPWA	Multichannel
$\Delta(2200) \rightarrow N\gamma$, helicity-3/2 amplitude $A_{3/2}$				
MODULUS ($\text{GeV}^{-1/2}$)	PHASE ($^\circ$)	DOCUMENT ID	TECN	COMMENT
0.021 ± 0.013	-180 ± 20	ROENCHEN 22	DPWA	Multichannel
••• We do not use the following data for averages, fits, limits, etc. •••				
0.157	-60	ROENCHEN 15A	DPWA	Multichannel

$\Delta(2200)$ REFERENCES

ROENCHEN 22	EPJ A58 229	D. Roenchen et al.	(JULI, GWU, BONN+)
ANISOVICH 17	PL B766 357	A.V. Anisovich et al.	
ROENCHEN 15A	EPJ A51 70	D. Roenchen et al.	
CUTKOSKY 80	Toronto Conf. 19	R.E. Cutkosky et al.	(CMU, LBL) IJP
Also	PR D20 2839	R.E. Cutkosky et al.	(CMU, LBL) IJP
HOEHLER 79	PDAT 12-1	G. Hoehler et al.	(KARLT) IJP
Also	Toronto Conf. 3	R. Koch	(KARLT) IJP

$\Delta(2300) 9/2^+$

 $I(J^P) = \frac{3}{2}(\frac{9}{2}^+)$ Status: **
 OMITTED FROM SUMMARY TABLE

$\Delta(2300)$ POLE POSITION

REAL PART	DOCUMENT ID	TECN	COMMENT
VALUE (MeV)			
2370 ± 80	CUTKOSKY 80	IPWA	$\pi N \rightarrow \pi N$
-2xIMAGINARY PART			
VALUE (MeV)	DOCUMENT ID	TECN	COMMENT
420 ± 160	CUTKOSKY 80	IPWA	$\pi N \rightarrow \pi N$

$\Delta(2300)$ ELASTIC POLE RESIDUE

MODULUS $ r $	DOCUMENT ID	TECN	COMMENT
VALUE (MeV)			
10 ± 4	CUTKOSKY 80	IPWA	$\pi N \rightarrow \pi N$

PHASE θ

VALUE ($^\circ$)	DOCUMENT ID	TECN	COMMENT
-20 ± 30	CUTKOSKY 80	IPWA	$\pi N \rightarrow \pi N$

$\Delta(2300)$ BREIT-WIGNER MASS

VALUE (MeV)	DOCUMENT ID	TECN	COMMENT
2400 ± 125	CUTKOSKY 80	IPWA	$\pi N \rightarrow \pi N$
2217 ± 80	HOEHLER 79	IPWA	$\pi N \rightarrow \pi N$

$\Delta(2300)$ BREIT-WIGNER WIDTH

VALUE (MeV)	DOCUMENT ID	TECN	COMMENT
425 ± 150	CUTKOSKY 80	IPWA	$\pi N \rightarrow \pi N$
300 ± 100	HOEHLER 79	IPWA	$\pi N \rightarrow \pi N$

$\Delta(2300)$ DECAY MODES

Mode	Fraction (Γ_i/Γ)
Γ_1 $N\pi$	1-8 %

$\Delta(2300)$ BRANCHING RATIOS

$\Gamma(N\pi)/\Gamma_{total}$	DOCUMENT ID	TECN	COMMENT	Γ_1/Γ
VALUE (%)				
6 ± 2	CUTKOSKY 80	IPWA	$\pi N \rightarrow \pi N$	
3 ± 2	HOEHLER 79	IPWA	$\pi N \rightarrow \pi N$	

$\Delta(2300)$ REFERENCES

CUTKOSKY 80	Toronto Conf. 19	R.E. Cutkosky et al.	(CMU, LBL) IJP
Also	PR D20 2839	R.E. Cutkosky et al.	(CMU, LBL) IJP
HOEHLER 79	PDAT 12-1	G. Hoehler et al.	(KARLT) IJP
Also	Toronto Conf. 3	R. Koch	(KARLT) IJP

$\Delta(2350) 5/2^-$

 $I(J^P) = \frac{3}{2}(\frac{5}{2}^-)$ Status: *
 OMITTED FROM SUMMARY TABLE

$\Delta(2350)$ POLE POSITION

REAL PART	DOCUMENT ID	TECN	COMMENT
VALUE (MeV)			
2400 ± 125	CUTKOSKY 80	IPWA	$\pi N \rightarrow \pi N$
••• We do not use the following data for averages, fits, limits, etc. •••			
2427	VRANA 00	DPWA	Multichannel
-2xIMAGINARY PART			
VALUE (MeV)	DOCUMENT ID	TECN	COMMENT
400 ± 150	CUTKOSKY 80	IPWA	$\pi N \rightarrow \pi N$
••• We do not use the following data for averages, fits, limits, etc. •••			
458	VRANA 00	DPWA	Multichannel

$\Delta(2350)$ ELASTIC POLE RESIDUE

MODULUS $ r $	DOCUMENT ID	TECN	COMMENT
VALUE (MeV)			
15 ± 8	CUTKOSKY 80	IPWA	$\pi N \rightarrow \pi N$

PHASE θ	DOCUMENT ID	TECN	COMMENT
VALUE ($^\circ$)			
-70 ± 70	CUTKOSKY 80	IPWA	$\pi N \rightarrow \pi N$

$\Delta(2350)$ BREIT-WIGNER MASS

VALUE (MeV)	DOCUMENT ID	TECN	COMMENT
2400 ± 125	CUTKOSKY 80	IPWA	$\pi N \rightarrow \pi N$
2305 ± 26	HOEHLER 79	IPWA	$\pi N \rightarrow \pi N$
••• We do not use the following data for averages, fits, limits, etc. •••			
2459 ± 100	VRANA 00	DPWA	Multichannel

$\Delta(2350)$ BREIT-WIGNER WIDTH

VALUE (MeV)	DOCUMENT ID	TECN	COMMENT
400 ± 150	CUTKOSKY 80	IPWA	$\pi N \rightarrow \pi N$
300 ± 70	HOEHLER 79	IPWA	$\pi N \rightarrow \pi N$
••• We do not use the following data for averages, fits, limits, etc. •••			
480 ± 360	VRANA 00	DPWA	Multichannel

Baryon Particle Listings

 $\Delta(2350)$, $\Delta(2390)$, $\Delta(2400)$ $\Delta(2350)$ DECAY MODES

Mode	Fraction (Γ_i/Γ)
Γ_1 $N\pi$	4-30 %

 $\Delta(2350)$ BRANCHING RATIOS

$\Gamma(N\pi)/\Gamma_{\text{total}}$	DOCUMENT ID	TECN	COMMENT	Γ_1/Γ
20±10	CUTKOSKY 80	IPWA	$\pi N \rightarrow \pi N$	
4±2	HOEHLER 79	IPWA	$\pi N \rightarrow \pi N$	
7±14	VRANA 00	DPWA	Multichannel	

••• We do not use the following data for averages, fits, limits, etc. •••

 $\Delta(2350)$ REFERENCES

VRANA 00	PRPL 328 181	T.P. Vrana, S.A. Dytman, T.-S.H. Lee	(PITT, ANL)
CUTKOSKY 80	Toronto Conf. 19	R.E. Cutkosky et al.	(CMU, LBL) IJP
Also	PR D20 2839	R.E. Cutkosky et al.	(CMU, LBL)
HOEHLER 79	PDAT 12-1	G. Hohler et al.	(KARLT) IJP
Also	Toronto Conf. 3	R. Koch	(KARLT) IJP

 $\Delta(2390)$ 7/2⁺

$$I(J^P) = \frac{3}{2}(\frac{7}{2}^+) \text{ Status: } *$$

OMITTED FROM SUMMARY TABLE

 $\Delta(2390)$ POLE POSITION

REAL PART	DOCUMENT ID	TECN	COMMENT
2223 ± 15 ± 19	¹ SVARC 14	L+P	$\pi N \rightarrow \pi N$
2350 ± 100	CUTKOSKY 80	IPWA	$\pi N \rightarrow \pi N$

-2xIMAGINARY PART	DOCUMENT ID	TECN	COMMENT
431 ± 26 ± 7	¹ SVARC 14	L+P	$\pi N \rightarrow \pi N$
260 ± 100	CUTKOSKY 80	IPWA	$\pi N \rightarrow \pi N$

 $\Delta(2390)$ ELASTIC POLE RESIDUE

MODULUS r	DOCUMENT ID	TECN	COMMENT
26 ± 2 ± 1	¹ SVARC 14	L+P	$\pi N \rightarrow \pi N$
12 ± 6	CUTKOSKY 80	IPWA	$\pi N \rightarrow \pi N$

PHASE θ	DOCUMENT ID	TECN	COMMENT
-160 ± 5 ± 11	¹ SVARC 14	L+P	$\pi N \rightarrow \pi N$
-90 ± 60	CUTKOSKY 80	IPWA	$\pi N \rightarrow \pi N$

 $\Delta(2390)$ BREIT-WIGNER MASS

VALUE (MeV)	DOCUMENT ID	TECN	COMMENT
2350 ± 100	CUTKOSKY 80	IPWA	$\pi N \rightarrow \pi N$
2425 ± 60	HOEHLER 79	IPWA	$\pi N \rightarrow \pi N$

 $\Delta(2390)$ BREIT-WIGNER WIDTH

VALUE (MeV)	DOCUMENT ID	TECN	COMMENT
300 ± 100	CUTKOSKY 80	IPWA	$\pi N \rightarrow \pi N$
300 ± 80	HOEHLER 79	IPWA	$\pi N \rightarrow \pi N$

 $\Delta(2390)$ DECAY MODES

Mode	Fraction (Γ_i/Γ)
Γ_1 $N\pi$	3-12 %

 $\Delta(2390)$ BRANCHING RATIOS

$\Gamma(N\pi)/\Gamma_{\text{total}}$	DOCUMENT ID	TECN	COMMENT	Γ_1/Γ
8±4	CUTKOSKY 80	IPWA	$\pi N \rightarrow \pi N$	
7±4	HOEHLER 79	IPWA	$\pi N \rightarrow \pi N$	

 $\Delta(2390)$ FOOTNOTES¹ Fit to the amplitudes of HOEHLER 79. $\Delta(2390)$ REFERENCES

SVARC 14	PR C89 045205	A. Svarc et al.	(RB) Zagreb, UNI Tuzla)
CUTKOSKY 80	Toronto Conf. 19	R.E. Cutkosky et al.	(CMU, LBL) IJP
Also	PR D20 2839	R.E. Cutkosky et al.	(CMU, LBL)
HOEHLER 79	PDAT 12-1	G. Hohler et al.	(KARLT) IJP
Also	Toronto Conf. 3	R. Koch	(KARLT) IJP

 $\Delta(2400)$ 9/2⁻

$$I(J^P) = \frac{3}{2}(\frac{9}{2}^-) \text{ Status: } **$$

OMITTED FROM SUMMARY TABLE

 $\Delta(2400)$ POLE POSITION

REAL PART

VALUE (MeV)	DOCUMENT ID	TECN	COMMENT
2458 ± 2	ROENCHEN 22	DPWA	Multichannel
2260 ± 60	CUTKOSKY 80	IPWA	$\pi N \rightarrow \pi N$
1931	ROENCHEN 15A	DPWA	Multichannel
1983	ARNDT 06	DPWA	$\pi N \rightarrow \pi N, \eta N$

••• We do not use the following data for averages, fits, limits, etc. •••

-2xIMAGINARY PART

VALUE (MeV)	DOCUMENT ID	TECN	COMMENT
280 ± 2	ROENCHEN 22	DPWA	Multichannel
320 ± 160	CUTKOSKY 80	IPWA	$\pi N \rightarrow \pi N$
442	ROENCHEN 15A	DPWA	Multichannel
878	ARNDT 06	DPWA	$\pi N \rightarrow \pi N, \eta N$

••• We do not use the following data for averages, fits, limits, etc. •••

 $\Delta(2400)$ ELASTIC POLE RESIDUE

MODULUS |r|

VALUE (MeV)	DOCUMENT ID	TECN	COMMENT
5.4 ± 2.7	ROENCHEN 22	DPWA	Multichannel
8 ± 4	CUTKOSKY 80	IPWA	$\pi N \rightarrow \pi N$
13	ROENCHEN 15A	DPWA	Multichannel
24	ARNDT 06	DPWA	$\pi N \rightarrow \pi N, \eta N$

••• We do not use the following data for averages, fits, limits, etc. •••

PHASE θ

VALUE (°)	DOCUMENT ID	TECN	COMMENT
8.4 ± 17	ROENCHEN 22	DPWA	Multichannel
-25 ± 15	CUTKOSKY 80	IPWA	$\pi N \rightarrow \pi N$
-96	ROENCHEN 15A	DPWA	Multichannel
-139	ARNDT 06	DPWA	$\pi N \rightarrow \pi N, \eta N$

••• We do not use the following data for averages, fits, limits, etc. •••

 $\Delta(2400)$ INELASTIC POLE RESIDUEThe "normalized residue" is the residue divided by $\Gamma_{\text{pole}}/2$.Normalized residue in $N\pi \rightarrow \Delta(2400) \rightarrow \Sigma K$

MODULUS	PHASE (°)	DOCUMENT ID	TECN	COMMENT
0.004 ± 0.003	17 ± 15	ROENCHEN 22	DPWA	Multichannel
0.009	25	ROENCHEN 15A	DPWA	Multichannel

••• We do not use the following data for averages, fits, limits, etc. •••

Normalized residue in $N\pi \rightarrow \Delta(2400) \rightarrow \Delta\pi, G\text{-wave}$

MODULUS	PHASE (°)	DOCUMENT ID	TECN	COMMENT
0.10 ± 0.05	17 ± 11	ROENCHEN 22	DPWA	Multichannel
0.18	-110	ROENCHEN 15A	DPWA	Multichannel

••• We do not use the following data for averages, fits, limits, etc. •••

Normalized residue in $N\pi \rightarrow \Delta(2400) \rightarrow \Delta\pi, I\text{-wave}$

MODULUS	PHASE (°)	DOCUMENT ID	TECN	COMMENT
0.019 ± 0.003	-120 ± 25	ROENCHEN 22	DPWA	Multichannel
0.012	-1.0	ROENCHEN 15A	DPWA	Multichannel

••• We do not use the following data for averages, fits, limits, etc. •••

 $\Delta(2400)$ BREIT-WIGNER MASS

VALUE (MeV)	DOCUMENT ID	TECN	COMMENT
2643 ± 141	¹ ARNDT 06	DPWA	$\pi N \rightarrow \pi N, \eta N$
2300 ± 100	CUTKOSKY 80	IPWA	$\pi N \rightarrow \pi N$
2468 ± 50	HOEHLER 79	IPWA	$\pi N \rightarrow \pi N$

¹ Statistical error only. $\Delta(2400)$ BREIT-WIGNER WIDTH

VALUE (MeV)	DOCUMENT ID	TECN	COMMENT
895 ± 432	² ARNDT 06	DPWA	$\pi N \rightarrow \pi N, \eta N$
330 ± 100	CUTKOSKY 80	IPWA	$\pi N \rightarrow \pi N$
480 ± 100	HOEHLER 79	IPWA	$\pi N \rightarrow \pi N$

² Statistical error only.

See key on page 1171

Baryon Particle Listings

$\Delta(2400)$, $\Delta(2420)$, $\Delta(2750)$

$\Delta(2400)$ DECAY MODES

Mode	Fraction (Γ_j/Γ)
$\Gamma_1 \quad N\pi$	3-9 %

$\Delta(2400)$ BRANCHING RATIOS

$\Gamma(N\pi)/\Gamma_{total}$	DOCUMENT ID	TECN	COMMENT	Γ_1/Γ
6.4±2.2	³ ARNDT	06	DPWA $\pi N \rightarrow \pi N, \eta N$	
5 ±2	CUTKOSKY	80	IPWA $\pi N \rightarrow \pi N$	
6 ±3	HOEHLER	79	IPWA $\pi N \rightarrow \pi N$	

³ Statistical error only.

$\Delta(2400)$ PHOTON DECAY AMPLITUDES AT THE POLE

$\Delta(2400) \rightarrow N\gamma$, helicity-1/2 amplitude $A_{1/2}$

MODULUS ($\text{GeV}^{-1/2}$)	PHASE ($^\circ$)	DOCUMENT ID	TECN	COMMENT
0.021±0.007	-67 ± 12	ROENCHEN	22	DPWA Multichannel
-0.034	63	ROENCHEN	15A	DPWA Multichannel

••• We do not use the following data for averages, fits, limits, etc. •••

$\Delta(2400) \rightarrow N\gamma$, helicity-3/2 amplitude $A_{3/2}$

MODULUS ($\text{GeV}^{-1/2}$)	PHASE ($^\circ$)	DOCUMENT ID	TECN	COMMENT
0.022±0.007	122 ± 7	ROENCHEN	22	DPWA Multichannel
0.054	-75	ROENCHEN	15A	DPWA Multichannel

••• We do not use the following data for averages, fits, limits, etc. •••

$\Delta(2400)$ REFERENCES

ROENCHEN	22	EPJ A58 229	D. Roenchen et al.	(JULI, GWU, BONN+)
ROENCHEN	15A	EPJ A51 70	D. Roenchen et al.	
ARNDT	06	PR C74 045205	R.A. Arndt et al.	(GWU)
CUTKOSKY	80	Toronto Conf. 19	R.E. Cutkosky et al.	(CMU, LBL) IJP
Also		PR D20 2839	R.E. Cutkosky et al.	(CMU, LBL)
HOEHLER	79	PDAT 12-1	G. Hohler et al.	(KARLT) IJP
Also		Toronto Conf. 3	R. Koch	(KARLT) IJP

$\Delta(2420) \ 11/2^+$

 $I(J^P) = \frac{3}{2}(\frac{1}{2}^+) \text{Status: } ***$

Older and obsolete values are listed and referenced in the 2014 edition, Chinese Physics C38 070001 (2014).

$\Delta(2420)$ POLE POSITION

REAL PART

VALUE (MeV)	DOCUMENT ID	TECN	COMMENT
2300 to 2500 (≈ 2400) OUR ESTIMATE			
2454 ± 4 ± 11	¹ SVARC	14	L+P $\pi N \rightarrow \pi N$
2360 ± 100	CUTKOSKY	80	IPWA $\pi N \rightarrow \pi N$
••• We do not use the following data for averages, fits, limits, etc. •••			
2529	ARNDT	06	DPWA $\pi N \rightarrow \pi N, \eta N$
2300	HOEHLER	93	ARGD $\pi N \rightarrow \pi N$

¹ Fit to the amplitudes of HOEHLER 79.

-2xIMAGINARY PART

VALUE (MeV)	DOCUMENT ID	TECN	COMMENT
350 to 550 (≈ 450) OUR ESTIMATE			
462 ± 8 ± 50	¹ SVARC	14	L+P $\pi N \rightarrow \pi N$
420 ± 100	CUTKOSKY	80	IPWA $\pi N \rightarrow \pi N$
••• We do not use the following data for averages, fits, limits, etc. •••			
621	ARNDT	06	DPWA $\pi N \rightarrow \pi N, \eta N$
620	HOEHLER	93	ARGD $\pi N \rightarrow \pi N$

¹ Fit to the amplitudes of HOEHLER 79.

$\Delta(2420)$ ELASTIC POLE RESIDUE

MODULUS |r|

VALUE (MeV)	DOCUMENT ID	TECN	COMMENT
20 to 40 (≈ 30) OUR ESTIMATE			
30 ± 1 ± 7	¹ SVARC	14	L+P $\pi N \rightarrow \pi N$
18 ± 6	CUTKOSKY	80	IPWA $\pi N \rightarrow \pi N$
••• We do not use the following data for averages, fits, limits, etc. •••			
33	ARNDT	06	DPWA $\pi N \rightarrow \pi N, \eta N$
39	HOEHLER	93	ARGD $\pi N \rightarrow \pi N$

¹ Fit to the amplitudes of HOEHLER 79.

PHASE θ

VALUE ($^\circ$)	DOCUMENT ID	TECN	COMMENT
-60 to 20 (≈ -20) OUR ESTIMATE			
11 ± 1 ± 8	¹ SVARC	14	L+P $\pi N \rightarrow \pi N$
-30 ± 40	CUTKOSKY	80	IPWA $\pi N \rightarrow \pi N$

••• We do not use the following data for averages, fits, limits, etc. •••

-45	ARNDT	06	DPWA $\pi N \rightarrow \pi N, \eta N$
-60	HOEHLER	93	ARGD $\pi N \rightarrow \pi N$

¹ Fit to the amplitudes of HOEHLER 79.

$\Delta(2420)$ BREIT-WIGNER MASS

VALUE (MeV)	DOCUMENT ID	TECN	COMMENT
2300 to 2600 (≈ 2450) OUR ESTIMATE			
2633 ± 29	¹ ARNDT	06	DPWA $\pi N \rightarrow \pi N, \eta N$
2400 ± 125	CUTKOSKY	80	IPWA $\pi N \rightarrow \pi N$
2416 ± 17	HOEHLER	79	IPWA $\pi N \rightarrow \pi N$

¹ Statistical error only.

$\Delta(2420)$ BREIT-WIGNER WIDTH

VALUE (MeV)	DOCUMENT ID	TECN	COMMENT
300 to 700 (≈ 500) OUR ESTIMATE			
692 ± 47	¹ ARNDT	06	DPWA $\pi N \rightarrow \pi N, \eta N$
450 ± 150	CUTKOSKY	80	IPWA $\pi N \rightarrow \pi N$
340 ± 28	HOEHLER	79	IPWA $\pi N \rightarrow \pi N$

¹ Statistical error only.

$\Delta(2420)$ DECAY MODES

The following branching fractions are our estimates, not fits or averages.

Mode	Fraction (Γ_j/Γ)
$\Gamma_1 \quad N\pi$	5-10 %

$\Delta(2420)$ BRANCHING RATIOS

$\Gamma(N\pi)/\Gamma_{total}$	DOCUMENT ID	TECN	COMMENT	Γ_1/Γ
5 to 10 (≈ 8) OUR ESTIMATE				
8.5 ± 0.8	¹ ARNDT	06	DPWA $\pi N \rightarrow \pi N, \eta N$	
8 ± 3	CUTKOSKY	80	IPWA $\pi N \rightarrow \pi N$	
8.0 ± 1.5	HOEHLER	79	IPWA $\pi N \rightarrow \pi N$	

¹ Statistical error only.

$\Delta(2420)$ REFERENCES

PDG	14	CP C38 070001	K. Olive et al.	(PDG Collab.)
SVARC	14	PR C89 045205	A. Svarc et al.	(RBI Zagreb, UNI Tuzla)
ARNDT	06	PR C74 045205	R.A. Arndt et al.	(GWU)
HOEHLER	93	πN Newsletter 9 1	G. Hohler	(KARLT)
CUTKOSKY	80	Toronto Conf. 19	R.E. Cutkosky et al.	(CMU, LBL) IJP
Also		PR D20 2839	R.E. Cutkosky et al.	(CMU, LBL)
HOEHLER	79	PDAT 12-1	G. Hohler et al.	(KARLT) IJP
Also		Toronto Conf. 3	R. Koch	(KARLT) IJP

$\Delta(2750) \ 13/2^-$

 $I(J^P) = \frac{3}{2}(\frac{1}{2}^-) \text{Status: } **$

OMITTED FROM SUMMARY TABLE

$\Delta(2750)$ BREIT-WIGNER MASS

VALUE (MeV)	DOCUMENT ID	TECN	COMMENT
2794 ± 80	HOEHLER	79	IPWA $\pi N \rightarrow \pi N$

$\Delta(2750)$ BREIT-WIGNER WIDTH

VALUE (MeV)	DOCUMENT ID	TECN	COMMENT
350 ± 100	HOEHLER	79	IPWA $\pi N \rightarrow \pi N$

$\Delta(2750)$ DECAY MODES

Mode	Fraction (Γ_j/Γ)
$\Gamma_1 \quad N\pi$	2-6 %

$\Delta(2750)$ BRANCHING RATIOS

$\Gamma(N\pi)/\Gamma_{total}$	DOCUMENT ID	TECN	COMMENT	Γ_1/Γ
4.0 ± 1.5	HOEHLER	79	IPWA $\pi N \rightarrow \pi N$	

$\Delta(2750)$ REFERENCES

HOEHLER	79	PDAT 12-1	G. Hohler et al.	(KARLT) IJP
Also		Toronto Conf. 3	R. Koch	(KARLT) IJP

Baryon Particle Listings

 $\Delta(2950)$, $\Delta(\sim 3000)$ $\Delta(2950) 15/2^+$ $I(J^P) = \frac{3}{2}(\frac{15}{2}^+)$ Status: **

OMITTED FROM SUMMARY TABLE

 $\Delta(2950)$ BREIT-WIGNER MASS

VALUE (MeV)	DOCUMENT ID	TECN	COMMENT
2990±100	HOEHLER 79	IPWA	$\pi N \rightarrow \pi N$

 $\Delta(2950)$ BREIT-WIGNER WIDTH

VALUE (MeV)	DOCUMENT ID	TECN	COMMENT
330±100	HOEHLER 79	IPWA	$\pi N \rightarrow \pi N$

 $\Delta(2950)$ DECAY MODES

Mode	Fraction (Γ_i/Γ)
$\Gamma_1 \quad N\pi$	2-6 %

 $\Delta(2950)$ BRANCHING RATIOS

$\Gamma(N\pi)/\Gamma_{\text{total}}$	DOCUMENT ID	TECN	COMMENT	Γ_1/Γ
4±2	HOEHLER 79	IPWA	$\pi N \rightarrow \pi N$	

 $\Delta(2950)$ REFERENCES

HOEHLER 79	PDAT 12-1	G. Hohler et al.	(KARLT) IJP
Also	Toronto Conf. 3	R. Koch	(KARLT) IJP

 $\Delta(\sim 3000)$ Region
Partial-Wave Analyses

OMITTED FROM SUMMARY TABLE

We list here miscellaneous high-mass candidates for isospin-3/2 resonances found in partial-wave analyses.

Our 1982 edition also had a $\Delta(2850)$ and a $\Delta(3230)$. The evidence for them was deduced from total cross-section and 180° elastic cross-section measurements. The $\Delta(2850)$ has been resolved into the $\Delta(2750) I_{3,13}$ and $\Delta(2950) K_{3,15}$. The $\Delta(3230)$ is perhaps related to the $K_{3,13}$ of HENDRY 78 and to the $L_{3,17}$ of KOCH 80.

 $\Delta(\sim 3000)$ BREIT-WIGNER MASS

VALUE (MeV)	DOCUMENT ID	TECN	COMMENT
3300	¹ KOCH 80	IPWA	$\pi N \rightarrow \pi N$ $L_{3,17}$ wave
3500	¹ KOCH 80	IPWA	$\pi N \rightarrow \pi N$ $M_{3,19}$ wave
2850±150	HENDRY 78	MPWA	$\pi N \rightarrow \pi N$ $I_{3,11}$ wave
3200±200	HENDRY 78	MPWA	$\pi N \rightarrow \pi N$ $K_{3,13}$ wave
3300±200	HENDRY 78	MPWA	$\pi N \rightarrow \pi N$ $L_{3,17}$ wave
3700±200	HENDRY 78	MPWA	$\pi N \rightarrow \pi N$ $M_{3,19}$ wave
4100±300	HENDRY 78	MPWA	$\pi N \rightarrow \pi N$ $N_{3,21}$ wave

 $\Delta(\sim 3000)$ BREIT-WIGNER WIDTH

VALUE (MeV)	DOCUMENT ID	TECN	COMMENT
700±200	HENDRY 78	MPWA	$\pi N \rightarrow \pi N$ $I_{3,11}$ wave
1000±300	HENDRY 78	MPWA	$\pi N \rightarrow \pi N$ $K_{3,13}$ wave
1100±300	HENDRY 78	MPWA	$\pi N \rightarrow \pi N$ $L_{3,17}$ wave
1300±400	HENDRY 78	MPWA	$\pi N \rightarrow \pi N$ $M_{3,19}$ wave
1600±500	HENDRY 78	MPWA	$\pi N \rightarrow \pi N$ $N_{3,21}$ wave

 $\Delta(\sim 3000)$ DECAY MODES

Mode	Fraction (Γ_i/Γ)
$\Gamma_1 \quad N\pi$	1-8%

 $\Delta(\sim 3000)$ BRANCHING RATIOS

$\Gamma(N\pi)/\Gamma_{\text{total}}$	DOCUMENT ID	TECN	COMMENT	Γ_1/Γ
1-8% OUR ESTIMATE				
6±2	HENDRY 78	MPWA	$\pi N \rightarrow \pi N$ $I_{3,11}$ wave	
5±2	HENDRY 78	MPWA	$\pi N \rightarrow \pi N$ $K_{3,13}$ wave	
3±1	HENDRY 78	MPWA	$\pi N \rightarrow \pi N$ $L_{3,17}$ wave	
3±1	HENDRY 78	MPWA	$\pi N \rightarrow \pi N$ $M_{3,19}$ wave	
2±1	HENDRY 78	MPWA	$\pi N \rightarrow \pi N$ $N_{3,21}$ wave	

 $\Delta(\sim 3000)$ FOOTNOTES

¹In addition, KOCH 80 reports some evidence for an $S_{31} \Delta(2700)$ and a $P_{33} \Delta(2800)$.

 $\Delta(\sim 3000)$ REFERENCES

KOCH 80	Toronto Conf. 3	R. Koch	(KARLT) IJP
HENDRY 78	PRL 41 222	A.W. Hendry	(IND, LBL) IJP
Also	ANP 136 1	A.W. Hendry	(IND)

See key on page 1171

Λ

Λ BARYONS

$(S = -1, I = 0)$

$\Lambda^0 = uds$

Λ

$I(J^P) = 0(\frac{1}{2}^+)$ Status: ****

We have omitted some results that have been superseded by later experiments. See our earlier editions.

Λ MASS

The fit uses Λ, Σ⁺, Σ⁰, Σ⁻ mass and mass-difference measurements.

VALUE (MeV)	EVTs	DOCUMENT ID	TECN	COMMENT
1115.683 ± 0.006 OUR FIT				
1115.683 ± 0.006 OUR AVERAGE				
1115.678 ± 0.006 ± 0.006	20k	HARTOUNI 94	SPEC	pp 27.5 GeV/c
1115.690 ± 0.008 ± 0.006	18k	¹ HARTOUNI 94	SPEC	pp 27.5 GeV/c
• • • We do not use the following data for averages, fits, limits, etc. • • •				
1115.59 ± 0.08	935	HYMAN 72	HEBC	
1115.39 ± 0.12	195	MAYEUR 67	EMUL	
1115.6 ± 0.4		LONDON 66	HBC	
1115.65 ± 0.07	488	² SCHMIDT 65	HBC	
1115.44 ± 0.12		³ BHOWMIK 63	RVUE	

- ¹We assume CPT invariance: this is the $\bar{\Lambda}$ mass as measured by HARTOUNI 94. See below for the fractional mass difference, testing CPT.
- ²The SCHMIDT 65 masses have been reevaluated using our April 1973 proton and K^\pm and π^\pm masses. P. Schmidt, private communication (1974).
- ³The mass has been raised 35 keV to take into account a 46 keV increase in the proton mass and an 11 keV decrease in the π^\pm mass (note added Reviews of Modern Physics **39** 1 (1967)).

$(m_\Lambda - m_{\bar{\Lambda}}) / m_\Lambda$

A test of CPT invariance.

VALUE (units 10 ⁻⁵)	EVTs	DOCUMENT ID	TECN	COMMENT
- 0.1 ± 1.1 OUR AVERAGE				Error includes scale factor of 1.6.
+ 1.3 ± 1.2	31k	¹ RYBICKI 96	NA32	π^- Cu, 230 GeV
- 1.08 ± 0.90		HARTOUNI 94	SPEC	pp 27.5 GeV/c
4.5 ± 5.4		CHIEN 66	HBC	6.9 GeV/c $\bar{p}p$
• • • We do not use the following data for averages, fits, limits, etc. • • •				
-26 ± 13		BADIER 67	HBC	2.4 GeV/c $\bar{p}p$

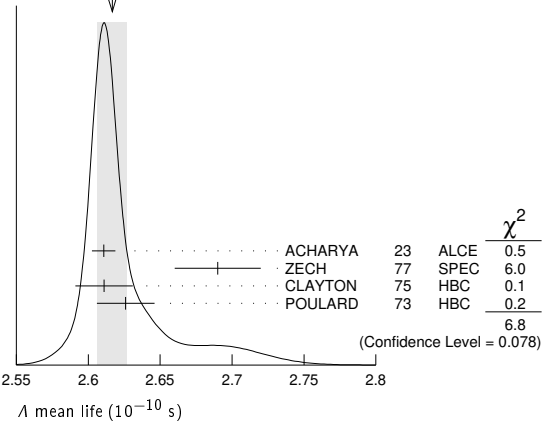
¹RYBICKI 96 is an analysis of old ACCMOR (NA32) data.

Λ MEAN LIFE

Measurements with an error $\geq 0.1 \times 10^{-10}$ s have been omitted altogether, and only the highest-statistics are used.

VALUE (10 ⁻¹⁰ s)	EVTs	DOCUMENT ID	TECN	COMMENT
2.617 ± 0.010 OUR AVERAGE				Error includes scale factor of 1.5. See the ideogram below.
2.6107 ± 0.0037 ± 0.0072	188M	ACHARYA 23	ALCE	Pb-Pb → ΛX or $\bar{\Lambda}X$ at 5.02 TeV
2.69 ± 0.03	53k	ZECH 77	SPEC	Neutral hyperon beam
2.611 ± 0.020	34k	CLAYTON 75	HBC	0.96-1.4 GeV/c K^-p
2.626 ± 0.020	36k	POULARD 73	HBC	0.4-2.3 GeV/c K^-p
• • • We do not use the following data for averages, fits, limits, etc. • • •				
2.69 ± 0.05	6582	ALTHOFF 73B	OSPK	$\pi^+ n \rightarrow \Lambda K^+$
2.54 ± 0.04	4572	BALTAY 71B	HBC	K^-p at rest
2.535 ± 0.035	8342	GRIMM 68	HBC	
2.47 ± 0.08	2600	HEPP 68	HBC	
2.35 ± 0.09	916	BURAN 66	HLBC	
2.452 \pm $\begin{smallmatrix} +0.056 \\ -0.054 \end{smallmatrix}$	2213	ENGELMANN 66	HBC	
2.59 ± 0.09	794	HUBBARD 64	HBC	
2.59 ± 0.07	1378	SCHWARTZ 64	HBC	
2.36 ± 0.06	2239	BLOCK 63	HEBC	

WEIGHTED AVERAGE
2.617 ± 0.010 (Error scaled by 1.5)



$(\tau_\Lambda - \tau_{\bar{\Lambda}}) / \tau_\Lambda$

A test of CPT invariance.

VALUE (units 10 ⁻³)	EVTs	DOCUMENT ID	TECN	COMMENT
0.9 ± 3.2 OUR AVERAGE				
1.3 ± 2.8 ± 2.1	188M	ACHARYA 23	ALCE	Pb-Pb → ΛX or $\bar{\Lambda}X$ at 5.02 TeV
- 1.8 ± 6.6 ± 5.6		BARNES 96	CNTR	LEAR $\bar{p}p \rightarrow \bar{\Lambda}\Lambda$
44 ± 85		BADIER 67	HBC	2.4 GeV/c $\bar{p}p$

Λ MAGNETIC MOMENT

See the "Quark Model" review. Measurements with an error $\geq 0.15 \mu_N$ have been omitted.

VALUE (μN)	EVTs	DOCUMENT ID	TECN	COMMENT
-0.613 ± 0.004 OUR AVERAGE				
-0.606 ± 0.015	200k	COX 81	SPEC	
-0.6138 ± 0.0047	3M	SCHACHIN... 78	SPEC	
-0.59 ± 0.07	350k	HELLER 77	SPEC	
-0.57 ± 0.05	1.2M	BUNCE 76	SPEC	
-0.66 ± 0.07	1300	DAHL-JENSEN 71	EMUL	200 kG field

Λ ELECTRIC DIPOLE MOMENT

A nonzero value is forbidden by both T invariance and P invariance.

VALUE (10 ⁻¹⁶ e-cm)	CL%	DOCUMENT ID	TECN
< 1.5	95	¹ PONDROM 81	SPEC
• • • We do not use the following data for averages, fits, limits, etc. • • •			
<100	95	² BARONI 71	EMUL
<500	95	GIBSON 66	EMUL

¹PONDROM 81 measures $(-3.0 \pm 7.4) \times 10^{-17}$ e-cm.
²BARONI 71 measures $(-5.9 \pm 2.9) \times 10^{-15}$ e-cm.

Λ DECAY MODES

Mode	Fraction (Γ _i /Γ)	Confidence level
Γ ₁ $p\pi^-$	(64.1 ± 0.5) %	
Γ ₂ $n\pi^0$	(35.9 ± 0.5) %	
Γ ₃ $n\gamma$	(8.3 ± 0.7) × 10 ⁻⁴	
Γ ₄ $p\pi^-\gamma$	[a] (8.5 ± 1.4) × 10 ⁻⁴	
Γ ₅ $p e^- \bar{\nu}_e$	(8.34 ± 0.14) × 10 ⁻⁴	
Γ ₆ $p\mu^- \bar{\nu}_\mu$	(1.51 ± 0.19) × 10 ⁻⁴	
Lepton (L) and/or Baryon (B) number violating decay modes		
Γ ₇ $\pi^+ e^-$	L,B < 6 × 10 ⁻⁷	90%
Γ ₈ $\pi^+ \mu^-$	L,B < 6 × 10 ⁻⁷	90%
Γ ₉ $\pi^- e^+$	L,B < 4 × 10 ⁻⁷	90%
Γ ₁₀ $\pi^- \mu^+$	L,B < 6 × 10 ⁻⁷	90%
Γ ₁₁ $K^+ e^-$	L,B < 2 × 10 ⁻⁶	90%
Γ ₁₂ $K^+ \mu^-$	L,B < 3 × 10 ⁻⁶	90%
Γ ₁₃ $K^- e^+$	L,B < 2 × 10 ⁻⁶	90%
Γ ₁₄ $K^- \mu^+$	L,B < 3 × 10 ⁻⁶	90%
Γ ₁₅ $K_S^0 \nu$	L,B < 2 × 10 ⁻⁵	90%
Γ ₁₆ $\bar{p}\pi^+$	B < 9 × 10 ⁻⁷	90%
Γ ₁₇ invisible	< 7.4 × 10 ⁻⁵	90%

[a] See the Listings below for the pion momentum range used in this measurement.

Baryon Particle Listings

Λ

CONSTRAINED FIT INFORMATION

An overall fit to 4 branching ratios uses 11 measurements and one constraint to determine 3 parameters. The overall fit has a $\chi^2 = 6.9$ for 9 degrees of freedom.

The following *off-diagonal* array elements are the correlation coefficients $\langle \delta x_i \delta x_j \rangle / (\delta x_i \delta x_j)$, in percent, from the fit to the branching fractions, $x_i \equiv \Gamma_i / \Gamma_{\text{total}}$. The fit constrains the x_i whose labels appear in this array to sum to one.

x_2	-100	
x_6	0	0
	x_1	x_2

Λ BRANCHING RATIOS

Γ($p\pi^-$)/Γ($N\pi$) Γ₁/(Γ₁+Γ₂)

VALUE	EVTs	DOCUMENT ID	TECN	COMMENT
0.641 ± 0.005 OUR FIT				
0.640 ± 0.005 OUR AVERAGE				
0.646 ± 0.008	4572	BALTAY	71B	HBC $K^- p$ at rest
0.635 ± 0.007	6736	DOYLE	69	HBC $\pi^- p \rightarrow \Lambda K^0$
0.643 ± 0.016	903	HUMPHREY	62	HBC
0.624 ± 0.030		CRAWFORD	59B	HBC $\pi^- p \rightarrow \Lambda K^0$

Γ($n\pi^0$)/Γ($N\pi$) Γ₂/(Γ₁+Γ₂)

VALUE	EVTs	DOCUMENT ID	TECN	COMMENT
0.359 ± 0.005 OUR FIT				
0.310 ± 0.028 OUR AVERAGE				
0.35 ± 0.05		BROWN	63	HLBC
0.291 ± 0.034	75	CHRETIEN	63	HLBC

Γ($n\gamma$)/Γ_{total} Γ₃/Γ

VALUE (units 10^{-3})	EVTs	DOCUMENT ID	TECN	COMMENT
0.832 ± 0.038 ± 0.054	13889	¹ ABLIKIM	22AJ	BES3 $J/\psi \rightarrow \Lambda \bar{\Lambda}$
• • • We do not use the following data for averages, fits, limits, etc. • • •				
1.75 ± 0.15	1816	LARSON	93	SPEC $K^- p$ at rest
1.78 ± 0.24 ^{+0.14} / _{-0.16}	287	NOBLE	92	SPEC See LARSON 93

¹ This ABLIKIM 22AJ value is a factor of 2.1 smaller and differs by 5.6σ from the previous LARSON 93 value.

Γ($n\gamma$)/Γ($n\pi^0$) Γ₃/Γ₂

VALUE (units 10^{-3})	EVTs	DOCUMENT ID	TECN	COMMENT
• • • We do not use the following data for averages, fits, limits, etc. • • •				
2.86 ± 0.74 ± 0.57	24	BIAGI	86	SPEC SPS hyperon beam

Γ($p\pi^- \gamma$)/Γ($p\pi^-$) Γ₄/Γ₁

VALUE (units 10^{-3})	EVTs	DOCUMENT ID	TECN	COMMENT
1.32 ± 0.22	72	BAGGETT	72c	HBC $\pi^- < 95$ MeV/c

Γ($p e^- \bar{\nu}_e$)/Γ($p\pi^-$) Γ₅/Γ₁

VALUE (units 10^{-3})	EVTs	DOCUMENT ID	TECN	COMMENT
1.301 ± 0.019 OUR AVERAGE				
1.335 ± 0.056	7111	BOURQUIN	83	SPEC SPS hyperon beam
1.313 ± 0.024	10k	WISE	80	SPEC
1.23 ± 0.11	544	LINDQUIST	77	SPEC $\pi^- p \rightarrow K^0 \Lambda$
1.27 ± 0.07	1089	KATZ	73	HBC
1.31 ± 0.06	1078	ALTHOFF	71	OSPK
1.17 ± 0.13	86	¹ CANTER	71	HBC $K^- p$ at rest
1.20 ± 0.12	143	² MALONEY	69	HBC
1.17 ± 0.18	120	² BAGLIN	64	FBC K^- freon 1.45 GeV/c
1.23 ± 0.20	150	² ELY	63	FBC

• • • We do not use the following data for averages, fits, limits, etc. • • •

1.32 ± 0.15 218 ¹ LINDQUIST 71 OSPK See LINDQUIST 77

¹ Changed by us from $\Gamma(p e^- \bar{\nu}_e) / \Gamma(N\pi)$ assuming the authors used $\Gamma(\Lambda \rightarrow p\pi^-) / \Gamma(\text{total}) = 2/3$.

² Changed by us from $\Gamma(p e^- \bar{\nu}_e) / \Gamma(N\pi)$ because $\Gamma(p e^- \nu) / \Gamma(p\pi^-)$ is the directly measured quantity.

Γ($p\mu^- \bar{\nu}_\mu$)/Γ_{total} Γ₆/Γ

VALUE (units 10^{-4})	EVTs	DOCUMENT ID	TECN	COMMENT
1.51 ± 0.19 OUR FIT				
1.48 ± 0.21 ± 0.08	64	¹ ABLIKIM	21AG	BES3 $J/\psi \rightarrow \Lambda \bar{\Lambda}$

¹ ABLIKIM 21AG use $\bar{\Lambda} \rightarrow \bar{p}\pi^+$ decay mode as the double tag identifier and thus as indirect normalization.

Γ($p\mu^- \bar{\nu}_\mu$)/Γ($N\pi$) Γ₆/(Γ₁+Γ₂)

VALUE (units 10^{-4})	EVTs	DOCUMENT ID	TECN	COMMENT
1.51 ± 0.19 OUR FIT				
1.57 ± 0.35 OUR AVERAGE				
1.4 ± 0.5	14	BAGGETT	72B	HBC $K^- p$ at rest
2.4 ± 0.8	9	CANTER	71B	HBC $K^- p$ at rest

1.3 ± 0.7	3	LIND	64	RVUE
1.5 ± 1.2	2	RONNE	64	FBC

Lepton (L) and/or Baryon (B) number violating decay modes

Γ($\pi^+ e^-$)/Γ_{total} Γ₇/Γ

VALUE	CL%	DOCUMENT ID	TECN	COMMENT
<6 × 10⁻⁷	90	¹ MCCracken	15	CLAS $\gamma p \rightarrow K^+ \Lambda$

¹ Uses $B(\Lambda \rightarrow p\pi^-) = (63.9 \pm 0.5)\%$ for normalization mode.

Γ($\pi^+ \mu^-$)/Γ_{total} Γ₈/Γ

VALUE	CL%	DOCUMENT ID	TECN	COMMENT
<6 × 10⁻⁷	90	¹ MCCracken	15	CLAS $\gamma p \rightarrow K^+ \Lambda$

¹ Uses $B(\Lambda \rightarrow p\pi^-) = (63.9 \pm 0.5)\%$ for normalization mode.

Γ($\pi^- e^+$)/Γ_{total} Γ₉/Γ

VALUE	CL%	DOCUMENT ID	TECN	COMMENT
<4 × 10⁻⁷	90	¹ MCCracken	15	CLAS $\gamma p \rightarrow K^+ \Lambda$

¹ Uses $B(\Lambda \rightarrow p\pi^-) = (63.9 \pm 0.5)\%$ for normalization mode.

Γ($\pi^- \mu^+$)/Γ_{total} Γ₁₀/Γ

VALUE	CL%	DOCUMENT ID	TECN	COMMENT
<6 × 10⁻⁷	90	¹ MCCracken	15	CLAS $\gamma p \rightarrow K^+ \Lambda$

¹ Uses $B(\Lambda \rightarrow p\pi^-) = (63.9 \pm 0.5)\%$ for normalization mode.

Γ($K^+ e^-$)/Γ_{total} Γ₁₁/Γ

VALUE	CL%	DOCUMENT ID	TECN	COMMENT
<2 × 10⁻⁶	90	¹ MCCracken	15	CLAS $\gamma p \rightarrow K^+ \Lambda$

¹ Uses $B(\Lambda \rightarrow p\pi^-) = (63.9 \pm 0.5)\%$ for normalization mode.

Γ($K^+ \mu^-$)/Γ_{total} Γ₁₂/Γ

VALUE	CL%	DOCUMENT ID	TECN	COMMENT
<3 × 10⁻⁶	90	¹ MCCracken	15	CLAS $\gamma p \rightarrow K^+ \Lambda$

¹ Uses $B(\Lambda \rightarrow p\pi^-) = (63.9 \pm 0.5)\%$ for normalization mode.

Γ($K^- e^+$)/Γ_{total} Γ₁₃/Γ

VALUE	CL%	DOCUMENT ID	TECN	COMMENT
<2 × 10⁻⁶	90	¹ MCCracken	15	CLAS $\gamma p \rightarrow K^+ \Lambda$

¹ Uses $B(\Lambda \rightarrow p\pi^-) = (63.9 \pm 0.5)\%$ for normalization mode.

Γ($K^- \mu^+$)/Γ_{total} Γ₁₄/Γ

VALUE	CL%	DOCUMENT ID	TECN	COMMENT
<3 × 10⁻⁶	90	¹ MCCracken	15	CLAS $\gamma p \rightarrow K^+ \Lambda$

¹ Uses $B(\Lambda \rightarrow p\pi^-) = (63.9 \pm 0.5)\%$ for normalization mode.

Γ($K_S^0 \nu$)/Γ_{total} Γ₁₅/Γ

VALUE	CL%	DOCUMENT ID	TECN	COMMENT
<2 × 10⁻⁵	90	¹ MCCracken	15	CLAS $\gamma p \rightarrow K^+ \Lambda$

¹ Uses $B(\Lambda \rightarrow p\pi^-) = (63.9 \pm 0.5)\%$ for normalization mode.

Γ($\bar{p}\pi^+$)/Γ_{total} Γ₁₆/Γ

VALUE	CL%	DOCUMENT ID	TECN	COMMENT
<9 × 10⁻⁷	90	¹ MCCracken	15	CLAS $\gamma p \rightarrow K^+ \Lambda$

¹ Uses $B(\Lambda \rightarrow p\pi^-) = (63.9 \pm 0.5)\%$ for normalization mode.

Γ(invisible)/Γ_{total} Γ₁₇/Γ

VALUE	CL%	DOCUMENT ID	TECN	COMMENT
<7.4 × 10⁻⁵	90	ABLIKIM	22P	BES3 $J/\psi \rightarrow \Lambda \bar{\Lambda}$

Λ CP-violating decay-rate asymmetries

This is the difference between Λ and $\bar{\Lambda}$ decay rates to state f and \bar{f} divided by the sum of the rates:

$$A_{CP}(f) = [B(\Lambda \rightarrow f) - B(\bar{\Lambda} \rightarrow \bar{f})] / S_{\text{sum}}$$

A_{CP}($p\mu^- \bar{\nu}_\mu$) in $\Lambda \rightarrow p\mu^- \bar{\nu}_\mu, \bar{\Lambda} \rightarrow \bar{p}\mu^+ \nu_\mu$

VALUE	DOCUMENT ID	TECN	COMMENT
0.02 ± 0.14 ± 0.02	ABLIKIM	21AG	BES3 $J/\psi \rightarrow \Lambda \bar{\Lambda}$

Limit on $\bar{\Lambda}\Lambda$ oscillations

Upper limit for the oscillation rate of ($\bar{\Lambda} \rightarrow \Lambda$) hyperons. A test of baryon number nonconservation. We quote the oscillation parameter $\delta m_{\bar{\Lambda}\Lambda}$, deduced from the oscillation rate $P(\Lambda)$ and the hyperon lifetime τ_Λ , as $(\delta m_{\bar{\Lambda}\Lambda})^2 = P(\Lambda) / 2\tau_\Lambda^2$.

VALUE (GeV)	CL%	DOCUMENT ID	TECN	COMMENT
<3.8 × 10⁻¹⁸	90	¹ ABLIKIM	23BM	BES3 $J/\psi \rightarrow pK^-\bar{\Lambda}$

¹ ABLIKIM 23BM quote the oscillation rate limit $P(\Lambda) < 4.4 \times 10^{-6}$ and calculate the oscillation parameter $\delta m_{\bar{\Lambda}\Lambda}$ given here.

See key on page 1171

Baryon Particle Listings

Λ

Λ DECAY PARAMETERS

See the "Note on Baryon Decay Parameters" in the neutron Listings. Some early results have been omitted.

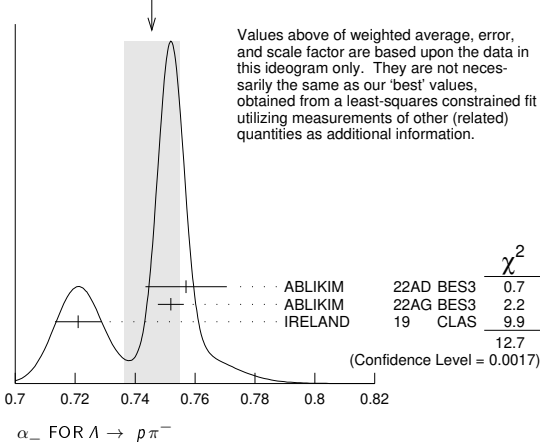
α₋ FOR Λ → pπ⁻

OUR FIT value is obtained from measurements of α(Ξ⁻), α₋(Λ), and α(Ξ⁻)α₋(Λ).

VALUE	EVTS	DOCUMENT ID	TECN	COMMENT
0.747 ± 0.009 OUR FIT				Error includes scale factor of 2.5.
0.746 ± 0.009 OUR AVERAGE				Error includes scale factor of 2.5. See the ideogram below.
0.757 ± 0.011 ± 0.008	73k	ABLIKIM 22AD BES3	J/ψ → ΞΞ̄ → ΛΛ̄ππ	
0.7519 ± 0.0036 ± 0.0024	3.2M	ABLIKIM 22AG BES3	J/ψ → ΛΛ̄	
0.721 ± 0.006 ± 0.005		¹ IRELAND 19 CLAS	K production	
• • • We do not use the following data for averages, fits, limits, etc. • • •				
0.74 +0.04 -0.03		AAIJ 20o LHCb	Λ _b → J/ψΛ	
0.750 ± 0.009 ± 0.004	420k	ABLIKIM 19Bj BES3	J/ψ → ΛΛ̄	
0.584 ± 0.046	8500	ASTBURY 75 SPEC		
0.649 ± 0.023	10325	CLELAND 72 OSPK		
0.67 ± 0.06	3520	DAUBER 69 HBC	From Ξ decay	
0.645 ± 0.017	10130	OVERSETH 67 OSPK	Λ from π ⁻ p	
0.62 ± 0.07	1156	CRONIN 63 CNTR	Λ from π ⁻ p	

¹ This is a new analysis based on existing kaon photoproduction data of the CLAS collaboration and using spin algebra constraints.

WEIGHTED AVERAGE
0.746±0.009 (Error scaled by 2.5)



Values above of weighted average, error, and scale factor are based upon the data in this ideogram only. They are not necessarily the same as our 'best' values, obtained from a least-squares constrained fit utilizing measurements of other (related) quantities as additional information.

α₊ FOR Λ → p̄π⁺

VALUE	EVTS	DOCUMENT ID	TECN	COMMENT
-0.757 ± 0.004 OUR AVERAGE				
-0.763 ± 0.011 ± 0.007	73k	ABLIKIM 22AD BES3	J/ψ → ΞΞ̄ → ΛΛ̄ππ	
-0.7559 ± 0.0036 ± 0.0030	3.2M	ABLIKIM 22AG BES3	J/ψ → ΛΛ̄	
• • • We do not use the following data for averages, fits, limits, etc. • • •				
-0.758 ± 0.010 ± 0.007	420k	ABLIKIM 19Bj BES3	J/ψ → ΛΛ̄	
-0.755 ± 0.083 ± 0.063	8.7k	ABLIKIM 10 BES	J/ψ → ΛΛ̄	
-0.63 ± 0.13	770	TIXIER 88 DM2	J/ψ → ΛΛ̄	

α₀ FOR Λ → ππ⁰

VALUE	EVTS	DOCUMENT ID	TECN	COMMENT
-0.692 ± 0.016 ± 0.006	47k	ABLIKIM 19Bj BES3	J/ψ to ΛΛ̄	

α_γ FOR Λ → nγ

VALUE	EVTS	DOCUMENT ID	TECN	COMMENT
-0.16 ± 0.10 ± 0.05	13889	ABLIKIM 22Aj BES3	J/ψ → ΛΛ̄	

φ ANGLE FOR Λ → pπ⁻

(tan φ = β / γ)

VALUE (°)	EVTS	DOCUMENT ID	TECN	COMMENT
- 6.5 ± 3.5 OUR AVERAGE				
- 7.0 ± 4.5	10325	CLELAND 72 OSPK	Λ from π ⁻ p	
- 8.0 ± 6.0	10130	OVERSETH 67 OSPK	Λ from π ⁻ p	
13.0 ± 17.0	1156	CRONIN 63 OSPK	Λ from π ⁻ p	

α₀ / α₋ = α(Λ → nπ⁰) / α(Λ → pπ⁻)

VALUE	EVTS	DOCUMENT ID	TECN	COMMENT
1.01 ± 0.07 OUR AVERAGE				
1.000 ± 0.068	4760	¹ OLSEN 70 OSPK	π ⁺ n → ΛK ⁺	
1.10 ± 0.27		CORK 60 CNTR		

¹ OLSEN 70 compares proton and neutron distributions from Λ decay.

α₀ / α₊ in Λ → π̄π⁰, Λ → p̄π⁺

VALUE	EVTS	DOCUMENT ID	TECN	COMMENT
0.913 ± 0.028 ± 0.012	47k	ABLIKIM 19Bj BES3	J/ψ to ΛΛ̄	

(α₋ + α₊) / (α₋ - α₊) in Λ → pπ⁻, Λ → p̄π⁺

Zero if CP is conserved; α₋ and α₊ are the asymmetry parameters for Λ → pπ⁻ and Λ → p̄π⁺ decay. See also the Ξ⁻ for a similar test involving the decay chain Ξ⁻ → Λπ⁻, Λ → pπ⁻ and the corresponding antiparticle chain.

VALUE (units 10 ⁻²)	EVTS	DOCUMENT ID	TECN	COMMENT
-0.1 ± 0.4 OUR AVERAGE				
1.3 ± 0.7 ± 1.1	369k	¹ LI 23c BELL	J/ψ → ΞΞ̄ → ΛΛ̄ππ	
-0.4 ± 1.2 ± 0.9	73k	ABLIKIM 22AD BES3	J/ψ → ΞΞ̄ → ΛΛ̄ππ	
-0.25 ± 0.46 ± 0.12	3.2M	ABLIKIM 22AG BES3	J/ψ → ΛΛ̄	
-8.1 ± 5.5 ± 5.9	8.7k	ABLIKIM 10 BES	J/ψ → ΛΛ̄	
1.3 ± 2.2	96k	BARNES 96 CNTR	LEAR p̄p → ΛΛ̄	
1 ± 10	770	TIXIER 88 DM2	J/ψ → ΛΛ̄	
-2 ± 14	10k	² CHAUVAT 85 CNTR	p̄p, p̄p ISR	
• • • We do not use the following data for averages, fits, limits, etc. • • •				
-0.6 ± 1.2 ± 0.7	420k	³ ABLIKIM 19Bj BES3	J/ψ → ΛΛ̄	
-7 ± 9	4063	BARNES 87 CNTR	See BARNES 96	

¹ LI 23c quote the average Λ-hyperon asymmetry A_{CP}^Λ from 264k Λ_c⁺ → Λπ⁺ decays and 105k Λ_c⁺ → Σ⁰π⁺ decays, under the assumption of no CP violation in the SM for Λ_c⁺, i.e. α_{Λ_c⁺} = -α_{Λ_c⁻}.

² CHAUVAT 85 actually gives α₊(Λ̄)/α₋(Λ) = -1.04 ± 0.29. Assumes polarization is same in p̄p → ΛX and pp → ΛX. Tests of this assumption, based on C-invariance and fragmentation, are satisfied by the data.

³ Superseded by ABLIKIM 22AG.

R = |G_E/G_M| in Λ → pπ⁻, Λ → p̄π⁺

VALUE	DOCUMENT ID	TECN	COMMENT
0.96 ± 0.14 ± 0.02	¹ ABLIKIM 19Bf BES3		e ⁺ e ⁻ → ΛΛ̄ at √s = 2.396 GeV

¹ Determined using the latest BES-III value on the asymmetry parameter α = 0.750 ± 0.010.

Δφ = φ_E - φ_M in Λ → pπ⁻, Λ → p̄π⁺

VALUE (degrees)	DOCUMENT ID	TECN	COMMENT
37 ± 12 ± 6	¹ ABLIKIM 19Bf BES3		e ⁺ e ⁻ → ΛΛ̄ at √s = 2.396 GeV

¹ Relative phase between GE and GM, determined using the latest BES-III value on the asymmetry parameter α = 0.750 ± 0.010.

g_A / g_V FOR Λ → p̄e⁻ν̄_e

Measurements with fewer than 500 events have been omitted. Where necessary, signs have been changed to agree with our conventions, which are given in the "Note on Baryon Decay Parameters" in the neutron Listings. The measurements all assume that the form factor g₂ = 0. See also the footnote on DWORKIN 90.

VALUE	EVTS	DOCUMENT ID	TECN	COMMENT
-0.718 ± 0.015 OUR AVERAGE				
-0.719 ± 0.016 ± 0.012	37k	¹ DWORKIN 90	SPEC	eν angular corr.
-0.70 ± 0.03	7111	BOURQUIN 83	SPEC	Ξ → Λπ ⁻
-0.734 ± 0.031	10k	² WISE 81	SPEC	eν angular correl.
• • • We do not use the following data for averages, fits, limits, etc. • • •				
-0.63 ± 0.06	817	ALTHOFF 73	OSPK	Polarized Λ

¹ The tabulated result assumes the weak-magnetism coupling w ≡ g_W(0)/g_V(0) to be 0.97, as given by the CVC hypothesis and as assumed by the other listed measurements. However, DWORKIN 90 measures w to be 0.15 ± 0.30, and then g_A/g_V = -0.731 ± 0.016.

² This experiment measures only the absolute value of g_A/g_V.

Λ REFERENCES

We have omitted some papers that have been superseded by later experiments. See our earlier editions.

ABLIKIM 23BM PRL 131 121801	M. Ablikim et al.	(BESIII Collab.)
ACHARYA 23 PR D108 032009	S. Acharya et al.	(ALICE Collab.)
LI 23c SCIB 68 583	L.K. Li et al.	(BELLE Collab.)
ABLIKIM 22AD NAT 606 64	M. Ablikim et al.	(BESIII Collab.)
ABLIKIM 22AG PRL 129 131801	M. Ablikim et al.	(BESIII Collab.)
ABLIKIM 22AJ PRL 129 212002	M. Ablikim et al.	(BESIII Collab.)
ABLIKIM 22P PR D105 1071101	M. Ablikim et al.	(BESIII Collab.)
ABLIKIM 21AG PRL 127 121802	M. Ablikim et al.	(BESIII Collab.)
AAIJ 20o JHEP 2006 110	R. Aaij et al.	(LHCb Collab.)
ABLIKIM 19BF PRL 123 122003	M. Ablikim et al.	(BESIII Collab.)
ABLIKIM 19Bj NATP 15 631	M. Ablikim et al.	(BESIII Collab.)
IRELAND 19 PRL 123 182301	D.C. Ireland et al.	(GLAS, GWU, JULI+)
MCCRACKEN 15 PR D92 072002	M.E. McCracken et al.	(JLab CLAS Collab.)
ABLIKIM 10 PR D81 012003	M. Ablikim et al.	(BES Collab.)
BARNES 96 PR C54 1877	P.D. Barnes et al.	(CERN PS-185 Collab.)
RYBICKI 96 APP B27 2155	K. Rybicki	(BNL E766 Collab.)
HARTOUNI 94 PRL 72 1322	E.P. Hartouni et al.	(BNL E766 Collab.)
Also PRL 72 2821 (errat.)	E.P. Hartouni et al.	(BNL-811 Collab.)
LARSON 93 PR D47 799	K.D. Larson et al.	(BNL-811 Collab.)
NOBLE 92 PRL 69 414	A.J. Noble et al.	(BIRM, BOST, BRCO+)
DWORKIN 90 PR D41 780	J. Dworkin et al.	(MICH, WIS C, RUTG+)
TIXIER 88 PL B212 523	M.H. Tixier et al.	(DM2 Collab.)
BARNES 87 PL B199 147	P.D. Barnes et al.	(CMU, SA CL, LANL+)
BIAGI 86 ZPHY C30 201	S.F. Biagi et al.	(BRIS, CERN, GEVA+)
CHAUVAT 85 PL 163B 273	P. Chauvat et al.	(CERN, CLER, UCLA+)
BOURQUIN 83 ZPHY C21 1	M.H. Bourquin et al.	(BRIS, GEVA, HEIDP+)
COX 81 PRL 46 877	P.T. Cox et al.	(MICH, WIS C, RUTG, MINN+)
PONDROM 81 PR D23 814	L. Pondrom et al.	(WISC, MICH, RUTG+)
WISE 81 PL 98B 123	J.E. Wise et al.	(MASA, BNL)
WISE 80 PL 91B 165	J.E. Wise et al.	(MASA, BNL)
SCHACHIN... 78 PRL 41 1348	L. Schachinger et al.	(MICH, RUTG, WISC)
HELLER 77 PL 68B 480	K. Heller et al.	(MICH, WIS C, HEIDH)

Baryon Particle Listings

Λ , Λ 's and Σ 's, $\Lambda(1380)$, $\Lambda(1405)$

LINDQUIST	77	PR D16 2104	J. Lindquist <i>et al.</i>	(EFI, OSU, ANL)
Also		JP G2 L211	J. Lindquist <i>et al.</i>	(EFI, WUSL, OSU+)
ZECH	77	NP B124 413	G. Zech <i>et al.</i>	(SIEG, CERN, DORT, HEIDH)
BUNCE	76	PRL 36 1113	G.R.M. Bunce <i>et al.</i>	(WISC, MICH, RUTG)
ASTBURY	75	NP B99 30	P. Astbury <i>et al.</i>	(LOIC, CERN, ETH+)
CLAYTON	75	NP B95 130	E.F. Clayton <i>et al.</i>	(LOIC, RHEL)
ALTHOFF	73	PL 43B 237	K.H. Althoff <i>et al.</i>	(CERN, HEID)
ALTHOFF	73B	NP B66 29	K.H. Althoff <i>et al.</i>	(CERN, HEID)
KATZ	73	Thesis MDDP-TR-74-044	C.N. Katz	(UMD)
POULARD	73	PL 46B 135	G. Poulard, A. Givernaud, A.C. Borg	(SACL)
BAGGETT	72B	ZPHY 252 362	M.J. Baggett <i>et al.</i>	(HEID)
BAGGETT	72C	PL 42B 379	M.J. Baggett <i>et al.</i>	(HEID)
CLELAND	72	NP B40 221	W.E. Cleland <i>et al.</i>	(CERN, GEVA, LUND)
HYMAN	72	PR D5 1063	L.G. Hyman <i>et al.</i>	(ANL, CMU)
ALTHOFF	71	PL 37B 531	K.H. Althoff <i>et al.</i>	(CERN, HEID)
BALTAY	71B	PR D4 670	C. Baltay <i>et al.</i>	(COLU, BING)
BARONI	71	LNC 2 1256	G. Baroni, S. Petrer, G. Romano	(ROMA)
CANTER	71	PRL 26 868	J. Canter <i>et al.</i>	(STON, COLU)
CANTER	71B	PRL 27 59	J. Canter <i>et al.</i>	(STON, COLU)
DAHL-JENSEN	71	NC 3A 1	E. Dahl-Jensen <i>et al.</i>	(CERN, ANKA, LAUS+)
LINDQUIST	71	PRL 27 612	J. Lindquist <i>et al.</i>	(EFI, WUSL, OSU+)
OLSEN	70	PRL 24 843	S.L. Olsen <i>et al.</i>	(WISC, MICH)
DAUBER	69	PR 179 1262	P.M. Dauber <i>et al.</i>	(LRL)
DOYLE	69	Thesis UCRL 18139	J.C. Doyle	(LRL)
MALONEY	69	PRL 23 425	J.E. Maloney, B. Sechi-Zorn	(UMD)
GRIMM	68	NC 54A 187	H.J. Grimm	(HEID)
HEPP	68	ZPHY 214 71	V. Hepp, H. Schleich	(HEID)
BADIER	67	PL 25B 152	J. Badier <i>et al.</i>	(EPOL)
MAYEUR	67	U.Libr.Brux.Bul. 32	C. Mayeur, E. Tompa, J.H. Wickens	(BELG, LOUC)
OVERSETH	67	PRL 19 391	O.E. Overseth, R.F. Roth	(MICH, PRIN)
PDC	67	RMP 39 1	A.H. Rosenfeld <i>et al.</i>	(LRL, CERN, YALE)
BURAN	66	PL 20 318	T. Buran <i>et al.</i>	(OSLO)
CHIEN	66	PR 152 1171	C.Y. Chien <i>et al.</i>	(YALE, BNL)
ENGELMANN	66	NC 45A 1038	R. Engelmann <i>et al.</i>	(HEID, REHO)
GIBSON	66	NC 45A 882	W.M. Gibson, K. Green	(BRIS)
LONDON	66	PR 143 1034	G.W. London <i>et al.</i>	(BNL, SYRA)
SCHMIDT	65	PR 140 B1328	P. Schmidt	(COLU)
BAGLIN	64	NC 35 977	C. Baglin <i>et al.</i>	(EPOL, CERN, LOUC, RHEL+)
HUBBARD	64	PR 135 B183	J.R. Hubbard <i>et al.</i>	(LRL)
LIND	64	PR 135 B1483	V.G. Lind <i>et al.</i>	(WISC)
RONNE	64	PL 11 357	B.E. Ronne <i>et al.</i>	(CERN, EPOL, LOUC+)
SCHWARTZ	64	Thesis UCRL 11360	J.A. Schwartz	(LRL)
BHOWMIK	63	NC 28 1494	B. Bhowmik, D.P. Goyal	(DELH)
BLOCK	63	PR 130 766	M.M. Block <i>et al.</i>	(NWES, BGNA, SYRA+)
BROWN	63	PR 130 769	J.L. Brown <i>et al.</i>	(LRL, MICH)
CHRETIEN	63	PR 131 2208	M. Chretien <i>et al.</i>	(BRAN, BROW, HARV+)
CRONIN	63	PR 129 1795	J.W. Cronin, O.E. Overseth	(PRIN)
ELY	63	PR 131 868	R.P. Ely <i>et al.</i>	(LRL)
HUMPHREY	62	PR 127 1305	W.E. Humphrey, R.R. Ross	(LRL)
CORK	60	PR 120 1000	B. Cork <i>et al.</i>	(LRL, PRIN, BNL)
CRAWFORD	59B	PRL 2 266	F.S. Crawford <i>et al.</i>	(LRL)

See the related review(s):
 Λ and Σ Resonances

$\Lambda(1380) 1/2^-$ $J^P = 1/2^-$ Status: **

OMITTED FROM SUMMARY TABLE
See the related review on "Pole Structure of the $\Lambda(1405)$ Region."

$\Lambda(1380)$ POLE POSITION

REAL PART	DOCUMENT ID	TECN
1325 ± 15	¹ MAI	15 DPWA
1330 $\pm \frac{4}{5}$	² MAI	15 DPWA
1388 ± 9	GUO	13 DPWA
1381 $\pm \frac{18}{6}$	IKEDA	12 DPWA

¹ Solution number 4.
² Solution number 2.

-2xIMAGINARY PART

VALUE (MeV)	DOCUMENT ID	TECN
180 $\pm \frac{24}{36}$	¹ MAI	15 DPWA
112 $\pm \frac{34}{22}$	² MAI	15 DPWA
228 $\pm \frac{48}{50}$	GUO	13 DPWA
162 $\pm \frac{38}{16}$	IKEDA	12 DPWA

¹ Solution number 4.
² Solution number 2.

$\Lambda(1380)$ REFERENCES

MAI	15	EPJ A51 30	M. Mai, U.-G. Meissner	(BONN, JULI)
GUO	13	PR C87 035202	Z.-H. Guo, J. Oller	
IKEDA	12	NP A881 98	Y. Ikeda, T. Hyodo, W. Weise	(TUM, RIKEN, TINT)

$\Lambda(1405) 1/2^-$

$I(J^P) = 0(\frac{1}{2}^-)$ Status: ***

In the 1998 Note on the $\Lambda(1405)$ in PDG 98, R.H. Dalitz discussed the S-shaped cusp behavior of the intensity at the $N\bar{K}$ threshold observed in THOMAS 73 and HEMINGWAY 85. He commented that this behavior "is characteristic of S-wave coupling; the other below threshold hyperon, the $\Sigma(1385)$, has no such threshold distortion because its $N\bar{K}$ coupling is P-wave. For $\Lambda(1405)$ this asymmetry is the sole direct evidence that $J^P = 1/2^-$."

A recent measurement by the CLAS collaboration, MORIYA 14, definitively established the long-assumed $J^P = 1/2^-$ spin-parity assignment of the $\Lambda(1405)$. The experiment produced the $\Lambda(1405)$ spin-polarized in the photoproduction process $\gamma p \rightarrow K^+ \Lambda(1405)$ and measured the decay of the $\Lambda(1405)$ (polarized) $\rightarrow \Sigma^+ (\text{polarized}) \pi^-$. The observed isotropic decay of $\Lambda(1405)$ is consistent with spin $J = 1/2$. The polarization transfer to the Σ^+ (polarized) direction revealed negative parity, and thus established $J^P = 1/2^-$.

See the related review(s):
Pole Structure of the $\Lambda(1405)$ Region

$\Lambda(1405)$ POLE POSITION

REAL PART	DOCUMENT ID	TECN
1417.7 $\pm \frac{6.0+1.1}{7.4-1.0}$	AIKAWA	23 DPWA
1429 $\pm \frac{8}{7}$	¹ MAI	15 DPWA
1434 ± 2	² MAI	15 DPWA
1421 $\pm \frac{3}{2}$	GUO	13 DPWA
1424 $\pm \frac{7}{23}$	IKEDA	12 DPWA

¹ Solution number 4.
² Solution number 2.

-2xIMAGINARY PART

VALUE (MeV)	DOCUMENT ID	TECN
52.2 $\pm \frac{12.0+3.4}{15.8-4.0}$	AIKAWA	23 DPWA
24 $\pm \frac{4}{6}$	¹ MAI	15 DPWA
20 $\pm \frac{4}{2}$	² MAI	15 DPWA
38 $\pm \frac{16}{10}$	GUO	13 DPWA
52 $\pm \frac{6}{28}$	IKEDA	12 DPWA

¹ Solution number 4.
² Solution number 2.

$\Lambda(1405)$ MASS

PRODUCTION EXPERIMENTS

VALUE (MeV)	EVTS	DOCUMENT ID	TECN	COMMENT
1405.1 $\pm \frac{1.3}{1.0}$		OUR AVERAGE		
1405 $\pm \frac{11}{9}$		HASSANVAND 13	SPEC	$pp \rightarrow p\Lambda(1405) K^+$
1405 $\pm \frac{1.4}{1.0}$		ESMAILI 10	RVUE	$^4\text{He} K^- \rightarrow \Sigma^\pm \pi^\mp X$ at rest
1406.5 ± 4.0		¹ DALITZ 91		M-matrix fit
1391 ± 1	700	¹ HEMINGWAY 85	HBC	$K^- p 4.2 \text{ GeV}/c$
~ 1405	400	² THOMAS 73	HBC	$\pi^- p 1.69 \text{ GeV}/c$
1405	120	BARBARO... 68B	DBC	$K^- d 2.1-2.7 \text{ GeV}/c$
1400 ± 5	67	BIRMINGHAM 66	HBC	$K^- p 3.5 \text{ GeV}/c$
1382 ± 8		ENGLER 65	HDDB	$\pi^- p, \pi^+ d 1.68 \text{ GeV}/c$
1400 ± 24		MUSGRAVE 65	HBC	$\bar{p} p 3-4 \text{ GeV}/c$
1410		ALEXANDER 62	HBC	$\pi^- p 2.1 \text{ GeV}/c$
1405		ALSTON 62	HBC	$K^- p 1.2-0.5 \text{ GeV}/c$
1405		ALSTON 61B	HBC	$K^- p 1.15 \text{ GeV}/c$

¹ DALITZ 91 fits the HEMINGWAY 85 data.
² THOMAS 73 data is fit by CHAO 73 (see next section).

See key on page 1171

Baryon Particle Listings

$\Lambda(1405), \Lambda(1520)$

EXTRAPOLATIONS BELOW $N\bar{K}$ THRESHOLD

VALUE (MeV)	DOCUMENT ID	TECN	COMMENT
••• We do not use the following data for averages, fits, limits, etc. •••			
1407.56 or 1407.50	1 KIMURA 00		potential model
1411	2 MARTIN 81		K-matrix fit
1406	3 CHAO 73	DPWA	0-range fit (sol. B)
1421	MARTIN 70	RVUE	Constant K-matrix
1416 ± 4	MARTIN 69	HBC	Constant K-matrix
1403 ± 3	KIM 67	HBC	K-matrix fit
1407.5 ± 1.2	4 KITTEL 66	HBC	0-effective-range fit
1410.7 ± 1.0	KIM 65	HBC	0-effective-range fit
1409.6 ± 1.7	4 SAKITT 65	HBC	0-effective-range fit

¹The KIMURA 00 values are from fits A and B from a coupled-channel potential model using low-energy $\bar{K}N$ and $\Sigma\pi$ data, kaonic-hydrogen x-ray measurements, and our $\Lambda(1405)$ mass and width. The results bear mainly on the nature of the $\Lambda(1405)$: three-quark state or $\bar{K}N$ bound state.

²The MARTIN 81 fit includes the $K^\pm p$ forward scattering amplitudes and the dispersion relations they must satisfy.

³See also the accompanying paper of THOMAS 73.

⁴Data of SAKITT 65 are used in the fit by KITTEL 66.

$\Lambda(1405)$ WIDTH

PRODUCTION EXPERIMENTS

VALUE (MeV)	EVTS	DOCUMENT ID	TECN	COMMENT
50.5 ± 2.0 OUR AVERAGE				
62 ± 10		HASSANVAND 13	SPEC	$pp \rightarrow p\Lambda(1405)K^+$
50 ± 2		1 DALITZ 91		M-matrix fit
••• We do not use the following data for averages, fits, limits, etc. •••				
24 ± 4		ESMAILI 10	RVUE	$^4\text{He } K^- \rightarrow \Sigma^\pm \pi^\mp X$ at rest
32 ± 1	700	1 HEMINGWAY 85	HBC	$K^- p$ 4.2 GeV/c
45 to 55	400	2 THOMAS 73	HBC	$\pi^- p$ 1.69 GeV/c
35	120	BARBARO... 68B	DBC	$K^- d$ 2.1-2.7 GeV/c
50 ± 10	67	BIRMINGHAM 66	HBC	$K^- p$ 3.5 GeV/c
89 ± 20		ENGLER 65	HDBC	
60 ± 20		MUSGRAVE 65	HBC	
35 ± 5		ALEXANDER 62	HBC	
50		ALSTON 62	HBC	
20		ALSTON 61B	HBC	

¹DALITZ 91 fits the HEMINGWAY 85 data.

²THOMAS 73 data is fit by CHAO 73 (see next section).

EXTRAPOLATIONS BELOW $N\bar{K}$ THRESHOLD

VALUE (MeV)	DOCUMENT ID	TECN	COMMENT
••• We do not use the following data for averages, fits, limits, etc. •••			
50.24 or 50.26	1 KIMURA 00		potential model
30	2 MARTIN 81		K-matrix fit
55	3,4 CHAO 73	DPWA	0-range fit (sol. B)
20	MARTIN 70	RVUE	Constant K-matrix
29 ± 6	MARTIN 69	HBC	Constant K-matrix
50 ± 5	KIM 67	HBC	K-matrix fit
34.1 ± 4.1	5 KITTEL 66	HBC	
37.0 ± 3.2	KIM 65	HBC	
28.2 ± 4.1	5 SAKITT 65	HBC	

¹The KIMURA 00 values are from fits A and B from a coupled-channel potential model using low-energy $\bar{K}N$ and $\Sigma\pi$ data, kaonic-hydrogen x-ray measurements, and our $\Lambda(1405)$ mass and width. The results bear mainly on the nature of the $\Lambda(1405)$: three-quark state or $\bar{K}N$ bound state.

²The MARTIN 81 fit includes the $K^\pm p$ forward scattering amplitudes and the dispersion relations they must satisfy.

³An asymmetric shape, with $\Gamma/2 = 41$ MeV below resonance, 14 MeV above.

⁴See also the accompanying paper of THOMAS 73.

⁵Data of SAKITT 65 are used in the fit by KITTEL 66.

$\Lambda(1405)$ DECAY MODES

Mode	Fraction (Γ_i/Γ)
$\Gamma_1 \Sigma\pi$	100 %
$\Gamma_2 \Lambda\gamma$	
$\Gamma_3 \Sigma^0\gamma$	
$\Gamma_4 N\bar{K}$	

$\Lambda(1405)$ PARTIAL WIDTHS

$\Gamma(\Lambda\gamma)$	DOCUMENT ID	COMMENT
VALUE (keV)		
••• We do not use the following data for averages, fits, limits, etc. •••		
27 ± 8	BURKHARDT 91	Isobar model fit

$\Gamma(\Sigma^0\gamma)$	DOCUMENT ID	COMMENT
VALUE (keV)		
••• We do not use the following data for averages, fits, limits, etc. •••		
10 ± 4 or 23 ± 7	BURKHARDT 91	Isobar model fit

$\Lambda(1405)$ BRANCHING RATIOS

$\Gamma(N\bar{K})/\Gamma(\Sigma\pi)$	CL%	DOCUMENT ID	TECN	COMMENT
••• We do not use the following data for averages, fits, limits, etc. •••				
<3	95	HEMINGWAY 85	HBC	$K^- p$ 4.2 GeV/c

$\Lambda(1405)$ REFERENCES

AIKAWA 23	PL B837 137637	S. Aikawa et al.	(J-PARC E31 Collab.)
MAI 15	EPJ A51 30	M. Mai, U.-G. Meissner	(BONN, JULI)
MORIYA 14	PRL 112 082004	K. Moriya et al.	(CLAS Collab.)
GUO 13	PR C87 035202	Z.-H. Guo, J. Oller	
HASSANVAND 13	PR C87 055202	M. Hassanvand et al.	
Also	PR C88 019905 (err.)	M. Hassanvand et al.	
IKEDA 12	NP A881 98	Y. Ikeda, T. Hyodo, W. Weise	(TUM, RIKEN, TINT)
ESMAILI 10	PL B686 23	J. Esmaili, Y. Akaishi, T. Yamazaki	(RIKEN, ISUT+)
KIMURA 00	PR C62 015206	M. Kimura et al.	
PDG 98	EPJ C3 1	C. Caso et al.	(PDG Collab.)
BURKHARDT 91	PR C44 607	H. Burkhardt, J. Lowe	(NOTT, UMM, BIRM)
DALITZ 91	JP G17 289	R.H. Dalitz, A. Deloff	(OXFTF, WINR)
HEMINGWAY 85	NP B253 742	R.J. Hemingway	(CERN J)
MARTIN 81	NP B179 33	A.D. Martin	(DURH)
CHAO 73	NP B56 46	Y.A. Chao et al.	(RHEL, CMU, LOUC)
THOMAS 73	NP B56 15	D.W. Thomas et al.	(CMU J)
MARTIN 70	NP B16 479	A.D. Martin, G.G. Ross	(DURH)
MARTIN 69	PR 183 1352	B.R. Martin, M. Sakitt	(LOUC, BNL)
Also	PR 183 1345	B.R. Martin, M. Sakitt	(LOUC, BNL)
BARBARO... 68B	PRL 21 573	A. Barbaro-Galileri et al.	(LRL, SLAC)
KIM 67	PRL 19 1074	J.K. Kim	(YALE)
BIRMINGHAM 66	PR 152 1148	M. Hauge et al.	(BIRM, GLAS, LOIC, OXF+)
KITTEL 66	PL 21 349	W. Kittel, G. Otter, I. Wacek	(VIEN)
ENGLER 65	PRL 15 224	A. Engler et al.	(CMU, BNL J)
KIM 65	PRL 14 29	J.K. Kim	(COLU)
MUSGRAVE 65	NC 35 735	B. Musgrave et al.	(BIRM, CERN, EPOL+)
SAKITT 65	PR 139 B719	M. Sakitt et al.	(UMD, LRL)
ALEXANDER 62	PRL 8 447	G. Alexander et al.	(LRL I)
ALSTON 62	CERN Conf. 311	M.H. Alston et al.	(LRL I)
ALSTON 61B	PRL 6 698	M.H. Alston et al.	(LRL I)

OTHER RELATED PAPERS

IWASAKI 97	PRL 78 3067	M. Iwasaki et al.	(KEK 228 Collab.)
FINK 90	PR C41 2720	P.J.Jr. Fink et al.	(IBM Y, ORST, ANSM)
LEINWEBER 90	ANP 198 203	D.B. Leinweber	(MCM5)
MUELLER-GR... 90	NP A513 557	A. Mueller-Groeling, K. Holinde, J. Speth	(JULI)
BARRETT 89	NC 102A 179	R.C. Barrett	(SURR)
BATTY 89	NC 102A 255	C.J. Batty, A. Gal	(RAL, HEBR)
CAPSTICK 89	Excited Baryons 88, p.32	S. Capstick	(GUEL)
LOWE 89	NC 102A 157	J. Lowe	(BIRM)
WHITEHOUSE 89	PRL 63 1352	D.A. Whitehouse et al.	(BIRM, BOST, BRCC+)
SIEGEL 88	PR C38 2221	P.B. Siegel, W. Weise	(REGE)
WORKMAN 88	PR D37 3117	R.L. Workman, H.W. Fearing	(TRIU)
SCHNICK 87	PRL 58 1719	J. Schnick, R.H. Landau	(ORST)
CAPSTICK 86	PR D34 2809	S. Capstick, N. Isgur	(TNTO)
JENNINGS 86	PL B176 229	B.K. Jennings	(TRIU)
MALTMAN 86	PR D34 1372	K. Maltman, N. Isgur	(LANL, TNTO)
ZHONG 86	PL B171 471	Y.S. Zhong et al.	(ADLD, TRIU, SURR)
BURKHARDT 85	NP A440 653	H. Burkhardt, J. Lowe, A.S. Rosenthal	(NOTT+)
DAREWYCH 85	PR D32 1765	J.W. Darewych, R. Konik, N. Isgur	(YORK, TNTO)
VEIT 85	PR D31 1033	E.A. Veit et al.	(TRIU, ADLD, SURR)
KIANG 84	PR C30 1638	D. Kiang et al.	(DALH, MCM5)
MILLER 84	Conference paper	D.J. Miller	(LOUC)
Conf. Intersections between Particle and Nuclear Physics, p. 783			
VANDUJK 84	PR D30 937	W. van Dijk	(MCM5)
VEIT 84	PL 137B 415	E.A. Veit et al.	(TRIU, SURR, CERN)
DALITZ 82	Heid. Conf.	R.H. Dalitz et al.	(OXFTF)
Heidelberg Conf., p. 201			
DALITZ 81	Kaon Conf.	R.H. Dalitz, J.G. McGinley	(OXFTF)
Low and Intermediate Energy Kaon-Nucleon Physics, p.381			
MARTIN 81B	Kaon Conf.	A.D. Martin	(DURH)
Low and Intermediate Energy Kaon-Nucleon Physics, p. 97			
OADES 77	NC 42A 462	G.C. Oades, G. Rasche	(AARH, ZURI)
SHAW 73	Purdue Conf. 417	G.L. Shaw	(UCI)
BARBARO... 72	LBL-555	A. Barbaro-Galileri	(LBL)
DOBS ON 72	PR D6 3256	P.N. Dobson, R. McElhaney	(HAWA)
RAJASEKA... 72	PR D5 610	G. Rajasekaran	(TATA)
Earlier papers also cited in RAJASEKARAN 72			
CLINE 71	PRL 26 1194	D. Cline, R. Laumann, J. Mapp	(WISC)
MARTIN 71	PL 35B 62	A.D. Martin, A.D. Martin, G.G. Ross	(DURH, LOUC+)
DALITZ 67	PR 153 1617	R.H. Dalitz, T.C. Wong, G. Rajasekaran	(OXFTF+)
DONALD 66	PL 22 711	R.A. Donald et al.	(LVP)
KADYK 66	PRL 17 599	J.A. Kadyk et al.	(LRL)
ABRAMS 65	PR 139 B454	G.S. Abrams, B. Sechi-Zorn	(UMD)

$\Lambda(1520) 3/2^-$

 $I(J^P) = 0(\frac{3}{2}^-)$ Status: ***

Discovered by FERRO-LUZZI 62; the elaboration in WATSON 63 is the classic paper on the Breit-Wigner analysis of a multichannel resonance.

The measurements of the mass, width, and elasticity published before 1975 are now obsolete and have been omitted. They were last listed in our 1982 edition Physics Letters **111B** 1 (1982).

Production and formation experiments agree quite well, so they are listed together here.

$\Lambda(1520)$ POLE POSITION

REAL PART	DOCUMENT ID	TECN	COMMENT
VALUE (MeV)			
1517 to 1518 (≈ 1517.5) OUR ESTIMATE			
1517.5 ± 0.4 OUR AVERAGE			
1517.5 ± 0.4	SARANTSEV 19	DPWA	$\bar{K}N$ multichannel
1517 ± 4	1 KAMANO 15	DPWA	$\bar{K}N$ multichannel
1517 ± 4			

Baryon Particle Listings

 $\Lambda(1520)$

••• We do not use the following data for averages, fits, limits, etc. •••

1518	ZHANG	13A	DPWA	$\bar{K}N$ multichannel
1518.8	QIANG	10	SPEC	$e p \rightarrow e' K^+ X$ (fit to X)

¹ From the preferred solution A in KAMANO 15.

-2xIMAGINARY PART

VALUE (MeV)	DOCUMENT ID	TECN	COMMENT
14 to 18 (≈ 16) OUR ESTIMATE			
15.3\pm 0.9 OUR AVERAGE			

15.3 \pm 0.9	SARANTSEV	19	DPWA	$\bar{K}N$ multichannel
15 \pm $\frac{10}{8}$	¹ KAMANO	15	DPWA	$\bar{K}N$ multichannel

••• We do not use the following data for averages, fits, limits, etc. •••

16	ZHANG	13A	DPWA	$\bar{K}N$ multichannel
17.2	QIANG	10	SPEC	$e p \rightarrow e' K^+ X$ (fit to X)

¹ From the preferred solution A in KAMANO 15.

 $\Lambda(1520)$ POLE RESIDUES

The normalized residue is the residue divided by $\Gamma_{pole}/2$.

Normalized residue in $N\bar{K} \rightarrow \Lambda(1520) \rightarrow N\bar{K}$

MODULUS	PHASE ($^\circ$)	DOCUMENT ID	TECN	COMMENT
0.45 \pm 0.01	-10 \pm 3	SARANTSEV	19	DPWA $\bar{K}N$ multichannel
0.431	-11	¹ KAMANO	15	DPWA $\bar{K}N$ multichannel

¹ From the preferred solution A in KAMANO 15.

Normalized residue in $N\bar{K} \rightarrow \Lambda(1520) \rightarrow \Sigma\pi$

MODULUS	PHASE ($^\circ$)	DOCUMENT ID	TECN	COMMENT
0.44 \pm 0.01	-15 \pm 3	SARANTSEV	19	DPWA $\bar{K}N$ multichannel
0.435	-10	¹ KAMANO	15	DPWA $\bar{K}N$ multichannel

¹ From the preferred solution A in KAMANO 15.

Normalized residue in $N\bar{K} \rightarrow \Lambda(1520) \rightarrow \Lambda\eta$

MODULUS	PHASE ($^\circ$)	DOCUMENT ID	TECN	COMMENT
0.013\pm0.003	116 \pm 3	SARANTSEV	19	DPWA $\bar{K}N$ multichannel

Normalized residue in $N\bar{K} \rightarrow \Lambda(1520) \rightarrow \Sigma(1385)\pi, S\text{-wave}$

MODULUS	PHASE ($^\circ$)	DOCUMENT ID	TECN	COMMENT
0.431	-123	¹ KAMANO	15	DPWA $\bar{K}N$ multichannel

¹ From the preferred solution A in KAMANO 15.

Normalized residue in $N\bar{K} \rightarrow \Lambda(1520) \rightarrow \Sigma(1385)\pi, D\text{-wave}$

MODULUS	PHASE ($^\circ$)	DOCUMENT ID	TECN	COMMENT
0.0141	122	¹ KAMANO	15	DPWA $\bar{K}N$ multichannel

¹ From the preferred solution A in KAMANO 15.

 $\Lambda(1520)$ MASS

VALUE (MeV)	EVTS	DOCUMENT ID	TECN	COMMENT
1518 to 1520 (≈ 1519) OUR ESTIMATE				
1519.42\pm0.19 OUR AVERAGE				Error includes scale factor of 1.1.
1518.5 \pm 0.5		SARANTSEV	19	DPWA $\bar{K}N$ multichannel
1519.6 \pm 0.5		ZHANG	13A	DPWA $\bar{K}N$ multichannel
1520.4 \pm 0.6 \pm 1.5		QIANG	10	SPEC $e p \rightarrow e' K^+ X$ (fit to X)
1517.3 \pm 1.5	300	BARBER	80D	SPEC $\gamma p \rightarrow \Lambda(1520) K^+$
1517.8 \pm 1.2	5k	BARLAG	79	HBC $K^- p$ 4.2 GeV/c
1520.0 \pm 0.5		ALSTON-...	78	DPWA $\bar{K}N \rightarrow \bar{K}N$
1519.7 \pm 0.3	4k	CAMERON	77	HBC $K^- p$ 0.96-1.36 GeV/c
1519 \pm 1		GOPAL	77	DPWA $\bar{K}N$ multichannel
1519.4 \pm 0.3	2000	CORDEN	75	DBC $K^- d$ 1.4-1.8 GeV/c

 $\Lambda(1520)$ WIDTH

VALUE (MeV)	EVTS	DOCUMENT ID	TECN	COMMENT
15 to 17 (≈ 16) OUR ESTIMATE				
15.73\pm0.26 OUR AVERAGE				
15.7 \pm 1.0		SARANTSEV	19	DPWA $\bar{K}N$ multichannel
17 \pm 1		ZHANG	13A	DPWA $\bar{K}N$ multichannel
18.6 \pm 1.9 \pm 1.0		QIANG	10	SPEC $e p \rightarrow e' K^+ X$ (fit to X)
16.3 \pm 3.3	300	BARBER	80D	SPEC $\gamma p \rightarrow \Lambda(1520) K^+$
16 \pm 1		GOPAL	80	DPWA $\bar{K}N \rightarrow \bar{K}N$
14 \pm 3	677	¹ BARLAG	79	HBC $K^- p$ 4.2 GeV/c
15.4 \pm 0.5		ALSTON-...	78	DPWA $\bar{K}N \rightarrow \bar{K}N$
16.3 \pm 0.5	4k	CAMERON	77	HBC $K^- p$ 0.96-1.36 GeV/c
15.0 \pm 0.5		GOPAL	77	DPWA $\bar{K}N$ multichannel
15.5 \pm 1.6	2000	CORDEN	75	DBC $K^- d$ 1.4-1.8 GeV/c

¹ From the best-resolution sample of $\Lambda\pi\pi$ events only.

 $\Lambda(1520)$ DECAY MODES

Mode	Fraction (Γ_i/Γ)
Γ_1 $N\bar{K}$	(45 \pm 1) %
Γ_2 $\Sigma\pi$	(42 \pm 1) %
Γ_3 $\Lambda\pi\pi$	(10 \pm 1) %
Γ_4 $\Sigma(1385)\pi, S\text{-wave}$	
Γ_5 $\Sigma(1385)\pi, D\text{-wave}$	
Γ_6 $\Sigma(1385)\pi$	
Γ_7 $\Sigma(1385)\pi(\rightarrow \Lambda\pi\pi)$	
Γ_8 $\Lambda(\pi\pi)S\text{-wave}$	
Γ_9 $\Sigma\pi\pi$	(0.9 \pm 0.1) %
Γ_{10} $\Lambda\gamma$	(0.85 \pm 0.15) %
Γ_{11} $\Sigma^0\gamma$	

 $\Lambda(1520)$ BRANCHING RATIOS

See "Sign conventions for resonance couplings" in the Note on Λ and Σ Resonances.

$\Gamma(N\bar{K})/\Gamma_{total}$	VALUE	DOCUMENT ID	TECN	COMMENT	Γ_1/Γ
0.45 to 0.47 OUR ESTIMATE					
0.45 \pm 0.01		SARANTSEV	19	DPWA $\bar{K}N$ multichannel	
0.47 \pm 0.04		ZHANG	13A	DPWA $\bar{K}N$ multichannel	
0.47 \pm 0.02		GOPAL	80	DPWA $\bar{K}N \rightarrow \bar{K}N$	
0.45 \pm 0.03		ALSTON-...	78	DPWA $\bar{K}N \rightarrow \bar{K}N$	
0.448 \pm 0.014		CORDEN	75	DBC $K^- d$ 1.4-1.8 GeV/c	
0.43		¹ KAMANO	15	DPWA $\bar{K}N$ multichannel	
0.47 \pm 0.01		GOPAL	77	DPWA See GOPAL 80	
0.42		MAST	76	HBC $K^- p \rightarrow \bar{K}^0 n$	

¹ From the preferred solution A in KAMANO 15.

$\Gamma(\Sigma\pi)/\Gamma_{total}$	VALUE	DOCUMENT ID	TECN	COMMENT	Γ_2/Γ
0.42 to 0.46 OUR ESTIMATE					
0.43 \pm 0.01		SARANTSEV	19	DPWA $\bar{K}N$ multichannel	
0.47 \pm 0.05		ZHANG	13A	DPWA $\bar{K}N$ multichannel	
0.426 \pm 0.014		CORDEN	75	DBC $K^- d$ 1.4-1.8 GeV/c	
0.418 \pm 0.017		BARBARO-...	69B	HBC $K^- p$ 0.28-0.45 GeV/c	
0.446		¹ KAMANO	15	DPWA $\bar{K}N$ multichannel	
0.46		KIM	71	DPWA K-matrix analysis	

¹ From the preferred solution A in KAMANO 15.

$\Gamma(\Sigma\pi)/\Gamma(N\bar{K})$	VALUE	DOCUMENT ID	TECN	COMMENT	Γ_2/Γ_1
0.9 to 1.0 OUR ESTIMATE					
0.98 \pm 0.03		¹ GOPAL	77	DPWA $\bar{K}N$ multichannel	
0.82 \pm 0.08		BURKHARDT	69	HBC $K^- p$ 0.8-1.2 GeV/c	
1.06 \pm 0.14		SCHEUER	68	DBC $K^- N$ 3 GeV/c	
0.96 \pm 0.20		DAHL	67	HBC $\pi^- p$ 1.6-4 GeV/c	
0.73 \pm 0.11		DAUBER	67	HBC $K^- p$ 2 GeV/c	
1.06 \pm 0.12		BERTHON	74	HBC Quasi-2-body σ	
1.72 \pm 0.78		MUSGRAVE	65	HBC	

¹ The $\bar{K}N \rightarrow \Sigma\pi$ amplitude at resonance is $+0.46 \pm 0.01$.

$\Gamma(\Lambda\pi\pi)/\Gamma_{total}$	VALUE	DOCUMENT ID	TECN	COMMENT	Γ_3/Γ
0.09 to 0.11 OUR ESTIMATE					
0.091 \pm 0.006		CORDEN	75	DBC $K^- d$ 1.4-1.8 GeV/c	
0.11 \pm 0.01		¹ MAST	73B	IPWA $K^- p \rightarrow \Lambda\pi\pi$	

¹ Assumes $\Gamma(N\bar{K})/\Gamma_{total} = 0.46 \pm 0.02$.

$\Gamma(\Lambda\pi\pi)/\Gamma(N\bar{K})$	VALUE	DOCUMENT ID	TECN	COMMENT	Γ_3/Γ_1
0.18 to 0.22 OUR ESTIMATE					
0.22 \pm 0.03		BURKHARDT	69	HBC $K^- p$ 0.8-1.2 GeV/c	
0.19 \pm 0.04		SCHEUER	68	DBC $K^- N$ 3 GeV/c	
0.17 \pm 0.05		DAHL	67	HBC $\pi^- p$ 1.6-4 GeV/c	
0.21 \pm 0.18		DAUBER	67	HBC $K^- p$ 2 GeV/c	
0.27 \pm 0.13		¹ BERTHON	74	HBC Quasi-2-body σ	
0.2		KIM	71	DPWA K-matrix analysis	

$\Gamma(\Sigma\pi)/\Gamma(\Lambda\pi\pi)$	VALUE	DOCUMENT ID	TECN	COMMENT	Γ_2/Γ_3
3.4 to 4.4 OUR ESTIMATE					
3.9 \pm 1.0		UHLIG	67	HBC $K^- p$ 0.9-1.0 GeV/c	
3.3 \pm 1.1		BIRMINGHAM	66	HBC $K^- p$ 3.5 GeV/c	
4.5 \pm 1.0		ARMENTEROS65c		HBC	

See key on page 1171

Baryon Particle Listings
 $\Lambda(1520)$, $\Lambda(1600)$ $\Gamma(\Sigma(1385)\pi, S\text{-wave})/\Gamma_{\text{total}}$ Γ_4/Γ

VALUE	DOCUMENT ID	TECN	COMMENT
0.121	¹ KAMANO 15	DPWA	$\bar{K}N$ multichannel

¹ From the preferred solution A in KAMANO 15. $\Gamma(\Sigma(1385)\pi, D\text{-wave})/\Gamma_{\text{total}}$ Γ_5/Γ

VALUE	DOCUMENT ID	TECN	COMMENT
0.003	¹ KAMANO 15	DPWA	Multichannel

¹ From the preferred solution A in KAMANO 15. $\Gamma(\Sigma(1385)\pi)/\Gamma_{\text{total}}$ Γ_6/Γ

VALUE	DOCUMENT ID	TECN	COMMENT
0.041 ± 0.005	CHAN 72	HBC	$K^- p \rightarrow \Lambda \pi \pi$

 $\Gamma(\Sigma(1385)\pi \rightarrow \Lambda \pi \pi)/\Gamma(\Lambda \pi \pi)$ Γ_7/Γ_3

The $\Lambda \pi \pi$ mode is largely due to $\Sigma(1385)\pi$. Only the values of $(\Sigma(1385)\pi)/\Gamma(\Lambda \pi \pi)$ given by MAST 73B and CORDEN 75 are based on real 3-body partial-wave analyses. The discrepancy between the two results is essentially due to the different hypotheses made concerning the shape of the $(\pi\pi)_{S\text{-wave}}$ state.

VALUE	CL%	DOCUMENT ID	TECN	COMMENT
0.58 ± 0.22		CORDEN 75	DBC	$K^- d$ 1.4–1.8 GeV/c
0.82 ± 0.10		¹ MAST 73B	IPWA	$K^- p \rightarrow \Lambda \pi \pi$

• • • We do not use the following data for averages, fits, limits, etc. • • •

<0.44	90	WIELAND 11	SPHR	$\gamma p \rightarrow K^+ \Lambda(1520)$
0.39 ± 0.10		² BURKHARDT 71	HBC	$K^- p \rightarrow (\Lambda \pi \pi) \pi$

¹ Both $\Sigma(1385)\pi DS_{03}$ and $\Sigma(\pi\pi) DP_{03}$ contribute.² The central bin (1514–1524 MeV) gives 0.74 ± 0.10 ; other bins are lower by 2-to-5 standard deviations. $\Gamma(\Lambda(\pi\pi)_{S\text{-wave}})/\Gamma(\Lambda \pi \pi)$ Γ_8/Γ_3

VALUE	DOCUMENT ID	TECN	COMMENT
0.20 ± 0.08	CORDEN 75	DBC	$K^- d$ 1.4–1.8 GeV/c

 $\Gamma(\Sigma \pi \pi)/\Gamma_{\text{total}}$ Γ_9/Γ

VALUE	DOCUMENT ID	TECN	COMMENT
0.007 to 0.011 OUR ESTIMATE			
0.007 ± 0.002	¹ CORDEN 75	DBC	$K^- d$ 1.4–1.8 GeV/c
0.0085 ± 0.0006	² MAST 73	MPWA	$K^- p \rightarrow \Sigma \pi \pi$
0.010 ± 0.0015	BARBARO... 69B	HBC	$K^- p$ 0.28–0.45 GeV/c

¹ Much of the $\Sigma \pi \pi$ decay proceeds via $\Sigma(1385)\pi$.² Assumes $\Gamma(N\bar{K})/\Gamma_{\text{total}} = 0.46$. $\Gamma(\Lambda \gamma)/\Gamma_{\text{total}}$ Γ_{10}/Γ

VALUE (units 10^{-3})	EVTS	DOCUMENT ID	TECN	COMMENT
7 to 11 OUR ESTIMATE				
$10.7 \pm 2.9^{+1.5}_{-0.4}$	32	TAYLOR 05	CLAS	$\gamma p \rightarrow K^+ \Lambda \gamma$
$10.2 \pm 2.1 \pm 1.5$	290	ANTIPOV 04A	SPNX	$p N(C) \rightarrow \Lambda(1520) K^+ N(C)$
8.0 ± 1.4	238	MAST 68B	HBC	Using $\Gamma(N\bar{K})/\Gamma_{\text{total}} = 0.45$

 $\Gamma(\Sigma^0 \gamma)/\Gamma_{\text{total}}$ Γ_{11}/Γ

VALUE	DOCUMENT ID	TECN	COMMENT
0.02 ± 0.0035	¹ MAST 68B	HBC	Not measured; see note

¹ Calculated from $\Gamma(\Lambda \gamma)/\Gamma_{\text{total}}$, assuming SU(3). Needed to constrain the sum of all the branching ratios to be unity. $\Lambda(1520)$ REFERENCES

SARANTSEV 19	EPJ A55 180	A.V. Sarantsev et al.	(BONN, PNPI)
KAMANO 15	PR C92 025205	H. Kamano et al.	(ANL, OSAK)
ZHANG 13A	PR C98 035205	H. Zhang et al.	(KSU)
WIELAND 11	EPJ A47 47	F. Wieland et al.	(ELSA SAPHIR Collab.)
QIANG 10	PL B694 123	Y. Qiang et al.	(DUKE, JEFF, PNPI, GWU+)
TAYLOR 05	PR C71 054609	S. Taylor et al.	(JLab CLAS Collab.)
Also	PR C72 039902 (errata)	S. Taylor et al.	(JLab CLAS Collab.)
ANTIPOV 04A	PL B604 22	Yu.M. Antipov et al.	(HEP SPHINX Collab.)
PDG 82	PL 111B 1	M. Roos et al.	(HELS, CIT, CERN)
BARBER 80D	ZPHY C7 17	D.P. Barber et al.	(DARE, LANC, SHEF)
GOPAL 80	Toronto Conf. 159	G.P. Gopal	(RHEL IJP)
BARLAG 79	NP B149 220	S.J.M. Barlag et al.	(AMST, CERN, NIJM+)
ALSTON... 78	PR D18 182	M. Alston-Garnjost et al.	(LBL, MTHO+ IJP)
Also	PR C38 1007	M. Alston-Garnjost et al.	(LBL, MTHO+ IJP)
CAMERON 77	NP B131 399	W. Cameron et al.	(RHEL, LOIC IJP)
GOPAL 77	NP B119 362	G.P. Gopal et al.	(LOIC, RHEL IJP)
MAST 76	PR D14 13	T.S. Mast et al.	(LBL)
CORDEN 75	NP B84 306	M.J. Corden et al.	(BIRM)
BERTHON 74	NC 21A 146	A. Berthon et al.	(CDEF, RHEL, SACL+)
MAST 73	PR D7 3212	T.S. Mast et al.	(LBL IJP)
MAST 73B	PR D7 5	T.S. Mast et al.	(LBL IJP)
CHAN 72	PRL 28 256	S.B. Chan et al.	(MASA, YALE)
BURKHARDT 71	NP B27 64	E. Burkhardt et al.	(HEID, CERN, SACL)
KIM 71	PRL 27 356	J.K. Kim	(HARV IJP)
Also	Duke Conf. 161	J.K. Kim	(HARV IJP)
Hyperon Resonances, 1970			
BARBARO... 69B	Lund Conf. 352	A. Barbaro-Galtri et al.	(LRL)
Also	Duke Conf. 95	R.D. Tripp	(LRL)
Hyperon Resonances 1970			
BURKHARDT 69	NP B14 106	E. Burkhardt et al.	(HEID, EFI, CERN+)

MAST 68B	PRL 21 1715	T.S. Mast et al.	(LRL)
SCHUEER 68	NP B8 503	J.C. Scheuer et al.	(SABRE Collab.)
DAHL 67	PR 163 1377	O.I. Dahl et al.	(LRL)
DAUBER 67	PL 24B 525	P.M. Dauber et al.	(UCLA)
UHLIG 67	PR 155 1448	R.P. Uhlig et al.	(UMD, NRL)
BIRMINGHAM 66	PR 152 1148	M. Haque et al.	(BIRM, GLAS, LOIC, OXF+)
ARMENTEROS 65C	PL 19 338	R. Armenteros et al.	(CERN, HEID, SACL)
MUSGRAVE 65	NC 35 735	B. Musgrave et al.	(BIRM, CERN, EPOL+)
WATSON 63	PR 131 2248	M.B. Watson, M. Ferro-Luzzi, R.D. Tripp	(LRL) IJP
FERRO-LUZZI 62	PRL 8 28	M. Ferro-Luzzi, R.D. Tripp, M.B. Watson	(LRL) IJP

 $\Lambda(1600) 1/2^+$ $I(J^P) = 0(\frac{1}{2}^+)$ Status: *** $\Lambda(1600)$ POLE POSITION

REAL PART

VALUE (MeV)	DOCUMENT ID	TECN	COMMENT
1540 to 1560 (≈ 1550) OUR ESTIMATE			
1546 ± 6 OUR AVERAGE			Error includes scale factor of 2.1.
1562 ± 8	SARANTSEV 19	DPWA	$\bar{K}N$ multichannel
1544^{+3}_{-3}	¹ KAMANO 15	DPWA	Multichannel

• • • We do not use the following data for averages, fits, limits, etc. • • •

1572	ZHANG 13A	DPWA	Multichannel
------	-----------	------	--------------

¹ From the preferred solution A in KAMANO 15.

−2×IMAGINARY PART

VALUE (MeV)	DOCUMENT ID	TECN	COMMENT
120 to 240 (≈ 180) OUR ESTIMATE			
159⁺⁶⁰_{−12} OUR AVERAGE			Error includes scale factor of 6.2.

232 ± 15	SARANTSEV 19	DPWA	$\bar{K}N$ multichannel
--------------	--------------	------	-------------------------

112^{+12}_{-2}	¹ KAMANO 15	DPWA	Multichannel
------------------	------------------------	------	--------------

• • • We do not use the following data for averages, fits, limits, etc. • • •

138	ZHANG 13A	DPWA	Multichannel
-----	-----------	------	--------------

¹ From the preferred solution A in KAMANO 15. $\Lambda(1600)$ POLE RESIDUESThe normalized residue is the residue divided by $\Gamma_{\text{pole}/2}$.Normalized residue in $N\bar{K} \rightarrow \Lambda(1600) \rightarrow N\bar{K}$

MODULUS	PHASE (°)	DOCUMENT ID	TECN	COMMENT
0.36 ± 0.07	−63 ± 10	SARANTSEV 19	DPWA	$\bar{K}N$ multichannel
0.105	−80	¹ KAMANO 15	DPWA	Multichannel

• • • We do not use the following data for averages, fits, limits, etc. • • •

¹ From the preferred solution A in KAMANO 15.Normalized residue in $N\bar{K} \rightarrow \Lambda(1600) \rightarrow \Sigma \pi$

MODULUS	PHASE (°)	DOCUMENT ID	TECN	COMMENT
0.39 ± 0.08	148 ± 10	SARANTSEV 19	DPWA	$\bar{K}N$ multichannel
0.232	108	¹ KAMANO 15	DPWA	Multichannel

• • • We do not use the following data for averages, fits, limits, etc. • • •

¹ From the preferred solution A in KAMANO 15.Normalized residue in $N\bar{K} \rightarrow \Lambda(1600) \rightarrow \Lambda \eta$

MODULUS	PHASE (°)	DOCUMENT ID	TECN	COMMENT
0.22 ± 0.13	180 ± 20	SARANTSEV 19	DPWA	$\bar{K}N$ multichannel

Normalized residue in $N\bar{K} \rightarrow \Lambda(1600) \rightarrow \Lambda \sigma$

MODULUS	PHASE (°)	DOCUMENT ID	TECN	COMMENT
0.30 ± 0.06	−70 ± 10	SARANTSEV 19	DPWA	$\bar{K}N$ multichannel

Normalized residue in $N\bar{K} \rightarrow \Lambda(1600) \rightarrow \Sigma(1385)\pi$

MODULUS	PHASE (°)	DOCUMENT ID	TECN	COMMENT
0.37 ± 0.07	103 ± 12	SARANTSEV 19	DPWA	$\bar{K}N$ multichannel
0.183	77	¹ KAMANO 15	DPWA	Multichannel

• • • We do not use the following data for averages, fits, limits, etc. • • •

¹ From the preferred solution A in KAMANO 15.Normalized residue in $N\bar{K} \rightarrow \Lambda(1600) \rightarrow N\bar{K}^*(892), S=1/2, P\text{-wave}$

MODULUS	PHASE (°)	DOCUMENT ID	TECN	COMMENT
0.02 ± 0.01	126 ± 45	SARANTSEV 19	DPWA	$\bar{K}N$ multichannel

Normalized residue in $N\bar{K} \rightarrow \Lambda(1600) \rightarrow N\bar{K}^*(892), S=3/2, P\text{-wave}$

MODULUS	PHASE (°)	DOCUMENT ID	TECN	COMMENT
0.02 ± 0.01	−135 ± 45	SARANTSEV 19	DPWA	$\bar{K}N$ multichannel

Baryon Particle Listings

$\Lambda(1600), \Lambda(1670)$

$\Lambda(1600)$ MASS

VALUE (MeV)	DOCUMENT ID	TECN	COMMENT
1570 to 1630 (≈ 1600) OUR ESTIMATE			
1605 \pm 8	SARANTSEV 19	DPWA	$\bar{K}N$ multichannel
1592 \pm 10	ZHANG 13A	DPWA	Multichannel
1568 \pm 20	GOPAL 80	DPWA	$\bar{K}N \rightarrow \bar{K}N$
1703 \pm 100	ALSTON-... 78	DPWA	$\bar{K}N \rightarrow \bar{K}N$
1573 \pm 25	GOPAL 77	DPWA	$\bar{K}N$ multichannel
1596 \pm 6	KANE 74	DPWA	$K^-p \rightarrow \Sigma\pi$
1620 \pm 10	LANGBEIN 72	IPWA	$\bar{K}N$ multichannel
••• We do not use the following data for averages, fits, limits, etc. •••			
1572 or 1617	¹ MARTIN 77	DPWA	$\bar{K}N$ multichannel
1646 \pm 7	² CARROLL 76	DPWA	Isospin-0 total σ
1570	KIM 71	DPWA	K-matrix analysis
¹ The two MARTIN 77 values are from a T-matrix pole and from a Breit-Wigner fit.			
² A total cross-section bump with $(J+1/2) \Gamma_{el} / \Gamma_{total} = 0.04$.			

$\Lambda(1600)$ WIDTH

VALUE (MeV)	DOCUMENT ID	TECN	COMMENT
150 to 250 (≈ 200) OUR ESTIMATE			
245 \pm 15	SARANTSEV 19	DPWA	$\bar{K}N$ multichannel
150 \pm 28	ZHANG 13A	DPWA	Multichannel
116 \pm 20	GOPAL 80	DPWA	$\bar{K}N \rightarrow \bar{K}N$
593 \pm 200	ALSTON-... 78	DPWA	$\bar{K}N \rightarrow \bar{K}N$
147 \pm 50	GOPAL 77	DPWA	$\bar{K}N$ multichannel
175 \pm 20	KANE 74	DPWA	$K^-p \rightarrow \Sigma\pi$
60 \pm 10	LANGBEIN 72	IPWA	$\bar{K}N$ multichannel
••• We do not use the following data for averages, fits, limits, etc. •••			
247 or 271	¹ MARTIN 77	DPWA	$\bar{K}N$ multichannel
20	² CARROLL 76	DPWA	Isospin-0 total σ
50	KIM 71	DPWA	K-matrix analysis
¹ The two MARTIN 77 values are from a T-matrix pole and from a Breit-Wigner fit.			
² A total cross-section bump with $(J+1/2) \Gamma_{el} / \Gamma_{total} = 0.04$.			

$\Lambda(1600)$ DECAY MODES

Mode	Fraction (Γ_i/Γ)
Γ_1 $N\bar{K}$	15-30 %
Γ_2 $\Sigma\pi$	10-60 %
Γ_3 $\Lambda\sigma$	(19 \pm 4) %
Γ_4 $\Sigma(1385)\pi$	(9 \pm 4) %

$\Lambda(1600)$ BRANCHING RATIOS

See "Sign conventions for resonance couplings" in the Note on Λ and Σ Resonances.

$\Gamma(N\bar{K})/\Gamma_{total}$	DOCUMENT ID	TECN	COMMENT	Γ_1/Γ
0.14 to 0.28 OUR ESTIMATE				
0.29 \pm 0.06	SARANTSEV 19	DPWA	$\bar{K}N$ multichannel	
0.14 \pm 0.04	ZHANG 13A	DPWA	Multichannel	
0.23 \pm 0.04	GOPAL 80	DPWA	$\bar{K}N \rightarrow \bar{K}N$	
0.14 \pm 0.05	ALSTON-... 78	DPWA	$\bar{K}N \rightarrow \bar{K}N$	
0.25 \pm 0.15	LANGBEIN 72	IPWA	$\bar{K}N$ multichannel	
••• We do not use the following data for averages, fits, limits, etc. •••				
0.064	¹ KAMANO 15	DPWA	Multichannel	
0.24 \pm 0.04	GOPAL 77	DPWA	See GOPAL 80	
0.30 or 0.29	² MARTIN 77	DPWA	$\bar{K}N$ multichannel	
¹ From the preferred solution A in KAMANO 15.				
² The two MARTIN 77 values are from a T-matrix pole and from a Breit-Wigner fit.				

$\Gamma(\Sigma\pi)/\Gamma_{total}$	DOCUMENT ID	TECN	COMMENT	Γ_2/Γ
0.37 \pm 0.07				
	SARANTSEV 19	DPWA	$\bar{K}N$ multichannel	
••• We do not use the following data for averages, fits, limits, etc. •••				
0.851	¹ KAMANO 15	DPWA	Multichannel	
¹ From the preferred solution A in KAMANO 15.				

$\Gamma(\Lambda\sigma)/\Gamma_{total}$	DOCUMENT ID	TECN	COMMENT	Γ_3/Γ
0.19 \pm 0.04				
	SARANTSEV 19	DPWA	$\bar{K}N$ multichannel	

$\Gamma(\Sigma(1385)\pi)/\Gamma_{total}$	DOCUMENT ID	TECN	COMMENT	Γ_4/Γ
0.09 \pm 0.04				
	SARANTSEV 19	DPWA	$\bar{K}N$ multichannel	
••• We do not use the following data for averages, fits, limits, etc. •••				
0.085	¹ KAMANO 15	DPWA	Multichannel	
¹ From the preferred solution A in KAMANO 15.				

$(\Gamma_1/\Gamma)_{1/2} / \Gamma_{total}$ in $N\bar{K} \rightarrow \Lambda(1600) \rightarrow \Sigma\pi$	DOCUMENT ID	TECN	COMMENT	$(\Gamma_1/\Gamma_2)_{1/2} / \Gamma$
-0.23 \pm 0.03	ZHANG 13A	DPWA	Multichannel	
-0.16 \pm 0.04	GOPAL 77	DPWA	$\bar{K}N$ multichannel	
-0.33 \pm 0.11	KANE 74	DPWA	$K^-p \rightarrow \Sigma\pi$	
0.28 \pm 0.09	LANGBEIN 72	IPWA	$\bar{K}N$ multichannel	
••• We do not use the following data for averages, fits, limits, etc. •••				
-0.39 or -0.39	¹ MARTIN 77	DPWA	$\bar{K}N$ multichannel	
not seen	HEPP 76B	DPWA	$K^-N \rightarrow \Sigma\pi$	
¹ The two MARTIN 77 values are from a T-matrix pole and from a Breit-Wigner fit.				

$\Lambda(1600)$ REFERENCES

SARANTSEV 19	EPJ A55 180	A.V. Sarantsev et al.	(BONN, PNPI)
KAMANO 15	PR C92 025205	H. Kamano et al.	(ANL, OSAK)
ZHANG 13A	PR C88 035205	H. Zhang et al.	(KSU)
GOPAL 80	Toronto Conf. 159	G.P. Gopal	(RHEL) IJP
ALSTON-... 78	PR D18 182	M. Alston-Garnjost et al.	(LBL, MTHO+) IJP
Also	PRL 38 1007	M. Alston-Garnjost et al.	(LBL, MTHO+) IJP
GOPAL 77	NP B119 362	G.P. Gopal et al.	(LOIC, RHEL) IJP
MARTIN 77	NP B127 349	B.R. Martin, M.K. Pidcock, R.G. Moorhouse	(LOUC+) IJP
Also	NP B126 266	B.R. Martin, M.K. Pidcock	(LOUC) IJP
Also	NP B126 285	B.R. Martin, M.K. Pidcock	(LOUC) IJP
CARROLL 76	PRL 37 806	A.S. Carroll et al.	(BNL) I
HEPP 76B	PL 65B 487	V. Hepp et al.	(CERN, HEID, MPIM) IJP
KANE 74	LBL-2452	D.F. Kane	(LBL) IJP
LANGBEIN 72	NP B47 477	W. Langbein, F. Wagner	(MPIM) IJP
KIM 71	PRL 27 356	J.K. Kim	(HARV) IJP

$\Lambda(1670)$ 1/2-

$$I(J^P) = 0(\frac{1}{2}^-) \text{ Status: } ***$$

The measurements of the mass, width, and elasticity published before 1974 are now obsolete and have been omitted. They were last listed in our 1982 edition Physics Letters **111B** 1 (1982).

$\Lambda(1670)$ POLE POSITIONS

REAL PART

VALUE (MeV)	DOCUMENT ID	TECN	COMMENT
1670 to 1678 (≈ 1674) OUR ESTIMATE			
1676 \pm 2	SARANTSEV 19	DPWA	$\bar{K}N$ multichannel
1669 \pm 3	¹ KAMANO 15	DPWA	$\bar{K}N$ multichannel
-8			
1677.5 \pm 0.8	GARCIA-REC...03	DPWA	$\bar{K}N$ multichannel
••• We do not use the following data for averages, fits, limits, etc. •••			
1667	ZHANG 13A	DPWA	$\bar{K}N$ multichannel
¹ From the preferred solution A in KAMANO 15.			

-2xIMAGINARY PART

VALUE (MeV)	DOCUMENT ID	TECN	COMMENT
28 to 36 (≈ 32) OUR ESTIMATE			
33 \pm 4	SARANTSEV 19	DPWA	$\bar{K}N$ multichannel
19 \pm 18	¹ KAMANO 15	DPWA	$\bar{K}N$ multichannel
-2			
29.2 \pm 1.4	GARCIA-REC...03	DPWA	$\bar{K}N$ multichannel
••• We do not use the following data for averages, fits, limits, etc. •••			
26	ZHANG 13A	DPWA	$\bar{K}N$ multichannel
¹ From the preferred solution A in KAMANO 15.			

$\Lambda(1670)$ POLE RESIDUES

The normalized residue is the residue divided by $\Gamma_{pole}/2$.

Normalized residue in $\bar{K}N \rightarrow \Lambda(1670) \rightarrow \bar{K}N$

MODULUS	PHASE ($^\circ$)	DOCUMENT ID	TECN	COMMENT
0.30 \pm 0.06	-145 \pm 11	SARANTSEV 19	DPWA	$\bar{K}N$ multichannel
••• We do not use the following data for averages, fits, limits, etc. •••				
0.351	164	¹ KAMANO 15	DPWA	$\bar{K}N$ multichannel
¹ From the preferred solution A in KAMANO 15.				

Normalized residue in $N\bar{K} \rightarrow \Lambda(1670) \rightarrow \Sigma\pi$

MODULUS	PHASE ($^\circ$)	DOCUMENT ID	TECN	COMMENT
0.19 \pm 0.06	145 \pm 14	SARANTSEV 19	DPWA	$\bar{K}N$ multichannel
••• We do not use the following data for averages, fits, limits, etc. •••				
0.327	125	¹ KAMANO 15	DPWA	$\bar{K}N$ multichannel
¹ From the preferred solution A in KAMANO 15.				

Normalized residue in $N\bar{K} \rightarrow \Lambda(1670) \rightarrow \Lambda\eta$

MODULUS	PHASE ($^\circ$)	DOCUMENT ID	TECN	COMMENT
0.26 \pm 0.09	104 \pm 14	SARANTSEV 19	DPWA	$\bar{K}N$ multichannel
••• We do not use the following data for averages, fits, limits, etc. •••				
0.474	59	¹ KAMANO 15	DPWA	Multichannel
¹ From the preferred solution A in KAMANO 15.				

Normalized residue in $N\bar{K} \rightarrow \Lambda(1670) \rightarrow \Xi K$

MODULUS	PHASE (°)	DOCUMENT ID	TECN	COMMENT
0.02 ± 0.02	100 ± 25	SARANTSEV 19	DPWA	$\bar{K}N$ multichannel

Normalized residue in $N\bar{K} \rightarrow \Lambda(1670) \rightarrow \Lambda\omega, S=1/2, S\text{-wave}$

MODULUS	PHASE (°)	DOCUMENT ID	TECN	COMMENT
0.09 ± 0.04	-60 ± 35	SARANTSEV 19	DPWA	$\bar{K}N$ multichannel

Normalized residue in $N\bar{K} \rightarrow \Lambda(1670) \rightarrow \Lambda\omega, S=3/2, D\text{-wave}$

MODULUS	PHASE (°)	DOCUMENT ID	TECN	COMMENT
0.05 ± 0.04		SARANTSEV 19	DPWA	$\bar{K}N$ multichannel

Normalized residue in $N\bar{K} \rightarrow \Lambda(1670) \rightarrow N\bar{K}^*(892), S=1/2, S\text{-wave}$

MODULUS	PHASE (°)	DOCUMENT ID	TECN	COMMENT
0.31 ± 0.14	100 ± 45	SARANTSEV 19	DPWA	$\bar{K}N$ multichannel

Normalized residue in $N\bar{K} \rightarrow \Lambda(1670) \rightarrow N\bar{K}^*(892), S=3/2, D\text{-wave}$

MODULUS	PHASE (°)	DOCUMENT ID	TECN	COMMENT
0.06 ± 0.03	-85 ± 40	SARANTSEV 19	DPWA	$\bar{K}N$ multichannel

Normalized residue in $N\bar{K} \rightarrow \Lambda(1670) \rightarrow \Lambda\sigma$

MODULUS	PHASE (°)	DOCUMENT ID	TECN	COMMENT
0.25 ± 0.08	160 ± 15	SARANTSEV 19	DPWA	$\bar{K}N$ multichannel

Normalized residue in $N\bar{K} \rightarrow \Lambda(1670) \rightarrow \Sigma(1385)\pi$

MODULUS	PHASE (°)	DOCUMENT ID	TECN	COMMENT
0.13 ± 0.06	110 ± 12	SARANTSEV 19	DPWA	$\bar{K}N$ multichannel

• • • We do not use the following data for averages, fits, limits, etc. • • •
0.0988 -104 ¹KAMANO 15 DPWA Multichannel

¹From the preferred solution A in KAMANO 15.

 $\Lambda(1670)$ MASS

VALUE (MeV)	DOCUMENT ID	TECN	COMMENT
1670 to 1678 (≈ 1674) OUR ESTIMATE			
$1674.3 \pm 0.8 \pm 4.9$	LEE 21A	BELL	$\Lambda_C^+ \rightarrow \Lambda(1670)\pi^+$
1677 ± 2	SARANTSEV 19	DPWA	$\bar{K}N$ multichannel
1672 ± 3	ZHANG 13A	DPWA	Multichannel
1670.8 ± 1.7	KOISO 85	DPWA	$K^-p \rightarrow \Sigma\pi$
1667 ± 5	GOPAL 80	DPWA	$\bar{K}N \rightarrow \bar{K}N$
1671 ± 3	ALSTON... 78	DPWA	$\bar{K}N \rightarrow \bar{K}N$
1675 ± 2	HEPP 76B	DPWA	$K^-N \rightarrow \Sigma\pi$
1679 ± 1	KANE 74	DPWA	$K^-p \rightarrow \Sigma\pi$
1665 ± 5	PREVOST 74	DPWA	$K^-N \rightarrow \Sigma(1385)\pi$
• • • We do not use the following data for averages, fits, limits, etc. • • •			
1673 ± 2	MANLEY 02	DPWA	$\bar{K}N$ multichannel
1668.9 ± 2.0	ABAEV 96	DPWA	$K^-p \rightarrow \Lambda\eta$
1670 ± 5	GOPAL 77	DPWA	$\bar{K}N$ multichannel
1664	¹ MARTIN 77	DPWA	$\bar{K}N$ multichannel

¹MARTIN 77 obtains identical resonance parameters from a T-matrix pole and from a Breit-Wigner fit.

 $\Lambda(1670)$ WIDTH

VALUE (MeV)	DOCUMENT ID	TECN	COMMENT
25 to 35 (≈ 30) OUR ESTIMATE			
$36.1 \pm 2.4 \pm 4.8$	LEE 21A	BELL	$\Lambda_C^+ \rightarrow \Lambda(1670)\pi^+$
33 ± 4	SARANTSEV 19	DPWA	$\bar{K}N$ multichannel
29 ± 5	ZHANG 13A	DPWA	$\bar{K}N$ multichannel
34.1 ± 3.7	KOISO 85	DPWA	$K^-p \rightarrow \Sigma\pi$
29 ± 5	GOPAL 80	DPWA	$\bar{K}N \rightarrow \bar{K}N$
29 ± 5	ALSTON... 78	DPWA	$\bar{K}N \rightarrow \bar{K}N$
46 ± 5	HEPP 76B	DPWA	$K^-N \rightarrow \Sigma\pi$
40 ± 3	KANE 74	DPWA	$K^-p \rightarrow \Sigma\pi$
19 ± 5	PREVOST 74	DPWA	$K^-N \rightarrow \Sigma(1385)\pi$
• • • We do not use the following data for averages, fits, limits, etc. • • •			
23 ± 6	MANLEY 02	DPWA	$\bar{K}N$ multichannel
21.1 ± 3.6	ABAEV 96	DPWA	$K^-p \rightarrow \Lambda\eta$
45 ± 10	GOPAL 77	DPWA	$\bar{K}N$ multichannel
12	¹ MARTIN 77	DPWA	$\bar{K}N$ multichannel

¹MARTIN 77 obtains identical resonance parameters from a T-matrix pole and from a Breit-Wigner fit.

 $\Lambda(1670)$ DECAY MODES

Mode	Fraction (Γ_i/Γ)
Γ_1 $N\bar{K}$	20–30 %
Γ_2 $\Sigma\pi$	25–55 %
Γ_3 $\Lambda\eta$	10–25 %
Γ_4 $\Sigma(1385)\pi, D\text{-wave}$	(6.0 ± 2.0) %
Γ_5 $N\bar{K}^*(892), S=1/2, S\text{-wave}$	
Γ_6 $N\bar{K}^*(892), S=3/2, D\text{-wave}$	(5 ± 4) %
Γ_7 $\Lambda\sigma$	(20 ± 8) %

 $\Lambda(1670)$ BRANCHING RATIOS

See "Sign conventions for resonance couplings" in the Note on Λ and Σ Resonances.

 $\Gamma(N\bar{K})/\Gamma_{\text{total}}$

VALUE	DOCUMENT ID	TECN	COMMENT	Γ_1/Γ
0.20 to 0.30 OUR ESTIMATE				
0.33 ± 0.07	SARANTSEV 19	DPWA	$\bar{K}N$ multichannel	
0.26 ± 0.25	ZHANG 13A	DPWA	$\bar{K}N$ multichannel	
0.18 ± 0.03	GOPAL 80	DPWA	$\bar{K}N \rightarrow \bar{K}N$	
0.17 ± 0.03	ALSTON... 78	DPWA	$\bar{K}N \rightarrow \bar{K}N$	
• • • We do not use the following data for averages, fits, limits, etc. • • •				
0.318	¹ KAMANO 15	DPWA	$\bar{K}N$ multichannel	
0.37 ± 0.07	MANLEY 02	DPWA	$\bar{K}N$ multichannel	
0.20 ± 0.03	GOPAL 77	DPWA	See GOPAL 80	
0.15	² MARTIN 77	DPWA	$\bar{K}N$ multichannel	

¹From the preferred solution A in KAMANO 15.

²MARTIN 77 obtains identical resonance parameters from a T-matrix pole and from a Breit-Wigner fit.

 $\Gamma(\Sigma\pi)/\Gamma_{\text{total}}$

VALUE	DOCUMENT ID	TECN	COMMENT	Γ_2/Γ
0.12 ± 0.03	SARANTSEV 19	DPWA	$\bar{K}N$ multichannel	
• • • We do not use the following data for averages, fits, limits, etc. • • •				
0.289	¹ KAMANO 15	DPWA	Multichannel	

¹From the preferred solution A in KAMANO 15.

 $\Gamma(\Lambda\eta)/\Gamma_{\text{total}}$

VALUE	DOCUMENT ID	TECN	COMMENT	Γ_3/Γ
0.20 ± 0.08	SARANTSEV 19	DPWA	$\bar{K}N$ multichannel	
• • • We do not use the following data for averages, fits, limits, etc. • • •				
0.373	KAMANO 15	DPWA	Multichannel	
0.30 ± 0.08	ABAEV 96	DPWA	$K^-p \rightarrow \Lambda\eta$	

 $\Gamma(\Sigma(1385)\pi, D\text{-wave})/\Gamma_{\text{total}}$

VALUE	DOCUMENT ID	TECN	COMMENT	Γ_4/Γ
0.06 ± 0.02	SARANTSEV 19	DPWA	$\bar{K}N$ multichannel	
• • • We do not use the following data for averages, fits, limits, etc. • • •				
0.019	KAMANO 15	DPWA	Multi-channel	

 $\Gamma(\Lambda\sigma)/\Gamma_{\text{total}}$

VALUE	DOCUMENT ID	TECN	COMMENT	Γ_7/Γ
0.20 ± 0.08	SARANTSEV 19	DPWA	$\bar{K}N$ multichannel	

 $\Gamma(N\bar{K}^*(892), S=1/2, S\text{-wave})/\Gamma_{\text{total}}$

VALUE	DOCUMENT ID	TECN	COMMENT	Γ_5/Γ
• • • We do not use the following data for averages, fits, limits, etc. • • •				
not seen	¹ KAMANO 15	DPWA	Multichannel	

¹Not seen in the preferred solution A in KAMANO 15.

 $\Gamma(N\bar{K}^*(892), S=3/2, D\text{-wave})/\Gamma_{\text{total}}$

VALUE	DOCUMENT ID	TECN	COMMENT	Γ_6/Γ
0.05 ± 0.04	ZHANG 13A	DPWA	Multichannel	
• • • We do not use the following data for averages, fits, limits, etc. • • •				
not seen	¹ KAMANO 15	DPWA	Multichannel	

¹Not seen in the preferred solution A in KAMANO 15.

 $(\Gamma_1\Gamma_7)^{1/2}/\Gamma_{\text{total}}$ in $N\bar{K} \rightarrow \Lambda(1670) \rightarrow \Sigma\pi$

VALUE	DOCUMENT ID	TECN	COMMENT	$(\Gamma_1\Gamma_7)^{1/2}/\Gamma$
-0.29 ± 0.06	ZHANG 13A	DPWA	Multichannel	
-0.26 ± 0.02	KOISO 85	DPWA	$K^-p \rightarrow \Sigma\pi$	
-0.31 ± 0.03	GOPAL 77	DPWA	$\bar{K}N$ multichannel	
-0.29 ± 0.03	HEPP 76B	DPWA	$K^-N \rightarrow \Sigma\pi$	
-0.23 ± 0.03	LONDON 75	HLBC	$K^-p \rightarrow \Sigma^0\pi^0$	
-0.27 ± 0.02	KANE 74	DPWA	$K^-p \rightarrow \Sigma\pi$	
• • • We do not use the following data for averages, fits, limits, etc. • • •				
-0.38 ± 0.03	MANLEY 02	DPWA	$\bar{K}N$ multichannel	
-0.13	¹ MARTIN 77	DPWA	$\bar{K}N$ multichannel	

¹MARTIN 77 obtains identical resonance parameters from a T-matrix pole and from a Breit-Wigner fit.

 $(\Gamma_1\Gamma_7)^{1/2}/\Gamma_{\text{total}}$ in $N\bar{K} \rightarrow \Lambda(1670) \rightarrow \Lambda\eta$

VALUE	DOCUMENT ID	TECN	COMMENT	$(\Gamma_1\Gamma_7)^{1/2}/\Gamma$
-0.30 ± 0.10	ZHANG 13A	DPWA	Multichannel	
$+0.20 \pm 0.05$	BAXTER 73	DPWA	$K^-p \rightarrow \text{neutrals}$	
• • • We do not use the following data for averages, fits, limits, etc. • • •				
$+0.24 \pm 0.04$	MANLEY 02	DPWA	$\bar{K}N$ multichannel	
0.24	KIM 71	DPWA	K-matrix analysis	
0.26	ARMENTEROS69C	HBC		
0.20 or 0.23	BERLEY 65	HBC		

Baryon Particle Listings

$\Lambda(1670)$, $\Lambda(1690)$

$(\Gamma_1 \Gamma_2)^{1/2} / \Gamma_{\text{total}}$ in $N\bar{K} \rightarrow \Lambda(1670) \rightarrow \Sigma(1385)\pi$, D-wave **$(\Gamma_1 \Gamma_4)^{1/2} / \Gamma$**

VALUE	DOCUMENT ID	TECN	COMMENT
-0.17 ± 0.06	MANLEY 02	DPWA	$\bar{K}N$ multichannel
-0.18 ± 0.05	PREVOST 74	DPWA	$K^-N \rightarrow \Sigma(1385)\pi$

$\Lambda(1670)$ REFERENCES

LEE 21A	PR D103 052005	J.Y. Lee <i>et al.</i>	(BELLE Collab.)
SARANTSEV 19	EPJ A55 180	A.V. Sarantsev <i>et al.</i>	(BONN, PNPI)
KAMANO 15	PR C92 025205	H. Kamano <i>et al.</i>	(ANL, OSAK)
ZHANG 13A	PR C88 035205	H. Zhang <i>et al.</i>	(KSU)
GARCIA-RECIO... 03	PR D67 075009	C. Garcia-Recio <i>et al.</i>	(GRAN, VALE)
MANLEY 02	PRL 88 012002	D.M. Manley <i>et al.</i>	(BNL Crystal Ball Collab.)
ABEY 96	PR C53 385	V.Y. Abey, B.M.K. Nefkens	(UCLA)
KOISO 85	NP A433 619	H. Koiso <i>et al.</i>	(TOKY, MASA)
PDG 82	PL 111B 1	M. Roos <i>et al.</i>	(HEL5, CIT, CERN)
GOPAL 80	Toronto Conf. 159	G.P. Gopal	(RHEL) IJP
ALSTON-... 78	PR D18 182	M. Alston-Garnjost <i>et al.</i>	(LBL, MTHO+) IJP
Also	PRL 38 1007	M. Alston-Garnjost <i>et al.</i>	(LBL, MTHO+) IJP
GOPAL 77	NP B119 362	G.P. Gopal <i>et al.</i>	(LOIC, RHEL) IJP
MARTIN 77	NP B127 349	B.R. Martin, M.K. Pidcock, R.G. Moorhouse	(LOUC+) IJP
Also	NP B126 266	B.R. Martin, M.K. Pidcock	(LOUC) IJP
Also	NP B126 285	B.R. Martin, M.K. Pidcock	(LOUC) IJP
HEPP 76B	PL 65B 487	V. Hepp <i>et al.</i>	(CERN, HEID, MPIM) IJP
LONDON 75	NP B85 289	G.W. London <i>et al.</i>	(BNL, CERN, EPOL+) IJP
KANE 74	LBL-2452	D.F. Kane	(LBL) IJP
PREVOST 74	NP B69 246	J. Prevost <i>et al.</i>	(SACL, CERN, HEID)
BAXTER 73	NP B67 125	D.F. Baxter <i>et al.</i>	(OXF) IJP
KIM 71	PRL 27 356	J.K. Kim	(HARV) IJP
Also	Duke Conf. 161	J.K. Kim	(HARV) IJP
Hyperon Resonances, 1970			
ARMENTEROS 69C	Lund Paper 229	R. Armenteros <i>et al.</i>	(CERN, HEID, SACL) IJP
Values are quoted in LEVI-SETTI 69.			
BERLEY 65	PRL 15 641	D. Berley <i>et al.</i>	(BNL) IJP

$\Lambda(1690) \ 3/2^-$

 $I(J^P) = 0(\frac{3}{2}^-)$ Status: * * * *

The measurements of the mass, width, and elasticity published before 1974 are now obsolete and have been omitted. They were last listed in our 1982 edition Physics Letters **111B** 1 (1982).

$\Lambda(1690)$ POLE POSITION

REAL PART

VALUE (MeV)	DOCUMENT ID	TECN	COMMENT
1680 to 1700 (≈ 1690) OUR ESTIMATE			
1683 ± 3	SARANTSEV 19	DPWA	$\bar{K}N$ multichannel
1697 ± $\frac{6}{6}$	¹ KAMANO 15	DPWA	$\bar{K}N$ multichannel
• • • We do not use the following data for averages, fits, limits, etc. • • •			
1689	ZHANG 13A	DPWA	$\bar{K}N$ multichannel
¹ From the preferred solution A in KAMANO 15.			
-2xIMAGINARY PART			
VALUE (MeV)	DOCUMENT ID	TECN	COMMENT
60 to 80 (≈ 70) OUR ESTIMATE			
72 ± 5	SARANTSEV 19	DPWA	$\bar{K}N$ multichannel
65 ± 14	¹ KAMANO 15	DPWA	$\bar{K}N$ multichannel
• • • We do not use the following data for averages, fits, limits, etc. • • •			
53	ZHANG 13A	DPWA	$\bar{K}N$ multichannel
¹ From the preferred solution A in KAMANO 15.			

$\Lambda(1690)$ POLE RESIDUES

The normalized residue is the residue divided by $\Gamma_{\text{pole}}/2$.

Normalized residue in $N\bar{K} \rightarrow \Lambda(1690) \rightarrow N\bar{K}$

MODULUS	PHASE (°)	DOCUMENT ID	TECN	COMMENT
0.24 ± 0.05	-28 ± 5	SARANTSEV 19	DPWA	$\bar{K}N$ multichannel
• • • We do not use the following data for averages, fits, limits, etc. • • •				
0.251	3	¹ KAMANO 15	DPWA	Multichannel
¹ From the preferred solution A in KAMANO 15.				
Normalized residue in $N\bar{K} \rightarrow \Lambda(1690) \rightarrow \Sigma\pi$				
MODULUS	PHASE (°)	DOCUMENT ID	TECN	COMMENT
0.35 ± 0.07	175 ± 6	SARANTSEV 19	DPWA	$\bar{K}N$ multichannel
• • • We do not use the following data for averages, fits, limits, etc. • • •				
0.315	-173	¹ KAMANO 15	DPWA	$\bar{K}N$ multichannel
¹ From the preferred solution A in KAMANO 15.				
Normalized residue in $N\bar{K} \rightarrow \Lambda(1690) \rightarrow \Lambda\eta$				
MODULUS	PHASE (°)	DOCUMENT ID	TECN	COMMENT
0.05 ± 0.02	88 ± 8	SARANTSEV 19	DPWA	$\bar{K}N$ multichannel
• • • We do not use the following data for averages, fits, limits, etc. • • •				
0.00567	81	¹ KAMANO 15	DPWA	Multichannel
¹ From the preferred solution A in KAMANO 15.				
Normalized residue in $N\bar{K} \rightarrow \Lambda(1690) \rightarrow \Lambda\sigma$				
MODULUS	PHASE (°)	DOCUMENT ID	TECN	COMMENT
0.08 ± 0.02	-10 ± 6	SARANTSEV 19	DPWA	$\bar{K}N$ multichannel

Normalized residue in $N\bar{K} \rightarrow \Lambda(1690) \rightarrow \Sigma(1385)\pi$, S-wave

MODULUS	PHASE (°)	DOCUMENT ID	TECN	COMMENT
0.11 ± 0.06	170 ± 70	SARANTSEV 19	DPWA	$\bar{K}N$ multichannel
• • • We do not use the following data for averages, fits, limits, etc. • • •				
0.134	168	¹ KAMANO 15	DPWA	$\bar{K}N$ multichannel
¹ From the preferred solution A in KAMANO 15.				

Normalized residue in $N\bar{K} \rightarrow \Lambda(1690) \rightarrow \Sigma(1385)\pi$, D-wave

MODULUS	PHASE (°)	DOCUMENT ID	TECN	COMMENT
0.06 ± 0.04	164 ± 15	SARANTSEV 19	DPWA	$\bar{K}N$ multichannel
• • • We do not use the following data for averages, fits, limits, etc. • • •				
0.319	-22	¹ KAMANO 15	DPWA	$\bar{K}N$ multichannel
¹ From the preferred solution A in KAMANO 15.				

Normalized residue in $N\bar{K} \rightarrow \Lambda(1690) \rightarrow N\bar{K}^*(892)$, S-wave

VALUE	DOCUMENT ID	TECN	COMMENT
0.05 ± 0.04	SARANTSEV 19	DPWA	$\bar{K}N$ multichannel

Normalized residue in $N\bar{K} \rightarrow \Lambda(1690) \rightarrow N\bar{K}^*(892)$, D-wave

VALUE	DOCUMENT ID	TECN	COMMENT
0.18+ -0.05@-110+ -45	SARANTSEV 19	DPWA	$\bar{K}N$ multichannel

$\Lambda(1690)$ MASS

VALUE (MeV)	DOCUMENT ID	TECN	COMMENT
1685 to 1695 (≈ 1690) OUR ESTIMATE			
1689 ± 3	SARANTSEV 19	DPWA	$\bar{K}N$ multichannel
1691 ± 3	ZHANG 13A	DPWA	$\bar{K}N$ multichannel
1695.7 ± 2.6	KOISO 85	DPWA	$K^-p \rightarrow \Sigma\pi$
1690 ± 5	GOPAL 80	DPWA	$\bar{K}N \rightarrow \bar{K}N$
1692 ± 5	ALSTON-... 78	DPWA	$\bar{K}N \rightarrow \bar{K}N$
1690 ± 3	HEPP 76B	DPWA	$K^-N \rightarrow \Sigma\pi$
1689 ± 1	KANE 74	DPWA	$K^-p \rightarrow \Sigma\pi$
• • • We do not use the following data for averages, fits, limits, etc. • • •			
1690 ± 5	GOPAL 77	DPWA	$\bar{K}N$ multichannel
1687 or 1689	¹ MARTIN 77	DPWA	$\bar{K}N$ multichannel
1692 ± 4	CARROLL 76	DPWA	Isospin-0 total σ
¹ The two MARTIN 77 values are from a T-matrix pole and from a Breit-Wigner fit. Another $D_{03} \Lambda$ at 1966 MeV is also suggested by MARTIN 77, but is very uncertain.			

$\Lambda(1690)$ WIDTH

VALUE (MeV)	DOCUMENT ID	TECN	COMMENT
60 to 80 (≈ 70) OUR ESTIMATE			
75 ± 5	SARANTSEV 19	DPWA	$\bar{K}N$ multichannel
54 ± 5	ZHANG 13A	DPWA	$\bar{K}N$ multichannel
67.2 ± 5.6	KOISO 85	DPWA	$K^-p \rightarrow \Sigma\pi$
61 ± 5	GOPAL 80	DPWA	$\bar{K}N \rightarrow \bar{K}N$
64 ± 10	ALSTON-... 78	DPWA	$\bar{K}N \rightarrow \bar{K}N$
82 ± 8	HEPP 76B	DPWA	$K^-N \rightarrow \Sigma\pi$
60 ± 4	KANE 74	DPWA	$K^-p \rightarrow \Sigma\pi$
• • • We do not use the following data for averages, fits, limits, etc. • • •			
60 ± 5	GOPAL 77	DPWA	$\bar{K}N$ multichannel
62 or 62	¹ MARTIN 77	DPWA	$\bar{K}N$ multichannel
38	CARROLL 76	DPWA	Isospin-0 total σ
¹ The two MARTIN 77 values are from a T-matrix pole and from a Breit-Wigner fit. Another $D_{03} \Lambda$ at 1966 MeV is also suggested by MARTIN 77, but is very uncertain.			

$\Lambda(1690)$ DECAY MODES

Mode	Fraction (Γ_i/Γ)
$\Gamma_1 \ N\bar{K}$	20-30 %
$\Gamma_2 \ \Sigma\pi$	20-40 %
$\Gamma_3 \ \Lambda\sigma$	(5.0 ± 2.0) %
$\Gamma_4 \ \Lambda\pi\pi$	~ 25 %
$\Gamma_5 \ \Sigma\pi\pi$	~ 20 %
$\Gamma_6 \ \Lambda\eta$	
$\Gamma_7 \ \Sigma(1385)\pi$, S-wave	(9 ± 5) %
$\Gamma_8 \ \Sigma(1385)\pi$, D-wave	(3.0 ± 2.0) %
$\Gamma_9 \ N\bar{K}^*(892)$, S=1/2, D-wave	
$\Gamma_{10} \ N\bar{K}^*(892)$, S=3/2, S-wave	
$\Gamma_{11} \ N\bar{K}^*(892)$, S=3/2, D-wave	

$\Lambda(1690)$ BRANCHING RATIOS

$\Gamma(N\bar{K})/\Gamma_{\text{total}}$	DOCUMENT ID	TECN	COMMENT	Γ_1/Γ
0.20 to 0.28 OUR ESTIMATE				
0.23 ± 0.05	SARANTSEV 19	DPWA	$\bar{K}N$ multichannel	
0.25 ± 0.04	ZHANG 13A	DPWA	$\bar{K}N$ multichannel	
0.23 ± 0.03	GOPAL 80	DPWA	$\bar{K}N \rightarrow \bar{K}N$	
0.22 ± 0.03	ALSTON-... 78	DPWA	$\bar{K}N \rightarrow \bar{K}N$	

See key on page 1171

Baryon Particle Listings

$\Lambda(1690), \Lambda(1710)$

••• We do not use the following data for averages, fits, limits, etc. •••

0.239	¹ KAMANO	15	DPWA	$\bar{K}N$ multichannel
0.24 ± 0.03	GOPAL	77	DPWA	See GOPAL 80
0.28 or 0.26	² MARTIN	77	DPWA	$\bar{K}N$ multichannel

¹ From the preferred solution A in KAMANO 15.
² The two MARTIN 77 values are from a T-matrix pole and from a Breit-Wigner fit. Another $D_{03} \Lambda$ at 1966 MeV is also suggested by MARTIN 77, but is very uncertain.

$\Gamma(\Sigma\pi)/\Gamma_{total}$ Γ_2/Γ

VALUE	DOCUMENT ID	TECN	COMMENT
0.50 ± 0.10	SARANTSEV 19	DPWA	$\bar{K}N$ multichannel

••• We do not use the following data for averages, fits, limits, etc. •••

0.387	¹ KAMANO	15	DPWA	$\bar{K}N$ multichannel
-------	---------------------	----	------	-------------------------

¹ From the preferred solution A in KAMANO 15.

$\Gamma(\Lambda\eta)/\Gamma_{total}$ Γ_6/Γ

VALUE	DOCUMENT ID	TECN	COMMENT
~ 0.01	SARANTSEV 19	DPWA	$\bar{K}N$ multichannel

••• We do not use the following data for averages, fits, limits, etc. •••

not seen	¹ KAMANO	15	DPWA	Multichannel
----------	---------------------	----	------	--------------

¹ From the preferred solution A in KAMANO 15.

$\Gamma(\Lambda\sigma)/\Gamma_{total}$ Γ_3/Γ

VALUE	DOCUMENT ID	TECN	COMMENT
0.05 ± 0.02	SARANTSEV 19	DPWA	$\bar{K}N$ multichannel

$\Gamma(\Sigma(1385)\pi, S\text{-wave})/\Gamma_{total}$ Γ_7/Γ

VALUE	DOCUMENT ID	TECN	COMMENT
0.09 ± 0.05	SARANTSEV 19	DPWA	$\bar{K}N$ multichannel

••• We do not use the following data for averages, fits, limits, etc. •••

0.062	¹ KAMANO	15	DPWA	$\bar{K}N$ multichannel
-------	---------------------	----	------	-------------------------

¹ From the preferred solution A in KAMANO 15.

$\Gamma(\Sigma(1385)\pi, D\text{-wave})/\Gamma_{total}$ Γ_8/Γ

VALUE	DOCUMENT ID	TECN	COMMENT
0.03 ± 0.02	SARANTSEV 19	DPWA	$\bar{K}N$ multichannel

••• We do not use the following data for averages, fits, limits, etc. •••

0.308	¹ KAMANO	15	DPWA	$\bar{K}N$ multichannel
-------	---------------------	----	------	-------------------------

¹ From the preferred solution A in KAMANO 15.

$\Gamma(N\bar{K}^*(892), S=1/2, D\text{-wave})/\Gamma_{total}$ Γ_9/Γ

VALUE	DOCUMENT ID	TECN	COMMENT	
not seen	SARANTSEV 19	DPWA	$\bar{K}N$ multichannel	
not seen	¹ KAMANO	15	DPWA	$\bar{K}N$ multichannel

¹ From the preferred solution A in KAMANO 15.

$\Gamma(N\bar{K}^*(892), S=3/2, S\text{-wave})/\Gamma_{total}$ Γ_{10}/Γ

VALUE	DOCUMENT ID	TECN	COMMENT	
0.003	KAMANO	15	DPWA	Multichannel

$\Gamma(N\bar{K}^*(892), S=3/2, D\text{-wave})/\Gamma_{total}$ Γ_{11}/Γ

VALUE	DOCUMENT ID	TECN	COMMENT	
not seen	¹ KAMANO	15	DPWA	Multichannel

¹ From the preferred solution A in KAMANO 15.

$(\Gamma_1\Gamma_f)^{1/2}/\Gamma_{total}$ in $N\bar{K} \rightarrow \Lambda(1690) \rightarrow \Sigma\pi$ $(\Gamma_1\Gamma_2)^{1/2}/\Gamma$

VALUE	DOCUMENT ID	TECN	COMMENT	
-0.27 ± 0.03	ZHANG	13A	DPWA	Multichannel
-0.34 ± 0.02	KOISO	85	DPWA	$K^-p \rightarrow \Sigma\pi$
-0.25 ± 0.03	GOPAL	77	DPWA	$\bar{K}N$ multichannel
-0.29 ± 0.03	HEPP	76B	DPWA	$K^-N \rightarrow \Sigma\pi$
-0.28 ± 0.03	LONDON	75	HLBC	$K^-p \rightarrow \Sigma^0\pi^0$
-0.28 ± 0.02	KANE	74	DPWA	$K^-p \rightarrow \Sigma\pi$

••• We do not use the following data for averages, fits, limits, etc. •••

-0.30 or -0.28	¹ MARTIN	77	DPWA	$\bar{K}N$ multichannel
----------------	---------------------	----	------	-------------------------

¹ The two MARTIN 77 values are from a T-matrix pole and from a Breit-Wigner fit. Another $D_{03} \Lambda$ at 1966 MeV is also suggested by MARTIN 77, but is very uncertain.

$(\Gamma_1\Gamma_f)^{1/2}/\Gamma_{total}$ in $N\bar{K} \rightarrow \Lambda(1690) \rightarrow \Lambda\pi\pi$ $(\Gamma_1\Gamma_4)^{1/2}/\Gamma$

VALUE	DOCUMENT ID	TECN	COMMENT	
0.25 ± 0.02	¹ BARTLEY	68	HDBC	$K^-p \rightarrow \Lambda\pi\pi$

¹ BARTLEY 68 uses only cross-section data. The enhancement is not seen by PREVOST 71.

$(\Gamma_1\Gamma_f)^{1/2}/\Gamma_{total}$ in $N\bar{K} \rightarrow \Lambda(1690) \rightarrow \Sigma\pi\pi$ $(\Gamma_1\Gamma_5)^{1/2}/\Gamma$

VALUE	DOCUMENT ID	TECN	COMMENT
0.21	ARMENTEROS68C	HDBC	$K^-N \rightarrow \Sigma\pi\pi$

$(\Gamma_1\Gamma_f)^{1/2}/\Gamma_{total}$ in $N\bar{K} \rightarrow \Lambda(1690) \rightarrow \Lambda\eta$ $(\Gamma_1\Gamma_6)^{1/2}/\Gamma$

VALUE	DOCUMENT ID	TECN	COMMENT	
0.00 ± 0.03	BAXTER	73	DPWA	$K^-p \rightarrow$ neutrals

$(\Gamma_1\Gamma_f)^{1/2}/\Gamma_{total}$ in $N\bar{K} \rightarrow \Lambda(1690) \rightarrow \Sigma(1385)\pi, S\text{-wave}$ $(\Gamma_1\Gamma_7)^{1/2}/\Gamma$

VALUE	DOCUMENT ID	TECN	COMMENT	
-0.28 ± 0.06	ZHANG	13A	DPWA	Multichannel
+0.27 ± 0.04	PREVOST	74	DPWA	$K^-N \rightarrow \Sigma(1385)\pi$

$\Lambda(1690)$ REFERENCES

SARANTSEV 19	EPJ A55 180	A.V. Sarantsev et al.	(BONN, PNPI)
KAMANO 15	PR C92 025205	H. Kamano et al.	(ANL, OSAK)
ZHANG 13A	PR C88 035205	H. Zhang et al.	(KSU)
KOISO 85	NP A433 619	H. Koiso et al.	(TOKY, MASA)
PDG 82	PL 111B 1	M. Roos et al.	(HELS, CIT, CERN)
GOPAL 80	Toronto Conf. 159	G.P. Gopal	(RHEL) IJP
ALSTON... 78	PR D18 182	M. Alston-Garnjost et al.	(LBL, MTHO+) IJP
Also	PRL 38 1007	M. Alston-Garnjost et al.	(LBL, MTHO+) IJP
GOPAL 77	NP B119 362	G.P. Gopal et al.	(LOIC, RHEL) IJP
MARTIN 77	NP B127 349	B.R. Martin, M.K. Pidcock, R.G. Moorhouse	(LOUC) IJP
Also	NP B126 266	B.R. Martin, M.K. Pidcock	(LOUC) IJP
Also	NP B126 285	B.R. Martin, M.K. Pidcock	(LOUC) IJP
CARROLL 76	PRL 37 806	A.S. Carroll et al.	(BNL) I
HEPP 76B	PL 65B 487	V. Hepp et al.	(CERN, HEIDH, MPM) I
LONDON 75	NP B85 289	G.W. London et al.	(BNL, CERN, EPOL+) I
KANE 74	LBL-2452	D.F. Kane	(LBL) IJP
PREVOST 74	NP B69 246	J. Prevost et al.	(SACL, CERN, HEID) I
BAXTER 73	NP B67 125	D.F. Baxter et al.	(OXF) IJP
PREVOST 71	Amsterdam Conf.	J. Prevost	(CERN, HEID, SACL) I
ARMENTEROS 68C	NP B8 216	R. Armenteros et al.	(CERN, HEID, SACL) I
BARTLEY 68	PRL 21 1111	J.H. Bartley et al.	(TUFTS, FSU, BRAN) I

$\Lambda(1710) 1/2^+$

$I(J^P) = 0(\frac{1}{2}^+)$ Status: *

OMITTED FROM SUMMARY TABLE

$\Lambda(1710)$ MASS

VALUE (MeV)	DOCUMENT ID	TECN	COMMENT	
1713 ± 13	ZHANG	13A	DPWA	Multichannel

$\Lambda(1710)$ WIDTH

VALUE (MeV)	DOCUMENT ID	TECN	COMMENT	
180 ± 42	ZHANG	13A	DPWA	Multichannel

$\Lambda(1710)$ DECAY MODES

Mode	Fraction (Γ_i/Γ)
Γ_1 $N\bar{K}$	(43 ± 4) %
Γ_2 $\Sigma\pi$	(21 ± 5) %
Γ_3 $\Sigma^*(1385)\pi, P\text{-wave}$	(20 ± 8) %
Γ_4 $N\bar{K}^*(892)$	
Γ_5 $N\bar{K}^*(892), S=1/2$	(5 ± 4) %
Γ_6 $N\bar{K}^*(892), S=3/2, P\text{-wave}$	(10 ± 8) %

$\Lambda(1710)$ BRANCHING RATIOS

$\Gamma(N\bar{K})/\Gamma_{total}$ Γ_1/Γ

VALUE	DOCUMENT ID	TECN	COMMENT	
0.43 ± 0.04	ZHANG	13A	DPWA	Multichannel

$\Gamma(\Sigma\pi)/\Gamma_{total}$ Γ_2/Γ

VALUE	DOCUMENT ID	TECN	COMMENT	
0.21 ± 0.05	ZHANG	13A	DPWA	Multichannel

$\Gamma(\Sigma^*(1385)\pi, P\text{-wave})/\Gamma_{total}$ Γ_3/Γ

VALUE	DOCUMENT ID	TECN	COMMENT	
0.20 ± 0.08	ZHANG	13A	DPWA	Multichannel

$\Gamma(N\bar{K}^*(892), S=1/2)/\Gamma_{total}$ Γ_5/Γ

VALUE	DOCUMENT ID	TECN	COMMENT	
0.05 ± 0.04	ZHANG	13A	DPWA	Multichannel

$\Gamma(N\bar{K}^*(892), S=3/2, P\text{-wave})/\Gamma_{total}$ Γ_6/Γ

VALUE	DOCUMENT ID	TECN	COMMENT	
0.10 ± 0.08	ZHANG	13A	DPWA	Multichannel

$\Lambda(1710)$ REFERENCES

ZHANG 13A	PR C88 035205	H. Zhang et al.	(KSU)
-----------	---------------	-----------------	-------

Baryon Particle Listings

 $\Lambda(1800)$ $\Lambda(1800) 1/2^-$ $I(J^P) = 0(\frac{1}{2}^-)$ Status: *** $\Lambda(1800)$ POLE POSITION

REAL PART

VALUE (MeV)	DOCUMENT ID	TECN	COMMENT
1809 ± 9	SARANTSEV 19	DPWA	$\bar{K}N$ multichannel
••• We do not use the following data for averages, fits, limits, etc. •••			
1729	ZHANG 13A	DPWA	Multichannel

-2xIMAGINARY PART

VALUE (MeV)	DOCUMENT ID	TECN	COMMENT
205 ± 16	SARANTSEV 19	DPWA	$\bar{K}N$ multichannel
••• We do not use the following data for averages, fits, limits, etc. •••			
198	ZHANG 13A	DPWA	Multichannel

 $\Lambda(1800)$ POLE RESIDUESThe normalized residue is the residue divided by $\Gamma_{pole}/2$.Normalized residue in $N\bar{K} \rightarrow \Lambda(1800) \rightarrow N\bar{K}$

MODULUS	PHASE (°)	DOCUMENT ID	TECN	COMMENT
0.34 ± 0.07	103 ± 8	SARANTSEV 19	DPWA	$\bar{K}N$ multichannel

Normalized residue in $N\bar{K} \rightarrow \Lambda(1800) \rightarrow \Sigma\pi$

MODULUS	PHASE (°)	DOCUMENT ID	TECN	COMMENT
0.30 ± 0.06	-123 ± 8	SARANTSEV 19	DPWA	$\bar{K}N$ multichannel

Normalized residue in $N\bar{K} \rightarrow \Lambda(1800) \rightarrow \Lambda\eta$

MODULUS	PHASE (°)	DOCUMENT ID	TECN	COMMENT
0.06 ± 0.03	75 ± 10	SARANTSEV 19	DPWA	$\bar{K}N$ multichannel

Normalized residue in $N\bar{K} \rightarrow \Lambda(1800) \rightarrow \Lambda\sigma$

MODULUS	PHASE (°)	DOCUMENT ID	TECN	COMMENT
0.24 ± 0.05	25 ± 10	SARANTSEV 19	DPWA	$\bar{K}N$ multichannel

Normalized residue in $N\bar{K} \rightarrow \Lambda(1800) \rightarrow \Lambda\omega, S=1/2, S\text{-wave}$

MODULUS	PHASE (°)	DOCUMENT ID	TECN	COMMENT
0.12 ± 0.04	-114 ± 30	SARANTSEV 19	DPWA	$\bar{K}N$ multichannel

Normalized residue in $N\bar{K} \rightarrow \Lambda(1800) \rightarrow \Lambda\omega, S=3/2, D\text{-wave}$

MODULUS	PHASE (°)	DOCUMENT ID	TECN	COMMENT
0.08 ± 0.03	-90 ± 17	SARANTSEV 19	DPWA	$\bar{K}N$ multichannel

Normalized residue in $N\bar{K} \rightarrow \Lambda(1800) \rightarrow \Sigma(1385)\pi$

MODULUS	PHASE (°)	DOCUMENT ID	TECN	COMMENT
0.16 ± 0.06	-140 ± 35	SARANTSEV 19	DPWA	$\bar{K}N$ multichannel

Normalized residue in $N\bar{K} \rightarrow \Lambda(1800) \rightarrow N\bar{K}^*(892), S=1/2, S\text{-wave}$

MODULUS	PHASE (°)	DOCUMENT ID	TECN	COMMENT
0.18 ± 0.06	65 ± 40	SARANTSEV 19	DPWA	$\bar{K}N$ multichannel

Normalized residue in $N\bar{K} \rightarrow \Lambda(1800) \rightarrow N\bar{K}^*(892), S=3/2, D\text{-wave}$

MODULUS	PHASE (°)	DOCUMENT ID	TECN	COMMENT
0.09 ± 0.07		SARANTSEV 19	DPWA	$\bar{K}N$ multichannel

 $\Lambda(1800)$ MASS

VALUE (MeV)	DOCUMENT ID	TECN	COMMENT
1750 to 1850 (≈ 1800) OUR ESTIMATE			
1811 ± 10	SARANTSEV 19	DPWA	$\bar{K}N$ multichannel
1783 ± 19	ZHANG 13A	DPWA	$\bar{K}N$ multichannel
1841 ± 10	GOPAL 80	DPWA	$\bar{K}N \rightarrow \bar{K}N$
1725 ± 20	ALSTON-... 78	DPWA	$\bar{K}N \rightarrow \bar{K}N$
1830 ± 20	LANGBEIN 72	IPWA	$\bar{K}N$ multichannel
••• We do not use the following data for averages, fits, limits, etc. •••			
1845 ± 10	MANLEY 02	DPWA	$\bar{K}N$ multichannel
1825 ± 20	GOPAL 77	DPWA	$\bar{K}N$ multichannel
1767 or 1842	¹ MARTIN 77	DPWA	$\bar{K}N$ multichannel
1780	KIM 71	DPWA	K-matrix analysis
1872 ± 10	BRICMAN 70B	DPWA	$\bar{K}N \rightarrow \bar{K}N$

 $\Lambda(1800)$ WIDTH

VALUE (MeV)	DOCUMENT ID	TECN	COMMENT
150 to 250 (≈ 200) OUR ESTIMATE			
209 ± 18	SARANTSEV 19	DPWA	$\bar{K}N$ multichannel
256 ± 35	ZHANG 13A	DPWA	$\bar{K}N$ multichannel
228 ± 20	GOPAL 80	DPWA	$\bar{K}N \rightarrow \bar{K}N$
185 ± 20	ALSTON-... 78	DPWA	$\bar{K}N \rightarrow \bar{K}N$
70 ± 15	LANGBEIN 72	IPWA	$\bar{K}N$ multichannel

••• We do not use the following data for averages, fits, limits, etc. •••

518 ± 84	MANLEY 02	DPWA	$\bar{K}N$ multichannel
230 ± 20	GOPAL 77	DPWA	$\bar{K}N$ multichannel
435 or 473	¹ MARTIN 77	DPWA	$\bar{K}N$ multichannel
40	KIM 71	DPWA	K-matrix analysis
100 ± 20	BRICMAN 70B	DPWA	$\bar{K}N \rightarrow \bar{K}N$

 $\Lambda(1800)$ DECAY MODES

Mode	Fraction (Γ_i/Γ)
Γ_1 $N\bar{K}$	25-40 %
Γ_2 $\Sigma\pi$	seen
Γ_3 $\Lambda\sigma$	(15 ± 4) %
Γ_4 $\Sigma(1385)\pi$	seen
Γ_5 $\Lambda\eta$	0.01 to 0.10
Γ_6 $N\bar{K}^*(892)$	seen
Γ_7 $N\bar{K}^*(892), S=1/2, S\text{-wave}$	
Γ_8 $N\bar{K}^*(892), S=3/2, D\text{-wave}$	

 $\Lambda(1800)$ BRANCHING RATIOSSee "Sign conventions for resonance couplings" in the Note on Λ and Σ Resonances.

$\Gamma(N\bar{K})/\Gamma_{total}$	DOCUMENT ID	TECN	COMMENT	Γ_1/Γ
0.25 to 0.40 OUR ESTIMATE				
0.35 ± 0.07	SARANTSEV 19	DPWA	$\bar{K}N$ multichannel	
0.13 ± 0.06	ZHANG 13A	DPWA	$\bar{K}N$ multichannel	
0.36 ± 0.04	GOPAL 80	DPWA	$\bar{K}N \rightarrow \bar{K}N$	
0.28 ± 0.05	ALSTON-... 78	DPWA	$\bar{K}N \rightarrow \bar{K}N$	
0.35 ± 0.15	LANGBEIN 72	IPWA	$\bar{K}N$ multichannel	

••• We do not use the following data for averages, fits, limits, etc. •••

0.24 ± 0.10	MANLEY 02	DPWA	$\bar{K}N$ multichannel	
0.37 ± 0.05	GOPAL 77	DPWA	See GOPAL 80	
1.21 or 0.70	¹ MARTIN 77	DPWA	$\bar{K}N$ multichannel	
0.80	KIM 71	DPWA	K-matrix analysis	
0.18 ± 0.02	BRICMAN 70B	DPWA	$\bar{K}N \rightarrow \bar{K}N$	

$\Gamma(\Sigma\pi)/\Gamma_{total}$	DOCUMENT ID	TECN	COMMENT	Γ_2/Γ
0.27 ± 0.06				
	SARANTSEV 19	DPWA	$\bar{K}N$ multichannel	

$\Gamma(\Lambda\sigma)/\Gamma_{total}$	DOCUMENT ID	TECN	COMMENT	Γ_3/Γ
0.15 ± 0.04				
	SARANTSEV 19	DPWA	$\bar{K}N$ multichannel	

$\Gamma(\Sigma(1385)\pi)/\Gamma_{total}$	DOCUMENT ID	TECN	COMMENT	Γ_4/Γ
0.09 ± 0.04				
	SARANTSEV 19	DPWA	$\bar{K}N$ multichannel	

$\Gamma(\Lambda\eta)/\Gamma_{total}$	DOCUMENT ID	TECN	COMMENT	Γ_5/Γ
0.01 to 0.10 OUR ESTIMATE				
0.010 ± 0.005	SARANTSEV 19	DPWA	$\bar{K}N$ multichannel	
0.06 ± 0.05	ZHANG 13A	DPWA	Multichannel	

$(\Gamma_1\Gamma_7)^{1/2}/\Gamma_{total}$ in $N\bar{K} \rightarrow \Lambda(1800) \rightarrow \Sigma\pi$	DOCUMENT ID	TECN	COMMENT	$(\Gamma_1\Gamma_2)^{1/2}/\Gamma$
0.01 to 0.10 OUR ESTIMATE				
-0.07 ± 0.02	ZHANG 13A	DPWA	Multichannel	
-0.08 ± 0.05	GOPAL 77	DPWA	$\bar{K}N$ multichannel	

••• We do not use the following data for averages, fits, limits, etc. •••

-0.74 or -0.43	¹ MARTIN 77	DPWA	$\bar{K}N$ multichannel	
0.24	KIM 71	DPWA	K-matrix analysis	

$(\Gamma_1\Gamma_7)^{1/2}/\Gamma_{total}$ in $N\bar{K} \rightarrow \Lambda(1800) \rightarrow \Sigma(1385)\pi$	DOCUMENT ID	TECN	COMMENT	$(\Gamma_1\Gamma_4)^{1/2}/\Gamma$
0.01 to 0.10 OUR ESTIMATE				
-0.09 ± 0.05	ZHANG 13A	DPWA	Multichannel	
+0.056 ± 0.028	² CAMERON 78	DPWA	$K^-\rho \rightarrow \Sigma(1385)\pi$	

$(\Gamma_1\Gamma_7)^{1/2}/\Gamma_{total}$ in $N\bar{K} \rightarrow \Lambda(1800) \rightarrow N\bar{K}^*(892), S=1/2, S\text{-wave}$	DOCUMENT ID	TECN	COMMENT	$(\Gamma_1\Gamma_7)^{1/2}/\Gamma$
0.01 to 0.10 OUR ESTIMATE				
-0.13 ± 0.02	ZHANG 13A	DPWA	Multichannel	
-0.17 ± 0.03	² CAMERON 78B	DPWA	$K^-\rho \rightarrow N\bar{K}^*$	

$(\Gamma_1\Gamma_7)^{1/2}/\Gamma_{total}$ in $N\bar{K} \rightarrow \Lambda(1800) \rightarrow N\bar{K}^*(892), S=3/2, D\text{-wave}$	DOCUMENT ID	TECN	COMMENT	$(\Gamma_1\Gamma_8)^{1/2}/\Gamma$
0.01 to 0.10 OUR ESTIMATE				
-0.13 ± 0.04	CAMERON 78B	DPWA	$K^-\rho \rightarrow N\bar{K}^*$	

 $\Lambda(1800)$ FOOTNOTES¹ The two MARTIN 77 values are from a T-matrix pole and from a Breit-Wigner fit.² The published sign has been changed to be in accord with the baryon-first convention.

$\Lambda(1800)$ REFERENCES

SARANTSEV	19	EPJ A55 180	A.V. Sarantsev et al.	(BONN, PNPI)
ZHANG	13A	PR C08 035205	H. Zhang et al.	(KSU)
MANLEY	02	PRL 88 012002	D.M. Manley et al.	(BNL Crystal Ball Collab.)
GOPAL	80	Toronto Conf. 159	G.P. Gopal	(RHEL) IJP
ALSTON...	78	PR D18 182	M. Alston-Garnjost et al.	(LBL, MTHO+) IJP
Also		PRL 38 1007	M. Alston-Garnjost et al.	(LBL, MTHO+) IJP
CAMERON	78	NP B143 189	W. Cameron et al.	(RHEL, LOIC) IJP
CAMERON	78B	NP B146 327	W. Cameron et al.	(RHEL, LOIC) IJP
GOPAL	77	NP B119 362	G.P. Gopal et al.	(LOIC, RHEL) IJP
MARTIN	77	NP B127 349	B.R. Martin, M.K. Pldcock, R.G. Moorhouse	(LOUC+) IJP
Also		NP B126 266	B.R. Martin, M.K. Pldcock	(LOUC) IJP
Also		NP B126 285	B.R. Martin, M.K. Pldcock	(LOUC) IJP
LANGBEIN	72	NP B47 477	W. Langbein, F. Wagner	(MPIM) IJP
KIM	71	PRL 27 356	J.K. Kim	(HARV) IJP
Also		Duke Conf. 161	J.K. Kim	(HARV) IJP
		Hyperon Resonances, 1970		
BRICMAN	70B	PL 33B 511	C. Bricman, M. Ferro-Luzzi, J.P. Lagnaux	(CERN) IJP

 $\Lambda(1810) 1/2^+$ $I(J^P) = 0(\frac{1}{2}^+)$ Status: *** $\Lambda(1810)$ POLE POSITION

REAL PART

VALUE (MeV)	DOCUMENT ID	TECN	COMMENT
1773 ± 7	SARANTSEV 19	DPWA	$\bar{K}N$ multichannel
••• We do not use the following data for averages, fits, limits, etc. •••			
2097 ⁺⁴⁰ ₋₁	¹ KAMANO 15	DPWA	Multichannel
1780	ZHANG 13A	DPWA	Multichannel
¹ From the preferred solution A in KAMANO 15. Solution B reports $M = 1841 \pm \frac{3}{-4}$ MeV.			

-2xIMAGINARY PART

VALUE (MeV)	DOCUMENT ID	TECN	COMMENT
38 ± 14	SARANTSEV 19	DPWA	$\bar{K}N$ multichannel
••• We do not use the following data for averages, fits, limits, etc. •••			
166 ⁺⁶⁴ ₋₁₂	¹ KAMANO 15	DPWA	Multichannel
64	ZHANG 13A	DPWA	Multichannel
¹ From the preferred solution A in KAMANO 15. Solution B Reports $\Gamma = 62 \pm \frac{6}{-4}$ MeV.			

 $\Lambda(1810)$ POLE RESIDUESThe normalized residue is the residue divided by $\Gamma_{pole}/2$.Normalized residue in $N\bar{K} \rightarrow \Lambda(1810) \rightarrow N\bar{K}$

MODULUS	PHASE (°)	DOCUMENT ID	TECN	COMMENT
0.018 ± 0.008	65 ± 26	SARANTSEV 19	DPWA	$\bar{K}N$ multichannel
••• We do not use the following data for averages, fits, limits, etc. •••				
0.205	-63	¹ KAMANO 15	DPWA	Multichannel
¹ From the preferred solution A in KAMANO 15.				

Normalized residue in $N\bar{K} \rightarrow \Lambda(1810) \rightarrow \Sigma\pi$

MODULUS	PHASE (°)	DOCUMENT ID	TECN	COMMENT
0.045 ± 0.020	-143 ± 24	SARANTSEV 19	DPWA	$\bar{K}N$ multichannel
••• We do not use the following data for averages, fits, limits, etc. •••				
0.0325	29	¹ KAMANO 15	DPWA	Multichannel
¹ From the preferred solution A in KAMANO 15.				

Normalized residue in $N\bar{K} \rightarrow \Lambda(1810) \rightarrow \Lambda\eta$

MODULUS	PHASE (°)	DOCUMENT ID	TECN	COMMENT
••• We do not use the following data for averages, fits, limits, etc. •••				
0.155	165	¹ KAMANO 15	DPWA	Multichannel
¹ From the preferred solution A in KAMANO 15.				

Normalized residue in $N\bar{K} \rightarrow \Lambda(1810) \rightarrow \Lambda\sigma$

MODULUS	PHASE (°)	DOCUMENT ID	TECN	COMMENT
0.055 ± 0.020	30 ± 16	SARANTSEV 19	DPWA	$\bar{K}N$ multichannel

Normalized residue in $N\bar{K} \rightarrow \Lambda(1810) \rightarrow \Xi K$

MODULUS	PHASE (°)	DOCUMENT ID	TECN	COMMENT
••• We do not use the following data for averages, fits, limits, etc. •••				
0.0937	-64	¹ KAMANO 15	DPWA	Multichannel
¹ From the preferred solution A in KAMANO 15.				

Normalized residue in $N\bar{K} \rightarrow \Lambda(1810) \rightarrow \Sigma(1385)\pi$

MODULUS	PHASE (°)	DOCUMENT ID	TECN	COMMENT
0.08 ± 0.03	-50 ± 30	SARANTSEV 19	DPWA	$\bar{K}N$ multichannel
••• We do not use the following data for averages, fits, limits, etc. •••				
0.244	-10	¹ KAMANO 15	DPWA	Multichannel
¹ From the preferred solution A in KAMANO 15.				

Normalized residue in $N\bar{K} \rightarrow \Lambda(1810) \rightarrow N\bar{K}^*(892)$, $S=1/2$, P -wave

MODULUS	PHASE (°)	DOCUMENT ID	TECN	COMMENT
0.03 ± 0.03		SARANTSEV 19	DPWA	$\bar{K}N$ multichannel
••• We do not use the following data for averages, fits, limits, etc. •••				
0.159	-97	¹ KAMANO 15	DPWA	Multichannel
¹ From the preferred solution A in KAMANO 15.				

Normalized residue in $N\bar{K} \rightarrow \Lambda(1810) \rightarrow N\bar{K}^*(892)$, $S=3/2$, P -wave

MODULUS	PHASE (°)	DOCUMENT ID	TECN	COMMENT
0.05 ± 0.04		SARANTSEV 19	DPWA	$\bar{K}N$ multichannel
••• We do not use the following data for averages, fits, limits, etc. •••				
0.0497	2	¹ KAMANO 15	DPWA	Multichannel
¹ From the preferred solution A in KAMANO 15.				

 $\Lambda(1810)$ MASS

VALUE (MeV)	DOCUMENT ID	TECN	COMMENT
1740 to 1840 (≈ 1790) OUR ESTIMATE			
1773 ± 7	SARANTSEV 19	DPWA	$\bar{K}N$ multichannel
1821 ± 10	ZHANG 13A	DPWA	Multichannel
1841 ± 20	GOPAL 80	DPWA	$\bar{K}N \rightarrow \bar{K}N$
1735 ± 5	CARROLL 76	DPWA	Isospin-0 total σ
1746 ± 10	PREVOST 74	DPWA	$K^-N \rightarrow \Sigma(1385)\pi$
1780 ± 20	LANGBEIN 72	IPWA	$\bar{K}N$ multichannel
••• We do not use the following data for averages, fits, limits, etc. •••			
1853 ± 20	GOPAL 77	DPWA	$\bar{K}N$ multichannel
1861 or 1953	¹ MARTIN 77	DPWA	$\bar{K}N$ multichannel
1755	KIM 71	DPWA	K-matrix analysis
1800	ARMENTEROS70	HBC	$\bar{K}N \rightarrow \bar{K}N$
1750	ARMENTEROS70	HBC	$\bar{K}N \rightarrow \Sigma\pi$
1690 ± 10	BARBARO... 70	HBC	$\bar{K}N \rightarrow \Sigma\pi$
1740	BAILEY 69	DPWA	$\bar{K}N \rightarrow \bar{K}N$
1745	ARMENTEROS68B	HBC	$\bar{K}N \rightarrow \bar{K}N$
¹ The two MARTIN 77 values are from a T-matrix pole and from a Breit-Wigner fit.			

 $\Lambda(1810)$ WIDTH

VALUE (MeV)	DOCUMENT ID	TECN	COMMENT
50 to 170 (≈ 110) OUR ESTIMATE			
39 ± 15	SARANTSEV 19	DPWA	$\bar{K}N$ multichannel
174 ± 50	ZHANG 13A	DPWA	Multichannel
164 ± 20	GOPAL 80	DPWA	$\bar{K}N \rightarrow \bar{K}N$
90 ± 20	CAMERON 78B	DPWA	$K^-p \rightarrow N\bar{K}^*$
46 ± 20	PREVOST 74	DPWA	$K^-N \rightarrow \Sigma(1385)\pi$
120 ± 10	LANGBEIN 72	IPWA	$\bar{K}N$ multichannel
••• We do not use the following data for averages, fits, limits, etc. •••			
166 ± 20	GOPAL 77	DPWA	$\bar{K}N$ multichannel
535 or 585	¹ MARTIN 77	DPWA	$\bar{K}N$ multichannel
28	CARROLL 76	DPWA	Isospin-0 total σ
35	KIM 71	DPWA	K-matrix analysis
30	ARMENTEROS70	HBC	$\bar{K}N \rightarrow \bar{K}N$
70	ARMENTEROS70	HBC	$\bar{K}N \rightarrow \Sigma\pi$
22	BARBARO... 70	HBC	$\bar{K}N \rightarrow \Sigma\pi$
300	BAILEY 69	DPWA	$\bar{K}N \rightarrow \bar{K}N$
147	ARMENTEROS68B	HBC	$\bar{K}N \rightarrow \bar{K}N$
¹ The two MARTIN 77 values are from a T-matrix pole and from a Breit-Wigner fit.			

 $\Lambda(1810)$ DECAY MODES

Mode	Fraction (Γ_i/Γ)
Γ_1 $N\bar{K}$	0.05 to 0.35
Γ_2 $\Sigma\pi$	(16 ± 5) %
Γ_3 $\Lambda\eta$	
Γ_4 ΞK	
Γ_5 $\Sigma(1385)\pi$	(40 ± 15) %
Γ_6 $N\bar{K}^*(892)$	30-60 %
Γ_7 $N\bar{K}^*(892)$, $S=1/2$, P -wave	
Γ_8 $N\bar{K}^*(892)$, $S=3/2$, P -wave	

 $\Lambda(1810)$ BRANCHING RATIOS

$\Gamma(N\bar{K})/\Gamma_{total}$	DOCUMENT ID	TECN	COMMENT	Γ_1/Γ
0.05 to 0.35 OUR ESTIMATE				
0.025 ± 0.013	SARANTSEV 19	DPWA	$\bar{K}N$ multichannel	
0.19 ± 0.08	ZHANG 13A	DPWA	$\bar{K}N$ multichannel	
0.24 ± 0.04	GOPAL 80	DPWA	$\bar{K}N \rightarrow \bar{K}N$	
0.36 ± 0.05	LANGBEIN 72	IPWA	$\bar{K}N$ multichannel	

Baryon Particle Listings

 $\Lambda(1810), \Lambda(1820)$

• • • We do not use the following data for averages, fits, limits, etc. • • •

0.225	¹ KAMANO 15	DPWA	$\bar{K}N$ multichannel
0.21 \pm 0.04	GOPAL 77	DPWA	See GOPAL 80
0.52 or 0.49	² MARTIN 77	DPWA	$\bar{K}N$ multichannel
0.30	KIM 71	DPWA	K-matrix analysis
0.15	ARMENTEROS70	DPWA	$\bar{K}N \rightarrow \bar{K}N$
0.55	BAILEY 69	DPWA	$\bar{K}N \rightarrow \bar{K}N$
0.4	ARMENTEROS68B	DPWA	$\bar{K}N \rightarrow \bar{K}N$

¹ From the preferred solution A in KAMANO 15.

² The two MARTIN 77 values are from a T-matrix pole and from a Breit-Wigner fit.

$\Gamma(\Sigma\pi)/\Gamma_{\text{total}}$	DOCUMENT ID	TECN	COMMENT
0.16 \pm 0.05	SARANTSEV 19	DPWA	$\bar{K}N$ multichannel

• • • We do not use the following data for averages, fits, limits, etc. • • •

0.009	¹ KAMANO 15	DPWA	Multichannel
-------	------------------------	------	--------------

¹ From the preferred solution A in KAMANO 15.

$\Gamma(\Lambda\eta)/\Gamma_{\text{total}}$	DOCUMENT ID	TECN	COMMENT
0.111	¹ KAMANO 15	DPWA	Multichannel

¹ From the preferred solution A in KAMANO 15.

$\Gamma(\Xi K)/\Gamma_{\text{total}}$	DOCUMENT ID	TECN	COMMENT
0.051	¹ KAMANO 15	DPWA	Multichannel

• • • We do not use the following data for averages, fits, limits, etc. • • •

0.051	¹ KAMANO 15	DPWA	Multichannel
-------	------------------------	------	--------------

¹ From the preferred solution A in KAMANO 15.

$\Gamma(\Sigma(1385)\pi)/\Gamma_{\text{total}}$	DOCUMENT ID	TECN	COMMENT
0.40 \pm 0.15	SARANTSEV 19	DPWA	$\bar{K}N$ multichannel

• • • We do not use the following data for averages, fits, limits, etc. • • •

0.600	¹ KAMANO 15	DPWA	Multichannel
-------	------------------------	------	--------------

¹ From the preferred solution A in KAMANO 15.

$\Gamma(N\bar{K}^*(892), S=1/2, P\text{-wave})/\Gamma_{\text{total}}$	DOCUMENT ID	TECN	COMMENT
0.003	¹ KAMANO 15	DPWA	Multichannel

• • • We do not use the following data for averages, fits, limits, etc. • • •

0.003	¹ KAMANO 15	DPWA	Multichannel
-------	------------------------	------	--------------

¹ From the preferred solution A in KAMANO 15.

$(\Gamma_1\Gamma_7)^{1/2}/\Gamma_{\text{total}}$ in $N\bar{K} \rightarrow \Lambda(1810) \rightarrow \Sigma\pi$	DOCUMENT ID	TECN	COMMENT
-0.08 \pm 0.05	ZHANG 13A	DPWA	Multichannel
-0.24 \pm 0.04	GOPAL 77	DPWA	$\bar{K}N$ multichannel

• • • We do not use the following data for averages, fits, limits, etc. • • •

+0.25 or +0.23	¹ MARTIN 77	DPWA	$\bar{K}N$ multichannel
< 0.01	LANGBEIN 72	IPWA	$\bar{K}N$ multichannel
0.17	KIM 71	DPWA	K-matrix analysis
+0.20	² ARMENTEROS70	DPWA	$\bar{K}N \rightarrow \Sigma\pi$
-0.13 \pm 0.03	BARBARO... 70	DPWA	$\bar{K}N \rightarrow \Sigma\pi$

¹ The two MARTIN 77 values are from a T-matrix pole and from a Breit-Wigner fit.

² The published sign has been changed to be in accord with the baryon-first convention.

$(\Gamma_1\Gamma_7)^{1/2}/\Gamma_{\text{total}}$ in $N\bar{K} \rightarrow \Lambda(1810) \rightarrow \Sigma(1385)\pi$	DOCUMENT ID	TECN	COMMENT
+0.18 \pm 0.10	PREVOST 74	DPWA	$K^-N \rightarrow \Sigma(1385)\pi$

• • • We do not use the following data for averages, fits, limits, etc. • • •

-0.14 \pm 0.03	¹ CAMERON 78B	DPWA	$K^-p \rightarrow N\bar{K}^*$
------------------	--------------------------	------	-------------------------------

¹ The published sign has been changed to be in accord with the baryon-first convention.

$(\Gamma_1\Gamma_7)^{1/2}/\Gamma_{\text{total}}$ in $N\bar{K} \rightarrow \Lambda(1810) \rightarrow N\bar{K}^*(892), S=1/2, P\text{-wave}$	DOCUMENT ID	TECN	COMMENT
-0.14 \pm 0.03	¹ CAMERON 78B	DPWA	$K^-p \rightarrow N\bar{K}^*$

• • • We do not use the following data for averages, fits, limits, etc. • • •

0.00111	70	¹ KAMANO 15	DPWA $\bar{K}N$ multichannel
---------	----	------------------------	------------------------------

¹ From the preferred solution A in KAMANO 15.

$(\Gamma_1\Gamma_7)^{1/2}/\Gamma_{\text{total}}$ in $N\bar{K} \rightarrow \Lambda(1810) \rightarrow \Sigma(1385)\pi, P\text{-wave}$	DOCUMENT ID	TECN	COMMENT
+0.38 \pm 0.06	ZHANG 13A	DPWA	Multichannel
+0.35 \pm 0.06	CAMERON 78B	DPWA	$K^-p \rightarrow N\bar{K}^*$

 $\Lambda(1810)$ REFERENCES

SARANTSEV 19	EPJ A55 180	A.V. Sarantsev et al.	(BONN, PNPI)
KAMANO 15	PR C92 025205	H. Kamano et al.	(ANL, OSAK)
ZHANG 13A	PR C88 035205	H. Zhang et al.	(KSU)
GOPAL 80	Toronto Conf. 159	G.P. Gopal	(RHEL) IJP
CAMERON 78B	NP B146 327	W. Cameron et al.	(RHEL, LOIC) IJP
GOPAL 77	NP B119 362	G.P. Gopal et al.	(LOIC, RHEL) IJP
MARTIN 77	NP B127 349	B.R. Martin, M.K. Piddcock, R.G. Moorhouse	(LOUC+) IJP
Also	NP B126 266	B.R. Martin, M.K. Piddcock	(LOUC) IJP
Also	NP B126 285	B.R. Martin, M.K. Piddcock	(LOUC) IJP
CARROLL 76	PRL 37 806	A.S. Carroll et al.	(BNL) I

PREVOST 74	NP B69 246	J. Prevost et al.	(SACL, CERN, HEID)
LANGBEIN 72	NP B47 477	W. Langbein, F. Wagner	(MPIM) IJP
KIM 71	PRL 27 356	J.K. Kim	(HARV) IJP
Also	Duke Conf. 161	J.K. Kim	(HARV) IJP
ARMENTEROS 70	Hyperon Resonances, 1970	R. Armenteros et al.	(CERN, HEID, SACL) IJP
BARBARO... 70	Duke Conf. 173	A. Barbaro-Galtieri	(LRL) IJP
BAILEY 69	Thesis UCRL 50617	J.M. Bailey	(LLL) IJP
ARMENTEROS 68B	NP B8 195	R. Armenteros et al.	(CERN, HEID, SACL) IJP

 $\Lambda(1820) 5/2^+$

$$I(J^P) = 0(\frac{5}{2}^+) \text{ Status: } ***$$

This resonance is the cornerstone for all partial-wave analyses in this region. Most of the results published before 1973 are now obsolete and have been omitted. They may be found in our 1982 edition Physics Letters **111B** 1 (1982).

 $\Lambda(1820)$ POLE POSITION

REAL PART

VALUE (MeV)	DOCUMENT ID	TECN	COMMENT
-------------	-------------	------	---------

1812 to 1825 (\approx 1818) OUR ESTIMATE

1813 \pm 3	SARANTSEV 19	DPWA	$\bar{K}N$ multichannel
--------------	--------------	------	-------------------------

1824 \pm $\frac{2}{1}$	¹ KAMANO 15	DPWA	$\bar{K}N$ multichannel
--------------------------	------------------------	------	-------------------------

• • • We do not use the following data for averages, fits, limits, etc. • • •

1814	ZHANG 13A	DPWA	$\bar{K}N$ multichannel
------	-----------	------	-------------------------

¹ From the preferred solution A in KAMANO 15.

-2xIMAGINARY PART

VALUE (MeV)	DOCUMENT ID	TECN	COMMENT
-------------	-------------	------	---------

75 to 80 (\approx 77) OUR ESTIMATE

78 \pm 7	SARANTSEV 19	DPWA	$\bar{K}N$ multichannel
------------	--------------	------	-------------------------

77 \pm 2	¹ KAMANO 15	DPWA	$\bar{K}N$ multichannel
------------	------------------------	------	-------------------------

• • • We do not use the following data for averages, fits, limits, etc. • • •

85	ZHANG 13A	DPWA	$\bar{K}N$ multichannel
----	-----------	------	-------------------------

¹ From the preferred solution A in KAMANO 15.

 $\Lambda(1820)$ POLE RESIDUES

The normalized residue is the residue divided by $\Gamma_{\text{pole}}/2$.

Normalized residue in $N\bar{K} \rightarrow \Lambda(1820) \rightarrow N\bar{K}$

MODULUS	PHASE ($^\circ$)	DOCUMENT ID	TECN	COMMENT
---------	--------------------	-------------	------	---------

0.60 \pm 0.12	-22 \pm 5	SARANTSEV 19	DPWA	$\bar{K}N$ multichannel
-----------------------------------	-------------------------------	--------------	------	-------------------------

• • • We do not use the following data for averages, fits, limits, etc. • • •

0.558	-13	¹ KAMANO 15	DPWA	$\bar{K}N$ multichannel
-------	-----	------------------------	------	-------------------------

¹ From the preferred solution A in KAMANO 15.

Normalized residue in $N\bar{K} \rightarrow \Lambda(1820) \rightarrow \Sigma\pi$

MODULUS	PHASE ($^\circ$)	DOCUMENT ID	TECN	COMMENT
---------	--------------------	-------------	------	---------

0.34 \pm 0.07	174 \pm 5	SARANTSEV 19	DPWA	$\bar{K}N$ multichannel
-----------------------------------	-------------------------------	--------------	------	-------------------------

• • • We do not use the following data for averages, fits, limits, etc. • • •

0.357	168	¹ KAMANO 15	DPWA	$\bar{K}N$ multichannel
-------	-----	------------------------	------	-------------------------

¹ From the preferred solution A in KAMANO 15.

Normalized residue in $N\bar{K} \rightarrow \Lambda(1820) \rightarrow \Lambda\eta$

MODULUS	PHASE ($^\circ$)	DOCUMENT ID	TECN	COMMENT
---------	--------------------	-------------	------	---------

• • • We do not use the following data for averages, fits, limits, etc. • • •

0.0184	-3	¹ KAMANO 15	DPWA	$\bar{K}N$ multichannel
--------	----	------------------------	------	-------------------------

¹ From the preferred solution A in KAMANO 15.

Normalized residue in $N\bar{K} \rightarrow \Lambda(1820) \rightarrow \Xi K$

MODULUS	PHASE ($^\circ$)	DOCUMENT ID	TECN	COMMENT
---------	--------------------	-------------	------	---------

~ 0

• • • We do not use the following data for averages, fits, limits, etc. • • •

0.00111	70	¹ KAMANO 15	DPWA	$\bar{K}N$ multichannel
---------	----	------------------------	------	-------------------------

¹ From the preferred solution A in KAMANO 15.

Normalized residue in $N\bar{K} \rightarrow \Lambda(1820) \rightarrow \Sigma(1385)\pi, P\text{-wave}$

MODULUS	PHASE ($^\circ$)	DOCUMENT ID	TECN	COMMENT
---------	--------------------	-------------	------	---------

0.07 \pm 0.02	-60 \pm 50	SARANTSEV 19	DPWA	$\bar{K}N$ multichannel
-----------------------------------	--------------------------------	--------------	------	-------------------------

• • • We do not use the following data for averages, fits, limits, etc. • • •

0.340	161	¹ KAMANO 15	DPWA	$\bar{K}N$ multichannel
-------	-----	------------------------	------	-------------------------

¹ From the preferred solution A in KAMANO 15.

Normalized residue in $N\bar{K} \rightarrow \Lambda(1820) \rightarrow \Sigma(1385)\pi, F\text{-wave}$

MODULUS	PHASE ($^\circ$)	DOCUMENT ID	TECN	COMMENT
---------	--------------------	-------------	------	---------

0.11 \pm 0.04	5 \pm 45	SARANTSEV 19	DPWA	$\bar{K}N$ multichannel
-----------------------------------	------------------------------	--------------	------	-------------------------

• • • We do not use the following data for averages, fits, limits, etc. • • •

0.201	151	¹ KAMANO 15	DPWA	$\bar{K}N$ multichannel
-------	-----	------------------------	------	-------------------------

¹ From the preferred solution A in KAMANO 15.

Normalized residue in $N\bar{K} \rightarrow \Lambda(1820) \rightarrow N\bar{K}^*(892)$, $S=1/2$, F -wave

MODULUS	PHASE (°)	DOCUMENT ID	TECN	COMMENT
0.02 ± 0.02		SARANTSEV 19	DPWA	$\bar{K}N$ multichannel
0.00750	41	¹ KAMANO 15	DPWA	$\bar{K}N$ multichannel

• • • We do not use the following data for averages, fits, limits, etc. • • •

¹ From the preferred solution A in KAMANO 15.

Normalized residue in $N\bar{K} \rightarrow \Lambda(1820) \rightarrow N\bar{K}^*(892)$, $S=3/2$, P -wave

MODULUS	PHASE (°)	DOCUMENT ID	TECN	COMMENT
0.35 ± 0.15	-30 ± 45	SARANTSEV 19	DPWA	$\bar{K}N$ multichannel
0.171	-139	¹ KAMANO 15	DPWA	$\bar{K}N$ multichannel

• • • We do not use the following data for averages, fits, limits, etc. • • •

¹ From the preferred solution A in KAMANO 15.

Normalized residue in $N\bar{K} \rightarrow \Lambda(1820) \rightarrow N\bar{K}^*(892)$, $S=3/2$, F -wave

MODULUS	PHASE (°)	DOCUMENT ID	TECN	COMMENT
0.02 ± 0.02		SARANTSEV 19	DPWA	$\bar{K}N$ multichannel
0.000517	161	¹ KAMANO 15	DPWA	$\bar{K}N$ multichannel

• • • We do not use the following data for averages, fits, limits, etc. • • •

¹ From the preferred solution A in KAMANO 15.

 $\Lambda(1820)$ MASS

VALUE (MeV)	DOCUMENT ID	TECN	COMMENT
1815 to 1825 (≈ 1820) OUR ESTIMATE			
1822 ± 4	SARANTSEV 19	DPWA	$\bar{K}N$ multichannel
1823.5 ± 0.8	ZHANG 13A	DPWA	$\bar{K}N$ multichannel
1823 ± 3	GOPAL 80	DPWA	$\bar{K}N \rightarrow \bar{K}N$
1819 ± 2	ALSTON-... 78	DPWA	$\bar{K}N \rightarrow \bar{K}N$
1821 ± 2	KANE 74	DPWA	$K^-p \rightarrow \Sigma\pi$
• • • We do not use the following data for averages, fits, limits, etc. • • •			
1830	DECLAIS 77	DPWA	$\bar{K}N \rightarrow \bar{K}N$
1822 ± 2	GOPAL 77	DPWA	$\bar{K}N$ multichannel
1817 or 1819	¹ MARTIN 77	DPWA	$\bar{K}N$ multichannel

¹ The two MARTIN 77 values are from a T-matrix pole and from a Breit-Wigner fit.

 $\Lambda(1820)$ WIDTH

VALUE (MeV)	DOCUMENT ID	TECN	COMMENT
70 to 90 (≈ 80) OUR ESTIMATE			
80 ± 8	SARANTSEV 19	DPWA	$\bar{K}N$ multichannel
89 ± 2	ZHANG 13A	DPWA	$\bar{K}N$ multichannel
77 ± 5	GOPAL 80	DPWA	$\bar{K}N \rightarrow \bar{K}N$
72 ± 5	ALSTON-... 78	DPWA	$\bar{K}N \rightarrow \bar{K}N$
87 ± 3	KANE 74	DPWA	$K^-p \rightarrow \Sigma\pi$
• • • We do not use the following data for averages, fits, limits, etc. • • •			
82	DECLAIS 77	DPWA	$\bar{K}N \rightarrow \bar{K}N$
81 ± 5	GOPAL 77	DPWA	$\bar{K}N$ multichannel
76 or 76	¹ MARTIN 77	DPWA	$\bar{K}N$ multichannel

¹ The two MARTIN 77 values are from a T-matrix pole and from a Breit-Wigner fit.

 $\Lambda(1820)$ DECAY MODES

Mode	Fraction (Γ_i/Γ)
Γ_1 $N\bar{K}$	55–65 %
Γ_2 $\Sigma\pi$	8–14 %
Γ_3 $\Sigma(1385)\pi$	5–10 %
Γ_4 $\Sigma(1385)\pi, P$ -wave	
Γ_5 $\Sigma(1385)\pi, F$ -wave	(2.0 ± 1.0) %
Γ_6 $\Lambda\eta$	
Γ_7 ΞK	
Γ_8 $\Sigma\pi\pi$	
Γ_9 $N\bar{K}^*(892), S=1/2, F$ -wave	
Γ_{10} $N\bar{K}^*(892), S=3/2, P$ -wave	(3.0 ± 1.0) %
Γ_{11} $N\bar{K}^*(892), S=3/2, F$ -wave	

 $\Lambda(1820)$ BRANCHING RATIOS

Errors quoted do not include uncertainties in the parametrizations used in the partial-wave analyses and are thus too small. See also "Sign conventions for resonance couplings" in the Note on Λ and Σ Resonances.

$\Gamma(N\bar{K})/\Gamma_{\text{total}}$	DOCUMENT ID	TECN	COMMENT	Γ_1/Γ
0.55 to 0.65 OUR ESTIMATE				
0.58 ± 0.12	SARANTSEV 19	DPWA	$\bar{K}N$ multichannel	
0.54 ± 0.01	ZHANG 13A	DPWA	$\bar{K}N$ multichannel	
0.58 ± 0.02	GOPAL 80	DPWA	$\bar{K}N \rightarrow \bar{K}N$	
0.60 ± 0.03	ALSTON-... 78	DPWA	$\bar{K}N \rightarrow \bar{K}N$	

0.547	¹ KAMANO 15	DPWA	$\bar{K}N$ multichannel
0.51	DECLAIS 77	DPWA	$\bar{K}N \rightarrow \bar{K}N$
0.57 ± 0.02	GOPAL 77	DPWA	See GOPAL 80
0.59 or 0.58	² MARTIN 77	DPWA	$\bar{K}N$ multichannel

¹ From the preferred solution A in KAMANO 15.
² The two MARTIN 77 values are from a T-matrix pole and from a Breit-Wigner fit.

$\Gamma(\Sigma\pi)/\Gamma_{\text{total}}$	DOCUMENT ID	TECN	COMMENT	Γ_2/Γ
0.19 ± 0.04	SARANTSEV 19	DPWA	$\bar{K}N$ multichannel	
0.218	¹ KAMANO 15	DPWA	$\bar{K}N$ multichannel	

• • • We do not use the following data for averages, fits, limits, etc. • • •

¹ From the preferred solution A in KAMANO 15.

$\Gamma(\Sigma(1385)\pi, P$ -wave)/ Γ_{total}	DOCUMENT ID	TECN	COMMENT	Γ_4/Γ
~ 0.01	SARANTSEV 19	DPWA	$\bar{K}N$ multichannel	
0.173	¹ KAMANO 15	DPWA	$\bar{K}N$ multichannel	

• • • We do not use the following data for averages, fits, limits, etc. • • •

¹ From the preferred solution A in KAMANO 15.

$\Gamma(\Sigma(1385)\pi, F$ -wave)/ Γ_{total}	DOCUMENT ID	TECN	COMMENT	Γ_5/Γ
0.02 ± 0.01	SARANTSEV 19	DPWA	$\bar{K}N$ multichannel	
0.055	¹ KAMANO 15	DPWA	$\bar{K}N$ multichannel	

• • • We do not use the following data for averages, fits, limits, etc. • • •

¹ From the preferred solution A in KAMANO 15.

$\Gamma(\Lambda\eta)/\Gamma_{\text{total}}$	DOCUMENT ID	TECN	COMMENT	Γ_6/Γ
0.001	¹ KAMANO 15	DPWA	Multichannel	

• • • We do not use the following data for averages, fits, limits, etc. • • •

¹ From the preferred solution A in KAMANO 15.

$\Gamma(\Xi K)/\Gamma_{\text{total}}$	DOCUMENT ID	TECN	COMMENT	Γ_7/Γ
not seen	¹ KAMANO 15	DPWA	Multichannel	

• • • We do not use the following data for averages, fits, limits, etc. • • •

¹ From the preferred solution A in KAMANO 15.

$\Gamma(\Sigma\pi\pi)/\Gamma_{\text{total}}$	DOCUMENT ID	TECN	COMMENT	Γ_8/Γ
no clear signal	¹ ARMENTEROS68C	HDBC	$K^-N \rightarrow \Sigma\pi\pi$	

• • • We do not use the following data for averages, fits, limits, etc. • • •

¹ There is a suggestion of a bump, enough to be consistent with what is expected from $\Sigma(1385) \rightarrow \Sigma\pi$ decay.

$\Gamma(N\bar{K}^*(892), S=1/2, F$ -wave)/ Γ_{total}	DOCUMENT ID	TECN	COMMENT	Γ_9/Γ
not seen	¹ KAMANO 15	DPWA	Multichannel	

• • • We do not use the following data for averages, fits, limits, etc. • • •

¹ From the preferred solution A in KAMANO 15.

$\Gamma(N\bar{K}^*(892), S=3/2, P$ -wave)/ Γ_{total}	DOCUMENT ID	TECN	COMMENT	Γ_{10}/Γ
0.03 ± 0.01	ZHANG 13A	DPWA	Multichannel	
0.006	¹ KAMANO 15	DPWA	Multichannel	

• • • We do not use the following data for averages, fits, limits, etc. • • •

¹ From the preferred solution A in KAMANO 15.

$\Gamma(N\bar{K}^*(892), S=3/2, F$ -wave)/ Γ_{total}	DOCUMENT ID	TECN	COMMENT	Γ_{11}/Γ
not seen	¹ KAMANO 15	DPWA	Multichannel	

• • • We do not use the following data for averages, fits, limits, etc. • • •

¹ From the preferred solution A in KAMANO 15.

$(\Gamma_1\Gamma_2)^{1/2}/\Gamma_{\text{total}}$ in $N\bar{K} \rightarrow \Lambda(1820) \rightarrow \Sigma\pi$	DOCUMENT ID	TECN	COMMENT	$(\Gamma_1\Gamma_2)^{1/2}/\Gamma$
-0.28 ± 0.01	ZHANG 13A	DPWA	Multichannel	
-0.28 ± 0.03	GOPAL 77	DPWA	$\bar{K}N$ multichannel	
-0.28 ± 0.01	KANE 74	DPWA	$K^-p \rightarrow \Sigma\pi$	
-0.25 or -0.25	¹ MARTIN 77	DPWA	$\bar{K}N$ multichannel	

• • • We do not use the following data for averages, fits, limits, etc. • • •

¹ The two MARTIN 77 values are from a T-matrix pole and from a Breit-Wigner fit.

$(\Gamma_1\Gamma_4)^{1/2}/\Gamma_{\text{total}}$ in $N\bar{K} \rightarrow \Lambda(1820) \rightarrow \Sigma(1385)\pi, P$ -wave	DOCUMENT ID	TECN	COMMENT	$(\Gamma_1\Gamma_4)^{1/2}/\Gamma$
-0.20 ± 0.02	ZHANG 13A	DPWA	Multichannel	
-0.167 ± 0.054	¹ CAMERON 78	DPWA	$K^-p \rightarrow \Sigma(1385)\pi$	
+0.27 ± 0.03	PREVOST 74	DPWA	$K^-N \rightarrow \Sigma(1385)\pi$	

• • • We do not use the following data for averages, fits, limits, etc. • • •

¹ The published sign has been changed to be in accord with the baryon-first convention.

Baryon Particle Listings

 $\Lambda(1820)$, $\Lambda(1830)$

$(\Gamma_1 \Gamma_2)^{1/2} / \Gamma_{\text{total}}$ in $N\bar{K} \rightarrow \Lambda(1820) \rightarrow \Sigma(1385)\pi$, F -wave				$(\Gamma_1 \Gamma_2)^{1/2} / \Gamma$
VALUE	DOCUMENT ID	TECN	COMMENT	
$+0.065 \pm 0.029$	¹ CAMERON 78	DPWA	$K^- p \rightarrow \Sigma(1385)\pi$	

¹ The published sign has been changed to be in accord with the baryon-first convention.

$(\Gamma_1 \Gamma_2)^{1/2} / \Gamma_{\text{total}}$ in $N\bar{K} \rightarrow \Lambda(1820) \rightarrow \Lambda\eta$				$(\Gamma_1 \Gamma_2)^{1/2} / \Gamma$
VALUE	DOCUMENT ID	TECN	COMMENT	
-0.096 ± 0.040 -0.020	RADER 73	MPWA		

 $\Lambda(1820)$ REFERENCES

SARANTSEV 19	EPJ A55 180	A.V. Sarantsev et al.	(BONN, PNPI)
KAMANO 15	PR C92 025205	H. Kamano et al.	(ANL, OSAK)
ZHANG 13A	PR C88 035205	H. Zhang et al.	(KSU)
PDG 82	PL 111B 1	M. Roos et al.	(HEL5, CIT, CERN)
GOPAL 80	Toronto Conf. 159	G.P. Gopal	(RHEL) IJP
ALSTON-... 78	PR D18 182	M. Alston-Garnjost et al.	(LBL, MTHO+) IJP
Also	PRL 38 1007	M. Alston-Garnjost et al.	(LBL, MTHO+) IJP
CAMERON 78	NP B143 189	W. Cameron et al.	(RHEL, LOIC) IJP
DECLAIS 77	CERN 77-16	Y. Declais et al.	(CAEN, CERN) IJP
GOPAL 77	NP B119 362	G.P. Gopal et al.	(LOIC, RHEL) IJP
MARTIN 77	NP B127 349	B.R. Martin, M.K. Pidcock, R.G. Moorhouse	(LOUC+) IJP
Also	NP B126 266	B.R. Martin, M.K. Pidcock	(LOUC)
Also	NP B126 285	B.R. Martin, M.K. Pidcock	(LOUC) IJP
KANE 74	LBL-2452	D.F. Kane	(LBL) IJP
PREVOST 74	NP B69 246	J. Prevost et al.	(SACL, CERN, HEID)
RADER 73	NC 16A 178	R.K. Rader et al.	(SACL, HEID, CERN+)
ARMENTEROS 68C	NP B8 216	R. Armenteros et al.	(CERN, HEID, SACL) I

$\Lambda(1830) 5/2^-$	$I(J^P) = 0(\frac{5}{2}^-)$ Status: * * * *
-----------------------	---

For results published before 1973 (they are now obsolete), see our 1982 edition Physics Letters **111B** 1 (1982).

The best evidence for this resonance is in the $\Sigma\pi$ channel.

 $\Lambda(1830)$ POLE POSITION

REAL PART

VALUE (MeV)	DOCUMENT ID	TECN	COMMENT
1800 to 1860 (\approx 1830) OUR ESTIMATE			
1819.5 ± 3.0	SARANTSEV 19	DPWA	$\bar{K}N$ multichannel
1899 ± 35 -37	¹ KAMANO 15	DPWA	Multichannel
• • • We do not use the following data for averages, fits, limits, etc. • • •			
1766 ± 37 -34	² KAMANO 15	DPWA	Multichannel
1809	ZHANG 13A	DPWA	Multichannel

¹ The preferred solution A in KAMANO 15 reports two poles. This entry is from the preferred solution A.

² From the preferred solution A in KAMANO 15. Not seen in solution B.

-2xIMAGINARY PART

VALUE (MeV)	DOCUMENT ID	TECN	COMMENT
50 to 80 (\approx 65) OUR ESTIMATE			
62 ± 5	SARANTSEV 19	DPWA	$\bar{K}N$ multichannel
80 ± 100 -34	¹ KAMANO 15	DPWA	Multichannel
• • • We do not use the following data for averages, fits, limits, etc. • • •			
212 ± 94 -62	² KAMANO 15	DPWA	Multichannel
109	ZHANG 13A	DPWA	Multichannel

¹ The preferred solution A in KAMANO 15 reports two poles. This entry is from the preferred solution A.

² From the preferred solution A in KAMANO 15. Not seen in solution B.

 $\Lambda(1830)$ POLE RESIDUES

The normalized residue is the residue divided by $\Gamma_{\text{pole}}/2$.

Normalized residue in $N\bar{K} \rightarrow \Lambda(1830) \rightarrow N\bar{K}$

MODULUS	PHASE ($^\circ$)	DOCUMENT ID	TECN	COMMENT
0.055 \pm 0.010 20 \pm 14		SARANTSEV 19	DPWA	$\bar{K}N$ multichannel
• • • We do not use the following data for averages, fits, limits, etc. • • •				
0.00502	-80	¹ KAMANO 15	DPWA	Multichannel

¹ From the preferred solution A in KAMANO 15.

Normalized residue in $N\bar{K} \rightarrow \Lambda(1830) \rightarrow \Sigma\pi$

MODULUS	PHASE ($^\circ$)	DOCUMENT ID	TECN	COMMENT
0.15 \pm 0.03 180 \pm 10		SARANTSEV 19	DPWA	$\bar{K}N$ multichannel
• • • We do not use the following data for averages, fits, limits, etc. • • •				
0.00581	179	¹ KAMANO 15	DPWA	Multichannel

¹ From the preferred solution A in KAMANO 15.

Normalized residue in $N\bar{K} \rightarrow \Lambda(1830) \rightarrow \Lambda\eta$

MODULUS	PHASE ($^\circ$)	DOCUMENT ID	TECN	COMMENT
• • • We do not use the following data for averages, fits, limits, etc. • • •				
0.00941	-65	¹ KAMANO 15	DPWA	Multichannel

¹ From the preferred solution A in KAMANO 15.

Normalized residue in $N\bar{K} \rightarrow \Lambda(1830) \rightarrow \Xi K$

MODULUS	PHASE ($^\circ$)	DOCUMENT ID	TECN	COMMENT
0.010 \pm 0.005 65 \pm 20		SARANTSEV 19	DPWA	$\bar{K}N$ multichannel
• • • We do not use the following data for averages, fits, limits, etc. • • •				
0.0477	94	¹ KAMANO 15	DPWA	Multichannel

¹ From the preferred solution A in KAMANO 15.

Normalized residue in $N\bar{K} \rightarrow \Lambda(1830) \rightarrow \Sigma(1385)\pi$, D -wave

MODULUS	PHASE ($^\circ$)	DOCUMENT ID	TECN	COMMENT
0.10 \pm 0.04 10 \pm 25		SARANTSEV 19	DPWA	$\bar{K}N$ multichannel
• • • We do not use the following data for averages, fits, limits, etc. • • •				
0.0237	113	¹ KAMANO 15	DPWA	Multichannel

¹ From the preferred solution A in KAMANO 15.

Normalized residue in $N\bar{K} \rightarrow \Lambda(1830) \rightarrow \Sigma(1385)\pi$, G -wave

MODULUS	PHASE ($^\circ$)	DOCUMENT ID	TECN	COMMENT
0.03 \pm 0.02		SARANTSEV 19	DPWA	$\bar{K}N$ multichannel
• • • We do not use the following data for averages, fits, limits, etc. • • •				
0.000726	127	¹ KAMANO 15	DPWA	Multichannel

¹ From the preferred solution A in KAMANO 15.

Normalized residue in $N\bar{K} \rightarrow \Lambda(1830) \rightarrow N\bar{K}^*(892)$, $S=1/2$, D -wave

MODULUS	PHASE ($^\circ$)	DOCUMENT ID	TECN	COMMENT
• • • We do not use the following data for averages, fits, limits, etc. • • •				
0.0278	-177	¹ KAMANO 15	DPWA	Multichannel

¹ From the preferred solution A in KAMANO 15.

Normalized residue in $N\bar{K} \rightarrow \Lambda(1830) \rightarrow N\bar{K}^*(892)$, $S=3/2$, D -wave

MODULUS	PHASE ($^\circ$)	DOCUMENT ID	TECN	COMMENT
• • • We do not use the following data for averages, fits, limits, etc. • • •				
0.0255	3	¹ KAMANO 15	DPWA	Multichannel

¹ From the preferred solution A in KAMANO 15.

Normalized residue in $N\bar{K} \rightarrow \Lambda(1830) \rightarrow N\bar{K}^*(892)$, $S=3/2$, G -wave

MODULUS	PHASE ($^\circ$)	DOCUMENT ID	TECN	COMMENT
• • • We do not use the following data for averages, fits, limits, etc. • • •				
0.00773	-17	¹ KAMANO 15	DPWA	Multichannel

¹ From the preferred solution A in KAMANO 15.

Normalized residue in $N\bar{K} \rightarrow \Lambda(1830) \rightarrow \Lambda\omega$, $S=1/2$, D -wave

MODULUS	PHASE ($^\circ$)	DOCUMENT ID	TECN	COMMENT
0.04 \pm 0.03		SARANTSEV 19	DPWA	$\bar{K}N$ multichannel

Normalized residue in $N\bar{K} \rightarrow \Lambda(1830) \rightarrow \Lambda\omega$, $S=3/2$, D -wave

MODULUS	PHASE ($^\circ$)	DOCUMENT ID	TECN	COMMENT
0.05 \pm 0.03 -110 \pm 35		SARANTSEV 19	DPWA	$\bar{K}N$ multichannel

 $\Lambda(1830)$ MASS

VALUE (MeV)	DOCUMENT ID	TECN	COMMENT
1820 to 1830 (\approx 1825) OUR ESTIMATE			
1821 ± 3	SARANTSEV 19	DPWA	$\bar{K}N$ multichannel
1820 ± 4	ZHANG 13A	DPWA	Multichannel
1831 ± 10	GOPAL 80	DPWA	$\bar{K}N \rightarrow \bar{K}N$
1825 ± 10	GOPAL 77	DPWA	$\bar{K}N$ multichannel
1825 ± 1	KANE 74	DPWA	$K^- p \rightarrow \Sigma\pi$
• • • We do not use the following data for averages, fits, limits, etc. • • •			
1817 or 1818	¹ MARTIN 77	DPWA	$\bar{K}N$ multichannel

¹ The two MARTIN 77 values are from a T-matrix pole and from a Breit-Wigner fit.

 $\Lambda(1830)$ WIDTH

VALUE (MeV)	DOCUMENT ID	TECN	COMMENT
60 to 120 (\approx 90) OUR ESTIMATE			
64 ± 7	SARANTSEV 19	DPWA	$\bar{K}N$ multichannel
114 ± 10	ZHANG 13A	DPWA	Multichannel
100 ± 10	GOPAL 80	DPWA	$\bar{K}N \rightarrow \bar{K}N$
94 ± 10	GOPAL 77	DPWA	$\bar{K}N$ multichannel
119 ± 3	KANE 74	DPWA	$K^- p \rightarrow \Sigma\pi$
• • • We do not use the following data for averages, fits, limits, etc. • • •			
56 or 56	¹ MARTIN 77	DPWA	$\bar{K}N$ multichannel

¹ The two MARTIN 77 values are from a T-matrix pole and from a Breit-Wigner fit.

See key on page 1171

Baryon Particle Listings
 $\Lambda(1830), \Lambda(1890)$

$\Lambda(1830)$ DECAY MODES

Mode	Fraction (Γ_i/Γ)	Scale factor
Γ_1 $N\bar{K}$	0.04 to 0.08	
Γ_2 $\Sigma\pi$	35-75 %	
Γ_3 ΞK		
Γ_4 $\Sigma(1385)\pi$	>15 %	
Γ_5 $\Sigma(1385)\pi, D\text{-wave}$	(40 \pm 15) %	3.2
Γ_6 $\Sigma(1385)\pi, G\text{-wave}$		
Γ_7 $\Lambda\eta$		
Γ_8 $N\bar{K}^*(892), S=1/2, D\text{-wave}$		
Γ_9 $N\bar{K}^*(892), S=3/2, D\text{-wave}$		
Γ_{10} $N\bar{K}^*(892), S=3/2, G\text{-wave}$		

$\Lambda(1830)$ BRANCHING RATIOS

See "Sign conventions for resonance couplings" in the Note on Λ and Σ Resonances.

$\Gamma(N\bar{K})/\Gamma_{\text{total}}$	DOCUMENT ID	TECN	COMMENT	Γ_1/Γ
0.04 to 0.08 OUR ESTIMATE				

0.055 \pm 0.010	SARANTSEV	19	DPWA	$\bar{K}N$ multichannel
0.041 \pm 0.005	ZHANG	13A	DPWA	Multichannel
0.08 \pm 0.03	GOPAL	80	DPWA	$\bar{K}N \rightarrow \bar{K}N$
0.02 \pm 0.02	ALSTON...	78	DPWA	$\bar{K}N \rightarrow \bar{K}N$
••• We do not use the following data for averages, fits, limits, etc. •••				
0.006	¹ KAMANO	15	DPWA	Multichannel
0.04 \pm 0.03	GOPAL	77	DPWA	See GOPAL 80
0.04 or 0.04	² MARTIN	77	DPWA	$\bar{K}N$ multichannel
¹ From the preferred solution A in KAMANO 15.				
² The two MARTIN 77 values are from a T-matrix pole and from a Breit-Wigner fit.				

$\Gamma(\Sigma\pi)/\Gamma_{\text{total}}$	DOCUMENT ID	TECN	COMMENT	Γ_2/Γ
0.42 \pm 0.08	SARANTSEV	19	DPWA	$\bar{K}N$ multichannel
••• We do not use the following data for averages, fits, limits, etc. •••				

0.017	¹ KAMANO	15	DPWA	Multichannel
¹ From the preferred solution A in KAMANO 15.				

$\Gamma(\Xi K)/\Gamma_{\text{total}}$	DOCUMENT ID	TECN	COMMENT	Γ_3/Γ
••• We do not use the following data for averages, fits, limits, etc. •••				
0.562	¹ KAMANO	15	DPWA	Multichannel
¹ From the preferred solution A in KAMANO 15.				

$\Gamma(\Sigma(1385)\pi, D\text{-wave})/\Gamma_{\text{total}}$	DOCUMENT ID	TECN	COMMENT	Γ_5/Γ
0.40 \pm 0.15 OUR AVERAGE	Error includes scale factor of 3.2.			

0.20 \pm 0.08	SARANTSEV	19	DPWA	$\bar{K}N$ multichannel
0.52 \pm 0.06	ZHANG	13A	DPWA	Multichannel
••• We do not use the following data for averages, fits, limits, etc. •••				
0.134	¹ KAMANO	15	DPWA	Multichannel
¹ From the preferred solution A in KAMANO 15.				

$\Gamma(\Sigma(1385)\pi, G\text{-wave})/\Gamma_{\text{total}}$	DOCUMENT ID	TECN	COMMENT	Γ_6/Γ
0.020 \pm 0.015	SARANTSEV	19	DPWA	$\bar{K}N$ multichannel

$\Gamma(\Lambda\eta)/\Gamma_{\text{total}}$	DOCUMENT ID	TECN	COMMENT	Γ_7/Γ
••• We do not use the following data for averages, fits, limits, etc. •••				
0.024	¹ KAMANO	15	DPWA	Multichannel
¹ From the preferred solution A in KAMANO 15.				

$\Gamma(N\bar{K}^*(892), S=1/2, D\text{-wave})/\Gamma_{\text{total}}$	DOCUMENT ID	TECN	COMMENT	Γ_8/Γ
••• We do not use the following data for averages, fits, limits, etc. •••				
0.134	¹ KAMANO	15	DPWA	Multichannel
¹ From the preferred solution A in KAMANO 15.				

$\Gamma(N\bar{K}^*(892), S=3/2, D\text{-wave})/\Gamma_{\text{total}}$	DOCUMENT ID	TECN	COMMENT	Γ_9/Γ
••• We do not use the following data for averages, fits, limits, etc. •••				
0.115	¹ KAMANO	15	DPWA	Multichannel
¹ From the preferred solution A in KAMANO 15.				

$\Gamma(N\bar{K}^*(892), S=3/2, G\text{-wave})/\Gamma_{\text{total}}$	DOCUMENT ID	TECN	COMMENT	Γ_{10}/Γ
••• We do not use the following data for averages, fits, limits, etc. •••				
0.009	¹ KAMANO	15	DPWA	Multichannel
¹ From the preferred solution A in KAMANO 15.				

$(\Gamma_i\Gamma_f)^{1/2}/\Gamma_{\text{total}}$ in $N\bar{K} \rightarrow \Lambda(1830) \rightarrow \Sigma\pi$ $(\Gamma_1\Gamma_2)^{1/2}/\Gamma$

VALUE	DOCUMENT ID	TECN	COMMENT
-0.13 \pm 0.01	ZHANG	13A	DPWA Multichannel
-0.17 \pm 0.03	GOPAL	77	DPWA $\bar{K}N$ multichannel
-0.15 \pm 0.01	KANE	74	DPWA $K^-p \rightarrow \Sigma\pi$
••• We do not use the following data for averages, fits, limits, etc. •••			
-0.17 or -0.17	¹ MARTIN	77	DPWA $\bar{K}N$ multichannel
¹ The two MARTIN 77 values are from a T-matrix pole and from a Breit-Wigner fit.			

$(\Gamma_i\Gamma_f)^{1/2}/\Gamma_{\text{total}}$ in $N\bar{K} \rightarrow \Lambda(1830) \rightarrow \Sigma(1385)\pi$ $(\Gamma_1\Gamma_4)^{1/2}/\Gamma$

VALUE	DOCUMENT ID	TECN	COMMENT
0.20 to 0.50 OUR ESTIMATE			
+0.141 \pm 0.014	¹ CAMERON	78	DPWA $K^-p \rightarrow \Sigma(1385)\pi$
+0.13 \pm 0.03	PREVOST	74	DPWA $K^-N \rightarrow \Sigma(1385)\pi$
¹ The CAMERON 78 upper limit on G-wave decay is 0.03. The published sign has been changed to be in accord with the baryon-first convention.			

$(\Gamma_i\Gamma_f)^{1/2}/\Gamma_{\text{total}}$ in $N\bar{K} \rightarrow \Lambda(1830) \rightarrow \Lambda\eta$ $(\Gamma_1\Gamma_7)^{1/2}/\Gamma$

VALUE	DOCUMENT ID	TECN	COMMENT
-0.044 \pm 0.020	RADER	73	MPWA

$\Lambda(1830)$ REFERENCES

SARANTSEV	19	EPJ A55 180	A.V. Sarantsev et al.	(BONN, PNPI)
KAMANO	15	PR C92 025205	H. Kamano et al.	(ANL, OSAK)
ZHANG	13A	PR C88 035205	H. Zhang et al.	(KSU)
PDG	82	PL 111B 1	M. Roos et al.	(HEL5, CIT, CERN)
GOPAL	80	Toronto Conf. 159	G.P. Gopal	(RHEL) IJP
ALSTON...	78	PR D18 182	M. Alston-Garnjost et al.	(LBL, MTHO+) IJP
Also		PRL 38 1007	M. Alston-Garnjost et al.	(LBL, MTHO+) IJP
CAMERON	78	NP B143 189	W. Cameron et al.	(RHEL, LOIC) IJP
GOPAL	77	NP B119 362	G.P. Gopal et al.	(RHEL, LOIC) IJP
MARTIN	77	NP B127 349	B.R. Martin, M.K. Pidcock, R.G. Moorhouse	(LOIC, RHEL) IJP
Also		NP B126 266	B.R. Martin, M.K. Pidcock	(LOIC)
Also		NP B126 285	B.R. Martin, M.K. Pidcock	(LOIC) IJP
KANE	74	LBL-2452	D.F. Kane	(LBL) IJP
PREVOST	74	NP B69 246	J. Prevost et al.	(SACL, CERN, HEID)
RADER	73	NC 16A 178	R.K. Rader et al.	(SACL, HEID, CERN+)

$\Lambda(1890) 3/2^+$

$I(J^P) = 0(\frac{3}{2}^+)$ Status: ***

For results published before 1974 (they are now obsolete), see our 1982 edition Physics Letters **111B** 1 (1982).

$\Lambda(1890)$ POLE POSITION

REAL PART

VALUE (MeV)	DOCUMENT ID	TECN	COMMENT
1872 \pm 5	SARANTSEV	19	DPWA $\bar{K}N$ multichannel
••• We do not use the following data for averages, fits, limits, etc. •••			

1859 $^{+5}_{-7}$	¹ KAMANO	15	DPWA Multichannel
1876	ZHANG	13A	DPWA Multichannel
¹ From the preferred solution A in KAMANO 15, incompatible with solution B.			

-2xIMAGINARY PART

VALUE (MeV)	DOCUMENT ID	TECN	COMMENT
101 \pm 10	SARANTSEV	19	DPWA $\bar{K}N$ multichannel
••• We do not use the following data for averages, fits, limits, etc. •••			

113 $^{+20}_{-4}$	¹ KAMANO	15	DPWA $\bar{K}N$ multichannel
145	ZHANG	13A	DPWA $\bar{K}N$ multichannel
¹ From the preferred solution A in KAMANO 15, incompatible with solution B.			

$\Lambda(1890)$ POLE RESIDUE

The "normalized residue" is the residue divided by $\Gamma_{\text{pole}}/2$.

Normalized residue in $K\bar{N} \rightarrow \Lambda(1890) \rightarrow K\bar{N}$

MODULUS	PHASE ($^\circ$)	DOCUMENT ID	TECN	COMMENT
0.30 \pm 0.06	0 \pm 10	SARANTSEV	19	DPWA $\bar{K}N$ multichannel
••• We do not use the following data for averages, fits, limits, etc. •••				

0.241	-23	¹ KAMANO	15	DPWA $\bar{K}N$ multichannel
¹ From the preferred solution A in KAMANO 15.				

Normalized residue in $N\bar{K} \rightarrow \Lambda(1890) \rightarrow \Sigma\pi$

MODULUS	PHASE ($^\circ$)	DOCUMENT ID	TECN	COMMENT
0.14 \pm 0.05	148 \pm 12	SARANTSEV	19	DPWA $\bar{K}N$ multichannel
••• We do not use the following data for averages, fits, limits, etc. •••				

0.101	104	¹ KAMANO	15	DPWA $\bar{K}N$ multichannel
¹ From the preferred solution A in KAMANO 15.				

Baryon Particle Listings

 $\Lambda(1890)$ Normalized residue in $N\bar{K} \rightarrow \Lambda(1890) \rightarrow \Lambda\eta$

MODULUS	PHASE (°)	DOCUMENT ID	TECN	COMMENT
0.0485	-54	¹ KAMANO 15	DPWA	Multichannel

¹ From the preferred solution A in KAMANO 15.

Normalized residue in $N\bar{K} \rightarrow \Lambda(1890) \rightarrow \Xi K$

MODULUS	PHASE (°)	DOCUMENT ID	TECN	COMMENT
0.065 ± 0.020	160 ± 30	SARANTSEV 19	DPWA	$\bar{K}N$ multichannel
0.0562	-85	¹ KAMANO 15	DPWA	$\bar{K}N$ multichannel

¹ From the preferred solution A in KAMANO 15.

Normalized residue in $N\bar{K} \rightarrow \Lambda(1890) \rightarrow \Sigma(1385)\pi, P\text{-wave}$

MODULUS	PHASE (°)	DOCUMENT ID	TECN	COMMENT
0.11 ± 0.05	-160 ± 45	SARANTSEV 19	DPWA	$\bar{K}N$ multichannel
0.295	-40	¹ KAMANO 15	DPWA	$\bar{K}N$ multichannel

¹ From the preferred solution A in KAMANO 15.

Normalized residue in $N\bar{K} \rightarrow \Lambda(1890) \rightarrow \Sigma(1385)\pi, F\text{-wave}$

MODULUS	PHASE (°)	DOCUMENT ID	TECN	COMMENT
0.10 ± 0.04	10 ± 50	SARANTSEV 19	DPWA	$\bar{K}N$ multichannel
0.064	127	¹ KAMANO 15	DPWA	$\bar{K}N$ multichannel

¹ From the preferred solution A in KAMANO 15.

Normalized residue in $N\bar{K} \rightarrow \Lambda(1890) \rightarrow N\bar{K}^*(892), S=1/2, P\text{-wave}$

MODULUS	PHASE (°)	DOCUMENT ID	TECN	COMMENT
0.03 ± 0.03		SARANTSEV 19	DPWA	$\bar{K}N$ multichannel
0.188	-160	¹ KAMANO 15	DPWA	$\bar{K}N$ multichannel

¹ From the preferred solution A in KAMANO 15.

Normalized residue in $N\bar{K} \rightarrow \Lambda(1890) \rightarrow N\bar{K}^*(892), S=3/2, P\text{-wave}$

MODULUS	PHASE (°)	DOCUMENT ID	TECN	COMMENT
0.05 ± 0.03	180 ± 40	SARANTSEV 19	DPWA	$\bar{K}N$ multichannel
0.209	15	¹ KAMANO 15	DPWA	$\bar{K}N$ multichannel

¹ From the preferred solution A in KAMANO 15.

Normalized residue in $N\bar{K} \rightarrow \Lambda(1890) \rightarrow N\bar{K}^*(892), S=3/2, F\text{-wave}$

MODULUS	PHASE (°)	DOCUMENT ID	TECN	COMMENT
0.0141	129	¹ KAMANO 15	DPWA	Multichannel

¹ From the preferred solution A in KAMANO 15.

Normalized residue in $N\bar{K} \rightarrow \Lambda(1890) \rightarrow \Lambda\omega, S=1/2, P\text{-wave}$

MODULUS	PHASE (°)	DOCUMENT ID	TECN	COMMENT
0.24 ± 0.06	15 ± 20	SARANTSEV 19	DPWA	$\bar{K}N$ multichannel

Normalized residue in $N\bar{K} \rightarrow \Lambda(1890) \rightarrow \Lambda\omega, S=3/2, P\text{-wave}$

MODULUS	PHASE (°)	DOCUMENT ID	TECN	COMMENT
0.15 ± 0.08	-165 ± 20	SARANTSEV 19	DPWA	$\bar{K}N$ multichannel

 $\Lambda(1890)$ MASS

VALUE (MeV)	DOCUMENT ID	TECN	COMMENT
1870 to 1910 (≈ 1890) OUR ESTIMATE			
1873 ± 5	SARANTSEV 19	DPWA	$\bar{K}N$ multichannel
1900 ± 5	ZHANG 13A	DPWA	$\bar{K}N$ multichannel
1897 ± 5	GOPAL 80	DPWA	$\bar{K}N \rightarrow \bar{K}N$
1908 ± 10	ALSTON... 78	DPWA	$\bar{K}N \rightarrow \bar{K}N$
1894 ± 10	HEMINGWAY 75	DPWA	$K^-p \rightarrow \bar{K}N$
••• We do not use the following data for averages, fits, limits, etc. •••			
1900 ± 5	GOPAL 77	DPWA	$\bar{K}N$ multichannel
1856 or 1868	¹ MARTIN 77	DPWA	$\bar{K}N$ multichannel
1900	² NAKKASYAN 75	DPWA	$K^-p \rightarrow \Lambda\omega$

¹ The two MARTIN 77 values are from a T-matrix pole and from a Breit-Wigner fit.
² Found in one of two best solutions.

 $\Lambda(1890)$ WIDTH

VALUE (MeV)	DOCUMENT ID	TECN	COMMENT
80 to 160 (≈ 120) OUR ESTIMATE			
103 ± 10	SARANTSEV 19	DPWA	$\bar{K}N$ multichannel
161 ± 15	ZHANG 13A	DPWA	$\bar{K}N$ multichannel
74 ± 10	GOPAL 80	DPWA	$\bar{K}N \rightarrow \bar{K}N$
119 ± 20	ALSTON... 78	DPWA	$\bar{K}N \rightarrow \bar{K}N$
107 ± 10	HEMINGWAY 75	DPWA	$K^-p \rightarrow \bar{K}N$

••• We do not use the following data for averages, fits, limits, etc. •••

72 ± 10	GOPAL 77	DPWA	$\bar{K}N$ multichannel
191 or 193	¹ MARTIN 77	DPWA	$\bar{K}N$ multichannel
100	² NAKKASYAN 75	DPWA	$K^-p \rightarrow \Lambda\omega$

¹ The two MARTIN 77 values are from a T-matrix pole and from a Breit-Wigner fit.
² Found in one of two best solutions.

 $\Lambda(1890)$ DECAY MODES

Mode	Fraction (Γ_i/Γ)
Γ_1 $N\bar{K}$	0.24 to 0.36
Γ_2 $\Sigma\pi$	3-10 %
Γ_3 $\Lambda\eta$	
Γ_4 ΞK	
Γ_5 $\Sigma(1385)\pi$	seen
Γ_6 $\Sigma(1385)\pi, P\text{-wave}$	(6.0 ± 3.0) %
Γ_7 $\Sigma(1385)\pi, F\text{-wave}$	(4.0 ± 2.0) %
Γ_8 $N\bar{K}^*(892)$	seen
Γ_9 $N\bar{K}^*(892), S=1/2$	
Γ_{10} $N\bar{K}^*(892), S=1/2, P\text{-wave}$	
Γ_{11} $N\bar{K}^*(892), S=3/2, P\text{-wave}$	
Γ_{12} $N\bar{K}^*(892), S=3/2, F\text{-wave}$	
Γ_{13} $\Lambda\omega$	

 $\Lambda(1890)$ BRANCHING RATIOS

See "Sign conventions for resonance couplings" in the Note on Λ and Σ Resonances.

$\Gamma(N\bar{K})/\Gamma_{\text{total}}$	DOCUMENT ID	TECN	COMMENT	Γ_1/Γ
0.24 to 0.36 OUR ESTIMATE				
0.30 ± 0.06	SARANTSEV 19	DPWA	$\bar{K}N$ multichannel	
0.37 ± 0.03	ZHANG 13A	DPWA	$\bar{K}N$ multichannel	
0.20 ± 0.02	GOPAL 80	DPWA	$\bar{K}N \rightarrow \bar{K}N$	
0.34 ± 0.05	ALSTON... 78	DPWA	$\bar{K}N \rightarrow \bar{K}N$	
0.24 ± 0.04	HEMINGWAY 75	DPWA	$K^-p \rightarrow \bar{K}N$	
••• We do not use the following data for averages, fits, limits, etc. •••				
0.305	¹ KAMANO 15	DPWA	$\bar{K}N$ multichannel	
0.18 ± 0.02	GOPAL 77	DPWA	See GOPAL 80	
0.36 or 0.34	² MARTIN 77	DPWA	$\bar{K}N$ multichannel	

¹ From the preferred solution A in KAMANO 15.

² The two MARTIN 77 values are from a T-matrix pole and from a Breit-Wigner fit.

$\Gamma(\Sigma\pi)/\Gamma_{\text{total}}$	DOCUMENT ID	TECN	COMMENT	Γ_2/Γ
6 ± 2	SARANTSEV 19	DPWA	$\bar{K}N$ multichannel	
<0.03	LANGBEIN 72	IPWA	$\bar{K}N$ multichannel	
••• We do not use the following data for averages, fits, limits, etc. •••				
0.04	¹ KAMANO 15	DPWA	$\bar{K}N$ multichannel	
¹ From the preferred solution A in KAMANO 15.				

$\Gamma(\Lambda\eta)/\Gamma_{\text{total}}$	DOCUMENT ID	TECN	COMMENT	Γ_3/Γ
••• We do not use the following data for averages, fits, limits, etc. •••				
0.012	¹ KAMANO 15	DPWA	$\bar{K}N$ multichannel	
¹ From the preferred solution A in KAMANO 15.				

$\Gamma(\Xi K)/\Gamma_{\text{total}}$	DOCUMENT ID	TECN	COMMENT	Γ_4/Γ
~0.01	SARANTSEV 19	DPWA	$\bar{K}N$ multichannel	
••• We do not use the following data for averages, fits, limits, etc. •••				
0.009	¹ KAMANO 15	DPWA	$\bar{K}N$ multichannel	
¹ From the preferred solution A in KAMANO 15.				

$\Gamma(\Sigma(1385)\pi, P\text{-wave})/\Gamma_{\text{total}}$	DOCUMENT ID	TECN	COMMENT	Γ_6/Γ
••• We do not use the following data for averages, fits, limits, etc. •••				
0.453	¹ KAMANO 15	DPWA	$\bar{K}N$ multichannel	
¹ From the preferred solution A in KAMANO 15.				

$\Gamma(\Sigma(1385)\pi, F\text{-wave})/\Gamma_{\text{total}}$	DOCUMENT ID	TECN	COMMENT	Γ_7/Γ
••• We do not use the following data for averages, fits, limits, etc. •••				
0.019	¹ KAMANO 15	DPWA	$\bar{K}N$ multichannel	
¹ From the preferred solution A in KAMANO 15.				

See key on page 1171

Baryon Particle Listings
 $\Lambda(1890)$, $\Lambda(2000)$, $\Lambda(2050)$ $\Gamma(N\bar{K}^*(892), S=1/2, P\text{-wave})/\Gamma_{\text{total}}$ Γ_{10}/Γ

VALUE	DOCUMENT ID	TECN	COMMENT
<0.01	SARANTSEV 19	DPWA	$\bar{K}N$ multichannel
••• We do not use the following data for averages, fits, limits, etc. •••			
0.073	¹ KAMANO 15	DPWA	$\bar{K}N$ multichannel
	¹ From the preferred solution A in KAMANO 15.		

 $\Gamma(N\bar{K}^*(892), S=3/2, P\text{-wave})/\Gamma_{\text{total}}$ Γ_{11}/Γ

VALUE	DOCUMENT ID	TECN	COMMENT
~ 0.01	SARANTSEV 19	DPWA	$\bar{K}N$ multichannel
••• We do not use the following data for averages, fits, limits, etc. •••			
0.088	¹ KAMANO 15	DPWA	$\bar{K}N$ multichannel
	¹ From the preferred solution A in KAMANO 15.		

 $\Gamma(N\bar{K}^*(892), S=3/2, F\text{-wave})/\Gamma_{\text{total}}$ Γ_{12}/Γ

VALUE	DOCUMENT ID	TECN	COMMENT
••• We do not use the following data for averages, fits, limits, etc. •••			
0.001	¹ KAMANO 15	DPWA	$\bar{K}N$ multichannel
	¹ From the preferred solution A in KAMANO 15.		

 $(\Gamma_i\Gamma_f)^{1/2}/\Gamma_{\text{total}}$ in $N\bar{K} \rightarrow \Lambda(1890) \rightarrow \Sigma\pi$ $(\Gamma_1\Gamma_2)^{1/2}/\Gamma$

VALUE	DOCUMENT ID	TECN	COMMENT
-0.09 ± 0.02	ZHANG 13A	DPWA	$\bar{K}N$ multichannel
-0.09 ± 0.03	GOPAL 77	DPWA	$\bar{K}N$ multichannel
••• We do not use the following data for averages, fits, limits, etc. •••			
+0.15 or +0.14	¹ MARTIN 77	DPWA	$\bar{K}N$ multichannel
	¹ The two MARTIN 77 values are from a T-matrix pole and from a Breit-Wigner fit.		

 $(\Gamma_i\Gamma_f)^{1/2}/\Gamma_{\text{total}}$ in $N\bar{K} \rightarrow \Lambda(1890) \rightarrow \Sigma(1385)\pi, P\text{-wave}$ $(\Gamma_1\Gamma_6)^{1/2}/\Gamma$

VALUE	DOCUMENT ID	TECN	COMMENT
<0.03	CAMERON 78	DPWA	$K^-p \rightarrow \Sigma(1385)\pi$

 $(\Gamma_i\Gamma_f)^{1/2}/\Gamma_{\text{total}}$ in $N\bar{K} \rightarrow \Lambda(1890) \rightarrow \Sigma(1385)\pi, F\text{-wave}$ $(\Gamma_1\Gamma_7)^{1/2}/\Gamma$

VALUE	DOCUMENT ID	TECN	COMMENT
-0.31 ± 0.04	ZHANG 13A	DPWA	$\bar{K}N$ multichannel
-0.126 ± 0.055	¹ CAMERON 78	DPWA	$K^-p \rightarrow \Sigma(1385)\pi$
	¹ The published sign has been changed to be in accord with the baryon-first convention.		

 $(\Gamma_i\Gamma_f)^{1/2}/\Gamma_{\text{total}}$ in $N\bar{K} \rightarrow \Lambda(1890) \rightarrow N\bar{K}^*(892), S=1/2$ $(\Gamma_1\Gamma_9)^{1/2}/\Gamma$

VALUE	DOCUMENT ID	TECN	COMMENT
-0.17 ± 0.05	ZHANG 13A	DPWA	$\bar{K}N$ multichannel
-0.07 ± 0.03	^{1,2} CAMERON 78B	DPWA	$K^-p \rightarrow N\bar{K}^*$
	¹ Upper limits on the P_3 and F_3 waves are each 0.03.		
	² The published sign has been changed to be in accord with the baryon-first convention.		

 $(\Gamma_i\Gamma_f)^{1/2}/\Gamma_{\text{total}}$ in $N\bar{K} \rightarrow \Lambda(1890) \rightarrow N\bar{K}^*(892), S=3/2, F\text{-wave}$ $(\Gamma_1\Gamma_{12})^{1/2}/\Gamma$

VALUE	DOCUMENT ID	TECN	COMMENT
-0.11 ± 0.03	ZHANG 13A	DPWA	$\bar{K}N$ multichannel

 $(\Gamma_i\Gamma_f)^{1/2}/\Gamma_{\text{total}}$ in $N\bar{K} \rightarrow \Lambda(1890) \rightarrow \Lambda\omega$ $(\Gamma_1\Gamma_{13})^{1/2}/\Gamma$

VALUE	DOCUMENT ID	TECN	COMMENT
seen	BACCARI 77	IPWA	$K^-p \rightarrow \Lambda\omega$
0.032	¹ NAKKASYAN 75	DPWA	$K^-p \rightarrow \Lambda\omega$
	¹ Found in one of two best solutions.		

 $\Lambda(1890)$ REFERENCES

SARANTSEV 19	EPJ A55 180	A.V. Sarantsev et al.	(BONN, PNPI)
KAMANO 15	PR C92 025205	H. Kamano et al.	(ANL, OSAK)
ZHANG 13A	PR C88 035205	H. Zhang et al.	(KSU)
PDG 82	PL 111B 1	M. Roos et al.	(HELS, CIT, CERN)
GOPAL 80	Toronto Conf. 159	G.P. Gopal	(RHEL) IJP
ALSTON... 78	PR D18 182	M. Alston-Garnjost et al.	(LBL, MTHO+) IJP
Also	PRL 38 1007	M. Alston-Garnjost et al.	(LBL, MTHO+) IJP
CAMERON 78	NP B143 189	W. Cameron et al.	(RHEL, LOIC) IJP
CAMERON 78B	NP B146 327	W. Cameron et al.	(RHEL, LOIC) IJP
BACCARI 77	NC 41A 96	B. Baccari et al.	(SACL, CDEF) IJP
GOPAL 77	NP B119 362	G.P. Gopal et al.	(LOIC, RHEL) IJP
MARTIN 77	NP B127 349	B.R. Martin, M.K. Pidcock, R.G. Moorhouse	(LOUC+) IJP
Also	NP B126 266	B.R. Martin, M.K. Pidcock	(LOUC) IJP
Also	NP B126 285	B.R. Martin, M.K. Pidcock	(LOUC) IJP
HEMINGWAY 75	NP B91 12	R.J. Hemingway et al.	(CERN, HEIDH, MPIM) IJP
NAKKASYAN 75	NP B93 85	A. Nakkasyan	(CERN) IJP
LANGBEIN 72	NP B47 477	W. Langbein, F. Wagner	(MPIM) IJP

 $\Lambda(2000) 1/2^-$ $I(J^P) = 0(\frac{1}{2}^-)$ Status: *

OMITTED FROM SUMMARY TABLE

BARBARO-GALTIERI 70 (in $\Sigma\pi$) and BRANDSTETTER 72 (in $\Lambda\omega$) proposed a state at about this mass. Those analyses are considered to be obsolete, see NAKKASYAN 75 and PDG 18. $\Lambda(2000)$ MASS

VALUE (MeV)	DOCUMENT ID	TECN	COMMENT
≈ 2000 OUR ESTIMATE			
2020 ± 16	ZHANG 13A	DPWA	Multichannel
2030 ± 30	CAMERON 78B	DPWA	$K^-p \rightarrow N\bar{K}^*$

 $\Lambda(2000)$ WIDTH

VALUE (MeV)	DOCUMENT ID	TECN	COMMENT
255 ± 63	ZHANG 13A	DPWA	Multichannel
125 ± 25	CAMERON 78B	DPWA	$K^-p \rightarrow N\bar{K}^*$

 $\Lambda(2000)$ DECAY MODES

Mode	Fraction (Γ_i/Γ)
Γ_1 $N\bar{K}$	(27±6) %
Γ_2 $\Sigma\pi$	
Γ_3 $\Lambda\eta$	(16±7) %
Γ_4 $N\bar{K}^*(892), S=1/2, S\text{-wave}$	
Γ_5 $N\bar{K}^*(892), S=3/2, D\text{-wave}$	

 $\Lambda(2000)$ BRANCHING RATIOSSee "Sign conventions for resonance couplings" in the Note on Λ and Σ Resonances.

$\Gamma(N\bar{K})/\Gamma_{\text{total}}$	DOCUMENT ID	TECN	COMMENT
0.27 ± 0.06	ZHANG 13A	DPWA	Multichannel

 $(\Gamma_i\Gamma_f)^{1/2}/\Gamma_{\text{total}}$ in $N\bar{K} \rightarrow \Lambda(2000) \rightarrow \Sigma\pi$ $(\Gamma_1\Gamma_2)^{1/2}/\Gamma$

VALUE	DOCUMENT ID	TECN	COMMENT
-0.07 ± 0.03	ZHANG 13A	DPWA	Multichannel

 $\Gamma(\Lambda\eta)/\Gamma_{\text{total}}$ Γ_3/Γ

VALUE	DOCUMENT ID	TECN	COMMENT
0.16 ± 0.07	ZHANG 13A	DPWA	Multichannel

 $(\Gamma_i\Gamma_f)^{1/2}/\Gamma_{\text{total}}$ in $N\bar{K} \rightarrow \Lambda(2000) \rightarrow N\bar{K}^*(892), S=1/2, S\text{-wave}$ $(\Gamma_1\Gamma_4)^{1/2}/\Gamma$

VALUE	DOCUMENT ID	TECN	COMMENT
-0.12 ± 0.03	¹ CAMERON 78B	DPWA	$K^-p \rightarrow N\bar{K}^*$
	¹ The published sign has been changed to be in accord with the baryon-first convention.		

 $(\Gamma_i\Gamma_f)^{1/2}/\Gamma_{\text{total}}$ in $N\bar{K} \rightarrow \Lambda(2000) \rightarrow N\bar{K}^*(892), S=3/2, D\text{-wave}$ $(\Gamma_1\Gamma_5)^{1/2}/\Gamma$

VALUE	DOCUMENT ID	TECN	COMMENT
$+0.34 \pm 0.05$	ZHANG 13A	DPWA	Multichannel
$+0.09 \pm 0.03$	CAMERON 78B	DPWA	$K^-p \rightarrow N\bar{K}^*$

 $\Lambda(2000)$ REFERENCES

PDG 18	PR D98 030001	M. Tanabashi et al.	(PDG Collab.)
ZHANG 13A	PR C88 035205	H. Zhang et al.	(KSU)
CAMERON 78B	NP B146 327	W. Cameron et al.	(RHEL, LOIC) IJP
NAKKASYAN 75	NP B93 85	A. Nakkasyan	(CERN) IJP
BRANDSTETTER... 72	NP B39 13	A.A. Brandstetter et al.	(RHEL, CDEF+)
BARBARO... 70	Duke Conf. 173	A. Barbaro-Galtieri	(LRL) IJP
	Hyperon Resonances, 1970		

 $\Lambda(2050) 3/2^-$ $I(J^P) = 0(\frac{3}{2}^-)$ Status: *

OMITTED FROM SUMMARY TABLE

 $\Lambda(2050)$ MASS

VALUE (MeV)	DOCUMENT ID	TECN	COMMENT
2056 ± 22	ZHANG 13A	DPWA	Multichannel

Baryon Particle Listings

 $\Lambda(2050)$, $\Lambda(2070)$ $\Lambda(2050)$ WIDTH

VALUE (MeV)	DOCUMENT ID	TECN	COMMENT
493±61	ZHANG	13A	DPWA Multichannel

 $\Lambda(2050)$ DECAY MODES

Mode	Fraction (Γ_i/Γ)
Γ_1 $N\bar{K}$	(19 ± 4) %
Γ_2 $\Sigma\pi$	(6.0 ± 3.0) %
Γ_3 $\Sigma^*(1385)\pi$, S-wave	(8 ± 6) %
Γ_4 $\Sigma^*(1385)\pi$, D-wave	(4.0 ± 3.0) %
Γ_5 $N\bar{K}^*(892)$, S=1/2	(23 ± 7) %

 $\Lambda(2050)$ BRANCHING RATIOS

$\Gamma(N\bar{K})/\Gamma_{\text{total}}$	Γ_1/Γ		
VALUE	DOCUMENT ID	TECN	COMMENT
0.19±0.04	ZHANG	13A	DPWA Multichannel
$\Gamma(\Sigma\pi)/\Gamma_{\text{total}}$	Γ_2/Γ		
VALUE	DOCUMENT ID	TECN	COMMENT
0.06±0.03	ZHANG	13A	DPWA Multichannel
$\Gamma(\Sigma^*(1385)\pi, \text{S-wave})/\Gamma_{\text{total}}$	Γ_3/Γ		
VALUE	DOCUMENT ID	TECN	COMMENT
0.08±0.06	ZHANG	13A	DPWA Multichannel
$\Gamma(\Sigma^*(1385)\pi, \text{D-wave})/\Gamma_{\text{total}}$	Γ_4/Γ		
VALUE	DOCUMENT ID	TECN	COMMENT
0.04±0.03	ZHANG	13A	DPWA Multichannel
$\Gamma(N\bar{K}^*(892), \text{S}=1/2)/\Gamma_{\text{total}}$	Γ_5/Γ		
VALUE	DOCUMENT ID	TECN	COMMENT
0.23±0.07	ZHANG	13A	DPWA Multichannel

 $\Lambda(2050)$ REFERENCES

ZHANG 13A PR C88 035205 H. Zhang et al. (KSU)

$\Lambda(2070)$ $3/2^+$ $J^P = \frac{3}{2}^+$ Status: *

OMITTED FROM SUMMARY TABLE

 $\Lambda(2070)$ POLE POSITION

REAL PART	DOCUMENT ID	TECN	COMMENT
VALUE (MeV)	SARANTSEV	19	DPWA $\bar{K}N$ multichannel
2044±20			
-2×IMAGINARY PART	DOCUMENT ID	TECN	COMMENT
VALUE (MeV)	SARANTSEV	19	DPWA $\bar{K}N$ multichannel
360±45			

 $\Lambda(2070)$ POLE RESIDUES

Normalized residue in $N\bar{K} \rightarrow \Lambda(2070) \rightarrow N\bar{K}$	DOCUMENT ID	TECN	COMMENT
MODULUS	SARANTSEV	19	DPWA $\bar{K}N$ multichannel
PHASE (°)			
0.15±0.05			
-37 ± 10			
Normalized residue in $N\bar{K} \rightarrow \Lambda(2070) \rightarrow \Sigma\pi$	DOCUMENT ID	TECN	COMMENT
MODULUS	SARANTSEV	19	DPWA $\bar{K}N$ multichannel
PHASE (°)			
0.10±0.03			
-47 ± 8			
Normalized residue in $N\bar{K} \rightarrow \Lambda(2070) \rightarrow \Xi K$	DOCUMENT ID	TECN	COMMENT
MODULUS	SARANTSEV	19	DPWA $\bar{K}N$ multichannel
PHASE (°)			
0.11±0.03			
0 ± 25			
Normalized residue in $N\bar{K} \rightarrow \Lambda(2070) \rightarrow \Lambda\omega, \text{S}=1/2, \text{P-wave}$	DOCUMENT ID	TECN	COMMENT
MODULUS	SARANTSEV	19	DPWA $\bar{K}N$ multichannel
PHASE (°)			
0.10±0.04			
150 ± 17			
Normalized residue in $N\bar{K} \rightarrow \Lambda(2070) \rightarrow \Lambda\omega, \text{S}=3/2, \text{P-wave}$	DOCUMENT ID	TECN	COMMENT
MODULUS	SARANTSEV	19	DPWA $\bar{K}N$ multichannel
PHASE (°)			
0.08±0.04			
20 ± 30			
Normalized residue in $N\bar{K} \rightarrow \Lambda(2070) \rightarrow \Lambda\omega, \text{S}=3/2, \text{F-wave}$	DOCUMENT ID	TECN	COMMENT
MODULUS	SARANTSEV	19	DPWA $\bar{K}N$ multichannel
PHASE (°)			
0.04±0.02			
-175 ± 35			

Normalized residue in $N\bar{K} \rightarrow \Lambda(2070) \rightarrow \Sigma(1385)\pi, \text{P-wave}$

MODULUS	PHASE (°)	DOCUMENT ID	TECN	COMMENT
0.12±0.07	-160 ± 55	SARANTSEV	19	DPWA $\bar{K}N$ multichannel

Normalized residue in $N\bar{K} \rightarrow \Lambda(2070) \rightarrow \Sigma(1385)\pi, \text{F-wave}$

MODULUS	PHASE (°)	DOCUMENT ID	TECN	COMMENT
0.07±0.04	-145 ± 50	SARANTSEV	19	DPWA $\bar{K}N$ multichannel

Normalized residue in $N\bar{K} \rightarrow \Lambda(2070) \rightarrow N\bar{K}^*(892), \text{S}=1/2, \text{P-wave}$

MODULUS	PHASE (°)	DOCUMENT ID	TECN	COMMENT
0.36±0.07	-45 ± 30	SARANTSEV	19	DPWA $\bar{K}N$ multichannel

Normalized residue in $N\bar{K} \rightarrow \Lambda(2070) \rightarrow N\bar{K}^*(892), \text{S}=3/2, \text{P-wave}$

MODULUS	PHASE (°)	DOCUMENT ID	TECN	COMMENT
0.16±0.05	150 ± 35	SARANTSEV	19	DPWA $\bar{K}N$ multichannel

Normalized residue in $N\bar{K} \rightarrow \Lambda(2070) \rightarrow N\bar{K}^*(892), \text{S}=3/2, \text{F-wave}$

MODULUS	PHASE (°)	DOCUMENT ID	TECN	COMMENT
0.14±0.08	-50 ± 30	SARANTSEV	19	DPWA $\bar{K}N$ multichannel

 $\Lambda(2070)$ MASS

VALUE (MeV)	DOCUMENT ID	TECN	COMMENT
2070±24	SARANTSEV	19	DPWA $\bar{K}N$ multichannel

 $\Lambda(2070)$ WIDTH

VALUE (MeV)	DOCUMENT ID	TECN	COMMENT
370±50	SARANTSEV	19	DPWA $\bar{K}N$ multichannel

 $\Lambda(2070)$ DECAY MODES

Mode	Fraction (Γ_i/Γ)
Γ_1 $N\bar{K}$	(12 ± 5) %
Γ_2 $\Sigma\pi$	(7.0 ± 3.0) %
Γ_3 ΞK	(7.0 ± 3.0) %
Γ_4 $\Lambda\omega, \text{S}=1/2, \text{P-wave}$	(7 ± 4) %
Γ_5 $\Lambda\omega, \text{S}=3/2, \text{P-wave}$	(3.0 ± 2.0) %
Γ_6 $\Lambda\omega, \text{S}=3/2, \text{F-wave}$	(1.0 ± 1.0) %
Γ_7 $\Sigma(1385)\pi, \text{P-wave}$	(10 ± 5) %
Γ_8 $\Sigma(1385)\pi, \text{F-wave}$	(2.0 ± 2.0) %
Γ_9 $N\bar{K}^*(892), \text{S}=1/2, \text{P-wave}$	(42 ± 8) %
Γ_{10} $N\bar{K}^*(892), \text{S}=3/2, \text{P-wave}$	(14 ± 6) %
Γ_{11} $N\bar{K}^*(892), \text{S}=3/2, \text{F-wave}$	(10 ± 6) %

 $\Lambda(2070)$ BRANCHING RATIOS

$\Gamma(N\bar{K})/\Gamma_{\text{total}}$	Γ_1/Γ		
VALUE	DOCUMENT ID	TECN	COMMENT
0.12±0.05	SARANTSEV	19	DPWA $\bar{K}N$ multichannel
$\Gamma(\Sigma\pi)/\Gamma_{\text{total}}$	Γ_2/Γ		
VALUE	DOCUMENT ID	TECN	COMMENT
0.07±0.03	SARANTSEV	19	DPWA $\bar{K}N$ multichannel
$\Gamma(\Xi K)/\Gamma_{\text{total}}$	Γ_3/Γ		
VALUE	DOCUMENT ID	TECN	COMMENT
0.07±0.03	SARANTSEV	19	DPWA $\bar{K}N$ multichannel
$\Gamma(\Lambda\omega, \text{S}=1/2, \text{P-wave})/\Gamma_{\text{total}}$	Γ_4/Γ		
VALUE	DOCUMENT ID	TECN	COMMENT
0.07±0.04	SARANTSEV	19	DPWA $\bar{K}N$ multichannel
$\Gamma(\Lambda\omega, \text{S}=3/2, \text{P-wave})/\Gamma_{\text{total}}$	Γ_5/Γ		
VALUE	DOCUMENT ID	TECN	COMMENT
0.03±0.02	SARANTSEV	19	DPWA $\bar{K}N$ multichannel
$\Gamma(\Lambda\omega, \text{S}=3/2, \text{F-wave})/\Gamma_{\text{total}}$	Γ_6/Γ		
VALUE	DOCUMENT ID	TECN	COMMENT
0.01±0.01	SARANTSEV	19	DPWA $\bar{K}N$ multichannel
$\Gamma(\Sigma(1385)\pi, \text{P-wave})/\Gamma_{\text{total}}$	Γ_7/Γ		
VALUE	DOCUMENT ID	TECN	COMMENT
0.10±0.05	SARANTSEV	19	DPWA $\bar{K}N$ multichannel
$\Gamma(\Sigma(1385)\pi, \text{F-wave})/\Gamma_{\text{total}}$	Γ_8/Γ		
VALUE	DOCUMENT ID	TECN	COMMENT
0.02±0.02	SARANTSEV	19	DPWA $\bar{K}N$ multichannel
$\Gamma(N\bar{K}^*(892), \text{S}=1/2, \text{P-wave})/\Gamma_{\text{total}}$	Γ_9/Γ		
VALUE	DOCUMENT ID	TECN	COMMENT
0.42±0.08	SARANTSEV	19	DPWA $\bar{K}N$ multichannel

See key on page 1171

Baryon Particle Listings
 $\Lambda(2070)$, $\Lambda(2080)$, $\Lambda(2085)$

$\Gamma(N\bar{K}^*(892), S=3/2, P\text{-wave})/\Gamma_{\text{total}}$				Γ_{10}/Γ
VALUE	DOCUMENT ID	TECN	COMMENT	
0.14 ± 0.06	SARANTSEV 19	DPWA	$\bar{K}N$ multichannel	

$\Gamma(N\bar{K}^*(892), S=3/2, F\text{-wave})/\Gamma_{\text{total}}$				Γ_{11}/Γ
VALUE	DOCUMENT ID	TECN	COMMENT	
0.10 ± 0.06	SARANTSEV 19	DPWA	$\bar{K}N$ multichannel	

 $\Lambda(2070)$ REFERENCES

SARANTSEV 19 EPJ A55 180 A.V. Sarantsev et al. (BONN, PNPI)

$\Lambda(2080) 5/2^-$	$J^P = \frac{5}{2}^-$	Status: *
-----------------------	-----------------------	-----------

OMITTED FROM SUMMARY TABLE

 $\Lambda(2080)$ POLE POSITION

REAL PART			
VALUE (MeV)	DOCUMENT ID	TECN	COMMENT
2070 ± 15	SARANTSEV 19	DPWA	$\bar{K}N$ multichannel

-2xIMAGINARY PART			
VALUE (MeV)	DOCUMENT ID	TECN	COMMENT
172 ± 28	SARANTSEV 19	DPWA	$\bar{K}N$ multichannel

 $\Lambda(2080)$ POLE RESIDUES

Normalized residue in $N\bar{K} \rightarrow \Lambda(2080) \rightarrow N\bar{K}$				
MODULUS	PHASE ($^\circ$)	DOCUMENT ID	TECN	COMMENT
0.12 ± 0.03	-35 ± 22	SARANTSEV 19	DPWA	$\bar{K}N$ multichannel

Normalized residue in $N\bar{K} \rightarrow \Lambda(2080) \rightarrow \Sigma\pi$				
MODULUS	PHASE ($^\circ$)	DOCUMENT ID	TECN	COMMENT
0.07 ± 0.03	11 ± 16	SARANTSEV 19	DPWA	$\bar{K}N$ multichannel

Normalized residue in $N\bar{K} \rightarrow \Lambda(2080) \rightarrow \Xi K$				
MODULUS	PHASE ($^\circ$)	DOCUMENT ID	TECN	COMMENT
0.06 ± 0.02	115 ± 20	SARANTSEV 19	DPWA	$\bar{K}N$ multichannel

Normalized residue in $N\bar{K} \rightarrow \Lambda(2080) \rightarrow \Lambda\omega, S=1/2, D\text{-wave}$				
MODULUS	PHASE ($^\circ$)	DOCUMENT ID	TECN	COMMENT
0.06 ± 0.03	115 ± 25	SARANTSEV 19	DPWA	$\bar{K}N$ multichannel

Normalized residue in $N\bar{K} \rightarrow \Lambda(2080) \rightarrow \Lambda\omega, S=3/2, D\text{-wave}$				
MODULUS	PHASE ($^\circ$)	DOCUMENT ID	TECN	COMMENT
0.09 ± 0.03	-10 ± 35	SARANTSEV 19	DPWA	$\bar{K}N$ multichannel

Normalized residue in $N\bar{K} \rightarrow \Lambda(2080) \rightarrow \Sigma(1385)\pi, D\text{-wave}$				
MODULUS	PHASE ($^\circ$)	DOCUMENT ID	TECN	COMMENT
0.14 ± 0.04	155 ± 45	SARANTSEV 19	DPWA	$\bar{K}N$ multichannel

Normalized residue in $N\bar{K} \rightarrow \Lambda(2080) \rightarrow \Sigma(1385)\pi, G\text{-wave}$				
MODULUS	PHASE ($^\circ$)	DOCUMENT ID	TECN	COMMENT
0.05 ± 0.03	30 ± 45	SARANTSEV 19		$\bar{K}N$ multichannel

Normalized residue in $N\bar{K} \rightarrow \Lambda(2080) \rightarrow N\bar{K}^*(892), S=1/2, D\text{-wave}$				
MODULUS	PHASE ($^\circ$)	DOCUMENT ID	TECN	COMMENT
0.16 ± 0.08	-120 ± 50	SARANTSEV 19	DPWA	$\bar{K}N$ multichannel

Normalized residue in $N\bar{K} \rightarrow \Lambda(2080) \rightarrow N\bar{K}^*(892), S=3/2, D\text{-wave}$				
MODULUS	PHASE ($^\circ$)	DOCUMENT ID	TECN	COMMENT
0.20 ± 0.14	60 ± 50	SARANTSEV 19	DPWA	$\bar{K}N$ multichannel

 $\Lambda(2080)$ MASS

VALUE (MeV)	DOCUMENT ID	TECN	COMMENT
2082 ± 13	SARANTSEV 19	DPWA	$\bar{K}N$ multichannel

 $\Lambda(2080)$ WIDTH

VALUE (MeV)	DOCUMENT ID	TECN	COMMENT
181 ± 29	SARANTSEV 19	DPWA	$\bar{K}N$ multichannel

 $\Lambda(2080)$ DECAY MODES

Mode	Fraction (Γ_i/Γ)
$\Gamma_1 N\bar{K}$	$(11.0 \pm 3.0) \%$
$\Gamma_2 \Sigma\pi$	$(5.0 \pm 2.0) \%$
$\Gamma_3 \Xi K$	$(4.0 \pm 1.0) \%$
$\Gamma_4 \Lambda\omega, S=1/2, D\text{-wave}$	$(4.0 \pm 2.0) \%$

$\Gamma_5 \Lambda\omega, S=3/2, D\text{-wave}$	$(8.0 \pm 3.0) \%$
$\Gamma_6 \Sigma(1385)\pi, D\text{-wave}$	$(15 \pm 5) \%$
$\Gamma_7 \Sigma(1385)\pi, G\text{-wave}$	$(3.0 \pm 2.0) \%$
$\Gamma_8 N\bar{K}^*(892), S=1/2, D\text{-wave}$	$(17 \pm 9) \%$
$\Gamma_9 N\bar{K}^*(892), S=3/2, D\text{-wave}$	$(25 \pm 16) \%$

 $\Lambda(2080)$ BRANCHING RATIOS

$\Gamma(N\bar{K})/\Gamma_{\text{total}}$	Γ_1/Γ			
VALUE	DOCUMENT ID	TECN	COMMENT	
0.11 ± 0.03	SARANTSEV 19	DPWA	$\bar{K}N$ multichannel	

$\Gamma(\Sigma\pi)/\Gamma_{\text{total}}$	Γ_2/Γ			
VALUE	DOCUMENT ID	TECN	COMMENT	
0.05 ± 0.02	SARANTSEV 19	DPWA	$\bar{K}N$ multichannel	

$\Gamma(\Xi K)/\Gamma_{\text{total}}$	Γ_3/Γ			
VALUE	DOCUMENT ID	TECN	COMMENT	
0.04 ± 0.01	SARANTSEV 19	DPWA	$\bar{K}N$ multichannel	

$\Gamma(\Lambda\omega, S=1/2, D\text{-wave})/\Gamma_{\text{total}}$	Γ_4/Γ			
VALUE	DOCUMENT ID	TECN	COMMENT	
0.04 ± 0.02	SARANTSEV 19	DPWA	$\bar{K}N$ multichannel	

$\Gamma(\Lambda\omega, S=3/2, D\text{-wave})/\Gamma_{\text{total}}$	Γ_5/Γ			
VALUE	DOCUMENT ID	TECN	COMMENT	
0.08 ± 0.03	SARANTSEV 19	DPWA	$\bar{K}N$ multichannel	

$\Gamma(\Sigma(1385)\pi, D\text{-wave})/\Gamma_{\text{total}}$	Γ_6/Γ			
VALUE	DOCUMENT ID	TECN	COMMENT	
0.15 ± 0.05	SARANTSEV 19	DPWA	$\bar{K}N$ multichannel	

$\Gamma(\Sigma(1385)\pi, G\text{-wave})/\Gamma_{\text{total}}$	Γ_7/Γ			
VALUE	DOCUMENT ID	TECN	COMMENT	
0.03 ± 0.02	SARANTSEV 19	DPWA	$\bar{K}N$ multichannel	

$\Gamma(N\bar{K}^*(892), S=1/2, D\text{-wave})/\Gamma_{\text{total}}$	Γ_8/Γ			
VALUE	DOCUMENT ID	TECN	COMMENT	
0.17 ± 0.09	SARANTSEV 19	DPWA	$\bar{K}N$ multichannel	

$\Gamma(N\bar{K}^*(892), S=3/2, D\text{-wave})/\Gamma_{\text{total}}$	Γ_9/Γ			
VALUE	DOCUMENT ID	TECN	COMMENT	
0.25 ± 0.16	SARANTSEV 19	DPWA	$\bar{K}N$ multichannel	

 $\Lambda(2080)$ REFERENCES

SARANTSEV 19 EPJ A55 180 A.V. Sarantsev et al. (BONN, PNPI)

$\Lambda(2085) 7/2^+$	$J^P = 0(\frac{7}{2}^+)$	Status: **
-----------------------	--------------------------	------------

OMITTED FROM SUMMARY TABLE
was $\Lambda(2020)$

In LITCHFIELD 71, need for the state rests solely on a possibly inconsistent polarization measurement at 1.784 GeV/c. HEMINGWAY 75 does not require this state. GOPAL 77 does not need it in either $N\bar{K}$ or $\Sigma\pi$. With new K^-n angular distributions included, DECLAIS 77 sees it. However, this and other new data are included in GOPAL 80 and the state is not required. BACCARI 77 weakly supports it.

 $\Lambda(2085)$ POLE POSITION

REAL PART			
VALUE	DOCUMENT ID	TECN	COMMENT
••• We do not use the following data for averages, fits, limits, etc. •••			
1757	¹ KAMANO 15	DPWA	Multichannel
	¹ From the preferred solution A in KAMANO 15. Solution B reports $M = 2041^{+80}_{-82}$ MeV.		

-2xIMAGINARY PART			
VALUE	DOCUMENT ID	TECN	COMMENT
••• We do not use the following data for averages, fits, limits, etc. •••			
146	¹ KAMANO 15	DPWA	Multichannel
	¹ From the preferred solution A in KAMANO 15. Solution B reports $M = 238^{+114}_{-34}$ MeV.		

 $\Lambda(2085)$ POLE RESIDUESThe normalized residue is the residue divided by $\Gamma_{\text{pole}}/2$.

Normalized residue in $N\bar{K} \rightarrow \Lambda(2085) \rightarrow N\bar{K}$				
MODULUS	PHASE ($^\circ$)	DOCUMENT ID	TECN	COMMENT
••• We do not use the following data for averages, fits, limits, etc. •••				
0.000145	-77	¹ KAMANO 15	DPWA	Multichannel
		¹ From the preferred solution A in KAMANO 15.		

Baryon Particle Listings

 $\Lambda(2085), \Lambda(2100)$ Normalized residue in $N\bar{K} \rightarrow \Lambda(2085) \rightarrow \Sigma\pi$

MODULUS	PHASE ($^\circ$)	DOCUMENT ID	TECN	COMMENT
0.0112	120	¹ KAMANO 15	DPWA	Multichannel
¹ From the preferred solution A in KAMANO 15.				

Normalized residue in $N\bar{K} \rightarrow \Lambda(2085) \rightarrow \Lambda\eta$

MODULUS	PHASE ($^\circ$)	DOCUMENT ID	TECN	COMMENT
0.000786	-100	¹ KAMANO 15	DPWA	Multichannel
¹ From the preferred solution A in KAMANO 15.				

Normalized residue in $N\bar{K} \rightarrow \Lambda(2085) \rightarrow \Sigma(1385)\pi, F\text{-wave}$

MODULUS	PHASE ($^\circ$)	DOCUMENT ID	TECN	COMMENT
0.00451	-82	¹ KAMANO 15	DPWA	Multichannel
¹ From the preferred solution A in KAMANO 15.				

Normalized residue in $N\bar{K} \rightarrow \Lambda(2085) \rightarrow \Sigma(1385)\pi, H\text{-wave}$

MODULUS	PHASE ($^\circ$)	DOCUMENT ID	TECN	COMMENT
0.0000298	-128	¹ KAMANO 15	DPWA	Multichannel
¹ From the preferred solution A in KAMANO 15.				

 $\Lambda(2085)$ MASS

VALUE (MeV)	DOCUMENT ID	TECN	COMMENT
≈ 2020 OUR ESTIMATE			
2043 \pm 22	ZHANG 13A	DPWA	Multichannel
2140	BACCARI 77	DPWA	$K^-p \rightarrow \Lambda\omega$
2117	DECLAIS 77	DPWA	$\bar{K}N \rightarrow \bar{K}N$
2100 \pm 30	LITCHFIELD 71	DPWA	$K^-p \rightarrow \bar{K}N$
2020 \pm 20	BARBARO... 70	DPWA	$K^-p \rightarrow \Sigma\pi$

 $\Lambda(2085)$ WIDTH

VALUE (MeV)	DOCUMENT ID	TECN	COMMENT
200 \pm 75	ZHANG 13A	DPWA	Multichannel
128	BACCARI 77	DPWA	$K^-p \rightarrow \Lambda\omega$
167	DECLAIS 77	DPWA	$\bar{K}N \rightarrow \bar{K}N$
120 \pm 30	LITCHFIELD 71	DPWA	$K^-p \rightarrow \bar{K}N$
160 \pm 30	BARBARO... 70	DPWA	$K^-p \rightarrow \Sigma\pi$

 $\Lambda(2085)$ DECAY MODES

Mode	Fraction (Γ_i/Γ)
Γ_1 $N\bar{K}$	
Γ_2 $\Sigma\pi$	
Γ_3 $\Lambda\eta$	
Γ_4 $\Sigma(1385)\pi, F\text{-wave}$	
Γ_5 $\Sigma(1385)\pi, H\text{-wave}$	
Γ_6 $N\bar{K}^*(892), S=1/2$	(30 \pm 9) %
Γ_7 $N\bar{K}^*(892), S=1/2, F\text{-wave}$	
Γ_8 $N\bar{K}^*(892), S=3/2, F\text{-wave}$	
Γ_9 $N\bar{K}^*(892), S=3/2, H\text{-wave}$	
Γ_{10} $\Lambda\omega$	

 $\Lambda(2085)$ BRANCHING RATIOS

See "Sign conventions for resonance couplings" in the Note on Λ and Σ Resonances.

$\Gamma(N\bar{K})/\Gamma_{\text{total}}$	DOCUMENT ID	TECN	COMMENT	Γ_1/Γ
0.028 \pm 0.005	ZHANG 13A	DPWA	Multichannel	
0.05	DECLAIS 77	DPWA	$\bar{K}N \rightarrow \bar{K}N$	
0.05 \pm 0.02	LITCHFIELD 71	DPWA	$K^-p \rightarrow \bar{K}N$	
not seen	¹ KAMANO 15	DPWA	Multichannel	
¹ From the preferred solution A in KAMANO 15.				

$\Gamma(\Sigma\pi)/\Gamma_{\text{total}}$	DOCUMENT ID	TECN	COMMENT	Γ_2/Γ
0.891	¹ KAMANO 15	DPWA	Multichannel	
¹ From the preferred solution A in KAMANO 15.				

$\Gamma(\Lambda\eta)/\Gamma_{\text{total}}$	DOCUMENT ID	TECN	COMMENT	Γ_3/Γ
0.002	¹ KAMANO 15	DPWA	Multichannel	
¹ From the preferred solution A in KAMANO 15.				

$\Gamma(\Sigma(1385)\pi, F\text{-wave})/\Gamma_{\text{total}}$	DOCUMENT ID	TECN	COMMENT	Γ_4/Γ
0.105	¹ KAMANO 15	DPWA	Multichannel	
¹ From the preferred solution A in KAMANO 15.				

$\Gamma(\Sigma(1385)\pi, H\text{-wave})/\Gamma_{\text{total}}$	DOCUMENT ID	TECN	COMMENT	Γ_5/Γ
not seen	¹ KAMANO 15	DPWA	Multichannel	
¹ From the preferred solution A in KAMANO 15.				

$\Gamma(N\bar{K}^*(892), S=1/2, F\text{-wave})/\Gamma_{\text{total}}$	DOCUMENT ID	TECN	COMMENT	Γ_7/Γ
not seen	¹ KAMANO 15	DPWA	Multichannel	
¹ From the preferred solution A in KAMANO 15.				

$\Gamma(N\bar{K}^*(892), S=3/2, F\text{-wave})/\Gamma_{\text{total}}$	DOCUMENT ID	TECN	COMMENT	Γ_8/Γ
0.001	¹ KAMANO 15	DPWA	Multichannel	
¹ From the preferred solution A in KAMANO 15.				

$\Gamma(N\bar{K}^*(892), S=3/2, H\text{-wave})/\Gamma_{\text{total}}$	DOCUMENT ID	TECN	COMMENT	Γ_9/Γ
not seen	¹ KAMANO 15	DPWA	Multichannel	
¹ From the preferred solution A in KAMANO 15.				

$\Gamma(N\bar{K}^*(892), S=1/2)/\Gamma_{\text{total}}$	DOCUMENT ID	TECN	COMMENT	Γ_6/Γ
0.30 \pm 0.09	ZHANG 13A	DPWA	Multichannel	

$(\Gamma_i\Gamma_j)^{1/2}/\Gamma_{\text{total}}$ in $N\bar{K} \rightarrow \Lambda(2085) \rightarrow \Sigma\pi$	DOCUMENT ID	TECN	COMMENT	$(\Gamma_1\Gamma_2)^{1/2}/\Gamma$
+0.02 \pm 0.01	ZHANG 13A	DPWA	Multichannel	
-0.15 \pm 0.02	BARBARO... 70	DPWA	$K^-p \rightarrow \Sigma\pi$	

$(\Gamma_i\Gamma_j)^{1/2}/\Gamma_{\text{total}}$ in $N\bar{K} \rightarrow \Lambda(2085) \rightarrow \Lambda\omega$	DOCUMENT ID	TECN	COMMENT	$(\Gamma_1\Gamma_{10})^{1/2}/\Gamma$
<0.05	BACCARI 77	DPWA	$K^-p \rightarrow \Lambda\omega$	

 $\Lambda(2085)$ REFERENCES

KAMANO 15	PR C92 025205	H. Kamano <i>et al.</i>	(ANL, OSAK)
ZHANG 13A	PR C88 035205	H. Zhang <i>et al.</i>	(KSU)
GOPAL 80	Toronto Conf. 159	G.P. Gopal	(RHEL)
BACCARI 77	NC 41A 96	B. Baccari <i>et al.</i>	(SACL, CDEF) IJP
DECLAIS 77	CERN 77-16	Y. Declais <i>et al.</i>	(CAEN, CERN) IJP
GOPAL 77	NP B19 362	G.P. Gopal <i>et al.</i>	(LOIC, RHEL)
HEMINGWAY 75	NP B91 12	R.J. Hemingway <i>et al.</i>	(CERN, HEIDH, MFM) IJP
LITCHFIELD 71	NP B30 125	P.J. Litchfield <i>et al.</i>	(RHEL, CDEF, SACL) IJP
BARBARO... 70	Duke Conf. 173	A. Barbaro-Galieri	(LRL) IJP
Hyperon Resonances, 1970			

 $\Lambda(2100) 7/2^-$

$$I(J^P) = 0(\frac{7}{2}^-) \text{ Status: } ***$$

Most of the results published before 1973 are now obsolete and have been omitted. They may be found in our 1982 edition Physics Letters **111B** 1 (1982).

This entry only includes results from partial-wave analyses. Parameters of peaks seen in cross sections and in invariant-mass distributions around 2100 MeV used to be listed in a separate entry immediately following. It may be found in our 1986 edition Physics Letters **170B** 1 (1986).

 $\Lambda(2100)$ POLE POSITION

REAL PART	DOCUMENT ID	TECN	COMMENT
2040 \pm 14	SARANTSEV 19	DPWA	$\bar{K}N$ multichannel
2023	ZHANG 13A	DPWA	Multichannel

See key on page 1171

Baryon Particle Listings

 $\Lambda(2100)$ $-2\times$ IMAGINARY PART

VALUE (MeV)	DOCUMENT ID	TECN	COMMENT
215 ± 29	SARANTSEV 19	DPWA	$\bar{K}N$ multichannel
• • • We do not use the following data for averages, fits, limits, etc. • • •			
239	ZHANG 13A	DPWA	Multichannel

 $\Lambda(2100)$ POLE RESIDUEThe "normalized residue" is the residue divided by $\Gamma_{pole}/2$.Normalized residue in $N\bar{K} \rightarrow \Lambda(2100) \rightarrow N\bar{K}$

MODULUS	PHASE (°)	DOCUMENT ID	TECN	COMMENT
0.28 ± 0.06	-40 ± 10	SARANTSEV 19	DPWA	$\bar{K}N$ multichannel

Normalized residue in $N\bar{K} \rightarrow \Lambda(2100) \rightarrow \Sigma\pi$

MODULUS	PHASE (°)	DOCUMENT ID	TECN	COMMENT
0.09 ± 0.02	-35 ± 15	SARANTSEV 19	DPWA	$\bar{K}N$ multichannel

Normalized residue in $N\bar{K} \rightarrow \Lambda(2100) \rightarrow \Sigma(1385)\pi, D$ -wave

MODULUS	PHASE (°)	DOCUMENT ID	TECN	COMMENT
0.04 ± 0.03		SARANTSEV 19	DPWA	$\bar{K}N$ multichannel

Normalized residue in $N\bar{K} \rightarrow \Lambda(2100) \rightarrow \Sigma(1385)\pi, G$ -wave

MODULUS	PHASE (°)	DOCUMENT ID	TECN	COMMENT
0.06 ± 0.03	-45 ± 15	SARANTSEV 19	DPWA	$\bar{K}N$ multichannel

Normalized residue in $N\bar{K} \rightarrow \Lambda(2100) \rightarrow N\bar{K}^*(892), S=3/2, D$ -wave

MODULUS	PHASE (°)	DOCUMENT ID	TECN	COMMENT
0.11 ± 0.06	-30 ± 30	SARANTSEV 19	DPWA	$\bar{K}N$ multichannel

 $\Lambda(2100)$ MASS

VALUE (MeV)	DOCUMENT ID	TECN	COMMENT
2090 to 2110 (≈ 2100) OUR ESTIMATE			
2090 ± 15	SARANTSEV 19	DPWA	$\bar{K}N$ multichannel
2086 ± 6	ZHANG 13A	DPWA	Multichannel
2104 ± 10	GOPAL 80	DPWA	$\bar{K}N \rightarrow \bar{K}N$
2106 ± 30	DEBELLEFON 78	DPWA	$\bar{K}N \rightarrow \bar{K}N$
2110 ± 10	GOPAL 77	DPWA	$\bar{K}N$ multichannel
2105 ± 10	HEMINGWAY 75	DPWA	$K^-p \rightarrow \bar{K}N$
2115 ± 10	KANE 74	DPWA	$K^-p \rightarrow \Sigma\pi$
• • • We do not use the following data for averages, fits, limits, etc. • • •			
2094	BACCARI 77	DPWA	$K^-p \rightarrow \Lambda\omega$
2094	DECLAIS 77	DPWA	$\bar{K}N \rightarrow \bar{K}N$
2110 or 2089	¹ NAKKASYAN 75	DPWA	$K^-p \rightarrow \Lambda\omega$

 $\Lambda(2100)$ WIDTH

VALUE (MeV)	DOCUMENT ID	TECN	COMMENT
100 to 250 (≈ 200) OUR ESTIMATE			
290 ± 30	SARANTSEV 19	DPWA	$\bar{K}N$ multichannel
305 ± 16	ZHANG 13A	DPWA	Multichannel
157 ± 40	DEBELLEFON 78	DPWA	$\bar{K}N \rightarrow \bar{K}N$
250 ± 30	GOPAL 77	DPWA	$\bar{K}N$ multichannel
241 ± 30	HEMINGWAY 75	DPWA	$K^-p \rightarrow \bar{K}N$
152 ± 15	KANE 74	DPWA	$K^-p \rightarrow \Sigma\pi$
• • • We do not use the following data for averages, fits, limits, etc. • • •			
98	BACCARI 77	DPWA	$K^-p \rightarrow \Lambda\omega$
250	DECLAIS 77	DPWA	$\bar{K}N \rightarrow \bar{K}N$
244 or 302	¹ NAKKASYAN 75	DPWA	$K^-p \rightarrow \Lambda\omega$

 $\Lambda(2100)$ DECAY MODES

Mode	Fraction (Γ_i/Γ)
Γ_1 $N\bar{K}$	25–35 %
Γ_2 $\Sigma\pi$	~ 5 %
Γ_3 $\Lambda\eta$	<3 %
Γ_4 ΞK	<3 %
Γ_5 $\Lambda\omega$	<8 %
Γ_6 $\Sigma(1385)\pi, D$ -wave	
Γ_7 $\Sigma(1385)\pi, G$ -wave	(1.0 ± 1.0) %
Γ_8 $N\bar{K}^*(892)$	10–20 %
Γ_9 $N\bar{K}^*(892), S=3/2, D$ -wave	(4.0 ± 2.0) %
Γ_{10} $N\bar{K}^*(892), S=1/2, G$ -wave	
Γ_{11} $N\bar{K}^*(892), S=3/2, G$ -wave	

 $\Lambda(2100)$ BRANCHING RATIOSSee "Sign conventions for resonance couplings" in the Note on Λ and Σ Resonances. $\Gamma(N\bar{K})/\Gamma_{total}$

VALUE	DOCUMENT ID	TECN	COMMENT	Γ_1/Γ
0.25 to 0.35 (≈ 0.30) OUR ESTIMATE				
0.24 ± 0.05	SARANTSEV 19	DPWA	$\bar{K}N$ multichannel	
0.23 ± 0.01	ZHANG 13A	DPWA	Multichannel	
0.34 ± 0.03	GOPAL 80	DPWA	$\bar{K}N \rightarrow \bar{K}N$	
0.24 ± 0.06	DEBELLEFON 78	DPWA	$\bar{K}N \rightarrow \bar{K}N$	
0.31 ± 0.03	HEMINGWAY 75	DPWA	$K^-p \rightarrow \bar{K}N$	
• • • We do not use the following data for averages, fits, limits, etc. • • •				
0.29	DECLAIS 77	DPWA	$\bar{K}N \rightarrow \bar{K}N$	
0.30 ± 0.03	GOPAL 77	DPWA	See GOPAL 80	

 $\Gamma(\Sigma\pi)/\Gamma_{total}$

VALUE	DOCUMENT ID	TECN	COMMENT	Γ_2/Γ
0.030 ± 0.015	SARANTSEV 19	DPWA	$\bar{K}N$ multichannel	

 $\Gamma(\Sigma(1385)\pi, D$ -wave)/ Γ_{total}

VALUE	DOCUMENT ID	TECN	COMMENT	Γ_6/Γ
<0.01	SARANTSEV 19	DPWA	$\bar{K}N$ multichannel	

 $\Gamma(\Sigma(1385)\pi, G$ -wave)/ Γ_{total}

VALUE	DOCUMENT ID	TECN	COMMENT	Γ_7/Γ
0.01 ± 0.01	SARANTSEV 19	DPWA	$\bar{K}N$ multichannel	

 $\Gamma(N\bar{K}^*(892), S=3/2, D$ -wave)/ Γ_{total}

VALUE	DOCUMENT ID	TECN	COMMENT	Γ_9/Γ
0.04 ± 0.02	SARANTSEV 19	DPWA	$\bar{K}N$ multichannel	

 $(\Gamma_i\Gamma_f)^{1/2}/\Gamma_{total}$ in $N\bar{K} \rightarrow \Lambda(2100) \rightarrow \Sigma\pi$

VALUE	DOCUMENT ID	TECN	COMMENT	$(\Gamma_1\Gamma_2)^{1/2}/\Gamma$
+0.03 ± 0.01	ZHANG 13A	DPWA	Multichannel	
+0.12 ± 0.04	GOPAL 77	DPWA	$\bar{K}N$ multichannel	
+0.11 ± 0.01	KANE 74	DPWA	$K^-p \rightarrow \Sigma\pi$	

 $(\Gamma_i\Gamma_f)^{1/2}/\Gamma_{total}$ in $N\bar{K} \rightarrow \Lambda(2100) \rightarrow \Lambda\eta$

VALUE	DOCUMENT ID	TECN	COMMENT	$(\Gamma_1\Gamma_3)^{1/2}/\Gamma$
-0.050 ± 0.020	RADER 73	MPWA	$K^-p \rightarrow \Lambda\eta$	

 $(\Gamma_i\Gamma_f)^{1/2}/\Gamma_{total}$ in $N\bar{K} \rightarrow \Lambda(2100) \rightarrow \Xi K$

VALUE	DOCUMENT ID	TECN	COMMENT	$(\Gamma_1\Gamma_4)^{1/2}/\Gamma$
0.035 ± 0.018	LITCHEFIELD 71	DPWA	$K^-p \rightarrow \Xi K$	
• • • We do not use the following data for averages, fits, limits, etc. • • •				
0.003	MULLER 69B	DPWA	$K^-p \rightarrow \Xi K$	
0.05	TRIPP 67	RVUE	$K^-p \rightarrow \Xi K$	

 $(\Gamma_i\Gamma_f)^{1/2}/\Gamma_{total}$ in $N\bar{K} \rightarrow \Lambda(2100) \rightarrow \Lambda\omega$

VALUE	DOCUMENT ID	TECN	COMMENT	$(\Gamma_1\Gamma_5)^{1/2}/\Gamma$
-0.070	² BACCARI 77	DPWA	GD_{37} wave	
+0.011	² BACCARI 77	DPWA	GG_{17} wave	
+0.008	² BACCARI 77	DPWA	GG_{37} wave	
0.122 or 0.154	¹ NAKKASYAN 75	DPWA	$K^-p \rightarrow \Lambda\omega$	

 $(\Gamma_i\Gamma_f)^{1/2}/\Gamma_{total}$ in $N\bar{K} \rightarrow \Lambda(2100) \rightarrow N\bar{K}^*(892), S=3/2, D$ -wave

VALUE	DOCUMENT ID	TECN	COMMENT	$(\Gamma_1\Gamma_9)^{1/2}/\Gamma$
+0.16 ± 0.02	ZHANG 13A	DPWA	Multichannel	
+0.21 ± 0.04	CAMERON 78B	DPWA	$K^-p \rightarrow N\bar{K}^*$	

 $(\Gamma_i\Gamma_f)^{1/2}/\Gamma_{total}$ in $N\bar{K} \rightarrow \Lambda(2100) \rightarrow N\bar{K}^*(892), S=1/2, G$ -wave

VALUE	DOCUMENT ID	TECN	COMMENT	$(\Gamma_1\Gamma_{10})^{1/2}/\Gamma$
-0.03 ± 0.02	ZHANG 13A	DPWA	Multichannel	
-0.04 ± 0.03	³ CAMERON 78B	DPWA	$K^-p \rightarrow N\bar{K}^*$	

 $(\Gamma_i\Gamma_f)^{1/2}/\Gamma_{total}$ in $N\bar{K} \rightarrow \Lambda(2100) \rightarrow N\bar{K}^*(892), S=3/2, G$ -wave

VALUE	DOCUMENT ID	TECN	COMMENT	$(\Gamma_1\Gamma_{11})^{1/2}/\Gamma$
+0.08 ± 0.02	ZHANG 13A	DPWA	Multichannel	

 $\Lambda(2100)$ FOOTNOTES¹ The NAKKASYAN 75 values are from the two best solutions found. Each has the $\Lambda(2100)$ and one additional resonance (P_3 or F_5).² Note that the three for BACCARI 77 entries are for three different waves.³ The published sign has been changed to be in accord with the baryon-sign convention. The upper limit on the G_3 wave is 0.03.

Baryon Particle Listings

 $\Lambda(2100), \Lambda(2110)$ $\Lambda(2100)$ REFERENCES

SARANTSEV	19	EPJ A55 180	A.V. Sarantsev et al.	(BONN, PNPI)
ZHANG	13A	PR C08 035205	H. Zhang et al.	(KSU)
PDG	86	PL 170B 1	M. Aguilar-Benitez et al.	(CERN, CIT+)
PDG	82	PL 111B 1	M. Roos et al.	(HEL5, CIT, CERN)
GOPAL	80	Toronto Conf. 159	G.P. Gopal	(RHEL) IJP
CAMERON	78B	NP B146 327	W. Cameron et al.	(RHEL, LOIC) IJP
DEBELLEFON	78	NC 42A 403	A. de Bellefon et al.	(CDEF, SA CL) IJP
BACCARI	77	NC 41A 96	B. Baccari et al.	(SACL, CDEF) IJP
DECLAIS	77	CERN 77-16	Y. Declais et al.	(CAEN, CERN) IJP
GOPAL	77	NP B119 362	G.P. Gopal et al.	(LOIC, RHEL) IJP
HEMINGWAY	75	NP B91 12	R.J. Hemingway et al.	(CERN, HEIDH, MPIM) IJP
NAKKASYAN	75	NP B93 85	A. Nakkasyan	(CERN) IJP
KANE	74	LBL-2452	D.F. Kane	(LBL) IJP
RADER	73	NC 16A 178	R.K. Rader et al.	(SACL, HEID, CERN+) IJP
LITCHFIELD	71	NP B30 125	P.J. Litchfield et al.	(RHEL, CDEF, SA CL) IJP
MULLER	69B	Thesis UCRL 19372	R.A. Muller	(LRL)
TRIPP	67	NP B3 10	R.D. Tripp et al.	(LRL, SLAC, CERN+)

 $\Lambda(2110) 5/2^+$

$$I(J^P) = 0(\frac{5}{2}^+) \text{ Status: } ***$$

For results published before 1974 (they are now obsolete), see our 1982 edition Physics Letters **111B 1** (1982). All the references have been retained.

This resonance is in the Baryon Summary Table, but the evidence for it could be better.

 $\Lambda(2110)$ POLE POSITION

REAL PART

VALUE (MeV)	DOCUMENT ID	TECN	COMMENT
2048 ± 10	SARANTSEV 19	DPWA	$\bar{K}N$ multichannel
••• We do not use the following data for averages, fits, limits, etc. •••			
1970	ZHANG 13A	DPWA	$\bar{K}N$ multichannel

-2xIMAGINARY PART

VALUE (MeV)	DOCUMENT ID	TECN	COMMENT
255 ± 20	SARANTSEV 19	DPWA	$\bar{K}N$ multichannel
••• We do not use the following data for averages, fits, limits, etc. •••			
350	ZHANG 13A	DPWA	$\bar{K}N$ multichannel

 $\Lambda(2110)$ POLE RESIDUE

The "normalized residue" is the residue divided by $\Gamma_{pole}/2$.

Normalized residue in $N\bar{K} \rightarrow \Lambda(2110) \rightarrow N\bar{K}$

MODULUS	PHASE (°)	DOCUMENT ID	TECN	COMMENT
0.020 ± 0.005	5 ± 15	SARANTSEV 19	DPWA	$\bar{K}N$ multichannel

Normalized residue in $N\bar{K} \rightarrow \Lambda(2110) \rightarrow \Sigma\pi$

MODULUS	PHASE (°)	DOCUMENT ID	TECN	COMMENT
0.13 ± 0.03	0 ± 15	SARANTSEV 19	DPWA	$\bar{K}N$ multichannel

Normalized residue in $N\bar{K} \rightarrow \Lambda(2110) \rightarrow \Xi K$

MODULUS	PHASE (°)	DOCUMENT ID	TECN	COMMENT
0.005 ± 0.005		SARANTSEV 19	DPWA	$\bar{K}N$ multichannel

Normalized residue in $N\bar{K} \rightarrow \Lambda(2110) \rightarrow \Lambda\omega, S=1/2, P\text{-wave}$

MODULUS	PHASE (°)	DOCUMENT ID	TECN	COMMENT
0.01 ± 0.01		SARANTSEV 19	DPWA	$\bar{K}N$ multichannel

Normalized residue in $N\bar{K} \rightarrow \Lambda(2110) \rightarrow \Lambda\omega, S=3/2, P\text{-wave}$

MODULUS	PHASE (°)	DOCUMENT ID	TECN	COMMENT
0.03 ± 0.01	-7 ± 16	SARANTSEV 19	DPWA	$\bar{K}N$ multichannel

Normalized residue in $N\bar{K} \rightarrow \Lambda(2110) \rightarrow \Lambda\omega, S=3/2, F\text{-wave}$

MODULUS	PHASE (°)	DOCUMENT ID	TECN	COMMENT
0.01 ± 0.01		SARANTSEV 19	DPWA	$\bar{K}N$ multichannel

 $\Lambda(2110)$ MASS

VALUE (MeV)	DOCUMENT ID	TECN	COMMENT
2050 to 2130 (≈ 2090) OUR ESTIMATE			
2086 ± 12	SARANTSEV 19	DPWA	$\bar{K}N$ multichannel
2036 ± 13	ZHANG 13A	DPWA	$\bar{K}N$ multichannel
2092 ± 25	GOPAL 80	DPWA	$\bar{K}N \rightarrow \bar{K}N$
2125 ± 25	CAMERON 78B	DPWA	$K^-p \rightarrow N\bar{K}^*$
2106 ± 50	DEBELLEFON 78	DPWA	$\bar{K}N \rightarrow \bar{K}N$
2140 ± 20	DEBELLEFON 77	DPWA	$K^-p \rightarrow \Sigma\pi$
2100 ± 50	GOPAL 77	DPWA	$\bar{K}N$ multichannel
2112 ± 7	KANE 74	DPWA	$K^-p \rightarrow \Sigma\pi$
••• We do not use the following data for averages, fits, limits, etc. •••			
2137	BACCARI 77	DPWA	$K^-p \rightarrow \Lambda\omega$
2103	¹ NAKKASYAN 75	DPWA	$K^-p \rightarrow \Lambda\omega$

 $\Lambda(2110)$ WIDTH

VALUE (MeV)	DOCUMENT ID	TECN	COMMENT
200 to 300 (≈ 250) OUR ESTIMATE			
274 ± 25	SARANTSEV 19	DPWA	$\bar{K}N$ multichannel
400 ± 38	ZHANG 13A	DPWA	$\bar{K}N$ multichannel
245 ± 25	GOPAL 80	DPWA	$\bar{K}N \rightarrow \bar{K}N$
160 ± 30	CAMERON 78B	DPWA	$K^-p \rightarrow N\bar{K}^*$
251 ± 50	DEBELLEFON 78	DPWA	$\bar{K}N \rightarrow \bar{K}N$
140 ± 20	DEBELLEFON 77	DPWA	$K^-p \rightarrow \Sigma\pi$
200 ± 50	GOPAL 77	DPWA	$\bar{K}N$ multichannel
190 ± 30	KANE 74	DPWA	$K^-p \rightarrow \Sigma\pi$
••• We do not use the following data for averages, fits, limits, etc. •••			
132	BACCARI 77	DPWA	$K^-p \rightarrow \Lambda\omega$
391	¹ NAKKASYAN 75	DPWA	$K^-p \rightarrow \Lambda\omega$

 $\Lambda(2110)$ DECAY MODES

Mode	Fraction (Γ_i/Γ)
Γ_1 $N\bar{K}$	5-25 %
Γ_2 $\Sigma\pi$	10-40 %
Γ_3 $\Lambda\omega$	seen
Γ_4 $\Lambda\omega, S=1/2, P\text{-wave}$	
Γ_5 $\Lambda\omega, S=3/2, P\text{-wave}$	(5.0 ± 2.0) %
Γ_6 $\Lambda\omega, S=3/2, F\text{-wave}$	
Γ_7 ΞK	
Γ_8 $\Sigma(1385)\pi$	seen
Γ_9 $\Sigma(1385)\pi, P\text{-wave}$	
Γ_{10} $N\bar{K}^*(892)$	10-60 %
Γ_{11} $N\bar{K}^*(892), S=1/2$	
Γ_{12} $N\bar{K}^*(892), S=3/2, P\text{-wave}$	

 $\Lambda(2110)$ BRANCHING RATIOS

See "Sign conventions for resonance couplings" in the Note on Λ and Σ Resonances.

$\Gamma(N\bar{K})/\Gamma_{total}$	DOCUMENT ID	TECN	COMMENT	Γ_1/Γ
0.05 to 0.25 OUR ESTIMATE				
0.020 ± 0.005	SARANTSEV 19	DPWA	$\bar{K}N$ multichannel	
0.083 ± 0.005	ZHANG 13A	DPWA	$\bar{K}N$ multichannel	
0.07 ± 0.03	GOPAL 80	DPWA	$\bar{K}N \rightarrow \bar{K}N$	
0.27 ± 0.06	² DEBELLEFON 78	DPWA	$\bar{K}N \rightarrow \bar{K}N$	
••• We do not use the following data for averages, fits, limits, etc. •••				
0.07 ± 0.03	GOPAL 77	DPWA	See GOPAL 80	
$\Gamma(\Sigma\pi)/\Gamma_{total}$	DOCUMENT ID	TECN	COMMENT	Γ_2/Γ
0.88 ± 0.20	SARANTSEV 19	DPWA	$\bar{K}N$ multichannel	
$\Gamma(\Lambda\omega, S=1/2, P\text{-wave})/\Gamma_{total}$	DOCUMENT ID	TECN	COMMENT	Γ_4/Γ
<0.01	SARANTSEV 19	DPWA	$\bar{K}N$ multichannel	
$\Gamma(\Lambda\omega, S=3/2, P\text{-wave})/\Gamma_{total}$	DOCUMENT ID	TECN	COMMENT	Γ_5/Γ
0.05 ± 0.02	SARANTSEV 19	DPWA	$\bar{K}N$ multichannel	
$\Gamma(\Lambda\omega, S=3/2, F\text{-wave})/\Gamma_{total}$	DOCUMENT ID	TECN	COMMENT	Γ_6/Γ
<0.01	SARANTSEV 19	DPWA	$\bar{K}N$ multichannel	
$\Gamma(\Xi K)/\Gamma_{total}$	DOCUMENT ID	TECN	COMMENT	Γ_7/Γ
~0	SARANTSEV 19	DPWA	$\bar{K}N$ multichannel	

$(\Gamma_1\Gamma_2)^{1/2}/\Gamma_{total}$ in $N\bar{K} \rightarrow \Lambda(2110) \rightarrow \Sigma\pi$	DOCUMENT ID	TECN	COMMENT	$(\Gamma_1\Gamma_2)^{1/2}/\Gamma$
0.04 ± 0.01	ZHANG 13A	DPWA	Multichannel	
+0.14 ± 0.01	DEBELLEFON 77	DPWA	$K^-p \rightarrow \Sigma\pi$	
+0.20 ± 0.03	KANE 74	DPWA	$K^-p \rightarrow \Sigma\pi$	
••• We do not use the following data for averages, fits, limits, etc. •••				
+0.10 ± 0.03	GOPAL 77	DPWA	$\bar{K}N$ multichannel	
$(\Gamma_1\Gamma_3)^{1/2}/\Gamma_{total}$ in $N\bar{K} \rightarrow \Lambda(2110) \rightarrow \Lambda\omega$	DOCUMENT ID	TECN	COMMENT	$(\Gamma_1\Gamma_3)^{1/2}/\Gamma$
<0.05	BACCARI 77	DPWA	$K^-p \rightarrow \Lambda\omega$	
0.112	¹ NAKKASYAN 75	DPWA	$K^-p \rightarrow \Lambda\omega$	

See key on page 1171

Baryon Particle Listings

$\Lambda(2110)$, $\Lambda(2325)$, $\Lambda(2350)$

$(\Gamma_i \Gamma_f)^{1/2} / \Gamma_{\text{total}}$ in $N\bar{K} \rightarrow \Lambda(2110) \rightarrow \Sigma(1385)\pi$, P-wave				$(\Gamma_1 \Gamma_9)^{1/2} / \Gamma$
VALUE	DOCUMENT ID	TECN	COMMENT	
+0.04 ± 0.01	ZHANG	13A	DPWA	Multichannel
+0.071 ± 0.025	3 CAMERON	78	DPWA	$K^- p \rightarrow \Sigma(1385)\pi$

$(\Gamma_i \Gamma_f)^{1/2} / \Gamma_{\text{total}}$ in $N\bar{K} \rightarrow \Lambda(2110) \rightarrow N\bar{K}^*(892)$, S=1/2				$(\Gamma_1 \Gamma_{11})^{1/2} / \Gamma$
VALUE	DOCUMENT ID	TECN	COMMENT	
-0.09 ± 0.01	ZHANG	13A	DPWA	Multichannel
-0.17 ± 0.04	4 CAMERON	78B	DPWA	$K^- p \rightarrow N\bar{K}^*$

$(\Gamma_i \Gamma_f)^{1/2} / \Gamma_{\text{total}}$ in $N\bar{K} \rightarrow \Lambda(2110) \rightarrow N\bar{K}^*(892)$, S=3/2, P-wave				$(\Gamma_1 \Gamma_{12})^{1/2} / \Gamma$
VALUE	DOCUMENT ID	TECN	COMMENT	
0.24 ± 0.01	ZHANG	13A	DPWA	Multichannel

 $\Lambda(2110)$ FOOTNOTES

- 1 Found in one of two best solutions.
- 2 The published error of 0.6 was a misprint.
- 3 The CAMERON 78 upper limit on F-wave decay is 0.03. The sign here has been changed to be in accord with the baryon-first convention.
- 4 The published sign has been changed to be in accord with the baryon-first convention. The CAMERON 78B upper limits on the P_3 and F_3 waves are each 0.03.

 $\Lambda(2110)$ REFERENCES

SARANTSEV	19	EPJ A55 180	A.V. Sarantsev et al.	(BONN, PNPI)
ZHANG	13A	PR C88 035205	H. Zhang et al.	(KSU)
PDG	82	PL 111B 1	M. Roos et al.	(HELS, CIT, CERN)
GOPAL	80	Toronto Conf. 159	G.P. Gopal	(RHEL) IJP
CAMERON	78	NP B143 189	W. Cameron et al.	(RHEL, LOIC) IJP
CAMERON	78B	NP B146 327	W. Cameron et al.	(RHEL, LOIC) IJP
DEBELLEFON	78	NC 42A 403	A. de Bellefon et al.	(CDEF, SAACL) IJP
BACCARI	77	NC 41A 96	B. Baccari et al.	(SACL, CDEF) IJP
DEBELLEFON	77	NC 37A 175	A. de Bellefon et al.	(CDEF, SAACL) IJP
GOPAL	77	NP B119 362	G.P. Gopal et al.	(LOIC, RHEL) IJP
NAKKASYAN	75	NP B93 85	A. Nakkasyan	(CERN) IJP
KANE	74	LBL-2452	D.F. Kane	(LBL) IJP

$\Lambda(2325)$ 3/2 ⁻	$I(J^P) = 0(\frac{3}{2}^-)$ Status: *
----------------------------------	---------------------------------------

OMITTED FROM SUMMARY TABLE

BACCARI 77 finds this state with either $J^P = 3/2^-$ or $3/2^+$ in an energy-dependent partial-wave analyses of $K^- p \rightarrow \Lambda\omega$ from 2070 to 2436 MeV. A subsequent semi-energy-independent analysis from threshold to 2436 MeV selects $3/2^-$. DEBELLEFON 78 (same group) also sees this state in an energy-dependent partial-wave analysis of $K^- p \rightarrow \bar{K}N$ data, and finds $J^P = 3/2^-$ or $3/2^+$. They again prefer $J^P = 3/2^-$, but only on the basis of model-dependent considerations.

 $\Lambda(2325)$ MASS

VALUE (MeV)	DOCUMENT ID	TECN	COMMENT
≈ 2325 OUR ESTIMATE			
2342 ± 30	DEBELLEFON 78	DPWA	$\bar{K}N \rightarrow \bar{K}N$
2327 ± 20	BACCARI 77	DPWA	$K^- p \rightarrow \Lambda\omega$

 $\Lambda(2325)$ WIDTH

VALUE (MeV)	DOCUMENT ID	TECN	COMMENT
177 ± 40	DEBELLEFON 78	DPWA	$\bar{K}N \rightarrow \bar{K}N$
160 ± 40	BACCARI 77	IPWA	$K^- p \rightarrow \Lambda\omega$

 $\Lambda(2325)$ DECAY MODES

Mode	Fraction (Γ_i/Γ)
Γ_1 $N\bar{K}$	~ 12 %
Γ_2 $\Lambda\omega$	~ 10 %

 $\Lambda(2325)$ BRANCHING RATIOS

$\Gamma(N\bar{K})/\Gamma_{\text{total}}$	Γ_1/Γ		
VALUE	DOCUMENT ID	TECN	COMMENT
0.19 ± 0.06	DEBELLEFON 78	DPWA	$\bar{K}N \rightarrow \bar{K}N$

$(\Gamma_i \Gamma_f)^{1/2} / \Gamma_{\text{total}}$ in $N\bar{K} \rightarrow \Lambda(2325) \rightarrow \Lambda\omega$				$(\Gamma_1 \Gamma_2)^{1/2} / \Gamma$
VALUE	DOCUMENT ID	TECN	COMMENT	
0.06 ± 0.02	1 BACCARI	77	IPWA	DS_{33} wave
0.05 ± 0.02	1 BACCARI	77	DPWA	DD_{13} wave
0.08 ± 0.03	1 BACCARI	77	DPWA	DD_{33} wave

 $\Lambda(2325)$ FOOTNOTES

- 1 Note that the three BACCARI 77 entries are for three different waves.

 $\Lambda(2325)$ REFERENCES

DEBELLEFON	78	NC 42A 403	A. de Bellefon et al.	(CDEF, SAACL) IJP
BACCARI	77	NC 41A 96	B. Baccari et al.	(SACL, CDEF) IJP

 $\Lambda(2350)$ 9/2⁺

$$I(J^P) = 0(\frac{9}{2}^+) \text{ Status: } ***$$

DAUM 68 favors $J^P = 7/2^-$ or $9/2^+$. BRICMAN 70 favors $9/2^+$. LASINSKI 71 suggests three states in this region using a Pomeron + resonances model. There are now also three formation experiments from the College de France-Saclay group, DEBELLEFON 77, BACCARI 77, and DEBELLEFON 78, which find $9/2^+$ in energy-dependent partial-wave analyses of $\bar{K}N \rightarrow \Sigma\pi$, $\Lambda\omega$, and $N\bar{K}$.

 $\Lambda(2350)$ MASS

VALUE (MeV)	DOCUMENT ID	TECN	COMMENT
2340 to 2370 (≈ 2350) OUR ESTIMATE			
2370 ± 50	DEBELLEFON 78	DPWA	$\bar{K}N \rightarrow \bar{K}N$
2365 ± 20	DEBELLEFON 77	DPWA	$K^- p \rightarrow \Sigma\pi$
2358 ± 6	BRICMAN 70	CNTR	Total, charge exchange
• • • We do not use the following data for averages, fits, limits, etc. • • •			
2372	BACCARI 77	DPWA	$K^- p \rightarrow \Lambda\omega$
2344 ± 15	COOL 70	CNTR	$K^- p$, $K^- d$ total
2360 ± 20	LU 70	CNTR	$\gamma p \rightarrow K^+ Y^*$
2340 ± 7	BUGG 68	CNTR	$K^- p$, $K^- d$ total

 $\Lambda(2350)$ WIDTH

VALUE (MeV)	DOCUMENT ID	TECN	COMMENT
100 to 250 (≈ 150) OUR ESTIMATE			
204 ± 50	DEBELLEFON 78	DPWA	$\bar{K}N \rightarrow \bar{K}N$
110 ± 20	DEBELLEFON 77	DPWA	$K^- p \rightarrow \Sigma\pi$
324 ± 30	BRICMAN 70	CNTR	Total, charge exchange
• • • We do not use the following data for averages, fits, limits, etc. • • •			
257	BACCARI 77	DPWA	$K^- p \rightarrow \Lambda\omega$
190	COOL 70	CNTR	$K^- p$, $K^- d$ total
55	LU 70	CNTR	$\gamma p \rightarrow K^+ Y^*$
140 ± 20	BUGG 68	CNTR	$K^- p$, $K^- d$ total

 $\Lambda(2350)$ DECAY MODES

Mode	Fraction (Γ_i/Γ)
Γ_1 $N\bar{K}$	~ 12 %
Γ_2 $\Sigma\pi$	~ 10 %
Γ_3 $\Lambda\omega$	

 $\Lambda(2350)$ BRANCHING RATIOS

See "Sign conventions for resonance couplings" in the Note on Λ and Σ Resonances.

$\Gamma(N\bar{K})/\Gamma_{\text{total}}$	Γ_1/Γ		
VALUE	DOCUMENT ID	TECN	COMMENT
~ 0.12 OUR ESTIMATE			
0.12 ± 0.04	DEBELLEFON 78	DPWA	$\bar{K}N \rightarrow \bar{K}N$

$(\Gamma_i \Gamma_f)^{1/2} / \Gamma_{\text{total}}$ in $N\bar{K} \rightarrow \Lambda(2350) \rightarrow \Sigma\pi$				$(\Gamma_1 \Gamma_2)^{1/2} / \Gamma$
VALUE	DOCUMENT ID	TECN	COMMENT	
-0.11 ± 0.02	DEBELLEFON 77	DPWA	$K^- p \rightarrow \Sigma\pi$	

$(\Gamma_i \Gamma_f)^{1/2} / \Gamma_{\text{total}}$ in $N\bar{K} \rightarrow \Lambda(2350) \rightarrow \Lambda\omega$				$(\Gamma_1 \Gamma_3)^{1/2} / \Gamma$
VALUE	DOCUMENT ID	TECN	COMMENT	
< 0.05	BACCARI 77	DPWA	$K^- p \rightarrow \Lambda\omega$	

 $\Lambda(2350)$ REFERENCES

DEBELLEFON	78	NC 42A 403	A. de Bellefon et al.	(CDEF, SAACL) IJP
BACCARI	77	NC 41A 96	B. Baccari et al.	(SACL, CDEF) IJP
DEBELLEFON	77	NC 37A 175	A. de Bellefon et al.	(CDEF, SAACL) IJP
LASINSKI	71	NP B29 125	T.A. Lasinski	(EFI) IJP
BRICMAN	70	PL 31B 152	C. Bricman et al.	(CERN, CAEN, SAACL)
COOL	70	PR D1 1887	R.L. Cool et al.	(BNL) I
	Also	PRL 16 1228	R.L. Cool et al.	(BNL) I
LU	70	PR D2 1846	D.C. Lu et al.	(YALE)
BUGG	68	PR 168 1466	D.V. Bugg et al.	(RHEL, BIRM, CAVE) I
DAUM	68	NP B7 19	C. Daum et al.	(CERN) IJP

Baryon Particle Listings

$\Lambda(2585)$ Bumps

$\Lambda(2585)$ Bumps $I(J^P) = 0(?^?)$ Status: *

OMITTED FROM SUMMARY TABLE

$\Lambda(2585)$ MASS (BUMPS)

VALUE (MeV)	DOCUMENT ID	TECN	COMMENT
≈ 2585 OUR ESTIMATE			
25 85 ± 45	ABRAMS 70	CNTR	$K^- p, K^- d$ total
25 30 ± 25	LU 70	CNTR	$\gamma p \rightarrow K^+ Y^*$

$\Lambda(2585)$ WIDTH (BUMPS)

VALUE (MeV)	DOCUMENT ID	TECN	COMMENT
300	ABRAMS 70	CNTR	$K^- p, K^- d$ total
150	LU 70	CNTR	$\gamma p \rightarrow K^+ Y^*$

$\Lambda(2585)$ DECAY MODES (BUMPS)

Mode
$\Gamma_1 \quad N\bar{K}$

$\Lambda(2585)$ BRANCHING RATIOS (BUMPS)

$(J+\frac{1}{2}) \times \Gamma(N\bar{K}) / \Gamma_{\text{total}}$ Γ_1 / Γ

J is not known, so only $(J+\frac{1}{2}) \times \Gamma(N\bar{K}) / \Gamma_{\text{total}}$ can be given.

VALUE	DOCUMENT ID	TECN	COMMENT
1	ABRAMS 70	CNTR	$K^- p, K^- d$ total
0.12 ± 0.12	¹ BRICMAN 70	CNTR	Total, charge exchange

$\Lambda(2585)$ FOOTNOTES (BUMPS)

¹ The resonance is at the end of the region analyzed — no clear signal.

$\Lambda(2585)$ REFERENCES (BUMPS)

ABRAMS 70	PR D1 1917	R.J. Abrams <i>et al.</i>	(BNL)1
Also	PRL 16 1228	R.L. Cool <i>et al.</i>	(BNL)1
BRICMAN 70	PL 31B 152	C. Bricman <i>et al.</i>	(CERN, CAEN, SACL)
LU 70	PR D2 1846	D.C. Lu <i>et al.</i>	(YALE)

Σ BARYONS

($S = -1, I = 1$)

$\Sigma^+ = uus, \Sigma^0 = uds, \Sigma^- = dds$

Σ^+

$$I(J^P) = 1(\frac{1}{2}^+)$$
 Status: * * * *

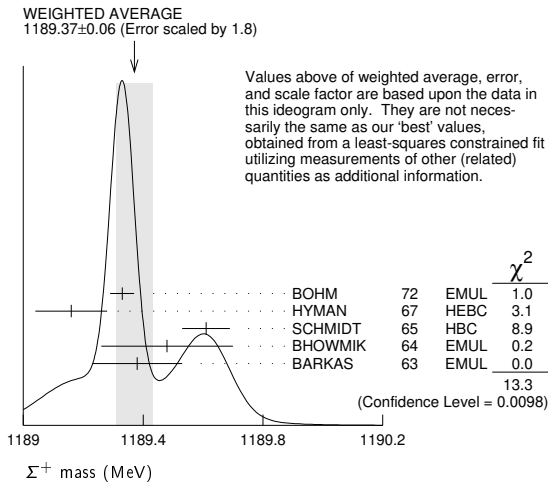
We have omitted some results that have been superseded by later experiments. See our earlier editions.

Σ^+ MASS

The fit uses $\Sigma^+, \Sigma^0, \Sigma^-$, and Λ mass and mass-difference measurements.

VALUE (MeV)	EVTS	DOCUMENT ID	TECN	COMMENT
1189.37 ± 0.07 OUR FIT				Error includes scale factor of 2.2.
1189.37 ± 0.06 OUR AVERAGE				Error includes scale factor of 1.8. See the ideogram below.
1189.33 ± 0.04	607	¹ BOHM	72 EMUL	
1189.16 ± 0.12		HYMAN	67 HBC	
1189.61 ± 0.08	4205	SCHMIDT	65 HBC	See note with Λ mass
1189.48 ± 0.22	58	² BHOWMIK	64 EMUL	
1189.38 ± 0.15	144	² BARKAS	63 EMUL	

¹ BOHM 72 is updated with our 1973 $K^-, \pi^-,$ and π^0 masses (Reviews of Modern Physics **45** 51 (1973)).
² These masses have been raised 30 keV to take into account a 46 keV increase in the proton mass and a 21 keV decrease in the π^0 mass (note added 1967 edition, Reviews of Modern Physics **39** 1 (1967)).



Values above of weighted average, error, and scale factor are based upon the data in this ideogram only. They are not necessarily the same as our 'best' values, obtained from a least-squares constrained fit utilizing measurements of other (related) quantities as additional information.

Σ^+ MEAN LIFE

Measurements with fewer than 1000 events have been omitted.

VALUE (10^{-10} s)	EVTS	DOCUMENT ID	TECN	COMMENT
0.8018 ± 0.0026 OUR AVERAGE				
0.8038 ± 0.0040 ± 0.0014		BARBOSA	00 E761	hyperons, 375 GeV
0.8043 ± 0.0080 ± 0.0014		¹ BARBOSA	00 E761	hyperons, 375 GeV
0.798 ± 0.005	30k	MARRAFFINO	80 HBC	$K^- p$ 0.42-0.5 GeV/c
0.807 ± 0.013	5719	CONFORTO	76 HBC	$K^- p$ 1-1.4 GeV/c
0.795 ± 0.010	20k	EISELE	70 HBC	$K^- p$ at rest
0.803 ± 0.008	10664	BARLOUTAUD	69 HBC	$K^- p$ 0.4-1.2 GeV/c
0.83 ± 0.032	1300	² CHANG	66 HBC	

¹ This is a measurement of the Σ^- lifetime. Here we assume CPT invariance; see below for the fractional $\Sigma^+ - \Sigma^-$ lifetime difference obtained by BARBOSA 00.
² We have increased the CHANG 66 error of 0.018; see our 1970 edition, Reviews of Modern Physics **42** 87 (1970).

$$(\tau_{\Sigma^+} - \tau_{\Sigma^-}) / \tau_{\Sigma^+}$$

A test of CPT invariance.

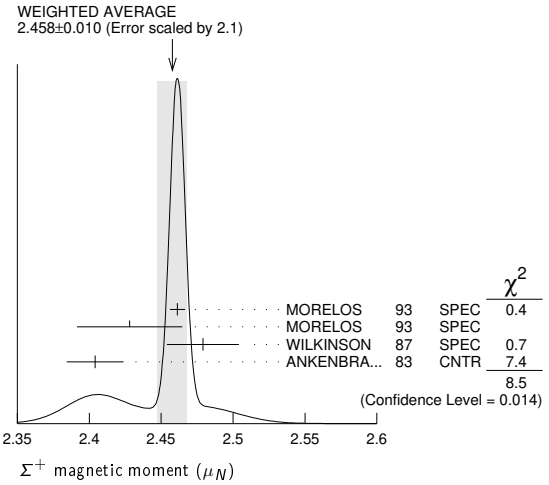
VALUE	DOCUMENT ID	TECN	COMMENT
(-6 ± 12) × 10⁻⁴	BARBOSA	00 E761	hyperons, 375 GeV

Σ^+ MAGNETIC MOMENT

See the "Quark Model" review. Measurements with an error $\geq 0.1 \mu_N$ have been omitted.

VALUE (μ_N)	EVTS	DOCUMENT ID	TECN	COMMENT
2.458 ± 0.010 OUR AVERAGE				Error includes scale factor of 2.1. See the ideogram below.
2.4613 ± 0.0034 ± 0.0040	250k	MORELOS	93 SPEC	p Cu 800 GeV
2.428 ± 0.036 ± 0.007	12k	¹ MORELOS	93 SPEC	p Cu 800 GeV
2.479 ± 0.012 ± 0.022	137k	WILKINSON	87 SPEC	p Be 400 GeV
2.4040 ± 0.0198	44k	² ANKENBRA...	83 CNTR	p Cu 400 GeV

¹ We assume CPT invariance: this is (minus) the Σ^- magnetic moment as measured by MORELOS 93. See below for the moment difference testing CPT .
² ANKENBRANDT 83 gives the value $2.38 \pm 0.02 \mu_N$. MORELOS 93 uses the same hyperon magnet and channel and claims to determine the field integral better, leading to the revised value given here.



$$(\mu_{\Sigma^+} + \mu_{\Sigma^-}) / \mu_{\Sigma^+}$$

A test of CPT invariance.

VALUE	DOCUMENT ID	TECN	COMMENT
0.014 ± 0.015	¹ MORELOS	93 SPEC	p Cu 800 GeV

¹ This is our calculation from the MORELOS 93 measurements of the Σ^+ and Σ^- magnetic moments given above. The statistical error on μ_{Σ^-} dominates the error here.

Σ^+ DECAY MODES

Mode	Fraction (Γ_i / Γ)	Confidence level
Γ_1 $p \pi^0$	(51.57 ± 0.30) %	
Γ_2 $n \pi^+$	(48.31 ± 0.30) %	
Γ_3 $p \gamma$	(1.23 ± 0.05) × 10 ⁻³	
Γ_4 $n \pi^+ \gamma$	[a] (4.5 ± 0.5) × 10 ⁻⁴	
Γ_5 $\Lambda e^+ \nu_e$	(2.3 ± 0.4) × 10 ⁻⁵	

$\Delta S = \Delta Q$ (SQ) violating modes or $\Delta S = 1$ weak neutral current (S1) modes

Mode	Fraction	Confidence level
Γ_6 $n e^+ \nu_e$	SQ < 5 × 10 ⁻⁶	90%
Γ_7 $n \mu^+ \nu_\mu$	SQ < 3.0 × 10 ⁻⁵	90%
Γ_8 $p e^+ e^-$	S1 < 7 × 10 ⁻⁶	
Γ_9 $p \mu^+ \mu^-$	S1 (2.4 ± 1.7 / -1.3) × 10 ⁻⁸	

[a] See the Listings below for the pion momentum range used in this measurement.

CONSTRAINED FIT INFORMATION

An overall fit to 2 branching ratios uses 14 measurements and one constraint to determine 3 parameters. The overall fit has a $\chi^2 = 7.7$ for 12 degrees of freedom.

The following *off-diagonal* array elements are the correlation coefficients $\langle \delta x_i \delta x_j \rangle / (\delta x_i \delta x_j)$, in percent, from the fit to the branching fractions, $x_i \equiv \Gamma_i / \Gamma_{\text{total}}$. The fit constrains the x_i whose labels appear in this array to sum to one.

x_2	-100	
x_3	12	-14
	x_1	x_2

Baryon Particle Listings

 Σ^+ Σ^+ BRANCHING RATIOS $\Gamma(n\pi^+)/\Gamma(N\pi)$

VALUE	EVTs	DOCUMENT ID	TECN	COMMENT
0.4836 ± 0.0030 OUR FIT				
0.4836 ± 0.0030 OUR AVERAGE				
0.4828 ± 0.0036	10k	¹ MARRAFFINO 80	HBC	$K^- p$ 0.42–0.5 GeV/c
0.488 ± 0.008	1861	NOWAK 78	HBC	
0.484 ± 0.015	537	TOVEE 71	EMUL	
0.488 ± 0.010	1331	BARLOUTAUD 69	HBC	$K^- p$ 0.4–1.2 GeV/c
0.46 ± 0.02	534	CHANG 66	HBC	
0.490 ± 0.024	308	HUMPHREY 62	HBC	

¹ MARRAFFINO 80 actually gives $\Gamma(p\pi^0)/\Gamma(\text{total}) = 0.5172 \pm 0.0036$. $\Gamma(p\gamma)/\Gamma(p\pi^0)$

VALUE (units 10^{-3})	EVTs	DOCUMENT ID	TECN	COMMENT
2.38 ± 0.10 OUR FIT				
2.38 ± 0.10 OUR AVERAGE				
2.32 ± 0.11 ± 0.10	32k	TIMM 95	E761	Σ^+ 375 GeV
2.81 ± 0.39 ± 0.21 -0.43	408	HESSEY 89	CNTR	$K^- p \rightarrow \Sigma^+ \pi^-$ at rest
2.52 ± 0.28	190	¹ KOBAYASHI 87	CNTR	$\pi^+ p \rightarrow \Sigma^+ K^+$
2.46 ± 0.30 -0.35	155	BIAGI 85	CNTR	CERN hyperon beam
2.11 ± 0.38	46	MANZ 80	HBC	$K^- p \rightarrow \Sigma^+ \pi^-$
2.1 ± 0.3	45	ANG 69B	HBC	$K^- p$ at rest
2.76 ± 0.51	31	GERSHWIN 69B	HBC	$K^- p \rightarrow \Sigma^+ \pi^-$
3.7 ± 0.8	24	BAZIN 65	HBC	$K^- p$ at rest

¹ KOBAYASHI 87 actually gives $\Gamma(p\gamma)/\Gamma(\text{total}) = (1.30 \pm 0.15) \times 10^{-3}$. $\Gamma(p\gamma)/\Gamma_{\text{total}}$

VALUE (units 10^{-3})	EVTs	DOCUMENT ID	TECN	COMMENT
0.996 ± 0.021 ± 0.18	2.5k	¹ ABLIKIM 23Y	BES3	$e^+ e^- \rightarrow J/\psi \rightarrow \Sigma^+ \bar{\Sigma}^-$

¹ This value is quoted by ABLIKIM 23Y for the simultaneous fit to $\Sigma^+ \rightarrow p\gamma$ and $\bar{\Sigma}^- \rightarrow \bar{p}\gamma$ assuming no CP violation. Individual values for the branching fractions are given as $(1.005 \pm 0.032) \times 10^{-3}$ and $(0.993 \pm 0.030) \times 10^{-3}$, respectively. $\Gamma(n\pi^+ \gamma)/\Gamma(n\pi^+)$ The π^+ momentum cuts differ, so we do not average the results but simply use the latest value in the Summary Table.

VALUE (units 10^{-3})	EVTs	DOCUMENT ID	TECN	COMMENT
0.93 ± 0.10	180	EBENHOH 73	HBC	$\pi^+ < 150$ MeV/c
0.27 ± 0.05	29	ANG 69B	HBC	$\pi^+ < 110$ MeV/c
~1.8		BAZIN 65B	HBC	$\pi^+ < 116$ MeV/c

 $\Gamma(\Lambda e^+ \nu_e)/\Gamma_{\text{total}}$

VALUE (units 10^{-5})	EVTs	DOCUMENT ID	TECN	COMMENT
2.3 ± 0.4 OUR AVERAGE				
2.93 ± 0.74 ± 0.13	16	ABLIKIM 23AA	BES3	$e^+ e^- \rightarrow J/\psi \rightarrow \Sigma^+ \bar{\Sigma}^-$
1.6 ± 0.7	5	BALTAY 69	HBC	$K^- p$ at rest
2.9 ± 1.0	10	EISELE 69	HBC	$K^- p$ at rest
2.0 ± 0.8	6	BARASH 67	HBC	$K^- p$ at rest

 $\Gamma(ne^+ \nu_e)/\Gamma(n\pi^+)$ Test of $\Delta S = \Delta Q$ rule. Experiments with an effective denominator less than 100,000 have been omitted.

EFFECTIVE DENOM.	EVTs	DOCUMENT ID	TECN	COMMENT
< 1.1 × 10⁻⁵ OUR LIMIT				Our 90% CL limit = (2.3 events)/(effective denominator sum). [Number of events increased to 2.3 for a 90% confidence level.]
111000	0	¹ EBENHOH 74	HBC	$K^- p$ at rest
105000	0	¹ SECHI-ZORN 73	HBC	$K^- p$ at rest

¹ Effective denominator calculated by us. $\Gamma(n\mu^+ \nu_\mu)/\Gamma(n\pi^+)$

EFFECTIVE DENOM.	EVTs	DOCUMENT ID	TECN	COMMENT
< 6.2 × 10⁻⁵ OUR LIMIT				Our 90% CL limit = (6.7 events)/(effective denominator sum). [Number of events increased to 6.7 for a 90% confidence level.]
33800	0	BAGGETT 69B	HBC	
62000	2	EISELE 69B	HBC	
10150	0	² COURANT 64	HBC	
1710	0	² NAUENBERG 64	HBC	
120	1	GALTIERI 62	EMUL	

¹ Effective denominator calculated by us.² Effective denominator taken from EISELE 67. $\Gamma(pe^+ e^-)/\Gamma_{\text{total}}$

VALUE (units 10^{-6})	DOCUMENT ID	TECN	COMMENT
< 7	¹ ANG 69B	HBC	$K^- p$ at rest

¹ ANG 69B found three $pe^+ e^-$ events in agreement with $\gamma \rightarrow e^+ e^-$ conversion from $\Sigma^+ \rightarrow p\gamma$. The limit given here is for neutral currents. $\Gamma(\rho\mu^+ \mu^-)/\Gamma_{\text{total}}$ A test for a $\Delta S = 1$ weak neutral current, but also allowed by higher-order electroweak interactions.

VALUE (units 10^{-8})	EVTs	DOCUMENT ID	TECN	COMMENT
2.4 ± 1.7 -1.3 OUR AVERAGE				
2.2 ± 0.9 ± 1.5 -0.8 -1.1	10.2	¹ AAIJ 18E	LHCB	pp at 7, 8 TeV
8.6 ± 6.6 ± 5.5 -5.4	3	² PARK 05	HYCP	p Cu, 800 GeV

¹ AAIJ 18E sees no structure in the dimuon mass distribution, contrary to PARK 05.² The masses of the three dimuons of PARK 05 are within 1 MeV of one another, perhaps indicating the existence of a new state P^0 with mass 214.3 ± 0.5 MeV. In that case, the decay is $\Sigma^+ \rightarrow pP^0, P^0 \rightarrow \mu^+ \mu^-$, with a branching fraction of $(3.1^{+2.4}_{-1.9} \pm 1.5) \times 10^{-8}$. $\Gamma(\Sigma^+ \rightarrow ne^+ \nu_e)/\Gamma(\Sigma^- \rightarrow ne^- \bar{\nu}_e)$

VALUE	CL%	EVTs	DOCUMENT ID	TECN	COMMENT
< 0.009 OUR LIMIT					Our 90% CL limit, using $\Gamma(ne^+ \nu_e)/\Gamma(n\pi^+)$ above.
< 0.019	90	0	EBENHOH 74	HBC	$K^- p$ at rest
< 0.018	90	0	SECHI-ZORN 73	HBC	$K^- p$ at rest
< 0.12	95	0	COLE 71	HBC	$K^- p$ at rest
< 0.03	90	0	EISELE 69B	HBC	See EBENHOH 74

 $\Gamma(\Sigma^+ \rightarrow n\mu^+ \nu_\mu)/\Gamma(\Sigma^- \rightarrow n\mu^- \bar{\nu}_\mu)$

VALUE	EVTs	DOCUMENT ID	TECN	COMMENT
< 0.12 OUR LIMIT				Our 90% CL limit, using $\Gamma(n\mu^+ \nu_\mu)/\Gamma(n\pi^+)$ above.
0.06 ± 0.045 -0.03	2	EISELE 69B	HBC	$K^- p$ at rest

 $\Gamma(\Sigma^+ \rightarrow n\ell^+ \nu)/\Gamma(\Sigma^- \rightarrow n\ell^- \bar{\nu}_\ell)$

VALUE	EVTs	DOCUMENT ID	TECN	COMMENT
< 0.043 OUR LIMIT				Our 90% CL limit, using $[\Gamma(\Sigma^+ \rightarrow n\mu^+ \nu_\mu) + \Gamma(\Sigma^+ \rightarrow ne^+ \nu_e)]/\Gamma(\Sigma^+ \rightarrow n\pi^+)$.
< 0.08	1	NORTON 69	HBC	
< 0.034	0	BAGGETT 67	HBC	

 Σ^+ DECAY PARAMETERS

See the "Note on Baryon Decay Parameters" in the neutron Listings. A few early results have been omitted.

 α_0 FOR $\Sigma^+ \rightarrow p\pi^0$

VALUE	EVTs	DOCUMENT ID	TECN	COMMENT
-0.982 ± 0.014 OUR FIT				
-0.982 ± 0.016 -0.013 OUR AVERAGE				
-0.998 ± 0.037 ± 0.009	93k	¹ ABLIKIM 20x	BES3	$J/\psi/\psi(2S) \rightarrow \Sigma^+ \bar{\Sigma}^-$
-0.945 ± 0.055 -0.042	1259	² LIPMAN 73	OSPK	$\pi^+ p \rightarrow \Sigma^+$
-0.940 ± 0.045	16k	BELLAMY 72	ASPK	$\pi^+ p \rightarrow \Sigma^+ K^+$
-0.98 ± 0.05 -0.02	1335	³ HARRIS 70	OSPK	$\pi^+ p \rightarrow \Sigma^+ K^+$
-0.999 ± 0.022	32k	BANGERTER 69	HBC	$K^- p$ 0.4 GeV/c

¹ ABLIKIM 20x uses production through $e^+ e^- \rightarrow J/\psi \rightarrow \Sigma^+ \bar{\Sigma}^-$ and $e^+ e^- \rightarrow \psi(2S) \rightarrow \Sigma^+ \bar{\Sigma}^-$, with 87,815 and 5,327 events, respectively. Note that the reported values of decay parameters α_0 of Σ^+ and $\bar{\alpha}_0$ of $\bar{\Sigma}^-$ are correlated.² Decay protons scattered off aluminum.³ Decay protons scattered off carbon. $\bar{\alpha}_0$ FOR $\bar{\Sigma}^- \rightarrow \bar{p}\pi^0$

VALUE	EVTs	DOCUMENT ID	TECN	COMMENT
0.990 ± 0.037 ± 0.011	93k	¹ ABLIKIM 20x	BES3	$J/\psi/\psi(2S) \rightarrow \Sigma^+ \bar{\Sigma}^-$
< 6.2 × 10 ⁻⁵ OUR LIMIT				Our 90% CL limit = (6.7 events)/(effective denominator sum). [Number of events increased to 6.7 for a 90% confidence level.]
33800	0	BAGGETT 69B	HBC	
62000	2	EISELE 69B	HBC	
10150	0	² COURANT 64	HBC	
1710	0	² NAUENBERG 64	HBC	
120	1	GALTIERI 62	EMUL	

¹ ABLIKIM 20x uses production through $e^+ e^- \rightarrow J/\psi \rightarrow \Sigma^+ \bar{\Sigma}^-$ and $e^+ e^- \rightarrow \psi(2S) \rightarrow \Sigma^+ \bar{\Sigma}^-$, with 87,815 and 5,327 events, respectively. Note that the reported values of decay parameters α_0 of Σ^+ and $\bar{\alpha}_0$ of $\bar{\Sigma}^-$ are correlated. $(\alpha_0 + \bar{\alpha}_0) / (\alpha_0 - \bar{\alpha}_0)$

VALUE	EVTs	DOCUMENT ID	TECN	COMMENT
0.004 ± 0.037 ± 0.010	93k	¹ ABLIKIM 20x	BES3	$J/\psi/\psi(2S) \rightarrow \Sigma^+ \bar{\Sigma}^-$
< 6.2 × 10 ⁻⁵ OUR LIMIT				Our 90% CL limit = (6.7 events)/(effective denominator sum). [Number of events increased to 6.7 for a 90% confidence level.]

¹ ABLIKIM 20x uses production through $e^+ e^- \rightarrow J/\psi \rightarrow \Sigma^+ \bar{\Sigma}^-$ and $e^+ e^- \rightarrow \psi(2S) \rightarrow \Sigma^+ \bar{\Sigma}^-$, with 87,815 and 5,327 events, respectively. Note that the reported values of decay parameters α_0 of Σ^+ and $\bar{\alpha}_0$ of $\bar{\Sigma}^-$ are correlated. ϕ_0 ANGLE FOR $\Sigma^+ \rightarrow p\pi^0$

VALUE (°)	EVTs	DOCUMENT ID	TECN	COMMENT
36 ± 34 OUR AVERAGE				
38.1 ± 35.7 -37.1	1259	¹ LIPMAN 73	OSPK	$\pi^+ p \rightarrow \Sigma^+ K^+$
22 ± 90		² HARRIS 70	OSPK	$\pi^+ p \rightarrow \Sigma^+ K^+$

¹ Decay proton scattered off aluminum.² Decay protons scattered off carbon.

See key on page 1171

Baryon Particle Listings

Σ^+, Σ^0

α_+ / α_0

Older results have been omitted.

VALUE (units 10^{-2})	EVTS	DOCUMENT ID	TECN	COMMENT
-4.98 ± 0.27 OUR FIT				
-5.0 ± 0.4 OUR AVERAGE				
-4.90 ± 0.32 ± 0.21	754k	¹ ABLIKIM 23BN BES3	J/ψ → Σ ⁺ Σ ⁻	
-7.3 ± 2.1	23k	MARRAFFINO 80 HBC	K ⁻ p 0.42-0.5 GeV/c	
¹ ABLIKIM 23BN uses production through e ⁺ e ⁻ → J/ψ → Σ ⁺ Σ ⁻ with 10G J/ψ events.				

α_+ FOR Σ⁺ → nπ⁺

VALUE (units 10^{-2})	EVTS	DOCUMENT ID	TECN	COMMENT
4.89 ± 0.26 OUR FIT				
4.9 ± 0.4 OUR AVERAGE				Error includes scale factor of 1.2.
4.81 ± 0.31 ± 0.19	754k	¹ ABLIKIM 23BN BES3	J/ψ → Σ ⁺ Σ ⁻	
3.7 ± 4.9	4101	BERLEY 70B HBC		
6.9 ± 1.7	35k	BANGERTER 69 HBC	K ⁻ p 0.4 GeV/c	
¹ ABLIKIM 23BN uses production through e ⁺ e ⁻ → J/ψ → Σ ⁺ Σ ⁻ with 10G J/ψ events.				

ϕ_+ ANGLE FOR Σ⁺ → nπ⁺

(tan φ₊ = β/γ)

VALUE (°)	EVTS	DOCUMENT ID	TECN	COMMENT
167 ± 20 OUR AVERAGE				Error includes scale factor of 1.1.
184 ± 24	1054	¹ BERLEY 70B HBC		
143 ± 29	560	BANGERTER 69B HBC	K ⁻ p 0.4 GeV/c	
¹ Changed from 176 to 184° to agree with our sign convention.				

$\bar{\alpha}_-$ FOR Σ⁻ → n̄π⁻

VALUE (units 10^{-2})	EVTS	DOCUMENT ID	TECN	COMMENT
-5.65 ± 0.47 ± 0.22	1.1M	¹ ABLIKIM 23BN BES3	J/ψ → Σ ⁺ Σ ⁻	
¹ ABLIKIM 23BN uses production through e ⁺ e ⁻ → J/ψ → Σ ⁺ Σ ⁻ with 10G J/ψ events.				

$\bar{\alpha}_-$ / $\bar{\alpha}_0$

VALUE (units 10^{-2})	DOCUMENT ID	TECN	COMMENT
-5.71 ± 0.53 ± 0.32	ABLIKIM 23BN BES3	J/ψ → Σ ⁺ Σ ⁻	

$(\alpha_+ + \bar{\alpha}_-) / (\alpha_+ - \bar{\alpha}_-)$

VALUE (units 10^{-2})	DOCUMENT ID	TECN	COMMENT
-8.0 ± 5.2 ± 2.8	ABLIKIM 23BN BES3	J/ψ → Σ ⁺ Σ ⁻	

α_γ FOR Σ⁺ → pγ

VALUE	EVTS	DOCUMENT ID	TECN	COMMENT
-0.69 ± 0.05 OUR AVERAGE				
-0.652 ± 0.056 ± 0.020	2.5k	¹ ABLIKIM 23Y BES3	e ⁺ e ⁻ → J/ψ → Σ ⁺ Σ ⁻	
-0.720 ± 0.086 ± 0.045	35k	² FOUCHER 92 SPEC	Σ ⁺ 375 GeV	
-0.86 ± 0.13 ± 0.04	190	KOBAYASHI 87 CNTR	π ⁺ p → Σ ⁺ K ⁺	
-0.53 ^{+0.38} _{-0.36}	46	MANZ 80 HBC	K ⁻ p → Σ ⁺ π ⁻	
-1.03 ^{+0.52} _{-0.42}	61	GERSHWIN 69B HBC	K ⁻ p → Σ ⁺ π ⁻	

¹ This value is quoted by ABLIKIM 23Y for the simultaneous fit to Σ⁺ → pγ and Σ⁻ → p̄γ assuming no CP violation. Individual values are given as -0.587 ± 0.082 and 0.710 ± 0.076, respectively.

² See TIMM 95 for a detailed description of the analysis.

Σ⁺ REFERENCES

We have omitted some papers that have been superseded by later experiments. See our earlier editions.

ABLIKIM 23AA PR D107 072010	M. Ablikim et al.	(BESIII Collab.)
ABLIKIM 23BN PRL 131 191802	M. Ablikim et al.	(BESIII Collab.)
ABLIKIM 23Y PRL 130 211901	M. Ablikim et al.	(BESIII Collab.)
ABLIKIM 20X PRL 125 052004	M. Ablikim et al.	(BESIII Collab.)
AAIJ 18E PRL 120 221803	R. Aaij et al.	(LHCb Collab.)
PARK 05 PRL 94 021801	H.K. Park et al.	(FNAL HyperCP Collab.)
BARBOSA 00 PR D61 031101	R.F. Barbosa et al.	(FNAL E761 Collab.)
TIMM 95 PR D51 4638	S. Timm et al.	(FNAL E761 Collab.)
MORELOS 93 PRL 71 3417	A. Morelos et al.	(FNAL E761 Collab.)
FOUCHER 92 PRL 68 3004	M. Foucher et al.	(FNAL E761 Collab.)
HESSEY 89 ZPHY C42 175	N.P. Hessey et al.	(BNL-811 Collab.)
KOBAYASHI 87 PRL 59 868	M. Kobayashi et al.	(KYOT)
WILKINSON 87 PRL 58 855	C.A. Wilkinson et al.	(WISC, MICH, RUTG+)
BIAGI 85 ZPHY C28 495	S.F. Biagi et al.	(CERN WA62 Collab.)
ANKENBRANDT... 83 PRL 51 863	C.M. Ankenbrandt et al.	(FNAL IOWA, ISU+)
MANZ 80 PL 96B 217	A. Manz et al.	(MIPM, VAND)
MARRAFFINO 80 PR D21 2501	J. Marraffino et al.	(VAND, MIPM)
NOWAK 78 NP B139 61	R.J. Nowak et al.	(VAND, MIPM)
CONFORTO 76 NP B105 189	B. Conforto et al.	(LOUC, BELG, DURH+)
EBENHOH 74 ZPHY 266 367	H. Ebenhoh et al.	(RHEL, LOIC)
EBENHOH 73 ZPHY 264 413	W. Ebenhoh et al.	(HEIDT)
LIPMAN 73 PL 43B 89	N.H. Lipman et al.	(RHEL, SUSS, LOWC)
PDG 73 RMP 45 51	T.A. Lasinski et al.	(LBL, BRAN, CERN+)
SECHI-ZORN 73 PR D8 12	B. Sechi-Zorn, G.A. Snow	(UMD)
BELLAMY 72 PL 39B 299	E.H. Bellamy et al.	(LOWC, RHEL, SUSS)
BOHM 72 NP B48 1	G. Bohm et al.	(BERL, KIDR, BRUX, IASD+)
Also IHE-73.2 Nov	G. Bohm	(BERL, KIDR, BRUX, IASD, DUUC+)
COLE 71 PR D4 631	J. Cole et al.	(VAND, MIPM)
TOWEE 71 NP B33 493	D.N. Towe et al.	(STON, COLU)
BERLEY 70B PR D1 2015	D. Berley et al.	(LOUC, KIDR, BERL+)
EISELE 70 ZPHY 238 372	F. Eisele et al.	(BNL, MASA, YALE)
HARRIS 70 PRL 24 165	F. Harris et al.	(HEID)
PDG 70 RMP 42 87	A. Barbaro-Gatti et al.	(MICH, WIS C)
ANG 69B ZPHY 228 151	G. Ang et al.	(LRL, BRAN+)
		(HEID)

BAGGETT 69B Thesis MDDP-TR-973	N.V. Baggett	(UMD)
BALTAY 69 PRL 22 615	C. Baltay et al.	(COLU, STON)
BANGERTER 69 Thesis UCRL 19244	R.O. Bangarter	(LRL)
BANGERTER 69B PR 187 1821	R.O. Bangarter et al.	(LRL)
BARLOUTAUD 69 NP B14 153	R. Barloutaud et al.	(SACL, CERN, HEID)
EISELE 69 ZPHY 221 1	F. Eisele et al.	(HEID)
Also PRL 13 291	W. Willis et al.	(BNL, CERN, HEID, UMD)
EISELE 69B ZPHY 221 401	F. Eisele et al.	(HEID)
GERSHWIN 69B PR 188 2077	L.K. Gershwin et al.	(LRL)
Also Thesis UCRL 19246	L.K. Gershwin	(LRL)
NORTON 69 Thesis Nevis 175	H. Norton	(COLU)
BAGGETT 67 PRL 19 1458	N. Baggett et al.	(UMD)
Also Vienna Abs. 374	N.V. Baggett, B. Kehoe	(UMD)
Also Private Comm.	N.V. Baggett	(UMD)
BARASH 67 PRL 19 181	N. Barash et al.	(UMD)
EISELE 67 ZPHY 205 409	F. Eisele et al.	(HEID)
HYMAN 67 PL 25B 376	L.G. Hyman et al.	(ANL, CMU, NWES)
PDG 67 RMP 39 1	A.H. Rosenfeld et al.	(LRL, CERN, YALE)
CHANG 66 PR 151 1081	C.Y. Chang	(COLU)
Also Thesis Nevis 145	C.Y. Chang	(COLU)
BAZIN 65 PRL 14 154	M. Bazin et al.	(PRIN, COLU)
BAZIN 65B PR 140 B1358	M. Bazin et al.	(PRIN, RUTG, COLU)
SCHMIDT 65 PR 140 B1328	P. Schmidt	(COLU)
BHOWMIK 64 NP 53 22	B. Bhowmik et al.	(DELH)
COURANT 64 PR 136 B1791	H. Courant et al.	(CERN, HEID, UMD+)
NAUENBERG 64 PRL 12 679	U. Nauenberg et al.	(COLU, RUTG, PRIN)
BARKAS 63 PRL 11 26	W.H. Barkas, J.N. Dyer, H.H. Heckman	(LRL)
Also Thesis UCRL 9450	J.N. Dyer	(LRL)
GALTIERI 62 PRL 9 26	A. Barbaro-Gatti et al.	(LRL)
HUMPHREY 62 PR 127 1305	W.E. Humphrey, R.R. Ross	(LRL)

Σ⁰

I(J^P) = 1(½⁺) Status: ***

COURANT 63 and ALFF 65, using Σ⁰ → Λe⁺e⁻ decays (Dalitz decays), determined the Σ⁰ parity to be positive, given that J = 1/2 and that certain very reasonable assumptions about form factors are true. The results of experiments involving the Primakoff effect, from which the Σ⁰ mean life and Σ⁰ → Λ transition magnetic moment come (see below), strongly support J = 1/2.

Σ⁰ MASS

The fit uses Σ⁺, Σ⁰, Σ⁻, and Λ mass and mass-difference measurements.

VALUE (MeV)	EVTS	DOCUMENT ID	TECN	COMMENT
1192.642 ± 0.024 OUR FIT				
••• We do not use the following data for averages, fits, limits, etc. •••				
1192.65 ± 0.020 ± 0.014	3327	¹ WANG 97 SPEC	Σ ⁰ → Λγ → (ρπ ⁻)(e ⁺ e ⁻)	
¹ This WANG 97 result is redundant with the Σ ⁰ -Λ mass-difference measurement below.				

m_{Σ⁻} - m_{Σ⁰}

VALUE (MeV)	EVTS	DOCUMENT ID	TECN	COMMENT
4.807 ± 0.035 OUR FIT				Error includes scale factor of 1.1.
4.86 ± 0.08 OUR AVERAGE				Error includes scale factor of 1.2.
4.87 ± 0.12	37	DOSCH 65 HBC		
5.01 ± 0.12	12	SCHMIDT 65 HBC		See note with Λ mass
4.75 ± 0.1	18	BURNSTEIN 64 HBC		

m_{Σ⁰} - m_Λ

VALUE (MeV)	EVTS	DOCUMENT ID	TECN	COMMENT
76.959 ± 0.023 OUR FIT				
76.966 ± 0.020 ± 0.013	3327	WANG 97 SPEC	Σ ⁰ → Λγ → (ρπ ⁻)(e ⁺ e ⁻)	
••• We do not use the following data for averages, fits, limits, etc. •••				
76.23 ± 0.55	109	COLAS 75 HLBC	Σ ⁰ → Λγ	
76.63 ± 0.28	208	SCHMIDT 65 HBC		See note with Λ mass

Σ⁰ MEAN LIFE

These lifetimes are deduced from measurements of the cross sections for the Primakoff process Λ → Σ⁰ in nuclear Coulomb fields. An alternative expression of the same information is the Σ⁰-Λ transition magnetic moment given in the following section. The relation is (μ_{ΣΛ}/μ_N)² τ = 1.92951 × 10⁻¹⁹ s (see DEVLIN 86).

VALUE (10 ⁻²⁰ s)	DOCUMENT ID	TECN	COMMENT
7.4 ± 0.7 OUR EVALUATION	Using μ _{ΣΛ} (see the above note).		
6.5 ^{+1.7} _{-1.1}	² DEVLIN 86	SPEC	Primakoff effect
7.6 ± 0.5 ± 0.7	³ PETERSEN 86	SPEC	Primakoff effect
••• We do not use the following data for averages, fits, limits, etc. •••			
5.8 ± 1.3	² DYDAK 77	SPEC	See DEVLIN 86
² DEVLIN 86 is a recalculation of the results of DYDAK 77 removing a numerical approximation made in that work.			
³ An additional uncertainty of the Primakoff formalism is estimated to be < 5%.			

Baryon Particle Listings

Σ^0, Σ^-

$|\mu(\Sigma^0 \rightarrow \Lambda)|$ TRANSITION MAGNETIC MOMENT

See the note in the Σ^0 mean-life section above. Also, See the "Quark Model" review.

VALUE (μ_N)	DOCUMENT ID	TECN	COMMENT
1.61 ± 0.08 OUR AVERAGE			
1.72 ^{+0.17} _{-0.19}	4 DEVLIN	86	SPEC Primakoff effect
1.59 ± 0.05 ± 0.07	5 PETERSEN	86	SPEC Primakoff effect
• • • We do not use the following data for averages, fits, limits, etc. • • •			
1.82 ^{+0.25} _{-0.18}	4 DYDAK	77	SPEC See DEVLIN 86
4 DEVLIN 86 is a recalculation of the results of DYDAK 77 removing a numerical approximation made in that work.			
5 An additional uncertainty of the Primakoff formalism is estimated to be < 2.5%.			

Σ^0 DECAY MODES

Mode	Fraction (Γ_i/Γ)	Confidence level
$\Gamma_1 \Lambda \gamma$	100 %	
$\Gamma_2 \Lambda \gamma \gamma$	< 3 %	90%
$\Gamma_3 \Lambda e^+ e^-$	[a] 5×10^{-3}	

[a] A theoretical value using QED.

Σ^0 BRANCHING RATIOS

VALUE	CL%	DOCUMENT ID	TECN	Γ_2/Γ
< 0.03	90	COLAS	75	HLBC

VALUE	DOCUMENT ID	COMMENT	Γ_3/Γ
0.00545	FEINBERG	58 Theoretical QED calculation	

See COURANT 63 and ALFF 65 for measurements of the invariant-mass spectrum of the Dalitz pairs.

Σ^0 REFERENCES

WANG	97	PR D56 2544	M.H.L.S. Wang et al. (BNL-E766 Collab.)
DEVLIN	86	PR D34 1626	T. Devlin, P.C. Petersen, A. Beretvas (RUTG)
PETERSEN	86	PRL 57 949	P.C. Petersen et al. (RUTG, WISC, MICH+)
DYDAK	77	NP B118 1	F. Dydak et al. (CERN, DORT, HEIDH)
COLAS	75	NP B91 253	J. Colas et al. (ORSAY)
ALFF	65	PR 137 B1105	C. Alff et al. (COLU, RUTG, BNL)P
DOSCH	65	PL 14 239	H.C. Dosch et al. (HEID)
SCHMIDT	65	PR 140 B1328	P. Schmidt (COLU)
BURNSTEIN	64	PRL 13 66	R.A. Burnstein et al. (UMD)
COURANT	63	PRL 10 409	H. Courant et al. (CERN, UMD)P
FEINBERG	58	PR 109 1019	G. Feinberg (BNL)

Σ^-

$I(J^P) = 1(\frac{1}{2}^+)$ Status: * * * *

We have omitted some results that have been superseded by later experiments. See our earlier editions.

Σ^- MASS

The fit uses Σ^+ , Σ^0 , Σ^- , and Λ mass and mass-difference measurements.

VALUE (MeV)	EVTS	DOCUMENT ID	TECN	COMMENT
1197.449 ± 0.029 OUR FIT				Error includes scale factor of 1.1.
1197.45 ± 0.04 OUR AVERAGE				Error includes scale factor of 1.2.
1197.417 ± 0.040		GUREV	93	SPEC Σ^- C atom, crystal diff.
1197.532 ± 0.057		GALL	88	CNTR Σ^- Pb, Σ^- W atoms
1197.43 ± 0.08	3000	SCHMIDT	65	HBC See note with Λ mass
• • • We do not use the following data for averages, fits, limits, etc. • • •				
1197.24 ± 0.15		1 DUGAN	75	CNTR Exotic atoms
1 GALL 88 concludes that the DUGAN 75 mass needs to be reevaluated.				

$m_{\Sigma^-} - m_{\Sigma^+}$

VALUE (MeV)	EVTS	DOCUMENT ID	TECN
8.08 ± 0.08 OUR FIT			
8.09 ± 0.16 OUR AVERAGE			
7.91 ± 0.23	86	BOHM	72
8.25 ± 0.25	2500	DOSCH	65
8.25 ± 0.40	87	BARKAS	63

$m_{\Sigma^-} - m_{\Lambda}$

VALUE (MeV)	EVTS	DOCUMENT ID	TECN	COMMENT
81.766 ± 0.029 OUR FIT				Error includes scale factor of 1.1.
81.69 ± 0.07 OUR AVERAGE				
81.64 ± 0.09	2279	HEPP	68	HBC

81.80 ± 0.13	85	SCHMIDT	65	HBC	See note with Λ mass
81.70 ± 0.19		BURNSTEIN	64	HBC	

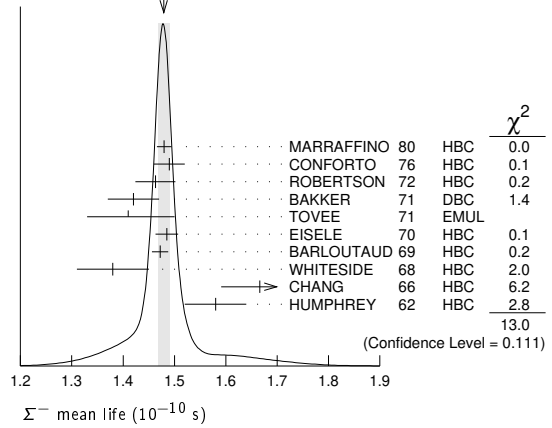
Σ^- MEAN LIFE

Measurements with an error $\geq 0.2 \times 10^{-10}$ s have been omitted.

VALUE (10^{-10} s)	EVTS	DOCUMENT ID	TECN	COMMENT
1.479 ± 0.011 OUR AVERAGE				Error includes scale factor of 1.3. See the ideogram below.
1.480 ± 0.014	16k	MARRAFFINO	80	HBC $K^- p$ 0.42-0.5 GeV/c
1.49 ± 0.03	8437	CONFORTO	76	HBC $K^- p$ 1-1.4 GeV/c
1.463 ± 0.039	2400	ROBERTSON	72	HBC $K^- p$ 0.25 GeV/c
1.42 ± 0.05	1383	BAKKER	71	DBC $K^- N \rightarrow \Sigma^- \pi \pi$
1.41 ^{+0.09} _{-0.08}		TOVEE	71	EMUL
1.485 ± 0.022	100k	EISELE	70	HBC $K^- p$ at rest
1.472 ± 0.016	10k	BARLOUTAUD	69	HBC $K^- p$ 0.4-1.2 GeV/c
1.38 ± 0.07	506	WHITESIDE	68	HBC $K^- p$ at rest
1.666 ± 0.075	3267	1 CHANG	66	HBC $K^- p$ at rest
1.58 ± 0.06	1208	HUMPHREY	62	HBC $K^- p$ at rest

1 We have increased the CHANG 66 error of 0.026; see our 1970 edition, Reviews of Modern Physics 42 87 (1970).

WEIGHTED AVERAGE
1.479 ± 0.011 (Error scaled by 1.3)

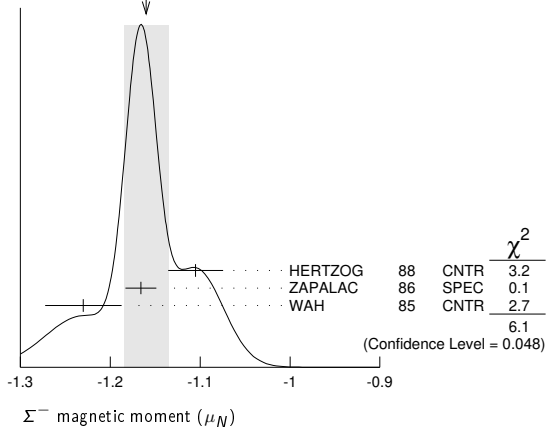


Σ^- MAGNETIC MOMENT

See the "Quark Model" review. Measurements with an error $\geq 0.3 \mu_N$ have been omitted.

VALUE (μ_N)	EVTS	DOCUMENT ID	TECN	COMMENT
-1.160 ± 0.025 OUR AVERAGE				Error includes scale factor of 1.7. See the ideogram below.
-1.105 ± 0.029 ± 0.010		HERTZOG	88	CNTR Σ^- Pb, Σ^- W atoms
-1.166 ± 0.014 ± 0.010	671k	ZAPALAC	86	SPEC $ne^- \nu, n\pi^-$ decays
-1.23 ± 0.03 ± 0.03		WAH	85	CNTR $pCu \rightarrow \Sigma^- X$
• • • We do not use the following data for averages, fits, limits, etc. • • •				
-0.89 ± 0.14	516k	DECK	83	SPEC $pBe \rightarrow \Sigma^- X$

WEIGHTED AVERAGE
-1.160 ± 0.025 (Error scaled by 1.7)



Σ^- CHARGE RADIUS

VALUE (fm)	DOCUMENT ID	TECN	COMMENT
0.780 ± 0.080 ± 0.060	¹ ESCHRICH 01	SELX	$\Sigma^- e \rightarrow \Sigma^- e$
¹ ESCHRICH 01 actually gives $\langle r^2 \rangle = (0.61 \pm 0.12 \pm 0.09) \text{ fm}^2$.			

 Σ^- DECAY MODES

Mode	Fraction (Γ_i/Γ)	Confidence level
Γ_1 $n\pi^-$	(99.848 ± 0.005) %	
Γ_2 $n\pi^-\gamma$	[a] (4.6 ± 0.6) × 10 ⁻⁴	
Γ_3 $ne^-\bar{\nu}_e$	(1.017 ± 0.034) × 10 ⁻³	
Γ_4 $n\mu^-\bar{\nu}_\mu$	(4.5 ± 0.4) × 10 ⁻⁴	
Γ_5 $\Lambda e^-\bar{\nu}_e$	(5.73 ± 0.27) × 10 ⁻⁵	
Γ_6 $\Sigma^+ X$	< 1.2 × 10 ⁻⁴	90%

Lepton number (L) violating modes

Γ_7 pe^-e^-	L < 6.7 × 10 ⁻⁵	90%
----------------------	----------------------------	-----

[a] See the Listings below for the pion momentum range used in this measurement.

CONSTRAINED FIT INFORMATION

An overall fit to 3 branching ratios uses 16 measurements and one constraint to determine 4 parameters. The overall fit has a $\chi^2 = 8.7$ for 13 degrees of freedom.

The following *off-diagonal* array elements are the correlation coefficients $\langle \delta x_i \delta x_j \rangle / (\delta x_i \delta x_j)$, in percent, from the fit to the branching fractions, $x_i \equiv \Gamma_i / \Gamma_{\text{total}}$. The fit constrains the x_i whose labels appear in this array to sum to one.

x_3	-64		
x_4	-77	0	
x_5	-5	0	0
	x_1	x_3	x_4

 Σ^- BRANCHING RATIOS $\Gamma(n\pi^-\gamma)/\Gamma(n\pi^-)$ Γ_2/Γ_1

The π^+ momentum cuts differ, so we do not average the results but simply use the latest value for the Summary Table.

VALUE (units 10 ⁻³)	EVTS	DOCUMENT ID	TECN	COMMENT
0.46 ± 0.06	292	EBENHOH 73	HBC	$\pi^+ < 150 \text{ MeV}/c$
• • • We do not use the following data for averages, fits, limits, etc. • • •				
0.10 ± 0.02	23	ANG 69B	HBC	$\pi^- < 110 \text{ MeV}/c$
~ 1.1		BAZIN 65B	HBC	$\pi^- < 166 \text{ MeV}/c$

 $\Gamma(ne^-\bar{\nu}_e)/\Gamma(n\pi^-)$ Γ_3/Γ_1

Measurements with an error $\geq 0.2 \times 10^{-3}$ have been omitted.

VALUE (units 10 ⁻³)	EVTS	DOCUMENT ID	TECN	COMMENT
1.019 ± 0.035 OUR FIT				
1.019 + 0.031 - 0.040 OUR AVERAGE				
0.96 ± 0.05	2847	BOURQUIN 83c	SPEC	SPS hyperon beam
1.09 + 0.06 - 0.08	601	¹ EBENHOH 74	HBC	$K^- p$ at rest
1.05 + 0.07 - 0.13	455	¹ SECHI-ZORN 73	HBC	$K^- p$ at rest
0.97 ± 0.15	57	COLE 71	HBC	$K^- p$ at rest
1.11 ± 0.09	180	BIERMAN 68	HBC	

¹ An additional negative systematic error is included for internal radiative corrections and latest form factors; see BOURQUIN 83c.

 $\Gamma(n\mu^-\bar{\nu}_\mu)/\Gamma(n\pi^-)$ Γ_4/Γ_1

VALUE (units 10 ⁻³)	EVTS	DOCUMENT ID	TECN	COMMENT
0.45 ± 0.04 OUR FIT				
0.45 ± 0.04 OUR AVERAGE				
0.38 ± 0.11	13	COLE 71	HBC	$K^- p$ at rest
0.43 ± 0.06	72	ANG 69	HBC	$K^- p$ at rest
0.43 ± 0.09	56	BAGGETT 69	HBC	$K^- p$ at rest
0.56 ± 0.20	11	BAZIN 65B	HBC	$K^- p$ at rest
0.66 ± 0.15	22	COURANT 64	HBC	

 $\Gamma(\Lambda e^-\bar{\nu}_e)/\Gamma(n\pi^-)$ Γ_5/Γ_1

VALUE (units 10 ⁻⁴)	EVTS	DOCUMENT ID	TECN	COMMENT
0.574 ± 0.027 OUR FIT				
0.574 ± 0.027 OUR AVERAGE				
0.561 ± 0.031	1620	¹ BOURQUIN 82	SPEC	SPS hyperon beam
0.63 ± 0.11	114	THOMPSON 80	ASP K	Hyperon beam
0.52 ± 0.09	31	BALTAY 69	HBC	$K^- p$ at rest
0.69 ± 0.12	31	EISELE 69	HBC	$K^- p$ at rest
0.64 ± 0.12	35	BARASH 67	HBC	$K^- p$ at rest
0.75 ± 0.28	11	COURANT 64	HBC	$K^- p$ at rest

¹ The value is from BOURQUIN 83b, and includes radiation corrections and new acceptance.

 $\Gamma(\Sigma^+ X)/\Gamma_{\text{total}}$ Γ_6/Γ

Here mode X can be any particle combination.

VALUE	CL%	DOCUMENT ID	TECN	COMMENT
< 1.2 × 10⁻⁴		ABLIIKIM 21F	BES	1,311 M J/ψ decays

Lepton number (L) violating modes

 $\Gamma(pe^-e^-)/\Gamma_{\text{total}}$ Γ_7/Γ

This decay violates lepton number conservation with $\Delta Q = \Delta L = 2$.

VALUE	CL%	DOCUMENT ID	TECN	COMMENT
< 6.7 × 10⁻⁵		ABLIIKIM 21F	BES	1,311 M J/ψ decays

 Σ^- DECAY PARAMETERS

See the "Note on Baryon Decay Parameters" in the neutron Listings. Older, outdated results have been omitted.

 α_- FOR $\Sigma^- \rightarrow n\pi^-$

VALUE	EVTS	DOCUMENT ID	TECN	COMMENT
-0.068 ± 0.008 OUR AVERAGE				
-0.062 ± 0.024	28k	HANSL 78	HBC	$K^- p \rightarrow \Sigma^- \pi^+$
-0.067 ± 0.011	60k	BOGERT 70	HBC	$K^- p$ 0.4 GeV/c
-0.071 ± 0.012	51k	BANGERTER 69	HBC	$K^- p$ 0.4 GeV/c

 ϕ ANGLE FOR $\Sigma^- \rightarrow n\pi^-$ (tan $\phi = \beta / \gamma$)

VALUE (°)	EVTS	DOCUMENT ID	TECN	COMMENT
10 ± 15 OUR AVERAGE				
+ 5 ± 23	1092	¹ BERLEY 70B	HBC	n rescattering
14 ± 19	1385	BANGERTER 69B	HBC	$K^- p$ 0.4 GeV/c

¹ BERLEY 70B changed from -5 to +5° to agree with our sign convention.

 g_A/g_V FOR $\Sigma^- \rightarrow ne^-\bar{\nu}_e$

Measurements with fewer than 500 events have been omitted. Where necessary, signs have been changed to agree with our conventions, which are given in the "Note on Baryon Decay Parameters" in the neutron Listings. What is actually listed is $|g_1/f_1 - 0.237g_2/f_1|$. This reduces to $g_A/g_V \equiv g_1(0)/f_1(0)$ on making the usual assumption that $g_2 = 0$. See also the note on HSUEH 88.

VALUE	EVTS	DOCUMENT ID	TECN	COMMENT
0.340 ± 0.017 OUR AVERAGE				
+ 0.327 ± 0.007 ± 0.019	50k	¹ HSUEH 88	SPEC	Σ^- 250 GeV
+ 0.34 ± 0.05	4456	² BOURQUIN 83c	SPEC	SPS hyperon beam
0.385 ± 0.037	3507	³ TANENBAUM 74	ASP K	
• • • We do not use the following data for averages, fits, limits, etc. • • •				
0.29 ± 0.07	25k	HSUEH 85	SPEC	See HSUEH 88
0.17 + 0.07 - 0.09	519	DECAMP 77	ELEC	Hyperon beam

¹ The sign is, with our conventions, unambiguously positive. The value assumes, as usual, that $g_2 = 0$. If g_2 is included in the fit, then (with our sign convention) $g_2 = -0.56 \pm 0.37$, with a corresponding reduction of g_A/g_V to $+0.20 \pm 0.08$.

² BOURQUIN 83c favors the positive sign by at least 2.6 standard deviations.

³ TANENBAUM 74 gives 0.435 ± 0.035 , assuming no q^2 dependence in g_A and g_V . The listed result allows q^2 dependence, and is taken from HSUEH 88.

 $f_2(0)/f_1(0)$ FOR $\Sigma^- \rightarrow ne^-\bar{\nu}_e$

The signs have been changed to be in accord with our conventions, given in the "Note on Baryon Decay Parameters" in the neutron Listings.

VALUE	EVTS	DOCUMENT ID	TECN	COMMENT
0.97 ± 0.14 OUR AVERAGE				
+ 0.96 ± 0.07 ± 0.13	50k	HSUEH 88	SPEC	Σ^- 250 GeV
+ 1.02 ± 0.34	4456	BOURQUIN 83c	SPEC	SPS hyperon beam

TRIPLE CORRELATION COEFFICIENT D for $\Sigma^- \rightarrow ne^-\bar{\nu}_e$

The coefficient D of the term $D \mathbf{P} \cdot (\mathbf{p}_e \times \mathbf{p}_\nu)$ in the $\Sigma^- \rightarrow ne^-\bar{\nu}$ decay angular distribution. A nonzero value would indicate a violation of time-reversal invariance.

VALUE	EVTS	DOCUMENT ID	TECN	COMMENT
0.11 ± 0.10	50k	HSUEH 88	SPEC	Σ^- 250 GeV

Baryon Particle Listings

$\Sigma^-, \Sigma(1385)$

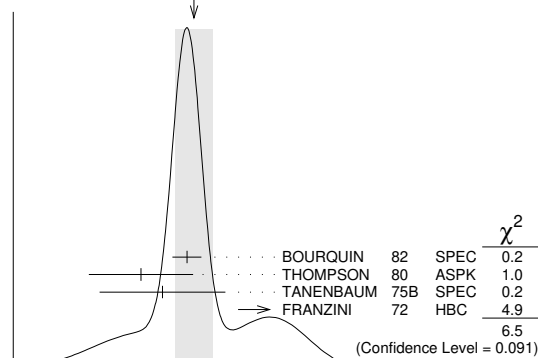
g_V/g_A FOR $\Sigma^- \rightarrow \Lambda e^- \bar{\nu}_e$

For the sign convention, see the "Note on Baryon Decay Parameters" in the neutron Listings. The value is predicted to be zero by conserved vector current theory. The values averaged assume CVC-SU(3) weak magnetism term.

VALUE	EVTs	DOCUMENT ID	TECN	COMMENT
0.01 ± 0.10 OUR AVERAGE		Error includes scale factor of 1.5. See the ideogram below.		
-0.034 ± 0.080	1620	¹ BOURQUIN 82	SPEC	SPS hyperon beam
-0.29 ± 0.29	114	THOMPSON 80	ASPK	BNL hyperon beam
-0.17 ± 0.35	55	TANENBAUM 75B	SPEC	BNL hyperon beam
+0.45 ± 0.20	186	^{1,2} FRANZINI 72	HBC	

¹ The sign has been changed to agree with our convention.
² The FRANZINI 72 value includes the events of earlier papers.

WEIGHTED AVERAGE
 0.01±0.10 (Error scaled by 1.5)



g_{WM}/g_A FOR $\Sigma^- \rightarrow \Lambda e^- \bar{\nu}_e$

The values quoted assume the CVC prediction $g_V = 0$.

VALUE	EVTs	DOCUMENT ID	TECN	COMMENT
2.4 ± 1.7 OUR AVERAGE				
1.75 ± 3.5	114	THOMPSON 80	ASPK	BNL hyperon beam
3.5 ± 4.5	55	TANENBAUM 75B	SPEC	BNL hyperon beam
2.4 ± 2.1	186	FRANZINI 72	HBC	

Σ^- REFERENCES

We have omitted some papers that have been superseded by later experiments. See our earlier editions.

ABLIKIM 21F	PR D103 052011	M. Ablikim <i>et al.</i>	(BESII Collab.)
ESCHRICH 01	PL B52 233	I. Eschrich <i>et al.</i>	(FNAL SELEX Collab.)
GUREV 93	JETPL 57 400	M.P. Gurev <i>et al.</i>	(PNPI)
Translated from ZETFP 57 389.			
GALL 88	PRL 60 186	K.P. Gall <i>et al.</i>	(BOST, MIT, WILL, CIT+)
HERTZOG 88	PR D37 1142	D.W. Hertzog <i>et al.</i>	(WILL, BOST, MIT+)
HSUEH 88	PR D38 2056	S.Y. Hsueh <i>et al.</i>	(CHIC, ELMT, FNAL+)
ZAPALAC 86	PRL 57 1526	G. Zapalac <i>et al.</i>	(EFI, ELMT, FNAL+)
HSUEH 85	PRL 54 2399	S.Y. Hsueh <i>et al.</i>	(CHIC, ELMT, FNAL+)
WAH 85	PRL 55 2551	Y.W. Wah <i>et al.</i>	(FNAL, IOWA, ISU)
BOURQUIN 83B	ZPHY C21 27	M.H. Bourquin <i>et al.</i>	(BRIS, GEVA, HEIDP+)
BOURQUIN 83C	ZPHY C21 17	M.H. Bourquin <i>et al.</i>	(BRIS, GEVA, HEIDP+)
DECK 83	PR D28 1	L. Deck <i>et al.</i>	(RUTG, WIS C, MICH, MINN)
BOURQUIN 82	ZPHY C12 307	M.H. Bourquin <i>et al.</i>	(BRIS, GEVA, HEIDP+)
MARRAFFINO 80	PR D21 2501	J. Marraffino <i>et al.</i>	(VAND, MPIM)
THOMPSON 80	PR D21 25	J.A. Thompson <i>et al.</i>	(PITT, BNL)
HANSL 78	NP B132 45	T. Hansl <i>et al.</i>	(MPIM, VAND)
DECAMP 77	PL 66B 295	D. Decamp <i>et al.</i>	(LALO, EPOL)
CONFORTO 76	NP B105 189	B. Conforto <i>et al.</i>	(RHEL, LOIC)
DUGAN 75	NP A254 396	G. Dugan <i>et al.</i>	(COLU, YALE)
TANENBAUM 75B	PR D12 1871	W. Tanenbaum <i>et al.</i>	(YALE, FNAL, BNL)
EBENHOH 74	ZPHY 266 367	H. Ebenhoh <i>et al.</i>	(HEIDT)
TANENBAUM 74	PRL 33 175	W. Tanenbaum <i>et al.</i>	(YALE, FNAL, BNL)
EBENHOH 73	ZPHY 264 413	W. Ebenhoh <i>et al.</i>	(HEIDT)
SECHI-ZORN 73	PR D8 12	B. Sechi-Zorn, G.A. Snow	(UMD)
BOHM 72	NP B48 1	G. Bohm <i>et al.</i>	(BERL, KIDR, BRUX, IASD+)
FRANZINI 72	PR D6 2417	P. Franzini <i>et al.</i>	(COLU, HEID, UMD+)
ROBERTSON 72	Thesis UMI 78-00877	R.M. Robertson	(IIT)
BAKKER 71	LNC 1 37	A.M. Bakker <i>et al.</i>	(SABRE Collab.)
COLE 71	PR D4 631	J. Cole <i>et al.</i>	(STON, COLU)
Also			
TOVEE 71	NP B33 493	H. Tovee <i>et al.</i>	(LOUC, KIDR, BERL+)
BERLEY 70B	PR D1 2015	D. Berley <i>et al.</i>	(BNL, MASA, YALE)
BOGERT 70	PR D2 6	D.V. Bogert <i>et al.</i>	(BNL, MASA, YALE)
EISELE 70	ZPHY 238 372	F. Eisele <i>et al.</i>	(HEID)
PDG 70	RMP 42 87	A. Barbaro-Galtieri <i>et al.</i>	(LRL, BRAN+)
ANG 69	ZPHY 223 103	G. Ang <i>et al.</i>	(HEID)
ANG 69B	ZPHY 228 151	G. Ang <i>et al.</i>	(HEID)
BAGGETT 69	PRL 23 249	N.V. Baggett, B. Kehoe, G.A. Snow	(UMD)
BALTAY 69	PR 22 615	E. Baltay <i>et al.</i>	(COLU, STON)
BANGERTER 69	Thesis UCRL 19244	R.O. Bangertter	(LRL)
BANGERTER 69B	PR 187 1821	R.O. Bangertter <i>et al.</i>	(LRL)
BARLOUTAUD 69	NP B14 153	R. Barloutaud <i>et al.</i>	(SACL, CERN, HEID)
EISELE 69	ZPHY 221 1	F. Eisele <i>et al.</i>	(HEID)
BIERMAN 68	PRL 20 1459	E. Bierman <i>et al.</i>	(PRIN)
HEPP 68	ZPHY 214 71	V. Hepp, H. Schleich	(HEID)
WHITESIDE 68	NC 54A 537	H. Whiteside, J. Gollub	(OBER)

BARASH 67	PRL 19 181	N. Barash <i>et al.</i>	(UMD)
CHANG 66	PR 151 1081	C.Y. Chang	(COLU)
BAZIN 65B	PR 140 B1358	M. Bazin <i>et al.</i>	(PRIN, RUTG, COLU)
DOSCH 65	PL 14 239	H.C. Dosch <i>et al.</i>	(HEID)
Also			
SCHMIDT 65	PR 151 1081	C.Y. Chang	(COLU)
BURNSTEIN 64	PR 140 B1328	P. Schmidt	(COLU)
COURANT 64	PRL 13 66	R.A. Burnstein <i>et al.</i>	(UMD)
BARKAS 63	PR 136 B1791	H. Courant <i>et al.</i>	(CERN, HEID, UMD+)
HUMPHREY 62	PRL 11 26	W.H. Barkas, J.N. Dyer, H.H. Heckman	(LRL)
	PR 127 1305	W.E. Humphrey, R.R. Ross	(LRL)

$\Sigma(1385) 3/2^+$

$$I(J^P) = 1(\frac{3}{2}^+) \text{ Status: } ***$$

Discovered by ALSTON 60. Early measurements of the mass and width for combined charge states have been omitted. They may be found in our 1984 edition Reviews of Modern Physics 56 S1 (1984).

We average only the most significant determinations. We do not average results from inclusive experiments with large backgrounds or results which are not accompanied by some discussion of experimental resolution. Nevertheless systematic differences between experiments remain. (See the ideograms in the Listings below.) These differences could arise from interference effects that change with production mechanism and/or beam momentum. They can also be accounted for in part by differences in the parametrizations employed. (See BORENSTEIN 74 for a discussion on this point.) Thus BORENSTEIN 74 uses a Breit-Wigner with energy-independent width, since a P -wave was found to give unsatisfactory fits. CAMERON 78 uses the same form. On the other hand HOLMGREN 77 obtains a good fit to their $\Lambda\pi$ spectrum with a P -wave Breit-Wigner, but includes the partial width for the $\Sigma\pi$ decay mode in the parametrization. AGUILAR-BENITEZ 81D gives masses and widths for five different Breit-Wigner shapes. The results vary considerably. Only the best-fit S -wave results are given here.

$\Sigma(1385)$ POLE POSITIONS

$\Sigma(1385)^+$ REAL PART

VALUE	DOCUMENT ID	COMMENT
1379 ± 1	LICHTENBERG74	Extrapolates HABIBI 73

$\Sigma(1385)^+$ -IMAGINARY PART

VALUE	DOCUMENT ID	COMMENT
17.5 ± 1.5	LICHTENBERG74	Extrapolates HABIBI 73

$\Sigma(1385)^-$ REAL PART

VALUE	DOCUMENT ID	COMMENT
1383 ± 1	LICHTENBERG74	Extrapolates HABIBI 73

$\Sigma(1385)^-$ -IMAGINARY PART

VALUE	DOCUMENT ID	COMMENT
22.5 ± 1.5	LICHTENBERG74	Extrapolates HABIBI 73

$\Sigma(1385)$ MASSES

$\Sigma(1385)^+$ MASS

VALUE (MeV)	EVTs	DOCUMENT ID	TECN	COMMENT
1382.83 ± 0.34 OUR AVERAGE		Error includes scale factor of 1.9. See the ideogram below.		
1384.8 ± 0.3 ± 1.4		LEE 21A	BELL	$\Lambda_C^+ \rightarrow \eta \Sigma(1385)^+$
1383.2 ± 0.9 ^{+0.1} _{-1.5}		AGAKISHIEV 12	SPEC	$p p \rightarrow \Sigma(1385)^+ K^+ n$, 3.5 GeV
1384.1 ± 0.7	1897	BAUBILLIER 84	HBC	$K^- p \rightarrow 8.25 \text{ GeV}/c$
1384.5 ± 0.5	5256	AGUILAR... 81D	HBC	$K^- p \rightarrow \Lambda \pi \pi 4.2 \text{ GeV}/c$
1383.0 ± 0.4	9361	AGUILAR... 81D	HBC	$K^- p \rightarrow \Lambda 3\pi 4.2 \text{ GeV}/c$
1381.9 ± 0.3	6900	CAMERON 78	HBC	$K^- p 0.96\text{-}1.36 \text{ GeV}/c$
1381 ± 1	6846	BORENSTEIN 74	HBC	$K^- p 2.18 \text{ GeV}/c$
1383.5 ± 0.85	2300	HABIBI 73	HBC	$K^- p \rightarrow \Lambda \pi \pi$
1382 ± 2	400	AGUILAR... 72B	HBC	$K^- p \rightarrow \Lambda \pi \pi$
1384.4 ± 1.0	1260	SIEGEL 67	HBC	$K^- p 2.1 \text{ GeV}/c$
1382 ± 1	750	ARMENTEROS65B	HBC	$K^- p 0.9\text{-}1.2 \text{ GeV}/c$
1381.0 ± 1.6	859	HUWE 64	HBC	$K^- p 1.22 \text{ GeV}/c$
••• We do not use the following data for averages, fits, limits, etc. •••				
1385.1 ± 1.2	600	BAKER 80	HYBR	$\pi^+ p 7 \text{ GeV}/c$
1383.2 ± 1.0	750	BAKER 80	HYBR	$K^- p 7 \text{ GeV}/c$
1381 ± 2	7k	¹ BAUBILLIER 79B	HBC	$K^- p 8.25 \text{ GeV}/c$
1391 ± 2	2k	CAUTIS 79	HYBR	$\pi^+ p / K^- p 11.5 \text{ GeV}$
1390 ± 2	100	¹ SUGAHARA 79B	HBC	$\pi^- p 6 \text{ GeV}/c$
1385 ± 3	22k	^{1,2} BARREIRO 77B	HBC	$K^- p 4.2 \text{ GeV}/c$
1385 ± 1	2594	HOLMGREN 77	HBC	See AGUILAR-BENITEZ 81D
1380 ± 2		¹ BARDADIN... 75	HBC	$K^- p 14.3 \text{ GeV}/c$
1382 ± 1	3740	³ BERTHON 74	HBC	$K^- p 1263\text{-}1843 \text{ MeV}/c$
1390 ± 6	46	AGUILAR... 70B	HBC	$K^- p \rightarrow \Sigma \pi \pi 4 \text{ GeV}/c$
1383 ± 8	62	⁴ BIRMINGHAM 66	HBC	$K^- p 3.5 \text{ GeV}/c$

See key on page 1171

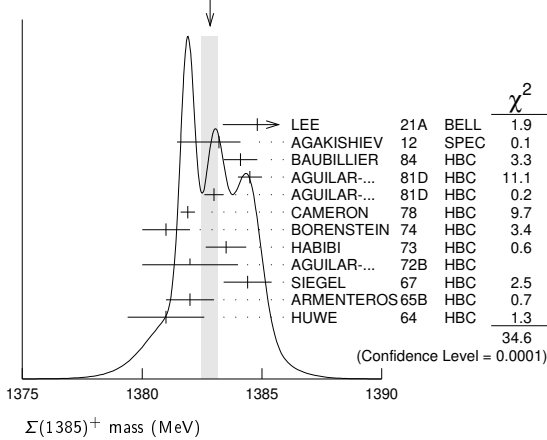
Baryon Particle Listings

$\Sigma(1385)$

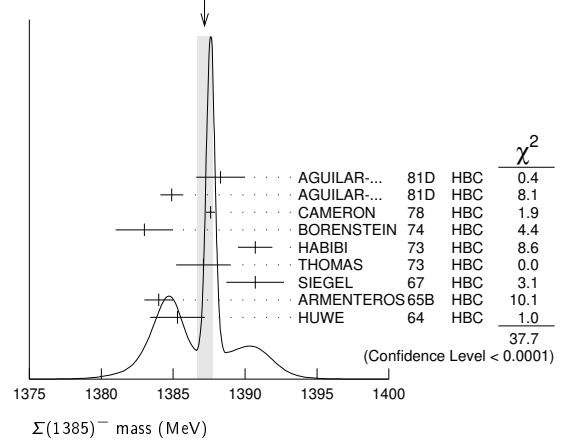
1378 ±5	135	LONDON	66	HBC	K^-p 2.24 GeV/c
1384.3 ±1.9	250	⁴ SMITH	65	HBC	K^-p 1.8 GeV/c
1382.6 ±2.1	250	⁴ SMITH	65	HBC	K^-p 1.95 GeV/c
1375.0 ±3.9	170	COOPER	64	HBC	K^-p 1.45 GeV/c
1376.0 ±3.9	154	⁴ ELY	61	HLBC	K^-p 1.11 GeV/c

1389 ±9	15	LONDON	66	HBC	K^-p 2.24 GeV/c
1391.5 ±2.6	120	⁴ SMITH	65	HBC	K^-p 1.8 GeV/c
1399.8 ±2.2	58	⁴ SMITH	65	HBC	K^-p 1.95 GeV/c
1392.0 ±6.2	200	COOPER	64	HBC	K^-p 1.45 GeV/c
1382 ±3	93	DAHL	61	DBC	K^-d 0.45 GeV/c
1376.0 ±4.4	224	⁴ ELY	61	HLBC	K^-p 1.11 GeV/c

WEIGHTED AVERAGE
1382.83±0.34 (Error scaled by 1.9)



WEIGHTED AVERAGE
1387.2±0.5 (Error scaled by 2.2)

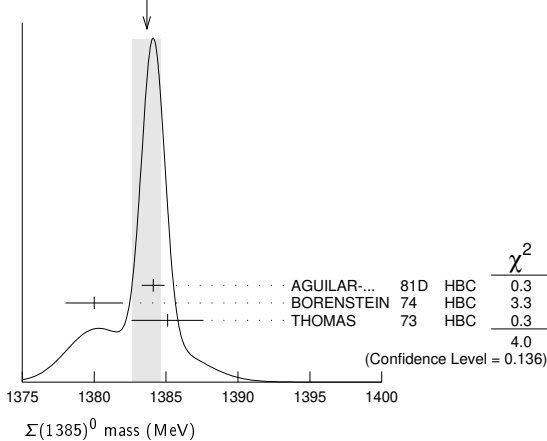


$\Sigma(1385)^0$ MASS

VALUE (MeV)	EVTs	DOCUMENT ID	TECN	COMMENT
1383.7 ± 1.0 OUR AVERAGE		Error includes scale factor of 1.4. See the ideogram below.		
1384.1 ± 0.8	5722	AGUILAR...	81D HBC	$K^-p \rightarrow \Lambda 3\pi$ 4.2 GeV/c
1380 ± 2	3100	⁵ BORENSTEIN	74 HBC	$K^-p \rightarrow \Lambda 3\pi$ 2.18 GeV/c
1385.1 ± 2.5	240	⁴ THOMAS	73 HBC	$\pi^-p \rightarrow \Lambda \pi^0 K^0$
1389 ± 3	500	⁶ BAUBILLIER	79B HBC	K^-p 8.25 GeV/c

• • • We do not use the following data for averages, fits, limits, etc. • • •

WEIGHTED AVERAGE
1383.7±1.0 (Error scaled by 1.4)



$m_{\Sigma(1385)^-} - m_{\Sigma(1385)^+}$

VALUE (MeV)	CL%	DOCUMENT ID	TECN	COMMENT
• • • We do not use the following data for averages, fits, limits, etc. • • •				
- 2 to +6	95	⁷ BORENSTEIN	74 HBC	K^-p 2.18 GeV/c
7.2 ± 1.4		⁷ HABIBI	73 HBC	$K^-p \rightarrow \Lambda \pi \pi$
6.3 ± 2.0		⁷ SIEGEL	67 HBC	K^-p 2.1 GeV/c
11 ± 9		⁷ LONDON	66 HBC	K^-p 2.24 GeV/c
9 ± 6		LONDON	66 HBC	$\Lambda 3\pi$ events
2.0 ± 1.5		⁷ ARMENTEROS65B	HBC	K^-p 0.9-1.2 GeV/c
7.2 ± 2.1		⁷ SMITH	65 HBC	K^-p 1.8 GeV/c
17.2 ± 2.0		⁷ SMITH	65 HBC	K^-p 1.95 GeV/c
17 ± 7		⁷ COOPER	64 HBC	K^-p 1.45 GeV/c
4.3 ± 2.2		⁷ HUWE	64 HBC	K^-p 1.22 GeV/c
0.0 ± 4.2		⁷ ELY	61 HLBC	K^-p 1.11 GeV/c

$m_{\Sigma(1385)^0} - m_{\Sigma(1385)^+}$

VALUE (MeV)	CL%	DOCUMENT ID	TECN	COMMENT
• • • We do not use the following data for averages, fits, limits, etc. • • •				
-4 to +4	95	⁷ BORENSTEIN	74 HBC	K^-p 2.18 GeV/c

$m_{\Sigma(1385)^-} - m_{\Sigma(1385)^0}$

VALUE (MeV)	DOCUMENT ID	TECN	COMMENT
• • • We do not use the following data for averages, fits, limits, etc. • • •			
2.0 ± 2.4	⁷ THOMAS	73 HBC	$\pi^-p \rightarrow \Lambda \pi^- K^+$

$\Sigma(1385)$ WIDTHS

$\Sigma(1385)^-$ MASS

VALUE (MeV)	EVTs	DOCUMENT ID	TECN	COMMENT
1387.2 ± 0.5 OUR AVERAGE		Error includes scale factor of 2.2. See the ideogram below.		
1388.3 ± 1.7	620	AGUILAR...	81D HBC	$K^-p \rightarrow \Lambda \pi \pi$ 4.2 GeV/c
1384.9 ± 0.8	3346	AGUILAR...	81D HBC	$K^-p \rightarrow \Lambda 3\pi$ 4.2 GeV/c
1387.6 ± 0.3	9720	CAMERON	78 HBC	K^-p 0.96-1.36 GeV/c
1383 ± 2	2303	BORENSTEIN	74 HBC	K^-p 2.18 GeV/c
1390.7 ± 1.2	1900	HABIBI	73 HBC	$K^-p \rightarrow \Lambda \pi \pi$
1387.1 ± 1.9	630	⁴ THOMAS	73 HBC	$\pi^-p \rightarrow \Lambda \pi^- K^+$
1390.7 ± 2.0	370	SIEGEL	67 HBC	K^-p 2.1 GeV/c
1384 ± 1	1380	ARMENTEROS65B	HBC	K^-p 0.9-1.2 GeV/c
1385.3 ± 1.9	1086	⁴ HUWE	64 HBC	K^-p 1.15-1.30 GeV/c
• • • We do not use the following data for averages, fits, limits, etc. • • •				
1383 ± 1	4.5k	¹ BAUBILLIER	79B HBC	K^-p 8.25 GeV/c
1380 ± 6	150	¹ SUGAHARA	79B HBC	π^-p 6 GeV/c
1387 ± 3	12k	^{1,2} BARREIRO	77B HBC	K^-p 4.2 GeV/c
1391 ± 3	193	HOLMGREN	77 HBC	See AGUILAR-BENITEZ 81D
1383 ± 2		¹ BARDADIN...	75 HBC	K^-p 14.3 GeV/c
1389 ± 1	3060	³ BERTHON	74 HBC	K^-p 1263-1843 MeV/c

$\Sigma(1385)^+$ WIDTH

VALUE (MeV)	EVTs	DOCUMENT ID	TECN	COMMENT
36.2 ± 0.7 OUR AVERAGE				
38.1 ± 1.5 ± 2.1		LEE	21A BELL	$\Lambda_c^+ \rightarrow \eta \Sigma(1385)^+$
40.2 ± 2.1 ^{+1.2} / _{-2.8}		AGAKISHIEV	12 SPEC	$pp \rightarrow \Sigma(1385)^+ K^+ n$, 3.5 GeV
37.2 ± 2.0	1897	BAUBILLIER	84 HBC	K^-p 8.25 GeV/c
35.1 ± 1.7	5256	AGUILAR...	81D HBC	$K^-p \rightarrow \Lambda \pi \pi$ 4.2 GeV/c
37.5 ± 2.0	9361	AGUILAR...	81D HBC	$K^-p \rightarrow \Lambda 3\pi$ 4.2 GeV/c
35.5 ± 1.9	6900	CAMERON	78 HBC	K^-p 0.96-1.36 GeV/c
34.0 ± 1.6	6846	⁸ BORENSTEIN	74 HBC	K^-p 2.18 GeV/c
38.3 ± 3.2	2300	⁹ HABIBI	73 HBC	$K^-p \rightarrow \Lambda \pi \pi$
32.5 ± 6.0	400	AGUILAR...	72B HBC	$K^-p \rightarrow \Lambda \pi$'s
36 ± 4	1260	⁹ SIEGEL	67 HBC	K^-p 2.1 GeV/c
32.0 ± 4.7	750	⁹ ARMENTEROS65B	HBC	K^-p 0.95-1.20 GeV/c
46.5 ± 6.4	859	⁹ HUWE	64 HBC	K^-p 1.15-1.30 GeV/c
• • • We do not use the following data for averages, fits, limits, etc. • • •				
40 ± 3	600	BAKER	80 HYBR	$\pi^+ p$ 7 GeV/c
37 ± 2	750	BAKER	80 HYBR	K^-p 7 GeV/c
37 ± 2	7k	¹ BAUBILLIER	79B HBC	K^-p 8.25 GeV/c
30 ± 4	2k	CAUTIS	79 HYBR	$\pi^+ p / K^-p$ 11.5 GeV

Baryon Particle Listings

$\Sigma(1385)$

30 ± 6	100	¹ SUGAHARA	79B	HBC	$\pi^- p$ 6 GeV/c
43 ± 5	22k	^{1,2} BARREIRO	77B	HBC	$K^- p$ 4.2 GeV/c
34 ± 2	2594	HOLMGREN	77	HBC	See AGUILAR-BENITEZ 81D
40.0 ± 3.2		¹ BARDADIN...	75	HBC	$K^- p$ 14.3 GeV/c
48 ± 3	3740	³ BERTHON	74	HBC	$K^- p$ 1263-1843 MeV/c
33 ± 20	46	⁹ AGUILAR...	70B	HBC	$K^- p \rightarrow \Sigma \pi$'s 4 GeV/c
25 ± 32	62	⁹ BIRMINGHAM	66	HBC	$K^- p$ 3.5 GeV/c
30.3 ± 7.5	250	⁹ SMITH	65	HBC	$K^- p$ 1.8 GeV/c
33.1 ± 8.3	250	⁹ SMITH	65	HBC	$K^- p$ 1.95 GeV/c
51 ± 16	170	⁹ COOPER	64	HBC	$K^- p$ 1.45 GeV/c
48 ± 16	154	⁹ ELY	61	HLBC	$K^- p$ 1.11 GeV/c

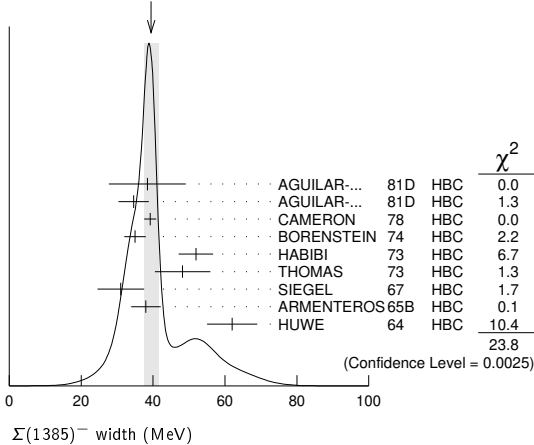
$\Sigma(1385)^0$ WIDTH

VALUE (MeV)	EVTs	DOCUMENT ID	TECN	COMMENT
36 ± 5 OUR AVERAGE				
34.8 ± 5.6	5722	AGUILAR...	81D	HBC $K^- p \rightarrow \Lambda \pi$ 4.2 GeV/c
39.3 ± 10.2	240	⁹ THOMAS	73	HBC $\pi^- p \rightarrow \Lambda \pi^0 K^0$
••• We do not use the following data for averages, fits, limits, etc. •••				
53 ± 8	3100	¹⁰ BORENSTEIN	74	HBC $K^- p \rightarrow \Lambda \pi$ 2.18 GeV/c
30 ± 9	106	CURTIS	63	OSPK $\pi^- p$ 1.5 GeV/c

$\Sigma(1385)^-$ WIDTH

VALUE (MeV)	EVTs	DOCUMENT ID	TECN	COMMENT
39.4 ± 2.1 OUR AVERAGE				Error includes scale factor of 1.7. See the ideogram below.
38.4 ± 10.7	620	AGUILAR...	81D	HBC $K^- p \rightarrow \Lambda \pi \pi$ 4.2 GeV/c
34.6 ± 4.2	3346	AGUILAR...	81D	HBC $K^- p \rightarrow \Lambda \pi$ 4.2 GeV/c
39.2 ± 1.7	9720	CAMERON	78	HBC $K^- p$ 0.96-1.36 GeV/c
35 ± 3	2303	⁸ BORENSTEIN	74	HBC $K^- p$ 2.18 GeV/c
51.9 ± 4.8	1900	⁹ HABIBI	73	HBC $K^- p \rightarrow \Lambda \pi \pi$
48.2 ± 7.7	630	⁹ THOMAS	73	HBC $\pi^- p \rightarrow \Lambda \pi^- K^0$
31.0 ± 6.5	370	⁹ SIEGEL	67	HBC $K^- p$ 2.1 GeV/c
38.0 ± 4.1	1382	⁹ ARMENTEROS65B	HBC	$K^- p$ 0.95-1.20 GeV/c
62 ± 7	1086	HUWE	64	HBC $K^- p$ 1.15-1.30 GeV/c
••• We do not use the following data for averages, fits, limits, etc. •••				
44 ± 4	4.5k	¹ BAUBILLIER	79B	HBC $K^- p$ 8.25 GeV/c
58 ± 4	150	¹ SUGAHARA	79B	HBC $\pi^- p$ 6 GeV/c
45 ± 5	12k	^{1,2} BARREIRO	77B	HBC $K^- p$ 4.2 GeV/c
35 ± 10	193	HOLMGREN	77	HBC See AGUILAR-BENITEZ 81D
47 ± 6		¹ BARDADIN...	75	HBC $K^- p$ 14.3 GeV/c
40 ± 3	3060	³ BERTHON	74	HBC $K^- p$ 1263-1843 MeV/c
29.2 ± 10.6	120	⁹ SMITH	65	HBC $K^- p$ 1.80 GeV/c
17.1 ± 8.9	58	⁹ SMITH	65	HBC $K^- p$ 1.95 GeV/c
88 ± 24	200	⁹ COOPER	64	HBC $K^- p$ 1.45 GeV/c
40		DAHL	61	DBC $K^- d$ 0.45 GeV/c
66 ± 18	224	⁹ ELY	61	HLBC $K^- p$ 1.11 GeV/c

WEIGHTED AVERAGE
39.4 ± 2.1 (Error scaled by 1.7)



$\Sigma(1385)$ DECAY MODES

Mode	Fraction (Γ_i/Γ)	Confidence level
Γ_1 $\Lambda \pi$	(87.0 ± 1.5) %	
Γ_2 $\Sigma \pi$	(11.7 ± 1.5) %	
Γ_3 $\Lambda \gamma$	(1.25 ^{+0.13} _{-0.12}) %	
Γ_4 $\Sigma^+ \gamma$	(7.0 ± 1.7) × 10 ⁻³	
Γ_5 $\Sigma^- \gamma$	< 2.4 × 10 ⁻⁴	90%
Γ_6 $N \bar{K}$		

$\Sigma(1385)$ BRANCHING RATIOS

$\Gamma(\Sigma \pi)/\Gamma(\Lambda \pi)$	VALUE	DOCUMENT ID	TECN	CHG	COMMENT	Γ_2/Γ_1
0.135 ± 0.011 OUR AVERAGE						
	0.20 ± 0.06	DIONISI	78B	HBC	± $K^- p \rightarrow \gamma^* K \bar{K}$	
	0.16 ± 0.03	BERTHON	74	HBC	+ $K^- p$ 1.26-1.84 GeV/c	
	0.11 ± 0.02	BERTHON	74	HBC	- $K^- p$ 1.26-1.84 GeV/c	
	0.21 ± 0.05	BORENSTEIN	74	HBC	+ $K^- p \rightarrow \Lambda \pi^+ \pi^-$, $\Sigma^0 \pi^+ \pi^-$	
	0.18 ± 0.04	MAST	73	MPWA	± $K^- p \rightarrow \Lambda \pi^+ \pi^-$, $\Sigma^0 \pi^+ \pi^-$	
	0.10 ± 0.05	THOMAS	73	HBC	- $\pi^- p \rightarrow \Lambda K \pi$, $\Sigma K \pi$	
	0.16 ± 0.07	AGUILAR...	72B	HBC	+ $K^- p$ 3.9, 4.6 GeV/c	
	0.13 ± 0.04	COLLEY	71B	DBC	-0 $K^- N$ 1.5 GeV/c	
	0.13 ± 0.04	PAN	69	HBC	+ $\pi^+ p \rightarrow \Lambda K \pi$, $\Sigma K \pi$	
	0.08 ± 0.06	LONDON	66	HBC	+ $K^- p$ 2.24 GeV/c	
	0.163 ± 0.041	ARMENTEROS65B	HBC	± $K^- p$ 0.95-1.20 GeV/c		
	0.09 ± 0.04	HUWE	64	HBC	± $K^- p$ 1.2-1.7 GeV	
••• We do not use the following data for averages, fits, limits, etc. •••						
	< 0.04	ALSTON	62	HBC	± 0 $K^- p$ 1.15 GeV/c	
	0.04 ± 0.04	BASTIEN	61	HBC	±	

$\Gamma(\Lambda \gamma)/\Gamma(\Lambda \pi)$

This ratio is of course for $\Sigma(1385)^0 \rightarrow \Lambda \gamma$ and $\Lambda \pi^0$.

$\Gamma(\Lambda \gamma)/\Gamma(\Lambda \pi)$	VALUE (units 10 ⁻²)	EVTs	DOCUMENT ID	TECN	COMMENT	Γ_3/Γ_1
1.43^{+0.15}_{-0.13} OUR AVERAGE						
	1.42 ± 0.12 ^{+0.11} _{-0.07}	624 ± 25	KELLER	11	CLAS $\gamma p \rightarrow K^+ \Lambda \gamma$, E_γ 1.6-3.8 GeV	
	1.53 ± 0.39 ^{+0.15} _{-0.24}	61	TAYLOR	05	CLAS $\gamma p \rightarrow K^+ \Lambda \gamma$	

$\Gamma(\Sigma^+ \gamma)/\Gamma(\Sigma \pi)$

This ratio is for $\Sigma(1385)^+ \rightarrow \Sigma^+ \gamma$ over $\Sigma(1385)^+ \rightarrow \Sigma \pi$.

$\Gamma(\Sigma^+ \gamma)/\Gamma(\Sigma \pi)$	VALUE (%)	DOCUMENT ID	TECN	COMMENT	Γ_4/Γ_2
5.98 ± 1.11^{+0.27}_{-0.61}		11 KELLER	12	CLAS $\gamma p \rightarrow K^0 \Sigma(1385)^+$	

$\Gamma(\Sigma^- \gamma)/\Gamma_{total}$

$\Gamma(\Sigma^- \gamma)/\Gamma_{total}$	VALUE	CL%	DOCUMENT ID	TECN	CHG	COMMENT	Γ_5/Γ
< 2.4 × 10⁻⁴		90	12 MOLCHANOV	04	SELX	- $\Sigma^- p \rightarrow \Sigma(1385)^- p$, 600 GeV	
••• We do not use the following data for averages, fits, limits, etc. •••							
< 6.1 × 10 ⁻⁴		90	13 ARIK	77	SPEC	- $\Sigma^- p \rightarrow \Sigma(1385)^- p$, 23 GeV	

$(\Gamma_1 \Gamma_2)^{1/2}/\Gamma_{total}$ in $N \bar{K} \rightarrow \Sigma(1385) \rightarrow \Lambda \pi$

$(\Gamma_1 \Gamma_2)^{1/2}/\Gamma_{total}$	VALUE	DOCUMENT ID	CHG	COMMENT	$(\Gamma_6 \Gamma_1)^{1/2}/\Gamma$	
+0.586 ± 0.319		14 DEVENISH	74B	0	Fixed-t dispersion rel.	

$\Sigma(1385)$ FOOTNOTES

- From fit to inclusive $\Lambda \pi$ spectrum.
- Includes data of HOLMGREN 77.
- The errors are statistical only. The resolution is not unfolded.
- The error is enlarged to Γ/\sqrt{N} . See the note on the $K^*(892)$ mass in the 1984 edition.
- From a fit to $\Lambda \pi^0$ with the width fixed at 34 MeV.
- From fit to inclusive $\Lambda \pi^0$ spectrum with the width fixed at 40 MeV.
- Redundant with data in the mass Listings.
- Results from $\Lambda \pi^+ \pi^-$ and $\Lambda \pi^+ \pi^- \pi^0$ combined by us.
- The error is enlarged to $4\Gamma/\sqrt{N}$. See the note on the $K^*(892)$ mass in the 1984 edition.
- Consistent with +, 0, and - widths equal.
- KELLER 12 gives $\Gamma(\Sigma^+ \gamma)/\Gamma(\Sigma^+ \pi^0) = (11.95 \pm 2.21 + 0.53)_{-1.21}$ %, using 1/2 our total $\Sigma(1385) \rightarrow \Sigma \pi$ fraction for $\Sigma^+ \pi^0$. We divide the KELLER 12 value by two.
- We calculate this from the MOLCHANOV 04 upper limit of 9.5 keV on the $\Sigma^- \gamma$ width.
- We calculate this from the ARIK 77 upper limit of 24 keV on the $\Sigma^- \gamma$ width.
- An extrapolation of the parametrized amplitude below threshold.

$\Sigma(1385)$ REFERENCES

LEE	21A	PR D103 052005	J.Y. Lee et al.	(BELLE Collab.)
AGAKISHIEV	12	PR C85 035203	G. Agakishiev et al.	(HADES Collab.)
KELLER	12	PR D85 052004	D. Keller et al.	(JLab CLAS Collab.)
KELLER	11	PR D83 072004	D. Keller et al.	(JLab CLAS Collab.)
TAYLOR	05	PR C71 054609	S. Taylor et al.	(JLab CLAS Collab.)
		Also PR C72 039902 (errata.)	S. Taylor et al.	(JLab CLAS Collab.)
MOLCHANOV	04	PL B590 161	V.V. Molchanov et al.	(FNAL SELEX Collab.)
BAUBILLIER	84	ZPHY C23 213	M. Baubillier et al.	(BIRM, CERN, GLAS+)
PDG	84	RMP 56 51	C.G. Wohl et al.	(LBL, CIT, CERN)
AGUILAR...	81D	AFIS A77 144	M. Aguilar-Benitez, J. Salicio	(MADR)
BAKER	80	NP B166 207	P.A. Baker et al.	(LOIC)
BAUBILLIER	79B	NP B148 18	M. Baubillier et al.	(BIRM, CERN, GLAS+)
CAUTIS	79	NP B156 507	C.V. Cautis et al.	(SIAC)
SUGAHARA	79B	NP B156 237	R. Sugahara et al.	(KEK, OSKC, KINK)
CAMERON	78	NP B143 189	W. Cameron et al.	(RHEL, LOIC)
DIONISI	78B	PL 78B 154	C. Dionisi, R. Armenteros, J. Diaz	(CERN, AMST+)
ARIK	77	PRL 38 1000	E. Arik et al.	(PITT, BNL, MASA)
BARREIRO	77B	NP B126 319	F. Barreiro et al.	(CERN, AMST, NIJM)
HOLMGREN	77	NP B119 261	S.O. Holmgren et al.	(CERN, AMST, NIJM)
BARDADIN...	75	NP B98 418	M. Bardadin-Otwinowska et al.	(SACL, EPOL+)
BERTHON	74	NC 21A 146	A. Berthon et al.	(CDEF, RHEL, SACL+)
BORENSTEIN	74	PR D9 3006	S.R. Borenstein et al.	(BNL, MICH)

Baryon Particle Listings
 $\Sigma(1385), \Sigma(1580)$

DEVENISH 74B	NP B81 330	R.C.E. Devenish, C.D. Froggatt, B.R. Martin (DESY+)
LICHTENBERG 74	PR D10 3865	D.B. Lichtenberg (IND)
Also	Private Comm.	D.B. Lichtenberg (IND)
HABIBI 73	Thesis Nevis 199	M. Habibi (COLU)
Also	Purdue Conf. 387	C. Baltay <i>et al.</i> (COLU, BING)
MAST 73	PR D7 3212	T.S. Mast <i>et al.</i> (LBL) IJP
Also	PR D7 5	(LBL) IJP
THOMAS 73	NP B56 15	D.W. Thomas <i>et al.</i> (CMU) JP
AGUILAR... 72B	PR D5 29	M. Aguilar-Benitez <i>et al.</i> (BNL)
COLLEY 71B	NP B31 61	D.C. Colley <i>et al.</i> (BIRM, EDIN, GLAS+)
AGUILAR... 70B	PRL 25 58	M. Aguilar-Benitez <i>et al.</i> (BNL, SYRA)
PAN 69	PRL 23 808	Y.L. Pan, F.L. Forman (PENN) I
SIEGEL 67	Thesis UCRL 18041	D.M. Siegel (LRL)
BIRMINGHAM 66	PR 152 1148	M. Haque <i>et al.</i> (BIRM, GLAS, LOIC, OXF+)
LONDON 66	PR 143 1034	G.W. London <i>et al.</i> (BNL, SYRA) J
ARMENTEROS 65B	PL 19 75	R. Armenteros <i>et al.</i> (CERN, HEID, SACL)
SMITH 65	Thesis UCLA	L.T. Smith (UCLA)
COOPER 64	PL 8 365	W.A. Cooper <i>et al.</i> (CERN, AMST)
HUWE 64	Thesis UCRL 11291	D.O. Huwe (LRL) JP
Also	PR 181 1824	(LRL)
CURTIS 63	PR 132 1771	L.J. Curtis <i>et al.</i> (MICH) J
ALSTON 62	CERN Conf. 311	M.H. Alston <i>et al.</i> (LRL)
BASTIEN 61	PRL 6 702	P.L. Bastien, M. Ferro-Luzzi, A.H. Rosenfeld (LRL)
DAHL 61	PRL 6 142	O.I. Dahl <i>et al.</i> (LRL)
ELY 61	PRL 7 461	R.P. Ely <i>et al.</i> (LRL) J
ALSTON 60	PRL 5 520	M.H. Alston <i>et al.</i> (LRL) I

$\Sigma(1580) 3/2^-$

$I(J^P) = 1(\frac{3}{2}^-)$ Status: *

OMITTED FROM SUMMARY TABLE

Seen in the isospin-1 $\bar{K}N$ cross section at BNL (LI 73, CARROLL 76) and in a partial-wave analysis of $K^-p \rightarrow \Lambda\pi^0$ for c.m. energies 1560–1600 MeV by LITCHFIELD 74. LITCHFIELD 74 finds $J^P = 3/2^-$. Not seen by ENGLER 78, CAMERON 78C, OLMSTED 04, nor by PRAKHOV 04.

Neither ZHANG 13A nor SARANTSEV 19 see any evidence for this state.

$\Sigma(1580)$ POLE POSITION

REAL PART

VALUE (MeV)	DOCUMENT ID	TECN	COMMENT
1607^{+13}_{-11}	¹ KAMANO	15	DPWA Multichannel
¹ From the preferred solution A in KAMANO 15. Solution B reports $M = 1492^{+4}_{-7}$ MeV.			

-2xIMAGINARY PART

VALUE (MeV)	DOCUMENT ID	TECN	COMMENT
253^{+30}_{-18}	² KAMANO	15	DPWA Multichannel
² From the preferred solution A in KAMANO 15. Solution B reports $M = 138^{+8}_{-14}$ MeV.			

$\Sigma(1580)$ POLE RESIDUES

The "normalized residue" is the residue divided by $\Gamma_{pole}/2$.

Normalized residue in $N\bar{K} \rightarrow \Sigma(1580) \rightarrow N\bar{K}$

MODULUS	PHASE (°)	DOCUMENT ID	TECN	COMMENT
0.00778	51	³ KAMANO	15	DPWA Multichannel
³ From the preferred solution A in KAMANO 15.				

Normalized residue in $N\bar{K} \rightarrow \Sigma(1580) \rightarrow \Sigma\pi$

MODULUS	PHASE (°)	DOCUMENT ID	TECN	COMMENT
0.0625	-6	⁴ KAMANO	15	DPWA Multichannel
⁴ From the preferred solution A in KAMANO 15.				

Normalized residue in $N\bar{K} \rightarrow \Sigma(1580) \rightarrow \Lambda\pi$

MODULUS	PHASE (°)	DOCUMENT ID	TECN	COMMENT
0.059	156	⁵ KAMANO	15	DPWA Multichannel
⁵ From the preferred solution A in KAMANO 15.				

Normalized residue in $N\bar{K} \rightarrow \Sigma(1580) \rightarrow \Sigma(1385)\pi, S\text{-wave}$

MODULUS	PHASE (°)	DOCUMENT ID	TECN	COMMENT
0.0368	-18	⁶ KAMANO	15	DPWA Multichannel
⁶ From the preferred solution A in KAMANO 15.				

Normalized residue in $N\bar{K} \rightarrow \Sigma(1580) \rightarrow \Sigma(1385)\pi, D\text{-wave}$

MODULUS	PHASE (°)	DOCUMENT ID	TECN	COMMENT
0.0103	123	⁷ KAMANO	15	DPWA Multichannel
⁷ From the preferred solution A in KAMANO 15.				

$\Sigma(1580)$ MASS

VALUE (MeV)	DOCUMENT ID	TECN	COMMENT
1583 ± 4	⁸ CARROLL	76	DPWA Isospin-1 total σ
1582 ± 4	⁹ LITCHFIELD	74	DPWA $K^-p \rightarrow \Lambda\pi^0$
⁸ CARROLL 76 sees a total-cross-section bump with $(J+1/2) \Gamma_{el} / \Gamma_{total} = 0.06$.			
⁹ The main effect observed by LITCHFIELD 74 is in the $\Lambda\pi$ final state; the $\bar{K}N$ and $\Sigma\pi$ couplings are estimated from a multichannel fit including total-cross-section data of LI 73.			

$\Sigma(1580)$ WIDTH

VALUE (MeV)	DOCUMENT ID	TECN	COMMENT
15	¹⁰ CARROLL	76	DPWA Isospin-1 total σ
11 ± 4	¹¹ LITCHFIELD	74	DPWA $K^-p \rightarrow \Lambda\pi^0$
¹⁰ CARROLL 76 sees a total-cross-section bump with $(J+1/2) \Gamma_{el} / \Gamma_{total} = 0.06$.			
¹¹ The main effect observed by LITCHFIELD 74 is in the $\Lambda\pi$ final state; the $\bar{K}N$ and $\Sigma\pi$ couplings are estimated from a multichannel fit including total-cross-section data of LI 73.			

$\Sigma(1580)$ DECAY MODES

Mode
$\Gamma_1 N\bar{K}$
$\Gamma_2 \Lambda\pi$
$\Gamma_3 \Sigma\pi$
$\Gamma_4 \Sigma(1385)\pi, S\text{-wave}$
$\Gamma_5 \Sigma(1385)\pi, D\text{-wave}$
$\Gamma_6 N\bar{K}^*(892), S=1/2, D\text{-wave}$
$\Gamma_7 N\bar{K}^*(892), S=3/2, S\text{-wave}$
$\Gamma_8 N\bar{K}^*(892), S=3/2, D\text{-wave}$

$\Sigma(1580)$ BRANCHING RATIOS

See "Sign conventions for resonance couplings" in the Note on Λ and Σ Resonances.

$\Gamma(N\bar{K})/\Gamma_{total}$	DOCUMENT ID	TECN	COMMENT	Γ_1/Γ
$+0.03 \pm 0.01$	¹² LITCHFIELD	74	DPWA $\bar{K}N$ multichannel	
0.003	¹³ KAMANO	15	DPWA Multichannel	

¹² The main effect observed by LITCHFIELD 74 is in the $\Lambda\pi$ final state; the $\bar{K}N$ and $\Sigma\pi$ couplings are estimated from a multichannel fit including total-cross-section data of LI 73.

¹³ From the preferred solution A in KAMANO 15.

$\Gamma(\Lambda\pi)/\Gamma_{total}$	DOCUMENT ID	TECN	COMMENT	Γ_2/Γ
0.490	¹⁴ KAMANO	15	DPWA Multichannel	
¹⁴ From the preferred solution A in KAMANO 15.				

$\Gamma(\Sigma\pi)/\Gamma_{total}$	DOCUMENT ID	TECN	COMMENT	Γ_3/Γ
0.387	¹⁵ KAMANO	15	DPWA Multichannel	
¹⁵ From the preferred solution A in KAMANO 15.				

$\Gamma(\Sigma(1385)\pi, S\text{-wave})/\Gamma_{total}$	DOCUMENT ID	TECN	COMMENT	Γ_4/Γ
0.12	¹⁶ KAMANO	15	DPWA Multichannel	
¹⁶ From the preferred solution A in KAMANO 15.				

$\Gamma(\Sigma(1385)\pi, D\text{-wave})/\Gamma_{total}$	DOCUMENT ID	TECN	COMMENT	Γ_5/Γ
0.001	¹⁷ KAMANO	15	DPWA Multichannel	
¹⁷ From the preferred solution A in KAMANO 15.				

Baryon Particle Listings

$\Sigma(1580), \Sigma(1620)$

$\Gamma(N\bar{K}^*(892), S=1/2, D\text{-wave})/\Gamma_{\text{total}}$ Γ_6/Γ

VALUE	DOCUMENT ID	TECN	COMMENT
••• We do not use the following data for averages, fits, limits, etc. •••			
not seen	18 KAMANO	15	DPWA Multichannel

¹⁸ From the preferred solution A in KAMANO 15.

$\Gamma(N\bar{K}^*(892), S=3/2, S\text{-wave})/\Gamma_{\text{total}}$ Γ_7/Γ

VALUE	DOCUMENT ID	TECN	COMMENT
••• We do not use the following data for averages, fits, limits, etc. •••			
not seen	19 KAMANO	15	DPWA Multichannel

¹⁹ From the preferred solution A in KAMANO 15.

$\Gamma(N\bar{K}^*(892), S=3/2, D\text{-wave})/\Gamma_{\text{total}}$ Γ_8/Γ

VALUE	DOCUMENT ID	TECN	COMMENT
••• We do not use the following data for averages, fits, limits, etc. •••			
not seen	20 KAMANO	15	DPWA Multichannel

²⁰ From the preferred solution A in KAMANO 15.

$(\Gamma_i/\Gamma)^{1/2}/\Gamma_{\text{total}}$ in $N\bar{K} \rightarrow \Sigma(1580) \rightarrow \Lambda\pi$ $(\Gamma_1\Gamma_2)^{1/2}/\Gamma$

VALUE	DOCUMENT ID	TECN	COMMENT
not seen	CAMERON	78c	HBC $K_L^0 p \rightarrow \Lambda\pi^+$
not seen	ENGLER	78	HBC $K_L^0 p \rightarrow \Lambda\pi^+$
+0.10±0.02	21 LITCHFIELD	74	DPWA $K^- p \rightarrow \Lambda\pi^0$

²¹ The main effect observed by LITCHFIELD 74 is in the $\Lambda\pi$ final state; the $\bar{K}N$ and $\Sigma\pi$ couplings are estimated from a multichannel fit including total-cross-section data of LI 73.

$(\Gamma_i/\Gamma)^{1/2}/\Gamma_{\text{total}}$ in $N\bar{K} \rightarrow \Sigma(1580) \rightarrow \Sigma\pi$ $(\Gamma_1\Gamma_3)^{1/2}/\Gamma$

VALUE	DOCUMENT ID	TECN	COMMENT
not seen	CAMERON	78c	HBC $K_L^0 p \rightarrow \Sigma^0\pi^+$
not seen	ENGLER	78	HBC $K_L^0 p \rightarrow \Sigma^0\pi^+$
+0.03±0.04	22 LITCHFIELD	74	DPWA $\bar{K}N$ multichannel

²² The main effect observed by LITCHFIELD 74 is in the $\Lambda\pi$ final state; the $\bar{K}N$ and $\Sigma\pi$ couplings are estimated from a multichannel fit including total-cross-section data of LI 73.

$\Sigma(1580)$ REFERENCES

SARANTSEV	19	EPJ A55 180	A.V. Sarantsev et al.	(BONN, PNPI)
KAMANO	15	PR C92 025205	H. Kamano et al.	(ANL, OSAK)
ZHANG	13A	PR C88 035205	H. Zhang et al.	(KSU)
OLMSTED	04	PL B588 29	J. Olmsted et al.	(BNL Crystal Ball Collab.)
PRAKHOV	04	PR C69 042202	S. Prakhov et al.	(BNL Crystal Ball Collab.)
CAMERON	78c	NP B132 189	W. Cameron et al.	(BONNA, EDIN, GLAS+)
ENGLER	78	PR D18 3061	A. Engler et al.	(CMU, ANL)
CARROLL	76	PRL 37 806	A.S. Carroll et al.	(BNL)1
LITCHFIELD	74	PL 51B 509	P.J. Litchfield	(CERN)1UP
LI	73	Purdue Conf. 283	K.K. Li	(BNL)1

$\Sigma(1620) 1/2^-$

 $I(J^P) = 1(\frac{1}{2}^-)$ Status: *

OMITTED FROM SUMMARY TABLE

The S_{11} state at 1697 MeV reported by VANHORN 75 is tentatively listed under the $\Sigma(1750)$. CARROLL 76 sees two bumps in the isospin-1 total cross section near this mass. GAO 12 sees no evidence for this resonance.

Production experiments are listed separately in the next entry.

$\Sigma(1620)$ POLE POSITION

REAL PART	DOCUMENT ID	TECN	COMMENT
1680±8	SARANTSEV 19	DPWA	$\bar{K}N$ multichannel
••• We do not use the following data for averages, fits, limits, etc. •••			
1501	ZHANG 13A	DPWA	$\bar{K}N$ multichannel
-2xIMAGINARY PART	DOCUMENT ID	TECN	COMMENT
39±11	SARANTSEV 19	DPWA	$\bar{K}N$ multichannel
••• We do not use the following data for averages, fits, limits, etc. •••			
171	ZHANG 13A	DPWA	$\bar{K}N$ multichannel

$\Sigma(1620)$ POLE RESIDUE

The "normalized residue" is the residue divided by $\Gamma_{\text{pole}}/2$.

Normalized residue in $N\bar{K} \rightarrow \Sigma(1620) \rightarrow \Sigma\pi$	DOCUMENT ID	TECN	COMMENT
0.14±0.03	SARANTSEV 19	DPWA	$\bar{K}N$ multichannel
MODULUS PHASE (°)			
-90 ± 25			

Normalized residue in $N\bar{K} \rightarrow \Sigma(1620) \rightarrow \Lambda\pi$	DOCUMENT ID	TECN	COMMENT
0.10±0.03	SARANTSEV 19	DPWA	$\bar{K}N$ multichannel
MODULUS PHASE (°)			
75 ± 20			

Normalized residue in $N\bar{K} \rightarrow \Sigma(1620) \rightarrow \Xi K$

MODULUS	PHASE (°)	DOCUMENT ID	TECN	COMMENT
0.02±0.01	120 ± 20	SARANTSEV 19	DPWA	$\bar{K}N$ multichannel

Normalized residue in $N\bar{K} \rightarrow \Sigma(1620) \rightarrow \Lambda(1520)\pi$

MODULUS	PHASE (°)	DOCUMENT ID	TECN	COMMENT
0.12±0.05	140 ± 40	SARANTSEV 19	DPWA	$\bar{K}N$ multichannel

Normalized residue in $N\bar{K} \rightarrow \Sigma(1620) \rightarrow \Sigma(1385)\pi$

MODULUS	PHASE (°)	DOCUMENT ID	TECN	COMMENT
0.015±0.010	155 ± 40	SARANTSEV 19	DPWA	$\bar{K}N$ multichannel

Normalized residue in $N\bar{K} \rightarrow \Sigma(1620) \rightarrow N\bar{K}^*(892), S\text{-wave}$

MODULUS	PHASE (°)	DOCUMENT ID	TECN	COMMENT
0.05±0.04		SARANTSEV 19	DPWA	$\bar{K}N$ multichannel

Normalized residue in $N\bar{K} \rightarrow \Sigma(1620) \rightarrow N\bar{K}^*(892), D\text{-wave}$

MODULUS	PHASE (°)	DOCUMENT ID	TECN	COMMENT
0.01±0.01		SARANTSEV 19	DPWA	$\bar{K}N$ multichannel

Normalized residue in $N\bar{K} \rightarrow \Sigma(1620) \rightarrow N\bar{K}$

VALUE	DOCUMENT ID	TECN	COMMENT
0.11±0.03@43+20	SARANTSEV 19	DPWA	$\bar{K}N$ multichannel

$\Sigma(1620)$ MASS

VALUE (MeV)	DOCUMENT ID	TECN	COMMENT
1600 to 1650 (≈ 1620) OUR ESTIMATE			
1681±6	SARANTSEV 19	DPWA	$\bar{K}N$ multichannel
1600±15	ZHANG 13A	DPWA	$\bar{K}N$ multichannel
1600±6	1 MORRIS 78	DPWA	$K^- n \rightarrow \Lambda\pi^-$
1608±5	2 CARROLL 76	DPWA	Isospin-1 total σ
1630±10	LANGBEIN 72	IPWA	$\bar{K}N$ multichannel
1620	KIM 71	DPWA	K-matrix analysis
••• We do not use the following data for averages, fits, limits, etc. •••			
1633±10	3 CARROLL 76	DPWA	Isospin-1 total σ

$\Sigma(1620)$ WIDTH

VALUE (MeV)	DOCUMENT ID	TECN	COMMENT
40 to 100 (≈ 70) OUR ESTIMATE			
40±12	SARANTSEV 19	DPWA	$\bar{K}N$ multichannel
400±152	ZHANG 13A	DPWA	$\bar{K}N$ multichannel
87±19	1 MORRIS 78	DPWA	$K^- n \rightarrow \Lambda\pi^-$
15	2 CARROLL 76	DPWA	Isospin-1 total σ
65±20	LANGBEIN 72	IPWA	$\bar{K}N$ multichannel
40	KIM 71	DPWA	K-matrix analysis
••• We do not use the following data for averages, fits, limits, etc. •••			
10	3 CARROLL 76	DPWA	Isospin-1 total σ

$\Sigma(1620)$ DECAY MODES

Mode	Fraction (Γ_i/Γ)
$\Gamma_1 N\bar{K}$	0.10 to 0.60
$\Gamma_2 \Lambda\pi$	(9.0 ± 3.0) %
$\Gamma_3 \Sigma\pi$	(17 ± 5) %
$\Gamma_4 \Xi K$	
$\Gamma_5 \Lambda(1520)\pi$	(10 ± 5) %
$\Gamma_6 \Sigma(1385)\pi$	

$\Sigma(1620)$ BRANCHING RATIOS

$\Gamma(N\bar{K})/\Gamma_{\text{total}}$	DOCUMENT ID	TECN	COMMENT	Γ_1/Γ
0.10 to 0.60 OUR ESTIMATE				
0.11±0.03	SARANTSEV 19	DPWA	$\bar{K}N$ multichannel	
0.59±0.10	ZHANG 13A	DPWA	$\bar{K}N$ multichannel	
0.22±0.02	LANGBEIN 72	IPWA	$\bar{K}N$ multichannel	
0.05	KIM 71	DPWA	K-matrix analysis	

$\Gamma(\Sigma\pi)/\Gamma_{\text{total}}$	DOCUMENT ID	TECN	COMMENT	Γ_3/Γ
0.17±0.05	SARANTSEV 19	DPWA	$\bar{K}N$ multichannel	

$\Gamma(\Lambda\pi)/\Gamma_{\text{total}}$	DOCUMENT ID	TECN	COMMENT	Γ_2/Γ
0.09±0.03	SARANTSEV 19	DPWA	$\bar{K}N$ multichannel	

$\Gamma(\Xi K)/\Gamma_{\text{total}}$	DOCUMENT ID	TECN	COMMENT	Γ_4/Γ
~ 0	SARANTSEV 19	DPWA	$\bar{K}N$ multichannel	

See key on page 1171

Baryon Particle Listings

$\Sigma(1620), \Sigma(1660)$

$\Gamma(\Lambda(1520)\pi)/\Gamma_{total}$				Γ_5/Γ
VALUE	DOCUMENT ID	TECN	COMMENT	
0.10 ± 0.05	SARANTSEV 19	DPWA	$\bar{K}N$ multichannel	

$\Gamma(\Sigma(1385)\pi)/\Gamma_{total}$				Γ_6/Γ
VALUE	DOCUMENT ID	TECN	COMMENT	
<0.01	SARANTSEV 19	DPWA	$\bar{K}N$ multichannel	

$(\Gamma_1\Gamma_2)^{1/2}/\Gamma_{total}$ in $N\bar{K} \rightarrow \Sigma(1620) \rightarrow \Lambda\pi$				$(\Gamma_1\Gamma_2)^{1/2}/\Gamma$
VALUE	DOCUMENT ID	TECN	COMMENT	
0.12 ± 0.02	¹ MORRIS 78	DPWA	$K^-n \rightarrow \Lambda\pi^-$	
not seen	BAILLON 75	IPWA	$\bar{K}N \rightarrow \Lambda\pi$	
0.15	KIM 71	DPWA	K-matrix analysis	

$(\Gamma_1\Gamma_3)^{1/2}/\Gamma_{total}$ in $N\bar{K} \rightarrow \Sigma(1620) \rightarrow \Sigma\pi$				$(\Gamma_1\Gamma_3)^{1/2}/\Gamma$
VALUE	DOCUMENT ID	TECN	COMMENT	
+0.32 ± 0.03	ZHANG 13A	DPWA	Multichannel	
not seen	HEPP 76B	DPWA	$K^-N \rightarrow \Sigma\pi$	
+0.40 ± 0.06	LANGBEIN 72	IPWA	$\bar{K}N$ multichannel	
+0.08	KIM 71	DPWA	K-matrix analysis	

$\Sigma(1620)$ FOOTNOTES

- ¹ MORRIS 78 obtains an equally good fit without including this resonance.
- ² Total cross-section bump with $(J+1/2)\Gamma_{el}/\Gamma_{total}$ is 0.06 seen by CARROLL 76.
- ³ Total cross-section bump with $(J+1/2)\Gamma_{el}/\Gamma_{total}$ is 0.04 seen by CARROLL 76.

$\Sigma(1620)$ REFERENCES

SARANTSEV 19	EPJ A55 180	A.V. Sarantsev et al.	(BONN, PNPI)
ZHANG 13A	PR C88 035205	H. Zhang et al.	(KSU)
GAO 12	PR C86 025201	P. Gao, J. Shi, B.S. Zou	(BHEP, BEIJ)
Also	NP A847 41	P. Gao, B.S. Zou, A. Sibirtsev	(BHEP, BEIJ+)
MORRIS 78	PR D17 55	W.A. Morris et al.	(FSU) IJF
CARROLL 76	PRL 37 806	A.S. Carroll et al.	(BNL) I
HEPP 76B	PL 65B 487	Y. Hepp et al.	(CERN, HEIDH, MPIM) IJF
BAILLON 75	NP B94 39	P.H. Baillon, P.J. Litchfield	(CERN, RHEL) IJF
VANHORN 75	NP B87 145	A.J. van Horn	(LBL) IJF
Also	NP B87 157	A.J. van Horn	(LBL) IJF
LANGBEIN 72	NP B47 477	W. Langbein, F. Wagner	(MPIM) IJF
KIM 71	PRL 27 356	J.K. Kim	(HARV) IJF
Also	Duke Conf. 161	J.K. Kim	(HARV) IJF
Hyperon Resonances, 1970			

$\Sigma(1660) 1/2^+$

$$I(J^P) = 1(\frac{1}{2}^+) \text{ Status: } ***$$

For results published before 1974 (they are now obsolete), see our 1982 edition Physics Letters **111B** 1 (1982).

$\Sigma(1660)$ POLE POSITION

REAL PART			
VALUE (MeV)	DOCUMENT ID	TECN	COMMENT
1585 ± 20	SARANTSEV 19	DPWA	$\bar{K}N$ multichannel

••• We do not use the following data for averages, fits, limits, etc. •••			
1547 ⁺¹¹¹ ₋₅₉	¹ KAMANO 15	DPWA	$\bar{K}N$ multichannel
¹ From the preferred solution A in KAMANO 15. Solution B reports $M = 1457^{+5}_{-1}$ MeV.			

-2xIMAGINARY PART			
VALUE (MeV)	DOCUMENT ID	TECN	COMMENT

290⁺¹⁴⁰ ₋₄₀	SARANTSEV 19	DPWA	$\bar{K}N$ multichannel
••• We do not use the following data for averages, fits, limits, etc. •••			
183 ⁺⁸⁶ ₋₇₈	¹ KAMANO 15	DPWA	$\bar{K}N$ multichannel
¹ From the preferred solution A in KAMANO 15. Solution B reports $\Gamma = 78^{+2}_{-8}$ MeV.			

$\Sigma(1660)$ POLE RESIDUES

The normalized residue is the residue divided by $\Gamma_{pole}/2$.

Normalized residue in $N\bar{K} \rightarrow \Sigma(1660) \rightarrow N\bar{K}$			
MODULUS	PHASE (°)	DOCUMENT ID	TECN COMMENT

0.07 ± 0.03	-165 ± 35	SARANTSEV 19	DPWA $\bar{K}N$ multichannel
••• We do not use the following data for averages, fits, limits, etc. •••			
0.0247	168	¹ KAMANO 15	DPWA $\bar{K}N$ multichannel
¹ From the preferred solution A in KAMANO 15.			

Normalized residue in $N\bar{K} \rightarrow \Sigma(1660) \rightarrow \Sigma\pi$			
MODULUS	PHASE (°)	DOCUMENT ID	TECN COMMENT

0.17 ± 0.04	150 ± 20	SARANTSEV 19	DPWA $\bar{K}N$ multichannel
••• We do not use the following data for averages, fits, limits, etc. •••			
0.16	78	¹ KAMANO 15	DPWA $\bar{K}N$ multichannel
¹ From the preferred solution A in KAMANO 15.			

Normalized residue in $N\bar{K} \rightarrow \Sigma(1660) \rightarrow \Lambda\pi$			
MODULUS	PHASE (°)	DOCUMENT ID	TECN COMMENT

0.16 ± 0.05	0 ± 25	SARANTSEV 19	DPWA $\bar{K}N$ multichannel
••• We do not use the following data for averages, fits, limits, etc. •••			
0.0614	-84	¹ KAMANO 15	DPWA $\bar{K}N$ multichannel
¹ From the preferred solution A in KAMANO 15.			

Normalized residue in $N\bar{K} \rightarrow \Sigma(1660) \rightarrow \Sigma\sigma$			
MODULUS	PHASE (°)	DOCUMENT ID	TECN COMMENT

0.14 ± 0.06	-150 ± 30	SARANTSEV 19	DPWA $\bar{K}N$ multichannel
••• We do not use the following data for averages, fits, limits, etc. •••			
0.0513	-44	¹ KAMANO 15	DPWA Multichannel
¹ From the preferred solution A in KAMANO 15.			

Normalized residue in $N\bar{K} \rightarrow \Sigma(1660) \rightarrow \Sigma(1385)\pi$			
MODULUS	PHASE (°)	DOCUMENT ID	TECN COMMENT

0.06 ± 0.03	-90 ± 25	SARANTSEV 19	DPWA $\bar{K}N$ multichannel
••• We do not use the following data for averages, fits, limits, etc. •••			
0.0513	-44	¹ KAMANO 15	DPWA Multichannel
¹ From the preferred solution A in KAMANO 15.			

Normalized residue in $N\bar{K} \rightarrow \Sigma(1660) \rightarrow \Lambda(1405)\pi$			
MODULUS	PHASE (°)	DOCUMENT ID	TECN COMMENT

0.04 ± 0.02	5 ± 20	SARANTSEV 19	DPWA $\bar{K}N$ multichannel
••• We do not use the following data for averages, fits, limits, etc. •••			

$\Sigma(1660)$ MASS

VALUE (MeV)	DOCUMENT ID	TECN	COMMENT
-------------	-------------	------	---------

1640 to 1680 (≈ 1660) OUR ESTIMATE			
1665 ± 20	SARANTSEV 19	DPWA	$\bar{K}N$ multichannel
1633 ± 3	GAO 12	DPWA	$\bar{K}N \rightarrow \Lambda\pi$
1665.1 ± 11.2	¹ KOISO 85	DPWA	$K^-p \rightarrow \Sigma\pi$
1670 ± 10	GOPAL 80	DPWA	$\bar{K}N \rightarrow \bar{K}N$
1679 ± 10	ALSTON-... 78	DPWA	$\bar{K}N \rightarrow \bar{K}N$
1668 ± 25	VANHORN 75	DPWA	$K^-p \rightarrow \Lambda\pi^0$
1670 ± 20	KANE 74	DPWA	$K^-p \rightarrow \Sigma\pi$
••• We do not use the following data for averages, fits, limits, etc. •••			
1676 ± 15	GOPAL 77	DPWA	$\bar{K}N$ multichannel
1565 or 1597	² MARTIN 77	DPWA	$\bar{K}N$ multichannel
1660 ± 30	³ BAILLON 75	IPWA	$\bar{K}N \rightarrow \Lambda\pi$
1671 ± 2	⁴ PONTE 75	DPWA	$K^-p \rightarrow \Lambda\pi^0$

- ¹ The evidence of KOISO 85 is weak.
- ² The two MARTIN 77 values are from a T-matrix pole and from a Breit-Wigner fit.
- ³ From solution 1 of BAILLON 75; not present in solution 2.
- ⁴ From solution 2 of PONTE 75; not present in solution 1.

$\Sigma(1660)$ WIDTH

VALUE (MeV)	DOCUMENT ID	TECN	COMMENT
-------------	-------------	------	---------

100 to 300 (≈ 200) OUR ESTIMATE			
300 ⁺¹⁴⁰ ₋₄₀	SARANTSEV 19	DPWA	$\bar{K}N$ multichannel
121 ⁺⁴ ₋₇	GAO 12	DPWA	$\bar{K}N \rightarrow \Lambda\pi$
81.5 ± 22.2	¹ KOISO 85	DPWA	$K^-p \rightarrow \Sigma\pi$
152 ± 20	GOPAL 80	DPWA	$\bar{K}N \rightarrow \bar{K}N$
38 ± 10	ALSTON-... 78	DPWA	$\bar{K}N \rightarrow \bar{K}N$
230 ⁺¹⁶⁵ ₋₆₀	VANHORN 75	DPWA	$K^-p \rightarrow \Lambda\pi^0$
250 ± 110	KANE 74	DPWA	$K^-p \rightarrow \Sigma\pi$
••• We do not use the following data for averages, fits, limits, etc. •••			
120 ± 20	GOPAL 77	DPWA	$\bar{K}N$ multichannel
202 or 217	² MARTIN 77	DPWA	$\bar{K}N$ multichannel
80 ± 40	³ BAILLON 75	IPWA	$\bar{K}N \rightarrow \Lambda\pi$
81 ± 10	⁴ PONTE 75	DPWA	$K^-p \rightarrow \Lambda\pi^0$

- ¹ The evidence of KOISO 85 is weak.
- ² The two MARTIN 77 values are from a T-matrix pole and from a Breit-Wigner fit.
- ³ From solution 1 of BAILLON 75; not present in solution 2.
- ⁴ From solution 2 of PONTE 75; not present in solution 1.

$\Sigma(1660)$ DECAY MODES

Mode	Fraction (Γ_i/Γ)
$\Gamma_1 N\bar{K}$	0.05 to 0.15 (≈ 010)
$\Gamma_2 \Lambda\pi$	(35 ± 12) %
$\Gamma_3 \Sigma\pi$	(37 ± 10) %
$\Gamma_4 \Sigma\sigma$	(20 ± 8) %
$\Gamma_5 \Sigma(1385)\pi$	
$\Gamma_6 \Lambda(1405)\pi$	(4.0 ± 2.0) %
$\Gamma_7 \Lambda(1520)\pi$	

Baryon Particle Listings

 $\Sigma(1660), \Sigma(1670)$ $\Sigma(1660)$ BRANCHING RATIOS

See "Sign conventions for resonance couplings" in the Note on Λ and Σ Resonances.

 $\Gamma(N\bar{K})/\Gamma_{\text{total}}$ Γ_1/Γ

VALUE	DOCUMENT ID	TECN	COMMENT
0.05 to 0.15 (≈ 0.10) OUR ESTIMATE			
0.07 \pm 0.03	SARANTSEV 19	DPWA	$\bar{K}N$ multichannel
0.12 \pm 0.03	GOPAL 80	DPWA	$\bar{K}N \rightarrow \bar{K}N$
0.10 \pm 0.05	ALSTON... 78	DPWA	$\bar{K}N \rightarrow \bar{K}N$
••• We do not use the following data for averages, fits, limits, etc. •••			
0.005	¹ KAMANO 15	DPWA	$\bar{K}N$ multichannel
< 0.04	GOPAL 77	DPWA	See GOPAL 80
0.27 or 0.29	² MARTIN 77	DPWA	$\bar{K}N$ multichannel
¹ From the preferred solution A in KAMANO 15.			
² The two MARTIN 77 values are from a T-matrix pole and from a Breit-Wigner fit.			

 $\Gamma(\Lambda\pi)/\Gamma_{\text{total}}$ Γ_2/Γ

VALUE	DOCUMENT ID	TECN	COMMENT
0.35 \pm 0.12	SARANTSEV 19	DPWA	$\bar{K}N$ multichannel
••• We do not use the following data for averages, fits, limits, etc. •••			
0.128	¹ KAMANO 15	DPWA	$\bar{K}N$ multichannel
¹ From the preferred solution A in KAMANO 15.			

 $\Gamma(\Sigma\pi)/\Gamma_{\text{total}}$ Γ_3/Γ

VALUE	DOCUMENT ID	TECN	COMMENT
0.37 \pm 0.10	SARANTSEV 19	DPWA	$\bar{K}N$ multichannel
••• We do not use the following data for averages, fits, limits, etc. •••			
0.865	¹ KAMANO 15	DPWA	$\bar{K}N$ multichannel
¹ From the preferred solution A in KAMANO 15.			

 $\Gamma(\Sigma\sigma)/\Gamma_{\text{total}}$ Γ_4/Γ

VALUE	DOCUMENT ID	TECN	COMMENT
0.20 \pm 0.08	SARANTSEV 19	DPWA	$\bar{K}N$ multichannel

 $\Gamma(\Sigma(1385)\pi)/\Gamma_{\text{total}}$ Γ_5/Γ

VALUE	DOCUMENT ID	TECN	COMMENT
••• We do not use the following data for averages, fits, limits, etc. •••			
0.001	¹ KAMANO 15	DPWA	Multichannel
¹ From the preferred solution A in KAMANO 15.			

 $\Gamma(\Lambda(1405)\pi)/\Gamma_{\text{total}}$ Γ_6/Γ

VALUE	DOCUMENT ID	TECN	COMMENT
0.04 \pm 0.02	SARANTSEV 19	DPWA	$\bar{K}N$ multichannel

 $\Gamma(\Lambda(1520)\pi)/\Gamma_{\text{total}}$ Γ_7/Γ

VALUE	DOCUMENT ID	TECN	COMMENT
< 0.01	SARANTSEV 19	DPWA	$\bar{K}N$ multichannel

 $(\Gamma_1\Gamma_2)^{1/2}/\Gamma_{\text{total}}$ in $N\bar{K} \rightarrow \Sigma(1660) \rightarrow \Lambda\pi$ $(\Gamma_1\Gamma_2)^{1/2}/\Gamma$

VALUE	DOCUMENT ID	TECN	COMMENT
-0.064 \pm 0.005 -0.003	GAO 12	DPWA	$\bar{K}N \rightarrow \Lambda\pi$
< 0.04	GOPAL 77	DPWA	$\bar{K}N$ multichannel
0.12 \pm 0.12 -0.04	VANHORN 75	DPWA	$K^-p \rightarrow \Lambda\pi^0$
••• We do not use the following data for averages, fits, limits, etc. •••			
-0.10 or -0.11	¹ MARTIN 77	DPWA	$\bar{K}N$ multichannel
-0.04 \pm 0.02	² BAILLON 75	IPWA	$\bar{K}N \rightarrow \Lambda\pi$
+0.16 \pm 0.01	³ PONTE 75	DPWA	$K^-p \rightarrow \Lambda\pi^0$
¹ The two MARTIN 77 values are from a T-matrix pole and from a Breit-Wigner fit.			
² From solution 1 of BAILLON 75; not present in solution 2.			
³ From solution 2 of PONTE 75; not present in solution 1.			

 $(\Gamma_1\Gamma_2)^{1/2}/\Gamma_{\text{total}}$ in $N\bar{K} \rightarrow \Sigma(1660) \rightarrow \Sigma\pi$ $(\Gamma_1\Gamma_3)^{1/2}/\Gamma$

VALUE	DOCUMENT ID	TECN	COMMENT
-0.13 \pm 0.04	¹ KOISO 85	DPWA	$K^-p \rightarrow \Sigma\pi$
-0.16 \pm 0.03	GOPAL 77	DPWA	$\bar{K}N$ multichannel
-0.11 \pm 0.01	KANE 74	DPWA	$K^-p \rightarrow \Sigma\pi$
••• We do not use the following data for averages, fits, limits, etc. •••			
-0.34 or -0.37	² MARTIN 77	DPWA	$\bar{K}N$ multichannel
not seen	HEPP 76B	DPWA	$K^-N \rightarrow \Sigma\pi$
¹ The evidence of KOISO 85 is weak.			
² The two MARTIN 77 values are from a T-matrix pole and from a Breit-Wigner fit.			

 $\Sigma(1660)$ REFERENCES

SARANTSEV 19	EPJ A55 180	A.V. Sarantsev et al.	(BONN, PNPI)
KAMANO 15	PR C92 025205	H. Kamano et al.	(ANL, OSAK)
GAO 12	PR C86 025201	P. Gao, J. Shi, B.S. Zou	(BHEP, BEIJT)
Also	NP A867 41	P. Gao, B.S. Zou, A. Sibirtsev	(BHEP, BEIJT+)
KOISO 85	NP A433 619	H. Koiso et al.	(TOKY, MASA)
PDG 82	PL 111B 1	M. Roos et al.	(HELVS, CIT, CERN)
GOPAL 80	Toronto Conf. 159	G.P. Gopal	(RHEL) IJP
ALSTON... 78	PR D18 182	M. Alston-Garnjost et al.	(LBL, MTHO+) IJP
Also	PR L 38 1007	M. Alston-Garnjost et al.	(LBL, MTHO+) IJP

GOPAL 77	NP B119 362	G.P. Gopal et al.	(LOIC, RHEL) IJP
MARTIN 77	NP B127 349	B.R. Martin, M.K. Pidcock, R.G. Moorhouse	(LOUC+) IJP
Also	NP B126 266	B.R. Martin, M.K. Pidcock	(LOUC)
Also	NP B126 285	B.R. Martin, M.K. Pidcock	(LOUC) IJP
HEPP 76B	PL 65B 487	V. Hepp et al.	(CERN, HEIDH, MPIM) IJP
BAILLON 75	NP B94 39	P.H. Baillon, P.J. Litchfield	(CERN, RHEL) IJP
PONTE 75	PR D12 2597	R.A. Ponte et al.	(MASA, TENN, UCR) IJP
VANHORN 75	NP B87 145	A.J. van Horn	(LBL) IJP
Also	NP B87 157	A.J. van Horn	(LBL) IJP
KANE 74	LBL-2452	D.F. Kane	(LBL) IJP

 $\Sigma(1670) 3/2^-$

$$I(J^P) = 1(\frac{3}{2}^-) \text{ Status: } ***$$

For most results published before 1974 (they are now obsolete), see our 1982 edition Physics Letters **111B** 1 (1982).

Results from production experiments are listed separately in the next entry.

 $\Sigma(1670)$ POLE POSITION

REAL PART

VALUE (MeV)	DOCUMENT ID	TECN	COMMENT
1655 to 1675 (≈ 1662) OUR ESTIMATE			
1661 \pm 3	SARANTSEV 19	DPWA	$\bar{K}N$ multichannel
1669 \pm 7	¹ KAMANO 15	DPWA	$\bar{K}N$ multichannel
••• We do not use the following data for averages, fits, limits, etc. •••			
1674	ZHANG 13A	DPWA	$\bar{K}N$ multichannel
¹ From the preferred solution A in KAMANO 15.			

-2xIMAGINARY PART

VALUE (MeV)	DOCUMENT ID	TECN	COMMENT
45 to 65 (≈ 55) OUR ESTIMATE			
52 \pm 6	SARANTSEV 19	DPWA	$\bar{K}N$ multichannel
64 \pm 10 -14	¹ KAMANO 15	DPWA	$\bar{K}N$ multichannel
••• We do not use the following data for averages, fits, limits, etc. •••			
54	ZHANG 13A	DPWA	$\bar{K}N$ multichannel
¹ From the preferred solution A in KAMANO 15.			

 $\Sigma(1670)$ POLE RESIDUES

The normalized residue is the residue divided by $\Gamma_{\text{pole}}/2$.

Normalized residue in $N\bar{K} \rightarrow \Sigma(1670) \rightarrow N\bar{K}$

MODULUS	PHASE ($^\circ$)	DOCUMENT ID	TECN	COMMENT
0.10 \pm 0.02	-31 \pm 12	SARANTSEV 19	DPWA	$\bar{K}N$ multichannel
••• We do not use the following data for averages, fits, limits, etc. •••				
0.129	-20	¹ KAMANO 15	DPWA	$\bar{K}N$ multichannel
¹ From the preferred solution A in KAMANO 15.				

Normalized residue in $N\bar{K} \rightarrow \Sigma(1670) \rightarrow \Sigma\pi$

MODULUS	PHASE ($^\circ$)	DOCUMENT ID	TECN	COMMENT
0.25 \pm 0.05	-25 \pm 10	SARANTSEV 19	DPWA	$\bar{K}N$ multichannel
••• We do not use the following data for averages, fits, limits, etc. •••				
0.249	-21	¹ KAMANO 15	DPWA	$\bar{K}N$ multichannel
¹ From the preferred solution A in KAMANO 15.				

Normalized residue in $N\bar{K} \rightarrow \Sigma(1670) \rightarrow \Lambda\pi$

MODULUS	PHASE ($^\circ$)	DOCUMENT ID	TECN	COMMENT
0.09 \pm 0.03	-52 \pm 12	SARANTSEV 19	DPWA	$\bar{K}N$ multichannel
••• We do not use the following data for averages, fits, limits, etc. •••				
0.0818	-7	¹ KAMANO 15	DPWA	$\bar{K}N$ multichannel
¹ From the preferred solution A in KAMANO 15.				

Normalized residue in $N\bar{K} \rightarrow \Sigma(1670) \rightarrow \Xi K$

MODULUS	PHASE ($^\circ$)	DOCUMENT ID	TECN	COMMENT
0.02 \pm 0.01	160 \pm 20	SARANTSEV 19	DPWA	$\bar{K}N$ multichannel

Normalized residue in $N\bar{K} \rightarrow \Sigma(1670) \rightarrow \Sigma\sigma$

MODULUS	PHASE ($^\circ$)	DOCUMENT ID	TECN	COMMENT
0.08 \pm 0.03	-25 \pm 15	SARANTSEV 19	DPWA	$\bar{K}N$ multichannel

Normalized residue in $N\bar{K} \rightarrow \Sigma(1670) \rightarrow \Sigma(1385)\pi, S\text{-wave}$

MODULUS	PHASE ($^\circ$)	DOCUMENT ID	TECN	COMMENT
••• We do not use the following data for averages, fits, limits, etc. •••				
0.228	167	¹ KAMANO 15	DPWA	$\bar{K}N$ multichannel
¹ From the preferred solution A in KAMANO 15.				

Normalized residue in $N\bar{K} \rightarrow \Sigma(1670) \rightarrow \Sigma(1385)\pi, D\text{-wave}$

MODULUS	PHASE ($^\circ$)	DOCUMENT ID	TECN	COMMENT
••• We do not use the following data for averages, fits, limits, etc. •••				
0.0915	141	KAMANO 15	DPWA	$\bar{K}N$ multichannel

Normalized residue in $N\bar{K} \rightarrow \Sigma(1670) \rightarrow \Lambda(1405)\pi$

MODULUS	PHASE (°)	DOCUMENT ID	TECN	COMMENT
0.03 ± 0.02	160 ± 15	SARANTSEV 19	DPWA	$\bar{K}N$ multichannel

Normalized residue in $N\bar{K} \rightarrow \Sigma(1670) \rightarrow \Lambda(1520)\pi, P\text{-wave}$

MODULUS	PHASE (°)	DOCUMENT ID	TECN	COMMENT
0.04 ± 0.02	120 ± 20	SARANTSEV 19	DPWA	$\bar{K}N$ multichannel

Normalized residue in $N\bar{K} \rightarrow \Sigma(1670) \rightarrow \Lambda(1520)\pi, F\text{-wave}$

MODULUS	PHASE (°)	DOCUMENT ID	TECN	COMMENT
0.01 ± 0.01		SARANTSEV 19	DPWA	$\bar{K}N$ multichannel

Normalized residue in $N\bar{K} \rightarrow \Sigma(1670) \rightarrow \Delta\bar{K}, S\text{-wave}$

MODULUS	PHASE (°)	DOCUMENT ID	TECN	COMMENT
0.01 ± 0.01		SARANTSEV 19	DPWA	$\bar{K}N$ multichannel

Normalized residue in $N\bar{K} \rightarrow \Sigma(1670) \rightarrow N\bar{K}^*(892), S=3/2, S\text{-wave}$

VALUE	DOCUMENT ID	TECN	COMMENT
0.05 ± 0.03	SARANTSEV 19	DPWA	$\bar{K}N$ multichannel

Normalized residue in $N\bar{K} \rightarrow \Sigma(1670) \rightarrow N\bar{K}^*(892), S=3/2, D\text{-wave}$

MODULUS	PHASE (°)	DOCUMENT ID	TECN	COMMENT
0.01 ± 0.01		SARANTSEV 19	DPWA	$\bar{K}N$ multichannel

Normalized residue in $N\bar{K} \rightarrow \Sigma(1670) \rightarrow N\bar{K}^*(892), S=1/2, D\text{-wave}$

MODULUS	PHASE (°)	DOCUMENT ID	TECN	COMMENT
0.03 ± 0.02		SARANTSEV 19	DPWA	$\bar{K}N$ multichannel

 $\Sigma(1670)$ MASS

VALUE (MeV)	DOCUMENT ID	TECN	COMMENT
1665 to 1685 (≈ 1675) OUR ESTIMATE			
1665 ± 3	SARANTSEV 19	DPWA	$\bar{K}N$ multichannel
1678 ± 2	ZHANG 13A	DPWA	$\bar{K}N$ multichannel
1673 ± 1	GAO 12	DPWA	$\bar{K}N \rightarrow \Lambda\pi$
1665.1 ± 4.1	KOISO 85	DPWA	$K^-p \rightarrow \Sigma\pi$
1682 ± 5	GOPAL 80	DPWA	$\bar{K}N \rightarrow \bar{K}N$
1679 ± 10	ALSTON... 78	DPWA	$\bar{K}N \rightarrow \bar{K}N$
1670 ± 5	GOPAL 77	DPWA	$\bar{K}N$ multichannel
1670 ± 6	HEPP 76B	DPWA	$K^-N \rightarrow \Sigma\pi$
1685 ± 20	BAILLON 75	IPWA	$\bar{K}N \rightarrow \Lambda\pi$
1659 ± 12	VANHORN 75	DPWA	$K^-p \rightarrow \Lambda\pi^0$
1670 ± 2	KANE 74	DPWA	$K^-p \rightarrow \Sigma\pi$
••• We do not use the following data for averages, fits, limits, etc. •••			
1667 or 1668	¹ MARTIN 77	DPWA	$\bar{K}N$ multichannel
1650	DEBELLEFON 76	IPWA	$K^-p \rightarrow \Lambda\pi^0$
1671 ± 3	PONTE 75	DPWA	$K^-p \rightarrow \Lambda\pi^0$ (sol. 1)
1655 ± 2	PONTE 75	DPWA	$K^-p \rightarrow \Lambda\pi^0$ (sol. 2)

¹The two MARTIN 77 values are from a T-matrix pole and from a Breit-Wigner fit.

 $\Sigma(1670)$ WIDTH

VALUE (MeV)	DOCUMENT ID	TECN	COMMENT
40 to 100 (≈ 70) OUR ESTIMATE			
54 ± 6	SARANTSEV 19	DPWA	$\bar{K}N$ multichannel
55 ± 4	ZHANG 13A	DPWA	$\bar{K}N$ multichannel
52 ± 5	GAO 12	DPWA	$\bar{K}N \rightarrow \Lambda\pi$
65.0 ± 7.3	KOISO 85	DPWA	$K^-p \rightarrow \Sigma\pi$
79 ± 10	GOPAL 80	DPWA	$\bar{K}N \rightarrow \bar{K}N$
56 ± 20	ALSTON... 78	DPWA	$\bar{K}N \rightarrow \bar{K}N$
50 ± 5	GOPAL 77	DPWA	$\bar{K}N$ multichannel
56 ± 3	HEPP 76B	DPWA	$K^-N \rightarrow \Sigma\pi$
85 ± 25	BAILLON 75	IPWA	$\bar{K}N \rightarrow \Lambda\pi$
32 ± 11	VANHORN 75	DPWA	$K^-p \rightarrow \Lambda\pi^0$
79 ± 6	KANE 74	DPWA	$K^-p \rightarrow \Sigma\pi$
••• We do not use the following data for averages, fits, limits, etc. •••			
46 or 46	¹ MARTIN 77	DPWA	$\bar{K}N$ multichannel
80	DEBELLEFON 76	IPWA	$K^-p \rightarrow \Lambda\pi^0$
44 ± 11	PONTE 75	DPWA	$K^-p \rightarrow \Lambda\pi^0$ (sol. 1)
76 ± 5	PONTE 75	DPWA	$K^-p \rightarrow \Lambda\pi^0$ (sol. 2)

¹The two MARTIN 77 values are from a T-matrix pole and from a Breit-Wigner fit.

 $\Sigma(1670)$ DECAY MODES

Mode	Fraction (Γ_j/Γ)
Γ_1 $N\bar{K}$	0.06 to 0.12
Γ_2 $\Lambda\pi$	5–15 %
Γ_3 $\Sigma\pi$	30–60 %
Γ_4 $\Lambda\pi\pi$	
Γ_5 $\Sigma\pi\pi$	
Γ_6 $\Sigma\sigma$	(7.0 \pm 3.0) %

Γ_7	$\Sigma(1385)\pi$
Γ_8	$\Sigma(1385)\pi, S\text{-wave}$
Γ_9	$\Sigma(1385)\pi, D\text{-wave}$
Γ_{10}	$N\bar{K}^*(892), S=1/2, D\text{-wave}$
Γ_{11}	$N\bar{K}^*(892), S=3/2, S\text{-wave}$
Γ_{12}	$N\bar{K}^*(892), S=3/2, D\text{-wave}$
Γ_{13}	$\Lambda(1405)\pi$
Γ_{14}	$\Lambda(1520)\pi$

 $\Sigma(1670)$ BRANCHING RATIOS

See "Sign conventions for resonance couplings" in the Note on Λ and Σ Resonances.

 $\Gamma(N\bar{K})/\Gamma_{\text{total}}$

VALUE	DOCUMENT ID	TECN	COMMENT	Γ_1/Γ
0.06 to 0.12 OUR ESTIMATE				
0.10 ± 0.02	SARANTSEV 19	DPWA	$\bar{K}N$ multichannel	
0.062 ± 0.007	ZHANG 13A	DPWA	$\bar{K}N$ multichannel	
0.10 ± 0.03	GOPAL 80	DPWA	$\bar{K}N \rightarrow \bar{K}N$	
0.11 ± 0.03	ALSTON... 78	DPWA	$\bar{K}N \rightarrow \bar{K}N$	
••• We do not use the following data for averages, fits, limits, etc. •••				
0.121	¹ KAMANO 15	DPWA	$\bar{K}N$ multichannel	
0.08 ± 0.03	GOPAL 77	DPWA	See GOPAL 80	
0.07 or 0.07	² MARTIN 77	DPWA	$\bar{K}N$ multichannel	

¹ From the preferred solution A in KAMANO 15.

² The two MARTIN 77 values are from a T-matrix pole and from a Breit-Wigner fit.

 $\Gamma(\Lambda\pi)/\Gamma_{\text{total}}$

VALUE	DOCUMENT ID	TECN	COMMENT	Γ_2/Γ
0.09 \pm 0.02				
	SARANTSEV 19	DPWA	$\bar{K}N$ multichannel	
••• We do not use the following data for averages, fits, limits, etc. •••				
0.058	¹ KAMANO 15	DPWA	$\bar{K}N$ multichannel	

¹ From the preferred solution A in KAMANO 15.

 $\Gamma(\Sigma\pi)/\Gamma_{\text{total}}$

VALUE	DOCUMENT ID	TECN	COMMENT	Γ_3/Γ
0.70 \pm 0.15				
	SARANTSEV 19	DPWA	$\bar{K}N$ multichannel	
••• We do not use the following data for averages, fits, limits, etc. •••				
0.465	¹ KAMANO 15	DPWA	$\bar{K}N$ multichannel	

¹ From the preferred solution A in KAMANO 15.

 $\Gamma(\Lambda\pi\pi)/\Gamma_{\text{total}}$

VALUE	DOCUMENT ID	TECN	COMMENT	Γ_4/Γ
••• We do not use the following data for averages, fits, limits, etc. •••				
< 0.11	ARMENTEROS68E HBC		K^-p ($\Gamma_1=0.09$)	

 $\Gamma(\Sigma\pi\pi)/\Gamma_{\text{total}}$

VALUE	DOCUMENT ID	TECN	COMMENT	Γ_5/Γ
••• We do not use the following data for averages, fits, limits, etc. •••				
< 0.14	¹ ARMENTEROS68E HBC		K^-p, K^-d ($\Gamma_1=0.09$)	

¹ Ratio only for $\Sigma 2\pi$ system in $l=1$, which cannot be $\Sigma(1385)$.

 $\Gamma(\Sigma\sigma)/\Gamma_{\text{total}}$

VALUE	DOCUMENT ID	TECN	COMMENT	Γ_6/Γ
0.07 \pm 0.03				
	SARANTSEV 19	DPWA	$\bar{K}N$ multichannel	

 $\Gamma(\Sigma(1385)\pi, S\text{-wave})/\Gamma_{\text{total}}$

VALUE	DOCUMENT ID	TECN	COMMENT	Γ_8/Γ
••• We do not use the following data for averages, fits, limits, etc. •••				
0.309	¹ KAMANO 15	DPWA	Multichannel	

¹ From the preferred solution A in KAMANO 15.

 $\Gamma(\Sigma(1385)\pi, D\text{-wave})/\Gamma_{\text{total}}$

VALUE	DOCUMENT ID	TECN	COMMENT	Γ_9/Γ
••• We do not use the following data for averages, fits, limits, etc. •••				
0.044	¹ KAMANO 15	DPWA	Multichannel	

¹ From the preferred solution A in KAMANO 15.

 $\Gamma(N\bar{K}^*(892), S=1/2, D\text{-wave})/\Gamma_{\text{total}}$

VALUE	DOCUMENT ID	TECN	COMMENT	Γ_{10}/Γ
••• We do not use the following data for averages, fits, limits, etc. •••				
0.001	¹ KAMANO 15	DPWA	Multichannel	

¹ From the preferred solution A in KAMANO 15.

 $\Gamma(N\bar{K}^*(892), S=3/2, S\text{-wave})/\Gamma_{\text{total}}$

VALUE	DOCUMENT ID	TECN	COMMENT	Γ_{11}/Γ
••• We do not use the following data for averages, fits, limits, etc. •••				
0.002	¹ KAMANO 15	DPWA	Multichannel	

¹ From the preferred solution A in KAMANO 15.

Baryon Particle Listings

 $\Sigma(1670)$, $\Sigma(1750)$ $\Gamma(N\bar{K}^*(892), S=3/2, D\text{-wave})/\Gamma_{\text{total}}$ Γ_{12}/Γ

VALUE	DOCUMENT ID	TECN	COMMENT
••• We do not use the following data for averages, fits, limits, etc. •••			
0.001	¹ KAMANO 15	DPWA	Multichannel

¹ From the preferred solution A in KAMANO 15.

 $\Gamma(\Lambda(1405)\pi)/\Gamma_{\text{total}}$ Γ_{13}/Γ

VALUE	DOCUMENT ID	TECN	COMMENT
0.01 ± 0.01	SARANTSEV 19	DPWA	$\bar{K}N$ multichannel
••• We do not use the following data for averages, fits, limits, etc. •••			
<0.06	ARMENTEROS68e	HBC	K^-p, K^-d ($\Gamma_1=0.09$)

 $\Gamma(\Lambda(1405)\pi)/\Gamma(\Sigma(1385)\pi)$ Γ_{13}/Γ_7

VALUE	DOCUMENT ID	TECN	COMMENT
0.23 ± 0.08	BRUCKER 70	DBC	$K^-N \rightarrow \Sigma\pi\pi$

 $(\Gamma_1\Gamma_7)^{1/2}/\Gamma_{\text{total}}$ in $N\bar{K} \rightarrow \Sigma(1670) \rightarrow \Lambda\pi$ $(\Gamma_1\Gamma_2)^{1/2}/\Gamma$

VALUE	DOCUMENT ID	TECN	COMMENT
+0.08 ± 0.01	ZHANG 13A	DPWA	Multichannel
+0.081 ^{+0.002} _{-0.004}	GAO 12	DPWA	$\bar{K}N \rightarrow \Lambda\pi$
+0.17 ± 0.03	¹ MORRIS 78	DPWA	$K^-n \rightarrow \Lambda\pi^-$
+0.13 ± 0.02	¹ MORRIS 78	DPWA	$K^-n \rightarrow \Lambda\pi^-$
+0.10 ± 0.02	GOPAL 77	DPWA	$\bar{K}N$ multichannel
+0.06 ± 0.02	BAILLON 75	IPWA	$\bar{K}N \rightarrow \Lambda\pi$
+0.09 ± 0.02	VANHORN 75	DPWA	$K^-p \rightarrow \Lambda\pi^0$
+0.018 ± 0.060	DEVENISH 74B		Fixed-t dispersion rel.
••• We do not use the following data for averages, fits, limits, etc. •••			
+0.08 or +0.08	² MARTIN 77	DPWA	$\bar{K}N$ multichannel
+0.05	DEBELLEFON 76	IPWA	$K^-p \rightarrow \Lambda\pi^0$
+0.08 ± 0.01	PONTE 75	DPWA	$K^-p \rightarrow \Lambda\pi^0$ (sol. 1)
+0.17 ± 0.01	PONTE 75	DPWA	$K^-p \rightarrow \Lambda\pi^0$ (sol. 2)

¹ Results are with and without an S_{11} $\Sigma(1620)$ in the fit.

² The two MARTIN 77 values are from a T-matrix pole and from a Breit-Wigner fit.

 $(\Gamma_1\Gamma_7)^{1/2}/\Gamma_{\text{total}}$ in $N\bar{K} \rightarrow \Sigma(1670) \rightarrow \Sigma\pi$ $(\Gamma_1\Gamma_3)^{1/2}/\Gamma$

VALUE	DOCUMENT ID	TECN	COMMENT
+0.20 ± 0.01	ZHANG 13A	DPWA	Multichannel
+0.20 ± 0.02	KOISO 85	DPWA	$K^-p \rightarrow \Sigma\pi$
+0.21 ± 0.02	GOPAL 77	DPWA	$\bar{K}N$ multichannel
+0.20 ± 0.01	HEPP 76B	DPWA	$K^-N \rightarrow \Sigma\pi$
+0.21 ± 0.03	KANE 74	DPWA	$K^-p \rightarrow \Sigma\pi$
••• We do not use the following data for averages, fits, limits, etc. •••			
+0.18 or +0.17	¹ MARTIN 77	DPWA	$\bar{K}N$ multichannel

¹ The two MARTIN 77 values are from a T-matrix pole and from a Breit-Wigner fit.

 $(\Gamma_1\Gamma_7)^{1/2}/\Gamma_{\text{total}}$ in $N\bar{K} \rightarrow \Sigma(1670) \rightarrow \Sigma(1385)\pi, S\text{-wave}$ $(\Gamma_1\Gamma_8)^{1/2}/\Gamma$

VALUE	DOCUMENT ID	TECN	COMMENT
+0.11 ± 0.03	PREVOST 74	DPWA	$K^-N \rightarrow \Sigma(1385)\pi$
••• We do not use the following data for averages, fits, limits, etc. •••			
0.17 ± 0.02	¹ SIMS 68	DBC	$K^-N \rightarrow \Lambda\pi\pi$

¹ SIMS 68 uses only cross-section data. Result used as upper limit only.

 $\Gamma_1\Gamma_7/\Gamma_{\text{total}}^2$ in $N\bar{K} \rightarrow \Sigma(1670) \rightarrow \Lambda(1405)\pi$ Γ_{13}/Γ_7^2

VALUE	DOCUMENT ID	TECN	COMMENT
0.007 ± 0.002	¹ BRUCKER 70	DBC	$K^-N \rightarrow \Sigma\pi\pi$
••• We do not use the following data for averages, fits, limits, etc. •••			
<0.03	BERLEY 69	HBC	K^-p 0.6-0.82 GeV/c

¹ Assuming the $\Lambda(1405)\pi$ cross-section bump is due only to $3/2^-$ resonance.

 $(\Gamma_1\Gamma_7)^{1/2}/\Gamma_{\text{total}}$ in $N\bar{K} \rightarrow \Sigma(1670) \rightarrow \Lambda(1520)\pi$ $(\Gamma_1\Gamma_{14})^{1/2}/\Gamma$

VALUE	DOCUMENT ID	TECN	COMMENT
0.081 ± 0.016	¹ CAMERON 77	DPWA	P-wave decay

¹ The CAMERON 77 upper limit on F-wave decay is 0.03.

 $\Sigma(1670)$ REFERENCES

SARANTSEV 19	EPJ A55 180	A.V. Sarantsev et al.	(BONN, PNPI)
KAMANO 15	PR C92 025205	H. Kamano et al.	(ANL, OSAK)
ZHANG 13A	PR C88 035205	H. Zhang et al.	(KSU)
GAO 12	PR C86 025201	P. Gao, J. Shi, B.S. Zou	(BHEP, BEIJT)
Also	NP A867 41	P. Gao, B.S. Zou, A. Sibirtsev	(BHEP, BEIJT+)
KOISO 85	NP A433 619	H. Koiso et al.	(TOKY, MASA)
PDG 82	PL 111B 1	M. Roos et al.	(HEL5, CIT, CERN)
GOPAL 80	Toronto Conf. 159	G.P. Gopal	(RHEL) IJP
ALSTON... 78	PR D18 182	M. Alston-Garnjost et al.	(LBL, MTHO+) IJP
Also	PRL 38 1007	M. Alston-Garnjost et al.	(LBL, MTHO+) IJP
MORRIS 78	PR D17 55	W.A. Morris et al.	(FSU) IJP
CAMERON 77	NP B131 399	W. Cameron et al.	(RHEL, LOIC) IJP
GOPAL 77	NP B119 362	G.P. Gopal et al.	(LOIC, RHEL) IJP
MARTIN 77	NP B127 349	B.R. Martin, M.K. Pidcock, R.G. Moorhouse	(LOUC+) IJP
Also	NP B126 266	B.R. Martin, M.K. Pidcock	(LOUC) IJP
Also	NP B126 285	B.R. Martin, M.K. Pidcock	(LOUC) IJP
DEBELLEFON 76	NP B109 129	A. de Bellefon, A. Berthon	(CDFE) IJP
HEPP 76B	PL 65B 487	V. Hepp et al.	(CERN, HEIDH, MPIM) IJP
BAILLON 75	NP B94 39	P.H. Baillon, P.J. Litchfield	(CERN, RHEL) IJP
PONTE 75	PR D12 2597	R.A. Ponte et al.	(MASA, TENN, UCR) IJP

VANHORN 75	NP B87 145	A.J. van Horn	(LBL) IJP
Also	NP B87 157	A.J. van Horn	(LBL) IJP
DEVENISH 74B	NP B81 330	R.C.E. Devenish, C.D. Froggatt, B.R. Martin	(DESY+) IJP
KANE 74	LBL-2452	D.F. Kane	(LBL) IJP
PREVOST 74	NP B69 246	J. Prevost et al.	(SACL, CERN, HEID)
BRUCKER 70	Duke Conf. 155	E.B. Brucker et al.	(FSU) IJP
Hyperon Resonances, 1970			
BERLEY 69	PL 30B 430	D. Berley et al.	(BNL)
ARMENTEROS 68e	PL 28B 521	R. Armenteros et al.	(CERN, HEID, SACL) IJP
SIMS 68	PRL 21 1413	W.H. Sims et al.	(FSU, TUFTS, BRAN)

 $\Sigma(1750) 1/2^-$

$$I(J^P) = I(\frac{1}{2}^-) \text{ Status: } ***$$

For most results published before 1974 (they are now obsolete), see our 1982 edition Physics Letters **111B** 1 (1982).

There is evidence for this state in many partial-wave analyses, but with wide variations in the mass, width, and couplings. The latest analyses indicated significant couplings to $N\bar{K}$ and $\Lambda\pi$, as well as to $\Sigma\eta$ whose threshold is at 1746 MeV (JONES 74).

 $\Sigma(1750)$ POLE POSITION

REAL PART

VALUE (MeV)	DOCUMENT ID	TECN	COMMENT
1689 ± 11	SARANTSEV 19	DPWA	$\bar{K}N$ multichannel
••• We do not use the following data for averages, fits, limits, etc. •••			
1704 ⁺³ ₋₆	¹ KAMANO 15	DPWA	$\bar{K}N$ multichannel
1708	ZHANG 13A	DPWA	$\bar{K}N$ multichannel

¹ From the preferred solution A in KAMANO 15. Solution B reports two poles at $M = 1551^{+2}_-9$ MeV and 1940^{+2}_-2 MeV.

-2xIMAGINARY PART

VALUE (MeV)	DOCUMENT ID	TECN	COMMENT
206 ± 18	SARANTSEV 19	DPWA	$\bar{K}N$ multichannel
••• We do not use the following data for averages, fits, limits, etc. •••			
86 ⁺¹⁴ ₋₄	¹ KAMANO 15	DPWA	$\bar{K}N$ multichannel
158	ZHANG 13A	DPWA	$\bar{K}N$ multichannel

¹ From the preferred solution A in KAMANO 15. Solution B Reports two poles with $\Gamma = 376^{+12}_-2$ and 172^{+4}_-4 MeV.

 $\Sigma(1750)$ POLE RESIDUES

The normalized residue is the residue divided by $\Gamma_{\text{pole}}/2$.

Normalized residue in $N\bar{K} \rightarrow \Sigma(1750) \rightarrow N\bar{K}$

MODULUS	PHASE (°)	DOCUMENT ID	TECN	COMMENT
0.46 ± 0.09	-144 ± 15	SARANTSEV 19	DPWA	$\bar{K}N$ multichannel
••• We do not use the following data for averages, fits, limits, etc. •••				
0.0982	178	¹ KAMANO 15	DPWA	$\bar{K}N$ multichannel

¹ From the preferred solution A in KAMANO 15.

Normalized residue in $N\bar{K} \rightarrow \Sigma(1750) \rightarrow \Sigma\pi$

MODULUS	PHASE (°)	DOCUMENT ID	TECN	COMMENT
0.27 ± 0.05	100 ± 18	SARANTSEV 19	DPWA	$\bar{K}N$ multichannel
••• We do not use the following data for averages, fits, limits, etc. •••				
0.192	137	¹ KAMANO 15	DPWA	Multichannel

¹ From the preferred solution A in KAMANO 15.

Normalized residue in $N\bar{K} \rightarrow \Sigma(1750) \rightarrow \Sigma\eta$

MODULUS	PHASE (°)	DOCUMENT ID	TECN	COMMENT
0.05 ± 0.03		SARANTSEV 19	DPWA	$\bar{K}N$ multichannel

Normalized residue in $N\bar{K} \rightarrow \Sigma(1750) \rightarrow \Lambda\pi$

MODULUS	PHASE (°)	DOCUMENT ID	TECN	COMMENT
0.26 ± 0.06	115 ± 15	SARANTSEV 19	DPWA	$\bar{K}N$ multichannel
••• We do not use the following data for averages, fits, limits, etc. •••				
0.207	169	¹ KAMANO 15	DPWA	$\bar{K}N$ multichannel

¹ From the preferred solution A in KAMANO 15.

Normalized residue in $N\bar{K} \rightarrow \Sigma(1750) \rightarrow \Xi K$

MODULUS	PHASE (°)	DOCUMENT ID	TECN	COMMENT
0.02 ± 0.02		SARANTSEV 19	DPWA	$\bar{K}N$ multichannel

Normalized residue in $N\bar{K} \rightarrow \Sigma(1750) \rightarrow \Sigma(1385)\pi, D\text{-wave}$

MODULUS	PHASE (°)	DOCUMENT ID	TECN	COMMENT
0.04 ± 0.03		SARANTSEV 19	DPWA	$\bar{K}N$ multichannel
••• We do not use the following data for averages, fits, limits, etc. •••				
0.0536	73	¹ KAMANO 15	DPWA	$\bar{K}N$ multichannel

¹ From the preferred solution A in KAMANO 15.

See key on page 1171

Baryon Particle Listings

 $\Sigma(1750)$ Normalized residue in $N\bar{K} \rightarrow \Sigma(1750) \rightarrow \Lambda(1520)\pi$

MODULUS	PHASE (°)	DOCUMENT ID	TECN	COMMENT
0.15 ± 0.07	-25 ± 40	SARANTSEV 19	DPWA	$\bar{K}N$ multichannel

Normalized residue in $N\bar{K} \rightarrow \Sigma(1750) \rightarrow N\bar{K}^*(892)$, $S=1/2$, S -wave

MODULUS	PHASE (°)	DOCUMENT ID	TECN	COMMENT
0.05 ± 0.03	-100 ± 35	SARANTSEV 19	DPWA	$\bar{K}N$ multichannel

 $\Sigma(1750)$ MASS

VALUE (MeV)	DOCUMENT ID	TECN	COMMENT
1700 to 1800 (≈ 1750) OUR ESTIMATE			
1692 ± 11	SARANTSEV 19	DPWA	$\bar{K}N$ multichannel
1739 ± 8	ZHANG 13A	DPWA	$\bar{K}N$ multichannel
1756 ± 10	GOPAL 80	DPWA	$\bar{K}N \rightarrow \bar{K}N$
1770 ± 10	ALSTON-... 78	DPWA	$\bar{K}N \rightarrow \bar{K}N$
• • • We do not use the following data for averages, fits, limits, etc. • • •			
1770 ± 15	GOPAL 77	DPWA	$\bar{K}N$ multichannel
1800 or 1813	¹ MARTIN 77	DPWA	$\bar{K}N$ multichannel
1715 ± 10	² CARROLL 76	DPWA	Isospin-1 total σ
1730	DEBELLEFON 76	IPWA	$K^- p \rightarrow \Lambda\pi^0$
1780 ± 30	BAILLON 75	IPWA	$\bar{K}N \rightarrow \Lambda\pi$ (sol. 1)
1700 ± 30	BAILLON 75	IPWA	$\bar{K}N \rightarrow \Lambda\pi$ (sol. 2)
1697^{+20}_{-10}	VANHORN 75	DPWA	$K^- p \rightarrow \Lambda\pi^0$
1785 ± 12	CHU 74	DBC	Fits $\sigma(K^- n \rightarrow \Sigma^- \eta)$
1760 ± 5	³ JONES 74	HBC	Fits $\sigma(K^- p \rightarrow \Sigma^0 \eta)$
1739 ± 10	PREVOST 74	DPWA	$K^- N \rightarrow \Sigma(1385)\pi$

¹ The two MARTIN 77 values are from a T-matrix pole and from a Breit-Wigner fit.² A total cross-section bump with $(J+1/2) \Gamma_{el} / \Gamma_{total} = 0.30$.³ An S-wave Breit-Wigner fit to the threshold cross section with no background and errors statistical only. $\Sigma(1750)$ WIDTH

VALUE (MeV)	DOCUMENT ID	TECN	COMMENT
100 to 200 (≈ 150) OUR ESTIMATE			
208 ± 18	SARANTSEV 19	DPWA	$\bar{K}N$ multichannel
182 ± 60	ZHANG 13A	DPWA	$\bar{K}N$ multichannel
64 ± 10	GOPAL 80	DPWA	$\bar{K}N \rightarrow \bar{K}N$
161 ± 20	ALSTON-... 78	DPWA	$\bar{K}N \rightarrow \bar{K}N$
• • • We do not use the following data for averages, fits, limits, etc. • • •			
60 ± 10	GOPAL 77	DPWA	$\bar{K}N$ multichannel
117 or 119	¹ MARTIN 77	DPWA	$\bar{K}N$ multichannel
10	² CARROLL 76	DPWA	Isospin-1 total σ
110	DEBELLEFON 76	IPWA	$K^- p \rightarrow \Lambda\pi^0$
140 ± 30	BAILLON 75	IPWA	$\bar{K}N \rightarrow \Lambda\pi$ (sol. 1)
160 ± 50	BAILLON 75	IPWA	$\bar{K}N \rightarrow \Lambda\pi$ (sol. 2)
66^{+14}_{-12}	VANHORN 75	DPWA	$K^- p \rightarrow \Lambda\pi^0$
89 ± 33	CHU 74	DBC	Fits $\sigma(K^- n \rightarrow \Sigma^- \eta)$
92 ± 7	³ JONES 74	HBC	Fits $\sigma(K^- p \rightarrow \Sigma^0 \eta)$
108 ± 20	PREVOST 74	DPWA	$K^- N \rightarrow \Sigma(1385)\pi$

¹ The two MARTIN 77 values are from a T-matrix pole and from a Breit-Wigner fit.² A total cross-section bump with $(J+1/2) \Gamma_{el} / \Gamma_{total} = 0.30$.³ An S-wave Breit-Wigner fit to the threshold cross section with no background and errors statistical only. $\Sigma(1750)$ DECAY MODES

Mode	Fraction (Γ_i/Γ)
Γ_1 $N\bar{K}$	0.06 to 0.12
Γ_2 $\Lambda\pi$	(14 ± 5) %
Γ_3 $\Sigma\pi$	(16 ± 4) %
Γ_4 $\Sigma\eta$	15-55 %
Γ_5 $\Sigma(1385)\pi$, D-wave	< 1 %
Γ_6 $\Lambda(1520)\pi$	(2.0 ± 1.0) %
Γ_7 $N\bar{K}^*(892)$, $S=1/2$	(8 ± 4) %
Γ_8 $N\bar{K}^*(892)$, $S=3/2$, D-wave	

 $\Sigma(1750)$ BRANCHING RATIOSSee "Sign conventions for resonance couplings" in the Note on Λ and Σ Resonances.

$\Gamma(N\bar{K})/\Gamma_{total}$	DOCUMENT ID	TECN	COMMENT	Γ_1/Γ
0.06 to 0.12 OUR ESTIMATE				
0.46 ± 0.09	SARANTSEV 19	DPWA	$\bar{K}N$ multichannel	
0.09 ± 0.07	ZHANG 13A	DPWA	Multichannel	
0.14 ± 0.03	GOPAL 80	DPWA	$\bar{K}N \rightarrow \bar{K}N$	
0.33 ± 0.05	ALSTON-... 78	DPWA	$\bar{K}N \rightarrow \bar{K}N$	

• • • We do not use the following data for averages, fits, limits, etc. • • •

0.154	¹ KAMANO 15	DPWA	Multichannel
0.15 ± 0.03	GOPAL 77	DPWA	See GOPAL 80
0.06 or 0.05	² MARTIN 77	DPWA	$\bar{K}N$ multichannel

¹ From the preferred solution A in KAMANO 15.² The two MARTIN 77 values are from a T-matrix pole and from a Breit-Wigner fit.

$\Gamma(\Lambda\pi)/\Gamma_{total}$	DOCUMENT ID	TECN	COMMENT	Γ_2/Γ
0.14 ± 0.05				
	SARANTSEV 19	DPWA	$\bar{K}N$ multichannel	

• • • We do not use the following data for averages, fits, limits, etc. • • •

0.435	¹ KAMANO 15	DPWA	$\bar{K}N$ multichannel
-------	------------------------	------	-------------------------

¹ From the preferred solution A in KAMANO 15.

$\Gamma(\Sigma\pi)/\Gamma_{total}$	DOCUMENT ID	TECN	COMMENT	Γ_3/Γ
0.16 ± 0.04				
	SARANTSEV 19	DPWA	$\bar{K}N$ multichannel	

• • • We do not use the following data for averages, fits, limits, etc. • • •

0.373	¹ KAMANO 15	DPWA	$\bar{K}N$ multichannel
-------	------------------------	------	-------------------------

¹ From the preferred solution A in KAMANO 15.

$\Gamma(\Lambda(1520)\pi)/\Gamma_{total}$	DOCUMENT ID	TECN	COMMENT	Γ_6/Γ
0.02 ± 0.01				
	SARANTSEV 19	DPWA	$\bar{K}N$ multichannel	

• • • We do not use the following data for averages, fits, limits, etc. • • •

0.024	¹ KAMANO 15	DPWA	$\bar{K}N$ multichannel
-------	------------------------	------	-------------------------

¹ From the preferred solution A in KAMANO 15.

$\Gamma(\Sigma(1385)\pi, D\text{-wave})/\Gamma_{total}$	DOCUMENT ID	TECN	COMMENT	Γ_5/Γ
< 0.01				
	SARANTSEV 19	DPWA	$\bar{K}N$ multichannel	

• • • We do not use the following data for averages, fits, limits, etc. • • •

0.024	¹ KAMANO 15	DPWA	$\bar{K}N$ multichannel
-------	------------------------	------	-------------------------

¹ From the preferred solution A in KAMANO 15.

$\Gamma(N\bar{K}^*(892), S=1/2)/\Gamma_{total}$	DOCUMENT ID	TECN	COMMENT	Γ_7/Γ
~ 0				
	SARANTSEV 19	DPWA	$\bar{K}N$ multichannel	
	ZHANG 13A	DPWA	$\bar{K}N$ multichannel	

• • • We do not use the following data for averages, fits, limits, etc. • • •

0.004	¹ KAMANO 15	DPWA	$\bar{K}N$ multichannel
-------	------------------------	------	-------------------------

¹ From the preferred solution A in KAMANO 15.

$\Gamma(N\bar{K}^*(892), S=3/2, D\text{-wave})/\Gamma_{total}$	DOCUMENT ID	TECN	COMMENT	Γ_8/Γ
~ 0				
	SARANTSEV 19	DPWA	$\bar{K}N$ multichannel	

• • • We do not use the following data for averages, fits, limits, etc. • • •

0.01	¹ KAMANO 15	DPWA	Multichannel
------	------------------------	------	--------------

¹ From the preferred solution A in KAMANO 15.

$(\Gamma_i \Gamma_f)^{1/2}/\Gamma_{total}$ in $N\bar{K} \rightarrow \Sigma(1750) \rightarrow \Lambda\pi$	DOCUMENT ID	TECN	COMMENT	$(\Gamma_1 \Gamma_2)^{1/2}/\Gamma$
~ 0				
	SARANTSEV 19	DPWA	$\bar{K}N$ multichannel	
	ZHANG 13A	DPWA	$\bar{K}N$ multichannel	

• • • We do not use the following data for averages, fits, limits, etc. • • •

$+0.10 \pm 0.04$	ZHANG 13A	DPWA	Multichannel
0.04 ± 0.03	GOPAL 77	DPWA	$\bar{K}N$ multichannel

• • • We do not use the following data for averages, fits, limits, etc. • • •

-0.10 or -0.09	¹ MARTIN 77	DPWA	$\bar{K}N$ multichannel
-0.12	DEBELLEFON 76	IPWA	$K^- p \rightarrow \Lambda\pi^0$
-0.12 ± 0.02	BAILLON 75	IPWA	$\bar{K}N \rightarrow \Lambda\pi$ (sol. 1)
-0.13 ± 0.03	BAILLON 75	IPWA	$\bar{K}N \rightarrow \Lambda\pi$ (sol. 2)
-0.13 ± 0.04	VANHORN 75	DPWA	$K^- p \rightarrow \Lambda\pi^0$
-0.120 ± 0.077	DEVENISH 74B		Fixed- t dispersion rel.

¹ The two MARTIN 77 values are from a T-matrix pole and from a Breit-Wigner fit.

$(\Gamma_i \Gamma_f)^{1/2}/\Gamma_{total}$ in $N\bar{K} \rightarrow \Sigma(1750) \rightarrow \Sigma\pi$	DOCUMENT ID	TECN	COMMENT	$(\Gamma_1 \Gamma_3)^{1/2}/\Gamma$
~ 0				
	SARANTSEV 19	DPWA	$\bar{K}N$ multichannel	
	ZHANG 13A	DPWA	Multichannel	

• • • We do not use the following data for averages, fits, limits, etc. • • •

$+0.17 \pm 0.07$	ZHANG 13A	DPWA	Multichannel
-0.09 ± 0.05	GOPAL 77	DPWA	$\bar{K}N$ multichannel

• • • We do not use the following data for averages, fits, limits, etc. • • •

$+0.06$ or $+0.06$	¹ MARTIN 77	DPWA	$\bar{K}N$ multichannel
0.13 ± 0.02	LANGBEIN 72	IPWA	$\bar{K}N$ multichannel

¹ The two MARTIN 77 values are from a T-matrix pole and from a Breit-Wigner fit.

$(\Gamma_i \Gamma_f)^{1/2}/\Gamma_{total}$ in $N\bar{K} \rightarrow \Sigma(1750) \rightarrow \Sigma\eta$	DOCUMENT ID	TECN	COMMENT	$(\Gamma_1 \Gamma_4)^{1/2}/\Gamma$
~ 0				
	SARANTSEV 19	DPWA	$\bar{K}N$ multichannel	

• • • We do not use the following data for averages, fits, limits, etc. • • •

0.23 ± 0.01	¹ JONES 74	HBC	Fits $\sigma(K^- p \rightarrow \Sigma^0 \eta)$
-----------------	-----------------------	-----	--

• • • We do not use the following data for averages, fits, limits, etc. • • •

seen	CLINE 69	DBC	Threshold bump
------	----------	-----	----------------

¹ An S-wave Breit-Wigner fit to the threshold cross section with no background and errors statistical only.

$(\Gamma_i \Gamma_f)^{1/2}/\Gamma_{total}$ in $N\bar{K} \rightarrow \Sigma(1750) \rightarrow \Sigma(1385)\pi, D\text{-wave}$	DOCUMENT ID	TECN	COMMENT	$(\Gamma_1 \Gamma_5)^{1/2}/\Gamma$
~ 0				
	SARANTSEV 19	DPWA	$\bar{K}N$ multichannel	
	ZHANG 13A	DPWA	Multichannel	
	PREVOST 74	DPWA	$K^- N \rightarrow \Sigma(1385)\pi$	

Baryon Particle Listings

 $\Sigma(1750), \Sigma(1775)$

$(\Gamma_i/\Gamma_{\text{total}})^{1/2}/\Gamma_{\text{total}}$ in $N\bar{K} \rightarrow \Sigma(1750) \rightarrow \Lambda(1520)\pi$		$(\Gamma_i/\Gamma_6)^{1/2}/\Gamma$	
VALUE	DOCUMENT ID	TECN	COMMENT
0.032±0.021	CAMERON 77	DPWA	<i>P</i> -wave decay

 $\Sigma(1750)$ REFERENCES

SARANTSEV 19	EPJ A55 180	A.V. Sarantsev et al.	(BONN, PNPI)
KAMANO 15	PR C92 025205	H. Kamano et al.	(ANL, OSAK)
ZHANG 13A	PR C88 035205	H. Zhang et al.	(KSU)
PDG 82	PL 111B 1	M. Roos et al.	(HEL5, CIT, CERN)
GOPAL 80	Toronto Conf. 159	G.P. Gopal	(RHEL) IJP
ALSTON... 78	PR D18 182	M. Alston-Garnjost et al.	(LBL, MTHO+) IJP
Also	PRL 38 1007	M. Alston-Garnjost et al.	(LBL, MTHO+) IJP
CAMERON 77	NP B131 399	W. Cameron et al.	(RHEL, LOIC) IJP
GOPAL 77	NP B119 362	G.P. Gopal et al.	(LOIC, RHEL) IJP
MARTIN 77	NP B127 349	B.R. Martin, M.K. Pidcock, R.G. Moorhouse	(LOUC+) IJP
Also	NP B126 266	B.R. Martin, M.K. Pidcock	(LOUC) IJP
Also	NP B126 285	B.R. Martin, M.K. Pidcock	(LOUC) IJP
CARROLL 76	PRL 37 806	A.S. Carroll et al.	(BNL) I
DEBELLEFON 76	NP B109 129	A. de Bellefon, A. Berthon	(CDEF) IJP
BAILLON 75	NP B94 39	P.H. Baillon, P.J. Litchfield	(CERN, RHEL) IJP
VANHORN 75	NP B87 145	A.J. van Horn	(LBL) IJP
Also	NP B87 157	A.J. van Horn	(LBL) IJP
CHU 74	NC 20A 35	R.Y.L. Chu et al.	(PLAT, TUFTS, BRAN) IJP
DEVENISH 74B	NP B81 330	R.C.E. Devenish, C.D. Froggatt, B.R. Martin	(DESY+) IJP
JONES 74	NP B73 141	M.D. Jones	(CHIC) IJP
PREVOST 74	NP B69 246	J. Prevost et al.	(SACL, CERN, HEID) IJP
LANGBEIN 72	NP B47 477	W. Langbein, F. Wagner	(MPIM) IJP
CLINE 69	LNC 2 407	D. Cline, R. Laumann, J. Mapp	(WISC) IJP

$$\Sigma(1775) 5/2^-$$

$$J(P) = 1(\frac{5}{2}^-) \text{ Status: } ****$$

Discovered by GALTIERI 63, this resonance plays the same role as cornerstone for isospin-1 analyses in this region as the $\Lambda(1820)F_{05}$ does in the isospin-0 channel.

For most results published before 1974 (they are now obsolete), see our 1982 edition Physics Letters **111B** 1 (1982).

 $\Sigma(1775)$ POLE POSITION

REAL PART

VALUE (MeV)	DOCUMENT ID	TECN	COMMENT
-------------	-------------	------	---------

1760 to 1780 (≈ 1770) OUR ESTIMATE

1767±4	SARANTSEV 19	DPWA	$\bar{K}N$ multichannel
--------	--------------	------	-------------------------

1767 \pm $\frac{+2}{-2}$	¹ KAMANO 15	DPWA	$\bar{K}N$ multichannel
----------------------------	------------------------	------	-------------------------

••• We do not use the following data for averages, fits, limits, etc. •••

1759	ZHANG 13A	DPWA	$\bar{K}N$ multichannel
------	-----------	------	-------------------------

¹ From the preferred solution A in KAMANO 15.

-2xIMAGINARY PART

VALUE (MeV)	DOCUMENT ID	TECN	COMMENT
-------------	-------------	------	---------

45 to 65 (≈ 55) OUR ESTIMATE

122±8	SARANTSEV 19	DPWA	$\bar{K}N$ multichannel
-------	--------------	------	-------------------------

128 \pm $\frac{+4}{-2}$	¹ KAMANO 15	DPWA	$\bar{K}N$ multichannel
---------------------------	------------------------	------	-------------------------

••• We do not use the following data for averages, fits, limits, etc. •••

118	ZHANG 13A	DPWA	$\bar{K}N$ multichannel
-----	-----------	------	-------------------------

¹ From the preferred solution A in KAMANO 15.

 $\Sigma(1775)$ POLE RESIDUES

The normalized residue is the residue divided by $\Gamma_{\text{pole}}/2$.

Normalized residue in $N\bar{K} \rightarrow \Sigma(1775) \rightarrow N\bar{K}$

MODULUS	PHASE (°)	DOCUMENT ID	TECN	COMMENT
---------	-----------	-------------	------	---------

0.44 ±0.09	-17 ±10	SARANTSEV 19	DPWA	$\bar{K}N$ multichannel
------------	---------	--------------	------	-------------------------

••• We do not use the following data for averages, fits, limits, etc. •••

0.371	-32	¹ KAMANO 15	DPWA	$\bar{K}N$ multichannel
-------	-----	------------------------	------	-------------------------

¹ From the preferred solution A in KAMANO 15.

Normalized residue in $N\bar{K} \rightarrow \Sigma(1775) \rightarrow \Sigma\pi$

MODULUS	PHASE (°)	DOCUMENT ID	TECN	COMMENT
---------	-----------	-------------	------	---------

0.13 ±0.03	10 ±12	SARANTSEV 19	DPWA	$\bar{K}N$ multichannel
------------	--------	--------------	------	-------------------------

••• We do not use the following data for averages, fits, limits, etc. •••

0.115	-24	¹ KAMANO 15	DPWA	$\bar{K}N$ multichannel
-------	-----	------------------------	------	-------------------------

¹ From the preferred solution A in KAMANO 15.

Normalized residue in $N\bar{K} \rightarrow \Sigma(1775) \rightarrow \Lambda\pi$

MODULUS	PHASE (°)	DOCUMENT ID	TECN	COMMENT
---------	-----------	-------------	------	---------

0.47 ±0.10	130 ±15	SARANTSEV 19	DPWA	$\bar{K}N$ multichannel
------------	---------	--------------	------	-------------------------

••• We do not use the following data for averages, fits, limits, etc. •••

0.325	157	¹ KAMANO 15	DPWA	$\bar{K}N$ multichannel
-------	-----	------------------------	------	-------------------------

¹ From the preferred solution A in KAMANO 15.

Normalized residue in $N\bar{K} \rightarrow \Sigma(1775) \rightarrow \Sigma(1385)\pi, D$ -wave

MODULUS	PHASE (°)	DOCUMENT ID	TECN	COMMENT
---------	-----------	-------------	------	---------

••• We do not use the following data for averages, fits, limits, etc. •••

0.391	137	¹ KAMANO 15	DPWA	$\bar{K}N$ multichannel
-------	-----	------------------------	------	-------------------------

¹ From the preferred solution A in KAMANO 15.

Normalized residue in $N\bar{K} \rightarrow \Sigma(1775) \rightarrow \Sigma(1385)\pi, G$ -wave

MODULUS	PHASE (°)	DOCUMENT ID	TECN	COMMENT
---------	-----------	-------------	------	---------

••• We do not use the following data for averages, fits, limits, etc. •••

0.0129	-58	¹ KAMANO 15	DPWA	$\bar{K}N$ multichannel
--------	-----	------------------------	------	-------------------------

¹ From the preferred solution A in KAMANO 15.

Normalized residue in $N\bar{K} \rightarrow \Sigma(1775) \rightarrow N\bar{K}^*(892), S=1/2, D$ -wave

MODULUS	PHASE (°)	DOCUMENT ID	TECN	COMMENT
---------	-----------	-------------	------	---------

0.04 ±0.02	-100 ±60	SARANTSEV 19	DPWA	$\bar{K}N$ multichannel
------------	----------	--------------	------	-------------------------

Normalized residue in $N\bar{K} \rightarrow \Sigma(1775) \rightarrow N\bar{K}^*(892), S=3/2, D$ -wave

MODULUS	PHASE (°)	DOCUMENT ID	TECN	COMMENT
---------	-----------	-------------	------	---------

0.09 ±0.06	10 ±50	SARANTSEV 19	DPWA	$\bar{K}N$ multichannel
------------	--------	--------------	------	-------------------------

Normalized residue in $N\bar{K} \rightarrow \Sigma(1775) \rightarrow N\bar{K}^*(892), S=3/2, G$ -wave

MODULUS	PHASE (°)	DOCUMENT ID	TECN	COMMENT
---------	-----------	-------------	------	---------

0.04 ±0.02	-100 ±60	SARANTSEV 19	DPWA	$\bar{K}N$ multichannel
------------	----------	--------------	------	-------------------------

Normalized residue in $N\bar{K} \rightarrow \Sigma(1775) \rightarrow \Xi K$

MODULUS	PHASE (°)	DOCUMENT ID	TECN	COMMENT
---------	-----------	-------------	------	---------

0.02 ±0.01	-90 ±35	SARANTSEV 19	DPWA	$\bar{K}N$ multichannel
------------	---------	--------------	------	-------------------------

Normalized residue in $N\bar{K} \rightarrow \Sigma(1775) \rightarrow \Lambda(1520)\pi, P$ -wave

MODULUS	PHASE (°)	DOCUMENT ID	TECN	COMMENT
---------	-----------	-------------	------	---------

0.09 ±0.03	10 ±30	SARANTSEV 19	DPWA	$\bar{K}N$ multichannel
------------	--------	--------------	------	-------------------------

Normalized residue in $N\bar{K} \rightarrow \Sigma(1775) \rightarrow \Lambda(1520)\pi, F$ -wave

VALUE	DOCUMENT ID	TECN	COMMENT
-------	-------------	------	---------

0.01 ±0.01	SARANTSEV 19	DPWA	$\bar{K}N$ multichannel
------------	--------------	------	-------------------------

Normalized residue in $N\bar{K} \rightarrow \Sigma(1775) \rightarrow \Delta\bar{K}, D$ -wave

VALUE	DOCUMENT ID	TECN	COMMENT
-------	-------------	------	---------

0.02 ±0.02	SARANTSEV 19	DPWA	$\bar{K}N$ multichannel
------------	--------------	------	-------------------------

 $\Sigma(1775)$ MASS

VALUE (MeV)	DOCUMENT ID	TECN	COMMENT
-------------	-------------	------	---------

1770 to 1780 (≈ 1775) OUR ESTIMATE

1776 ± 4	SARANTSEV 19	DPWA	$\bar{K}N$ multichannel
----------	--------------	------	-------------------------

1778 ± 1	ZHANG 13A	DPWA	$\bar{K}N$ multichannel
----------	-----------	------	-------------------------

1778 ± 5	GOPAL 80	DPWA	$\bar{K}N \rightarrow \bar{K}N$
----------	----------	------	---------------------------------

1777 ± 5	ALSTON... 78	DPWA	$\bar{K}N \rightarrow \bar{K}N$
----------	--------------	------	---------------------------------

1775 ±10	BAILLON 75	IPWA	$\bar{K}N \rightarrow \Lambda\pi$
----------	------------	------	-----------------------------------

1774 ±10	VANHORN 75	DPWA	$K^-\rho \rightarrow \Lambda\pi^0$
----------	------------	------	------------------------------------

1772 ± 6	KANE 74	DPWA	$K^-\rho \rightarrow \Sigma\pi$
----------	---------	------	---------------------------------

••• We do not use the following data for averages, fits, limits, etc. •••

1774 ± 5	GOPAL 77	DPWA	$\bar{K}N$ multichannel
----------	----------	------	-------------------------

1772 or 1777	¹ MARTIN 77	DPWA	$\bar{K}N$ multichannel
--------------	------------------------	------	-------------------------

1765	DEBELLEFON 76	IPWA	$K^-\rho \rightarrow \Lambda\pi^0$
------	---------------	------	------------------------------------

¹ The two MARTIN 77 values are from a T-matrix pole and from a Breit-Wigner fit.

 $\Sigma(1775)$ WIDTH

VALUE (MeV)	DOCUMENT ID	TECN	COMMENT
-------------	-------------	------	---------

105 to 135 (≈ 120) OUR ESTIMATE

124 ± 8	SARANTSEV 19	DPWA	$\bar{K}N$ multichannel
---------	--------------	------	-------------------------

131 ± 3	ZHANG 13A	DPWA	$\bar{K}N$ multichannel
---------	-----------	------	-------------------------

137 ±10	GOPAL 80	DPWA	$\bar{K}N \rightarrow \bar{K}N$
---------	----------	------	---------------------------------

116 ±10	ALSTON... 78	DPWA	$\bar{K}N \rightarrow \bar{K}N$
---------	--------------	------	---------------------------------

125 ±15	BAILLON 75	IPWA	$\bar{K}N \rightarrow \Lambda\pi$
---------	------------	------	-----------------------------------

146 ±18	VANHORN 75	DPWA	$K^-\rho \rightarrow \Lambda\pi^0$
---------	------------	------	------------------------------------

154 ±10	KANE 74	DPWA	$K^-\rho \rightarrow \Sigma\pi$
---------	---------	------	---------------------------------

••• We do not use the following data for averages, fits, limits, etc. •••

130 ±10	GOPAL 77	DPWA	$\bar{K}N$ multichannel
---------	----------	------	-------------------------

102 or 103	¹ MARTIN 77	DPWA	$\bar{K}N$ multichannel
------------	------------------------	------	-------------------------

120	DEBELLEFON 76	IPWA	$K^-\rho \rightarrow \Lambda\pi^0$
-----	---------------	------	------------------------------------

¹ The two MARTIN 77 values are from a T-matrix pole and from a Breit-Wigner fit.

 $\Sigma(1775)$ DECAY MODES

Mode	Fraction (Γ_i/Γ)
------	--------------------------------

Γ_1 $N\bar{K}$	37–43%
-----------------------	--------

Γ_2 $\Lambda\pi$	14–20%
-------------------------	--------

Γ_3 $\Sigma\pi$	2–5%
------------------------	------

Γ_4 $\Sigma(1385)\pi$	8–12%
------------------------------	-------

Γ_5 $\Sigma(1385)\pi, D$ -wave	
---------------------------------------	--

Γ_6 $\Sigma(1385)\pi, G$ -wave	
---------------------------------------	--

Γ_7	$\Lambda(1520)\pi$, <i>P</i> -wave	17–23%
Γ_8	$\Sigma\pi\pi$	
Γ_9	$\Delta(1232)\bar{K}$, <i>D</i> -wave	
Γ_{10}	$N\bar{K}^*(892)$, $S=1/2$	
Γ_{11}	$N\bar{K}^*(892)$, $S=1/2$, <i>D</i> -wave	
Γ_{12}	$N\bar{K}^*(892)$, $S=3/2$, <i>D</i> -wave	
Γ_{13}	$N\bar{K}^*(892)$, $S=3/2$, <i>G</i> -wave	

 $\Sigma(1775)$ BRANCHING RATIOS

See “Sign conventions for resonance couplings” in the Note on Λ and Σ Resonances. Also, the errors quoted do not include uncertainties due to the parametrization used in the partial-wave analyses and are thus too small.

$\Gamma(N\bar{K})/\Gamma_{\text{total}}$				Γ_1/Γ
VALUE	DOCUMENT ID	TECN	COMMENT	
0.37 to 0.43 OUR ESTIMATE				
0.43 ± 0.09	SARANTSEV 19	DPWA	$\bar{K}N$ multichannel	
0.40 ± 0.01	ZHANG 13A	DPWA	$\bar{K}N$ multichannel	
0.40 ± 0.02	GOPAL 80	DPWA	$\bar{K}N \rightarrow \bar{K}N$	
0.37 ± 0.03	ALSTON... 78	DPWA	$\bar{K}N \rightarrow \bar{K}N$	
••• We do not use the following data for averages, fits, limits, etc. •••				
0.402	¹ KAMANO 15	DPWA	Multichannel	
0.41 ± 0.03	GOPAL 77	DPWA	See GOPAL 80	
0.37 or 0.36	² MARTIN 77	DPWA	$\bar{K}N$ multichannel	

¹ From the preferred solution A in KAMANO 15.
² The two MARTIN 77 values are from a T-matrix pole and from a Breit-Wigner fit.

$\Gamma(\Lambda\pi)/\Gamma_{\text{total}}$				Γ_2/Γ
VALUE	DOCUMENT ID	TECN	COMMENT	
0.49 ± 0.10	SARANTSEV 19	DPWA	$\bar{K}N$ multichannel	
••• We do not use the following data for averages, fits, limits, etc. •••				
0.244	¹ KAMANO 15	DPWA	$\bar{K}N$ multichannel	
¹ From the preferred solution A in KAMANO 15.				

$\Gamma(\Lambda\pi)/\Gamma(N\bar{K})$				Γ_2/Γ_1
VALUE	DOCUMENT ID	TECN	COMMENT	
0.33 ± 0.05	UHLIG 67	HBC	$K^-\rho$ 0.9 GeV/c	

$\Gamma(\Sigma\pi)/\Gamma_{\text{total}}$				Γ_3/Γ
VALUE	DOCUMENT ID	TECN	COMMENT	
0.035 ± 0.010	SARANTSEV 19	DPWA	$\bar{K}N$ multichannel	
••• We do not use the following data for averages, fits, limits, etc. •••				
0.042	¹ KAMANO 15	DPWA	$\bar{K}N$ multichannel	
¹ From the preferred solution A in KAMANO 15.				

$\Gamma(\Sigma(1385)\pi)/\Gamma(N\bar{K})$				Γ_4/Γ_1
VALUE	DOCUMENT ID	TECN	COMMENT	
0.25 ± 0.09	UHLIG 67	HBC	$K^-\rho$ 0.9 GeV/c	

$\Gamma(\Sigma(1385)\pi, D\text{-wave})/\Gamma_{\text{total}}$				Γ_5/Γ
VALUE	DOCUMENT ID	TECN	COMMENT	
••• We do not use the following data for averages, fits, limits, etc. •••				
0.309	¹ KAMANO 15	DPWA	Multichannel	
¹ From the preferred solution A in KAMANO 15.				

$\Gamma(\Sigma(1385)\pi, G\text{-wave})/\Gamma_{\text{total}}$				Γ_6/Γ
VALUE	DOCUMENT ID	TECN	COMMENT	
••• We do not use the following data for averages, fits, limits, etc. •••				
not seen	¹ KAMANO 15	DPWA	Multichannel	
¹ From the preferred solution A in KAMANO 15.				

$\Gamma(\Lambda(1520)\pi, P\text{-wave})/\Gamma_{\text{total}}$				Γ_7/Γ
VALUE	DOCUMENT ID	TECN	COMMENT	
0.02 ± 0.01	SARANTSEV 19	DPWA	$\bar{K}N$ multichannel	

$\Gamma(\Lambda(1520)\pi, P\text{-wave})/\Gamma(N\bar{K})$				Γ_7/Γ_1
VALUE	DOCUMENT ID	TECN	COMMENT	
0.28 ± 0.05	UHLIG 67	HBC	$K^-\rho$ 0.9 GeV/c	

$\Gamma(\Sigma\pi\pi)/\Gamma_{\text{total}}$				Γ_8/Γ
VALUE	DOCUMENT ID	TECN	COMMENT	
••• We do not use the following data for averages, fits, limits, etc. •••				
0.12	¹ ARMENTEROS68c	HDBC	$K^-N \rightarrow \Sigma\pi\pi$	

¹ For about 3/4 of this, the $\Sigma\pi$ system has $l=0$ and is almost entirely $\Lambda(1520)$. For the rest, the $\Sigma\pi$ has $l=1$, which is about what is expected from the known $\Sigma(1775) \rightarrow \Sigma(1385)\pi$ rate, as seen in $\Lambda\pi\pi$.

$\Gamma(N\bar{K}^*(892), S=1/2, D\text{-wave})/\Gamma_{\text{total}}$				Γ_{11}/Γ
VALUE	DOCUMENT ID	TECN	COMMENT	
••• We do not use the following data for averages, fits, limits, etc. •••				
not seen	¹ KAMANO 15	DPWA	Multichannel	
¹ From the preferred solution A in KAMANO 15.				

$\Gamma(N\bar{K}^*(892), S=3/2, D\text{-wave})/\Gamma_{\text{total}}$				Γ_{12}/Γ
VALUE	DOCUMENT ID	TECN	COMMENT	
••• We do not use the following data for averages, fits, limits, etc. •••				
0.003	¹ KAMANO 15	DPWA	Multichannel	
¹ From the preferred solution A in KAMANO 15.				

$\Gamma(N\bar{K}^*(892), S=3/2, G\text{-wave})/\Gamma_{\text{total}}$				Γ_{13}/Γ
VALUE	DOCUMENT ID	TECN	COMMENT	
••• We do not use the following data for averages, fits, limits, etc. •••				
not seen	¹ KAMANO 15	DPWA	Multichannel	
¹ From the preferred solution A in KAMANO 15.				

$(\Gamma_1\Gamma_7)^{1/2}/\Gamma_{\text{total}}$ in $N\bar{K} \rightarrow \Sigma(1775) \rightarrow \Lambda\pi$				$(\Gamma_1\Gamma_2)^{1/2}/\Gamma$
VALUE	DOCUMENT ID	TECN	COMMENT	
−0.31 ± 0.01	ZHANG 13A	DPWA	Multichannel	
−0.28 ± 0.03	GOPAL 77	DPWA	$\bar{K}N$ multichannel	
−0.25 ± 0.02	BAILLON 75	IPWA	$\bar{K}N \rightarrow \Lambda\pi$	
−0.28 +0.04 −0.05	VANHORN 75	DPWA	$K^-\rho \rightarrow \Lambda\pi^0$	
−0.259 ± 0.048	DEVENISH 74B		Fixed- t dispersion rel.	
••• We do not use the following data for averages, fits, limits, etc. •••				
−0.29 or −0.28	¹ MARTIN 77	DPWA	$\bar{K}N$ multichannel	
−0.30	DEBELLEFON 76	IPWA	$K^-\rho \rightarrow \Lambda\pi^0$	
¹ The two MARTIN 77 values are from a T-matrix pole and from a Breit-Wigner fit.				

$(\Gamma_1\Gamma_7)^{1/2}/\Gamma_{\text{total}}$ in $N\bar{K} \rightarrow \Sigma(1775) \rightarrow \Sigma\pi$				$(\Gamma_1\Gamma_3)^{1/2}/\Gamma$
VALUE	DOCUMENT ID	TECN	COMMENT	
+0.08 ± 0.01	ZHANG 13A	DPWA	Multichannel	
+0.13 ± 0.02	GOPAL 77	DPWA	$\bar{K}N$ multichannel	
0.09 ± 0.01	KANE 74	DPWA	$K^-\rho \rightarrow \Sigma\pi$	
••• We do not use the following data for averages, fits, limits, etc. •••				
+0.08 or +0.08	¹ MARTIN 77	DPWA	$\bar{K}N$ multichannel	
¹ The two MARTIN 77 values are from a T-matrix pole and from a Breit-Wigner fit.				

$(\Gamma_1\Gamma_7)^{1/2}/\Gamma_{\text{total}}$ in $N\bar{K} \rightarrow \Sigma(1775) \rightarrow \Sigma(1385)\pi, D\text{-wave}$				$(\Gamma_1\Gamma_5)^{1/2}/\Gamma$
VALUE	DOCUMENT ID	TECN	COMMENT	
−0.12 ± 0.01	ZHANG 13A	DPWA	Multichannel	
−0.184 ± 0.011	¹ CAMERON 78	DPWA	$K^-\rho \rightarrow \Sigma(1385)\pi$	
+0.20 ± 0.02	PREVOST 74	DPWA	$K^-N \rightarrow \Sigma(1385)\pi$	
••• We do not use the following data for averages, fits, limits, etc. •••				
0.32 ± 0.06	SIMS 68	DBC	$K^-N \rightarrow \Lambda\pi\pi$	
0.24 ± 0.03	ARMENTEROS67c	HBC	$K^-\rho \rightarrow \Lambda\pi\pi$	
¹ The CAMERON 78 upper limit on <i>G</i> -wave decay is 0.03.				

$(\Gamma_1\Gamma_7)^{1/2}/\Gamma_{\text{total}}$ in $N\bar{K} \rightarrow \Sigma(1775) \rightarrow \Lambda(1520)\pi, P\text{-wave}$				$(\Gamma_1\Gamma_7)^{1/2}/\Gamma$
VALUE	DOCUMENT ID	TECN	COMMENT	
−0.06 ± 0.01	ZHANG 13A	DPWA	Multichannel	
−0.305 ± 0.010	¹ CAMERON 77	DPWA	$K^-\rho \rightarrow \Lambda(1520)\pi^0$	
0.31 ± 0.02	BARLETTA 72	DPWA	$K^-\rho \rightarrow \Lambda(1520)\pi^0$	
0.27 ± 0.03	ARMENTEROS65c	HBC	$K^-\rho \rightarrow \Lambda(1520)\pi^0$	
¹ This rate combines <i>P</i> -wave- and <i>F</i> -wave decays. The CAMERON 77 results for the separate <i>P</i> -wave- and <i>F</i> -wave decays are -0.303 ± 0.010 and -0.037 ± 0.014 . The published signs have been changed here to be in accord with the baryon-first convention.				

$(\Gamma_1\Gamma_7)^{1/2}/\Gamma_{\text{total}}$ in $N\bar{K} \rightarrow \Sigma(1775) \rightarrow \Delta(1232)\bar{K}, D\text{-wave}$				$(\Gamma_1\Gamma_9)^{1/2}/\Gamma$
VALUE	DOCUMENT ID	TECN	COMMENT	
+0.06 ± 0.03	ZHANG 13A	DPWA	Multichannel	

$(\Gamma_1\Gamma_7)^{1/2}/\Gamma_{\text{total}}$ in $N\bar{K} \rightarrow \Sigma(1775) \rightarrow N\bar{K}^*(892), S=1/2$				$(\Gamma_1\Gamma_{10})^{1/2}/\Gamma$
VALUE	DOCUMENT ID	TECN	COMMENT	
+0.04 ± 0.01	ZHANG 13A	DPWA	Multichannel	

$(\Gamma_1\Gamma_7)^{1/2}/\Gamma_{\text{total}}$ in $N\bar{K} \rightarrow \Sigma(1775) \rightarrow N\bar{K}^*(892), S=3/2, D\text{-wave}$				$(\Gamma_1\Gamma_{12})^{1/2}/\Gamma$
VALUE	DOCUMENT ID	TECN	COMMENT	
+0.04 ± 0.01	ZHANG 13A	DPWA	Multichannel	

 $\Sigma(1775)$ REFERENCES

SARANTSEV 19	EPJ A55 180	A.V. Sarantsev et al.	(BONN, PNPI)
KAMANO 15	PR C92 025205	H. Kamano et al.	(ANL, OSAK)
ZHANG 13A	PR C08 035205	H. Zhang et al.	(KSU)
PDG 82	PL 111B 1	M. Roos et al.	(HELS, CIT, CERN)
GOPAL 80	Toronto Conf. 159	G.P. Gopal et al.	(RHEL) IJP
ALSTON... 78	PR D18 182	M. Alston-Garnjost et al.	(LBL, MTHO) IJP
Also	PRL 38 1007	M. Alston-Garnjost et al.	(LBL, MTHO) IJP
CAMERON 78	NP B143 189	W. Cameron et al.	(RHEL, LOIC) IJP
CAMERON 77	NP B131 399	W. Cameron et al.	(RHEL, LOIC) IJP
GOPAL 77	NP B119 362	G.P. Gopal et al.	(LOIC, RHEL) IJP
MARTIN 77	NP B127 349	B.R. Martin, M.K. Pidcock, R.G. Moorhouse	(LOUC+) IJP
Also	NP B126 266	B.R. Martin, M.K. Pidcock	(LOUC)
Also	NP B126 285	B.R. Martin, M.K. Pidcock	(LOUC) IJP
DEBELLEFON 76	NP B109 129	A. de Bellefon, A. Berthon	(CDFE) IJP
BAILLON 75	NP B94 39	P.H. Baillon, P.J. Litchfield	(CERN, RHEL) IJP

Baryon Particle Listings

 $\Sigma(1775)$, $\Sigma(1780)$, $\Sigma(1880)$

VANHORN	75	NP B87 145	A.J. van Horn	(LBL) IJP
Also		NP B87 157	A.J. van Horn	(LBL) IJP
DEVENISH	74B	NP B81 330	R.C.E. Devenish, C.D. Froggatt, B.R. Martin	(DESY+)
KANE	74	LBL-2452	D.F. Kane	(LBL) IJP
PREVOST	74	NP B69 246	J. Prevost <i>et al.</i>	(SACL, CERN, HEID)
BARLETTA	72	NP B40 45	W.A. Barletta	(EFI) IJP
Also		PRL 17 841	S. Fenster <i>et al.</i>	(CHIC, ANL, CERN) IJP
ARMENTEROS	68C	NP B8 216	R. Armenteros <i>et al.</i>	(CERN, HEID, SAFL) I
SIMS	68	PRL 21 1413	W.H. Sims <i>et al.</i>	(FSU, TUFTS, BRAN)
ARMENTEROS	67C	ZPHY 202 486	R. Armenteros <i>et al.</i>	(CERN, HEID, SAFL)
UHLIG	67	PR 155 1448	R.P. Uhlig <i>et al.</i>	(UMD, NRL)
ARMENTEROS	65C	PL 19 338	R. Armenteros <i>et al.</i>	(CERN, HEID, SAFL) IJP
GALTIERI	63	PL 6 296	A. Galtieri, A. Hussain, R. Tripp	(LRL) IJ

 $\Sigma(1780) 3/2^+$

$$I(J^P) = 1(\frac{3}{2}^+) \text{ Status: } *$$

OMITTED FROM SUMMARY TABLE
was $\Sigma(1730)$

 $\Sigma(1780)$ MASS

VALUE (MeV)	DOCUMENT ID	TECN	COMMENT
1730 to 1830 (≈ 1780) OUR ESTIMATE			
1727 \pm 27	ZHANG	13A	DPWA Multichannel
1798 or 1802	¹ MARTIN	77	DPWA $\bar{K}N$ multichannel
1720 \pm 30	² BAILLON	75	IPWA $\bar{K}N \rightarrow \Lambda\pi$
1840 \pm 10	LANGBEIN	72	IPWA $\bar{K}N$ multichannel

¹ The two MARTIN 77 values are from a T-matrix pole and from a Breit-Wigner fit.
² From solution 1 of BAILLON 75; not present in solution 2.

 $\Sigma(1780)$ WIDTH

VALUE (MeV)	DOCUMENT ID	TECN	COMMENT
100 to 300 (≈ 200) OUR ESTIMATE			
276 \pm 87	ZHANG	13A	DPWA Multichannel
93 or 93	¹ MARTIN	77	DPWA $\bar{K}N$ multichannel
120 \pm 30	² BAILLON	75	IPWA $\bar{K}N \rightarrow \Lambda\pi$
120 \pm 10	LANGBEIN	72	IPWA $\bar{K}N$ multichannel

¹ The two MARTIN 77 values are from a T-matrix pole and from a Breit-Wigner fit.
² From solution 1 of BAILLON 75; not present in solution 2.

 $\Sigma(1780)$ DECAY MODES

Mode	Fraction (Γ_i/Γ)
Γ_1 $N\bar{K}$	(2.0 \pm 1.0) %
Γ_2 $\Lambda\pi$	(70 \pm 17) %
Γ_3 $\Sigma\pi$	(12 \pm 6) %

 $\Sigma(1780)$ BRANCHING RATIOS

$\Gamma(N\bar{K})/\Gamma_{\text{total}}$ Γ_1/Γ

VALUE	DOCUMENT ID	TECN	COMMENT
0.02 \pm 0.01	ZHANG	13A	DPWA Multichannel

$\Gamma(\Lambda\pi)/\Gamma_{\text{total}}$ Γ_2/Γ

VALUE	DOCUMENT ID	TECN	COMMENT
0.70 \pm 0.17	ZHANG	13A	DPWA Multichannel

$\Gamma(\Sigma\pi)/\Gamma_{\text{total}}$ Γ_3/Γ

VALUE	DOCUMENT ID	TECN	COMMENT
0.12 \pm 0.06	ZHANG	13A	DPWA Multichannel

 $\Sigma(1780)$ REFERENCES

ZHANG	13A	PR C88 035205	H. Zhang <i>et al.</i>	(KSU)
MARTIN	77	NP B127 349	B.R. Martin, M.K. Pidcock, R.G. Moorhouse	(LOUC+)
BAILLON	75	NP B94 39	P.H. Baillon, P.J. Litchfield	(CERN, RHEL)
LANGBEIN	72	NP B47 477	W. Langbein, F. Wagner	(MPIM)

 $\Sigma(1880) 1/2^+$

$$I(J^P) = 1(\frac{1}{2}^+) \text{ Status: } **$$

OMITTED FROM SUMMARY TABLE

A P_{11} resonance is suggested by several partial-wave analyses, but with wide variations in the mass and other parameters. We list here all claims which lie well above the P_{11} $\Sigma(1770)$.

 $\Sigma(1880)$ POLE POSITION

REAL PART

VALUE (MeV)	DOCUMENT ID	TECN	COMMENT
1776	ZHANG	13A	DPWA Multichannel

• • • We do not use the following data for averages, fits, limits, etc. • • •

-2xIMAGINARY PART

VALUE (MeV)	DOCUMENT ID	TECN	COMMENT
270	ZHANG	13A	DPWA Multichannel

• • • We do not use the following data for averages, fits, limits, etc. • • •

 $\Sigma(1880)$ MASS

VALUE (MeV)	DOCUMENT ID	TECN	COMMENT
1820 to 1940 (≈ 1880) OUR ESTIMATE			
1821 \pm 17	ZHANG	13A	DPWA Multichannel
1826 \pm 20	GOPAL	80	DPWA $\bar{K}N \rightarrow \bar{K}N$
1870 \pm 10	CAMERON	78B	DPWA $K^-p \rightarrow N\bar{K}^*$
1847 or 1863	¹ MARTIN	77	DPWA $\bar{K}N$ multichannel
1960 \pm 30	² BAILLON	75	IPWA $\bar{K}N \rightarrow \Lambda\pi$
1985 \pm 50	VANHORN	75	DPWA $K^-p \rightarrow \Lambda\pi^0$
1898	³ LEA	73	DPWA Multichannel K-matrix
~ 1850	ARMENTEROSTO	70	IPWA $\bar{K}N \rightarrow \bar{K}N$
1950 \pm 50	BARBARO...	70	DPWA $K^-N \rightarrow \Lambda\pi$
1920 \pm 30	LITCHFIELD	70	DPWA $K^-N \rightarrow \Lambda\pi$
1850	BAILEY	69	DPWA $\bar{K}N \rightarrow \bar{K}N$
1882 \pm 40	SMART	68	DPWA $K^-N \rightarrow \Lambda\pi$

 $\Sigma(1880)$ WIDTH

VALUE (MeV)	DOCUMENT ID	TECN	COMMENT
100 to 300 (≈ 200) OUR ESTIMATE			
300 \pm 59	ZHANG	13A	DPWA Multichannel
86 \pm 15	GOPAL	80	DPWA $\bar{K}N \rightarrow \bar{K}N$
80 \pm 10	CAMERON	78B	DPWA $K^-p \rightarrow N\bar{K}^*$
216 or 220	¹ MARTIN	77	DPWA $\bar{K}N$ multichannel
260 \pm 40	² BAILLON	75	IPWA $\bar{K}N \rightarrow \Lambda\pi$
220 \pm 140	VANHORN	75	DPWA $K^-p \rightarrow \Lambda\pi^0$
222	³ LEA	73	DPWA Multichannel K-matrix
~ 30	ARMENTEROSTO	70	IPWA $\bar{K}N \rightarrow \bar{K}N$
200 \pm 50	BARBARO...	70	DPWA $K^-N \rightarrow \Lambda\pi$
170 \pm 40	LITCHFIELD	70	DPWA $K^-N \rightarrow \Lambda\pi$
200	BAILEY	69	DPWA $\bar{K}N \rightarrow \bar{K}N$
222 \pm 150	SMART	68	DPWA $K^-N \rightarrow \Lambda\pi$

 $\Sigma(1880)$ DECAY MODES

Mode	Fraction (Γ_i/Γ)
Γ_1 $N\bar{K}$	0.10 to 0.30 (≈ 0.20)
Γ_2 $\Lambda\pi$	
Γ_3 $\Sigma\pi$	
Γ_4 $\Lambda(1520)\pi$, D-wave	(2.0 \pm 1.0) %
Γ_5 $N\bar{K}^*(892)$, S=1/2, P-wave	
Γ_6 $N\bar{K}^*(892)$, S=3/2, P-wave	
Γ_7 $\Delta(1232)\bar{K}$, P-wave	(39 \pm 8) %

 $\Sigma(1880)$ BRANCHING RATIOS

See "Sign conventions for resonance couplings" in the Note on Λ and Σ Resonances.

$\Gamma(N\bar{K})/\Gamma_{\text{total}}$ Γ_1/Γ

VALUE	DOCUMENT ID	TECN	COMMENT
0.10 to 0.30 (≈ 0.20) OUR ESTIMATE			
0.10 \pm 0.03	ZHANG	13A	DPWA Multichannel
0.06 \pm 0.02	GOPAL	80	DPWA $\bar{K}N \rightarrow \bar{K}N$
0.27 or 0.27	¹ MARTIN	77	DPWA $\bar{K}N$ multichannel
0.31	³ LEA	73	DPWA Multichannel K-matrix
0.20	ARMENTEROSTO	70	IPWA $\bar{K}N \rightarrow \bar{K}N$
0.22	BAILEY	69	DPWA $\bar{K}N \rightarrow \bar{K}N$

$(\Gamma_1\Gamma_2)^{1/2}/\Gamma_{\text{total}}$ in $N\bar{K} \rightarrow \Sigma(1880) \rightarrow \Lambda\pi$

$(\Gamma_1\Gamma_2)^{1/2}/\Gamma$

VALUE	DOCUMENT ID	TECN	COMMENT
-0.24 or -0.24	¹ MARTIN	77	DPWA $\bar{K}N$ multichannel
-0.12 \pm 0.02	² BAILLON	75	IPWA $\bar{K}N \rightarrow \Lambda\pi$
+0.05 \pm 0.07	VANHORN	75	DPWA $K^-p \rightarrow \Lambda\pi^0$
-0.169 \pm 0.119	DEVENISH	74B	Fixed-t dispersion rel.
-0.30	³ LEA	73	DPWA Multichannel K-matrix
-0.09 \pm 0.04	BARBARO...	70	DPWA $K^-N \rightarrow \Lambda\pi$
-0.14 \pm 0.03	LITCHFIELD	70	DPWA $K^-N \rightarrow \Lambda\pi$
-0.11 \pm 0.03	SMART	68	DPWA $K^-N \rightarrow \Lambda\pi$

$(\Gamma_1\Gamma_3)^{1/2}/\Gamma_{\text{total}}$ in $N\bar{K} \rightarrow \Sigma(1880) \rightarrow \Sigma\pi$

$(\Gamma_1\Gamma_3)^{1/2}/\Gamma$

VALUE	DOCUMENT ID	TECN	COMMENT
+0.30 or +0.29	¹ MARTIN	77	DPWA $\bar{K}N$ multichannel
not seen	³ LEA	73	DPWA Multichannel K-matrix

See key on page 1171

Baryon Particle Listings
 $\Sigma(1880), \Sigma(1900)$

$\Gamma(\Lambda(1520)\pi, D\text{-wave})/\Gamma_{\text{total}}$		Γ_4/Γ	
VALUE	DOCUMENT ID	TECN	COMMENT
0.02 ± 0.01	ZHANG	13A	DPWA Multichannel

$(\Gamma_1/\Gamma_7)^{1/2}/\Gamma_{\text{total}}$ in $N\bar{K} \rightarrow \Sigma(1880) \rightarrow N\bar{K}^*(892), S=1/2, P\text{-wave} (\Gamma_1/\Gamma_5)^{1/2}/\Gamma$			
VALUE	DOCUMENT ID	TECN	COMMENT
-0.05 ± 0.03	4 CAMERON	78B	DPWA $K^- p \rightarrow N\bar{K}^*$

$(\Gamma_1/\Gamma_7)^{1/2}/\Gamma_{\text{total}}$ in $N\bar{K} \rightarrow \Sigma(1880) \rightarrow N\bar{K}^*(892), S=3/2, P\text{-wave} (\Gamma_1/\Gamma_6)^{1/2}/\Gamma$			
VALUE	DOCUMENT ID	TECN	COMMENT
$+0.11 \pm 0.03$	CAMERON	78B	DPWA $K^- p \rightarrow N\bar{K}^*$

$\Gamma(\Delta(1232)\bar{K}, P\text{-wave})/\Gamma_{\text{total}}$		Γ_7/Γ	
VALUE	DOCUMENT ID	TECN	COMMENT
0.39 ± 0.08	ZHANG	13A	DPWA Multichannel

 $\Sigma(1880)$ FOOTNOTES

- The two MARTIN 77 values are from a T-matrix pole and from a Breit-Wigner fit.
- From solution 1 of BAILLON 75; not present in solution 2.
- Only unconstrained states from table 1 of LEA 73 are listed.
- The published sign has been changed to be in accord with the baryon-first convention.

 $\Sigma(1880)$ REFERENCES

ZHANG	13A	PR C88 035205	H. Zhang et al.	(KSU)
GOPAL	80	Toronto Conf. 159	G.P. Gopal	(RHEL) IJP
CAMERON	78B	NP B146 327	W. Cameron et al.	(RHEL, LOIC) IJP
MARTIN	77	NP B127 349	B.R. Martin, M.K. Pidcock, R.G. Moorhouse	(LOUC+) IJP
		Also NP B126 266	B.R. Martin, M.K. Pidcock	(LOUC) IJP
		Also NP B126 285	B.R. Martin, M.K. Pidcock	(LOUC) IJP
BAILLON	75	NP B94 39	P.H. Baillon, P.J. Litchfield	(CERN, RHEL) IJP
VANHORN	75	NP B87 145	A.J. van Horn	(LBL) IJP
		Also NP B87 157	A.J. van Horn	(LBL) IJP
DEVENISH	74B	NP B81 330	R.C.E. Devenish, C.D. Froggatt, B.R. Martin	(DESY+) IJP
LEA	73	NP B56 77	A.T. Lea et al.	(RHEL, LOUC, GLAS, AARH) IJP
ARMENTEROS	70	Duke Conf. 123	R. Armenteros et al.	(CERN, HEID, SACL) IJP
		Hyperon Resonances, 1970		
BARBARO...	70	Duke Conf. 173	A. Barbaro-Galiteri	(LRL) IJP
		Hyperon Resonances, 1970		
LITCHFIELD	70	NP B22 269	P.J. Litchfield	(RHEL) IJP
BAILEY	69	Thesis UCRL 50617	J.M. Bailey	(LLL) IJP
SMART	68	PR 169 1330	W.M. Smart	(LRL) IJP

 $\Sigma(1900) 1/2^-$

$$I(J^P) = 1(\frac{1}{2}^-) \text{ Status: **}$$

OMITTED FROM SUMMARY TABLE

 $\Sigma(1900)$ POLE POSITION

REAL PART			
VALUE	DOCUMENT ID	TECN	COMMENT
1936 ± 10	SARANTSEV	19	DPWA $\bar{K}N$ multichannel

-2xIMAGINARY PART			
VALUE	DOCUMENT ID	TECN	COMMENT
150 ± 25	SARANTSEV	19	DPWA $\bar{K}N$ multichannel

 $\Sigma(1900)$ POLE RESIDUESThe normalized residue is the residue divided by $\Gamma_{\text{pole}}/2$.

Normalized residue in $N\bar{K} \rightarrow \Sigma(1900) \rightarrow N\bar{K}$			
MODULUS	PHASE ($^\circ$)	DOCUMENT ID	TECN
0.45 ± 0.09	90 ± 25	SARANTSEV	19
		DPWA	$\bar{K}N$ multichannel

Normalized residue in $N\bar{K} \rightarrow \Sigma(1900) \rightarrow \Sigma\pi$			
MODULUS	PHASE ($^\circ$)	DOCUMENT ID	TECN
0.38 ± 0.08	95 ± 20	SARANTSEV	19
		DPWA	$\bar{K}N$ multichannel

Normalized residue in $N\bar{K} \rightarrow \Sigma(1900) \rightarrow \Sigma\eta$			
MODULUS	PHASE ($^\circ$)	DOCUMENT ID	TECN
0.03 ± 0.01	20 ± 20	SARANTSEV	19
		DPWA	$\bar{K}N$ multichannel

Normalized residue in $N\bar{K} \rightarrow \Sigma(1900) \rightarrow \Lambda\pi$			
MODULUS	PHASE ($^\circ$)	DOCUMENT ID	TECN
0.14 ± 0.05	-160 ± 50	SARANTSEV	19
		DPWA	$\bar{K}N$ multichannel

Normalized residue in $N\bar{K} \rightarrow \Sigma(1900) \rightarrow \Xi K$			
MODULUS	PHASE ($^\circ$)	DOCUMENT ID	TECN
0.08 ± 0.05	75 ± 25	SARANTSEV	19
		DPWA	$\bar{K}N$ multichannel

Normalized residue in $N\bar{K} \rightarrow \Sigma(1900) \rightarrow \Sigma(1385)\pi$			
MODULUS	PHASE ($^\circ$)	DOCUMENT ID	TECN
0.16 ± 0.05	40 ± 30	SARANTSEV	19
		DPWA	$\bar{K}N$ multichannel

Normalized residue in $N\bar{K} \rightarrow \Sigma(1900) \rightarrow \Lambda(1520)\pi$			
MODULUS	PHASE ($^\circ$)	DOCUMENT ID	TECN
0.04 ± 0.02	-25 ± 40	SARANTSEV	19
		DPWA	$\bar{K}N$ multichannel

Normalized residue in $N\bar{K} \rightarrow \Sigma(1900) \rightarrow \Delta\bar{K}$			
MODULUS	PHASE ($^\circ$)	DOCUMENT ID	TECN
0.11 ± 0.04	60 ± 30	SARANTSEV	19
		DPWA	$\bar{K}N$ multichannel

Normalized residue in $N\bar{K} \rightarrow \Sigma(1900) \rightarrow N\bar{K}^*(892), S=1/2, S\text{-wave}$			
MODULUS	PHASE ($^\circ$)	DOCUMENT ID	TECN
0.17 ± 0.06	50 ± 50	SARANTSEV	19
		DPWA	$\bar{K}N$ multichannel

Normalized residue in $N\bar{K} \rightarrow \Sigma(1900) \rightarrow N\bar{K}^*(892), S=3/2, D\text{-wave}$			
MODULUS	PHASE ($^\circ$)	DOCUMENT ID	TECN
0.05 ± 0.04		SARANTSEV	19
		DPWA	$\bar{K}N$ multichannel

 $\Sigma(1900)$ MASS

VALUE (MeV)	DOCUMENT ID	TECN	COMMENT
1900 to 1950 (≈ 1925) OUR ESTIMATE			
1938 ± 12	SARANTSEV	19	DPWA $\bar{K}N$ multichannel
1900 ± 21	ZHANG	13A	DPWA $\bar{K}N$ multichannel
1944 ± 15	GOPAL	80	DPWA $\bar{K}N \rightarrow \bar{K}N$
$1755 \text{ or } 1834$	1 MARTIN	77	DPWA $\bar{K}N$ multichannel
2004 ± 40	VANHORN	75	DPWA $K^- p \rightarrow \Lambda\pi^0$
• • • We do not use the following data for averages, fits, limits, etc. • • •			
1955 ± 15	GOPAL	77	DPWA $\bar{K}N$ multichannel

1 The two MARTIN 77 values are from a T-matrix pole and from a Breit-Wigner fit.

 $\Sigma(1900)$ WIDTH

VALUE (MeV)	DOCUMENT ID	TECN	COMMENT
140 to 190 (≈ 165) OUR ESTIMATE			
155 ± 30	SARANTSEV	19	DPWA $\bar{K}N$ multichannel
191 ± 47	ZHANG	13A	DPWA $\bar{K}N$ multichannel
215 ± 25	GOPAL	80	DPWA $\bar{K}N \rightarrow \bar{K}N$
$413 \text{ or } 450$	1 MARTIN	77	DPWA $\bar{K}N$ multichannel
116 ± 40	VANHORN	75	DPWA $K^- p \rightarrow \Lambda\pi^0$
• • • We do not use the following data for averages, fits, limits, etc. • • •			
170 ± 40	GOPAL	77	DPWA $\bar{K}N$ multichannel

1 The two MARTIN 77 values are from a T-matrix pole and from a Breit-Wigner fit.

 $\Sigma(1900)$ DECAY MODES

Mode	Fraction (Γ_i/Γ)
$\Gamma_1 N\bar{K}$	0.40 to 0.70 (≈ 0.55)
$\Gamma_2 \Sigma\pi$	0.10 to 0.40 (≈ 0.25)
$\Gamma_3 \Sigma\eta$	(1.0 \pm 1.0) %
$\Gamma_4 \Lambda\pi$	(6.0 \pm 2.0) %
$\Gamma_5 \Xi K$	(3.0 \pm 2.0) %
$\Gamma_6 \Sigma(1385)\pi$	(7.0 \pm 3.0) %
$\Gamma_7 \Lambda(1520)\pi$	
$\Gamma_8 \Delta\bar{K}$	(2.5 \pm 1.0) %
$\Gamma_9 N\bar{K}^*(892), S=1/2, S\text{-wave}$	(7.0 \pm 3.0) %
$\Gamma_{10} N\bar{K}^*(892), S=3/2, D\text{-wave}$	

 $\Sigma(1900)$ BRANCHING RATIOS

$\Gamma(N\bar{K})/\Gamma_{\text{total}}$		Γ_1/Γ	
VALUE	DOCUMENT ID	TECN	COMMENT
0.40 to 0.70 (≈ 0.55) OUR ESTIMATE			
0.45 ± 0.09	SARANTSEV	19	DPWA $\bar{K}N$ multichannel
0.67 ± 0.17	ZHANG	13A	DPWA $\bar{K}N$ multichannel

$\Gamma(\Sigma\pi)/\Gamma_{\text{total}}$		Γ_2/Γ	
VALUE	DOCUMENT ID	TECN	COMMENT
0.10 to 0.40 (≈ 0.25) OUR ESTIMATE			
0.33 ± 0.07	SARANTSEV	19	DPWA $\bar{K}N$ multichannel
0.10 ± 0.05	ZHANG	13A	DPWA $\bar{K}N$ multichannel

$\Gamma(\Sigma\eta)/\Gamma_{\text{total}}$		Γ_3/Γ	
VALUE	DOCUMENT ID	TECN	COMMENT
0.01 ± 0.01	SARANTSEV	19	DPWA $\bar{K}N$ multichannel

$\Gamma(\Lambda\pi)/\Gamma_{\text{total}}$		Γ_4/Γ	
VALUE	DOCUMENT ID	TECN	COMMENT
0.06 ± 0.02	SARANTSEV	19	DPWA $\bar{K}N$ multichannel

$\Gamma(\Xi K)/\Gamma_{\text{total}}$		Γ_5/Γ	
VALUE	DOCUMENT ID	TECN	COMMENT
0.03 ± 0.02	SARANTSEV	19	DPWA $\bar{K}N$ multichannel

$\Gamma(\Sigma(1385)\pi)/\Gamma_{\text{total}}$		Γ_6/Γ	
VALUE	DOCUMENT ID	TECN	COMMENT
0.07 ± 0.03	SARANTSEV	19	DPWA $\bar{K}N$ multichannel

Baryon Particle Listings

 $\Sigma(1900)$, $\Sigma(1910)$

$\Gamma(\Lambda(1520)\pi)/\Gamma_{\text{total}}$	DOCUMENT ID	TECN	COMMENT	Γ_7/Γ
VALUE				
<0.01	SARANTSEV	19	DPWA $\bar{K}N$ multichannel	

$\Gamma(\Delta\bar{K})/\Gamma_{\text{total}}$	DOCUMENT ID	TECN	COMMENT	Γ_8/Γ
VALUE				
0.025 ± 0.010	SARANTSEV	19	DPWA $\bar{K}N$ multichannel	

$\Gamma(N\bar{K}^*(892), S=1/2, S\text{-wave})/\Gamma_{\text{total}}$	DOCUMENT ID	TECN	COMMENT	Γ_9/Γ
VALUE				
0.07 ± 0.03	SARANTSEV	19	DPWA $\bar{K}N$ multichannel	

$\Gamma(N\bar{K}^*(892), S=3/2, D\text{-wave})/\Gamma_{\text{total}}$	DOCUMENT ID	TECN	COMMENT	Γ_{10}/Γ
VALUE				
<0.01	SARANTSEV	19	DPWA $\bar{K}N$ multichannel	

 $\Sigma(1900)$ REFERENCES

SARANTSEV	19	EPJ A55 180	A.V. Sarantsev et al.	(BONN, PNPI)
ZHANG	13A	PR C88 035205	H. Zhang et al.	(KSU)
GOPAL	80	Toronto Conf. 159	G.P. Gopal	(RHEL)
GOPAL	77	NP B119 362	G.P. Gopal et al.	(LOIC, RHEL)
MARTIN	77	NP B127 349	B.R. Martin, M.K. Pldcock, R.G. Moorhouse	(LOUC+)
VANHORN	75	NP B87 145	A.J. van Horn	(LBL)

$$\Sigma(1910) 3/2^- \quad I(J^P) = 1(\frac{3}{2}^-) \text{ Status: } ***$$

was $\Sigma(1940)$

For results published before 1974 (they are now obsolete), see our 1982 edition Physics Letters **111B** 1 (1982).

Not all analyses require this state. It is not required by the GOYAL 77 analysis of $K^-n \rightarrow (\Sigma\pi)^-$ nor by the GOPAL 80 analysis of $K^-n \rightarrow K^-n$. See also HEMINGWAY 75.

 $\Sigma(1910)$ POLE RESIDUES

The normalized residue is the residue divided by $\Gamma_{\text{pole}}/2$.

Normalized residue in $N\bar{K} \rightarrow \Sigma(1910) \rightarrow N\bar{K}$	DOCUMENT ID	TECN	COMMENT
MODULUS			
0.03 ± 0.02	SARANTSEV	19	DPWA $\bar{K}N$ multichannel
PHASE ($^\circ$)			
-95 ± 60			

Normalized residue in $N\bar{K} \rightarrow \Sigma(1910) \rightarrow \Sigma\pi$	DOCUMENT ID	TECN	COMMENT
MODULUS			
0.16 ± 0.04	SARANTSEV	19	DPWA $\bar{K}N$ multichannel
PHASE ($^\circ$)			
-160 ± 15			

Normalized residue in $N\bar{K} \rightarrow \Sigma(1910) \rightarrow \Lambda\pi$	DOCUMENT ID	TECN	COMMENT
MODULUS			
0.04 ± 0.03	SARANTSEV	19	DPWA $\bar{K}N$ multichannel
PHASE ($^\circ$)			
25 ± 25			

Normalized residue in $N\bar{K} \rightarrow \Sigma(1910) \rightarrow \Xi\pi$	DOCUMENT ID	TECN	COMMENT
MODULUS			
0.01 ± 0.01	SARANTSEV	19	DPWA $\bar{K}N$ multichannel
PHASE ($^\circ$)			

Normalized residue in $N\bar{K} \rightarrow \Sigma(1910) \rightarrow \Lambda(1520)\pi, P\text{-wave}$	DOCUMENT ID	TECN	COMMENT
MODULUS			
0.01 ± 0.01	SARANTSEV	19	DPWA $\bar{K}N$ multichannel
PHASE ($^\circ$)			

Normalized residue in $N\bar{K} \rightarrow \Sigma(1910) \rightarrow \Lambda(1520)\pi, F\text{-wave}$	DOCUMENT ID	TECN	COMMENT
MODULUS			
~ 0	SARANTSEV	19	DPWA $\bar{K}N$ multichannel
PHASE ($^\circ$)			

Normalized residue in $N\bar{K} \rightarrow \Sigma(1910) \rightarrow \Delta\bar{K}, S\text{-wave}$	DOCUMENT ID	TECN	COMMENT
MODULUS			
0.03 ± 0.01	SARANTSEV	19	DPWA $\bar{K}N$ multichannel
PHASE ($^\circ$)			
120 ± 20			

Normalized residue in $N\bar{K} \rightarrow \Sigma(1910) \rightarrow N\bar{K}^*(892), S=3/2, S\text{-wave}$	DOCUMENT ID	TECN	COMMENT
MODULUS			
0.03 ± 0.02	SARANTSEV	19	DPWA $\bar{K}N$ multichannel
PHASE ($^\circ$)			
20 ± 35			

Normalized residue in $N\bar{K} \rightarrow \Sigma(1910) \rightarrow N\bar{K}^*(892), S=1/2, D\text{-wave}$	DOCUMENT ID	TECN	COMMENT
MODULUS			
0.02 ± 0.01	SARANTSEV	19	DPWA $\bar{K}N$ multichannel
PHASE ($^\circ$)			

Normalized residue in $N\bar{K} \rightarrow \Sigma(1910) \rightarrow N\bar{K}^*(892), S=3/2, D\text{-wave}$	DOCUMENT ID	TECN	COMMENT
MODULUS			
0.01 ± 0.01	SARANTSEV	19	DPWA $\bar{K}N$ multichannel
PHASE ($^\circ$)			

 $\Sigma(1910)$ MASS

VALUE (MeV)	DOCUMENT ID	TECN	COMMENT
1870 to 1950 (≈ 1910) OUR ESTIMATE			
1878 ± 12	SARANTSEV	19	DPWA $\bar{K}N$ multichannel
1920 ± 50	GOPAL	77	DPWA $\bar{K}N$ multichannel

1950 ± 30	BAILLON	75	IPWA $\bar{K}N \rightarrow \Lambda\pi$
1949 ± 40	VANHORN	75	DPWA $K^-p \rightarrow \Lambda\pi^0$
1935 ± 80	KANE	74	DPWA $K^-p \rightarrow \Sigma\pi$
1940 ± 20	LITCHFIELD	74B	DPWA $K^-p \rightarrow \Lambda(1520)\pi^0$
1950 ± 20	LITCHFIELD	74C	DPWA $K^-p \rightarrow \Delta(1232)\bar{K}$
• • • We do not use the following data for averages, fits, limits, etc. • • •			
1886 or 1893	¹ MARTIN	77	DPWA $\bar{K}N$ multichannel
1940	DEBELLEFON	76	IPWA $K^-p \rightarrow \Lambda\pi^0, F_{17}$ wave

 $\Sigma(1910)$ WIDTH

VALUE (MeV)	DOCUMENT ID	TECN	COMMENT
150 to 300 (≈ 220) OUR ESTIMATE			
224 ± 25	SARANTSEV	19	DPWA $\bar{K}N$ multichannel
170 ± 25	CAMERON	78B	DPWA $K^-p \rightarrow N\bar{K}^*$
300 ± 80	GOPAL	77	DPWA $\bar{K}N$ multichannel
150 ± 75	BAILLON	75	IPWA $\bar{K}N \rightarrow \Lambda\pi$
160 ± 70	VANHORN	75	DPWA $K^-p \rightarrow \Lambda\pi^0$
160 ± 40			
330 ± 80	KANE	74	DPWA $K^-p \rightarrow \Sigma\pi$
60 ± 20	LITCHFIELD	74B	DPWA $K^-p \rightarrow \Lambda(1520)\pi^0$
70 ± 30	LITCHFIELD	74C	DPWA $K^-p \rightarrow \Delta(1232)\bar{K}$
-20			
• • • We do not use the following data for averages, fits, limits, etc. • • •			
157 or 159	¹ MARTIN	77	DPWA $\bar{K}N$ multichannel

 $\Sigma(1910)$ DECAY MODES

Mode	Fraction (Γ_i/Γ)
Γ_1 $N\bar{K}$	0.01 to 0.05 (≈ 0.02)
Γ_2 $\Lambda\pi$	(6 \pm 4) %
Γ_3 $\Sigma\pi$	(86 \pm 21) %
Γ_4 ΞK	
Γ_5 $\Sigma(1385)\pi$	seen
Γ_6 $\Sigma(1385)\pi, S\text{-wave}$	
Γ_7 $\Lambda(1520)\pi$	seen
Γ_8 $\Lambda(1520)\pi, P\text{-wave}$	
Γ_9 $\Lambda(1520)\pi, F\text{-wave}$	
Γ_{10} $\Delta(1232)\bar{K}$	(3.0 \pm 1.0) %
Γ_{11} $\Delta(1232)\bar{K}, S\text{-wave}$	
Γ_{12} $\Delta(1232)\bar{K}, D\text{-wave}$	
Γ_{13} $N\bar{K}^*(892)$	seen
Γ_{14} $N\bar{K}^*(892), S=3/2, S\text{-wave}$	
Γ_{15} $N\bar{K}^*(892), S=1/2, D\text{-wave}$	(1.0 \pm 1.0) %
Γ_{16} $N\bar{K}^*(892), S=3/2, D\text{-wave}$	

 $\Sigma(1910)$ BRANCHING RATIOS

See "Sign conventions for resonance couplings" in the Note on Λ and Σ Resonances.

$\Gamma(N\bar{K})/\Gamma_{\text{total}}$	DOCUMENT ID	TECN	COMMENT	Γ_1/Γ
VALUE				
0.01 to 0.05 (≈ 0.02) OUR ESTIMATE				
0.03 ± 0.02	SARANTSEV	19	DPWA $\bar{K}N$ multichannel	
<0.04	GOPAL	77	DPWA $\bar{K}N$ multichannel	
0.14 or 0.13	¹ MARTIN	77	DPWA $\bar{K}N$ multichannel	

$\Gamma(\Lambda\pi)/\Gamma_{\text{total}}$	DOCUMENT ID	TECN	COMMENT	Γ_2/Γ
VALUE				
0.06 \pm 0.04	SARANTSEV	19	DPWA $\bar{K}N$ multichannel	

$\Gamma(\Sigma\pi)/\Gamma_{\text{total}}$	DOCUMENT ID	TECN	COMMENT	Γ_3/Γ
VALUE				
0.86 \pm 0.21	SARANTSEV	19	DPWA $\bar{K}N$ multichannel	

$\Gamma(\Xi K)/\Gamma_{\text{total}}$	DOCUMENT ID	TECN	COMMENT	Γ_4/Γ
VALUE				
~ 0	SARANTSEV	19	DPWA $\bar{K}N$ multichannel	

$\Gamma(\Lambda(1520)\pi, P\text{-wave})/\Gamma_{\text{total}}$	DOCUMENT ID	TECN	COMMENT	Γ_8/Γ
VALUE				
~ 0	SARANTSEV	19	DPWA $\bar{K}N$ multichannel	

$\Gamma(\Lambda(1520)\pi, F\text{-wave})/\Gamma_{\text{total}}$	DOCUMENT ID	TECN	COMMENT	Γ_9/Γ
VALUE				
~ 0	SARANTSEV	19	DPWA $\bar{K}N$ multichannel	

$\Gamma(\Delta(1232)\bar{K})/\Gamma_{\text{total}}$	DOCUMENT ID	TECN	COMMENT	Γ_{10}/Γ
VALUE				
0.03 \pm 0.01	SARANTSEV	19	DPWA $\bar{K}N$ multichannel	

See key on page 1171

Baryon Particle Listings
 $\Sigma(1910), \Sigma(1915)$

$\Gamma(N\bar{K}^*(892))/\Gamma_{\text{total}}$	DOCUMENT ID	TECN	COMMENT	Γ_{13}/Γ
0.03 ± 0.02	SARANTSEV	19	DPWA $\bar{K}N$ multichannel	

$\Gamma(N\bar{K}^*(892), S=1/2, D\text{-wave})/\Gamma_{\text{total}}$	DOCUMENT ID	TECN	COMMENT	Γ_{15}/Γ
0.01 ± 0.01	SARANTSEV	19	DPWA $\bar{K}N$ multichannel	

$\Gamma(N\bar{K}^*(892), S=3/2, D\text{-wave})/\Gamma_{\text{total}}$	DOCUMENT ID	TECN	COMMENT	Γ_{16}/Γ
~ 0	SARANTSEV	19	DPWA $\bar{K}N$ multichannel	

$(\Gamma_1 \Gamma_f)^{1/2}/\Gamma_{\text{total}}$ in $N\bar{K} \rightarrow \Sigma(1910) \rightarrow \Lambda\pi$	DOCUMENT ID	TECN	COMMENT	$(\Gamma_1 \Gamma_2)^{1/2}/\Gamma$
-0.06 ± 0.03	GOPAL	77	DPWA $\bar{K}N$ multichannel	
-0.04 ± 0.02	BAILLON	75	IPWA $\bar{K}N \rightarrow \Lambda\pi$	
-0.05 ± 0.03 -0.02	VANHORN	75	DPWA $K^-p \rightarrow \Lambda\pi^0$	
-0.153 ± 0.070	DEVENISH	74B	Fixed- t dispersion rel.	
••• We do not use the following data for averages, fits, limits, etc. •••				
-0.15 or -0.14	¹ MARTIN	77	DPWA $\bar{K}N$ multichannel	

$(\Gamma_1 \Gamma_f)^{1/2}/\Gamma_{\text{total}}$ in $N\bar{K} \rightarrow \Sigma(1910) \rightarrow \Sigma\pi$	DOCUMENT ID	TECN	COMMENT	$(\Gamma_1 \Gamma_3)^{1/2}/\Gamma$
-0.08 ± 0.04	GOPAL	77	DPWA $\bar{K}N$ multichannel	
-0.14 ± 0.04	KANE	74	DPWA $K^-p \rightarrow \Sigma\pi$	
••• We do not use the following data for averages, fits, limits, etc. •••				
+0.16 or +0.16	¹ MARTIN	77	DPWA $\bar{K}N$ multichannel	

$(\Gamma_1 \Gamma_f)^{1/2}/\Gamma_{\text{total}}$ in $N\bar{K} \rightarrow \Sigma(1910) \rightarrow \Sigma(1385)\pi$	DOCUMENT ID	TECN	COMMENT	$(\Gamma_1 \Gamma_5)^{1/2}/\Gamma$
+0.066 ± 0.025	² CAMERON	78	DPWA $K^-p \rightarrow \Sigma(1385)\pi$	

$(\Gamma_1 \Gamma_f)^{1/2}/\Gamma_{\text{total}}$ in $N\bar{K} \rightarrow \Sigma(1910) \rightarrow \Lambda(1520)\pi, P\text{-wave}$	DOCUMENT ID	TECN	COMMENT	$(\Gamma_1 \Gamma_8)^{1/2}/\Gamma$
< 0.03	CAMERON	77	DPWA $K^-p \rightarrow \Lambda(1520)\pi^0$	
-0.11 ± 0.04	LITCHFIELD	74B	DPWA $K^-p \rightarrow \Lambda(1520)\pi^0$	

$(\Gamma_1 \Gamma_f)^{1/2}/\Gamma_{\text{total}}$ in $N\bar{K} \rightarrow \Sigma(1910) \rightarrow \Lambda(1520)\pi, F\text{-wave}$	DOCUMENT ID	TECN	COMMENT	$(\Gamma_1 \Gamma_9)^{1/2}/\Gamma$
0.062 ± 0.021	CAMERON	77	DPWA $K^-p \rightarrow \Lambda(1520)\pi^0$	
-0.08 ± 0.04	LITCHFIELD	74B	DPWA $K^-p \rightarrow \Lambda(1520)\pi^0$	

$(\Gamma_1 \Gamma_f)^{1/2}/\Gamma_{\text{total}}$ in $N\bar{K} \rightarrow \Sigma(1910) \rightarrow \Delta(1232)\bar{K}, S\text{-wave}$	DOCUMENT ID	TECN	COMMENT	$(\Gamma_1 \Gamma_{11})^{1/2}/\Gamma$
-0.16 ± 0.05	LITCHFIELD	74C	DPWA $K^-p \rightarrow \Delta(1232)\bar{K}$	

$(\Gamma_1 \Gamma_f)^{1/2}/\Gamma_{\text{total}}$ in $N\bar{K} \rightarrow \Sigma(1910) \rightarrow \Delta(1232)\bar{K}, D\text{-wave}$	DOCUMENT ID	TECN	COMMENT	$(\Gamma_1 \Gamma_{12})^{1/2}/\Gamma$
-0.14 ± 0.05	LITCHFIELD	74C	DPWA $K^-p \rightarrow \Delta(1232)\bar{K}$	

$(\Gamma_1 \Gamma_f)^{1/2}/\Gamma_{\text{total}}$ in $N\bar{K} \rightarrow \Sigma(1910) \rightarrow N\bar{K}^*(892)$	DOCUMENT ID	TECN	COMMENT	$(\Gamma_1 \Gamma_{13})^{1/2}/\Gamma$
-0.09 ± 0.02	³ CAMERON	78B	DPWA $K^-p \rightarrow N\bar{K}^*$	

 $\Sigma(1910)$ FOOTNOTES

- ¹ The two MARTIN 77 values are from a T-matrix pole and from a Breit-Wigner fit.
² The published sign has been changed to be in accord with the baryon-first convention.
³ Upper limits on the D_1 and D_3 waves are each 0.03.

 $\Sigma(1910)$ REFERENCES

SARANTSEV 19	EPJ A55 180	A.V. Sarantsev et al.	(BONN, PNPI)
PDG 82	PL 111B 1	M. Roos et al.	(HELS, CIT, CERN)
GOPAL 80	Toronto Conf. 159	G.P. Gopal	(RHEL)
CAMERON 78	NP B143 189	W. Cameron et al.	(RHEL, LOIC) IJP
CAMERON 78B	NP B146 327	W. Cameron et al.	(RHEL, LOIC) IJP
CAMERON 77	NP B131 399	W. Cameron et al.	(RHEL, LOIC) IJP
GOPAL 77	NP B119 362	G.P. Gopal et al.	(LOIC, RHEL) IJP
GOYAL 77	PR D16 2746	D.P. Goyal, A.V. Sodhi	(DELH)
MARTIN 77	NP B127 349	B.R. Martin, M.K. Pidcock, R.G. Moorhouse	(LOUC+) IJP
Also	NP B126 266	B.R. Martin, M.K. Pidcock	(LOUC)
Also	NP B126 285	B.R. Martin, M.K. Pidcock	(LOUC) IJP
DEBELLEFON 76	NP B109 129	A. de Bellefon, A. Berthon	(CDEF) IJP
BAILLON 75	NP B94 39	P.H. Baillon, P.J. Litchfield	(CERN, RHEL) IJP
HEMINGWAY 75	NP B91 12	R.J. Hemingway et al.	(CERN, HEIDH, MPIM) IJP
VANHORN 75	NP B87 145	A.J. van Horn	(LBL) IJP
Also	NP B87 157	A.J. van Horn	(LBL) IJP
DEVENISH 74B	NP B81 330	R.C.E. Devenish, C.D. Froggatt, B.R. Martin	(DESY+) IJP
KANE 74	LBL-2452	D.F. Kane	(LBL) IJP
LITCHFIELD 74B	NP B74 19	P.J. Litchfield et al.	(CERN, HEIDH) IJP
LITCHFIELD 74C	NP B74 39	P.J. Litchfield et al.	(CERN, HEIDH) IJP

 $\Sigma(1915) 5/2^+$ $I(J^P) = 1(\frac{5}{2}^+)$ Status: ***

Discovered by COOL 66. For results published before 1974 (they are now obsolete), see our 1982 edition Physics Letters **111B** 1 (1982).

This entry only includes results from partial-wave analyses. Parameters of peaks seen in cross sections and invariant-mass distributions in this region used to be listed in a separate entry immediately following. They may be found in our 1986 edition Physics Letters **170B** 1 (1986).

 $\Sigma(1915)$ POLE POSITION

REAL PART

VALUE (MeV)	DOCUMENT ID	TECN	COMMENT
1885 to 1915 (≈ 1900) OUR ESTIMATE			
1908 ± 7	SARANTSEV	19	DPWA $\bar{K}N$ multichannel
1890 ± ³ / ₂	¹ KAMANO	15	DPWA $\bar{K}N$ multichannel
••• We do not use the following data for averages, fits, limits, etc. •••			
1897	ZHANG	13A	DPWA $\bar{K}N$ multichannel
¹ From the preferred solution A in KAMANO 15.			

-2xIMAGINARY PART

VALUE (MeV)	DOCUMENT ID	TECN	COMMENT
90 to 110 (≈ 100) OUR ESTIMATE			
98 ± 12	SARANTSEV	19	DPWA $\bar{K}N$ multichannel
97 ± ⁴ / ₆	¹ KAMANO	15	DPWA $\bar{K}N$ multichannel
••• We do not use the following data for averages, fits, limits, etc. •••			
133	ZHANG	13A	DPWA $\bar{K}N$ multichannel
¹ From the preferred solution A in KAMANO 15.			

 $\Sigma(1915)$ POLE RESIDUES

The normalized residue is the residue divided by $\Gamma_{\text{pole}}/2$.

Normalized residue in $N\bar{K} \rightarrow \Sigma(1915) \rightarrow N\bar{K}$

MODULUS	PHASE (°)	DOCUMENT ID	TECN	COMMENT
0.08 ± 0.02	-33 ± 15	SARANTSEV	19	DPWA $\bar{K}N$ multichannel
••• We do not use the following data for averages, fits, limits, etc. •••				
0.0391	-15	¹ KAMANO	15	DPWA $\bar{K}N$ multichannel
¹ From the preferred solution A in KAMANO 15.				

Normalized residue in $N\bar{K} \rightarrow \Sigma(1915) \rightarrow \Sigma\pi$

MODULUS	PHASE (°)	DOCUMENT ID	TECN	COMMENT
0.09 ± 0.02	180 ± 12	SARANTSEV	19	DPWA $\bar{K}N$ multichannel
••• We do not use the following data for averages, fits, limits, etc. •••				
0.157	157	¹ KAMANO	15	DPWA $\bar{K}N$ multichannel
¹ From the preferred solution A in KAMANO 15.				

Normalized residue in $N\bar{K} \rightarrow \Sigma(1915) \rightarrow \Lambda\pi$

MODULUS	PHASE (°)	DOCUMENT ID	TECN	COMMENT
0.07 ± 0.02	-170 ± 20	SARANTSEV	19	DPWA $\bar{K}N$ multichannel
••• We do not use the following data for averages, fits, limits, etc. •••				
0.0757	166	¹ KAMANO	15	DPWA $\bar{K}N$ multichannel
¹ From the preferred solution A in KAMANO 15.				

Normalized residue in $N\bar{K} \rightarrow \Sigma(1915) \rightarrow \Xi K$

MODULUS	PHASE (°)	DOCUMENT ID	TECN	COMMENT
0.02 ± 0.01	-65 ± 35	SARANTSEV	19	DPWA $\bar{K}N$ multichannel
••• We do not use the following data for averages, fits, limits, etc. •••				
0.002	-88	¹ KAMANO	15	DPWA $\bar{K}N$ multichannel
¹ From the preferred solution A in KAMANO 15.				

Normalized residue in $N\bar{K} \rightarrow \Lambda(1915) \rightarrow \Sigma(1385)\pi, P\text{-wave}$

MODULUS	PHASE (°)	DOCUMENT ID	TECN	COMMENT
0.02 ± 0.02		SARANTSEV	19	DPWA $\bar{K}N$ multichannel
••• We do not use the following data for averages, fits, limits, etc. •••				
0.0724	161	¹ KAMANO	15	DPWA $\bar{K}N$ multichannel
¹ From the preferred solution A in KAMANO 15.				

Normalized residue in $N\bar{K} \rightarrow \Lambda(1915) \rightarrow \Sigma(1385)\pi, F\text{-wave}$

MODULUS	PHASE (°)	DOCUMENT ID	TECN	COMMENT
0.05 ± 0.03	-30 ± 50	SARANTSEV	19	DPWA $\bar{K}N$ multichannel
••• We do not use the following data for averages, fits, limits, etc. •••				
0.0162	-163	¹ KAMANO	15	DPWA $\bar{K}N$ multichannel
¹ From the preferred solution A in KAMANO 15.				

Normalized residue in $N\bar{K} \rightarrow \Sigma(1915) \rightarrow \Lambda(1520)\pi, D\text{-wave}$

MODULUS	PHASE (°)	DOCUMENT ID	TECN	COMMENT
0.08 ± 0.02	-105 ± 50	SARANTSEV	19	DPWA $\bar{K}N$ multichannel

Baryon Particle Listings

 $\Sigma(1915)$ Normalized residue in $N\bar{K} \rightarrow \Sigma(1915) \rightarrow \Delta\bar{K}$, P -wave

MODULUS	PHASE (°)	DOCUMENT ID	TECN	COMMENT
0.12 ± 0.03	-10 ± 20	SARANTSEV 19	DPWA	$\bar{K}N$ multichannel

Normalized residue in $N\bar{K} \rightarrow \Sigma(1915) \rightarrow \Delta\bar{K}$, F -wave

MODULUS	PHASE (°)	DOCUMENT ID	TECN	COMMENT
0.07 ± 0.02	-35 ± 25	SARANTSEV 19	DPWA	$\bar{K}N$ multichannel

Normalized residue in $N\bar{K} \rightarrow \Sigma(1915) \rightarrow \Lambda(1520)\pi$, G -wave

MODULUS	PHASE (°)	DOCUMENT ID	TECN	COMMENT
0.01 ± 0.01		SARANTSEV 19	DPWA	$\bar{K}N$ multichannel

Normalized residue in $N\bar{K} \rightarrow \Sigma(1915) \rightarrow N\bar{K}^*(892)$, $S=1/2$, F -wave

MODULUS	PHASE (°)	DOCUMENT ID	TECN	COMMENT
0.07 ± 0.04	-60 ± 45	SARANTSEV 19	DPWA	$\bar{K}N$ multichannel

• • • We do not use the following data for averages, fits, limits, etc. • • •

0.00476	4	¹ KAMANO 15	DPWA	$\bar{K}N$ multichannel
---------	---	------------------------	------	-------------------------

¹ From the preferred solution A in KAMANO 15.

Normalized residue in $N\bar{K} \rightarrow \Sigma(1915) \rightarrow N\bar{K}^*(892)$, $S=3/2$, P -wave

MODULUS	PHASE (°)	DOCUMENT ID	TECN	COMMENT
0.0494	51	¹ KAMANO 15	DPWA	$\bar{K}N$ multichannel

¹ From the preferred solution A in KAMANO 15.

Normalized residue in $N\bar{K} \rightarrow \Sigma(1915) \rightarrow N\bar{K}^*(892)$, $S=3/2$, F -wave

MODULUS	PHASE (°)	DOCUMENT ID	TECN	COMMENT
0.07 ± 0.03	-40 ± 45	SARANTSEV 19	DPWA	$\bar{K}N$ multichannel

• • • We do not use the following data for averages, fits, limits, etc. • • •

0.000314	16	¹ KAMANO 15	DPWA	$\bar{K}N$ multichannel
----------	----	------------------------	------	-------------------------

¹ From the preferred solution A in KAMANO 15.

 $\Sigma(1915)$ MASS

VALUE (MeV)	DOCUMENT ID	TECN	COMMENT
1900 to 1935 (≈ 1915) OUR ESTIMATE			

1918 \pm 6	SARANTSEV 19	DPWA	$\bar{K}N$ multichannel
1920 \pm 7	ZHANG 13A	DPWA	$\bar{K}N$ multichannel
1937 \pm 20	ALSTON-... 78	DPWA	$\bar{K}N \rightarrow \bar{K}N$
1894 \pm 5	¹ CORDEN 77c		$K^- n \rightarrow \Sigma\pi$
1909 \pm 5	¹ CORDEN 77c		$K^- n \rightarrow \Sigma\pi$
1920 \pm 10	GOPAL 77	DPWA	$\bar{K}N$ multichannel
1920 \pm 30	BAILLON 75	IPWA	$\bar{K}N \rightarrow \Lambda\pi$
1914 \pm 10	HEMINGWAY 75	DPWA	$K^- p \rightarrow \bar{K}N$
1920 \pm 15	VANHORN 75	DPWA	$K^- p \rightarrow \Lambda\pi^0$
1920 \pm 5	KANE 74	DPWA	$K^- p \rightarrow \Sigma\pi$

• • • We do not use the following data for averages, fits, limits, etc. • • •

not seen	DECLAIS 77	DPWA	$\bar{K}N \rightarrow \bar{K}N$
1925 or 1933	² MARTIN 77	DPWA	$\bar{K}N$ multichannel
1900 \pm 4	³ CORDEN 76	DPWA	$K^- n \rightarrow \Lambda\pi^-$
1915	DEBELLEFON 76	IPWA	$K^- p \rightarrow \Lambda\pi^0$

¹ The two entries for CORDEN 77c are from two different acceptable solutions.

² The two MARTIN 77 values are from a T-matrix pole and from a Breit-Wigner fit.

³ Preferred solution 3; see CORDEN 76 for other possibilities.

 $\Sigma(1915)$ WIDTH

VALUE (MeV)	DOCUMENT ID	TECN	COMMENT
80 to 160 (≈ 120) OUR ESTIMATE			

102 \pm 12	SARANTSEV 19	DPWA	$\bar{K}N$ multichannel
149 \pm 17	ZHANG 13A	DPWA	Multichannel
161 \pm 20	ALSTON-... 78	DPWA	$\bar{K}N \rightarrow \bar{K}N$
107 \pm 14	¹ CORDEN 77c		$K^- n \rightarrow \Sigma\pi$
85 \pm 13	¹ CORDEN 77c		$K^- n \rightarrow \Sigma\pi$
130 \pm 10	GOPAL 77	DPWA	$\bar{K}N$ multichannel
70 \pm 20	BAILLON 75	IPWA	$\bar{K}N \rightarrow \Lambda\pi$
85 \pm 15	HEMINGWAY 75	DPWA	$K^- p \rightarrow \bar{K}N$
102 \pm 18	VANHORN 75	DPWA	$K^- p \rightarrow \Lambda\pi^0$
162 \pm 25	KANE 74	DPWA	$K^- p \rightarrow \Sigma\pi$

• • • We do not use the following data for averages, fits, limits, etc. • • •

171 or 173	² MARTIN 77	DPWA	$\bar{K}N$ multichannel
75 \pm 14	³ CORDEN 76	DPWA	$K^- n \rightarrow \Lambda\pi^-$
60	DEBELLEFON 76	IPWA	$K^- p \rightarrow \Lambda\pi^0$

¹ The two entries for CORDEN 77c are from two different acceptable solutions.

² The two MARTIN 77 values are from a T-matrix pole and from a Breit-Wigner fit.

³ Preferred solution 3; see CORDEN 76 for other possibilities.

 $\Sigma(1915)$ DECAY MODES

Mode	Fraction (Γ_i/Γ)
Γ_1 $N\bar{K}$	0.05 to 0.15
Γ_2 $\Lambda\pi$	(6.0 \pm 2.0) %
Γ_3 $\Sigma\pi$	(10.0 \pm 2.0) %
Γ_4 ΞK	
Γ_5 $\Sigma(1385)\pi$	
Γ_6 $\Sigma(1385)\pi$, P -wave	(2.0 \pm 2.0) %
Γ_7 $\Sigma(1385)\pi$, F -wave	(4.0 \pm 2.0) %
Γ_8 $\Lambda(1520)\pi$, D -wave	(8.0 \pm 2.0) %
Γ_9 $\Lambda(1520)\pi$, G -wave	
Γ_{10} $N\bar{K}^*(892)$, $S=1/2$, F -wave	(5.0 \pm 3.0) %
Γ_{11} $N\bar{K}^*(892)$, $S=3/2$, P -wave	
Γ_{12} $N\bar{K}^*(892)$, $S=3/2$, F -wave	(5.0 \pm 2.0) %
Γ_{13} $\Delta\bar{K}$, P -wave	(16 \pm 5) %
Γ_{14} $\Delta\bar{K}$, F -wave	(5.0 \pm 3.0) %

 $\Sigma(1915)$ BRANCHING RATIOS

See "Sign conventions for resonance couplings" in the Note on Λ and Σ Resonances.

$\Gamma(N\bar{K})/\Gamma_{\text{total}}$	VALUE	DOCUMENT ID	TECN	COMMENT	Γ_1/Γ
0.05 to 0.15 OUR ESTIMATE					
	0.08 \pm 0.02	SARANTSEV 19	DPWA	$\bar{K}N$ multichannel	
	0.026 \pm 0.004	ZHANG 13A	DPWA	$\bar{K}N$ multichannel	
	0.03 \pm 0.02	¹ GOPAL 80	DPWA	$\bar{K}N \rightarrow \bar{K}N$	
	0.14 \pm 0.05	ALSTON-... 78	DPWA	$\bar{K}N \rightarrow \bar{K}N$	
	0.11 \pm 0.04	HEMINGWAY 75	DPWA	$K^- p \rightarrow \bar{K}N$	
	0.036	² KAMANO 15	DPWA	$\bar{K}N$ multichannel	
	0.05 \pm 0.03	GOPAL 77	DPWA	See GOPAL 80	
	0.08 or 0.08	³ MARTIN 77	DPWA	$\bar{K}N$ multichannel	

¹ The mass and width are fixed to the GOPAL 77 values due to the low elasticity.

² From the preferred solution A in KAMANO 15.

³ The two MARTIN 77 values are from a T-matrix pole and from a Breit-Wigner fit.

$\Gamma(\Lambda\pi)/\Gamma_{\text{total}}$	VALUE	DOCUMENT ID	TECN	COMMENT	Γ_2/Γ
0.06 \pm 0.02					
		SARANTSEV 19	DPWA	$\bar{K}N$ multichannel	
	0.127	¹ KAMANO 15	DPWA	$\bar{K}N$ multichannel	
					¹ From the preferred solution A in KAMANO 15.

$\Gamma(\Sigma\pi)/\Gamma_{\text{total}}$	VALUE	DOCUMENT ID	TECN	COMMENT	Γ_3/Γ
0.10 \pm 0.02					
		SARANTSEV 19	DPWA	$\bar{K}N$ multichannel	
	0.678	¹ KAMANO 15	DPWA	$\bar{K}N$ multichannel	
					¹ From the preferred solution A in KAMANO 15.

$\Gamma(\Xi K)/\Gamma_{\text{total}}$	VALUE	DOCUMENT ID	TECN	COMMENT	Γ_4/Γ
<0.01					
		SARANTSEV 19	DPWA	$\bar{K}N$ multichannel	
	not seen	¹ KAMANO 15	DPWA	Multichannel	
					¹ From the preferred solution A in KAMANO 15.

$\Gamma(\Sigma(1385)\pi, P\text{-wave})/\Gamma_{\text{total}}$	VALUE	DOCUMENT ID	TECN	COMMENT	Γ_6/Γ
0.02 \pm 0.02					
		SARANTSEV 19	DPWA	$\bar{K}N$ multichannel	
	0.112	¹ KAMANO 15	DPWA	$\bar{K}N$ multichannel	
					¹ From the preferred solution A in KAMANO 15.

$\Gamma(\Sigma(1385)\pi, F\text{-wave})/\Gamma_{\text{total}}$	VALUE	DOCUMENT ID	TECN	COMMENT	Γ_7/Γ
0.04 \pm 0.02					
		SARANTSEV 19	DPWA	$\bar{K}N$ multichannel	
	0.004	¹ KAMANO 15	DPWA	$\bar{K}N$ multichannel	
					¹ From the preferred solution A in KAMANO 15.

$\Gamma(\Lambda(1520)\pi, D\text{-wave})/\Gamma_{\text{total}}$	VALUE	DOCUMENT ID	TECN	COMMENT	Γ_8/Γ
0.08 \pm 0.02					
		SARANTSEV 19	DPWA	$\bar{K}N$ multichannel	

$\Gamma(\Lambda(1520)\pi, G\text{-wave})/\Gamma_{\text{total}}$	VALUE	DOCUMENT ID	TECN	COMMENT	Γ_9/Γ
def 0					
		SARANTSEV 19	DPWA	$\bar{K}N$ multichannel	

See key on page 1171

Baryon Particle Listings

$\Sigma(1915)$, $\Sigma(1940)$, $\Sigma(2010)$

$\Gamma(N\bar{K}^*(892), S=1/2, F\text{-wave})/\Gamma_{\text{total}}$ Γ_{10}/Γ

VALUE	DOCUMENT ID	TECN	COMMENT
0.05 ± 0.03	SARANTSEV 19	DPWA	$\bar{K}N$ multichannel
••• We do not use the following data for averages, fits, limits, etc. •••			
0.001	¹ KAMANO 15	DPWA	Multichannel

¹ From the preferred solution A in KAMANO 15.

$\Gamma(N\bar{K}^*(892), S=3/2, P\text{-wave})/\Gamma_{\text{total}}$ Γ_{11}/Γ

VALUE	DOCUMENT ID	TECN	COMMENT
••• We do not use the following data for averages, fits, limits, etc. •••			
0.042	¹ KAMANO 15	DPWA	Multichannel

¹ From the preferred solution A in KAMANO 15.

$\Gamma(N\bar{K}^*(892), S=3/2, F\text{-wave})/\Gamma_{\text{total}}$ Γ_{12}/Γ

VALUE	DOCUMENT ID	TECN	COMMENT
0.05 ± 0.02	SARANTSEV 19	DPWA	$\bar{K}N$ multichannel
••• We do not use the following data for averages, fits, limits, etc. •••			
not seen	¹ KAMANO 15	DPWA	Multichannel

¹ From the preferred solution A in KAMANO 15.

$\Gamma(\Delta\bar{K}, P\text{-wave})/\Gamma_{\text{total}}$ Γ_{13}/Γ

VALUE	DOCUMENT ID	TECN	COMMENT
0.16 ± 0.05	SARANTSEV 19	DPWA	$\bar{K}N$ multichannel

$\Gamma(\Delta\bar{K}, F\text{-wave})/\Gamma_{\text{total}}$ Γ_{14}/Γ

VALUE	DOCUMENT ID	TECN	COMMENT
0.05 ± 0.03	SARANTSEV 19	DPWA	$\bar{K}N$ multichannel

$(\Gamma_1\Gamma_2)^{1/2}/\Gamma_{\text{total}}$ in $N\bar{K} \rightarrow \Sigma(1915) \rightarrow \Lambda\pi$ $(\Gamma_1\Gamma_2)^{1/2}/\Gamma$

VALUE	DOCUMENT ID	TECN	COMMENT
-0.09 ± 0.03	GOPAL 77	DPWA	$\bar{K}N$ multichannel
-0.10 ± 0.01	¹ CORDEN 76	DPWA	$K^-n \rightarrow \Lambda\pi^-$
-0.06 ± 0.02	BAILLON 75	IPWA	$\bar{K}N \rightarrow \Lambda\pi$
-0.09 ± 0.02	VANHORN 75	DPWA	$K^-p \rightarrow \Lambda\pi^0$
-0.087 ± 0.056	DEVENISH 74B		Fixed- t dispersion rel.
••• We do not use the following data for averages, fits, limits, etc. •••			
-0.09 or -0.09	² MARTIN 77	DPWA	$\bar{K}N$ multichannel
-0.10	DEBELLEFON 76	IPWA	$K^-p \rightarrow \Lambda\pi^0$

¹ Preferred solution 3; see CORDEN 76 for other possibilities.² The two MARTIN 77 values are from a T-matrix pole and from a Breit-Wigner fit.

$(\Gamma_1\Gamma_2)^{1/2}/\Gamma_{\text{total}}$ in $N\bar{K} \rightarrow \Sigma(1915) \rightarrow \Sigma\pi$ $(\Gamma_1\Gamma_3)^{1/2}/\Gamma$

VALUE	DOCUMENT ID	TECN	COMMENT
-0.14 ± 0.01	ZHANG 13A	DPWA	Multichannel
-0.17 ± 0.01	¹ CORDEN 77C		$K^-n \rightarrow \Sigma\pi$
-0.15 ± 0.02	¹ CORDEN 77C		$K^-n \rightarrow \Sigma\pi$
-0.19 ± 0.03	GOPAL 77	DPWA	$\bar{K}N$ multichannel
-0.16 ± 0.03	KANE 74	DPWA	$K^-p \rightarrow \Sigma\pi$
••• We do not use the following data for averages, fits, limits, etc. •••			
-0.05 or -0.05	² MARTIN 77	DPWA	$\bar{K}N$ multichannel

¹ The two entries for CORDEN 77C are from two different acceptable solutions.² The two MARTIN 77 values are from a T-matrix pole and from a Breit-Wigner fit.

$(\Gamma_1\Gamma_2)^{1/2}/\Gamma_{\text{total}}$ in $N\bar{K} \rightarrow \Sigma(1915) \rightarrow \Sigma(1385)\pi, P\text{-wave}$ $(\Gamma_1\Gamma_6)^{1/2}/\Gamma$

VALUE	DOCUMENT ID	TECN	COMMENT
<0.01	CAMERON 78	DPWA	$K^-p \rightarrow \Sigma(1385)\pi$

$(\Gamma_1\Gamma_2)^{1/2}/\Gamma_{\text{total}}$ in $N\bar{K} \rightarrow \Sigma(1915) \rightarrow \Sigma(1385)\pi, F\text{-wave}$ $(\Gamma_1\Gamma_7)^{1/2}/\Gamma$

VALUE	DOCUMENT ID	TECN	COMMENT
+0.06 ± 0.02	ZHANG 13A	DPWA	Multichannel
+0.039 ± 0.009	¹ CAMERON 78	DPWA	$K^-p \rightarrow \Sigma(1385)\pi$

¹ The published sign has been changed to be in accord with the baryon-first convention.

$\Sigma(1915)$ REFERENCES

SARANTSEV 19	EPJ A55 180	A.V. Sarantsev et al.	(BONN, PNPI)
KAMANO 15	PR C92 025205	H. Kamano et al.	(ANL, OSAK)
ZHANG 13A	PR C88 035205	H. Zhang et al.	(KSU)
PDG 86	PL 170B 1	M. Aguilar-Benitez et al.	(CERN, CIT+)
PDG 82	PL 111B 1	M. Roos et al.	(HELS, CIT, CERN)
GOPAL 80	Toronto Conf. 159	G.P. Gopal	(RHEL) IJP
ALSTON... 78	PR D18 182	M. Alston-Garnjost et al.	(LBL, MTHO+) IJP
Also	PRL 38 1007	M. Alston-Garnjost et al.	(LBL, MTHO+) IJP
CAMERON 78	NP B143 189	W. Cameron et al.	(RHEL, LOIC) IJP
CORDEN 77C	NP B125 61	M.J. Corden et al.	(BIRM) IJP
DECLAIS 77	CERN 77-16	Y. Declais et al.	(CAEN, CERN) IJP
GOPAL 77	NP B119 362	G.P. Gopal et al.	(LOIC, RHEL) IJP
MARTIN 77	NP B127 349	B.R. Martin, M.K. Pidcock, R.G. Moorhouse	(LOUC+) IJP
Also	NP B126 266	B.R. Martin, M.K. Pidcock	(LOUC) IJP
Also	NP B126 285	B.R. Martin, M.K. Pidcock	(LOUC) IJP
CORDEN 76	NP B104 382	M.J. Corden et al.	(BIRM) IJP
DEBELLEFON 76	NP B109 129	A. de Bellefon, A. Berthon	(CDEF) IJP
BAILLON 75	NP B94 39	P.H. Baillon, P.J. Litchfield	(CERN, RHEL) IJP
Hemingway 75	NP B91 12	R.J. Hemingway et al.	(CERN, HEIDH, MPIM) IJP
VANHORN 75	NP B87 145	A.J. van Horn	(LBL) IJP
Also	NP B87 157	A.J. van Horn	(LBL) IJP
DEVENISH 74B	NP B81 330	R.C.E. Devensh, C.D. Froggatt, B.R. Martin	(DESY+) IJP
KANE 74	LBL-2452	D.F. Kane	(LBL) IJP
COOL 66	PRL 16 1228	R.L. Cool et al.	(BNL)

$\Sigma(1940) 3/2^+$

 $I(J^P) = 1(\frac{3}{2}^+)$ Status: *

OMITTED FROM SUMMARY TABLE

$\Sigma(1940)$ MASS

VALUE (MeV)	DOCUMENT ID	TECN	COMMENT
100 to 1960 (≈ 1940) OUR ESTIMATE			
1941 ± 18	ZHANG 13A	DPWA	$\bar{K}N$ multichannel
1925 ± 200	VANHORN 75	DPWA	$K^-p \rightarrow \Lambda\pi^0$

$\Sigma(1940)$ WIDTH

VALUE (MeV)	DOCUMENT ID	TECN	COMMENT
100 to 400 (≈ 250) OUR ESTIMATE			
400 ± 49	ZHANG 13A	DPWA	$\bar{K}N$ multichannel
65 +5.0 -2.0	VANHORN 75	DPWA	$K^-p \rightarrow \Lambda\pi^0$

$\Sigma(1940)$ DECAY MODES

Mode	Fraction (Γ_i/Γ)
$\Gamma_1 N\bar{K}$	(13.0 ± 2.0) %
$\Gamma_2 \Sigma\pi$	(4.0 ± 2.0) %
$\Gamma_3 \Sigma(1385)\pi, P\text{-wave}$	(22 ± 7) %
$\Gamma_4 \Lambda(1520)\pi, S\text{-wave}$	(5.0 ± 2.0) %

$\Sigma(1940)$ BRANCHING RATIOS

$\Gamma(N\bar{K})/\Gamma_{\text{total}}$	DOCUMENT ID	TECN	COMMENT	Γ_1/Γ
0.13 ± 0.02	ZHANG 13A	DPWA	$\bar{K}N$ multichannel	

$\Gamma(\Sigma\pi)/\Gamma_{\text{total}}$	DOCUMENT ID	TECN	COMMENT	Γ_2/Γ
0.04 ± 0.02	ZHANG 13A	DPWA	$\bar{K}N$ multichannel	

$\Gamma(\Sigma(1385)\pi, P\text{-wave})/\Gamma_{\text{total}}$	DOCUMENT ID	TECN	COMMENT	Γ_3/Γ
0.22 ± 0.07	ZHANG 13A	DPWA	$\bar{K}N$ multichannel	

$\Gamma(\Lambda(1520)\pi, S\text{-wave})/\Gamma_{\text{total}}$	DOCUMENT ID	TECN	COMMENT	Γ_4/Γ
0.05 ± 0.02	ZHANG 13A	DPWA	$\bar{K}N$ multichannel	

$\Sigma(1940)$ REFERENCES

ZHANG 13A	PR C88 035205	H. Zhang et al.	(KSU)
VANHORN 75	NP B87 145	A.J. van Horn	(LBL)

$\Sigma(2010) 3/2^-$

 $I(J^P) = 1(\frac{3}{2}^-)$ Status: *

OMITTED FROM SUMMARY TABLE

was $\Sigma(2000)$

$\Sigma(2010)$ POLE POSITION

REAL PART

VALUE (MeV)	DOCUMENT ID	TECN	COMMENT
1995 ± 12	SARANTSEV 19	DPWA	$\bar{K}N$ multichannel

-2*x*IMAGINARY PART

VALUE (MeV)	DOCUMENT ID	TECN	COMMENT
175 ± 24	SARANTSEV 19	DPWA	$\bar{K}N$ multichannel

$\Sigma(2010)$ POLE RESIDUES

The normalized residue is the residue divided by $\Gamma_{\text{pole}}/2$.

Normalized residue in $N\bar{K} \rightarrow \Sigma(2010) \rightarrow N\bar{K}$

MODULUS	PHASE (°)	DOCUMENT ID	TECN	COMMENT
0.07 ± 0.03	-115 ± 25	SARANTSEV 19	DPWA	$\bar{K}N$ multichannel

Normalized residue in $N\bar{K} \rightarrow \Sigma(2010) \rightarrow \Sigma\pi$

MODULUS	PHASE (°)	DOCUMENT ID	TECN	COMMENT
0.04 ± 0.02	130 ± 22	SARANTSEV 19	DPWA	$\bar{K}N$ multichannel

Normalized residue in $N\bar{K} \rightarrow \Sigma(2010) \rightarrow \Lambda\pi$

MODULUS	PHASE (°)	DOCUMENT ID	TECN	COMMENT
0.06 ± 0.03	170 ± 25	SARANTSEV 19	DPWA	$\bar{K}N$ multichannel

Baryon Particle Listings

 $\Sigma(2010)$, $\Sigma(2030)$ Normalized residue in $N\bar{K} \rightarrow \Sigma(2010) \rightarrow \Xi K$

MODULUS	PHASE (°)	DOCUMENT ID	TECN	COMMENT
0.04 ± 0.02	-120 ± 45	SARANTSEV 19	DPWA	$\bar{K}N$ multichannel

Normalized residue in $N\bar{K} \rightarrow \Sigma(2010) \rightarrow \Lambda(1520)\pi$, P -wave

MODULUS	PHASE (°)	DOCUMENT ID	TECN	COMMENT
0.08 ± 0.02	80 ± 35	SARANTSEV 19	DPWA	$\bar{K}N$ multichannel

Normalized residue in $N\bar{K} \rightarrow \Sigma(2010) \rightarrow \Lambda(1520)\pi$, F -wave

MODULUS	PHASE (°)	DOCUMENT ID	TECN	COMMENT
0.08 ± 0.05	150 ± 65	SARANTSEV 19	DPWA	$\bar{K}N$ multichannel

Normalized residue in $N\bar{K} \rightarrow \Sigma(2010) \rightarrow \Sigma(1385)\pi$, P -wave

VALUE	DOCUMENT ID	TECN	COMMENT
$0.04 + -0.02 \text{ @ } 25 + -45$	SARANTSEV 19	DPWA	$\bar{K}N$ multichannel

Normalized residue in $N\bar{K} \rightarrow \Sigma(2010) \rightarrow \Sigma(1385)\pi$, F -wave

VALUE	DOCUMENT ID	TECN	COMMENT
0.02 ± 0.02	SARANTSEV 19	DPWA	$\bar{K}N$ multichannel

Normalized residue in $N\bar{K} \rightarrow \Sigma(2010) \rightarrow \Delta\bar{K}$, S -wave

MODULUS	PHASE (°)	DOCUMENT ID	TECN	COMMENT
0.08 ± 0.04	0 ± 30	SARANTSEV 19	DPWA	$\bar{K}N$ multichannel

Normalized residue in $N\bar{K} \rightarrow \Sigma(2010) \rightarrow \Delta\bar{K}$, D -wave

MODULUS	PHASE (°)	DOCUMENT ID	TECN	COMMENT
0.02 ± 0.02		SARANTSEV 19	DPWA	$\bar{K}N$ multichannel

Normalized residue in $N\bar{K} \rightarrow \Sigma(2010) \rightarrow N\bar{K}^*(892)$, S -wave

VALUE	DOCUMENT ID	TECN	COMMENT
$0.12 + -0.03 \text{ @ } -60 + -60$	SARANTSEV 19	DPWA	$\bar{K}N$ multichannel

Normalized residue in $N\bar{K} \rightarrow \Sigma(2010) \rightarrow N\bar{K}^*(892)$, $S=1/2$, D -wave

MODULUS	PHASE (°)	DOCUMENT ID	TECN	COMMENT
0.08 ± 0.04	55 ± 60	SARANTSEV 19	DPWA	$\bar{K}N$ multichannel

Normalized residue in $N\bar{K} \rightarrow \Sigma(2010) \rightarrow N\bar{K}^*(892)$, $S=3/2$, D -wave

MODULUS	PHASE (°)	DOCUMENT ID	TECN	COMMENT
0.08 ± 0.04	15 ± 60	SARANTSEV 19	DPWA	$\bar{K}N$ multichannel

 $\Sigma(2010)$ MASS

VALUE (MeV)	DOCUMENT ID	TECN	COMMENT
2005 ± 14	SARANTSEV 19	DPWA	$\bar{K}N$ multichannel

 $\Sigma(2010)$ WIDTH

VALUE (MeV)	DOCUMENT ID	TECN	COMMENT
178 ± 23	SARANTSEV 19	DPWA	$\bar{K}N$ multichannel

 $\Sigma(2010)$ DECAY MODES

Mode	Fraction (Γ_i/Γ)
Γ_1 $N\bar{K}$	(7.0 ± 3.0) %
Γ_2 $\Lambda\pi$	(5.0 ± 2.0) %
Γ_3 $\Sigma\pi$	(3.0 ± 2.0) %
Γ_4 ΞK	(3.0 ± 2.0) %
Γ_5 $\Sigma(1385)\pi$, P -wave	(3.0 ± 2.0) %
Γ_6 $\Sigma(1385)\pi$, F -wave	(2.0 ± 2.0) %
Γ_7 $\Lambda(1520)\pi$, P -wave	(2.0 ± 2.0) %
Γ_8 $\Lambda(1520)\pi$, F -wave	(12 ± 6) %
Γ_9 $\Delta\bar{K}$, S -wave	(11 ± 5) %
Γ_{10} $\Delta\bar{K}$, D -wave	(1.0 ± 1.0) %
Γ_{11} $N\bar{K}^*(892)$, $S=1/2$, S -wave	(27 ± 7) %
Γ_{12} $N\bar{K}^*(892)$, $S=1/2$, D -wave	(13 ± 6) %
Γ_{13} $N\bar{K}^*(892)$, $S=3/2$, D -wave	(13 ± 6) %

 $\Sigma(2010)$ BRANCHING RATIOS

See "Sign conventions for resonance couplings" in the Note on Λ and Σ Resonances.

$\Gamma(N\bar{K})/\Gamma_{\text{total}}$	DOCUMENT ID	TECN	COMMENT	Γ_1/Γ
0.07 ± 0.03	SARANTSEV 19	DPWA	$\bar{K}N$ multichannel	

$\Gamma(\Lambda\pi)/\Gamma_{\text{total}}$	DOCUMENT ID	TECN	COMMENT	Γ_2/Γ
0.05 ± 0.02	SARANTSEV 19	DPWA	$\bar{K}N$ multichannel	

$\Gamma(\Sigma\pi)/\Gamma_{\text{total}}$	DOCUMENT ID	TECN	COMMENT	Γ_3/Γ
0.03 ± 0.02	SARANTSEV 19	DPWA	$\bar{K}N$ multichannel	

$\Gamma(\Xi K)/\Gamma_{\text{total}}$	DOCUMENT ID	TECN	COMMENT	Γ_4/Γ
0.03 ± 0.02	SARANTSEV 19	DPWA	$\bar{K}N$ multichannel	

$\Gamma(\Sigma(1385)\pi, P\text{-wave})/\Gamma_{\text{total}}$	DOCUMENT ID	TECN	COMMENT	Γ_5/Γ
0.03 ± 0.02	SARANTSEV 19	DPWA	$\bar{K}N$ multichannel	

$\Gamma(\Sigma(1385)\pi, F\text{-wave})/\Gamma_{\text{total}}$	DOCUMENT ID	TECN	COMMENT	Γ_6/Γ
0.02 ± 0.02	SARANTSEV 19	DPWA	$\bar{K}N$ multichannel	

$\Gamma(\Lambda(1520)\pi, P\text{-wave})/\Gamma_{\text{total}}$	DOCUMENT ID	TECN	COMMENT	Γ_7/Γ
0.02 ± 0.02	SARANTSEV 19	DPWA	$\bar{K}N$ multichannel	

$\Gamma(\Lambda(1520)\pi, F\text{-wave})/\Gamma_{\text{total}}$	DOCUMENT ID	TECN	COMMENT	Γ_8/Γ
0.12 ± 0.06	SARANTSEV 19	DPWA	$\bar{K}N$ multichannel	

$\Gamma(\Delta\bar{K}, S\text{-wave})/\Gamma_{\text{total}}$	DOCUMENT ID	TECN	COMMENT	Γ_9/Γ
0.11 ± 0.05	SARANTSEV 19	DPWA	$\bar{K}N$ multichannel	

$\Gamma(\Delta\bar{K}, D\text{-wave})/\Gamma_{\text{total}}$	DOCUMENT ID	TECN	COMMENT	Γ_{10}/Γ
0.01 ± 0.01	SARANTSEV 19	DPWA	$\bar{K}N$ multichannel	

$\Gamma(N\bar{K}^*(892), S=1/2, S\text{-wave})/\Gamma_{\text{total}}$	DOCUMENT ID	TECN	COMMENT	Γ_{11}/Γ
0.27 ± 0.07	SARANTSEV 19	DPWA	$\bar{K}N$ multichannel	

$\Gamma(N\bar{K}^*(892), S=1/2, D\text{-wave})/\Gamma_{\text{total}}$	DOCUMENT ID	TECN	COMMENT	Γ_{12}/Γ
0.13 ± 0.06	SARANTSEV 19	DPWA	$\bar{K}N$ multichannel	

$\Gamma(N\bar{K}^*(892), S=3/2, D\text{-wave})/\Gamma_{\text{total}}$	DOCUMENT ID	TECN	COMMENT	Γ_{13}/Γ
0.13 ± 0.06	SARANTSEV 19	DPWA	$\bar{K}N$ multichannel	

 $\Sigma(2010)$ REFERENCES

SARANTSEV 19 EPJ A55 180 A.V. Sarantsev et al. (BONN, PNPI)

 $\Sigma(2030) 7/2^+$

$I(J^P) = 1(\frac{7}{2}^+)$ Status: * * * *

Discovered by COOL 66 and by WOHL 66. For most results published before 1974 (they are now obsolete), see our 1982 edition Physics Letters **111B** 1 (1982).

This entry only includes results from partial-wave analyses. Parameters of peaks seen in cross sections and invariant-mass distributions around 2030 MeV may be found in our 1984 edition, Reviews of Modern Physics **56** S1 (1984).

 $\Sigma(2030)$ POLE POSITION

REAL PART

VALUE (MeV)	DOCUMENT ID	TECN	COMMENT
2010 to 2030 (\approx 2020) OUR ESTIMATE			
2014 ± 6	SARANTSEV 19	DPWA	$\bar{K}N$ multichannel
$2025 \pm_{-5}^{+10}$	¹ KAMANO 15	DPWA	$\bar{K}N$ multichannel
• • • We do not use the following data for averages, fits, limits, etc. • • •			
1993	ZHANG 13A	DPWA	$\bar{K}N$ multichannel
¹ From the preferred solution A in KAMANO 15.			

-2xIMAGINARY PART

VALUE (MeV)	DOCUMENT ID	TECN	COMMENT
130 to 190 (\approx 160) OUR ESTIMATE			
172 ± 12	SARANTSEV 19	DPWA	$\bar{K}N$ multichannel
$130 \pm_{-24}^{+6}$	¹ KAMANO 15	DPWA	$\bar{K}N$ multichannel
• • • We do not use the following data for averages, fits, limits, etc. • • •			
176	ZHANG 13A	DPWA	$\bar{K}N$ multichannel
¹ From the preferred solution A in KAMANO 15.			

 $\Sigma(2030)$ POLE RESIDUES

The normalized residue is the residue divided by $\Gamma_{\text{pole}}/2$.

Normalized residue in $N\bar{K} \rightarrow \Sigma(2030) \rightarrow N\bar{K}$

MODULUS	PHASE (°)	DOCUMENT ID	TECN	COMMENT
0.20 ± 0.04	-38 ± 8	SARANTSEV 19	DPWA	$\bar{K}N$ multichannel
• • • We do not use the following data for averages, fits, limits, etc. • • •				
0.220	-38	¹ KAMANO 15	DPWA	$\bar{K}N$ multichannel
¹ From the preferred solution A in KAMANO 15.				

Normalized residue in $N\bar{K} \rightarrow \Sigma(2030) \rightarrow \Sigma\pi$

MODULUS	PHASE (°)	DOCUMENT ID	TECN	COMMENT
0.07 ± 0.02	165 ± 12	SARANTSEV 19	DPWA	$\bar{K}N$ multichannel
••• We do not use the following data for averages, fits, limits, etc. •••				
0.0807	135	¹ KAMANO 15	DPWA	$\bar{K}N$ multichannel
¹ From the preferred solution A in KAMANO 15.				

Normalized residue in $N\bar{K} \rightarrow \Sigma(2030) \rightarrow \Lambda\pi$

MODULUS	PHASE (°)	DOCUMENT ID	TECN	COMMENT
0.18 ± 0.04	-22 ± 12	SARANTSEV 19	DPWA	$\bar{K}N$ multichannel
••• We do not use the following data for averages, fits, limits, etc. •••				
0.138	-24	¹ KAMANO 15	DPWA	$\bar{K}N$ multichannel
¹ From the preferred solution A in KAMANO 15.				

Normalized residue in $N\bar{K} \rightarrow \Sigma(2030) \rightarrow \Xi K$

MODULUS	PHASE (°)	DOCUMENT ID	TECN	COMMENT
0.01 ± 0.01		SARANTSEV 19	DPWA	$\bar{K}N$ multichannel
••• We do not use the following data for averages, fits, limits, etc. •••				
0.0348	129	¹ KAMANO 15	DPWA	$\bar{K}N$ multichannel
¹ From the preferred solution A in KAMANO 15.				

Normalized residue in $N\bar{K} \rightarrow \Sigma(2030) \rightarrow \Sigma(1385)\pi, F\text{-wave}$

MODULUS	PHASE (°)	DOCUMENT ID	TECN	COMMENT
0.04 ± 0.03		SARANTSEV 19	DPWA	$\bar{K}N$ multichannel
••• We do not use the following data for averages, fits, limits, etc. •••				
0.089	-23	¹ KAMANO 15	DPWA	$\bar{K}N$ multichannel
¹ From the preferred solution A in KAMANO 15.				

Normalized residue in $N\bar{K} \rightarrow \Sigma(2030) \rightarrow \Sigma(1385)\pi, H\text{-wave}$

MODULUS	PHASE (°)	DOCUMENT ID	TECN	COMMENT
0.0245	132	¹ KAMANO 15	DPWA	Multichannel
¹ From the preferred solution A in KAMANO 15.				

Normalized residue in $N\bar{K} \rightarrow \Sigma(2030) \rightarrow \Lambda(1520)\pi, D\text{-wave}$

MODULUS	PHASE (°)	DOCUMENT ID	TECN	COMMENT
0.03 ± 0.02	-100 ± 40	SARANTSEV 19	DPWA	$\bar{K}N$ multichannel

Normalized residue in $N\bar{K} \rightarrow \Sigma(2030) \rightarrow \Lambda(1520)\pi, G\text{-wave}$

MODULUS	PHASE (°)	DOCUMENT ID	TECN	COMMENT
0.02 ± 0.02		SARANTSEV 19	DPWA	$\bar{K}N$ multichannel

Normalized residue in $N\bar{K} \rightarrow \Sigma(2030) \rightarrow \Delta\bar{K}, F\text{-wave}$

MODULUS	PHASE (°)	DOCUMENT ID	TECN	COMMENT
0.16 ± 0.06	-130 ± 20	SARANTSEV 19	DPWA	$\bar{K}N$ multichannel

Normalized residue in $N\bar{K} \rightarrow \Sigma(2030) \rightarrow \Delta\bar{K}, H\text{-wave}$

MODULUS	PHASE (°)	DOCUMENT ID	TECN	COMMENT
0.04 ± 0.02	-130 ± 35	SARANTSEV 19	DPWA	$\bar{K}N$ multichannel

Normalized residue in $N\bar{K} \rightarrow \Sigma(2030) \rightarrow N\bar{K}^*(892), S=1/2, F\text{-wave}$

MODULUS	PHASE (°)	DOCUMENT ID	TECN	COMMENT
0.02 ± 0.02		SARANTSEV 19	DPWA	$\bar{K}N$ multichannel
••• We do not use the following data for averages, fits, limits, etc. •••				
0.193	38	¹ KAMANO 15	DPWA	$\bar{K}N$ multichannel
¹ From the preferred solution A in KAMANO 15.				

Normalized residue in $N\bar{K} \rightarrow \Sigma(2030) \rightarrow N\bar{K}^*(892), S=3/2, F\text{-wave}$

MODULUS	PHASE (°)	DOCUMENT ID	TECN	COMMENT
0.16 ± 0.09	-160 ± 40	SARANTSEV 19	DPWA	$\bar{K}N$ multichannel
••• We do not use the following data for averages, fits, limits, etc. •••				
0.320	37	¹ KAMANO 15	DPWA	$\bar{K}N$ multichannel
¹ From the preferred solution A in KAMANO 15.				

Normalized residue in $N\bar{K} \rightarrow \Sigma(2030) \rightarrow N\bar{K}^*(892), S=3/2, H\text{-wave}$

MODULUS	PHASE (°)	DOCUMENT ID	TECN	COMMENT
0.00358	22	¹ KAMANO 15	DPWA	Multichannel
¹ From the preferred solution A in KAMANO 15.				

 $\Sigma(2030)$ MASS

VALUE (MeV)	DOCUMENT ID	TECN	COMMENT
2025 to 2040 (≈ 2030) OUR ESTIMATE			
2032 ± 6	SARANTSEV 19	DPWA	$\bar{K}N$ multichannel
2030 ± 5	ZHANG 13A	DPWA	$\bar{K}N$ multichannel
2036 ± 5	GOPAL 80	DPWA	$\bar{K}N \rightarrow \bar{K}N$
2038 ± 10	CORDEN 77B		$K^-N \rightarrow N\bar{K}^*$
2030 ± 3	¹ CORDEN 76	DPWA	$K^-n \rightarrow \Lambda\pi^-$
2035 ± 15	BAILLON 75	IPWA	$\bar{K}N \rightarrow \bar{K}N$
2038 ± 10	HEMINGWAY 75	DPWA	$K^-p \rightarrow \bar{K}N$
2042 ± 11	VANHORN 75	DPWA	$K^-p \rightarrow \Lambda\pi^0$
2020 ± 6	KANE 74	DPWA	$K^-p \rightarrow \Sigma\pi$
2035 ± 10	LITCHFIELD 74B	DPWA	$K^-p \rightarrow \Lambda(1520)\pi^0$
2020 ± 30	LITCHFIELD 74C	DPWA	$K^-p \rightarrow \Delta(1232)\bar{K}$
2025 ± 10	LITCHFIELD 74D	DPWA	$K^-p \rightarrow \Lambda(1820)\pi^0$

••• We do not use the following data for averages, fits, limits, etc. •••

2040 ± 5	GOPAL 77	DPWA	$\bar{K}N$ multichannel
2027 to 2057	GOYAL 77	DPWA	$K^-N \rightarrow \Sigma\pi$
2030	DEBELLEFON 76	IPWA	$K^-p \rightarrow \Lambda\pi^0$
¹ Preferred solution 3; see CORDEN 76 for other possibilities.			

 $\Sigma(2030)$ WIDTH

VALUE (MeV)	DOCUMENT ID	TECN	COMMENT
150 to 200 (≈ 180) OUR ESTIMATE			
177 ± 12	SARANTSEV 19	DPWA	$\bar{K}N$ multichannel
207 ± 17	ZHANG 13A	DPWA	$\bar{K}N$ multichannel
172 ± 10	GOPAL 80	DPWA	$\bar{K}N \rightarrow \bar{K}N$
137 ± 40	CORDEN 77B		$K^-N \rightarrow N\bar{K}^*$
201 ± 9	¹ CORDEN 76	DPWA	$K^-n \rightarrow \Lambda\pi^-$
180 ± 20	BAILLON 75	IPWA	$\bar{K}N \rightarrow \Lambda\pi$
172 ± 15	HEMINGWAY 75	DPWA	$K^-p \rightarrow \bar{K}N$
178 ± 13	VANHORN 75	DPWA	$K^-p \rightarrow \Lambda\pi^0$
111 ± 5	KANE 74	DPWA	$K^-p \rightarrow \Sigma\pi$
160 ± 20	LITCHFIELD 74B	DPWA	$K^-p \rightarrow \Lambda(1520)\pi^0$
200 ± 30	LITCHFIELD 74C	DPWA	$K^-p \rightarrow \Delta(1232)\bar{K}$
••• We do not use the following data for averages, fits, limits, etc. •••			
260	DECLAIS 77	DPWA	$\bar{K}N \rightarrow \bar{K}N$
190 ± 10	GOPAL 77	DPWA	$\bar{K}N$ multichannel
126 to 195	GOYAL 77	DPWA	$K^-N \rightarrow \Sigma\pi$
160	DEBELLEFON 76	IPWA	$K^-p \rightarrow \Lambda\pi^0$
70 to 125	LITCHFIELD 74D	DPWA	$K^-p \rightarrow \Lambda(1820)\pi^0$
¹ Preferred solution 3; see CORDEN 76 for other possibilities.			

 $\Sigma(2030)$ DECAY MODES

Mode	Fraction (Γ_i/Γ)
Γ_1 $N\bar{K}$	17–23 %
Γ_2 $\Lambda\pi$	17–23 %
Γ_3 $\Sigma\pi$	5–10 %
Γ_4 ΞK	<2 %
Γ_5 $\Sigma(1385)\pi$	5–15 %
Γ_6 $\Sigma(1385)\pi, F\text{-wave}$	(1.0 ± 1.0) %
Γ_7 $\Sigma(1385)\pi, H\text{-wave}$	
Γ_8 $\Lambda(1520)\pi$	10–20 %
Γ_9 $\Lambda(1520)\pi, D\text{-wave}$	
Γ_{10} $\Lambda(1520)\pi, G\text{-wave}$	
Γ_{11} $\Delta(1232)\bar{K}$	10–20 %
Γ_{12} $\Delta(1232)\bar{K}, F\text{-wave}$	(15 ± 5) %
Γ_{13} $\Delta(1232)\bar{K}, H\text{-wave}$	(1.0 ± 1.0) %
Γ_{14} $N\bar{K}^*(892)$	
Γ_{15} $N\bar{K}^*(892), S=1/2, F\text{-wave}$	
Γ_{16} $N\bar{K}^*(892), S=3/2, F\text{-wave}$	(14 ± 8) %
Γ_{17} $N\bar{K}^*(892), S=3/2, H\text{-wave}$	
Γ_{18} $\Lambda(1820)\pi, P\text{-wave}$	

 $\Sigma(2030)$ BRANCHING RATIOSSee "Sign conventions for resonance couplings" in the Note on Λ and Σ Resonances.

$\Gamma(N\bar{K})/\Gamma_{\text{total}}$	DOCUMENT ID	TECN	COMMENT	Γ_1/Γ
0.17 to 0.23 OUR ESTIMATE				
0.20 ± 0.04	SARANTSEV 19	DPWA	$\bar{K}N$ multichannel	
0.13 ± 0.01	ZHANG 13A	DPWA	$\bar{K}N$ multichannel	
0.19 ± 0.03	GOPAL 80	DPWA	$\bar{K}N \rightarrow \bar{K}N$	
0.18 ± 0.03	HEMINGWAY 75	DPWA	$K^-p \rightarrow \bar{K}N$	
••• We do not use the following data for averages, fits, limits, etc. •••				
0.269	¹ KAMANO 15	DPWA	Multichannel	
0.15	DECLAIS 77	DPWA	$\bar{K}N \rightarrow \bar{K}N$	
0.24 ± 0.02	GOPAL 77	DPWA	See GOPAL 80	
¹ From the preferred solution A in KAMANO 15.				

$\Gamma(\Lambda\pi)/\Gamma_{\text{total}}$	DOCUMENT ID	TECN	COMMENT	Γ_2/Γ
0.17 ± 0.04				
••• We do not use the following data for averages, fits, limits, etc. •••				
0.080	¹ KAMANO 15	DPWA	$\bar{K}N$ multichannel	
¹ From the preferred solution A in KAMANO 15.				

$\Gamma(\Sigma\pi)/\Gamma_{\text{total}}$	DOCUMENT ID	TECN	COMMENT	Γ_3/Γ
0.025 ± 0.008				
••• We do not use the following data for averages, fits, limits, etc. •••				
0.037	¹ KAMANO 15	DPWA	$\bar{K}N$ multichannel	
¹ From the preferred solution A in KAMANO 15.				

Baryon Particle Listings

 $\Sigma(2030)$ $\Gamma(\Xi K)/\Gamma_{\text{total}}$ Γ_4/Γ

VALUE	DOCUMENT ID	TECN	COMMENT
<0.01	SARANTSEV 19	DPWA	$\bar{K}N$ multichannel
••• We do not use the following data for averages, fits, limits, etc. •••			
0.006	¹ KAMANO 15	DPWA	$\bar{K}N$ multichannel
			¹ From the preferred solution A in KAMANO 15.

 $\Gamma(\Lambda(1520)\pi, D\text{-wave})/\Gamma_{\text{total}}$ Γ_9/Γ

VALUE	DOCUMENT ID	TECN	COMMENT
~ 0.01	SARANTSEV 19	DPWA	$\bar{K}N$ multichannel

 $\Gamma(\Lambda(1520)\pi, G\text{-wave})/\Gamma_{\text{total}}$ Γ_{10}/Γ

VALUE	DOCUMENT ID	TECN	COMMENT
<0.01	SARANTSEV 19	DPWA	$\bar{K}N$ multichannel

 $\Gamma(\Sigma(1385)\pi, F\text{-wave})/\Gamma_{\text{total}}$ Γ_6/Γ

VALUE	DOCUMENT ID	TECN	COMMENT
0.01 \pm 0.01	SARANTSEV 19	DPWA	$\bar{K}N$ multichannel
••• We do not use the following data for averages, fits, limits, etc. •••			
0.030	¹ KAMANO 15	DPWA	$\bar{K}N$ multichannel
			¹ From the preferred solution A in KAMANO 15.

 $\Gamma(\Sigma(1385)\pi, H\text{-wave})/\Gamma_{\text{total}}$ Γ_7/Γ

VALUE	DOCUMENT ID	TECN	COMMENT
••• We do not use the following data for averages, fits, limits, etc. •••			
0.003	¹ KAMANO 15	DPWA	Multichannel
			¹ From the preferred solution A in KAMANO 15.

 $\Gamma(\Delta(1232)\bar{K}, F\text{-wave})/\Gamma_{\text{total}}$ Γ_{12}/Γ

VALUE	DOCUMENT ID	TECN	COMMENT
0.15 \pm 0.05	SARANTSEV 19	DPWA	$\bar{K}N$ multichannel

 $\Gamma(\Delta(1232)\bar{K}, H\text{-wave})/\Gamma_{\text{total}}$ Γ_{13}/Γ

VALUE	DOCUMENT ID	TECN	COMMENT
0.01 \pm 0.01	SARANTSEV 19	DPWA	$\bar{K}N$ multichannel

 $\Gamma(N\bar{K}^*(892), S=1/2, F\text{-wave})/\Gamma_{\text{total}}$ Γ_{15}/Γ

VALUE	DOCUMENT ID	TECN	COMMENT
<0.01	SARANTSEV 19	DPWA	$\bar{K}N$ multichannel
••• We do not use the following data for averages, fits, limits, etc. •••			
0.154	¹ KAMANO 15	DPWA	$\bar{K}N$ multichannel
			¹ From the preferred solution A in KAMANO 15.

 $\Gamma(N\bar{K}^*(892), S=3/2, F\text{-wave})/\Gamma_{\text{total}}$ Γ_{16}/Γ

VALUE	DOCUMENT ID	TECN	COMMENT
0.14 \pm 0.08	SARANTSEV 19	DPWA	$\bar{K}N$ multichannel
••• We do not use the following data for averages, fits, limits, etc. •••			
0.422	¹ KAMANO 15	DPWA	$\bar{K}N$ multichannel
			¹ From the preferred solution A in KAMANO 15.

 $\Gamma(N\bar{K}^*(892), S=3/2, H\text{-wave})/\Gamma_{\text{total}}$ Γ_{17}/Γ

VALUE	DOCUMENT ID	TECN	COMMENT
••• We do not use the following data for averages, fits, limits, etc. •••			
not seen	¹ KAMANO 15	DPWA	$\bar{K}N$ multichannel
			¹ From the preferred solution A in KAMANO 15.

 $(\Gamma_1\Gamma_7)^{1/2}/\Gamma_{\text{total}}$ in $N\bar{K} \rightarrow \Sigma(2030) \rightarrow \Lambda\pi$ $(\Gamma_1\Gamma_2)^{1/2}/\Gamma$

VALUE	DOCUMENT ID	TECN	COMMENT
+0.15 \pm 0.01	ZHANG 13A	DPWA	Multichannel
+0.18 \pm 0.02	GOPAL 77	DPWA	$\bar{K}N$ multichannel
+0.20 \pm 0.01	¹ CORDEN 76	DPWA	$K^-n \rightarrow \Lambda\pi^-$
+0.18 \pm 0.02	BAILLON 75	IPWA	$\bar{K}N \rightarrow \Lambda\pi$
+0.20 \pm 0.01	VANHORN 75	DPWA	$K^-p \rightarrow \Lambda\pi^0$
+0.195 \pm 0.053	DEVENISH 74B		Fixed- t dispersion rel.
••• We do not use the following data for averages, fits, limits, etc. •••			
0.20	DEBELLEFON 76	IPWA	$K^-p \rightarrow \Lambda\pi^0$

¹ Preferred solution 3; see CORDEN 76 for other possibilities.

 $(\Gamma_1\Gamma_7)^{1/2}/\Gamma_{\text{total}}$ in $N\bar{K} \rightarrow \Sigma(2030) \rightarrow \Sigma\pi$ $(\Gamma_1\Gamma_3)^{1/2}/\Gamma$

VALUE	DOCUMENT ID	TECN	COMMENT
-0.08 \pm 0.01	ZHANG 13A	DPWA	Multichannel
-0.09 \pm 0.01	¹ CORDEN 77C		$K^-n \rightarrow \Sigma\pi$
-0.06 \pm 0.01	¹ CORDEN 77C		$K^-n \rightarrow \Sigma\pi$
-0.15 \pm 0.03	GOPAL 77	DPWA	$\bar{K}N$ multichannel
-0.10 \pm 0.01	KANE 74	DPWA	$K^-p \rightarrow \Sigma\pi$
••• We do not use the following data for averages, fits, limits, etc. •••			
-0.085 \pm 0.02	² GOYAL 77	DPWA	$K^-N \rightarrow \Sigma\pi$

¹ The two entries for CORDEN 77C are from two different acceptable solutions.

² This coupling is extracted from unnormalized data.

 $(\Gamma_1\Gamma_7)^{1/2}/\Gamma_{\text{total}}$ in $N\bar{K} \rightarrow \Sigma(2030) \rightarrow \Xi K$ $(\Gamma_1\Gamma_4)^{1/2}/\Gamma$

VALUE	DOCUMENT ID	TECN	COMMENT
0.023	MULLER 69B	DPWA	$K^-p \rightarrow \Xi K$
<0.05	BURGUN 68	DPWA	$K^-p \rightarrow \Xi K$
<0.05	TRIPP 67	RVUE	$K^-p \rightarrow \Xi K$

 $(\Gamma_1\Gamma_7)^{1/2}/\Gamma_{\text{total}}$ in $N\bar{K} \rightarrow \Sigma(2030) \rightarrow \Sigma(1385)\pi, F\text{-wave}$ $(\Gamma_1\Gamma_6)^{1/2}/\Gamma$

VALUE	DOCUMENT ID	TECN	COMMENT
+0.16 \pm 0.01	ZHANG 13A	DPWA	Multichannel
+0.153 \pm 0.026	¹ CAMERON 78	DPWA	$K^-p \rightarrow \Sigma(1385)\pi$
			¹ The published sign has been changed to be in accord with the baryon-first convention.

 $(\Gamma_1\Gamma_7)^{1/2}/\Gamma_{\text{total}}$ in $N\bar{K} \rightarrow \Sigma(2030) \rightarrow \Lambda(1520)\pi, D\text{-wave}$ $(\Gamma_1\Gamma_9)^{1/2}/\Gamma$

VALUE	DOCUMENT ID	TECN	COMMENT
+0.114 \pm 0.010	¹ CAMERON 77	DPWA	$\Lambda(1520)\pi^0$
0.14 \pm 0.03	LITCHFIELD 74B	DPWA	$K^-p \rightarrow \Lambda(1520)\pi^0$
••• We do not use the following data for averages, fits, limits, etc. •••			
0.10 \pm 0.03	² CORDEN 75B	DBC	$K^-n \rightarrow N\bar{K}\pi^-$
			¹ The published sign has been changed to be in accord with the baryon-first convention.
			² An upper limit.

 $(\Gamma_1\Gamma_7)^{1/2}/\Gamma_{\text{total}}$ in $N\bar{K} \rightarrow \Sigma(2030) \rightarrow \Lambda(1520)\pi, G\text{-wave}$ $(\Gamma_1\Gamma_{10})^{1/2}/\Gamma$

VALUE	DOCUMENT ID	TECN	COMMENT
+0.146 \pm 0.010	¹ CAMERON 77	DPWA	$K^-p \rightarrow \Lambda(1520)\pi^0$
0.02 \pm 0.02	LITCHFIELD 74B	DPWA	$K^-p \rightarrow \Lambda(1520)\pi^0$
			¹ The published sign has been changed to be in accord with the baryon-first convention.

 $(\Gamma_1\Gamma_7)^{1/2}/\Gamma_{\text{total}}$ in $N\bar{K} \rightarrow \Sigma(2030) \rightarrow \Delta(1232)\bar{K}, F\text{-wave}$ $(\Gamma_1\Gamma_{12})^{1/2}/\Gamma$

VALUE	DOCUMENT ID	TECN	COMMENT
+0.12 \pm 0.02	ZHANG 13A	DPWA	Multichannel
0.16 \pm 0.03	LITCHFIELD 74C	DPWA	$K^-p \rightarrow \Delta(1232)\bar{K}$
••• We do not use the following data for averages, fits, limits, etc. •••			
0.17 \pm 0.03	¹ CORDEN 75B	DBC	$K^-n \rightarrow N\bar{K}\pi^-$
			¹ An upper limit.

 $(\Gamma_1\Gamma_7)^{1/2}/\Gamma_{\text{total}}$ in $N\bar{K} \rightarrow \Sigma(2030) \rightarrow \Delta(1232)\bar{K}, H\text{-wave}$ $(\Gamma_1\Gamma_{13})^{1/2}/\Gamma$

VALUE	DOCUMENT ID	TECN	COMMENT
0.00 \pm 0.02	LITCHFIELD 74C	DPWA	$K^-p \rightarrow \Delta(1232)\bar{K}$

 $(\Gamma_1\Gamma_7)^{1/2}/\Gamma_{\text{total}}$ in $N\bar{K} \rightarrow \Sigma(2030) \rightarrow N\bar{K}^*(892), S=1/2, F\text{-wave}$ $(\Gamma_1\Gamma_{15})^{1/2}/\Gamma$

VALUE	DOCUMENT ID	TECN	COMMENT
+0.06 \pm 0.02	ZHANG 13A	DPWA	Multichannel
+0.06 \pm 0.03	¹ CAMERON 78B	DPWA	$K^-p \rightarrow N\bar{K}^*$
-0.02 \pm 0.01	CORDEN 77B		$K^-d \rightarrow NN\bar{K}^*$
			¹ The published sign has been changed to be in accord with the baryon-first convention.

 $(\Gamma_1\Gamma_7)^{1/2}/\Gamma_{\text{total}}$ in $N\bar{K} \rightarrow \Sigma(2030) \rightarrow N\bar{K}^*(892), S=3/2, F\text{-wave}$ $(\Gamma_1\Gamma_{16})^{1/2}/\Gamma$

VALUE	DOCUMENT ID	TECN	COMMENT
+0.05 \pm 0.01	ZHANG 13A	DPWA	Multichannel
+0.04 \pm 0.03	¹ CAMERON 78B	DPWA	$K^-p \rightarrow N\bar{K}^*$
-0.12 \pm 0.02	CORDEN 77B		$K^-d \rightarrow NN\bar{K}^*$
			¹ The upper limit on the G_3 wave is 0.03.

 $(\Gamma_1\Gamma_7)^{1/2}/\Gamma_{\text{total}}$ in $N\bar{K} \rightarrow \Sigma(2030) \rightarrow \Lambda(1820)\pi, P\text{-wave}$ $(\Gamma_1\Gamma_{18})^{1/2}/\Gamma$

VALUE	DOCUMENT ID	TECN	COMMENT
0.14 \pm 0.02	CORDEN 75B	DBC	$K^-n \rightarrow N\bar{K}\pi^-$
0.18 \pm 0.04	LITCHFIELD 74D	DPWA	$K^-p \rightarrow \Lambda(1820)\pi^0$

 $\Sigma(2030)$ REFERENCES

SARANTSEV 19	EPI A55 180	A.V. Sarantsev et al.	(BONN, PNPI)
KAMANO 15	PR C92 025205	H. Kamano et al.	(ANL, OSAK)
ZHANG 13A	PR C88 035205	H. Zhang et al.	(KSU)
PDG 84	RMP 56 51	C.G. Wohl et al.	(LBL, CIT, CERN)
PDG 82	PL 111B 1	M. Roos et al.	(HELS, CIT, CERN)
GOPAL 80	Toronto Conf. 159	G.P. Gopal	(RHEL) IJP
CAMERON 78	NP B143 189	W. Cameron et al.	(RHEL, LOIC) IJP
CAMERON 78B	NP B146 327	W. Cameron et al.	(RHEL, LOIC) IJP
CAMERON 77	NP B131 399	W. Cameron et al.	(RHEL, LOIC) IJP
CORDEN 77B	NP B121 365	M.J. Corden et al.	(BIRM) IJP
CORDEN 77C	NP B125 61	M.J. Corden et al.	(BIRM) IJP
DECLAIS 77	CERN 77-16	Y. Declais et al.	(CAEN, CERN) IJP
GOPAL 77	NP B119 362	G.P. Gopal et al.	(LOIC, RHEL) IJP
GOYAL 77	PR D16 2746	D.P. Goyal, A.V. Sodhi	(DELH) IJP
CORDEN 76	NP B104 382	M.J. Corden et al.	(BIRM) IJP
DEBELLEFON 76	NP B109 129	A. de Bellefon, A. Berthon	(CDEF) IJP
BAILLON 75	NP B94 39	P.H. Bailion, P.J. Litchfield	(CERN, RHEL) IJP
CORDEN 75B	NP B92 365	M.J. Corden et al.	(BIRM) IJP
HEMINGWAY 75	NP B91 12	R.J. Hemingway et al.	(CERN, HEIDH, MPMI) IJP
VANHORN 75	NP B87 145	A.J. van Horn	(LBL) IJP
Also	NP B87 157	A.J. van Horn	(LBL) IJP

See key on page 1171

Baryon Particle Listings

$\Sigma(2030)$, $\Sigma(2070)$, $\Sigma(2080)$, $\Sigma(2100)$

DEVENISH	74B	NP B81 330	R.C.E. Devenish, C.D. Froggatt, B.R. Martin (DESY+)
KANE	74	LBL-2452	D.F. Kane (LBL) IJP
LITCHFIELD	74B	NP B74 19	P.J. Litchfield <i>et al.</i> (CERN, HEIDH) IJP
LITCHFIELD	74C	NP B74 39	P.J. Litchfield <i>et al.</i> (CERN, HEIDH) IJP
LITCHFIELD	74D	NP B74 12	P.J. Litchfield <i>et al.</i> (CERN, HEIDH) IJP
MULLER	69B	Thesis UCRL 19372	R.A. Muller (LRL) IJP
BURGUN	68	NP B8 447	G. Burgun <i>et al.</i> (SACL, CDEF, RHEL)
TRIPP	67	NP B3 10	R.D. Tripp <i>et al.</i> (LRL, SLAC, CERN+)
COOL	66	PRL 16 1228	R.L. Cool <i>et al.</i> (BNL)
WOHL	66	PRL 17 107	C.G. Wohl, F.T. Solmitz, M.L. Stevenson (LRL) IJP

$$\Sigma(2070) 5/2^+ \quad I(J^P) = 1(\frac{5}{2}^+) \text{ Status: } *$$

OMITTED FROM SUMMARY TABLE

This state suggested by BERTHON 70B finds support in GOPAL 80 with new $K^- p$ polarization and $K^- n$ angular distributions. The very broad state seen in KANE 72 is not required in the later (KANE 74) analysis of $\bar{K} N \rightarrow \Sigma \pi$.

 $\Sigma(2070)$ MASS

VALUE (MeV)	DOCUMENT ID	TECN	COMMENT
2020 to 2100 (≈ 2060) OUR ESTIMATE			
2051 \pm 25	GOPAL 80	DPWA	$\bar{K} N \rightarrow \bar{K} N$
2070 \pm 10	BERTHON 70B	DPWA	$K^- p \rightarrow \Sigma \pi$
• • • We do not use the following data for averages, fits, limits, etc. • • •			
2057	KANE 72	DPWA	$K^- p \rightarrow \Sigma \pi$

 $\Sigma(2070)$ WIDTH

VALUE (MeV)	DOCUMENT ID	TECN	COMMENT
100 to 300 (≈ 200) OUR ESTIMATE			
300 \pm 30	GOPAL 80	DPWA	$\bar{K} N \rightarrow \bar{K} N$
140 \pm 20	BERTHON 70B	DPWA	$K^- p \rightarrow \Sigma \pi$
• • • We do not use the following data for averages, fits, limits, etc. • • •			
906	KANE 72	DPWA	$K^- p \rightarrow \Sigma \pi$

 $\Sigma(2070)$ DECAY MODES

Mode
Γ_1 $N\bar{K}$
Γ_2 $\Sigma \pi$

 $\Sigma(2070)$ BRANCHING RATIOS

See "Sign conventions for resonance couplings" in the Note on Λ and Σ Resonances.

$\Gamma(N\bar{K})/\Gamma_{\text{total}}$	DOCUMENT ID	TECN	COMMENT	Γ_1/Γ
0.08 \pm 0.03	GOPAL 80	DPWA	$\bar{K} N \rightarrow \bar{K} N$	
$(\Gamma_1\Gamma_2)^{1/2}/\Gamma_{\text{total}}$ in $N\bar{K} \rightarrow \Sigma(2070) \rightarrow \Sigma \pi$ $(\Gamma_1\Gamma_2)^{1/2}/\Gamma$				
VALUE	DOCUMENT ID	TECN	COMMENT	
0.12 \pm 0.02	BERTHON 70B	DPWA	$K^- p \rightarrow \Sigma \pi$	
• • • We do not use the following data for averages, fits, limits, etc. • • •				
0.104	KANE 72	DPWA	$K^- p \rightarrow \Sigma \pi$	

 $\Sigma(2070)$ REFERENCES

GOPAL	80	Toronto Conf. 159	G.P. Gopal (RHEL) IJP
KANE	74	LBL-2452	D.F. Kane (LBL)
KANE	72	PR D5 1583	D.F.J. Kane (LBL)
BERTHON	70B	NP B24 417	A. Berthon <i>et al.</i> (CDEF, RHEL, SACL) IJP

$$\Sigma(2080) 3/2^+ \quad I(J^P) = 1(\frac{3}{2}^+) \text{ Status: } *$$

OMITTED FROM SUMMARY TABLE

Suggested by some but not all partial-wave analyses across this region.

 $\Sigma(2080)$ MASS

VALUE (MeV)	DOCUMENT ID	TECN	COMMENT
2060 to 2120 (≈ 2090) OUR ESTIMATE			
2091 \pm 7	¹ CORDEN 76	DPWA	$K^- n \rightarrow \Lambda \pi^-$
2070 to 2120	DEBELLEFON 76	IPWA	$K^- p \rightarrow \Lambda \pi^0$
2120 \pm 40	BAILLON 75	IPWA	$\bar{K} N \rightarrow \Lambda \pi$ (sol. 1)
2140 \pm 40	BAILLON 75	IPWA	$\bar{K} N \rightarrow \Lambda \pi$ (sol. 2)
2082 \pm 4	COX 70	DPWA	See CORDEN 76
2070 \pm 30	LITCHFIELD 70	DPWA	$K^- N \rightarrow \Lambda \pi$

 $\Sigma(2080)$ WIDTH

VALUE (MeV)	DOCUMENT ID	TECN	COMMENT
100 to 240 (≈ 170) OUR ESTIMATE			
186 \pm 48	¹ CORDEN 76	DPWA	$K^- n \rightarrow \Lambda \pi^-$
100	DEBELLEFON 76	IPWA	$K^- p \rightarrow \Lambda \pi^0$
240 \pm 50	BAILLON 75	IPWA	$\bar{K} N \rightarrow \Lambda \pi$ (sol. 1)
200 \pm 50	BAILLON 75	IPWA	$\bar{K} N \rightarrow \Lambda \pi$ (sol. 2)
87 \pm 20	COX 70	DPWA	See CORDEN 76
250 \pm 40	LITCHFIELD 70	DPWA	$K^- N \rightarrow \Lambda \pi$

 $\Sigma(2080)$ DECAY MODES

Mode
Γ_1 $N\bar{K}$
Γ_2 $\Lambda \pi$

 $\Sigma(2080)$ BRANCHING RATIOS

See "Sign conventions for resonance couplings" in the Note on Λ and Σ Resonances.

$(\Gamma_1\Gamma_2)^{1/2}/\Gamma_{\text{total}}$ in $N\bar{K} \rightarrow \Sigma(2080) \rightarrow \Lambda \pi$	DOCUMENT ID	TECN	COMMENT	$(\Gamma_1\Gamma_2)^{1/2}/\Gamma$
VALUE				
-0.10 \pm 0.03	¹ CORDEN 76	DPWA	$K^- n \rightarrow \Lambda \pi^-$	
-0.10	DEBELLEFON 76	IPWA	$K^- p \rightarrow \Lambda \pi^0$	
-0.13 \pm 0.04	BAILLON 75	IPWA	$\bar{K} N \rightarrow \Lambda \pi$ (sol. 1 and 2)	
-0.16 \pm 0.03	COX 70	DPWA	See CORDEN 76	
-0.09 \pm 0.03	LITCHFIELD 70	DPWA	$K^- N \rightarrow \Lambda \pi$	

 $\Sigma(2080)$ FOOTNOTES

¹ Preferred solution 3; see CORDEN 76 for other possibilities, including a D_{15} at this mass.

 $\Sigma(2080)$ REFERENCES

CORDEN	76	NP B104 382	M.J. Corden <i>et al.</i> (BIRM) IJP
DEBELLEFON	76	NP B109 129	A. de Bellefon, A. Berthon (CDEF) IJP
		Also NP B90 1	A. de Bellefon <i>et al.</i> (CDEF, SACL) IJP
BAILLON	75	NP B94 39	P.H. Baillon, P.J. Litchfield (CERN, RHEL) IJP
COX	70	NP B19 61	G.F. Cox <i>et al.</i> (BIRM, EDIN, GLAS, LOIC) IJP
LITCHFIELD	70	NP B22 269	P.J. Litchfield (RHEL) IJP

$$\Sigma(2100) 7/2^- \quad I(J^P) = 1(\frac{7}{2}^-) \text{ Status: } *$$

OMITTED FROM SUMMARY TABLE

 $\Sigma(2100)$ POLE POSITION

REAL PART	DOCUMENT ID	TECN	COMMENT
VALUE (MeV)			
2093 \pm 16	SARANTSEV 19	DPWA	$\bar{K} N$ multichannel
-2xIMAGINARY PART			
VALUE (MeV)	DOCUMENT ID	TECN	COMMENT
210 \pm 35	SARANTSEV 19	DPWA	$\bar{K} N$ multichannel

 $\Sigma(2100)$ POLE RESIDUES

Normalized residue in $N\bar{K} \rightarrow \Sigma(2100) \rightarrow N\bar{K}$	DOCUMENT ID	TECN	COMMENT
MODULUS PHASE ($^\circ$)			
0.09 \pm 0.02 -110 \pm 15	SARANTSEV 19	DPWA	$\bar{K} N$ multichannel
Normalized residue in $N\bar{K} \rightarrow \Sigma(2100) \rightarrow \Sigma \pi$			
MODULUS PHASE ($^\circ$)			
0.04 \pm 0.02 -50 \pm 20	SARANTSEV 19	DPWA	$\bar{K} N$ multichannel
Normalized residue in $N\bar{K} \rightarrow \Sigma(2100) \rightarrow \Lambda \pi$			
MODULUS PHASE ($^\circ$)			
0.03 \pm 0.02 -100 \pm 25	SARANTSEV 19	DPWA	$\bar{K} N$ multichannel
Normalized residue in $N\bar{K} \rightarrow \Sigma(2100) \rightarrow \Xi K$			
MODULUS PHASE ($^\circ$)			
0.010 \pm 0.005 -120 \pm 35	SARANTSEV 19	DPWA	$\bar{K} N$ multichannel
Normalized residue in $N\bar{K} \rightarrow \Sigma(2100) \rightarrow \Lambda(1520)\pi$, F-wave			
MODULUS PHASE ($^\circ$)			
0.02 \pm 0.01 -100 \pm 30	SARANTSEV 19	DPWA	$\bar{K} N$ multichannel
Normalized residue in $N\bar{K} \rightarrow \Sigma(2100) \rightarrow \Lambda(1520)\pi$, H-wave			
MODULUS PHASE ($^\circ$)			
0.01 \pm 0.01	SARANTSEV 19	DPWA	$\bar{K} N$ multichannel

Baryon Particle Listings

 $\Sigma(2100)$, $\Sigma(2110)$

Normalized residue in $N\bar{K} \rightarrow \Sigma(2100) \rightarrow \Sigma(1385)\pi$, <i>D-wave</i>			
MODULUS	PHASE (°)	DOCUMENT ID	TECN COMMENT
0.10 ± 0.03	-60 ± 30	SARANTSEV 19	DPWA $\bar{K}N$ multichannel
Normalized residue in $N\bar{K} \rightarrow \Sigma(2100) \rightarrow \Sigma(1385)\pi$, <i>G-wave</i>			
MODULUS	PHASE (°)	DOCUMENT ID	TECN COMMENT
0.03 ± 0.01	-50 ± 30	SARANTSEV 19	DPWA $\bar{K}N$ multichannel
Normalized residue in $N\bar{K} \rightarrow \Sigma(2100) \rightarrow \Delta\bar{K}$, <i>G-wave</i>			
MODULUS	PHASE (°)	DOCUMENT ID	TECN COMMENT
0.04 ± 0.02	75 ± 35	SARANTSEV 19	DPWA $\bar{K}N$ multichannel
Normalized residue in $N\bar{K} \rightarrow \Sigma(2100) \rightarrow N\bar{K}^*(892)$, <i>S=3/2, D-wave</i>			
MODULUS	PHASE (°)	DOCUMENT ID	TECN COMMENT
0.08 ± 0.04	20 ± 50	SARANTSEV 19	DPWA $\bar{K}N$ multichannel

 $\Sigma(2100)$ MASS

VALUE (MeV)	DOCUMENT ID	TECN	COMMENT
≈ 2100 OUR ESTIMATE			
2146 ± 17	SARANTSEV 19	DPWA	$\bar{K}N$ multichannel
2060 ± 20	BARBARO... 70	DPWA	$K^-p \rightarrow \Lambda\pi^0$
2120 ± 30	BARBARO... 70	DPWA	$K^-p \rightarrow \Sigma\pi$

 $\Sigma(2100)$ WIDTH

VALUE (MeV)	DOCUMENT ID	TECN	COMMENT
260 ± 40	SARANTSEV 19	DPWA	$\bar{K}N$ multichannel
70 ± 30	BARBARO... 70	DPWA	$K^-p \rightarrow \Lambda\pi^0$
135 ± 30	BARBARO... 70	DPWA	$K^-p \rightarrow \Sigma\pi$

 $\Sigma(2100)$ DECAY MODES

Mode	Fraction (Γ_i/Γ)
Γ_1 $N\bar{K}$	(8.0 ± 2.0) %
Γ_2 $\Lambda\pi$	(1.5 ± 1.0) %
Γ_3 $\Sigma\pi$	(2.0 ± 1.0) %
Γ_4 ΞK	
Γ_5 $\Sigma(1385)\pi$, <i>D-wave</i>	(12 ± 6) %
Γ_6 $\Sigma(1385)\pi$, <i>G-wave</i>	
Γ_7 $\Lambda(1520)\pi$, <i>F-wave</i>	(1.0 ± 1.0) %
Γ_8 $\Lambda(1520)\pi$, <i>H-wave</i>	
Γ_9 $N\bar{K}^*(892)$, <i>S=3/2, D-wave</i>	(6.0 ± 3.0) %
Γ_{10} $\Delta\bar{K}$, <i>G-wave</i>	(1.0 ± 1.0) %

 $\Sigma(2100)$ BRANCHING RATIOS

See "Sign conventions for resonance couplings" in the Note on Λ and Σ Resonances.

$(\Gamma_1\Gamma_2)^{1/2}/\Gamma_{\text{total}}$ in $N\bar{K} \rightarrow \Sigma(2100) \rightarrow \Lambda\pi$	$(\Gamma_1\Gamma_2)^{1/2}/\Gamma$		
VALUE	DOCUMENT ID	TECN	COMMENT
-0.07 ± 0.02	BARBARO... 70	DPWA	$K^-p \rightarrow \Lambda\pi^0$
$(\Gamma_1\Gamma_3)^{1/2}/\Gamma_{\text{total}}$ in $N\bar{K} \rightarrow \Sigma(2100) \rightarrow \Sigma\pi$	$(\Gamma_1\Gamma_3)^{1/2}/\Gamma$		
VALUE	DOCUMENT ID	TECN	COMMENT
$+0.13 \pm 0.02$	BARBARO... 70	DPWA	$K^-p \rightarrow \Sigma\pi$
$\Gamma(N\bar{K})/\Gamma_{\text{total}}$	Γ_1/Γ		
VALUE	DOCUMENT ID	TECN	COMMENT
0.08 ± 0.02	SARANTSEV 19	DPWA	$\bar{K}N$ multichannel
$\Gamma(\Lambda\pi)/\Gamma_{\text{total}}$	Γ_2/Γ		
VALUE	DOCUMENT ID	TECN	COMMENT
0.015 ± 0.01	SARANTSEV 19	DPWA	$\bar{K}N$ multichannel
$\Gamma(\Sigma\pi)/\Gamma_{\text{total}}$	Γ_3/Γ		
VALUE	DOCUMENT ID	TECN	COMMENT
0.02 ± 0.01	SARANTSEV 19	DPWA	$\bar{K}N$ multichannel
$\Gamma(\Xi K)/\Gamma_{\text{total}}$	Γ_4/Γ		
VALUE	DOCUMENT ID	TECN	COMMENT
< 0.01	SARANTSEV 19	DPWA	$\bar{K}N$ multichannel
$\Gamma(\Sigma(1385)\pi, \text{D-wave})/\Gamma_{\text{total}}$	Γ_5/Γ		
VALUE	DOCUMENT ID	TECN	COMMENT
0.12 ± 0.06	SARANTSEV 19	DPWA	$\bar{K}N$ multichannel
$\Gamma(\Sigma(1385)\pi, \text{G-wave})/\Gamma_{\text{total}}$	Γ_6/Γ		
VALUE	DOCUMENT ID	TECN	COMMENT
~ 0.01	SARANTSEV 19	DPWA	$\bar{K}N$ multichannel

$\Gamma(\Lambda(1520)\pi, \text{F-wave})/\Gamma_{\text{total}}$	Γ_7/Γ		
VALUE	DOCUMENT ID	TECN	COMMENT
0.01 ± 0.01	SARANTSEV 19	DPWA	$\bar{K}N$ multichannel
$\Gamma(\Lambda(1520)\pi, \text{H-wave})/\Gamma_{\text{total}}$	Γ_8/Γ		
VALUE	DOCUMENT ID	TECN	COMMENT
~ 0	SARANTSEV 19	DPWA	$\bar{K}N$ multichannel
$\Gamma(N\bar{K}^*(892), \text{S=3/2, D-wave})/\Gamma_{\text{total}}$	Γ_9/Γ		
VALUE	DOCUMENT ID	TECN	COMMENT
0.06 ± 0.03	SARANTSEV 19	DPWA	$\bar{K}N$ multichannel
$\Gamma(\Delta\bar{K}, \text{G-wave})/\Gamma_{\text{total}}$	Γ_{10}/Γ		
VALUE	DOCUMENT ID	TECN	COMMENT
0.01 ± 0.01	SARANTSEV 19	DPWA	$\bar{K}N$ multichannel

 $\Sigma(2100)$ REFERENCES

SARANTSEV 19	EPJ A55 180	A.V. Sarantsev et al.	(BONN, PNPI)
BARBARO... 70	Duke Conf. 173	A. Barbaro-Galtri	(LRL) IUP
	Hyperon Resonances, 1970		

$\Sigma(2110) 1/2^-$

$I(J^P) = 1(\frac{1}{2}^-)$ Status: *

OMITTED FROM SUMMARY TABLE
was $\Sigma(2160)$

 $\Sigma(2110)$ POLE POSITION

REAL PART	DOCUMENT ID	TECN	COMMENT
VALUE (MeV)			
2158 ± 25	SARANTSEV 19	DPWA	$\bar{K}N$ multichannel
-2xIMAGINARY PART	DOCUMENT ID	TECN	COMMENT
VALUE (MeV)			
$300 - \frac{300}{60}$	SARANTSEV 19	DPWA	$\bar{K}N$ multichannel

 $\Sigma(2110)$ POLE RESIDUES

Normalized residue in $N\bar{K} \rightarrow \Sigma(2110) \rightarrow N\bar{K}$			
MODULUS	PHASE (°)	DOCUMENT ID	TECN COMMENT
0.29 ± 0.08	-20 ± 35	SARANTSEV 19	DPWA $\bar{K}N$ multichannel
Normalized residue in $N\bar{K} \rightarrow \Sigma(2110) \rightarrow \Sigma\pi$			
MODULUS	PHASE (°)	DOCUMENT ID	TECN COMMENT
0.14 ± 0.04	-5 ± 35	SARANTSEV 19	DPWA $\bar{K}N$ multichannel
Normalized residue in $N\bar{K} \rightarrow \Sigma(2110) \rightarrow \Lambda\pi$			
MODULUS	PHASE (°)	DOCUMENT ID	TECN COMMENT
0.39 ± 0.08	85 ± 25	SARANTSEV 19	DPWA $\bar{K}N$ multichannel
Normalized residue in $N\bar{K} \rightarrow \Sigma(2110) \rightarrow \Xi K$			
MODULUS	PHASE (°)	DOCUMENT ID	TECN COMMENT
0.05 ± 0.02	-85 ± 35	SARANTSEV 19	DPWA $\bar{K}N$ multichannel
Normalized residue in $N\bar{K} \rightarrow \Sigma(2110) \rightarrow \Lambda(1520)\pi$			
MODULUS	PHASE (°)	DOCUMENT ID	TECN COMMENT
0.025 ± 0.015		SARANTSEV 19	DPWA $\bar{K}N$ multichannel
Normalized residue in $N\bar{K} \rightarrow \Sigma(2110) \rightarrow \Sigma(1385)\pi$			
MODULUS	PHASE (°)	DOCUMENT ID	TECN COMMENT
0.03 ± 0.02		SARANTSEV 19	DPWA $\bar{K}N$ multichannel
Normalized residue in $N\bar{K} \rightarrow \Sigma(2110) \rightarrow \Delta\bar{K}$			
MODULUS	PHASE (°)	DOCUMENT ID	TECN COMMENT
0.035 ± 0.02	-30 ± 40	SARANTSEV 19	DPWA $\bar{K}N$ multichannel
Normalized residue in $N\bar{K} \rightarrow \Sigma(2110) \rightarrow N\bar{K}^*(892)$, <i>S-wave</i>			
MODULUS	PHASE (°)	DOCUMENT ID	TECN COMMENT
0.09 ± 0.03	-40 ± 50	SARANTSEV 19	DPWA $\bar{K}N$ multichannel
Normalized residue in $N\bar{K} \rightarrow \Sigma(2110) \rightarrow N\bar{K}^*(892)$, <i>D-wave</i>			
MODULUS	PHASE (°)	DOCUMENT ID	TECN COMMENT
0.04 ± 0.03		SARANTSEV 19	DPWA $\bar{K}N$ multichannel

 $\Sigma(2110)$ MASS

VALUE (MeV)	DOCUMENT ID	TECN	COMMENT
2110 ± 50 OUR AVERAGE			Error includes scale factor of 3.4.
2165 ± 23	SARANTSEV 19	DPWA	$\bar{K}N$ multichannel
2060 ± 20	ZHANG 13A	DPWA	$\bar{K}N$ multichannel

See key on page 1171

Baryon Particle Listings
 $\Sigma(2110), \Sigma(2230)$ $\Sigma(2110)$ WIDTH

VALUE (MeV)	DOCUMENT ID	TECN	COMMENT
310_{-120}^{+120} OUR AVERAGE			
320_{-60}^{+300}	SARANTSEV 19	DPWA	$\bar{K}N$ multichannel
300 ± 134	ZHANG 13A	DPWA	$\bar{K}N$ multichannel

 $\Sigma(2110)$ DECAY MODES

Mode	Fraction (Γ_i/Γ)
Γ_1 $N\bar{K}$	(29 \pm 7) %
Γ_2 $\Sigma\pi$	(7.0 \pm 2.0) %
Γ_3 $\Lambda\pi$	(54 \pm 12) %
Γ_4 $N\bar{K}^*(892)$, S-wave	(3.0 \pm 1.0) %
Γ_5 $N\bar{K}^*(892)$, D-wave	

 $\Sigma(2110)$ BRANCHING RATIOS

$\Gamma(N\bar{K})/\Gamma_{\text{total}}$	DOCUMENT ID	TECN	COMMENT	Γ_1/Γ
0.29 ± 0.07	SARANTSEV 19	DPWA	$\bar{K}N$ multichannel	
$\Gamma(\Sigma\pi)/\Gamma_{\text{total}}$	DOCUMENT ID	TECN	COMMENT	Γ_2/Γ
0.07 ± 0.02	SARANTSEV 19	DPWA	$\bar{K}N$ multichannel	
$\Gamma(\Lambda\pi)/\Gamma_{\text{total}}$	DOCUMENT ID	TECN	COMMENT	Γ_3/Γ
0.54 ± 0.12	SARANTSEV 19	DPWA	$\bar{K}N$ multichannel	
$\Gamma(N\bar{K}^*(892), \text{S-wave})/\Gamma_{\text{total}}$	DOCUMENT ID	TECN	COMMENT	Γ_4/Γ
0.03 ± 0.01	SARANTSEV 19	DPWA	$\bar{K}N$ multichannel	
$\Gamma(N\bar{K}^*(892), \text{D-wave})/\Gamma_{\text{total}}$	DOCUMENT ID	TECN	COMMENT	Γ_5/Γ
~ 0.01	SARANTSEV 19	DPWA	$\bar{K}N$ multichannel	

••• We do not use the following data for averages, fits, limits, etc. •••
~ 0.01

 $\Sigma(2110)$ REFERENCES

SARANTSEV 19	EPJ A55 180	A.V. Sarantsev et al.	(BONN, PNPI)
ZHANG 13A	PR C88 035205	H. Zhang et al.	(KSU)

 $\Sigma(2230) 3/2^+$ $I(J^P) = 1(\frac{3}{2}^+)$ Status: *

OMITTED FROM SUMMARY TABLE

 $\Sigma(2230)$ POLE POSITION

REAL PART	DOCUMENT ID	TECN	COMMENT
2234 ± 25	SARANTSEV 19	DPWA	$\bar{K}N$ multichannel
$-2 \times$ IMAGINARY PART	DOCUMENT ID	TECN	COMMENT
340 ± 45	SARANTSEV 19	DPWA	$\bar{K}N$ multichannel

 $\Sigma(2230)$ POLE RESIDUES

Normalized residue in $N\bar{K} \rightarrow \Sigma(2230) \rightarrow N\bar{K}$			
MODULUS	PHASE ($^\circ$)	DOCUMENT ID	TECN COMMENT
0.07 ± 0.02	25 ± 15	SARANTSEV 19	DPWA $\bar{K}N$ multichannel
Normalized residue in $N\bar{K} \rightarrow \Sigma(2230) \rightarrow \Sigma\pi$			
MODULUS	PHASE ($^\circ$)	DOCUMENT ID	TECN COMMENT
0.03 ± 0.02	180 ± 25	SARANTSEV 19	DPWA $\bar{K}N$ multichannel
Normalized residue in $N\bar{K} \rightarrow \Sigma(2030) \rightarrow \Lambda\pi$			
MODULUS	PHASE ($^\circ$)	DOCUMENT ID	TECN COMMENT
0.11 ± 0.05	-16 ± 10	SARANTSEV 19	DPWA $\bar{K}N$ multichannel
Normalized residue in $N\bar{K} \rightarrow \Sigma(2230) \rightarrow \Xi K$			
MODULUS	PHASE ($^\circ$)	DOCUMENT ID	TECN COMMENT
0.04 ± 0.02	155 ± 20	SARANTSEV 19	DPWA $\bar{K}N$ multichannel
Normalized residue in $N\bar{K} \rightarrow \Sigma(2230) \rightarrow \Lambda(1520)\pi, \text{S-wave}$			
MODULUS	PHASE ($^\circ$)	DOCUMENT ID	TECN COMMENT
0.12 ± 0.05	-80 ± 25	SARANTSEV 19	DPWA $\bar{K}N$ multichannel

Normalized residue in $N\bar{K} \rightarrow \Sigma(2230) \rightarrow \Lambda(1520)\pi, \text{D-wave}$

MODULUS	PHASE ($^\circ$)	DOCUMENT ID	TECN	COMMENT
0.03 ± 0.02	160 ± 30	SARANTSEV 19	DPWA	$\bar{K}N$ multichannel

Normalized residue in $N\bar{K} \rightarrow \Sigma(2230) \rightarrow \Sigma(1385)\pi, \text{P-wave}$

MODULUS	PHASE ($^\circ$)	DOCUMENT ID	TECN	COMMENT
0.05 ± 0.02	60 ± 25	SARANTSEV 19	DPWA	$\bar{K}N$ multichannel

Normalized residue in $N\bar{K} \rightarrow \Sigma(2230) \rightarrow \Sigma(1385)\pi, \text{F-wave}$

MODULUS	PHASE ($^\circ$)	DOCUMENT ID	TECN	COMMENT
0.05 ± 0.03	-70 ± 20	SARANTSEV 19	DPWA	$\bar{K}N$ multichannel

Normalized residue in $N\bar{K} \rightarrow \Sigma(2230) \rightarrow \Delta\bar{K}, \text{P-wave}$

MODULUS	PHASE ($^\circ$)	DOCUMENT ID	TECN	COMMENT
0.11 ± 0.04	60 ± 15	SARANTSEV 19	DPWA	$\bar{K}N$ multichannel

Normalized residue in $N\bar{K} \rightarrow \Sigma(2230) \rightarrow \Delta\bar{K}, \text{F-wave}$

MODULUS	PHASE ($^\circ$)	DOCUMENT ID	TECN	COMMENT
0.07 ± 0.03	90 ± 25	SARANTSEV 19	DPWA	$\bar{K}N$ multichannel

Normalized residue in $N\bar{K} \rightarrow \Sigma(2230) \rightarrow N\bar{K}^*(892), \text{S}=1/2, \text{P-wave}$

MODULUS	PHASE ($^\circ$)	DOCUMENT ID	TECN	COMMENT
0.08 ± 0.04	40 ± 45	SARANTSEV 19	DPWA	$\bar{K}N$ multichannel

Normalized residue in $N\bar{K} \rightarrow \Sigma(2230) \rightarrow N\bar{K}^*(892), \text{S}=3/2, \text{P-wave}$

MODULUS	PHASE ($^\circ$)	DOCUMENT ID	TECN	COMMENT
0.14 ± 0.03	-40 ± 45	SARANTSEV 19	DPWA	$\bar{K}N$ multichannel

Normalized residue in $N\bar{K} \rightarrow \Sigma(2230) \rightarrow N\bar{K}^*(892), \text{S}=3/2, \text{F-wave}$

MODULUS	PHASE ($^\circ$)	DOCUMENT ID	TECN	COMMENT
0.05 ± 0.03	35 ± 30	SARANTSEV 19	DPWA	$\bar{K}N$ multichannel

 $\Sigma(2230)$ MASS

VALUE (MeV)	DOCUMENT ID	TECN	COMMENT
2240 ± 27	SARANTSEV 19	DPWA	$\bar{K}N$ multichannel

 $\Sigma(2230)$ WIDTH

VALUE (MeV)	DOCUMENT ID	TECN	COMMENT
345 ± 50	SARANTSEV 19	DPWA	$\bar{K}N$ multichannel

 $\Sigma(2230)$ DECAY MODES

Mode	Fraction (Γ_i/Γ)
Γ_1 $N\bar{K}$	(6.0 \pm 2.0) %
Γ_2 $\Sigma\pi$	(2.0 \pm 1.0) %
Γ_3 $\Lambda\pi$	(12 \pm 6) %
Γ_4 ΞK	(2.0 \pm 1.0) %
Γ_5 $\Lambda(1520)\pi, \text{S-wave}$	(14 \pm 5) %
Γ_6 $\Lambda(1520)\pi, \text{D-wave}$	
Γ_7 $\Sigma(1385)\pi, \text{P-wave}$	(4 \pm 4) %
Γ_8 $\Sigma(1385)\pi, \text{F-wave}$	(3.0 \pm 2.0) %
Γ_9 $\Delta\bar{K}, \text{P-wave}$	(14 \pm 5) %
Γ_{10} $\Delta\bar{K}, \text{F-wave}$	(8.0 \pm 2.0) %
Γ_{11} $N\bar{K}^*(892), \text{S}=1/2, \text{F-wave}$	(8.0 \pm 3.0) %
Γ_{12} $N\bar{K}^*(892), \text{S}=3/2, \text{F-wave}$	(26 \pm 5) %

 $\Sigma(2230)$ BRANCHING RATIOS

$\Gamma(N\bar{K})/\Gamma_{\text{total}}$	DOCUMENT ID	TECN	COMMENT	Γ_1/Γ
0.06 ± 0.02	SARANTSEV 19	DPWA	$\bar{K}N$ multichannel	
$\Gamma(\Sigma\pi)/\Gamma_{\text{total}}$	DOCUMENT ID	TECN	COMMENT	Γ_2/Γ
0.02 ± 0.01	SARANTSEV 19	DPWA	$\bar{K}N$ multichannel	
$\Gamma(\Lambda\pi)/\Gamma_{\text{total}}$	DOCUMENT ID	TECN	COMMENT	Γ_3/Γ
0.12 ± 0.06	SARANTSEV 19	DPWA	$\bar{K}N$ multichannel	
$\Gamma(\Xi K)/\Gamma_{\text{total}}$	DOCUMENT ID	TECN	COMMENT	Γ_4/Γ
0.02 ± 0.01	SARANTSEV 19	DPWA	$\bar{K}N$ multichannel	
$\Gamma(\Lambda(1520)\pi, \text{S-wave})/\Gamma_{\text{total}}$	DOCUMENT ID	TECN	COMMENT	Γ_5/Γ
0.14 ± 0.05	SARANTSEV 19	DPWA	$\bar{K}N$ multichannel	

Baryon Particle Listings

 $\Sigma(2230)$, $\Sigma(2250)$ $\Gamma(\Lambda(1520)\pi, D\text{-wave})/\Gamma_{\text{total}}$

VALUE	DOCUMENT ID	TECN	COMMENT	Γ_6/Γ
••• We do not use the following data for averages, fits, limits, etc. •••				
~ 1	SARANTSEV 19	DPWA	$\bar{K}N$ multichannel	

 $\Gamma(\Sigma(1385)\pi, P\text{-wave})/\Gamma_{\text{total}}$

VALUE	DOCUMENT ID	TECN	COMMENT	Γ_7/Γ
0.04 ± 0.04	SARANTSEV 19	DPWA	$\bar{K}N$ multichannel	

 $\Gamma(\Sigma(1385)\pi, F\text{-wave})/\Gamma_{\text{total}}$

VALUE	DOCUMENT ID	TECN	COMMENT	Γ_8/Γ
0.03 ± 0.02	SARANTSEV 19	DPWA	$\bar{K}N$ multichannel	

 $\Gamma(\Delta\bar{K}, P\text{-wave})/\Gamma_{\text{total}}$

VALUE	DOCUMENT ID	TECN	COMMENT	Γ_9/Γ
0.14 ± 0.05	SARANTSEV 19	DPWA	$\bar{K}N$ multichannel	

 $\Gamma(\Delta\bar{K}, F\text{-wave})/\Gamma_{\text{total}}$

VALUE	DOCUMENT ID	TECN	COMMENT	Γ_{10}/Γ
0.08 ± 0.02	SARANTSEV 19	DPWA	$\bar{K}N$ multichannel	

 $\Gamma(N\bar{K}^*(892), S=1/2, F\text{-wave})/\Gamma_{\text{total}}$

VALUE	DOCUMENT ID	TECN	COMMENT	Γ_{11}/Γ
0.08 ± 0.03	SARANTSEV 19	DPWA	$\bar{K}N$ multichannel	

 $\Gamma(N\bar{K}^*(892), S=3/2, F\text{-wave})/\Gamma_{\text{total}}$

VALUE	DOCUMENT ID	TECN	COMMENT	Γ_{12}/Γ
0.26 ± 0.05	SARANTSEV 19	DPWA	$\bar{K}N$ multichannel	

 $\Sigma(2230)$ REFERENCES

SARANTSEV 19 EPJ A55 180 A.V. Sarantsev et al. (BONN, PNPI)

 $\Sigma(2250)$

$$J(J^P) = 1(?)^? \quad \text{Status: } **$$

OMITTED FROM SUMMARY TABLE

Results from partial-wave analyses are too weak to warrant separating them from the production and cross-section experiments. LASINSKI 71 in $\bar{K}N$ using a Pomeron + resonances model, and DEBELLEFON 76, DEBELLEFON 77, and DEBELLEFON 78 in energy-dependent partial-wave analyses of $\bar{K}N \rightarrow \Lambda\pi$, $\Sigma\pi$, and $N\bar{K}$, respectively, suggest two resonances around this mass.

 $\Sigma(2250)$ MASS

VALUE (MeV)	DOCUMENT ID	TECN	COMMENT
2210 to 2280 (≈ 2250) OUR ESTIMATE			
2270 ± 50	DEBELLEFON 78	DPWA	D_5 wave
2210 ± 30	DEBELLEFON 78	DPWA	G_9 wave
2275 ± 20	DEBELLEFON 77	DPWA	D_5 wave
2215 ± 20	DEBELLEFON 77	DPWA	G_9 wave
2300 ± 30	¹ DEBELLEFON 75B	HBC	$K^-p \rightarrow \Xi^{*0}K^0$
2251^{+30}_{-20}	VANHORN 75	DPWA	$K^-p \rightarrow \Lambda\pi^0, F_5$ wave
2280 ± 14	AGUILAR-... 70B	HBC	K^-p 3.9, 4.6 GeV/c
2237 ± 11	BRICMAN 70	CNTR	Total, charge exchange
2255 ± 10	COOL 70	CNTR	K^-p, K^-d total
2250 ± 7	BUGG 68	CNTR	K^-p, K^-d total
••• We do not use the following data for averages, fits, limits, etc. •••			
2260	DEBELLEFON 76	IPWA	D_5 wave
2215	DEBELLEFON 76	IPWA	G_9 wave
2250 ± 20	LU 70	CNTR	$\gamma p \rightarrow K^+Y^*$
2245	BLANPIED 65	CNTR	$\gamma p \rightarrow K^+Y^*$
2299 ± 6	BOCK 65	HBC	$\bar{p}p$ 5.7 GeV/c

 $\Sigma(2250)$ WIDTH

VALUE (MeV)	DOCUMENT ID	TECN	COMMENT
60 to 150 (≈ 100) OUR ESTIMATE			
120 ± 40	DEBELLEFON 78	DPWA	D_5 wave
80 ± 20	DEBELLEFON 78	DPWA	G_9 wave
70 ± 20	DEBELLEFON 77	DPWA	D_5 wave
60 ± 20	DEBELLEFON 77	DPWA	G_9 wave
130 ± 20	¹ DEBELLEFON 75B	HBC	$K^-p \rightarrow \Xi^{*0}K^0$
192 ± 30	VANHORN 75	DPWA	$K^-p \rightarrow \Lambda\pi^0, F_5$ wave
100 ± 20	AGUILAR-... 70B	HBC	K^-p 3.9, 4.6 GeV/c
164 ± 50	BRICMAN 70	CNTR	Total, charge exchange
230 ± 20	BUGG 68	CNTR	K^-p, K^-d total

••• We do not use the following data for averages, fits, limits, etc. •••				
100	DEBELLEFON 76	IPWA	D_5 wave	
140	DEBELLEFON 76	IPWA	G_9 wave	
170	COOL 70	CNTR	K^-p, K^-d total	
125	LU 70	CNTR	$\gamma p \rightarrow K^+Y^*$	
150	BLANPIED 65	CNTR	$\gamma p \rightarrow K^+Y^*$	
21^{+17}_{-21}	BOCK 65	HBC	$\bar{p}p$ 5.7 GeV/c	

 $\Sigma(2250)$ DECAY MODES

Mode	Fraction (Γ_i/Γ)
Γ_1 $N\bar{K}$	<10 %
Γ_2 $\Lambda\pi$	seen
Γ_3 $\Sigma\pi$	seen
Γ_4 $\Xi(1530)K$	

 $\Sigma(2250)$ BRANCHING RATIOSSee "Sign conventions for resonance couplings" in the Note on Λ and Σ Resonances. $\Gamma(N\bar{K})/\Gamma_{\text{total}}$

VALUE	DOCUMENT ID	TECN	COMMENT	Γ_1/Γ
<0.1 OUR ESTIMATE				
0.08 ± 0.02	DEBELLEFON 78	DPWA	D_5 wave	
0.02 ± 0.01	DEBELLEFON 78	DPWA	G_9 wave	

 $(J+\frac{1}{2}) \times \Gamma(N\bar{K})/\Gamma_{\text{total}}$

VALUE	DOCUMENT ID	TECN	COMMENT	Γ_1/Γ
••• We do not use the following data for averages, fits, limits, etc. •••				
0.16 ± 0.12	BRICMAN 70	CNTR	Total, charge exchange	
0.42	COOL 70	CNTR	K^-p, K^-d total	
0.47	BUGG 68	CNTR		

 $(\Gamma_1\Gamma_2)^{1/2}/\Gamma_{\text{total}}$ in $N\bar{K} \rightarrow \Sigma(2250) \rightarrow \Lambda\pi$

VALUE	DOCUMENT ID	TECN	COMMENT	$(\Gamma_1\Gamma_2)^{1/2}/\Gamma$
-0.16 ± 0.03	VANHORN 75	DPWA	$K^-p \rightarrow \Lambda\pi^0, F_5$ wave	
••• We do not use the following data for averages, fits, limits, etc. •••				
+0.11	DEBELLEFON 76	IPWA	D_5 wave	
-0.10	DEBELLEFON 76	IPWA	G_9 wave	
-0.18	BARBARO-... 70	DPWA	$K^-p \rightarrow \Lambda\pi^0, G_9$ wave	

 $(\Gamma_1\Gamma_3)^{1/2}/\Gamma_{\text{total}}$ in $N\bar{K} \rightarrow \Sigma(2250) \rightarrow \Sigma\pi$

VALUE	DOCUMENT ID	TECN	COMMENT	$(\Gamma_1\Gamma_3)^{1/2}/\Gamma$
+0.06 \pm 0.02	DEBELLEFON 77	DPWA	D_5 wave	
-0.03 \pm 0.02	DEBELLEFON 77	DPWA	G_9 wave	
+0.07	BARBARO-... 70	DPWA	$K^-p \rightarrow \Sigma\pi, G_9$ wave	

 $\Gamma(N\bar{K})/\Gamma(\Sigma\pi)$

VALUE	DOCUMENT ID	TECN	COMMENT	Γ_1/Γ_3
••• We do not use the following data for averages, fits, limits, etc. •••				
<0.18	BARNES 69	HBC	1 standard dev. limit	

 $\Gamma(\Lambda\pi)/\Gamma(\Sigma\pi)$

VALUE	DOCUMENT ID	TECN	COMMENT	Γ_2/Γ_3
••• We do not use the following data for averages, fits, limits, etc. •••				
<0.18	BARNES 69	HBC	1 standard dev. limit	

 $(\Gamma_1\Gamma_4)^{1/2}/\Gamma_{\text{total}}$ in $N\bar{K} \rightarrow \Sigma(2250) \rightarrow \Xi(1530)K$

VALUE	DOCUMENT ID	TECN	COMMENT	$(\Gamma_1\Gamma_4)^{1/2}/\Gamma$
0.18 ± 0.04	¹ DEBELLEFON 75B	HBC	$K^-p \rightarrow \Xi^{*0}K^0$	

 $\Sigma(2250)$ FOOTNOTES¹ Seen in the (initial and final state) D_5 wave. Isospin not determined. $\Sigma(2250)$ REFERENCES

DEBELLEFON 78	NC 42A 403	A. de Bellefon et al.	(CDEF, SACL) IJP
DEBELLEFON 77	NC 37A 175	A. de Bellefon et al.	(CDEF, SACL) IJP
DEBELLEFON 76	NP B109 129	A. de Bellefon, A. Berthon	(CDEF) IJP
Also	NP B90 1	A. de Bellefon et al.	(CDEF, SACL) IJP
DEBELLEFON 75B	NC 28A 289	A. de Bellefon et al.	(CDEF, SACL) IJP
VANHORN 75	NP B87 145	A.J. van Horn	(LBL) IJP
Also	NP B87 157	A.J. van Horn	(LBL) IJP
LASINSKI 71	NP B29 125	T.A. Lasinski	(TIF) IJP
AGUILAR-... 70B	PRL 25 58	M. Aguilar-Benitez et al.	(BNL, SYR) A
BARBARO-... 70	Duke Conf. 173	A. Barbaro-Galleri	(LRL) IJP
Hyperon Resonances, 1970			
BRICMAN 70	PL 31B 152	C. Bricman et al.	(CERN, CAEN, SACL)
COOL 70	PR D1 1887	R.L. Cool et al.	(BNL) I
Also	PRL 16 1228	R.L. Cool et al.	(BNL) I
LU 70	PR D2 1846	D.C. Lu et al.	(YALE)
BARNES 69	PRL 22 479	V.E. Barnes et al.	(BNL, SYR) A
BUGG 68	PR 168 1466	D.V. Bugg et al.	(RHEL, BIRM, CAVE) I
BLANPIED 65	PRL 14 741	W.A. Blanpied et al.	(YALE, CE) A
BOCK 65	PL 17 166	R.K. Bock et al.	(CERN, SACL)

See key on page 1171

Baryon Particle Listings

$\Sigma(2455)$ Bumps, $\Sigma(2620)$ Bumps, $\Sigma(3000)$ Bumps, $\Sigma(3170)$ Bumps

$\Sigma(2455)$ Bumps $I(J^P) = 1(?^?)$ Status: *

OMITTED FROM SUMMARY TABLE
There is also some slight evidence for Y^* states in this mass region from the reaction $\gamma p \rightarrow K^+ X$ — see GREENBERG 68.

$\Sigma(2455)$ MASS

VALUE (MeV)	DOCUMENT ID	TECN	COMMENT
≈ 2455 OUR ESTIMATE			
2455 ± 10	ABRAMS 70	CNTR	$K^- p, K^- d$ total
2455 ± 7	BUGG 68	CNTR	$K^- p, K^- d$ total

$\Sigma(2455)$ WIDTH

VALUE (MeV)	DOCUMENT ID	TECN	COMMENT
140	ABRAMS 70	CNTR	$K^- p, K^- d$ total
100 ± 20	BUGG 68	CNTR	

$\Sigma(2455)$ DECAY MODES

Mode	Γ_1
$N\bar{K}$	

$\Sigma(2455)$ BRANCHING RATIOS

$(J+\frac{1}{2}) \times \Gamma(N\bar{K}) / \Gamma_{total}$	VALUE	DOCUMENT ID	TECN	COMMENT	Γ_1 / Γ
	0.39	ABRAMS 70	CNTR	$K^- p, K^- d$ total	
	0.05 ± 0.05	¹ BRICMAN 70	CNTR	Total, charge exchange	
	0.3	BUGG 68	CNTR		

$\Sigma(2455)$ FOOTNOTES
¹ Fit of total cross section given by BRICMAN 70 is poor in this region.

$\Sigma(2455)$ REFERENCES

ABRAMS 70	PR D1 1917	R.J. Abrams et al.	(BNL) ¹
Also	PRL 19 678	R.J. Abrams et al.	(BNL)
BRICMAN 70	PL 31B 152	C. Bricean et al.	(CERN, CAEN, SAACL)
BUGG 68	PR 168 1466	D.V. Bugg et al.	(RHEL, BIRM, CAVE) ¹
GREENBERG 68	PRL 20 221	J.S. Greenberg et al.	(YALE)

$\Sigma(2620)$ Bumps $I(J^P) = 1(?^?)$ Status: *

OMITTED FROM SUMMARY TABLE

$\Sigma(2620)$ MASS

VALUE (MeV)	DOCUMENT ID	TECN	COMMENT
≈ 2620 OUR ESTIMATE			
2542 ± 22	DIBIANCA 75	DBC	$K^- N \rightarrow \Xi K\pi$
2620 ± 15	ABRAMS 70	CNTR	$K^- p, K^- d$ total

$\Sigma(2620)$ WIDTH

VALUE (MeV)	DOCUMENT ID	TECN	COMMENT
221 ± 81	DIBIANCA 75	DBC	$K^- N \rightarrow \Xi K\pi$
175	ABRAMS 70	CNTR	$K^- p, K^- d$ total

$\Sigma(2620)$ DECAY MODES

Mode	Γ_1
$N\bar{K}$	

$\Sigma(2620)$ BRANCHING RATIOS

$(J+\frac{1}{2}) \times \Gamma(N\bar{K}) / \Gamma_{total}$	VALUE	DOCUMENT ID	TECN	COMMENT	Γ_1 / Γ
	0.32	ABRAMS 70	CNTR	$K^- p, K^- d$ total	
	0.36 ± 0.12	BRICMAN 70	CNTR	Total, charge exchange	

$\Sigma(2620)$ REFERENCES

DIBIANCA 75	NP B98 137	F.A. Dibiaccia, R.J. Endorf	(CMU)
ABRAMS 70	PR D1 1917	R.J. Abrams et al.	(BNL) ¹
Also	PRL 19 678	R.J. Abrams et al.	(BNL)
BRICMAN 70	PL 31B 152	C. Bricean et al.	(CERN, CAEN, SAACL)

$\Sigma(3000)$ Bumps $I(J^P) = 1(?^?)$ Status: *

OMITTED FROM SUMMARY TABLE
Seen as an enhancement in $\Lambda\pi$ and $\bar{K}N$ invariant mass spectra and in the missing mass of neutrals recoiling against a K^0 .

$\Sigma(3000)$ MASS

VALUE (MeV)	DOCUMENT ID	TECN	CHG	COMMENT
≈ 3000 OUR ESTIMATE				
3000	EHRlich 66	HBC	0	$\pi^- p$ 7.91 GeV/c

$\Sigma(3000)$ DECAY MODES

Mode	Γ_1	Γ_2
$N\bar{K}$		
$\Lambda\pi$		

$\Sigma(3000)$ REFERENCES
EHRlich 66 PR 152 1194 R. Ehrlich, W. Selove, H. Yuta (PENN)¹

$\Sigma(3170)$ Bumps $I(J^P) = 1(?^?)$ Status: *

OMITTED FROM SUMMARY TABLE
Seen by AMIRZADEH 79 as a narrow 6.5-standard-deviation enhancement in the reaction $K^- p \rightarrow Y^{*+} \pi^-$ using data from independent high statistics bubble chamber experiments at 8.25 and 6.5 GeV/c. The dominant decay modes are multibody, multistrange final states and the production is via isospin-3/2 baryon exchange. Isospin 1 is favored.

Not seen in a $K^- p$ experiment in LASS at 11 GeV/c (ASTON 85B).

$\Sigma(3170)$ MASS (PRODUCTION EXPERIMENTS)

VALUE (MeV)	EVTS	DOCUMENT ID	TECN	COMMENT
≈ 3170 OUR ESTIMATE				
3170 ± 5	35	AMIRZADEH 79	HBC	$K^- p \rightarrow Y^{*+} \pi^-$

$\Sigma(3170)$ WIDTH (PRODUCTION EXPERIMENTS)

VALUE (MeV)	EVTS	DOCUMENT ID	TECN	COMMENT
<20	35	¹ AMIRZADEH 79	HBC	$K^- p \rightarrow Y^{*+} \pi^-$

$\Sigma(3170)$ DECAY MODES (PRODUCTION EXPERIMENTS)

Mode	Fraction (Γ_i / Γ)
$\Lambda K \bar{K} \pi$'s	seen
$\Sigma K \bar{K} \pi$'s	seen
$\Xi K \pi$'s	seen

$\Sigma(3170)$ BRANCHING RATIOS (PRODUCTION EXPERIMENTS)

$\Gamma(\Lambda K \bar{K} \pi \text{'s}) / \Gamma_{total}$	VALUE	DOCUMENT ID	TECN	COMMENT	Γ_1 / Γ
	seen	AMIRZADEH 79	HBC	$K^- p \rightarrow Y^{*+} \pi^-$	
$\Gamma(\Sigma K \bar{K} \pi \text{'s}) / \Gamma_{total}$	VALUE	DOCUMENT ID	TECN	COMMENT	Γ_2 / Γ
	seen	AMIRZADEH 79	HBC	$K^- p \rightarrow Y^{*+} \pi^-$	
$\Gamma(\Xi K \pi \text{'s}) / \Gamma_{total}$	VALUE	DOCUMENT ID	TECN	COMMENT	Γ_3 / Γ
	seen	AMIRZADEH 79	HBC	$K^- p \rightarrow Y^{*+} \pi^-$	

$\Sigma(3170)$ FOOTNOTES (PRODUCTION EXPERIMENTS)
¹ Observed width consistent with experimental resolution.

$\Sigma(3170)$ REFERENCES (PRODUCTION EXPERIMENTS)

ASTON 85B	PR D32 2270	D. Aston et al.	(SLAC, CARL, CNRC, CINC)
AMIRZADEH 79	PL 89B 125	J. Amirzadeh et al.	(BIRM, CERN, GLAS+) ¹
Also	Toronto Conf. 263	J.B. Kinson et al.	(BIRM, CERN, GLAS+) ¹

Baryon Particle Listings

 Ξ^0

Ξ BARYONS

$(S = -2, I = 1/2)$

$$\Xi^0 = uss, \Xi^- = dss$$

 Ξ^0

$$I(J^P) = \frac{1}{2}(\frac{1}{2}^+) \text{ Status: } ****$$

The parity has not actually been measured, but + is of course expected.

 Ξ^0 MASS

The fit uses the Ξ^0 , Ξ^- , and Ξ^+ masses and the $\Xi^- - \Xi^0$ mass difference. It assumes that the Ξ^- and Ξ^+ masses are the same.

VALUE (MeV)	EVTS	DOCUMENT ID	TECN	COMMENT
1314.86 ± 0.20 OUR FIT				
1314.82 ± 0.06 ± 0.20	3120	FANTI	00 NA48	p Be, 450 GeV
• • • We do not use the following data for averages, fits, limits, etc. • • •				
1315.2 ± 0.92	49	WILQUET	72 HLBC	
1313.4 ± 1.8	1	PALMER	68 HBC	

 $m_{\Xi^-} - m_{\Xi^0}$

The fit uses the Ξ^0 , Ξ^- , and Ξ^+ masses and the $\Xi^- - \Xi^0$ mass difference. It assumes that the Ξ^- and Ξ^+ masses are the same.

VALUE (MeV)	EVTS	DOCUMENT ID	TECN	COMMENT
6.85 ± 0.21 OUR FIT				
6.3 ± 0.7 OUR AVERAGE				
6.9 ± 2.2	29	LONDON	66 HBC	
6.1 ± 0.9	88	PJERROU	65B HBC	
6.8 ± 1.6	23	JAUNEAU	63 FBC	
• • • We do not use the following data for averages, fits, limits, etc. • • •				
6.1 ± 1.6	45	CARMONY	64B HBC	See PJERROU 65B

 Ξ^0 MEAN LIFE

VALUE (10^{-10} s)	EVTS	DOCUMENT ID	TECN	COMMENT
2.90 ± 0.09 OUR AVERAGE				
2.83 ± 0.16	6300	¹ ZECH	77 SPEC	Neutral hyperon beam
2.88 ^{+0.21} _{-0.19}	652	BALTAY	74 HBC	1.75 GeV/c $K^- p$
2.90 ^{+0.32} _{-0.27}	157	² MAYEUR	72 HLBC	2.1 GeV/c K^-
3.07 ^{+0.22} _{-0.20}	340	DAUBER	69 HBC	
3.0 ± 0.5	80	PJERROU	65B HBC	
2.5 ^{+0.4} _{-0.3}	101	HUBBARD	64 HBC	
3.9 ^{+1.4} _{-0.8}	24	JAUNEAU	63 FBC	
• • • We do not use the following data for averages, fits, limits, etc. • • •				
3.5 ^{+1.0} _{-0.8}	45	CARMONY	64B HBC	See PJERROU 65B

¹ The ZECH 77 result is $\tau_{\Xi^0} = [2.77 - (\tau_A - 2.69)] \times 10^{-10}$ s, in which we use $\tau_A = 2.63 \times 10^{-10}$ s.

² The MAYEUR 72 value is modified by the erratum.

 Ξ^0 MAGNETIC MOMENT

See the "Quark Model" review.

VALUE (μ_N)	EVTS	DOCUMENT ID	TECN	COMMENT
-1.250 ± 0.014 OUR AVERAGE				
-1.253 ± 0.014	270k	COX	81 SPEC	
-1.20 ± 0.06	42k	BUNCE	79 SPEC	

 Ξ^0 DECAY MODES

Mode	Fraction (Γ_i/Γ)	Confidence level
$\Gamma_1 \Lambda\pi^0$	(99.524 ± 0.012) %	
$\Gamma_2 \Lambda\gamma$	(1.17 ± 0.07) × 10 ⁻³	
$\Gamma_3 \Lambda e^+ e^-$	(7.6 ± 0.6) × 10 ⁻⁶	
$\Gamma_4 \Sigma^0 \gamma$	(3.33 ± 0.10) × 10 ⁻³	
$\Gamma_5 \Sigma^+ e^- \bar{\nu}_e$	(2.52 ± 0.08) × 10 ⁻⁴	
$\Gamma_6 \Sigma^+ \mu^- \bar{\nu}_\mu$	(2.33 ± 0.35) × 10 ⁻⁶	

 $\Delta S = \Delta Q$ (SQ) violating modes or $\Delta S = 2$ forbidden (S_2) modes

$\Gamma_7 \Sigma^- e^+ \nu_e$	SQ	< 1.6	× 10 ⁻⁴	90%
$\Gamma_8 \Sigma^- \mu^+ \nu_\mu$	SQ	< 9	× 10 ⁻⁴	90%
$\Gamma_9 p \pi^-$	S2	< 8	× 10 ⁻⁶	90%
$\Gamma_{10} p e^- \bar{\nu}_e$	S2	< 1.3	× 10 ⁻³	
$\Gamma_{11} p \mu^- \bar{\nu}_\mu$	S2	< 1.3	× 10 ⁻³	
$\Gamma_{12} K^- e^+$				
$\Gamma_{13} K^+ e^-$				

CONSTRAINED FIT INFORMATION

An overall fit to 5 branching ratios uses 11 measurements and one constraint to determine 5 parameters. The overall fit has a $\chi^2 = 7.5$ for 7 degrees of freedom.

The following *off-diagonal* array elements are the correlation coefficients $\langle \delta x_i \delta x_j \rangle / (\delta x_i \delta x_j)$, in percent, from the fit to the branching fractions, $x_i \equiv \Gamma_i/\Gamma_{\text{total}}$. The fit constrains the x_i whose labels appear in this array to sum to one.

x_2	-57				
x_4	-82	0			
x_5	-7	0	0		
x_6	0	0	0	1	
	x_1	x_2	x_4	x_5	

 Ξ^0 BRANCHING RATIOS

$\Gamma(\Lambda\gamma)/\Gamma(\Lambda\pi^0)$	VALUE (units 10 ⁻³)	EVTS	DOCUMENT ID	TECN	COMMENT	Γ_2/Γ_1
1.17 ± 0.07 OUR FIT						
1.17 ± 0.07 OUR AVERAGE						
1.17 ± 0.05 ± 0.06	672	¹ LAI	04A NA48	p Be, 450 GeV		
1.91 ± 0.34 ± 0.19	31	² FANTI	00 NA48	p Be, 450 GeV		
1.06 ± 0.12 ± 0.11	116	JAMES	90 SPEC	FNAL hyperons		

¹ LAI 04A used our 2002 value of 99.5% for the $\Xi^0 \rightarrow \Lambda\pi^0$ branching fraction to get $\Gamma(\Xi^0 \rightarrow \Lambda\gamma)/\Gamma_{\text{total}} = (1.16 \pm 0.05 \pm 0.06) \times 10^{-3}$. We adjust slightly to go back to what was directly measured.

² FANTI 00 used our 1998 value of 99.5% for the $\Xi^0 \rightarrow \Lambda\pi^0$ branching fraction to get $\Gamma(\Xi^0 \rightarrow \Lambda\gamma)/\Gamma_{\text{total}} = (1.90 \pm 0.34 \pm 0.19) \times 10^{-3}$. We adjust slightly to go back to what was directly measured.

$\Gamma(\Lambda e^+ e^-)/\Gamma_{\text{total}}$	VALUE (units 10 ⁻⁶)	EVTS	DOCUMENT ID	TECN	COMMENT	Γ_3/Γ
7.6 ± 0.4 ± 0.5	397 ± 21	¹ BATLEY	07c NA48	p Be, 400 GeV		

¹ This BATLEY 07c result is consistent with internal bremsstrahlung.

$\Gamma(\Sigma^0 \gamma)/\Gamma(\Lambda\pi^0)$	VALUE (units 10 ⁻³)	EVTS	DOCUMENT ID	TECN	COMMENT	Γ_4/Γ_1
3.35 ± 0.10 OUR FIT						
3.35 ± 0.10 OUR AVERAGE						
3.34 ± 0.05 ± 0.09	4045	ALAVI-HARATI	01c KTEV	p nucleus, 800 GeV		
3.16 ± 0.76 ± 0.32	17	¹ FANTI	00 NA48	p Be, 450 GeV		
3.56 ± 0.42 ± 0.10	85	TEIGE	89 SPEC	FNAL hyperons		

¹ FANTI 00 used our 1998 value of 99.5% for the $\Xi^0 \rightarrow \Lambda\pi^0$ branching fraction to get $\Gamma(\Xi^0 \rightarrow \Sigma^0 \gamma)/\Gamma_{\text{total}} = (3.14 \pm 0.76 \pm 0.32) \times 10^{-3}$. We adjust slightly to go back to what was directly measured.

$\Gamma(\Sigma^+ e^- \bar{\nu}_e)/\Gamma_{\text{total}}$	VALUE (units 10 ⁻⁴)	EVTS	DOCUMENT ID	TECN	COMMENT	Γ_5/Γ
2.52 ± 0.08 OUR FIT						
2.53 ± 0.08 OUR AVERAGE						
2.51 ± 0.03 ± 0.09	6101	BATLEY	07 NA48	p Be, 400 GeV		
2.55 ± 0.14 ± 0.10	419	¹ BATLEY	07 NA48	p Be, 400 GeV		
2.71 ± 0.22 ± 0.31	176	AFFOLDER	99 KTEV	p nucleus, 800 GeV		

¹ This BATLEY 07 result is for $\Xi^0 \rightarrow \Sigma^- e^+ \nu_e$ events.

$\Gamma(\Sigma^+ \mu^- \bar{\nu}_\mu)/\Gamma_{\text{total}}$	VALUE (units 10 ⁻⁶)	EVTS	DOCUMENT ID	TECN	COMMENT	Γ_6/Γ
2.3 ± 0.4 OUR FIT						
2.17 ± 0.32 ± 0.17	66	¹ BATLEY	13 NA48	p Be, 400 GeV		

¹ BATLEY 13 used $\Xi^0 \rightarrow \Sigma^+ e^- \bar{\nu}_e$ decay as a normalization mode and its branching fraction value of $(2.51 \pm 0.03 \pm 0.09) \times 10^{-4}$ from BATLEY 07.

$\Gamma(\Sigma^+ \mu^- \bar{\nu}_\mu)/\Gamma(\Sigma^+ e^- \bar{\nu}_e)$	VALUE	EVTS	DOCUMENT ID	TECN	COMMENT	Γ_6/Γ_5
0.0092 ± 0.0015 OUR FIT						
0.018^{+0.007}_{-0.005} ± 0.002	9	ABOUZAID	05 KTEV	p nucleus 800 GeV		

$\Gamma(\Sigma^- e^+ \nu_e)/\Gamma_{\text{total}}$					Γ_7/Γ
VALUE	CL%	DOCUMENT ID	TECN	COMMENT	
$<1.6 \times 10^{-4}$	90	ABLIKIM	23B BES3	$J/\psi \rightarrow \Xi^0 \Xi^0$	

$\Gamma(\Sigma^- e^+ \nu_e)/\Gamma(\Lambda\pi^0)$					Γ_7/Γ_1
Test of $\Delta S = \Delta Q$ rule.					
VALUE (units 10^{-3})	CL%	DOCUMENT ID	TECN	COMMENT	
••• We do not use the following data for averages, fits, limits, etc. •••					
<0.9	90	YEH	74 HBC	Effective denom.=2500	
<1.5		DAUBER	69 HBC		
<6		HUBBARD	66 HBC		

$\Gamma(\Sigma^- \mu^+ \nu_\mu)/\Gamma(\Lambda\pi^0)$					Γ_8/Γ_1
Test of $\Delta S = \Delta Q$ rule.					
VALUE (units 10^{-3})	CL%	DOCUMENT ID	TECN	COMMENT	
<0.9	90	YEH	74 HBC	Effective denom.=2500	
••• We do not use the following data for averages, fits, limits, etc. •••					
<1.5		DAUBER	69 HBC		
<6		HUBBARD	66 HBC		

$\Gamma(p\pi^-)/\Gamma(\Lambda\pi^0)$					Γ_9/Γ_1
$\Delta S=2$. Forbidden in first-order weak interaction.					
VALUE (units 10^{-6})	CL%	DOCUMENT ID	TECN	COMMENT	
< 8.2	90	WHITE	05 HYCP	p Cu, 800 GeV	
••• We do not use the following data for averages, fits, limits, etc. •••					
< 36	90	GEWENIGER	75 SPEC		
<1800	90	YEH	74 HBC	Effective denom.=1300	
< 900		DAUBER	69 HBC		
<5000		HUBBARD	66 HBC		

$\Gamma(p e^- \bar{\nu}_e)/\Gamma(\Lambda\pi^0)$					Γ_{10}/Γ_1
$\Delta S=2$. Forbidden in first-order weak interaction.					
VALUE (units 10^{-3})	CL%	DOCUMENT ID	TECN	COMMENT	
<1.3		DAUBER	69 HBC		
••• We do not use the following data for averages, fits, limits, etc. •••					
<3.4	90	YEH	74 HBC	Effective denom.=670	
<6		HUBBARD	66 HBC		

$\Gamma(p\mu^- \bar{\nu}_\mu)/\Gamma(\Lambda\pi^0)$					Γ_{11}/Γ_1
$\Delta S=2$. Forbidden in first-order weak interaction.					
VALUE (units 10^{-3})	CL%	DOCUMENT ID	TECN	COMMENT	
<1.3		DAUBER	69 HBC		
••• We do not use the following data for averages, fits, limits, etc. •••					
<3.5	90	YEH	74 HBC	Effective denom.=664	
<6		HUBBARD	66 HBC		

$\Gamma(K^- e^+)/\Gamma_{\text{total}}$					Γ_{12}/Γ
VALUE	CL%	DOCUMENT ID	TECN	COMMENT	
$<3.6 \times 10^{-6}$	90	¹ ABLIKIM	23AP BES3	$J/\psi \rightarrow \Xi^0 \Xi^0$	
¹ This decay mode violates baryon and lepton number conservation with $ \Delta(B-L) =0$.					

$\Gamma(K^+ e^-)/\Gamma_{\text{total}}$					Γ_{13}/Γ
VALUE	CL%	DOCUMENT ID	TECN	COMMENT	
$<1.9 \times 10^{-6}$	90	¹ ABLIKIM	23AP BES3	$J/\psi \rightarrow \Xi^0 \Xi^0$	
¹ This decay mode violates baryon and lepton number conservation with $ \Delta(B-L) =2$.					

Ξ^0 DECAY PARAMETERS

See the "Note on Baryon Decay Parameters" in the neutron Listings.

$\alpha(\Xi^0) \alpha_-(\Lambda)$

This is a product of the $\Xi^0 \rightarrow \Lambda\pi^0$ and $\Lambda \rightarrow p\pi^-$ asymmetries.

VALUE	EVTS	DOCUMENT ID	TECN	COMMENT
-0.261 ± 0.006	OUR AVERAGE			
$-0.276 \pm 0.001 \pm 0.035$	4M	BATLEY	10B NA48	p Be, 400 GeV
$-0.260 \pm 0.004 \pm 0.005$	300k	HANDLER	82 SPEC	FNAL hyperons
••• We do not use the following data for averages, fits, limits, etc. •••				
-0.317 ± 0.027	6075	BUNCE	78 SPEC	FNAL hyperons
-0.35 ± 0.06	505	BALTAY	74 HBC	$K^- p$ 1.75 GeV/c
-0.28 ± 0.06	739	DAUBER	69 HBC	$K^- p$ 1.7–2.6 GeV/c

α FOR $\Xi^0 \rightarrow \Lambda\pi^0$

The PDG 22 average $\alpha(\Xi^0)\alpha_-(\Lambda) = -0.261 \pm 0.006$ divided by the PDG 22 average $\alpha_-(\Lambda) = 0.748 \pm 0.007$ gives $\alpha(\Xi^0) = -0.349 \pm 0.009$.

VALUE	EVTS	DOCUMENT ID	TECN	COMMENT
-0.349 ± 0.009	OUR EVALUATION			
$-0.3750 \pm 0.0034 \pm 0.0016$	327k	ABLIKIM	23AU BES3	$J/\psi \rightarrow \Xi^0 \Xi^0$
••• We do not use the following data for averages, fits, limits, etc. •••				
$-0.358 \pm 0.042 \pm 0.013$	1.9k	ABLIKIM	23AD BES3	$\psi(2S) \rightarrow \Xi^0 \Xi^0$

α FOR $\Xi^0 \rightarrow \bar{\Lambda}\pi^0$

VALUE	EVTS	DOCUMENT ID	TECN	COMMENT
$0.3790 \pm 0.0034 \pm 0.0021$	327k	ABLIKIM	23AU BES3	$J/\psi \rightarrow \Xi^0 \Xi^0$
••• We do not use the following data for averages, fits, limits, etc. •••				
$0.363 \pm 0.042 \pm 0.013$	1.9k	ABLIKIM	23AD BES3	$\psi(2S) \rightarrow \Xi^0 \Xi^0$

ϕ ANGLE FOR $\Xi^0 \rightarrow \Lambda\pi^0$

($\tan\phi = \beta/\gamma$)

VALUE (°)	EVTS	DOCUMENT ID	TECN	COMMENT
$0.292 \pm 0.550 \pm 0.103$	327k	¹ ABLIKIM	23AU BES3	$J/\psi \rightarrow \Xi^0 \Xi^0$
••• We do not use the following data for averages, fits, limits, etc. •••				
$1.55 \pm 6.70 \pm 0.63$	1.9k	ABLIKIM	23AD BES3	$\psi(2S) \rightarrow \Xi^0 \Xi^0$
16 ± 17	652	BALTAY	74 HBC	1.75 GeV/c $K^- p$
38 ± 19	739	² DAUBER	69 HBC	
-8 ± 30	146	³ BERGE	66 HBC	

¹ Converted from radians to degrees.

² DAUBER 69 uses $\alpha_\Lambda = 0.647 \pm 0.020$.

³ The errors have been multiplied by 1.2 due to approximations used for the Ξ polarization; see DAUBER 69 for a discussion.

ϕ ANGLE FOR $\Xi^0 \rightarrow \bar{\Lambda}\pi^0$ with $\tan\phi = \beta/\gamma$

VALUE (degrees)	EVTS	DOCUMENT ID	TECN	COMMENT
$-0.304 \pm 0.556 \pm 0.109$	327k	ABLIKIM	23AU BES3	$J/\psi \rightarrow \Xi^0 \Xi^0$
••• We do not use the following data for averages, fits, limits, etc. •••				
$-10.60 \pm 6.65 \pm 0.97$	1.9k	ABLIKIM	23AD BES3	$\psi(2S) \rightarrow \Xi^0 \Xi^0$

$\Delta\phi_{CP}(\Xi^0) = (\phi_{\Xi^0} + \phi_{\Xi^0})/2$

VALUE (degrees)	EVTS	DOCUMENT ID	TECN	COMMENT
$-0.006 \pm 0.395 \pm 0.052$	327k	¹ ABLIKIM	23AU BES3	$J/\psi \rightarrow \Xi^0 \Xi^0$
••• We do not use the following data for averages, fits, limits, etc. •••				
$-4.53 \pm 4.70 \pm 0.57$	1.9k	¹ ABLIKIM	23AD BES3	$\psi(2S) \rightarrow \Xi^0 \Xi^0$
¹ Converted from radians to degrees.				

A_{CP} FOR $\Xi^0 \rightarrow \Lambda\pi^0, \Xi^0 \rightarrow \bar{\Lambda}\pi^0$

$A_{CP} = (\alpha + \bar{\alpha}) / (\alpha - \bar{\alpha})$

VALUE (units 10^{-3})	EVTS	DOCUMENT ID	TECN	COMMENT
$-5.4 \pm 6.5 \pm 3.1$	327k	¹ ABLIKIM	23AU BES3	$J/\psi \rightarrow \Xi^0 \Xi^0$
••• We do not use the following data for averages, fits, limits, etc. •••				
$-7 \pm 82 \pm 25$	1.9k	¹ ABLIKIM	23AD BES3	$\psi(2S) \rightarrow \Xi^0 \Xi^0$
¹ Probing CP symmetry and weak phases with entangled double-strange baryons.				

RADIATIVE HYPERON DECAYS

Revised July 2011 by J.D. Jackson (LBNL).

The weak radiative decays of spin-1/2 hyperons, $B_i \rightarrow B_f \gamma$, yield information about matrix elements (form factors) similar to that gained from weak hadronic decays. For a polarized spin-1/2 hyperon decaying radiatively via a $\Delta Q = 0, \Delta S = 1$ transition, the angular distribution of the direction $\hat{\mathbf{p}}$ of the final spin-1/2 baryon in the hyperon rest frame is

$$\frac{dN}{d\Omega} = \frac{N}{4\pi} (1 + \alpha_\gamma \mathbf{P}_i \cdot \hat{\mathbf{p}}). \quad (1)$$

Here \mathbf{P}_i is the polarization of the decaying hyperon, and α_γ is the asymmetry parameter. In terms of the form factors $F_1(q^2)$, $F_2(q^2)$, and $G(q^2)$ of the effective hadronic weak electromagnetic vertex,

$$F_1(q^2)\gamma_\lambda + iF_2(q^2)\sigma_{\lambda\mu}q^\mu + G(q^2)\gamma_\lambda\gamma_5,$$

α_γ is

$$\alpha_\gamma = \frac{2 \operatorname{Re}[G(0)F_M^*(0)]}{|G(0)|^2 + |F_M(0)|^2}, \quad (2)$$

where $F_M = (m_i - m_f)[F_2 - F_1/(m_i + m_f)]$. If the decaying hyperon is unpolarized, the decay baryon has a longitudinal polarization given by $P_f = -\alpha_\gamma$ [1].

The angular distribution for the weak hadronic decay, $B_i \rightarrow B_f \pi$, has the same form as Eq. (1), but of course with a different asymmetry parameter, α_π . Now, however, if the decaying hyperon is unpolarized, the decay baryon has a

Baryon Particle Listings

 Ξ^0

longitudinal polarization given by $P_f = +\alpha_\pi$ [2,3]. The difference of sign is because the spins of the pion and photon are different.

$\Xi^0 \rightarrow \Lambda\gamma$ *decay*—The radiative decay $\Xi^0 \rightarrow \Lambda\gamma$ of an unpolarized Ξ^0 uses the hadronic decay $\Lambda \rightarrow p\pi^-$ as the analyzer. As noted above, the longitudinal polarization of the Λ will be $P_\Lambda = -\alpha_{\Xi\Lambda\gamma}$. Let α_- be the $\Lambda \rightarrow p\pi^-$ asymmetry parameter and $\theta_{\Lambda p}$ be the angle, as seen in the Λ rest frame, between the Λ line of flight and the proton momentum. Then the hadronic version of Eq. (1) applied to the $\Lambda \rightarrow p\pi^-$ decay gives

$$\frac{dN}{d\cos\theta_{\Lambda p}} = \frac{N}{2} (1 - \alpha_{\Xi\Lambda\gamma} \alpha_- \cos\theta_{\Lambda p}) \quad (3)$$

for the angular distribution of the proton in the Λ frame. Our current value, from the CERN NA48/1 experiment [4], is $\alpha_{\Xi\Lambda\gamma} = -0.704 \pm 0.019 \pm 0.064$.

$\Xi^0 \rightarrow \Sigma^0\gamma$ *decay*—The asymmetry parameter here, $\alpha_{\Xi\Sigma\gamma}$, is measured by following the decay chain $\Xi^0 \rightarrow \Sigma^0\gamma$, $\Sigma^0 \rightarrow \Lambda\gamma$, $\Lambda \rightarrow p\pi^-$. Again, for an unpolarized Ξ^0 , the longitudinal polarization of the Σ^0 will be $P_\Sigma = -\alpha_{\Xi\Sigma\gamma}$. In the $\Sigma^0 \rightarrow \Lambda\gamma$ decay, a parity-conserving magnetic-dipole transition, the polarization of the Σ^0 is transferred to the Λ , as may be seen as follows. Let $\theta_{\Sigma\Lambda}$ be the angle seen in the Σ^0 rest frame between the Σ^0 line of flight and the Λ momentum. For Σ^0 helicity $+1/2$, the probability amplitudes for positive and negative spin states of the Σ^0 along the Λ momentum are $\cos(\theta_{\Sigma\Lambda}/2)$ and $\sin(\theta_{\Sigma\Lambda}/2)$. Then the amplitude for a negative helicity photon and a negative helicity Λ is $\cos(\theta_{\Sigma\Lambda}/2)$, while the amplitude for positive helicities for the photon and Λ is $\sin(\theta_{\Sigma\Lambda}/2)$. For Σ^0 helicity $-1/2$, the amplitudes are interchanged. If the Σ^0 has longitudinal polarization P_Σ , the probabilities for Λ helicities $\pm 1/2$ are therefore

$$p(\pm 1/2) = \frac{1}{2} (1 \mp P_\Sigma) \cos^2(\theta_{\Sigma\Lambda}/2) + \frac{1}{2} (1 \pm P_\Sigma) \sin^2(\theta_{\Sigma\Lambda}/2), \quad (4)$$

and the longitudinal polarization of the Λ is

$$P_\Lambda = -P_\Sigma \cos\theta_{\Sigma\Lambda} = +\alpha_{\Xi\Sigma\gamma} \cos\theta_{\Sigma\Lambda}. \quad (5)$$

Using Eq. (1) for the $\Lambda \rightarrow p\pi^-$ decay again, we get for the joint angular distribution of the $\Sigma^0 \rightarrow \Lambda\gamma$, $\Lambda \rightarrow p\pi^-$ chain,

$$\frac{d^2N}{d\cos\theta_{\Sigma\Lambda} d\cos\theta_{\Lambda p}} = \frac{N}{4} (1 + \alpha_{\Xi\Sigma\gamma} \cos\theta_{\Sigma\Lambda} \alpha_- \cos\theta_{\Lambda p}). \quad (6)$$

Our current average for $\alpha_{\Xi\Sigma\gamma}$ is -0.69 ± 0.06 [4,5].

References

1. R.E. Behrends, Phys. Rev. **111**, 1691 (1958); see Eq. (7) or (8).
2. In ancient times, the signs of the asymmetry term in the angular distributions of radiative and hadronic decays of polarized hyperons were sometimes opposite. For roughly 50 years, however, the overwhelming convention has been to make them the same. The aim, not always achieved, is to remove ambiguities.
3. For the definition of α_π , see the note on “Baryon Decay Parameters” in the Neutron Listings.
4. J.R. Batley *et al.*, Phys. Lett. **B693**, 241 (2010).
5. A. Alavi-Harati *et al.*, Phys. Rev. Lett. **86**, 3239 (2001).

 α FOR $\Xi^0 \rightarrow \Lambda\gamma$

See the note above on “Radiative Hyperon Decays.”

VALUE	EVTS	DOCUMENT ID	TECN	COMMENT
$-0.704 \pm 0.019 \pm 0.064$	52k	¹ BATLEY	10B NA48	p Be, 400 GeV
• • • We do not use the following data for averages, fits, limits, etc. • • •				
$-0.78 \pm 0.18 \pm 0.06$	672	LAI	04A NA48	See BATLEY 10B
-0.43 ± 0.44	87	² JAMES	90 SPEC	FNAL hyperons
¹ BATLEY 10B also measured the $\Xi^0 \rightarrow \bar{\Lambda}\gamma$ asymmetry to be -0.798 ± 0.064 (no systematic error given) with 4769 events.				
² The sign has been changed; see the erratum, JAMES 02.				

 α FOR $\Xi^0 \rightarrow \Lambda e^+ e^-$

VALUE	EVTS	DOCUMENT ID	TECN	COMMENT
-0.8 ± 0.2	397 \pm 21	¹ BATLEY	07C NA48	p Be, 400 GeV
¹ This BATLEY 07C result is consistent with the asymmetry α for $\Xi^0 \rightarrow \Lambda\gamma$, as expected if the mechanism is internal bremsstrahlung.				

 α FOR $\Xi^0 \rightarrow \Sigma^0\gamma$

See the note above on “Radiative Hyperon Decays.”

VALUE	EVTS	DOCUMENT ID	TECN	COMMENT
-0.69 ± 0.06 OUR AVERAGE				
$-0.729 \pm 0.030 \pm 0.076$	15k	¹ BATLEY	10B NA48	p Be, 400 GeV
$-0.63 \pm 0.08 \pm 0.05$	4045	ALAVI-HARATI01C	KTEV	p nucleus, 800 GeV
• • • We do not use the following data for averages, fits, limits, etc. • • •				
$+0.20 \pm 0.32 \pm 0.05$	85	² TEIGE	89 SPEC	FNAL hyperons
¹ BATLEY 10B also measured the $\Xi^0 \rightarrow \bar{\Sigma}^0\gamma$ asymmetry to be -0.786 ± 0.104 (no systematic error given) with 1404 events.				
² This result has been withdrawn, due to an error. See the erratum, TEIGE 02.				

 $g_1(0)/f_1(0)$ FOR $\Xi^0 \rightarrow \Sigma^+ e^- \bar{\nu}_e$

VALUE	EVTS	DOCUMENT ID	TECN	COMMENT
1.22 ± 0.05 OUR AVERAGE				
1.21 ± 0.05		BATLEY	13 NA48	p Be, 400 GeV
$1.32^{+0.21}_{-0.17} \pm 0.05$	487	¹ ALAVI-HARATI01I	KTEV	p nucleus, 800 GeV
• • • We do not use the following data for averages, fits, limits, etc. • • •				
$1.20 \pm 0.04 \pm 0.03$	6520	² BATLEY	07 NA48	See BATLEY 13
¹ ALAVI-HARATI 01I assumes here that the second-class current is zero and that the weak-magnetism term takes its exact SU(3) value.				
² This BATLEY 07 result uses our 2006 value of V_{US} from semileptonic kaon decays as input.				

 $g_2(0)/f_1(0)$ FOR $\Xi^0 \rightarrow \Sigma^+ e^- \bar{\nu}_e$

VALUE	EVTS	DOCUMENT ID	TECN	COMMENT
$-1.7^{+2.1}_{-2.0} \pm 0.5$	487	¹ ALAVI-HARATI01I	KTEV	p nucleus, 800 GeV
¹ ALAVI-HARATI 01I thus assumes that $g_2 = 0$ in calculating g_1/f_1 , above.				

 $f_2(0)/f_1(0)$ FOR $\Xi^0 \rightarrow \Sigma^+ e^- \bar{\nu}_e$

VALUE	EVTS	DOCUMENT ID	TECN	COMMENT
2.0 ± 0.9 OUR AVERAGE				
2.0 ± 1.3		BATLEY	13 NA48	p Be, 400 GeV
$2.0 \pm 1.2 \pm 0.5$	487	ALAVI-HARATI01I	KTEV	p nucleus, 800 GeV

 Ξ^0 REFERENCES

ABLIKIM	23AD	PR D108 L011101	M. Ablikim <i>et al.</i>	(BESIII Collab.)
ABLIKIM	23AP	PR D108 L012006	M. Ablikim <i>et al.</i>	(BESIII Collab.)
ABLIKIM	23AU	PR D108 L031106	M. Ablikim <i>et al.</i>	(BESIII Collab.)
ABLIKIM	23B	PR D107 012002	M. Ablikim <i>et al.</i>	(BESIII Collab.)
PDG	22	PTEP 2022 083C01	R.L. Workman <i>et al.</i>	(PDG Collab.)
BATLEY	13	PL B720 105	J.R. Batley <i>et al.</i>	(CERN NA48/1 Collab.)
BATLEY	10B	PL B693 241	J.R. Batley <i>et al.</i>	(CERN NA48/1 Collab.)
BATLEY	07C	PL B645 36	J.R. Batley <i>et al.</i>	(CERN NA48/1 Collab.)
BATLEY	07C	PL B650 1	J.R. Batley <i>et al.</i>	(CERN NA48 Collab.)
ABOUZAID	05	PRL 95 081801	E. Abouzaid <i>et al.</i>	(FNAL KTeV Collab.)
WHITE	05	PRL 94 101804	C.G. White <i>et al.</i>	(FNAL HyperCP Collab.)
LAI	04A	PL B584 251	A. Lai <i>et al.</i>	(CERN NA48 Collab.)
JAMES	02	PRL 89 169901 (err.)	C. James <i>et al.</i>	(MINN, MICH, WISC, RUTG)
TEIGE	02	PRL 89 169902 (err.)	S. Teige <i>et al.</i>	(RUTG, MICH, MINN)
ALAVI-HARATI 01C		PRL 86 3239	A. Alavi-Harati <i>et al.</i>	(FNAL KTeV Collab.)
ALAVI-HARATI 01I		PRL 87 132001	A. Alavi-Harati <i>et al.</i>	(FNAL KTeV Collab.)
FANTI	00	EPJ C12 69	V. Fanti <i>et al.</i>	(CERN NA48 Collab.)
AFFOLDER	99	PRL 82 3751	A. Affolder <i>et al.</i>	(FNAL KTeV Collab.)
JAMES	90	PRL 64 843	C. James <i>et al.</i>	(MINN, MICH, WISC, RUTG)
TEIGE	89	PRL 63 2717	S. Teige <i>et al.</i>	(RUTG, MICH, MINN)
HANDLER	82	PR D25 639	R. Handler <i>et al.</i>	(WISC, MICH, MINN+)
COX	81	PRL 46 877	P.T. Cox <i>et al.</i>	(MICH, WISC, RUTG, MINN+)
BUNCE	79	PL B68 386	G.R.M. Bunce <i>et al.</i>	(BNL, MICH, RUTG+)
BUNCE	78	PR D18 633	G.R.M. Bunce <i>et al.</i>	(WISC, MICH, RUTG)
ZECH	77	NP B124 413	G. Zech <i>et al.</i>	(SIEG, CERN, DORT, HEIDH)
GEWENIGER	75	PL 57B 193	C. Geweniger <i>et al.</i>	(CERN, HEIDH)
BALTAY	74	PR D9 419	C. Baltay <i>et al.</i>	(COLU, BING, J)
YEH	74	PR D10 3545	N. Yeh <i>et al.</i>	(BING, COLU)
MAYEUR	72	NP B47 333	C. Mayeur <i>et al.</i>	(BRUX, CERN, TUFTS, LOUC)
Also		NP B53 268 (err.)	C. Mayeur	
WILQUET	72	PL 42B 372	G. Wilquet <i>et al.</i>	(BRUX, CERN, TUFTS+)
DAUBER	69	PR 179 1262	P.M. Dauber <i>et al.</i>	(LRL)
PALMER	68	PL 26B 323	R.B. Palmer <i>et al.</i>	(BNL, SYRA)
BERGE	66	PR 147 945	J.P. Berge <i>et al.</i>	(LRL)
HUBBARD	66	Thesis UCRL 11510	J.R. Hubbard	(BNL, SYRA)
LONDON	66	PR 143 1034	G.W. London <i>et al.</i>	(BNL, SYRA)
PJERROU	65B	PR 14 275	G.M. Pjerrou <i>et al.</i>	(UCLA)
Also		Thesis	G.M. Pjerrou	(UCLA)
CARMONY	64B	PRL 12 482	D.D. Carmony <i>et al.</i>	(UCLA)
HUBBARD	64	PR 135 B183	J.R. Hubbard <i>et al.</i>	(LRL)
JAUNEAU	63	PL 4 49	L. Jauneau <i>et al.</i>	(EPOL, CERN, LOUC+)
Also		Siena Conf. 1 1	L. Jauneau <i>et al.</i>	(EPOL, CERN, LOUC+)



$$I(J^P) = \frac{1}{2}(\frac{1}{2}^+) \text{ Status: } ****$$

$$(\tau_{\Xi^-} - \tau_{\Xi^+}) / \tau_{\Xi^-}$$

A test of CPT invariance.

The parity has not actually been measured, but + is of course expected.

We have omitted some results that have been superseded by later experiments. See our earlier editions.

VALUE	DOCUMENT ID	TECN	COMMENT
-0.01 ± 0.07	ABDALLAH	06E	DLPH from Z decays

Ξ⁻ MASS

The fit uses the Ξ⁻, Ξ⁺, and Ξ⁰ masses and the Ξ⁻ - Ξ⁺ mass difference. It assumes that the Ξ⁻ and Ξ⁺ masses are the same.

VALUE (MeV)	EVTS	DOCUMENT ID	TECN	COMMENT
1321.71 ± 0.07 OUR FIT				
1321.70 ± 0.08 ± 0.05	2478 ± 68	ABDALLAH	06E	DLPH from Z decays
• • • We do not use the following data for averages, fits, limits, etc. • • •				
1321.46 ± 0.34	632	DIBIANCA	75	DBC 4.9 GeV/c K⁻ d
1321.12 ± 0.41	268	WILQUET	72	HLBC
1321.87 ± 0.51	195	¹ GOLDWASSER	70	HBC 5.5 GeV/c K⁻ p
1321.67 ± 0.52	6	CHIEN	66	HBC 6.9 GeV/c p̄ p
1321.4 ± 1.1	299	LONDON	66	HBC
1321.3 ± 0.4	149	PJERROU	65B	HBC
1321.1 ± 0.3	241	² BADIER	64	HBC
1321.4 ± 0.4	517	² JAUNEAU	63D	FBC
1321.1 ± 0.65	62	² SCHNEIDER	63	HBC

¹ GOLDWASSER 70 uses m_Λ = 1115.58 MeV.

² These masses have been increased 0.09 MeV because the Λ mass increased.

Ξ⁺ MASS

The fit uses the Ξ⁻, Ξ⁺, and Ξ⁰ masses and the Ξ⁻ - Ξ⁺ mass difference. It assumes that the Ξ⁻ and Ξ⁺ masses are the same.

VALUE (MeV)	EVTS	DOCUMENT ID	TECN	COMMENT
1321.71 ± 0.07 OUR FIT				
1321.73 ± 0.08 ± 0.05	2256 ± 63	ABDALLAH	06E	DLPH from Z decays
• • • We do not use the following data for averages, fits, limits, etc. • • •				
1321.6 ± 0.8	35	VOTRUBA	72	HBC 10 GeV/c K⁺ p
1321.2 ± 0.4	34	STONE	70	HBC
1320.69 ± 0.93	5	CHIEN	66	HBC 6.9 GeV/c p̄ p

$$(m_{\Xi^-} - m_{\Xi^+}) / m_{\Xi^-}$$

A test of CPT invariance.

VALUE	DOCUMENT ID	TECN	COMMENT
(-2.5 ± 8.7) × 10⁻⁵	ABDALLAH	06E	DLPH from Z decays

Ξ⁻ MEAN LIFE

Measurements with an error > 0.2 × 10⁻¹⁰ s or with systematic errors not included have been omitted.

VALUE (10 ⁻¹⁰ s)	EVTS	DOCUMENT ID	TECN	COMMENT
1.639 ± 0.015 OUR AVERAGE				
1.65 ± 0.07 ± 0.12	2478 ± 68	ABDALLAH	06E	DLPH from Z decays
1.652 ± 0.051	32k	BOURQUIN	84	SPEC Hyperon beam
1.665 ± 0.065	41k	BOURQUIN	79	SPEC Hyperon beam
1.609 ± 0.028	4286	HEMINGWAY	78	HBC 4.2 GeV/c K⁻ p
1.67 ± 0.08		DIBIANCA	75	DBC 4.9 GeV/c K⁻ d
1.63 ± 0.03	4303	BALTAY	74	HBC 1.75 GeV/c K⁻ p
1.73 ^{+0.08} _{-0.07}	680	MAYEUR	72	HLBC 2.1 GeV/c K⁻
1.61 ± 0.04	2610	DAUBER	69	HBC
1.80 ± 0.16	299	LONDON	66	HBC
1.70 ± 0.12	246	PJERROU	65B	HBC
1.69 ± 0.07	794	HUBBARD	64	HBC
1.86 ^{+0.15} _{-0.14}	517	JAUNEAU	63D	FBC

Ξ⁺ MEAN LIFE

VALUE (10 ⁻¹⁰ s)	EVTS	DOCUMENT ID	TECN	COMMENT
1.70 ± 0.08 ± 0.12	2256 ± 63	ABDALLAH	06E	DLPH from Z decays
• • • We do not use the following data for averages, fits, limits, etc. • • •				
1.55 ^{+0.35} _{-0.20}	35	¹ VOTRUBA	72	HBC 10 GeV/c K⁺ p
1.6 ± 0.3	34	STONE	70	HBC
1.9 ^{+0.7} _{-0.5}	12	¹ SHEN	67	HBC
1.51 ± 0.55	5	¹ CHIEN	66	HBC 6.9 GeV/c p̄ p

¹ The error is statistical only.

Ξ⁻ MAGNETIC MOMENT

See the "Quark Model" review.

VALUE (μ _N)	EVTS	DOCUMENT ID	TECN	COMMENT
-0.6507 ± 0.0025 OUR AVERAGE				
-0.6505 ± 0.0025	4.36M	DURYEA	92	SPEC 800 GeV p Be
-0.661 ± 0.036 ± 0.036	44k	TROST	89	SPEC Ξ⁻ ~ 250 GeV
-0.69 ± 0.04	218k	RAMEIKA	84	SPEC 400 GeV p Be
• • • We do not use the following data for averages, fits, limits, etc. • • •				
-0.674 ± 0.021 ± 0.020	122k	HO	90	SPEC See DURYEA 92
-2.1 ± 0.8	2436	COOL	74	OSPK 1.8 GeV/c K⁻ p
-0.1 ± 2.1	2724	BINGHAM	70B	OSPK 1.8 GeV/c K⁻ p

Ξ⁺ MAGNETIC MOMENT

See the "Quark Model" review.

VALUE (μ _N)	EVTS	DOCUMENT ID	TECN	COMMENT
+0.657 ± 0.028 ± 0.020	70k	HO	90	SPEC 800 GeV p Be

$$(\mu_{\Xi^-} + \mu_{\Xi^+}) / |\mu_{\Xi^-}|$$

A test of CPT invariance. We calculate this from the Ξ⁻ and Ξ⁺ magnetic moments above.

VALUE	DOCUMENT ID
+0.01 ± 0.05 OUR EVALUATION	

Ξ⁻ DECAY MODES

Mode	Fraction (Γ _i /Γ)	Confidence level
Γ ₁ Λπ⁻	(99.887 ± 0.035) %	
Γ ₂ Σ⁻ γ	(1.27 ± 0.23) × 10 ⁻⁴	
Γ ₃ Λe⁻ ν̄ _e	(5.63 ± 0.31) × 10 ⁻⁴	
Γ ₄ Λμ⁻ ν̄ _μ	(3.5 ^{+3.5} _{-2.2}) × 10 ⁻⁴	
Γ ₅ Σ ⁰ e⁻ ν̄ _e	(8.7 ± 1.7) × 10 ⁻⁵	
Γ ₆ Σ ⁰ μ⁻ ν̄ _μ	< 8 × 10 ⁻⁴	90%
Γ ₇ Ξ ⁰ e⁻ ν̄ _e	< 2.59 × 10 ⁻⁴	90%

ΔS = 2 forbidden (S2) modes

Γ ₈ nπ⁻	S2 < 1.9	× 10 ⁻⁵	90%
Γ ₉ ne⁻ ν̄ _e	S2 < 3.2	× 10 ⁻³	90%
Γ ₁₀ nμ⁻ ν̄ _μ	S2 < 1.5	%	90%
Γ ₁₁ pπ⁻ π⁻	S2 < 4	× 10 ⁻⁴	90%
Γ ₁₂ pπ⁻ e⁻ ν̄ _e	S2 < 4	× 10 ⁻⁴	90%
Γ ₁₃ pπ⁻ μ⁻ ν̄ _μ	S2 < 4	× 10 ⁻⁴	90%
Γ ₁₄ pμ⁻ μ⁻	L < 4	× 10 ⁻⁸	90%

CONSTRAINED FIT INFORMATION

An overall fit to 4 branching ratios uses 5 measurements and one constraint to determine 5 parameters. The overall fit has a χ² = 1.0 for 1 degrees of freedom.

The following off-diagonal array elements are the correlation coefficients <δx_iδx_j>/((δx_iδx_j)), in percent, from the fit to the branching fractions, x_i ≡ Γ_i/Γ_{total}. The fit constrains the x_i whose labels appear in this array to sum to one.

x ₂	-6			
x ₃	-8	0		
x ₄	-99	0	-1	
x ₅	-5	0	0	0
	x ₁	x ₂	x ₃	x ₄

Baryon Particle Listings



Ξ^- BRANCHING RATIOS

A number of early results have been omitted.

$\Gamma(\Sigma^-\gamma)/\Gamma(\Lambda\pi^-)$ Γ_2/Γ_1

VALUE (units 10^{-4})	CL%	EVTS	DOCUMENT ID	TECN	COMMENT
1.27 ± 0.24 OUR FIT					
1.27 ± 0.23 OUR AVERAGE					
1.22 ± 0.23 ± 0.06		211	¹ DUBBS	94 E761	Ξ^- 375 GeV
2.27 ± 1.02		9	BIAGI	87B SPEC	SPS hyperon beam

¹DUBBS 94 also finds weak evidence that the asymmetry parameter α_γ is positive ($\alpha_\gamma = 1.0 \pm 1.3$).

$\Gamma(\Lambda e^- \bar{\nu}_e)/\Gamma(\Lambda\pi^-)$ Γ_3/Γ_1

VALUE (units 10^{-3})	CL%	EVTS	DOCUMENT ID	TECN	COMMENT
0.564 ± 0.031 OUR FIT					
0.564 ± 0.031		2857	BOURQUIN	83 SPEC	SPS hyperon beam
0.30 ± 0.13		11	THOMPSON	80 ASPK	Hyperon beam

••• We do not use the following data for averages, fits, limits, etc. •••

$\Gamma(\Lambda\mu^- \bar{\nu}_\mu)/\Gamma(\Lambda\pi^-)$ Γ_4/Γ_1

VALUE (units 10^{-3})	CL%	EVTS	DOCUMENT ID	TECN	COMMENT
0.35 ± 0.35 OUR FIT					
0.35 ± 0.35		1	YEH	74 HBC	Effective denom.=2859
< 2.3		90	THOMPSON	80 ASPK	Effective denom.=1017
< 1.3			DAUBER	69 HBC	
< 12			BERGE	66 HBC	

••• We do not use the following data for averages, fits, limits, etc. •••

$\Gamma(\Sigma^0 e^- \bar{\nu}_e)/\Gamma(\Lambda\pi^-)$ Γ_5/Γ_1

VALUE (units 10^{-3})	CL%	EVTS	DOCUMENT ID	TECN	COMMENT
0.087 ± 0.017 OUR FIT					
0.087 ± 0.017		154	BOURQUIN	83 SPEC	SPS hyperon beam

$[\Gamma(\Lambda e^- \bar{\nu}_e) + \Gamma(\Sigma^0 e^- \bar{\nu}_e)]/\Gamma(\Lambda\pi^-)$ $(\Gamma_3 + \Gamma_5)/\Gamma_1$

VALUE (units 10^{-3})	CL%	EVTS	DOCUMENT ID	TECN	COMMENT
0.651 ± 0.031		3011	¹ BOURQUIN	83 SPEC	SPS hyperon beam
0.68 ± 0.22		17	² DUCLOS	71 OSPK	

¹ See the separate BOURQUIN 83 values for $\Gamma(\Lambda e^- \bar{\nu}_e)/\Gamma(\Lambda\pi^-)$ and $\Gamma(\Sigma^0 e^- \bar{\nu}_e)/\Gamma(\Lambda\pi^-)$ above.

² DUCLOS 71 cannot distinguish Σ^0 's from Λ 's. The Cabibbo theory predicts the Σ^0 rate is about a factor 6 smaller than the Λ rate.

$\Gamma(\Sigma^0 \mu^- \bar{\nu}_\mu)/\Gamma(\Lambda\pi^-)$ Γ_6/Γ_1

VALUE (units 10^{-3})	CL%	EVTS	DOCUMENT ID	TECN	COMMENT
< 0.76		90	YEH	74 HBC	Effective denom.=3026
< 5			BERGE	66 HBC	

••• We do not use the following data for averages, fits, limits, etc. •••

$\Gamma(\Xi^0 e^- \bar{\nu}_e)/\Gamma_{total}$ Γ_7/Γ

VALUE	CL%	DOCUMENT ID	TECN	COMMENT
< 2.59 × 10⁻⁴	90	ABLIKIM	21AH BES3	$J/\psi \rightarrow \Xi\bar{\Xi}$

$\Gamma(\Xi^0 e^- \bar{\nu}_e)/\Gamma(\Lambda\pi^-)$ Γ_7/Γ_1

VALUE	CL%	DOCUMENT ID	TECN	COMMENT
< 2.3 × 10⁻³	90	YEH	74 HBC	Effective denom.=1000

••• We do not use the following data for averages, fits, limits, etc. •••

$\Gamma(n\pi^-)/\Gamma(\Lambda\pi^-)$ Γ_8/Γ_1

$\Delta S=2$. Forbidden in first-order weak interaction.

VALUE (units 10^{-3})	CL%	EVTS	DOCUMENT ID	TECN	COMMENT
< 0.019		90	BIAGI	82B SPEC	SPS hyperon beam
< 3.0		90	YEH	74 HBC	Effective denom.=760
< 1.1			DAUBER	69 HBC	
< 5.0			FERRO-LUZZI	63 HBC	

••• We do not use the following data for averages, fits, limits, etc. •••

$\Gamma(ne^- \bar{\nu}_e)/\Gamma(\Lambda\pi^-)$ Γ_9/Γ_1

$\Delta S=2$. Forbidden in first-order weak interaction.

VALUE (units 10^{-3})	CL%	EVTS	DOCUMENT ID	TECN	COMMENT
< 3.2		90	YEH	74 HBC	Effective denom.=715
< 10		90	BINGHAM	65 RVUE	

••• We do not use the following data for averages, fits, limits, etc. •••

$\Gamma(n\mu^- \bar{\nu}_\mu)/\Gamma(\Lambda\pi^-)$ Γ_{10}/Γ_1

$\Delta S=2$. Forbidden in first-order weak interaction.

VALUE (units 10^{-3})	CL%	EVTS	DOCUMENT ID	TECN	COMMENT
< 15.3		90	YEH	74 HBC	Effective denom.=150

$\Gamma(\rho\pi^-\pi^-)/\Gamma(\Lambda\pi^-)$ Γ_{11}/Γ_1

$\Delta S=2$. Forbidden in first-order weak interaction.

VALUE (units 10^{-4})	CL%	EVTS	DOCUMENT ID	TECN	COMMENT
< 3.7	90	0	YEH	74 HBC	Effective denom.=6200

$\Gamma(\rho\pi^- e^- \bar{\nu}_e)/\Gamma(\Lambda\pi^-)$ Γ_{12}/Γ_1

$\Delta S=2$. Forbidden in first-order weak interaction.

VALUE (units 10^{-4})	CL%	EVTS	DOCUMENT ID	TECN	COMMENT
< 3.7	90	0	YEH	74 HBC	Effective denom.=6200

$\Gamma(\rho\pi^- \mu^- \bar{\nu}_\mu)/\Gamma(\Lambda\pi^-)$ Γ_{13}/Γ_1

$\Delta S=2$. Forbidden in first-order weak interaction.

VALUE (units 10^{-4})	CL%	EVTS	DOCUMENT ID	TECN	COMMENT
< 3.7	90	0	YEH	74 HBC	Effective denom.=6200

$\Gamma(\rho\mu^- \mu^-)/\Gamma(\Lambda\pi^-)$ Γ_{14}/Γ_1

$\Delta L=2$ decay, forbidden by total lepton number conservation.

VALUE (units 10^{-8})	CL%	DOCUMENT ID	TECN	COMMENT
< 4.0	90	RAJARAM	05 HYCP	p Cu, 800 GeV
< 3.7 × 10 ⁴	90	¹ LITTENBERG	92B HBC	Uses YEH 74 data

••• We do not use the following data for averages, fits, limits, etc. •••

¹ This LITTENBERG 92B limit and the identical YEH 74 limits for the preceding three modes all result from nonobservance of any 3-prong decays of the Ξ^- . One could as well apply the limit to the *sum* of the four modes.

Ξ^- DECAY PARAMETERS

See the "Note on Baryon Decay Parameters" in the neutron Listings.

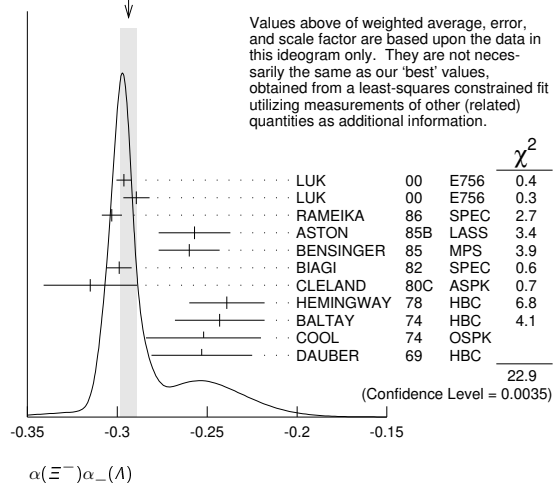
$\alpha(\Xi^-)\alpha_-(\Lambda)$

OUR FIT value is obtained from measurements of $\alpha(\Xi^-)$, $\alpha_-(\Lambda)$, and $\alpha(\Xi^-)\alpha_-(\Lambda)$.

VALUE	CL%	EVTS	DOCUMENT ID	TECN	COMMENT
-0.291 ± 0.004 OUR FIT					Error includes scale factor of 1.8.
-0.294 ± 0.005 OUR AVERAGE					Error includes scale factor of 1.7. See the ideogram below.
-0.2963 ± 0.0042		189k	LUK	00 E756	p Be, 800 GeV
-0.2894 ± 0.0073		63k	¹ LUK	00 E756	p Be, 800 GeV
-0.303 ± 0.004 ± 0.004		192k	RAMEIKA	86 SPEC	400 GeV p Be
-0.257 ± 0.020		11k	ASTON	85B LASS	11 GeV/c K^-p
-0.260 ± 0.017		21k	BENSINGER	85 MPS	5 GeV/c K^-p
-0.299 ± 0.007		150k	BIAGI	82 SPEC	SPS hyperon beam
-0.315 ± 0.026		9046	CLELAND	80C ASPK	BNL hyperon beam
-0.239 ± 0.021		6599	HEMINGWAY	78 HBC	4.2 GeV/c K^-p
-0.243 ± 0.025		4303	BALTAY	74 HBC	1.75 GeV/c K^-p
-0.252 ± 0.032		2436	COOL	74 OSPK	1.8 GeV/c K^-p
-0.253 ± 0.028		2781	DAUBER	69 HBC	

¹ This LUK 00 value is for $\alpha(\Xi^+)\alpha_+(\bar{\Lambda})$. We assume CP conservation here by including it in the average for $\alpha(\Xi^-)\alpha_-(\Lambda)$. But see the second data block below for the CP test.

WEIGHTED AVERAGE
-0.294 ± 0.005 (Error scaled by 1.7)



$\alpha(\Xi^-)$ for $\Xi^- \rightarrow \Lambda\pi^-$

OUR FIT value is obtained from measurements of $\alpha(\Xi^-)$, $\alpha_-(\Lambda)$, and $\alpha(\Xi^-)\alpha_-(\Lambda)$.

VALUE	CL%	EVTS	DOCUMENT ID	TECN	COMMENT
-0.390 ± 0.007 OUR FIT					Error includes scale factor of 2.0.
-0.376 ± 0.007 ± 0.003		73k	ABLIKIM	22AD BES3	$J/\psi \rightarrow \Xi\bar{\Xi} \rightarrow \Lambda\bar{\Lambda}\pi\pi$
-0.344 ± 0.025 ± 0.007		5.4k	ABLIKIM	22BE BES3	$\psi(3686) \rightarrow \Xi\bar{\Xi} \rightarrow \Lambda\bar{\Lambda}\pi\pi$

••• We do not use the following data for averages, fits, limits, etc. •••

See key on page 1171

Baryon Particle Listings

Ξ^- , Ξ^0 , Ξ^+

$\alpha(\Xi^+)$ for $\Xi^+ \rightarrow \Lambda\pi^+$

VALUE	EVTS	DOCUMENT ID	TECN	COMMENT
$0.371 \pm 0.007 \pm 0.002$	73k	ABLIKIM	22AD BES3	$J/\psi \rightarrow \Xi^+ \rightarrow \Lambda\bar{\Lambda}\pi\pi$
••• We do not use the following data for averages, fits, limits, etc. •••				
$0.355 \pm 0.025 \pm 0.002$	5.4k	ABLIKIM	22BE BES3	$\psi(3686) \rightarrow \Xi^+ \rightarrow \Lambda\bar{\Lambda}\pi\pi$

$(\alpha + \bar{\alpha}) / (\alpha - \bar{\alpha})$ for $\Xi^- \rightarrow \Lambda\pi^-$, $\Xi^+ \rightarrow \Lambda\pi^+$

VALUE (units 10^{-3})	EVTS	DOCUMENT ID	TECN	COMMENT
$6 \pm 13 \pm 6$	73k	ABLIKIM	22AD BES3	$J/\psi \rightarrow \Xi^+ \rightarrow \Lambda\bar{\Lambda}\pi\pi$
••• We do not use the following data for averages, fits, limits, etc. •••				
$-15 \pm 51 \pm 10$	5.4k	ABLIKIM	22BE BES3	$\psi(3686) \rightarrow \Xi^+ \rightarrow \Lambda\bar{\Lambda}\pi\pi$

$\frac{[\alpha(\Xi^-)\alpha_-(\Lambda) - \alpha(\Xi^+)\alpha_+(\Lambda)]}{[\alpha(\Xi^-)\alpha_-(\Lambda) + \alpha(\Xi^+)\alpha_+(\Lambda)]}$

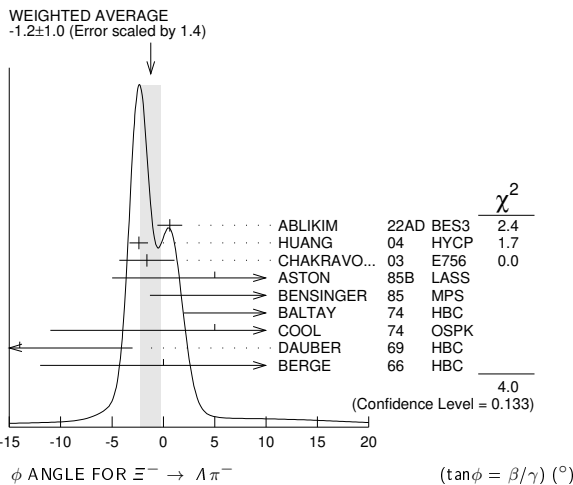
This is zero if CP is conserved. The α 's are the decay-asymmetry parameters for $\Xi^- \rightarrow \Lambda\pi^-$ and $\Lambda \rightarrow p\pi^-$ and for $\Xi^+ \rightarrow \Lambda\pi^+$ and $\Lambda \rightarrow \bar{p}\pi^+$.

VALUE (units 10^{-4})	EVTS	DOCUMENT ID	TECN	COMMENT
$0.0 \pm 5.1 \pm 4.4$	158M	HOLMSTROM	04 HYCP	p Cu, 800 GeV
••• We do not use the following data for averages, fits, limits, etc. •••				
$+120 \pm 140$	252k	LUK	00 E756	p Be, 800 GeV

ϕ ANGLE FOR $\Xi^- \rightarrow \Lambda\pi^-$

VALUE ($^\circ$)	EVTS	DOCUMENT ID	TECN	COMMENT
-1.2 ± 1.0 OUR AVERAGE				Error includes scale factor of 1.4. See the ideogram below.
$0.63 \pm 1.09 \pm 0.52$	73k	1 ABLIKIM	22AD BES3	$J/\psi \rightarrow \Xi^+ \rightarrow \Lambda\bar{\Lambda}\pi\pi$
$-2.39 \pm 0.64 \pm 0.64$	144M	2 HUANG	04 HYCP	p Cu, 800 GeV
$-1.61 \pm 2.66 \pm 0.37$	1.35M	3 CHAKRAVO...	03 E756	p Be, 800 GeV
5 ± 10	11k	4 ASTON	85B LASS	$K^- p$
14.7 ± 16.0	21k	4 BENSINGER	85 MPS	5 GeV/c $K^- p$
11 ± 9	4303	BALTAY	74 HBC	1.75 GeV/c $K^- p$
5 ± 16	2436	COOL	74 OSPK	1.8 GeV/c $K^- p$
-14 ± 11	2781	DAUBER	69 HBC	Uses $\alpha_\Lambda = 0.647 \pm 0.020$
0 ± 12	1004	5 BERGE	66 HBC	
••• We do not use the following data for averages, fits, limits, etc. •••				
$1.32 \pm 4.24 \pm 0.17$	5.4k	6 ABLIKIM	22BE BES3	$\psi(3686) \rightarrow \Xi^+ \rightarrow \Lambda\bar{\Lambda}\pi\pi$
-26 ± 30	2724	BINGHAM	70B OSPK	
0 ± 20.4	364	5 LONDON	66 HBC	Using $\alpha_\Lambda = 0.62$
54 ± 30	356	5 CARMONY	64B HBC	

- Converted from radians to degrees. ABLIKIM 22AD reports a value of $0.011 \pm 0.019 \pm 0.009$ radians.
- From this result and α_Ξ , HUANG 04 gets $\beta_\Xi = -0.037 \pm 0.011 \pm 0.010$ and $\gamma_\Xi = 0.888 \pm 0.0004 \pm 0.006$. And the strong p-s phase difference for $\Lambda\pi^-$ scattering is $(4.6 \pm 1.4 \pm 1.2)^\circ$.
- From this result and α_Ξ , CHAKRAVORTY 03 obtains $\beta_\Xi = -0.025 \pm 0.042 \pm 0.006$ and $\gamma_\Xi = 0.889 \pm 0.001 \pm 0.007$. And the strong p-s phase difference for $\Lambda\pi^-$ scattering is $(3.17 \pm 5.28 \pm 0.73)^\circ$.
- BENSINGER 85 used $\alpha_\Lambda = 0.642 \pm 0.013$.
- The errors have been multiplied by 1.2 due to approximations used for the Ξ polarization; see DAUBER 69 for a discussion.
- Converted from radians to degrees. ABLIKIM 22BE reports a value of $0.023 \pm 0.074 \pm 0.003$ radians.



ϕ ANGLE FOR $\Xi^+ \rightarrow \Lambda\pi^+$

VALUE ($^\circ$)	EVTS	DOCUMENT ID	TECN	COMMENT
$-1.20 \pm 1.09 \pm 0.40$	73k	1 ABLIKIM	22AD BES3	$J/\psi \rightarrow \Xi^+ \rightarrow \Lambda\bar{\Lambda}\pi\pi$
••• We do not use the following data for averages, fits, limits, etc. •••				
$-7.05 \pm 4.18 \pm 0.23$	5.4k	2 ABLIKIM	22BE BES3	$\psi(3686) \rightarrow \Xi^+ \rightarrow \Lambda\bar{\Lambda}\pi\pi$
1 Converted from radians to degrees. ABLIKIM 22AD reports a value of $-0.021 \pm 0.019 \pm 0.007$ radians.				
2 Converted from radians to degrees. ABLIKIM 22BE reports a value of $-0.123 \pm 0.073 \pm 0.004$ radians.				

$\Delta\Phi_{CP} = (\Phi_- + \Phi_+)/2$

VALUE ($^\circ$)	EVTS	DOCUMENT ID	TECN	COMMENT
$-0.28 \pm 0.78 \pm 0.17$	73k	1 ABLIKIM	22AD BES3	$J/\psi \rightarrow \Xi^+ \rightarrow \Lambda\bar{\Lambda}\pi\pi$
••• We do not use the following data for averages, fits, limits, etc. •••				
$-2.86 \pm 2.98 \pm 0.17$	5.4k	2 ABLIKIM	22BE BES3	$\psi(3686) \rightarrow \Xi^+ \rightarrow \Lambda\bar{\Lambda}\pi\pi$

- Converted from radians to degrees. ABLIKIM 22AD reports a value of $(-0.5 \pm 1.4 \pm 0.3) \times 10^{-2}$ radians.
- Converted from radians to degrees. ABLIKIM 22BE reports a value of $(-5.0 \pm 5.2 \pm 0.3) \times 10^{-2}$ radians.

g_A / g_V FOR $\Xi^- \rightarrow \Lambda e^- \bar{\nu}_e$

VALUE	EVTS	DOCUMENT ID	TECN	COMMENT
-0.25 ± 0.05	1992	1 BOURQUIN	83 SPEC	SPS hyperon beam
1 BOURQUIN 83 assumes that $g_2 = 0$. Also, the sign has been changed to agree with our conventions, given in the "Note on Baryon Decay Parameters" in the neutron Listings.				

Ξ^- REFERENCES

We have omitted some papers that have been superseded by later experiments. See our earlier editions.

ABLIKIM 22AD NAT 606 64	M. Ablikim et al.	(BESIII Collab.)
ABLIKIM 22BE PR D106 L091101	M. Ablikim et al.	(BESIII Collab.)
ABLIKIM 21AH PR D104 072007	M. Ablikim et al.	(BESIII Collab.)
ABDALLAH 06E PL B639 179	J. Abdallah et al.	(DELPHI Collab.)
RAJARAM 05E PRL 94 181801	D. Rajaram et al.	(FNAL HyperCP Collab.)
HOLMSTROM 04 PRL 93 262001	T. Holmstrom et al.	(FNAL HyperCP Collab.)
HUANG 04 PRL 93 011802	M. Huang et al.	(FNAL HyperCP Collab.)
CHAKRAVO... 03 PRL 91 031601	A. Chakravorty et al.	(FNAL E756 Collab.)
LUK 00 PRL 85 4860	K.B. Luk et al.	(FNAL E756 Collab.)
DUBBS 94 PRL 72 8008	T. Dubbs et al.	(FNAL E756 Collab.)
DURVEA 92 PRL 68 768	J. Durvea et al.	(MINN, FNAL, MICH, RUTG)
LITTEBERG 92B PR D46 892	L.S. Littenberg, R.E. Shrock	(BNL, STON)
HO 90 PRL 65 1713	P.M. Ho et al.	(MICH, FNAL, MINN, RUTG)
Also PR D44 3402	P.M. Ho et al.	(MICH, FNAL, MINN, RUTG)
TROST 89 PR D40 1703	L.H. Trost et al.	(FNAL-715 Collab.)
BIAGI 87B ZPHY C35 143	S.F. Biagi et al.	(BRIS, CERN, GEVA+)
RAMEIKA 86 PR D33 3172	R. Rameika et al.	(RUTG, MICH, WISC+)
ASTON 85B PR D32 2270	D. Aston et al.	(SLAC, CARL, CNRC, CINC)
BENSINGER 85 NP B252 561	J.R. Bensingier et al.	(CHIC, ELMT, FNAL+)
BOURQUIN 84 NP B241 1	M.H. Bourquin et al.	(BRIS, GEVA, HEIDP+)
RAMEIKA 84 PRL 52 581	R. Rameika et al.	(RUTG, MICH, WISC+)
BOURQUIN 83 ZPHY C21 1	M.H. Bourquin et al.	(BRIS, GEVA, HEIDP+)
BIAGI 82 PL 112B 265	S.F. Biagi et al.	(BRIS, CAVE, GEVA+)
BIAGI 82B PL 112B 277	S.F. Biagi et al.	(LOQM, GEVA, RL+)
CLELAND 80C PR D21 12	W.E. Cleland et al.	(PITT, BNL)
THOMPSON 80 PR D21 25	J.A. Thompson et al.	(PITT, BNL)
BOURQUIN 79 PL 87B 297	M.H. Bourquin et al.	(BRIS, GEVA, HEIDP+)
HEMINGWAY 78 NP B142 205	R.J. Hemingway et al.	(CERN, ZEEM, NIJM+)
DIBIANCA 75 NP B98 137	F.A. Dibianca, R.J. Endorf	(CMU)
BALTAY 74 PR D9 49	C. Baltay et al.	(COLU, BING J)
COOL 74 PR D10 792	R.L. Cool et al.	(BNL)
Also PRL 29 1630	R.L. Cool et al.	(BNL)
YEH 74 PR D10 3545	N. Yeh et al.	(BING, COLU)
MAYEUR 72 NP B47 333	C. Mayeur et al.	(BRUX, CERN, TUFTS, LOUC)
VOTRUBA 72 NP B45 77	M.F. Votruba, A. Sailer, T.M. Ratcliffe	(BRIM+)
WILQUET 72 PL 42B 372	G. Wilquet et al.	(BRUX, CERN, TUFTS+)
DUCLOS 71 NP B32 493	J. Duclos et al.	(CERN)
BINGHAM 70B PR D1 3010	G.M. Bingham et al.	(UCSD, WASH)
GOLDWASSER 70 PR D1 1960	E.L. Goldwasser, P.F. Schultz	(ILL)
STONE 70 PL 32B 515	S.L. Stone et al.	(ROCH)
DAUBER 69 PR 179 1262	P.M. Dauber et al.	(LRL J)
SHEN 67 PL 25B 443	B.C. Shen, A. Firestone, G. Goldhaber	(UCB+)
BERGE 66 PR 147 945	J.P. Berge et al.	(LRL)
CHIEN 66 PR 152 1171	C.Y. Chien et al.	(YALE, BNL)
LONDON 66 PR 143 1034	G.W. London et al.	(BNL, SYRA)
BINGHAM 65 PRSL 285 202	H.H. Bingham	(CERN)
PJERROU 65B PRL 14 275	G.M. Pjerrou et al.	(UCLA)
Also Thesis	G.M. Pjerrou	(UCLA)
BADIER 64 Dubna Conf. 1 593	J. Badier et al.	(EPOL, SAEL, ZEEM)
CARMONY 64B PRL 12 482	D.D. Carmony et al.	(UCLA J)
HUBBARD 64 PR 135 B183	J.R. Hubbard et al.	(LRL)
FERRO-LUZZI 63 PR 130 1568	M. Ferro-Luzzi et al.	(LRL)
JAUNEAU 63D Siena Conf. 4	L. Jauneau et al.	(EPOL, CERN, LOUC+)
Also PL 5 261	L. Jauneau et al.	(EPOL, CERN, LOUC+)
SCHNEIDER 63 PL 4 360	J. Schneider	(CERN)

Ξ RESONANCES

Revised 2023 by V. Crede (FSU), U. Thoma (U. Bonn)

Most of our present knowledge of Ξ resonances stems from the low-statistics data samples recorded in the 1960s–1980s using K^- beams and in the 1980s and 1990s using hyperon (Σ^-, Ξ^-) beams. This is because (1) they could only be produced as a part of a final state, and so the analysis is more complicated than if direct formation were possible, (2) the production cross sections are small (typically a few μb), and (3) the final states are topologically complicated and difficult to study with electronic techniques. Thus, early information about Ξ resonances came entirely from bubble chamber experiments, where the numbers of events are small, and only in the 1980s did electronic experiments make any significant contributions.

Baryon Particle Listings

Ξ 's, $\Xi(1530)$

In recent years, significant contributions have come from collider experiments. Excited Ξ baryons are produced and have been studied in the decay of the charmed Λ_c^+ into $(\Sigma^+ K^-)_{\Xi(1690)} K^+$ by the Belle Collaboration [1] and into $(\Xi^- \pi^+)_{\Xi^*} K^+$ by the BaBar Collaboration [2]. Belle measures the decay $\Xi_c^+ \rightarrow (\Xi^- \pi^+)_{\Xi^*} \pi^+$ [3] with unprecedented statistical quality.

Table 1. Our estimate of the status of the Ξ resonances. Only those with an overall status of *** or **** are included in the Baryon Summary Table.

Particle	J^P	Overall status	Status as seen in —				
			$\Xi\pi$	ΛK	ΣK	$\Xi(1530)\pi$	Other channels
$\Xi(1318)$	$1/2^+$	****					Decays weakly
$\Xi(1530)$	$3/2^+$	****	****				
$\Xi(1620)$		**	**				
$\Xi(1690)$		***	**	***	**		
$\Xi(1820)$	$3/2^-$	***	**	***	**	**	
$\Xi(1950)$		***	**	**		*	
$\Xi(2030)$		***		**	***		
$\Xi(2120)$		*		*			
$\Xi(2250)$		**					3-body decays
$\Xi(2370)$		**					3-body decays
$\Xi(2500)$		*		*	*		3-body decays

**** Existence is certain, and properties are at least fairly well explored.
 *** Existence ranges from very likely to certain, but further confirmation is desirable and/or quantum numbers, branching fractions, etc. are not well determined.
 ** Evidence of existence is only fair.
 * Evidence of existence is poor.

Reference

1. K. Abe *et al.* [Belle Collaboration], Phys. Lett. B **524**, 33-43 (2002).
2. B. Aubert *et al.* [BaBar Collaboration], Phys. Rev. D **78**, 034008 (2008).
3. M. Sumihama *et al.* [Belle Collaboration], Phys. Rev. Lett. **122**, 072501 (2019).

$\Xi(1530) 3/2^+$

 $I(J^P) = \frac{1}{2}(\frac{3}{2}^+) \text{ Status: } ****$

This is the only Ξ resonance whose properties are all reasonably well known. Assuming that the Λ_c^+ has $J^P = 1/2^+$, AUBERT 08AK, in a study of $\Lambda_c^+ \rightarrow \Xi^- \pi^+ K^+$, finds conclusively that the spin of the $\Xi(1530)^0$ is $3/2$. In conjunction with SCHLEIN 63B and BUTTON-SHAFER 66, this proves also that the parity is +.

We use only those determinations of the mass and width that are accompanied by some discussion of systematics and resolution.

$\Xi(1530)$ POLE POSITIONS

$\Xi(1530)^0$ REAL PART		
VALUE	DOCUMENT ID	COMMENT
1531.6 ± 0.4	LICHTENBERG74	Using HABIBI 73

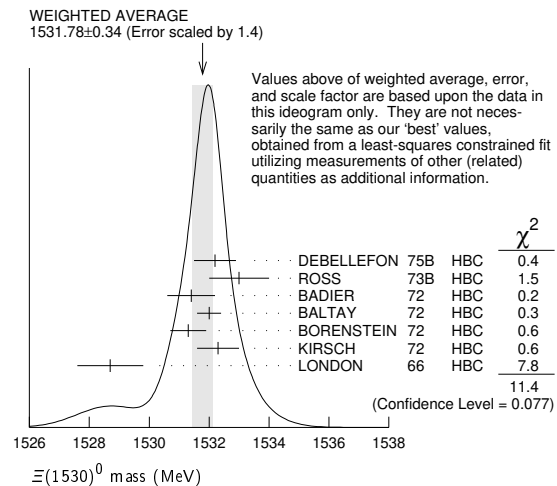
$\Xi(1530)^0$ IMAGINARY PART		
VALUE	DOCUMENT ID	COMMENT
4.45 ± 0.35	LICHTENBERG74	Using HABIBI 73

$\Xi(1530)^-$ REAL PART		
VALUE	DOCUMENT ID	COMMENT
1534.4 ± 1.1	LICHTENBERG74	Using HABIBI 73

$\Xi(1530)^-$ IMAGINARY PART		
VALUE	DOCUMENT ID	COMMENT
3.9 ± 1.75 -3.9	LICHTENBERG74	Using HABIBI 73

$\Xi(1530)$ MASSES

$\Xi(1530)^0$ MASS					
VALUE (MeV)	EVTS	DOCUMENT ID	TECN	COMMENT	
1531.80 ± 0.32 OUR FIT				Error includes scale factor of 1.3.	
1531.78 ± 0.34 OUR AVERAGE				Error includes scale factor of 1.4. See the ideogram below.	
1532.2 ± 0.7		DEBELLEFON 75B	HBC	$K^- p \rightarrow \Xi^- \bar{K} \pi$	
1533 ± 1		ROSS 73B	HBC	$K^- p \rightarrow \Xi \bar{K} \pi(\pi)$	
1531.4 ± 0.8	59	BADIER 72	HBC	$K^- p$ 3.95 GeV/c	
1532.0 ± 0.4	1262	BALTAY 72	HBC	$K^- p$ 1.75 GeV/c	
1531.3 ± 0.6	324	BORENSTEIN 72	HBC	$K^- p$ 2.2 GeV/c	
1532.3 ± 0.7	286	KIRSCH 72	HBC	$K^- p$ 2.87 GeV/c	
1528.7 ± 1.1	76	LONDON 66	HBC	$K^- p$ 2.24 GeV/c	
••• We do not use the following data for averages, fits, limits, etc. •••					
1532.1 ± 0.4	1244	ASTON 85B	LASS	$K^- p$ 11 GeV/c	
1532.1 ± 0.6	2700	¹ BAUBILLIER 81B	HBC	$K^- p$ 8.25 GeV/c	
1530 ± 1	450	BIAGI 81	SPEC	SPS hyperon beam	
1527 ± 6	80	SIXEL 79	HBC	$K^- p$ 10 GeV/c	
1535 ± 4	100	SIXEL 79	HBC	$K^- p$ 16 GeV/c	
1533.6 ± 1.4	97	BERTHON 74	HBC	Quasi-2-body σ	



$\Xi(1530)^-$ MASS					
VALUE (MeV)	EVTS	DOCUMENT ID	TECN	COMMENT	
1535.0 ± 0.6 OUR FIT					
1535.2 ± 0.8 OUR AVERAGE					
1534.5 ± 1.2		DEBELLEFON 75B	HBC	$K^- p \rightarrow \Xi^- \bar{K} \pi$	
1535.3 ± 2.0		ROSS 73B	HBC	$K^- p \rightarrow \Xi \bar{K} \pi(\pi)$	
1536.2 ± 1.6	185	KIRSCH 72	HBC	$K^- p$ 2.87 GeV/c	
1535.7 ± 3.2	38	LONDON 66	HBC	$K^- p$ 2.24 GeV/c	
••• We do not use the following data for averages, fits, limits, etc. •••					
1540 ± 3	48	BERTHON 74	HBC	Quasi-2-body σ	
1534.7 ± 1.1	334	BALTAY 72	HBC	$K^- p$ 1.75 GeV/c	

$m_{\Xi(1530)^-} - m_{\Xi(1530)}$

VALUE (MeV)	DOCUMENT ID	TECN	COMMENT
3.2 ± 0.6 OUR FIT			
2.9 ± 0.9 OUR AVERAGE			
2.7 ± 1.0	BALTAY 72	HBC	$K^- p$ 1.75 GeV/c
2.0 ± 3.2	MERRILL 66	HBC	$K^- p$ 1.7-2.7 GeV/c
5.7 ± 3.0	PJERROU 65B	HBC	$K^- p$ 1.8-1.95 GeV/c
••• We do not use the following data for averages, fits, limits, etc. •••			
3.9 ± 1.8	² KIRSCH 72	HBC	$K^- p$ 2.87 GeV/c
7 ± 4	² LONDON 66	HBC	$K^- p$ 2.24 GeV/c

$\Xi(1530)$ WIDTHS

$\Xi(1530)^0$ WIDTH					
VALUE (MeV)	EVTS	DOCUMENT ID	TECN	COMMENT	
9.1 ± 0.5 OUR AVERAGE					
9.5 ± 1.2		DEBELLEFON 75B	HBC	$K^- p \rightarrow \Xi^- \bar{K} \pi$	
9.1 ± 2.4		ROSS 73B	HBC	$K^- p \rightarrow \Xi \bar{K} \pi(\pi)$	
11 ± 2		BADIER 72	HBC	$K^- p$ 3.95 GeV/c	
9.0 ± 0.7		BALTAY 72	HBC	$K^- p$ 1.75 GeV/c	
8.4 ± 1.4		BORENSTEIN 72	HBC	$\Xi^- \pi^+$	
11.0 ± 1.8		KIRSCH 72	HBC	$\Xi^- \pi^+$	
7 ± 7		BERGE 66	HBC	$K^- p$ 15-1.7 GeV/c	
8.5 ± 3.5		LONDON 66	HBC	$K^- p$ 2.24 GeV/c	
7 ± 2		SCHLEIN 63B	HBC	$K^- p$ 1.8, 1.95 GeV/c	

See key on page 1171

Baryon Particle Listings

$\Xi(1530), \Xi(1620), \Xi(1690)$

••• We do not use the following data for averages, fits, limits, etc. •••

12.8 ± 1.0	2700	¹ BAUBILLIER	81B	HBC	$K^- p$ 8.25 GeV/c
19 ± 6	80	³ SIXEL	79	HBC	$K^- p$ 10 GeV/c
14 ± 5	100	³ SIXEL	79	HBC	$K^- p$ 16 GeV/c

$\Xi(1530)^-$ WIDTH

VALUE (MeV)	DOCUMENT ID	TECN	COMMENT
9.9^{+1.7}_{-1.9} OUR AVERAGE			
9.6 ± 2.8	DEBELLEFON 75B	HBC	$K^- p \rightarrow \Xi^- \bar{K} \pi$
8.3 ± 3.6	ROSS 73B	HBC	$K^- p \rightarrow \Xi^- \bar{K} \pi(\pi)$
7.8 ^{+3.5} _{-7.8}	BALTAY 72	HBC	$K^- p$ 1.75 GeV/c
16.2 ± 4.6	KIRSCH 72	HBC	$\Xi^- \pi^0, \Xi^0 \pi^-$

$\Xi(1530)$ DECAY MODES

Mode	Fraction (Γ_i/Γ)	Confidence level
$\Gamma_1 \Xi \pi$	100 %	
$\Gamma_2 \Xi \gamma$	<3.7 %	90%

$\Xi(1530)$ BRANCHING RATIOS

$\Gamma(\Xi \gamma)/\Gamma_{total}$	CL%	DOCUMENT ID	TECN	COMMENT	Γ_2/Γ
<0.037	90	ABLKIM 20	BES3	$J/\psi \rightarrow \Xi(1530)^- \Xi^+$	
••• We do not use the following data for averages, fits, limits, etc. •••					
<0.04	90	KALBFLEISCH 75	HBC	$K^- p$ 2.18 GeV/c	

$\Xi(1530)$ FOOTNOTES

- ¹ BAUBILLIER 81B is a fit to the inclusive spectrum. The resolution (5 MeV) is not unfolded.
- ² Redundant with data in the mass Listings.
- ³ SIXEL 79 doesn't unfold the experimental resolution of 15 MeV.

$\Xi(1530)$ REFERENCES

ABLKIM 20	PR D101 012004	M. Ablikim et al.	(BESIII Collab.)
AUBERT 08AK	PR D78 034008	B. Aubert et al.	(BABAR Collab.)
ASTON 85B	PR D32 2270	D. Aston et al.	(SLAC, CARL, CNRC, CINC)
BAUBILLIER 81B	NP B192 1	M. Baubillier et al.	(BIRM, CERN, GLAS+)
BIAGI 81	ZPHY C9 305	S.F. Biagi et al.	(BRIS, CAVE, GEVA+)
SIXEL 79	NP B159 125	P. Sixel et al.	(AACH3, BERL, CERN, LOIC+)
DEBELLEFON 75B	NC 28A 289	A. de Bellefon et al.	(CDEF, SACL)
KALBFLEISCH 75	PR D11 987	G.R. Kalbfleisch, R.C. Strand, J.W. Chapman	(BNL+)
BERTHON 74	NC 21A 146	A. Berthon et al.	(CDEF, RHEL, SACL+)
LICHTENBERG 74	PR D10 3865	D.B. Lichtenberg	(IND)
	Also Private Comm.	J.B. Lichtenberg	(IND)
HABIBI 73	Thesis Nevis 199	M. Habibi	(COLU)
ROSS 73B	Purdue Conf. 355	R.T. Ross, J.L. Lloyd, D. Radojicic	(OXF)
BADIER 72	NP B37 429	J. Badier et al.	(EPOL)
BALTAY 72	PL 42B 129	C. Baltay et al.	(COLU, BING)
BORENSTEIN 72	PR D5 1559	S.R. Borenstein et al.	(BNL, MICH)I
KIRSCH 72	NP B40 349	L.E. Kirsch et al.	(BRAN, UMD, SYRA+)
BERGE 66	PR 147 945	J.P. Berge et al.	(LRL)I
BUTTON... 66	PR 142 883	J. Button-Shafer et al.	(LRL)JP
LONDON 66	PR 143 1034	G.W. London et al.	(BNL, SYRA)IJ
MERRILL 66	Thesis UCRL 16455	D.W. Merrill	(LRL)JP
PJERROU 65B	PRL 14 275	G.M. Pjerrou et al.	(UCLA)
SCHLEIN 63B	PRL 11 167	P.E. Schlein et al.	(UCLA)IJP

OTHER RELATED PAPERS

MAZZUCATO 81	NP B178 1	M. Mazzucato et al.	(AMST, CERN, NUM+)
BRIEFEL 77	PR D16 2706	E. Briefel et al.	(BRAN, UMD, SYRA+)
BRIEFEL 75	PR D12 1859	E. Briefel et al.	(BRAN, UMD, SYRA+)
HUNGERBU... 74	PR D10 2051	V. Hungerbuhler et al.	(YALE, FNAL, BNL+)
BUTTON... 66	PR 142 883	J. Button-Shafer et al.	(LRL)JP

$\Xi(1620)$

$J(P) = \frac{1}{2}(?)$ Status: **
J, P need confirmation.

OMITTED FROM SUMMARY TABLE

The clearest evidence is a peak in $\Xi^- \pi^+$ seen by SUMIHAMA 19. Older low-statistics experiments (e.g., BORENSTEIN 72 and HASSALL 81) have looked for the state but have not seen any effect.

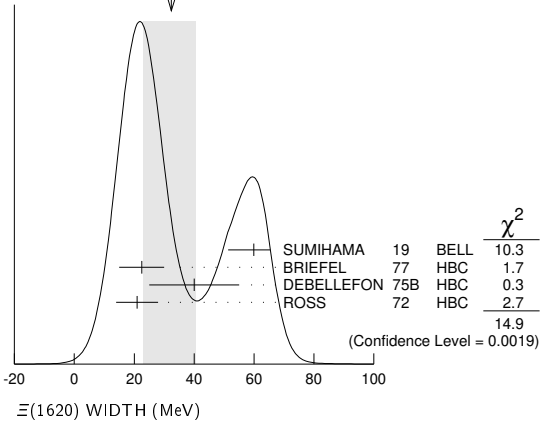
$\Xi(1620)$ MASS

VALUE (MeV)	EVTS	DOCUMENT ID	TECN	COMMENT
≈ 1620 OUR ESTIMATE				
1610.4 ± 6.0 ^{+6.1} _{-4.2}		SUMIHAMA 19	BELL	$\Xi_c^+ \rightarrow \Xi(1620) \pi^+$
1624 ± 3	31	BRIEFEL 77	HBC	$K^- p$ 2.87 GeV/c
1633 ± 12	34	DEBELLEFON 75B	HBC	$K^- p \rightarrow \Xi^- \bar{K} \pi$
1606 ± 6	29	ROSS 72	HBC	$K^- p$ 3.1-3.7 GeV/c

$\Xi(1620)$ WIDTH

VALUE (MeV)	EVTS	DOCUMENT ID	TECN	COMMENT
32⁺⁸₋₉ OUR AVERAGE				Error includes scale factor of 2.2. See the ideogram below.
59.9 ± 4.8 ^{+2.8} _{-7.1}		SUMIHAMA 19	BELL	$\Xi_c^+ \rightarrow \Xi(1620) \pi^+$
22.5 ± 7.5	31	¹ BRIEFEL 77	HBC	$K^- p$ 2.87 GeV/c
40 ± 15	34	DEBELLEFON 75B	HBC	$K^- p \rightarrow \Xi^- \bar{K} \pi$
21 ± 7	29	ROSS 72	HBC	$K^- p \rightarrow \Xi^- \pi^+ K^0(892)$

WEIGHTED AVERAGE
32+8-9 (Error scaled by 2.2)



$\Xi(1620)$ DECAY MODES

Mode

$\Gamma_1 \Xi \pi$

$\Xi(1620)$ FOOTNOTES

- ¹ The fit is insensitive to values between 15 and 30 MeV.

$\Xi(1620)$ REFERENCES

SUMIHAMA 19	PRL 122 072501	M. Sumihama et al.	(BELLE Collab.)
HASSALL 81	NP B189 397	J.K. Hassall et al.	(CAVE, MSU)
BRIEFEL 77	PR D16 2706	E. Briefel et al.	(BRAN, UMD, SYRA+)
	Also Duke Conf. 317	E. Briefel et al.	(BRAN, UMD, SYRA+)
	Hyperon Resonances, 1970		
	Also PR D12 1859	E. Briefel et al.	(BRAN, UMD, SYRA+)
DEBELLEFON 75B	NC 28A 289	A. de Bellefon et al.	(CDEF, SACL)
BORENSTEIN 72	PR D5 1559	S.R. Borenstein et al.	(BNL, MICH)I
ROSS 72	PL 38B 177	R.T. Ross et al.	(OXF)I

OTHER RELATED PAPERS

HUNGERBU... 74	PR D10 2051	V. Hungerbuhler et al.	(YALE, FNAL, BNL+)
SCHMIDT 73	Purdue Conf. 363	P.E. Schmidt	(BRAN)
KALBFLEISCH 70	Duke Conf. 331	G.R. Kalbfleisch	(BNL)I
	Hyperon Resonances 1970		
APSELL 69	PRL 23 884	S.P. Appell et al.	(BRAN, UMD, SYRA+)
BARTSCH 69	PL 28B 439	J. Bartsch et al.	(AACH, BERL, CERN+)

$\Xi(1690)$

$J(P) = \frac{1}{2}(?)$ Status: ** *

AUBERT 08AK, in a study of $\Lambda_c^+ \rightarrow \Xi^- \pi^+ K^+$, finds some evidence that the $\Xi(1690)$ has $J^P = 1/2^-$.

DIONISI 78 sees a threshold enhancement in both the neutral and negatively charged $\Sigma \bar{K}$ mass spectra in $K^- p \rightarrow (\Sigma \bar{K}) K \pi$ at 4.2 GeV/c. The data from the $\Sigma \bar{K}$ channels alone cannot distinguish between a resonance and a large scattering length. Weaker evidence at the same mass is seen in the corresponding $\Lambda \bar{K}$ channels, and a coupled-channel analysis yields results consistent with a new Ξ .

BIAGI 81 sees an enhancement at 1700 MeV in the diffractively produced ΛK^- system. A peak is also observed in the ΛK^0 mass spectrum at 1660 MeV that is consistent with a 1720 MeV resonance decaying to $\Sigma^0 \bar{K}^0$, with the γ from the Σ^0 decay not detected.

BIAGI 87 provides further confirmation of this state in diffractive dissociation of Ξ^- into ΛK^- . The significance claimed is 6.7 standard deviations.

ADAMOVICH 98 sees a peak of 1400 ± 300 events in the $\Xi^- \pi^+$ spectrum produced by 345 GeV/c Σ^- -nucleus interactions.

SUMIHAMA 19 observes a peak in the $\Xi^- \pi^+$ spectrum with a significance of 4.0 standard deviations.

Baryon Particle Listings

 $\Xi(1690), \Xi(1820)$ $\Xi(1690)$ MASSES

MIXED CHARGES

VALUE (MeV) DOCUMENT ID
1690±10 OUR ESTIMATE This is only an educated guess; the error given is larger than the error on the average of the published values.

 $\Xi(1690)^0$ MASS

VALUE (MeV)	EVTS	DOCUMENT ID	TECN	COMMENT
1686±4	1400	ADAMOVICH	98 WA89	Σ^- nucleus, 345 GeV/c
1699±5	175	¹ DIONISI	78 HBC	$K^- p$ 4.2 GeV/c
1684±5	183	² DIONISI	78 HBC	$K^- p$ 4.2 GeV/c

 $\Xi(1690)^-$ MASS

VALUE (MeV)	EVTS	DOCUMENT ID	TECN	COMMENT
1691.1±1.9±2.0	104	BIAGI	87 SPEC	Ξ^- Be 116 GeV
1700±10	150	³ BIAGI	81 SPEC	Ξ^- H 100, 135 GeV
1694±6	45	⁴ DIONISI	78 HBC	$K^- p$ 4.2 GeV/c

 $\Xi(1690)$ WIDTHS

MIXED CHARGES

VALUE (MeV) DOCUMENT ID
20±15 OUR ESTIMATE

 $\Xi(1690)^0$ WIDTH

VALUE (MeV)	EVTS	DOCUMENT ID	TECN	COMMENT
10±6	1400	ADAMOVICH	98 WA89	Σ^- nucleus, 345 GeV/c
44±23	175	¹ DIONISI	78 HBC	$K^- p$ 4.2 GeV/c
20±4	183	² DIONISI	78 HBC	$K^- p$ 4.2 GeV/c

 $\Xi(1690)^-$ WIDTH

VALUE (MeV)	CL%	EVTS	DOCUMENT ID	TECN	COMMENT
< 8	90	104	BIAGI	87 SPEC	Ξ^- Be 116 GeV
47±14		150	³ BIAGI	81 SPEC	Ξ^- H 100, 135 GeV
26±6		45	⁴ DIONISI	78 HBC	$K^- p$ 4.2 GeV/c

 $\Xi(1690)$ DECAY MODES

Mode	Fraction (Γ_i/Γ)
Γ_1 $\Lambda\bar{K}$	seen
Γ_2 $\Sigma\bar{K}$	seen
Γ_3 $\Xi\pi$	seen
Γ_4 $\Xi^- \pi^+ \pi^0$	
Γ_5 $\Xi^- \pi^+ \pi^-$	possibly seen
Γ_6 $\Xi(1530)\pi$	

 $\Xi(1690)$ BRANCHING RATIOS

$\Gamma(\Lambda\bar{K})/\Gamma_{\text{total}}$	Γ_1/Γ
VALUE EVTS DOCUMENT ID TECN CHG COMMENT	
seen 104 BIAGI 87 SPEC - Ξ^- Be 116 GeV	

$\Gamma(\Sigma\bar{K})/\Gamma(\Lambda\bar{K})$	Γ_2/Γ_1
VALUE EVTS DOCUMENT ID TECN CHG COMMENT	
0.75±0.39 75 ABE 02c BELL $e^+e^- \approx \Upsilon(4S)$	
2.7±0.9 DIONISI 78 HBC 0 $K^- p$ 4.2 GeV/c	
3.1±1.4 DIONISI 78 HBC - $K^- p$ 4.2 GeV/c	

$\Gamma(\Xi\pi)/\Gamma(\Sigma\bar{K})$	Γ_3/Γ_2
VALUE DOCUMENT ID TECN CHG COMMENT	
<0.09 DIONISI 78 HBC 0 $K^- p$ 4.2 GeV/c	

$\Gamma(\Xi\pi)/\Gamma_{\text{total}}$	Γ_3/Γ
VALUE DOCUMENT ID TECN COMMENT	
seen ADAMOVICH 98 WA89 Σ^- nucleus, 345 GeV/c	

$\Gamma(\Xi^- \pi^+ \pi^0)/\Gamma(\Sigma\bar{K})$	Γ_4/Γ_2
VALUE DOCUMENT ID TECN CHG COMMENT	
<0.04 DIONISI 78 HBC 0 $K^- p$ 4.2 GeV/c	

$\Gamma(\Xi^- \pi^+ \pi^-)/\Gamma_{\text{total}}$	Γ_5/Γ
VALUE EVTS DOCUMENT ID TECN CHG COMMENT	
possibly seen 4 BIAGI 87 SPEC - Ξ^- Be 116 GeV	

$\Gamma(\Xi^- \pi^+ \pi^-)/\Gamma(\Sigma\bar{K})$	Γ_5/Γ_2
VALUE DOCUMENT ID TECN CHG COMMENT	
<0.03 DIONISI 78 HBC - $K^- p$ 4.2 GeV/c	

 $\Gamma(\Xi(1530)\pi)/\Gamma(\Sigma\bar{K})$

VALUE	DOCUMENT ID	TECN	CHG	COMMENT	Γ_6/Γ_2
<0.06	DIONISI	78 HBC	-	$K^- p$ 4.2 GeV/c	

 $\Xi(1690)$ FOOTNOTES

- From a fit to the $\Sigma^+ K^-$ spectrum.
- From a coupled-channel analysis of the $\Sigma^+ K^-$ and $\Lambda\bar{K}^0$ spectra.
- A fit to the inclusive spectrum from $\Xi^- N \rightarrow \Lambda K^- X$.
- From a coupled-channel analysis of the $\Sigma^0 K^-$ and ΛK^- spectra.

 $\Xi(1690)$ REFERENCES

SUMIHAMA 19 PRL 122 072501	M. Sumihama et al.	(BELLE Collab.)
AUBERT 08AK PR D78 034008	B. Aubert et al.	(BABAR Collab.)
ABE 02C PL B524 33	K. Abe et al.	(KEK BELLE Collab.)
ADAMOVICH 98 EPJ C5 621	M.I. Adamovich et al.	(CERN WA89 Collab.)
BIAGI 87 ZPHY C34 15	S.F. Biagi et al.	(BRIS, CERN, GEVA+)
BIAGI 81 ZPHY C9 305	S.F. Biagi et al.	(BRIS, CAVE, GEVA+)
DIONISI 78 PL 80B 145	C. Dionisi et al.	(CERN, AMST, NIJ+)

 $\Xi(1820) 3/2^-$

$$I(J^P) = \frac{1}{2}(3/2^-) \text{ Status: } ***$$

The clearest evidence is an 8-standard-deviation peak in ΛK^- seen by GAY 76C. TEODORO 78 favors $J = 3/2$, but cannot make a parity discrimination. BIAGI 87C is consistent with $J = 3/2$ and favors negative parity for this J value.

 $\Xi(1820)$ MASS

We only average the measurements that appear to us to be most significant and best determined.

VALUE (MeV)	EVTS	DOCUMENT ID	TECN	CHG	COMMENT
1823 ± 5 OUR ESTIMATE					
1823.5 ± 1.4 OUR AVERAGE					
1825.5 ± 4.7±4.7	288	ABLIKIM	20c BES3	-	$e^+e^- \rightarrow \Xi(1820)^- \Xi^+$
1819.4 ± 3.1±2.0	280	¹ BIAGI	87 SPEC 0		$\Xi^- \text{Be} \rightarrow (\Lambda K^-) X$
1826 ± 3 ± 1	54	BIAGI	87c SPEC 0		$\Xi^- \text{Be} \rightarrow (\Lambda\bar{K}^0) X$
1822 ± 6		JENKINS	83 MPS -		$K^- p \rightarrow K^+ (MM)$
1830 ± 6	300	BIAGI	81 SPEC -		SPS hyperon beam
1823 ± 2	130	GAY	76c HBC -		$K^- p$ 4.2 GeV/c
••• We do not use the following data for averages, fits, limits, etc. •••					
1817 ± 3		ADAMOVICH	99B WA89		Σ^- nucleus, 345 GeV
1797 ± 19	74	BRIEFEL	77 HBC 0		$K^- p$ 2.87 GeV/c
1829 ± 9	68	BRIEFEL	77 HBC -0		$\Xi(1530)\pi$
1860 ± 14	39	BRIEFEL	77 HBC -		$\Sigma^- \bar{K}^0$
1870 ± 9	44	BRIEFEL	77 HBC 0		$\Lambda\bar{K}^0$
1813 ± 4	57	BRIEFEL	77 HBC -		ΛK^-
1807 ± 27		DIBIANCA	75 DBC -0		$\Xi\pi, \Xi^*\pi$
1762 ± 8	28	² BADIÉ	72 HBC -0		$\Xi\pi, \Xi\pi\pi, YK$
1838 ± 5	38	² BADIÉ	72 HBC -0		$\Xi\pi, \Xi\pi\pi, YK$
1830 ± 10	25	³ CRENNELL	70B DBC -0		3.6, 3.9 GeV/c
1826 ± 12		⁴ CRENNELL	70B DBC -0		3.6, 3.9 GeV/c
1830 ± 10	40	ALITTI	69 HBC -		$\Lambda, \Sigma\bar{K}$
1814 ± 4	30	BADIÉ	65 HBC 0		$\Lambda\bar{K}^0$
1817 ± 7	29	SMITH	65c HBC -0		$\Lambda\bar{K}^0, \Lambda K^-$
1770		HALSTEINSLID63	FBC -0		K^- freon 3.5 GeV/c

 $\Xi(1820)$ WIDTH

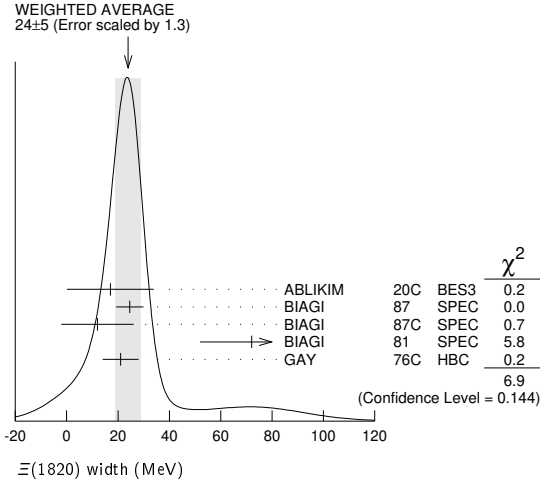
VALUE (MeV)	EVTS	DOCUMENT ID	TECN	CHG	COMMENT
24 ⁺¹⁵ -10 OUR ESTIMATE					
24 ± 5 OUR AVERAGE					Error includes scale factor of 1.3. See the ideogram below.
17.0±15.0±7.9	288	ABLIKIM	20c BES3	-	$e^+e^- \rightarrow \Xi(1820)^- \Xi^+$
24.6 ± 5.3	280	¹ BIAGI	87 SPEC 0		$\Xi^- \text{Be} \rightarrow (\Lambda K^-) X$
12 ± 14 ± 1.7	54	BIAGI	87c SPEC 0		$\Xi^- \text{Be} \rightarrow (\Lambda\bar{K}^0) X$
72 ± 20	300	BIAGI	81 SPEC -		SPS hyperon beam
² ± 7	130	GAY	76c HBC -		$K^- p$ 4.2 GeV/c
••• We do not use the following data for averages, fits, limits, etc. •••					
23 ± 13		ADAMOVICH	99B WA89		Σ^- nucleus, 345 GeV
99 ± 57	74	BRIEFEL	77 HBC 0		$K^- p$ 2.87 GeV/c
52 ± 34	68	BRIEFEL	77 HBC -0		$\Xi(1530)\pi$
72 ± 17	39	BRIEFEL	77 HBC -		$\Sigma^- \bar{K}^0$
44 ± 11	44	BRIEFEL	77 HBC 0		$\Lambda\bar{K}^0$
26 ± 11	57	BRIEFEL	77 HBC -		ΛK^-
85 ± 58		DIBIANCA	75 DBC -0		$\Xi\pi, \Xi^*\pi$
51 ± 13		² BADIÉ	72 HBC -0		Lower mass
58 ± 13		² BADIÉ	72 HBC -0		Higher mass

See key on page 1171

Baryon Particle Listings

$\Xi(1820), \Xi(1950)$

103	+38 -24	3	CRENNELL	70B	DBC	-0	3.6, 3.9 GeV/c
48	+36 -19	4	CRENNELL	70B	DBC	-0	3.6, 3.9 GeV/c
55	+40 -20		ALITTI	69	HBC	-	$\Lambda, \Sigma \bar{K}$
12	± 4		BADIER	65	HBC	0	$\Lambda \bar{K}^0$
30	± 7		SMITH	65B	HBC	-0	$\Lambda \bar{K}$
<80			HALSTEINSLID63	FBC	-0		K^- freon 3.5 GeV/c



$\Xi(1820)$ DECAY MODES

Mode	Fraction (Γ_i/Γ)
Γ_1 $\Lambda \bar{K}$	large
Γ_2 $\Sigma \bar{K}$	small
Γ_3 $\Xi \pi$	small
Γ_4 $\Xi(1530)\pi$	small
Γ_5 $\Xi \pi \pi$ (not $\Xi(1530)\pi$)	

$\Xi(1820)$ BRANCHING RATIOS

The dominant modes seem to be $\Lambda \bar{K}$ and (perhaps) $\Xi(1530)\pi$, but the branching fractions are very poorly determined.

$\Gamma(\Lambda \bar{K})/\Gamma_{total}$	DOCUMENT ID	TECN	CHG	COMMENT	Γ_1/Γ
0.25 ± 0.05 OUR AVERAGE					
0.24 ± 0.05	ANISOVICH 12A	DPWA	-	Multichannel	
0.30 ± 0.15	ALITTI 69	HBC	-	$K^- p$ 3.9-5 GeV/c	

$\Gamma(\Xi \pi)/\Gamma_{total}$	DOCUMENT ID	TECN	CHG	COMMENT	Γ_3/Γ
0.10 ± 0.10					
	ALITTI 69	HBC	-	$K^- p$ 3.9-5 GeV/c	

$\Gamma(\Xi \pi)/\Gamma(\Xi(1530)\pi)$	DOCUMENT ID	TECN	CHG	COMMENT	Γ_3/Γ_4
0.20 ± 0.20					
	GAY 76c	HBC	-	$K^- p$ 4.2 GeV/c	
	BADIER 65	HBC	0	$K^- p$ 3 GeV/c	

$\Gamma(\Xi \pi)/\Gamma(\Xi(1530)\pi)$	DOCUMENT ID	TECN	CHG	COMMENT	Γ_3/Γ_4
1.5 ± 0.6 -0.4					
	APSELL 70	HBC	0	$K^- p$ 2.87 GeV/c	

$\Gamma(\Sigma \bar{K})/\Gamma_{total}$	DOCUMENT ID	TECN	CHG	COMMENT	Γ_2/Γ
0.30 ± 0.15					
	ALITTI 69	HBC	-	$K^- p$ 3.9-5 GeV/c	
••• We do not use the following data for averages, fits, limits, etc. •••					
<0.02	TRIPP 67	RVUE	-	Use SMITH 65c	

$\Gamma(\Sigma \bar{K})/\Gamma(\Lambda \bar{K})$	DOCUMENT ID	TECN	CHG	COMMENT	Γ_2/Γ_1
0.24 ± 0.10					
	GAY 76c	HBC	-	$K^- p$ 4.2 GeV/c	

$\Gamma(\Xi(1530)\pi)/\Gamma_{total}$	DOCUMENT ID	TECN	CHG	COMMENT	Γ_4/Γ
0.30 ± 0.15					
	ALITTI 69	HBC	-	$K^- p$ 3.9-5 GeV/c	
••• We do not use the following data for averages, fits, limits, etc. •••					
seen	ASTON 85B	LASS	-	$K^- p$ 11 GeV/c	
not seen	5 HASSALL 81	HBC	-	$K^- p$ 6.5 GeV/c	
<0.25	6 DAUBER 69	HBC	-	$K^- p$ 2.7 GeV/c	

$\Gamma(\Xi(1530)\pi)/\Gamma(\Lambda \bar{K})$	DOCUMENT ID	TECN	CHG	COMMENT	Γ_4/Γ_1
0.38 ± 0.27 OUR AVERAGE				Error includes scale factor of 2.3.	
1.0 ± 0.3	GAY 76c	HBC	-	$K^- p$ 4.2 GeV/c	
0.26 ± 0.13	SMITH 65c	HBC	-0	$K^- p$ 2.45-2.7 GeV/c	

$\Gamma(\Xi \pi \pi \text{ (not } \Xi(1530)\pi))/\Gamma(\Lambda \bar{K})$	DOCUMENT ID	TECN	CHG	COMMENT	Γ_5/Γ_1
0.30 ± 0.20					
	BIAGI 87	SPEC	-	Ξ^- Be 116 GeV	
••• We do not use the following data for averages, fits, limits, etc. •••					
<0.14	7 BADIER 65	HBC	0	1 st. dev. limit	
>0.1	SMITH 65c	HBC	-0	$K^- p$ 2.45-2.7 GeV/c	

$\Gamma(\Xi \pi \pi \text{ (not } \Xi(1530)\pi))/\Gamma(\Xi(1530)\pi)$	DOCUMENT ID	TECN	CHG	COMMENT	Γ_5/Γ_4
consistent with zero					
	GAY 76c	HBC	-	$K^- p$ 4.2 GeV/c	
••• We do not use the following data for averages, fits, limits, etc. •••					
0.3 ± 0.5	8 APSELL 70	HBC	0	$K^- p$ 2.87 GeV/c	

$\Xi(1820)$ FOOTNOTES

- BIAGI 87 also sees weak signals in the in the $\Xi^- \pi^+ \pi^-$ channel at 1782.6 ± 1.4 MeV ($\Gamma = 6.0 \pm 1.5$ MeV) and 1831.9 ± 2.8 MeV ($\Gamma = 9.6 \pm 9.9$ MeV).
- BADIER 72 adds all channels and divides the peak into lower and higher mass regions. The data can also be fitted with a single Breit-Wigner of mass 1800 MeV and width 150 MeV.
- From a fit to inclusive $\Xi \pi, \Xi \pi \pi,$ and ΛK^- spectra.
- From a fit to inclusive $\Xi \pi$ and $\Xi \pi \pi$ spectra only.
- Including $\Xi \pi \pi$.
- DAUBER 69 uses in part the same data as SMITH 65c.
- For the decay mode $\Xi^- \pi^+ \pi^0$ only. This limit includes $\Xi(1530)\pi$.
- Or less. Upper limit for the 3-body decay.

$\Xi(1820)$ REFERENCES

ABLIKIM 20C	PRL 124 032002	M. Ablikim et al.	(BESIII Collab.)
ANISOVICH 12A	EPJ A48 15	A.V. Anisovich et al.	(BONN, PNPI)
ADAMOVICH 99B	EPJ C11 271	M.I. Adamovich et al.	(CERN WA89 Collab.)
BIAGI 87	ZPHY C34 15	S.F. Biagi et al.	(BRIS, CERN, GEVA+)
BIAGI 87C	ZPHY C34 175	S.F. Biagi et al.	(BRIS, CERN, GEVA+)
ASTON 85B	PR D32 2270	D. Aston et al.	(SLAC, CARL, CNRC, CINC)
JENKINS 83	PRL 51 951	C.M. Jenkins et al.	(FSU, BRAN, LBL+)
BIAGI 81	ZPHY C9 305	S.F. Biagi et al.	(BRIS, CAVE, GEVA+)
HASSALL 81	NP B189 397	J.K. Hassall et al.	(CAVE, MSU)
TEODORO 78	PL 77B 451	D. Teodoro et al.	(AMST, CERN, NIJM+)
BRIEFEL 77	PR D16 2706	E. Briefel et al.	(BRAN, UMD, SYRA+)
Also	PRL 23 884	S.P. Appell et al.	(BRAN, UMD, SYRA+)
GAY 76c	PL 62B 477	J.B. Gay et al.	(AMST, CERN, NIJM)
DIBIANCA 75	NP B98 137	F.A. Dibiaccia, R.J. Endorf	(CMU)
BADIER 72	NP B37 429	J. Badier et al.	(EPOL)
APSELL 70	PRL 24 777	S.P. Appell et al.	(BRAN, UMD, SYRA+)
CRENNELL 70B	PR D1 847	D.J. Crennell et al.	(BNL)
ALITTI 69	PRL 22 79	J. Alitti et al.	(BNL, SYRA)
DAUBER 69	PR 179 1262	P.M. Dauber et al.	(LRL)
TRIPP 67	NP B3 10	R.D. Tripp et al.	(LRL, SLAC, CERN+)
BADIER 65	PL 16 171	J. Badier et al.	(EPOL, SACL, AMST)
SMITH 65B	Athens Conf. 251	G.A. Smith, J.S. Lindsey	(LRL)
SMITH 65C	PRL 14 25	G.A. Smith et al.	(LRL)
HALSTEINSLID 63	Siena Conf. 1 73	A. Halsteinslid et al.	(BERG, CERN, EPOL+)

OTHER RELATED PAPERS

TEODORO 78	PL 77B 451	D. Teodoro et al.	(AMST, CERN, NIJM+)
BRIEFEL 75	PR D12 1859	E. Briefel et al.	(BRAN, UMD, SYRA+)
SCHMIDT 73	Purdue Conf. 363	P.E. Schmidt	(BRAN)
MERRILL 68	PR 167 1202	D.W. Merrill, J. Button-Shafer	(LRL)
SMITH 64	PRL 13 61	G.A. Smith et al.	(LRL)

$\Xi(1950)$

$$I(J^P) = \frac{1}{2}(?)^? \text{ Status: } ** *$$

We list here everything reported between 1875 and 2000 MeV. The accumulated evidence for a Ξ near 1950 MeV seems strong enough to include a $\Xi(1950)$ in the main Baryon Table, but not much can be said about its properties. In fact, there may be more than one Ξ near this mass.

$\Xi(1950)$ MASS

VALUE (MeV)	EVTS	DOCUMENT ID	TECN	COMMENT
1950 ± 15 OUR ESTIMATE				
1955 ± 6		ADAMOVICH 99B	WA89	Σ^- nucleus, 345 GeV
1944 ± 9	129	BIAGI 87	SPEC	Ξ^- Be \rightarrow ($\Xi^- \pi^+$) $\pi^- X$
1963 ± 5 ± 2	63	BIAGI 87c	SPEC	Ξ^- Be \rightarrow ($\Lambda \bar{K}^0$) X
1937 ± 7	150	BIAGI 81	SPEC	SPS hyperon beam
1961 ± 18	139	BRIEFEL 77	HBC	2.87 $K^- p \rightarrow$ $\Xi^- \pi^+ X$
1936 ± 22	44	BRIEFEL 77	HBC	2.87 $K^- p \rightarrow \Xi^0 \pi^- X$
1964 ± 10	56	BRIEFEL 77	HBC	$\Xi(1530)\pi$
1900 ± 12		DIBIANCA 75	DBC	$\Xi \pi$
1952 ± 11	25	ROSS 73c		($\Xi \pi$) $^-$
1956 ± 6	29	BADIER 72	HBC	$\Xi \pi, \Xi \pi \pi, \gamma K$

Baryon Particle Listings

$\Xi(1950), \Xi(2030)$

1955 ± 14	21	GOLDWASSER 70	HBC	$\Xi \pi$
1894 ± 18	66	DAUBER 69	HBC	$\Xi \pi$
1930 ± 20	27	ALITTI 68	HBC	$\Xi^- \pi^+$
1933 ± 16	35	BADIER 65	HBC	$\Xi^- \pi^+$

$\Xi(1950)$ WIDTH

VALUE (MeV)	EVTS	DOCUMENT ID	TECN	COMMENT
60 ± 20 OUR ESTIMATE				
68 ± 22		ADAMOVICH 99B	WA 89	Σ^- nucleus, 345 GeV
100 ± 31	129	BIAGI 87	SPEC	$\Xi^- \text{Be} \rightarrow (\Xi^- \pi^+) \pi^- X$
25 ± 15 ± 1.2	63	BIAGI 87c	SPEC	$\Xi^- \text{Be} \rightarrow (\Lambda \bar{K}^0) X$
60 ± 8	150	BIAGI 81	SPEC	SPS hyperon beam
159 ± 57	139	BRIEFEL 77	HBC	$2.87 K^- p \rightarrow \Xi^- \pi^+ X$
87 ± 26	44	BRIEFEL 77	HBC	$2.87 K^- p \rightarrow \Xi^0 \pi^- X$
60 ± 39	56	BRIEFEL 77	HBC	$\Xi(1530) \pi$
63 ± 78		DIBIANCA 75	DBC	$\Xi \pi$
38 ± 10		ROSS 73c		$(\Xi \pi)^-$
35 ± 11	29	BADIER 72	HBC	$\Xi \pi, \Xi \pi \pi, \gamma K$
56 ± 26	21	GOLDWASSER 70	HBC	$\Xi \pi$
98 ± 23	66	DAUBER 69	HBC	$\Xi \pi$
80 ± 40	27	ALITTI 68	HBC	$\Xi^- \pi^+$
140 ± 35	35	BADIER 65	HBC	$\Xi^- \pi^+$

$\Xi(1950)$ DECAY MODES

Mode	Fraction (Γ_i/Γ)
Γ_1 $\Lambda \bar{K}$	seen
Γ_2 $\Sigma \bar{K}$	possibly seen
Γ_3 $\Xi \pi$	seen
Γ_4 $\Xi(1530) \pi$	
Γ_5 $\Xi \pi \pi$ (not $\Xi(1530) \pi$)	

$\Xi(1950)$ BRANCHING RATIOS

VALUE	CL%	EVTS	DOCUMENT ID	TECN	COMMENT	Γ_2/Γ_1
<2.3	90	0	BIAGI 87c	SPEC	$\Xi^- \text{Be} 116 \text{ GeV}$	
$\Gamma(\Sigma \bar{K})/\Gamma_{\text{total}}$						
possibly seen						
17						
HASSALL 81 HBC $K^- p 6.5 \text{ GeV}/c$						
$\Gamma(\Xi \pi)/\Gamma(\Xi(1530) \pi)$						
2.8^{+0.7}_{-0.6}						
APSELL 70 HBC						
$\Gamma(\Xi \pi \pi \text{ (not } \Xi(1530) \pi))/\Gamma(\Xi(1530) \pi)$						
0.0 ± 0.3						
APSELL 70 HBC						

$\Xi(1950)$ REFERENCES

ADAMOVICH 99B	EPJ C11 271	M.I. Adamovich et al.	(CERN WA89 Collab.)
BIAGI 87	ZPHY C34 15	S.F. Biagi et al.	(BRIS, CERN, GEVA+)
BIAGI 87c	ZPHY C34 175	S.F. Biagi et al.	(BRIS, CERN, GEVA+)
BIAGI 81	ZPHY C9 305	S.F. Biagi et al.	(BRIS, CAVE, GEVA+)
HASSALL 81	NP B189 397	J.K. Hassall et al.	(CAVE, MSU)
BRIEFEL 77	PR D16 2706	E. Briefel et al.	(BRAN, UMD, SYRA+)
Also Hyperon Resonances, 1970			
DIBIANCA 75	NP B98 137	F.A. Dibianca, R.J. Endorf	(CMU)
ROSS 73c	Purdue Conf. 345	R.T. Ross, J.L. Lloyd, D. Radojicic	(OXF)
BADIER 72	NP B37 429	J. Badier et al.	(EPOL)
APSELL 70	PRL 24 777	S.P. Appell et al.	(BRAN, UMD, SYRA+)
GOLDWASSER 70	PR D1 1960	E.L. Goldwasser, P.F. Schultz	(ILL)
DAUBER 69	PR 179 1262	P.M. Dauber et al.	(LRL)
ALITTI 68	PRL 21 1119	J. Alitti et al.	(BNL, SYRA)
BADIER 65	PL 16 171	J. Badier et al.	(EPOL, SACL, AMST)

$\Xi(2030)$

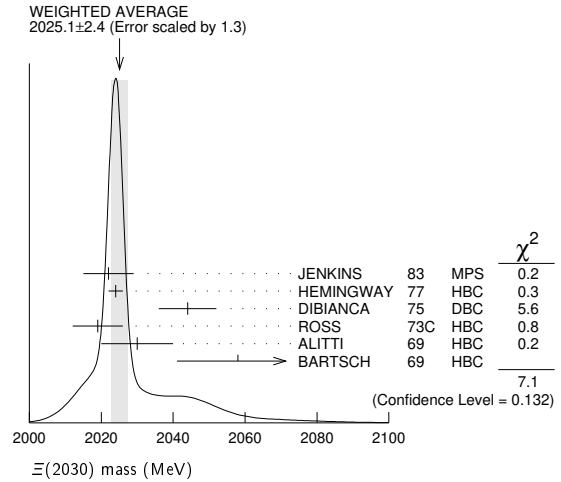
$$I(J^P) = \frac{1}{2} (\geq \frac{5}{2}^?) \text{status: } ***$$

The evidence for this state has been much improved by HEMINGWAY 77, who see an eight standard deviation enhancement in $\Sigma \bar{K}$ and a weaker coupling to $\Lambda \bar{K}$. ALITTI 68 and HEMINGWAY 77 observe no signals in the $\Xi \pi \pi$ (or $\Xi(1530) \pi$) channel, in contrast to DIBIANCA 75. The decay $(\Lambda/\Sigma) \bar{K} \pi$ reported by BARTSCH 69 is also not confirmed by HEMINGWAY 77.

A moments analysis of the HEMINGWAY 77 data indicates at a level of three standard deviations that $J \geq 5/2$.

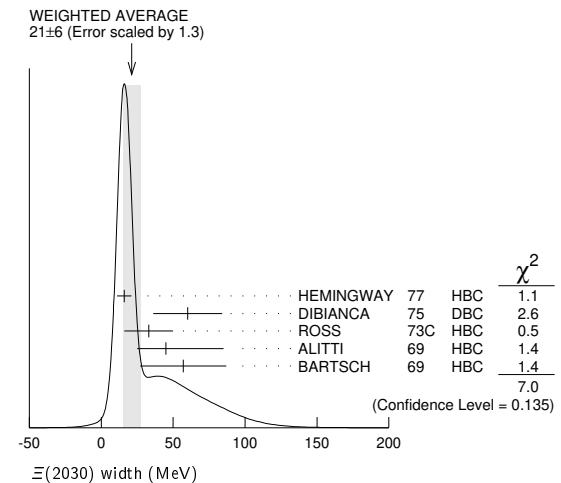
$\Xi(2030)$ MASS

VALUE (MeV)	EVTS	DOCUMENT ID	TECN	CHG	COMMENT
2025 ± 5 OUR ESTIMATE					
2025.1 ± 2.4 OUR AVERAGE					
Error includes scale factor of 1.3. See the ideogram below.					
2022 ± 7		JENKINS 83	MPS	-	$K^- p \rightarrow K^+ \text{MM}$
2024 ± 2	200	HEMINGWAY 77	HBC	-	$K^- p 4.2 \text{ GeV}/c$
2044 ± 8		DIBIANCA 75	DBC	-0	$\Xi \pi \pi, \Xi^* \pi$
2019 ± 7	15	ROSS 73c	HBC	-0	$\Sigma \bar{K}$
2030 ± 10	42	ALITTI 69	HBC	-	$K^- p 3.9-5 \text{ GeV}/c$
2058 ± 17	40	BARTSCH 69	HBC	-0	$K^- p 10 \text{ GeV}/c$



$\Xi(2030)$ WIDTH

VALUE (MeV)	EVTS	DOCUMENT ID	TECN	CHG	COMMENT
20 ± 15 OUR ESTIMATE					
21 ± 6 OUR AVERAGE					
Error includes scale factor of 1.3. See the ideogram below.					
16 ± 5	200	HEMINGWAY 77	HBC	-	$K^- p 4.2 \text{ GeV}/c$
60 ± 24		DIBIANCA 75	DBC	-0	$\Xi \pi \pi, \Xi^* \pi$
33 ± 17	15	ROSS 73c	HBC	-0	$\Sigma \bar{K}$
45 ± 40		ALITTI 69	HBC	-	$K^- p 3.9-5 \text{ GeV}/c$
57 ± 30		BARTSCH 69	HBC	-0	$K^- p 10 \text{ GeV}/c$



$\Xi(2030)$ DECAY MODES

Mode	Fraction (Γ_i/Γ)
Γ_1 $\Lambda \bar{K}$	~ 20 %
Γ_2 $\Sigma \bar{K}$	~ 80 %
Γ_3 $\Xi \pi$	small
Γ_4 $\Xi(1530) \pi$	small
Γ_5 $\Xi \pi \pi$ (not $\Xi(1530) \pi$)	small
Γ_6 $\Lambda \bar{K} \pi$	small
Γ_7 $\Sigma \bar{K} \pi$	small

See key on page 1171

Baryon Particle Listings

$\Xi(2030)$, $\Xi(2120)$, $\Xi(2250)$

 $\Xi(2030)$ BRANCHING RATIOS

$$\frac{\Gamma(\Xi\pi)}{\Gamma(\Lambda\bar{K}) + \Gamma(\Sigma\bar{K}) + \Gamma(\Xi\pi) + \Gamma(\Xi(1530)\pi)} \quad \Gamma_3/(\Gamma_1+\Gamma_2+\Gamma_3+\Gamma_4)$$

VALUE	DOCUMENT ID	TECN	CHG	COMMENT
<0.30	ALITTI 69	HBC	—	1 standard dev. limit

••• We do not use the following data for averages, fits, limits, etc. •••

$$\frac{\Gamma(\Xi\pi)}{\Gamma(\Sigma\bar{K})} \quad \Gamma_3/\Gamma_2$$

VALUE	CL%	DOCUMENT ID	TECN	CHG	COMMENT
<0.19	95	HEMINGWAY 77	HBC	—	$K^- p$ 4.2 GeV/c

$$\frac{\Gamma(\Lambda\bar{K})}{\Gamma(\Lambda\bar{K}) + \Gamma(\Sigma\bar{K}) + \Gamma(\Xi\pi) + \Gamma(\Xi(1530)\pi)} \quad \Gamma_1/(\Gamma_1+\Gamma_2+\Gamma_3+\Gamma_4)$$

VALUE	DOCUMENT ID	TECN	CHG	COMMENT
0.25 ± 0.15	ALITTI 69	HBC	—	$K^- p$ 3.9–5 GeV/c

$$\frac{\Gamma(\Lambda\bar{K})}{\Gamma(\Sigma\bar{K})} \quad \Gamma_1/\Gamma_2$$

VALUE	DOCUMENT ID	TECN	CHG	COMMENT
0.22 ± 0.09	HEMINGWAY 77	HBC	—	$K^- p$ 4.2 GeV/c

$$\frac{\Gamma(\Sigma\bar{K})}{\Gamma(\Lambda\bar{K}) + \Gamma(\Sigma\bar{K}) + \Gamma(\Xi\pi) + \Gamma(\Xi(1530)\pi)} \quad \Gamma_2/(\Gamma_1+\Gamma_2+\Gamma_3+\Gamma_4)$$

VALUE	DOCUMENT ID	TECN	CHG	COMMENT
0.75 ± 0.20	ALITTI 69	HBC	—	$K^- p$ 3.9–5 GeV/c

$$\frac{\Gamma(\Xi(1530)\pi)}{\Gamma(\Lambda\bar{K}) + \Gamma(\Sigma\bar{K}) + \Gamma(\Xi\pi) + \Gamma(\Xi(1530)\pi)} \quad \Gamma_4/(\Gamma_1+\Gamma_2+\Gamma_3+\Gamma_4)$$

VALUE	DOCUMENT ID	TECN	CHG	COMMENT
<0.15	ALITTI 69	HBC	—	1 standard dev. limit

••• We do not use the following data for averages, fits, limits, etc. •••

$$\frac{\Gamma(\Xi(1530)\pi) + \Gamma(\Xi\pi(\text{not } \Xi(1530)\pi))}{\Gamma(\Sigma\bar{K})} \quad (\Gamma_4+\Gamma_5)/\Gamma_2$$

VALUE	CL%	DOCUMENT ID	TECN	CHG	COMMENT
<0.11	95	1 HEMINGWAY 77	HBC	—	$K^- p$ 4.2 GeV/c

$$\frac{\Gamma(\Lambda\bar{K}\pi)}{\Gamma_{\text{total}}} \quad \Gamma_6/\Gamma$$

VALUE	DOCUMENT ID	TECN	COMMENT
seen	BARTSCH 69	HBC	$K^- p$ 10 GeV

••• We do not use the following data for averages, fits, limits, etc. •••

$$\frac{\Gamma(\Lambda\bar{K}\pi)}{\Gamma(\Sigma\bar{K})} \quad \Gamma_6/\Gamma_2$$

VALUE	CL%	DOCUMENT ID	TECN	CHG	COMMENT
<0.32	95	HEMINGWAY 77	HBC	—	$K^- p$ 4.2 GeV/c

$$\frac{\Gamma(\Sigma\bar{K}\pi)}{\Gamma_{\text{total}}} \quad \Gamma_7/\Gamma$$

VALUE	DOCUMENT ID	TECN	COMMENT
seen	BARTSCH 69	HBC	$K^- p$ 10 GeV

••• We do not use the following data for averages, fits, limits, etc. •••

$$\frac{\Gamma(\Sigma\bar{K}\pi)}{\Gamma(\Sigma\bar{K})} \quad \Gamma_7/\Gamma_2$$

VALUE	CL%	DOCUMENT ID	TECN	CHG	COMMENT
<0.04	95	2 HEMINGWAY 77	HBC	—	$K^- p$ 4.2 GeV/c

 $\Xi(2030)$ FOOTNOTES

¹ For the decay mode $\Xi^- \pi^+ \pi^-$ only.

² For the decay mode $\Sigma^\pm K^- \pi^\mp$ only.

 $\Xi(2030)$ REFERENCES

JENKINS 83	PRL 51 951	C.M. Jenkins <i>et al.</i>	(FSU, BRAN, LBL+)
HEMINGWAY 77	PL 68B 197	R.J. Hemingway <i>et al.</i>	(AMST, CERN, NIJM+)
Also	PL 62B 477	J.B. Gay <i>et al.</i>	(AMST, CERN, NIJM)
DIBIANCA 75	NP B98 137	F.A. Dibianca, R.J. Endorf	(CMU)
ROSS 73C	Purdue Conf. 345	R.T. Ross, J.L. Lloyd, D. Radojčić	(OXF)
ALITTI 69	PRL 22 79	J. Alitti <i>et al.</i>	(BNL, SYRA)
BARTSCH 69	PL 28B 439	J. Bartsch <i>et al.</i>	(AACH, BERL, CERN+)
ALITTI 68	PRL 21 1119	J. Alitti <i>et al.</i>	(BNL, SYRA)

 $\Xi(2120)$

$I(J^P) = \frac{1}{2}(?)^?$ Status: *
J, P need confirmation.

OMITTED FROM SUMMARY TABLE

 $\Xi(2120)$ MASS

VALUE (MeV)	EVTS	DOCUMENT ID	TECN	COMMENT
≈ 2120 OUR ESTIMATE				
2137 ± 4	18	1 CHLIAPNIK... 79	HBC	$K^+ p$ 32 GeV/c
2123 ± 7		2 GAY 76c	HBC	$K^- p$ 4.2 GeV/c

 $\Xi(2120)$ WIDTH

VALUE (MeV)	EVTS	DOCUMENT ID	TECN	COMMENT
<20	18	1 CHLIAPNIK... 79	HBC	$K^+ p$ 32 GeV/c
25 ± 12		2 GAY 76c	HBC	$K^- p$ 4.2 GeV/c

 $\Xi(2120)$ DECAY MODES

Mode	Fraction (Γ_i/Γ)
Γ_1 $\Lambda\bar{K}$	seen

 $\Xi(2120)$ BRANCHING RATIOS

$\Gamma(\Lambda\bar{K})/\Gamma_{\text{total}}$	DOCUMENT ID	TECN	COMMENT	Γ_1/Γ
seen	1 CHLIAPNIK... 79	HBC	$K^+ p \rightarrow (\bar{K} K^+) X$	
seen	2 GAY 76c	HBC	$K^- p$ 4.2 GeV/c	

 $\Xi(2120)$ FOOTNOTES

¹ CHLIAPNIKOV 79 does not uniquely identify the K^+ in the $(\bar{K} K^+) X$ final state. It also reports bumps with fewer events at 2240, 2540, and 2830 MeV.

² GAY 76c sees a 4-standard deviation signal. However, HEMINGWAY 77, with more events from the same experiment points out that the signal is greatly reduced if a cut is made on the 4-momentum u . This suggests an anomalous production mechanism if the $\Xi(2120)$ is real.

 $\Xi(2120)$ REFERENCES

CHLIAPNIK... 79	NP B158 253	P.V. Chliapnikov <i>et al.</i>	(CERN, BELG, MONS)
HEMINGWAY 77	PL 68B 197	R.J. Hemingway <i>et al.</i>	(AMST, CERN, NIJM+)
GAY 76c	PL 62B 477	J.B. Gay <i>et al.</i>	(AMST, CERN, NIJM)

 $\Xi(2250)$

$I(J^P) = \frac{1}{2}(?)^?$ Status: **
J, P need confirmation.

OMITTED FROM SUMMARY TABLE

The evidence for this state is mixed. BARTSCH 69 sees a bump of not much statistical significance in $\Lambda\bar{K}\pi$, $\Sigma\bar{K}\pi$, and $\Xi\pi\pi$ mass spectra. GOLDWASSER 70 sees a narrower bump in $\Xi\pi\pi$ at a higher mass. Not seen by HASSALL 81 with 45 events/ μb at 6.5 GeV/c. Seen by JENKINS 83. Perhaps seen by BIAGI 87.

 $\Xi(2250)$ MASS

VALUE (MeV)	EVTS	DOCUMENT ID	TECN	CHG	COMMENT
≈ 2250 OUR ESTIMATE					
2189 ± 7	66	BIAGI 87	SPEC	—	$\Xi^- \text{Be} \rightarrow (\Xi^- \pi^+ \pi^-) X$
2214 ± 5		JENKINS 83	MPS	—	$K^- p \rightarrow K^+ \text{MM}$
2295 ± 15	18	GOLDWASSER 70	HBC	—	$K^- p$ 5.5 GeV/c
2244 ± 52	35	BARTSCH 69	HBC	—	$K^- p$ 10 GeV/c

 $\Xi(2250)$ WIDTH

VALUE (MeV)	EVTS	DOCUMENT ID	TECN	CHG	COMMENT
46 ± 27	66	BIAGI 87	SPEC	—	$\Xi^- \text{Be} \rightarrow (\Xi^- \pi^+ \pi^-) X$
< 30		GOLDWASSER 70	HBC	—	$K^- p$ 5.5 GeV/c
130 ± 80		BARTSCH 69	HBC	—	

 $\Xi(2250)$ DECAY MODES

Mode	Fraction (Γ_i/Γ)
Γ_1 $\Xi\pi\pi$	
Γ_2 $\Lambda\bar{K}\pi$	
Γ_3 $\Sigma\bar{K}\pi$	

 $\Xi(2250)$ REFERENCES

BIAGI 87	ZPHY C34 15	S.F. Biagi <i>et al.</i>	(BRIS, CERN, GEVA+)
JENKINS 83	PRL 51 951	C.M. Jenkins <i>et al.</i>	(FSU, BRAN, LBL+)
HASSALL 81	NP B189 397	J.K. Hassall <i>et al.</i>	(CAVE, MSU)
GOLDWASSER 70	PR D1 1960	E.L. Goldwasser, P.F. Schultz	(ILL)
BARTSCH 69	PL 28B 439	J. Bartsch <i>et al.</i>	(AACH, BERL, CERN+)

Baryon Particle Listings

 $\Xi(2370)$, $\Xi(2500)$ $\Xi(2370)$

$I(J^P) = \frac{1}{2}(??)$ Status: **
J, P need confirmation.

OMITTED FROM SUMMARY TABLE

 $\Xi(2370)$ MASS

VALUE (MeV)	EVTS	DOCUMENT ID	TECN	CHG	COMMENT
≈ 2370 OUR ESTIMATE					
2356 \pm 10		JENKINS 83	MPS	-	$K^- p \rightarrow K^+ \Lambda$
2370	50	HASSALL 81	HBC	-0	$K^- p$ 6.5 GeV/c
2373 \pm 8	94	AMIRZADEH 80	HBC	-0	$K^- p$ 8.25 GeV/c
2392 \pm 27		DIBIANCA 75	DBC		$\Xi 2\pi$

 $\Xi(2370)$ WIDTH

VALUE (MeV)	EVTS	DOCUMENT ID	TECN	CHG	COMMENT
80	50	HASSALL 81	HBC	-0	$K^- p$ 6.5 GeV/c
80 \pm 25	94	AMIRZADEH 80	HBC	-0	$K^- p$ 8.25 GeV/c
75 \pm 69		DIBIANCA 75	DBC		$\Xi 2\pi$

 $\Xi(2370)$ DECAY MODES

Mode	Fraction (Γ_j/Γ)
Γ_1 $\Lambda \bar{K} \pi$ Includes $\Gamma_4 + \Gamma_6$.	seen
Γ_2 $\Sigma \bar{K} \pi$ Includes $\Gamma_5 + \Gamma_6$.	seen
Γ_3 $\Omega^- K$	
Γ_4 $\Lambda \bar{K}^*(892)$	
Γ_5 $\Sigma \bar{K}^*(892)$	
Γ_6 $\Sigma(1385) \bar{K}$	

 $\Xi(2370)$ BRANCHING RATIOS

$\Gamma(\Lambda \bar{K} \pi)/\Gamma_{\text{total}}$	Γ_1/Γ			
VALUE	DOCUMENT ID	TECN	CHG	COMMENT
seen	AMIRZADEH 80	HBC	-0	$K^- p$ 8.25 GeV/c

$\Gamma(\Sigma \bar{K} \pi)/\Gamma_{\text{total}}$	Γ_2/Γ			
VALUE	DOCUMENT ID	TECN	CHG	COMMENT
seen	AMIRZADEH 80	HBC	-0	$K^- p$ 8.25 GeV/c

$[\Gamma(\Lambda \bar{K} \pi) + \Gamma(\Sigma \bar{K} \pi)]/\Gamma_{\text{total}}$	$(\Gamma_1 + \Gamma_2)/\Gamma$				
VALUE	EVTS	DOCUMENT ID	TECN	CHG	COMMENT
seen	50	HASSALL 81	HBC	-0	$K^- p$ 6.5 GeV/c

$\Gamma(\Omega^- K)/\Gamma_{\text{total}}$	Γ_3/Γ				
VALUE	DOCUMENT ID	TECN	CHG	COMMENT	
0.09 \pm 0.04	1	KINSON 80	HBC	-	$K^- p$ 8.25 GeV/c

$[\Gamma(\Lambda \bar{K}^*(892)) + \Gamma(\Sigma \bar{K}^*(892))]/\Gamma_{\text{total}}$	$(\Gamma_4 + \Gamma_5)/\Gamma$				
VALUE	DOCUMENT ID	TECN	CHG	COMMENT	
0.22 \pm 0.13	1	KINSON 80	HBC	-	$K^- p$ 8.25 GeV/c

$\Gamma(\Sigma(1385) \bar{K})/\Gamma_{\text{total}}$	Γ_6/Γ				
VALUE	DOCUMENT ID	TECN	CHG	COMMENT	
0.12 \pm 0.08	1	KINSON 80	HBC	-	$K^- p$ 8.25 GeV/c

 $\Xi(2370)$ FOOTNOTES

¹ KINSON 80 is a reanalysis of AMIRZADEH 80 with 50% more events.

 $\Xi(2370)$ REFERENCES

JENKINS 83	PRL 51 951	C.M. Jenkins et al.	(FSU, BRAN, LBL+)
HASSALL 81	NP B189 397	J.K. Hassall et al.	(CAVE, MSU)
AMIRZADEH 80	PL 90B 324	J. Amirzadeh et al.	(BIRM, CERN, GLAS+) ¹
KINSON 80	Toronto Conf. 263	J.B. Kinson et al.	(BIRM, CERN, GLAS+) ¹
DIBIANCA 75	NP B98 137	F.A. Dibianna, R.J. Endorf	(CMU)

 $\Xi(2500)$

$I(J^P) = \frac{1}{2}(??)$ Status: *
J, P need confirmation.

OMITTED FROM SUMMARY TABLE

The ALITTI 69 peak might be instead the $\Xi(2370)$ or might be neither the $\Xi(2370)$ nor the $\Xi(2500)$.

 $\Xi(2500)$ MASS

VALUE (MeV)	EVTS	DOCUMENT ID	TECN	CHG	COMMENT
≈ 2500 OUR ESTIMATE					
2505 \pm 10		JENKINS 83	MPS	-	$K^- p \rightarrow K^+ \Lambda$ MM
2430 \pm 20	30	ALITTI 69	HBC	-	$K^- p$ 4.6-5 GeV/c
2500 \pm 10	45	BARTSCH 69	HBC	-0	$K^- p$ 10 GeV/c

 $\Xi(2500)$ WIDTH

VALUE (MeV)	DOCUMENT ID	TECN	CHG
150 ⁺⁶⁰ -40	ALITTI 69	HBC	-
59 \pm 27	BARTSCH 69	HBC	-0

 $\Xi(2500)$ DECAY MODES

Mode	Fraction (Γ_j/Γ)
Γ_1 $\Xi \pi$	
Γ_2 $\Lambda \bar{K}$	
Γ_3 $\Sigma \bar{K}$	
Γ_4 $\Xi \pi \pi$	seen
Γ_5 $\Xi(1530) \pi$	
Γ_6 $\Lambda \bar{K} \pi + \Sigma \bar{K} \pi$	seen

 $\Xi(2500)$ BRANCHING RATIOS

$\Gamma(\Xi \pi)/[\Gamma(\Xi \pi) + \Gamma(\Lambda \bar{K}) + \Gamma(\Sigma \bar{K}) + \Gamma(\Xi(1530) \pi)]$	$\Gamma_1/(\Gamma_1 + \Gamma_2 + \Gamma_3 + \Gamma_5)$		
VALUE	DOCUMENT ID	TECN	COMMENT
<0.5	ALITTI 69	HBC	1 standard dev. limit

$\Gamma(\Lambda \bar{K})/[\Gamma(\Xi \pi) + \Gamma(\Lambda \bar{K}) + \Gamma(\Sigma \bar{K}) + \Gamma(\Xi(1530) \pi)]$	$\Gamma_2/(\Gamma_1 + \Gamma_2 + \Gamma_3 + \Gamma_5)$		
VALUE	DOCUMENT ID	TECN	CHG
0.5 \pm 0.2	ALITTI 69	HBC	-

$\Gamma(\Sigma \bar{K})/[\Gamma(\Xi \pi) + \Gamma(\Lambda \bar{K}) + \Gamma(\Sigma \bar{K}) + \Gamma(\Xi(1530) \pi)]$	$\Gamma_3/(\Gamma_1 + \Gamma_2 + \Gamma_3 + \Gamma_5)$		
VALUE	DOCUMENT ID	TECN	CHG
0.5 \pm 0.2	ALITTI 69	HBC	-

$\Gamma(\Xi(1530) \pi)/[\Gamma(\Xi \pi) + \Gamma(\Lambda \bar{K}) + \Gamma(\Sigma \bar{K}) + \Gamma(\Xi(1530) \pi)]$	$\Gamma_5/(\Gamma_1 + \Gamma_2 + \Gamma_3 + \Gamma_5)$		
VALUE	DOCUMENT ID	TECN	COMMENT
<0.2	ALITTI 69	HBC	1 standard dev. limit

$\Gamma(\Xi \pi \pi)/\Gamma_{\text{total}}$	Γ_4/Γ		
VALUE	DOCUMENT ID	TECN	CHG
seen	BARTSCH 69	HBC	-0

$[\Gamma(\Lambda \bar{K} \pi) + \Gamma(\Sigma \bar{K} \pi)]/\Gamma_{\text{total}}$	Γ_6/Γ		
VALUE	DOCUMENT ID	TECN	CHG
seen	BARTSCH 69	HBC	-0

 $\Xi(2500)$ REFERENCES

JENKINS 83	PRL 51 951	C.M. Jenkins et al.	(FSU, BRAN, LBL+)
ALITTI 69	PRL 22 79	J. Alitti et al.	(BNL, SYR) ¹
BARTSCH 69	PL 28B 439	J. Bartsch et al.	(AACH, BERL, CERN+)

Ω^- BARYONS

($S = -3, I = 0$)

$\Omega^- = sss$



$I(J^P) = 0(\frac{3}{2}^+)$ Status: * * * *

The unambiguous discovery in both production and decay was by BARNES 64. The quantum numbers follow from the assignment of the particle to the baryon decuplet. DEUTSCHMANN 78 and BAUBILLIER 78 rule out $J = 1/2$ and find consistency with $J = 3/2$. AUBERT, BE 06 finds from the decay angular distributions of $\Xi_c^0 \rightarrow \Omega^- K^+$ and $\Omega_c^0 \rightarrow \Omega^- K^+$ that $J = 3/2$; this depends on the spins of the Ξ_c^0 and Ω_c^0 being $J = 1/2$, their supposed values. ABLIKIM 21E determines the Ω^- spin to be $J = 3/2$ from the decay angular distributions of the complete decay chain $\psi(3686) \rightarrow \Omega^- \bar{\Omega}^+$, with subsequent decays $\Omega^- \rightarrow K^- \Lambda$ and $\bar{\Omega}^+ \rightarrow K^+ \bar{\Lambda}$.

We have omitted some results that have been superseded by later experiments. See our earlier editions.

Ω^- MASS

The fit assumes the Ω^- and $\bar{\Omega}^+$ masses are the same, and averages them together.

VALUE (MeV)	EVTS	DOCUMENT ID	TECN	COMMENT
1672.45 ± 0.29 OUR FIT				
1672.43 ± 0.32 OUR AVERAGE				
1673 ± 1	100	HARTOUNI 85	SPEC	80-280 GeV $K_L^0 C$
1673.0 ± 0.8	41	BAUBILLIER 78	HBC	8.25 GeV/c $K^- p$
1671.7 ± 0.6	27	HEMINGWAY 78	HBC	4.2 GeV/c $K^- p$
1673.4 ± 1.7	4	¹ DIBIANCA 75	DBC	4.9 GeV/c $K^- d$
1673.3 ± 1.0	3	PALMER 68	HBC	$K^- p$ 4.6, 5 GeV/c
1671.8 ± 0.8	3	SCHULTZ 68	HBC	$K^- p$ 5.5 GeV/c
1674.2 ± 1.6	5	SCOTTER 68	HBC	$K^- p$ 6 GeV/c
1672.1 ± 1.0	1	² FRY 55	EMUL	
• • • We do not use the following data for averages, fits, limits, etc. • • •				
1671.43 ± 0.78	13	³ DEUTSCH... 73	HBC	$K^- p$ 10 GeV/c
1671.9 ± 1.2	6	³ SPETH 69	HBC	See DEUTSCHMANN 73
1673.0 ± 0.8	1	ABRAMS 64	HBC	$\rightarrow \Xi^- \pi^0$
1670.6 ± 1.0	1	² FRY 55B	EMUL	
1672.1 ± 1.0	1	⁴ EISENBERG 54	EMUL	

¹DIBIANCA 75 gives a mass for each event. We quote the average.
²The FRY 55 and FRY 55B events were identified as Ω^- by ALVAREZ 73. The masses assume decay to ΛK^- at rest. For FRY 55B, decay from an atomic orbit could Doppler shift the K^- energy and the resulting Ω^- mass by several MeV. This shift is negligible for FRY 55 because the Ω^- decay is approximately perpendicular to its orbital velocity, as is known because the Λ strikes the nucleus (L.Alvarez, private communication 1973). We have calculated the error assuming that the orbital n is 4 or larger.
³Excluded from the average; the Ω^- lifetimes measured by the experiments differ significantly from other measurements.
⁴The EISENBERG 54 mass was calculated for decay in flight. ALVAREZ 73 has shown that the Ω^- interacted with an Ag nucleus to give $K^- \Xi Ag$.

$\bar{\Omega}^+$ MASS

The fit assumes the Ω^- and $\bar{\Omega}^+$ masses are the same, and averages them together.

VALUE (MeV)	EVTS	DOCUMENT ID	TECN	COMMENT
1672.45 ± 0.29 OUR FIT				
1672.5 ± 0.7 OUR AVERAGE				
1672 ± 1	72	HARTOUNI 85	SPEC	80-280 GeV $K_L^0 C$
1673.1 ± 1.0	1	FIRESTONE 71B	HBC	12 GeV/c $K^+ d$

$(m_{\Omega^-} - m_{\bar{\Omega}^+}) / m_{\Omega^-}$

A test of CPT invariance.

VALUE (units 10^{-5})	DOCUMENT ID	TECN	COMMENT
-1.44 ± 7.98	CHAN 98	E756	p Be, 800 GeV

Ω^- MEAN LIFE

Measurements with an error $> 0.1 \times 10^{-10}$ s have been omitted. The fit assumes the Ω^- and $\bar{\Omega}^+$ mean lives are the same, and averages them together.

VALUE (10^{-10} s)	EVTS	DOCUMENT ID	TECN	COMMENT
0.821 ± 0.011 OUR FIT				
0.821 ± 0.011 OUR AVERAGE				
0.817 ± 0.013 ± 0.018	6934	CHAN 98	E756	p Be, 800 GeV
0.811 ± 0.037	1096	LUK 88	SPEC	p Be 400 GeV
0.823 ± 0.013	12k	BOURQUIN 84	SPEC	SPS hyperon beam
• • • We do not use the following data for averages, fits, limits, etc. • • •				
0.822 ± 0.028	2437	BOURQUIN 79B	SPEC	See BOURQUIN 84

$\bar{\Omega}^+$ MEAN LIFE

The fit assumes the Ω^- and $\bar{\Omega}^+$ mean lives are the same, and averages them together.

VALUE (10^{-10} s)	EVTS	DOCUMENT ID	TECN	COMMENT
0.821 ± 0.011 OUR FIT				
0.823 ± 0.031 ± 0.022	1801	CHAN 98	E756	p Be, 800 GeV

$(\tau_{\Omega^-} - \tau_{\bar{\Omega}^+}) / \tau_{\Omega^-}$

A test of CPT invariance. Our calculation, from the averages in the preceding two data blocks.

VALUE	DOCUMENT ID
0.00 ± 0.05 OUR ESTIMATE	

Ω^- MAGNETIC MOMENT

VALUE (μ_N)	EVTS	DOCUMENT ID	TECN	COMMENT
-2.02 ± 0.05 OUR AVERAGE				
-2.024 ± 0.056	235k	WALLACE 95	SPEC	Ω^- 300-550 GeV
-1.94 ± 0.17 ± 0.14	25k	DIEHL 91	SPEC	Spin-transfer production

Ω^- DECAY MODES

Mode	Fraction (Γ_i/Γ)	Scale factor/ Confidence level
$\Gamma_1 \Lambda K^-$	(67.7 ± 0.7) %	
$\Gamma_2 \Xi^0 \pi^-$	(24.3 ± 0.7) %	S=1.5
$\Gamma_3 \Xi^- \pi^0$	(8.55 ± 0.33) %	
$\Gamma_4 \Xi^- \pi^+ \pi^-$	(3.7 ^{+0.7} _{-0.6}) × 10 ⁻⁴	
$\Gamma_5 \Xi(1530)^0 \pi^-$	< 7 × 10 ⁻⁵	CL=90%
$\Gamma_6 \Xi^0 e^- \bar{\nu}_e$	(5.6 ± 2.8) × 10 ⁻³	
$\Gamma_7 \Xi^- \gamma$	< 4.6 × 10 ⁻⁴	CL=90%
$\Delta S = 2$ forbidden (S_2) modes		
$\Gamma_8 \Lambda \pi^-$	S_2 < 2.9 × 10 ⁻⁶	CL=90%

Ω^- BRANCHING RATIOS

The BOURQUIN 84 values (which include results of BOURQUIN 79B, a separate experiment) are much more accurate than any other results, and so the other results have been omitted.

$\Gamma(AK^-)/\Gamma_{total}$	Γ_1/Γ
67.7 ± 0.7 OUR AVERAGE	
66.3 ± 0.8 ± 2.0	9.0k
67.8 ± 0.7	14k
• • • We do not use the following data for averages, fits, limits, etc. • • •	
68.6 ± 1.3	1920

$\Gamma(\Xi^0 \pi^-)/\Gamma_{total}$	Γ_2/Γ
24.3 ± 0.7 OUR AVERAGE	
25.03 ± 0.44 ± 0.53	5.4k
23.6 ± 0.7	1947
• • • We do not use the following data for averages, fits, limits, etc. • • •	
23.4 ± 1.3	317

$\Gamma(\Xi^- \pi^0)/\Gamma_{total}$	Γ_3/Γ
8.55 ± 0.33 OUR AVERAGE	
8.43 ± 0.52 ± 0.28	794
8.6 ± 0.4	759
• • • We do not use the following data for averages, fits, limits, etc. • • •	
8.0 ± 0.8	145

Baryon Particle Listings

$\Omega^-, \Omega(2012)^-$

$\Gamma(\Xi^-\pi^+\pi^-)/\Gamma_{\text{total}}$		Γ_4/Γ	
VALUE (units 10^{-4})	EVTS	DOCUMENT ID	TECN COMMENT

$3.74^{+0.67}_{-0.56}$ 100 ⁵ KAMAEV 10 HYCP *p* Cu, 800 GeV

••• We do not use the following data for averages, fits, limits, etc. •••

4.3 $^{+3.4}_{-1.3}$ 4 BOURQUIN 84 SPEC SPS hyperon beam

⁵ This KAMAEV 10 value uses 76 $\Omega^- \rightarrow \Xi^-\pi^+\pi^-$ and 24 $\bar{\Omega}^+ \rightarrow \Xi^+\pi^-\pi^+$ decays. The Ω^- and $\bar{\Omega}^+$ branching fractions measurements are statistically equal. The errors given combine statistical and systematic contributions. The *CP* branching-fraction asymmetry, $(\Omega^- - \bar{\Omega}^+)/\text{sum}$, is $+0.12 \pm 0.20$.

$\Gamma(\Xi(1530)^0\pi^-)/\Gamma_{\text{total}}$		Γ_5/Γ	
VALUE (units 10^{-4})	CL% EVTS	DOCUMENT ID	TECN COMMENT

<0.7 90 KAMAEV 10 HYCP *p* Cu, 800 GeV

••• We do not use the following data for averages, fits, limits, etc. •••

$6.4^{+5.1}_{-2.0}$ 4 ⁶ BOURQUIN 84 SPEC SPS hyperon beam

⁶ The same 4 events as in the previous mode, with the isospin factor to take into account $\Xi(1530)^0 \rightarrow \Xi^0\pi^0$ decays included. BOURQUIN 84 adopted a theoretical assumption that $\Xi(1530)^0\pi^-$ would dominate $\Xi^-\pi^+\pi^-$ decay.

$\Gamma(\Xi^0 e^- \bar{\nu}_e)/\Gamma_{\text{total}}$		Γ_6/Γ	
VALUE (units 10^{-3})	EVTS	DOCUMENT ID	TECN COMMENT

5.6 ± 2.8 14 BOURQUIN 84 SPEC SPS hyperon beam

••• We do not use the following data for averages, fits, limits, etc. •••

~ 10 3 BOURQUIN 79B SPEC See BOURQUIN 84

$\Gamma(\Xi^-\gamma)/\Gamma_{\text{total}}$		Γ_7/Γ	
VALUE (units 10^{-4})	CL% EVTS	DOCUMENT ID	TECN COMMENT

<4.6 90 0 ALBUQUERQ...94 E761 Ω^- 375 GeV

••• We do not use the following data for averages, fits, limits, etc. •••

<22 90 9 BOURQUIN 84 SPEC SPS hyperon beam

<31 90 0 BOURQUIN 79B SPEC See BOURQUIN 84

$\Gamma(\Lambda\pi^-)/\Gamma_{\text{total}}$		Γ_8/Γ	
VALUE (units 10^{-6})	CL% EVTS	DOCUMENT ID	TECN COMMENT

$\Delta S=2$. Forbidden in first-order weak interaction.

<2.9 90 WHITE 05 HYCP *p* Cu, 800 GeV

••• We do not use the following data for averages, fits, limits, etc. •••

<190 90 BOURQUIN 84 SPEC SPS hyperon beam

<1300 90 BOURQUIN 79B SPEC See BOURQUIN 84

Ω^- DECAY PARAMETERS

$\alpha(\Omega^-)\alpha_-(\Lambda)$ FOR $\Omega^- \rightarrow \Lambda K^-$

Some early results have been omitted.

VALUE	EVTS	DOCUMENT ID	TECN	COMMENT
-------	------	-------------	------	---------

0.0115 ± 0.0015 OUR AVERAGE

$0.0133 \pm 0.0033 \pm 0.0052$ 960k ⁷ CHEN 05 HYCP *p* Cu, 800 GeV

$0.0114 \pm 0.0012 \pm 0.0010$ 4.5M ⁷ LU 05A HYCP *p* Cu, 800 GeV

••• We do not use the following data for averages, fits, limits, etc. •••

-0.018 ± 0.030 6953 CHAN 98 E756 *p* Be, 800 GeV

-0.022 ± 0.051 1743 LUK 88 SPEC *p* Be 400 GeV

-0.016 ± 0.018 12k BOURQUIN 84 SPEC SPS hyperon beam

⁷ The results of CHEN 05 and LU 05A are from different experimental runs.

α FOR $\Omega^- \rightarrow \Lambda K^-$

The above average, $\alpha(\Omega^-)\alpha_-(\Lambda) = 0.0115 \pm 0.0015$, divided by our current average

$\alpha_-(\Lambda) = 0.747 \pm 0.009$ gives $\alpha(\Omega^-)$:

VALUE	DOCUMENT ID
-------	-------------

0.0154 ± 0.0020 OUR EVALUATION

$\bar{\alpha}$ FOR $\bar{\Omega}^+ \rightarrow \bar{\Lambda} K^+$

VALUE	EVTS	DOCUMENT ID	TECN	COMMENT
-------	------	-------------	------	---------

$-0.0181 \pm 0.0028 \pm 0.0026$ 1.89M LU 06 HYCP *p* Cu, 800 GeV

••• We do not use the following data for averages, fits, limits, etc. •••

$+0.017 \pm 0.077$ 1823 CHAN 98 E756 *p* Be, 800 GeV

$(\alpha + \bar{\alpha})/(\alpha - \bar{\alpha})$ in $\Omega^- \rightarrow \Lambda K^-, \bar{\Omega}^+ \rightarrow \bar{\Lambda} K^+$

Zero if *CP* is conserved.

VALUE	DOCUMENT ID	TECN	COMMENT
-------	-------------	------	---------

$-0.016 \pm 0.092 \pm 0.089$ ⁸ LU 06 HYCP *p* Cu, 800 GeV

⁸ This value uses the results of CHEN 05, LU 05A, and LU 06.

α FOR $\Omega^- \rightarrow \Xi^0\pi^-$

VALUE	EVTS	DOCUMENT ID	TECN	COMMENT
-------	------	-------------	------	---------

$+0.09 \pm 0.14$ 1630 BOURQUIN 84 SPEC SPS hyperon beam

α FOR $\Omega^- \rightarrow \Xi^-\pi^0$

VALUE	EVTS	DOCUMENT ID	TECN	COMMENT
-------	------	-------------	------	---------

$+0.05 \pm 0.21$ 614 BOURQUIN 84 SPEC SPS hyperon beam

Ω^- REFERENCES

We have omitted some papers that have been superseded by later experiments. See our earlier editions.

ABLIKIM 23BJ PR D108 L091101	M. Ablikim <i>et al.</i>	(BESIII Collab.)
ABLIKIM 21E PRL 126 092002	M. Ablikim <i>et al.</i>	(BESIII Collab.)
KAMAEV 10 PL B693 236	O. Kamnev <i>et al.</i>	(FNAL HyperCP Collab.)
AUBERT_BE 06 PRL 97 112001	B. Aubert <i>et al.</i>	(BABAR Collab.)
LU 06 PRL 96 242001	L.C. Lu <i>et al.</i>	(FNAL HyperCP Collab.)
CHEN 05 PR D71 051102	Y.C. Chen <i>et al.</i>	(FNAL HyperCP Collab.)
LU 05A PL B617 11	L.C. Lu <i>et al.</i>	(FNAL HyperCP Collab.)
WHITE 05 PRL 94 101804	C.G. White <i>et al.</i>	(FNAL HyperCP Collab.)
CHAN 98 PR D58 072002	A.W. Chan <i>et al.</i>	(FNAL E756 Collab.)
WALLACE 95 PRL 74 3732	N.B. Wallace <i>et al.</i>	(MINN, ARIZ, MICH+)
ALBUQUERQ... 94 PR D50 18	I.F. Albuquerque <i>et al.</i>	(FNAL E761 Collab.)
DIHL 91 PRL 67 804	H.T. Diehl <i>et al.</i>	(RUTG, FNAL, MICH+)
LUK 88 PR D38 19	K.B. Luk <i>et al.</i>	(RUTG, WIS C, MICH, MINN)
HARTOUNI 85 PRL 54 628	E.P. Hartouni <i>et al.</i>	(COLU, ILL, FNAL)
BOURQUIN 84 NP B241 1	M.H. Bourquin <i>et al.</i>	(BRIS, GEVA, HEIDP+)
Also 84 PL B7B 297	M.H. Bourquin <i>et al.</i>	(BRIS, GEVA, HEIDP+)
BOURQUIN 79B PL B8B 192	M.H. Bourquin <i>et al.</i>	(BRIS, GEVA, HEIDP+)
BAUBILLIER 78 PL B7B 342	M. Baubillier <i>et al.</i>	(BIRM, CERN, GLAS+J)
DEUTSCH... 78 PL B7B 96	M. Deuschmann <i>et al.</i>	(AACH3, BERL, CERN+J)
HEMINGWAY 78 NP B142 205	R.J. Hemingway <i>et al.</i>	(CERN, ZEEM, NIJM+)
DIBIAN CA 75 NP B98 137	F.A. Dibiaanca, R.J. Endorf	(CMU)
ALVAREZ 73 PR D8 702	L.W. Alvarez	(LBL)
DEUTSCH... 73 NP B61 102	M. Deuschmann <i>et al.</i>	(ABCLV Collab.)
FIRESTONE 71B PRL 26 410	I. Firestone <i>et al.</i>	(LRL)
SPEITH 69 PL B9B 252	R. Speith <i>et al.</i>	(AACH, BERL, CERN, LOIC+)
PALMER 68 PL B6B 323	R.B. Palmer <i>et al.</i>	(BNL, SYR)
SCHULTZ 68 PR 168 1509	P.F. Schultz <i>et al.</i>	(ILL, ANL, NWES+)
SCOTTER 68 PL B6B 474	D. Scotter <i>et al.</i>	(BIRM, GLAS, LOIC+)
ABRAMS 64 PRL 13 670	G.S. Abrams <i>et al.</i>	(UMD, NRL)
BARNES 64 PRL 12 204	V.E. Barnes <i>et al.</i>	(BNL)
FRY 55 PR 97 1189	W.F. Fry, J. Schneps, M.S. Swami	(WISC)
FRY 55B NC 2 346	W.F. Fry, J. Schneps, M.S. Swami	(WISC)
EISENBERG 54 PR 96 541	Y. Eisenberg	(CORN)

$\Omega(2012)^-$

$I(J^P) = 0(?^-)$ Status: ***

Seen in $\Xi^0 K^-$ and $\Xi^- K_S^0$ decays with a combined significance of 8.3 standard deviations.

$\Omega(2012)^-$ MASS

VALUE (MeV)	EVTS	DOCUMENT ID	TECN	COMMENT
-------------	------	-------------	------	---------

$2012.4 \pm 0.7 \pm 0.6$ 520 YELTON 18A BELL In $\Upsilon(1S), \Upsilon(2S), \Upsilon(3S)$

$\Omega(2012)^-$ WIDTH

VALUE (MeV)	EVTS	DOCUMENT ID	TECN	COMMENT
-------------	------	-------------	------	---------

$6.4^{+2.5}_{-2.0} \pm 1.6$ 520 YELTON 18A BELL In $\Upsilon(1S), \Upsilon(2S), \Upsilon(3S)$

$\Omega(2012)^-$ DECAY MODES

Branching fractions are given relative to the one DEFINED AS 1.

Mode	Fraction (Γ_i/Γ)	Confidence level
------	--------------------------------	------------------

$\Gamma_1 \Xi K$

$\Gamma_2 (\Xi\pi) K$

$\Gamma_3 \Xi^0 K^-$ **DEFINED AS 1**

$\Gamma_4 \Xi^- \bar{K}^0$ 0.83 ± 0.21

$\Gamma_5 \Xi^0 \pi^0 K^-$ <0.30 90%

$\Gamma_6 \Xi^0 \pi^- \bar{K}^0$ <0.21 90%

$\Gamma_7 \Xi^- \pi^0 \bar{K}^0$ <0.7 90%

$\Gamma_8 \Xi^- \pi^+ K^-$ <0.08 90%

$\Omega(2012)^-$ BRANCHING RATIOS

$\Gamma((\Xi\pi)K)/\Gamma(\Xi K)$		Γ_2/Γ_1	
VALUE	CL%	DOCUMENT ID	TECN COMMENT

<0.119 90 JIA 19 BELL In $\Upsilon(1S, 2S, 3S)$

$\Gamma(\Xi^0 K^-)/\Gamma(\Xi^- \bar{K}^0)$		Γ_3/Γ_4	
VALUE	CL%	DOCUMENT ID	TECN COMMENT

1.2 ± 0.3 YELTON 18A BELL In $\Upsilon(1S, 2S, 3S)$

$\Gamma(\Xi^0 \pi^0 K^-)/\Gamma(\Xi^0 K^-)$		Γ_5/Γ_3	
VALUE	CL%	DOCUMENT ID	TECN COMMENT

<0.304 90 JIA 19 BELL In $\Upsilon(1S, 2S, 3S)$

$\Gamma(\Xi^0 \pi^- \bar{K}^0)/\Gamma(\Xi^0 K^-)$		Γ_6/Γ_3	
VALUE	CL%	DOCUMENT ID	TECN COMMENT

<0.213 90 JIA 19 BELL In $\Upsilon(1S, 2S, 3S)$

$\Gamma(\Xi^0 \pi^- \bar{K}^0)/\Gamma(\Xi^- \bar{K}^0)$		Γ_6/Γ_4	
VALUE	CL%	DOCUMENT ID	TECN COMMENT

<0.256 90 JIA 19 BELL In $\Upsilon(1S, 2S, 3S)$

See key on page 1171

Baryon Particle Listings

 $\Omega(2012)^-$, $\Omega(2250)^-$, $\Omega(2380)^-$, $\Omega(2470)^-$

$\Gamma(\Xi^-\pi^0\bar{K}^0)/\Gamma(\Xi^-\bar{K}^0)$		Γ_7/Γ_4		
VALUE	CL%	DOCUMENT ID	TECN	COMMENT
<0.811	90	JIA	19	BELL In $\Upsilon(1S, 2S, 3S)$

$\Gamma(\Xi^-\pi^+K^-)/\Gamma(\Xi^0K^-)$		Γ_8/Γ_3		
VALUE	CL%	DOCUMENT ID	TECN	COMMENT
<0.078	90	JIA	19	BELL In $\Upsilon(1S, 2S, 3S)$

$\Gamma(\Xi^-\pi^+K^-)/\Gamma(\Xi^-\bar{K}^0)$		Γ_8/Γ_4		
VALUE	CL%	DOCUMENT ID	TECN	COMMENT
<0.093	90	JIA	19	BELL In $\Upsilon(1S, 2S, 3S)$

 $\Omega(2012)^-$ REFERENCES

JIA	19	PR D100 032006	S. Jia et al.	(BELLE Collab.)
YELTON	18A	PRL 121 052003	J. Yelton et al.	(BELLE Collab.)

 $\Omega(2250)^-$ $I(J^P) = 0(?)^?$ Status: *** $\Omega(2250)^-$ MASS

VALUE (MeV)	EVTS	DOCUMENT ID	TECN	COMMENT
2252 ± 9 OUR AVERAGE				
2253 ± 13	44	ASTON	87B	LASS $K^-\rho$ 11 GeV/c
2251 ± 9 ± 8	78	BIAGI	86B	SPEC SPS Ξ^- beam

 $\Omega(2250)^-$ WIDTH

VALUE (MeV)	EVTS	DOCUMENT ID	TECN	COMMENT
55 ± 18 OUR AVERAGE				
41 ± 38	44	ASTON	87B	LASS $K^-\rho$ 11 GeV/c
48 ± 20	78	BIAGI	86B	SPEC SPS Ξ^- beam

 $\Omega(2250)^-$ DECAY MODES

Mode	Fraction (Γ_i/Γ)
Γ_1 $\Xi^-\pi^+K^-$	seen
Γ_2 $\Xi(1530)^0K^-$	seen

 $\Omega(2250)^-$ BRANCHING RATIOS

$\Gamma(\Xi(1530)^0K^-)/\Gamma(\Xi^-\pi^+K^-)$		Γ_2/Γ_1		
VALUE	EVTS	DOCUMENT ID	TECN	COMMENT
~ 1.0	44	ASTON	87B	LASS $K^-\rho$ 11 GeV/c
0.70 ± 0.20	49	BIAGI	86B	SPEC Ξ^- Be 116 GeV/c

 $\Omega(2250)^-$ REFERENCES

ASTON	87B	PL B194 579	D. Aston et al.	(SLAC, NAGO, CINC, INUS)
BIAGI	86B	ZPHY C31 33	S.F. Biagi et al.	(LOQM, GEVA, RAL+)

 $\Omega(2380)^-$

Status: **

OMITTED FROM SUMMARY TABLE

 $\Omega(2380)^-$ MASS

VALUE (MeV)	EVTS	DOCUMENT ID	TECN	COMMENT
≈ 2380 OUR ESTIMATE				
2384 ± 9 ± 8	45	BIAGI	86B	SPEC SPS Ξ^- beam

 $\Omega(2380)^-$ WIDTH

VALUE (MeV)	EVTS	DOCUMENT ID	TECN	COMMENT
26 ± 23	45	BIAGI	86B	SPEC SPS Ξ^- beam

 $\Omega(2380)^-$ DECAY MODES

Mode	Fraction (Γ_i/Γ)
Γ_1 $\Xi^-\pi^+K^-$	
Γ_2 $\Xi(1530)^0K^-$	seen
Γ_3 $\Xi^-\bar{K}^*(892)^0$	

 $\Omega(2380)^-$ BRANCHING RATIOS

$\Gamma(\Xi(1530)^0K^-)/\Gamma(\Xi^-\pi^+K^-)$		Γ_2/Γ_1			
VALUE	CL%	EVTS	DOCUMENT ID	TECN	COMMENT
<0.44	90	9	BIAGI	86B	SPEC Ξ^- Be 116 GeV/c

$\Gamma(\Xi^-\bar{K}^*(892)^0)/\Gamma(\Xi^-\pi^+K^-)$		Γ_3/Γ_1		
VALUE	EVTS	DOCUMENT ID	TECN	COMMENT
0.5 ± 0.3	21	BIAGI	86B	SPEC Ξ^- Be 116 GeV/c

 $\Omega(2380)^-$ REFERENCES

BIAGI	86B	ZPHY C31 33	S.F. Biagi et al.	(LOQM, GEVA, RAL+)
-------	-----	-------------	-------------------	--------------------

 $\Omega(2470)^-$

Status: **

OMITTED FROM SUMMARY TABLE

A peak in the $\Omega^-\pi^+\pi^-$ mass spectrum with a signal significance claimed to be at least 5.5 standard deviations. There is no reason to seriously doubt the existence of this state, but unless the evidence is overwhelming we usually wait for confirmation from a second experiment before elevating peaks to the Summary Table.

 $\Omega(2470)^-$ MASS

VALUE (MeV)	EVTS	DOCUMENT ID	TECN	COMMENT
2474 ± 12	59	ASTON	88G	LASS $K^-\rho$ 11 GeV/c

 $\Omega(2470)^-$ WIDTH

VALUE (MeV)	EVTS	DOCUMENT ID	TECN	COMMENT
72 ± 33	59	ASTON	88G	LASS $K^-\rho$ 11 GeV/c

 $\Omega(2470)^-$ DECAY MODES

Mode	Fraction (Γ_i/Γ)
Γ_1 $\Omega^-\pi^+\pi^-$	

 $\Omega(2470)^-$ REFERENCES

ASTON	88G	PL B215 799	D. Aston et al.	(SLAC, NAGO, CINC, INUS)
-------	-----	-------------	-----------------	--------------------------

Baryon Particle Listings

Charmed Baryons, Λ_c^+

CHARMED BARYONS (C = +1)

$$\Lambda_c^+ = udc, \quad \Sigma_c^{++} = uuc, \quad \Sigma_c^+ = udc, \quad \Sigma_c^0 = ddc, \\ \Xi_c^+ = usc, \quad \Xi_c^0 = dsc, \quad \Omega_c^0 = ssc$$

Λ_c^+

$$I(J^P) = 0(\frac{1}{2}^+) \text{ Status: } ****$$

The parity of the Λ_c^+ is defined to be positive (as are the parities of the proton, neutron, and Λ). The quark content is udc . Results of an analysis of $pK^-\pi^+$ decays (JEZABEK 92) are consistent with $J = 1/2$. ABLIKIM 21N determines the Λ_c^+ spin to be $J = 1/2$, from an angular analysis of various 2-body Λ_c^+ decays in $e^+e^- \rightarrow \Lambda_c^+ \bar{\Lambda}_c^-$.

We have omitted some results that have been superseded by later experiments. The omitted results may be found in earlier editions.

Λ_c^+ MASS

Our value in 2004, 2284.9 ± 0.6 MeV, was the average of the measurements now filed below as "not used." The BABAR measurement is so much better that we use it alone. Note that it is about 2.6 (old) standard deviations above the 2004 value.

The fit also includes $\Sigma_c^-\Lambda_c^+$ and $\Lambda_c^{*+}\Lambda_c^+$ mass-difference measurements, but this doesn't affect the Λ_c^+ mass. The new (in 2006) Λ_c^+ mass simply pushes all those other masses higher.

VALUE (MeV)	EVTS	DOCUMENT ID	TECN	COMMENT
2286.46 ± 0.14 OUR FIT				
2286.46 ± 0.14	4891	¹ AUBERT,B	05s BABR	$\Lambda_c^0 K_S^+ K^+$ and $\Sigma^0 K_S^0 K^+$
• • • We do not use the following data for averages, fits, limits, etc. • • •				
2284.7 ± 0.6 ± 0.7	1134	AVERY	91 CLEO	Six modes
2281.7 ± 2.7 ± 2.6	29	ALVAREZ	90b NA14	$pK^-\pi^+$
2285.8 ± 0.6 ± 1.2	101	BARLAG	89 NA32	$pK^-\pi^+$
2284.7 ± 2.3 ± 0.5	5	AGUILAR...	88b LEBE	$pK^-\pi^+$
2283.1 ± 1.7 ± 2.0	628	ALBRECHT	88c ARG	$pK^-\pi^+$, $p\bar{K}^0$, $\Lambda_3\pi$
2286.2 ± 1.7 ± 0.7	97	ANJOS	88b E691	$pK^-\pi^+$
2281 ± 3	2	JONES	87 HBC	$pK^-\pi^+$
2283 ± 3	3	BOSETTI	82 HBC	$pK^-\pi^+$
2290 ± 3	1	CALICCHIO	80 HYBR	$pK^-\pi^+$

¹ AUBERT,B 05s uses low-Q $\Lambda_c^0 K_S^+ K^+$ and $\Sigma^0 K_S^0 K^+$ decays to minimize systematic errors. The error above includes systematic as well as statistical errors. Many cross checks and adjustments to properties of the BABAR detector, as well as the large number of clean events, make this by far the best measurement of the Λ_c^+ mass.

Λ_c^+ MEAN LIFE

Measurements with an error $\geq 100 \times 10^{-15}$ s or with fewer than 20 events have been omitted from the Listings.

VALUE (10^{-15} s)	EVTS	DOCUMENT ID	TECN	COMMENT
202.6 ± 1.0 OUR AVERAGE				
203.20 ± 0.89 ± 0.77	107k	ABUDINEN	23A BEL2	$\Lambda_c^+ \rightarrow pK^-\pi^+$, e^+e^- near $\Upsilon(4S)$
202.1 ± 1.7 ± 0.9	304k	¹ AAIJ	19AG LHCB	$\Lambda_c^+ \rightarrow pK^-\pi^+$
204.6 ± 3.4 ± 2.5	8034	LINK	02c FOCS	$\Lambda_c^+ \rightarrow pK^-\pi^+$
198.1 ± 7.0 ± 5.6	1630	KUSHNIR...	01 SELX	$\Lambda_c^+ \rightarrow pK^-\pi^+$
179.6 ± 6.9 ± 4.4	4749	MAHMOOD	01 CLE2	$e^+e^- \approx \Upsilon(4S)$
215 ± 16 ± 8	1340	FRABETTI	93D E687	γBe , $\Lambda_c^+ \rightarrow pK^-\pi^+$
• • • We do not use the following data for averages, fits, limits, etc. • • •				
180 ± 30 ± 30	29	ALVAREZ	90 NA14	γ , $\Lambda_c^+ \rightarrow pK^-\pi^+$
200 ± 30 ± 30	90	FRABETTI	90 E687	γBe , $\Lambda_c^+ \rightarrow pK^-\pi^+$
196 $^{+23}_{-20}$	101	BARLAG	89 NA32	$pK^-\pi^+$ + c.c.
220 ± 30 ± 20	97	ANJOS	88b E691	$pK^-\pi^+$ + c.c.

¹ AAIJ 19AG reports $[\Lambda_c^+ \text{ MEAN LIFE}] / [D^{\pm} \text{ MEAN LIFE}] = 0.1956 \pm 0.0010 \pm 0.0013$ which we multiply by our best value $D^{\pm} \text{ MEAN LIFE} = (1.033 \pm 0.005) \times 10^{-12}$ s. Our first error is their experiment's error and our second error is the systematic error from using our best value.

Λ_c^+ DECAY MODES

Branching fractions marked with a footnote, e.g. [a], have been corrected for decay modes not observed in the experiments. For example, the sub-mode fraction $\Lambda_c^+ \rightarrow p\bar{K}^*(892)^0$ seen in $\Lambda_c^+ \rightarrow pK^-\pi^+$ has been multiplied up to include $\bar{K}^*(892)^0 \rightarrow \bar{K}^0\pi^0$ decays.

Mode	Fraction (Γ_i/Γ)	Scale factor/ Confidence level
Hadronic modes with a p or n: S = -1 final states		
Γ_1 pK_S^0	(1.59 ± 0.07) %	S=1.1
Γ_2 $pK^-\pi^+$	(6.24 ± 0.28) %	S=1.4
Γ_3 $p\bar{K}_S^0(700)^0$	(1.9 ± 0.6) × 10 ⁻³	
Γ_4 $p\bar{K}^*(892)^0$	[a] (1.39 ± 0.07) %	
Γ_5 $p\bar{K}_S^0(1430)$	(9.2 ± 1.8) × 10 ⁻³	
Γ_6 $\Delta(1232)^{++}K^-$	(1.76 ± 0.09) %	
Γ_7 $\Delta(1600)^{++}K^-$	(2.8 ± 1.0) × 10 ⁻³	
Γ_8 $\Delta(1700)^{++}K^-$	(2.4 ± 0.6) × 10 ⁻³	
Γ_9 $\Lambda(1405)^0\pi^+$	(4.8 ± 1.9) × 10 ⁻³	
Γ_{10} $\Lambda(1520)\pi^+$	[a] (1.16 ± 0.16) × 10 ⁻³	
Γ_{11} $\Lambda(1600)\pi^+$	(3.2 ± 1.2) × 10 ⁻³	
Γ_{12} $\Lambda(1670)\pi^+$	(7.4 ± 2.1) × 10 ⁻⁴	
Γ_{13} $\Lambda(1690)\pi^+$	(7.4 ± 2.2) × 10 ⁻⁴	
Γ_{14} $\Lambda(2000)\pi^+$	(6.0 ± 0.7) × 10 ⁻³	
Γ_{15} $pK^-\pi^+$ nonresonant	(3.5 ± 0.4) %	
Γ_{16} $pK_S^0\pi^0$	(1.96 ± 0.12) %	
Γ_{17} $nK_S^0\pi^+$	(1.82 ± 0.25) %	
Γ_{18} $nK^-\pi^+\pi^+$	(1.90 ± 0.12) %	
Γ_{19} $p\bar{K}^0\eta$	(8.8 ± 0.6) × 10 ⁻³	S=1.1
Γ_{20} $pK_S^0\pi^+\pi^-$	(1.59 ± 0.11) %	S=1.1
Γ_{21} $pK^-\pi^+\pi^0$	(4.43 ± 0.28) %	S=1.5
Γ_{22} $pK^*(892)^-\pi^+$	[a] (1.4 ± 0.5) %	
Γ_{23} $p(K^-\pi^+)$ nonresonant π^0	(4.6 ± 0.8) %	
Γ_{24} $\Delta(1232)\bar{K}^*(892)$	seen	
Γ_{25} $pK^-2\pi^+\pi^-$	(1.4 ± 0.9) × 10 ⁻³	
Γ_{26} $pK^-\pi^+2\pi^0$	(10 ± 5) × 10 ⁻³	
Hadronic modes with a p or n: S = 0 final states		
Γ_{27} $p\pi^0$	< 8 × 10 ⁻⁵	CL=90%
Γ_{28} $n\pi^+$	(6.6 ± 1.3) × 10 ⁻⁴	
Γ_{29} $p\eta$	(1.57 ± 0.12) × 10 ⁻³	
Γ_{30} $p\eta'$	(4.8 ± 0.9) × 10 ⁻⁴	
Γ_{31} $p\omega(782)^0$	(1.11 ± 0.21) × 10 ⁻³	
Γ_{32} $p\pi^+\pi^-$	(4.59 ± 0.25) × 10 ⁻³	
Γ_{33} $p\phi(980)$	[a] (3.4 ± 2.3) × 10 ⁻³	
Γ_{34} $n\pi^+\pi^0$	(6.4 ± 0.9) × 10 ⁻³	
Γ_{35} $n\pi^+\pi^-\pi^+$	(4.5 ± 0.8) × 10 ⁻³	
Γ_{36} $p2\pi^+2\pi^-$	(2.2 ± 1.4) × 10 ⁻³	
Γ_{37} pK^+K^-	(1.06 ± 0.05) × 10 ⁻³	
Γ_{38} $p\phi$	[a] (1.06 ± 0.14) × 10 ⁻³	
Γ_{39} pK^+K^- non- ϕ	(5.2 ± 1.1) × 10 ⁻⁴	
Γ_{40} $pK_S^0K_S^0$	(2.35 ± 0.18) × 10 ⁻⁴	
Γ_{41} $p\phi\pi^0$	(10 ± 4) × 10 ⁻⁵	
Γ_{42} $pK^+K^-\pi^0$ nonresonant	< 6.3 × 10 ⁻⁵	CL=90%
Hadronic modes with a hyperon: S = -1 final states		
Γ_{43} $\Lambda\pi^+$	(1.29 ± 0.05) %	S=1.1
Γ_{44} $\Lambda(1670)\pi^+$, $\Lambda(1670) \rightarrow \eta\Lambda$	(3.5 ± 0.5) × 10 ⁻³	
Γ_{45} $\Lambda\pi^+\pi^0$	(7.02 ± 0.35) %	S=1.1
Γ_{46} $\Lambda\rho^+$	(4.0 ± 0.5) %	
Γ_{47} $\Sigma(1385)^+\pi^0$, $\Sigma^+ \rightarrow \Lambda\pi^+$	(5.0 ± 0.7) × 10 ⁻³	
Γ_{48} $\Sigma(1385)^0\pi^+$, $\Sigma^0 \rightarrow \Lambda\pi^0$	(5.6 ± 0.8) × 10 ⁻³	
Γ_{49} $\Lambda\pi^-2\pi^+$	(3.61 ± 0.26) %	S=1.4
Γ_{50} $\Sigma(1385)^+\pi^+\pi^-$, $\Sigma^{*+} \rightarrow \Lambda\pi^+$	(1.0 ± 0.5) %	
Γ_{51} $\Sigma(1385)^-2\pi^+$, $\Sigma^{*-} \rightarrow \Lambda\pi^-$	(7.6 ± 1.4) × 10 ⁻³	
Γ_{52} $\Lambda\pi^+\rho^0$	(1.4 ± 0.6) %	
Γ_{53} $\Sigma(1385)^+\rho^0$, $\Sigma^{*+} \rightarrow \Lambda\pi^+$	(5 ± 4) × 10 ⁻³	
Γ_{54} $\Lambda\pi^-2\pi^+$ nonresonant	< 1.1 %	CL=90%
Γ_{55} $\Lambda\pi^-2\pi^+$ total	(2.2 ± 0.8) %	
Γ_{56} $\Lambda\pi^+\eta$	[a] (1.84 ± 0.11) %	S=1.1
Γ_{57} $\Sigma(1385)^+\eta$	[a] (9.1 ± 2.0) × 10 ⁻³	
Γ_{58} $\Lambda\pi^+\omega$	[a] (1.5 ± 0.5) %	
Γ_{59} $\Lambda\pi^-\pi^02\pi^+$, no η or ω	< 8 × 10 ⁻³	CL=90%
Γ_{60} $\Lambda K^+\bar{K}^0$	(5.6 ± 1.1) × 10 ⁻³	S=1.9

Baryon Particle Listings

 Λ_C^+ $\Gamma(\rho K^- \pi^+)/\Gamma_{\text{total}}$ Γ_2/Γ

VALUE (%)	EVTS	DOCUMENT ID	TECN	COMMENT
6.24 ± 0.28 OUR FIT				Error includes scale factor of 1.4.
6.3 ± 0.5 OUR AVERAGE				Error includes scale factor of 2.0.
5.84 ± 0.27 ± 0.23	6.3k	ABLIKIM	16 BES3	$e^+ e^- \rightarrow \Lambda_C \bar{\Lambda}_C$, 4.599 GeV
6.84 ± 0.24 ± $\begin{smallmatrix} 0.21 \\ -0.27 \end{smallmatrix}$	1.4k	¹ ZUPANC	14 BELL	$e^+ e^- \rightarrow D^{(*)-} \bar{p} \pi^+$ recoil

• • • We do not use the following data for averages, fits, limits, etc. • • •

5.0 ± 1.3		² PDG	02	See footnote
-----------	--	------------------	----	--------------

¹This ZUPANC 14 value is the FIRST-EVER model-independent measurement of a Λ_C^+ branching fraction.

²See the note by P. Burchat, "A $^+$ Branching Fractions," in any edition of the Review from 2002 through 2014 for how this value was obtained. It is now obsolete.

 $\Gamma(\rho K_S^0(700)^0)/\Gamma(\rho K^- \pi^+)$ Γ_3/Γ_2

VALUE (units 10 ⁻²)	DOCUMENT ID	TECN	COMMENT
3.02 ± 0.16 ± 0.18 ± 0.92	¹ AAIJ	23z LHCb	1.7fb ⁻¹ , pp at 13 TeV

¹AAIJ 23z uses an amplitude analysis of 400k $\Lambda_C \rightarrow \rho K^- \pi^+$ decays, the last uncertainty is due to the amplitude model.

 $\Gamma(\rho \bar{K}^*(892)^0)/\Gamma(\rho K^- \pi^+)$ Γ_4/Γ_2

Unseen decay modes of the $\bar{K}^*(892)^0$ are included.

VALUE (units 10 ⁻²)	EVTS	DOCUMENT ID	TECN	COMMENT
22.3 ± 0.7 OUR AVERAGE				
22.14 ± 0.23 ± 0.04 ± 0.64		¹ AAIJ	23z LHCb	1.7fb ⁻¹ , pp at 13 TeV
29 ± 4 ± 3		² AITALA	00 E791	$\pi^- N$, 500 GeV

• • • We do not use the following data for averages, fits, limits, etc. • • •

35 ± $\begin{smallmatrix} 6 \\ -7 \end{smallmatrix}$ ± 3	39	BOZEK	93 NA32	$\pi^- \text{Cu}$ 230 GeV
35 ± 11		BARLAG	90d NA32	See BOZEK 93
42 ± 24	12	BASILE	81b CNTR	pp → $\Lambda_C^+ e^- X$

¹AAIJ 23z uses an amplitude analysis of 400k $\Lambda_C \rightarrow \rho K^- \pi^+$ decays, the last uncertainty is due to the amplitude model.

²AITALA 00 makes a coherent 5-dimensional amplitude analysis of 946 ± 38 $\Lambda_C^+ \rightarrow \rho K^- \pi^+$ decays.

 $\Gamma(\rho \bar{K}_S^0(1430))/\Gamma(\rho K^- \pi^+)$ Γ_5/Γ_2

VALUE (units 10 ⁻²)	DOCUMENT ID	TECN	COMMENT
14.7 ± 0.6 ± 0.1 ± 2.7	¹ AAIJ	23z LHCb	1.7fb ⁻¹ , pp at 13 TeV

¹AAIJ 23z uses an amplitude analysis of 400k $\Lambda_C \rightarrow \rho K^- \pi^+$ decays, the last uncertainty is due to the amplitude model.

 $\Gamma(\Delta(1232)^{++} K^-)/\Gamma(\rho K^- \pi^+)$ Γ_6/Γ_2

VALUE (units 10 ⁻²)	EVTS	DOCUMENT ID	TECN	COMMENT
28.2 ± 0.8 OUR AVERAGE				
28.60 ± 0.29 ± 0.16 ± 0.76		¹ AAIJ	23z LHCb	1.7fb ⁻¹ , pp at 13 TeV
18 ± 3 ± 3		² AITALA	00 E791	$\pi^- N$, 500 GeV

• • • We do not use the following data for averages, fits, limits, etc. • • •

12 ± $\begin{smallmatrix} 4 \\ -5 \end{smallmatrix}$ ± 5	14	BOZEK	93 NA32	$\pi^- \text{Cu}$ 230 GeV
40 ± 17	17	BASILE	81b CNTR	pp → $\Lambda_C^+ e^- X$

¹AAIJ 23z uses an amplitude analysis of 400k $\Lambda_C \rightarrow \rho K^- \pi^+$ decays, the last uncertainty is due to the amplitude model.

²AITALA 00 makes a coherent 5-dimensional amplitude analysis of 946 ± 38 $\Lambda_C^+ \rightarrow \rho K^- \pi^+$ decays.

 $\Gamma(\Delta(1600)^{++} K^-)/\Gamma(\rho K^- \pi^+)$ Γ_7/Γ_2

VALUE (units 10 ⁻²)	DOCUMENT ID	TECN	COMMENT
4.5 ± 0.3 ± 0.1 ± 1.5	¹ AAIJ	23z LHCb	1.7fb ⁻¹ , pp at 13 TeV

¹AAIJ 23z uses an amplitude analysis of 400k $\Lambda_C \rightarrow \rho K^- \pi^+$ decays, the last uncertainty is due to the amplitude model.

 $\Gamma(\Delta(1700)^{++} K^-)/\Gamma(\rho K^- \pi^+)$ Γ_8/Γ_2

VALUE (units 10 ⁻²)	DOCUMENT ID	TECN	COMMENT
3.90 ± 0.20 ± 0.07 ± 0.94	¹ AAIJ	23z LHCb	1.7fb ⁻¹ , pp at 13 TeV

¹AAIJ 23z uses an amplitude analysis of 400k $\Lambda_C \rightarrow \rho K^- \pi^+$ decays, the last uncertainty is due to the amplitude model.

 $\Gamma(\Lambda(1405)^0 \pi^+)/\Gamma(\rho K^- \pi^+)$ Γ_9/Γ_2

VALUE (units 10 ⁻²)	DOCUMENT ID	TECN	COMMENT
7.7 ± 0.2 ± 0.2 ± 3.0	¹ AAIJ	23z LHCb	1.7fb ⁻¹ , pp at 13 TeV

¹AAIJ 23z uses an amplitude analysis of 400k $\Lambda_C \rightarrow \rho K^- \pi^+$ decays, the last uncertainty is due to the amplitude model.

 $\Gamma(\Lambda(1520) \pi^+)/\Gamma(\rho K^- \pi^+)$ Γ_{10}/Γ_2

Unseen decay modes of the $\Lambda(1520)$ are included.

VALUE (units 10 ⁻²)	EVTS	DOCUMENT ID	TECN	COMMENT
1.86 ± 0.09 ± 0.03 ± 0.23		¹ AAIJ	23z LHCb	1.7fb ⁻¹ , pp at 13 TeV

¹AAIJ 23z uses an amplitude analysis of 400k $\Lambda_C \rightarrow \rho K^- \pi^+$ decays, the last uncertainty is due to the amplitude model.

• • • We do not use the following data for averages, fits, limits, etc. • • •

34 ± 8 ± 5		² AITALA	00 E791	$\pi^- N$, 500 GeV
40 ± $\begin{smallmatrix} +18 \\ -13 \end{smallmatrix}$ ± 9	12	BOZEK	93 NA32	$\pi^- \text{Cu}$ 230 GeV

¹AAIJ 23z uses an amplitude analysis of 400k $\Lambda_C \rightarrow \rho K^- \pi^+$ decays, the last uncertainty is due to the amplitude model.

²AITALA 00 makes a coherent 5-dimensional amplitude analysis of 946 ± 38 $\Lambda_C^+ \rightarrow \rho K^- \pi^+$ decays.

 $\Gamma(\Lambda(1600) \pi^+)/\Gamma(\rho K^- \pi^+)$ Γ_{11}/Γ_2

VALUE (units 10 ⁻²)	DOCUMENT ID	TECN	COMMENT
5.2 ± 0.2 ± 0.1 ± 1.9	¹ AAIJ	23z LHCb	1.7fb ⁻¹ , pp at 13 TeV

¹AAIJ 23z uses an amplitude analysis of 400k $\Lambda_C \rightarrow \rho K^- \pi^+$ decays, the last uncertainty is due to the amplitude model.

 $\Gamma(\Lambda(1670) \pi^+)/\Gamma(\rho K^- \pi^+)$ Γ_{12}/Γ_2

VALUE (units 10 ⁻²)	DOCUMENT ID	TECN	COMMENT
1.18 ± 0.06 ± 0.01 ± 0.32	¹ AAIJ	23z LHCb	1.7fb ⁻¹ , pp at 13 TeV

¹AAIJ 23z uses an amplitude analysis of 400k $\Lambda_C \rightarrow \rho K^- \pi^+$ decays, the last uncertainty is due to the amplitude model.

 $\Gamma(\Lambda(1690) \pi^+)/\Gamma(\rho K^- \pi^+)$ Γ_{13}/Γ_2

VALUE (units 10 ⁻²)	DOCUMENT ID	TECN	COMMENT
1.19 ± 0.09 ± 0.01 ± 0.34	¹ AAIJ	23z LHCb	1.7fb ⁻¹ , pp at 13 TeV

¹AAIJ 23z uses an amplitude analysis of 400k $\Lambda_C \rightarrow \rho K^- \pi^+$ decays, the last uncertainty is due to the amplitude model.

 $\Gamma(\Lambda(2000) \pi^+)/\Gamma(\rho K^- \pi^+)$ Γ_{14}/Γ_2

VALUE (units 10 ⁻²)	DOCUMENT ID	TECN	COMMENT
9.58 ± 0.27 ± 0.23 ± 0.93	¹ AAIJ	23z LHCb	1.7fb ⁻¹ , pp at 13 TeV

¹AAIJ 23z uses an amplitude analysis of 400k $\Lambda_C \rightarrow \rho K^- \pi^+$ decays, the last uncertainty is due to the amplitude model.

 $\Gamma(\rho K^- \pi^+ \text{ nonresonant})/\Gamma(\rho K^- \pi^+)$ Γ_{15}/Γ_2

VALUE	EVTS	DOCUMENT ID	TECN	COMMENT
0.55 ± 0.06 OUR AVERAGE				
0.55 ± 0.06 ± 0.04		¹ AITALA	00 E791	$\pi^- N$, 500 GeV
0.56 ± $\begin{smallmatrix} +0.07 \\ -0.09 \end{smallmatrix}$ ± 0.05	71	BOZEK	93 NA32	$\pi^- \text{Cu}$ 230 GeV

¹AITALA 00 makes a coherent 5-dimensional amplitude analysis of 946 ± 38 $\Lambda_C^+ \rightarrow \rho K^- \pi^+$ decays.

 $\Gamma(\rho K_S^0 \pi^0)/\Gamma_{\text{total}}$ Γ_{16}/Γ

VALUE (%)	EVTS	DOCUMENT ID	TECN	COMMENT
1.96 ± 0.12 OUR FIT				
1.87 ± 0.13 ± 0.05	558	ABLIKIM	16 BES3	$e^+ e^- \rightarrow \Lambda_C \bar{\Lambda}_C$, 4.599 GeV

Measurements given as a \bar{K}^0 ratio have been divided by 2 to convert to a K_S^0 ratio.

VALUE	EVTS	DOCUMENT ID	TECN	COMMENT
0.33 ± 0.03 ± 0.04	774	ALAM	98 CLE2	$e^+ e^- \approx \Upsilon(4S)$

¹AITALA 00 makes a coherent 5-dimensional amplitude analysis of 946 ± 38 $\Lambda_C^+ \rightarrow \rho K^- \pi^+$ decays.

 $\Gamma(n K^- \pi^+ \pi^+)/\Gamma_{\text{total}}$ Γ_{17}/Γ

VALUE (%)	EVTS	DOCUMENT ID	TECN	COMMENT
1.82 ± 0.23 ± 0.11	83	ABLIKIM	17H BES3	$e^+ e^-$ at 4.6 GeV

¹ABLIKIM 17H measures $B(\Lambda_C^+ \rightarrow \rho K_S^0 \eta)/B(\Lambda_C^+ \rightarrow \rho K_S^0 \pi^+) = (0.414 \pm 0.084 \pm 0.028)\%$.

 $\Gamma(n K_S^0 \pi^+)/\Gamma_{\text{total}}$ Γ_{18}/Γ

VALUE (%)	EVTS	DOCUMENT ID	TECN	COMMENT
1.90 ± 0.08 ± 0.09	810	ABLIKIM	23A BES	4.5 fb ⁻¹ , $e^+ e^-$ at 4.600-4.699 GeV

¹ABLIKIM 23A measures $B(\Lambda_C^+ \rightarrow \rho K_S^0 \eta)/B(\Lambda_C^+ \rightarrow \rho K_S^0 \pi^+) = 0.273 \pm 0.006 \pm 0.013$.

 $\Gamma(\rho \bar{K}^0 \eta)/\Gamma_{\text{total}}$ Γ_{19}/Γ

VALUE (%)	EVTS	DOCUMENT ID	TECN	COMMENT
0.88 ± 0.06 OUR FIT				Error includes scale factor of 1.1.
0.828 ± 0.168 ± 0.056	42	¹ ABLIKIM	21H BES3	$e^+ e^-$ at 4.6 GeV

¹ABLIKIM 21H measures $B(\Lambda_C^+ \rightarrow \rho K_S^0 \eta)/B(\Lambda_C^+ \rightarrow \rho K_S^0 \pi^+) = (0.414 \pm 0.084 \pm 0.028)\%$.

 $\Gamma(\rho \bar{K}^0 \eta)/\Gamma(\rho K_S^0 \pi^+)$ Γ_{19}/Γ_1

VALUE	EVTS	DOCUMENT ID	TECN	COMMENT
0.551 ± 0.029 OUR FIT				
0.546 ± 0.012 ± 0.026	12.6k	¹ LI	23B BELL	$e^+ e^- \rightarrow \Upsilon(nS)$

¹LI 23B measures $B(\Lambda_C^+ \rightarrow \rho K_S^0 \eta)/B(\Lambda_C^+ \rightarrow \rho K_S^0 \pi^+) = 0.273 \pm 0.006 \pm 0.013$.

 $\Gamma(\rho \bar{K}^0 \eta)/\Gamma(\rho K^- \pi^+)$ Γ_{19}/Γ_2

VALUE	EVTS	DOCUMENT ID	TECN	COMMENT
0.141 ± 0.009 OUR FIT				Error includes scale factor of 1.1.
0.25 ± 0.04 ± 0.04	57	AMMAR	95 CLE2	$e^+ e^- \approx \Upsilon(4S)$

¹AMMAR 95 measures $B(\Lambda_C^+ \rightarrow \rho K_S^0 \eta)/B(\Lambda_C^+ \rightarrow \rho K_S^0 \pi^+) = 0.273 \pm 0.006 \pm 0.013$.

$\Gamma(\rho K_S^0 \pi^+ \pi^-)/\Gamma_{\text{total}}$					Γ_{20}/Γ
VALUE (%)	EVTS	DOCUMENT ID	TECN	COMMENT	
1.59 ± 0.11 OUR FIT				Error includes scale factor of 1.1.	
1.53 ± 0.11 ± 0.09	485	ABLIKIM	16 BES3	$e^+e^- \rightarrow \Lambda_C \bar{\Lambda}_C$, 4.599 GeV	

$\Gamma(\rho K_S^0 \pi^+ \pi^-)/\Gamma(\rho K^- \pi^+)$					Γ_{20}/Γ_2
VALUE	EVTS	DOCUMENT ID	TECN	COMMENT	
0.255 ± 0.014 OUR FIT					
0.257 ± 0.031 OUR AVERAGE					
0.26 ± 0.02 ± 0.03	985	ALAM	98 CLE2	$e^+e^- \approx \Upsilon(4S)$	
0.22 ± 0.06 ± 0.02	83	AVERY	91 CLEO	e^+e^- 10.5 GeV	
0.49 ± 0.18 ± 0.04	12	BARLAG	90D NA32	π^- 230 GeV	

$\Gamma(\rho K^- \pi^+ \pi^0)/\Gamma_{\text{total}}$					Γ_{21}/Γ
VALUE (%)	EVTS	DOCUMENT ID	TECN	COMMENT	
4.43 ± 0.28 OUR FIT				Error includes scale factor of 1.5.	
4.53 ± 0.23 ± 0.30	1849	ABLIKIM	16 BES3	$e^+e^- \rightarrow \Lambda_C \bar{\Lambda}_C$, 4.599 GeV	

$\Gamma(\rho K^- \pi^+ \pi^0)/\Gamma(\rho K^- \pi^+)$					Γ_{21}/Γ_2
VALUE	EVTS	DOCUMENT ID	TECN	COMMENT	
0.71 ± 0.04 OUR FIT				Error includes scale factor of 2.3.	
0.685 ± 0.019 OUR AVERAGE					
0.685 ± 0.007 ± 0.018	242k	PAL	17 BELL	$e^+e^- \approx \Upsilon(4S), \Upsilon(5S)$	
0.67 ± 0.04 ± 0.11	2.6k	ALAM	98 CLE2	$e^+e^- \approx \Upsilon(4S)$	

$\Gamma(\rho K^*(892)^- \pi^+)/\Gamma(\rho K_S^0 \pi^+ \pi^-)$					Γ_{22}/Γ_{20}
VALUE	EVTS	DOCUMENT ID	TECN	COMMENT	
0.88 ± 0.28	17	ALEEV	94 BIS2	$n N$ 20–70 GeV	

$\Gamma(\rho(K^- \pi^+)_{\text{nonresonant}} \pi^0)/\Gamma(\rho K^- \pi^+)$					Γ_{23}/Γ_2
VALUE	EVTS	DOCUMENT ID	TECN	COMMENT	
0.73 ± 0.12 ± 0.05	67	BOZEK	93 NA32	π^- Cu 230 GeV	

$\Gamma(\Delta(1232) \bar{K}^*(892))/\Gamma_{\text{total}}$					Γ_{24}/Γ
VALUE	EVTS	DOCUMENT ID	TECN	COMMENT	
seen	35	AMENDOLIA	87 SPEC	γ Ge-Si	

$\Gamma(\rho K^- 2\pi^+ \pi^-)/\Gamma(\rho K^- \pi^+)$					Γ_{25}/Γ_2
VALUE	DOCUMENT ID	TECN	COMMENT		
0.022 ± 0.015	BARLAG	90D NA32	π^- 230 GeV		

$\Gamma(\rho K^- \pi^+ 2\pi^0)/\Gamma(\rho K^- \pi^+)$					Γ_{26}/Γ_2
VALUE	EVTS	DOCUMENT ID	TECN	COMMENT	
0.16 ± 0.07 ± 0.03	15	BOZEK	93 NA32	π^- Cu 230 GeV	

Hadronic modes with a p and n : $S = 0$ final states

$\Gamma(\rho \pi^0)/\Gamma_{\text{total}}$					Γ_{27}/Γ
VALUE	CL%	DOCUMENT ID	TECN	COMMENT	
•••				We do not use the following data for averages, fits, limits, etc. •••	
$< 2.7 \times 10^{-4}$	90	ABLIKIM	17Q BES3	e^+e^- at 4.6 GeV	

$\Gamma(\rho \pi^0)/\Gamma(\rho K^- \pi^+)$					Γ_{27}/Γ_2
VALUE	CL%	EVTS	DOCUMENT ID	TECN	COMMENT
$< 1.273 \times 10^{-3}$	90	7.7k	¹ LI	21 BELL	e^+e^- at $\Upsilon(\text{nS})$
					¹ Uses $B(\pi^0 \rightarrow \gamma\gamma) = 0.9882 \pm 0.0003$.

$\Gamma(n \pi^+)/\Gamma_{\text{total}}$					Γ_{28}/Γ
VALUE (units 10^{-4})	EVTS	DOCUMENT ID	TECN	COMMENT	
6.6 ± 1.2 ± 0.4	50	ABLIKIM	22s BES3	e^+e^- at 4.612–4.699 GeV	

$\Gamma(\rho \eta)/\Gamma_{\text{total}}$					Γ_{29}/Γ
VALUE (units 10^{-3})	EVTS	DOCUMENT ID	TECN	COMMENT	
1.57 ± 0.11 ± 0.04	507	¹ ABLIKIM	23CB BES3	$\eta \rightarrow 2\gamma, \pi^+ \pi^0 \pi^-$	
•••				We do not use the following data for averages, fits, limits, etc. •••	
1.24 ± 0.28 ± 0.10	52	ABLIKIM	17Q BES3	$\eta \rightarrow 2\gamma, \pi^+ \pi^0 \pi^-$	
					¹ ABLIKIM 23CB report a significance of 10σ .

$\Gamma(\rho \eta)/\Gamma(\rho K^- \pi^+)$					Γ_{29}/Γ_2
VALUE (units 10^{-2})	EVTS	DOCUMENT ID	TECN	COMMENT	
2.258 ± 0.077 ± 0.122	7.7k	¹ LI	21 BELL	e^+e^- at $\Upsilon(\text{nS})$	
					¹ Uses $B(\eta \rightarrow \gamma\gamma) = 0.3941 \pm 0.0020$.

$\Gamma(\rho \eta')/\Gamma_{\text{total}}$					Γ_{30}/Γ
VALUE (units 10^{-4})	EVTS	DOCUMENT ID	TECN	COMMENT	
4.8 ± 0.9 OUR FIT					
5.62 ^{+2.46} _{-2.04} ± 0.26	9	¹ ABLIKIM	22AN BES3	e^+e^- at 4.600–4.699 GeV	

¹ Observed with 3.6σ statistical significance with 4.5 fb^{-1} of e^+e^- collisions between 4.600 and 4.699 GeV. The η' is reconstructed in the two decay modes $\eta' \rightarrow \pi^+ \pi^- \eta$ and $\eta' \rightarrow \pi^+ \pi^- \gamma$, with signal yields $4.9^{+3.2}_{-2.6}$ and $4.3^{+2.6}_{-2.2}$ events, respectively.

$\Gamma(\rho \eta')/\Gamma(\rho K^- \pi^+)$					Γ_{30}/Γ_2
VALUE (units 10^{-3})	DOCUMENT ID	TECN	COMMENT		
7.8 ± 1.4 OUR FIT					
7.54 ± 1.32 ± 0.73	LI	22B BELL	e^+e^- at $\Upsilon(\text{nS})$		

$\Gamma(\rho \omega(782)^0)/\Gamma_{\text{total}}$					Γ_{31}/Γ
VALUE (units 10^{-4})	EVTS	DOCUMENT ID	TECN	COMMENT	
11.1 ± 2.0 ± 0.7	234	¹ ABLIKIM	23CB BES3	$\omega \rightarrow \pi^+ \pi^- \pi^0$	
•••				We do not use the following data for averages, fits, limits, etc. •••	
9.4 ± 3.2 ± 2.2	13	AAIJ	18N LHCb	Seen in $\Lambda_C^+ \rightarrow p \mu^+ \mu^-$	
					¹ ABLIKIM 23CB report a significance of 5.7 σ .

$\Gamma(\rho \omega(782)^0)/\Gamma(\rho K^- \pi^+)$					Γ_{31}/Γ_2
VALUE (units 10^{-2})	EVTS	DOCUMENT ID	TECN	COMMENT	
1.32 ± 0.12 ± 0.10	1.8k	¹ LI	21E BELL	e^+e^- at $\Upsilon(\text{nS})$	
					¹ LI 21E reconstructs the $\omega(782)$ via $\omega \rightarrow \pi^+ \pi^- \pi^0$ and $\pi^0 \rightarrow \gamma\gamma$.

$\Gamma(\rho \pi^+ \pi^-)/\Gamma(\rho K^- \pi^+)$					Γ_{32}/Γ_2
VALUE (units 10^{-2})	EVTS	DOCUMENT ID	TECN	COMMENT	
7.35 ± 0.24 OUR AVERAGE				Error includes scale factor of 1.3.	
7.44 ± 0.08 ± 0.18	20k	AAIJ	18v LHCb	$\Lambda_b^0 \rightarrow \Lambda_C^+ \mu^- X$	
6.70 ± 0.48 ± 0.25	495	ABLIKIM	16U BES3	e^+e^- at 4.599 GeV	
6.9 ± 3.6	5	BARLAG	90D NA32	π^- 230 GeV	

$\Gamma(\rho f_0(980))/\Gamma(\rho K^- \pi^+)$					Γ_{33}/Γ_2
VALUE	DOCUMENT ID	TECN	COMMENT		
0.055 ± 0.036	BARLAG	90D NA32	π^- 230 GeV		

$\Gamma(n \pi^+ \pi^0)/\Gamma_{\text{total}}$					Γ_{34}/Γ
VALUE (%)	EVTS	DOCUMENT ID	TECN	COMMENT	
0.64 ± 0.09 ± 0.02	150	ABLIKIM	23A BES	$4.5 \text{ fb}^{-1}, e^+e^-$ at 4.600–4.699 GeV	

$\Gamma(n \pi^+ \pi^- \pi^+)/\Gamma_{\text{total}}$					Γ_{35}/Γ
VALUE (%)	EVTS	DOCUMENT ID	TECN	COMMENT	
0.45 ± 0.07 ± 0.03	120	ABLIKIM	23A BES	$4.5 \text{ fb}^{-1}, e^+e^-$ at 4.600–4.699 GeV	

$\Gamma(\rho 2\pi^+ 2\pi^-)/\Gamma(\rho K^- \pi^+)$					Γ_{36}/Γ_2
VALUE	DOCUMENT ID	TECN	COMMENT		
0.036 ± 0.023	BARLAG	90D NA32	π^- 230 GeV		

$\Gamma(\rho K^+ K^-)/\Gamma(\rho K^- \pi^+)$					Γ_{37}/Γ_2
VALUE (units 10^{-2})	EVTS	DOCUMENT ID	TECN	COMMENT	
1.70 ± 0.04 OUR AVERAGE					
1.70 ± 0.03 ± 0.03	3.4k	AAIJ	18v LHCb	$\Lambda_b^0 \rightarrow \Lambda_C^+ \mu^- X$	
1.4 ± 0.2 ± 0.2	676	ABE	02c BELL	$e^+e^- \approx \Upsilon(4S)$	
3.9 ± 0.9 ± 0.7	214	ALEXANDER	96c CLE2	$e^+e^- \approx \Upsilon(4S)$	
•••				We do not use the following data for averages, fits, limits, etc. •••	
9.6 ± 2.9 ± 1.0	30	FRABETTI	93H E687	γ Be, \bar{E}_γ 220 GeV	
4.8 ± 2.7		BARLAG	90D NA32	π^- 230 GeV	

$\Gamma(\rho \phi)/\Gamma(\rho K^- \pi^+)$					Γ_{38}/Γ_2
VALUE (units 10^{-2})	EVTS	DOCUMENT ID	TECN	COMMENT	
1.70 ± 0.21 OUR AVERAGE					
1.81 ± 0.33 ± 0.13	44	ABLIKIM	16U BES3	e^+e^- at 4.599 GeV	
1.5 ± 0.2 ± 0.2	345	ABE	02c BELL	$e^+e^- \approx \Upsilon(4S)$	
2.4 ± 0.6 ± 0.3	54	ALEXANDER	96c CLE2	$e^+e^- \approx \Upsilon(4S)$	
•••				We do not use the following data for averages, fits, limits, etc. •••	
4.0 ± 2.7		BARLAG	90D NA32	π^- 230 GeV	

$\Gamma(\rho K^+ K^- \text{non-}\phi)/\Gamma(\rho K^- \pi^+)$					Γ_{39}/Γ_2
VALUE (units 10^{-3})	EVTS	DOCUMENT ID	TECN	COMMENT	
8.4 ± 1.8 OUR AVERAGE					
9.36 ± 2.22 ± 0.71	38	ABLIKIM	16U BES3	e^+e^- at 4.599 GeV	
7 ± 2 ± 2	344	ABE	02c BELL	$e^+e^- \approx \Upsilon(4S)$	

$\Gamma(\rho K_S^0 K_S^0)/\Gamma(\rho K_S^0)$					Γ_{40}/Γ_1
VALUE (units 10^{-2})	EVTS	DOCUMENT ID	TECN	COMMENT	
1.48 ± 0.08 ± 0.04	2.4k	LI	23B BELL	e^+e^- at $\Upsilon(\text{nS})$	

$\Gamma(\rho \phi \pi^0)/\Gamma(\rho K^- \pi^+)$					Γ_{41}/Γ_2
VALUE (units 10^{-3})	DOCUMENT ID	TECN	COMMENT		
1.538 ± 0.641^{+0.077}_{-0.100}	PAL	17 BELL	$e^+e^- \approx \Upsilon(4S), \Upsilon(5S)$		

$\Gamma(\rho K^+ K^- \pi^0 \text{nonresonant})/\Gamma_{\text{total}}$					Γ_{42}/Γ
VALUE	CL%	DOCUMENT ID	TECN	COMMENT	
$< 6.3 \times 10^{-5}$	90	PAL	17 BELL	$e^+e^- \approx \Upsilon(4S), \Upsilon(5S)$	

Baryon Particle Listings

 Λ_C^+ Hadronic modes with a hyperon: $S = -1$ final states $\Gamma(\Lambda\pi^+)/\Gamma_{\text{total}}$ Γ_{43}/Γ

VALUE (%)	EVTS	DOCUMENT ID	TECN	COMMENT
1.29±0.05 OUR FIT				Error includes scale factor of 1.1.
1.27±0.06 OUR AVERAGE				
1.31±0.08±0.05	376	ABLIKIM	22S BES3	e^+e^- at 4.612-4.699 GeV
1.24±0.07±0.03	706	ABLIKIM	16 BES3	$e^+e^- \rightarrow \Lambda_C \bar{\Lambda}_C$, 4.599 GeV

 $\Gamma(\Lambda\pi^+)/\Gamma(\rho K^- \pi^+)$ Γ_{43}/Γ_2

VALUE	EVTS	DOCUMENT ID	TECN	COMMENT
0.207±0.008 OUR FIT				Error includes scale factor of 1.2.
0.204±0.019 OUR AVERAGE				
0.217±0.013±0.020	750	LINK	05F FOCUS	γ nucleus, $\bar{E}_\gamma \approx 180$ GeV
0.18±0.03±0.04		ALBRECHT	92 ARG	$e^+e^- \approx 10.4$ GeV
0.18±0.03±0.03	87	AVERY	91 CLEO	e^+e^- 10.5 GeV

 $\Gamma(\Lambda(1670)\pi^+, \Lambda(1670) \rightarrow \eta\Lambda)/\Gamma(\rho K^- \pi^+)$ Γ_{44}/Γ_2

VALUE (units 10^{-2})	EVTS	DOCUMENT ID	TECN	COMMENT
5.54±0.29±0.73	9.7k	LEE	21A BELL	$e^+e^- \approx \Upsilon(nS)$

 $\Gamma(\Lambda\pi^+\pi^0)/\Gamma_{\text{total}}$ Γ_{45}/Γ

VALUE (%)	EVTS	DOCUMENT ID	TECN	COMMENT
7.02±0.35 OUR FIT				Error includes scale factor of 1.1.
7.01±0.37±0.19	1497	ABLIKIM	16 BES3	$e^+e^- \rightarrow \Lambda_C \bar{\Lambda}_C$, 4.599 GeV

 $\Gamma(\Lambda\pi^+\pi^0)/\Gamma(\rho K^- \pi^+)$ Γ_{45}/Γ_2

VALUE	EVTS	DOCUMENT ID	TECN	COMMENT
1.12±0.06 OUR FIT				Error includes scale factor of 1.1.
0.73±0.09±0.16	464	AVERY	94 CLE2	$e^+e^- \approx \Upsilon(3S), \Upsilon(4S)$

 $\Gamma(\Lambda\rho^+)/\Gamma(\rho K^- \pi^+)$ Γ_{46}/Γ_2

VALUE	CL%	DOCUMENT ID	TECN	COMMENT
•••				We do not use the following data for averages, fits, limits, etc. •••
<0.95	95	AVERY	94 CLE2	$e^+e^- \approx \Upsilon(3S), \Upsilon(4S)$

 $\Gamma(\Lambda\rho^+)/\Gamma(\Lambda\pi^+\pi^0)$ Γ_{46}/Γ_{45}

These results are fit fraction from an amplitude / partial wave analysis.

VALUE (units 10^{-2})	EVTS	DOCUMENT ID	TECN	COMMENT
57.2±4.2±4.9	8.9k	ABLIKIM	22BA BES3	e^+e^- at 4.6-4.7 GeV

 $\Gamma(\Sigma(1385)^+\pi^0, \Sigma^+ \rightarrow \Lambda\pi^+)/\Gamma(\Lambda\pi^+\pi^0)$ Γ_{47}/Γ_{45}

These results are fit fraction from an amplitude / partial wave analysis.

VALUE (units 10^{-2})	EVTS	DOCUMENT ID	TECN	COMMENT
7.18±0.60±0.64	8.9k	ABLIKIM	22BA BES3	e^+e^- at 4.6-4.7 GeV

 $\Gamma(\Sigma(1385)^0\pi^+, \Sigma^0 \rightarrow \Lambda\pi^0)/\Gamma(\Lambda\pi^+\pi^0)$ Γ_{48}/Γ_{45}

These results are fit fraction from an amplitude / partial wave analysis.

VALUE (units 10^{-2})	EVTS	DOCUMENT ID	TECN	COMMENT
7.92±0.72±0.80	8.9k	ABLIKIM	22BA BES3	e^+e^- at 4.6-4.7 GeV

 $\Gamma(\Lambda\pi^-2\pi^+)/\Gamma_{\text{total}}$ Γ_{49}/Γ

VALUE (%)	EVTS	DOCUMENT ID	TECN	COMMENT
3.61±0.26 OUR FIT				Error includes scale factor of 1.4.
3.81±0.24±0.18	609	ABLIKIM	16 BES3	$e^+e^- \rightarrow \Lambda_C \bar{\Lambda}_C$, 4.599 GeV

 $\Gamma(\Lambda\pi^-2\pi^+)/\Gamma(\rho K^- \pi^+)$ Γ_{49}/Γ_2

VALUE	EVTS	DOCUMENT ID	TECN	COMMENT
0.58±0.04 OUR FIT				Error includes scale factor of 1.8.
0.522±0.032 OUR AVERAGE				
0.508±0.024±0.024	1356	LINK	05F FOCUS	γ nucleus, $\bar{E}_\gamma \approx 180$ GeV
0.65±0.11±0.12	289	AVERY	91 CLEO	e^+e^- 10.5 GeV
0.82±0.29±0.27	44	ANJOS	90 E691	γ Be 70-260 GeV
0.94±0.41±0.13	10	BARLAG	90D NA32	π^- 230 GeV
0.61±0.16±0.04	105	ALBRECHT	88c ARG	e^+e^- 10 GeV

 $\Gamma(\Sigma(1385)^+\pi^+\pi^-, \Sigma^{*+} \rightarrow \Lambda\pi^+)/\Gamma(\Lambda\pi^-2\pi^+)$ Γ_{50}/Γ_{49}

VALUE	DOCUMENT ID	TECN	COMMENT
0.28±0.10±0.08	LINK	05F FOCUS	γ nucleus, $\bar{E}_\gamma \approx 180$ GeV

 $\Gamma(\Sigma(1385)^-2\pi^+, \Sigma^{*-} \rightarrow \Lambda\pi^-)/\Gamma(\Lambda\pi^-2\pi^+)$ Γ_{51}/Γ_{49}

VALUE	DOCUMENT ID	TECN	COMMENT
0.21±0.03±0.02	LINK	05F FOCUS	γ nucleus, $\bar{E}_\gamma \approx 180$ GeV

 $\Gamma(\Lambda\pi^+\rho^0)/\Gamma(\Lambda\pi^-2\pi^+)$ Γ_{52}/Γ_{49}

VALUE	DOCUMENT ID	TECN	COMMENT
0.40±0.12±0.12	LINK	05F FOCUS	γ nucleus, $\bar{E}_\gamma \approx 180$ GeV

 $\Gamma(\Sigma(1385)^+\rho^0, \Sigma^{*+} \rightarrow \Lambda\pi^+)/\Gamma(\Lambda\pi^-2\pi^+)$ Γ_{53}/Γ_{49}

VALUE	DOCUMENT ID	TECN	COMMENT
0.14±0.09±0.07	LINK	05F FOCUS	γ nucleus, $\bar{E}_\gamma \approx 180$ GeV

 $\Gamma(\Lambda\pi^-2\pi^+ \text{ nonresonant})/\Gamma(\Lambda\pi^-2\pi^+)$ Γ_{54}/Γ_{49}

VALUE	CL%	DOCUMENT ID	TECN	COMMENT
<0.3	90	LINK	05F FOCUS	γ nucleus, $\bar{E}_\gamma \approx 180$ GeV

 $\Gamma(\Lambda\pi^- \pi^0 2\pi^+ \text{ total})/\Gamma(\rho K^- \pi^+)$ Γ_{55}/Γ_2

VALUE	EVTS	DOCUMENT ID	TECN	COMMENT
0.36±0.09±0.09	50	1 CRONIN-HEN..03	CLE3	$e^+e^- \approx \Upsilon(4S)$
				1 CRONIN-HENNESSY 03 finds this channel to be dominantly $\Lambda\eta\pi^+$ and $\Lambda\omega\pi^+$; see below.

 $\Gamma(\Lambda\pi^+\eta)/\Gamma_{\text{total}}$ Γ_{56}/Γ

VALUE (units 10^{-2})	EVTS	DOCUMENT ID	TECN	COMMENT
1.84±0.11 OUR FIT				Error includes scale factor of 1.1.
1.84±0.21±0.15	154	ABLIKIM	19Y BES3	e^+e^- at 4.6 GeV

 $\Gamma(\Lambda\pi^+\eta)/\Gamma(\rho K^- \pi^+)$ Γ_{56}/Γ_2 Unseen decay modes of the η are included.

VALUE	EVTS	DOCUMENT ID	TECN	COMMENT
0.295±0.014 OUR FIT				
0.295±0.014 OUR AVERAGE				
0.293±0.003±0.014	51k	LEE	21A BELL	$e^+e^- \approx \Upsilon(nS)$
0.41±0.17±0.10	11	CRONIN-HEN..03	CLE3	$e^+e^- \approx \Upsilon(4S)$
0.35±0.05±0.06	116	AMMAR	95 CLE2	$e^+e^- \approx \Upsilon(4S)$

 $\Gamma(\Sigma(1385)^+\eta)/\Gamma_{\text{total}}$ Γ_{57}/Γ

VALUE (units 10^{-2})	EVTS	DOCUMENT ID	TECN	COMMENT
0.91±0.18±0.09	54	ABLIKIM	19Y BES3	e^+e^- at 4.6 GeV

 $\Gamma(\Sigma(1385)^+\eta)/\Gamma(\rho K^- \pi^+)$ Γ_{57}/Γ_2 Unseen decay modes of the $\Sigma(1385)^+$ and η are included.

VALUE	EVTS	DOCUMENT ID	TECN	COMMENT
0.190±0.016 OUR FIT				
0.295±0.014 OUR AVERAGE				
0.192±0.006±0.016	29k	LEE	21A BELL	$e^+e^- \approx \Upsilon(nS)$
0.17±0.04±0.03	54	AMMAR	95 CLE2	$e^+e^- \approx \Upsilon(4S)$

 $\Gamma(\Lambda\pi^+\omega)/\Gamma(\rho K^- \pi^+)$ Γ_{58}/Γ_2 Unseen decay modes of the ω are included.

VALUE	EVTS	DOCUMENT ID	TECN	COMMENT
0.24±0.06±0.06	32	CRONIN-HEN..03	CLE3	$e^+e^- \approx \Upsilon(4S)$

 $\Gamma(\Lambda\pi^- \pi^0 2\pi^+, \text{ no } \eta \text{ or } \omega)/\Gamma(\rho K^- \pi^+)$ Γ_{59}/Γ_2

VALUE	CL%	DOCUMENT ID	TECN	COMMENT
<0.13	90	CRONIN-HEN..03	CLE3	$e^+e^- \approx \Upsilon(4S)$

 $\Gamma(\Lambda K^+ \bar{K}^0)/\Gamma(\rho K^- \pi^+)$ Γ_{60}/Γ_2

VALUE	EVTS	DOCUMENT ID	TECN	COMMENT
0.090±0.017 OUR FIT				Error includes scale factor of 1.9.
0.131±0.020 OUR AVERAGE				
0.142±0.018±0.022	251	LINK	05F FOCUS	γ nucleus, $\bar{E}_\gamma \approx 180$ GeV
0.12±0.02±0.02	59	AMMAR	95 CLE2	$e^+e^- \approx \Upsilon(4S)$

 $\Gamma(\Lambda K^+ \bar{K}^0)/\Gamma(\Lambda\pi^+)$ Γ_{60}/Γ_{43}

VALUE	EVTS	DOCUMENT ID	TECN	COMMENT
0.44±0.08 OUR FIT				Error includes scale factor of 2.0.
0.395±0.026±0.036	460±30	AUBERT	07U BABR	$e^+e^- \approx \Upsilon(4S)$

 $\Gamma(\Xi(1690)^0 K^+, \Xi^{*0} \rightarrow \Lambda \bar{K}^0)/\Gamma(\Lambda K^+ \bar{K}^0)$ Γ_{61}/Γ_{60}

VALUE	EVTS	DOCUMENT ID	TECN	COMMENT
0.28±0.07 OUR AVERAGE				
0.32±0.10±0.04	84±24	LINK	05F FOCUS	γ nucleus, $\bar{E}_\gamma \approx 180$ GeV
0.26±0.08±0.03	93	ABE	02c BELL	$e^+e^- \approx \Upsilon(4S)$

 $\Gamma(\Sigma^0\pi^+)/\Gamma_{\text{total}}$ Γ_{62}/Γ

VALUE (%)	EVTS	DOCUMENT ID	TECN	COMMENT
1.27±0.06 OUR FIT				Error includes scale factor of 1.1.
1.25±0.07 OUR AVERAGE				
1.22±0.08±0.07	343	ABLIKIM	22S BES3	e^+e^- at 4.612-4.699 GeV
1.27±0.08±0.03	522	ABLIKIM	16 BES3	$e^+e^- \rightarrow \Lambda_C \bar{\Lambda}_C$, 4.599 GeV

 $\Gamma(\Sigma^0\pi^+)/\Gamma(\rho K^- \pi^+)$ Γ_{62}/Γ_2

VALUE	EVTS	DOCUMENT ID	TECN	COMMENT
0.204±0.010 OUR FIT				Error includes scale factor of 1.2.
0.20±0.04 OUR AVERAGE				
0.21±0.02±0.04	196	AVERY	94 CLE2	$e^+e^- \approx \Upsilon(3S), \Upsilon(4S)$
0.17±0.06±0.04		ALBRECHT	92 ARG	$e^+e^- \approx 10.4$ GeV

 $\Gamma(\Sigma^0\pi^+)/\Gamma(\Lambda\pi^+)$ Γ_{62}/Γ_{43}

VALUE	EVTS	DOCUMENT ID	TECN	COMMENT
0.99±0.04 OUR FIT				
0.98±0.05 OUR AVERAGE				
0.977±0.015±0.051	33k	AUBERT	07U BABR	$e^+e^- \approx \Upsilon(4S)$
1.09±0.11±0.19	750	LINK	05F FOCUS	γ nucleus, $\bar{E}_\gamma \approx 180$ GeV

 $\Gamma(\Sigma^0\pi^+\eta)/\Gamma(\rho K^- \pi^+)$ Γ_{63}/Γ_2

VALUE	EVTS	DOCUMENT ID	TECN	COMMENT
0.120±0.006±0.010	17k	LEE	21A BELL	$e^+e^- \approx \Upsilon(nS)$

 $\Gamma(\Sigma^+\pi^0)/\Gamma_{\text{total}}$ Γ_{64}/Γ

VALUE (%)	EVTS	DOCUMENT ID	TECN	COMMENT
1.24±0.09 OUR FIT				
1.18±0.10±0.03	309	ABLIKIM	16 BES3	$e^+e^- \rightarrow \Lambda_C \bar{\Lambda}_C$, 4.599 GeV

$\Gamma(\Sigma^+\pi^0)/\Gamma(\rho K^-\pi^+)$ Γ_{64}/Γ_2
 VALUE EVTS DOCUMENT ID TECN COMMENT

0.200±0.015 OUR FIT
 0.20 ±0.03 ±0.03 93 KUBOTA 93 CLE2 $e^+e^- \approx \mathcal{T}(4S)$

$\Gamma(\Sigma^+\eta)/\Gamma(\rho K^-\pi^+)$ Γ_{65}/Γ_2
 Unseen decay modes of the η are included.
 VALUE EVTS DOCUMENT ID TECN COMMENT

0.11±0.03±0.02 26 AMMAR 95 CLE2 $e^+e^- \approx \mathcal{T}(4S)$

$\Gamma(\Sigma^+\eta)/\Gamma(\Sigma^+\pi^0)$ Γ_{65}/Γ_{64}
 VALUE EVTS DOCUMENT ID TECN COMMENT

0.254±0.031 OUR AVERAGE
 0.25 ±0.03 ±0.01 700 LI 23A BELL e^+e^- at/near $\mathcal{T}(nS)$,
 $n=1,\dots,5$

0.35 ±0.16 ±0.02 15 ¹ABLIKIM 19x BES3 e^+e^- at 4.6 GeV

¹ABLIKIM 19x report evidence for the observation of the decay $\Lambda_c^+ \rightarrow \Sigma^+\eta$ at 2.5 σ significance.

$\Gamma(\Sigma^+\eta')/\Gamma(\Sigma^+\pi^0)$ Γ_{66}/Γ_{64}
 VALUE EVTS DOCUMENT ID TECN COMMENT

0.33±0.06±0.02 300 LI 23A BELL e^+e^- at/near $\mathcal{T}(nS)$,
 $n=1,\dots,5$

$\Gamma(\Sigma^+\eta')/\Gamma(\Sigma^+\omega)$ Γ_{66}/Γ_{73}
 VALUE EVTS DOCUMENT ID TECN COMMENT

0.86±0.34±0.04 13 ¹ABLIKIM 19x BES3 e^+e^- at 4.6 GeV

¹ABLIKIM 19x report evidence for the observation of the decay $\Lambda_c^+ \rightarrow \Sigma^+\eta'$ at 3.2 σ significance.

$\Gamma(\Sigma^+\pi^+\pi^-)/\Gamma_{total}$ Γ_{67}/Γ
 VALUE(%) EVTS DOCUMENT ID TECN COMMENT

4.47±0.22 OUR FIT Error includes scale factor of 1.2.
4.25±0.24±0.20 1156 ABLIKIM 16 BES3 $e^+e^- \rightarrow \Lambda_c\bar{\Lambda}_c$, 4.599 GeV

$\Gamma(\Sigma^+\pi^+\pi^-)/\Gamma(\rho K^-\pi^+)$ Γ_{67}/Γ_2
 VALUE EVTS DOCUMENT ID TECN COMMENT

0.716±0.019 OUR FIT
0.720±0.024 OUR AVERAGE

0.719±0.003±0.024 2.7M BERGER 18 BELL $e^+e^- \approx \mathcal{T}(4S)$
 0.74 ±0.07 ±0.09 487 KUBOTA 93 CLE2 $e^+e^- \approx \mathcal{T}(4S)$

••• We do not use the following data for averages, fits, limits, etc. •••

0.72 ±0.14 47 ±9 VAZQUEZ-JA...08 SELX Σ^- nucleus, 600 GeV
 0.54 ^{+0.18}_{-0.15} 11 BARLAG 92 NA32 π^- Cu 230 GeV

$\Gamma(\Sigma^+\rho^0)/\Gamma(\rho K^-\pi^+)$ Γ_{68}/Γ_2
 VALUE CL% DOCUMENT ID TECN COMMENT

<0.27 95 KUBOTA 93 CLE2 $e^+e^- \approx \mathcal{T}(4S)$

$\Gamma(\Sigma^-2\pi^+)/\Gamma_{total}$ Γ_{69}/Γ
 VALUE(%) EVTS DOCUMENT ID TECN COMMENT

1.86±0.18 OUR FIT
1.81±0.17±0.09 161 ABLIKIM 17Y BES3 e^+e^- at 4.6 GeV

$\Gamma(\Sigma^-2\pi^+)/\Gamma(\rho K^-\pi^+)$ Γ_{69}/Γ_2
 VALUE EVTS DOCUMENT ID TECN COMMENT

0.299±0.030 OUR FIT
0.314±0.067 30 ±6 VAZQUEZ-JA...08 SELX Σ^- nucleus, 600 GeV

$\Gamma(\Sigma^-2\pi^+)/\Gamma(\Sigma^+\pi^+\pi^-)$ Γ_{69}/Γ_{67}
 VALUE EVTS DOCUMENT ID TECN COMMENT

0.42±0.04 OUR FIT
0.53±0.15±0.07 56 FRABETTI 94E E687 γ Be, \bar{E}_γ 220 GeV

$\Gamma(\Sigma^0\pi^+\pi^0)/\Gamma(\rho K^-\pi^+)$ Γ_{70}/Γ_2
 VALUE EVTS DOCUMENT ID TECN COMMENT

0.56 ±0.05 OUR AVERAGE Error includes scale factor of 1.5.
 0.575±0.005±0.036 2.7M BERGER 18 BELL $e^+e^- \approx \mathcal{T}(4S)$
 0.36 ±0.09 ±0.10 117 AVERY 94 CLE2 $e^+e^- \approx \mathcal{T}(3S), \mathcal{T}(4S)$

$\Gamma(\Sigma^+\pi^0\pi^0)/\Gamma(\rho K^-\pi^+)$ Γ_{71}/Γ_2
 VALUE EVTS DOCUMENT ID TECN COMMENT

0.247±0.006±0.019 925k BERGER 18 BELL $e^+e^- \approx \mathcal{T}(4S)$

$\Gamma(\Sigma^0\pi^-2\pi^+)/\Gamma(\rho K^-\pi^+)$ Γ_{72}/Γ_2
 VALUE EVTS DOCUMENT ID TECN COMMENT

0.18±0.05 OUR FIT
0.21±0.05±0.05 90 AVERY 94 CLE2 $e^+e^- \approx \mathcal{T}(3S), \mathcal{T}(4S)$

$\Gamma(\Sigma^0\pi^-2\pi^+)/\Gamma(\Lambda\pi^-2\pi^+)$ Γ_{72}/Γ_{49}
 VALUE EVTS DOCUMENT ID TECN COMMENT

0.31±0.08 OUR FIT
0.26±0.06±0.09 480 LINK 05F FOCS γ nucleus, $\bar{E}_\gamma \approx 180$ GeV

$\Gamma(\Sigma^+\omega)/\Gamma_{total}$ Γ_{73}/Γ
 VALUE(%) EVTS DOCUMENT ID TECN COMMENT

1.69±0.20 OUR FIT
1.56±0.20±0.07 157 ABLIKIM 16 BES3 $e^+e^- \rightarrow \Lambda_c\bar{\Lambda}_c$, 4.599 GeV

$\Gamma(\Sigma^+\omega)/\Gamma(\rho K^-\pi^+)$ Γ_{73}/Γ_2
 Unseen decay modes of the ω are included.
 VALUE EVTS DOCUMENT ID TECN COMMENT

0.271±0.031 OUR FIT
0.54 ±0.13 ±0.06 107 KUBOTA 93 CLE2 $e^+e^- \approx \mathcal{T}(4S)$

$\Gamma(\Sigma^-\pi^02\pi^+)/\Gamma_{total}$ Γ_{74}/Γ
 VALUE(%) EVTS DOCUMENT ID TECN COMMENT

2.11±0.33±0.14 88 ABLIKIM 17Y BES3 e^+e^- at 4.6 GeV

$\Gamma(\Sigma^+K^+K^-)/\Gamma(\rho K^-\pi^+)$ Γ_{75}/Γ_2
 VALUE EVTS DOCUMENT ID TECN COMMENT

0.057±0.005 OUR FIT
0.070±0.011±0.011 59 AVERY 93 CLE2 $e^+e^- \approx 10.5$ GeV

$\Gamma(\Sigma^+K^+K^-)/\Gamma(\Sigma^+\pi^+\pi^-)$ Γ_{75}/Γ_{67}
 VALUE (units 10^{-2}) EVTS DOCUMENT ID TECN COMMENT

8.0 ±0.7 OUR FIT
7.8 ±0.7 OUR AVERAGE

8.38±0.93±0.44 110 ABLIKIM 23BY BES3 e^+e^- at 4.600–4.699 GeV
 7.6 ±0.7 ±0.9 246 ABE 02c BELL $e^+e^- \approx \mathcal{T}(4S)$
 7.1 ±1.1 ±1.1 103 LINK 02g FOCS γ nucleus, ≈ 180 GeV

$\Gamma(\Sigma^+K^+K^-(non-\phi))/\Gamma(\Sigma^+\pi^+\pi^-)$ Γ_{76}/Γ_{67}
 VALUE EVTS DOCUMENT ID TECN COMMENT

••• We do not use the following data for averages, fits, limits, etc. •••

4.38±0.79±0.21 75 ¹ABLIKIM 23BY BES3 e^+e^- at 4.600–4.699 GeV

¹We do not include this measurement in our average because it is highly correlated to the relative branching fractions $B(\Lambda_c \rightarrow \Sigma^+K^+K^-) / B(\Lambda_c \rightarrow \Sigma^+\pi^+\pi^-)$ and $B(\Lambda_c \rightarrow \Sigma^+\phi) / B(\Lambda_c \rightarrow \Sigma^+\pi^+\pi^-)$ measured in the same analysis (which we do use). Although the measurements are done on the same data, ABLIKIM 23BY do not obtain exactly $B(\Lambda_c \rightarrow \Sigma^+\phi)B(\phi \rightarrow K^+K^-) / B(\Lambda_c \rightarrow \Sigma^+\pi^+\pi^-) + B(\Lambda_c^+ \rightarrow \Sigma^+K^+K^-(non-\phi)) / B(\Lambda_c \rightarrow \Sigma^+\pi^+\pi^-) = B(\Lambda_c \rightarrow \Sigma^+K^+K^-) / B(\Lambda_c \rightarrow \Sigma^+\pi^+\pi^-)$.

$\Gamma(\Sigma^+\phi)/\Gamma(\rho K^-\pi^+)$ Γ_{77}/Γ_2
 Unseen decay modes of the ϕ are included.
 VALUE EVTS DOCUMENT ID TECN COMMENT

0.063±0.007 OUR FIT
0.069±0.023±0.016 26 AVERY 93 CLE2 $e^+e^- \approx 10.5$ GeV

$\Gamma(\Sigma^+\phi)/\Gamma(\Sigma^+\pi^+\pi^-)$ Γ_{77}/Γ_{67}
 Unseen decay modes of the ϕ are included.
 VALUE (units 10^{-2}) EVTS DOCUMENT ID TECN COMMENT

8.8±1.0 OUR FIT
8.8±1.0 OUR AVERAGE

9.2±1.8±0.7 119 ABLIKIM 23BY BES3 e^+e^- at 4.600–4.699 GeV
 8.5±1.2±1.2 129 ABE 02c BELL $e^+e^- \approx \mathcal{T}(4S)$
 8.7±1.6±0.6 57 LINK 02g FOCS γ nucleus, ≈ 180 GeV

$\Gamma(\Xi(1690)^0K^+, \Xi^{*0} \rightarrow \Sigma^+K^-)/\Gamma(\Sigma^+\pi^+\pi^-)$ Γ_{78}/Γ_{67}
 VALUE EVTS DOCUMENT ID TECN COMMENT

0.023±0.005 OUR AVERAGE
 0.023±0.005±0.005 75 ABE 02c BELL $e^+e^- \approx \mathcal{T}(4S)$
 0.022±0.006±0.006 34 LINK 02g FOCS γ nucleus, ≈ 180 GeV

$\Gamma(\Sigma^+K^+K^-(nonresonant))/\Gamma(\Sigma^+\pi^+\pi^-)$ Γ_{79}/Γ_{67}
 VALUE CL% DOCUMENT ID TECN COMMENT

<0.018 90 ABE 02c BELL $e^+e^- \approx \mathcal{T}(4S)$

••• We do not use the following data for averages, fits, limits, etc. •••

<0.028 90 LINK 02g FOCS γ nucleus, ≈ 180 GeV

$\Gamma(\Xi^0K^+)/\Gamma_{total}$ Γ_{80}/Γ
 VALUE (units 10^{-3}) EVTS DOCUMENT ID TECN COMMENT

5.5 ±0.7 OUR FIT
5.90±0.86±0.39 68 ABLIKIM 18Y BES3 e^+e^- at 4.6 GeV

$\Gamma(\Xi^0K^+)/\Gamma(\rho K^-\pi^+)$ Γ_{80}/Γ_2
 VALUE EVTS DOCUMENT ID TECN COMMENT

0.088±0.012 OUR FIT
0.078±0.013±0.013 56 AVERY 93 CLE2 $e^+e^- \approx 10.5$ GeV

$\Gamma(\Xi^-K^+\pi^+)/\Gamma(\rho K^-\pi^+)$ Γ_{81}/Γ_2
 VALUE EVTS DOCUMENT ID TECN COMMENT

0.099±0.009 OUR FIT Error includes scale factor of 1.1.
0.098±0.021 OUR AVERAGE Error includes scale factor of 1.3. See the ideogram below.

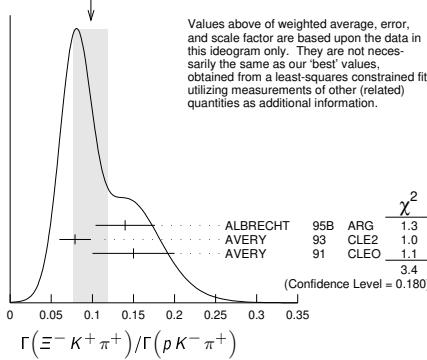
0.14 ±0.03 ±0.02 34 ALBRECHT 95B ARG $e^+e^- \approx 10.4$ GeV

Baryon Particle Listings

 Λ_C^+

$0.079 \pm 0.013 \pm 0.014$	60	AVERY	93	CLE2	$e^+e^- \approx 10.5$ GeV
$0.15 \pm 0.04 \pm 0.03$	30	AVERY	91	CLEO	$e^+e^- 10.5$ GeV

WEIGHTED AVERAGE
 0.098 ± 0.021 (Error scaled by 1.3)



$\Gamma(\Xi^- K^+ \pi^+) / \Gamma(\Lambda \pi^+)$ $\Gamma_{81} / \Gamma_{43}$

VALUE	EVTS	DOCUMENT ID	TECN	COMMENT
0.48 ± 0.04 OUR FIT				
$0.480 \pm 0.016 \pm 0.039$	2665 ± 84	AUBERT	07U BABR	$e^+e^- \approx \Upsilon(4S)$

$\Gamma(\Xi(1530)^0 K^+) / \Gamma_{\text{total}}$ Γ_{82} / Γ

VALUE (units 10^{-3})	EVTS	DOCUMENT ID	TECN	COMMENT
4.3 ± 0.9 OUR FIT				Error includes scale factor of 1.1.
$5.02 \pm 0.99 \pm 0.31$	60	ABLIKIM	18Y BES3	e^+e^- at 4.6 GeV

$\Gamma(\Xi(1530)^0 K^+) / \Gamma(\rho K^- \pi^+)$ Γ_{82} / Γ_2

VALUE	EVTS	DOCUMENT ID	TECN	COMMENT
0.068 ± 0.014 OUR FIT				Error includes scale factor of 1.1.
$0.053 \pm 0.016 \pm 0.010$	24	AVERY	93 CLE2	$e^+e^- \approx 10.5$ GeV
••• We do not use the following data for averages, fits, limits, etc. •••				
$0.05 \pm 0.02 \pm 0.01$	11	ALBRECHT	95B ARG	$e^+e^- \approx 10.4$ GeV

Hadronic modes with a hyperon: S = 0 final states

$\Gamma(\Lambda K^+) / \Gamma(\Lambda \pi^+)$ $\Gamma_{83} / \Gamma_{43}$

VALUE (units 10^{-2})	EVTS	DOCUMENT ID	TECN	COMMENT
4.96 ± 0.14 OUR AVERAGE				
$5.05 \pm 0.13 \pm 0.09$	11k	LI	23C BELL	e^+e^- at/near $\Upsilon(nS)$, $n=1, \dots, 5$
$4.78 \pm 0.34 \pm 0.20$		ABLIKIM	22Bc BES3	$6.44 \text{ fb}^{-1} e^+e^-$ at 4.599–4.950 GeV
$4.4 \pm 0.4 \pm 0.3$	1.1k	AUBERT	07U BABR	$e^+e^- \approx \Upsilon(4S)$
••• We do not use the following data for averages, fits, limits, etc. •••				
$7.4 \pm 1.0 \pm 1.2$	265	ABE	02c BELL	$e^+e^- \approx \Upsilon(4S)$

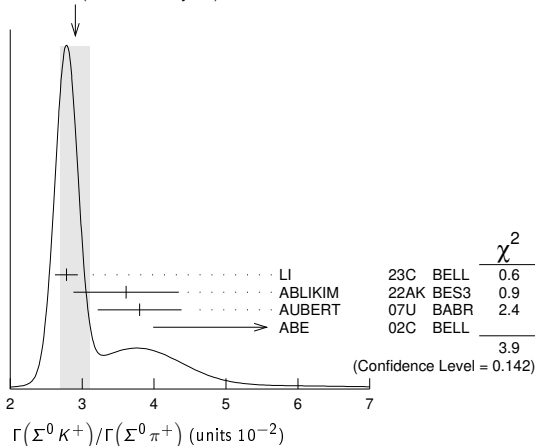
$\Gamma(\Lambda K^+ \pi^+) / \Gamma(\Lambda \pi^+)$ $\Gamma_{84} / \Gamma_{43}$

VALUE	CL%	DOCUMENT ID	TECN	COMMENT
$< 4.1 \times 10^{-2}$	90	AUBERT	07U BABR	$e^+e^- \approx \Upsilon(4S)$

$\Gamma(\Sigma^0 K^+) / \Gamma(\Sigma^0 \pi^+)$ $\Gamma_{85} / \Gamma_{62}$

VALUE (units 10^{-2})	EVTS	DOCUMENT ID	TECN	COMMENT
2.90 ± 0.21 OUR AVERAGE				Error includes scale factor of 1.4. See the ideogram below.
$2.78 \pm 0.15 \pm 0.05$	2.4k	LI	23C BELL	e^+e^- at/near $\Upsilon(nS)$, $n=1, \dots, 5$
$3.61 \pm 0.73 \pm 0.05$	43	ABLIKIM	22AK BES3	e^+e^- at 4.178–4.226 GeV
$3.8 \pm 0.5 \pm 0.3$	366 ± 52	AUBERT	07U BABR	$e^+e^- \approx \Upsilon(4S)$
$5.6 \pm 1.4 \pm 0.8$	75	ABE	02c BELL	$e^+e^- \approx \Upsilon(4S)$

WEIGHTED AVERAGE
 2.90 ± 0.21 (Error scaled by 1.4)



$\Gamma(\Sigma^+ K_S^0) / \Gamma(\Sigma^+ \pi^+ \pi^-)$ $\Gamma_{86} / \Gamma_{67}$

VALUE (units 10^{-2})	EVTS	DOCUMENT ID	TECN	COMMENT
$1.06 \pm 0.31 \pm 0.04$	44	ABLIKIM	22AK BES3	e^+e^- at 4.178–4.226 GeV

$\Gamma(\Sigma^0 K^+ \pi^+) / \Gamma(\Sigma^0 \pi^+)$ $\Gamma_{87} / \Gamma_{62}$

VALUE	CL%	DOCUMENT ID	TECN	COMMENT
$< 2.0 \times 10^{-2}$	90	AUBERT	07U BABR	$e^+e^- \approx \Upsilon(4S)$

$\Gamma(\Sigma^+ K^+ \pi^-) / \Gamma(\Sigma^+ \pi^+ \pi^-)$ $\Gamma_{88} / \Gamma_{67}$

VALUE (units 10^{-2})	EVTS	DOCUMENT ID	TECN	COMMENT
4.5 ± 0.5 OUR AVERAGE				
$4.44 \pm 0.52 \pm 0.25$	224	ABLIKIM	23BY BES3	e^+e^- at 4.600–4.699 GeV
$4.7 \pm 1.1 \pm 0.8$	105	ABE	02c BELL	$e^+e^- \approx \Upsilon(4S)$

$\Gamma(\Sigma^+ K^*(892)^0) / \Gamma(\Sigma^+ \pi^+ \pi^-)$ $\Gamma_{89} / \Gamma_{67}$

VALUE	EVTS	DOCUMENT ID	TECN	COMMENT
Unseen decay modes of the $K^*(892)^0$ are included.				
$0.078 \pm 0.018 \pm 0.013$	49	LINK	02G FOCUS	γ nucleus, ≈ 180 GeV

$\Gamma(\Sigma^+ K^+ \pi^-) / \Gamma(\Sigma^+ \pi^+ \pi^-)$ $\Gamma_{90} / \Gamma_{67}$

VALUE	CL%	DOCUMENT ID	TECN	COMMENT
$< 2.5 \times 10^{-2}$	90	ABLIKIM	23BY BES3	e^+e^- at 4.600–4.699 GeV

$\Gamma(\Sigma^- K^+ \pi^+) / \Gamma(\Sigma^+ K^*(892)^0)$ $\Gamma_{91} / \Gamma_{89}$

VALUE	CL%	DOCUMENT ID	TECN	COMMENT
< 0.35	90	LINK	02G FOCUS	γ nucleus, ≈ 180 GeV

Doubly Cabibbo-suppressed modes

$\Gamma(\rho K^+ \pi^-) / \Gamma(\rho K^- \pi^+)$ Γ_{92} / Γ_2

VALUE (units 10^{-3})	EVTS	DOCUMENT ID	TECN	COMMENT
1.77 ± 0.27 OUR AVERAGE				Error includes scale factor of 1.9.
$1.65 \pm 0.15 \pm 0.05$	392	AAIJ	18V LHCb	$\Lambda_b^0 \rightarrow \Lambda_c^+ \mu^- X$
$2.35 \pm 0.27 \pm 0.21$	3379	YANG	16 BELL	At or near Υ 's

Semileptonic modes

$\Gamma(\Lambda e^+ \nu_e) / \Gamma_{\text{total}}$ Γ_{93} / Γ

VALUE (%)	EVTS	DOCUMENT ID	TECN	COMMENT
$3.56 \pm 0.11 \pm 0.07$		1 ABLIKIM	22AT BES3	4.5 fb^{-1} in e^+e^- at 4.600–4.699 GeV
••• We do not use the following data for averages, fits, limits, etc. •••				
$3.63 \pm 0.38 \pm 0.20$	104	2 ABLIKIM	15Y BES3	567 pb^{-1} , 4.599 GeV
1 Using Lattice QCD calculations for the form factors yields $ V_{cs} = 0.936 \pm 0.030$.				
2 Superseded by ABLIKIM 22AT.				

$\Gamma(\Lambda e^+ \nu_e) / \Gamma(\rho K^- \pi^+)$ Γ_{93} / Γ_2

VALUE	DOCUMENT ID	TECN	COMMENT
••• We do not use the following data for averages, fits, limits, etc. •••			
0.43 ± 0.08	1,2 BERGFELD	94 CLE2	$e^+e^- \approx \Upsilon(4S)$
0.38 ± 0.14	2,3 ALBRECHT	91G ARG	$e^+e^- \approx 10.4$ GeV
1 BERGFELD 94 measures $\sigma(e^+e^- \rightarrow \Lambda_c^+ X) \cdot B(\Lambda_c^+ \rightarrow \Lambda e^+ \nu_e) = (4.87 \pm 0.28 \pm 0.69) \text{ pb}$.			
2 To extract $\Gamma(\Lambda_c^+ \rightarrow \Lambda e^+ \nu_e) / \Gamma(\Lambda_c^+ \rightarrow \rho K^- \pi^+)$, we use $\sigma(e^+e^- \rightarrow \Lambda_c^+ X) \cdot B(\Lambda_c \rightarrow \rho K^- \pi^+) = (11.2 \pm 1.3) \text{ pb}$, which is the weighted average of measurements from ARGUS (ALBRECHT 96E) and CLEO (AVERY 91).			
3 ALBRECHT 91G measures $\sigma(e^+e^- \rightarrow \Lambda_c^+ X) \cdot B(\Lambda_c^+ \rightarrow \Lambda e^+ \nu_e) = (4.20 \pm 1.28 \pm 0.71) \text{ pb}$.			

$\Gamma(\Lambda \pi^+ \pi^- e^+ \nu_e) / \Gamma_{\text{total}}$ Γ_{94} / Γ

VALUE	CL%	DOCUMENT ID	TECN	COMMENT
$< 3.9 \times 10^{-4}$	90	ABLIKIM	23AB BES3	4.5 fb^{-1} , e^+e^- at 4.600–4.699 GeV

$\Gamma(\rho K^- e^+ \nu_e) / \Gamma_{\text{total}}$ Γ_{95} / Γ

VALUE (units 10^{-3})	DOCUMENT ID	TECN	COMMENT
$0.88 \pm 0.17 \pm 0.07$	ABLIKIM	22BB BES	4.5 fb^{-1} in e^+e^- at 4.600–4.699 GeV

$\Gamma(\rho K_S^0 \pi^- e^+ \nu_e) / \Gamma_{\text{total}}$ Γ_{96} / Γ

VALUE	CL%	DOCUMENT ID	TECN	COMMENT
$< 3.3 \times 10^{-4}$	90	ABLIKIM	23AB BES3	4.5 fb^{-1} , e^+e^- at 4.600–4.699 GeV

$\Gamma(\Lambda(1520) e^+ \nu_e) / \Gamma_{\text{total}}$ Γ_{97} / Γ

VALUE (units 10^{-3})	DOCUMENT ID	TECN	COMMENT
$1.02 \pm 0.52 \pm 0.11$	1 ABLIKIM	22BB BES	4.5 fb^{-1} e^+e^- at 4.600–4.699 GeV
1 ABLIKIM 22BB reports $B(\Lambda_c^+ \rightarrow \Lambda(1520) e^+ \nu_e) \cdot B(\Lambda(1520) \rightarrow \rho K^-) = (2.3 \pm 1.2 \pm 0.2) \times 10^{-4}$, which is divided by the best value for $B(\Lambda(1520) \rightarrow \rho K^-)$ assuming the isospin limit $2 \cdot B(\Lambda(1520) \rightarrow \rho K^-) = B(\Lambda(1520) \rightarrow N \bar{K}) = 0.45 \pm 0.01$.			

$\Gamma(\Lambda(1405)^0 e^+ \nu_e, \Lambda^0 \rightarrow p K^-)/\Gamma_{\text{total}}$				Γ_{98}/Γ
VALUE (units 10^{-3})	EVTS	DOCUMENT ID	TECN	COMMENT
$0.42 \pm 0.19 \pm 0.04$		ABLIKIM	22BB BES	4.5 fb^{-1} in $e^+ e^-$ at 4.600–4.699 GeV

$\Gamma(\Lambda\mu^+ \nu_\mu)/\Gamma_{\text{total}}$				Γ_{99}/Γ
VALUE (%)	EVTS	DOCUMENT ID	TECN	COMMENT
$3.48 \pm 0.14 \pm 0.10$	752	ABLIKIM	23AT BES3	$e^+ e^-$ at 4.600–4.699 GeV

• • • We do not use the following data for averages, fits, limits, etc. • • •
 $3.49 \pm 0.46 \pm 0.27$ 79 ¹ABLIKIM 17D BES3 $e^+ e^-$ at 4.6 GeV
¹ Superseded by ABLIKIM 23AT.

$\Gamma(\Lambda\mu^+ \nu_\mu)/\Gamma(p K^- \pi^+)$				Γ_{99}/Γ_2
VALUE	EVTS	DOCUMENT ID	TECN	COMMENT
0.40 ± 0.09		1,2 BERGFELD	94 CLE2	$e^+ e^- \approx \Upsilon(4S)$
0.35 ± 0.20		2,3 ALBRECHT	91G ARG	$e^+ e^- \approx 10.4 \text{ GeV}$

• • • We do not use the following data for averages, fits, limits, etc. • • •
¹ BERGFELD 94 measures $\sigma(e^+ e^- \rightarrow \Lambda_C^+ X) \cdot B(\Lambda_C^+ \rightarrow \Lambda\mu^+ \nu_\mu) = (4.43 \pm 0.51 \pm 0.64) \text{ pb}$.

² To extract $\Gamma(\Lambda_C^+ \rightarrow \Lambda\mu^+ \nu_\mu)/\Gamma(\Lambda_C^+ \rightarrow p K^- \pi^+)$, we use $\sigma(e^+ e^- \rightarrow \Lambda_C^+ X) \cdot B(\Lambda_C^+ \rightarrow p K^- \pi^+) = (11.2 \pm 1.3) \text{ pb}$, which is the weighted average of measurements from ARGUS (ALBRECHT 96E) and CLEO (AVERY 91).

³ ALBRECHT 91G measures $\sigma(e^+ e^- \rightarrow \Lambda_C^+ X) \cdot B(\Lambda_C^+ \rightarrow \Lambda\mu^+ \nu_\mu) = (3.91 \pm 2.02 \pm 0.90) \text{ pb}$.

$\Gamma(\Lambda\mu^+ \nu_\mu)/\Gamma(\Lambda e^+ \nu_e)$				Γ_{99}/Γ_{93}
VALUE	EVTS	DOCUMENT ID	TECN	COMMENT
$0.96 \pm 0.16 \pm 0.04$		1 ABLIKIM	17D BES3	$e^+ e^-$ at 4.6 GeV

¹ This is the ratio of the ABLIKIM 17D $\Lambda\mu^+ \nu_e$ branching fraction and the ABLIKIM 15V $\Lambda e^+ \nu_e$ branching fraction (see above), and so is not an independent measurement.

Inclusive modes

$\Gamma(e^+ \text{ anything})/\Gamma_{\text{total}}$				Γ_{100}/Γ
VALUE (%)	EVTS	DOCUMENT ID	TECN	COMMENT
$4.06 \pm 0.10 \pm 0.09$	4692	ABLIKIM	23AK BES3	$e^+ e^-$ at 4.6–4.698 GeV

• • • We do not use the following data for averages, fits, limits, etc. • • •
 $3.95 \pm 0.34 \pm 0.09$ 214 ¹ABLIKIM 18AF BES3 $e^+ e^-$ 4.6 GeV

¹ Superseded by ABLIKIM 23AK.

$\Gamma(p \text{ anything})/\Gamma_{\text{total}}$				Γ_{101}/Γ
VALUE	EVTS	DOCUMENT ID	TECN	COMMENT
$0.50 \pm 0.08 \pm 0.14$		1 CRAWFORD	92 CLEO	$e^+ e^-$ 10.5 GeV

¹ This CRAWFORD 92 value includes protons from Λ decay. The value is model dependent, but account is taken of this in the systematic error.

$\Gamma(n \text{ anything})/\Gamma_{\text{total}}$				Γ_{102}/Γ
VALUE (units 10^{-2})	EVTS	DOCUMENT ID	TECN	COMMENT
32.6 ± 1.6 OUR AVERAGE				
$32.4 \pm 0.7 \pm 1.5$	3105	1 ABLIKIM	23AS BES3	$e^+ e^-$ at 4.6–4.698 GeV
$50 \pm 8 \pm 14$		2 CRAWFORD	92 CLEO	$e^+ e^-$ 10.5 GeV

¹ ABLIKIM 23AS measures the antiparticle decay $\bar{\Lambda}_C^- \rightarrow \bar{n} X$.

² This CRAWFORD 92 value includes neutrons from Λ decay. The value is model dependent, but account is taken of this in the systematic error.

$\Gamma(\Lambda \text{ anything})/\Gamma_{\text{total}}$				Γ_{103}/Γ
VALUE (%)	EVTS	DOCUMENT ID	TECN	COMMENT
$38.2 \pm 2.8 \pm 0.9$	700	ABLIKIM	18E BES3	$e^+ e^-$ at 4.6 GeV

$\Gamma(K_S^0 \text{ anything})/\Gamma_{\text{total}}$				Γ_{104}/Γ
VALUE (%)	EVTS	DOCUMENT ID	TECN	COMMENT
$9.9 \pm 0.6 \pm 0.4$	478	ABLIKIM	20AJ BES3	$e^+ e^-$ at 4.6 GeV

$\Gamma(3\text{prongs})/\Gamma_{\text{total}}$				Γ_{105}/Γ
VALUE	EVTS	DOCUMENT ID	TECN	COMMENT
$0.24 \pm 0.07 \pm 0.04$		KAYIS-TOPAK.03	CHRS	ν_μ emulsion, $\bar{E}=27 \text{ GeV}$

Rare or forbidden modes

$\Gamma(p e^+ e^-)/\Gamma_{\text{total}}$				Γ_{106}/Γ	
VALUE	CL%	EVTS	DOCUMENT ID	TECN	COMMENT
$< 5.5 \times 10^{-6}$	90	4.0 ± 7.1	LEES	11G BABR	$e^+ e^- \approx \Upsilon(4S)$

$\Gamma(p\mu^+ \mu^- \text{ non-resonant})/\Gamma_{\text{total}}$				Γ_{107}/Γ	
VALUE	CL%	EVTS	DOCUMENT ID	TECN	COMMENT
$< 7.7 \times 10^{-8}$	90		AAIJ	18N LHCB	Ratio to $p\phi, \phi \rightarrow \mu^+ \mu^-$

• • • We do not use the following data for averages, fits, limits, etc. • • •

$< 4.4 \times 10^{-5}$	90	LEES	11G BABR	$e^+ e^- \approx \Upsilon(4S)$
$< 3.4 \times 10^{-4}$	90	KODAMA	95 E653	π^- emulsion 600 GeV

$\Gamma(p e^+ \mu^-)/\Gamma_{\text{total}}$				Γ_{108}/Γ	
VALUE	CL%	EVTS	DOCUMENT ID	TECN	COMMENT
$< 9.9 \times 10^{-6}$	90	-0.7 ± 3.0	LEES	11G BABR	$e^+ e^- \approx \Upsilon(4S)$

$\Gamma(p e^- \mu^+)/\Gamma_{\text{total}}$				Γ_{109}/Γ	
VALUE	CL%	EVTS	DOCUMENT ID	TECN	COMMENT
$< 19 \times 10^{-6}$	90	6.2 ± 4.9	LEES	11G BABR	$e^+ e^- \approx \Upsilon(4S)$

$\Gamma(\bar{p} 2e^+)/\Gamma_{\text{total}}$				Γ_{110}/Γ	
VALUE	CL%	EVTS	DOCUMENT ID	TECN	COMMENT
$< 2.7 \times 10^{-6}$	90	-1.5 ± 4.5	LEES	11G BABR	$e^+ e^- \approx \Upsilon(4S)$

$\Gamma(\bar{p} 2\mu^+)/\Gamma_{\text{total}}$				Γ_{111}/Γ	
VALUE	CL%	EVTS	DOCUMENT ID	TECN	COMMENT
$< 9.4 \times 10^{-6}$	90	0.0 ± 2.2	LEES	11G BABR	$e^+ e^- \approx \Upsilon(4S)$

$\Gamma(\bar{p} e^+ \mu^+)/\Gamma_{\text{total}}$				Γ_{112}/Γ	
VALUE	CL%	EVTS	DOCUMENT ID	TECN	COMMENT
$< 16 \times 10^{-6}$	90	10.1 ± 6.8	LEES	11G BABR	$e^+ e^- \approx \Upsilon(4S)$

$\Gamma(\Sigma^- \mu^+ \mu^+)/\Gamma_{\text{total}}$				Γ_{113}/Γ	
VALUE	CL%	EVTS	DOCUMENT ID	TECN	COMMENT
$< 7.0 \times 10^{-4}$	90	0	KODAMA	95 E653	π^- emulsion 600 GeV

$\Gamma(\Sigma^+ \gamma)/\Gamma_{\text{total}}$				Γ_{114}/Γ	
VALUE	CL%	EVTS	DOCUMENT ID	TECN	COMMENT
$< 4.4 \times 10^{-4}$	90		ABLIKIM	23Z BES3	$e^+ e^-$ at 4.600–4.699 GeV

Radiative modes

$\Gamma(\Sigma^+ \gamma)/\Gamma(p K^- \pi^+)$				Γ_{114}/Γ_2	
VALUE	CL%	EVTS	DOCUMENT ID	TECN	COMMENT
$< 4.0 \times 10^{-3}$	90		LI	23 BELL	$e^+ e^- \rightarrow \Upsilon(nS)$

Exotic modes

$\Gamma(p\gamma_D)/\Gamma_{\text{total}}$				Γ_{115}/Γ	
VALUE	CL%	EVTS	DOCUMENT ID	TECN	COMMENT
$< 8.0 \times 10^{-5}$	90		ABLIKIM	22AR BES	4.5 fb^{-1} $e^+ e^-$ at 4.600–4.699 GeV

Λ_C^+ DECAY PARAMETERS

See the review on “Baryon Decay Parameters.”

α FOR $\Lambda_C^+ \rightarrow \Lambda \pi^+$

VALUE	EVTS	DOCUMENT ID	TECN	COMMENT
-0.755 ± 0.006 OUR AVERAGE				
$-0.755 \pm 0.005 \pm 0.003$	264k	¹ LI	23c BELL	$e^+ e^-$ at/near $\Upsilon(nS)$, $n=1, \dots, 5$
$-0.80 \pm 0.11 \pm 0.02$		ABLIKIM	19AX BES3	$e^+ e^-$ at 4.6 GeV
$-0.78 \pm 0.16 \pm 0.19$		LINK	06A FOCUS	$\gamma A, \bar{E}_{\gamma} \approx 180 \text{ GeV}$
$-0.94 \pm 0.21 \pm 0.12$	414	² BISHAI	95 CLE2	$e^+ e^- \approx \Upsilon(4S)$
-0.96 ± 0.42		ALBRECHT	92 ARG	$e^+ e^- \approx 10.4 \text{ GeV}$
-1.1 ± 0.4	86	AVERY	90B CLEO	$e^+ e^- \approx 10.6 \text{ GeV}$

¹ LI 23c obtained the value by a fit for the product $\alpha \times \alpha_{\Lambda}^{\text{avg}}$, and dividing by the value $\alpha_{\Lambda}^{\text{avg}} = 0.7542 \pm 0.0026$ reported in ABLIKIM 22Ac.

² BISHAI 95 actually gives $\alpha = -0.94 \pm 0.21 \pm 0.12$, chopping the errors at the physical limit -1.0 . However, for $\alpha \approx -1.0$, some experiments should get unphysical values ($\alpha < -1.0$), and for averaging with other measurements such values (or errors that extend below -1.0) should *not* be chopped.

α FOR $\Lambda_C^+ \rightarrow \Lambda p^+$

VALUE	EVTS	DOCUMENT ID	TECN	COMMENT
$-0.763 \pm 0.053 \pm 0.045$	8.9k	ABLIKIM	22BA BES3	$e^+ e^-$ at 4.6–4.7 GeV

α FOR $\Lambda_C^+ \rightarrow \Sigma^+ \pi^0$

VALUE	EVTS	DOCUMENT ID	TECN	COMMENT
-0.484 ± 0.027 OUR AVERAGE				
$-0.48 \pm 0.02 \pm 0.02$	7k	LI	23A BELL	$e^+ e^-$ at/near $\Upsilon(nS)$, $n=1, \dots, 5$
$-0.57 \pm 0.10 \pm 0.07$		ABLIKIM	19AX BES3	$e^+ e^-$ at 4.6 GeV
$-0.45 \pm 0.31 \pm 0.06$	89	BISHAI	95 CLE2	$e^+ e^- \approx \Upsilon(4S)$

Baryon Particle Listings

 Λ_c^+ α FOR $\Lambda_c^+ \rightarrow \Sigma^+ \eta$

VALUE	EVTS	DOCUMENT ID	TECN	COMMENT
$-0.99 \pm 0.03 \pm 0.05$	700	LI	23A	BELL $e^+ e^-$ at/near $\Upsilon(nS)$, $n=1, \dots, 5$

 α FOR $\Lambda_c^+ \rightarrow \Sigma^+ \eta'$

VALUE	EVTS	DOCUMENT ID	TECN	COMMENT
$-0.46 \pm 0.06 \pm 0.03$	300	LI	23A	BELL $e^+ e^-$ at/near $\Upsilon(nS)$, $n=1, \dots, 5$

 α FOR $\Lambda_c^+ \rightarrow \Sigma^0 \pi^+$

VALUE	EVTS	DOCUMENT ID	TECN	COMMENT
-0.466 ± 0.018 OUR AVERAGE				
$-0.463 \pm 0.016 \pm 0.008$	105k	¹ LI	23C	BELL $e^+ e^-$ at/near $\Upsilon(nS)$, $n=1, \dots, 5$
$-0.73 \pm 0.17 \pm 0.07$		ABLIKIM	19AX	BES3 $e^+ e^-$ at 4.6 GeV

¹ LI 23C obtained the value by a fit for the product $\alpha \times \alpha_{\Lambda}^{avg}$, and dividing by the value $\alpha_{\Lambda}^{avg} = 0.7542 \pm 0.0026$ reported in ABLIKIM 22AG.

 α FOR $\Lambda_c^+ \rightarrow \Sigma(1385)^+ \pi^0$

VALUE	EVTS	DOCUMENT ID	TECN	COMMENT
$-0.917 \pm 0.069 \pm 0.056$	8.9k	ABLIKIM	22BA	BES3 $e^+ e^-$ at 4.6–4.7 GeV

 α FOR $\Lambda_c^+ \rightarrow \Sigma(1385)^0 \pi^+$

VALUE	EVTS	DOCUMENT ID	TECN	COMMENT
$-0.789 \pm 0.098 \pm 0.056$	8.9k	ABLIKIM	22BA	BES3 $e^+ e^-$ at 4.6–4.7 GeV

 α FOR $\Lambda_c^+ \rightarrow \Lambda \ell^+ \nu_{\ell}$

The experiments don't cover the complete (or same incomplete) $M(\Lambda \ell^+)$ range, but we average them together anyway.

VALUE	EVTS	DOCUMENT ID	TECN	COMMENT
-0.875 ± 0.033 OUR AVERAGE				
$-0.94 \pm 0.07 \pm 0.03$	752	¹ ABLIKIM	23AT	BES3 $e^+ e^-$, 4.600–4.699 GeV
$-0.86 \pm 0.03 \pm 0.02$	3201	² HINSON	05	CLEO $e^+ e^- \approx \Upsilon(4S)$
$-0.91 \pm 0.42 \pm 0.25$		³ ALBRECHT	94B	ARG $e^+ e^- \approx 10$ GeV
• • • We do not use the following data for averages, fits, limits, etc. • • •				
$-0.82 \pm 0.09 \pm 0.06$	700	⁴ CRAWFORD	95	CLE2 See HINSON 05
$-0.89 \pm 0.17 \pm 0.09$	350	⁵ BERGFELD	94	CLE2 See CRAWFORD 95

¹ ABLIKIM 23AT measures α of $\Lambda_c^+ \rightarrow \Lambda \mu^+ \nu_{\mu}$ decay over eight q^2 bins from zero to the kinematic endpoint. The value provided here is $\langle \alpha \rangle$, averaged over q^2 . The analysis uses form factors extracted from a simultaneous fit to electron and muon mode data.

² HINSON 05 measures the form-factor ratio $R \equiv f_2/f_1$ for $\Lambda_c^+ \rightarrow \Lambda e^+ \nu_e$ events to be $-0.31 \pm 0.05 \pm 0.04$ and the pole mass to be $2.21 \pm 0.08 \pm 0.14$ GeV/ c^2 , and from these calculates α , averaged over q^2 , where $\langle q^2 \rangle = 0.67$ (GeV/ c^2).

³ ALBRECHT 94B uses Λe^+ and $\Lambda \mu^+$ events in the mass range $1.85 < M(\Lambda \ell^+) < 2.20$ GeV.

⁴ CRAWFORD 95 measures the form-factor ratio $R \equiv f_2/f_1$ for $\Lambda_c^+ \rightarrow \Lambda e^+ \nu_e$ events to be $-0.25 \pm 0.14 \pm 0.08$ and from this calculates α , averaged over q^2 , to be the above.

⁵ BERGFELD 94 uses Λe^+ events.

 α FOR $\Lambda_c^+ \rightarrow p K_S^0$

VALUE	DOCUMENT ID	TECN	COMMENT
$0.18 \pm 0.43 \pm 0.14$	ABLIKIM	19AX	BES3 $e^+ e^-$ at 4.6 GeV

 α FOR $\Lambda_c^+ \rightarrow \Lambda K^+$

VALUE	EVTS	DOCUMENT ID	TECN	COMMENT
$-0.585 \pm 0.049 \pm 0.018$	11k	¹ LI	23C	BELL $e^+ e^-$ at/near $\Upsilon(nS)$, $n=1, \dots, 5$

¹ LI 23C obtained the value by a fit for the product $\alpha \times \alpha_{\Lambda}^{avg}$, and dividing by the value $\alpha_{\Lambda}^{avg} = 0.7542 \pm 0.0026$ reported in ABLIKIM 22AG.

 α FOR $\Lambda_c^+ \rightarrow \Sigma^0 K^+$

VALUE	EVTS	DOCUMENT ID	TECN	COMMENT
$-0.54 \pm 0.18 \pm 0.09$	2.4k	¹ LI	23C	BELL $e^+ e^-$ at/near $\Upsilon(nS)$, $n=1, \dots, 5$

¹ LI 23C obtained the value by a fit for the product $\alpha \times \alpha_{\Lambda}^{avg}$, and dividing by the value $\alpha_{\Lambda}^{avg} = 0.7542 \pm 0.0026$ reported in ABLIKIM 22AG.

 α FOR $\Lambda_c^+ \rightarrow \Lambda(1405)^+ \pi^+$

The polarization is defined with respect to the daughter baryon momentum in the parent rest frame. See "Baryon Decay Parameters" review.

VALUE	DOCUMENT ID	TECN	COMMENT
$0.58 \pm 0.05 \pm 0.01 \pm 0.28$	¹ AAIJ	23Z	LHCB 1.7fb^{-1} , pp at 13 TeV

¹ AAIJ 23Z uses an amplitude analysis of 400k $\Lambda_c \rightarrow p K^- \pi^+$ decays, the last uncertainty is due to the amplitude model. Sign determined per authors; see also AAIJ 23AJ.

 α FOR $\Lambda_c^+ \rightarrow \Lambda(1520)^+ \pi^+$

The polarization is defined with respect to the daughter baryon momentum in the parent rest frame. See "Baryon Decay Parameters" review.

VALUE	DOCUMENT ID	TECN	COMMENT
$0.925 \pm 0.025 \pm 0.005 \pm 0.084$	¹ AAIJ	23Z	LHCB 1.7fb^{-1} , pp at 13 TeV

¹ AAIJ 23Z uses an amplitude analysis of 400k $\Lambda_c \rightarrow p K^- \pi^+$ decays, the last uncertainty is due to the amplitude model. Sign determined per authors; see also AAIJ 23AJ.

 α FOR $\Lambda_c^+ \rightarrow \Lambda(1600)^+ \pi^+$

The polarization is defined with respect to the daughter baryon momentum in the parent rest frame. See "Baryon Decay Parameters" review.

VALUE	DOCUMENT ID	TECN	COMMENT
$0.20 \pm 0.06 \pm 0.03 \pm 0.50$	¹ AAIJ	23Z	LHCB 1.7fb^{-1} , pp at 13 TeV

¹ AAIJ 23Z uses an amplitude analysis of 400k $\Lambda_c \rightarrow p K^- \pi^+$ decays, the last uncertainty is due to the amplitude model. Sign determined per authors; see also AAIJ 23AJ.

 α FOR $\Lambda_c^+ \rightarrow \Lambda(1670)^+ \pi^+$

The polarization is defined with respect to the daughter baryon momentum in the parent rest frame. See "Baryon Decay Parameters" review.

VALUE	DOCUMENT ID	TECN	COMMENT
$0.817 \pm 0.042 \pm 0.006 \pm 0.073$	¹ AAIJ	23Z	LHCB 1.7fb^{-1} , pp at 13 TeV

¹ AAIJ 23Z uses an amplitude analysis of 400k $\Lambda_c \rightarrow p K^- \pi^+$ decays, the last uncertainty is due to the amplitude model. Sign determined per authors; see also AAIJ 23AJ.

 α FOR $\Lambda_c^+ \rightarrow \Lambda(1690)^+ \pi^+$

The polarization is defined with respect to the daughter baryon momentum in the parent rest frame. See "Baryon Decay Parameters" review.

VALUE	DOCUMENT ID	TECN	COMMENT
$0.958 \pm 0.020 \pm 0.006 \pm 0.027$	¹ AAIJ	23Z	LHCB 1.7fb^{-1} , pp at 13 TeV

¹ AAIJ 23Z uses an amplitude analysis of 400k $\Lambda_c \rightarrow p K^- \pi^+$ decays, the last uncertainty is due to the amplitude model. Sign determined per authors; see also AAIJ 23AJ.

 α FOR $\Lambda_c^+ \rightarrow \Lambda(2000)^+ \pi^+$

VALUE	DOCUMENT ID	TECN	COMMENT
$-0.57 \pm 0.03 \pm 0.01 \pm 0.19$	¹ AAIJ	23Z	LHCB 1.7fb^{-1} , pp at 13 TeV

¹ AAIJ 23Z uses an amplitude analysis of 400k $\Lambda_c \rightarrow p K^- \pi^+$ decays, the last uncertainty is due to the amplitude model. Sign determined per authors; see also AAIJ 23AJ.

 α FOR $\Lambda_c^+ \rightarrow \Delta(1232)^{++} K^-$

The polarization is defined with respect to the daughter baryon momentum in the parent rest frame. See "Baryon Decay Parameters" review.

VALUE	DOCUMENT ID	TECN	COMMENT
$0.548 \pm 0.014 \pm 0.004 \pm 0.036$	¹ AAIJ	23Z	LHCB 1.7fb^{-1} , pp at 13 TeV

¹ AAIJ 23Z uses an amplitude analysis of 400k $\Lambda_c \rightarrow p K^- \pi^+$ decays, the last uncertainty is due to the amplitude model. Sign determined per authors; see also AAIJ 23AJ.

 α FOR $\Lambda_c^+ \rightarrow \Delta(1600)^{++} K^-$

The polarization is defined with respect to the daughter baryon momentum in the parent rest frame. See "Baryon Decay Parameters" review.

VALUE	DOCUMENT ID	TECN	COMMENT
$-0.50 \pm 0.05 \pm 0.01 \pm 0.17$	¹ AAIJ	23Z	LHCB 1.7fb^{-1} , pp at 13 TeV

¹ AAIJ 23Z uses an amplitude analysis of 400k $\Lambda_c \rightarrow p K^- \pi^+$ decays, the last uncertainty is due to the amplitude model. Sign determined per authors; see also AAIJ 23AJ.

 α FOR $\Lambda_c^+ \rightarrow \Delta(1700)^{++} K^-$

The polarization is defined with respect to the daughter baryon momentum in the parent rest frame. See "Baryon Decay Parameters" review.

VALUE	DOCUMENT ID	TECN	COMMENT
$0.216 \pm 0.036 \pm 0.011 \pm 0.075$	¹ AAIJ	23Z	LHCB 1.7fb^{-1} , pp at 13 TeV

¹ AAIJ 23Z uses an amplitude analysis of 400k $\Lambda_c \rightarrow p K^- \pi^+$ decays, the last uncertainty is due to the amplitude model. Sign determined per authors; see also AAIJ 23AJ.

 α FOR $\Lambda_c^+ \rightarrow \bar{K}_0^*(700)^0 \rho$

The polarization is defined with respect to the daughter baryon momentum in the parent rest frame. See "Baryon Decay Parameters" review.

VALUE	DOCUMENT ID	TECN	COMMENT
$-0.06 \pm 0.66 \pm 0.23 \pm 0.24$	¹ AAIJ	23Z	LHCB 1.7fb^{-1} , pp at 13 TeV

¹ AAIJ 23Z uses an amplitude analysis of 400k $\Lambda_c \rightarrow p K^- \pi^+$ decays, the last uncertainty is due to the amplitude model. Sign determined per authors; see also AAIJ 23AJ.

 α FOR $\Lambda_c^+ \rightarrow \bar{K}_0^*(1430)^0 \rho$

The polarization is defined with respect to the daughter baryon momentum in the parent rest frame. See "Baryon Decay Parameters" review.

VALUE	DOCUMENT ID	TECN	COMMENT
$0.34 \pm 0.03 \pm 0.01 \pm 0.14$	¹ AAIJ	23Z	LHCB 1.7fb^{-1} , pp at 13 TeV

¹ AAIJ 23Z uses an amplitude analysis of 400k $\Lambda_c \rightarrow p K^- \pi^+$ decays, the last uncertainty is due to the amplitude model. Sign determined per authors; see also AAIJ 23AJ.

 $\Lambda_c^+, \bar{\Lambda}_c^-$ CP-VIOLATING DECAY ASYMMETRIES $(\alpha + \bar{\alpha})/(\alpha - \bar{\alpha})$ in $\Lambda_c^+ \rightarrow \Lambda \pi^+, \bar{\Lambda}_c^- \rightarrow \bar{\Lambda} \pi^-$

This is zero if CP is conserved.

VALUE	EVTS	DOCUMENT ID	TECN	COMMENT
0.020 ± 0.016 OUR AVERAGE				
$0.020 \pm 0.007 \pm 0.014$	264k	LI	23C	BELL $e^+ e^-$ at/near $\Upsilon(nS)$, $n=1, \dots, 5$
$-0.07 \pm 0.19 \pm 0.24$		LINK	06A	FOCS $\gamma A, \bar{E}_{\gamma} \approx 180$ GeV

 $(\alpha + \bar{\alpha})/(\alpha - \bar{\alpha})$ in $\Lambda_c^+ \rightarrow \Sigma^0 \pi^+, \bar{\Lambda}_c^- \rightarrow \bar{\Sigma}^0 \pi^-$

VALUE	EVTS	DOCUMENT ID	TECN	COMMENT
$-0.023 \pm 0.034 \pm 0.030$	105k	LI	23C	BELL $e^+ e^-$ at/near $\Upsilon(nS)$, $n=1, \dots, 5$

See key on page 1171

Baryon Particle Listings

Λ_c^+ , $\Lambda_c(2595)^+$

$(\alpha + \bar{\alpha})/(\alpha - \bar{\alpha})$ in $\Lambda_c^+ \rightarrow \Lambda e^+ \nu_e, \bar{\Lambda}_c^- \rightarrow \bar{\Lambda} e^- \bar{\nu}_e$
This is zero if CP is conserved.

VALUE	DOCUMENT ID	TECN	COMMENT
$0.00 \pm 0.03 \pm 0.02$	HINSON 05 CLEO		$e^+ e^- \approx \mathcal{T}(4S)$

$(\alpha + \bar{\alpha})/(\alpha - \bar{\alpha})$ in $\Lambda_c^+ \rightarrow \Lambda K^+, \bar{\Lambda}_c^- \rightarrow \bar{\Lambda} K^-$

VALUE	EVTS	DOCUMENT ID	TECN	COMMENT
$-0.23 \pm 0.086 \pm 0.071$	11k	LI 23c BELL		$e^+ e^-$ at/near $\mathcal{T}(nS)$, $n=1, \dots, 5$

$(\alpha + \bar{\alpha})/(\alpha - \bar{\alpha})$ in $\Lambda_c^+ \rightarrow \Sigma^0 K^+, \bar{\Lambda}_c^- \rightarrow \bar{\Sigma}^0 K^-$

VALUE	EVTS	DOCUMENT ID	TECN	COMMENT
$0.08 \pm 0.35 \pm 0.14$	2.4k	LI 23c BELL		$e^+ e^-$ at/near $\mathcal{T}(nS)$, $n=1, \dots, 5$

$A_{CP}(\Lambda X)$ in $\Lambda_c \rightarrow \Lambda X, \bar{\Lambda}_c \rightarrow \bar{\Lambda} X$

VALUE (%)	EVTS	DOCUMENT ID	TECN	COMMENT
$2.1^+_{-6.6} \pm 1.6$	700	ABLIKIM 18E BES3		$e^+ e^-$ at 4.6 GeV

$A_{CP}(\Lambda K^+)$ in $\Lambda_c \rightarrow \Lambda K^+, \bar{\Lambda}_c \rightarrow \bar{\Lambda} K^-$

VALUE	EVTS	DOCUMENT ID	TECN	COMMENT
$0.021 \pm 0.026 \pm 0.001$	11k	LI 23c BELL		$e^+ e^-$ at/near $\mathcal{T}(nS)$, $n=1, \dots, 5$

$A_{CP}(\Sigma^0 K^+)$ in $\Lambda_c \rightarrow \Sigma^0 K^+, \bar{\Lambda}_c \rightarrow \bar{\Sigma}^0 K^-$

VALUE	EVTS	DOCUMENT ID	TECN	COMMENT
$0.025 \pm 0.054 \pm 0.004$	2.4k	LI 23c BELL		$e^+ e^-$ at/near $\mathcal{T}(nS)$, $n=1, \dots, 5$

$\Delta A_{CP} = A_{CP}(\Lambda_c^+ \rightarrow p K^+ K^-) - A_{CP}(\Lambda_c^+ \rightarrow p \pi^+ \pi^-)$

VALUE (%)	DOCUMENT ID	TECN	COMMENT
$0.30 \pm 0.91 \pm 0.61$	¹ AAIJ 18R	LHCB	$p p \bar{7}, 8 \text{ TeV}$

¹AAIJ 18R applies phase-space-dependent weights to the $\Lambda_c^+ \rightarrow p \pi^+ \pi^-$ sample to align its kinematics with the $\Lambda_c^+ \rightarrow p K^+ K^-$ sample.

Λ_c^+ REFERENCES

We have omitted some papers that have been superseded by later experiments. The omitted papers may be found in our 1992 edition (Physical Review D45, 1 June, Part II) or in earlier editions.

AAIJ	23AJ	JHEP 2307 228	R. Aaij et al.	(LHCb Collab.)
AAIJ	23Z	PR D108 012023	R. Aaij et al.	(LHCb Collab.)
ABLIKIM	23A	CP C47 023001	M. Ablikim et al.	(BESIII Collab.)
ABLIKIM	23AB	PL B843 137993	M. Ablikim et al.	(BESIII Collab.)
ABLIKIM	23AK	PR D107 052005	M. Ablikim et al.	(BESIII Collab.)
ABLIKIM	23AS	PR D108 L031101	M. Ablikim et al.	(BESIII Collab.)
ABLIKIM	23AT	PR D108 L031105	M. Ablikim et al.	(BESIII Collab.)
ABLIKIM	23BY	JHEP 2309 125	M. Ablikim et al.	(BESIII Collab.)
ABLIKIM	23CB	JHEP 2311 137	M. Ablikim et al.	(BESIII Collab.)
ABLIKIM	23Z	PR D107 052002	M. Ablikim et al.	(BESIII Collab.)
ABUDINEN	23A	PRL 130 071802	F. Abudinén et al.	(BELLE II Collab.)
LI	23	PR D107 032001	Y. Li et al.	(BELLE Collab.)
LI	23A	PR D107 032003	S.X. Li et al.	(BELLE Collab.)
LI	23B	PR D107 032004	L.K. Li et al.	(BELLE Collab.)
LI	23C	SCIB 68 583	L.K. Li et al.	(BELLE Collab.)
ABLIKIM	22AG	PRL 129 131801	M. Ablikim et al.	(BESIII Collab.)
ABLIKIM	22AK	PR D106 052003	M. Ablikim et al.	(BESIII Collab.)
ABLIKIM	22AN	PR D106 072002	M. Ablikim et al.	(BESIII Collab.)
ABLIKIM	22AR	PR D106 072008	M. Ablikim et al.	(BESIII Collab.)
ABLIKIM	22AT	PRL 129 231803	M. Ablikim et al.	(BESIII Collab.)
ABLIKIM	22BA	JHEP 2212 033	M. Ablikim et al.	(BESIII Collab.)
ABLIKIM	22BB	PR D106 112010	M. Ablikim et al.	(BESIII Collab.)
ABLIKIM	22BC	PR D106 L111101	M. Ablikim et al.	(BESIII Collab.)
ABLIKIM	22S	PRL 128 142001	M. Ablikim et al.	(BESIII Collab.)
LI	22B	JHEP 2203 090	S.X. Li et al.	(BELLE Collab.)
ABLIKIM	21H	PL B817 136327	M. Ablikim et al.	(BESIII Collab.)
ABLIKIM	21N	PR D103 L091101	M. Ablikim et al.	(BESIII Collab.)
LEE	21A	PR D103 052005	J.Y. Lee et al.	(BELLE Collab.)
LI	21	PR D103 072004	S.X. Li et al.	(BELLE Collab.)
LI	21E	PR D104 072008	S.X. Li et al.	(BELLE Collab.)
ABLIKIM	20AJ	EPJ C80 935	M. Ablikim et al.	(BESIII Collab.)
AAIJ	19AG	PR D100 032001	R. Aaij et al.	(LHCb Collab.)
ABLIKIM	19AX	PR D100 072004	M. Ablikim et al.	(BESIII Collab.)
ABLIKIM	19X	CP C43 063002	M. Ablikim et al.	(BESIII Collab.)
ABLIKIM	19Y	PR D99 032010	M. Ablikim et al.	(BESIII Collab.)
AAIJ	18N	PR D97 091101	R. Aaij et al.	(LHCb Collab.)
AAIJ	18R	JHEP 1803 182	R. Aaij et al.	(LHCb Collab.)
AAIJ	18V	JHEP 1803 043	R. Aaij et al.	(LHCb Collab.)
ABLIKIM	18AF	PRL 121 251801	M. Ablikim et al.	(BESIII Collab.)
ABLIKIM	18E	PRL 121 062003	M. Ablikim et al.	(BESIII Collab.)
ABLIKIM	18Y	PL B783 200	M. Ablikim et al.	(BESIII Collab.)
BERGER	18	PR D98 112006	M. Berger et al.	(BELLE Collab.)
ABLIKIM	17D	PL B767 42	M. Ablikim et al.	(BESIII Collab.)
ABLIKIM	17X	PRL 118 112001	M. Ablikim et al.	(BESIII Collab.)
ABLIKIM	17Q	PR D95 111102	M. Ablikim et al.	(BESIII Collab.)
ABLIKIM	17Y	PL B772 389	M. Ablikim et al.	(BESIII Collab.)
PAL	17	PR D96 051102	B. Pal et al.	(BELLE Collab.)
ABLIKIM	16	PRL 116 052001	M. Ablikim et al.	(BESIII Collab.)
ABLIKIM	16U	PRL 117 232002	M. Ablikim et al.	(BESIII Collab.)
YANG	16	PRL 117 011801	S.B. Yang et al.	(BELLE Collab.)
ABLIKIM	15Y	PRL 115 221805	M. Ablikim et al.	(BESIII Collab.)
ZUPANEC	14	PRL 113 042002	A. Zupanc et al.	(BELLE Collab.)
LEES	11G	PR D84 072006	J.P. Lees et al.	(BABAR Collab.)
VÁZQUEZ-JA...	08	PL B666 299	E. Vazquez-Jauregui et al.	(SELEX Collab.)
AUBERT	07U	PR D75 052002	B. Aubert et al.	(BABAR Collab.)
LINK	06A	PL B634 145	J.M. Link et al.	(FNAL FOCUS Collab.)
AUBERT,B	05S	PR D72 052006	B. Aubert et al.	(BABAR Collab.)
HINSON	05	PRL 94 191801	J.W. Hinson et al.	(CLEO Collab.)
LINK	05F	PL B624 22	J.M. Link et al.	(FNAL FOCUS Collab.)
CRONIN-HEN...	03	PR D67 012001	D. Cronin-Hennessy et al.	(CLEO Collab.)
KAYIS-TOPAK...	03	PL B555 156	A. Kayis-Topaksu et al.	(CERN CHORUS Collab.)

ABE	02C	PL B524 33	K. Abe et al.	(KEK BELLE Collab.)
LINK	02C	PRL 88 161801	J.M. Link et al.	(FNAL FOCUS Collab.)
LINK	02G	PL B540 25	J.M. Link et al.	(FNAL FOCUS Collab.)
PDG	02	PR D66 010001	K. Hagiwara et al.	(PDG Collab.)
KUSHNIR...	01	PRL 86 5243	A. Kushnirenko et al.	(FNAL SELEX Collab.)
MAHMOOD	01	PRL 86 2232	A.H. Mahmood et al.	(CLEO Collab.)
AITALA	00	PL B471 449	E.M. Ait'ala et al.	(FNAL E791 Collab.)
ALAM	98	PR D57 4467	M.S. Alam et al.	(CLEO Collab.)
ALBRECHT	96E	PRPL 276 223	H. Albrecht et al.	(ARGUS Collab.)
ALEXANDER	96C	PR D53 1013	J.P. Alexander et al.	(CLEO Collab.)
ALBRECHT	95B	PL B342 397	H. Albrecht et al.	(ARGUS Collab.)
AMMAR	95	PRL 74 3534	R. Ammar et al.	(CLEO Collab.)
BISHAI	95	PL B350 256	M. Bishai et al.	(CLEO Collab.)
CRAWFORD	95	PRL 75 624	G. Crawford et al.	(CLEO Collab.)
KODAMA	95	PL B345 85	K. Kodama et al.	(FNAL E653 Collab.)
ALBRECHT	94B	PL B326 320	H. Albrecht et al.	(ARGUS Collab.)
ALEEV	94	PAN 57 1370	A.N. Aleev et al.	(Serpukhov BIS-2 Collab.)
AVERY	94	PL B325 257	P. Avery et al.	(CLEO Collab.)
BERGFELD	94	PL B323 219	T. Bergfeld et al.	(CLEO Collab.)
FRABETTI	94E	PL B328 193	P.L. Frabetti et al.	(FNAL E687 Collab.)
AVERY	93	PRL 71 2391	P. Avery et al.	(CLEO Collab.)
BOZEK	93	PL B312 247	A. Bozek et al.	(CERN NA32 Collab.)
FRABETTI	93D	PRL 70 1755	P.L. Frabetti et al.	(FNAL E687 Collab.)
FRABETTI	93H	PL B314 477	P.L. Frabetti et al.	(FNAL E687 Collab.)
KUBOTA	93	PRL 71 3255	Y. Kubota et al.	(CLEO Collab.)
ALBRECHT	92	PL B274 239	H. Albrecht et al.	(ARGUS Collab.)
BARLAG	92	PL B283 465	S. Barlag et al.	(ACCMOR Collab.)
CRAWFORD	92	PR D45 752	G. Crawford et al.	(CLEO Collab.)
JEZABEK	92	PL B286 175	M. Jezabek, K. Rybicki, R. Rylko	(CRAC Collab.)
ALBRECHT	91G	PL B269 234	H. Albrecht et al.	(ARGUS Collab.)
AVERY	91	PR D43 3599	P. Avery et al.	(CLEO Collab.)
ALVAREZ	90	ZPHY C47 539	M.P. Alvarez et al.	(CERN NA14/2 Collab.)
ALVAREZ	90B	PL B246 256	M.P. Alvarez et al.	(CERN NA14/2 Collab.)
ANJOS	90	PR D41 801	J.C. Anjos et al.	(FNAL E691 Collab.)
AVERY	90B	PRL 65 2842	P. Avery et al.	(CLEO Collab.)
BARLAG	90D	ZPHY C48 29	S. Barlag et al.	(ACCMOR Collab.)
FRABETTI	90	PL B251 639	P.L. Frabetti et al.	(FNAL E687 Collab.)
BARLAG	89B	PL B218 374	S. Barlag et al.	(ACCMOR Collab.)
AGUILAR...	88B	ZPHY C40 321	M. Aguilar-Benitez et al.	(LEBC-EHS Collab.)
Also	Also	PL B189 254	M. Aguilar-Benitez et al.	(LEBC-EHS Collab.)
Also	Also	PL B199 462	M. Aguilar-Benitez et al.	(LEBC-EHS Collab.)
Also	Also	SJNP 48 833	M. Begalli et al.	(LEBC-EHS Collab.)
ALBRECHT	88C	PL B207 109	H. Albrecht et al.	(ARGUS Collab.)
ANJOS	88B	PRL 60 1379	J.C. Anjos et al.	(FNAL E691 Collab.)
AMENDOLIA	87	ZPHY C36 513	S.R. Amendolia et al.	(CERN NA1 Collab.)
JONES	87	ZPHY C36 593	G.T. Jones et al.	(CERN WA21 Collab.)
BOSETTI	82	PL 109B 234	P.C. Bosetti et al.	(AACH3, BONN, CERN+)
BASILE	81B	NC 62A 14	M. Basile et al.	(CERN, BONA, PGIA, FRAS)
CALICCHIO	80	PL 93B 521	M. Calicchio et al.	(BARI, BIRM, BRUX+)

OTHER RELATED PAPERS

MIGLIOZZI	99	PL B462 217	P. Migliozi et al.
DUNIETZ	98	PR D58 094010	I. Dunietz

$\Lambda_c(2595)^+$

$$I(J^P) = 0(\frac{1}{2}^-) \text{ Status: } ***$$

The $\Lambda_c^+ \pi^+ \pi^-$ mode is largely, and perhaps entirely, $\Sigma_c \pi$, which is just at threshold; since the Σ_c has $J^P = 1/2^+$, the J^P here is almost certainly $1/2^-$. This result is in accord with the theoretical expectation that this is the charm counterpart of the strange $\Lambda(1405)$.

$\Lambda_c(2595)^+$ MASS

The mass is obtained from the $\Lambda_c(2595)^+ - \Lambda_c^+$ mass-difference measurements below.

VALUE (MeV)	DOCUMENT ID
2592.25 ± 0.28 OUR FIT	

$\Lambda_c(2595)^+ - \Lambda_c^+$ MASS DIFFERENCE

VALUE (MeV)	EVTS	DOCUMENT ID	TECN	COMMENT
305.79 ± 0.24 OUR FIT				
$305.79 \pm 0.14 \pm 0.20$	3.5k	AALTONEN	11H CDF	$p\bar{p}$ at 1.96 TeV
• • • We do not use the following data for averages, fits, limits, etc. • • •				
305.6 \pm 0.3		¹ BLECHMAN	03	Threshold shift
309.7 \pm 0.9 \pm 0.4	19	ALBRECHT	97 ARG	$e^+ e^- \approx 10$ GeV
309.2 \pm 0.7 \pm 0.3	14 \pm 4.5	FRABETTI	96 E687	$\gamma Be, \bar{E}_\gamma \approx 220$ GeV
307.5 \pm 0.4 \pm 1.0	112 \pm 17	EDWARDS	95 CLE2	$e^+ e^- \approx 10.5$ GeV

¹BLECHMAN 03 finds that a more sophisticated treatment than a simple Breit-Wigner for the proximity of the threshold of the dominant decay, $\Sigma_c(2455)\pi$, lowers the $\Lambda_c(2595)^+ - \Lambda_c^+$ mass difference by 2 or 3 MeV. The analysis of AALTONEN 11H bears this out.

$\Lambda_c(2595)^+$ WIDTH

VALUE (MeV)	EVTS	DOCUMENT ID	TECN	COMMENT
$2.59 \pm 0.30 \pm 0.47$	3.5k	² AALTONEN	11H CDF	$p\bar{p}$ at 1.96 TeV
• • • We do not use the following data for averages, fits, limits, etc. • • •				
2.9 $+2.9$ -2.1 -1.4	19	ALBRECHT	97 ARG	$e^+ e^- \approx 10$ GeV
3.9 $+1.4$ -1.2 $+2.0$ -1.0	112 \pm 17	EDWARDS	95 CLE2	$e^+ e^- \approx 10.5$ GeV

Baryon Particle Listings

 $\Lambda_c(2595)^+$, $\Lambda_c(2625)^+$

²AALTONEN 11H treats the three charged modes $\Lambda_c(2595)^+ \rightarrow \Sigma_c(2455)^{++}\pi^-$, $\Sigma_c(2455)^+\pi^0$, $\Sigma_c(2455)^0\pi^+$ separately in terms of a common coupling constant h_2 and obtains $h_2^2 = 0.36 \pm 0.08$. From this the width is determined.

 $\Lambda_c(2595)^+$ DECAY MODES

$\Lambda_c^+\pi\pi$ and its submode $\Sigma_c(2455)\pi$ — the latter just barely — are the only strong decays allowed to an excited Λ_c^+ having this mass; and the submode seems to dominate.

Mode	Fraction (Γ_i/Γ)
Γ_1 $\Lambda_c^+\pi^+\pi^-$	[a] —
Γ_2 $\Sigma_c(2455)^{++}\pi^-$	$24 \pm 7\%$
Γ_3 $\Sigma_c(2455)^0\pi^+$	$24 \pm 7\%$
Γ_4 $\Lambda_c^+\pi^+\pi^-$ 3-body	$18 \pm 10\%$
Γ_5 $\Lambda_c^+\pi^0$	[b] not seen
Γ_6 $\Lambda_c^+\gamma$	not seen

[a] See AALTONEN 11H, Fig. 8, for the calculated ratio of $\Lambda_c^+\pi^0\pi^0$ and $\Lambda_c^+\pi^+\pi^-$ partial widths as a function of the $\Lambda_c(2595)^+ - \Lambda_c^+$ mass difference. At our value of the mass difference, the ratio is about 4.

[b] A test that the isospin is indeed 0, so that the particle is indeed a Λ_c^+ .

 $\Lambda_c(2595)^+$ BRANCHING RATIOS

$\Gamma(\Sigma_c(2455)^{++}\pi^-)/\Gamma(\Lambda_c^+\pi^+\pi^-)$	Γ_2/Γ_1		
VALUE	DOCUMENT ID	TECN	COMMENT
0.36 ± 0.10 OUR AVERAGE			
$0.37 \pm 0.12 \pm 0.13$	ALBRECHT	97	ARG $e^+e^- \approx 10$ GeV
$0.36 \pm 0.09 \pm 0.09$	EDWARDS	95	CLE2 $e^+e^- \approx 10.5$ GeV

$\Gamma(\Sigma_c(2455)^0\pi^+)/\Gamma(\Lambda_c^+\pi^+\pi^-)$	Γ_3/Γ_1		
VALUE	DOCUMENT ID	TECN	COMMENT
0.37 ± 0.10 OUR AVERAGE			
$0.29 \pm 0.10 \pm 0.11$	ALBRECHT	97	ARG $e^+e^- \approx 10$ GeV
$0.42 \pm 0.09 \pm 0.09$	EDWARDS	95	CLE2 $e^+e^- \approx 10.5$ GeV

$[\Gamma(\Sigma_c(2455)^{++}\pi^-) + \Gamma(\Sigma_c(2455)^0\pi^+)]/\Gamma(\Lambda_c^+\pi^+\pi^-)$	$(\Gamma_2 + \Gamma_3)/\Gamma_1$			
VALUE	CL%	DOCUMENT ID	TECN	COMMENT
••• We do not use the following data for averages, fits, limits, etc. ••••				
$0.66^{+0.13}_{-0.16} \pm 0.07$		ALBRECHT	97	ARG $e^+e^- \approx 10$ GeV
> 0.51	90	³ FRABETTI	96	E687 γBe , $\overline{E}_\gamma \approx 220$ GeV

³The results of FRABETTI 96 are consistent with this ratio being 100%.

$\Gamma(\Lambda_c^+\pi^0)/\Gamma(\Lambda_c^+\pi^+\pi^-)$	Γ_5/Γ_1			
VALUE	CL%	DOCUMENT ID	TECN	COMMENT
< 3.53	90	EDWARDS	95	CLE2 $e^+e^- \approx 10.5$ GeV

$\Lambda_c^+\pi^0$ decay is forbidden by isospin conservation if this state is in fact a Λ_c .

$\Gamma(\Lambda_c^+\gamma)/\Gamma(\Lambda_c^+\pi^+\pi^-)$	Γ_6/Γ_1			
VALUE	CL%	DOCUMENT ID	TECN	COMMENT
< 0.98	90	EDWARDS	95	CLE2 $e^+e^- \approx 10.5$ GeV

 $\Lambda_c(2595)^+$ REFERENCES

AALTONEN	11H	PR D84 012003	T. Aaltonen <i>et al.</i>	(CDF Collab.)
BLECHMAN	03	PR D67 074033	A.E. Blechman <i>et al.</i>	(JHU, FLOR)
ALBRECHT	97	PL B402 207	H. Albrecht <i>et al.</i>	(ARGUS Collab.)
FRABETTI	96	PL B365 461	P.L. Frabetti <i>et al.</i>	(FNAL E687 Collab.)
EDWARDS	95	PRL 74 3331	K.W. Edwards <i>et al.</i>	(CLEO Collab.)

 $\Lambda_c(2625)^+$

$$I(J^P) = 0(\frac{3}{2}^-) \text{ Status: } ***$$

The spin-parity has not been measured but is expected to be $3/2^-$: this is presumably the charm counterpart of the strange $\Lambda(1520)$.

 $\Lambda_c(2625)^+$ MASS

The mass is obtained from the $\Lambda_c(2625)^+ - \Lambda_c^+$ mass-difference measurements below.

VALUE (MeV)	EVTS	DOCUMENT ID	TECN	COMMENT
2628.00 ± 0.15 OUR FIT				
••• We do not use the following data for averages, fits, limits, etc. ••••				
$2626.6 \pm 0.5 \pm 1.5$	42 ± 9	ALBRECHT	93F	ARG See ALBRECHT 97

 $\Lambda_c(2625)^+ - \Lambda_c^+$ MASS DIFFERENCE

VALUE (MeV)	EVTS	DOCUMENT ID	TECN	COMMENT
341.54 ± 0.05 OUR FIT				
341.54 ± 0.05 OUR AVERAGE				
$341.518 \pm 0.006 \pm 0.049$	30.3k	WANG	23	BELL e^+e^- at/near $\Upsilon(4S)$
$341.65 \pm 0.04 \pm 0.12$	6.2k	AALTONEN	11H	CDF $p\overline{p}$ at 1.96 TeV
$342.1 \pm 0.5 \pm 0.5$	51	ALBRECHT	97	ARG $e^+e^- \approx 10$ GeV
$342.2 \pm 0.2 \pm 0.5$	245	EDWARDS	95	CLE2 $e^+e^- \approx 10.5$ GeV
$340.4 \pm 0.6 \pm 0.3$	40	FRABETTI	94	E687 γBe , $\overline{E}_\gamma \approx 220$ GeV

 $\Lambda_c(2625)^+$ WIDTH

VALUE (MeV)	CL%	EVTS	DOCUMENT ID	TECN	COMMENT
< 0.52	90	30.3k	WANG	23	BELL e^+e^- at/near $\Upsilon(4S)$
••• We do not use the following data for averages, fits, limits, etc. ••••					
< 0.97	90	6.2k	AALTONEN	11H	CDF $p\overline{p}$ at 1.96 TeV
< 1.9	90	245 ± 19	EDWARDS	95	CLE2 $e^+e^- \approx 10.5$ GeV
< 3.2	90		ALBRECHT	93F	ARG $e^+e^- \approx \Upsilon(4S)$

 $\Lambda_c(2625)^+$ DECAY MODES

$\Lambda_c^+\pi\pi$ and its submode $\Sigma(2455)\pi$ are the only strong decays allowed to an excited Λ_c^+ having this mass.

Mode	Fraction (Γ_i/Γ)	Confidence level
Γ_1 $\Lambda_c^+\pi^+\pi^-$	[a] 66.67	%
Γ_2 $\Sigma_c(2455)^{++}\pi^-$	(3.42 ± 0.27)	%
Γ_3 $\Sigma_c(2455)^0\pi^+$	(3.46 ± 0.31)	%
Γ_4 $\Lambda_c^+\pi^+\pi^-$ 3-body	large	
Γ_5 $\Lambda_c^+\pi^0$	[b] < 60	% 90%
Γ_6 $\Lambda_c^+\gamma$	< 35	% 90%

[a] Assuming isospin conservation, so that the other third is $\Lambda_c^+\pi^0\pi^0$.

[b] A test that the isospin is indeed 0, so that the particle is indeed a Λ_c^+ .

 $\Lambda_c(2625)^+$ BRANCHING RATIOS

$\Gamma(\Sigma_c(2455)^{++}\pi^-)/\Gamma(\Lambda_c^+\pi^+\pi^-)$	Γ_2/Γ_1				
VALUE (units 10^{-2})	CL%	EVTS	DOCUMENT ID	TECN	COMMENT
$5.13 \pm 0.26 \pm 0.32$		467	¹ WANG	23	BELL e^+e^- at/near $\Upsilon(4S)$
••• We do not use the following data for averages, fits, limits, etc. ••••					
< 8	90		EDWARDS	95	CLE2 $e^+e^- \approx 10.5$ GeV

¹From a Dalitz plot fit, recovered simultaneously with $\Lambda_c(2625)^+ \rightarrow \Sigma_c(2455)^0\pi^+$.

$\Gamma(\Sigma_c(2455)^0\pi^+)/\Gamma(\Lambda_c^+\pi^+\pi^-)$	Γ_3/Γ_1				
VALUE (units 10^{-2})	CL%	EVTS	DOCUMENT ID	TECN	COMMENT
$5.19 \pm 0.23 \pm 0.40$		391	² WANG	23	BELL e^+e^- at/near $\Upsilon(4S)$
••• We do not use the following data for averages, fits, limits, etc. ••••					
< 7	90		EDWARDS	95	CLE2 $e^+e^- \approx 10.5$ GeV

²From a Dalitz plot fit, recovered simultaneously with $\Lambda_c(2625)^+ \rightarrow \Sigma_c(2455)^{++}\pi^-$.

$[\Gamma(\Sigma_c(2455)^{++}\pi^-) + \Gamma(\Sigma_c(2455)^0\pi^+)]/\Gamma(\Lambda_c^+\pi^+\pi^-)$	$(\Gamma_2 + \Gamma_3)/\Gamma_1$				
VALUE	CL%	EVTS	DOCUMENT ID	TECN	COMMENT
••• We do not use the following data for averages, fits, limits, etc. ••••					
< 0.36	90		FRABETTI	94	E687 γBe , $\overline{E}_\gamma \approx 220$ GeV
0.46 ± 0.14		21	ALBRECHT	93F	ARG $e^+e^- \approx \Upsilon(4S)$

$\Gamma(\Lambda_c^+\pi^+\pi^- \text{ 3-body})/\Gamma(\Lambda_c^+\pi^+\pi^-)$	Γ_4/Γ_1			
VALUE	EVTS	DOCUMENT ID	TECN	COMMENT
••• We do not use the following data for averages, fits, limits, etc. ••••				
0.54 ± 0.14	16	ALBRECHT	93F	ARG $e^+e^- \approx \Upsilon(4S)$

$\Gamma(\Lambda_c^+\pi^0)/\Gamma(\Lambda_c^+\pi^+\pi^-)$	Γ_5/Γ_1			
VALUE	CL%	DOCUMENT ID	TECN	COMMENT
< 0.91	90	EDWARDS	95	CLE2 $e^+e^- \approx 10.5$ GeV

$\Lambda_c^+\pi^0$ decay is forbidden by isospin conservation if this state is in fact a Λ_c .

$\Gamma(\Lambda_c^+\gamma)/\Gamma(\Lambda_c^+\pi^+\pi^-)$	Γ_6/Γ_1			
VALUE	CL%	DOCUMENT ID	TECN	COMMENT
< 0.52	90	EDWARDS	95	CLE2 $e^+e^- \approx 10.5$ GeV

 $\Lambda_c(2625)^+$ REFERENCES

WANG	23	PR D107 032008	D. Wang <i>et al.</i>	(BELLE Collab.)
AALTONEN	11H	PR D84 012003	T. Aaltonen <i>et al.</i>	(CDF Collab.)
ALBRECHT	97	PL B402 207	H. Albrecht <i>et al.</i>	(ARGUS Collab.)
EDWARDS	95	PRL 74 3331	K.W. Edwards <i>et al.</i>	(CLEO Collab.)
FRABETTI	94	PL 72 961	P.L. Frabetti <i>et al.</i>	(FNAL E687 Collab.)
ALBRECHT	93F	PL B317 227	H. Albrecht <i>et al.</i>	(ARGUS Collab.)

See key on page 1171

Baryon Particle Listings

$\Lambda_c(2765)^+$, $\Lambda_c(2860)^+$, $\Lambda_c(2880)^+$

$\Lambda_c(2765)^+$ or $\Sigma_c(2765)$ $I(J^P) = ?(??)$ Status: *

OMITTED FROM SUMMARY TABLE

A broad, statistically significant peak (997^{+141}_{-129} events) seen in $\Lambda_c^+ \pi^+ \pi^-$. However, nothing at all is known about its quantum numbers, including whether it is a Λ_c^+ or a Σ_c , or whether the width might be due to overlapping states.

 $\Lambda_c(2765)^+$ MASS

The mass is obtained from the $\Lambda_c(2765)^+ - \Lambda_c^+$ mass-difference measurement below.

VALUE (MeV)	DOCUMENT ID
2766.6 ± 2.4 OUR FIT	

 $\Lambda_c(2765)^+ - \Lambda_c^+$ MASS DIFFERENCE

VALUE (MeV)	EVTS	DOCUMENT ID	TECN	COMMENT
480.1 ± 2.4 OUR FIT				
480.1 ± 2.4	997^{+141}_{-129}	ARTUSO	01	CLE2 $e^+ e^- \approx \Upsilon(4S)$

 $\Lambda_c(2765)^+$ WIDTH

VALUE (MeV)	DOCUMENT ID	TECN	COMMENT
50	ARTUSO	01	CLE2 $e^+ e^- \approx \Upsilon(4S)$

 $\Lambda_c(2765)^+$ DECAY MODES

Mode	Fraction (Γ_i/Γ)
Γ_1 $\Lambda_c^+ \pi^+ \pi^-$	seen

 $\Lambda_c(2765)^+$ REFERENCES

ARTUSO	01	PRL 86 4479	M. Artuso et al.	(CLEO Collab.)
--------	----	-------------	------------------	----------------

$\Lambda_c(2860)^+$ $I(J^P) = 0(\frac{3}{2}^+)$ Status: ***

 $\Lambda_c(2860)^+$ MASS

VALUE (MeV)	DOCUMENT ID	TECN	COMMENT
2856.1 ± 2.0 ± 1.7 ± 0.5 ± 1.1 ± 5.6	¹ AAIJ	17s	LHCB in $\Lambda_b^0 \rightarrow D^0 p \pi^-$

¹ The third AAIJ 17s uncertainty comes from modeling the resonant shape of the nearby $\Lambda_c(2880)^+$ and the background (non-resonant) amplitudes.

 $\Lambda_c(2860)^+$ WIDTH

VALUE (MeV)	DOCUMENT ID	TECN	COMMENT
67.6 ± 10.1 ± 1.4 ± 5.9 ± 8.1 ± 20.0	¹ AAIJ	17s	LHCB in $\Lambda_b^0 \rightarrow D^0 p \pi^-$

¹ The third AAIJ 17s uncertainty comes from modeling the resonant shape of the nearby $\Lambda_c(2880)^+$ and the background (non-resonant) amplitudes.

 $\Lambda_c(2860)^+$ DECAY MODES

Mode	Fraction (Γ_i/Γ)
Γ_1 $D^0 p$	seen

 $\Lambda_c(2860)^+$ BRANCHING RATIOS

$\Gamma(D^0 p)/\Gamma_{\text{total}}$	Γ_1/Γ
seen	

VALUE	DOCUMENT ID	TECN	COMMENT
seen	AAIJ	17s	LHCB in $\Lambda_b^0 \rightarrow D^0 p \pi^-$

 $\Lambda_c(2860)^+$ REFERENCES

AAIJ	17s	JHEP 1705 030	R. Aaij et al.	(LHCb Collab.) JP
------	-----	---------------	----------------	-------------------

$\Lambda_c(2880)^+$ $I(J^P) = 0(\frac{5}{2}^+)$ Status: ***

A narrow peak seen in $\Lambda_c^+ \pi^+ \pi^-$ and in $p D^0$. It is not seen in $p D^+$, and therefore it is a Λ_c^+ and not a Σ_c .

 $\Lambda_c(2880)^+$ MASS

VALUE (MeV)	EVTS	DOCUMENT ID	TECN	COMMENT
2881.63 ± 0.24 OUR FIT				
2881.62 ± 0.24 OUR AVERAGE				
$2881.75 \pm 0.29 \pm 0.07^{+0.14}_{-0.20}$	¹ AAIJ	17s	LHCB	in $\Lambda_b^0 \rightarrow D^0 p \pi^-$
$2881.9 \pm 0.1 \pm 0.5$	2.8k	AUBERT	07	BABR in $p D^0$
$2881.2 \pm 0.2 \pm 0.4$	690	MIZUK	07	BELL in $\Sigma_c(2455)^{0,++} \pi^\pm$

¹ The third AAIJ 17s uncertainty comes from modeling the resonant shape of the $\Lambda_c(2880)^+$ and the background (non-resonant) amplitudes.

 $\Lambda_c(2880)^+ - \Lambda_c^+$ MASS DIFFERENCE

VALUE (MeV)	EVTS	DOCUMENT ID	TECN	COMMENT
595.17 ± 0.28 OUR FIT				
596 ± 1 ± 2	350	ARTUSO	01	CLE2 in $\Lambda_c^+ \pi^+ \pi^-$

 $\Lambda_c(2880)^+$ WIDTH

VALUE (MeV)	CL%	EVTS	DOCUMENT ID	TECN	COMMENT
5.6 ± 0.8 ± 0.6 OUR AVERAGE					
$5.43^{+0.77+0.81}_{-0.71-0.29}$		² AAIJ	17s	LHCB	in $\Lambda_b^0 \rightarrow D^0 p \pi^-$
$5.8 \pm 1.5 \pm 1.1$	2.8k	AUBERT	07	BABR in $p D^0$	
$5.8 \pm 0.7 \pm 1.1$	690	MIZUK	07	BELL in $\Sigma_c(2455)^{0,++} \pi^\pm$	
••• We do not use the following data for averages, fits, limits, etc. •••					
<8	90	ARTUSO	01	CLEO	in $\Lambda_c^+ \pi^+ \pi^-$

² AAIJ 17s reports $5.43^{+0.77}_{-0.71} \pm 0.29^{+0.75}_{-0.00}$ MeV value where the third uncertainty comes from modeling the resonant shape of the $\Lambda_c(2880)^+$ and the background (non-resonant) amplitudes. We have combined in quadrature the systematic uncertainties.

 $\Lambda_c(2880)^+$ DECAY MODES

Mode	Fraction (Γ_i/Γ)
Γ_1 $\Lambda_c^+ \pi^+ \pi^-$	seen
Γ_2 $\Sigma_c(2455)^{0,++} \pi^\pm$	seen
Γ_3 $\Sigma_c(2520)^{0,++} \pi^\pm$	seen
Γ_4 $p D^0$	seen

 $\Lambda_c(2880)^+$ BRANCHING RATIOS

$\Gamma(\Sigma_c(2455)^{0,++} \pi^\pm)/\Gamma(\Lambda_c^+ \pi^+ \pi^-)$	Γ_2/Γ_1			
0.392 ± 0.031 OUR AVERAGE	Error includes scale factor of 1.3.			
$0.404 \pm 0.021 \pm 0.014$	MIZUK	07	BELL	in $\Sigma_c(2455)^{0,++} \pi^\pm$
$0.31 \pm 0.06 \pm 0.03$	96	ARTUSO	01	CLE2 $e^+ e^- \approx \Upsilon(4S)$

$\Gamma(\Sigma_c(2520)^{0,++} \pi^\pm)/\Gamma(\Lambda_c^+ \pi^+ \pi^-)$	Γ_3/Γ_1			
0.091 ± 0.025 ± 0.010				
<0.11	90			
	ARTUSO	01	CLE2	$e^+ e^- \approx \Upsilon(4S)$

••• We do not use the following data for averages, fits, limits, etc. •••

$\Gamma(\Sigma_c(2520)^{0,++} \pi^\pm)/\Gamma(\Sigma_c(2455)^{0,++} \pi^\pm)$	Γ_3/Γ_2			
0.225 ± 0.062 ± 0.025				
	³ MIZUK	07	BELL	in $\Sigma_c(2455)^{0,++} \pi^\pm$
	³ This MIZUK 07 ratio is redundant with MIZUK 07 ratios given above.			

 $\Lambda_c(2880)^+$ REFERENCES

AAIJ	17s	JHEP 1705 030	R. Aaij et al.	(LHCb Collab.) JP
AUBERT	07	PRL 98 012001	B. Aubert et al.	(BABAR Collab.)
MIZUK	07	PRL 98 262001	R. Mizuk et al.	(BELLE Collab.)
ARTUSO	01	PRL 86 4479	M. Artuso et al.	(CLEO Collab.)

Baryon Particle Listings

 $\Lambda_c(2910)^+$, $\Lambda_c(2940)^+$, $\Sigma_c(2455)$ $\Lambda_c(2910)^+$

$I(J^P) = ?(??) \text{ Status: } *$

OMITTED FROM SUMMARY TABLE

A candidate heavy quark symmetry doublet partner to the $\Lambda_c(2940)$. Further study is needed to confirm whether this state is an excited Λ_c or Σ_c .

 $\Lambda_c(2910)^+$ MASS

VALUE (MeV)	EVTS	DOCUMENT ID	TECN	COMMENT
2913.8 ± 5.6 ± 3.8	150	¹ LI	23E	BELL $\bar{B}^0 \rightarrow \Sigma_c(2455)^{0,++} \pi^\pm \bar{p}$

¹ LI 23E observes evidence for the $\Lambda_c(2910)^+$ at 4.2 σ significance.

 $\Lambda_c(2910)^+$ WIDTH

VALUE (MeV)	EVTS	DOCUMENT ID	TECN	COMMENT
51.8 ± 20.0 ± 18.8	150	¹ LI	23E	BELL $\bar{B}^0 \rightarrow \Sigma_c(2455)^{0,++} \pi^\pm \bar{p}$

¹ LI 23E observes evidence for the $\Lambda_c(2910)^+$ at 4.2 σ significance.

 $\Lambda_c(2910)^+$ DECAY MODES

Mode	Fraction (Γ_i/Γ)
Γ_1 $\Sigma_c(2455)^0 \pi^+$	seen
Γ_2 $\Sigma_c(2455)^{++} \pi^-$	seen

 $\Lambda_c(2910)^+$ BRANCHING RATIOS

$\Gamma(\Sigma_c(2455)^0 \pi^+)/\Gamma_{\text{total}}$	Γ_1/Γ
seen	seen

$\Gamma(\Sigma_c(2455)^{++} \pi^-)/\Gamma_{\text{total}}$	Γ_2/Γ
seen	seen

 $\Lambda_c(2910)^+$ REFERENCES

LI	23E	PRL 130 031901	Y.B. Li et al.	(BELLE Collab.)
----	-----	----------------	----------------	-----------------

 $\Lambda_c(2940)^+$

$I(J^P) = 0(\frac{3}{2}^-) \text{ Status: } ***$

A narrow peak seen in pD^0 and in $\Lambda_c^+ \pi^+ \pi^-$. It is not seen in pD^+ , and therefore it is a Λ_c^+ and not a Σ_c . $J^P = 3/2^-$ is favored, but not certain.

 $\Lambda_c(2940)^+$ MASS

VALUE (MeV)	EVTS	DOCUMENT ID	TECN	COMMENT
2939.6 ± 1.3 OUR AVERAGE				
2944.8 ± 3.5 ± 0.4 ± 0.1 -2.5 -4.6		¹ AAIJ	17S	LHCB in $\Lambda_b^0 \rightarrow D^0 p \pi^-$
2939.8 ± 1.3 ± 1.0	2.2k	AUBERT	07	BABR in pD^0
2938.0 ± 1.3 ± 2.0 -4.0	220	MIZUK	07	BELL in $\Sigma_c(2455)^{0,++} \pi^\pm$

¹ The third AAIJ 17S uncertainty comes from modeling the resonant shape of the nearby $\Lambda_c(2880)^+$ and the background (non-resonant) amplitudes.

 $\Lambda_c(2940)^+$ WIDTH

VALUE (MeV)	EVTS	DOCUMENT ID	TECN	COMMENT
20 ± 6 OUR AVERAGE				
27.7 ± 8.2 ± 0.9 ± 5.2 -6.0 -10.4		² AAIJ	17S	LHCB in $\Lambda_b^0 \rightarrow D^0 p \pi^-$
17.5 ± 5.2 ± 5.9	2.2k	AUBERT	07	BABR in pD^0
13 ± 8 ± 27 -5 -7	220	MIZUK	07	BELL in $\Sigma_c(2455)^{0,++} \pi^\pm$

² The third AAIJ 17S uncertainty comes from modeling the resonant shape of the nearby $\Lambda_c(2880)^+$ and the background (non-resonant) amplitudes.

 $\Lambda_c(2940)^+$ DECAY MODES

Mode	Fraction (Γ_i/Γ)
Γ_1 pD^0	seen
Γ_2 $\Sigma_c(2455)^{0,++} \pi^\pm$	seen

 $\Lambda_c(2940)^+$ REFERENCES

AAIJ	17S	JHEP 1705 030	R. Aaij et al.	(LHCb Collab.) JP
AUBERT	07	PRL 98 012001	B. Aubert et al.	(BABAR Collab.)
MIZUK	07	PRL 98 262001	R. Mizuk et al.	(BELLE Collab.)

 $\Sigma_c(2455)$

$I(J^P) = 1(\frac{1}{2}^+) \text{ Status: } ***$

The angular distribution of $B^- \rightarrow \Sigma_c(2455)^0 \bar{p}$ favors $J = 1/2$ (as the quark model predicts). $J = 3/2$ is excluded by more than four standard deviations; see AUBERT 08BN.

 $\Sigma_c(2455)$ MASSES

The masses are obtained from the mass-difference measurements that follow.

 $\Sigma_c(2455)^{++}$ MASS

VALUE (MeV)	DOCUMENT ID
2453.97 ± 0.14 OUR FIT	

 $\Sigma_c(2455)^+$ MASS

VALUE (MeV)	DOCUMENT ID
2452.65 ± 0.22 OUR FIT	

 $\Sigma_c(2455)^0$ MASS

VALUE (MeV)	DOCUMENT ID
2453.75 ± 0.14 OUR FIT	

 $\Sigma_c(2455) - \Lambda_c^+$ MASS DIFFERENCES $m_{\Sigma_c(2455)^{++}} - m_{\Lambda_c^+}$

VALUE (MeV)	EVTS	DOCUMENT ID	TECN	COMMENT
167.510 ± 0.017 OUR FIT				
167.510 ± 0.022 OUR AVERAGE				
167.51 ± 0.01 ± 0.02	36k	LEE	14	BELL e^+e^- at $\Upsilon(4S)$
167.44 ± 0.04 ± 0.12	13.8k	AALTONEN	11H	CDF $p\bar{p}$ at 1.96 TeV
167.4 ± 0.1 ± 0.2	2k	ARTUSO	02	CLE2 $e^+e^- \approx \Upsilon(4S)$
167.35 ± 0.19 ± 0.12	461	LINK	00C	FOCS $\gamma A, \bar{E}_\gamma$ 180 GeV
167.76 ± 0.29 ± 0.15	122	AITALA	96B	E791 $\pi^- N, 500$ GeV
167.6 ± 0.6 ± 0.6	56	FRABETTI	96	E687 $\gamma\text{Be}, \bar{E}_\gamma \approx 220$ GeV
168.2 ± 0.3 ± 0.2	126	CRAWFORD	93	CLE2 $e^+e^- \approx \Upsilon(4S)$
167.8 ± 0.4 ± 0.3	54	BOWCOCK	89	CLEO $e^+e^- 10$ GeV
168.2 ± 0.5 ± 1.6	92	ALBRECHT	88D	ARG $e^+e^- 10$ GeV
167.4 ± 0.5 ± 2.0	46	DIESBURG	87	SPEC $nA \sim 600$ GeV
• • • We do not use the following data for averages, fits, limits, etc. • • •				
167 ± 1	2	JONES	87	HBC νp in BEBC
166 ± 1	1	BOSETTI	82	HBC See JONES 87
168 ± 3	6	BALTAY	79	HLBC ν Ne-H in 15-ft
166 ± 15	1	CAZZOLI	75	HBC νp in BNL 7-ft

 $m_{\Sigma_c(2455)^+} - m_{\Lambda_c^+}$

VALUE (MeV)	EVTS	DOCUMENT ID	TECN	COMMENT
166.19 ± 0.16 OUR FIT				
166.19 ± 0.15 OUR AVERAGE				
166.17 ± 0.05 ± 0.16 -0.07		YELTON	21	BELL e^+e^- at $\Upsilon(nS)$
166.4 ± 0.2 ± 0.3	661	AMMAR	01	CLE2 $e^+e^- \approx \Upsilon(4S)$
• • • We do not use the following data for averages, fits, limits, etc. • • •				
168.5 ± 0.4 ± 0.2	111	CRAWFORD	93	CLE2 See AMMAR 01
168 ± 3	1	CALICCHIO	80	HBC νp in BEBC-TST

 $m_{\Sigma_c(2455)^0} - m_{\Lambda_c^+}$

VALUE (MeV)	EVTS	DOCUMENT ID	TECN	COMMENT
167.290 ± 0.017 OUR FIT				
167.290 ± 0.022 OUR AVERAGE				
167.29 ± 0.01 ± 0.02	32k	LEE	14	BELL e^+e^- at $\Upsilon(4S)$
167.28 ± 0.03 ± 0.12	15.9k	AALTONEN	11H	CDF $p\bar{p}$ at 1.96 TeV
167.2 ± 0.1 ± 0.2	2k	ARTUSO	02	CLE2 $e^+e^- \approx \Upsilon(4S)$
167.38 ± 0.21 ± 0.13	362	LINK	00C	FOCS $\gamma A, \bar{E}_\gamma$ 180 GeV
167.38 ± 0.29 ± 0.15	143	AITALA	96B	E791 $\pi^- N, 500$ GeV
167.8 ± 0.6 ± 0.2		ALEEV	96	SPEC n nucleus, 50 GeV/c
166.6 ± 0.5 ± 0.6	69	FRABETTI	96	E687 $\gamma\text{Be}, \bar{E}_\gamma \approx 220$ GeV
167.1 ± 0.3 ± 0.2	124	CRAWFORD	93	CLE2 $e^+e^- \approx \Upsilon(4S)$
168.4 ± 1.0 ± 0.3	14	ANJOS	89D	E691 $\gamma\text{Be} 90\text{--}260$ GeV
• • • We do not use the following data for averages, fits, limits, etc. • • •				
167.9 ± 0.5 ± 0.3	48	¹ BOWCOCK	89	CLEO $e^+e^- 10$ GeV
167.0 ± 0.5 ± 1.6	70	¹ ALBRECHT	88D	ARG $e^+e^- 10$ GeV

See key on page 1171

Baryon Particle Listings

$\Sigma_c(2455), \Sigma_c(2520)$

178.2 ± 0.4 ± 2.0	85	² DIESBURG	87	SPEC	$nA \sim 600$ GeV
163 ± 2	1	AMMAR	86	EMUL	νA

¹ This result enters the fit through $m_{\Sigma_c^{++}} - m_{\Sigma_c^0}$ given below.

² See the note on DIESBURG 87 in the $m_{\Sigma_c^{++}} - m_{\Sigma_c^0}$ section below.

$\Sigma_c(2455)$ MASS DIFFERENCES

$m_{\Sigma_c(2455)^{++}} - m_{\Sigma_c(2455)^0}$

VALUE (MeV)	DOCUMENT ID	TECN	COMMENT
0.220 ± 0.013 OUR FIT			
0.221 ± 0.014 OUR AVERAGE			
0.22 ± 0.01 ± 0.01	LEE	14	BELL e^+e^- at $\Upsilon(4S)$
0.2 ± 0.1 ± 0.1	ARTUSO	02	CLE2 $e^+e^- \approx \Upsilon(4S)$
- 0.03 ± 0.28 ± 0.11	LINK	00C	FOCS $\gamma A, \bar{E}_\gamma \approx 180$ GeV
0.38 ± 0.40 ± 0.15	AITALA	96B	E791 $\pi^- N, 500$ GeV
1.1 ± 0.4 ± 0.1	CRAWFORD	93	CLE2 $e^+e^- \approx \Upsilon(4S)$
- 0.1 ± 0.6 ± 0.1	BOWCOCK	89	CLEO $e^+e^- \approx 10$ GeV
1.2 ± 0.7 ± 0.3	ALBRECHT	88D	ARG $e^+e^- \approx 10$ GeV

- • • We do not use the following data for averages, fits, limits, etc. • • •
- 10.8 ± 2.9 ³ DIESBURG 87 SPEC $nA \sim 600$ GeV
- ³ DIESBURG 87 is completely incompatible with the other experiments, which is surprising since it agrees with them about $m_{\Sigma_c(2455)^{++}} - m_{\Lambda_c^+}$. We go with the majority here.

$m_{\Sigma_c(2455)^+} - m_{\Sigma_c(2455)^0}$

VALUE (MeV)	DOCUMENT ID	TECN	COMMENT
-1.10 ± 0.16 OUR FIT			
-1.10 ± 0.16 OUR AVERAGE			
1.4 ± 0.5 ± 0.3	CRAWFORD	93	CLE2 See AMMAR 01

- • • We do not use the following data for averages, fits, limits, etc. • • •

$\Sigma_c(2455)$ WIDTHS

$\Sigma_c(2455)^{++}$ WIDTH

VALUE (MeV)	EVTS	DOCUMENT ID	TECN	COMMENT
1.89 ± 0.09 OUR AVERAGE				Error includes scale factor of 1.1.
1.84 ± 0.04 ± 0.07	36k	LEE	14	BELL e^+e^- at $\Upsilon(4S)$
2.34 ± 0.13 ± 0.45	13.8k	AALTONEN	11H	CDF $p\bar{p}$ at 1.96 TeV
2.3 ± 0.2 ± 0.3	2k	ARTUSO	02	CLE2 $e^+e^- \approx \Upsilon(4S)$
2.05 ± 0.41 ± 0.38	1110	LINK	02	FOCS $\gamma A, \bar{E}_\gamma \approx 180$ GeV

$\Sigma_c(2455)^+$ WIDTH

VALUE (MeV)	CL%	EVTS	DOCUMENT ID	TECN	COMMENT
2.3 ± 0.3 ± 0.3			YELTON	21	BELL e^+e^- at $\Upsilon(nS)$
<4.6		90 661	AMMAR	01	CLE2 $e^+e^- \approx \Upsilon(4S)$

$\Sigma_c(2455)^0$ WIDTH

VALUE (MeV)	EVTS	DOCUMENT ID	TECN	COMMENT
1.83 ± 0.11 OUR AVERAGE				Error includes scale factor of 1.2.
1.76 ± 0.04 ± 0.09	32k	LEE	14	BELL e^+e^- at $\Upsilon(4S)$
1.65 ± 0.11 ± 0.49	15.9k	AALTONEN	11H	CDF $p\bar{p}$ at 1.96 TeV
2.6 ± 0.5 ± 0.3		AUBERT	08BN	BABR $B^- \rightarrow \bar{p}\Lambda_c^+ \pi^-$
2.5 ± 0.2 ± 0.3	2k	ARTUSO	02	CLE2 $e^+e^- \approx \Upsilon(4S)$
1.55 ± 0.41 ± 0.37	913	LINK	02	FOCS $\gamma A, \bar{E}_\gamma \approx 180$ GeV

$\Sigma_c(2455)$ DECAY MODES

$\Lambda_c^+ \pi$ is the only strong decay allowed to a Σ_c having this mass.

Mode	Fraction (Γ_i/Γ)
$\Gamma_1 \Lambda_c^+ \pi$	$\approx 100\%$

$\Sigma_c(2455)$ REFERENCES

YELTON	21	PR D104 052003	J. Yelton et al.	(BELLE Collab.)
LEE	14	PR D89 091102	S.-H. Lee et al.	(BELLE Collab.)
AALTONEN	11H	PR D84 012003	T. Aaltonen et al.	(CDF Collab.)
AUBERT	08BN	PR D78 112003	B. Aubert et al.	(BABAR Collab.)
ARTUSO	02	PR D65 071101	M. Artuso et al.	(CLEO Collab.)
LINK	02	PL B525 205	J.M. Link et al.	(FNAL FOCUS Collab.)
AMMAR	01	PR L 86 1167	R. Ammar et al.	(CLEO Collab.)
LINK	00C	PL B488 218	J.M. Link et al.	(FNAL FOCUS Collab.)
AITALA	96B	PL B379 292	E.M. Aitala et al.	(FNAL E791 Collab.)
ALEV	96	JINRRC 3-77 31	A.N. Alev et al.	(Serpukhov EXCHARM Collab.)
FRABETTI	96	PL B365 461	P.L. Frabetti et al.	(FNAL E687 Collab.)

CRAWFORD	93	PRL 71 3259	G. Crawford et al.	(CLEO Collab.)
ANJOS	89D	PRL 62 1721	J.C. Anjos et al.	(FNAL E691 Collab.)
BOWCOCK	89	PRL 62 1240	T.J.V. Bowcock et al.	(CLEO Collab.)
ALBRECHT	88D	PL B211 489	H. Albrecht et al.	(ARGUS Collab.)
DIESBURG	87	PRL 59 2711	M. Diesburg et al.	(FNAL E400 Collab.)
JONES	87	ZPHY C36 593	G.T. Jones et al.	(CERN WA21 Collab.)
AMMAR	86	JETPL 43 515	R. Ammar et al.	(ITEP)
		Translated from ZETFP 43 401		
BOSETTI	82	PL 109B 234	P.C. Bosetti et al.	(AACH3, BONN, CERN+)
CALICCHIO	80	PL 93B 521	M. Calicchio et al.	(BARI, BIRM, BRUX+)
BALTAY	79	PRL 42 1721	C. Baltay et al.	(COLU, BNL)
CAZZOLI	75	PRL 34 1125	E.G. Cazzoli et al.	(BNL)

$\Sigma_c(2520)$

$I(J^P) = 1(\frac{3}{2}^+)$ Status: ***

Seen in the $\Lambda_c^+ \pi^+$ mass spectrum. The natural assignment is that this is the $J^P = 3/2^+$ excitation of the $\Sigma_c(2455)$, the charm counterpart of the $\Sigma(1385)$, but neither J nor P has been measured.

$\Sigma_c(2520)$ MASSES

The masses are obtained from the mass-difference measurements that follow.

$\Sigma_c(2520)^{++}$ MASS

VALUE (MeV)	EVTS	DOCUMENT ID	TECN	COMMENT
2518.41 ± 0.22 OUR FIT				Error includes scale factor of 1.3.
2530 ± 5 ± 5	6	¹ AMMOSOV 93	HLBC	$\nu p \rightarrow \mu^- \Sigma_c(2530)^{++}$
		¹ AMMOSOV 93		sees a cluster of 6 events and estimates the background to be 1 event.

$\Sigma_c(2520)^+$ MASS

VALUE (MeV)	DOCUMENT ID
2517.4 ± 0.7 OUR FIT	
2517.4 ± 0.7 ± 0.5	

$\Sigma_c(2520)^0$ MASS

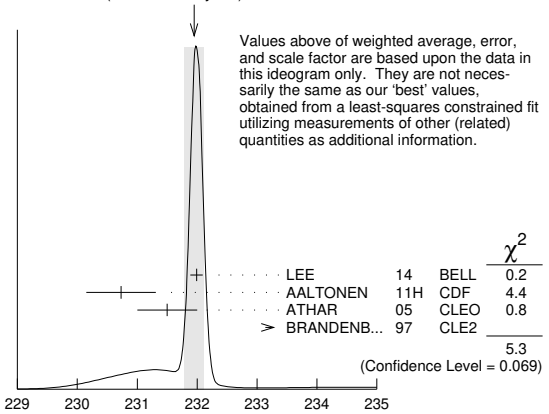
VALUE (MeV)	DOCUMENT ID
2518.48 ± 0.21 OUR FIT	
2518.48 ± 0.21 ± 0.2	

$\Sigma_c(2520)$ MASS DIFFERENCES

$m_{\Sigma_c(2520)^{++}} - m_{\Lambda_c^+}$

VALUE (MeV)	EVTS	DOCUMENT ID	TECN	COMMENT
231.95 ± 0.18 OUR FIT				Error includes scale factor of 1.8.
231.95 ± 0.16 OUR AVERAGE				Error includes scale factor of 1.6. See the ideogram below.
231.99 ± 0.10 ± 0.02	44k	LEE	14	BELL e^+e^- at $\Upsilon(4S)$
230.73 ± 0.56 ± 0.16	8.8k	AALTONEN	11H	CDF $p\bar{p}$ at 1.96 TeV
231.5 ± 0.4 ± 0.3	1.3k	ATHAR	05	CLEO e^+e^- , 9.4-11.5 GeV
234.5 ± 1.1 ± 0.8	677	BRANDENB...	97	CLE2 $e^+e^- \approx \Upsilon(4S)$

WEIGHTED AVERAGE
231.95 ± 0.16 (Error scaled by 1.6)



$m_{\Sigma_c(2520)^+} - m_{\Lambda_c^+}$

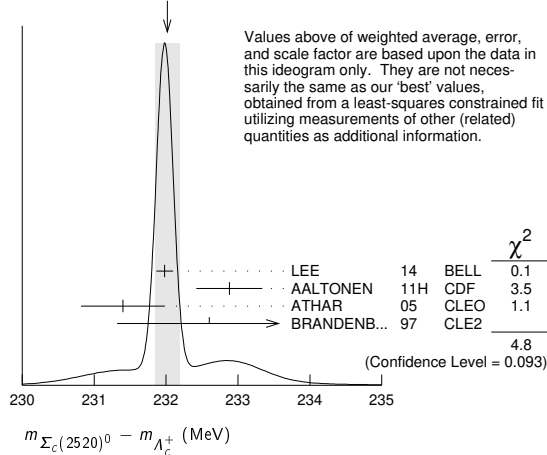
VALUE (MeV)	EVTS	DOCUMENT ID	TECN	COMMENT
230.9 ± 0.7 OUR FIT				
230.9 ± 0.7 OUR AVERAGE				
230.9 ± 0.5 ± 0.5		YELTON	21	BELL e^+e^- at $\Upsilon(nS)$
231.0 ± 1.1 ± 2.0	327	AMMAR	01	CLE2 $e^+e^- \approx \Upsilon(4S)$

Baryon Particle Listings

 $\Sigma_c(2520), \Sigma_c(2800)$ $m_{\Sigma_c(2520)^0} - m_{\Lambda_c^+}$

VALUE (MeV)	EVTS	DOCUMENT ID	TECN	COMMENT
232.02 ± 0.15 OUR FIT	Error	includes scale factor of 1.4.		
232.02 ± 0.17 OUR AVERAGE	Error	includes scale factor of 1.5. See the ideogram below.		
231.98 ± 0.11 ± 0.04	41k	LEE	14	BELL e^+e^- at $\Upsilon(4S)$
232.88 ± 0.43 ± 0.16	9.0k	AALTONEN	11H	CDF $p\bar{p}$ at 1.96 TeV
231.4 ± 0.5 ± 0.3	1.3k	ATHAR	05	CLEO e^+e^- , 9.4–11.5 GeV
232.6 ± 1.0 ± 0.8	504	BRANDENB...	97	CLE2 $e^+e^- \approx \Upsilon(4S)$

WEIGHTED AVERAGE
232.02 ± 0.17 (Error scaled by 1.5)

 $m_{\Sigma_c(2520)^{++}} - m_{\Sigma_c(2520)^0}$

VALUE (MeV)	EVTS	DOCUMENT ID	TECN	COMMENT
0.01 ± 0.15 ± 0.03	44/41k	LEE	14	BELL e^+e^- at $\Upsilon(4S)$
• • • We do not use the following data for averages, fits, limits, etc. • • •				
0.1 ± 0.8 ± 0.3		² ATHAR	05	CLEO e^+e^- , 9.4–11.5 GeV
1.9 ± 1.4 ± 1.0		³ BRANDENB...	97	CLE2 $e^+e^- \approx \Upsilon(4S)$
		² This ATHAR 05 result is redundant with measurements in earlier entries.		
		³ This BRANDENBURG 97 result is redundant with measurements in earlier entries.		

 $\Sigma_c(2520)$ WIDTHS $\Sigma_c(2520)^{++}$ WIDTH

VALUE (MeV)	EVTS	DOCUMENT ID	TECN	COMMENT
14.78 ± 0.30 OUR AVERAGE				
14.77 ± 0.25 ± 0.18	44k	LEE	14	BELL e^+e^- at $\Upsilon(4S)$
15.03 ± 2.12 ± 1.36	8.8k	AALTONEN	11H	CDF $p\bar{p}$ at 1.96 TeV
14.4 ± 1.6 ± 1.4	1.3k	ATHAR	05	CLEO e^+e^- , 9.4–11.5 GeV
17.9 ± 3.8 ± 3.2	677	BRANDENB...	97	CLE2 $e^+e^- \approx \Upsilon(4S)$

 $\Sigma_c(2520)^+$ WIDTH

VALUE (MeV)	CL%	EVTS	DOCUMENT ID	TECN	COMMENT
17.2 ± 2.3 ± 3.1			YELTON	21	BELL e^+e^- at $\Upsilon(ns)$
• • • We do not use the following data for averages, fits, limits, etc. • • •					
<17	90	327	AMMAR	01	CLE2 $e^+e^- \approx \Upsilon(4S)$

 $\Sigma_c(2520)^0$ WIDTH

VALUE (MeV)	EVTS	DOCUMENT ID	TECN	COMMENT
15.3 ± 0.4 OUR AVERAGE				
15.41 ± 0.41 ± 0.20	41k	LEE	14	BELL e^+e^- at $\Upsilon(4S)$
12.51 ± 1.82 ± 1.37	9.0k	AALTONEN	11H	CDF $p\bar{p}$ at 1.96 TeV
16.6 ± 1.9 ± 1.4	1.3k	ATHAR	05	CLEO e^+e^- , 9.4–11.5 GeV
13.0 ± 3.7 ± 3.0	504	BRANDENB...	97	CLE2 $e^+e^- \approx \Upsilon(4S)$

 $\Sigma_c(2520)$ DECAY MODES

$\Lambda_c^+ \pi$ is the only strong decay allowed to a Σ_c having this mass.

Mode	Fraction (Γ_i/Γ)
$\Gamma_1 \Lambda_c^+ \pi$	≈ 100 %

 $\Sigma_c(2520)$ REFERENCES

YELTON	21	PR D104 052003	J. Yelton <i>et al.</i>	(BELLE Collab.)
LEE	14	PR D89 091102	S.-H. Lee <i>et al.</i>	(BELLE Collab.)
AALTONEN	11H	PR D84 012003	T. Aaltonen <i>et al.</i>	(CDF Collab.)
ATHAR	05	PR D71 051101	S.B. Athar <i>et al.</i>	(CLEO Collab.)
AMMAR	01	PRL 86 1167	R. Ammar <i>et al.</i>	(CLEO Collab.)
BRANDENB...	97	PRL 78 2304	G. Brandenburg <i>et al.</i>	(CLEO Collab.)
AMMOS OV	93	JETPL 58 247	V.V. Ammosov <i>et al.</i>	(SERP)
Translated from ZETFP 58 241.				

 $\Sigma_c(2800)$

$I(J^P) = 1(?)^?$ Status: ***

Seen in the $\Lambda_c^+ \pi^+$, $\Lambda_c^+ \pi^0$, and $\Lambda_c^+ \pi^-$ mass spectra.

 $\Sigma_c(2800)$ MASSES

The charged ++ and + masses are obtained from the mass-difference measurements that follow. The neutral mass is dominated by the mass-difference measurement, but is pulled up somewhat by the less well-determined but considerably higher direct-mass measurement. It is possible, in fact, that AUBERT 08BN is seeing a different Σ_c .

 $\Sigma_c(2800)^{++}$ MASS

VALUE (MeV)	DOCUMENT ID
2801 ± 4 OUR FIT	

 $\Sigma_c(2800)^+$ MASS

VALUE (MeV)	DOCUMENT ID
2792 ± 14 OUR FIT	

 $\Sigma_c(2800)^0$ MASS

VALUE (MeV)	DOCUMENT ID	TECN	COMMENT
2806 ± 5 OUR FIT	Error	includes scale factor of 1.3.	
2846 ± 8 ± 10	AUBERT	08BN BABR	$B^- \rightarrow \bar{p} \Lambda_c^+ \pi^-$

 $\Sigma_c(2800)$ MASS DIFFERENCES $m_{\Sigma_c(2800)^{++}} - m_{\Lambda_c^+}$

VALUE (MeV)	EVTS	DOCUMENT ID	TECN	COMMENT
514 ± 4 OUR FIT				
514.5 ± 3.4 ± 2.8	2810 ± 1090	MIZUK	05	BELL $e^+e^- \approx \Upsilon(4S)$

 $m_{\Sigma_c(2800)^+} - m_{\Lambda_c^+}$

VALUE (MeV)	EVTS	DOCUMENT ID	TECN	COMMENT
505 ± 14 OUR FIT				
505.4 ± 5.8 ± 12.4	1540 ± 1750	MIZUK	05	BELL $e^+e^- \approx \Upsilon(4S)$
	4.6 ± 2.0			

 $m_{\Sigma_c(2800)^0} - m_{\Lambda_c^+}$

VALUE (MeV)	EVTS	DOCUMENT ID	TECN	COMMENT
519 ± 5 OUR FIT	Error	includes scale factor of 1.3.		
515.4 ± 3.2 ± 2.1	2240 ± 1300	MIZUK	05	BELL $e^+e^- \approx \Upsilon(4S)$
	3.1 ± 6.0			

 $\Sigma_c(2800)$ WIDTHS $\Sigma_c(2800)^{++}$ WIDTH

VALUE (MeV)	EVTS	DOCUMENT ID	TECN	COMMENT
75 ± 18 ± 12	2810 ± 1090	MIZUK	05	BELL $e^+e^- \approx \Upsilon(4S)$
	13 ± 11			

 $\Sigma_c(2800)^+$ WIDTH

VALUE (MeV)	EVTS	DOCUMENT ID	TECN	COMMENT
62 ± 37 ± 52	1540 ± 1750	MIZUK	05	BELL $e^+e^- \approx \Upsilon(4S)$
	23 ± 38			

 $\Sigma_c(2800)^0$ WIDTH

VALUE (MeV)	EVTS	DOCUMENT ID	TECN	COMMENT
72 ± 22 OUR AVERAGE				
86 ± 33 ± 12		AUBERT	08BN BABR	$B^- \rightarrow \bar{p} \Lambda_c^+ \pi^-$
61 ± 18 ± 22	2240 ± 1300	MIZUK	05	BELL $e^+e^- \approx \Upsilon(4S)$
	13 ± 13			

$\Sigma_c(2800)$ DECAY MODES

Mode	Fraction (Γ_i/Γ)
$\Gamma_1 \Lambda_c^+ \pi$	seen

$\Sigma_c(2800)$ REFERENCES

AUBERT MIZUK	08BN PR D78 112003 05 PRL 94 122002	B. Aubert et al. R. Mizuk et al.	(BABAR Collab.) (BELLE Collab.)
-----------------	--	-------------------------------------	------------------------------------



$I(J^P) = \frac{1}{2}(\frac{1}{2}^+)$ Status: * * *

Neither of J or P has actually been measured.

Ξ_c^+ MASS

The fit uses the Ξ_c^+ and Ξ_c^0 mass and mass-difference measurements.

VALUE (MeV)	EVTS	DOCUMENT ID	TECN	COMMENT
2467.71 ± 0.23 OUR FIT				Error includes scale factor of 1.3.
2467.95 ± 0.19 OUR AVERAGE				
2467.97 ± 0.14 ± 0.17	3.8k	¹ AAIJ	14Z LHCb	$p\bar{p}$ at 7, 8 TeV
2468.00 ± 0.18 ± 0.51	5.1k	AALTONEN	14B CDF	$p\bar{p}$ at 1.96 TeV
2468.1 ± 0.4 ± 0.2	4.9k	² LESIAK	05 BELL	e^+e^- , $\Upsilon(4S)$
2465.8 ± 1.9 ± 2.5	90	FRABETTI	98 E687	γ Be, $\bar{E}_\gamma = 220$ GeV
2467.0 ± 1.6 ± 2.0	147	EDWARDS	96 CLE2	$e^+e^- \approx \Upsilon(4S)$
2465.1 ± 3.6 ± 1.9	30	ALBRECHT	90F ARG	e^+e^- at $\Upsilon(4S)$
2467 ± 3 ± 4	23	ALAM	89 CLEO	e^+e^- 10.6 GeV
2466.5 ± 2.7 ± 1.2	5	BARLAG	89c ACCM	π^- Cu 230 GeV
• • • We do not use the following data for averages, fits, limits, etc. • • •				
2464.4 ± 2.0 ± 1.4	30	FRABETTI	93B E687	See FRABETTI 98
2459 ± 5 ± 30	56	³ COTEUS	87 SPEC	$nA \approx 600$ GeV
2460 ± 25	82	BIAGI	83 SPEC	Σ^- Be 135 GeV

¹ AAIJ 14Z systematic error includes in quadrature the 0.14 MeV uncertainty from the $m(\Lambda_c^+)$ mass value.
² The systematic error was (wrongly) given the other way round in LESIAK 05; see the erratum.
³ Although COTEUS 87 claims to agree well with BIAGI 83 on the mass and width, there appears to be a discrepancy between the two experiments. BIAGI 83 sees a single peak (stated significance about 6 standard deviations) in the $\Lambda K^- \pi^+ \pi^+$ mass spectrum. COTEUS 87 sees two peaks in the same spectrum, one at the Ξ_c^+ mass, the other 75 MeV lower. The latter is attributed to $\Xi_c^+ \rightarrow \Sigma^0 K^- \pi^+ \pi^+ \rightarrow (\Lambda \gamma) K^- \pi^+ \pi^+$, with the γ unseen. The combined significance of the double peak is stated to be 5.5 standard deviations. But the absence of any trace of a lower peak in BIAGI 83 seems to us to throw into question the interpretation of the lower peak of COTEUS 87.

Ξ_c^+ MEAN LIFE

VALUE (10^{-15} s)	EVTS	DOCUMENT ID	TECN	COMMENT
453 ± 5 OUR AVERAGE				
454 ± 5 ± 2	56k	¹ AAIJ	19AG LHCb	$\Xi_c^+ \rightarrow p K^- \pi^+$
503 ± 47 ± 18	250	MAHMOOD	02 CLE2	$e^+e^- \approx \Upsilon(4S)$
439 ± 22 ± 9	532	LINK	01D FOCUS	γ nucleus, $\bar{E}_\gamma \approx 180$ GeV
340 ⁺ ₋₅₀ ± 20	56	FRABETTI	98 E687	γ Be, $\bar{E}_\gamma = 220$ GeV
400 ⁺ ₋₁₂₀ ± 100	102	COTEUS	87 SPEC	$nA \approx 600$ GeV
480 ⁺ ₋₁₅₀ ± 200	53	BIAGI	85c SPEC	Σ^- Be 135 GeV
• • • We do not use the following data for averages, fits, limits, etc. • • •				
410 ⁺ ₋₈₀ ± 20	30	FRABETTI	93B E687	See FRABETTI 98
200 ⁺ ₋₆₀ ± 110	6	BARLAG	89c ACCM	$\pi^- (K^-)$ Cu 230 GeV

¹ AAIJ 19AG reports $[\Xi_c^+ \text{ MEAN LIFE}] / [D^\pm \text{ MEAN LIFE}] = 0.4392 \pm 0.0034 \pm 0.0028$ which we multiply by our best value $D^\pm \text{ MEAN LIFE} = (1.033 \pm 0.005) \times 10^{-12}$ s. Our first error is their experiment's error and our second error is the systematic error from using our best value.

Ξ_c^+ DECAY MODES

Branching fractions marked with a footnote, e.g. [a], have been corrected for decay modes not observed in the experiments. For example, the sub-mode fraction $\Xi_c^+ \rightarrow \Sigma^+ \bar{K}^*(892)^0$ seen in $\Xi_c^+ \rightarrow \Sigma^+ K^- \pi^+$ has been multiplied up to include $\bar{K}^*(892)^0 \rightarrow \bar{K}^0 \pi^0$ decays.

Mode	Fraction (Γ_i/Γ)	Scale factor/ Confidence level
------	--------------------------------	-----------------------------------

Cabibbo-favored ($S = -2$) decays

Γ_1	$p 2K_S^0$	$(2.5 \pm 1.3) \times 10^{-3}$	
Γ_2	$\Lambda \bar{K}^0 \pi^+$	—	
Γ_3	$\Sigma(1385)^+ \bar{K}^0$	[a] $(2.9 \pm 2.0) \%$	
Γ_4	$\Lambda K^- 2\pi^+$	$(9 \pm 4) \times 10^{-3}$	
Γ_5	$\Lambda \bar{K}^*(892)^0 \pi^+$	[a] $< 5 \times 10^{-3}$	CL=90%
Γ_6	$\Sigma(1385)^+ K^- \pi^+$	[a] $< 6 \times 10^{-3}$	CL=90%
Γ_7	$\Sigma^+ K^- \pi^+$	$(2.7 \pm 1.2) \%$	
Γ_8	$\Sigma^+ \bar{K}^*(892)^0$	[a] $(2.3 \pm 1.1) \%$	
Γ_9	$\Sigma^0 K^- 2\pi^+$	$(8 \pm 5) \times 10^{-3}$	
Γ_{10}	$\Xi^0 \pi^+$	$(1.6 \pm 0.8) \%$	
Γ_{11}	$\Xi^- 2\pi^+$	$(2.9 \pm 1.3) \%$	
Γ_{12}	$\Xi(1530)^0 \pi^+$	[a] $< 2.9 \times 10^{-3}$	CL=90%
Γ_{13}	$\Xi(1620)^0 \pi^+$	seen	
Γ_{14}	$\Xi(1690)^0 \pi^+$	seen	
Γ_{15}	$\Xi^0 \pi^+ \pi^0$	$(6.7 \pm 3.5) \%$	
Γ_{16}	$\Xi^0 \pi^- 2\pi^+$	$(5.0 \pm 2.6) \%$	
Γ_{17}	$\Xi^0 e^+ \nu_e$	$(7 \pm 4) \%$	
Γ_{18}	$\Omega^- K^+ \pi^+$	$(2.0 \pm 1.5) \times 10^{-3}$	

Cabibbo-suppressed decays

Γ_{19}	$p K^- \pi^+$	$(6.2 \pm 3.0) \times 10^{-3}$	S=1.5
Γ_{20}	$p \bar{K}^*(892)^0$	[a] $(3.3 \pm 1.7) \times 10^{-3}$	
Γ_{21}	$\Sigma^+ \pi^+ \pi^-$	$(1.4 \pm 0.8) \%$	
Γ_{22}	$\Sigma^- 2\pi^+$	$(5.1 \pm 3.4) \times 10^{-3}$	
Γ_{23}	$\Sigma^+ K^+ K^-$	$(4.3 \pm 2.5) \times 10^{-3}$	
Γ_{24}	$\Sigma^+ \phi$	[a] $< 3.2 \times 10^{-3}$	CL=90%
Γ_{25}	$\Xi(1690)^0 K^+, \Xi^0 \rightarrow \Sigma^+ K^-$	$< 1.3 \times 10^{-3}$	CL=90%
Γ_{26}	$p \phi(1020)$	$(1.2 \pm 0.6) \times 10^{-4}$	

[a] This branching fraction includes all the decay modes of the final-state resonance.

Ξ_c^+ BRANCHING RATIOS

Cabibbo-favored ($S = -2$) decays

$\Gamma(p 2K_S^0)/\Gamma(\Xi^- 2\pi^+)$	Γ_1/Γ_{11}			
VALUE	EVTS	DOCUMENT ID	TECN	COMMENT
0.087 ± 0.016 ± 0.014	168 ± 27	LESIAK	05 BELL	e^+e^- , $\Upsilon(4S)$

$\Gamma(\Sigma(1385)^+ \bar{K}^0)/\Gamma(\Xi^- 2\pi^+)$	Γ_3/Γ_{11}			
VALUE	EVTS	DOCUMENT ID	TECN	COMMENT
1.00 ± 0.49 ± 0.24	20	LINK	03E FOCUS	$< 1.72, 90\% \text{ CL}$

$\Gamma(\Lambda K^- 2\pi^+)/\Gamma(\Xi^- 2\pi^+)$	Γ_4/Γ_{11}			
VALUE	EVTS	DOCUMENT ID	TECN	COMMENT
0.323 ± 0.033 OUR AVERAGE				
0.32 ± 0.03 ± 0.02	1177 ± 55	LESIAK	05 BELL	e^+e^- , $\Upsilon(4S)$
0.28 ± 0.06 ± 0.06	58	LINK	03E FOCUS	γ nucleus, $\bar{E}_\gamma \approx 180$ GeV
0.58 ± 0.16 ± 0.07	61	BERGFELD	96 CLE2	$e^+e^- \approx \Upsilon(4S)$

$\Gamma(\Lambda \bar{K}^*(892)^0 \pi^+)/\Gamma(\Lambda K^- 2\pi^+)$	Γ_5/Γ_4			
VALUE	CL%	DOCUMENT ID	TECN	COMMENT
< 0.5	90	BERGFELD	96 CLE2	$e^+e^- \approx \Upsilon(4S)$

$\Gamma(\Sigma(1385)^+ K^- \pi^+)/\Gamma(\Lambda K^- 2\pi^+)$	Γ_6/Γ_4			
VALUE	CL%	DOCUMENT ID	TECN	COMMENT
< 0.7	90	BERGFELD	96 CLE2	$e^+e^- \approx \Upsilon(4S)$

$\Gamma(\Sigma^+ K^- \pi^+)/\Gamma(\Xi^- 2\pi^+)$	Γ_7/Γ_{11}			
VALUE	EVTS	DOCUMENT ID	TECN	COMMENT
0.94 ± 0.10 OUR AVERAGE				
0.91 ± 0.11 ± 0.04	251	LINK	03E FOCUS	γ nucleus, $\bar{E}_\gamma \approx 180$ GeV
0.92 ± 0.20 ± 0.07		¹ JUN	00 SELX	Σ^- nucleus, 600 GeV
1.18 ± 0.26 ± 0.17	119	BERGFELD	96 CLE2	$e^+e^- \approx \Upsilon(4S)$

¹ This JUN 00 result is redundant with other results given below.

$\Gamma(\Sigma^+ \bar{K}^*(892)^0)/\Gamma(\Xi^- 2\pi^+)$	Γ_8/Γ_{11}			
VALUE	EVTS	DOCUMENT ID	TECN	COMMENT
0.81 ± 0.15 OUR AVERAGE				
0.78 ± 0.16 ± 0.06	119	LINK	03E FOCUS	γ nucleus, $\bar{E}_\gamma \approx 180$ GeV
0.92 ± 0.27 ± 0.14	61	BERGFELD	96 CLE2	$e^+e^- \approx \Upsilon(4S)$

Baryon Particle Listings

$$\Xi_c^+, \Xi_c^0$$

$\Gamma(\Sigma^0 K^- 2\pi^+)/\Gamma(\Lambda K^- 2\pi^+)$		Γ_9/Γ_4	
VALUE	EVTS	DOCUMENT ID	TECN COMMENT
0.84 ± 0.36	47	¹ COTEUS 87	SPEC nA ≈ 600 GeV

¹ See, however, the note on the COTEUS 87 Ξ_c^+ mass measurement.

$\Gamma(\Xi^0 \pi^+)/\Gamma(\Xi^- 2\pi^+)$		Γ_{10}/Γ_{11}	
VALUE	EVTS	DOCUMENT ID	TECN COMMENT
0.55 ± 0.13 ± 0.09	39	EDWARDS 96	CLE2 e ⁺ e ⁻ ≈ $\mathcal{T}(45)$

$\Gamma(\Xi^- 2\pi^+)/\Gamma_{total}$		Γ_{11}/Γ	
VALUE (units 10 ⁻²)	EVTS	DOCUMENT ID	TECN COMMENT
2.86 ± 1.21 ± 0.38	24	¹ LI 19c	BELL e ⁺ e ⁻ ≈ $\mathcal{T}(45)$

• • • We do not use the following data for averages, fits, limits, etc. • • •

seen	131	BERGFELD 96	CLE2 e ⁺ e ⁻ ≈ $\mathcal{T}(45)$
seen	160	AVERY 95	CLE2 e ⁺ e ⁻ ≈ $\mathcal{T}(45)$
seen	30	FRABETTI 93B	E687 γ Be, $\bar{E}_\gamma \approx 220$ GeV
seen	30	ALBRECHT 90F	ARG e ⁺ e ⁻ at $\mathcal{T}(45)$
seen	23	ALAM 89	CLEO e ⁺ e ⁻ 10.6 GeV

¹ LI 19c report a significance of 6.8 σ for the observation of this decay mode, observed in Ξ_c^+ from $\bar{B}^0 \rightarrow \bar{\Lambda}_c^- \Xi_c^+$.

$\Gamma(\Xi(1530)^0 \pi^+)/\Gamma(\Xi^- 2\pi^+)$		Γ_{12}/Γ_{11}	
VALUE	CL%	DOCUMENT ID	TECN COMMENT
<0.1	90	LINK 03E	FOCS γ nucleus, $\bar{E}_\gamma \approx 180$ GeV

• • • We do not use the following data for averages, fits, limits, etc. • • •

<0.2	90	BERGFELD 96	CLE2 e ⁺ e ⁻ ≈ $\mathcal{T}(45)$
------	----	-------------	--

$\Gamma(\Xi(1620)^0 \pi^+)/\Gamma_{total}$		Γ_{13}/Γ	
VALUE	DOCUMENT ID	TECN	COMMENT
seen	SUMIHAMA 19	BELL	e ⁺ e ⁻ mostly at $\mathcal{T}(45)$

$\Gamma(\Xi(1690)^0 \pi^+)/\Gamma_{total}$		Γ_{14}/Γ	
VALUE	DOCUMENT ID	TECN	COMMENT
seen	SUMIHAMA 19	BELL	e ⁺ e ⁻ mostly at $\mathcal{T}(45)$

$\Gamma(\Xi^0 \pi^+ \pi^0)/\Gamma(\Xi^- 2\pi^+)$		Γ_{15}/Γ_{11}	
VALUE	EVTS	DOCUMENT ID	TECN COMMENT
2.34 ± 0.57 ± 0.37	81	EDWARDS 96	CLE2 e ⁺ e ⁻ ≈ $\mathcal{T}(45)$

$\Gamma(\Xi(1530)^0 \pi^+)/\Gamma(\Xi^0 \pi^+ \pi^0)$		Γ_{12}/Γ_{15}	
VALUE	CL%	DOCUMENT ID	TECN COMMENT
<0.3	90	EDWARDS 96	CLE2 e ⁺ e ⁻ ≈ $\mathcal{T}(45)$

• • • We do not use the following data for averages, fits, limits, etc. • • •

$\Gamma(\Xi^0 \pi^- 2\pi^+)/\Gamma(\Xi^- 2\pi^+)$		Γ_{16}/Γ_{11}	
VALUE	EVTS	DOCUMENT ID	TECN COMMENT
1.74 ± 0.42 ± 0.27	57	EDWARDS 96	CLE2 e ⁺ e ⁻ ≈ $\mathcal{T}(45)$

$\Gamma(\Xi^0 e^+ \nu_e)/\Gamma(\Xi^- 2\pi^+)$		Γ_{17}/Γ_{11}	
VALUE	EVTS	DOCUMENT ID	TECN COMMENT
2.3 ± 0.6^{+0.3}_{-0.6}	41	ALEXANDER 95B	CLE2 e ⁺ e ⁻ ≈ $\mathcal{T}(45)$

$\Gamma(\Omega^- K^+ \pi^+)/\Gamma(\Xi^- 2\pi^+)$		Γ_{18}/Γ_{11}	
VALUE	EVTS	DOCUMENT ID	TECN COMMENT
0.07 ± 0.03 ± 0.03	14	LINK 03E	FOCS < 0.12, 90% CL

$\Gamma(p K^- \pi^+)/\Gamma_{total}$		Γ_{19}/Γ	
VALUE (units 10 ⁻³)	EVTS	DOCUMENT ID	TECN COMMENT
6.2 ± 3.0 OUR AVERAGE		Error includes scale factor of 1.5.	
11.35 ± 0.02 ± 3.87	1.6M	¹ AAIJ 20AH	LHCB pp at 13 TeV
4.5 ± 2.1 ± 0.7	24	² LI 19c	BELL e ⁺ e ⁻ ≈ $\mathcal{T}(45)$

¹ AAIJ 20AH extracts $B(\Xi_c^+ \rightarrow p K^- \pi^+)$ assuming production fraction ratios $f_{\Xi_c^+}/f_{\Lambda_c^+} = (9.7 \pm 0.9 \pm 3.1) \times 10^{-2}$ (from AAIJ 19AB plus heavy quark symmetry arguments) as well as $f_{\Xi_c^0}/f_{\Xi_c^+} = 1.00 \pm 0.01$, and uses the input $B(\Lambda_c^+ \rightarrow p K^- \pi^+) = (6.23 \pm 0.33) \times 10^{-2}$. Its correlation with $B(\Xi_c^0 \rightarrow \Lambda_c^+ \pi^-)$, as measured in AAIJ 20AH, is 0.414.

² LI 19c report a significance of 4.4 σ for the observation of this decay mode, observed in Ξ_c^+ from $\bar{B}^0 \rightarrow \bar{\Lambda}_c^- \Xi_c^+$.

Cabibbo-suppressed decays

$\Gamma(p K^- \pi^+)/\Gamma(\Xi^- 2\pi^+)$		Γ_{19}/Γ_{11}	
VALUE	EVTS	DOCUMENT ID	TECN COMMENT
0.21 ± 0.04 OUR AVERAGE		Error includes scale factor of 1.5.	
0.194 ± 0.054	47 ± 11	VAZQUEZ-JA...08	SELX Σ^- nucleus, 600 GeV
0.234 ± 0.047 ± 0.022	202	LINK 01B	FOCS γ nucleus

• • • We do not use the following data for averages, fits, limits, etc. • • •

0.20 ± 0.04 ± 0.02	76	JUN 00	SELX See VAZQUEZ-JAUREGUI 08
--------------------	----	--------	------------------------------

$\Gamma(p \bar{K}^*(892)^0)/\Gamma(p K^- \pi^+)$		Γ_{20}/Γ_{19}	
VALUE	DOCUMENT ID	TECN	COMMENT
0.54 ± 0.09 ± 0.05	LINK 01B	FOCS	γ nucleus

Unseen decay modes of the $\bar{K}^*(892)^0$ are included.

$\Gamma(\Sigma^+ \pi^+ \pi^-)/\Gamma(\Xi^- 2\pi^+)$		Γ_{21}/Γ_{11}	
VALUE	EVTS	DOCUMENT ID	TECN COMMENT
0.48 ± 0.20	21 ± 8	VAZQUEZ-JA...08	SELX Σ^- nucleus, 600 GeV

$\Gamma(\Sigma^- 2\pi^+)/\Gamma(\Xi^- 2\pi^+)$		Γ_{22}/Γ_{11}	
VALUE	EVTS	DOCUMENT ID	TECN COMMENT
0.18 ± 0.09	10 ± 4	VAZQUEZ-JA...08	SELX Σ^- nucleus, 600 GeV

$\Gamma(\Sigma^+ K^+ K^-)/\Gamma(\Sigma^+ K^- \pi^+)$		Γ_{23}/Γ_7	
VALUE	EVTS	DOCUMENT ID	TECN COMMENT
0.16 ± 0.06 ± 0.01	17	LINK 03E	FOCS γ nucleus, $\bar{E}_\gamma \approx 180$ GeV

$\Gamma(\Sigma^+ \phi)/\Gamma(\Sigma^+ K^- \pi^+)$		Γ_{24}/Γ_7	
VALUE	CL%	DOCUMENT ID	TECN COMMENT
<0.12	90	LINK 03E	FOCS γ nucleus, $\bar{E}_\gamma \approx 180$ GeV

Unseen decay modes of the ϕ are included.

$\Gamma(p \phi(1020))/\Gamma(p K^- \pi^+)$		Γ_{26}/Γ_{19}	
VALUE (units 10 ⁻³)	EVTS	DOCUMENT ID	TECN COMMENT
19.8 ± 0.7 ± 0.9 ± 0.2	3.4k	¹ AAIJ 19I	LHCB pp at 8 TeV

¹ The last uncertainty is due to the uncertainty in the $\phi \rightarrow K^+ K^-$ branching fraction.

$\Gamma(\Xi(1690)^0 K^+ \times B(\Xi(1690)^0 \rightarrow \Sigma^+ K^-))/\Gamma(\Sigma^+ K^- \pi^+)$		Γ_{25}/Γ_7	
VALUE	CL%	DOCUMENT ID	TECN COMMENT
<0.05	90	LINK 03E	FOCS γ nucleus, $\bar{E}_\gamma \approx 180$ GeV

 Ξ_c^+ REFERENCES

AAIJ 20AH	PR D102 071101	R. Aaij et al.	(LHCb Collab.)
AAIJ 19AB	PR D99 052006	R. Aaij et al.	(LHCb Collab.)
AAIJ 19AG	PR D100 032001	R. Aaij et al.	(LHCb Collab.)
AAIJ 19I	JHEP 1904 084	R. Aaij et al.	(LHCb Collab.)
LI 19C	PR D100 031101	Y.B. Li et al.	(BELLE Collab.)
SUMIHAMA 19	PRL 122 072501	M. Sumihama et al.	(BELLE Collab.)
AAIJ 14Z	PRL 113 032001	R. Aaij et al.	(LHCb Collab.)
AALTONEN 14B	PR D89 072014	T. Aaltonen et al.	(CDF Collab.)
VAZQUEZ-JA...08	PL B666 299	E. Vazquez-Jauregui et al.	(SELEX Collab.)
LESIAK 05	PL B605 237	T. Lesiak et al.	(BELLE Collab.)
Also	PL B617 198 (errat.)	T. Lesiak et al.	(BELLE Collab.)
LINK 03E	PL B571 139	J.M. Link et al.	(FNAL FOCUS Collab.)
MAHMOOD 02	PR D65 031102	A.H. Mahmood et al.	(CLEO Collab.)
LINK 01B	PL B512 277	J.M. Link et al.	(FNAL FOCUS Collab.)
LINK 01D	PL B523 53	J.M. Link et al.	(FNAL FOCUS Collab.)
JUN 00	PRL 84 1857	S.Y. Jun et al.	(FNAL SELEX Collab.)
FRABETTI 98	PL B427 211	P.L. Frabetti et al.	(FNAL E687 Collab.)
BERGFELD 96	PL B365 431	T. Bergfeld et al.	(CLEO Collab.)
EDWARDS 96	PL B373 261	K.W. Edwards et al.	(CLEO Collab.)
ALEXANDER 95B	PRL 74 3113	J. Alexander et al.	(CLEO Collab.)
Also	PRL 75 4155 (errat.)	J. Alexander et al.	(CLEO Collab.)
AVERY 95	PRL 75 4364	P. Avery et al.	(CLEO Collab.)
FRABETTI 93B	PRL 70 1381	P.L. Frabetti et al.	(FNAL E687 Collab.)
ALBRECHT 90F	PL B247 121	H. Albrecht et al.	(ARGUS Collab.)
ALAM 89	PL B226 401	M.S. Alam et al.	(CLEO Collab.)
BARLAG 89C	PL B233 522	S. Barlag et al.	(ACCMOR Collab.)
COTEUS 87	PRL 59 1530	P. Coteus et al.	(FNAL E400 Collab.)
BIAGI 85C	PL 150B 230	S.F. Biagi et al.	(CERN WA62 Collab.)
BIAGI 83	PL 122B 455	S.F. Biagi et al.	(CERN WA62 Collab.)

$$\Xi_c^0$$

$$I(J^P) = \frac{1}{2}(\frac{1}{2}^+) \text{ Status: } ***$$

Neither J or P has actually been measured.

 Ξ_c^0 MASS

The fit uses the Ξ_c^0 and Ξ_c^+ mass and mass-difference measurements.

VALUE (MeV)	EVTS	DOCUMENT ID	TECN COMMENT
2470.44 ± 0.28 OUR FIT		Error includes scale factor of 1.2.	
2470.99^{+0.30}_{-0.50} OUR AVERAGE			

2470.85 ± 0.24 ± 0.55	3.4k	AALTONEN 14B	CDF $p\bar{p}$ at 1.96 TeV
2471.0 ± 0.3 ^{+0.2} _{-1.4}	8.6k	¹ LESIAK 05	BELL e ⁺ e ⁻ , $\mathcal{T}(45)$

2470.0 ± 2.8 ± 2.6	85	FRABETTI 98B	E687 γ Be, $\bar{E}_\gamma \approx 220$ GeV
2469 ± 2 ± 3	9	HENDERSON 92B	CLEO $\Omega^- K^+$
2472.1 ± 2.7 ± 1.6	54	ALBRECHT 90F	ARG e ⁺ e ⁻ at $\mathcal{T}(45)$
2473.3 ± 1.9 ± 1.2	4	BARLAG 90	ACCMOR $\pi^- (K^-)$ Cu 230 GeV
2472 ± 3 ± 4	19	ALAM 89	CLEO e ⁺ e ⁻ 10.6 GeV

• • • We do not use the following data for averages, fits, limits, etc. • • •

2462.1 ± 3.1 ± 1.4	42	² FRABETTI 93C	E687 See FRABETTI 98B
2471 ± 3 ± 4	14	AVERY 89	CLEO See ALAM 89

¹ The systematic error was (wrongly) given the other way round in LESIAK 05.

² The FRABETTI 93C mass is well below the other measurements.

$\Xi_c^0 - \Xi_c^+$ MASS DIFFERENCE

VALUE (MeV)	EVTS	DOCUMENT ID	TECN	COMMENT
2.72±0.23 OUR FIT				Error includes scale factor of 1.1.
2.91±0.26 OUR AVERAGE				
2.85±0.30±0.04	5.1/3.4k	AALTONEN	14B	CDF $p\bar{p}$ at 1.96 TeV
2.9 ±0.5		LESIAK	05	BELL e^+e^- , $\Upsilon(4S)$
7.0 ±4.5 ±2.2		ALBRECHT	90F	ARG e^+e^- at $\Upsilon(4S)$
6.8 ±3.3 ±0.5		BARLAG	90	ACCM $\pi^- (K^-)$ Cu 230 GeV
5 ±4 ±1		ALAM	89	CLEO $\Xi_c^0 \rightarrow \Xi^- \pi^+, \Xi_c^+ \rightarrow \Xi^- \pi^+ \pi^+$

 Ξ_c^0 MEAN LIFE

VALUE (10^{-15} s)	EVTS	DOCUMENT ID	TECN	COMMENT
150.4± 2.8 OUR AVERAGE				Error includes scale factor of 1.4.
148.0± 2.3±2.2		¹ AAIJ	22Y	LHCB $pp \rightarrow \Xi_c^0 + X, \Xi_c^0 \rightarrow p K^- K^- \pi^+$
153.4± 2.4±0.7	22k	^{2,3} AAIJ	19AG	LHCB $\Xi_b^- \rightarrow \Xi_c^0 \mu^- \bar{\nu}_\mu + X, \Xi_c^0 \rightarrow p K^- K^- \pi^+$
118 $\begin{smallmatrix} +14 \\ -12 \end{smallmatrix}$ ±5	110	LINK	02H	FOCS γ nucleus, ≈ 180 GeV
101 $\begin{smallmatrix} +25 \\ -17 \end{smallmatrix}$ ±5	42	FRABETTI	93c	E687 γ Be, $\bar{E}_\gamma = 220$ GeV
82 $\begin{smallmatrix} +59 \\ -30 \end{smallmatrix}$	4	BARLAG	90	ACCM $\pi^- (K^-)$ Cu 230 GeV

¹ Measured in Ξ_c^0 produced promptly in pp collisions, using $D^0 \rightarrow K^+ K^- \pi^+ \pi^-$ as normalisation mode. AAIJ 22Y reports this lifetime value as $(148.0 \pm 2.3 \pm 2.2 \pm 0.2) \times 10^{-15}$ s where the last uncertainty is due to the uncertainty on the D^0 lifetime value from PDG 20 average, $\tau_{D^0} = (410.1 \pm 1.5)$ fs.

² AAIJ 19AG reports $[\Xi_c^0 \text{ MEAN LIFE}] / [D^\pm \text{ MEAN LIFE}] = 0.1485 \pm 0.0017 \pm 0.0016$ which we multiply by our best value $D^\pm \text{ MEAN LIFE} = (1.033 \pm 0.005) \times 10^{-12}$ s. Our first error is their experiment's error and our second error is the systematic error from using our best value.

³ Measured in Ξ_c^0 produced in semileptonic Ξ_b^- decays.

 Ξ_c^0 DECAY MODES

Mode	Fraction (Γ_i/Γ)	Confidence level	
Cabibbo-favored decays			
Γ_1	$p K^- K^- \pi^+$	$(4.9 \pm 1.0) \times 10^{-3}$	
Γ_2	$p K^- \bar{K}^*(892)^0, \bar{K}^{*0} \rightarrow K^- \pi^+$	$(2.0 \pm 0.6) \times 10^{-3}$	
Γ_3	$p K^- K^- \pi^+$ (no \bar{K}^{*0})	$(3.0 \pm 0.8) \times 10^{-3}$	
Γ_4	ΛK_S^0	$(3.2 \pm 0.6) \times 10^{-3}$	
Γ_5	$\Lambda K^- \pi^+$	$(1.45 \pm 0.28) \%$	
Γ_6	$\Lambda \bar{K}^*(892)^0$	$(2.6 \pm 0.6) \times 10^{-3}$	
Γ_7	$\Lambda \bar{K}^0 \pi^+ \pi^-$	seen	
Γ_8	$\Lambda K^- \pi^+ \pi^+ \pi^-$	seen	
Γ_9	$\Sigma^0 K_S^0$	$(5.4 \pm 1.4) \times 10^{-4}$	
Γ_{10}	$\Sigma^+ K^-$	$(1.8 \pm 0.4) \times 10^{-3}$	
Γ_{11}	$\Sigma^0 \bar{K}^*(892)^0$	$(9.9 \pm 1.9) \times 10^{-3}$	
Γ_{12}	$\Sigma^+ K^*(892)^-$	$(4.9 \pm 1.3) \times 10^{-3}$	
Γ_{13}	$\Xi^- \pi^+$	$(1.43 \pm 0.27) \%$	
Γ_{14}	$\Xi^- \pi^+ \pi^+ \pi^-$	$(4.8 \pm 2.3) \%$	
Γ_{15}	$\Xi^0 K^+ K^-$		
Γ_{16}	$\Xi^0 \phi, \phi \rightarrow K^+ K^-$	$(5.2 \pm 1.2) \times 10^{-4}$	
Γ_{17}	$\Xi^0 K^+ K^-$ nonresonant	$(5.6 \pm 1.2) \times 10^{-4}$	
Γ_{18}	$\Omega^- K^+$	$(4.2 \pm 0.9) \times 10^{-3}$	
Γ_{19}	$\Xi^- e^+ \nu_e$	$(1.05 \pm 0.20) \%$	
Γ_{20}	$\Xi^- \mu^+ \nu_\mu$	$(1.01 \pm 0.21) \%$	
Γ_{21}	$\Xi^0 \gamma$	$< 1.7 \times 10^{-4}$	90%
Cabibbo-suppressed decays			
Γ_{22}	$\Lambda_c^+ \pi^-$	$(5.5 \pm 1.1) \times 10^{-3}$	
Γ_{23}	$\Xi^- K^+$	$(3.9 \pm 1.1) \times 10^{-4}$	
Γ_{24}	$\Lambda K^+ K^-$ (no ϕ)	$(4.1 \pm 1.3) \times 10^{-4}$	
Γ_{25}	$\Lambda \phi$	$(4.9 \pm 1.3) \times 10^{-4}$	

FIT INFORMATION

An overall fit to 7 branching ratios uses 8 measurements to determine 4 parameters. The overall fit has a $\chi^2 = 1.4$ for 4 degrees of freedom.

The following *off-diagonal* array elements are the correlation coefficients $\langle \delta x_i \delta x_j \rangle / (\delta x_i \delta x_j)$, in percent, from the fit to the branching fractions, $x_i \equiv \Gamma_i / \Gamma_{\text{total}}$.

x_5	64		
x_{13}	86	74	
x_{22}	64	55	75
	x_1	x_5	x_{13}

 Ξ_c^0 BRANCHING RATIOSCabibbo-favored ($S = -2$) decays

$\Gamma(p K^- K^- \pi^+) / \Gamma_{\text{total}}$	Γ_1 / Γ			
VALUE (%)	EVTS	DOCUMENT ID	TECN	COMMENT
0.49±0.10 OUR FIT				
0.58±0.23±0.05	17 ± 5	LI	19A	BELL e^+e^- at $\Upsilon(4S)$
$\Gamma(p K^- K^- \pi^+) / \Gamma(\Xi^- \pi^+)$ <td>Γ_1 / Γ_{13}</td>	Γ_1 / Γ_{13}			
VALUE	EVTS	DOCUMENT ID	TECN	COMMENT
0.339±0.035 OUR FIT				
0.34 ±0.04 OUR AVERAGE				
0.33 ±0.03 ±0.03	1908 ± 62	LESIAK	05	BELL e^+e^- , $\Upsilon(4S)$
0.35 ±0.06 ±0.03	148 ± 18	DANKO	04	CLEO e^+e^-
$\Gamma(p K^- \bar{K}^*(892)^0, \bar{K}^{*0} \rightarrow K^- \pi^+) / \Gamma(\Xi^- \pi^+)$ <td>Γ_2 / Γ_{13} </td>	Γ_2 / Γ_{13}			
VALUE	DOCUMENT ID	TECN	COMMENT	
0.14±0.03±0.01	DANKO	04	CLEO e^+e^-	
$\Gamma(p K^- K^- \pi^+ \text{ (no } \bar{K}^{*0} \text{)}) / \Gamma(\Xi^- \pi^+)$ <td>Γ_3 / Γ_{13} </td>	Γ_3 / Γ_{13}			
VALUE	DOCUMENT ID	TECN	COMMENT	
0.21±0.04±0.02	DANKO	04	CLEO e^+e^-	
$\Gamma(\Lambda K_S^0) / \Gamma(\Xi^- \pi^+)$ <td>Γ_4 / Γ_{13} </td>	Γ_4 / Γ_{13}			
VALUE	EVTS	DOCUMENT ID	TECN	COMMENT
0.225±0.013 OUR AVERAGE				
0.229±0.008±0.012	5.6k	LI	21F	BELL e^+e^- at $\Upsilon(\text{nS})$
0.21 ±0.02 ±0.02	465 ± 37	LESIAK	05	BELL e^+e^- , $\Upsilon(4S)$
$\Gamma(\Lambda K^- \pi^+) / \Gamma_{\text{total}}$ <td>Γ_5 / Γ </td>	Γ_5 / Γ			
VALUE (%)	EVTS	DOCUMENT ID	TECN	COMMENT
1.45±0.28 OUR FIT				
1.17±0.37±0.09	24 ± 6	LI	19A	BELL e^+e^- at $\Upsilon(4S)$
$\Gamma(\Lambda K^- \pi^+) / \Gamma(\Xi^- \pi^+)$ <td>Γ_5 / Γ_{13} </td>	Γ_5 / Γ_{13}			
VALUE	EVTS	DOCUMENT ID	TECN	COMMENT
1.02±0.14 OUR FIT				Error includes scale factor of 1.1.
1.07±0.12±0.07	2979 ± 211	LESIAK	05	BELL e^+e^- , $\Upsilon(4S)$
$\Gamma(\Lambda \bar{K}^*(892)^0) / \Gamma(\Xi^- \pi^+)$ <td>Γ_6 / Γ_{13} </td>	Γ_6 / Γ_{13}			
VALUE	EVTS	DOCUMENT ID	TECN	COMMENT
0.18±0.02±0.01	4k	JIA	21	BELL e^+e^- at $\Upsilon(\text{nS})$
$\Gamma(\Lambda \bar{K}^0 \pi^+ \pi^-) / \Gamma_{\text{total}}$ <td>Γ_7 / Γ </td>	Γ_7 / Γ			
VALUE	DOCUMENT ID	TECN	COMMENT	
seen	FRABETTI	98b	E687	γ Be, $\bar{E}_\gamma = 220$ GeV
$\Gamma(\Lambda K^- \pi^+ \pi^+ \pi^-) / \Gamma_{\text{total}}$ <td>Γ_8 / Γ </td>	Γ_8 / Γ			
VALUE	DOCUMENT ID	TECN	COMMENT	
seen	FRABETTI	98b	E687	γ Be, $\bar{E}_\gamma = 220$ GeV
$\Gamma(\Sigma^0 K_S^0) / \Gamma(\Xi^- \pi^+)$ <td>Γ_9 / Γ_{13} </td>	Γ_9 / Γ_{13}			
VALUE (units 10^{-2})	EVTS	DOCUMENT ID	TECN	COMMENT
3.8±0.6±0.4	279	LI	21F	BELL e^+e^- at $\Upsilon(\text{nS})$
$\Gamma(\Sigma^+ K^-) / \Gamma(\Xi^- \pi^+)$ <td>$\Gamma_{10} / \Gamma_{13}$ </td>	$\Gamma_{10} / \Gamma_{13}$			
VALUE (units 10^{-2})	EVTS	DOCUMENT ID	TECN	COMMENT
12.3±0.7±1.0	889	LI	21F	BELL e^+e^- at $\Upsilon(\text{nS})$
$\Gamma(\Sigma^0 \bar{K}^*(892)^0) / \Gamma(\Xi^- \pi^+)$ <td>$\Gamma_{11} / \Gamma_{13}$ </td>	$\Gamma_{11} / \Gamma_{13}$			
VALUE	EVTS	DOCUMENT ID	TECN	COMMENT
0.69±0.03±0.03	6.3k	JIA	21	BELL e^+e^- at $\Upsilon(\text{nS})$
$\Gamma(\Sigma^+ K^*(892)^-) / \Gamma(\Xi^- \pi^+)$ <td>$\Gamma_{12} / \Gamma_{13}$ </td>	$\Gamma_{12} / \Gamma_{13}$			
VALUE	EVTS	DOCUMENT ID	TECN	COMMENT
0.34±0.06±0.02	373	JIA	21	BELL e^+e^- at $\Upsilon(\text{nS})$
$\Gamma(\Xi^- \pi^+) / \Gamma_{\text{total}}$ <td>Γ_{13} / Γ </td>	Γ_{13} / Γ			
VALUE (%)	EVTS	DOCUMENT ID	TECN	COMMENT
1.43±0.27 OUR FIT				
1.80±0.50±0.14	45 ± 7	LI	19A	BELL e^+e^- at $\Upsilon(4S)$
$\Gamma(\Xi^- \pi^+) / \Gamma(\Xi^- \pi^+ \pi^+ \pi^-)$ <td>$\Gamma_{13} / \Gamma_{14}$ </td>	$\Gamma_{13} / \Gamma_{14}$			
VALUE	DOCUMENT ID	TECN	COMMENT	
0.30±0.12±0.05		ALBRECHT	90F	ARG e^+e^- at $\Upsilon(4S)$

Baryon Particle Listings

$$\Xi_c^0, \Xi_c^{\prime+}$$

$\Gamma(\Omega^- K^+)/\Gamma(\Xi^- \pi^+)$		Γ_{18}/Γ_{13}	
VALUE	EVTS	DOCUMENT ID	TECN COMMENT
$0.294 \pm 0.018 \pm 0.016$	650	AUBERT,B	05M BABR $e^+ e^- \approx \Upsilon(4S)$

$\Gamma(\Xi_c^0 \phi, \phi \rightarrow K^+ K^-)/\Gamma(\Xi^- \pi^+)$		Γ_{16}/Γ_{13}	
VALUE	EVTS	DOCUMENT ID	TECN COMMENT
$0.036 \pm 0.004 \pm 0.002$	311	¹ MCNEIL	21 BELL $e^+ e^-$ at $\Upsilon(nS)$

¹ MCNEIL 21 assumes an azimuthally symmetric amplitude model to recover resonant and nonresonant contributions to $\Xi_c^0 \rightarrow \Xi^0 K^+ K^-$.

$\Gamma(\Xi^0 K^+ K^- \text{ nonresonant})/\Gamma(\Xi^- \pi^+)$		Γ_{17}/Γ_{13}	
VALUE	EVTS	DOCUMENT ID	TECN COMMENT
$0.039 \pm 0.004 \pm 0.002$	311	¹ MCNEIL	21 BELL $e^+ e^-$ at $\Upsilon(nS)$

¹ MCNEIL 21 assumes an azimuthally symmetric amplitude model to recover resonant and nonresonant contributions to $\Xi_c^0 \rightarrow \Xi^0 K^+ K^-$.

$\Gamma(\Xi^- e^+ \nu_e)/\Gamma(\Xi^- \pi^+)$		Γ_{19}/Γ_{13}	
VALUE	EVTS	DOCUMENT ID	TECN COMMENT
$0.730 \pm 0.021 \pm 0.039$		¹ LI	21C BELL $e^+ e^-$ at 10.52, 10.58 GeV

••• We do not use the following data for averages, fits, limits, etc. •••

$1.38 \pm 0.14 \pm 0.22$		ACHARYA	21A ALCE pp at 13 TeV
$3.1 \pm 1.0 \pm 0.3 \pm 0.5$	54	ALEXANDER	95B CLE2 $e^+ e^- \approx \Upsilon(4S)$
$0.96 \pm 0.43 \pm 0.18$	18	² ALBRECHT	93B ARG $e^+ e^- \approx 10.4$ GeV

¹ LI 21C measures ratio $B(\Xi_c^0 \rightarrow \Xi^- e^+ \nu_e) / B(\Xi_c^0 \rightarrow \Xi^- \mu^+ \nu_\mu) = 1.03 \pm 0.05 \pm 0.07$.

² This ALBRECHT 93B value is the average of the $(\Xi^- e^+ \text{ anything})/\Xi^- \pi^+$ and $(\Xi^- \mu^+ \text{ anything})/\Xi^- \pi^+$ ratios. Here we average it with the $\Xi^- e^+ \nu_e/\Xi^- \pi^+$ ratio.

$\Gamma(\Xi^- e^+ \nu_e)/\Gamma(\Xi^- \mu^+ \nu_\mu)$		Γ_{19}/Γ_{20}	
VALUE	DOCUMENT ID	TECN	COMMENT
$1.03 \pm 0.05 \pm 0.07$	¹ LI	21C BELL	$e^+ e^-$ at 10.52, 10.58 GeV

¹ LI 21C value is not independent from other quoted measurements.

$\Gamma(\Xi^- \mu^+ \nu_\mu)/\Gamma(\Xi^- \pi^+)$		Γ_{20}/Γ_{13}	
VALUE	DOCUMENT ID	TECN	COMMENT
$0.708 \pm 0.033 \pm 0.056$	¹ LI	21C BELL	$e^+ e^-$ at 10.52, 10.58 GeV

¹ LI 21C measures ratio $B(\Xi_c^0 \rightarrow \Xi^- e^+ \nu_e) / B(\Xi_c^0 \rightarrow \Xi^- \mu^+ \nu_\mu) = 1.03 \pm 0.05 \pm 0.07$.

$\Gamma(\Xi^0 \gamma)/\Gamma(\Xi^- \pi^+)$		Γ_{21}/Γ_{13}	
VALUE	CL%	DOCUMENT ID	TECN COMMENT
$< 1.2 \times 10^{-2}$	90	LI	23 BELL $e^+ e^- \rightarrow \Upsilon(nS)$

Cabibbo-suppressed decays

$\Gamma(\Lambda_c^+ \pi^-)/\Gamma_{\text{total}}$		Γ_{22}/Γ	
VALUE (units 10^{-3})	EVTS	DOCUMENT ID	TECN COMMENT
5.5 ± 1.1 OUR FIT			
$5.5 \pm 0.2 \pm 1.8$	6.3k	¹ AAIJ	20AH LHCB pp at 13 TeV

¹ AAIJ 20AH extracts $B(\Xi_c^0 \rightarrow \Lambda_c^+ \pi^-)$ using two different normalization modes: $\Lambda_c^+ \rightarrow p K^- \pi^+$ and $\Xi_c^+ \rightarrow p K^- \pi^+$. The mean value of both results, taking their correlations into account, is presented as the final result. The measurement assumes production fraction ratios $f_{\Xi_c^0}/f_{\Lambda_c^+} = (9.7 \pm 0.9 \pm 3.1) \times 10^{-2}$ (from AAIJ 19AB plus heavy quark symmetry arguments) as well as $f_{\Xi_c^0}/f_{\Xi_c^+} = 1.00 \pm 0.01$. It further uses the inputs $B(\Lambda_c^+ \rightarrow p K^- \pi^+) = (6.23 \pm 0.33) \times 10^{-2}$ and $B(\Xi_c^+ \rightarrow p K^- \pi^+) = (4.5 \pm 2.1 \pm 0.7) \times 10^{-3}$ (from LI 19C). Its correlation with $B(\Xi_c^+ \rightarrow p K^- \pi^+)$, as measured in AAIJ 20AH, is 0.414.

$\Gamma(\Lambda_c^+ \pi^-)/\Gamma(\Xi^- \pi^+)$		Γ_{22}/Γ_{13}	
VALUE	EVTS	DOCUMENT ID	TECN COMMENT
0.38 ± 0.05 OUR FIT			
$0.38 \pm 0.04 \pm 0.04$	1468	¹ TANG	23 BELL $e^+ e^- \rightarrow \Upsilon(nS)$

¹ TANG 23 reports fitted masses $m_{\Lambda_c^+} = 2286.55 \pm 0.03$ MeV and $m_{\Xi_c^0} = 2470.43 \pm 0.06$ MeV.

$\Gamma(\Xi^- K^+)/\Gamma(\Xi^- \pi^+)$		Γ_{23}/Γ_{13}	
VALUE (units 10^{-2})	EVTS	DOCUMENT ID	TECN COMMENT
$2.75 \pm 0.51 \pm 0.25$	314 \pm 58	CHISTOV	13 BELL $e^+ e^- \approx \Upsilon(4S)$

$\Gamma(\Lambda K^+ K^- \text{ (no } \phi))/\Gamma(\Xi^- \pi^+)$		Γ_{24}/Γ_{13}	
VALUE (units 10^{-2})	EVTS	DOCUMENT ID	TECN COMMENT
$2.86 \pm 0.61 \pm 0.37$	510 \pm 110	CHISTOV	13 BELL $e^+ e^- \approx \Upsilon(4S)$

$\Gamma(\Lambda \phi)/\Gamma(\Xi^- \pi^+)$		Γ_{25}/Γ_{13}	
VALUE (units 10^{-2})	EVTS	DOCUMENT ID	TECN COMMENT
$3.43 \pm 0.58 \pm 0.32$	316 \pm 54	CHISTOV	13 BELL $e^+ e^- \approx \Upsilon(4S)$

 Ξ_c^0 DECAY PARAMETERS

See the note on "Baryon Decay Parameters" in the neutron Listings.

α FOR $\Xi_c^0 \rightarrow \Xi^- \pi^+$			
VALUE	EVTS	DOCUMENT ID	TECN COMMENT
$-0.64 \pm 0.05 \pm 0.01$		LI	21C BELL $e^+ e^-$ at 10.52, 10.58 GeV
•••			We do not use the following data for averages, fits, limits, etc. •••
$-0.56 \pm 0.39 \pm 0.10 \pm 0.09$	138	CHAN	01 CLE2 $e^+ e^- \approx \Upsilon(4S)$

α FOR $\Xi_c^0 \rightarrow \Xi^0 \pi^-$			
VALUE	EVTS	DOCUMENT ID	TECN COMMENT
$0.61 \pm 0.05 \pm 0.01$		LI	21C BELL $e^+ e^-$ at 10.52, 10.58 GeV

α FOR $\Xi_c^0 \rightarrow \Lambda \bar{K}^*(892)^0$			
VALUE	EVTS	DOCUMENT ID	TECN COMMENT
$0.15 \pm 0.22 \pm 0.04$	4k	¹ JIA	21 BELL $e^+ e^-$ at $\Upsilon(nS)$
		¹ JIA	21 measures $\alpha(\Xi_c^0 \rightarrow \Lambda \bar{K}^*(892)^0) \alpha(\Lambda \rightarrow p \pi^-) = 0.115 \pm 0.164 \pm 0.031$, and uses $\alpha(\Lambda \rightarrow p \pi^-) = 0.747 \pm 0.010$.

α FOR $\Xi_c^0 \rightarrow \Sigma^+ K^*(892)^-$			
VALUE	EVTS	DOCUMENT ID	TECN COMMENT
$-0.52 \pm 0.30 \pm 0.02$	373	¹ JIA	21 BELL $e^+ e^-$ at $\Upsilon(nS)$
		¹ JIA	21 measures $\alpha(\Xi_c^0 \rightarrow \Sigma^+ \bar{K}^*(892)^-) \alpha(\Sigma^+ \rightarrow p \pi^0) = 0.514 \pm 0.295 \pm 0.012$, and uses $\alpha(\Sigma^+ \rightarrow p \pi^0) = -0.980 \pm 0.017$.

 Ξ_c^0 REFERENCES

LI	23	PR D107 032001	Y. Li <i>et al.</i>	(BELLE Collab.)
TANG	23	PR D107 032005	S.S. Tang <i>et al.</i>	(BELLE Collab.)
AAIJ	22Y	SCIB 67 479	R. Aaij <i>et al.</i>	(LHCb Collab.)
ACHARYA	21A	PRL 127 272001	S. Acharya <i>et al.</i>	(ALICE Collab.)
JIA	21	JHEP 2106 160	S. Jia <i>et al.</i>	(BELLE Collab.)
LI	21C	PRL 127 121803	Y.B. Li <i>et al.</i>	(BELLE Collab.)
LI	21F	PR D105 L011102	Y. Li <i>et al.</i>	(BELLE Collab.)
MCNEIL	21	PR D103 112002	J.T. McNeil <i>et al.</i>	(BELLE Collab.)
AAIJ	20AH	PR D102 071101	R. Aaij <i>et al.</i>	(LHCb Collab.)
PDG	20	PTEP 2020 083CD1	P.A. Zyla <i>et al.</i>	(PDG Collab.)
AAIJ	19AB	PR D99 052006	R. Aaij <i>et al.</i>	(LHCb Collab.)
AAIJ	19AG	PR D100 032001	R. Aaij <i>et al.</i>	(LHCb Collab.)
LI	19A	PRL 122 082001	Y.B. Li <i>et al.</i>	(BELLE Collab.)
LI	19C	PR D100 031101	Y.B. Li <i>et al.</i>	(BELLE Collab.)
AALTONEN	14B	PR D89 072014	T. Aaltonen <i>et al.</i>	(CDF Collab.)
CHISTOV	13	PR D88 071103	R. Chistov <i>et al.</i>	(BELLE Collab.)
AUBERT,B	05M	PRL 95 142003	B. Aubert <i>et al.</i>	(BABAR Collab.)
LESIAK	05	PL B605 237	T. Lesiak <i>et al.</i>	(BELLE Collab.)
Also		PL B617 198 (errata.)	T. Lesiak <i>et al.</i>	(BELLE Collab.)
DANKO	04	PR D69 052004	I. Danko <i>et al.</i>	(CLEO Collab.)
LINK	02H	PL B541 211	J.M. Link <i>et al.</i>	(FNAL FOCUS Collab.)
CHAN	01	PR D63 111102	S. Chan <i>et al.</i>	(CLEO Collab.)
FRABETTI	98B	PL B426 403	P.L. Frabetti <i>et al.</i>	(FNAL E687 Collab.)
ALEXANDER	95B	PRL 74 3113	J. Alexander <i>et al.</i>	(CLEO Collab.)
Also		PRL 75 4155 (errata.)	J. Alexander <i>et al.</i>	(CLEO Collab.)
ALBRECHT	93B	PL B303 368	H. Albrecht <i>et al.</i>	(ARGUS Collab.)
FRABETTI	93C	PRL 70 2058	P.L. Frabetti <i>et al.</i>	(FNAL E687 Collab.)
HENDERS-ON	92B	PL B283 161	S. Henderson <i>et al.</i>	(CLEO Collab.)
ALBRECHT	90F	PL B247 121	H. Albrecht <i>et al.</i>	(ARGUS Collab.)
BARLAG	90	PL B236 495	S. Barlag <i>et al.</i>	(ACCMOR Collab.)
ALAM	89	PL B226 401	M.S. Alam <i>et al.</i>	(CLEO Collab.)
AVERY	89	PRL 62 863	P. Avery <i>et al.</i>	(CLEO Collab.)

$$\Xi_c^{\prime+} \quad I(J^P) = \frac{1}{2}(\frac{1}{2}^+) \text{ Status: } ** *$$

The $\Xi_c^{\prime+}$ and $\Xi_c^{\prime0}$ presumably complete the SU(3) sextet whose other members are the Σ_c^{++} , Σ_c^+ , Σ_c^0 , and Ω_c^0 ; see Fig. 5 in the "Quark Model" review. The quantum numbers given above come from this presumption but have not been measured.

 $\Xi_c^{\prime+}$ MASS

The mass is obtained from the mass-difference measurement that follows.

VALUE (MeV)	DOCUMENT ID
2578.2 ± 0.5 OUR FIT	Error includes scale factor of 1.1.

 $\Xi_c^{\prime+} - \Xi_c^+$ MASS DIFFERENCE

VALUE (MeV)	EVTS	DOCUMENT ID	TECN	COMMENT
110.5 ± 0.4 OUR FIT				
$110.5 \pm 0.1 \pm 0.4$	7k	YELTON	16 BELL	$e^+ e^-$, Υ regions
•••				We do not use the following data for averages, fits, limits, etc. •••
$107.8 \pm 1.7 \pm 2.5$	25	JESSOP	99 CLE2	$e^+ e^- \approx \Upsilon(4S)$

 $\Xi_c^{\prime+} - \Xi_c^{\prime0}$ MASS DIFFERENCE

VALUE (MeV)	DOCUMENT ID	TECN	COMMENT
-0.5 ± 0.6 OUR FIT			
•••			We do not use the following data for averages, fits, limits, etc. •••
$-0.8 \pm 0.1 \pm 0.5$	YELTON	16 BELL	7055 and 11,560 evts

See key on page 1171

Baryon Particle Listings

 $\Xi_c^{'+}, \Xi_c^0, \Xi_c(2645), \Xi_c(2790)$ $\Xi_c^{'+}$ DECAY MODESThe $\Xi_c^{'+} - \Xi_c^+$ mass difference is too small for any strong decay to occur.

Mode	Fraction (Γ_i/Γ)
$\Gamma_1 \Xi_c^+ \gamma$	seen

 $\Xi_c^{'+}$ REFERENCES

YELTON	16	PR D94 052011	J. Yelton <i>et al.</i>	(BELLE Collab.)
JESSOP	99	PRL 82 492	C.P. Jessop <i>et al.</i>	(CLEO Collab.)



$$I(J^P) = \frac{1}{2}(\frac{1}{2}^+) \text{ Status: } ***$$

The Ξ_c^0 and Ξ_c^+ presumably complete the SU(3) sextet whose other members are the $\Sigma_c^{++}, \Sigma_c^+, \Sigma_c^0$, and Ω_c^0 ; see Fig. 5 in the "Quark Model" review. The quantum numbers given above come from this presumption but have not been measured.

 Ξ_c^0 MASS

The mass is obtained from the mass-difference measurement that follows.

VALUE (MeV)	DOCUMENT ID
2578.7 ± 0.5 OUR FIT	

 $\Xi_c^0 - \Xi_c^+$ MASS DIFFERENCE

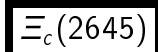
VALUE (MeV)	EVTs	DOCUMENT ID	TECN	COMMENT
108.3 ± 0.4 OUR FIT				
108.3 ± 0.1 ± 0.4	11.5k	YELTON	16	BELL e^+e^- , Υ regions
• • • We do not use the following data for averages, fits, limits, etc. • • •				
107.0 ± 1.4 ± 2.5	28	JESSOP	99	CLE2 $e^+e^- \approx \Upsilon(4S)$

 Ξ_c^0 DECAY MODESThe $\Xi_c^0 - \Xi_c^+$ mass difference is too small for any strong decay to occur.

Mode	Fraction (Γ_i/Γ)
$\Gamma_1 \Xi_c^0 \gamma$	seen

 Ξ_c^0 REFERENCES

YELTON	16	PR D94 052011	J. Yelton <i>et al.</i>	(BELLE Collab.)
JESSOP	99	PRL 82 492	C.P. Jessop <i>et al.</i>	(CLEO Collab.)



$$I(J^P) = \frac{1}{2}(\frac{3}{2}^+) \text{ Status: } ***$$

The natural assignment is that this is the $J^P = 3/2^+$ excitation of the Ξ_c in the same SU(4) multiplet as the $\Delta(1232)$, but the quantum numbers have not been measured.

 $\Xi_c(2645)$ MASSES $\Xi_c(2645)^+$ MASS

VALUE (MeV)	EVTs	DOCUMENT ID	TECN	COMMENT
2645.10 ± 0.30 OUR FIT				Error includes scale factor of 1.2.
2645.6 ± 0.2 ± 0.6 - 0.8	578 ± 32	LESIAK	08	BELL $e^+e^- \approx \Upsilon(4S)$

 $\Xi_c(2645)^0$ MASS

VALUE (MeV)	EVTs	DOCUMENT ID	TECN	COMMENT
2646.16 ± 0.25 OUR FIT				Error includes scale factor of 1.3.
2645.7 ± 0.2 ± 0.6 - 0.7	611 ± 32	LESIAK	08	BELL $e^+e^- \approx \Upsilon(4S)$

 $\Xi_c(2645) - \Xi_c$ MASS DIFFERENCES $m_{\Xi_c(2645)^+} - m_{\Xi_c^+}$

VALUE (MeV)	EVTs	DOCUMENT ID	TECN	COMMENT
174.67 ± 0.09 OUR FIT				
174.66 ± 0.06 ± 0.07	1260	YELTON	16	BELL e^+e^- in Υ regions
• • • We do not use the following data for averages, fits, limits, etc. • • •				
177.1 ± 0.5 ± 1.1	47	FRABETTI	98B	E687 γ Be, $\overline{E}_\gamma = 220$ GeV
174.3 ± 0.5 ± 1.0	34	GIBBONS	96	CLE2 $e^+e^- \approx \Upsilon(4S)$

 $m_{\Xi_c(2645)^0} - m_{\Xi_c^+}$

VALUE (MeV)	EVTs	DOCUMENT ID	TECN	COMMENT
178.45 ± 0.10 OUR FIT				
178.46 ± 0.07 ± 0.07	975	YELTON	16	BELL e^+e^- in Υ regions
• • • We do not use the following data for averages, fits, limits, etc. • • •				
178.2 ± 0.5 ± 1.0	55	AVERY	95	CLE2 $e^+e^- \approx \Upsilon(4S)$

 $\Xi_c(2645)^+ - \Xi_c(2645)^0$ MASS DIFFERENCE

VALUE (MeV)	DOCUMENT ID	TECN	COMMENT
-1.06 ± 0.27 OUR FIT			Error includes scale factor of 1.1.
• • • We do not use the following data for averages, fits, limits, etc. • • •			
-0.85 ± 0.09 ± 0.49	YELTON	16	BELL 1260 and 975 evts
-0.1 ± 0.3 ± 0.6	LESIAK	08	BELL ≈ 600 evts each

 $\Xi_c(2645)$ WIDTHS $\Xi_c(2645)^+$ WIDTH

VALUE (MeV)	CL%	EVTs	DOCUMENT ID	TECN	COMMENT
2.14 ± 0.19 OUR AVERAGE					Error includes scale factor of 1.1.
2.06 ± 0.13 ± 0.13	1260	YELTON	16	BELL	e^+e^- in Υ regions
2.6 ± 0.2 ± 0.4	3.7k	KATO	14	BELL	$e^+e^- \Upsilon(1S) - \Upsilon(5S)$
• • • We do not use the following data for averages, fits, limits, etc. • • •					
<3.1	90	GIBBONS	96	CLE2	$e^+e^- \approx \Upsilon(4S)$

 $\Xi_c(2645)^0$ WIDTH

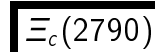
VALUE (MeV)	CL%	EVTs	DOCUMENT ID	TECN	COMMENT
2.35 ± 0.18 ± 0.13					
2.35 ± 0.18 ± 0.13	975	YELTON	16	BELL	e^+e^- in Υ regions
• • • We do not use the following data for averages, fits, limits, etc. • • •					
<5.5	90	55	AVERY	95	CLE2 $e^+e^- \approx \Upsilon(4S)$

 $\Xi_c(2645)$ DECAY MODES $\Xi_c \pi$ is the only strong decay allowed to a Ξ_c resonance having this mass.

Mode	Fraction (Γ_i/Γ)
$\Gamma_1 \Xi_c^0 \pi^+$	seen
$\Gamma_2 \Xi_c^+ \pi^-$	seen

 $\Xi_c(2645)$ REFERENCES

YELTON	16	PR D94 052011	J. Yelton <i>et al.</i>	(BELLE Collab.)
KATO	14	PR D89 052003	Y. Kato <i>et al.</i>	(BELLE Collab.)
LESIAK	08	PL B665 9	T. Lesiak <i>et al.</i>	(BELLE Collab.)
FRABETTI	98B	PL B426 403	P.L. Frabetti <i>et al.</i>	(FNAL E687 Collab.)
GIBBONS	96	PRL 77 810	L.K. Gibbons <i>et al.</i>	(CLEO Collab.)
AVERY	95	PRL 75 4364	P. Avery <i>et al.</i>	(CLEO Collab.)



$$I(J^P) = \frac{1}{2}(\frac{1}{2}^-) \text{ Status: } ***$$

Seen in $\Xi_c' \pi$ decays. The simplest assignment, based on the mass, width, and decay mode, is that this belongs in the same SU(4) multiplet as the $\Lambda(1405)$ and the $\Lambda_c(2595)^+$, but the spin and parity have not been measured.

 $\Xi_c(2790)$ MASSES

The masses are obtained from the mass-difference measurements that follow.

 $\Xi_c(2790)^+$ MASS

VALUE (MeV)	DOCUMENT ID
2791.9 ± 0.5 OUR FIT	

 $\Xi_c(2790)^0$ MASS

VALUE (MeV)	DOCUMENT ID
2793.9 ± 0.5 OUR FIT	

 $\Xi_c(2790) - \Xi_c'$ MASS DIFFERENCES $m_{\Xi_c(2790)^+} - m_{\Xi_c^+}$

VALUE (MeV)	EVTs	DOCUMENT ID	TECN	COMMENT
213.20 ± 0.22 OUR FIT				
213.2 ± 0.2 ± 0.1				
• • • We do not use the following data for averages, fits, limits, etc. • • •				
211.2 ± 1.3 ± 1.0	18	CSORNA	01	CLEO $e^+e^- \approx \Upsilon(4S)$

Baryon Particle Listings

 $\Xi_c(2790), \Xi_c(2815)$ $m_{\Xi_c(2790)^0} - m_{\Xi_c^+}$

VALUE (MeV)	EVTs	DOCUMENT ID	TECN	COMMENT
215.70 ± 0.22 OUR FIT				
215.7 ± 0.2 ± 0.1		YELTON	16	BELL 1241 and 7055 evts
• • • We do not use the following data for averages, fits, limits, etc. • • •				
216.2 ± 1.3 ± 1.0	14	CSORNA	01	CLEO $e^+e^- \approx \Upsilon(4S)$

 $\Xi_c(2790)^+ - \Xi_c(2790)^0$ MASS DIFFERENCE

VALUE (MeV)	DOCUMENT ID	TECN	COMMENT
-2.0 ± 0.7 OUR FIT			
-3.3 ± 0.4 ± 0.5	YELTON	16	BELL 2231 and 1241 evts
• • • We do not use the following data for averages, fits, limits, etc. • • •			

 $\Xi_c(2790)$ WIDTHS $\Xi_c(2790)^+$ WIDTH

VALUE (MeV)	CL%	EVTs	DOCUMENT ID	TECN	COMMENT
8.9 ± 0.6 ± 0.8		2231	YELTON	16	BELL e^+e^- , Υ regions
• • • We do not use the following data for averages, fits, limits, etc. • • •					
<15	90		CSORNA	01	CLEO $e^+e^- \approx \Upsilon(4S)$

 $\Xi_c(2790)^0$ WIDTH

VALUE (MeV)	CL%	EVTs	DOCUMENT ID	TECN	COMMENT
10.0 ± 0.7 ± 0.8		1241	YELTON	16	BELL e^+e^- , Υ regions
• • • We do not use the following data for averages, fits, limits, etc. • • •					
<12	90		CSORNA	01	CLEO $e^+e^- \approx \Upsilon(4S)$

 $\Xi_c(2790)$ DECAY MODES

Mode	Fraction (Γ_i/Γ)
Γ_1 $\Xi_c^- \pi$	seen
Γ_2 $\Xi_c^0 \gamma$	
Γ_3 $\Xi_c^+ \gamma$	
Γ_4 $\Lambda_c^+ K^-$	seen

 $\Xi_c(2790)$ BRANCHING RATIOS

$\Gamma(\Xi_c^- \pi)/\Gamma_{\text{total}}$	DOCUMENT ID	TECN	COMMENT	Γ_1/Γ
seen	YELTON	16	BELL e^+e^- , Υ regions	
seen	CSORNA	01	CLEO $e^+e^- \approx \Upsilon(4S)$	

$\Gamma(\Xi_c^0 \gamma)/\Gamma(\Xi_c^- \pi)$	DOCUMENT ID	TECN	CHG	COMMENT	Γ_2/Γ_1	
0.13 ± 0.03 ± 0.02	401	1	YELTON	20	BELL 0 e^+e^- at $\Upsilon(4S)$	

¹ Assumes $B(\Xi_c^+ \rightarrow \Xi_c^+ \gamma) = 100\%$, noting no strong decay of the Ξ_c^+ is permitted in the available phase space. YELTON 20 measures $B(\Xi_c(2790)^0 \rightarrow \Xi_c^0 \gamma)/B(\Xi_c(2790)^0 \rightarrow \Xi_c^+ \pi^- \rightarrow \Xi_c^+ \gamma \pi^-)$.

$\Gamma(\Xi_c^+ \gamma)/\Gamma(\Xi_c^- \pi)$	DOCUMENT ID	TECN	CHG	COMMENT	Γ_3/Γ_1	
<0.06	90	1	YELTON	20	BELL + e^+e^- at $\Upsilon(4S)$	

¹ Assumes $B(\Xi_c^0 \rightarrow \Xi_c^0 \gamma) = 100\%$, noting no strong decay of the Ξ_c^0 is permitted in the available phase space. YELTON 20 measures $B(\Xi_c(2790)^+ \rightarrow \Xi_c^+ \gamma)/B(\Xi_c(2790)^+ \rightarrow \Xi_c^0 \pi^+ \rightarrow \Xi_c^0 \gamma \pi^+)$.

$\Gamma(\Lambda_c^+ K^-)/\Gamma_{\text{total}}$	DOCUMENT ID	TECN	COMMENT	Γ_4/Γ	
seen	1.5k	1	AAIJ	23x	LHCB $B^- \rightarrow \Lambda_c^+ \bar{K}^-$

¹ AAIJ 23x observes this decay mode at 3.7σ significance from a study of the $\Lambda_c^+ K^-$ system within $B^- \rightarrow \Lambda_c^+ \bar{K}^-$ decays.

 $\Xi_c(2790)$ REFERENCES

AAIJ	23x	PR D108 012020	R. Aaij et al.	(LHCb Collab.)
YELTON	20	PR D102 071103	J. Yelton et al.	(BELLE Collab.)
YELTON	16	PR D94 052011	J. Yelton et al.	(BELLE Collab.)
CSORNA	01	PRL 86 4243	S.E. Csorna et al.	(CLEO Collab.)

 $\Xi_c(2815)$

$$I(J^P) = \frac{1}{2}(\frac{3}{2}^-) \text{ Status: } ***$$

Seen in both $\Xi_c' \pi$ and $\Xi_c \pi \pi$ decays. The simplest assignment is that this belongs to the same SU(4) multiplet as the $\Lambda(1520)$ and the $\Lambda_c(2625)$, but the spin and parity have not been measured.

 $\Xi_c(2815)$ MASSES

The masses are obtained from the mass-difference measurements that follow.

 $\Xi_c(2815)^+$ MASS

VALUE (MeV)	EVTs	DOCUMENT ID	TECN	COMMENT
2816.51 ± 0.25 OUR FIT				Error includes scale factor of 1.2.
• • • We do not use the following data for averages, fits, limits, etc. • • •				
2817.0 ± 1.2 $\pm_{-0.6}^{+0.7}$	73 ± 10	LESIAK	08	BELL $e^+e^- \approx \Upsilon(4S)$

 $\Xi_c(2815)^0$ MASS

VALUE (MeV)	EVTs	DOCUMENT ID	TECN	COMMENT
2819.79 ± 0.30 OUR FIT				Error includes scale factor of 1.1.
• • • We do not use the following data for averages, fits, limits, etc. • • •				
2820.4 ± 1.4 $\pm_{-1.0}^{+0.9}$	48 ± 8	LESIAK	08	BELL $e^+e^- \approx \Upsilon(4S)$

 $\Xi_c(2815) - \Xi_c$ MASS DIFFERENCES $m_{\Xi_c(2815)^+} - m_{\Xi_c^+}$

VALUE (MeV)	EVTs	DOCUMENT ID	TECN	COMMENT
348.80 ± 0.10 OUR FIT				
348.80 ± 0.08 ± 0.06	941	YELTON	16	BELL e^+e^- , Υ regions
• • • We do not use the following data for averages, fits, limits, etc. • • •				
348.6 ± 0.6 ± 1.0	20	ALEXANDER	99b	CLE2 $e^+e^- \approx \Upsilon(4S)$

 $m_{\Xi_c(2815)^0} - m_{\Xi_c^0}$

VALUE (MeV)	EVTs	DOCUMENT ID	TECN	COMMENT
349.35 ± 0.11 OUR FIT				
349.35 ± 0.08 ± 0.07	1258	YELTON	16	BELL e^+e^- , Υ regions
• • • We do not use the following data for averages, fits, limits, etc. • • •				
347.2 ± 0.7 ± 2.0	9	ALEXANDER	99b	CLE2 $e^+e^- \approx \Upsilon(4S)$

 $\Xi_c(2815)^+ - \Xi_c(2815)^0$ MASS DIFFERENCE $m_{\Xi_c(2815)^+} - m_{\Xi_c(2815)^0}$

VALUE (MeV)	DOCUMENT ID	TECN	COMMENT
-3.27 ± 0.27 OUR FIT			
• • • We do not use the following data for averages, fits, limits, etc. • • •			
-3.47 ± 0.12 ± 0.48	YELTON	16	BELL 941 and 1258 evts
-3.4 ± 1.9 ± 0.9	LESIAK	08	BELL 73 & 48 events

 $\Xi_c(2815)$ WIDTHS $\Xi_c(2815)^+$ WIDTH

VALUE (MeV)	CL%	EVTs	DOCUMENT ID	TECN	COMMENT
2.43 ± 0.20 ± 0.17		941	YELTON	16	BELL e^+e^- , Υ regions
• • • We do not use the following data for averages, fits, limits, etc. • • •					
<3.5	90		ALEXANDER	99b	CLE2 $e^+e^- \approx \Upsilon(4S)$

 $\Xi_c(2815)^0$ WIDTH

VALUE (MeV)	CL%	EVTs	DOCUMENT ID	TECN	COMMENT
2.54 ± 0.18 ± 0.17		1258	YELTON	16	BELL e^+e^- , Υ regions
• • • We do not use the following data for averages, fits, limits, etc. • • •					
<6.5	90		ALEXANDER	99b	CLE2 $e^+e^- \approx \Upsilon(4S)$

 $\Xi_c(2815)$ DECAY MODES

The $\Xi_c \pi \pi$ modes are consistent with being entirely via $\Xi_c(2645) \pi$.

Mode	Fraction (Γ_i/Γ)
Γ_1 $\Xi_c^- \pi$	seen
Γ_2 $\Xi_c^-(2645) \pi$	seen
Γ_3 $\Xi_c^0 \gamma$	seen
Γ_4 $\Xi_c^+ \gamma$	

$\Gamma(\Xi_c^- \pi)/\Gamma_{\text{total}}$	DOCUMENT ID	TECN	COMMENT	Γ_1/Γ
seen	YELTON	16	BELL e^+e^- , Υ regions	
seen	ALEXANDER	99b	CLE2 $e^+e^- \approx \Upsilon(4S)$	

See key on page 1171

Baryon Particle Listings

 $\Xi_c(2815)$, $\Xi_c(2882)$, $\Xi_c(2923)$, $\Xi_c(2930)$

$\Gamma(\Xi_c(2645)\pi)/\Gamma_{\text{total}}$		Γ_2/Γ	
VALUE	DOCUMENT ID	TECN	COMMENT
seen	YELTON	16	BELL e^+e^- , Υ regions
seen	LESIAK	08	BELL $e^+e^- \approx \Upsilon(4S)$

$\Gamma(\Xi_c^0\gamma)/\Gamma(\Xi_c(2645)\pi)$		Γ_3/Γ_2			
VALUE	EVTS	DOCUMENT ID	TECN	CHG	COMMENT
$0.41 \pm 0.05 \pm 0.03$	222	¹ YELTON	20	BELL	0 e^+e^- at $\Upsilon(4S)$

¹ Assumes $B(\Xi_c(2645)^+ \rightarrow \Xi_c^0\pi^+) = 100\%$, which is the only strong decay of the $\Xi_c(2645)$ permitted in the available phase space. YELTON 20 measures $B(\Xi_c(2815)^0 \rightarrow \Xi_c^0\gamma)/B(\Xi_c(2815)^0 \rightarrow \Xi_c(2645)^+\pi^- \rightarrow \Xi_c^0\pi^+\pi^-)$.

$\Gamma(\Xi_c^+\gamma)/\Gamma(\Xi_c(2645)\pi)$		Γ_4/Γ_2			
VALUE	CL%	DOCUMENT ID	TECN	CHG	COMMENT
<0.09	90	¹ YELTON	20	BELL	+ e^+e^- at $\Upsilon(4S)$

¹ Assumes $B(\Xi_c(2645)^0 \rightarrow \Xi_c^+\pi^-) = 100\%$, which is the only strong decay of the $\Xi_c(2645)$ permitted in the available phase space. YELTON 20 measures $B(\Xi_c(2815)^+ \rightarrow \Xi_c^+\gamma)/B(\Xi_c(2815)^+ \rightarrow \Xi_c(2645)^0\pi^+ \rightarrow \Xi_c^+\pi^+\pi^-)$.

 $\Xi_c(2815)$ REFERENCES

YELTON	20	PR D102 071103	J. Yelton et al.	(BELLE Collab.)
YELTON	16	PR D94 052011	J. Yelton et al.	(BELLE Collab.)
LESIAK	08	PL B665 9	T. Lesiak et al.	(BELLE Collab.)
ALEXANDER	99B	PRL 83 3390	J.P. Alexander et al.	(CLEO Collab.)

$\Xi_c(2882)$ $I(J^P) = ?(??)$ Status: *

OMITTED FROM SUMMARY TABLE

 $\Xi_c(2882)$ MASS

VALUE (MeV)	EVTS	DOCUMENT ID	TECN	COMMENT
$2881.8 \pm 3.1 \pm 0.5$	1.5k	¹ AAIJ	23x	LHCB $B^- \rightarrow \Lambda_c^+\bar{\Lambda}_c^- K^-$

¹ AAIJ 23x finds evidence of this state with a local significance of 3.8σ .

 $\Xi_c(2882)$ WIDTH

VALUE (MeV)	EVTS	DOCUMENT ID	TECN	COMMENT
$12.4 \pm 5.3 \pm 5.8$	1.5k	¹ AAIJ	23x	LHCB $B^- \rightarrow \Lambda_c^+\bar{\Lambda}_c^- K^-$

¹ AAIJ 23x finds evidence of this state with a local significance of 3.8σ .

 $\Xi_c(2882)$ DECAY MODES

Mode	Fraction (Γ_i/Γ)
Γ_1 $\Lambda_c^+ K^-$	seen

 $\Xi_c(2882)$ BRANCHING RATIOS

$\Gamma(\Lambda_c^+ K^-)/\Gamma_{\text{total}}$		Γ_1/Γ		
VALUE	EVTS	DOCUMENT ID	TECN	COMMENT
seen	1.5k	AAIJ	23x	LHCB $B^- \rightarrow \Lambda_c^+\bar{\Lambda}_c^- K^-$

 $\Xi_c(2882)$ REFERENCES

AAIJ	23X	PR D108 012020	R. Aaij et al.	(LHCb Collab.)
------	-----	----------------	----------------	----------------

$\Xi_c(2923)$ $I(J^P) = ?(??)$ Status: **

OMITTED FROM SUMMARY TABLE

 $\Xi_c(2923)$ MASSES

$\Xi_c(2923)^0$ MASS		$\Xi_c(2923)^+$ MASS		
VALUE (MeV)	EVTS	DOCUMENT ID	TECN	COMMENT
2923.2 ± 0.4	OUR AVERAGE	Error includes scale factor of 1.2.		
$2924.5 \pm 0.4 \pm 1.1$	1.5k	¹ AAIJ	23x	LHCB $B^- \rightarrow \Lambda_c^+\bar{\Lambda}_c^- K^-$
$2923.04 \pm 0.25 \pm 0.24$	5.4k	² AAIJ	20x	LHCB pp at 13 TeV

¹ AAIJ 23x studies the $\Lambda_c^+ K^-$ system within $B^- \rightarrow \Lambda_c^+\bar{\Lambda}_c^- K^-$ decays.
² AAIJ 20x uses a prompt $\Lambda_c^+ K^-$ sample, and reports $2923.04 \pm 0.25 \pm 0.20 \pm 0.14$ MeV where the last uncertainty is due to the Λ_c^+ mass.

 $\Xi_c(2923)$ WIDTHS

$\Xi_c(2923)^0$ WIDTH		$\Xi_c(2923)^+$ WIDTH		
VALUE (MeV)	EVTS	DOCUMENT ID	TECN	COMMENT
5.8 ± 1.3	OUR AVERAGE			
$4.8 \pm 0.9 \pm 1.5$	1.5k	¹ AAIJ	23x	LHCB $B^- \rightarrow \Lambda_c^+\bar{\Lambda}_c^- K^-$
$7.1 \pm 0.8 \pm 1.8$	5.4k	² AAIJ	20x	LHCB pp at 13 TeV

¹ AAIJ 23x studies the $\Lambda_c^+ K^-$ system within $B^- \rightarrow \Lambda_c^+\bar{\Lambda}_c^- K^-$ decays.
² AAIJ 20x uses a prompt $\Lambda_c^+ K^-$ sample

 $\Xi_c(2923)$ DECAY MODES

Mode	Fraction (Γ_i/Γ)
Γ_1 $\Lambda_c^+ K^-$	seen

 $\Xi_c(2923)$ BRANCHING RATIOS

$\Gamma(\Lambda_c^+ K^-)/\Gamma_{\text{total}}$		Γ_1/Γ		
VALUE	EVTS	DOCUMENT ID	TECN	COMMENT
seen	1.5k	AAIJ	23x	LHCB $B^- \rightarrow \Lambda_c^+\bar{\Lambda}_c^- K^-$
seen	5.4k	AAIJ	20x	LHCB pp at 13 TeV

 $\Xi_c(2923)$ REFERENCES

AAIJ	23X	PR D108 012020	R. Aaij et al.	(LHCb Collab.)
AAIJ	20X	PRL 124 222001	R. Aaij et al.	(LHCb Collab.)

$\Xi_c(2930)$ $I(J^P) = ?(??)$ Status: **

OMITTED FROM SUMMARY TABLE

 $\Xi_c(2930)$ MASSES

$\Xi_c(2930)^+$ MASS		$\Xi_c(2930)^0$ MASS		
VALUE (MeV)	EVTS	DOCUMENT ID	TECN	COMMENT
$2942.3 \pm 4.4 \pm 1.5$	21	LI	18D	BELL e^+e^- at $\Upsilon(4S)$

 $\Xi_c(2930)^0$ MASS

VALUE (MeV)	EVTS	DOCUMENT ID	TECN	COMMENT
2938.55 ± 0.30	OUR AVERAGE			
$2938.5 \pm 0.9 \pm 2.3$	1.5k	¹ AAIJ	23x	LHCB $B^- \rightarrow \Lambda_c^+\bar{\Lambda}_c^- K^-$
$2938.55 \pm 0.21 \pm 0.22$	10.4k	² AAIJ	20x	LHCB pp at 13 TeV

••• We do not use the following data for averages, fits, limits, etc. •••

2928.9 ± 3.0	± 0.9 ± 12.0	61	LI	18A	BELL e^+e^- at $\Upsilon(4S)$
2931	± 3	± 5	34	AUBERT	08H BABR $\Upsilon(4S) \rightarrow B\bar{B}$

¹ AAIJ 23x studies the $\Lambda_c^+ K^-$ system within $B^- \rightarrow \Lambda_c^+\bar{\Lambda}_c^- K^-$ decays.
² AAIJ 20x uses a prompt $\Lambda_c^+ K^-$ sample and reports $2938.55 \pm 0.21 \pm 0.17 \pm 0.14$ MeV where the last uncertainty is due to the Λ_c^+ mass. Observes that the broader resonance at 2930 MeV seen in $B^- \rightarrow K^- \Lambda_c^+\bar{\Lambda}_c^-$ by LI 18A and AUBERT 08H resolves into two narrower peaks at approximately 2939 MeV and 2923 MeV.

 $\Xi_c(2930)^+ - \Xi_c(2930)^0$ MASS DIFFERENCE

VALUE (MeV)	EVTS	DOCUMENT ID	TECN	COMMENT	
13.4 ± 5.3	± 1.7 ± 12.1	21	¹ LI	18D	BELL e^+e^- at $\Upsilon(4S)$

¹ This LI 18D value is not independent of the mass measurements.

 $\Xi_c(2930)$ WIDTHS

$\Xi_c(2930)^+$ WIDTH		$\Xi_c(2930)^0$ WIDTH		
VALUE (MeV)	EVTS	DOCUMENT ID	TECN	COMMENT
$14.8 \pm 8.8 \pm 2.5$	21	LI	18D	BELL e^+e^- at $\Upsilon(4S)$

 $\Xi_c(2930)^0$ WIDTH

VALUE (MeV)	EVTS	DOCUMENT ID	TECN	COMMENT	
$10.2 \pm 0.8 \pm 1.1$	10.4k	¹ AAIJ	20x	LHCB pp at 13 TeV	
$11.0 \pm 1.9 \pm 7.5$	1.5k	² AAIJ	23x	LHCB $B^- \rightarrow \Lambda_c^+\bar{\Lambda}_c^- K^-$	
19.5 ± 8.4	± 5.9 ± 7.9	61	LI	18A	BELL e^+e^- at $\Upsilon(4S)$
36 ± 7	± 11	34	AUBERT	08H	BABR $\Upsilon(4S) \rightarrow B\bar{B}$

¹ AAIJ 20x uses a prompt $\Lambda_c^+ K^-$ sample and observes that the broader resonance at 2930 MeV seen in $B^- \rightarrow K^- \Lambda_c^+\bar{\Lambda}_c^-$ by LI 18A and AUBERT 08H resolves into two narrower peaks at approximately 2939 MeV and 2923 MeV.
² AAIJ 23x studies the $\Lambda_c^+ K^-$ system within $B^- \rightarrow \Lambda_c^+\bar{\Lambda}_c^- K^-$ decays.

Baryon Particle Listings

$\Xi_c(2930)$, $\Xi_c(2970)$

$\Xi_c(2930)$ DECAY MODES

Mode	Fraction (Γ_i/Γ)
$\Gamma_1 \Lambda_c^+ K^-$	seen
$\Gamma_2 \Lambda_c^+ K_S^0$	seen

$\Xi_c(2930)$ BRANCHING RATIOS

$\Gamma(\Lambda_c^+ K^-)/\Gamma_{\text{total}}$					Γ_1/Γ
VALUE	EVTs	DOCUMENT ID	TECN	COMMENT	
seen	1.5k	AAIJ	23x LHCB	$B^- \rightarrow \Lambda_c^+ \bar{K}^- K^-$	
seen	10.4k	AAIJ	20x LHCB	pp at 13 TeV	
seen	61	LI	18A BELL	Significance 5.1 std	
seen	34	AUBERT	08H BABR	e^+e^- at $\Upsilon(4S)$	

$\Gamma(\Lambda_c^+ K_S^0)/\Gamma_{\text{total}}$					Γ_2/Γ
VALUE	EVTs	DOCUMENT ID	TECN	COMMENT	
seen	21	LI	18D BELL	Significance 4.1 std	

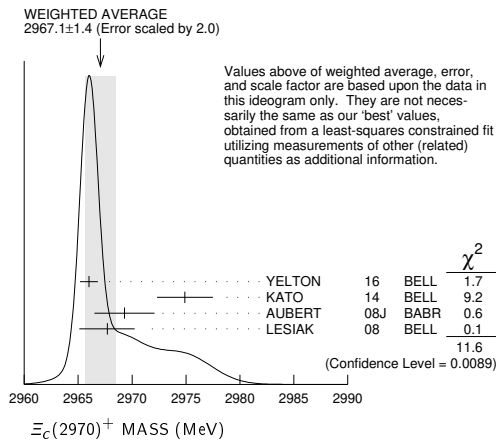
$\Xi_c(2930)$ REFERENCES

AAIJ	23X	PR D108 012020	R. Aaij <i>et al.</i>	(LHCb Collab.)
AAIJ	20X	PRL 124 222001	R. Aaij <i>et al.</i>	(LHCb Collab.)
LI	18A	EPJ C78 252	Y.B. Li <i>et al.</i>	(BELLE Collab.)
LI	18D	EPJ C78 928	Y.B. Li <i>et al.</i>	(BELLE Collab.)
AUBERT	08H	PR D77 031101	B. Aubert <i>et al.</i>	(BABAR Collab.)

$\Xi_c(2970)$ $J(P) = \frac{1}{2}(\frac{1}{2}^+)$ Status: ***
 was $\Xi_c(2980)$
 $J^P = 1/2^+$ is favored by MOON 21.

$\Xi_c(2970)$ MASSES

$\Xi_c(2970)^+$ MASS				
VALUE (MeV)	EVTs	DOCUMENT ID	TECN	COMMENT
2964.3 ± 1.5 OUR FIT				Error includes scale factor of 3.9.
2967.1 ± 1.4 OUR AVERAGE				Error includes scale factor of 2.0. See the ideogram below.
2966.0 ± 0.8 ± 0.2	0.9k	YELTON	16 BELL	$e^+e^- \rightarrow \Upsilon(4S), \Upsilon(5S)$ and continuum
2974.9 ± 1.5 ± 2.1	244 ± 39	KATO	14 BELL	$e^+e^- \rightarrow \Upsilon(1S)$ to $\Upsilon(5S)$
2969.3 ± 2.2 ± 1.7	756 ± 206	AUBERT	08J BABR	$e^+e^- \approx 10.58$ GeV
2967.7 ± 2.3 ± 1.1 ± 1.2	78 ± 13	LESIAK	08 BELL	$e^+e^- \approx \Upsilon(4S)$
• • • We do not use the following data for averages, fits, limits, etc. • • •				
2978.5 ± 2.1 ± 2.0	405 ± 51	CHISTOV	06 BELL	See KATO 14



$\Xi_c(2970)^0$ MASS

The evidence is statistically weaker for this charge state.

VALUE (MeV)	EVTs	DOCUMENT ID	TECN	COMMENT
2967.1 ± 1.7 OUR FIT				Error includes scale factor of 6.7.
2965.9 ± 2.2 OUR AVERAGE				Error includes scale factor of 7.4.
2964.88 ± 0.26 ± 0.20	11.7k	¹ AAIJ	20x LHCB	pp at 13 TeV
2970.8 ± 0.7 ± 0.2	1.4k	YELTON	16 BELL	$e^+e^- \rightarrow \Upsilon(4S), \Upsilon(5S)$, continuum
2972.9 ± 4.4 ± 1.6	67 ± 44	AUBERT	08J BABR	$e^+e^- \approx 10.58$ GeV
2965.7 ± 2.4 ± 1.1 ± 1.2	57 ± 13	LESIAK	08 BELL	$e^+e^- \approx \Upsilon(4S)$
2977.1 ± 8.8 ± 3.5	42 ± 24	CHISTOV	06 BELL	$e^+e^- \approx \Upsilon(4S)$

¹AAIJ 20x reports 2964.88 ± 0.26 ± 0.14 ± 0.14 MeV where the last uncertainty is due to the Λ_c^+ mass. Further studies are required to establish whether the narrow resonance at 2965 MeV is a different baryon from the narrow resonance at 2970 MeV seen by YELTON 16.

$\Xi_c(2970) - \Xi_c$ MASS DIFFERENCES

$m_{\Xi_c(2970)^+} - m_{\Xi_c^+}$				
VALUE (MeV)	EVTs	DOCUMENT ID	TECN	COMMENT
496.6 ± 1.5 OUR FIT				Error includes scale factor of 3.7.
498.1 ± 0.8 ± 0.2	916	YELTON	16 BELL	e^+e^- , Υ regions

$m_{\Xi_c(2970)^0} - m_{\Xi_c^0}$				
VALUE (MeV)	EVTs	DOCUMENT ID	TECN	COMMENT
496.7 ± 1.8 OUR FIT				Error includes scale factor of 5.3.
499.9 ± 0.7 ± 0.2	1.4k	YELTON	16 BELL	e^+e^- , Υ regions

$\Xi_c(2970)^+ - \Xi_c(2970)^0$ MASS DIFFERENCE

VALUE (MeV)	DOCUMENT ID	TECN	COMMENT
-2.8 ± 1.9 OUR FIT			Error includes scale factor of 4.8.
-4.8 ± 0.1 ± 0.5	YELTON	16 BELL	916 and 1443 evts

$\Xi_c(2970)$ WIDTHS

$\Xi_c(2970)^+$ WIDTH

VALUE (MeV)	EVTs	DOCUMENT ID	TECN	COMMENT
20.9 ± 2.4 ± 3.5 OUR AVERAGE				Error includes scale factor of 1.2.
28.1 ± 2.4 ± 1.0 ± 5.0	916	YELTON	16 BELL	e^+e^- , Υ regions
14.8 ± 2.5 ± 4.1	244 ± 39	KATO	14 BELL	$e^+e^- \Upsilon(1S)$ to $\Upsilon(5S)$
27 ± 8 ± 2	756 ± 206	AUBERT	08J BABR	$e^+e^- \approx 10.58$ GeV
18 ± 6 ± 3	78 ± 13	LESIAK	08 BELL	$e^+e^- \approx \Upsilon(4S)$
• • • We do not use the following data for averages, fits, limits, etc. • • •				
43.5 ± 7.5 ± 7.0	405 ± 51	CHISTOV	06 BELL	See KATO 14

$\Xi_c(2970)^0$ WIDTH

VALUE (MeV)	EVTs	DOCUMENT ID	TECN	COMMENT
14.1 ± 0.9 ± 1.3	11.7k	¹ AAIJ	20x LHCB	pp at 13 TeV
30.3 ± 2.3 ± 1.0 ± 1.8	1443	YELTON	16 BELL	e^+e^- , Υ regions
• • • We do not use the following data for averages, fits, limits, etc. • • •				
31 ± 7 ± 8	67 ± 44	AUBERT	08J BABR	$e^+e^- \approx 10.58$ GeV
15 ± 6 ± 3	57 ± 13	LESIAK	08 BELL	$e^+e^- \approx \Upsilon(4S)$

¹Further studies are required to establish whether the narrow resonance at 2965 MeV is a different baryon from the narrow resonance at 2970 MeV seen by YELTON 16.

$\Xi_c(2970)$ DECAY MODES

Mode	Fraction (Γ_i/Γ)
$\Gamma_1 \Lambda_c^+ \bar{K} \pi$	seen
$\Gamma_2 \Sigma_c(2455) \bar{K}$	seen
$\Gamma_3 \Lambda_c^+ \bar{K}$	not seen
$\Gamma_4 \Lambda_c^+ K^-$	seen
$\Gamma_5 \Xi_c 2\pi$	seen
$\Gamma_6 \Xi_c' \pi$	seen
$\Gamma_7 \Xi_c(2645) \pi$	seen

$\Xi_c(2970)$ BRANCHING RATIOS

$\Gamma(\Lambda_c^+ \bar{K} \pi)/\Gamma_{\text{total}}$				Γ_1/Γ
VALUE	DOCUMENT ID	TECN	COMMENT	
seen	AUBERT	08J BABR	$e^+e^- \approx \Upsilon(4S)$	
seen	CHISTOV	06 BELL	$e^+e^- \approx \Upsilon(4S)$	

$\Gamma(\Lambda_c^+ K^-)/\Gamma_{\text{total}}$				Γ_4/Γ
VALUE	EVTs	DOCUMENT ID	TECN	COMMENT
seen	11.7k	¹ AAIJ	20x LHCB	pp at 13 TeV

¹Further studies are required to establish whether the narrow resonance at 2965 MeV is a different baryon from the narrow resonance at 2970 MeV seen by YELTON 16.

$\Gamma(\Sigma_c(2455) \bar{K})/\Gamma(\Lambda_c^+ \bar{K} \pi)$			Γ_2/Γ_1
VALUE	DOCUMENT ID	TECN	COMMENT
0.55 ± 0.07 ± 0.13	AUBERT	08J BABR	$e^+e^- \approx \Upsilon(4S)$

$\Gamma(\Xi_c' \pi)/\Gamma_{\text{total}}$				Γ_6/Γ
VALUE	DOCUMENT ID	TECN	COMMENT	
seen	YELTON	16 BELL	e^+e^- , Υ regions	

$\Gamma(\Xi_c(2645) \pi)/\Gamma_{\text{total}}$				Γ_7/Γ
VALUE	DOCUMENT ID	TECN	COMMENT	
seen	LESIAK	08 BELL	$e^+e^- \approx \Upsilon(4S)$	

See key on page 1171

Baryon Particle Listings

$\Xi_c(2970)$, $\Xi_c(3055)$, $\Xi_c(3080)$, $\Xi_c(3123)$

$\Gamma(\Xi_c^+ \pi)/\Gamma(\Xi_c(2645)\pi)$ Γ_6/Γ_7

VALUE	EVTS	DOCUMENT ID	TECN	COMMENT
$1.67 \pm 0.29 \pm 0.15$ -0.09 ± 0.25	778	1 MOON	21 BELL	e^+e^- at $\Upsilon(nS)$

¹ Measurement of the ratio of $\Xi_c(2970)^+ \rightarrow \Xi_c(2645)^0 \pi^+$ versus $\Xi_c(2970)^+ \rightarrow \Xi_c^0 \pi^+$. The last uncertainty is from possible isospin-symmetry-breaking effects. MOON 21 determines from an angular analysis of the $\Xi_c^+ \pi^+ \pi^-$ final state that the spin of the $\Xi_c(2970)^+$ is strongly compatible with $J = 1/2$, assuming domination by the lowest partial wave in $\Xi_c(2970)^+ \rightarrow \Xi_c(2645)^0 \pi^+$. When further combined with the size of this ratio, MOON 21 determines from heavy quark symmetry that the spin-parity of the $\Xi_c(2970)^+$ is favored to be $J^P = 1/2^+$, with light degrees of freedom in the 0^+ state.

$\Xi_c(2970)$ REFERENCES

MOON	21	PR D103 L111101	T. J. Moon <i>et al.</i>	(BELLE Collab.)	JP
AAIJ	20X	PRL 124 222001	R. Aaij <i>et al.</i>	(LHCb Collab.)	
YELTON	16	PR D94 052011	J. Yelton <i>et al.</i>	(BELLE Collab.)	
KATO	14	PR D89 052003	Y. Kato <i>et al.</i>	(BELLE Collab.)	
AUBERT	08J	PR D77 012002	B. Aubert <i>et al.</i>	(BABAR Collab.)	
LESIAK	08	PL B665 9	T. Lesiak <i>et al.</i>	(BELLE Collab.)	
CHISTOV	06	PRL 97 162001	R. Chistov <i>et al.</i>	(BELLE Collab.)	

$\Xi_c(3055)$ $I(J^P) = ?(??)$ Status: ***

$\Xi_c(3055)$ MASSES

$\Xi_c(3055)^+$ MASS

VALUE (MeV)	EVTS	DOCUMENT ID	TECN	COMMENT
3055.9 ± 0.4	894	KATO	16 BELL	$e^+e^- \Upsilon$ region
• • • We do not use the following data for averages, fits, limits, etc. • • •				
$3058.1 \pm 1.0 \pm 2.1$	199 ± 46	KATO	14 BELL	See KATO 16
$3054.2 \pm 1.2 \pm 0.5$	218 ± 95	AUBERT	08J BABR	$e^+e^- \approx 10.58$ GeV

$\Xi_c(3055)$ WIDTHS

$\Xi_c(3055)^+$ WIDTH

VALUE (MeV)	EVTS	DOCUMENT ID	TECN	COMMENT
$7.8 \pm 1.2 \pm 1.5$		KATO	16 BELL	$e^+e^- \Upsilon$ region
• • • We do not use the following data for averages, fits, limits, etc. • • •				
$9.7 \pm 3.4 \pm 3.3$	199 ± 46	KATO	14 BELL	$e^+e^- \Upsilon(1S)$ to $\Upsilon(5S)$
$17 \pm 6 \pm 11$	218 ± 95	AUBERT	08J BABR	$e^+e^- \approx 10.58$ GeV

$\Xi_c(3055)$ DECAY MODES

Mode	Fraction (Γ_i/Γ)
Γ_1 $\Sigma^{++} K^-$	seen
Γ_2 ΛD^+	seen

$\Xi_c(3055)$ BRANCHING RATIOS

$\Gamma(\Lambda D^+)/\Gamma(\Sigma^{++} K^-)$ Γ_2/Γ_1

VALUE	DOCUMENT ID	TECN	COMMENT
$5.09 \pm 1.01 \pm 0.76$	KATO	16 BELL	721 and 103 evts

$\Xi_c(3055)$ REFERENCES

KATO	16	PR D94 032002	Y. Kato <i>et al.</i>	(BELLE Collab.)
KATO	14	PR D89 052003	Y. Kato <i>et al.</i>	(BELLE Collab.)
AUBERT	08J	PR D77 012002	B. Aubert <i>et al.</i>	(BABAR Collab.)

$\Xi_c(3080)$ $I(J^P) = \frac{1}{2}(??)$ Status: ***

$\Xi_c(3080)$ MASSES

$\Xi_c(3080)^+$ MASS

VALUE (MeV)	EVTS	DOCUMENT ID	TECN	COMMENT
3077.2 ± 0.4 OUR AVERAGE				
3077.9 ± 0.9	596	KATO	16 BELL	$e^+e^- \Upsilon$ region
$3077.0 \pm 0.4 \pm 0.2$	403 ± 60	AUBERT	08J BABR	$e^+e^- \approx 10.58$ GeV
• • • We do not use the following data for averages, fits, limits, etc. • • •				
$3076.9 \pm 0.3 \pm 0.2$	210 ± 30	KATO	14 BELL	See KATO 16
$3076.7 \pm 0.9 \pm 0.5$	326 ± 40	CHISTOV	06 BELL	See KATO 14

$\Xi_c(3080)^0$ MASS

VALUE (MeV)	EVTS	DOCUMENT ID	TECN	COMMENT
3079.9 ± 1.4 OUR AVERAGE				Error includes scale factor of 1.3.
$3079.3 \pm 1.1 \pm 0.2$	90 ± 27	AUBERT	08J BABR	$e^+e^- \approx 10.58$ GeV
$3082.8 \pm 1.8 \pm 1.5$	67 ± 20	CHISTOV	06 BELL	$e^+e^- \approx \Upsilon(4S)$

$\Xi_c(3080)$ WIDTHS

$\Xi_c(3080)^+$ WIDTH

VALUE (MeV)	EVTS	DOCUMENT ID	TECN	COMMENT
3.6 ± 1.1 OUR AVERAGE				Error includes scale factor of 1.5.
$3.0 \pm 0.7 \pm 0.4$	596	KATO	16 BELL	$e^+e^- \Upsilon$ region
$5.5 \pm 1.3 \pm 0.6$	403 ± 60	AUBERT	08J BABR	$e^+e^- \approx 10.58$ GeV
• • • We do not use the following data for averages, fits, limits, etc. • • •				
$2.4 \pm 0.9 \pm 1.6$	210 ± 30	KATO	14 BELL	See KATO 16
$6.2 \pm 1.2 \pm 0.8$	326 ± 40	CHISTOV	06 BELL	See KATO 14

$\Xi_c(3080)^0$ WIDTH

VALUE (MeV)	EVTS	DOCUMENT ID	TECN	COMMENT
5.6 ± 2.2 OUR AVERAGE				
$5.9 \pm 2.3 \pm 1.5$	90 ± 27	AUBERT	08J BABR	$e^+e^- \approx 10.58$ GeV
$5.2 \pm 3.1 \pm 1.8$	67 ± 20	CHISTOV	06 BELL	$e^+e^- \approx \Upsilon(4S)$

$\Xi_c(3080)$ DECAY MODES

Mode	Fraction (Γ_i/Γ)
Γ_1 $\Lambda_c^+ \bar{K} \pi$	seen
Γ_2 $\Sigma_c(2455) \bar{K}$	seen
Γ_3 $\Sigma_c(2455)^{++} K^-$	seen
Γ_4 $\Sigma_c(2520)^{++} K^-$	seen
Γ_5 $\Sigma_c(2455) \bar{K} + \Sigma_c(2520) \bar{K}$	seen
Γ_6 $\Lambda_c^+ \bar{K}$	not seen
Γ_7 $\Lambda_c^+ \bar{K} \pi^+ \pi^-$	not seen
Γ_8 ΛD^+	seen

$\Xi_c(3080)$ BRANCHING RATIOS

$\Gamma(\Sigma_c(2455) \bar{K})/\Gamma(\Lambda_c^+ \bar{K} \pi)$ Γ_2/Γ_1

VALUE	DOCUMENT ID	TECN	COMMENT
0.45 ± 0.06 OUR AVERAGE			
$0.45 \pm 0.05 \pm 0.05$	AUBERT	08J BABR	in $\Lambda_c^+ K^- \pi^+$
$0.44 \pm 0.12 \pm 0.07$	AUBERT	08J BABR	in $\Lambda_c^+ K_S^0 \pi^-$

$\Gamma(\Sigma_c(2520)^{++} K^-)/\Gamma(\Sigma_c(2455)^{++} K^-)$ Γ_4/Γ_3

VALUE	DOCUMENT ID	TECN	COMMENT
$1.07 \pm 0.27 \pm 0.04$	KATO	16 BELL	234 and 176 evts

$[\Gamma(\Sigma_c(2455) \bar{K}) + \Gamma(\Sigma_c(2520) \bar{K})]/\Gamma(\Lambda_c^+ \bar{K} \pi)$ Γ_5/Γ_1

VALUE	DOCUMENT ID	TECN	COMMENT
0.89 ± 0.12 OUR AVERAGE			
$0.95 \pm 0.14 \pm 0.06$	AUBERT	08J BABR	in $\Lambda_c^+ K^- \pi^+$
$0.78 \pm 0.21 \pm 0.05$	AUBERT	08J BABR	in $\Lambda_c^+ K_S^0 \pi^-$

$\Gamma(\Lambda D^+)/\Gamma(\Sigma_c(2455)^{++} K^-)$ Γ_8/Γ_3

VALUE	DOCUMENT ID	TECN	COMMENT
$1.29 \pm 0.30 \pm 0.15$	KATO	16 BELL	186 and 176 evts

$\Xi_c(3080)$ REFERENCES

KATO	16	PR D94 032002	Y. Kato <i>et al.</i>	(BELLE Collab.)
KATO	14	PR D89 052003	Y. Kato <i>et al.</i>	(BELLE Collab.)
AUBERT	08J	PR D77 012002	B. Aubert <i>et al.</i>	(BABAR Collab.)
CHISTOV	06	PRL 97 162001	R. Chistov <i>et al.</i>	(BELLE Collab.)

$\Xi_c(3123)$ $I(J^P) = ?(??)$ Status: *

OMITTED FROM SUMMARY TABLE

A peak in the $\Sigma_c(2520)^{++} K^- \rightarrow \Lambda_c^+ K^- \pi^+$ mass spectrum with a significance of 3.6 standard deviations. KATO 14 finds no evidence for this state.

$\Xi_c(3123)$ MASSES

$\Xi_c(3123)^+$ MASS

VALUE (MeV)	EVTS	DOCUMENT ID	TECN	COMMENT
$3122.9 \pm 1.3 \pm 0.3$	101 ± 35	AUBERT	08J BABR	$e^+e^- \approx 10.58$ GeV

$\Xi_c(3123)$ WIDTHS

$\Xi_c(3123)^+$ WIDTH

VALUE (MeV)	EVTS	DOCUMENT ID	TECN	COMMENT
$4.4 \pm 3.4 \pm 1.7$	101 ± 35	AUBERT	08J BABR	$e^+e^- \approx 10.58$ GeV

$\Xi_c(3123)$ REFERENCES

KATO	14	PR D89 052003	Y. Kato <i>et al.</i>	(BELLE Collab.)
AUBERT	08J	PR D77 012002	B. Aubert <i>et al.</i>	(BABAR Collab.)

Baryon Particle Listings

Ω_c^0



$I(J^P) = 0(\frac{1}{2}^+)$ Status: ***

The quantum numbers have not been measured, but are simply assigned in accord with the quark model, in which the Ω_c^0 is the ssc ground state. No absolute branching fractions have been measured.

Ω_c^0 MASS

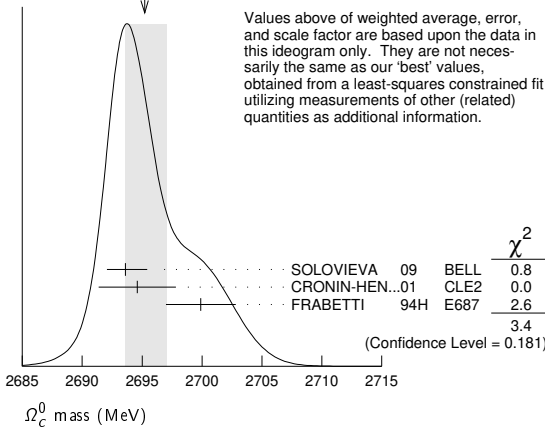
VALUE (MeV) EVTS DOCUMENT ID TECN COMMENT
2695.2 ± 1.7 OUR FIT Error includes scale factor of 1.3.

2695.2^{+1.8}_{-1.6} OUR AVERAGE Error includes scale factor of 1.3. See the ideogram below.

VALUE (MeV)	EVTS	DOCUMENT ID	TECN	COMMENT
2693.6 ± 0.3 ^{+1.8} _{-1.5}	725	SOLOVIEVA 09	BELL	$\Omega_c^- \pi^+$ in $e^+ e^- \rightarrow \Upsilon(4S)$
2694.6 ± 2.6 ± 1.9	40	¹ CRONIN-HEN...01	CLE2	$e^+ e^- \approx 10.6$ GeV
2699.9 ± 1.5 ± 2.5	42	² FRABETTI 94H	E687	γ Be, $\bar{E}_\gamma = 221$ GeV
2705.9 ± 3.3 ± 2.0	10	³ FRABETTI 93	E687	γ Be, $\bar{E}_\gamma = 221$ GeV
2719.0 ± 7.0 ± 2.5	11	⁴ ALBRECHT 92H	ARG	$e^+ e^- \approx 10.6$ GeV
2740 ± 20	3	BIAGI 85B	SPEC	Σ^- Be 135 GeV/c

- • • We do not use the following data for averages, fits, limits, etc. • • •
- ¹ CRONIN-HENNESSY 01 sees 40.4 ± 9.0 events in a sum over five channels.
- ² FRABETTI 94H claims a signal of 42.5 ± 8.8 $\Sigma^+ K^- K^- \pi^+$ events. The background is about 24 events.
- ³ FRABETTI 93 claims a signal of 10.3 ± 3.9 $\Omega^- \pi^+$ events above a background of 5.8 events.
- ⁴ ALBRECHT 92H claims a signal of 11.5 ± 4.3 $\Xi^- K^- \pi^+ \pi^+$ events. The background is about 5 events.

WEIGHTED AVERAGE
 2695.2+1.8-1.6 (Error scaled by 1.3)



Values above of weighted average, error, and scale factor are based upon the data in this ideogram only. They are not necessarily the same as our 'best' values, obtained from a least-squares constrained fit utilizing measurements of other (related) quantities as additional information.

Ω_c^0 MEAN LIFE

VALUE (10^{-15} s) EVTS DOCUMENT ID TECN COMMENT

VALUE (10^{-15} s)	EVTS	DOCUMENT ID	TECN	COMMENT
273 ± 12 OUR AVERAGE				
243 ± 48 ± 11	88	ABUDINEN 23	BEL2	$e^+ e^- \rightarrow \Omega_c^0 + X$, $\Omega_c^0 \rightarrow \Omega^- \pi^+$
276.5 ± 13.4 ± 4.5	1,2	AAIJ 22Y	LHCB	$pp \rightarrow \Omega_c X$, $\Omega_c \rightarrow p K^- K^- \pi^+$
268 ± 24 ± 10	978	^{1,3} AAIJ 18J	LHCB	$\Omega_b \rightarrow \Omega_c \mu \nu + X$, $\Omega_c \rightarrow p K^- K^- \pi^+$
72 ± 11 ± 11	64	LINK 03C	FOCS	$\Omega^- \pi^+$, $\Xi^- K^- \pi^+ \pi^+$
55 ⁺¹³ ₋₁₁ ± 18 ⁺¹⁸ ₋₂₃	86	ADAMOVIICH 95B	WA89	$\Omega^- \pi^- \pi^+ \pi^+$, $\Xi^- K^- \pi^+ \pi^+$
86 ⁺²⁷ ₋₂₀ ± 28	25	FRABETTI 95D	E687	$\Sigma^+ K^- K^- \pi^+$

- • • We do not use the following data for averages, fits, limits, etc. • • •
- ¹ Recent measurements by AAIJ 18J, AAIJ 22Y, and ABUDINEN 23 obtain consistent results that are nearly four times larger than the average result of previous experiments, $(69 \pm 12) \times 10^{-15}$ s. We go with the more recent results, mostly obtained with much larger data samples, and also note the positive correlation between the measured value and the inverse of the estimated statistical uncertainty in lifetime measurements.
- ² AAIJ 22Y reports this measurement as $(276.5 \pm 13.4 \pm 4.4 \pm 0.7) \times 10^{-15}$ s. The last uncertainty is due to the uncertainty on the D^0 lifetime $\tau_{D^0} = (410.1 \pm 1.5)$ fs from PDG 20. Measured in Ω_c produced promptly in pp collisions, using $D^0 \rightarrow K^+ K^- \pi^+ \pi^-$ as normalisation mode.
- ³ Measured using Ω_c produced in semileptonic Ω_b decays.

Ω_c^0 DECAY MODES

No absolute branching fractions have been measured. The following are branching ratios relative to $\Omega^- \pi^+$.

Mode Fraction (Γ_i/Γ) Confidence level

Cabibbo-favored ($S = -3$) decays — relative to $\Omega^- \pi^+$

Mode	Fraction (Γ_i/Γ)	Confidence level
$\Omega^- \pi^+$	DEFINED AS 1	
$\Omega^- \pi^+ \pi^0$	1.80 ± 0.33	
$\Omega^- \rho^+$	>1.3	90%
$\Omega^- \pi^- 2\pi^+$	0.31 ± 0.05	
$\Omega^- e^+ \nu_e$	1.98 ± 0.15	
$\Omega^- \mu^+ \nu_\mu$	1.94 ± 0.21	
$\Xi^0 \bar{K}^0$	1.64 ± 0.29	
$\Xi^0 K^- \pi^+$	1.20 ± 0.18	
$\Xi^0 \bar{K}^{*0}, \bar{K}^{*0} \rightarrow K^- \pi^+$	0.68 ± 0.16	
$\Omega(2012)^- \pi^+, \Omega(2012)^- \rightarrow \Xi^0 K^-$	0.12 ± 0.05	
$\Xi^- \bar{K}^0 \pi^+$	2.12 ± 0.28	
$\Omega(2012)^- \pi^+, \Omega(2012)^- \rightarrow \Xi^- \bar{K}^0$	0.12 ± 0.06	
$\Xi^- K^- 2\pi^+$	0.63 ± 0.09	
$\Xi(1530)^0 K^- \pi^+, \Xi^{*0} \rightarrow \Xi^- \pi^+$	0.21 ± 0.06	
$\Xi^- \bar{K}^{*0} \pi^+$	0.34 ± 0.11	
$p K^- K^- \pi^+$	seen	
$\Sigma^+ K^- K^- \pi^+$	<0.32	90%
$\Lambda \bar{K}^0 \bar{K}^0$	1.72 ± 0.35	

Singly Cabibbo-suppressed modes — relative to $\Omega^- \pi^+$

$\Xi^- \pi^+$	0.25 ± 0.06	
$\Omega^- K^+$	<0.29	90%

Doubly Cabibbo-suppressed modes — relative to $\Omega^- \pi^+$

$\Xi^- K^+$	<0.07	90%
-------------	-------	-----

Ω_c^0 BRANCHING RATIOS

A few early but now obsolete measurements have been omitted. See K.A. Olive, et al. (Particle Data Group), Chinese Physics **C38** 070001 (2014).

$\Gamma(\Omega^- \pi^+ \pi^0)/\Gamma(\Omega^- \pi^+)$ Γ_2/Γ_1

VALUE	EVTS	DOCUMENT ID	TECN	COMMENT
1.80 ± 0.33 OUR AVERAGE				Error includes scale factor of 1.9.
2.00 ± 0.17 ± 0.11	403	YELTON 18	BELL	$e^+ e^- \rightarrow \Upsilon(4S)$, +higher
1.27 ± 0.31 ± 0.11	64	AUBERT 07AH	BABR	$e^+ e^- \approx \Upsilon(4S)$

$\Gamma(\Omega^- \rho^+)/\Gamma(\Omega^- \pi^+ \pi^0)$ Γ_3/Γ_2

VALUE	CL%	DOCUMENT ID	TECN	COMMENT
>0.71	90	¹ YELTON 18	BELL	$e^+ e^- \rightarrow \Upsilon(4S)$, +higher

¹ This submode fraction is evaluated from a background-subtracted signal in a mass plot. Result ignores interference effects and systematic uncertainties, which YELTON 18 claim are both small.

$\Gamma(\Omega^- \pi^- 2\pi^+)/\Gamma(\Omega^- \pi^+)$ Γ_4/Γ_1

VALUE	EVTS	DOCUMENT ID	TECN	COMMENT
0.31 ± 0.05 OUR AVERAGE				
0.32 ± 0.05 ± 0.02	108	YELTON 18	BELL	$e^+ e^- \rightarrow \Upsilon(4S)$, +higher
0.28 ± 0.09 ± 0.01	25	AUBERT 07AH	BABR	$e^+ e^- \approx \Upsilon(4S)$

$\Gamma(\Omega^- e^+ \nu_e)/\Gamma(\Omega^- \pi^+)$ Γ_5/Γ_1

VALUE	EVTS	DOCUMENT ID	TECN	COMMENT
1.98 ± 0.13 ± 0.08		LI 22A	BELL	$e^+ e^-$ at $\Upsilon(4S)$
2.4 ± 1.1 ± 0.2	11	¹ AMMAR 02	CLE2	$e^+ e^- \approx \Upsilon(4S)$

¹ AMMAR 02 reported 0.41 ± 0.19 ± 0.04 for the inverse of this branching fraction.

$\Gamma(\Omega^- \mu^+ \nu_\mu)/\Gamma(\Omega^- \pi^+)$ Γ_6/Γ_1

VALUE	DOCUMENT ID	TECN	COMMENT
1.94 ± 0.18 ± 0.10	LI 22A	BELL	$e^+ e^-$ at $\Upsilon(4S)$

$\Gamma(\Omega^- e^+ \nu_e)/\Gamma(\Omega^- \mu^+ \nu_\mu)$ Γ_5/Γ_6

VALUE	DOCUMENT ID	TECN	COMMENT
1.02 ± 0.10 ± 0.02	LI 22A	BELL	$e^+ e^-$ at $\Upsilon(4S)$

$\Gamma(\Xi^0 \bar{K}^0)/\Gamma(\Omega^- \pi^+)$ Γ_7/Γ_1

VALUE	EVTS	DOCUMENT ID	TECN	COMMENT
1.64 ± 0.26 ± 0.12	98	YELTON 18	BELL	$e^+ e^- \rightarrow \Upsilon(4S)$, +higher

See key on page 1171

Baryon Particle Listings

$$\Omega_c^0, \Omega_c(2770)^0, \Omega_c(3000)^0$$

$\Gamma(\Xi^0 K^- \pi^+)/\Gamma(\Omega^- \pi^+)$		Γ_8/Γ_1	
VALUE	EVTS	DOCUMENT ID	TECN COMMENT
$1.20 \pm 0.16 \pm 0.08$	168	YELTON 18	BELL $e^+e^- \rightarrow \Upsilon(4S)$, +higher

$\Gamma(\Xi^0 \bar{K}^{*0}, \bar{K}^{*0} \rightarrow K^- \pi^+)/\Gamma(\Xi^0 K^- \pi^+)$		Γ_9/Γ_8	
VALUE	EVTS	DOCUMENT ID	TECN COMMENT
0.57 ± 0.10	95	¹ YELTON 18	BELL $e^+e^- \rightarrow \Upsilon(4S)$, +higher

¹ This submode fraction is evaluated from a background-subtracted signal in a mass plot. Result ignores interference effects and systematic uncertainties, which YELTON 18 claim are both small.

$\Gamma(\Omega(2012)^- \pi^+, \Omega(2012)^- \rightarrow \Xi^0 K^-)/\Gamma(\Xi^0 K^- \pi^+)$		Γ_{10}/Γ_8	
VALUE (units 10^{-2})	EVTS	DOCUMENT ID	TECN COMMENT
$9.6 \pm 3.2 \pm 1.8$	28	¹ LI 21D	BELL e^+e^- at $\Upsilon(nS)$

¹ LI 21D reports the significance of the $\Omega(2012)$ signal is 4.2σ including systematic uncertainties. Also measures $B(\Omega_c^0 \rightarrow \Omega(2012)^- \pi^+, \Omega(2012)^- \rightarrow (\bar{K}\Xi^-))/B(\Omega_c^0 \rightarrow \Xi^0 K^- \pi^+) = 0.220 \pm 0.059 \pm 0.035$.

$\Gamma(\Xi^- \bar{K}^0 \pi^+)/\Gamma(\Omega^- \pi^+)$		Γ_{11}/Γ_1	
VALUE	EVTS	DOCUMENT ID	TECN COMMENT
$2.12 \pm 0.24 \pm 0.14$	349	YELTON 18	BELL $e^+e^- \rightarrow \Upsilon(4S)$, +higher

$\Gamma(\Omega(2012)^- \pi^+, \Omega(2012)^- \rightarrow \Xi^- \bar{K}^0)/\Gamma(\Xi^- \bar{K}^0 \pi^+)$		Γ_{12}/Γ_{11}	
VALUE (units 10^{-2})	EVTS	DOCUMENT ID	TECN COMMENT
$5.5 \pm 2.8 \pm 0.7$	18	¹ LI 21D	BELL e^+e^- at $\Upsilon(nS)$

¹ LI 21D reports the significance of the $\Omega(2012)$ signal is 4.2σ including systematic uncertainties. Also measures $B(\Omega_c^0 \rightarrow \Omega(2012)^- \pi^+, \Omega(2012)^- \rightarrow (\bar{K}\Xi^-))/B(\Omega_c^0 \rightarrow \Xi^0 K^- \pi^+) = 0.220 \pm 0.059 \pm 0.035$.

$\Gamma(\Xi^- K^- 2\pi^+)/\Gamma(\Omega^- \pi^+)$		Γ_{13}/Γ_1	
VALUE	EVTS	DOCUMENT ID	TECN COMMENT
0.63 ± 0.09 OUR AVERAGE			Error includes scale factor of 1.4.
$0.68 \pm 0.07 \pm 0.03$	278	YELTON 18	BELL $e^+e^- \rightarrow \Upsilon(4S)$, +higher
$0.46 \pm 0.13 \pm 0.03$	45	AUBERT 07AH	BABR $e^+e^- \approx \Upsilon(4S)$

$\Gamma(\Xi(1530)^0 K^- \pi^+, \Xi^0 \rightarrow \Xi^- \pi^+)/\Gamma(\Xi^- K^- 2\pi^+)$		Γ_{14}/Γ_{13}	
VALUE	EVTS	DOCUMENT ID	TECN COMMENT
0.33 ± 0.09	74	¹ YELTON 18	BELL $e^+e^- \rightarrow \Upsilon(4S)$, +higher

¹ This submode fraction is evaluated from a background-subtracted signal in a mass plot. Result ignores interference effects and systematic uncertainties, which YELTON 18 claim are both small.

$\Gamma(\Xi^- \bar{K}^{*0} \pi^+)/\Gamma(\Xi^- K^- 2\pi^+)$		Γ_{15}/Γ_{13}	
VALUE	EVTS	DOCUMENT ID	TECN COMMENT
0.55 ± 0.16	136	¹ YELTON 18	BELL $e^+e^- \rightarrow \Upsilon(4S)$, +higher

¹ This submode fraction is evaluated from a background-subtracted signal in a mass plot. Result ignores interference effects and systematic uncertainties, which YELTON 18 claim are both small.

$\Gamma(p K^- K^- \pi^+)/\Gamma_{\text{total}}$		Γ_{16}/Γ	
VALUE	DOCUMENT ID	TECN	COMMENT
seen	AAIJ 160	LHCb	pp at 7, 8 TeV

$\Gamma(\Sigma^+ K^- K^- \pi^+)/\Gamma(\Omega^- \pi^+)$		Γ_{17}/Γ_1	
VALUE	CL% EVTS	DOCUMENT ID	TECN COMMENT
<0.32	90 17	YELTON 18	BELL $e^+e^- \rightarrow \Upsilon(4S)$, +higher

$\Gamma(\Lambda \bar{K}^0 \bar{K}^0)/\Gamma(\Omega^- \pi^+)$		Γ_{18}/Γ_1	
VALUE	EVTS	DOCUMENT ID	TECN COMMENT
$1.72 \pm 0.32 \pm 0.14$	95	YELTON 18	BELL $e^+e^- \rightarrow \Upsilon(4S)$, +higher

$\Gamma(\Xi^- \pi^+)/\Gamma(\Omega^- \pi^+)$		Γ_{19}/Γ_1	
VALUE	EVTS	DOCUMENT ID	TECN COMMENT
$0.253 \pm 0.052 \pm 0.030$	208	HAN 23	BELL $e^+e^- \rightarrow \Upsilon(nS)$

$\Gamma(\Omega^- K^+)/\Gamma(\Omega^- \pi^+)$		Γ_{20}/Γ_1	
VALUE	CL%	DOCUMENT ID	TECN COMMENT
<0.29	90	HAN 23	BELL $e^+e^- \rightarrow \Upsilon(nS)$

$\Gamma(\Xi^- K^+)/\Gamma(\Omega^- \pi^+)$		Γ_{21}/Γ_1	
VALUE	CL%	DOCUMENT ID	TECN COMMENT
<0.070	90	HAN 23	BELL $e^+e^- \rightarrow \Upsilon(nS)$

 Ω_c^0 REFERENCES

ABUDINEN 23	PR D107 L031103	F. Abudinen et al.	(BELLE II Collab.)
HAN 23	JHEP 2301 055	X. Han et al.	(BELLE Collab.)
AAIJ 22Y	SCIB 67 479	R. Aaij et al.	(LHCb Collab.)
LI 22A	PR D105 L091101	Y.B. Li et al.	(BELLE Collab.)
LI 21D	PR D104 052005	Y.B. Li et al.	(BELLE Collab.)
PDG 20	PTEP 2020 083C01	P.A. Zyla et al.	(PDG Collab.)
AAIJ 18J	PRL 121 092003	R. Aaij et al.	(LHCb Collab.)
YELTON 18	PR D97 032001	J. Yelton et al.	(BELLE Collab.)

AAIJ 16O	PR D93 092007	R. Aaij et al.	(LHCb Collab.)
PDG 14	CP C38 070001	K. Olive et al.	(PDG Collab.)
SOLOVIEVA 09	PL B672 1	E. Solovieva et al.	(BELLE Collab.)
AUBERT 07AH	PRL 99 062001	B. Aubert et al.	(BABAR Collab.)
LINK 03C	PL B561 41	J.M. Link et al.	(FNAL FOCUS Collab.)
AMMAR 02	PRL 89 171803	R. Ammar et al.	(CLEO Collab.)
CRONIN-HEN... 01	PRL 86 3730	D. Cronin-Hennessy et al.	(CLEO Collab.)
ADAMOVIICH 95B	PL B358 151	M.I. Adamovich et al.	(CERN WA89 Collab.)
FRABETTI 95D	PL B357 678	P.L. Frabetti et al.	(FNAL E687 Collab.)
FRABETTI 94H	PL B338 106	P.L. Frabetti et al.	(FNAL E687 Collab.)
FRABETTI 93	PL B300 190	P.L. Frabetti et al.	(FNAL E687 Collab.)
ALBRECHT 92H	PL B288 367	H. Albrecht et al.	(ARGUS Collab.)
BIAGI 85B	ZPHY C28 175	S.F. Biagi et al.	(CERN WA62 Collab.)

$$\Omega_c(2770)^0$$

$$I(J^P) = 0(\frac{3}{2}^+) \text{ Status: } ***$$

The natural assignment is that this goes with the $\Sigma_c(2520)$ and $\Xi_c(2645)$ to complete the lowest mass $J^P = \frac{3}{2}^+$ SU(3) sextet, part of the SU(4) 20-plet that includes the $\Delta(1232)$. But J and P have not been measured.

 $\Omega_c(2770)^0$ MASS

The mass is obtained from the mass-difference measurement that follows.

VALUE (MeV)	DOCUMENT ID
2765.9 ± 2.0 OUR FIT	Error includes scale factor of 1.2.

 $\Omega_c(2770)^0 - \Omega_c^0$ MASS DIFFERENCE

VALUE (MeV)	EVTS	DOCUMENT ID	TECN	COMMENT
$70.7^{+0.8}_{-0.9}$ OUR FIT				
$70.7^{+0.8}_{-1.0}$ OUR AVERAGE				
$70.7 \pm 0.9^{+0.1}_{-0.9}$	54 ± 9	SOLOVIEVA 09	BELL	$\Omega_c^0 \gamma$ in $e^+e^- \rightarrow \Upsilon(4S)$
$70.8 \pm 1.0 \pm 1.1$	105 ± 22	AUBERT, BE 06i	BABR	$e^+e^- \approx \Upsilon(4S)$

 $\Omega_c(2770)^0$ DECAY MODES

The $\Omega_c(2770)^0 - \Omega_c^0$ mass difference is too small for any strong decay to occur.

Mode	Fraction (Γ_i/Γ)
$\Gamma_1 \Omega_c^0 \gamma$	presumably 100%

 $\Omega_c(2770)^0$ REFERENCES

SOLOVIEVA 09	PL B672 1	E. Solovieva et al.	(BELLE Collab.)
AUBERT, BE 06i	PRL 97 232001	B. Aubert et al.	(BABAR Collab.)

$$\Omega_c(3000)^0$$

$$I(J^P) = ?(??) \text{ Status: } ***$$

 $\Omega_c(3000)^0$ MASS

VALUE (MeV)	EVTS	DOCUMENT ID	TECN	COMMENT
3000.46 ± 0.25 OUR AVERAGE				
$3000.44 \pm 0.07^{+0.07}_{-0.13} \pm 0.23$	8.8k	¹ AAIJ 23As	LHCb	pp at 7, 8, 13 TeV
$3000.7 \pm 1.0 \pm 0.2$	38	YELTON 18B	BELL	e^+e^- at $\Upsilon(4S)$
• • • We do not use the following data for averages, fits, limits, etc. • • •				
$2999.2 \pm 0.9 \pm 0.9^{+0.19}_{-0.22}$	24	² AAIJ 21Ac	LHCb	pp at 7, 8, 13 TeV
$3000.4 \pm 0.2 \pm 0.1$	1.3k	³ AAIJ 17Ah	LHCb	pp at 7, 8, 13 TeV

¹ The third uncertainty is due to the uncertainty in the Ξ_c^+ mass, taken to be the PDG 22 fit result 2467.71 ± 0.23 MeV.

² Measured via $\Omega_b^- \rightarrow \Omega_c^{*0} \pi^- \rightarrow \Xi_c^+ K^- \pi^-$. The third uncertainty is due to the uncertainty in the Ξ_c^+ mass.

³ See AAJ 23As

 $\Omega_c(3000)^0$ WIDTH

VALUE (MeV)	EVTS	DOCUMENT ID	TECN	COMMENT
$3.83 \pm 0.23^{+1.59}_{-0.29}$	8.8k	AAIJ 23As	LHCb	pp at 7, 8, 13 TeV

• • • We do not use the following data for averages, fits, limits, etc. • • •

$4.8 \pm 2.1 \pm 2.5$	24	AAIJ 21Ac	LHCb	pp at 7, 8, 13 TeV
$4.5 \pm 0.6 \pm 0.3$	1.3k	¹ AAIJ 17Ah	LHCb	pp at 7, 8, 13 TeV

¹ See AAJ 23As.

Baryon Particle Listings

 $\Omega_c(3000)^0, \Omega_c(3050)^0, \Omega_c(3065)^0, \Omega_c(3090)^0$ $\Omega_c(3000)^0$ DECAY MODES

Mode	Fraction (Γ_i/Γ)
$\Gamma_1 \Xi_c^+ K^-$	seen

 $\Omega_c(3000)^0$ BRANCHING RATIOS

$\Gamma(\Xi_c^+ K^-)/\Gamma_{\text{total}}$	Γ_1/Γ			
VALUE	EVTS	DOCUMENT ID	TECN	COMMENT
seen	8.8k	AAIJ	23AS LHCb	pp at 7, 8, 13 TeV
seen	24	¹ AAIJ	21AC LHCb	pp at 7, 8, 13 TeV
seen	38	² YELTON	18B BELL	e^+e^- at $\Upsilon(4S)$
••• We do not use the following data for averages, fits, limits, etc. •••				
seen	1.3k	^{3,4} AAIJ	17AH LHCb	pp at 7, 8, 13 TeV

- ¹AAIJ 21AC report a significance of 6.2 σ .
²YELTON 18B report a significance of 3.9 σ .
³AAIJ 17AH report a significance of 20.4 σ .
⁴See AAIJ 23As.

 $\Omega_c(3000)^0$ REFERENCES

AAIJ	23AS	PRL 131 131902	R. Aaij <i>et al.</i>	(LHCb Collab.)
PDG	22	PTEP 2022 083C01	R.L. Workman <i>et al.</i>	(PDG Collab.)
AAIJ	21AC	PR D104 L091102	R. Aaij <i>et al.</i>	(LHCb Collab.)
YELTON	18B	PR D97 051102	J. Yelton <i>et al.</i>	(BELLE Collab.)
AAIJ	17AH	PRL 118 182001	R. Aaij <i>et al.</i>	(LHCb Collab.)

 $\Omega_c(3050)^0$

$I(J^P) = ?(??)$ Status: ***

AAIJ 21AC rejects $J = 1/2$ hypothesis at 2.2 σ . $\Omega_c(3050)^0$ MASS

VALUE (MeV)	CL%	EVTS	DOCUMENT ID	TECN	COMMENT
3050.17 \pm 0.19 OUR AVERAGE					
3050.18 \pm 0.04 \pm 0.06 \pm 0.07 \pm 0.23	8.5k	¹ AAIJ	23AS LHCb	pp at 7, 8, 13 TeV	
3050.1 \pm 0.3 \pm 0.2 \pm 0.19 \pm 0.22	33	² AAIJ	21AC LHCb	pp at 7, 8, 13 TeV	
3050.2 \pm 0.4 \pm 0.2	28	YELTON	18B BELL	e^+e^- at $\Upsilon(4S)$	
••• We do not use the following data for averages, fits, limits, etc. •••					
3050.2 \pm 0.1 \pm 0.1	970	³ AAIJ	17AH LHCb	pp at 7, 8, 13 TeV	

- ¹The third uncertainty is due to the uncertainty in the Ξ_c^+ mass, taken to be the PDG 22 fit result 2467.71 \pm 0.23 MeV.
²Measured via $\Omega_b^- \rightarrow \Omega_c^{*0} \pi^- \rightarrow \Xi_c^+ K^- \pi^-$. The third uncertainty is due to the uncertainty in the Ξ_c^+ mass.
³See AAIJ 23As.

 $\Omega_c(3050)^0$ WIDTH

VALUE (MeV)	CL%	EVTS	DOCUMENT ID	TECN	COMMENT
<1.8	95	8.5k	¹ AAIJ	23AS LHCb	pp at 7, 8, 13 TeV
••• We do not use the following data for averages, fits, limits, etc. •••					
<1.6	95	33	AAIJ	21AC LHCb	pp at 7, 8, 13 TeV
<1.2	95	970	² AAIJ	17AH LHCb	pp at 7, 8, 13 TeV

- ¹AAIJ 23As also report a central value of 0.67 \pm 0.17 \pm 0.64 MeV.
²See AAIJ 23As.

 $\Omega_c(3050)^0$ DECAY MODES

Mode	Fraction (Γ_i/Γ)
$\Gamma_1 \Xi_c^+ K^-$	seen

 $\Omega_c(3050)^0$ BRANCHING RATIOS

$\Gamma(\Xi_c^+ K^-)/\Gamma_{\text{total}}$	Γ_1/Γ			
VALUE	EVTS	DOCUMENT ID	TECN	COMMENT
seen	8.5k	AAIJ	23AS LHCb	pp at 7, 8, 13 TeV
seen	33	¹ AAIJ	21AC LHCb	pp at 7, 8, 13 TeV
seen	28	² YELTON	18B BELL	e^+e^- at $\Upsilon(4S)$
••• We do not use the following data for averages, fits, limits, etc. •••				
seen	970	^{3,4} AAIJ	17AH LHCb	pp at 7, 8, 13 TeV

- ¹AAIJ 21AC report a significance of 9.9 σ .
²YELTON 18B report a significance of 4.6 σ .
³AAIJ 17AH report a significance of 20.4 σ .
⁴See AAIJ 23As.

 $\Omega_c(3050)^0$ REFERENCES

AAIJ	23AS	PRL 131 131902	R. Aaij <i>et al.</i>	(LHCb Collab.)
PDG	22	PTEP 2022 083C01	R.L. Workman <i>et al.</i>	(PDG Collab.)
AAIJ	21AC	PR D104 L091102	R. Aaij <i>et al.</i>	(LHCb Collab.)
YELTON	18B	PR D97 051102	J. Yelton <i>et al.</i>	(BELLE Collab.)
AAIJ	17AH	PRL 118 182001	R. Aaij <i>et al.</i>	(LHCb Collab.)

 $\Omega_c(3065)^0$

$I(J^P) = ?(??)$ Status: ***

AAIJ 21AC rejects $J = 1/2$ hypothesis at 3.6 σ . $\Omega_c(3065)^0$ MASS

VALUE (MeV)	CL%	EVTS	DOCUMENT ID	TECN	COMMENT
3065.58 \pm 0.21 OUR AVERAGE					
3065.63 \pm 0.06 \pm 0.06 \pm 0.23	15k	¹ AAIJ	23AS LHCb	pp at 7, 8, 13 TeV	
3065.9 \pm 0.4 \pm 0.4 \pm 0.19 \pm 0.22	51	² AAIJ	21AC LHCb	pp at 7, 8, 13 TeV	
3064.9 \pm 0.6 \pm 0.2	82	YELTON	18B BELL	e^+e^- at $\Upsilon(4S)$	
••• We do not use the following data for averages, fits, limits, etc. •••					
3065.6 \pm 0.1 \pm 0.3	1.74k	³ AAIJ	17AH LHCb	pp at 7, 8, 13 TeV	

- ¹The third uncertainty is due to the uncertainty in the Ξ_c^+ mass, taken to be the PDG 22 fit result 2467.71 \pm 0.23 MeV.
²Measured via $\Omega_b^- \rightarrow \Omega_c^{*0} \pi^- \rightarrow \Xi_c^+ K^- \pi^-$. The third uncertainty is due to the uncertainty in the Ξ_c^+ mass.
³See AAIJ 23As.

 $\Omega_c(3065)^0$ WIDTH

VALUE (MeV)	CL%	EVTS	DOCUMENT ID	TECN	COMMENT
3.4 \pm 0.7 \pm 0.8 OUR AVERAGE					Error includes scale factor of 1.7.
3.79 \pm 0.20 \pm 0.38 \pm 0.47	15k	AAIJ	23AS LHCb	pp at 7, 8, 13 TeV	
1.7 \pm 1.0 \pm 0.5	51	AAIJ	21AC LHCb	pp at 7, 8, 13 TeV	
••• We do not use the following data for averages, fits, limits, etc. •••					
3.5 \pm 0.4 \pm 0.2	1.74k	¹ AAIJ	17AH LHCb	pp at 7, 8, 13 TeV	

- ¹See AAIJ 23As.

 $\Omega_c(3065)^0$ DECAY MODES

Mode	Fraction (Γ_i/Γ)
$\Gamma_1 \Xi_c^+ K^-$	seen

 $\Omega_c(3065)^0$ BRANCHING RATIOS

$\Gamma(\Xi_c^+ K^-)/\Gamma_{\text{total}}$	Γ_1/Γ			
VALUE	EVTS	DOCUMENT ID	TECN	COMMENT
seen	15k	AAIJ	23AS LHCb	pp at 7, 8, 13 TeV
seen	51	¹ AAIJ	21AC LHCb	pp at 7, 8, 13 TeV
seen	82	YELTON	18B BELL	e^+e^- at $\Upsilon(4S)$
••• We do not use the following data for averages, fits, limits, etc. •••				
seen	1.74k	^{2,3} AAIJ	17AH LHCb	pp at 7, 8, 13 TeV

- ¹AAIJ 21AC report a significance of 11.9 σ .
²AAIJ 17AH report a significance of 23.9 σ .
³See AAIJ 23As.

 $\Omega_c(3065)^0$ REFERENCES

AAIJ	23AS	PRL 131 131902	R. Aaij <i>et al.</i>	(LHCb Collab.)
PDG	22	PTEP 2022 083C01	R.L. Workman <i>et al.</i>	(PDG Collab.)
AAIJ	21AC	PR D104 L091102	R. Aaij <i>et al.</i>	(LHCb Collab.)
YELTON	18B	PR D97 051102	J. Yelton <i>et al.</i>	(BELLE Collab.)
AAIJ	17AH	PRL 118 182001	R. Aaij <i>et al.</i>	(LHCb Collab.)

 $\Omega_c(3090)^0$

$I(J^P) = ?(??)$ Status: ***

 $\Omega_c(3090)^0$ MASS

VALUE (MeV)	CL%	EVTS	DOCUMENT ID	TECN	COMMENT
3090.15 \pm 0.26 OUR AVERAGE					
3090.16 \pm 0.11 \pm 0.06 \pm 0.23	17k	¹ AAIJ	23AS LHCb	pp at 7, 8, 13 TeV	
3091.0 \pm 1.1 \pm 1.0 \pm 0.19 \pm 0.22	41	² AAIJ	21AC LHCb	pp at 7, 8, 13 TeV	
3089.3 \pm 1.2 \pm 0.2	87	YELTON	18B BELL	e^+e^- at $\Upsilon(4S)$	
••• We do not use the following data for averages, fits, limits, etc. •••					
3090.2 \pm 0.3 \pm 0.5	2.0k	³ AAIJ	17AH LHCb	pp at 7, 8, 13 TeV	

- ¹The third uncertainty is due to the uncertainty in the Ξ_c^+ mass, taken to be the PDG 22 fit result 2467.71 \pm 0.23 MeV.
²Measured via $\Omega_b^- \rightarrow \Omega_c^{*0} \pi^- \rightarrow \Xi_c^+ K^- \pi^-$. The third uncertainty is due to the uncertainty in the Ξ_c^+ mass.
³See AAIJ 23As.

See key on page 1171

Baryon Particle Listings

 $\Omega_c(3090)^0, \Omega_c(3120)^0, \Omega_c(3185)^0, \Omega_c(3327)^0$ $\Omega_c(3090)^0$ WIDTH

VALUE (MeV)	EVTS	DOCUMENT ID	TECN	COMMENT
$8.48 \pm 0.44 \pm 0.61$ -1.62	17k	AAIJ	23As LHCb	pp at 7, 8, 13 TeV
• • • We do not use the following data for averages, fits, limits, etc. • • •				
$7.4 \pm 3.1 \pm 2.8$	41	AAIJ	21Ac LHCb	pp at 7, 8, 13 TeV
$8.7 \pm 1.0 \pm 0.8$	2.0k	¹ AAIJ	17Ah LHCb	pp at 7, 8, 13 TeV
¹ See AAIJ 23As.				

 $\Omega_c(3090)^0$ DECAY MODES

Mode	Fraction (Γ_i/Γ)
$\Gamma_1 \Xi_c^+ K^-$	seen

 $\Omega_c(3090)^0$ BRANCHING RATIOS

$\Gamma(\Xi_c^+ K^-)/\Gamma_{\text{total}}$	EVTS	DOCUMENT ID	TECN	COMMENT	Γ_1/Γ
seen	17k	AAIJ	23As LHCb	pp at 7, 8, 13 TeV	
seen	41	¹ AAIJ	21Ac LHCb	pp at 7, 8, 13 TeV	
seen	87	YELTON	18B BELLE	e^+e^- at $\Upsilon(4S)$	
• • • We do not use the following data for averages, fits, limits, etc. • • •					
seen	2.0k	^{2,3} AAIJ	17Ah LHCb	pp at 7, 8, 13 TeV	
¹ AAIJ 21Ac report a significance of 7.8 σ .					
² AAIJ 17Ah report a significance of 21.1 σ .					
³ See AAIJ 23As.					

 $\Omega_c(3090)^0$ REFERENCES

AAIJ	23As	PRL 131 131902	R. Aaij <i>et al.</i>	(LHCb Collab.)
PDG	22	PTEP 2022 083C01	R.L. Workman <i>et al.</i>	(PDG Collab.)
AAIJ	21Ac	PR D104 L091102	R. Aaij <i>et al.</i>	(LHCb Collab.)
YELTON	18B	PR D97 051102	J. Yelton <i>et al.</i>	(BELLE Collab.)
AAIJ	17Ah	PRL 118 182001	R. Aaij <i>et al.</i>	(LHCb Collab.)

 $\Omega_c(3120)^0$ $I(J^P) = ?(??)$ Status: *** $\Omega_c(3120)^0$ MASS

VALUE (MeV)	EVTS	DOCUMENT ID	TECN	COMMENT
$3118.98 \pm 0.12 \pm 0.09 \pm 0.23$	3.7k	¹ AAIJ	23As LHCb	pp at 7, 8, 13 TeV
• • • We do not use the following data for averages, fits, limits, etc. • • •				
$3119.1 \pm 0.3 \pm 0.9 \pm 0.3$	480	^{2,3} AAIJ	17Ah LHCb	pp at 7, 8, 13 TeV
¹ The third uncertainty is due to the uncertainty in the Ξ_c^+ mass, taken to be the PDG 22 fit result 2467.71 ± 0.23 MeV.				
² The third error is the uncertainty on the Ξ_c^+ mass. (AAIJ 17Ah gave $+0.3$ MeV here, but as of 2018 it is ± 0.3 .)				
³ See AAIJ 23As.				

 $\Omega_c(3120)^0$ WIDTH

VALUE (MeV)	CL%	EVTS	DOCUMENT ID	TECN	COMMENT
<2.5	95	3.7k	¹ AAIJ	23As LHCb	pp at 7, 8, 13 TeV
• • • We do not use the following data for averages, fits, limits, etc. • • •					
<2.6	95	480	² AAIJ	17Ah LHCb	pp at 7, 8, 13 TeV
¹ AAIJ 23As also report a central value of $0.60 \pm 0.63^{+0.90}_{-1.05}$.					
² See AAIJ 23As.					

 $\Omega_c(3120)^0$ DECAY MODES

Mode	Fraction (Γ_i/Γ)
$\Gamma_1 \Xi_c^+ K^-$	seen

 $\Omega_c(3120)^0$ BRANCHING RATIOS

$\Gamma(\Xi_c^+ K^-)/\Gamma_{\text{total}}$	EVTS	DOCUMENT ID	TECN	COMMENT	Γ_1/Γ
seen	3.7k	AAIJ	23As LHCb	pp at 7, 8, 13 TeV	
• • • We do not use the following data for averages, fits, limits, etc. • • •					
seen	480	^{1,2} AAIJ	17Ah LHCb	pp at 7, 8, 13 TeV	
¹ AAIJ 17Ah report a significance of 10.4 σ .					
² See AAIJ 23As.					

 $\Omega_c(3120)^0$ REFERENCES

AAIJ	23As	PRL 131 131902	R. Aaij <i>et al.</i>	(LHCb Collab.)
PDG	22	PTEP 2022 083C01	R.L. Workman <i>et al.</i>	(PDG Collab.)
AAIJ	17Ah	PRL 118 182001	R. Aaij <i>et al.</i>	(LHCb Collab.)

 $\Omega_c(3185)^0$ $I(J^P) = ?(??)$ Status: *** $\Omega_c(3185)^0$ MASS

VALUE (MeV)	EVTS	DOCUMENT ID	TECN	COMMENT
$3185 \pm 1.7 \pm 7.4 \pm 0.2$	12k	¹ AAIJ	23As LHCb	pp at 7, 8, 13 TeV
¹ The third uncertainty is due to the uncertainty in the Ξ_c^+ mass, taken to be the PDG 22 fit result 2467.71 ± 0.23 MeV.				

 $\Omega_c(3185)^0$ WIDTH

VALUE (MeV)	EVTS	DOCUMENT ID	TECN	COMMENT
$50 \pm 7 \pm 10$ -20	12k	AAIJ	23As LHCb	pp at 7, 8, 13 TeV

 $\Omega_c(3185)^0$ DECAY MODES

Mode	Fraction (Γ_i/Γ)
$\Gamma_1 \Xi_c^+ K^-$	seen

 $\Omega_c(3185)^0$ BRANCHING RATIOS

$\Gamma(\Xi_c^+ K^-)/\Gamma_{\text{total}}$	EVTS	DOCUMENT ID	TECN	COMMENT	Γ_1/Γ
seen	12k	¹ AAIJ	23As LHCb	pp at 7, 8, 13 TeV	
¹ AAIJ 23As report a significance of 12 σ .					

 $\Omega_c(3185)^0$ REFERENCES

AAIJ	23As	PRL 131 131902	R. Aaij <i>et al.</i>	(LHCb Collab.)
PDG	22	PTEP 2022 083C01	R.L. Workman <i>et al.</i>	(PDG Collab.)

 $\Omega_c(3327)^0$ $I(J^P) = ?(??)$ Status: *** $\Omega_c(3327)^0$ MASS

VALUE (MeV)	EVTS	DOCUMENT ID	TECN	COMMENT
$3327.1 \pm 1.2 \pm 0.1 \pm 0.2$	4.1k	¹ AAIJ	23As LHCb	pp at 7, 8, 13 TeV
¹ The third uncertainty is due to the uncertainty in the Ξ_c^+ mass, taken to be the PDG 22 fit result 2467.71 ± 0.23 MeV.				

 $\Omega_c(3327)^0$ WIDTH

VALUE (MeV)	EVTS	DOCUMENT ID	TECN	COMMENT
$20 \pm 5 \pm 13$ -1	4.1k	AAIJ	23As LHCb	pp at 7, 8, 13 TeV

 $\Omega_c(3327)^0$ DECAY MODES

Mode	Fraction (Γ_i/Γ)
$\Gamma_1 \Xi_c^+ K^-$	seen

 $\Omega_c(3327)^0$ BRANCHING RATIOS

$\Gamma(\Xi_c^+ K^-)/\Gamma_{\text{total}}$	EVTS	DOCUMENT ID	TECN	COMMENT	Γ_1/Γ
seen	4.1k	¹ AAIJ	23As LHCb	pp at 7, 8, 13 TeV	
¹ AAIJ 23As report a significance of 10 σ .					

 $\Omega_c(3327)^0$ REFERENCES

AAIJ	23As	PRL 131 131902	R. Aaij <i>et al.</i>	(LHCb Collab.)
PDG	22	PTEP 2022 083C01	R.L. Workman <i>et al.</i>	(PDG Collab.)

Baryon Particle Listings

 Ξ_{cc}^+ Ξ_{cc}^{++} DOUBLY CHARMED BARYONS
($C = +2$) $\Xi_{cc}^{++} = ucc$, $\Xi_{cc}^+ = dcc$, $\Omega_{cc}^+ = scc$ Ξ_{cc}^+ $I(J^P) = ?(?^?)$ Status: *

OMITTED FROM SUMMARY TABLE

Nominally the isospin partner of the Ξ_{cc}^{++} (ccu). While the SELEX experiment (MATTSON 02, OCHERASHVILI 05) claimed an observation of this state, subsequent searches by BABAR (AUBERT, B 06D), Belle (CHISTOV 06, KATO 14), and LHCb (AAIJ 13CD, AAIJ 20AX) did not find any significant signal or evidence for the Ξ_{cc}^+ . However, AAIJ 21AE reports that its search for $\Xi_{cc}^+ \rightarrow \Xi_c^+ \pi^+ \pi^-$, when combined with a prior search for $\Xi_{cc}^+ \rightarrow \Lambda_c^+ K^- \pi^+$ decays in AAIJ 20AX, yields a signal at 2.9 σ global significance (4.0 σ local).

 Ξ_{cc}^+ MASS

VALUE (MeV)	EVTS	DOCUMENT ID	TECN	COMMENT
3518.9 ± 0.9 OUR AVERAGE				
3518 ± 3	6	¹ OCHERASHVILI.05	SELX	Σ^- nucleus \approx 600 GeV
3519 ± 1	16	² MATTSON 02	SELX	Σ^- nucleus \approx 600 GeV
••• We do not use the following data for averages, fits, limits, etc. •••				
3623.0 ± 1.4	368 ± 193	³ AAIJ	21AE LHCb	pp at 7, 8, 13 TeV

¹ OCHERASHVILI 05 claims "an excess of 5.62 events over ... 1.38 ± 0.13 events" for a significance of 4.8 σ in $pD^+ K^-$ events.

² MATTSON 02 claims "an excess of 15.9 events over an expected background of 6.1 ± 0.5 events, a statistical significance of 6.3 σ " in the $\Lambda_c^+ K^- \pi^+$ invariant-mass spectrum. The probability that the peak is a fluctuation increases from 1.0 × 10⁻⁶ to 1.1 × 10⁻⁴ when the number of bins searched is considered.

³ Uncertainties are statistical only. Because of undetermined systematic uncertainties in the extraction of this result it cannot be considered a mass measurement. AAIJ 21AE performs a combined fit to its $\Xi_{cc}^+ \rightarrow \Xi_c^+ \pi^+ \pi^-$ data and the $\Xi_{cc}^+ \rightarrow \Lambda_c^+ K^- \pi^+$ data from AAIJ 20AX, finding a global significance of 2.9 σ (4.0 σ local).

 Ξ_{cc}^+ MEAN LIFE

VALUE (10 ⁻¹⁵ s)	CL%	DOCUMENT ID	TECN	COMMENT
••• We do not use the following data for averages, fits, limits, etc. •••				
<33	90	MATTSON 02	SELX	Σ^- nucleus, \approx 600 GeV

 Ξ_{cc}^+ DECAY MODES

Mode	Fraction (Γ_i/Γ)
Γ_1 $\Lambda_c^+ K^- \pi^+$	not seen
Γ_2 $\Xi_c^+ \pi^+ \pi^-$	not seen
Γ_3 $p D^+ K^-$	

$\Gamma(pD^+ K^-)/\Gamma(\Lambda_c^+ K^- \pi^+)$	Γ_3/Γ_1			
VALUE	EVTS	DOCUMENT ID	TECN	COMMENT
••• We do not use the following data for averages, fits, limits, etc. •••				
0.36 ± 0.21	6	UCHERASHVILI.05	SELX	$\Sigma^- \approx$ 600 GeV

$\Gamma(\Lambda_c^+ K^- \pi^+)/\Gamma_{total}$	Γ_1/Γ		
VALUE	DOCUMENT ID	TECN	COMMENT
not seen	¹ AAIJ	20AX LHCb	pp at 7, 8, 13 TeV
¹ No significant signal is observed in the mass range 3.4–3.8 GeV			

$\Gamma(\Xi_c^+ \pi^+ \pi^-)/\Gamma_{total}$	Γ_2/Γ				
VALUE	CL%	EVTS	DOCUMENT ID	TECN	COMMENT
not seen	95	145 ± 139	¹ AAIJ	21AE LHCb	pp at 7, 8, 13 TeV
¹ No significant signal is seen in the mass range 3.4–3.8 GeV. AAIJ 21AE performs a combined fit to its $\Xi_{cc}^+ \rightarrow \Xi_c^+ \pi^+ \pi^-$ data and the $\Xi_{cc}^+ \rightarrow \Lambda_c^+ K^- \pi^+$ data from AAIJ 20AX, finding a global significance of 2.9 σ (4.0 σ local).					

 Ξ_{cc}^+ REFERENCES

AAIJ	21AE	JHEP 2112 107	R. Aaij et al.	(LHCb Collab.)
AAIJ	20AX	SCPPA 63 221062	R. Aaij et al.	(LHCb Collab.)
KATO	14	PR D89 052003	Y. Kato et al.	(BELLE Collab.)
AAIJ	13CD	JHEP 1312 090	R. Aaij et al.	(LHCb Collab.)
AUBERT, B	06D	PR D74 011103	B. Aubert et al.	(BABAR Collab.)
CHISTOV	06	PRL 97 162001	R. Chistov et al.	(BELLE Collab.)
UCHERASHVILI.05	PL	B628 18	A. Ocherashvili et al.	(FNAL SELEX Collab.)
MATTSON	02	PRL 89 112001	M. Mattson et al.	(FNAL SELEX Collab.)

 Ξ_{cc}^{++} $I(J^P) = ?(?^?)$ Status: *** Ξ_{cc}^{++} MASS

VALUE (MeV)	EVTS	DOCUMENT ID	TECN	COMMENT
3621.55 ± 0.23 ± 0.30	2k	¹ AAIJ	20J LHCb	pp at 13 TeV
••• We do not use the following data for averages, fits, limits, etc. •••				
3620.6 ± 1.5 ± 0.4 ± 0.3	91	² AAIJ	18BA LHCb	pp at 13 TeV
3621.40 ± 0.72 ± 0.27 ± 0.14	313	³ AAIJ	17bc LHCb	pp at 13 TeV

¹ AAIJ 20J combines mass measurements 3621.53 ± 0.24 ± 0.29 MeV from $\Xi_{cc}^{++} \rightarrow \Lambda_c^+ K^- \pi^+ \pi^+$ and 3621.95 ± 0.60 ± 0.49 MeV from $\Xi_{cc}^{++} \rightarrow \Xi_c^+ \pi^+$. Supersedes AAIJ 18BA and AAIJ 17BC.

² The third error in AAIJ 18BA value is from the uncertainty of the Ξ_c^+ mass.

³ The third error in AAIJ 17BC value is from the uncertainty of the Λ_c^+ mass. The width of the signal is 6.6 ± 0.8 MeV, consistent with the experimental resolution.

 Ξ_{cc}^{++} MEAN LIFE

VALUE (10 ⁻¹⁵ s)	EVTS	DOCUMENT ID	TECN	COMMENT
256 ⁺²⁴ ₋₂₂ ± 14	304	AAIJ	18G LHCb	pp at 13 TeV

 Ξ_{cc}^{++} DECAY MODES

Mode	Fraction (Γ_i/Γ)	Confidence level
Γ_1 $\Lambda_c^+ K^- \pi^+ \pi^+$	DEFINED AS 1	
Γ_2 $\Xi_c^+ \pi^+$, $\Xi_c^+ \rightarrow p K^- \pi^+$	0.0022 ± 0.0006	
Γ_3 $\Xi_c^+ \pi^+$, $\Xi_c^+ \rightarrow \Xi_c^+ \gamma$, $\Xi_c^+ \rightarrow p K^- \pi^+$	0.0031 ± 0.0009	
Γ_4 $D^+ p K^- \pi^+$	<0.017	90%

$\Gamma(\Lambda_c^+ K^- \pi^+ \pi^+)/\Gamma_{total}$	Γ_1/Γ		
VALUE	DOCUMENT ID	TECN	COMMENT
••• We do not use the following data for averages, fits, limits, etc. •••			
seen	AAIJ	17bc LHCb	12 std significance

$\Gamma(\Xi_c^+ \pi^+, \Xi_c^+ \rightarrow p K^- \pi^+)/\Gamma_{total}$	Γ_2/Γ			
VALUE	EVTS	DOCUMENT ID	TECN	COMMENT
••• We do not use the following data for averages, fits, limits, etc. •••				
seen	91	AAIJ	18BA LHCb	5.9 std significance

$\Gamma(\Xi_c^+ \pi^+, \Xi_c^+ \rightarrow p K^- \pi^+)/\Gamma(\Lambda_c^+ K^- \pi^+ \pi^+)$	Γ_2/Γ_1		
VALUE (units 10 ⁻³)	DOCUMENT ID	TECN	COMMENT
2.2 ± 0.6 ± 0.1	¹ AAIJ	18BA LHCb	Ratio 91 over 289 events

¹ AAIJ 18BA reports $[\Gamma(\Xi_{cc}^{++} \rightarrow \Xi_c^+ \pi^+, \Xi_c^+ \rightarrow p K^- \pi^+)/\Gamma(\Xi_{cc}^{++} \rightarrow \Lambda_c^+ K^- \pi^+ \pi^+)] / [B(\Lambda_c^+ \rightarrow p K^- \pi^+)] = (3.5 \pm 0.9 \pm 0.3) \times 10^{-2}$ which we multiply by our best value $B(\Lambda_c^+ \rightarrow p K^- \pi^+) = (6.24 \pm 0.28) \times 10^{-2}$. Our first error is their experiment's error and our second error is the systematic error from using our best value.

$\Gamma(\Xi_c^+ \pi^+, \Xi_c^+ \rightarrow \Xi_c^+ \gamma, \Xi_c^+ \rightarrow p K^- \pi^+)/\Gamma(\Xi_c^+ \pi^+, \Xi_c^+ \rightarrow p K^- \pi^+)$	Γ_3/Γ_2			
VALUE	EVTS	DOCUMENT ID	TECN	COMMENT
1.41 ± 0.17 ± 0.10	756	¹ AAIJ	22G LHCb	pp at 13 TeV

¹ The photon in the $\Xi_c^+ \rightarrow \Xi_c^+ \gamma$ process is not reconstructed. Analysis uses two disjoint subsamples triggered on and independently from the signal.

$\Gamma(D^+ p K^- \pi^+)/\Gamma(\Lambda_c^+ K^- \pi^+ \pi^+)$	Γ_4/Γ_1			
VALUE	CL%	DOCUMENT ID	TECN	COMMENT
<1.7 × 10⁻²	90	AAIJ	19A0 LHCb	pp at 13 TeV

 Ξ_{cc}^{++} REFERENCES

AAIJ	22G	JHEP 2205 038	R. Aaij et al.	(LHCb Collab.)
AAIJ	20J	JHEP 2002 049	R. Aaij et al.	(LHCb Collab.)
AAIJ	19A0	JHEP 1910 124	R. Aaij et al.	(LHCb Collab.)
AAIJ	18BA	PRL 121 162002	R. Aaij et al.	(LHCb Collab.)
AAIJ	18G	PRL 121 052002	R. Aaij et al.	(LHCb Collab.)
AAIJ	17BC	PRL 119 112001	R. Aaij et al.	(LHCb Collab.)

See key on page 1171

Baryon Particle Listings

Λ_b^0

BOTTOM BARYONS
($B = -1$)

$$\Lambda_b^0 = udb, \Sigma_b^0 = udb, \Sigma_b^+ = uub, \Sigma_b^- = ddb$$

$$\Xi_b^0 = usb, \Xi_b^- = dsb, \Omega_b^- = ssb$$

Λ_b^0

$$I(J^P) = 0(\frac{1}{2}^+) \text{ Status: } ***$$

In the quark model, a Λ_b^0 is an isospin-0 udb state. The lowest Λ_b^0 ought to have $J^P = 1/2^+$. None of $I, J,$ or P have actually been measured.

Λ_b^0 MASS

$m_{\Lambda_b^0}$	VALUE (MeV)	EVTs	DOCUMENT ID	TECN	COMMENT
5619.60 ± 0.17 OUR AVERAGE					
5619.62 ± 0.16 ± 0.13			1 AAIJ	17AM LHCb	pp at 7, 8 TeV
5619.30 ± 0.34			2 AAIJ	14AA LHCb	pp at 7 TeV
5620.15 ± 0.31 ± 0.47			3 AALTONEN	14B CDF	$p\bar{p}$ at 1.96 TeV
5619.7 ± 0.7 ± 1.1			3 AAD	13U ATLS	pp at 7 TeV
5621 ± 4 ± 3			4 ABE	97B CDF	$p\bar{p}$ at 1.8 TeV
5668 ± 16 ± 8		4	5 ABREU	96N DLPH	$e^+e^- \rightarrow Z$
5614 ± 21 ± 4		4	5 BUSKULIC	96L ALEP	$e^+e^- \rightarrow Z$
••• We do not use the following data for averages, fits, limits, etc. •••					
5619.65 ± 0.17 ± 0.17			6 AAIJ	16Y LHCb	Repl. by AAIJ 17AM
5619.44 ± 0.13 ± 0.38			3 AAIJ	13AV LHCb	Repl. by AAIJ 17AM
5619.19 ± 0.70 ± 0.30			3 AAIJ	12E LHCb	Repl. by AAIJ 13AV
5619.7 ± 1.2 ± 1.2			7 ACOSTA	06 CDF	Repl. by AALTONEN 14B
not seen			8 ABE	93B CDF	Repl. by ABE 97B
5640 ± 50 ± 30		16	9 ALBAJAR	91E UA1	$p\bar{p}$ 630 GeV
5640 +100 -210		52	BARI	91 SFM	$\Lambda_b^0 \rightarrow pD^0\pi^-$
5650 +150 -200		90	BARI	91 SFM	$\Lambda_b^0 \rightarrow \Lambda_c^+\pi^+\pi^-\pi^-$

- 1 Uses $\Lambda_b^0 \rightarrow \chi_{c1}pK^-, \Lambda_b^0 \rightarrow \chi_{c2}pK^-, \Lambda_b^0 \rightarrow J/\psi\Lambda, \Lambda_b^0 \rightarrow p\psi(2S)K^-, \Lambda_b^0 \rightarrow pJ/\psi\pi^+\pi^-K^-,$ and $\Lambda_b^0 \rightarrow pJ/\psi K^-$ decays.
- 2 Uses exclusively reconstructed final states $\Lambda_b^0 \rightarrow \Lambda_c^+D_s^-, \Lambda_c^+D^-$ and $\bar{B}^0 \rightarrow D^+D_s^-$ decays. The uncertainty includes both statistical and systematic contributions.
- 3 Uses $\Lambda_b^0 \rightarrow J/\psi\Lambda$ fully reconstructed decays.
- 4 ABE 97B observed 38 events with a background of 18 ± 1.6 events in the mass range 5.60–5.65 GeV/ c^2 , a significance of > 3.4 standard deviations.
- 5 Uses 4 fully reconstructed Λ_b^0 events.
- 6 Uses $\Lambda_b^0 \rightarrow p\psi(2S)K^-, \Lambda_b^0 \rightarrow pJ/\psi\pi^+\pi^-K^-,$ and $\Lambda_b^0 \rightarrow pJ/\psi K^-$ decays.
- 7 Uses exclusively reconstructed final states containing a $J/\psi \rightarrow \mu^+\mu^-$ decays.
- 8 ABE 93B states that, based on the signal claimed by ALBAJAR 91E, CDF should have found $30 \pm 23 \Lambda_b^0 \rightarrow J/\psi(1S)\Lambda$ events. Instead, CDF found not more than 2 events.
- 9 ALBAJAR 91E claims 16 ± 5 events above a background of 9 ± 1 events, a significance of about 5 standard deviations.

$m_{\Lambda_b^0} - m_{B^0}$

VALUE (MeV)	DOCUMENT ID	TECN	COMMENT
339.2 ± 1.4 ± 0.1	1 ACOSTA	06 CDF	$p\bar{p}$ at 1.96 TeV

- 1 Uses exclusively reconstructed final states containing $J/\psi \rightarrow \mu^+\mu^-$ decays.

$m_{\Lambda_b^0} - m_{B^+}$

VALUE (MeV)	DOCUMENT ID	TECN	COMMENT
339.72 ± 0.28 OUR AVERAGE			
339.72 ± 0.24 ± 0.18	1 AAIJ	14AA LHCb	pp at 7 TeV
339.71 ± 0.71 ± 0.09	2 AAIJ	12E LHCb	pp at 7 TeV

- 1 Uses exclusively reconstructed final states $\Lambda_b^0 \rightarrow \Lambda_c^+D_s^-, \Lambda_c^+D^-$ and $\bar{B}^0 \rightarrow D^+D_s^-$ decays.
- 2 Uses exclusively reconstructed final states containing $J/\psi \rightarrow \mu^+\mu^-$ decays.

Λ_b^0 MEAN LIFE

See b -baryon Admixture section for data on b -baryon mean life average over species of b -baryon particles.

VALUE (10^{-12} s)	EVTs	DOCUMENT ID	TECN	COMMENT
1.471 ± 0.009 OUR EVALUATION				(Produced by HFLAV)
1.477 ± 0.027 ± 0.009		1 SIRUNYAN	18BY CMS	pp at 8 TeV
1.415 ± 0.027 ± 0.006		2 AAIJ	14E LHCb	pp at 7 TeV
1.479 ± 0.009 ± 0.010		3 AAIJ	14U LHCb	pp at 7, 8 TeV
1.565 ± 0.035 ± 0.020		2 AALTONEN	14B CDF	$p\bar{p}$ at 1.96 TeV
1.449 ± 0.036 ± 0.017		2 AAD	13U ATLS	pp at 7 TeV
1.503 ± 0.052 ± 0.031		2 CHATRCHYAN	13AC CMS	pp at 7 TeV
1.303 ± 0.075 ± 0.035		2 ABAZOV	12U D0	$p\bar{p}$ at 1.96 TeV
1.401 ± 0.046 ± 0.035		4 AALTONEN	10B CDF	$p\bar{p}$ at 1.96 TeV

••• We do not use the following data for averages, fits, limits, etc. •••

1.482 ± 0.018 ± 0.012	5 AAIJ	13BB LHCb	Repl. by AAIJ 14U
1.537 ± 0.045 ± 0.014	2 AALTONEN	11 CDF	Repl. by AALTONEN 14B
1.218 +0.130 -0.115 ± 0.042	2 ABAZOV	07S D0	Repl. by ABAZOV 12U
1.290 +0.119 +0.087 -0.110 -0.091	6 ABAZOV	07U D0	$p\bar{p}$ at 1.96 TeV
1.593 +0.083 ± 0.033	2 ABULENCIA	07A CDF	Repl. by AALTONEN 11
1.22 +0.22 ± 0.04	2 ABAZOV	05C D0	Repl. by ABAZOV 07S
1.11 +0.19 ± 0.05	7 ABREU	99W DLPH	$e^+e^- \rightarrow Z$
1.29 +0.24 ± 0.06	7 ACKERSTAFF	98G OPAL	$e^+e^- \rightarrow Z$
1.21 ± 0.11	7 BARATE	98D ALEP	$e^+e^- \rightarrow Z$
1.32 ± 0.15 ± 0.07	8 ABE	96M CDF	$p\bar{p}$ at 1.8 TeV
1.19 +0.21 ± 0.07 -0.18 -0.08	ABREU	96D DLPH	Repl. by ABREU 99W
1.27 +0.35 ± 0.09 -0.29	ABREU	95S DLPH	Repl. by ABREU 99W
1.14 +0.22 ± 0.07 -0.19	69 AKERS	95K OPAL	Repl. by ACKERSTAFF 98G
1.02 +0.23 ± 0.06 -0.18	44 BUSKULIC	95L ALEP	Repl. by BARATE 98D

- 1 Measured using $\Lambda_b^0 \rightarrow J/\psi\Lambda$ decays.
- 2 Measured mean life using fully reconstructed $\Lambda_b^0 \rightarrow J/\psi\Lambda$ decays.
- 3 Used $\Lambda_b^0 \rightarrow J/\psi pK^-$ decays.
- 4 Measured mean life using fully reconstructed $\Lambda_b^0 \rightarrow \Lambda_c^+\pi^-$ decays.
- 5 Measured the lifetime ratio of decays $\Lambda_b^0 \rightarrow J/\psi pK^-$ to $B^0 \rightarrow J/\psi\pi^+K^-$ to be $0.976 \pm 0.012 \pm 0.006$ with $\tau_{B^0} = 1.519 \pm 0.007$ ps.
- 6 Measured using semileptonic decays $\Lambda_b^0 \rightarrow \Lambda_c^+\mu\nu X$ and $\Lambda_c^+ \rightarrow K_S^0 p$.
- 7 Measured using $\Lambda_c\ell^-$ and $\Lambda\ell^+\ell^-$.
- 8 Excess $\Lambda_c\ell^-$, decay lengths.

$\tau_{\Lambda_b^0}/\tau_{B^0}$

VALUE	DOCUMENT ID	TECN	COMMENT
0.940 ± 0.035 ± 0.006	1 AAIJ	14E LHCb	pp at 7 TeV

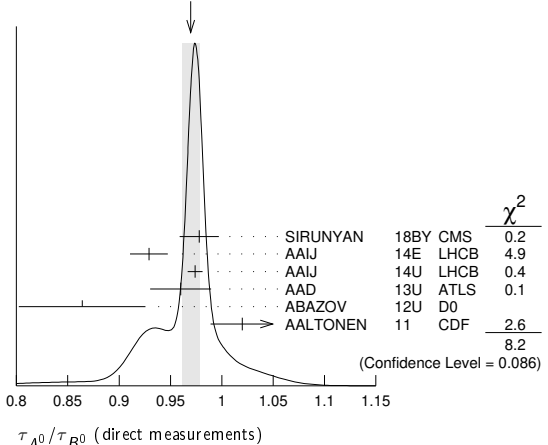
- 1 Measured using $\Lambda_b^0 \rightarrow J/\psi\Lambda$ decays.

$\tau_{\Lambda_b^0}/\tau_{B^0}$ MEAN LIFE RATIO

$\tau_{\Lambda_b^0}/\tau_{B^0}$ (direct measurements)

VALUE	DOCUMENT ID	TECN	COMMENT
0.964 ± 0.007 OUR EVALUATION			(Produced by HFLAV)
0.970 ± 0.009 OUR AVERAGE			Error includes scale factor of 1.4. See the ideogram below.
0.978 ± 0.018 ± 0.006	1 SIRUNYAN	18BY CMS	pp at 8 TeV
0.929 ± 0.018 ± 0.004	1 AAIJ	14E LHCb	pp at 7 TeV
0.974 ± 0.006 ± 0.004	2 AAIJ	14U LHCb	pp at 7, 8 TeV
0.960 ± 0.025 ± 0.016	3 AAD	13U ATLS	pp at 7 TeV
0.864 ± 0.052 ± 0.033	4,5 ABAZOV	12U D0	$p\bar{p}$ at 1.96 TeV
1.020 ± 0.030 ± 0.008	4 AALTONEN	11 CDF	$p\bar{p}$ at 1.96 TeV
••• We do not use the following data for averages, fits, limits, etc. •••			
0.976 ± 0.012 ± 0.006	6 AAIJ	13BB LHCb	Repl. by AAIJ 14U
0.811 +0.096 ± 0.034 -0.087	4,5 ABAZOV	07S D0	Repl. by ABAZOV 12U
1.041 ± 0.057	7 ABULENCIA	07A CDF	Repl. by AALTONEN 11
0.87 +0.17 ± 0.03 -0.14	7 ABAZOV	05C D0	Repl. by ABAZOV 07S

WEIGHTED AVERAGE
0.970 ± 0.009 (Error scaled by 1.4)



- 1 Measured using $\Lambda_b^0 \rightarrow J/\psi\Lambda$ and $B^0 \rightarrow J/\psi K^*(892)^0$ decays.
- 2 Used $\Lambda_b^0 \rightarrow J/\psi pK^-$ and $B^0 \rightarrow J/\psi K^*(892)^0$ decays.

Baryon Particle Listings

Λ_b^0

³ Measured with $\Lambda_b^0 \rightarrow J/\psi(\mu^+\mu^-)\Lambda^0(p\pi^-)$ decays.
⁴ Uses fully reconstructed $\Lambda_b \rightarrow J/\psi\Lambda$ decays.
⁵ Uses $B^0 \rightarrow J/\psi K_S^0$ decays for denominator.
⁶ Measures $1/\tau_{\Lambda_b^0} - 1/\tau_{B^0}$ and uses $\tau_{B^0} = 1.519 \pm 0.007$ ps to extract lifetime ratio.
⁷ Measured mean life ratio using fully reconstructed decays.

Λ_b^0 DECAY MODES

The branching fractions $B(b\text{-baryon} \rightarrow \Lambda\ell^-\bar{\nu}_\ell\text{anything})$ and $B(\Lambda_b^0 \rightarrow \Lambda_c^+\ell^-\bar{\nu}_\ell\text{anything})$ are not pure measurements because the underlying measured products of these with $B(b \rightarrow b\text{-baryon})$ were used to determine $B(b \rightarrow b\text{-baryon})$, as described in the note "Production and Decay of b -Flavored Hadrons."

For inclusive branching fractions, e.g., $\Lambda_b \rightarrow \bar{\Lambda}_c\text{anything}$, the values usually are multiplicities, not branching fractions. They can be greater than one.

Mode	Fraction (Γ_i/Γ)	Scale factor/ Confidence level
Γ_1 $J/\psi(1S)\Lambda \times B(b \rightarrow \Lambda_b^0)$	$(5.8 \pm 0.8) \times 10^{-5}$	
Γ_2 $J/\psi(1S)\Lambda$		
Γ_3 $J/\psi(1S)\Lambda\phi$		
Γ_4 $\psi(2S)\Lambda$		
Γ_5 $pD^0\pi^-$	$(6.2 \pm 0.6) \times 10^{-4}$	
Γ_6 $pD^+\pi^-\pi^-$	$(2.7 \pm 0.4) \times 10^{-4}$	
Γ_7 $pD^*(2010)^+\pi^-\pi^-$	$(5.2 \pm 1.0) \times 10^{-4}$	
Γ_8 $\Lambda_c(2860)^+\pi^-, \Lambda_c^+ \rightarrow D^0p$		
Γ_9 $\Lambda_c(2880)^+\pi^-, \Lambda_c^+ \rightarrow D^0p$		
Γ_{10} $\Lambda_c(2940)^+\pi^-, \Lambda_c^+ \rightarrow D^0p$		
Γ_{11} pD^0K^-	$(4.5 \pm 0.8) \times 10^{-5}$	
Γ_{12} $pDK^-, D \rightarrow K^-\pi^+$		
Γ_{13} $pDK^-, D \rightarrow K^+\pi^-$		
Γ_{14} $pJ/\psi\pi^-$	$(2.6^{+0.5}_{-0.4}) \times 10^{-5}$	
Γ_{15} $p\pi^- J/\psi, J/\psi \rightarrow \mu^+\mu^-$	$(1.6 \pm 0.8) \times 10^{-6}$	
Γ_{16} $pJ/\psi K^-$	$(3.2^{+0.6}_{-0.5}) \times 10^{-4}$	
Γ_{17} $p\eta_c(1S)K^-$	$(1.06 \pm 0.26) \times 10^{-4}$	
Γ_{18} $P_{c\bar{c}}(4312)^+K^-, P_{c\bar{c}}^+ \rightarrow p\eta_c(1S)$	$< 2.5 \times 10^{-5}$	CL=95%
Γ_{19} $P_{c\bar{c}}(4380)^+K^-, P_{c\bar{c}}^+ \rightarrow pJ/\psi$	[a] $(2.7 \pm 1.4) \times 10^{-5}$	
Γ_{20} $P_c(4450)^+K^-, P_c \rightarrow pJ/\psi$	[a] $(1.3 \pm 0.4) \times 10^{-5}$	
Γ_{21} $\chi_{c1}(1P)pK^-$	$(7.6^{+1.5}_{-1.3}) \times 10^{-5}$	
Γ_{22} $\chi_{c1}(1P)p\pi^-$	$(5.0^{+1.3}_{-1.1}) \times 10^{-6}$	
Γ_{23} $\chi_{c2}(1P)pK^-$	$(7.7^{+1.6}_{-1.4}) \times 10^{-5}$	
Γ_{24} $\chi_{c2}(1P)p\pi^-$	$(4.8 \pm 1.9) \times 10^{-6}$	
Γ_{25} $pJ/\psi(1S)\pi^+\pi^-K^-$	$(6.6^{+1.3}_{-1.1}) \times 10^{-5}$	
Γ_{26} $p\psi(2S)K^-$	$(6.6^{+1.2}_{-1.0}) \times 10^{-5}$	
Γ_{27} $\chi_{c1}(3872)pK^-$	$(3.5 \pm 1.3) \times 10^{-5}$	
Γ_{28} $\chi_{c1}(3872)\Lambda(1520)$	$(2.0 \pm 0.9) \times 10^{-5}$	
Γ_{29} $\psi(2S)p\pi^-$	$(7.5^{+1.6}_{-1.4}) \times 10^{-6}$	
Γ_{30} $p\bar{K}^0\pi^-$	$(1.3 \pm 0.4) \times 10^{-5}$	
Γ_{31} pK^0K^-	$< 3.5 \times 10^{-6}$	CL=90%
Γ_{32} $\Lambda_c^+\pi^-$	$(4.9 \pm 0.4) \times 10^{-3}$	S=1.2
Γ_{33} $\Lambda_c^+K^-$	$(3.56 \pm 0.28) \times 10^{-4}$	S=1.2
Γ_{34} $\Lambda_c^+a_1(1260)^-$	seen	
Γ_{35} $\Lambda_c^+D^-$	$(4.6 \pm 0.6) \times 10^{-4}$	
Γ_{36} $\Lambda_c^+D_s^-$	$(1.10 \pm 0.10) \%$	
Γ_{37} $\Lambda_c^+\pi^+\pi^-\pi^-$	$(7.6 \pm 1.1) \times 10^{-3}$	S=1.1
Γ_{38} $\Lambda_c(2595)^+\pi^-, \Lambda_c(2595)^+ \rightarrow \Lambda_c^+\pi^+\pi^-$	$(3.4 \pm 1.4) \times 10^{-4}$	
Γ_{39} $\Lambda_c(2625)^+\pi^-, \Lambda_c(2625)^+ \rightarrow \Lambda_c^+\pi^+\pi^-$	$(3.3 \pm 1.3) \times 10^{-4}$	
Γ_{40} $\Sigma_c(2455)^0\pi^+\pi^-, \Sigma_c^0 \rightarrow \Lambda_c^+\pi^-$	$(5.7 \pm 2.2) \times 10^{-4}$	
Γ_{41} $\Sigma_c(2455)^{++}\pi^-\pi^-, \Sigma_c^{++} \rightarrow \Lambda_c^+\pi^+$	$(3.2 \pm 1.5) \times 10^{-4}$	
Γ_{42} $\Lambda_c^+K^+K^-\pi^-$	$(1.02 \pm 0.11) \times 10^{-3}$	
Γ_{43} $\Lambda_c^+p\bar{p}\pi^-$	$(2.63 \pm 0.27) \times 10^{-4}$	

Γ_{44} $\Sigma_c(2455)^0p\bar{p}, \Sigma_c^0 \rightarrow \Lambda^+\pi^-$	$(2.3 \pm 0.5) \times 10^{-5}$	
Γ_{45} $\Sigma_c(2520)^0p\bar{p}, \Sigma_c(2520)^0 \rightarrow \Lambda_c^+\pi^-$	$(3.1 \pm 0.7) \times 10^{-5}$	
Γ_{46} $\Lambda K^0 2\pi^+ 2\pi^-$		
Γ_{47} $\Lambda_c^+\ell^-\bar{\nu}_\ell\text{anything}$	[b] $(10.9 \pm 2.2) \%$	
Γ_{48} $\Lambda_c^+\ell^-\bar{\nu}_\ell$	$(6.2^{+1.4}_{-1.3}) \%$	
Γ_{49} $\Lambda_c^+\tau^-\bar{\nu}_\tau$	$(1.9 \pm 0.5) \%$	
Γ_{50} $\Lambda_c^+\pi^+\pi^-\ell^-\bar{\nu}_\ell$	$(5.6 \pm 3.1) \%$	
Γ_{51} $\Lambda_c(2595)^+\ell^-\bar{\nu}_\ell$	$(7.9^{+4.0}_{-3.5}) \times 10^{-3}$	
Γ_{52} $\Lambda_c(2625)^+\ell^-\bar{\nu}_\ell$	$(1.3^{+0.6}_{-0.5}) \%$	
Γ_{53} $\Sigma_c(2455)^0\pi^+\ell^-\bar{\nu}_\ell$		
Γ_{54} $\Sigma_c(2455)^{++}\pi^-\ell^-\bar{\nu}_\ell$		
Γ_{55} $p h^-$	[c] $< 2.3 \times 10^{-5}$	CL=90%
Γ_{56} $p\pi^-$	$(4.6 \pm 0.8) \times 10^{-6}$	
Γ_{57} pK^-	$(5.5 \pm 1.0) \times 10^{-6}$	
Γ_{58} pD_s^-	$(1.25 \pm 0.13) \times 10^{-5}$	
Γ_{59} $p\mu^-\bar{\nu}_\mu$	$(4.1 \pm 1.0) \times 10^{-4}$	
Γ_{60} $\Lambda\mu^+\mu^-$	$(1.08 \pm 0.28) \times 10^{-6}$	
Γ_{61} $p\pi^-\mu^+\mu^-$	$(6.9 \pm 2.5) \times 10^{-8}$	
Γ_{62} $pK^-e^+e^-$	$(3.1 \pm 0.6) \times 10^{-7}$	
Γ_{63} $pK^-\mu^+\mu^-$	$(2.6^{+0.5}_{-0.4}) \times 10^{-7}$	
Γ_{64} $\Lambda(1520)^0\mu^+\mu^-$		
Γ_{65} $\Lambda\gamma$	$(7.1 \pm 1.7) \times 10^{-6}$	
Γ_{66} $\Lambda\eta$	$(9^{+7}_{-5}) \times 10^{-6}$	
Γ_{67} $\Lambda\eta'(958)$	$< 3.1 \times 10^{-6}$	CL=90%
Γ_{68} $\Lambda\pi^+\pi^-$	$(4.6 \pm 1.9) \times 10^{-6}$	
Γ_{69} $\Lambda K^+\pi^-$	$(5.6 \pm 1.2) \times 10^{-6}$	
Γ_{70} ΛK^+K^-	$(1.60 \pm 0.21) \times 10^{-5}$	
Γ_{71} $\Lambda\phi$	$(9.8 \pm 2.6) \times 10^{-6}$	
Γ_{72} $p\pi^-\pi^+\pi^-$	$(2.08 \pm 0.21) \times 10^{-5}$	
Γ_{73} $pK^-K^+\pi^-$	$(4.0 \pm 0.6) \times 10^{-6}$	
Γ_{74} $pK^-\pi^+\pi^-$	$(5.0 \pm 0.5) \times 10^{-5}$	
Γ_{75} $pK^-K^+K^-$	$(1.25 \pm 0.13) \times 10^{-5}$	

[a] $P_{c\bar{c}}^+$ is a pentaquark-charmonium state.

[b] Not a pure measurement. See note at head of Λ_b^0 Decay Modes.

[c] Here h^- means π^- or K^- .

FIT INFORMATION

An overall fit to 10 branching ratios uses 12 measurements to determine 6 parameters. The overall fit has a $\chi^2 = 10.8$ for 6 degrees of freedom.

The following *off-diagonal* array elements are the correlation coefficients $\langle \delta x_i \delta x_j \rangle / (\delta x_i \delta x_j)$, in percent, from the fit to the branching fractions, $x_i \equiv \Gamma_i/\Gamma_{\text{total}}$.

x_{33}	92				
x_{37}	46	43			
x_{48}	13	12	6		
x_{56}	0	0	0	0	
x_{57}	0	0	0	0	82
	x_{32}	x_{33}	x_{37}	x_{48}	x_{56}

Λ_b^0 BRANCHING RATIOS

$\Gamma(J/\psi(1S)\Lambda \times B(b \rightarrow \Lambda_b^0))/\Gamma_{\text{total}}$	Γ_1/Γ			
VALUE (units 10^{-5})	EVTS	DOCUMENT ID	TECN	COMMENT
5.8 ± 0.8 OUR AVERAGE				
6.01 ± 0.60 ± 0.58 ± 0.28		1 ABAZOV	11o D0	$p\bar{p}$ at 1.96 TeV
4.7 ± 2.3 ± 0.2		2 ABE	97B CDF	$p\bar{p}$ at 1.8 TeV
••• We do not use the following data for averages, fits, limits, etc. •••				
180 ± 60 ± 90	16	ALBAJAR	91E UA1	$p\bar{p}$ at 630 GeV
¹ ABAZOV 11o uses $B(B^0 \rightarrow J/\psi K_S^0) \times B(b \rightarrow B^0) = (1.74 \pm 0.08) \times 10^{-4}$ to obtain the result. The $(\pm 0.08) \times 10^{-4}$ uncertainty of this product is listed as the last uncertainty of the measurement, $(\pm 0.28) \times 10^{-5}$.				
² ABE 97B reports $[B(\Lambda_b^0 \rightarrow J/\psi\Lambda) \times B(b \rightarrow \Lambda_b^0)] / [B(B^0 \rightarrow J/\psi K_S^0) \times B(b \rightarrow B^0)] = 0.27 \pm 0.12 \pm 0.05$. We multiply by our best value $B(B^0 \rightarrow J/\psi K_S^0) \times B(b \rightarrow B^0) = (1.74 \pm 0.08) \times 10^{-4}$. Our first error is their experiment error and our second error is the systematic error from using our best value.				

$\Gamma(\psi(2S)\Lambda)/\Gamma(J/\psi(1S)\Lambda)$

VALUE	DOCUMENT ID	TECN	COMMENT
0.508±0.023 OUR AVERAGE			
0.513±0.023±0.019	¹ AAIJ	19F LHCB	pp at 7, 8 TeV
0.50 ± 0.03 ± 0.02	² AAD	15CH ATLS	pp at 8 TeV

¹ AAIJ 19F uses $B(J/\psi \rightarrow \mu^+\mu^-) = (5.961 \pm 0.033) \times 10^{-2}$ and $B(\psi(2S) \rightarrow e^+e^-) = (7.93 \pm 0.17) \times 10^{-3}$ from PDG 18 with assumption of lepton universality. AAIJ 19F reports this result as $0.513 \pm 0.023 \pm 0.016 \pm 0.011$, where the last uncertainty is the contribution due to the external input of branching fractions used in the analysis.

² AAD 15CH uses $B(J/\psi \rightarrow \mu^+\mu^-) = (5.961 \pm 0.033) \times 10^{-2}$ and $B(\psi(2S) \rightarrow \mu^+\mu^-) = (7.89 \pm 0.17) \times 10^{-3}$ from PDG 14 with assumption of lepton universality.

 $\Gamma(J/\psi(1S)\Lambda\phi)/\Gamma(\psi(2S)\Lambda)$

VALUE (units 10^{-2})	DOCUMENT ID	TECN	COMMENT
8.26±0.90±0.69	SIRUNYAN	20H CMS	pp at 13 TeV

 $\Gamma(\rho D^0 \pi^-)/\Gamma_{\text{total}}$

VALUE	EVTS	DOCUMENT ID	TECN	COMMENT
•••				
seen	52	BARJ	91 SFM	$D^0 \rightarrow K^-\pi^+$
seen		BASILE	81 SFM	$D^0 \rightarrow K^-\pi^+$

 $\Gamma(\rho D^+ \pi^- \pi^-)/\Gamma(\Lambda_c^+ \pi^+ \pi^- \pi^-)$

VALUE (%)	DOCUMENT ID	TECN	COMMENT
3.56±0.18±0.17	¹ AAIJ	22R LHCB	pp at 7 and 8 TeV

¹ AAIJ 22R reports $[\Gamma(\Lambda_b^0 \rightarrow \rho D^+ \pi^- \pi^-)/\Gamma(\Lambda_b^0 \rightarrow \Lambda_c^+ \pi^+ \pi^- \pi^-)] \times [B(D^+ \rightarrow K^- 2\pi^+)] / [B(\Lambda_c^+ \rightarrow \rho K^- \pi^+)] = 5.35 \pm 0.21 \pm 0.16\%$ which we multiply or divide by our best values $B(D^+ \rightarrow K^- 2\pi^+) = (9.38 \pm 0.16) \times 10^{-2}$, $B(\Lambda_c^+ \rightarrow \rho K^- \pi^+) = (6.24 \pm 0.28) \times 10^{-2}$. Our first error is their experiment's error and our second error is the systematic error from using our best values.

 $\Gamma(\rho D^* (2010)^+ \pi^- \pi^-)/\Gamma(\rho D^+ \pi^- \pi^-)$

VALUE	DOCUMENT ID	TECN	COMMENT
1.90±0.19	¹ AAIJ	22R LHCB	pp at 7 and 8 TeV

¹ AAIJ 22R uses partial reconstruction of $\rho D^+ \pi^- \pi^-$ final state.

 $\Gamma(\Lambda_c(2860)^+ \pi^-, \Lambda_c^+ \rightarrow D^0 \rho)/\Gamma(\Lambda_c(2880)^+ \pi^-, \Lambda_c^+ \rightarrow D^0 \rho)$

VALUE	DOCUMENT ID	TECN	COMMENT
4.54^{+0.51+0.21}_{-0.39-0.59}	AAIJ	17s LHCB	pp at 7, 8 TeV

 $\Gamma(\Lambda_c(2940)^+ \pi^-, \Lambda_c^+ \rightarrow D^0 \rho)/\Gamma(\Lambda_c(2880)^+ \pi^-, \Lambda_c^+ \rightarrow D^0 \rho)$

VALUE	DOCUMENT ID	TECN	COMMENT
0.83^{+0.31+0.18}_{-0.10-0.43}	AAIJ	17s LHCB	pp at 7, 8 TeV

 $\Gamma(\rho D^0 K^-)/\Gamma(\rho D^0 \pi^-)$

VALUE (units 10^{-2})	DOCUMENT ID	TECN	COMMENT
7.3±0.8^{+0.5}_{-0.6}	AAIJ	14H LHCB	pp at 7 TeV

 $\Gamma(\rho DK^-, D \rightarrow K^- \pi^+)/\Gamma(\rho DK^-, D \rightarrow K^+ \pi^-)$

VALUE	DOCUMENT ID	TECN	COMMENT
7.1±0.8^{+0.4}_{-0.3}	¹ AAIJ	21AD LHCB	pp at 7, 8, 13 TeV

¹ Measured in the full phase space.

 $\Gamma(\rho J/\psi \pi^-)/\Gamma(\rho J/\psi K^-)$

VALUE (units 10^{-2})	DOCUMENT ID	TECN	COMMENT
8.24±0.25±0.42	AAIJ	14K LHCB	pp at 7, 8 TeV

 $\Gamma(\rho J/\psi K^-)/\Gamma_{\text{total}}$

VALUE (units 10^{-4})	DOCUMENT ID	TECN	COMMENT
3.17±0.04^{+0.57}_{-0.45}	¹ AAIJ	16A LHCB	pp at 7, 8 TeV

¹ AAIJ 16A reported the measurement of $(3.17 \pm 0.04 \pm 0.07 \pm 0.34^{+0.45}_{-0.28}) \times 10^{-4}$ where the first uncertainty is statistical, the second is systematic, the third is due to the branching fraction of $B^0 \rightarrow J/\psi K^*(892)^0$, and the fourth is due to the knowledge of f_{Λ_b}/f_D . We combined in quadrature second to fourth uncertainties to a total systematic uncertainty.

 $\Gamma(\rho \eta_c(1S) K^-)/\Gamma(\rho J/\psi K^-)$

VALUE	DOCUMENT ID	TECN	COMMENT
0.333±0.050±0.037	¹ AAIJ	20AK LHCB	pp at 13 TeV

¹ AAIJ 20AK reported the measurement of $0.333 \pm 0.050 \pm 0.019 \pm 0.032$, where the last uncertainty is due to uncertainties of the used branching fractions of $J/\psi \rightarrow \rho \bar{p}$ and $\eta_c \rightarrow \rho \bar{p}$ decays. We combined in quadrature the systematic uncertainties.

 $\Gamma(P_{cc}(4312)^+ K^-, P_{cc}^+ \rightarrow \rho \eta_c(1S))/\Gamma(\rho \eta_c(1S) K^-)$

VALUE	CL%	DOCUMENT ID	TECN	COMMENT
<0.24	95	AAIJ	20AK LHCB	pp at 13 TeV

 $\Gamma(P_{cc}(4380)^+ K^-, P_{cc}^+ \rightarrow \rho J/\psi)/\Gamma_{\text{total}}$

VALUE (units 10^{-5})	DOCUMENT ID	TECN	COMMENT
2.66±0.22^{+1.41}_{-1.38}	¹ AAIJ	16A LHCB	pp at 7, 8 TeV

¹ AAIJ 16 total systematic includes the uncertainties on $f(P_{cc}^+)$ and $B(\Lambda_b \rightarrow \rho J/\psi K^-)$.

 $\Gamma(P_{cc}(4450)^+ K^-, P_c \rightarrow \rho J/\psi)/\Gamma_{\text{total}}$

VALUE (units 10^{-5})	DOCUMENT ID	TECN	COMMENT
1.30±0.16^{+0.42}_{-0.39}	¹ AAIJ	16A LHCB	pp at 7, 8 TeV

¹ AAIJ 16 total systematic includes the uncertainties on $f(P_c^+)$ and $B(\Lambda_b \rightarrow \rho J/\psi K^-)$.

 $\Gamma(\chi_{c1}(1P) \rho K^-)/\Gamma(\rho J/\psi K^-)$

VALUE	DOCUMENT ID	TECN	COMMENT
0.239±0.019±0.009	¹ AAIJ	17AM LHCB	pp at 7, 8 TeV

¹ AAIJ 17AM reports $0.242 \pm 0.014 \pm 0.016$ from a measurement of $[\Gamma(\Lambda_b^0 \rightarrow \chi_{c1}(1P) \rho K^-)/\Gamma(\Lambda_b^0 \rightarrow \rho J/\psi K^-)] \times [B(\chi_{c1}(1P) \rightarrow \gamma J/\psi(1S))]$ assuming $B(\chi_{c1}(1P) \rightarrow \gamma J/\psi(1S)) = (33.9 \pm 1.2) \times 10^{-2}$, which we rescale to our best value $B(\chi_{c1}(1P) \rightarrow \gamma J/\psi(1S)) = (34.3 \pm 1.3) \times 10^{-2}$. Our first error is their experiment's error and our second error is the systematic error from using our best value.

 $\Gamma(\chi_{c1}(1P) \rho \pi^-)/\Gamma(\chi_{c1}(1P) \rho K^-)$

VALUE (units 10^{-2})	DOCUMENT ID	TECN	COMMENT
6.59±1.01±0.22	AAIJ	21R LHCB	pp at 13 TeV

 $\Gamma(\chi_{c2}(1P) \rho K^-)/\Gamma(\rho J/\psi K^-)$

VALUE	DOCUMENT ID	TECN	COMMENT
0.244±0.024±0.009	¹ AAIJ	17AM LHCB	pp at 7, 8 TeV

¹ AAIJ 17AM reports $0.248 \pm 0.02 \pm 0.017$ from a measurement of $[\Gamma(\Lambda_b^0 \rightarrow \chi_{c2}(1P) \rho K^-)/\Gamma(\Lambda_b^0 \rightarrow \rho J/\psi K^-)] \times [B(\chi_{c2}(1P) \rightarrow \gamma J/\psi(1S))]$ assuming $B(\chi_{c2}(1P) \rightarrow \gamma J/\psi(1S)) = (19.2 \pm 0.7) \times 10^{-2}$, which we rescale to our best value $B(\chi_{c2}(1P) \rightarrow \gamma J/\psi(1S)) = (19.5 \pm 0.8) \times 10^{-2}$. Our first error is their experiment's error and our second error is the systematic error from using our best value.

 $\Gamma(\chi_{c2}(1P) \rho K^-)/\Gamma(\chi_{c1}(1P) \rho K^-)$

VALUE	DOCUMENT ID	TECN	COMMENT
1.06±0.05±0.04±0.04	¹ AAIJ	21R LHCB	pp at 13 TeV

¹ The first uncertainty is statistical, the second is systematic and the third is related to the uncertainties in the branching fractions of the $\chi_{cJ} \rightarrow J/\psi \gamma$ decays.

 $\Gamma(\chi_{c2}(1P) \rho \pi^-)/\Gamma(\chi_{c1}(1P) \rho \pi^-)$

VALUE	DOCUMENT ID	TECN	COMMENT
0.95±0.30±0.04±0.04	¹ AAIJ	21R LHCB	pp at 13 TeV

¹ Evidence for the $\Lambda_b^0 \rightarrow \chi_{c2} \rho \pi^-$ decay is obtained with a significance of 3.5 standard deviations. The first uncertainty is statistical, the second is systematic and the third is related to the uncertainties in the branching fractions of the $\chi_{cJ} \rightarrow J/\psi \gamma$ decays.

 $\Gamma(\rho J/\psi(1S) \pi^+ \pi^- K^-)/\Gamma(\rho J/\psi K^-)$

VALUE	DOCUMENT ID	TECN	COMMENT
0.2086±0.0096±0.0134	¹ AAIJ	16Y LHCB	pp at 7, 8 TeV

¹ Excludes $\psi(2S) \rightarrow J/\psi \pi^+ \pi^-$.

 $\Gamma(\rho \psi(2S) K^-)/\Gamma(\rho J/\psi K^-)$

VALUE	DOCUMENT ID	TECN	COMMENT
0.2070±0.0076±0.0059	¹ AAIJ	16Y LHCB	pp at 7, 8 TeV

¹ AAIJ 16Y reports a measurement of $0.2070 \pm 0.0076 \pm 0.0046 \pm 0.0037$ where the third uncertainty is due to the knowledge of J/ψ and $\psi(2S)$ branching fractions. We have combined both systematic uncertainties in quadrature.

 $\Gamma(\chi_{c1}(3872) \Lambda(1520))/\Gamma(\chi_{c1}(3872) \rho K^-)$

VALUE	DOCUMENT ID	TECN	COMMENT
0.58±0.15	AAIJ	19AN LHCB	pp at 7, 8, 13 TeV

 $\Gamma(\chi_{c1}(3872) \rho K^-)/\Gamma(\rho \psi(2S) K^-)$

VALUE	DOCUMENT ID	TECN	COMMENT
0.53±0.11±0.14	¹ AAIJ	19AN LHCB	pp at 7, 8, 13 TeV

¹ AAIJ 19AN reports $[\Gamma(\Lambda_b^0 \rightarrow \chi_{c1}(3872) \rho K^-)/\Gamma(\Lambda_b^0 \rightarrow \rho \psi(2S) K^-)] \times [B(\chi_{c1}(3872) \rightarrow \pi^+ \pi^- J/\psi(1S))] / [B(\psi(2S) \rightarrow J/\psi(1S) \pi^+ \pi^-)] = (5.4 \pm 1.1 \pm 0.2) \times 10^{-2}$ which we multiply or divide by our best values $B(\chi_{c1}(3872) \rightarrow \pi^+ \pi^- J/\psi(1S)) = (3.5 \pm 0.9) \times 10^{-2}$, $B(\psi(2S) \rightarrow J/\psi(1S) \pi^+ \pi^-) = (34.69 \pm 0.34) \times 10^{-2}$. Our first error is their experiment's error and our second error is the systematic error from using our best values.

 $\Gamma(\psi(2S) \rho \pi^-)/\Gamma(\rho \psi(2S) K^-)$

VALUE (%)	DOCUMENT ID	TECN	COMMENT
11.4±1.3±0.2	AAIJ	18AF LHCB	pp at 7, 8, 13 TeV

Baryon Particle Listings

Λ_b^0			
$\Gamma(p\bar{K}^0\pi^-)/\Gamma_{\text{total}}$		Γ_{30}/Γ	
<u>VALUE (units 10^{-5})</u>	<u>DOCUMENT ID</u>	<u>TECN</u>	<u>COMMENT</u>
1.26 ± 0.19 ± 0.36	¹ AAIJ	14Q	LHCB pp at 7 TeV
¹ Used the normalizing mode branching fraction value of $B(B^0 \rightarrow K^0\pi^+\pi^-) = (4.96 \pm 0.20) \times 10^{-5}$.			
$\Gamma(pK^0K^-)/\Gamma_{\text{total}}$		Γ_{31}/Γ	
<u>VALUE</u>	<u>CL%</u>	<u>DOCUMENT ID</u>	<u>TECN</u>
<3.5 × 10⁻⁶	90	AAIJ	14Q LHCB pp at 7 TeV
$\Gamma(\Lambda_c^+ \pi^-)/\Gamma_{\text{total}}$		Γ_{32}/Γ	
<u>VALUE (units 10^{-3})</u>	<u>EVTS</u>	<u>DOCUMENT ID</u>	<u>TECN</u>
4.9 ± 0.4 OUR FIT	Error includes scale factor of 1.2.		
4.8 ± 0.5 OUR AVERAGE	Error includes scale factor of 1.5.		
4.60 ^{+0.31} _{-0.30} ± 0.14	¹ AAIJ	14I	LHCB pp at 7 TeV
5.97 ± 0.28 ± 0.81	² AAIJ	14Q	LHCB pp at 7 TeV
8.8 ± 2.8 ± 1.5	³ ABULENCIA	07B	CDF $p\bar{p}$ at 1.96 TeV
• • • We do not use the following data for averages, fits, limits, etc. • • •			
seen	3	ABREU	96N DLPH $\Lambda_c^+ \rightarrow pK^-\pi^+$
seen	4	BUSKULIC	96L ALEP $\Lambda_c^+ \rightarrow pK^-\pi^+$, $p\bar{K}^0, \Lambda\pi^+\pi^+\pi^-$
¹ AAIJ 14I reports $(4.30 \pm 0.03^{+0.12}_{-0.11} \pm 0.26 \pm 0.21) \times 10^{-3}$ from a measurement of $[\Gamma(\Lambda_b^0 \rightarrow \Lambda_c^+\pi^-)/\Gamma_{\text{total}}] \times [B(B^0 \rightarrow D^-\pi^+)]$ assuming $B(B^0 \rightarrow D^-\pi^+) = (2.68 \pm 0.13) \times 10^{-3}$, which we rescale to our best value $B(B^0 \rightarrow D^-\pi^+) = (2.51 \pm 0.08) \times 10^{-3}$. Our first error is their experiment's error and our second error is the systematic error from using our best value. Uses information on f_{baryon}/f_d from measurement in semileptonic decays by the same authors.			
² Obtained using the branching fraction of $\Lambda_c^+ \rightarrow pK^-\pi^+$ decay.			
³ The result is obtained from $(f_{\text{baryon}}/f_d) (B(\Lambda_b^0 \rightarrow \Lambda_c^+\pi^-)/B(\bar{B}^0 \rightarrow D^+\pi^-)) = 0.82 \pm 0.08 \pm 0.11 \pm 0.22$, assuming $f_{\text{baryon}}/f_d = 0.25 \pm 0.04$ and $B(\bar{B}^0 \rightarrow D^+\pi^-) = (2.68 \pm 0.13) \times 10^{-3}$.			
$\Gamma(pD^0\pi^-)/\Gamma(\Lambda_c^+\pi^-)$		Γ_5/Γ_{32}	
<u>VALUE</u>	<u>DOCUMENT ID</u>	<u>TECN</u>	<u>COMMENT</u>
0.127 ± 0.007 ± 0.006	¹ AAIJ	14H	LHCB pp at 7 TeV
¹ AAIJ 14H reports $[\Gamma(\Lambda_b^0 \rightarrow pD^0\pi^-)/\Gamma(\Lambda_b^0 \rightarrow \Lambda_c^+\pi^-)] \times [B(D^0 \rightarrow K^-\pi^+)] / [B(\Lambda_c^+ \rightarrow pK^-\pi^+)] = (8.06 \pm 0.23 \pm 0.35) \times 10^{-2}$ which we multiply or divide by our best values $B(D^0 \rightarrow K^-\pi^+) = (3.947 \pm 0.030) \times 10^{-2}$, $B(\Lambda_c^+ \rightarrow pK^-\pi^+) = (6.24 \pm 0.28) \times 10^{-2}$. Our first error is their experiment's error and our second error is the systematic error from using our best values.			
$\Gamma(\Lambda_c^+ K^-)/\Gamma_{\text{total}}$		Γ_{33}/Γ	
<u>VALUE (units 10^{-4})</u>	<u>DOCUMENT ID</u>	<u>TECN</u>	<u>COMMENT</u>
3.56 ± 0.28 OUR FIT	Error includes scale factor of 1.2.		
3.55 ± 0.44 ± 0.50	¹ AAIJ	14Q	LHCB pp at 7 TeV
¹ Obtained using the branching fraction of $\Lambda_c^+ \rightarrow pK^-\pi^+$ decay.			
$\Gamma(\Lambda_c^+ K^-)/\Gamma(\Lambda_c^+\pi^-)$		Γ_{33}/Γ_{32}	
<u>VALUE (units 10^{-2})</u>	<u>DOCUMENT ID</u>	<u>TECN</u>	<u>COMMENT</u>
7.31 ± 0.22 OUR FIT			
7.31 ± 0.16 ± 0.16	AAIJ	14H	LHCB pp at 7 TeV
$\Gamma(\Lambda_c^+ a_1(1260)^-)/\Gamma_{\text{total}}$		Γ_{34}/Γ	
<u>VALUE</u>	<u>EVTS</u>	<u>DOCUMENT ID</u>	<u>TECN</u>
seen	1	ABREU	96N DLPH $\Lambda_c^+ \rightarrow pK^-\pi^+, a_1^- \rightarrow \rho^0\pi^- \rightarrow \pi^+\pi^-\pi^-$
$\Gamma(\Lambda_c^+ D_s^-)/\Gamma_{\text{total}}$		Γ_{36}/Γ	
<u>VALUE (units 10^{-2})</u>	<u>DOCUMENT ID</u>	<u>TECN</u>	<u>COMMENT</u>
1.1 ± 0.1	¹ AAIJ	14AA	LHCB pp at 7 TeV
¹ Uses $B(\bar{B}^0 \rightarrow D^+D_s^-) = (7.2 \pm 0.8) \times 10^{-3}$ and their measured $B(\Lambda_b^0 \rightarrow \Lambda_c^+\pi^-)/B(\bar{B}^0 \rightarrow D^+\pi^-)$ values.			
$\Gamma(\Lambda_c^+ D^-)/\Gamma(\Lambda_c^+ D_s^-)$		Γ_{35}/Γ_{36}	
<u>VALUE</u>	<u>DOCUMENT ID</u>	<u>TECN</u>	<u>COMMENT</u>
0.042 ± 0.003 ± 0.003	AAIJ	14AA	LHCB pp at 7 TeV
$\Gamma(\Lambda_c^+ \pi^+\pi^-\pi^-)/\Gamma_{\text{total}}$		Γ_{37}/Γ	
<u>VALUE (units 10^{-3})</u>	<u>EVTS</u>	<u>DOCUMENT ID</u>	<u>TECN</u>
7.6 ± 1.1 OUR FIT	Error includes scale factor of 1.1.		
14.8^{+3.8}_{-3.1} ± 1.1	¹ AALTONEN	12A	CDF $p\bar{p}$ at 1.96 TeV
• • • We do not use the following data for averages, fits, limits, etc. • • •			
seen	90	BARJ	91 SFM $\Lambda_c^+ \rightarrow pK^-\pi^+$
¹ AALTONEN 12A reports $[\Gamma(\Lambda_b^0 \rightarrow \Lambda_c^+\pi^+\pi^-\pi^-)/\Gamma_{\text{total}}] / [B(\Lambda_b^0 \rightarrow \Lambda_c^+\pi^-)] = 3.04 \pm 0.33^{+0.70}_{-0.55}$ which we multiply by our best value $B(\Lambda_b^0 \rightarrow \Lambda_c^+\pi^-) = (4.9 \pm 0.4) \times 10^{-3}$. Our first error is their experiment's error and our second error is the systematic error from using our best value.			
$\Gamma(\Lambda_c^+ \pi^+\pi^-\pi^-)/\Gamma(\Lambda_c^+\pi^-)$		Γ_{37}/Γ_{32}	
<u>VALUE</u>	<u>DOCUMENT ID</u>	<u>TECN</u>	<u>COMMENT</u>
1.57 ± 0.21 OUR FIT			
1.43 ± 0.16 ± 0.13	AAIJ	11E	LHCB pp at 7 TeV
$\Gamma(\Lambda_c(2595)^+\pi^-, \Lambda_c(2595)^+ \rightarrow \Lambda_c^+\pi^+\pi^-)/\Gamma(\Lambda_c^+\pi^-\pi^-)$		Γ_{38}/Γ_{37}	
<u>VALUE (units 10^{-2})</u>	<u>DOCUMENT ID</u>	<u>TECN</u>	<u>COMMENT</u>
4.4 ± 1.7^{+0.6}_{-0.4}	AAIJ	11E	LHCB pp at 7 TeV
$\Gamma(\Lambda_c(2625)^+\pi^-, \Lambda_c(2625)^+ \rightarrow \Lambda_c^+\pi^+\pi^-)/\Gamma(\Lambda_c^+\pi^-\pi^-)$		Γ_{39}/Γ_{37}	
<u>VALUE (units 10^{-2})</u>	<u>DOCUMENT ID</u>	<u>TECN</u>	<u>COMMENT</u>
4.3 ± 1.5 ± 0.4	AAIJ	11E	LHCB pp at 7 TeV
$\Gamma(\Sigma_c(2455)^0\pi^+\pi^-, \Sigma_c^0 \rightarrow \Lambda_c^+\pi^-)/\Gamma(\Lambda_c^+\pi^-\pi^-)$		Γ_{40}/Γ_{37}	
<u>VALUE (units 10^{-2})</u>	<u>DOCUMENT ID</u>	<u>TECN</u>	<u>COMMENT</u>
7.4 ± 2.4 ± 1.2	AAIJ	11E	LHCB pp at 7 TeV
$\Gamma(\Sigma_c(2455)^{++}\pi^-\pi^-, \Sigma_c^{++} \rightarrow \Lambda_c^+\pi^+)/\Gamma(\Lambda_c^+\pi^-\pi^-)$		Γ_{41}/Γ_{37}	
<u>VALUE (units 10^{-2})</u>	<u>DOCUMENT ID</u>	<u>TECN</u>	<u>COMMENT</u>
4.2 ± 1.8 ± 0.7	AAIJ	11E	LHCB pp at 7 TeV
$\Gamma(\Lambda_c^+ K^+K^-\pi^-)/\Gamma(\Lambda_c^+ D_s^-)$		Γ_{42}/Γ_{36}	
<u>VALUE (units 10^{-2})</u>	<u>DOCUMENT ID</u>	<u>TECN</u>	<u>COMMENT</u>
9.26 ± 0.29 ± 0.53	¹ AAIJ	21B	LHCB pp at 7 and 8 TeV
¹ AAIJ 21B systematic uncertainty includes the contribution from the $D_s^- \rightarrow K^+K^-\pi^-$ branching fraction.			
$\Gamma(\Lambda_c^+ p\bar{p}\pi^-)/\Gamma(\Lambda_c^+\pi^-)$		Γ_{43}/Γ_{32}	
<u>VALUE (units 10^{-2})</u>	<u>DOCUMENT ID</u>	<u>TECN</u>	<u>COMMENT</u>
5.40 ± 0.23 ± 0.32	AAIJ	18AW	LHCB pp at 7 and 8 TeV
$\Gamma(\Sigma_c(2455)^0 p\bar{p}, \Sigma_c^0 \rightarrow \Lambda_c^+\pi^-)/\Gamma(\Lambda_c^+ p\bar{p}\pi^-)$		Γ_{44}/Γ_{43}	
<u>VALUE (units 10^{-2})</u>	<u>DOCUMENT ID</u>	<u>TECN</u>	<u>COMMENT</u>
8.9 ± 1.5 ± 0.6	AAIJ	18AW	LHCB pp at 7 and 8 TeV
$\Gamma(\Sigma_c(2520)^0 p\bar{p}, \Sigma_c(2520)^0 \rightarrow \Lambda_c^+\pi^-)/\Gamma(\Lambda_c^+ p\bar{p}\pi^-)$		Γ_{45}/Γ_{43}	
<u>VALUE</u>	<u>DOCUMENT ID</u>	<u>TECN</u>	<u>COMMENT</u>
0.119 ± 0.020 ± 0.014	AAIJ	18AW	LHCB pp at 7 and 8 TeV
$\Gamma(\Lambda K^0 2\pi^+ 2\pi^-)/\Gamma_{\text{total}}$		Γ_{46}/Γ	
<u>VALUE</u>	<u>EVTS</u>	<u>DOCUMENT ID</u>	<u>TECN</u>
• • • We do not use the following data for averages, fits, limits, etc. • • •			
seen	4	¹ ARENTON	86 FMPS $\Lambda K_S^0 2\pi^+ 2\pi^-$
¹ See the footnote to the ARENTON 86 mass value.			
$\Gamma(\Lambda_c^+ \ell^- \bar{\nu}_\ell \text{ anything})/\Gamma_{\text{total}}$		Γ_{47}/Γ	
<u>VALUE</u>	<u>EVTS</u>	<u>DOCUMENT ID</u>	<u>TECN</u>
0.109 ± 0.022 OUR AVERAGE			
0.102 ± 0.019 ± 0.013	¹ BARATE	98D	ALEP $e^+e^- \rightarrow Z$
0.14 ^{+0.05} _{-0.04} ± 0.02	² ABREU	95S	DLPH $e^+e^- \rightarrow Z$
• • • We do not use the following data for averages, fits, limits, etc. • • •			
0.090 ± 0.022 ± 0.012	³ BUSKULIC	95L	ALEP Repl. by BARATE 98D
0.18 ± 0.07 ± 0.02	⁴ BUSKULIC	92E	ALEP $\Lambda_c^+ \rightarrow pK^-\pi^+$
¹ BARATE 98D reports $[\Gamma(\Lambda_b^0 \rightarrow \Lambda_c^+ \ell^- \bar{\nu}_\ell \text{ anything})/\Gamma_{\text{total}}] \times [B(\bar{B} \rightarrow b\text{-baryon})] = 0.0086 \pm 0.0007 \pm 0.0014$ which we divide by our best value $B(\bar{B} \rightarrow b\text{-baryon}) = (8.4 \pm 1.1) \times 10^{-2}$. Our first error is their experiment's error and our second error is the systematic error from using our best value. Measured using $\Lambda_c \ell^-$ and $\Lambda \ell^+ \ell^-$.			
² ABREU 95S reports $[\Gamma(\Lambda_b^0 \rightarrow \Lambda_c^+ \ell^- \bar{\nu}_\ell \text{ anything})/\Gamma_{\text{total}}] \times [B(\bar{B} \rightarrow b\text{-baryon})] = 0.0118 \pm 0.0026^{+0.0031}_{-0.0021}$ which we divide by our best value $B(\bar{B} \rightarrow b\text{-baryon}) = (8.4 \pm 1.1) \times 10^{-2}$. Our first error is their experiment's error and our second error is the systematic error from using our best value.			
³ BUSKULIC 95L reports $[\Gamma(\Lambda_b^0 \rightarrow \Lambda_c^+ \ell^- \bar{\nu}_\ell \text{ anything})/\Gamma_{\text{total}}] \times [B(\bar{B} \rightarrow b\text{-baryon})] = 0.00755 \pm 0.0014 \pm 0.0012$ which we divide by our best value $B(\bar{B} \rightarrow b\text{-baryon}) = (8.4 \pm 1.1) \times 10^{-2}$. Our first error is their experiment's error and our second error is the systematic error from using our best value.			
⁴ BUSKULIC 92E reports $[\Gamma(\Lambda_b^0 \rightarrow \Lambda_c^+ \ell^- \bar{\nu}_\ell \text{ anything})/\Gamma_{\text{total}}] \times [B(\bar{B} \rightarrow b\text{-baryon})] = 0.015 \pm 0.0035 \pm 0.0045$ which we divide by our best value $B(\bar{B} \rightarrow b\text{-baryon}) = (8.4 \pm 1.1) \times 10^{-2}$. Our first error is their experiment's error and our second error is the systematic error from using our best value. Superseded by BUSKULIC 95L.			
$\Gamma(\Lambda_c^+ \ell^- \bar{\nu}_\ell)/\Gamma_{\text{total}}$		Γ_{48}/Γ	
<u>VALUE</u>	<u>DOCUMENT ID</u>	<u>TECN</u>	<u>COMMENT</u>
0.062 ± 0.014			
-0.013 OUR FIT			
0.050 ± 0.011 ± 0.016	¹ ABDALLAH	04A	DLPH $e^+e^- \rightarrow Z^0$
-0.008 ± 0.012			
¹ Derived from a combined likelihood and event rate fit to the distribution of the l_{sgur} -wise variable and using HQET. The slope of the form factor is measured to be $\rho^2 = 2.03 \pm 0.46^{+0.72}_{-1.00}$.			

See key on page 1171

Baryon Particle Listings

 Λ_b^0 $\Gamma(\Lambda_c^+ \ell^- \bar{\nu}_\ell) / \Gamma(\Lambda_c^+ \pi^-)$ $\Gamma_{48} / \Gamma_{32}$

VALUE	DOCUMENT ID	TECN	COMMENT
$12.8^{+3.0}_{-2.7}$ OUR FIT			
$16.6 \pm 3.0^{+2.8}_{-3.6}$	AALTONEN	09E	CDF $p\bar{p}$ at 1.96 TeV

 $\Gamma(\Lambda_c^+ \tau^- \bar{\nu}_\tau) / \Gamma(\Lambda_c^+ \pi^+ \pi^- \pi^-)$ $\Gamma_{49} / \Gamma_{37}$

VALUE	DOCUMENT ID	TECN	COMMENT
$2.46 \pm 0.27 \pm 0.40$	¹ AAIJ	22K	LHCB pp at 7, 8 TeV

¹ Uses $\tau^- \rightarrow \pi^- \pi^+ \pi^- (\pi^0) \nu_\tau$ decays. $\Gamma(\Lambda_c^+ \pi^+ \pi^- \ell^- \bar{\nu}_\ell) / \Gamma_{\text{total}}$ Γ_{50} / Γ

VALUE	DOCUMENT ID	TECN	COMMENT
$0.056^{+0.031}_{-0.030}$	¹ ABDALLAH	04A	DLPH $e^+ e^- \rightarrow Z^0$

¹ Derived from the fraction of $\Gamma(\Lambda_b^0 \rightarrow \Lambda_c^+ \ell^- \bar{\nu}_\ell) / (\Gamma(\Lambda_b^0 \rightarrow \Lambda_c^+ \ell^- \bar{\nu}_\ell) + \Gamma(\Lambda_b^0 \rightarrow \Lambda_c^+ \pi^+ \pi^- \ell^- \bar{\nu}_\ell)) = 0.47^{+0.10+0.07}_{-0.08-0.06}$. $\Gamma(\Lambda_c^+ \ell^- \bar{\nu}_\ell) / [\Gamma(\Lambda_c^+ \ell^- \bar{\nu}_\ell) + \Gamma(\Lambda_c^+ \pi^+ \pi^- \ell^- \bar{\nu}_\ell)]$ $\Gamma_{48} / (\Gamma_{48} + \Gamma_{50})$

VALUE	DOCUMENT ID	TECN	COMMENT
$0.47^{+0.10+0.07}_{-0.08-0.06}$	ABDALLAH	04A	DLPH $e^+ e^- \rightarrow Z^0$

 $\Gamma(\Lambda_c(2595)^+ \ell^- \bar{\nu}_\ell) / \Gamma(\Lambda_c^+ \ell^- \bar{\nu}_\ell)$ $\Gamma_{51} / \Gamma_{48}$

VALUE	DOCUMENT ID	TECN	COMMENT
$0.126 \pm 0.033^{+0.047}_{-0.038}$	¹ AALTONEN	09E	CDF $p\bar{p}$ at 1.96 TeV

¹ AALTONEN 09E assumes isospin conservation for $\Lambda_c(2595) \rightarrow \Lambda_c \pi^+ \pi^+$ and $\Lambda_c(2595) \rightarrow \Lambda_c \pi^0 \pi^0$. Significant isospin violation from thresholds in $\Lambda_c(2595) \rightarrow \Sigma_c(2455) \pi \rightarrow \Lambda_c \pi \pi$ may alter the recovered ratio. $\Gamma(\Lambda_c(2625)^+ \ell^- \bar{\nu}_\ell) / \Gamma(\Lambda_c^+ \ell^- \bar{\nu}_\ell)$ $\Gamma_{52} / \Gamma_{48}$

VALUE	DOCUMENT ID	TECN	COMMENT
$0.210 \pm 0.042^{+0.071}_{-0.050}$	AALTONEN	09E	CDF $p\bar{p}$ at 1.96 TeV

 $[\frac{1}{2}\Gamma(\Sigma_c(2455)^0 \pi^+ \ell^- \bar{\nu}_\ell) + \frac{1}{2}\Gamma(\Sigma_c(2455)^{++} \pi^- \ell^- \bar{\nu}_\ell)] / \Gamma(\Lambda_c^+ \ell^- \bar{\nu}_\ell)$ $(\frac{1}{2}\Gamma_{53} + \frac{1}{2}\Gamma_{54}) / \Gamma_{48}$

VALUE	DOCUMENT ID	TECN	COMMENT
$0.054 \pm 0.022^{+0.021}_{-0.018}$	AALTONEN	09E	CDF $p\bar{p}$ at 1.96 TeV

 $\Gamma(p h^-) / \Gamma_{\text{total}}$ Γ_{55} / Γ

VALUE	CL%	DOCUMENT ID	TECN	COMMENT
$< 2.3 \times 10^{-5}$	90	¹ ACOSTA	05O	CDF $p\bar{p}$ at 1.96 TeV

¹ Assumes $f_A / f_d = 0.25$, and equal momentum distribution for Λ_b and B mesons. $\Gamma(p \pi^-) / \Gamma_{\text{total}}$ Γ_{56} / Γ

VALUE (units 10^{-6})	CL%	DOCUMENT ID	TECN	COMMENT
4.6 ± 0.8 OUR FIT				
$4.1 \pm 0.9 \pm 0.5$		¹ AALTONEN	09c	CDF $p\bar{p}$ at 1.96 TeV

• • • We do not use the following data for averages, fits, limits, etc. • • •

VALUE	CL%	DOCUMENT ID	TECN	COMMENT
< 50	90	² BUSKULIC	96v	ALEP $e^+ e^- \rightarrow Z$

¹ AALTONEN 09c reports $[\Gamma(\Lambda_b^0 \rightarrow p \pi^-) / \Gamma_{\text{total}}] / [B(B^0 \rightarrow K^+ \pi^-)] \times [B(\bar{B} \rightarrow b\text{-baryon})] / [B(\bar{B} \rightarrow B^0)] = 0.042 \pm 0.007 \pm 0.006$ which we multiply or divide by our best values $B(B^0 \rightarrow K^+ \pi^-) = (2.00 \pm 0.04) \times 10^{-5}$, $B(\bar{B} \rightarrow b\text{-baryon}) = (8.4 \pm 1.1) \times 10^{-2}$, $B(\bar{B} \rightarrow B^0) = (40.8 \pm 0.7) \times 10^{-2}$. Our first error is their experiment's error and our second error is the systematic error from using our best values.² BUSKULIC 96v assumes PDG 96 production fractions for B^0 , B^+ , B_s , b baryons. $\Gamma(p K^-) / \Gamma_{\text{total}}$ Γ_{57} / Γ

VALUE (units 10^{-6})	CL%	DOCUMENT ID	TECN	COMMENT
5.5 ± 1.0 OUR FIT				
$6.4 \pm 1.2 \pm 0.9$		¹ AALTONEN	09c	CDF $p\bar{p}$ at 1.96 TeV

• • • We do not use the following data for averages, fits, limits, etc. • • •

VALUE	CL%	DOCUMENT ID	TECN	COMMENT
< 360	90	² ADAM	96D	DLPH $e^+ e^- \rightarrow Z$
< 50	90	³ BUSKULIC	96v	ALEP $e^+ e^- \rightarrow Z$

¹ AALTONEN 09c reports $[\Gamma(\Lambda_b^0 \rightarrow p K^-) / \Gamma_{\text{total}}] / [B(B^0 \rightarrow K^+ \pi^-)] \times [B(\bar{B} \rightarrow b\text{-baryon})] / [B(\bar{B} \rightarrow B^0)] = 0.066 \pm 0.009 \pm 0.008$ which we multiply or divide by our best values $B(B^0 \rightarrow K^+ \pi^-) = (2.00 \pm 0.04) \times 10^{-5}$, $B(\bar{B} \rightarrow b\text{-baryon}) = (8.4 \pm 1.1) \times 10^{-2}$, $B(\bar{B} \rightarrow B^0) = (40.8 \pm 0.7) \times 10^{-2}$. Our first error is their experiment's error and our second error is the systematic error from using our best values.² ADAM 96D assumes $f_{B^0} = f_{B^-} = 0.39$ and $f_{B_s} = 0.12$.³ BUSKULIC 96v assumes PDG 96 production fractions for B^0 , B^+ , B_s , b baryons. $\Gamma(p \pi^-) / \Gamma(p K^-)$ $\Gamma_{56} / \Gamma_{57}$

VALUE	DOCUMENT ID	TECN	COMMENT
0.84 ± 0.09 OUR FIT			
$0.86 \pm 0.08 \pm 0.05$	AAIJ	12AR	LHCB pp at 7 TeV

 $\Gamma(p D_s^-) / \Gamma_{\text{total}}$ Γ_{58} / Γ

VALUE	CL%	DOCUMENT ID	TECN	COMMENT
$< 4.8 \times 10^{-4}$	90	AAIJ	14Q	LHCB pp at 7 TeV

• • • We do not use the following data for averages, fits, limits, etc. • • •

 $\Gamma(p D_s^-) / \Gamma(\Lambda_c^+ \pi^-)$ $\Gamma_{58} / \Gamma_{32}$

VALUE (units 10^{-3})	DOCUMENT ID	TECN	COMMENT
$2.56 \pm 0.10 \pm 0.15$	¹ AAIJ	23K	LHCB pp at 13 TeV

¹ AAIJ 23K reports this measurement as $(2.56 \pm 0.10 \pm 0.05 \pm 0.14) \times 10^{-3}$ where the last uncertainty is due to the branching fractions $B(D_s^- \rightarrow K^- K^+ \pi^-)$ and $B(\Lambda_c^+ \rightarrow p K^- \pi^+)$ uncertainties. $\Gamma(p \mu^- \bar{\nu}_\mu) / \Gamma_{\text{total}}$ Γ_{59} / Γ

VALUE (units 10^{-4})	DOCUMENT ID	TECN	COMMENT
4.1 ± 1.0	¹ AAIJ	15B6	LHCB pp at 8 TeV

¹ The ratio of $B(\Lambda_b^0 \rightarrow p \mu^- \bar{\nu}_\mu)$ to $B(\Lambda_b^0 \rightarrow \Lambda_c^+ \mu^- \bar{\nu}_\mu)$ is measured within a restricted q^2 region. Combined with theoretical calculations of the form factors and the previously measured value of $|V_{cb}|$, the first $|V_{ub}| = (3.27 \pm 0.15 \pm 0.16 \pm 0.06) \times 10^{-3}$ measurement from the Λ_b decay is obtained, consistent with the exclusively measured world averages. $\Gamma(p \mu^- \bar{\nu}_\mu) / \Gamma(\Lambda_c^+ \ell^- \bar{\nu}_\ell)$ $\Gamma_{59} / \Gamma_{48}$

VALUE (units 10^{-2})	DOCUMENT ID	TECN	COMMENT
$1.0 \pm 0.04 \pm 0.08$	¹ AAIJ	15B6	LHCB pp at 8 TeV

¹ This measurement is a ratio of $\Gamma(\Lambda_b^0 \rightarrow p \mu^- \bar{\nu}_\mu)[q^2 > 15 \text{ GeV}/c^2]$ to $\Gamma(\Lambda_b^0 \rightarrow \Lambda_c^+ \mu^- \bar{\nu}_\mu)[q^2 > 7 \text{ GeV}/c^2]$ within a restricted q^2 region. Combined with theoretical calculations of the form factors and the previously measured value of $|V_{cb}|$, the first $|V_{ub}| = (3.27 \pm 0.15 \pm 0.16 \pm 0.06) \times 10^{-3}$ measurement from the Λ_b decay is obtained, consistent with the exclusively measured world averages. $\Gamma(\Lambda \mu^+ \mu^-) / \Gamma_{\text{total}}$ Γ_{60} / Γ

VALUE (units 10^{-7})	DOCUMENT ID	TECN	COMMENT
10.8 ± 2.8 OUR AVERAGE			
$9.6 \pm 1.6 \pm 2.5$	¹ AAIJ	13A1	LHCB pp at 7 TeV
$17.3 \pm 4.2 \pm 5.5$	AALTONEN	11A1	CDF $p\bar{p}$ at 1.96 TeV

¹ Uses $B(\Lambda_b^0 \rightarrow J/\psi \Lambda) = (6.2 \pm 1.4) \times 10^{-4}$. This measurement comes from the sum of the differential rates in q^2 regions excluding those corresponding to J/ψ and $\psi(2S)$ ($[8.68, 10.09]$ and $[12.86, 14.18] \text{ GeV}^2/c^4$). $\Gamma(p \pi^- \mu^+ \mu^-) / \Gamma_{\text{total}}$ Γ_{61} / Γ

VALUE (units 10^{-8})	DOCUMENT ID	TECN	COMMENT
$6.9 \pm 1.9^{+1.7}_{-1.5}$	¹ AAIJ	17P	LHCB pp at 7, 8 TeV

¹ Excludes J/ψ and $\psi(2S)$ decays to $\mu^+ \mu^-$. $\Gamma(p \pi^- \mu^+ \mu^-) / \Gamma(p \pi^- J/\psi, J/\psi \rightarrow \mu^+ \mu^-)$ $\Gamma_{61} / \Gamma_{15}$

VALUE (units 10^{-2})	DOCUMENT ID	TECN	COMMENT
$4.4 \pm 1.2 \pm 0.7$	¹ AAIJ	17P	LHCB pp at 7, 8 TeV

¹ The $p \pi^- \mu^+ \mu^-$ mode excludes J/ψ and $\psi(2S)$ decays to $\mu^+ \mu^-$. $\Gamma(p K^- e^+ e^-) / \Gamma_{\text{total}}$ Γ_{62} / Γ

VALUE (units 10^{-6})	DOCUMENT ID	TECN	COMMENT
$0.310 \pm 0.040^{+0.054}_{-0.047}$	^{1,2} AAIJ	20M	LHCB pp at 7, 8, 13 TeV

¹ Measured over $0.1 < q^2 < 6.0 \text{ GeV}/c^2$, and $m_{pK} < 2.6 \text{ GeV}/c^2$.² The first uncertainty is the statistical uncertainty and the second is the combination of all systematic uncertainties including those related to the normalization of $\Lambda_b^0 \rightarrow J/\psi p K^-$. $\Gamma(p K^- \mu^+ \mu^-) / \Gamma_{\text{total}}$ Γ_{63} / Γ

VALUE (units 10^{-6})	DOCUMENT ID	TECN	COMMENT
$0.265 \pm 0.014^{+0.049}_{-0.039}$	^{1,2} AAIJ	20M	LHCB pp at 7, 8, 13 TeV

¹ Measured over $0.1 < q^2 < 6.0 \text{ GeV}/c^2$, and $m_{pK} < 2.6 \text{ GeV}/c^2$.² The first uncertainty is the statistical uncertainty and the second is the combination of all systematic uncertainties including those related to the normalization of $\Lambda_b^0 \rightarrow J/\psi p K^-$. $\Gamma(p K^- \mu^+ \mu^-) / \Gamma(p K^- e^+ e^-)$ $\Gamma_{63} / \Gamma_{62}$

VALUE	DOCUMENT ID	TECN	COMMENT
$0.86^{+0.14}_{-0.11} \pm 0.05$	¹ AAIJ	20M	LHCB pp at 7, 8, 13 TeV

¹ Measured over $0.1 < q^2 < 6.0 \text{ GeV}/c^2$, and $m_{pK} < 2.6 \text{ GeV}/c^2$. $\Gamma(p K^- e^+ e^-) / \Gamma(p J/\psi K^-)$ $\Gamma_{62} / \Gamma_{16}$

VALUE (units 10^{-4})	DOCUMENT ID	TECN	COMMENT
$9.8^{+1.4}_{-1.3} \pm 0.8$	¹ AAIJ	20M	LHCB pp at 7, 8, 13 TeV

¹ Measured over $0.1 < q^2 < 6.0 \text{ GeV}/c^2$, and $m_{pK} < 2.6 \text{ GeV}/c^2$.

Baryon Particle Listings

 Λ_b^0 $\Gamma(pK^-\mu^+\mu^-)/\Gamma(pJ/\psi K^-)$ Γ_{63}/Γ_{16}

VALUE (units 10^{-4})	DOCUMENT ID	TECN	COMMENT
$8.4 \pm 0.4 \pm 0.4$	¹ AAIJ	20M LHCb	pp at 7, 8, 13 TeV

¹ Measured over $0.1 < q^2 < 6.0$ GeV/c², and $m_{pK} < 2.6$ GeV/c².

 $\Gamma(\Lambda\gamma)/\Gamma_{\text{total}}$ Γ_{65}/Γ

VALUE (units 10^{-6})	CL%	DOCUMENT ID	TECN	COMMENT
$7.1 \pm 1.5 \pm 0.9$		¹ AAIJ	19Z LHCb	pp at 13 TeV

• • • We do not use the following data for averages, fits, limits, etc. • • •

VALUE (units 10^{-6})	CL%	DOCUMENT ID	TECN	COMMENT
<1300	90	ACOSTA	02G CDF	$p\bar{p}$ at 1.8 TeV

¹ AAIJ 19Z normalized to $B^0 \rightarrow K^*0\gamma$ and used an integrated luminosity of 1.7 fb⁻¹.

 $\Gamma(\Lambda\eta)/\Gamma_{\text{total}}$ Γ_{66}/Γ

VALUE (units 10^{-6})	DOCUMENT ID	TECN	COMMENT
$9 \pm 7 \pm 1$	¹ AAIJ	15AH LHCb	pp at 7, 8 TeV

¹ AAIJ 15AH reports $[\Gamma(\Lambda_b^0 \rightarrow \Lambda\eta)/\Gamma_{\text{total}}] / [B(B^0 \rightarrow \eta'K^0)] = 0.14 \pm 0.11 \pm 0.08$ which we multiply by our best value $B(B^0 \rightarrow \eta'K^0) = (6.6 \pm 0.4) \times 10^{-5}$. Our first error is their experiment's error and our second error is the systematic error from using our best value. The single uncertainty quoted with the original measurement combines in quadrature statistical and systematic uncertainties.

 $\Gamma(\Lambda\eta(958))/\Gamma_{\text{total}}$ Γ_{67}/Γ

VALUE	CL%	DOCUMENT ID	TECN	COMMENT
$<3.1 \times 10^{-6}$	90	¹ AAIJ	15AH LHCb	pp at 7, 8 TeV

¹ AAIJ 15AH reports $[\Gamma(\Lambda_b^0 \rightarrow \Lambda\eta(958))/\Gamma_{\text{total}}] / [B(B^0 \rightarrow \eta'K^0)] < 0.047$ which we multiply by our best value $B(B^0 \rightarrow \eta'K^0) = 6.6 \times 10^{-5}$.

 $\Gamma(\Lambda\pi^+\pi^-)/\Gamma(\Lambda_c^+\pi^-)$ Γ_{68}/Γ_{32}

VALUE (units 10^{-4})	DOCUMENT ID	TECN	COMMENT
$9.4 \pm 3.8 \pm 0.4$	¹ AAIJ	16W LHCb	pp at 7, 8 TeV

¹ AAIJ 16W reports $[\Gamma(\Lambda_b^0 \rightarrow \Lambda\pi^+\pi^-)/\Gamma(\Lambda_b^0 \rightarrow \Lambda_c^+\pi^-)] / [B(\Lambda_c^+ \rightarrow \Lambda\pi^+)] = (7.3 \pm 1.9 \pm 2.2) \times 10^{-2}$ which we multiply by our best value $B(\Lambda_c^+ \rightarrow \Lambda\pi^+) = (1.29 \pm 0.05) \times 10^{-2}$. Our first error is their experiment's error and our second error is the systematic error from using our best value.

 $\Gamma(\Lambda K^+\pi^-)/\Gamma(\Lambda_c^+\pi^-)$ Γ_{69}/Γ_{32}

VALUE (units 10^{-4})	DOCUMENT ID	TECN	COMMENT
$11.5 \pm 2.3 \pm 0.5$	¹ AAIJ	16W LHCb	pp at 7, 8 TeV

¹ AAIJ 16W reports $[\Gamma(\Lambda_b^0 \rightarrow \Lambda K^+\pi^-)/\Gamma(\Lambda_b^0 \rightarrow \Lambda_c^+\pi^-)] / [B(\Lambda_c^+ \rightarrow \Lambda\pi^+)] = (8.9 \pm 1.2 \pm 1.3) \times 10^{-2}$ which we multiply by our best value $B(\Lambda_c^+ \rightarrow \Lambda\pi^+) = (1.29 \pm 0.05) \times 10^{-2}$. Our first error is their experiment's error and our second error is the systematic error from using our best value.

 $\Gamma(\Lambda K^+K^-)/\Gamma(\Lambda_c^+\pi^-)$ Γ_{70}/Γ_{32}

VALUE (units 10^{-3})	DOCUMENT ID	TECN	COMMENT
$3.27 \pm 0.35 \pm 0.13$	¹ AAIJ	16W LHCb	pp at 7, 8 TeV

¹ AAIJ 16W reports $[\Gamma(\Lambda_b^0 \rightarrow \Lambda K^+K^-)/\Gamma(\Lambda_b^0 \rightarrow \Lambda_c^+\pi^-)] / [B(\Lambda_c^+ \rightarrow \Lambda\pi^+)] = (25.3 \pm 1.9 \pm 1.9) \times 10^{-2}$ which we multiply by our best value $B(\Lambda_c^+ \rightarrow \Lambda\pi^+) = (1.29 \pm 0.05) \times 10^{-2}$. Our first error is their experiment's error and our second error is the systematic error from using our best value.

 $\Gamma(\Lambda\phi)/\Gamma_{\text{total}}$ Γ_{71}/Γ

VALUE (units 10^{-6})	DOCUMENT ID	TECN	COMMENT
$9.8 \pm 2.1 \pm 1.6 \pm 1.5$	¹ AAIJ	16J LHCb	pp at 7, 8 TeV

¹ AAIJ 16J reports $[\Gamma(\Lambda_b^0 \rightarrow \Lambda\phi)/\Gamma_{\text{total}}] / [B(B^0 \rightarrow K^0\phi)] \times [B(\bar{B} \rightarrow b\text{-baryon})] / [B(\bar{B} \rightarrow B^0)] = 0.275 \pm 0.055 \pm 0.020$ which we multiply or divide by our best values $B(B^0 \rightarrow K^0\phi) = (7.3 \pm 0.7) \times 10^{-6}$, $B(\bar{B} \rightarrow b\text{-baryon}) = (8.4 \pm 1.1) \times 10^{-2}$, $B(\bar{B} \rightarrow B^0) = (40.8 \pm 0.7) \times 10^{-2}$. Our first error is their experiment's error and our second error is the systematic error from using our best values.

 $\Gamma(p\pi^-\pi^+\pi^-)/\Gamma(\Lambda_c^+\pi^-)$ Γ_{72}/Γ_{32}

VALUE (units 10^{-3})	DOCUMENT ID	TECN	COMMENT
$4.27 \pm 0.24 \pm 0.18 \pm 0.19$	¹ AAIJ	18Q LHCb	pp at 7, 8 TeV

¹ AAIJ 18Q reports $[\Gamma(\Lambda_b^0 \rightarrow p\pi^-\pi^+\pi^-)/\Gamma(\Lambda_b^0 \rightarrow \Lambda_c^+\pi^-)] / [B(\Lambda_c^+ \rightarrow pK^-\pi^+)] = (6.85 \pm 0.19 \pm 0.08 \pm 0.32) \times 10^{-2}$ which we multiply by our best value $B(\Lambda_c^+ \rightarrow pK^-\pi^+) = (6.24 \pm 0.28) \times 10^{-2}$. Our first error is their experiment's error and our second error is the systematic error from using our best value.

 $\Gamma(pK^-K^+\pi^-)/\Gamma(\Lambda_c^+\pi^-)$ Γ_{73}/Γ_{32}

VALUE (units 10^{-3})	DOCUMENT ID	TECN	COMMENT
$0.82 \pm 0.10 \pm 0.04$	¹ AAIJ	18Q LHCb	pp at 7, 8 TeV

¹ AAIJ 18Q reports $[\Gamma(\Lambda_b^0 \rightarrow pK^-K^+\pi^-)/\Gamma(\Lambda_b^0 \rightarrow \Lambda_c^+\pi^-)] / [B(\Lambda_c^+ \rightarrow pK^-\pi^+)] = (1.32 \pm 0.09 \pm 0.09 \pm 0.10) \times 10^{-2}$ which we multiply by our best value $B(\Lambda_c^+ \rightarrow pK^-\pi^+) = (6.24 \pm 0.28) \times 10^{-2}$. Our first error is their experiment's error and our second error is the systematic error from using our best value.

 $\Gamma(pK^-\pi^+\pi^-)/\Gamma(\Lambda_c^+\pi^-)$ Γ_{74}/Γ_{32}

VALUE (units 10^{-3})	DOCUMENT ID	TECN	COMMENT
$10.2 \pm 0.5 \pm 0.4 \pm 0.5$	¹ AAIJ	18Q LHCb	pp at 7, 8 TeV

¹ AAIJ 18Q reports $[\Gamma(\Lambda_b^0 \rightarrow pK^-\pi^+\pi^-)/\Gamma(\Lambda_b^0 \rightarrow \Lambda_c^+\pi^-)] / [B(\Lambda_c^+ \rightarrow pK^-\pi^+)] = (16.4 \pm 0.3 \pm 0.2 \pm 0.7) \times 10^{-2}$ which we multiply by our best value $B(\Lambda_c^+ \rightarrow pK^-\pi^+) = (6.24 \pm 0.28) \times 10^{-2}$. Our first error is their experiment's error and our second error is the systematic error from using our best value.

 $\Gamma(pK^-K^+K^-)/\Gamma(\Lambda_c^+\pi^-)$ Γ_{75}/Γ_{32}

VALUE (units 10^{-3})	DOCUMENT ID	TECN	COMMENT
$2.56 \pm 0.15 \pm 0.11 \pm 0.12$	¹ AAIJ	18Q LHCb	pp at 7, 8 TeV

¹ AAIJ 18Q reports $[\Gamma(\Lambda_b^0 \rightarrow pK^-K^+K^-)/\Gamma(\Lambda_b^0 \rightarrow \Lambda_c^+\pi^-)] / [B(\Lambda_c^+ \rightarrow pK^-\pi^+)] = (4.11 \pm 0.12 \pm 0.06 \pm 0.19) \times 10^{-2}$ which we multiply by our best value $B(\Lambda_c^+ \rightarrow pK^-\pi^+) = (6.24 \pm 0.28) \times 10^{-2}$. Our first error is their experiment's error and our second error is the systematic error from using our best value.

PARTIAL BRANCHING FRACTIONS

 $B(\Lambda_b \rightarrow \Lambda\mu^+\mu^-)$ ($q^2 < 2.0$ GeV²/c⁴)

VALUE (units 10^{-7})	DOCUMENT ID	TECN	COMMENT
0.71 ± 0.27 OUR AVERAGE			
$0.72 \pm 0.24 \pm 0.14$	¹ AAIJ	15AE LHCb	pp at 7, 8 TeV
$0.15 \pm 2.01 \pm 0.05$	AALTONEN	11AI CDF	$p\bar{p}$ at 1.96 TeV

• • • We do not use the following data for averages, fits, limits, etc. • • •

VALUE (units 10^{-7})	DOCUMENT ID	TECN	COMMENT
$0.56 \pm 0.76 \pm 0.80$	² AAIJ	13AJ LHCb	Repl. by AAIJ 15AE

¹ AAIJ 15AE measurement covers $0.1 < q^2 < 2.0$ GeV²/c⁴.
² Uses $B(\Lambda_b^0 \rightarrow J/\psi\Lambda) = (6.2 \pm 1.4) \times 10^{-4}$.

 $B(\Lambda_b \rightarrow \Lambda\mu^+\mu^-)$ ($2.0 < q^2 < 4.3$ GeV²/c⁴)

VALUE (units 10^{-7})	DOCUMENT ID	TECN	COMMENT
$0.28 \pm 0.28 \pm 0.21$ OUR AVERAGE			
$0.253 \pm 0.276 \pm 0.046$	¹ AAIJ	15AE LHCb	pp at 7, 8 TeV
$1.8 \pm 1.7 \pm 0.6$	AALTONEN	11AI CDF	$p\bar{p}$ at 1.96 TeV

• • • We do not use the following data for averages, fits, limits, etc. • • •

VALUE (units 10^{-7})	DOCUMENT ID	TECN	COMMENT
$0.71 \pm 0.60 \pm 0.23$	² AAIJ	13AJ LHCb	Repl. by AAIJ 15AE

¹ AAIJ 15AE measurement covers $2.0 < q^2 < 4.0$ GeV²/c⁴.
² Uses $B(\Lambda_b^0 \rightarrow J/\psi\Lambda) = (6.2 \pm 1.4) \times 10^{-4}$.

 $B(\Lambda_b \rightarrow \Lambda\mu^+\mu^-)$ ($q^2 < 4.3$ GeV²/c⁴)

VALUE (units 10^{-7})	DOCUMENT ID	TECN	COMMENT
$2.7 \pm 2.5 \pm 0.9$	AALTONEN	11AI CDF	$p\bar{p}$ at 1.96 TeV

 $B(\Lambda_b \rightarrow \Lambda\mu^+\mu^-)$ ($4.0 < q^2 < 6.0$ GeV²/c⁴)

VALUE (units 10^{-7})	DOCUMENT ID	TECN	COMMENT
$0.04 \pm 0.18 \pm 0.02$	AAIJ	15AE LHCb	pp at 7, 8 TeV

 $B(\Lambda_b \rightarrow \Lambda\mu^+\mu^-)$ ($1.0 < q^2 < 6.0$ GeV²/c⁴)

VALUE (units 10^{-7})	DOCUMENT ID	TECN	COMMENT
$0.47 \pm 0.31 \pm 0.27$ OUR AVERAGE			
$0.45 \pm 0.30 \pm 0.10$	¹ AAIJ	15AE LHCb	pp at 7 and 8 TeV
$1.3 \pm 2.1 \pm 0.4$	AALTONEN	11AI CDF	$p\bar{p}$ at 1.96 TeV

¹ AAIJ 15AE measurement covers $1.1 < q^2 < 6.0$ GeV²/c⁴.

 $B(\Lambda_b \rightarrow \Lambda\mu^+\mu^-)$ ($6.0 < q^2 < 8.0$ GeV²/c⁴)

VALUE (units 10^{-7})	DOCUMENT ID	TECN	COMMENT
$0.50 \pm 0.24 \pm 0.10$	AAIJ	15AE LHCb	pp at 7, 8 TeV

 $B(\Lambda_b \rightarrow \Lambda\mu^+\mu^-)$ ($4.3 < q^2 < 8.68$ GeV²/c⁴)

VALUE (units 10^{-7})	DOCUMENT ID	TECN	COMMENT
0.5 ± 0.7 OUR AVERAGE			
$0.66 \pm 0.74 \pm 0.18$	¹ AAIJ	13AJ LHCb	pp at 7 TeV
$-0.2 \pm 1.6 \pm 0.1$	AALTONEN	11AI CDF	$p\bar{p}$ at 1.96 TeV

¹ Uses $B(\Lambda_b^0 \rightarrow J/\psi\Lambda) = (6.2 \pm 1.4) \times 10^{-4}$.

 $B(\Lambda_b \rightarrow \Lambda\mu^+\mu^-)$ ($10.09 < q^2 < 12.86$ GeV²/c⁴)

VALUE (units 10^{-7})	DOCUMENT ID	TECN	COMMENT
2.2 ± 0.6 OUR AVERAGE			
$2.08 \pm 0.42 \pm 0.35 \pm 0.42$	¹ AAIJ	15AE LHCb	pp at 7, 8 TeV
$3.0 \pm 1.5 \pm 1.0$	AALTONEN	11AI CDF	$p\bar{p}$ at 1.96 TeV

• • • We do not use the following data for averages, fits, limits, etc. • • •

VALUE (units 10^{-7})	DOCUMENT ID	TECN	COMMENT
$1.55 \pm 0.58 \pm 0.55$	² AAIJ	13AJ LHCb	Repl. by AAIJ 15AE

¹ AAIJ 15AE measurement covers $11.0 < q^2 < 12.5$ GeV²/c⁴.
² Uses $B(\Lambda_b^0 \rightarrow J/\psi\Lambda) = (6.2 \pm 1.4) \times 10^{-4}$.

$B(\Lambda_b \rightarrow \Lambda \mu^+ \mu^-)$ ($14.18 < q^2 < 16.0 \text{ GeV}^2/c^4$)

VALUE (units 10^{-7})	DOCUMENT ID	TECN	COMMENT
1.7 ± 0.5 OUR AVERAGE			Error includes scale factor of 1.1.
$2.04^{+0.35}_{-0.33} \pm 0.42$	¹ AAIJ	15AE LHCb	pp at 7, 8 TeV
$1.0 \pm 0.7 \pm 0.3$	AALTONEN	11AI CDF	$p\bar{p}$ at 1.96 TeV
• • • We do not use the following data for averages, fits, limits, etc. • • •			
$1.44 \pm 0.44 \pm 0.42$	² AAIJ	13AJ LHCb	Repl. by AAIJ 15AE
¹ AAIJ 15AE measurement covers $15.0 < q^2 < 16.0 \text{ GeV}^2/c^4$.			
² Uses $B(\Lambda_b^0 \rightarrow J/\psi \Lambda) = (6.2 \pm 1.4) \times 10^{-4}$.			

 $B(\Lambda_b \rightarrow \Lambda \mu^+ \mu^-)$ ($16.0 < q^2 < 20.0 \text{ GeV}^2/c^4$)

VALUE (units 10^{-7})	DOCUMENT ID	TECN	COMMENT
$7.0 \pm 1.9 \pm 2.2$	AALTONEN	11AI CDF	$p\bar{p}$ at 1.96 TeV
• • • We do not use the following data for averages, fits, limits, etc. • • •			
$4.73 \pm 0.77 \pm 1.25$	^{1,2} AAIJ	13AJ LHCb	Repl. by AAIJ 15AE
¹ Uses $B(\Lambda_b^0 \rightarrow J/\psi \Lambda) = (6.2 \pm 1.4) \times 10^{-4}$.			
² Requires $16.00 < q^2 < 20.30 \text{ GeV}^2/c^4$.			

 $B(\Lambda_b \rightarrow \Lambda \mu^+ \mu^-)$ ($18.0 < q^2 < 20.0 \text{ GeV}^2/c^4$)

VALUE (units 10^{-7})	DOCUMENT ID	TECN	COMMENT
$2.44 \pm 0.28 \pm 0.50$	AAIJ	15AE LHCb	pp at 7, 8 TeV

 $B(\Lambda_b \rightarrow \Lambda \mu^+ \mu^-)$ ($15.0 < q^2 < 20.0 \text{ GeV}^2/c^4$)

VALUE (units 10^{-7})	DOCUMENT ID	TECN	COMMENT
$6.00 \pm 0.45 \pm 1.25$	AAIJ	15AE LHCb	pp at 7, 8 TeV

 $B(\Lambda_b \rightarrow \Lambda(1520)^0 \mu^+ \mu^-)$ ($1.1 < q^2 < 6.0 \text{ GeV}^2/c^4$)

VALUE (units 10^{-8})	DOCUMENT ID	TECN	COMMENT
$9.56 \pm 1.13 \pm 0.78 \pm 1.81$	¹ AAIJ	23BB LHCb	pp at 7, 8, 13 TeV
¹ Uses $B(\Lambda_b \rightarrow J/\psi p K^-) = (3.2 \pm 0.6) \times 10^{-4}$. The last uncertainty is due to uncertainties of $B(\Lambda_b^0 \rightarrow p K^- J/\psi)$ and $B(J/\psi \rightarrow \mu^+ \mu^-)$ values.			

 $B(\Lambda_b \rightarrow \Lambda(1520)^0 \mu^+ \mu^-)$ ($15.0 < q^2 < 17.0 \text{ GeV}^2/c^4$)

VALUE (units 10^{-8})	DOCUMENT ID	TECN	COMMENT
$1.14 \pm 0.48 \pm 0.26 \pm 0.22$	¹ AAIJ	23BB LHCb	pp at 7, 8, 13 TeV
¹ Uses $B(\Lambda_b \rightarrow J/\psi p K^-) = (3.2 \pm 0.6) \times 10^{-4}$. The last uncertainty is due to uncertainties of $B(\Lambda_b^0 \rightarrow p K^- J/\psi)$ and $B(J/\psi \rightarrow \mu^+ \mu^-)$ values.			

CP VIOLATION

A_{CP} is defined as

$$A_{CP} = \frac{B(\Lambda_b^0 \rightarrow f) - B(\bar{\Lambda}_b^0 \rightarrow \bar{f})}{B(\Lambda_b^0 \rightarrow f) + B(\bar{\Lambda}_b^0 \rightarrow \bar{f})},$$

the CP-violation asymmetry of exclusive Λ_b^0 and $\bar{\Lambda}_b^0$ decay.

 $A_{CP}(\Lambda_b \rightarrow p \pi^-)$

VALUE	DOCUMENT ID	TECN	COMMENT
-0.025 ± 0.029 OUR AVERAGE			Error includes scale factor of 1.2.
$-0.035 \pm 0.017 \pm 0.020$	AAIJ	18AX LHCb	pp at 7 and 8 TeV
$0.06 \pm 0.07 \pm 0.03$	AALTONEN	14P CDF	$p\bar{p}$ at 1.96 TeV
• • • We do not use the following data for averages, fits, limits, etc. • • •			
$0.03 \pm 0.17 \pm 0.05$	AALTONEN	11N CDF	Repl. by AALTONEN 14P

 $A_{CP}(\Lambda_b \rightarrow p K^-)$

VALUE	DOCUMENT ID	TECN	COMMENT
-0.025 ± 0.022 OUR AVERAGE			
$-0.020 \pm 0.013 \pm 0.019$	AAIJ	18AX LHCb	pp at 7 and 8 TeV
$-0.10 \pm 0.08 \pm 0.04$	AALTONEN	14P CDF	$p\bar{p}$ at 1.96 TeV
• • • We do not use the following data for averages, fits, limits, etc. • • •			
$0.37 \pm 0.17 \pm 0.03$	AALTONEN	11N CDF	Repl. by AALTONEN 14P

 $A_{CP}(\Lambda_b \rightarrow D \rho K^-)$

VALUE	DOCUMENT ID	TECN	COMMENT
$0.12 \pm 0.09 \pm 0.02$ -0.03	¹ AAIJ	21AD LHCb	pp at 7, 8, 13 TeV
¹ A_{CP} is measured from $(B(\Lambda_b^0 \rightarrow [K^+ \pi^-]_D \rho K^-) - B(\bar{\Lambda}_b^0 \rightarrow [K^- \pi^+]_D \bar{\rho} K^+)) / (B(\Lambda_b^0 \rightarrow [K^+ \pi^-]_D \rho K^-) + B(\bar{\Lambda}_b^0 \rightarrow [K^- \pi^+]_D \bar{\rho} K^+))$ in the full phase space.			

 $\Delta A_{CP}(\rho K^- / \pi^-)$

VALUE	DOCUMENT ID	TECN	COMMENT
$\Delta A_{CP} \equiv A_{CP}(\rho K^-) - A_{CP}(\pi^-)$			
$0.014 \pm 0.022 \pm 0.010$	AAIJ	18AX LHCb	pp at 7 and 8 TeV

 $A_{CP}(\Lambda_b \rightarrow \rho \bar{K}^0 \pi^-)$

VALUE	DOCUMENT ID	TECN	COMMENT
$0.22 \pm 0.13 \pm 0.03$	AAIJ	14Q LHCb	pp at 7 TeV

 $\Delta A_{CP}(J/\psi p \pi^- / K^-)$

VALUE (units 10^{-2})	DOCUMENT ID	TECN	COMMENT
$\Delta A_{CP} \equiv A_{CP}(J/\psi p \pi^-) - A_{CP}(J/\psi p K^-)$			
$5.7 \pm 2.4 \pm 1.2$	AAIJ	14K LHCb	pp at 7, 8 TeV

 $A_{CP}(\Lambda_b \rightarrow \Lambda K^+ \pi^-)$

VALUE	DOCUMENT ID	TECN	COMMENT
$-0.53 \pm 0.23 \pm 0.11$	¹ AAIJ	16W LHCb	pp at 7, 8 TeV
¹ Measured relative to $\Lambda_b^0 \rightarrow \Lambda_c^+ \pi^-$ decay.			

 $A_{CP}(\Lambda_b \rightarrow \Lambda K^+ K^-)$

VALUE	DOCUMENT ID	TECN	COMMENT
$-0.28 \pm 0.10 \pm 0.07$	¹ AAIJ	16W LHCb	pp at 7, 8 TeV
¹ Measured relative to $\Lambda_b^0 \rightarrow \Lambda_c^+ \pi^-$ decay.			

 $\Delta A_{CP}(\Lambda_b^0 \rightarrow \rho K^- \mu^+ \mu^-)$

VALUE (units 10^{-2})	DOCUMENT ID	TECN	COMMENT
$\Delta A_{CP} \equiv A_{CP}(\rho K^- \mu^+ \mu^-) - A_{CP}(\rho K^- J/\psi)$			
$-3.5 \pm 5.0 \pm 0.2$	AAIJ	17T LHCb	pp at 7, 8 TeV

 $\Delta A_{CP}(\Lambda_b^0 \rightarrow \rho \pi^- \pi^+ \pi^-)$

VALUE (units 10^{-2})	DOCUMENT ID	TECN	COMMENT
$\Delta A_{CP} \equiv A_{CP}(\Lambda_b^0 \rightarrow \rho \pi^- \pi^+ \pi^-) - A_{CP}(\Lambda_b^0 \rightarrow (\Lambda_c^+ \rightarrow p \pi^- \pi^+) \pi^-)$			
$1.1 \pm 2.5 \pm 0.6$	¹ AAIJ	19AH LHCb	pp at 7 and 8 TeV
¹ Full phase space.			

 $\Delta A_{CP}(\Lambda_b^0 \rightarrow (\rho \pi^- \pi^+ \pi^-)_{LBM})$

VALUE (units 10^{-2})	DOCUMENT ID	TECN	COMMENT
$\Delta A_{CP} \equiv A_{CP}(\Lambda_b^0 \rightarrow (\rho \pi^- \pi^+ \pi^-)_{LBM}) - A_{CP}(\Lambda_b^0 \rightarrow (\Lambda_c^+ \rightarrow p \pi^- \pi^+) \pi^-)$			
$3.7 \pm 4.1 \pm 0.5$	¹ AAIJ	19AH LHCb	pp at 7 and 8 TeV
¹ Two-body low invariant-mass region (LBM): $m(\rho \pi^-) < 2000 \text{ MeV}$ and $m(\pi^+ \pi^-) < 1640 \text{ MeV}$.			

VALUE (units 10^{-2})	DOCUMENT ID	TECN	COMMENT
$3.7 \pm 4.1 \pm 0.5$	¹ AAIJ	19AH LHCb	pp at 7 and 8 TeV
¹ Measurement done with $m(\rho \pi^-) < 2000 \text{ MeV}/c^2$ and $m(\pi^+ \pi^-) < 1640 \text{ MeV}/c^2$.			

 $\Delta A_{CP}(\Lambda_b^0 \rightarrow \rho a_1(1260)^-)$

VALUE (units 10^{-2})	DOCUMENT ID	TECN	COMMENT
$\Delta A_{CP} \equiv A_{CP}(\Lambda_b^0 \rightarrow \rho a_1(1260)^-) - A_{CP}(\Lambda_b^0 \rightarrow (\Lambda_c^+ \rightarrow p \pi^- \pi^+) \pi^-)$			
$-1.5 \pm 4.2 \pm 0.6$	AAIJ	19AH LHCb	pp at 7 and 8 TeV
¹ $419 < m(\pi^+ \pi^-) < 1500 \text{ MeV}$.			

 $\Delta A_{CP}(\Lambda_b^0 \rightarrow N(1520)^0 \rho(770)^0)$

VALUE (units 10^{-2})	DOCUMENT ID	TECN	COMMENT
$\Delta A_{CP} \equiv A_{CP}(\Lambda_b^0 \rightarrow N(1520)^0 \rho(770)^0) - A_{CP}(\Lambda_b^0 \rightarrow (\Lambda_c^+ \rightarrow p \pi^- \pi^+) \pi^-)$			
$2.0 \pm 4.9 \pm 0.4$	AAIJ	19AH LHCb	pp at 7 and 8 TeV
¹ $1078 < m(\rho \pi^-) < 1800 \text{ MeV}$ and $m(\pi^+ \pi^-) < 1100 \text{ MeV}$.			

 $\Delta A_{CP}(\Lambda_b^0 \rightarrow \Delta(1232)^{++} \pi^- \pi^-)$

VALUE (units 10^{-2})	DOCUMENT ID	TECN	COMMENT
$\Delta A_{CP} \equiv A_{CP}(\Lambda_b^0 \rightarrow \Delta(1232)^{++} \pi^- \pi^-) - A_{CP}(\Lambda_b^0 \rightarrow (\Lambda_c^+ \rightarrow p \pi^- \pi^+) \pi^-)$			
$0.1 \pm 3.2 \pm 0.6$	AAIJ	19AH LHCb	pp at 7 and 8 TeV
¹ $1078 < m(\rho \pi^+) < 1432 \text{ MeV}$.			

 $\Delta A_{CP}(\Lambda_b^0 \rightarrow \rho K^- \pi^+ \pi^-)$

VALUE (units 10^{-2})	DOCUMENT ID	TECN	COMMENT
$\Delta A_{CP} \equiv A_{CP}(\Lambda_b^0 \rightarrow \rho K^- \pi^+ \pi^-) - A_{CP}(\Lambda_b^0 \rightarrow (\Lambda_c^+ \rightarrow p K^- \pi^+) \pi^-)$			
$3.2 \pm 1.1 \pm 0.6$	¹ AAIJ	19AH LHCb	pp at 7 and 8 TeV
¹ Full phase space.			

 $\Delta A_{CP}(\Lambda_b^0 \rightarrow (\rho K^- \pi^+ \pi^-)_{LBM})$

VALUE (units 10^{-2})	DOCUMENT ID	TECN	COMMENT
$\Delta A_{CP} \equiv A_{CP}(\Lambda_b^0 \rightarrow (\rho K^- \pi^+ \pi^-)_{LBM}) - A_{CP}(\Lambda_b^0 \rightarrow (\Lambda_c^+ \rightarrow p K^- \pi^+) \pi^-)$			
$3.5 \pm 1.5 \pm 0.5$	¹ AAIJ	19AH LHCb	pp at 7 and 8 TeV
¹ Two-body low invariant-mass region (LBM): $m(\rho K^-) < 2000 \text{ MeV}$ and $m(\pi^+ \pi^-) < 1640 \text{ MeV}$.			
¹ Measurement done with $m(\rho K^-) < 2000 \text{ MeV}/c^2$ and $m(\pi^+ \pi^-) < 1640 \text{ MeV}/c^2$.			

 $\Delta A_{CP}(\Lambda_b^0 \rightarrow N(1520)^0 K^*(892)^0)$

VALUE (units 10^{-2})	DOCUMENT ID	TECN	COMMENT
$\Delta A_{CP} \equiv A_{CP}(\Lambda_b^0 \rightarrow N(1520)^0 K^*(892)^0) - A_{CP}(\Lambda_b^0 \rightarrow (\Lambda_c^+ \rightarrow p K^- \pi^+) \pi^-)$			
$5.5 \pm 2.5 \pm 0.5$	AAIJ	19AH LHCb	pp at 7 and 8 TeV
¹ $1078 < m(\rho \pi^-) < 1800 \text{ MeV}$ and $750 < m(\pi^+ \pi^-) < 1100 \text{ MeV}$.			

 $\Delta A_{CP}(\Lambda_b^0 \rightarrow \Lambda(1520) \rho(770)^0)$

VALUE (units 10^{-2})	DOCUMENT ID	TECN	COMMENT
$\Delta A_{CP} \equiv A_{CP}(\Lambda_b^0 \rightarrow \Lambda(1520) \rho(770)^0) - A_{CP}(\Lambda_b^0 \rightarrow (\Lambda_c^+ \rightarrow p K^- \pi^+) \pi^-)$			
$0.6 \pm 6.0 \pm 0.5$	AAIJ	19AH LHCb	pp at 7 and 8 TeV
¹ $1460 < m(\rho K^-) < 1580 \text{ MeV}$ and $m(\pi^+ \pi^-) < 1100 \text{ MeV}$.			

Baryon Particle Listings

 Λ_b^0 $\Delta A_{CP}(\Lambda_b^0 \rightarrow \Delta(1232)^{++} K^- \pi^-)$

$$\Delta A_{CP} \equiv A_{CP}(\Lambda_b^0 \rightarrow \Delta(1232)^{++} K^- \pi^-) - A_{CP}(\Lambda_b^0 \rightarrow (\Lambda_c^+ \rightarrow p K^- \pi^+) \pi^-)$$

$$1078 < m(p\pi^+) < 1432 \text{ MeV.}$$

VALUE (units 10^{-2})	DOCUMENT ID	TECN	COMMENT
$4.4 \pm 2.6 \pm 0.6$	AAIJ	19AH LHCb	pp at 7 and 8 TeV

 $\Delta A_{CP}(\Lambda_b^0 \rightarrow p K_1(1410)^-)$

$$\Delta A_{CP} \equiv A_{CP}(\Lambda_b^0 \rightarrow p K_1(1410)^-) - A_{CP}(\Lambda_b^0 \rightarrow (\Lambda_c^+ \rightarrow p K^- \pi^+) \pi^-)$$

$$1200 < m(K^- \pi^+) < 1600 \text{ MeV.}$$

VALUE (units 10^{-2})	DOCUMENT ID	TECN	COMMENT
$4.7 \pm 3.5 \pm 0.8$	AAIJ	19AH LHCb	pp at 7 and 8 TeV

 $\Delta A_{CP}(\Lambda_b^0 \rightarrow p K^- K^+ \pi^-)$

$$\Delta A_{CP} \equiv A_{CP}(\Lambda_b^0 \rightarrow p K^- K^+ \pi^-) - A_{CP}(\Lambda_b^0 \rightarrow (\Lambda_c^+ \rightarrow p \pi^- \pi^+) \pi^-)$$

VALUE (units 10^{-2})	DOCUMENT ID	TECN	COMMENT
$-6.9 \pm 4.9 \pm 0.8$	1 AAIJ	19AH LHCb	pp at 7 and 8 TeV

¹ Full phase space.
 $\Delta A_{CP}(\Lambda_b^0 \rightarrow p K^- K^+ K^-)$

$$\Delta A_{CP} \equiv A_{CP}(\Lambda_b^0 \rightarrow p K^- K^+ K^-) - A_{CP}(\Lambda_b^0 \rightarrow (\Lambda_c^+ \rightarrow p K^- \pi^+) \pi^-)$$

VALUE (units 10^{-2})	DOCUMENT ID	TECN	COMMENT
$0.2 \pm 1.8 \pm 0.6$	1 AAIJ	19AH LHCb	pp at 7 and 8 TeV

¹ Full phase space.
 $\Delta A_{CP}(\Lambda_b^0 \rightarrow \Lambda(1520) \phi(1020))$

$$\Delta A_{CP} \equiv A_{CP}(\Lambda_b^0 \rightarrow \Lambda(1520) \phi(1020)) - A_{CP}(\Lambda_b^0 \rightarrow (\Lambda_c^+ \rightarrow p K^- \pi^+) \pi^-)$$

$$1460 < m(pK^-) < 1600 \text{ MeV and } 1005 < m(K^+ K^-) < 1040 \text{ MeV.}$$

VALUE (units 10^{-2})	DOCUMENT ID	TECN	COMMENT
$4.3 \pm 5.6 \pm 0.4$	AAIJ	19AH LHCb	pp at 7 and 8 TeV

 $\Delta A_{CP}(\Lambda_b^0 \rightarrow (pK^-)_{\text{highmass}} \phi(1020))$

$$\Delta A_{CP} \equiv A_{CP}(\Lambda_b^0 \rightarrow (pK^-)_{\text{highmass}} \phi(1020)) - A_{CP}(\Lambda_b^0 \rightarrow (\Lambda_c p K^- \pi^+) \pi^-)$$

$$m(pK^-) > 1600 \text{ MeV and } 1005 < m(K^+ K^-) < 1040 \text{ MeV.}$$

VALUE (units 10^{-2})	DOCUMENT ID	TECN	COMMENT
$-0.7 \pm 3.3 \pm 0.7$	1 AAIJ	19AH LHCb	pp at 7 and 8 TeV

¹ Measurement done with $m(pK^-) > 1600 \text{ MeV}/c^2$.
 $\Delta A_{CP}(\Lambda_b^0 \rightarrow (pK^- K^+ K^-)_{\text{LBM}})$

$$\Delta A_{CP} \equiv A_{CP}(\Lambda_b^0 \rightarrow (pK^- K^+ K^-)_{\text{LBM}}) - A_{CP}(\Lambda_b^0 \rightarrow (\Lambda_c^+ \rightarrow p K^- \pi^+) \pi^-)$$

$$\text{Two-body low invariant-mass region (LBM): } m(pK^-) < 2000 \text{ MeV and } m(K^+ K^-) < 1675 \text{ MeV.}$$

VALUE (units 10^{-2})	DOCUMENT ID	TECN	COMMENT
$2.7 \pm 2.3 \pm 0.6$	1 AAIJ	19AH LHCb	pp at 7 and 8 TeV

¹ Measurement done with $m(pK^-) < 2000 \text{ MeV}/c^2$ and $m(K^+ K^-) < 1675 \text{ MeV}/c^2$.

CP AND T VIOLATION PARAMETERS

Measured values of the triple-product asymmetry parameters, odd under time-reversal, are defined as $A_{c(s)}(\Lambda/\phi) = (N_{c(s)}^+ - N_{c(s)}^-) / (\text{sum})$

where $N_{c(s)}^+$, $N_{c(s)}^-$ are the number of Λ or ϕ candidates for which the $\cos(\phi)$ and $\sin(\phi)$ observables are positive and negative, respectively. Angles $\cos(\phi)$ and $\sin(\phi)$ are defined as in LEITNER 07.

 $A_c(\Lambda)$

VALUE	DOCUMENT ID	TECN	COMMENT
$-0.22 \pm 0.12 \pm 0.06$	AAIJ	16J LHCb	pp at 7, 8 TeV

 $A_s(\Lambda)$

VALUE	DOCUMENT ID	TECN	COMMENT
$0.13 \pm 0.12 \pm 0.05$	AAIJ	16J LHCb	pp at 7, 8 TeV

 $A_c(\phi)$

VALUE	DOCUMENT ID	TECN	COMMENT
$-0.01 \pm 0.12 \pm 0.03$	AAIJ	16J LHCb	pp at 7, 8 TeV

 $A_s(\phi)$

VALUE	DOCUMENT ID	TECN	COMMENT
$-0.07 \pm 0.12 \pm 0.01$	AAIJ	16J LHCb	pp at 7, 8 TeV

 $a_{CP}(\Lambda_b^0 \rightarrow p \pi^- \pi^+ \pi^-)$

Observable calculated as half of the difference between triple products for Λ_b^0 and $\bar{\Lambda}_b^0$, which is sensitive to CP violation.

VALUE (%)	DOCUMENT ID	TECN	COMMENT
$-0.7 \pm 0.7 \pm 0.2$	1 AAIJ	20AB LHCb	pp at 7, 8, 13 TeV

- • • We do not use the following data for averages, fits, limits, etc. • • •

¹ 1.15 ± 1.45 ± 0.32

² 2 AAIJ 17H LHCb Repl. by AAIJ 20AB

¹ Used both triple product asymmetries and the unbinned energy test method.

² Measured over full phase space of the decay.
 $a_{CP}(\Lambda_b^0 \rightarrow p K^- \pi^+ \pi^-)$

Observable calculated as half of the difference between triple products for Λ_b^0 and $\bar{\Lambda}_b^0$, which is sensitive to CP violation.

VALUE (%)	DOCUMENT ID	TECN	COMMENT
$-0.81 \pm 0.84 \pm 0.31$	1 AAIJ	18AG LHCb	pp at 7, 8 TeV

¹ Measured over full phase space of the decay.
 $a_{CP}(\Lambda_b^0 \rightarrow p K^- K^+ \pi^-)$

Observable calculated as half of the difference between triple products for Λ_b^0 and $\bar{\Lambda}_b^0$, which is sensitive to CP violation.

VALUE (%)	DOCUMENT ID	TECN	COMMENT
$-0.93 \pm 4.54 \pm 0.42$	1 AAIJ	17H LHCb	pp at 7, 8 TeV

¹ Measured over full phase space of the decay.
 $a_{CP}(\Lambda_b^0 \rightarrow p K^- K^+ K^-)$

Observable calculated as half of the difference between triple products for Λ_b^0 and $\bar{\Lambda}_b^0$, which is sensitive to CP violation.

VALUE (%)	DOCUMENT ID	TECN	COMMENT
$1.12 \pm 1.51 \pm 0.32$	1 AAIJ	18AG LHCb	pp at 7, 8 TeV

¹ Measured over full phase space of the decay.
 $a_{CP}(\Lambda_b^0 \rightarrow p K^- \mu^+ \mu^-)$

VALUE (%)	DOCUMENT ID	TECN	COMMENT
$1.2 \pm 5.0 \pm 0.7$	AAIJ	17T LHCb	pp at 7, 8 TeV

P VIOLATION PARAMETERS

Observables calculated as average of the triple products for Λ_b^0 and $\bar{\Lambda}_b^0$, which is sensitive to parity violation.

 $a_P(\Lambda_b^0 \rightarrow p \pi^- \pi^+ \pi^-)$

VALUE (%)	DOCUMENT ID	TECN	COMMENT
$-4.0 \pm 0.7 \pm 0.2$	1 AAIJ	20AB LHCb	pp at 7, 8, 13 TeV

- • • We do not use the following data for averages, fits, limits, etc. • • •

¹ -3.71 ± 1.45 ± 0.32

² 2 AAIJ 17H LHCb Repl. by AAIJ 20AB

¹ Used both triple product asymmetries and the unbinned energy test method.

² Measured over full phase space of the decay.
 $a_P(\Lambda_b^0 \rightarrow p K^- \pi^+ \pi^-)$

VALUE (%)	DOCUMENT ID	TECN	COMMENT
$-0.60 \pm 0.84 \pm 0.31$	1 AAIJ	18AG LHCb	pp at 7, 8 TeV

¹ Measured over full phase space of the decay.
 $a_P(\Lambda_b^0 \rightarrow p K^- K^+ \pi^-)$

VALUE (%)	DOCUMENT ID	TECN	COMMENT
$3.62 \pm 4.54 \pm 0.42$	1 AAIJ	17H LHCb	pp at 7, 8 TeV

¹ Measured over full phase space of the decay.
 $a_P(\Lambda_b^0 \rightarrow p K^- K^+ K^-)$

VALUE (%)	DOCUMENT ID	TECN	COMMENT
$-1.56 \pm 1.51 \pm 0.32$	1 AAIJ	18AG LHCb	pp at 7, 8 TeV

¹ Measured over full phase space of the decay.
 $a_P(\Lambda_b^0 \rightarrow p K^- \mu^+ \mu^-)$

VALUE (%)	DOCUMENT ID	TECN	COMMENT
$-4.8 \pm 5.0 \pm 0.7$	AAIJ	17T LHCb	pp at 7, 8 TeV

 Λ_b^0 DECAY PARAMETERS

See the note on "Baryon Decay Parameters" in the neutron Listings.

 α decay parameter for $\Lambda_b \rightarrow J/\psi \Lambda$

VALUE	DOCUMENT ID	TECN	COMMENT
-0.017 ± 0.026 OUR AVERAGE			

¹ -0.022 +0.027 -0.026

² 1 AAIJ 20c LHCb pp at 7, 8, 13 TeV

³ -0.14 ± 0.14 ± 0.10

² SJRUNYAN 18R CMS pp at 7, 8 TeV

³ 0.30 ± 0.16 ± 0.06

³ AAD 14L ATLS pp at 7 TeV

- • • We do not use the following data for averages, fits, limits, etc. • • •

⁴ 0.05 ± 0.17 ± 0.07

⁴ AAIJ 13AG LHCb Repl. by AAIJ 20c

¹ Extracted using a Bayesian analysis. The most probable value is given as -0.022, with a 68% credibility interval [-0.048, 0.005]. Transverse polarizations of Λ_b^0 of -0.004 (68% credibility interval [-0.064, 0.051]), 0.001 (68% credibility interval [-0.035, 0.045]), and 0.032 (68% credibility interval [-0.011, 0.065]) are also reported at 7 TeV, 8 TeV and 13 TeV, respectively. Note that both statistical and systematic uncertainties are included.

² An angular analysis of $\Lambda_b \rightarrow J/\psi \Lambda$ decay is performed. Note that the sign of α in CMS definition is the opposite to that used by AAIJ 13AG and AAD 14L. Λ_b transverse production polarization of $0.00 \pm 0.06 \pm 0.06$ is also reported, as well as squares of the helicity amplitudes.

³ An angular analysis of $\Lambda_b \rightarrow J/\psi \Lambda$ decay is performed and magnitudes of all helicity amplitudes are also reported.

⁴ An angular analysis of $\Lambda_b \rightarrow J/\psi \Lambda$ decay is performed and a Λ_b transverse production polarization of $0.06 \pm 0.07 \pm 0.02$ is also reported.

See key on page 1171

Baryon Particle Listings

$\Lambda_b^0, \Lambda_b(5912)^0$

α_γ decay parameter for $\Lambda_b \rightarrow \Lambda\gamma$

Measures asymmetry between left- and right-handed photons in the decay.

VALUE	DOCUMENT ID	TECN	COMMENT
$0.82^{+0.17+0.04}_{-0.26-0.13}$	¹ AAIJ	22M LHCb	pp at 13 TeV

¹ AAIJ 22M provides a combined measurement as well as measured $\alpha_\gamma^- = 1.26 \pm 0.42 \pm 0.20$ and $\alpha_\gamma^+ = 0.55 \pm 0.32 \pm 0.16$ for Λ_b^0 and $\bar{\Lambda}_b^0$ separately.

$f_L(\mu\mu)$ longitudinal polarization fraction in $\Lambda_b \rightarrow \Lambda\mu^+\mu^-$

VALUE	DOCUMENT ID	TECN	COMMENT
$0.61^{+0.11}_{-0.14} \pm 0.03$	¹ AAIJ	15AE LHCb	pp at 7, 8 TeV

¹ AAIJ 15AE measurement covers $15.0 < q^2 < 20.0 \text{ GeV}^2/c^4$.

FORWARD-BACKWARD ASYMMETRIES

The forward-backward asymmetry is defined as $A_{FB}(\Lambda_b^0) = [N(F) - N(B)] / [N(F) + N(B)]$, where the forward (F) direction corresponds to a particle (Λ_b^0 or $\bar{\Lambda}_b^0$) sharing valence quark flavors with a beam particle with the same sign of rapidity.

$A_{FB}(\Lambda_b^0 \rightarrow J/\psi\Lambda)$

VALUE	DOCUMENT ID	TECN	COMMENT
$0.04 \pm 0.07 \pm 0.02$	¹ ABAZOV	15I D0	pp at 1.96 TeV

¹ The measured asymmetry integrated over rapidity y in the range of $0.1 < |y| < 2.0$.

$A_{FB}^{\ell}(\mu\mu)$ in $\Lambda_b \rightarrow \Lambda\mu^+\mu^-$

VALUE	DOCUMENT ID	TECN	COMMENT
$-0.39 \pm 0.04 \pm 0.01$	¹ AAIJ	18AP LHCb	pp at 7, 8, 13 TeV

• • • We do not use the following data for averages, fits, limits, etc. • • •

$-0.05 \pm 0.09 \pm 0.03$	² AAIJ	15AE LHCb	Repl. by AAIJ 18AP.
---------------------------	-------------------	-----------	---------------------

¹ The measurement covers $15.0 < q^2 < 20.0 \text{ GeV}^2/c^4$.

² AAIJ 15AE measurement covers $15.0 < q^2 < 20.0 \text{ GeV}^2/c^4$.

$\Delta(A_{FB}^{\ell}(\mu\mu))$ in $\Lambda_b \rightarrow \Lambda\mu^+\mu^-$

Difference of asymmetries $A_{FB}^{\ell}(\mu\mu)$ in $\Lambda_b \rightarrow \Lambda\mu^+\mu^-$ between Λ_b and $\bar{\Lambda}_b$ decays

VALUE	DOCUMENT ID	TECN	COMMENT
$-0.05 \pm 0.09 \pm 0.03$	AAIJ	18AO LHCb	pp at 7, 8 TeV

$A_{FB}^h(\rho\pi)$ in $\Lambda_b \rightarrow \Lambda(\rho\pi)\mu^+\mu^-$

VALUE	DOCUMENT ID	TECN	COMMENT
$-0.30 \pm 0.05 \pm 0.02$	¹ AAIJ	18AP LHCb	pp at 7, 8, 13 TeV

• • • We do not use the following data for averages, fits, limits, etc. • • •

$-0.29 \pm 0.07 \pm 0.03$	² AAIJ	15AE LHCb	Repl. by AAIJ 18AP.
---------------------------	-------------------	-----------	---------------------

¹ The measurement covers $15.0 < q^2 < 20.0 \text{ GeV}^2/c^4$.

² AAIJ 15AE measurement covers $15.0 < q^2 < 20.0 \text{ GeV}^2/c^4$.

$A_{FB}^{\ell h}$ in $\Lambda_b \rightarrow \Lambda\mu^+\mu^-$

VALUE	DOCUMENT ID	TECN	COMMENT
$0.25 \pm 0.04 \pm 0.01$	¹ AAIJ	18AP LHCb	pp at 7, 8, 13 TeV

¹ The measurement covers $15.0 < q^2 < 20.0 \text{ GeV}^2/c^4$.

$\Lambda_b^0 - \bar{\Lambda}_b^0$ Production Asymmetry

$$A_P(\Lambda_b^0) = [\sigma(\Lambda_b^0) - \sigma(\bar{\Lambda}_b^0)] / [\sigma(\Lambda_b^0) + \sigma(\bar{\Lambda}_b^0)]$$

$A_P(\Lambda_b^0)$

VALUE (units 10^{-2})	DOCUMENT ID	TECN	COMMENT
1.4 ± 0.4 OUR AVERAGE	Error includes scale factor of 1.8.		
1.92 ± 0.35	¹ AAIJ	21AJ LHCb	pp at 7 TeV
1.09 ± 0.29	¹ AAIJ	21AJ LHCb	pp at 8 TeV
-0.11 ± 2.53 ± 1.08	² AAIJ	17BF LHCb	pp at 7 TeV
3.44 ± 1.61 ± 0.76	² AAIJ	17BF LHCb	pp at 8 TeV

¹ Integrated over the kinematic range $2 < p_T < 27 \text{ GeV}/c$ and $2.15 < y < 4.10$.

² Indirect determination in kinematic range $2 < p_T < 30 \text{ GeV}/c$ and $2.1 < \eta < 4.5$ from production asymmetries of B^+ , B^0 and B_s^0 .

Λ_b^0 REFERENCES

AAIJ	23BB PRL 131 151801	R. Aaij et al.	(LHCb Collab.)
AAIJ	23K JHEP 2307 075	R. Aaij et al.	(LHCb Collab.)
AAIJ	22K PRL 128 191803	R. Aaij et al.	(LHCb Collab.)
AAIJ	22M PR D105 L051104	R. Aaij et al.	(LHCb Collab.)
AAIJ	22R JHEP 2203 153	R. Aaij et al.	(LHCb Collab.)
AAIJ	21AD PR D104 112008	R. Aaij et al.	(LHCb Collab.)
AAIJ	21AJ JHEP 2110 060	R. Aaij et al.	(LHCb Collab.)
AAIJ	21B PL B815 136172	R. Aaij et al.	(LHCb Collab.)
AAIJ	21R JHEP 2105 095	R. Aaij et al.	(LHCb Collab.)
AAIJ	20AB PR D102 051101	R. Aaij et al.	(LHCb Collab.)
AAIJ	20AK PR D102 112012	R. Aaij et al.	(LHCb Collab.)
AAIJ	20M JHEP 2005 040	R. Aaij et al.	(LHCb Collab.)
AAIJ	20O JHEP 2006 110	R. Aaij et al.	(LHCb Collab.)
SIRUNYAN	20H PL B802 135203	A.M. Sirunyan et al.	(CMS Collab.)
AAIJ	19AH EPJ C79 745	R. Aaij et al.	(LHCb Collab.)
AAIJ	19AN JHEP 1909 028	R. Aaij et al.	(LHCb Collab.)
AAIJ	19F JHEP 1903 126	R. Aaij et al.	(LHCb Collab.)

AAIJ	19Z PRL 123 031801	R. Aaij et al.	(LHCb Collab.)
AAIJ	18AF JHEP 1808 131	R. Aaij et al.	(LHCb Collab.)
AAIJ	18AG JHEP 1808 039	R. Aaij et al.	(LHCb Collab.)
AAIJ	18AO JHEP 1809 145 (errata.)	R. Aaij et al.	(LHCb Collab.)
AAIJ	18AP JHEP 1809 146	R. Aaij et al.	(LHCb Collab.)
AAIJ	18AW PL B784 101	R. Aaij et al.	(LHCb Collab.)
AAIJ	18AX PL B787 124	R. Aaij et al.	(LHCb Collab.)
AAIJ	18Q JHEP 1802 098	R. Aaij et al.	(LHCb Collab.)
PDG	18 PR D98 030001	M. Tanabashi et al.	(PDG Collab.)
SIRUNYAN	18BY EPJ C78 457	A.M. Sirunyan et al.	(CMS Collab.)
SIRUNYAN	18R PR D97 072010	A.M. Sirunyan et al.	(CMS Collab.)
AAIJ	17AM PRL 119 062001	R. Aaij et al.	(LHCb Collab.)
AAIJ	17BF PL B774 139	R. Aaij et al.	(LHCb Collab.)
AAIJ	17H NATP 13 391	R. Aaij et al.	(LHCb Collab.)
AAIJ	17P JHEP 1704 029	R. Aaij et al.	(LHCb Collab.)
AAIJ	17S JHEP 1705 030	R. Aaij et al.	(LHCb Collab.)
AAIJ	17T JHEP 1706 108	R. Aaij et al.	(LHCb Collab.)
AAIJ	16 JHEP 1601 012	R. Aaij et al.	(LHCb Collab.)
AAIJ	16A CP C40 011001	R. Aaij et al.	(LHCb Collab.)
AAIJ	16J PL B759 282	R. Aaij et al.	(LHCb Collab.)
AAIJ	16W JHEP 1605 081	R. Aaij et al.	(LHCb Collab.)
AAIJ	16Y JHEP 1605 132	R. Aaij et al.	(LHCb Collab.)
AAD	15CH PL B751 63	G. Aad et al.	(ATLAS Collab.)
AAIJ	15AE JHEP 1506 115	R. Aaij et al.	(LHCb Collab.)
Also	JHEP 1809 145 (errata.)	R. Aaij et al.	(LHCb Collab.)
AAIJ	15AH JHEP 1509 006	R. Aaij et al.	(LHCb Collab.)
AAIJ	15BG NATP 11 743	R. Aaij et al.	(LHCb Collab.)
ABAZOV	15I PR D91 072008	V.M. Abazov et al.	(D0 Collab.)
AAD	14L PR D89 092009	G. Aad et al.	(ATLAS Collab.)
AAIJ	14AA PRL 112 202001	R. Aaij et al.	(LHCb Collab.)
AAIJ	14E JHEP 1404 114	R. Aaij et al.	(LHCb Collab.)
AAIJ	14H PR D89 032001	R. Aaij et al.	(LHCb Collab.)
AAIJ	14I JHEP 1408 143	R. Aaij et al.	(LHCb Collab.)
AAIJ	14K JHEP 1407 103	R. Aaij et al.	(LHCb Collab.)
AAIJ	14Q JHEP 1404 087	R. Aaij et al.	(LHCb Collab.)
AAIJ	14U PL B734 122	R. Aaij et al.	(LHCb Collab.)
AALTONEN	14B PR D89 072014	T. Aaltonen et al.	(CDF Collab.)
AALTONEN	14P PRL 113 242001	T. Aaltonen et al.	(CDF Collab.)
PDG	14 CP C38 070001	K. Olive et al.	(PDG Collab.)
AAD	13U PR D87 032002	G. Aad et al.	(ATLAS Collab.)
AAIJ	13AG PL B724 27	R. Aaij et al.	(LHCb Collab.)
AAIJ	13AJ PL B725 25	R. Aaij et al.	(LHCb Collab.)
AAIJ	13AV PRL 110 182001	R. Aaij et al.	(LHCb Collab.)
AAIJ	13BB PRL 111 102003	R. Aaij et al.	(LHCb Collab.)
CHATRCHYAN	13AC JHEP 1307 163	S. Chatrchyan et al.	(CMS Collab.)
AAIJ	12AR JHEP 1210 037	R. Aaij et al.	(LHCb Collab.)
AAIJ	12E PL B708 241	R. Aaij et al.	(LHCb Collab.)
AALTONEN	12A PR D85 032003	T. Aaltonen et al.	(CDF Collab.)
ABAZOV	12U PR D85 112003	V.M. Abazov et al.	(D0 Collab.)
AAIJ	11E PR D84 092001	R. Aaij et al.	(LHCb Collab.)
Also	PR D85 039904 (errata.)	R. Aaij et al.	(LHCb Collab.)
AALTONEN	11I PRL 106 121804	T. Aaltonen et al.	(CDF Collab.)
AALTONEN	11AI PRL 107 201802	T. Aaltonen et al.	(CDF Collab.)
AALTONEN	11N PRL 106 181802	T. Aaltonen et al.	(CDF Collab.)
ABAZOV	11O PR D84 031102	V.M. Abazov et al.	(D0 Collab.)
AALTONEN	10B PRL 104 102002	T. Aaltonen et al.	(CDF Collab.)
AALTONEN	09C PRL 103 031801	T. Aaltonen et al.	(CDF Collab.)
AALTONEN	09E PR D79 032001	T. Aaltonen et al.	(CDF Collab.)
ABAZOV	07S PRL 99 142001	V.M. Abazov et al.	(D0 Collab.)
ABAZOV	07U PRL 99 182001	V.M. Abazov et al.	(D0 Collab.)
ABULENCIA	07A PRL 98 122001	A. Abulencia et al.	(FNAL CDF Collab.)
ABULENCIA	07B PRL 98 122002	A. Abulencia et al.	(FNAL CDF Collab.)
LEITNER	07 NPBP5 174 169	O. Leitner, Z.J. Ajaltouni	
ACOSTA	06 PR 96 202001	D. Acosta et al.	(CDF Collab.)
ABAZOV	05C PRL 94 102001	V.M. Abazov et al.	(D0 Collab.)
ACOSTA	05A PR D72 051104	D. Acosta et al.	(CDF Collab.)
ABDALLAH	04O PL B585 63	J. Abdallah et al.	(DELPHI Collab.)
ACOSTA	02G PR D66 112002	D. Acosta et al.	(CDF Collab.)
ABREU	99W EPJ C10 185	P. Abreu et al.	(DELPHI Collab.)
ACKERSTAFF	98G PL B426 161	K. Ackerstaff et al.	(OPAL Collab.)
BARATE	98D EPJ C2 197	R. Barate et al.	(ALEPH Collab.)
ABE	97B PR D55 1142	F. Abe et al.	(CDF Collab.)
ABE	96M PRL 77 1439	F. Abe et al.	(CDF Collab.)
ABREU	96D ZPHY C71 199	P. Abreu et al.	(DELPHI Collab.)
ABREU	96N PL B374 351	P. Abreu et al.	(DELPHI Collab.)
ADAM	96D ZPHY C72 207	N. Adam et al.	(DELPHI Collab.)
BUSKULIC	96L PL B380 442	D. Buskulic et al.	(ALEPH Collab.)
BUSKULIC	96V PL B384 471	D. Buskulic et al.	(ALEPH Collab.)
PDG	96 PR D54 1	R. M. Barnett et al.	(PDG Collab.)
ABREU	95S ZPHY C68 375	P. Abreu et al.	(DELPHI Collab.)
AKERS	95L PL B353 402	R. Akers et al.	(OPAL Collab.)
BUSKULIC	95L PL B357 685	D. Buskulic et al.	(ALEPH Collab.)
ABE	93B PR D47 2639	F. Abe et al.	(CDF Collab.)
BUSKULIC	92E PL B294 145	D. Buskulic et al.	(ALEPH Collab.)
ALBAJAR	91E PL B273 540	C. Albajar et al.	(UA1 Collab.)
BARI	91I NC 104A 1787	G. Bari et al.	(CERN R422 Collab.)
ARENTOV	86 NP B274 707	M.W. Arenton et al.	(ARIZ, NDAM, VAND)
BASILE	81 LNC 31 97	M. Basile et al.	(CERN R415 Collab.)

$\Lambda_b(5912)^0$

$J^P = \frac{1}{2}^-$ Status: * * *

Quantum numbers are based on quark model expectations.

$\Lambda_b(5912)^0$ MASS

VALUE (MeV)	DOCUMENT ID	TECN	COMMENT
5912.19 ± 0.17 OUR AVERAGE			
5912.19 ± 0.03 ± 0.17	¹ AAIJ	20Q LHCb	pp at 7, 8, 13 TeV
5912.32 ± 0.12 ± 0.17	² SIRUNYAN	20K CMS	pp at 13 TeV
• • • We do not use the following data for averages, fits, limits, etc. • • •			
5912.20 ± 0.13 ± 0.17	^{3,4} AAIJ	12AL LHCb	Repl. by AAIJ 20Q

¹ AAIJ 20Q measures $m(\Lambda_b(5912)^0) - m(\Lambda_b^0) = 292.589 \pm 0.029 \pm 0.010 \text{ MeV}$. We have adjusted the measurement to our best value of $m(\Lambda_b^0) = 5619.60 \pm 0.17 \text{ MeV}$. Our first error is their experiment's error and our second error is the systematic error from using our best values.

² SIRUNYAN 20K measures $m(\Lambda_b(5912)^0) - m(\Lambda_b^0) = 292.72 \pm 0.12 \pm 0.01 \text{ MeV}$. We have adjusted the measurement to our best value of $m(\Lambda_b^0) = 5619.60 \pm 0.17 \text{ MeV}$. Our first error is their experiment's error and our second error is the systematic error from using our best values.

Baryon Particle Listings

 $\Lambda_b(5912)^0$, $\Lambda_b(5920)^0$, $\Lambda_b(6070)^0$, $\Lambda_b(6146)^0$

³ Observed in $\Lambda_b(5912)^0 \rightarrow \Lambda_b^0 \pi^+ \pi^-$ decays with 17.6 ± 4.8 candidates with a significance of 5.2 sigma.

⁴ AAIJ 12AL measures $m(\Lambda_b(5912)^0) - m(\Lambda_b^0) = 292.60 \pm 0.12 \pm 0.04$ MeV. We have adjusted the measurement to our best value of $m(\Lambda_b^0) = 5619.60 \pm 0.17$ MeV. Our first error is their experiment's error and our second error is the systematic error from using our best values.

 $\Lambda_b(5912)^0$ WIDTH

VALUE (MeV)	CL%	DOCUMENT ID	TECN	COMMENT
<0.25	90	AAIJ	20Q LHCb	pp at 7, 8, 13 TeV
• • • We do not use the following data for averages, fits, limits, etc. • • •				
<0.66	90	AAIJ	12AL LHCb	Repl. by AAIJ 20Q

 $\Lambda_b(5912)^0$ DECAY MODES

Mode	Fraction (Γ_i/Γ)
Γ_1 $\Lambda_b^0 \pi^+ \pi^-$	seen

 $\Lambda_b(5912)^0$ BRANCHING RATIOS

$\Gamma(\Lambda_b^0 \pi^+ \pi^-)/\Gamma_{\text{total}}$	DOCUMENT ID	TECN	COMMENT	Γ_1/Γ
seen	AAIJ	20Q LHCb	pp at 7, 8, 13 TeV	
seen	SIRUNYAN	20K CMS	pp at 13 TeV	
seen	AAIJ	12AL LHCb	pp at 7 TeV	

 $\Lambda_b(5912)^0$ REFERENCES

AAIJ	20Q	JHEP 2006 136	R. Aaij <i>et al.</i>	(LHCb Collab.)
SIRUNYAN	20K	PL B803 135345	A.M. Sirunyan <i>et al.</i>	(CMS Collab.)
AAIJ	12AL	PRL 109 172003	R. Aaij <i>et al.</i>	(LHCb Collab.)

$$\Lambda_b(5920)^0 \quad J^P = \frac{3}{2}^- \quad \text{Status: } ***$$

Quantum numbers are based on quark model expectations.

 $\Lambda_b(5920)^0$ MASS

VALUE (MeV)	DOCUMENT ID	TECN	COMMENT
5920.09 ± 0.17 OUR AVERAGE			
5920.09 ± 0.02 ± 0.17	¹ AAIJ	20Q LHCb	pp at 7, 8, 13 TeV
5920.16 ± 0.07 ± 0.17	² SIRUNYAN	20K CMS	pp at 13 TeV
• • • We do not use the following data for averages, fits, limits, etc. • • •			
5919.4 ± 0.5 ± 0.2	^{3,4} AALTONEN	13V CDF	$p\bar{p}$ at 1.96 TeV
5920.00 ± 0.09 ± 0.17	^{5,6} AAIJ	12AL LHCb	Repl. by AAIJ 20Q

¹ AAIJ 20Q measures $m(\Lambda_b(5920)^0) - m(\Lambda_b^0) = 300.492 \pm 0.019 \pm 0.010$ MeV. We have adjusted the measurement to our best value of $m(\Lambda_b^0) = 5619.60 \pm 0.17$ MeV. Our first error is their experiment's error and our second error is the systematic error from using our best values.

² SIRUNYAN 20K measures $m(\Lambda_b(5920)^0) - m(\Lambda_b^0) = 300.56 \pm 0.07 \pm 0.01$ MeV. We have adjusted the measurement to our best value of $m(\Lambda_b^0) = 5619.60 \pm 0.17$ MeV. Our first error is their experiment's error and our second error is the systematic error from using our best values.

³ Measured in $\Lambda_b(5920)^0 \rightarrow \Lambda_b^0 \pi^+ \pi^-$ decays with $17.3^{+5.3}_{-4.6}$ events, with a significance of 3.5 sigma.

⁴ AALTONEN 13V measures $m(\Lambda_b(5920)^0) - m(\Lambda_b^0) - 2m(\pi) = 20.68 \pm 0.35 \pm 0.30$ MeV. We have adjusted the measurement to our best values of $m(\Lambda_b^0) = 5619.60 \pm 0.17$ MeV and $m(\pi) = 139.57039 \pm 0.00018$ MeV. Our first error is their experiment's error and our second error is the systematic error from using our best values.

⁵ Observed in $\Lambda_b(5920)^0 \rightarrow \Lambda_b^0 \pi^+ \pi^-$ decays with 52.5 ± 8.1 candidates with a significance of 10.2 sigma.

⁶ AAIJ 12AL measures $m(\Lambda_b(5920)^0) - m(\Lambda_b^0) = 300.40 \pm 0.08 \pm 0.04$ MeV. We have adjusted the measurement to our best value of $m(\Lambda_b^0) = 5619.60 \pm 0.17$ MeV. Our first error is their experiment's error and our second error is the systematic error from using our best values.

 $\Lambda_b(5920)^0$ WIDTH

VALUE (MeV)	CL%	DOCUMENT ID	TECN	COMMENT
<0.19	90	AAIJ	20Q LHCb	pp at 7, 8, 13 TeV
• • • We do not use the following data for averages, fits, limits, etc. • • •				
<0.63	90	AAIJ	12AL LHCb	Repl. by AAIJ 20Q

 $\Lambda_b(5920)^0$ DECAY MODES

Mode	Fraction (Γ_i/Γ)
Γ_1 $\Lambda_b^0 \pi^+ \pi^-$	seen

 $\Lambda_b(5920)^0$ BRANCHING RATIOS

$\Gamma(\Lambda_b^0 \pi^+ \pi^-)/\Gamma_{\text{total}}$	DOCUMENT ID	TECN	COMMENT	Γ_1/Γ
seen	AAIJ	20Q LHCb	pp at 7, 8, 13 TeV	
seen	SIRUNYAN	20K LHCb	pp at 13 TeV	
seen	AALTONEN	13V CDF	$p\bar{p}$ at 1.96 TeV	
seen	AAIJ	12AL LHCb	pp at 7 TeV	

 $\Lambda_b(5920)^0$ REFERENCES

AAIJ	20Q	JHEP 2006 136	R. Aaij <i>et al.</i>	(LHCb Collab.)
SIRUNYAN	20K	PL B803 135345	A.M. Sirunyan <i>et al.</i>	(CMS Collab.)
AALTONEN	13V	PR D88 071101	T. Aaltonen <i>et al.</i>	(CDF Collab.)
AAIJ	12AL	PRL 109 172003	R. Aaij <i>et al.</i>	(LHCb Collab.)

$$\Lambda_b(6070)^0 \quad J^P = \frac{1}{2}^+ \quad \text{Status: } ***$$

Quantum numbers are based on quark model expectations.

 $\Lambda_b(6070)^0$ MASS

VALUE (MeV)	DOCUMENT ID	TECN	COMMENT
6072.3 ± 2.9 ± 0.2	¹ AAIJ	20Q LHCb	pp at 7, 8, 13 TeV
¹ AAIJ 20Q measures $m(\Lambda_b(6070)^0) - m(\Lambda_b^0) = 452.7 \pm 2.9 \pm 0.5$ MeV. We have adjusted the measurement to our best value of $m(\Lambda_b^0) = 5619.60 \pm 0.17$ MeV. Our first error is their experiment's error and our second error is the systematic error from using our best values.			

 $\Lambda_b(6070)^0$ WIDTH

VALUE (MeV)	DOCUMENT ID	TECN	COMMENT
72 ± 11 ± 2	AAIJ	20Q LHCb	pp at 7, 8, 13 TeV

 $\Lambda_b(6070)^0$ DECAY MODES

Mode	Fraction (Γ_i/Γ)
Γ_1 $\Lambda_b^0 \pi^+ \pi^-$	seen

 $\Lambda_b(6070)^0$ BRANCHING RATIOS

$\Gamma(\Lambda_b^0 \pi^+ \pi^-)/\Gamma_{\text{total}}$	DOCUMENT ID	TECN	COMMENT	Γ_1/Γ
seen	AAIJ	20Q LHCb	pp at 7, 8, 13 TeV	

 $\Lambda_b(6070)^0$ REFERENCES

AAIJ	20Q	JHEP 2006 136	R. Aaij <i>et al.</i>	(LHCb Collab.)
------	-----	---------------	-----------------------	----------------

$$\Lambda_b(6146)^0 \quad J^P = \frac{3}{2}^+ \quad \text{Status: } ***$$

Quantum numbers are based on quark model expectations.

 $\Lambda_b(6146)^0$ MASS

VALUE (MeV)	DOCUMENT ID	TECN	COMMENT
6146.2 ± 0.4 OUR AVERAGE			
6146.5 ± 2.1 ± 0.2	¹ SIRUNYAN	20K CMS	pp at 13 TeV
6146.17 ± 0.33 ± 0.27	² AAIJ	19AJ LHCb	pp at 7, 8, 13 TeV
¹ SIRUNYAN 20K measures $m(\Lambda_b(6146)^0) - m(\Lambda_b^0) = 526.9 \pm 1.9 \pm 0.8$ MeV. We have adjusted the measurement to our best value of $m(\Lambda_b^0) = 5619.60 \pm 0.17$ MeV. Our first error is their experiment's error and our second error is the systematic error from using our best values.			
² Observed in $\Lambda_b^0 \pi^+ \pi^-$ mode.			

 $m_{\Lambda_b(6146)^0} - m_{\Lambda_b^0}$

VALUE (MeV)	DOCUMENT ID	TECN	COMMENT
526.55 ± 0.33 ± 0.10	¹ AAIJ	19AJ LHCb	pp at 7, 8, 13 TeV
¹ Observed in $\Lambda_b^0 \pi^+ \pi^-$ mode.			

 $\Lambda_b(6146)^0$ WIDTH

VALUE (MeV)	DOCUMENT ID	TECN	COMMENT
2.9 ± 1.3 ± 0.3	¹ AAIJ	19AJ LHCb	pp at 7, 8, 13 TeV
¹ Observed in $\Lambda_b^0 \pi^+ \pi^-$ mode.			

See key on page 1171

Baryon Particle Listings

$\Lambda_b(6146)^0$, $\Lambda_b(6152)^0$, Σ_b , Σ_b^*

$\Lambda_b(6146)^0$ DECAY MODES

Mode	Fraction (Γ_i/Γ)
$\Gamma_1 \Lambda_b^0 \pi^+ \pi^-$	seen

$\Lambda_b(6146)^0$ BRANCHING RATIOS

$\Gamma(\Lambda_b^0 \pi^+ \pi^-)/\Gamma_{\text{total}}$	DOCUMENT ID	TECN	COMMENT	Γ_1/Γ
seen	SIRUNYAN	20K LHCb	pp at 13 TeV	
seen	AAIJ	19AJ LHCb	pp at 7, 8, 13 TeV	

$\Lambda_b(6146)^0$ REFERENCES

SIRUNYAN	20K	PL B803 135345	A.M. Sirunyan et al.	(CMS Collab.)
AAIJ	19AJ	PRL 123 152001	R. Aaij et al.	(LHCb Collab.)

$\Lambda_b(6152)^0$ $J^P = \frac{5}{2}^+$ Status: ***

Quantum numbers are based on quark model expectations.

$\Lambda_b(6152)^0$ MASS

$\Lambda_b(6152)^0$ MASS

VALUE (MeV)	DOCUMENT ID	TECN	COMMENT
6152.5 ± 0.4 OUR AVERAGE			
6152.7 ± 1.2 ± 0.2	¹ SIRUNYAN	20K CMS	pp at 13 TeV
6152.51 ± 0.26 ± 0.27	² AAIJ	19AJ LHCb	pp at 7, 8, 13 TeV

¹ SIRUNYAN 20K measures $m(\Lambda_b(6152)^0) - m(\Lambda_b^0) = 533.1 \pm 1.1 \pm 0.4$ MeV. We have adjusted the measurement to our best value of $m(\Lambda_b^0) = 5619.60 \pm 0.17$ MeV. Our first error is their experiment's error and our second error is the systematic error from using our best values.

² Observed in $\Lambda_b^0 \pi^+ \pi^-$ mode.

$m_{\Lambda_b(6152)^0} - m_{\Lambda_b^0}$

VALUE (MeV)	DOCUMENT ID	TECN	COMMENT
532.89 ± 0.26 ± 0.10	¹ AAIJ	19AJ LHCb	pp at 7, 8, 13 TeV

¹ Observed in $\Lambda_b^0 \pi^+ \pi^-$ mode.

$m_{\Lambda_b(6152)^0} - m_{\Lambda_b(6146)^0}$

VALUE (MeV)	DOCUMENT ID	TECN	COMMENT
6.34 ± 0.32 ± 0.02	AAIJ	19AJ LHCb	pp at 7, 8, 13 TeV

$\Lambda_b(6152)^0$ WIDTH

VALUE (MeV)	DOCUMENT ID	TECN	COMMENT
2.1 ± 0.8 ± 0.3	¹ AAIJ	19AJ LHCb	pp at 7, 8, 13 TeV

¹ Observed in $\Lambda_b^0 \pi^+ \pi^-$ mode.

$\Lambda_b(6152)^0$ DECAY MODES

Mode	Fraction (Γ_i/Γ)
$\Gamma_1 \Lambda_b^0 \pi^+ \pi^-$	seen

$\Lambda_b(6152)^0$ BRANCHING RATIOS

$\Gamma(\Lambda_b^0 \pi^+ \pi^-)/\Gamma_{\text{total}}$	DOCUMENT ID	TECN	COMMENT	Γ_1/Γ
seen	SIRUNYAN	20K LHCb	pp at 13 TeV	
seen	AAIJ	19AJ LHCb	pp at 7, 8, 13 TeV	

$\Lambda_b(6152)^0$ REFERENCES

SIRUNYAN	20K	PL B803 135345	A.M. Sirunyan et al.	(CMS Collab.)
AAIJ	19AJ	PRL 123 152001	R. Aaij et al.	(LHCb Collab.)

Σ_b $I(J^P) = 1(\frac{3}{2}^+)$ Status: ***
 I, J, P need confirmation.

In the quark model Σ_b^+ , Σ_b^0 , Σ_b^- are an isotriplet (uub , udb , ddb) state. The lowest Σ_b ought to have $J^P = 1/2^+$. None of I, J , or P have actually been measured.

Σ_b MASS

Σ_b^+ MASS

VALUE (MeV)	DOCUMENT ID	TECN	COMMENT
5810.56 ± 0.25 OUR AVERAGE			
5810.55 ± 0.11 ± 0.23	¹ AAIJ	19A LHCb	pp at 7, 8 TeV
5811.3 ± 0.9 ± 1.7	² AALTONEN	12F CDF	$p\bar{p}$ at 1.96 TeV

••• We do not use the following data for averages, fits, limits, etc. •••

5807.8 $^{+2.0}_{-2.2} \pm 1.7$ ³ AALTONEN 07K CDF Repl. by AALTONEN 12F

¹ Measured using fully reconstructed $\Lambda_b^0 \rightarrow \Lambda_c^+ \pi^-$ and $\Lambda_c^+ \rightarrow p K^- \pi^+$ decays.

² Measured using fully reconstructed $\Lambda_b^0 \rightarrow \Lambda_c^+ \pi^-$ and $\Lambda_c^+ \rightarrow K^- \pi^+$ decays.

³ Observed four $\Lambda_b^0 \pi^\pm$ resonances in the fully reconstructed decay mode $\Lambda_b^0 \rightarrow \Lambda_c^+ \pi^-$, where $\Lambda_c^+ \rightarrow p K^- \pi^+$.

Σ_b^- MASS

VALUE (MeV)	DOCUMENT ID	TECN	COMMENT
5815.64 ± 0.27 OUR AVERAGE			
5815.64 ± 0.14 ± 0.24	¹ AAIJ	19A LHCb	pp at 7, 8 TeV
5815.5 $^{+0.6}_{-0.5} \pm 1.7$	² AALTONEN	12F CDF	$p\bar{p}$ at 1.96 TeV

••• We do not use the following data for averages, fits, limits, etc. •••

5815.2 ± 1.0 ± 1.7 ³ AALTONEN 07K CDF Repl. by AALTONEN 12F

¹ Measured using fully reconstructed $\Lambda_b^0 \rightarrow \Lambda_c^+ \pi^-$ and $\Lambda_c^+ \rightarrow p K^- \pi^+$ decays.

² Measured using fully reconstructed $\Lambda_b^0 \rightarrow \Lambda_c^+ \pi^-$ and $\Lambda_c^+ \rightarrow K^- \pi^+$ decays.

³ Observed four $\Lambda_b^0 \pi^\pm$ resonances in the fully reconstructed decay mode $\Lambda_b^0 \rightarrow \Lambda_c^+ \pi^-$, where $\Lambda_c^+ \rightarrow p K^- \pi^+$.

$m_{\Sigma_b^+} - m_{\Sigma_b^-}$

VALUE (MeV)	DOCUMENT ID	TECN	COMMENT
-5.06 ± 0.18 OUR AVERAGE			
-5.09 ± 0.18 ± 0.01	¹ AAIJ	19A LHCb	pp at 7, 8 TeV
-4.2 $^{+1.1}_{-1.0} \pm 0.1$	² AALTONEN	12F CDF	$p\bar{p}$ at 1.96 TeV

¹ Measured using fully reconstructed $\Lambda_b^0 \rightarrow \Lambda_c^+ \pi^-$ and $\Lambda_c^+ \rightarrow p K^- \pi^+$ decays.

² Measured using fully reconstructed $\Lambda_b^0 \rightarrow \Lambda_c^+ \pi^-$ and $\Lambda_c^+ \rightarrow K^- \pi^+$ decays.

Σ_b WIDTH

Σ_b^+ WIDTH

VALUE (MeV)	DOCUMENT ID	TECN	COMMENT
5.0 ± 0.5 OUR AVERAGE			
4.83 ± 0.31 ± 0.37	¹ AAIJ	19A LHCb	pp at 7, 8 TeV
9.7 $^{+3.8}_{-2.8} \pm 1.2$	² AALTONEN	12F CDF	$p\bar{p}$ at 1.96 TeV

¹ Measured using fully reconstructed $\Lambda_b^0 \rightarrow \Lambda_c^+ \pi^-$ and $\Lambda_c^+ \rightarrow p K^- \pi^+$ decays.

² Measured using fully reconstructed $\Lambda_b^0 \rightarrow \Lambda_c^+ \pi^-$ and $\Lambda_c^+ \rightarrow K^- \pi^+$ decays.

Σ_b^- WIDTH

VALUE (MeV)	DOCUMENT ID	TECN	COMMENT
5.3 ± 0.5 OUR AVERAGE			
5.33 ± 0.42 ± 0.37	¹ AAIJ	19A LHCb	pp at 7, 8 TeV
4.9 $^{+3.1}_{-2.1} \pm 1.1$	² AALTONEN	12F CDF	$p\bar{p}$ at 1.96 TeV

¹ Measured using fully reconstructed $\Lambda_b^0 \rightarrow \Lambda_c^+ \pi^-$ and $\Lambda_c^+ \rightarrow p K^- \pi^+$ decays.

² Measured using fully reconstructed $\Lambda_b^0 \rightarrow \Lambda_c^+ \pi^-$ and $\Lambda_c^+ \rightarrow K^- \pi^+$ decays.

Σ_b DECAY MODES

Mode	Fraction (Γ_i/Γ)
$\Gamma_1 \Lambda_b^0 \pi$	dominant

Σ_b BRANCHING RATIOS

$\Gamma(\Lambda_b^0 \pi)/\Gamma_{\text{total}}$	DOCUMENT ID	TECN	COMMENT	Γ_1/Γ
dominant	AALTONEN	07K CDF	$p\bar{p}$ at 1.96 TeV	

Σ_b REFERENCES

AAIJ	19A	PRL 122 012001	R. Aaij et al.	(LHCb Collab.)
AALTONEN	12F	PR D85 092011	T. Aaltonen et al.	(CDF Collab.)
AALTONEN	07K	PRL 99 202001	T. Aaltonen et al.	(CDF Collab.)

Σ_b^* $I(J^P) = 1(\frac{3}{2}^+)$ Status: ***
 I, J, P need confirmation.

I, J, P need confirmation. Quantum numbers shown are quark-model predictions.

Σ_b^* MASS

Σ_b^{*+} MASS

VALUE (MeV)	DOCUMENT ID	TECN	COMMENT
5830.32 ± 0.27 OUR AVERAGE			
5830.28 ± 0.14 ± 0.24	¹ AAIJ	19A LHCb	pp at 7, 8 TeV
5832.1 ± 0.7 $^{+1.7}_{-1.6}$	² AALTONEN	12F CDF	$p\bar{p}$ at 1.96 TeV

¹ Measured using fully reconstructed $\Lambda_b^0 \rightarrow \Lambda_c^+ \pi^-$ and $\Lambda_c^+ \rightarrow p K^- \pi^+$ decays.

² Measured using fully reconstructed $\Lambda_b^0 \rightarrow \Lambda_c^+ \pi^-$ and $\Lambda_c^+ \rightarrow K^- \pi^+$ decays.

Baryon Particle Listings

 Σ_b^* , $\Sigma_b(6097)^+$, $\Sigma_b(6097)^-$ Σ_b^{*-} MASS

VALUE (MeV)	DOCUMENT ID	TECN	COMMENT
5834.73 ± 0.30 OUR AVERAGE			
5834.73 ± 0.17 ± 0.25	¹ AAIJ	19A	LHCB pp at 7, 8 TeV
5835.1 ± 0.6 $^{+1.7}_{-1.8}$	² AALTONEN	12F	CDF $p\bar{p}$ at 1.96 TeV

- ¹ Measured using fully reconstructed $\Lambda_b^0 \rightarrow \Lambda_c^+ \pi^-$ and $\Lambda_c^+ \rightarrow p K^- \pi^+$ decays.
² Measured using fully reconstructed $\Lambda_b^0 \rightarrow \Lambda_c^+ \pi^-$ and $\Lambda_c^+ \rightarrow K^- \pi^+$ decays.

 $m_{\Sigma_b^{*+}} - m_{\Sigma_b^{*-}}$

VALUE (MeV)	DOCUMENT ID	TECN	COMMENT
-4.37 ± 0.33 OUR AVERAGE			
-4.45 ± 0.22 ± 0.01	¹ AAIJ	19A	LHCB pp at 7, 8 TeV
-3.0 $^{+1.0}_{-0.9}$ ± 0.1	² AALTONEN	12F	CDF $p\bar{p}$ at 1.96 TeV

- ¹ Measured using fully reconstructed $\Lambda_b^0 \rightarrow \Lambda_c^+ \pi^-$ and $\Lambda_c^+ \rightarrow p K^- \pi^+$ decays.
² Measured using fully reconstructed $\Lambda_b^0 \rightarrow \Lambda_c^+ \pi^-$ and $\Lambda_c^+ \rightarrow K^- \pi^+$ decays.

 $m_{\Sigma_b^{*+}} - m_{\Sigma_b^+}$

VALUE	DOCUMENT ID	TECN	COMMENT
19.73 ± 0.18 ± 0.01			
	¹ AAIJ	19A	LHCB pp at 7, 8 TeV
	² AALTONEN	12F	CDF $p\bar{p}$ at 1.96 TeV

- ¹ Measured using fully reconstructed $\Lambda_b^0 \rightarrow \Lambda_c^+ \pi^-$ and $\Lambda_c^+ \rightarrow p K^- \pi^+$ decays.

 $m_{\Sigma_b^{*-}} - m_{\Sigma_b^-}$

VALUE	DOCUMENT ID	TECN	COMMENT
19.09 ± 0.22 ± 0.02			
	¹ AAIJ	19A	LHCB pp at 7, 8 TeV
	² AALTONEN	12F	CDF $p\bar{p}$ at 1.96 TeV

- ¹ Measured using fully reconstructed $\Lambda_b^0 \rightarrow \Lambda_c^+ \pi^-$ and $\Lambda_c^+ \rightarrow p K^- \pi^+$ decays.

 Σ_b^* WIDTH Σ_b^{*+} WIDTH

VALUE (MeV)	DOCUMENT ID	TECN	COMMENT
9.4 ± 0.5 OUR AVERAGE			
9.34 ± 0.47 ± 0.26	¹ AAIJ	19A	LHCB pp at 7, 8 TeV
11.5 $^{+2.7}_{-2.2}$ $^{+1.0}_{-1.5}$	² AALTONEN	12F	CDF $p\bar{p}$ at 1.96 TeV

- ¹ Measured using fully reconstructed $\Lambda_b^0 \rightarrow \Lambda_c^+ \pi^-$ and $\Lambda_c^+ \rightarrow p K^- \pi^+$ decays.
² Measured using fully reconstructed $\Lambda_b^0 \rightarrow \Lambda_c^+ \pi^-$ and $\Lambda_c^+ \rightarrow K^- \pi^+$ decays.

 Σ_b^{*-} WIDTH

VALUE (MeV)	DOCUMENT ID	TECN	COMMENT
10.4 ± 0.8 OUR AVERAGE			
10.68 ± 0.60 ± 0.33	¹ AAIJ	19A	LHCB pp at 7, 8 TeV
7.5 $^{+2.2}_{-1.8}$ $^{+0.9}_{-1.4}$	² AALTONEN	12F	CDF $p\bar{p}$ at 1.96 TeV

- ¹ Measured using fully reconstructed $\Lambda_b^0 \rightarrow \Lambda_c^+ \pi^-$ and $\Lambda_c^+ \rightarrow p K^- \pi^+$ decays.
² Measured using fully reconstructed $\Lambda_b^0 \rightarrow \Lambda_c^+ \pi^-$ and $\Lambda_c^+ \rightarrow K^- \pi^+$ decays.

 $m_{\Sigma_b^{*+}} - m_{\Sigma_b}$

VALUE (MeV)	DOCUMENT ID	TECN	COMMENT
21.2 $^{+2.0}_{-1.9}$ ± 0.4 ± 0.3			
	¹ AALTONEN	07K	CDF $p\bar{p}$ at 1.96 TeV

- ¹ Observed four $\Lambda_b^0 \pi^\pm$ resonances in the fully reconstructed decay mode $\Lambda_b^0 \rightarrow \Lambda_c^+ \pi^-$, where $\Lambda_c^+ \rightarrow p K^- \pi^+$. Assumes $m_{\Sigma_b^{*+}} - m_{\Sigma_b^+} = m_{\Sigma_b^{*-}} - m_{\Sigma_b^-}$.

 Σ_b^* DECAY MODES

Mode	Fraction (Γ_i/Γ)
Γ_1 $\Lambda_b^0 \pi$	dominant

 Σ_b^* BRANCHING RATIOS

$\Gamma(\Lambda_b^0 \pi)/\Gamma_{\text{total}}$	DOCUMENT ID	TECN	COMMENT	Γ_1/Γ
dominant	AALTONEN	07K	CDF $p\bar{p}$ at 1.96 TeV	

 Σ_b^* REFERENCES

AAIJ	19A	PRL 122 012001	R. Aaij et al.	(LHCb Collab.)
AALTONEN	12F	PR D85 092011	T. Aaltonen et al.	(CDF Collab.)
AALTONEN	07K	PRL 99 202001	T. Aaltonen et al.	(CDF Collab.)

 $\Sigma_b(6097)^+$ $J^P = ??$

Status: ***

 $\Sigma_b(6097)^+$ MASS

VALUE (MeV)	DOCUMENT ID	TECN	COMMENT
6095.8 ± 1.7 ± 0.4			
	¹ AAIJ	19A	LHCB pp at 7, 8 TeV

- ¹ Measured using fully reconstructed $\Lambda_b^0 \rightarrow \Lambda_c^+ \pi^-$ and $\Lambda_c^+ \rightarrow p K^- \pi^+$ decays.

 $m_{\Sigma_b(6097)^+} - m_{\Sigma_b(6097)^-}$

VALUE	DOCUMENT ID	TECN	COMMENT
-2.2 ± 2.4 ± 0.3 MeV			
	¹ AAIJ	19A	LHCB pp at 7, 8 TeV

- ¹ Measured using fully reconstructed $\Lambda_b^0 \rightarrow \Lambda_c^+ \pi^-$ and $\Lambda_c^+ \rightarrow p K^- \pi^+$ decays.

 $\Sigma_b(6097)^+$ WIDTH

VALUE (MeV)	DOCUMENT ID	TECN	COMMENT
31.0 ± 5.5 ± 0.7			
	¹ AAIJ	19A	LHCB pp at 7, 8 TeV

- ¹ Measured using fully reconstructed $\Lambda_b^0 \rightarrow \Lambda_c^+ \pi^-$ and $\Lambda_c^+ \rightarrow p K^- \pi^+$ decays.

 $\Sigma_b(6097)^+$ DECAY MODES

Mode	Fraction (Γ_i/Γ)
Γ_1 $\Lambda_b \pi^+ \times B(b \rightarrow \Sigma_b(6097)^+)$	seen

 $\Sigma_b(6097)^+$ BRANCHING RATIOS

$\Gamma(\Lambda_b \pi^+ \times B(b \rightarrow \Sigma_b(6097)^+))/\Gamma_{\text{total}}$	DOCUMENT ID	TECN	COMMENT	Γ_1/Γ
seen	AAIJ	19A	LHCB pp at 7, 8 TeV	

 $\Sigma_b(6097)^+$ REFERENCES

AAIJ	19A	PRL 122 012001	R. Aaij et al.	(LHCb Collab.)
------	-----	----------------	----------------	----------------

 $\Sigma_b(6097)^-$ $J^P = ??$

Status: ***

 $\Sigma_b(6097)^-$ MASS

VALUE (MeV)	DOCUMENT ID	TECN	COMMENT
6098.0 ± 1.7 ± 0.5			
	¹ AAIJ	19A	LHCB pp at 7, 8 TeV

- ¹ Measured using fully reconstructed $\Lambda_b^0 \rightarrow \Lambda_c^+ \pi^-$ and $\Lambda_c^+ \rightarrow p K^- \pi^+$ decays.

 $\Sigma_b(6097)^-$ WIDTH

VALUE (MeV)	DOCUMENT ID	TECN	COMMENT
28.9 ± 4.2 ± 0.9			
	¹ AAIJ	19A	LHCB pp at 7, 8 TeV

- ¹ Measured using fully reconstructed $\Lambda_b^0 \rightarrow \Lambda_c^+ \pi^-$ and $\Lambda_c^+ \rightarrow p K^- \pi^+$ decays.

 $\Sigma_b(6097)^-$ DECAY MODES

Mode	Fraction (Γ_i/Γ)
Γ_1 $\Lambda_b \pi^- \times B(b \rightarrow \Sigma_b(6097)^-)$	seen

 $\Sigma_b(6097)^-$ BRANCHING RATIOS

$\Gamma(\Lambda_b \pi^- \times B(b \rightarrow \Sigma_b(6097)^-))/\Gamma_{\text{total}}$	DOCUMENT ID	TECN	COMMENT	Γ_1/Γ
seen	AAIJ	19A	LHCB pp at 7, 8 TeV	

 $\Sigma_b(6097)^-$ REFERENCES

AAIJ	19A	PRL 122 012001	R. Aaij et al.	(LHCb Collab.)
------	-----	----------------	----------------	----------------



$$I(J^P) = \frac{1}{2}(\frac{1}{2}^+) \text{ Status: } ***$$

I, J, P need confirmation.

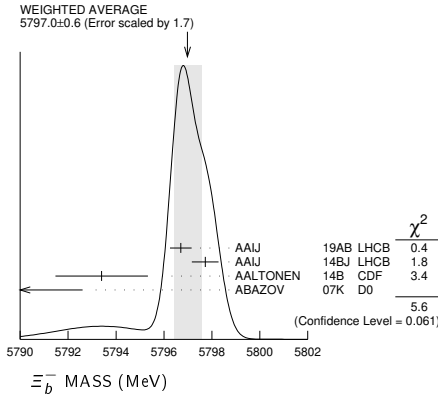
In the quark model, Ξ_b^0 and Ξ_b^- are an isodoublet (usb, dsb) state; the lowest Ξ_b^0 and Ξ_b^- ought to have $J^P = 1/2^+$. None of $I, J,$ or P have actually been measured.

Ξ_b^- MASS

Ξ_b^- MASS

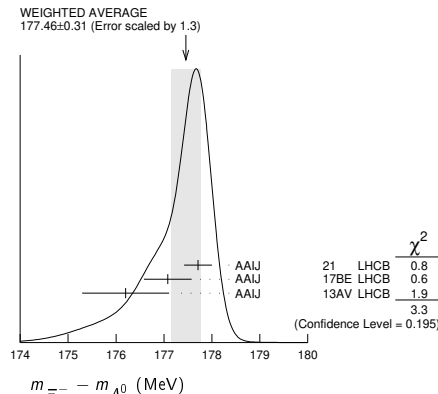
VALUE (MeV)	DOCUMENT ID	TECN	COMMENT
5797.0 ± 0.6 OUR AVERAGE	Error includes scale factor of 1.7. See the ideogram below.		
5796.70 ± 0.39 ± 0.23	AAIJ	19AB LHCB	pp at 7, 8 and 13 TeV
5797.72 ± 0.46 ± 0.31	1 AAIJ	14BJ LHCB	pp at 7, 8 TeV
5793.4 ± 1.8 ± 0.7	2 AALTONEN	14B CDF	$p\bar{p}$ at 1.96 TeV
5774 ± 11 ± 15	3 ABAZOV	07K D0	$p\bar{p}$ at 1.96 TeV
• • • We do not use the following data for averages, fits, limits, etc. • • •			
5795.8 ± 0.9 ± 0.4	4 AAIJ	13AV LHCB	Repl. by AAIJ 19AB
5796.7 ± 5.1 ± 1.4	5 AALTONEN	11X CDF	Repl. by AALTONEN 14B
5790.9 ± 2.6 ± 0.8	6 AALTONEN	09AP CDF	Repl. by AALTONEN 14B
5792.9 ± 2.5 ± 1.7	7 AALTONEN	07A CDF	Repl. by AALTONEN 09AP

- 1 Reconstructed in $\Xi_b^- \rightarrow \Xi_c^0 \pi^-, \Xi_c^0 \rightarrow p K^- K^- \pi^+$ decays. Reference Λ_b^0 mass 5619.30 ± 0.34 MeV from AAIJ 14AA.
- 2 Uses $\Xi_b^- \rightarrow J/\psi \Xi^-$ and $\Xi_c^0 \pi^-$ decays.
- 3 Observed in $\Xi_b^- \rightarrow J/\psi \Xi^-$ decays with $15.2 \pm 4.4^{+1.9}_{-0.4}$ candidates, a significance of 5.5 sigma.
- 4 Measured in $\Xi_b^- \rightarrow J/\psi \Xi^-$ decays.
- 5 Measured in $\Xi_b^- \rightarrow \Xi_c^0 \pi^-$ with $25.8^{+5.5}_{-5.2}$ candidates.
- 6 Measured in $\Xi_b^- \rightarrow J/\psi \Xi^-$ decays with 66^{+14}_9 candidates.
- 7 Observed in $\Xi_b^- \rightarrow J/\psi \Xi^-$ decays with 17.5 ± 4.3 candidates, a significance of 7.7 sigma.



$m_{\Xi_b^-} - m_{\Lambda_b^0}$

VALUE (MeV)	DOCUMENT ID	TECN	COMMENT
177.46 ± 0.31 OUR AVERAGE	Error includes scale factor of 1.3. See the ideogram below.		
177.71 ± 0.24 ± 0.16	1 AAIJ	21 LHCB	pp at 7, 8, 13 TeV
177.08 ± 0.47 ± 0.16	2 AAIJ	17BE LHCB	pp at 7, 8 TeV
176.2 ± 0.9 ± 0.1	3 AAIJ	13AV LHCB	pp at 7 TeV
• • • We do not use the following data for averages, fits, limits, etc. • • •			
177.73 ± 0.33 ± 0.14	4 AAIJ	17BE LHCB	pp at 7, 8 TeV
178.36 ± 0.46 ± 0.16	1.5 AAIJ	14BJ LHCB	Repl. by AAIJ 2021



- 1 Reconstructed in $\Xi_b^- \rightarrow \Xi_c^0 \pi^-, \Xi_c^0 \rightarrow p K^- K^- \pi^+$ decays. Reference decays $\Lambda_b^0 \rightarrow \Lambda_c^+ \pi^-$ were used.

- 2 Reconstructed in $\Xi_b^- \rightarrow J/\psi \Lambda K^-$ decays. Reference decays $\Lambda_b^0 \rightarrow J/\psi \Lambda$ were used.
- 3 Reconstructed in $\Xi_b^- \rightarrow J/\psi \Xi^-$ decays.
- 4 Combination of the original statistically independent measurements of AAIJ 17BE and AAIJ 14BJ taking into account correlation between systematic uncertainties.
- 5 Combined with AAIJ 17BE.

$m_{\Xi_b^-} - m_{\Xi_b^0}$

VALUE (MeV)	DOCUMENT ID	TECN	COMMENT
5.9 ± 0.6 OUR AVERAGE	Error includes scale factor of 1.7. See the ideogram below.		
5.92 ± 0.60 ± 0.23	1 AAIJ	14BJ LHCB	pp at 7, 8 TeV
3.1 ± 5.6 ± 1.3	2 AALTONEN	11X CDF	$p\bar{p}$ at 1.96 TeV

- 1 Reconstructed in $\Xi_b^- \rightarrow \Xi_c^0 \pi^-, \Xi_c^0 \rightarrow p K^- K^- \pi^+$ decays. Uses $m(\Xi_b^0) - m(\Lambda_b^0) = 172.44 \pm 0.39 \pm 0.17$ MeV from AAIJ 14Z.
- 2 Derived from measurements in $\Xi_b^0 \rightarrow \Xi_c^+ \pi^-$ and $\Xi_b^- \rightarrow J/\psi \Xi^-$ from AALTONEN 09AP taking correlated systematic uncertainties into account.

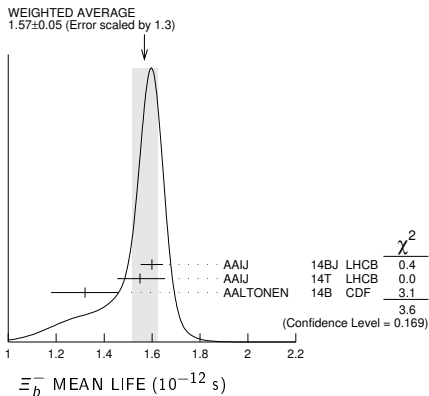
Ξ_b^- MEAN LIFE

“OUR EVALUATION” is an average using rescaled values of the data listed below. The average and rescaling were performed by the Heavy Flavor Averaging Group (HFLAV) and are described at <https://hflav.web.cern.ch/>. The averaging/rescaling procedure takes into account correlations between the measurements and asymmetric lifetime errors.

Ξ_b^- MEAN LIFE

VALUE (10^{-12} s)	DOCUMENT ID	TECN	COMMENT
1.572 ± 0.040 OUR EVALUATION	(Produced by HFLAV)		
1.57 ± 0.05 OUR AVERAGE	Error includes scale factor of 1.3. See the ideogram below.		
1.599 ± 0.041 ± 0.022	1 AAIJ	14BJ LHCB	pp at 7, 8 TeV
1.55 $^{+0.10}_{-0.09}$ ± 0.03	2 AAIJ	14T LHCB	pp at 7, 8 TeV
1.32 ± 0.14 ± 0.02	AALTONEN	14B CDF	$p\bar{p}$ at 1.96 TeV
• • • We do not use the following data for averages, fits, limits, etc. • • •			
1.56 $^{+0.27}_{-0.25}$ ± 0.02	3 AALTONEN	09AP CDF	Repl. by AALTONEN 14B

- 1 Reconstructed in $\Xi_b^- \rightarrow \Xi_c^0 \pi^-, \Xi_c^0 \rightarrow p K^- K^- \pi^+$ decays. Reference Λ_b^0 lifetime 1.479 ± 0.009 ± 0.010 ps from AAIJ 14U.
- 2 Measured in $\Xi_b^- \rightarrow J/\psi \Xi^-$ decays.
- 3 Measured in $\Xi_b^- \rightarrow J/\psi \Xi^-$ decays with 66^{+14}_9 candidates.



MEAN LIFE RATIOS

$\tau_{\Xi_b^-} / \tau_{\Lambda_b^0}$ mean life ratio

VALUE	DOCUMENT ID	TECN	COMMENT
1.089 ± 0.026 ± 0.011	1 AAIJ	14BJ LHCB	pp at 7, 8 TeV
1 Reconstructed in $\Xi_b^- \rightarrow \Xi_c^0 \pi^-, \Xi_c^0 \rightarrow p K^- K^- \pi^+$ decays. Reference $\Lambda_b^0 \rightarrow \Lambda_c^+ \pi^-$.			

$\tau_{\Xi_b^-} / \tau_{\Xi_b^0}$ mean life ratio

VALUE	DOCUMENT ID	TECN	COMMENT
1.083 ± 0.032 ± 0.016	1 AAIJ	14BJ LHCB	pp at 7, 8 TeV
1 Reconstructed in $\Xi_b^- \rightarrow \Xi_c^0 \pi^-, \Xi_c^0 \rightarrow p K^- K^- \pi^+$ decays. Uses Ξ_b^0 measurements from AAIJ 14Z.			

Ξ_b^- DECAY MODES

Mode	Fraction (Γ_i/Γ)	Confidence level
Γ_1 $J/\psi \Xi^- \times B(b \rightarrow \Xi_b^-)$	$(1.02^{+0.26}_{-0.21}) \times 10^{-5}$	
Γ_2 $J/\psi \Lambda K^- \times B(b \rightarrow \Xi_b^-)$	$(2.5 \pm 0.4) \times 10^{-6}$	
Γ_3 $p K^- K^- \times B(b \rightarrow \Xi_b^-)$	$(3.7 \pm 0.8) \times 10^{-8}$	
Γ_4 $p K^- K^-$	seen	
Γ_5 $p \pi^- \pi^-$		

Baryon Particle Listings

 Ξ_b^-

Γ_6	$pK^- \pi^-$	seen		
Γ_7	$\Lambda_b^0 \pi^- \times B(b \rightarrow \Xi_b^-) / B(b \rightarrow \Lambda_b^0)$	$(7.0 \pm 0.9) \times 10^{-4}$		
Γ_8	$\Xi_c^0 \pi^-$	seen		
Γ_9	$\Sigma(1385) K^-$	$(2.6 \pm 2.3) \times 10^{-7}$		
Γ_{10}	$\Lambda(1405) K^-$	$(1.9 \pm 1.2) \times 10^{-7}$		
Γ_{11}	$\Lambda(1520) K^-$	$(7.6 \pm 3.2) \times 10^{-7}$		
Γ_{12}	$\Lambda(1670) K^-$	$(4.5 \pm 2.3) \times 10^{-7}$		
Γ_{13}	$\Sigma(1775) K^-$	$(2.2 \pm 1.5) \times 10^{-7}$		
Γ_{14}	$\Sigma(1915) K^-$	$(2.6 \pm 2.5) \times 10^{-7}$		
Γ_{15}	$\Xi^- \gamma$	$< 1.3 \times 10^{-4}$	95%	

 Ξ_b^- BRANCHING RATIOS

$\Gamma(J/\psi \Xi^- \times B(b \rightarrow \Xi_b^-)) / \Gamma_{\text{total}}$ Γ_1 / Γ

VALUE (units 10^{-4})	DOCUMENT ID	TECN	COMMENT
--------------------------	-------------	------	---------

0.102 ± 0.026 OUR AVERAGE
-0.021

$0.098^{+0.023}_{-0.016} \pm 0.014$	¹ AALTONEN	09AP CDF	$p\bar{p}$ at 1.96 TeV
$0.16 \pm 0.07 \pm 0.02$	² ABAZOV	07k D0	$p\bar{p}$ at 1.96 TeV

¹ AALTONEN 09AP reports $[\Gamma(\Xi_b^- \rightarrow J/\psi \Xi^- \times B(b \rightarrow \Xi_b^-)) / \Gamma_{\text{total}}] / [B(\Lambda_b^0 \rightarrow J/\psi(1S) \Lambda \times B(b \rightarrow \Lambda_b^0))] = 0.167^{+0.037}_{-0.025} \pm 0.012$ which we multiply by our best value $B(\Lambda_b^0 \rightarrow J/\psi(1S) \Lambda \times B(b \rightarrow \Lambda_b^0)) = (5.8 \pm 0.8) \times 10^{-5}$. Our first error is their experiment's error and our second error is the systematic error from using our best value.

² ABAZOV 07k reports $[\Gamma(\Xi_b^- \rightarrow J/\psi \Xi^- \times B(b \rightarrow \Xi_b^-)) / \Gamma_{\text{total}}] / [B(\Lambda_b^0 \rightarrow J/\psi(1S) \Lambda \times B(b \rightarrow \Lambda_b^0))] = 0.28 \pm 0.09^{+0.09}_{-0.08}$ which we multiply by our best value $B(\Lambda_b^0 \rightarrow J/\psi(1S) \Lambda \times B(b \rightarrow \Lambda_b^0)) = (5.8 \pm 0.8) \times 10^{-5}$. Our first error is their experiment's error and our second error is the systematic error from using our best value.

$\Gamma(J/\psi \Lambda K^- \times B(b \rightarrow \Xi_b^-)) / \Gamma_{\text{total}}$ Γ_2 / Γ

VALUE (units 10^{-6})	DOCUMENT ID	TECN	COMMENT
--------------------------	-------------	------	---------

2.45 ± 0.19 ± 0.35 ^{1,2} AAIJ 17BE LHCb pp at 7 and 8 TeV

¹ AAIJ 17BE reports $[\Gamma(\Xi_b^- \rightarrow J/\psi \Lambda K^- \times B(b \rightarrow \Xi_b^-)) / \Gamma_{\text{total}}] / [B(\Lambda_b^0 \rightarrow J/\psi(1S) \Lambda \times B(b \rightarrow \Lambda_b^0))] = (4.19 \pm 0.29 \pm 0.15) \times 10^{-2}$ which we multiply by our best value $B(\Lambda_b^0 \rightarrow J/\psi(1S) \Lambda \times B(b \rightarrow \Lambda_b^0)) = (5.8 \pm 0.8) \times 10^{-5}$. Our first error is their experiment's error and our second error is the systematic error from using our best value.

² Integrated over the b -baryon transverse momentum $p_T < 25$ GeV and rapidity $2.0 < y < 4.5$.

$\Gamma(pK^- K^- \times B(b \rightarrow \Xi_b^-)) / \Gamma_{\text{total}}$ Γ_3 / Γ

VALUE (units 10^{-8})	DOCUMENT ID	TECN	COMMENT
--------------------------	-------------	------	---------

3.7 ± 0.8 ± 0.2 ¹ AAIJ 17F LHCb pp at 7, 8 TeV

¹ AAIJ 17F reports $[\Gamma(\Xi_b^- \rightarrow pK^- K^- \times B(\bar{b} \rightarrow \Xi_b^-)) / \Gamma_{\text{total}}] / [B(B^+ \rightarrow K^+ K^- K^+)] / [B(\bar{b} \rightarrow B^+)] = (2.65 \pm 0.35 \pm 0.47) \times 10^{-3}$ which we multiply by our best values $B(B^+ \rightarrow K^+ K^- K^+) = (3.40 \pm 0.14) \times 10^{-5}$, $B(\bar{b} \rightarrow B^+) = (40.8 \pm 0.7) \times 10^{-2}$. Our first error is their experiment's error and our second error is the systematic error from using our best values.

$\Gamma(pK^- K^-) / \Gamma_{\text{total}}$ Γ_4 / Γ

VALUE (units 10^{-6})	DOCUMENT ID	TECN	COMMENT
--------------------------	-------------	------	---------

2.3 ± 0.9 ¹ AAIJ 21AH LHCb pp at 7, 8, 13 TeV

¹ Obtained using the ratio of fragmentation and branching fractions relative to the $B^- \rightarrow K^+ K^- K^-$ decay.

$\Gamma(p\pi^- \pi^-) / \Gamma(pK^- K^-)$ Γ_5 / Γ_4

VALUE	CL%	DOCUMENT ID	TECN	COMMENT
-------	-----	-------------	------	---------

< 0.56 90 ¹ AAIJ 17F LHCb pp at 7, 8 TeV

¹ Measures the ratio as $0.28 \pm 0.16 \pm 0.13$.

$\Gamma(pK^- \pi^-) / \Gamma(pK^- K^-)$ Γ_6 / Γ_4

VALUE	DOCUMENT ID	TECN	COMMENT
-------	-------------	------	---------

0.98 ± 0.27 ± 0.09 AAIJ 17F LHCb pp at 7, 8 TeV

$\Gamma(\Lambda_b^0 \pi^- \times B(b \rightarrow \Xi_b^-) / B(b \rightarrow \Lambda_b^0)) / \Gamma_{\text{total}}$ Γ_7 / Γ

VALUE (units 10^{-4})	DOCUMENT ID	TECN	COMMENT
--------------------------	-------------	------	---------

7.0 ± 0.9 OUR AVERAGE

$7.3 \pm 0.8 \pm 0.6$ ¹ AAIJ 23AV LHCb pp at 13 TeV

$5.7 \pm 1.8^{+0.8}_{-0.9}$ ² AAIJ 15BA LHCb pp at 7, 8 TeV

¹ Measured in the decay chain of $\Xi_b^- \rightarrow \Lambda_b^0 \pi^-$, $\Lambda_b^0 \rightarrow \Lambda_c^+ \pi^-$ and $\Lambda_b^0 \rightarrow \Lambda_c^+ \pi^- \pi^+ \pi^-$, with $\Lambda_c^+ \rightarrow pK^- \pi^+$.

² A signal is reported with a significance of 3.2 standard deviations in the decay chain of $\Xi_b^- \rightarrow \Lambda_b^0 \pi^-$, $\Lambda_b^0 \rightarrow \Lambda_c^+ \pi^-$, and $\Lambda_c^+ \rightarrow pK^- \pi^+$.

$\Gamma(\Xi_c^0 \pi^-) / \Gamma_{\text{total}}$ Γ_8 / Γ

VALUE	DOCUMENT ID	TECN	COMMENT
-------	-------------	------	---------

seen AAIJ 16o LHCb pp at 7, 8 TeV

$\Gamma(\Sigma(1385) K^-) / \Gamma_{\text{total}}$ Γ_9 / Γ

VALUE (units 10^{-6})	DOCUMENT ID	TECN	COMMENT
--------------------------	-------------	------	---------

0.26 ± 0.11 ± 0.20 ¹ AAIJ 21AH LHCb pp at 7, 8 and 13 TeV

¹ Obtained from an amplitude analysis of quasi-two-body contributions to the $\Xi_b^- \rightarrow R K^-$ decay, with $R \rightarrow pK^-$.

$\Gamma(\Lambda(1405) K^-) / \Gamma_{\text{total}}$ Γ_{10} / Γ

VALUE (units 10^{-6})	DOCUMENT ID	TECN	COMMENT
--------------------------	-------------	------	---------

0.19 ± 0.06 ± 0.10 ¹ AAIJ 21AH LHCb pp at 7, 8 and 13 TeV

¹ Obtained from an amplitude analysis of quasi-two-body contributions to the $\Xi_b^- \rightarrow R K^-$ decay, with $R \rightarrow pK^-$.

$\Gamma(\Lambda(1520) K^-) / \Gamma_{\text{total}}$ Γ_{11} / Γ

VALUE (units 10^{-6})	DOCUMENT ID	TECN	COMMENT
--------------------------	-------------	------	---------

0.76 ± 0.09 ± 0.31 ¹ AAIJ 21AH LHCb pp at 7, 8 and 13 TeV

¹ Obtained from an amplitude analysis of quasi-two-body contributions to the $\Xi_b^- \rightarrow R K^-$ decay, with $R \rightarrow pK^-$.

$\Gamma(\Lambda(1670) K^-) / \Gamma_{\text{total}}$ Γ_{12} / Γ

VALUE (units 10^{-6})	DOCUMENT ID	TECN	COMMENT
--------------------------	-------------	------	---------

0.45 ± 0.07 ± 0.22 ¹ AAIJ 21AH LHCb pp at 7, 8 and 13 TeV

¹ Obtained from an amplitude analysis of quasi-two-body contributions to the $\Xi_b^- \rightarrow R K^-$ decay, with $R \rightarrow pK^-$.

$\Gamma(\Sigma(1775) K^-) / \Gamma_{\text{total}}$ Γ_{13} / Γ

VALUE (units 10^{-6})	DOCUMENT ID	TECN	COMMENT
--------------------------	-------------	------	---------

0.22 ± 0.08 ± 0.13 ¹ AAIJ 21AH LHCb pp at 7, 8 and 13 TeV

¹ Obtained from an amplitude analysis of quasi-two-body contributions to the $\Xi_b^- \rightarrow R K^-$ decay, with $R \rightarrow pK^-$.

$\Gamma(\Sigma(1915) K^-) / \Gamma_{\text{total}}$ Γ_{14} / Γ

VALUE (units 10^{-6})	DOCUMENT ID	TECN	COMMENT
--------------------------	-------------	------	---------

0.26 ± 0.09 ± 0.23 ¹ AAIJ 21AH LHCb pp at 7, 8 and 13 TeV

¹ Obtained from an amplitude analysis of quasi-two-body contributions to the $\Xi_b^- \rightarrow R K^-$ decay, with $R \rightarrow pK^-$.

$\Gamma(\Xi^- \gamma) / \Gamma_{\text{total}}$ Γ_{15} / Γ

VALUE	CL%	DOCUMENT ID	TECN	COMMENT
-------	-----	-------------	------	---------

< 1.3 × 10⁻⁴ 95 ¹ AAIJ 22F LHCb pp at 13 TeV

¹ Used $\Xi_b^- \rightarrow \Xi^- J/\psi$ as normalization and an integrated luminosity of 5.4 fb⁻¹.

P VIOLATION ASYMMETRY

$A_P(\Xi_b^-), \Xi_b^- - \Xi_b^+$ production asymmetry

$$A_P(\Xi_b^-) = [\sigma(\Xi_b^-) - \sigma(\Xi_b^+)] / [\sigma(\Xi_b^-) + \sigma(\Xi_b^+)]$$

VALUE (units 10^{-2})	DOCUMENT ID	TECN	COMMENT
--------------------------	-------------	------	---------

-2 ± 4 OUR AVERAGE

$1.1 \pm 5.6 \pm 1.9$ ^{1,2} AAIJ 19AB LHCb pp at 7 and 8 TeV

$-3.9 \pm 4.9 \pm 2.5$ ^{1,2} AAIJ 19AB LHCb pp at 13 TeV

¹ Baryon kinematic range $p_T < 20$ GeV/c and $2 < \eta < 6$.

² Measured using previous measurements of $A_P(\Lambda_b)$ in AAIJ 17BF.

CP VIOLATION in Ξ_b decays

$$A_{CP}(\Xi_b) = [B(\Xi_b^- \rightarrow f) - B(\Xi_b^+ \rightarrow \bar{f})] / \text{Sum}$$

$A_{CP}(\Xi_b^- \rightarrow \Sigma(1385) K^-)$

VALUE	DOCUMENT ID	TECN	COMMENT
-------	-------------	------	---------

(-27 ± 34 ± 73) × 10⁻² AAIJ 21AH LHCb pp at 7, 8, 13 TeV

$A_{CP}(\Xi_b^- \rightarrow \Lambda(1405) K^-)$

VALUE	DOCUMENT ID	TECN	COMMENT
-------	-------------	------	---------

(-1 ± 24 ± 32) × 10⁻² AAIJ 21AH LHCb pp at 7, 8, 13 TeV

$A_{CP}(\Xi_b^- \rightarrow \Lambda(1520) K^-)$

VALUE	DOCUMENT ID	TECN	COMMENT
-------	-------------	------	---------

(-5 ± 9 ± 8) × 10⁻² AAIJ 21AH LHCb pp at 7, 8, 13 TeV

$A_{CP}(\Xi_b^- \rightarrow \Lambda(1670) K^-)$

VALUE	DOCUMENT ID	TECN	COMMENT
-------	-------------	------	---------

(3 ± 14 ± 10) × 10⁻² AAIJ 21AH LHCb pp at 7, 8, 13 TeV

$A_{CP}(\Xi_b^- \rightarrow \Sigma(1775) K^-)$

VALUE	DOCUMENT ID	TECN	COMMENT
-------	-------------	------	---------

(-47 ± 26 ± 14) × 10⁻² AAIJ 21AH LHCb pp at 7, 8, 13 TeV

$A_{CP}(\Xi_b^- \rightarrow \Sigma(1915) K^-)$

VALUE	DOCUMENT ID	TECN	COMMENT
-------	-------------	------	---------

(11 ± 26 ± 22) × 10⁻² AAIJ 21AH LHCb pp at 7, 8, 13 TeV

$$\Xi_b^-, \Xi_b^0$$

Ξ_b^- REFERENCES

AAIJ	23AV	PR D108 072002	R. Aaij <i>et al.</i>	(LHCb Collab.)
AAIJ	22F	JHEP 2201 069	R. Aaij <i>et al.</i>	(LHCb Collab.)
AAIJ	21	PR D103 012004	R. Aaij <i>et al.</i>	(LHCb Collab.)
AAIJ	21AH	PR D104 052010	R. Aaij <i>et al.</i>	(LHCb Collab.)
AAIJ	19AB	PR D99 052006	R. Aaij <i>et al.</i>	(LHCb Collab.)
AAIJ	17BE	PL B772 265	R. Aaij <i>et al.</i>	(LHCb Collab.)
AAIJ	17BF	PL B774 139	R. Aaij <i>et al.</i>	(LHCb Collab.)
AAIJ	17F	PRL 118 071801	R. Aaij <i>et al.</i>	(LHCb Collab.)
AAIJ	16O	PR D93 092007	R. Aaij <i>et al.</i>	(LHCb Collab.)
AAIJ	15BA	PRL 115 241801	R. Aaij <i>et al.</i>	(LHCb Collab.)
AAIJ	14AA	PRL 112 202001	R. Aaij <i>et al.</i>	(LHCb Collab.)
AAIJ	14BJ	PRL 113 242002	R. Aaij <i>et al.</i>	(LHCb Collab.)
AAIJ	14T	PL B736 154	R. Aaij <i>et al.</i>	(LHCb Collab.)
AAIJ	14U	PL B734 122	R. Aaij <i>et al.</i>	(LHCb Collab.)
AAIJ	14Z	PRL 113 032001	R. Aaij <i>et al.</i>	(LHCb Collab.)
AALTONEN	14B	PR D89 072014	T. Aaltonen <i>et al.</i>	(CDF Collab.)
AAIJ	13AV	PRL 110 182001	R. Aaij <i>et al.</i>	(LHCb Collab.)
AALTONEN	11X	PRL 107 102001	T. Aaltonen <i>et al.</i>	(CDF Collab.)
AALTONEN	09AP	PR D80 072003	T. Aaltonen <i>et al.</i>	(CDF Collab.)
AALTONEN	07A	PRL 99 052002	T. Aaltonen <i>et al.</i>	(CDF Collab.)
ABAZOV	07K	PRL 99 052001	V.M. Abazov <i>et al.</i>	(DO Collab.)

$$\Xi_b^0$$

$I(J^P) = \frac{1}{2}(\frac{1}{2}^+)$ Status: ***
I, J, P need confirmation.

In the quark model, Ξ_b^0 and Ξ_b^- are an isodoublet (*usb*, *dsb*) state; the lowest Ξ_b^0 and Ξ_b^- ought to have $J^P = 1/2^+$. None of I, J, or P have actually been measured.

Ξ_b^0 MASS

Ξ_b^0 MASS

VALUE (MeV)	DOCUMENT ID	TECN	COMMENT
5791.9 ± 0.5 OUR AVERAGE			
5794.3 ± 2.4 ± 0.7	AAIJ	14H LHCb	<i>pp</i> at 7 TeV
5791.80 ± 0.39 ± 0.31	¹ AAIJ	14Z LHCb	<i>pp</i> at 7, 8 TeV
5788.7 ± 4.3 ± 1.4	² AALTONEN	14B CDF	<i>p</i> \bar{p} at 1.96 TeV
• • • We do not use the following data for averages, fits, limits, etc. • • •			
5787.8 ± 5.0 ± 1.3	³ AALTONEN	11X CDF	Repl. by AALTONEN 14B
¹ Uses $\Xi_b^0 \rightarrow \Xi_c^+ \pi^-$ and $\Xi_c^+ \rightarrow p K^- \pi^+$ decays. The measurement comes from the mass difference of Ξ_b^0 and Λ_b^0 .			
² Uses $\Xi_b^0 \rightarrow \Xi_c^+ \pi^-$ decays.			
³ Measured in $\Xi_b^0 \rightarrow \Xi_c^+ \pi^-$ with 25.3 $^{+5.6}_{-5.4}$ candidates.			

$m_{\Xi_b^0} - m_{\Lambda_b^0}$

VALUE (MeV)	DOCUMENT ID	TECN	COMMENT
172.5 ± 0.4 OUR AVERAGE			
174.8 ± 2.4 ± 0.5	AAIJ	14H LHCb	<i>pp</i> at 7 TeV
172.44 ± 0.39 ± 0.17	¹ AAIJ	14Z LHCb	<i>pp</i> at 7, 8 TeV
¹ Uses $\Xi_b^0 \rightarrow \Xi_c^+ \pi^-$ and $\Xi_c^+ \rightarrow p K^- \pi^+$ decays.			

Ξ_b^0 MEAN LIFE

"OUR EVALUATION" is an average using rescaled values of the data listed below. The average and rescaling were performed by the Heavy Flavor Averaging Group (HFLAV) and are described at <https://hflav.web.cern.ch/>. The averaging/rescaling procedure takes into account correlations between the measurements and asymmetric lifetime errors.

Ξ_b^0 MEAN LIFE

VALUE (10^{-12} s)	DOCUMENT ID	TECN	COMMENT
1.480 ± 0.030 OUR EVALUATION	(Produced by HFLAV)		
1.477 ± 0.026 ± 0.019	¹ AAIJ	14Z LHCb	<i>pp</i> at 7, 8 TeV
¹ Uses $\Xi_b^0 \rightarrow \Xi_c^+ \pi^-$ and $\Xi_c^+ \rightarrow p K^- \pi^+$ decays. The measurement comes from the value of relative lifetime of Ξ_b^0 to Λ_b^0 .			
$\tau_{mix} (1/2\pi)$ times the oscillation period			
VALUE (s)	DOCUMENT ID	TECN	COMMENT
>13 × 10 ⁻¹²	¹ AAIJ	17BH LHCb	<i>pp</i> at 7, 8 TeV
¹ Uses Ξ_b^{*-} and Ξ_b^- decays to $\Xi_b^0 \pi^-$, where $\Xi_b^0 \rightarrow \Xi_c^+ \pi^-$, $\Xi_c^+ \rightarrow p K^- \pi^+$.			

Ξ_b^0 DECAY MODES

Mode	Fraction (Γ_i/Γ)	Confidence level
Γ_1 $p D^0 K^- \times B(b \rightarrow \Xi_b^0)$	(1.7 ± 0.5) × 10 ⁻⁶	
Γ_2 $p \bar{K}^0 \pi^- \times B(b \rightarrow \Xi_b^0)/B(\bar{b} \rightarrow B^0)$	< 1.6 × 10 ⁻⁶	90%
Γ_3 $p K^0 K^- \times B(b \rightarrow \Xi_b^0)/B(\bar{b} \rightarrow B^0)$	< 1.1 × 10 ⁻⁶	90%
Γ_4 $\Lambda \pi^+ \pi^- \times B(b \rightarrow \Xi_b^0)/B(b \rightarrow \Lambda_b^0)$	< 1.7 × 10 ⁻⁶	90%

Γ_5 $\Lambda K^- \pi^+ \times B(b \rightarrow \Xi_b^0)/B(b \rightarrow \Lambda_b^0)$	< 8 × 10 ⁻⁷	90%
Γ_6 $\Lambda K^+ K^- \times B(b \rightarrow \Xi_b^0)/B(b \rightarrow \Lambda_b^0)$	< 3 × 10 ⁻⁷	90%
Γ_7 $J/\psi \Lambda$	seen	
Γ_8 $J/\psi \Xi^0$	seen	
Γ_9 $\Lambda_c^+ K^- \times B(b \rightarrow \Xi_b^0)$	(6 ± 4) × 10 ⁻⁷	
Γ_{10} $p K^- \pi^+ \pi^- \times B(b \rightarrow \Xi_b^0)/B(b \rightarrow \Lambda_b^0)$	(1.9 ± 0.4) × 10 ⁻⁶	
Γ_{11} $p K^- K^- \pi^+ \times B(b \rightarrow \Xi_b^0)/B(b \rightarrow \Lambda_b^0)$	(1.70 ± 0.30) × 10 ⁻⁶	
Γ_{12} $p K^- K^+ K^- \times B(b \rightarrow \Xi_b^0)/B(b \rightarrow \Lambda_b^0)$	(1.7 ± 0.9) × 10 ⁻⁷	

Ξ_b^0 BRANCHING RATIOS

$\Gamma(p D^0 K^- \times B(b \rightarrow \Xi_b^0))/\Gamma_{total}$	Γ_1/Γ		
VALUE (units 10 ⁻⁶)	DOCUMENT ID	TECN	COMMENT
1.7 ± 0.4 ± 0.4	¹ AAIJ	14H LHCb	<i>pp</i> at 7 TeV

¹AAIJ 14H reports [$\Gamma(\Xi_b \rightarrow p D^0 K^- \times B(\bar{b} \rightarrow \Xi_b^0))/\Gamma_{total}$] / [$B(\bar{b} \rightarrow b\text{-baryon})$] / [$B(\Lambda_b^0 \rightarrow p D^0 K^-)$] = 0.44 ± 0.09 ± 0.06 which we multiply by our best values $B(\bar{b} \rightarrow b\text{-baryon}) = (8.4 \pm 1.1) \times 10^{-2}$, $B(\Lambda_b^0 \rightarrow p D^0 K^-) = (4.5 \pm 0.8) \times 10^{-5}$. Our first error is their experiment's error and our second error is the systematic error from using our best values.

$\Gamma(p \bar{K}^0 \pi^- \times B(b \rightarrow \Xi_b^0)/B(\bar{b} \rightarrow B^0))/\Gamma_{total}$	Γ_2/Γ			
VALUE	CL%	DOCUMENT ID	TECN	COMMENT
<1.6 × 10 ⁻⁶	90	AAIJ	14Q LHCb	<i>pp</i> at 7 TeV

$\Gamma(p K^0 K^- \times B(b \rightarrow \Xi_b^0)/B(\bar{b} \rightarrow B^0))/\Gamma_{total}$	Γ_3/Γ			
VALUE	CL%	DOCUMENT ID	TECN	COMMENT
<1.1 × 10 ⁻⁶	90	AAIJ	14Q LHCb	<i>pp</i> at 7 TeV

$\Gamma(\Lambda \pi^+ \pi^- \times B(b \rightarrow \Xi_b^0)/B(b \rightarrow \Lambda_b^0))/\Gamma_{total}$	Γ_4/Γ			
VALUE	CL%	DOCUMENT ID	TECN	COMMENT
<1.7 × 10 ⁻⁶	90	AAIJ	16W LHCb	<i>pp</i> at 7, 8 TeV

$\Gamma(\Lambda K^- \pi^+ \times B(b \rightarrow \Xi_b^0)/B(b \rightarrow \Lambda_b^0))/\Gamma_{total}$	Γ_5/Γ			
VALUE	CL%	DOCUMENT ID	TECN	COMMENT
<0.8 × 10 ⁻⁶	90	AAIJ	16W LHCb	<i>pp</i> at 7, 8 TeV

$\Gamma(\Lambda K^+ K^- \times B(b \rightarrow \Xi_b^0)/B(b \rightarrow \Lambda_b^0))/\Gamma_{total}$	Γ_6/Γ			
VALUE	CL%	DOCUMENT ID	TECN	COMMENT
<0.3 × 10 ⁻⁶	90	AAIJ	16W LHCb	<i>pp</i> at 7, 8 TeV

$\Gamma(J/\psi \Lambda)/\Gamma(J/\psi \Xi^0)$	Γ_7/Γ_8		
VALUE (units 10 ⁻³)	DOCUMENT ID	TECN	COMMENT
8.2 ± 2.1 ± 0.9	¹ AAIJ	20U LHCb	<i>pp</i> at 7, 8 and 13 TeV

¹ The Cabibbo suppressed $\Xi_b \rightarrow J/\psi \Lambda$ decay is observed for the first time.

$\Gamma(\Lambda_c^+ K^- \times B(b \rightarrow \Xi_b^0))/\Gamma(p D^0 K^- \times B(b \rightarrow \Xi_b^0))$	Γ_9/Γ_1		
VALUE	DOCUMENT ID	TECN	COMMENT
0.36 ± 0.19 ± 0.02	¹ AAIJ	14H LHCb	<i>pp</i> at 7 TeV

¹AAIJ 14H reports [$\Gamma(\Xi_b \rightarrow \Lambda_c^+ K^- \times B(\bar{b} \rightarrow \Xi_b^0))/\Gamma(\Xi_b \rightarrow p D^0 K^- \times B(\bar{b} \rightarrow \Xi_b^0))$] / [$B(\Lambda_c^+ \rightarrow p K^- \pi^+)$] / [$B(D^0 \rightarrow K^- \pi^+)$] = 0.57 ± 0.22 ± 0.21 which we multiply or divide by our best values $B(\Lambda_c^+ \rightarrow p K^- \pi^+) = (6.24 \pm 0.28) \times 10^{-2}$, $B(D^0 \rightarrow K^- \pi^+) = (3.947 \pm 0.030) \times 10^{-2}$. Our first error is their experiment's error and our second error is the systematic error from using our best values.

$\Gamma(p K^- \pi^+ \pi^- \times B(b \rightarrow \Xi_b^0)/B(b \rightarrow \Lambda_b^0))/\Gamma_{total}$	Γ_{10}/Γ		
VALUE (units 10 ⁻⁶)	DOCUMENT ID	TECN	COMMENT
1.89 ± 0.35 ± 0.16	¹ AAIJ	18Q LHCb	<i>pp</i> at 7, 8 TeV

¹AAIJ 18Q reports [$\Gamma(\Xi_b \rightarrow p K^- \pi^+ \pi^- \times B(b \rightarrow \Xi_b^0)/B(b \rightarrow \Lambda_b^0))/\Gamma_{total}$] / [$B(\Lambda_c^+ \rightarrow p K^- \pi^+)$] / [$B(\Lambda_b^0 \rightarrow \Lambda_c^+ \pi^-)$] = (6.2 ± 0.8 ± 0.2 ± 0.8) × 10⁻³ which we multiply by our best values $B(\Lambda_c^+ \rightarrow p K^- \pi^+) = (6.24 \pm 0.28) \times 10^{-2}$, $B(\Lambda_b^0 \rightarrow \Lambda_c^+ \pi^-) = (4.9 \pm 0.4) \times 10^{-3}$. Our first error is their experiment's error and our second error is the systematic error from using our best values.

$\Gamma(p K^- K^- \pi^+ \times B(b \rightarrow \Xi_b^0)/B(b \rightarrow \Lambda_b^0))/\Gamma_{total}$	Γ_{11}/Γ		
VALUE (units 10 ⁻⁶)	DOCUMENT ID	TECN	COMMENT
1.70 ± 0.27 ± 0.15	¹ AAIJ	18Q LHCb	<i>pp</i> at 7, 8 TeV

¹AAIJ 18Q reports [$\Gamma(\Xi_b \rightarrow p K^- K^- \pi^+ \times B(b \rightarrow \Xi_b^0)/B(b \rightarrow \Lambda_b^0))/\Gamma_{total}$] / [$B(\Lambda_c^+ \rightarrow p K^- \pi^+)$] / [$B(\Lambda_b^0 \rightarrow \Lambda_c^+ \pi^-)$] = (5.6 ± 0.6 ± 0.4 ± 0.5) × 10⁻³ which we multiply by our best values $B(\Lambda_c^+ \rightarrow p K^- \pi^+) = (6.24 \pm 0.28) \times 10^{-2}$, $B(\Lambda_b^0 \rightarrow \Lambda_c^+ \pi^-) = (4.9 \pm 0.4) \times 10^{-3}$. Our first error is their experiment's error and our second error is the systematic error from using our best values.

Baryon Particle Listings

 $\Xi_b^0, \Xi_b'(5935)^-, \Xi_b(5945)^0$

$\Gamma(pK^-K^+ \times B(b \rightarrow \Xi_b^0)/B(b \rightarrow \Lambda_b^0))/\Gamma_{\text{total}}$	Γ_{12}/Γ		
VALUE (units 10^{-6})	DOCUMENT ID	TECN	COMMENT
$0.17 \pm 0.09 \pm 0.01$	^{1,2} AAIJ	18Q	LHCB pp at 7, 8 TeV
¹ AAIJ 18Q reports $[\Gamma(\Xi_b^- \rightarrow pK^-K^+K^- \times B(b \rightarrow \Xi_b^0)/B(b \rightarrow \Lambda_b^0))/\Gamma_{\text{total}}] / [B(\Lambda_c^+ \rightarrow pK^- \pi^+)] / [B(\Lambda_b^0 \rightarrow \Lambda_c^+ \pi^-)] = (0.57 \pm 0.28 \pm 0.08 \pm 0.10) \times 10^{-3}$ which we multiply by our best values $B(\Lambda_c^+ \rightarrow pK^- \pi^+) = (6.24 \pm 0.28) \times 10^{-2}$, $B(\Lambda_b^0 \rightarrow \Lambda_c^+ \pi^-) = (4.9 \pm 0.4) \times 10^{-3}$. Our first error is their experiment's error and our second error is the systematic error from using our best values. ² AAIJ 18Q sees excess with a significance of 2.3 σ . Using $B(\Lambda_b^0 \rightarrow \Lambda_c^+ \pi^-) = (0.430 \pm 0.036) \times 10^{-2}$ and $B(\Lambda_c^+ \rightarrow pK^- \pi^+) = (6.46 \pm 0.24) \times 10^{-2}$ the authors set two sided limit $[0.11-0.25]$ at 90% C.L.			

P AND CP VIOLATION ASYMMETRIES

$a_P(\Xi_b^0 \rightarrow pK^-K^+\pi^+)$
Observable calculated as average of the triple products for Ξ_b^0 and Ξ_b^0 , which is sensitive to parity violation.

VALUE (%)	DOCUMENT ID	TECN	COMMENT
$-3.04 \pm 5.19 \pm 0.36$	¹ AAIJ	18AG	LHCB pp at 7, 8 TeV

¹ Measured over full phase space of the decay.

$a_{CP}(\Xi_b^0 \rightarrow pK^-K^+\pi^+)$
Observable calculated as half of the difference between triple products for Ξ_b^0 and Ξ_b^0 , which is sensitive to CP violation.

VALUE (%)	DOCUMENT ID	TECN	COMMENT
$-3.58 \pm 5.19 \pm 0.36$	¹ AAIJ	18AG	LHCB pp at 7, 8 TeV

¹ Measured over full phase space of the decay.

$\Delta A_{CP}(\Xi_b^0 \rightarrow pK^- \pi^+ \pi^-)$
 $\Delta A_{CP} \equiv A_{CP}(\Xi_b^0 \rightarrow pK^- \pi^+ \pi^-) - A_{CP}(\Xi_b^0 \rightarrow (\Xi_c^+ \rightarrow pK^- \pi^+) \pi^-)$

VALUE (units 10^{-2})	DOCUMENT ID	TECN	COMMENT
$-17 \pm 11 \pm 1$	¹ AAIJ	19AH	LHCB pp at 7 and 8 TeV

¹ Full phase space.

$\Delta A_{CP}(\Xi_b^0 \rightarrow pK^- \pi^+ K^-)$
 $\Delta A_{CP} \equiv A_{CP}(\Xi_b^0 \rightarrow pK^- \pi^+ K^-) - A_{CP}(\Xi_b^0 \rightarrow (\Xi_c^+ \rightarrow pK^- \pi^+) \pi^-)$

VALUE (units 10^{-2})	DOCUMENT ID	TECN	COMMENT
$-6.8 \pm 8.0 \pm 0.8$	¹ AAIJ	19AH	LHCB pp at 7 and 8 TeV

¹ Full phase space.

 Ξ_b^0 REFERENCES

AAIJ	20U	PRL 124 111802	R. Aaij et al.	(LHCb Collab.)
AAIJ	19AH	EPJ C79 745	R. Aaij et al.	(LHCb Collab.)
AAIJ	18AG	JHEP 1808 039	R. Aaij et al.	(LHCb Collab.)
AAIJ	18Q	JHEP 1802 098	R. Aaij et al.	(LHCb Collab.)
AAIJ	17BH	PRL 119 181807	R. Aaij et al.	(LHCb Collab.)
AAIJ	16W	JHEP 1605 081	R. Aaij et al.	(LHCb Collab.)
AAIJ	14H	PR D89 032001	R. Aaij et al.	(LHCb Collab.)
AAIJ	14Q	JHEP 1404 087	R. Aaij et al.	(LHCb Collab.)
AAIJ	14Z	PRL 113 032001	R. Aaij et al.	(LHCb Collab.)
AALTONEN	14B	PR D89 072014	T. Aaltonen et al.	(CDF Collab.)
AALTONEN	11X	PRL 107 102001	T. Aaltonen et al.	(CDF Collab.)

$\Xi_b'(5935)^-$ $J^P = \frac{1}{2}^+$ Status: ***

 $\Xi_b'(5935)^-$ MASS

VALUE (MeV)	DOCUMENT ID	TECN	COMMENT
5935.1 ± 0.5 OUR AVERAGE			
$5935.09 \pm 0.01 \pm 0.49$	^{1,2} AAIJ	23AU	LHCB pp at 7, 8, 13 TeV
$5935.08 \pm 0.02 \pm 0.49$	^{1,3} AAIJ	15H	LHCB pp at 7, 8 TeV

¹ Observed in $\Xi_b^0 \pi^-$ channel with $\Xi_b^0 \rightarrow \Xi_c^+ \pi^-$ and $\Xi_c^+ \rightarrow pK^- \pi^+$.

² AAIJ 23AU measures $m(\Xi_b'(5935)^-) - m(\Xi_b^0) - m(\pi^-) = 3.66 \pm 0.01 \pm 0.00$ MeV. We have adjusted the measurement to our best values of $m(\Xi_b^0) = 5791.9 \pm 0.5$ MeV, $m(\pi^-) = 139.57039 \pm 0.00018$ MeV. Our first error is their experiment's error and our second error is the systematic error from using our best values.

³ AAIJ 15H measures $m(\Xi_b'(5935)^-) - m(\Xi_b^0) - m(\pi^-) = 3.653 \pm 0.018 \pm 0.006$ MeV. We have adjusted the measurement to our best values of $m(\Xi_b^0) = 5791.9 \pm 0.5$ MeV, $m(\pi^-) = 139.57039 \pm 0.00018$ MeV. Our first error is their experiment's error and our second error is the systematic error from using our best values.

 $\Xi_b'(5935)^-$ WIDTH

VALUE (MeV)	CL%	DOCUMENT ID	TECN	COMMENT
$0.03 \pm 0.01 \pm 0.03$		¹ AAIJ	23AU	LHCB pp at 7, 8, 13 TeV

• • • We do not use the following data for averages, fits, limits, etc. • • •

<0.08 95 ¹ AAIJ 15H LHCB pp at 7, 8 TeV

¹ Observed in $\Xi_b^0 \pi^-$ channel with $\Xi_b^0 \rightarrow \Xi_c^+ \pi^-$ and $\Xi_c^+ \rightarrow pK^- \pi^+$.

 $\Xi_b'(5935)^-$ DECAY MODES

Mode	Fraction (Γ_i/Γ)
$\Xi_b^0 \pi^- \times B(\bar{b} \rightarrow \Xi_b'(5935)^-)/B(\bar{b} \rightarrow \Xi_b^0)$	$(11.8 \pm 1.8) \%$

 $\Xi_b'(5935)^-$ BRANCHING RATIOS

$\Gamma(\Xi_b^0 \pi^- \times B(\bar{b} \rightarrow \Xi_b'(5935)^-)/B(\bar{b} \rightarrow \Xi_b^0))/\Gamma_{\text{total}}$	Γ_1/Γ		
VALUE	DOCUMENT ID	TECN	COMMENT
$0.118 \pm 0.017 \pm 0.007$	¹ AAIJ	15H	LHCB pp at 7, 8 TeV
¹ Observed in $\Xi_b^0 \pi^-$ channel with $\Xi_b^0 \rightarrow \Xi_c^+ \pi^-$ and $\Xi_c^+ \rightarrow pK^- \pi^+$.			

 $\Xi_b'(5935)^-$ REFERENCES

AAIJ	23AU	PRL 131 171901	R. Aaij et al.	(LHCb Collab.)
AAIJ	15H	PRL 114 062004	R. Aaij et al.	(LHCb Collab.)

$\Xi_b(5945)^0$

$J^P = \frac{3}{2}^+$ Status: ***

Quantum numbers are based on quark model expectations.

 $\Xi_b(5945)^0$ MASS

VALUE (MeV)	DOCUMENT ID	TECN	COMMENT
5952.3 ± 0.6 OUR AVERAGE			
$5952.35 \pm 0.02 \pm 0.58$	^{1,2} AAIJ	23AU	LHCB pp at 7, 8, 13 TeV
$5952.3 \pm 0.1 \pm 0.6$	³ AAIJ	16AE	LHCB pp at 7, 8 TeV
$5951.4 \pm 0.8 \pm 0.6$	⁴ CHATRCHYAN	12S	CMS pp at 7 TeV, 5.3 fb ⁻¹

¹ Measured using $\Xi_b(5945)^0 \rightarrow \Xi_b^- \pi^+, \Xi_b^- \rightarrow \Xi_c^0 \pi^-, \Xi_c^0 \rightarrow pK^- K^- \pi^+$ decays.

² AAIJ 23AU measures $m(\Xi_b(5945)^0) - m(\Xi_b^-) - m(\pi^+) = 15.80 \pm 0.02 \pm 0.01$ MeV.

We have adjusted the measurement to our best values of $m(\Xi_b^-) = 5797.0 \pm 0.6$ MeV, $m(\pi^+) = 139.57039 \pm 0.00018$ MeV. Our first error is their experiment's error and our second error is the systematic error from using our best values.

³ AAIJ 16AE measures $m(\Xi_b(5945)^0) - m(\Xi_b^-) - m(\pi^+) = 15.727 \pm 0.068 \pm 0.023$ MeV.

We have adjusted the measurement to our best values of $m(\Xi_b^-) = 5797.0 \pm 0.6$ MeV, $m(\pi^+) = 139.57039 \pm 0.00018$ MeV. Our first error is their experiment's error and our second error is the systematic error from using our best values.

⁴ CHATRCHYAN 12S measures $m(\Xi_b(5945)^0) - m(\Xi_b^-) - m(\pi^+) = 14.84 \pm 0.74 \pm 0.28$ MeV. We have adjusted the measurement to our best values of $m(\Xi_b^-) = 5797.0 \pm 0.6$ MeV, $m(\pi^+) = 139.57039 \pm 0.00018$ MeV. Our first error is their experiment's error and our second error is the systematic error from using our best values.

 $\Xi_b(5945)^0$ WIDTH

VALUE (MeV)	DOCUMENT ID	TECN	COMMENT
$0.87 \pm 0.06 \pm 0.05$	¹ AAIJ	23AU	LHCB pp at 7, 8, 13 TeV
• • • We do not use the following data for averages, fits, limits, etc. • • •			
$0.90 \pm 0.16 \pm 0.08$	¹ AAIJ	16AE	LHCB pp at 7, 8 TeV
2.1 ± 1.7	² CHATRCHYAN	12S	CMS pp at 7 TeV, 5.3 fb ⁻¹

¹ Measured using $\Xi_b(5945)^0 \rightarrow \Xi_b^- \pi^+, \Xi_b^- \rightarrow \Xi_c^0 \pi^-, \Xi_c^0 \rightarrow pK^- K^- \pi^+$ decays.

² Systematic uncertainty not evaluated.

 $\Xi_b(5945)^0$ DECAY MODES

Mode	Fraction (Γ_i/Γ)
$\Xi_b^- \pi^+$	seen

 $\Xi_b(5945)^0$ BRANCHING RATIOS

$\Gamma(\Xi_b^- \pi^+)/\Gamma_{\text{total}}$	Γ_1/Γ		
VALUE	DOCUMENT ID	TECN	COMMENT
seen	AAIJ	16AE	ATLS pp at 7, 8 TeV
seen	CHATRCHYAN	12S	CMS pp at 7 TeV, 5.3 fb ⁻¹

 $\Xi_b(5945)^0$ REFERENCES

AAIJ	23AU	PRL 131 171901	R. Aaij et al.	(LHCb Collab.)
AAIJ	16AE	JHEP 1605 161	R. Aaij et al.	(LHCb Collab.)
CHATRCHYAN	12S	PRL 108 252002	S. Chatrchyan et al.	(CMS Collab.)

See key on page 1171

Baryon Particle Listings

 $\Xi_b(5955)^-$, $\Xi_b(6087)^0$, $\Xi_b(6095)^0$, $\Xi_b(6100)^-$ $\Xi_b(5955)^-$ $J^P = \frac{3}{2}^+$ Status: *** $\Xi_b(5955)^-$ MASS

VALUE (MeV)	DOCUMENT ID	TECN	COMMENT
5955.7 ± 0.5 OUR AVERAGE			
5955.70 ± 0.03 ± 0.49	^{1,2} AAIJ	23AU LHCb	pp at 7, 8, 13 TeV
5955.4 ± 0.1 ± 0.5	^{1,3} AAIJ	15H LHCb	pp at 7, 8 TeV

- ¹ Observed in $\Xi_b^0 \pi^-$ channel with $\Xi_b^0 \rightarrow \Xi_c^+ \pi^-$ and $\Xi_c^+ \rightarrow p K^- \pi^+$.
- ² AAIJ 23AU measures $m(\Xi_b(5955)^-) - m(\Xi_b^0) - m(\pi^-) = 24.27 \pm 0.03 \pm 0.01$ MeV. We have adjusted the measurement to our best values of $m(\Xi_b^0) = 5791.9 \pm 0.5$ MeV, $m(\pi^-) = 139.57039 \pm 0.00018$ MeV. Our first error is their experiment's error and our second error is the systematic error from using our best values.
- ³ AAIJ 15H measures $m(\Xi_b(5955)^-) - m(\Xi_b^0) - m(\pi^-) = 24.96 \pm 0.12 \pm 0.06$ MeV. We have adjusted the measurement to our best values of $m(\Xi_b^0) = 5791.9 \pm 0.5$ MeV, $m(\pi^-) = 139.57039 \pm 0.00018$ MeV. Our first error is their experiment's error and our second error is the systematic error from using our best values.

 $\Xi_b(5955)^-$ WIDTH

VALUE (MeV)	DOCUMENT ID	TECN	COMMENT
1.43 ± 0.08 ± 0.08	¹ AAIJ	23AU LHCb	pp at 7, 8, 13 TeV
• • • We do not use the following data for averages, fits, limits, etc. • • •			
1.65 ± 0.31 ± 0.10	¹ AAIJ	15H LHCb	pp at 7, 8 TeV

- ¹ Observed in $\Xi_b^0 \pi^-$ channel with $\Xi_b^0 \rightarrow \Xi_c^+ \pi^-$ and $\Xi_c^+ \rightarrow p K^- \pi^+$.

 $\Xi_b(5955)^-$ DECAY MODES

Mode	Fraction (Γ_i/Γ)
$\Gamma_1 \quad \Xi_b^0 \pi^- \times B(\bar{b} \rightarrow \Xi_b^*(5955)^-)/B(\bar{b} \rightarrow \Xi_b^0)$	(20.7 ± 3.5) %

 $\Xi_b(5955)^-$ BRANCHING RATIOS

$\Gamma(\Xi_b^0 \pi^- \times B(\bar{b} \rightarrow \Xi_b^*(5955)^-)/B(\bar{b} \rightarrow \Xi_b^0))/\Gamma_{\text{total}}$	Γ_1/Γ
0.207 ± 0.032 ± 0.015	
¹ AAIJ	15H LHCb pp at 7, 8 TeV

- ¹ Observed in $\Xi_b^0 \pi^-$ channel with $\Xi_b^0 \rightarrow \Xi_c^+ \pi^-$ and $\Xi_c^+ \rightarrow p K^- \pi^+$.

 $\Xi_b(5955)^-$ REFERENCES

AAIJ	23AU PRL 131 171901	R. Aaij et al.	(LHCb Collab.)
AAIJ	15H PRL 114 062004	R. Aaij et al.	(LHCb Collab.)

 $\Xi_b(6087)^0$ $J^P = \frac{1}{2}(\frac{3}{2}^-)$ Status: ***
J, P need confirmation. $\Xi_b(6087)^0$ MASS

VALUE (MeV)	DOCUMENT ID	TECN	COMMENT
6087.2 ± 0.2 ± 0.5			
6087.9 ± 0.1 ± 0.6	^{1,2} AAIJ	23AU LHCb	pp at 7, 8, 13 TeV
6100.3 ± 0.2 ± 0.6	^{3,4} SIRUNYAN	21F CMS	pp at 13 TeV

- ¹ Observed in $\Xi_b^0 \pi^+ \pi^-$ channel with $\Xi_b^0 \rightarrow \Xi_c^+ \pi^-$ and $\Xi_c^+ \rightarrow \Xi_c^+ \pi^- \pi^+ \pi^-$ and $\Xi_c^+ \rightarrow p K^- \pi^+$. Measured as mass difference, listed separately.
- ² AAIJ 23AU measures $m(\Xi_b(6087)^0) - m(\Xi_b^0) - 2m(\pi^\pm) = 16.20 \pm 0.20 \pm 0.06$ MeV. We have adjusted the measurement to our best values of $m(\Xi_b^0) = 5791.9 \pm 0.5$ MeV, $m(\pi^\pm) = 139.57039 \pm 0.00018$ MeV. Our first error is their experiment's error and our second error is the systematic error from using our best values.
- ³ Observed in $\Xi_b(6100)^- \rightarrow \Xi_b^- \pi^+ \pi^-$ decays.
- ⁴ SIRUNYAN 21F measures $m(\Xi_b(6100)^-) - m(\Xi_b^-) - 2m(\pi^\pm) = 24.14 \pm 0.22 \pm 0.09$ MeV. We have adjusted the measurement to our best values of $m(\Xi_b^-) = 5797.0 \pm 0.6$ MeV, $m(\pi^\pm) = 139.57039 \pm 0.00018$ MeV. Our first error is their experiment's error and our second error is the systematic error from using our best values.

 $\Xi_b(6087)^0$ WIDTH

VALUE (MeV)	DOCUMENT ID	TECN	COMMENT
2.43 ± 0.51 ± 0.10	¹ AAIJ	23AU LHCb	pp at 7, 8, 13 TeV

- ¹ Observed in $\Xi_b^0 \pi^+ \pi^-$ channel with $\Xi_b^0 \rightarrow \Xi_c^+ \pi^-$ and $\Xi_c^+ \rightarrow \Xi_c^+ \pi^- \pi^+ \pi^-$ and $\Xi_c^+ \rightarrow p K^- \pi^+$.

 $\Xi_b(6087)^0$ DECAY MODES

Mode	Fraction (Γ_i/Γ)
$\Gamma_1 \quad \Xi_b^0 \pi^+ \pi^-$	seen

 $\Xi_b(6087)^0$ BRANCHING RATIOS

$\Gamma(\Xi_b^0 \pi^+ \pi^-)/\Gamma_{\text{total}}$	Γ_1/Γ
0.207 ± 0.032 ± 0.015	
AAIJ	23AU LHCb pp at 7, 8, 13 TeV

 $\Xi_b(6087)^0$ REFERENCES

AAIJ	23AU PRL 131 171901	R. Aaij et al.	(LHCb Collab.)
------	---------------------	----------------	----------------

 $\Xi_b(6095)^0$ $J^P = \frac{1}{2}(\frac{3}{2}^-)$ Status: ***
J, P need confirmation. $\Xi_b(6095)^0$ MASS

VALUE (MeV)	DOCUMENT ID	TECN	COMMENT
6095.3 ± 0.2 ± 0.5			
6099.7 ± 0.1 ± 0.6	^{1,2} AAIJ	23AU LHCb	pp at 7, 8, 13 TeV
6100.3 ± 0.2 ± 0.6	^{3,4} SIRUNYAN	21F CMS	pp at 13 TeV

- ¹ Observed in $\Xi_b^0 \pi^+ \pi^-$ channel with $\Xi_b^0 \rightarrow \Xi_c^+ \pi^-$ and $\Xi_c^+ \rightarrow \Xi_c^+ \pi^- \pi^+ \pi^-$ and $\Xi_c^+ \rightarrow p K^- \pi^+$. Measured as mass difference, listed separately.
- ² AAIJ 23AU measures $m(\Xi_b(6095)^0) - m(\Xi_b^0) - 2m(\pi^\pm) = 24.32 \pm 0.15 \pm 0.03$ MeV. We have adjusted the measurement to our best values of $m(\Xi_b^0) = 5791.9 \pm 0.5$ MeV, $m(\pi^\pm) = 139.57039 \pm 0.00018$ MeV. Our first error is their experiment's error and our second error is the systematic error from using our best values.
- ³ Observed in $\Xi_b(6100)^- \rightarrow \Xi_b^- \pi^+ \pi^-$ decays.
- ⁴ SIRUNYAN 21F measures $m(\Xi_b(6100)^-) - m(\Xi_b^-) - 2m(\pi^\pm) = 24.14 \pm 0.22 \pm 0.09$ MeV. We have adjusted the measurement to our best values of $m(\Xi_b^-) = 5797.0 \pm 0.6$ MeV, $m(\pi^\pm) = 139.57039 \pm 0.00018$ MeV. Our first error is their experiment's error and our second error is the systematic error from using our best values.

 $\Xi_b(6095)^0$ WIDTH

VALUE (MeV)	DOCUMENT ID	TECN	COMMENT
0.50 ± 0.33 ± 0.11	¹ AAIJ	23AU LHCb	pp at 7, 8, 13 TeV

- ¹ Observed in $\Xi_b^0 \pi^+ \pi^-$ channel with $\Xi_b^0 \rightarrow \Xi_c^+ \pi^-$ and $\Xi_c^+ \rightarrow \Xi_c^+ \pi^- \pi^+ \pi^-$ and $\Xi_c^+ \rightarrow p K^- \pi^+$.

 $\Xi_b(6095)^0$ DECAY MODES

Mode	Fraction (Γ_i/Γ)
$\Gamma_1 \quad \Xi_b^0 \pi^+ \pi^-$	seen

 $\Xi_b(6095)^0$ BRANCHING RATIOS

$\Gamma(\Xi_b^0 \pi^+ \pi^-)/\Gamma_{\text{total}}$	Γ_1/Γ
0.207 ± 0.032 ± 0.015	
AAIJ	23AU LHCb pp at 7, 8, 13 TeV

 $\Xi_b(6095)^0$ REFERENCES

AAIJ	23AU PRL 131 171901	R. Aaij et al.	(LHCb Collab.)
------	---------------------	----------------	----------------

 $\Xi_b(6100)^-$ $J^P = \frac{3}{2}^-$ Status: ***
J, P need confirmation. $\Xi_b(6100)^-$ MASS

VALUE (MeV)	DOCUMENT ID	TECN	COMMENT
6099.8 ± 0.6 OUR AVERAGE			
6099.7 ± 0.1 ± 0.6	^{1,2} AAIJ	23AU LHCb	pp at 7, 8, 13 TeV
6100.3 ± 0.2 ± 0.6	^{3,4} SIRUNYAN	21F CMS	pp at 13 TeV

- ¹ Observed in $\Xi_b^- \pi^+ \pi^-$ channel with $\Xi_b^- \rightarrow \Xi_c^0 \pi^-$ and $\Xi_c^0 \rightarrow \Xi_c^0 \pi^- \pi^+ \pi^-$ and $\Xi_c^0 \rightarrow p K^- K^- \pi^+$.
- ² AAIJ 23AU measures $m(\Xi_b(6100)^-) - m(\Xi_b^-) - 2m(\pi^\pm) = 23.60 \pm 0.11 \pm 0.12$ MeV. We have adjusted the measurement to our best values of $m(\Xi_b^-) = 5797.0 \pm 0.6$ MeV, $m(\pi^\pm) = 139.57039 \pm 0.00018$ MeV. Our first error is their experiment's error and our second error is the systematic error from using our best values.
- ³ Observed in $\Xi_b(6100)^- \rightarrow \Xi_b^- \pi^+ \pi^-$ decays.
- ⁴ SIRUNYAN 21F measures $m(\Xi_b(6100)^-) - m(\Xi_b^-) - 2m(\pi^\pm) = 24.14 \pm 0.22 \pm 0.09$ MeV. We have adjusted the measurement to our best values of $m(\Xi_b^-) = 5797.0 \pm 0.6$ MeV, $m(\pi^\pm) = 139.57039 \pm 0.00018$ MeV. Our first error is their experiment's error and our second error is the systematic error from using our best values.

 $\Xi_b(6100)^-$ WIDTH

VALUE (MeV)	CL%	DOCUMENT ID	TECN	COMMENT
0.94 ± 0.30 ± 0.08		¹ AAIJ	23AU LHCb	pp at 7, 8, 13 TeV
• • • We do not use the following data for averages, fits, limits, etc. • • •				
<1.9	95	² SIRUNYAN	21F CMS	pp at 13 TeV

- ¹ Observed in $\Xi_b^- \pi^+ \pi^-$ channel with $\Xi_b^- \rightarrow \Xi_c^0 \pi^-$ and $\Xi_c^0 \rightarrow \Xi_c^0 \pi^- \pi^+ \pi^-$ and $\Xi_c^0 \rightarrow p K^- K^- \pi^+$.
- ² Observed in $\Xi_b(6100)^- \rightarrow \Xi_b^- \pi^+ \pi^-$ decays.

Baryon Particle Listings

 $\Xi_b(6100)^-$, $\Xi_b(6227)^-$, $\Xi_b(6227)^0$, $\Xi_b(6327)^0$ $\Xi_b(6100)^-$ DECAY MODES

Mode	Fraction (Γ_i/Γ)
$\Gamma_1 \Xi_b^- \pi^+ \pi^-$	seen

 $\Xi_b(6100)^-$ BRANCHING RATIOS

$\Gamma(\Xi_b^- \pi^+ \pi^-)/\Gamma_{\text{total}}$		Γ_1/Γ	
VALUE	EVTS	DOCUMENT ID	TECN COMMENT
seen		AAIJ	23AU LHCb pp at 7, 8, 13 TeV
seen	60	SIRUNYAN	21F CMS pp at 13 TeV

 $\Xi_b(6100)^-$ REFERENCES

AAIJ	23AU	PRL 131 171901	R. Aaij <i>et al.</i>	(LHCb Collab.)
SIRUNYAN	21F	PRL 126 252003	A.M. Sirunyan <i>et al.</i>	(CMS Collab.)

$\Xi_b(6227)^-$ $J^P = ??$ Status: ***

 $\Xi_b(6227)^-$ MASS

VALUE (MeV)	DOCUMENT ID	TECN	COMMENT
6227.9 ± 0.9 ± 0.2	¹ AAIJ	21	LHCb pp at 7, 8, 13 TeV
• • • We do not use the following data for averages, fits, limits, etc. • • •			
6226.9 ± 2.0 ± 0.4	^{2,3} AAIJ	18H	LHCb Repl. by AAIJ 2021
¹ AAIJ 21 measures $m(\Xi_b(6227)^-) - m(\Lambda_b^0) = 608.3 \pm 0.8 \pm 0.4$ MeV. We have adjusted the measurement to our best value of $m(\Lambda_b^0) = 5619.60 \pm 0.17$ MeV. Our first error is their experiment's error and our second error is the systematic error from using our best values.			
² Uses $\Lambda_b^0 K^-$ and $\Xi_b^0 \pi^-$ modes.			
³ Measures mass difference $m(\Xi_b(6227)^-) - m(\Lambda_b^0) = 607.3 \pm 2.0 \pm 0.3$ MeV and uses $m(\Lambda_b^0) = 5619.58 \pm 0.17$ MeV.			

 $\Xi_b(6227)^-$ WIDTH

VALUE (MeV)	DOCUMENT ID	TECN	COMMENT
19.9 ± 2.1 ± 1.5	¹ AAIJ	21	LHCb pp at 7, 8, 13 TeV
• • • We do not use the following data for averages, fits, limits, etc. • • •			
18.1 ± 5.4 ± 1.8	² AAIJ	18H	LHCb Repl. by AAIJ 2021
¹ Uses $\Lambda_b^0 K^-$ decays.			
² Uses $\Lambda_b^0 K^-$ and $\Xi_b^0 \pi^-$ modes.			

 $\Xi_b(6227)^-$ DECAY MODES

Mode	Fraction (Γ_i/Γ)	Scale factor
$\Gamma_1 \Lambda_b^0 K^- \times B(b \rightarrow \Xi_b(6227)^-)/B(b \rightarrow \Lambda_b^0)$	$(3.20 \pm 0.35) \times 10^{-3}$	
$\Gamma_2 \Xi_b^0 \pi^- \times B(b \rightarrow \Xi_b(6227)^-)/B(b \rightarrow \Xi_b^0)$	$(2.8 \pm 1.1) \%$	1.8

 $\Xi_b(6227)^-$ BRANCHING RATIOS

$\Gamma(\Lambda_b^0 K^- \times B(b \rightarrow \Xi_b(6227)^-)/B(b \rightarrow \Lambda_b^0))/\Gamma_{\text{total}}$		Γ_1/Γ	
VALUE (units 10^{-3})	DOCUMENT ID	TECN	COMMENT
3.20 ± 0.35 OUR AVERAGE			
3.0 ± 0.3 ± 0.4	AAIJ	18H	LHCb pp at 7, 8 TeV
3.4 ± 0.3 ± 0.4	AAIJ	18H	LHCb pp at 13 TeV
$\Gamma(\Xi_b^0 \pi^- \times B(b \rightarrow \Xi_b(6227)^-)/B(b \rightarrow \Xi_b^0))/\Gamma_{\text{total}}$		Γ_2/Γ	
VALUE (units 10^{-3})	DOCUMENT ID	TECN	COMMENT
28 ± 11 OUR AVERAGE Error includes scale factor of 1.8.			
47 ± 10 ± 7	AAIJ	18H	LHCb pp at 7, 8 TeV
22 ± 6 ± 3	AAIJ	18H	LHCb pp at 13 TeV

 $\Xi_b(6227)^-$ REFERENCES

AAIJ	21	PR D103 012004	R. Aaij <i>et al.</i>	(LHCb Collab.)
AAIJ	18H	PRL 121 072002	R. Aaij <i>et al.</i>	(LHCb Collab.)

 $\Xi_b(6227)^0$ $J^P = ??$

Status: ***

 $\Xi_b(6227)^0$ MASS

VALUE (MeV)	DOCUMENT ID	TECN	COMMENT
6226.8 ± 1.4 ± 0.6	^{1,2} AAIJ	21	LHCb pp at 7, 8, 13 TeV
¹ AAIJ 21 measures $m(\Xi_b(6227)^0) - m(\Xi_b^-) = 429.8^{+1.4}_{-1.5} \pm 0.3$ MeV. We have adjusted the measurement to our best value of $m(\Xi_b^-) = 5797.0 \pm 0.6$ MeV. Our first error is their experiment's error and our second error is the systematic error from using our best values.			
² Uses $\Xi_b^- \pi^+$ decays.			

 $\Xi_b(6227)^0$ WIDTH

VALUE (MeV)	DOCUMENT ID	TECN	COMMENT
18.6 ± 5.0 ± 1.4	¹ AAIJ	21	LHCb pp at 7, 8, 13 TeV
¹ Uses $\Xi_b^- \pi^+$ decays.			

 $\Xi_b(6227)^0$ DECAY MODES

Mode	Fraction (Γ_i/Γ)
$\Gamma_1 \Xi_b^- \pi^+ \times B(b \rightarrow \Xi_b(6227)^0)/B(b \rightarrow \Xi_b^-)$	$(4.5 \pm 0.9) \%$

 $\Xi_b(6227)^0$ BRANCHING RATIOS

$\Gamma(\Xi_b^- \pi^+ \times B(b \rightarrow \Xi_b(6227)^0)/B(b \rightarrow \Xi_b^-))/\Gamma_{\text{total}}$		Γ_1/Γ	
VALUE (%)	DOCUMENT ID	TECN	COMMENT
4.5 ± 0.8 ± 0.4	AAIJ	21	LHCb pp at 7, 8, 13 TeV

 $\Xi_b(6227)^0$ REFERENCES

AAIJ	21	PR D103 012004	R. Aaij <i>et al.</i>	(LHCb Collab.)
------	----	----------------	-----------------------	----------------

 $\Xi_b(6327)^0$ $J^P = ??$

Status: ***

 $\Xi_b(6327)^0$ MASS

VALUE (MeV)	DOCUMENT ID	TECN	COMMENT
6327.28 ± 0.23 ± 0.27	AAIJ	22i	LHCb pp at 13 TeV

 $\Xi_b(6327)^0$ WIDTH

VALUE (MeV)	CL%	DOCUMENT ID	TECN	COMMENT
<2.56	95	AAIJ	22i	LHCb pp at 13 TeV

 $\Xi_b(6327)^0$ DECAY MODES

Mode	Fraction (Γ_i/Γ)
$\Gamma_1 \Lambda_b^0 K^- \pi^+$	seen

 $\Xi_b(6327)^0$ BRANCHING RATIOS

$\Gamma(\Lambda_b^0 K^- \pi^+)/\Gamma_{\text{total}}$		Γ_1/Γ	
VALUE	DOCUMENT ID	TECN	COMMENT
seen	AAIJ	22i	LHCb pp at 13 TeV

 $\Xi_b(6327)^0$ REFERENCES

AAIJ	22i	PRL 128 162001	R. Aaij <i>et al.</i>	(LHCb Collab.)
------	-----	----------------	-----------------------	----------------

See key on page 1171

Baryon Particle Listings

$$\Xi_b(6333)^0, \Xi_{bc}^0, \Omega_b^-$$

$\Xi_b(6333)^0$				$J^P = ??$	Status: ***
$\Xi_b(6333)^0$ MASS					
VALUE (MeV)	DOCUMENT ID	TECN	COMMENT		
$6332.69^{+0.17}_{-0.18} \pm 0.22$	AAIJ	22i	LHCB	pp	at 13 TeV
$\Xi_b(6333)^0$ WIDTH					
VALUE (MeV)	CL%	DOCUMENT ID	TECN	COMMENT	
<1.92	95	AAIJ	22i	LHCB	pp at 13 TeV
$\Xi_b(6333)^0$ DECAY MODES					
Mode	Fraction (Γ_i/Γ)				
Γ_1	$\Lambda_b^0 K^- \pi^+$	seen			
$\Xi_b(6333)^0$ BRANCHING RATIOS					
$\Gamma(\Lambda_b^0 K^- \pi^+)/\Gamma_{\text{total}}$	DOCUMENT ID	TECN	COMMENT	Γ_1/Γ	
seen	AAIJ	22i	LHCB	pp	at 13 TeV
$\Xi_b(6333)^0$ REFERENCES					
AAIJ	22i	PRL 128 162001	R. Aaij <i>et al.</i>	(LHCb Collab.)	

Ξ_{bc}^0				$J^P = \frac{1}{2}^+$	
OMITTED FROM SUMMARY TABLE					
Ξ_{bc}^0 DECAY MODES					
Mode	Fraction (Γ_i/Γ)		Confidence level		
Γ_1	$D^0 p K^- \times B(b \rightarrow \Xi_{bc}^0)/B(b \rightarrow \Lambda_b)$	$<1.4 \times 10^{-5}$	95%		
Ξ_{bc}^0 BRANCHING RATIOS					
$\Gamma(D^0 p K^- \times B(b \rightarrow \Xi_{bc}^0)/B(b \rightarrow \Lambda_b))/\Gamma_{\text{total}}$	DOCUMENT ID	TECN	COMMENT	Γ_1/Γ	
$<1.4 \times 10^{-5}$	95	1,2 AAIJ	20AMLHCB	pp	at 13 TeV
<p>¹ AAIJ 20AM reports upper limits for $[\Gamma(\Xi_{bc}^0 \rightarrow D^0 p K^- \times B(b \rightarrow \Xi_{bc}^0)/B(b \rightarrow \Lambda_b))/\Gamma_{\text{total}}] / [B(\Lambda_b^0 \rightarrow p D^0 K^-)] < 3.0 \times 10^{-1} - 1.7 \times 10^{-2}$ for the considered Ξ_{bc}^0 mass and lifetime hypotheses ranging from 6.7 to 7.2 GeV and from 100 to 500 fs. We use the 3.0×10^{-1} limit for the quoted result.</p> <p>² AAIJ 20AM reports $[\Gamma(\Xi_{bc}^0 \rightarrow D^0 p K^- \times B(b \rightarrow \Xi_{bc}^0)/B(b \rightarrow \Lambda_b))/\Gamma_{\text{total}}] / [B(\Lambda_b^0 \rightarrow p D^0 K^-)] < 3.0 \times 10^{-1}$ which we multiply by our best value $B(\Lambda_b^0 \rightarrow p D^0 K^-) = 4.5 \times 10^{-9}$.</p>					
Ξ_{bc}^0 REFERENCES					
AAIJ	20AM	JHEP 2011 095	R. Aaij <i>et al.</i>	(LHCb Collab.)	

Ω_b^-				$J^P = 0(\frac{1}{2}^+)$	Status: ***
<p>In the quark model Ω_b^- is ssb ground state. None of its quantum numbers has been measured.</p>					
Ω_b^- MASS					
VALUE (MeV)	DOCUMENT ID	TECN	COMMENT		
6045.8 ± 0.8 OUR AVERAGE					
$6045.7 \pm 0.5 \pm 0.6$	¹ AAIJ	23BD	LHCB	pp	at 7, 8, 13 TeV
$6047.5 \pm 3.8 \pm 0.6$	² AALTONEN	14B	CDF	$p\bar{p}$	at 1.96 TeV
<p>• • • We do not use the following data for averages, fits, limits, etc. • • •</p>					
$6045.9 \pm 0.5 \pm 0.6$	³ AAIJ	23BD	LHCB	pp	at 7, 8, 13 TeV
$6044.30 \pm 1.20 \pm 1.12$	⁴ AAIJ	21AC	LHCB	Repl. by AAIJ 23BD	
$6045.1 \pm 3.2 \pm 0.8$	⁵ AAIJ	16O	LHCB	Repl. by AAIJ 23BD	
$6046.0 \pm 2.2 \pm 0.5$	⁶ AAIJ	13AV	LHCB	Repl. by AAIJ 23BD	
$6054.4 \pm 6.8 \pm 0.9$	⁷ AALTONEN	09AP	CDF	Repl. by AALTONEN 14B	
$6165 \pm 10 \pm 13$	⁸ ABZOV	08AL	D0	$p\bar{p}$	at 1.96 TeV
<p>¹ Combines measurement using $\Omega_b^- \rightarrow J/\psi \Omega^-$ decays with results from AAIJ 16O and AAIJ 21AC taking into account correlations amongst systematic uncertainties. Uses Ξ_b^- mass $5797.33 \pm 0.24 \pm 0.29$ MeV from AAIJ 21.</p>					

² Uses $\Omega_b^- \rightarrow J/\psi \Omega^-$ and $\Omega_c^0 \pi^-$ decays, with the first evidence for $\Omega_b^- \rightarrow \Omega_c^0 \pi^-$ at 3.3 σ significance.					
³ Uses $\Omega_b^- \rightarrow J/\psi \Omega^-$ decays.					
⁴ Uses $\Omega_b^- \rightarrow \Xi_c^+ K^- \pi^-$ and $\Xi_c^+ \rightarrow p K^- \pi^+$ decays. Reports the value of $6044.3 \pm 1.2 \pm 1.1^{+0.19}_{-0.22}$ MeV where the last uncertainty is due to the mass of Ξ_c^+ . We have combined the two systematic uncertainties in quadrature.					
⁵ Reconstructed in $\Omega_b^- \rightarrow \Omega_c^0 \pi^-$, $\Omega_c^0 \rightarrow p K^- K^- \pi^+$ decays. Reference Ξ_b^- mass 5797.72 ± 0.6 MeV from AAIJ 14B.					
⁶ Measured in $\Omega_b^- \rightarrow J/\psi \Omega^-$ with 19 \pm 5 events.					
⁷ Observed in $\Omega_b^- \rightarrow J/\psi \Omega^-$ decays with 16^{+4}_{-4} candidates, a significance of 5.5 sigma from a combined mass-lifetime fit.					
⁸ Observed in $\Omega_b^- \rightarrow J/\psi \Omega^-$ decays with $17.8 \pm 4.9 \pm 0.8$ candidates, a significance of 5.4 sigma.					
$m_{\Omega_b^-} - m_{\Lambda_b^0}$					
VALUE (MeV)	DOCUMENT ID	TECN	COMMENT		
$426.4 \pm 2.2 \pm 0.4$	AAIJ	13AV	LHCB	pp	at 7 TeV
$m_{\Omega_b^-} - m_{\Xi_b^-}$					
VALUE (MeV)	DOCUMENT ID	TECN	COMMENT		
$248.50 \pm 0.51 \pm 0.37$	¹ AAIJ	23BD	LHCB	pp	at 7, 8, 13 TeV
<p>• • • We do not use the following data for averages, fits, limits, etc. • • •</p>					
$248.54 \pm 0.51 \pm 0.38$	² AAIJ	23BD	LHCB	pp	at 7, 8, 13 TeV
$247.3 \pm 3.2 \pm 0.5$	³ AAIJ	16O	LHCB	Repl. by AAIJ 23BD	
<p>¹ Uses $\Omega_b^- \rightarrow J/\psi \Omega^-$ decays combined with the result from AAIJ 16O obtained using $\Omega_b^- \rightarrow \Omega_c^0 \pi^-$, $\Omega_c^0 \rightarrow p K^- K^- \pi^+$ and $\Xi_b^- \rightarrow \Xi_c^0 \pi^-$, $\Xi_c^0 \rightarrow p K^- K^- \pi^+$ decays taking into account correlation of systematic uncertainties.</p> <p>² Uses $\Omega_b^- \rightarrow J/\psi \Omega^-$ decays.</p> <p>³ Uses $\Omega_b^- \rightarrow \Omega_c^0 \pi^-$, $\Omega_c^0 \rightarrow p K^- K^- \pi^+$ and $\Xi_b^- \rightarrow \Xi_c^0 \pi^-$, $\Xi_c^0 \rightarrow p K^- K^- \pi^+$ decays.</p>					

Ω_b^- MEAN LIFE					
VALUE (10^{-12} s)	DOCUMENT ID	TECN	COMMENT		
$1.64^{+0.18}_{-0.17}$ OUR EVALUATION	(Produced by HFLAV)				
$1.65^{+0.18}_{-0.16}$ OUR AVERAGE					
$1.78 \pm 0.26 \pm 0.05 \pm 0.06$	¹ AAIJ	16O	LHCB	pp	at 7, 8 TeV
$1.54^{+0.26}_{-0.21} \pm 0.05$	² AAIJ	14T	LHCB	pp	at 7, 8 TeV
$1.66^{+0.53}_{-0.40} \pm 0.02$	² AALTONEN	14B	CDF	$p\bar{p}$	at 1.96 TeV
<p>• • • We do not use the following data for averages, fits, limits, etc. • • •</p>					
$1.13^{+0.53}_{-0.40} \pm 0.02$	³ AALTONEN	09AP	CDF	Repl. by AALTONEN 14B	
<p>¹ Measured in $\Omega_b^- \rightarrow \Omega_c^0 \pi^-$, $\Omega_c^0 \rightarrow p K^- K^- \pi^+$ decays relative to $\Xi_b^- \rightarrow \Xi_c^0 \pi^-$, $\Xi_c^0 \rightarrow p K^- K^- \pi^+$ decays with reference Ξ_b^- mean life 1.599 ± 0.06 ps from AAIJ 14B.</p> <p>² Measured in $\Omega_b^- \rightarrow J/\psi \Omega^-$ decays.</p> <p>³ Observed in $\Omega_b^- \rightarrow J/\psi \Omega^-$ decays with 16^{+6}_{-4} candidates, a significance of 5.5 sigma from a combined mass-lifetime fit.</p>					
$\tau(\Omega_b^-)/\tau(\Xi_b^-)$ mean life ratio					
VALUE	DOCUMENT ID	TECN	COMMENT		
$1.11 \pm 0.16 \pm 0.03$	¹ AAIJ	16O	LHCB	pp	at 7, 8 TeV
<p>¹ Uses $\Omega_b^- \rightarrow \Omega_c^0 \pi^-$, $\Omega_c^0 \rightarrow p K^- K^- \pi^+$ and $\Xi_b^- \rightarrow \Xi_c^0 \pi^-$, $\Xi_c^0 \rightarrow p K^- K^- \pi^+$ decays.</p>					

Ω_b^- DECAY MODES			
Mode	Fraction (Γ_i/Γ)	Scale factor/ Confidence level	
Γ_1	$J/\psi \Omega^- \times B(b \rightarrow \Omega_b)$	$(1.4^{+0.5}_{-0.4}) \times 10^{-6}$	S=1.6
Γ_2	$p K^- K^- \times B(\bar{b} \rightarrow \Omega_b)$	$< 2.3 \times 10^{-9}$	CL=90%
Γ_3	$p \pi^- \pi^- \times B(\bar{b} \rightarrow \Omega_b)$	$< 1.5 \times 10^{-8}$	CL=90%
Γ_4	$p K^- \pi^- \times B(\bar{b} \rightarrow \Omega_b)$	$< 7 \times 10^{-9}$	CL=90%
Γ_5	$\Omega_c^0 \pi^-$	seen	
Γ_6	$\Omega_c^0 \pi^-$, $\Omega_c^0 \rightarrow p K^- K^- \pi^+$	seen	
Γ_7	$\Xi_c^+ K^- \pi^-$	seen	

Ω_b^- BRANCHING RATIOS					
$\Gamma(J/\psi \Omega^- \times B(b \rightarrow \Omega_b))/\Gamma_{\text{total}}$	DOCUMENT ID	TECN	COMMENT		
$1.4^{+0.5}_{-0.4}$ OUR AVERAGE	Error includes scale factor of 1.6.				
$1.22 \pm 0.12 \pm 0.31 \pm 0.26$	^{1,2} AAIJ	23BD	LHCB	pp	at 13 TeV

Baryon Particle Listings

$\Omega_b^-, \Omega_b(6316)^-, \Omega_b(6330)^-, \Omega_b(6340)^-$

2.6 $^{+1.0}_{-0.7} \pm 0.4$ ³ AALTONEN 09AP CDF $p\bar{p}$ at 1.96 TeV
 8 $\pm 4 \pm 2$ ⁴ ABAZOV 08AL D0 $p\bar{p}$ at 1.96 TeV
¹ AAIJ 23BD reports $[\Gamma(\Omega_b^- \rightarrow J/\psi \Omega^- \times B(b \rightarrow \Omega_b))/\Gamma_{\text{total}}] / [B(\Xi_b^- \rightarrow J/\psi \Xi^- \times B(b \rightarrow \Xi_b^-))] = 0.120 \pm 0.008 \pm 0.008$ which we multiply by our best value $B(\Xi_b^- \rightarrow J/\psi \Xi^- \times B(b \rightarrow \Xi_b^-)) = (1.02^{+0.26}_{-0.21}) \times 10^{-5}$. Our first error is their experiment's error and our second error is the systematic error from using our best value.
² Reconstructing beauty baryons in the kinematic region $2 < \eta < 6$ and $p_T < 20$ GeV/c with their decays to a J/ψ meson and a hyperon.
³ AALTONEN 09AP reports $[\Gamma(\Omega_b^- \rightarrow J/\psi \Omega^- \times B(b \rightarrow \Omega_b))/\Gamma_{\text{total}}] / [B(\Lambda_b^0 \rightarrow J/\psi(1S) \Lambda \times B(b \rightarrow \Lambda_b^0))] = 0.045^{+0.017}_{-0.012} \pm 0.004$ which we multiply by our best value $B(\Lambda_b^0 \rightarrow J/\psi(1S) \Lambda \times B(b \rightarrow \Lambda_b^0)) = (5.8 \pm 0.8) \times 10^{-5}$. Our first error is their experiment's error and our second error is the systematic error from using our best value.
⁴ ABAZOV 08AL reports $[\Gamma(\Omega_b^- \rightarrow J/\psi \Omega^- \times B(b \rightarrow \Omega_b))/\Gamma_{\text{total}}] / [B(\Xi_b^- \rightarrow J/\psi \Xi^- \times B(b \rightarrow \Xi_b^-))] = 0.80 \pm 0.32^{+0.14}_{-0.22}$ which we multiply by our best value $B(\Xi_b^- \rightarrow J/\psi \Xi^- \times B(b \rightarrow \Xi_b^-)) = (1.02^{+0.26}_{-0.21}) \times 10^{-5}$. Our first error is their experiment's error and our second error is the systematic error from using our best value.

$\Gamma(pK^- K^- \times B(\bar{b} \rightarrow \Omega_b))/\Gamma_{\text{total}}$ Γ_2/Γ

VALUE (units 10^{-5})	CL%	DOCUMENT ID	TECN	COMMENT
$<2.3 \times 10^{-4}$	90	¹ AAIJ	21AH LHCb	pp at 7, 8, 13 TeV
• • • We do not use the following data for averages, fits, limits, etc. • • •				
$<2.5 \times 10^{-4}$	90	² AAIJ	17F LHCb	pp at 7, 8 TeV
¹ AAIJ 21AH reports $[\Gamma(\Omega_b^- \rightarrow pK^- K^- \times B(\bar{b} \rightarrow \Omega_b))/\Gamma_{\text{total}}] / [B(\Xi_b^- \rightarrow pK^- K^- \times B(b \rightarrow \Xi_b^-))] < 62 \times 10^{-3}$ which we multiply by our best value $B(\Xi_b^- \rightarrow pK^- K^- \times B(b \rightarrow \Xi_b^-)) = 3.7 \times 10^{-8}$.				
² AAIJ 17F reports $[\Gamma(\Omega_b^- \rightarrow pK^- K^- \times B(\bar{b} \rightarrow \Omega_b))/\Gamma_{\text{total}}] / [B(B^+ \rightarrow K^+ K^- K^+)] / [B(\bar{b} \rightarrow B^+)] < 18 \times 10^{-5}$ which we multiply by our best values $B(B^+ \rightarrow K^+ K^- K^+) = 3.40 \times 10^{-5}$, $B(\bar{b} \rightarrow B^+) = 40.8 \times 10^{-2}$.				

$\Gamma(p\pi^- \pi^- \times B(\bar{b} \rightarrow \Omega_b))/\Gamma_{\text{total}}$ Γ_3/Γ

VALUE (units 10^{-5})	CL%	DOCUMENT ID	TECN	COMMENT
$<1.5 \times 10^{-3}$	90	¹ AAIJ	17F LHCb	pp at 7, 8 TeV
¹ AAIJ 17F reports $[\Gamma(\Omega_b^- \rightarrow p\pi^- \pi^- \times B(\bar{b} \rightarrow \Omega_b))/\Gamma_{\text{total}}] / [B(B^+ \rightarrow K^+ K^- K^+)] / [B(\bar{b} \rightarrow B^+)] < 109 \times 10^{-5}$ which we multiply by our best values $B(B^+ \rightarrow K^+ K^- K^+) = 3.40 \times 10^{-5}$, $B(\bar{b} \rightarrow B^+) = 40.8 \times 10^{-2}$.				

$\Gamma(pK^- \pi^- \times B(\bar{b} \rightarrow \Omega_b))/\Gamma_{\text{total}}$ Γ_4/Γ

VALUE (units 10^{-5})	CL%	DOCUMENT ID	TECN	COMMENT
$<7 \times 10^{-4}$	90	¹ AAIJ	17F LHCb	pp at 7, 8 TeV
¹ AAIJ 17F reports $[\Gamma(\Omega_b^- \rightarrow pK^- \pi^- \times B(\bar{b} \rightarrow \Omega_b))/\Gamma_{\text{total}}] / [B(B^+ \rightarrow K^+ K^- K^+)] / [B(\bar{b} \rightarrow B^+)] < 51 \times 10^{-5}$ which we multiply by our best values $B(B^+ \rightarrow K^+ K^- K^+) = 3.40 \times 10^{-5}$, $B(\bar{b} \rightarrow B^+) = 40.8 \times 10^{-2}$.				

$\Gamma(\Omega_c^0 \pi^-)/\Gamma_{\text{total}}$ Γ_5/Γ

VALUE	DOCUMENT ID	TECN	COMMENT
seen	AAIJ	16o LHCb	pp at 7, 8 TeV

$\Gamma(\Xi_c^+ K^- \pi^-)/\Gamma(\Omega_c^0 \pi^-), \Omega_c^0 \rightarrow pK^- K^- \pi^+$ Γ_7/Γ_6

VALUE (units 10^2)	DOCUMENT ID	TECN	COMMENT
$2.2 \pm 0.2 \pm 1.0$	¹ AAIJ	21AC LHCb	pp at 7, 8, 13 TeV
¹ AAIJ 21AC reports $[\Gamma(\Omega_b^- \rightarrow \Xi_c^+ K^- \pi^-)/\Gamma(\Omega_b^- \rightarrow \Omega_c^0 \pi^-), \Omega_c^0 \rightarrow pK^- K^- \pi^+] \times [B(\Xi_c^+ \rightarrow pK^- \pi^+)] = 1.35 \pm 0.11 \pm 0.05$ which we divide by our best value $B(\Xi_c^+ \rightarrow pK^- \pi^+) = (6.2 \pm 3.0) \times 10^{-3}$. Our first error is their experiment's error and our second error is the systematic error from using our best value.			

Ω_b^- REFERENCES

AAIJ	23BD PR D108 052008	R. Aaij et al.	(LHCb Collab.)
AAIJ	21 PR D103 012004	R. Aaij et al.	(LHCb Collab.)
AAIJ	21AC PR D104 L0911102	R. Aaij et al.	(LHCb Collab.)
AAIJ	21AH PR D104 052010	R. Aaij et al.	(LHCb Collab.)
AAIJ	17F PRL 118 071801	R. Aaij et al.	(LHCb Collab.)
AAIJ	16O PR D93 092007	R. Aaij et al.	(LHCb Collab.)
AAIJ	14B PL B728 234	R. Aaij et al.	(LHCb Collab.)
AAIJ	14T PL B736 154	R. Aaij et al.	(LHCb Collab.)
AALTONEN	14B PR D89 072014	T. Aaltonen et al.	(CDF Collab.)
AAIJ	13AV PRL 110 182001	R. Aaij et al.	(LHCb Collab.)
AALTONEN	09AP PR D80 072003	T. Aaltonen et al.	(CDF Collab.)
ABAZOV	08AL PRL 101 232002	V.M. Abazov et al.	(D0 Collab.)

$\Omega_b(6316)^-$

$I(J^P) = ?(??)$ Status: ***
l, J, P need confirmation.

$\Omega_b(6316)^-$ MASS

VALUE (MeV)	DOCUMENT ID	TECN	COMMENT
$6315.6 \pm 0.3 \pm 0.5$	¹ AAIJ	20T LHCb	pp at 7, 8, 13 TeV
¹ AAIJ 20T measures $m(\Omega_b(6316)^-) - m(\Xi_b^0) = 523.74 \pm 0.31 \pm 0.07$ MeV. We have adjusted the measurement to our best values of $m(\Xi_b^0) = 5791.9 \pm 0.5$ MeV. Our first error is their experiment's error and our second error is the systematic error from using our best values.			

$\Omega_b(6316)^-$ WIDTH

VALUE (MeV)	CL%	DOCUMENT ID	TECN	COMMENT
<4.2	95	AAIJ	20T LHCb	pp at 7, 8, 13 TeV

$\Omega_b(6316)^-$ DECAY MODES

Mode	Fraction (Γ_i/Γ)
$\Gamma_1 \Xi_b^0 K^-$	seen

$\Omega_b(6316)^-$ BRANCHING RATIOS

$\Gamma(\Xi_b^0 K^-)/\Gamma_{\text{total}}$	Γ_1/Γ
seen	seen
¹ AAIJ 20T establishes the decay at 2.1 σ significance level.	

$\Omega_b(6316)^-$ REFERENCES

AAIJ	20T PRL 124 082002	R. Aaij et al.	(LHCb Collab.)
------	--------------------	----------------	----------------

$\Omega_b(6330)^-$

$I(J^P) = ?(??)$ Status: ***
l, J, P need confirmation.

$\Omega_b(6330)^-$ MASS

VALUE (MeV)	DOCUMENT ID	TECN	COMMENT
$6330.3 \pm 0.3 \pm 0.5$	¹ AAIJ	20T LHCb	pp at 7, 8, 13 TeV
¹ AAIJ 20T measures $m(\Omega_b(6330)^-) - m(\Xi_b^0) = 538.40 \pm 0.28 \pm 0.07$ MeV. We have adjusted the measurement to our best values of $m(\Xi_b^0) = 5791.9 \pm 0.5$ MeV. Our first error is their experiment's error and our second error is the systematic error from using our best values.			

$\Omega_b(6330)^-$ WIDTH

VALUE (MeV)	CL%	DOCUMENT ID	TECN	COMMENT
<4.7	95	AAIJ	20T LHCb	pp at 7, 8, 13 TeV

$\Omega_b(6330)^-$ DECAY MODES

Mode	Fraction (Γ_i/Γ)
$\Gamma_1 \Xi_b^0 K^-$	seen

$\Omega_b(6330)^-$ BRANCHING RATIOS

$\Gamma(\Xi_b^0 K^-)/\Gamma_{\text{total}}$	Γ_1/Γ
seen	seen
¹ AAIJ 20T establishes the decay at 2.6 σ significance level.	

$\Omega_b(6330)^-$ REFERENCES

AAIJ	20T PRL 124 082002	R. Aaij et al.	(LHCb Collab.)
------	--------------------	----------------	----------------

$\Omega_b(6340)^-$

$I(J^P) = ?(??)$ Status: ***
l, J, P need confirmation.

$\Omega_b(6340)^-$ MASS

VALUE (MeV)	DOCUMENT ID	TECN	COMMENT
$6339.7 \pm 0.3 \pm 0.5$	¹ AAIJ	20T LHCb	pp at 7, 8, 13 TeV
¹ AAIJ 20T measures $m(\Omega_b(6340)^-) - m(\Xi_b^0) = 547.81 \pm 0.26 \pm 0.05$ MeV. We have adjusted the measurement to our best values of $m(\Xi_b^0) = 5791.9 \pm 0.5$ MeV. Our first error is their experiment's error and our second error is the systematic error from using our best values.			

$\Omega_b(6340)^-$ WIDTH

VALUE (MeV)	CL%	DOCUMENT ID	TECN	COMMENT
<1.8	95	AAIJ	20T LHCb	pp at 7, 8, 13 TeV

$\Omega_b(6340)^-$ DECAY MODES

Mode	Fraction (Γ_i/Γ)
$\Gamma_1 \Xi_b^0 K^-$	seen

See key on page 1171

Baryon Particle Listings

 $\Omega_b(6340)^-$, $\Omega_b(6350)^-$, b -baryon ADMIXTURE (Λ_b , Ξ_b , Ω_b) $\Omega_b(6340)^-$ BRANCHING RATIOS

$\Gamma(\Xi_b^0 K^-)/\Gamma_{\text{total}}$	DOCUMENT ID	TECN	COMMENT	Γ_1/Γ
seen	AAIJ	20T	LHCB	$p\bar{p}$ at 7, 8, 13 TeV

 $\Omega_b(6340)^-$ REFERENCES

AAIJ 20T PRL 124 082002 R. Aaij et al. (LHCb Collab.)

 $\Omega_b(6350)^-$ $I(J^P) = ?(??)$ Status: ***
 I, J, P need confirmation. $\Omega_b(6350)^-$ MASS

VALUE (MeV)	DOCUMENT ID	TECN	COMMENT
$6349.8 \pm 0.4 \pm 0.5$	¹ AAIJ	20T	LHCB $p\bar{p}$ at 7, 8, 13 TeV

¹AAIJ 20T measures $m(\Omega_b(6350)^-) - m(\Xi_b^0) = 557.98 \pm 0.35 \pm 0.05$ MeV. We have adjusted the measurement to our best values of $m(\Xi_b^0) = 5791.9 \pm 0.5$ MeV. Our first error is their experiment's error and our second error is the systematic error from using our best values.

 $\Omega_b(6350)^-$ WIDTH

VALUE (MeV)	CL%	DOCUMENT ID	TECN	COMMENT
<3.2	95	AAIJ	20T	LHCB $p\bar{p}$ at 7, 8, 13 TeV

 $\Omega_b(6350)^-$ DECAY MODES

Mode	Fraction (Γ_i/Γ)
$\Gamma_1 \Xi_b^0 K^-$	seen

 $\Omega_b(6350)^-$ BRANCHING RATIOS

$\Gamma(\Xi_b^0 K^-)/\Gamma_{\text{total}}$	DOCUMENT ID	TECN	COMMENT	Γ_1/Γ
seen	AAIJ	20T	LHCB	$p\bar{p}$ at 7, 8, 13 TeV

 $\Omega_b(6350)^-$ REFERENCES

AAIJ 20T PRL 124 082002 R. Aaij et al. (LHCb Collab.)

 b -baryon ADMIXTURE (Λ_b , Ξ_b , Ω_b) b -baryon ADMIXTURE MEAN LIFE

Each measurement of the b -baryon mean life is an average over an admixture of various b -baryons which decay weakly. Different techniques emphasize different admixtures of produced particles, which could result in a different b -baryon mean life. More b -baryon flavor specific channels are not included in the measurement.

VALUE (10^{-12} s)	EVTS	DOCUMENT ID	TECN	COMMENT
$1.218^{+0.130}_{-0.115} \pm 0.042$		¹ ABAZOV	07s	D0 Repl. by ABAZOV 12u
$1.22^{+0.22}_{-0.18} \pm 0.04$		¹ ABAZOV	05c	D0 Repl. by ABAZOV 07s
$1.16 \pm 0.20 \pm 0.08$		² ABREU	99w	DLPH $e^+e^- \rightarrow Z$
$1.19 \pm 0.14 \pm 0.07$		³ ABREU	99w	DLPH $e^+e^- \rightarrow Z$
$1.14 \pm 0.08 \pm 0.04$		⁴ ABREU	99w	DLPH $e^+e^- \rightarrow Z$
$1.11^{+0.19}_{-0.18} \pm 0.05$		⁵ ABREU	99w	DLPH $e^+e^- \rightarrow Z$
$1.29^{+0.24}_{-0.22} \pm 0.06$		⁵ ACKERSTAFF	98G	OPAL $e^+e^- \rightarrow Z$
$1.20 \pm 0.08 \pm 0.06$		⁶ BARATE	98D	ALEP $e^+e^- \rightarrow Z$
1.21 ± 0.11		⁵ BARATE	98D	ALEP $e^+e^- \rightarrow Z$
$1.32 \pm 0.15 \pm 0.07$		⁷ ABE	96M	CDF $p\bar{p}$ at 1.8 TeV
$1.46^{+0.22}_{-0.21} \pm 0.07$		ABREU	96D	DLPH Repl. by ABREU 99w
$1.10^{+0.19}_{-0.17} \pm 0.09$		⁵ ABREU	96D	DLPH $e^+e^- \rightarrow Z$
$1.16 \pm 0.11 \pm 0.06$		⁵ AKERS	96	OPAL $e^+e^- \rightarrow Z$
$1.27^{+0.35}_{-0.29} \pm 0.09$		ABREU	95s	DLPH Repl. by ABREU 99w
$1.05^{+0.12}_{-0.11} \pm 0.09$	290	BUSKULIC	95L	ALEP Repl. by BARATE 98D
$1.04^{+0.48}_{-0.38} \pm 0.10$	11	⁸ ABREU	93F	DLPH Excess $\Lambda\mu^-$, decay lengths
$1.05^{+0.23}_{-0.20} \pm 0.08$	157	⁹ AKERS	93	OPAL Excess $\Lambda\ell^-$, decay lengths
$1.12^{+0.32}_{-0.29} \pm 0.16$	101	¹⁰ BUSKULIC	92I	ALEP Excess $\Lambda\ell^-$, impact parameters

¹ Measured mean life using fully reconstructed $\Lambda_b^0 \rightarrow J/\psi\Lambda$ decays.

² Measured using $\Lambda\ell^-$ decay length.

³ Measured using $p\ell^-$ decay length.

⁴ This ABREU 99w result is the combined result of the $\Lambda\ell^-$, $p\ell^-$, and excess $\Lambda\mu^-$ impact parameter measurements.

⁵ Measured using $\Lambda_c\ell^-$ and $\Lambda\ell^+\ell^-$.

⁶ Measured using the excess of $\Lambda\ell^-$, lepton impact parameter.

⁷ Measured using $\Lambda_c\ell^-$.

⁸ ABREU 93F superseded by ABREU 96D.

⁹ AKERS 93 superseded by AKERS 96.

¹⁰ BUSKULIC 92I superseded by BUSKULIC 95L.

 b -baryon ADMIXTURE DECAY MODES (Λ_b , Ξ_b , Ω_b)

These branching fractions are actually an average over weakly decaying b -baryons weighted by their production rates at the LHC, LEP, and Tevatron, branching ratios, and detection efficiencies. They scale with the b -baryon production fraction $B(b \rightarrow b\text{-baryon})$.

The branching fractions $B(b\text{-baryon} \rightarrow \Lambda\ell^-\bar{\nu}_\ell\text{anything})$ and $B(\Lambda_b^0 \rightarrow \Lambda^+\ell^-\bar{\nu}_\ell\text{anything})$ are not pure measurements because the underlying measured products of these with $B(b \rightarrow b\text{-baryon})$ were used to determine $B(b \rightarrow b\text{-baryon})$, as described in the note "Production and Decay of b -Flavored Hadrons."

For inclusive branching fractions, e.g., $B \rightarrow D^\pm\text{anything}$, the values usually are multiplicities, not branching fractions. They can be greater than one.

Mode	Fraction (Γ_i/Γ)	Scale factor
$\Gamma_1 p\mu^-\bar{\nu}$ anything	$(5.8^{+2.3}_{-2.0})\%$	
$\Gamma_2 p\ell\bar{\nu}_\ell$ anything	$(5.6 \pm 1.2)\%$	
$\Gamma_3 p$ anything	$(70 \pm 22)\%$	
$\Gamma_4 \Lambda\ell^-\bar{\nu}_\ell$ anything	$(3.8 \pm 0.6)\%$	
$\Gamma_5 \Lambda\ell^+\nu_\ell$ anything	$(3.2 \pm 0.8)\%$	
$\Gamma_6 \Lambda$ anything	$(39 \pm 7)\%$	
$\Gamma_7 \Xi^-\ell^-\bar{\nu}_\ell$ anything	$(4.6 \pm 1.4) \times 10^{-3}$	1.2

 b -baryon ADMIXTURE (Λ_b , Ξ_b , Ω_b) BRANCHING RATIOS

$\Gamma(p\mu^-\bar{\nu}\text{anything})/\Gamma_{\text{total}}$	EVTS	DOCUMENT ID	TECN	COMMENT	Γ_1/Γ
$5.8^{+2.3}_{-1.9} \pm 0.8$	125	¹ ABREU	95s	DLPH $e^+e^- \rightarrow Z$	

¹ABREU 95s reports $[\Gamma(b\text{-baryon} \rightarrow p\mu^-\bar{\nu}\text{anything})/\Gamma_{\text{total}}] \times [B(\bar{b} \rightarrow b\text{-baryon})] = 0.0049 \pm 0.0011^{+0.0015}_{-0.0011}$ which we divide by our best value $B(\bar{b} \rightarrow b\text{-baryon}) = (8.4 \pm 1.1) \times 10^{-2}$. Our first error is their experiment's error and our second error is the systematic error from using our best value.

$\Gamma(p\ell\bar{\nu}_\ell\text{anything})/\Gamma_{\text{total}}$	DOCUMENT ID	TECN	COMMENT	Γ_2/Γ
$5.6 \pm 0.9 \pm 0.7$	¹ BARATE	98v	ALEP $e^+e^- \rightarrow Z$	

¹BARATE 98v reports $[\Gamma(b\text{-baryon} \rightarrow p\ell\bar{\nu}_\ell\text{anything})/\Gamma_{\text{total}}] \times [B(\bar{b} \rightarrow b\text{-baryon})] = (4.72 \pm 0.66 \pm 0.44) \times 10^{-3}$ which we divide by our best value $B(\bar{b} \rightarrow b\text{-baryon}) = (8.4 \pm 1.1) \times 10^{-2}$. Our first error is their experiment's error and our second error is the systematic error from using our best value.

$\Gamma(p\ell\bar{\nu}_\ell\text{anything})/\Gamma(p\text{anything})$	DOCUMENT ID	TECN	COMMENT	Γ_2/Γ_3
$8.0 \pm 1.2 \pm 1.4$	BARATE	98v	ALEP $e^+e^- \rightarrow Z$	

$\Gamma(\Lambda\ell^-\bar{\nu}_\ell\text{anything})/\Gamma_{\text{total}}$	DOCUMENT ID	TECN	COMMENT	Γ_4/Γ
--	-------------	------	---------	-------------------

The values and averages in this section serve only to show what values result if one assumes our $B(b \rightarrow b\text{-baryon})$. They cannot be thought of as measurements since the underlying product branching fractions were also used to determine $B(b \rightarrow b\text{-baryon})$ as described in the note on "Production and Decay of b -Flavored Hadrons."

VALUE (%)	EVTS	DOCUMENT ID	TECN	COMMENT
3.8 ± 0.6 OUR AVERAGE				
$3.9 \pm 0.5 \pm 0.5$		¹ BARATE	98D	ALEP $e^+e^- \rightarrow Z$
$3.5 \pm 0.4 \pm 0.5$		² AKERS	96	OPAL Excess of $\Lambda\ell^-$ over $\Lambda\ell^+$
$3.6 \pm 0.9 \pm 0.5$	262	³ ABREU	95s	DLPH Excess of $\Lambda\ell^-$ over $\Lambda\ell^+$
$7.3 \pm 1.4 \pm 1.0$	290	⁴ BUSKULIC	95L	ALEP Excess of $\Lambda\ell^-$ over $\Lambda\ell^+$
$\bullet \bullet \bullet$ We do not use the following data for averages, fits, limits, etc. $\bullet \bullet \bullet$				
seen	157	⁵ AKERS	93	OPAL Excess of $\Lambda\ell^-$ over $\Lambda\ell^+$
$8.3 \pm 2.5 \pm 1.1$	101	⁶ BUSKULIC	92I	ALEP Excess of $\Lambda\ell^-$ over $\Lambda\ell^+$

¹BARATE 98D reports $[\Gamma(b\text{-baryon} \rightarrow \Lambda\ell^-\bar{\nu}_\ell\text{anything})/\Gamma_{\text{total}}] \times [B(\bar{b} \rightarrow b\text{-baryon})] = 0.00326 \pm 0.00016 \pm 0.00039$ which we divide by our best value $B(\bar{b} \rightarrow b\text{-baryon}) = (8.4 \pm 1.1) \times 10^{-2}$. Our first error is their experiment's error and our second error is the systematic error from using our best value. Measured using the excess of $\Lambda\ell^-$, lepton impact parameter.

²AKERS 96 reports $[\Gamma(b\text{-baryon} \rightarrow \Lambda\ell^-\bar{\nu}_\ell\text{anything})/\Gamma_{\text{total}}] \times [B(\bar{b} \rightarrow b\text{-baryon})] = 0.00291 \pm 0.00023 \pm 0.00025$ which we divide by our best value $B(\bar{b} \rightarrow b\text{-baryon}) =$

Baryon Particle Listings

 b -baryon ADMIXTURE ($\Lambda_b, \Xi_b, \Omega_b$)

$(8.4 \pm 1.1) \times 10^{-2}$. Our first error is their experiment's error and our second error is the systematic error from using our best value.

³ ABREU 95s reports $[\Gamma(b\text{-baryon} \rightarrow \Lambda \ell^- \bar{\nu}_\ell \text{ anything})/\Gamma_{\text{total}}] \times [B(\bar{b} \rightarrow b\text{-baryon})] = 0.0030 \pm 0.0006 \pm 0.0004$ which we divide by our best value $B(\bar{b} \rightarrow b\text{-baryon}) = (8.4 \pm 1.1) \times 10^{-2}$. Our first error is their experiment's error and our second error is the systematic error from using our best value.

⁴ BUSKULIC 95L reports $[\Gamma(b\text{-baryon} \rightarrow \Lambda \ell^- \bar{\nu}_\ell \text{ anything})/\Gamma_{\text{total}}] \times [B(\bar{b} \rightarrow b\text{-baryon})] = 0.0061 \pm 0.0006 \pm 0.0010$ which we divide by our best value $B(\bar{b} \rightarrow b\text{-baryon}) = (8.4 \pm 1.1) \times 10^{-2}$. Our first error is their experiment's error and our second error is the systematic error from using our best value.

⁵ AKERS 93 superseded by AKERS 96.

⁶ BUSKULIC 92i reports $[\Gamma(b\text{-baryon} \rightarrow \Lambda \ell^- \bar{\nu}_\ell \text{ anything})/\Gamma_{\text{total}}] \times [B(\bar{b} \rightarrow b\text{-baryon})] = 0.0070 \pm 0.0010 \pm 0.0018$ which we divide by our best value $B(\bar{b} \rightarrow b\text{-baryon}) = (8.4 \pm 1.1) \times 10^{-2}$. Our first error is their experiment's error and our second error is the systematic error from using our best value. Superseded by BUSKULIC 95L.

 $\Gamma(\Lambda \ell^+ \nu_\ell \text{ anything})/\Gamma(\Lambda \text{ anything})$ Γ_5/Γ_6

VALUE (units 10^{-2})	DOCUMENT ID	TECN	COMMENT
$8.0 \pm 1.2 \pm 0.8$	ABBIENDI	99L	OPAL $e^+ e^- \rightarrow Z$
$7.0 \pm 1.2 \pm 0.7$	ACKERSTAFF	97N	OPAL Repl. by ABBIENDI 99L

 $\Gamma(\Lambda \text{ anything})/\Gamma_{\text{total}}$ Γ_6/Γ

VALUE (%)	DOCUMENT ID	TECN	COMMENT
39 ± 7 OUR AVERAGE			
$42 \pm 6 \pm 5$	¹ ABBIENDI	99L	OPAL $e^+ e^- \rightarrow Z$
$27 \pm 15 \pm 3$	² ABREU	95c	DLPH $e^+ e^- \rightarrow Z$

• • • We do not use the following data for averages, fits, limits, etc. • • •

$47 \pm 7 \pm 6$ ³ ACKERSTAFF 97N OPAL Repl. by ABBIENDI 99L

¹ ABBIENDI 99L reports $[\Gamma(b\text{-baryon} \rightarrow \Lambda \text{ anything})/\Gamma_{\text{total}}] \times [B(\bar{b} \rightarrow b\text{-baryon})] = 0.035 \pm 0.0032 \pm 0.0035$ which we divide by our best value $B(\bar{b} \rightarrow b\text{-baryon}) = (8.4 \pm 1.1) \times 10^{-2}$. Our first error is their experiment's error and our second error is the systematic error from using our best value.

² ABREU 95c reports 0.28 ± 0.17 from a measurement of $[\Gamma(b\text{-baryon} \rightarrow \Lambda \text{ anything})/\Gamma_{\text{total}}] \times [B(\bar{b} \rightarrow b\text{-baryon})]$ assuming $B(\bar{b} \rightarrow b\text{-baryon}) = 0.08 \pm 0.02$, which we rescale to our best value $B(\bar{b} \rightarrow b\text{-baryon}) = (8.4 \pm 1.1) \times 10^{-2}$. Our first error is their experiment's error and our second error is the systematic error from using our best value.

³ ACKERSTAFF 97N reports $[\Gamma(b\text{-baryon} \rightarrow \Lambda \text{ anything})/\Gamma_{\text{total}}] \times [B(\bar{b} \rightarrow b\text{-baryon})] = 0.0393 \pm 0.0046 \pm 0.0037$ which we divide by our best value $B(\bar{b} \rightarrow b\text{-baryon}) = (8.4 \pm 1.1) \times 10^{-2}$. Our first error is their experiment's error and our second error is the systematic error from using our best value.

 $\Gamma(\Xi^- \ell^- \bar{\nu}_\ell \text{ anything})/\Gamma_{\text{total}}$

VALUE (units 10^{-3})	DOCUMENT ID	TECN	COMMENT
4.6 ± 1.4 OUR AVERAGE			Error includes scale factor of 1.2.
$3.6 \pm 1.2 \pm 0.5$	¹ ABDALLAH	05c	DLPH $e^+ e^- \rightarrow Z^0$
$6.4 \pm 1.6 \pm 0.8$	² BUSKULIC	96T	ALEP Excess $\Xi^- \ell^-$ over $\Xi^- \ell^+$
$7.0 \pm 2.8 \pm 0.9$	³ ABREU	95v	DLPH Repl. by ABDALLAH 05c

• • • We do not use the following data for averages, fits, limits, etc. • • •

¹ ABDALLAH 05c reports $[\Gamma(b\text{-baryon} \rightarrow \Xi^- \ell^- \bar{\nu}_\ell \text{ anything})/\Gamma_{\text{total}}] \times [B(\bar{b} \rightarrow b\text{-baryon})] = (3.0 \pm 1.0 \pm 0.3) \times 10^{-4}$ which we divide by our best value $B(\bar{b} \rightarrow b\text{-baryon}) = (8.4 \pm 1.1) \times 10^{-2}$. Our first error is their experiment's error and our second error is the systematic error from using our best value.

² BUSKULIC 96T reports $[\Gamma(b\text{-baryon} \rightarrow \Xi^- \ell^- \bar{\nu}_\ell \text{ anything})/\Gamma_{\text{total}}] \times [B(\bar{b} \rightarrow b\text{-baryon})] = (5.4 \pm 1.1 \pm 0.8) \times 10^{-4}$ which we divide by our best value $B(\bar{b} \rightarrow b\text{-baryon}) = (8.4 \pm 1.1) \times 10^{-2}$. Our first error is their experiment's error and our second error is the systematic error from using our best value.

³ ABREU 95v reports $[\Gamma(b\text{-baryon} \rightarrow \Xi^- \ell^- \bar{\nu}_\ell \text{ anything})/\Gamma_{\text{total}}] \times [B(\bar{b} \rightarrow b\text{-baryon})] = (5.9 \pm 2.1 \pm 1.0) \times 10^{-4}$ which we divide by our best value $B(\bar{b} \rightarrow b\text{-baryon}) = (8.4 \pm 1.1) \times 10^{-2}$. Our first error is their experiment's error and our second error is the systematic error from using our best value.

 b -baryon ADMIXTURE ($\Lambda_b, \Xi_b, \Omega_b$) REFERENCES

ABAZOV	12U	PR D85 112003	V.M. Abazov <i>et al.</i>	(D0 Collab.)
ABAZOV	07S	PRL 99 142001	V.M. Abazov <i>et al.</i>	(D0 Collab.)
ABAZOV	05C	PRL 94 102001	V.M. Abazov <i>et al.</i>	(D0 Collab.)
ABDALLAH	05C	EPJ C44 299	J. Abdallah <i>et al.</i>	(DELPHI Collab.)
ABBIENDI	99L	EPJ C9 1	G. Abbiendi <i>et al.</i>	(OPAL Collab.)
ABREU	99W	EPJ C10 185	P. Abreu <i>et al.</i>	(DELPHI Collab.)
ACKERSTAFF	98G	PL B426 161	K. Ackerstaff <i>et al.</i>	(OPAL Collab.)
BARATE	98D	EPJ C2 197	R. Barate <i>et al.</i>	(ALEPH Collab.)
BARATE	98V	EPJ C5 205	R. Barate <i>et al.</i>	(ALEPH Collab.)
ACKERSTAFF	97N	ZPHY C74 423	K. Ackerstaff <i>et al.</i>	(OPAL Collab.)
ABE	96M	PRL 77 1439	F. ABE <i>et al.</i>	(CDF Collab.)
ABREU	96D	ZPHY C71 199	P. Abreu <i>et al.</i>	(DELPHI Collab.)
AKERS	96	ZPHY C69 195	R. Akers <i>et al.</i>	(OPAL Collab.)
BUSKULIC	96T	PL B384 449	D. Buskulic <i>et al.</i>	(ALEPH Collab.)
ABREU	95C	PL B347 447	P. Abreu <i>et al.</i>	(DELPHI Collab.)
ABREU	95S	ZPHY C68 375	P. Abreu <i>et al.</i>	(DELPHI Collab.)
ABREU	95V	ZPHY C68 541	P. Abreu <i>et al.</i>	(DELPHI Collab.)
BUSKULIC	95L	PL B357 685	D. Buskulic <i>et al.</i>	(ALEPH Collab.)
ABREU	93F	PL B311 379	P. Abreu <i>et al.</i>	(DELPHI Collab.)
AKERS	93	PL B316 435	R. Akers <i>et al.</i>	(OPAL Collab.)
BUSKULIC	92I	PL B297 449	D. Buskulic <i>et al.</i>	(ALEPH Collab.)

See key on page 1171

Baryon Particle Listings

Pentaquarks, $P_{c\bar{c}}(4312)^+$, $P_{c\bar{c}s}(4338)^0$, $P_{c\bar{c}}(4380)^+$, $P_{c\bar{c}}(4440)^+$ **EXOTIC BARYONS**

See the related review(s):

Pentaquarks

 $P_{c\bar{c}}(4312)^+$ $I(J^P) = \frac{1}{2}(?)^?$ Status: *OMITTED FROM SUMMARY TABLE
Was $P_c(4312)^+$. **$P_{c\bar{c}}(4312)^+$ MASS**

VALUE (MeV)	DOCUMENT ID	TECN	COMMENT
$4311.9 \pm 0.7 \pm 6.8$ -0.6	AAIJ	19w	LHCB pp at 7, 8, 13 TeV

 $P_{c\bar{c}}(4312)^+$ WIDTH

VALUE (MeV)	DOCUMENT ID	TECN	COMMENT
$9.8 \pm 2.7 \pm 3.7$ -4.5	AAIJ	19w	LHCB pp at 7, 8, 13 TeV

 $P_{c\bar{c}}(4312)^+$ DECAY MODES

Mode	Fraction (Γ_i/Γ)
Γ_1 $J/\psi p$	seen

 $P_{c\bar{c}}(4312)^+$ BRANCHING RATIOS

$\Gamma(J/\psi p)/\Gamma_{\text{total}}$	VALUE	EVTS	DOCUMENT ID	TECN	COMMENT	Γ_1/Γ
seen	246k	¹ AAIJ	19w	LHCB	pp at 7, 8, 13 TeV	
••• We do not use the following data for averages, fits, limits, etc. •••						
not seen	797	² AAIJ	22H	LHCB	pp at 7, 8, 13 TeV	
¹ Amplitude analysis of $\Lambda_b^0 \rightarrow J/\psi p K^-$.						
² Amplitude analysis of $B_s^0 \rightarrow J/\psi p \bar{p}$. AAIJ 22H finds evidence at just over 3σ for a $J/\psi p$ structure at $4337 \pm 7 \pm 2$ MeV.						

 $P_{c\bar{c}}(4312)^+$ REFERENCES

AAIJ	22H	PRL 128 062001	R. Aaij et al.	(LHCb Collab.)
AAIJ	19w	PRL 122 222001	R. Aaij et al.	(LHCb Collab.)

 $P_{c\bar{c}s}(4338)^0$ $I(J^P) = 0(\frac{1}{2}^-)$ Status: *AAIJ 23Q determines that spin-parity $J^P = 1/2^-$ is preferred, while spin-parity $J^P = 1/2^+$ is excluded at a 90% confidence level and spin $J = 3/2$ hypotheses are discarded. **$P_{c\bar{c}s}(4338)^0$ MASS**

VALUE (MeV)	EVTS	DOCUMENT ID	TECN	COMMENT
$4338.2 \pm 0.7 \pm 0.4$	4.4k	AAIJ	23Q	LHCB $B^- \rightarrow J/\psi \Lambda \bar{p}$

 $P_{c\bar{c}s}(4338)^0$ WIDTH

VALUE (MeV)	EVTS	DOCUMENT ID	TECN	COMMENT
$7.0 \pm 1.2 \pm 1.3$	4.4k	AAIJ	23Q	LHCB $B^- \rightarrow J/\psi \Lambda \bar{p}$

 $P_{c\bar{c}s}(4338)^0$ DECAY MODES

Mode	Fraction (Γ_i/Γ)
Γ_1 $J/\psi \Lambda$	seen

 $P_{c\bar{c}s}(4338)^0$ BRANCHING RATIOS

$\Gamma(J/\psi \Lambda)/\Gamma_{\text{total}}$	VALUE	EVTS	DOCUMENT ID	TECN	COMMENT	Γ_1/Γ
seen	4.4k	AAIJ	23Q	LHCB	$B^- \rightarrow J/\psi \Lambda \bar{p}$	

 $P_{c\bar{c}s}(4338)^0$ REFERENCES

AAIJ	23Q	PRL 131 031901	R. Aaij et al.	(LHCb Collab.)JP
------	-----	----------------	----------------	------------------

 $P_{c\bar{c}}(4380)^+$ $I(J^P) = \frac{1}{2}(?)^?$ Status: *OMITTED FROM SUMMARY TABLE
Was $P_c(4380)^+$.A resonance seen in $\Lambda_b^0 \rightarrow P_c^+ K^-$, then $P_c \rightarrow J/\psi p$, with a significance of 9 standard deviations. The $J/\psi p$ quark content is $uudc\bar{c}$, a pentaquark. See also the $P_c(4450)^+$. In the best amplitude fit, the two states have opposite parity, one having $J = 3/2$, the other $J = 5/2$.Extraction of the pentaquark signals requires some understanding of the dominant $K^- p$ background. AAIJ 15P used a model-dependent approach. AAIJ 16AG reanalyzed the data making minimal assumptions about the $K^- p$ background, and thus confirmed the strong significance of the pentaquark signals. **$P_{c\bar{c}}(4380)^+$ MASS**

VALUE (MeV)	DOCUMENT ID	TECN	COMMENT
$4380 \pm 8 \pm 29$	AAIJ	15P	LHCB pp at 7, 8 TeV

 $P_{c\bar{c}}(4380)^+$ WIDTH

VALUE (MeV)	DOCUMENT ID	TECN	COMMENT
$205 \pm 18 \pm 86$	AAIJ	15P	LHCB pp at 7, 8 TeV

 $P_{c\bar{c}}(4380)^+$ DECAY MODES

Mode	Fraction (Γ_i/Γ)
Γ_1 $J/\psi p$	seen

 $P_{c\bar{c}}(4380)^+$ BRANCHING RATIOS

$\Gamma(J/\psi p)/\Gamma_{\text{total}}$	VALUE	DOCUMENT ID	TECN	COMMENT	Γ_1/Γ
seen		AAIJ	15P	LHCB pp at 7, 8 TeV	

 $P_{c\bar{c}}(4380)^+$ REFERENCES

AAIJ	16AG	PRL 117 082002	R. Aaij et al.	(LHCb Collab.)
AAIJ	15P	PRL 115 072001	R. Aaij et al.	(LHCb Collab.)

 $P_{c\bar{c}}(4440)^+$ $I(J^P) = \frac{1}{2}(?)^?$ Status: *OMITTED FROM SUMMARY TABLE
Was $P_c(4440)^+$. **$P_{c\bar{c}}(4440)^+$ MASS**

VALUE (MeV)	DOCUMENT ID	TECN	COMMENT
$4440.3 \pm 1.3 \pm 4.1$ -4.7	AAIJ	19w	LHCB pp at 7, 8, 13 TeV

 $P_{c\bar{c}}(4440)^+$ WIDTH

VALUE (MeV)	DOCUMENT ID	TECN	COMMENT
$20.6 \pm 4.9 \pm 8.7$ -10.1	AAIJ	19w	LHCB pp at 7, 8, 13 TeV

 $P_{c\bar{c}}(4440)^+$ DECAY MODES

Mode	Fraction (Γ_i/Γ)
Γ_1 $J/\psi p$	seen

 $P_{c\bar{c}}(4440)^+$ BRANCHING RATIOS

$\Gamma(J/\psi p)/\Gamma_{\text{total}}$	VALUE	DOCUMENT ID	TECN	COMMENT	Γ_1/Γ
seen		¹ POPOV	21	D0 $p\bar{p}$ at 1.96 TeV	
seen		AAIJ	19w	LHCB pp at 7, 8, 13 TeV	

¹ Search for J/ψ inclusive production in association with a charged particle, assumed to be a proton. POPOV 21 observes a resonant signal consistent with a superposition of the $P_{c\bar{c}}(4440)^+$ and $P_{c\bar{c}}(4457)^+$, using masses and widths measured by AAIJ 19w, at significance of 3σ . **$P_{c\bar{c}}(4440)^+$ REFERENCES**

POPOV	21	PAN 83 1383	A.V. Popov et al.	(D0 Collab.)
AAIJ	19w	PRL 122 222001	R. Aaij et al.	(LHCb Collab.)

Baryon Particle Listings

 $P_{c\bar{c}}(4457)^+$, $P_{c\bar{c}s}(4459)^0$ $P_{c\bar{c}}(4457)^+$ $I(J^P) = \frac{1}{2}(??)$ Status: *OMITTED FROM SUMMARY TABLE
was $P_c(4450)$

A resonance seen in $\Lambda_b^0 \rightarrow P_c^+ K^-$, then $P_c \rightarrow J/\psi p$, with a significance of 12 standard deviations. The $J/\psi p$ quark content is $uudc\bar{c}$, a pentaquark. See also the $P_{c\bar{c}}(4380)^+$. In the best amplitude fit, the two states have opposite parity, one having $J = 3/2$, the other $J = 5/2$.

Extraction of the pentaquark signals requires some understanding of the dominant $K^- p$ background. AAIJ 15P used a model-dependent approach. AAIJ 16AG reanalyzed the data making minimal assumptions about the $K^- p$ background, and thus confirmed the strong significance of the pentaquark signals.

 $P_{c\bar{c}}(4457)^+$ MASS

VALUE (MeV)	DOCUMENT ID	TECN	COMMENT
$4457.3 \pm 0.6^{+4.1}_{-1.7}$	AAIJ	19W LHCb	pp at 7, 8, 13 TeV
• • • We do not use the following data for averages, fits, limits, etc. • • •			
$4449.8 \pm 1.7 \pm 2.5$	¹ AAIJ	15P LHCb	Repl. by AAIJ 19W
¹ Considering $P_{c\bar{c}}(4440)$ and $P_{c\bar{c}}(4457)$ as a single resonance.			

 $P_{c\bar{c}}(4457)^+$ WIDTH

VALUE (MeV)	DOCUMENT ID	TECN	COMMENT
$6.4 \pm 2.0^{+5.7}_{-1.9}$	AAIJ	19W LHCb	pp at 7, 8, 13 TeV
• • • We do not use the following data for averages, fits, limits, etc. • • •			
$39 \pm 5 \pm 19$	¹ AAIJ	15P LHCb	Repl. by AAIJ 19W
¹ Considering $P_{c\bar{c}}(4440)$ and $P_{c\bar{c}}(4457)$ as a single resonance.			

 $P_{c\bar{c}}(4457)^+$ DECAY MODES

Mode	Fraction (Γ_i/Γ)
Γ_1 $J/\psi p$	seen

 $P_{c\bar{c}}(4457)^+$ BRANCHING RATIOS

$\Gamma(J/\psi p)/\Gamma_{\text{total}}$	Γ_1/Γ		
VALUE	DOCUMENT ID	TECN	COMMENT
seen	¹ POPOV	21 D0	$p\bar{p}$ at 1.96 TeV
seen	AAIJ	19W LHCb	pp at 7, 8, 13 TeV
seen	AAIJ	15P LHCb	pp at 7, 8 TeV

¹ Search for J/ψ inclusive production in association with a charged particle, assumed to be a proton. POPOV 21 observes a resonant signal consistent with a superposition of the $P_{c\bar{c}}(4440)^+$ and $P_{c\bar{c}}(4457)^+$, using masses and widths measured by AAIJ 19W, at significance of 3σ .

 $P_{c\bar{c}}(4457)^+$ REFERENCES

POPOV	21	PAN 83 1383	A.V. Popov <i>et al.</i>	(D0 Collab.)
AAIJ	19W	PRL 122 222001	R. Aaij <i>et al.</i>	(LHCb Collab.)
AAIJ	16AG	PRL 117 082002	R. Aaij <i>et al.</i>	(LHCb Collab.)
AAIJ	15P	PRL 115 072001	R. Aaij <i>et al.</i>	(LHCb Collab.)

 $P_{c\bar{c}s}(4459)^0$ $I(J^P) = 0(??)$ Status: *

OMITTED FROM SUMMARY TABLE

 $P_{c\bar{c}s}(4459)^0$ MASS

VALUE (MeV)	EVTS	DOCUMENT ID	TECN	COMMENT
$4458.8 \pm 2.9^{+4.7}_{-1.1}$	1.8k	¹ AAIJ	21A0 LHCb	$\Xi_b^- \rightarrow J/\psi \Lambda K^-$
¹ AAIJ 21A0 sees evidence for the $P_{c\bar{c}s}(4459)$ at 3.1σ global significance.				

 $P_{c\bar{c}s}(4459)^0$ WIDTH

VALUE (MeV)	EVTS	DOCUMENT ID	TECN	COMMENT
$17.3 \pm 6.5^{+8.0}_{-5.7}$	1.8k	¹ AAIJ	21A0 LHCb	$\Xi_b^- \rightarrow J/\psi \Lambda K^-$
¹ AAIJ 21A0 sees evidence for the $P_{c\bar{c}s}(4459)$ at 3.1σ global significance.				

 $P_{c\bar{c}s}(4459)^0$ DECAY MODES

Mode	Fraction (Γ_i/Γ)
Γ_1 $J/\psi \Lambda$	seen

 $P_{c\bar{c}s}(4459)^0$ BRANCHING RATIOS

$\Gamma(J/\psi \Lambda)/\Gamma_{\text{total}}$	Γ_1/Γ			
VALUE	EVTS	DOCUMENT ID	TECN	COMMENT
seen	1.8k	¹ AAIJ	21A0 LHCb	$\Xi_b^- \rightarrow J/\psi \Lambda K^-$
¹ AAIJ 21A0 sees evidence for the $P_{c\bar{c}s}(4459)$ at 3.1σ global significance.				

 $P_{c\bar{c}s}(4459)^0$ REFERENCES

AAIJ	21A0	SCIB 66 1278	R. Aaij <i>et al.</i>	(LHCb Collab.)
------	------	--------------	-----------------------	----------------

MISCELLANEOUS SEARCHES

Magnetic Monopole Searches	2289
Supersymmetric Particle Searches	2292
Technicolor	2347
Quark and Lepton Compositeness	2348
Extra Dimensions	2352
WIMP and Dark Matter Searches	2359
Other Particle Searches	2374

SEARCHES IN OTHER SECTIONS

Neutral Higgs Bosons, Searches for	1237
Charged Higgs Bosons (H^\pm and $H^{\pm\pm}$), Searches for	1248
New Heavy Bosons	1253
Axions (A^0) and Other Very Light Bosons	1271
Heavy Charged Lepton Searches	1331
Double- β Decay	1343
Heavy Neutral Leptons, Searches for	1367
b' (Fourth Generation) Quark	1398
t' (Fourth Generation) Quark	1401
Free Quark Searches	1403

Related Reviews in Volume 1

85. Extra dimensions (rev.)	1021
86. W' -boson searches (rev.)	1029
87. Z' -boson searches (rev.)	1033
88. Supersymmetry: theory (rev.)	1038
89. Supersymmetry: experiment (rev.)	1058
90. Axions and other similar particles (rev.)	1079
91. Quark and lepton compositeness, searches for (rev.)	1098
92. Dynamical electroweak symmetry	1104
breaking: implications of the H^0 (rev.)	
93. Grand unified theories (rev.)	1119
94. Leptoquarks (rev.)	1134
95. Magnetic monopoles (rev.)	1138



See key on page 1171

Searches Particle Listings

Magnetic Monopole Searches

SEARCHES
not in other sections

Magnetic Monopole Searches

See the related review(s):
Magnetic Monopoles

Monopole Production Cross Section — Accelerator Searches

X-SECT (cm ²)	MASS (GeV)	CHG (g)	ENERGY (GeV)	BEAM	DOCUMENT ID	TECN
<4 E-41	200-4000	1-2	13000	pp	1 AAD	23Co ATLS
<4 E-38	590-1000	1-4	8000	pp	2 ACHARYA	22A INDU
<2 E-29	0-70	1-3	5020	PbPb	3 ACHARYA	22B INDU
<3 E-38	750-1910	1-5	13000	pp	4 ACHARYA	21 INDU
<1.3E-40	200-4000	1	13000	pp	5 AAD	20G ATLS
<5.6E-40	500-4000	2	13000	pp	5 AAD	20G ATLS
	200-5000	2	13000	pp	6 ACHARYA	19B INDU
	200-5000	1	13000	pp	7 ACHARYA	18A INDU
<2.5E-37	200-6000	1	13000	pp	8 ACHARYA	17 INDU
<2E-37	200-6000	2	13000	pp	8 ACHARYA	17 INDU
<4E-37	200-5000	3	13000	pp	8 ACHARYA	17 INDU
<1.5E-36	400-4000	4	13000	pp	8 ACHARYA	17 INDU
<7E-36	1000-3000	5	13000	pp	8 ACHARYA	17 INDU
<5E-40	200-2500	0.5-2.0	8000	pp	9 AAD	16AB ATLS
<2E-37	100-3500	1	8000	pp	10 ACHARYA	16 INDU
<2E-37	100-3500	2	8000	pp	10 ACHARYA	16 INDU
<6E-37	500-3000	3	8000	pp	10 ACHARYA	16 INDU
<7E-36	1000-2000	4	8000	pp	10 ACHARYA	16 INDU
<1.6E-38	200-1200	1	7000	pp	11 AAD	12CS ATLS
<5E-38	45-102	1	206	e ⁺ e ⁻	12 ABBIENDI	08 OPAL
<0.2E-36	200-700	1	1960	p \bar{p}	13 ABULENCIA	06K CNTR
< 2.E-36		1	300	e ⁺ p	14,15 AKTAS	05A INDU
< 0.2 E-36		2	300	e ⁺ p	14,15 AKTAS	05A INDU
< 0.09E-36		3	300	e ⁺ p	14,15 AKTAS	05A INDU
< 0.05E-36		≥ 6	300	e ⁺ p	14,15 AKTAS	05A INDU
< 2.E-36		1	300	e ⁺ p	14,16 AKTAS	05A INDU
< 0.2E-36		2	300	e ⁺ p	14,16 AKTAS	05A INDU
< 0.07E-36		3	300	e ⁺ p	14,16 AKTAS	05A INDU
< 0.06E-36		≥ 6	300	e ⁺ p	14,16 AKTAS	05A INDU
< 0.06E-36	>265	1	1800	p \bar{p}	17 KALBFLEISCH 04	INDU
< 0.2E-36	>355	2	1800	p \bar{p}	17 KALBFLEISCH 04	INDU
< 0.07E-36	>410	3	1800	p \bar{p}	17 KALBFLEISCH 04	INDU
< 0.2E-36	>375	6	1800	p \bar{p}	17 KALBFLEISCH 04	INDU
< 0.7E-36	>295	1	1800	p \bar{p}	18,19 KALBFLEISCH 00	INDU
< 7.8E-36	>260	2	1800	p \bar{p}	18,19 KALBFLEISCH 00	INDU
< 2.3E-36	>325	3	1800	p \bar{p}	18,20 KALBFLEISCH 00	INDU
< 0.11E-36	>420	6	1800	p \bar{p}	18,20 KALBFLEISCH 00	INDU
<0.65E-33	<3.3	≥ 2	11A	¹⁹⁷ Au	21,22 HE	97
<1.90E-33	<8.1	≥ 2	160A	²⁰⁸ Pb	21,22 HE	97
<3.E-37	<45.0	1.0	88-94	e ⁺ e ⁻	PINFOLD	93 PLAS
<3.E-37	<41.6	2.0	88-94	e ⁺ e ⁻	PINFOLD	93 PLAS
<7.E-35	<44.9	0.2-1.0	89-93	e ⁺ e ⁻	KINOSHITA	92 PLAS
<2.E-34	<85.0	≥ 0.5	1800	p \bar{p}	BERTANI	90 PLAS
<1.2E-33	<800	≥ 1	1800	p \bar{p}	PRICE	90 PLAS
<1.E-37	<29	1	50-61	e ⁺ e ⁻	KINOSHITA	89 PLAS
<1.E-37	<18	2	50-61	e ⁺ e ⁻	KINOSHITA	89 PLAS
<1.E-38	<17	<1	35	e ⁺ e ⁻	BRAUNSCH...	88B CNTR
<8.E-37	<24	1	50-52	e ⁺ e ⁻	KINOSHITA	88 PLAS
<1.3E-35	<22	2	50-52	e ⁺ e ⁻	KINOSHITA	88 PLAS
<9.E-37	<4	<0.15	10.6	e ⁺ e ⁻	GENTILE	87 CLEO
<3.E-32	<800	≥ 1	1800	p \bar{p}	PRICE	87 PLAS
<3.E-38	<3	29	e ⁺ e ⁻	FRYBERGER	84 PLAS	
<1.E-31	1.3	540	p \bar{p}	AUBERT	83B PLAS	
<4.E-38	<10	<6	34	e ⁺ e ⁻	MUSSET	83 PLAS
<8.E-36	<20	52	pp	DELL	82 CNTR	
<9.E-37	<30	<3	29	e ⁺ e ⁻	KINOSHITA	82 PLAS
<1.E-37	<20	<24	63	pp	CARRIGAN	78 CNTR
<1.E-37	<30	<3	56	pp	HOFFMANN	78 PLAS
			62	pp	DELL	76 SPRK
<4.E-33			300	p	23 STEVENS	76B SPRK
<1.E-40	<5	<2	70	p	24 ZRELOV	76 CNTR
<2.E-30			300	n	23 BURKE	75 OSPK
<1.E-38			8	ν	25 CARRIGAN	75 HLBC
<5.E-43	<12	<10	400	p	EBERHARD	75B INDU
<2.E-36	<30	<3	60	pp	GIACOMELLI	75 PLAS
<5.E-42	<13	<24	400	p	CARRIGAN	74 CNTR
<6.E-42	<12	<24	300	p	CARRIGAN	73 CNTR
<2.E-36		1	0.001	γ	24 BARTLETT	72 CNTR
<1.E-41	<5		70	p	GUREVICH	72 EMUL
<1.E-40	<3	<2	28	p	AMALDI	63 EMUL

<2.E-40	<3	<2	30	p	PURCELL	63	CNTR
<1.E-35	<3	<4	28	p	FIDECARO	61	CNTR
<2.E-35	<1	1	6	p	BRADNER	59	EMUL

- AAD 23Co limits given for monopoles pair produced via a Drell-Yan or photon-fusion mechanism. Spins 1/2 and 0 are considered. The quoted limit is representative of the lowest values that were achieved.
- ACHARYA 22A give limits for monopoles pair-produced via a Drell-Yan production. Spins 0, 1/2, and 1 are considered. The cross section limit is representative of the lowest values that were achieved. The experiment used a combination of nuclear track detectors to look evidence of passing monopoles and a SQUID magnetometer to look for stopped monopoles.
- ACHARYA 22B achieved limits on monopole (point-like included) production via the Schwinger mechanism in Pb-Pb collisions at 5.02 TeV centre-of-mass energy per nucleon pair. The upper cross section limit value quoted here is representative of the lowest values achieved.
- ACHARYA 21 search for dyons at LHC. Using a production model limits (we report the lowest) are set for dyons with magnetic charge up to 5 gD, electric charges up to 200 e and spins 0, 1/2, 1. The corresponding mass limits for magnetic monopoles are in the range 870-2040 GeV for magnetic charges in the same range.
- AAD 20G give limits for Drell-Yan production with spin-0 and spin-1/2 monopoles. The above limit is for spin = 0 at mass = 3 TeV.
- ACHARYA 19B limits both β-dependent and β-independent on monopoles with spins 0, 1/2, and 1 and with magnetic charges ranging from one to five times the Dirac charge in mass ranges between 200 GeV and 5000 GeV.
- ACHARYA 18A provide limits on monopoles with spins 0, 1/2, and 1 and with magnetic charges ranging from two to five times the Dirac charge.
- The search was sensitive to monopoles which had stopped in aluminium trapping volumes. Monopoles with spins 0 and 1/2 were considered; mass-dependent spin 1/2 monopole limits are quoted here.
- AAD 16AB model-independent 95% CL limits estimated using a fiducial region of approximately constant acceptance. Limits are mass-dependent.
- ACHARYA 16 limits at 95% CL estimated using a Drell-Yan-like production mechanism for scalar monopoles.
- AAD 12cs searched for monopoles as highly ionising objects. The cross section limits are based on an assumed Drell-Yan-like production process for spin 1/2 monopoles. The limits are mass- and scenario-dependent.
- ABBIENDI 08 assume production of spin 1/2 monopoles with effective charge gβ (n=1), via e⁺e⁻ → γ* → M \bar{M} , so that the cross section is proportional to (1 + cos²θ). There is no z information for such highly saturated tracks, so a parabolic track in the jet chamber is projected onto the xy plane. Charge per hit in the chamber produces a clean separation of signal and background.
- ABULENCIA 06k searches for high-ionizing signals in CDF central outer tracker and time-of-flight detector. For Drell-Yan M \bar{M} production, the cross section limit implies M > 360 GeV at 95% CL.
- AKTAS 05A model-dependent limits as a function of monopole mass shown for arbitrary mass of 60 GeV. Based on search for stopped monopoles in the H1 Al beam pipe.
- AKTAS 05A limits with assumed elastic spin 0 monopole pair production.
- AKTAS 05A limits with assumed inelastic spin 1/2 monopole pair production.
- KALBFLEISCH 04 reports searches for stopped magnetic monopoles in Be, Al, and Pb samples obtained from discarded material from the upgrading of DØ and CDF. A large-aperture warm-bore cryogenic detector was used. The approach was an extension of the methods of KALBFLEISCH 00. Cross section results moderately model dependent; interpretation as a mass lower limit depends on possibly invalid perturbation expansion.
- KALBFLEISCH 00 used an induction method to search for stopped monopoles in pieces of the DØ (FNAL) beryllium beam pipe and in extensions to the drift chamber aluminium support cylinder. Results are model dependent.
- KALBFLEISCH 00 result is for aluminum.
- KALBFLEISCH 00 result is for beryllium.
- HE 97 used a lead target and barium phosphate glass detectors. Cross-section limits are well below those predicted via the Drell-Yan mechanism.
- This work has also been reinterpreted in the framework of monopole production via the thermal Schwinger process (GOULD 17); this gives rise to lower mass limits.
- Two-photon events.
- Cherenkov radiation polarization.
- Re-examines CERN neutrino experiments.

Monopole Production — Other Accelerator Searches

MASS (GeV)	CHG (g)	SPIN	ENERGY (GeV)	BEAM	DOCUMENT ID	TECN
> 610	≥ 1	0	1800	p \bar{p}	1 ABBOTT	98k D0
> 870	≥ 1	1/2	1800	p \bar{p}	1 ABBOTT	98k D0
>1580	≥ 1	1	1800	p \bar{p}	1 ABBOTT	98k D0
> 510			88-94	e ⁺ e ⁻	2 ACCIARRI	95c L3

- ABBOTT 98k search for heavy pointlike Dirac monopoles via central production of a pair of photons with high transverse energies.
- ACCIARRI 95c finds a limit B(Z → γγ) < 0.8 × 10⁻⁵ (which is possible via a monopole loop) at 95% CL and sets the mass limit via a cross section model.

Monopole Flux — Cosmic Ray Searches

"Caty" in the charge column indicates a search for monopole-catalyzed nucleon decay.

FLUX (cm ⁻² sr ⁻¹ s ⁻¹)	MASS (GeV)	CHG (g)	COMMENTS (β = v/c)	DOCUMENT ID	TECN
<2E-19		1	0.86 < β < 0.995	1 ABBASI	22 ICCB
<2E-14	>5E8		6E-4 < β < 5E-3	2 ACERO	21 NOVA
<1E-17		Caty	1E-5 < β < 1E-3	3 GAPONENKO	21 BAIK
<1.5E-18		1	β > 0.6	4 ALBERT	17 ANTR
<2.5E-21		1	1E8 < γ < 1E13	5 AAB	16 AUGE
<1.55E-18			β > 0.51	6 AARTSEN	16B ICCB
<1E-17		Caty	1E-3 < β < 1E-2	7 AARTSEN	14 ICCB
<3E-18		1	β > 0.8	8 ABBASI	13 ICCB
<1.3E-17		1	β > 0.625	9 ADRIAN-MAR.	12A ANTR

Searches Particle Listings

Magnetic Monopole Searches

<6E-28	<1E17	Caty	1E-5 < β < 0.04	10 UENO	12 SKAM
<1E-19		1	γ > 1E10	11 DETRIXHE	11 ANIT
<3.8E-17		1	β > 0.76	8 ABBASI	10A ICCB
<1.3E-15	1E4 < M < 5E13	1	β > 0.05	12 BALESTRA	08 PLAS
<0.65E-15	> 5E13	1	β > 0.05	12 BALESTRA	08 PLAS
<1E-18		1	γ > 1E8	11 HOGAN	08 RICE
<1.4E-16		1	1.1E-4 < β < 1	13 AMBROSIO	02B MCRO
<3E-16		Caty	1.1E-4 < β < 5E-3	14 AMBROSIO	02C MCRO
<1.5E-15		1	5E-3 < β < 0.99	15 AMBROSIO	02D MCRO
<1E-15		1	1.1 × 10 ⁻⁴ -0.1	16 AMBROSIO	97 MCRO
<5.6E-15		1	(0.18-3.0)E-3	17 AHLEN	94 MCRO
<2.7E-15		Caty	β ~ 1 × 10 ⁻³	18 BECKER-SZ...	94 IMB
<8.7E-15		1	> 2.E-3	THRON	92 SOUD
<4.4E-12		1	all β	GARDNER	91 INDU
<7.2E-13		1	all β	HUBER	91 INDU
<3.7E-15	> E12	1	β = 1.E-4	19 ORITO	91 PLAS
<3.2E-16	> E10	1	β > 0.05	19 ORITO	91 PLAS
<3.2E-16	> E10-E12	2,3		19 ORITO	91 PLAS
<3.8E-13		1	all β	BERMON	90 INDU
<5E-16		Caty	β < 1.E-3	18 BEZRUKOV	90 CHER
<1.8E-14		1	β > 1.1E-4	20 BUCKLAND	90 HEPT
<1E-18		1	3.E-4 < β < 1.5E-3	21 GHOSH	90 MICA
<7.2E-13		1	all β	HUBER	90 INDU
<5E-12	> E7	1	3.E-4 < β < 5.E-3	BARISH	87 CNTR
<1.E-13		Caty	1.E-5 < β < 1	18 BARTELT	87 SOUD
<1.E-10		1	all β	EBISU	87 INDU
<2.E-13		1	1.E-4 < β < 6.E-4	MASEK	87 HEPT
<2.E-14		1	4.E-5 < β < 2.E-4	NAKAMURA	87 PLAS
<2.E-14		1	1.E-3 < β < 1	NAKAMURA	87 PLAS
<5E-14		1	9.E-4 < β < 1.E-2	SHEPKO	87 CNTR
<2.E-13		1	4.E-4 < β < 1	TSUKA MOTO	87 CNTR
<5E-14		1	all β	22 CAPLIN	86 INDU
<5E-12		1		CROMAR	86 INDU
<1.E-13		1	7.E-4 < β	HARA	86 CNTR
<7.E-11		1	all β	INCANDELA	86 INDU
<1.E-18		1	4.E-4 < β < 1.E-3	21 PRICE	86 MICA
<5E-12		1		BERMON	85 INDU
<6.E-12		1		CAPLIN	85 INDU
<6.E-10		1		EBISU	85 INDU
<3.E-15		Caty	5.E-5 ≤ β ≤ 1.E-3	18 KAJITA	85 KAMI
<2.E-21		Caty	β < 1.E-3	18,23 KAJITA	85 KAMI
<3.E-15		Caty	1.E-3 < β < 1.E-1	18 PARK	85B CNTR
<5E-12		1	1.E-4 < β < 1	BATTISTONI	84 NUSX
<7.E-12		1		INCANDELA	84 INDU
<7.E-13		1	3.E-4 < β	20 KAJINO	84 CNTR
<2.E-12		1	3.E-4 < β < 1.E-1	KAJINO	84B CNTR
<6.E-13		1	5.E-4 < β < 1	KAWAGOE	84 CNTR
<2.E-14		1	1.E-3 < β	18 KRISHNA...	84 CNTR
<4.E-13		1	6.E-4 < β < 2.E-3	LISS	84 CNTR
<1.E-16		1	3.E-4 < β < 1.E-3	21 PRICE	84 MICA
<1.E-13		1	1.E-4 < β	PRICE	84B PLAS
<4.E-13		1	6.E-4 < β < 2.E-3	TARLE	84 CNTR
<4.E-13		1	1.E-2 < β < 1.E-3	24 ANDERSON	83 EMUL
<1.E-12		1	7.E-3 < β < 1	BARTELT	83B CNTR
<3.E-13		1	1.E-3 < β < 4.E-1	BARWICK	83 PLAS
<3.E-12		Caty	5.E-4 < β < 5.E-2	BONARELLI	83 CNTR
<4.E-11		1		18 BOSETTI	83 CNTR
<5E-15		1	1.E-2 < β < 1	CABRERA	83 INDU
<8E-15		1	1.E-4 < β < 1.E-1	DOKE	83 PLAS
<5E-12		Caty	1.E-4 < β < 3.E-2	18 ERREDE	83 IMB
<2.E-12		1	6.E-4 < β < 1	GROOM	83 CNTR
<1.E-13		1	β = 3.E-3	MASHIMO	83 CNTR
<2.E-12		1	7.E-3 < β < 6.E-1	MASHIMO	83 CNTR
6.E-10		1	all β	25 BONARELLI	82 CNTR
<2E-11		1	1.E-2 < β < 1.E-1	CABRERA	82 INDU
<2E-15			concentrator	MASHIMO	82 CNTR
<1.E-13	> 1		1.E-3 < β	BARTLETT	81 PLAS
<5E-11	< E17		3.E-4 < β < 1.E-3	KINOSHITA	81B PLAS
<2E-11			concentrator	ULLMAN	81 CNTR
1.E-1	> 200	2		BARTLETT	78 PLAS
<2E-13		> 2		PRICE	75 PLAS
<1E-19		> 2	obsidian, mica	FLEISCHER	71 PLAS
<5E-15	< 15	< 3	concentrator	FLEISCHER	69C PLAS
<2E-11		< 1-3	concentrator	CARITHERS	66 ELEC
				MALKUS	51 EMUL

¹ ABBASI 22 search was based on Cherenkov light detection in an array of optical modules in the Antarctic ice cap. Limits are speed-dependent.
² ACERO 21 employ NOVA experiment to set reported 90% CL upper limit on the cosmic monopoles flux for velocity $6 \times 10^{-4} < \beta < 5 \times 10^{-3}$ and mass $> 5 \times 10^8$ GeV.
³ GAPONENKO 21 use data of NT200 two-year operation at Baikal to give speed-dependent limits for different assumed catalysis cross sections. Reported limit is for $\sigma = 10$ mb.
⁴ ALBERT 17 limits were estimated using a Cherenkov light in an array of optical modules under the Mediterranean Sea. The limits are for MM masses between 10^{10} and 10^{14} GeV. The limits are speed-dependent.
⁵ AAB 16 search was made with a set of telescopes sampling the longitudinal profile of fluorescence light emitted by extensive air showers. Limits are speed dependent.
⁶ AARTSEN 16B was based on a Cherenkov signature in an array of optical modules which were sunk in the Antarctic ice cap. Limits are speed-dependent.

⁷ Beyond the monopole speed, the limits of AARTSEN 14 depend on the catalysis cross section (σ) which corresponds to the monopole radiating \bar{l} times the light per track length compared to the Cherenkov light from a single electrically charged, relativistic particle. The values quoted here correspond to $\sigma = 1$ barn or $\bar{l} = 30$.
⁸ ABBASI 13 and ABBASI 10A were based on a Cherenkov signature in an array of optical modules which were sunk in the Antarctic ice cap. Limits are speed-dependent.
⁹ ADRIAN-MARTINEZ 12A measurements were based on a Cherenkov signature in an underwater telescope in the Western Mediterranean Sea. Limits are speed-dependent.
¹⁰ The limits from UENO 12 depend on the monopole speed and are also sensitive to assumed values of monopole mass and the catalysis cross section.
¹¹ HOGAN 08 and DETRIXHE 11 limits on relativistic monopoles are based on nonobservation of radio Cherenkov signals at the South Pole. Limits are speed-dependent.
¹² BALESTRA 08 exposed of nuclear track detector modules totaling 400 m² for 4 years at the Chacaltaya Laboratory (5230 m) in search for intermediate-mass monopoles with $\beta > 0.05$. The analysis is mainly based on three CR39 modules. For $M > 5 \times 10^{13}$ GeV there can be upward-going monopoles as well, hence the flux limit is half that obtained for less massive monopoles. Previous experiments (e.g. MACRO and OHYA (ORITO 91)) had set limits only for $M > 1 \times 10^9$ GeV.
¹³ AMBROSIO 02B direct search final result for $m \geq 10^{17}$ GeV, based upon 4.2 to 9.5 years of running, depending upon the subsystem. Limit with CR39 track-etch detector extends the limit from $\beta = 4 \times 10^{-5}$ (3.1×10^{-16} cm⁻² sr⁻¹ s⁻¹) to $\beta = 1 \times 10^{-4}$ (2.1×10^{-16} cm⁻² sr⁻¹ s⁻¹). Limit curve in paper is piecewise continuous due to different detection techniques for different β ranges.
¹⁴ AMBROSIO 02c limit for catalysis of nucleon decay with catalysis cross section of ≈ 1 mb. The flux limit increases by ~ 3 at the higher β limit, and increases to 1×10^{-14} cm⁻² sr⁻¹ s⁻¹ if the catalysis cross section is 0.01 mb. Based upon 71193 hr of data with the streamer detector, with an acceptance of 4250 m² sr.
¹⁵ AMBROSIO 02b result for "more than two years of data." Ionization search using several subsystems. Limit curve as a function of β not given. Included in AMBROSIO 02b.
¹⁶ AMBROSIO 97 global MACRO 90% CL is 0.78×10^{-15} at $\beta = 1.1 \times 10^{-4}$, goes through a minimum at 0.61×10^{-15} near $\beta = (1.1-2.7) \times 10^{-3}$, then rises to 0.84×10^{-15} at $\beta = 0.1$. The global limit in this region is below the Parker bound at 10^{-15} . Less stringent limits are established for $4 \times 10^{-5} < \beta < 1 \times 10^{-4}$. Limits set by various triggers and different subdetectors are given in the paper. All limits assume a catalysis cross section smaller than a few mb.
¹⁷ AHLEN 94 limit for dyons extends down to $\beta = 0.9E-4$ and a limit of $1.3E-14$ extends to $\beta = 0.8E-4$. Also see comment by PRICE 94 and reply of BARISH 94. One loophole in the AHLEN 94 result is that in the case of monopoles catalyzing nucleon decay, relativistic particles could veto the events. See AMBROSIO 97 for additional results.
¹⁸ Catalysis of nucleon decay; sensitive to assumed catalysis cross section.
¹⁹ ORITO 91 limits are functions of velocity. Lowest limits are given here.
²⁰ Used DKMPR mechanism and Penning effect.
²¹ Assumes monopole attaches fermion nucleus.
²² Limit from combining data of CAPLIN 86, BERMON 85, INCANDELA 84, and CABRERA 83. For a discussion of controversy about CAPLIN 86 observed event, see GUY 87. Also see SCHOUTEN 87.
²³ Based on lack of high-energy solar neutrinos from catalysis in the sun.
²⁴ Anomalous long-range α (⁴He) tracks.
²⁵ CABRERA 82 candidate event has single Dirac charge within $\pm 5\%$.
²⁶ ALVAREZ 75, FLEISCHER 75, and FRIEDLANDER 75 explain as fragmenting nucleus. EBERHARD 75 and ROSS 76 discuss conflict with other experiments. HAGSTROM 77 reinterprets as antinucleus. PRICE 78 reassesses.

Monopole Flux — Astrophysics				DOCUMENT ID	TECN
FLUX (cm ⁻² sr ⁻¹ s ⁻¹)	MASS (GeV)	CHG (g)	COMMENTS (β = v/c)		
< 1.2 × 10 ⁻²¹	> 10 ⁴	1	Parker	1 KOBAYASHI	23A COSM
< 1.3 × 10 ⁻²⁰			faint white dwarf	2 FREESE	99 ASTR
< 1 × 10 ⁻¹⁶	10 ¹⁷	1	galactic field	3 ADAMS	93 COSM
< 1 × 10 ⁻²³			Jovian planets	2 ARAFUNE	85 ASTR
< 1 × 10 ⁻¹⁶	10 ¹⁵		solar trapping	BRACCI	85B ASTR
< 1 × 10 ⁻¹⁸		1		2 HARVEY	84 COSM
< 3 × 10 ⁻²³			neutron stars	KOLB	84 ASTR
< 7 × 10 ⁻²²			pulsars	2 FREESE	83B ASTR
< 1 × 10 ⁻¹⁸	< 10 ¹⁸	1	intergalactic field	2 REPHAELI	83 COSM
< 1 × 10 ⁻²³			neutron stars	2 DIMOPOUL...	82 COSM
< 5 × 10 ⁻²²			neutron stars	2 KOLB	82 COSM
< 5 × 10 ⁻¹⁵	> 10 ²¹		galactic halo	SALPETER	82 COSM
< 1 × 10 ⁻¹²	10 ¹⁹	1	β = 3 × 10 ⁻³	4 TURNER	82 COSM
< 1 × 10 ⁻¹⁶		1	galactic field	PARKER	70 COSM

1 KOBAYASHI 23A found Parker-type bounds on magnetic monopoles with arbitrary magnetic charge based on the survival of galactic, seed, and primordial magnetic fields. Bounds are between 10^{-21} and 10^{-5} cm⁻²sr⁻¹s⁻¹ for masses between 10^4 and 10^{18} GeV. Reported bound is the most stringent one.
² Catalysis of nucleon decay.
³ ADAMS 93 limit based on "survival and growth of a small galactic seed field" is 10^{-16} (m/10¹⁷ GeV) cm⁻²s⁻¹sr⁻¹. Above 10¹⁷ GeV, limit 10^{-16} (10¹⁷ GeV/m) cm⁻²s⁻¹sr⁻¹ (from requirement that monopole density does not overclose the universe) is more stringent.
⁴ Re-evaluates PARKER 70 limit for GUT monopoles.

Monopole Density — Matter Searches				DOCUMENT ID	TECN
DENSITY	CHG (g)	MATERIAL			
< 9.8E-5/gram	≥ 1	Polar rock		BENDTZ	13 INDU
< 6.9E-6/gram	> 1/3	Meteorites and other		JEON	95 INDU
< 2.E-7/gram	> 0.6	Fe ore		1 EBISU	87 INDU
< 4.6E-6/gram	> 0.5	deep schist		KOVALIK	86 INDU
< 1.6E-6/gram	> 0.5	manganese nodules		2 KOVALIK	86 INDU
< 1.3E-6/gram	> 0.5	seawater		KOVALIK	86 INDU

See key on page 1171

Searches Particle Listings
Magnetic Monopole Searches

Table with columns: Energy/Flux, Material, Searcher, Experiment, Status. Includes entries like '>1.E+14/gram', '>1/3 iron aerosols', 'MIKHAILOV 83 SPEC', etc.

Monopole Density — Astrophysics

Table with columns: DENSITY, CHG, MATERIAL, DOCUMENT ID, TECN. Includes entries like '<1.E-9/gram', '1 sun, catalysis', '1 ARAFUNE 83 COSM', etc.

REFERENCES FOR Magnetic Monopole Searches

Extensive list of references for magnetic monopole searches, including authors like AAD, KOBAYASHI, ABBASI, etc., and their respective publications.

Continuation of references for magnetic monopole searches, including authors like CAPLIN, ARAFUNE, CROMAR, etc., and their respective publications.

OTHER RELATED PAPERS

References for other related papers, including GROOM 86 PRPL 140 323, D.E. Groom (UTAH).

Searches Particle Listings

Supersymmetric Particle Searches

Supersymmetric Particle Searches

The exclusion of particle masses within a mass range (m_1, m_2) will be denoted with the notation “none m_1 – m_2 ” in the VALUE column of the following Listings. The latest unpublished results are described in the “Supersymmetry: Experiment” review.

See the related review(s):

Supersymmetry, Part I (Theory)

Supersymmetry, Part II (Experiment)

CONTENTS:

- $\tilde{\chi}_1^0$ (Lightest Neutralino) mass limit
 - Accelerator limits for stable $\tilde{\chi}_1^0$
 - Bounds on $\tilde{\chi}_1^0$ from dark matter searches
 - $\tilde{\chi}_1^0$ - p elastic cross section
 - Spin-dependent interactions
 - Spin-independent interactions
 - Other bounds on $\tilde{\chi}_1^0$ from astrophysics and cosmology
 - Unstable $\tilde{\chi}_1^0$ (Lightest Neutralino) mass limit
- $\tilde{\chi}_2^0, \tilde{\chi}_3^0, \tilde{\chi}_4^0$ (Neutralinos) mass limits
- $\tilde{\chi}_1^\pm, \tilde{\chi}_2^\pm$ (Charginos) mass limits
- Long-lived $\tilde{\chi}^\pm$ (Chargino) mass limit
- $\tilde{\nu}$ (Sneutrino) mass limit
- Charged sleptons
 - R-parity conserving \tilde{e} (Selectron) mass limit
 - R-parity violating \tilde{e} (Selectron) mass limit
 - R-parity conserving $\tilde{\mu}$ (Smuon) mass limit
 - R-parity violating $\tilde{\mu}$ (Smuon) mass limit
 - R-parity conserving $\tilde{\tau}$ (Stau) mass limit
 - R-parity violating $\tilde{\tau}$ (Stau) mass limit
 - Long-lived $\tilde{\ell}$ (Slepton) mass limit
- \tilde{q} (Squark) mass limit
 - R-parity conserving \tilde{q} (Squark) mass limit
 - R-parity violating \tilde{q} (Squark) mass limit
- Long-lived \tilde{q} (Squark) mass limit
- \tilde{b} (Sbottom) mass limit
 - R-parity conserving \tilde{b} (Sbottom) mass limit
 - R-parity violating \tilde{b} (Sbottom) mass limit
- \tilde{t} (Stop) mass limit
 - R-parity conserving \tilde{t} (Stop) mass limit
 - R-parity violating \tilde{t} (Stop) mass limit
- Heavy \tilde{g} (Gluino) mass limit
 - R-parity conserving heavy \tilde{g} (Gluino) mass limit
 - R-parity violating heavy \tilde{g} (Gluino) mass limit
- Long-lived \tilde{g} (Gluino) mass limit
- Light \tilde{G} (Gravitino) mass limits from collider experiments
- Supersymmetry miscellaneous results

The results shown below, unless stated otherwise, are based on the Minimal Supersymmetric Standard Model (MSSM), as described in the Note on Supersymmetry. Unless otherwise indicated, this includes the assumption of common gaugino and scalar masses at the scale of Grand Unification (GUT), and use of the resulting relations in the spectrum and decay branching ratios. Unless otherwise indicated, it is also assumed that R -parity (R) is conserved and that:

- 1) The $\tilde{\chi}_1^0$ is the lightest supersymmetric particle (LSP),
- 2) $m_{\tilde{f}_L} = m_{\tilde{f}_R}$, where $\tilde{f}_{L,R}$ refer to the scalar partners of left- and right-handed fermions.

Limits involving different assumptions are identified in the Comments or in the Footnotes, in particular also the many simplified models, see definitions below. We summarize here the notations used in this Chapter to characterize some of the most common deviations from the MSSM (for further details, see the Note on Supersymmetry).

Theories with R -parity violation (RPV) are characterized by a superpotential of the form: $\lambda_{ijk} L_i L_j e_k^c + \lambda'_{ijk} L_i Q_j d_k^c + \lambda''_{ijk} u_i^c d_j^c d_k^c$, where i, j, k are generation indices. The presence of any of these couplings is often identified in the following by the symbols $LL\bar{E}$, $LQ\bar{D}$, and $U\bar{D}\bar{D}$. Mass limits in the presence

of RPV will often refer to “direct” and “indirect” decays. Direct refers to RPV decays of the particle in consideration. Indirect refers to cases where RPV appears in the decays of the LSP. The LSP need not be the $\tilde{\chi}_1^0$.

In several models, most notably in theories with so-called Gauge Mediated Supersymmetry Breaking (GMSB), the gravitino (\tilde{G}) is the LSP. It is usually much lighter than any other massive particle in the spectrum, and $m_{\tilde{G}}$ is then neglected in all decay processes involving gravitinos. In these scenarios, particles other than the neutralino are sometimes considered as the next-to-lightest supersymmetric particle (NLSP), and are assumed to decay to their even- R partner plus \tilde{G} . If the lifetime is short enough for the decay to take place within the detector, \tilde{G} is assumed to be undetected and to give rise to missing energy (E) or missing transverse energy (E_T) signatures.

When needed, specific assumptions on the eigenstate content of $\tilde{\chi}^0$ and $\tilde{\chi}^\pm$ states are indicated, using the notation $\tilde{\gamma}$ (photino), \tilde{H} (higgsino), \tilde{W} (wino), and \tilde{Z} (zino) to signal that the limit of pure states was used. The term gaugino is also used, to generically indicate wino-like charginos and zino-like neutralinos.

In the listings we have made use of the following abbreviations for simplified models employed by the experimental collaborations in supersymmetry searches published in the past year.

WARNING: Experimental lower mass limits determined within simplified models are to be treated with extreme care as they might not be directly applicable to realistic models. This is outlined in detail in the publications and we recommend consulting them before using bounds. For example, branching ratios, typically fixed to specific values in simplified models, can vary substantially in more elaborate models.

Simplified Models Table

Tglu1A: gluino pair production with $\tilde{g} \rightarrow q\bar{q}\tilde{\chi}_1^0$.

Tglu1B: gluino pair production with $\tilde{g} \rightarrow q\bar{q}'\tilde{\chi}_1^\pm, \tilde{\chi}_1^\pm \rightarrow W^\pm\tilde{\chi}_1^0$.

Tglu1C: gluino pair production with a 2/3 probability of having a $\tilde{g} \rightarrow q\bar{q}'\tilde{\chi}_1^\pm, \tilde{\chi}_1^\pm \rightarrow W^\pm\tilde{\chi}_1^0$ decay and a 1/3 probability of having a $\tilde{g} \rightarrow q\bar{q}\tilde{\chi}_2^0, \tilde{\chi}_2^0 \rightarrow Z^\pm\tilde{\chi}_1^0$ decay.

Tglu1D: gluino pair production with one gluino decaying to $q\bar{q}'\tilde{\chi}_1^\pm$ with $\tilde{\chi}_1^\pm \rightarrow W^\pm + \tilde{G}$, and the other gluino decaying to $q\bar{q}\tilde{\chi}_1^0$ with $\tilde{\chi}_1^0 \rightarrow \gamma + \tilde{G}$.

Tglu1E: gluino pair production with $\tilde{g} \rightarrow q\bar{q}'\tilde{\chi}_1^\pm, \tilde{\chi}_1^\pm \rightarrow W^\pm\tilde{\chi}_2^0$ and $\tilde{\chi}_2^0 \rightarrow Z^\pm\tilde{\chi}_1^0$ where $m_{\tilde{\chi}_1^\pm} = (m_{\tilde{g}} + m_{\tilde{\chi}_1^0})/2$, $m_{\tilde{\chi}_2^0} = (m_{\tilde{\chi}_1^\pm} + m_{\tilde{\chi}_1^0})/2$.

Tglu1F: gluino pair production with $\tilde{g} \rightarrow q\bar{q}'\tilde{\chi}_1^\pm$ or $\tilde{g} \rightarrow q\bar{q}\tilde{\chi}_2^0$ with equal branching ratios, where $\tilde{\chi}_1^\pm$ decays through an intermediate scalar tau lepton or sneutrino to $\tau\nu\tilde{\chi}_1^0$ and where $\tilde{\chi}_2^0$ decays through an intermediate scalar tau lepton or sneutrino to $\tau^+\tau^-\tilde{\chi}_1^0$ or $\nu\bar{\nu}\tilde{\chi}_1^0$; the mass hierarchy is such that $m_{\tilde{\chi}_1^\pm} \sim m_{\tilde{\chi}_2^0} = (m_{\tilde{g}} + m_{\tilde{\chi}_1^0})/2$ and $m_{\tilde{\tau},\tilde{\nu}} = (m_{\tilde{\chi}_1^\pm} + m_{\tilde{\chi}_1^0})/2$.

Tglu1G: gluino pair production with $\tilde{g} \rightarrow q\bar{q}\tilde{\chi}_2^0$, and $\tilde{\chi}_2^0$ decaying through an intermediate slepton or sneutrino to $l^+\nu\tilde{\chi}_1^0$ or $\nu\bar{\nu}\tilde{\chi}_1^0$ where $m_{\tilde{\chi}_2^0} = (m_{\tilde{g}} + m_{\tilde{\chi}_1^0})/2$ and $m_{\tilde{\nu},\tilde{e}} = (m_{\tilde{\chi}_2^0} + m_{\tilde{\chi}_1^0})/2$.

Tglu1H: gluino pair production with $\tilde{g} \rightarrow q\bar{q}\tilde{\chi}_2^0$, and $\tilde{\chi}_2^0 \rightarrow \tilde{\chi}_1^0 Z^{0(*)}$.

Tglu1I: gluino pair production with $\tilde{g} \rightarrow q\bar{q}\tilde{\chi}_2^0$, and $\tilde{\chi}_2^0 \rightarrow \tilde{\chi}_1^0 H$.

Tglu1J: gluino pair production with $\tilde{g} \rightarrow q\bar{q}\tilde{\chi}_2^0$, and $\text{BR}(\tilde{\chi}_2^0 \rightarrow \tilde{\chi}_1^0 Z^{0(*)}) = \text{BR}(\tilde{\chi}_2^0 \rightarrow \tilde{\chi}_1^0 H) = 0.5$.

Tglu1LL gluino pair production where $\tilde{g} \rightarrow q\bar{q}\tilde{\chi}_1^0$ happens with 1/3 probability and $\tilde{g} \rightarrow q\bar{q}'\tilde{\chi}_1^\pm$ happens with 2/3 probability. The

- $\tilde{\chi}_1^\pm$ is assumed to be few hundreds of MeV heavier than the $\tilde{\chi}_1^0$, and decays to $\tilde{\chi}_1^0$ via a pion.
- Tglu2A:** gluino pair production with $\tilde{g} \rightarrow b\tilde{b}\tilde{\chi}_1^0$.
- Tglu3A:** gluino pair production with $\tilde{g} \rightarrow t\tilde{t}\tilde{\chi}_1^0$.
- Tglu3B:** gluino pair production with $\tilde{g} \rightarrow \tilde{t}\tilde{t}$ where \tilde{t} decays exclusively to $t\tilde{\chi}_1^0$.
- Tglu3C:** gluino pair production with $\tilde{g} \rightarrow \tilde{t}\tilde{t}$ where \tilde{t} decays exclusively to $c\tilde{\chi}_1^0$.
- Tglu3D:** gluino pair production with $\tilde{g} \rightarrow \tilde{t}\tilde{b}\tilde{\chi}_1^\pm$ with $\tilde{\chi}_1^\pm \rightarrow W^\pm\tilde{\chi}_1^0$.
- Tglu3E:** gluino pair production where the gluino decays 25% of the time through $\tilde{g} \rightarrow \tilde{t}\tilde{\chi}_1^0$, 25% of the time through $\tilde{g} \rightarrow \tilde{b}\tilde{b}\tilde{\chi}_1^0$ and 50% of the time through $\tilde{g} \rightarrow \tilde{t}\tilde{b}\tilde{\chi}_1^\pm$ with $\tilde{\chi}_1^\pm \rightarrow W^\pm\tilde{\chi}_1^0$.
- Tglu3F:** gluino pair production with wino-like couplings to electroweakinos, that is: $\tilde{g} \rightarrow \tilde{t}\tilde{\chi}_{1,2}^0$ with BR 17%, $\tilde{g} \rightarrow \tilde{b}\tilde{\chi}_{1,2}^0$ with BR 17%, $\tilde{g} \rightarrow \tilde{t}\tilde{\chi}_1^\pm$ with BR 66%.
- Tglu3G:** gluino pair production with higgsino-like couplings to electroweakinos, that is: $\tilde{g} \rightarrow \tilde{t}\tilde{\chi}_{1,2}^0$ with BR 50%, $\tilde{g} \rightarrow \tilde{t}\tilde{\chi}_1^\pm$ with BR 50%.
- Tglu4A:** gluino pair production with one gluino decaying to $q\tilde{q}\tilde{\chi}_1^\pm$ with $\tilde{\chi}_1^\pm \rightarrow W^\pm + \tilde{G}$, and the other gluino decaying to $q\tilde{q}\tilde{\chi}_1^0$ with $\tilde{\chi}_1^0 \rightarrow \gamma + \tilde{G}$.
- Tglu4B:** gluino pair production with gluinos decaying to $q\tilde{q}\tilde{\chi}_1^0$ and $\tilde{\chi}_1^0 \rightarrow \gamma + \tilde{G}$.
- Tglu4C:** gluino pair production with gluinos decaying to $\tilde{g} \rightarrow q\tilde{q}\tilde{\chi}_1^0$ and $\tilde{\chi}_1^0 \rightarrow Z + \tilde{G}$.
- Tglu4D:** gluino pair production with $\tilde{g} \rightarrow q\tilde{q}\tilde{\chi}_1^0$ where the $\tilde{\chi}_1^0$ decays with equal probability to $\tilde{\chi}_1^0 \rightarrow \gamma + \tilde{G}$ or to $\tilde{\chi}_1^0 \rightarrow H + \tilde{G}$.
- Tglu4E:** gluino pair production with $\tilde{g} \rightarrow \tilde{b}\tilde{b}\tilde{\chi}_1^0$ where the $\tilde{\chi}_1^0$ decays with equal probability to $\tilde{\chi}_1^0 \rightarrow \gamma + \tilde{G}$ or to $\tilde{\chi}_1^0 \rightarrow Z + \tilde{G}$.
- Tglu4F:** gluino pair production with $\tilde{g} \rightarrow \tilde{t}\tilde{t}\tilde{\chi}_1^0$ where the $\tilde{\chi}_1^0$ decays with equal probability to $\tilde{\chi}_1^0 \rightarrow \gamma + \tilde{G}$ or to $\tilde{\chi}_1^0 \rightarrow Z + \tilde{G}$.
- Tglu4G:** gluino pair production with $\tilde{g} \rightarrow q\tilde{q}\tilde{\chi}_1^0$ where the $\tilde{\chi}_1^0$ decays with equal probability to $\tilde{\chi}_1^0 \rightarrow \gamma + \tilde{G}$ or to $\tilde{\chi}_1^0 \rightarrow Z + \tilde{G}$.
- Tglu1RPV:** gluino pair production with $\tilde{g} \rightarrow uds$ via RPV coupling λ''_{112} .
- Tglu2RPV:** gluino pair production with $\tilde{g} \rightarrow (tbd, tbs)$ via RPV coupling λ''_{313} or λ''_{323} .
- Tsqk1:** squark pair production with $\tilde{q} \rightarrow q\tilde{\chi}_1^0$.
- Tsqk1LL:** squark pair production where $\tilde{q} \rightarrow q\tilde{\chi}_1^0$ and $\tilde{q} \rightarrow q\tilde{\chi}_1^\pm$ each happen with 50% probability. The $\tilde{\chi}_1^\pm$ is assumed to be few hundreds of MeV heavier than the $\tilde{\chi}_1^0$, and decays to $\tilde{\chi}_1^0$ via a pion.
- Tsqk2:** squark pair production with $\tilde{q} \rightarrow q\tilde{\chi}_2^0$ and $\tilde{\chi}_2^0 \rightarrow Z + \tilde{\chi}_1^0$.
- Tsqk2A:** squark pair production with $\tilde{q} \rightarrow q\tilde{\chi}_2^0$, where one of the $\tilde{\chi}_2^0 \rightarrow Z^{(*)}\tilde{\chi}_1^0 \rightarrow f\tilde{f}\tilde{\chi}_1^0$ and the other $\tilde{\chi}_2^0 \rightarrow \tilde{\ell}\tilde{\ell}^+ \rightarrow \ell^+\ell^-\tilde{\chi}_1^0$.
- Tsqk3:** squark pair production with $\tilde{q} \rightarrow q'\tilde{\chi}_1^\pm$, $\tilde{\chi}_1^\pm \rightarrow W^\pm\tilde{\chi}_1^0$ (like Tglu1B but for squarks)
- Tsqk4:** squark pair production with squarks decaying to $q\tilde{\chi}_1^0$ and $\tilde{\chi}_1^0 \rightarrow \gamma + \tilde{G}$.
- Tsqk4A:** squark pair production with one squark decaying to $q\tilde{\chi}_1^\pm$ with $\tilde{\chi}_1^\pm \rightarrow W^\pm + \tilde{G}$, and the other squark decaying to $q\tilde{\chi}_1^0$ with $\tilde{\chi}_1^0 \rightarrow \gamma + \tilde{G}$.
- Tsqk4B:** squark pair production with squarks decaying to $q\tilde{\chi}_1^0$ and $\tilde{\chi}_1^0 \rightarrow \gamma + \tilde{G}$.
- Tstop1:** stop pair production with $\tilde{t} \rightarrow t\tilde{\chi}_1^0$.
- Tstop1LL:** stop pair production where $\tilde{t} \rightarrow t\tilde{\chi}_1^0$ and $\tilde{t} \rightarrow b\tilde{\chi}_1^\pm$ each happen with 50% probability. The $\tilde{\chi}_1^\pm$ is assumed to be few hundreds of MeV heavier than the $\tilde{\chi}_1^0$, and decays to $\tilde{\chi}_1^0$ via a pion.
- Tstop2:** stop pair production with $\tilde{t} \rightarrow b\tilde{\chi}_1^\pm$ with $\tilde{\chi}_1^\pm \rightarrow W^\pm\tilde{\chi}_1^0$.
- Tstop3:** stop pair production with the subsequent four-body decay $\tilde{t} \rightarrow bff'\tilde{\chi}_1^0$ where f represents a lepton or a quark.
- Tstop4:** stop pair production with $\tilde{t} \rightarrow c\tilde{\chi}_1^0$.
- Tstop5:** stop pair production with $\tilde{t} \rightarrow b\tilde{\nu}\tilde{\tau}$ with $\tilde{\tau} \rightarrow \tau\tilde{G}$.
- Tstop6:** stop pair production with $\tilde{t} \rightarrow t + \tilde{\chi}_2^0$, where $\tilde{\chi}_2^0 \rightarrow Z + \tilde{\chi}_1^0$ or $H + \tilde{\chi}_1^0$ each with BR 50%.
- Tstop7:** stop pair production with $\tilde{t}_2 \rightarrow \tilde{t}_1 + H/Z$, where $\tilde{t}_1 \rightarrow t + \tilde{\chi}_1^0$.
- Tstop8:** stop pair production with equal probability of the stop decaying via $\tilde{t} \rightarrow t\tilde{\chi}_1^0$ or via $\tilde{t} \rightarrow b\tilde{\chi}_1^\pm$ with $\tilde{\chi}_1^\pm \rightarrow W^\pm\tilde{\chi}_1^0$.
- Tstop9:** stop pair production with equal probability of the stop decaying via $\tilde{t} \rightarrow c\tilde{\chi}_1^0$ or via the four-body decay $\tilde{t} \rightarrow bff'\tilde{\chi}_1^0$ where f represents a lepton or a quark.
- Tstop10:** stop pair production with $\tilde{t} \rightarrow b\tilde{\chi}_1^\pm$ and $\tilde{\chi}_1^\pm \rightarrow W^\pm\tilde{\chi}_1^0 \rightarrow (f\tilde{f}') + \tilde{\chi}_1^0$ with a virtual W -boson.
- Tstop11:** stop pair production with $\tilde{t} \rightarrow b\tilde{\chi}_1^\pm$ with $\tilde{\chi}_1^\pm$ decaying through an intermediate slepton to $l\nu\tilde{\chi}_1^0$.
- Tstop12:** stop pair production with $\tilde{t} \rightarrow t\tilde{\chi}_1^0$ and $\tilde{\chi}_1^0 \rightarrow \gamma + \tilde{G}$.
- Tstop13:** stop pair production with $\tilde{t} \rightarrow t\tilde{\chi}_1^0$ where the $\tilde{\chi}_1^0$ can decay with equal probability to $\tilde{\chi}_1^0 \rightarrow \gamma + \tilde{G}$ or to $\tilde{\chi}_1^0 \rightarrow Z + \tilde{G}$.
- Tstop14:** stop pair production with wino-like couplings to electroweakinos, that is: $\tilde{t} \rightarrow t\tilde{\chi}_{1,2}^0$ with BR 33%, $\tilde{g} \rightarrow b\tilde{\chi}_1^\pm$ with BR 67%.
- Tstop15:** stop pair production with higgsino-like couplings to electroweakinos, that is: $\tilde{t} \rightarrow t\tilde{\chi}_{1,2}^0$ with BR 50%, $\tilde{g} \rightarrow b\tilde{\chi}_1^\pm$ with BR 50%.
- Tstop16:** stop pair production with $\tilde{t} \rightarrow b\tilde{\chi}_1^\pm$, followed either by $\tilde{\chi}_1^\pm \rightarrow \nu\tau\tilde{\tau}_1$ and $\tilde{\tau}_1 \rightarrow \tau\tilde{\chi}_1^0$, or by $\tilde{\chi}_1^\pm \rightarrow \tau\tilde{\nu}_\tau$ and $\tilde{\nu}_\tau \rightarrow \nu\tilde{\chi}_1^0$, each with BR 50%.
- Tstop1RPV:** stop pair production with $\tilde{t} \rightarrow \tilde{b}\tilde{s}$ via RPV coupling λ''_{323} .
- Tstop2RPV:** stop pair production with $\tilde{t} \rightarrow b\tilde{t}$, via RPV coupling λ''_{333} .
- Tstop3RPV:** stop pair production with $\tilde{t} \rightarrow q\mu$, via RPV coupling λ''_{23k} .
- Tstop4RPV:** stop pair production with $\tilde{t} \rightarrow b\tilde{\chi}_1^\pm$, $\tilde{\chi}_1^\pm \rightarrow bbs$ via RPV coupling λ''_{323} .
- Tstop5RPV:** stop pair production with $\tilde{t} \rightarrow t\tilde{\chi}_{1,2}^0$, $\tilde{\chi}_{1,2}^0 \rightarrow tbs$ via RPV coupling λ''_{323} .
- Tsbot1:** sbottom pair production with $\tilde{b} \rightarrow b\tilde{\chi}_1^0$.
- Tsbot2:** sbottom pair production with $\tilde{b} \rightarrow t\tilde{\chi}_1^-, \tilde{\chi}_1^- \rightarrow W^-\tilde{\chi}_1^0$.
- Tsbot3:** sbottom pair production with $\tilde{b} \rightarrow b\tilde{\chi}_2^0$, where one of the $\tilde{\chi}_2^0 \rightarrow Z^{(*)}\tilde{\chi}_1^0 \rightarrow f\tilde{f}\tilde{\chi}_1^0$ and the other $\tilde{\chi}_2^0 \rightarrow \tilde{\ell}\tilde{\ell}^+ \rightarrow \ell^+\ell^-\tilde{\chi}_1^0$.
- Tsbot4:** sbottom pair production with $\tilde{b} \rightarrow b\tilde{\chi}_2^0$, with $\tilde{\chi}_2^0 \rightarrow H\tilde{\chi}_1^0$.
- Tchi1chi1A:** electroweak pair and associated production of nearly mass-degenerate charginos $\tilde{\chi}_1^\pm$ and neutralinos $\tilde{\chi}_1^0$, where $\tilde{\chi}_1^\pm$ decays to $\tilde{\chi}_1^0$ plus soft radiation, and where one of the $\tilde{\chi}_1^0$ decays to $\gamma + \tilde{G}$ while the other one decays to $Z/H + \tilde{G}$ (with equal probability).
- Tchi1chi1B:** electroweak pair production of charginos $\tilde{\chi}_1^\pm$, where $\tilde{\chi}_1^\pm$ decays through an intermediate slepton or sneutrino to $l\nu\tilde{\chi}_1^0$ and where the slepton or sneutrino mass is 5%, 25%, 50%, 75% and 95% of the $\tilde{\chi}_1^\pm$ mass.
- Tchi1chi1C:** electroweak pair production of charginos $\tilde{\chi}_1^\pm$, where $\tilde{\chi}_1^\pm$ decays through an intermediate slepton or sneutrino to $l\nu\tilde{\chi}_1^0$ and where $m_{\tilde{l},\tilde{\nu}} = (m_{\tilde{\chi}_1^\pm} + m_{\tilde{\chi}_1^0})/2$.
- Tchi1chi1D:** electroweak associated pair production of charginos $\tilde{\chi}_1^\pm$, where $\tilde{\chi}_1^\pm$ decays through an intermediate scalar tau lepton or sneutrino to $\tau\nu\tilde{\chi}_1^0$ and where $m_{\tilde{\tau}}, m_{\tilde{\nu}} = (m_{\tilde{\chi}_1^\pm} + m_{\tilde{\chi}_1^0})/2$.
- Tchi1chi1F:** electroweak pair and associated production of nearly mass-degenerate charginos $\tilde{\chi}_1^\pm$ and neutralinos $\tilde{\chi}_1^0$ (i.e. $\tilde{\chi}_1^\pm\tilde{\chi}_1^\pm$ and $\tilde{\chi}_1^\pm\tilde{\chi}_1^0$ production) where the $\tilde{\chi}_1^\pm$ decays exclusively to $\tilde{\chi}_1^0$ plus soft radiation and the $\tilde{\chi}_1^0$ decays to $\gamma/Z + \tilde{G}$.
- Tchi1chi1G:** electroweak pair production of charginos $\tilde{\chi}_1^\pm$, which are nearly mass-degenerate with neutralinos $\tilde{\chi}_1^0$. The $\tilde{\chi}_1^\pm$ decays either to $W^\pm + \tilde{G}$, or to $\tilde{\chi}_1^0$ plus soft radiation. The $\tilde{\chi}_1^0$ decays exclusively to $\gamma + \tilde{G}$.
- Tchi1chi1H:** electroweak pair production of charginos $\tilde{\chi}_1^\pm$, with $\tilde{\chi}_1^\pm \rightarrow W^\pm + \tilde{\chi}_1^0$ and $W^\pm \rightarrow \ell^\pm + \nu$.
- Tchi1chi1I:** electroweak pair production of charginos $\tilde{\chi}_1^\pm$ with $\tilde{\chi}_1^\pm \rightarrow W^\pm\tilde{\chi}_1^0$ and $W^\pm \rightarrow q\tilde{q}'$.
- Tchi1n1A:** electroweak associated production of mass-degenerate charginos $\tilde{\chi}_1^\pm$ and neutralinos $\tilde{\chi}_1^0$, where $\tilde{\chi}_1^\pm$ decays exclusively to $W^\pm + \tilde{G}$ and $\tilde{\chi}_1^0$ decays exclusively to $\gamma + \tilde{G}$.
- Tchi1n2A:** electroweak associated production of mass-degenerate charginos $\tilde{\chi}_1^\pm$ and neutralinos $\tilde{\chi}_2^0$, where $\tilde{\chi}_1^\pm$ decays through an intermediate slepton or sneutrino to $l\nu\tilde{\chi}_1^0$ and where $\tilde{\chi}_2^0$ decays through an intermediate slepton or sneutrino to $l^+\ell^-\tilde{\chi}_1^0$ or $\nu\tilde{\nu}\tilde{\chi}_1^0$.
- Tchi1n2B:** electroweak associated production of mass-degenerate charginos $\tilde{\chi}_1^\pm$ and neutralinos $\tilde{\chi}_2^0$, where $\tilde{\chi}_1^\pm$ decays through an intermediate slepton or sneutrino to $l\nu\tilde{\chi}_1^0$ and where $\tilde{\chi}_2^0$ decays through an intermediate slepton or sneutrino to $l^+\ell^-\tilde{\chi}_1^0$ or $\nu\tilde{\nu}\tilde{\chi}_1^0$ and where the slepton or sneutrino mass is 5%, 25%, 50%, 75% and 95% of the $\tilde{\chi}_1^\pm$ mass.

Searches Particle Listings

Supersymmetric Particle Searches

- Tchi1n2C:** electroweak associated production of mass-degenerate charginos $\tilde{\chi}_1^\pm$ and neutralinos $\tilde{\chi}_2^0$, where $\tilde{\chi}_1^\pm$ decays through an intermediate slepton or sneutrino to $l\nu\tilde{\chi}_1^0$ and where $\tilde{\chi}_2^0$ decays through an intermediate slepton or sneutrino to $l^+l^-\tilde{\chi}_1^0$ or $\nu\bar{\nu}\tilde{\chi}_1^0$ and where $m_{\tilde{l},\tilde{\nu}} = (m_{\tilde{\chi}_1^\pm} + m_{\tilde{\chi}_1^0})/2$.
- Tchi1n2D:** electroweak associated production of mass-degenerate charginos $\tilde{\chi}_1^\pm$ and neutralinos $\tilde{\chi}_2^0$, where $\tilde{\chi}_1^\pm$ decays through an intermediate scalar tau lepton or sneutrino to $\tau\nu\tilde{\chi}_1^0$ and where $\tilde{\chi}_2^0$ decays through an intermediate scalar tau lepton or sneutrino to $\tau^+\tau^-\tilde{\chi}_1^0$ or $\nu\bar{\nu}\tilde{\chi}_1^0$ and where $m_{\tilde{\tau},\tilde{\nu}} = (m_{\tilde{\chi}_1^\pm} + m_{\tilde{\chi}_1^0})/2$.
- Tchi1n2E:** electroweak associated production of mass-degenerate charginos $\tilde{\chi}_1^\pm$ and neutralinos $\tilde{\chi}_2^0$, where $\tilde{\chi}_1^\pm \rightarrow W^\pm + \tilde{\chi}_1^0$ and $\tilde{\chi}_2^0 \rightarrow H + \tilde{\chi}_1^0$.
- Tchi1n2F:** electroweak associated production of mass-degenerate wino-like charginos $\tilde{\chi}_1^\pm$ and neutralinos $\tilde{\chi}_2^0$, where $\tilde{\chi}_1^\pm$ decays through an intermediate W^{**} to $l\nu\tilde{\chi}_1^0$ and where $\tilde{\chi}_2^0$ decays through an intermediate Z^* to $l^+l^-\tilde{\chi}_1^0$ or $\nu\bar{\nu}\tilde{\chi}_1^0$.
- Tchi1n2Fa:** electroweak associated production of mass-degenerate wino-like charginos $\tilde{\chi}_1^\pm$ and neutralinos $\tilde{\chi}_2^0$, where $\tilde{\chi}_1^\pm$ decays through an intermediate W^{**} to $q\bar{q}\tilde{\chi}_1^0$ and where $\tilde{\chi}_2^0$ decays through an intermediate Z^* to $l^+l^-\tilde{\chi}_1^0$ or $\nu\bar{\nu}\tilde{\chi}_1^0$.
- Tchi1n2Fb:** electroweak associated production of mass-degenerate wino-like charginos $\tilde{\chi}_1^\pm$ and neutralinos $\tilde{\chi}_2^0$, where $\tilde{\chi}_1^\pm$ decays through an intermediate $W^{(*)}$ to $q\bar{q}\tilde{\chi}_1^0$ and where $\tilde{\chi}_2^0$ decays through an intermediate $Z^{(*)}$ to $q\bar{q}\tilde{\chi}_1^0$.
- Tchi1n2Fc:** electroweak associated production of mass-degenerate wino-like charginos $\tilde{\chi}_1^\pm$ and neutralinos $\tilde{\chi}_2^0$, where $\tilde{\chi}_1^\pm$ decays through an intermediate $W^{(*)}$ to $q\bar{q}\tilde{\chi}_1^0$ and where $\tilde{\chi}_2^0$ decays through an intermediate $H^{(*)}$ to $q\bar{q}\tilde{\chi}_1^0$.
- Tchi1n2G:** electroweak associated production of Higgsino-like charginos $\tilde{\chi}_1^\pm$ and neutralinos $\tilde{\chi}_2^0$, and electroweak associated production of $\tilde{\chi}_2^0$ and $\tilde{\chi}_1^0$, where $m_{\tilde{\chi}_1^\pm} = (m_{\tilde{\chi}_2^0} + m_{\tilde{\chi}_1^0})/2$ and where $\tilde{\chi}_1^\pm$ decays through an intermediate W^{**} to $q\bar{q}\tilde{\chi}_1^0$ and where $\tilde{\chi}_2^0$ decays through an intermediate Z^* to $l^+l^-\tilde{\chi}_1^0$.
- Tchi1n2Ga:** electroweak associated production of Higgsino-like charginos $\tilde{\chi}_1^\pm$ and neutralinos $\tilde{\chi}_2^0$, and electroweak associated production of $\tilde{\chi}_2^0$ and $\tilde{\chi}_1^0$, where $m_{\tilde{\chi}_1^\pm} = (m_{\tilde{\chi}_2^0} + m_{\tilde{\chi}_1^0})/2$ and where $\tilde{\chi}_1^\pm$ decays through an intermediate W^{**} to $l\nu\tilde{\chi}_1^0$ and where $\tilde{\chi}_2^0$ decays through an intermediate Z^* to $l^+l^-\tilde{\chi}_1^0$.
- Tchi1n2H:** electroweak associated production of mass-degenerate charginos $\tilde{\chi}_1^\pm$ and neutralinos $\tilde{\chi}_2^0$, where $\tilde{\chi}_1^\pm$ decays through an intermediate slepton or sneutrino to $l\nu\tilde{\chi}_1^0$ and where $\tilde{\chi}_2^0$ decays through an intermediate scalar tau lepton or sneutrino to $\tau^+\tau^-\tilde{\chi}_1^0$ or $\nu\bar{\nu}\tilde{\chi}_1^0$.
- Tchi1n2I:** electroweak associated production of mass-degenerate charginos $\tilde{\chi}_1^\pm$ and neutralinos $\tilde{\chi}_2^0$, where $\tilde{\chi}_1^\pm$ decays to $W^\pm + \tilde{\chi}_1^0$ and where $\tilde{\chi}_2^0$ decays 50% of the time to $Z + \tilde{\chi}_1^0$ and 50% of the time to $H + \tilde{\chi}_1^0$.
- Tchi1n12_GGM:** in the framework of General Gauge Mediation (GGM): electroweak pair and associated production of nearly mass-degenerate charginos $\tilde{\chi}_1^\pm$ and neutralinos $\tilde{\chi}_1^0, \tilde{\chi}_2^0$ (i.e. $\tilde{\chi}_1^\pm\tilde{\chi}_1^0, \tilde{\chi}_1^\pm\tilde{\chi}_2^0$ production) where the $\tilde{\chi}_1^\pm$ decays exclusively to $W^\pm + \tilde{G}$, the $\tilde{\chi}_2^0$ decays to $Z/H + \tilde{G}$ and the $\tilde{\chi}_1^0$ decays to $\gamma/Z + \tilde{G}$. The branching ratios depend on the composition of the gauge eigenstates of the neutralinos in the GGM scenario.
- TwinoLSPBL:** Electroweak pair production of wino-like $\tilde{\chi}_1^\pm$ and $\tilde{\chi}_1^0$ (i.e. $\tilde{\chi}_1^\pm\tilde{\chi}_1^\pm$ and $\tilde{\chi}_1^0\tilde{\chi}_1^0$). The $\tilde{\chi}_1^\pm$ can decay via bi-linear RPV into Zl, Hl or $W\nu$; the $\tilde{\chi}_1^0$ can decay into $Z\nu, H\nu$ or Wl .
- Tn1n1A:** electroweak pair and associated production of nearly mass-degenerate Higgsino-like charginos $\tilde{\chi}_1^\pm$ and neutralinos $\tilde{\chi}_1^0$ and $\tilde{\chi}_2^0$, where $\tilde{\chi}_1^\pm$ and $\tilde{\chi}_2^0$ decay to $\tilde{\chi}_1^0$ plus soft radiation and where both of the $\tilde{\chi}_1^0$ decay to $H + \tilde{G}$.
- Tn1n1B:** electroweak pair and associated production of nearly mass-degenerate Higgsino-like charginos $\tilde{\chi}_1^\pm$ and neutralinos $\tilde{\chi}_1^0$ and $\tilde{\chi}_2^0$, where $\tilde{\chi}_1^\pm$ and $\tilde{\chi}_2^0$ decay to $\tilde{\chi}_1^0$ plus soft radiation and where the $\tilde{\chi}_1^0$ decays 50% of the time to $H + \tilde{G}$ and 50 % of the time to $Z + \tilde{G}$.
- Tn1n1C:** electroweak pair and associated production of nearly mass-degenerate Higgsino-like charginos $\tilde{\chi}_1^\pm$ and neutralinos $\tilde{\chi}_1^0$ and $\tilde{\chi}_2^0$, where $\tilde{\chi}_1^\pm$ and $\tilde{\chi}_2^0$ decay to $\tilde{\chi}_1^0$ plus soft radiation and where both of the $\tilde{\chi}_1^0$ decay to $Z + \tilde{G}$.

- Tn1n1D:** electroweak pair and associated production of nearly mass-degenerate Higgsino-like charginos $\tilde{\chi}_1^\pm$ and neutralinos $\tilde{\chi}_1^0, \tilde{\chi}_2^0$.
- Tn1n1E:** electroweak pair and associated production of nearly mass-degenerate wino-like charginos $\tilde{\chi}_1^\pm$ and neutralinos $\tilde{\chi}_1^0$.
- Tn1n2A:** electroweak associated production of nearly mass-degenerate neutralinos $\tilde{\chi}_2^0$ and $\tilde{\chi}_3^0$, where the $\tilde{\chi}_2^0$ always decays to $\gamma + \tilde{G}$ and $\tilde{\chi}_3^0$ 50% of the time to $H + \tilde{G}$ and 50 % of the time to $Z + \tilde{G}$.
- Tn2n3A:** electroweak associated production of mass-degenerate neutralinos $\tilde{\chi}_2^0$ and $\tilde{\chi}_3^0$, where $\tilde{\chi}_2^0$ and $\tilde{\chi}_3^0$ decay through intermediate sleptons to $l^+l^-\tilde{\chi}_1^0$ and where the slepton mass is 5%, 25%, 50%, 75% and 95% of the $\tilde{\chi}_2^0$ mass.
- Tn2n3B:** electroweak associated production of mass-degenerate neutralinos $\tilde{\chi}_2^0$ and $\tilde{\chi}_3^0$, where $\tilde{\chi}_2^0$ and $\tilde{\chi}_3^0$ decay through intermediate sleptons to $l^+l^-\tilde{\chi}_1^0$ and where $m_{\tilde{l}} = (m_{\tilde{\chi}_2^0} + m_{\tilde{\chi}_3^0})/2$.

- TWinoBinoA:** electroweak pair production of mass-degenerate wino-like doublet $(\tilde{\chi}_2^0, \tilde{\chi}_1^\pm)$ (including all pair-production mechanisms) decaying into a bino singlet ($\tilde{\chi}_1^0$). Decays happen via Standard Model bosons, assumed to decay via hadrons.
- TWinoHinoA:** electroweak pair production of mass-degenerate wino-like doublet $(\tilde{\chi}_3^0, \tilde{\chi}_2^\pm)$ (including all possible pair-production mechanisms) decaying into a quasi-mass-degenerate Higgsino triplet $(\tilde{\chi}_1^0, \tilde{\chi}_2^0, \tilde{\chi}_3^\pm)$. Decays happen via Standard Model bosons, assumed to decay via hadrons.
- THinoBinoA:** electroweak pair production of quasi-mass-degenerate higgsino-like triplet $(\tilde{\chi}_2^0, \tilde{\chi}_3^0, \tilde{\chi}_1^\pm)$ (including all possible pair-production mechanisms) decaying into a bino singlet ($\tilde{\chi}_1^0$). Decays happen via Standard Model bosons, assumed to decay via hadrons.
- THinoWinoA:** electroweak pair production of quasi-mass-degenerate higgsino-like triplet $(\tilde{\chi}_2^0, \tilde{\chi}_3^0, \tilde{\chi}_1^\pm)$ (including all possible pair-production mechanisms) decaying into a mass-degenerate wino doublet $(\tilde{\chi}_1^0, \tilde{\chi}_1^\pm)$. Decays happen via Standard Model bosons, assumed to decay via hadrons.

$\tilde{\chi}_1^0$ (Lightest Neutralino) mass limit

$\tilde{\chi}_1^0$ is often assumed to be the lightest supersymmetric particle (LSP). See also the $\tilde{\chi}_2^0, \tilde{\chi}_3^0, \tilde{\chi}_4^0$ section below.

We have divided the $\tilde{\chi}_1^0$ listings below into five sections:

- 1) Accelerator limits for stable $\tilde{\chi}_1^0$,
- 2) Bounds on $\tilde{\chi}_1^0$ from dark matter searches,
- 3) $\tilde{\chi}_1^0 - p$ elastic cross section (spin-dependent, spin-independent interactions),
- 4) Other bounds on $\tilde{\chi}_1^0$ from astrophysics and cosmology, and
- 5) Unstable $\tilde{\chi}_1^0$ (Lightest Neutralino) mass limit.

Accelerator limits for stable $\tilde{\chi}_1^0$

Unless otherwise stated, results in this section assume spectra, production rates, decay modes, and branching ratios as evaluated in the MSSM, with gaugino and sfermion mass unification at the GUT scale. These papers generally study production of $\tilde{\chi}_i^0\tilde{\chi}_j^0$ ($i \geq 1, j \geq 2$), $\tilde{\chi}_1^+\tilde{\chi}_1^-$, and (in the case of hadronic collisions) $\tilde{\chi}_1^+\tilde{\chi}_2^0$ pairs. The mass limits on $\tilde{\chi}_1^0$ are either direct, or follow indirectly from the constraints set by the non-observation of $\tilde{\chi}_1^\pm$ and $\tilde{\chi}_2^0$ states on the gaugino and higgsino MSSM parameters M_2 and μ . In some cases, information is used from the nonobservation of slepton decays.

Obsolete limits obtained from e^+e^- collisions up to $\sqrt{s}=184$ GeV have been removed from this compilation and can be found in the 2000 Edition (The European Physical Journal **C15** 1 (2000)) of this Review.
 $\Delta m = m_{\tilde{\chi}_2^0} - m_{\tilde{\chi}_1^0}$

VALUE (GeV)	CL%	DOCUMENT ID	TECN	COMMENT
none 0.5–4.29	95	1 LEES	23c	BABR $B + \text{charged track, RPV}$ $B \rightarrow \tilde{\chi}_1^0 p, \lambda_{113}^0$ of order $10^{-7}-10^{-6}$
>150	95	2 AAD	22E	ATLS $t\bar{u}_L$ production, RPV, $\bar{u}_L \rightarrow \mu\tilde{\chi}_1^0, \lambda_{231}^0 = 1, 200 \text{ GeV} < m_{\bar{u}_L} < 600 \text{ GeV}$.
none 125–175	95	3 TUMASYAN	22s	CMS 2 same-sign e or μ , 3 or 4 leptons, Tn1n1A, $m_{\tilde{G}} = 1 \text{ GeV}$
none 125–415	95	3 TUMASYAN	22s	CMS 2 same-sign e or μ , 3 or 4 leptons, Tn1n1B, $m_{\tilde{G}} = 1 \text{ GeV}$

none 100–625	95	³ TUMASYAN	22s	CMS	2 same-sign e or μ , 3 or 4 leptons, Tn1n1C, $m_{\tilde{G}} = 1$ GeV
none 175–1025	95	⁴ TUMASYAN	22v	CMS	3, 4 b -tag jets or 2 large-radius jets, \cancel{E}_T ; Tn1n1A; $m_{\tilde{G}} = 1$ GeV
none 450–930	95	⁵ AAD	21Ax	ATLS	jets + large-R jets + \cancel{E}_T , Tn1n1C
none 200–320	95	⁶ AAD	21BF	ATLS	$\ell^\pm + b$ -jets + many jets, Tn1n1D, RPV, λ'_{323} electroweakino decay, degenerate Higgsino triplet
none 200–370	95	⁶ AAD	21BF	ATLS	$\ell^\pm + b$ -jets + many jets, Tn1n1E, RPV, λ'_{323} electroweakino decay, degenerate Wino doublet
> 40	95	⁷ DREINER	09	THEO	
		⁸ ABBIENDI	04H	OPAL	all $\tan\beta$, $\Delta m > 5$ GeV, $m_0 > 500$ GeV, $A_0 = 0$
> 42.4	95	⁹ HEISTER	04	ALEP	all $\tan\beta$, all Δm , all m_0
> 39.2	95	¹⁰ ABDALLAH	03M	DLPH	all $\tan\beta$, $m_{\tilde{\nu}} > 500$ GeV
> 46	95	¹¹ ABDALLAH	03M	DLPH	all $\tan\beta$, all Δm , all m_0
> 32.5	95	¹² ACCIARRI	00D	L3	$\tan\beta > 0.7$, $\Delta m > 3$ GeV, all m_0
• • •		¹³ AAD	14K	ATLS	
> 24		¹⁴ CALIBBI	13		thermal relic abundance, MSSM particle content

¹ LEES 23c search in 398 fb^{-1} of e^+e^- annihilations at 10.58 GeV for SUSY in events with a tagged B meson and one and only one charged track that must be consistent with the hypothesis of being a proton. The results are interpreted in an RPV SUSY model, where a neutralino is produced in the decay of a B meson into a neutralino and a proton with the RPV coupling λ'_{113} . A branching fraction upper limit is determined for the λ'_{113} coupling, divided by the relevant squark mass squared as a function of the neutralino mass, see their figure 6. They also search for a new dark sector antibaryon that could be produced in decays of B mesons.

² AAD 22e searched in 139 fb^{-1} of pp collisions at $\sqrt{s} = 13$ TeV for supersymmetry by measuring the yield asymmetry between events containing $e^- \mu^+$ and those containing $e^+ \mu^-$. This was found in agreement with the standard model prediction of 1. Limits are set on the RPV production of $t \tilde{\mu}_L$ events with $\tilde{\mu}_L \rightarrow \mu \tilde{\chi}_1^0$ for various values of λ'_{231} , see their figures 6 and 7.

³ TUMASYAN 22s searched in 137 fb^{-1} of pp collisions at $\sqrt{s} = 13$ TeV for evidence of electroweakino pair production in events with three or four leptons, with up to two hadronically decaying τ leptons, or two same-sign light leptons (e or μ). No significant excess above the Standard Model expectations is observed. Limits are set on the mass of $\tilde{\chi}_2^0$ and $\tilde{\chi}_1^\pm$ in the models Tchi1n2B (in flavory-democratic and tau-enriched or -dominated scenarios), Tchi1n2E, Tchi1n2F, see their Figures 16–20, and on the mass of the higgsino-triplet $\tilde{\chi}_2^0$, $\tilde{\chi}_1^\pm$, and $\tilde{\chi}_1^0$ in the models Tn1n1A, Tn1n1B, and Tn1n1C, see their Figure 21.

⁴ TUMASYAN 22v searched in 137 fb^{-1} of pp collisions at $\sqrt{s} = 13$ TeV for evidence of electroweakino pair production with decay to two Higgs bosons H , with $H \rightarrow b\bar{b}$, resulting either in 4 resolved b -jets or two large-radius jets, and large \cancel{E}_T . No significant excess above the Standard Model expectations is observed. Limits are set on the mass of $\tilde{\chi}_2^0$ and $\tilde{\chi}_1^\pm$ in the models Tn1n1A, see their Figures 11 and 12, or in a model where higgsino-like nearly mass degenerate $\tilde{\chi}_2^0$ and $\tilde{\chi}_3^0$ are pair produced and each decay to H and a bino-like $\tilde{\chi}_1^0$, see their Figure 13. Limits are also set on the gluino mass in the model Tglu1l, see their Figure 14.

⁵ AAD 21Ax searched in 139 fb^{-1} of pp collisions at $\sqrt{s} = 13$ TeV for pair production of electroweakinos decaying to the LSP via the emission of Standard Model bosons (Higgs, W , Z) decaying into hadrons. The final state in all cases characterised by the presence of \cancel{E}_T , jets, and large-R jets tagged according to the boson of interest. Different assumptions (Higgsino, Wino, Bino) are made for the pair produced electroweakinos and for the LSP multiplet. No significant excess above the Standard Model predictions is observed. Limits are set on the electroweakino masses as a function of the model parameters (in particular $m_{\tilde{\chi}_3^0}$). See Fig. 16.

⁶ AAD 21BF searched in 139 fb^{-1} of pp collisions at $\sqrt{s} = 13$ TeV for pair production of gluinos, stops, electroweakinos decaying RPV either directly or indirectly via the LSP. The final state in all cases is one or two leptons, many jets (up to fifteen) and b -jets. Different models with different branching fractions of the gluino or stop follow from the assumptions on the nature of the electroweakinos. No significant excess above the Standard Model predictions is observed. Limits are set on the $gluino$, \tilde{t}_1 , electroweakino masses as a function of the $\tilde{\chi}_1^0$ mass in several scenarios of gluino, stop and electroweakino pair production.

⁷ DREINER 09 show that in the general MSSM with non-universal gaugino masses there exists no model-independent laboratory bound on the mass of the lightest neutralino. An essentially massless $\tilde{\chi}_1^0$ is allowed by the experimental and observational data, imposing some constraints on other MSSM parameters, including M_2 , μ and the slepton and squark masses.

⁸ ABBIENDI 04H search for charginos and neutralinos in events with acoplanar leptons+jets and multi-jet final states in the 192–209 GeV data, combined with the results on leptonic final states from ABBIENDI 04. The results hold for a scan over the parameter space covering the region $0 < M_2 < 5000$ GeV, $-1000 < \mu < 1000$ GeV and $\tan\beta$ from 1 to 40. This limit supersedes ABBIENDI 00H.

⁹ HEISTER 04 data collected up to 209 GeV. Updates earlier analysis of selectrons from HEISTER 02e, includes a new analysis of charginos and neutralinos decaying into stau and uses results on charginos with initial state radiation from HEISTER 02j. The limit is based on the direct search for charginos and neutralinos, the constraints from the slepton search and the Higgs mass limits from HEISTER 02 using a top mass of 175 GeV, interpreted in a framework with universal gaugino and sfermion masses. Assuming the mixing in the stau sector to be negligible, the limit improves to 43.1 GeV. Under the assumption of MSUGRA with unification of the Higgs and sfermion masses, the limit improves to 50 GeV, and reaches 53 GeV for $A_0 = 0$. These limits include and update the results of BARATE 01.

¹⁰ ABDALLAH 03M uses data from $\sqrt{s} = 192$ –208 GeV. A limit on the mass of $\tilde{\chi}_1^0$ is derived from direct searches for neutralinos combined with the chargino search. Neutralinos are searched in the production of $\tilde{\chi}_1^0 \tilde{\chi}_2^0$, $\tilde{\chi}_1^0 \tilde{\chi}_3^0$, as well as $\tilde{\chi}_2^0 \tilde{\chi}_3^0$ and $\tilde{\chi}_2^0 \tilde{\chi}_4^0$ giving rise to cascade decays, and $\tilde{\chi}_1^0 \tilde{\chi}_2^0$ and $\tilde{\chi}_1^0 \tilde{\chi}_3^0$, followed by the decay $\tilde{\chi}_2^0 \rightarrow \tilde{\tau} \tau$. The results hold for the parameter space defined by values of $M_2 < 1$ TeV, $|\mu| \leq 2$ TeV with the $\tilde{\chi}_1^0$ as LSP. The limit is obtained for $\tan\beta = 1$ and large m_0 , where $\tilde{\chi}_2^0 \tilde{\chi}_4^0$ and chargino pair production are important. If the constraint from Higgs searches is also imposed, the limit improves to 49.0 GeV in the m_h^{max} scenario with $m_t = 174.3$ GeV. These limits update the results of ABREU 00j.

¹¹ ABDALLAH 03M uses data from $\sqrt{s} = 192$ –208 GeV. An indirect limit on the mass of $\tilde{\chi}_1^0$ is derived by constraining the MSSM parameter space by the results from direct searches for neutralinos (including cascade decays and $\tilde{\tau} \tau$ final states), for charginos (for all Δm_+) and for sleptons, stop and sbottom. The results hold for the full parameter space defined by values of $M_2 < 1$ TeV, $|\mu| \leq 2$ TeV with the $\tilde{\chi}_1^0$ as LSP. Constraints from the Higgs search in the m_h^{max} scenario assuming $m_t = 174.3$ GeV are included. The limit is obtained for $\tan\beta \geq 5$ when stau mixing leads to mass degeneracy between $\tilde{\tau}_1$ and $\tilde{\chi}_1^0$ and the limit is based on $\tilde{\chi}_2^0$ production followed by its decay to $\tilde{\tau}_1 \tau$. In the pathological scenario where m_0 and $|\mu|$ are large, so that the $\tilde{\chi}_2^0$ production cross section is negligible, and where there is mixing in the stau sector but not in stop nor sbottom, the limit is based on charginos with soft decay products and an ISR photon. The limit then degrades to 39 GeV. See Figs. 40–42 for the dependence of the limit on $\tan\beta$ and $m_{\tilde{\nu}}$. These limits update the results of ABREU 00w.

¹² ACCIARRI 00D data collected at $\sqrt{s} = 189$ GeV. The results hold over the full parameter space defined by $0.7 \leq \tan\beta \leq 60$, $0 \leq M_2 \leq 2$ TeV, $m_0 \leq 500$ GeV, $|\mu| \leq 2$ TeV. The minimum mass limit is reached for $\tan\beta = 1$ and large m_0 . The results of slepton searches from ACCIARRI 99w are used to help set constraints in the region of small m_0 . The limit improves to 48 GeV for $m_0 \gtrsim 200$ GeV and $\tan\beta \gtrsim 10$. See their Figs. 6–8 for the $\tan\beta$ and m_0 dependence of the limits. Updates ACCIARRI 98f.

¹³ AAD 14k sets limits on the χ -nucleon spin-dependent and spin-independent cross sections out to $m_\chi = 10$ TeV.

¹⁴ CALIBBI 13 use the fact that if the relic abundance of $\tilde{\chi}_1^0$ does not overclose the universe, scalar lepton and Higgsino masses must be relatively small. Using 8 TeV ATLAS constraints on the scalar tau mass and on invisible Higgs decays, they estimate a lower bound for the $\tilde{\chi}_1^0$ mass.

Bounds on $\tilde{\chi}_1^0$ from dark matter searches

These papers generally exclude regions in the $M_2 - \mu$ parameter plane assuming that $\tilde{\chi}_1^0$ is the dominant form of dark matter in the galactic halo. These limits are based on the lack of detection in laboratory experiments, telescopes, or by the absence of a signal in underground neutrino detectors. The latter signal is expected if $\tilde{\chi}_1^0$ accumulates in the Sun or the Earth and annihilates into high-energy ν 's.

VALUE	DOCUMENT ID	TECN
-------	-------------	------

• • • We do not use the following data for averages, fits, limits, etc. • • •

1	ABE	23B	MGIC
2	FOSTER	23	FLAT
3	GUO	23A	ICCB
4	ABBASI	22B	ICCB
5	ABDALLA	22	HESS
6	ABDALLAH	21	HESS
7	ABAZAJIAN	20	FLAT
8	ABDALLAH	20	HESS
9	ABE	20G	SKAM
10	ALBERT	20	HAWC
11	ALBERT	20A	ANTR
12	ALBERT	20C	ANIC
13	ALVAREZ	20	FLAT
14	HOOF	20	FLAT
15	DI-MAURO	19	FLAT
16	JOHNSON	19	FLAT
17	LI	19D	FLAT
18	AHNEN	18	MGIC
19	ALBERT	18B	HAWC
20	ALBERT	18C	HAWC
21	AARTSEN	17	ICCB
22	AARTSEN	17A	ICCB
23	AARTSEN	17C	ICCB
24	ARCHAMBAU	17	VRTS
25	ADRIAN-MAR	16	ANTR
26	AHNEN	16	MGFL
27	AVRORIN	16	BAIK
28	CIRELLI	16	THEO
28	LEITE	16	THEO
29	ACKERMANN	15	FLAT
30	ACKERMANN	15A	FLAT
31	ACKERMANN	15B	FLAT
32	BUCKLEY	15	THEO
33	CHOI	15	SKAM
34	ALEKSI	14	MGIC
35	AVRORIN	14	BAIK
36	AARTSEN	13c	ICCB
37	BERGSTROM	13	COSM
38	BOLIEV	13	BAKS
37	JIN	13	ASTR

Searches Particle Listings

Supersymmetric Particle Searches

- | | | | | |
|--|----|------------|-----|------|
| | 37 | KOPP | 13 | COSM |
| | 39 | ACKERMANN | 10 | FLAT |
| | 40 | ACHTERBERG | 06 | AMND |
| | 41 | ACKERMANN | 06 | AMND |
| | 42 | DEBOER | 06 | RVUE |
| | 43 | DESAI | 04 | SKAM |
| | 43 | AMBROSIO | 99 | MCRO |
| | 44 | LOSECCO | 95 | RVUE |
| | 45 | MORI | 93 | KAMI |
| | 46 | BOTTINO | 92 | COSM |
| | 47 | BOTTINO | 91 | RVUE |
| | 48 | GELMINI | 91 | COSM |
| | 49 | KAMIONKOW. | 91 | RVUE |
| | 50 | MORI | 91B | KAMI |
| | 51 | OLIVE | 88 | COSM |
- none 4–15 GeV
- 1 ABE 23b sets limits on the dark matter annihilation cross section from line-like features in TeV gamma-rays in the direction of the Galactic center using the MAGIC stereoscopic telescope.
 - 2 FOSTER 23 sets limits on the dark matter annihilation cross section from monochromatic gamma-rays in the inner Milky Way using 14 years of data from Fermi-LAT.
 - 3 GUO 23A sets limits on the dark matter annihilation cross section from 10 years of IceCube muon-track data from 18 dwarf spheroidal galaxies.
 - 4 ABBASI 22b presents 7 years of data from a search of neutrinos from dark matter annihilations in the sun using the DeepCore sub-array of IceCube. Annihilation cross section limits applies to dark matter masses between 5–100 GeV.
 - 5 ABDALLA 22 uses gamma-ray observations in the Galactic center to constrain the dark matter annihilation cross section for annihilations into WW and $\tau\tau$ for dark matter masses between 200 GeV to 70 TeV. This updates ABDALLAH 18.
 - 6 ABDALLAH 21 places constraints on the dark matter annihilation cross section for annihilations into gamma-rays from the dwarf irregular galaxy WLM for masses between 0.15 to 10 TeV.
 - 7 ABAZAJIAN 20 sets constraints on the dark matter annihilation from gamma-ray searches from Fermi LAT observations of the Galactic center.
 - 8 ABDALLAH 20 places constraints on the dark matter annihilation cross section for annihilations into gamma-rays from Milky Way dwarf galaxy satellites for masses between 0.2 to 40 TeV.
 - 9 ABE 20G is based on SuperKamiokande data taken from 1996 to 2016 searching for neutrinos produced from dark matter annihilations in the galactic center or halo. They place constraints on the dark matter-nucleon scattering cross section for dark matter masses between 1 GeV and 10 TeV.
 - 10 ALBERT 20 sets limits on the annihilation cross section of dark matter with mass between 1 and 100 TeV from gamma-ray observations of the local dwarf spheroidal galaxies.
 - 11 ALBERT 20a set limits on the dark matter annihilation cross section from neutrinos observations in the Galactic center using 11 years of ANTARES data.
 - 12 ALBERT 20c set limits on the dark matter annihilation cross section from neutrinos observations in the Galactic center combining Antares and IceCube data.
 - 13 ALVAREZ 20 set limits on the dark matter annihilation from gamma-ray searches from Fermi LAT observations in the directions of dwarf spheroidal galaxies.
 - 14 HOOF 20 set limits on the dark matter annihilation from gamma-ray searches from Fermi LAT observations in the directions of dwarf spheroidal galaxies.
 - 15 DI-MAURO 19 sets limits on the dark matter annihilation from gamma-ray searches in M31 and M33 galaxies using Fermi LAT data.
 - 16 JOHNSON 19 sets limits on p-wave dark matter annihilations in the galactic center using Fermi data.
 - 17 LI 19d sets limits on dark matter annihilation cross sections searching for line-like signals in the all-sky Fermi data.
 - 18 AHNEN 18 uses observations of the dwarf satellite galaxy Ursa Major II to obtain upper limits on annihilation cross sections for dark matter in various channels for masses between 0.1–100 TeV.
 - 19 ALBERT 18b sets limits on the annihilation cross section of dark matter with mass between 1 and 100 TeV from gamma-ray observations of the Andromeda galaxy.
 - 20 ALBERT 18c sets limits on the spin-dependent coupling of dark matter to protons from dark matter annihilation in the Sun.
 - 21 AARTSEN 17 is based on data collected during 327 days of detector livetime with IceCube. They looked for interactions of ν 's resulting from neutralino annihilations in the Earth over a background of atmospheric neutrinos and set 90% CL limits on the spin independent neutralino-proton cross section for neutralino masses in the range 10–10000 GeV.
 - 22 AARTSEN 17A is based on data collected during 532 days of livetime with the IceCube 86-string detector including the DeepCore sub-array. They looked for interactions of ν 's from neutralino annihilations in the Sun over a background of atmospheric neutrinos and set 90% CL limits on the spin dependent neutralino-proton cross section for neutralino masses in the range 10–10000 GeV. This updates AARTSEN 16c.
 - 23 AARTSEN 17c is based on 1005 days of running with the IceCube detector. They set a limit on the annihilation cross section for dark matter with masses between 10–1000 GeV annihilating in the Galactic center assuming an NFW profile. The limit is of $1.2 \times 10^{23} \text{ cm}^3 \text{ s}^{-1}$ in the $\tau^+ \tau^-$ channel. Supercedes AARTSEN 15e.
 - 24 ARCHAMBAULT 17 performs a joint statistical analysis of four dwarf galaxies with VERITAS looking for gamma-ray emission from neutralino annihilation. They set limits on the neutralino annihilation cross section.
 - 25 ADRIAN-MARTINEZ 16 is based on data from the ANTARES neutrino telescope. They looked for interactions of ν 's from neutralino annihilations in the Sun over a background of atmospheric neutrinos and set 90% CL limits on the muon neutrino flux. They also obtain limits on the spin dependent and spin independent neutralino-proton cross section for neutralino masses in the range 50 to 5,000 GeV. This updates ADRIAN-MARTINEZ 13.
 - 26 AHNEN 16 combines 158 hours of Segue 1 observations with MAGIC with 6 year observations of 15 dwarf satellite galaxies by Fermi-LAT to set limits on annihilation cross sections for dark matter masses between 10 GeV and 100 TeV.
 - 27 AVRORIN 16 is based on 2.76 years with Lake Baikal neutrino telescope. They derive 90% upper limits on the annihilation cross section from dark matter annihilations in the Galactic center.
 - 28 CIRELLI 16 and LEITE 16 derive bounds on the annihilation cross section from radio observations.
 - 29 ACKERMANN 15 is based on 5.8 years of data with Fermi-LAT and search for monochromatic gamma-rays in the energy range of 0.2–500 GeV from dark matter annihilations. This updates ACKERMANN 13A.
 - 30 ACKERMANN 15A is based on 50 months of data with Fermi-LAT and search for dark matter annihilation signals in the isotropic gamma-ray background as well as galactic subhalos in the energy range of a few GeV to a few tens of TeV.
 - 31 ACKERMANN 15B is based on 6 years of data with Fermi-LAT observations of Milky Way dwarf spheroidal galaxies. Set limits on the annihilation cross section from $m_{\chi} = 2 \text{ GeV}$ to 10 TeV. This updates ACKERMANN 14.
 - 32 BUCKLEY 15 is based on 5 years of Fermi-LAT data searching for dark matter annihilation signals from Large Magellanic Cloud.
 - 33 CHOI 15 is based on 3903 days of SuperKamiokande data searching for neutrinos produced from dark matter annihilations in the sun. They place constraints on the dark matter-nucleon scattering cross section for dark matter masses between 4–200 GeV.
 - 34 ALEKSIC 14 is based on almost 160 hours of observations of Segue 1 satellite dwarf galaxy using the MAGIC telescopes between 2011 and 2013. Sets limits on the annihilation cross section out to $m_{\chi} = 10 \text{ TeV}$.
 - 35 AVRORIN 14 is based on almost 2.76 years with Lake Baikal neutrino telescope. They derive 90% upper limits on the fluxes of muons and muon neutrinos from dark matter annihilations in the Sun.
 - 36 AARTSEN 13c is based on data collected during 339.8 effective days with the IceCube 59-string detector. They looked for interactions of ν_{μ} 's from neutralino annihilations in nearby galaxies and galaxy clusters. They obtain limits on the neutralino annihilation cross section for neutralino masses in the range 30–100,000 GeV.
 - 37 BERGSTROM 13, JIN 13, and KOPP 13 derive limits on the mass and annihilation cross section using AMS-02 data. JIN 13 also sets a limit on the lifetime of the dark matter particle.
 - 38 BOLIEV 13 is based on data collected during 24.12 years of live time with the Bakson Underground Scintillator Telescope. They looked for interactions of ν_{μ} 's from neutralino annihilations in the Sun over a background of atmospheric neutrinos and set 90% CL limits on the muon flux. They also obtain limits on the spin dependent and spin independent neutralino-proton cross section for neutralino masses in the range 10–1000 GeV.
 - 39 ACKERMANN 10 place upper limits on the annihilation cross section with $b\bar{b}$ or $\mu^+ \mu^-$ final states.
 - 40 ACHTERBERG 06 is based on data collected during 421.9 effective days with the AMANDA detector. They looked for interactions of ν_{μ} 's from the centre of the Earth over a background of atmospheric neutrinos and set 90% CL limits on the muon flux. Their limit is compared with the muon flux expected from neutralino annihilations into $W^+ W^-$ and $b\bar{b}$ at the centre of the Earth for MSSM parameters compatible with the relic dark matter density, see their Fig. 7.
 - 41 ACKERMANN 06 is based on data collected during 143.7 days with the AMANDA-II detector. They looked for interactions of ν_{μ} 's from the Sun over a background of atmospheric neutrinos and set 90% CL limits on the muon flux. Their limit is compared with the muon flux expected from neutralino annihilations into $W^+ W^-$ in the Sun for SUSY model parameters compatible with the relic dark matter density, see their Fig. 3.
 - 42 DEBOER 06 interpret an excess of diffuse Galactic gamma rays observed with the EGRET satellite as originating from π^0 decays from the annihilation of neutralinos into quark jets. They analyze the corresponding parameter space in a supergravity inspired MSSM model with radiative electroweak symmetry breaking, see their Fig. 3 for the preferred region in the $(m_0, m_{1/2})$ plane of a scenario with large $\tan\beta$.
 - 43 AMBROSIO 99 and DESAI 04 set new neutrino flux limits which can be used to limit the parameter space in supersymmetric models based on neutralino annihilation in the Sun and the Earth.
 - 44 LOSECCO 95 reanalyzed the IMB data and places lower limit on $m_{\tilde{\chi}_1^0}$ of 18 GeV if the LSP is a photino and 10 GeV if the LSP is a higgsino based on LSP annihilation in the sun producing high-energy neutrinos and the limits on neutrino fluxes from the IMB detector.
 - 45 MORI 93 excludes some region in $M_2 - \mu$ parameter space depending on $\tan\beta$ and lightest scalar Higgs mass for neutralino dark matter $m_{\tilde{\chi}_1^0} > m_{\nu\tau}$, using limits on ongoing muons produced by energetic neutrinos from neutralino annihilation in the Sun and the Earth.
 - 46 BOTTINO 92 excludes some region $M_2 - \mu$ parameter space assuming that the lightest neutralino is the dark matter, using ongoing muons at Kamiokande, direct searches by Ge detectors, and by LEP experiments. The analysis includes top radiative corrections on Higgs parameters and employs two different hypotheses for nucleon-Higgs coupling. Effects of rescaling in the local neutralino density according to the neutralino relic abundance are taken into account.
 - 47 BOTTINO 91 excluded a region in $M_2 - \mu$ plane using ongoing muon data from Kamioka experiment, assuming that the dark matter surrounding us is composed of neutralinos and that the Higgs boson is not too heavy.
 - 48 GELMINI 91 exclude a region in $M_2 - \mu$ plane using dark matter searches.
 - 49 KAMIONKOWSKI 91 excludes a region in the $M_2 - \mu$ plane using IMB limit on ongoing muons originated by energetic neutrinos from neutralino annihilation in the sun, assuming that the dark matter is composed of neutralinos and that $m_{H_1^0} \lesssim 50 \text{ GeV}$. See Fig. 8 in the paper.
 - 50 MORI 91B exclude a part of the region in the $M_2 - \mu$ plane with $m_{\tilde{\chi}_1^0} \lesssim 80 \text{ GeV}$ using a limit on ongoing muons originated by energetic neutrinos from neutralino annihilation in the earth, assuming that the dark matter surrounding us is composed of neutralinos and that $m_{H_1^0} \lesssim 80 \text{ GeV}$.
 - 51 OLIVE 88 result assumes that photinos make up the dark matter in the galactic halo. Limit is based on annihilations in the sun and is due to an absence of high energy neutrinos detected in underground experiments. The limit is model dependent.

$\tilde{\chi}_1^0 - p$ elastic cross section

Experimental results on the $\tilde{\chi}_1^0 - p$ elastic cross section are evaluated at $m_{\tilde{\chi}_1^0} = 100 \text{ GeV}$. The experimental results on the cross section are often mass dependent. Therefore, the mass and cross section results are also given where the limit is strongest, when appropriate. Results are quoted separately for spin-dependent interactions (based on an effective 4-Fermi Lagrangian of the form $\overline{\chi}_1^0 \mu \gamma^5 \chi \overline{q} \gamma_\mu \gamma^5 q$) and spin-independent interactions ($\overline{\chi}_1^0 q q$). For calculational details see GRIEST 88b, ELLIS 88b, BARBIERI 89c, DREES 93b, ARNOWITT 96, BERGSTROM 96, and BAER 97 in addition to the theory papers listed in the Tables. For a description of the theoretical assumptions and experimental techniques underlying most

See key on page 1171

Searches Particle Listings Supersymmetric Particle Searches

of the listed papers, see the review on "Dark matter" in this "Review of Particle Physics," and references therein. Most of the following papers use galactic halo and nuclear interaction assumptions from (LEWIN 96).

Spin-dependent interactions

VALUE (pb)	CL%	DOCUMENT ID	TECN	COMMENT
< 1.9 × 10 ⁻⁴	90	1 AALBERS 23 LZ	Xe	
< 3.3 × 10 ⁻⁴	90	2 APRILE 23A XENT	Xe	
< 2 × 10 ⁻⁴	90	3 HUANG 22 PNDX	Xe	
< 4 × 10 ⁻⁵	90	4 AMOLE 19 PICO	C ₃ F ₈	
< 5 × 10 ⁻⁴	90	5 APRILE 19A XE1T	Xe	
< 8 × 10 ⁻⁴	90	6 AKERIB 17A LUX	Xe	
< 0.28	90	7 BATTAT 17 DRFT	CS ₂ ; CF ₄	
< 0.027	90	8 BEHNKE 17 PICA	C ₄ F ₁₀	
< 5 × 10 ⁻⁴	90	9 AMOLE 16 PICO	CF ₃ I	
< 6.8 × 10 ⁻³	90	10 APRILE 16B X100	Xe	
< 6.3 × 10 ⁻³	90	11 FELIZARDO 14 SMPL	C ₂ ClF ₅	
< 0.01	90	12 AKIMOV 12 ZEP3	Xe	
< 7 × 10 ⁻³	90	13 BEHNKE 12 COUP	CF ₃ I	
< 8.5 × 10 ⁻³	90	14 FELIZARDO 12 SMPL	C ₂ ClF ₅	
< 0.016	90	15 KIM 12 KIMS	Csl	
5 × 10 ⁻¹⁰ to 10 ⁻⁵	95	16 BUCHMUEL... 11B	THEO	
< 1	90	17 ANGLE 08A XE10	Xe	
< 0.055	90	18 BEDNYAKOV 08 HDMS	Ge	
< 0.33	90	19 BEHNKE 08 COUP	CF ₃ I	
< 5	90	20 AKERIB 06 CDMS	Ge	
< 2	90	21 SHIMIZU 06A CNTR	CaF ₂	
< 0.4	90	22 ALNER 05 NAIA	Nal Spin Dep.	
< 2	90	23 BARNABE-HE...05	PICA C	
2 × 10 ⁻¹¹ to 1 × 10 ⁻⁴	90	24 ELLIS 04 THEO	μ > 0	
< 0.8	90	25 AHMED 03 NAIA	Nal Spin Dep.	
< 40	90	26 TAKEDA 03 BOLO	NaF Spin Dep.	
< 10	90	27 ANGLOHER 02 CRES	Sapphire	
8 × 10 ⁻⁷ to 2 × 10 ⁻⁵	90	28 ELLIS 01c THEO	tanβ ≤ 10	
< 3.8	90	29 BERNABEI 00D DAMA	Xe	
< 0.8	90	30 SPOONER 00 UKDM	Nal	
< 4.8	90	31 BELL 99c DAMA	F	
< 100	90	31 OOTANI 99 BOLO	LIF	
< 0.6	90	31 BERNABEI 98c DAMA	Xe	
< 5	90	30 BERNABEI 97 DAMA	F	

- 1 The strongest upper limit is 4.2 × 10⁻⁵ pb at 32 GeV. The limit for scattering on neutrons is 4 × 10⁻⁶ pb at 100 GeV and is 1.5 × 10⁻⁶ pb at 30 GeV.
- 2 The strongest upper limit is 1.4 × 10⁻⁴ pb at 28 GeV. The limit for scattering on neutrons is 1.1 × 10⁻⁵ pb at 100 GeV and is 4.3 × 10⁻⁶ pb at 28 GeV.
- 3 The strongest limit is < 1.7 × 10⁻⁴ pb at m_χ = 40 GeV. This updates FU 17 and XIA 19A.
- 4 The strongest limit is < 3.2 × 10⁻⁵ pb at m_χ = 25 GeV. This updates AMOLE 17.
- 5 The strongest limit is < 2 × 10⁻⁴ pb at m_χ = 30 GeV. For scatterings on neutrons, the strongest limit is < 6.3 × 10⁻⁶ pb at m_χ = 30 GeV.
- 6 The strongest limit is 5 × 10⁻⁴ pb at m_χ = 35 GeV. The limit for scattering on neutrons is 3 × 10⁻⁵ pb at 100 GeV and is 1.6 × 10⁻⁵ pb at 35 GeV. This updates AKERIB 16A.
- 7 Directional recoil detector. This updates DAW 12.
- 8 This result updates ARCHAMBAULT 12. The strongest limit is 0.013 pb at m_χ = 20 GeV.
- 9 The strongest limit is 5 × 10⁻⁴ pb at m_χ = 80 GeV.
- 10 The strongest limit is 5.2 × 10⁻³ pb at 50 GeV. The limit for scattering on neutrons is 2.8 × 10⁻⁴ pb at 100 GeV and the strongest limit is 2.0 × 10⁻⁴ pb at 50 GeV. This updates APRILE 13.
- 11 The strongest limit is 0.0043 pb and occurs at m_χ = 35 GeV. FELIZARDO 14 also presents limits for the scattering on neutrons. At m_χ = 100 GeV, the upper limit is 0.13 pb and the strongest limit is 0.066 pb at m_χ = 35 GeV.
- 12 This result updates LEBEDENKO 09A. The strongest limit is 8 × 10⁻³ pb at m_χ = 50 GeV. Limit applies to the neutralino neutron elastic cross section.
- 13 The strongest limit is 6 × 10⁻³ pb at m_χ = 60 GeV.
- 14 The strongest limit is 5.7 × 10⁻³ pb at m_χ = 35 GeV.
- 15 This result updates LEE 07A. The strongest limit is at m_χ = 80 GeV.
- 16 Predictions for the spin-dependent elastic cross section based on a frequentist approach to electroweak observables in the framework of N = 1 supergravity models with radiative breaking of the electroweak gauge symmetry.
- 17 The strongest limit is 0.6 pb and occurs at m_χ = 30 GeV. The limit for scattering on neutrons is 0.01 pb at m_χ = 100 GeV, and the strongest limit is 0.0045 pb at m_χ = 30 GeV.
- 18 Limit applies to neutron elastic cross section.
- 19 The strongest upper limit is 0.25 pb and occurs at m_χ ≈ 40 GeV.
- 20 The strongest upper limit is 4 pb and occurs at m_χ ≈ 60 GeV. The limit on the neutron spin-dependent elastic cross section is 0.07 pb. This latter limit is improved in AHMED 09, where a limit of 0.02 pb is obtained at m_χ = 100 GeV. The strongest limit in AHMED 09 is 0.018 pb and occurs at m_χ = 60 GeV.
- 21 The strongest upper limit is 1.2 pb and occurs at m_χ ≈ 40 GeV. The limit on the neutron spin-dependent cross section is 35 pb.
- 22 The strongest upper limit is 0.35 pb and occurs at m_χ ≈ 60 GeV.
- 23 The strongest upper limit is 1.2 pb and occurs m_χ ≈ 30 GeV.

- 24 ELLIS 04 calculates the χp elastic scattering cross section in the framework of N=1 supergravity models with radiative breaking of the electroweak gauge symmetry, but without universal scalar masses. In the case of universal squark and slepton masses, but non-universal Higgs masses, the limit becomes 2 × 10⁻⁴, see ELLIS 03c.
- 25 The strongest upper limit is 0.75 pb and occurs at m_χ ≈ 70 GeV.
- 26 The strongest upper limit is 30 pb and occurs at m_χ ≈ 20 GeV.
- 27 The strongest upper limit is 8 pb and occurs at m_χ ≈ 30 GeV.
- 28 ELLIS 01c calculates the χ-p elastic scattering cross section in the framework of N=1 supergravity models with radiative breaking of the electroweak gauge symmetry. In models with nonuniversal Higgs masses, the upper limit to the cross section is 6 × 10⁻⁴.
- 29 The strongest upper limit is 3 pb and occurs at m_χ ≈ 60 GeV. The limits are for inelastic scattering X⁰ + 129Xe → X⁰ + 129Xe* (39.58 keV).
- 30 The strongest upper limit is 4.4 pb and occurs at m_χ ≈ 60 GeV.
- 31 The strongest upper limit is about 35 pb and occurs at m_χ ≈ 15 GeV.

Spin-independent interactions

VALUE (pb)	CL%	DOCUMENT ID	TECN	COMMENT
< 3 × 10 ⁻¹¹	90	1 AALBERS 23 LZ	Xe	
< 6.1 × 10 ⁻¹¹	90	2 APRILE 23A XENT	Xe	
< 6.5 × 10 ⁻¹¹	90	3 MENG 21B PNDX	Xe	
< 5 × 10 ⁻¹⁰	90	4 WANG 20G PNDX	Xe	
< 2.5 × 10 ⁻⁸	90	5 ABE 19 XMAS	Xe	
< 3.9 × 10 ⁻⁹	90	6 AJAJ 19 DEAP	Ar	
< 2 × 10 ⁻⁸	90	7 AMOLE 19 PICO	C ₃ F ₈	
< 2.25 × 10 ⁻⁶	90	8 ADHIKARI 18 C100	Nal	
< 1.14 × 10 ⁻⁸	90	9 AGNES 18A DS50	Ar	
< 1.6 × 10 ⁻⁸	90	10 AGNESE 18A CDMS	Ge	
< 9 × 10 ⁻¹¹	90	11 APRILE 18 XE1T	Xe	
< 1.8 × 10 ⁻¹⁰	90	12 AKERIB 17 LUX	Xe	
< 1.5 × 10 ⁻⁹	90	13 APRILE 16B X100	Xe	
< 1.5 × 10 ⁻⁹	90	14 AKERIB 14 LUX	Xe	
10 ⁻¹¹ -10 ⁻⁷	95	15 BUCHMUEL... 14A	THEO	
< 4.6 × 10 ⁻⁶	90	16 FELIZARDO 14 SMPL	C ₂ ClF ₅	
10 ⁻¹¹ -10 ⁻⁸	95	17 ROSZKOWSKI 14 THEO		
< 2.2 × 10 ⁻⁶	90	18 AGNESE 13 CDMS	Si	
< 5 × 10 ⁻⁸	90	19 AKIMOV 12 ZEP3	Xe	
1.6 × 10 ⁻⁶ ; 3.7 × 10 ⁻⁵	90	20 ANGLOHER 12 CRES	CaWO ₄	
3 × 10 ⁻¹² to 3 × 10 ⁻⁹	95	21 BECHTLE 12 THEO		
< 1.6 × 10 ⁻⁷	90	22 BEHNKE 12 COUP	CF ₃ I	
< 2.3 × 10 ⁻⁷	90	23 KIM 12 KIMS	Csl	
< 3.3 × 10 ⁻⁸	90	24 AHMED 11A	Ge	
< 4.4 × 10 ⁻⁸	90	25 ARMENGAUD 11 EDE2	Ge	
< 1 × 10 ⁻⁷	90	26 ANGLE 08 XE10	Xe	
< 1 × 10 ⁻⁶	90	27 BENETTI 08 WARP	Ar	
< 7.5 × 10 ⁻⁷	90	27 ALNER 07A ZEP2	Xe	
< 2 × 10 ⁻⁷	90	28 AKERIB 06A CDMS	Ge	
< 90 × 10 ⁻⁷	90	28 ALNER 05 NAIA	Nal Spin Indep.	
< 12 × 10 ⁻⁷	90	29 ALNER 05A ZEPL		
< 14 × 10 ⁻⁷	90	30 SANGIARD 05 EDEL	Ge	
< 4 × 10 ⁻⁷	90	30 AKERIB 04 CDMS	Ge	
2 × 10 ⁻¹¹ to 1.5 × 10 ⁻⁷	95	31 BALTZ 04 THEO		
2 × 10 ⁻¹¹ to 8 × 10 ⁻⁶	32,33	31 ELLIS 04 THEO	μ > 0	
< 5 × 10 ⁻⁸	90	34 PIERCE 04A THEO		
< 2 × 10 ⁻⁵	90	35 AHMED 03 NAIA	Nal Spin Indep.	
< 3 × 10 ⁻⁶	90	36 AKERIB 03 CDMS	Ge	
2 × 10 ⁻¹³ to 2 × 10 ⁻⁷	90	37 BAER 03A THEO		
< 1.4 × 10 ⁻⁵	90	38 KLAPDOR-K...03	HDMS Ge	
< 6 × 10 ⁻⁶	90	39 ABRAMS 02 CDMS	Ge	
1 × 10 ⁻¹² to 7 × 10 ⁻⁶	90	32 KIM 02b THEO		
< 3 × 10 ⁻⁵	90	40 MORALES 02b CSME	Ge	
< 1 × 10 ⁻⁵	90	41 MORALES 02c IGEX	Ge	
< 1 × 10 ⁻⁶	90	BALTZ 01 THEO		
< 3 × 10 ⁻⁵	90	42 BAUDIS 01 HDMS	Ge	
< 7 × 10 ⁻⁶	90	43 BOTTINO 01 THEO		
< 1 × 10 ⁻⁸	90	44 CORSETTI 01 THEO	tanβ ≤ 25	
5 × 10 ⁻¹⁰ to 1.5 × 10 ⁻⁸	90	45 ELLIS 01c THEO	tanβ ≤ 10	
< 4 × 10 ⁻⁶	90	44 GOMEZ 01 THEO		
2 × 10 ⁻¹⁰ to 1 × 10 ⁻⁷	90	44 LAHANAS 01 THEO		
< 3 × 10 ⁻⁶	90	46 ABUSAIID 00 CDMS	Ge, Si	
< 6 × 10 ⁻⁷	90	46 ACCOMANDO 00 THEO		
2.5 × 10 ⁻⁹ to 3.5 × 10 ⁻⁸	90	47 BERNABEI 00 DAMA	Nal	
< 1.5 × 10 ⁻⁵	90	48 FENG 00 THEO	tanβ=10	
< 4 × 10 ⁻⁵	90	MORALES 00 IGEX	Ge	
< 7 × 10 ⁻⁶	90	SPOONER 00 UKDM	Nal	
< 7 × 10 ⁻⁶	90	BAUDIS 99 HDMO	⁷⁶ Ge	
< 7 × 10 ⁻⁶	90	BERNABEI 98c DAMA	Xe	

- 1 The strongest upper limit is 9.2 × 10⁻¹² pb at 36 GeV.
- 2 The strongest upper limit is 2.6 × 10⁻¹¹ pb at 28 GeV.
- 3 Commissioning Run for PandaX-4T. The strongest limit is 3.8 × 10⁻¹¹ pb at m_χ = 40 GeV.
- 4 WANG 20g strongest limit is 2.2 × 10⁻¹⁰ pb at 30 GeV using 132 ton-day full exposure of PandaX-II. This updates CUI 17A, though the results here provide weaker constraints.
- 5 The strongest upper limit is 2.2 × 10⁻⁸ pb at 60 GeV.
- 6 This updates AMAUDRUZ 18.

Searches Particle Listings

Supersymmetric Particle Searches

- ⁷ This updates AMOLE 16.
- ⁸ The strongest limit is 2.05×10^{-6} at $m = 60$ GeV.
- ⁹ The strongest limit is 1.09×10^{-8} pb at $m_\chi = 126$ GeV. This updates AGNES 15.
- ¹⁰ The strongest limit is 1.0×10^{-8} pb at $m_\chi = 46$ GeV. This updates AGNESE 15B.
- ¹¹ Based on 278.8 days of data collection. The strongest limit is 4.1×10^{-11} pb at $m_\chi = 30$ GeV. This updates APRILE 17G.
- ¹² AKERIB 17. The strongest limit is 1.1×10^{-10} pb at 50 GeV. This updates AKERIB 16.
- ¹³ The strongest limit is 1.1×10^{-9} pb at 50 GeV. This updates APRILE 12.
- ¹⁴ The strongest upper limit is 7.6×10^{-10} at $m_\chi = 33$ GeV.
- ¹⁵ Predictions for the spin-independent elastic cross section based on a frequentist approach to electroweak observables in the framework of $N = 1$ supergravity models with radiative breaking of the electroweak gauge symmetry using the 20 fb⁻¹ LHC data and the 5 fb⁻¹ 7 TeV LHC data and the LUX data.
- ¹⁶ The strongest limit is 3.6×10^{-6} pb and occurs at $m_\chi = 35$ GeV. Felizardo 2014 updates Felizardo 2012.
- ¹⁷ Predictions for the spin-independent elastic cross section based on a Bayesian approach to electroweak observables in the framework of $N = 1$ supergravity models with radiative breaking of the electroweak gauge symmetry using the 20 fb⁻¹ LHC data and LUX.
- ¹⁸ AGNESE 13 presents 90% CL limits on the elastic cross section for masses in the range 7–100 GeV using the Si based detector. The strongest upper limit is 1.8×10^{-6} pb at $m_\chi = 50$ GeV. This limit is improved to 7×10^{-7} pb in AGNESE 13A.
- ¹⁹ This result updates LEBEDENKO 09. The strongest limit is 3.9×10^{-8} pb at $m_\chi = 52$ GeV.
- ²⁰ ANGLÖHER 12 presents results of 730 kg days from the CRESST-II dark matter detector. They find two maxima in the likelihood function corresponding to best fit WIMP masses of 25.3 and 11.6 GeV with elastic cross sections of 1.6×10^{-6} and 3.7×10^{-5} pb respectively, see their Table 4. The statistical significance is more than 4σ . ANGLÖHER 12 updates ANGLÖHER 09
- ²¹ Predictions for the spin-independent elastic cross section based on a frequentist approach to electroweak observables in the framework of $N = 1$ supergravity models with radiative breaking of the electroweak gauge symmetry using the 5 fb⁻¹ LHC data and XENON100.
- ²² The strongest limit is 1.4×10^{-7} at $m_\chi = 60$ GeV.
- ²³ This result updates LEE 07A. The strongest limit is 2.1×10^{-7} at $m_\chi = 70$ GeV.
- ²⁴ AHMED 11A gives combined results from CDMS and EDELWEISS. The strongest limit is at $m_\chi = 90$ GeV.
- ²⁵ ARMENGAUD 11 updates result of ARMENGAUD 10. Strongest limit at $m_\chi = 85$ GeV.
- ²⁶ The strongest upper limit is 5.1×10^{-8} pb and occurs at $m_\chi \simeq 30$ GeV. The values quoted here are based on the analysis performed in ANGLE 08 with the update from SORENSEN 09.
- ²⁷ The strongest upper limit is 6.6×10^{-7} pb and occurs at $m_\chi \simeq 65$ GeV.
- ²⁸ AKERIB 06A updates the results of AKERIB 05. The strongest upper limit is 1.6×10^{-7} pb and occurs at $m_\chi \simeq 60$ GeV.
- ²⁹ The strongest upper limit is also close to 1.0×10^{-6} pb and occurs at $m_\chi \simeq 70$ GeV. BENOIT 06 claim that the discrimination power of ZEPLIN-I measurement (ALNER 05A) is not reliable enough to obtain a limit better than 1×10^{-3} pb. However, SMITH 06 do not agree with the criticisms of BENOIT 06.
- ³⁰ AKERIB 04 is incompatible with BERNABEI 00 most likely value, under the assumption of standard WIMP-halo interactions. The strongest upper limit is 4×10^{-7} pb and occurs at $m_\chi \simeq 60$ GeV.
- ³¹ Predictions for the spin-independent elastic cross section in the framework of $N = 1$ supergravity models with radiative breaking of the electroweak gauge symmetry.
- ³² KIM 02 and ELLIS 04 calculate the χp elastic scattering cross section in the framework of $N=1$ supergravity models with radiative breaking of the electroweak gauge symmetry, but without universal scalar masses.
- ³³ In the case of universal squark and slepton masses, but non-universal Higgs masses, the limit becomes 2×10^{-6} (2×10^{-11} when constraint from the BNL $g-2$ experiment are included), see ELLIS 03E. ELLIS 05 display the sensitivity of the elastic scattering cross section to the π -Nucleon Σ term.
- ³⁴ PIERCE 04A calculates the χp elastic scattering cross section in the framework of models with very heavy scalar masses. See Fig. 2 of the paper.
- ³⁵ The strongest upper limit is 1.8×10^{-5} pb and occurs at $m_\chi \simeq 80$ GeV.
- ³⁶ Under the assumption of standard WIMP-halo interactions, Akerib 03 is incompatible with BERNABEI 00 most likely value at the 99.98% CL. See Fig. 4.
- ³⁷ BAER 03A calculates the χp elastic scattering cross section in several models including the framework of $N=1$ supergravity models with radiative breaking of the electroweak gauge symmetry.
- ³⁸ The strongest upper limit is 7×10^{-6} pb and occurs at $m_\chi \simeq 30$ GeV.
- ³⁹ ABRAMS 02 is incompatible with the DAMA most likely value at the 99.9% CL. The strongest upper limit is 3×10^{-6} pb and occurs at $m_\chi \simeq 30$ GeV.
- ⁴⁰ The strongest upper limit is 2×10^{-5} pb and occurs at $m_\chi \simeq 40$ GeV.
- ⁴¹ The strongest upper limit is 7×10^{-6} pb and occurs at $m_\chi \simeq 46$ GeV.
- ⁴² The strongest upper limit is 1.8×10^{-5} pb and occurs at $m_\chi \simeq 32$ GeV
- ⁴³ BOTTINO 01 calculates the χ - p elastic scattering cross section in the framework of the following supersymmetric models: $N=1$ supergravity with the radiative breaking of the electroweak gauge symmetry, $N=1$ supergravity with nonuniversal scalar masses and an effective MSSM model at the electroweak scale.
- ⁴⁴ Calculates the χ - p elastic scattering cross section in the framework of $N=1$ supergravity models with radiative breaking of the electroweak gauge symmetry.
- ⁴⁵ ELLIS 01c calculates the χ - p elastic scattering cross section in the framework of $N=1$ supergravity models with radiative breaking of the electroweak gauge symmetry. ELLIS 02b find a range 2×10^{-8} – 1.5×10^{-7} at $\tan\beta=50$. In models with nonuniversal Higgs masses, the upper limit to the cross section is 4×10^{-7} .
- ⁴⁶ ACCOMANDO 00 calculate the χ - p elastic scattering cross section in the framework of minimal $N=1$ supergravity models with radiative breaking of the electroweak gauge symmetry. The limit is relaxed by at least an order of magnitude when models with nonuniversal scalar masses are considered. A subset of the authors in ARNOWITT 02 updated the limit to $< 9 \times 10^{-8}$ ($\tan\beta < 55$).
- ⁴⁷ BERNABEI 00 search for annual modulation of the WIMP signal. The data favor the hypothesis of annual modulation at 4σ and are consistent, for a particular model framework quoted there, with $m_{\chi_0} = 44 \pm 12$ GeV and a spin-independent χ^0 -proton cross section of $(5.4 \pm 1.0) \times 10^{-6}$ pb. See also BERNABEI 01 and BERNABEI 00c.
- ⁴⁸ FENG 00 calculate the χ - p elastic scattering cross section in the framework of $N=1$ supergravity models with radiative breaking of the electroweak gauge symmetry with a particular emphasis on focus point models. At $\tan\beta=50$, the range is 8×10^{-8} – 4×10^{-7} .

Other bounds on $\tilde{\chi}_1^0$ from astrophysics and cosmology

Most of these papers generally exclude regions in the $M_2 - \mu$ parameter plane by requiring that the $\tilde{\chi}_1^0$ contribution to the overall cosmological density is less than some maximal value to avoid overclosure of the Universe. Those not based on the cosmological density are indicated. Many of these papers also include LEP and/or other bounds.

VALUE	DOCUMENT ID	TECN	COMMENT
>46 GeV	1 ELLIS	00	RVUE
• • • We do not use the following data for averages, fits, limits, etc. • • •			
	2 ATHRON	17B	COSM
	3 BECHTLE	16	COSM
	4 BAGNASCHI	15	COSM
	5 BUCHMUEL...	14	COSM
	6 BUCHMUEL...	14A	COSM
	7 ROSZKOWSKI	14	COSM
	8 CABRERA	13	COSM
	9 ELLIS	13B	COSM
	8 STREGE	13	COSM
	5 AKULA	12	COSM
	5 ARBEY	12A	COSM
	5 BAER	12	COSM
	10 BALAZS	12	COSM
	11 BECHTLE	12	COSM
	12 BESKIDT	12	COSM
	13 BOTTINO	12	COSM
	5 BUCHMUEL...	12	COSM
	5 CAO	12A	COSM
	5 ELLIS	12B	COSM
	14 FENG	12B	COSM
	5 KADASTIK	12	COSM
	10 STREGE	12	COSM
	15 BUCHMUEL...	11	COSM
	16 ROSZKOWSKI	11	COSM
	17 ELLIS	10	COSM
	18 BUCHMUEL...	09	COSM
	19 DREINER	09	THEO
	20 BUCHMUEL...	08	COSM
	16 ELLIS	08	COSM
	21 CALIBBI	07	COSM
	22 ELLIS	07	COSM
	23 ALLANACH	06	COSM
	24 DE-AUSTRI	06	COSM
	16 BAER	05	COSM
	25 BALTZ	04	COSM
	13,26 BELANGER	04	THEO
	27 ELLIS	04B	COSM
	28 PIERCE	04A	COSM
	29 BAER	03	COSM
	13 BOTTINO	03	COSM
	29 CHATTOPAD...	03	COSM
	30 ELLIS	03	COSM
	16 ELLIS	03B	COSM
	29 ELLIS	03C	COSM
	29 LAHANAS	03	COSM
	31 LAHANAS	02	COSM
	32 BARGER	01c	COSM
	33 ELLIS	01B	COSM
	30 BOEHM	00B	COSM
	34 FENG	00	COSM
	35 ELLIS	98B	COSM
	36 EDSJO	97	COSM Co-annihilation
	37 BAER	96	COSM
	16 BEREZINSKY	95	COSM
	38 FALK	95	COSM CP-violating phases
	39 DREES	93	COSM Minimal supergravity
	40 FALK	93	COSM Sfermion mixing
	39 KELLEY	93	COSM Minimal supergravity
	41 MIZUTA	93	COSM Co-annihilation
	42 LOPEZ	92	COSM Minimal supergravity, $m_0=A=0$
	43 MCDONALD	92	COSM
	44 GRIEST	91	COSM
	45 NOJIRI	91	COSM Minimal supergravity
	46 OLIVE	91	COSM
	47 ROSZKOWSKI	91	COSM
	48 GRIEST	90	COSM
	46 OLIVE	89	COSM
none 100 eV – 15 GeV	SREDNICKI	88	COSM $\tilde{\tau}; m_{\tilde{\tau}}=100$ GeV

none 100 eV–5 GeV ELLIS 84 COSM $\tilde{\gamma}$; for $m_{\tilde{f}}=100$ GeV
 GOLDBERG 83 COSM $\tilde{\gamma}$
 49 KRAUSS 83 COSM $\tilde{\gamma}$
 VYSOTSKII 83 COSM $\tilde{\gamma}$

- 1 ELLIS 00 updates ELLIS 98. Uses LEP e^+e^- data at $\sqrt{s}=202$ and 204 GeV to improve bound on neutralino mass to 51 GeV when scalar mass universality is assumed and 46 GeV when Higgs mass universality is relaxed. Limits on $\tan\beta$ improve to > 2.7 ($\mu > 0$), > 2.2 ($\mu < 0$) when scalar mass universality is assumed and > 1.9 (both signs of μ) when Higgs mass universality is relaxed.
- 2 ATHRON 17b places constraints on the SUSY parameter space in the framework of $N=1$ supergravity models with radiative breaking of the electroweak gauge symmetry using all Run I and the 13 fb $^{-1}$ 13 TeV Run II LHC searches and other experimental data.
- 3 BECHTLE 16 places constraints on the SUSY parameter space in the framework of $N=1$ supergravity models with radiative breaking of the electroweak gauge symmetry using all Run I LHC searches.
- 4 BAGNASCHI 15 places constraints on the SUSY parameter space in the framework of $N=1$ supergravity models with radiative breaking of the electroweak gauge symmetry using all Run I LHC searches.
- 5 Implications of the LHC result on the Higgs mass and on the SUSY parameter space in the framework of $N=1$ supergravity models with radiative breaking of the electroweak gauge symmetry.
- 6 BUCHMUELLER 14A places constraints on the SUSY parameter space in the framework of $N=1$ supergravity models with radiative breaking of the electroweak gauge symmetry using indirect experimental searches using the 20 fb $^{-1}$ 8 TeV and the 5 fb $^{-1}$ 7 TeV LHC and the LUX data.
- 7 ROSZKOWSKI 14 places constraints on the SUSY parameter space in the framework of $N=1$ supergravity models with radiative breaking of the electroweak gauge symmetry using Bayesian statistics and indirect experimental searches using the 20 fb $^{-1}$ LHC and the LUX data.
- 8 CABRERA 13 and STREGE 13 place constraints on the SUSY parameter space in the framework of $N=1$ supergravity models with radiative breaking of the electroweak gauge symmetry with and without non-universal Higgs masses using the 5.8 fb $^{-1}$, $\sqrt{s}=7$ TeV ATLAS supersymmetry searches and XENON100 results.
- 9 ELLIS 13b place constraints on the SUSY parameter space in the framework of $N=1$ supergravity models with radiative breaking of the electroweak gauge symmetry with and without Higgs mass universality. Models with universality below the GUT scale are also considered.
- 10 BALAZS 12 and STREGE 12 place constraints on the SUSY parameter space in the framework of $N=1$ supergravity models with radiative breaking of the electroweak gauge symmetry using the 1 fb $^{-1}$ LHC supersymmetry searches, the 5 fb $^{-1}$ Higgs mass constraints, both with $\sqrt{s}=7$ TeV, and XENON100 results.
- 11 BECHTLE 12 places constraints on the SUSY parameter space in the framework of $N=1$ supergravity models with radiative breaking of the electroweak gauge symmetry using indirect experimental searches, using the 5 fb $^{-1}$ LHC and XENON100 data.
- 12 BESKIDT 12 places constraints on the SUSY parameter space in the framework of $N=1$ supergravity models with radiative breaking of the electroweak gauge symmetry using indirect experimental searches, the 5 fb $^{-1}$ LHC and the XENON100 data.
- 13 BELANGER 04 and BOTTINO 12 (see also BOTTINO 03, BOTTINO 03A and BOTTINO 04) do not assume gaugino or scalar mass unification.
- 14 FENG 12b places constraints on the SUSY parameter space in the framework of $N=1$ supergravity models with radiative breaking of the electroweak gauge symmetry and large sfermion masses using the 1 fb $^{-1}$ LHC supersymmetry searches, the 5 fb $^{-1}$ LHC Higgs mass constraints both with $\sqrt{s}=7$ TeV, and XENON100 results.
- 15 BUCHMUELLER 11 places constraints on the SUSY parameter space in the framework of $N=1$ supergravity models with radiative breaking of the electroweak gauge symmetry using indirect experimental searches and including supersymmetry breaking relations between A and B parameters.
- 16 Places constraints on the SUSY parameter space in the framework of $N=1$ supergravity models with radiative breaking of the electroweak gauge symmetry but non-Universal Higgs masses.
- 17 ELLIS 10 places constraints on the SUSY parameter space in the framework of $N=1$ supergravity models with radiative breaking of the electroweak gauge symmetry with universality above the GUT scale.
- 18 BUCHMUELLER 09 places constraints on the SUSY parameter space in the framework of $N=1$ supergravity models with radiative breaking of the electroweak gauge symmetry using indirect experimental searches.
- 19 DREINER 09 show that in the general MSSM with non-universal gaugino masses there exists no model-independent laboratory bound on the mass of the lightest neutralino. An essentially massless $\tilde{\chi}_1^0$ is allowed by the experimental and observational data, imposing some constraints on other MSSM parameters, including M_2 , μ and the slepton and squark masses.
- 20 BUCHMUELLER 08 places constraints on the SUSY parameter space in the framework of $N=1$ supergravity models with radiative breaking of the electroweak gauge symmetry using indirect experimental searches.
- 21 CALIBBI 07 places constraints on the SUSY parameter space in the framework of $N=1$ supergravity models with radiative breaking of the electroweak gauge symmetry with universality above the GUT scale including the effects of right-handed neutrinos.
- 22 ELLIS 07 places constraints on the SUSY parameter space in the framework of $N=1$ supergravity models with radiative breaking of the electroweak gauge symmetry with universality below the GUT scale.
- 23 ALLANACH 06 places constraints on the SUSY parameter space in the framework of $N=1$ supergravity models with radiative breaking of the electroweak gauge symmetry.
- 24 DE-AUSTRI 06 places constraints on the SUSY parameter space in the framework of $N=1$ supergravity models with radiative breaking of the electroweak gauge symmetry.
- 25 BALTZ 04 places constraints on the SUSY parameter space in the framework of $N=1$ supergravity models with radiative breaking of the electroweak gauge symmetry.
- 26 Limit assumes a pseudo scalar mass < 200 GeV. For larger pseudo scalar masses, $m_{\tilde{\chi}} > 18(29)$ GeV for $\tan\beta = 50(10)$. Bounds from WMAP, $(g-2)_\mu$, $b \rightarrow s\gamma$, LEP.
- 27 ELLIS 04b places constraints on the SUSY parameter space in the framework of $N=1$ supergravity models with radiative breaking of the electroweak gauge symmetry including supersymmetry breaking relations between A and B parameters. See also ELLIS 03d.
- 28 PIERCE 04a places constraints on the SUSY parameter space in the framework of models with very heavy scalar masses.

- 29 BAER 03, CHATTOPADHYAY 03, ELLIS 03c and LAHANAS 03 place constraints on the SUSY parameter space in the framework of $N=1$ supergravity models with radiative breaking of the electroweak gauge symmetry based on WMAP results for the cold dark matter density.
- 30 BOEHM 00b and ELLIS 03 place constraints on the SUSY parameter space in the framework of minimal $N=1$ supergravity models with radiative breaking of the electroweak gauge symmetry. Includes the effect of χ - t co-annihilations.
- 31 LAHANAS 02 places constraints on the SUSY parameter space in the framework of minimal $N=1$ supergravity models with radiative breaking of the electroweak gauge symmetry. Focuses on the role of pseudo-scalar Higgs exchange.
- 32 BARGER 01c use the cosmic relic density inferred from recent CMB measurements to constrain the parameter space in the framework of minimal $N=1$ supergravity models with radiative breaking of the electroweak gauge symmetry.
- 33 ELLIS 01b places constraints on the SUSY parameter space in the framework of minimal $N=1$ supergravity models with radiative breaking of the electroweak gauge symmetry. Focuses on models with large $\tan\beta$.
- 34 FENG 00 explores cosmologically allowed regions of MSSM parameter space with multi-TeV masses.
- 35 ELLIS 98b assumes a universal scalar mass and radiative supersymmetry breaking with universal gaugino masses. The upper limit to the LSP mass is increased due to the inclusion of $\chi - \tilde{\tau}_R$ coannihilations.
- 36 EDSJO 97 included all coannihilation processes between neutralinos and charginos for any neutralino mass and composition.
- 37 Notes the location of the neutralino Z resonance and h resonance annihilation corridors in minimal supergravity models with radiative electroweak breaking.
- 38 Mass of the bino (=LSP) is limited to $m_{\tilde{B}} \lesssim 350$ GeV for $m_t = 174$ GeV.
- 39 DREES 93, KELLEY 93 compute the cosmic relic density of the LSP in the framework of minimal $N=1$ supergravity models with radiative breaking of the electroweak gauge symmetry.
- 40 FALK 93 relax the upper limit to the LSP mass by considering sfermion mixing in the MSSM.
- 41 MIZUTA 93 include coannihilations to compute the relic density of Higgsino dark matter.
- 42 LOPEZ 92 calculate the relic LSP density in a minimal SUSY GUT model.
- 43 MCDONALD 92 calculate the relic LSP density in the MSSM including exact tree-level annihilation cross sections for all two-body final states.
- 44 GRIEST 91 improve relic density calculations to account for coannihilations, pole effects, and threshold effects.
- 45 NOJIRI 91 uses minimal supergravity mass relations between squarks and sleptons to narrow cosmologically allowed parameter space.
- 46 Mass of the bino (=LSP) is limited to $m_{\tilde{B}} \lesssim 350$ GeV for $m_t \leq 200$ GeV. Mass of the higgsino (=LSP) is limited to $m_{\tilde{H}} \lesssim 1$ TeV for $m_t \leq 200$ GeV.
- 47 ROSZKOWSKI 91 calculates LSP relic density in mixed gaugino/higgsino region.
- 48 Mass of the bino (=LSP) is limited to $m_{\tilde{B}} \lesssim 550$ GeV. Mass of the higgsino (=LSP) is limited to $m_{\tilde{H}} \lesssim 3.2$ TeV.
- 49 KRAUSS 83 finds $m_{\tilde{\nu}}$ not 30 eV to 2.5 GeV. KRAUSS 83 takes into account the gravitino decay. Find that limits depend strongly on reheated temperature. For example a new allowed region $m_{\tilde{\nu}} = 4-20$ MeV exists if $m_{\text{gravitino}} < 40$ TeV. See figure 2.

Unstable $\tilde{\chi}_1^0$ (Lightest Neutralino) mass limit

Unless otherwise stated, results in this section assume spectra and production rates as evaluated in the MSSM. Unless otherwise stated, the goldstino or gravitino mass $m_{\tilde{G}}$ is assumed to be negligible relative to all other masses. In the following, \tilde{G} is assumed to be undetected and to give rise to a missing energy (\cancel{E}) signature.

Some earlier papers are now obsolete and have been omitted. They were last listed in our PDG 14 edition: K. Olive, *et al.* (Particle Data Group), Chinese Physics **C38** 070001 (2014) (<http://pdg.lbl.gov>).

VALUE (GeV)	CL%	DOCUMENT ID	TECN	COMMENT
> 900	95	1 AAD	23AE ATLS	2 SFOS ℓ , jets, \cancel{E}_T , Tn1n1C, $m_{\tilde{\chi}_1^0}$
> 365	95	2 AAD	23AM ATLS	= 1 GeV $\tilde{\chi}_1^0$, displaced diphoton vertex, Tn1n1A, $\tau = 2$ ns
> 605	95	2 AAD	23AM ATLS	long-lived $\tilde{\chi}_1^0$, displaced diphoton vertex, Tn1n1B, $\tau = 2$ ns
> 705	95	2 AAD	23AM ATLS	long-lived $\tilde{\chi}_1^0$, displaced diphoton vertex, Tn1n1C, $\tau = 2$ ns
> 440	95	3 AAD	23CP ATLS	2 same-sign or 3 ℓ , Tn1n1D, bRPV higgsino decays to νW , ℓW
> 1180	95	4 TUMASYAN	23AO CMS	long-lived $\tilde{\chi}_1^0$, ≥ 2 trackless delayed jets + \cancel{E}_T , Tn1n1B, $c\tau = 0.5$ m
> 990	95	4 TUMASYAN	23AO CMS	long-lived $\tilde{\chi}_1^0$, ≥ 2 trackless delayed jets + \cancel{E}_T , Tn1n1B, $c\tau = 3$ m
> 540	95	5 AAD	21Y ATLS	$\geq 4\ell$, Tchi1n12-GGM, $\tilde{\chi}_1^0 \rightarrow Z\tilde{G}$
none 7–50	95	6 AAIJ	21V LHCB	$e^\pm\mu^\mp$, RPV $\tilde{\chi}_1^0 \rightarrow e^\pm\mu^\mp$, 2 ps $< \tau < 50$ ps
> 1100	95	7 SIRUNYAN	21AF CMS	long-lived $\tilde{\chi}_1^0$, RPV $\tilde{\chi}_1^0 \rightarrow tbs$, χ_{323} coupling, 0.6 mm $< c\tau < 70$ mm
> 800	95	8 SIRUNYAN	21M CMS	$\ell^\pm\ell^\mp + \cancel{E}_T$, Tn1n1C
> 650	95	8 SIRUNYAN	21M CMS	$\ell^\pm\ell^\mp + \cancel{E}_T$, Tn1n1B
> 380	95	9 AAD	20AN ATLS	$2\gamma + \cancel{E}_T$, Tn1n1A, GMSB
> 525	95	10 SIRUNYAN	19CA CMS	$\tilde{\chi}_1^0 \rightarrow \gamma\tilde{G}$, GMSB, SP58, $c\tau = 1$ m
> 290	95	11 SIRUNYAN	19ci CMS	≥ 1 H ($\rightarrow \gamma\gamma$) + jets + \cancel{E}_T , Tn1n1A, GMSB
> 230	95	11 SIRUNYAN	19ci CMS	≥ 1 H ($\rightarrow \gamma\gamma$) + jets + \cancel{E}_T , Tn1n1B, GMSB

Searches Particle Listings

Supersymmetric Particle Searches

> 930	95	12	SIRUNYAN	19K	CMS	$\gamma + \text{lepton} + \cancel{E}_T, \text{TchIn1A}$
none 130-230, 290-880	95	13	AABOUD	18CK	ATLS	$2H (\rightarrow bb) + \cancel{E}_T, \text{Tn1n1A, GMSB}$
> 295	95	14	AABOUD	18Z	ATLS	$\geq 4\ell, \text{GMSB, Tn1n1C}$
> 180	95	15	SIRUNYAN	18AO	CMS	$\ell^\pm \ell^\pm \text{ or } \geq 3\ell, \text{Tn1n1A}$
> 260	95	15	SIRUNYAN	18AO	CMS	$\ell^\pm \ell^\pm \text{ or } \geq 3\ell, \text{Tn1n1B}$
> 450	95	15	SIRUNYAN	18AO	CMS	$\ell^\pm \ell^\pm \text{ or } \geq 3\ell, \text{Tn1n1C}$
> 750	95	16	SIRUNYAN	18AP	CMS	Combination of searches, GMSB, Tn1n1A
> 650	95	16	SIRUNYAN	18AP	CMS	Combination of searches, GMSB, Tn1n1B
> 690	95	16	SIRUNYAN	18AP	CMS	Combination of searches, GMSB, Tn1n1C
> 500	95	17	SIRUNYAN	18AR	CMS	$\ell^\pm \ell^\mp + \text{jets} + \cancel{E}_T, \text{GMSB, Tn1n1B}$
> 650	95	17	SIRUNYAN	18AR	CMS	$\ell^\pm \ell^\mp + \text{jets} + \cancel{E}_T, \text{GMSB, Tn1n1C}$
none 230-770	95	18	SIRUNYAN	18O	CMS	$2H (\rightarrow bb) + \cancel{E}_T, \text{Tn1n1A, GMSB}$
> 205	95	19	SIRUNYAN	18X	CMS	$\geq 1H (\rightarrow \gamma\gamma) + \text{jets} + \cancel{E}_T, \text{Tn1n1A, GMSB}$
> 130	95	19	SIRUNYAN	18X	CMS	$\geq 1H (\rightarrow \gamma\gamma) + \text{jets} + \cancel{E}_T, \text{Tn1n1B, GMSB}$
> 380	95	20	KHACHATRYAN	14L	CMS	$\tilde{\chi}_1^0 \rightarrow Z\tilde{G}$ simplified models, GMSB, RPV
• • • We do not use the following data for averages, fits, limits, etc. • • •						
		21	AAD	20D		$\tilde{q} \rightarrow q\tilde{\chi}_1^0, \tilde{\chi}_1^0 \rightarrow \ell\ell\nu, \text{RPV}, \lambda_{121}$ or $\lambda_{122} \neq 0$
none 300-1000	95	22	AABOUD	19G	ATLS	$\tilde{\chi}_1^0 \rightarrow Z\tilde{G}$ from gluinos as in Tglu1A, GMSB, depending on c_T
		23	AAIJ	17Z		displaced vertex with associated μ
		24	KHACHATRYAN	16BX	CMS	$\geq 3\ell^\pm, \text{RPV}, \lambda \text{ or } \lambda' \text{ couplings, wino- or higgsino-like neutralinos}$
		25	AAD	14BH	ATLS	$2\gamma + \cancel{E}_T, \text{GMSB, SPS8}$
		26	AAD	13AP	ATLS	$2\gamma + \cancel{E}_T, \text{GMSB, SPS8}$
none 220-380	95	27	AAD	13Q	ATLS	$\gamma + b + \cancel{E}_T, \text{higgsino-like neutralino, GMSB}$
		28	AAD	13R	ATLS	$\tilde{\chi}_1^0 \rightarrow \mu\tilde{j}, \text{RPV}, \lambda'_{211} \neq 0$
		29	AALTONEN	13I	CDF	$\tilde{\chi}_1^0 \rightarrow \gamma\tilde{G}, \cancel{E}_T, \text{GMSB}$
> 220	95	30	CHATRCHYAN	13AH	CMS	$\tilde{\chi}_1^0 \rightarrow \gamma\tilde{G}, \text{GMSB, SPS8}, c_T < 500 \text{ mm}$
		31	AAD	12CP	ATLS	$2\gamma + \cancel{E}_T, \text{GMSB}$
		32	AAD	12CT	ATLS	$\geq 4\ell^\pm, \text{RPV}$
		33	AAD	12R	ATLS	$\tilde{\chi}_1^0 \rightarrow \mu\tilde{j}, \text{RPV}, \lambda'_{211} \neq 0$
		34	ABAZOV	12AD	DO	$\tilde{\chi}_1^0 \rightarrow \gamma Z\tilde{G}, \text{GMSB}$
		35	CHATRCHYAN	12BK	CMS	$2\gamma + \cancel{E}_T, \text{GMSB}$
		36	CHATRCHYAN	11B	CMS	$\tilde{W}^0 \rightarrow \gamma\tilde{G}, \tilde{W}^\pm \rightarrow \ell^\pm\tilde{G}, \text{GMSB}$
> 149	95	37	AALTONEN	10	CDF	$p\bar{p} \rightarrow \tilde{\chi}\tilde{\chi}, \tilde{\chi} = \tilde{\chi}_2^0, \tilde{\chi}_1^\pm, \tilde{\chi}_1^0 \rightarrow \gamma\tilde{G}, \text{GMSB}$
> 175	95	38	ABAZOV	10P	DO	$\tilde{\chi}_1^0 \rightarrow \gamma\tilde{G}, \text{GMSB}$
> 125	95	39	ABAZOV	08F	DO	$p\bar{p} \rightarrow \tilde{\chi}\tilde{\chi}, \tilde{\chi} = \tilde{\chi}_2^0, \tilde{\chi}_1^\pm, \tilde{\chi}_1^0 \rightarrow \gamma\tilde{G}, \text{GMSB}$
		40	ABULENCIA	07H	CDF	RPV, $L\tilde{L}\tilde{E}$
> 96.8	95	41	ABBIENDI	06B	OPAL	$e^+e^- \rightarrow \tilde{B}\tilde{B}, (\tilde{B} \rightarrow \tilde{G}\gamma)$
		42	ABDALLAH	05B	DLPH	$e^+e^- \rightarrow \tilde{G}\tilde{\chi}_1^0, (\tilde{\chi}_1^0 \rightarrow \tilde{G}\gamma)$
> 96	95	43	ABDALLAH	05B	DLPH	$e^+e^- \rightarrow \tilde{B}\tilde{B}, (\tilde{B} \rightarrow \tilde{G}\gamma)$

1 AAD 23AE searched in 139 fb^{-1} of pp collisions at $\sqrt{s} = 13 \text{ TeV}$ for events with 2ℓ with same flavour and opposite sign, plus jets and \cancel{E}_T , defining signal region with the dilepton invariant mass both on- and off-shell with respect to the Z boson. No significant excess above the Standard Model predictions is observed. Limits are set on models of strong and electroweak production. In this case, limits are placed on production of mass-degenerate, higgsino triplet NLSF with $\tilde{\chi}_1^0 \rightarrow Z\tilde{G}$ in a GGM-like scenario, see figure 15.

2 AAD 23AM searched in 139 fb^{-1} of pp collisions at $\sqrt{s} = 13 \text{ TeV}$ for events containing electron/photon pairs with invariant mass compatible with h/Z and originating from a common displaced vertex. No significant excess above the Standard Model predictions is observed. Limits are set on a model where members of a nearly degenerate higgsino triplet are pair-produced, yielding long-lived $\tilde{\chi}_1^0$ followed by $\tilde{\chi}_1^0 \rightarrow h/Z\tilde{G}$. Limits are set on $m_{\tilde{\chi}_1^0}$ as a function of its lifetime and of the $B(\tilde{\chi}_1^0 \rightarrow h\tilde{G})$ assuming $B(\tilde{\chi}_1^0 \rightarrow h\tilde{G}) + B(\tilde{\chi}_1^0 \rightarrow Z\tilde{G}) = 1$, see Figure 10.

3 AAD 23CP searched in 139 fb^{-1} of pp collisions at $\sqrt{s} = 13 \text{ TeV}$ for events with 2ℓ with same charge or 3ℓ plus at least one jet and \cancel{E}_T , defining signal region based on 'transverse mass' of the dilepton system, \cancel{E}_T significance and effective mass. No significant excess above the Standard Model predictions is observed. Limits are set on the mass of a mass-degenerate higgsino triplet decaying into a lepton (neutral or charged) and a W via a bilinear RPV coupling, see figure 14.

4 TUMASYAN 23AO searched in 138 fb^{-1} of pp collisions at $\sqrt{s} = 13 \text{ TeV}$ for evidence of neutralino-chargino production in events with nearly trackless and out-of-time jets that are used to identify decays of long-lived particles. No significant excess above the Standard Model expectations is observed. Limits are set on the mass of the long-lived $\tilde{\chi}_1^0$ in the model Tn1n1B, see their figures 8-10.

5 AAD 21V searched in 139 fb^{-1} of pp collisions at $\sqrt{s} = 13 \text{ TeV}$ for supersymmetry in events with four or more leptons (electrons, muons and tau-leptons). No significant excess above the Standard Model expectations is observed. Limits are set on Tchi1n2-GGM, and RPV models similar to Tchi1n2L, Tglu1A (with $q = u, d, s, c, b$, with equal branching fractions), and $\tilde{\ell}_L/\tilde{\nu} \rightarrow \ell/\nu\tilde{\chi}_1^0$ (mass-degenerate $\tilde{\ell}_L$ and $\tilde{\nu}$ of all 3 generations), all with $\tilde{\chi}_1^0 \rightarrow \ell^\pm\tilde{\tau}\nu$ via λ_{12k} or λ_{133} (where $i, k = 1, 2$), see their Figure 11.

6 AAIJ 21V searched in 5.38 fb^{-1} of pp collisions at $\sqrt{s} = 13 \text{ TeV}$ for long-lived particles (LLP) decaying to $e^\pm\mu^\mp\nu$. The LLP can be a $\tilde{\chi}_1^0$ in RPV SUSY, or a right-handed neutrino, and can be produced in pairs, in the decay of the Higgs boson, or from charged

current processes. No significant excess above the Standard Model expectations is observed. Limits are set on the cross section times branching ratio for all three production mechanisms, see their Figures 6-8.

7 SIRUNYAN 21AF searched in 140 fb^{-1} of pp collisions at $\sqrt{s} = 13 \text{ TeV}$ for supersymmetry in events with two displaced vertices from long-lived particles decaying into multijet or dijet final states. No significant excess above the Standard Model expectations is observed. Limits are set on the gluino mass in the simplified model Tglu2RPV with λ'_{323} coupling, on the $\tilde{\chi}_1^0$ mass in an RPV model with $\tilde{\chi}_1^0$ pair production and the RPV decay $\tilde{\chi}_1^0 \rightarrow tbs$ with λ'_{323} coupling and on the $\tilde{\tau}$ mass in an RPV model with top squark pair production and the RPV decay $\tilde{\tau} \rightarrow \tilde{d}_i\tilde{d}_j$ with λ'_{3ij} coupling, see their Figure 7.

8 SIRUNYAN 21M searched in 137 fb^{-1} of pp collisions at $\sqrt{s} = 13 \text{ TeV}$ for supersymmetry in events with two opposite-sign same-flavour leptons (electrons, muons) and \cancel{E}_T . No significant excess above the Standard Model expectations is observed. Limits are set on the gluino mass in the simplified model Tglu4C, see their Figure 10, on the $\tilde{\chi}_2^0$ and $\tilde{\chi}_1^\pm$ mass in Tchi1n2Fa, see their Figure 11, on the $\tilde{\chi}_1^0$ mass in Tn1n1C and Tn1n1B for $m_{\tilde{\chi}_2^0} = m_{\tilde{\chi}_1^\pm} = m_{\tilde{\chi}_1^0}$, see their Figure 12. Limits are also set on the light squark mass for the simplified model Tsqk2A, on the sbottom mass in Tsbot3, see their Figure 13, and on the slepton mass in direct electroweak pair production of mass-degenerate left- and right-handed sleptons (selectrons and smuons), see their Figure 14.

9 AAD 20AN searched in 139 fb^{-1} of pp collisions at $\sqrt{s} = 13 \text{ TeV}$ for events with two photons and missing transverse momentum. Events are further categorised in terms of lepton or jet multiplicity. No significant excess over the expected background is observed. Limits at 95% C.L. are set on the Higgsino mass in the Tn1n1A simplified model, see their Figure 11.

10 SIRUNYAN 19CA searched in 77.4 fb^{-1} of pp collisions at $\sqrt{s} = 13 \text{ TeV}$ for events containing delayed photons in both single and diphoton plus \cancel{E}_T final states. No excess is observed above the background expected from Standard Model processes. The results are used to set 95% C.L. exclusion limits in the context of GMSB, using the SPS8 benchmark model. For neutralino proper decay lengths of 0.1, 1, 10, and 100 m, masses up to about 320, 525, 360, and 215 GeV are excluded, respectively. See their Fig. 5. The searches involve the simplified models Tglu1D, Tglu4A,B,C, Tsqk4,4A,4B.

11 SIRUNYAN 19CI searched in 77.5 fb^{-1} of pp collisions at $\sqrt{s} = 13 \text{ TeV}$ for events with one or more high-momentum Higgs bosons, decaying to pairs of photons, jets and \cancel{E}_T . No significant excess above the Standard Model expectations is observed. Limits are set on the sbottom mass in the Tsbot4 simplified model, see Figure 3, and on the wino mass in the Tchi1n2E simplified model, see their Figure 4. Limits are also set on the higgsino mass in the Tn1n1A and Tn1n1B simplified models, see their Figure 5.

12 SIRUNYAN 19K searched in 35.9 fb^{-1} of pp collisions at $\sqrt{s} = 13 \text{ TeV}$ for events with a photon, an electron or muon, and large \cancel{E}_T . No significant excess above the Standard Model expectations is observed. In the framework of GMSB, limits are set on the chargino and neutralino mass in the Tchi1n1A simplified model, see their Figure 6. Limits are also set on the gluino mass in the Tglu4A simplified model, and on the squark mass in the Tsqk4A simplified model, see their Figure 7.

13 AABOUD 18CK searched for events with at least 3 b -jets and large missing transverse energy in two datasets of pp collisions at $\sqrt{s} = 13 \text{ TeV}$ of 36.1 fb^{-1} and 24.3 fb^{-1} depending on the trigger requirements. The analyses aimed to reconstruct two Higgs bosons decaying to pairs of b -quarks. No significant excess above the Standard Model expectations is observed. Limits are set on the Higgsino mass in the Tn1n1A simplified model, see their Figure 15(a). Constraints are also presented as a function of the BR of Higgsino decaying into an higgs boson and a gravitino, see their Figure 15(b).

14 AABOUD 18Z searched in 36.1 fb^{-1} of pp collisions at $\sqrt{s} = 13 \text{ TeV}$ for events containing four or more charged leptons (electrons, muons and tau) to two hadronically decaying taus). No significant deviation from the expected SM background is observed. Limits are set on the Higgsino mass in simplified models of general gauge mediated supersymmetry Tn1n1A/Tn1n1B/Tn1n1C, see their Figure 9. Limits are also set on the wino, slepton, neutralino and gluino mass in a simplified model of NLSF pair production with R-parity violating decays of the LSP via λ_{12k} or λ_{133} to charged leptons, see their Figures 7, 8.

15 SIRUNYAN 18AO searched in 35.9 fb^{-1} of pp collisions at $\sqrt{s} = 13 \text{ TeV}$ for direct electroweak production of charginos and neutralinos in events with either two or more leptons (electrons or muons) of the same electric charge, or with three or more leptons, which can include up to two hadronically decaying tau leptons. No significant excess above the Standard Model expectations is observed. Limits are set on the chargino/neutralino mass in the Tchi1n2A, Tchi1n2H, Tchi1n2D, Tchi1n2E and Tchi1n2F simplified models, see their Figures 14, 15, 16, 17 and 18. Limits are also set on the higgsino mass in the Tn1n1A, Tn1n1B and Tn1n1C simplified models, see their Figure 19.

16 SIRUNYAN 18AP searched in 35.9 fb^{-1} of pp collisions at $\sqrt{s} = 13 \text{ TeV}$ for direct electroweak production of charginos and neutralinos by combining a number of previous and new searches. No significant excess above the Standard Model expectations is observed. Limits are set on the chargino/neutralino mass in the Tchi1n2E, Tchi1n2F and Tchi1n2I simplified models, see their Figures 7, 8, 9 and 10. Limits are also set on the higgsino mass in the Tn1n1A, Tn1n1B and Tn1n1C simplified models, see their Figure 11, 12, 13 and 14.

17 SIRUNYAN 18AR searched in 35.9 fb^{-1} of pp collisions at $\sqrt{s} = 13 \text{ TeV}$ for events containing two opposite-charge, same-flavour leptons (electrons or muons), jets and \cancel{E}_T . No significant excess above the Standard Model expectations is observed. Limits are set on the gluino mass in the Tglu4C simplified model, see their Figure 7. Limits are also set on the chargino/neutralino mass in the Tchi1n2F simplified models, see their Figure 8, and on the higgsino mass in the Tn1n1B and Tn1n1C simplified models, see their Figure 9. Finally, limits are set on the sbottom mass in the Tsbot3 simplified model, see their Figure 10.

18 SIRUNYAN 18O searched in 35.9 fb^{-1} of pp collisions at $\sqrt{s} = 13 \text{ TeV}$ for events with two Higgs bosons, decaying to pairs of b -quarks, and large \cancel{E}_T . No significant excess above the Standard Model expectations is observed. Limits are set on the Higgsino mass in the Tn1n1A simplified model, see their Figure 9.

19 SIRUNYAN 18X searched in 35.9 fb^{-1} of pp collisions at $\sqrt{s} = 13 \text{ TeV}$ for events with one or more high-momentum Higgs bosons, decaying to pairs of photons, jets and \cancel{E}_T . The razor variables (M_R and R^2) are used to categorise the events. No significant excess above the Standard Model expectations is observed. Limits are set on the sbottom mass in the Tsbot4 simplified model and on the wino mass in the Tchi1n2E simplified model, see their Figure 5. Limits are also set on the higgsino mass in the Tn1n1A and Tn1n1B simplified models, see their Figure 6.

20 KHACHATRYAN 14L searched in 19.5 fb^{-1} of pp collisions at $\sqrt{s} = 8 \text{ TeV}$ for evidence of direct pair production of neutralinos with Higgs or Z -bosons in the decay chain, leading to HH, HZ and ZZ final states with missing transverse energy. The decays of 16-20

- a Higgs boson to a b -quark pair, to a photon pair, and to final states with leptons are considered in conjunction with hadronic and leptonic decay modes of the Z and W bosons. No significant excesses over the expected SM backgrounds are observed. The results are interpreted in the context of GMSB simplified models where the decays $\tilde{\chi}_1^0 \rightarrow H\bar{G}$ or $\tilde{\chi}_1^0 \rightarrow Z\bar{G}$ take place either 100% or 50% of the time, see Figs. 16–20.
- 21 AAD 20b searched in 32.8 fb^{-1} of pp collisions at $\sqrt{s} = 13 \text{ TeV}$ for events containing an oppositely charge lepton pair ($e\bar{e}, \mu\bar{\mu}$ or $e\mu$) coming from long-lived neutralinos decaying through the R -parity-violating decay $\tilde{\chi}_1^0 \rightarrow \ell\ell\nu$ with $\lambda_{121} \neq 0$ or $\lambda_{122} \neq 0$. No excess over the expected background is observed. Limits are derived for decay lengths of the neutralino between 1 mm and 10 m in a scenario where a squark-antisquark pair is produced, with the squark decaying to a quark and a $\tilde{\chi}_1^0$, with either $\tilde{\chi}_1^0 \rightarrow e\bar{e}\nu/e\mu\nu$ ($\lambda_{121} \neq 0$) or $\tilde{\chi}_1^0 \rightarrow e\mu\nu/\mu\mu\nu$ ($\lambda_{122} \neq 0$), see their Figures 4 and 5.
- 22 AABOU 19c searched in 32.9 fb^{-1} of pp collisions at $\sqrt{s} = 13 \text{ TeV}$ for evidence of neutralinos decaying into a Z -boson and a gravitino, in events characterized by the presence of dimuon vertices with displacements from the pp interaction point in the range of 1400 cm. Neutralinos are assumed to be produced in the decay chain of gluinos as in Tglu1A models. No significant excess is observed in the number of vertices relative to the predicted background. In GGM with a gluino mass of 1100 GeV, neutralino masses in the range 300–1000 GeV are excluded for certain values of $c\tau$, see their Figure 7.
- 23 AAIJ 17z searched in 1 fb^{-1} of pp collisions at $\sqrt{s} = 7 \text{ TeV}$ and in 2 fb^{-1} of pp collisions at $\sqrt{s} = 8 \text{ TeV}$ for events containing a displaced vertex with one associated high transverse momentum μ . No excess is observed above the background expected from Standard Model processes. The results are used to set 95% C.L. upper limits on the cross section times branching fractions of pair-produced neutralinos decaying non-promptly into a muon and two quarks. Long-lived particles in a mass range 23–198 GeV are considered, see their Fig. 5 and Fig. 6.
- 24 KHACHATRYAN 16bx searched in 19.5 fb^{-1} of pp collisions at $\sqrt{s} = 8 \text{ TeV}$ for events containing 3 or more leptons coming from the electroweak production of wino- or higgsino-like neutralinos, assuming non-zero R -parity-violating leptonic couplings λ_{122} , λ_{123} , and λ_{233} or semileptonic couplings λ'_{131} , λ'_{233} , λ'_{331} , and λ'_{333} . No excess over the expected background is observed and limits are derived on the neutralino mass, see Figs. 24 and 25.
- 25 AAD 14Bh searched in 20.3 fb^{-1} of pp collisions at $\sqrt{s} = 8 \text{ TeV}$ for events containing non-pointing photons in a diphoton plus missing transverse energy final state. No excess is observed above the background expected from Standard Model processes. The results are used to set 95% C.L. exclusion limits in the contact of gauge-mediated supersymmetric breaking models, with the lightest neutralino being the next-to-lightest supersymmetric particle and decaying with a lifetime in the range from 0.25 ns to about 100 ns into a photon and a gravitino. For limits on the NLSF lifetime versus Λ plane, for the SPS8 model, see their Fig. 7.
- 26 AAD 13Ap searched in 4.8 fb^{-1} of pp collisions at $\sqrt{s} = 7 \text{ TeV}$ for events containing non-pointing photons in a diphoton plus missing transverse energy final state. No excess is observed above the background expected from Standard Model processes. The results are used to set 95% C.L. exclusion limits in the context of gauge-mediated supersymmetric breaking models, with the lightest neutralino being the next-to-lightest supersymmetric particle and decaying with a lifetime in excess of 0.25 ns into a photon and a gravitino. For limits in the NLSF lifetime versus Λ plane, for the SPS8 model, see their Fig. 8.
- 27 AAD 13Q searched in 4.7 fb^{-1} of pp collisions at $\sqrt{s} = 7 \text{ TeV}$ for events containing a high- p_T isolated photon, at least one jet identified as originating from a bottom quark, and high missing transverse momentum. Such signatures may originate from supersymmetric models with gauge-mediated supersymmetry breaking in events in which one of a pair of higgsino-like neutralinos decays into a photon and a gravitino while the other decays into a Higgs boson and a gravitino. No significant excess above the expected background was found and limits were set on the neutralino mass in a generalized GMSB model (GGM) with a higgsino-like neutralino NLSF, see their Fig. 4. Intermediate neutralino masses between 220 and 380 GeV are excluded at 95% C.L., regardless of the squark and gluino masses, purely on the basis of the expected weak production.
- 28 AAD 13R looked in 4.4 fb^{-1} of pp collisions at $\sqrt{s} = 7 \text{ TeV}$ for events containing new, heavy particles that decay at a significant distance from their production point into a final state containing a high-momentum muon and charged hadrons. No excess over the expected background is observed and limits are placed on the production cross-section of neutralinos via squarks for various $m_{\tilde{q}}, m_{\tilde{\chi}_1^0}$ in an R -parity violating scenario with $\lambda'_{211} \neq 0$, as a function of the neutralino lifetime, see their Fig. 6.
- 29 AALTONEN 13i searched in 6.3 fb^{-1} of $p\bar{p}$ collisions at $\sqrt{s} = 1.96 \text{ TeV}$ for events containing \cancel{E}_T and a delayed photon that arrives late in the detector relative to the time expected from prompt production. No evidence of delayed photon production is observed.
- 30 CHATRCHYAN 13AH searched in 4.9 fb^{-1} of pp collisions at $\sqrt{s} = 7 \text{ TeV}$ for events containing \cancel{E}_T and a delayed photon that arrives late in the detector relative to the time expected from prompt production. No significant excess above the expected background was found and limits were set on the pair production of $\tilde{\chi}_1^0$ depending on the neutralino proper decay length, see Fig. 8. Supersedes CHATRCHYAN 12Bk.
- 31 AAD 12CP searched in 4.8 fb^{-1} of pp collisions at $\sqrt{s} = 7 \text{ TeV}$ for events with two photons and large \cancel{E}_T due to $\tilde{\chi}_1^0 \rightarrow \gamma\bar{G}$ decays in a GMSB framework. No significant excess above the expected background was found and limits were set on the neutralino mass in a generalized GMSB model (GGM) with a bino-like neutralino NLSF, see Figs. 6 and 7. The other sparticle masses were decoupled, $\tan\beta = 2$ and $c\tau_{NLSF} < 0.1 \text{ mm}$. Also, in the framework of the SPS8 model, limits are presented in Fig. 8.
- 32 AAD 12CT searched in 4.7 fb^{-1} of pp collisions at $\sqrt{s} = 7 \text{ TeV}$ for events containing four or more leptons (electrons or muons) and either moderate values of missing transverse momentum or large effective mass. No significant excess is found in the data. Limits are presented in a simplified model of R -parity violating supersymmetry in which charginos are pair-produced and then decay into a W -boson and a $\tilde{\chi}_1^0$, which in turn decays through an RPV coupling into two charged leptons ($e^\pm e^\mp$ or $\mu^\pm \mu^\mp$) and a neutrino. In this model, limits are set on the neutralino mass as a function of the chargino mass, see Fig. 3a. Limits are also set in an R -parity violating mSUGRA model, see Fig. 3b.
- 33 AAD 12R looked in 33 pb^{-1} of pp collisions at $\sqrt{s} = 7 \text{ TeV}$ for events containing new, heavy particles that decay at a significant distance from their production point into a final state containing a high-momentum muon and charged hadrons. No excess over the expected background is observed and limits are placed on the production cross-section of neutralinos via squarks for various $(m_{\tilde{q}}, m_{\tilde{\chi}_1^0})$ in an R -parity violating scenario with $\lambda'_{211} \neq 0$, as a function of the neutralino lifetime, see their Fig. 8. Supersedes by AAD 13R.
- 34 ABZOV 12AD looked in 6.2 fb^{-1} of pp collisions at $\sqrt{s} = 1.96 \text{ TeV}$ for events with a photon, a Z -boson, and large \cancel{E}_T in the final state. This topology corresponds to a GMSB model where pairs of neutralino NLSFs are either pair produced promptly or from decays of other supersymmetric particles and then decay to either $Z\bar{G}$ or $\gamma\bar{G}$. No significant excess over the SM expectation is observed and a limit at 95% C.L. on the cross section is derived as a function of the effective SUSY breaking scale Λ , see Fig. 3. Assuming $N_{mes} = 2$, $M_{mes} = 3 \Lambda$, $\tan\beta = 3$, $\mu = 0.75 M_1$, and $C_{grav} = 1$, the model is excluded at 95% C.L. for values of $\Lambda < 87 \text{ TeV}$.
- 35 CHATRCHYAN 12Bk searched in 2.23 fb^{-1} of pp collisions at $\sqrt{s} = 7 \text{ TeV}$ for events with two photons and large \cancel{E}_T due to $\tilde{\chi}_1^0 \rightarrow \gamma\bar{G}$ decays in a GMSB framework. No significant excess above the expected background was found and limits were set on the pair production of $\tilde{\chi}_1^0$ depending on the neutralino lifetime, see Fig. 6.
- 36 CHATRCHYAN 11B looked in 35 pb^{-1} of pp collisions at $\sqrt{s} = 7 \text{ TeV}$ for events with an isolated lepton (e or μ), a photon and \cancel{E}_T which may arise in a generalized gauge mediated model from the decay of Wino-like NLSFs. No evidence for an excess over the expected background is observed. Limits are derived in the plane of squark/gluino mass versus Wino mass (see Fig. 4). Mass degeneracy of the produced squarks and gluinos is assumed.
- 37 AALTONEN 10 searched in 2.6 fb^{-1} of $p\bar{p}$ collisions at $\sqrt{s} = 1.96 \text{ TeV}$ for diphoton events with large \cancel{E}_T . They may originate from the production of $\tilde{\chi}^\pm$ in pairs or associated to a $\tilde{\chi}_1^0$, decaying into $\tilde{\chi}_1^0$ which itself decays in GMSB to $\gamma\bar{G}$. There is no excess of events beyond expectation. An upper limit on the cross section is calculated in the GMSB model as a function of the $\tilde{\chi}_1^0$ mass and lifetime, see their Fig. 2. A limit is derived on the $\tilde{\chi}_1^0$ mass of 149 GeV for $\tau_{\tilde{\chi}_1^0} \ll 1 \text{ ns}$, which improves the results of previous searches.
- 38 ABZOV 10P looked in 6.3 fb^{-1} of $p\bar{p}$ collisions at $\sqrt{s} = 1.96 \text{ TeV}$ for events with at least two isolated γ s and large \cancel{E}_T . These could be the signature of $\tilde{\chi}_2^0$ and $\tilde{\chi}_1^\pm$ production, decaying to $\tilde{\chi}_1^0$ and finally $\tilde{\chi}_1^0 \rightarrow \gamma\bar{G}$ in a GMSB framework. No significant excess over the SM expectation is observed, and a limit at 95% C.L. on the cross section is derived for $N_{mes} = 1$, $\tan\beta = 15$ and $\mu > 0$, see their Fig. 2. This allows them to set a limit on the effective SUSY breaking scale $\Lambda > 124 \text{ TeV}$, from which the excluded $\tilde{\chi}_1^0$ mass range is obtained.
- 39 ABZOV 08f looked in 1.1 fb^{-1} of $p\bar{p}$ collisions at $\sqrt{s} = 1.96 \text{ TeV}$ for diphoton events with large \cancel{E}_T . They may originate from the production of $\tilde{\chi}^\pm$ in pairs or associated to a $\tilde{\chi}_1^0$, decaying to a $\tilde{\chi}_1^0$ which itself decays promptly in GMSB to $\gamma\bar{G}$. No significant excess was found compared to the background expectation. A limit is derived on the masses of SUSY particles in the GMSB framework for $M = 2\Lambda$, $N = 1$, $\tan\beta = 15$ and $\mu > 0$, see Figure 2. It also excludes $\Lambda < 91.5 \text{ TeV}$. Supersedes the results of ABZOV 05A. Superseded by ABZOV 10P.
- 40 ABULENCIA 07H searched in 346 pb^{-1} of $p\bar{p}$ collisions at $\sqrt{s} = 1.96 \text{ TeV}$ for events with at least three leptons (e or μ) from the decay of $\tilde{\chi}_1^0$ via $L\bar{L}E$ couplings. The results are consistent with the hypothesis of no signal. Upper limits on the cross-section are extracted and a limit is derived in the framework of mSUGRA on the masses of $\tilde{\chi}_1^0$ and $\tilde{\chi}_1^\pm$, see e.g. their Fig. 3 and Tab. II.
- 41 ABBIENDI 06b use 600 pb^{-1} of data from $\sqrt{s} = 189\text{--}209 \text{ GeV}$. They look for events with diphotons + \cancel{E} final states originating from prompt decays of pair-produced neutralinos in a GMSB scenario with $\tilde{\chi}_1^0$ NLSF. Limits on the cross-section are computed as a function of $m(\tilde{\chi}_1^0)$, see their Fig. 14. The limit on the $\tilde{\chi}_1^0$ mass is for a pure Bino state assuming a prompt decay, with lifetimes up to 10^{-9} s . Supersedes the results of ABBIENDI 04N.
- 42 ABDALLAH 05B use data from $\sqrt{s} = 180\text{--}209 \text{ GeV}$. They look for events with single photons + \cancel{E} final states. Limits are computed in the plane $(m(\tilde{G}), m(\tilde{\chi}_1^0))$, shown in their Fig. 9b for a pure Bino state in the GMSB framework and in Fig. 9c for a no-scale supergravity model. Supersedes the results of ABREU 00Z.
- 43 ABDALLAH 05B use data from $\sqrt{s} = 130\text{--}209 \text{ GeV}$. They look for events with diphotons + \cancel{E} final states and single photons not pointing to the vertex, expected in GMSB when the $\tilde{\chi}_1^0$ is the NLSF. Limits are computed in the plane $(m(\tilde{G}), m(\tilde{\chi}_1^0))$, see their Fig. 10. The lower limit is derived on the $\tilde{\chi}_1^0$ mass for a pure Bino state assuming a prompt decay and $m_{\tilde{e}_R} = m_{\tilde{e}_L} = 2 m_{\tilde{\chi}_1^0}$. It improves to 100 GeV for $m_{\tilde{e}_R} = m_{\tilde{e}_L} = 1.1 m_{\tilde{\chi}_1^0}$ and the limit in the plane $(m(\tilde{\chi}_1^0), m(\tilde{e}_R))$ is shown in Fig. 10b. For long-lived neutralinos, cross-section limits are displayed in their Fig. 11. Supersedes the results of ABREU 00Z.

$\tilde{\chi}_2^0, \tilde{\chi}_3^0, \tilde{\chi}_4^0$ (Neutralinos) mass limits

Neutralinos are unknown mixtures of photinos, z -inos, and neutral higgsinos (the supersymmetric partners of photons and of Z and Higgs bosons). The limits here apply only to $\tilde{\chi}_2^0, \tilde{\chi}_3^0$, and $\tilde{\chi}_4^0$. $\tilde{\chi}_1^0$ is the lightest supersymmetric particle (LSP); see $\tilde{\chi}_1^0$ Mass Limits. It is not possible to quote rigorous mass limits because they are extremely model dependent; i.e. they depend on branching ratios of various $\tilde{\chi}_i^0$ decay modes, on the masses of decay products ($\tilde{e}, \tilde{\nu}, \tilde{q}, \tilde{g}$), and on the \tilde{e} mass exchanged in $e^+e^- \rightarrow \tilde{\chi}_i^0\tilde{\chi}_j^0$. Limits arise either from direct searches, or from the MSSM constraints set on the gaugino and higgsino mass parameters M_2 and μ through searches for lighter charginos and neutralinos. Often limits are given as contour plots in the $m_{\tilde{\chi}_0} - m_{\tilde{e}}$ plane vs other parameters. When specific assumptions are made, e.g. the neutralino is a pure photino ($\tilde{\gamma}$), pure z -ino (\tilde{Z}), or pure neutral higgsino (\tilde{H}^0), the neutralinos will be labelled as such.

Limits obtained from e^+e^- collisions at energies up to 136 GeV, as well as other limits from different techniques, are now superseded and have not been included in this compilation. They can be found in the 1998 Edition (The European Physical Journal **C3** 1 (1998)) of this Review. Some later papers are now obsolete and have been omitted. They were last listed in our PDG 14 edition: K. Olive, *et al.* (Particle Data Group), Chinese Physics **C38** 070001 (2014) (<http://pdg.lbl.gov>).

VALUE (GeV)	CL%	DOCUMENT ID	TECN	COMMENT
> 820	95	1 AAD	23AE ATLS	2 SFOS ℓ , jets, \cancel{E}_T , TchiIn2Fa, $m_{\tilde{\chi}_1^0} = 1 \text{ GeV}$
none 260–420	95	2 AAD	23CI ATLS	1 ℓ + jets + \cancel{E}_T , TchiIn2J, $m_{\tilde{\chi}_1^0} = 0 \text{ GeV}$

Searches Particle Listings

Supersymmetric Particle Searches

> 230	95	³ AAD	23CI ATLS	$1\ell + \text{jets} + \cancel{E}_T$, Tchi1n2E, $m_{\tilde{\chi}_2^0} - m_{\tilde{\chi}_1^0} = 133 \text{ GeV}$	> 650	95	⁹ TUMASYAN	22s CMS	2 same-sign e or μ , 3 or 4 leptons, Tchi1n2F, $m_{\tilde{\chi}_1^0} = 0 \text{ GeV}$
> 450	95	³ AAD	23CI ATLS	$1\ell + \text{jets} + \cancel{E}_T$, Tchi1n2E, $m_{\tilde{\chi}_2^0} - m_{\tilde{\chi}_1^0} = 260 \text{ GeV}$	> 260	95	⁹ TUMASYAN	22s CMS	2 same-sign e or μ , 3 or 4 leptons, Tchi1n2E, $m_{\tilde{\chi}_1^0} = 0 \text{ GeV}$
> 525	95	⁴ AAD	23CP ATLS	2 same-sign ℓ , Tchi1n2E, wino-bino, $m_{\tilde{\chi}_1^0} = 1 \text{ GeV}$	none 265-305	95	¹⁰ TUMASYAN	22v CMS	3, 4 b -tagged or 2 large-radius jets, \cancel{E}_T ; higgsino $\tilde{\chi}_2^0 \tilde{\chi}_3^0$ prod. with $\tilde{\chi}_{2,3}^0 \rightarrow H\tilde{\chi}_1^0$; $m_{\tilde{\chi}_1^0} = 1 \text{ GeV}$
none 200-250	95	⁴ AAD	23CP ATLS	2 same-sign ℓ , Tchi1n2F, wino-bino, $m_{\tilde{\chi}_1^0} = 1 \text{ GeV}$	> 640	95	¹¹ AAD	21BG ATLS	$3\ell + \cancel{E}_T$, Tchi1n2F, wino cross section, $m_{\tilde{\chi}_1^0} = 0 \text{ GeV}$
none 200-585	95	⁵ AAD	23CR ATLS	RPV, 2 same-sign, 3, 4 ℓ , 1, 2 b -jets, higgsino production with $\tilde{\chi} \rightarrow b + \ell/\nu + t/b$ via λ'_{j33} coupling	> 300	95	¹¹ AAD	21BG ATLS	$3\ell + \cancel{E}_T$, Tchi1n2F, wino cross section, $m_{\tilde{\chi}_2^0} - m_{\tilde{\chi}_1^0} = m_Z$
none 200-670	95	⁵ AAD	23CR ATLS	RPV, 2 same-sign, 3, 4 ℓ , 1, 2 b -jets, wino production with $\tilde{\chi} \rightarrow b + \ell/\nu + t/b$ via λ'_{j33} coupling	> 240	95	¹¹ AAD	21BG ATLS	$3\ell + \cancel{E}_T$, Tchi1n2F, wino cross section, $m_{\tilde{\chi}_2^0} - m_{\tilde{\chi}_1^0} = 10 \text{ GeV}$
>1050	95	⁶ HAYRAPETY...23E	CMS	$\gamma + \text{jets} + \cancel{E}_T$, Tchi1chi1A	> 195	95	¹¹ AAD	21BG ATLS	$3\ell + \cancel{E}_T$, Tchi1n2Ga, higgsino cross section, $m_{\tilde{\chi}_2^0} - m_{\tilde{\chi}_1^0} = 10 \text{ GeV}$
> 450	95	⁶ HAYRAPETY...23E	CMS	$\gamma + \text{jets} + \cancel{E}_T$, Tn1n2A	> 190	95	¹¹ AAD	21BG ATLS	$3\ell + \cancel{E}_T$, Tchi1n2E, wino cross section, $m_{\tilde{\chi}_1^0} = 0 \text{ GeV}$
none 290-670	95	⁷ TUMASYAN	23B CMS	2 AK8 jets + 2-6 AK4 jets + \cancel{E}_T , Tchi1chi1l, $m_{\tilde{\chi}_1^0} = 1 \text{ GeV}$	>1600	95	¹² AAD	21Y ATLS	$\geq 4\ell$, RPV Tchi1n2l with $\tilde{\chi}_1^0 \rightarrow \ell^\pm \ell^\mp \nu$, $\lambda_{12k} \neq 0$, $m_{\tilde{\chi}_1^0} = 1200 \text{ GeV}$
none 230-760	95	⁷ TUMASYAN	23B CMS	2 AK8 jets + 2-6 AK4 jets + \cancel{E}_T , Tchi1n2Fb, $m_{\tilde{\chi}_1^0} = 1 \text{ GeV}$	>1100	95	¹² AAD	21Y ATLS	$\geq 4\ell$, RPV Tchi1n2l with $\tilde{\chi}_1^0 \rightarrow \ell^\pm \ell^\mp \nu$, $\lambda_{j33} \neq 0$, $m_{\tilde{\chi}_1^0} = 1000 \text{ GeV}$
none 240-970	95	⁷ TUMASYAN	23B CMS	2 AK8 jets + 2-6 AK4 jets + \cancel{E}_T , Tchi1n2Fc, $m_{\tilde{\chi}_1^0} = 1 \text{ GeV}$	> 750	95	¹³ SIRUNYAN	21M CMS	$\ell^\pm \ell^\mp + \cancel{E}_T$, Tchi1n2Fa, $m_{\tilde{\chi}_1^0} < 100 \text{ GeV}$
none 300-650	95	⁷ TUMASYAN	23B CMS	2 AK8 jets + 2-6 AK4 jets + \cancel{E}_T , THinoBinoA, $m_{\tilde{\chi}_1^0} = 1 \text{ GeV}$	none 400-820	95	¹⁴ TUMASYAN	21c CMS	$1\ell^\pm + 2b$ -jets + \cancel{E}_T , Tchi1n2E, $m_{\tilde{\chi}_1^0} = 200 \text{ GeV}$
> 275	95	⁸ TUMASYAN	22Q CMS	2 or 3 ℓ (soft), \cancel{E}_T ; Tchi1n2F, wino-bino, $m_{\tilde{\chi}_2^0} - m_{\tilde{\chi}_1^0} = 10 \text{ GeV}$	none 160-820	95	¹⁴ TUMASYAN	21c CMS	$1\ell^\pm + 2b$ -jets + \cancel{E}_T , Tchi1n2E, $m_{\tilde{\chi}_1^0} = 0 \text{ GeV}$
> 205	95	⁸ TUMASYAN	22Q CMS	2 or 3 ℓ (soft), \cancel{E}_T ; higgsino model with $\tilde{\chi}_2^0 \tilde{\chi}_1^\pm$ and $\tilde{\chi}_2^0 \tilde{\chi}_1^0$ prod., $m_{\tilde{\chi}_2^0} - m_{\tilde{\chi}_1^0} = 7.5 \text{ GeV}$	> 380	95	¹⁵ AAD	20AN ATLS	$2\gamma + \cancel{E}_T$, Tn1n1A, GMSB
> 150	95	⁸ TUMASYAN	22Q CMS	2 or 3 ℓ (soft), \cancel{E}_T ; higgsino model with $\tilde{\chi}_2^0 \tilde{\chi}_1^\pm$ and $\tilde{\chi}_2^0 \tilde{\chi}_1^0$ prod., $m_{\tilde{\chi}_2^0} - m_{\tilde{\chi}_1^0} = 3 \text{ GeV}$	> 193	95	¹⁶ AAD	20i ATLS	2ℓ (soft), jets, \cancel{E}_T ; Tchi1n2Ga, higgsino, $m_{\tilde{\chi}_2^0} - m_{\tilde{\chi}_1^0} = 9.3 \text{ GeV}$
>1450	95	⁹ TUMASYAN	22s CMS	2 same-sign e or μ , 3 or 4 leptons, Tchi1n2B (flavor-democratic), $m_{\tilde{\ell}} = 1/2(m_{\tilde{\chi}_1^\pm} + m_{\tilde{\chi}_1^0})$, $m_{\tilde{\chi}_1^0} = 850 \text{ GeV}$	> 240	95	¹⁷ AAD	20i ATLS	2ℓ (soft), jets, \cancel{E}_T ; Tchi1n2Fa, wino, $m_{\tilde{\chi}_2^0} - m_{\tilde{\chi}_1^0} = 7 \text{ GeV}$
>1360	95	⁹ TUMASYAN	22s CMS	2 same-sign e or μ , 3 or 4 leptons, Tchi1n2B (flavor-democratic), $m_{\tilde{\ell}} = 1/2(m_{\tilde{\chi}_1^\pm} + m_{\tilde{\chi}_1^0})$, $m_{\tilde{\chi}_1^0} = 0 \text{ GeV}$	> 345	95	¹⁸ AAD	20k ATLS	$3\ell + \cancel{E}_T$, Tchi1n2F, $m_{\tilde{\chi}_1^0} = 0 \text{ GeV}$
>1290	95	⁹ TUMASYAN	22s CMS	2 same-sign e or μ , 3 or 4 leptons, Tchi1n2B (flavor-democratic), $m_{\tilde{\ell}} = 0.05m_{\tilde{\chi}_1^\pm} + 0.95m_{\tilde{\chi}_1^0}$, $m_{\tilde{\chi}_1^0} = 0 \text{ GeV}$	> 740	95	¹⁹ AAD	20R ATLS	$1\ell + 2b$ -jets + \cancel{E}_T , Tchi1n2E, $m_{\tilde{\chi}_1^0} = 0 \text{ GeV}$
>1440	95	⁹ TUMASYAN	22s CMS	2 same-sign e or μ , 3 or 4 leptons, Tchi1n2B (flavor-democratic), $m_{\tilde{\ell}} = 0.95m_{\tilde{\chi}_1^\pm} + 0.05m_{\tilde{\chi}_1^0}$, $m_{\tilde{\chi}_1^0} = 0 \text{ GeV}$	> 290	95	²⁰ SIRUNYAN	20AU CMS	soft $\tau + \text{jet} + \cancel{E}_T$, Tchi1n2D, wino, $m_{\tilde{\chi}_1^\pm} - m_{\tilde{\chi}_1^0} = 50 \text{ GeV}$
>1140	95	⁹ TUMASYAN	22s CMS	2 same-sign e or μ , 3 or 4 leptons, Tchi1n2B (lepton in $\tilde{\chi}_1^\pm$ decay is τ), $m_{\tilde{\ell}} = 1/2(m_{\tilde{\chi}_1^\pm} + m_{\tilde{\chi}_1^0})$, $m_{\tilde{\chi}_1^0} = 0 \text{ GeV}$	> 680	95	²¹ AABOUD	19AU ATL	0, 1, 2 or more ℓ , H ($\rightarrow \gamma\gamma, b\bar{b}, W W^*, Z Z^*, \tau\tau$) (various searches), Tchi1n2E, $m_{\tilde{\chi}_1^0} = 0 \text{ GeV}$
>1140	95	⁹ TUMASYAN	22s CMS	2 same-sign e or μ , 3 or 4 leptons, Tchi1n2B (lepton in $\tilde{\chi}_1^\pm$ decay is τ), $m_{\tilde{\ell}} = 1/2(m_{\tilde{\chi}_1^\pm} + m_{\tilde{\chi}_1^0})$, $m_{\tilde{\chi}_1^0} = 0 \text{ GeV}$	> 112	95	²² SIRUNYAN	19BU CMS	$pp \rightarrow \tilde{\chi}_1^+ \tilde{\chi}_2^0 + 2 \text{ jets}$, $\tilde{\chi}_2^0 \rightarrow \ell^+ \ell^- \tilde{\chi}_1^0$, heavy sleptons, $m_{\tilde{\chi}_2^0} - m_{\tilde{\chi}_1^0} = 1 \text{ GeV}$, $m_{\tilde{\chi}_2^0} = m_{\tilde{\chi}_1^+}$
>1110	95	⁹ TUMASYAN	22s CMS	2 same-sign e or μ , 3 or 4 leptons, Tchi1n2B (lepton in $\tilde{\chi}_1^\pm$ decay is τ), $m_{\tilde{\ell}} = 1/2(m_{\tilde{\chi}_1^\pm} + m_{\tilde{\chi}_1^0})$, $m_{\tilde{\chi}_1^0} = 0 \text{ GeV}$	> 215	95	²² SIRUNYAN	19BU CMS	$pp \rightarrow \tilde{\chi}_1^+ \tilde{\chi}_2^0 + 2 \text{ jets}$, $\tilde{\chi}_2^0 \rightarrow \ell^+ \ell^- \tilde{\chi}_1^0$, heavy sleptons, $m_{\tilde{\chi}_2^0} - m_{\tilde{\chi}_1^0} = 30 \text{ GeV}$, $m_{\tilde{\chi}_2^0} = m_{\tilde{\chi}_1^+}$
>980	95	⁹ TUMASYAN	22s CMS	2 same-sign e or μ , 3 or 4 leptons, Tchi1n2B (leptons in $\tilde{\chi}_1^\pm$ and $\tilde{\chi}_2^0$ decays are τ), $m_{\tilde{\ell}} = 1/2(m_{\tilde{\chi}_1^\pm} + m_{\tilde{\chi}_1^0})$, $m_{\tilde{\chi}_1^0} = 0 \text{ GeV}$	> 760	95	²³ AABOUD	18AY ATLS	$2\tau + \cancel{E}_T$, Tchi1n2D and $\tilde{\tau}_L$ -only, $m_{\tilde{\chi}_1^0} = 0 \text{ GeV}$
>905	95	⁹ TUMASYAN	22s CMS	2 same-sign e or μ , 3 or 4 leptons, Tchi1n2B (leptons in $\tilde{\chi}_1^\pm$ and $\tilde{\chi}_2^0$ decays are τ), $m_{\tilde{\ell}} = 0.05m_{\tilde{\chi}_1^\pm} + 0.95m_{\tilde{\chi}_1^0}$, $m_{\tilde{\chi}_1^0} = 0 \text{ GeV}$	>1125	95	²⁴ AABOUD	18BT ATLS	$2,3\ell + \cancel{E}_T$, Tchi1n2C, $m_{\tilde{\chi}_1^0} = 0 \text{ GeV}$
> 875	95	⁹ TUMASYAN	22s CMS	2 same-sign e or μ , 3 or 4 leptons, Tchi1n2B (leptons in $\tilde{\chi}_1^\pm$ and $\tilde{\chi}_2^0$ decays are τ), $m_{\tilde{\ell}} = 0.95m_{\tilde{\chi}_1^\pm} + 0.05m_{\tilde{\chi}_1^0}$, $m_{\tilde{\chi}_1^0} = 0 \text{ GeV}$	> 580	95	²⁵ AABOUD	18BT ATLS	$2,3\ell + \cancel{E}_T$, Tchi1n2F, $m_{\tilde{\chi}_1^0} = 0 \text{ GeV}$
> 875	95	⁹ TUMASYAN	22s CMS	2 same-sign e or μ , 3 or 4 leptons, Tchi1n2B (leptons in $\tilde{\chi}_1^\pm$ and $\tilde{\chi}_2^0$ decays are τ), $m_{\tilde{\ell}} = 0.95m_{\tilde{\chi}_1^\pm} + 0.05m_{\tilde{\chi}_1^0}$, $m_{\tilde{\chi}_1^0} = 0 \text{ GeV}$	none 130-230, 290-880	95	²⁶ AABOUD	18CK ATLS	$2H$ ($\rightarrow b\bar{b}$) + \cancel{E}_T , Tn1n1A, GMSB
> 875	95	⁹ TUMASYAN	22s CMS	2 same-sign e or μ , 3 or 4 leptons, Tchi1n2B (leptons in $\tilde{\chi}_1^\pm$ and $\tilde{\chi}_2^0$ decays are τ), $m_{\tilde{\ell}} = 0.95m_{\tilde{\chi}_1^\pm} + 0.05m_{\tilde{\chi}_1^0}$, $m_{\tilde{\chi}_1^0} = 0 \text{ GeV}$	none 220-600	95	²⁷ AABOUD	18CO ATLS	$2,3\ell + \cancel{E}_T$, recursive jigsaw, Tchi1n2F, $m_{\tilde{\chi}_1^0} = 0 \text{ GeV}$
> 875	95	⁹ TUMASYAN	22s CMS	2 same-sign e or μ , 3 or 4 leptons, Tchi1n2B (leptons in $\tilde{\chi}_1^\pm$ and $\tilde{\chi}_2^0$ decays are τ), $m_{\tilde{\ell}} = 0.95m_{\tilde{\chi}_1^\pm} + 0.05m_{\tilde{\chi}_1^0}$, $m_{\tilde{\chi}_1^0} = 0 \text{ GeV}$	> 145	95	²⁸ AABOUD	18R ATLS	2ℓ (soft) + \cancel{E}_T , Tchi1n2G, higgsino, $m_{\tilde{\chi}_2^0} - m_{\tilde{\chi}_1^0} = 5 \text{ GeV}$
> 875	95	⁹ TUMASYAN	22s CMS	2 same-sign e or μ , 3 or 4 leptons, Tchi1n2B (leptons in $\tilde{\chi}_1^\pm$ and $\tilde{\chi}_2^0$ decays are τ), $m_{\tilde{\ell}} = 0.95m_{\tilde{\chi}_1^\pm} + 0.05m_{\tilde{\chi}_1^0}$, $m_{\tilde{\chi}_1^0} = 0 \text{ GeV}$	> 175	95	²⁹ AABOUD	18R ATLS	2ℓ (soft) + \cancel{E}_T , Tchi1n2F, wino, $m_{\tilde{\chi}_2^0} - m_{\tilde{\chi}_1^0} = 10 \text{ GeV}$
> 875	95	⁹ TUMASYAN	22s CMS	2 same-sign e or μ , 3 or 4 leptons, Tchi1n2B (leptons in $\tilde{\chi}_1^\pm$ and $\tilde{\chi}_2^0$ decays are τ), $m_{\tilde{\ell}} = 0.95m_{\tilde{\chi}_1^\pm} + 0.05m_{\tilde{\chi}_1^0}$, $m_{\tilde{\chi}_1^0} = 0 \text{ GeV}$	>1060	95	³⁰ AABOUD	18U ATLS	$2\gamma + \cancel{E}_T$, GGM, Tchi1chi1A, any NLSP mass
> 875	95	⁹ TUMASYAN	22s CMS	2 same-sign e or μ , 3 or 4 leptons, Tchi1n2B (leptons in $\tilde{\chi}_1^\pm$ and $\tilde{\chi}_2^0$ decays are τ), $m_{\tilde{\ell}} = 0.95m_{\tilde{\chi}_1^\pm} + 0.05m_{\tilde{\chi}_1^0}$, $m_{\tilde{\chi}_1^0} = 0 \text{ GeV}$	> 167	95	³¹ SIRUNYAN	18AJ CMS	2ℓ (soft) + \cancel{E}_T , Tchi1n2G, higgsino, $m_{\tilde{\chi}_2^0} - m_{\tilde{\chi}_1^0} = 15 \text{ GeV}$
> 875	95	⁹ TUMASYAN	22s CMS	2 same-sign e or μ , 3 or 4 leptons, Tchi1n2B (leptons in $\tilde{\chi}_1^\pm$ and $\tilde{\chi}_2^0$ decays are τ), $m_{\tilde{\ell}} = 0.95m_{\tilde{\chi}_1^\pm} + 0.05m_{\tilde{\chi}_1^0}$, $m_{\tilde{\chi}_1^0} = 0 \text{ GeV}$	> 710	95	³² SIRUNYAN	18DP CMS	$2\tau + \cancel{E}_T$, Tchi1n2D, $m_{\tilde{\chi}_1^0} = 0 \text{ GeV}$
> 875	95	⁹ TUMASYAN	22s CMS	2 same-sign e or μ , 3 or 4 leptons, Tchi1n2B (leptons in $\tilde{\chi}_1^\pm$ and $\tilde{\chi}_2^0$ decays are τ), $m_{\tilde{\ell}} = 0.95m_{\tilde{\chi}_1^\pm} + 0.05m_{\tilde{\chi}_1^0}$, $m_{\tilde{\chi}_1^0} = 0 \text{ GeV}$	none 220-490	95	³³ SIRUNYAN	17AW CMS	$1\ell + 2 b$ -jets + \cancel{E}_T , Tchi1n2E, $m_{\tilde{\chi}_1^0} = 0 \text{ GeV}$
> 875	95	⁹ TUMASYAN	22s CMS	2 same-sign e or μ , 3 or 4 leptons, Tchi1n2B (leptons in $\tilde{\chi}_1^\pm$ and $\tilde{\chi}_2^0$ decays are τ), $m_{\tilde{\ell}} = 0.95m_{\tilde{\chi}_1^\pm} + 0.05m_{\tilde{\chi}_1^0}$, $m_{\tilde{\chi}_1^0} = 0 \text{ GeV}$	> 600	95	³⁴ AAD	16AA ATLS	$3,4\ell + \cancel{E}_T$, Tn2n3A, $m_{\tilde{\chi}_1^0} = 0 \text{ GeV}$
> 875	95	⁹ TUMASYAN	22s CMS	2 same-sign e or μ , 3 or 4 leptons, Tchi1n2B (leptons in $\tilde{\chi}_1^\pm$ and $\tilde{\chi}_2^0$ decays are τ), $m_{\tilde{\ell}} = 0.95m_{\tilde{\chi}_1^\pm} + 0.05m_{\tilde{\chi}_1^0}$, $m_{\tilde{\chi}_1^0} = 0 \text{ GeV}$	> 670	95	³⁴ AAD	16AA ATLS	$3,4\ell + \cancel{E}_T$, Tn2n3B, $m_{\tilde{\chi}_1^0} < 200 \text{ GeV}$

See key on page 1171

Searches Particle Listings

Supersymmetric Particle Searches

> 250	95	35	AAD	15BA ATLAS	$m_{\tilde{\chi}_1^\pm} = m_{\tilde{\chi}_2^0}, m_{\tilde{\chi}_1^0} = 0$ GeV
> 380	95	36	AAD	14H ATLAS	$\tilde{\chi}_1^\pm \tilde{\chi}_2^0 \rightarrow \tau^\pm \nu \lambda_1^0 \tau^\pm \tau^\mp \tilde{\chi}_1^0$, simplified model, $m_{\tilde{\chi}_1^\pm} = m_{\tilde{\chi}_2^0}$, $m_{\tilde{\chi}_1^0} = 0$ GeV
> 700	95	36	AAD	14H ATLAS	$\tilde{\chi}_1^\pm \tilde{\chi}_2^0 \rightarrow \ell^\pm \nu \tilde{\chi}_1^0 \ell^\pm \ell^\mp \tilde{\chi}_1^0$, simplified model, $m_{\tilde{\chi}_1^\pm} = m_{\tilde{\chi}_2^0}$, $m_{\tilde{\chi}_1^0} = 0$ GeV
> 345	95	36	AAD	14H ATLAS	$\tilde{\chi}_1^\pm \tilde{\chi}_2^0 \rightarrow W \tilde{\chi}_1^0 Z \tilde{\chi}_1^0$, simplified model, $m_{\tilde{\chi}_1^\pm} = m_{\tilde{\chi}_2^0}, m_{\tilde{\chi}_1^0} = 0$
> 148	95	36	AAD	14H ATLAS	$\tilde{\chi}_1^\pm \tilde{\chi}_2^0 \rightarrow W \tilde{\chi}_1^0 H \tilde{\chi}_1^0$, simplified model, $m_{\tilde{\chi}_1^\pm} = m_{\tilde{\chi}_2^0}, m_{\tilde{\chi}_1^0} = 0$
> 620	95	37	AAD	14x ATLAS	$\geq 4\ell^\pm, \tilde{\chi}_{2,3}^0 \rightarrow \ell^\pm \ell^\mp \tilde{\chi}_1^0, m_{\tilde{\chi}_1^0} = 0$ GeV
		38	AAD	13 ATLAS	$3\ell^\pm + \cancel{E}_T$, pMSSM, SMS
		39	CHATRCHYAN12BJ	CMS	$\geq 2\ell$, jets + \cancel{E}_T , $pp \rightarrow \tilde{\chi}_1^\pm \tilde{\chi}_2^0$
> 62.4	95	40	ABREU	00W DLPH	$\tilde{\chi}_3^0, 1 \leq \tan\beta \leq 40$, all Δm , all m_0
> 99.9	95	40	ABREU	00W DLPH	$\tilde{\chi}_3^0, 1 \leq \tan\beta \leq 40$, all Δm , all m_0
> 116.0	95	40	ABREU	00W DLPH	$\tilde{\chi}_4^0, 1 \leq \tan\beta \leq 40$, all Δm , all m_0
• • • We do not use the following data for averages, fits, limits, etc. • • •					
> 310	95	41	AAD	20AN ATLAS	$2\gamma + \cancel{E}_T$, Tchi1n2E, $m_{\tilde{\chi}_1^0} = 0$ GeV
none 180–355	95	42	AAD	14G ATLAS	$\tilde{\chi}_1^\pm \tilde{\chi}_2^0 \rightarrow W \tilde{\chi}_1^0 Z \tilde{\chi}_1^0$, simplified model, $m_{\tilde{\chi}_1^\pm} = m_{\tilde{\chi}_2^0}, m_{\tilde{\chi}_1^0} = 0$
		43	KHACHATRYAN14I	CMS	$\tilde{\chi}_2^0 \rightarrow (Z, H) \tilde{\chi}_1^0 \ell \ell$, simplified model
		44	AAD	12As ATLAS	$3\ell^\pm + \cancel{E}_T$, pMSSM
		45	AAD	12T ATLAS	$\ell^\pm \ell^\pm + \cancel{E}_T, pp \rightarrow \tilde{\chi}_1^\pm \tilde{\chi}_2^0$

¹ AAD 23AE searched in 139 fb^{-1} of pp collisions at $\sqrt{s} = 13 \text{ TeV}$ for events with 2 ℓ with same flavour and opposite sign, plus jets and \cancel{E}_T , defining signal region with the dilepton invariant mass both on- and off-shell with respect to the Z boson. No significant excess above the Standard Model predictions is observed. Limits are set on models of strong and electroweak production. For electroweak production, limits are placed on production of mass-degenerate, wino-like $\tilde{\chi}_2^0 \tilde{\chi}_1^0$ with $\tilde{\chi}_2^0 \rightarrow Z \tilde{\chi}_1^0$ and $\tilde{\chi}_1^0 \rightarrow W \tilde{\chi}_1^0$, see figure 15.

² AAD 23CI searched in 139 fb^{-1} of pp collisions for events containing 1 ℓ (e or μ), jets, and \cancel{E}_T . Final states consistent with the production of a diboson system plus \cancel{E}_T were identified also by making use of large-R jet tagging techniques. No excess on top of the Standard Model background was observed. Limits were set on the production of $\tilde{\chi}_1^\pm \tilde{\chi}_2^0$ and $\tilde{\chi}_1^\pm \tilde{\chi}_1^\pm$ (assuming wino cross sections) decaying to $WZ \tilde{\chi}_1^0 \tilde{\chi}_1^0$ or $WW \tilde{\chi}_1^0 \tilde{\chi}_1^0$. See their figure 9.

³ AAD 23CI searched in 139 fb^{-1} of pp collisions for events containing 1 ℓ (e or μ), jets, and \cancel{E}_T . Final states consistent with the production of a boson + Higgs system plus \cancel{E}_T were identified via a BDT. No excess on top of the Standard Model background was observed. Limits were set on the production of degenerate $\tilde{\chi}_1^\pm \tilde{\chi}_2^0$ (assuming wino cross sections) decaying into $Wh \tilde{\chi}_1^0 \tilde{\chi}_1^0$. See their figure 10.

⁴ AAD 23CP searched in 139 fb^{-1} of pp collisions at $\sqrt{s} = 13 \text{ TeV}$ for events with 2 ℓ with same charge plus at least one jet and \cancel{E}_T , defining signal region based on 'stransverse mass' of the dilepton system, \cancel{E}_T significance and effective mass. No significant excess above the Standard Model predictions is observed. Limits are set on the mass of mass-degenerate $\tilde{\chi}_1^\pm$ and $\tilde{\chi}_2^0$ for the wino-like production of $\tilde{\chi}_1^\pm \tilde{\chi}_2^0$ followed by the decay into either $WZ \tilde{\chi}_1^0 \tilde{\chi}_1^0$ or $Wh \tilde{\chi}_1^0 \tilde{\chi}_1^0$, see figure 13.

⁵ AAD 23CR searched in 139 fb^{-1} of pp collisions at $\sqrt{s} = 13 \text{ TeV}$ for RPV SUSY in final states with multiple leptons and b -tagged jets. No significant excess above the Standard Model expectations is observed. Limits are set on the production of electroweakinos (wino or higgsino) that decay via RPV coupling λ'_{133} to a charged lepton or a neutrino, a b quark, and an additional t or b quark, see their figure 16. A second model addresses direct $\tilde{\mu}_{L,R}$ production and decay to a muon and a bino-like neutralino, which decays in the same way as in the first model, see their figure 17.

⁶ HAYRAPETYAN 23E searched in 137 fb^{-1} of pp collisions at $\sqrt{s} = 13 \text{ TeV}$ for evidence of gluino, top squark and electroweakino pair production in events with at least one photon, multiple jets, and large \cancel{E}_T . No significant excess above the Standard Model expectations is observed. Limits are set in models for strong production, Tglu4D, Tglu4E, Tglu4F and Tstop13, see their figure 9. They also interpret the results in the models for electroweak production, shown in their figure 10. Tchi1n1A assumes wino-like $\tilde{\chi}_1^\pm \tilde{\chi}_1^0$ production, while Tchi1chi1A assumes higgsino-like cross sections and includes $\tilde{\chi}_1^\pm \tilde{\chi}_1^\pm, \tilde{\chi}_1^0 \tilde{\chi}_2^0$ and $\tilde{\chi}_{1,2}^0 \tilde{\chi}_1^\pm$ production. For $\tilde{\chi}_1^0 \tilde{\chi}_2^0$ alone no mass point can be excluded in the model Tchi1chi1A, but in another model for $\tilde{\chi}_1^0 \tilde{\chi}_2^0$ production, Tn1n2A.

⁷ TUMASYAN 23B searched in 137 fb^{-1} of pp collisions at $\sqrt{s} = 13 \text{ TeV}$ for evidence of electroweakino pair production with decays including hadronically decaying bosons, WW, WZ, WH , or ZH , identified with a DNN classifying large-area (AK8) jets. No significant excess above the Standard Model expectations is observed. Limits are set on the mass of the nearly mass degenerate wino-like $\tilde{\chi}_2^0$ and $\tilde{\chi}_1^\pm$ in the models Tchi1chi1I, Tchi1n2Fb, and Tchi1n2Fc, see their figure 4. They also consider a model that contains both $\tilde{\chi}_2^0 \tilde{\chi}_1^\pm$ and $\tilde{\chi}_1^\pm \tilde{\chi}_1^\pm$ production, see their figure 5 (upper). Results are also interpreted in the model THinoBinoA with nearly mass-degenerate higgsino-like $\tilde{\chi}_3^0, \tilde{\chi}_2^0, \tilde{\chi}_1^\pm$, and a lighter bino-like $\tilde{\chi}_1^0$, see their figure 5 (lower).

⁸ TUMASYAN 22Q searched in up to 137 fb^{-1} of pp collisions at $\sqrt{s} = 13 \text{ TeV}$ for evidence of electroweakino and top squark pair production with a small mass difference between the produced supersymmetric particles and the lightest neutralino in events with two or three low-momentum leptons and missing transverse momentum. No significant excess above the Standard Model expectations is observed. Limits are set on the mass of $\tilde{\chi}_2^0$ and $\tilde{\chi}_1^\pm$ in the model Tchi1n2F, see their Figure 8. Limits are also set in a higgsino simplified model with both $\tilde{\chi}_2^0 \tilde{\chi}_1^\pm$ and $\tilde{\chi}_2^0 \tilde{\chi}_1^0$ production, where $\tilde{\chi}_2^0 \rightarrow Z \tilde{\chi}_1^0$ and $m_{\tilde{\chi}_1^\pm} = 1/2(m_{\tilde{\chi}_2^0} + m_{\tilde{\chi}_1^0})$. A model inspired by the pMSSM is used for further interpretations in the case of a higgsino LSP, see their Figure 9. Limits are also set on the mass of the top squark in the models Tstop2 and Tstop3, see their Figure 10.

⁹ TUMASYAN 22s searched in 137 fb^{-1} of pp collisions at $\sqrt{s} = 13 \text{ TeV}$ for evidence of electroweakino pair production in events with three or four leptons, with up to two hadronically decaying τ leptons, or two same-sign light leptons (e or μ). No significant excess above the Standard Model expectations is observed. Limits are set on the mass of $\tilde{\chi}_2^0$ and $\tilde{\chi}_1^\pm$ in the models Tchi1n2B (in flavour-democratic and tau-enriched or -dominated scenarios), Tchi1n2E, Tchi1n2F, see their Figures 16–20, and on the mass of the higgsino-triplet $\tilde{\chi}_2^0, \tilde{\chi}_1^\pm$, and $\tilde{\chi}_1^0$ in the models Tn1n1A, Tn1n1B, and Tn1n1C, see their Figure 21.

¹⁰ TUMASYAN 22v searched in 137 fb^{-1} of pp collisions at $\sqrt{s} = 13 \text{ TeV}$ for evidence of electroweakino pair production with decay to two Higgs bosons H , with $H \rightarrow b\bar{b}$, resulting either in 4 resolved b -jets or two large-radius jets, and large \cancel{E}_T . No significant excess above the Standard Model expectations is observed. Limits are set on the mass of $\tilde{\chi}_2^0$ and $\tilde{\chi}_1^\pm$ in the models Tn1n1A, see their Figures 11 and 12, or in a model where higgsino-like nearly mass degenerate $\tilde{\chi}_2^0$ and $\tilde{\chi}_3^0$ are pair produced and each decay to H and a bino-like $\tilde{\chi}_1^0$, see their Figure 13. Limits are also set on the gluino mass in the model Tglu1I, see their Figure 14.

¹¹ AAD 21BG searched in 139 fb^{-1} of pp collisions at $\sqrt{s} = 13 \text{ TeV}$ for pair production $\tilde{\chi}_2^0 \tilde{\chi}_1^\pm$ in final states with three leptons, with and without assuming the presence of a $Z \rightarrow \ell\ell$ decay. No significant excess above the Standard Model predictions is observed. Limits are set on the $\tilde{\chi}_2^0$ and $\tilde{\chi}_1^\pm$ mass in Tchi1n2E, Tchi1n2F and Tchi1n2Ga. See their Fig. 16.

¹² AAD 21Y searched in 139 fb^{-1} of pp collisions at $\sqrt{s} = 13 \text{ TeV}$ for supersymmetry in events with four or more leptons (electrons, muons and tau-leptons). No significant excess above the Standard Model expectations is observed. Limits are set on Tchi1n12-GGM, and RPV models similar to Tchi1n2I, Tglu1A (with $q = u, d, s, c, b$, with equal branching fractions), and $\tilde{\ell}_L/\tilde{\nu} \rightarrow \ell/\nu \tilde{\chi}_1^0$ (mass-degenerate $\tilde{\ell}_L$ and $\tilde{\nu}$ of all 3 generations), all with $\tilde{\chi}_1^0 \rightarrow \ell^\pm \ell^\mp \nu$ via λ_{12k} or λ_{133} (where $i, k \in 1, 2$), see their Figure 11.

¹³ SIRUNYAN 21M searched in 137 fb^{-1} of pp collisions at $\sqrt{s} = 13 \text{ TeV}$ for supersymmetry in events with two opposite-sign same-flavor leptons (electrons, muons) and \cancel{E}_T . No significant excess above the Standard Model expectations is observed. Limits are set on the gluino mass in the simplified model Tglu4C, see their Figure 10, on the $\tilde{\chi}_2^0$ and $\tilde{\chi}_1^\pm$ mass in Tchi1n2Fa, see their Figure 11, on the $\tilde{\chi}_1^0$ mass in Tn1n1C and Tn1n1B for $m_{\tilde{\chi}_2^0} = m_{\tilde{\chi}_1^\pm} = m_{\tilde{\chi}_1^0}$, see their Figure 12. Limits are also set on the light squark mass for the simplified model Tsqk2A, on the sbottom mass in Tsbott3, see their Figure 13, and on the slepton mass in direct electroweak pair production of mass-degenerate left- and right-handed sleptons (selectrons and smuons), see their Figure 14.

¹⁴ TUMASYAN 21c searched in 137 fb^{-1} of pp collisions at $\sqrt{s} = 13 \text{ TeV}$ for supersymmetry in events with one lepton, a Higgs boson decaying to a pair of bottom quarks, and large \cancel{E}_T . No significant excess above the Standard Model expectations is observed. Lower limits are set on the masses of $\tilde{\chi}_2^0$ and $\tilde{\chi}_1^\pm$ in the simplified model Tchi1n2E, see their Figure 6.

¹⁵ AAD 20AN searched in 139 fb^{-1} of pp collisions at $\sqrt{s} = 13 \text{ TeV}$ for events with two photons and missing transverse momentum. Events are further categorised in terms of lepton or jet multiplicity. No significant excess over the expected background is observed. Limits at 95% C.L. are set on the Higgsino mass in the Tn1n1A simplified model, see their Figure 11.

¹⁶ AAD 20I reported on ATLAS searches for electroweak production in models with compressed mass spectra as Tchi1n2Ga. A dataset of pp collisions at $\sqrt{s} = 13 \text{ TeV}$ corresponding to an integrated luminosity of 139 fb^{-1} was used. Events with \cancel{E}_T , two same-flavour, opposite-charge, low-transverse-momentum leptons, and jets from initial-state radiation or characteristic of vector-boson fusion production are selected. Constraints at 95% C.L. are placed in Higgsino models on the mass of the $\tilde{\chi}_2^0$ (the $\tilde{\chi}_1^\pm$ mass is halfway between the $\tilde{\chi}_2^0$ and $\tilde{\chi}_1^0$ masses) at 193 GeV for a mass splitting between $\tilde{\chi}_2^0$ and $\tilde{\chi}_1^0$ of 9.3 GeV and extend down to a mass splitting of 2.4 GeV at the LEP chargino mass limit. See their Fig. 14(a).

¹⁷ AAD 20I reported on ATLAS searches for electroweak production in models with compressed mass spectra as Tchi1n2Fa. A dataset of pp collisions at $\sqrt{s} = 13 \text{ TeV}$ corresponding to an integrated luminosity of 139 fb^{-1} was used. Events with \cancel{E}_T , two same-flavour, opposite-charge, low-transverse-momentum leptons, and jets from initial-state radiation or characteristic of vector-boson fusion production are selected. Constraints at 95% C.L. are placed in Wino-Bino models on the mass of the $\tilde{\chi}_2^0$ (degenerate with $\tilde{\chi}_1^\pm$) at 240 GeV for a mass splitting between $\tilde{\chi}_2^0$ and $\tilde{\chi}_1^0$ of 7 GeV and extend down to a mass splitting of 1.5 GeV at the LEP chargino mass limit of 92.4 GeV. See their Fig. 14(b,c).

¹⁸ AAD 20K reported on a search for electroweak production in models with mass splittings near the electroweak scale as Tchi1n2F and exploiting three-lepton final state events with an emulated recursive jigsaw reconstruction method. The analysis uses a dataset of pp collisions at $\sqrt{s} = 13 \text{ TeV}$ corresponding to an integrated luminosity of 139 fb^{-1} . Exclusion limits at 95% C.L. are derived on next-to-lightest neutralinos and charginos with masses up to 345 GeV for a massless lightest neutralino, see their Fig. 7.

¹⁹ AAD 20R searched for electroweak production in the model Tchi1n2E, selecting events with a pair of b -tagged jets consistent with those from a Higgs boson decay, either an electron or a muon from the W boson decay and \cancel{E}_T . The analysis uses a dataset of pp collisions at $\sqrt{s} = 13 \text{ TeV}$ corresponding to an integrated luminosity of 139 fb^{-1} . Exclusion limits at 95% C.L. are derived on next-to-lightest neutralinos and charginos with masses up to 740 GeV for a massless lightest neutralino, assuming pure wino cross-sections. See their Fig. 6.

Searches Particle Listings

Supersymmetric Particle Searches

- ²⁰ SIRUNYAN 20AU searched in 77.2 fb^{-1} of pp collisions at $\sqrt{s} = 13 \text{ TeV}$ for events containing one soft, hadronically decaying tau lepton, one energetic jet from initial-state radiation, and large $E_{T\cancel{}}$. No excess over the expected background is observed. Limits are derived on the wino mass in the Tchi1n2D simplified model, see their Figure 2.
- ²¹ AABOUD 19AU searched in 36.1 fb^{-1} of pp collisions at $\sqrt{s} = 13 \text{ TeV}$ for direct electroweak production of charginos and next-to-lightest neutralinos decaying into lightest neutralinos and a W and a Higgs boson, respectively. Fully hadronic, semileptonic, diphoton, and multilepton (electrons, muons) final states with missing transverse momentum are considered in this search. Observations are consistent with the Standard Model expectations, and 95% confidence-level limits of up to 680 GeV on the chargino/next-to-lightest neutralino masses are set (Tchi1n2E model). See their Figure 14 for an overlay of exclusion contours from all searches.
- ²² SIRUNYAN 19BU searched for pair production of gauginos via vector boson fusion assuming the gaugino spectrum is compressed, in 35.9 fb^{-1} of pp collisions at $\sqrt{s} = 13 \text{ TeV}$. The final states explored included zero leptons plus two jets, one lepton plus two jets, and one hadronic tau plus two jets. A similar bound is obtained in the light slepton limit.
- ²³ AABOUD 18AY searched in 36.1 fb^{-1} of pp collisions at $\sqrt{s} = 13 \text{ TeV}$ for direct electroweak production of charginos and neutralinos as in Tchi1n2D models, in events characterised by the presence of at least two hadronically decaying tau leptons and large missing transverse energy. No significant deviation from the expected SM background is observed. Assuming decays via intermediate $\tilde{\tau}_1$ and $m_{\tilde{\chi}_1^\pm} = m_{\tilde{\chi}_2^0}$, the observed limits rule out $\tilde{\chi}_2^0$ masses up to 760 GeV for a massless $\tilde{\chi}_1^0$. See their Fig. 7 (right). Interpretations are also provided in Fig 8 (bottom) for different assumptions on the ratio between $m_{\tilde{\tau}}$ and $m_{\tilde{\chi}_2^0} + m_{\tilde{\chi}_1^0}$.
- ²⁴ AABOUD 18BT searched in 36.1 fb^{-1} of pp collisions at $\sqrt{s} = 13 \text{ TeV}$ for direct electroweak production of charginos, chargino and next-to-lightest neutralinos and sleptons in events with two or three leptons (electrons or muons), with or without jets, and large missing transverse energy. No significant excess above the Standard Model expectations is observed. Limits are set on the next-to-lightest neutralino mass up to 1100 GeV for massless $\tilde{\chi}_1^0$ in the Tchi1n2C simplified model exploiting the 3ℓ signature, see their Figure 8(c).
- ²⁵ AABOUD 18BT searched in 36.1 fb^{-1} of pp collisions at $\sqrt{s} = 13 \text{ TeV}$ for direct electroweak production of charginos, chargino and next-to-lightest neutralinos and sleptons in events with two or three leptons (electrons or muons), with or without jets, and large missing transverse energy. No significant excess above the Standard Model expectations is observed. Limits are set on the next-to-lightest neutralino mass up to 580 GeV for massless $\tilde{\chi}_1^0$ in the Tchi1n2F simplified model exploiting the $2\ell+2$ jets and 3ℓ signatures, see their Figure 8(d).
- ²⁶ AABOUD 18CK searched for events with at least 3 b -jets and large missing transverse energy in two datasets of pp collisions at $\sqrt{s} = 13 \text{ TeV}$ of 36.1 fb^{-1} and 24.3 fb^{-1} depending on the trigger requirements. The analyses aimed to reconstruct two Higgs bosons decaying to pairs of b -quarks. No significant excess above the Standard Model expectations is observed. Limits are set on the Higgsino mass in the T1n1n1A simplified model, see their Figure 15(a). Constraints are also presented as a function of the BR of Higgsino decaying into a higgs boson and a gravitino, see their Figure 15(b).
- ²⁷ AABOUD 18CO searched in 36.1 fb^{-1} of pp collisions at $\sqrt{s} = 13 \text{ TeV}$ for direct electroweak production of mass-degenerate charginos and next-to-lightest neutralinos in events with two or three leptons (electrons or muons), with or without jets, and large missing transverse energy. The search channels are based on recursive jigsaw reconstruction. Limits are set on the next-to-lightest neutralinos mass up to 600 GeV for massless neutralinos in the Tchi1n2F simplified model exploiting the statistical combination of $2\ell+2$ jets and 3ℓ channels. Next-to-lightest neutralinos masses below 220 GeV are not excluded due to an excess of events above the SM prediction in the dedicated regions. See their Figure 13(d).
- ²⁸ AABOUD 18R searched in 36.1 fb^{-1} of pp collisions at $\sqrt{s} = 13 \text{ TeV}$ for electroweak production in scenarios with compressed mass spectra in final states with two low-momentum leptons and missing transverse momentum. The data are found to be consistent with the SM prediction. Results are interpreted in Tchi1n2G higgsino models, and $\tilde{\chi}_2^0$ masses are excluded up to 145 GeV for $m_{\tilde{\chi}_2^0} - m_{\tilde{\chi}_1^0} = 5 \text{ GeV}$. The exclusion limits extend down to mass splittings of 2.5 GeV, see their Fig. 10 (top). Results are also interpreted in terms of exclusion bounds on the production cross-sections for the NUHM2 scenario as a function of the universal gaugino mass $m_{1/2}$ and $m_{\tilde{\chi}_2^0} - m_{\tilde{\chi}_1^0}$, see their Fig. 12.
- ²⁹ AABOUD 18R searched in 36.1 fb^{-1} of pp collisions at $\sqrt{s} = 13 \text{ TeV}$ for electroweak production in scenarios with compressed mass spectra in final states with two low-momentum leptons and missing transverse momentum. The data are found to be consistent with the SM prediction. Results are interpreted in Tchi1n2F wino models, and $\tilde{\chi}_2^0$ masses are excluded up to 175 GeV for $m_{\tilde{\chi}_2^0} - m_{\tilde{\chi}_1^0} = 10 \text{ GeV}$. The exclusion limits extend down to mass splittings of 2 GeV, see their Fig. 10 (bottom). Results are also interpreted in terms of exclusion bounds on the production cross-sections for the NUHM2 scenario as a function of the universal gaugino mass $m_{1/2}$ and $m_{\tilde{\chi}_2^0} - m_{\tilde{\chi}_1^0}$, see their Fig. 12.
- ³⁰ AABOUD 18U searched in 36.1 fb^{-1} of pp collisions at $\sqrt{s} = 13 \text{ TeV}$ in events with at least one isolated photon, possibly jets and significant transverse momentum targeting generalised models of gauge-mediated SUSY breaking. No significant excess of events is observed above the SM prediction. Results of the diphoton channel are interpreted in terms of lower limits on the masses of gauginos Tchi1n1A models, which reach as high as 1.3 TeV. Gaugino masses below 1060 GeV are excluded for any NLSP mass, see their Fig. 10.
- ³¹ SIRUNYAN 18AJ searched in 35.9 fb^{-1} of pp collisions at $\sqrt{s} = 13 \text{ TeV}$ for events containing two low-momentum, oppositely charged leptons (electrons or muons) and $E_{T\cancel{}}$. No excess over the expected background is observed. Limits are derived on the wino mass in the Tchi1n2F simplified model, see their Figure 5. Limits are also set on the stop mass in the Tstop10 simplified model, see their Figure 6. Finally, limits are set on the Higgsino mass in the Tchi1n2G simplified model, see Figure 8 and in the pMSSM, see Figure 7.
- ³² SIRUNYAN 18DP searched in 35.9 fb^{-1} of pp collisions at $\sqrt{s} = 13 \text{ TeV}$ for direct electroweak production of charginos and neutralinos or of chargino pairs in events with a tau lepton pair and significant missing transverse momentum. Both hadronic and leptonic decay modes are considered for the tau lepton. No significant excess above the Standard Model expectations is observed. Limits are set on the chargino mass in the Tchi1ch1D and Tchi1n2 simplified models, see their Figures 14 and 15. Also, excluded stau pair production cross sections are shown in Figures 11, 12, and 13.
- ³³ SIRUNYAN 17AW searched in 35.9 fb^{-1} of pp collisions at $\sqrt{s} = 13 \text{ TeV}$ for events with a charged lepton (electron or muon), two jets identified as originating from a b -quark, and large $E_{T\cancel{}}$. No significant excess above the Standard Model expectations is observed. Limits are set on the mass of the chargino and the next-to-lightest neutralino in the Tchi1n2E simplified model, see their Figure 6.
- ³⁴ AAD 16AA summarized and extended ATLAS searches for electroweak supersymmetry in final states containing several charged leptons, $E_{T\cancel{}}$, with or without hadronic jets, in 20 fb^{-1} of pp collisions at $\sqrt{s} = 8 \text{ TeV}$. The paper reports the results of new interpretations and statistical combinations of previously published analyses, as well as new analyses. Exclusion limits at 95% C.L. are set on mass-degenerate $\tilde{\chi}_2^0$ and $\tilde{\chi}_3^0$ masses in the Tn2n3A and Tn2n3B simplified models. See their Fig. 15.
- ³⁵ AAD 15BA searched in 20.3 fb^{-1} of pp collisions at $\sqrt{s} = 8 \text{ TeV}$ for electroweak production of charginos and neutralinos decaying to a final state containing a W boson and a 125 GeV Higgs boson, plus missing transverse momentum. No excess beyond the Standard Model expectation is observed. Exclusion limits are derived in simplified models of direct chargino and next-to-lightest neutralino production, with the decays $\tilde{\chi}_1^\pm \rightarrow W^\pm \tilde{\chi}_1^0$ and $\tilde{\chi}_2^0 \rightarrow H \tilde{\chi}_1^0$ having 100% branching fraction, see Fig. 8. A combination of the multiple final states for the Higgs decay yields the best limits (Fig. 8d).
- ³⁶ AAD 14H searched in 20.3 fb^{-1} of pp collisions at $\sqrt{s} = 8 \text{ TeV}$ for electroweak production of charginos and neutralinos decaying to a final state with three leptons and missing transverse momentum. No excess beyond the Standard Model expectation is observed. Exclusion limits are derived in simplified models of direct chargino and next-to-lightest neutralino production, with decays to the lightest neutralino via either all three generations of leptons, staus only, gauge bosons, or Higgs bosons, see Fig. 7. An interpretation in the pMSSM is also given, see Fig. 8.
- ³⁷ AAD 14X searched in 20.3 fb^{-1} of pp collisions at $\sqrt{s} = 8 \text{ TeV}$ for events with at least four leptons (electrons, muons, taus) in the final state. No significant excess above the Standard Model expectations is observed. Limits are set on the neutralino mass in an R-parity conserving simplified model where the decay $\tilde{\chi}_{2,3}^0 \rightarrow \ell^\pm \ell^\mp \tilde{\chi}_1^0$ takes place with a branching ratio of 100%, see Fig. 10.
- ³⁸ AAD 13 searched in 4.7 fb^{-1} of pp collisions at $\sqrt{s} = 7 \text{ TeV}$ for charginos and neutralinos decaying to a final state with three leptons (e and μ) and missing transverse energy. No excess beyond the Standard Model expectation is observed. Exclusion limits are derived in the phenomenological MSSM, see Fig. 2 and 3, and in simplified models, see Fig. 4. For the simplified models with intermediate slepton decays, degenerate $\tilde{\chi}_2^\pm$ and $\tilde{\chi}_2^0$ masses up to 500 GeV are excluded at 95% C.L. for very large mass differences with the $\tilde{\chi}_1^0$. Supersedes AAD 12As.
- ³⁹ CHATRCHYAN 12BJ searched in 4.98 fb^{-1} of pp collisions at $\sqrt{s} = 7 \text{ TeV}$ for direct electroweak production of charginos and neutralinos in events with at least two leptons, jets and missing transverse momentum. No significant excesses over the expected SM backgrounds are observed and 95% C.L. limits on the production cross section of $\tilde{\chi}_1^\pm \tilde{\chi}_2^0$ pair production were set in a number of simplified models, see Figs. 7 to 12. Most limits are for exactly 3 jets.
- ⁴⁰ ABREU 00w combines data collected at $\sqrt{s}=189 \text{ GeV}$ with results from lower energies. The mass limit is obtained by constraining the MSSM parameter space with gaugino and stfermion mass universality at the GUT scale, using the results of negative direct searches for neutralinos (including cascade decays and $\tilde{\tau}\tilde{\tau}$ final states) from ABREU 01, for charginos from ABREU 00j and ABREU 00T (for all Δm_\pm), and for charged sleptons from ABREU 01b. The results hold for the full parameter space defined by all values of M_2 and $|\mu| \leq 2 \text{ TeV}$ with the $\tilde{\chi}_1^0$ as LSP.
- ⁴¹ AAD 20AN searched in 139 fb^{-1} of pp collisions at $\sqrt{s} = 13 \text{ TeV}$ for events with two photons and missing transverse momentum. Events are further categorised in terms of lepton or jet multiplicity. No significant excess over the expected background is observed. Limits at 95% C.L. are derived in Tchi1n2E simplified models. Next-to-lightest neutralinos and charginos with masses up to 310 GeV for a massless lightest neutralino are excluded. See their Fig. 10.
- ⁴² AAD 14G searched in 20.3 fb^{-1} of pp collisions at $\sqrt{s} = 8 \text{ TeV}$ for electroweak production of chargino-neutralino pairs, decaying to a final state with two leptons (e and μ) and missing transverse momentum. No excess beyond the Standard Model expectation is observed. Exclusion limits are derived in simplified models of chargino and next-to-lightest neutralino production, with decays to the lightest neutralino via gauge bosons, see Fig. 7. An interpretation in the pMSSM is also given, see Fig. 10.
- ⁴³ KHACHATRYAN 14I searched in 19.5 fb^{-1} of pp collisions at $\sqrt{s} = 8 \text{ TeV}$ for electroweak production of charginos and neutralinos decaying to a final state with three leptons (e or μ) and missing transverse momentum, or with a Z -boson, dijets and missing transverse momentum. No excess beyond the Standard Model expectation is observed. Exclusion limits are derived in simplified models, see Figs. 12–16.
- ⁴⁴ AAD 12As searched in 2.06 fb^{-1} of pp collisions at $\sqrt{s} = 7 \text{ TeV}$ for charginos and neutralinos decaying to a final state with three leptons (e and μ) and missing transverse energy. No excess beyond the Standard Model expectation is observed. Exclusion limits are derived in the phenomenological MSSM, see Fig. 2 (top), and in simplified models, see Fig. 2 (bottom).
- ⁴⁵ AAD 12T looked in 1 fb^{-1} of pp collisions at $\sqrt{s} = 7 \text{ TeV}$ for the production of supersymmetric particles decaying into final states with missing transverse momentum and exactly two isolated leptons (e or μ). Same-sign dilepton events were separately studied. Additionally, in opposite-sign events, a search was made for an excess of same-flavor over different-flavor lepton pairs. No excess over the expected background is observed and limits are placed on the effective production cross section of opposite-sign dilepton events with $E_{T\cancel{}} > 250 \text{ GeV}$ and on same-sign dilepton events with $E_{T\cancel{}} > 100 \text{ GeV}$. The latter limit is interpreted in a simplified electroweak gaugino production model.

$\tilde{\chi}_1^\pm, \tilde{\chi}_2^\pm$ (Charginos) mass limits

Charginos are unknown mixtures of w -inos and charged higgsinos (the supersymmetric partners of W and Higgs bosons). A lower mass limit for the lightest chargino ($\tilde{\chi}_1^\pm$) of approximately 45 GeV, independent of the field composition and of the decay mode, has been obtained by the LEP experiments from the analysis of the Z width and decays. These results, as well as other now superseded limits from e^+e^- collisions at energies below 136 GeV, and from hadronic collisions, can be found in the 1998 Edition (The European Physical Journal **C3** 1 (1998)) of this Review.

Unless otherwise stated, results in this section assume spectra, production rates, decay modes and branching ratios as evaluated in the MSSM, with gaugino and sfermion mass unification at the GUT scale. These papers generally study production of $\tilde{\chi}_1^0 \tilde{\chi}_2^0$, $\tilde{\chi}_1^+ \tilde{\chi}_1^-$ and (in the case of hadronic collisions) $\tilde{\chi}_1^+ \tilde{\chi}_2^0$ pairs, including the effects of cascade decays. The mass limits on $\tilde{\chi}_1^\pm$ are either direct, or follow indirectly from the constraints set by the non-observation of $\tilde{\chi}_2^0$ states on the gaugino and higgsino MSSM parameters M_2 and μ . For generic values of the MSSM parameters, limits from high-energy e^+e^- collisions coincide with the highest value of the mass allowed by phase-space, namely $m_{\tilde{\chi}_1^\pm} \lesssim \sqrt{s}/2$. The still unpublished combination of the results of the four LEP collaborations from the 2000 run of LEP2 at \sqrt{s} up to ≈ 209 GeV yields a lower mass limit of 103.5 GeV valid for general MSSM models. The limits become however weaker in certain regions of the MSSM parameter space where the detection efficiencies or production cross sections are suppressed. For example, this may happen when: (i) the mass differences $\Delta m_{\pm} = m_{\tilde{\chi}_1^\pm} - m_{\tilde{\chi}_1^0}$ or $\Delta m_{\nu} = m_{\tilde{\chi}_1^\pm} - m_{\tilde{\nu}}$ are very small, and the detection efficiency is reduced; (ii) the electron sneutrino mass is small, and the $\tilde{\chi}_1^\pm$ production rate is suppressed due to a destructive interference between s and t channel exchange diagrams. The regions of MSSM parameter space where the following limits are valid are indicated in the comment lines or in the footnotes.

Some earlier papers are now obsolete and have been omitted. They were last listed in our PDG 14 edition: K. Olive, *et al.* (Particle Data Group), Chinese Physics **C38** 070001 (2014) (<http://pdg.lbl.gov>).

VALUE (GeV)	CL%	DOCUMENT ID	TECN	COMMENT	>1440	95	10	TUMASYAN	22s	CMS	2 same-sign e or μ , 3 or 4 leptons, Tchi1n2B (flavor-democratic), $m_{\tilde{\ell}} = 0.95m_{\tilde{\chi}_1^\pm} + 0.05m_{\tilde{\chi}_1^0}$, $m_{\tilde{\chi}_1^0} = 0$ GeV
> 820	95	1 AAD	23AE ATLS	2 SFOS ℓ , jets, \cancel{E}_T , Tchi1n2Fa, $m_{\tilde{\chi}_1^0} = 1$ GeV	>1140	95	10	TUMASYAN	22s	CMS	2 same-sign e or μ , 3 or 4 leptons, Tchi1n2B (lepton in $\tilde{\chi}_1^\pm$ decay is τ), $m_{\tilde{\ell}} = 1/2(m_{\tilde{\chi}_1^\pm} + m_{\tilde{\chi}_1^0})$, $m_{\tilde{\chi}_1^0} = 0$ GeV
none 260-420	95	2 AAD	23CI ATLS	1ℓ + jets + \cancel{E}_T , Tchi1n2J, $m_{\tilde{\chi}_1^0} = 0$ GeV	>1110	95	10	TUMASYAN	22s	CMS	2 same-sign e or μ , 3 or 4 leptons, Tchi1n2B (lepton in $\tilde{\chi}_1^\pm$ decay is τ), $m_{\tilde{\ell}} = 0.05m_{\tilde{\chi}_1^\pm} + 0.95m_{\tilde{\chi}_1^0}$, $m_{\tilde{\chi}_1^0} = 0$ GeV
none 260-520	95	2 AAD	23CI ATLS	1ℓ + jets + \cancel{E}_T , Tchi1chi1J, $m_{\tilde{\chi}_1^0} = 0$ GeV	>1140	95	10	TUMASYAN	22s	CMS	2 same-sign e or μ , 3 or 4 leptons, Tchi1n2B (lepton in $\tilde{\chi}_1^\pm$ decay is τ), $m_{\tilde{\ell}} = 0.95m_{\tilde{\chi}_1^\pm} + 0.05m_{\tilde{\chi}_1^0}$, $m_{\tilde{\chi}_1^0} = 0$ GeV
> 230	95	3 AAD	23CI ATLS	1ℓ + jets + \cancel{E}_T , Tchi1n2E, $m_{\tilde{\chi}_2^0} - m_{\tilde{\chi}_1^0} = 133$ GeV	> 980	95	10	TUMASYAN	22s	CMS	2 same-sign e or μ , 3 or 4 leptons, Tchi1n2B (leptons in $\tilde{\chi}_1^\pm$ and $\tilde{\chi}_2^0$ decays are τ), $m_{\tilde{\ell}} = 1/2(m_{\tilde{\chi}_1^\pm} + m_{\tilde{\chi}_1^0})$, $m_{\tilde{\chi}_1^0} = 0$ GeV
> 450	95	3 AAD	23CI ATLS	1ℓ + jets + \cancel{E}_T , Tchi1n2E, $m_{\tilde{\chi}_2^0} - m_{\tilde{\chi}_1^0} = 260$ GeV	> 905	95	10	TUMASYAN	22s	CMS	2 same-sign e or μ , 3 or 4 leptons, Tchi1n2B (leptons in $\tilde{\chi}_1^\pm$ and $\tilde{\chi}_2^0$ decays are τ), $m_{\tilde{\ell}} = 0.05m_{\tilde{\chi}_1^\pm} + 0.95m_{\tilde{\chi}_1^0}$, $m_{\tilde{\chi}_1^0} = 0$ GeV
none 200-250	95	4 AAD	23CP ATLS	2 same-sign ℓ , Tchi1n2F, wino-bino, $m_{\tilde{\chi}_1^0} = 1$ GeV	> 875	95	10	TUMASYAN	22s	CMS	2 same-sign e or μ , 3 or 4 leptons, Tchi1n2B (leptons in $\tilde{\chi}_1^\pm$ and $\tilde{\chi}_2^0$ decays are τ), $m_{\tilde{\ell}} = 0.95m_{\tilde{\chi}_1^\pm} + 0.05m_{\tilde{\chi}_1^0}$, $m_{\tilde{\chi}_1^0} = 0$ GeV
> 525	95	4 AAD	23CP ATLS	2 same-sign ℓ , Tchi1n2E, wino-bino, $m_{\tilde{\chi}_1^0} = 1$ GeV	> 650	95	10	TUMASYAN	22s	CMS	2 same-sign e or μ , 3 or 4 leptons, Tchi1n2F, $m_{\tilde{\chi}_1^0} = 0$ GeV
none 200-585	95	5 AAD	23CR ATLS	RPV, 2 same-sign, 3, 4 ℓ , 1, 2 b -jets, higgsino production with $\tilde{\chi} \rightarrow b + \ell/\nu + t/b$ via λ'_{33} coupling	> 260	95	10	TUMASYAN	22s	CMS	2 same-sign e or μ , 3 or 4 leptons, Tchi1n2E, $m_{\tilde{\chi}_1^0} = 0$ GeV
none 200-670	95	5 AAD	23CR ATLS	RPV, 2 same-sign, 3, 4 ℓ , 1, 2 b -jets, wino production with $\tilde{\chi} \rightarrow b + \ell/\nu + t/b$ via λ'_{33} coupling	>1080	95	11	AAD	21AX ATLS		jets + large-R jets + \cancel{E}_T , TWinoBinoA, nearly independent of $B(\tilde{\chi}_2^0 \rightarrow Z\tilde{\chi}_1^0)$, $m_{\tilde{\chi}_1^0} = 0$ GeV
> 150	95	6 AAD	23M ATLS	2 ℓ , Tchi1chi1H, $m_{\tilde{\chi}_1^\pm} - m_{\tilde{\chi}_1^0} > 110$ GeV	>1060	95	11	AAD	21AX ATLS		jets + large-R jets + \cancel{E}_T , THinoBinoA, nearly independent of $B(\tilde{\chi}_2^0 \rightarrow Z\tilde{\chi}_1^0)$, $m_{\tilde{\chi}_1^0} = 0$ GeV
> 104	95	6 AAD	23M ATLS	2 ℓ , Tchi1chi1H, $m_{\tilde{\chi}_1^\pm} - m_{\tilde{\chi}_1^0} > 90$ GeV	> 900	95	11	AAD	21AX ATLS		jets + large-R jets + \cancel{E}_T , THinoBinoA, nearly independent of $B(\tilde{\chi}_2^0 \rightarrow Z\tilde{\chi}_1^0)$, $m_{\tilde{\chi}_1^0} = 0$ GeV
>1230	95	7 HAYRAPETY...23E	CMS	γ + jets + \cancel{E}_T , Tchi1n1A	> 900	95	11	AAD	21AX ATLS		jets + large-R jets + \cancel{E}_T , THinoWinoA, $\tan \beta = 10$, $\mu > 0$, $m_{\tilde{\chi}_1^0} = 0$ GeV
>1050	95	7 HAYRAPETY...23E	CMS	γ + jets + \cancel{E}_T , Tchi1chi1A	>1060	95	11	AAD	21AX ATLS		jets + large-R jets + \cancel{E}_T , Tchi1n2E, full hadronic final state, $m_{\tilde{\chi}_1^0} = 0$ GeV
none 290-670	95	8 TUMASYAN	23B CMS	2 AK8 jets + 2-6 AK4 jets + \cancel{E}_T , Tchi1chi1I, $m_{\tilde{\chi}_1^0} = 1$ GeV	> 960	95	11	AAD	21AX ATLS		jets + large-R jets + \cancel{E}_T , Tchi1n2Fb, $m_{\tilde{\chi}_1^0} = 0$ GeV
none 230-760	95	8 TUMASYAN	23B CMS	2 AK8 jets + 2-6 AK4 jets + \cancel{E}_T , Tchi1n2Fb, $m_{\tilde{\chi}_1^0} = 1$ GeV	none 620-740	95	11	AAD	21AX ATLS		jets + large-R jets + \cancel{E}_T , Tchi1chi1I, $m_{\tilde{\chi}_1^0} = 0$ GeV
none 240-970	95	8 TUMASYAN	23B CMS	2 AK8 jets + 2-6 AK4 jets + \cancel{E}_T , Tchi1n2Fc, $m_{\tilde{\chi}_1^0} = 1$ GeV	> 640	95	12	AAD	21BG ATLS		3 ℓ + \cancel{E}_T , Tchi1n2F, wino cross section, $m_{\tilde{\chi}_1^0} = 0$ GeV
none 300-650	95	8 TUMASYAN	23B CMS	2 AK8 jets + 2-6 AK4 jets + \cancel{E}_T , THinoBinoA, $m_{\tilde{\chi}_1^0} = 1$ GeV	> 300	95	12	AAD	21BG ATLS		3 ℓ + \cancel{E}_T , Tchi1n2F, wino cross section, $m_{\tilde{\chi}_2^0} - m_{\tilde{\chi}_1^0} = m_Z$
> 275	95	9 TUMASYAN	22Q CMS	2 or 3 ℓ (soft), \cancel{E}_T ; Tchi1n2F, wino-bino, $m_{\tilde{\chi}_2^0} - m_{\tilde{\chi}_1^0} = 10$ GeV	> 240	95	12	AAD	21BG ATLS		3 ℓ + \cancel{E}_T , Tchi1n2F, wino cross section, $m_{\tilde{\chi}_2^0} - m_{\tilde{\chi}_1^0} = 10$ GeV
> 205	95	9 TUMASYAN	22Q CMS	2 or 3 ℓ (soft), \cancel{E}_T ; higgsino model with $\tilde{\chi}_2^0 \tilde{\chi}_1^\pm$ and $\tilde{\chi}_2^0 \tilde{\chi}_1^0$ prod., $m_{\tilde{\chi}_2^0} - m_{\tilde{\chi}_1^0} = 7.5$ GeV	> 190	95	12	AAD	21BG ATLS		3 ℓ + \cancel{E}_T , Tchi1n2E, wino cross section, $m_{\tilde{\chi}_1^0} = 0$ GeV
> 150	95	9 TUMASYAN	22Q CMS	2 or 3 ℓ (soft), \cancel{E}_T ; higgsino model with $\tilde{\chi}_2^0 \tilde{\chi}_1^\pm$ and $\tilde{\chi}_2^0 \tilde{\chi}_1^0$ prod., $m_{\tilde{\chi}_2^0} - m_{\tilde{\chi}_1^0} = 3$ GeV	>1100	95	13	AAD	21E ATLS		3 ℓ , Z ℓ resonances, TWinoL-SPBL, RPV, $B(\tilde{\chi}_1^\pm \rightarrow Z e) = B(\tilde{\chi}_1^0 \rightarrow Z \nu) = 1$
>1450	95	10 TUMASYAN	22s CMS	2 same-sign e or μ , 3 or 4 leptons, Tchi1n2B (flavor-democratic), $m_{\tilde{\ell}} = 1/2(m_{\tilde{\chi}_1^\pm} + m_{\tilde{\chi}_1^0})$, $m_{\tilde{\chi}_1^0} = 850$ GeV	>1050	95	13	AAD	21E ATLS		3 ℓ , Z ℓ resonances, TWinoL-SPBL, RPV, $B(\tilde{\chi}_1^\pm \rightarrow Z \mu) = B(\tilde{\chi}_1^0 \rightarrow Z \nu) = 1$
>1360	95	10 TUMASYAN	22s CMS	2 same-sign e or μ , 3 or 4 leptons, Tchi1n2B (flavor-democratic), $m_{\tilde{\ell}} = 1/2(m_{\tilde{\chi}_1^\pm} + m_{\tilde{\chi}_1^0})$, $m_{\tilde{\chi}_1^0} = 0$ GeV	> 625	95	13	AAD	21E ATLS		3 ℓ , Z ℓ resonances, TWinoL-SPBL, RPV, $B(\tilde{\chi}_1^\pm \rightarrow Z \tau) = B(\tilde{\chi}_1^0 \rightarrow Z \nu) = 1$
>1290	95	10 TUMASYAN	22s CMS	2 same-sign e or μ , 3 or 4 leptons, Tchi1n2B (flavor-democratic), $m_{\tilde{\ell}} = 0.05m_{\tilde{\chi}_1^\pm} + 0.95m_{\tilde{\chi}_1^0}$, $m_{\tilde{\chi}_1^0} = 0$ GeV							

Searches Particle Listings

Supersymmetric Particle Searches

> 975	95	13	AAD	21E	ATLS	3ℓ, Zℓ resonances, TwinO-SPBL, RPV, B($\tilde{\chi}_1^\pm \rightarrow Z\ell$) = B($\tilde{\chi}_1^0 \rightarrow Z\nu$) = 1 and $\ell = e, \mu, \tau$	> 780	95	40	SIRUNYAN	18AA	CMS	$\geq 1\gamma + \cancel{E}_T$, Tchi1n1A
> 950	95						> 950	95	40	SIRUNYAN	18AA	CMS	$\geq 1\gamma + \cancel{E}_T$, Tchi1chi1A
> 230	95						> 230	95	41	SIRUNYAN	18AJ	CMS	2ℓ (soft) + \cancel{E}_T , Tchi1n2F, wino, $m_{\tilde{\chi}_2^0} - m_{\tilde{\chi}_1^0} = 20$ GeV
>1600	95	14	AAD	21Y	ATLS	$\geq 4\ell$, RPV Tchi1n2l with $\tilde{\chi}_1^0 \rightarrow \ell^\pm \ell^\mp \nu$, $\lambda_{12k} \neq 0$, $m_{\tilde{\chi}_1^0} = 1200$ GeV	>1150	95	42	SIRUNYAN	18AO	CMS	$\ell^\pm \ell^\pm$ or $\geq 3\ell$, Tchi1n2A, $m_{\tilde{\ell}} = m_{\tilde{\nu}} = m_{\tilde{\chi}_1^0} + 0.5 (m_{\tilde{\chi}_1^\pm} - m_{\tilde{\chi}_1^0})$, $m_{\tilde{\chi}_1^0} = 0$ GeV
>1100	95	14	AAD	21Y	ATLS	$\geq 4\ell$, RPV Tchi1n2l with $\tilde{\chi}_1^0 \rightarrow \ell^\pm \ell^\mp \nu$, $\lambda_{j33} \neq 0$, $m_{\tilde{\chi}_1^0} = 1000$ GeV	>1120	95	42	SIRUNYAN	18AO	CMS	$\ell^\pm \ell^\pm$ or $\geq 3\ell$, Tchi1n2A, $m_{\tilde{\ell}} = m_{\tilde{\nu}} = m_{\tilde{\chi}_1^0} + 0.05 (m_{\tilde{\chi}_1^\pm} - m_{\tilde{\chi}_1^0})$, $m_{\tilde{\chi}_1^0} = 0$ GeV
> 750	95	15	SIRUNYAN	21M	CMS	$\ell^\pm \ell^\mp + \cancel{E}_T$, Tchi1n2Fa, $m_{\tilde{\chi}_1^0} < 100$ GeV	>1050	95	42	SIRUNYAN	18AO	CMS	$\ell^\pm \ell^\pm$ or $\geq 3\ell$, Tchi1n2A, $m_{\tilde{\ell}} = m_{\tilde{\nu}} = m_{\tilde{\chi}_1^0} + 0.95 (m_{\tilde{\chi}_1^\pm} - m_{\tilde{\chi}_1^0})$, $m_{\tilde{\chi}_1^0} = 0$ GeV
none 400-820	95	16	TUMASYAN	21C	CMS	1 $\ell^\pm + 2b$ -jets + \cancel{E}_T , Tchi1n2E, $m_{\tilde{\chi}_1^0} = 200$ GeV	>1080	95	42	SIRUNYAN	18AO	CMS	$\ell^\pm \ell^\pm$ or $\geq 3\ell$, Tchi1n2H, $m_{\tilde{\ell}} = m_{\tilde{\nu}} = m_{\tilde{\chi}_1^0} + 0.5 (m_{\tilde{\chi}_1^\pm} - m_{\tilde{\chi}_1^0})$, $m_{\tilde{\chi}_1^0} = 0$ GeV
none 160-820	95	16	TUMASYAN	21C	CMS	1 $\ell^\pm + 2b$ -jets + \cancel{E}_T , Tchi1n2E, $m_{\tilde{\chi}_1^0} = 0$ GeV	>1030	95	42	SIRUNYAN	18AO	CMS	$\ell^\pm \ell^\pm$ or $\geq 3\ell$, Tchi1n2H, $m_{\tilde{\ell}} = m_{\tilde{\nu}} = m_{\tilde{\chi}_1^0} + 0.05 (m_{\tilde{\chi}_1^\pm} - m_{\tilde{\chi}_1^0})$, $m_{\tilde{\chi}_1^0} = 0$ GeV
> 380	95	17	AAD	20AN	ATLS	2 γ + \cancel{E}_T , Tn1n1A, GMSB	>1030	95	42	SIRUNYAN	18AO	CMS	$\ell^\pm \ell^\pm$ or $\geq 3\ell$, Tchi1n2H, $m_{\tilde{\ell}} = m_{\tilde{\nu}} = m_{\tilde{\chi}_1^0} + 0.5 (m_{\tilde{\chi}_1^\pm} - m_{\tilde{\chi}_1^0})$, $m_{\tilde{\chi}_1^0} = 0$ GeV
> 240	95	18	AAD	20I	ATLS	2ℓ (soft), jets, \cancel{E}_T ; Tchi1n2Fa, wino, $m_{\tilde{\chi}_1^\pm} - m_{\tilde{\chi}_1^0} = 7$ GeV	>1050	95	42	SIRUNYAN	18AO	CMS	$\ell^\pm \ell^\pm$ or $\geq 3\ell$, Tchi1n2H, $m_{\tilde{\ell}} = m_{\tilde{\nu}} = m_{\tilde{\chi}_1^0} + 0.95 (m_{\tilde{\chi}_1^\pm} - m_{\tilde{\chi}_1^0})$, $m_{\tilde{\chi}_1^0} = 0$ GeV
> 345	95	19	AAD	20K	ATLS	3ℓ + \cancel{E}_T , Tchi1n2F, $m_{\tilde{\chi}_1^0} = 0$ GeV	> 625	95	42	SIRUNYAN	18AO	CMS	$\ell^\pm \ell^\pm$ or $\geq 3\ell$, Tchi1n2D, $m_{\tilde{\ell}} = m_{\tilde{\nu}} = m_{\tilde{\chi}_1^0} + 0.5 (m_{\tilde{\chi}_1^\pm} - m_{\tilde{\chi}_1^0})$, $m_{\tilde{\chi}_1^0} = 0$ GeV
> 420	95	20	AAD	20O	ATLS	2ℓ + \cancel{E}_T , Tchi1chi1H, $m_{\tilde{\chi}_1^0} = 0$ GeV	> 180	95	42	SIRUNYAN	18AO	CMS	$\ell^\pm \ell^\pm$ or $\geq 3\ell$, Tchi1n2E, $m_{\tilde{\chi}_1^0} = 0$ GeV
>1000	95	21	AAD	20O	ATLS	2ℓ + \cancel{E}_T , Tchi1chi1C, $m_{\tilde{\chi}_1^0} = 0$ GeV	> 450	95	42	SIRUNYAN	18AO	CMS	$\ell^\pm \ell^\pm$ or $\geq 3\ell$, Tchi1n2F, $m_{\tilde{\chi}_1^0} = 0$ GeV
> 740	95	22	AAD	20R	ATLS	1ℓ + 2b-jets + \cancel{E}_T , Tchi1n2E, $m_{\tilde{\chi}_1^0} = 0$ GeV	> 480	95	43	SIRUNYAN	18AP	CMS	Combination of searches, Tchi1n2E, $m_{\tilde{\chi}_1^0} = 0$ GeV
> 290	95	23	SIRUNYAN	20AU	CMS	soft τ + jet + \cancel{E}_T , Tchi1n2D, wino, $m_{\tilde{\chi}_1^\pm} - m_{\tilde{\chi}_1^0} = 50$ GeV	> 650	95	43	SIRUNYAN	18AP	CMS	Combination of searches, Tchi1n2F, $m_{\tilde{\chi}_1^0} = 0$ GeV
>1050	95	24	SIRUNYAN	20B	CMS	$\geq 1\gamma + \cancel{E}_T$, Tchi1chi1F, $\tilde{\chi}_1^0 \rightarrow \gamma \tilde{G}$	> 535	95	43	SIRUNYAN	18AP	CMS	Combination of searches, Tchi1n2l, $m_{\tilde{\chi}_1^0} = 0$ GeV
> 825	95	24	SIRUNYAN	20B	CMS	$\geq 1\gamma + \cancel{E}_T$, Tchi1chi1G, $\tilde{\chi}_1^\pm \rightarrow \tilde{\chi}_1^0 + \text{soft}$	none 160-610	95	44	SIRUNYAN	18AR	CMS	$\ell^\pm \ell^\mp + \text{jets} + \cancel{E}_T$, Tchi1n2F, $m_{\tilde{\chi}_1^0} = 0$ GeV
> 840	95	24	SIRUNYAN	20B	CMS	$\geq 1\gamma + \cancel{E}_T$, Tchi1n12-GGM, 120 GeV < $m_{\tilde{\chi}_1^0} < 720$ GeV	none 170-200	95	45	SIRUNYAN	18DN	CMS	$\ell^\pm \ell^\mp$, Tchi1chi1E, $m_{\tilde{\chi}_1^0} = 1$ GeV
> 680	95	25	AABOUD	19AU	ATL	0, 1, 2 or more ℓ , H ($\rightarrow \gamma\gamma, bb, WW^*, ZZ^*, \tau\tau$) (various searches), Tchi1n2E, $m_{\tilde{\chi}_1^0} = 0$ GeV	> 810	95	45	SIRUNYAN	18DN	CMS	$\ell^\pm \ell^\mp$, Tchi1chi1C, $m_{\tilde{\chi}_1^0} = 0$ GeV
> 112	95	26	SIRUNYAN	19BU	CMS	$pp \rightarrow \tilde{\chi}_1^+ \tilde{\chi}_2^0 + 2$ jets, $\tilde{\chi}_1^+ \rightarrow \ell^+ \nu \tilde{\chi}_1^0$, heavy sleptons, $m_{\tilde{\chi}_1^\pm} - m_{\tilde{\chi}_1^0} = 1$ GeV, $m_{\tilde{\chi}_1^\pm} = m_{\tilde{\chi}_2^0}$	> 630	95	46	SIRUNYAN	18DP	CMS	2 τ + \cancel{E}_T , Tchi1chi1D, $m_{\tilde{\chi}_1^0} = 0$ GeV
> 215	95	26	SIRUNYAN	19BU	CMS	$pp \rightarrow \tilde{\chi}_1^+ \tilde{\chi}_2^0 + 2$ jets, $\tilde{\chi}_1^+ \rightarrow \ell^+ \nu \tilde{\chi}_1^0$, heavy sleptons, $m_{\tilde{\chi}_1^\pm} - m_{\tilde{\chi}_1^0} = 30$ GeV, $m_{\tilde{\chi}_1^\pm} = m_{\tilde{\chi}_2^0}$	> 710	95	46	SIRUNYAN	18DP	CMS	2 τ + \cancel{E}_T , Tchi1n2D, $m_{\tilde{\chi}_1^0} = 0$ GeV
> 235	95	27	SIRUNYAN	19CI	CMS	≥ 1 H ($\rightarrow \gamma\gamma$) + jets + \cancel{E}_T , Tchi1n2E, $m_{\tilde{\chi}_1^0} = 1$ GeV	> 170	95	47	SIRUNYAN	18X	CMS	≥ 1 H ($\rightarrow \gamma\gamma$) + jets + \cancel{E}_T , Tchi1n2E, $m_{\tilde{\chi}_1^0} < 25$ GeV
> 930	95	28	SIRUNYAN	19K	CMS	γ + lepton + \cancel{E}_T , Tchi1n1A	> 420	95	48	KHACHATRY...17L	CMS	2 τ + \cancel{E}_T , Tchi1chi1C and $\tilde{\tau}$ -only, $m_{\tilde{\chi}_1^0} = 0$ GeV	
> 630	95	29	AABOUD	18AY	ATLS	2 τ + \cancel{E}_T , Tchi1chi1D and $\tilde{\tau}_L$ -only, $m_{\tilde{\chi}_1^0} = 0$ GeV	none 220-490	95	49	SIRUNYAN	17AW	CMS	1ℓ + 2b-jets + \cancel{E}_T , Tchi1n2E, $m_{\tilde{\chi}_1^0} = 0$ GeV
> 760	95	30	AABOUD	18AY	ATLS	2 τ + \cancel{E}_T , Tchi1n2D and $\tilde{\tau}_L$ -only, $m_{\tilde{\chi}_1^0} = 0$ GeV	> 500	95	50	AAD	16AA	ATLS	2ℓ $^\pm$ + \cancel{E}_T , Tchi1chi1B, $m_{\tilde{\chi}_1^0} = 0$ GeV
> 740	95	31	AABOUD	18BT	ATLS	2ℓ + \cancel{E}_T , Tchi1chi1C, $m_{\tilde{\chi}_1^0} = 0$ GeV	> 220	95	50	AAD	16AA	ATLS	2ℓ $^\pm$ + \cancel{E}_T , Tchi1chi1C, low Δm for $\tilde{\chi}_1^\pm, \tilde{\chi}_1^0$
>1125	95	32	AABOUD	18BT	ATLS	2,3ℓ + \cancel{E}_T , Tchi1n2C, $m_{\tilde{\chi}_1^0} = 0$ GeV	> 700	95	51	AAD	16AA	ATLS	3,4ℓ + \cancel{E}_T , Tchi1n2B, $m_{\tilde{\chi}_1^0} = 0$ GeV
> 580	95	33	AABOUD	18BT	ATLS	2,3ℓ + \cancel{E}_T , Tchi1n2F, $m_{\tilde{\chi}_1^0} = 0$ GeV	> 700	95	51	AAD	16AA	ATLS	3,4ℓ + \cancel{E}_T , Tchi1n2C, $m_{\tilde{\ell}} = m_{\tilde{\chi}_1^0} + 0.5$ (or 0.95) $(m_{\tilde{\chi}_1^\pm} - m_{\tilde{\chi}_1^0})$
none 130-230, 290-880	95	34	AABOUD	18CK	ATLS	2H ($\rightarrow bb$) + \cancel{E}_T , Tn1n1A, GMSB	> 400	95	51	AAD	16AA	ATLS	2 hadronic τ + \cancel{E}_T & 3ℓ + \cancel{E}_T combination, Tchi1n2D, $m_{\tilde{\chi}_1^0} = 0$ GeV
none 220-600	95	35	AABOUD	18CO	ATLS	2,3ℓ + \cancel{E}_T , recursive jigsaw, Tchi1n2F, $m_{\tilde{\chi}_1^0} = 0$ GeV	> 540	95	52	KHACHATRY...16R	CMS	$\geq 1\gamma + 1$ e or μ + \cancel{E}_T , Tchi1n1A	
> 175	95	36	AABOUD	18R	ATLS	2ℓ (soft) + \cancel{E}_T , Tchi1n2F, wino, $m_{\tilde{\chi}_1^\pm} - m_{\tilde{\chi}_1^0} = 10$ GeV	> 250	95	53	AAD	15BA	ATLS	$m_{\tilde{\chi}_1^\pm} = m_{\tilde{\chi}_2^0}$, $m_{\tilde{\chi}_1^0} = 0$ GeV
> 145	95	37	AABOUD	18R	ATLS	2ℓ (soft) + \cancel{E}_T , Tchi1n2G, higgsino, $m_{\tilde{\chi}_1^\pm} - m_{\tilde{\chi}_1^0} = 5$ GeV	> 590	95	54	AAD	15CA	ATLS	$\geq 2\gamma + \cancel{E}_T$, GGM, bino-like NLSP, any NLSP mass
>1060	95	38	AABOUD	18U	ATLS	2 γ + \cancel{E}_T , GGM, Tchi1chi1A, any NLSP mass	none 124-361	95	54	AAD	15CA	ATLS	$\geq 1\gamma + e, \mu + \cancel{E}_T$, GGM, wino-like NLSP
>1400	95	39	AABOUD	18Z	ATLS	$\geq 4\ell$, RPV, $\lambda_{12k} \neq 0$, $m_{\tilde{\chi}_1^0} > 500$ GeV	> 700	95	55	AAD	14H	ATLS	$\tilde{\chi}_1^\pm \tilde{\chi}_2^0 \rightarrow \ell^\pm \nu \tilde{\chi}_1^0 \ell^\pm \ell^\mp \tilde{\chi}_1^0$, simplified model, $m_{\tilde{\chi}_1^\pm} = m_{\tilde{\chi}_2^0}$, $m_{\tilde{\chi}_1^0} = 0$ GeV
>1320	95	39	AABOUD	18Z	ATLS	$\geq 4\ell$, RPV, $\lambda_{12k} \neq 0$, $m_{\tilde{\chi}_1^0} > 50$ GeV							
> 980	95	39	AABOUD	18Z	ATLS	$\geq 4\ell$, RPV, $\lambda_{j33} \neq 0$, 400 GeV < $m_{\tilde{\chi}_1^0} < 700$ GeV							
> 980	95	40	SIRUNYAN	18AA	CMS	$\geq 1\gamma + \cancel{E}_T$, GGM, wino-like $\tilde{\chi}_2^0 \tilde{\chi}_1^\pm$ pair production, nearly degenerate wino and bino masses							

See key on page 1171

Searches Particle Listings

Supersymmetric Particle Searches

> 345	95	55	AAD	14H	ATLS	$\tilde{\chi}_1^\pm \tilde{\chi}_2^0 \rightarrow W \tilde{\chi}_1^0 Z \tilde{\chi}_1^0$, simplified model, $m_{\tilde{\chi}_1^\pm} = m_{\tilde{\chi}_2^0}$, $m_{\tilde{\chi}_1^0} = 0$ GeV	4	AAD 23CP searched in 139 fb ⁻¹ of pp collisions at $\sqrt{s} = 13$ TeV for events with 2 ℓ with same charge plus at least one jet and E_T , defining signal region based on 'stransverse mass' of the dilepton system, E_T significance and effective mass. No significant excess above the Standard Model predictions is observed. Limits are set on the mass of mass-degenerate $\tilde{\chi}_1^\pm$ and $\tilde{\chi}_2^0$ for the wino-like production of $\tilde{\chi}_1^\pm \tilde{\chi}_2^0$ followed by the decay into either $WZ \tilde{\chi}_1^0 \tilde{\chi}_1^0$ or $Wh \tilde{\chi}_1^0 \tilde{\chi}_1^0$, see figure 13.
> 148	95	55	AAD	14H	ATLS	$\tilde{\chi}_1^\pm \tilde{\chi}_2^0 \rightarrow W \tilde{\chi}_1^0 H \tilde{\chi}_1^0$, simplified model, $m_{\tilde{\chi}_1^\pm} = m_{\tilde{\chi}_2^0}$, $m_{\tilde{\chi}_1^0} = 0$ GeV	5	AAD 23CR searched in 139 fb ⁻¹ of pp collisions at $\sqrt{s} = 13$ TeV for RPV SUSY in final states with multiple leptons and b -tagged jets. No significant excess above the Standard Model expectations is observed. Limits are set on the production of electroweakinos (wino or higgsino) that decay via RPV coupling λ'_{i33} to a charged lepton or a neutrino, a b quark, and an additional t or b quark, see their figure 16. A second model addresses direct $\tilde{\mu}_{L,R}$ production and decay to a muon and a bino-like neutralino, which decays in the same way as in the first model, see their figure 17.
> 380	95	55	AAD	14H	ATLS	$\tilde{\chi}_1^\pm \tilde{\chi}_2^0 \rightarrow \tau^\pm \nu \tilde{\chi}_1^0 \tau^\pm \tau^\mp \tilde{\chi}_1^0$, simplified model, $m_{\tilde{\chi}_1^\pm} = m_{\tilde{\chi}_2^0}$, $m_{\tilde{\chi}_1^0} = 0$ GeV	6	AAD 23M searched in 139 fb ⁻¹ of pp collisions at $\sqrt{s} = 13$ TeV for $\tilde{\chi}_1^\pm$ pair production, followed by $\tilde{\chi}_1^\pm \rightarrow W^\pm \tilde{\chi}_1^0 \rightarrow \ell^\pm \nu \tilde{\chi}_1^0$ in events with two leptons. The focus is on models where $m_{\tilde{\chi}_1^\pm} - m_{\tilde{\chi}_1^0}$ is close to the W mass. No significant excess above the Standard Model predictions is observed. Limits are set on the $\tilde{\chi}_1^\pm$ mass as a function of $m_{\tilde{\chi}_1^0}$, see Figure 9.
> 750	95	56	AAD	14X	ATLS	RPV, $\geq 4\ell^\pm$, $\tilde{\chi}_1^\pm \rightarrow W^{(*)\pm} \tilde{\chi}_1^0$, $\tilde{\chi}_1^0 \rightarrow \ell^\pm \ell^\mp \nu$	7	HAYRAPETYAN 23E searched in 137 fb ⁻¹ of pp collisions at $\sqrt{s} = 13$ TeV for evidence of gluino, top squark and electroweakino pair production in events with at least one photon, multiple jets, and large E_T . No significant excess above the Standard Model expectations is observed. Limits are set in models for strong production, Tglu4D, Tglu4E, Tglu4F and Tstop13, see their figure 9. They also interpret the results in the models for electroweak production, shown in their figure 10. Tchi1n1A assumes wino-like $\tilde{\chi}_1^\pm \tilde{\chi}_1^0$ production, while Tchi1chi1A assumes higgsino-like cross sections and includes $\tilde{\chi}_1^\pm \tilde{\chi}_1^\pm$, $\tilde{\chi}_1^0 \tilde{\chi}_2^0$ and $\tilde{\chi}_1^0 \tilde{\chi}_2^\pm$ production. For $\tilde{\chi}_1^0 \tilde{\chi}_2^0$ alone no production can be excluded in the model Tchi1chi1A, but in another model for $\tilde{\chi}_1^0 \tilde{\chi}_2^0$ production, Tn1n2A.
> 210	95	57	KHACHATRY...14L	CMS	$\tilde{\chi}_2^0 \rightarrow H \tilde{\chi}_1^0$ and $\tilde{\chi}_1^\pm \rightarrow W^\pm \tilde{\chi}_1^0$ simplified models, $m_{\tilde{\chi}_2^0} = m_{\tilde{\chi}_1^\pm}$, $m_{\tilde{\chi}_1^0} = 0$ GeV	8	TUMASYAN 23B searched in 137 fb ⁻¹ of pp collisions at $\sqrt{s} = 13$ TeV for evidence of electroweakino pair production with decays including hadronically decaying bosons, WW , WZ , WH , or ZH , identified with a DNN classifying large-area (AK8) jets. No significant excess above the Standard Model expectations is observed. Limits are set on the mass of the nearly mass degenerate wino-like $\tilde{\chi}_2^0$ and $\tilde{\chi}_1^\pm$ in the models Tchi1chi1I, Tchi1n2Fb, and Tchi1n2Fc, see their figure 4. They also consider a model that contains both $\tilde{\chi}_2^0 \tilde{\chi}_1^\pm$ and $\tilde{\chi}_1^\pm \tilde{\chi}_1^\pm$ production, see their figure 5 (upper). Results are also interpreted in the model THinoBinoA with nearly mass-degenerate higgsino-like $\tilde{\chi}_3^0$, $\tilde{\chi}_2^0$, $\tilde{\chi}_1^\pm$, and a lighter bino-like $\tilde{\chi}_1^0$, see their figure 5 (lower).	
> 540	95	58	AAD	13	ATLS	$3\ell^\pm + E_T$, pMSSM, SMS	9	TUMASYAN 22Q searched in up to 137 fb ⁻¹ of pp collisions at $\sqrt{s} = 13$ TeV for evidence of electroweakino and top squark pair production with a small mass difference between the produced supersymmetric particles and the lightest neutralino in events with two or three low-momentum leptons and missing transverse momentum. No significant excess above the Standard Model expectations is observed. Limits are set on the mass of $\tilde{\chi}_2^0$ and $\tilde{\chi}_1^\pm$ in the model Tchi1n2F, see their Figure 8. Limits are also set in a higgsino simplified model with both $\tilde{\chi}_2^0 \tilde{\chi}_1^\pm$ and $\tilde{\chi}_2^0 \tilde{\chi}_1^0$ production, where $\tilde{\chi}_2^0 \rightarrow Z \tilde{\chi}_1^0$ and $m_{\tilde{\chi}_1^\pm} = 1/2(m_{\tilde{\chi}_2^0} + m_{\tilde{\chi}_1^0})$. A model inspired by the pMSSM is used for further interpretations in the case of a higgsino LSP, see their Figure 9. Limits are also set on the mass of the top squark in the models Tstop2 and Tstop3, see their Figure 10.
> 540	95	59	AAD	13B	ATLS	$2\ell^\pm + E_T$, pMSSM, SMS	10	TUMASYAN 22s searched in 137 fb ⁻¹ of pp collisions at $\sqrt{s} = 13$ TeV for evidence of electroweakino pair production in events with three or four leptons, with up to two hadronically decaying τ leptons, or two same-sign light leptons (e or μ). No significant excess above the Standard Model expectations is observed. Limits are set on the mass of $\tilde{\chi}_2^0$ and $\tilde{\chi}_1^\pm$ in the models Tchi1n2B (in flavor-democratic and tau-enriched or -dominated scenarios), Tchi1n2E, Tchi1n2F, see their Figures 16–20, and on the mass of the higgsino-triplet $\tilde{\chi}_2^0$, $\tilde{\chi}_1^\pm$, and $\tilde{\chi}_1^0$ in the models Tn1n1A, Tn1n1B, and Tn1n1C, see their Figure 21.
> 540	95	60	AAD	12Ct	ATLS	$\geq 4\ell^\pm$, RPV, $m_{\tilde{\chi}_1^0} > 300$ GeV	11	AAD 21Ax searched in 139 fb ⁻¹ of pp collisions at $\sqrt{s} = 13$ TeV for pair production of electroweakinos decaying to the LSP via the emission of Standard Model bosons (Higgs, W , Z) decaying into hadrons. The final state in all cases characterised by the presence of E_T , jets, and large- R jets tagged according to the boson of interest. Different assumptions (Higgsino, Wino, Bino) are made for the pair produced electroweakinos and for the LSP multiplet. No significant excess above the Standard Model predictions is observed. Limits are set on the electroweakino masses as a function of the model parameters (in particular $m_{\tilde{\chi}_1^0}$). See Figs. 12, 14, 15.
> 94	95	61	CHATRCHYAN 12Bj	CMS	$\geq 2\ell$, jets + E_T , $pp \rightarrow \tilde{\chi}_1^\pm \tilde{\chi}_2^0$	12	AAD 21Bg searched in 139 fb ⁻¹ of pp collisions at $\sqrt{s} = 13$ TeV for pair production $\tilde{\chi}_2^0 \tilde{\chi}_1^\pm$ in final states with three leptons, with and without assuming the presence of a $Z \rightarrow \ell\ell$ decay. No significant excess above the Standard Model predictions is observed. Limits are set on the $\tilde{\chi}_2^0$ and $\tilde{\chi}_1^\pm$ mass in Tchi1n2E, Tchi1n2F and Tchi1n2Ga. See their Fig. 16.	
• • •						We do not use the following data for averages, fits, limits, etc. • • •		
> 310	95	63	AAD	20AN	ATLS	$2\gamma + E_T$, Tchi1n2E, $m_{\tilde{\chi}_1^0} = 0$ GeV	13	AAD 21E searched in 139 fb ⁻¹ of pp collisions at $\sqrt{s} = 13$ TeV for production of wino-like $\tilde{\chi}_1^\pm \tilde{\chi}_1^\pm$ and $\tilde{\chi}_1^\pm \tilde{\chi}_1^0$, followed by the RPV decay of $\tilde{\chi}_1^\pm$ into $Z\ell$, $H\ell$ or $W\nu$ and of $\tilde{\chi}_1^0$ into $Z\nu$, $H\nu$ or $W\ell$, in events with three leptons, looking for $Z\ell$ resonances. No significant excess above the Standard Model predictions is observed. Limits are set on the common $m_{\tilde{\chi}_1^\pm}/m_{\tilde{\chi}_1^0}$ mass in the TwinoLSPRPV simplified model, as a function of the common $\tilde{\chi}_1^\pm/\tilde{\chi}_1^0$ branching fraction to a Z boson. See Figure 9.
> 570	95	64	KHACHATRY...16AA	CMS	$\geq 1\gamma + \text{jets} + E_T$, Tchi1chi1A			
> 680	95	64	KHACHATRY...16AA	CMS	$\geq 1\gamma + \text{jets} + E_T$, Tchi1n1A			
> 710	95	64	KHACHATRY...16AA	CMS	$\geq 1\gamma + \text{jets} + E_T$, GGM, $\tilde{\chi}_2^0 \tilde{\chi}_1^\pm$ pair production, wino-like NLSP			
>1000	95	65	KHACHATRY...16R	CMS	$\geq 1\gamma + 1e$ or $\mu + E_T$, Tglu1F, $m_{\tilde{\chi}_1^\pm} = m_{\tilde{\chi}_2^0} > 200$ GeV			
> 307	95	66	KHACHATRY...16Y	CMS	1,2 soft $\ell^\pm + \text{jets} + E_T$, Tchi1n2A, $m_{\tilde{\chi}_1^\pm} - m_{\tilde{\chi}_1^0} = 20$ GeV			
> 410	95	67	AAD	14AV	ATLS	$\geq 2\tau + E_T$, direct $\tilde{\chi}_1^\pm \tilde{\chi}_2^0$, $\tilde{\chi}_1^\pm \tilde{\chi}_1^\mp$ production, $m_{\tilde{\chi}_2^0} = m_{\tilde{\chi}_1^\pm}$, $m_{\tilde{\chi}_1^0} = 0$ GeV		
> 345	95	68	AAD	14AV	ATLS	$\geq 2\tau + E_T$, direct $\tilde{\chi}_1^\pm \tilde{\chi}_1^\mp$ production, $m_{\tilde{\chi}_1^0} = 0$ GeV		
none 100–105, 120–135, 145–160	95	69	AAD	14G	ATLS	$\tilde{\chi}_1^\pm \tilde{\chi}_1^\mp \rightarrow W^\pm \tilde{\chi}_1^0 W^- \tilde{\chi}_1^0$, simplified model, $m_{\tilde{\chi}_1^0} = 0$ GeV		
none 140–465	95	69	AAD	14G	ATLS	$\tilde{\chi}_1^\pm \tilde{\chi}_1^\mp \rightarrow \ell^\pm \nu \tilde{\chi}_1^0 \ell^- \bar{\nu} \tilde{\chi}_1^0$, simplified model, $m_{\tilde{\chi}_1^0} = 0$ GeV		
none 180–355	95	69	AAD	14G	ATLS	$\tilde{\chi}_1^\pm \tilde{\chi}_2^0 \rightarrow W \tilde{\chi}_1^0 Z \tilde{\chi}_1^0$, simplified model, $m_{\tilde{\chi}_1^\pm} = m_{\tilde{\chi}_2^0}$, $m_{\tilde{\chi}_1^0} = 0$ GeV		
> 168	95	70	AALTONEN	14	CDF	$3\ell^\pm + E_T$, $\tilde{\chi}_1^\pm \rightarrow \ell\nu \tilde{\chi}_1^0$, mSUGRA with $m_0=60$ GeV		
		71	KHACHATRY...14i	CMS	$\tilde{\chi}_1^\pm \rightarrow W \tilde{\chi}_1^0$, $\ell\nu$, $\bar{\ell}\nu$, simplified model			
		72	AALTONEN	13Q	CDF	$\tilde{\chi}_1^\pm \rightarrow \tau X$, simplified gravity- and gauge-mediated models		
		73	AAD	12AS	ATLS	$3\ell^\pm + E_T$, pMSSM		
		74	AAD	12T	ATLS	$\ell^\pm \ell^\mp + E_T$, $\ell^\pm \ell^\pm + E_T$, $pp \rightarrow \tilde{\chi}_1^\pm \tilde{\chi}_2^0$		
		75	CHATRCHYAN 11B	CMS	$\tilde{W}^0 \rightarrow \gamma \tilde{G}, \tilde{W}^\pm \rightarrow \ell^\pm \tilde{G}, \text{GMSB}$			
> 163	95	76	CHATRCHYAN 11V	CMS	$\tan\beta=3$, $m_0=60$ GeV, $A_0=0$, $\mu > 0$			

¹ AAD 23AE searched in 139 fb⁻¹ of pp collisions at $\sqrt{s} = 13$ TeV for events with 2 ℓ with same flavour and opposite sign, plus jets and E_T , defining signal region with the dilepton invariant mass both on- and off-shell with respect to the Z boson. No significant excess above the Standard Model predictions is observed. Limits are set on models of strong and electroweak production. For electroweak production, limits are placed on production of mass-degenerate, wino-like $\tilde{\chi}_2^0 \tilde{\chi}_1^\pm$ with $\tilde{\chi}_2^0 \rightarrow Z \tilde{\chi}_1^0$ and $\tilde{\chi}_1^\pm \rightarrow W \tilde{\chi}_1^0$, see figure 15.

² AAD 23Ci searched in 139 fb⁻¹ of pp collisions for events containing 1 ℓ (e or μ), jets, and E_T . Final states consistent with the production of a diboson system plus E_T were identified also by making use of large- R jet tagging techniques. No excess on top of the Standard Model background was observed. Limits were set on the production of $\tilde{\chi}_1^\pm \tilde{\chi}_2^0$ and $\tilde{\chi}_1^\pm \tilde{\chi}_1^\pm$ (assuming wino cross sections) decaying to $WZ \tilde{\chi}_1^0 \tilde{\chi}_1^0$ or $WW \tilde{\chi}_1^0 \tilde{\chi}_1^0$. See their figure 9.

³ AAD 23Ci searched in 139 fb⁻¹ of pp collisions for events containing 1 ℓ (e or μ), jets, and E_T . Final states consistent with the production of a boson + Higgs system plus E_T were identified via a BDT. No excess on top of the Standard Model background was observed. Limits were set on the production of degenerate $\tilde{\chi}_1^\pm \tilde{\chi}_2^0$ (assuming wino cross sections) decaying into $Wh \tilde{\chi}_1^0 \tilde{\chi}_1^0$. See their figure 10.

¹² AAD 21Bg searched in 139 fb⁻¹ of pp collisions at $\sqrt{s} = 13$ TeV for pair production $\tilde{\chi}_2^0 \tilde{\chi}_1^\pm$ in final states with three leptons, with and without assuming the presence of a $Z \rightarrow \ell\ell$ decay. No significant excess above the Standard Model predictions is observed. Limits are set on the $\tilde{\chi}_2^0$ and $\tilde{\chi}_1^\pm$ mass in Tchi1n2E, Tchi1n2F and Tchi1n2Ga. See their Fig. 16.

¹³ AAD 21E searched in 139 fb⁻¹ of pp collisions at $\sqrt{s} = 13$ TeV for production of wino-like $\tilde{\chi}_1^\pm \tilde{\chi}_1^\pm$ and $\tilde{\chi}_1^\pm \tilde{\chi}_1^0$, followed by the RPV decay of $\tilde{\chi}_1^\pm$ into $Z\ell$, $H\ell$ or $W\nu$ and of $\tilde{\chi}_1^0$ into $Z\nu$, $H\nu$ or $W\ell$, in events with three leptons, looking for $Z\ell$ resonances. No significant excess above the Standard Model predictions is observed. Limits are set on the common $m_{\tilde{\chi}_1^\pm}/m_{\tilde{\chi}_1^0}$ mass in the TwinoLSPRPV simplified model, as a function of the common $\tilde{\chi}_1^\pm/\tilde{\chi}_1^0$ branching fraction to a Z boson. See Figure 9.

¹⁴ AAD 21v searched in 139 fb⁻¹ of pp collisions at $\sqrt{s} = 13$ TeV for supersymmetry in events with four or more leptons (electrons, muons and tau-leptons). No significant excess above the Standard Model expectations is observed. Limits are set on Tchi1n12-GGM, and RPV models similar to Tchi1n2I, Tglu1A (with $q = u, d, s, c, b$, with equal branching fractions), and $\tilde{\ell}_L/\tilde{\nu} \rightarrow \ell/\nu \tilde{\chi}_1^0$ (mass-degenerate $\tilde{\ell}_L$ and $\tilde{\nu}$ of all 3 generations), all with $\tilde{\chi}_1^0 \rightarrow \ell^\pm \ell^\mp \nu$ via λ_{12k} or λ_{i33} (where $i, k \in \{1, 2\}$), see their Figure 11.

Searches Particle Listings

Supersymmetric Particle Searches

- 15 SIRUNYAN 21M searched in 137 fb^{-1} of pp collisions at $\sqrt{s} = 13 \text{ TeV}$ for supersymmetry in events with two opposite-sign same-flavor leptons (electrons, muons) and \cancel{E}_T . No significant excess above the Standard Model expectations is observed. Limits are set on the gluino mass in the simplified model Tglu4C, see their Figure 10, on the $\tilde{\chi}_2^0$ and $\tilde{\chi}_1^\pm$ mass in Tchi1n2Fa, see their Figure 11, on the $\tilde{\chi}_1^0$ mass in Tn1n1C and Tn1n1B for $m_{\tilde{\chi}_2^0} = m_{\tilde{\chi}_1^\pm} = m_{\tilde{\chi}_1^0}$, see their Figure 12. Limits are also set on the light squark mass for the simplified model Tsqk2A, on the sbottom mass in Tsb0t3, see their Figure 13, and on the slepton mass in direct electroweak pair production of mass-degenerate left- and right-handed sleptons (selectrons and smuons), see their Figure 14.
- 16 TUMASYAN 21c searched in 137 fb^{-1} of pp collisions at $\sqrt{s} = 13 \text{ TeV}$ for supersymmetry in events with with one lepton, a Higgs boson decaying to a pair of bottom quarks, and large \cancel{E}_T . No significant excess above the Standard Model expectations is observed. Lower limits are set on the masses of $\tilde{\chi}_2^0$ and $\tilde{\chi}_1^\pm$ in the simplified model Tchi1n2E, see their Figure 6.
- 17 AAD 20AN searched in 139 fb^{-1} of pp collisions at $\sqrt{s} = 13 \text{ TeV}$ for events with two photons and missing transverse momentum. Events are further categorised in terms of lepton or jet multiplicity. No significant excess over the expected background is observed. Limits at 95% C.L. are set on the Higgsino mass in the T1n1n1A simplified model, see their Figure 11.
- 18 AAD 20I reported on ATLAS searches for electroweak production in models with compressed mass spectra as Tchi1n2Fa. A dataset of pp collisions at $\sqrt{s} = 13 \text{ TeV}$ corresponding to an integrated luminosity of 139 fb^{-1} was used. Events with \cancel{E}_T , two same-flavour, opposite-charge, low-transverse-momentum leptons, and jets from initial-state radiation or characteristic of vector-boson fusion production are selected. Constraints at 95% C.L. are placed on the mass of the $\tilde{\chi}_1^\pm$ (degenerate with $\tilde{\chi}_2^0$) at 240 GeV for a mass splitting between $\tilde{\chi}_1^\pm$ and $\tilde{\chi}_1^0$ of 7 GeV and extend down to a mass splitting of 1.5 GeV at the LEP chargino mass limit of 92.4 GeV. See their Fig. 14(b,c).
- 19 AAD 20K reported on a search for electroweak production in models with mass splittings near the electroweak scale as Tchi1n2F and exploiting three-lepton final state events with an emulated recursive jigsaw reconstruction method. The analysis uses a dataset of pp collisions at $\sqrt{s} = 13 \text{ TeV}$ corresponding to an integrated luminosity of 139 fb^{-1} . Exclusion limits at 95% C.L. are derived on next-to-lightest neutralinos and charginos with masses up to 345 GeV for a massless lightest neutralino, see their Fig. 7.
- 20 AAD 20O reported on a search for electroweak production in models with charginos and sleptons decaying into final states with exactly two oppositely charged leptons and missing transverse momentum. A dataset of pp collisions at $\sqrt{s} = 13 \text{ TeV}$ corresponding to an integrated luminosity of 139 fb^{-1} was used. Exclusion limits at 95% C.L. are derived on $m_{\tilde{\chi}_1^\pm}$ decaying according to the Tchi1chi1H simplified model. Chargino masses up to 420 GeV are excluded for a massless lightest neutralino, see their Fig. 7(a).
- 21 AAD 20Q reported on a search for electroweak production in models with charginos and sleptons decaying into final states with exactly two oppositely charged leptons and missing transverse momentum. A dataset of pp collisions at $\sqrt{s} = 13 \text{ TeV}$ corresponding to an integrated luminosity of 139 fb^{-1} was used. Exclusion limits at 95% C.L. are derived on $m_{\tilde{\chi}_1^\pm}$ decaying according to the Tchi1chi1C simplified model. Chargino masses up to 1000 GeV are excluded for a massless lightest neutralino, see their Fig. 7(b).
- 22 AAD 20R searched for electroweak production in the model Tchi1n2E, selecting events with a pair of b -tagged jets consistent with those from a Higgs boson decay, either an electron or a muon from the W boson decay and \cancel{E}_T . The analysis uses a dataset of pp collisions at $\sqrt{s} = 13 \text{ TeV}$ corresponding to an integrated luminosity of 139 fb^{-1} . Exclusion limits at 95% C.L. are derived on next-to-lightest neutralinos and charginos with masses up to 740 GeV for a massless lightest neutralino, assuming pure wino cross-sections. See their Fig. 6.
- 23 SIRUNYAN 20AU searched in 77.2 fb^{-1} of pp collisions at $\sqrt{s} = 13 \text{ TeV}$ for events containing one soft, hadronically decaying tau lepton, one energetic jet from initial-state radiation, and large \cancel{E}_T . No excess over the expected background is observed. Limits are derived on the wino mass in the Tchi1n2D simplified model, see their Figure 2.
- 24 SIRUNYAN 20B searched in 35.9 fb^{-1} of pp collisions at $\sqrt{s} = 13 \text{ TeV}$ for events with at least one photon and large \cancel{E}_T . No significant excess above the Standard Model expectations is observed. Limits are set on chargino masses in a general gauge-mediated SUSY breaking (GGM) scenario Tchi1n12-GGM, see Figure 4. Limits are also set on the NLSP mass in the Tchi1chi1F and Tchi1chi1G simplified models, see their Figure 5. Finally, limits are set on the gluino mass in the Tglu4A simplified model, see Figure 6.
- 25 AABOUD 19AU searched in 36.1 fb^{-1} of pp collisions at $\sqrt{s} = 13 \text{ TeV}$ for direct electroweak production of charginos and next-to-lightest neutralinos decaying into lightest neutralinos and a W , and a Higgs boson, respectively. Fully hadronic, semileptonic, diphoton, and multilepton (electrons, muons) final states with missing transverse momentum are considered in this search. Observations are consistent with the Standard Model expectations, and 95% confidence-level limits of up to 680 GeV on the chargino/next-to-lightest neutralino masses are set (Tchi1n2E model). See their Figure 14 for an overlay of exclusion contours from all searches.
- 26 SIRUNYAN 19BU searched for pair production of gauginos via vector boson fusion assuming the gaugino spectrum is compressed, in 35.9 fb^{-1} of pp collisions at $\sqrt{s} = 13 \text{ TeV}$. The final states explored included zero leptons plus two jets, one lepton plus two jets, and one hadronic tau plus two jets. A similar bound is obtained in the light slepton limit.
- 27 SIRUNYAN 19CI searched in 77.5 fb^{-1} of pp collisions at $\sqrt{s} = 13 \text{ TeV}$ for events with one or more high-momentum Higgs bosons, decaying to pairs of photons, jets and \cancel{E}_T . No significant excess above the Standard Model expectations is observed. Limits are set on the sbottom mass in the Tsb0t4 simplified model, see Figure 3, and on the wino mass in the Tchi1n2E simplified model, see their Figure 4. Limits are also set on the higgsino mass in the Tn1n1A and Tn1n1B simplified models, see their Figure 5.
- 28 SIRUNYAN 19K searched in 35.9 fb^{-1} of pp collisions at $\sqrt{s} = 13 \text{ TeV}$ for events with a photon, an electron or muon, and large \cancel{E}_T . No significant excess above the Standard Model expectations is observed. In the framework of GMSB, limits are set on the chargino and neutralino mass in the Tchi1n1A simplified model, see their Figure 6. Limits are also set on the gluino mass in the Tglu4A simplified model, and on the squark mass in the Tsqk4A simplified model, see their Figure 7.
- 29 AABOUD 18AY searched in 36.1 fb^{-1} of pp collisions at $\sqrt{s} = 13 \text{ TeV}$ for direct electroweak production of charginos as in Tchi1chi1D models in events characterised by the presence of at least two hadronically decaying tau leptons and large missing transverse energy. No significant deviation from the expected SM background is observed. In the Tchi1chi1D model, assuming decays via intermediate $\tilde{\tau}_L$, the observed limits rule out $\tilde{\chi}_1^\pm$ masses up to 630 GeV for a massless $\tilde{\chi}_1^0$. See their Fig.7 (left). Interpretations are also provided in Fig 8 (top) for different assumptions on the ratio between $m_{\tilde{\tau}}$ and $m_{\tilde{\chi}_1^\pm} + m_{\tilde{\chi}_1^0}$.
- 30 AABOUD 18AY searched in 36.1 fb^{-1} of pp collisions at $\sqrt{s} = 13 \text{ TeV}$ for direct electroweak production of charginos and neutralinos as in Tchi1n2D models, in events characterised by the presence of at least two hadronically decaying tau leptons and large missing transverse energy. No significant deviation from the expected SM background is observed. Assuming decays via intermediate $\tilde{\tau}_L$ and $m_{\tilde{\chi}_1^\pm} = m_{\tilde{\chi}_1^0}$, the observed limits rule out $\tilde{\chi}_1^\pm$ masses up to 760 GeV for a massless $\tilde{\chi}_1^0$. See their Fig.7 (right). Interpretations are also provided in Fig 8 (bottom) for different assumptions on the ratio between $m_{\tilde{\tau}}$ and $m_{\tilde{\chi}_1^\pm} + m_{\tilde{\chi}_1^0}$.
- 31 AABOUD 18BT searched in 36.1 fb^{-1} of pp collisions at $\sqrt{s} = 13 \text{ TeV}$ for direct electroweak production of charginos, chargino and next-to-lightest neutralinos and sleptons in events with two or three leptons (electrons or muons), with or without jets and large missing transverse energy. No significant excess above the Standard Model expectations is observed. Limits are set on the chargino mass up to 750 GeV for massless neutralinos in the Tchi1chi1C simplified model exploiting $2\ell + 0$ jets signatures, see their Figure 8(a).
- 32 AABOUD 18BT searched in 36.1 fb^{-1} of pp collisions at $\sqrt{s} = 13 \text{ TeV}$ for direct electroweak production of charginos, chargino and next-to-lightest neutralinos and sleptons in events with two or three leptons (electrons or muons), with or without jets, and large missing transverse energy. No significant excess above the Standard Model expectations is observed. Limits are set on the chargino mass up to 1100 GeV for massless neutralinos in the Tchi1n2C simplified model exploiting 3ℓ signature, see their Figure 8(c).
- 33 AABOUD 18BT searched in 36.1 fb^{-1} of pp collisions at $\sqrt{s} = 13 \text{ TeV}$ for direct electroweak production of charginos, chargino and next-to-lightest neutralinos and sleptons in events with two or three leptons (electrons or muons), with or without jets, and large missing transverse energy. No significant excess above the Standard Model expectations is observed. Limits are set on the chargino mass up to 580 GeV for massless neutralinos in the Tchi1n2F simplified model exploiting $2\ell + 2$ jets and 3ℓ signatures, see their Figure 8(d).
- 34 AABOUD 18CK searched for events with at least 3 b -jets and large missing transverse energy in two datasets of pp collisions at $\sqrt{s} = 13 \text{ TeV}$ of 36.1 fb^{-1} and 24.3 fb^{-1} depending on the trigger requirements. The analyses aimed to reconstruct two Higgs bosons decaying to pairs of b -quarks. No significant excess above the Standard Model expectations is observed. Limits are set on the Higgsino mass in the T1n1n1A simplified model, see their Figure 15(a). Constraints are also presented as a function of the BR of Higgsino decaying into a higgs boson and a gravitino, see their Figure 15(b).
- 35 AABOUD 18CO searched in 36.1 fb^{-1} of pp collisions at $\sqrt{s} = 13 \text{ TeV}$ for direct electroweak production of mass-degenerate charginos and next-to-lightest neutralinos in events with two or three leptons (electrons or muons), with or without jets, and large missing transverse energy. The search channels are based on recursive jigsaw reconstruction. Limits are set on the chargino mass up to 600 GeV for massless neutralinos in the Tchi1n2F simplified model exploiting the statistical combination of $2\ell + 2$ jets and 3ℓ channels. Chargino masses below 220 GeV are not excluded due to an excess of events above the SM prediction in the dedicated regions. See their Figure 13(d).
- 36 AABOUD 18R searched in 36.1 fb^{-1} of pp collisions at $\sqrt{s} = 13 \text{ TeV}$ for electroweak production in scenarios with compressed mass spectra in final states with two low-momentum leptons and missing transverse momentum. The data are found to be consistent with the SM prediction. Results are interpreted in Tchi1n2G wino models and $\tilde{\chi}_1^\pm$ masses are excluded up to 175 GeV for $m_{\tilde{\chi}_1^\pm} - m_{\tilde{\chi}_1^0} = 10 \text{ GeV}$. The exclusion limits extend down to mass splittings of 2 GeV, see their Fig. 10 (bottom).
- 37 AABOUD 18R searched in 36.1 fb^{-1} of pp collisions at $\sqrt{s} = 13 \text{ TeV}$ for electroweak production in scenarios with compressed mass spectra in final states with two low-momentum leptons and missing transverse momentum. The data are found to be consistent with the SM prediction. Results are interpreted in Tchi1n2G higgsino models and $\tilde{\chi}_1^\pm$ masses are excluded up to 145 GeV for $m_{\tilde{\chi}_1^\pm} - m_{\tilde{\chi}_1^0} = 5 \text{ GeV}$. The exclusion limits extend down to mass splittings of 2.5 GeV, see their Fig. 10 (top).
- 38 AABOUD 18U searched in 36.1 fb^{-1} of pp collisions at $\sqrt{s} = 13 \text{ TeV}$ in events with at least one isolated photon, possibly jets and significant transverse momentum targeting generalised models of gauge-mediated SUSY breaking. No significant excess of events is observed above the SM prediction. Results of the diphoton channel are interpreted in terms of lower limits on the masses of gauginos Tchi1chi1A models, which reach as high as 1.3 TeV. Gaugino masses below 1060 GeV are excluded for any NLSP mass, see their Fig. 10.
- 39 AABOUD 18Z searched in 36.1 fb^{-1} of pp collisions at $\sqrt{s} = 13 \text{ TeV}$ for events containing four or more charged leptons (electrons, muons and up to two hadronically decaying taus). No significant deviation from the expected SM background is observed. Limits are set on the Higgsino mass in simplified models of general gauge mediated supersymmetry Tn1n1A/Tn1n1B/Tn1n1C, see their Figure 9. Limits are also set on the wino, slepton, sneutrino and gluino mass in a simplified model of NLSP pair production with R-parity violating decays of the LSP via λ_{12k} or λ_{133} to charged leptons, see their Figures 7, 8.
- 40 SIRUNYAN 18AA searched in 35.9 fb^{-1} of pp collisions at $\sqrt{s} = 13 \text{ TeV}$ for events with at least one photon and large \cancel{E}_T . No significant excess above the Standard Model expectations is observed. Limits are set on wino masses in a general gauge-mediated SUSY breaking (GGM) scenario with bino-like $\tilde{\chi}_1^0$ and wino-like $\tilde{\chi}_1^\pm$ and $\tilde{\chi}_2^0$, see Figure 7. Limits are also set on the NLSP mass in the Tchi1n1A and Tchi1chi1A simplified models, see their Figure 8. Finally, limits are set on the gluino mass in the Tglu4A and Tglu4B simplified models, see their Figure 9, and on the squark mass in the Tsqk4A and Tsqk4B simplified models, see their Figure 10.
- 41 SIRUNYAN 18AJ searched in 35.9 fb^{-1} of pp collisions at $\sqrt{s} = 13 \text{ TeV}$ for events containing two low-momentum, oppositely charged leptons (electrons or muons) and \cancel{E}_T . No excess over the expected background is observed. Limits are derived on the wino mass in the Tchi1n2F simplified model, see their Figure 5. Limits are also set on the stop mass in the Tstop10 simplified model, see their Figure 6. Finally, limits are set on the Higgsino mass in the Tchi1n2G simplified model, see Figure 8 and in the pMSSM, see Figure 7.
- 42 SIRUNYAN 18AO searched in 35.9 fb^{-1} of pp collisions at $\sqrt{s} = 13 \text{ TeV}$ for direct electroweak production of charginos and neutralinos in events with either two or more leptons (electrons or muons) of the same electric charge, or with three or more leptons, which can include up to two hadronically decaying tau leptons. No significant excess above the Standard Model expectations is observed. Limits are set on the chargino/neutralino mass in the Tchi1n2A, Tchi1n2H, Tchi1n2D, Tchi1n2E and Tchi1n2F simplified models,

- see their Figures 14, 15, 16, 17 and 18. Limits are also set on the higgsino mass in the Tn1n1A, Tn1n1B and Tn1n1C simplified models, see their Figure 19.
- 43 SIRUNYAN 18AP searched in 35.9 fb^{-1} of pp collisions at $\sqrt{s} = 13 \text{ TeV}$ for direct electroweak production of charginos and neutralinos by combining a number of previous and new searches. No significant excess above the Standard Model expectations is observed. Limits are set on the chargino/neutralino mass in the Tchi1n2E, Tchi1n2F and Tchi1n2I simplified models, see their Figures 7, 8, 9 and 10. Limits are also set on the higgsino mass in the Tn1n1A, Tn1n1B and Tn1n1C simplified models, see their Figure 11, 12, 13 and 14.
- 44 SIRUNYAN 18AR searched in 35.9 fb^{-1} of pp collisions at $\sqrt{s} = 13 \text{ TeV}$ for events containing two opposite-charge, same-flavour leptons (electrons or muons), jets and \cancel{E}_T . No significant excess above the Standard Model expectations is observed. Limits are set on the gluino mass in the Tglu4C simplified model, see their Figure 7. Limits are also set on the chargino/neutralino mass in the Tchi1n2F simplified models, see their Figure 8, and on the higgsino mass in the Tn1n1B and Tn1n1C simplified models, see their Figure 9. Finally, limits are set on the sbottom mass in the Tsb0t3 simplified model, see their Figure 10.
- 45 SIRUNYAN 18DN searched in 35.9 fb^{-1} of pp collisions at $\sqrt{s} = 13 \text{ TeV}$ for direct electroweak production of charginos and for pair production of top squarks in events with two leptons (electrons or muons) of the opposite electric charge. No significant excess above the Standard Model expectations is observed. Limits are set on the chargino mass in the Tchi1chi1C and Tchi1chi1E simplified models, see their Figure 8. Limits are also set on the stop mass in the Tstop1 and Tstop2 simplified models, see their Figure 9.
- 46 SIRUNYAN 18DP searched in 35.9 fb^{-1} of pp collisions at $\sqrt{s} = 13 \text{ TeV}$ for direct electroweak production of charginos and neutralinos or of chargino pairs in events with a tau lepton pair and significant missing transverse momentum. Both hadronic and leptonic decay modes are considered for the tau lepton. No significant excess above the Standard Model expectations is observed. Limits are set on the chargino mass in the Tchi1chi1D and Tchi1n2 simplified models, see their Figures 14 and 15. Also, excluded stau pair production cross sections are shown in Figures 11, 12, and 13.
- 47 SIRUNYAN 18X searched in 35.9 fb^{-1} of pp collisions at $\sqrt{s} = 13 \text{ TeV}$ for events with one or more high-momentum Higgs bosons, decaying to pairs of photons, jets and \cancel{E}_T . The razor variables (M_R and R^2) are used to categorise the events. No significant excess above the Standard Model expectations is observed. Limits are set on the sbottom mass in the Tsb0t4 simplified model and on the wino mass in the Tchi1n2E simplified model, see their Figure 5. Limits are also set on the higgsino mass in the Tn1n1A and Tn1n1B simplified models, see their Figure 6.
- 48 KHACHATRYAN 17L searched in about 19 fb^{-1} of pp collisions at $\sqrt{s} = 8 \text{ TeV}$ for events with two τ (at least one decaying hadronically) and \cancel{E}_T . In the Tchi1chi1C model, assuming decays via intermediate $\tilde{\tau}$ or ν_τ with equivalent mass, the observed limits rule out $\tilde{\chi}_1^\pm$ masses up to 420 GeV for a branching $\tilde{\chi}_1^0$. See their Fig. 5.
- 49 SIRUNYAN 17AW searched in 35.9 fb^{-1} of pp collisions at $\sqrt{s} = 13 \text{ TeV}$ for events with a charged lepton (electron or muon), two jets identified as originating from a b -quark, and large \cancel{E}_T . No significant excess above the Standard Model expectations is observed. Limits are set on the mass of the chargino and the next-to-lightest neutralino in the Tchi1n2E simplified model, see their Figure 6.
- 50 AAD 16AA summarized and extended ATLAS searches for electroweak supersymmetry in final states containing several charged leptons, \cancel{E}_T , with or without hadronic jets, in 20 fb^{-1} of pp collisions at $\sqrt{s} = 8 \text{ TeV}$. The paper reports the results of new interpretations and statistical combinations of previously published analyses, as well as new analyses. Exclusion limits at 95% C.L. are set on the $\tilde{\chi}_1^\pm$ mass in the Tchi1chi1B and Tchi1chi1C simplified models. See their Fig. 13.
- 51 AAD 16AA summarized and extended ATLAS searches for electroweak supersymmetry in final states containing several charged leptons, \cancel{E}_T , with or without hadronic jets, in 20 fb^{-1} of pp collisions at $\sqrt{s} = 8 \text{ TeV}$. The paper reports the results of new interpretations and statistical combinations of previously published analyses, as well as new analyses. Exclusion limits at 95% C.L. are set on mass-degenerate $\tilde{\chi}_1^\pm$ and $\tilde{\chi}_2^0$ masses in the Tchi1n2B, Tchi1n2C, and Tchi1n2D simplified models. See their Figs. 16, 17, and 18. Interpretations in phenomenological-MSSM, two-parameter Non Universal Higgs Masses (NUHM2), and gauge-mediated symmetry breaking (GMSB) models are also given in their Figs. 20, 21 and 22.
- 52 KHACHATRYAN 16R searched in 19.7 fb^{-1} of pp collisions at $\sqrt{s} = 8 \text{ TeV}$ for events with one or more photons, one electron or muon, and \cancel{E}_T . No significant excess above the Standard Model expectations is observed. Limits are set on wino masses in a general gauge-mediated SUSY breaking model (GGM), for a wino-like neutralino NLSP scenario, see Fig. 5. Limits are also set in the Tglu1D and Tchi1n1A simplified models, see Fig. 6. The Tchi1n1A limit is reduced to 340 GeV for a branching ratio reduced by the weak mixing angle.
- 53 AAD 15BA searched in 20.3 fb^{-1} of pp collisions at $\sqrt{s} = 8 \text{ TeV}$ for electroweak production of charginos and neutralinos decaying to a final state containing a W boson and a 125 GeV Higgs boson, plus missing transverse momentum. No excess beyond the Standard Model expectation is observed. Exclusion limits are derived in simplified models of direct chargino and next-to-lightest neutralino production, with the decays $\tilde{\chi}_1^\pm \rightarrow W^\pm \tilde{\chi}_1^0$ and $\tilde{\chi}_2^0 \rightarrow H \tilde{\chi}_1^0$ having 100% branching fraction, see Fig. 8. A combination of the multiple final states for the Higgs decay yields the best limits (Fig. 8d).
- 54 AAD 15CA searched in 20.3 fb^{-1} of pp collisions at $\sqrt{s} = 8 \text{ TeV}$ for events with one or more photons and \cancel{E}_T , with or without leptons (e, μ). No significant excess above the Standard Model expectations is observed. Limits are set on wino masses in the general gauge-mediated SUSY breaking model (GGM), for wino-like NLSP, see Fig. 9, 12.
- 55 AAD 14X searched in 20.3 fb^{-1} of pp collisions at $\sqrt{s} = 8 \text{ TeV}$ for electroweak production of charginos and neutralinos decaying to a final state with three leptons and missing transverse momentum. No excess beyond the Standard Model expectation is observed. Exclusion limits are derived in simplified models of direct chargino and next-to-lightest neutralino production, with decays to the lightest neutralino via either all three generations of leptons, staus only, gauge bosons, or Higgs bosons, see Fig. 7. An interpretation in the pMSSM is also given, see Fig. 8.
- 56 AAD 14X searched in 20.3 fb^{-1} of pp collisions at $\sqrt{s} = 8 \text{ TeV}$ for events with at least four leptons (electrons, muons, taus) in the final state. No significant excess above the Standard Model expectations is observed. Limits are set on the wino-like chargino mass in an R-parity violating simplified model where the decay $\tilde{\chi}_1^\pm \rightarrow W^{(*)} \tilde{\chi}_1^0$, with $\tilde{\chi}_1^0 \rightarrow \ell^\pm \ell^\mp \nu$, takes place with a branching ratio of 100%, see Fig. 8.
- 57 KHACHATRYAN 14L searched in 19.5 fb^{-1} of pp collisions at $\sqrt{s} = 8 \text{ TeV}$ for evidence of chargino-neutralino $\tilde{\chi}_1^\pm \tilde{\chi}_2^0$ pair production with Higgs or W -bosons in the decay chain, leading to HW final states with missing transverse energy. The decays of a Higgs boson to a photon pair are considered in conjunction with hadronic and leptonic decay modes of the W bosons. No significant excesses over the expected SM backgrounds are observed. The results are interpreted in the context of simplified models where the decays $\tilde{\chi}_2^0 \rightarrow H \tilde{\chi}_1^0$ and $\tilde{\chi}_1^\pm \rightarrow W^\pm \tilde{\chi}_1^0$ take place 100% of the time, see Figs. 22–23.
- 58 AAD 13 searched in 4.7 fb^{-1} of pp collisions at $\sqrt{s} = 7 \text{ TeV}$ for charginos and neutralinos decaying to a final state with three leptons (e and μ) and missing transverse energy. No excess beyond the Standard Model expectation is observed. Exclusion limits are derived in the phenomenological MSSM, see Fig. 2 and 3, and in simplified models, see Fig. 4. For the simplified models with intermediate slepton decays, degenerate $\tilde{\chi}_1^\pm$ and $\tilde{\chi}_2^0$ masses up to 500 GeV are excluded at 95% C.L. for very large mass differences with the $\tilde{\chi}_1^0$. Supersedes AAD 12As.
- 59 AAD 13B searched in 4.7 fb^{-1} of pp collisions at $\sqrt{s} = 7 \text{ TeV}$ for gauginos decaying to a final state with two leptons (e and μ) and missing transverse energy. No excess beyond the Standard Model expectation is observed. Limits are derived in a simplified model of wino-like chargino pair production, where the chargino always decays to the lightest neutralino via an intermediate on-shell charged slepton, see Fig. 2(b). Chargino masses between 110 and 340 GeV are excluded at 95% C.L. for $m_{\tilde{\chi}_1^0} = 10 \text{ GeV}$. Exclusion limits are also derived in the phenomenological MSSM, see Fig. 3.
- 60 AAD 12CT searched in 4.7 fb^{-1} of pp collisions at $\sqrt{s} = 7 \text{ TeV}$ for events containing four or more leptons (electrons or muons) and either moderate values of missing transverse momentum or large effective mass. No significant excess is found in the data. Limits are presented in a simplified model of R-parity violating supersymmetry in which charginos are pair-produced and then decay into a W -boson and a $\tilde{\chi}_1^0$, which in turn decays through an RPV coupling into two charged leptons ($e^\pm e^\mp$ or $e^\pm \mu^\mp$) and a neutrino. In this model, chargino masses up to 540 GeV are excluded at 95% C.L. for $m_{\tilde{\chi}_1^0}$ above 300 GeV, see Fig. 3a. The limit deteriorates for lighter $\tilde{\chi}_1^0$. Limits are also set in an R-parity violating mSUGRA model, see Fig. 3b.
- 61 KHACHATRYAN 12BJ searched in 4.98 fb^{-1} of pp collisions at $\sqrt{s} = 7 \text{ TeV}$ for direct electroweak production of charginos and neutralinos in events with at least two leptons, jets and missing transverse momentum. No significant excesses over the expected SM backgrounds are observed and 95% C.L. limits on the production cross section of $\tilde{\chi}_1^\pm \tilde{\chi}_2^0$ pair production were set in a number of simplified models, see Figs. 7 to 12.
- 62 ABDALLAH 03M uses data from $\sqrt{s} = 192\text{--}208 \text{ GeV}$ to obtain limits in the framework of the MSSM with gaugino and sfermion mass universality at the GUT scale. An indirect limit on the mass of charginos is derived by constraining the MSSM parameter space by the results from direct searches for neutralinos (including cascade decays), for charginos and for sleptons. These limits are valid for values of $M_2 < 1 \text{ TeV}$, $|\mu| \leq 2 \text{ TeV}$ with the $\tilde{\chi}_1^0$ as LSP. Constraints from the Higgs search in the m_h^{max} scenario assuming $m_t = 174.3 \text{ GeV}$ are included. The quoted limit applies if there is no mixing in the third family or when $m_{\tilde{\tau}_1} - m_{\tilde{\chi}_1^0} > 6 \text{ GeV}$. If mixing is included the limit degrades to 90 GeV. See Fig. 43 for the mass limits as a function of $\tan\beta$. These limits update the results of ABREU 00w.
- 63 AAD 20AN searched in 139 fb^{-1} of pp collisions at $\sqrt{s} = 13 \text{ TeV}$ for events with two photons and missing transverse momentum. Events are further categorised in terms of lepton or jet multiplicity. No significant excess over the expected background is observed. Limits at 95% C.L. are derived in Tchi1n2E simplified models. Next-to-lightest neutralinos and charginos with masses up to 310 GeV for a massless lightest neutralino are excluded. See their Fig. 10.
- 64 KHACHATRYAN 16AA searched in 7.4 fb^{-1} of pp collisions at $\sqrt{s} = 8 \text{ TeV}$ for events with one or more photons, hadronic jets and \cancel{E}_T . No significant excess above the Standard Model expectations is observed. Limits are set on wino masses in the general gauge-mediated SUSY breaking model (GGM), for a wino-like neutralino NLSP scenario and with the wino mass fixed at 10 GeV above the bino mass, see Fig. 4. Limits are also set in the Tchi1chi1A and Tchi1n1A simplified models, see Fig. 3.
- 65 KHACHATRYAN 16R searched in 19.7 fb^{-1} of pp collisions at $\sqrt{s} = 8 \text{ TeV}$ for events with one or more photons, one electron or muon, and \cancel{E}_T . No significant excess above the Standard Model expectations is observed. Limits are also set in the Tglu1F simplified model, see Fig. 6.
- 66 KHACHATRYAN 16Y searched in 19.7 fb^{-1} of pp collisions at $\sqrt{s} = 8 \text{ TeV}$ for events with one or two soft isolated leptons, hadronic jets, and \cancel{E}_T . No significant excess above the Standard Model expectations is observed. Limits are set on the $\tilde{\chi}_1^\pm$ mass (which is degenerate with the $\tilde{\chi}_2^0$) in the Tchi1n2A simplified model, see Fig. 4.
- 67 AAD 14AV searched in 20.3 fb^{-1} of pp collisions at $\sqrt{s} = 8 \text{ TeV}$ for the direct production of charginos, neutralinos and staus in events containing at last two hadronically decaying τ -leptons, large missing transverse momentum and low jet activity. The quoted limit was derived for direct $\tilde{\chi}_1^\pm \tilde{\chi}_2^0$ and $\tilde{\chi}_1^\pm \tilde{\chi}_1^\mp$ production with $\tilde{\chi}_2^0 \rightarrow \tilde{\tau} \tau \rightarrow \tau \tau \tilde{\chi}_1^0$ and $\tilde{\chi}_1^\pm \rightarrow \tilde{\tau} \nu(\tilde{\nu}_\tau) \rightarrow \tau \nu \tilde{\chi}_1^0$, $m_{\tilde{\chi}_2^0} = m_{\tilde{\chi}_1^\pm}$, $m_{\tilde{\tau}} = 0.5 (m_{\tilde{\chi}_1^\pm} + m_{\tilde{\chi}_1^0})$, $m_{\tilde{\chi}_1^0} = 0 \text{ GeV}$. No excess over the expected SM background is observed. Exclusion limits are set in simplified models of $\tilde{\chi}_1^\pm \tilde{\chi}_1^\mp$ and $\tilde{\chi}_1^\pm \tilde{\chi}_2^0$ pair production, see their Figure 7. Upper limits on the cross section and signal strength for direct di-stau production are derived, see Figures 8 and 9. Also, limits are derived in a pMSSM model where the only light slepton is the $\tilde{\tau}_R$, see Figure 10.
- 68 AAD 14AV searched in 20.3 fb^{-1} of pp collisions at $\sqrt{s} = 8 \text{ TeV}$ for the direct production of charginos, neutralinos and staus in events containing at last two hadronically decaying τ -leptons, large missing transverse momentum and low jet activity. The quoted limit was derived for direct $\tilde{\chi}_1^\pm \tilde{\chi}_1^\mp$ production with $\tilde{\chi}_1^\pm \rightarrow \tilde{\tau} \nu(\tilde{\nu}_\tau) \rightarrow \tau \nu \tilde{\chi}_1^0$, $m_{\tilde{\tau}} = 0.5 (m_{\tilde{\chi}_1^\pm} + m_{\tilde{\chi}_1^0})$, $m_{\tilde{\chi}_1^0} = 0 \text{ GeV}$. No excess over the expected SM background is observed. Exclusion limits are set in simplified models of $\tilde{\chi}_1^\pm \tilde{\chi}_1^\mp$ and $\tilde{\chi}_1^\pm \tilde{\chi}_2^0$ pair production, see their Figure 7. Upper limits on the cross section and signal strength for direct di-stau production are derived, see Figures 8 and 9. Also, limits are derived in a pMSSM model where the only light slepton is the $\tilde{\tau}_R$, see Figure 10.
- 69 AAD 14G searched in 20.3 fb^{-1} of pp collisions at $\sqrt{s} = 8 \text{ TeV}$ for electroweak production of chargino pairs, or chargino-neutralino pairs, decaying to a final state with two leptons (e and μ) and missing transverse momentum. No excess beyond the Standard Model expectation is observed. Exclusion limits are derived in simplified models of chargino pair production, with chargino decays to the lightest neutralino via either sleptons or gauge bosons, see Fig. 5; or in simplified models of chargino and next-to-lightest neutralino

Searches Particle Listings

Supersymmetric Particle Searches

production, with decays to the lightest neutralino via gauge bosons, see Fig. 7. An interpretation in the pMSSM is also given, see Fig. 10.

- 70 AALTONEN 14 searched in 5.8 fb^{-1} of $p\bar{p}$ collisions at $\sqrt{s} = 1.96 \text{ TeV}$ for evidence of chargino and next-to-lightest neutralino associated production in final states consisting of three leptons (electrons, muons or taus) and large missing transverse momentum. The results are consistent with the Standard Model predictions within 1.85σ . Limits on the chargino mass are derived in an mSUGRA model with $m_0 = 60 \text{ GeV}$, $\tan\beta = 3$, $A_0 = 0$ and $\mu > 0$, see their Fig. 2.
- 71 KHACHATRYAN 14i searched in 19.5 fb^{-1} of pp collisions at $\sqrt{s} = 8 \text{ TeV}$ for electroweak production of chargino pairs decaying to a final state with opposite-sign lepton pairs (e or μ) and missing transverse momentum. No excess beyond the Standard Model expectation is observed. Exclusion limits are derived in simplified models, see Fig. 18.
- 72 AALTONEN 13Q searched in 6.0 fb^{-1} of $p\bar{p}$ collisions at $\sqrt{s} = 1.96 \text{ TeV}$ for evidence of chargino-neutralino associated production in like-sign dilepton final states. One lepton is identified as the hadronic decay of a tau lepton, while the other is an electron or muon. Good agreement with the Standard Model predictions is observed and limits are set on the chargino-neutralino cross section for simplified gravity- and gauge-mediated models, see their Figs. 2 and 3.
- 73 AAD 12As searched in 2.06 fb^{-1} of pp collisions at $\sqrt{s} = 7 \text{ TeV}$ for charginos and neutralinos decaying to a final state with three leptons (e and μ) and missing transverse energy. No excess beyond the Standard Model expectation is observed. Exclusion limits are derived in the phenomenological MSSM, see Fig. 2 (top), and in simplified models, see Fig. 2 (bottom).
- 74 AAD 12T looked in 1 fb^{-1} of pp collisions at $\sqrt{s} = 7 \text{ TeV}$ for the production of supersymmetric particles decaying into final states with missing transverse momentum and exactly two isolated leptons (e or μ). Opposite-sign and same-sign dilepton events were separately studied. Additionally, in opposite-sign events, a search was made for an excess of same-flavor over different-flavor lepton pairs. No excess over the expected background is observed and limits are placed on the effective production cross section of opposite-sign dilepton events with $E_{T\gamma} > 250 \text{ GeV}$ and on same-sign dilepton events with $E_{T\gamma} > 100 \text{ GeV}$. The latter limit is interpreted in a simplified electroweak gaugino production model as a lower chargino mass limit.
- 75 CHATRCHYAN 11B looked in 35 pb^{-1} of pp collisions at $\sqrt{s} = 7 \text{ TeV}$ for events with an isolated lepton (e or μ), a photon and $E_{T\gamma}$ which may arise in a generalized gauge mediated model from the decay of Wino-like NLSPs. No evidence for an excess over the expected background is observed. Limits are derived in the plane of squark/gluino mass versus Wino mass (see Fig. 4). Mass degeneracy of the produced squarks and gluinos is assumed.
- 76 CHATRCHYAN 11v looked in 35 pb^{-1} of pp collisions at $\sqrt{s} = 7 \text{ TeV}$ for events with ≥ 3 isolated leptons (e , μ or τ), with or without jets and $E_{T\gamma}$. No evidence for an excess over the expected background is observed. Limits are derived in the CMSSM ($m_0, m_{1/2}$) plane for $\tan\beta = 3$ (see Fig. 5).

Long-lived $\tilde{\chi}^\pm$ (Chargino) mass limit

Limits on charginos which leave the detector before decaying.

VALUE (GeV)	CL%	DOCUMENT ID	TECN	COMMENT
>1050	95	1 AAD	23G ATLS	$\tilde{\chi}^\pm \rightarrow \tilde{\chi}_1^0 \pi^\pm$, wino LSP, $\tau = 20 \text{ ns}$
>1050	95	1 AAD	23G ATLS	$\tilde{\chi}^\pm \rightarrow \tilde{\chi}_1^0 \pi^\pm$, wino LSP, stable
> 660	95	2 AAD	22U ATLS	$\tilde{\chi}^\pm \rightarrow \tilde{\chi}_1^0 \pi^\pm$, wino LSP, AMSB, $\tan\beta = 5, \mu > 0, \tau = 0.2 \text{ ns}$
> 860	95	2 AAD	22U ATLS	$\tilde{\chi}^\pm \rightarrow \tilde{\chi}_1^0 \pi^\pm$, wino LSP, AMSB, $\tan\beta = 5, \mu > 0, \tau = 1.5 \text{ ns}$
> 220	95	2 AAD	22U ATLS	$\tilde{\chi}^\pm \rightarrow \tilde{\chi}_1^0 \pi^\pm$, higgsino LSP, $\tau = 0.04 \text{ ns}$
> 710	95	2 AAD	22U ATLS	$\tilde{\chi}^\pm \rightarrow \tilde{\chi}_1^0 \pi^\pm$, higgsino LSP, $\tau = 1 \text{ ns}$
> 884	95	3 SIRUNYAN	20N CMS	$\tilde{\chi}^\pm \rightarrow \tilde{\chi}_1^0 \pi^\pm$, wino LSP, AMSB, $\tan\beta = 5, \mu > 0, \tau = 3 \text{ ns}$
> 474	95	3 SIRUNYAN	20N CMS	$\tilde{\chi}^\pm \rightarrow \tilde{\chi}_1^0 \pi^\pm$, wino LSP, AMSB, $\tan\beta = 5, \mu > 0, \tau = 0.2 \text{ ns}$
> 750	95	3 SIRUNYAN	20N CMS	$\tilde{\chi}^\pm \rightarrow \tilde{\chi}_1^0 \pi^\pm$, higgsino LSP, AMSB, $\tan\beta = 5, \mu > 0, \tau = 3 \text{ ns}$
> 175	95	3 SIRUNYAN	20N CMS	$\tilde{\chi}^\pm \rightarrow \tilde{\chi}_1^0 \pi^\pm$, higgsino LSP, AMSB, $\tan\beta = 5, \mu > 0, \tau = 0.05 \text{ ns}$
>1090	95	4 AABOUD	19AT ATLS	long-lived $\tilde{\chi}_1^\pm$ mAMSB
> 460	95	5 AABOUD	18As ATLS	$\tilde{\chi}^\pm \rightarrow \tilde{\chi}_1^0 \pi^\pm$, lifetime 0.2 ns, $m_{\tilde{\chi}^\pm} - m_{\tilde{\chi}_1^0} = 160 \text{ MeV}$
> 715	95	6 SIRUNYAN	18BR CMS	$\tilde{\chi}^\pm \rightarrow \tilde{\chi}_1^0 \pi^\pm$, AMSB, $\tan\beta = 5$ and $\mu > 0, \tau = 3 \text{ ns}$
> 695	95	6 SIRUNYAN	18BR CMS	$\tilde{\chi}^\pm \rightarrow \tilde{\chi}_1^0 \pi^\pm$, AMSB, $\tan\beta = 5$ and $\mu > 0, \tau = 7 \text{ ns}$
> 505	95	6 SIRUNYAN	18BR CMS	$\tilde{\chi}^\pm \rightarrow \tilde{\chi}_1^0 \pi^\pm$, AMSB, $\tan\beta = 5, \mu > 0, 0.5 \text{ ns} > \tau > 60 \text{ ns}$
> 620	95	7 AAD	15AE ATLS	stable $\tilde{\chi}^\pm$
> 534	95	8 AAD	15BMATLS	stable $\tilde{\chi}^\pm$
> 239	95	8 AAD	15BMATLS	$\tilde{\chi}^\pm \rightarrow \tilde{\chi}_1^0 \pi^\pm$, lifetime 1 ns, $m_{\tilde{\chi}^\pm} - m_{\tilde{\chi}_1^0} = 0.14 \text{ GeV}$
> 482	95	8 AAD	15BMATLS	$\tilde{\chi}^\pm \rightarrow \tilde{\chi}_1^0 \pi^\pm$, lifetime 15 ns, $m_{\tilde{\chi}^\pm} - m_{\tilde{\chi}_1^0} = 0.14 \text{ GeV}$
> 103	95	9 AAD	13H ATLS	long-lived $\tilde{\chi}^\pm \rightarrow \tilde{\chi}_1^0 \pi^\pm$, mAMSB, $\Delta m_{\tilde{\chi}_1^0} = 160 \text{ MeV}$
> 92	95	10 AAD	12BJ ATLS	long-lived $\tilde{\chi}^\pm \rightarrow \pi^\pm \tilde{\chi}_1^0$, mAMSB
> 171	95	11 ABAZOV	09M D0	\tilde{H}
> 102	95	12 ABBIENDI	03L OPAL	$m_{\tilde{\nu}} > 500 \text{ GeV}$
none 2-93.0	95	13 ABREU	00T DLPH	\tilde{H}^\pm or $m_{\tilde{\nu}} > m_{\tilde{\chi}^\pm}$

• • • We do not use the following data for averages, fits, limits, etc. • • •

> 260	95	14 KHACHATRY...15AB CMS	$\tilde{\chi}_1^\pm \rightarrow \tilde{\chi}_1^0 \pi^\pm, \tau_{\tilde{\chi}_1^\pm} = 0.2 \text{ ns}$, AMSB
> 800	95	15 KHACHATRY...15A0 CMS	long-lived $\tilde{\chi}_1^\pm$, mAMSB, $\tau > 100 \text{ ns}$
> 100	95	15 KHACHATRY...15A0 CMS	long-lived $\tilde{\chi}_1^\pm$, mAMSB, $\tau > 3 \text{ ns}$
		16 KHACHATRY...15W CMS	long-lived $\tilde{\chi}^0, \tilde{q} \rightarrow q\tilde{\chi}^0, \tilde{\chi}^0 \rightarrow \ell^+ \ell^- \nu, \text{RPV}$
> 270	95	17 AAD	13BD ATLS disappearing-track signature, AMSB
> 278	95	18 ABAZOV	13B D0 long-lived $\tilde{\chi}^\pm$, gaugino-like
> 244	95	18 ABAZOV	13B D0 long-lived $\tilde{\chi}^\pm$, higgsino-like

- 1 AAD 23G searched in 139 fb^{-1} of pp collisions at $\sqrt{s} = 13 \text{ TeV}$ for chargino/neutralino pair production (wino-like LSP) in events with high- p_T tracks with large ionisation in the pixel detector. No significant excess above the Standard Model predictions is observed. Limits are set on the chargino mass as a function of its lifetime, see Figure 19.
- 2 AAD 22U searched for the signature of disappearing track from a long-lived chargino in 139 fb^{-1} of pp collisions at $\sqrt{s} = 13 \text{ TeV}$. Long-lived charginos decay into quasi-degenerate neutralino emitting a low-momentum particle whose identification is not attempted. The signal is identified by requiring short tracklets in the four pixel layers with no continuation in the SCT (strip) detector. The main background from fake tracklets is estimated directly with the data. No significant excess above the background prediction is found. The results are interpreted in an AMSB scenario (wino LSP), on $pp \rightarrow \tilde{\chi}^\pm \tilde{\chi}^\pm$ and $pp \rightarrow \tilde{\chi}^\pm \tilde{\chi}_1^0$, assuming $B(\tilde{\chi}^\pm \rightarrow \tilde{\chi}_1^0 \pi^\pm) = 100\%$, see their figure 7. Results are also interpreted in a higgsino-LSP model, with $pp \rightarrow \tilde{\chi}^\pm \tilde{\chi}^\mp$, and $pp \rightarrow \tilde{\chi}^\pm \tilde{\chi}_{1,2}^0$, assuming $B(\tilde{\chi}^\pm \rightarrow \tilde{\chi}_1^0 \pi^\pm) = 95.5\%$, $B(\tilde{\chi}^\pm \rightarrow \tilde{\chi}_1^0 e^\pm) = 3\%$, $B(\tilde{\chi}^\pm \rightarrow \tilde{\chi}_1^0 \mu^\pm) = 1.5\%$, see their figure 8. Finally, results are interpreted in a simplified model of gluino pair production, with $pp \rightarrow \tilde{g}\tilde{g}$ and $B(\tilde{g} \rightarrow qq\tilde{\chi}_1^0) = B(\tilde{g} \rightarrow qq\tilde{\chi}^+) = B(\tilde{g} \rightarrow qq\tilde{\chi}^-) = 1/3$, see their figure 9.
- 3 SIRUNYAN 20N searched in 101 fb^{-1} of pp collisions at $\sqrt{s} = 13 \text{ TeV}$ for direct electroweak production of long-lived charginos in events containing isolated tracks with missing hits in the outer layer of the silicon tracker and little or no associated calorimetric energy deposits (disappearing tracks). No significant excess above the Standard Model expectations is observed. In an AMSB context and assuming a wino LSP, limits are set on the cross section of direct chargino production through $pp \rightarrow \tilde{\chi}^\pm \tilde{\chi}^\mp$ and $pp \rightarrow \tilde{\chi}^\pm \tilde{\chi}_1^0$, assuming $B(\tilde{\chi}^\pm \rightarrow \tilde{\chi}_1^0 \pi^\pm) = 100\%$, as a function of the chargino mass and mean proper lifetime, see Figure 2. In the case of a Higgsino LSP, limits are set on the cross section of direct chargino production through $pp \rightarrow \tilde{\chi}^\pm \tilde{\chi}^\mp$ and $pp \rightarrow \tilde{\chi}^\pm \tilde{\chi}_{1,2}^0$, assuming $B(\tilde{\chi}^\pm \rightarrow \tilde{\chi}_1^0 \pi^\pm) = 95.5\%$, $B(\tilde{\chi}^\pm \rightarrow \tilde{\chi}_1^0 e^\pm) = 3\%$, $B(\tilde{\chi}^\pm \rightarrow \tilde{\chi}_1^0 \mu^\pm) = 1.5\%$, as a function of the chargino mass and mean proper lifetime, see Figure 3.
- 4 AABOUD 19AT searched in 36.1 fb^{-1} of pp collisions at $\sqrt{s} = 13 \text{ TeV}$ for metastable R -hadrons. Multiple search strategies for a wide range of lifetimes, corresponding to path lengths of a few meters, are defined. No significant deviations from the expected Standard Model background are observed. Results are interpreted in terms of direct electroweak production of long-lived charginos in the context of AMSB scenarios. Chargino masses are excluded at 95% C.L. below 1090 GeV. See their Figure 10 (right).
- 5 AABOUD 18As searched in 36.1 fb^{-1} of pp collisions at $\sqrt{s} = 13 \text{ TeV}$ for direct electroweak production of long-lived charginos in the context of AMSB or phenomenological MSSM scenarios with wino-like LSP. Events with a disappearing track due to a low-momentum pion accompanied by at least one jet with high transverse momentum from initial-state radiation are considered. No significant excess above the Standard Model expectations is observed. Exclusion limits are set at 95% confidence level on the mass of charginos for different chargino lifetimes. For a pure wino with a lifetime of about 0.2 ns, corresponding to a mass-splitting between the charged and neutral wino of around 160 MeV, chargino masses up to 460 GeV are excluded, see their Fig. 8.
- 6 SIRUNYAN 18BR searched in 38.4 fb^{-1} of pp collisions at $\sqrt{s} = 13 \text{ TeV}$ for direct electroweak production of long-lived charginos in events containing isolated tracks with missing hits in the outer layer of the silicon tracker and little or no associated calorimetric energy deposits (disappearing tracks). No significant excess above the Standard Model expectations is observed. In an AMSB context, limits are set on the cross section of direct chargino production through $pp \rightarrow \tilde{\chi}^\pm \tilde{\chi}^\mp$ and $pp \rightarrow \tilde{\chi}^\pm \tilde{\chi}_1^0$, assuming $BR(\tilde{\chi}^\pm \rightarrow \tilde{\chi}_1^0 \pi^\pm) = 100\%$, as a function of the chargino mass and mean proper lifetime, see Figures 3, 4 and 5.
- 7 AAD 15AE searched in 19.1 fb^{-1} of pp collisions at $\sqrt{s} = 8 \text{ TeV}$ for heavy long-lived charged particles, measured through their specific ionization energy loss in the ATLAS pixel detector or their time-of-flight in the ATLAS muon system. In the absence of an excess of events above the expected backgrounds, limits are set on stable charginos, see Fig. 10.
- 8 AAD 15BM searched in 18.4 fb^{-1} of pp collisions at $\sqrt{s} = 8 \text{ TeV}$ for stable and metastable non-relativistic charged particles through their anomalous specific ionization energy loss in the ATLAS pixel detector. In absence of an excess of events above the expected backgrounds, limits are set on stable charginos (see Table 5) and on metastable charginos decaying to $\tilde{\chi}_1^0 \pi^\pm$, see Fig. 11.
- 9 AAD 13H searched in 4.7 fb^{-1} of pp collisions at $\sqrt{s} = 7 \text{ TeV}$ for direct electroweak production of long-lived charginos in the context of AMSB scenarios. The search is based on the signature of a high-momentum isolated track with few associated hits in the outer part of the tracking system, arising from a chargino decay into a neutralino and a low-momentum pion. The p_T spectrum of the tracks was found to be consistent with the SM expectations. Constraints on the lifetime and the production cross section were obtained, see Fig. 6. In the minimal AMSB framework with $\tan\beta = 5$, and $\mu > 0$, a chargino having a mass below 103 (85) GeV for a chargino-neutralino mass splitting $\Delta m_{\tilde{\chi}_1^0}$ of 160 (170) MeV is excluded at the 95% C.L. See Fig. 7 for more precise bounds.
- 10 AAD 12BJ looked in 1.02 fb^{-1} of pp collisions at $\sqrt{s} = 7 \text{ TeV}$ for signatures of decaying charginos resulting in isolated tracks with few associated hits in the outer region of the tracking system. The p_T spectrum of the tracks was found to be consistent with the SM expectations. Constraints on the lifetime and the production cross section were obtained. In the minimal AMSB framework with $m_{3/2} < 32 \text{ TeV}$, $m_0 < 1.5 \text{ TeV}$, $\tan\beta = 5$, and $\mu > 0$, a chargino having a mass below 92 GeV and a lifetime between 0.5 ns and 2 ns is excluded at the 95% C.L. See their Fig. 8 for more precise bounds.
- 11 ABAZOV 09M searched in 1.1 fb^{-1} of $p\bar{p}$ collisions at $\sqrt{s} = 1.96 \text{ TeV}$ for events with direct production of a pair of charged massive stable particles identified by their TOF.

See key on page 1171

Searches Particle Listings Supersymmetric Particle Searches

- The number of the observed events is consistent with the predicted background. The data are used to constrain the production cross section as a function of the $\tilde{\chi}_1^\pm$ mass, see their Fig. 2. The quoted limit improves to 206 GeV for gaugino-like charginos.
- ¹²ABBIENDI 03L used e^+e^- data at $\sqrt{s} = 130\text{--}209$ GeV to select events with two high momentum tracks with anomalous dE/dx . The excluded cross section is compared to the theoretical expectation as a function of the heavy particle mass in their Fig. 3. The bounds are valid for colorless fermions with lifetime longer than 10^{-6} s. Supersedes the results from ACKERSTAFF 98P.
- ¹³ABREU 00T searches for the production of heavy stable charged particles, identified by their ionization or Cherenkov radiation, using data from $\sqrt{s} = 130$ to 189 GeV. These limits include and update the results of ABREU 98P.
- ¹⁴KHACHATRYAN 15AB searched in 19.5 fb^{-1} of pp collisions at $\sqrt{s} = 8$ TeV for events containing tracks with little or no associated calorimeter energy deposits and with missing hits in the outer layers of the tracking system (disappearing-track signature). Such disappearing tracks can result from the decay of charginos that are nearly mass degenerate with the lightest neutralino. The number of observed events is in agreement with the background expectation. Limits are set on the cross section of electroweak chargino production in terms of the chargino mass and mean proper lifetime, see Fig. 4. In the minimal AMSB model, a chargino mass below 260 GeV is excluded at 95% C.L., see their Fig. 5.
- ¹⁵KHACHATRYAN 15O searched in 18.8 fb^{-1} of pp collisions at $\sqrt{s} = 8$ TeV for evidence of long-lived charginos in the context of AMSB and pMSSM scenarios. The results are based on a previously published search for heavy stable charged particles at 7 and 8 TeV. In the minimal AMSB framework with $\tan\beta = 5$ and $\mu \geq 0$, constraints on the chargino mass and lifetime were placed, see Fig. 5. Charginos with a mass below 800 (100) GeV are excluded at the 95% C.L. for lifetimes above 100 ns (3 ns). Constraints are also placed on the pMSSM parameter space, see Fig. 3.
- ¹⁶KHACHATRYAN 15W searched in up to 20.5 fb^{-1} of pp collisions at $\sqrt{s} = 8$ TeV for evidence of long-lived neutralinos produced through $\bar{q}q$ -pair production, with $\bar{q} \rightarrow q\tilde{\chi}^0$ and $\tilde{\chi}^0 \rightarrow \ell^+\ell^-\nu$ (RPV: $\lambda_{121}, \lambda_{122} \neq 0$). 95% C.L. exclusion limits on cross section times branching ratio are set as a function of mean proper decay length of the neutralino, see Figs. 6 and 9.
- ¹⁷AAD 13BD searched in 20.3 fb^{-1} of pp collisions at $\sqrt{s} = 8$ TeV for events containing tracks with no associated hits in the outer region of the tracking system resulting from the decay of charginos that are nearly mass degenerate with the lightest neutralino, as is often the case in AMSB scenarios. No significant excess above the background expectation is observed for candidate tracks with large transverse momentum. Constraints on chargino properties are obtained and in the minimal AMSB model, a chargino mass below 270 GeV is excluded at 95% C.L., see their Fig. 7.
- ¹⁸ABAZOV 13B looked in 6.3 fb^{-1} of $p\bar{p}$ collisions at $\sqrt{s} = 1.96$ TeV for charged massive long-lived particles in events with muon-like particles that have both speed and ionization energy loss inconsistent with muons produced in beam collisions. In the absence of an excess, limits are set at 95% C.L. on gaugino- and higgsino-like charginos, see their Table 20 and Fig. 23.

>1700	95	⁷ SIRUNYAN	18AT CMS	RPV, $\tilde{\nu}_\tau \rightarrow e\mu, \lambda_{132} = \lambda_{231} = \lambda'_{311} = 0.01$
>3800	95	⁷ SIRUNYAN	18AT CMS	RPV, $\tilde{\nu}_\tau \rightarrow e\mu, \lambda_{132} = \lambda_{231} = \lambda'_{311} = 0.1$
>2300	95	⁸ AABOUD	16P ATLS	RPV, $\tilde{\nu}_\tau \rightarrow e\mu, \lambda'_{311} = 0.11$
>2200	95	⁸ AABOUD	16P ATLS	RPV, $\tilde{\nu}_\tau \rightarrow e\tau, \lambda'_{311} = 0.11$
>1900	95	⁸ AABOUD	16P ATLS	RPV, $\tilde{\nu}_\tau \rightarrow \mu\tau, \lambda'_{311} = 0.11$
> 400	95	⁹ AAD	14X ATLS	RPV, $\geq 4\ell^\pm, \tilde{\nu} \rightarrow \nu\tilde{\chi}_1^0, \tilde{\chi}_1^0 \rightarrow \ell^\pm\ell^\mp\nu$
> 94	95	¹⁰ AAD	11Z ATLS	RPV, $\tilde{\nu}_\tau \rightarrow e\mu$
> 84	95	¹¹ ABDALLAH	03M DLPH	$1 \leq \tan\beta \leq 40, \tilde{m}_{\tilde{e}_R} - \tilde{m}_{\tilde{\chi}_1^0} > 10$ GeV
> 41	95	¹² HEISTER	02N ALEP	$\tilde{\nu}_e$, any Δm
	95	¹³ DECAMP	92 ALEP	$\Gamma(Z \rightarrow \text{invisible}); M(\tilde{\nu})=3$, model independent
• • • We do not use the following data for averages, fits, limits, etc. • • •				
		¹⁴ SIRUNYAN	19A0	RPV, $\mu^\pm\mu^\pm + \geq 2$ jets, $\lambda'_{211} \neq 0, \tilde{\nu}_\mu \rightarrow \mu\tilde{\chi}_1^\pm, \tilde{\chi}_1^\pm \rightarrow \mu q\bar{q}q\bar{q}$
>1280	95	¹⁵ KHACHATRY..16BE	CMS	RPV, $\tilde{\nu}_\tau \rightarrow e\mu, \lambda_{132} = \lambda_{231} = \lambda'_{311} = 0.01$
>2300	95	¹⁵ KHACHATRY..16BE	CMS	RPV, $\tilde{\nu}_\tau \rightarrow e\mu, \lambda_{132} = \lambda_{231} = 0.07, \lambda'_{311} = 0.11$
>2000	95	¹⁶ AAD	15O ATLS	RPV ($e\mu$), $\tilde{\nu}_\tau, \lambda_{311} = 0.11, \lambda_{33k} = 0.07$
>1700	95	¹⁶ AAD	15O ATLS	RPV ($\tau\mu, e\tau$), $\tilde{\nu}_\tau, \lambda'_{311} = 0.11, \lambda_{33k} = 0.07$
> 95	95	¹⁷ AAD	13A1 ATLS	RPV, $\tilde{\nu}_\tau \rightarrow e\mu, e\tau, \mu\tau$
> 37.1	95	¹⁸ AAD	11H ATLS	RPV, $\tilde{\nu}_\tau \rightarrow e\mu$
> 36	95	¹⁹ AALTONEN	10Z CDF	RPV, $\tilde{\nu}_\tau \rightarrow e\mu, e\tau, \mu\tau$
> 31.2	95	²⁰ ABAZOV	10M D0	RPV, $\tilde{\nu}_\tau \rightarrow e\mu$
	95	²¹ ABDALLAH	04H DLPH	AMSB, $\mu > 0$
	95	²² ADRIANI	93M L3	$\Gamma(Z \rightarrow \text{invisible}); M(\tilde{\nu})=1$
	95	²³ ABREU	91F DLPH	$\Gamma(Z \rightarrow \text{invisible}); M(\tilde{\nu})=1$
	95	²³ ALEXANDER	91F OPAL	$\Gamma(Z \rightarrow \text{invisible}); M(\tilde{\nu})=1$

- ¹AAD 23CB searched in 139 fb^{-1} of pp collisions at $\sqrt{s} = 13$ TeV for heavy particles decaying into an $e\mu, e\tau, \mu\tau$ final state. No significant deviation from the expected SM background is observed. Limits are set on the mass of a stau neutrino with R-parity-violating couplings, with decays $\tilde{\nu}_\tau \rightarrow e\mu, \tilde{\nu}_\tau \rightarrow e\tau, \tilde{\nu}_\tau \rightarrow \mu\tau$, see figures 4b, 5b, 6b.
- ²TUMASYAN 23H searched in 138 fb^{-1} of pp collisions at $\sqrt{s} = 13$ TeV for evidence of resonant $\tilde{\nu}_\tau$ production in events with two charged leptons, $e\mu, e\tau, \mu\tau$. No significant excess above the Standard Model expectations is observed. Limits are set on the mass of $\tilde{\nu}_\tau$ in an RPV model for resonant sneutrino production, where all RPV couplings vanish, except for those that are connected to the production and decay of the $\tilde{\nu}_\tau$, considering a SUSY mass hierarchy with $\tilde{\nu}_\tau$ as the LSP. The $\tilde{\nu}_\tau$ is produced resonantly through λ'_{311} coupling, and decays via λ_{33k} coupling to two leptons, see their figure 3 for couplings of 0.1 and 0.01. Exclusion limits are also shown in the plane of $\tilde{\nu}_\tau$ mass and λ' coupling, for four values of λ couplings, see their figure 6. In addition, limits are set on heavy Z' gauge bosons with lepton flavor violating decays, see their figure 4, and on nonresonant quantum black hole production in models with extra spatial dimensions, see their figure 5. Model-independent upper limits on the product of the cross section, the branching fraction, acceptance, and efficiency are given as well, see their figure 7.
- ³AABOUD 18CM searched in 36.1 fb^{-1} of pp collisions at $\sqrt{s} = 13$ TeV for heavy particles decaying into an $e\mu, e\tau, \mu\tau$ final state. No significant deviation from the expected SM background is observed. Limits are set on the mass of a stau neutrino with R-parity-violating couplings. For $\tilde{\nu}_\tau \rightarrow e\mu$, masses below 3.4 TeV are excluded at 95% CL, see their Figure 4(b). Upper limits on the RPV couplings $|\lambda_{312}|$ versus $|\lambda'_{311}|$ are also performed, see their Figure 8(a-b).
- ⁴AABOUD 18CM searched in 36.1 fb^{-1} of pp collisions at $\sqrt{s} = 13$ TeV for heavy particles decaying into an $e\mu, e\tau, \mu\tau$ final state. No significant deviation from the expected SM background is observed. Limits are set on the mass of a stau neutrino with R-parity-violating couplings. For $\tilde{\nu}_\tau \rightarrow e\tau$, masses below 2.9 TeV are excluded at 95% CL, see their Figure 5(b). Upper limits on the RPV couplings $|\lambda_{313}|$ versus $|\lambda'_{311}|$ are also performed, see their Figure 8(c).
- ⁵AABOUD 18CM searched in 36.1 fb^{-1} of pp collisions at $\sqrt{s} = 13$ TeV for heavy particles decaying into an $e\mu, e\tau, \mu\tau$ final state. No significant deviation from the expected SM background is observed. Limits are set on the mass of a stau neutrino with R-parity-violating couplings. For $\tilde{\nu}_\tau \rightarrow \mu\tau$, masses below 2.6 TeV are excluded at 95% CL, see their Figure 6(b). Upper limits on the RPV couplings $|\lambda_{323}|$ versus $|\lambda'_{311}|$ are also performed, see their Figure 8(d).
- ⁶AABOUD 18Z searched in 36.1 fb^{-1} of pp collisions at $\sqrt{s} = 13$ TeV for events containing four or more charged leptons (electrons, muons and up to two hadronically decaying taus). No significant deviation from the expected SM background is observed. Limits are set on the Higgsino mass in simplified models of general gauge mediated supersymmetry Tn1n1A/Tn1n1B/Tn1n1C, see their Figure 9. Limits are also set on the wino, slepton, sneutrino and gluino mass in a simplified model of NLSP pair production with R-parity violating decays of the LSP via λ_{12k} or λ_{333} to charged leptons, see their Figures 7, 8.
- ⁷SIRUNYAN 18AT searched in 35.9 fb^{-1} of pp collisions at $\sqrt{s} = 13$ TeV for heavy resonances decaying into $e\mu$ final states. No significant excess above the Standard Model expectation is observed and 95% C.L. exclusions are placed on the cross section times branching ratio for the R-parity-violating production and decay of a supersymmetric tau sneutrino, see their Fig. 3.

$\tilde{\nu}$ (Sneutrino) mass limit

The limits may depend on the number, $M(\tilde{\nu})$, of sneutrinos assumed to be degenerate in mass. Only $\tilde{\nu}_L$ (not $\tilde{\nu}_R$) is assumed to exist. It is possible that $\tilde{\nu}$ could be the lightest supersymmetric particle (LSP).

We report here, but do not include in the Listings, the limits obtained from the fit of the final results obtained by the LEP Collaborations on the invisible width of the Z boson ($\Delta\Gamma_{\text{inv}} < 2.0$ MeV, LEP-SLC 06): $m_{\tilde{\nu}} > 43.7$ GeV ($M(\tilde{\nu})=1$) and $m_{\tilde{\nu}} > 44.7$ GeV ($M(\tilde{\nu})=3$).

Some earlier papers are now obsolete and have been omitted. They were last listed in our PDG 14 edition: K. Olive, et al. (Particle Data Group), Chinese Physics **C38** 070001 (2014) (<http://pdg.lbl.gov>).

VALUE (GeV)	CL%	DOCUMENT ID	TECN	COMMENT
>3900	95	¹ AAD	23CB ATLS	RPV, $\tilde{\nu}_\tau \rightarrow e\mu, \lambda_{312} = \lambda_{321} = 0.07, \lambda'_{311} = 0.11$
>2800	95	¹ AAD	23CB ATLS	RPV, $\tilde{\nu}_\tau \rightarrow e\tau, \lambda_{313} = 0.07, \lambda'_{311} = 0.11$
>2700	95	¹ AAD	23CB ATLS	RPV, $\tilde{\nu}_\tau \rightarrow \mu\tau, \lambda_{323} = 0.07, \lambda'_{311} = 0.11$
> 4200	95	² TUMASYAN	23H CMS	$1e + 1\mu, \text{RPV } \nu_\tau \rightarrow e\mu, \lambda = \lambda' = 0.1$
>3700	95	² TUMASYAN	23H CMS	$1e + 1\tau, \text{RPV } \nu_\tau \rightarrow e\tau, \lambda = \lambda' = 0.1$
>3600	95	² TUMASYAN	23H CMS	$1\mu + 1\tau, \text{RPV } \nu_\tau \rightarrow \mu\tau, \lambda = \lambda' = 0.1$
>2200	95	² TUMASYAN	23H CMS	$1e + 1\mu, \text{RPV } \nu_\tau \rightarrow e\mu, \lambda = \lambda' = 0.01$
>1600	95	² TUMASYAN	23H CMS	$1e + 1\tau, \text{RPV } \nu_\tau \rightarrow e\tau, \lambda = \lambda' = 0.01$
>1600	95	² TUMASYAN	23H CMS	$1\mu + 1\tau, \text{RPV } \nu_\tau \rightarrow \mu\tau, \lambda = \lambda' = 0.01$
>3400	95	³ AABOUD	18cm ATLS	RPV, $\tilde{\nu}_\tau \rightarrow e\mu, \lambda_{312} = \lambda_{321} = 0.07, \lambda'_{311} = 0.11$
>2900	95	⁴ AABOUD	18cm ATLS	RPV, $\tilde{\nu}_\tau \rightarrow e\tau, \lambda_{313} = \lambda_{331} = 0.07, \lambda'_{311} = 0.11$
>2600	95	⁵ AABOUD	18cm ATLS	RPV, $\tilde{\nu}_\tau \rightarrow \mu\tau, \lambda_{323} = \lambda_{332} = 0.07, \lambda'_{311} = 0.11$
>1060	95	⁶ AABOUD	18z ATLS	RPV, $\geq 4\ell, \lambda_{12k} \neq 0, m_{\tilde{\nu}_0} = 600$ GeV (mass-degenerate left-handed sleptons and sneutrinos of all 3 generations)
> 780	95	⁶ AABOUD	18z ATLS	RPV, $\geq 4\ell, \lambda_{333} \neq 0, m_{\tilde{\nu}_0} = 300$ GeV (mass-degenerate left-handed sleptons and sneutrinos of all 3 generations)

Searches Particle Listings

Supersymmetric Particle Searches

- ⁸ AABOUD 16P searched in 3.2 fb^{-1} of pp collisions at $\sqrt{s} = 13 \text{ TeV}$ for events with different flavour dilepton pairs ($e\mu, e\tau, \mu\tau$) from the production of $\tilde{\nu}_\tau$ via an RPV λ'_{311} coupling and followed by a decay via $\lambda_{312} = \lambda_{321} = 0.07$ for $e + \mu$, via $\lambda_{313} = \lambda_{331} = 0.07$ for $e + \tau$ and via $\lambda_{323} = \lambda_{332} = 0.07$ for $\mu + \tau$. No evidence for a dilepton resonance over the SM expectation is observed, and limits are derived on $m_{\tilde{\nu}_\tau}$ at 95% CL, see their Figs. 2(b), 3(b), 4(b), and Table 3.
- ⁹ AAD 14x searched in 20.3 fb^{-1} of pp collisions at $\sqrt{s} = 8 \text{ TeV}$ for events with at least four leptons (electrons, muons, taus) in the final state. No significant excess above the Standard Model expectations is observed. Limits are set on the sneutrino mass in an R-parity violating simplified model where the decay $\tilde{\nu} \rightarrow \nu \tilde{\chi}_1^0$, with $\tilde{\chi}_1^0 \rightarrow \ell^\pm \tilde{\tau} \nu$, takes place with a branching ratio of 100%, see Fig. 9.
- ¹⁰ AAD 11z looked in 1.07 fb^{-1} of pp collisions at $\sqrt{s} = 7 \text{ TeV}$ for events with one electron and one muon of opposite charge from the production of $\tilde{\nu}_\tau$ via an RPV λ'_{311} coupling and followed by a decay via λ_{312} into $e + \mu$. No evidence for an (e, μ) resonance over the SM expectation is observed, and a limit is derived in the plane of λ'_{311} versus $m_{\tilde{\nu}_\tau}$ for three values of λ_{312} , see their Fig. 2. Masses $m_{\tilde{\nu}_\tau} < 1.32$ (1.45) TeV are excluded for $\lambda'_{311} = 0.10$ and $\lambda_{312} = 0.05$ ($\lambda'_{311} = 0.11$ and $\lambda_{312} = 0.07$).
- ¹¹ ABDALLAH 03M uses data from $\sqrt{s} = 192\text{--}208 \text{ GeV}$ to obtain limits in the framework of the MSSM with gaugino and sfermion mass universality at the GUT scale. An indirect limit on the mass is derived by constraining the MSSM parameter space by the results from direct searches for neutralinos (including cascade decays) and for sleptons. These limits are valid for values of $M_2 < 1 \text{ TeV}$, $|\mu| \leq 1 \text{ TeV}$ with the $\tilde{\chi}_1^0$ as LSP. The quoted limit is obtained when there is no mixing in the third family. See Fig. 43 for the mass limits as a function of $\tan\beta$. These limits update the results of ABREU 00W.
- ¹² HEISTER 02N derives a bound on $m_{\tilde{\nu}_e}$ by exploiting the mass relation between the $\tilde{\nu}_e$ and \tilde{e} , based on the assumption of universal GUT scale gaugino and scalar masses $m_{1/2}$ and m_0 and the search described in the \tilde{e} section. In the MSUGRA framework with radiative electroweak symmetry breaking, the limit improves to $m_{\tilde{\nu}_e} > 130 \text{ GeV}$, assuming a trilinear coupling $A_0=0$ at the GUT scale. See Figs. 5 and 7 for the dependence of the limits on $\tan\beta$.
- ¹³ DECAMP 92 limit is from $\Gamma(\text{invisible})/\Gamma(\ell\ell) = 5.91 \pm 0.15$ ($N_\nu = 2.97 \pm 0.07$).
- ¹⁴ SIRUNYAN 19A0 searched in 35.9 fb^{-1} of pp collisions at $\sqrt{s} = 13 \text{ TeV}$ for events containing two same-sign muons and at last two jets, originating from resonant production of second-generation sleptons ($\tilde{\mu}_L, \tilde{\nu}_\mu$) via the R-parity violating coupling λ'_{211} to quarks. No significant excess above the Standard Model expectations is observed. Upper limits on cross sections are derived in the context of two simplified models, see their Figure 4. The cross section limits are translated into limits on λ'_{211} for a modified CMSSM, see their Figure 5.
- ¹⁵ KHACHATRYAN 16BE searched in 19.7 fb^{-1} of pp collisions at $\sqrt{s} = 8 \text{ TeV}$ for evidence of narrow resonances decaying into $e\mu$ final states. No significant excess above the Standard Model expectation is observed and 95% C.L. exclusions are placed on the cross section times branching ratio for the production of an R-parity-violating supersymmetric tau sneutrino, applicable to any sneutrino flavour, see their Fig. 2.
- ¹⁶ AAD 15o searched in 20.3 fb^{-1} of pp collisions at $\sqrt{s} = 8 \text{ TeV}$ for evidence of heavy particles decaying into $e\mu, e\tau$ or $\mu\tau$ final states. No significant excess above the Standard Model expectation is observed, and 95% C.L. exclusions are placed on the cross section times branching ratio for the production of an R-parity-violating supersymmetric tau sneutrino, see their Fig. 2. For couplings $\lambda'_{311} = 0.10$ and $\lambda_{33k} = 0.05$, the lower limits on the $\tilde{\nu}_\tau$ mass are 1610, 1110, 1100 GeV in the $e\mu, e\tau$, and $\mu\tau$ channels, respectively.
- ¹⁷ AAD 13A searched in 4.6 fb^{-1} of pp collisions at $\sqrt{s} = 7 \text{ TeV}$ for evidence of heavy particles decaying into $e\mu, e\tau$ or $\mu\tau$ final states. No significant excess above the Standard Model expectation is observed, and 95% C.L. exclusions are placed on the cross section times branching ratio for the production of an R-parity-violating supersymmetric tau sneutrino, see their Fig. 2. For couplings $\lambda'_{311} = 0.10$ and $\lambda_{33k} = 0.05$, the lower limits on the $\tilde{\nu}_\tau$ mass are 1610, 1110, 1100 GeV in the $e\mu, e\tau$, and $\mu\tau$ channels, respectively.
- ¹⁸ AAD 11h looked in 35 pb^{-1} of pp collisions at $\sqrt{s} = 7 \text{ TeV}$ for events with one electron and one muon of opposite charge from the production of $\tilde{\nu}_\tau$ via an RPV λ'_{311} coupling and followed by a decay via λ_{312} into $e + \mu$. No evidence for an excess over the SM expectation is observed, and a limit is derived in the plane of λ'_{311} versus $m_{\tilde{\nu}_\tau}$ for several values of λ_{312} , see their Fig. 2. Superseded by AAD 11z.
- ¹⁹ AALTONEN 10Z searched in 1 fb^{-1} of $p\bar{p}$ collisions at $\sqrt{s} = 1.96 \text{ TeV}$ for events from the production $d\bar{d} \rightarrow \tilde{\nu}_\tau$ with the subsequent decays $\tilde{\nu}_\tau \rightarrow e\mu, \mu\tau, e\tau$ in the MSSM framework with RPV. Two isolated leptons of different flavor and opposite charges are required, with τ s identified by their hadronic decay. No statistically significant excesses are observed over the SM background. Upper limits on λ'_{311} times the branching ratio are listed in their Table III for various $\tilde{\nu}_\tau$ masses. Limits on the cross section times branching ratio for $\lambda'_{311} = 0.10$ and $\lambda_{33k} = 0.05$, displayed in Fig. 2, are used to set limits on the $\tilde{\nu}_\tau$ mass of 558 GeV for the $e\mu$, 441 GeV for the $e\tau$ and 442 GeV for the $e\tau$ channels.
- ²⁰ ABAZOV 10M looked in 5.3 fb^{-1} of $p\bar{p}$ collisions at $\sqrt{s} = 1.96 \text{ TeV}$ for events with exactly one pair of high p_T isolated $e\mu$ and a veto against hard jets. No evidence for an excess over the SM expectation is observed, and a limit at 95% C.L. on the cross section times branching ratio is derived, see their Fig. 3. These limits are translated into limits on couplings as a function of $m_{\tilde{\nu}_\tau}$ as shown on their Fig. 4. As an example, for $m_{\tilde{\nu}_\tau} = 100 \text{ GeV}$ and $\lambda_{312} \leq 0.07$, couplings $\lambda'_{311} > 7.7 \times 10^{-4}$ are excluded.
- ²¹ ABDALLAH 04H use data from LEP 1 and $\sqrt{s} = 192\text{--}208 \text{ GeV}$. They re-use results or re-analyze the data from ABDALLAH 03M to put limits on the parameter space of anomaly-mediated supersymmetry breaking (AMSB), which is scanned in the region $1 < m_{3/2} < 50 \text{ TeV}$, $0 < m_0 < 1000 \text{ GeV}$, $1.5 < \tan\beta < 35$, both signs of μ . The constraints are obtained from the searches for mass degenerate chargino and neutralino, for SM-like and invisible Higgs, for leptonically decaying charginos and from the limit on non-SM Z width of 3.2 MeV. The limit is for $m_t = 174.3 \text{ GeV}$ (see Table 2 for other m_t values). The limit improves to 114 GeV for $\mu < 0$.
- ²² ADRIANI 93M limit from $\Delta\Gamma(Z)(\text{invisible}) < 16.2 \text{ MeV}$.
- ²³ ALEXANDER 91F limit is for one species of $\tilde{\nu}$ and is derived from $\Gamma(\text{invisible, new})/\Gamma(\ell\ell) < 0.38$.

Charged sleptons

This section contains limits on charged scalar leptons ($\tilde{\ell}$, with $\ell=e,\mu,\tau$). Studies of width and decays of the Z boson (use is made here of $\Delta\Gamma_{\text{inv}} < 2.0 \text{ MeV}$, LEP 00) conclusively rule out $m_{\tilde{\ell}_R} < 40 \text{ GeV}$ (41 GeV for $\tilde{\ell}_L$), independently of decay modes, for each individual slepton. The limits improve to 43 GeV (43.5 GeV for $\tilde{\ell}_L$) assuming all 3 flavors to be degenerate. Limits on higher mass sleptons depend on model assumptions and on the mass splitting $\Delta m = m_{\tilde{\ell}} - m_{\tilde{\chi}_1^0}$. The mass and composition of $\tilde{\chi}_1^0$ may affect the slepton production rate in e^+e^- collisions through t-channel exchange diagrams. Production rates are also affected by the potentially large mixing angle of the lightest mass eigenstate $\tilde{\ell}_1 = \tilde{\ell}_R \sin\theta_{\tilde{\ell}} + \tilde{\ell}_L \cos\theta_{\tilde{\ell}}$. It is generally assumed that only $\tilde{\tau}$ may have significant mixing. The coupling to the Z vanishes for $\theta_{\tilde{\ell}}=0.82$. In the high-energy limit of e^+e^- collisions the interference between γ and Z exchange leads to a minimal cross section for $\theta_{\tilde{\ell}}=0.91$, a value which is sometimes used in the following entries relative to data taken at LEP2. When limits on $m_{\tilde{\ell}_R}$ are quoted, it is understood that limits on $m_{\tilde{\ell}_L}$ are usually at least as strong.

Possibly open decays involving gauginos other than $\tilde{\chi}_1^0$ will affect the detection efficiencies. Unless otherwise stated, the limits presented here result from the study of $\tilde{\ell}^+\tilde{\ell}^-$ production, with production rates and decay properties derived from the MSSM. Limits made obsolete by the recent analyses of e^+e^- collisions at high energies can be found in previous Editions of this Review.

For decays with final state gravitinos (\tilde{G}), $m_{\tilde{G}}$ is assumed to be negligible relative to all other masses.

R-parity conserving \tilde{e} (Selectron) mass limit

Some earlier papers are now obsolete and have been omitted. They were last listed in our PDG 14 edition: K. Olive, et al. (Particle Data Group), Chinese Physics **C38** 070001 (2014) (<http://pdg.lbl.gov>).

VALUE (GeV)	CL%	DOCUMENT ID	TECN	COMMENT
>270	95	1 AAD	23M ATLS	$2\ell, \tilde{\ell}$ pair production, $m_{\tilde{\ell}_L} = m_{\tilde{\ell}_R}$, $m_{\tilde{\chi}_1^0} = 0 \text{ GeV}$
> 90	95	1 AAD	23M ATLS	$2\ell, \tilde{\ell}$ pair production, $m_{\tilde{\ell}_L} = m_{\tilde{\ell}_R}$, $m_{\tilde{e}} - m_{\tilde{\chi}_1^0} = 26 \text{ GeV}$
>700	95	2 SIRUNYAN	21M CMS	$\ell^\pm \tilde{\ell}^\mp + \cancel{E}_T, m_{\tilde{\ell}_R} = m_{\tilde{\ell}_L}$ and $\tilde{\ell} = \tilde{e}, \tilde{\mu}, m_{\tilde{\chi}_1^0} = 0 \text{ GeV}$
>700	95	3 AAD	20o ATLS	$2\ell + \cancel{E}_T, m_{\tilde{\ell}_R} = m_{\tilde{\ell}_L}$ and $\tilde{\ell} = \tilde{e}, \tilde{\mu}, m_{\tilde{\chi}_1^0} = 0 \text{ GeV}$
>250	95	4 SIRUNYAN	19AW CMS	$\ell^\pm \tilde{\ell}^\mp + \cancel{E}_T, \tilde{e}_R, m_{\tilde{\chi}_1^0} = 0 \text{ GeV}$
>310	95	4 SIRUNYAN	19AW CMS	$\ell^\pm \tilde{\ell}^\mp + \cancel{E}_T, \tilde{e}_L, m_{\tilde{\chi}_1^0} = 0 \text{ GeV}$
>350	95	4 SIRUNYAN	19AW CMS	$\ell^\pm \tilde{\ell}^\mp + \cancel{E}_T, m_{\tilde{e}_R} = m_{\tilde{e}_L}, m_{\tilde{\chi}_1^0} = 0 \text{ GeV}$
>290	95	4 SIRUNYAN	19AW CMS	$\ell^\pm \tilde{\ell}^\mp + \cancel{E}_T, \tilde{\ell}_R$ and $\tilde{\ell} = \tilde{e}, \tilde{\mu}, m_{\tilde{\chi}_1^0} = 0 \text{ GeV}$
>400	95	4 SIRUNYAN	19AW CMS	$\ell^\pm \tilde{\ell}^\mp + \cancel{E}_T, \tilde{\ell}_L$ and $\tilde{\ell} = \tilde{e}, \tilde{\mu}, m_{\tilde{\chi}_1^0} = 0 \text{ GeV}$
>450	95	4 SIRUNYAN	19AW CMS	$\ell^\pm \tilde{\ell}^\mp + \cancel{E}_T, m_{\tilde{\ell}_R} = m_{\tilde{\ell}_L}$ and $\tilde{\ell} = \tilde{e}, \tilde{\mu}, m_{\tilde{\chi}_1^0} = 0 \text{ GeV}$
>500	95	5 AABOUD	18BT ATLS	$2\ell + \cancel{E}_T, m_{\tilde{\ell}_R} = m_{\tilde{\ell}_L}$ and $\tilde{\ell} = \tilde{e}, \tilde{\mu}, \tilde{\tau}$, with $m_{\tilde{\chi}_1^0} = 0 \text{ GeV}$
>190	95	6 AABOUD	18R ATLS	2ℓ (soft) + $\cancel{E}_T, m_{\tilde{e}} = m_{\tilde{\mu}}, m_{\tilde{e}} - m_{\tilde{\chi}_1^0} = 5 \text{ GeV}$
> 97.5		7 CHATRCHYAN 14R	CMS	$\geq 3\ell^\pm, \tilde{\ell} \rightarrow \ell^\pm \tau^\mp \tau^\mp \tilde{G}$ simplified model, GMSB, stau (N)NLSP scenario
> 94.4		8 AAD	13B ATLS	$2\ell^\pm + \cancel{E}_T, \text{SMS, pMSSM}$
> 94.4		9 ABBIENDI	04 OPAL	$\tilde{e}_R, \Delta m > 11 \text{ GeV}, \mu > 100 \text{ GeV}, \tan\beta = 1.5$
> 71.3		10 ACHARD	04 L3	$\tilde{e}_R, \Delta m > 10 \text{ GeV}, \mu > 200 \text{ GeV}, \tan\beta \geq 2$
none 30–94	95	10 ACHARD	04 L3	\tilde{e}_R , all Δm
> 94	95	11 ABDALLAH	03M DLPH	$\Delta m > 15 \text{ GeV}, \tilde{e}_R^+ \tilde{e}_R^-$
> 95	95	12 ABDALLAH	03M DLPH	$\tilde{e}_R, 1 < \tan\beta \leq 40, \Delta m > 10 \text{ GeV}$
> 94	95	13 HEISTER	02E ALEP	$\Delta m > 15 \text{ GeV}, \tilde{e}_R^+ \tilde{e}_R^-$
> 73	95	14 HEISTER	02N ALEP	\tilde{e}_R , any Δm
>107	95	14 HEISTER	02N ALEP	\tilde{e}_L , any Δm
>101	95	15 AAD	20i ATLS	2ℓ (soft), jets, $\cancel{E}_T, \tilde{e}_R$ only, $m_{\tilde{e}_R} - m_{\tilde{\chi}_1^0} = 7.5 \text{ GeV}$
>169	95	16 AAD	20i ATLS	2ℓ (soft), jets, $\cancel{E}_T, \tilde{e}_L$ only, $m_{\tilde{e}_L} - m_{\tilde{\chi}_1^0} = 7.1 \text{ GeV}$

••• We do not use the following data for averages, fits, limits, etc. •••

- none 90–325 95 17 AAD 14G ATLS $\bar{\ell}\bar{\ell} \rightarrow \ell^{\pm}\bar{\chi}_1^0\ell^{\pm}\bar{\chi}_1^0$, simplified model, $m_{\tilde{\ell}_L}^2 = m_{\tilde{\ell}_R}^2 = m_{\tilde{\chi}_1^0}^2 = 0$ GeV, simplified model
- 18 KHACHATRYAN 14i CMS $\bar{\ell}\bar{\ell} \rightarrow \ell^{\pm}\bar{\chi}_1^0\ell^{\pm}\bar{\chi}_1^0$, simplified model
- 1 AAD 23M searched in 139 fb^{-1} of pp collisions at $\sqrt{s} = 13 \text{ TeV}$ for $\tilde{\ell}^{\pm}$ pair production, followed by $\tilde{\ell}^{\pm} \rightarrow \ell^{\pm}\bar{\chi}_1^0$ in events with two leptons. The focus is on models where $m_{\tilde{\ell}^{\pm}} - m_{\tilde{\chi}_1^0}$ is close to the W mass. No significant excess above the Standard Model predictions is observed. Limits were set on the $\tilde{\ell}$ mass (assuming $\tilde{e} - \tilde{\mu}$ and $L - R$ degeneracy), as a function of $m_{\tilde{\chi}_1^0}$, see Figure 6. Limits were also derived for single \tilde{e} or $\tilde{\mu}$, and for L and R independently, see Figure 7.
- 2 SIRUNYAN 21M searched in 137 fb^{-1} of pp collisions at $\sqrt{s} = 13 \text{ TeV}$ for supersymmetry in events with two opposite-sign same-flavour leptons (electrons, muons) and \cancel{E}_T . No significant excess above the Standard Model expectations is observed. Limits are set on the gluino mass in the simplified model Tglu4C, see their Figure 10, on the $\tilde{\chi}_2^0$ and $\tilde{\chi}_1^{\pm}$ mass in Tchi1n2Fa, see their Figure 11, on the $\tilde{\chi}_1^0$ mass in Tn1n1C and Tn1n1B for $m_{\tilde{\chi}_2^0} = m_{\tilde{\chi}_1^{\pm}} = m_{\tilde{\chi}_1^0}$, see their Figure 12. Limits are also set on the light squark mass for the simplified model Tsqk2A, on the sbottom mass in Tsb0t3, see their Figure 13, and on the slepton mass in direct electroweak pair production of mass-degenerate left- and right-handed sleptons (selectrons and smuons), see their Figure 14.
- 3 AAD 20i reported on a search for electroweak production in models with charginos and sleptons decaying into final states with exactly two oppositely charged leptons and missing transverse momentum. A dataset of pp collisions at $\sqrt{s} = 13 \text{ TeV}$ corresponding to an integrated luminosity of 139 fb^{-1} was used. Light-flavour sleptons \tilde{e} and $\tilde{\mu}$ are constrained at 95% C.L. to have masses above 700 GeV for massless lightest neutralino, see their Fig. 7(c). Exclusion limits are also set for selectrons and smuons separately, considering either right- or left-handed components, by including only the di-electron and di-muon same-flavour signal regions defined in the search, see their Fig. 8.
- 4 SIRUNYAN 19Aw searched in 35.9 fb^{-1} of pp collisions at $\sqrt{s} = 13 \text{ TeV}$ for direct electroweak pair production of selectrons or smuons in events with two leptons (electrons or muons) of the opposite electric charge and same flavour, no jets and large \cancel{E}_T . No significant excess above the Standard Model expectations is observed. Limits are set on the slepton mass assuming left-handed, right-handed or both left- and right-handed (mass degenerate) production, see their Figure 6. Similarly, limits are set on the smuon mass, see their Figure 7. Limits are also set on slepton masses under the assumption that the selectron and smuon are mass degenerate, see their Figure 5.
- 5 AABOUD 18Bt searched in 36.1 fb^{-1} of pp collisions at $\sqrt{s} = 13 \text{ TeV}$ for direct electroweak production of charginos, chargino and next-to-lightest neutralinos and sleptons in events with two or three leptons (electrons or muons), with or without jets, and large missing transverse energy. No significant excess above the Standard Model expectations is observed. Limits are set on the slepton mass up to 500 GeV for massless $\tilde{\chi}_1^0$, assuming degeneracy of \tilde{e} , $\tilde{\mu}$, and $\tilde{\tau}$ and exploiting the 2ℓ signature, see their Figure 8(b).
- 6 AABOUD 18r searched in 36.1 fb^{-1} of pp collisions at $\sqrt{s} = 13 \text{ TeV}$ for electroweak production in scenarios with compressed mass spectra in final states with two low-momentum leptons and missing transverse momentum. The data are found to be consistent with the SM prediction. Results are interpreted in slepton pair production models with a fourfold degeneracy assumed in selectron and smuon masses. The \tilde{e} masses are excluded up to 190 GeV for $m_{\tilde{e}} - m_{\tilde{\chi}_1^0} = 5 \text{ GeV}$. The exclusion limits extend down to mass splittings of 1 GeV, see their Fig. 11.
- 7 CHATRCHYAN 14R searched in 19.5 fb^{-1} of pp collisions at $\sqrt{s} = 8 \text{ TeV}$ for events with at least three leptons (electrons, muons, taus) in the final state. No significant excess above the Standard Model expectations is observed. Limits are set on the slepton mass in a stau (N)NLSP simplified model (GMSB) where the decay $\tilde{\ell} \rightarrow \ell^{\pm}\tau^{\pm}\tilde{\tau}^{\pm}\tilde{G}$ takes place with a branching ratio of 100%, see Fig. 8.
- 8 AAD 13b searched in 4.7 fb^{-1} of pp collisions at $\sqrt{s} = 7 \text{ TeV}$ for sleptons decaying to a final state with two leptons (e and μ) and missing transverse energy. No excess beyond the Standard Model expectation is observed. Limits are derived in a simplified model of direct left-handed slepton pair production, where left-handed slepton masses between 85 and 195 GeV are excluded at 95% C.L. for $m_{\tilde{\chi}_1^0} = 20 \text{ GeV}$. See also Fig. 2(a). Exclusion limits are also derived in the phenomenological MSSM, see Fig. 3.
- 9 ABBIENDI 04 search for $\tilde{e}_R\tilde{e}_R$ production in acoplanar di-electron final states in the 183–208 GeV data. See Fig. 13 for the dependence of the limits on $m_{\tilde{\chi}_1^0}$ and for the limit at $\tan\beta=35$. This limit supersedes ABBIENDI 00g.
- 10 ACHARD 04 search for $\tilde{e}_R\tilde{e}_L$ and $\tilde{e}_R\tilde{e}_R$ production in single- and acoplanar di-electron final states in the 192–209 GeV data. Absolute limits on $m_{\tilde{e}_R}$ are derived from a scan over the MSSM parameter space with universal GUT scale gaugino and scalar masses $m_{1/2}$ and m_0 , $1 \leq \tan\beta \leq 60$ and $-2 \leq \mu \leq 2 \text{ TeV}$. See Fig. 4 for the dependence of the limits on $m_{\tilde{\chi}_1^0}$. This limit supersedes ACCIARRI 99w.
- 11 ABDALLAH 03M looked for acoplanar dielectron + \cancel{E}_T final states at $\sqrt{s} = 189\text{--}208 \text{ GeV}$. The limit assumes $\mu = -200 \text{ GeV}$ and $\tan\beta=1.5$ in the calculation of the production cross section and $B(\tilde{e} \rightarrow e\tilde{\chi}_1^0)=1$. See Fig. 15 for limits in the $(m_{\tilde{e}_R}, m_{\tilde{\chi}_1^0})$ plane. These limits include and update the results of ABREU 01.
- 12 ABDALLAH 03M uses data from $\sqrt{s} = 192\text{--}208 \text{ GeV}$ to obtain limits in the framework of the MSSM with gaugino and sfermion mass universality at the GUT scale. An indirect limit on the mass is derived by constraining the MSSM parameter space by the results from direct searches for neutralinos (including cascade decays) and for sleptons. These limits are valid for values of $M_2 < 1 \text{ TeV}$, $|\mu| \leq 1 \text{ TeV}$ with the $\tilde{\chi}_1^0$ as LSP. The quoted limit is obtained when there is no mixing in the third family. See Fig. 43 for the mass limits as a function of $\tan\beta$. These limits update the results of ABREU 00w.
- 13 HEISTER 02e looked for acoplanar dielectron + \cancel{E}_T final states from e^+e^- interactions between 183 and 209 GeV. The mass limit assumes $\mu < -200 \text{ GeV}$ and $\tan\beta=2$ for the production cross section and $B(\tilde{e} \rightarrow e\tilde{\chi}_1^0)=1$. See their Fig. 4 for the dependence of the limit on Δm . These limits include and update the results of BARATE 01.
- 14 HEISTER 02n search for $\tilde{e}_R\tilde{e}_L$ and $\tilde{e}_R\tilde{e}_R$ production in single- and acoplanar di-electron final states in the 183–208 GeV data. Absolute limits on $m_{\tilde{e}_R}$ are derived from a scan over the MSSM parameter space with universal GUT scale gaugino and scalar masses $m_{1/2}$ and m_0 , $1 \leq \tan\beta \leq 50$ and $-10 \leq \mu \leq 10 \text{ TeV}$. The region of small $|\mu|$, where cascade decays are important, is covered by a search for $\tilde{\chi}_1^0\tilde{\chi}_3^0$ in final states with

leptons and possibly photons. Limits on $m_{\tilde{e}_L}$ are derived by exploiting the mass relation between the \tilde{e}_L and \tilde{e}_R , based on universal m_0 and $m_{1/2}$. When the constraint from the mass limit of the lightest Higgs from HEISTER 02 is included, the bounds improve to $m_{\tilde{e}_R} > 77(75) \text{ GeV}$ and $m_{\tilde{e}_L} > 115(115) \text{ GeV}$ for a top mass of 175(180) GeV. In the MSUGRA framework with radiative electroweak symmetry breaking, the limits improve further to $m_{\tilde{e}_R} > 95 \text{ GeV}$ and $m_{\tilde{e}_L} > 152 \text{ GeV}$, assuming a trilinear coupling $A_0=0$ at the GUT scale. See Figs. 4, 5, 7 for the dependence of the limits on $\tan\beta$.

- 15 AAD 20i reported on ATLAS searches for slepton pair production in models with compressed mass spectra. A dataset of pp collisions at $\sqrt{s} = 13 \text{ TeV}$ corresponding to an integrated luminosity of 139 fb^{-1} was used. Events with \cancel{E}_T , two same-flavour, opposite-charge, low-transverse-momentum leptons, and jets from initial-state radiation or characteristic of vector-boson fusion production are selected. Light-flavour sleptons \tilde{e} and $\tilde{\mu}$ are constrained at 95% C.L. to have masses above 251 GeV for a mass splitting slepton- $\tilde{\chi}_1^0$ of 10 GeV, with constraints extending down to mass splittings of 550 MeV at the LEP slepton limits (73 GeV), see their Fig. 16(a). If only selectrons are considered, and $\tilde{e} = \tilde{e}_R$, masses below 101 GeV are excluded for mass splitting $\tilde{e}_R, \tilde{\chi}_1^0$ of 7.5 GeV. See their Fig. 16(b).
- 16 AAD 20i reported on ATLAS searches for slepton pair production in models with compressed mass spectra. A dataset of pp collisions at $\sqrt{s} = 13 \text{ TeV}$ corresponding to an integrated luminosity of 139 fb^{-1} was used. Events with \cancel{E}_T , two same-flavour, opposite-charge, low-transverse-momentum leptons, and jets from initial-state radiation or characteristic of vector-boson fusion production are selected. Light-flavour sleptons \tilde{e} and $\tilde{\mu}$ are constrained at 95% C.L. to have masses above 251 GeV for a mass splitting slepton- $\tilde{\chi}_1^0$ of 10 GeV, with constraints extending down to mass splittings of 550 MeV at the LEP slepton limits (73 GeV). See their Fig. 16(a). If only selectron are considered, and $\tilde{e} = \tilde{e}_L$, masses below 169 GeV are excluded for mass splitting $\tilde{e}_L, \tilde{\chi}_1^0$ of 7.1 GeV. See their Fig. 16(b).
- 17 AAD 14G searched in 20.3 fb^{-1} of pp collisions at $\sqrt{s} = 8 \text{ TeV}$ for electroweak production of slepton pairs, decaying to a final state with two leptons (e and μ) and missing transverse momentum. No excess beyond the Standard Model expectation is observed. Exclusion limits are derived in simplified models of slepton pair production, see Fig. 8. An interpretation in the pMSSM is also given, see Fig. 10.
- 18 KHACHATRYAN 14i searched in 19.5 fb^{-1} of pp collisions at $\sqrt{s} = 8 \text{ TeV}$ for electroweak production of slepton pairs decaying to a final state with opposite-sign lepton pairs (e or μ) and missing transverse momentum. No excess beyond the Standard Model expectation is observed. Exclusion limits are derived in simplified models, see Fig. 18.

R-parity violating \tilde{e} (Selectron) mass limit

Some earlier papers are now obsolete and have been omitted. They were last listed in our PDG 14 edition: K. Olive, *et al.* (Particle Data Group), Chinese Physics **C38** 070001 (2014) (<http://pdg.lbl.gov>).

VALUE (GeV)	CL%	DOCUMENT ID	TECN	COMMENT
>1200	95	1 AAD	21Y ATLS	$\geq 4\ell, \lambda_{12k} \neq 0, m_{\tilde{\chi}_1^0} = 900$ GeV (mass-degenerate \tilde{e}_L and $\tilde{\nu}$ of all 3 generations)
> 870	95	1 AAD	21Y ATLS	$\geq 4\ell, \lambda_{i33} \neq 0, m_{\tilde{\chi}_1^0} = 450$ GeV (mass-degenerate \tilde{e}_L and $\tilde{\nu}$ of all 3 generations)
>1065	95	2 AABOUD	18Z ATLS	$\geq 4\ell, \lambda_{12k} \neq 0, m_{\tilde{\chi}_1^0} = 600$ GeV (mass-degenerate left-handed sleptons and sneutrinos of all 3 generations)
> 780	95	2 AABOUD	18Z ATLS	$\geq 4\ell, \lambda_{i33} \neq 0, m_{\tilde{\chi}_1^0} = 300$ GeV (mass-degenerate left-handed sleptons and sneutrinos of all 3 generations)
> 410	95	3 AAD	14X ATLS	$\geq 4\ell^{\pm}, \tilde{e} \rightarrow l\tilde{\chi}_1^0, \tilde{\chi}_1^0 \rightarrow \ell^{\pm}\tilde{\ell}^{\mp}\nu$
•••				We do not use the following data for averages, fits, limits, etc. •••
> 89	95	4 ABBIENDI	04F OPAL	\tilde{e}_L
> 92	95	5 ABDALLAH	04M DLPH	\tilde{e}_R , indirect, $\Delta m > 5 \text{ GeV}$

- 1 AAD 21Y searched in 139 fb^{-1} of pp collisions at $\sqrt{s} = 13 \text{ TeV}$ for supersymmetry in events with four or more leptons (electrons, muons and tau-leptons). No significant excess above the Standard Model expectations is observed. Limits are set on Tchi1n12-GGM, and RPV models similar to Tchi1n2L, Tglu1A (with $q = u, d, s, c, b$, with equal branching fractions), and $\tilde{e}_L/\tilde{\nu} \rightarrow \ell/\nu\tilde{\chi}_1^0$ (mass-degenerate \tilde{e}_L and $\tilde{\nu}$ of all 3 generations), all with $\tilde{\chi}_1^0 \rightarrow \ell^{\pm}\tilde{\ell}^{\mp}\nu$ via λ_{12k} or λ_{i33} (where $i, k \in 1, 2$), see their Figure 11.
- 2 AABOUD 18Z searched in 36.1 fb^{-1} of pp collisions at $\sqrt{s} = 13 \text{ TeV}$ for events containing four or more charged leptons (electrons, muons and up to two hadronically decaying taus). No significant deviation from the expected SM background is observed. Limits are set on the Higgsino mass in simplified models of general gauge mediated supersymmetry Tn1n1A/Tn1n1B/Tn1n1C, see their Figure 9. Limits are also set on the wino, slepton, sneutrino and gluino mass in a simplified model of NLSP pair production with R-parity violating decays of the LSP via λ_{12k} or λ_{i33} to charged leptons, see their Figures 7, 8.
- 3 AAD 14x searched in 20.3 fb^{-1} of pp collisions at $\sqrt{s} = 8 \text{ TeV}$ for events with at least four leptons (electrons, muons, taus) in the final state. No significant excess above the Standard Model expectations is observed. Limits are set on the slepton mass in an R-parity violating simplified model where the decay $\tilde{\ell} \rightarrow \ell^{\pm}\tilde{\chi}_1^0$, with $\tilde{\chi}_1^0 \rightarrow \ell^{\pm}\tilde{\ell}^{\mp}\nu$, takes place with a branching ratio of 100%, see Fig. 9.
- 4 ABBIENDI 04F use data from $\sqrt{s} = 189\text{--}209 \text{ GeV}$. They derive limits on sparticle masses under the assumption of RPV with $LL\tilde{E}$ or $LQ\tilde{D}$ couplings. The results are valid for $\tan\beta = 1.5$, $\mu = -200 \text{ GeV}$, with, in addition, $\Delta m > 5 \text{ GeV}$ for indirect decays via $L\tilde{Q}\tilde{D}$. The limit quoted applies to direct decays via $LL\tilde{E}$ or $LQ\tilde{D}$ couplings. For indirect decays, the limits on the \tilde{e}_R mass are respectively 99 and 92 GeV for $LL\tilde{E}$ and $LQ\tilde{D}$ couplings and $m_{\tilde{\chi}_1^0} = 10 \text{ GeV}$ and degrade slightly for larger $\tilde{\chi}_1^0$ mass. Supersedes the results of ABBIENDI 00.
- 5 ABDALLAH 04M use data from $\sqrt{s} = 192\text{--}208 \text{ GeV}$ to derive limits on sparticle masses under the assumption of RPV with $LL\tilde{E}$ or $U\tilde{D}\tilde{D}$ couplings. The results are valid for μ

Searches Particle Listings

Supersymmetric Particle Searches

$= -200$ GeV, $\tan\beta = 1.5$, $\Delta m > 5$ GeV and assuming a BR of 1 for the given decay. The limit quoted is for indirect \overline{UDD} decays using the neutralino constraint of 39.5 GeV for $L\overline{L}\overline{E}$ and of 38.0 GeV for \overline{UDD} couplings, also derived in ABDALLAH 04M. For indirect decays via $L\overline{L}\overline{E}$ the limit improves to 95 GeV if the constraint from the neutralino is used and to 94 GeV if it is not used. For indirect decays via \overline{UDD} couplings it remains unchanged when the neutralino constraint is not used. Supersedes the result of ABREU 00u.

R-parity conserving $\tilde{\mu}$ (Smuon) mass limit

VALUE (GeV)	CL%	DOCUMENT ID	TECN	COMMENT
none 220-460	95	¹ AAD	23CR ATLS	2 same-sign, 3, 4 ℓ , 1, 2 b-jets, $\tilde{\mu}_{L,R}$ pair production with $\tilde{\mu}_{L,R} \rightarrow \mu\tilde{\chi}_1^0, \tilde{\chi}_1^0 \rightarrow b + \ell/\nu + t/b$ via χ'_{133} coupling
>240	95	² AAD	23M ATLS	$2\ell, \tilde{\ell}$ pair production, $m_{\tilde{\mu}_L} = m_{\tilde{\mu}_R}, m_{\tilde{\chi}_1^0} = 0$ GeV
> 90	95	² AAD	23M ATLS	$2\ell, \tilde{\ell}$ pair production, $m_{\tilde{\mu}_L} = m_{\tilde{\mu}_R}, m_{\tilde{\mu}} - m_{\tilde{\chi}_1^0} = 32$ GeV
>700	95	³ SIRUNYAN	21M CMS	$\ell^\pm \ell^\mp + \cancel{E}_T, m_{\tilde{\tau}_R} = m_{\tilde{\tau}_L}$ and $\tilde{\ell} = \tilde{e}, \tilde{\mu}, m_{\tilde{\chi}_1^0} = 0$ GeV
>150	95	⁴ AAD	20I ATLS	2ℓ (soft), jets, $\cancel{E}_T, \tilde{\mu}_R$ only, $m_{\tilde{\mu}_R} - m_{\tilde{\chi}_1^0} = 8.2$ GeV
>216	95	⁵ AAD	20I ATLS	2ℓ (soft), jets, $\cancel{E}_T, \tilde{\mu}_L$ only, $m_{\tilde{\mu}_L} - m_{\tilde{\chi}_1^0} = 10$ GeV
>700	95	⁶ AAD	20o ATLS	$2\ell + \cancel{E}_T, m_{\tilde{\ell}_R} = m_{\tilde{\ell}_L}$ and $\tilde{\ell} = \tilde{e}, \tilde{\mu}, m_{\tilde{\chi}_1^0} = 0$ GeV
>210	95	⁷ SIRUNYAN	19AW CMS	$\ell^\pm \ell^\mp + \cancel{E}_T, \tilde{\mu}_R, m_{\tilde{\chi}_1^0} = 0$ GeV
>280	95	⁷ SIRUNYAN	19AW CMS	$\ell^\pm \ell^\mp + \cancel{E}_T, \tilde{\mu}_L, m_{\tilde{\chi}_1^0} = 0$ GeV
>290	95	⁷ SIRUNYAN	19AW CMS	$\ell^\pm \ell^\mp + \cancel{E}_T, \tilde{\ell}_L$ and $\tilde{\ell} = \tilde{e}, \tilde{\mu}, m_{\tilde{\chi}_1^0} = 0$ GeV
>400	95	⁷ SIRUNYAN	19AW CMS	$\ell^\pm \ell^\mp + \cancel{E}_T, \tilde{\ell}_L$ and $\tilde{\ell} = \tilde{e}, \tilde{\mu}, m_{\tilde{\chi}_1^0} = 0$ GeV
>450	95	⁷ SIRUNYAN	19AW CMS	$\ell^\pm \ell^\mp + \cancel{E}_T, m_{\tilde{\tau}_R} = m_{\tilde{\tau}_L}$ and $\tilde{\ell} = \tilde{e}, \tilde{\mu}, m_{\tilde{\chi}_1^0} = 0$ GeV
>310	95	⁷ SIRUNYAN	19AW CMS	$\ell^\pm \ell^\mp + \cancel{E}_T, m_{\tilde{\mu}_R} = m_{\tilde{\mu}_L}, m_{\tilde{\chi}_1^0} = 0$ GeV
>190	95	⁸ AABOUD	18R ATLS	2ℓ (soft) + $\cancel{E}_T, m_{\tilde{e}} = m_{\tilde{\mu}}, m_{\tilde{\mu}} - m_{\tilde{\chi}_1^0} = 5$ GeV
		⁹ CHATRCHYAN 14R	CMS	$\geq 3\ell^\pm, \tilde{\ell} \rightarrow \ell^\pm \tau^\mp \tau^\mp \tilde{G}$ simplified model, GMSB, stau (N)NLSP scenario
		¹⁰ AAD	13B ATLS	$2\ell^\pm + \cancel{E}_T, SMS, pMSSM$
> 91.0		¹¹ ABBIENDI	04 OPAL	$\Delta m > 3$ GeV, $\tilde{\mu}_R^+ \tilde{\mu}_R^-, \mu > 100$ GeV, $\tan\beta = 1.5$
> 86.7		¹² ACHARD	04 L3	$\Delta m > 10$ GeV, $\tilde{\mu}_R^+ \tilde{\mu}_R^-, \mu > 200$ GeV, $\tan\beta \geq 2$
none 30-88	95	¹³ ABDALLAH	03M DLPH	$\Delta m > 5$ GeV, $\tilde{\mu}_R^+ \tilde{\mu}_R^-$
> 94	95	¹⁴ ABDALLAH	03M DLPH	$\tilde{\mu}_R, 1 \leq \tan\beta \leq 40, \Delta m > 10$ GeV
> 88	95	¹⁵ HEISTER	02E ALEP	$\Delta m > 15$ GeV, $\tilde{\mu}_R^+ \tilde{\mu}_R^-$
• • • We do not use the following data for averages, fits, limits, etc. • • •				
>500	95	¹⁶ AABOUD	18BT ATLS	$2\ell + \cancel{E}_T, m_{\tilde{\tau}_R} = m_{\tilde{\tau}_L}$ and $\tilde{\ell} = \tilde{e}, \tilde{\mu}, \tilde{\tau}, \tilde{\nu}$, with $m_{\tilde{\chi}_1^0} = 0$ GeV
none 90-325	95	¹⁷ AAD	14G ATLS	$\tilde{\ell}\tilde{\ell} \rightarrow \ell^+ \tilde{\chi}_1^0 \ell^- \tilde{\chi}_1^0$ simplified model, $m_{\tilde{\tau}_L} = m_{\tilde{\tau}_R}, m_{\tilde{\chi}_1^0} = 0$ GeV
		¹⁸ KHACHATRY...14I	CMS	$\tilde{\ell} \rightarrow \ell \tilde{\chi}_1^0$ simplified model
> 80	95	¹⁹ ABREU	00V DLPH	$\tilde{\mu}_R \tilde{\mu}_R (\tilde{\mu}_R \rightarrow \mu \tilde{G}), m_{\tilde{G}} > 8$ eV

¹ AAD 23CR searched in 139 fb^{-1} of pp collisions at $\sqrt{s} = 13$ TeV for RPV SUSY in final states with multiple leptons and b-tagged jets. No significant excess above the Standard Model expectations is observed. Limits are set on the production of electroweakinos (wino or higgsino) that decay via RPV coupling χ'_{133} to a charged lepton or a neutrino, a b quark, and an additional t or b quark, see their figure 16. A second model addresses direct $\tilde{\mu}_{L,R}$ production and decay to a muon and a bino-like neutralino, which decays in the same way as in the first model, see their figure 17.

² AAD 23M searched in 139 fb^{-1} of pp collisions at $\sqrt{s} = 13$ TeV for \tilde{e}^\pm pair production, followed by $\tilde{e}^\pm \rightarrow \ell^\pm \tilde{\chi}_1^0$ in events with two leptons. The focus is on models where $m_{\tilde{e}^\pm} - m_{\tilde{\chi}_1^0}$ is close to the W mass. No significant excess above the Standard Model predictions is observed. Limits were set on the $\tilde{\ell}$ mass (assuming $\tilde{e} - \tilde{\mu}$ and $L - R$ degeneracy), as a function of $m_{\tilde{\chi}_1^0}$, see Figure 6. Limits were also derived for single \tilde{e} or $\tilde{\mu}$, and for L and R independently, see Figure 7.

³ SIRUNYAN 21M searched in 137 fb^{-1} of pp collisions at $\sqrt{s} = 13$ TeV for supersymmetry in events with two opposite-sign same-flavor leptons (electrons, muons) and \cancel{E}_T . No significant excess above the Standard Model expectations is observed. Limits are set on the gluino mass in the simplified model Tglu4C, see their Figure 10, on the $\tilde{\chi}_2^0$ and $\tilde{\chi}_1^\pm$ mass in Tchi1n2Fa, see their Figure 11, on the $\tilde{\chi}_1^0$ mass in Tn1n1C and Tn1n1B for

$m_{\tilde{\chi}_2^0} = m_{\tilde{\chi}_1^\pm} = m_{\tilde{\chi}_1^0}$, see their Figure 12. Limits are also set on the light squark mass for the simplified model Tsqk2A, on the sbottom mass in Tsb0t3, see their Figure 13, and on the slepton mass in direct electroweak pair production of mass-degenerate left- and right-handed sleptons (selectrons and smuons), see their Figure 14.

⁴ AAD 20i reported on ATLAS searches for slepton pair production in models with compressed mass spectra. A dataset of pp collisions at $\sqrt{s} = 13$ TeV corresponding to an integrated luminosity of 139 fb^{-1} was used. Events with \cancel{E}_T , two same-flavour, opposite-charge, low-transverse-momentum leptons, and jets from initial-state radiation or characteristic of vector-boson fusion production are selected. Light-flavour sleptons \tilde{e} and $\tilde{\mu}$ are constrained at 95% C.L. to have masses above 251 GeV for a mass splitting slepton $-\tilde{\chi}_1^0$ of 10 GeV, with constraints extending down to mass splittings of 550 MeV at the LEP slepton limits (73 GeV). See their Fig. 16(a). If only smuon are considered, and $\tilde{\mu} = \tilde{\mu}_R$, masses below 150 GeV are excluded for mass splitting $\tilde{\mu}_R, \tilde{\chi}_1^0$ of 8.2 GeV. See their Fig. 16(b).

⁵ AAD 20i reported on ATLAS searches for slepton pair production in models with compressed mass spectra. A dataset of pp collisions at $\sqrt{s} = 13$ TeV corresponding to an integrated luminosity of 139 fb^{-1} was used. Events with \cancel{E}_T , two same-flavour, opposite-charge, low-transverse-momentum leptons, and jets from initial-state radiation or characteristic of vector-boson fusion production are selected. Light-flavour sleptons \tilde{e} and $\tilde{\mu}$ are constrained at 95% C.L. to have masses above 251 GeV for a mass splitting slepton $-\tilde{\chi}_1^0$ of 10 GeV, with constraints extending down to mass splittings of 550 MeV at the LEP slepton limits (73 GeV). See their Fig. 16(a). If only smuon are considered, and $\tilde{\mu} = \tilde{\mu}_L$, masses below 216 GeV are excluded for mass splitting $\tilde{\mu}_L, \tilde{\chi}_1^0$ of 10 GeV. See their Fig. 16(b).

⁶ AAD 20o reported on a search for electroweak production in models with charginos and sleptons decaying into final states with exactly two oppositely charged leptons and missing transverse momentum. A dataset of pp collisions at $\sqrt{s} = 13$ TeV corresponding to an integrated luminosity of 139 fb^{-1} was used. Light-flavour sleptons \tilde{e} and $\tilde{\mu}$ are constrained at 95% C.L. to have masses above 700 GeV for massless lightest neutralino, see their Fig. 7(c). Exclusion limits are also set for selectrons and smuons separately, considering either right- or left-handed components, by including only the di-electron and di-muon same-flavour signal regions defined in the search, see their Fig. 8.

⁷ SIRUNYAN 19AW searched in 35.9 fb^{-1} of pp collisions at $\sqrt{s} = 13$ TeV for direct electroweak pair production of selectrons or smuons in events with two leptons (electrons or muons) of the opposite electric charge and same flavour, no jets and large \cancel{E}_T . No significant excess above the Standard Model expectations is observed. Limits are set on the slepton mass assuming left-handed, right-handed or both left- and right-handed (mass degenerate) production, see their Figure 6. Similarly, limits are set on the smuon mass, see their Figure 7. Limits are also set on slepton masses under the assumption that the selection and smuon are mass degenerate, see their Figure 5.

⁸ AABOUD 18R searched in 36.1 fb^{-1} of pp collisions at $\sqrt{s} = 13$ TeV for electroweak production in scenarios with compressed mass spectra in final states with two low-momentum leptons and missing transverse momentum. The data are found to be consistent with the SM prediction. Results are interpreted in slepton pair production models with a fourfold degeneracy assumed in selection and smuon masses. The $\tilde{\mu}$ masses are excluded up to 190 GeV for $m_{\tilde{\mu}} - m_{\tilde{\chi}_1^0} = 5$ GeV. The exclusion limits extend down to mass splittings of 1 GeV, see their Fig. 11.

⁹ CHATRCHYAN 14R searched in 19.5 fb^{-1} of pp collisions at $\sqrt{s} = 8$ TeV for events with at least three leptons (electrons, muons, taus) in the final state. No significant excess above the Standard Model expectations is observed. Limits are set on the slepton mass in a stau (N)NLSP simplified model (GMSB) where the decay $\tilde{\ell} \rightarrow \ell^\pm \tau^\pm \tau^\mp \tilde{G}$ takes place with a branching ratio of 100%, see Fig. 8.

¹⁰ AAD 13b searched in 4.7 fb^{-1} of pp collisions at $\sqrt{s} = 7$ TeV for sleptons decaying to a final state with two leptons (e and μ) and missing transverse energy. No excess beyond the Standard Model expectation is observed. Limits are derived in a simplified model of direct left-handed slepton pair production, where left-handed slepton masses between 85 and 195 GeV are excluded at 95% C.L. for $m_{\tilde{\chi}_1^0} = 20$ GeV. See also Fig. 2(a). Exclusion limits are also derived in the phenomenological MSSM, see Fig. 3.

¹¹ ABBIENDI 04 search for $\tilde{\mu}_R \tilde{\mu}_R$ production in acoplanar di-muon final states in the 183-208 GeV data. See Fig. 14 for the dependence of the limits on $m_{\tilde{\chi}_1^0}$ and for the limit at $\tan\beta = 35$. Under the assumption of 100% branching ratio for $\tilde{\mu}_R \rightarrow \mu \tilde{\chi}_1^0$, the limit improves to 94.0 GeV for $\Delta m > 4$ GeV. See Fig. 11 for the dependence of the limits on $m_{\tilde{\chi}_1^0}$ at several values of the branching ratio. This limit supersedes ABBIENDI 00G.

¹² ACHARD 04 search for $\tilde{\mu}_R \tilde{\mu}_R$ production in acoplanar di-muon final states in the 192-209 GeV data. Limits on $m_{\tilde{\mu}_R}$ are derived from a scan over the MSSM parameter space with universal GUT scale gaugino and scalar masses $m_{1/2}$ and m_0 , $1 \leq \tan\beta \leq 60$ and $-2 \leq \mu \leq 2$ TeV. See Fig. 4 for the dependence of the limits on $m_{\tilde{\chi}_1^0}$. This limit supersedes ACCIARRI 99w.

¹³ ABDALLAH 03M looked for acoplanar dimuon + \cancel{E} final states at $\sqrt{s} = 189-208$ GeV. The limit assumes $B(\tilde{\mu} \rightarrow \mu \tilde{\chi}_1^0) = 100\%$. See Fig. 16 for limits on the $(m_{\tilde{\mu}_R}, m_{\tilde{\chi}_1^0})$ plane. These limits include and update the results of ABREU 01.

¹⁴ ABDALLAH 03M uses data from $\sqrt{s} = 192-208$ GeV to obtain limits in the framework of the MSSM with gaugino and sfermion mass universality at the GUT scale. An indirect limit on the mass is derived by constraining the MSSM parameter space by the results from direct searches for neutralinos (including cascade decays) and for sleptons. These limits are valid for values of $M_2 < 1$ TeV, $|\mu| \leq 1$ TeV with the $\tilde{\chi}_1^0$ as LSP. The quoted limit is obtained when there is no mixing in the third family. See Fig. 43 for the mass limits as a function of $\tan\beta$. These limits update the results of ABREU 00w.

¹⁵ HEISTER 02E looked for acoplanar dimuon + \cancel{E}_T final states from e^+e^- interactions between 183 and 209 GeV. The mass limit assumes $B(\tilde{\mu} \rightarrow \mu \tilde{\chi}_1^0) = 1$. See their Fig. 4 for the dependence of the limit on Δm . These limits include and update the results of BARATE 01.

¹⁶ AABOUD 18BT searched in 36.1 fb^{-1} of pp collisions at $\sqrt{s} = 13$ TeV for direct electroweak production of charginos, chargino and next-to-lightest neutralinos and sleptons in events with two or three leptons (electrons or muons), with or without jets, and large missing transverse energy. No significant excess above the Standard Model expectations is observed. Limits are set on the slepton mass up to 500 GeV for massless $\tilde{\chi}_1^0$, assuming degeneracy of $\tilde{e}, \tilde{\mu}$, and $\tilde{\tau}$ and exploiting the 2ℓ signature, see their Figure 8(b).

See key on page 1171

Searches Particle Listings Supersymmetric Particle Searches

- 17** AAD 14g searched in 20.3 fb^{-1} of pp collisions at $\sqrt{s} = 8 \text{ TeV}$ for electroweak production of slepton pairs, decaying to a final state with two leptons (e and μ) and missing transverse momentum. No excess beyond the Standard Model expectation is observed. Exclusion limits are derived in simplified models of slepton pair production, see Fig. 8. An interpretation in the pMSSM is also given, see Fig. 10.
- 18** KHACHATRYAN 14t searched in 19.5 fb^{-1} of pp collisions at $\sqrt{s} = 8 \text{ TeV}$ for electroweak production of slepton pairs decaying to a final state with opposite-sign lepton pairs (e or μ) and missing transverse momentum. No excess beyond the Standard Model expectation is observed. Exclusion limits are derived in simplified models, see Fig. 18.
- 19** ABREU 00v use data from $\sqrt{s} = 130\text{--}189 \text{ GeV}$ to search for tracks with large impact parameter or visible decay vertices. Limits are obtained as function of $m_{\tilde{G}}$, after combining these results with the search for slepton pair production in the SUGRA framework from ABREU 01 to cover prompt decays and on stable particle searches from ABREU 00q. For limits at different $m_{\tilde{G}}$, see their Fig. 12.

R-parity violating $\tilde{\mu}$ (Smuon) mass limit

VALUE (GeV)	CL%	DOCUMENT ID	TECN	COMMENT
none 120–645	95	1 AAD	22E ATLS	$t\tilde{\mu}_L$ production, RPV, $\tilde{\mu}_L \rightarrow \mu\tilde{\chi}_1^0, \lambda'_{231} = 1, m_{\tilde{\chi}_1^0} = 0 \text{ GeV}$.
>1200	95	2 AAD	21Y ATLS	$\geq 4\ell, \lambda_{12k} \neq 0, m_{\tilde{\chi}_1^0} = 900 \text{ GeV}$ (mass-degenerate $\tilde{\ell}_L$ and $\tilde{\nu}$ of all 3 generations)
> 870	95	2 AAD	21Y ATLS	$\geq 4\ell, \lambda_{i33} \neq 0, m_{\tilde{\chi}_1^0} = 450 \text{ GeV}$ (mass-degenerate $\tilde{\ell}_L$ and $\tilde{\nu}$ of all 3 generations)
> 780	95	3 AABOUD	18z ATLS	$\geq 4\ell, \lambda_{12k} \neq 0, m_{\tilde{\chi}_1^0} = 300 \text{ GeV}$ (mass-degenerate left-handed sleptons and sneutrinos of all 3 generations)
>1060	95	3 AABOUD	18z ATLS	$\geq 4\ell, \lambda_{12k} \neq 0, m_{\tilde{\chi}_1^0} = 600 \text{ GeV}$ (mass-degenerate left-handed sleptons and sneutrinos of all 3 generations)
> 410	95	4 AAD	14x ATLS	RPV, $\geq 4\ell^\pm, \tilde{\ell} \rightarrow \ell\tilde{\chi}_1^0, \tilde{\chi}_1^0 \rightarrow \ell^\pm\tilde{\ell}^\mp\nu$
••• We do not use the following data for averages, fits, limits, etc. •••				
		5 SIRUNYAN	19Ao	$\mu^\pm\mu^\pm + \geq 2\text{jets}, \lambda'_{211} \neq 0, \tilde{\mu}_L \rightarrow \mu\tilde{\chi}_1^0, \tilde{\chi}_1^0 \rightarrow \mu q\bar{q}$
> 87	95	6 ABDALLAH	04M DLPH	RPV, $\tilde{\mu}_R$, indirect, $\Delta m > 5 \text{ GeV}$
> 81	95	7 HEISTER	03G ALEP	RPV, $\tilde{\mu}_L$

- 1** AAD 22e searched in 139 fb^{-1} of pp collisions at $\sqrt{s} = 13 \text{ TeV}$ for supersymmetry by measuring the yield asymmetry between events containing $e^-\mu^+$ and those containing $e^+\mu^-$. This was found in agreement with the standard model prediction of 1. Limits are set on the RPV production of $t\tilde{\mu}_L$ events with $\tilde{\mu}_L \rightarrow \mu\tilde{\chi}_1^0$ for various values of λ'_{231} , see their figures 6 and 7.
- 2** AAD 21y searched in 139 fb^{-1} of pp collisions at $\sqrt{s} = 13 \text{ TeV}$ for supersymmetry in events with four or more leptons (electrons, muons and tau-leptons). No significant excess above the Standard Model expectations is observed. Limits are set on Tch1n12-GGM, and RPV models similar to Tch1n2l, Tglu1A (with $q = u, d, s, c, b$, with equal branching fractions), and $\tilde{\ell}_L/\tilde{\nu} \rightarrow \ell/\nu\tilde{\chi}_1^0$ (mass-degenerate $\tilde{\ell}_L$ and $\tilde{\nu}$ of all 3 generations), all with $\tilde{\chi}_1^0 \rightarrow \ell^\pm\tilde{\ell}^\mp\nu$ via λ_{12k} or λ_{i33} (where $i, k = 1, 2$), see their Figure 11.
- 3** AABOUD 18z searched in 36.1 fb^{-1} of pp collisions at $\sqrt{s} = 13 \text{ TeV}$ for events containing four or more charged leptons (electrons, muons and up to two hadronically decaying taus). No significant deviation from the expected SM background is observed. Limits are set on the Higgsino mass in simplified models of general gauge mediated supersymmetry Tn1n1A/Tn1n1B/Tn1n1C, see their Figure 9. Limits are also set on the wino, slepton, sneutrino and gluino mass in a simplified model of NLSP pair production with R-parity violating decays of the LSP via λ_{12k} or λ_{i33} to charged leptons, see their Figures 7, 8.
- 4** AAD 14x searched in 20.3 fb^{-1} of pp collisions at $\sqrt{s} = 8 \text{ TeV}$ for events with at least four leptons (electrons, muons, taus) in the final state. No significant excess above the Standard Model expectations is observed. Limits are set on the slepton mass in an R-parity violating simplified model where the decay $\tilde{\ell} \rightarrow \ell\tilde{\chi}_1^0$, with $\tilde{\chi}_1^0 \rightarrow \ell^\pm\tilde{\ell}^\mp\nu$, takes place with a branching ratio of 100%, see Fig. 9.
- 5** SIRUNYAN 19Ao searched in 35.9 fb^{-1} of pp collisions at $\sqrt{s} = 13 \text{ TeV}$ for events containing two same-sign muons and at least two jets, originating from resonant production of second-generation sleptons ($\tilde{\mu}_L, \tilde{\nu}_\mu$) via the R-parity violating coupling λ'_{211} to quarks. No significant excess above the Standard Model expectations is observed. Upper limits on cross sections are derived in the context of two simplified models, see their Figure 4. The cross section limits are translated into limits on λ'_{211} for a modified CMSSM, see their Figure 5.
- 6** ABDALLAH 04M use data from $\sqrt{s} = 192\text{--}208 \text{ GeV}$ to derive limits on sparticle masses under the assumption of RPV with $L\tilde{L}\tilde{E}$ or $U\tilde{D}\tilde{D}$ couplings. The results are valid for $\mu = -200 \text{ GeV}, \tan\beta = 1.5, \Delta m \geq 5 \text{ GeV}$ and assuming a BR of 1 for the given decay. The limit quoted is for indirect $U\tilde{D}\tilde{D}$ decays using the neutralino constraint of 39.5 GeV for $L\tilde{L}\tilde{E}$ and of 38.0 GeV for $U\tilde{D}\tilde{D}$ couplings, also derived in ABDALLAH 04M. For indirect decays via $L\tilde{L}\tilde{E}$ the limit improves to 90 GeV if the constraint from the neutralino is used and remains at 87 GeV if it is not used. For indirect decays via $U\tilde{D}\tilde{D}$ couplings it degrades to 85 GeV when the neutralino constraint is not used. Supersedes the result of ABREU 00u.
- 7** HEISTER 03G searches for the production of smuons in the case of RPV prompt decays with $L\tilde{L}\tilde{E}, L\tilde{Q}\tilde{D}$ or $U\tilde{D}\tilde{D}$ couplings at $\sqrt{s} = 189\text{--}209 \text{ GeV}$. The search is performed for direct and indirect decays, assuming one coupling at a time to be non-zero. The limit holds for direct decays mediated by RPV $L\tilde{Q}\tilde{D}$ couplings and improves to 90 GeV for indirect decays (for $\Delta m > 10 \text{ GeV}$). Limits are also given for $L\tilde{L}\tilde{E}$ direct ($m_{\tilde{\mu}R} > 87 \text{ GeV}$) and indirect decays ($m_{\tilde{\mu}R} > 96 \text{ GeV}$ for $m(\tilde{\chi}_1^0) > 23 \text{ GeV}$ from BARATE 98s) and for $U\tilde{D}\tilde{D}$ indirect decays ($m_{\tilde{\mu}R} > 85 \text{ GeV}$ for $\Delta m > 10 \text{ GeV}$). Supersedes the results from BARATE 01b.

R-parity conserving $\tilde{\tau}$ (Stau) mass limit

Some earlier papers are now obsolete and have been omitted. They were last listed in our PDG 14 edition: K. Olive, et al. (Particle Data Group), Chinese Physics **C38** 070001 (2014) (<http://pdg.lbl.gov>).

VALUE (GeV)	CL%	DOCUMENT ID	TECN	COMMENT
>400	95	1 TUMASYAN	23AG CMS	2 hadronic $\tau + \cancel{E}_T, \tilde{\tau}_{R/L} \rightarrow \tau\tilde{\chi}_1^0, m_{\tilde{\chi}_1^0} = 1 \text{ GeV}$
none 115–340	95	1 TUMASYAN	23AG CMS	2 hadronic $\tau + \cancel{E}_T, \tilde{\tau}_L \rightarrow \tau\tilde{\chi}_1^0, m_{\tilde{\chi}_1^0} = 1 \text{ GeV}$
none 120–390	95	2 AAD	20H	2 hadronic $\tau + \cancel{E}_T, \tilde{\tau}_{R/L} \rightarrow \tau\tilde{\chi}_1^0, m_{\tilde{\chi}_1^0} = 0 \text{ GeV}$
none 90–150	95	3 SIRUNYAN	20P CMS	2 $\tau + \cancel{E}_T, \tau_h\tilde{\tau}_h$ and $\ell\tau_h, m_{\tilde{\tau}_R} = m_{\tilde{\tau}_L}, m_{\tilde{\chi}_1^0} = 1 \text{ GeV}$
> 85.2	95	4 ABBIENDI	04 OPAL	$\Delta m > 6 \text{ GeV}, \theta_\tau = \pi/2, \mu > 100 \text{ GeV}, \tan\beta = 1.5$
> 78.3	95	5 ACHARD	04 L3	$\Delta m > 15 \text{ GeV}, \theta_\tau = \pi/2, \mu > 200 \text{ GeV}, \tan\beta \geq 2$
> 81.9	95	6 ABDALLAH	03M DLPH	$\Delta m > 15 \text{ GeV}, \text{all } \theta_\tau$
> 79	95	7 HEISTER	02E ALEP	$\Delta m > 15 \text{ GeV}, \theta_\tau = \pi/2$
> 76	95	7 HEISTER	02E ALEP	$\Delta m > 15 \text{ GeV}, \theta_\tau = 0.91$
••• We do not use the following data for averages, fits, limits, etc. •••				
>500	95	8 AABOUD	18bT ATLS	$2\ell + \cancel{E}_T, m_{\tilde{\tau}} = m_{\tilde{\ell}}, \tilde{\ell} = \tilde{e}, \tilde{\mu}, \tilde{\tau}, m_{\tilde{\chi}_1^0} = 0 \text{ GeV}$
none 109	95	9 KHACHATRYAN 17L	CMS	2 $\tau + \cancel{E}_T, \tilde{\tau}_L \rightarrow \tau\tilde{\chi}_1^0, m_{\tilde{\chi}_1^0} = 0 \text{ GeV}$
none 109	95	10 AAD	16AA ATLS	2 hadronic $\tau + \cancel{E}_T, \tilde{\tau}_{R/L} \rightarrow \tau\tilde{\chi}_1^0, m_{\tilde{\chi}_1^0} = 0 \text{ GeV}$
		11 AAD	12AF ATLS	$2\tau + \text{jets} + \cancel{E}_T, \text{GMSB}$
		12 AAD	12AG ATLS	$\geq 1\tau_h + \text{jets} + \cancel{E}_T, \text{GMSB}$
		13 AAD	12CM ATLS	$\geq 1\tau + \text{jets} + \cancel{E}_T, \text{GMSB}$
> 87.4	95	14 ABBIENDI	06B OPAL	$\tilde{\tau}_R \rightarrow \tau\tilde{G}, \text{all } \tau(\tilde{\tau}_R)$
> 68	95	15 ABDALLAH	04H DLPH	AMS, $\mu > 0$
none $m_{\tilde{\tau}} - 26.3$	95	6 ABDALLAH	03M DLPH	$\Delta m > m_{\tilde{\tau}}, \text{all } \theta_\tau$

- 1** TUMASYAN 23AG searched in 138 fb^{-1} of pp collisions at $\sqrt{s} = 13 \text{ TeV}$ for or direct pair production of tau sleptons in events with two hadronically decaying tau leptons. No significant excess above the Standard Model expectations is observed. Limits are set on the mass of the tau slepton in models with $\tilde{\tau} \rightarrow \tau\tilde{\chi}_1^0$ for mass-degenerate, pure left-handed and pure right-handed tau sleptons, see their figures 4–7. Limits are also set for the maximally mixed scenario with long-lived tau sleptons and $\tilde{\tau}$ lifetimes of 0.01 mm to 2.5 mm, see their figure 8.
- 2** AAD 20H presented ATLAS searches for direct production for $\tilde{\tau}$ in final states with two hadronically decaying leptons and \cancel{E}_T . The analysis uses a dataset of pp collisions at $\sqrt{s} = 13 \text{ TeV}$ corresponding to an integrated luminosity of 139 fb^{-1} . Exclusion limits at 95% C.L. are derived in scenarios of direct production of $\tilde{\tau}$ pairs with each $\tilde{\tau}$ decaying into a τ and the lightest neutralino $\tilde{\chi}_1^0$ in simplified models where the $\tilde{\tau}_R$ and $\tilde{\tau}_L$ mass eigenstates are degenerate. Stau masses from 120 GeV to 390 GeV are excluded for a massless lightest neutralino, see their Fig. 7(a). If $\tilde{\tau}$ -only pair production is considered, the exclusion region extends between 155 GeV to 310 GeV, see their Fig. 7(b).
- 3** SIRUNYAN 20P searched in 77.2 fb^{-1} of pp collisions at $\sqrt{s} = 13 \text{ TeV}$ for direct pair production of tau sleptons in events with a tau lepton pair and significant missing transverse momentum. Final states with two double hadronic decay of the tau leptons are considered, as well as where one of the tau leptons decays into an electron or a muon. No significant excess above the Standard Model expectations is observed. Limits are set on the stau mass in a simplified model where two tau sleptons are pair produced and decay to a tau lepton and the lightest neutralino, assuming either only left-handed stau production, see Figure 8, or assuming degenerate left- and right-handed stau production, see Figure 9.
- 4** ABBIENDI 04 search for $\tilde{\tau}\tilde{\tau}$ production in acoplanar di-tau final states in the 183–208 GeV data. See Fig. 15 for the dependence of the limits on $m_{\tilde{\chi}_1^0}$ and for the limit at $\tan\beta = 35$. Under the assumption of 100% branching ratio for $\tilde{\tau}_R \rightarrow \tau\tilde{\chi}_1^0$, the limit improves to 89.8 GeV for $\Delta m > 8 \text{ GeV}$. See Fig. 12 for the dependence of the limits on $m_{\tilde{\chi}_1^0}$ at several values of the branching ratio and for their dependence on θ_τ . This limit supersedes ABBIENDI 00g.
- 5** ACHARD 04 search for $\tilde{\tau}\tilde{\tau}$ production in acoplanar di-tau final states in the 192–209 GeV data. Limits on $m_{\tilde{\tau}_R}$ are derived from a scan over the MSSM parameter space with universal GUT scale gaugino and scalar masses $m_{1/2}$ and $m_0, 1 \leq \tan\beta \leq 60$ and $-2 \leq \mu \leq 2 \text{ TeV}$. See Fig. 4 for the dependence of the limits on $m_{\tilde{\chi}_1^0}$.
- 6** ABDALLAH 03M looked for acoplanar ditau and \cancel{E}_T final states at $\sqrt{s} = 130\text{--}208 \text{ GeV}$. A dedicated search was made for low mass $\tilde{\tau}$ s decoupling from the Z^0 . The limit assumes $B(\tilde{\tau} \rightarrow \tau\tilde{\chi}_1^0) = 100\%$. See Fig. 20 for limits on the $(m_{\tilde{\tau}}, m_{\tilde{\chi}_1^0})$ plane and as function of the $\tilde{\chi}_1^0$ mass and of the branching ratio. The limit in the low-mass region improves to 29.6 and 31.1 GeV for $\tilde{\tau}_R$ and $\tilde{\tau}_L$, respectively, at $\Delta m > m_{\tilde{\tau}}$. The limit in the high-mass region improves to 84.7 GeV for $\tilde{\tau}_R$ and $\Delta m > 15 \text{ GeV}$. These limits include and update the results of ABREU 01.
- 7** HEISTER 02E looked for acoplanar ditau and \cancel{E}_T final states from e^+e^- interactions between 183 and 209 GeV. The mass limit assumes $B(\tilde{\tau} \rightarrow \tau\tilde{\chi}_1^0) = 1$. See their Fig. 4 for the dependence of the limit on Δm . These limits include and update the results of BARATE 01.
- 8** AABOUD 18bT searched in 36.1 fb^{-1} of pp collisions at $\sqrt{s} = 13 \text{ TeV}$ for direct electroweak production of charginos, chargino and next-to-lightest neutralinos and sleptons in events with two or three leptons (electrons or muons), with or without jets, and large missing transverse energy. No significant excess above the Standard Model expectations

Searches Particle Listings

Supersymmetric Particle Searches

is observed. Limits are set on the slepton mass up to 500 GeV for massless $\tilde{\chi}_1^0$, assuming degeneracy of \tilde{e} , $\tilde{\mu}$, and $\tilde{\tau}$ and exploiting the 2ℓ signature, see their Figure 8(b).

- ⁹ KHACHATRYAN 17L searched in about 19 fb^{-1} of pp collisions at $\sqrt{s} = 8 \text{ TeV}$ for events with two τ (at least one decaying hadronically) and \cancel{E}_T . Results were interpreted to set constraints on the cross section for production of $\tilde{\tau}_L$ pairs for $m_{\tilde{\chi}_1^0} = 1 \text{ GeV}$. No mass constraints are set, see their Fig. 7.
- ¹⁰ AAD 16AA summarized and extended ATLAS searches for electroweak supersymmetry in final states containing several charged leptons, \cancel{E}_T , with or without hadronic jets, in 20 fb^{-1} of pp collisions at $\sqrt{s} = 8 \text{ TeV}$. The paper reports 95% C.L. exclusion limits on the cross-section for production of $\tilde{\tau}_R$ and $\tilde{\tau}_L$ pairs for various $m_{\tilde{\chi}_1^0}$, using the 2 hadronic $\tau + \cancel{E}_T$ analysis. The $m_{\tilde{\tau}_{R/L}} = 109 \text{ GeV}$ is excluded for $m_{\tilde{\chi}_1^0} = 0 \text{ GeV}$, with the constraints being stronger for $\tilde{\tau}_R$. See their Fig. 12.
- ¹¹ AAD 12AF searched in 2 fb^{-1} of pp collisions at $\sqrt{s} = 7 \text{ TeV}$ for events with two tau leptons, jets and large \cancel{E}_T in a GMSB framework. No significant excess above the expected background was found and an upper limit on the visible cross section for new phenomena is set. A 95% C.L. lower limit of 32 TeV on the mGMSB breaking scale Λ is set for $M_{mess} = 250 \text{ TeV}$, $N_S = 3$, $\mu > 0$ and $C_{grav} = 1$, independent of $\tan\beta$.
- ¹² AAD 12AG searched in 2.05 fb^{-1} of pp collisions at $\sqrt{s} = 7 \text{ TeV}$ for events with at least one hadronically decaying tau lepton, jets, and large \cancel{E}_T in a GMSB framework. No significant excess above the expected background was found and an upper limit on the visible cross section for new phenomena is set. A 95% C.L. lower limit of 30 TeV on the mGMSB breaking scale Λ is set for $M_{mess} = 250 \text{ TeV}$, $N_S = 3$, $\mu > 0$ and $C_{grav} = 1$, independent of $\tan\beta$. For large values of $\tan\beta$, the limit on Λ increases to 43 TeV.
- ¹³ AAD 12CM searched in 4.7 fb^{-1} of pp collisions at $\sqrt{s} = 7 \text{ TeV}$ for events with at least one tau lepton, zero or one additional light lepton (e/μ) jets, and large \cancel{E}_T in a GMSB framework. No significant excess above the expected background was found and an upper limit on the visible cross section for new phenomena is set. A 95% C.L. lower limit of 54 TeV on the mGMSB breaking scale Λ is set for $M_{mess} = 250 \text{ TeV}$, $N_S = 3$, $\mu > 0$ and $C_{grav} = 1$, for $\tan\beta > 20$. Here the $\tilde{\tau}_1$ is the NLSP.
- ¹⁴ ABBIENDI 06b use 600 pb^{-1} of data from $\sqrt{s} = 189\text{--}209 \text{ GeV}$. They look for events from pair-produced staus in a GMSB scenario with $\tilde{\tau}$ NLSP including prompt $\tilde{\tau}$ decays to t quarks + \cancel{E} final states, large impact parameters, kinked tracks and heavy stable charged particles. Limits on the cross-section are computed as a function of $m(\tilde{\tau})$ and the lifetime, see their Fig. 7. The limit is compared to the $\sigma \cdot BR^2$ from a scan over the GMSB parameter space.
- ¹⁵ ABDALLAH 04H use data from LEP 1 and $\sqrt{s} = 192\text{--}208 \text{ GeV}$. They re-use results or re-analyze the data from ABDALLAH 03M to put limits on the parameter space of anomaly-mediated supersymmetry breaking (AMSB), which is scanned in the region $1 < m_{3/2} < 50 \text{ TeV}$, $0 < m_0 < 1000 \text{ GeV}$, $1.5 < \tan\beta < 35$, both signs of μ . The constraints are obtained from the searches for mass degenerate chargino and neutralino, for SM-like and invisible Higgs, for leptonically decaying charginos and from the limit on non-SM Z width of 3.2 MeV. The limit is for $m_{\tilde{t}} = 174.3 \text{ GeV}$ (see Table 2 for other $m_{\tilde{t}}$ values). The limit improves to 75 GeV for $\mu < 0$.

R-parity violating $\tilde{\tau}$ (Stau) mass limit

Some earlier papers are now obsolete and have been omitted. They were last listed in our PDG 14 edition: K. Olive, *et al.* (Particle Data Group), Chinese Physics **C38** 070001 (2014) (<http://pdg.lbl.gov>).

VALUE (GeV)	CL%	DOCUMENT ID	TECN	COMMENT
>1200	95	¹ AAD	21Y ATLS	$\geq 4\ell, \lambda_{12k} \neq 0, m_{\tilde{\chi}_1^0} = 900 \text{ GeV}$ (mass-degenerate $\tilde{\ell}_L$ and $\tilde{\nu}$ of all 3 generations)
> 870	95	¹ AAD	21Y ATLS	$\geq 4\ell, \lambda_{i33} \neq 0, m_{\tilde{\chi}_1^0} = 450 \text{ GeV}$ (mass-degenerate $\tilde{\ell}_L$ and $\tilde{\nu}$ of all 3 generations)
>1060	95	² AABOUD	18Z ATLS	$\geq 4\ell, \lambda_{12k} \neq 0, m_{\tilde{\chi}_1^0} = 600 \text{ GeV}$ (mass-degenerate left-handed sleptons and sneutrinos of all 3 generations)
> 780	95	² AABOUD	18Z ATLS	$\geq 4\ell, \lambda_{i33} \neq 0, m_{\tilde{\chi}_1^0} = 300 \text{ GeV}$ (mass-degenerate left-handed sleptons and sneutrinos of all 3 generations)
> 90	95	³ ABDALLAH	04M DLPH	$\tilde{\tau}_R$, indirect, $\Delta m > 5 \text{ GeV}$
• • •				We do not use the following data for averages, fits, limits, etc. • • •
> 74	95	⁴ ABBIENDI	04F OPAL	$\tilde{\tau}_L$

- ¹ AAD 21Y searched in 139 fb^{-1} of pp collisions at $\sqrt{s} = 13 \text{ TeV}$ for supersymmetry in events with four or more leptons (electrons, muons and tau-leptons). No significant excess above the Standard Model expectations is observed. Limits are set on $T\text{ch}1n12\text{-GGM}$, and RPV models similar to $T\text{ch}1n21$, $T\text{glu}1A$ (with $q = u, d, s, c, b$, with equal branching fractions), and $\tilde{\ell}_L/\tilde{\nu} \rightarrow \ell/\nu\tilde{\chi}_1^0$ (mass-degenerate $\tilde{\ell}_L$ and $\tilde{\nu}$ of all 3 generations), all with $\tilde{\chi}_1^0 \rightarrow \ell^\pm \tilde{E}^\mp \nu$ via λ_{12k} or λ_{i33} (where $i, k \in 1, 2$), see their Figure 11.
- ² AABOUD 18Z searched in 36.1 fb^{-1} of pp collisions at $\sqrt{s} = 13 \text{ TeV}$ for events containing four or more charged leptons (electrons, muons and up to two hadronically decaying taus). No significant deviation from the expected SM background is observed. Limits are set on the Higgsino mass in simplified models of general gauge mediated supersymmetry $Tn1n1A/Tn1n1B/Tn1n1C$, see their Figure 9. Limits are also set on the wino, slepton, sneutrino and gluino mass in a simplified model of NLSP pair production with R-parity violating decays of the LSP via λ_{12k} or λ_{i33} to charged leptons, see their Figures 7, 8.
- ³ ABDALLAH 04M use data from $\sqrt{s} = 192\text{--}208 \text{ GeV}$ to derive limits on sparticle masses under the assumption of RPV with $LL\bar{E}$ couplings. The results are valid for $\mu = -200 \text{ GeV}$, $\tan\beta = 1.5$, $\Delta m > 5 \text{ GeV}$ and assuming a BR of 1 for the given decay. The limit quoted is for indirect decays using the neutralino constraint of 39.5 GeV, also derived in ABDALLAH 04M. For indirect decays via $LL\bar{E}$ the limit decreases to 86 GeV if the constraint from the neutralino is not used. Supersedes the result of ABREU 00U.
- ⁴ ABBIENDI 04F use data from $\sqrt{s} = 189\text{--}209 \text{ GeV}$. They derive limits on sparticle masses under the assumption of RPV with $LL\bar{E}$ or $LQ\bar{D}$ couplings. The results are valid for

$\tan\beta = 1.5$, $\mu = -200 \text{ GeV}$, with, in addition, $\Delta m > 5 \text{ GeV}$ for indirect decays via $LQ\bar{D}$. The limit quoted applies to direct decays with $LL\bar{E}$ couplings and improves to 75 GeV for $LQ\bar{D}$ couplings. The limit on the $\tilde{\tau}_R$ mass for indirect decays is 92 GeV for $LL\bar{E}$ couplings at $m_{\tilde{\chi}_1^0} = 10 \text{ GeV}$ and no exclusion is obtained for $LQ\bar{D}$ couplings. Supersedes the results of ABBIENDI 00.

Long-lived $\tilde{\ell}$ (Slepton) mass limit

Limits on scalar leptons which leave detector before decaying. Limits from Z decays are independent of lepton flavor. Limits from continuum e^+e^- annihilation are also independent of flavor for smuons and staus. Selection limits from e^+e^- collisions in the continuum depend on MSSM parameters because of the additional neutralino exchange contribution.

VALUE (GeV)	CL%	DOCUMENT ID	TECN	COMMENT
>520	95	¹ AAD	23BQ ATLS	2ℓ slightly displaced, long-lived $\tilde{\mu}, \tilde{\mu} \rightarrow \mu\tilde{G}, m_{\tilde{\mu}_R} = m_{\tilde{\mu}_L}, \tau_{\tilde{\mu}} = 10 \text{ ps}$
>190	95	¹ AAD	23BQ ATLS	2ℓ slightly displaced, long-lived $\tilde{\mu}, \tilde{\mu} \rightarrow \mu\tilde{G}, m_{\tilde{\mu}_R} = m_{\tilde{\mu}_L}, \tau_{\tilde{\mu}} = 1 \text{ ps}$
none 220–360	95	² AAD	23G ATLS	direct $\tilde{\tau}$ pair, $\tilde{\tau} \rightarrow \tau\tilde{G}, \tau = 10 \text{ ns}$
none 150–220	95	³ TUMASYAN	23AG CMS	2 hadronic $\tau + \cancel{E}_T, \tilde{\tau} \rightarrow \tau\tilde{\chi}_1^0$, maximally mixed scenario with $c\tau = 0.1 \text{ mm}, m_{\tilde{\chi}_1^0} = 1 \text{ GeV}$
>610	95	⁴ TUMASYAN	22AF CMS	2ℓ displaced, long-lived $\tilde{e}, \tilde{e} \rightarrow e\tilde{G}, m_{\tilde{e}_R} = m_{\tilde{e}_L}, c\tau = 0.7 \text{ cm}$
>610	95	⁴ TUMASYAN	22AF CMS	2ℓ displaced, long-lived $\tilde{\mu}, \tilde{\mu} \rightarrow \mu\tilde{G}, m_{\tilde{\mu}_R} = m_{\tilde{\mu}_L}, c\tau = 3 \text{ cm}$
>405	95	⁴ TUMASYAN	22AF CMS	2ℓ displaced, long-lived $\tilde{\tau}, \tilde{\tau} \rightarrow \tau\tilde{G}, m_{\tilde{\tau}_R} = m_{\tilde{\tau}_L}, c\tau = 2 \text{ cm}$
>270	95	⁴ TUMASYAN	22AF CMS	2ℓ displaced, long-lived $\tilde{\ell}, \tilde{\ell} \rightarrow \tilde{G}, m_{\tilde{\ell}_R} = m_{\tilde{\ell}_L}, m_{\tilde{e}} = m_{\tilde{\mu}} = m_{\tilde{\tau}}, 0.005 \text{ cm} < c\tau < 265 \text{ cm}$
>680	95	⁴ TUMASYAN	22AF CMS	2ℓ displaced, long-lived $\tilde{\ell}, \tilde{\ell} \rightarrow \tilde{G}, m_{\tilde{\ell}_R} = m_{\tilde{\ell}_L}, m_{\tilde{e}} = m_{\tilde{\mu}} = m_{\tilde{\tau}}, c\tau = 2 \text{ cm}$
>720	95	⁵ AAD	21AL ATLS	2ℓ displaced, long-lived $\tilde{e}, \tilde{e} \rightarrow e\tilde{G}, m_{\tilde{e}_R} = m_{\tilde{e}_L}, \tau_{\tilde{e}} = 0.1 \text{ ns}$
>680	95	⁵ AAD	21AL ATLS	2ℓ displaced, long-lived $\tilde{\mu}, \tilde{\mu} \rightarrow \mu\tilde{G}, m_{\tilde{\mu}_R} = m_{\tilde{\mu}_L}, \tau_{\tilde{\mu}} = 0.1 \text{ ns}$
>340	95	⁵ AAD	21AL ATLS	2ℓ displaced, long-lived $\tilde{\tau}, \tilde{\tau} \rightarrow \tau\tilde{G}, \text{mixing } \sin\theta_{\tilde{\tau}} = 0.95, \tau_{\tilde{\tau}} = 0.1 \text{ ns}$
>820	95	⁵ AAD	21AL ATLS	2ℓ displaced, long-lived $\tilde{\ell}, \tilde{\ell} \rightarrow \tilde{G}, m_{\tilde{\ell}_R} = m_{\tilde{\ell}_L}, m_{\tilde{e}} = m_{\tilde{\mu}} = m_{\tilde{\tau}}, \tau_{\tilde{\ell}} = 0.1 \text{ ns}$
>430	95	⁶ AABOUD	19AT ATLS	long-lived $\tilde{\tau}$, GMSB
>490	95	⁷ KHACHATRY...	16BW CMS	long-lived $\tilde{\tau}$ from inclusive production, mGMSB SPS line 7 scenario
>240	95	⁷ KHACHATRY...	16BW CMS	long-lived $\tilde{\tau}$ from direct pair production, mGMSB SPS line 7 scenario
>440	95	⁸ AAD	15AE ATLS	mGMSB, $M_{mess} = 250 \text{ TeV}, N_S = 3, \mu > 0, C_{grav} = 5000, \tan\beta = 10$
>385	95	⁸ AAD	15AE ATLS	mGMSB, $M_{mess} = 250 \text{ TeV}, N_S = 3, \mu > 0, C_{grav} = 5000, \tan\beta = 50$
>286	95	⁸ AAD	15AE ATLS	direct $\tilde{\tau}$ production
none 124–309	95	⁹ AAIJ	15BD LHCB	long-lived $\tilde{\tau}$, mGMSB, SPS7
> 98	95	¹⁰ ABBIENDI	03L OPAL	$\tilde{\mu}_R, \tilde{\tau}_R$
none 2–87.5	95	¹¹ ABREU	00Q DLPH	$\tilde{\mu}_R, \tilde{\tau}_R$
> 81.2	95	¹² ACCIARRI	99H L3	$\tilde{\mu}_R, \tilde{\tau}_R$
> 81	95	¹³ BARATE	98K ALEP	$\tilde{\mu}_R, \tilde{\tau}_R$
• • •				We do not use the following data for averages, fits, limits, etc. • • •
>300	95	¹⁴ AAD	13AA ATLS	long-lived $\tilde{\tau}$, GMSB, $\tan\beta = 5\text{--}20$
>339	95	¹⁵ ABAZOV	13B D0	long-lived $\tilde{\tau}, 100 < m_{\tilde{\tau}} < 300 \text{ GeV}$
>500	95	^{16,17} CHATRCHYAN	13AB CMS	long-lived $\tilde{\tau}$, direct $\tilde{\tau}_1$ pair prod., minimal GMSB, SPS line 7
>500	95	^{16,18} CHATRCHYAN	13AB CMS	long-lived $\tilde{\tau}, \tilde{\tau}_1$ from direct pair prod. and from decay of heavier SUSY particles, minimal GMSB, SPS line 7
>314	95	¹⁹ CHATRCHYAN	12L CMS	long-lived $\tilde{\tau}, \tilde{\tau}_1$ from decay of heavier SUSY particles, minimal GMSB, SPS line 7
>136	95	²⁰ AAD	11P ATLS	stable $\tilde{\tau}$, GMSB scenario, $\tan\beta = 5$

- ¹ AAD 23BQ searched in 139 fb^{-1} of pp collisions at $\sqrt{s} = 13 \text{ TeV}$ for pair production of long-lived $\tilde{\mu}$ in events with muons with impact parameters in the millimeter range. No significant excess above the Standard Model predictions is observed. Limits are set on $m_{\tilde{\mu}}$ as a function of the $\tilde{\mu}$ lifetime, assuming the $\tilde{\mu} \rightarrow \mu\tilde{G}$ decay and mass-degenerate $\tilde{\mu}_L$ and $\tilde{\mu}_R$. See Figure 4.
- ² AAD 23c searched in 139 fb^{-1} of pp collisions at $\sqrt{s} = 13 \text{ TeV}$ for stau pair production in events with high-pt tracks with large ionisation in the pixel detector. No significant excess above the Standard Model predictions is observed. Limits are set on the stau mass as a function of its lifetime, see Figure 19.

- ³ TUMASYAN 23AG searched in 138 fb^{-1} of pp collisions at $\sqrt{s} = 13 \text{ TeV}$ for direct pair production of tau sleptons in events with two hadronically decaying tau leptons. No significant excess above the Standard Model expectations is observed. Limits are set for the maximally mixed scenario with long-lived tau sleptons and $\tilde{\tau}$ lifetimes of 0.01 mm to 2.5 mm, see their figure 8. Limits are also set on the mass of the tau slepton in models with $\tilde{\tau} \rightarrow \tau \tilde{\chi}_1^0$ for mass-degenerate, pure left-handed and pure right-handed tau sleptons, see their figures 4–7.
- ⁴ TUMASYAN 22AF searched for evidence of new long-lived particles decaying to leptons in pp collisions at $\sqrt{s} = 13 \text{ TeV}$, corresponding to $118 (113) \text{ fb}^{-1}$ in the $e\mu$ and $\mu\mu$ channels. The leptons are required to have transverse impact parameter values between 0.01 and 10 cm and are not required to form a common vertex. No significant excess above the Standard Model expectations is observed. Limits are set on the mass of the top squark in RPV models with top squark pair production and $\tilde{t} \rightarrow b\tilde{\ell}$ and $\tilde{t} \rightarrow d\tilde{\ell}$, see their Figure 4, which contains a wider range of lifetime limits. Limits are also set on a gauge-mediated SUSY breaking model, where the next-to-lightest SUSY particle is a slepton and the lightest SUSY particle a gravitino \tilde{G} , see their Figure 5, which also contains a wider range of lifetime limits. Limits are also set in a model that produces BSM Higgs bosons (H) with a mass of 125 GeV through gluon fusion, where the H decays to two long-lived scalars S , each of which decays to two oppositely charged and same-flavor leptons.
- ⁵ AAD 21AL searched in 139 fb^{-1} of pp collisions at $\sqrt{s} = 13 \text{ TeV}$ for pair production of long-lived sleptons in events with highly displaced leptons. No significant excess above the Standard Model predictions is observed. Limits are set on $m_{\tilde{e}}, m_{\tilde{\mu}}, m_{\tilde{\tau}}$ as a function of the slepton lifetime, assuming the $\tilde{\ell} \rightarrow \ell \tilde{G}$ decay and mass-degenerate $\tilde{\ell}_L$ and $\tilde{\ell}_R$. See Figures 2.
- ⁶ AABOUD 19AT searched in 36.1 fb^{-1} of pp collisions at $\sqrt{s} = 13 \text{ TeV}$ for metastable and stable R -hadrons. Multiple search strategies for a wide range of lifetimes, corresponding to path lengths of a few meters, are defined. No significant deviations from the expected Standard Model background are observed. Results are interpreted in terms of exclusion limits on long-lived stau in the context of GMSB models. Lower limits on the mass for direct production of staus are set at 430 GeV, see their Fig. 10 (left).
- ⁷ KHACHATRYAN 16BW searched in 2.5 fb^{-1} of pp collisions at $\sqrt{s} = 13 \text{ TeV}$ for events with heavy stable charged particles, identified by their anomalously high energy deposits in the silicon tracker and/or long time-of-flight measurements by the muon system. No evidence for an excess over the expected background is observed. Limits are derived for pair production of tau sleptons as a function of mass, depending on their direct or inclusive production in a minimal GMSB scenario along the Snowmass Points and Slopes (SPS) line 7, see Fig. 4 and Table 7.
- ⁸ AAD 15AE searched in 19.1 fb^{-1} of pp collisions at $\sqrt{s} = 8 \text{ TeV}$ for heavy long-lived charged particles, measured through their specific ionization energy loss in the ATLAS pixel detector or their time-of-flight in the ALTAS muon system. In the absence of an excess of events above the expected backgrounds, limits are set on stable $\tilde{\tau}$ sleptons in various scenarios, see Figs. 5–7.
- ⁹ AAIJ 15BD searched in 3.0 fb^{-1} of pp collisions at $\sqrt{s} = 7$ and 8 TeV for evidence of Drell-Yan pair production of long-lived $\tilde{\tau}$ particles. No evidence for such particles is observed and 95% C.L. upper limits on the cross section of $\tilde{\tau}$ pair production are derived, see Fig. 7. In the mGMSB, assuming the SPST benchmark scenario $\tilde{\tau}$ masses between 124 and 309 GeV are excluded at 95% C.L.
- ¹⁰ ABBIENDI 03L used e^+e^- data at $\sqrt{s} = 130\text{--}209 \text{ GeV}$ to select events with two high momentum tracks with anomalous dE/dx . The excluded cross section is compared to the theoretical expectation as a function of the heavy particle mass in their Fig. 3. The limit improves to 98.5 GeV for $\tilde{\mu}_L$ and $\tilde{\tau}_L$. The bounds are valid for colorless spin 0 particles with lifetimes longer than 10^{-6} s . Supersedes the results from ACKERSTAFF 98P.
- ¹¹ ABREU 00Q searches for the production of pairs of heavy, charged stable particles in e^+e^- annihilation at $\sqrt{s} = 130\text{--}189 \text{ GeV}$. The upper bound improves to 88 GeV for $\tilde{\mu}_L$, $\tilde{\tau}_L$. These limits include and update the results of ABREU 98P.
- ¹² ACCIARRI 99H searched for production of pairs of back-to-back heavy charged particles at $\sqrt{s} = 130\text{--}183 \text{ GeV}$. The upper bound improves to 82.2 GeV for $\tilde{\mu}_L$, $\tilde{\tau}_L$.
- ¹³ The BARATE 98k mass limit improves to 82 GeV for $\tilde{\mu}_L, \tilde{\tau}_L$. Data collected at $\sqrt{s} = 161\text{--}184 \text{ GeV}$.
- ¹⁴ AAD 13AA searched in 4.7 fb^{-1} of pp collisions at $\sqrt{s} = 7 \text{ TeV}$ for events containing long-lived massive particles in a GMSB framework. No significant excess above the expected background was found. A 95% C.L. lower limit of 300 GeV is placed on long-lived $\tilde{\tau}$'s in the GMSB model with $M_{\text{mess}} = 250 \text{ TeV}$, $N_\zeta = 3$, $\mu > 0$, for $\tan\beta = 5\text{--}20$. The lower limit on the GMSB breaking scale Λ was found to be 99–110 TeV, for $\tan\beta$ values between 5 and 40, see Fig. 4 (top). Also, directly produced long-lived sleptons, or sleptons decaying to long-lived ones, are excluded at 95% C.L. up to a $\tilde{\tau}$ mass of 278 GeV for models with slepton splittings smaller than 50 GeV.
- ¹⁵ ABAZOV 13B looked in 6.3 fb^{-1} of $p\bar{p}$ collisions at $\sqrt{s} = 1.96 \text{ TeV}$ for charged massive long-lived particles in events with muon-like particles that have both speed and ionization energy loss inconsistent with muons produced in beam collisions. In the absence of an excess, limits are set at 95% C.L. on the production cross section of stau leptons in the mass range 100–300 GeV, see their Table 20 and Fig. 23.
- ¹⁶ CHATRCHYAN 13AB looked in 5.0 fb^{-1} of pp collisions at $\sqrt{s} = 7 \text{ TeV}$ and in 18.8 fb^{-1} of pp collisions at $\sqrt{s} = 8 \text{ TeV}$ for events with heavy stable particles, identified by their anomalous dE/dx in the tracker or additionally requiring that it be identified as muon in the muon chambers, from pair production of $\tilde{\tau}_1$'s. No evidence for an excess over the expected background is observed. Supersedes CHATRCHYAN 12L.
- ¹⁷ CHATRCHYAN 13AB limits are derived for pair production of $\tilde{\tau}_1$ as a function of mass in minimal GMSB scenarios along the Snowmass Points and Slopes (SPS) line 7 (see Fig. 8 and Table 7). The limit given here is valid for direct pair $\tilde{\tau}_1$ production.
- ¹⁸ CHATRCHYAN 13AB limits are derived for the production of $\tilde{\tau}_1$ as a function of mass in minimal GMSB scenarios along the Snowmass Points and Slopes (SPS) line 7 (see Fig. 8 and Table 7). The limit given here is valid for the production of $\tilde{\tau}_1$ from both direct pair production and from the decay of heavier supersymmetric particles.
- ¹⁹ CHATRCHYAN 12L looked in 5.0 fb^{-1} of pp collisions at $\sqrt{s} = 7 \text{ TeV}$ for events with heavy stable particles, identified by their anomalous dE/dx in the tracker or additionally requiring that it be identified as muon in the muon chambers, from pair production of $\tilde{\tau}_1$'s. No evidence for an excess over the expected background is observed. Limits are derived for the production of $\tilde{\tau}_1$ as a function of mass in minimal GMSB scenarios along the Snowmass Points and Slopes (SPS) line 7 (see Fig. 3). The limit given here is valid for the production of $\tilde{\tau}_1$ in the decay of heavier supersymmetric particles.
- ²⁰ AAD 11P looked in 37 pb^{-1} of pp collisions at $\sqrt{s} = 7 \text{ TeV}$ for events with two heavy stable particles, reconstructed in the Inner tracker and the Muon System and identified by their time of flight in the Muon System. No evidence for an excess over the SM expectation is observed. Limits on the mass are derived, see Fig. 3, for $\tilde{\tau}$ in a GMSB

scenario and for sleptons produced by electroweak processes only, in which case the limit degrades to 110 GeV.

\tilde{q} (Squark) mass limit

For $m_{\tilde{q}} > 60\text{--}70 \text{ GeV}$, it is expected that squarks would undergo a cascade decay via a number of neutralinos and/or charginos rather than undergo a direct decay to photinos as assumed by some papers. Limits obtained when direct decay is assumed are usually higher than limits when cascade decays are included.

Limits from e^+e^- collisions depend on the mixing angle of the lightest mass eigenstate $\tilde{q}_1 = \tilde{q}_R \sin\theta_q + \tilde{q}_L \cos\theta_q$. It is usually assumed that only the sbottom and stop squarks have non-trivial mixing angles (see the stop and sbottom sections). Here, unless otherwise noted, squarks are always taken to be either left/right degenerate, or purely of left or right type. Data from Z decays have set squark mass limits above 40 GeV, in the case of $\tilde{q} \rightarrow q \tilde{\chi}_1^0$ decays if $\Delta m = m_{\tilde{q}} - m_{\tilde{\chi}_1^0} \gtrsim 5 \text{ GeV}$. For smaller values of Δm , current constraints on the invisible width of the Z ($\Delta\Gamma_{\text{inv}} < 2.0 \text{ MeV}$, LEP 00) exclude $m_{\tilde{u}_{L,R}} < 44 \text{ GeV}$, $m_{\tilde{d}_R} < 33 \text{ GeV}$, $m_{\tilde{d}_L} < 44 \text{ GeV}$ and, assuming all squarks degenerate, $m_{\tilde{q}} < 45 \text{ GeV}$.

Some earlier papers are now obsolete and have been omitted. They were last listed in our PDG 14 edition: K. Olive, *et al.* (Particle Data Group), Chinese Physics **C38** 070001 (2014) (<http://pdg.lbl.gov>).

R-parity conserving \tilde{q} (Squark) mass limit

VALUE (GeV)	CL%	DOCUMENT ID	TECN	COMMENT
>1550	95	1 AAD	23AE ATLS	2 SFOS ℓ , jets, \cancel{E}_T , Tsqk2, $m_{\tilde{\chi}_2^0} = (m_{\tilde{q}} + m_{\tilde{\chi}_1^0})/2$, $m_{\tilde{\chi}_1^0} = 100 \text{ GeV}$
none 1200–2500	95	2 TUMASYAN	23x CMS	2 AK8 jets + 1 AK4 jet, $\tilde{q} \rightarrow q \tilde{\chi}_1^0$ and $\tilde{\chi}_2^0 \rightarrow H_1 \tilde{\chi}_1^0$, $40 < m_{H_1} < 120 \text{ GeV}$
>1400	95	3 AAD	21AK ATLS	ℓ^\pm + jets + \cancel{E}_T , Tsqk3, 4 degenerate light \tilde{q}_ℓ , $m_{\tilde{\chi}_1^\pm} = (m_{\tilde{q}} + m_{\tilde{\chi}_1^0})/2$, $m_{\tilde{\chi}_1^0} < 200 \text{ GeV}$
>1040	95	3 AAD	21AK ATLS	ℓ^\pm + jets + \cancel{E}_T , Tsqk3, 1 light \tilde{q}_ℓ , $m_{\tilde{\chi}_1^\pm} = (m_{\tilde{q}} + m_{\tilde{\chi}_1^0})/2$, $m_{\tilde{\chi}_1^0} < 200 \text{ GeV}$
> 925	95	4 AAD	21F ATLS	$\geq 1 \text{ jet} + \cancel{E}_T$, Tsqk1, $m_{\tilde{q}} - m_{\tilde{\chi}_1^0} = 5 \text{ GeV}$
> 550	95	4 AAD	21F ATLS	$\geq 1 \text{ jet} + \cancel{E}_T$, Tstop3, $m_{\tilde{t}} - m_{\tilde{\chi}_1^0} = 5 \text{ GeV}$
> 550	95	4 AAD	21F ATLS	$\geq 1 \text{ jet} + \cancel{E}_T$, Tstop4, $m_{\tilde{t}} - m_{\tilde{\chi}_1^0} = 5 \text{ GeV}$
> 545	95	4 AAD	21F ATLS	$\geq 1 \text{ jet} + \cancel{E}_T$, Tsb01, $m_{\tilde{b}} - m_{\tilde{\chi}_1^0} = 5 \text{ GeV}$
>1850	95	5 AAD	21L ATLS	jets + \cancel{E}_T , Tsqk1, 8 degenerate \tilde{q} , $m_{\tilde{\chi}_1^0} = 0 \text{ GeV}$
>1220	95	5 AAD	21L ATLS	jets + \cancel{E}_T , Tsqk1, 1 non-degenerate \tilde{q} , $m_{\tilde{\chi}_1^0} = 0 \text{ GeV}$
>1310	95	5 AAD	21L ATLS	jets + \cancel{E}_T , Tsqk3, 4 degenerate \tilde{q}_j , $m_{\tilde{\chi}_1^\pm} = (m_{\tilde{q}} + m_{\tilde{\chi}_1^0})/2$, $m_{\tilde{\chi}_1^0} = 0 \text{ GeV}$
>3000	95	5 AAD	21L ATLS	jets + \cancel{E}_T , combined $\tilde{g}\tilde{g}$, $\tilde{g}\tilde{q}$, $\tilde{q}\tilde{q}$ production, $\tilde{g} \rightarrow q q' \tilde{\chi}_1^0$, $\tilde{q} \rightarrow q \tilde{\chi}_1^0$, $m_{\tilde{q}} = m_{\tilde{g}}$, $m_{\tilde{\chi}_1^0} = 0 \text{ GeV}$
>1800	95	6 SIRUNYAN	21M CMS	$\ell^\pm \cancel{E}_T + \cancel{E}_T$, Tsqk2A, $m_{\tilde{\chi}_2^0} = 1500 \text{ GeV}$, $m_{\tilde{\chi}_1^0} = 100 \text{ GeV}$
>1590	95	7 SIRUNYAN	19Ag CMS	$2\gamma + \cancel{E}_T$, Tsqk4B, 500 GeV $< m_{\tilde{\chi}_1^0} < 1500 \text{ GeV}$
>1130	95	8 SIRUNYAN	19Ch CMS	jets + \cancel{E}_T , Tsqk1, 1 light flavour, $m_{\tilde{\chi}_1^0} = 0 \text{ GeV}$
>1630	95	8 SIRUNYAN	19Ch CMS	jets + \cancel{E}_T , Tsqk1, 8 degenerate light flavours, $m_{\tilde{\chi}_1^0} = 0 \text{ GeV}$
>1430	95	9 SIRUNYAN	19K CMS	$\gamma + \ell + \cancel{E}_T$, Tsqk4A, $m_{\tilde{\chi}_1^0} = 1200 \text{ GeV}$
>1200	95	10 AABOUD	18Bj ATLS	$\ell^\pm \cancel{E}_T + \text{jets} + \cancel{E}_T$, Tsqk2, $m_{\tilde{\chi}_2^0} = 1 \text{ GeV}$, any $m_{\tilde{\chi}_1^0}$
> 850	95	11 AABOUD	18Bv ATLS	c-jets + \cancel{E}_T , Tsqk1 (charm only), $m_{\tilde{\chi}_1^0} = 0 \text{ GeV}$
> 710	95	12 AABOUD	18l ATLS	$\geq 1 \text{ jets} + \cancel{E}_T$, Tsqk1, $m_{\tilde{q}} \sim m_{\tilde{\chi}_1^0}$

Searches Particle Listings

Supersymmetric Particle Searches

>1820	95	13	AABOUD	18U	ATLS	$2\gamma + \cancel{E}_T$, GGM, Tsqk4B, any NLSFP mass	>1430	95	39	CHATRCHYAN13H	CMS	$2\gamma + \geq 4$ jets + low \cancel{E}_T , stealth SUSY model	
>1550	95	14	AABOUD	18V	ATLS	jets + \cancel{E}_T , Tsqk1, $m_{\tilde{\chi}_1^0} = 0$ GeV	> 750	95	40	CHATRCHYAN13T	CMS	jets + \cancel{E}_T , $\tilde{q} \rightarrow q\tilde{\chi}_1^0$ simplified model, $m_{\tilde{\chi}_1^0} = 0$ GeV	
>1150	95	15	AABOUD	18V	ATLS	jets + \cancel{E}_T , Tsqk3, $m_{\tilde{\chi}_1^\pm} = 0.5(m_{\tilde{q}} + m_{\tilde{\nu}_\tau})$, $m_{\tilde{\chi}_1^0} = 0$ GeV	> 820	95	41	AAD	12AX	ATLS	$\ell +$ jets + \cancel{E}_T , CMSSM, $m_{\tilde{q}} = m_{\tilde{g}}$
>1650	95	16	SIRUNYAN	18AA	CMS	$\geq 1\gamma + \cancel{E}_T$, Tsqk4A	>1200	95	42	AAD	12CJ	ATLS	$\ell^\pm +$ jets + \cancel{E}_T , CMSSM, $m_{\tilde{q}} = m_{\tilde{g}}$
>1750	95	16	SIRUNYAN	18AA	CMS	$\geq 1\gamma + \cancel{E}_T$, Tsqk4B	> 870	95	43	AAD	12CP	ATLS	$2\gamma + \cancel{E}_T$, GMSB, bino NLSFP, $m_{\tilde{\chi}_1^0} > 50$ GeV
> 675	95	17	SIRUNYAN	18AY	CMS	jets + \cancel{E}_T , Tsqk1, 1 light flavor state, $m_{\tilde{\chi}_1^0} = 0$ GeV	> 950	95	44	AAD	12W	ATLS	jets + \cancel{E}_T , CMSSM, $m_{\tilde{q}} = m_{\tilde{g}}$
>1320	95	17	SIRUNYAN	18AY	CMS	jets + \cancel{E}_T , Tsqk1, 8 degenerate light flavor states, $m_{\tilde{\chi}_1^0} = 0$ GeV	> 760	95	45	CHATRCHYAN12	CMS	e, μ , jets, razor, CMSSM	
>1220	95	18	AABOUD	17AR	ATLS	$1\ell +$ jets + \cancel{E}_T , Tsqk3, $m_{\tilde{\chi}_1^0} = 0$ GeV	> 1110	95	46	CHATRCHYAN12AE	CMS	jets + \cancel{E}_T , $\tilde{q} \rightarrow q\tilde{\chi}_1^0$, $m_{\tilde{\chi}_1^0} < 200$ GeV	
>1000	95	19	AABOUD	17N	ATLS	2 same-flavour, opposite-sign $\ell +$ jets + \cancel{E}_T , Tsqk2, $m_{\tilde{\chi}_1^0} = 0$ GeV	>1180	95	47	CHATRCHYAN12AT	CMS	jets + \cancel{E}_T , CMSSM	
>1150	95	20	KHACHATRY...17P	CMS	1 or more jets + \cancel{E}_T , Tsqk1, 4(flavor) x 2(isospin) = 8 mass degenerate states, $m_{\tilde{\chi}_1^0} = 0$ GeV	>1080	95	47	CHATRCHYAN12AT	CMS	jets + \cancel{E}_T , CMSSM, $m_{\tilde{q}} = m_{\tilde{g}}$		
> 575	95	20	KHACHATRY...17P	CMS	1 or more jets + \cancel{E}_T , Tsqk1, one light flavor state, $m_{\tilde{\chi}_1^0} = 0$ GeV	>1080	95	48	AABOUD	18V	ATLS	jets + \cancel{E}_T , Tsqk5, $(m_{\tilde{\chi}_2^0} - m_{\tilde{\chi}_1^0}) / (m_{\tilde{q}} - m_{\tilde{\chi}_1^0}) < 0.95$, $m_{\tilde{\chi}_1^0} = 60$ GeV	
>1370	95	21	KHACHATRY...17V	CMS	$2\gamma + \cancel{E}_T$, GGM, Tsqk4, any NLSFP mass	>1650	95	49	KHACHATRY...16BT	CMS	19-parameter pMSSM model, global Bayesian analysis, flat prior		
>1600	95	22	SIRUNYAN	17AY	CMS	$\gamma +$ jets + \cancel{E}_T , Tsqk4B, $m_{\tilde{\chi}_1^0} = 0$ GeV	> 790	95	50	AAD	15AI	ATLS	$\ell^\pm +$ jets + \cancel{E}_T
>1370	95	22	SIRUNYAN	17AY	CMS	$\gamma +$ jets + \cancel{E}_T , Tsqk4A, $m_{\tilde{\chi}_1^0} = 0$ GeV	> 820	95	28	AAD	15BV	ATLS	jets + \cancel{E}_T , $m_{\tilde{g}} = m_{\tilde{q}}$, $m_{\tilde{\chi}_1^0} = 1$ GeV
>1050	95	23	SIRUNYAN	17AZ	CMS	≥ 1 jets + \cancel{E}_T , Tsqk1, single light flavor state, $m_{\tilde{\chi}_1^0} = 0$ GeV	> 820	95	28	AAD	15BV	ATLS	jets + \cancel{E}_T , $\tilde{q} \rightarrow qW\tilde{\chi}_1^0$, $m_{\tilde{\chi}_1^0} = 100$ GeV
>1550	95	23	SIRUNYAN	17AZ	CMS	≥ 1 jets + \cancel{E}_T , Tsqk1, 4(flavor) x 2(isospin) = 8 degenerate mass states, $m_{\tilde{\chi}_1^0} = 0$ GeV	> 850	95	28	AAD	15BV	ATLS	2 or 3 leptons + jets, \tilde{q} decays via sleptons, $m_{\tilde{\chi}_1^0} = 100$ GeV
>1390	95	24	SIRUNYAN	17P	CMS	jets + \cancel{E}_T , Tsqk1, 4(flavor) x 2(isospin) = 8 degenerate mass states, $m_{\tilde{\chi}_1^0} = 0$ GeV	> 700	95	28	AAD	15BV	ATLS	τ, \tilde{q} decays via staus, $m_{\tilde{\chi}_1^0} = 50$ GeV
> 950	95	24	SIRUNYAN	17P	CMS	jets + \cancel{E}_T , Tsqk1, one light flavor state, $m_{\tilde{\chi}_1^0} = 0$ GeV	> 700	95	51	KHACHATRY...15AR	CMS	$\tilde{q} \rightarrow q\tilde{\chi}_1^0, \tilde{\chi}_1^0 \rightarrow \tilde{S}g, \tilde{S} \rightarrow \tilde{S}\tilde{G}, \tilde{S} \rightarrow gg, m_{\tilde{S}} = 100$ GeV, $m_{\tilde{S}} = 90$ GeV	
> 608	95	25	AABOUD	16D	ATLS	≥ 1 jet + \cancel{E}_T , Tsqk1, $m_{\tilde{q}} - m_{\tilde{\chi}_1^0} \geq 5$ GeV	> 550	95	51	KHACHATRY...15AR	CMS	$\ell^\pm, \tilde{q} \rightarrow q\tilde{\chi}_1^\pm, \tilde{\chi}_1^\pm \rightarrow \tilde{S}W^\pm, \tilde{S} \rightarrow \tilde{S}\tilde{G}, \tilde{S} \rightarrow gg, m_{\tilde{S}} = 100$ GeV, $m_{\tilde{S}} = 90$ GeV	
>1030	95	26	AABOUD	16N	ATLS	≥ 2 jets + \cancel{E}_T , Tsqk1, $m_{\tilde{\chi}_1^0} = 0$ GeV	>1500	95	52	KHACHATRY...15AZ	CMS	$\geq 2\gamma, \geq 1$ jet, (Razor), bino-like NLSFP, $m_{\tilde{\chi}_1^0} = 375$ GeV	
> 600	95	27	KHACHATRY...16BS	CMS	jets + \cancel{E}_T , Tsqk1, single light squark, $m_{\tilde{\chi}_1^0} = 0$ GeV	>1000	95	52	KHACHATRY...15AZ	CMS	$\geq 1\gamma, \geq 2$ jet, wino-like NLSFP, $m_{\tilde{\chi}_1^0} = 375$ GeV		
>1260	95	27	KHACHATRY...16BS	CMS	jets + \cancel{E}_T , Tsqk1, 8 degenerate light squarks, $m_{\tilde{\chi}_1^0} = 0$ GeV	> 670	95	53	AAD	14E	ATLS	$\ell^\pm \ell^\pm (\ell^\mp) +$ jets, $\tilde{q} \rightarrow q'\tilde{\chi}_1^\pm, \tilde{\chi}_1^\pm \rightarrow W^{(*)\pm}\tilde{\chi}_2^0, \tilde{\chi}_2^0 \rightarrow Z^{(*)}\tilde{\chi}_1^0$ simplified model, $m_{\tilde{\chi}_1^0} < 300$ GeV	
> 850	95	28	AAD	15BV	ATLS	jets + $\cancel{E}_T, \tilde{q} \rightarrow q\tilde{\chi}_1^0, m_{\tilde{\chi}_1^0} = 100$ GeV	> 780	95	53	AAD	14E	ATLS	$\ell^\pm \ell^\pm (\ell^\mp) +$ jets, $\tilde{q} \rightarrow q'\tilde{\chi}_1^\pm/\tilde{\chi}_2^0, \tilde{\chi}_1^\pm \rightarrow \ell^\pm \nu\tilde{\chi}_1^0, \tilde{\chi}_2^0 \rightarrow \ell^\pm \ell^\mp (\nu\nu)\tilde{\chi}_1^0$ simplified model
> 250	95	29	AAD	15CS	ATLS	photon + $\cancel{E}_T, pp \rightarrow \tilde{q}\tilde{q}^*\gamma, \tilde{q} \rightarrow q\tilde{\chi}_1^0, m_{\tilde{q}} - m_{\tilde{\chi}_1^0} = m_c$	> 700	95	54	CHATRCHYAN13A0	CMS	$\ell^\pm \ell^\mp +$ jets + \cancel{E}_T , CMSSM, $m_0 < 700$ GeV	
> 490	95	30	AAD	15K	ATLS	$\tilde{c} \rightarrow c\tilde{\chi}_1^0, m_{\tilde{\chi}_1^0} < 200$ GeV	>1350	95	55	CHATRCHYAN13AV	CMS	jets (+ leptons) + \cancel{E}_T , CMSSM, $m_{\tilde{g}} = m_{\tilde{q}}$	
> 875	95	31	KHACHATRY...15AF	CMS	$\tilde{q} \rightarrow q\tilde{\chi}_1^0$, simplified model, 8 degenerate light $\tilde{q}, m_{\tilde{\chi}_1^0} = 0$	> 800	95	56	CHATRCHYAN13W	CMS	≥ 1 photons + jets + \cancel{E}_T , GGM, wino-like NLSFP, $m_{\tilde{\chi}_1^0} = 375$ GeV		
> 520	95	31	KHACHATRY...15AF	CMS	$\tilde{q} \rightarrow q\tilde{\chi}_1^0$, simplified model, single light squark, $m_{\tilde{\chi}_1^0} = 0$	>1000	95	56	CHATRCHYAN13W	CMS	≥ 2 photons + jets + \cancel{E}_T , GGM, bino-like NLSFP, $m_{\tilde{\chi}_1^0} = 375$ GeV		
>1450	95	31	KHACHATRY...15AF	CMS	CMSSM, $\tan\beta = 30, A_0 = -2\max(m_0, m_1/2), \mu > 0$	> 340	95	57	DREINER	12A	THEO	$m_{\tilde{q}} \sim m_{\tilde{\chi}_1^0}$	
> 850	95	32	AAD	14AE	ATLS	jets + $\cancel{E}_T, \tilde{q} \rightarrow q\tilde{\chi}_1^0$ simplified model, mass degenerate first and second generation squarks, $m_{\tilde{\chi}_1^0} = 0$ GeV	> 650	95	58	DREINER	12A	THEO	$m_{\tilde{q}} = m_{\tilde{g}} \sim m_{\tilde{\chi}_1^0}$
> 440	95	32	AAD	14AE	ATLS	jets + $\cancel{E}_T, \tilde{q} \rightarrow q\tilde{\chi}_1^0$ simplified model, single light-flavour squark, $m_{\tilde{\chi}_1^0} = 0$ GeV							
>1700	95	32	AAD	14AE	ATLS	jets + \cancel{E}_T, m SUGRA/CMSSM, $m_{\tilde{q}} = m_{\tilde{g}}$							
> 800	95	33	CHATRCHYAN14AH	CMS	jets + $\cancel{E}_T, \tilde{q} \rightarrow q\tilde{\chi}_1^0$ simplified model, $m_{\tilde{\chi}_1^0} = 50$ GeV								
> 780	95	34	CHATRCHYAN14I	CMS	multijets + $\cancel{E}_T, \tilde{q} \rightarrow q\tilde{\chi}_1^0$ simplified model, $m_{\tilde{\chi}_1^0} < 200$ GeV								
>1360	95	35	AAD	13L	ATLS	jets + \cancel{E}_T , CMSSM, $m_{\tilde{g}} = m_{\tilde{q}}$							
>1200	95	36	AAD	13Q	ATLS	$\gamma + b + \cancel{E}_T$, higgsino-like neutralino, $m_{\tilde{\chi}_1^0} > 220$ GeV, GMSB							
>1250	95	37	CHATRCHYAN13	CMS	$\ell^\pm \ell^\mp +$ jets + \cancel{E}_T , CMSSM								
		38	CHATRCHYAN13G	CMS	$0, 1, 2, \geq 3$ b-jets + \cancel{E}_T , CMSSM, $m_{\tilde{q}} = m_{\tilde{g}}$								

• • • We do not use the following data for averages, fits, limits, etc. • • •

1 AAD 23AE searched in 139 fb^{-1} of pp collisions at $\sqrt{s} = 13$ TeV for events with 2ℓ with same flavour and opposite sign, plus jets and \cancel{E}_T , defining signal region with the dilepton invariant mass both on- and off-shell with respect to the Z boson. No significant excess above the Standard Model predictions is observed. Limits are set on models of strong and electroweak production. In this case, limits are placed on the mass of pair-produced squarks, assuming a scenario like in Tsqk2, see figure 16.

2 TUMASYAN 23x searched in 138 fb^{-1} of pp collisions at $\sqrt{s} = 13$ TeV for squark pair production with cascade decays to CP-even singlet-like Higgs bosons (H_1), leading to final states with small missing transverse momentum. This search targets H_1 decays to $b\bar{b}$ -pairs that are reconstructed in large-area (AK8) jets. No significant excess above the Standard Model expectations is observed. Limits are set in the next-to-minimal supersymmetric extension of the SM, where a singlino of small mass leads to squark and gluino cascade decays that can predominantly end in a highly Lorentz-boosted singlet-like H_1 and a singlino-like neutralino $\tilde{\chi}_2^0$ of small transverse momentum. The eight first- and second-generation squarks are assumed mass-degenerate, and the gluino mass is set at 1% larger.

3 AAD 21AK searched in 139 fb^{-1} of pp collisions at $\sqrt{s} = 13$ TeV for pair production of gluinos and squarks in events with a single isolated electron or muon, originating from the decay of a W boson, multiple jets and significant \cancel{E}_T . No significant excess above the Standard Model expectations is observed. Limits are set on the gluino mass in the Tglu1B simplified model and on the squark mass in the Tsqk3 simplified model, see their Figure 8.

See key on page 1171

Searches Particle Listings Supersymmetric Particle Searches

- 4 AAD 21F searched in 139 fb^{-1} of pp collisions at $\sqrt{s} = 13 \text{ TeV}$ for pair production of squarks in events with a high- p_T jet and \cancel{E}_T . No significant excess above the Standard Model predictions is observed. Limits are set on the \tilde{t} mass in the Tstop3 and Tstop4, on the \tilde{b} mass in the Tsb0t1, and on the \tilde{q} mass in the Tsqk1 simplified model (four-flavour, two chirality states degeneracy).
- 5 AAD 21L searched in 139 fb^{-1} of pp collisions at $\sqrt{s} = 13 \text{ TeV}$ for pair production of gluinos and squarks in events with jets, large missing transverse momentum but no electrons or muons. No significant excess above the Standard Model expectations is observed. Limits are set on the gluino mass in the Tglu1A and Tglu1B simplified models, on the squark mass in the Tsqk1 and Tsqk3 simplified models and in a simplified model for gluino-squark production, see their Figures 13-17.
- 6 SIRUNYAN 21M searched in 137 fb^{-1} of pp collisions at $\sqrt{s} = 13 \text{ TeV}$ for supersymmetry in events with two opposite-sign same-flavor leptons (electrons, muons) and \cancel{E}_T . No significant excess above the Standard Model expectations is observed. Limits are set on the gluino mass in the simplified model Tglu4C, see their Figure 10, on the $\tilde{\chi}_2^0$ and $\tilde{\chi}_1^\pm$ mass in Tchi1n2Fa, see their Figure 11, on the $\tilde{\chi}_1^0$ mass in Tn1n1C and Tn1n1B for $m_{\tilde{\chi}_2^0} = m_{\tilde{\chi}_1^\pm} = m_{\tilde{\chi}_1^0}$, see their Figure 12. Limits are also set on the light squark mass for the simplified model Tsqk2A, on the sbottom mass in Tsb0t3, see their Figure 13, and on the slepton mass in direct electroweak pair production of mass-degenerate left- and right-handed sleptons (selectrons and smuons), see their Figure 14.
- 7 SIRUNYAN 19AG searched in 35.9 fb^{-1} of pp collisions at $\sqrt{s} = 13 \text{ TeV}$ for events with two photons and large \cancel{E}_T . No significant excess above the Standard Model expectations is observed. Limits are set on the gluino mass in the Tglu4B simplified model and on the squark mass in the Tsqk4B simplified model, see their Figure 3.
- 8 SIRUNYAN 19CH searched in 137 fb^{-1} of pp collisions at $\sqrt{s} = 13 \text{ TeV}$ for events containing multiple jets and large \cancel{E}_T . No significant excess above the Standard Model expectations is observed. Limits are set on the gluino mass in the Tglu1A, Tglu1C, Tglu2A and Tglu3A simplified models, see their Figure 13. Limits are also set on squark, sbottom and stop masses in the Tsqk1, Tsb0t1, Tstop1 simplified models, see their Figure 14.
- 9 SIRUNYAN 19K searched in 35.9 fb^{-1} of pp collisions at $\sqrt{s} = 13 \text{ TeV}$ for events with a photon, an electron or muon, and large \cancel{E}_T . No significant excess above the Standard Model expectations is observed. In the framework of GMSB, limits are set on the chargino and neutralino mass in the Tchi1n1A simplified model, see their Figure 6. Limits are also set on the gluino mass in the Tglu4A simplified model, and on the squark mass in the Tsqk4A simplified model, see their Figure 7.
- 10 AABOUD 18BJ searched in 36.1 fb^{-1} of pp collisions at $\sqrt{s} = 13 \text{ TeV}$ in events with two opposite-sign charged leptons (electrons and muons), jets and missing transverse momentum, with various requirements to be sensitive to signals with different kinematic endpoint values in the dilepton invariant mass distribution. The data are found to be consistent with the SM expectation. Results are interpreted in the Tsqk2 model in case of $m_{\tilde{\chi}_1^0} = 1 \text{ GeV}$: for any $m_{\tilde{\chi}_2^0}$, squark masses below 1200 GeV are excluded, see their Fig. 14(b).
- 11 AABOUD 18BV searched in 36.1 fb^{-1} of pp collisions at $\sqrt{s} = 13 \text{ TeV}$ for events with at least one jet identified as c -jet, large missing transverse energy and no leptons. Good agreement is observed between the number of events in data and Standard Model predictions. The results are translated into exclusion limits in Tsqk1 models considering only \tilde{c}_1 . In scenarios with massless neutralinos, scharm masses below 850 GeV are excluded. If the differences of the \tilde{c}_1 and $\tilde{\chi}_1^0$ masses is below 100 GeV , scharm masses below 500 GeV are excluded. See their Fig.6 and Fig.7.
- 12 AABOUD 18I searched in 36.1 fb^{-1} of pp collisions at $\sqrt{s} = 13 \text{ TeV}$ for events with at least one jet with a transverse momentum above 250 GeV and no leptons. Good agreement is observed between the number of events in data and Standard Model predictions. The results are translated into exclusion limits in Tsqk1 models. In the compressed scenario with similar squark and neutralino masses, squark masses below 710 GeV are excluded. See their Fig.10(b).
- 13 AABOUD 18U searched in 36.1 fb^{-1} of pp collisions at $\sqrt{s} = 13 \text{ TeV}$ in events with at least one isolated photon, possibly jets and significant transverse momentum targeting generalised models of gauge-mediated SUSY breaking. No significant excess of events is observed above the SM prediction. Results are interpreted in terms of lower limits on the masses of squark in Tsqk4B models. Masses below 1820 GeV are excluded for any NLSP mass, see their Fig. 9.
- 14 AABOUD 18V searched in 36.1 fb^{-1} of pp collisions at $\sqrt{s} = 13 \text{ TeV}$ in events with no charged leptons, jets and missing transverse momentum. The data are found to be consistent with the SM expectation. Results are interpreted in the Tsqk1 model: squark masses below 1550 GeV are excluded for massless LSP, see their Fig. 13(a).
- 15 AABOUD 18V searched in 36.1 fb^{-1} of pp collisions at $\sqrt{s} = 13 \text{ TeV}$ in events with no charged leptons, jets and missing transverse momentum. The data are found to be consistent with the SM expectation. Results are interpreted in the Tsqk3 model. Assuming that $m_{\tilde{\chi}_1^\pm} = 0.5 (m_{\tilde{q}} + m_{\tilde{\chi}_1^0})$, squark masses below 1150 GeV are excluded for massless LSP, see their Fig. 14(a). Exclusions are also shown assuming $m_{\tilde{\chi}_1^0} = 60 \text{ GeV}$, see their Fig. 14(b).
- 16 SIRUNYAN 18AA searched in 35.9 fb^{-1} of pp collisions at $\sqrt{s} = 13 \text{ TeV}$ for events with at least one photon and large \cancel{E}_T . No significant excess above the Standard Model expectations is observed. Limits are set on wino masses in a general gauge-mediated SUSY breaking (GGM) scenario with bino-like $\tilde{\chi}_1^0$ and wino-like $\tilde{\chi}_1^\pm$ and $\tilde{\chi}_2^0$, see Figure 7. Limits are also set on the NLSP mass in the Tchi1n1A and Tchi1ch1A simplified models, see their Figure 8. Finally, limits are set on the gluino mass in the Tglu4A and Tglu4B simplified models, see their Figure 9, and on the squark mass in the Tsqk4A and Tsqk4B simplified models, see their Figure 10.
- 17 SIRUNYAN 18AY searched in 35.9 fb^{-1} of pp collisions at $\sqrt{s} = 13 \text{ TeV}$ for events containing one or more jets and significant \cancel{E}_T . No significant excess above the Standard Model expectations is observed. Limits are set on the gluino mass in the Tglu1A, Tglu2A and Tglu3A simplified models, see their Figure 3. Limits are also set on squark, sbottom and stop masses in the Tsqk1, Tsb0t1, Tstop1 and Tstop4 simplified models, see their Figure 3. Finally, limits are set on long-lived gluino masses in a Tglu1A simplified model where the gluino is metastable or long-lived with proper decay lengths in the range $10^{-3} \text{ mm} < c\tau < 10^5 \text{ mm}$, see their Figure 4.
- 18 AABOUD 17AR searched in 36.1 fb^{-1} of pp collisions at $\sqrt{s} = 13 \text{ TeV}$ for events with one isolated lepton, at least two jets and large missing transverse momentum. No significant excess above the Standard Model expectations is observed. Limits up to 1.25 TeV are set on the 1st and 2nd generation squark masses in Tsqk3 simplified models, with $x = (m_{\tilde{\chi}_1^\pm} - m_{\tilde{\chi}_1^0}) / (m_{\tilde{q}} - m_{\tilde{\chi}_1^0}) = 1/2$. Similar limits are obtained for variable x and fixed neutralino mass, $m_{\tilde{\chi}_1^0} = 60 \text{ GeV}$. See their Figure 13.
- 19 AABOUD 17N searched in 14.7 fb^{-1} of pp collisions at $\sqrt{s} = 13 \text{ TeV}$ for events with 2 same-flavour, opposite-sign leptons (electrons or muons), jets and large missing transverse momentum. The results are interpreted as 95% C.L. limits in Tsqk2 models, assuming $m_{\tilde{\chi}_1^0} = 0 \text{ GeV}$ and $m_{\tilde{\chi}_2^0} = 600 \text{ GeV}$. See their Fig. 12 for exclusion limits as a function of $m_{\tilde{\chi}_1^0} / m_{\tilde{\chi}_2^0}$.
- 20 KHACHATRYAN 17P searched in 2.3 fb^{-1} of pp collisions at $\sqrt{s} = 13 \text{ TeV}$ for events with one or more jets and large \cancel{E}_T . No significant excess above the Standard Model expectations is observed. Limits are set on the gluino mass in the Tglu1A, Tglu2A, Tglu3A, Tglu3B, Tglu3C and Tglu3D simplified models, see their Figures 7 and 8. Limits are also set on the squark mass in the Tsqk1 simplified model, see their Fig. 7, and on the sbottom mass in the Tsb0t1 simplified model, see Fig. 8. Finally, limits are set on the stop mass in the Tstop1, Tstop3, Tstop4, Tstop6 and Tstop7 simplified models, see Fig. 8.
- 21 KHACHATRYAN 17V searched in 2.3 fb^{-1} of pp collisions at $\sqrt{s} = 13 \text{ TeV}$ for events with two photons and large \cancel{E}_T . No significant excess above the Standard Model expectations is observed. Limits are set on the gluino and squark mass in the context of general gauge mediation models Tglu4B and Tsqk4, see their Fig. 4.
- 22 SIRUNYAN 17AY searched in 35.9 fb^{-1} of pp collisions at $\sqrt{s} = 13 \text{ TeV}$ for events with at least one photon, jets and large \cancel{E}_T . No significant excess above the Standard Model expectations is observed. Limits are set on the gluino mass in the Tglu4A and Tglu4B simplified models, and on the squark mass in the Tsqk4A and Tsqk4B simplified models, see their Figure 6.
- 23 SIRUNYAN 17AZ searched in 35.9 fb^{-1} of pp collisions at $\sqrt{s} = 13 \text{ TeV}$ for events with one or more jets and large \cancel{E}_T . No significant excess above the Standard Model expectations is observed. Limits are set on the gluino mass in the Tglu1A, Tglu2A, Tglu3A simplified models, see their Figures 6. Limits are also set on the squark mass in the Tsqk1 simplified model (for single light squark and for 8 degenerate light squarks), on the sbottom mass in the Tsb0t1 simplified model and on the stop mass in the Tstop1 simplified model, see their Fig. 7. Finally, limits are set on the stop mass in the Tstop2, Tstop4 and Tstop8 simplified models, see Fig. 8.
- 24 SIRUNYAN 17P searched in 35.9 fb^{-1} of pp collisions at $\sqrt{s} = 13 \text{ TeV}$ for events with multiple jets and large \cancel{E}_T . No significant excess above the Standard Model expectations is observed. Limits are set on the gluino mass in the Tglu1A, Tglu1C, Tglu2A, Tglu3A and Tglu3D simplified models, see their Fig. 12. Limits are also set on the squark mass in the Tsqk1 simplified model, on the stop mass in the Tstop1 simplified model, and on the sbottom mass in the Tsb0t1 simplified model, see Fig. 13.
- 25 AABOUD 16D searched in 3.2 fb^{-1} of pp collisions at $\sqrt{s} = 13 \text{ TeV}$ for events with an energetic jet and large missing transverse momentum. The results are interpreted as 95% C.L. limits on masses of first and second generation squarks decaying into a quark and the lightest neutralino in scenarios with $m_{\tilde{q}} - m_{\tilde{\chi}_1^0} < 25 \text{ GeV}$. See their Fig. 6.
- 26 AABOUD 16N searched in 3.2 fb^{-1} of pp collisions at $\sqrt{s} = 13 \text{ TeV}$ for events containing hadronic jets, large \cancel{E}_T , and no electrons or muons. No significant excess above the Standard Model expectations is observed. First- and second-generation squark masses below 1030 GeV are excluded at the 95% C.L. decaying to quarks and a massless lightest neutralino. See their Fig. 7a.
- 27 KHACHATRYAN 16BS searched in 2.3 fb^{-1} of pp collisions at $\sqrt{s} = 13 \text{ TeV}$ for events with at least one energetic jet, no isolated leptons, and significant \cancel{E}_T , using the transverse mass variable M_{T2} to discriminate between signal and background processes. No significant excess above the Standard Model expectations is observed. Limits are set on the squark mass in the Tsqk1 simplified model, both in the assumption of a single light squark and of 8 degenerate squarks, see Fig. 11 and Table 3.
- 28 AAD 15Bv summarized and extended ATLAS searches for gluinos and first- and second-generation squarks in final states containing jets and missing transverse momentum, with or without leptons or b -jets in the $\sqrt{s} = 8 \text{ TeV}$ data set collected in 2012. The paper reports the results of new interpretations and statistical combinations of previously published analyses, as well as new analyses. Exclusion limits at 95% C.L. are set on the squark mass in several R-parity conserving models. See their Figs. 9, 11, 18, 22, 24, 27, 28.
- 29 AAD 15Cs searched in 20.3 fb^{-1} of pp collisions at $\sqrt{s} = 8 \text{ TeV}$ for evidence of pair production of squarks, decaying into a quark and a neutralino, where a photon was radiated either from an initial-state quark, from an intermediate squark, or from a final-state quark. No evidence was found for an excess above the expected level of Standard Model background and a 95% C.L. exclusion limit was set on the squark mass as a function of the squark-neutralino mass difference, see Fig. 19.
- 30 AAD 15k searched in 20.3 fb^{-1} of pp collisions at $\sqrt{s} = 8 \text{ TeV}$ for events containing at least two jets, where the two leading jets are each identified as originating from c -quarks, and large missing transverse momentum. No excess of events above the expected level of Standard Model background was found. Exclusion limits at 95% C.L. are set on the mass of superpartners of charm quarks (\tilde{c}). Assuming that the decay $\tilde{c} \rightarrow c\tilde{\chi}_1^0$ takes place 100% of the time, a scalar charm mass below 490 GeV is excluded for $m_{\tilde{\chi}_1^0} < 200 \text{ GeV}$. For more details, see their Fig. 2.
- 31 KHACHATRYAN 15AF searched in 19.5 fb^{-1} of pp collisions at $\sqrt{s} = 8 \text{ TeV}$ for events with at least two energetic jets and significant \cancel{E}_T , using the transverse mass variable M_{T2} to discriminate between signal and background processes. No significant excess above the Standard Model expectations is observed. Limits are set on the squark mass in simplified models where the decay $\tilde{q} \rightarrow q\tilde{\chi}_1^0$ takes place with a branching ratio of 100%, both for the case of a single light squark or 8 degenerate squarks, see Fig. 12. See also Table 5. Exclusions in the CMSSM, assuming $\tan\beta = 30$, $A_0 = -2 \max(m_0, m_{1/2})$ and $\mu > 0$, are also presented, see Fig. 15.
- 32 AAD 14AE searched in 20.3 fb^{-1} of pp collisions at $\sqrt{s} = 8 \text{ TeV}$ for strongly produced supersymmetric particles in events containing jets and large missing transverse momentum, and no electrons or muons. No excess over the expected SM background is observed. Exclusion limits are derived in simplified models containing squarks that decay via $\tilde{q} \rightarrow q\tilde{\chi}_1^0$, where either a single light state or two degenerate generations of squarks are assumed, see Fig. 10.
- 33 CHATRACHYAN 14AH searched in 4.7 fb^{-1} of pp collisions at $\sqrt{s} = 7 \text{ TeV}$ for events with at least two energetic jets and significant \cancel{E}_T , using the razor variables (M_R and R_2) to discriminate between signal and background processes. No significant excess above the Standard Model expectations is observed. Limits are set on squark masses in simplified models where the decay $\tilde{q} \rightarrow q\tilde{\chi}_1^0$ takes place with a branching ratio of 100%,

Searches Particle Listings

Supersymmetric Particle Searches

- see Fig. 28. Exclusions in the CMSSM, assuming $\tan\beta = 10$, $A_0 = 0$ and $\mu > 0$, are also presented, see Fig. 26.
- 34 CHATRCHYAN 14I searched in 19.5 fb^{-1} of pp collisions at $\sqrt{s} = 8 \text{ TeV}$ for events containing multijets and large E_T . No excess over the expected SM background is observed. Exclusion limits are derived in simplified models containing squarks that decay via $\tilde{q} \rightarrow q\tilde{\chi}_1^0$, where either a single light state or two degenerate generations of squarks are assumed, see Fig. 7a.
- 35 AAD 13L searched in 4.7 fb^{-1} of pp collisions at $\sqrt{s} = 7 \text{ TeV}$ for the production of squarks and gluinos in events containing jets, missing transverse momentum and no high- p_T electrons or muons. No excess over the expected SM background is observed. In mSUGRA/CMSSM models with $\tan\beta = 10$, $A_0 = 0$ and $\mu > 0$, squarks and gluinos of equal mass are excluded for masses below 1360 GeV at 95% C.L. In a simplified model containing only squarks of the first two generations, a gluino octet and a massless neutralino, squark masses below 1320 GeV are excluded at 95% C.L. for gluino masses below 2 TeV. See Figures 10–15 for more precise bounds.
- 36 AAD 13Q searched in 4.7 fb^{-1} of pp collisions at $\sqrt{s} = 7 \text{ TeV}$ for events containing a high- p_T isolated photon, at least one jet identified as originating from a bottom quark, and high missing transverse momentum. Such signatures may originate from supersymmetric models with gauge-mediated supersymmetry breaking in events in which one of a pair of higgsino-like neutralinos decays into a photon and a gravitino while the other decays into a Higgs boson and a gravitino. No significant excess above the expected background was found and limits were set on the squark mass as a function of the neutralino mass in a generalized GMSB model (GGM) with a higgsino-like neutralino NLSP, see their Fig. 4. For neutralino masses greater than 220 GeV, squark masses below 1020 GeV are excluded at 95% C.L.
- 37 CHATRCHYAN 13 looked in 4.98 fb^{-1} of pp collisions at $\sqrt{s} = 7 \text{ TeV}$ for events with two opposite-sign leptons (e, μ, τ), jets and missing transverse energy. No excess beyond the Standard Model expectation is observed. Exclusion limits are derived in the mSUGRA/CMSSM model with $\tan\beta = 10$, $A_0 = 0$ and $\mu > 0$, see Fig. 6.
- 38 CHATRCHYAN 13G searched in 4.98 fb^{-1} of pp collisions at $\sqrt{s} = 7 \text{ TeV}$ for the production of squarks and gluinos in events containing $0, 1, 2, \geq 3$ b-jets, missing transverse momentum and no electrons or muons. No excess over the expected SM background is observed. In mSUGRA/CMSSM models with $\tan\beta = 10$, $A_0 = 0$, and $\mu > 0$, squarks and gluinos of equal mass are excluded for masses below 1250 GeV at 95% C.L. Exclusions are also derived in various simplified models, see Fig. 7.
- 39 CHATRCHYAN 13H searched in 4.96 fb^{-1} of pp collisions at $\sqrt{s} = 7 \text{ TeV}$ for events with two photons, ≥ 4 jets and low E_T due to $\tilde{q} \rightarrow \gamma\tilde{\chi}_1^0$ decays in a stealth SUSY framework, where the $\tilde{\chi}_1^0$ decays through a singlino (\tilde{S}) intermediate state to $\gamma S \tilde{G}$, with the singlet state S decaying to two jets. No significant excess above the expected background was found and limits were set in a particular R-parity conserving stealth SUSY model. The model assumes $m_{\tilde{\chi}_1^0} = 0.5 m_{\tilde{q}}$, $m_{\tilde{S}} = 100 \text{ GeV}$ and $m_S = 90 \text{ GeV}$. Under these assumptions, squark masses less than 1430 GeV were excluded at the 95% C.L.
- 40 CHATRCHYAN 13T searched in 11.7 fb^{-1} of pp collisions at $\sqrt{s} = 8 \text{ TeV}$ for events with at least two energetic jets and significant E_T , using the α_T variable to discriminate between processes with genuine and misreconstructed E_T . No significant excess above the Standard Model expectations is observed. Limits are set on squark masses in simplified models where the decay $\tilde{q} \rightarrow q\tilde{\chi}_1^0$ takes place with a branching ratio of 100%, assuming an eightfold degeneracy of the masses of the first two generation squarks, see Fig. 8 and Table 9. Also limits in the case of a single light squark are given.
- 41 AAD 12AX searched in 1.04 fb^{-1} of pp collisions at $\sqrt{s} = 7 \text{ TeV}$ for supersymmetry in events containing jets, missing transverse momentum and one isolated electron or muon. No excess over the expected SM background is observed and model-independent limits are set on the cross section of new physics contributions to the signal regions. In mSUGRA/CMSSM models with $\tan\beta = 10$, $A_0 = 0$ and $\mu > 0$, squarks and gluinos of equal mass are excluded for masses below 820 GeV at 95% C.L. Limits are also set on simplified models for squark production and decay via an intermediate chargino and on supersymmetric models with bilinear R-parity violation. Supersedes AAD 11c.
- 42 AAD 12CJ searched in 4.7 fb^{-1} of pp collisions at $\sqrt{s} = 7 \text{ TeV}$ for events containing one or more isolated leptons (electrons or muons), jets and E_T . The observations are in good agreement with the SM expectations and exclusion limits have been set in number of SUSY models. In the mSUGRA/CMSSM model with $\tan\beta = 10$, $A_0 = 0$, and $\mu > 0$, 95% C.L. exclusion limits have been derived for $m_{\tilde{q}} < 1200 \text{ GeV}$, assuming equal squark and gluino masses. In minimal GMSB, values of the effective SUSY breaking scale $\Lambda < 50 \text{ TeV}$ are excluded at 95% C.L. for $\tan\beta < 45$. Also exclusion limits in a number of simplified models have been presented, see Figs. 10 and 12.
- 43 AAD 12CP searched in 4.8 fb^{-1} of pp collisions at $\sqrt{s} = 7 \text{ TeV}$ for events with two photons and large E_T due to $\tilde{\chi}_1^0 \rightarrow \gamma\tilde{G}$ decays in a GMSB framework. No significant excess above the expected background was found and limits were set on the squark mass as a function of the neutralino mass in a generalized GMSB model (GGM) with a bino-like neutralino NLSP. The other sparticle masses were decoupled, $\tan\beta = 2$ and $c\tau_{\text{NLSP}} < 0.1 \text{ mm}$. Also, in the framework of the SP58 model, a 95% C.L. lower limit was set on the breaking scale Λ of 196 TeV.
- 44 AAD 12W searched in 1.04 fb^{-1} of pp collisions at $\sqrt{s} = 7 \text{ TeV}$ for the production of squarks and gluinos in events containing jets, missing transverse momentum and no electrons or muons. No excess over the expected SM background is observed. In mSUGRA/CMSSM models with $\tan\beta = 10$, $A_0 = 0$ and $\mu > 0$, squarks and gluinos of equal mass are excluded for masses below 950 GeV at 95% C.L. In a simplified model containing only squarks of the first two generations, a gluino octet and a massless neutralino, squark masses below 875 GeV are excluded at 95% C.L.
- 45 CHATRCHYAN 12 looked in 35 pb^{-1} of pp collisions at $\sqrt{s} = 7 \text{ TeV}$ for events with e and/or μ and/or jets, a large total transverse energy, and E_T . The event selection is based on the dimensionless razor variable R , related to the E_T and $M_{\tilde{q}}$, an indicator of the heavy particle mass scale. No evidence for an excess over the expected background is observed. Limits are derived in the CMSSM ($m_0, m_{1/2}$) plane for $\tan\beta = 3, 10$ and 50 (see Fig. 7 and 8). Limits are also obtained for Simplified Model Spectra.
- 46 CHATRCHYAN 12AE searched in 4.98 fb^{-1} of pp collisions at $\sqrt{s} = 7 \text{ TeV}$ for events with at least three jets and large missing transverse momentum. No significant excesses over the expected SM backgrounds are observed and 95% C.L. limits on the production cross section of squarks in a scenario where $\tilde{q} \rightarrow q\tilde{\chi}_1^0$ with a 100% branching ratio, see Fig. 3. For $m_{\tilde{\chi}_1^0} < 200 \text{ GeV}$, values of $m_{\tilde{q}}$ below 760 GeV are excluded at 95% C.L. Also limits in the CMSSM are presented, see Fig. 2.
- 47 CHATRCHYAN 12AT searched in 4.73 fb^{-1} of pp collisions at $\sqrt{s} = 7 \text{ TeV}$ for the production of squarks and gluinos in events containing jets, missing transverse momentum and no electrons or muons. No excess over the expected SM background is observed. In mSUGRA/CMSSM models with $\tan\beta = 10$, $A_0 = 0$ and $\mu > 0$, squarks with masses below 1110 GeV are excluded at 95% C.L. Squarks and gluinos of equal mass are excluded for masses below 1180 GeV at 95% C.L. Exclusions are also derived in various simplified models, see Fig. 6.
- 48 AABOUD 18V searched in 36.1 fb^{-1} of pp collisions at $\sqrt{s} = 13 \text{ TeV}$ in events with no charged leptons, jets and missing transverse momentum. The data are found to be consistent with the SM expectation. Results are interpreted in the Tsq5k model. Squark masses below 1100 GeV are excluded if $(m_{\tilde{\chi}_2^0} - m_{\tilde{\chi}_1^0})/(m_{\tilde{q}} - m_{\tilde{\chi}_1^0}) < 0.95$ and $m_{\tilde{\chi}_1^0} = 60 \text{ GeV}$, see their Fig. 16(a).
- 49 KHACHATRYAN 16BT performed a global Bayesian analysis of a wide range of CMS results obtained with data samples corresponding to 5.0 fb^{-1} of pp collisions at $\sqrt{s} = 7 \text{ TeV}$ and in 19.5 fb^{-1} of pp collisions at $\sqrt{s} = 8 \text{ TeV}$. The set of searches considered, both individually and in combination, includes those with all-hadronic final states, same-sign and opposite-sign dileptons, and multi-lepton final states. An interpretation was given in a scan of the 19-parameter pMSSM. No scan points with a gluino mass less than 500 GeV survived and 98% of models with a squark mass less than 300 GeV were excluded.
- 50 AAD 15AI searched in 20 fb^{-1} of pp collisions at $\sqrt{s} = 8 \text{ TeV}$ for events containing at least one isolated lepton (electron or muon), jets, and large missing transverse momentum. No excess of events above the expected level of Standard Model background was found. Exclusion limits at 95% C.L. are set on the squark masses in the CMSSM/mSUGRA, see Fig. 15, in the NUHM2, see Fig. 16, and in various simplified models, see Figs. 19–21.
- 51 KHACHATRYAN 15AR searched in 19.7 fb^{-1} of pp collisions at $\sqrt{s} = 8 \text{ TeV}$ for events containing jets, either a charged lepton or a photon, and low missing transverse momentum. No significant excess above the Standard Model expectations is observed. Limits are set on the squark mass in a stealth SUSY model where the decays $\tilde{q} \rightarrow q\tilde{\chi}_1^\pm$, $\tilde{\chi}_1^\pm \rightarrow \tilde{S} W^\pm$, $\tilde{S} \rightarrow S \tilde{G}$ and $S \rightarrow g g$, with $m_{\tilde{S}} = 100 \text{ GeV}$ and $m_S = 90 \text{ GeV}$, take place with a branching ratio of 100%. See Fig. 6 for γ or Fig. 7 for e^\pm analyses.
- 52 KHACHATRYAN 15AZ searched in 19.7 fb^{-1} of pp collisions at $\sqrt{s} = 8 \text{ TeV}$ for events with either at least one photon, hadronic jets and E_T (single photon channel) or with at least two photons and at least one jet and using the razor variables. No significant excess above the Standard Model expectations is observed. Limits are set on gluino masses in the general gauge-mediated SUSY breaking model (GGM), for both a bino-like and wino-like neutralino NLSP scenario, see Fig. 8 and 9.
- 53 AAD 14E searched in 20.3 fb^{-1} of pp collisions at $\sqrt{s} = 8 \text{ TeV}$ for strongly produced supersymmetric particles in events containing jets and two same-sign leptons or three leptons. The search also utilises jets originating from b -quarks, missing transverse momentum and other variables. No excess over the expected SM background is observed. Exclusion limits are derived in simplified models containing gluinos and squarks, see Figures 5 and 6. In the $\tilde{q} \rightarrow q'\tilde{\chi}_1^\pm$, $\tilde{\chi}_1^\pm \rightarrow W^{(*)}\tilde{\chi}_2^0$, $\tilde{\chi}_2^0 \rightarrow Z^{(*)}\tilde{\chi}_1^0$ simplified model, the following assumptions have been made: $m_{\tilde{\chi}_1^\pm} = 0.5 m_{\tilde{\chi}_2^0} + m_{\tilde{g}}$, $m_{\tilde{\chi}_2^0} = 0.5 (m_{\tilde{\chi}_1^\pm} + m_{\tilde{q}})$. In the $\tilde{q} \rightarrow q'\tilde{\chi}_1^\pm$ or $\tilde{q} \rightarrow q'\tilde{\chi}_2^0$, $\tilde{\chi}_1^\pm \rightarrow e^\pm \nu \tilde{\chi}_1^0$ or $\tilde{\chi}_2^0 \rightarrow e^\pm \nu (\nu) \tilde{\chi}_1^0$ simplified model, the following assumptions have been made: $m_{\tilde{\chi}_1^\pm} = m_{\tilde{\chi}_2^0} = 0.5 (m_{\tilde{\chi}_1^\pm} + m_{\tilde{q}})$, $m_{\tilde{\chi}_2^0} < 460 \text{ GeV}$. Limits are also derived in the mSUGRA/CMSSM, bRPV and GMSB models, see their Fig. 8.
- 54 CHATRCHYAN 13AO searched in 4.98 fb^{-1} of pp collisions at $\sqrt{s} = 7 \text{ TeV}$ for events with two opposite-sign isolated leptons accompanied by hadronic jets and E_T . No significant excesses over the expected SM backgrounds are observed and 95% C.L. exclusion limits are derived in the mSUGRA/CMSSM model with $\tan\beta = 10$, $A_0 = 0$ and $\mu > 0$, see Fig. 8.
- 55 CHATRCHYAN 13AV searched in 4.7 fb^{-1} of pp collisions at $\sqrt{s} = 7 \text{ TeV}$ for new heavy particle pairs decaying into jets (possibly b -tagged), leptons and E_T using the Razor variables. No significant excesses over the expected SM backgrounds are observed and 95% C.L. exclusion limits are derived in the mSUGRA/CMSSM model with $\tan\beta = 10$, $A_0 = 0$ and $\mu > 0$, see Fig. 3. The results are also interpreted in various simplified models, see Fig. 4.
- 56 CHATRCHYAN 13W searched in 4.93 fb^{-1} of pp collisions at $\sqrt{s} = 7 \text{ TeV}$ for events with one or more photons, hadronic jets and E_T . No significant excess above the Standard Model expectations is observed. Limits are set on squark masses in the general gauge-mediated SUSY breaking model (GGM), for both a wino-like and bino-like neutralino NLSP scenario, see Fig. 5.
- 57 DREINER 12A reassesses constraints from CMS (at 7 TeV, $\sim 4.4 \text{ fb}^{-1}$) under the assumption that the first and second generation squarks and the lightest SUSY particle are quasi-degenerate in mass (compressed spectrum).
- 58 DREINER 12A reassesses constraints from CMS (at 7 TeV, $\sim 4.4 \text{ fb}^{-1}$) under the assumption that the first and second generation squarks, the gluino, and the lightest SUSY particle are quasi-degenerate in mass (compressed spectrum).

R-parity violating \tilde{q} (Squark) mass limit

VALUE (GeV)	CL%	DOCUMENT ID	TECN	COMMENT
none	100–720	95	1 SIRUNYAN 18EA CMS	2 large jets with four-parton substructure, $\tilde{q} \rightarrow 4q$
>1600	95	2 KHACHATRYAN...16BX CMS		$\tilde{q} \rightarrow q\tilde{\chi}_1^0, \tilde{\chi}_1^0 \rightarrow \ell\ell\nu, \lambda_{121}$ or $\lambda_{122} \neq 0, m_{\tilde{g}} = 2400 \text{ GeV}$
>1000	95	3 AAD 15CB ATLS		jets, $\tilde{q} \rightarrow q\tilde{\chi}_1^0, \tilde{\chi}_1^0 \rightarrow \ell q q$, $m_{\tilde{\chi}_1^0} = 108 \text{ GeV}$ and $2.5 < c\tau_{\tilde{\chi}_1^0} < 200 \text{ mm}$
		4 AAD 12AX ATLS		ℓ + jets + E_T , CMSSM, $m_{\tilde{q}} = m_{\tilde{g}}$
		5 CHATRCHYAN 12AL CMS		$\geq 3e^\pm$

¹ SIRUNYAN 18EA searched in 38.2 fb^{-1} of pp collisions at $\sqrt{s} = 13 \text{ TeV}$ for the pair production of resonances, each decaying to at least four quarks. Reconstructed particles are clustered into two large jets of similar mass, each consistent with four-parton substructure. No statistically significant excess over the Standard Model expectation is observed. Limits are set on the squark and gluino mass in RPV supersymmetry models where squarks (gluinos) decay, through intermediate higgsinos, to four (five) quarks, see their Figure 4.

² KHACHATRYAN 16BX searched in 19.5 fb^{-1} of pp collisions at $\sqrt{s} = 8 \text{ TeV}$ for events containing 4 leptons coming from R-parity-violating decays of $\tilde{\chi}_1^0 \rightarrow \ell\ell\nu$ with $\lambda_{121} \neq$

0 or $\lambda_{122} \neq 0$. No excess over the expected background is observed. Limits are derived on the gluino, squark and stop masses, see Fig. 23.

³AAD 15CB searched for events containing at least one long-lived particle that decays at a significant distance from its production point (displaced vertex, DV) into two leptons or into five or more charged particles in 20.3 fb^{-1} of pp collisions at $\sqrt{s} = 8 \text{ TeV}$. The dilepton signature is characterised by DV formed from at least two lepton candidates. Four different final states were considered for the multitrack signature, in which the DV must be accompanied by a high-transverse momentum muon or electron candidate that originates from the DV, jets or missing transverse momentum. No events were observed in any of the signal regions. Results were interpreted in SUSY scenarios involving R-parity violation, split supersymmetry, and gauge mediation. See their Fig. 14–20.

⁴AAD 12AX searched in 1.04 fb^{-1} of pp collisions at $\sqrt{s} = 7 \text{ TeV}$ for supersymmetry in events containing jets, missing transverse momentum and one isolated electron or muon. No excess over the expected SM background is observed and model-independent limits are set on the cross section of new physics contributions to the signal regions. In mSUGRA/CMSSM models with $\tan\beta = 10$, $A_0 = 0$ and $\mu > 0$, squarks and gluinos of equal mass are excluded for masses below 820 GeV at 95% C.L. Limits are also set on simplified models for squark production and decay via an intermediate chargino and on supersymmetric models with bilinear R-parity violation. Supersedes AAD 11G.

⁵CHATRCHYAN 12AL looked in 4.98 fb^{-1} of pp collisions at $\sqrt{s} = 7 \text{ TeV}$ for anomalous production of events with three or more isolated leptons. Limits on squark and gluino masses are set in RPV SUSY models with leptonic $LL\bar{E}$ couplings, $\lambda_{123} > 0.05$, and hadronic \overline{UDD} couplings, $\lambda_{112}^{\prime\prime} > 0.05$, see their Fig. 5. In the \overline{UDD} case the leptons arise from supersymmetric cascade decays. A very specific supersymmetric spectrum is assumed. All decays are prompt.

Long-lived \tilde{q} (Squark) mass limit

The following are bounds on long-lived scalar quarks, assumed to hadronise into hadrons with lifetime long enough to escape the detector prior to a possible decay. Limits may depend on the mixing angle of mass eigenstates: $\tilde{q}_1 = \tilde{q}_L \cos\theta_q + \tilde{q}_R \sin\theta_q$.

The coupling to the Z^0 boson vanishes for up-type squarks when $\theta_u = 0.98$, and for down type squarks when $\theta_d = 1.17$.

VALUE (GeV)	CL%	DOCUMENT ID	TECN	COMMENT
>1250	95	¹ AABOUD 19AT ATLS	19AT ATLS	\tilde{b} R-hadrons
>1340	95	² AABOUD 19AT ATLS	19AT ATLS	\tilde{t} R-hadrons
>1600	95	³ SIRUNYAN 19BH CMS	19BH CMS	long-lived \tilde{t} , RPV, $\tilde{t} \rightarrow \bar{d}\bar{d}, 10 \text{ mm} < c\tau < 110 \text{ mm}$
>1350	95	³ SIRUNYAN 19BH CMS	19BH CMS	long-lived \tilde{t} , RPV, $\tilde{t} \rightarrow b\bar{l}, 7 \text{ mm} < c\tau < 110 \text{ mm}$
> 805	95	⁴ AABOUD 16B ATLS	16B ATLS	\tilde{b} R-hadrons
> 890	95	⁵ AABOUD 16B ATLS	16B ATLS	\tilde{t} R-hadrons
>1040	95	⁶ KHACHATRY..16BW CMS	16BW CMS	\tilde{t} R-hadrons, cloud interaction model
>1000	95	⁶ KHACHATRY..16BW CMS	16BW CMS	\tilde{t} R-hadrons, charge-suppressed interaction model
> 845	95	⁷ AAD 15AE ATLS	15AE ATLS	\tilde{b} R-hadron, stable, Regge model
> 900	95	⁷ AAD 15AE ATLS	15AE ATLS	\tilde{t} R-hadron, stable, Regge model
>1500	95	⁷ AAD 15AE ATLS	15AE ATLS	\tilde{g} decaying to 300 GeV stable sleptons, LeptoSUSY model
> 751	95	⁸ AAD 15BM ATLS	15BM ATLS	\tilde{b} R-hadron, stable, Regge model
> 766	95	⁸ AAD 15BM ATLS	15BM ATLS	\tilde{t} R-hadron, stable, Regge model
> 525	95	⁹ KHACHATRY..15AK CMS	15AK CMS	\tilde{t} R-hadrons, $10 \mu\text{s} < \tau < 1000 \text{ s}$
> 470	95	⁹ KHACHATRY..15AK CMS	15AK CMS	\tilde{t} R-hadrons, $1 \mu\text{s} < \tau < 1000 \text{ s}$

••• We do not use the following data for averages, fits, limits, etc. •••

> 683	95	¹⁰ AAD 13AA ATLS	13AA ATLS	\tilde{t} , R-hadrons, generic interaction model
> 612	95	¹¹ AAD 13AA ATLS	13AA ATLS	\tilde{b} , R-hadrons, generic interaction model
> 344	95	¹² AAD 13BC ATLS	13BC ATLS	R-hadrons, $\tilde{t} \rightarrow b\tilde{\chi}_1^0$, Regge model, lifetime between 10^{-5} and 10^3 s , $m_{\tilde{\chi}_1^0} = 100 \text{ GeV}$
> 379	95	¹³ AAD 13BC ATLS	13BC ATLS	R-hadrons, $\tilde{t} \rightarrow t\tilde{\chi}_1^0$, Regge model, lifetime between 10^{-5} and 10^3 s , $m_{\tilde{\chi}_1^0} = 100 \text{ GeV}$
> 935	95	¹⁴ CHATRCHYAN 13AB CMS	13AB CMS	long-lived \tilde{t} forming R-hadrons, cloud interaction model

¹AABOUD 19AT searched in 36.1 fb^{-1} of pp collisions at $\sqrt{s} = 13 \text{ TeV}$ for metastable and stable R-hadrons. Multiple search strategies for a wide range of lifetimes, corresponding to path lengths of a few meters, are defined. No significant deviations from the expected Standard Model background are observed. Sbottom R-hadrons are excluded at 95% C.L. for masses below 1250 GeV. Less stringent constraints are achieved with the muon-spectrometer agnostic analysis. See their Figure 9 (bottom-left).

²AABOUD 19AT searched in 36.1 fb^{-1} of pp collisions at $\sqrt{s} = 13 \text{ TeV}$ for metastable and stable R-hadrons. Multiple search strategies for a wide range of lifetimes, corresponding to path lengths of a few meters, are defined. No significant deviations from the expected Standard Model background are observed. Stop R-hadrons are excluded at 95% C.L. for masses below 1340 GeV. Similar constraints are achieved with the muon-spectrometer agnostic analysis. See their Figure 9 (bottom-right).

³SIRUNYAN 19BH searched in 35.9 fb^{-1} of pp collisions at $\sqrt{s} = 13 \text{ TeV}$ for long-lived particles decaying into jets, with each long-lived particle having a decay vertex well displaced from the production vertex. The selected events are found to be consistent with standard model predictions. Limits are set on the gluino mass in a GMSB model where the gluino is decaying via $\tilde{g} \rightarrow g\tilde{G}$, see their Figure 4 and in an RPV model of supersymmetry where the gluino is decaying via $\tilde{g} \rightarrow \tilde{t}\tilde{b}$, see their Figures 5. Limits are also set on the stop mass in two RPV models, see their Figure 6 (for $\tilde{t} \rightarrow b\bar{l}$ decays) and Figure 7 (for $\tilde{t} \rightarrow \bar{d}\bar{d}$ decays).

⁴AABOUD 16B searched in 3.2 fb^{-1} of pp collisions at $\sqrt{s} = 13 \text{ TeV}$ for long-lived R-hadrons using observables related to large ionization losses and slow propagation velocities, which are signatures of heavy charged particles traveling significantly slower than the speed of light. Exclusion limits at 95% C.L. are set on the long-lived sbottom masses exceeding 805 GeV. See their Fig. 5.

⁵AABOUD 16B searched in 3.2 fb^{-1} of pp collisions at $\sqrt{s} = 13 \text{ TeV}$ for long-lived R-hadrons using observables related to large ionization losses and slow propagation velocities, which are signatures of heavy charged particles traveling significantly slower than the speed of light. Exclusion limits at 95% C.L. are set on the long-lived stop masses exceeding 890 GeV. See their Fig. 5.

⁶KHACHATRYAN 16BW searched in 2.5 fb^{-1} of pp collisions at $\sqrt{s} = 13 \text{ TeV}$ for events with heavy stable charged particles, identified by their anomalously high energy deposits in the silicon tracker and/or long time-of-flight measurements by the muon system. No evidence for an excess over the expected background is observed. Limits are derived for pair production of top squarks as a function of mass, depending on the interaction model, see Fig. 4 and Table 7.

⁷AAD 15AE searched in 19.1 fb^{-1} of pp collisions at $\sqrt{s} = 8 \text{ TeV}$ for heavy long-lived charged particles, measured through their specific ionization energy loss in the ATLAS pixel detector or their time-of-flight in the ALTAS muon system. In the absence of an excess of events above the expected backgrounds, limits are set R-hadrons in various scenarios, see Fig. 11. Limits are also set in LeptoSUSY models where the gluino decays to stable 300 GeV leptons, see Fig. 9.

⁸AAD 15BM searched in 18.4 fb^{-1} of pp collisions at $\sqrt{s} = 8 \text{ TeV}$ for stable and metastable non-relativistic charged particles through their anomalously specific ionization energy loss in the ATLAS pixel detector. In absence of an excess of events above the expected backgrounds, limits are set on stable bottom and top squark R-hadrons, see Table 5.

⁹KHACHATRYAN 15AK looked in a data set corresponding to fb^{-1} of pp collisions at $\sqrt{s} = 8 \text{ TeV}$, and a search interval corresponding to 281 h of trigger lifetime, for long-lived particles that have stopped in the CMS detector. No evidence for an excess over the expected background in a cloud interaction model is observed. Assuming the decay $\tilde{t} \rightarrow t\tilde{\chi}_1^0$ and lifetimes between $1 \mu\text{s}$ and 1000 s , limits are derived on \tilde{t} production as a function of $m_{\tilde{\chi}_1^0}$, see Figs. 4 and 7. The exclusions require that $m_{\tilde{\chi}_1^0}$ is kinematically consistent with the minimum values of the jet energy thresholds used.

¹⁰AAD 13AA searched in 4.7 fb^{-1} of pp collisions at $\sqrt{s} = 7 \text{ TeV}$ for events containing colored long-lived particles that hadronize forming R-hadrons. No significant excess above the expected background was found. Long-lived R-hadrons containing a \tilde{t} are excluded for masses up to 683 GeV at 95% C.L. in a general interaction model. Also, limits independent of the fraction of R-hadrons that arrive charged in the muon system were derived, see Fig. 6.

¹¹AAD 13AA searched in 4.7 fb^{-1} of pp collisions at $\sqrt{s} = 7 \text{ TeV}$ for events containing colored long-lived particles that hadronize forming R-hadrons. No significant excess above the expected background was found. Long-lived R-hadrons containing a \tilde{b} are excluded for masses up to 612 GeV at 95% C.L. in a general interaction model. Also, limits independent of the fraction of R-hadrons that arrive charged in the muon system were derived, see Fig. 6.

¹²AAD 13BC searched in 5.0 fb^{-1} of pp collisions at $\sqrt{s} = 7 \text{ TeV}$ and in 22.9 fb^{-1} of pp collisions at $\sqrt{s} = 8 \text{ TeV}$ for bottom squark R-hadrons that have come to rest within the ATLAS calorimeter and decay at some later time to hadronic jets and a neutralino. In absence of an excess of events above the expected backgrounds, limits are set on sbottom masses for the decay $\tilde{b} \rightarrow b\tilde{\chi}_1^0$ for different lifetimes, and for a neutralino mass of 100 GeV, see their Table 6 and Fig 10.

¹³AAD 13BC searched in 5.0 fb^{-1} of pp collisions at $\sqrt{s} = 7 \text{ TeV}$ and in 22.9 fb^{-1} of pp collisions at $\sqrt{s} = 8 \text{ TeV}$ for bottom squark R-hadrons that have come to rest within the ATLAS calorimeter and decay at some later time to hadronic jets and a neutralino. In absence of an excess of events above the expected backgrounds, limits are set on stop masses for the decay $\tilde{t} \rightarrow t\tilde{\chi}_1^0$ for different lifetimes, and for a neutralino mass of 100 GeV, see their Table 6 and Fig 10.

¹⁴CHATRCHYAN 13AB looked in 5.0 fb^{-1} of pp collisions at $\sqrt{s} = 7 \text{ TeV}$ and in 18.8 fb^{-1} of pp collisions at $\sqrt{s} = 8 \text{ TeV}$ for events with heavy stable particles, identified by their anomalously dE/dx in the tracker or additionally requiring that it be identified as muon in the muon chambers, from pair production of \tilde{t}_1 's. No evidence for an excess over the expected background is observed. Limits are derived for pair production of stops as a function of mass in the cloud interaction model (see Fig. 8 and Table 6). In the charge-suppressed model, the limit decreases to 818 GeV.

\tilde{b} (Sbottom) mass limit

Limits in e^+e^- depend on the mixing angle of the mass eigenstate $\tilde{b}_1 = \tilde{b}_L \cos\theta_b + \tilde{b}_R \sin\theta_b$. Coupling to the Z vanishes for $\theta_b \sim 1.17$. As a consequence, no absolute constraint in the mass region $\lesssim 40 \text{ GeV}$ is available in the literature at this time from e^+e^- collisions. In the Listings below, we use $\Delta m = m_{\tilde{b}_1} - m_{\tilde{\chi}_1^0}$.

Some earlier papers are now obsolete and have been omitted. They were last listed in our PDG 14 edition: K. Olive, et al. (Particle Data Group), Chinese Physics **C38** 070001 (2014) (<http://pdg.lbl.gov>).

R-parity conserving \tilde{b} (Sbottom) mass limit

VALUE (GeV)	CL%	DOCUMENT ID	TECN	COMMENT
> 850	95	¹ AAD 21AM ATLS	21AM ATLS	$\tau^{\pm}s + b\text{-jets} + \cancel{E}_T$, Tsb0t4, $m_{\tilde{\chi}_2^0} - m_{\tilde{\chi}_1^0} = 130 \text{ GeV}$, $m_{\tilde{\chi}_2^0} < 180 \text{ GeV}$
>1270	95	² AAD 21S ATLS	21S ATLS	$b\text{-jets} + \cancel{E}_T$, Tsb0t1, $m_{\tilde{\chi}_1^0} = 0 \text{ GeV}$
> 660	95	² AAD 21S ATLS	21S ATLS	$b\text{-jets} + \cancel{E}_T$, Tsb0t1, $m_{\tilde{b}_1} - m_{\tilde{\chi}_1^0} = 10 \text{ GeV}$
>1600	95	³ SIRUNYAN 21M CMS	21M CMS	$\ell^{\pm}\ell^{\mp} + \cancel{E}_T$, Tsb0t3, $m_{\tilde{\chi}_2^0} = 1500 \text{ GeV}$, $m_{\tilde{\chi}_1^0} = 100 \text{ GeV}$
> 750	95	⁴ AAD 20V ATLS	20V ATLS	same-sign $\ell^{\pm}\ell^{\pm} + \text{jets}$, Tsb0t2, $m_{\tilde{\chi}_2^0} = m_{\tilde{\chi}_1^0} + 100 \text{ GeV}$, $m_{\tilde{\chi}_1^0} \sim 50 \text{ GeV}$

Searches Particle Listings

Supersymmetric Particle Searches

> 850	95	5	SIRUNYAN	20T	CMS	same-sign $\ell^\pm \ell^\pm$ or $\geq 3\ell^\pm$ + jets, $T_{\text{stop}2}, m_{\tilde{\chi}_1^\pm} < 800$ GeV, $m_{\tilde{\chi}_1^0} = 50$ GeV	> 400	95	36	CHATRCHYAN14AH	CMS	jets + $\cancel{E}_T, \tilde{b} \rightarrow b\tilde{\chi}_1^0$ simplified model, $m_{\tilde{\chi}_1^0} = 50$ GeV	
>1500	95	6	AAD	19H	ATLS	≥ 3 b-jets + $\cancel{E}_T, T_{\text{stop}4}, \geq 1$ $h(\rightarrow b\bar{b}), m_{\tilde{\chi}_1^0} = 60$ GeV			37	CHATRCHYAN14R	CMS	$\geq 3\ell^\pm, \tilde{b} \rightarrow t\tilde{\chi}_1^\pm, \tilde{\chi}_1^\pm \rightarrow W^\pm \tilde{\chi}_1^0$ simplified model, $m_{\tilde{\chi}_1^0} = 50$ GeV	
>1300	95	7	AAD	19H	ATLS	≥ 3 b-jets + $\cancel{E}_T, T_{\text{stop}4}, \geq 1h(\rightarrow b\bar{b}), m_{\tilde{\chi}_1^0} = m_{\tilde{\chi}_1^\pm} + 130$ GeV			••• We do not use the following data for averages, fits, limits, etc. •••				
>1220	95	8	SIRUNYAN	19CH	CMS	jets + $\cancel{E}_T, T_{\text{stop}1}, m_{\tilde{\chi}_1^0} = 0$ GeV			38	KHACHATRY...15AD	CMS	$\ell^\pm \ell^\mp$ + jets + $\cancel{E}_T, \tilde{b} \rightarrow b\ell^\pm \ell^\mp \tilde{\chi}_1^0$	
> 530	95	9	SIRUNYAN	19CI	CMS	≥ 1 $H(\rightarrow \gamma\gamma)$ + jets + $\cancel{E}_T, T_{\text{stop}4}, m_{\tilde{\chi}_1^0} = m_{\tilde{\chi}_1^\pm} + 130$ GeV, $m_{\tilde{\chi}_1^0} = 1$ GeV	none 340–600	95	39	AAD	14AX	ATLS	≥ 3 b-jets + $\cancel{E}_T, \tilde{b} \rightarrow b\tilde{\chi}_1^0$ simplified model with $\tilde{\chi}_2^0 \rightarrow h\tilde{\chi}_1^0, m_{\tilde{\chi}_1^0} = 60$ GeV, $m_{\tilde{\chi}_2^0} = 300$ GeV
> 430	95	10	AABOUD	18I	ATLS	≥ 1 jets + $\cancel{E}_T, T_{\text{stop}1}, m_{\tilde{b}} - m_{\tilde{\chi}_1^0} \sim m_b$	> 440	95	40	AAD	14E	ATLS	$\ell^\pm \ell^\pm(\ell^\mp)$ + jets, $\tilde{b}_1 \rightarrow t\tilde{\chi}_1^\pm$ with $\tilde{\chi}_1^\pm \rightarrow W^{(*)\pm} \tilde{\chi}_1^0$ simplified model, $m_{\tilde{\chi}_1^\pm} = 2$ $m_{\tilde{\chi}_1^0}$
> 840	95	11	SIRUNYAN	18AL	CMS	$\geq 3\ell^\pm$ + jets + $\cancel{E}_T, T_{\text{stop}2}, m_{\tilde{\chi}_1^0} = 50$ GeV	> 500	95	41	CHATRCHYAN14H	CMS	same-sign $\ell^\pm \ell^\pm, \tilde{b} \rightarrow t\tilde{\chi}_1^\pm, \tilde{\chi}_1^\pm \rightarrow W^\pm \tilde{\chi}_1^0$ simplified model, $m_{\tilde{\chi}_1^\pm} = 2$ GeV, $m_{\tilde{\chi}_1^0} = 100$ GeV	
> 975	95	12	SIRUNYAN	18AR	CMS	$\ell^\pm \ell^\mp$ + jets + $\cancel{E}_T, T_{\text{stop}3}, m_{\tilde{b}} = (m_{\tilde{\chi}_2^0} + m_{\tilde{\chi}_1^0})/2, m_{\tilde{\chi}_1^0} = 100$ GeV	> 620	95	42	AAD	13AU	ATLS	2 b-jets + $\cancel{E}_T, \tilde{b}_1 \rightarrow b\tilde{\chi}_1^0, m_{\tilde{\chi}_1^0} < 120$ GeV
>1060	95	13	SIRUNYAN	18AY	CMS	jets + $\cancel{E}_T, T_{\text{stop}1}, m_{\tilde{\chi}_1^0} = 0$ GeV	> 550	95	43	CHATRCHYAN13AT	CMS	jets + $\cancel{E}_T, \tilde{b} \rightarrow b\tilde{\chi}_1^0$ simplified model, $m_{\tilde{\chi}_1^0} = 50$ GeV	
>1230	95	14	SIRUNYAN	18B	CMS	jets + $\cancel{E}_T, T_{\text{stop}1}, m_{\tilde{\chi}_1^0} = 0$ GeV	> 600	95	44	CHATRCHYAN13T	CMS	jets + $\cancel{E}_T, \tilde{b} \rightarrow b\tilde{\chi}_1^0$ simplified model, $m_{\tilde{\chi}_1^0} = 0$ GeV	
> 420	95	15	SIRUNYAN	18X	CMS	≥ 1 $H(\rightarrow \gamma\gamma)$ + jets + $\cancel{E}_T, T_{\text{stop}4}, m_{\tilde{\chi}_1^0} = m_{\tilde{\chi}_1^\pm} + 130$ GeV, $m_{\tilde{\chi}_1^0} < 225$ GeV	> 450	95	45	CHATRCHYAN13V	CMS	same-sign $\ell^\pm \ell^\pm + \geq 2$ b-jets, $\tilde{b} \rightarrow t\tilde{\chi}_1^\pm, \tilde{\chi}_1^\pm \rightarrow W^\pm \tilde{\chi}_1^0$ simplified model, $m_{\tilde{\chi}_1^0} = 50$ GeV	
> 700	95	16	AABOUD	17AJ	ATLS	same-sign $\ell^\pm \ell^\pm / 3$ ℓ + jets + $\cancel{E}_T, T_{\text{stop}2}, m_{\tilde{\chi}_1^0} = 0$ GeV	> 390		46	AAD	12AN	ATLS	$\tilde{b}_1 \rightarrow b\tilde{\chi}_1^0$, simplified model, $m_{\tilde{\chi}_1^0} < 60$ GeV
> 950	95	17	AABOUD	17AX	ATLS	2 b-jets + $\cancel{E}_T, T_{\text{stop}1}, m_{\tilde{\chi}_1^0} = 0$ GeV	> 410	95	47	CHATRCHYAN12AI	CMS	$\ell^\pm \ell^\pm$ + b-jets + \cancel{E}_T	
> 880	95	18	AABOUD	17AX	ATLS	2 b-jets + \cancel{E}_T , mixture $T_{\text{stop}1}$ and $T_{\text{stop}2}$ BR=50%, $m_{\tilde{\chi}_1^0} = 0$ GeV, $m_{\tilde{\chi}_1^\pm} - m_{\tilde{\chi}_1^0} = 1$ GeV	> 294	95	48	CHATRCHYAN12BO	CMS	$\tilde{b}_1 \rightarrow b\tilde{\chi}_1^0$, simplified model, $m_{\tilde{\chi}_1^0} = 50$ GeV	
> 315	95	19	KHACHATRY...17A	CMS	2 VBF jets + $\cancel{E}_T, T_{\text{stop}1}, m_{\tilde{b}} - m_{\tilde{\chi}_1^0} = 5$ GeV	> 230	95	49	AAD	11K	ATLS	stable \tilde{b}	
> 450	95	20	KHACHATRY...17AW	CMS	$\geq 3\ell^\pm, 2$ jets, $T_{\text{stop}2}, m_{\tilde{\chi}_1^0} = 50$ GeV, $m_{\tilde{\chi}_1^\pm} = 200$ GeV	> 247	95	50	AAD	11O	ATLS	$\tilde{g} \rightarrow \tilde{b}_1 b, \tilde{b}_1 \rightarrow b\tilde{\chi}_1^0, m_{\tilde{\chi}_1^0} = 60$ GeV	
> 800	95	21	KHACHATRY...17P	CMS	1 or more jets + $\cancel{E}_T, T_{\text{stop}1}, m_{\tilde{\chi}_1^0} = 0$ GeV	> 230	95	51	CHATRCHYAN11D	CMS	$\tilde{b}, \tilde{t} \rightarrow b$		
>1175	95	22	SIRUNYAN	17AZ	CMS	≥ 1 jets + $\cancel{E}_T, T_{\text{stop}1}, m_{\tilde{\chi}_1^0} = 0$ GeV	> 247	95	52	AALTONEN	10R	CDF	$\tilde{b}_1 \rightarrow b\tilde{\chi}_1^0, m_{\tilde{\chi}_1^0} < 70$ GeV
> 890	95	23	SIRUNYAN	17K	CMS	jets + $\cancel{E}_T, T_{\text{stop}1}, m_{\tilde{\chi}_1^0} = 0$ GeV			53	ABAZOV	10L	D0	$\tilde{b}_1 \rightarrow b\tilde{\chi}_1^0, m_{\tilde{\chi}_1^0} = 0$ GeV
> 810	95	24	SIRUNYAN	17S	CMS	same-sign $\ell^\pm \ell^\pm$ + jets + $\cancel{E}_T, T_{\text{stop}2}, m_{\tilde{\chi}_1^0} = 50$ GeV, $m_{\tilde{\chi}_1^\pm} = 100$ GeV			1 AAD 21AM searched in 139 fb^{-1} of pp collisions at $\sqrt{s} = 13$ TeV for pair production of bottom squarks in events with hadronically decaying τ^\pm -leptons, b-tagged jets, and large \cancel{E}_T . No significant excess above the Standard Model expectations is observed. Limits are set on the bottom squark mass in the $T_{\text{stop}4}$ simplified model, assuming $m_{\tilde{\chi}_2^0} - m_{\tilde{\chi}_1^0} = 130$ GeV, see their Figure 8.				
> 323	95	25	AABOUD	16D	ATLS	≥ 1 jet + $\cancel{E}_T, T_{\text{stop}1}, m_{\tilde{b}_1} - m_{\tilde{\chi}_1^0} = 5$ GeV			2 AAD 21S searched in 139 fb^{-1} of pp collisions at $\sqrt{s} = 13$ TeV for pair production of sbottoms, LQ or dark matter in events with b-jets and \cancel{E}_T , also using dedicated secondary-vertex-finding techniques. No significant excess above the Standard Model predictions is observed. Limits are set on $m_{\tilde{b}_1}$ in the $T_{\text{stop}1}$ simplified model, on the LQ masses depending on the BR in $b\nu$, on scalar and pseudoscalar dark matter mediator masses. See Figures 8, 9, 10.				
> 840	95	26	AABOUD	16Q	ATLS	2 b-jets + $\cancel{E}_T, T_{\text{stop}1}, m_{\tilde{\chi}_1^0} = 100$ GeV			3 SIRUNYAN 21M searched in 137 fb^{-1} of pp collisions at $\sqrt{s} = 13$ TeV for supersymmetry in events with two opposite-sign same-flavor leptons (electrons, muons) and \cancel{E}_T . No significant excess above the Standard Model expectations is observed. Limits are set on the gluino mass in the simplified model Tglu4C, see their Figure 10, on the $\tilde{\chi}_2^0$ and $\tilde{\chi}_1^\pm$ mass in Tchi1n2Fa, see their Figure 11, on the $\tilde{\chi}_1^0$ mass in Tn1n1C and Tn1n1B for $m_{\tilde{\chi}_2^0} = m_{\tilde{\chi}_1^\pm} = m_{\tilde{\chi}_1^0}$, see their Figure 12. Limits are also set on the light squark mass for the simplified model Tsqk2A, on the sbottom mass in $T_{\text{stop}3}$, see their Figure 13, and on the slepton mass in direct electroweak pair production of mass-degenerate left- and right-handed sleptons (selectrons and smuons), see their Figure 14.				
> 540	95	27	AAD	16BB	ATLS	2 same-sign $\ell^\pm \ell^\pm / 3\ell$ + jets + $\cancel{E}_T, T_{\text{stop}2}, m_{\tilde{\chi}_1^0} < 55$ GeV			4 AAD 20V searched in 139 fb^{-1} of pp collisions at $\sqrt{s} = 13$ TeV for events with two same-sign charged leptons (electrons or muons) and jets. No significant excess above the Standard Model expectations is observed. Exclusion limits at 95% C.L. are set on the bottom squark masses in the $T_{\text{stop}2}$ simplified model for $m_{\tilde{\chi}_1^\pm} = m_{\tilde{\chi}_1^0} + 100$ GeV, see their Fig. 8(a).				
> 680	95	28	KHACHATRY...16BJ	CMS	same-sign $\ell^\pm \ell^\pm, T_{\text{stop}2}, m_{\tilde{\chi}_1^\pm} < 550$ GeV, $m_{\tilde{\chi}_1^0} = 50$ GeV			5 SIRUNYAN 20T searched in 137 fb^{-1} of pp collisions at $\sqrt{s} = 13$ TeV for events with at least two jets, and two isolated same-sign or three or more charged leptons (electrons or muons). No significant excess above the Standard Model expectations is observed. Limits are set on the gluino mass in the Tglu3A, Tglu3B, Tglu3C and Tglu3D simplified models, see their Figure 7, and in the Tglu1C and Tglu1B simplified models, see their Figures 8 and 9. Limits are also set on the sbottom mass in the $T_{\text{stop}2}$ simplified model, see their Figure 10, and on the stop mass in the $T_{\text{stop}7}$ simplified model, see their Figure 11. Finally, limits are set on the gluino mass in RPV simplified models where the gluino decays either via $\tilde{g} \rightarrow qq\bar{q}\bar{q} + e/\mu/\tau$ or via $\tilde{g} \rightarrow tbs$, see Figure 12.					
> 500	95	28	KHACHATRY...16BJ	CMS	same-sign $\ell^\pm \ell^\pm, T_{\text{stop}2}, m_{\tilde{b}} - m_{\tilde{\chi}_1^\pm} < 100$ GeV, $m_{\tilde{\chi}_1^0} = 50$ GeV			6 AAD 19H searched in 139 fb^{-1} of pp collisions at $\sqrt{s} = 13$ TeV for events with no charged leptons, three or more b-jets, and large \cancel{E}_T . Higgs boson candidates are reconstructed as b-jet pairs. No significant excess above the Standard Model expectations is observed. Limits up to 1500 GeV are set on the sbottom mass in the $T_{\text{stop}4}$ simplified model, see Figure 8(a), for fixed $m_{\tilde{\chi}_1^0} = 60$ GeV and for $m_{\tilde{\chi}_2^0}$ up to 1200 GeV.					
> 880	95	29	KHACHATRY...16BS	CMS	jets + $\cancel{E}_T, T_{\text{stop}1}, m_{\tilde{\chi}_1^0} = 0$ GeV								
> 550	95	30	KHACHATRY...16BY	CMS	opposite-sign $\ell^\pm \ell^\pm, T_{\text{stop}3}, m_{\tilde{\chi}_1^0} = 100$ GeV								
> 600	95	31	AAD	15CJ	ATLS	$\tilde{b} \rightarrow b\tilde{\chi}_1^0, m_{\tilde{\chi}_1^0} < 250$ GeV							
> 440	95	31	AAD	15CJ	ATLS	$\tilde{b} \rightarrow t\tilde{\chi}_1^\pm, \tilde{\chi}_1^\pm \rightarrow W^{(*)\pm} \tilde{\chi}_1^0, m_{\tilde{\chi}_1^0} = 60$ GeV, $m_{\tilde{b}} - m_{\tilde{\chi}_1^\pm} < m_{\tilde{t}}$							
none 300–650	95	31	AAD	15CJ	ATLS	$\tilde{b} \rightarrow \tilde{b}\tilde{\chi}_2^0, \tilde{\chi}_2^0 \rightarrow h\tilde{\chi}_1^0, m_{\tilde{\chi}_1^0} = 60$ GeV, $m_{\tilde{\chi}_2^0} > 250$ GeV							
> 640	95	32	KHACHATRY...15AF	CMS	$\tilde{b} \rightarrow b\tilde{\chi}_1^0, m_{\tilde{\chi}_1^0} = 0$								
> 650	95	33	KHACHATRY...15AH	CMS	$\tilde{b} \rightarrow b\tilde{\chi}_1^0, m_{\tilde{\chi}_1^0} = 0$								
> 250	95	33	KHACHATRY...15AH	CMS	$\tilde{b} \rightarrow b\tilde{\chi}_1^0, m_{\tilde{b}} - m_{\tilde{\chi}_1^0} < 10$ GeV								
> 570	95	34	KHACHATRY...15I	CMS	$\tilde{b} \rightarrow t\tilde{\chi}_1^\pm, \tilde{\chi}_1^\pm \rightarrow W^\pm \tilde{\chi}_1^0, m_{\tilde{\chi}_1^0} = 50$ GeV, $150 < m_{\tilde{\chi}_1^\pm} < 300$ GeV								
> 255	95	35	AAD	14T	ATLS	$\tilde{b}_1 \rightarrow b\tilde{\chi}_1^0, m_{\tilde{b}_1} - m_{\tilde{\chi}_1^0} \approx m_b$							

- 7 AAD 19H searched in 139 fb^{-1} of pp collisions at $\sqrt{s} = 13 \text{ TeV}$ for events with no charged leptons, three or more b -jets, and large \cancel{E}_T . Higgs boson candidates are reconstructed as b -jet pairs. No significant excess above the Standard Model expectations is observed. Limits up to 1300 GeV are set on the sbottom mass in the Tsb04 simplified model, see Figure 8(b), for $m_{\tilde{\chi}_2^0} = m_{\tilde{\chi}_1^0} + 130 \text{ GeV}$ and $m_{\tilde{\chi}_2^0}$ from 200 to 750 GeV .
- 8 SIRUNYAN 19CH searched in 137 fb^{-1} of pp collisions at $\sqrt{s} = 13 \text{ TeV}$ for events containing multiple jets and large \cancel{E}_T . No significant excess above the Standard Model expectations is observed. Limits are set on the gluino mass in the Tglu1A, Tglu1C, Tglu2A and Tglu3A simplified models, see their Figure 13. Limits are also set on squark, sbottom and stop masses in the Tsqk1, Tsb01, Tstop1 simplified models, see their Figure 14.
- 9 SIRUNYAN 19CI searched in 77.5 fb^{-1} of pp collisions at $\sqrt{s} = 13 \text{ TeV}$ for events with one or more high-momentum Higgs bosons, decaying to pairs of photons, jets and \cancel{E}_T . No significant excess above the Standard Model expectations is observed. Limits are set on the sbottom mass in the Tsb04 simplified model, see Figure 3, and on the wino mass in the Tch1n2E simplified model, see their Figure 4. Limits are also set on the higgsino mass in the Tn1n1A and Tn1n1B simplified models, see their Figure 5.
- 10 AABOUD 18I searched in 36.1 fb^{-1} of pp collisions at $\sqrt{s} = 13 \text{ TeV}$ for events with at least one jet with a transverse momentum above 250 GeV and no leptons. Good agreement is observed between the number of events in data and Standard Model predictions. The results are translated into exclusion limits in Tsb01 models. In the compressed scenario with sbottom and neutralino masses differing by m_b , sbottom masses below 430 GeV are excluded. For $m_{\tilde{\chi}_1^0} = 0$ they exclude sbottom masses up to 610 GeV . See their Fig.10(a).
- 11 SIRUNYAN 18AL searched in 35.9 fb^{-1} of pp collisions at $\sqrt{s} = 13 \text{ TeV}$ for events with at least three charged leptons, in any combination of electrons and muons, jets and significant \cancel{E}_T . No significant excess above the Standard Model expectations is observed. Limits are set on the gluino mass in the Tglu3A and Tglu1C simplified models, see their Figure 5. Limits are also set on the sbottom mass in the Tsb02 simplified model, see their Figure 6, and on the stop mass in the Tstop7 simplified model, see their Figure 7.
- 12 SIRUNYAN 18AR searched in 35.9 fb^{-1} of pp collisions at $\sqrt{s} = 13 \text{ TeV}$ for events containing two opposite-charge, same-flavour leptons (electrons or muons), jets and \cancel{E}_T . No significant excess above the Standard Model expectations is observed. Limits are set on the gluino mass in the Tglu4C simplified model, see their Figure 7. Limits are also set on the chargino/neutralino mass in the Tch1n2F simplified model, see their Figure 8, and on the neutralino mass in the Tn1n1B and Tn1n1C simplified models, see their Figure 9. Finally, limits are set on the sbottom mass in the Tsb03 simplified model, see their Figure 10.
- 13 SIRUNYAN 18AV searched in 35.9 fb^{-1} of pp collisions at $\sqrt{s} = 13 \text{ TeV}$ for events containing one or more jets and significant \cancel{E}_T . No significant excess above the Standard Model expectations is observed. Limits are set on the gluino mass in the Tglu1A, Tglu2A and Tglu3A simplified models, see their Figure 3. Limits are also set on squark, sbottom and stop masses in the Tsqk1, Tsb01, Tstop1 and Tstop4 simplified models, see their Figure 3. Finally, limits are set on long-lived gluino masses in a Tglu1A simplified model where the gluino is metastable or long-lived with proper decay lengths in the range $10^{-3} \text{ mm} < c\tau < 10^5 \text{ mm}$, see their Figure 4.
- 14 SIRUNYAN 18B searched in 35.9 fb^{-1} of pp collisions at $\sqrt{s} = 13 \text{ TeV}$ for the pair production of third-generation squarks in events with jets and large \cancel{E}_T . No significant excess above the Standard Model expectations is observed. Limits are set on the sbottom mass in the Tsb01 simplified model, see their Figure 5, and on the stop mass in the Tstop4 simplified model, see their Figure 6.
- 15 SIRUNYAN 18X searched in 35.9 fb^{-1} of pp collisions at $\sqrt{s} = 13 \text{ TeV}$ for events with one or more high-momentum Higgs bosons, decaying to pairs of photons, jets and \cancel{E}_T . The razor variables (M_R and R^2) are used to categorise the events. No significant excess above the Standard Model expectations is observed. Limits are set on the sbottom mass in the Tsb04 simplified model and on the wino mass in the Tch1n2E simplified model, see their Figure 5. Limits are also set on the higgsino mass in the Tn1n1A and Tn1n1B simplified models, see their Figure 6.
- 16 AABOUD 17AJ searched in 36.1 fb^{-1} of pp collisions at $\sqrt{s} = 13 \text{ TeV}$ for events with two same-sign or three leptons, jets and large missing transverse momentum. No significant excess above the Standard Model expectations is observed. Limits up to 700 GeV are set on the bottom squark mass in Tsb02 simplified models assuming $m_{\tilde{\chi}_1^0} = 0 \text{ GeV}$. See their Figure 4(d).
- 17 AABOUD 17AX searched in 36 fb^{-1} of pp collisions at $\sqrt{s} = 13 \text{ TeV}$ for events containing two jets identified as originating from b -quarks and large missing transverse momentum. No excess of events above the expected level of Standard Model background was found. Exclusion limits at 95% C.L. are set on the masses of bottom squarks. In the Tsb01 simplified model, a \tilde{b}_1 mass below 950 GeV is excluded for $m_{\tilde{\chi}_1^0} = 0$ ($<420 \text{ GeV}$). See their Fig. 7(a).
- 18 AABOUD 17AX searched in 36 fb^{-1} of pp collisions at $\sqrt{s} = 13 \text{ TeV}$ for events containing two jets identified as originating from b -quarks and large missing transverse momentum, with or without leptons. No excess of events above the expected level of Standard Model background was found. Exclusion limits at 95% C.L. are set on the masses of bottom squarks. Assuming 50% BR for Tsb01 and Tsb02 simplified models, a \tilde{b}_1 mass below 880 (860) GeV is excluded for $m_{\tilde{\chi}_1^0} = 0$ (<250) GeV. See their Fig. 7(b).
- 19 KHACHATRYAN 17A searched in 18.5 fb^{-1} of pp collisions at $\sqrt{s} = 8 \text{ TeV}$ for events with two forward jets, produced through vector boson fusion, and missing transverse momentum. No significant excess above the Standard Model expectations is observed. A limit is set on sbottom masses in the Tsb01 simplified model, see Fig. 3.
- 20 KHACHATRYAN 17AW searched in 2.3 fb^{-1} of pp collisions at $\sqrt{s} = 13 \text{ TeV}$ for events with at least three charged leptons, in any combination of electrons and muons, and significant \cancel{E}_T . No significant excess above the Standard Model expectations is observed. Limits are set on the gluino mass in the Tglu3A and Tglu1C simplified models, and on the sbottom mass in the Tsb02 simplified model, see their Figure 4.
- 21 KHACHATRYAN 17P searched in 2.3 fb^{-1} of pp collisions at $\sqrt{s} = 13 \text{ TeV}$ for events with one or more jets and large \cancel{E}_T . No significant excess above the Standard Model expectations is observed. Limits are set on the gluino mass in the Tglu1A, Tglu2A, Tglu3A, Tglu3B, Tglu3C and Tglu3D simplified models, see their Figures 7 and 8. Limits are also set on the squark mass in the Tsqk1 simplified model, see their Fig. 7, and on the sbottom mass in the Tsb01 simplified model, see Fig. 8. Finally, limits are set on the stop mass in the Tstop1, Tstop3, Tstop4, Tstop6 and Tstop7 simplified models, see Fig. 8.
- 22 SIRUNYAN 17AZ searched in 35.9 fb^{-1} of pp collisions at $\sqrt{s} = 13 \text{ TeV}$ for events with one or more jets and large \cancel{E}_T . No significant excess above the Standard Model expectations is observed. Limits are set on the gluino mass in the Tglu1A, Tglu2A, Tglu3A simplified models, see their Figures 6. Limits are also set on the squark mass in the Tsqk1 simplified model (for single light squark and for 8 degenerate light squarks), on the sbottom mass in the Tsb01 simplified model and on the stop mass in the Tstop1 simplified model, see their Fig. 7. Finally, limits are set on the stop mass in the Tstop2, Tstop4 and Tstop8 simplified models, see Fig. 8.
- 23 SIRUNYAN 17K searched in 2.3 fb^{-1} of pp collisions at $\sqrt{s} = 13 \text{ TeV}$ for direct production of stop or sbottom pairs in events with multiple jets and significant \cancel{E}_T . A second search also requires an isolated lepton and is combined with the all-hadronic search. No significant excess above the Standard Model expectations is observed. Limits are set on the stop mass in the Tstop1, Tstop8 and Tstop4 simplified models, see their Figures 7, 8 and 9 (for the Tstop4 limits, only the results of the all-hadronic search are used). Limits are also set on the sbottom mass in the Tsb01 simplified model, see Fig. 10 (also here, only the results of the all-hadronic search are used).
- 24 SIRUNYAN 17S searched in 35.9 fb^{-1} of pp collisions at $\sqrt{s} = 13 \text{ TeV}$ for events with two isolated same-sign leptons, jets, and large \cancel{E}_T . No significant excess above the Standard Model expectations is observed. Limits are set on the mass of the gluino mass in the Tglu3A, Tglu3B, Tglu3C, Tglu3D and Tglu1B simplified models, see their Figures 5 and 6, and on the sbottom mass in the Tsb02 simplified model, see their Figure 6.
- 25 AABOUD 16D searched in 3.2 fb^{-1} of pp collisions at $\sqrt{s} = 13 \text{ TeV}$ for events with an energetic jet and large missing transverse momentum. The results are interpreted as 95% C.L. limits on mass of sbottom decaying into a b -quark and the lightest neutralino in scenarios with $m_{\tilde{b}_1} - m_{\tilde{\chi}_1^0}$ between 5 and 20 GeV . See their Fig. 6.
- 26 AABOUD 16Q searched in 3.2 fb^{-1} of pp collisions at $\sqrt{s} = 13 \text{ TeV}$ for events containing two jets identified as originating from b -quarks and large missing transverse momentum. No excess of events above the expected level of Standard Model background was found. Exclusion limits at 95% C.L. are set on the masses of third-generation squarks. Assuming that the decay $\tilde{b}_1 \rightarrow b\tilde{\chi}_1^0$ (Tsb01) takes place 100% of the time, a \tilde{b}_1 mass below 840 (800) GeV is excluded for $m_{\tilde{\chi}_1^0} < 100$ (360) GeV. Differences in mass above 100 GeV between the \tilde{b}_1 and the $\tilde{\chi}_1^0$ are excluded up to a \tilde{b}_1 mass of 500 GeV . For more details, see their Fig. 4.
- 27 AAD 16BB searched in 3.2 fb^{-1} of pp collisions at $\sqrt{s} = 13 \text{ TeV}$ for events with exactly two same-sign leptons or at least three leptons, multiple hadronic jets, b -jets, and \cancel{E}_T . No significant excess over the Standard Model expectation is found. Exclusion limits at 95% C.L. are set on the sbottom mass for the Tsb02 model, assuming $m_{\tilde{\chi}_1^0} = m_{\tilde{\chi}_1^0} + 100 \text{ GeV}$. See their Fig. 4c.
- 28 KHACHATRYAN 16BJ searched in 2.3 fb^{-1} of pp collisions at $\sqrt{s} = 13 \text{ TeV}$ for events with two isolated same-sign dileptons and jets in the final state. No significant excess above the Standard Model expectations is observed. Limits are set on the sbottom mass in the Tsb02 simplified model, see Fig. 6.
- 29 KHACHATRYAN 16BS searched in 2.3 fb^{-1} of pp collisions at $\sqrt{s} = 13 \text{ TeV}$ for events with at least one energetic jet, no isolated leptons, and significant \cancel{E}_T , using the transverse mass variable M_{T2} to discriminate between signal and background processes. No significant excess above the Standard Model expectations is observed. Limits are set on the sbottom mass in the Tsb01 simplified model, see Fig. 11 and Table 3.
- 30 KHACHATRYAN 16BY searched in 2.3 fb^{-1} of pp collisions at $\sqrt{s} = 13 \text{ TeV}$ for events with two opposite-sign, same-flavour leptons, jets, and missing transverse momentum. No significant excess above the Standard Model expectations is observed. Limits are set on the gluino mass in the Tglu4C simplified model, see Fig. 4, and on sbottom masses in the Tsb03 simplified model, see Fig. 5.
- 31 AAD 15CJ searched in 20 fb^{-1} of pp collisions at $\sqrt{s} = 8 \text{ TeV}$ for evidence of third generation squarks by combining a large number of searches covering various final states. Limits on the sbottom mass are shown, either assuming the $\tilde{b} \rightarrow b\tilde{\chi}_1^0$ decay, see Fig. 11, or assuming the $\tilde{b} \rightarrow t\tilde{\chi}_1^\pm$ decay, with $\tilde{\chi}_1^\pm \rightarrow W^{(*)}\tilde{\chi}_1^0$, see Fig. 12a, or assuming the $\tilde{b} \rightarrow b\tilde{\chi}_2^0$ decay, with $\tilde{\chi}_2^0 \rightarrow h\tilde{\chi}_1^0$, see Fig. 12b. Interpretations in the pMSSM are also discussed, see Figures 13–15.
- 32 KHACHATRYAN 15AF searched in 19.5 fb^{-1} of pp collisions at $\sqrt{s} = 8 \text{ TeV}$ for events with at least two energetic jets and significant \cancel{E}_T , using the transverse mass variable M_{T2} to discriminate between signal and background processes. No significant excess above the Standard Model expectations is observed. Limits are set on the sbottom mass in simplified models where the decay $\tilde{b} \rightarrow b\tilde{\chi}_1^0$ takes place with a branching ratio of 100%, see Fig. 12. See also Table 5. Exclusions in the CMSSM, assuming $\tan\beta = 30$, $A_0 = -2 \max(m_0, m_{1/2})$ and $\mu > 0$, are also presented, see Fig. 15.
- 33 KHACHATRYAN 15AH searched in 19.4 or 19.7 fb^{-1} of pp collisions at $\sqrt{s} = 8 \text{ TeV}$ for events containing either a fully reconstructed top quark, or events containing dijets requiring one or both jets to originate from b -quarks, or events containing a mono-jet. No significant excess above the Standard Model expectations is observed. Limits are set on the sbottom mass in simplified models where the decay $\tilde{b} \rightarrow b\tilde{\chi}_1^0$ takes place with a branching ratio of 100%, see Fig. 12. Limits are also set in a simplified model where the decay $\tilde{b} \rightarrow c\tilde{\chi}_1^0$ takes place with a branching ratio of 100%, see Fig. 12.
- 34 KHACHATRYAN 15I searched in 19.5 fb^{-1} of pp collisions at $\sqrt{s} = 8 \text{ TeV}$ for events in which b -jets and four W -bosons are produced. Five individual search channels are combined (fully hadronic, single lepton, same-sign dilepton, opposite-sign dilepton, multi-lepton). No significant excess above the Standard Model expectations is observed. Limits are set on the sbottom mass in a simplified model where the decay $\tilde{b} \rightarrow t\tilde{\chi}_1^\pm$, with $\tilde{\chi}_1^\pm \rightarrow W^\pm\tilde{\chi}_1^0$, takes place with a branching ratio of 100%, see Fig. 7.
- 35 AAD 14T searched in 20.3 fb^{-1} of pp collisions at $\sqrt{s} = 8 \text{ TeV}$ for monojet-like events. No excess of events above the expected level of Standard Model background was found. Exclusion limits at 95% C.L. are set on the masses of third-generation squarks in simplified models which assume that the decay $\tilde{b}_1 \rightarrow b\tilde{\chi}_1^0$ takes place 100% of the time, see Fig. 12.
- 36 KHACHATRYAN 14AH searched in 4.7 fb^{-1} of pp collisions at $\sqrt{s} = 7 \text{ TeV}$ for events with at least two energetic jets and significant \cancel{E}_T , using the razor variables (M_R and R^2) to discriminate between signal and background processes. A second analysis requires at least one of the jets to be originating from a b -quark. No significant excess above the Standard Model expectations is observed. Limits are set on sbottom masses in simplified models where the decay $\tilde{b} \rightarrow b\tilde{\chi}_1^0$ takes place with a branching ratio of 100%, see Figs. 28 and 29. Exclusions in the CMSSM, assuming $\tan\beta = 10$, $A_0 = 0$ and $\mu > 0$, are also presented, see Fig. 26.
- 37 KHACHATRYAN 14R searched in 19.5 fb^{-1} of pp collisions at $\sqrt{s} = 8 \text{ TeV}$ for events with at least three leptons (electrons, muons, taus) in the final state. No significant

Searches Particle Listings

Supersymmetric Particle Searches

- excess above the Standard Model expectations is observed. Limits are set on the gluino mass in a simplified model where the decay $\tilde{b} \rightarrow t\tilde{\chi}_1^\pm$, with $\tilde{\chi}_1^\pm \rightarrow W^\pm\tilde{\chi}_1^0$, takes place with a branching ratio of 100%, see Fig. 11.
- 38 KHACHATRYAN 15AD searched in 19.4 fb^{-1} of pp collisions at $\sqrt{s} = 8 \text{ TeV}$ for events with two opposite-sign same flavor isolated leptons featuring either a kinematic edge, or a peak at the Z-boson mass, in the invariant mass spectrum. No evidence for a statistically significant excess over the expected SM backgrounds is observed and 95% C.L. exclusion limits are derived in a simplified model of sbottom pair production where the sbottom decays into a b -quark, two opposite-sign dileptons and a neutralino LSP, through an intermediate state containing either an off-shell Z-boson or a slepton, see Fig. 8.
- 39 AAD 14AX searched in 20.1 fb^{-1} of pp collisions at $\sqrt{s} = 8 \text{ TeV}$ for the strong production of supersymmetric particles in events containing either zero or at last one high- p_T lepton, large missing transverse momentum, high jet multiplicity and at least three jets identified as originating from b -quarks. No excess over the expected SM background is observed. Limits are derived in mSUGRA/CMSSM models with $\tan\beta = 30$, $A_0 = -2 m_0$ and $\mu > 0$, see their Fig. 14. Also, exclusion limits are set in simplified models containing scalar bottom quarks, where the decay $\tilde{b} \rightarrow b\tilde{\chi}_2^0$ and $\tilde{\chi}_2^0 \rightarrow h\tilde{\chi}_1^0$ takes place with a branching ratio of 100%, see their Figures 11.
- 40 AAD 14E searched in 20.3 fb^{-1} of pp collisions at $\sqrt{s} = 8 \text{ TeV}$ for strongly produced supersymmetric particles in events containing jets and two same-sign leptons or three leptons. The search also utilises jets originating from b -quarks, missing transverse momentum and other variables. No excess over the expected SM background is observed. Exclusion limits are derived in simplified models containing bottom, see Fig. 7. Limits are also derived in the mSUGRA/CMSSM, bRPV and GMSB models, see their Fig. 8.
- 41 CHATRCHYAN 14H searched in 19.5 fb^{-1} of pp collisions at $\sqrt{s} = 8 \text{ TeV}$ for events with two isolated same-sign dileptons and jets in the final state. No significant excess above the Standard Model expectations is observed. Limits are set on the sbottom mass in a simplified models where the decay $\tilde{b} \rightarrow t\tilde{\chi}_1^\pm$, $\tilde{\chi}_1^\pm \rightarrow W^\pm\tilde{\chi}_1^0$ takes place with a branching ratio of 100%, with varying mass of the $\tilde{\chi}_1^\pm$, for $m_{\tilde{\chi}_1^0} = 50 \text{ GeV}$, see Fig. 6.
- 42 AAD 13AU searched in 20.1 fb^{-1} of pp collisions at $\sqrt{s} = 8 \text{ TeV}$ for events containing two jets identified as originating from b -quarks and large missing transverse momentum. No excess of events above the expected level of Standard Model background was found. Exclusion limits at 95% C.L. are set on the masses of third-generation squarks. Assuming that the decay $\tilde{b}_1 \rightarrow b\tilde{\chi}_1^0$ takes place 100% of the time, a \tilde{b}_1 mass below 620 GeV is excluded for $m_{\tilde{\chi}_1^0} < 120 \text{ GeV}$. For more details, see their Fig. 5.
- 43 CHATRCHYAN 13AT provides interpretations of various searches for supersymmetry by the CMS experiment based on $4.73\text{--}4.98 \text{ fb}^{-1}$ of pp collisions at $\sqrt{s} = 7 \text{ TeV}$ in the framework of simplified models. Limits are set on the sbottom mass in a simplified models where sbottom quarks are pair-produced and the decay $\tilde{b} \rightarrow b\tilde{\chi}_1^0$ takes place with a branching ratio of 100%, see Fig. 4.
- 44 CHATRCHYAN 13T searched in 11.7 fb^{-1} of pp collisions at $\sqrt{s} = 8 \text{ TeV}$ for events with at least two energetic jets and significant \cancel{E}_T , using the α_T variable to discriminate between processes with genuine and misreconstructed \cancel{E}_T . No significant excess above the Standard Model expectations is observed. Limits are set on sbottom masses in simplified models where the decay $\tilde{b} \rightarrow b\tilde{\chi}_1^0$ takes place with a branching ratio of 100%, see Fig. 8 and Table 9.
- 45 CHATRCHYAN 13v searched in 10.5 fb^{-1} of pp collisions at $\sqrt{s} = 8 \text{ TeV}$ for events with two isolated same-sign dileptons and at least two b -jets in the final state. No significant excess above the Standard Model expectations is observed. Limits are set on the bottom mass in a simplified models where the decay $\tilde{b} \rightarrow t\tilde{\chi}_1^\pm$, $\tilde{\chi}_1^\pm \rightarrow W^\pm\tilde{\chi}_1^0$ takes place with a branching ratio of 100%, with varying mass of the $\tilde{\chi}_1^\pm$, for $m_{\tilde{\chi}_1^0} = 50 \text{ GeV}$, see Fig. 4.
- 46 AAD 12AN searched in 2.05 fb^{-1} of pp collisions at $\sqrt{s} = 7 \text{ TeV}$ for scalar bottom quarks in events with large missing transverse momentum and two b -jets in the final state. The data are found to be consistent with the Standard Model expectations. Limits are set in an R-parity conserving minimal supersymmetric scenario, assuming $B(\tilde{b}_1 \rightarrow b\tilde{\chi}_1^0) = 100\%$, see their Fig. 2.
- 47 CHATRCHYAN 12Al looked in 4.98 fb^{-1} of pp collisions at $\sqrt{s} = 7 \text{ TeV}$ for events with two same-sign leptons (e, μ), but not necessarily same flavor, at least 2 b -jets and missing transverse energy. No excess beyond the Standard Model expectation is observed. Exclusion limits are derived in a simplified model for sbottom pair production, where the sbottom decays through $\tilde{b}_1 \rightarrow t\tilde{\chi}_1 W$, see Fig. 8.
- 48 CHATRCHYAN 12Bo searched in 4.7 fb^{-1} of pp collisions at $\sqrt{s} = 7 \text{ TeV}$ for scalar bottom quarks in events with large missing transverse momentum and two b -jets in the final state. The data are found to be consistent with the Standard Model expectations. Limits are set in an R-parity conserving minimal supersymmetric scenario, assuming $B(\tilde{b}_1 \rightarrow b\tilde{\chi}_1^0) = 100\%$, see their Fig. 2.
- 49 AAD 11K looked in 34 pb^{-1} of pp collisions at $\sqrt{s} = 7 \text{ TeV}$ for events with heavy stable particles, identified by their anomalous dE/dx in the tracker or time of flight in the tile calorimeter, from pair production of \tilde{b} . No evidence for an excess over the SM expectation is observed and limits on the mass are derived for pair production of sbottom, see Fig. 4.
- 50 AAD 11o looked in 35 pb^{-1} of pp collisions at $\sqrt{s} = 7 \text{ TeV}$ for events with jets, of which at least one is a b -jet, and \cancel{E}_T . No excess above the Standard Model was found. Limits are derived in the $(m_{\tilde{g}}, m_{\tilde{b}_1})$ plane (see Fig. 2) under the assumption of 100% branching ratios and \tilde{b}_1 being the lightest squark. The quoted limit is valid for $m_{\tilde{b}_1} < 500 \text{ GeV}$. A similar approach for \tilde{t}_1 as the lightest squark with $\tilde{g} \rightarrow \tilde{t}_1 t$ and $\tilde{t}_1 \rightarrow b\tilde{\chi}_1^\pm$ with 100% branching ratios leads to a gluino mass limit of 520 GeV for $130 < m_{\tilde{t}_1} < 300 \text{ GeV}$. Limits are also derived in the CMSSM $(m_0, m_{1/2})$ plane for $\tan\beta = 40$, see Fig. 4, and in scenarios based on the gauge group $SO(10)$.
- 51 CHATRCHYAN 11D looked in 35 pb^{-1} of pp collisions at $\sqrt{s} = 7 \text{ TeV}$ for events with ≥ 2 jets, at least one of which is b -tagged, and \cancel{E}_T , where the b -jets are decay products of \tilde{t} or \tilde{b} . No evidence for an excess over the expected background is observed. Limits are derived in the CMSSM $(m_0, m_{1/2})$ plane for $\tan\beta = 50$ (see Fig. 2).
- 52 AALTONEN 10R searched in 2.65 fb^{-1} of $p\bar{p}$ collisions at $\sqrt{s} = 1.96 \text{ TeV}$ for events with \cancel{E}_T and exactly two jets, at least one of which is b -tagged. The results are in agreement with the SM prediction, and a limit on the cross section of 0.1 pb is obtained for the

range of masses $80 < m_{\tilde{b}_1} < 280 \text{ GeV}$ assuming that the sbottom decays exclusively to $b\tilde{\chi}_1^0$. The excluded mass region in the framework of conserved R_p is shown in a plane of $(m_{\tilde{b}_1}, m_{\tilde{\chi}_1^0})$, see their Fig. 2.

- 53 ABAZOV 10L looked in 5.2 fb^{-1} of $p\bar{p}$ collisions at $\sqrt{s} = 1.96 \text{ TeV}$ for events with at least 2 b -jets and \cancel{E}_T from the production of $\tilde{b}_1\tilde{b}_1$. No evidence for an excess over the SM expectation is observed, and a limit on the cross section is derived under the assumption of 100% branching ratio. The excluded mass region in the framework of conserved R_p is shown in a plane of $(m_{\tilde{b}_1}, m_{\tilde{\chi}_1^0})$, see their Fig. 3b. The exclusion also extends to $m_{\tilde{\chi}_1^0} = 110 \text{ GeV}$ for $160 < m_{\tilde{b}_1} < 200 \text{ GeV}$.

R-parity violating \tilde{b} (Sbottom) mass limit

VALUE (GeV)	CL%	DOCUMENT ID	TECN	COMMENT
>307	95	1 KHACHATRY...16BX CMS		RPV, $\tilde{b} \rightarrow td$ or ts , λ''_{332} or λ''_{331} coupling

• • • We do not use the following data for averages, fits, limits, etc. • • •

- 2 AAD 14E ATLS $\ell^\pm\ell^\pm(\ell\bar{\nu}) + \text{jets}, \tilde{b}_1 \rightarrow t\tilde{\chi}_1^\pm$ with $\tilde{\chi}_1^\pm \rightarrow W^{(*)\pm}\tilde{\chi}_1^0$ simplified model, $m_{\tilde{\chi}_1^\pm} = 2 m_{\tilde{\chi}_1^0}$
- 1 KHACHATRYAN 16BX searched in 19.5 fb^{-1} of pp collisions at $\sqrt{s} = 8 \text{ TeV}$ for events containing 2 leptons coming from R-parity-violating decays of supersymmetric particles. No excess over the expected background is observed. Limits are derived on the sbottom mass, assuming the RPV $\tilde{b} \rightarrow td$ or $\tilde{b} \rightarrow ts$ decay, see Fig. 15.
- 2 AAD 14E searched in 20.3 fb^{-1} of pp collisions at $\sqrt{s} = 8 \text{ TeV}$ for strongly produced supersymmetric particles in events containing jets and two same-sign leptons or three leptons. The search also utilises jets originating from b -quarks, missing transverse momentum and other variables. No excess over the expected SM background is observed. Exclusion limits are derived in simplified models containing bottom, see Fig. 7. Limits are also derived in the mSUGRA/CMSSM, bRPV and GMSB models, see their Fig. 8.

\tilde{t} (Stop) mass limit

Limits depend on the decay mode. In e^+e^- collisions they also depend on the mixing angle of the mass eigenstate $\tilde{t}_1 = \tilde{t}_L \cos\theta_t + \tilde{t}_R \sin\theta_t$. The coupling to the Z vanishes when $\theta_t = 0.9\pi$. In the Listings below, we use $\Delta m \equiv m_{\tilde{t}_1} - m_{\tilde{\chi}_1^0}$ or $\Delta m \equiv m_{\tilde{t}_1} - m_{\tilde{\nu}_\tau}$, depending on relevant decay mode. See also bounds in "q (Squark) MASS LIMIT."

Some earlier papers are now obsolete and have been omitted. They were last listed in our PDG 14 edition: K. Olive, *et al.* (Particle Data Group), Chinese Physics **C38** 070001 (2014) (<http://pdg.lbl.gov>).

R-parity conserving \tilde{t} (Stop) mass limit

VALUE (GeV)	CL%	DOCUMENT ID	TECN	COMMENT
>1430	95	1 HAYRAPETY...23E CMS		$\gamma + \text{jets} + \cancel{E}_T$, Tstop13, $m_{\tilde{\chi}_1^0} \geq 1170 \text{ GeV}$
>1150	95	2 TUMASYAN 23AB CMS		$\geq 1 \tau^\pm + \cancel{E}_T$, Tstop16, $m_{\tilde{\chi}_1^0} = 1 \text{ GeV}$
> 480	95	3 TUMASYAN 23K CMS		1 high- p_T jet, 1 low- p_T e or μ , Tstop3, $m_{\tilde{t}} - m_{\tilde{\chi}_1^0} = 10 \text{ GeV}$
> 700	95	3 TUMASYAN 23K CMS		1 high- p_T jet, 1 low- p_T e or μ , Tstop3, $m_{\tilde{t}} - m_{\tilde{\chi}_1^0} = 80 \text{ GeV}$
> 480	95	4 TUMASYAN 22Q CMS		2 or 3 ℓ (soft), \cancel{E}_T ; Tstop2, $m_{\tilde{t}} - m_{\tilde{\chi}_1^0} = 30 \text{ GeV}$
> 540	95	4 TUMASYAN 22Q CMS		2 or 3 ℓ (soft), \cancel{E}_T ; Tstop3, $m_{\tilde{t}} - m_{\tilde{\chi}_1^0} = 30 \text{ GeV}$
>1400	95	5 AAD 21AW ATLS		$\tau^\pm + \text{jets} + b\text{-jets} + \cancel{E}_T$, Tstop5, $m_{\tilde{t}_1} = 1200 \text{ GeV}$
>1200	95	6 AAD 21o ATLS		$\ell^\pm + \text{jet} + \cancel{E}_T$, Tstop1, $m_{\tilde{\chi}_1^0} = 0 \text{ GeV}$
> 710	95	6 AAD 21o ATLS		$\ell^\pm + \text{jet} + \cancel{E}_T$, Tstop1, $m_{\tilde{\chi}_1^0} = 580 \text{ GeV}$
> 640	95	6 AAD 21o ATLS		$\ell^\pm + \text{jet} + \cancel{E}_T$, Tstop3, $m_{\tilde{\chi}_1^0} = 580 \text{ GeV}$
>1000	95	7 AAD 21P ATLS		$\ell^\pm\ell^\pm + \text{jets} + \cancel{E}_T$, Tstop1, $m_{\tilde{\chi}_1^0} = 0 \text{ GeV}$
> 600	95	7 AAD 21P ATLS		$\ell^\pm\ell^\pm + \text{jets} + \cancel{E}_T$, Tstop2, $m_{\tilde{\chi}_1^0} = 500 \text{ GeV}$
> 550	95	7 AAD 21P ATLS		$\ell^\pm\ell^\pm + \text{jets} + \cancel{E}_T$, Tstop3, $m_{\tilde{\chi}_1^0} = 500 \text{ GeV}$
>1310	95	8 SIRUNYAN 21AD CMS		jets + \cancel{E}_T , Tstop1, $m_{\tilde{\chi}_1^0} < 300 \text{ GeV}$
>1170	95	8 SIRUNYAN 21AD CMS		jets + \cancel{E}_T , Tstop2, $m_{\tilde{\chi}_1^\pm} = (m_{\tilde{t}} + m_{\tilde{\chi}_1^0})/2$, $m_{\tilde{\chi}_1^0} < 100 \text{ GeV}$
>1150	95	8 SIRUNYAN 21AD CMS		jets + \cancel{E}_T , Tstop1 (50%) or Tstop2 (50%), $m_{\tilde{\chi}_1^\pm} - m_{\tilde{\chi}_1^0} = 5 \text{ GeV}$, $m_{\tilde{\chi}_1^0} = 100 \text{ GeV}$

See key on page 1171

Searches Particle Listings
Supersymmetric Particle Searches

> 640	95	⁸ SIRUNYAN	21AD CMS	jets + \cancel{E}_T , Tstop3, $m_{\tilde{t}} - m_{\tilde{\chi}_1^0} = 50$ GeV	>1070	95	¹⁷ SIRUNYAN	20AH CMS	$\ell^\pm + \text{jet} + \cancel{E}_T$, Tstop8, $m_{\tilde{\chi}_1^\pm} - m_{\tilde{\chi}_1^0} = 5$ GeV, $m_{\tilde{\chi}_1^0} = 0$ GeV
> 620	95	⁸ SIRUNYAN	21AD CMS	jets + \cancel{E}_T , Tstop3, 10 GeV < $m_{\tilde{t}} - m_{\tilde{\chi}_1^0} < 60$ GeV	>1050	95	¹⁷ SIRUNYAN	20AH CMS	$\ell^\pm + \text{jet} + \cancel{E}_T$, Tstop8, $m_{\tilde{\chi}_1^\pm} - m_{\tilde{\chi}_1^0} = 5$ GeV, $m_{\tilde{\chi}_1^0} < 350$ GeV
> 740	95	⁸ SIRUNYAN	21AD CMS	jets + \cancel{E}_T , Tstop2, $m_{\tilde{t}} - m_{\tilde{\chi}_1^0} = 80$ GeV	> 730	95	¹⁸ SIRUNYAN	20T CMS	same-sign $\ell^\pm \ell^\pm$ or $\geq 3\ell^\pm + \text{jets}$, Tstop7, $m_{\tilde{t}_1} - m_{\tilde{\chi}_1^0} = 175$ GeV, $m_{\tilde{t}_1} = 200$ GeV, $B(\tilde{t}_2 \rightarrow \tilde{t}_1 H) = 100\%$
> 720	95	⁸ SIRUNYAN	21AD CMS	jets + \cancel{E}_T , Tstop2, 40 GeV < $m_{\tilde{t}} - m_{\tilde{\chi}_1^0} < 80$ GeV	> 730	95	¹⁸ SIRUNYAN	20T CMS	same-sign $\ell^\pm \ell^\pm$ or $\geq 3\ell^\pm + \text{jets}$, Tstop7, $m_{\tilde{t}_1} - m_{\tilde{\chi}_1^0} = 175$ GeV, $m_{\tilde{t}_1} = 200$ GeV, $B(\tilde{t}_2 \rightarrow \tilde{t}_1 Z) = 100\%$
> 595	95	⁸ SIRUNYAN	21AD CMS	jets + \cancel{E}_T , Tstop2, $m_{\tilde{t}} - m_{\tilde{\chi}_1^0} = 10$ GeV	> 890	95	¹⁸ SIRUNYAN	20T CMS	same-sign $\ell^\pm \ell^\pm$ or $\geq 3\ell^\pm + \text{jets}$, Tstop7, $m_{\tilde{t}_1} - m_{\tilde{\chi}_1^0} = 175$ GeV, $m_{\tilde{t}_1} = 200$ GeV, $B(\tilde{t}_2 \rightarrow \tilde{t}_1 H) = 50\%$
> 630	95	⁸ SIRUNYAN	21AD CMS	jets + \cancel{E}_T , Tstop4, $m_{\tilde{t}} - m_{\tilde{\chi}_1^0} = 20$ GeV	> 890	95	¹⁸ SIRUNYAN	20T CMS	same-sign $\ell^\pm \ell^\pm$ or $\geq 3\ell^\pm + \text{jets}$, Tstop7, $m_{\tilde{t}_1} - m_{\tilde{\chi}_1^0} = 175$ GeV, $m_{\tilde{t}_1} = 200$ GeV, $B(\tilde{t}_2 \rightarrow \tilde{t}_1 Z) = 50\%$
none 200-920	95	⁹ SIRUNYAN	21B CMS	$\ell^\pm \ell^\mp + b\text{-jets} + \cancel{E}_T$, Tstop1, $m_{\tilde{\chi}_1^0} = 0$ GeV	> 760	95	¹⁸ SIRUNYAN	20T CMS	same-sign $\ell^\pm \ell^\pm$ or $\geq 3\ell^\pm + \text{jets}$, Tstop7, $m_{\tilde{t}_1} - m_{\tilde{\chi}_1^0} = 175$ GeV, $m_{\tilde{t}_1} = 200$ GeV, $B(\tilde{t}_2 \rightarrow \tilde{t}_1 Z) = 100\%$
none 250-810	95	⁹ SIRUNYAN	21B CMS	$\ell^\pm \ell^\mp + b\text{-jets} + \cancel{E}_T$, Tstop2, $m_{\tilde{\chi}_1^\pm} = (m_{\tilde{t}} + m_{\tilde{\chi}_1^0})/2$, $m_{\tilde{\chi}_1^0} = 0$ GeV	> 760	95	¹⁸ SIRUNYAN	20T CMS	same-sign $\ell^\pm \ell^\pm$ or $\geq 3\ell^\pm + \text{jets}$, Tstop7, $m_{\tilde{t}_1} - m_{\tilde{\chi}_1^0} = 175$ GeV, $m_{\tilde{t}_1} = 200$ GeV, $B(\tilde{t}_2 \rightarrow \tilde{t}_1 Z) = 100\%$
>1300	95	⁹ SIRUNYAN	21B CMS	$\ell^\pm \ell^\mp + b\text{-jets} + \cancel{E}_T$, Tstop11, $m_{\tilde{\chi}_1^\pm} = (m_{\tilde{t}} + m_{\tilde{\chi}_1^0})/2$, $m_{\tilde{\chi}_1^0} = (m_{\tilde{\chi}_1^\pm} - m_{\tilde{\chi}_1^0})/2 + m_{\tilde{\chi}_1^0}$, $m_{\tilde{\chi}_1^0} = 0$	>1100	95	¹⁹ SIRUNYAN	20U CMS	$\tau^\pm \tau^\mp + b\text{-jets} + \cancel{E}_T$, Tstop11, $m_{\tilde{\chi}_1^\pm} = 0.5 (m_{\tilde{t}} + m_{\tilde{\chi}_1^0})$, $m_{\tilde{\chi}_1^0} = 0.5 m_{\tilde{\chi}_1^\pm}$, $m_{\tilde{\chi}_1^0} = 0$
none 400-1180	95	⁹ SIRUNYAN	21B CMS	$\ell^\pm \ell^\mp + b\text{-jets} + \cancel{E}_T$, Tstop11, $m_{\tilde{\chi}_1^\pm} = (m_{\tilde{t}} + m_{\tilde{\chi}_1^0})/2$, $m_{\tilde{\chi}_1^0} = 0.05 (m_{\tilde{\chi}_1^\pm} - m_{\tilde{\chi}_1^0}) + m_{\tilde{\chi}_1^0}$, $m_{\tilde{\chi}_1^0} = 0$	>1110	95	²⁰ SIRUNYAN	19AU CMS	$\gamma + \text{jets} + b\text{-jets} + \cancel{E}_T$, Tstop13, $m_{\tilde{\chi}_1^0} = 1$ GeV
>1400	95	⁹ SIRUNYAN	21B CMS	$\ell^\pm \ell^\mp + b\text{-jets} + \cancel{E}_T$, Tstop11, $m_{\tilde{\chi}_1^\pm} = (m_{\tilde{t}} + m_{\tilde{\chi}_1^0})/2$, $m_{\tilde{\chi}_1^0} = 0.95 (m_{\tilde{\chi}_1^\pm} - m_{\tilde{\chi}_1^0}) + m_{\tilde{\chi}_1^0}$, $m_{\tilde{\chi}_1^0} = 0$	>1230	95	²⁰ SIRUNYAN	19AU CMS	$\gamma + \text{jets} + b\text{-jets} + \cancel{E}_T$, Tstop13, $m_{\tilde{\chi}_1^0} = 800$ GeV
>1325	95	¹⁰ TUMASYAN	21I CMS	≥ 2 jets + $\cancel{E}_T + 0,1,2 \ell$, Tstop1, $m_{\tilde{\chi}_1^0} = 0$ GeV	>1190	95	²¹ SIRUNYAN	19CH CMS	jets + \cancel{E}_T , Tstop1, $m_{\tilde{\chi}_1^0} = 0$ GeV
>1150	95	¹⁰ TUMASYAN	21I CMS	≥ 2 jets + $\cancel{E}_T + 0,1,2 \ell$, Tstop1, $m_{\tilde{\chi}_1^0} = 700$ GeV	>1140	95	²² SIRUNYAN	19s CMS	1 or 2 $\ell + \text{jets} + \cancel{E}_T$, Tstop1, $m_{\tilde{\chi}_1^0} < 200$ GeV
>1260	95	¹⁰ TUMASYAN	21I CMS	≥ 2 jets + $\cancel{E}_T + 0,1,2 \ell$, Tstop2, $m_{\tilde{\chi}_1^0} = 0$ GeV	> 208	95	²³ SIRUNYAN	19U CMS	$e^\pm \mu^\mp + \geq 1b\text{-jet}$, Tstop1, $m_{\tilde{t}_1} - m_{\tilde{\chi}_1^0} = 175$ GeV
>1000	95	¹⁰ TUMASYAN	21I CMS	≥ 2 jets + $\cancel{E}_T + 0,1,2 \ell$, Tstop2, $m_{\tilde{\chi}_1^0} < 575$ GeV	> 235	95	²³ SIRUNYAN	19U CMS	$e^\pm \mu^\mp + \geq 1b\text{-jet}$, Tstop1, $m_{\tilde{t}_1} - m_{\tilde{\chi}_1^0} = 182.5$ GeV
>1175	95	¹⁰ TUMASYAN	21I CMS	≥ 2 jets + $\cancel{E}_T + 0,1,2 \ell$, Tstop1 (50%) or Tstop2 (50%), $m_{\tilde{\chi}_1^0} = 0$ GeV	> 242	95	²³ SIRUNYAN	19U CMS	$e^\pm \mu^\mp + \geq 1b\text{-jet}$, Tstop1, $m_{\tilde{t}_1} - m_{\tilde{\chi}_1^0} = 167.5$ GeV
>1000	95	¹⁰ TUMASYAN	21I CMS	≥ 2 jets + $\cancel{E}_T + 0,1,2 \ell$, Tstop1 (50%) or Tstop2 (50%), $m_{\tilde{\chi}_1^0} = 570$ GeV	> 940	95	²⁴ AABOUD	18AQ ATLS	$1\ell + \text{jets} + \cancel{E}_T$, Tstop1, $m_{\tilde{\chi}_1^0} = 0$ GeV
none 145-295	95	¹⁰ TUMASYAN	21I CMS	$\ell^\pm \ell^\mp + \text{jets} + \cancel{E}_T$, Tstop1, $ m_{\tilde{t}} - m_{\tilde{\chi}_1^0} - 175 \text{ GeV} < 30$ GeV	> 270	95	²⁵ AABOUD	18AQ ATLS	$1\ell + \text{jets} + \cancel{E}_T$, Tstop3, $m_{\tilde{t}_1} - m_{\tilde{\chi}_1^0} = 20$ GeV
none, 170-230	95	¹¹ AABOUD	20 ATLS	$e^\pm \mu^\mp + \geq 1b\text{-jet}$, Tstop1, $m_{\tilde{\chi}_1^0} = 0.5$ GeV	> 840	95	²⁶ AABOUD	18AQ ATLS	$1\ell + \text{jets} + \cancel{E}_T$, Tstop2, $m_{\tilde{t}_1} - m_{\tilde{\chi}_1^0} = 10$ GeV
none, 170-220	95	¹¹ AABOUD	20 ATLS	$e^\pm \mu^\mp + \geq 1b\text{-jet}$, Tstop1, $m_{\tilde{\chi}_1^0} < 62$ GeV	> 500	95	²⁷ AABOUD	18BV ATLS	$c\text{-jets} + \cancel{E}_T$, Tstop4, $m_{\tilde{t}_1} - m_{\tilde{\chi}_1^0} < 100$ GeV
>1220	95	¹² AAD	20AS ATLS	$\ell^\pm \ell^\mp$ or 2 $b\text{-jets}$ and \cancel{E}_T , Tstop6, $m_{\tilde{\chi}_2^0} = 900$ GeV	> 850	95	²⁸ AABOUD	18BV ATLS	$c\text{-jets} + \cancel{E}_T$, Tstop4, $m_{\tilde{\chi}_1^0} = 0$ GeV
> 860	95	¹³ AAD	20AS ATLS	$\ell^\pm \ell^\mp$ or 2 $b\text{-jets}$ and \cancel{E}_T , \tilde{t}_2 with $\tilde{t}_2 \rightarrow \tilde{t}_1 Z$, $\tilde{t}_1 \rightarrow b f f' \tilde{\chi}_1^0$, $\Delta m(\tilde{t}_1, \tilde{\chi}_1^0) = 40$ GeV	> 390	95	²⁹ AABOUD	18I ATLS	≥ 1 jets + \cancel{E}_T , Tstop3, $m_{\tilde{t}_1} \sim m_{\tilde{\chi}_1^0}$
none 400-1250	95	¹⁴ AAD	20s ATLS	jets + \cancel{E}_T , Tstop1, $m_{\tilde{\chi}_1^0} = 0$ GeV	> 430	95	³⁰ AABOUD	18I ATLS	≥ 1 jets + \cancel{E}_T , Tstop4, $m_{\tilde{t}_1} - m_{\tilde{\chi}_1^0} = 5$ GeV
none 300-660	95	¹⁵ AAD	20s ATLS	jets + \cancel{E}_T , Tstop3, $m_{\tilde{\chi}_1^0} = 0$ GeV	>1160	95	³¹ AABOUD	18Y ATLS	$2\ell (\geq 1 \text{ hadronic } \tau) + b\text{-jets} + \cancel{E}_T$, Tstop5, $m_{\tilde{\tau}} \sim 800$ GeV
> 765	95	¹⁶ AAD	20v ATLS	same-sign $\ell^\pm \ell^\pm + \text{jets}$, $\tilde{t}_1 \rightarrow t \tilde{\chi}_2^0$, $\tilde{\chi}_2^0 \rightarrow \tilde{\chi}_1^\pm W$, $\tilde{\chi}_1^\pm \rightarrow \tilde{\chi}_1^0 W$, $m_{\tilde{\chi}_1^\pm} \sim m_{\tilde{\chi}_1^0}$	> 450	95	³² SIRUNYAN	18AJ CMS	$2\ell (\text{soft}) + \cancel{E}_T$, Tstop10, $m_{\tilde{\chi}_1^\pm} = (m_{\tilde{t}} + m_{\tilde{\chi}_1^0})/2$, $m_{\tilde{t}_1} - m_{\tilde{\chi}_1^0} = 40$ GeV
>1200	95	¹⁷ SIRUNYAN	20AH CMS	$\ell^\pm + \text{jet} + \cancel{E}_T$, Tstop1, $m_{\tilde{\chi}_1^0} = 0$ GeV	> 720	95	³³ SIRUNYAN	18AL CMS	$\geq 3\ell^\pm + \text{jets} + \cancel{E}_T$, Tstop7, $m_{\tilde{t}_1} - m_{\tilde{\chi}_1^0} = 175$ GeV, $m_{\tilde{t}_1} = 200$ GeV, $BR(\tilde{t}_2 \rightarrow \tilde{t}_1 H) = 100\%$
>1175	95	¹⁷ SIRUNYAN	20AH CMS	$\ell^\pm + \text{jet} + \cancel{E}_T$, Tstop1, $m_{\tilde{\chi}_1^0} < 425$ GeV	> 780	95	³³ SIRUNYAN	18AL CMS	$\geq 3\ell^\pm + \text{jets} + \cancel{E}_T$, Tstop7, $m_{\tilde{t}_1} - m_{\tilde{\chi}_1^0} = 175$ GeV, $m_{\tilde{t}_1} = 200$ GeV, $BR(\tilde{t}_2 \rightarrow \tilde{t}_1 Z) = 100\%$
none 230-1140	95	¹⁷ SIRUNYAN	20AH CMS	$\ell^\pm + \text{jet} + \cancel{E}_T$, Tstop2, $m_{\tilde{\chi}_1^\pm} = (m_{\tilde{t}} + m_{\tilde{\chi}_1^0})/2$, $m_{\tilde{\chi}_1^0} = 0$ GeV	> 710	95	³³ SIRUNYAN	18AL CMS	$\geq 3\ell^\pm + \text{jets} + \cancel{E}_T$, Tstop7, $m_{\tilde{t}_1} - m_{\tilde{\chi}_1^0} = 175$ GeV, $m_{\tilde{t}_1} = 200$ GeV, $BR(\tilde{t}_2 \rightarrow \tilde{t}_1 Z) = 50\%$
>1100	95	¹⁷ SIRUNYAN	20AH CMS	$\ell^\pm + \text{jet} + \cancel{E}_T$, Tstop2, $m_{\tilde{\chi}_1^\pm} = (m_{\tilde{t}} + m_{\tilde{\chi}_1^0})/2$, $50 < m_{\tilde{\chi}_1^0} < 425$ GeV	> 730	95	³⁴ SIRUNYAN	18AN CMS	1 or 2 $\gamma + \ell + \text{jets}$, GGM, Tstop12, $m_{\tilde{\chi}_1^0} = 150$ GeV
	95	¹⁷ SIRUNYAN	20AH CMS	$\ell^\pm + \text{jet} + \cancel{E}_T$, Tstop2, $m_{\tilde{\chi}_1^\pm} = (m_{\tilde{t}} + m_{\tilde{\chi}_1^0})/2$, $50 < m_{\tilde{\chi}_1^0} < 425$ GeV	> 650	95	³⁴ SIRUNYAN	18AN CMS	1 or 2 $\gamma + \ell + \text{jets}$, GGM, Tstop12, $m_{\tilde{\chi}_1^0} = 500$ GeV
	95	¹⁷ SIRUNYAN	20AH CMS	$\ell^\pm + \text{jet} + \cancel{E}_T$, Tstop1, $m_{\tilde{\chi}_1^0} = 0$ GeV	>1000	95	³⁵ SIRUNYAN	18AY CMS	jets + \cancel{E}_T , Tstop1, $m_{\tilde{\chi}_1^0} = 0$ GeV
	95	¹⁷ SIRUNYAN	20AH CMS	jets + \cancel{E}_T , Tstop4, $m_{\tilde{\chi}_1^0} = 420$ GeV	> 500	95	³⁵ SIRUNYAN	18AY CMS	jets + \cancel{E}_T , Tstop4, $m_{\tilde{\chi}_1^0} = 420$ GeV

Searches Particle Listings

Supersymmetric Particle Searches

> 510	95	36	SIRUNYAN	18B	CMS	jets+ \cancel{E}_T , Tstop4, $m_{\tilde{t}} - m_{\tilde{\chi}_1^0} =$	> 610	95	51	KHACHATRY...17AD	CMS	jets+b-jets+ \cancel{E}_T , mixture	
> 800	95	37	SIRUNYAN	18C	CMS	$\ell^\pm \ell^\mp + b$ -jets + \cancel{E}_T , Tstop1, $m_{\tilde{\chi}_1^0} = 0$	> 590	95	52	KHACHATRY...17P	CMS	1 or more jets+ \cancel{E}_T , Tstop8, $m_{\tilde{\chi}_1^\pm} - m_{\tilde{\chi}_1^0} = 5$ GeV, $m_{\tilde{\chi}_1^0} = 100$ GeV	
> 750	95	37	SIRUNYAN	18C	CMS	$\ell^\pm \ell^\mp + b$ -jets + \cancel{E}_T , Tstop2, $m_{\tilde{\chi}_1^\pm} = (m_{\tilde{t}} + m_{\tilde{\chi}_1^0})/2$, $m_{\tilde{\chi}_1^0} = 0$	none 280-640	95	52	KHACHATRY...17P	CMS	1 or more jets+ \cancel{E}_T , Tstop1, $m_{\tilde{\chi}_1^0} = 0$ GeV	
>1050	95	37	SIRUNYAN	18C	CMS	Combination of all-hadronic, 1 ℓ^\pm and $\ell^\pm \ell^\mp$ searches, Tstop1, $m_{\tilde{\chi}_1^0} = 0$	> 350	95	52	KHACHATRY...17P	CMS	1 or more jets+ \cancel{E}_T , Tstop4, 10 GeV < $m_{\tilde{t}} - m_{\tilde{\chi}_1^0} < 80$ GeV	
>1000	95	37	SIRUNYAN	18C	CMS	Combination of all-hadronic, 1 ℓ^\pm and $\ell^\pm \ell^\mp$ searches, Tstop2, $m_{\tilde{\chi}_1^\pm} = (m_{\tilde{t}} + m_{\tilde{\chi}_1^0})/2$, $m_{\tilde{\chi}_1^0} = 0$	> 280	95	52	KHACHATRY...17P	CMS	1 or more jets+ \cancel{E}_T , Tstop3, 10 GeV < $m_{\tilde{t}} - m_{\tilde{\chi}_1^0} < 80$ GeV	
>1200	95	37	SIRUNYAN	18C	CMS	$\ell^\pm \ell^\mp + b$ -jets + \cancel{E}_T , Tstop11, $m_{\tilde{\chi}_1^\pm} = 0.5 (m_{\tilde{t}} + m_{\tilde{\chi}_1^0})$, $m_{\tilde{\ell}} = 0.5 m_{\tilde{\chi}_1^\pm}$, $m_{\tilde{\chi}_1^0} = 0$	> 240	95	53	KHACHATRY...17s	CMS	jets+ \cancel{E}_T , Tstop4, $m_{\tilde{t}} - m_{\tilde{\chi}_1^0} = 10$ GeV	
>1300	95	37	SIRUNYAN	18C	CMS	$\ell^\pm \ell^\mp + b$ -jets + \cancel{E}_T , Tstop11, $m_{\tilde{\chi}_1^\pm} = 0.5 (m_{\tilde{t}} + m_{\tilde{\chi}_1^0})$, $m_{\tilde{\ell}} = 0.95 m_{\tilde{\chi}_1^\pm}$, $m_{\tilde{\chi}_1^0} = 0$	> 225	95	54	KHACHATRY...17s	CMS	jets+ \cancel{E}_T , Tstop3, $m_{\tilde{t}} - m_{\tilde{\chi}_1^0} = 10$ GeV	
none 460-1060	95	37	SIRUNYAN	18C	CMS	$\ell^\pm \ell^\mp + b$ -jets + \cancel{E}_T , Tstop11, $m_{\tilde{\chi}_1^\pm} = 0.5 (m_{\tilde{t}} + m_{\tilde{\chi}_1^0})$, $m_{\tilde{\ell}} = 0.05 m_{\tilde{\chi}_1^\pm}$, $m_{\tilde{\chi}_1^0} = 0$	> 400	95	55	KHACHATRY...17s	CMS	jets+ \cancel{E}_T , Tstop2, $m_{\tilde{\chi}_1^\pm} = 0.25 m_{\tilde{t}} + 0.75 m_{\tilde{\chi}_1^0}$, $m_{\tilde{\chi}_1^0} = 225$ GeV	
>1020	95	38	SIRUNYAN	18D	CMS	top quark (hadronically decaying) + jets + \cancel{E}_T , Tstop1, $m_{\tilde{\chi}_1^0} = 0$ GeV	> 500	95	56	KHACHATRY...17s	CMS	jets+ \cancel{E}_T , Tstop2, $m_{\tilde{\chi}_1^\pm} = 0.75 m_{\tilde{t}} + 0.25 m_{\tilde{\chi}_1^0}$, $m_{\tilde{\chi}_1^0} = 0$ GeV	
> 420	95	39	SIRUNYAN	18DI	CMS	$\ell^\pm + \text{jet} + \cancel{E}_T$, Tstop3, $m_{\tilde{t}} - m_{\tilde{\chi}_1^0} = 10$ GeV	>1120	95	57	KHACHATRY...17s	CMS	jets+ \cancel{E}_T , Tstop1, $m_{\tilde{\chi}_1^0} = 0$ GeV	
> 560	95	39	SIRUNYAN	18DI	CMS	$\ell^\pm + \text{jet} + \cancel{E}_T$, Tstop3, $m_{\tilde{t}} - m_{\tilde{\chi}_1^0} = 80$ GeV	>1000	95	58	SIRUNYAN	17As	CMS	1 ℓ +jets+ \cancel{E}_T , Tstop1, $m_{\tilde{\chi}_1^0} = 0$ GeV
> 540	95	39	SIRUNYAN	18DI	CMS	ℓ^\pm , Tstop10, $m_{\tilde{\chi}_1^\pm} = (m_{\tilde{t}} + m_{\tilde{\chi}_1^0})/2$, $m_{\tilde{t}} - m_{\tilde{\chi}_1^0} = 40$ GeV	> 980	95	58	SIRUNYAN	17As	CMS	1 ℓ +jets+ \cancel{E}_T , Tstop2, $m_{\tilde{\chi}_1^\pm} = (m_{\tilde{t}} + m_{\tilde{\chi}_1^0})/2$, $m_{\tilde{\chi}_1^0} = 0$ GeV
> 590	95	39	SIRUNYAN	18DI	CMS	Combination of all-hadronic and 1 ℓ^\pm searches, Tstop3, $m_{\tilde{t}} - m_{\tilde{\chi}_1^0} = 30$ GeV	>1040	95	59	SIRUNYAN	17AT	CMS	jets+ \cancel{E}_T , Tstop1, $m_{\tilde{\chi}_1^0} = 0$ GeV
> 670	95	39	SIRUNYAN	18DI	CMS	Combination of all-hadronic and 1 ℓ^\pm searches, Tstop10, $m_{\tilde{\chi}_1^\pm} = (m_{\tilde{t}} + m_{\tilde{\chi}_1^0})/2$, $m_{\tilde{t}} - m_{\tilde{\chi}_1^0} = 60$ GeV	> 750	95	59	SIRUNYAN	17AT	CMS	jets+ \cancel{E}_T , Tstop2, $m_{\tilde{\chi}_1^\pm} = (m_{\tilde{t}} + m_{\tilde{\chi}_1^0})/2$, $m_{\tilde{\chi}_1^0} = 0$ GeV
> 450	95	40	SIRUNYAN	18DN	CMS	$\ell^\pm \ell^\mp$, Tstop1, $m_{\tilde{t}} - m_{\tilde{\chi}_1^0} = m_W$	> 540	95	59	SIRUNYAN	17AT	CMS	jets+ \cancel{E}_T , Tstop3, 10 GeV < $m_{\tilde{t}} - m_{\tilde{\chi}_1^0} < 80$ GeV
none 225-325	95	40	SIRUNYAN	18DN	CMS	$\ell^\pm \ell^\mp$, Tstop2, $m_{\tilde{\chi}_1^\pm} = (m_{\tilde{t}} + m_{\tilde{\chi}_1^0})/2$, $m_{\tilde{t}} - m_{\tilde{\chi}_1^0} = 2 m_W$	> 480	95	59	SIRUNYAN	17AT	CMS	jets+ \cancel{E}_T , Tstop4, 10 GeV < $m_{\tilde{t}} - m_{\tilde{\chi}_1^0} < 80$ GeV
none 210-690	95	40	SIRUNYAN	18DN	CMS	$\ell^\pm \ell^\mp$, Tstop1, $m_{\tilde{\chi}_1^0} = 0$ GeV	> 530	95	59	SIRUNYAN	17AT	CMS	jets+ \cancel{E}_T , Tstop10, $m_{\tilde{\chi}_1^\pm} = (m_{\tilde{t}} + m_{\tilde{\chi}_1^0})/2$, 10 GeV < $m_{\tilde{t}} - m_{\tilde{\chi}_1^0} < 80$ GeV
none 250-600	95	40	SIRUNYAN	18DN	CMS	$\ell^\pm \ell^\mp$, Tstop2, $m_{\tilde{\chi}_1^\pm} = (m_{\tilde{t}} + m_{\tilde{\chi}_1^0})/2$, $m_{\tilde{\chi}_1^0} = 0$ GeV	>1070	95	60	SIRUNYAN	17AZ	CMS	≥ 1 jets+ \cancel{E}_T , Tstop1, $m_{\tilde{\chi}_1^0} = 0$ GeV
> 700	95	41	AABOUD	17AJ	ATLS	same-sign $\ell^\pm \ell^\pm / 3 \ell + \text{jets} + \cancel{E}_T$, Tstop11, $m_{\tilde{\chi}_2^0} = m_{\tilde{\chi}_1^0}$	> 900	95	60	SIRUNYAN	17AZ	CMS	≥ 1 jets+ \cancel{E}_T , Tstop2, $m_{\tilde{\chi}_1^\pm} = (m_{\tilde{t}} + m_{\tilde{\chi}_1^0})/2$, $m_{\tilde{\chi}_1^0} = 0$ GeV
> 880	95	42	AABOUD	17AX	ATLS	b-jets+ \cancel{E}_T , mixture Tstop1 and Tstop2 with BR=50%, $m_{\tilde{\chi}_1^0} = 0$ GeV, $m_{\tilde{\chi}_1^\pm} - m_{\tilde{\chi}_1^0} = 1$ GeV	>1020	95	60	SIRUNYAN	17AZ	CMS	≥ 1 jets+ \cancel{E}_T , Tstop8, $m_{\tilde{\chi}_1^\pm} - m_{\tilde{\chi}_1^0} = 5$ GeV, $m_{\tilde{\chi}_1^0} = 100$ GeV
none 250-1000	95	43	AABOUD	17AY	ATLS	jets+ \cancel{E}_T , Tstop1, $m_{\tilde{\chi}_1^0} = 0$ GeV	> 540	95	60	SIRUNYAN	17AZ	CMS	≥ 1 jets+ \cancel{E}_T , Tstop4, 10 GeV < $m_{\tilde{t}} - m_{\tilde{\chi}_1^0} < 80$ GeV
none 450-850	95	44	AABOUD	17AY	ATLS	jets+ \cancel{E}_T , mixture of Tstop1 and Tstop2 with BR=50%, $m_{\tilde{\chi}_1^\pm} - m_{\tilde{\chi}_1^0} = 1$ GeV	none 280-830	95	61	SIRUNYAN	17K	CMS	0, 1 ℓ^\pm +jets+ \cancel{E}_T (combination), Tstop1, $m_{\tilde{\chi}_1^0} = 0$ GeV
> 720	95	45	AABOUD	17BE	ATLS	$\ell^\pm \ell^\mp + \cancel{E}_T$, Tstop1, $m_{\tilde{\chi}_1^0} = 0$ GeV	> 700	95	61	SIRUNYAN	17K	CMS	0, 1 ℓ^\pm +jets+ \cancel{E}_T (combination), Tstop8, $m_{\tilde{\chi}_1^\pm} - m_{\tilde{\chi}_1^0} = 5$ GeV, $m_{\tilde{\chi}_1^0} = 100$ GeV
> 400	95	46	AABOUD	17BE	ATLS	$\ell^\pm \ell^\mp + \cancel{E}_T$, Tstop3, $m_{\tilde{t}} - m_{\tilde{\chi}_1^0} = 40$ GeV	> 160	95	61	SIRUNYAN	17K	CMS	jets+ \cancel{E}_T , Tstop4, 10 < $m_{\tilde{t}} - m_{\tilde{\chi}_1^0} < 80$ GeV
> 430	95	47	AABOUD	17BE	ATLS	$\ell^\pm \ell^\mp + \cancel{E}_T$, Tstop1 (offshell t), $m_{\tilde{t}} - m_{\tilde{\chi}_1^0} \sim m_W$	none 230-960	95	62	SIRUNYAN	17P	CMS	jets+ \cancel{E}_T , Tstop1, $m_{\tilde{\chi}_1^0} = 0$ GeV
> 700	95	48	AABOUD	17BE	ATLS	$\ell^\pm \ell^\mp + \cancel{E}_T$, Tstop2, $m_{\tilde{t}} - m_{\tilde{\chi}_1^\pm} = 10$ GeV, $m_{\tilde{\chi}_1^0} = 0$ GeV	> 990	95	62	SIRUNYAN	17P	CMS	jets+ \cancel{E}_T , Tstop1, $m_{\tilde{\chi}_1^0} = 0$ GeV
> 750	95	49	KHACHATRY...17	CMS	jets+ \cancel{E}_T , Tstop1, $m_{\tilde{\chi}_1^0} = 100$ GeV	> 323	95	63	AABOUD	16D	ATLS	≥ 1 jet + \cancel{E}_T , Tstop4, $m_{\tilde{t}} - m_{\tilde{\chi}_1^0} = 5$ GeV	
none 250-740	95	50	KHACHATRY...17AD	CMS	jets+b-jets+ \cancel{E}_T , Tstop1, $m_{\tilde{\chi}_1^0} = 0$ GeV	none, 745-780	95	64	AABOUD	16J	ATLS	1 $\ell^\pm + \geq 4$ jets + \cancel{E}_T , Tstop1, $m_{\tilde{\chi}_1^0} = 0$ GeV	

See key on page 1171

Searches Particle Listings

Supersymmetric Particle Searches

> 490–650	95	65	AAD	16AY ATLS	2ℓ (including hadronic τ) + \cancel{E}_T , Tstop5, $87 \text{ GeV} < m_{\tilde{\tau}} < m_{\tilde{\chi}_1^0}$	> 880	95	84	AABOUD	17AF ATLS	2ℓ +jets+ b -jets+ \cancel{E}_T , Tstop7 with 100% decays via higgs, $m_{\tilde{\chi}_1^0} = 50 \text{ GeV}$
> 700	95	66	KHACHATRY...16AV	CMS	1 or 2 ℓ^\pm +jets+ b -jets+ \cancel{E}_T , Tstop1, $m_{\tilde{\chi}_1^0} < 250 \text{ GeV}$			85	AABOUD	17AY ATLS	jets+ \cancel{E}_T , pMSSM-inspired
> 700	95	66	KHACHATRY...16AV	CMS	1 or 2 ℓ^\pm +jets+ b -jets \cancel{E}_T , Tstop2, $m_{\tilde{\chi}_1^0} = 0 \text{ GeV}$, $m_{\tilde{\chi}_1^\pm} = 0.75 m_{\tilde{\tau}_1} + 0.25 m_{\tilde{\chi}_1^0}$	> 230		15	ROLBIECKI	THEO	WW xsection, $\tilde{\tau}_1 \rightarrow b W \tilde{\chi}_1^0$, $m_{\tilde{\tau}_1} \simeq m_b + m_W + m_{\tilde{\chi}_1^0}$
> 775	95	67	KHACHATRY...16BK	CMS	jets+ \cancel{E}_T , Tstop1, $m_{\tilde{\chi}_1^0} < 200 \text{ GeV}$	> 600	95	86	AAD	14B ATLS	$Z+b \cancel{E}_T$, $\tilde{\tau}_2 \rightarrow Z \tilde{\tau}_1, \tilde{\tau}_1 \rightarrow t \tilde{\chi}_1^0$, $m_{\tilde{\chi}_1^0} < 200 \text{ GeV}$
> 620	95	67	KHACHATRY...16BK	CMS	jets+ \cancel{E}_T , Tstop2, $m_{\tilde{\chi}_1^0} = 0 \text{ GeV}$	> 540	95	86	AAD	14B ATLS	$Z+b \cancel{E}_T$, $\tilde{\tau}_1 \rightarrow t \tilde{\chi}_1^0, \tilde{\chi}_1^0 \rightarrow Z \tilde{G}$, natural GMSB, 100 GeV $< m_{\tilde{\chi}_1^0} < m_{\tilde{\tau}_1} - 10 \text{ GeV}$
> 800	95	68	KHACHATRY...16BS	CMS	jets+ \cancel{E}_T , Tstop1, $m_{\tilde{\chi}_1^0} = 0 \text{ GeV}$	> 360	95	87	CHATRCHYAN14U	CMS	$\tilde{\tau}_1 \rightarrow b \tilde{\chi}_1^\pm, \tilde{\chi}_1^\pm \rightarrow f f' \tilde{\chi}_1^0$, $\tilde{\chi}_1^0 \rightarrow H \tilde{G}$ simplified model, $m_{\tilde{\chi}_1^\pm} - m_{\tilde{\chi}_1^0} = 5 \text{ GeV}$, GMSB
> 316	95	69	KHACHATRY...16Y	CMS	1 or 2 soft ℓ^\pm + jets + \cancel{E}_T , Tstop3, $m_{\tilde{\tau}} - m_{\tilde{\chi}_1^0} = 25 \text{ GeV}$	> 215	95	88	CZAKON	14C	$\tilde{\tau} \rightarrow t \tilde{\chi}_1^0, m_{\tilde{\chi}_1^0} < 10 \text{ GeV}$
> 250	95	70	AAD	15CJ ATLS	$B(\tilde{\tau} \rightarrow c \tilde{\chi}_1^0) + B(\tilde{\tau} \rightarrow b f f' \tilde{\chi}_1^0) = 1$, $m_{\tilde{\tau}} - m_{\tilde{\chi}_1^0} = 10 \text{ GeV}$			88	KHACHATRY...14C	CMS	$\tilde{\tau}_2 \rightarrow H \tilde{\tau}_1$ or $\tilde{\tau}_2 \rightarrow Z \tilde{\tau}_1$ simplified model
> 270	95	70	AAD	15CJ ATLS	$\tilde{\tau} \rightarrow c \tilde{\chi}_1^0, m_{\tilde{\tau}} - m_{\tilde{\chi}_1^0} = 80 \text{ GeV}$						
none, 200–700	95	70	AAD	15CJ ATLS	$\tilde{\tau} \rightarrow t \tilde{\chi}_1^0, m_{\tilde{\chi}_1^0} = 0$						
> 500	95	70	AAD	15CJ ATLS	$B(\tilde{\tau} \rightarrow t \tilde{\chi}_1^0) + B(\tilde{\tau} \rightarrow b \tilde{\chi}_1^\pm) = 1$, $\tilde{\chi}_1^\pm \rightarrow W^{(*)} \tilde{\chi}_1^0, m_{\tilde{\chi}_1^\pm} = 2m_{\tilde{\chi}_1^0}, m_{\tilde{\chi}_1^0} < 160 \text{ GeV}$						
> 600	95	70	AAD	15CJ ATLS	$\tilde{\tau}_2 \rightarrow Z \tilde{\tau}_1, m_{\tilde{\tau}_1} - m_{\tilde{\chi}_1^0} = 180 \text{ GeV}, m_{\tilde{\chi}_1^0} = 0$						
> 600	95	70	AAD	15CJ ATLS	$\tilde{\tau}_2 \rightarrow h \tilde{\tau}_1, m_{\tilde{\tau}_1} - m_{\tilde{\chi}_1^0} = 180 \text{ GeV}, m_{\tilde{\chi}_1^0} = 0$						
none, 172.5–191	95	71	AAD	15J ATLS	$\tilde{\tau} \rightarrow t \tilde{\chi}_1^0, m_{\tilde{\chi}_1^0} = 1 \text{ GeV}$						
> 450	95	72	KHACHATRY...15AF	CMS	$\tilde{\tau} \rightarrow t \tilde{\chi}_1^0, m_{\tilde{\chi}_1^0} = 0, m_{\tilde{\tau}} > m_t + m_{\tilde{\chi}_1^0}$						
> 560	95	73	KHACHATRY...15AH	CMS	$\tilde{\tau} \rightarrow t \tilde{\chi}_1^0, m_{\tilde{\chi}_1^0} = 0, m_{\tilde{\tau}} > m_t + m_{\tilde{\chi}_1^0}$						
> 250	95	74	KHACHATRY...15AH	CMS	$\tilde{\tau} \rightarrow c \tilde{\chi}_1^0, m_{\tilde{\tau}} - m_{\tilde{\chi}_1^0} < 10 \text{ GeV}$						
> 730	95	75	KHACHATRY...15X	CMS	$\tilde{\tau} \rightarrow t \tilde{\chi}_1^0, m_{\tilde{\chi}_1^0} = 100 \text{ GeV}, m_{\tilde{\tau}} > m_t + m_{\tilde{\chi}_1^0}$						
none 400–645	95	75	KHACHATRY...15X	CMS	$\tilde{\tau} \rightarrow t \tilde{\chi}_1^0$ or $\tilde{\tau} \rightarrow b \tilde{\chi}_1^\pm, m_{\tilde{\chi}_1^0} = 100 \text{ GeV}, m_{\tilde{\chi}_1^\pm} - m_{\tilde{\chi}_1^0} = 5 \text{ GeV}$						
none 270–645	95	76	AAD	14AJ ATLS	≥ 4 jets + $\cancel{E}_T, \tilde{\tau}_1 \rightarrow t \tilde{\chi}_1^0, m_{\tilde{\chi}_1^0} < 30 \text{ GeV}$						
none 250–550	95	76	AAD	14AJ ATLS	≥ 4 jets + $\cancel{E}_T, B(\tilde{\tau}_1 \rightarrow b \tilde{\chi}_1^\pm) = 50\%$, $m_{\tilde{\chi}_1^\pm} = 2 m_{\tilde{\chi}_1^0}, m_{\tilde{\chi}_1^0} < 60 \text{ GeV}$						
none 210–640	95	77	AAD	14BD ATLS	ℓ^\pm + jets + $\cancel{E}_T, \tilde{\tau}_1 \rightarrow t \tilde{\chi}_1^0, m_{\tilde{\chi}_1^0} = 0 \text{ GeV}$						
> 500	95	77	AAD	14BD ATLS	ℓ^\pm + jets + $\cancel{E}_T, \tilde{\tau}_1 \rightarrow b \tilde{\chi}_1^\pm, m_{\tilde{\chi}_1^\pm} = 2 m_{\tilde{\chi}_1^0}, 100 \text{ GeV} < m_{\tilde{\chi}_1^0} < 150 \text{ GeV}$						
none 150–445	95	78	AAD	14F ATLS	$\ell^\pm \ell^\mp$ final state, $\tilde{\tau}_1 \rightarrow b \tilde{\chi}_1^\pm, m_{\tilde{\tau}_1} - m_{\tilde{\chi}_1^\pm} = 10 \text{ GeV}, m_{\tilde{\chi}_1^0} = 1 \text{ GeV}$						
none 215–530	95	78	AAD	14F ATLS	$\ell^\pm \ell^\mp$ final state, $\tilde{\tau}_1 \rightarrow t \tilde{\chi}_1^0, m_{\tilde{\chi}_1^0} = 1 \text{ GeV}$						
> 270	95	79	AAD	14T ATLS	$\tilde{\tau}_1 \rightarrow c \tilde{\chi}_1^0, m_{\tilde{\chi}_1^0} = 200 \text{ GeV}$						
> 240	95	79	AAD	14T ATLS	$\tilde{\tau}_1 \rightarrow c \tilde{\chi}_1^0, m_{\tilde{\tau}_1} - m_{\tilde{\chi}_1^0} < 85 \text{ GeV}$						
> 255	95	79	AAD	14T ATLS	$\tilde{\tau}_1 \rightarrow b f f' \tilde{\chi}_1^0, m_{\tilde{\tau}_1} - m_{\tilde{\chi}_1^0} \approx m_b$						
> 400	95	80	CHATRCHYAN14AH	CMS	jets + $\cancel{E}_T, \tilde{\tau} \rightarrow t \tilde{\chi}_1^0$ simplified model, $m_{\tilde{\chi}_1^0} = 50 \text{ GeV}$						
		81	CHATRCHYAN14R	CMS	$\geq 3\ell^\pm, \tilde{\tau} \rightarrow (b \tilde{\chi}_1^\pm / t \tilde{\chi}_1^0), \tilde{\chi}_1^\pm \rightarrow (q q' / \ell \nu) \tilde{\chi}_1^0, \tilde{\chi}_1^0 \rightarrow (H/Z) \tilde{G}$, GMSB, natural higgsino NLSP scenario						
• • • We do not use the following data for averages, fits, limits, etc. • • •											
> 850	95	82	AABOUD	17AF ATLS	2ℓ +jets+ b -jets+ \cancel{E}_T , Tstop6, $m_{\tilde{\chi}_1^0} = 0$						
> 800	95	83	AABOUD	17AF ATLS	2ℓ +jets+ b -jets+ \cancel{E}_T , Tstop7 with 100% decays via Z , $m_{\tilde{\chi}_1^0} = 50 \text{ GeV}$						

¹ HAYRAPETYAN 23E searched in 137 fb^{-1} of pp collisions at $\sqrt{s} = 13 \text{ TeV}$ for evidence of gluino, top squark and electroweakino pair production in events with at least one photon, multiple jets, and large \cancel{E}_T . No significant excess above the Standard Model expectations is observed. Limits are set in models for strong production, Tglu4D, Tglu4E, Tglu4F and Tstop13, see their figure 9. They also interpret the results in the models for electroweak production, shown in their figure 10. Tch1n1A assumes wino-like $\tilde{\chi}_1^\pm \tilde{\chi}_1^0$ production, while Tch1ch1A assumes higgsino-like cross sections and includes $\tilde{\chi}_1^\pm \tilde{\chi}_1^\pm, \tilde{\chi}_1^0 \tilde{\chi}_2^0$ and $\tilde{\chi}_1^0 \tilde{\chi}_2^\pm$ production. For $\tilde{\chi}_1^0 \tilde{\chi}_2^0$ alone no mass point can be excluded in the model Tch1ch1A, but in another model for $\tilde{\chi}_1^0 \tilde{\chi}_2^0$ production, Tn1n2A.

² TUMASYAN 23AB searched in 138 fb^{-1} of pp collisions at $\sqrt{s} = 13 \text{ TeV}$ for evidence of top squark pair production in a final state with at least one hadronically decaying tau lepton and large missing transverse momentum. No significant excess above the Standard Model expectations is observed. Limits are set on the mass of \tilde{t} for the model Tstop16, see their Figure 9. The exclusion limits are not very sensitive to the choice of the $\tilde{\tau}$ mass parameter, chosen between $0.25 < (m_{\tilde{\tau}^\pm} - m_{\tilde{\chi}_1^0}) / (m_{\tilde{\chi}_1^\pm} - m_{\tilde{\chi}_1^0}) < 0.75$ because of the complementary nature of the signal diagrams.

³ TUMASYAN 23K searched in 138 fb^{-1} of pp collisions at $\sqrt{s} = 13 \text{ TeV}$ for evidence of top squark pair production in events with a high-momentum jet, an electron or muon with low transverse momentum, and significant \cancel{E}_T . No significant excess above the Standard Model expectations is observed. Limits are set on the top squark mass in the simplified model Tstop3 for $10 \text{ GeV} < m_{\tilde{t}} - m_{\tilde{\chi}_1^0} < 80 \text{ GeV}$, see their Figure 10.

⁴ TUMASYAN 22Q searched in up to 137 fb^{-1} of pp collisions at $\sqrt{s} = 13 \text{ TeV}$ for evidence of electroweakino and top squark pair production with a small mass difference between the produced supersymmetric particles and the lightest neutralino in events with two or three low-momentum leptons and missing transverse momentum. No significant excess above the Standard Model expectations is observed. Limits are set on the mass of $\tilde{\chi}_2^0$ and $\tilde{\chi}_1^\pm$ in the model Tch1n2F, see their Figure 8. Limits are also set in a higgsino simplified model with both $\tilde{\chi}_2^0 \tilde{\chi}_1^\pm$ and $\tilde{\chi}_2^0 \tilde{\chi}_1^0$ production, where $\tilde{\chi}_2^0 \rightarrow Z \tilde{\chi}_1^0$ and $m_{\tilde{\chi}_1^\pm} = 1/2(m_{\tilde{\chi}_2^0} + m_{\tilde{\chi}_1^0})$. A model inspired by the pMSSM is used for further interpretations in the case of a higgsino LSP, see their Figure 9. Limits are also set on the mass of the top squark in the models Tstop2 and Tstop3, see their Figure 10.

⁵ AAD 21AW searched in 139 fb^{-1} of pp collisions at $\sqrt{s} = 13 \text{ TeV}$ for pair production of stops in events with one or two hadronically decaying τ leptons, jets, b -jets and \cancel{E}_T . No significant excess above the Standard Model predictions is observed. Limits are set on the \tilde{t}_1 mass as a function of the $\tilde{\tau}_1$ in the Tstop5 scenario. See their Fig. 8.

⁶ AAD 21o searched in 139 fb^{-1} of pp collisions at $\sqrt{s} = 13 \text{ TeV}$ for pair production of top squarks in events with one electron or muon, jets, and large missing transverse momentum. No significant excess above the Standard Model expectations is observed. Limits are set on the top squark mass in the Tstop1 and Tstop3 simplified models and dark matter models, see their Figures 13, 14 and 15.

⁷ AAD 21F searched in 139 fb^{-1} of pp collisions at $\sqrt{s} = 13 \text{ TeV}$ for pair production of top squarks in events with two opposite-sign leptons, jets, and large missing transverse momentum. No significant excess above the Standard Model expectations is observed. Limits are set on the top squark mass in the Tstop1, Tstop2, and Tstop3 simplified models, see their Figures 14.

⁸ SIRUNYAN 21AD searched in 137 fb^{-1} of pp collisions at $\sqrt{s} = 13 \text{ TeV}$ for supersymmetry in events with multiple jets, no leptons, and large \cancel{E}_T . No significant excess above the Standard Model expectations is observed. Limits are set on the top squark mass in the simplified models Tstop1, Tstop2 with $m_{\tilde{\chi}_1^\pm} = (m_{\tilde{t}} + m_{\tilde{\chi}_1^0})/2$, and a 50:50 mixture of these with $m_{\tilde{\chi}_1^\pm} - m_{\tilde{\chi}_1^0} = 5 \text{ GeV}$, see their Figure 8. Limits are also set on the top squark mass for $10 \text{ GeV} < m_{\tilde{t}} - m_{\tilde{\chi}_1^\pm} < 80 \text{ GeV}$ in the simplified models Tstop2, Tstop 3, and Tstop4, see their Figure 9. For indirect top squark production, limits are set on the gluino mass in the simplified models Tglu3A, Tglu3C with $m_{\tilde{t}} - m_{\tilde{\chi}_1^0} = 20 \text{ GeV}$, and Tglu3D with $m_{\tilde{\chi}_1^\pm} - m_{\tilde{\chi}_1^0} = 5 \text{ GeV}$, see their Figure 10.

⁹ SIRUNYAN 21B searched in 137 fb^{-1} of pp collisions at $\sqrt{s} = 13 \text{ TeV}$ for the pair production of top squarks in events with two oppositely charged leptons (electrons or muons), jets identified as originating from a b -quark and significant \cancel{E}_T . No significant excess above the Standard Model expectations is observed. Limits are set on the stop mass in the Tstop1, Tstop2 and Tstop11 simplified models, see their Figures 6 and 7.

¹⁰ TUMASYAN 21i searched in 137 fb^{-1} of pp collisions at $\sqrt{s} = 13 \text{ TeV}$ for evidence of top squarks in events with at least two jets and large \cancel{E}_T , categorized into events with 0, 1, or 2 leptons. No significant excess above the Standard Model expectations is observed. Limits are set on the top squark mass in the simplified model Tstop1 in the top corridor $|m_{\tilde{t}} - m_{\tilde{\chi}_1^0} - 175 \text{ GeV}| < 30 \text{ GeV}$ using dilepton events, see their Figure 7. Limits are also set for a combination of earlier searches with 0, 1, and 2 leptons in

Searches Particle Listings

Supersymmetric Particle Searches

- the models Tstop1, Tstop2 and a 50:50 mixture of these models, see their Figure 9. The results are interpreted in an alternative signal model of dark matter production via a spin-0 mediator in association with a top quark pair as well.
- 11 AABOUD 20 searched in 36.1 fb^{-1} of pp collisions at $\sqrt{s} = 13 \text{ TeV}$ for events containing one electron-muon pair with opposite charge. The search targets a region of parameter space where the kinematics of top squark pair production and top quark pair production is very similar and makes use of the double-differential angular distributions of the leptons. No excess above the Standard Model expectations is observed. Limits are set on the stop mass in the Tstop1 model, see Figures 16 and 17.
 - 12 AAD 20As searched in 139 fb^{-1} of pp collisions at $\sqrt{s} = 13 \text{ TeV}$ for evidence of top squarks in events containing either a pair of jets consistent with SM Higgs boson decay into b -quarks or a same-flavour opposite-sign dilepton pair with an invariant mass consistent with a Z boson. No significant excess over the expected background is observed. Limits at 95% C.L. are set in Tstop6 simplified model. Assuming $m_{\tilde{\chi}_1^0} = 0 \text{ GeV}$, \tilde{t}_1 masses up to 1220 GeV are excluded for $m_{\tilde{\chi}_2^0}$ around 900 GeV. Limits reduce down to \tilde{t}_1 masses up to 900 GeV for $m_{\tilde{\chi}_2^0} = 130 \text{ GeV}$. See their Fig. 10. Limits are presented also in case of $B(\tilde{\chi}_2^0 \rightarrow \tilde{\chi}_1^0 h) = 0$ and 1, see their Fig. 11.
 - 13 AAD 20As searched in 139 fb^{-1} of pp collisions at $\sqrt{s} = 13 \text{ TeV}$ for evidence of top squarks in events containing either a pair of jets consistent with SM Higgs boson decay into b -quarks or a same-flavour opposite-sign dilepton pair with an invariant mass consistent with a Z boson. No significant excess over the expected background is observed. Limits at 95% C.L. are set in simplified model featuring \tilde{t}_2 pair production, $\tilde{t}_2 \rightarrow \tilde{t}_1 Z$ and $\tilde{t}_1 \rightarrow b f f \tilde{\chi}_1^0$. Assuming $m_{\tilde{\chi}_1^0} = 300 \text{ GeV}$, and a mass difference between \tilde{t}_1 and $\tilde{\chi}_1^0$ of 40 GeV, \tilde{t}_2 masses up to 860 GeV are excluded. See their Fig. 12.
 - 14 AAD 20s searched in 139 fb^{-1} of pp collisions at $\sqrt{s} = 13 \text{ TeV}$ for events containing multiple jets and large \cancel{E}_T . No significant excess above the Standard Model expectations is observed. Exclusion limits at 95% C.L. are set on top squark masses in the Tstop1 model up to 1250 GeV for lightest neutralino masses below 200 GeV. Additional constraints are set in the case where $m_{\tilde{t}} - m_{\tilde{\chi}_1^0} \sim m_t$ for which top squark masses in the range 300–630 GeV are excluded. See their Fig. 13.
 - 15 AAD 20s searched in 139 fb^{-1} of pp collisions at $\sqrt{s} = 13 \text{ TeV}$ for events containing multiple jets and large \cancel{E}_T . No significant excess above the Standard Model expectations is observed. Exclusion limits at 95% C.L. are set on top squark masses in the Tstop3 model in the range 300–660 GeV. In case $m_{\tilde{t}} - m_{\tilde{\chi}_1^0} \sim 5 \text{ GeV}$ or above, $m_{\tilde{t}}$ below 500 GeV are excluded. See their Fig. 13(b).
 - 16 AAD 20v searched in 139 fb^{-1} of pp collisions at $\sqrt{s} = 13 \text{ TeV}$ for events with two same-sign charged leptons (electrons or muons) and jets. No significant excess above the Standard Model expectations is observed. Exclusion limits at 95% C.L. are set on the top squark mass up to 765 GeV assuming $\tilde{t}_1 \rightarrow t \tilde{\chi}_2^0$ with $\tilde{\chi}_2^0 \rightarrow \tilde{\chi}_1^\pm W$ and $\tilde{\chi}_1^\pm \rightarrow \tilde{\chi}_1^0 W$. Masses of the charginos and lightest neutralinos are set as $m_{\tilde{\chi}_1^0} = m_{\tilde{t}_1} - 275 \text{ GeV}$, $m_{\tilde{\chi}_2^0} = m_{\tilde{\chi}_1^0} + 100 \text{ GeV}$ and $m_{\tilde{\chi}_1^\pm} \sim m_{\tilde{\chi}_1^0}$. See their Fig. 8(b).
 - 17 SIRUNYAN 20AH searched in 137 fb^{-1} of pp collisions at $\sqrt{s} = 13 \text{ TeV}$ for pair production of top squarks in events with a single isolated electron or muon, multiple jets and large \cancel{E}_T . No significant excess above the Standard Model expectations is observed. Limits are set on the stop mass in the Tstop1, Tstop2 and Tstop8 simplified models, see Figures 6, 7 and 8, respectively.
 - 18 SIRUNYAN 20T searched in 137 fb^{-1} of pp collisions at $\sqrt{s} = 13 \text{ TeV}$ for events with at least two jets, and two isolated same-sign or three or more charged leptons (electrons or muons). No significant excess above the Standard Model expectations is observed. Limits are set on the gluino mass in the Tglu3A, Tglu3B, Tglu3C and Tglu3D simplified models, see their Figure 7, and in the Tglu1C and Tglu1B simplified models, see their Figures 8 and 9. Limits are also set on the sbottom mass in the Tstop2 simplified model, see their Figure 10, and on the stop mass in the Tstop7 simplified model, see their Figure 11. Finally, limits are set on the gluino mass in RPV simplified models where the gluino decays either via $\tilde{g} \rightarrow qq\bar{q}\bar{q} + e\mu\tau$ or via $\tilde{g} \rightarrow tbs$, see Figure 12.
 - 19 SIRUNYAN 20U searched in 77.2 fb^{-1} of pp collisions at $\sqrt{s} = 13 \text{ TeV}$ for the pair production of top squarks in events with two hadronically decaying taus, jets identified as originating from a b -quark and large \cancel{E}_T . No significant excess above the Standard Model expectations is observed. Limits are set on the stop mass in the Tstop11 simplified model assuming the final state leptons are taus. Different values of the scalar tau mass are considered; the impact on the lower bound is negligible.
 - 20 SIRUNYAN 19AU searched in 35.9 fb^{-1} of pp collisions at $\sqrt{s} = 13 \text{ TeV}$ for events with at least one photon, jets, some of which are identified as originating from b -quarks, and large \cancel{E}_T . No significant excess above the Standard Model expectations is observed. In the framework of GMSB, limits are set on the gluino mass in the Tglu4C, Tglu4D and Tglu4E simplified models, and on the top squark mass in the Tstop13 simplified model, see their Figure 5.
 - 21 SIRUNYAN 19CH searched in 137 fb^{-1} of pp collisions at $\sqrt{s} = 13 \text{ TeV}$ for events containing multiple jets and large \cancel{E}_T . No significant excess above the Standard Model expectations is observed. Limits are set on the gluino mass in the Tglu1A, Tglu1C, Tglu2A and Tglu3A simplified models, see their Figure 13. Limits are also set on squark, sbottom and stop masses in the Tsqk1, Tstop1, Tstop1 simplified models, see their Figure 14.
 - 22 SIRUNYAN 19s searched in 35.9 fb^{-1} of pp collisions at $\sqrt{s} = 13 \text{ TeV}$ for events with zero or one charged leptons, jets and \cancel{E}_T . The razor variables (M_R and R^2) are used to categorize the events. No significant excess above the Standard Model expectations is observed. Limits are set on the gluino mass in the Tglu3A and Tglu3C simplified models, see Figures 22 and 23, and on the stop mass in the Tstop1 simplified model, see their Figure 24.
 - 23 SIRUNYAN 19U searched in 35.9 fb^{-1} of pp collisions at $\sqrt{s} = 13 \text{ TeV}$ for events containing one electron-muon pair with opposite charge. The search targets a region of parameter space where the kinematics of top squark pair production and top quark pair production is very similar, due to the mass difference between the top squark and the neutralino being close to the top quark mass. No excess above the Standard Model expectations is observed. Limits are set on the stop mass in the Tstop1 model, with $m_{\tilde{t}_1} - m_{\tilde{\chi}_1^0}$ close to m_t , see Figure 5.
 - 24 AABOUD 18AQ searched in 36.1 fb^{-1} of pp collisions at $\sqrt{s} = 13 \text{ TeV}$ for top squark pair production in final states with one isolated electron or muon, several energetic jets, and missing transverse momentum. No significant excess over the Standard Model prediction is observed. In case of Tstop1 models, top squark masses up to 940 GeV are excluded assuming $m_{\tilde{\chi}_1^0} = 0 \text{ GeV}$, see their Fig. 20. If the top quark is not on-shell (3-body) decay, exclusions up to 500 GeV are obtained for $m_{\tilde{\chi}_1^0} = 300 \text{ GeV}$. Exclusions as a function of $m_{\tilde{t}_1} - m_{\tilde{\chi}_1^0}$ are given in their Fig. 21.
 - 25 AABOUD 18AQ searched in 36.1 fb^{-1} of pp collisions at $\sqrt{s} = 13 \text{ TeV}$ for top squark pair production in final states with one isolated electron or muon, several energetic jets, and missing transverse momentum. No significant excess over the Standard Model prediction is observed. In case of Tstop3 models (4-body), top squark masses up to 370 GeV are excluded for $m_{\tilde{t}} - m_{\tilde{\chi}_1^0}$ as low as 20 GeV. Top squark masses below 195 GeV are excluded for all $m_{\tilde{\chi}_1^0}$, see their Fig. 20 and Fig. 21.
 - 26 AABOUD 18AQ searched in 36.1 fb^{-1} of pp collisions at $\sqrt{s} = 13 \text{ TeV}$ for top squark pair production in final states with one isolated electron or muon, several energetic jets, and missing transverse momentum. No significant excess over the Standard Model prediction is observed. In case of Tstop2 models, top squark masses up to 840 GeV are excluded for $m_{\tilde{t}} - m_{\tilde{\chi}_1^\pm} = 10 \text{ GeV}$. See their Fig. 23. Exclusion limits for this decay mode are presented also in the context of Higgsino-LSP phenomenological MSSM models, where $m_{\tilde{\chi}_1^\pm} - m_{\tilde{\chi}_1^0} = 5 \text{ GeV}$, see their Fig. 26.
 - 27 AABOUD 18BV searched in 36.1 fb^{-1} of pp collisions at $\sqrt{s} = 13 \text{ TeV}$ for events with at least one jet identified as c -jet, large missing transverse energy and no leptons. Good agreement is observed between the number of events in data and Standard Model predictions. The results are translated into exclusion limits in Tstop4 models. In scenarios with differences of the stop and neutralino masses below 100 GeV, stop masses below 500 GeV are excluded. See their Fig. 6 and Fig. 7.
 - 28 AABOUD 18BV searched in 36.1 fb^{-1} of pp collisions at $\sqrt{s} = 13 \text{ TeV}$ for events with at least one jet identified as c -jet, large missing transverse energy and no leptons. Good agreement is observed between the number of events in data and Standard Model predictions. The results are translated into exclusion limits in Tstop1 models. In scenarios with massless neutralinos, top squark masses below 850 GeV are excluded. See their Fig. 6.
 - 29 AABOUD 18I searched in 36.1 fb^{-1} of pp collisions at $\sqrt{s} = 13 \text{ TeV}$ for events with at least one jet with a transverse momentum above 250 GeV and no leptons. Good agreement is observed between the number of events in data and Standard Model predictions. The results are translated into exclusion limits in Tstop3 models. Stop masses below 390 GeV are excluded for $m_{\tilde{t}} - m_{\tilde{\chi}_1^0} = m_b$. See their Fig. 9(b).
 - 30 AABOUD 18I searched in 36.1 fb^{-1} of pp collisions at $\sqrt{s} = 13 \text{ TeV}$ for events with at least one jet with a transverse momentum above 250 GeV and no leptons. Good agreement is observed between the number of events in data and Standard Model predictions. The results are translated into exclusion limits in Tstop4 models. In scenarios with differences of the stop and neutralino masses around 5 GeV, stop masses below 430 GeV are excluded. See their Fig. 9(a).
 - 31 AABOUD 18Y searched in 36.1 fb^{-1} of pp collisions at $\sqrt{s} = 13 \text{ TeV}$ for direct pair production of top squarks in final states with two tau leptons, b -jets, and missing transverse momentum. At least one hadronic τ is required. No significant deviation from the SM predictions is observed in the data. The analysis results are interpreted in Tstop5 models with a nearly massless gravitino. Top squark masses up to 1.16 TeV and tau slepton masses up to 1 TeV are excluded, see their Fig. 7.
 - 32 SIRUNYAN 18AJ searched in 35.9 fb^{-1} of pp collisions at $\sqrt{s} = 13 \text{ TeV}$ for events containing two low-momentum, oppositely charged leptons (electrons or muons) and \cancel{E}_T . No excess over the expected background is observed. Limits are derived on the wino mass in the Tch1n2F simplified model, see their Figure 5. Limits are also set on the stop mass in the Tstop10 simplified model, see their Figure 6. Finally, limits are set on the Higgsino mass in the Tch1n2G simplified model, see Figure 8 and in the pMSSM, see their Figure 7.
 - 33 SIRUNYAN 18AL searched in 35.9 fb^{-1} of pp collisions at $\sqrt{s} = 13 \text{ TeV}$ for events with at least three charged leptons, in any combination of electrons and muons, jets and significant \cancel{E}_T . No significant excess above the Standard Model expectations is observed. Limits are set on the gluino mass in the Tglu3A and Tglu1C simplified models, see their Figure 5. Limits are also set on the sbottom mass in the Tstop2 simplified model, see their Figure 6, and on the stop mass in the Tstop7 simplified model, see their Figure 7.
 - 34 SIRUNYAN 18AN searched in 19.7 fb^{-1} of pp collisions at $\sqrt{s} = 8 \text{ TeV}$ for events containing one or two photons and a pair of top quarks from the decay of a pair of top squark in a natural gauge-mediated scenario. The final state consists of a lepton (electron or muon), jets and one or two photons. No significant excess above the Standard Model expectations is observed. Limits are set on the stop mass in the Tstop12 simplified model, see their Figure 6.
 - 35 SIRUNYAN 18AV searched in 35.9 fb^{-1} of pp collisions at $\sqrt{s} = 13 \text{ TeV}$ for events containing one or more jets and significant \cancel{E}_T . No significant excess above the Standard Model expectations is observed. Limits are set on the gluino mass in the Tglu1A, Tglu2A and Tglu3A simplified models, see their Figure 3. Limits are also set on squark, sbottom and stop masses in the Tsqk1, Tstop1, Tstop1 and Tstop4 simplified models, see their Figure 3. Finally, limits are set on long-lived gluino masses in a Tglu1A simplified model where the gluino is metastable or long-lived with proper decay lengths in the range $10^{-3} \text{ mm} < c\tau < 10^5 \text{ mm}$, see their Figure 4.
 - 36 SIRUNYAN 18B searched in 35.9 fb^{-1} of pp collisions at $\sqrt{s} = 13 \text{ TeV}$ for the pair production of third-generation squarks in events with jets and large \cancel{E}_T . No significant excess above the Standard Model expectations is observed. Limits are set on the sbottom mass in the Tstop1 simplified model, see their Figure 5, and on the stop mass in the Tstop4 simplified model, see their Figure 6.
 - 37 SIRUNYAN 18C searched in 35.9 fb^{-1} of pp collisions at $\sqrt{s} = 13 \text{ TeV}$ for the pair production of top squarks in events with two oppositely charged leptons (electrons or muons), jets identified as originating from a b -quark and large \cancel{E}_T . No significant excess above the Standard Model expectations is observed. Limits are set on the stop mass in the Tstop1, Tstop2 and Tstop11 simplified models, see their Figures 11 and 12. The Tstop1 and Tstop2 results are combined with complementary searches in the all-hadronic and single lepton channels, see their Figures 13 and 14.
 - 38 SIRUNYAN 18D searched in 35.9 fb^{-1} of pp collisions at $\sqrt{s} = 13 \text{ TeV}$ for events containing identified hadronically decaying top quarks, no leptons, and \cancel{E}_T . No significant excess above the Standard Model expectations is observed. Limits are set on the stop mass in the Tstop1 simplified model, see their Figure 8, and on the gluino mass in the Tglu3A, Tglu3B, Tglu3C and Tglu3E simplified models, see their Figure 9.
 - 39 SIRUNYAN 18DI searched in 35.9 fb^{-1} of pp collisions at $\sqrt{s} = 13 \text{ TeV}$ for pair production of top squarks in events with a low transverse momentum lepton (electron or muon), a high-momentum jet and significant missing transverse momentum. No significant excess above the Standard Model expectations is observed. Limits are set on the

- stop mass in the Tstop3 and Tstop10 simplified models, see their Figures 7 and 8. A combination of this search with the all-hadronic search is presented in Figure 9.
- 40 SIRUNYAN 18DN searched in 35.9 fb^{-1} of pp collisions at $\sqrt{s} = 13 \text{ TeV}$ for direct electroweak production of charginos and for pair production of top squarks in events with two leptons (electrons or muons) of the opposite electric charge. No significant excess above the Standard Model expectations is observed. Limits are set on the chargino mass in the Tch1chi1C and Tch1chi1E simplified models, see their Figure 8. Limits are also set on the stop mass in the Tstop1 and Tstop2 simplified models, see their Figure 9.
- 41 AABOUD 17AJ searched in 36.1 fb^{-1} of pp collisions at $\sqrt{s} = 13 \text{ TeV}$ for events with two same-sign or three leptons, jets and large missing transverse momentum. No significant excess above the Standard Model expectations is observed. Limits up to 700 GeV are set on the top squark mass in Tstop11 simplified models, assuming $m_{\tilde{\chi}_1^0} = m_{\tilde{\tau}} - 275 \text{ GeV}$ and $m_{\tilde{\chi}_2^0} = m_{\tilde{\chi}_1^0} + 100 \text{ GeV}$. See their Figure 4(e).
- 42 AABOUD 17AX searched in 36 fb^{-1} of pp collisions at $\sqrt{s} = 13 \text{ TeV}$ for events containing two jets identified as originating from b -quarks and large missing transverse momentum, with or without leptons. No excess of events above the expected level of Standard Model background was found. Exclusion limits at 95% C.L. are set on the masses of top squarks. Assuming 50% BR for Tstop1 and Tstop2 simplified models, a \tilde{t}_1 mass below 880 (860) GeV is excluded for $m_{\tilde{\chi}_1^0} = 0$ (<250) GeV. See their Fig. 7(b).
- 43 AABOUD 17AY searched in 36.1 fb^{-1} of pp collisions at $\sqrt{s} = 13 \text{ TeV}$ for events with at least four jets and large missing transverse momentum. No significant excess above the Standard Model expectations is observed. Limits in the range 250–1000 GeV are set on the top squark mass in Tstop1 simplified models. For the first time, additional constraints are set for the region $m_{\tilde{t}_1} \sim m_{\tilde{t}} + m_{\tilde{\chi}_1^0}$, with exclusion of the \tilde{t}_1 mass range 235–590 GeV. See their Figure 8.
- 44 AABOUD 17AZ searched in 36.1 fb^{-1} of pp collisions at $\sqrt{s} = 13 \text{ TeV}$ for events with at least four jets and large missing transverse momentum. No significant excess above the Standard Model expectations is observed. Limits in the range 450–850 GeV are set on the top squark mass in a mixture of Tstop1 and Tstop2 simplified models with BR=50% and assuming $m_{\tilde{\chi}_1^\pm} - m_{\tilde{\chi}_1^0} = 1 \text{ GeV}$ and $m_{\tilde{\chi}_1^0} < 240 \text{ GeV}$. Constraints are given for various values of the BR. See their Figure 9.
- 45 AABOUD 17BE searched in 36.1 fb^{-1} of pp collisions at $\sqrt{s} = 13 \text{ TeV}$ for events with two opposite-charge leptons (electrons and muons) and large missing transverse momentum. No significant excess above the Standard Model expectations is observed. Limits up to 720 GeV are set on the top squark mass in Tstop1 simplified models, assuming massless neutralinos. See their Figure 9 (2-body area).
- 46 AABOUD 17BE searched in 36.1 fb^{-1} of pp collisions at $\sqrt{s} = 13 \text{ TeV}$ for events with two opposite-charge leptons (electrons and muons) and large missing transverse momentum. No significant excess above the Standard Model expectations is observed. Limits up to 400 GeV are set on the top squark mass in Tstop3 simplified models, assuming $m_{\tilde{t}_1} - m_{\tilde{\chi}_1^0} = 40 \text{ GeV}$. See their Figure 9 (4-body area).
- 47 AABOUD 17BE searched in 36.1 fb^{-1} of pp collisions at $\sqrt{s} = 13 \text{ TeV}$ for events with two opposite-charge leptons (electrons and muons) and large missing transverse momentum. No significant excess above the Standard Model expectations is observed. Limits up to 430 GeV are set on the top squark mass in Tstop1 simplified models where top quarks are offshell, assuming $m_{\tilde{t}_1} - m_{\tilde{\chi}_1^0}$ close to the W mass. See their Figure 9 (3-body area).
- 48 AABOUD 17BE searched in 36.1 fb^{-1} of pp collisions at $\sqrt{s} = 13 \text{ TeV}$ for events with two opposite-charge leptons (electrons and muons) and large missing transverse momentum. No significant excess above the Standard Model expectations is observed. Limits up to 700 GeV are set on the top squark mass in Tstop2 simplified models, assuming $m_{\tilde{t}_1} - m_{\tilde{\chi}_1^\pm} = 10 \text{ GeV}$ and massless neutralinos. See their Figure 10.
- 49 KHACHATRYAN 17 searched in 2.3 fb^{-1} of pp collisions at $\sqrt{s} = 13 \text{ TeV}$ for events containing four or more jets, no more than one lepton, and missing transverse momentum, using the razor variables ($M_{\tilde{R}^2}$ and R^2) to discriminate between signal and background processes. No evidence for an excess over the expected background is observed. Limits are derived on the stop mass in the Tstop1 simplified model, see Fig. 17.
- 50 KHACHATRYAN 17AD searched in 2.3 fb^{-1} of pp collisions at $\sqrt{s} = 13 \text{ TeV}$ for events containing at least four jets (including b -jets), missing transverse momentum and tagged top quarks. No evidence for an excess over the expected background is observed. Top squark masses in the range 250–740 GeV and neutralino masses up to 240 GeV are excluded at 95% C.L. See Fig. 12.
- 51 KHACHATRYAN 17AD searched in 2.3 fb^{-1} of pp collisions at $\sqrt{s} = 13 \text{ TeV}$ for events containing at least four jets (including b -jets), missing transverse momentum and tagged top quarks. No evidence for an excess over the expected background is observed. Limits are derived on the \tilde{t} mass in simplified models that are a mixture of Tstop1 and Tstop2 with branching fractions 50% for each of the two decay modes: top squark masses of up to 610 GeV and neutralino masses up to 190 GeV are excluded at 95% C.L. The $\tilde{\chi}_1^\pm$ and the $\tilde{\chi}_1^0$ are assumed to be nearly degenerate in mass, with a 5 GeV difference between their masses. See Fig. 12.
- 52 KHACHATRYAN 17P searched in 2.3 fb^{-1} of pp collisions at $\sqrt{s} = 13 \text{ TeV}$ for events with one or more jets and large $E_{\cancel{T}}$. No significant excess above the Standard Model expectations is observed. Limits are set on the gluino mass in the Tglu1A, Tglu2A, Tglu3A, Tglu3B, Tglu3C and Tglu3D simplified models, see their Figures 7 and 8. Limits are also set on the squark mass in the Tsqk1 simplified model, see their Fig. 7, and on the sbottom mass in the Tsb01 simplified model, see Fig. 8. Finally, limits are set on the stop mass in the Tstop1, Tstop3, Tstop4, Tstop6 and Tstop7 simplified models, see Fig. 8.
- 53 KHACHATRYAN 17S searched in 18.5 fb^{-1} of pp collisions at $\sqrt{s} = 8 \text{ TeV}$ for events containing multiple jets and missing transverse momentum, using the α_T variable to discriminate between signal and background processes. No evidence for an excess over the expected background is observed. Limits are derived on the stop mass in the Tstop4 model: for $\Delta m = m_{\tilde{\tau}} - m_{\tilde{\chi}_1^0}$ equal to 10 and 80 GeV, masses of stop below 240 and 260 GeV are excluded, respectively. See their Fig.3.
- 54 KHACHATRYAN 17S searched in 18.5 fb^{-1} of pp collisions at $\sqrt{s} = 8 \text{ TeV}$ for events containing multiple jets and missing transverse momentum, using the α_T variable to discriminate between signal and background processes. No evidence for an excess over the expected background is observed. Limits are derived on the stop mass in the Tstop3 model: for $\Delta m = m_{\tilde{\tau}} - m_{\tilde{\chi}_1^0}$ equal to 10 and 80 GeV, masses of stop below 225 and 130 GeV are excluded, respectively. See their Fig.3.
- 55 KHACHATRYAN 17S searched in 18.5 fb^{-1} of pp collisions at $\sqrt{s} = 8 \text{ TeV}$ for events containing multiple jets and missing transverse momentum, using the α_T variable to discriminate between signal and background processes. No evidence for an excess over the expected background is observed. Limits are derived on the stop mass in the Tstop2 model: assuming $m_{\tilde{\chi}_1^\pm} = 0.25 m_{\tilde{\tau}} + 0.75 m_{\tilde{\chi}_1^0}$, masses of stop up to 325 GeV and masses of the neutralino up to 225 GeV are excluded. See their Fig.3.
- 56 KHACHATRYAN 17S searched in 18.5 fb^{-1} of pp collisions at $\sqrt{s} = 8 \text{ TeV}$ for events containing multiple jets and missing transverse momentum, using the α_T variable to discriminate between signal and background processes. No evidence for an excess over the expected background is observed. Limits are derived on the stop mass in the Tstop2 model: assuming $m_{\tilde{\chi}_1^\pm} = 0.75 m_{\tilde{\tau}} + 0.25 m_{\tilde{\chi}_1^0}$, masses of stop up to 400 GeV are excluded for low neutralino masses. See their Fig.3.
- 57 KHACHATRYAN 17S searched in 18.5 fb^{-1} of pp collisions at $\sqrt{s} = 8 \text{ TeV}$ for events containing multiple jets and missing transverse momentum, using the α_T variable to discriminate between signal and background processes. No evidence for an excess over the expected background is observed. Limits are derived on the stop mass in the Tstop1 model: assuming masses of stop up to 500 GeV and masses of the neutralino up to 105 GeV are excluded. See their Fig.3.
- 58 SIRUNYAN 17As searched in 35.9 fb^{-1} of pp collisions at $\sqrt{s} = 13 \text{ TeV}$ for events with a single lepton (electron or muon), jets, and large $E_{\cancel{T}}$. No significant excess above the Standard Model expectations is observed. Limits are set on the stop mass in the Tstop1, Tstop2 and Tstop8 simplified models, see their Figures 5, 6 and 7.
- 59 SIRUNYAN 17AT searched in 35.9 fb^{-1} of pp collisions at $\sqrt{s} = 13 \text{ TeV}$ for direct production of top squarks in events with jets and large $E_{\cancel{T}}$. No significant excess above the Standard Model expectations is observed. Limits are set on the stop mass in the Tstop1, Tstop2, Tstop3, Tstop4, Tstop8 and Tstop10 simplified models, see their Figures 9 to 14.
- 60 SIRUNYAN 17AZ searched in 35.9 fb^{-1} of pp collisions at $\sqrt{s} = 13 \text{ TeV}$ for events with one or more jets and large $E_{\cancel{T}}$. No significant excess above the Standard Model expectations is observed. Limits are set on the gluino mass in the Tglu1A, Tglu2A, Tglu3A and Tglu3D simplified models, see their Figures 6. Limits are also set on the squark mass in the Tsqk1 simplified model (for single light squark and for 8 degenerate light squarks), on the sbottom mass in the Tsb01 simplified model and on the stop mass in the Tstop1 simplified model, see their Fig. 7. Finally, limits are set on the stop mass in the Tstop2, Tstop4 and Tstop8 simplified models, see Fig. 8.
- 61 SIRUNYAN 17k searched in 2.3 fb^{-1} of pp collisions at $\sqrt{s} = 13 \text{ TeV}$ for direct production of stop or sbottom pairs in events with multiple jets and significant $E_{\cancel{T}}$. A second search also requires an isolated lepton and is combined with the all-hadronic search. No significant excess above the Standard Model expectations is observed. Limits are set on the stop mass in the Tstop1, Tstop8 and Tstop4 simplified models, see their Figures 7, 8 and 9 (for the Tstop4 limits, only the results of the all-hadronic search are used). Limits are also set on the sbottom mass in the Tsb01 simplified model, see Fig. 10 (also here, only the results of the all-hadronic search are used).
- 62 SIRUNYAN 17P searched in 35.9 fb^{-1} of pp collisions at $\sqrt{s} = 13 \text{ TeV}$ for events with multiple jets and large $E_{\cancel{T}}$. No significant excess above the Standard Model expectations is observed. Limits are set on the gluino mass in the Tglu1A, Tglu1C, Tglu2A, Tglu3A and Tglu3D simplified models, see their Fig. 12. Limits are also set on the squark mass in the Tsqk1 simplified model, on the stop mass in the Tstop1 simplified model, and on the sbottom mass in the Tsb01 simplified model, see Fig. 13.
- 63 AABOUD 16D searched in 3.2 fb^{-1} of pp collisions at $\sqrt{s} = 13 \text{ TeV}$ in events with an energetic jet and large missing transverse momentum. The results are interpreted as 95% C.L. limits on mass of stop decaying into a charm-quark and the lightest neutralino in scenarios with $m_{\tilde{t}_1} - m_{\tilde{\chi}_1^0}$ between 5 and 20 GeV. See their Fig. 5.
- 64 AABOUD 16J searched in 3.2 fb^{-1} of pp collisions at $\sqrt{s} = 13 \text{ TeV}$ in final states with one isolated electron or muon, jets, and missing transverse momentum. For the direct stop pair production model where the stop decays via top and lightest neutralino, the results exclude at 95% C.L. stop masses between 745 GeV and 780 GeV for a massless $\tilde{\chi}_1^0$. See their Fig. 8.
- 65 AAD 16AY searched in 20 fb^{-1} of pp collisions at $\sqrt{s} = 8 \text{ TeV}$ for events with either two hadronically decaying tau leptons, one hadronically decaying tau and one light lepton, or two light leptons. No significant excess over the Standard Model expectation is found. Exclusion limits at 95% C.L. on the mass of top squarks decaying via $\tilde{\tau}$ to a nearly massless gravitino are placed depending on $m_{\tilde{\tau}}$ which is ranging from the 87 GeV LEP limit to $m_{\tilde{t}_1}$. See their Figs. 9 and 10.
- 66 KHACHATRYAN 16AV searched in 19.7 fb^{-1} of pp collisions at $\sqrt{s} = 8 \text{ TeV}$ for events with one or two isolated leptons, hadronic jets, b -jets and $E_{\cancel{T}}$. No significant excess above the Standard Model expectations is observed. Limits are set on the stop mass in the Tstop1 and Tstop2 simplified models, see Fig. 11.
- 67 KHACHATRYAN 16BK searched in 18.9 fb^{-1} of pp collisions at $\sqrt{s} = 8 \text{ TeV}$ for events with hadronic jets and $E_{\cancel{T}}$. No significant excess above the Standard Model expectations is observed. Limits are set on the stop mass in the Tstop1 and Tstop2 simplified models, see Fig. 16.
- 68 KHACHATRYAN 16BS searched in 2.3 fb^{-1} of pp collisions at $\sqrt{s} = 13 \text{ TeV}$ for events with at least one energetic jet, no isolated leptons, and significant $E_{\cancel{T}}$, using the transverse mass variable M_{T2} to discriminate between signal and background processes. No significant excess above the Standard Model expectations is observed. Limits are set on the stop mass in the Tstop1 simplified model, see Fig. 11 and Table 3.
- 69 KHACHATRYAN 16V searched in 19.7 fb^{-1} of pp collisions at $\sqrt{s} = 8 \text{ TeV}$ for events with one or two soft isolated leptons, hadronic jets, and $E_{\cancel{T}}$. No significant excess above the Standard Model expectations is observed. Limits are set on the stop mass in the Tstop3 simplified model, see Fig. 3.
- 70 AAD 15CJ searched in 20 fb^{-1} of pp collisions at $\sqrt{s} = 8 \text{ TeV}$ for evidence of third generation squarks by combining a large number of searches covering various final states. Stop decays with and without charginos in the decay chain are considered and summaries of all ATLAS Run 1 searches for direct stop production can be found in Fig. 4 (no intermediate charginos) and Fig. 7 (intermediate charginos). Limits are set on stop masses in compressed mass regions regions, with $B(\tilde{t} \rightarrow c\tilde{\chi}_1^0) + B(\tilde{t} \rightarrow b\tilde{f}'\tilde{\chi}_1^0) = 1$, see Fig. 5. Limits are also set on stop masses assuming that both the decay $\tilde{t} \rightarrow t\tilde{\chi}_1^0$ and $\tilde{t} \rightarrow b\tilde{\chi}_1^\pm$ are possible, with both their branching ratios summing up to 1, assuming $\tilde{\chi}_1^\pm \rightarrow W^{(*)}\tilde{\chi}_1^0$ and $m_{\tilde{\chi}_1^\pm} = 2 m_{\tilde{\chi}_1^0}$, see Fig. 6. Limits on the mass of the next-to-lightest stop \tilde{t}_2 , decaying either to $Z\tilde{t}_1$, $h\tilde{t}_1$ or $t\tilde{\chi}_1^0$, are also presented, see Figs. 9 and 10. Interpretations in the pMSSM are also discussed, see Figs 13–15.

Searches Particle Listings

Supersymmetric Particle Searches

- 71** AAD 15J interpreted the measurement of spin correlations in $t\bar{t}$ production using 20.3 fb⁻¹ of pp collisions at $\sqrt{s} = 8$ TeV in exclusion limits on the pair production of light \tilde{t}_1 squarks with masses similar to the top quark mass. The \tilde{t}_1 is assumed to decay through $\tilde{t}_1 \rightarrow t\tilde{\chi}_1^0$ with predominantly right-handed top and a 100% branching ratio. The data are found to be consistent with the Standard Model expectations and masses between the top quark mass and 191 GeV are excluded, see their Fig. 2
- 72** KHACHATRYAN 15AF searched in 19.5 fb⁻¹ of pp collisions at $\sqrt{s} = 8$ TeV for events with at least two energetic jets and significant \cancel{E}_T , using the transverse mass variable M_{T2} to discriminate between signal and background processes. No significant excess above the Standard Model expectations is observed. Limits are set on the stop mass in simplified models where the decay $\tilde{t} \rightarrow t\tilde{\chi}_1^0$ takes place with a branching ratio of 100%, see Fig. 12. See also Table 5. Exclusions in the CMSSM, assuming $\tan\beta = 30$, $A_0 = -2 \max(m_0, m_{1/2})$ and $\mu > 0$, are also presented, see Fig. 15.
- 73** KHACHATRYAN 15AH searched in 19.4 or 19.7 fb⁻¹ of pp collisions at $\sqrt{s} = 8$ TeV for events containing either a fully reconstructed top quark, or events containing dijets requiring one or both jets to originate from b -quarks, or events containing a mono-jet. No significant excess above the Standard Model expectations is observed. Limits are set on the stop mass in simplified models where the decay $\tilde{t} \rightarrow t\tilde{\chi}_1^0$ takes place with a branching ratio of 100%, see Fig. 9. Limits are also set in simplified models where the decays $\tilde{t} \rightarrow t\tilde{\chi}_1^0$ and $\tilde{t} \rightarrow b\tilde{\chi}_1^\pm$, with $m_{\tilde{\chi}_1^\pm} - m_{\tilde{\chi}_1^0} = 5$ GeV, each take place with a branching ratio of 50%, see Fig. 10, or with other fractions, see Fig. 11. Finally, limits are set in a simplified model where the decay $\tilde{t} \rightarrow c\tilde{\chi}_1^0$ takes place with a branching ratio of 100%, see Figs. 9, 10 and 11.
- 74** KHACHATRYAN 15AH searched in 19.4 or 19.7 fb⁻¹ of pp collisions at $\sqrt{s} = 8$ TeV for events containing either a fully reconstructed top quark, or events containing dijets requiring one or both jets to originate from b -quarks, or events containing a mono-jet. No significant excess above the Standard Model expectations is observed. Limits are set on the stop mass in simplified models where the decay $\tilde{t} \rightarrow t\tilde{\chi}_1^0$ takes place with a branching ratio of 100%, see Fig. 9. Limits are also set in simplified models where the decays $\tilde{t} \rightarrow t\tilde{\chi}_1^0$ and $\tilde{t} \rightarrow b\tilde{\chi}_1^\pm$, with $m_{\tilde{\chi}_1^\pm} - m_{\tilde{\chi}_1^0} = 5$ GeV, each take place with a branching ratio of 50%, see Fig. 10, or with other fractions, see Fig. 11. Finally, limits are set in a simplified model where the decay $\tilde{t} \rightarrow c\tilde{\chi}_1^0$ takes place with a branching ratio of 100%, see Figs. 9, 10, and 11.
- 75** KHACHATRYAN 15x searched in 19.3 fb⁻¹ of pp collisions at $\sqrt{s} = 8$ TeV for events with at least two energetic jets, at least one of which is required to originate from a b quark, possibly a lepton, and significant \cancel{E}_T , using the razor variables (M_R and R^2) to discriminate between signal and background processes. No significant excess above the Standard Model expectations is observed. Limits are set on the stop mass in simplified models where the decay $\tilde{t} \rightarrow t\tilde{\chi}_1^0$ and the decay $\tilde{t} \rightarrow b\tilde{\chi}_1^\pm$, with $m_{\tilde{\chi}_1^\pm} - m_{\tilde{\chi}_1^0} = 5$ GeV, take place with branching ratios varying between 0 and 100%, see Figs. 15, 16 and 17.
- 76** AAD 14AJ searched in 20.1 fb⁻¹ of pp collisions at $\sqrt{s} = 8$ TeV for events containing four or more jets and large missing transverse momentum. No excess of events above the expected level of Standard Model background was found. Exclusion limits at 95% C.L. are set on the masses of third-generation squarks in simplified models which either assume that the decay $\tilde{t}_1 \rightarrow t\tilde{\chi}_1^0$ takes place 100% of the time, see Fig. 8, or that this decay takes place 50% of the time, while the decay $\tilde{t}_1 \rightarrow b\tilde{\chi}_1^\pm$ takes place the other 50% of the time, see Fig. 9.
- 77** AAD 14BD searched in 20 fb⁻¹ of pp collisions at $\sqrt{s} = 8$ TeV for events containing one isolated lepton, jets and large missing transverse momentum. No excess of events above the expected level of Standard Model background was found. Exclusion limits at 95% C.L. are set on the masses of third-generation squarks in simplified models which either assume that the decay $\tilde{t}_1 \rightarrow t\tilde{\chi}_1^0$ takes place 100% of the time, see Fig. 15, or the decay $\tilde{t}_1 \rightarrow b\tilde{\chi}_1^\pm$ takes place 100% of the time, see Fig. 16–22. For the mixed decay scenario, see Fig. 23.
- 78** AAD 14F searched in 20.3 fb⁻¹ of pp collisions at $\sqrt{s} = 8$ TeV for events containing two leptons (e or μ), and possibly jets and missing transverse momentum. No excess of events above the expected level of Standard Model background was found. Exclusion limits at 95% C.L. are set on the masses of third-generation squarks in simplified models which either assume that the decay $\tilde{t}_1 \rightarrow b\tilde{\chi}_1^\pm$ takes place 100% of the time, see Figs. 14–17 and 20, or that the decay $\tilde{t}_1 \rightarrow t\tilde{\chi}_1^0$ takes place 100% of the time, see Figs. 18 and 19.
- 79** AAD 14T searched in 20.3 fb⁻¹ of pp collisions at $\sqrt{s} = 8$ TeV for monojet-like and c -tagged events. No excess of events above the expected level of Standard Model background was found. Exclusion limits at 95% C.L. are set on the masses of third-generation squarks in simplified models which assume that the decay $\tilde{t}_1 \rightarrow c\tilde{\chi}_1^0$ takes place 100% of the time, see Fig. 9 and 10. The results of the monojet-like analysis are also interpreted in terms of stop pair production in the four-body decay $\tilde{t}_1 \rightarrow b\tilde{t}'\tilde{\chi}_1^0$, see Fig. 11.
- 80** CHATRCHYAN 14AH searched in 4.7 fb⁻¹ of pp collisions at $\sqrt{s} = 7$ TeV for events with at least two energetic jets and significant \cancel{E}_T , using the razor variables (M_R and R^2) to discriminate between signal and background processes. A second analysis requires at least one of the jets to be originating from a b -quark. No significant excess above the Standard Model expectations is observed. Limits are set on sbottom masses in simplified models where the decay $\tilde{t} \rightarrow t\tilde{\chi}_1^0$ takes place with a branching ratio of 100%, see Figs. 28 and 29. Exclusions in the CMSSM, assuming $\tan\beta = 10$, $A_0 = 0$ and $\mu > 0$, are also presented, see Fig. 26.
- 81** CHATRCHYAN 14R searched in 19.5 fb⁻¹ of pp collisions at $\sqrt{s} = 8$ TeV for events with at least three leptons (electrons, muons, taus) in the final state. No significant excess above the Standard Model expectations is observed. Limits are set on the stop mass in a natural higgsino NLSP simplified model (GMSB) where the decay $\tilde{t} \rightarrow b\tilde{\chi}_1^\pm$, with $\tilde{\chi}_1^\pm \rightarrow (qq'/\ell\nu)H$, $Z\tilde{G}$, takes place with a branching ratio of 100% (the particles between brackets have a soft p_T spectrum), see Figs. 4–6.
- 82** AABOUD 17AF searched in 36 fb⁻¹ of pp collisions at $\sqrt{s} = 13$ TeV for evidence of top squarks in events containing 2 leptons, jets, b -jets and \cancel{E}_T . In Tstop6 model, assuming $m_{\tilde{\chi}_1^0} = 0$ GeV, \tilde{t}_1 masses up to 850 GeV are excluded for $m_{\tilde{\chi}_2^0} > 200$ GeV.
- 83** AABOUD 17AF searched in 36 fb⁻¹ of pp collisions at $\sqrt{s} = 13$ TeV for evidence of \tilde{t}_2 in events containing 2 leptons, jets, b -jets and \cancel{E}_T . In Tstop7 model, assuming $m_{\tilde{\chi}_1^0} = 50$ GeV and 100% decays via Z boson, \tilde{t}_2 masses up to 800 GeV are excluded. Exclusion limits are also shown as a function of the \tilde{t}_2 branching ratios in their Figure 7.
- 84** AABOUD 17AF searched in 36 fb⁻¹ of pp collisions at $\sqrt{s} = 13$ TeV for evidence of \tilde{t}_2 in events containing 2 leptons, jets, b -jets and \cancel{E}_T . In Tstop7 model, assuming $m_{\tilde{\chi}_1^0} = 50$ GeV and 100% decays via higgs boson, \tilde{t}_2 masses up to 880 GeV are excluded. Exclusion limits are also shown as a function of the \tilde{t}_2 branching ratios in their Figure 7.
- 85** AABOUD 17AY searched in 36.1 fb⁻¹ of pp collisions at $\sqrt{s} = 13$ TeV for events with at least four jets and large missing transverse momentum. No significant excess above the Standard Model expectations is observed. Limits are set on the top quark mass assuming three pMSSM-inspired models. The first one, referred to as Higgsino LSP model, assumes $m_{\tilde{\chi}_1^\pm} - m_{\tilde{\chi}_1^0} = 5$ GeV and $m_{\tilde{\chi}_2^0} - m_{\tilde{\chi}_1^0} = 10$ GeV, with a mixture of decay modes as in Tstop1, Tstop2 and Tstop6. See their Figure 10. The second and third models are referred to as Wino NLSP and well-tempered pMSSM models, respectively. See their Figure 11 and Figure 12, and text for details on assumptions.
- 86** AAD 14B searched in 20.3 fb⁻¹ of pp collisions at $\sqrt{s} = 8$ TeV for events containing a Z boson, with or without additional leptons, plus jets originating from b -quarks and significant missing transverse momentum. No excess over the expected SM background is observed. Limits are derived in simplified models featuring \tilde{t}_2 production, with $\tilde{t}_2 \rightarrow Z\tilde{t}_1$, $\tilde{t}_1 \rightarrow t\tilde{\chi}_1^0$ with a 100% branching ratio, see Fig. 4, and in the framework of natural GMSB, see Fig. 6.
- 87** CHATRCHYAN 14U searched in 19.7 fb⁻¹ of pp collisions at $\sqrt{s} = 8$ TeV for evidence of direct pair production of top squarks, with Higgs bosons in the decay chain. The search is performed using a selection of events containing two Higgs bosons, each decaying to a photon pair, missing transverse energy and possibly b -quark jets. No significant excesses over the expected SM backgrounds are observed. The results are interpreted in the context of a “natural SUSY” simplified model where the decays $\tilde{t}_1 \rightarrow b\tilde{\chi}_1^\pm$, with $\tilde{\chi}_1^\pm \rightarrow f'\tilde{\chi}_1^0$, and $\tilde{\chi}_1^0 \rightarrow H\tilde{G}$, all happen with 100% branching ratio, see Fig. 4.
- 88** KHACHATRYAN 14C searched in 19.5 fb⁻¹ of pp collisions at $\sqrt{s} = 8$ TeV for evidence of direct pair production of top squarks, with Higgs or Z -bosons in the decay chain. The search is performed using a selection of events containing leptons and b -quark jets. No significant excesses over the expected SM backgrounds are observed. The results are interpreted in the context of a simplified model with pair production of a heavier top-squark mass eigenstate \tilde{t}_2 decaying to a lighter top-squark eigenstate \tilde{t}_1 via either $\tilde{t}_2 \rightarrow H\tilde{t}_1$ or $\tilde{t}_2 \rightarrow Z\tilde{t}_1$, followed in both cases by $\tilde{t}_1 \rightarrow t\tilde{\chi}_1^0$. The interpretation is performed in the region where the mass difference between the \tilde{t}_1 and $\tilde{\chi}_1^0$ is approximately equal to the top-quark mass, which is not probed by searches for direct \tilde{t}_1 pair production, see Figs. 5 and 6. The analysis excludes top squarks with masses $m_{\tilde{t}_2} < 575$ GeV and $m_{\tilde{t}_1} < 400$ GeV at 95% C.L.

R-parity violating \tilde{t} (Stop) mass limit

VALUE (GeV)	CL%	DOCUMENT ID	TECN	COMMENT
none 500–520, 580–770	95	1 TUMASYAN	23L CMS	4 jets with dijet masses > 350 GeV, Tstop1aRPV
>1500	95	2 TUMASYAN	22AF CMS	long-lived \tilde{t} , $\tilde{t} \rightarrow b\tilde{t}$, $c\tau = 2$ cm
>1500	95	2 TUMASYAN	22AF CMS	long-lived \tilde{t} , $\tilde{t} \rightarrow d\tilde{t}$, $c\tau = 2$ cm
> 460	95	2 TUMASYAN	22AF CMS	long-lived \tilde{t} , $\tilde{t} \rightarrow b\tilde{t}$, $0.01 \text{ cm} < c\tau < 1000$ cm
> 460	95	2 TUMASYAN	22AF CMS	long-lived \tilde{t} , $\tilde{t} \rightarrow d\tilde{t}$, $0.01 \text{ cm} < c\tau < 1000$ cm
>1100	95	3 AAD	21BF ATLS	$\ell^\pm + b$ -jets + many jets, Tstop14, λ_{323}'' electroweakino decay, 500 GeV < $m_{\tilde{\chi}_1^0} < 800$ GeV
>1150	95	3 AAD	21BF ATLS	$\ell^\pm + b$ -jets + many jets, Tstop15, λ_{323}'' electroweakino decay, 600 GeV < $m_{\tilde{\chi}_1^0} < 900$ GeV
>1300	95	3 AAD	21BF ATLS	$\ell^\pm + b$ -jets + many jets, Tstop1, λ_{323}'' electroweakino decay, 500 GeV < $m_{\tilde{\chi}_1^0} < 1000$ GeV
>1600	95	4 SIRUNYAN	21AF CMS	long-lived \tilde{t} , $\tilde{t} \rightarrow \bar{d}\bar{d}$, λ_{313}'' coupling, $0.4 \text{ mm} < c\tau < 80 \text{ mm}$
>1600	95	5 SIRUNYAN	21U CMS	long-lived \tilde{t} , $\tilde{t} \rightarrow b\tilde{t}$, $5 < c\tau < 240 \text{ mm}$
>1600	95	5 SIRUNYAN	21U CMS	long-lived \tilde{t} , $\tilde{t} \rightarrow d\tilde{t}$, λ_{331}'' coupling, $3 < c\tau < 360 \text{ mm}$
>1600	95	5 SIRUNYAN	21U CMS	long-lived \tilde{t} , $\tilde{t} \rightarrow \bar{d}\bar{d}$, η_{311}'' coupling, $2 < c\tau < 1320 \text{ mm}$
> 670	95	6 SIRUNYAN	21V CMS	$\ell^\pm + \geq 7$ jets, Tstop1 with $\tilde{\chi}_1^0 \rightarrow qqg$, λ_{abc}'' coupling, $a,b,c = 1,2$
> 870	95	6 SIRUNYAN	21V CMS	$\ell^\pm + \geq 7$ jets, stealth SYY model
>1700	95	7 AAD	20M ATLS	$\tilde{t} \rightarrow q\mu$, long-lived, Tstop3RPV, $\tau = 0.1$ ns
>1150	95	8 SIRUNYAN	19Bi ATLS	$\tilde{t} \rightarrow b\mu$, long-lived, Tstop2RPV, $c\tau = 0.1$ cm
>1100	95	9 SIRUNYAN	19Bj CMS	$\tilde{t} \rightarrow be$, Tstop2RPV, prompt
none 100–410	95	10 AABOUD	18BB ATLS	4 jets, Tstop1RPV with $\tilde{t} \rightarrow d s$, λ_{312}'' coupling

See key on page 1171

Searches Particle Listings

Supersymmetric Particle Searches

none 100–470, 480–610	95	11 AABOUD	18BB ATLS	4 jets, Tstop1RPV, λ''_{323} coupling
≥ 600 –1500	95	12 AABOUD	18P ATLS	$2\ell + b$ -jets, Tstop2RPV, depending on λ''_{333} coupling ($i = 1, 2, 3$)
>1130	95	13 SIRUNYAN	18AD CMS	$\tilde{t} \rightarrow b\ell$, long-lived, $c\tau = 70$ –100 mm
> 550	95	13 SIRUNYAN	18AD CMS	$\tilde{t} \rightarrow b\ell$, long-lived, $c\tau = 1$ –1000 mm
>1400	95	14 SIRUNYAN	18DV CMS	long-lived \tilde{t} , $\tilde{t} \rightarrow \bar{d}\bar{d}$, 0.6 mm $< c\tau < 80$ mm
none 80–520	95	15 SIRUNYAN	18DY CMS	2, 4 jets, Tstop3RPV, λ''_{312} coupling
none 80–270, 285–340, 400–525	95	15 SIRUNYAN	18DY CMS	2, 4 jets, Tstop1RPV, λ''_{323} coupling
>1200	95	16 AABOUD	17AI ATLS	$\geq 1\ell + \geq 8$ jets, Tstop1 with $\tilde{\chi}_1^0 \rightarrow tbs$, λ''_{323} coupling, $m_{\tilde{\chi}_1^0} = 500$ GeV
none, 100–315	95	17 AAD	16AMATLS	2 large-radius jets, Tstop1RPV
none, 200–350	95	18 KHACHATRYAN...15L	CMS	$\tilde{t} \rightarrow qq$, $\lambda''_{312} \neq 0$
none, 200–385	95	18 KHACHATRYAN...15L	CMS	$\tilde{t} \rightarrow qb$, $\lambda''_{323} \neq 0$
> 740	95	19 KHACHATRYAN...14T	CMS	$\tau + b$ -jets, $LQ\bar{D}$, $\lambda''_{333} \neq 0$, $\tilde{t} \rightarrow \tau b$ simplified model
> 580	95	19 KHACHATRYAN...14T	CMS	$\tau + b$ -jets, $LQ\bar{D}$, $\lambda''_{333} \neq 0$ ($j \neq 3$), $\tilde{t} \rightarrow \tilde{\chi}^{\pm} b$, $\tilde{\chi}^{\pm} \rightarrow qq\tau^{\pm}$ simplified model
• • • We do not use the following data for averages, fits, limits, etc. • • •				
> 770	95	20 AAD	21B ATLS	≥ 8 jets, ≥ 5 b -jets, Tstop4RPV
> 890	95	21 KHACHATRYAN...16AC	CMS	$e^+e^- + \geq 5$ jets; $\tilde{t} \rightarrow b\tilde{\chi}_1^{\pm}$; $\tilde{\chi}_1^{\pm} \rightarrow \ell^{\pm}jj$, λ''_{ijk}
>1000	95	21 KHACHATRYAN...16AC	CMS	$\mu^+\mu^- + \geq 5$ jets; $\tilde{t} \rightarrow b\tilde{\chi}_1^{\pm}$; $\tilde{\chi}_1^{\pm} \rightarrow \ell^{\pm}jj$, λ''_{ijk}
> 950	95	22 KHACHATRYAN...16BX	CMS	$\tilde{t} \rightarrow t\tilde{\chi}_1^0$, $\tilde{\chi}_1^0 \rightarrow \ell\ell\nu$, λ_{121} or $\lambda_{122} \neq 0$
> 790	95	23 KHACHATRYAN...15E	CMS	$\tilde{t}_1 \rightarrow b\ell$, $c\tau = 2$ cm

¹ TUMASYAN 23L searched in 138 fb^{-1} of pp collisions at $\sqrt{s} = 13$ TeV for pairs of dijet resonances with the same mass in final states with at least four jets, for the case where the four-jet production proceeds via an intermediate resonant state and for nonresonant production. No significant excess above the Standard Model expectations is observed. Limits are set in the nonresonant search on the top squark mass in the simplified model Tstop1aRPV with λ_{312} coupling, assuming $B(d/s) = 1$, see their figure 12. Limits are also set on resonant pair production of dijet resonances via high mass intermediate states and compared to a signal model of diquarks that decay into pairs of vector-like quarks, see their figures 10 and 11.

² TUMASYAN 22AF searched for evidence of new long-lived particles decaying to leptons in pp collisions at $\sqrt{s} = 13$ TeV, corresponding to 118 (113) fb^{-1} in the ee ($e\mu$ and $\mu\mu$) channels. The leptons are required to have transverse impact parameter values between 0.01 and 10 cm and are not required to form a common vertex. No significant excess above the Standard Model expectations is observed. Limits are set on the mass of the top squark in RPV models with top squark pair production and $\tilde{t} \rightarrow b\bar{\ell}$ and $\tilde{t} \rightarrow d\bar{\ell}$, see their Figure 4, which contains a wide range of lifetime limits. Limits are also set on a gauge-mediated SUSY breaking model, where the next-to-lightest SUSY particle is a stjepton and the lightest SUSY particle a gravitino \tilde{G} , see their Figure 5, which also contains a wider range of lifetime limits. Limits are also set in a model that produces BSM Higgs bosons (H) with a mass of 125 GeV through gluon-gluon fusion, where the H decays to two long-lived scalars S_i , each of which decays to two oppositely charged and same-flavor leptons.

³ AAD 21BF searched in 139 fb^{-1} of pp collisions at $\sqrt{s} = 13$ TeV for pair production of gluinos, stops, electroweakinos decaying RPV either directly or indirectly via the LSP. The final state in all cases is one or two leptons, many jets (up to fifteen) and b -jets. Different models with different branching fractions of the gluino or stop follow from the assumptions on the nature of the electroweakinos. No significant excess above the Standard Model predictions is observed. Limits are set on the *gluino*, \tilde{t}_1 , electroweakino masses as a function of the $\tilde{\chi}_1^0$ mass in several scenarios of gluino, stop and electroweakino pair production.

⁴ SIRUNYAN 21AF searched in 140 fb^{-1} of pp collisions at $\sqrt{s} = 13$ TeV for supersymmetry in events with two displaced vertices from long-lived particles decaying into multijet or dijet final states. No significant excess above the Standard Model expectations is observed. Limits are set on the gluino mass in the simplified model Tglu2RPV with λ''_{323} coupling, on the $\tilde{\chi}_1^0$ mass in an RPV model with $\tilde{\chi}_1^0$ pair production and the RPV decay $\tilde{\chi}_1^0 \rightarrow tbs$ with λ''_{323} coupling and on the \tilde{t} mass in an RPV model with top squark pair production and the RPV decay $\tilde{t} \rightarrow \bar{d}_i \bar{d}_j$ with λ''_{3ij} coupling, see their Figure 7.

⁵ SIRUNYAN 21U searched in 132 fb^{-1} of pp collisions at $\sqrt{s} = 13$ TeV for supersymmetry in events with displaced tracks and displaced vertices associated with a dijet system. No significant excess above the Standard Model expectations is observed. Limits are set on long-lived gluinos in an RPC GMSB SUSY model of gluino pair production, with $\tilde{g} \rightarrow g\tilde{G}$, see their Figure 9, in Tglu1A in a mini-split model, see their Figure 10, and in an RPV model of gluino pair production, with $\tilde{g} \rightarrow tbs$ with coupling λ''_{323} , see their Figure 11. Limits are also set on long-lived top squarks in Tstop2RPV, see their Figure 12, in an RPV model with $\tilde{t} \rightarrow d\bar{\ell}$ and λ''_{331} coupling, see their Figure 13, and in a dynamical RPV model with $\tilde{t} \rightarrow \bar{d}\bar{d}$ via a nonholomorphic RPV coupling λ''_{311} , see their Figure 14. The best mass limit is achieved in all cases at $c\tau = 30$ mm.

⁶ SIRUNYAN 21V searched in 137 fb^{-1} of pp collisions at $\sqrt{s} = 13$ TeV for supersymmetry in events with one charged lepton (e^{\pm} or μ^{\pm}) and ≥ 7 jets. No significant excess above the Standard Model expectations is observed. Limits are set on an RPV SUSY model like Tstop1 with the additional decay $\tilde{\chi}_1^0 \rightarrow qq\bar{q}$ with coupling λ''_{abc} , with $a, b, c \in 1, 2$, and

on a stealth SUSY model called SY, with one scalar particle S with even R-parity and its superpartner \tilde{S} , both singlets under all SM interactions, and with a portal mediated by loop interactions involving a new vectorlike messenger field (Y), where pair produced top squarks decay as $\tilde{t} \rightarrow t\tilde{g}S$, and $\tilde{S} \rightarrow \tilde{G}S$, and $S \rightarrow gg$, see their Figure 6 and 7.

⁷ AAD 20M searched for long-lived particles decaying into hadrons and at least one muon in events containing a displaced muon track and a displaced vertex. The analysis uses a dataset of pp collisions at $\sqrt{s} = 13$ TeV corresponding to an integrated luminosity of 136 fb^{-1} . Using the Tstop3RPV simplified model, top squarks with masses up to 1.7 TeV are excluded for a lifetime of 0.1 ns, and masses below 1.3 TeV are excluded for lifetimes between 0.01 ns and 30 ns, see their Fig. 7. The dependence on the RPV coupling λ''_{23k} multiplied by $\cos\theta_t$, with θ_t the mixing angle between the left- and right-handed \tilde{t} squarks, is also shown, see their Fig. 7.

⁸ SIRUNYAN 19BI searched in 35.9 fb^{-1} of pp collisions at $\sqrt{s} = 13$ TeV in final states with two muons and two jets, or with one muon, two jets, and missing transverse momentum. Limits are set in a model of pair-produced, prompt or long-lived top squarks with R-parity violating decays to a b -quark and a lepton (Tstop2RPV), branching fraction of $\tilde{t} \rightarrow b\mu$ equal to 1/3 and $c\tau$ between 0.1 cm and 10 cm in the case of long-lived top squarks. See their Fig. 10.

⁹ SIRUNYAN 19BJ searched in 35.9 fb^{-1} of pp collisions at $\sqrt{s} = 13$ TeV in final states with two electrons and two jets, or with one electron, two jets, and missing transverse momentum. Limits are set in a model of pair-produced, prompt top squarks with R-parity violating decays to a b -quark and a lepton (Tstop2RPV), assuming branching fraction of $\tilde{t} \rightarrow be$ equal to 1/3 and $c\tau = 0$ cm. See their Fig. 10.

¹⁰ AABOUD 18BB searched in 36.7 fb^{-1} of pp collisions at $\sqrt{s} = 13$ TeV for massive colored resonances which are pair-produced and decay into two jets. No significant deviation from the background prediction is observed. Results are interpreted in a SUSY simplified model as Tstop1RPV with $\tilde{t} \rightarrow ds$. Top squarks with masses in the range 100–410 GeV are excluded, see their Figure 9(a). The λ''_{312} coupling is assumed to be sufficiently large for the decays to be prompt, but small enough to neglect the single-top-squark resonant production through RPV couplings.

¹¹ AABOUD 18BB searched in 36.7 fb^{-1} of pp collisions at $\sqrt{s} = 13$ TeV for massive coloured resonances which are pair-produced and decay into two jets. No significant deviation from the background prediction is observed. Results are interpreted in Tstop1RPV. Top squarks with masses in the range 100–470 GeV or 480–610 GeV are excluded, see their Figure 9(b). The λ''_{323} coupling is assumed to be sufficiently large for the decays to be prompt, but small enough to neglect the single-top-squark resonant production through RPV couplings.

¹² AABOUD 18P searched in 36.1 fb^{-1} of pp collisions at $\sqrt{s} = 13$ TeV for pair-produced top squarks that decay through RPV λ''_{333} ($i = 1, 2, 3$) couplings to a final state with two leptons and two jets, at least one of which is identified as a b -jet. No significant excess is observed over the SM background. In the Tstop2RPV model, lower limits on the top squark masses between 600 and 1500 GeV are set depending on the branching fraction to be , $b\mu$, and $b\tau$ final states. See their Figs 6 and 7.

¹³ SIRUNYAN 18AD searched in 2.6 fb^{-1} of pp collisions at $\sqrt{s} = 13$ TeV for long-lived particles by exploiting the multiplicity of displaced jets to search for the presence of signal decays occurring at distances between 1 and 1000 mm. Limits are set in a model of pair-produced, long-lived top squarks with R-parity violating decays to a b -quark and a lepton, see their Figure 3.

¹⁴ SIRUNYAN 18DV searched in 38.5 fb^{-1} of pp collisions at $\sqrt{s} = 13$ TeV for long-lived particles in events with multiple jets and two displaced vertices composed of many tracks. No events with two well-separated high-track-multiplicity vertices were observed. Limits are set on the stop and the gluino mass in RPV models of supersymmetry where the stop (gluino) is decaying solely into dijet (multijet) final states, see their Figures 6 and 7.

¹⁵ SIRUNYAN 18DY searched in 35.9 fb^{-1} of pp collisions at $\sqrt{s} = 13$ TeV for the pair production of resonances, each decaying to two quarks. The search is conducted separately in a boosted (two-jet) and resolved (four-jet) jet topology. The mass spectra are found to be consistent with the Standard Model expectations. Limits are set on the stop mass in the Tstop3RPV and Tstop1RPV simplified models, see their Figure 11.

¹⁶ AABOUD 17AI searched in 36.1 fb^{-1} of pp collisions at $\sqrt{s} = 13$ TeV for events with one or more isolated lepton, at least eight jets, either zero or many b -jets, for evidence of R-parity violating decays of the top squark. No significant excess above the Standard Model expectations is observed. Limits up to 1.25 (1.10) TeV are set on the top squark mass in R-parity-violating supersymmetry models where \tilde{t}_1 decays for a bino LSP as: $\tilde{t} \rightarrow t\tilde{\chi}_1^0$ and for a higgsino LSP as $\tilde{t} \rightarrow t\tilde{\chi}_{1,2}^0/b\tilde{\chi}_1^{\pm}$. These is followed by the decays through the non-zero λ''_{323} coupling $\tilde{\chi}_1^{\pm} \rightarrow tbs$, $\tilde{\chi}_1^{\pm} \rightarrow bbs$. See their Figure 10 and text for details on model assumptions.

¹⁷ AAD 16AM searched in 17.4 fb^{-1} of pp collisions at $\sqrt{s} = 8$ TeV for events containing two large-radius hadronic jets. No deviation from the background prediction is observed. Top squarks with masses between 100 and 315 GeV are excluded at 95% C.L. in the hypothesis that they both decay via R-parity violating coupling λ''_{323} to b - and s -quarks. See their Fig. 10.

¹⁸ KHACHATRYAN 15L searched in 19.4 fb^{-1} of pp collisions at $\sqrt{s} = 8$ TeV for pair production of heavy resonances decaying to pairs of jets in four jet events. No significant excess above the Standard Model expectations is observed. Limits are set on the stop mass in R-parity-violating supersymmetry models where $\tilde{t} \rightarrow qq$ ($\lambda''_{312} \neq 0$), see Fig. 6 (top) and $\tilde{t} \rightarrow qb$ ($\lambda''_{323} \neq 0$), see Fig. 6 (bottom).

¹⁹ KHACHATRYAN 14T searched in 19.7 fb^{-1} of pp collisions at $\sqrt{s} = 8$ TeV for events with τ -leptons and b -quark jets, possibly with extra light-flavour jets. No excess above the Standard Model expectations is observed. Limits are set on stop masses in RPV SUSY models with $LQ\bar{D}$ couplings, in two simplified models. In the first model, the decay $\tilde{t} \rightarrow \tau b$ is considered, with $\lambda''_{333} \neq 0$, see Fig. 3. In the second model, the decay $\tilde{t} \rightarrow \tilde{\chi}^{\pm} b$, with the subsequent decay $\tilde{\chi}^{\pm} \rightarrow qq\tau^{\pm}$ is considered, with $\lambda''_{3jk} \neq 0$ and the mass splitting between the top squark and the chargino chosen to be 100 GeV, see Fig. 4.

²⁰ AAD 21B searched in 139 fb^{-1} of pp collisions at $\sqrt{s} = 13$ TeV for events with at least eight jets and at least 5 b -jets, for evidence of R-parity violating decays of the top squark. No significant excess above the Standard Model expectations is observed. Limits up to 950 GeV are set on the top squark mass in Tstop4RPV simplified model. See their Figure 7 for more detailed mass bounds.

²¹ KHACHATRYAN 16AC searched in 19.7 fb^{-1} of pp collisions at $\sqrt{s} = 8$ TeV for events with low missing transverse momentum, two oppositely charged electrons or muons, and at least five jets, at least one of which is a b -jet, for evidence of R-parity violating,

Searches Particle Listings

Supersymmetric Particle Searches

charging-mediated decays of the top squark. No significant excess above the Standard Model expectations is observed. Limits are set on the stop mass in R-parity-violating supersymmetry models where $\tilde{t} \rightarrow b\tilde{\chi}_1^\pm \rightarrow \ell^\pm jj, \lambda'_{ijk} \neq 0 (i, j, k \leq 2)$, and with $m_{\tilde{t}} - m_{\tilde{\chi}_1^\pm} = 100$ GeV, see Fig. 3.

22 KHACHATRYAN 16BX searched in 19.5 fb^{-1} of pp collisions at $\sqrt{s} = 8$ TeV for events containing 4 leptons coming from R-parity-violating decays of $\tilde{\chi}_1^0 \rightarrow \ell\ell\nu$ with $\lambda_{121} \neq 0$ or $\lambda_{122} \neq 0$. No excess over the expected background is observed. Limits are derived on the gluino, squark and stop masses, see Fig. 23.

23 KHACHATRYAN 15E searched for long-lived particles decaying to leptons in 19.7 fb^{-1} of pp collisions at $\sqrt{s} = 8$ TeV. Events were selected with an electron and muon with opposite charges and each with transverse impact parameter values between 0.02 and 2 cm. Limits are set on SUSY benchmark models with pair production of top squarks decaying into an $e\mu$ final state via RPV interactions. See their Fig. 2

Heavy \tilde{g} (Gluino) mass limit

For $m_{\tilde{g}} > 60\text{--}70$ GeV, it is expected that gluinos would undergo a cascade decay via a number of neutralinos and/or charginos rather than undergo a direct decay to photinos as assumed by some papers. Limits obtained when direct decay is assumed are usually higher than limits when cascade decays are included.

Some earlier papers are now obsolete and have been omitted. They were last listed in our PDG 14 edition: K. Olive, *et al.* (Particle Data Group), Chinese Physics **C38** 070001 (2014) (<http://pdg.lbl.gov>).

R-parity conserving heavy \tilde{g} (Gluino) mass limit

VALUE (GeV)	CL%	DOCUMENT ID	TECN	COMMENT
>2200	95	1 AAD	23AB ATLS	$\geq 1 \gamma + \text{jets} + \cancel{E}_T$, GGM-like, Tglu4D, $\tilde{\chi}_1^0$ NLSP, $m_{\tilde{\chi}_1^0} > 300$ GeV
>2200	95	1 AAD	23AB ATLS	$\geq 1 \gamma + \text{jets} + \cancel{E}_T$, GGM-like, Tglu4G, $\tilde{\chi}_1^0$ NLSP, $m_{\tilde{\chi}_1^0} > 350$ GeV
>2250	95	2 AAD	23AE ATLS	2 SFOS ℓ , jets, \cancel{E}_T , Tglu1G, $m_{\tilde{\chi}_1^0} = 100$ GeV
>1950	95	3 AAD	23AE ATLS	2 SFOS ℓ , jets, \cancel{E}_T , Tglu1H, $m_{\tilde{\chi}_2^0} = (m_{\tilde{g}} + m_{\tilde{\chi}_1^0})/2$, $m_{\tilde{\chi}_1^0} = 100$ GeV
>2440	95	4 AAD	23AL ATLS	At least 3 b -tagged jets, 0 or 1 lepton, Tglu3B, $m_{\tilde{\chi}_1^0} = 1$ GeV
>2350	95	4 AAD	23AL ATLS	At least 3 b -tagged jets, 0 or 1 lepton, Tglu2A, $m_{\tilde{\chi}_1^0} = 1$ GeV
>2050	95	5 AAD	23AL ATLS	At least 3 b -tagged jets, 0 or 1 lepton, Tglu3E, $m_{\tilde{\chi}_1^\pm} - m_{\tilde{\chi}_1^0} = 2$ GeV, $m_{\tilde{\chi}_1^0} = 1$ GeV
>2320	95	6 HAYRAPETY...23E	CMS	$\gamma + \text{jets} + \cancel{E}_T$, Tglu4E, $m_{\tilde{\chi}_1^0} = 1700$ GeV
>2375	95	6 HAYRAPETY...23E	CMS	$\gamma + \text{jets} + \cancel{E}_T$, Tglu4D, $m_{\tilde{\chi}_1^0} = 1700$ GeV
>2260	95	6 HAYRAPETY...23E	CMS	$\gamma + \text{jets} + \cancel{E}_T$, Tglu4F, $m_{\tilde{\chi}_1^0} = 1700$ GeV
>2120	95	7 TUMASYAN	23AY CMS	$\ell^\pm + \geq 6$ jets + ≥ 1 b -jet, Tglu3A, $m_{\tilde{\chi}_1^0} = 0$ GeV
>2050	95	7 TUMASYAN	23AY CMS	$\ell^\pm + \geq 5$ jets, 0 b -jets, Tglu1B, $m_{\tilde{\chi}_1^0} = 0$ GeV, $m_{\tilde{\chi}_1^\pm} = 0.5(m_{\tilde{g}} + m_{\tilde{\chi}_1^0})$
>2200	95	8 AAD	22U ATLS	$\tilde{g} \rightarrow qq\tilde{\chi}_1^0, qq\tilde{\chi}_1^\pm, m_{\tilde{\chi}_1^\pm} = 1000$ GeV, $\tau(\tilde{\chi}_1^\pm) = 1$ ns
>2330	95	9 TUMASYAN	22V CMS	3 or 4 b -tagged jets or 2 large-radius jets, \cancel{E}_T ; Tglu1I; $m_{\tilde{\chi}_1^0} = 1$ GeV
>2200	95	10 AAD	21AK ATLS	$\ell^\pm + \text{jets} + \cancel{E}_T$, Tglu1B, $m_{\tilde{\chi}_1^\pm} = (m_{\tilde{g}} + m_{\tilde{\chi}_1^0})/2, m_{\tilde{\chi}_1^0} < 400$ GeV
none 1300–2050	95	10 AAD	21AK ATLS	$\ell^\pm + \text{jets} + \cancel{E}_T$, Tglu1B, $m_{\tilde{\chi}_1^\pm} = (m_{\tilde{g}} + m_{\tilde{\chi}_1^0})/2, m_{\tilde{\chi}_1^0} < 1000$ GeV
>2300	95	11 AAD	21L ATLS	jets + \cancel{E}_T , Tglu1A, $m_{\tilde{\chi}_1^0} < 200$ GeV
>3000	95	11 AAD	21L ATLS	jets + \cancel{E}_T , combined $\tilde{g}\tilde{g}, \tilde{g}\tilde{q}, \tilde{q}\tilde{q}$ production, $\tilde{g} \rightarrow qq'\tilde{\chi}_1^0, \tilde{q} \rightarrow q\tilde{\chi}_1^0, m_{\tilde{q}} = m_{\tilde{g}}, m_{\tilde{\chi}_1^0} = 0$ GeV
>2200	95	11 AAD	21L ATLS	jets + \cancel{E}_T , Tglu1B, $m_{\tilde{\chi}_1^0} = 0$ GeV
>1400	95	12 AAD	21X ATLS	jets in empty bunch crossings, Tglu1A, long-lived R-hadron, $m_{\tilde{\chi}_1^0} = 100$ GeV, $10^{-5} \text{ s} < \tau_{\text{R-hadron}} < 10^3 \text{ s}$

> 870	95	12 AAD	21X ATLS	jets in empty bunch crossings, Tglu1A, long-lived R-hadron, $m_{\tilde{g}} - m_{\tilde{\chi}_1^0} = 100$ GeV, $10^{-5} \text{ s} < \tau_{\text{R-hadron}} < 10^3 \text{ s}$
>2260	95	13 SIRUNYAN	21AD CMS	jets + \cancel{E}_T , Tglu3A, $m_{\tilde{\chi}_1^0} < 1050$ GeV
>2150	95	13 SIRUNYAN	21AD CMS	jets + \cancel{E}_T , Tglu3C, $m_{\tilde{\chi}_1^0} = 600$ GeV, $m_{\tilde{t}} - m_{\tilde{\chi}_1^0} = 20$ GeV
>2250	95	13 SIRUNYAN	21AD CMS	jets + \cancel{E}_T , Tglu3D, $m_{\tilde{\chi}_1^0} = 700$ GeV, $m_{\tilde{t}} - m_{\tilde{\chi}_1^0} = 5$ GeV
>1870	95	14 SIRUNYAN	21M CMS	$\ell^\pm \ell^\mp + \cancel{E}_T$, Tglu4C, $m_{\tilde{\chi}_1^0} = 1100$ GeV
>1980	95	15 AAD	20AL ATLS	8 or more jets + \cancel{E}_T , Tglu1E, $m_{\tilde{\chi}_1^0} = 100$ GeV
>1820	95	15 AAD	20AL ATLS	8 or more jets + \cancel{E}_T , Tglu3A, $m_{\tilde{\chi}_1^0} = 100$ GeV
>1600	95	16 AAD	20V ATLS	same-sign $\ell^\pm \ell^\pm + \text{jets}$, Tglu1E, $m_{\tilde{\chi}_1^0} = 100$ GeV
>1975	95	17 SIRUNYAN	20B CMS	$\geq 1\gamma + \cancel{E}_T$, Tglu4A, BR($\tilde{g} \rightarrow qq\tilde{\chi}_1^\pm$)=0.5, $m_{\tilde{\chi}_1^0} \simeq m_{\tilde{g}}$
>1920	95	18 SIRUNYAN	20BJ CMS	jets+ \cancel{E}_T , Tglu1H, $m_{\tilde{g}} - m_{\tilde{\chi}_2^0} = 50$ GeV, $m_{\tilde{\chi}_1^0} = 1$ GeV
>2150	95	19 SIRUNYAN	20E CMS	1 ℓ +jets, Tglu3A, $m_{\tilde{\chi}_1^0} < 700$ GeV
>2050	95	19 SIRUNYAN	20E CMS	1 ℓ +jets, Tglu3A, $m_{\tilde{\chi}_1^0} < 1100$ GeV
>1650	95	19 SIRUNYAN	20E CMS	1 ℓ + jets, Tglu3C, $m_{\tilde{t}} - m_{\tilde{\chi}_1^0} = 175$ GeV, $m_{\tilde{\chi}_1^0} < 1150$ GeV
>1700	95	20 SIRUNYAN	20T CMS	same-sign $\ell^\pm \ell^\pm$ or $\geq 3\ell^\pm + \text{jets}$, Tglu3A, $m_{\tilde{\chi}_1^0} = 0$ GeV
>1610	95	20 SIRUNYAN	20T CMS	same-sign $\ell^\pm \ell^\pm$ or $\geq 3\ell^\pm + \text{jets}$, Tglu3B, $m_{\tilde{t}} - m_{\tilde{\chi}_1^0} = 175$ GeV, $m_{\tilde{\chi}_1^0} = 0$ GeV
>1300	95	20 SIRUNYAN	20T CMS	same-sign $\ell^\pm \ell^\pm$ or $\geq 3\ell^\pm + \text{jets}$, Tglu3C, $m_{\tilde{t}} - m_{\tilde{\chi}_1^0} = 20$ GeV, $m_{\tilde{\chi}_1^0} = 0$ GeV
>1500	95	20 SIRUNYAN	20T CMS	same-sign $\ell^\pm \ell^\pm$ or $\geq 3\ell^\pm + \text{jets}$, Tglu3D, $m_{\tilde{\chi}_1^\pm} = m_{\tilde{\chi}_1^0} + 5$ GeV, $m_{\tilde{\chi}_1^0} = 0$ GeV
>1350	95	20 SIRUNYAN	20T CMS	same-sign $\ell^\pm \ell^\pm$ or $\geq 3\ell^\pm + \text{jets}$, Tglu1C, $m_{\tilde{\chi}_2^0} = m_{\tilde{\chi}_1^\pm} = (m_{\tilde{g}} + m_{\tilde{\chi}_1^0})/2, m_{\tilde{\chi}_1^0} = 0$ GeV
>1250	95	20 SIRUNYAN	20T CMS	same-sign $\ell^\pm \ell^\pm$ or $\geq 3\ell^\pm + \text{jets}$, Tglu1C, $m_{\tilde{\chi}_2^0} = m_{\tilde{\chi}_1^\pm} = m_{\tilde{\chi}_1^0} + 20$ GeV, $m_{\tilde{\chi}_1^0} = 0$ GeV
>1425	95	20 SIRUNYAN	20T CMS	same-sign $\ell^\pm \ell^\pm$ or $\geq 3\ell^\pm + \text{jets}$, Tglu1B, $m_{\tilde{\chi}_1^\pm} = (m_{\tilde{g}} + m_{\tilde{\chi}_1^0})/2, m_{\tilde{\chi}_1^0} = 0$ GeV
>1425	95	20 SIRUNYAN	20T CMS	same-sign $\ell^\pm \ell^\pm$ or $\geq 3\ell^\pm + \text{jets}$, Tglu1B, $m_{\tilde{\chi}_1^\pm} = m_{\tilde{\chi}_1^0} + 20$ GeV, $m_{\tilde{\chi}_1^0} = 0$ GeV
>2000	95	21 AABOUD	19I ATL	≥ 2 jets + 1 or 2 $\tau + \cancel{E}_T$, Tglu1F, $m_{\tilde{\chi}_1^0} = 100$ GeV
>1860	95	22 SIRUNYAN	19AG CMS	$2\gamma + \cancel{E}_T$, Tglu4B, 500 GeV $< m_{\tilde{\chi}_1^0} < 1500$ GeV
>1920	95	23 SIRUNYAN	19AU CMS	$\gamma + \text{jets} + b\text{-jets} + \cancel{E}_T$, Tglu4D, $m_{\tilde{\chi}_1^0} = 127$ GeV
>1950	95	23 SIRUNYAN	19AU CMS	$\gamma + \text{jets} + b\text{-jets} + \cancel{E}_T$, Tglu4E, $m_{\tilde{\chi}_1^0} = 1$ GeV
>1800	95	23 SIRUNYAN	19AU CMS	$\gamma + \text{jets} + b\text{-jets} + \cancel{E}_T$, Tglu4F, $m_{\tilde{\chi}_1^0} = 1$ GeV
>2090	95	23 SIRUNYAN	19AU CMS	$\gamma + \text{jets} + b\text{-jets} + \cancel{E}_T$, Tglu4D, $m_{\tilde{\chi}_1^0} = 1200$ GeV
>2120	95	23 SIRUNYAN	19AU CMS	$\gamma + \text{jets} + b\text{-jets} + \cancel{E}_T$, Tglu4E, $m_{\tilde{\chi}_1^0} = 1200$ GeV
>1970	95	23 SIRUNYAN	19AU CMS	$\gamma + \text{jets} + b\text{-jets} + \cancel{E}_T$, Tglu4F, $m_{\tilde{\chi}_1^0} = 1200$ GeV
>1700	95	24 SIRUNYAN	19CE CMS	2 jets, Stealth SUSY, Tglu1A and $\tilde{\chi}_1^0 \rightarrow \tilde{S}\gamma (\tilde{S} \rightarrow S\tilde{G}), m_{\tilde{\chi}_1^0} = 200$ GeV
>2000	95	25 SIRUNYAN	19CH CMS	jets+ \cancel{E}_T , Tglu1A, $m_{\tilde{\chi}_1^0} = 0$ GeV

See key on page 1171

Searches Particle Listings
Supersymmetric Particle Searches

>2030	95	25	SIRUNYAN	19CH CMS	jets+ \cancel{E}_T , Tglu1C, $m_{\tilde{\chi}_1^\pm} = m_{\tilde{\chi}_2^0} = 0.5(m_{\tilde{g}} + m_{\tilde{\chi}_1^0})$, $m_{\tilde{\chi}_1^0} = 0$ GeV	>1860	95	47	AABOUD	17AJ ATLS	same-sign $\ell^\pm \ell^\pm / 3 \ell +$ jets + \cancel{E}_T , Tglu1G, $m_{\tilde{\chi}_1^0} = 200$ GeV
>2270	95	25	SIRUNYAN	19CH CMS	jets+ \cancel{E}_T , Tglu2A, $m_{\tilde{\chi}_1^0} = 0$ GeV	>2100	95	48	AABOUD	17AR ATLS	1 ℓ +jets+ \cancel{E}_T , Tglu1B, $m_{\tilde{\chi}_1^0} = 0$ GeV
>2180	95	25	SIRUNYAN	19CH CMS	jets+ \cancel{E}_T , Tglu3A, $m_{\tilde{\chi}_1^0} = 0$ GeV	>1740	95	49	AABOUD	17AR ATLS	1 ℓ +jets+ \cancel{E}_T , Tglu1E, $m_{\tilde{\chi}_1^0} = 0$ GeV
>1750	95	26	SIRUNYAN	19K CMS	$\gamma + \ell + \cancel{E}_T$, Tglu4A, $m_{\tilde{\chi}_1^0} = 1500$ GeV	>1800	95	50	AABOUD	17AY ATLS	jets+ \cancel{E}_T , Tglu3A, $m_{\tilde{\tau}_1} - m_{\tilde{\chi}_1^0} = 5$ GeV
>2000	95	27	SIRUNYAN	19s CMS	1 or 2 $\ell +$ jets + \cancel{E}_T , Tglu3A, $m_{\tilde{\chi}_1^0} < 700$ GeV	>1800	95	51	AABOUD	17AZ ATLS	≥ 7 jets+ \cancel{E}_T , large R-jets and/or b-jets, Tglu1E, $m_{\tilde{\chi}_1^0} = 100$ GeV
>1900	95	27	SIRUNYAN	19s CMS	1 or 2 $\ell +$ jets + \cancel{E}_T , Tglu3C, $150 \text{ GeV} < m_{\tilde{\chi}_1^0} < 950 \text{ GeV}$	>1540	95	52	AABOUD	17AZ ATLS	≥ 7 jets+ \cancel{E}_T , large R-jets and/or b-jets, Tglu3A, $m_{\tilde{\chi}_1^0} = 0$ GeV
>1970	95	28	AABOUD	18AR ATLS	jets+ $\geq 3b$ -jets+ \cancel{E}_T , Tglu3A, $m_{\tilde{\chi}_1^0} < 300$ GeV	>1340	95	53	AABOUD	17N ATLS	2 same-flavor, opposite-sign $\ell +$ jets + \cancel{E}_T , Tglu1H, $m_{\tilde{\chi}_1^0} = 0$ GeV
>1920	95	29	AABOUD	18AR ATLS	jets+ $\geq 3b$ -jets+ \cancel{E}_T , Tglu2A, $m_{\tilde{\chi}_1^0} < 600$ GeV	>1310	95	54	AABOUD	17N ATLS	2 same-flavor, opposite-sign $\ell +$ jets + \cancel{E}_T , Tglu1H, $m_{\tilde{\chi}_2^0} = (m_{\tilde{g}} + m_{\tilde{\chi}_1^0})/2$, $m_{\tilde{\chi}_1^0} < 400$ GeV
>1650	95	30	AABOUD	18As ATLS	≥ 4 jets and disappearing tracks from $\tilde{\chi}^\pm \rightarrow \tilde{\chi}_1^0 \pi^\pm$, modified Tglu1A or Tglu1B, $\tilde{\chi}^\pm$ lifetime 0.2 ns, $m_{\tilde{\chi}^\pm} = 460$ GeV	>1700	95	55	AABOUD	17N ATLS	2 same-flavor, opposite-sign $\ell +$ jets + \cancel{E}_T , Tglu1G, $m_{\tilde{\chi}_1^0} \sim 1$ GeV
>1850	95	31	AABOUD	18BJ ATLS	$\ell^\pm \ell^\mp +$ jets + \cancel{E}_T , Tglu1G, $m_{\tilde{\chi}_1^0} = 100$ GeV	>1400	95	56	KHACHATRY...17	CMS	jets+ \cancel{E}_T , Tglu1A, $m_{\tilde{\chi}_1^0} = 200$ GeV
>1650	95	32	AABOUD	18BJ ATLS	$\ell^\pm \ell^\mp +$ jets + \cancel{E}_T , Tglu1H, $m_{\tilde{\chi}_1^0} = 100$ GeV	>1650	95	56	KHACHATRY...17	CMS	jets+ \cancel{E}_T , Tglu2A, $m_{\tilde{\chi}_1^0} = 200$ GeV
>2150	95	33	AABOUD	18U ATLS	2 $\gamma + \cancel{E}_T$, GGM, Tglu4B, any NLSP mass	>1600	95	56	KHACHATRY...17	CMS	jets+ \cancel{E}_T , Tglu3A, $m_{\tilde{\chi}_1^0} = 200$ GeV
>1600	95	34	AABOUD	18U ATLS	$\gamma +$ jets + \cancel{E}_T , GGM higgsino-bino, mix of Tglu4B and Tglu4C, any NLSP mass	>1550	95	57	KHACHATRY...17AD	CMS	jets+b-jets+ \cancel{E}_T , Tglu3A, $m_{\tilde{\chi}_1^0} = 0$ GeV
>2030	95	35	AABOUD	18v ATLS	jets+ \cancel{E}_T , Tglu1A, $m_{\tilde{\chi}_1^0} = 0$ GeV	>1450	95	58	KHACHATRY...17AD	CMS	jets+b-jets+ \cancel{E}_T , Tglu3C, $200 < m_{\tilde{\chi}_1^0} < 400$ GeV
>1980	95	36	AABOUD	18v ATLS	jets+ \cancel{E}_T , Tglu1B, $m_{\tilde{\chi}_1^\pm} = 0.5(m_{\tilde{g}} + m_{\tilde{\chi}_1^0})$, $m_{\tilde{\chi}_1^0} = 0$ GeV	>1570	95	59	KHACHATRY...17As	CMS	1 ℓ , Tglu3A, $m_{\tilde{\chi}_1^0} < 600$ GeV
>1750	95	37	AABOUD	18v ATLS	jets+ \cancel{E}_T , Tglu1C, $m_{\tilde{\chi}_1^0} = 1$ GeV, any $m_{\tilde{\chi}_2^0} > 100$ GeV	>1500	95	59	KHACHATRY...17As	CMS	1 ℓ , Tglu3A, $m_{\tilde{\chi}_1^0} < 775$ GeV
>2000	95	38	SIRUNYAN	18AA CMS	$\geq 1\gamma + \cancel{E}_T$, Tglu4A	>1400	95	59	KHACHATRY...17As	CMS	1 ℓ , Tglu1B, $m_{\tilde{\chi}_1^\pm} = (m_{\tilde{g}} + m_{\tilde{\chi}_1^0})/2$, $m_{\tilde{\chi}_1^0} < 725$ GeV
>2100	95	38	SIRUNYAN	18AA CMS	$\geq 1\gamma + \cancel{E}_T$, Tglu4B	none	95	59	KHACHATRY...17As	CMS	1 ℓ , Tglu1B, $m_{\tilde{\chi}_1^\pm} = (m_{\tilde{g}} + m_{\tilde{\chi}_1^0})/2$, $m_{\tilde{\chi}_1^0} < 850$ GeV
>1800	95	39	SIRUNYAN	18AC CMS	1 ℓ +jets, Tglu3A, $m_{\tilde{\chi}_1^0} < 650$ GeV	1050-1350	95	60	KHACHATRY...17Aw	CMS	$\geq 3\ell^\pm$, 2 jets, Tglu3A, $m_{\tilde{\chi}_1^0} = 0$ GeV
>1700	95	39	SIRUNYAN	18AC CMS	1 ℓ +jets, Tglu3A, $m_{\tilde{\chi}_1^0} < 1040$ GeV	>1175	95	60	KHACHATRY...17Aw	CMS	$\geq 3\ell^\pm$, 2 jets, Tglu1C, $m_{\tilde{\chi}_1^\pm} = (m_{\tilde{g}} + m_{\tilde{\chi}_1^0})/2$, $m_{\tilde{\chi}_1^0} = 0$ GeV
>1900	95	39	SIRUNYAN	18AC CMS	1 $\ell +$ jets, Tglu1B, $m_{\tilde{\chi}_1^\pm} = (m_{\tilde{g}} + m_{\tilde{\chi}_1^0})/2$, $m_{\tilde{\chi}_1^0} < 300$ GeV	> 825	95	60	KHACHATRY...17Aw	CMS	1 or more jets+ \cancel{E}_T , Tglu1A, $m_{\tilde{\chi}_1^0} = 0$ GeV
>1250	95	39	SIRUNYAN	18AC CMS	1 $\ell +$ jets, Tglu1B, $m_{\tilde{\chi}_1^\pm} = (m_{\tilde{g}} + m_{\tilde{\chi}_1^0})/2$, $m_{\tilde{\chi}_1^0} < 950$ GeV	>1545	95	61	KHACHATRY...17P	CMS	1 or more jets+ \cancel{E}_T , Tglu2A, $m_{\tilde{\chi}_1^0} = 0$ GeV
>1610	95	40	SIRUNYAN	18AL CMS	$\geq 3\ell^\pm +$ jets + \cancel{E}_T , Tglu3A, $m_{\tilde{\chi}_1^0} = 0$ GeV	>1120	95	61	KHACHATRY...17P	CMS	1 or more jets+ \cancel{E}_T , Tglu3A, $m_{\tilde{\chi}_1^0} = 0$ GeV
>1160	95	40	SIRUNYAN	18AL CMS	$\geq 3\ell^\pm +$ jets + \cancel{E}_T , Tglu1C, $m_{\tilde{\chi}_2^0} = m_{\tilde{\chi}_1^\pm} = (m_{\tilde{g}} + m_{\tilde{\chi}_1^0})/2$, $m_{\tilde{\chi}_1^0} = 0$ GeV	>1300	95	61	KHACHATRY...17P	CMS	1 or more jets+ \cancel{E}_T , Tglu3D, $m_{\tilde{\chi}_1^\pm} = m_{\tilde{\chi}_1^0} + 5$ GeV, $m_{\tilde{\chi}_1^0} = 100$ GeV
>1500	95	41	SIRUNYAN	18AR CMS	$\ell^\pm \ell^\mp +$ jets + \cancel{E}_T , GMSB, Tglu4C, $m_{\tilde{\chi}_1^0} = 100$ GeV	> 780	95	61	KHACHATRY...17P	CMS	1 or more jets+ \cancel{E}_T , Tglu3B, $m_{\tilde{\tau}_1} - m_{\tilde{\chi}_1^0} = 175$ GeV, $m_{\tilde{\chi}_1^0} = 50$ GeV
>1770	95	41	SIRUNYAN	18AR CMS	$\ell^\pm \ell^\mp +$ jets + \cancel{E}_T , GMSB, Tglu4C, $m_{\tilde{\chi}_1^0} = 1400$ GeV	> 790	95	61	KHACHATRY...17P	CMS	1 or more jets+ \cancel{E}_T , Tglu3C, $m_{\tilde{\tau}_1} - m_{\tilde{\chi}_1^0} = 20$ GeV, $m_{\tilde{\chi}_1^0} = 0$ GeV
>1625	95	42	SIRUNYAN	18AY CMS	jets+ \cancel{E}_T , Tglu1A, $m_{\tilde{\chi}_1^0} = 0$ GeV	>1650	95	62	KHACHATRY...17V	CMS	2 $\gamma + \cancel{E}_T$, GGM, Tglu4B, any NLSP mass
>1825	95	42	SIRUNYAN	18AY CMS	jets+ \cancel{E}_T , Tglu2A, $m_{\tilde{\chi}_1^0} = 0$ GeV	>1900	95	63	SIRUNYAN	17AF CMS	1 ℓ +jets+b-jets+ \cancel{E}_T , Tglu3A, $m_{\tilde{\chi}_1^0} = 0$ GeV
>1625	95	42	SIRUNYAN	18AY CMS	jets+ \cancel{E}_T , Tglu3A, $m_{\tilde{\chi}_1^0} = 0$ GeV	>1600	95	63	SIRUNYAN	17AF CMS	1 ℓ +jets+b-jets+ \cancel{E}_T , Tglu3B, $m_{\tilde{\tau}_1} - m_{\tilde{\chi}_1^0} = 175$ GeV, $m_{\tilde{\chi}_1^0} = 200$ GeV
>2040	95	43	SIRUNYAN	18D CMS	top quark (hadronically decaying) + jets + \cancel{E}_T , Tglu3A, $m_{\tilde{\chi}_1^0} = 0$ GeV	>1800	95	64	SIRUNYAN	17AY CMS	$\gamma +$ jets+ \cancel{E}_T , Tglu4B, $m_{\tilde{\chi}_1^0} = 0$ GeV
>1930	95	43	SIRUNYAN	18D CMS	top quark (hadronically decaying) + jets + \cancel{E}_T , Tglu3B, $m_{\tilde{\tau}_1} - m_{\tilde{\chi}_1^0} = 175$ GeV, $m_{\tilde{\chi}_1^0} = 200$ GeV	>1600	95	64	SIRUNYAN	17AY CMS	$\gamma +$ jets+ \cancel{E}_T , Tglu4A, $m_{\tilde{\chi}_1^0} = 0$ GeV
>1690	95	43	SIRUNYAN	18D CMS	top quark (hadronically decaying) + jets + \cancel{E}_T , Tglu3C, $m_{\tilde{\tau}_1} - m_{\tilde{\chi}_1^0} = 20$ GeV, $m_{\tilde{\chi}_1^0} = 0$ GeV	>1860	95	65	SIRUNYAN	17AZ CMS	≥ 1 jets + \cancel{E}_T , Tglu1A, $m_{\tilde{\chi}_1^0} = 0$ GeV
>1990	95	43	SIRUNYAN	18D CMS	top quark (hadronically decaying) + jets + \cancel{E}_T , Tglu3E, $m_{\tilde{\chi}_1^\pm} = m_{\tilde{\chi}_1^0} + 5$ GeV, $m_{\tilde{\chi}_1^0} = 100$ GeV	>2025	95	65	SIRUNYAN	17AZ CMS	≥ 1 jets+ \cancel{E}_T , Tglu2A, $m_{\tilde{\chi}_1^0} = 0$ GeV
>2010	95	44	SIRUNYAN	18M CMS	$\geq 1 H (\rightarrow bb) + \cancel{E}_T$, Tglu1I	>1900	95	65	SIRUNYAN	17AZ CMS	≥ 1 jets+ \cancel{E}_T , Tglu3A, $m_{\tilde{\chi}_1^0} = 0$ GeV
>1825	95	44	SIRUNYAN	18M CMS	$\geq 1 H (\rightarrow bb) + \cancel{E}_T$, Tglu1J	>1825	95	66	SIRUNYAN	17P CMS	jets+ \cancel{E}_T , Tglu1A, $m_{\tilde{\chi}_1^0} = 0$ GeV
>1750	95	45	AABOUD	17AJ ATLS	same-sign $\ell^\pm \ell^\pm / 3 \ell +$ jets + \cancel{E}_T , Tglu3A, $m_{\tilde{\chi}_1^0} = 100$ GeV	>1950	95	66	SIRUNYAN	17P CMS	jets+ \cancel{E}_T , Tglu2A, $m_{\tilde{\chi}_1^0} = 0$ GeV
>1570	95	46	AABOUD	17AJ ATLS	same-sign $\ell^\pm \ell^\pm / 3 \ell +$ jets + \cancel{E}_T , Tglu1E, $m_{\tilde{\chi}_1^0} = 100$ GeV	>1960	95	66	SIRUNYAN	17P CMS	jets+ \cancel{E}_T , Tglu3A, $m_{\tilde{\chi}_1^0} = 0$ GeV

Searches Particle Listings

Supersymmetric Particle Searches

>1800	95	66	SIRUNYAN	17P	CMS	jets+ \cancel{E}_T , Tglu1C, $m_{\tilde{\chi}_1^\pm} = m_{\tilde{\chi}_2^0}$ $= (m_{\tilde{g}} + m_{\tilde{\chi}_1^0})/2, m_{\tilde{\chi}_1^0} = 0$ GeV	>1050	95	79	KHACHATRY...16BJ	CMS	same-sign $\ell^\pm \ell^\pm$, Tglu3B, $m_{\tilde{\tau}^-} - m_{\tilde{\chi}_1^0} = m_t, m_{\tilde{\chi}_1^0} < 800$ GeV	
>1870	95	66	SIRUNYAN	17P	CMS	jets+ \cancel{E}_T , Tglu3D, $m_{\tilde{\chi}_1^\pm} = m_{\tilde{\chi}_1^0}$ $+ 5$ GeV, $m_{\tilde{\chi}_1^0} = 1000$ GeV	>1725	95	80	KHACHATRY...16Bs	CMS	jets + \cancel{E}_T , Tglu1A, $m_{\tilde{\chi}_1^0} = 0$	
>1520	95	67	SIRUNYAN	17s	CMS	same-sign $\ell^\pm \ell^\pm$ + jets + \cancel{E}_T , Tglu3A, $m_{\tilde{\chi}_1^0} = 0$ GeV	>1750	95	80	KHACHATRY...16Bs	CMS	jets + \cancel{E}_T , Tglu2A, $m_{\tilde{\chi}_1^0} = 0$	
>1200	95	67	SIRUNYAN	17s	CMS	same-sign $\ell^\pm \ell^\pm$ + jets + \cancel{E}_T , Tglu3D, $m_{\tilde{\chi}_1^\pm} = m_{\tilde{\chi}_1^0} + 5$ GeV, $m_{\tilde{\chi}_1^0} = 100$ GeV	>1550	95	80	KHACHATRY...16Bs	CMS	jets + \cancel{E}_T , Tglu3A, $m_{\tilde{\chi}_1^0} = 0$	
>1370	95	67	SIRUNYAN	17s	CMS	same-sign $\ell^\pm \ell^\pm$ + jets + \cancel{E}_T , Tglu3B, $m_{\tilde{\tau}^-} - m_{\tilde{\chi}_1^0} = 175$ GeV, $m_{\tilde{\chi}_1^0} = 50$ GeV	>1280	95	81	KHACHATRY...16BY	CMS	opposite-sign $\ell^\pm \ell^\pm$, Tglu4C, $m_{\tilde{\chi}_1^0} = 1000$ GeV	
>1180	95	67	SIRUNYAN	17s	CMS	same-sign $\ell^\pm \ell^\pm$ + jets + \cancel{E}_T , Tglu3C, $m_{\tilde{\tau}^-} - m_{\tilde{\chi}_1^0} = 20$ GeV, $m_{\tilde{\chi}_1^0} = 0$ GeV	>1030	95	81	KHACHATRY...16BY	CMS	opposite-sign $\ell^\pm \ell^\pm$, Tglu4C, $m_{\tilde{\chi}_1^0} = 0$ GeV	
>1280	95	67	SIRUNYAN	17s	CMS	same-sign $\ell^\pm \ell^\pm$ + jets + \cancel{E}_T , Tglu1B, $m_{\tilde{\chi}_1^\pm} = (m_{\tilde{g}} + m_{\tilde{\chi}_1^0})/2$, $m_{\tilde{\chi}_1^0} = 0$ GeV	>1440	95	82	KHACHATRY...16v	CMS	jets + \cancel{E}_T , Tglu1A, $m_{\tilde{\chi}_1^0} = 0$	
>1300	95	67	SIRUNYAN	17s	CMS	same-sign $\ell^\pm \ell^\pm$ + jets + \cancel{E}_T , Tglu1B, $m_{\tilde{\tau}^-} - m_{\tilde{\chi}_1^0} = 20$ GeV, $m_{\tilde{\chi}_1^0} = 100$ GeV	>1600	95	82	KHACHATRY...16v	CMS	jets + \cancel{E}_T , Tglu2A, $m_{\tilde{\chi}_1^0} = 0$	
>1570	95	68	AABOUD	16AC	ATLS	≥ 2 jets + 1 or 2 τ + \cancel{E}_T , Tglu1F, $m_{\tilde{\chi}_1^0} = 100$ GeV	>1550	95	82	KHACHATRY...16v	CMS	jets + \cancel{E}_T , Tglu3A, $m_{\tilde{\chi}_1^0} = 0$	
>1460	95	69	AABOUD	16J	ATLS	1 ℓ^\pm + ≥ 4 jets + \cancel{E}_T , Tglu3C, $m_{\tilde{\tau}^-} - m_{\tilde{\chi}_1^0} = 5$ GeV	>1450	95	82	KHACHATRY...16v	CMS	jets + \cancel{E}_T , Tglu1C, $m_{\tilde{\chi}_1^0} = 0$	
>1650	95	70	AABOUD	16M	ATLS	2 γ + \cancel{E}_T , Tglu1D, any NLSP mass	> 820	95	83	AAD	15Bg	ATLS	GGM, $\tilde{g} \rightarrow q\bar{q}Z\tilde{G}$, $\tan\beta = 30$, $\mu > 600$ GeV
>1510	95	71	AABOUD	16N	ATLS	≥ 4 jets + \cancel{E}_T , Tglu1A, $m_{\tilde{\chi}_1^0} = 0$ GeV	> 850	95	83	AAD	15Bg	ATLS	GGM, $\tilde{g} \rightarrow q\bar{q}Z\tilde{G}$, $\tan\beta = 1.5$, $\mu > 450$ GeV
>1500	95	72	AABOUD	16N	ATLS	≥ 4 jets + \cancel{E}_T , Tglu1B, $m_{\tilde{\chi}_1^\pm} = (m_{\tilde{g}} + m_{\tilde{\chi}_1^0})/2$, $m_{\tilde{\chi}_1^0} = 200$ GeV	>1150	95	84	AAD	15BV	ATLS	general RPC \tilde{g} decays, $m_{\tilde{\chi}_1^0} < 100$ GeV $\tilde{g} \rightarrow X\tilde{\chi}_1^0$, independent of $m_{\tilde{\chi}_1^0}$
>1780	95	73	AAD	16AD	ATLS	0 ℓ , ≥ 3 b-jets + \cancel{E}_T , Tglu2A, $m_{\tilde{\chi}_1^0} < 800$ GeV	> 700	95	85	AAD	15BX	ATLS	$\tilde{g} \rightarrow 2\gamma + \cancel{E}_T$, GGM, bino-like NLSP, any NLSP mass
>1760	95	74	AAD	16AD	ATLS	1 ℓ , ≥ 3 b-jets + \cancel{E}_T , Tglu3A, $m_{\tilde{\chi}_1^0} < 700$ GeV	>1290	95	86	AAD	15CA	ATLS	$\geq 1\gamma + b$ -jets + \cancel{E}_T , GGM, higgsino-bino admix. NLSP and $\mu < 0$, $m(\text{NLSP}) > 450$ GeV
>1300	95	75	AAD	16BB	ATLS	2 same-sign/ 3ℓ + jets + \cancel{E}_T , Tglu1D, $m_{\tilde{\chi}_1^0} < 600$ GeV	>1260	95	86	AAD	15CA	ATLS	$\geq 1\gamma + \text{jets} + \cancel{E}_T$, GGM, higgsino-bino admixture NLSP, all $\mu > 0$
>1100	95	75	AAD	16BB	ATLS	2 same-sign/ 3ℓ + jets + \cancel{E}_T , Tglu1E, $m_{\tilde{\chi}_1^0} < 300$ GeV	>1225	95	87	KHACHATRY...15AF	CMS	$\tilde{g} \rightarrow q\bar{q}\tilde{\chi}_1^0$, $m_{\tilde{\chi}_1^0} = 0$	
>1200	95	75	AAD	16BB	ATLS	2 same-sign/ 3ℓ + jets + \cancel{E}_T , Tglu3A, $m_{\tilde{\chi}_1^0} < 600$ GeV	>1300	95	87	KHACHATRY...15AF	CMS	$\tilde{g} \rightarrow b\bar{b}\tilde{\chi}_1^0$, $m_{\tilde{\chi}_1^0} = 0$	
>1600	95	76	AAD	16BG	ATLS	1 ℓ , ≥ 4 jets, \cancel{E}_T , Tglu1B, $m_{\tilde{\chi}_1^\pm} = (m_{\tilde{g}} + m_{\tilde{\chi}_1^0})/2$, $m_{\tilde{\chi}_1^0} = 100$ GeV	>1225	95	87	KHACHATRY...15AF	CMS	$\tilde{g} \rightarrow t\bar{t}\tilde{\chi}_1^0$, $m_{\tilde{\chi}_1^0} = 0$	
>1400	95	77	AAD	16V	ATLS	≥ 7 to ≥ 10 jets + \cancel{E}_T , Tglu1E, $m_{\tilde{\chi}_1^0} < 200$ GeV	>1550	95	87	KHACHATRY...15AF	CMS	CMSSM, $\tan\beta=30$, $m_{\tilde{g}}=m_{\tilde{q}}$, $A_0 = -2\max(m_0, m_{1/2})$, $\mu > 0$	
>1400	95	77	AAD	16V	ATLS	≥ 7 to ≥ 10 jets + \cancel{E}_T , pMSSM $M_1 = 60$ GeV, $M_2 = 3$ TeV, $\tan\beta=10$, $\mu < 0$	>1150	95	87	KHACHATRY...15AF	CMS	CMSSM, $\tan\beta=30$, $A_0 = -2\max(m_0, m_{1/2})$, $\mu > 0$	
>1100	95	78	KHACHATRY...16AM	CMS	boosted $W+b$, Tglu3C, $m_{\tilde{\tau}^-} - m_{\tilde{\chi}_1^0} < 80$ GeV, $m_{\tilde{\chi}_1^0} < 400$ GeV	>1280	95	88	KHACHATRY...15I	CMS	$\tilde{g} \rightarrow t\bar{t}\tilde{\chi}_1^0$, $m_{\tilde{\chi}_1^0} = 0$		
> 700	95	78	KHACHATRY...16AM	CMS	boosted $W+b$, Tglu3B, $m_{\tilde{\tau}^-} - m_{\tilde{\chi}_1^0} = 175$ GeV, $m_{\tilde{\chi}_1^0} = 0$ GeV	>1310	95	89	KHACHATRY...15X	CMS	$\tilde{g} \rightarrow b\bar{b}\tilde{\chi}_1^0$, $m_{\tilde{\chi}_1^0} = 100$ GeV		
>1050	95	79	KHACHATRY...16BJ	CMS	same-sign $\ell^\pm \ell^\pm$, Tglu3A, $m_{\tilde{\chi}_1^0} < 800$ GeV	>1175	95	89	KHACHATRY...15X	CMS	$\tilde{g} \rightarrow t\bar{t}\tilde{\chi}_1^0$, $m_{\tilde{\chi}_1^0} = 100$ GeV		
>1300	95	79	KHACHATRY...16BJ	CMS	same-sign $\ell^\pm \ell^\pm$, Tglu3A, $m_{\tilde{\chi}_1^0} = 0$	>1330	95	90	AAD	14AE	ATLS	jets + \cancel{E}_T , $\tilde{g} \rightarrow q\bar{q}\tilde{\chi}_1^0$ simplified model, $m_{\tilde{\chi}_1^0} = 0$ GeV	
>1140	95	79	KHACHATRY...16BJ	CMS	same-sign $\ell^\pm \ell^\pm$, Tglu3B, $m_{\tilde{\tau}^-} - m_{\tilde{\chi}_1^0} = 20$ GeV, $m_{\tilde{\chi}_1^0} = 0$	>1700	95	90	AAD	14AE	ATLS	jets + \cancel{E}_T , mSUGRA/CMSSM, $m_{\tilde{q}} = m_{\tilde{g}}$	
> 850	95	79	KHACHATRY...16BJ	CMS	same-sign $\ell^\pm \ell^\pm$, Tglu3B, $m_{\tilde{\tau}^-} - m_{\tilde{\chi}_1^0} = 20$ GeV, $m_{\tilde{\chi}_1^0} < 700$ GeV	>1090	95	91	AAD	14AG	ATLS	τ + jets + \cancel{E}_T , natural Gauge Mediation	
> 950	95	79	KHACHATRY...16BJ	CMS	same-sign $\ell^\pm \ell^\pm$, Tglu3D, $m_{\tilde{\chi}_1^\pm} = m_{\tilde{\chi}_1^0} + 5$ GeV	>1600	95	91	AAD	14AG	ATLS	τ + jets + \cancel{E}_T , mGMSB, $M_{\text{mess}} = 250$ GeV, $N_5 = 3$, $\mu > 0$, $C_{\text{grav}} = 1$	
>1100	95	79	KHACHATRY...16BJ	CMS	same-sign $\ell^\pm \ell^\pm$, Tglu1B, $m_{\tilde{\chi}_1^\pm} = 0.5(m_{\tilde{g}} + m_{\tilde{\chi}_1^0})$, $m_{\tilde{\chi}_1^0} < 400$ GeV	> 640	95	92	AAD	14X	ATLS	$\geq 4\ell^\pm$, $\tilde{g} \rightarrow q\bar{q}\tilde{\chi}_1^0$, $\tilde{\chi}_1^0 \rightarrow \ell^\pm \ell^\mp \tilde{G}$, $\tan\beta = 30$, GGM	
> 830	95	79	KHACHATRY...16BJ	CMS	same-sign $\ell^\pm \ell^\pm$, Tglu1B, $m_{\tilde{\chi}_1^\pm} = 0.5(m_{\tilde{g}} + m_{\tilde{\chi}_1^0})$, $m_{\tilde{\chi}_1^0} < 700$ GeV	>1000	95	93	CHATRCHYAN 14AH	CMS	jets + \cancel{E}_T , $\tilde{g} \rightarrow q\bar{q}\tilde{\chi}_1^0$ simplified model, $m_{\tilde{\chi}_1^0} = 50$ GeV		
>1300	95	79	KHACHATRY...16BJ	CMS	same-sign $\ell^\pm \ell^\pm$, Tglu3B, $m_{\tilde{\tau}^-} - m_{\tilde{\chi}_1^0} = m_t$, $m_{\tilde{\chi}_1^0} = 0$	>1350	95	93	CHATRCHYAN 14AH	CMS	jets + \cancel{E}_T , CMSSM, $m_{\tilde{g}} = m_{\tilde{q}}$		
>1140	95	79	KHACHATRY...16BJ	CMS	same-sign $\ell^\pm \ell^\pm$, Tglu3B, $m_{\tilde{\tau}^-} - m_{\tilde{\chi}_1^0} = 20$ GeV, $m_{\tilde{\chi}_1^0} = 0$	>1000	95	94	CHATRCHYAN 14AH	CMS	jets + \cancel{E}_T , $\tilde{g} \rightarrow b\bar{b}\tilde{\chi}_1^0$ simplified model, $m_{\tilde{\chi}_1^0} = 50$ GeV		
> 850	95	79	KHACHATRY...16BJ	CMS	same-sign $\ell^\pm \ell^\pm$, Tglu3B, $m_{\tilde{\tau}^-} - m_{\tilde{\chi}_1^0} = 20$ GeV, $m_{\tilde{\chi}_1^0} < 700$ GeV	>1160	95	95	CHATRCHYAN 14AH	CMS	jets + \cancel{E}_T , $\tilde{g} \rightarrow t\bar{t}\tilde{\chi}_1^0$ simplified model, $m_{\tilde{\chi}_1^0} = 50$ GeV		
> 950	95	79	KHACHATRY...16BJ	CMS	same-sign $\ell^\pm \ell^\pm$, Tglu3D, $m_{\tilde{\chi}_1^\pm} = m_{\tilde{\chi}_1^0} + 5$ GeV	>1130	95	96	CHATRCHYAN 14I	CMS	jets + \cancel{E}_T , $\tilde{g} \rightarrow q\bar{q}\tilde{\chi}_1^0$ simplified model, $m_{\tilde{\chi}_1^0} < 100$ GeV		
>1100	95	79	KHACHATRY...16BJ	CMS	same-sign $\ell^\pm \ell^\pm$, Tglu1B, $m_{\tilde{\chi}_1^\pm} = 0.5(m_{\tilde{g}} + m_{\tilde{\chi}_1^0})$, $m_{\tilde{\chi}_1^0} < 400$ GeV	>1210	95	96	CHATRCHYAN 14I	CMS	multijets + \cancel{E}_T , $\tilde{g} \rightarrow t\bar{t}\tilde{\chi}_1^0$ simplified model, $m_{\tilde{\chi}_1^0} < 100$ GeV		
> 830	95	79	KHACHATRY...16BJ	CMS	same-sign $\ell^\pm \ell^\pm$, Tglu1B, $m_{\tilde{\chi}_1^\pm} = 0.5(m_{\tilde{g}} + m_{\tilde{\chi}_1^0})$, $m_{\tilde{\chi}_1^0} < 700$ GeV	>1260	95	96	CHATRCHYAN 14I	CMS	multijets + \cancel{E}_T , $\tilde{g} \rightarrow q\bar{q}W/Z\tilde{\chi}_1^0$ simplified model, $m_{\tilde{\chi}_1^0} < 100$ GeV		
>1300	95	79	KHACHATRY...16BJ	CMS	same-sign $\ell^\pm \ell^\pm$, Tglu3B, $m_{\tilde{\tau}^-} - m_{\tilde{\chi}_1^0} = m_t$, $m_{\tilde{\chi}_1^0} = 0$		95	97	CHATRCHYAN 14N	CMS	1 ℓ^\pm + jets + $\geq 2b$ -jets, $\tilde{g} \rightarrow t\bar{t}\tilde{\chi}_1^0$ simplified model, $m_{\tilde{\chi}_1^0} = 0$ GeV, $m_{\tilde{\tau}^-} > m_{\tilde{g}}$		
								98	CHATRCHYAN 14R	CMS	$\geq 3\ell^\pm$, $(\tilde{g}/\tilde{q}) \rightarrow q\ell^\pm \ell^\mp \tilde{G}$ simplified model, GMSB, slep- ton co-NLSP scenario		
								99	CHATRCHYAN 14R	CMS	$\geq 3\ell^\pm$, $\tilde{g} \rightarrow t\bar{t}\tilde{\chi}_1^0$ simplified model		

See key on page 1171

Searches Particle Listings
Supersymmetric Particle Searches

• • • We do not use the following data for averages, fits, limits, etc. • • •

>1500	95	100	AABOUD	18BJ ATLS	$\ell^\pm \ell^\mp + \text{jets} + \cancel{E}_T, T_{\text{glu1H}}, m_{\tilde{\chi}_1^0} = 1 \text{ GeV}, \text{any } m_{\tilde{\chi}_2^0}$	>1180	95	110	AAD	14AX ATLS	$\geq 3 \text{ } b\text{-jets} + \cancel{E}_T, \tilde{g} \rightarrow \tilde{t}_1 t \tilde{\chi}_1^0$ simplified model, $\tilde{t}_1 \rightarrow b \tilde{\chi}_1^\pm$, $m_{\tilde{\chi}_1^\pm} = 2m_{\tilde{\chi}_1^0}, m_{\tilde{\chi}_1^0} = 60 \text{ GeV},$ $m_{\tilde{t}_1} < 1000 \text{ GeV}$
>1770	95	101	AABOUD	18V ATLS	$\text{jets} + \cancel{E}_T, T_{\text{glu1C-like}}, 1/2$ BR per decay mode, any $m_{\tilde{\chi}_2^0} - m_{\tilde{\chi}_1^0}, m_{\tilde{\chi}_1^0} = 60 \text{ GeV}$	>1250	95	110	AAD	14AX ATLS	$\geq 3 \text{ } b\text{-jets} + \cancel{E}_T, \tilde{g} \rightarrow b \tilde{\chi}_1^0$ simplified model, $m_{\tilde{\chi}_1^0} < 400$ GeV
>1600	95	102	AABOUD	17AZ ATLS	$\geq 7 \text{ jets} + \cancel{E}_T, \text{large } R\text{-jets}$ and/or $b\text{-jets}, p\text{MSSM}, m_{\tilde{\chi}_1^\pm}$ $= 200 \text{ GeV}$	>1340	95	110	AAD	14AX ATLS	$\geq 3 \text{ } b\text{-jets} + \cancel{E}_T, \tilde{g} \rightarrow t \tilde{\chi}_1^0$ simplified model, $m_{\tilde{\chi}_1^0} < 400$ GeV
>1600	95	103	KHACHATRY...	16AY CMS	$1\ell^\pm + \text{jets} + b\text{-jets} + \cancel{E}_T,$ Tglu3A, $m_{\tilde{\chi}_1^0} = 0 \text{ GeV}$	>1300	95	110	AAD	14AX ATLS	$\geq 3 \text{ } b\text{-jets} + \cancel{E}_T, \tilde{g} \rightarrow t \tilde{b} \tilde{\chi}_1^\pm$ simplified model, $\tilde{\chi}_1^\pm \rightarrow$ $f' \ell' \tilde{\chi}_1^0, m_{\tilde{\chi}_1^\pm} - m_{\tilde{\chi}_1^0} = 2 \text{ GeV},$ $m_{\tilde{\chi}_1^0} < 300 \text{ GeV}$
> 500	95	104	KHACHATRY...	16BT CMS	19-parameter pMSSM model, global Bayesian analysis, flat prior	> 950	95	111	AAD	14E ATLS	$\ell^\pm \ell^\pm (\ell^\mp) + \text{jets}, \tilde{g} \rightarrow t \tilde{\chi}_1^0$ simplified model
		105	AAD	15AB ATLS	$\tilde{g} \rightarrow \tilde{S} g, c\tau = 1 \text{ m}, \tilde{S} \rightarrow S \tilde{G}$ and $\tilde{S} \rightarrow g g, \text{BR} = 100\%$	>1000	95	111	AAD	14E ATLS	$\ell^\pm \ell^\pm (\ell^\mp) + \text{jets}, \tilde{g} \rightarrow t \tilde{t}_1$ with $\tilde{t}_1 \rightarrow b \tilde{\chi}_1^\pm$ simplified model, $m_{\tilde{t}_1} < 200 \text{ GeV}, m_{\tilde{\chi}_1^\pm}$ $= 118 \text{ GeV}, m_{\tilde{\chi}_1^0} = 60 \text{ GeV}$
>1600	95	106	AAD	15AI ATLS	$\ell^\pm + \text{jets} + \cancel{E}_T$	> 640	95	111	AAD	14E ATLS	$\ell^\pm \ell^\pm (\ell^\mp) + \text{jets}, \tilde{g} \rightarrow t \tilde{t}_1$ with $\tilde{t}_1 \rightarrow c \tilde{\chi}_1^0$ simplified model, $m_{\tilde{t}_1} = m_{\tilde{\chi}_1^0} + 20 \text{ GeV}$
		84	AAD	15BV ATLS	pMSSM, $M_1 = 60 \text{ GeV}, m_{\tilde{q}} <$ 1500 GeV	> 860	95	111	AAD	14E ATLS	$\ell^\pm \ell^\pm (\ell^\mp) + \text{jets}, \tilde{g} \rightarrow q q' \tilde{\chi}_1^\pm,$ $\tilde{\chi}_1^\pm \rightarrow W^{(*)\pm} \tilde{\chi}_1^0$ simpli- fied model, $m_{\tilde{\chi}_1^\pm} = 2 m_{\tilde{\chi}_1^0},$ $m_{\tilde{\chi}_1^0} < 400 \text{ GeV}$
>1280	95	84	AAD	15BV ATLS	mSUGRA, $m_0 > 2 \text{ TeV}$	>1040	95	111	AAD	14E ATLS	$\ell^\pm \ell^\pm (\ell^\mp) + \text{jets}, \tilde{g} \rightarrow q q' \tilde{\chi}_1^\pm,$ $\tilde{\chi}_1^\pm \rightarrow W^{(*)\pm} \tilde{\chi}_2^0, \tilde{\chi}_2^0 \rightarrow$ $Z^{(*)} \tilde{\chi}_1^0$ simplified model, $m_{\text{widetilde}x_1^0} < 520 \text{ GeV}$
>1100	95	84	AAD	15BV ATLS	via $\tilde{\tau}, \text{natural GMSB}, \text{all } m_{\tilde{\tau}}$	>1200	95	111	AAD	14E ATLS	$\ell^\pm \ell^\pm (\ell^\mp) + \text{jets}, \tilde{g} \rightarrow$ $q q' \tilde{\chi}_1^\pm / \tilde{\chi}_2^0, \tilde{\chi}_1^\pm \rightarrow \ell^\pm \nu \tilde{\chi}_1^0,$ $\tilde{\chi}_2^0 \rightarrow \ell^\pm \ell^\mp (\nu \nu) \tilde{\chi}_1^0$ simpli- fied model
>1330	95	84	AAD	15BV ATLS	$\text{jets} + \cancel{E}_T, \tilde{g} \rightarrow q \tilde{q} \tilde{\chi}_1^0, m_{\tilde{\chi}_1^0} =$ 1 GeV	>1050	95	112	CHATRCHYAN 14H	CMS	same-sign $\ell^\pm \ell^\pm, \tilde{g} \rightarrow t \tilde{\chi}_1^0$ simplified model, massless $\tilde{\chi}_1^0$
>1500	95	84	AAD	15BV ATLS	$\text{jets} + \cancel{E}_T, \tilde{g} \rightarrow \tilde{q} q, \tilde{q} \rightarrow q \tilde{\chi}_1^0,$ $m_{\tilde{\chi}_1^0} = 1 \text{ GeV}$	> 900	95	113	CHATRCHYAN 14H	CMS	same-sign $\ell^\pm \ell^\pm, \tilde{g} \rightarrow q q' \tilde{\chi}_1^\pm,$ $\tilde{\chi}_1^\pm \rightarrow W^\pm \tilde{\chi}_1^0$ simplified model, $m_{\tilde{\chi}_1^\pm} = 0.5 m_{\tilde{g}}, \text{mass-}$ less $\tilde{\chi}_1^0$
>1650	95	84	AAD	15BV ATLS	$\text{jets} + \cancel{E}_T, m_{\tilde{g}} = m_{\tilde{q}}, m_{\tilde{\chi}_1^0} = 1$ GeV	>1050	95	114	CHATRCHYAN 14H	CMS	same-sign $\ell^\pm \ell^\pm, \tilde{g} \rightarrow b \tilde{\chi}_1^\pm,$ $\tilde{\chi}_1^\pm \rightarrow W^\pm \tilde{\chi}_1^0$ simplified model, $m_{\tilde{\chi}_1^\pm} = 300 \text{ GeV}, m_{\tilde{\chi}_1^0}$ $= 50 \text{ GeV}$
> 850	95	84	AAD	15BV ATLS	$\text{jets} + \cancel{E}_T, \tilde{g} \rightarrow g \tilde{\chi}_1^0, m_{\tilde{\chi}_1^0} <$ 550 GeV						
>1270	95	84	AAD	15BV ATLS	$\text{jets} + \cancel{E}_T, \tilde{g} \rightarrow q \tilde{q} W \tilde{\chi}_1^0, m_{\tilde{\chi}_1^0}$ $= 100 \text{ GeV}$						
>1150	95	84	AAD	15BV ATLS	$\text{jets} + \ell^\pm \ell^\pm, \tilde{g} \rightarrow q \tilde{q} W Z \tilde{\chi}_1^0,$ $m_{\tilde{\chi}_1^0} = 100 \text{ GeV}$						
>1320	95	84	AAD	15BV ATLS	$\text{jets} + \ell^\pm \ell^\pm, \tilde{g} \text{ decays via slep-}$ tons, $m_{\tilde{\chi}_1^0} = 100 \text{ GeV}$						
>1220	95	84	AAD	15BV ATLS	$\tau, \tilde{q} \text{ decays via staus}, m_{\tilde{\chi}_1^0} = 100$ GeV						
>1310	95	84	AAD	15BV ATLS	$b\text{-jets}, \tilde{g} \rightarrow t \tilde{\chi}_1^0, m_{\tilde{\chi}_1^0} < 400$ GeV						
>1220	95	84	AAD	15BV ATLS	$b\text{-jets}, \tilde{g} \rightarrow \tilde{t}_1 t \text{ and } \tilde{t}_1 \rightarrow t \tilde{\chi}_1^0,$ $m_{\tilde{\tau}_1} < 1000 \text{ GeV}$						
>1180	95	84	AAD	15BV ATLS	$b\text{-jets}, \tilde{g} \rightarrow \tilde{t}_1 t \text{ and } \tilde{t}_1 \rightarrow$ $b \tilde{\chi}_1^\pm, m_{\tilde{\tau}_1} < 1000 \text{ GeV},$ $m_{\tilde{\chi}_1^0} = 60 \text{ GeV}$						
>1260	95	84	AAD	15BV ATLS	$b\text{-jets}, \tilde{g} \rightarrow \tilde{t}_1 t \text{ and } \tilde{g} \rightarrow c \tilde{\chi}_1^0$						
>1200	95	84	AAD	15BV ATLS	$b\text{-jets}, \tilde{g} \rightarrow \tilde{b}_1 b \text{ and } \tilde{b}_1 \rightarrow$ $b \tilde{\chi}_1^0, m_{\tilde{b}_1} < 1000 \text{ GeV}$						
>1250	95	84	AAD	15BV ATLS	$b\text{-jets}, \tilde{g} \rightarrow b \tilde{\chi}_1^0, m_{\tilde{\chi}_1^0} < 400$ GeV						
none, 750-1250	95	84	AAD	15BV ATLS	$b\text{-jets}, \tilde{g} \text{ decay via offshell } \tilde{t}_1 \text{ and}$ $\tilde{b}_1, m_{\tilde{\chi}_1^0} < 500 \text{ GeV}$						
>1100	95	107	AAD	15CB ATLS	$\text{jets}, \tilde{g} \rightarrow q q \tilde{\chi}_1^0, \tilde{\chi}_1^0 \rightarrow Z \tilde{G},$ GGM, $m_{\tilde{\chi}_1^0} = 400 \text{ GeV}$ and 3 $< c\tau_{\tilde{\chi}_1^0} < 500 \text{ mm}$						
>1400	95	107	AAD	15CB ATLS	$\text{jets or } \cancel{E}_T, \tilde{g} \rightarrow q q \tilde{\chi}_1^0, \text{Split}$ SUSY, $m_{\tilde{\chi}_1^0} = 100 \text{ GeV}$ and $15 < c\tau < 300 \text{ mm}$						
>1500	95	107	AAD	15CB ATLS	$\cancel{E}_T, \tilde{g} \rightarrow q q \tilde{\chi}_1^0, \text{Split SUSY},$ $m_{\tilde{\chi}_1^0} = 100 \text{ GeV}$ and 20 < $c\tau < 250 \text{ mm}$						
>1300	95	109	KHACHATRY...	15AD CMS	$\ell^\pm \ell^\mp + \text{jets} + \cancel{E}_T, \text{GMSB}, \tilde{g} \rightarrow$ $q \tilde{q} Z \tilde{G}$						
> 800	95	109	KHACHATRY...	15AZ CMS	$\geq 2 \gamma, \geq 1 \text{ jet}, (\text{Razor}), \text{bino-}$ like NLSP, $m_{\tilde{\chi}_1^0} = 375 \text{ GeV}$						
>1280	95	110	AAD	14AX ATLS	$\geq 3 \text{ } b\text{-jets} + \cancel{E}_T, \text{CMSSM}$						
>1250	95	110	AAD	14AX ATLS	$\geq 3 \text{ } b\text{-jets} + \cancel{E}_T, \tilde{g} \rightarrow \tilde{b}_1 b \tilde{\chi}_1^0$ simplified model, $\tilde{b}_1 \rightarrow b \tilde{\chi}_1^0,$ $m_{\tilde{\chi}_1^0} = 60 \text{ GeV}, m_{\tilde{b}_1} < 900$ GeV						
>1190	95	110	AAD	14AX ATLS	$\geq 3 \text{ } b\text{-jets} + \cancel{E}_T, \tilde{g} \rightarrow \tilde{t}_1 t \tilde{\chi}_1^0$ simplified model, $\tilde{t}_1 \rightarrow t \tilde{\chi}_1^0,$ $m_{\tilde{\chi}_1^0} = 60 \text{ GeV}, m_{\tilde{t}_1} < 1000$ GeV						

¹ AAD 23AB searched in 139 fb^{-1} of pp collisions at $\sqrt{s} = 13 \text{ TeV}$ for an excess of events with one photon, jets and \cancel{E}_T . No significant excess above the Standard Model predictions is observed. Limits are set on the mass of pair produced gluinos decaying to $\tilde{g} \rightarrow q q \tilde{\chi}_1^0$ followed by $\tilde{\chi}_1^0 \rightarrow \gamma \tilde{G}$ or $\tilde{\chi}_1^0 \rightarrow X \tilde{G}$ with equal probability, see Figure 4. X can be Z (left figure) or h (right figure).

² AAD 23AE searched in 139 fb^{-1} of pp collisions at $\sqrt{s} = 13 \text{ TeV}$ for events with 2 ℓ with same flavour and opposite sign, plus jets and \cancel{E}_T , defining signal region with the dilepton invariant mass both on- and off-shell with respect to the Z boson. No significant excess above the Standard Model predictions is observed. Limits are set on models of strong and electroweak production. In this case, limits are placed on the mass of pair-produced gluinos, assuming a scenario like in Tglu1G, see figure 16.

³ AAD 23AE searched in 139 fb^{-1} of pp collisions at $\sqrt{s} = 13 \text{ TeV}$ for events with 2 ℓ with same flavour and opposite sign, plus jets and \cancel{E}_T , defining signal region with the dilepton invariant mass both on- and off-shell with respect to the Z boson. No significant excess above the Standard Model predictions is observed. Limits are set on models of strong and electroweak production. In this case, limits are placed on the gluino mass assuming gluino pair production, assuming a scenario like in Tglu1H, see figure 16.

⁴ AAD 23AL searched in 139 fb^{-1} of pp collisions at $\sqrt{s} = 13 \text{ TeV}$ for events with 0 or 1 lepton and at least three b -tagged jets. No significant excess above the Standard Model prediction is observed. Results are interpreted in terms of gluino pair production followed by the decay of gluinos into off-shell third generation squarks, yielding final states with top and bottom quarks, and missing transverse momentum from a $\tilde{\chi}_1^0$ LSP. Limits are set on the mass of the gluino as a function of the $\tilde{\chi}_1^0$ assuming $B(\tilde{g} \rightarrow \tilde{t} t) = 100\%$ or $B(\tilde{g} \rightarrow \tilde{b} b) = 100\%$, see figure 10.

⁵ AAD 23AL searched in 139 fb^{-1} of pp collisions at $\sqrt{s} = 13 \text{ TeV}$ for events with 0 or 1 lepton and at least three b -tagged jets. No significant excess above the Standard Model prediction is observed. Results are interpreted in terms of gluino pair production followed by the decay of gluinos into off-shell third generation squarks, yielding final states with top and bottom quarks, and missing transverse momentum from a $\tilde{\chi}_1^0$ LSP. Limits are set on the mass of the gluino as a function of $m_{\tilde{\chi}_1^0}$, assuming $B(\tilde{g} \rightarrow \tilde{t} t) + B(\tilde{g} \rightarrow \tilde{b} b) + B(\tilde{g} \rightarrow t b \tilde{\chi}_1^\pm) = 100\%$, and $m_{\tilde{\chi}_1^\pm} - m_{\tilde{\chi}_1^0} = 2 \text{ GeV}$, see figures 11-13.

Searches Particle Listings

Supersymmetric Particle Searches

- 6** HAYRAPETYAN 23E searched in 137 fb⁻¹ of pp collisions at $\sqrt{s} = 13$ TeV for evidence of gluino, top squark and electroweakino pair production in events with at least one photon, multiple jets, and large \cancel{E}_T . No significant excess above the Standard Model expectations is observed. Limits are set in models for strong production, Tglu4D, Tglu4E, Tglu4F and Tstop13, see their figure 9. They also interpret the results in the models for electroweak production, shown in their figure 10. Tchi1n1A assumes wino-like $\tilde{\chi}_1^\pm \tilde{\chi}_1^0$ production, while Tchi1chi1A assumes higgsino-like cross sections and includes $\tilde{\chi}_1^\pm \tilde{\chi}_1^\pm$, $\tilde{\chi}_1^0 \tilde{\chi}_2^0$ and $\tilde{\chi}_{1,2}^0 \tilde{\chi}_1^\pm$ production. For $\tilde{\chi}_1^0 \tilde{\chi}_2^0$ alone no mass point can be excluded in the model Tchi1chi1A, but in another model for $\tilde{\chi}_1^0 \tilde{\chi}_2^0$ production, Tn1n2A.
- 7** TUMASYAN 23AY searched in 138 fb⁻¹ of pp collisions at $\sqrt{s} = 13$ TeV for evidence of gluino pair production in events with a single electron or muon and multiple hadronic jets. No significant excess above the Standard Model expectations is observed. Limits are set in the models Tglu3A and Tglu1B, see their figure 11. For Tglu1B, the chargino mass is set to $m_{\tilde{\chi}_1^\pm} = 0.5 (m_{\tilde{g}} + m_{\tilde{\chi}_1^0})$.
- 8** AAD 22U searched for the signature of disappearing track from a long-lived chargino in 139 fb⁻¹ of pp collisions at $\sqrt{s} = 13$ TeV. Long-lived charginos decay into quasi-degenerate neutralino emitting a low-momentum particle whose identification is not attempted. The signal is identified by requiring short tracklets in the four pixel layers with no continuation in the SCT (strip) detector. The main background from fake tracklets is estimated directly with the data. No significant excess above the background prediction is found. The results are interpreted in an AMSB scenario (win LSP), on $pp \rightarrow \tilde{\chi}^\pm \tilde{\chi}^\pm$ and $pp \rightarrow \tilde{\chi}^\pm \tilde{\chi}_1^0$, assuming $B(\tilde{\chi}^\pm \rightarrow \tilde{\chi}_1^0 \pi^\pm) = 100\%$, see their figure 7. Results are also interpreted in a higgsino-LSP model, with $pp \rightarrow \tilde{\chi}^\pm \tilde{\chi}^\mp$, and $pp \rightarrow \tilde{\chi}^\pm \tilde{\chi}_{1,2}^0$, assuming $B(\tilde{\chi}^\pm \rightarrow \tilde{\chi}_1^0 \pi^\pm) = 95.5\%$, $B(\tilde{\chi}^\pm \rightarrow \tilde{\chi}_1^0 e^\pm) = 3\%$, $B(\tilde{\chi}^\pm \rightarrow \tilde{\chi}_1^0 \mu^\pm) = 1.5\%$, see their figure 8. Finally, results are interpreted in a simplified model of gluino pair production, with $pp \rightarrow \tilde{g} \tilde{g}$ and $B(\tilde{g} \rightarrow qq\tilde{\chi}_1^0) = B(\tilde{g} \rightarrow qq\tilde{\chi}^\pm) = B(\tilde{g} \rightarrow qq\tilde{\chi}^\mp) = 1/3$, see their figure 9.
- 9** TUMASYAN 22v searched in 137 fb⁻¹ of pp collisions at $\sqrt{s} = 13$ TeV for evidence of electroweakino pair production with decay to two Higgs bosons H , with $H \rightarrow b\bar{b}$, resulting either in 4 resolved b -jets or two large-radius jets, and large \cancel{E}_T . No significant excess above the Standard Model expectations is observed. Limits are set on the mass of $\tilde{\chi}_2^0$ and $\tilde{\chi}_3^0$ in the models Tn1n1A, see their Figures 11 and 12, or in a model where higgsino-like nearly mass degenerate $\tilde{\chi}_2^0$ and $\tilde{\chi}_3^0$ are pair produced and each decay to H and a bino-like $\tilde{\chi}_1^0$, see their Figure 13. Limits are also set on the gluino mass in the model Tglu1I, see their Figure 14.
- 10** AAD 21AK searched in 139 fb⁻¹ of pp collisions at $\sqrt{s} = 13$ TeV for pair production of gluinos and squarks in events with a single isolated electron or muon, originating from the decay of a W boson, multiple jets and significant \cancel{E}_T . No significant excess above the Standard Model expectations is observed. Limits are set on the gluino mass in the Tglu1B simplified model and on the squark mass in the Tsqk3 simplified model, see their Figure 8.
- 11** AAD 21L searched in 139 fb⁻¹ of pp collisions at $\sqrt{s} = 13$ TeV for pair production of gluinos and squarks in events with jets, large missing transverse momentum but no electrons or muons. No significant excess above the Standard Model expectations is observed. Limits are set on the gluino mass in the Tglu1A and Tglu1B simplified models, on the squark mass in the Tsqk1 and Tsqk3 simplified models and in a simplified model for gluino-squark production, see their Figures 13-17.
- 12** AAD 21x searched in 139 fb⁻¹ of pp collisions at $\sqrt{s} = 13$ TeV for the decay of long-lived R -hadrons stopped by the calorimeter, producing high-momentum jets resulting in large out-of-time energy deposits in the calorimeters. These decays are detected using data collected during periods in the LHC bunch structure when collisions are absent. No significant excess above the predicted background is observed. Limits are set on the R -hadron mass in the Tglu1A simplified model as a function of the R -hadron lifetime, for different $m_{\tilde{\chi}_1^0}$. See Figures 9, 10.
- 13** SIRUNYAN 21AD searched in 137 fb⁻¹ of pp collisions at $\sqrt{s} = 13$ TeV for supersymmetry in events with multiple jets, no leptons, and large \cancel{E}_T . No significant excess above the Standard Model expectations is observed. Limits are set on the top squark mass in the simplified models Tstop1, Tstop2 with $m_{\tilde{\chi}_1^\pm} = (m_T + m_{\tilde{\chi}_1^0})/2$, and a 50:50 mixture of these with $m_{\tilde{\chi}_1^\pm} - m_{\tilde{\chi}_1^0} = 5$ GeV, see their Figure 8. Limits are also set on the top squark mass for $10 \text{ GeV} < m_{\tilde{t}} - m_{\tilde{\chi}_1^0} < 80 \text{ GeV}$ in the simplified models Tstop2, Tstop 3, and Tstop4, see their Figure 9. For indirect top squark production, limits are set on the gluino mass in the simplified models Tglu3A, Tglu3C with $m_{\tilde{t}} - m_{\tilde{\chi}_1^0} = 20 \text{ GeV}$, and Tglu3D with $m_{\tilde{\chi}_1^\pm} - m_{\tilde{\chi}_1^0} = 5 \text{ GeV}$, see their Figure 10.
- 14** SIRUNYAN 21M searched in 137 fb⁻¹ of pp collisions at $\sqrt{s} = 13$ TeV for supersymmetry in events with two opposite-sign same-flavor leptons (electrons, muons) and \cancel{E}_T . No significant excess above the Standard Model expectations is observed. Limits are set on the gluino mass in the simplified model Tglu4C, see their Figure 10, on the $\tilde{\chi}_2^0$ and $\tilde{\chi}_3^0$ mass in Tchi1n2Fa, see their Figure 11, on the $\tilde{\chi}_1^0$ mass in Tn1n1C and Tn1n1B for $m_{\tilde{\chi}_2^0} = m_{\tilde{\chi}_3^0} = m_{\tilde{\chi}_1^0}$, see their Figure 12. Limits are also set on the light squark mass for the simplified model Tsqk2A, on the sbottom mass in Tstop3, see their Figure 13, and on the slepton mass in direct electroweak pair production of mass-degenerate left- and right-handed sleptons (selectrons and smuons), see their Figure 14.
- 15** AAD 20AL searched in 139 fb⁻¹ of pp collisions at $\sqrt{s} = 13$ TeV for events with 8 or more jets and moderate missing transverse momentum. The selection makes requirements according to the number of b -tagged jets and the scalar sum of masses of large-radius jets. No significant excess above the Standard Model expectations is observed. Limits up to about 2 TeV are set on the gluino mass in Tglu1E simplified model. Limits up to about 1.8 TeV are set on the gluino mass in Tglu3A simplified model. See their Fig. 10(a).
- 16** AAD 20v searched in 139 fb⁻¹ of pp collisions at $\sqrt{s} = 13$ TeV in final states with same-sign charged leptons (electrons or muons) and jets. No significant excess over the Standard Model expectation is observed. In the Tglu1E model, considering off-shell intermediate W and Z bosons in the decay chains, gluino masses are excluded at 95% C.L. up to 1600 GeV for neutralino masses of 100 GeV or above (up to 1000 GeV). See their Fig. 7(a).
- 17** SIRUNYAN 20b searched in 35.9 fb⁻¹ of pp collisions at $\sqrt{s} = 13$ TeV for events with at least one photon and large \cancel{E}_T . No significant excess above the Standard Model expectations is observed. Limits are set on chargino masses in a general gauge-mediated SUSY breaking (GGM) scenario Tchi1n12-GGM, see Figure 4. Limits are also set on the NLSP mass in the Tchi1chi1F and Tchi1chi1G simplified models, see their Figure 5. Finally, limits are set on the gluino mass in the Tglu4A simplified model, see Figure 6.
- 18** SIRUNYAN 20Bj searched in 137 fb⁻¹ of pp collisions at $\sqrt{s} = 13$ TeV for events containing two hadronically decaying, highly energetic Z bosons and large \cancel{E}_T . No significant excess above the Standard Model expectations is observed. Limits are set on the gluino mass in the Tglu1H simplified model, see their Figure 9.
- 19** SIRUNYAN 20E searched in 137 fb⁻¹ of pp collisions at $\sqrt{s} = 13$ TeV for events with a single electron or muon and multiple jets, including at least one identified as originating from a b -quark, and large \cancel{E}_T . No significant excess above the Standard Model expectations is observed. Limits are set on the gluino mass in the Tglu3A simplified model, see their Fig. 10, and the Tglu3C simplified model, see their Fig. 11.
- 20** SIRUNYAN 20r searched in 137 fb⁻¹ of pp collisions at $\sqrt{s} = 13$ TeV for events with at least two jets, and two isolated same-sign or three or more charged leptons (electrons or muons). No significant excess above the Standard Model expectations is observed. Limits are set on the gluino mass in the Tglu3A, Tglu3B, Tglu3C and Tglu3D simplified models, see their Figure 7, and in the Tglu1C and Tglu1B simplified models, see their Figures 8 and 9. Limits are also set on the sbottom mass in the Tstop2 simplified model, see their Figure 10, and on the stop mass in the Tstop7 simplified model, see their Figure 11. Finally, limits are set on the gluino mass in RPV simplified models where the gluino decays either via $\tilde{g} \rightarrow qq\tilde{q}\tilde{q} + e/\mu/\tau$ or via $\tilde{g} \rightarrow tbs$, see Figure 12.
- 21** AABOU 19i searched in 36.1 fb⁻¹ of pp collisions at $\sqrt{s} = 13$ TeV in final states with hadronic jets, 1 or two hadronically decaying τ and \cancel{E}_T . In Tglu1F, gluino masses are excluded at 95% C.L. up to 2000 GeV for neutralino masses of 100 GeV or below. Neutralino masses up to 1000 GeV are excluded for all gluino masses below 1400 GeV. See their Fig. 9. Limits are also presented in the context of Gauge-Mediated Symmetry Breaking models: in this case, values of A below 110 TeV are excluded at the 95% CL for all values of $\tan\beta$ in the range $2 < \tan\beta < 60$, see their Fig. 10.
- 22** SIRUNYAN 19AG searched in 35.9 fb⁻¹ of pp collisions at $\sqrt{s} = 13$ TeV for events with two photons and large \cancel{E}_T . No significant excess above the Standard Model expectations is observed. Limits are set on the gluino mass in the Tglu4B simplified model and on the squark mass in the Tsqk4B simplified model, see their Figure 13.
- 23** SIRUNYAN 19AU searched in 35.9 fb⁻¹ of pp collisions at $\sqrt{s} = 13$ TeV for events with at least one photon, jets, some of which are identified as originating from b -quarks, and large \cancel{E}_T . No significant excess above the Standard Model expectations is observed. In the framework of GMSB, limits are set on the gluino mass in the Tglu4C, Tglu4D and Tglu4E simplified models, and on the top squark mass in the Tstop13 simplified model, see their Figure 5.
- 24** SIRUNYAN 19CE searched in 35.9 fb⁻¹ of pp collisions at $\sqrt{s} = 13$ TeV for new particles decaying to a photon and two gluons in events with at least three large-radius jets of which two have substructure and are composed of a photon and two gluons. No statistically significant excess is observed above the SM background expectation. Upper limits at 95% confidence level on the cross section for gluino pair production are set, using a simplified Tglu1A-like stealth SUSY model. Gluino masses up to 1500-1700 GeV are excluded, depending on the neutralino mass, with the highest exclusion set for $m_{\tilde{\chi}_1^0} = 200$ GeV. See their Fig. 4.
- 25** SIRUNYAN 19CH searched in 137 fb⁻¹ of pp collisions at $\sqrt{s} = 13$ TeV for events containing multiple jets and large \cancel{E}_T . No significant excess above the Standard Model expectations is observed. Limits are set on the gluino mass in the Tglu1A, Tglu1C, Tglu2A and Tglu3A simplified models, see their Figure 13. Limits are also set on squark, sbottom and stop masses in the Tsqk1, Tstop1, Tstop1 simplified models, see their Figure 14.
- 26** SIRUNYAN 19k searched in 35.9 fb⁻¹ of pp collisions at $\sqrt{s} = 13$ TeV for events with a photon, an electron or muon, and large \cancel{E}_T . No significant excess above the Standard Model expectations is observed. In the framework of GMSB, limits are set on the chargino and neutralino mass in the Tchi1n1A simplified model, see their Figure 6. Limits are also set on the gluino mass in the Tglu4A simplified model, and on the squark mass in the Tsqk4A simplified model, see their Figure 7.
- 27** SIRUNYAN 19s searched in 35.9 fb⁻¹ of pp collisions at $\sqrt{s} = 13$ TeV for events with zero or one charged leptons, jets and \cancel{E}_T . The razor variables (M_P and R^2) are used to categorize the events. No significant excess above the Standard Model expectations is observed. Limits are set on the gluino mass in the Tglu3A and Tglu3C simplified models, see Figures 22 and 23, and on the stop mass in the Tstop1 simplified model, see their Figure 24.
- 28** AABOU 18AR searched in 36.1 fb⁻¹ of pp collisions at $\sqrt{s} = 13$ TeV for gluino pair production in events containing large missing transverse momentum and several energetic jets, at least three of which must be identified as originating from b -quarks. No excess is found above the predicted background. In Tglu3A models, gluino masses of less than 1.97 TeV are excluded for $m_{\tilde{\chi}_1^0}$ below 300 GeV, see their Fig. 10(a). Interpretations are also provided for scenarios where Tglu3A modes mix with Tglu2A and Tglu3D, see their Fig. 11.
- 29** AABOU 18AR searched in 36.1 fb⁻¹ of pp collisions at $\sqrt{s} = 13$ TeV for gluino pair production in events containing large missing transverse momentum and several energetic jets, at least three of which must be identified as originating from b -quarks. No excess is found above the predicted background. In Tglu2A models, gluino masses of less than 1.92 TeV are excluded for $m_{\tilde{\chi}_1^0}$ below 600 GeV, see their Fig. 10(b). Interpretations are also provided for scenarios where Tglu2A modes mix with Tglu3A and Tglu3D, see their Fig. 11.
- 30** AABOU 18AS searched for in 36.1 fb⁻¹ of pp collisions at $\sqrt{s} = 13$ TeV for gluino pair production in the context of AMSB or phenomenological MSSM scenarios with wino-like LSP and long-lived charginos. Events with a disappearing track due to a low-momentum pion accompanied by at least four jets are considered. No significant excess above the Standard Model expectations is observed. Exclusion limits are set at 95% confidence level on the mass of gluinos for different chargino lifetimes. Gluino masses up to 1.65 TeV are excluded assuming a chargino mass of 460 GeV and lifetime of 0.2 ns, corresponding to a mass-splitting between the charged and neutral wino of around 160 MeV. See their Fig. 9.
- 31** AABOU 18Bj searched in 36.1 fb⁻¹ of pp collisions at $\sqrt{s} = 13$ TeV in events with two opposite-sign charged leptons (electrons and muons), jets and missing transverse momentum, with various requirements to be sensitive to signals with different kinematic endpoint values in the dilepton invariant mass distribution. The data are found to be consistent with the SM expectation. Results are interpreted in the Tglu1G model: gluino masses below 1850 GeV are excluded for $m_{\tilde{\chi}_1^0} = 100$ GeV, see their Fig. 12(a).

- ³² AABOUD 18BJ searched in 36.1 fb^{-1} of pp collisions at $\sqrt{s} = 13 \text{ TeV}$ in events with two opposite-sign charged leptons (electrons and muons), jets and missing transverse momentum, with various requirements to be sensitive to signals with different kinematic endpoint values in the dilepton invariant mass distribution. The data are found to be consistent with the SM expectation. Results are interpreted in the Tglu1H model: gluino masses below 1650 GeV are excluded for $m_{\tilde{\chi}_1^0} = 100 \text{ GeV}$, see their Fig. 13(a).
- ³³ AABOUD 18U searched in 36.1 fb^{-1} of pp collisions at $\sqrt{s} = 13 \text{ TeV}$ in events with at least one isolated photon, possibly jets and significant transverse momentum targeting generalised models of gauge-mediated SUSY breaking. No significant excess of events is observed above the SM prediction. Results for the di-photon channel are interpreted in terms of lower limits on the masses of gluinos in GGM higgsino-bino models (mix of Tglu4B and Tglu4C), which reach as high as 2050 GeV. Gluino masses below 1600 GeV are excluded for any NLSP mass provided that $m_{\tilde{g}} - m_{\tilde{\chi}_1^0} > 50 \text{ GeV}$. See their Fig. 11.
- ³⁴ AABOUD 18U searched in 36.1 fb^{-1} of pp collisions at $\sqrt{s} = 13 \text{ TeV}$ in events with at least one isolated photon, possibly jets and significant transverse momentum targeting generalised models of gauge-mediated SUSY breaking. No significant excess of events is observed above the SM prediction. Results of the $\gamma + \text{jets} + \cancel{E}_T$ channel are interpreted in terms of lower limits on the masses of gluinos in GGM higgsino-bino models (mix of Tglu4B and Tglu4C), which reach as high as 2050 GeV. Gluino masses below 1600 GeV are excluded for any NLSP mass provided that $m_{\tilde{g}} - m_{\tilde{\chi}_1^0} > 50 \text{ GeV}$. See their Fig. 11.
- ³⁵ AABOUD 18V searched in 36.1 fb^{-1} of pp collisions at $\sqrt{s} = 13 \text{ TeV}$ in events with no charged leptons, jets and missing transverse momentum. The data are found to be consistent with the SM expectation. Results are interpreted in the Tglu1A model: gluino masses below 2030 GeV are excluded for massless LSP, see their Fig. 13(b).
- ³⁶ AABOUD 18V searched in 36.1 fb^{-1} of pp collisions at $\sqrt{s} = 13 \text{ TeV}$ in events with no charged leptons, jets and missing transverse momentum. The data are found to be consistent with the SM expectation. Results are interpreted in the Tglu1B model. Assuming that $m_{\tilde{\chi}_1^\pm} = 0.5 (m_{\tilde{g}} + m_{\tilde{\chi}_1^0})$, gluino masses below 1980 GeV are excluded for massless LSP, see their Fig. 14(c). Exclusions are also shown assuming $m_{\tilde{\chi}_1^0} = 60 \text{ GeV}$, see their Fig. 14(d).
- ³⁷ AABOUD 18V searched in 36.1 fb^{-1} of pp collisions at $\sqrt{s} = 13 \text{ TeV}$ in events with no charged leptons, jets and missing transverse momentum. The data are found to be consistent with the SM expectation. Results are interpreted in the Tglu1E model: gluino masses below 1750 GeV are excluded for $m_{\tilde{\chi}_1^0} = 1 \text{ GeV}$ and any $m_{\tilde{\chi}_2^0}$ above 100 GeV, see their Fig. 15. Gluino mass exclusion up to 2 TeV is found for $m_{\tilde{\chi}_2^0} = 1 \text{ TeV}$.
- ³⁸ SIRUNYAN 18AA searched in 35.9 fb^{-1} of pp collisions at $\sqrt{s} = 13 \text{ TeV}$ for events with at least one photon and large \cancel{E}_T . No significant excess above the Standard Model expectations is observed. Limits are set on wino masses in a general gauge-mediated SUSY breaking (GGM) scenario with bino-like $\tilde{\chi}_1^0$ and wino-like $\tilde{\chi}_1^\pm$ and $\tilde{\chi}_2^0$, see Figure 7. Limits are also set on the NLSP mass in the Tchl1n1A and Tchl1ch1A simplified models, see their Figure 8. Finally, limits are set on the gluino mass in the Tglu4A and Tglu4B simplified models, see their Figure 9, and on the squark mass in the Tsq4kA and Tsq4kB simplified models, see their Figure 10.
- ³⁹ SIRUNYAN 18AC searched in 35.9 fb^{-1} of pp collisions at $\sqrt{s} = 13 \text{ TeV}$ for events with a single electron or muon and multiple jets. No significant excess above the Standard Model expectations is observed. Limits are set on the gluino mass in the Tglu3A and Tglu1B simplified models, see their Figure 5.
- ⁴⁰ SIRUNYAN 18AL searched in 35.9 fb^{-1} of pp collisions at $\sqrt{s} = 13 \text{ TeV}$ for events with at least three charged leptons, in any combination of electrons and muons, jets and significant \cancel{E}_T . No significant excess above the Standard Model expectations is observed. Limits are set on the gluino mass in the Tglu3A and Tglu1C simplified models, see their Figure 5. Limits are also set on the sbottom mass in the Tsb02 simplified model, see their Figure 6, and on the stop mass in the Tstop7 simplified model, see their Figure 7.
- ⁴¹ SIRUNYAN 18AR searched in 35.9 fb^{-1} of pp collisions at $\sqrt{s} = 13 \text{ TeV}$ for events containing two opposite-charge, same-flavour leptons (electrons or muons), jets and \cancel{E}_T . No significant excess above the Standard Model expectations is observed. Limits are set on the gluino mass in the Tglu4C simplified model, see their Figure 7. Limits are also set on the chargino/neutralino mass in the Tchl1n2F simplified models, see their Figure 8, and on the higgsino mass in the Tn1n1B and Tn1n1C simplified models, see their Figure 9. Finally, limits are set on the sbottom mass in the Tsb03 simplified model, see their Figure 10.
- ⁴² SIRUNYAN 18AY searched in 35.9 fb^{-1} of pp collisions at $\sqrt{s} = 13 \text{ TeV}$ for events containing one or more jets and significant \cancel{E}_T . No significant excess above the Standard Model expectations is observed. Limits are set on the gluino mass in the Tglu1A, Tglu2A and Tglu3A simplified models, see their Figure 3. Limits are also set on squark, sbottom and stop masses in the Tsqk1, Tsb01, Tstop1 and Tstop4 simplified models, see their Figure 3. Finally, limits are set on long-lived gluino masses in a Tglu1A simplified model where the gluino is metastable or long-lived with proper decay lengths in the range $10^{-3} \text{ mm} < c\tau < 10^5 \text{ mm}$, see their Figure 4.
- ⁴³ SIRUNYAN 18D searched in 35.9 fb^{-1} of pp collisions at $\sqrt{s} = 13 \text{ TeV}$ for events containing identified hadronically decaying top quarks, no leptons, and \cancel{E}_T . No significant excess above the Standard Model expectations is observed. Limits are set on the stop mass in the Tstop1 simplified model, see their Figure 8, and on the gluino mass in the Tglu3A, Tglu3B, Tglu3C and Tglu3E simplified models, see their Figure 9.
- ⁴⁴ SIRUNYAN 18M searched in 35.9 fb^{-1} of pp collisions at $\sqrt{s} = 13 \text{ TeV}$ for events with one or more high-momentum Higgs bosons, decaying to pairs of b -quarks, and large \cancel{E}_T . No significant excess above the Standard Model expectations is observed. Limits are set on the gluino mass in the Tglu1I and Tglu1J simplified models, see their Figure 3.
- ⁴⁵ AABOUD 17AJ searched in 36.1 fb^{-1} of pp collisions at $\sqrt{s} = 13 \text{ TeV}$ for events with two same-sign or three leptons, jets and large missing transverse momentum. No significant excess above the Standard Model expectations is observed. Limits up to 1.75 TeV are set on the gluino mass in Tglu3A simplified models in case of off-shell top squarks and for $m_{\tilde{\chi}_1^0} = 100 \text{ GeV}$. See their Figure 4(a).
- ⁴⁶ AABOUD 17AJ searched in 36.1 fb^{-1} of pp collisions at $\sqrt{s} = 13 \text{ TeV}$ for events with two same-sign or three leptons, jets and large missing transverse momentum. No significant excess above the Standard Model expectations is observed. Limits up to 1.57 TeV are set on the gluino mass in Tglu1E simplified models (2-step models) for $m_{\tilde{\chi}_1^0} = 100 \text{ GeV}$. See their Figure 4(b).
- ⁴⁷ AABOUD 17AJ searched in 36.1 fb^{-1} of pp collisions at $\sqrt{s} = 13 \text{ TeV}$ for events with two same-sign or three leptons, jets and large missing transverse momentum. No significant excess above the Standard Model expectations is observed. Limits up to 1.86 TeV are set on the gluino mass in Tglu1G simplified models for $m_{\tilde{\chi}_1^0} = 200 \text{ GeV}$. See their Figure 4(c).
- ⁴⁸ AABOUD 17AR searched in 36.1 fb^{-1} of pp collisions at $\sqrt{s} = 13 \text{ TeV}$ for events with one isolated lepton, at least two jets and large missing transverse momentum. No significant excess above the Standard Model expectations is observed. Limits up to 2.1 TeV are set on the gluino mass in Tglu1B simplified models, with $x = (m_{\tilde{\chi}_1^\pm} - m_{\tilde{\chi}_1^0}) / (m_{\tilde{g}} - m_{\tilde{\chi}_1^0}) = 1/2$. Similar limits are obtained for variable x and fixed neutralino mass, $m_{\tilde{\chi}_1^0} = 60 \text{ GeV}$. See their Figure 13.
- ⁴⁹ AABOUD 17AR searched in 36.1 fb^{-1} of pp collisions at $\sqrt{s} = 13 \text{ TeV}$ for events with one isolated lepton, at least two jets and large missing transverse momentum. No significant excess above the Standard Model expectations is observed. Limits up to 1.74 TeV are set on the gluino mass in Tglu1E simplified model. Limits up to 1.7 TeV are also set on pMSSM models leading to similar signal event topologies. See their Figure 13.
- ⁵⁰ AABOUD 17AY searched in 36.1 fb^{-1} of pp collisions at $\sqrt{s} = 13 \text{ TeV}$ for events with at least four jets and large missing transverse momentum. No significant excess above the Standard Model expectations is observed. Limits up to 1.8 TeV are set on the gluino mass in Tglu3A simplified models assuming $m_{\tilde{t}_1} - m_{\tilde{\chi}_1^0} = 5 \text{ GeV}$. See their Figure 13.
- ⁵¹ AABOUD 17AZ searched in 36.1 fb^{-1} of pp collisions at $\sqrt{s} = 13 \text{ TeV}$ for events with at least seven jets and large missing transverse momentum. Selected events are further classified based on the presence of large R -jets or b -jets and no leptons. No significant excess above the Standard Model expectations is observed. Limits up to 1.8 TeV are set on the gluino mass in Tglu1E simplified models. See their Figure 6b.
- ⁵² AABOUD 17AZ searched in 36.1 fb^{-1} of pp collisions at $\sqrt{s} = 13 \text{ TeV}$ for events with at least seven jets and large missing transverse momentum. Selected events are further classified based on the presence of large R -jets or b -jets and no leptons. No significant excess above the Standard Model expectations is observed. Limits up to 1.54 TeV are set on the gluino mass in Tglu3A simplified models. See their Figure 7a.
- ⁵³ AABOUD 17N searched in 14.7 fb^{-1} of pp collisions at $\sqrt{s} = 13 \text{ TeV}$ in final states with 2 same-flavor, opposite-sign leptons (electrons or muons), jets and large missing transverse momentum. In Tglu1J models, gluino masses are excluded at 95% C.L. up to 1300 GeV for $m_{\tilde{\chi}_1^0} = 0 \text{ GeV}$ and $m_{\tilde{\chi}_2^0} = 1100 \text{ GeV}$. See their Fig. 12 for exclusion limits as a function of $m_{\tilde{\chi}_2^0}$. Limits are also presented assuming $m_{\tilde{\chi}_2^0} = m_{\tilde{\chi}_1^0} + 100 \text{ GeV}$, see their Fig. 13.
- ⁵⁴ AABOUD 17N searched in 14.7 fb^{-1} of pp collisions at $\sqrt{s} = 13 \text{ TeV}$ in final states with 2 same-flavor, opposite-sign leptons (electrons or muons), jets and large missing transverse momentum. In Tglu1H models, gluino masses are excluded at 95% C.L. up to 1310 GeV for $m_{\tilde{\chi}_1^0} < 400 \text{ GeV}$ and assuming $m_{\tilde{\chi}_2^0} = (m_{\tilde{g}} + m_{\tilde{\chi}_1^0})/2$. See their Fig. 15.
- ⁵⁵ AABOUD 17N searched in 14.7 fb^{-1} of pp collisions at $\sqrt{s} = 13 \text{ TeV}$ in final states with 2 same-flavor, opposite-sign leptons (electrons or muons), jets and large missing transverse momentum. In Tglu1G models, gluino masses are excluded at 95% C.L. up to 1700 GeV for small $m_{\tilde{\chi}_1^0}$. The results probe kinematic endpoints as small as $m_{\tilde{\chi}_2^0} - m_{\tilde{\chi}_1^0} = (m_{\tilde{g}} - m_{\tilde{\chi}_1^0})/2 = 50 \text{ GeV}$. See their Fig. 14.
- ⁵⁶ KHACHATRYAN 17 searched in 2.3 fb^{-1} of pp collisions at $\sqrt{s} = 13 \text{ TeV}$ for events containing four or more jets, no more than one lepton, and missing transverse momentum, using the razor variables (M_R and R^2) to discriminate between signal and background processes. No evidence for an excess over the expected background is observed. Limits are derived on the gluino mass in the Tglu1A, Tglu2A and Tglu3A simplified models, see Figs. 16 and 17. Also, assuming gluinos decay only via three-body processes involving third-generation quarks plus a neutralino/chargino, and assuming $m_{\tilde{\chi}_1^\pm} = m_{\tilde{\chi}_1^0} + 5 \text{ GeV}$, a branching ratio-independent limit on the gluino mass is given, see Fig. 16.
- ⁵⁷ KHACHATRYAN 17AD searched in 2.3 fb^{-1} of pp collisions at $\sqrt{s} = 13 \text{ TeV}$ for events containing at least four jets (including b -jets), missing transverse momentum and tagged top quarks. No evidence for an excess over the expected background is observed. Gluino masses up to 1550 GeV and neutralino masses up to 900 GeV are excluded at 95% C.L. See Fig. 13.
- ⁵⁸ KHACHATRYAN 17AD searched in 2.3 fb^{-1} of pp collisions at $\sqrt{s} = 13 \text{ TeV}$ for events containing at least four jets (including b -jets), missing transverse momentum and tagged top quarks. No evidence for an excess over the expected background is observed. Gluino masses up to 1450 GeV and neutralino masses up to 820 GeV are excluded at 95% C.L. See Fig. 13.
- ⁵⁹ KHACHATRYAN 17AS searched in 2.3 fb^{-1} of pp collisions at $\sqrt{s} = 13 \text{ TeV}$ for events with a single electron or muon and multiple jets. No significant excess above the Standard Model expectations is observed. Limits are set on the gluino mass in the Tglu3A and Tglu1B simplified models, see their Fig. 7.
- ⁶⁰ KHACHATRYAN 17AW searched in 2.3 fb^{-1} of pp collisions at $\sqrt{s} = 13 \text{ TeV}$ for events with at least three charged leptons, in any combination of electrons and muons, and significant \cancel{E}_T . No significant excess above the Standard Model expectations is observed. Limits are set on the gluino mass in the Tglu3A and Tglu1C simplified models, and on the sbottom mass in the Tsb02 simplified model, see their Figure 4.
- ⁶¹ KHACHATRYAN 17P searched in 2.3 fb^{-1} of pp collisions at $\sqrt{s} = 13 \text{ TeV}$ for events with one or more jets and large \cancel{E}_T . No significant excess above the Standard Model expectations is observed. Limits are set on the gluino mass in the Tglu1A, Tglu2A, Tglu3A, Tglu3B, Tglu3C and Tglu3D simplified models, see their Figures 7 and 8. Limits are also set on the squark mass in the Tsqk1 simplified model, see their Fig. 7, and on the sbottom mass in the Tsb01 simplified model, see Fig. 8. Finally, limits are set on the stop mass in the Tstop1, Tstop3, Tstop4, Tstop6 and Tstop7 simplified models, see Fig. 8.
- ⁶² KHACHATRYAN 17V searched in 2.3 fb^{-1} of pp collisions at $\sqrt{s} = 13 \text{ TeV}$ for events with two photons and large \cancel{E}_T . No significant excess above the Standard Model expectations is observed. Limits are set on the gluino and squark mass in the context of general gauge mediation models Tglu4B and Tsq4k, see their Fig. 4.
- ⁶³ SIRUNYAN 17AF searched in 35.9 fb^{-1} of pp collisions at $\sqrt{s} = 13 \text{ TeV}$ for events with a single lepton (electron or muon), jets, including at least one jet originating from a b -quark, and large \cancel{E}_T . No significant excess above the Standard Model expectations is observed. Limits are set on the gluino mass in the Tglu3A and Tglu3B simplified models, see their Figure 2.
- ⁶⁴ SIRUNYAN 17AY searched in 35.9 fb^{-1} of pp collisions at $\sqrt{s} = 13 \text{ TeV}$ for events with at least one photon, jets and large \cancel{E}_T . No significant excess above the Standard Model expectations is observed. Limits are set on the gluino mass in the Tglu4A and Tglu4B

Searches Particle Listings

Supersymmetric Particle Searches

- simplified models, and on the squark mass in the Tskq4A and Tskq4B simplified models, see their Figure 6.
- 65 SIRUNYAN 17AZ searched in 35.9 fb^{-1} of pp collisions at $\sqrt{s} = 13 \text{ TeV}$ for events with one or more jets and large \cancel{E}_T . No significant excess above the Standard Model expectations is observed. Limits are set on the gluino mass in the Tglu1A, Tglu2A, Tglu3A simplified models, see their Figures 6. Limits are also set on the squark mass in the Tskq1 simplified model (for single light squark and for 8 degenerate light squarks), on the sbottom mass in the Tsb01 simplified model and on the stop mass in the Tstop1 simplified model, see their Fig. 7. Finally, limits are set on the stop mass in the Tstop2, Tstop4 and Tstop8 simplified models, see Fig. 8.
- 66 SIRUNYAN 17P searched in 35.9 fb^{-1} of pp collisions at $\sqrt{s} = 13 \text{ TeV}$ for events with multiple jets and large \cancel{E}_T . No significant excess above the Standard Model expectations is observed. Limits are set on the gluino mass in the Tglu1A, Tglu1C, Tglu2A, Tglu3A and Tglu3D simplified models, see their Fig. 12. Limits are also set on the squark mass in the Tskq1 simplified model, on the stop mass in the Tstop1 simplified model, and on the sbottom mass in the Tsb01 simplified model, see Fig. 13.
- 67 SIRUNYAN 17S searched in 35.9 fb^{-1} of pp collisions at $\sqrt{s} = 13 \text{ TeV}$ for events with two isolated same-sign leptons, jets, and large \cancel{E}_T . No significant excess above the Standard Model expectations is observed. Limits are set on the mass of the gluino mass in the Tglu3A, Tglu3B, Tglu3C, Tglu3D and Tglu1B simplified models, see their Figures 5 and 6, and on the sbottom mass in the Tsb02 simplified model, see their Figure 6.
- 68 AABOUD 16AC searched in 3.2 fb^{-1} of pp collisions at $\sqrt{s} = 13 \text{ TeV}$ in final states with hadronic jets, 1 or two hadronically decaying τ and \cancel{E}_T . In Tglu1F, gluino masses are excluded at 95% C.L. up to 1570 GeV for neutralino masses of 100 GeV or below. Neutralino masses up to 700 GeV are excluded for all gluino masses between 800 GeV and 1500 GeV, while the strongest neutralino-mass exclusion of 750 GeV is achieved for gluino masses around 1400 GeV. See their Fig. 8. Limits are also presented in the context of Gauge-Mediated Symmetry Breaking models: in this case, values of A below 92 TeV are excluded at the 95% C.L. corresponding to gluino masses below 2000 GeV. See their Fig. 9.
- 69 AABOUD 16J searched in 3.2 fb^{-1} of pp collisions at $\sqrt{s} = 13 \text{ TeV}$ in final states with one isolated electron or muon, hadronic jets, and \cancel{E}_T . Gluino-mediated pair production of stops with a nearly mass-degenerate stop and neutralino are targeted and gluino masses are excluded at 95% C.L. up to 1460 GeV. A 100% of stops decaying via $\chi_{\tilde{t}_1}^{\pm}$ + neutralino is assumed. The results are also valid in case of 4-body decays $\tilde{t}_1 \rightarrow f f' b \tilde{\chi}_{\tilde{t}_1}^0$. See their Fig. 8.
- 70 AABOUD 16M searched in 3.2 fb^{-1} of pp collisions at $\sqrt{s} = 13 \text{ TeV}$ for events with two photons, hadronic jets and \cancel{E}_T . No significant excess above the Standard Model expectations is observed. Exclusion limits at 95% C.L. are set on gluino masses in the general gauge-mediated SUSY breaking model (GGM), for bino-like NLSP. See their Fig. 3.
- 71 AABOUD 16N searched in 3.2 fb^{-1} of pp collisions at $\sqrt{s} = 13 \text{ TeV}$ for events containing hadronic jets, large \cancel{E}_T , and no electrons or muons. No significant excess above the Standard Model expectations is observed. Gluino masses below 1510 GeV are excluded at the 95% C.L. in a simplified model with only gluinos and the lightest neutralino. See their Fig. 7b.
- 72 AABOUD 16N searched in 3.2 fb^{-1} of pp collisions at $\sqrt{s} = 13 \text{ TeV}$ for events containing hadronic jets, large \cancel{E}_T , and no electrons or muons. No significant excess above the Standard Model expectations is observed. Gluino masses below 1500 GeV are excluded at the 95% C.L. in a simplified model with gluinos decaying via an intermediate $\tilde{\chi}_{\tilde{t}_1}^{\pm}$ to two quarks, a W boson and a $\tilde{\chi}_{\tilde{t}_1}^0$ for $m_{\tilde{\chi}_{\tilde{t}_1}^0} = 200 \text{ GeV}$. See their Fig. 8.
- 73 AAD 16AD searched in 3.2 fb^{-1} of pp collisions at $\sqrt{s} = 13 \text{ TeV}$ for events containing several energetic jets, of which at least three must be identified as b -jets, large \cancel{E}_T and no electrons or muons. No significant excess above the Standard Model expectations is observed. For $\tilde{\chi}_{\tilde{t}_1}^0$ below 800 GeV, gluino masses below 1780 GeV are excluded at 95% C.L. for gluinos decaying via bottom squarks. See their Fig. 7a.
- 74 AAD 16AD searched in 3.2 fb^{-1} of pp collisions at $\sqrt{s} = 13 \text{ TeV}$ for events containing several energetic jets, of which at least three must be identified as b -jets, large \cancel{E}_T and one electron or muon. Large-radius jets with a high mass are also used to identify highly boosted top quarks. No significant excess above the Standard Model expectations is observed. For $\tilde{\chi}_{\tilde{t}_1}^0$ below 700 GeV, gluino masses below 1760 GeV are excluded at 95% C.L. for gluinos decaying via top squarks. See their Fig. 7b.
- 75 AAD 16BB searched in 3.2 fb^{-1} of pp collisions at $\sqrt{s} = 13 \text{ TeV}$ for events with exactly two same-sign leptons or at least three leptons, multiple hadronic jets, b -jets, and \cancel{E}_T . No significant excess over the Standard Model expectation is found. Exclusion limits at 95% C.L. are set on the gluino mass in various simplified models (Tglu1D, Tglu1E, Tglu3A). See their Figs. 4.a, 4.b, and 4.d.
- 76 AAD 16BG searched in 3.2 fb^{-1} of pp collisions at $\sqrt{s} = 13 \text{ TeV}$ in final states with one isolated electron or muon, hadronic jets, and \cancel{E}_T . The data agree with the SM background expectation in the six signal selections defined in the search, and the largest deviation is a 2.1 standard deviation excess. Gluinos are excluded at 95% C.L. up to 1600 GeV assuming they decay via the lightest chargino to the lightest neutralino as in the model Tglu1B for $m_{\tilde{\chi}_{\tilde{t}_1}^0} = 100 \text{ GeV}$, assuming $m_{\tilde{\chi}_{\tilde{t}_1}^{\pm}} = (m_{\tilde{g}} + m_{\tilde{\chi}_{\tilde{t}_1}^0})/2$. See their Fig. 6.
- 77 AAD 16V searched in 3.2 fb^{-1} of pp collisions at $\sqrt{s} = 13 \text{ TeV}$ for events with \cancel{E}_T various hadronic jet multiplicities from ≥ 7 to ≥ 10 and with various b -jet multiplicity requirements. No significant excess over the Standard Model expectation is found. Exclusion limits at 95% C.L. are set on the gluino mass in one simplified model (Tglu1E) and a pMSSM-inspired model. See their Fig. 5.
- 78 KHACHATRYAN 16AM searched in 19.7 fb^{-1} of pp collisions at $\sqrt{s} = 8 \text{ TeV}$ for events with highly boosted W -bosons and b -jets, using the razor variables (M_R and R^2) to discriminate between signal and background processes. No significant excess above the Standard Model expectations is observed. Limits are set on the gluino mass in the Tglu3C and Tglu3B simplified models, see Fig. 12.
- 79 KHACHATRYAN 16BJ searched in 2.3 fb^{-1} of pp collisions at $\sqrt{s} = 13 \text{ TeV}$ for events with two isolated same-sign dileptons and jets in the final state. No significant excess above the Standard Model expectations is observed. Limits are set on the gluino mass in the following simplified models: Tglu3A and Tglu3D, see Fig. 4, Tglu3B and Tglu3C, see Fig. 5, and Tglu1B, see Fig. 7.
- 80 KHACHATRYAN 16BS searched in 2.3 fb^{-1} of pp collisions at $\sqrt{s} = 13 \text{ TeV}$ for events with at least one energetic jet, no isolated leptons, and significant \cancel{E}_T , using the transverse mass variable M_{T2} to discriminate between signal and background processes. No significant excess above the Standard Model expectations is observed. Limits are set on the gluino mass in the Tglu1A, Tglu2A and Tglu3A simplified models, see Fig. 10 and Table 3.
- 81 KHACHATRYAN 16BY searched in 2.3 fb^{-1} of pp collisions at $\sqrt{s} = 13 \text{ TeV}$ for events with two opposite-sign, same-flavour leptons, jets, and missing transverse momentum. No significant excess above the Standard Model expectations is observed. Limits are set on the gluino mass in the Tglu4C simplified model, see Fig. 4, and on sbottom masses in the Tsb03 simplified model, see Fig. 5.
- 82 KHACHATRYAN 16V searched in 2.3 fb^{-1} of pp collisions at $\sqrt{s} = 13 \text{ TeV}$ for events with at least four energetic jets and significant \cancel{E}_T , no identified isolated electron or muon or charged track. No significant excess above the Standard Model expectations is observed. Limits are set on the gluino mass in the Tglu1A, Tglu1C, Tglu2A, and Tglu3A simplified models, see Fig. 8.
- 83 AAD 15BG searched in 20.3 fb^{-1} of pp collisions at $\sqrt{s} = 8 \text{ TeV}$ for events with jets, missing E_T , and two opposite-sign same flavour isolated leptons featuring either a kinematic edge, or a peak at the Z -boson mass, in the invariant mass spectrum. No evidence for a statistically significant excess over the expected SM backgrounds are observed and 95% C.L. exclusion limits are derived in a GGM simplified model of gluino pair production where the gluino decays into quarks, a Z -boson, and a massless gravitino LSP, see Fig. 12. Also, limits are set in simplified models with slepton/sneutrino intermediate states, see Fig. 13.
- 84 AAD 15BV summarized and extended ATLAS searches for gluinos and first- and second-generation squarks in final states containing jets and missing transverse momentum, with or without leptons or b -jets in the $\sqrt{s} = 8 \text{ TeV}$ data set collected in 2012. The paper reports the results of new interpretations and statistical combinations of previously published analyses, as well as new analyses. Exclusion limits at 95% C.L. are set on the gluino mass in several R-parity conserving models, leading to a generalized constraint on gluino masses exceeding 1150 GeV for lightest supersymmetric particle masses below 100 GeV. See their Figs. 10, 19, 20, 21, 23, 25, 26, 29-37.
- 85 AAD 15BX interpreted the results of a wide range of ATLAS direct searches for supersymmetry, during the first run of the LHC using the $\sqrt{s} = 7 \text{ TeV}$ and $\sqrt{s} = 8 \text{ TeV}$ data set collected in 2012, within the wider framework of the phenomenological MSSM (pMSSM). The integrated luminosity was up to 20.3 fb^{-1} . From an initial random sampling of 500 million pMSSM points, generated from the 19-parameter pMSSM, a total of 310,327 model points with $\tilde{\chi}_{\tilde{t}_1}^0$ LSP were selected each of which satisfies constraints from previous collider searches, precision measurements, cold dark matter energy density measurements and direct dark matter searches. The impact of the ATLAS Run 1 searches on this space was presented, considering the fraction of model points surviving, after projection into two-dimensional spaces of sparticle masses. Good complementarity is observed between different ATLAS analyses, with almost all showing regions of unique sensitivity. ATLAS searches have good sensitivity at LSP mass below 800 GeV.
- 86 AAD 15CA searched in 20.3 fb^{-1} of pp collisions at $\sqrt{s} = 8 \text{ TeV}$ for events with one or more photons, hadronic jets or b -jets and \cancel{E}_T . No significant excess above the Standard Model expectations is observed. Limits are set on gluino masses in the general gauge-mediated SUSY breaking model (GGM), for bino-like or higgsino-bino admixtures NLSP, see Fig. 8, 10, 11.
- 87 KHACHATRYAN 15AF searched in 19.5 fb^{-1} of pp collisions at $\sqrt{s} = 8 \text{ TeV}$ for events with at least two energetic jets and significant \cancel{E}_T , using the transverse mass variable M_{T2} to discriminate between signal and background processes. No significant excess above the Standard Model expectations is observed. Limits are set on the gluino mass in simplified models where the decay $\tilde{g} \rightarrow q\bar{q}\tilde{\chi}_{\tilde{t}_1}^0$ takes place with a branching ratio of 100%, see Fig. 13(a), or where the decay $\tilde{g} \rightarrow b\bar{b}\tilde{\chi}_{\tilde{t}_1}^0$ takes place with a branching ratio of 100%, see Fig. 13(b), or where the decay $\tilde{g} \rightarrow t\bar{t}\tilde{\chi}_{\tilde{t}_1}^0$ takes place with a branching ratio of 100%, see Fig. 13(c). See also Table 5. Exclusions in the CMSSM, assuming $\tan\beta = 30$, $A_0 = -2 \max(m_0, m_{1/2})$ and $\mu > 0$, are also presented, see Fig. 15.
- 88 KHACHATRYAN 15I searched in 19.5 fb^{-1} of pp collisions at $\sqrt{s} = 8 \text{ TeV}$ for events in which b -jets and four W -bosons are produced. Five individual search channels are combined (fully hadronic, single lepton, same-sign dilepton, opposite-sign dilepton, multilepton). No significant excess above the Standard Model expectations is observed. Limits are set on the gluino mass in a simplified model where the decay $\tilde{g} \rightarrow t\bar{t}\tilde{\chi}_{\tilde{t}_1}^0$ takes place with a branching ratio of 100%, see Fig. 5. Also a simplified model with gluinos decaying into on-shell top squarks is considered, see Fig. 6.
- 89 KHACHATRYAN 15X searched in 19.3 fb^{-1} of pp collisions at $\sqrt{s} = 8 \text{ TeV}$ for events with at least two energetic jets, at least one of which is required to originate from a b quark, and significant \cancel{E}_T , using the razor variables (M_R and R^2) to discriminate between signal and background processes. No significant excess above the Standard Model expectations is observed. Limits are set on the gluino mass in simplified models where the decay $\tilde{g} \rightarrow b\bar{b}\tilde{\chi}_{\tilde{t}_1}^0$ and the decay $\tilde{g} \rightarrow t\bar{t}\tilde{\chi}_{\tilde{t}_1}^0$ take place with branching ratios varying between 0, 50 and 100%, see Figs. 13 and 14.
- 90 AAD 14AE searched in 20.3 fb^{-1} of pp collisions at $\sqrt{s} = 8 \text{ TeV}$ for strongly produced supersymmetric particles in events containing jets and large missing transverse momentum, and no electrons or muons. No excess over the expected SM background is observed. Exclusion limits are derived in simplified models containing gluinos and squarks, see Figures 5, 6 and 7. Limits are also derived in the mSUGRA/CMSSM with parameters $\tan\beta = 30$, $A_0 = -2 m_0$ and $\mu > 0$, see their Fig. 8.
- 91 AAD 14AG searched in 20.3 fb^{-1} of pp collisions at $\sqrt{s} = 8 \text{ TeV}$ for events containing one hadronically decaying τ -lepton, zero or one additional light leptons (electrons or muons), jets and large missing transverse momentum. No excess of events above the expected level of Standard Model background was found. Exclusion limits at 95% C.L. are set in several SUSY scenarios. For an interpretation in the minimal GMSB model, see their Fig. 8. For an interpretation in the mSUGRA/CMSSM with parameters $\tan\beta = 30$, $A_0 = -2 m_0$ and $\mu > 0$, see their Fig. 9. For an interpretation in the framework of natural Gauge Mediation, see Fig. 10. For an interpretation in the bRPV scenario, see their Fig. 11.
- 92 AAD 14X searched in 20.3 fb^{-1} of pp collisions at $\sqrt{s} = 8 \text{ TeV}$ for events with at least four leptons (electrons, muons, taus) in the final state. No significant excess above the Standard Model expectations is observed. Limits are set on the gluino mass in a general gauge-mediation model (GGM) where the decay $\tilde{g} \rightarrow q\bar{q}\tilde{\chi}_{\tilde{t}_1}^0$, with $\tilde{\chi}_{\tilde{t}_1}^0 \rightarrow \ell^{\pm}\ell^{\mp}\tilde{G}$, takes place with a branching ratio of 100%, for two choices of $\tan\beta = 1.5$ and 30, see Fig. 11. Also some constraints on the higgsino mass parameter μ are discussed.
- 93 KHACHATRYAN 14AH searched in 4.7 fb^{-1} of pp collisions at $\sqrt{s} = 7 \text{ TeV}$ for events with at least two energetic jets and significant \cancel{E}_T , using the razor variables (M_R and R^2) to discriminate between signal and background processes. No significant excess above the Standard Model expectations is observed. Limits are set on sbottom masses in simplified models where the decay $\tilde{g} \rightarrow q\bar{q}\tilde{\chi}_{\tilde{t}_1}^0$ takes place with a branching ratio of 100%, see Fig. 28. Exclusions in the CMSSM, assuming $\tan\beta = 10$, $A_0 = 0$ and $\mu > 0$, are also presented, see Fig. 26.

- 94 CHATRCHYAN 14AH searched in 4.7 fb^{-1} of pp collisions at $\sqrt{s} = 7 \text{ TeV}$ for events with at least two energetic jets and significant \cancel{E}_T , using the razor variables (M_R and R^2) to discriminate between signal and background processes. A second analysis requires at least one of the jets to be originating from a b -quark. No significant excess above the Standard Model expectations is observed. Limits are set on sbottom masses in simplified models where the decay $\tilde{g} \rightarrow b\bar{b}\tilde{\chi}_1^0$ takes place with a branching ratio of 100%, see Figs. 28 and 29. Exclusions in the CMSSM, assuming $\tan\beta = 10$, $A_0 = 0$ and $\mu > 0$, are also presented, see Fig. 26.
- 95 CHATRCHYAN 14AH searched in 4.7 fb^{-1} of pp collisions at $\sqrt{s} = 7 \text{ TeV}$ for events with at least two energetic jets and significant \cancel{E}_T , using the razor variables (M_R and R^2) to discriminate between signal and background processes. A second analysis requires at least one of the jets to be originating from a b -quark. No significant excess above the Standard Model expectations is observed. Limits are set on sbottom masses in simplified models where the decay $\tilde{g} \rightarrow t\bar{t}\tilde{\chi}_1^0$ takes place with a branching ratio of 100%, see Figs. 28 and 29. Exclusions in the CMSSM, assuming $\tan\beta = 10$, $A_0 = 0$ and $\mu > 0$, are also presented, see Fig. 26.
- 96 CHATRCHYAN 14I searched in 19.5 fb^{-1} of pp collisions at $\sqrt{s} = 8 \text{ TeV}$ for events containing multijets and large \cancel{E}_T . No excess over the expected SM background is observed. Exclusion limits are derived in simplified models containing gluinos that decay via $\tilde{g} \rightarrow q\bar{q}\tilde{\chi}_1^0$ with a 100% branching ratio, see Fig. 7b, or via $\tilde{g} \rightarrow t\bar{t}\tilde{\chi}_1^0$ with a 100% branching ratio, see Fig. 7c, or via $\tilde{g} \rightarrow q\bar{q}W/Z\tilde{\chi}_1^0$, see Fig. 7d.
- 97 CHATRCHYAN 14N searched in 19.3 fb^{-1} of pp collisions at $\sqrt{s} = 8 \text{ TeV}$ for events containing a single isolated electron or muon and multiple jets, at least two of which are identified as originating from a b -quark. No significant excesses over the expected SM backgrounds are observed. The results are interpreted in three simplified models of gluino pair production with subsequent decay into virtual or on-shell top squarks, where each of the top squarks decays in turn into a top quark and a $\tilde{\chi}_1^0$, see Fig. 4. The models differ in which masses are allowed to vary.
- 98 CHATRCHYAN 14R searched in 19.5 fb^{-1} of pp collisions at $\sqrt{s} = 8 \text{ TeV}$ for events with at least three leptons (electrons, muons, taus) in the final state. No significant excess above the Standard Model expectations is observed. Limits are set on the gluino mass in a slepton co-NLSP simplified model (GMSB) where the decay $\tilde{g} \rightarrow q\ell^\pm\ell^\mp\tilde{G}$ takes place with a branching ratio of 100%, see Fig. 8.
- 99 CHATRCHYAN 14R searched in 19.5 fb^{-1} of pp collisions at $\sqrt{s} = 8 \text{ TeV}$ for events with at least three leptons (electrons, muons, taus) in the final state. No significant excess above the Standard Model expectations is observed. Limits are set on the gluino mass in a simplified model where the decay $\tilde{g} \rightarrow t\bar{t}\tilde{\chi}_1^0$ takes place with a branching ratio of 100%, see Fig. 11.
- 100 AABOUD 18BJ searched in 36.1 fb^{-1} of pp collisions at $\sqrt{s} = 13 \text{ TeV}$ in events with two opposite-sign charged leptons (electrons and muons), jets and missing transverse momentum, with various requirements to be sensitive to signals with different kinematic endpoint values in the dilepton invariant mass distribution. The data are found to be consistent with the SM expectation. Results are interpreted in the Tglu1H model in case of $m_{\tilde{\chi}_1^0} = 1 \text{ GeV}$: for any $m_{\tilde{\chi}_2^0}$, gluino masses below 1500 GeV are excluded, see their Fig. 14(a).
- 101 AABOUD 18v searched in 36.1 fb^{-1} of pp collisions at $\sqrt{s} = 13 \text{ TeV}$ in events with no charged leptons, jets and missing transverse momentum. The data are found to be consistent with the SM expectation. Results are interpreted in a Tglu1C-like model, assuming 50% BR for each gluino decay mode. Gluino masses below 1770 GeV are excluded for any $m_{\tilde{\chi}_2^0} - m_{\tilde{\chi}_1^0}$ and $m_{\tilde{\chi}_1^0} = 60 \text{ GeV}$, see their Fig. 16(b).
- 102 AABOUD 17AZ searched in 36.1 fb^{-1} of pp collisions at $\sqrt{s} = 13 \text{ TeV}$ for events with at least seven jets and large missing transverse momentum. Selected events are further classified based on the presence of large R -jets or b -jets and no leptons. No significant excess above the Standard Model expectations is observed. Limits are set for pMSSM models with $M_1 = 60 \text{ GeV}$, $\tan(\beta) = 10$, $\mu < 0$ varying the soft-breaking parameters M_3 and μ . Gluino masses up to 1600 GeV are excluded for $m_{\tilde{\chi}_1^\pm} = 200 \text{ GeV}$. See their Figure 6a and text for details on the model.
- 103 KHACHATRYAN 16AY searched in 2.3 fb^{-1} of pp collisions at $\sqrt{s} = 13 \text{ TeV}$ for events with one isolated high transverse momentum lepton (e or μ), hadronic jets of which at least one is identified as coming from a b -quark, and large \cancel{E}_T . No significant excess above the Standard Model expectations is observed. Limits are set on the gluino mass in the Tglu3A simplified model, see Fig. 10, and in the Tglu3B model, see Fig. 11.
- 104 KHACHATRYAN 16BT performed a global Bayesian analysis of a wide range of CMS results obtained with data samples corresponding to 5.0 fb^{-1} of pp collisions at $\sqrt{s} = 7 \text{ TeV}$ and in 19.5 fb^{-1} of pp collisions at $\sqrt{s} = 8 \text{ TeV}$. The set of searches considered, both individually and in combination, includes those with all-hadronic final states, same-sign and opposite-sign dileptons, and multi-lepton final states. An interpretation was given in a scan of the 19-parameter pMSSM. No scan points with a gluino mass less than 500 GeV survived and 98% of models with a squark mass less than 300 GeV were excluded.
- 105 AAD 15AB searched for the decay of neutral, weakly interacting, long-lived particles in 20.3 fb^{-1} of pp collisions at $\sqrt{s} = 8 \text{ TeV}$. Signal events require at least two reconstructed vertices possibly originating from long-lived particles decaying to jets in the inner tracking detector and muon spectrometer. No significant excess of events over the expected background was found. Results were interpreted in Stealth SUSY benchmark models where a pair of gluinos decay to long-lived singlinos, \tilde{S} , which in turn each decay to a low-mass gravitino and a pair of jets. The 95% confidence-level limits are set on the cross section \times branching ratio for the decay $\tilde{g} \rightarrow \tilde{S}g$, as a function of the singlino proper lifetime ($c\tau$). See their Fig. 10(f).
- 106 AAD 15AI searched in 20 fb^{-1} of pp collisions at $\sqrt{s} = 8 \text{ TeV}$ for events containing at least one isolated lepton (electron or muon), jets, and large missing transverse momentum. No excess of events above the expected level of Standard Model background was found. Exclusion limits at 95% C.L. are set on the gluino mass in the CMSSM/mSUGRA, see Fig. 15, in the NUHMG, see Fig. 16, and in various simplified models, see Figs. 18–22.
- 107 AAD 15CB searched for events containing at least one long-lived particle that decays at a significant distance from its production point (displaced vertex, DV) into two leptons or into five or more charged particles in 20.3 fb^{-1} of pp collisions at $\sqrt{s} = 8 \text{ TeV}$. The dilepton signature is characterised by DV formed from at least two lepton candidates. Four different final states were considered for the multitrak signature, in which the DV must be accompanied by a high-transverse momentum muon or electron candidate that originates from the DV, jets or missing transverse momentum. No events were observed in any of the signal regions. Results were interpreted in SUSY scenarios involving R -parity violation, split supersymmetry, and gauge mediation. See their Fig. 12–20.
- 108 KHACHATRYAN 15AD searched in 19.4 fb^{-1} of pp collisions at $\sqrt{s} = 8 \text{ TeV}$ for events with two opposite-sign same flavor isolated leptons featuring either a kinematic edge, or a peak at the Z -boson mass, in the invariant mass spectrum. No evidence for a statistically significant excess over the expected SM backgrounds is observed and 95% C.L. exclusion limits are derived in a simplified model of gluino pair production where the gluino decays into quarks, a Z -boson, and a massless gravitino LSP, see Fig. 9.
- 109 KHACHATRYAN 15AZ searched in 19.7 fb^{-1} of pp collisions at $\sqrt{s} = 8 \text{ TeV}$ for events with either at least one photon, hadronic jets and \cancel{E}_T (single photon channel) or with at least two photons and at least one jet and using the razor variables. No significant excess above the Standard Model expectations is observed. Limits are set on gluino masses in the general gauge-mediated SUSY breaking model (GGM), for both a bino-like and wino-like neutralino NLSP scenario, see Fig. 8 and 9.
- 110 AAD 14AX searched in 20.1 fb^{-1} of pp collisions at $\sqrt{s} = 8 \text{ TeV}$ for the strong production of supersymmetric particles in events containing either zero or at least one high- p_T lepton, large missing transverse momentum, high jet multiplicity and at least three jets identified as originating from b -quarks. No excess over the expected SM background is observed. Limits are derived in mSUGRA/CMSSM models with $\tan\beta = 30$, $A_0 = -2m_0$ and $\mu > 0$, see their Fig. 14. Also, exclusion limits in simplified models containing gluinos and scalar top and bottom quarks are set, see their Figures 12, 13.
- 111 AAD 14E searched in 20.3 fb^{-1} of pp collisions at $\sqrt{s} = 8 \text{ TeV}$ for strongly produced supersymmetric particles in events containing jets and two same-sign leptons or three leptons. The search also utilises jets originating from b -quarks, missing transverse momentum and other variables. No excess over the expected SM background is observed. Exclusion limits are derived in simplified models containing gluinos and squarks, see Figures 5 and 6. In the $\tilde{g} \rightarrow qq'\tilde{\chi}_1^\pm, \tilde{\chi}_1^\pm \rightarrow W^{(*)}\tilde{\chi}_2^0, \tilde{\chi}_2^0 \rightarrow Z^{(*)}\tilde{\chi}_1^0$ simplified model, the following assumptions have been made: $m_{\tilde{\chi}_1^\pm} = 0.5 m_{\tilde{\chi}_2^0} + m_{\tilde{g}}$, $m_{\tilde{\chi}_2^0} = 0.5 (m_{\tilde{\chi}_1^0} + m_{\tilde{\chi}_1^\pm})$, $m_{\tilde{\chi}_1^0} < 520 \text{ GeV}$. In the $\tilde{g} \rightarrow qq'\tilde{\chi}_1^\pm, \tilde{\chi}_1^\pm \rightarrow \ell^\pm\nu\tilde{\chi}_1^0$ or $\tilde{g} \rightarrow qq'\tilde{\chi}_2^0, \tilde{\chi}_2^0 \rightarrow \ell^\pm\ell^\mp(\nu\nu)\tilde{\chi}_1^0$ simplified model, the following assumptions have been made: $m_{\tilde{\chi}_1^\pm} = m_{\tilde{\chi}_2^0} = 0.5 (m_{\tilde{\chi}_1^0} + m_{\tilde{g}})$, $m_{\tilde{\chi}_1^0} < 660 \text{ GeV}$. Limits are also derived in the mSUGRA/CMSSM, bRPV and GMSB models, see their Fig. 8.
- 112 CHATRCHYAN 14H searched in 19.5 fb^{-1} of pp collisions at $\sqrt{s} = 8 \text{ TeV}$ for events with two isolated same-sign dileptons and jets in the final state. No significant excess above the Standard Model expectations is observed. Limits are set on the gluino mass in simplified models where the decay $\tilde{g} \rightarrow t\bar{t}\tilde{\chi}_1^0$ takes place with a branching ratio of 100%, or where the decay $\tilde{g} \rightarrow \tilde{t}t, \tilde{t} \rightarrow t\tilde{\chi}_1^0$ takes place with a branching ratio of 100%, with varying mass of the $\tilde{\chi}_1^0$, or where the decay $\tilde{g} \rightarrow \tilde{b}b, \tilde{b} \rightarrow t\tilde{\chi}_1^\pm, \tilde{\chi}_1^\pm \rightarrow W^\pm\tilde{\chi}_1^0$ takes place with a branching ratio of 100%, with varying mass of the $\tilde{\chi}_1^\pm$, see Fig. 5.
- 113 CHATRCHYAN 14H searched in 19.5 fb^{-1} of pp collisions at $\sqrt{s} = 8 \text{ TeV}$ for events with two isolated same-sign dileptons and jets in the final state. No significant excess above the Standard Model expectations is observed. Limits are set on the gluino mass in simplified models where the decay $\tilde{g} \rightarrow qq'\tilde{\chi}_1^\pm, \tilde{\chi}_1^\pm \rightarrow W^\pm\tilde{\chi}_1^0$ takes place with a branching ratio of 100%, with varying mass of the $\tilde{\chi}_1^\pm$ and $\tilde{\chi}_1^0$, see Fig. 7.
- 114 CHATRCHYAN 14H searched in 19.5 fb^{-1} of pp collisions at $\sqrt{s} = 8 \text{ TeV}$ for events with two isolated same-sign dileptons and jets in the final state. No significant excess above the Standard Model expectations is observed. Limits are set on the gluino mass in simplified models where the decay $\tilde{g} \rightarrow b\bar{t}\tilde{\chi}_1^\pm, \tilde{\chi}_1^\pm \rightarrow W^\pm\tilde{\chi}_1^0$ takes place with a branching ratio of 100%, for two choices of $m_{\tilde{\chi}_1^\pm}$ and fixed $m_{\tilde{\chi}_1^0}$, see Fig. 6.

R-parity violating heavy \tilde{g} (Gluino) mass limit

VALUE (GeV)	CL%	DOCUMENT ID	TECN	COMMENT
>2200	95	1 AAD	21BF ATLS	$\ell^\pm + b$ -jets + many jets, Tglu3F, λ_{323}'' electroweakino decay, $500 \text{ GeV} < m_{\tilde{\chi}_1^0} < 1600 \text{ GeV}$
>2250	95	1 AAD	21BF ATLS	$\ell^\pm + b$ -jets + many jets, Tglu3G, λ_{323}'' electroweakino decay, $600 \text{ GeV} < m_{\tilde{\chi}_1^0} < 1600 \text{ GeV}$
>2200	95	1 AAD	21BF ATLS	$\ell^\pm + b$ -jets + many jets, Tglu3B, λ_{323}'' electroweakino decay, $600 \text{ GeV} < m_{\tilde{\chi}_1^0} < 1600 \text{ GeV}$
>1800	95	1 AAD	21BF ATLS	$\ell^\pm + b$ -jets + many jets, Tglu3B, λ_{323}'' , \tilde{t} decay, $m_{\tilde{t}} < 1200 \text{ GeV}$
>2200	95	1 AAD	21BF ATLS	$\ell^\pm + b$ -jets + many jets, Tglu1A, $\lambda', \tilde{\chi}_1^0$ decay with equal probability into e, μ, ν_e, ν_μ , $400 \text{ GeV} < m_{\tilde{\chi}_1^0} < 1700 \text{ GeV}$
>2500	95	2 AAD	21Y ATLS	$\geq 4\ell$, Tglu1A with $\tilde{\chi}_1^0 \rightarrow \ell^\pm\ell^\mp\nu, \lambda_{12k} \neq 0, m_{\tilde{\chi}_1^0}$
>1900	95	2 AAD	21Y ATLS	$\geq 2200 \text{ GeV}$, $\geq 4\ell$, Tglu1A with $\tilde{\chi}_1^0 \rightarrow \ell^\pm\ell^\mp\nu, \lambda_{j33} \neq 0, m_{\tilde{\chi}_1^0} = 1550 \text{ GeV}$
>1600	95	3 AAD	20AL ATLS	8 or more jets + \cancel{E}_T , Tglu2RPV
>1600	95	4 AAD	20V ATLS	same-sign $\ell^\pm\ell^\pm +$ jets, $\tilde{g} \rightarrow t\bar{b}$ simplified model
>2150	95	5 SIRUNYAN	20T CMS	same-sign $\ell^\pm\ell^\pm$ or $\geq 3\ell^\pm +$ jets, $\tilde{g} \rightarrow qq\bar{q}\bar{q} + e/\mu/\tau$ simplified model

Searches Particle Listings

Supersymmetric Particle Searches

>1725	95	5	SIRUNYAN	20T	CMS	same-sign $\ell^\pm \ell^\pm$ or $> 3\ell^\pm$ + jets, $\tilde{g} \rightarrow tbs$ simplified model	>1220	95	23	AAD	15BV ATLS	b -jets, $\tilde{g} \rightarrow \tilde{t}_1 t$ and $\tilde{t}_1 \rightarrow t \tilde{\chi}_1^0$, $m_{\tilde{T}_1} < 1000$ GeV
>1500	95	6	SIRUNYAN	19F	CMS	$\tilde{g} \rightarrow jjj$	>1180	95	23	AAD	15BV ATLS	b -jets, $\tilde{g} \rightarrow \tilde{t}_1 t$ and $\tilde{t}_1 \rightarrow b \tilde{\chi}_1^\pm$, $m_{\tilde{T}_1} < 1000$ GeV, $m_{\tilde{\chi}_1^0} = 60$ GeV
>2260	95	7	AABOUD	18Z	ATLS	$\geq 4\ell$, $\lambda_{12k} \neq 0$, $m_{\tilde{\chi}_1^0} > 1000$ GeV	> 880	95	23	AAD	15BV ATLS	jets, $\tilde{g} \rightarrow \tilde{t}_1 t$ and $\tilde{t}_1 \rightarrow sb$, $400 < m_{\tilde{T}_1} < 1000$ GeV
>1650	95	7	AABOUD	18Z	ATLS	$\geq 4\ell$, $\lambda_{133} \neq 0$, $m_{\tilde{\chi}_1^0} > 500$ GeV	> 600	95	28	AAD	15CB ATLS	$\ell, \tilde{g} \rightarrow (e/\mu)qq$, benchmark gluino, neutralino masses
>1610	95	8	SIRUNYAN	18AK	CMS	$\tilde{g} \rightarrow tbs$, λ''_{332} coupling	> 600	95	28	AAD	15CB ATLS	$\ell\ell/Z, \tilde{g} \rightarrow (e/e/\mu/\mu/e/\mu)qq$, $m_{\tilde{\chi}_1^0} = 400$ GeV and $0.7 < c\tau_{\tilde{\chi}_1^0} < 3 \times 10^5$ mm
>1690	95	9	SIRUNYAN	18D	CMS	top quark (hadronically decaying) + jets + \cancel{E}_T , Tglu3C, $m_{\tilde{T}_1} - m_{\tilde{\chi}_1^0} = 20$ GeV, $m_{\tilde{\chi}_1^0} = 0$ GeV	>1000	95	29	AAD	15X ATLS	≥ 10 jets, $\tilde{g} \rightarrow q\bar{q}\tilde{\chi}_1^0, \tilde{\chi}_1^0 \rightarrow qq\bar{q}, m_{\tilde{\chi}_1^0} = 500$ GeV
none 100-1410	95	10	SIRUNYAN	18EA	CMS	2 large jets with four-parton sub-structure, $\tilde{g} \rightarrow 5q$	> 917	95	29	AAD	15X ATLS	$\geq 6,7$ jets, $\tilde{g} \rightarrow qq\bar{q}$, (light-quark, λ'' couplings)
>2100	95	11	AABOUD	17AI	ATLS	$\geq 1\ell + \geq 8$ jets, Tglu3A and $\tilde{\chi}_1^0 \rightarrow uds$, λ''_{112} coupling, $m_{\tilde{\chi}_1^0} = 1000$ GeV	> 929	95	29	AAD	15X ATLS	$\geq 6,7$ jets, $\tilde{g} \rightarrow qq\bar{q}$, (b-quark, λ'' couplings)
>1650	95	12	AABOUD	17AI	ATLS	$\geq 1\ell + \geq 8$ jets, $\tilde{g} \rightarrow t\bar{t}, \tilde{t} \rightarrow bs$, λ''_{323} coupling, $m_{\tilde{T}_1} = 1000$ GeV	>1180	95	30	AAD	14AX ATLS	≥ 3 b-jets + \cancel{E}_T , $\tilde{g} \rightarrow \tilde{t}_1 t \tilde{\chi}_1^0$ simplified model, $\tilde{t}_1 \rightarrow b \tilde{\chi}_1^\pm$, $m_{\tilde{\chi}_1^\pm} = 2m_{\tilde{\chi}_1^0}$, $m_{\tilde{\chi}_1^0} = 60$ GeV, $m_{\tilde{t}_1} < 1000$ GeV
>1800	95	13	AABOUD	17AI	ATLS	$\geq 1\ell + \geq 8$ jets, Tglu1A and $\tilde{\chi}_1^0 \rightarrow qq\ell$, λ' coupling, $m_{\tilde{\chi}_1^0} = 1000$ GeV	> 850	95	31	AAD	14E ATLS	$\ell^\pm \ell^\pm (\ell\bar{\nu}) +$ jets, $\tilde{g} \rightarrow t\bar{t}_1$ with $\tilde{t}_1 \rightarrow bs$ simplified model
>1800	95	14	AABOUD	17AJ	ATLS	same-sign $\ell^\pm \ell^\pm / 3\ell +$ jets + \cancel{E}_T , Tglu3A, λ''_{112} coupling, $m_{\tilde{\chi}_1^0} = 50$ GeV	> 900	95	32	CHATRCHYAN14H	CMS	same-sign $\ell^\pm \ell^\pm, \tilde{g} \rightarrow tbs$ simplified model
>1750	95	15	AABOUD	17AJ	ATLS	same-sign $\ell^\pm \ell^\pm / 3\ell +$ jets + \cancel{E}_T , Tglu1A and $\tilde{\chi}_1^0 \rightarrow qq\ell$, λ' coupling						
>1450	95	16	AABOUD	17AJ	ATLS	same-sign $\ell^\pm \ell^\pm / 3\ell +$ jets + \cancel{E}_T , $\tilde{g} \rightarrow t\bar{t}_1$ and $\tilde{t}_1 \rightarrow sd$, λ''_{321} coupling						
>1450	95	17	AABOUD	17AJ	ATLS	same-sign $\ell^\pm \ell^\pm / 3\ell +$ jets + \cancel{E}_T , $\tilde{g} \rightarrow t\bar{t}_1$ and $\tilde{t}_1 \rightarrow bd$, λ''_{313} coupling						
> 400	95	18	AABOUD	17AJ	ATLS	same-sign $\ell^\pm \ell^\pm / 3\ell +$ jets + $\cancel{E}_T, \tilde{d}_R \rightarrow tb(t)s$, λ''_{313} (λ''_{321}) coupling						
none 625-1375	95	19	AABOUD	17AZ	ATLS	≥ 7 jets + \cancel{E}_T , large R-jets and/or b-jets, $\tilde{g} \rightarrow t\bar{t}_1$ and $\tilde{t}_1 \rightarrow bs$, λ''_{323} coupling						
none 600-650	95	20	KHACHATRY...17Y	CMS	$\tilde{g} \rightarrow qq\bar{q}q, \lambda''_{212}$ coupling, $m_{\tilde{q}} = 100$ GeV							
none 600-1030	95	20	KHACHATRY...17Y	CMS	$\tilde{g} \rightarrow qq\bar{q}q, \lambda''_{112}$ coupling, $m_{\tilde{q}} = 900$ GeV							
none 600-650	95	20	KHACHATRY...17Y	CMS	$\tilde{g} \rightarrow qq\bar{q}q, \lambda''_{113}$ coupling, $m_{\tilde{q}} = 100$ GeV							
none 600-1080	95	20	KHACHATRY...17Y	CMS	$\tilde{g} \rightarrow qq\bar{q}q, \lambda''_{213}$ coupling, $m_{\tilde{q}} = 900$ GeV							
none 600-680	95	20	KHACHATRY...17Y	CMS	$\tilde{g} \rightarrow qq\bar{q}b, \lambda''_{112}$ coupling, $m_{\tilde{q}} = 100$ GeV							
none 600-1080	95	20	KHACHATRY...17Y	CMS	$\tilde{g} \rightarrow qq\bar{q}b, \lambda''_{212}$ coupling, $m_{\tilde{q}} = 900$ GeV							
none 600-650	95	20	KHACHATRY...17Y	CMS	$\tilde{g} \rightarrow qq\bar{q}b, \lambda''_{213}$ coupling, $m_{\tilde{q}} = 100$ GeV							
none 600-1100	95	20	KHACHATRY...17Y	CMS	$\tilde{g} \rightarrow qq\bar{q}b, \lambda''_{313}$ coupling, $m_{\tilde{q}} = 900$ GeV							
>1050	95	21	KHACHATRY...16BJ	CMS	same-sign $\ell^\pm \ell^\pm$, Tglu3A, $m_{\tilde{\chi}_1^0} < 800$ GeV							
>1140	95	21	KHACHATRY...16BJ	CMS	same-sign $\ell^\pm \ell^\pm$, Tglu3B, $m_{\tilde{T}_1} - m_{\tilde{\chi}_1^0} = 20$ GeV, $m_{\tilde{\chi}_1^0} = 0$							
>1030	95	22	KHACHATRY...16BX	CMS	$\tilde{g} \rightarrow tbs$, λ''_{332} coupling							
>1150	95	23	AAD	15BV	ATLS	general RPC \tilde{g} decays, $m_{\tilde{\chi}_1^0} < 100$ GeV						
>1350	95	24	AAD	14X	ATLS	$\geq 4\ell^\pm, \tilde{g} \rightarrow q\bar{q}\tilde{\chi}_1^0, \tilde{\chi}_1^0 \rightarrow \ell^\pm \ell^\mp \nu$						
> 650	95	25	CHATRCHYAN14P	CMS	$\tilde{g} \rightarrow jjj$							
none 200-835	95	25	CHATRCHYAN14P	CMS	$\tilde{g} \rightarrow bjj$							
••• We do not use the following data for averages, fits, limits, etc. •••												
>1875	95	26	AABOUD	18CF	ATLS	jets and large R-jets, Tglu2RPV and $\tilde{\chi}_1^0 \rightarrow qq\bar{q}, \lambda''$ coupling, $m_{\tilde{\chi}_1^0} = 1000$ GeV						
>1400	95	27	KHACHATRY...16BX	CMS	$\tilde{g} \rightarrow qq\tilde{\chi}_1^0, \tilde{\chi}_1^0 \rightarrow \ell\ell\nu, \lambda_{121}$ or $\lambda_{122} \neq 0, m_{\tilde{\chi}_1^0} > 400$ GeV							
>1600	95	23	AAD	15BV	ATLS	pMSSM, $M_1 = 60$ GeV, $m_{\tilde{q}} < 1500$ GeV						
>1280	95	23	AAD	15BV	ATLS	mSUGRA, $m_0 > 2$ TeV						
>1100	95	23	AAD	15BV	ATLS	via $\tilde{\tau}$, natural GMSB, all $m_{\tilde{\tau}}$						

1 AAD 21BF searched in 139 fb^{-1} of pp collisions at $\sqrt{s} = 13$ TeV for pair production of gluinos, stops, electroweakinos decaying RPV either directly or indirectly via the LSP. The final state in all cases is one or two leptons, many jets (up to fifteen) and b -jets. Different models with different branching fractions of the gluino or stop follow from the assumptions on the nature of the electroweakinos. No significant excess above the Standard Model predictions is observed. Limits are set on the gluino, \tilde{t}_1 , electroweakino masses as a function of the $\tilde{\chi}_1^0$ mass in several scenarios of gluino, stop and electroweakino pair production.

2 AAD 21V searched in 139 fb^{-1} of pp collisions at $\sqrt{s} = 13$ TeV for supersymmetry in events with four or more leptons (electrons, muons and tau-leptons). No significant excess above the Standard Model expectations is observed. Limits are set on Tchl1n12-GGM, and RPV models similar to Tchl1n2l, Tglu1A (with $q = u, d, s, c, b$ with equal branching fractions), and $\tilde{t}_1/\tilde{\nu} \rightarrow \ell/\nu\tilde{\chi}_1^0$ (mass-degenerate \tilde{t}_1 and $\tilde{\nu}$ of all 3 generations), all with $\tilde{\chi}_1^0 \rightarrow \ell^\pm e^\mp \nu$ via λ_{12k} or λ_{133} (where $i, k \in \{1, 2\}$), see their Figure 11.

3 AAD 20AL searched in 139 fb^{-1} of pp collisions at $\sqrt{s} = 13$ TeV for events with 8 or more jets and moderate missing transverse momentum. The selection makes requirements according to the number of b -tagged jets and the scalar sum of masses of large-radius jets. No significant excess above the Standard Model expectations is observed. Exclusion limits at 95% C.L. are set on the gluino mass in RPV simplified models where the gluino decays via $\tilde{g} \rightarrow tbd$ or $\tilde{g} \rightarrow tbs$. They extend up to almost 1.6 TeV for a \tilde{t}_1 mass of 900 GeV. See their Fig. 10(c).

4 AAD 20V searched in 139 fb^{-1} of pp collisions at $\sqrt{s} = 13$ TeV for events with two same-sign charged leptons (electrons or muons) and jets. No significant excess above the Standard Model expectations is observed. Exclusion limits at 95% C.L. are set on the gluino mass in RPV simplified models where the gluino decays via $\tilde{g} \rightarrow tbd$, see Figure 7(b).

5 SIRUNYAN 20T searched in 137 fb^{-1} of pp collisions at $\sqrt{s} = 13$ TeV for events with at least two jets, and two isolated same-sign or three or more charged leptons (electrons or muons). No significant excess above the Standard Model expectations is observed. Limits are set on the gluino mass in the Tglu3A, Tglu3B, Tglu3C and Tglu3D simplified models, see their Figure 7, and in the Tglu1C and Tglu1B simplified models, see their Figures 8 and 9. Limits are also set on the sbottom mass in the Tstbot2 simplified model, see their Figure 10, and on the stop mass in the Tstop7 simplified model, see their Figure 11. Finally, limits are set on the gluino mass in RPV simplified models where the gluino decays either via $\tilde{g} \rightarrow qq\bar{q} + e/\mu/\tau$ or via $\tilde{g} \rightarrow tbs$, see Figure 12.

6 SIRUNYAN 19F searched in 35.9 fb^{-1} of pp collisions at $\sqrt{s} = 13$ TeV for three-jet resonances produced in the decay of a gluino in R-parity violating supersymmetric models. The mass range from 200 to 2000 GeV is explored in four separate mass regions. The observations show agreement with standard model expectations. The results are interpreted within the framework of R-parity violating SUSY, where pair-produced gluinos decay to a six quark final state. Gluino masses below 1500 GeV are excluded at 95% C.L. See their Figure 5.

7 AABOUD 18Z searched in 36.1 fb^{-1} of pp collisions at $\sqrt{s} = 13$ TeV for events containing four or more charged leptons (electrons, muons and up to two hadronically decaying taus). No significant deviation from the expected SM background is observed. Limits are set on the Higgsino mass in simplified models of general gauge mediated supersymmetry Tn1n1A/Tn1n1B/Tn1n1C, see their Figure 9. Limits are also set on the wino, slepton, sneutrino and gluino mass in a simplified model of NLSF pair production with R-parity violating decays of the LSP via λ_{12k} or λ_{133} to charged leptons, see their Figures 7, 8.

8 SIRUNYAN 18AK searched in 35.9 fb^{-1} of pp collisions at $\sqrt{s} = 13$ TeV for events containing a single lepton, large jet and b -quark jet multiplicities, coming from R-parity-violating decays of gluinos. No excess over the expected background is observed. Limits are derived on the gluino mass, assuming the RPV $\tilde{g} \rightarrow tbs$ decay, see their Figure 9.

9 SIRUNYAN 18D searched in 35.9 fb^{-1} of pp collisions at $\sqrt{s} = 13$ TeV for events containing identified hadronically decaying top quarks, no leptons, and \cancel{E}_T . No significant excess above the Standard Model expectations is observed. Limits are set on the stop mass in the Tstop1 simplified model, see their Figure 8, and on the gluino mass in the Tglu3A, Tglu3B, Tglu3C and Tglu3E simplified models, see their Figure 9.

10 SIRUNYAN 18EA searched in 38.2 fb^{-1} of pp collisions at $\sqrt{s} = 13$ TeV for the pair production of resonances, each decaying to at least four quarks. Reconstructed particles are clustered into two large jets of similar mass, each consistent with four-parton

- substructure. No statistically significant excess over the Standard Model expectation is observed. Limits are set on the squark and gluino mass in RPV supersymmetry models where squarks (gluinos) decay, through intermediate higgsinos, to four (five) quarks, see their Figure 4.
- 11 AABOUD 17A1 searched in 36.1 fb^{-1} of pp collisions at $\sqrt{s} = 13 \text{ TeV}$ for events with one or more isolated lepton, at least eight jets, either zero or many b -jets, for evidence of R-parity violating decays of the gluino. No significant excess above the Standard Model expectations is observed. Limits up to 2.1 TeV are set on the gluino mass in R-parity-violating supersymmetry models as Tglu3A with LSP decay through the non-zero λ''_{112} coupling as $\tilde{\chi}_1^0 \rightarrow uds$. See their Figure 9.
- 12 AABOUD 17A1 searched in 36.1 fb^{-1} of pp collisions at $\sqrt{s} = 13 \text{ TeV}$ for events with one or more isolated lepton, at least eight jets, either zero or many b -jets, for evidence of R-parity violating decays of the gluino. No significant excess above the Standard Model expectations is observed. Limits up to 1.65 TeV are set on the gluino mass in R-parity-violating supersymmetry models with $\tilde{g} \rightarrow t\bar{t}, \bar{t} \rightarrow b\bar{s}$ through the non-zero λ''_{323} coupling. See their Figure 9.
- 13 AABOUD 17A1 searched in 36.1 fb^{-1} of pp collisions at $\sqrt{s} = 13 \text{ TeV}$ for events with one or more isolated lepton, at least eight jets, either zero or many b -jets, for evidence of R-parity violating decays of the gluino. No significant excess above the Standard Model expectations is observed. Limits up to 1.8 TeV are set on the gluino mass in R-parity-violating supersymmetry models as Tglu1A with the LSP decay through the non-zero λ' coupling as $\tilde{\chi}_1^0 \rightarrow qq\ell$. See their Figure 9.
- 14 AABOUD 17A1 searched in 36.1 fb^{-1} of pp collisions at $\sqrt{s} = 13 \text{ TeV}$ for events with two same-sign or three leptons, jets and large missing transverse momentum. No significant excess above the Standard Model expectations is observed. Limits up to 1.8 TeV are set on the gluino mass in R-parity-violating supersymmetry models as Tglu3A with LSP decaying through the non-zero λ''_{112} coupling as $\tilde{\chi}_1^0 \rightarrow uds$. See their Figure 5(d).
- 15 AABOUD 17A1 searched in 36.1 fb^{-1} of pp collisions at $\sqrt{s} = 13 \text{ TeV}$ for events with two same-sign or three leptons, jets and large missing transverse momentum. No significant excess above the Standard Model expectations is observed. Limits up to 1.75 TeV are set on the gluino mass in R-parity-violating supersymmetry models as Tglu1A with LSP decaying through the non-zero λ' coupling as $\tilde{\chi}_1^0 \rightarrow qq\ell$. See their Figure 5(c).
- 16 AABOUD 17A1 searched in 36.1 fb^{-1} of pp collisions at $\sqrt{s} = 13 \text{ TeV}$ for events with two same-sign or three leptons, jets and large missing transverse momentum. No significant excess above the Standard Model expectations is observed. Limits up to 1.45 TeV are set on the gluino mass in R-parity-violating supersymmetry models where $\tilde{g} \rightarrow t\bar{t}_1$ and $\bar{t}_1 \rightarrow s\bar{d}$ through the non-zero λ''_{321} coupling. See their Figure 5(b).
- 17 AABOUD 17A1 searched in 36.1 fb^{-1} of pp collisions at $\sqrt{s} = 13 \text{ TeV}$ for events with two same-sign or three leptons, jets and large missing transverse momentum. No significant excess above the Standard Model expectations is observed. Limits up to 1.45 TeV are set on the gluino mass in R-parity-violating supersymmetry models where $\tilde{g} \rightarrow t\bar{t}_1$ and $\bar{t}_1 \rightarrow b\bar{d}$ through the non-zero λ''_{313} coupling. See their Figure 5(a).
- 18 AABOUD 17A1 searched in 36.1 fb^{-1} of pp collisions at $\sqrt{s} = 13 \text{ TeV}$ for events with two same-sign or three leptons, jets and large missing transverse momentum. No significant excess above the Standard Model expectations is observed. Limits up to 400 GeV are set on the down type squark (\tilde{d}_R mass in R-parity-violating supersymmetry models where $\tilde{d}_R \rightarrow t\bar{b}$ through the non-zero λ''_{313} coupling or $\tilde{d}_R \rightarrow t\bar{s}$ through the non-zero λ''_{321} . See their Figure 5(e) and 5(f).
- 19 AABOUD 17AZ searched in 36.1 fb^{-1} of pp collisions at $\sqrt{s} = 13 \text{ TeV}$ for events with at least seven jets and large missing transverse momentum. Selected events are further classified based on the presence of large R-jets or b -jets and no leptons. No significant excess above the Standard Model expectations is observed. Limits are set for R-parity violating decays of the gluino assuming $\tilde{g} \rightarrow t\bar{t}_1$ and $\bar{t}_1 \rightarrow b\bar{s}$ through the non-zero λ''_{223} couplings. The range 625–1375 GeV is excluded for $m_{\tilde{t}_1} = 400 \text{ GeV}$. See their Figure 7b.
- 20 KHACHATRYAN 17Y searched in 19.7 fb^{-1} of pp collisions at $\sqrt{s} = 8 \text{ TeV}$ for events containing at least 8 or 10 jets, possibly b -tagged, coming from R-parity-violating decays of supersymmetric particles. No excess over the expected background is observed. Limits are derived on the gluino mass, assuming various RPV decay modes, see Fig. 7.
- 21 KHACHATRYAN 16BJ searched in 2.3 fb^{-1} of pp collisions at $\sqrt{s} = 13 \text{ TeV}$ for events with two isolated same-sign dileptons and jets in the final state. No significant excess above the Standard Model expectations is observed. Limits are set on the gluino mass in the following simplified models: Tglu3A and Tglu3D, see Fig. 4, Tglu3B and Tglu3C, see Fig. 5, and Tglu1B, see Fig. 7.
- 22 KHACHATRYAN 16BX searched in 19.5 fb^{-1} of pp collisions at $\sqrt{s} = 8 \text{ TeV}$ for events containing 0 or 1 leptons and b -tagged jets, coming from R-parity-violating decays of supersymmetric particles. No excess over the expected background is observed. Limits are derived on the gluino mass, assuming the RPV $\tilde{g} \rightarrow t\bar{b}s$ decay, see Fig. 7 and 10.
- 23 AAD 15BV summarized and extended ATLAS searches for gluinos and first- and second-generation squarks in final states containing jets and missing transverse momentum, with or without leptons or b -jets in the $\sqrt{s} = 8 \text{ TeV}$ data set collected in 2012. The paper reports the results of new interpretations and statistical combinations of previously published analyses, as well as new analyses. Exclusion limits at 95% C.L. are set on the gluino mass in several R-parity conserving models, leading to a generalized constraint on gluino masses exceeding 1150 GeV for lightest supersymmetric particle masses below 100 GeV. See their Figs. 10, 19, 20, 21, 23, 25, 26, 29–37.
- 24 AAD 14X searched in 20.3 fb^{-1} of pp collisions at $\sqrt{s} = 8 \text{ TeV}$ for events with at least four leptons (electrons, muons, taus) in the final state. No significant excess above the Standard Model expectations is observed. Limits are set on the gluino mass in an R-parity violating simplified model where the decay $\tilde{g} \rightarrow q\bar{q}\tilde{\chi}_1^0$, with $\tilde{\chi}_1^0 \rightarrow \ell^\pm\ell^\mp\nu$, takes place with a branching ratio of 100%, see Fig. 8.
- 25 CHATRCHYAN 14P searched in 19.4 fb^{-1} of pp collisions at $\sqrt{s} = 8 \text{ TeV}$ for three-jet resonances produced in the decay of a gluino in R-parity violating supersymmetric models. No excess over the expected SM background is observed. Assuming a 100% branching ratio for the gluino decay into three light-flavour jets, limits are set on the cross section of gluino pair production, see Fig. 7, and gluino masses below 650 GeV are excluded at 95% C.L. Assuming a 100% branching ratio for the gluino decaying to one b -quark jet and two light-flavour jets, gluino masses between 200 GeV and 835 GeV are excluded at 95% C.L.
- 26 AABOUD 18CF searched in 36.1 fb^{-1} of pp collisions at $\sqrt{s} = 13 \text{ TeV}$ for events with several jets, possibly b -jets, and large-radius jets for evidence of R-parity violating decays of the gluino. No significant excess above the Standard Model expectations is observed. Limits between 1000 and 1875 GeV are set on the gluino mass in R-parity-violating supersymmetry models as Tglu2RPV with the LSP decay through the non-zero λ'' coupling as $\tilde{\chi}_1^0 \rightarrow qq\ell$. The most stringent limit is obtained for $m_{\tilde{\chi}_1^0} = 1000 \text{ GeV}$, the weakest for $m_{\tilde{\chi}_1^0} = 50 \text{ GeV}$. See their Figure 7(b). Figure 7(a) presents results for gluinos directly decaying into 3 quarks, Tglu1RPV.
- 27 KHACHATRYAN 16BX searched in 19.5 fb^{-1} of pp collisions at $\sqrt{s} = 8 \text{ TeV}$ for events containing 4 leptons coming from R-parity-violating decays of $\tilde{\chi}_1^0 \rightarrow \ell\ell\nu$ with $\lambda_{122} \neq 0$ or $\lambda_{122} \neq 0$. No excess over the expected background is observed. Limits are derived on the gluino, squark and stop masses, see Fig. 23.
- 28 AAD 15CB searched for events containing at least one long-lived particle that decays at a significant distance from its production point (displaced vertex, DV) into two leptons or into five or more charged particles in 20.3 fb^{-1} of pp collisions at $\sqrt{s} = 8 \text{ TeV}$. The dilepton signature is characterised by DV formed from at least two lepton candidates. Four different final states were considered for the multitrack signature, in which the DV must be accompanied by a high-transverse momentum muon or electron candidate that originates from the DV, jets or missing transverse momentum. No events were observed in any of the signal regions. Results were interpreted in SUSY scenarios involving R-parity violation, split supersymmetry, and gauge mediation. See their Fig. 12–20.
- 29 AAD 15X searched in 20.3 fb^{-1} of pp collisions at $\sqrt{s} = 8 \text{ TeV}$ for events containing large number of jets, no requirements on missing transverse momentum and no isolated electrons or muons. The sensitivity of the search is enhanced by considering the number of b -tagged jets and the scalar sum of masses of large-radius jets in an event. No evidence was found for excesses above the expected level of Standard Model background. Exclusion limits at 95% C.L. are set on the gluino mass assuming the gluino decays to various quark flavors, and for various neutralino masses. See their Fig. 11–16.
- 30 AAD 14AX searched in 20.1 fb^{-1} of pp collisions at $\sqrt{s} = 8 \text{ TeV}$ for the strong production of supersymmetric particles in events containing either zero or at least one high p_T lepton, large missing transverse momentum, high jet multiplicity and at least three jets identified as originating from b -quarks. No excess over the expected SM background is observed. Limits are derived in mSUGRA/CMSSM models with $\tan\beta = 30$, $A_0 = -2m_0$ and $\mu > 0$, see their Fig. 14. Also, exclusion limits in simplified models containing gluinos and scalar top and bottom quarks are set, see their Figures 12, 13.
- 31 AAD 14E searched in 20.3 fb^{-1} of pp collisions at $\sqrt{s} = 8 \text{ TeV}$ for strongly produced supersymmetric particles in events containing jets and two same-sign leptons or three leptons. The search also utilises jets originating from b -quarks, missing transverse momentum and other variables. No excess over the expected SM background is observed. Exclusion limits are derived in simplified models containing gluinos and squarks, see Figures 5 and 6. In the $\tilde{g} \rightarrow q\bar{q}\tilde{\chi}_1^\pm, \tilde{\chi}_1^\pm \rightarrow W^{(*)}\tilde{\chi}_2^0, \tilde{\chi}_2^0 \rightarrow Z^{(*)}\tilde{\chi}_1^0$ simplified model, the following assumptions have been made: $m_{\tilde{\chi}_1^\pm} = 0.5 m_{\tilde{\chi}_1^0} + m_{\tilde{g}}, m_{\tilde{\chi}_2^0} = 0.5 (m_{\tilde{\chi}_1^0} + m_{\tilde{\chi}_1^\pm}), m_{\tilde{\chi}_1^0} < 520 \text{ GeV}$. In the $\tilde{g} \rightarrow q\bar{q}\tilde{\chi}_1^\pm, \tilde{\chi}_1^\pm \rightarrow \ell^\pm\nu\tilde{\chi}_1^0$ or $\tilde{g} \rightarrow q\bar{q}\tilde{\chi}_2^0, \tilde{\chi}_2^0 \rightarrow \ell^\pm\ell^\mp(\nu\nu)\tilde{\chi}_1^0$ simplified model, the following assumptions have been made: $m_{\tilde{\chi}_1^\pm} = m_{\tilde{\chi}_2^0} = 0.5 (m_{\tilde{\chi}_1^0} + m_{\tilde{g}}), m_{\tilde{\chi}_1^0} < 660 \text{ GeV}$. Limits are also derived in the mSUGRA/CMSSM, bRPV and GMSB models, see their Fig. 8.
- 32 CHATRCHYAN 14H searched in 19.5 fb^{-1} of pp collisions at $\sqrt{s} = 8 \text{ TeV}$ for events with two isolated same-sign dileptons and jets in the final state. No significant excess above the Standard Model expectations is observed. Limits are set on the gluino mass in simplified models where the R-parity violating decay $\tilde{g} \rightarrow t\bar{b}s$ takes place with a branching ratio of 100%, see Fig. 8.

Long-lived \tilde{g} (Gluino) mass limit

Limits on light gluinos ($m_{\tilde{g}} < 5 \text{ GeV}$) were last listed in our PDG 14 edition: K. Olive, *et al.* (Particle Data Group), Chinese Physics **C38** 070001 (2014) (<http://pdg.lbl.gov>).

VALUE (GeV)	CL%	DOCUMENT ID	TECN	COMMENT
>2050	95	1 AAD	23G ATLS	R-hadrons, Tglu1A, stable, $m_{\tilde{g}} = 100 \text{ GeV}$
>2270	95	1 AAD	23G ATLS	R-hadrons, Tglu1A, $\tau = 20 \text{ ns}, m_{\tilde{\chi}_1^0} = 100 \text{ GeV}$
>2050	95	1 AAD	23G ATLS	R-hadrons, Tglu1A, stable, $m_{\tilde{g}} - m_{\tilde{\chi}_1^0} = 30 \text{ GeV}$
>2050	95	1 AAD	23G ATLS	R-hadrons, Tglu1A, $\tau = 20 \text{ ns}, m_{\tilde{g}} - m_{\tilde{\chi}_1^0} = 30 \text{ GeV}$
>2500	95	2 SIRUNYAN	21AF CMS	long-lived \tilde{g} , Tglu2RPV, λ''_{323} coupling, $0.6 \text{ mm} < c\tau < 90 \text{ mm}$
>2450	95	3 SIRUNYAN	21U CMS	long-lived \tilde{g} , $pp \rightarrow \tilde{g}\tilde{g}, \tilde{g} \rightarrow g\tilde{G}, \text{GMSB}, 6 < c\tau < 550 \text{ mm}$
>2500	95	3 SIRUNYAN	21U CMS	long-lived \tilde{g} , $pp \rightarrow \tilde{g}\tilde{g}, \tilde{g} \rightarrow q\bar{q}\tilde{\chi}_1^0$, mini-split, $m_{\tilde{\chi}_1^0} = 100 \text{ GeV}, 7 < c\tau < 360 \text{ mm}$
>2500	95	3 SIRUNYAN	21U CMS	long-lived \tilde{g} , $pp \rightarrow \tilde{g}\tilde{g}, \tilde{g} \rightarrow t\bar{b}s, \lambda''_{323}$ coupling, $3 < c\tau < 1000 \text{ mm}$
>1980	95	4 AABOUD	19AT ATLS	R-hadrons, Tglu1A, metastable
>2060	95	5 AABOUD	19C ATLS	R-hadrons, Tglu1A, $\tau \geq 10 \text{ ns}, m_{\tilde{\chi}_1^0} = 100 \text{ GeV}$
>1890	95	5 AABOUD	19C ATLS	R-hadrons, Tglu1A, stable
>2400	95	6 SIRUNYAN	19BH CMS	long-lived \tilde{g} , RPV, $\tilde{g} \rightarrow \bar{t}\bar{b}s, 10 \text{ mm} < c\tau < 250 \text{ mm}$
>2300	95	6 SIRUNYAN	19BH CMS	long-lived \tilde{g} , GMSB, $\tilde{g} \rightarrow g\tilde{G}, 20 \text{ mm} < c\tau < 110 \text{ mm}$
>2100	95	7 SIRUNYAN	19BT CMS	long-lived \tilde{g} , GMSB, $\tilde{g} \rightarrow g\tilde{G}, 0.3 \text{ mm} < c\tau < 30 \text{ mm}$

Searches Particle Listings

Supersymmetric Particle Searches

>2500	95	7	SIRUNYAN	19BT CMS	long-lived \tilde{g} , GMSB, $\tilde{g} \rightarrow g\tilde{G}$, $c\tau = 1$ m	>1098	95	23	CHATRCHYAN12L CMS	long-lived \tilde{g} forming R-hadrons, $f = 0.1$	
>1900	95	7	SIRUNYAN	19BT CMS	long-lived \tilde{g} , GMSB, $\tilde{g} \rightarrow g\tilde{G}$, $c\tau = 100$ m	> 586	95	24	AAD	11K ATLS	stable \tilde{g}
>2370	95	8	AABOUD	18s ATLS	displaced vertex + \cancel{E}_T , long-lived Tglu1A, $m_{\tilde{\chi}_1^0} = 100$ GeV, and $\tau = 0.17$ ns	> 544	95	25	AAD	11P ATLS	stable \tilde{g} , GMSB scenario, $\tan\beta = 5$
>1600	95	9	SIRUNYAN	18AY CMS	jets+ \cancel{E}_T , Tglu1A, $c\tau < 0.1$ mm, $m_{\tilde{\chi}_1^0} = 100$ GeV	> 370	95	26	KHACHATRY...11	CMS	long-lived \tilde{g}
>1750	95	9	SIRUNYAN	18AY CMS	jets+ \cancel{E}_T , Tglu1A, $c\tau = 1$ mm, $m_{\tilde{\chi}_1^0} = 100$ GeV	> 398	95	27	KHACHATRY...11c	CMS	stable \tilde{g}
>1640	95	9	SIRUNYAN	18AY CMS	jets+ \cancel{E}_T , Tglu1A, $c\tau = 10$ mm, $m_{\tilde{\chi}_1^0} = 100$ GeV	1 AAD 23G searched in 139 fb ⁻¹ of pp collisions at $\sqrt{s} = 13$ TeV for R-hadron pair production in events with high-pt tracks with large ionisation in the pixel detector. No significant excess above the Standard Model predictions is observed. Limits are set on the R-hadron mass for different masses of the LSP and for different R-hadron lifetimes, see Figure 18.					
>1490	95	9	SIRUNYAN	18AY CMS	jets+ \cancel{E}_T , Tglu1A, $c\tau = 100$ mm, $m_{\tilde{\chi}_1^0} = 100$ GeV	2 SIRUNYAN 21Af searched in 140 fb ⁻¹ of pp collisions at $\sqrt{s} = 13$ TeV for supersymmetry in events with two displaced vertices from long-lived particles decaying into multijet or dijet final states. No significant excess above the Standard Model expectations is observed. Limits are set on the gluino mass in the simplified model Tglu2RPV with λ_{323}^0 coupling, on the $\tilde{\chi}_1^0$ mass in an RPV model with $\tilde{\chi}_1^0$ pair production and the RPV decay $\tilde{\chi}_1^0 \rightarrow tbs$ with λ_{323}^0 coupling and on the \tilde{t} mass in an RPV model with top squark pair production and the RPV decay $\tilde{t} \rightarrow \bar{d}_i \tilde{d}_j$ with λ_{3ij}^0 coupling, see their Figure 7.					
>1300	95	9	SIRUNYAN	18AY CMS	jets+ \cancel{E}_T , Tglu1A, $c\tau = 1$ m, $m_{\tilde{\chi}_1^0} = 100$ GeV	3 SIRUNYAN 21u searched in 132 fb ⁻¹ of pp collisions at $\sqrt{s} = 13$ TeV for supersymmetry in events with displaced tracks and displaced vertices associated with a dijet system. No significant excess above the Standard Model expectations is observed. Limits are set on long-lived gluinos in an RPC GMSB SUSY model of gluino pair production, with $\tilde{g} \rightarrow g\tilde{G}$, see their Figure 9, in Tglu1A in a mini-split model, see their Figure 10, and in an RPV model of gluino pair production, with $\tilde{g} \rightarrow tbs$ with coupling λ_{323}^0 , see their Figure 11. Limits are also set on long-lived top squarks in Tstop2RPV, see their Figure 12, in an RPV model with $\tilde{t} \rightarrow d\tilde{e}$ and λ_{331}^0 coupling, see their Figure 13, and in a dynamical RPV model with $\tilde{t} \rightarrow \bar{d}\tilde{d}$ via a nonholomorphic RPV coupling η_{311}^0 , see their Figure 14. The best mass limit is achieved in all cases at $c\tau = 30$ mm.					
> 960	95	9	SIRUNYAN	18AY CMS	jets+ \cancel{E}_T , Tglu1A, $c\tau = 10$ m, $m_{\tilde{\chi}_1^0} = 100$ GeV	4 AABOUD 19AT searched in 36.1 fb ⁻¹ of pp collisions at $\sqrt{s} = 13$ TeV for metastable and stable R-hadrons. Multiple search strategies for a wide range of lifetimes, corresponding to path lengths of a few meters, are defined. No significant deviations from the expected Standard Model background are observed. Gluino R-hadrons with lifetimes of the order of 50 ns are excluded at 95% C.L. for masses below 1980 GeV using the muon-spectrometer agnostic analysis. Using the full-detector search, the observed lower limits on the mass are 2000 GeV. See their Figure 9 (top).					
> 900	95	9	SIRUNYAN	18AY CMS	jets+ \cancel{E}_T , Tglu1A, $c\tau = 100$ m, $m_{\tilde{\chi}_1^0} = 100$ GeV	5 AABOUD 19C searched in 36.1 fb ⁻¹ of pp collisions at $\sqrt{s} = 13$ TeV for metastable and stable R-hadrons arising as excesses in the mass distribution of reconstructed tracks with high transverse momentum and large dE/dx . Gluino R-hadrons with lifetimes above 10 ns are excluded at 95% C.L. with lower mass limit range between 1000 GeV and 2060 GeV, see their Figure 5(a). Masses smaller than 1290 GeV are excluded for a lifetime of 1 ns, see their Figure 6. In the case of stable R-hadrons, the lower mass limit is 1890 GeV, see their Figure 5(b).					
>2200	95	10	SIRUNYAN	18DV CMS	long-lived \tilde{g} , RPV, $\tilde{g} \rightarrow \bar{t}b\tilde{s}$, 0.6 mm $< c\tau < 80$ mm	6 SIRUNYAN 19BH searched in 35.9 fb ⁻¹ of pp collisions at $\sqrt{s} = 13$ TeV for long-lived particles decaying into jets, with each long-lived particle having a decay vertex well displaced from the production vertex. The selected events are found to be consistent with standard model predictions. Limits are set on the gluino mass in a GMSB model where the gluino is decaying via $\tilde{g} \rightarrow g\tilde{G}$, see their Figure 4 and in an RPV model of supersymmetry where the gluino is decaying via $\tilde{g} \rightarrow \bar{t}b\tilde{s}$, see their Figures 5. Limits are also set on the stop mass in two RPV models, see their Figure 6 (for $t \rightarrow b\tilde{l}$ decays) and Figure 7 (for $\tilde{t} \rightarrow \bar{d}\tilde{d}$ decays).					
>1000	95	11	KHACHATRY...17AR	CMS	long-lived \tilde{g} , RPV, $\tilde{g} \rightarrow \bar{t}b\tilde{s}$, $c\tau = 0.3$ mm	7 SIRUNYAN 19BT searched in 137 fb ⁻¹ of pp collisions at $\sqrt{s} = 13$ TeV for long-lived particles decaying to displaced, nonprompt jets and missing transverse momentum. Candidate signal events are identified using the timing capabilities of the CMS electromagnetic calorimeter. The results of the search are found to be consistent with the background predictions. Limits are set on the gluino mass in a GMSB model where long-lived gluinos are pair produced and decaying via $\tilde{g} \rightarrow g\tilde{G}$, see their Figures 4 and 5.					
>1300	95	11	KHACHATRY...17AR	CMS	long-lived \tilde{g} , RPV, $\tilde{g} \rightarrow \bar{t}b\tilde{s}$, $c\tau = 1.0$ mm	8 AABOUD 18s searched in 32.8 fb ⁻¹ of pp collisions at $\sqrt{s} = 13$ TeV for long-lived gluinos in final states with large missing transverse momentum and at least one high-mass displaced vertex with five or more tracks. The observed yield is consistent with the expected background. Exclusion limits are derived for Tglu1A models predicting the existence of long-lived gluinos reaching roughly $m(\tilde{g}) = 2000$ GeV to 2370 GeV for $m(\tilde{\chi}_1^0) = 100$ GeV and gluino lifetimes between 0.02 and 10 ns, see their Fig. 8. Limits are presented also as a function of the lifetime (for a fixed gluino-neutralino mass difference of 100 GeV) and of the gluino and neutralino masses (for a fixed lifetime of 1 ns). See their Fig. 9 and 10 respectively.					
>1400	95	11	KHACHATRY...17AR	CMS	long-lived \tilde{g} , RPV, $\tilde{g} \rightarrow \bar{t}b\tilde{s}$, 2 mm $< c\tau < 30$ mm	9 SIRUNYAN 18AY searched in 35.9 fb ⁻¹ of pp collisions at $\sqrt{s} = 13$ TeV for events containing one or more jets and significant \cancel{E}_T . No significant excess above the Standard Model expectations is observed. Limits are set on the gluino mass in the Tglu1A, Tglu2A and Tglu3A simplified models, see their Figure 3. Limits are also set on squark, sbottom and stop masses in the Tsqk1, Tsb01, Tstop1 and Tstop4 simplified models, see their Figure 3. Finally, limits are set on long-lived gluino masses in a Tglu1A simplified model where the gluino is metastable or long-lived with proper decay lengths in the range 10^{-3} mm $< c\tau < 10^5$ mm, see their Figure 4.					
>1580	95	12	AABOUD	16B ATLS	long-lived R-hadrons	10 SIRUNYAN 18DV searched in 38.5 fb ⁻¹ of pp collisions at $\sqrt{s} = 13$ TeV for long-lived particles in events with multiple jets and two displaced vertices composed of many tracks. No events with two well-separated high-track-multiplicity vertices were observed. Limits are set on the stop and the gluino mass in RPV models of supersymmetry where the stop (gluino) is decaying solely into dijet (multijet) final states, see their Figures 6 and 7.					
> 740-1590	95	13	AABOUD	16C ATLS	R-hadrons, Tglu1A, $\tau \geq 0.4$ ns, $m_{\tilde{\chi}_1^0} = 100$ GeV	11 KHACHATRYAN 17AR searched in 17.6 fb ⁻¹ of pp collisions at $\sqrt{s} = 8$ TeV for R-parity-violating SUSY in which long-lived neutralinos or gluinos decay into multijet final states. No significant excess above the Standard Model expectations is observed. Limits are set on the gluino mass for a range of mean proper decay lengths ($c\tau$), see their Fig. 7. The upper limits on the production cross section times branching ratio squared (Fig. 7) are also applicable to long-lived neutralinos.					
>1570	95	13	AABOUD	16C ATLS	R-hadrons, Tglu1A, stable	12 AABOUD 16B searched in 3.2 fb ⁻¹ of pp collisions at $\sqrt{s} = 13$ TeV for long-lived R-hadrons using observables related to large ionization losses and slow propagation velocities, which are signatures of heavy charged particles traveling significantly slower than the speed of light. Exclusion limits at 95% C.L. are set on the long-lived gluino masses exceeding 1580 GeV. See their Fig. 5.					
>1610	95	14	KHACHATRY...16BW	CMS	long-lived \tilde{g} forming R-hadrons, $f = 0.1$, cloud interaction model	13 AABOUD 16c searched in 3.2 fb ⁻¹ of pp collisions at $\sqrt{s} = 13$ TeV for long-lived and stable R-hadrons identified by anomalous specific ionization energy loss in the ATLAS					
>1580	95	14	KHACHATRY...16BW	CMS	long-lived \tilde{g} forming R-hadrons, $f = 0.1$, charge-suppressed interaction model						
>1520	95	14	KHACHATRY...16BW	CMS	long-lived \tilde{g} forming R-hadrons, $f = 0.5$, cloud interaction model						
>1540	95	14	KHACHATRY...16BW	CMS	long-lived \tilde{g} forming R-hadrons, $f = 0.5$, charge-suppressed interaction model						
>1270	95	15	AAD	15AE ATLS	\tilde{g} R-hadron, generic R-hadron model						
>1360	95	15	AAD	15AE ATLS	\tilde{g} decaying to 300 GeV stable sleptons, LeptoSUSY model						
>1115	95	16	AAD	15BMATLS	\tilde{g} R-hadron, stable						
>1185	95	16	AAD	15BMATLS	$\tilde{g} \rightarrow (g/q\bar{q})\tilde{\chi}_1^0$, lifetime 10 ns, $m_{\tilde{\chi}_1^0} = 100$ GeV						
>1099	95	16	AAD	15BMATLS	$\tilde{g} \rightarrow (g/q\bar{q})\tilde{\chi}_1^0$, lifetime 10 ns, $m_{\tilde{g}} - m_{\tilde{\chi}_1^0} = 100$ GeV						
>1182	95	16	AAD	15BMATLS	$\tilde{g} \rightarrow t\bar{t}\tilde{\chi}_1^0$, lifetime 10 ns, $m_{\tilde{\chi}_1^0} = 100$ GeV						
>1157	95	16	AAD	15BMATLS	$\tilde{g} \rightarrow t\bar{t}\tilde{\chi}_1^0$, lifetime 10 ns, $m_{\tilde{g}} - m_{\tilde{\chi}_1^0} = 480$ GeV						
> 869	95	16	AAD	15BMATLS	$\tilde{g} \rightarrow (g/q\bar{q})\tilde{\chi}_1^0$, lifetime 1 ns, $m_{\tilde{\chi}_1^0} = 100$ GeV						
> 821	95	16	AAD	15BMATLS	$\tilde{g} \rightarrow (g/q\bar{q})\tilde{\chi}_1^0$, lifetime 1 ns, $m_{\tilde{g}} - m_{\tilde{\chi}_1^0} = 100$ GeV						
> 836	95	16	AAD	15BMATLS	$\tilde{g} \rightarrow t\bar{t}\tilde{\chi}_1^0$, lifetime 1 ns, $m_{\tilde{\chi}_1^0} = 100$ GeV						
> 836	95	16	AAD	15BMATLS	$\tilde{g} \rightarrow t\bar{t}\tilde{\chi}_1^0$, lifetime 10 ns, $m_{\tilde{g}} - m_{\tilde{\chi}_1^0} = 480$ GeV						
>1000	95	17	KHACHATRY...15AK	CMS	\tilde{g} R-hadrons, $10 \mu\text{s} < \tau < 1000$ s						
> 880	95	17	KHACHATRY...15AK	CMS	\tilde{g} R-hadrons, $1 \mu\text{s} < \tau < 1000$ s						
••• We do not use the following data for averages, fits, limits, etc. •••											
> 985	95	18	AAD	13AA ATLS	\tilde{g} , R-hadrons, generic interaction model						
> 832	95	19	AAD	13BC ATLS	R-hadrons, $\tilde{g} \rightarrow g/q\bar{q}\tilde{\chi}_1^0$, generic R-hadron model, lifetime between 10^{-5} and 10^3 s, $m_{\tilde{\chi}_1^0} = 100$ GeV						
>1322	95	20	CHATRCHYAN13AB	CMS	long-lived \tilde{g} forming R-hadrons, $f = 0.1$, cloud interaction model						
none 200-341	95	21	AAD	12P ATLS	long-lived $\tilde{g} \rightarrow g\tilde{\chi}_1^0$, $m_{\tilde{\chi}_1^0} = 100$ GeV						
> 640	95	22	CHATRCHYAN12AN	CMS	long-lived $\tilde{g} \rightarrow g\tilde{\chi}_1^0$						

- Pixel detector. Gluino R -hadrons with lifetimes above 0.4 ns are excluded at 95% C.L. with lower mass limit range between 740 GeV and 1590 GeV. In the case of stable R -hadrons, the lower mass limit is 1570 GeV. See their Figs. 5 and 6.
- 14 KHACHATRYAN 16BW searched in 2.5 fb^{-1} of pp collisions at $\sqrt{s} = 13 \text{ TeV}$ for events with heavy stable charged particles, identified by their anomalously high energy deposits in the silicon tracker and/or long time-of-flight measurements by the muon system. No evidence for an excess over the expected background is observed. Limits are derived for pair production of gluinos as a function of mass, depending on the interaction model and on the fraction f , of produced gluinos hadronizing into a \tilde{g} -gluon state, see Fig. 4 and Table 7.
- 15 AAD 15AE searched in 19.1 fb^{-1} of pp collisions at $\sqrt{s} = 8 \text{ TeV}$ for heavy long-lived charged particles, measured through their specific ionization energy loss in the ATLAS pixel detector or their time-of-flight in the ALTA5 muon system. In the absence of an excess of events above the expected backgrounds, limits are set R -hadrons in various scenarios, see Fig. 11. Limits are also set in LeptoSUSY models where the gluino decays to stable 300 GeV leptons, see Fig. 9.
- 16 AAD 15BM searched in 18.4 fb^{-1} of pp collisions at $\sqrt{s} = 8 \text{ TeV}$ for stable and metastable non-relativistic charged particles through their anomalous specific ionization energy loss in the ATLAS pixel detector. In absence of an excess of events above the expected backgrounds, limits are set within a generic R -hadron model, on stable gluino R -hadrons (see Table 5) and on metastable gluino R -hadrons decaying to $(g/q\bar{q})$ plus a light $\tilde{\chi}_1^0$ (see Fig. 7) and decaying to $t\bar{t}$ plus a light $\tilde{\chi}_1^0$ (see Fig. 9).
- 17 KHACHATRYAN 15AK looked in a data set corresponding to 18.6 fb^{-1} of pp collisions at $\sqrt{s} = 8 \text{ TeV}$, and a search interval corresponding to 281 h of trigger lifetime, for long-lived particles that have stopped in the CMS detector. No evidence for an excess over the expected background in a cloud interaction model is observed. Assuming the decay $\tilde{g} \rightarrow g\tilde{\chi}_1^0$ and lifetimes between 1 μs and 1000 s, limits are derived on \tilde{g} production as a function of $m_{\tilde{\chi}_1^0}$, see Figs. 4 and 6. The exclusions require that $m_{\tilde{\chi}_1^0}$ is kinematically consistent with the minimum values of the jet energy thresholds used.
- 18 AAD 13AA searched in 4.7 fb^{-1} of pp collisions at $\sqrt{s} = 7 \text{ TeV}$ for events containing colored long-lived particles that hadronize forming R -hadrons. No significant excess above the expected background was found. Long-lived R -hadrons containing a \tilde{g} are excluded for masses up to 985 GeV at 95% C.L. in a general interaction model. Also, limits independent of the fraction of R -hadrons that arrive charged in the muon system were derived, see Fig. 6.
- 19 AAD 13BC searched in 5.0 fb^{-1} of pp collisions at $\sqrt{s} = 7 \text{ TeV}$ and in 22.9 fb^{-1} of pp collisions at $\sqrt{s} = 8 \text{ TeV}$ for bottom squark R -hadrons that have come to rest within the ATLAS calorimeter and decay at some later time to hadronic jets and a neutralino. In absence of an excess of events above the expected backgrounds, limits are set on gluino masses for different decays, lifetimes, and neutralino masses, see their Table 6 and Fig. 10.
- 20 CHATRCHYAN 13AB looked in 5.0 fb^{-1} of pp collisions at $\sqrt{s} = 7 \text{ TeV}$ and in 18.8 fb^{-1} of pp collisions at $\sqrt{s} = 8 \text{ TeV}$ for events with heavy stable particles, identified by their anomalous dE/dx in the tracker or additionally requiring that it be identified as muon in the muon chambers, from pair production of \tilde{g} 's. No evidence for an excess over the expected background is observed. Limits are derived for pair production of gluinos as a function of mass (see Fig. 8 and Table 5), depending on the fraction, f , of formation of \tilde{g} - \tilde{g} (R -gluonball) states. The quoted limit is for $f = 0.1$, while for $f = 0.5$ it degrades to 1276 GeV. In the conservative scenario where every hadronic interaction causes it to become neutral, the limit decreases to 928 GeV for $f = 0.1$.
- 21 AAD 12P looked in 31 pb^{-1} of pp collisions at $\sqrt{s} = 7 \text{ TeV}$ for events with pair production of long-lived gluinos. The hadronization of the gluinos leads to R -hadrons which may stop inside the detector and later decay via $\tilde{g} \rightarrow g\tilde{\chi}_1^0$ during gaps between the proton bunches. No significant excess over the expected background is observed. From a counting experiment, a limit at 95% C.L. on the cross section as a function of $m_{\tilde{g}}$ is derived for $m_{\tilde{\chi}_1^0} = 100 \text{ GeV}$, see Fig. 4. The limit is valid for lifetimes between 10^{-5} and 10^3 seconds and assumes the *Generic* matter interaction model for the production cross section.
- 22 CHATRCHYAN 12AN looked in 4.0 fb^{-1} of pp collisions at $\sqrt{s} = 7 \text{ TeV}$ for events with pair production of long-lived gluinos. The hadronization of the gluinos leads to R -hadrons which may stop inside the detector and later decay via $\tilde{g} \rightarrow g\tilde{\chi}_1^0$ during gaps between the proton bunches. No significant excess over the expected background is observed. From a counting experiment, a limit at 95% C.L. on the cross section as a function of $m_{\tilde{g}}$ is derived, see Fig. 3. The mass limit is valid for lifetimes between 10^{-5} and 10^3 seconds, for what they call "the daughter gluon energy $E_{\tilde{g}} > 100 \text{ GeV}$ and assuming the *cloud* interaction model for R -hadrons. Supersedes KHACHATRYAN 11.
- 23 CHATRCHYAN 12L looked in 5.0 fb^{-1} of pp collisions at $\sqrt{s} = 7 \text{ TeV}$ for events with heavy stable particles, identified by their anomalous dE/dx in the tracker or additionally requiring that it be identified as muon in the muon chambers, from pair production of \tilde{g} 's. No evidence for an excess over the expected background is observed. Limits are derived for pair production of gluinos as a function of mass (see Fig. 3), depending on the fraction, f , of formation of \tilde{g} - \tilde{g} (R -glueball) states. The quoted limit is for $f = 0.1$, while for $f = 0.5$ it degrades to 1046 GeV. In the conservative scenario where every hadronic interaction causes it to become neutral, the limit decreases to 928 GeV for $f = 0.1$. Supersedes KHACHATRYAN 11c.
- 24 AAD 11K looked in 34 pb^{-1} of pp collisions at $\sqrt{s} = 7 \text{ TeV}$ for events with heavy stable particles, identified by their anomalous dE/dx in the tracker or time of flight in the tile calorimeter, from pair production of \tilde{g} . No evidence for an excess over the SM expectation is observed. Limits are derived for pair production of gluinos as a function of mass (see Fig. 4), for a fraction, $f = 10\%$, of formation of \tilde{g} - \tilde{g} (R -gluonball). If instead of a phase space driven approach for the hadronic scattering of the R -hadrons, a triple-Regge model or a bag-model is used, the limit degrades to 566 and 562 GeV, respectively.
- 25 AAD 11P looked in 37 pb^{-1} of pp collisions at $\sqrt{s} = 7 \text{ TeV}$ for events with heavy stable particles, reconstructed and identified by their time of flight in the Muon System. There is no requirement on their observation in the tracker to increase the sensitivity to cases where gluinos have a large fraction, f , of formation of neutral \tilde{g} - \tilde{g} (R -gluonball). No evidence for an excess over the SM expectation is observed. Limits are derived as a function of mass (see Fig. 4), for $f = 0.1$. For fractions $f = 0.5$ and $f = 1.0$ the limit degrades to 537 and 530 GeV, respectively.
- 26 KHACHATRYAN 11 looked in 10 pb^{-1} of pp collisions at $\sqrt{s} = 7 \text{ TeV}$ for events with pair production of long-lived gluinos. The hadronization of the gluinos leads to R -hadrons which may stop inside the detector and later decay via $\tilde{g} \rightarrow g\tilde{\chi}_1^0$ during gaps between the proton bunches. No significant excess over the expected background is observed.

From a counting experiment, a limit at 95% C.L. on the cross section times branching ratio is derived for $m_{\tilde{g}} - m_{\tilde{\chi}_1^0} > 100 \text{ GeV}$, see their Fig. 2. Assuming 100% branching

ratio, lifetimes between 75 ns and $3 \times 10^5 \text{ s}$ are excluded for $m_{\tilde{g}} = 300 \text{ GeV}$. The \tilde{g} mass exclusion is obtained with the same assumptions for lifetimes between 10 μs and 1000 s, but shows some dependence on the model for R -hadron interactions with matter, illustrated in Fig. 3. From a time-profile analysis, the mass exclusion is 382 GeV for a lifetime of 10 μs under the same assumptions as above.

- 27 KHACHATRYAN 11C looked in 3.1 pb^{-1} of pp collisions at $\sqrt{s} = 7 \text{ TeV}$ for events with heavy stable particles, identified by their anomalous dE/dx in the tracker or additionally requiring that it be identified as muon in the muon chambers, from pair production of \tilde{g} . No evidence for an excess over the expected background is observed. Limits are derived for pair production of gluinos as a function of mass (see Fig. 3), depending on the fraction, f , of formation of \tilde{g} - \tilde{g} (R -gluonball). The quoted limit is for $f = 0.1$, while for $f = 0.5$ it degrades to 357 GeV. In the conservative scenario where every hadronic interaction causes it to become neutral, the limit decreases to 311 GeV for $f = 0.1$.

Light \tilde{G} (Gravitino) mass limits from collider experiments

The following are bounds on light ($\ll 1 \text{ eV}$) gravitino indirectly inferred from its coupling to matter suppressed by the gravitino decay constant.

Unless otherwise stated, all limits assume that other supersymmetric particles besides the gravitino are too heavy to be produced. The gravitino is assumed to be undetected and to give rise to a missing energy (\cancel{E}) signature.

Some earlier papers are now obsolete and have been omitted. They were last listed in our PDG 14 edition: K. Olive, et al. (Particle Data Group), Chinese Physics **C38** 070001 (2014) (<http://pdg.lbl.gov>).

VALUE (eV)	CL%	DOCUMENT ID	TECN	COMMENT
• • • We do not use the following data for averages, fits, limits, etc. • • •				
$> 3.5 \times 10^{-4}$	95	¹ AAD	15BH ATLS	jet + \cancel{E}_T , $pp \rightarrow (\tilde{q}/\tilde{g})\tilde{G}$, $m_{\tilde{q}} = m_{\tilde{g}} = 500 \text{ GeV}$
$> 3 \times 10^{-4}$	95	¹ AAD	15BH ATLS	jet + \cancel{E}_T , $pp \rightarrow (\tilde{q}/\tilde{g})\tilde{G}$, $m_{\tilde{q}} = m_{\tilde{g}} = 1000 \text{ GeV}$
$> 2 \times 10^{-4}$	95	¹ AAD	15BH ATLS	jet + \cancel{E}_T , $pp \rightarrow (\tilde{q}/\tilde{g})\tilde{G}$, $m_{\tilde{q}} = m_{\tilde{g}} = 1500 \text{ GeV}$
$> 1.09 \times 10^{-5}$	95	² ABDALLAH	05B DLPH	$e^+e^- \rightarrow \tilde{G}\tilde{G}\gamma$
$> 1.35 \times 10^{-5}$	95	³ ACHARD	04E L3	$e^+e^- \rightarrow \tilde{G}\tilde{G}\gamma$
$> 1.3 \times 10^{-5}$	95	⁴ HEISTER	03C ALEP	$e^+e^- \rightarrow \tilde{G}\tilde{G}\gamma$
$> 11.7 \times 10^{-6}$	95	⁵ ACOSTA	02H CDF	$p\bar{p} \rightarrow \tilde{G}\tilde{G}\gamma$
$> 8.7 \times 10^{-6}$	95	⁶ ABBIENDI,G	00D OPAL	$e^+e^- \rightarrow \tilde{G}\tilde{G}\gamma$

- ¹ AAD 15BH searched in 20.3 fb^{-1} of pp collisions at $\sqrt{s} = 8 \text{ TeV}$ for associated production of a light gravitino and a squark or gluino. The squark (gluino) is assumed to decay exclusively to a quark (gluon) and a gravitino. No evidence was found for an excess above the expected level of Standard Model background and 95% C.L. lower limits were set on the gravitino mass as a function of the squark/gluino mass, both in the case of degenerate and non-degenerate squark/gluino masses, see Figs. 14 and 15.

- ² ABDALLAH 05B use data from $\sqrt{s} = 180$ -208 GeV. They look for events with a single photon + \cancel{E} final states from which a cross section limit of $\sigma < 0.18 \text{ pb}$ at 208 GeV is obtained, allowing a limit on the mass to be set. Supersedes the results of ABREU 00z.

- ³ ACHARD 04E use data from $\sqrt{s} = 189$ -209 GeV. They look for events with a single photon + \cancel{E} final states from which a limit on the Gravitino mass is set corresponding to $\sqrt{F} > 238 \text{ GeV}$. Supersedes the results of ACCIARRI 99R.

- ⁴ HEISTER 03c use the data from $\sqrt{s} = 189$ -209 GeV to search for $\gamma\cancel{E}_T$ final states.

- ⁵ ACOSTA 02h looked in 87 pb^{-1} of $p\bar{p}$ collisions at $\sqrt{s} = 1.8 \text{ TeV}$ for events with a high- E_T photon and \cancel{E}_T . They compared the data with a GMSB model where the final state could arise from $q\bar{q} \rightarrow \tilde{G}\tilde{G}\gamma$. Since the cross section for this process scales as $1/|F|^4$, a limit at 95% CL is derived on $|F|^{1/2} > 221 \text{ GeV}$. A model independent limit for the above topology is also given in the paper.

- ⁶ ABBIENDI,G 00D searches for $\gamma\cancel{E}$ final states from $\sqrt{s} = 189 \text{ GeV}$.

Supersymmetry miscellaneous results

Results that do not appear under other headings or that make nonminimal assumptions.

Some earlier papers are now obsolete and have been omitted. They were last listed in our PDG 14 edition: K. Olive, et al. (Particle Data Group), Chinese Physics **C38** 070001 (2014) (<http://pdg.lbl.gov>).

VALUE	CL%	DOCUMENT ID	TECN	COMMENT
• • • We do not use the following data for averages, fits, limits, etc. • • •				
		¹ AAD	20c ATLS	habemus MSSM, m_A - $\tan\beta$ plane
none 450-1400	95	² AAD	20L ATLS	heavy neutral Higgs bosons, hMSSM, m_A - $\tan\beta$ plane
> 65	95	³ AABOUD	16AF ATLS	selected ATLAS searches on EWK sector
none 0-2	95	⁴ AAD	16AG ATLS	dark photon, γ_d , in SUSY- and Higgs-portal models
		⁵ AAD	13P ATLS	dark γ , hidden valley
		⁶ AALTONEN	12AB CDF	hidden-valley Higgs
		⁷ AAD	11AA ATLS	scalar gluons
none 100-185	95	⁸ CHATRCHYAN 11E	CMS	$\mu\mu$ resonances
		⁹ ABAZOV	10E D0	γ_d , hidden valley

- ¹ AAD 20c uses a statistical combination of six final states $b\bar{b}b\bar{b}$, $b\bar{b}W W$, $b\bar{b}\tau\tau$, $W W W W$, $b\bar{b}\gamma\gamma$, and $W W\gamma\gamma$ to search for non-resonant and resonant production of Higgs boson pairs. The search uses 36.1 fb^{-1} of pp collisions data at $\sqrt{s} = 13 \text{ TeV}$. Constraints in the habemus Minimal Supersymmetric Standard Model in the $(m_A, \tan\beta)$ parameter space are placed, see their Figure 7(b).

- ² AAD 20L used 27.8 fb^{-1} of pp collision data at $\sqrt{s} = 13 \text{ TeV}$ to search for heavy neutral Higgs bosons produced in association with at least one b -quark and decaying into a pair

Searches Particle Listings

Supersymmetric Particle Searches

of b -quarks. The data are compatible with SM expectations, yielding no significant excess of events in the mass range 450–1400 GeV, see their Fig. 11. Exclusion limits at 95% C.L. were derived in hMSSM scenarios as a function of m_A and $\tan\beta$, see their Fig. 9 and 10.

³ ABOUD 16AF uses a selection of searches by ATLAS for the electroweak production of SUSY particles studying resulting constraints on dark matter candidates. They use 20 fb⁻¹ of pp collisions at $\sqrt{s} = 8$ TeV. A likelihood-driven scan of an effective model focusing on the gaugino-higgsino and Higgs sector of the pMSSM is performed. The ATLAS searches impact models where $m_0 < 65$ GeV, excluding 86% of them. See their Figs. 2, 4, and 6.

⁴ AAD 16AG searches for prompt lepton-jets using 20 fb⁻¹ of pp collisions at $\sqrt{s} = 8$ TeV collected with the ATLAS detector. Lepton-jets are expected from decays of low-mass dark photons in SUSY-portal and Higgs-portal models. No significant excess of events is observed and 95% CL upper limits are computed on the production cross section times branching ratio for two prompt lepton-jets in models predicting 2 or 4 γ_D via SUSY-portal topologies, for γ_D mass values between 0 and 2 GeV. See their Figs 9 and 10. The results are also interpreted in terms of a 90% CL exclusion region in kinetic mixing and dark-photon mass parameter space. See their Fig. 13.

⁵ AAD 13P searched in 5 fb⁻¹ of pp collisions at $\sqrt{s} = 7$ TeV for single lepton-jets with at least four muons; pairs of lepton-jets, each with two or more muons; and pairs of lepton-jets with two or more electrons. All of these could be signatures of Hidden Valley supersymmetric models. No statistically significant deviations from the Standard Model expectations are found. 95% C.L. limits are placed on the production cross section times branching ratio of dark photons for several parameter sets of a Hidden Valley model.

⁶ AALTONEN 12AB looked in 5.1 fb⁻¹ of $p\bar{p}$ collisions at $\sqrt{s} = 1.96$ TeV for anomalous production of multiple low-energy leptons in association with a W or Z boson. Such events may occur in hidden valley models in which a supersymmetric Higgs boson is produced in association with a W or Z boson, with $H \rightarrow \tilde{\chi}_1^0 \tilde{\chi}_1^0$ pair and with the $\tilde{\chi}_1^0$ further decaying into a dark photon (γ_D) and the unobservable lightest SUSY particle of the hidden sector. As the γ_D is expected to be light, it may decay into a lepton pair. No significant excess over the SM expectation is observed and a limit at 95% C.L. is set on the cross section for a benchmark model of supersymmetric hidden-valley Higgs production.

⁷ AAD 11AA looked in 34 pb⁻¹ of pp collisions at $\sqrt{s} = 7$ TeV for events with ≥ 4 jets originating from pair production of scalar gluons, each decaying to two gluons. No two-jet resonances are observed over the SM background. Limits are derived on the cross section times branching ratio (see Fig. 3). Assuming 100% branching ratio for the decay to two gluons, the quoted exclusion range is obtained, except for a 5 GeV mass window around 140 GeV.

⁸ CHATRACHYAN 11E looked in 35 pb⁻¹ of pp collisions at $\sqrt{s} = 7$ TeV for events with collimated μ pairs (leptonic jets) from the decay of hidden sector states. No evidence for new resonance production is found. Limits are derived and compared to various SUSY models (see Fig. 4) where the LSP, either the $\tilde{\chi}_1^0$ or a \tilde{q} , decays to dark sector particles.

⁹ ABAZOV 10N looked in 5.8 fb⁻¹ of $p\bar{p}$ collisions at $\sqrt{s} = 1.96$ TeV for events from hidden valley models in which a $\tilde{\chi}_1^0$ decays into a dark photon, γ_D , and the unobservable lightest SUSY particle of the hidden sector. As the γ_D is expected to be light, it may decay into a tightly collimated lepton pair, called lepton jet. They searched for events with B_T and two isolated lepton jets observable by an opposite charged lepton pair e, e, μ, μ . No significant excess over the SM expectation is observed, and a limit at 95% C.L. on the cross section times branching ratio is derived, see their Table I. They also examined the invariant mass of the lepton jets for a narrow resonance, see their Fig. 4, but found no evidence for a signal.

REFERENCES FOR Supersymmetric Particle Searches

AAD	23AB	JHEP 2307 021	G. Aad et al.	(ATLAS Collab.)
AAD	23AE	EPJ C83 515	G. Aad et al.	(ATLAS Collab.)
AAD	23AL	EPJ C83 561	G. Aad et al.	(ATLAS Collab.)
AAD	23AM	PR D108 012012	G. Aad et al.	(ATLAS Collab.)
AAD	23BQ	PL B846 138172	G. Aad et al.	(ATLAS Collab.)
AAD	23CB	JHEP 2310 082	G. Aad et al.	(ATLAS Collab.)
AAD	23CI	JHEP 2312 167	G. Aad et al.	(ATLAS Collab.)
AAD	23CP	JHEP 2311 150	G. Aad et al.	(ATLAS Collab.)
AAD	23CR	JHEP 2312 081	G. Aad et al.	(ATLAS Collab.)
AAD	23G	JHEP 2306 158	G. Aad et al.	(ATLAS Collab.)
AAD	23M	JHEP 2306 031	G. Aad et al.	(ATLAS Collab.)
AALBERS	23	PRL 131 041002	J. Aalbers et al.	(LZ Collab.)
ABE	23B	PRL 130 051002	H. Abe et al.	(MAGIC Collab.)
APRILE	23A	PRL 131 041003	E. Aprile et al.	(XENONnT Collab.)
FOSTER	23	PR D107 103047	J.W. Foster et al.	(MIT, UCB, LBL+)
GUO	23A	PR D108 043001	X.-K. Guo et al.	(CMS Collab.)
HAYRAPETYAN...	23E	JHEP 2310 046	A. Hayrapetyan et al.	(BABAR Collab.)
LEES	23C	PRL 131 201801	J.P. Lees et al.	(CMS Collab.)
TUMASYAN	23AB	JHEP 2307 110	A. Tumasyan et al.	(CMS Collab.)
TUMASYAN	23AG	PR D108 012011	A. Tumasyan et al.	(CMS Collab.)
TUMASYAN	23AO	JHEP 2307 210	A. Tumasyan et al.	(CMS Collab.)
TUMASYAN	23AY	JHEP 2309 149	A. Tumasyan et al.	(CMS Collab.)
TUMASYAN	23B	PL B842 137460	A. Tumasyan et al.	(CMS Collab.)
TUMASYAN	23H	JHEP 2305 227	A. Tumasyan et al.	(CMS Collab.)
TUMASYAN	23K	JHEP 2306 060	A. Tumasyan et al.	(CMS Collab.)
TUMASYAN	23L	JHEP 2307 161	A. Tumasyan et al.	(CMS Collab.)
TUMASYAN	23X	EPJ C83 571	A. Tumasyan et al.	(CMS Collab.)
AAD	22E	PL B830 137106	G. Aad et al.	(ATLAS Collab.)
AAD	22U	EPJ C82 606	G. Aad et al.	(ATLAS Collab.)
ABBASI	22B	PR D105 062004	R. Abbasi et al.	(IceCube Collab.)
ABDALLA	22	PRL 129 111101	H. Abdalla et al.	(H.E.S.S. Collab.)
HUANG	22	PL B834 137487	Z. Huang et al.	(PandaX-4T Collab.)
TUMASYAN	22AF	EPJ C82 153	A. Tumasyan et al.	(CMS Collab.)
TUMASYAN	22Q	JHEP 2204 091	A. Tumasyan et al.	(CMS Collab.)
TUMASYAN	22S	JHEP 2204 147	A. Tumasyan et al.	(CMS Collab.)
TUMASYAN	22V	JHEP 2205 014	A. Tumasyan et al.	(CMS Collab.)
AAD	21AK	EPJ C81 600	G. Aad et al.	(ATLAS Collab.)
AAD	21AL	PRL 127 051802	G. Aad et al.	(ATLAS Collab.)
AAD	21AM	PR D104 032014	G. Aad et al.	(ATLAS Collab.)
AAD	21AW	PR D104 112005	G. Aad et al.	(ATLAS Collab.)
AAD	21AX	PR D104 112010	G. Aad et al.	(ATLAS Collab.)
AAD	21B	EPJ C81 11	G. Aad et al.	(ATLAS Collab.)
Also	EPJ	C81 249 (errata.)	G. Aad et al.	(ATLAS Collab.)
AAD	21BF	EPJ C81 1023	G. Aad et al.	(ATLAS Collab.)
AAD	21BG	EPJ C81 1118	G. Aad et al.	(ATLAS Collab.)
AAD	21E	PR D103 112003	G. Aad et al.	(ATLAS Collab.)
AAD	21F	PR D103 112006	G. Aad et al.	(ATLAS Collab.)
AAD	21L	JHEP 2102 143	G. Aad et al.	(ATLAS Collab.)
AAD	21O	JHEP 2104 174	G. Aad et al.	(ATLAS Collab.)
AAD	21P	JHEP 2104 165	G. Aad et al.	(ATLAS Collab.)
AAD	21S	JHEP 2105 093	G. Aad et al.	(ATLAS Collab.)

AAD	21X	JHEP 2107 173	G. Aad et al.	(ATLAS Collab.)
AAD	21Y	JHEP 2107 167	G. Aad et al.	(ATLAS Collab.)
AAIJ	21V	EPJ C81 261	R. Aaij et al.	(LHCb Collab.)
ABDALLAH	21	PR D103 102002	H. Abdallah et al.	(H.E.S.S. Collab.)
MENG	21B	PRL 127 261802	Y. Meng et al.	(PandaX-4T Collab.)
SIRUNYAN	21AD	PR D104 052001	A.M. Sirunyan et al.	(CMS Collab.)
SIRUNYAN	21AF	PR D104 052011	A.M. Sirunyan et al.	(CMS Collab.)
SIRUNYAN	21B	EPJ C81 3	A.M. Sirunyan et al.	(CMS Collab.)
SIRUNYAN	21M	JHEP 2104 123	A.M. Sirunyan et al.	(CMS Collab.)
SIRUNYAN	21U	PR D104 012015	A.M. Sirunyan et al.	(CMS Collab.)
SIRUNYAN	21V	PR D104 032006	A.M. Sirunyan et al.	(CMS Collab.)
TUMASYAN	21C	JHEP 2110 045	A. Tumasyan et al.	(CMS Collab.)
TUMASYAN	21I	EPJ C81 970	A. Tumasyan et al.	(CMS Collab.)
AABOUD	20	EPJ C80 754	M. Aaboud et al.	(ATLAS Collab.)
AAD	20AL	JHEP 2010 062	G. Aad et al.	(ATLAS Collab.)
AAD	20AN	JHEP 2010 005	G. Aad et al.	(ATLAS Collab.)
AAD	20AS	EPJ C80 1080	G. Aad et al.	(ATLAS Collab.)
AAD	20C	PL B800 135113	G. Aad et al.	(ATLAS Collab.)
AAD	20D	PL B801 135114	G. Aad et al.	(ATLAS Collab.)
AAD	20H	PR D101 032009	G. Aad et al.	(ATLAS Collab.)
AAD	20I	PR D101 052005	G. Aad et al.	(ATLAS Collab.)
AAD	20K	PR D101 072001	G. Aad et al.	(ATLAS Collab.)
AAD	20L	PR D102 032004	G. Aad et al.	(ATLAS Collab.)
AAD	20M	PR D102 032006	G. Aad et al.	(ATLAS Collab.)
AAD	20O	EPJ C80 123	G. Aad et al.	(ATLAS Collab.)
AAD	20R	EPJ C80 691	G. Aad et al.	(ATLAS Collab.)
AAD	20S	EPJ C80 737	G. Aad et al.	(ATLAS Collab.)
AAD	20V	JHEP 2006 046	G. Aad et al.	(ATLAS Collab.)
ABAZAJIAN	20	PR D102 043012	K.M. Abazajian et al.	(UCI, VPI, TOKY+)
ABDALLAH	20	PR D102 052001	H. Abdallah et al.	(H.E.S.S. Collab.)
ABE	20G	PR D102 072002	K. Abe et al.	(Super-Kamiokande Collab.)
ALBERT	20	PR D101 103001	A. Albert et al.	(HAWC Collab.)
ALBERT	20A	PL B805 135439	A. Albert et al.	(ANTARES Collab.)
ALBERT	20C	PR D102 082002	A. Albert et al.	(ANTARES and IceCube Collab.)
ALVAREZ	20	JCAP 2009 004	A. Alvarez et al.	(GOET+)
HOOF	20	JCAP 2002 012	S. Hoof, A. Geringer-Sameth, R. Trotta	(GOET+)
SIRUNYAN	20AH	JHEP 2005 032	A.M. Sirunyan et al.	(CMS Collab.)
SIRUNYAN	20AU	PRL 124 041803	A.M. Sirunyan et al.	(CMS Collab.)
SIRUNYAN	20B	PL B801 135183	A.M. Sirunyan et al.	(CMS Collab.)
SIRUNYAN	20BJ	JHEP 2009 149	A.M. Sirunyan et al.	(CMS Collab.)
SIRUNYAN	20E	PR D101 052010	A.M. Sirunyan et al.	(CMS Collab.)
SIRUNYAN	20F	PL B806 135502	A.M. Sirunyan et al.	(CMS Collab.)
SIRUNYAN	20P	EPJ C80 189	A.M. Sirunyan et al.	(CMS Collab.)
SIRUNYAN	20T	EPJ C80 752	A.M. Sirunyan et al.	(CMS Collab.)
SIRUNYAN	20U	JHEP 2002 015	A.M. Sirunyan et al.	(CMS Collab.)
WANG	20	CP C44 125001	Q. Wang et al.	(PandaX-II Collab.)
AABOUD	19AT	PR D99 092007	M. Aaboud et al.	(ATLAS Collab.)
AABOUD	19U	PR D100 012006	M. Aaboud et al.	(ATLAS Collab.)
AABOUD	19C	PL B788 96	M. Aaboud et al.	(ATLAS Collab.)
AABOUD	19G	PR D99 012001	M. Aaboud et al.	(ATLAS Collab.)
AABOUD	19I	PR D99 012009	M. Aaboud et al.	(ATLAS Collab.)
AAD	19H	JHEP 1912 060	G. Aad et al.	(ATLAS Collab.)
ABE	19	PL B778 45	K. Abe et al.	(XMASS Collab.)
AIAJ	19	PR D100 022004	R. Aaij et al.	(DEAP-3600 Collab.)
AMOLE	19	PR D100 022001	C. Amole et al.	(PICO Collab.)
APRILE	19A	PRL 122 141301	E. Aprile et al.	(XENONIT Collab.)
DI-MAURO	19	PR D99 123027	M. Di Mauro et al.	(CMS Collab.)
JOHNSON	19	PR D99 103007	C. Johnson et al.	(CMS Collab.)
LI	19D	PR D99 123519	S. Li et al.	(CMS Collab.)
SIRUNYAN	19AG	JHEP 1906 143	A.M. Sirunyan et al.	(CMS Collab.)
SIRUNYAN	19AO	EPJ C79 305	A.M. Sirunyan et al.	(CMS Collab.)
SIRUNYAN	19AU	EPJ C79 444	A.M. Sirunyan et al.	(CMS Collab.)
SIRUNYAN	19AW	PL B790 140	A.M. Sirunyan et al.	(CMS Collab.)
SIRUNYAN	19BH	PR D99 032011	A.M. Sirunyan et al.	(CMS Collab.)
SIRUNYAN	19BI	PR D99 032014	A.M. Sirunyan et al.	(CMS Collab.)
SIRUNYAN	19BJ	PR D99 052002	A.M. Sirunyan et al.	(CMS Collab.)
SIRUNYAN	19BT	PL B797 134876	A.M. Sirunyan et al.	(CMS Collab.)
SIRUNYAN	19BU	JHEP 1908 150	A.M. Sirunyan et al.	(CMS Collab.)
SIRUNYAN	19CA	PR D100 112003	A.M. Sirunyan et al.	(CMS Collab.)
SIRUNYAN	19CE	PRL 123 241801	A.M. Sirunyan et al.	(CMS Collab.)
SIRUNYAN	19CH	JHEP 1910 244	A.M. Sirunyan et al.	(CMS Collab.)
SIRUNYAN	19CI	JHEP 1911 109	A.M. Sirunyan et al.	(CMS Collab.)
SIRUNYAN	19CF	PR D99 012010	A.M. Sirunyan et al.	(CMS Collab.)
SIRUNYAN	19Q	JHEP 1901 154	A.M. Sirunyan et al.	(CMS Collab.)
SIRUNYAN	19S	JHEP 1903 031	A.M. Sirunyan et al.	(CMS Collab.)
SIRUNYAN	19U	JHEP 1903 101	A.M. Sirunyan et al.	(CMS Collab.)
XIA	19A	PL B792 193	J. Xia et al.	(PandaX-II Collab.)
AABOUD	18AQ	JHEP 1806 108	M. Aaboud et al.	(ATLAS Collab.)
AABOUD	18AR	JHEP 1806 107	M. Aaboud et al.	(ATLAS Collab.)
AABOUD	18AS	JHEP 1806 022	M. Aaboud et al.	(ATLAS Collab.)
AABOUD	18AV	EPJ C78 154	M. Aaboud et al.	(ATLAS Collab.)
AABOUD	18BB	EPJ C78 250	M. Aaboud et al.	(ATLAS Collab.)
AABOUD	18BT	EPJ C78 625	M. Aaboud et al.	(ATLAS Collab.)
AABOUD	18BT	EPJ C78 995	M. Aaboud et al.	(ATLAS Collab.)
AABOUD	18BV	JHEP 1809 050	M. Aaboud et al.	(ATLAS Collab.)
AABOUD	18CF	PL B785 136	M. Aaboud et al.	(ATLAS Collab.)
AABOUD	18CK	PR D98 092002	M. Aaboud et al.	(ATLAS Collab.)
AABOUD	18CM	PR D98 092008	M. Aaboud et al.	(ATLAS Collab.)
AABOUD	18CO	PR D98 092012	M. Aaboud et al.	(ATLAS Collab.)
AABOUD	18I	JHEP 1801 126	M. Aaboud et al.	(ATLAS Collab.)
AABOUD	18P	PR D97 032003	M. Aaboud et al.	(ATLAS Collab.)
AABOUD	18R	PR D97 052010	M. Aaboud et al.	(ATLAS Collab.)
AABOUD	18U	PR D97 092006	M. Aaboud et al.	(ATLAS Collab.)
AABOUD	18V	PR D97 112001	M. Aaboud et al.	(ATLAS Collab.)
AABOUD	18Y	PR D98 032008	M. Aaboud et al.	(ATLAS Collab.)
AABOUD	18Z	PR D98 032009	M. Aaboud et al.	(ATLAS Collab.)
ABDALLAH	18	PRL 120 201101	H. Abdallah et al.	(H.E.S.S. Collab.)
ADHIKARI	18	NAT 564 83	G. Adhikari et al.	(COSINE-100 Collab.)
AGNES	18A	PR D98 102006	P. Agnes et al.	(DarkSide-50 Collab.)
AGNESE	18A	PRL 120 061802	R. Agnese et al.	(SuperCDMS Collab.)
AHNEN	18	JCAP 1803 009	M.L. Ahnen et al.	(MAGIC Collab.)
ALBERT	18B	JCAP 1806 043	A. Albert et al.	(HAWC Collab.)
ALBERT	18C	PR D98 123012	A. Albert et al.	(HAWC Collab.)
AMAUDRUZ	18	PRL 121 071801	P.A. Amaudruz et al.	(DEAP-3600 Collab.)
APRILE	18	PRL 121 111302	E. Aprile et al.	(XENONIT Collab.)
SIRUNYAN	18AA	PL B780 118	A.M. Sirunyan et al.	(CMS Collab.)
SIRUNYAN	18AC	PL B780 384	A.M. Sirunyan et al.	(CMS Collab.)
SIRUNYAN	18AD	PL B780 432	A.M. Sirunyan et al.	(CMS Collab.)
SIRUNYAN	18AJ	PL B782 440	A.M. Sirunyan et al.	(CMS Collab.)
SIRUNYAN	18AK	PL B783 114	A.M. Sirunyan et al.	(CMS Collab.)
SIRUNYAN	18AL	JHEP 1802 067	A.M. Sirunyan et al.	(CMS Collab.)
SIRUNYAN	18AN	JHEP 1803 167	A.M. Sirunyan et al.	(CMS Collab.)
SIRUNYAN	18AO	JHEP 1803 166	A.M. Sirunyan et al.	(CMS Collab.)
SIRUNYAN	18AP	JHEP 1803 160	A.M. Sirunyan et al.	(CMS Collab.)
SIRUNYAN	18AR	JHEP 1803 076	A.M. Sirunyan et al.	(CMS Collab.)
SIRUNYAN	18AT	JHEP 1804 073	A.M. Sirunyan et al.	(CMS Collab.)
SIRUNYAN	18AY	JHEP 1805 025	A.M. Sirunyan et al.	(CMS Collab.)
SIRUNYAN	18B	PL B778 263	A.M. Sirunyan et al.	(CMS Collab.)
SIRUNYAN	18BR	JHEP 1808 016	A.M. Sirunyan et al.	(CMS Collab.)
SIRUNYAN	18C	PR D97 032009	A.M. Sirunyan et al.	(CMS Collab.)
SIRUNYAN	18D	PR D97 012007	A.M. Sirunyan et al.	(CMS Collab.)

See key on page 1171

Searches Particle Listings

Supersymmetric Particle Searches

SIRUNYAN	18DI	JHEP	1809	065	A.M. Sirunyan et al.	(CMS Collab.)	ACKERMANN	15	PR	D91	122002	M. Ackermann et al.	(Fermi-LAT Collab.)
SIRUNYAN	18DN	JHEP	1811	079	A.M. Sirunyan et al.	(CMS Collab.)	ACKERMANN	15A	JCAP	1509	008	M. Ackermann et al.	(Fermi-LAT Collab.)
SIRUNYAN	18DP	JHEP	1811	151	A.M. Sirunyan et al.	(CMS Collab.)	ACKERMANN	15B	PRL	115	231301	M. Ackermann et al.	(Fermi-LAT Collab.)
SIRUNYAN	18DV	PR	D98	092011	A.M. Sirunyan et al.	(CMS Collab.)	AGNES	15	PL	B743	456	P. Agnes et al.	(DarkSide-50 Collab.)
SIRUNYAN	18DY	PR	D98	112014	A.M. Sirunyan et al.	(CMS Collab.)	AGNES E	15B	PR	D92	072003	R. Agnese et al.	(SuperCDMS Collab.)
SIRUNYAN	18EA	PRL	121	141802	A.M. Sirunyan et al.	(CMS Collab.)	BAGNASCHI	15	EPJ	C75	500	E.A. Bagnaschi et al.	
SIRUNYAN	18M	PRL	120	241801	A.M. Sirunyan et al.	(CMS Collab.)	BUCKLEY	15	PR	D91	102001	M.R. Buckley et al.	
SIRUNYAN	18O	PR	D97	032007	A.M. Sirunyan et al.	(CMS Collab.)	CHOI	15	PRL	114	141301	K. Choi et al.	(Super-Kamiokande Collab.)
SIRUNYAN	18X	PL	B779	166	A.M. Sirunyan et al.	(CMS Collab.)	KHACHATRYAN	15AB	JHEP	1501	096	V. Khachatryan et al.	(CMS Collab.)
AABOUD	17AF	JHEP	1708	006	M. Aboud et al.	(ATLAS Collab.)	KHACHATRYAN	15AD	JHEP	1504	124	V. Khachatryan et al.	(CMS Collab.)
AABOUD	17AI	JHEP	1709	088	M. Aboud et al.	(ATLAS Collab.)	KHACHATRYAN	15AF	JHEP	1505	078	V. Khachatryan et al.	(CMS Collab.)
AABOUD	17AJ	JHEP	1709	084	M. Aboud et al.	(ATLAS Collab.)	KHACHATRYAN	15AH	JHEP	1506	116	V. Khachatryan et al.	(CMS Collab.)
	Also	JHEP	1908	121	(err.)	M. Aboud et al.	KHACHATRYAN	15AK	EPJ	C75	151	V. Khachatryan et al.	(CMS Collab.)
AABOUD	17AR	PR	D96	112010	M. Aboud et al.	(ATLAS Collab.)	KHACHATRYAN	15AO	EPJ	C75	325	V. Khachatryan et al.	(CMS Collab.)
AABOUD	17AX	JHEP	1711	195	M. Aboud et al.	(ATLAS Collab.)	KHACHATRYAN	15AR	PL	B743	503	V. Khachatryan et al.	(CMS Collab.)
AABOUD	17AY	JHEP	1712	085	M. Aboud et al.	(ATLAS Collab.)	KHACHATRYAN	15AZ	PR	D92	072006	V. Khachatryan et al.	(CMS Collab.)
AABOUD	17AZ	JHEP	1712	034	M. Aboud et al.	(ATLAS Collab.)	KHACHATRYAN	15B	PRL	114	061801	V. Khachatryan et al.	(CMS Collab.)
AABOUD	17BE	EPJ	C77	898	M. Aboud et al.	(ATLAS Collab.)	KHACHATRYAN	15I	PL	B745	5	V. Khachatryan et al.	(CMS Collab.)
AABOUD	17N	EPJ	C77	144	M. Aboud et al.	(ATLAS Collab.)	KHACHATRYAN	15L	PL	B747	98	V. Khachatryan et al.	(CMS Collab.)
AALU	17Z	EPJ	C77	224	R. Aaij et al.	(LHCb Collab.)	KHACHATRYAN	15O	PL	B749	255	V. Khachatryan et al.	(CMS Collab.)
AARTSEN	17	EPJ	C77	82	M.G. Aartsen et al.	(IceCube Collab.)	KHACHATRYAN	15W	PR	D91	052012	V. Khachatryan et al.	(CMS Collab.)
AARTSEN	17A	EPJ	C77	146	M.G. Aartsen et al.	(IceCube Collab.)	KHACHATRYAN	15X	PR	D91	052018	V. Khachatryan et al.	(CMS Collab.)
	Also	EPJ	C79	214	(err.)	M.G. Aartsen et al.	ROLBIECKI	15	PL	B750	247	K. Rolbiecki, J. Tattersall	(MADE, HEID)
AARTSEN	17C	EPJ	C77	627	M.G. Aartsen et al.	(IceCube Collab.)	AAD	14AE	JHEP	1409	176	G. Aad et al.	(ATLAS Collab.)
AKERIB	17	PRL	118	021303	D.S. Akerib et al.	(LUX Collab.)	AAD	14AG	JHEP	1409	103	G. Aad et al.	(ATLAS Collab.)
AKERIB	17A	PRL	118	251302	D.S. Akerib et al.	(LUX Collab.)	AAD	14AJ	JHEP	1409	015	G. Aad et al.	(ATLAS Collab.)
AMOLE	17	PRL	118	251301	C. Amole et al.	(PICO Collab.)	AAD	14AV	JHEP	1410	096	G. Aad et al.	(ATLAS Collab.)
APRILE	17G	PRL	119	181301	E. Aprile et al.	(XENON Collab.)	AAD	14AX	JHEP	1410	024	G. Aad et al.	(ATLAS Collab.)
ARCHAMBAULT	17	PR	D95	082001	S. Archambault et al.	(VERITAS Collab.)	AAD	14B	EPJ	C74	2883	G. Aad et al.	(ATLAS Collab.)
ATHRON	17B	EPJ	C77	824	P. Athron et al.	(GAMBIT Collab.)	AAD	14BD	JHEP	1411	118	G. Aad et al.	(ATLAS Collab.)
BATTAT	17	ASP	91	65	J.B.R. Battat et al.	(DRIFT Collab.)	AAD	14BH	PR	D90	01005	G. Aad et al.	(ATLAS Collab.)
BEHNKE	17	ASP	90	85	J. Behnke et al.	(PICASSO Collab.)	AAD	14E	JHEP	1406	035	G. Aad et al.	(ATLAS Collab.)
CUI	17A	PRL	119	181302	X. Cui et al.	(PandaX-II Collab.)	AAD	14F	JHEP	1406	124	G. Aad et al.	(ATLAS Collab.)
FU	17	PR	118	071301	C. Fu et al.	(PandaX-II Collab.)	AAD	14G	JHEP	1405	071	G. Aad et al.	(ATLAS Collab.)
	Also	PRL	120	049902	(err.)	C. Fu et al.	AAD	14H	JHEP	1404	169	G. Aad et al.	(ATLAS Collab.)
KHACHATRYAN	17	PR	D95	012003	V. Khachatryan et al.	(CMS Collab.)	AAD	14K	PR	D90	012004	G. Aad et al.	(ATLAS Collab.)
KHACHATRYAN	17A	PRL	118	021802	V. Khachatryan et al.	(CMS Collab.)	AAD	14T	PR	D90	052008	G. Aad et al.	(ATLAS Collab.)
KHACHATRYAN	17AD	PR	D96	012004	V. Khachatryan et al.	(CMS Collab.)	AAD	14X	PR	D90	052001	G. Aad et al.	(ATLAS Collab.)
KHACHATRYAN	17AR	PR	D95	012009	V. Khachatryan et al.	(CMS Collab.)	AALTONEN	14	PR	D90	012011	T. Aaltonen et al.	(CDF Collab.)
KHACHATRYAN	17AS	PR	D95	012011	V. Khachatryan et al.	(CMS Collab.)	ACKERMANN	14	PR	D89	042001	M. Ackermann et al.	(Fermi-LAT Collab.)
KHACHATRYAN	17AW	EPJ	C77	635	V. Khachatryan et al.	(CMS Collab.)	AKERIB	14	PRL	112	091303	D.S. Akerib et al.	(LUX Collab.)
KHACHATRYAN	17L	JHEP	1704	018	V. Khachatryan et al.	(CMS Collab.)	AKHSIC	14	JCAP	1402	008	J. Akhsic et al.	(MAGIC Collab.)
KHACHATRYAN	17P	EPJ	C77	294	V. Khachatryan et al.	(CMS Collab.)	AVRORIN	14	ASP	62	12	A.D. Avrorin et al.	(BAIKAL Collab.)
KHACHATRYAN	17S	PL	B767	403	V. Khachatryan et al.	(CMS Collab.)	BUCHMUELLER	14	EPJ	C74	2809	O. Buchmüller et al.	
KHACHATRYAN	17V	PL	B769	391	V. Khachatryan et al.	(CMS Collab.)	BUCHMUELLER	14A	EPJ	C74	2922	O. Buchmüller et al.	
KHACHATRYAN	17Y	PL	B770	257	V. Khachatryan et al.	(CMS Collab.)	CHATRCHYAN	14AH	PR	D90	112001	S. Chatrchyan et al.	(CMS Collab.)
SIRUNYAN	17AF	PRL	119	151802	A.M. Sirunyan et al.	(CMS Collab.)	CHATRCHYAN	14H	JHEP	1401	163	S. Chatrchyan et al.	(CMS Collab.)
SIRUNYAN	17AS	JHEP	1710	019	A.M. Sirunyan et al.	(CMS Collab.)	CHATRCHYAN	14I	JHEP	1406	055	S. Chatrchyan et al.	(CMS Collab.)
SIRUNYAN	17AT	JHEP	1710	005	A.M. Sirunyan et al.	(CMS Collab.)	CHATRCHYAN	14N	PL	B733	328	S. Chatrchyan et al.	(CMS Collab.)
SIRUNYAN	17AW	JHEP	1711	029	A.M. Sirunyan et al.	(CMS Collab.)	CHATRCHYAN	14P	PL	B730	193	S. Chatrchyan et al.	(CMS Collab.)
SIRUNYAN	17AY	JHEP	1712	142	A.M. Sirunyan et al.	(CMS Collab.)	CHATRCHYAN	14R	PR	D90	032006	S. Chatrchyan et al.	(CMS Collab.)
SIRUNYAN	17AZ	EPJ	C77	710	A.M. Sirunyan et al.	(CMS Collab.)	CHATRCHYAN	14U	PRL	112	161802	S. Chatrchyan et al.	(CMS Collab.)
SIRUNYAN	17K	EPJ	C77	327	A.M. Sirunyan et al.	(CMS Collab.)	CZAKON	14	PRL	113	201803	S.M. Czakon et al.	(LEP Collab.)
SIRUNYAN	17P	PR	D96	032003	A.M. Sirunyan et al.	(CMS Collab.)	FELIZARDO	14	PR	D89	072013	M. Felizardo et al.	(AACH, CAMB Collab.)
SIRUNYAN	17S	EPJ	C77	578	A.M. Sirunyan et al.	(CMS Collab.)	KHACHATRYAN	14C	PL	B736	371	V. Khachatryan et al.	(CMS Collab.)
AABOUD	16AC	EPJ	C76	683	M. Aboud et al.	(ATLAS Collab.)	KHACHATRYAN	14I	EPJ	C74	3036	V. Khachatryan et al.	(CMS Collab.)
AABOUD	16AF	JHEP	1609	175	M. Aboud et al.	(ATLAS Collab.)	KHACHATRYAN	14L	PR	D90	092007	V. Khachatryan et al.	(CMS Collab.)
AABOUD	16B	PL	B760	647	M. Aboud et al.	(ATLAS Collab.)	KHACHATRYAN	14T	PL	B739	229	V. Khachatryan et al.	(CMS Collab.)
AABOUD	16C	PR	D93	112015	M. Aboud et al.	(ATLAS Collab.)	PDG	14	CP	C38	070001	K. Olive et al.	(PDG Collab.)
AABOUD	16D	PR	D94	032005	M. Aboud et al.	(ATLAS Collab.)	ROSKZKOWSKI	14	JHEP	1408	067	L. Roszkowski, E.M. Sessolo, A.J. Williams	(WINR)
AABOUD	16J	PR	D94	052009	M. Aboud et al.	(ATLAS Collab.)	AAD	13	PL	B718	841	G. Aad et al.	(ATLAS Collab.)
AABOUD	16M	EPJ	C76	517	M. Aboud et al.	(ATLAS Collab.)	AAD	13AA	PL	B720	277	G. Aad et al.	(ATLAS Collab.)
AABOUD	16N	EPJ	C76	392	M. Aboud et al.	(ATLAS Collab.)	AAD	13AI	PL	B723	15	G. Aad et al.	(ATLAS Collab.)
AABOUD	16P	EPJ	C76	541	M. Aboud et al.	(ATLAS Collab.)	AAD	13AP	PR	D89	012001	G. Aad et al.	(ATLAS Collab.)
AABOUD	16Q	EPJ	C76	547	M. Aboud et al.	(ATLAS Collab.)	AAD	13AU	JHEP	1310	189	G. Aad et al.	(ATLAS Collab.)
AAD	16AA	PR	D93	052002	G. Aad et al.	(ATLAS Collab.)	AAD	13B	PL	B718	879	G. Aad et al.	(ATLAS Collab.)
AAD	16AD	PR	D94	032003	G. Aad et al.	(ATLAS Collab.)	AAD	13BC	PR	D88	112003	G. Aad et al.	(ATLAS Collab.)
AAD	16AG	JHEP	1602	062	G. Aad et al.	(ATLAS Collab.)	AAD	13BD	PR	D88	112006	G. Aad et al.	(ATLAS Collab.)
AAD	16AM	JHEP	1606	067	G. Aad et al.	(ATLAS Collab.)	AAD	13H	JHEP	1301	131	G. Aad et al.	(ATLAS Collab.)
AAD	16AY	EPJ	C76	81	G. Aad et al.	(ATLAS Collab.)	AAD	13L	PR	D87	012008	G. Aad et al.	(ATLAS Collab.)
AAD	16BB	EPJ	C76	259	G. Aad et al.	(ATLAS Collab.)	AAD	13P	PL	B719	299	G. Aad et al.	(ATLAS Collab.)
AAD	16BG	EPJ	C76	565	G. Aad et al.	(ATLAS Collab.)	AAD	13Q	PL	B719	261	G. Aad et al.	(ATLAS Collab.)
AAD	16V	PL	B757	334	G. Aad et al.	(ATLAS Collab.)	AAD	13R	PL	B719	280	G. Aad et al.	(ATLAS Collab.)
AARTSEN	16C	JCAP	1604	022	M.G. Aartsen et al.	(IceCube Collab.)	AALTONEN	13I	PR	D88	031103	T. Aaltonen et al.	(CDF Collab.)
ADRIAN-MAR.	15	PR	B759	327	S. Adrian-Martinez et al.	(ANTARES Collab.)	AALTONEN	13J	PR	110	201802	T. Aaltonen et al.	(CDF Collab.)
AHNEN	15	JCAP	1602	039	M.L. Ahnen et al.	(MAGIC and Fermi-LAT Collab.)	AARTSEN	13Q	PR	D88	122001	M.L. Aartsen et al.	(IceCube Collab.)
AKERIB	16	PRL	116	161301	D.S. Akerib et al.	(LUX Collab.)	ABAZOV	13B	PR	D87	052011	V.M. Abazov et al.	(DO Collab.)
AKERIB	16A	PRL	116	161302	D.S. Akerib et al.	(LUX Collab.)	ACKERMANN	13A	PR	D88	082002	M. Ackermann et al.	(Fermi-LAT Collab.)
AMOLE	16	PR	D93	052014	C. Amole et al.	(PICO Collab.)	ADRIAN-MAR.	13	JCAP	1311	032	S. Adrian-Martinez et al.	(ANTARES Collab.)
APRILE	16B	PR	D94	122001	E. Aprile et al.	(XENON100 Collab.)	AGNES E	13	PR	D88	031104	R. Agnese et al.	(CMS Collab.)
AVRORIN	16	ASP	81	12	A.D. Avrorin et al.	(BAIKAL Collab.)	AGNES E	13A	PRL	111	251301	R. Agnese et al.	(CMS Collab.)
BECHTLE	16	EPJ	C76	96	P. Bechtle et al.	(BAIKAL Collab.)	APRILE	13	PRL	111	021301	E. Aprile et al.	(XENON100 Collab.)
CIRELLI	16	JCAP	1607	041	M. Cirelli, M. Taoso	(LPNHE, MADE)	BERGSTROM	13	PRL	111	171101	L. Bergstrom et al.	
KHACHATRYAN	16AA	PL	B759	479	V. Khachatryan et al.	(CMS Collab.)	BOLEV	13	JCAP	1309	019	M. Boлев et al.	
KHACHATRYAN	16AC	PL	B760	178	V. Khachatryan et al.	(CMS Collab.)	CABRERA	13	JHEP	1307	182	M. Cabrera, J. Casas, R. de Austri	
KHACHATRYAN	16AM	PR	D93	092009	V. Khachatryan et al.	(CMS Collab.)	ALIBISI	13	JHEP	1310	132	L. Alibisi et al.	
KHACHATRYAN	16AV	JHEP	1607	027	V. Khachatryan et al.	(CMS Collab.)	CHATRCHYAN	13	PL	B718	815	S. Chatrchyan et al.	(CMS Collab.)
KHACHATRYAN	16AY	JHEP	1608	122									

Searches Particle Listings

Supersymmetric Particle Searches

ANGLOHER	12	EPJ C72 1971	G. Angloher et al. (CRESS-T-II Collab.)
APRILE	12	PRL 109 181301	E. Aprile et al. (XENON100 Collab.)
ARBEY	12A	PL B708 162	A. Arbey et al.
ARCHAMBAULT	12	PL B711 153	S. Archambault et al. (PICASSO Collab.)
BAER	12	JHEP 1205 091	H. Baer, V. Barger, A. Mustafayev (OKLA, WIS+)
BALAZS	12	EPJ C73 2563	C. Balazs et al.
BECHTLE	12	JHEP 1206 098	P. Bechtle et al. (COUAPP Collab.)
BEHNKE	12	PR D86 052001	E. Behnke et al. (COUAPP Collab.)
Also		PR D90 079902 (errat.)	
BESKIDT	12	EPJ C72 2166	C. Beskidt et al. (KARLE, JINR, ITEP)
BOTTINO	12	PR D85 095013	A. Bottino, N. Fornengo, S. Scopel (TORI, SOGA)
BUCHMUELLER	12	EPJ C72 2020	O. Buchmüller et al.
CAO	12A	PL B710 665	J. Cao et al.
CHATRCHYAN	12	PR D85 012004	S. Chatrchyan et al. (CMS Collab.)
CHATRCHYAN	12A	PRL 109 171803	S. Chatrchyan et al. (CMS Collab.)
CHATRCHYAN	12A	JHEP 1208 110	S. Chatrchyan et al. (CMS Collab.)
CHATRCHYAN	12A	JHEP 1206 169	S. Chatrchyan et al. (CMS Collab.)
CHATRCHYAN	12A	JHEP 1208 026	S. Chatrchyan et al. (CMS Collab.)
CHATRCHYAN	12A	JHEP 1210 018	S. Chatrchyan et al. (CMS Collab.)
CHATRCHYAN	12B	JHEP 1211 147	S. Chatrchyan et al. (CMS Collab.)
CHATRCHYAN	12B	JHEP 1211 172	S. Chatrchyan et al. (CMS Collab.)
CHATRCHYAN	12B	JHEP 1212 055	S. Chatrchyan et al. (CMS Collab.)
CHATRCHYAN	12L	PL B713 408	S. Chatrchyan et al. (CMS Collab.)
DAW	12	ASP 35 397	E. Daw et al. (DRIFT-III Collab.)
DREINER	12A	EPL 99 61001	H.K. Dreiner, M. Kramer, J. Tattersall (BONN+)
ELLIS	12B	EPJ C72 2005	J. Ellis, K. Olive
FELIZARDO	12	PRL 108 201302	M. Felizardo et al. (SIMPLE Collab.)
FENG	12B	PR D85 075007	J. Feng, K. Matchev, D. Sanford
KADASTIK	12	JHEP 1205 061	M. Kadastik et al.
KIM	12	PRL 108 181301	S.C. Kim et al. (KIMS Collab.)
STREGGE	12	ICAP 1203 020	C. Stregge et al. (LOIC, AMST, MADU, GRAN+)
AAD	11A	EPJ C71 1828	G. Aad et al. (ATLAS Collab.)
AAD	11G	PRL 106 131802	G. Aad et al. (ATLAS Collab.)
AAD	11H	PRL 106 251801	G. Aad et al. (ATLAS Collab.)
AAD	11K	PL B701 1	G. Aad et al. (ATLAS Collab.)
AAD	11O	PL B701 398	G. Aad et al. (ATLAS Collab.)
AAD	11P	PL B703 428	G. Aad et al. (ATLAS Collab.)
AAD	11Z	EPJ C71 1809	G. Aad et al. (ATLAS Collab.)
AHMED	11A	PR D84 011102	Z. Ahmed et al. (CDMS and EDELWEISS Collabs.)
ARMENGAUD	11	PL B702 329	E. Armengaud et al. (EDELWEISS-II Collab.)
BUCHMUELLER	11	EPJ C71 1583	O. Buchmüller et al.
BUCHMUELLER	11B	EPJ C71 1722	O. Buchmüller et al.
CHATRCHYAN	11B	JHEP 1106 093	S. Chatrchyan et al. (CMS Collab.)
CHATRCHYAN	11D	JHEP 1107 113	S. Chatrchyan et al. (CMS Collab.)
CHATRCHYAN	11E	JHEP 1107 098	S. Chatrchyan et al. (CMS Collab.)
CHATRCHYAN	11V	PL B704 411	S. Chatrchyan et al. (CMS Collab.)
KHACHATRYAN	11	PRL 106 011801	V. Khachatryan et al. (CMS Collab.)
KHACHATRYAN	11C	JHEP 1103 024	V. Khachatryan et al. (CMS Collab.)
ROSKOWSKI	11	PR D83 015014	L. Roszkowski et al.
AALTONEN	10	PRL 104 011801	T. Aaltonen et al. (CDF Collab.)
AALTONEN	10R	PRL 105 081802	T. Aaltonen et al. (CDF Collab.)
AALTONEN	10Z	PRL 105 191801	T. Aaltonen et al. (CDF Collab.)
ABAZOV	10	PL B693 95	V.M. Abazov et al. (DO Collab.)
ABAZOV	10M	PRL 105 191802	V.M. Abazov et al. (DO Collab.)
ABAZOV	10N	PRL 105 211802	V.M. Abazov et al. (DO Collab.)
ABAZOV	10P	PRL 105 221802	V.M. Abazov et al. (DO Collab.)
ACKERMANN	10	JCAP 1005 025	M. Ackermann (Fermi-LAT Collab.)
ARMENGAUD	10	PL B687 294	E. Armengaud et al. (EDELWEISS-II Collab.)
ELLIS	10	EPJ C69 201	J. Ellis, A. Mustafayev, K. Olive
ABAZOV	09M	PRL 102 161802	V.M. Abazov et al. (DO Collab.)
AHMED	09	PRL 102 011301	Z. Ahmed et al. (CDMS Collab.)
ANGLOHER	09	ASP 31 270	G. Angloher et al. (CRESS-T Collab.)
BUCHMUELLER	09	EPJ C64 391	O. Buchmüller et al. (LOIC, FNAL, CERN+)
DREINER	09	EPJ C62 547	H. Dreiner et al.
LEBEDENKO	09	PR D80 052010	V.N. Lebedenko et al. (ZEPLIN-III Collab.)
LEBEDENKO	09A	PRL 103 151302	V.N. Lebedenko et al. (ZEPLIN-III Collab.)
SORENSEN	09	NIM A601 339	P. Sorensen et al. (XENON10 Collab.)
ABAZOV	08F	PL B659 856	V.M. Abazov et al. (DO Collab.)
ANGLE	08	PRL 100 021303	J. Angle et al. (XENON10 Collab.)
ANGLE	08A	PRL 101 091301	J. Angle et al. (XENON10 Collab.)
BEDNYAKOV	08	PAN 71 111	V.A. Bednyakov, H.P. Klapdor-Kleingrothaus, I.V. Krivosheina
Translated from YAF 71 112			
BEHNKE	08	SCI 319 933	E. Behnke (COUAPP Collab.)
BENNETTI	08	ASP 28 495	P. Benetti et al. (WARP Collab.)
BUCHMUELLER	08	JHEP 0809 117	O. Buchmüller et al.
ELLIS	08	PR D78 075012	J. Ellis, K. Olive, P. Sandick (CERN, MINN)
ABULENCIA	07H	PRL 98 131804	A. Abulencia et al. (CDF Collab.)
ALNER	07A	ASP 28 287	G.J. Alner et al. (ZEPLIN-II Collab.)
CALIBBI	07	JHEP 0709 081	L. Calibbi et al.
ELLIS	07	JHEP 0706 079	J. Ellis, K. Olive, P. Sandick (CERN, MINN)
LEE	07A	PRL 99 091301	H.S. Lee et al. (KIMS Collab.)
ABBIENDI	06B	EPJ C46 307	G. Abbiendi et al. (OPAL Collab.)
ACHTERBERG	06	ASP 26 129	A. Achterberg et al. (AMANDA Collab.)
ACKERMANN	06	ASP 24 459	M. Ackermann et al. (AMANDA Collab.)
AKERIB	06	PR D73 011102	D.S. Akerib et al. (CDMS Collab.)
AKERIB	06A	PRL 96 011302	D.S. Akerib et al. (CDMS Collab.)
ALLANACH	06	PR D73 015013	B.C. Allanach et al.
BENOIT	06	PL B637 156	A. Benoit et al.
DE-AUSTRI	06	JHEP 0605 002	R.R. de Austri, R. Trotta, L. Roszkowski
DEBOER	06	PL B636 13	W. de Boer et al.
LEP-SLC	06	PRPL 427 257	ALEPH, DELPHI, L3, OPAL, SLD and working groups
SHIMIZU	06A	PL B633 195	Y. Shimizu et al.
SMITH	06	PL B642 567	N.J.T. Smith, A.S. Murphy, T.J. Sumner (DO Collab.)
ABAZOV	05A	PRL 94 041801	V.M. Abazov et al. (DELPHI Collab.)
ABDALLAH	05B	EPJ C38 395	J. Abdallah et al. (CDMS Collab.)
AKERIB	05	PR D72 052009	D.S. Akerib et al. (UK Dark Matter Collab.)
ALNER	05	PL B616 17	G.J. Alner et al. (UK Dark Matter Collab.)
ALNER	05A	ASP 23 444	G.J. Alner et al. (FSU, MSU, HAWA)
BAER	05	JHEP 0507 065	H. Baer et al. (PICASSO Collab.)
BARNABE-HEIDER	05	PL B624 186	M. Barnabe-Heider et al.
ELLIS	05	PR D71 095007	J. Ellis et al.
SANGLARD	05	PR D71 122002	V. Sanglard et al. (EDELWEISS Collab.)
ABBIENDI	04	EPJ C32 453	G. Abbiendi et al. (OPAL Collab.)
ABBIENDI	04F	EPJ C33 149	G. Abbiendi et al. (OPAL Collab.)
ABBIENDI	04H	EPJ C35 1	G. Abbiendi et al. (OPAL Collab.)
ABBIENDI	04N	PL B602 167	G. Abbiendi et al. (OPAL Collab.)
ABDALLAH	04	EPJ C34 145	J. Abdallah et al. (DELPHI Collab.)
ABDALLAH	04M	EPJ C36 1	J. Abdallah et al. (DELPHI Collab.)
Also		EPJ C37 129 (errat.)	
ACHARD	04	PL B580 37	P. Achard et al. (L3 Collab.)
ACHARD	04E	PL B587 16	P. Achard et al. (L3 Collab.)
AKERIB	04	PRL 93 211301	D.S. Akerib et al. (CDMS II Collab.)
BALTZ	04	JHEP 0410 052	E. Baltz, P. Gondolo
BELANGER	04	JHEP 0403 012	G. Belanger et al.
BOTTINO	04	PR D69 037302	A. Bottino et al. (Super-Kamiokande Collab.)
DESAI	04	PR D70 083232	S. Desai et al. (Super-Kamiokande Collab.)
ELLIS	04	EPJ C38 395	J. Ellis et al.
ELLIS	04B	PR D70 055005	J. Ellis et al. (ALEPH Collab.)
AHEISTER	04	PL B583 247	A. Heister et al. (ALEPH Collab.)
PIERCE	04A	PR D70 075006	A. Pierce (OPAL Collab.)
ABBIENDI	03L	PL B572 8	G. Abbiendi et al. (OPAL Collab.)
ABDALLAH	03M	EPJ C31 421	J. Abdallah et al. (DELPHI Collab.)
AHMED	03	ASP 19 691	B. Ahmed et al. (UK Dark Matter Collab.)
AKERIB	03	PR D68 082002	D.S. Akerib et al. (CDMS Collab.)
BAER	03	JCAP 0305 006	H. Baer, C. Balazs
BAER	03A	JCAP 0309 007	H. Baer et al.
BOTTINO	03	PR D68 043506	A. Bottino et al.
BOTTINO	03A	PR D67 063519	A. Bottino, N. Fornengo, S. Scopel
CHATTOPADHYAY	03	PR D68 035005	U. Chattopadhyay, A. Corsetti, P. Nath
ELLIS	03	ASP 18 395	J. Ellis, K.A. Olive, Y. Santoso
ELLIS	03B	NP B552 259	J. Ellis et al.
ELLIS	03C	PL B565 176	J. Ellis et al.
ELLIS	03D	PL B573 162	J. Ellis et al.
ELLIS	03E	PR D67 123502	J. Ellis et al.
HEISTER	03C	EPJ C28 1	A. Heister et al. (ALEPH Collab.)
HEISTER	03G	EPJ C31 1	A. Heister et al. (ALEPH Collab.)
KLAPDOR-KLEINGROTHAUS	03	ASP 18 525	H.V. Klapdor-Kleingrothaus et al.
LAHANAS	03	PL B568 55	A. Lahanas, D. Nanopoulos
TAKEDA	03	PL B572 145	A. Takeda et al.
ABRAMS	02	PR D66 122003	D. Abrams et al. (CDMS Collab.)
ACOSTA	02H	PRL 89 261801	D. Acosta et al. (CDF Collab.)
ANGLOHER	02	ASP 18 43	G. Angloher et al. (CRESS-T Collab.)
ARNOWITT	02	hep-ph/0211417	R. Arnowitt, B. Dutta
ELLIS	02B	PL B532 318	J. Ellis, A. Ferstl, K.A. Olive
HEISTER	02	PL B526 191	A. Heister et al. (ALEPH Collab.)
HEISTER	02E	PL B526 206	A. Heister et al. (ALEPH Collab.)
HEISTER	02J	PL B533 223	A. Heister et al. (ALEPH Collab.)
HEISTER	02N	PL B544 73	A. Heister et al. (ALEPH Collab.)
KIM	02	PL B527 18	H.B. Kim et al.
KIM	02B	JHEP 0212 034	Y.G. Kim et al.
LAHANAS	02	EPJ C23 185	A. Lahanas, V.C. Spanos
MORALES	02B	ASP 16 325	A. Morales et al. (COSME Collab.)
MORALES	02C	PL B532 9	A. Morales et al. (DELPHI Collab.)
ABREU	01	EPJ C19 29	P. Abreu et al. (DELPHI Collab.)
ABREU	01B	EPJ C19 201	P. Abreu et al. (DELPHI Collab.)
BALTZ	01	PRL 86 5004	E. Baltz, P. Gondolo
BARATE	01	PL B499 67	R. Barate et al. (ALEPH Collab.)
BARATE	01B	EPJ C19 415	R. Barate et al. (ALEPH Collab.)
BARGER	01C	PL B518 117	V. Barger, C. Kao
BAUDIS	01	PR D63 022001	L. Baudis et al. (Heidelberg-Moscow Collab.)
BERNABEI	01	PL B509 197	R. Bernabei et al. (DAMA Collab.)
BOTTINO	01	PR D63 125003	A. Bottino et al.
CORSETTI	01	PR D64 125010	A. Corsetti, P. Nath
ELLIS	01B	PL B510 236	J. Ellis et al. (IGEX Collab.)
ELLIS	01C	PR D63 050101	J. Ellis, A. Ferstl, K.A. Olive
GOMEZ	01	PL B512 252	M.E. Gomez, J.D. Vergados
LAHANAS	01	PL B518 94	A. Lahanas, D.V. Nanopoulos, V. Spanos
ABBIENDI	00	EPJ C12 1	G. Abbiendi et al. (OPAL Collab.)
ABBIENDI	00G	EPJ C14 51	G. Abbiendi et al. (OPAL Collab.)
ABBIENDI	00H	EPJ C14 187	G. Abbiendi et al. (OPAL Collab.)
Also		EPJ C16 707 (errat.)	
ABBIENDI G	00D	EPJ C18 253	G. Abbiendi et al. (OPAL Collab.)
ABREU	00J	PL B479 129	P. Abreu et al. (DELPHI Collab.)
ABREU	00Q	PL B478 65	P. Abreu et al. (DELPHI Collab.)
ABREU	00T	PL B485 95	P. Abreu et al. (DELPHI Collab.)
ABREU	00U	PL B487 36	P. Abreu et al. (DELPHI Collab.)
ABREU	00V	EPJ C16 211	P. Abreu et al. (DELPHI Collab.)
ABREU	00W	PL B489 38	P. Abreu et al. (DELPHI Collab.)
ABREU	00Z	EPJ C17 53	P. Abreu et al. (DELPHI Collab.)
ABUSAUDI	00	PRL 84 5699	R. Abusaudi et al. (CDMS Collab.)
ACCIARRI	00D	PL B472 420	M. Acciarri et al. (L3 Collab.)
ACCOMANDO	00	NP B585 124	E. Accomando et al.
BERNABEI	00	PL B480 23	R. Bernabei et al. (DAMA Collab.)
BERNABEI	00C	EPJ C18 283	R. Bernabei et al. (DAMA Collab.)
BERNABEI	00D	NPJ 2 15	R. Bernabei et al. (DAMA Collab.)
BOEHM	00B	PL D62 035012	J. Boehm, A. Djoudi, M. Drees
ELLIS	00	PR D62 075010	J. Ellis et al.
FENG	00	PL B482 388	J.L. Feng, K.T. Matchev, F. Wilczek
LEP	00	CERN-EP-2000-016	LEP Collabs (ALEPH, DELPHI, L3, OPAL, SLD+)
MORALES	00	PL B489 268	A. Morales et al. (IGEX Collab.)
PDG	00	EPJ C15 1	D.E. Groom et al. (PDG Collab.)
SPOONER	00	PL B473 330	N.J.C. Spooner et al. (UK Dark Matter Col.)
ACCIARRI	99H	PL B456 283	M. Acciarri et al. (L3 Collab.)
ACCIARRI	99P	PL B470 268	M. Acciarri et al. (L3 Collab.)
ACCIARRI	99W	PL B471 280	M. Acciarri et al. (L3 Collab.)
AMBROSIO	99	PR D60 082002	M. Ambrosio et al. (Macro Collab.)
BAUDIS	99	PR D63 022001	L. Baudis et al. (Heidelberg-Moscow Collab.)
BELLI	99C	NP B563 97	P. Belli et al. (DAMA Collab.)
OOTANI	99	PL B461 371	W. Ootani et al.
ABREU	98P	PL B444 491	P. Abreu et al. (DELPHI Collab.)
ACCIARRI	98F	EPJ C4 207	M. Acciarri et al. (L3 Collab.)
ACKERSTAFF	98P	PL B433 195	K. Ackerstaff et al. (OPAL Collab.)
BARATE	98K	PL B433 176	R. Barate et al. (ALEPH Collab.)
BARATE	98S	EPJ C4 433	R. Barate et al. (ALEPH Collab.)
BERNABEI	98C	PL B436 379	R. Bernabei et al. (DAMA Collab.)
ELLIS	98	PR D58 095002	J. Ellis et al.
ELLIS	98B	PL B444 367	J. Ellis, T. Falk, K. Olive
PDG	98	EPJ C3 1	C. Caso et al. (PDG Collab.)
BAER	97	PR D57 567	H. Baer, M. Brhlik
BERNABEI	97	ASP 7 73	R. Bernabei et al. (DAMA Collab.)
EDSJO	97	PR D56 1879	J. Edsjo, P. Gondolo
ARNOWITT	96	PR D54 2374	R. Arnowitt, P. Nath
BAER	96	PR D53 597	H. Baer, M. Brhlik
BERGSTROM	96	ASP 5 263	L. Bergstrom, P. Gondolo
LEWIN	96	ASP 6 87	J.D. Lewin, P.F. Smith
BEREZINSKY	95	ASP 5 1	V. Berezinsky et al.
FALK	95	PL B354 99	T. Falk, K.A. Olive, M. Srednicki (MINN, UCSB)
LOSECCO	95	PL B342 392	J.M. LoSecco (NDAM)
ADRIANI	93M	PRL 236 1	O. Adriani et al. (L3 Collab.)
DREES	93	PR D47 376	M. Drees, M.M. Nojiri (DESY, SLAC)
DREES	93B	PR D48 3483	M. Drees, M.M. Nojiri
FALK	93	PL B318 354	T. Falk et al. (UCB, UCSB, MINN)
KELLEY	93	PR D47 2461	S. Kelley et al. (TAMU, ALAH)
MIZUTA	93	PL B298 120	S. Mizuta, M. Yamaguchi (TOHO)
MORI	93	PR D48 5505	M. Mori et al. (KEK, NIIG, TOKY, TOKA+)
BOTTINO	92	MPL A7 733	A. Bottino et al. (TORI, ZARA)
Also		PL B265 57	
DECAMP	92	PRPL 216 253	A. Bottino et al. (TORI, INFN)
LOPEZ	92	NP B370 445	D. Decamp et al. (ALEPH Collab.)
MCDONALD	92	PL B283 80	J.L. Lopez, D.V. Nanopoulos, K.J. Yuan (TAMU)
ABREU	91F	NP B367 511	J. McDonald, K.A. Olive, M. Srednicki (LIS-B+)
ALEXANDER	91F	ZPHY C52 175	P. Abreu et al. (DELPHI Collab.)
BOTTINO	91	PL B265 57	G. Alexander et al. (OPAL Collab.)
GELMINI	91	NP B351 623	

GRIEST	88B	PR D38 2357	K. Griest	
OLIVE	88	PL B205 553	K.A. Olive, M. Srednicki	(MINN, UCSB)
SREDNICKI	88	NP B310 693	M. Srednicki, R. Watkins, K.A. Olive	(MINN, UCSB)
ELLIS	84	NP B238 453	J. Ellis et al.	(CERN)
GOLDBERG	83	PRL 50 1419	H. Goldberg	(NEAS)
KRAUSS	83	NP B227 556	L.M. Krauss	(HARV)
VYSOTSKII	83	SJNP 37 948	M.I. Vysotsky	(ITEP)
		Translated from YAF 37 1597.		

Technicolor

See the related review(s):

Dynamical Electroweak Symmetry Breaking: Implications of the H^0

The latest unpublished results are described in "Dynamical Electroweak Symmetry Breaking" review.

MASS LIMITS for Resonances in Models of Dynamical Electroweak Symmetry Breaking

VALUE (GeV)	CL%	DOCUMENT ID	TECN	COMMENT
• • • We do not use the following data for averages, fits, limits, etc. • • •				
>3900	95	1 AAD 20AM ATLS	top-color Z'	
		2 AAD 20W ATLS	$\rho_T \rightarrow W\pi_T \rightarrow \ell\nu q\bar{q}$	
		3 AAD 16W ATLS	color octet vector resonance	
>2400	95	4 KHACHATRYAN...16E CMS	top-color Z'	
		5 AAD 15AB ATLS	$h \rightarrow \pi_V \pi_V$	
>1800	95	6 AAD 15AO ATLS	top-color Z'	
		7 AAD 15BB ATLS	$\rho\rho \rightarrow \rho_T/\omega_T \rightarrow Wh$ or Zh	
		8 AAD 15Q ATLS	$h \rightarrow \pi_V \pi_V$	
		9 AAIJ 15AN LHCB	$h \rightarrow \pi_V \pi_V$	
>1140	95	10 KHACHATRYAN...15C CMS	$\rho_T \rightarrow WZ$	
		11 KHACHATRYAN...15W CMS	$H \rightarrow \pi_V \pi_V$	
none 200-700, 750-890	95	12 AAD 14AT ATLS	$\rho\rho \rightarrow \omega_T \rightarrow Z\gamma$	
none 275-960	95	12 AAD 14AT ATLS	$\rho\rho \rightarrow a_T \rightarrow W\gamma$	
		13 AAD 14V ATLS	color singlet techni-vector	
> 703		14 AAD 13AN ATLS	$\rho\rho \rightarrow a_T \rightarrow W\gamma$	
> 494		15 AAD 13AN ATLS	$\rho\rho \rightarrow \omega_T \rightarrow Z\gamma$	
none 500-1740	95	16 AAD 13AQ ATLS	top-color Z'	
>1300	95	17 CHATRCHYAN13AP CMS	top-color Z'	
>2100	95	16 CHATRCHYAN13BM CMS	top-color Z'	
		18 BAAK 12 RVUE	QCD-like technicolor	
none 167-687	95	19 CHATRCHYAN12AF CMS	$\rho_T \rightarrow WZ$	
> 805	95	16 AALTONEN 11AD CDF	top-color Z'	
> 805	95	16 AALTONEN 11AE CDF	top-color Z'	
		20 CHIVUKULA 11 RVUE	top-Higgs	
		21 CHIVUKULA 11A RVUE	techni- π	
		22 AALTONEN 10I CDF	$\rho\bar{\rho} \rightarrow \rho_T/\omega_T \rightarrow W\pi_T$	
none 208-408	95	23 ABAZOV 10A D0	$\rho_T \rightarrow WZ$	
		24 ABAZOV 07I D0	$\rho\bar{\rho} \rightarrow \rho_T/\omega_T \rightarrow W\pi_T$	
> 280	95	25 ABULENCIA 05A CDF	$\rho_T \rightarrow e^+e^-, \mu^+\mu^-$	
		26 CHEKANOV 02B ZEUS	color octet techni- π	
> 207	95	27 ABAZOV 01B D0	$\rho_T \rightarrow e^+e^-$	
none 90-206.7	95	28 ABDALLAH 01 DLPH	$e^+e^- \rightarrow \rho_T$	
		29 AFFOLDER 00F CDF	color-singlet techni- ρ , $\rho_T \rightarrow W\pi_T, 2\pi_T$	
> 600	95	30 AFFOLDER 00K CDF	color-octet techni- ρ , $\rho_T \rightarrow 2\pi_L Q$	
none 350-440	95	31 ABE 99F CDF	color-octet techni- ρ , $\rho_T \rightarrow \bar{b}b$	
		32 ABE 99N CDF	techni- ω , $\omega_T \rightarrow \gamma\bar{b}b$	
none 260-480	95	33 ABE 97G CDF	color-octet techni- ρ , $\rho_T \rightarrow 2j$ ets	

- 1 AAD 20AM search for a top-color Z' decaying to $t\bar{t}$ in pp collisions at $\sqrt{s} = 13$ TeV. The quoted limit is for $\Gamma_{Z'}/M_{Z'} = 0.01$. The limit becomes $M_{Z'} > 4700$ GeV for $\Gamma_{Z'}/M_{Z'} = 0.03$.
- 2 AAD 20W search for techni- ρ decaying to $\pi_T W$ in pp collisions at $\sqrt{s} = 13$ TeV. See their Fig. 5a for limits on σ_B .
- 3 AAD 16W search for color octet vector resonance decaying to $b\bar{b}$ in pp collisions at $\sqrt{s} = 8$ TeV. The vector like quark B is assumed to decay to bH . See their Fig.3 and Fig.4 for limits on σ_B .
- 4 KHACHATRYAN 16E search for top-color Z' decaying to $t\bar{t}$. The quoted limit is for $\Gamma_{Z'}/M_{Z'} = 0.012$. Also exclude $M_{Z'} < 2.9$ TeV for wider topcolor Z' with $\Gamma_{Z'}/M_{Z'} = 0.1$.
- 5 AAD 15AB search for long-lived hidden valley π_V particles which are produced in pairs by the decay of a scalar boson. π_V is assumed to decay into dijets. See their Fig. 10 for the limit on σ_B .
- 6 AAD 15AO search for top-color Z' decaying to $t\bar{t}$. The quoted limit is for $\Gamma_{Z'}/M_{Z'} = 0.012$.
- 7 AAD 15BB search for minimal walking technicolor (MWT) isotriplet vector and axial-vector resonances decaying to Wh or Zh . See their Fig. 3 for the exclusion limit in the MWT parameter space.
- 8 AAD 15Q search for long-lived hidden valley π_V particles which are produced in pairs by the decay of scalar boson. π_V is assumed to decay into dijets. See their Fig. 5 and Fig. 6 for the limit on σ_B .

- 9 AAIJ 15AN search for long-lived hidden valley π_V particles which are produced in pairs by the decay of scalar boson with a mass of 120GeV. π_V is assumed to decay into dijets. See their Fig. 4 for the limit on σ_B .
- 10 KHACHATRYAN 15c search for a vector techni-resonance decaying to WZ . The limit assumes $M_{\rho_T} = (3/4) M_{\rho_T} - 25$ GeV. See their Fig.3 for the limit in $M_{\rho_T} - M_{\rho_T}$ plane of the low scale technicolor model.
- 11 KHACHATRYAN 15W search for long-lived hidden valley π_V particles which are produced in pairs in the decay of heavy higgs boson H . π_V is assumed to decay into $\ell^+ \ell^-$. See their Fig. 7 and Fig. 8 for the limits on σ_B .
- 12 AAD 14AT search for techni- ω and techni- a resonances decaying to $V\gamma$ with $V = W(\rightarrow \ell\nu)$ or $Z(\rightarrow \ell^+ \ell^-)$.
- 13 AAD 14V search for vector techni-resonances decaying into electron or muon pairs in pp collisions at $\sqrt{s} = 8$ TeV. See their table IX for exclusion limits with various assumptions.
- 14 AAD 13AN search for vector techni-resonance a_T decaying into $W\gamma$.
- 15 AAD 13AN search for vector techni-resonance ω_T decaying into $Z\gamma$.
- 16 Search for top-color Z' decaying to $t\bar{t}$. The quoted limit is for $\Gamma_{Z'}/M_{Z'} = 0.012$.
- 17 CHATRCHYAN 13AP search for top-color leptophobic Z' decaying to $t\bar{t}$. The quoted limit is for $\Gamma_{Z'}/M_{Z'} = 0.012$.
- 18 BAAK 12 give electroweak oblique parameter constraints on the QCD-like technicolor models. See their Fig. 28.
- 19 CHATRCHYAN 12AF search for a vector techni-resonance decaying to WZ . The limit assumes $M_{\rho_T} = (3/4) M_{\rho_T} - 25$ GeV. See their Fig. 3 for the limit in $M_{\rho_T} - M_{\rho_T}$ plane of the low scale technicolor model.
- 20 Using the LHC limit on the Higgs boson production cross section, CHIVUKULA 11 obtain a limit on the top-Higgs mass > 300 GeV at 95% CL assuming 150 GeV top-pion mass.
- 21 Using the LHC limit on the Higgs boson production cross section, CHIVUKULA 11A obtain a limit on the technipion mass ruling out the region $110 \text{ GeV} < m_P < 2m_T$. Existence of color techni-fermions, top-color mechanism, and $N_{TC} \geq 3$ are assumed.
- 22 AALTONEN 10I search for the vector techni-resonances (ρ_T, ω_T) decaying into $W\pi_T$ with $W \rightarrow \ell\nu$ and $\pi_T \rightarrow b\bar{b}, b\bar{c}$, or $b\bar{u}$. See their Fig.3 for the exclusion plot in $M_{\rho_T} - M_{\rho_T}$ plane.
- 23 ABAZOV 10A search for a vector techni-resonance decaying into WZ . The limit assumes $M_{\rho_T} < M_{\rho_T} + MW$.
- 24 ABAZOV 07I search for the vector techni-resonances (ρ_T, ω_T) decaying into $W\pi_T$ with $W \rightarrow e\nu$ and $\pi_T \rightarrow b\bar{b}$ or $b\bar{c}$. See their Fig. 2 for the exclusion plot in $M_{\rho_T} - M_{\rho_T}$ plane.
- 25 ABULENCIA 05A search for resonances decaying to electron or muon pairs in $p\bar{p}$ collisions. at $\sqrt{s} = 1.96$ TeV. The limit assumes Technicolor-scale mass parameters $M_V = M_A = 500$ GeV.
- 26 CHEKANOV 02B search for color octet techni- π P decaying into dijets in ep collisions. See their Fig. 5 for the limit on $\sigma(ep \rightarrow ePX) \cdot B(P \rightarrow 2j)$.
- 27 ABAZOV 01B searches for vector techni-resonances (ρ_T, ω_T) decaying to e^+e^- . The limit assumes $M_{\rho_T} = M_{\omega_T} < M_{\rho_T} + MW$.
- 28 The limit is independent of the π_T mass. See their Fig. 9 and Fig. 10 for the exclusion plot in the $M_{\rho_T} - M_{\rho_T}$ plane. ABDALLAH 01 limit on the technipion mass is $M_{\pi_T} > 79.8$ GeV for $N_D = 2$, assuming its point-like coupling to gauge bosons.
- 29 AFFOLDER 00F search for ρ_T decaying into $W\pi_T$ or $\pi_T\pi_T$ with $W \rightarrow \ell\nu$ and $\pi_T \rightarrow \bar{b}b, \bar{b}c$. See Fig. 1 in the above Note on "Dynamical Electroweak Symmetry Breaking" for the exclusion plot in the $M_{\rho_T} - M_{\rho_T}$ plane.
- 30 AFFOLDER 00K search for the ρ_T decaying into $\pi_L Q \pi_L Q$ with $\pi_L Q \rightarrow b\nu$. For $\pi_L Q \rightarrow c\nu$, the limit is $M_{\rho_T} > 510$ GeV. See their Fig. 2 and Fig. 3 for the exclusion plot in the $M_{\rho_T} - M_{\rho_T}$ plane.
- 31 ABE 99F search for a new particle X decaying into $b\bar{b}$ in $p\bar{p}$ collisions at $E_{cm} = 1.8$ TeV. See Fig. 7 in the above Note on "Dynamical Electroweak Symmetry Breaking" for the upper limit on $\sigma(p\bar{p} \rightarrow X) \times B(X \rightarrow b\bar{b})$. ABE 99F also exclude top gluons of width $\Gamma = 0.3M$ in the mass interval $280 < M < 670$ GeV, of width $\Gamma = 0.5M$ in the mass interval $340 < M < 640$ GeV, and of width $\Gamma = 0.7M$ in the mass interval $375 < M < 560$ GeV.
- 32 ABE 99N search for the techni- ω decaying into $\gamma\pi_T$. The technipion is assumed to decay $\pi_T \rightarrow b\bar{b}$. See Fig. 2 in the above Note on "Dynamical Electroweak Symmetry Breaking" for the exclusion plot in the $M_{\omega_T} - M_{\omega_T}$ plane.
- 33 ABE 97G search for a new particle X decaying into dijets in $p\bar{p}$ collisions at $E_{cm} = 1.8$ TeV. See Fig. 5 in the above Note on "Dynamical Electroweak Symmetry Breaking" for the upper limit on $\sigma(p\bar{p} \rightarrow X) \times B(X \rightarrow 2j)$.

REFERENCES FOR Technicolor

AAD	20AM	JHEP 2010 061	G. Aad et al.	(ATLAS Collab.)
AAD	20W	JHEP 2006 151	G. Aad et al.	(ATLAS Collab.)
AAD	16W	PL B758 249	G. Aad et al.	(ATLAS Collab.)
KHACHATRYAN...	16E	PR D93 012001	V. Khachatryan et al.	(CMS Collab.)
AAD	15AB	PR D92 012010	G. Aad et al.	(ATLAS Collab.)
AAD	15AO	JHEP 1508 148	G. Aad et al.	(ATLAS Collab.)
AAD	15BB	EPJ C75 263	G. Aad et al.	(ATLAS Collab.)
AAD	15Q	PL B743 15	G. Aad et al.	(ATLAS Collab.)
AAIJ	15AN	EPJ C75 152	R. Aaij et al.	(LHCb Collab.)
KHACHATRYAN...	15C	PL B740 83	V. Khachatryan et al.	(CMS Collab.)
KHACHATRYAN...	15W	PR D91 052012	V. Khachatryan et al.	(CMS Collab.)
AAD	14AT	PL B738 428	G. Aad et al.	(ATLAS Collab.)
AAD	14V	PR D90 052005	G. Aad et al.	(ATLAS Collab.)
AAD	13AN	PR D87 112003	G. Aad et al.	(ATLAS Collab.)
	Also	PR D91 119901 (errat.)	G. Aad et al.	(ATLAS Collab.)
AAD	13AQ	PR D88 012004	G. Aad et al.	(ATLAS Collab.)
CHATRCHYAN	13AP	PR D87 072002	S. Chatrchyan et al.	(CMS Collab.)
CHATRCHYAN	13BM	PRL 111 211804	S. Chatrchyan et al.	(CMS Collab.)
	Also	PRL 112 119903 (errat.)	S. Chatrchyan et al.	(CMS Collab.)
BAAK	12	EPJ C72 2003	M. Baak et al.	(Glitter Group)
CHATRCHYAN	12AF	PRL 109 141801	S. Chatrchyan et al.	(CMS Collab.)
AALTONEN	11AD	PR D84 072003	T. Aaltonen et al.	(CDF Collab.)
AALTONEN	11AE	PR D84 072004	T. Aaltonen et al.	(CDF Collab.)
CHIVUKULA	11	PR D84 095022	R.S. Chivukula et al.	(ATLAS Collab.)
CHIVUKULA	11A	PR D84 115025	R.S. Chivukula et al.	(ATLAS Collab.)
AALTONEN	10I	PRL 104 111802	T. Aaltonen et al.	(CDF Collab.)

Searches Particle Listings

Technicolor, Quark and Lepton Compositeness

ABAZOV	10A	PRL 104 061801	V.M. Abazov et al.	(DO Collab.)
ABAZOV	07I	PRL 98 221801	V.M. Abazov et al.	(DO Collab.)
ABULENCIA	05A	PRL 95 252001	A. Abulencia et al.	(CDF Collab.)
CHEKANOV	02B	PL B531 9	S. Chekanov et al.	(ZEUS Collab.)
ABAZOV	01B	PRL 87 061802	V.M. Abazov et al.	(DO Collab.)
ABDALLAH	01	EPJ C22 17	J. Abdallah et al.	(DELPHI Collab.)
AFFOLDER	00F	PRL 84 1110	T. Affolder et al.	(CDF Collab.)
AFFOLDER	00K	PRL 85 2056	T. Affolder et al.	(CDF Collab.)
ABE	99F	PRL 82 2038	F. Abe et al.	(CDF Collab.)
ABE	99N	PRL 83 3124	F. Abe et al.	(CDF Collab.)
ABE	97G	PR D55 5263	F. Abe et al.	(CDF Collab.)

Quark and Lepton Compositeness, Searches for

The latest unpublished results are described in the "Quark and Lepton Compositeness" review.

See the related review(s):

Searches for Quark and Lepton Compositeness

CONTENTS:

Scale Limits for Contact Interactions: $\Lambda(eeee)$

Scale Limits for Contact Interactions: $\Lambda(ee\mu\mu)$

Scale Limits for Contact Interactions: $\Lambda(ee\tau\tau)$

Scale Limits for Contact Interactions: $\Lambda(\ell\ell\ell\ell)$

Scale Limits for Contact Interactions: $\Lambda(eeqq)$

Scale Limits for Contact Interactions: $\Lambda(\mu\mu qq)$

Scale Limits for Contact Interactions: $\Lambda(\ell\nu\ell\nu)$

Scale Limits for Contact Interactions: $\Lambda(e\nu qq)$

Scale Limits for Contact Interactions: $\Lambda(qqqq)$

Scale Limits for Contact Interactions: $\Lambda(\nu\nu qq)$

Mass Limits for Excited e (e^*)

- Limits for Excited e (e^*) from Pair Production
- Limits for Excited e (e^*) from Single Production
- Limits for Excited e (e^*) from $e^+e^- \rightarrow \gamma\gamma$
- Indirect Limits for Excited e (e^*)

Mass Limits for Excited μ (μ^*)

- Limits for Excited μ (μ^*) from Pair Production
- Limits for Excited μ (μ^*) from Single Production
- Indirect Limits for Excited μ (μ^*)

Mass Limits for Excited τ (τ^*)

- Limits for Excited τ (τ^*) from Pair Production
- Limits for Excited τ (τ^*) from Single Production

Mass Limits for Excited Neutrino (ν^*)

- Limits for Excited ν (ν^*) from Pair Production
- Limits for Excited ν (ν^*) from Single Production

Mass Limits for Excited q (q^*)

- Limits for Excited q (q^*) from Pair Production
- Limits for Excited q (q^*) from Single Production

Mass Limits for Color Sextet Quarks (q_6)

Mass Limits for Color Octet Charged Leptons (ℓ_8)

Mass Limits for Color Octet Neutrinos (ν_8)

Mass Limits for W_8 (Color Octet W Boson)

SCALE LIMITS for Contact Interactions: $\Lambda(eeee)$

Limits are for Λ_{LL}^{\pm} only. For other cases, see each reference.

$\Lambda_{LL}^+(TeV)$	$\Lambda_{LL}^-(TeV)$	CL%	DOCUMENT ID	TECN	COMMENT
>8.3	>10.3	95	¹ BOURILKOV 01	RVUE	$E_{cm} = 192-208$ GeV
•••			We do not use the following data for averages, fits, limits, etc. •••		
>4.5	>7.0	95	² SCHAEEL 07A	ALEP	$E_{cm} = 189-209$ GeV
>5.3	>6.8	95	ABDALLAH 06c	DLPH	$E_{cm} = 130-207$ GeV
>4.7	>6.1	95	³ ABBIENDI 04G	OPAL	$E_{cm} = 130-207$ GeV
>4.3	>4.9	95	ACCIARRI 00P	L3	$E_{cm} = 130-189$ GeV

¹ A combined analysis of the data from ALEPH, DELPHI, L3, and OPAL.

² SCHAEEL 07A limits are from $R_{e^+e^-}$, Q_{FB}^{depl} , and hadronic cross section measurements.

³ ABBIENDI 04G limits are from $e^+e^- \rightarrow e^+e^-$ cross section at $\sqrt{s} = 130-207$ GeV.

SCALE LIMITS for Contact Interactions: $\Lambda(ee\mu\mu)$

Limits are for Λ_{LL}^{\pm} only. For other cases, see each reference.

$\Lambda_{LL}^+(TeV)$	$\Lambda_{LL}^-(TeV)$	CL%	DOCUMENT ID	TECN	COMMENT
>6.6	>9.5	95	¹ SCHAEEL 07A	ALEP	$E_{cm} = 189-209$ GeV
> 8.5	>3.8	95	ACCIARRI 00P	L3	$E_{cm} = 130-189$ GeV
•••			We do not use the following data for averages, fits, limits, etc. •••		
>7.3	>7.6	95	ABDALLAH 06c	DLPH	$E_{cm} = 130-207$ GeV
>8.1	>7.3	95	² ABBIENDI 04G	OPAL	$E_{cm} = 130-207$ GeV

¹ SCHAEEL 07A limits are from $R_{e^+e^-}$, Q_{FB}^{depl} , and hadronic cross section measurements.

² ABBIENDI 04G limits are from $e^+e^- \rightarrow \mu\mu$ cross section at $\sqrt{s} = 130-207$ GeV.

SCALE LIMITS for Contact Interactions: $\Lambda(ee\tau\tau)$

Limits are for Λ_{LL}^{\pm} only. For other cases, see each reference.

$\Lambda_{LL}^+(TeV)$	$\Lambda_{LL}^-(TeV)$	CL%	DOCUMENT ID	TECN	COMMENT
>7.9	>5.8	95	¹ SCHAEEL 07A	ALEP	$E_{cm} = 189-209$ GeV
>7.9	>4.6	95	ABDALLAH 06c	DLPH	$E_{cm} = 130-207$ GeV
>4.9	>7.2	95	² ABBIENDI 04G	OPAL	$E_{cm} = 130-207$ GeV
•••			We do not use the following data for averages, fits, limits, etc. •••		
>5.4	>4.7	95	ACCIARRI 00P	L3	$E_{cm} = 130-189$ GeV

¹ SCHAEEL 07A limits are from $R_{e^+e^-}$, Q_{FB}^{depl} , and hadronic cross section measurements.

² ABBIENDI 04G limits are from $e^+e^- \rightarrow \tau\tau$ cross section at $\sqrt{s} = 130-207$ GeV.

SCALE LIMITS for Contact Interactions: $\Lambda(\ell\ell\ell\ell)$

Lepton universality assumed. Limits are for Λ_{LL}^{\pm} only. For other cases, see each reference.

$\Lambda_{LL}^+(TeV)$	$\Lambda_{LL}^-(TeV)$	CL%	DOCUMENT ID	TECN	COMMENT
>7.9	> 10.3	95	¹ SCHAEEL 07A	ALEP	$E_{cm} = 189-209$ GeV
>9.1	>8.2	95	ABDALLAH 06c	DLPH	$E_{cm} = 130-207$ GeV
•••			We do not use the following data for averages, fits, limits, etc. •••		
>7.7	>9.5	95	² ABBIENDI 04G	OPAL	$E_{cm} = 130-207$ GeV
			³ BABICH 03	RVUE	
>9.0	>5.2	95	ACCIARRI 00P	L3	$E_{cm} = 130-189$ GeV

¹ SCHAEEL 07A limits are from $R_{e^+e^-}$, Q_{FB}^{depl} , and hadronic cross section measurements.

² ABBIENDI 04G limits are from $e^+e^- \rightarrow \ell^+\ell^-$ cross section at $\sqrt{s} = 130-207$ GeV.

³ BABICH 03 obtain a bound $-0.175 \text{ TeV}^{-2} < 1/\Lambda_{LL}^2 < 0.095 \text{ TeV}^{-2}$ (95%CL) in a model independent analysis allowing all of $\Lambda_{LL}, \Lambda_{LR}, \Lambda_{RL}, \Lambda_{RR}$ to coexist.

SCALE LIMITS for Contact Interactions: $\Lambda(eeqq)$

Limits are for Λ_{LL}^{\pm} only. For other cases, see each reference.

$\Lambda_{LL}^+(TeV)$	$\Lambda_{LL}^-(TeV)$	CL%	DOCUMENT ID	TECN	COMMENT
>24	>37	95	¹ AABOUD 17AT	ATLS	($eeqq$)
> 8.4	>10.2	95	² ABDALLAH 09	DLPH	($eebb$)
> 9.4	>5.6	95	³ SCHAEEL 07A	ALEP	($eecc$)
> 9.4	>4.9	95	² SCHAEEL 07A	ALEP	($eebb$)
>23.3	>12.5	95	⁴ CHEUNG 01B	RVUE	($eeuu$)
>11.1	>26.4	95	⁴ CHEUNG 01B	RVUE	($eedd$)
•••			We do not use the following data for averages, fits, limits, etc. •••		
> 7.1	>7.1	95	⁵ AAD 21AU	ATLS	($eebs$)
>23.5	>26.1	95	⁶ AAD 21Q	ATLS	($eeqq$)
>19.5	>24.0	95	⁷ SIRUNYAN 21N	CMS	($eeqq$)
>23.5	>26.1	95	⁸ AAD 20AP	ATLS	($eeqq$)
> 4.5	>12.8	95	⁹ ABRAMOWICZ19	ZEUS	($eeqq$)
>16.8	>23.9	95	¹⁰ SIRUNYAN 19AC	CMS	($eeqq$)
>15.5	>19.5	95	¹¹ AABOUD 16U	ATLS	($eeqq$)
>13.5	>18.3	95	¹² KHACHATRYAN 15AE	CMS	($eeqq$)
>16.4	>20.7	95	¹³ AAD 14BE	ATLS	($eeqq$)
> 9.5	>12.1	95	¹⁴ AAD 13E	ATLS	($eeqq$)
>10.1	>9.4	95	¹⁵ AAD 12AB	ATLS	($eeqq$)
> 4.2	>4.0	95	¹⁶ AARON 11C	H1	($eeqq$)
> 3.8	>3.8	95	¹⁷ ABDALLAH 11	DLPH	($ee\tau c$)
>12.9	>7.2	95	¹⁸ SCHAEEL 07A	ALEP	($eeqq$)
> 3.7	>5.9	95	¹⁹ ABULENCIA 06L	CDF	($eeqq$)

¹ AABOUD 17AT limits are from pp collisions at $\sqrt{s} = 13$ TeV. The quoted limit uses a uniform positive prior in $1/\Lambda^2$.

² ABDALLAH 09 and SCHAEEL 07A limits are from R_b, A_{FB}^b .

³ SCHAEEL 07A limits are from $R_{e^+e^-}$, Q_{FB}^{depl} , and hadronic cross section measurements.

⁴ CHEUNG 01B is an update of BARGER 98E.

⁵ AAD 21AU search for new phenomena in final states with e^+e^- and one or no b -tagged jets in pp collisions at $\sqrt{s} = 13$ TeV. The quoted limits assume $g_*^2 = 4$.

⁶ AAD 21Q limits are from pp collisions at $\sqrt{s} = 13$ TeV. A frequentist statistical framework is used to remove the prior dependence.

⁷ SIRUNYAN 21N limits are from e^+e^- mass distribution in pp collisions at $\sqrt{s} = 13$ TeV.

⁸ AAD 20AP limits are from e^+e^- mass distribution in pp collisions at $\sqrt{s} = 13$ TeV.

⁹ ABRAMOWICZ 19 limits are from Q^2 spectrum measurements of $e^\pm p \rightarrow e^\pm X$.

¹⁰ SIRUNYAN 19AC limits are from e^+e^- mass distribution in pp collisions at $\sqrt{s} = 13$ TeV.

¹¹ AABOUD 16U limits are from pp collisions at $\sqrt{s} = 13$ TeV. The quoted limit uses a uniform positive prior in $1/\Lambda^2$.

¹² KHACHATRYAN 15AE limit is from e^+e^- mass distribution in pp collisions at $E_{cm} = 8$ TeV.

¹³ AAD 14BE limits are from pp collisions at $\sqrt{s} = 8$ TeV. The quoted limit uses a uniform positive prior in $1/\Lambda^2$.

¹⁴ AAD 13E limits are from e^+e^- mass distribution in pp collisions at $E_{cm} = 7$ TeV.

¹⁵ AAD 12AB limits are from e^+e^- mass distribution in pp collisions at $E_{cm} = 7$ TeV.

¹⁶ AARON 11C limits are from Q^2 spectrum measurements of $e^\pm p \rightarrow e^\pm X$.

¹⁷ ABDALLAH 11 limit is from $e^+e^- \rightarrow t\bar{c}$ cross section. $\Lambda_{LL} = \Lambda_{LR} = \Lambda_{RL} = \Lambda_{RR}$ is assumed.

¹⁸ SCHAEEL 07A limit assumes quark flavor universality of the contact interactions.

¹⁹ ABULENCIA 06L limits are from $p\bar{p}$ collisions at $\sqrt{s} = 1.96$ TeV.

See key on page 1171

Searches Particle Listings

Quark and Lepton Compositeness

SCALE LIMITS for Contact Interactions: $\Lambda(\mu\mu q\bar{q})$

$\Lambda_{LL}^+(TeV)$	$\Lambda_{LL}^-(TeV)$	CL%	DOCUMENT ID	TECN	COMMENT
>23.3	>40.0	95	1 SIRUNYAN 21N	CMS	($\mu\mu q\bar{q}$)
•••	•••	•••	•••	•••	••• We do not use the following data for averages, fits, limits, etc. •••
> 8.5	>8.5	95	2 AAD	21AU ATLS	($\mu\mu b\bar{s}$)
>22.3	>32.7	95	3 AAD	21Q ATLS	($\mu\mu q\bar{q}$)
>22.3	>32.7	95	4 AAD	20AP ATLS	($\mu\mu q\bar{q}$)
>20.4	>30.4	95	5 SIRUNYAN	19AC CMS	($\mu\mu q\bar{q}$)
>20	>30	95	6 AABOUD	17AT ATLS	($\mu\mu q\bar{q}$)
>15.8	>21.8	95	7 AABOUD	16U ATLS	($\mu\mu q\bar{q}$)
>12.0	>15.2	95	8 KHACHATRYAN	15AE CMS	($\mu\mu q\bar{q}$)
>12.5	>16.7	95	9 AAD	14BE ATLS	($\mu\mu q\bar{q}$)
> 9.6	>12.9	95	10 AAD	13E ATLS	($\mu\mu q\bar{q}$) (isosinglet)
> 9.5	>13.1	95	11 CHATRCHYAN	13K CMS	($\mu\mu q\bar{q}$) (isosinglet)
> 8.0	>7.0	95	12 AAD	12AB ATLS	($\mu\mu q\bar{q}$) (isosinglet)

- 1 SIRUNYAN 21N limits are from $\mu^+\mu^-$ mass distribution in pp collisions at $\sqrt{s} = 13$ TeV.
- 2 AAD 21AU search for new phenomena in final states with $\mu^+\mu^-$ and one or no b -tagged jets in pp collisions at $\sqrt{s} = 13$ TeV. The quoted limits assume $g_*^2 = 4\pi$.
- 3 AAD 21Q limits are from pp collisions at $\sqrt{s} = 13$ TeV. A frequentist statistical framework is used to remove the prior dependence.
- 4 AAD 20AP limits are from $\mu^+\mu^-$ mass distribution in pp collisions at $\sqrt{s} = 13$ TeV.
- 5 SIRUNYAN 19AC limits are from $\mu^+\mu^-$ mass distribution in pp collisions at $\sqrt{s} = 13$ TeV.
- 6 AABOUD 17AT limits are from pp collisions at $\sqrt{s} = 13$ TeV. The quoted limit uses a uniform positive prior in $1/\Lambda^2$.
- 7 AABOUD 16U limits are from pp collisions at $\sqrt{s} = 13$ TeV. The quoted limit uses a uniform positive prior in $1/\Lambda^2$.
- 8 KHACHATRYAN 15AE limit is from $\mu^+\mu^-$ mass distribution in pp collisions at $E_{cm} = 8$ TeV.
- 9 AAD 14BE limits are from pp collisions at $\sqrt{s} = 8$ TeV. The quoted limit uses a uniform positive prior in $1/\Lambda^2$.
- 10 AAD 13E limits are from $\mu^+\mu^-$ mass distribution in pp collisions at $E_{cm} = 7$ TeV.
- 11 CHATRCHYAN 13K limits are from $\mu^+\mu^-$ mass distribution in pp collisions at $E_{cm} = 7$ TeV.
- 12 AAD 12AB limits are from $\mu^+\mu^-$ mass distribution in pp collisions at $E_{cm} = 7$ TeV.

SCALE LIMITS for Contact Interactions: $\Lambda(\ell\nu\ell\nu)$

VALUE (TeV)	CL%	DOCUMENT ID	TECN	COMMENT
>3.10	90	1 JODIDIO 86	SPEC	$\Lambda_{LR}^\pm(\nu_\mu\nu_e\mu e)$
•••	•••	•••	•••	••• We do not use the following data for averages, fits, limits, etc. •••
>3.8		2 DIAZCRUZ 94	RVUE	$\Lambda_{LL}^+(\tau\nu_\tau e\nu_e)$
>8.1		2 DIAZCRUZ 94	RVUE	$\Lambda_{LL}^-(\tau\nu_\tau e\nu_e)$
>4.1		3 DIAZCRUZ 94	RVUE	$\Lambda_{LL}^+(\tau\nu_\tau\mu\nu_\mu)$
>6.5		3 DIAZCRUZ 94	RVUE	$\Lambda_{LL}^-(\tau\nu_\tau\mu\nu_\mu)$

- 1 JODIDIO 86 limit is from $\mu^+ \rightarrow \nu_\mu e^+ \nu_e$. Chirality invariant interactions $L = (g^2/\Lambda^2)$ [$\eta_{LL} (\overline{\nu}_\mu L \gamma^\alpha \mu_L) (\overline{e} L \gamma_\alpha \nu_e) + \eta_{LR} (\overline{\nu}_\mu L \gamma^\alpha \nu_e) (\overline{e} R \gamma_\alpha \mu_R)$] with $g^2/4\pi = 1$ and (η_{LL}, η_{LR}) = (0, ±1) are taken. No limits are given for Λ_{LL}^\pm with (η_{LL}, η_{LR}) = (±1, 0). For more general constraints with right-handed neutrinos and chirality nonconserving contact interactions, see their text.
- 2 DIAZCRUZ 94 limits are from $\Gamma(\tau \rightarrow e\nu\nu)$ and assume flavor-dependent contact interactions with $\Lambda(\tau\nu_\tau e\nu_e) \ll \Lambda(\mu\nu_\mu e\nu_e)$.
- 3 DIAZCRUZ 94 limits are from $\Gamma(\tau \rightarrow \mu\nu\nu)$ and assume flavor-dependent contact interactions with $\Lambda(\tau\nu_\tau\mu\nu_\mu) \ll \Lambda(\mu\nu_\mu e\nu_e)$.

SCALE LIMITS for Contact Interactions: $\Lambda(e\nu q\bar{q})$

VALUE (TeV)	CL%	DOCUMENT ID	TECN	COMMENT
>2.81	95	1 AFFOLDER 01I	CDF	

- 1 AFFOLDER 00I bound is for a scalar interaction $\overline{q}_R q_L \overline{\nu}_e \nu_L$.

SCALE LIMITS for Contact Interactions: $\Lambda(qq\bar{q}\bar{q})$

$\Lambda_{LL}^+(TeV)$	$\Lambda_{LL}^-(TeV)$	CL%	DOCUMENT ID	TECN	COMMENT
>13.1 none	17.4–29.5	>21.8	95	1 AABOUD 17AK	ATLS pp dijet angl.
•••	•••	•••	•••	•••	••• We do not use the following data for averages, fits, limits, etc. •••
>12.8	>17.5	95	2 AABOUD	18AV ATLS	$pp \rightarrow t\bar{t}t\bar{t}$
>11.5	>14.7	95	3 SIRUNYAN	18DD CMS	pp dijet angl.
>12.0	>17.5	95	4 SIRUNYAN	17F CMS	pp dijet angl.
			5 AAD	16S ATLS	pp dijet angl.
			6 AAD	15AR ATLS	$pp \rightarrow t\bar{t}t\bar{t}$
			7 AAD	15BY ATLS	$pp \rightarrow t\bar{t}t\bar{t}$
> 8.1	>12.0	95	8 AAD	15L ATLS	pp dijet angl.
> 9.0	>11.7	95	9 KHACHATRYAN	15J CMS	pp dijet angl.
> 5		95	10 FABBRICHESI	14 RVUE	$q\bar{q}t\bar{t}$

- 1 AABOUD 17AK limit is from dijet angular distribution in pp collisions at $\sqrt{s} = 13$ TeV. $u, d,$ and s quarks are assumed to be composite.
- 2 AABOUD 18AV obtain limit on t_R compositeness $2\pi/\Lambda_{RR}^2 < 1.6$ TeV $^{-2}$ at 95% CL from $t\bar{t}t\bar{t}$ production in the pp collisions at $E_{cm} = 13$ TeV.
- 3 SIRUNYAN 18DD limit is from dijet angular distribution in pp collisions at $\sqrt{s} = 13$ TeV.

- 4 SIRUNYAN 17F limit is from dijet angular cross sections in pp collisions at $E_{cm} = 13$ TeV. All quarks are assumed to be composite.
- 5 AAD 16S limit is from dijet angular selections in pp collisions at $E_{cm} = 13$ TeV. $u, d,$ and s quarks are assumed to be composite.
- 6 AAD 15AR obtain limit on the t_R compositeness $2\pi/\Lambda_{RR}^2 < 6.6$ TeV $^{-2}$ at 95% CL from the $t\bar{t}t\bar{t}$ production in the pp collisions at $E_{cm} = 8$ TeV.
- 7 AAD 15BY obtain limit on the t_R compositeness $2\pi/\Lambda_{RR}^2 < 15.1$ TeV $^{-2}$ at 95% CL from the $t\bar{t}t\bar{t}$ production in the pp collisions at $E_{cm} = 8$ TeV.
- 8 AAD 15L limit is from dijet angular distribution in pp collisions at $E_{cm} = 8$ TeV. $u, d,$ and s quarks are assumed to be composite.
- 9 KHACHATRYAN 15J limit is from dijet angular distribution in pp collisions at $E_{cm} = 8$ TeV. $u, d, s, c,$ and b quarks are assumed to be composite.
- 10 FABBRICHESI 14 obtain bounds on chromoelectric and chromomagnetic form factors of the top-quark using $pp \rightarrow t\bar{t}$ and $p\bar{p} \rightarrow t\bar{t}$ cross sections. The quoted limit on the $q\bar{q}t\bar{t}$ contact interaction is derived from their bound on the chromoelectric form factor.

SCALE LIMITS for Contact Interactions: $\Lambda(\nu\nu q\bar{q})$

Limits are for Λ_{LL}^\pm only. For other cases, see each reference.

$\Lambda_{LL}^+(TeV)$	$\Lambda_{LL}^-(TeV)$	CL%	DOCUMENT ID	TECN	COMMENT
>5.0	>5.4	95	1 MCFARLAND 98	CCFR	νN scattering

- 1 MCFARLAND 98 assumed a flavor universal interaction. Neutrinos were mostly of muon type.

MASS LIMITS for Excited e (e^*)

Most e^+e^- experiments assume one-photon or Z exchange. The limits from some e^+e^- experiments which depend on λ have assumed transition couplings which are chirality violating ($\eta_L = \eta_R$). However they can be interpreted as limits for chirality-conserving interactions after multiplying the coupling value λ by $\sqrt{2}$; see Note.

Excited leptons have the same quantum numbers as other ortholeptons. See also the searches for ortholeptons in the "Searches for Heavy Leptons" section.

Limits for Excited e (e^*) from Pair Production

These limits are obtained from $e^+e^- \rightarrow e^*e^*$ and thus rely only on the (electroweak) charge of e^* . Form factor effects are ignored unless noted. For the case of limits from Z decay, the e^* coupling is assumed to be of sequential type. Possible t channel contribution from transition magnetic coupling is neglected. All limits assume a dominant $e^* \rightarrow e\gamma$ decay except the limits from $\Gamma(Z)$.

For limits prior to 1987, see our 1992 edition (Physical Review **D45** S1 (1992)).

VALUE (GeV)	CL%	DOCUMENT ID	TECN	COMMENT
>103.2	95	1 ABBIENDI 02G	OPAL	$e^+e^- \rightarrow e^*e^*$ Homodoublet type
•••	•••	•••	•••	••• We do not use the following data for averages, fits, limits, etc. •••
>102.8	95	2 ACHARD 03B	L3	$e^+e^- \rightarrow e^*e^*$ Homodoublet type

- 1 From e^+e^- collisions at $\sqrt{s} = 183$ –209 GeV. $f = f'$ is assumed.
- 2 From e^+e^- collisions at $\sqrt{s} = 189$ –209 GeV. $f = f'$ is assumed. ACHARD 03B also obtain limit for $f = -f'$. $m_{e^*} > 96.6$ GeV.

Limits for Excited e (e^*) from Single Production

These limits are from $e^+e^- \rightarrow e^*e, W \rightarrow e^*\nu, \text{ or } ep \rightarrow e^*X$ and depend on transition magnetic coupling between e and e^* . All limits assume $e^* \rightarrow e\gamma$ decay except as noted. Limits from LEP, UA2, and H1 are for chiral coupling, whereas all other limits are for nonchiral coupling, $\eta_L = \eta_R = 1$. In most papers, the limit is expressed in the form of an excluded region in the λ – m_{e^*} plane. See the original papers.

For limits prior to 1987, see our 1992 edition (Physical Review **D45** S1 (1992)).

VALUE (GeV)	CL%	DOCUMENT ID	TECN	COMMENT
>5600	95	1 SIRUNYAN 20AJ	CMS	$pp \rightarrow e^*e^*X$
•••	•••	•••	•••	••• We do not use the following data for averages, fits, limits, etc. •••
>4800	95	2 AABOUD	19AZ ATLS	$pp \rightarrow e^*e^*X$
>3900	95	3 SIRUNYAN	19Z CMS	$pp \rightarrow e^*e^*X$
>2450	95	4 KHACHATRYAN	16AQ CMS	$pp \rightarrow e^*e^*X$
>3000	95	5 AAD	15AP ATLS	$pp \rightarrow e^{(*)}e^*X$
>2200	95	6 AAD	13BB ATLS	$pp \rightarrow e^*e^*X$
>1900	95	7 CHATRCHYAN	13AE CMS	$pp \rightarrow e^*e^*X$
>1870	95	8 AAD	12AZ ATLS	$pp \rightarrow e^{(*)}e^*X$

- 1 SIRUNYAN 20AJ search for e^* production in $2e2\gamma$ final states in pp collisions at $\sqrt{s} = 13$ TeV. The quoted limit assumes $\Lambda = m_{e^*}$, $f = f' = 1$. The contact interaction is included. See their Fig.11 for exclusion limits in m_{e^*} – Λ plane.
- 2 AABOUD 19AZ search for single e^* production in pp collisions at $\sqrt{s} = 13$ TeV. The limit quoted above is from $e^* \rightarrow e q\bar{q}$ and $e^* \rightarrow \nu W$ decays assuming $f = f' = 1$ and $m_{e^*} = \Lambda$. The contact interaction is included in e^* production and decay amplitudes. See their Fig.6 for exclusion limits in m_{e^*} – Λ plane.
- 3 SIRUNYAN 19Z search for e^* production in $\ell\ell\gamma$ final states in pp collisions at $\sqrt{s} = 13$ TeV. The quoted limit assumes $\Lambda = m_{e^*}$, $f = f' = 1$. The contact interaction is included in the e^* production and decay amplitudes.
- 4 KHACHATRYAN 16AQ search for single e^* production in pp collisions at $\sqrt{s} = 8$ TeV. The limit above is from the $e^* \rightarrow e\gamma$ search channel assuming $f = f' = 1$, $m_{e^*} = \Lambda$. See their Table 7 for limits in other search channels or with different assumptions.

Searches Particle Listings

Quark and Lepton Compositeness

- ⁵ AAD 15AP search for e^* production in evens with three or more charged leptons in pp collisions at $\sqrt{s} = 8$ TeV. The quoted limit assumes $\Lambda = m_{e^*}$, $f = f' = 1$. The contact interaction is included in the e^* production and decay amplitudes.
- ⁶ AAD 13BB search for single e^* production in pp collisions with $e^* \rightarrow e\gamma$ decay. $f = f' = 1$, and e^* production via contact interaction with $\Lambda = m_{e^*}$ are assumed.
- ⁷ CHATRCHYAN 13AE search for single e^* production in pp collisions with $e^* \rightarrow e\gamma$ decay. $f = f' = 1$, and e^* production via contact interaction with $\Lambda = m_{e^*}$ are assumed.
- ⁸ AAD 12AZ search for e^* production via four-fermion contact interaction in pp collisions with $e^* \rightarrow e\gamma$ decay. The quoted limit assumes $\Lambda = m_{e^*}$. See their Fig. 8 for the exclusion plot in the mass-coupling plane.

Limits for Excited e (e^*) from $e^+e^- \rightarrow \gamma\gamma$

These limits are derived from indirect effects due to e^* exchange in the t channel and depend on transition magnetic coupling between e and e^* . All limits are for $\lambda_\gamma = 1$. All limits except ABE 89J and ACHARD 02D are for nonchiral coupling with $\eta_L = \eta_R = 1$. We choose the chiral coupling limit as the best limit and list it in the Summary Table.

For limits prior to 1987, see our 1992 edition (Physical Review **D45** S1 (1992)).

VALUE (GeV)	CL%	DOCUMENT ID	TECN	COMMENT
>356	95	¹ ABDALLAH 04N	DLPH	$\sqrt{s} = 161\text{--}208$ GeV
•••				We do not use the following data for averages, fits, limits, etc. •••
>310	95	ACHARD 02D	L3	$\sqrt{s} = 192\text{--}209$ GeV

- ¹ ABDALLAH 04N also obtain a limit on the excited electron mass with e^* chiral coupling, $m_{e^*} > 295$ GeV at 95% CL.

Indirect Limits for Excited e (e^*)

These limits make use of loop effects involving e^* and are therefore subject to theoretical uncertainty.

VALUE (GeV)	DOCUMENT ID	TECN	COMMENT
•••			We do not use the following data for averages, fits, limits, etc. •••
	¹ DORENBOS... 89	CHRM	$\mathcal{P}_\mu e \rightarrow \mathcal{P}_\mu e, \nu_\mu e \rightarrow \nu_\mu e$
	² GRIFOLS 86	THEO	$\nu_\mu e \rightarrow \nu_\mu e$
	³ RENARD 82	THEO	$g-2$ of electron

- ¹ DORENBOSCH 89 obtain the limit $\lambda_\gamma^2 \Lambda_{\text{cut}}^2 / m_{e^*}^2 < 2.6$ (95% CL), where Λ_{cut} is the cutoff scale, based on the one-loop calculation by GRIFOLS 86. If one assumes that $\Lambda_{\text{cut}} = 1$ TeV and $\lambda_\gamma = 1$, one obtains $m_{e^*} > 620$ GeV. However, one generally expects $\lambda_\gamma \approx m_{e^*} / \Lambda_{\text{cut}}$ in composite models.
- ² GRIFOLS 86 uses $\nu_\mu e \rightarrow \nu_\mu e$ and $\mathcal{P}_\mu e \rightarrow \mathcal{P}_\mu e$ data from CHARM Collaboration to derive mass limits which depend on the scale of compositeness.
- ³ RENARD 82 derived from $g-2$ data limits on mass and couplings of e^* and μ^* . See figures 2 and 3 of the paper.

MASS LIMITS for Excited μ (μ^*)

Limits for Excited μ (μ^*) from Pair Production

These limits are obtained from $e^+e^- \rightarrow \mu^* \mu^*$ and thus rely only on the (electroweak) charge of μ^* . Form factor effects are ignored unless noted. For the case of limits from Z decay, the μ^* coupling is assumed to be of sequential type. All limits assume a dominant $\mu^* \rightarrow \mu\gamma$ decay except the limits from $\Gamma(Z)$.

For limits prior to 1987, see our 1992 edition (Physical Review **D45** S1 (1992)).

VALUE (GeV)	CL%	DOCUMENT ID	TECN	COMMENT
>103.2	95	¹ ABBIENDI 02G	OPAL	$e^+e^- \rightarrow \mu^* \mu^*$ Homodoublet type
•••				We do not use the following data for averages, fits, limits, etc. •••
>102.8	95	² ACHARD 03B	L3	$e^+e^- \rightarrow \mu^* \mu^*$ Homodoublet type
				¹ From e^+e^- collisions at $\sqrt{s} = 183\text{--}209$ GeV. $f = f'$ is assumed.
				² From e^+e^- collisions at $\sqrt{s} = 189\text{--}209$ GeV. $f = f'$ is assumed. ACHARD 03B also obtain limit for $f = -f'$: $m_{\mu^*} > 96.6$ GeV.

Limits for Excited μ (μ^*) from Single Production

These limits are from $e^+e^- \rightarrow \mu^* \mu$ and depend on transition magnetic coupling between μ and μ^* . All limits assume $\mu^* \rightarrow \mu\gamma$ decay. Limits from LEP are for chiral coupling, whereas all other limits are for nonchiral coupling, $\eta_L = \eta_R = 1$. In most papers, the limit is expressed in the form of an excluded region in the $\lambda\text{--}m_{\mu^*}$ plane. See the original papers.

For limits prior to 1987, see our 1992 edition (Physical Review **D45** S1 (1992)).

VALUE (GeV)	CL%	DOCUMENT ID	TECN	COMMENT
>5700	95	¹ SIRUNYAN 20AJ	CMS	$pp \rightarrow \mu \mu^* X$
•••				We do not use the following data for averages, fits, limits, etc. •••
>3800	95	² SIRUNYAN 19Z	CMS	$pp \rightarrow \mu \mu^* X$
>2800	95	³ AAD 16BMATLS		$pp \rightarrow \mu \mu^* X$
>2470	95	⁴ KHACHATRY...16AQ	CMS	$pp \rightarrow \mu \mu^* X$
>3000	95	⁵ AAD 15AP	ATLS	$pp \rightarrow \mu^{(*)} \mu^* X$
>2200	95	⁶ AAD 13BB	ATLS	$pp \rightarrow \mu \mu^* X$
>1900	95	⁷ CHATRCHYAN13AE	CMS	$pp \rightarrow \mu \mu^* X$
>1750	95	⁸ AAD 12AZ	ATLS	$pp \rightarrow \mu^{(*)} \mu^* X$

- ¹ SIRUNYAN 20AJ search for μ^* production in $2\mu 2j$ final states in pp collisions at $\sqrt{s} = 13$ TeV. The quoted limit assumes $\Lambda = m_{\mu^*}$, $f = f' = 1$. The contact interaction is included. See their Fig.11 for exclusion limits in $m_{\mu^*}\text{--}\Lambda$ plane.

- ² SIRUNYAN 19Z search for μ^* production in $\ell\ell\gamma$ final states in pp collisions at $\sqrt{s} = 13$ TeV. The quoted limit assumes $\Lambda = m_{\mu^*}$, $f = f' = 1$. The contact interaction is included in the μ^* production and decay amplitudes.
- ³ AAD 16BM search for μ^* production in $\mu\mu jj$ events in pp collisions at $\sqrt{s} = 8$ TeV. Both the production and decay are assumed to occur via a contact interaction with $\Lambda = m_{\mu^*}$.
- ⁴ KHACHATRYAN 16AQ search for single μ^* production in pp collisions at $\sqrt{s} = 8$ TeV. The limit above is from the $\mu^* \rightarrow \mu\gamma$ search channel assuming $f = f' = 1$, $m_{\mu^*} = \Lambda$. See their Table 7 for limits in other search channels or with different assumptions.
- ⁵ AAD 15AP search for μ^* production in evens with three or more charged leptons in pp collisions at $\sqrt{s} = 8$ TeV. The quoted limit assumes $\Lambda = m_{\mu^*}$, $f = f' = 1$. The contact interaction is included in the μ^* production and decay amplitudes.
- ⁶ AAD 13BB search for single μ^* production in pp collisions with $\mu^* \rightarrow \mu\gamma$ decay. $f = f' = 1$, and μ^* production via contact interaction with $\Lambda = m_{\mu^*}$ are assumed.
- ⁷ CHATRCHYAN 13AE search for single μ^* production in pp collisions with $\mu^* \rightarrow \mu\gamma$ decay. $f = f' = 1$, and μ^* production via contact interaction with $\Lambda = m_{\mu^*}$ are assumed.
- ⁸ AAD 12AZ search for μ^* production via four-fermion contact interaction in pp collisions with $\mu^* \rightarrow \mu\gamma$ decay. The quoted limit assumes $\Lambda = m_{\mu^*}$. See their Fig. 8 for the exclusion plot in the mass-coupling plane.

Indirect Limits for Excited μ (μ^*)

These limits make use of loop effects involving μ^* and are therefore subject to theoretical uncertainty.

VALUE (GeV)	DOCUMENT ID	TECN	COMMENT
•••			We do not use the following data for averages, fits, limits, etc. •••
	¹ RENARD 82	THEO	$g-2$ of muon
			¹ RENARD 82 derived from $g-2$ data limits on mass and couplings of e^* and μ^* . See figures 2 and 3 of the paper.

MASS LIMITS for Excited τ (τ^*)

Limits for Excited τ (τ^*) from Pair Production

These limits are obtained from $e^+e^- \rightarrow \tau^* \tau^*$ and thus rely only on the (electroweak) charge of τ^* . Form factor effects are ignored unless noted. For the case of limits from Z decay, the τ^* coupling is assumed to be of sequential type. All limits assume a dominant $\tau^* \rightarrow \tau\gamma$ decay except the limits from $\Gamma(Z)$.

For limits prior to 1987, see our 1992 edition (Physical Review **D45** S1 (1992)).

VALUE (GeV)	CL%	DOCUMENT ID	TECN	COMMENT
>103.2	95	¹ ABBIENDI 02G	OPAL	$e^+e^- \rightarrow \tau^* \tau^*$ Homodoublet type
•••				We do not use the following data for averages, fits, limits, etc. •••
>102.8	95	² ACHARD 03B	L3	$e^+e^- \rightarrow \tau^* \tau^*$ Homodoublet type
				¹ From e^+e^- collisions at $\sqrt{s} = 183\text{--}209$ GeV. $f = f'$ is assumed.
				² From e^+e^- collisions at $\sqrt{s} = 189\text{--}209$ GeV. $f = f'$ is assumed. ACHARD 03B also obtain limit for $f = -f'$: $m_{\tau^*} > 96.6$ GeV.

Limits for Excited τ (τ^*) from Single Production

These limits are from $e^+e^- \rightarrow \tau^* \tau$ and depend on transition magnetic coupling between τ and τ^* . All limits assume $\tau^* \rightarrow \tau\gamma$ decay. Limits from LEP are for chiral coupling, whereas all other limits are for nonchiral coupling, $\eta_L = \eta_R = 1$. In most papers, the limit is expressed in the form of an excluded region in the $\lambda\text{--}m_{\tau^*}$ plane. See the original papers.

VALUE (GeV)	CL%	DOCUMENT ID	TECN	COMMENT
>4600	95	¹ AAD 23BJ	ATLS	$pp \rightarrow \tau \tau^*$
•••				We do not use the following data for averages, fits, limits, etc. •••
>2500	95	² AAD 15AP	ATLS	$pp \rightarrow \tau^{(*)} \tau^* X$
>180	95	³ ACHARD 03B	L3	$e^+e^- \rightarrow \tau \tau^*$
>185	95	⁴ ABBIENDI 02G	OPAL	$e^+e^- \rightarrow \tau \tau^*$

- ¹ AAD 23BJ search for τ^* produced in association with τ and decaying into $\tau q\bar{q}$ via a contact interaction with $g_{\text{contact}}^2 = (4\pi)^2$. The limit quoted above assumes $\Lambda = m_{\tau^*}$.
- ² AAD 15AP search for τ^* production in events with three or more charged leptons in pp collisions at $\sqrt{s} = 8$ TeV. The quoted limit assumes $\Lambda = m_{\tau^*}$, $f = f' = 1$. The contact interaction is included in the τ^* production and decay amplitudes.
- ³ ACHARD 03B result is from e^+e^- collisions at $\sqrt{s} = 189\text{--}209$ GeV. $f = f' = \Lambda/m_{\tau^*}$ is assumed. See their Fig. 4 for the exclusion plot in the mass-coupling plane.
- ⁴ ABBIENDI 02G result is from e^+e^- collisions at $\sqrt{s} = 183\text{--}209$ GeV. $f = f' = \Lambda/m_{\tau^*}$ is assumed for τ^* coupling. See their Fig. 4c for the exclusion limit in the mass-coupling plane.

MASS LIMITS for Excited Neutrino (ν^*)

Limits for Excited ν (ν^*) from Pair Production

These limits are obtained from $e^+e^- \rightarrow \nu^* \nu^*$ and thus rely only on the (electroweak) charge of ν^* . Form factor effects are ignored unless noted. The ν^* coupling is assumed to be of sequential type unless otherwise noted. All limits assume a dominant $\nu^* \rightarrow \nu\gamma$ decay except the limits from $\Gamma(Z)$.

VALUE (GeV)	CL%	DOCUMENT ID	TECN	COMMENT
>1600	95	¹ AAD 15AP	ATLS	$pp \rightarrow \nu^* \nu^* X$

See key on page 1171

Searches Particle Listings

Quark and Lepton Compositeness

- • • We do not use the following data for averages, fits, limits, etc. • • •
- 2 ABBIENDI 04N OPAL
- > 102.6 95 3 ACHARD 03b L3 $e^+e^- \rightarrow \nu^*\nu^*$ Homodoublet type
- 1 AAD 15AP search for ν^* pair production in events with three or more charged leptons in pp collisions at $\sqrt{s} = 8$ TeV. The quoted limit assumes $\Lambda = m_{\nu^*}$, $f = f' = 1$. The contact interaction is included in the ν^* production and decay amplitudes.
- 2 From e^+e^- collisions at $\sqrt{s} = 192\text{--}209$ GeV, ABBIENDI 04N obtain limit on $\sigma(e^+e^- \rightarrow \nu^*\nu^*) B^2(\nu^* \rightarrow \nu\gamma)$. See their Fig.2. The limit ranges from 20 to 45 fb for $m_{\nu^*} > 45$ GeV.
- 3 From e^+e^- collisions at $\sqrt{s} = 189\text{--}209$ GeV. $f = -f'$ is assumed. ACHARD 03b also obtain limit for $f = f'$: $m_{\nu_e^*} > 101.7$ GeV, $m_{\nu_\mu^*} > 101.8$ GeV, and $m_{\nu_\tau^*} > 92.9$ GeV. See their Fig. 4 for the exclusion plot in the mass-coupling plane.

Limits for Excited ν (ν^*) from Single Production

These limits are from $e^+e^- \rightarrow \nu\nu^*$, $Z \rightarrow \nu\nu^*$, or $ep \rightarrow \nu^*X$ and depend on transition magnetic coupling between ν/e and ν^* . Assumptions about ν^* decay mode are given in footnotes.

VALUE (GeV)	CL%	DOCUMENT ID	TECN	COMMENT
> 213	95	1 AARON 08 H1	H1	$ep \rightarrow \nu^*X$
> 6000	95	2 TUMASYAN 23AL CMS	CMS	$pp \rightarrow \ell\nu^* \rightarrow \ell\ell q\bar{q}$, $\ell = e$
> 190	95	3 ACHARD 03b L3	L3	$e^+e^- \rightarrow \nu\nu^*$
none 50–150	95	4 ADLOFF 02 H1	H1	$ep \rightarrow \nu^*X$
> 158	95	5 CHEKANOV 02D ZEUS	ZEUS	$ep \rightarrow \nu^*X$

- • • We do not use the following data for averages, fits, limits, etc. • • •
- 1 AARON 08 search for single ν^* production in ep collisions with the decays $\nu^* \rightarrow \nu\gamma$, νZ , eW . The quoted limit assumes $f = -f' = \Lambda/m_{\nu^*}$. See their Fig. 3 and Fig. 4 for the exclusion plots in the mass-coupling plane.
- 2 TUMASYAN 23AL search for Majorana excited neutrino ν^* produced and decaying via gauge and contact interactions. The limit quoted above is for $\ell = e$ with $\Lambda = M_{\nu^*}$. The limit becomes $M_{\nu^*} > 6.1$ TeV for $\ell = \mu$.
- 3 ACHARD 03b result is from e^+e^- collisions at $\sqrt{s} = 189\text{--}209$ GeV. The quoted limit is for ν_e^* . $f = -f' = \Lambda/m_{\nu^*}$ is assumed. See their Fig. 4 for the exclusion plot in the mass-coupling plane.
- 4 ADLOFF 02 search for single ν^* production in ep collisions with the decays $\nu^* \rightarrow \nu\gamma$, νZ , eW . The quoted limit assumes $f = -f' = \Lambda/m_{\nu^*}$. See their Fig. 1 for the exclusion plots in the mass-coupling plane.
- 5 CHEKANOV 02d search for single ν^* production in ep collisions with the decays $\nu^* \rightarrow \nu\gamma$, νZ , eW . $f = -f' = \Lambda/m_{\nu^*}$ is assumed for the e^* coupling. CHEKANOV 02d also obtain limit for $f = f' = \Lambda/m_{\nu^*}$: $m_{\nu_e^*} > 135$ GeV. See their Fig. 5c and Fig. 5d for the exclusion plot in the mass-coupling plane.

MASS LIMITS for Excited q (q^*)

Limits for Excited q (q^*) from Pair Production

These limits are mostly obtained from $e^+e^- \rightarrow q^*\bar{q}^*$ and thus rely only on the (electroweak) charge of the q^* . Form factor effects are ignored unless noted. Assumptions about the q^* decay are given in the comments and footnotes.

VALUE (GeV)	CL%	DOCUMENT ID	TECN	COMMENT
> 338	95	1 AALTONEN 10H CDF	CDF	$q^* \rightarrow tW^-$
• • • We do not use the following data for averages, fits, limits, etc. • • •				
none 700–1200	95	2 SIRUNYAN 18v CMS	CMS	$pp \rightarrow t^*_{3/2}\bar{t}^*_{3/2} \rightarrow t\bar{t}g\bar{g}$
> 45.6	95	3 BARATE 98u ALEP	ALEP	$Z \rightarrow q^*q^*$
> 41.7	95	4 ADRIANI 93M L3	L3	u or d type, $Z \rightarrow q^*q^*$
> 44.7	95	5 BARDADIN... 92 RVUE	RVUE	u -type, $\Gamma(Z)$
> 40.6	95	6 BARDADIN... 92 RVUE	RVUE	d -type, $\Gamma(Z)$
> 44.2	95	7 DEACAMP 92 ALEP	ALEP	u -type, $\Gamma(Z)$
> 45	95	8 DEACAMP 92 ALEP	ALEP	d -type, $\Gamma(Z)$
> 45	95	9 DEACAMP 92 ALEP	ALEP	u or d type, $Z \rightarrow q^*q^*$
> 45	95	10 ABREU 91F DLPH	DLPH	u -type, $\Gamma(Z)$
> 45	95	11 ABREU 91F DLPH	DLPH	d -type, $\Gamma(Z)$

- 1 AALTONEN 10H obtain limits on the q^*q^* production cross section in $p\bar{p}$ collisions. See their Fig. 3.
- 2 SIRUNYAN 18v search for pair production of spin 3/2 excited top quarks. $B(t^*_{3/2} \rightarrow t\bar{g}) = 1$ is assumed.
- 3 BARATE 98u obtain limits on the form factor. See their Fig. 16 for limits in mass-form factor plane.
- 4 ADRIANI 93M limit is valid for $B(q^* \rightarrow qg) > 0.25$ (0.17) for up (down) type.
- 5 BARDADIN-OTWINOWSKA 92 limit based on $\Delta\Gamma(Z) < 36$ MeV.
- 6 These limits are independent of decay modes.
- 7 Limit is for $B(q^* \rightarrow qg) + B(q^* \rightarrow q\gamma) = 1$.

Limits for Excited q (q^*) from Single Production

These limits are from $e^+e^- \rightarrow q^*\bar{q}$, $p\bar{p} \rightarrow q^*X$, or $pp \rightarrow q^*X$ and depend on transition magnetic couplings between q and q^* . Assumptions about q^* decay mode are given in the footnotes and comments.

VALUE (GeV)	CL%	DOCUMENT ID	TECN	COMMENT
> 6700 (CL = 95%) OUR LIMIT				
none 1800–2500	95	1 TUMASYAN 23AF CMS	CMS	$pp \rightarrow b^*X$, $b^* \rightarrow b\bar{g}$
none 1000–6000	95	2 TUMASYAN 23bc CMS	CMS	$pp \rightarrow q^*X$, $q^* \rightarrow q\bar{g}$

none 1000–2200	95	3 TUMASYAN 23bc CMS	CMS	$pp \rightarrow b^*X$, $b^* \rightarrow b\bar{g}$
none 2000–6700	95	4 AAD 20T ATLS	ATLS	$pp \rightarrow q^*X$, $q^* \rightarrow q\bar{g}$
none 1250–3200	95	4 AAD 20T ATLS	ATLS	$pp \rightarrow b^*X$, $b^* \rightarrow b\bar{g}$, $b\bar{Z}$, tW
none 1800–6300	95	5 SIRUNYAN 20AI CMS	CMS	$pp \rightarrow q^*X$, $q^* \rightarrow q\bar{g}$
none 1500–2600	95	6 AABOUD 18AB ATLS	ATLS	$pp \rightarrow b^*X$, $b^* \rightarrow b\bar{g}$
none 1500–5300	95	7 AABOUD 18BA ATLS	ATLS	$pp \rightarrow q^*X$, $q^* \rightarrow q\bar{g}$
none 1000–5500	95	8 SIRUNYAN 18AG CMS	CMS	$pp \rightarrow q^*X$, $q^* \rightarrow q\bar{g}$
none 1000–1800	95	9 SIRUNYAN 18AG CMS	CMS	$pp \rightarrow b^*X$, $b^* \rightarrow b\bar{g}$
none 600–6000	95	10 SIRUNYAN 18BO CMS	CMS	$pp \rightarrow q^*X$, $q^* \rightarrow q\bar{g}$
none 1200–5000	95	11 SIRUNYAN 18P CMS	CMS	$pp \rightarrow q^*X$, $q^* \rightarrow qW$
none 1200–4700	95	11 SIRUNYAN 18P CMS	CMS	$pp \rightarrow q^*X$, $q^* \rightarrow qZ$
> 6000	95	12 AABOUD 17AK ATLS	ATLS	$pp \rightarrow q^*X$, $q^* \rightarrow q\bar{g}$
• • • We do not use the following data for averages, fits, limits, etc. • • •				
none 700–3000	95	13 TUMASYAN 22O CMS	CMS	$pp \rightarrow b^*X$, $b^* \rightarrow tW$
> 2600	95	14 SIRUNYAN 21AG CMS	CMS	$pp \rightarrow b^*X$, $b^* \rightarrow tW$
none 600–5400	95	15 KHACHATRY...17W CMS	CMS	$pp \rightarrow q^*X$, $q^* \rightarrow q\bar{g}$
none 1100–2100	95	16 AABOUD 16 ATLS	ATLS	$pp \rightarrow b^*X$, $b^* \rightarrow b\bar{g}$
> 1500	95	17 AAD 16AH ATLS	ATLS	$pp \rightarrow b^*X$, $b^* \rightarrow tW$
> 4400	95	18 AAD 16AI ATLS	ATLS	$pp \rightarrow q^*X$, $q^* \rightarrow q\bar{g}$
		19 AAD 16AV ATLS	ATLS	$pp \rightarrow q^*X$, $q^* \rightarrow Wb$
> 5200	95	20 AAD 16S ATLS	ATLS	$pp \rightarrow q^*X$, $q^* \rightarrow q\bar{g}$
> 1390	95	21 KHACHATRY...16I CMS	CMS	$pp \rightarrow b^*X$, $b^* \rightarrow tW$
> 5000	95	22 KHACHATRY...16K CMS	CMS	$pp \rightarrow q^*X$, $q^* \rightarrow q\bar{g}$
none 500–1600	95	23 KHACHATRY...16L CMS	CMS	$pp \rightarrow q^*X$, $q^* \rightarrow q\bar{g}$
> 4060	95	24 AAD 15V ATLS	ATLS	$pp \rightarrow q^*X$, $q^* \rightarrow q\bar{g}$
> 3500	95	25 KHACHATRY...15V CMS	CMS	$pp \rightarrow q^*X$, $q^* \rightarrow q\bar{g}$
> 3500	95	26 AAD 14A ATLS	ATLS	$pp \rightarrow q^*X$, $q^* \rightarrow q\bar{g}$
> 3200	95	27 KHACHATRY...14 CMS	CMS	$pp \rightarrow q^*X$, $q^* \rightarrow qW$
> 2900	95	28 KHACHATRY...14 CMS	CMS	$pp \rightarrow q^*X$, $q^* \rightarrow qZ$
none 700–3500	95	29 KHACHATRY...14J CMS	CMS	$pp \rightarrow q^*X$, $q^* \rightarrow q\bar{g}$
> 2380	95	30 CHATRCHYAN13AJ CMS	CMS	$pp \rightarrow q^*X$, $q^* \rightarrow qW$
> 2150	95	31 CHATRCHYAN13AJ CMS	CMS	$pp \rightarrow q^*X$, $q^* \rightarrow qZ$

- 1 TUMASYAN 23AF limit quoted above assumes $b\bar{g} \rightarrow b^*$ production. The limit becomes $m_{b^*} > 4$ TeV if contact interaction is included in the b^* production cross section. See their Fig. 5 for limits on σ_B .
- 2 TUMASYAN 23BC search for excited light flavor quark q^* in pp collisions at $\sqrt{s} = 13$ TeV. $f = 1.0$ is assumed.
- 3 TUMASYAN 23BC search for excited b quark b^* in pp collisions at $\sqrt{s} = 13$ TeV. b^* production via gauge interactions and $f = 1.0$ are assumed. The limit becomes $m_{b^*} > 3.8$ TeV if contact interaction is included in the b^* production cross section.
- 4 AAD 20T search for resonances decaying into dijets in pp collisions at $\sqrt{s} = 13$ TeV. Assume $\Lambda = m_{q^*}$, $f_5 = f = f' = 1$.
- 5 SIRUNYAN 20AI search for resonances decaying into dijets in pp collisions at $\sqrt{s} = 13$ TeV. Assume $\Lambda = m_{q^*}$, $f_5 = f = f' = 1$.
- 6 AABOUD 18AB assume $\Lambda = m_{b^*}$, $f_5 = f = f' = 1$. The contact interactions are not included in b^* production and decay amplitudes.
- 7 AABOUD 18BA search for first-generation excited quarks (u^* and d^*) with degenerate mass, assuming $\Lambda = m_{q^*}$, $f_5 = f = f' = 1$. The contact interactions are not included in q^* production and decay amplitudes.
- 8 SIRUNYAN 18AG search for first-generation excited quarks (u^* and d^*) with degenerate mass, assuming $\Lambda = m_{q^*}$, $f_5 = f = f' = 1$.
- 9 SIRUNYAN 18AG search for excited b quark assuming $\Lambda = m_{q^*}$, $f_5 = f = f' = 1$.
- 10 SIRUNYAN 18BO assume $\Lambda = m_{q^*}$, $f_5 = f = f' = 1$. The contact interactions are not included in q^* production and decay amplitudes.
- 11 SIRUNYAN 18P use the hadronic decay of W or Z , assuming $\Lambda = m_{q^*}$, $f_5 = f = f' = 1$.
- 12 AABOUD 17AK assume $\Lambda = m_{q^*}$, $f_5 = f = f' = 1$. The contact interactions are not included in q^* production and decay amplitudes. Only the decay of $q^* \rightarrow g\bar{u}$ and $q^* \rightarrow g\bar{d}$ is simulated as the benchmark signals in the analysis.
- 13 TUMASYAN 22O search for b^* decaying to tW in pp collisions at $\sqrt{s} = 13$ TeV. The limit quoted above assumes $\kappa_L^b = g_L = 1$, $\kappa_R^b = g_R = 0$. The limit becomes $m_{b^*} > 3.0$ TeV (> 3.2 TeV) if we assume $\kappa_L^b = g_L = 0$, $\kappa_R^b = g_R = 1$ ($\kappa_L^b = g_L = 1$, $\kappa_R^b = g_R = 1$). See their Fig. 3 for limits on σ_B .
- 14 SIRUNYAN 21AG search for b^* decaying to tW in pp collisions at $\sqrt{s} = 13$ TeV. The limit quoted above assumes $\kappa_L^b = g_L = 1$, $\kappa_R^b = g_R = 0$. The limit becomes $m_{b^*} > 2.8$ TeV (> 3.1 TeV) if we assume $\kappa_L^b = g_L = 0$, $\kappa_R^b = g_R = 1$ ($\kappa_L^b = g_L = \kappa_R^b = g_R = 1$). See their Fig. 5 for limits on σ_B .
- 15 KHACHATRYAN 17W assume $\Lambda = m_{q^*}$, $f_5 = f = f' = 1$. The contact interactions are not included in q^* production and decay amplitudes.
- 16 AABOUD 16 assume $\Lambda = m_{b^*}$, $f_5 = f = f' = 1$. The contact interactions are not included in the b^* production and decay amplitudes.
- 17 AAD 16AH search for b^* decaying to tW in pp collisions at $\sqrt{s} = 8$ TeV. $f_g = f_L = f_R = 1$ are assumed. See their Fig. 12b for limits on σ_B .
- 18 AAD 16AI assume $\Lambda = m_{q^*}$, $f_5 = f = f' = 1$.
- 19 AAD 16AV search for single production of vector-like quarks decaying to Wb in pp collisions. See their Fig. 8 for the limits on couplings and mixings.
- 20 AAD 16S assume $\Lambda = m_{q^*}$, $f_5 = f = f' = 1$. The contact interactions are not included in q^* production and decay amplitudes.

Searches Particle Listings

Quark and Lepton Compositeness, Extra Dimensions

- 21 KHACHATRYAN 16i search for b^* decaying to tW in pp collisions at $\sqrt{s} = 8$ TeV. $\kappa_R^b = g_L = 1$, $\kappa_R^b = g_R = 0$ are assumed. See their Fig. 8 for limits on $\sigma \cdot B$.
- 22 KHACHATRYAN 16k assume $\Lambda = m_{q^*}$, $f_S = f = f' = 1$. The contact interactions are not included in q^* production and decay amplitudes.
- 23 KHACHATRYAN 16l search for resonances decaying to dijets in pp collisions at $\sqrt{s} = 8$ TeV using the data scouting technique which increases the sensitivity to the low mass resonances.
- 24 AAD 15v assume $\Lambda = m_{q^*}$, $f_S = f = f' = 1$. The contact interactions are not included in q^* production and decay amplitudes.
- 25 KHACHATRYAN 15v assume $\Lambda = m_{q^*}$, $f_S = f = f' = 1$. The contact interactions are not included in q^* production and decay amplitudes.
- 26 AAD 14a assume $\Lambda = m_{q^*}$, $f_S = f = f' = 1$.
- 27 KHACHATRYAN 14 use the hadronic decay of W , assuming $\Lambda = m_{q^*}$, $f_S = f = f' = 1$.
- 28 KHACHATRYAN 14 use the hadronic decay of Z , assuming $\Lambda = m_{q^*}$, $f_S = f = f' = 1$.
- 29 KHACHATRYAN 14j assume $f_S = f = f' = \Lambda / m_{q^*}$.
- 30 CHATRCHYAN 13AJ use the hadronic decay of W .
- 31 CHATRCHYAN 13AJ use the hadronic decay of Z .

MASS LIMITS for Color Sextet Quarks (q_6)

VALUE (GeV)	CL%	DOCUMENT ID	TECN	COMMENT
>84	95	1 ABE	89D CDF	$p\bar{p} \rightarrow q_6 \bar{q}_6$

1 ABE 89D look for pair production of unit-charged particles which leave the detector before decaying. In the above limit the color sextet quark is assumed to fragment into a unit-charged or neutral hadron with equal probability and to have long enough lifetime not to decay within the detector. A limit of 121 GeV is obtained for a color decuplet.

MASS LIMITS for Color Octet Charged Leptons (ℓ_8)

VALUE (GeV)	CL%	DOCUMENT ID	TECN	COMMENT
>86	95	1 ABE	89D CDF	Stable ℓ_8 ; $p\bar{p} \rightarrow \ell_8 \bar{\ell}_8$

• • • We do not use the following data for averages, fits, limits, etc. • • •

2 ABT 93 H1 e_8 ; $e p \rightarrow e_8 X$

1 ABE 89D look for pair production of unit-charged particles which leave the detector before decaying. In the above limit the color octet lepton is assumed to fragment into a unit-charged or neutral hadron with equal probability and to have long enough lifetime not to decay within the detector. The limit improves to 99 GeV if it always fragments into a unit-charged hadron.

2 ABT 93 search for e_8 production via e -gluon fusion in ep collisions with $e_8 \rightarrow e g$. See their Fig. 3 for exclusion plot in the m_{e_8} - Λ plane for $m_{e_8} = 35$ –220 GeV.

MASS LIMITS for Color Octet Neutrinos (ν_8)

VALUE (GeV)	CL%	DOCUMENT ID	TECN	COMMENT
>110	90	1 BARGER	89 RVUE	ν_8 ; $p\bar{p} \rightarrow \nu_8 \bar{\nu}_8$

• • • We do not use the following data for averages, fits, limits, etc. • • •

none 3.8–29.8 95 2 KIM 90 AMY ν_8 ; $e^+e^- \rightarrow$ acoplanar jets

none 9–21.9 95 3 BARTEL 87B JADE ν_8 ; $e^+e^- \rightarrow$ acoplanar jets

1 BARGER 89 used ABE 89B limit for events with large missing transverse momentum. Two-body decay $\nu_8 \rightarrow \nu g$ is assumed.

2 KIM 90 is at $E_{cm} = 50$ –60.8 GeV. The same assumptions as in BARTEL 87B are used.

3 BARTEL 87B is at $E_{cm} = 46.3$ –46.78 GeV. The limit assumes the ν_8 pair production cross section to be eight times larger than that of the corresponding heavy neutrino pair production. This assumption is not valid in general for the weak couplings, and the limit can be sensitive to its $SU(2)_L \times U(1)_Y$ quantum numbers.

MASS LIMITS for W_8 (Color Octet W Boson)

VALUE (GeV)	DOCUMENT ID	TECN	COMMENT
>110	1 ALBAJAR	89 UA1	$p\bar{p} \rightarrow W_8 X, W_8 \rightarrow W g$

1 ALBAJAR 89 give $\sigma(W_8 \rightarrow W + \text{jet})/\sigma(W) < 0.019$ (90% CL) for $m_{W_8} > 220$ GeV.

REFERENCES FOR Searches for Quark and Lepton Compositeness

AAD	23BJ	JHEP 2306 199	G. Aad et al.	(ATLAS Collab.)
TUMASYAN	23AF	PR D108 012009	A. Tumasyan et al.	(CMS Collab.)
TUMASYAN	23AL	PL B843 137803	A. Tumasyan et al.	(CMS Collab.)
TUMASYAN	23BC	JHEP 2312 189	A. Tumasyan et al.	(CMS Collab.)
TUMASYAN	22O	JHEP 2204 048	A. Tumasyan et al.	(CMS Collab.)
AAD	21AU	PRL 127 141801	G. Aad et al.	(ATLAS Collab.)
AAD	21Q	JHEP 2104 142	G. Aad et al.	(ATLAS Collab.)
SIRUNYAN	21AG	JHEP 2112 106	A.M. Sirunyan et al.	(CMS Collab.)
SIRUNYAN	21N	JHEP 2107 208	A.M. Sirunyan et al.	(CMS Collab.)
AAD	20AP	JHEP 2011 005	G. Aad et al.	(ATLAS Collab.)
AAD	20T	JHEP 2003 145	G. Aad et al.	(ATLAS Collab.)
SIRUNYAN	20AI	JHEP 2005 033	A.M. Sirunyan et al.	(CMS Collab.)
SIRUNYAN	20AJ	JHEP 2005 052	A.M. Sirunyan et al.	(CMS Collab.)
AABOUD	19AZ	EPJ C79 803	M. Aaboud et al.	(ATLAS Collab.)
ABRAMOWICZ	19	PR D99 092006	H. Abramowitz et al.	(ZEUS Collab.)
SIRUNYAN	19AC	JHEP 1904 114	A.M. Sirunyan et al.	(CMS Collab.)
SIRUNYAN	19Z	JHEP 1904 015	A.M. Sirunyan et al.	(CMS Collab.)
AABOUD	18AB	PR D98 032016	M. Aaboud et al.	(ATLAS Collab.)
AABOUD	18AV	JHEP 1807 089	M. Aaboud et al.	(ATLAS Collab.)
AABOUD	18BA	EPJ C78 102	M. Aaboud et al.	(ATLAS Collab.)

SIRUNYAN	18AG	PL B781 390	A.M. Sirunyan et al.	(CMS Collab.)
SIRUNYAN	18BO	JHEP 1808 130	A.M. Sirunyan et al.	(CMS Collab.)
SIRUNYAN	18DD	EPJ C78 789	A.M. Sirunyan et al.	(CMS Collab.)
SIRUNYAN	18P	PR D97 072006	A.M. Sirunyan et al.	(CMS Collab.)
SIRUNYAN	18V	PL B778 349	A.M. Sirunyan et al.	(CMS Collab.)
AABOUD	17AK	PR D96 052004	M. Aaboud et al.	(ATLAS Collab.)
AABOUD	17AT	JHEP 1710 182	M. Aaboud et al.	(ATLAS Collab.)
KHACHATRYAN	17W	PL B769 520	V. Khachatryan et al.	(CMS Collab.)
SIRUNYAN	17F	JHEP 1707 013	A.M. Sirunyan et al.	(CMS Collab.)
AABOUD	16	PL B759 229	M. Aaboud et al.	(ATLAS Collab.)
AABOUD	16U	PL B761 372	M. Aaboud et al.	(ATLAS Collab.)
AAD	16AH	JHEP 1602 110	G. Aad et al.	(ATLAS Collab.)
AAD	16AI	JHEP 1603 041	G. Aad et al.	(ATLAS Collab.)
AAD	16AV	EPJ C76 442	G. Aad et al.	(ATLAS Collab.)
AAD	16BM	NJP 18 073021	G. Aad et al.	(ATLAS Collab.)
AAD	16S	PL B754 302	G. Aad et al.	(ATLAS Collab.)
KHACHATRYAN	16AQ	JHEP 1603 125	V. Khachatryan et al.	(CMS Collab.)
KHACHATRYAN	16I	JHEP 1601 166	V. Khachatryan et al.	(CMS Collab.)
KHACHATRYAN	16K	PRL 116 071801	V. Khachatryan et al.	(CMS Collab.)
KHACHATRYAN	16L	PRL 117 091802	V. Khachatryan et al.	(CMS Collab.)
AAD	15AP	JHEP 1508 138	G. Aad et al.	(ATLAS Collab.)
AAD	15AR	JHEP 1508 105	G. Aad et al.	(ATLAS Collab.)
AAD	15BY	JHEP 1510 150	G. Aad et al.	(ATLAS Collab.)
AAD	15L	PRL 114 221802	G. Aad et al.	(ATLAS Collab.)
AAD	15V	PR D91 052007	G. Aad et al.	(ATLAS Collab.)
KHACHATRYAN	15AE	JHEP 1504 025	V. Khachatryan et al.	(CMS Collab.)
KHACHATRYAN	15J	PL B746 79	V. Khachatryan et al.	(CMS Collab.)
KHACHATRYAN	15V	PR D91 052009	V. Khachatryan et al.	(CMS Collab.)
AAD	14A	PL B728 562	G. Aad et al.	(ATLAS Collab.)
AAD	14BE	EPJ C74 3134	G. Aad et al.	(ATLAS Collab.)
FABBRICHESI	14	PR D99 074028	M. Fabbrichesi, M. Pinamonti, A. Tonerio	(ATLAS Collab.)
KHACHATRYAN	14	JHEP 1408 173	V. Khachatryan et al.	(CMS Collab.)
KHACHATRYAN	14J	PL B738 274	V. Khachatryan et al.	(CMS Collab.)
AAD	13BB	NJP 15 093011	G. Aad et al.	(ATLAS Collab.)
AAD	13E	PR D87 015010	G. Aad et al.	(ATLAS Collab.)
CHATRCHYAN	13AE	PL B720 309	S. Chatrchyan et al.	(CMS Collab.)
CHATRCHYAN	13AJ	PL B723 280	S. Chatrchyan et al.	(CMS Collab.)
CHATRCHYAN	13K	PR D87 032001	S. Chatrchyan et al.	(CMS Collab.)
AAD	12AB	PL B712 40	G. Aad et al.	(ATLAS Collab.)
AAD	12AZ	PR D85 072003	G. Aad et al.	(ATLAS Collab.)
AARON	11C	PL B705 52	F. D. Aaron et al.	(H1 Collab.)
ABDALLAH	10	PRL C71 1555	J. Abdallah et al.	(DELPHI Collab.)
AALTONEN	10H	PRL 104 091801	T. Aaltonen et al.	(CDF Collab.)
ABDALLAH	09	EPJ C60 1	J. Abdallah et al.	(DELPHI Collab.)
AARON	08	PL B663 382	F.D. Aaron et al.	(H1 Collab.)
SCHAEF	07A	EPJ C49 411	S. Schaefer et al.	(ALEPH Collab.)
ABDALLAH	06C	EPJ C45 589	J. Abdallah et al.	(DELPHI Collab.)
ABULENCIA	06L	PRL 96 211801	A. Abulencia et al.	(CDF Collab.)
ABBIENDI	04G	EPJ C33 173	G. Abbiendi et al.	(OPAL Collab.)
ABBIENDI	04N	PL B602 167	G. Abbiendi et al.	(OPAL Collab.)
ABDALLAH	04N	EPJ C37 405	J. Abdallah et al.	(DELPHI Collab.)
ACHARD	03B	PL B568 23	P. Achard et al.	(L3 Collab.)
BABICH	03	EPJ C29 103	A.A. Babich et al.	(OPAL Collab.)
ABBIENDI	02G	PL B544 57	G. Abbiendi et al.	(OPAL Collab.)
ACHARD	02D	PL B531 28	P. Achard et al.	(L3 Collab.)
ADLOFF	02	PL B525 9	C. Adloff et al.	(H1 Collab.)
CHEKANOV	02D	PL B549 32	S. Chekanov et al.	(ZEUS Collab.)
AFFOLDER	01I	PRL 87 231803	T. Affolder et al.	(CDF Collab.)
BOURILKOV	01	PR D64 071701	D. Bourilkov	(CDF Collab.)
CHEUNG	01B	PL B517 167	K. Cheung	(L3 Collab.)
ACCARIARI	00P	PL B489 81	M. Acciarri et al.	(L3 Collab.)
AFFOLDER	00I	PR D62 012004	T. Affolder et al.	(CDF Collab.)
BARATE	98U	EPJ C4 571	R. Barate et al.	(ALEPH Collab.)
BARGER	98E	PR D57 391	V. Barger et al.	(CCFR/NuTeV Collab.)
MC FARLAND	98	EPJ C1 509	K.S. McFarland et al.	(CERN Collab.)
DIACRUZ	94	PR D49 2149	J.L. Diaz Cruz, O.A. Sampayo	(CERN Collab.)
ABT	93	NP B396 3	I. Abt et al.	(H1 Collab.)
ADRIANI	93M	PRPL 236 1	O. Adriani et al.	(L3 Collab.)
BARDADIN	92	ZPHY C55 163	M. Bardadin-Ottwinowska	(CLER)
DECAMP	92	PRPL 216 253	D. Decamp et al.	(ALEPH Collab.)
PDG	92	PR D45 51	K. Hikasa et al.	(KEK, LBL, BOST+)
ABREU	91F	NP B367 511	P. Abreu et al.	(DELPHI Collab.)
KIM	90	PL B240 243	G.N. Kim et al.	(AMY Collab.)
ABE	89B	PRL 62 1825	F. Abe et al.	(CDF Collab.)
ABE	89D	PRL 63 1447	F. Abe et al.	(CDF Collab.)
ABE	89J	ZPHY C45 175	K. Abe et al.	(VENUS Collab.)
ALBAJAR	89	ZPHY C44 15	C. Albajar et al.	(UA1 Collab.)
BARGER	89	PL B220 464	V. Barger et al.	(WISC, KEK)
DORENBOSCH	89	ZPHY C41 567	J. Dorenbosch et al.	(CHARM Collab.)
BARTEL	87B	ZPHY C36 15	W. Bartel et al.	(JADE Collab.)
GRIFFIOS	86	PL B68B 264	J.A. Griffios, S. Peris	(BARC)
JODIDIO	86	PR D34 1967	A. Jodidio et al.	(LBL, NWES, TRIU)
Also	PR D37 237 (errata.)	A. Jodidio et al.	(LBL, NWES, TRIU)	
RENARD	82	PL 116B 264	F.M. Renard	(CERN)

Extra Dimensions

For explanation of terms used and discussion of significant model dependence of following limits, see the “Extra Dimensions” review. Footnotes describe originally quoted limit. δ indicates the number of extra dimensions.

Limits not encoded here are summarized in the “Extra Dimensions” review, where the latest unpublished results are also described.

See the related review(s):

Extra Dimensions

CONTENTS:

- Limits on R from Deviations in Gravitational Force Law
- Limits on R from On-Shell Production of Gravitons: $\delta = 2$
- Mass Limits on M_{Pl}
- Limits on $1/R = M_c$
- Limits on Kaluza-Klein Gravitons in Warped Extra Dimensions
- Limits on Kaluza-Klein Gluons in Warped Extra Dimensions
- Black Hole Production Limits
 - Semiclassical Black Holes
 - Quantum Black Holes

See key on page 1171

Searches Particle Listings Extra Dimensions

Limits on R from Deviations in Gravitational Force Law

This section includes limits on the size of extra dimensions from deviations in the Newtonian ($1/r^2$) gravitational force law at short distances. Deviations are parametrized by a gravitational potential of the form $V = -(G m m'/r) [1 + \alpha \exp(-r/R)]$. For δ toroidal extra dimensions of equal size, $\alpha = 8\delta/3$. Quoted bounds are for $\delta = 2$ unless otherwise noted.

VALUE (μm)	CL%	DOCUMENT ID	TECN	COMMENT
		• • • We do not use the following data for averages, fits, limits, etc. • • •		
		1 BLAKEMORE 21		Optical levitation
		2 HEACOCK 21		Neutron scattering
		3 LEE 20		Torsion pendulum
< 37	95	4 TAN 20A		Torsion pendulum
		5 BERGE 18	MICR	Space accelerometer
		6 FAYET 18A	MICR	Space accelerometer
		7 KLIMCHITSK...17A		Torsion oscillator
		8 XU 13		Nuclei properties
		9 BEZERRA 11		Torsion oscillator
		10 SUSHKOV 11		Torsion pendulum
		11 BEZERRA 10		Microcantilever
		12 MASUDA 09		Torsion pendulum
		13 GERACI 08		Microcantilever
		14 TRENKEL 08		Newton's constant
		15 DECCA 07A		Torsion oscillator
< 37	95	16 KAPNER 07		Torsion pendulum
< 47	95	17 TU 07		Torsion pendulum
		18 SMULLIN 05		Microcantilever
< 130	95	19 HOYLE 04		Torsion pendulum
		20 CHIAVERINI 03		Microcantilever
< 200	95	21 LONG 03		Microcantilever
< 190	95	22 HOYLE 01		Torsion pendulum
		23 HOSKINS 85		Torsion pendulum

- 1 BLAKEMORE 21 obtain constraints on non-Newtonian forces with strengths $|\alpha| \gtrsim 10^8$ and length scales $R > 10 \mu\text{m}$. See their Fig. 4 for more details including comparison with previous searches.
- 2 HEACOCK 21 obtain constraints on non-Newtonian forces with strengths $10^{18} \lesssim |\alpha| \lesssim 10^{25}$ and length scales $R \approx 0.02\text{--}10 \text{ nm}$. See their Figure 3 for more details. This improves the results of HADDOCK 18. These constraints do not place limits on the size of extra flat dimensions.
- 3 LEE 20 search for new forces probing a range of $|\alpha| \approx 0.1\text{--}10^5$ and length scales $R \approx 7\text{--}90 \mu\text{m}$. For $\delta = 1$ the bound on R is $30 \mu\text{m}$. See their Fig. 5 for details on the bound.
- 4 TAN 20A search for new forces probing a range of $|\alpha| \approx 4 \times 10^{-3}\text{--}1 \times 10^2$ and length scales $R \approx 40\text{--}350 \mu\text{m}$. See their Fig. 6 for details on the bound.
- 5 BERGE 18 uses results from the MICROSCOPE experiment to obtain constraints on non-Newtonian forces with strengths $10^{-11} \lesssim |\alpha| \lesssim 10^{-7}$ and length scales $R \gtrsim 10^5 \text{ m}$. See their Figure 1 for more details. These constraints do not place limits on the size of extra flat dimensions.
- 6 FAYET 18A uses results from the MICROSCOPE experiment to obtain constraints on an EP-violating force possibly arising from a new $U(1)$ gauge boson. For $R \gtrsim 10^7 \text{ m}$ the limits are $|\alpha| \lesssim$ a few 10^{-13} to a few 10^{-11} depending on the coupling, corresponding to $|e| \lesssim 10^{-24}$ for the coupling of the new spin-1 or spin-0 mediator. These constraints do not place limits on the size of extra flat dimensions. This extends the results of FAYET 18.
- 7 KLIMCHITSKAYA 17A uses an experiment that measures the difference of Casimir forces to obtain bounds on non-Newtonian forces with strengths $|\alpha| \approx 10^5\text{--}10^{17}$ and length scales $R = 0.03\text{--}10 \mu\text{m}$. See their Fig. 3. These constraints do not place limits on the size of extra flat dimensions.
- 8 XU 13 obtain constraints on non-Newtonian forces with strengths $|\alpha| \approx 10^{34}\text{--}10^{36}$ and length scales $R \approx 1\text{--}10 \text{ fm}$. See their Fig. 4 for more details. These constraints do not place limits on the size of extra flat dimensions.
- 9 BEZERRA 11 obtain constraints on non-Newtonian forces with strengths $10^{11} \lesssim |\alpha| \lesssim 10^{18}$ and length scales $R = 30\text{--}1260 \text{ nm}$. See their Fig. 2 for more details. These constraints do not place limits on the size of extra flat dimensions.
- 10 SUSHKOV 11 obtain improved limits on non-Newtonian forces with strengths $10^7 \lesssim |\alpha| \lesssim 10^{11}$ and length scales $0.4 \mu\text{m} < R < 4 \mu\text{m}$ (95% CL). See their Fig. 2. These bounds do not place limits on the size of extra flat dimensions. However, a model dependent bound of $M_* > 70 \text{ TeV}$ is obtained assuming gauge bosons that couple to baryon number also propagate in $(4 + \delta)$ dimensions.
- 11 BEZERRA 10 obtain improved constraints on non-Newtonian forces with strengths $10^{19} \lesssim |\alpha| \lesssim 10^{29}$ and length scales $R = 1.6\text{--}14 \text{ nm}$ (95% CL). See their Fig. 1. This bound does not place limits on the size of extra flat dimensions.
- 12 MASUDA 09 obtain improved constraints on non-Newtonian forces with strengths $10^9 \lesssim |\alpha| \lesssim 10^{11}$ and length scales $R = 1.0\text{--}2.9 \mu\text{m}$ (95% CL). See their Fig. 3. This bound does not place limits on the size of extra flat dimensions.
- 13 GERACI 08 obtain improved constraints on non-Newtonian forces with strengths $|\alpha| > 14,000$ and length scales $R = 5\text{--}15 \mu\text{m}$. See their Fig. 9. This bound does not place limits on the size of extra flat dimensions.
- 14 TRENKEL 08 uses two independent measurements of Newton's constant G to constrain new forces with strength $|\alpha| \approx 10^{-4}$ and length scales $R = 0.02\text{--}1 \text{ m}$. See their Fig. 1. This bound does not place limits on the size of extra flat dimensions.
- 15 DECCA 07A search for new forces and obtain bounds in the region with strengths $|\alpha| \approx 10^{13}\text{--}10^{18}$ and length scales $R = 20\text{--}86 \text{ nm}$. See their Fig. 6. This bound does not place limits on the size of extra flat dimensions.
- 16 KAPNER 07 search for new forces, probing a range of $|\alpha| \approx 10^{-3}\text{--}10^5$ and length scales $R \approx 10\text{--}1000 \mu\text{m}$. For $\delta = 1$ the bound on R is $44 \mu\text{m}$. For $\delta = 2$, the bound is expressed in terms of M_* , here translated to a bound on the radius. See their Fig. 6 for details on the bound.
- 17 TU 07 search for new forces probing a range of $|\alpha| \approx 10^{-1}\text{--}10^5$ and length scales $R \approx 20\text{--}1000 \mu\text{m}$. For $\delta = 1$ the bound on R is $53 \mu\text{m}$. See their Fig. 3 for details on the bound.

- 18 SMULLIN 05 search for new forces, and obtain bounds in the region with strengths $\alpha \approx 10^3\text{--}10^8$ and length scales $R = 6\text{--}20 \mu\text{m}$. See their Figs. 1 and 16 for details on the bound. This work does not place limits on the size of extra flat dimensions.
- 19 HOYLE 04 search for new forces, probing α down to 10^{-2} and distances down to $10 \mu\text{m}$. Quoted bound on R is for $\delta = 2$. For $\delta = 1$, bound goes to $160 \mu\text{m}$. See their Fig. 34 for details on the bound.
- 20 CHIAVERINI 03 search for new forces, probing α above 10^4 and λ down to $3 \mu\text{m}$, finding no signal. See their Fig. 4 for details on the bound. This bound does not place limits on the size of extra flat dimensions.
- 21 LONG 03 search for new forces, probing α down to 3, and distances down to about $10 \mu\text{m}$. See their Fig. 4 for details on the bound.
- 22 HOYLE 01 search for new forces, probing α down to 10^{-2} and distances down to $20 \mu\text{m}$. See their Fig. 4 for details on the bound. The quoted bound is for $\alpha \geq 3$.
- 23 HOSKINS 85 search for new forces, probing distances down to 4 mm . See their Fig. 13 for details on the bound. This bound does not place limits on the size of extra flat dimensions.

Limits on R from On-Shell Production of Gravitons: $\delta = 2$

This section includes limits on on-shell production of gravitons in collider and astrophysical processes. Bounds quoted are on R , the assumed common radius of the flat extra dimensions, for $\delta = 2$ extra dimensions. Studies often quote bounds in terms of derived parameter; experiments are actually sensitive to the masses of the KK gravitons: $m_{\vec{n}} = |\vec{n}|/R$. See the Review on "Extra Dimensions" for details. Bounds are given in μm for $\delta = 2$.

VALUE (μm)	CL%	DOCUMENT ID	TECN	COMMENT
< 3.8	95	1 AAD 21F	ATLS	$pp \rightarrow jG$
< 0.00016	95	2 HANNESTAD 03		Neutron star heating
		• • • We do not use the following data for averages, fits, limits, etc. • • •		
< 56	95	3 SIRUNYAN 21A	CMS	$pp \rightarrow ZG$
< 4.1	95	4 TUMASYAN 21D	CMS	$pp \rightarrow jG$
		5 SIRUNYAN 17AQ	CMS	$pp \rightarrow \gamma G$
		6 AABOUD 16F	ATLS	$pp \rightarrow \gamma G$
		7 KHACHATRYAN 16N	CMS	$pp \rightarrow \gamma G$
		8 AAD 15CS	ATLS	$pp \rightarrow \gamma G$
		9 AAD 13C	ATLS	$pp \rightarrow \gamma G$
		10 AAD 13D	ATLS	$pp \rightarrow jj$
< 127	95	11 AJELLO 12	FLAT	Neutron star γ sources
< 34.4	95	12 AALTONEN 08AC	CDF	$p\bar{p} \rightarrow \gamma G, jG$
< 0.0087	95	13 ABAZOV 08S	D0	$p\bar{p} \rightarrow \gamma G$
< 245	95	14 DAS 08		Supernova cooling
< 615	95	15 ABULENCIA, A 06	CDF	$p\bar{p} \rightarrow jG$
< 0.916	95	16 ABDALLAH 05B	DLPH	$e^+e^- \rightarrow \gamma G$
< 350	95	17 ACHARD 04E	L3	$e^+e^- \rightarrow \gamma G$
< 270	95	18 ACOSTA 04C	CDF	$p\bar{p} \rightarrow jG$
< 210	95	19 CASSE 04		Neutron star γ sources
< 480	95	20 ABAZOV 03	D0	$p\bar{p} \rightarrow jG$
< 0.00038	95	21 HANNESTAD 03		Supernova cooling
< 0.96	95	22 HANNESTAD 03		Diffuse γ background
< 0.096	95	23 HANNESTAD 03		Neutron star γ sources
< 0.051	95	24 HEISTER 03C	ALEP	$e^+e^- \rightarrow \gamma G$
< 300	95	25 FAIRBAIRN 01		Cosmology
		26 HANNHART 01		Supernova cooling
< 0.66	95	27 CASSISI 00		Red giants
< 1300	95	28 ACCIARRI 99S	L3	$e^+e^- \rightarrow ZG$

- 1 AAD 21F search for $pp \rightarrow jG$, using 139 fb^{-1} of data at $\sqrt{s} = 13 \text{ TeV}$ to place lower limits on M_D for two to six extra dimensions (see their Table X), from which this bound on R is derived. This limit supersedes that in AABOUD 18f.
- 2 HANNESTAD 03 obtain a limit on R from the heating of old neutron stars by the surrounding cloud of trapped KK gravitons. Limits for all $\delta \leq 7$ are given in their Tables V and VI. These limits supersede those in HANNESTAD 02.
- 3 SIRUNYAN 21A search for $pp \rightarrow ZG$, using 137 fb^{-1} of data at $\sqrt{s} = 13 \text{ TeV}$ to place lower limits on M_D for two to seven extra dimensions (see their Figure 12), from which this bound on R is derived. These limits supersede those obtained in SIRUNYAN 18bV.
- 4 TUMASYAN 21D search for $pp \rightarrow jG$, using 137 fb^{-1} of data at $\sqrt{s} = 13 \text{ TeV}$ to place lower limits on M_D for two to seven extra dimensions (see their Table 3), from which this bound on R is derived. This limit supersedes that in SIRUNYAN 18s.
- 5 SIRUNYAN 17AQ search for $pp \rightarrow \gamma G$, using 12.9 fb^{-1} of data at $\sqrt{s} = 13 \text{ TeV}$ to place limits on M_D for three to six extra dimensions (see their Table 3).
- 6 AABOUD 16F search for $pp \rightarrow \gamma G$, using 3.2 fb^{-1} of data at $\sqrt{s} = 13 \text{ TeV}$ to place limits on M_D for two to six extra dimensions (see their Figure 9), from which this bound on R is derived.
- 7 KHACHATRYAN 16N search for $pp \rightarrow \gamma G$, using 19.6 fb^{-1} of data at $\sqrt{s} = 8 \text{ TeV}$ to place limits on M_D for three to six extra dimensions (see their Table 5).
- 8 AAD 15CS search for $pp \rightarrow \gamma G$, using 20.3 fb^{-1} of data at $\sqrt{s} = 8 \text{ TeV}$ to place lower limits on M_D for two to six extra dimensions (see their Fig. 18).
- 9 AAD 13C search for $pp \rightarrow \gamma G$, using 4.6 fb^{-1} of data at $\sqrt{s} = 7 \text{ TeV}$ to place bounds on M_D for two to six extra dimensions, from which this bound on R is derived.
- 10 AAD 13D search for the dijet decay of quantum black holes in 4.8 fb^{-1} of data produced in pp collisions at $\sqrt{s} = 7 \text{ TeV}$ to place bounds on M_D for two to seven extra dimensions, from which these bounds on R are derived. Limits on M_D for all $\delta \leq 7$ are given in their Table 3.
- 11 AJELLO 12 obtain a limit on R from the gamma-ray emission of point γ sources that arise from the photon decay of KK gravitons which are gravitationally bound around neutron stars. Limits for all $\delta \leq 7$ are given in their Table 7.
- 12 AALTONEN 08AC search for $p\bar{p} \rightarrow \gamma G$ and $p\bar{p} \rightarrow jG$ at $\sqrt{s} = 1.96 \text{ TeV}$ with 2.0 fb^{-1} and 1.1 fb^{-1} respectively, in order to place bounds on the fundamental scale and size of the extra dimensions. See their Table III for limits on all $\delta \leq 6$.
- 13 ABAZOV 08S search for $p\bar{p} \rightarrow \gamma G$, using 1 fb^{-1} of data at $\sqrt{s} = 1.96 \text{ TeV}$ to place bounds on M_D for two to eight extra dimensions, from which these bounds on R are derived. See their paper for intermediate values of δ .

Searches Particle Listings

Extra Dimensions

- ¹⁴ DAS 08 obtain a limit on R from Kaluza-Klein graviton cooling of SN1987A due to plasmon-plasmon annihilation.
- ¹⁵ ABULENCIA, A 06 search for $p\bar{p} \rightarrow jG$ using 368 pb^{-1} of data at $\sqrt{s} = 1.96 \text{ TeV}$. See their Table II for bounds for all $\delta \leq 6$.
- ¹⁶ ABDALLAH 05B search for $e^+e^- \rightarrow \gamma G$ at $\sqrt{s} = 180\text{--}209 \text{ GeV}$ to place bounds on the size of extra dimensions and the fundamental scale. Limits for all $\delta \leq 6$ are given in their Table 6. These limits supersede those in ABREU 00Z.
- ¹⁷ ACHARD 04E search for $e^+e^- \rightarrow \gamma G$ at $\sqrt{s} = 189\text{--}209 \text{ GeV}$ to place bounds on the size of extra dimensions and the fundamental scale. See their Table 8 for limits with $\delta \leq 8$. These limits supersede those in ACCIARRI 99R.
- ¹⁸ ACOSTA 04C search for $p\bar{p} \rightarrow jG$ at $\sqrt{s} = 1.8 \text{ TeV}$ to place bounds on the size of extra dimensions and the fundamental scale. See their paper for bounds on $\delta = 4, 6$.
- ¹⁹ CASSE 04 obtain a limit on R from the gamma-ray emission of point γ sources that arises from the photon decay of gravitons around newly born neutron stars, applying the technique of HANNESTAD 03 to neutron stars in the galactic bulge. Limits for all $\delta \leq 7$ are given in their Table I.
- ²⁰ ABAZOV 03 search for $p\bar{p} \rightarrow jG$ at $\sqrt{s} = 1.8 \text{ TeV}$ to place bounds on M_D for 2 to 7 extra dimensions, from which these bounds on R are derived. See their paper for bounds on intermediate values of δ . We quote results without the approximate NLO scaling introduced in the paper.
- ²¹ HANNESTAD 03 obtain a limit on R from graviton cooling of supernova SN1987A. Limits for all $\delta \leq 7$ are given in their Tables V and VI.
- ²² HANNESTAD 03 obtain a limit on R from gravitons emitted in supernovae and which subsequently decay, contaminating the diffuse cosmic γ background. Limits for all $\delta \leq 7$ are given in their Tables V and VI. These limits supersede those in HANNESTAD 02.
- ²³ HANNESTAD 03 obtain a limit on R from gravitons emitted in two recent supernovae and which subsequently decay, creating point γ sources. Limits for all $\delta \leq 7$ are given in their Tables V and VI. These limits are corrected in the published erratum.
- ²⁴ HEISTER 03C use the process $e^+e^- \rightarrow \gamma G$ at $\sqrt{s} = 189\text{--}209 \text{ GeV}$ to place bounds on the size of extra dimensions and the scale of gravity. See their Table 4 for limits with $\delta \leq 6$ for derived limits on M_D .
- ²⁵ FAIRBAIRN 01 obtains bounds on R from over production of KK gravitons in the early universe. Bounds are quoted in paper in terms of fundamental scale of gravity. Bounds depend strongly on temperature of QCD phase transition and range from $R < 0.13 \mu\text{m}$ to $0.001 \mu\text{m}$ for $\delta=2$; bounds for $\delta=3,4$ can be derived from Table 1 in the paper.
- ²⁶ HANHART 01 obtain bounds on R from limits on graviton cooling of supernova SN1987A using numerical simulations of proto-neutron star neutrino emission.
- ²⁷ CASSISI 00 obtain rough bounds on M_D (and thus R) from red giant cooling for $\delta=2,3$. See their paper for details.
- ²⁸ ACCIARRI 99s search for $e^+e^- \rightarrow ZG$ at $\sqrt{s}=189 \text{ GeV}$. Limits on the gravity scale are found in their Table 2, for $\delta \leq 4$.

Mass Limits on M_{TT}

This section includes limits on the cut-off mass scale, M_{TT} , of dimension-8 operators from KK graviton exchange in models of large extra dimensions. Ambiguities in the UV-divergent summation are absorbed into the parameter λ , which is taken to be $\lambda = \pm 1$ in the following analyses. Bounds for $\lambda = -1$ are shown in parenthesis after the bound for $\lambda = +1$, if appropriate. Different papers use slightly different definitions of the mass scale. The definition used here is related to another popular convention by $M_{TT}^4 = (2/\pi) \Lambda_{*}^4$, as discussed in the above Review on "Extra Dimensions."

VALUE (TeV)	CL%	DOCUMENT ID	TECN	COMMENT
> 9.02	95	1 SIRUNYAN	18DD CMS	$p\bar{p} \rightarrow$ dijet, ang. distrib.
> 20.6	(> 15.7)	2 GIUDICE	03 RVUE	Dim-6 operators
> 6.7	95	3 SIRUNYAN	21N CMS	$p\bar{p} \rightarrow e^+e^-, \mu^+\mu^-$
> 6.9	95	4 SIRUNYAN	19AC CMS	$p\bar{p} \rightarrow e^+e^-, \mu^+\mu^-, \gamma\gamma$
> 7.0	(> 5.6)	5 SIRUNYAN	18DU CMS	$p\bar{p} \rightarrow \gamma\gamma$
> 6.5	95	6 AABOUD	17AP ATLS	$p\bar{p} \rightarrow \gamma\gamma$
> 3.8	95	7 AAD	14BE ATLS	$p\bar{p} \rightarrow e^+e^-, \mu^+\mu^-$
> 3.2	95	8 AAD	13E ATLS	$p\bar{p} \rightarrow e^+e^-, \mu^+\mu^-, \gamma\gamma$
		9 BAAK	12 RVUE	Electroweak
> 0.90	(> 0.92)	10 AARON	11c H1	$e^{\pm}p \rightarrow e^{\pm}X$
> 1.48	95	11 ABAZOV	09AE D0	$p\bar{p} \rightarrow$ dijet, ang. distrib.
> 1.45	95	12 ABAZOV	09D D0	$p\bar{p} \rightarrow e^+e^-, \gamma\gamma$
> 1.1	(> 1.0)	13 SCHAEEL	07A ALEP	$e^+e^- \rightarrow e^+e^-$
> 0.898	(> 0.998)	14 ABDALLAH	06C DLPH	$e^+e^- \rightarrow \ell^+\ell^-$
> 0.853	(> 0.939)	15 GERDES	06	$p\bar{p} \rightarrow e^+e^-, \gamma\gamma$
> 0.96	(> 0.93)	16 ABAZOV	05V D0	$p\bar{p} \rightarrow \mu^+\mu^-$
> 0.78	(> 0.79)	17 CHEKANOV	04B ZEUS	$e^{\pm}p \rightarrow e^{\pm}X$
> 0.805	(> 0.956)	18 ABBIENDI	03D OPAL	$e^+e^- \rightarrow \gamma\gamma$
> 0.7	(> 0.7)	19 ACHARD	03D L3	$e^+e^- \rightarrow ZZ$
> 0.82	(> 0.78)	20 ADLOFF	03 H1	$e^{\pm}p \rightarrow e^{\pm}X$
> 1.28	(> 1.25)	21 GIUDICE	03 RVUE	
> 0.80	(> 0.85)	22 HEISTER	03C ALEP	$e^+e^- \rightarrow \gamma\gamma$
> 0.84	(> 0.99)	23 ACHARD	02D L3	$e^+e^- \rightarrow \gamma\gamma$
> 1.2	(> 1.1)	24 ABBOTT	01 D0	$p\bar{p} \rightarrow e^+e^-, \gamma\gamma$
> 0.60	(> 0.63)	25 ABBIENDI	00R OPAL	$e^+e^- \rightarrow \mu^+\mu^-$
> 0.63	(> 0.50)	25 ABBIENDI	00R OPAL	$e^+e^- \rightarrow \tau^+\tau^-$
> 0.68	(> 0.61)	25 ABBIENDI	00R OPAL	$e^+e^- \rightarrow \mu^+\mu^-, \tau^+\tau^-$
		26 ABREU	00A DLPH	$e^+e^- \rightarrow \gamma\gamma$
		27 ABREU	00S DLPH	$e^+e^- \rightarrow \mu^+\mu^-, \tau^+\tau^-$
> 0.680	(> 0.542)	28 CHANG	00B RVUE	Electroweak
> 15-28	99.7	29 CHEUNG	00 RVUE	$e^+e^- \rightarrow \gamma\gamma$
> 0.98	95	30 GRAESSER	00 RVUE	$(g-2)_{\mu}$
> 0.29-0.38	95	31 HAN	00 RVUE	Electroweak
> 0.50-1.1	95	32 MATHEWS	00 RVUE	$\bar{p}p \rightarrow jj$
> 2.0	(> 2.0)			

> 1.0	(> 1.1)	95	33 MELE	00 RVUE	$e^+e^- \rightarrow VV$
			34 ABBIENDI	99P OPAL	
			35 ACCIARRI	99M L3	
			36 ACCIARRI	99S L3	
> 1.412	(> 1.077)	95	37 BOURILKOV	99	$e^+e^- \rightarrow e^+e^-$

- ¹ SIRUNYAN 18DD use dijet angular distributions in 35.9 fb^{-1} of data from $p\bar{p}$ collisions at $\sqrt{s} = 13 \text{ TeV}$ to place a lower bound on Λ_T , here converted to M_{TT} . This updates the results of SIRUNYAN 17F.
- ² GIUDICE 03 place bounds on Λ_6 , the coefficient of the gravitationally-induced dimension-6 operator $(2\pi\lambda/\Lambda_6^2)(\sum \bar{T}_\gamma \mu^{\gamma 5} \eta)(\sum \bar{T}_\gamma \mu^{\gamma 5} \eta)$, using data from a variety of experiments. Results are quoted for $\lambda = \pm 1$ and are independent of δ .
- ³ SIRUNYAN 21N use $137 (140) \text{ fb}^{-1}$ of data from $p\bar{p}$ collisions at $\sqrt{s} = 13 \text{ TeV}$ in the dilepton (dimuon) channels to place a lower limit on Λ_T , here converted to M_{TT} . Bounds on individual channels can be found in their Table 7.
- ⁴ SIRUNYAN 19AC use $35.9 (36.3) \text{ fb}^{-1}$ of data from $p\bar{p}$ collisions at $\sqrt{s} = 13 \text{ TeV}$ in the dilepton (dimuon) channels to place a lower limit on Λ_T , here converted to M_{TT} . The dilepton and dimuon channels are combined with previous results in the diphoton channel to set the best limit. Bounds on individual channels and different priors can be found in their Table 2. This updates the results in KHACHATRYAN 15AE.
- ⁵ SIRUNYAN 18DU use 35.9 fb^{-1} of data from $p\bar{p}$ collisions at $\sqrt{s} = 13 \text{ TeV}$ to place lower limits on M_{TT} (equivalent to their M_S). This updates the results of CHATRCHYAN 12R.
- ⁶ AABOUD 17AP use 36.7 fb^{-1} of data from $p\bar{p}$ collisions at $\sqrt{s} = 13 \text{ TeV}$ to place lower limits on M_{TT} (equivalent to their M_S). This updates the results of AAD 13AS.
- ⁷ AAD 14BE use 20 fb^{-1} of data from $p\bar{p}$ collisions at $\sqrt{s} = 8 \text{ TeV}$ in the dilepton channel to place lower limits on M_{TT} (equivalent to their M_S).
- ⁸ AAD 13E use 4.9 and 5.0 fb^{-1} of data from $p\bar{p}$ collisions at $\sqrt{s} = 7 \text{ TeV}$ in the dilepton and dimuon channels, respectively, to place lower limits on M_{TT} (equivalent to their M_S). The dilepton and dimuon channels are combined with previous results in the diphoton channel to set the best limit. Bounds on individual channels and different priors can be found in their Table VIII.
- ⁹ BAAK 12 use electroweak precision observables to place bounds on the ratio Λ_T/M_D as a function of M_D . See their Fig. 22 for constraints with a Higgs mass of 120 GeV .
- ¹⁰ AARON 11C search for deviations in the differential cross section of $e^{\pm}p \rightarrow e^{\pm}X$ in 446 pb^{-1} of data taken at $\sqrt{s} = 301$ and 319 GeV to place a bound on M_{TT} .
- ¹¹ ABAZOV 09AE use dijet angular distributions in 0.7 fb^{-1} of data from $p\bar{p}$ collisions at $\sqrt{s} = 1.96 \text{ TeV}$ to place lower bounds on Λ_T (equivalent to their M_S), here converted to M_{TT} .
- ¹² ABAZOV 09D use 1.05 fb^{-1} of data from $p\bar{p}$ collisions at $\sqrt{s} = 1.96 \text{ TeV}$ to place lower bounds on Λ_T (equivalent to their M_S), here converted to M_{TT} .
- ¹³ SCHAEEL 07A use e^+e^- collisions at $\sqrt{s} = 189\text{--}209 \text{ GeV}$ to place lower limits on Λ_T , here converted to limits on M_{TT} .
- ¹⁴ ABDALLAH 06C use e^+e^- collisions at $\sqrt{s} \sim 130\text{--}207 \text{ GeV}$ to place lower limits on M_{TT} , which is equivalent to their definition of M_S . Bound shown includes all possible final state leptons, $\ell = e, \mu, \tau$. Bounds on individual leptonic final states can be found in their Table 31.
- ¹⁵ GERDES 06 use 100 to 110 pb^{-1} of data from $p\bar{p}$ collisions at $\sqrt{s} = 1.8 \text{ TeV}$, as recorded by the CDF Collaboration during Run I of the Tevatron. Bound shown includes a K -factor of 1.3 . Bounds on individual e^+e^- and $\gamma\gamma$ final states are found in their Table 1.
- ¹⁶ ABAZOV 05V use 246 pb^{-1} of data from $p\bar{p}$ collisions at $\sqrt{s} = 1.96 \text{ TeV}$ to search for deviations in the differential cross section to $\mu^+\mu^-$ from graviton exchange.
- ¹⁷ CHEKANOV 04B search for deviations in the differential cross section of $e^{\pm}p \rightarrow e^{\pm}X$ with 130 pb^{-1} of combined data and Q^2 values up to $40,000 \text{ GeV}^2$ to place a bound on M_{TT} .
- ¹⁸ ABBIENDI 03D use e^+e^- collisions at $\sqrt{s}=181\text{--}209 \text{ GeV}$ to place bounds on the ultraviolet scale M_{TT} , which is equivalent to their definition of M_S .
- ¹⁹ ACHARD 03D look for deviations in the cross section for $e^+e^- \rightarrow ZZ$ from $\sqrt{s} = 200\text{--}209 \text{ GeV}$ to place a bound on M_{TT} .
- ²⁰ ADLOFF 03 search for deviations in the differential cross section of $e^{\pm}p \rightarrow e^{\pm}X$ at $\sqrt{s}=301$ and 319 GeV to place bounds on M_{TT} .
- ²¹ GIUDICE 03 review existing experimental bounds on M_{TT} and derive a combined limit.
- ²² HEISTER 03C use e^+e^- collisions at $\sqrt{s}=189\text{--}209 \text{ GeV}$ to place bounds on the scale of dim-8 gravitational interactions. Their M_S^{\pm} is equivalent to our M_{TT} with $\lambda = \pm 1$.
- ²³ ACHARD 02 search for s-channel graviton exchange effects in $e^+e^- \rightarrow \gamma\gamma$ at $E_{\text{cm}} = 192\text{--}209 \text{ GeV}$.
- ²⁴ ABBOTT 01 search for variations in differential cross sections to e^+e^- and $\gamma\gamma$ final states at the Tevatron.
- ²⁵ ABBIENDI 00R uses e^+e^- collisions at $\sqrt{s} = 189 \text{ GeV}$.
- ²⁶ ABREU 00A search for s-channel graviton exchange effects in $e^+e^- \rightarrow \gamma\gamma$ at $E_{\text{cm}} = 189\text{--}202 \text{ GeV}$.
- ²⁷ ABREU 00S uses e^+e^- collisions at $\sqrt{s}=183$ and 189 GeV . Bounds on μ and τ individual final states given in paper.
- ²⁸ CHANG 00B derive 3σ limit on M_{TT} of $(28,19,15) \text{ TeV}$ for $\delta=(2,4,6)$ respectively assuming the presence of a torsional coupling in the gravitational action. Highly model dependent.
- ²⁹ CHEUNG 00 obtains limits from anomalous diphoton production at OPAL due to graviton exchange. Original limit for $\delta=4$. However, unknown UV theory renders δ dependence unreliable. Original paper works in HLZ convention.
- ³⁰ GRAESSER 00 obtains a bound from graviton contributions to $g-2$ of the muon through loops of 0.29 TeV for $\delta=2$ and 0.38 TeV for $\delta=4,6$. Limits scale as $\lambda^{1/2}$. However calculational scheme not well-defined without specification of high-scale theory. See the "Extra Dimensions Review."
- ³¹ HAN 00 calculates corrections to gauge boson self-energies from KK graviton loops and constrain them using S and T . Bounds on M_{TT} range from 0.5 TeV ($\delta=6$) to 1.1 TeV ($\delta=2$); see text. Limits have strong dependence, $\lambda^{\delta+2}$, on unknown λ coefficient.
- ³² MATHEWS 00 search for evidence of graviton exchange in CDF and DØ dijet production data. See their Table 2 for slightly stronger δ -dependent bounds. Limits expressed in terms of $\tilde{M}_S^4 = M_{TT}^4/8$.
- ³³ MELE 00 obtains bound from KK graviton contributions to $e^+e^- \rightarrow VV$ ($V=\gamma, W, Z$) at LEP. Authors use Hewett conventions.

- ³⁴ ABBIENDI 99P search for s -channel graviton exchange effects in $e^+e^- \rightarrow \gamma\gamma$ at $E_{\text{cm}}=189$ GeV. The limits $G_{\pm} > 660$ GeV and $G_{\pm} > 634$ GeV are obtained from combined $E_{\text{cm}}=183$ and 189 GeV data, where G_{\pm} is a scale related to the fundamental gravity scale.
- ³⁵ ACCIARRI 99M search for the reaction $e^+e^- \rightarrow \gamma G$ and s -channel graviton exchange effects in $e^+e^- \rightarrow \gamma\gamma, W^+W^-, ZZ, e^+e^-, \mu^+\mu^-, \tau^+\tau^-, q\bar{q}$ at $E_{\text{cm}}=183$ GeV. Limits on the gravity scale are listed in their Tables 1 and 2.
- ³⁶ ACCIARRI 99S search for the reaction $e^+e^- \rightarrow ZG$ and s -channel graviton exchange effects in $e^+e^- \rightarrow \gamma\gamma, W^+W^-, ZZ, e^+e^-, \mu^+\mu^-, \tau^+\tau^-, q\bar{q}$ at $E_{\text{cm}}=189$ GeV. Limits on the gravity scale are listed in their Tables 1 and 2.
- ³⁷ BOURILKOV 99 performs global analysis of LEP data on e^+e^- collisions at $\sqrt{s}=183$ and 189 GeV. Bound is on Λ_T .

Limits on $1/R = M_C$

This section includes limits on $1/R = M_C$, the compactification scale in models with one TeV-sized extra dimension, due to exchange of Standard Model KK excitations. Bounds assume fermions are not in the bulk, unless stated otherwise. See the "Extra Dimensions" review for discussion of model dependence.

VALUE (TeV)	CL%	DOCUMENT ID	TECN	COMMENT
>4.16	95	1 AAD	12CC ATLS	$pp \rightarrow \ell\bar{\ell}$
>6.1		2 BARBIERI	04 RVUE	Electroweak
		3 FLORES	23 RVUE	minimal universal extra dims
		4 AVNISH	21 RVUE	$pp \rightarrow$ multijet
		5 AABOUD	18AV ATLS	$pp \rightarrow t\bar{t}\tau\bar{\tau}$
		6 AABOUD	18CE ATLS	$pp \rightarrow t\bar{t}t\bar{t}$
>3.8	95	7 ACCOMANDO	15 RVUE	Electroweak
>3.40	95	8 KHACHATRYAN	15T CMS	$pp \rightarrow \ell X$
		9 CHATRCHYAN	13AQ CMS	$pp \rightarrow \ell X$
>1.38	95	10 CHATRCHYAN	13W CMS	$pp \rightarrow \gamma\gamma, \delta=6, M_D=5$ TeV
>0.715	95	11 EDELHAUSER	13 RVUE	$pp \rightarrow \ell\bar{\ell} + X$
>1.40	95	12 AAD	12CP ATLS	$pp \rightarrow \gamma\gamma, \delta=6, M_D=5$ TeV
>1.23	95	13 AAD	12X ATLS	$pp \rightarrow \gamma\gamma, \delta=6, M_D=5$ TeV
>0.26	95	14 ABAZOV	12M D0	$p\bar{p} \rightarrow \mu\mu$
>0.75	95	15 BAAK	12 RVUE	Electroweak
		16 FLACKE	12 RVUE	Electroweak
>0.43	95	17 NISHIWAKI	12 RVUE	$H \rightarrow WW, \gamma\gamma$
>0.729	95	18 AAD	11F ATLS	$pp \rightarrow \gamma\gamma, \delta=6, M_D=5$ TeV
>0.961	95	19 AAD	11X ATLS	$pp \rightarrow \gamma\gamma, \delta=6, M_D=5$ TeV
>0.477	95	20 ABAZOV	10P D0	$p\bar{p} \rightarrow \gamma\gamma, \delta=6, M_D=5$ TeV
>1.59	95	21 ABAZOV	09AE D0	$p\bar{p} \rightarrow$ dijet, angular dist.
>0.6	95	22 HAISCH	07 RVUE	$\bar{B} \rightarrow X_s \gamma$
>0.6	90	23 GOGOLADZE	06 RVUE	Electroweak
>3.3	95	24 CORNET	00 RVUE	Electroweak
>3.3-3.8	95	25 RIZZO	00 RVUE	Electroweak

- ¹ AAD 12CC use 4.9 and 5.0 fb^{-1} of data from pp collisions at $\sqrt{s} = 7$ TeV in the dielectron and dimuon channels, respectively, to place a lower bound on the mass of the lightest KK Z/γ boson (equivalent to $1/R = M_C$). The limit quoted here assumes a flat prior corresponding to when the pure Z/γ KK cross section term dominates. See their Section 15 for more details.
- ² BARBIERI 04 use electroweak precision observables to place a lower bound on the compactification scale $1/R$. Both the gauge bosons and the Higgs boson are assumed to propagate in the bulk.
- ³ FLORES 23 use a number of 13 TeV Run 2 searches at the LHC to place constraints on the compactification scale $1/R$ and cutoff scale Λ in the minimal universal extra dimension model with Standard Model fields propagating in the bulk (see their Fig.6).
- ⁴ AVNISH 21 perform a study on the ATLAS collaboration search for multiple jets plus missing transverse energy from pp collisions at $\sqrt{s} = 13$ TeV and integrated luminosity of 139 fb^{-1} , to place constraints on the compactification scale and cutoff scale Λ in universal extra dimension models with Standard Model fields propagating in the bulk.
- ⁵ AABOUD 18AV use 36.1 fb^{-1} of data from pp collisions at $\sqrt{s} = 13$ TeV in final states with multiple b-jets, to place a lower bound on the compactification scale in a model with two universal extra dimensions. Assuming the radii of the two extra dimensions are equal, a lower limit of 1.8 TeV for the Kaluza-Klein mass is obtained.
- ⁶ AABOUD 18CE use 36.1 fb^{-1} of data from pp collisions at $\sqrt{s} = 13$ TeV in final states with same-charge leptons and b-jets, to place a lower bound on the compactification scale in a model with two universal extra dimensions. Assuming the radii of the two extra dimensions are equal, a lower limit of 1.45 TeV for the Kaluza-Klein mass is obtained.
- ⁷ ACCOMANDO 15 use electroweak precision observables to place a lower bound on the compactification scale $1/R$. See their Fig. 2 for the bound as a function of $\sin\beta$, which parametrizes the VEV contribution from brane and bulk Higgs fields. The quoted value is for the minimum bound which occurs at $\sin\beta = 0.45$.
- ⁸ KHACHATRYAN 15T use 19.7 fb^{-1} of data from pp collisions at $\sqrt{s} = 8$ TeV to place a lower bound on the compactification scale $1/R$.
- ⁹ CHATRCHYAN 13AQ use 5.0 fb^{-1} of data from pp collisions at $\sqrt{s} = 7$ TeV and a further 3.7 fb^{-1} of data at $\sqrt{s} = 8$ TeV to place a lower bound on the compactification scale $1/R$, in models with universal extra dimensions and Standard Model fields propagating in the bulk. See their Fig. 5 for the bound as a function of the universal bulk fermion mass parameter μ .
- ¹⁰ CHATRCHYAN 13W use diphoton events with large missing transverse momentum in 4.93 fb^{-1} of data produced from pp collisions at $\sqrt{s} = 7$ TeV to place a lower bound on the compactification scale in a universal extra dimension model with gravitational decays. The bound assumes that the cutoff scale Λ , for the radiative corrections to the Kaluza-Klein masses, satisfies $\Lambda/M_C = 20$. The model parameters are chosen such that the decay $\gamma^* \rightarrow G\gamma$ occurs with an appreciable branching fraction.
- ¹¹ EDELHAUSER 13 use 19.6 and 20.6 fb^{-1} of data from pp collisions at $\sqrt{s} = 8$ TeV analyzed by the CMS Collaboration in the dielectron and dimuon channels, respectively, to place a lower bound on the mass of the second lightest Kaluza-Klein Z/γ boson (converted to a limit on $1/R = M_C$). The bound assumes Standard Model fields propagating

in the bulk and that the cutoff scale Λ , for the radiative corrections to the Kaluza-Klein masses, satisfies $\Lambda/M_C = 20$.

- ¹² AAD 12CP use diphoton events with large missing transverse momentum in 4.8 fb^{-1} of data produced from pp collisions at $\sqrt{s} = 7$ TeV to place a lower bound on the compactification scale in a universal extra dimension model with gravitational decays. The bound assumes that the cutoff scale Λ , for the radiative corrections to the Kaluza-Klein masses, satisfies $\Lambda/M_C = 20$. The model parameters are chosen such that the decay $\gamma^* \rightarrow G\gamma$ occurs with an appreciable branching fraction.
- ¹³ AAD 12X use diphoton events with large missing transverse momentum in 1.07 fb^{-1} of data produced from pp collisions at $\sqrt{s} = 7$ TeV to place a lower bound on the compactification scale in a universal extra dimension model with gravitational decays. The bound assumes that the cutoff scale Λ , for the radiative corrections to the Kaluza-Klein masses, satisfies $\Lambda/M_C = 20$. The model parameters are chosen such that the decay $\gamma^* \rightarrow G\gamma$ occurs with an appreciable branching fraction.
- ¹⁴ ABAZOV 12M use same-sign dimuon events in 7.3 fb^{-1} of data from $p\bar{p}$ collisions at $\sqrt{s} = 1.96$ TeV to place a lower bound on the compactification scale $1/R$, in models with universal extra dimensions where all Standard Model fields propagate in the bulk.
- ¹⁵ BAAK 12 use electroweak precision observables to place a lower bound on the compactification scale $1/R$, in models with universal extra dimensions and Standard Model fields propagating in the bulk. Bound assumes a 125 GeV Higgs mass. See their Fig. 25 for the bound as a function of the Higgs mass.
- ¹⁶ FLACKE 12 use electroweak precision observables to place a lower bound on the compactification scale $1/R$, in models with universal extra dimensions and Standard Model fields propagating in the bulk. See their Fig. 1 for the bound as a function of the universal bulk fermion mass parameter μ .
- ¹⁷ NISHIWAKI 12 use up to 2 fb^{-1} of data from the ATLAS and CMS experiments that constrains the production cross section of a Higgs-like particle to place a lower bound on the compactification scale $1/R$ in universal extra dimension models. The quoted bound assumes Standard Model fields propagating in the bulk and a 125 GeV Higgs mass. See their Fig. 1 for the bound as a function of the Higgs mass.
- ¹⁸ AAD 11F use diphoton events with large missing transverse energy in 3.1 pb^{-1} of data produced from pp collisions at $\sqrt{s} = 7$ TeV to place a lower bound on the compactification scale in a universal extra dimension model with gravitational decays. The bound assumes that the cutoff scale Λ , for the radiative corrections to the Kaluza-Klein masses, satisfies $\Lambda/M_C = 20$. The model parameters are chosen such that the decay $\gamma^* \rightarrow G\gamma$ occurs with an appreciable branching fraction.
- ¹⁹ AAD 11X use diphoton events with large missing transverse energy in 36 pb^{-1} of data produced from pp collisions at $\sqrt{s} = 7$ TeV to place a lower bound on the compactification scale in a universal extra dimension model with gravitational decays. The bound assumes that the cutoff scale Λ , for the radiative corrections to the Kaluza-Klein masses, satisfies $\Lambda/M_C = 20$. The model parameters are chosen such that the decay $\gamma^* \rightarrow G\gamma$ occurs with an appreciable branching fraction.
- ²⁰ ABAZOV 10P use diphoton events with large missing transverse energy in 6.3 fb^{-1} of data produced from $p\bar{p}$ collisions at $\sqrt{s} = 1.96$ TeV to place a lower bound on the compactification scale in a universal extra dimension model with gravitational decays. The bound assumes that the cutoff scale Λ , for the radiative corrections to the Kaluza-Klein masses, satisfies $\Lambda/M_C = 20$. The model parameters are chosen such that the decay $\gamma^* \rightarrow G\gamma$ occurs with an appreciable branching fraction.
- ²¹ ABAZOV 09AE use dijet angular distributions in 0.7 fb^{-1} of data from $p\bar{p}$ collisions at $\sqrt{s} = 1.96$ TeV to place a lower bound on the compactification scale.
- ²² HAISCH 07 use inclusive \bar{B} -meson decays to place a Higgs mass independent bound on the compactification scale $1/R$ in the minimal universal extra dimension model.
- ²³ GOGOLADZE 06 use electroweak precision observables to place a lower bound on the compactification scale in models with universal extra dimensions. Bound assumes a 115 GeV Higgs mass. See their Fig. 3 for the bound as a function of the Higgs mass.
- ²⁴ CORNET 00 translates a bound on the coefficient of the 4-fermion operator $(\bar{\ell}\gamma_{\mu}\tau^{\alpha}\ell)(\bar{\ell}\gamma^{\mu}\tau^{\alpha}\ell)$ derived by Hagiwara and Matsumoto into a limit on the mass scale of KK W bosons.
- ²⁵ RIZZO 00 obtains limits from global electroweak fits in models with a Higgs in the bulk (3.8 TeV) or on the standard brane (3.3 TeV).

Limits on Kaluza-Klein Gravitons in Warped Extra Dimensions

This section places limits on the mass of the first Kaluza-Klein (KK) excitation of the graviton in the warped extra dimension model of Randall and Sundrum. Bounds in parenthesis assume Standard Model fields propagate in the bulk. Experimental bounds depend strongly on the warp parameter, k . See the "Extra Dimensions" review for a full discussion.

Here we list limits for the value of the warp parameter $k/\overline{M}_P = 0.1$.

VALUE (TeV)	CL%	DOCUMENT ID	TECN	COMMENT
>4.78	95	1 SIRUNYAN	21N CMS	$pp \rightarrow G \rightarrow e^+e^-, \mu^+\mu^-$
		2 TUMASYAN	23AP CMS	$pp \rightarrow G \rightarrow WW, ZZ$
		3 AAD	22F ATLS	$pp \rightarrow G \rightarrow HH$
		4 TUMASYAN	22D CMS	$pp \rightarrow G \rightarrow WW$
		5 TUMASYAN	22J CMS	$pp \rightarrow G \rightarrow ZZ$
		6 TUMASYAN	22R CMS	$pp \rightarrow G \rightarrow ZZ$
		7 TUMASYAN	22U CMS	$pp \rightarrow G \rightarrow HH$
		8 AAD	21AF ATLS	$pp \rightarrow G \rightarrow ZZ$
>4.5	95	9 AAD	21AY ATLS	$pp \rightarrow G \rightarrow \gamma\gamma$
		10 AAD	20AT ATLS	$pp \rightarrow G \rightarrow WW, ZZ$
		11 AAD	20C ATLS	$pp \rightarrow G \rightarrow HH$
		12 AAD	20T ATLS	$pp \rightarrow G \rightarrow b\bar{b}$
>2.6	95	13 SIRUNYAN	20AI CMS	$pp \rightarrow G \rightarrow jj$
		14 SIRUNYAN	20F CMS	$pp \rightarrow G \rightarrow HH$
		15 AABOUD	19O ATLS	$pp \rightarrow G \rightarrow HH$
		16 AAD	19D ATLS	$pp \rightarrow G \rightarrow WW, ZZ$
		17 SIRUNYAN	19 CMS	$pp \rightarrow G \rightarrow HH$
		18 SIRUNYAN	19BE CMS	$pp \rightarrow G \rightarrow HH$
		19 AABOUD	18B ATLS	$pp \rightarrow G \rightarrow t\bar{t}$
		20 AABOUD	18C ATLS	$pp \rightarrow G \rightarrow VV, VH, \ell\bar{\ell}$

• • • We do not use the following data for averages, fits, limits, etc. • • •

Searches Particle Listings

Extra Dimensions

		21	AABOUD	18CQ ATLS	$pp \rightarrow G \rightarrow HH$
		22	AABOUD	18CW ATLS	$pp \rightarrow G \rightarrow HH$
		23	SIRUNYAN	18AF CMS	$pp \rightarrow G \rightarrow HH$
		24	SIRUNYAN	18AS CMS	$pp \rightarrow G \rightarrow ZZ$
		25	SIRUNYAN	18CW CMS	$pp \rightarrow G \rightarrow HH$
>4.1	95	26	SIRUNYAN	18DU CMS	$pp \rightarrow G \rightarrow \gamma\gamma$
		27	SIRUNYAN	18I CMS	$pp \rightarrow G \rightarrow b\bar{b}$
		28	AAD	16R ATLS	$pp \rightarrow G \rightarrow WW, ZZ$
		29	AAD	15AZ ATLS	$pp \rightarrow G \rightarrow WW$
		30	AAD	15CP ATLS	$pp \rightarrow G \rightarrow WW, ZZ$
>2.68	95	31	AAD	14V ATLS	$pp \rightarrow G \rightarrow e^+e^-, \mu^+\mu^-$
>1.23 (>0.84)	95	32	AAD	13A ATLS	$pp \rightarrow G \rightarrow WW$
>0.94 (>0.71)	95	33	AAD	13AO ATLS	$pp \rightarrow G \rightarrow WW$
>2.23	95	34	AAD	13AS ATLS	$pp \rightarrow \gamma\gamma, e^+e^-, \mu^+\mu^-$
>0.845	95	35	AAD	12AD ATLS	$pp \rightarrow G \rightarrow ZZ$
		36	AALTONEN	12V CDF	$p\bar{p} \rightarrow G \rightarrow ZZ$
		37	BAAK	12 RVUE	Electroweak
		38	AALTONEN	11G CDF	$p\bar{p} \rightarrow G \rightarrow ZZ$
>1.058	95	39	AALTONEN	11R CDF	$p\bar{p} \rightarrow G \rightarrow e^+e^-, \gamma\gamma$
>0.754	95	40	ABAZOV	11H D0	$p\bar{p} \rightarrow G \rightarrow WW$
>0.607		41	AALTONEN	10N CDF	$p\bar{p} \rightarrow G \rightarrow WW$
>1.05		42	ABAZOV	10F D0	$p\bar{p} \rightarrow G \rightarrow e^+e^-, \gamma\gamma$
		43	AALTONEN	08S CDF	$p\bar{p} \rightarrow G \rightarrow ZZ$
>0.90		44	ABAZOV	08J D0	$p\bar{p} \rightarrow G \rightarrow e^+e^-, \gamma\gamma$
		45	AALTONEN	07G CDF	$p\bar{p} \rightarrow G \rightarrow \gamma\gamma$
>0.889		46	AALTONEN	07H CDF	$p\bar{p} \rightarrow G \rightarrow e\bar{e}$
>0.785		47	ABAZOV	05N D0	$p\bar{p} \rightarrow G \rightarrow \ell\ell, \gamma\gamma$
>0.71		48	ABULENCIA	05A CDF	$p\bar{p} \rightarrow G \rightarrow \ell\bar{\ell}$

- on the cross section times branching fraction as a function of the KK graviton mass for $k/\overline{M}_P = 1$ and $k/\overline{M}_P = 2$.
- 16 AAD 19d use 139 fb^{-1} of data from pp collisions at $\sqrt{s} = 13 \text{ TeV}$ to search for diboson resonances in the all-hadronic final state. See their Figure 9(b) for the limit on the cross section times branching fraction as a function of the KK graviton mass, including theoretical values for $k/\overline{M}_P = 1$. This updates the results of AABOUD 18F.
- 17 SIRUNYAN 19 use 35.9 fb^{-1} of data from pp collisions at $\sqrt{s} = 13 \text{ TeV}$ to search for Higgs boson pair production in the $\gamma\gamma b\bar{b}$ final state. See their Figure 9 for limits on the cross section times branching fraction as a function of the KK graviton mass. Assuming $k/\overline{M}_P = 1$, gravitons in the mass range 290–810 GeV are excluded. This updates the result of KHACHATRYAN 16BQ.
- 18 SIRUNYAN 19BE use 35.9 fb^{-1} of data from pp collisions at $\sqrt{s} = 13 \text{ TeV}$ to search for Higgs boson pair production by combining the results from four final states: $b\bar{b}\gamma\gamma$, $b\bar{b}\tau\tau$, $b\bar{b}b\bar{b}$, and $b\bar{b}VV$. See their Figure 7 for limits on the cross section times branching fraction as a function of the KK graviton mass.
- 19 AABOUD 18BI use 36.1 fb^{-1} of data from pp collisions at $\sqrt{s} = 13 \text{ TeV}$ to search for top-quark pairs decaying into the lepton-plus jets topology. See their Figure 16 for the limit on the KK graviton mass as a function of the cross section times branching fraction, including theoretical values for $k/\overline{M}_P = 1$.
- 20 AABOUD 18CJ combine the searches for heavy resonances decaying into bosonic and leptonic final states from 36.1 fb^{-1} of pp collision data at $\sqrt{s} = 13 \text{ TeV}$. The lower limit on the KK graviton mass, with $k/\overline{M}_P = 1$, is 2.3 TeV.
- 21 AABOUD 18CQ use 36.1 fb^{-1} of data from pp collisions at $\sqrt{s} = 13 \text{ TeV}$ to search for Higgs boson pair production in the $b\bar{b}\tau^+\tau^-$ final state. See their Figure 2 for limits on the cross section times branching fraction as a function of the KK graviton mass. Assuming $k/\overline{M}_P = 1$, gravitons in the mass range 325–885 GeV are excluded.
- 22 AABOUD 18CW use 36.1 fb^{-1} of data from pp collisions at $\sqrt{s} = 13 \text{ TeV}$ to search for Higgs boson pair production in the $\gamma\gamma b\bar{b}$ final state. See their Figure 7 for limits on the cross section times branching fraction as a function of the KK graviton mass.
- 23 SIRUNYAN 18AF use 35.9 fb^{-1} of data from pp collisions at $\sqrt{s} = 13 \text{ TeV}$ to search for Higgs boson pair production in the $b\bar{b}b\bar{b}$ final state. See their Figure 9 for limits on the cross section times branching fraction as a function of the KK graviton mass, including theoretical values for $k/\overline{M}_P = 0.5$. This updates the results of KHACHATRYAN 15R.
- 24 SIRUNYAN 18AS use 35.9 fb^{-1} of data from pp collisions at $\sqrt{s} = 13 \text{ TeV}$ to search for ZZ resonances in the $\ell\nu\ell\nu$ final state ($\ell = e, \mu$). See their Figure 5 for the limit on the KK graviton mass as a function of the cross section times branching fraction, including theoretical values for $k/\overline{M}_P = 0.1, 0.5, \text{ and } 1.0$.
- 25 SIRUNYAN 18CW use 35.9 fb^{-1} of data from pp collisions at $\sqrt{s} = 13 \text{ TeV}$ to search for Higgs boson pair production in the $b\bar{b}b\bar{b}$ final state. See their Figure 8 for limits on the cross section times branching fraction as a function of the KK graviton mass, including theoretical values for $k/\overline{M}_P = 0.5$.
- 26 SIRUNYAN 18DU use 35.9 fb^{-1} of data from pp collisions at $\sqrt{s} = 13 \text{ TeV}$, in the diphoton channel to place a lower limit on the mass of the lightest KK graviton. See their paper for limits with other warp parameter values $k/\overline{M}_P = 0.01 \text{ and } 0.2$. This updates the results of KHACHATRYAN 16M.
- 27 SIRUNYAN 18I use 19.7 fb^{-1} of data from pp collisions at $\sqrt{s} = 8 \text{ TeV}$ to search for narrow resonances decaying to bottom quark pairs. See their Figure 3 for the limit on the KK graviton mass as a function of the cross section times branching fraction in the mass range of 325–1200 GeV.
- 28 AAD 16R use 20.3 fb^{-1} of data from pp collisions at $\sqrt{s} = 8 \text{ TeV}$ to place a lower bound on the mass of the lightest KK graviton. See their Figure 4 for the limit on the KK graviton mass as a function of the cross section times branching fraction.
- 29 AAD 15AZ use 20.3 fb^{-1} of data from pp collisions at $\sqrt{s} = 8 \text{ TeV}$ to place a lower bound on the mass of the lightest KK graviton. See their Figure 2 for limits on the KK graviton mass as a function of the cross section times branching ratio.
- 30 AAD 15CP use 20.3 fb^{-1} of data from pp collisions at $\sqrt{s} = 8 \text{ TeV}$ to place a lower bound on the mass of the lightest KK graviton. See their Figures 6b and 6c for the limit on the KK graviton mass as a function of the cross section times branching fraction.
- 31 AAD 14V use $20.3 (20.5) \text{ fb}^{-1}$ of data from pp collisions at $\sqrt{s} = 8 \text{ TeV}$ in the dielectron (dimuon) channels to place a lower bound on the mass of the lightest KK graviton. This updates the results of AAD 12cc.
- 32 AAD 13A use 4.7 fb^{-1} of data from pp collisions at $\sqrt{s} = 7 \text{ TeV}$ in the $\ell\nu\ell\nu$ channel, to place a lower bound on the mass of the lightest KK graviton.
- 33 AAD 13AO use 4.7 fb^{-1} of data from pp collisions at $\sqrt{s} = 7 \text{ TeV}$ in the $\ell\nu jj$ channel, to place a lower bound on the mass of the lightest KK graviton.
- 34 AAD 13AS use 4.9 fb^{-1} of data from pp collisions at $\sqrt{s} = 7 \text{ TeV}$ in the diphoton channel to place lower limits on the mass of the lightest KK graviton. The diphoton channel is combined with previous results in the dielectron and dimuon channels to set the best limit. See their Table 2 for warp parameter values k/\overline{M}_P between 0.01 and 0.1. This updates the results of AAD 12y.
- 35 AAD 12AD use 1.02 fb^{-1} of data from pp collisions at $\sqrt{s} = 7 \text{ TeV}$ to search for KK gravitons in a warped extra dimension decaying to ZZ dibosons in the $lljj$ and $llll$ channels ($\ell = e, \mu$). The limit is quoted for the combined $lljj + llll$ channels. See their Figure 5 for limits on the cross section $\sigma(G \rightarrow ZZ)$ as a function of the graviton mass.
- 36 AALTONEN 12v use 6 fb^{-1} of data from $p\bar{p}$ collisions at $\sqrt{s} = 1.96 \text{ TeV}$ to search for KK gravitons in a warped extra dimension decaying to ZZ dibosons in the $lljj$ and $llll$ channels ($\ell = e, \mu$). It provides improved limits over the previous analysis in AALTONEN 11G. See their Figure 16 for limits from all channels combined on the cross section times branching ratio $\sigma(p\bar{p} \rightarrow G^* \rightarrow ZZ)$ as a function of the graviton mass.
- 37 BAAK 12 use electroweak precision observables to place a lower bound on the compactification scale $k e^{-\pi k R}$, assuming Standard Model fields propagate in the bulk and the Higgs is confined to the IR brane. See their Fig. 27 for more details.
- 38 AALTONEN 11G use $2.5\text{--}2.9 \text{ fb}^{-1}$ of data from $p\bar{p}$ collisions at $\sqrt{s} = 1.96 \text{ TeV}$ to search for KK gravitons in a warped extra dimension decaying to ZZ dibosons via the $e e e, e e \mu \mu, \mu \mu \mu \mu, e e j j$, and $\mu \mu j j$ channels. See their Fig. 20 for limits on the cross section $\sigma(G \rightarrow ZZ)$ as a function of the graviton mass.
- 39 AALTONEN 11R uses 5.7 fb^{-1} of data from $p\bar{p}$ collisions at $\sqrt{s} = 1.96 \text{ TeV}$ in the dielectron channel to place a lower bound on the mass of the lightest graviton. It provides combined limits with the diphoton channel analysis of AALTONEN 11U. For warp parameter values k/\overline{M}_P between 0.01 to 0.1 the lower limit on the mass of the lightest graviton is between 612 and 1058 GeV. See their Table 1 for more details.
- 40 ABAZOV 11H use 5.4 fb^{-1} of data from $p\bar{p}$ collisions at $\sqrt{s} = 1.96 \text{ TeV}$ to place a lower bound on the mass of the lightest graviton. Their 95% C.L. exclusion limit does not include masses less than 300 GeV.
- 1 SIRUNYAN 21N use $137 (140) \text{ fb}^{-1}$ of data from pp collisions at $\sqrt{s} = 13 \text{ TeV}$ to search for dilepton resonances in the dielectron (dimuon) channel. See Table 6 for other limits with warp parameter values $k/\overline{M}_P = 0.01$ and 0.05 . This updates the results of SIRUNYAN 18BB.
- 2 TUMASYAN 23AP use 138 fb^{-1} of data from pp collisions at $\sqrt{s} = 13 \text{ TeV}$ to search for WW, ZZ diboson resonances in $q\bar{q}q\bar{q}$ final states. See their Figure 7 for the limit on the cross section times branching fraction as a function of the KK graviton mass. Assuming $k/\overline{M}_P = 0.5$, a graviton mass is excluded below 1400 GeV. This updates the result of SIRUNYAN 20q.
- 3 AAD 22F use $126\text{--}139 \text{ fb}^{-1}$ of data from pp collisions at $\sqrt{s} = 13 \text{ TeV}$ to search for Higgs boson pair production in the $b\bar{b}b\bar{b}$ final state. See their Figure 14 for limits on the cross section times branching fraction as a function of the KK graviton mass. Assuming $k/\overline{M}_P = 1$, gravitons in the mass range 298–1460 GeV are excluded. This updates the results of AABOUD 19A.
- 4 TUMASYAN 22D use 137 fb^{-1} of data from pp collisions at $\sqrt{s} = 13 \text{ TeV}$ to search for WW resonances in $\ell\nu q\bar{q}$ final states ($\ell = e, \mu$). See their Figure 6 for the limit on the KK graviton mass as a function of the cross section times branching fraction, including theoretical values for $k/\overline{M}_P = 0.5$. This updates the results of SIRUNYAN 18AX.
- 5 TUMASYAN 22J use 137 fb^{-1} of data from pp collisions at $\sqrt{s} = 13 \text{ TeV}$ to search for ZZ resonances in the $\nu\tau q\bar{q}$ final state. See their Figure 10 for the limit on the KK graviton mass as a function of the cross section times branching fraction, assuming $k/\overline{M}_P = 0.5$. This updates the result of SIRUNYAN 18BK.
- 6 TUMASYAN 22R use 138 fb^{-1} of data from pp collisions at $\sqrt{s} = 13 \text{ TeV}$ to search for ZZ resonances in $2\ell 2q$ final states ($\ell = e, \mu$). See their Figure 8 for the limit on the KK graviton mass as a function of the cross section times branching fraction. Assuming $k/\overline{M}_P = 0.5$, a graviton mass is excluded below 1200 GeV. This updates the result of SIRUNYAN 18DJ.
- 7 TUMASYAN 22U use 138 fb^{-1} of data from pp collisions at $\sqrt{s} = 13 \text{ TeV}$ to search for Higgs boson pair production in the $b\bar{b}q\bar{q} \ell\nu, b\bar{b}\ell\nu\ell\nu$ and $b\bar{b}\ell\nu\nu\ell\nu$ final states ($\ell = e, \mu$). See their Figure 7 for limits on the cross section times branching fraction as a function of the KK graviton mass, including theoretical values for $k/\overline{M}_P = 0.3$ and 0.5 . This updates the results of SIRUNYAN 19CF and SIRUNYAN 18F.
- 8 AAD 21AF use 139 fb^{-1} of data from pp collisions at $\sqrt{s} = 13 \text{ TeV}$ to search for ZZ resonances in the $\ell\ell\ell\ell$ and $\ell\nu\ell\nu$ final states ($\ell = e, \mu$). See their Figure 8 for the limit on the cross section times branching fraction as a function of the KK graviton mass, including theoretical values for $k/\overline{M}_P = 1$. This updates the results of AAD 15AU and AABOUD 18BF.
- 9 AAD 21AY use 139 fb^{-1} of data from pp collisions at $\sqrt{s} = 13 \text{ TeV}$ in the diphoton channel to place a lower limit on the mass of the lightest KK graviton. This updates the results of AABOUD 17AP.
- 10 AAD 20AT use 139 fb^{-1} of data from pp collisions at $\sqrt{s} = 13 \text{ TeV}$ to search for diboson resonances in semileptonic final states ($\ell\nu q\bar{q}, \ell\ell q\bar{q}, \nu\nu q\bar{q}$). See their Figure 15 for the limit on the cross section times branching fraction as a function of the KK graviton mass. Lower limits on the graviton mass are also given for $k/\overline{M}_P = 1$. This updates the results of AABOUD 18AK and AABOUD 18AL.
- 11 AAD 20C use 36.1 fb^{-1} of data from pp collisions at $\sqrt{s} = 13 \text{ TeV}$ to search for Higgs boson pair production in the $b\bar{b}b\bar{b}, b\bar{b}W^+W^-, \text{ and } b\bar{b}\tau^+\tau^-$ final states. See their Figure 5(b)(c) for limits on the cross section as a function of the KK graviton mass. In the case of $k/\overline{M}_P = 1$ and 2, gravitons are excluded in the mass range 260–3000 GeV and 260–1760 GeV, respectively.
- 12 AAD 20T use 139 fb^{-1} of data from pp collisions at $\sqrt{s} = 13 \text{ TeV}$ to search for narrow resonances decaying to bottom quark pairs. See their Figure 7 for the limit on the product of the cross section, branching fraction, acceptance and b -tagging efficiency as a function of the KK graviton mass. In the case of $k/\overline{M}_P = 0.2$, KK gravitons in the mass range 1.25–2.8 TeV are excluded.
- 13 SIRUNYAN 20AI use 137 fb^{-1} of data from pp collisions at $\sqrt{s} = 13 \text{ TeV}$ to search for dijet resonances. See their Figure 6 for the limit on the product of the cross section, branching fraction and acceptance as a function of the KK graviton mass. This updates the results of SIRUNYAN 18BQ.
- 14 SIRUNYAN 20F use 35.9 fb^{-1} of data from pp collisions at $\sqrt{s} = 13 \text{ TeV}$ to search for Higgs boson pair production in the $b\bar{b}ZZ$ final state. See their Figure 4 for limits on the cross section times branching fraction as a function of the KK graviton mass, and Figure 5 for limits as a function of k/\overline{M}_P .

See key on page 1171

Searches Particle Listings Extra Dimensions

- ⁴¹ AALTONEN 10N use 2.9 fb^{-1} of data from $p\bar{p}$ collisions at $\sqrt{s} = 1.96 \text{ TeV}$ to place a lower bound on the mass of the lightest graviton.
- ⁴² ABAZOV 10F use 5.4 fb^{-1} of data from $p\bar{p}$ collisions at $\sqrt{s} = 1.96 \text{ TeV}$ to place a lower bound on the mass of the lightest graviton. For warp parameter values of k/\overline{M}_P between 0.01 and 0.1 the lower limit on the mass of the lightest graviton is between 560 and 1050 GeV. See their Fig. 3 for more details.
- ⁴³ AALTONEN 08s use $p\bar{p}$ collisions at $\sqrt{s} = 1.96 \text{ TeV}$ to search for KK gravitons in warped extra dimensions. They search for graviton resonances decaying to four electrons via two Z bosons using 1.1 fb^{-1} of data. See their Fig. 8 for limits on $\sigma \cdot \text{Br}(G \rightarrow ZZ)$ versus the graviton mass.
- ⁴⁴ ABAZOV 08j use $p\bar{p}$ collisions at $\sqrt{s} = 1.96 \text{ TeV}$ to search for KK gravitons in warped extra dimensions. They search for graviton resonances decaying to electrons and photons using 1 fb^{-1} of data. For warp parameter values of k/\overline{M}_P between 0.01 and 0.1 the lower limit on the mass of the lightest excitation is between 300 and 900 GeV. See their Fig. 4 for more details.
- ⁴⁵ AALTONEN 07G use $p\bar{p}$ collisions at $\sqrt{s} = 1.96 \text{ TeV}$ to search for KK gravitons in warped extra dimensions. They search for graviton resonances decaying to photons using 1.2 fb^{-1} of data. For warp parameter values of $k/\overline{M}_P = 0.1, 0.05,$ and 0.01 the bounds on the graviton mass are 850, 694, and 230 GeV, respectively. See their Fig. 3 for more details. See also AALTONEN 07H.
- ⁴⁶ AALTONEN 07H use $p\bar{p}$ collisions at $\sqrt{s} = 1.96 \text{ TeV}$ to search for KK gravitons in warped extra dimensions. They search for graviton resonances decaying to electrons using 1.3 fb^{-1} of data. For a warp parameter value of $k/\overline{M}_P = 0.1$ the bound on the graviton mass is 807 GeV. See their Fig. 4 for more details. A combined analysis with the diphoton data of AALTONEN 07G yields for $k/\overline{M}_P = 0.1$ a graviton mass lower bound of 889 GeV.
- ⁴⁷ ABAZOV 05N use $p\bar{p}$ collisions at $\sqrt{s} = 1.96 \text{ TeV}$ to search for KK gravitons in warped extra dimensions. They search for graviton resonances decaying to muons, electrons or photons, using 260 pb^{-1} of data. For warp parameter values of $k/\overline{M}_P = 0.1, 0.05,$ and $0.01,$ the bounds on the graviton mass are 785, 650 and 250 GeV respectively. See their Fig. 3 for more details.
- ⁴⁸ ABULENCIA 05A use $p\bar{p}$ collisions at $\sqrt{s} = 1.96 \text{ TeV}$ to search for KK gravitons in warped extra dimensions. They search for graviton resonances decaying to muons or electrons, using 200 pb^{-1} of data. For warp parameter values of $k/\overline{M}_P = 0.1, 0.05,$ and $0.01,$ the bounds on the graviton mass are 710, 510 and 170 GeV respectively.

Limits on Kaluza-Klein Gluons in Warped Extra Dimensions

This section places limits on the mass of the first Kaluza-Klein (KK) excitation of the gluon in warped extra dimension models with Standard Model fields propagating in the bulk. Bounds are given for a specific benchmark model with $\Gamma/m = 15.3\%$ where Γ is the width and m the mass of the KK gluon. See the "Extra Dimensions" review for more discussion.

VALUE (TeV)	CL%	DOCUMENT ID	TECN	COMMENT
>3.8	95	¹ AABOUD 18BI ATLS	$g_{KK} \rightarrow t\bar{t} \rightarrow \ell j$	
• • • We do not use the following data for averages, fits, limits, etc. • • •				
		² TUMASYAN 22c CMS	$g_{KK} \rightarrow Rj \rightarrow jjj$	
		³ AABOUD 19AS ATLS	$g_{KK} \rightarrow t\bar{t} \rightarrow jj$	
		⁴ SIRUNYAN 19AL CMS	$g_{KK} \rightarrow tT$	
>2.5	95	⁵ CHATRCHYAN 13BM CMS	$g_{KK} \rightarrow t\bar{t}$	
		⁶ CHEN 13A	$\overline{B} \rightarrow X_s \gamma$	
>1.5	95	⁷ AAD 12BV ATLS	$g_{KK} \rightarrow t\bar{t} \rightarrow \ell j$	

- ¹ AABOUD 18BI use 36.1 fb^{-1} of data from pp collisions at $\sqrt{s} = 13 \text{ TeV}$. This result updates AAD 13AQ.
- ² TUMASYAN 22c use 138 fb^{-1} of data from pp collisions at $\sqrt{s} = 13 \text{ TeV}$ to place limits on a KK gluon decaying to gluons via a spin-0 radion, R . See their Figure 5 for limits on the cross section times branching fraction as a function of the KK gluon mass and various values of the radion mass.
- ³ AABOUD 19AS use 36.1 fb^{-1} of data from pp collisions at $\sqrt{s} = 13 \text{ TeV}$. An upper bound of 3.4 TeV is placed on the KK gluon mass for $\Gamma/m = 30\%$.
- ⁴ SIRUNYAN 19AL use 35.9 fb^{-1} of data from pp collisions at $\sqrt{s} = 13 \text{ TeV}$ to place limits on a KK gluon decaying to a top quark and a heavy vector-like fermion, T . KK gluon masses between 1.5 and 2.3 TeV and between 2.0 and 2.4 TeV are excluded for T masses of 1.2 and 1.5 TeV, respectively.
- ⁵ CHATRCHYAN 13BM use 19.7 fb^{-1} of data from pp collisions at $\sqrt{s} = 8 \text{ TeV}$. Bound is for a width of approximately 15–20% of the KK gluon mass.
- ⁶ CHEN 13A place limits on the KK mass scale for a specific warped model with custodial symmetry and bulk fermions. See their Figures 4 and 5.
- ⁷ AAD 12BV use 2.05 fb^{-1} of data from pp collisions at $\sqrt{s} = 7 \text{ TeV}$.

Black Hole Production Limits

Semiclassical Black Holes

VALUE (GeV)	DOCUMENT ID	TECN	COMMENT
• • • We do not use the following data for averages, fits, limits, etc. • • •			
	¹ SIRUNYAN 18DA CMS	$pp \rightarrow \text{multijet}$	
	² AAD 16N ATLS	$pp \rightarrow \text{multijet}$	
	³ AAD 16O ATLS	$pp \rightarrow \ell + (\ell\ell/ j /jj)$	
	⁴ AAD 13AW ATLS	$pp \rightarrow \mu\mu$	

- ¹ SIRUNYAN 18DA use 35.9 fb^{-1} of data from pp collisions at $\sqrt{s} = 13 \text{ TeV}$ to search for semiclassical black holes decaying to multijet final states. No excess of events above the expected level of standard model background was observed. Exclusions at 95% CL are set on the mass threshold for black hole production as a function of the higher-dimensional Planck scale for rotating and nonrotating black holes under several model assumptions (ADD, 2, 4, 6 extra dimensions model) in the 7.1–10.3 TeV range. These limits supersede those in SIRUNYAN 17CP.
- ² AAD 16N use 3.6 fb^{-1} of data from pp collisions at $\sqrt{s} = 13 \text{ TeV}$ to search for semiclassical black hole decays to multijet final states. No excess of events above the expected level of Standard Model background was observed. Exclusion contours at 95% C.L. are set on the mass threshold for black hole production versus higher-dimensional Planck scale for rotating black holes (ADD, 6 extra dimensions model).

- ³ AAD 16O use 3.2 fb^{-1} of data from pp collisions at $\sqrt{s} = 13 \text{ TeV}$ to search for semiclassical black hole decays to high-mass final states with leptons and jets. No excess of events above the expected level of Standard Model background was observed. Exclusion contours at 95% C.L. are set on the mass threshold for black hole production versus higher-dimensional Planck scale for rotating black holes (ADD, 2 to 6 extra dimensions).
- ⁴ AAD 13AW use 20.3 fb^{-1} of data from pp collisions at $\sqrt{s} = 8 \text{ TeV}$ to search for semiclassical black hole decays to like-sign dimuon final states using large track multiplicity. No excess of events above the expected level of Standard Model background was observed. Exclusion contours at 95% C.L. are set on the mass threshold for black hole production versus higher-dimensional Planck scale in various extra dimensions, rotating and non-rotating models.

Quantum Black Holes

VALUE (GeV)	DOCUMENT ID	TECN	COMMENT
• • • We do not use the following data for averages, fits, limits, etc. • • •			
	¹ AAD 23CB ATLS	$pp \rightarrow e\mu, e\tau, \mu\tau$	
	² TUMASYAN 23AW CMS	$pp \rightarrow \tau\nu$	
	³ TUMASYAN 23BC CMS	$pp \rightarrow \gamma j$	
	⁴ TUMASYAN 23H CMS	$pp \rightarrow e\mu, e\tau, \mu\tau$	
	⁵ AAD 20T ATLS	$pp \rightarrow jj$	
	⁶ AABOUD 18BA ATLS	$pp \rightarrow \gamma j$	
	⁷ SIRUNYAN 18AT CMS	$pp \rightarrow e\mu$	
	⁸ SIRUNYAN 18DD CMS	$pp \rightarrow \text{dijet, ang. distrib.}$	
	⁹ SIRUNYAN 17CP CMS	$pp \rightarrow jj$	
	¹⁰ KHACHATRYAN 16BE CMS	$pp \rightarrow e\mu$	
	¹¹ KHACHATRYAN 15V CMS	$pp \rightarrow jj$	
	¹² AAD 14AL ATLS	$pp \rightarrow \ell j$	
	¹³ AAD 14V ATLS	$pp \rightarrow ee, \mu\mu$	
	¹⁴ CHATRCHYAN 13A CMS	$pp \rightarrow jj$	

- ¹ AAD 23CB use 139 fb^{-1} of data from pp collisions at $\sqrt{s} = 13 \text{ TeV}$ to search for quantum black hole decays with different-flavor high-mass dilepton final states. No excess of events above the expected level of Standard Model background was observed. Exclusion limits at 95% C.L. are set on mass thresholds for black hole production in ADD (6 extra dimensions) and RS1 models. Assuming the black hole mass threshold is equal to the higher-dimensional Planck scale, mass thresholds below 5.9 (3.8), 5.2 (3.0), and 5.1 (3.0) TeV are excluded in the $e\mu, e\tau$ and $\mu\tau$ channels for the ADD (RS1) models, respectively. These limits supersede those in AABOUD 18CM.
- ² TUMASYAN 23AW use 138 fb^{-1} of data from pp collisions at $\sqrt{s} = 13 \text{ TeV}$ to search for quantum black hole decays in the tau lepton plus missing transverse momentum final state. Assuming the black hole mass threshold is equal to the higher-dimensional Planck scale, threshold masses below 6.6 TeV are excluded in the ADD model with four extra dimensions (see their Figure 8).
- ³ TUMASYAN 23BC use 138 fb^{-1} of data from pp collisions at $\sqrt{s} = 13 \text{ TeV}$ to search for quantum black hole decays to final states with a photon and a jet. No excess of events above the expected level of Standard Model background was observed. Exclusion limits at 95% C.L. are set on mass thresholds for black hole production in ADD (6 extra dimensions) and RS1 models. Assuming the black hole mass threshold is equal to the higher-dimensional Planck scale, mass thresholds below 7.5 TeV and 5.2 TeV are excluded for the ADD and RS1 models, respectively (see their Figure 9).
- ⁴ TUMASYAN 23H use 138 fb^{-1} of data from pp collisions at $\sqrt{s} = 13 \text{ TeV}$ to search for quantum black hole decays with different-flavor high-mass dilepton final states. No excess of events above the expected level of Standard Model background was observed. Exclusion limits at 95% C.L. are set on mass thresholds for black hole production in the ADD model (with 4 extra dimensions). Assuming the black hole mass threshold is equal to the higher-dimensional Planck scale, mass thresholds below 5.6, 5.2, and 5.0 TeV are excluded in the $e\mu, e\tau$ and $\mu\tau$ channels, respectively.
- ⁵ AAD 20T use 139 fb^{-1} of data from pp collisions at $\sqrt{s} = 13 \text{ TeV}$ to search for quantum black hole decays to final states with dijets. No excess of events above the expected level of Standard Model background was observed. Exclusion limits at 95% C.L. are set on mass thresholds for black hole production in an ADD (6 extra dimensions) model. Assuming the black hole mass threshold is equal to the higher-dimensional Planck scale, mass thresholds below 9.4 TeV are excluded. This limit supersedes AABOUD 17AK.
- ⁶ AABOUD 18BA use 36.7 fb^{-1} of data from pp collisions at $\sqrt{s} = 13 \text{ TeV}$ to search for quantum black hole decays to final states with a photon and a jet. No excess of events above the expected level of Standard Model background was observed. Exclusion limits at 95% C.L. are set on mass thresholds for black hole production in ADD (6 extra dimensions) and RS1 models. Assuming the black hole mass threshold is equal to the Planck scale, mass thresholds below 7.1 TeV and 4.4 TeV are excluded for the ADD and RS1 models, respectively. These limits supersede those in AAD 16AL.
- ⁷ SIRUNYAN 18AT use 35.9 fb^{-1} of data from pp collisions at $\sqrt{s} = 13 \text{ TeV}$ to search for quantum black hole decays to $e\mu$ final states. In Figure 4, lower mass limits of 5.3, 5.5 and 5.6 TeV are placed in a model with 4, 5 and 6 extra dimensions, respectively, and a lower mass limit of 3.6 TeV is found for a single warped dimension.
- ⁸ SIRUNYAN 18DD use 35.9 fb^{-1} of data from pp collisions at $\sqrt{s} = 13 \text{ TeV}$ to search for quantum black hole decays in dijet angular distributions. A lower mass limit of 5.9 (8.2) TeV is placed in the RS (ADD) model with one (six) extra dimension(s).
- ⁹ SIRUNYAN 17CP use 2.3 fb^{-1} of data from pp collisions at $\sqrt{s} = 13 \text{ TeV}$ to search for quantum black holes decaying to dijet final states. No excess of events above the expected level of standard model background was observed. Limits on the quantum black hole mass threshold are set as a function of the higher-dimensional Planck scale, under the assumption that the mass threshold must exceed the above Planck scale. Depending on the model, mass thresholds in the range up to 5.1–9.0 TeV are excluded.
- ¹⁰ KHACHATRYAN 16BE use 19.7 fb^{-1} of data from pp collisions at $\sqrt{s} = 8 \text{ TeV}$ to search for quantum black holes undergoing lepton flavor violating decay to the $e\mu$ final state. No excess of events above the expected level of standard model background was observed. Exclusion limits at 95% CL are set on mass thresholds for black hole production in the ADD (2–6 flat extra dimensions), RS1 (1 warped extra dimension), and a model with a Planck scale at the TeV scale from a renormalization of the gravitational constant (no extra dimensions). Limits on the black hole mass threshold are set assuming that it is equal to the higher-dimensional Planck scale. Mass thresholds for quantum black holes in the range up to 3.15–3.63 TeV are excluded in the ADD model. In the RS1 model, mass thresholds below 2.81 TeV are excluded in the PDG convention for the Schwarzschild radius. In the model with no extra dimensions, mass thresholds below 1.99 TeV are excluded.
- ¹¹ KHACHATRYAN 15V use 19.7 fb^{-1} of data from pp collisions at $\sqrt{s} = 8 \text{ TeV}$ to search for quantum black holes decaying to dijet final states. No excess of events above

Searches Particle Listings

Extra Dimensions

the expected level of standard model background was observed. Exclusion limits at 95% CL are set on mass thresholds for black hole production in the ADD (2–6 flat extra dimensions) and RS1 (1 warped extra dimension) model. Limits on the black hole mass threshold are set as a function of the higher-dimensional Planck scale, under the assumption that the mass threshold must exceed the above Planck scale. Depending on the model, mass thresholds in the range up to 5.0–6.3 TeV are excluded. This paper supersedes CHATRCHYAN 13Ad.

12 AAD 14AL use 20.3 fb⁻¹ of data from *pp* collisions at $\sqrt{s} = 8$ TeV to search for quantum black hole decays to final states with high-invariant-mass lepton + jet. No excess of events above the expected level of Standard Model background was observed. Exclusion limits at 95% C.L. are set on mass thresholds for black hole production in an ADD (6 extra dimensions) model. Assuming the black hole mass threshold is equal to the higher-dimensional Planck scale, mass thresholds below 5.3 TeV are excluded.

13 AAD 14V use 20.3 (20.5) fb⁻¹ of data in the dielectron (dimuon) channels from *pp* collisions at $\sqrt{s} = 8$ TeV to search for quantum black hole decaying to dilepton resonances. No excess of events above the expected level of Standard Model background was observed. Exclusion limits at 95% C.L. are set on mass thresholds for black hole production in ADD (6 extra dimensions) and RS1 models. Assuming the black hole mass threshold is equal to the higher-dimensional Planck scale, mass thresholds below 3.65 TeV and 2.24 TeV are excluded for the ADD and RS1 models, respectively.

14 CHATRCHYAN 13A use 5 fb⁻¹ of data from *pp* collisions at $\sqrt{s} = 7$ TeV to search for quantum black holes decaying to dijet final states. No excess of events above the expected level of standard model background was observed. Exclusion limits at 95% CL are set on mass thresholds for black hole production in the ADD (2–6 flat extra dimensions) and RS (1 warped extra dimension) model. Limits on the black hole mass threshold are set as a function of the higher-dimensional Planck scale, under assumption that the mass threshold must exceed the above Planck scale. Depending on the model, mass thresholds in the range up to 4.0–5.3 TeV are excluded.

REFERENCES FOR Extra Dimensions

- AAD 23CB JHEP 2310 082 G. Aad et al. (ATLAS Collab.)
 FLORES 23 JUMP A38 2350002 M.M. Flores et al. (WITS, WARS, NIP-UPD+) (CMS Collab.)
 TUMASYAN 23AP PL B844 137813 A. Tumasyan et al. (CMS Collab.)
 TUMASYAN 23AW JHEP 2309 051 A. Tumasyan et al. (CMS Collab.)
 TUMASYAN 23BC JHEP 2312 189 A. Tumasyan et al. (CMS Collab.)
 TUMASYAN 23H JHEP 2305 227 A. Tumasyan et al. (CMS Collab.)
 AAD 22F PR D105 092002 G. Aad et al. (ATLAS Collab.)
 TUMASYAN 22C PL B832 137263 A. Tumasyan et al. (CMS Collab.)
 TUMASYAN 22D PR D105 032008 A. Tumasyan et al. (CMS Collab.)
 TUMASYAN 22J PR D106 012004 A. Tumasyan et al. (CMS Collab.)
 TUMASYAN 22R JHEP 2204 087 A. Tumasyan et al. (CMS Collab.)
 TUMASYAN 22U JHEP 2205 005 A. Tumasyan et al. (CMS Collab.)
 AAD 21AF EPJ C81 332 G. Aad et al. (ATLAS Collab.)
 AAD 21AY PL B822 136651 G. Aad et al. (ATLAS Collab.)
 AAD 21F PR D103 112006 G. Aad et al. (ATLAS Collab.)
 AVNISH 21 PR D103 115011 Avnish et al. (STAN)
 BLAKEMORE 21 PR D104 L061101 C.P. Blakemore et al. (NIST, RIKEN, NAGO+) (CMS Collab.)
 HEACOCK 21 SCI 373 1239 B. Heacock et al. (CMS Collab.)
 SIRUNYAN 21A EPJ C81 13 A.M. Sirunyan et al. (CMS Collab.)
 Also EPJ C81 333 (errata.) A.M. Sirunyan et al. (CMS Collab.)
 SIRUNYAN 21N JHEP 2107 200 A.M. Sirunyan et al. (CMS Collab.)
 TUMASYAN 21D JHEP 2111 153 A. Tumasyan et al. (CMS Collab.)
 AAD 20AT EPJ C80 1165 G. Aad et al. (ATLAS Collab.)
 AAD 20C PL B800 135103 G. Aad et al. (ATLAS Collab.)
 AAD 20T JHEP 2003 145 G. Aad et al. (ATLAS Collab.)
 LEE 20 PRL 124 101101 J.G. Lee et al. (WASH)
 SIRUNYAN 20AI JHEP 2005 033 A.M. Sirunyan et al. (CMS Collab.)
 SIRUNYAN 20F PR D102 032003 A.M. Sirunyan et al. (CMS Collab.)
 SIRUNYAN 20Q EPJ C80 237 A.M. Sirunyan et al. (CMS Collab.)
 TAN 20A PRL 124 051301 W.-H. Tan et al. (ATLAS Collab.)
 AABOUD 19A JHEP 1901 030 M. Aaboud et al. (ATLAS Collab.)
 AABOUD 19AS PR D99 092004 M. Aaboud et al. (ATLAS Collab.)
 AABOUD 19O JHEP 1904 092 M. Aaboud et al. (ATLAS Collab.)
 AAD 19D JHEP 1909 091 G. Aad et al. (ATLAS Collab.)
 Also JHEP 2006 042 (errata.) G. Aad et al. (ATLAS Collab.)
 SIRUNYAN 19 PL B788 7 A.M. Sirunyan et al. (CMS Collab.)
 SIRUNYAN 19AC JHEP 1904 114 A.M. Sirunyan et al. (CMS Collab.)
 SIRUNYAN 19AL EPJ C79 208 A.M. Sirunyan et al. (CMS Collab.)
 SIRUNYAN 19BE PRL 122 121803 A.M. Sirunyan et al. (CMS Collab.)
 SIRUNYAN 19CF JHEP 1910 125 A.M. Sirunyan et al. (CMS Collab.)
 AABOUD 18AK JHEP 1803 042 M. Aaboud et al. (ATLAS Collab.)
 AABOUD 18AL JHEP 1803 009 M. Aaboud et al. (ATLAS Collab.)
 AABOUD 18AV JHEP 1807 089 M. Aaboud et al. (ATLAS Collab.)
 AABOUD 18BA EPJ C78 102 M. Aaboud et al. (ATLAS Collab.)
 AABOUD 18BF EPJ C78 293 M. Aaboud et al. (ATLAS Collab.)
 AABOUD 18BI EPJ C78 565 M. Aaboud et al. (ATLAS Collab.)
 AABOUD 18CE JHEP 1812 039 M. Aaboud et al. (ATLAS Collab.)
 AABOUD 18CJ PR D98 052008 M. Aaboud et al. (ATLAS Collab.)
 AABOUD 18CM PR D98 092008 M. Aaboud et al. (ATLAS Collab.)
 AABOUD 18CQ PRL 121 191801 M. Aaboud et al. (ATLAS Collab.)
 AABOUD 18CW JHEP 1811 040 M. Aaboud et al. (ATLAS Collab.)
 AABOUD 18F PL B777 91 M. Aaboud et al. (ATLAS Collab.)
 AABOUD 18I JHEP 1801 126 M. Aaboud et al. (ATLAS Collab.)
 BERGE 18 PRL 120 141101 J. Berge et al. (MICROSCOPE Collab.)
 FAYET 18 PR D97 055039 P. Fayet (ENSP, EPOL)
 FAYET 18A PR D99 055043 P. Fayet (ENSP, EPOL)
 HADDOCK 18 PR D97 062002 C. Haddock et al. (NAGO, KEK, OSAK+) (CMS Collab.)
 SIRUNYAN 18AF PL B781 244 A.M. Sirunyan et al. (CMS Collab.)
 SIRUNYAN 18AS JHEP 1803 003 A.M. Sirunyan et al. (CMS Collab.)
 SIRUNYAN 18AT JHEP 1804 073 A.M. Sirunyan et al. (CMS Collab.)
 SIRUNYAN 18AX JHEP 1805 088 A.M. Sirunyan et al. (CMS Collab.)
 SIRUNYAN 18BB JHEP 1806 120 A.M. Sirunyan et al. (CMS Collab.)
 SIRUNYAN 18BK JHEP 1807 075 A.M. Sirunyan et al. (CMS Collab.)
 SIRUNYAN 18BO JHEP 1808 130 A.M. Sirunyan et al. (CMS Collab.)
 SIRUNYAN 18BV EPJ C78 291 A.M. Sirunyan et al. (CMS Collab.)
 SIRUNYAN 18CW JHEP 1808 152 A.M. Sirunyan et al. (CMS Collab.)
 SIRUNYAN 18DA JHEP 1811 042 A.M. Sirunyan et al. (CMS Collab.)
 SIRUNYAN 18DD EPJ C78 789 A.M. Sirunyan et al. (CMS Collab.)
 SIRUNYAN 18DJ JHEP 1809 101 A.M. Sirunyan et al. (CMS Collab.)
 SIRUNYAN 18DU PR D98 092001 A.M. Sirunyan et al. (CMS Collab.)
 SIRUNYAN 18F JHEP 1801 054 A.M. Sirunyan et al. (CMS Collab.)
 SIRUNYAN 18I PRL 120 201801 A.M. Sirunyan et al. (CMS Collab.)
 SIRUNYAN 18S PR D97 092005 A.M. Sirunyan et al. (CMS Collab.)
 AABOUD 17AK PR D96 052004 M. Aaboud et al. (ATLAS Collab.)
 AABOUD 17AQ PL B775 105 M. Aaboud et al. (ATLAS Collab.)
 KLIMCHITSK... 17A PR D95 123013 G.L. Klimchitskaya, V.M. Mostepanenko (CMS Collab.)
 SIRUNYAN 17AP JHEP 1710 073 A.M. Sirunyan et al. (CMS Collab.)
 SIRUNYAN 17CP PL B774 279 A.M. Sirunyan et al. (CMS Collab.)
 SIRUNYAN 17F JHEP 1707 013 A.M. Sirunyan et al. (CMS Collab.)
 AABOUD 16F JHEP 1606 059 M. Aaboud et al. (ATLAS Collab.)
 AAD 16AI JHEP 1603 041 G. Aad et al. (ATLAS Collab.)
 AAD 16N JHEP 1603 026 G. Aad et al. (ATLAS Collab.)
 AAD 16O PL B760 520 G. Aad et al. (ATLAS Collab.)
 AAD 16R PL B755 285 G. Aad et al. (ATLAS Collab.)
 KHACHATRY... 16BE EPJ C76 317 V. Khachatryan et al. (CMS Collab.)
 KHACHATRY... 16BQ PR D94 052012 V. Khachatryan et al. (CMS Collab.)
 KHACHATRY... 16M PRL 117 051802 V. Khachatryan et al. (CMS Collab.)
 KHACHATRY... 16N PL B755 102 V. Khachatryan et al. (CMS Collab.)
 AAD 15AU EPJ C75 69 G. Aad et al. (ATLAS Collab.)
 AAD 15AZ EPJ C75 209 G. Aad et al. (ATLAS Collab.)
 Also EPJ C75 370 (errata.) G. Aad et al. (ATLAS Collab.)
 AAD 15CP JHEP 1512 055 G. Aad et al. (ATLAS Collab.)
 AAD 15CS PR D91 012008 G. Aad et al. (ATLAS Collab.)
 Also PR D92 059903 (errata.) G. Aad et al. (ATLAS Collab.)
 ACCOMANDO 15 MPL A30 1540010 E. Accomando (SHMP)
 KHACHATRY... 15AE JHEP 1504 025 V. Khachatryan et al. (CMS Collab.)
 KHACHATRY... 15R PL B749 560 V. Khachatryan et al. (CMS Collab.)
 KHACHATRY... 15T PR D91 092005 V. Khachatryan et al. (CMS Collab.)
 KHACHATRY... 15V PR D91 052009 V. Khachatryan et al. (CMS Collab.)
 AAD 14AL PRL 112 091804 G. Aad et al. (ATLAS Collab.)
 AAD 14BE EPJ C74 3134 G. Aad et al. (ATLAS Collab.)
 AAD 14V PR D90 052005 G. Aad et al. (ATLAS Collab.)
 AAD 13A PL B718 860 G. Aad et al. (ATLAS Collab.)
 AAD 13AO PR D87 112006 G. Aad et al. (ATLAS Collab.)
 AAD 13AQ PR D88 012004 G. Aad et al. (ATLAS Collab.)
 AAD 13AS NJP 15 043007 G. Aad et al. (ATLAS Collab.)
 AAD 13AW PR D88 072001 G. Aad et al. (ATLAS Collab.)
 AAD 13C PRL 110 011802 G. Aad et al. (ATLAS Collab.)
 AAD 13D JHEP 1301 029 G. Aad et al. (ATLAS Collab.)
 AAD 13E PR D87 015010 G. Aad et al. (ATLAS Collab.)
 CHATRCHYAN 13A JHEP 1301 013 S. Chatrchyan et al. (CMS Collab.)
 CHATRCHYAN 13AD JHEP 1307 178 S. Chatrchyan et al. (CMS Collab.)
 CHATRCHYAN 13AQ PR D87 072005 S. Chatrchyan et al. (CMS Collab.)
 CHATRCHYAN 13BM PRL 111 211804 S. Chatrchyan et al. (CMS Collab.)
 Also PRL 112 119903 (errata.) S. Chatrchyan et al. (CMS Collab.)
 CHATRCHYAN 13W JHEP 1303 111 S. Chatrchyan et al. (CMS Collab.)
 CHEN 13A CP C37 063102 J.-B. Chen et al. (DALI)
 EDELHAUSER 13 JHEP 1308 091 L. Edelhauser, T. Flacke, M. Kramer (AACH, KAIST)
 XU 13 JP 640 035107 J. Xu et al. (ATLAS Collab.)
 AAD 12AD PL B712 331 G. Aad et al. (ATLAS Collab.)
 AAD 12BV JHEP 1209 041 G. Aad et al. (ATLAS Collab.)
 AAD 12CC JHEP 1211 138 G. Aad et al. (ATLAS Collab.)
 AAD 12CP PL B718 411 G. Aad et al. (ATLAS Collab.)
 AAD 12X PL B710 519 G. Aad et al. (ATLAS Collab.)
 AAD 12Y PL B710 538 G. Aad et al. (ATLAS Collab.)
 AALTONEN 12V PR D85 012008 T. Aaltonen et al. (CDF Collab.)
 ABAZOV 12M PRL 108 131802 V.M. Abazov et al. (DO Collab.)
 AJELLO 12 JCAP 1202 012 M. Ajello et al. (Fermi-LAT Collab.)
 BAAK 12 EPJ C72 2003 M. Baak et al. (Glitter Group)
 CHATRCHYAN 12R PRL 108 111801 S. Chatrchyan et al. (CMS Collab.)
 FLACKE 12 PR D85 126007 T. Flacke, C. Pasold (WURZ)
 NISHIWAKI 12 PL B707 506 K. Nishiwaki et al. (KOBE, OSAK)
 AAD 11F PRL 106 121803 G. Aad et al. (ATLAS Collab.)
 AAD 11X EPJ C71 1744 G. Aad et al. (ATLAS Collab.)
 AALTONEN 11G PR D83 112008 T. Aaltonen et al. (CDF Collab.)
 AALTONEN 11H PRL 107 051801 T. Aaltonen et al. (CDF Collab.)
 AALTONEN 11U PR D83 011102 T. Aaltonen et al. (CDF Collab.)
 AARON 11C PL B705 52 F. D. Aaron et al. (H1 Collab.)
 ABAZOV 11H PRL 107 011801 V.M. Abazov et al. (DO Collab.)
 BEZERRA 11 PR D83 075004 V.B. Bezerra et al. (DO Collab.)
 SUSHKOV 11 PRL 107 171101 A.O. Sushkov et al. (DO Collab.)
 AALTONEN 10P PRL 104 241801 T. Aaltonen et al. (CDF Collab.)
 ABAZOV 10F PRL 104 241802 V.M. Abazov et al. (DO Collab.)
 ABAZOV 10P PRL 105 221802 V.M. Abazov et al. (DO Collab.)
 BEZERRA 10 PR D81 055003 V.B. Bezerra et al. (DO Collab.)
 ABAZOV 09AE PRL 103 191803 V.M. Abazov et al. (DO Collab.)
 ABAZOV 09D PRL 102 051603 V.M. Abazov et al. (DO Collab.)
 MASUDA 09 PR 102 171101 M. Masuda, M. Sasaki (ICRR)
 AALTONEN 08AC PRL 101 181602 T. Aaltonen et al. (CDF Collab.)
 AALTONEN 08A PR D78 012008 T. Aaltonen et al. (CDF Collab.)
 ABAZOV 08B PRL 100 091802 V.M. Abazov et al. (DO Collab.)
 ABAZOV 08J PRL 101 011601 V.M. Abazov et al. (DO Collab.)
 DAS 08 PR D78 063011 P.K. Das, V.H.S. Kumar, P.K. Suresh (STAN)
 GERACI 08 PR D78 022002 A.A. Geraci et al. (STAN)
 TRENKEL 08 PR D77 122001 C. Trenkel (CDF Collab.)
 AALTONEN 07G PRL 99 171801 T. Aaltonen et al. (CDF Collab.)
 AALTONEN 07H PRL 99 171802 T. Aaltonen et al. (CDF Collab.)
 DECCA 07 PR D76 031901 R.S. Decca et al. (CDF Collab.)
 HAISCH 07 PR D76 034014 U. Haisch, A. Weiler (CDF Collab.)
 KAPNER 07 PR 98 021101 D.J. Kapner et al. (CDF Collab.)
 SCHAEF 07A EPJ C49 411 S. Schaefer et al. (ALEPH Collab.)
 TU 07 PRL 98 201101 L.-C. Tu et al. (CDF Collab.)
 ABDALLAH 06C EPJ C45 589 J. Abdallah et al. (DELPHI Collab.)
 ABULENCIA,A 06 PRL 97 171802 A. Abulencia et al. (CDF Collab.)
 GERDES 06 PR D73 112008 D. Gerdes et al. (CDF Collab.)
 GOGOLADZE 06 PR D74 093012 I. Gogoladze, C. Macesanu (DO Collab.)
 ABAZOV 05N PRL 95 091801 V.M. Abazov et al. (DO Collab.)
 ABAZOV 05V PRL 95 161602 V.M. Abazov et al. (DO Collab.)
 ABDALLAH 05B EPJ C38 395 J. Abdallah et al. (DELPHI Collab.)
 ABULENCIA 05A PRL 95 252001 A. Abulencia et al. (CDF Collab.)
 SMULLIN 05 PR D72 122001 S.J. Smullin et al. (CDF Collab.)
 ACHARD 04E PL B587 16 P. Achard et al. (L3 Collab.)
 ACOSTA 04C PRL 92 121802 D. Acosta et al. (CDF Collab.)
 BARBIERI 04 NP B703 127 R. Barbieri et al. (CDF Collab.)
 CASSE 04 PRL 92 111102 M. Casse et al. (ZEUS Collab.)
 CHEKANOV 04B PL B591 23 S. Chekanov et al. (ZEUS Collab.)
 HOYLE 04 PR D70 042004 C.D. Hoyle et al. (WASH)
 ABAZOV 03 PRL 90 251802 V.M. Abazov et al. (DO Collab.)
 ABBIENDI 03D EPJ C26 331 G. Abbiendi et al. (OPAL Collab.)
 ACHARD 03D PL B572 133 P. Achard et al. (L3 Collab.)
 ADLOFF 03 PR B568 35 C. Adloff et al. (H1 Collab.)
 CHIAVERINI 03 PRL 90 151101 J. Chiaverini et al. (CDF Collab.)
 GUIDICE 03 NP B663 377 G.F. Giudice, A. Strumia (CDF Collab.)
 HANNENSTAD 03 PR D67 125008 S. Hannestad, G.G. Raffelt (CDF Collab.)
 Also PR D69 029901 (errata.) S. Hannestad, G.G. Raffelt
 HEISTER 03C EPJ C28 1 A. Heister et al. (ALEPH Collab.)
 LONG 03 NAT 421 922 J.C. Long et al. (L3 Collab.)
 ACHARD 02D PL B524 65 P. Achard et al. (L3 Collab.)
 ACHARD 02D PL B531 28 P. Achard et al. (L3 Collab.)
 HANNENSTAD 02 PRL 88 071301 S. Hannestad, G. Raffelt (DO Collab.)
 ABBOTT 01 PRL 86 1156 B. Abbott et al. (DO Collab.)
 FAIRBAIRN 01 PL B508 335 M. Fairbairn (DO Collab.)
 HANHART 01 PL B509 1 C. Hanhart et al. (OPAL Collab.)
 HOYLE 01 PRL 86 1418 C.D. Hoyle et al. (OPAL Collab.)
 ABBIENDI 00R EPJ C13 553 G. Abbiendi et al. (DELPHI Collab.)
 ABREU 00A PL B491 67 P. Abreu et al. (DELPHI Collab.)
 ABREU 00E PL B485 45 P. Abreu et al. (DELPHI Collab.)
 ABREU 00Z EPJ C17 53 P. Abreu et al. (DELPHI Collab.)
 CASSISI 00 PR B481 323 S. Cassisi et al. (DELPHI Collab.)
 CHANG 00B PRL 85 3765 L.N. Chang et al. (DELPHI Collab.)
 CHEUNG 00 PR D61 015005 K. Cheung (DELPHI Collab.)
 CORNET 00 PR D61 031701 F. Cornet, M. Relano, J. Rico (DELPHI Collab.)
 GRAESSER 00 PR D61 074019 M.L. Graesser (DELPHI Collab.)
 HAN 00 PR D62 125018 T. Han, D. Marfatia, R.-J. Zhang (DELPHI Collab.)
 MATHEWS 00 JHEP 0007 008 P. Mathews, S. Raychaudhuri, K. Sridhar (DELPHI Collab.)

See key on page 1171

Searches Particle Listings

Extra Dimensions, WIMP and Dark Matter Searches

MELE	00	PR D61 117901	S. Mele, E. Sanchez
RIZZO	00	PR D61 016007	T. G. Rizzo, J.D. Wells
ABBIENDI	99P	PL B465 303	G. Abbiendi et al.
ACCIARRI	99M	PL B464 135	M. Acciari et al.
ACCIARRI	99R	PL B470 268	M. Acciari et al.
ACCIARRI	99S	PL B470 281	M. Acciari et al.
BOURILKOV	99	JHEP 9908 006	D. Bourilkov
HOSKINS	85	PR D32 3084	J.K. Hoskins et al.

(OPAL Collab.)
(L3 Collab.)
(L3 Collab.)
(L3 Collab.)

WIMP and Dark Matter Searches

We omit papers on CHAMP's, millicharged particles, and other exotic particles.

GALACTIC WIMP SEARCHES

These limits are for weakly-interacting stable particles that may constitute the invisible mass in the galaxy. Unless otherwise noted, a local mass density of $0.3 \text{ GeV}/\text{cm}^3$ is assumed; see each paper for velocity distribution assumptions. In the papers the limit is given as a function of the χ^0 mass. Here we list limits only for typical mass values of sub-GeV, GeV, 20 GeV, 100 GeV, and 1 TeV. Specific limits on supersymmetric dark matter particles may be found in the Supersymmetry section.

Spin-Independent Cross Section Limits for Dark Matter Particle (χ^0) on Nucleon

For m_{χ^0} in GeV range

We provide here limits for $m_{\chi^0} < 5 \text{ GeV}$

VALUE (pb)	CL%	DOCUMENT ID	TECN	COMMENT
$< 3 \times 10^{-3}$	90	1 AALBERS 23A	LZ	SI scatter on Xe
$< 4 \times 10^{-7}$	90	2 AGNES 23	DS50	LDM search via Migdal
$< 6 \times 10^{-7}$	90	3 AGNES 23B	DS50	LDM scatter on nucleons
< 0.5	90	4 ALBAKRY 23	SCDM	LDM via Migdal
< 1	95	5 AMBROSONE 23		DM distortion of CR spectra
< 70	90	6 ANGLOHER 23	CRES	LDM search
$< 8 \times 10^{-8}$	90	7 LI 23F	PNDX	SI light DM limits
$< 5 \times 10^{-10}$	90	8 MA 23A	PNDX	LDM search
< 10	90	9 ADHIKARI 22B	C100	sub-GeV WIMP via SI coupling/Migdal effect
$< 1.4 \times 10^4$	90	10 ARMENGAUD 22	EDEL	GeV-scale DM on Ge via Migdal effect
$< 5 \times 10^5$	90	11 CUI 22	PNDX	sub-GeV boosted DM
$< 6.5 \times 10^6$	90	12 XU 22	CDEX	sub-GeV DM
$< 2 \times 10^{-7}$	95	13 AKERIB 21A	LUX	low mass WIMPs
$< 5 \times 10^6$	90	14 ALKHATIB 21	SCDM	light DM
$< 1 \times 10^8$	95	15 ANDRIAMIR... 21A		sub-GeV DM on nucleon
$< 1 \times 10^{-8}$	90	16 APRILE 21	XE1T	GeV-scale DM
$< 8 \times 10^{-4}$	90	17 AGUILAR-AR... 20C	DMIC	WIMP SI scatter on Si
$< 8 \times 10^{-4}$	90	18 AKERIB 20A	LUX	GeV-scale WIMP search
$< 1 \times 10^{-2}$	90	19 ABDELHAME... 19A	CRES	CaWO ₄
$< 5.4 \times 10^{-6}$	90	20 AGNESE 19A	SCDM	GeV-scale WIMPs on Ge
< 1	90	21 AKERIB 19	LUX	light DM on Xe via Migdal/brem effect
$< 1 \times 10^{-6}$	90	22 AMOLE 19	PICO	C ₃ F ₈
$< 1.6 \times 10^{-3}$	90	23 APRILE 19C	XE1T	DM on Xe
$< 1 \times 10^{-7}$	90	24 APRILE 19D	XE1T	DM on Xe
< 0.1	90	25 ARMENGAUD 19	EDEL	GeV-scale WIMPs on Ge
$< 1.6 \times 10^3$	90	26 KOBAYASHI 19	XMAS	annual modulation Xe
$< 7 \times 10^2$	90	27 LIU 19B	CDEX	GeV-scale DM via Migdal
$< 7 \times 10^{-7}$	90	28 AGNES 18	DS50	GeV-scale WIMPs on Ar
$< 1.5 \times 10^{-5}$	95	29 AGNESE 18	SCDM	GeV-scale WIMPs on Ge
$< 2 \times 10^{-8}$	90	30 APRILE 18	XE1T	Xe, Si
$< 4.5 \times 10^{-3}$	90	31 ARNAUD 18	NEWS	low mass WIMP, Ne
$< 8 \times 10^{-6}$	90	32 JIANG 18	CDEX	GeV-scale WIMPs on Ge
$< 3 \times 10^{-5}$	90	33 YANG 18	CDEX	WIMPs on Ge
$< 1 \times 10^{-6}$	90	34 AKERIB 17	LUX	Xe
$< 1 \times 10^2$	90	35 ANGLOHER 17A	CRES	GeV-scale WIMPs
$< 7 \times 10^{-5}$	90	36 ANGLOHER 16	CRES	CaWO ₄
$< 3 \times 10^{-5}$	90	37 APRILE 16	X100	Xe
$< 4.3 \times 10^{-4}$	90	38 ARMENGAUD 16	EDE3	GeV-scale WIMPs on Ge
$< 7 \times 10^{-5}$	90	39 HEHN 16	EDE3	SI WIMP on Ge
$< 6 \times 10^{-5}$	90	40 ZHAO 16	CDEX	GeV-scale WIMPs on Ge
$< 1 \times 10^{-4}$	90	41 AMOLE 15	PICO	C ₃ F ₈
$< 8 \times 10^{-5}$	90	42 XIAO 15	PNDX	WIMPs on Xe
$< 3 \times 10^{-5}$	90	43 AGNESE 14	SCDM	GeV-scale WIMPs
$< 1 \times 10^{-3}$	90	44 AKERIB 14	LUX	WIMP on Xe
$< 9 \times 10^{-4}$	90	45 LI 13B	TEXO	WIMPs on Ge
$< 3 \times 10^{-4}$	90	46 AARCHA MBAU... 12	PICA	C ₄ F ₁₀
$< 2 \times 10^{-4}$	90	47 ALSETH 11	CGNT	GeV WIMPs on Ge
$< 5 \times 10^{-4}$	90	48 AHMED 11B	CDM2	GeV-scale WIMPs on Ge

$< 8 \times 10^{-5}$ 90 49 ANGLE 11 XE10 Xe
 $< 5 \times 10^{-4}$ 90 50 AKERIB 10 CDM2 WIMPs on Ge/Si

- AALBERS 23A search for e recoil events from GeV scale WIMP scatter on Xe. No signal observed. Limits placed on 6 different models including $\sigma^{SI} < 3 \times 10^{-3}$ for $m(\chi) \sim 1 \text{ GeV}$ via Migdal scattering.
- AGNES 23 for light DM via e recoil/Migdal effect. No signal observed. $\sigma^{SI}(\chi N) < 4 \times 10^{-7}$ pb for $m(\chi) = 3 \text{ GeV}$.
- AGNES 23B search for GeV-scale DM scatter on nucleons in Ar. No signal observed. Limit $\sigma^{SI}(\chi N) < 6 \times 10^{-7}$ pb for $m(\chi) = 3 \text{ GeV}$.
- ALBAKRY 23 search for light DM via Migdal effect. No signal observed. Allow $\sigma^{SI} < 0.5 \text{ pb}$ for $m(\chi)=1 \text{ GeV}$ (see e.g. Fig. 7).
- AMBROSONE 23 derive limits on $\sigma(\chi p)$ due to possible DM distortion of cosmic ray spectra in starburst galaxies. Limits placed in σ vs. mass (10^{-3} –10 MeV) plane, the most stringent given above being at 1 keV.
- ANGLOHER 23 search for light DM using Si target. No signal observed. Require $\sigma^{SI} < 70 \text{ pb}$ for $m(\chi) = 0.3 \text{ GeV}$ (see e.g. Fig. 5).
- LI 23F searches for SI light DM scatter from Xe. No signal observed. The quoted limit for $m(\chi) = 4 \text{ GeV}$.
- MA 23A search for GeV-scale DM using PandaX-4T. No signal observed. $\sigma(\chi p) < 5 \times 10^{-10}$ pb for $m(\chi) = 10 \text{ GeV}$.
- ADHIKARI 22B search for sub-GeV WIMPs via SI and SD detection; no signal detected; limits placed in $m(\chi)$ vs. σ plane for $m(\chi)$: 0.2–3 GeV; quoted limit is for $m(\chi) = 1 \text{ GeV}$.
- ARMENGAUD 22 search for GeV-scale DM scatter on Ge at EDELWEISS via Migdal effect; no signal observed; limits placed in $\sigma^{SI}(\chi N)$ vs. $m(\text{DM})$ plane; quoted limit is for $m(\text{DM}) = 100 \text{ MeV}$.
- CUI 22 search for sub-GeV boosted DM at PandaX-II at CJPL; no signal detected; limits set in $\sigma^{SI}(\chi p)$ vs. $m(\chi)$ plane; quoted limit for $m(\chi) = 0.1 \text{ GeV}$.
- XU 22 search for sub-GeV boosted DM in CDEX; no signal observed; limits placed in $\sigma(\chi N)$ vs. $m(\text{DM})$ plane; quoted limit is for $m(\text{DM}) = 0.1 \text{ GeV}$.
- AKERIB 21A present new technique for low mass WIMP detection. Require $\sigma^{SI}(\rho \chi) < 2 \times 10^{-7}$ pb for $m(\text{WIMP}) 10 \text{ GeV}$.
- ALKHATIB 21 search for light DM using SuperCDMS; require $\sigma^{SI}(\rho \chi) < 5 \times 10^6$ for $m(\text{DM}) = 0.1 \text{ GeV}$.
- ANDRIAMIRADO 21A search for upscattered (boosted) sub-GeV DM interacting with proton in PROSPECT detector. No signal observed. Limits placed in $\sigma(\chi N)$ vs. $m(\text{DM})$ plane for $m(\text{DM}) \sim 1 \text{ keV} - 0.5 \text{ GeV}$. The listed limit is for $m(\text{DM}) = 1 \text{ keV}$.
- APRILE 21 search for low recoil energy GeV-scale DM in XENON1T with 1.6 keV threshold. No signal in 0.6 t y exposure. Limits placed in $\sigma^{SI}(\chi N)$ vs. $m(\text{DM})$ plane for $m(\text{DM})$ between 3–12 GeV. The listed limit is for $m(\text{DM}) = 5 \text{ GeV}$.
- AGUILAR-AREVALO 20c search for WIMP SI scatter on Si using DAMIC at SNOLab; some excess; limits placed in σ vs $m(\text{DM})$ for $m(\text{DM})$ in 1.2–10 GeV; quoted limit for $m(\text{WIMP}) = 2 \text{ GeV}$.
- AKERIB 20A search for GeV-scale WIMPs via WIMP-nucleon scatter with single photon emission; no signal; limits placed in $m(\text{WIMP})$ vs σ^{SI} plane: for example $\sigma^{SI}(\chi n) < 8 \times 10^{-4}$ pb for $m(\text{WIMP}) = 2.5 \text{ GeV}$.
- ABDELHAMEED 19A search for GeV scale dark matter SI scatter on CaWO₄; no signal, limits placed in σ vs. mass plane for $m(\text{DM}) \sim 0.1$ –10 GeV. The listed limit is for $m(\text{DM}) = 1 \text{ GeV}$.
- AGNESE 19A search for 1.5–10 GeV WIMP scatter on Ge in CDMsLite dataset. Limits set in a likelihood analysis. No signal was observed. Limit reported for $m(\chi) = 5 \text{ GeV}$.
- AKERIB 19 search for 0.4–5 GeV DM using bremsstrahlung photons and "Migdal" electrons; $1.4 \times 10^4 \text{ kg d}$ exposure of liquid Xe; constraint $\sigma^{SI}(\chi N) < 1 \text{ pb}$ for $m(\chi) = 5 \text{ GeV}$ in light scalar mediator model.
- AMOLE 19 search for SI WIMP scatter on C₃F₈ in PICO-60 bubble chamber; no signal; set limit for spin independent coupling $\sigma^{SI}(\chi N) < 1 \times 10^{-6}$ pb for $m(\chi) = 5 \text{ GeV}$.
- APRILE 19c search for light DM scatter on Xe via atomic excitation, ionization (Migdal effect) or bremsstrahlung; no signal, limits placed in σ vs. $m(\text{DM})$ plane for $m(\text{DM}) \sim 0.085$ –2 GeV. The listed limit is for $m(\text{DM}) = 1 \text{ GeV}$.
- APRILE 19d search for light DM scatter on Xe via ionization to probe SI, SD, and χe cross sections; with 22 t d exposure, limits placed in various σ vs. $m(\text{DM})$ planes. Quoted limit is for $m(\text{DM}) = 5 \text{ GeV}$.
- ARMENGAUD 19 search for GeV scale WIMP scatter on Ge; limits placed in $\sigma^{SI}(\chi N)$ vs. $m(\chi)$ plane for $m(\chi) \sim 0.045$ –10 GeV; quoted limit is for $m(\chi) = 5 \text{ GeV}$.
- KOBAYASHI 19 search for sub-GeV WIMP annual modulation in Xe via brems; no signal; limits placed in $\sigma^{SI}(\chi N)$ vs. $m(\chi)$ plane for $m \sim 0.3$ –1 GeV; quoted limit is for $m(\chi) = 0.5 \text{ GeV}$.
- LIU 19B search for sub-GeV DM using Migdal effect on Ge at CDEX-IB; no signal, require $\sigma^{SI}(\chi M) < 7 \times 10^2$ pb for $m(\chi) = 0.1 \text{ GeV}$.
- AGNES 18 search for 1.8–20 GeV WIMP SI scatter on Ar; quoted limit is for $m(\chi) = 5 \text{ GeV}$.
- AGNESE 18 search for GeV scale WIMPs using CDMsLite; limits placed in $\sigma^{SI}(\chi N)$ vs. $m(\chi)$ plane for $m \sim 1.5$ –20 GeV; quoted limit is for $m(\chi) = 5 \text{ GeV}$.
- APRILE 18 search for WIMP scatter on 1 t yr Xe; no signal, limits set in $\sigma(\chi N)$ vs. $m(\chi)$ plane for $m(\chi) \sim 6$ –1000 GeV; quoted limit is for $m = 6 \text{ GeV}$.
- ARNAUD 18 search for low mass WIMP scatter on Ne via SPC at NEWS-G; limits set in $\sigma^{SI}(\chi N)$ vs. $m(\chi)$ plane for $m \sim 0.5$ –20 GeV; quoted limit is for $m = 5 \text{ GeV}$.
- JIANG 18 search for GeV scale WIMP scatter on Ge; limits placed in $\sigma^{SI}(\chi N)$ vs. $m(\chi)$ plane for $m(\chi) \sim 3$ –10 GeV; quoted limit is for $m(\chi) = 5 \text{ GeV}$.
- YANG 18 search for WIMP scatter on Ge; limits placed in $\sigma^{SI}(\chi N)$ vs. $m(\chi)$ plane for $m(\chi) \sim 2$ –10 GeV; quoted limit is for $m(\chi) = 5 \text{ GeV}$.
- AKERIB 17 search for WIMP scatter on Xe; limits placed in $\sigma^{SI}(\chi N)$ vs. $m(\chi)$ plane for $m(\chi) \sim 5$ – 1×10^5 GeV; quoted limit is for $m(\chi) = 5 \text{ GeV}$.
- ANGLOHER 17A search for GeV scale WIMP scatter on Al₂O₃ crystal; limits placed in $\sigma^{SI}(\chi N)$ vs. $m(\chi)$ plane for $m(\chi) \sim 0.15$ –10 GeV; quoted limit is for $m(\chi) = 5 \text{ GeV}$.
- ANGLOHER 16 search for GeV scale WIMP scatter on CaWO₄; limits placed in $\sigma^{SI}(\chi N)$ vs. $m(\chi)$ plane for $m(\chi) \sim 0.5$ –30 GeV; quoted limit is for $m(\chi) = 5 \text{ GeV}$.
- APRILE 16 search for low mass WIMPs via ionization at XENON100; limits placed in $\sigma^{SI}(\chi N)$ vs $m(\chi)$ plane for $m \sim 3.5$ –20 GeV; quoted limit is for $m(\chi) = 5 \text{ GeV}$.

Searches Particle Listings

WIMP and Dark Matter Searches

- 38 ARMENGAUD 16 search for GeV scale WIMP scatter on Ge; limits placed in $\sigma^{SI}(\chi N)$ vs. $m(\chi)$ plane for $m(\chi) \sim 4\text{--}30$ GeV; quoted limit is for $m(\chi) = 5$ GeV.
- 39 HEHN 16 search for low mass WIMPs via SI scatter on Ge target using profile likelihood analysis; limits placed in $\sigma^{SI}(\chi N)$ vs. $m(\chi)$ plane for $m(\chi) \sim 4\text{--}30$ GeV; quoted limit is for $m(\chi) = 5$ GeV.
- 40 ZHAO 16 search for GeV-scale WIMP scatter on Ge; limits placed in $\sigma^{SI}(\chi N)$ vs. $m(\chi)$ plane for $m(\chi) \sim 4\text{--}30$ GeV; quoted limit is for $m(\chi) = 5$ GeV.
- 41 AMOLE 15 search for WIMP scatter on C_3F_8 in PICO-2L; limits placed in $\sigma^{SI}(\chi N)$ vs. $m(\chi)$ plane for $m(\chi) \sim 4\text{--}25$ GeV; quoted limit is for $m(\chi) = 5$ GeV.
- 42 XIAO 15 search for WIMP scatter on Xe with PandaX-I; limits placed in $\sigma^{SI}(\chi N)$ vs. $m(\chi)$ plane for $m(\chi) \sim 5\text{--}100$ GeV; quoted limit is for $m(\chi) = 5$ GeV.
- 43 AGNESE 14 search for GeV scale WIMPs SI scatter at SuperCDMS; no signal, limits placed in $\sigma^{SI}(\chi N)$ vs. $m(\chi)$ plane for $m(\chi) \sim 3.5\text{--}30$ GeV; quoted limit is for $m(\chi) = 5$ GeV.
- 44 AKERIB 14 search for WIMP scatter on Xe; limits placed in $\sigma^{SI}(\chi N)$ vs. $m(\chi)$ plane for $m(\chi) \sim 3.5\text{--}5000$ GeV. Limit given for $m(\chi) = 5$ GeV.
- 45 LI 13B search for WIMP scatter on Ge; limits placed in $\sigma^{SI}(\chi N)$ vs. $m(\chi)$ plane for $m(\chi) \sim 4\text{--}100$ GeV; quoted limit is for $m(\chi) = 5$ GeV.
- 46 ARCHAMBAULT 12 search for low mass WIMP scatter on C_4F_{10} ; limits set in $\sigma^{SI}(\chi N)$ vs. $m(\chi)$ plane for $m \sim 4\text{--}12$ GeV; quoted limit is for $m = 5$ GeV.
- 47 AALSETH 11 search for GeV-scale SI WIMP scatter on Ge; limits placed on $\sigma^{SI}(\chi N)$ for $m(\chi) \sim 3.5\text{--}100$ GeV; quoted limit is for $m(\chi) = 5$ GeV.
- 48 AHMED 11B search for GeV scale WIMP scatter on Ge in CDMS II; limits placed in $\sigma^{SD}(\chi n)$ vs. $m(\chi)$ plane for $m \sim 4\text{--}12$ GeV.
- 49 ANGLE 11 search for GeV scale WIMPs in Xenon-10; limits placed in $\sigma^{SI}(\chi N)$ vs. $m(\chi)$ plane for $m(\chi) \sim 4\text{--}20$ GeV; quoted limit is for $m(\chi) = 5$ GeV.
- 50 AKERIB 10 search for WIMP scatter on Ge/Si in CDMS II; limits place in $\sigma_{SI}(\chi N)$ vs. $m(\chi)$ plane for $m \sim 3\text{--}100$ GeV. Limit given for $m(\text{DM}) = 5$ GeV.

For $m_{\chi_0} = 20$ GeV

For limits from X^0 annihilation in the Sun, the assumed annihilation final state is shown in parenthesis in the comment.

VALUE (pb)	CL%	DOCUMENT ID	TECN	COMMENT
<1 × 10 ⁻¹¹	90	1 AALBERS	23 LZ	SI scatter on Xe
<2 × 10 ⁻⁷	90	2 ABE	23E XMAS	WIMP search
<4 × 10 ⁻¹¹	90	3 APRILE	23A XENT	SI WIMP search
<5 × 10 ⁻¹¹	90	4 MENG	21B PNDX	Xe WIMP search
<5 × 10 ⁻⁵		5 FELIZARDO	20 SMPL	C ₂ F ₅
<2.2 × 10 ⁻¹⁰	90	6 WANG	20G PNDX	Xe TPC
		7 ANGLÖHER	19 CRES	CaWO ₄
<7 × 10 ⁻⁵	90	8 KIM	19A KIMS	Nal
<3 × 10 ⁻⁷	90	9 KOBAYASHI	19 XMAS	SI WIMP on Xe
		10 SEONG	19 BELL	$\tau \rightarrow \gamma A, A \rightarrow \chi\chi$
<3.5 × 10 ⁻⁵	90	11 YANG	19 CDEX	annual modulation Ge
<2 × 10 ⁻⁷	90	12 ABE	18C XMAS	X ⁰ -Xe modulation
<1.44 × 10 ⁻⁵	90	13 ADHIKARI	18 C100	Nal
<3 × 10 ⁻⁷	90	14 AGNES	18 DS50	X ⁰ -Ar
<5 × 10 ⁻⁶	95	15 AGNESE	18 SCDM	Ge
<4 × 10 ⁻⁸	90	16 AGNESE	18A SCDM	Ge
<6 × 10 ⁻¹¹	90	17 APRILE	18 XE1T	Xe, SI
<4.5 × 10 ⁻³	90	18 ARNAUD	18 NEWS	GeV WIMPs on Ne
<2 × 10 ⁻⁶	90	19 AARTSEN	17 ICCB	ν , earth
<2 × 10 ⁻¹⁰	90	20 AKERIB	17 LUX	Xe
<1 × 10 ⁻³	90	21 BARBOSA-D...	17 ICCB	Nal
<1.7 × 10 ⁻¹⁰	90	22 CUI	17A PNDX	WIMPs on Xe
<7.3 × 10 ⁻⁷	90		AGNES	16 DS50 Ar
<1 × 10 ⁻⁵	90	23 AGNESE	16 CDM2	Ge
<2 × 10 ⁻⁴	90	24 AGUILAR-AR...	16 DMIC	Si CCDs
<4.5 × 10 ⁻⁵	90	25 ANGLÖHER	16 CRES	CaWO ₄
<2 × 10 ⁻⁶	90	26 APRILE	16 X100	Xe
<9.4 × 10 ⁻⁸	90	27 ARMENGAUD	16 EDE3	Ge
<1.0 × 10 ⁻⁷	90	28 HEHN	16 EDE3	Ge
<5 × 10 ⁻⁶	90	29 ZHAO	16 CDEX	Ge
<1 × 10 ⁻⁵	90		AGNES	15 DS50 Ar
<1.5 × 10 ⁻⁶	90	30 AGNESE	15A CDM2	Ge
<1.5 × 10 ⁻⁷	90	31 AGNESE	15B CDM2	Ge
<2 × 10 ⁻⁶	90	32 AMOLE	15 PICO	C ₃ F ₈
<1.2 × 10 ⁻⁵	90		CHOI	15 SKAM H, solar ν ($b\bar{b}$)
<1.19 × 10 ⁻⁶	90		CHOI	15 SKAM H, solar ν ($\tau^+\tau^-$)
<2 × 10 ⁻⁸	90	33 XIAO	15 PNDX	Xe
<2.0 × 10 ⁻⁷	90	34 AGNESE	14 SCDM	Ge
<3.7 × 10 ⁻⁵	90	35 AGNESE	14A SCDM	Ge
<1 × 10 ⁻⁹	90	36 AKERIB	14 LUX	Xe
<2 × 10 ⁻⁶	90	37 ANGLÖHER	14 CRES	CaWO ₄
<5 × 10 ⁻⁶	90		FELIZARDO	14 SMPL C ₂ F ₅
<8 × 10 ⁻⁶	90	38 LEE	14A KIMS	Csl
<2 × 10 ⁻⁴	90	39 LIU	14A CDEX	Ge
<1 × 10 ⁻⁵	90	40 YUE	14 CDEX	Ge
<1.08 × 10 ⁻⁴	90	41 AARTSEN	13 ICCB	H, solar ν ($\tau^+\tau^-$)
<1.5 × 10 ⁻⁵	90	42 ABE	13B XMAS	Xe
<3.1 × 10 ⁻⁶	90	43 AGNESE	13 CDM2	Si
<3.4 × 10 ⁻⁶	90	44 AGNESE	13A CDM2	Si
<2.2 × 10 ⁻⁶	90	45 AGNESE	13A CDM2	Si
		46 BERNABEI	13A DAMA	Nal modulation
<1.2 × 10 ⁻⁴	90	47 LI	13B TEXO	Ge

<1.2 × 10 ⁻⁷	90	48 ZHAO	13 CDEX	Ge
			AKIMOV	12 ZEP3 Xe
		49 ANGLÖHER	12 CRES	CaWO ₄
<8 × 10 ⁻⁶	90	50 ANGLÖHER	12 CRES	CaWO ₄
<7 × 10 ⁻⁹	90	51 APRILE	12 X100	Xe
<7 × 10 ⁻⁷	90	52 ARMENGAUD	12 EDE2	Ge
		53 BARRETO	12 DMIC	CCD
<2 × 10 ⁻⁶	90		BEHNKE	12 COUP CF ₃ I
<7 × 10 ⁻⁶		54 FELIZARDO	12 SMPL	C ₂ F ₅
<1.5 × 10 ⁻⁶	90		KIM	12 KIMS Csl
<5 × 10 ⁻⁵	90	55 AALSETH	11 CGNT	Ge
		56 AALSETH	11A CGNT	Ge
<5 × 10 ⁻⁷	90	57 AHMED	11 CDM2	Ge, inelastic
<2.7 × 10 ⁻⁷	90	58 AHMED	11A RVUE	Ge
<3 × 10 ⁻⁶	90	59 ANGLE	11 XE10	Xe
<7 × 10 ⁻⁸	90	60 APRILE	11 X100	Xe
		61 APRILE	11A X100	Xe, inelastic
<2 × 10 ⁻⁸	90	51 APRILE	11B X100	Xe
		62 HORN	11 ZEP3	Xe
<2 × 10 ⁻⁷	90		AHMED	10 CDM2
<1 × 10 ⁻⁵	90	63 AKERIB	10 CDM2	Si, Ge, low threshold
<1 × 10 ⁻⁷	90		APRILE	10 X100
<2 × 10 ⁻⁶	90		ARMENGAUD	10 EDE2
<4 × 10 ⁻⁵	90		FELIZARDO	10 SMPL C ₂ F ₅
<1.5 × 10 ⁻⁷	90	64 AHMED	09 CDM2	Ge
<2 × 10 ⁻⁴	90	65 LIN	09 TEXO	Ge
		66 AALSETH	08 CGNT	Ge

- 1 AALBERS 23 present first limits for WIMP scatter on Xe. $\sigma^{SI}(\chi p) < 1 \times 10^{-11}$ pb for $m(\chi) = 20$ GeV.
- 2 ABE 23E search for WIMP scatter on Xe in XMAS. No signal observed. Require $\sigma^{SI} < 2 \times 10^{-7}$ pb for $m(\chi) = 20$ GeV.
- 3 APRILE 23A present first results from Xe-nton SI WIMP search. No signal observed. Quoted limit is for $m(\chi) = 20$ GeV.
- 4 MENG 21B search for SI WIMP interaction with 3.7 t Xe and 0.63 t yr exposure. No signal observed. Limits placed in $m(\text{DM})$ vs. σ^{SI} plane.
- 5 FELIZARDO 20 presents 2014 SIMPLE bounds on WIMP DM using C₂F₅ target.
- 6 WANG 20G search for SI WIMP scatter on Xe with 132 t d exposure of PANDAX-II.
- 7 ANGLÖHER 19 search for low mass WIMP scatter on CaWO₄; no signal; limits placed on Wilson coefficients for $m(\chi) = 0.6\text{--}60$ GeV.
- 8 KIM 19A search for WIMP scatter in Nal KIMS experiment; no signal; require $\sigma^{SI}(\chi n) < 7 \times 10^{-5}$ pb for $m(\chi) = 20$ GeV.
- 9 KOBAYASHI 19 search for WIMP scatter in XMAS single-phase liquid Xe detector; no signal; require $\sigma^{SI}(\chi N) < 3 \times 10^{-7}$ pb for $m(\chi) = 20$ GeV.
- 10 SEONG 19 search for $\tau \rightarrow \gamma A, A \rightarrow \chi\chi$ via CP-odd Higgs; no signal; limits on BF set; model dependent conversion to WIMP-nucleon scattering cross section limits $\sigma^{SI} < 10^{-36}$ cm² for $m(\chi) = 0.01\text{--}1$ GeV.
- 11 YANG 19 search for low mass wimps via annual modulation in Ge; no signal; require $\sigma^{SI}(\chi N) < 3.5 \times 10^{-5}$ pb for $m(\chi) = 20$ GeV.
- 12 ABE 18C search for WIMP annual modulation signal for $m(\text{WIMP})$: 6–20 GeV; limits set on SI WIMP-nucleon cross section: see Fig. 6.
- 13 ADHIKARI 18 search for WIMP scatter on Nal; no signal; require $\sigma^{SI} < 1.44 \times 10^{-5}$ pb for $m(\text{WIMP}) = 20$ GeV; inconsistent with DAMA/LIBRA result.
- 14 AGNES 18 search low mass $m(\text{WIMP})$: 1.8–20 GeV scatter on Ar; limits on SI WIMP-nucleon cross section set in Fig. 8.
- 15 AGNESE 18 give limits for $\sigma^{SI}(\chi N)$ for $m(\text{WIMP})$ between 1.5 and 20 GeV using CDMSlite mode data.
- 16 AGNESE 18A search for WIMP scatter on Ge at SuperCDMS; 1 event, consistent with expected background; set limit in $\sigma^{SI}(\chi N)$ vs. $m(\chi)$ plane for $m \sim 10\text{--}250$ GeV.
- 17 APRILE 18 search for WIMP scatter on 1 t yr Xe; no signal, limits placed in $\sigma^{SI}(\chi N)$ vs. $m(\chi)$ plane for $m(\chi) \sim 6\text{--}1000$ GeV.
- 18 ARNAUD 18 search for low mass WIMP scatter on Ne via SPC at NEWS-G; limits set in $\sigma^{SI}(\chi N)$ vs. $m(\chi)$ plane for $m \sim 0.5\text{--}20$ GeV.
- 19 AARTSEN 17 obtain $\sigma(\text{SI}) < 6 \times 10^{-6}$ pb for $m(\text{wimp}) = 20$ GeV from ν from earth.
- 20 AKERIB 17 search for WIMP scatter on Xe; limits placed in $\sigma^{SI}(\chi N)$ vs. $m(\chi)$ plane for $m(\chi) \sim 5\text{--}1 \times 10^5$ GeV.
- 21 BARBOSA-DE-SOUZA 17 search for annual modulation of WIMP scatter on Nal using an exposure of 61 kg yr of DM-Ice17 for recoil energy in the 4–20 keV range (DAMA found modulation for recoil energy < 5 keV). No modulation seen. Sensitivity insufficient to distinguish DAMA signal from null.
- 22 CUI 17A search for SI WIMP scatter; limits placed in $\sigma^{SI}(\chi N)$ vs. $m(\chi)$ plane for $m \sim 10\text{--}1 \times 10^4$ GeV using 54 ton-day exposure of Xe.
- 23 AGNESE 16 CDMSlite excludes low mass WIMPs 1.6–5.5 GeV and SI scattering cross section depending on $m(\text{WIMP})$; see Fig. 4.
- 24 AGUILAR-AREVALO 16 search low mass 1–10 GeV WIMP scatter on Si CCDs; set limits Fig. 11.
- 25 ANGLÖHER 16 search for GeV scale WIMP scatter on CaWO₄; limits placed in $\sigma^{SI}(\chi N)$ vs. $m(\chi)$ plane for $m(\chi) \sim 0.5\text{--}30$ GeV.
- 26 APRILE 16 search for low mass WIMPs via ionization at XENON100; limits placed in $\sigma^{SI}(\chi N)$ vs. $m(\chi)$ plane for $m \sim 3.5\text{--}20$ GeV.
- 27 ARMENGAUD 16 search for GeV scale WIMP scatter on Ge; limits placed in $\sigma^{SI}(\chi N)$ vs. $m(\chi)$ plane for $m(\chi) \sim 4\text{--}30$ GeV.
- 28 HEHN 16 search for low mass WIMPs via SI scatter on Ge target using profile likelihood analysis; limits placed in $\sigma^{SI}(\chi N)$ vs. $m(\chi)$ plane for $m(\chi) \sim 4\text{--}30$ GeV.
- 29 ZHAO 16 search for GeV-scale WIMP scatter on Ge; limits placed in $\sigma^{SI}(\chi N)$ vs. $m(\chi)$ plane for $m(\chi) \sim 4\text{--}30$ GeV.
- 30 AGNESE 15A reanalyse AHMED 11B low threshold data. See their Fig. 12 (left) for improved limits extending down to 5 GeV.
- 31 AGNESE 15B reanalyse AHMED 10 data.

See key on page 1171

Searches Particle Listings

WIMP and Dark Matter Searches

- 32 See their Fig. 7 for limits extending down to 4 GeV.
- 33 XIAO 15 search for WIMP scatter on Xe with PandaX-I; limits placed in $\sigma^{SI}(\chi N)$ vs. $m(\chi)$ plane for $m(\chi) \sim 5\text{--}100$ GeV.
- 34 This limit value is provided by the authors. See their Fig. 4 for limits extending down to $m_{\chi^0} = 3.5$ GeV.
- 35 This limit value is provided by the authors. AGNESE 14A result is from CDMSlite mode operation with enhanced sensitivity to low mass m_{χ^0} . See their Fig. 3 for limits extending down to $m_{\chi^0} = 3.5$ GeV (see also Fig. 4 in AGNESE 14).
- 36 See their Fig. 5 for limits extending down to $m_{\chi^0} = 5.5$ GeV.
- 37 See their Fig. 5 for limits extending down to $m_{\chi^0} = 1$ GeV.
- 38 See their Fig. 5 for limits extending down to $m_{\chi^0} = 5$ GeV.
- 39 LIU 14A result is based on prototype CDEX-0 detector. See their Fig. 13 for limits extending down to $m_{\chi^0} = 2$ GeV.
- 40 See their Fig. 4 for limits extending down to $m_{\chi^0} = 4.5$ GeV.
- 41 AARTSEN 13 search for neutrinos from the Sun arising from the pair annihilation of X^0 trapped by the sun in data taken between June 2010 and May 2011.
- 42 See their Fig. 8 for limits extending down to $m_{\chi^0} = 7$ GeV.
- 43 This limit value is provided by the authors. AGNESE 13 use data taken between Oct. 2006 and July 2007. See their Fig. 4 for limits extending down to $m_{\chi^0} = 7$ GeV.
- 44 This limit value is provided by the authors. AGNESE 13A use data taken between July 2007 and Sep. 2008. Three candidate events are seen. Assuming these events are real, the best fit parameters are $m_{\chi^0} = 8.6$ GeV and $\sigma = 1.9 \times 10^{-5}$ pb.
- 45 This limit value is provided by the authors. Limit from combined data of AGNESE 13 and AGNESE 13A. See their Fig. 4 for limits extending down to $m_{\chi^0} = 5.5$ GeV.
- 46 BERNABEI 13A search for annual modulation of counting rate in the 2–6 keV recoil energy interval, in a 14 yr live time exposure of 1.33 t yr. Find a modulation of 0.0112 ± 0.0012 counts/(day kg keV) with 9.3 sigma C.L. Find period and phase in agreement with expectations from DM particles.
- 47 LI 13b search for WIMP scatter on Ge; limits placed in $\sigma^{SI}(\chi N)$ vs. $m(\chi)$ plane for $m(\chi) \sim 4\text{--}100$ GeV.
- 48 See their Fig. 5 for limits for $m_{\chi^0} = 4\text{--}12$ GeV.
- 49 ANGLÖHER 12 observe excess events above the expected background which are consistent with X^0 with mass ~ 25 GeV (or 12 GeV) and spin-independent X^0 -nucleon cross section of 2×10^{-6} pb (or 4×10^{-5} pb).
- 50 Reanalysis of ANGLÖHER 09 data with all three nuclides. See also BROWN 12.
- 51 See also APRILE 14A.
- 52 See their Fig. 4 for limits extending down to $m_{\chi^0} = 7$ GeV.
- 53 See their Fig. 13 for cross section limits for m_{χ^0} between 1.2 and 10 GeV.
- 54 See also DAHL 12 for a criticism.
- 55 See their Fig. 4 for limits extending to $m_{\chi^0} = 3.5$ GeV.
- 56 AALSETH 11A find indications of annual modulation of the data, the energy spectrum being compatible with X^0 mass around 8 GeV. See also AALSETH 13.
- 57 AHMED 11 search for X^0 inelastic scattering. See their Fig. 8–10 for limits. The inelastic cross section reduces to the elastic cross section at the limit of zero mass splitting (Fig. 8, left).
- 58 AHMED 11A combine CDMS II and EDELWEISS data.
- 59 ANGLE 11 show limits down to $m_{\chi^0} = 4$ GeV on Fig. 3.
- 60 APRILE 11 reanalyze APRILE 10 data.
- 61 APRILE 11A search for X^0 inelastic scattering. See their Fig. 2 and 3 for limits. See also APRILE 14A.
- 62 HORN 11 perform detector calibration by neutrons. Earlier results are only marginally affected.
- 63 See their Fig. 10 and 12 for limits extending to X^0 mass of 1 GeV.
- 64 Superseded by AHMED 10.
- 65 See their Fig. 6(a) for cross section limits for m_{χ^0} extending down to 2 GeV.
- 66 See their Fig. 2 for cross section limits for m_{χ^0} between 4 and 10 GeV.

For $m_{\chi^0} = 100$ GeV

For limits from X^0 annihilation in the Sun, the assumed annihilation final state is shown in parenthesis in the comment.

VALUE (pb)	CL%	DOCUMENT ID	TECN	COMMENT
$<2.5 \times 10^{-11}$	90	1 AALBERS	23 LZ	SI scatter on Xe
$<2 \times 10^{-8}$	90	2 ABE	23E XMAS	WIMP search
$<6 \times 10^{-11}$	90	3 APRILE	23A XENT	SI WIMP search
$<6 \times 10^{-11}$	90	4 MENG	21B PNDX	Xe WIMP search
$<5 \times 10^{-5}$		5 ADHIKARI	20 DEAP	Ar
$<4.2 \times 10^{-10}$	90	6 FELIZARDO	20 SMPL	W
$<4 \times 10^{-8}$	90	7 WANG	20G PNDX	Xe TPC
$<3.9 \times 10^{-9}$	90	8 ABE	19 XMAS	Xe
$<2.3 \times 10^{-6}$	90	9 AJAJ	19 DEAP	Ar
$<1.14 \times 10^{-8}$	90	10 ADHIKARI	18 C100	Nal
$<2 \times 10^{-8}$	90	11 AGNES	18A DS50	Ar
$<1.2 \times 10^{-8}$	90	12 AGNESE	18A CDMS	Ge
$<9.12 \times 10^{-11}$	90	13 AMAUDRUZ	18 DEAP	Ar
		14 APRILE	18 XE1T	Xe
		15 REN	18 PNDX	SIDM at PDX-II
$<1.7 \times 10^{-10}$	90	16 AKERIB	17 LUX	Xe
$<1.2 \times 10^{-10}$	90	17 APRILE	17G XE1T	Xe
$<1.2 \times 10^{-10}$	90	18 CUI	17A PNDX	Xe
$<2.0 \times 10^{-8}$	90	19 AGNES	16 DS50	Ar
$<1 \times 10^{-9}$	90	20 AKERIB	16 LUX	Xe
$<1 \times 10^{-9}$	90	21 APRILE	16B X100	Xe
$<2 \times 10^{-8}$	90	22 TAN	16 PNDX	Xe
$<4 \times 10^{-10}$	90	23 TAN	16B PNDX	Xe
$<6 \times 10^{-8}$	90	24 AGNES	15 DS50	Ar

$<4 \times 10^{-8}$	90	23 AGNESE	15B CDM2	Ge
$<7.13 \times 10^{-6}$	90	24 CHOI	15 SKAM	H, solar ν ($b\bar{b}$)
$<6.26 \times 10^{-7}$	90	25 CHOI	15 SKAM	H, solar ν ($W^+ W^-$)
$<2.76 \times 10^{-7}$	90	26 CHOI	15 SKAM	H, solar ν ($\tau^+ \tau^-$)
$<1.5 \times 10^{-8}$	90	27 XIAO	15 PNDX	Xe
$<1 \times 10^{-9}$	90	28 AKERIB	14 LUX	Xe
$<4.0 \times 10^{-6}$	90	29 AVORIN	14 BAIK	H, solar ν ($W^+ W^-$)
$<1.0 \times 10^{-4}$	90	30 AVORIN	14 BAIK	H, solar ν ($b\bar{b}$)
$<1.6 \times 10^{-6}$	90	31 AVORIN	14 BAIK	H, solar ν ($\tau^+ \tau^-$)
$<5 \times 10^{-6}$	90	32 FELIZARDO	14 SMPL	C_2ClF_5
$<6.01 \times 10^{-7}$	90	33 AARTSEN	13 ICCB	H, solar ν ($W^+ W^-$)
$<3.30 \times 10^{-5}$	90	34 AARTSEN	13 ICCB	H, solar ν ($b\bar{b}$)
$<1.9 \times 10^{-6}$	90	35 ADRIAN-MAR.13	13 ANTR	H, solar ν ($W^+ W^-$)
$<1.2 \times 10^{-4}$	90	36 ADRIAN-MAR.13	13 ANTR	H, solar ν ($b\bar{b}$)
$<7.6 \times 10^{-7}$	90	37 ADRIAN-MAR.13	13 ANTR	H, solar ν ($\tau^+ \tau^-$)
$<2 \times 10^{-6}$	90	38 AGNESE	13 CDM2	Si
$<1.6 \times 10^{-6}$	90	39 BOLIEV	13 BAKS	H, solar ν ($W^+ W^-$)
$<1.9 \times 10^{-5}$	90	40 BOLIEV	13 BAKS	H, solar ν ($b\bar{b}$)
$<7.1 \times 10^{-7}$	90	41 BOLIEV	13 BAKS	H, solar ν ($\tau^+ \tau^-$)
$<3.2 \times 10^{-4}$	90	42 LI	13B TEXO	WIMPs on Ge
$<1.67 \times 10^{-6}$	90	43 ABBASI	12 ICCB	H, solar ν ($W^+ W^-$)
$<1.07 \times 10^{-4}$	90	44 ABBASI	12 ICCB	H, solar ν ($b\bar{b}$)
$<4 \times 10^{-8}$	90	45 AKIMOV	12 ZEP3	Xe
$<1.4 \times 10^{-6}$	90	46 ANGLÖHER	12 CRES	CaWO ₄
$<3 \times 10^{-9}$	90	47 APRILE	12 X100	Xe
$<3 \times 10^{-7}$	90	48 BEHNKE	12 COUP	Cf ₃ I
$<7 \times 10^{-6}$	90	49 FELIZARDO	12 SMPL	C_2ClF_5
$<2.5 \times 10^{-7}$	90	50 KIM	12 KIMS	Csl
$<2 \times 10^{-4}$	90	51 AALSETH	11 CGNT	Ge
$<3.3 \times 10^{-8}$	90	52 AHMED	11 CDM2	Ge, inelastic
		53 AHMED	11A RVUE	Ge
		54 AJELLO	11 FLAT	
		55 APRILE	11 X100	Xe
		56 APRILE	11A X100	Xe, inelastic
$<1 \times 10^{-8}$	90	57 APRILE	11B X100	Xe
$<5 \times 10^{-8}$	90	58 ARMENGAUD	11 EDE2	Ge
		59 HORN	11 ZEP3	Xe
$<4 \times 10^{-8}$	90	60 AHMED	10 CDM2	Ge
$<9 \times 10^{-6}$	90	61 AKERIB	10 CDM2	Si, Ge, low threshold
		62 AKIMOV	10 ZEP3	Xe, inelastic
$<5 \times 10^{-8}$	90	63 APRILE	10 X100	Xe
$<1 \times 10^{-7}$	90	64 ARMENGAUD	10 EDE2	Ge
$<3 \times 10^{-5}$	90	65 FELIZARDO	10 SMPL	C_2ClF_5
$<5 \times 10^{-8}$	90	66 AHMED	09 CDM2	Ge
		67 ANGLE	09 XE10	Xe, inelastic
$<3 \times 10^{-4}$	90	68 LIN	09 TEXO	Ge
		69 GIULIANI	05 RVUE	

- 1 AALBERS 23 present first LZ limits on SI WIMP-nucleon scatter from Xe. $\sigma^{SI}(\chi p) < 2.5 \times 10^{-11}$ pb for $m(\chi) = 100$ GeV.
- 2 ABE 23E search for WIMP scatter on Xe in XMAS. No signal observed. Require $\sigma^{SI} < 2 \times 10^{-7}$ pb for $m(\chi) = 100$ GeV.
- 3 APRILE 23A present first results from Xe-nton SI WIMP search. No signal observed. Quoted limit is for $m(\chi) = 100$ GeV.
- 4 MENG 21B search for SI WIMP interaction with 3.7 t Xe and 0.63 t yr exposure. No signal observed. Limits placed in $m(\text{DM})$ vs. σ^{SI} plane.
- 5 ADHIKARI 20 search for SI WIMP scatter from Ar in AJAJ 19 data. No signal observed. Limits placed on σ^p vs. $m(\text{WIMP})$ for various assumed operators and models.
- 6 FELIZARDO 20 presents 2014 SIMPLE bounds on WIMP DM using C_2ClF_5 target.
- 7 WANG 20G search for SI WIMP scatter on Xe with 132 t d exposure of PANDAX-II.
- 8 ABE 19 search for SI-DD in single phase Xe; no signal; require $\sigma^{SI}(\chi p) < 4 \times 10^{-8}$ pb for $m(\chi) \sim 100$ GeV.
- 9 AJAJ 19 search for SI WIMP-nucleon scatter with 758 tonne day exposure of single phase liquid Ar; no signal; require $\sigma^{SI}(\chi N) < 3.9 \times 10^{-9}$ pb for $m(\chi) = 100$ GeV.
- 10 ADHIKARI 18 search for WIMP scatter on NaI; limit set $\sigma^{SI}(\chi p) < 2.3 \times 10^{-6}$ pb for $m(\chi) = 100$ GeV.
- 11 AGNES 18A search for WIMP scatter on 46.4 kg Ar; no signal; require $\sigma^{SI}(\chi N) < 1.14 \times 10^{-8}$ pb for $m(\chi) = 100$ GeV.
- 12 AGNESE 18A set limit $\sigma^{SI}(\chi N) < 2 \times 10^{-8}$ pb for $m(\text{WIMP}) = 100$ GeV.
- 13 AMAUDRUZ 18 search for WIMP scatter on Ar with DEAP-3600; limits set: $\sigma^{SI}(\chi p) < 1.2 \times 10^{-8}$ pb for $m(\text{WIMP}) = 100$ GeV.
- 14 APRILE 18 search for WIMP scatter on 1.3 t liquid Xe; no signal; require $\sigma^{SI}(\chi p) < 9.12 \times 10^{-11}$ pb for $m(\chi) = 100$ GeV.
- 15 REN 18 search for self-interacting DM at PandaX-II with a total exposure of 54 ton day; limits set in $m(\text{DM})$ vs. $m(\text{mediator})$ plane.
- 16 AKERIB 17 exclude SI cross section $> 1.7 \times 10^{-10}$ pb for $m(\text{WIMP}) = 100$ GeV. Uses complete LUX data set.
- 17 APRILE 17G set limit $\sigma^{SI}(\chi p) < 1.2 \times 10^{-10}$ pb for $m(\text{WIMP}) = 100$ GeV using 1 ton fiducial mass Xe TPC. Exposure is 34.2 live days.
- 18 CUI 17A search for SI WIMP scatter; limits placed in $\sigma^{SI}(\chi N)$ vs. $m(\chi)$ plane for $m \sim 10\text{--}1 \times 10^4$ GeV using 54 ton-day exposure of Xe.
- 19 AKERIB 16 re-analysis of 2013 data exclude SI cross section $> 1 \times 10^{-9}$ pb for $m(\text{WIMP}) = 100$ GeV on Xe target.
- 20 APRILE 16B combined 447 live days using Xe target exclude $\sigma(\text{SI}) > 1.1 \times 10^{-9}$ pb for $m(\text{WIMP}) = 50$ GeV.
- 21 TAN 16 search for WIMP scatter off Xe target; see SI exclusion plot Fig. 6.
- 22 TAN 16B search for WIMP-p scatter off Xe target; see Fig. 5 for SI exclusion.

Searches Particle Listings

WIMP and Dark Matter Searches

- ²³ AGNESE 15B reanalyse AHMED 10 data.
- ²⁴ XIAO 15 search for WIMP scatter on Xe with PandaX-I; limits placed in $\sigma^{SI}(\chi N)$ vs. $m(\chi)$ plane for $m(\chi) \sim 5\text{--}100$ GeV.
- ²⁵ AVRORIN 14 search for neutrinos from the Sun arising from the pair annihilation of X^0 trapped by the Sun in data taken between 1998 and 2003. See their Table 1 for limits assuming annihilation into neutrino pairs.
- ²⁶ AARTSEN 13 search for neutrinos from the Sun arising from the pair annihilation of X^0 trapped by the sun in data taken between June 2010 and May 2011.
- ²⁷ ADRIAN-MARTINEZ 13 search for neutrinos from the Sun arising from the pair annihilation of X^0 trapped by the sun in data taken between Jan. 2007 and Dec. 2008.
- ²⁸ AGNESE 13 use data taken between Oct. 2006 and July 2007.
- ²⁹ BOLIEV 13 search for neutrinos from the Sun arising from the pair annihilation of X^0 trapped by the sun in data taken from 1978 to 2009. See also SUVOROVA 13 for an older analysis of the same data.
- ³⁰ LI 13B search for WIMP scatter on Ge; limits placed in $\sigma^{SI}(\chi N)$ vs. $m(\chi)$ plane for $m(\chi) \sim 4\text{--}100$ GeV.
- ³¹ ABBASI 12 search for neutrinos from the Sun arising from the pair annihilation of X^0 trapped by the Sun. The amount of X^0 depends on the X^0 -proton cross section.
- ³² Reanalysis of ANGIOHER 09 data with all three nuclides. See also BROWN 12.
- ³³ See also APRILE 14A.
- ³⁴ See their Fig. 6 for a limit on inelastically scattering X^0 for $m_{X^0} = 70$ GeV.
- ³⁵ AHMED 11 search for X^0 inelastic scattering. See their Fig. 8–10 for limits.
- ³⁶ AHMED 11A combine CDMS and EDELWEISS data.
- ³⁷ AJELLO 11 search for e^\pm flux from X^0 annihilations in the Sun. Models in which X^0 annihilates into an intermediate long-lived weakly interacting particles or X^0 scatter inelastically are constrained. See their Fig. 6–8 for limits.
- ³⁸ APRILE 11 reanalyse APRILE 10 data.
- ³⁹ APRILE 11A search for X^0 inelastic scattering. See their Fig. 2 and 3 for limits. See also APRILE 14A.
- ⁴⁰ Supersedes ARMENGAUD 10. A limit on inelastic cross section is also given.
- ⁴¹ HORN 11 perform detector calibration by neutrons. Earlier results are only marginally affected.
- ⁴² AKIMOV 10 give cross section limits for inelastically scattering dark matter. See their Fig. 4.
- ⁴³ Superseded by AHMED 10.
- ⁴⁴ ANGIOHER 09 search for X^0 inelastic scattering. See their Fig. 4 for limits.
- ⁴⁵ GIULIANI 05 analyzes the spin-independent X^0 -nucleon cross section limits with both isoscalar and isovector couplings. See their Fig. 3 and 4 for limits on the couplings.

For $m_{X^0} = 1$ TeV

For limits from X^0 annihilation in the Sun, the assumed annihilation final state is shown in parenthesis in the comment.

VALUE (pb)	CL%	DOCUMENT ID	TECN	COMMENT
••• We do not use the following data for averages, fits, limits, etc. •••				
$< 2.8 \times 10^{-10}$	90	1 AALBERS	23 LZ	SI scatter on Xe
$< 1 \times 10^{-7}$	90	2 ABE	23E XMAS	WIMP search
$< 5 \times 10^{-10}$	90	3 MENG	21B PNDX	Xe WIMP search
		4 ADHIKARI	20 DEAP	Ar
$< 4 \times 10^{-9}$	90	5 WANG	20G PNDX	Xe TPC
$< 3 \times 10^{-6}$	90	6 YAGUNA	19 Ar;	l-spin viol DM
$< 3.8 \times 10^{-8}$	90	7 AGNES	18A DS50	Ar
$< 8.24 \times 10^{-10}$	90	8 APRILE	18 XE1T	Xe
$< 2 \times 10^{-9}$	90	9 AKERIB	17 LUX	Xe
< 0.3	90	10 CHEN	17E PNDX	$\chi N \rightarrow \chi^* \rightarrow \chi \gamma$
$< 1.2 \times 10^{-9}$	90	11 CUI	17A PNDX	SI WIMPs on Xe
$< 8.6 \times 10^{-8}$	90	AGNES	16 DS50	Ar
$< 2 \times 10^{-7}$	90	AGNES	15 DS50	Ar
$< 2 \times 10^{-7}$	90	12 AGNESE	15B CDM2	Ge
$< 1 \times 10^{-8}$	90	AKERIB	14 LUX	Xe
$< 2.2 \times 10^{-6}$	90	13 AVRORIN	14 BAIK	H, solar ν ($W^+ W^-$)
$< 5.5 \times 10^{-5}$	90	13 AVRORIN	14 BAIK	H, solar ν ($b\bar{b}$)
$< 6.8 \times 10^{-7}$	90	13 AVRORIN	14 BAIK	H, solar ν ($\tau^+ \tau^-$)
$< 3.46 \times 10^{-7}$	90	14 AARTSEN	13 ICCB	H, solar ν ($W^+ W^-$)
$< 7.75 \times 10^{-6}$	90	14 AARTSEN	13 ICCB	H, solar ν ($b\bar{b}$)
$< 6.9 \times 10^{-7}$	90	15 ADRIAN-MAR..13	ANTR	H, solar ν ($W^+ W^-$)
$< 1.5 \times 10^{-5}$	90	15 ADRIAN-MAR..13	ANTR	H, solar ν ($b\bar{b}$)
$< 1.8 \times 10^{-7}$	90	15 ADRIAN-MAR..13	ANTR	H, solar ν ($\tau^+ \tau^-$)
$< 4.3 \times 10^{-6}$	90	16 BOLIEV	13 BAKS	H, solar ν ($W^+ W^-$)
$< 3.4 \times 10^{-5}$	90	16 BOLIEV	13 BAKS	H, solar ν ($b\bar{b}$)
$< 1.2 \times 10^{-6}$	90	16 BOLIEV	13 BAKS	H, solar ν ($\tau^+ \tau^-$)
$< 2.12 \times 10^{-7}$	90	17 ABBASI	12 ICCB	H, solar ν ($W^+ W^-$)
$< 6.56 \times 10^{-6}$	90	17 ABBASI	12 ICCB	H, solar ν ($b\bar{b}$)
$< 4 \times 10^{-7}$	90	AKIMOV	12 ZEP3	Xe
$< 1.1 \times 10^{-5}$	90	18 ANGIOHER	12 CRES	CaWO ₄
$< 2 \times 10^{-8}$	90	19 APRILE	12 X100	Xe
$< 2 \times 10^{-6}$	90	BEHNKE	12 COUP	CF ₃ I
$< 4 \times 10^{-6}$	90	FELIZARDO	12 SMPL	C ₂ ClF ₅
$< 1.5 \times 10^{-6}$	90	KIM	12 KIMS	Csl
		20 AHMED	11 CDM2	Ge, inelastic
$< 1.5 \times 10^{-7}$	90	21 AHMED	11A RVUE	Ge
$< 2 \times 10^{-7}$	90	22 APRILE	11 X100	Xe
$< 8 \times 10^{-8}$	90	19 APRILE	11B X100	Xe
$< 2 \times 10^{-7}$	90	23 ARMENGAUD	11 EDE2	Ge
		24 HORN	11 ZEP3	Xe
		AHMED	10 CDM2	Ge
$< 4 \times 10^{-7}$	90	APRILE	10 X100	Xe
$< 6 \times 10^{-7}$	90	ARMENGAUD	10 EDE2	Ge
$< 3.5 \times 10^{-7}$	90	25 AHMED	09 CDM2	Ge

¹ AALBERS 23 give first LZ limits on WIMP-nucleon scatter from Xe. $\sigma^{SI} < 2.8 \times 10^{-10}$ pb for $m(\chi) = 1$ TeV.

- ² ABE 23E search for WIMP scatter on Xe in XMASS. No signal observed. Require $\sigma^{SI} < 2 \times 10^{-7}$ pb for $m(\chi) = 1000$ GeV.
- ³ MENG 21B search for SI WIMP interaction with 3.7 t Xe and 0.63 t yr exposure. No signal observed. Limits placed in $m(\text{DM})$ vs. σ^{SI} plane.
- ⁴ ADHIKARI 20 search for SI WIMP scatter from Ar in AJAJ 19 data. No signal observed. Limits placed on σ^p vs. $m(\text{WIMP})$ for various assumed operators and models.
- ⁵ WANG 20G search for SI WIMP scatter on Xe with 132 t d exposure of PANDAX-II.
- ⁶ YAGUNA 19 recasts DEAP-3600 single-phase liquid argon results in limit for isospin violating DM; for $f_n/f_p = -0.69$, requires $\sigma^{SI}(\chi p) < 3 \times 10^{-6}$ pb for $m(\chi) = 1$ TeV.
- ⁷ AGNES 18A search for WIMP scatter on 46.4 kg Ar; no signal; require $\sigma^{SI}(\chi N) < 3.8 \times 10^{-8}$ pb for $m(\chi) = 1$ TeV.
- ⁸ APRILE 18 search for WIMP scatter on 1.3 t Xe; no signal seen; require $\sigma^{SI}(\chi p) < 8.24 \times 10^{-10}$ pb for $m(\chi) = 1$ TeV.
- ⁹ AKERIB 17 search for WIMP scatter on Xe using complete LUX data set; limits placed in $\sigma^{SI}(\chi N)$ vs. $m(\chi)$ plane for $m(\chi) \sim 5\text{--}1 \times 10^5$ GeV.
- ¹⁰ CHEN 17E search for inelastic WIMP scatter on Xe; require $\sigma^{SI}(\chi N) < 0.3$ pb for $m(\chi) = 1$ TeV and (mass difference) = 300 keV.
- ¹¹ CUI 17A search for WIMP scatter using 54 ton-day exposure of Xe; limits placed in $\sigma^{SI}(\chi N)$ vs. $m(\chi)$ plane for $m \sim 10\text{--}1 \times 10^4$ GeV.
- ¹² AGNESE 15B reanalyse AHMED 10 data.
- ¹³ AVRORIN 14 search for neutrinos from the Sun arising from the pair annihilation of X^0 trapped by the Sun in data taken between 1998 and 2003. See their Table 1 for limits assuming annihilation into neutrino pairs.
- ¹⁴ AARTSEN 13 search for neutrinos from the Sun arising from the pair annihilation of X^0 trapped by the sun in data taken between June 2010 and May 2011.
- ¹⁵ ADRIAN-MARTINEZ 13 search for neutrinos from the Sun arising from the pair annihilation of X^0 trapped by the sun in data taken between Jan. 2007 and Dec. 2008.
- ¹⁶ BOLIEV 13 search for neutrinos from the Sun arising from the pair annihilation of X^0 trapped by the sun in data taken from 1978 to 2009. See also SUVOROVA 13 for an older analysis of the same data.
- ¹⁷ ABBASI 12 search for neutrinos from the Sun arising from the pair annihilation of X^0 trapped by the Sun. The amount of X^0 depends on the X^0 -proton cross section.
- ¹⁸ Reanalysis of ANGIOHER 09 data with all three nuclides. See also BROWN 12.
- ¹⁹ See also APRILE 14A.
- ²⁰ AHMED 11 search for X^0 inelastic scattering. See their Fig. 8–10 for limits.
- ²¹ AHMED 11A combine CDMS and EDELWEISS data.
- ²² APRILE 11 reanalyse APRILE 10 data.
- ²³ Supersedes ARMENGAUD 10. A limit on inelastic cross section is also given.
- ²⁴ HORN 11 perform detector calibration by neutrons. Earlier results are only marginally affected.
- ²⁵ Superseded by AHMED 10.

For Super-heavy dark matter ($m_{X^0} > 10^{10}$ GeV)

VALUE	DOCUMENT ID	TECN	COMMENT
••• We do not use the following data for averages, fits, limits, etc. •••			
	1 ABREU	23 AUGÉ	DM decay to photons
	2 ACEVEDO	23	DM tracks in ancient mica
	¹ ABREU 23 search for superheavy DM X decay to $q\bar{q}$ pairs via instanton, then to $\gamma\gamma$. No signal detected. Exclude $m(X) > 3 \times 10^{13}$ GeV for dark gauge coupling $\alpha_X = 0.09$.		
	² ACEVEDO 23 re-examine data from ancient mica to place limits on superheavy DM in the mass range $10^7\text{--}10^{25}$ GeV. See Fig. 3 for σ^{SI} and σ^{SD} limits.		

Spin-Dependent Cross Section Limits for Dark Matter Particle (X^0) on Proton

For m_{X^0} in GeV range

We provide here limits for $m_{X^0} < 5$ GeV

VALUE (pb)	CL%	DOCUMENT ID	TECN	COMMENT
••• We do not use the following data for averages, fits, limits, etc. •••				
$< 1 \times 10^4$	90	1 AALBERS	23A LZ	SD scatter on Xe
$< 2 \times 10^5$	90	2 ADHIKARI	22B C100	sub-GeV WIMP via SD coupling/Migdal effect
$< 9 \times 10^4$	90	3 ANGIOHER	22 CRES	SD limit using Li
< 40	90	4 ANGIOHER	22A CRES	SD limit using Li and Al
$< 8 \times 10^4$	90	5 ABDELHAME..20A	CRES	LiAlO ₂
$< 1 \times 10^6$	95	6 ABDELHAME..19	CRES	GeV-scale WIMPs on Li
$< 3 \times 10^{-4}$	90	7 AMOLE	19 PICO	C ₃ F ₈
$< 1.7 \times 10^4$	90	8 APRILE	19C XE1T	light DM on Xe via Migdal/brem effect
$< 8 \times 10^6$	90	9 ARMENGAUD	19 EDEL	GeV-scale WIMPs on Ge
< 70	90	10 XIA	19A PNDX	SD WIMP on Xe
< 100	90	11 AGNESE	18 SCDM	GeV-scale WIMPs on Ge
< 1	90	12 AKERIB	17A LUX	Xe
< 0.6	90	13 FU	17 PNDX	SD WIMP on Xe
< 0.2	90	14 AMOLE	15 PICO	C ₃ F ₈
$< 1.6 \times 10^{-1}$	90	15 ARCHAMBAU..12	PICA	19F

- ¹ AALBERS 23A search for GeV-scale WIMP scatter on Xe. No signal observed. Limits placed in $\sigma^{SD}(\chi p)$ vs. $m(\chi)$ plane. Quoted limit is for $m(\chi) = 1$ GeV via Migdal scattering.
- ² ADHIKARI 22B search for sub-GeV WIMPs via SI and SD detection; no signal detected; limits placed in $m(\chi)$ vs. σ plane for $m(\chi)$: 0.2–3 GeV; quoted limit is for SD $m(\chi) = 1$ GeV.
- ³ ANGIOHER 22 search for SD WIMP-proton scatter from Li target; no signal detected; limits placed in σ vs. $m(\text{WIMP})$ plane; limit quoted for $m(\text{WIMP}) = 1$ GeV.
- ⁴ ANGIOHER 22A search for spin-dependent DM scatter on Li and Al for $m(\text{DM}) \sim 0.2\text{--}6$ GeV; no signal observed; limits set in $\sigma(\chi p)$ vs. $m(\text{DM})$ plane; quoted limit is for $m(\text{DM}) = 1$ GeV.
- ⁵ ABDELHAMEED 20A use LiAlO₂ target in CRESST to search for SD WIMP scatter on p; no signal; quoted limit is for $m(\text{DM}) = 1$ GeV.

- 6 ABDELHAMEED 19 search for SD WIMP scatter on ${}^7\text{Li}$; limits placed on $\sigma^{SD}(\chi p)$ for $m(\chi) \sim 0.8\text{--}20$ GeV; quoted limit is for $m(\chi) = 1$ GeV.
- 7 AMOLE 19 search for SD WIMP scatter on C_3F_8 in PICO-60 bubble chamber; no signal; set limit for spin dependent coupling $\sigma^{SD}(\chi p) < 2 \times 10^{-4}$ pb for $m(\chi) = 5$ GeV.
- 8 APRILE 19c search for light DM on Xe via Migdal/brem effect; no signal, require $\sigma^{SD}(\chi p) < 1.7 \times 10^4$ pb for $m(\chi) = 1$ GeV.
- 9 ARMENGAUD 19 search for GeV scale WIMP scatter on Ge; limits placed in $\sigma^{SD}(\chi p)$ vs. $m(\chi)$ plane for $m(\chi) \sim 0.5\text{--}10$ GeV; quoted limit is for $m(\chi) = 5$ GeV.
- 10 XIA 19a search for WIMP scatter on Xe in PandaX-II; limits placed in $\sigma^{SD}(\chi p)$ vs. $m(\chi)$ plane for $m(\chi) \sim 5\text{--}1 \times 10^5$ GeV; quoted limit is for $m(\chi) = 5$ GeV.
- 11 AGNESE 18 search for GeV scale WIMPs with CDMSlite; limits placed in $\sigma^{SD}(\chi p)$ vs. $m(\chi)$ plane for $m(\chi) \sim 1.5\text{--}20$ GeV; quoted limit is for $m(\chi) = 5$ GeV.
- 12 AKERIB 17a search for SD WIMP scatter on Xe using 129.5 kg yr exposure; limits placed in $\sigma^{SD}(\chi p)$ vs. $m(\chi)$ plane for $m(\chi) \sim 6\text{--}1 \times 10^5$ GeV.
- 13 FU 17 search for SD WIMP scatter on Xe; limits set in $\sigma^{SD}(\chi p)$ vs. $m(\chi)$ plane for $m(\chi) \sim 4\text{--}1 \times 10^3$ GeV.; quoted limit is for $m(\chi) = 5$ GeV.
- 14 AMOLE 15 search for WIMP scatter on C_3F_8 in PICO-2L; limits placed in $\sigma^{SD}(\chi p)$ vs. $m(\chi)$ plane for $m(\chi) \sim 4\text{--}1 \times 10^4$ GeV; quoted limit is for $m(\chi) = 5$ GeV.
- 15 ARCHAMBAULT 12 search for SD WIMP scatter in ${}^{19}\text{F}$ with PICASSO; limits set in $\sigma^{SD}(\chi p)$ vs. $m(\chi)$ plane for $m \sim 4\text{--}500$ GeV; quoted limit is for $m(\chi) = 5$ GeV.

For $m_{\chi 0} = 20$ GeV

For limits from X^0 annihilation in the Sun, the assumed annihilation final state is shown in parenthesis in the comment.

VALUE (pb)	CL%	DOCUMENT ID	TECN	COMMENT
< 6 × 10 ⁻⁵	90	1 AALBERS 23 LZ	SD	scatter on Xe
< 3.5 × 10 ⁻⁵	90	2 ABBASI 22B ICCB	IceCube	SD limit
< 1.5 × 10 ⁵	90	3 ANGLÖHER 22 CRES	SD	limit using Li
< 2 × 10 ⁻⁴	90	4 HUANG 22 PNDX	SD	DM limits
< 9 × 10 ⁻⁵	90	5 AARTSEN 20c ICCB	SD	WIMP on p
< 2 × 10 ⁵	90	6 ABDELHAMEED...20A CRES	LiAlO ₂	
< 5 × 10 ⁻³	90	7 FELIZARDO 20 SMPL	WIMPs	via SIMPLE
< 3 × 10 ⁵	95	8 ABDELHAMEED...19 CRES	${}^7\text{Li}$	
< 2.5 × 10 ⁻⁵	90	9 AMOLE 19 PICO	C_3F_8	
< 2.5 × 10 ⁻⁴	90	10 APRILE 19A XE1T	Xe, SD	
< 1 × 10 ⁻³	90	11 XIA 19A PNDX	SD	WIMP on Xe
< 30	95	12 AGNESE 18 SCDM	Ge	
< 1 × 10 ⁻³	90	13 AKERIB 17A LUX	Xe	
< 1.32 × 10 ⁻²	90	14 BEHNKE 17 PICA	C_4F_{10}	
< 2 × 10 ⁻³	90	15 FU 17 PNDX	SD	WIMP on Xe
< 5 × 10 ⁻⁴	90	16 AMOLE 16A PICO	C_3F_8	
< 2 × 10 ⁻⁶	90	17 KHACHATRYAN...16AJ CMS	8 TeV pp → Z+ $\cancel{e}\tau$;	
			Z → $\ell\bar{\ell}$	
< 1.2 × 10 ⁻³	90	AMOLE 15 PICO	C_3F_8	
< 1.43 × 10 ⁻³	90	CHOI 15 SKAM	H, solar ν ($b\bar{b}$)	
< 1.42 × 10 ⁻⁴	90	CHOI 15 SKAM	H, solar ν ($\tau^+\tau^-$)	
< 5 × 10 ⁻³	90	FELIZARDO 14 SMPL	C_2ClF_5	
< 1.29 × 10 ⁻²	90	18 AARTSEN 13 ICCB	H, solar ν ($\tau^+\tau^-$)	
< 3.17 × 10 ⁻²	90	19 APRILE 13 X100	Xe	
< 3 × 10 ⁻²	90	20 ARCHAMBAULT...12 PICA	F (C_4F_{10})	
< 6 × 10 ⁻²	90	BEHNKE 12 COUP	CF_3I	
< 20	90	DAW 12 DRFT	F (CF_4)	
< 7 × 10 ⁻³	90	FELIZARDO 12 SMPL	C_2ClF_5	
< 0.15	90	KIM 12 KIMS	Csl	
< 1 × 10 ⁵	90	21 AHLEN 11 DMTP	F (CF_4)	
< 0.1	90	21 BEHNKE 11 COUP	CF_3I	
< 1.5 × 10 ⁻²	90	22 TANAKA 11 SKAM	H, solar ν ($b\bar{b}$)	
< 0.2	90	ARCHAMBAULT...09 PICA	F	
< 4	90	LEBEDENKO 09A ZEP3	Xe	
< 0.6	90	ANGLE 08A XE10	Xe	
<100	90	ALNER 07 ZEP2	Xe	
< 1	90	LEE 07A KIMS	Csl	
< 20	90	23 AKERIB 06 CDMS	${}^{73}\text{Ge}$, ${}^{29}\text{Si}$	
< 2	90	SHIMIZU 06A CNTR	F (C_4F_2)	
< 0.5	90	ALNER 05 NAIA	NaI	
< 1.5	90	BARNABE-HE...05 PICA	F (C_4F_{10})	
< 1.5	90	GIRARD 05 SMPL	F (C_2ClF_5)	
< 35	90	MIUCHI 03 BOLO	LIF	
< 30	90	TAKEDA 03 BOLO	NaF	

1 AALBERS 23 yield first SD LZ limits on WIMP-p scatter using Xe. $\sigma^{SD}(\chi p) < 6 \times 10^{-5}$ pb for $m(\chi) = 20$ GeV.

2 ABBASI 22B search for WIMP annihilation to $b\bar{b}$, $\tau\bar{\tau}$, $\nu\bar{\nu}$ in Sun with 7 years data; no signal; limits set in $m(\chi)$ vs. $\sigma^{SD}(\chi p)$ plane for $m(\chi)$: 10–100 GeV; quoted limit for $\nu\bar{\nu}$ channel.

3 ANGLÖHER 22 search for SD WIMP-proton scatter from Li target; no signal detected; limits placed in σ vs. $m(\text{WIMP})$ plane.

4 HUANG 22 search for SD DM scatter on Xe; no signal observed; limits placed in $\sigma(\chi n)$ vs. $m(\text{DM})$ plane; quoted limit is for $m(\text{DM}) = 20$ GeV.

5 AARTSEN 20c place combined IceCube and Pico-60 velocity-independent limits on spin-dependent WIMP-p scatter $\sigma^{SD}(\chi p) < 9\text{--}5$ pb for $m(\text{WIMP}) = 20$ GeV assuming dominant annihilation to $\tau\bar{\tau}$.

6 ABDELHAMEED 20A use LiAlO₂ target in CRESST to search for spin-dependent WIMP scatter on p; limits set for $m(\text{WIMP})$: 0.3–30 GeV in Fig. 8. Quoted limit is for $M(\text{WIMP}) = 30$ GeV.

7 FELIZARDO 20 presents 2014 SIMPLE bounds on WIMP DM using C_2ClF_5 target.

8 ABDELHAMEED 19 uses Li₂MoO₄ target to set limit for spin dependent coupling $\sigma^{SD}(\chi p) < 3 \times 10^5$ pb for $m(\chi) = 20$ GeV.

9 AMOLE 19 search for SD WIMP scatter on C_3F_8 in PICO-60 bubble chamber; no signal; set limit for spin dependent coupling $\sigma^{SD}(\chi p) < 2.5 \times 10^{-5}$ pb for $m(\chi) = 20$ GeV.

10 APRILE 19a search for SD WIMP scatter on 1 t yr Xe; no signal, limits placed in $\sigma^{SD}(\chi p)$ vs. $m(\chi)$ plane for $m \sim 6\text{--}1000$ GeV.

11 XIA 19a search for WIMP scatter on Xe in PandaX-II; limits placed in $\sigma^{SD}(\chi p)$ vs. $m(\chi)$ plane for $m(\chi) \sim 5\text{--}1 \times 10^5$ GeV.

12 AGNESE 18 give limits for $\sigma^{SD}(\rho\chi)$ for $m(\text{WIMP})$ between 1.5 and 20 GeV using CDMSlite mode data.

13 AKERIB 17a search for SD WIMP scatter on Xe using 129.5 kg yr exposure; limits placed in $\sigma^{SD}(\chi p)$ vs. $m(\chi)$ plane for $m(\chi) \sim 6\text{--}1 \times 10^5$ GeV.

14 BEHNKE 17 show final Picasso results based on 231.4 kg d exposure at SNOLab for WIMP scatter on C_4F_{10} search via superheated droplet; require $\sigma(\text{SD}) < 1.32 \times 10^{-2}$ pb for $m(\text{WIMP}) = 20$ GeV.

15 FU 17 search for SD WIMP scatter on Xe; limits set in $\sigma^{SD}(\chi p)$ vs. $m(\chi)$ plane for $m(\chi) \sim 4\text{--}1 \times 10^3$ GeV.

16 AMOLE 16a require SD WIMP-p scattering $< 5 \times 10^{-4}$ pb for $m(\text{WIMP}) = 20$ GeV; bubbles from C_3F_8 target.

17 KHACHATRYAN 16AJ require SD WIMP-p $< 2 \times 10^{-6}$ pb for $m(\text{WIMP}) = 20$ GeV from $pp \rightarrow Z + \cancel{e}\tau$; Z → $\ell\bar{\ell}$ signal.

18 AARTSEN 13 search for neutrinos from the Sun arising from the pair annihilation of X^0 trapped by the sun in data taken between June 2010 and May 2011.

19 The value has been provided by the authors. APRILE 13 note that the proton limits on Xe are highly sensitive to the theoretical model used. See also APRILE 14A.

20 ARCHAMBAULT 12 search for WIMP scatter on C_4F_{10} ; limits set in $\sigma^{SD}(\chi p)$ vs. $m(\chi)$ plane for $m \sim 4\text{--}500$ GeV.

21 Use a direction-sensitive detector.

22 TANAKA 11 search for neutrinos from the Sun arising from the pair annihilation of X^0 trapped by the Sun. The amount of X^0 depends on the X^0 -proton cross section.

23 See also AKERIB 05.

For $m_{\chi 0} = 100$ GeV

For limits from X^0 annihilation in the Sun, the assumed annihilation final state is shown in parenthesis in the comment.

VALUE (pb)	CL%	DOCUMENT ID	TECN	COMMENT
< 1.5 × 10 ⁻⁴	90	1 AALBERS 23 LZ	SD	scatter on Xe
< 1	90	2 ADHIKARI 23c C100	SD	WIMP scatter on I
< 25.7	90	3 SHIMADA 23 NAGE	directional	WIMP search
< 2.5 × 10 ⁻⁵	90	4 ABBASI 22B ICCB	IceCube	SD limit
< 2 × 10 ⁻⁴	90	5 HUANG 22 PNDX	SD	DM limits
< 50	90	6 IKEDA 21 NAGE	directional	gas TPC
< 3.34 × 10 ⁻⁴	90	7 AARTSEN 20c ICCB	SD	WIMP on p
< 6.5 × 10 ⁻³	90	8 FELIZARDO 20 SMPL	WIMPs	via SIMPLE
< 4 × 10 ⁻⁵	90	9 AMOLE 19 PICO	C_3F_8	
< 4 × 10 ⁻⁴	90	10 APRILE 19A XE1T	Xe, SD	
< 8 × 10 ⁻⁴	90	11 XIA 19A PNDX	SD	WIMP on Xe
< 8 × 10 ⁻⁴	90	12 AKERIB 17A LUX	Xe	
< 5 × 10 ⁻⁵	90	13 AMOLE 17 PICO	C_3F_8	
< 3.3 × 10 ⁻²	90	14 APRILE 17A X100	Xe inelastic	
< 2.8 × 10 ⁻¹	90	15 BATTAT 17 DRFT	CS_2	
< 1.5 × 10 ⁻³	90	16 FU 17 PNDX	Xe	
< 0.553–0.019	95	17 AABOUD 16D ATLS	pp → j + $\cancel{e}\tau$	
< 1 × 10 ⁻⁵	90	18 AABOUD 16F ATLS	pp → γ + $\cancel{e}\tau$	
< 1 × 10 ⁻⁴	90	19 AARTSEN 16c ICCB	solar ν (W^+W^-)	
< 2 × 10 ⁻⁴	90	20 ADRIAN-MAR...16 ANTR	solar ν (W^+W^- , $b\bar{b}$, $\tau\bar{\tau}$)	
< 3 × 10 ⁻³	90	21 AKERIB 16A LUX	Xe	
< 5 × 10 ⁻⁴	90	22 AMOLE 16 PICO	CF_3I	
< 1.5 × 10 ⁻³	90	AMOLE 15 PICO	C_3F_8	
< 3.19 × 10 ⁻³	90	CHOI 15 SKAM	H, solar ν ($b\bar{b}$)	
< 2.80 × 10 ⁻⁴	90	CHOI 15 SKAM	H, solar ν (W^+W^-)	
< 1.24 × 10 ⁻⁴	90	CHOI 15 SKAM	H, solar ν ($\tau^+\tau^-$)	
< 8 × 10 ²	90	23 NAKAMURA 15 NAGE	CF_4	
< 1.7 × 10 ⁻³	90	24 AVRORIN 14 BAIK	H, solar ν (W^+W^-)	
< 4.5 × 10 ⁻²	90	24 AVRORIN 14 BAIK	H, solar ν ($b\bar{b}$)	
< 7.1 × 10 ⁻⁴	90	24 AVRORIN 14 BAIK	H, solar ν ($\tau^+\tau^-$)	
< 6 × 10 ⁻³	90	FELIZARDO 14 SMPL	C_2ClF_5	
< 2.68 × 10 ⁻⁴	90	25 AARTSEN 13 ICCB	H, solar ν (W^+W^-)	
< 1.47 × 10 ⁻²	90	25 AARTSEN 13 ICCB	H, solar ν ($b\bar{b}$)	
< 8.5 × 10 ⁻⁴	90	26 ADRIAN-MAR...13 ANTR	H, solar ν (W^+W^-)	
< 5.5 × 10 ⁻²	90	26 ADRIAN-MAR...13 ANTR	H, solar ν ($b\bar{b}$)	
< 3.4 × 10 ⁻⁴	90	26 ADRIAN-MAR...13 ANTR	H, solar ν ($\tau^+\tau^-$)	
< 1.00 × 10 ⁻²	90	27 APRILE 13 X100	Xe	
< 7.1 × 10 ⁻⁴	90	27 BOLIEV 13 BAKS	H, solar ν (W^+W^-)	
< 8.4 × 10 ⁻³	90	28 BOLIEV 13 BAKS	H, solar ν ($b\bar{b}$)	
< 3.1 × 10 ⁻⁴	90	28 BOLIEV 13 BAKS	H, solar ν ($\tau^+\tau^-$)	
< 7.07 × 10 ⁻⁴	90	29 ABBASI 12 ICCB	H, solar ν (W^+W^-)	
< 4.53 × 10 ⁻²	90	29 ABBASI 12 ICCB	H, solar ν ($b\bar{b}$)	
< 7 × 10 ⁻²	90	30 ARCHAMBAULT...12 PICA	F (C_4F_{10})	
< 1 × 10 ⁻²	90	BEHNKE 12 COUP	CF_3I	
< 1.8	90	DAW 12 DRFT	F (CF_4)	
< 9 × 10 ⁻³	90	FELIZARDO 12 SMPL	C_2ClF_5	
< 2 × 10 ⁻²	90	KIM 12 KIMS	Csl	
< 2 × 10 ³	90	23 AHLEN 11 DMTP	F (CF_4)	

Searches Particle Listings

WIMP and Dark Matter Searches

< 7 × 10 ⁻²	90	BEHNKE	11	COUP	CF ₃ I
< 2.7 × 10 ⁻⁴	90	³¹ TANAKA	11	SKAM	H, solar ν (W ⁺ W ⁻)
< 4.5 × 10 ⁻³	90	³¹ TANAKA	11	SKAM	H, solar ν (b \bar{b})
		³² FELIZARDO	10	SMPL	C ₂ ClF ₃
< 6 × 10 ³	90	²³ MIUCHI	10	NAGE	CF ₄
< 0.4	90	ARCHAMBAU.	09	PICA	F
< 0.8	90	LEBEDENKO	09A	ZEP3	Xe
< 1.0	90	ANGLE	08A	XE10	Xe
< 15	90	ALNER	07	ZEP2	Xe
< 0.2	90	LEE	07A	KIMS	Csl
< 1 × 10 ⁴	90	²³ MIUCHI	07	NAGE	F (CF ₄)
< 5	90	³³ AKERIB	06	CDMS	⁷³ Ge, ²⁹ Si
< 2	90	SHIMIZU	06A	CNTR	F (CaF ₂)
< 0.3	90	ALNER	05	NAIA	NaI
< 2	90	BARNABE-HE.	05	PICA	F (C ₄ F ₁₀)
<100	90	BENOIT	05	EDEL	⁷³ Ge
< 1.5	90	GIRARD	05	SMPL	F (C ₂ ClF ₅)
< 0.7		³⁴ GIULIANI	05A	RVUE	
		³⁵ GIULIANI	04	RVUE	
		³⁶ GIULIANI	04A	RVUE	
< 35	90	MIUCHI	03	BOLO	LIF
< 40	90	TAKEDA	03	BOLO	NaF

- AALBERS 23 yield first SD LZ limits on WIMP- p scatter using Xe. $\sigma^{SD}(\chi p) < 1.5 \times 10^{-4}$ pb for $m(\chi) = 100$ GeV.
- ADHIKARI 23c search for SD WIMP scatter on I. No signal observed. Require $\sigma^{SD}(\chi p) < 1$ pb for $m(\chi) = 100$ GeV.
- SHIMADA 23 search for WIMPs in NEWAGE directional detector. No signal observed. Limits placed in $\sigma^{SD}(\chi p)$ vs. mass plane. Quoted limit for $m(\chi) = 150$ GeV.
- ABBASI 22b search for WIMP annihilation to $b\bar{b}$, $\tau\bar{\tau}$, $\nu\bar{\nu}$ in Sun with 7 years data; no signal; limits set in $m(\chi)$ vs. $\sigma^{SD}(\chi p)$ plane for $m(\chi)$: 10-100 GeV; quoted limit for $\nu\bar{\nu}$ channel.
- HUANG 22 search for SD DM scatter on Xe; no signal observed; limits placed in $\sigma(\chi n)$ vs. $m(\text{DM})$ plane; quoted limit is for $m(\text{DM}) = 100$ GeV.
- IKEDA 21 use direction sensitive TPC NEWAGE to search for SD WIMPs. No signal observed. Limits set in $\sigma^{SD}(\chi p)$ vs. m plane; $\sigma^{SD}(\chi p) < 50$ pb for $m(\text{DM}) = 100$ GeV.
- AARTSEN 20c place combined IceCube and Pico-60 velocity-independent limits on spin-dependent WIMP- p scatter $\sigma^{SD}(\chi p) < 3.34 \times 10^{-4}$ pb for $m(\text{WIMP}) = 100$ GeV assuming dominant annihilation to $\tau\bar{\tau}$.
- FELIZARDO 20 presents 2014 SIMPLE bounds on WIMP DM using C₂ClF₅ target.
- AMOLE 19 search for SD WIMP scatter on C₃F₈ in PICO-60 bubble chamber; no signal; set limit for spin dependent coupling $\sigma^{SD}(\chi p) < 4 \times 10^{-5}$ pb for $m(\chi) = 100$ GeV.
- APRILE 19A search for SD WIMP scatter on 1 t yr Xe; no signal, limits placed in $\sigma^{SD}(\chi p)$ vs. $m(\chi)$ plane for $m \sim 6-1000$ GeV.
- XIA 19A search for WIMP scatter on Xe in PandaX-II; limits placed in $\sigma^{SD}(\chi p)$ vs. $m(\chi)$ plane for $m(\chi) \sim 5-1 \times 10^5$ GeV.
- AKERIB 17A search for SD WIMP scatter on Xe using 129.5 kg yr exposure; limits placed in $\sigma^{SD}(\chi p)$ vs. $m(\chi)$ plane for $m(\chi) \sim 6-1 \times 10^5$ GeV.
- AMOLE 17 require $\sigma(\text{WIMP-}p)^{SD} < 5 \times 10^{-5}$ pb for $m(\text{WIMP}) = 100$ GeV using PICO-60 1167 kg-days exposure at SNOLab.
- APRILE 17A require $\sigma(\text{WIMP-}p)(\text{inelastic})^{SD} < 3.3 \times 10^{-2}$ pb for $m(\text{WIMP}) = 100$ GeV, based on 7640 kg day exposure at LNGS.
- BATTAT 17 use directional detection of CS₂ ions to require $\sigma(\text{SD}) < 2.8 \times 10^{-1}$ pb for 100 GeV WIMP with a 55 days exposure at the Boulby Underground Science Facility.
- FU 17 from a 33000 kg d exposure at CJPL, PANDEX II derive for $m(\text{DM}) = 100$ GeV, $\sigma^{SD}(\text{WIMP-}p) < 2 \times 10^{-3}$ pb.
- AABOUD 16d use ATLAS 13 TeV 3.2 fb⁻¹ of data to search for monojet plus missing E_T ; agree with SM rates; present limits on large extra dimensions, compressed SUSY spectra and wimp pair production.
- AABOUD 16f search for monophoton plus missing E_T events at ATLAS with 13 TeV and 3.2 fb⁻¹; signal agrees with SM background; place limits on SD WIMP-proton scattering vs. mediator mass and large extra dimension models.
- AARTSEN 16c search for high energy ν s from WIMP annihilation in solar core; limits set on SD WIMP- p scattering (Fig. 8).
- ADRIAN-MARTINEZ 16 search for WIMP annihilation into ν s from solar core; exclude SD cross section < few 10⁻⁴ depending on $m(\text{WIMP})$.
- AKERIB 16A using 2013 data exclude SD WIMP-proton scattering > 3 × 10⁻³ pb for $m(\text{WIMP}) = 100$ GeV.
- AMOLE 16 use bubble technique on CF₃I target to exclude SD WIMP- p scattering > 5 × 10⁻⁴ pb for $m(\text{WIMP}) = 100$ GeV.
- Use a direction-sensitive detector.
- AVRORIN 14 search for neutrinos from the Sun arising from the pair annihilation of X⁰ trapped by the Sun in data taken between 1998 and 2003. See their Table 1 for limits assuming annihilation into neutrino pairs.
- AARTSEN 13 search for neutrinos from the Sun arising from the pair annihilation of X⁰ trapped by the sun in data taken between June 2010 and May 2011.
- ADRIAN-MARTINEZ 13 search for neutrinos from the Sun arising from the pair annihilation of X⁰ trapped by the sun in data taken between Jan. 2007 and Dec. 2008.
- The value has been provided by the authors. APRILE 13 note that the proton limits on Xe are highly sensitive to the theoretical model used. See also APRILE 14A.
- BOLIEV 13 search for neutrinos from the Sun arising from the pair annihilation of X⁰ trapped by the sun in data taken from 1978 to 2009. See also SUVOROVA 13 for an older analysis of the same data.
- ABBASI 12 search for neutrinos from the Sun arising from the pair annihilation of X⁰ trapped by the Sun. The amount of X⁰ depends on the X⁰-proton cross section.
- ARCHAMBAULT 12 search for WIMP scatter on C₄F₁₀; limits set in $\sigma^{SD}(\chi p)$ vs. $m(\chi)$ plane for $m \sim 4-500$ GeV.
- TANAKA 11 search for neutrinos from the Sun arising from the pair annihilation of X⁰ trapped by the Sun. The amount of X⁰ depends on the X⁰-proton cross section.

- See their Fig. 3 for limits on spin-dependent proton couplings for X⁰ mass of 50 GeV.
- See also AKERIB 05.
- GIULIANI 05A analyze available data and give combined limits.
- GIULIANI 04 reanalyze COLLAR 00 data and give limits for spin-dependent X⁰-proton coupling.
- GIULIANI 04A give limits for spin-dependent X⁰-proton couplings from existing data.

For $m_{X^0} = 1$ TeV

For limits from X⁰ annihilation in the Sun, the assumed annihilation final state is shown in parenthesis in the comment.

VALUE (pb)	CL%	DOCUMENT ID	TECN	COMMENT
• • • We do not use the following data for averages, fits, limits, etc. • • •				
< 1.5 × 10 ⁻³	90	¹ AALBERS	23	LZ SD scatter on Xe
< 0.2	90	² ADHIKARI	23c	C100 SD WIMP scatter on I
< 1.2 × 10 ⁻³	90	³ HUANG	22	PNDX SD DM limits
<200	90	⁴ IKEDA	21	NAGE directional gas TPC
< 4.81 × 10 ⁻³	90	⁵ AARTSEN	20c	ICCB SD WIMP on p
< 3 × 10 ⁻⁴	90	⁶ AMOLE	19	PICO C ₃ F ₈
< 4 × 10 ⁻³	90	⁷ APRILE	19A	XE1T Xe, SD
< 5 × 10 ⁻³	90	⁸ XIA	19A	PNDX SD WIMP on Xe
		⁹ ALBERT	18c	HAWC DM annihilation in Sun to long-lived mediator
< 2.05 × 10 ⁻⁵	90	¹⁰ AARTSEN	17A	ICCB ν , sun
< 7 × 10 ⁻³	90	¹¹ AKERIB	17A	LUX Xe
< 2 × 10 ⁻²	90	¹² FU	17	PNDX SD WIMP on Xe
		¹³ ADRIAN-MAR.	16b	ANTR solar μ from WIMP annih.
< 1 × 10 ⁻²	90	AMOLE	15	PICO C ₃ F ₈
< 1.5 × 10 ³	90	NAKAMURA	15	NAGE CF ₄
< 2.7 × 10 ⁻³	90	¹⁴ AVRORIN	14	BAIK H, solar ν (W ⁺ W ⁻)
< 6.9 × 10 ⁻²	90	¹⁴ AVRORIN	14	BAIK H, solar ν (b \bar{b})
< 8.4 × 10 ⁻⁴	90	¹⁴ AVRORIN	14	BAIK H, solar ν (τ ⁺ τ ⁻)
< 4.48 × 10 ⁻⁴	90	¹⁵ AARTSEN	13	ICCB H, solar ν (W ⁺ W ⁻)
< 1.00 × 10 ⁻²	90	¹⁵ AARTSEN	13	ICCB H, solar ν (b \bar{b})
< 8.9 × 10 ⁻⁴	90	¹⁶ ADRIAN-MAR.	13	ANTR H, solar ν (W ⁺ W ⁻)
< 2.0 × 10 ⁻²	90	¹⁶ ADRIAN-MAR.	13	ANTR H, solar ν (b \bar{b})
< 2.3 × 10 ⁻⁴	90	¹⁶ ADRIAN-MAR.	13	ANTR H, solar ν (τ ⁺ τ ⁻)
< 7.57 × 10 ⁻²	90	¹⁷ APRILE	13	X100 Xe
< 5.4 × 10 ⁻³	90	¹⁸ BOLIEV	13	BAKS H, solar ν (W ⁺ W ⁻)
< 4.2 × 10 ⁻²	90	¹⁸ BOLIEV	13	BAKS H, solar ν (b \bar{b})
< 1.5 × 10 ⁻³	90	¹⁸ BOLIEV	13	BAKS H, solar ν (τ ⁺ τ ⁻)
< 2.50 × 10 ⁻⁴	90	¹⁹ ABBASI	12	ICCB H, solar ν (W ⁺ W ⁻)
< 7.86 × 10 ⁻³	90	¹⁹ ABBASI	12	ICCB H, solar ν (b \bar{b})
< 8 × 10 ⁻²	90	BEHNKE	12	COUP CF ₃ I
< 8	90	DAW	12	DRFT F (CF ₄)
< 6 × 10 ⁻²		FELIZARDO	12	SMPL C ₂ ClF ₅
< 8 × 10 ⁻²	90	KIM	12	KIMS Csl
< 8 × 10 ³	90	²⁰ AHLEN	11	DMTP F (CF ₄)
< 0.4	90	BEHNKE	11	COUP CF ₃ I
< 2 × 10 ⁻³	90	²¹ TANAKA	11	SKAM H, solar ν (b \bar{b})
< 2 × 10 ⁻²	90	²¹ TANAKA	11	SKAM H, solar ν (W ⁺ W ⁻)
< 1 × 10 ⁻³	90	²² ABBASI	10	ICCB KK dark matter
< 2 × 10 ⁴	90	²⁰ MIUCHI	10	NAGE CF ₄
< 8.7 × 10 ⁻⁴	90	ABBASI	09b	ICCB H, solar ν (W ⁺ W ⁻)
< 2.2 × 10 ⁻²	90	ABBASI	09b	ICCB H, solar ν (b \bar{b})
< 3	90	ARCHAMBAU.	09	PICA F
< 6	90	LEBEDENKO	09A	ZEP3 Xe
< 9	90	ANGLE	08A	XE10 Xe
<100	90	ALNER	07	ZEP2 Xe
< 0.8	90	LEE	07A	KIMS Csl
< 4 × 10 ⁴	90	²⁰ MIUCHI	07	NAGE F (CF ₄)
< 30	90	²³ AKERIB	06	CDMS ⁷³ Ge, ²⁹ Si
< 1.5	90	ALNER	05	NAIA NaI
< 15	90	BARNABE-HE.	05	PICA F (C ₄ F ₁₀)
<600	90	BENOIT	05	EDEL ⁷³ Ge
< 10	90	GIRARD	05	SMPL F (C ₂ ClF ₅)
<260	90	MIUCHI	03	BOLO LIF
<150	90	TAKEDA	03	BOLO NaF

- AALBERS 23 yield first SD LZ limits on WIMP- p scatter using Xe. $\sigma^{SD}(\chi p) < 2 \times 10^{-3}$ pb for $m(\chi) = 1$ TeV.
- ADHIKARI 23c search for SD WIMP scatter on I. No signal observed. Require $\sigma^{SD}(\chi p) < 0.2$ pb for $m(\chi) = 1$ TeV.
- HUANG 22 search for SD DM scatter on Xe; no signal observed; limits placed in $\sigma(\chi n)$ vs. $m(\text{DM})$ plane; quoted limit is for $m(\text{DM}) = 1$ TeV.
- IKEDA 21 use direction sensitive TPC NEWAGE to search for SD WIMPs. No signal observed. Limits set in $\sigma^{SD}(\chi p)$ vs. m plane; $\sigma^{SD}(\chi p) < 200$ pb for $m(\text{DM}) = 1000$ GeV.
- AARTSEN 20c place combined IceCube and Pico-60 velocity-independent limits on spin-dependent WIMP- p scatter $\sigma^{SD}(\chi p) < 3 \times 10^{-3}$ pb for $m(\text{WIMP}) = 1$ TeV assuming dominant annihilation to $W W$.
- AMOLE 19 search for SD WIMP scatter on C₃F₈ in PICO-60 bubble chamber; no signal; set limit for spin dependent coupling $\sigma^{SD}(\chi p) < 3 \times 10^{-4}$ pb for $m(\chi) = 1000$ GeV.
- APRILE 19A search for SD WIMP scatter on 1 t yr Xe; no signal, limits placed in $\sigma^{SD}(\chi p)$ vs. $m(\chi)$ plane for $m \sim 6-1000$ GeV.
- XIA 19A search for WIMP scatter on Xe in PandaX-II; limits placed in $\sigma^{SD}(\chi p)$ vs. $m(\chi)$ plane for $m(\chi) \sim 5-1 \times 10^5$ GeV.

- ⁹ ALBERT 18c search for DM annihilation in Sun to long-lived mediator (LLM) which decays outside Sun, for DM masses above 1 TeV; assuming LLM, limits set on $\sigma^{SD}(\chi p)$.
- ¹⁰ AARTSEN 17A search for neutrinos from solar WIMP annihilation into $\tau^+ \tau^-$ in 532 days of live time.
- ¹¹ AKERIB 17A search for SD WIMP scatter on Xe using 129.5 kg yr exposure; limits placed in $\sigma^{SD}(\chi p)$ vs. $m(\chi)$ plane for $m(\chi) \sim 6-1 \times 10^5$ GeV.
- ¹² FU 17 search for SD WIMP scatter on Xe; limits set in $\sigma^{SD}(\chi p)$ vs. $m(\chi)$ plane for $m(\chi) \sim 4-1 \times 10^3$ GeV.
- ¹³ ADRIAN-MARTINEZ 16b search for secluded DM via WIMP annihilation in solar core into light mediator which later decays to μ or ν s; limits presented in Figures 3 and 4.
- ¹⁴ AVRORIN 14 search for neutrinos from the Sun arising from the pair annihilation of X^0 trapped by the Sun in data taken between 1998 and 2003. See their Table 1 for limits assuming annihilation into neutrino pairs.
- ¹⁵ AARTSEN 13 search for neutrinos from the Sun arising from the pair annihilation of X^0 trapped by the sun in data taken between June 2010 and May 2011.
- ¹⁶ ADRIAN-MARTINEZ 13 search for neutrinos from the Sun arising from the pair annihilation of X^0 trapped by the sun in data taken between Jan. 2007 and Dec. 2008.
- ¹⁷ The value has been provided by the authors. APRILE 13 note that the proton limits on Xe are highly sensitive to the theoretical model used. See also APRILE 14A.
- ¹⁸ BOLIEV 13 search for neutrinos from the Sun arising from the pair annihilation of X^0 trapped by the sun in data taken from 1978 to 2009. See also SUVOROVA 13 for an older analysis of the same data.
- ¹⁹ ABBASI 12 search for neutrinos from the Sun arising from the pair annihilation of X^0 trapped by the Sun. The amount of X^0 depends on the X^0 -proton cross section.
- ²⁰ Use a direction-sensitive detector.
- ²¹ TANAKA 11 search for neutrinos from the Sun arising from the pair annihilation of X^0 trapped by the Sun. The amount of X^0 depends on the X^0 -proton cross section.
- ²² ABBASI 10 search for ν_μ from annihilations of Kaluza-Klein photon dark matter in the Sun.
- ²³ See also AKERIB 05.

———— Spin-Dependent Cross Section Limits ————
———— for Dark Matter Particle (X^0) on Neutron ————

For m_{X^0} in GeV range

We provide here limits for $m_{X^0} < 5$ GeV

VALUE (pb)	CL%	DOCUMENT ID	TECN	COMMENT
• • • We do not use the following data for averages, fits, limits, etc. • • •				
$< 1 \times 10^2$	90	1 AALBERS 23A	LZ	SD scatter on Xe
$< 1 \times 10^6$	90	2 ANGLOHER 22	CRES	SD limit using Li
< 570	90	3 ANGLOHER 22A	CRES	SD limit using Li and Al
$< 1 \times 10^8$	90	4 ABDELHAMEED.20A	CRES	LiAlO ₂
$< 1 \times 10^{10}$	95	5 ABDELHAMEED.19	CRES	SD low mass DM on Li
$< 2.3 \times 10^2$	90	6 APRILE 19C	XE1T	light DM on Xe via Migdal/brem effect
$< 1 \times 10^{-2}$	90	7 APRILE 19D	XE1T	light DM on Xe via ionization
$< 4 \times 10^4$	90	8 ARMENGAUD 19	EDEL	GeV-scale WIMPs on Ge
$< 8 \times 10^{-2}$	90	9 XIA 19A	PNDX	SD WIMP on Xe
< 3	90	10 AGNESE 18	SCDM	GeV-scale WIMPs on Ge
< 3	90	11 JIANG 18	CDEX	GeV-scale WIMPs on Ge
< 10	90	12 YANG 18	CDEX	WIMPs on Ge
$< 1 \times 10^{-1}$	90	13 AKERIB 17A	LUX	Xe
< 0.1	90	14 FU 17	PNDX	SD WIMP on Xe
< 20	90	15 ZHAO 16	CDEX	GeV-scale WIMPs on Ge
< 150	90	16 AHMED 11B	CDM2	GeV-scale WIMPs on Ge

- ¹ AALBERS 23A search for GeV-scale WIMP scatter on Xe. No signal observed. Limits placed in $\sigma^{SD}(\chi n)$ vs. $m(\chi)$ plane. Quoted limit is for $m(\chi) = 1$ GeV via Migdal scattering.
- ² ANGLOHER 22 search for SD WIMP scatter on Li target; no signal detected; limits placed on WIMP-neutron SD scatter versus $m(\text{WIMP})$; limit quoted for $m(\text{WIMP}) = 1$ GeV.
- ³ ANGLOHER 22A search for spin-dependent DM scatter on Li and Al for $m(\text{DM}) \sim 0.2-6$ GeV; no signal observed; limits set in $\sigma(\chi n)$ vs. $m(\text{DM})$ plane; quoted limit is for $m(\text{DM}) = 1$ GeV.
- ⁴ ABDELHAMEED 20A use LiAlO₂ target in CRESST to search for SD WIMP scatter; no signal; quoted limit is for $m(\text{DM}) = 1$ GeV.
- ⁵ ABDELHAMEED 19 search for GeV-scale WIMP SD scatter on ⁷Li crystal; set limit $\sigma^{SD}(\chi n)$ for $m(\chi) \sim 0.8-20$ GeV; quoted limit for $m(\chi) = 1$ GeV.
- ⁶ APRILE 19C search for light DM on Xe via Migdal/bremsstrahlung effect; no signal, require $\sigma^{SD}(\chi n) < 230$ pb for $m(\chi) = 1$ GeV.
- ⁷ APRILE 19D search for light DM scatter on Xe via ionization; no signal, limits placed in σ vs. $m(\text{DM}) \sim 3-6$ GeV; quoted limit is for $m(\text{DM}) = 5$ GeV.
- ⁸ ARMENGAUD 19 search for GeV scale WIMP scatter on Ge; limits placed in $\sigma^{SD}(\chi n)$ vs. $m(\chi)$ plane for $m(\chi) \sim 0.5-10$ GeV; quoted limit is for $m(\chi) = 5$ GeV.
- ⁹ XIA 19A search for WIMP scatter on Xe in PandaX-II; limits placed in $\sigma^{SD}(\chi n)$ vs. $m(\chi)$ plane for $m(\chi) \sim 5-1 \times 10^5$ GeV; quoted limit is for $m(\chi) = 5$ GeV.
- ¹⁰ AGNESE 18 search for GeV scale WIMPs scatter at CDM2Site; limits placed in $\sigma^{SD}(\chi n)$ vs. $m(\chi)$ plane for $m \sim 1.5-20$ GeV; quoted limit is for $m(\chi) = 5$ GeV.
- ¹¹ JIANG 18 search for GeV scale WIMP scatter on Ge; limits placed in $\sigma^{SD}(\chi n)$ vs. $m(\chi)$ plane for $m(\chi) \sim 3-10$ GeV; quoted limit is for $m(\chi) = 5$ GeV.
- ¹² YANG 18 search for WIMP scatter on Ge; limits placed in $\sigma^{SD}(\chi n)$ vs. $m(\chi)$ plane for $m(\chi) \sim 2-10$ GeV; quoted limit is for $m(\chi) = 5$ GeV.
- ¹³ AKERIB 17A search for SD WIMP scatter on Xe with 129.5 kg yr exposure; limits placed in $\sigma^{SD}(\chi n)$ vs. $m(\chi)$ plane for $m(\chi) \sim 5-1 \times 10^5$ GeV; quoted limit is for $m(\chi) = 5$ GeV.
- ¹⁴ FU 17 search for SD WIMP scatter on Xe; limits set in $\sigma^{SD}(\chi n)$ vs. $m(\chi)$ plane for $m(\chi) \sim 4-1 \times 10^3$ GeV.; quoted limit is for $m(\chi) = 5$ GeV.
- ¹⁵ ZHAO 16 search for GeV-scale WIMP scatter on Ge; limits placed in $\sigma^{SD}(\chi n)$ vs. $m(\chi)$ plane for $m(\chi) \sim 4-30$ GeV; quoted limit is for $m(\chi) = 5$ GeV.
- ¹⁶ AHMED 11B search for GeV scale WIMP scatter on Ge in CDM2 II; limits placed in $\sigma^{SD}(\chi n)$ vs. $m(\chi)$ plane for $m \sim 4-12$ GeV. Limit given for $m(\chi) = 5$ GeV.

For $m_{X^0} = 20$ GeV

VALUE (pb)	CL%	DOCUMENT ID	TECN	COMMENT
• • • We do not use the following data for averages, fits, limits, etc. • • •				
$< 2 \times 10^{-6}$	90	1 AALBERS 23	LZ	SD scatter on Xe
$< 5 \times 10^6$	90	2 ANGLOHER 22	CRES	SD limit using Li
$< 7 \times 10^{-6}$	90	3 HUANG 22	PNDX	SD DM limits
$< 5 \times 10^7$	90	4 ABDELHAMEED.20A	CRES	LiAlO ₂
$< 1 \times 10^{-1}$	90	5 FELIZARDO 20	SMPLE	WIMPs via SIMPLE
$< 8 \times 10^{-6}$	90	6 APRILE 19A	XE1T	Xe, SD
$< 3 \times 10^{-5}$	90	7 XIA 19A	PNDX	SD WIMP on Xe
< 1.5	95	8 AGNESE 18	SCDM	Ge
$< 2.5 \times 10^{-5}$	90	9 AKERIB 17A	LUX	Xe
$< 7 \times 10^{-5}$	90	10 FU 17	PNDX	SD WIMP on Xe
< 2	90	11 ZHAO 16	CDEX	GeV-scale WIMPs on Ge
< 0.09	90	12 FELIZARDO 14	SMPLE	C ₂ F ₅
< 8	90	13 UCHIDA 14	XMAS	¹²⁹ Xe, inelastic
$< 1.13 \times 10^{-3}$	90	14 APRILE 13	X100	Xe
< 0.02	90	15 AKIMOV 12	ZEP3	Xe
< 0.06	90	16 AHMED 09	CDM2	Ge
< 0.04	90	17 LEBEDENKO 09A	ZEP3	Xe
< 50	90	18 LIN 09	TEXO	Ge
$< 6 \times 10^{-3}$	90	19 ANGLE 08A	XE10	Xe
< 0.5	90	20 ALNER 07	ZEP2	Xe
< 25	90	21 LEE 07A	KIMS	Csl
< 0.3	90	22 AKERIB 06	CDMS	⁷³ Ge, ²⁹ Si
< 30	90	23 SHIMIZU 06A	CNTR	F (CaF ₂)
< 60	90	24 ALNER 05	NAIA	Nal
< 20	90	25 BARNABE-HE.05	PICA	F (C ₄ F ₁₀)
< 10	90	26 BENOIT 05	EDEL	⁷³ Ge
< 4	90	27 KLAPDOR-K... 05	HDM5	⁷³ Ge (enriched)
< 600	90	28 TAKEDA 03	BOLO	NaF

- ¹ AALBERS 23 yield first LZ limits on SD WIMP-*n* scatter using Xe. $\sigma^{SD}(\chi n) < 2 \times 10^{-6}$ pb for $m(\chi) = 20$ GeV.
- ² ANGLOHER 22 search for SD WIMP-neutron scatter from Li target; no signal detected; limits placed in σ vs. $m(\text{WIMP})$ plane.
- ³ HUANG 22 search for SD DM scatter on Xe; no signal observed; limits placed in $\sigma(\chi n)$ vs. $m(\text{DM})$ plane; quoted limit is for $m(\text{DM}) = 20$ GeV.
- ⁴ ABDELHAMEED 20A use LiAlO₂ target in CRESST to search for SD WIMP scatter on *n*; limits placed for $m(\text{WIMP})$: 0.3-30 GeV in Fig. 8. Quoted limit is for $M(\text{WIMP}) = 30$ GeV.
- ⁵ FELIZARDO 20 presents 2014 SIMPLE bounds on WIMP DM using C₂F₅ target.
- ⁶ APRILE 19A search for SD WIMP scatter on 1 t yr Xe; no signal: limits placed in $\sigma^{SD}(\chi n)$ vs. $m(\chi)$ plane for $m \sim 6-1000$ GeV.
- ⁷ XIA 19A search for WIMP scatter on Xe in PandaX-II; limits placed in $\sigma^{SD}(\chi n)$ vs. $m(\chi)$ plane for $m(\chi) \sim 5-1 \times 10^5$ GeV.
- ⁸ AGNESE 18 give limits for $\sigma^{SD}(n\chi)$ for $m(\text{WIMP})$ between 1.5 and 20 GeV using CDM2Site mode data.
- ⁹ AKERIB 17A search for SD WIMP scatter on Xe with 129.5 kg yr exposure; limits placed in $\sigma^{SD}(\chi n)$ vs. $m(\chi)$ plane for $m(\chi) \sim 5-1 \times 10^5$ GeV.
- ¹⁰ FU 17 search for SD WIMP scatter on Xe; limits set in $\sigma^{SD}(\chi n)$ vs. $m(\chi)$ plane for $m(\chi) \sim 4-1 \times 10^3$ GeV.
- ¹¹ ZHAO 16 search for GeV-scale WIMP scatter on Ge; limits placed in $\sigma^{SD}(\chi n)$ vs. $m(\chi)$ plane for $m(\chi) \sim 4-30$ GeV.
- ¹² Derived limit from search for inelastic scattering $X^0 + ^{129}\text{Xe} \rightarrow X^0 + ^{129}\text{Xe}^*(39.58 \text{ keV})$.
- ¹³ The value has been provided by the authors. See also APRILE 14A.
- ¹⁴ See their Fig. 6(b) for cross section limits for m_{X^0} extending down to 2 GeV.
- ¹⁵ See also AKERIB 05.

For $m_{X^0} = 100$ GeV

VALUE (pb)	CL%	DOCUMENT ID	TECN	COMMENT
• • • We do not use the following data for averages, fits, limits, etc. • • •				
$< 5 \times 10^{-6}$	90	1 AALBERS 23	LZ	SD scatter on Xe
$< 1 \times 10^{-5}$	90	2 HUANG 22	PNDX	SD DM limits
$< 1.5 \times 10^{-1}$	90	3 FELIZARDO 20	SMPLE	WIMPs via SIMPLE
$< 1.5 \times 10^{-5}$	90	4 APRILE 19A	XE1T	Xe, SD
$< 4 \times 10^{-3}$	90	5 SUZUKI 19	XMAS	¹²⁹ Xe, inelastic
$< 2 \times 10^{-5}$	90	6 XIA 19A	PNDX	SD WIMP on Xe
$< 2.5 \times 10^{-5}$	90	7 AKERIB 17A	LUX	Xe
$< 7 \times 10^{-5}$	90	8 FU 17	PNDX	SD WIMP on Xe
< 0.1	90	9 FELIZARDO 14	SMPLE	C ₂ F ₅
< 0.05	90	10 UCHIDA 14	XMAS	¹²⁹ Xe, inelastic
$< 4.68 \times 10^{-4}$	90	11 APRILE 13	X100	Xe
< 0.01	90	12 AKIMOV 12	ZEP3	Xe
< 0.02	90	13 FELIZARDO 10	SMPLE	C ₂ F ₃
< 0.01	90	14 AHMED 09	CDM2	Ge
< 0.01	90	15 LEBEDENKO 09A	ZEP3	Xe
< 100	90	16 LIN 09	TEXO	Ge
< 0.01	90	17 ANGLE 08A	XE10	Xe
< 0.05	90	18 BEDNYAKOV 08	RVUE	Ge
< 0.08	90	19 ALNER 07	ZEP2	Xe
< 6	90	20 LEE 07A	KIMS	Csl
< 0.07	90	21 AKERIB 06	CDMS	⁷³ Ge, ²⁹ Si
< 30	90	22 SHIMIZU 06A	CNTR	F (CaF ₂)
< 10	90	23 ALNER 05	NAIA	Nal
< 30	90	24 BARNABE-HE.05	PICA	F (C ₄ F ₁₀)
< 0.7	90	25 BENOIT 05	EDEL	⁷³ Ge

Searches Particle Listings

WIMP and Dark Matter Searches

< 0.2		14 GIULIANI	05A	RVUE		4 AGOSTINI	22A	GERD	search for superWIMPs
< 1.5	90	KLAPDOR-K...	05	HDMS	⁷³ Ge (enriched)	5 APRILE	22	XE1T	WIMP-e scatter
		15 GIULIANI	04	RVUE		6 BATTAGLIERI	22		BDX-MINI search for light DM from beam dump
		16 GIULIANI	04A	RVUE		7 BOSE	22		DM-e limits from solar γ s
		17 MIUCHI	03	BOLO	LIF	8 GHOSH	22		boosted DM-e/DM- ν scatter
<800	90	TAKEDA	03	BOLO	NaF	9 HOCHBERG	22	SNSP	superconducting nanowire search for light DM
						10 ZHANG	22A	CDEX	light DM search on e in Ge
						11 CHENG	21	PNDX	MeV-scale DM on e
						12 AKERIB	20	LUX	mirror DM with Xe
						13 AMARAL	20	SCDM	light DM scatter on e in Si
						14 APRILE	20	XE1T	excess keV electron recoil in Xe
						15 ARNAUD	20	EDEL	MeV DM scatter on e in Ge
						16 BARAK	20	SENS	MeV scale DM scatter from e in Si
						17 ABRAMOFF	19	SENS	WIMP-e scatter on Si
						18 AGUILAR-AR...	19A	DMIC	MeV scale DM scatter on e in Si
						19 APRILE	19D	XE1T	light DM on Xe via ionization
						20 AGNES	18B	DS50	Ar
						21 AGNESE	18B	SCDM	e χ scatter
						22 CRISLER	18	SENS	Si CCD
						23 APRILE	17	X100	Xe, annual modulation

1 AALBERS 23 yield first LZ limits on SD WIMP-n scatter using Xe. $\sigma(\chi n) < 5 \times 10^{-6}$ pb for $m(\chi) = 100$ GeV.

2 HUANG 22 search for SD DM scatter on Xe; no signal observed; limits placed in $\sigma(\chi n)$ vs. $m(\text{DM})$ plane; quoted limit is for $m(\text{DM}) = 100$ GeV.

3 FELIZARDO 20 presents 2014 SIMPLE bounds on WIMP DM using C_2ClF_5 target.

4 APRILE 19A search for SD WIMP scatter on 1 t yr Xe; no signal, limits placed in $\sigma^{SD}(\chi n)$ vs. $m(\chi)$ plane for $m \sim 6$ -1000 GeV.

5 SUZUKI 19 search in single phase liquid xenon detector for inelastic scattering $\chi^0 + ^{129}\text{Xe} \rightarrow \chi^0 + ^{129}\text{Xe}^*$ (39.58 keV); no signal; require $\sigma(\chi n)^{SD} < 4 \times 10^{-3}$ pb for $m(\chi) = 100$ GeV.

6 XIA 19A search for WIMP scatter on Xe in PandaX-II; limits placed in $\sigma^{SD}(\chi n)$ vs. $m(\chi)$ plane for $m(\chi) \sim 5$ - 1×10^5 GeV.

7 AKERIB 17A search for SD WIMP scatter on Xe with 129.5 kg yr exposure; limits placed in $\sigma^{SD}(\chi n)$ vs. $m(\chi)$ plane for $m(\chi) \sim 5$ - 1×10^5 GeV.

8 FU 17 search for SD WIMP scatter on Xe; limits set in $\sigma^{SD}(\chi n)$ vs. $m(\chi)$ plane for $m(\chi) \sim 4$ - 1×10^3 GeV.

9 UCHIDA 14 derived limit from search for inelastic scattering $\chi^0 + ^{129}\text{Xe} \rightarrow \chi^0 + ^{129}\text{Xe}^*$ (39.58 keV).

10 The value has been provided by the authors. See also APRILE 14A.

11 See their Fig. 3 for limits on spin-dependent neutron couplings for X^0 mass of 50 GeV.

12 BEDNYAKOV 08 reanalyze KLAPDOR-KLEINGROTHAUS 05 and BAUDIS 01 data.

13 See also AKERIB 05.

14 GIULIANI 05A analyze available data and give combined limits.

15 GIULIANI 04 reanalyze COLLAR 00 data and give limits for spin-dependent X^0 -neutron coupling.

16 GIULIANI 04A give limits for spin-dependent X^0 -neutron couplings from existing data.

17 MIUCHI 03 give model-independent limit for spin-dependent X^0 -proton and neutron cross sections. See their Fig. 5.

For $m_{X^0} = 1$ TeV

VALUE (pb)	CL%	DOCUMENT ID	TECN	COMMENT
< 5 $\times 10^{-5}$	90	1 AALBERS 23	LZ	SD scatter on Xe
< 6 $\times 10^{-5}$	90	2 HUANG 22	PNDX	SD DM limits
< 7 $\times 10^{-1}$		3 FELIZARDO 20	SMPL	WIMPs via SIMPLE
< 1.2 $\times 10^{-4}$	90	4 APRILE 19A	XE1T	Xe, SD
< 2 $\times 10^{-4}$	90	5 XIA 19A	PNDX	Xe
< 2.5 $\times 10^{-4}$	90	6 AKERIB 17A	LUX	Xe
< 4 $\times 10^{-4}$	90	7 FU 17	PNDX	SD WIMP on Xe
< 0.07	90	8 FELIZARDO 14	SMPL	C_2ClF_5
< 0.2	90	9 UCHIDA 14	XMAS	¹²⁹ Xe, inelastic
< 3.64 $\times 10^{-3}$	90	10 APRILE 13	X100	Xe
< 0.08	90	11 AKIMOV 12	ZEP3	Xe
< 0.2	90	12 AHMED 09	CDM2	Ge
< 0.1	90	13 LEBEDENKO 09A	ZEP3	Xe
< 0.1	90	14 ANGLE 08A	XE10	Xe
< 0.25	90	15 BEDNYAKOV 08	RVUE	Ge
< 0.6	90	16 ALNER 07	ZEP2	Xe
< 30	90	17 LEE 07A	KIMS	Csl
< 0.5	90	18 AKERIB 06	CDMS	⁷³ Ge, ²⁹ Si
< 40	90	19 ALNER 05	NAIA	NaI
< 200	90	20 BARNABE-HE...05	PICA	F(C_4F_{10})
< 4	90	21 BENOIT 05	EDEL	⁷³ Ge
< 10	90	22 KLAPDOR-K... 05	HDMS	⁷³ Ge (enriched)
< 4 $\times 10^3$	90	23 TAKEDA 03	BOLO	NaF

- 1 AALBERS 23 yield first LZ SD limits on WIMP-n scatter on Xe. $\sigma^{SD}(\chi n) < 5 \times 10^{-5}$ pb for $m(\chi) = 1$ TeV.
- 2 HUANG 22 search for SD DM scatter on Xe; no signal observed; limits placed in $\sigma(\chi n)$ vs. $m(\text{DM})$ plane; quoted limit is for $m(\text{DM}) = 1$ TeV.
- 3 FELIZARDO 20 presents 2014 SIMPLE bounds on WIMP DM using C_2ClF_5 target.
- 4 APRILE 19A search for SD WIMP scatter on 1 t yr Xe; no signal, limits placed in $\sigma^{SD}(\chi n)$ vs. $m(\chi)$ plane for $m \sim 6$ -1000 GeV.
- 5 XIA 19A search for WIMP scatter on Xe in PandaX-II; limits placed in $\sigma^{SD}(\chi n)$ vs. $m(\chi)$ plane for $m(\chi) \sim 5$ - 1×10^5 GeV.
- 6 AKERIB 17A search for SD WIMP scatter on Xe with 129.5 kg yr exposure; limits placed in $\sigma^{SD}(\chi n)$ vs. $m(\chi)$ plane for $m(\chi) \sim 5$ - 1×10^5 GeV.
- 7 FU 17 search for SD WIMP scatter on Xe; limits set in $\sigma^{SD}(\chi n)$ vs. $m(\chi)$ plane for $m(\chi) \sim 4$ - 1×10^3 GeV.
- 8 Derived limit from search for inelastic scattering $\chi^0 + ^{129}\text{Xe} \rightarrow \chi^0 + ^{129}\text{Xe}^*$ (39.58 keV).
- 9 The value has been provided by the authors. See also APRILE 14A.
- 10 BEDNYAKOV 08 reanalyze KLAPDOR-KLEINGROTHAUS 05 and BAUDIS 01 data.
- 11 See also AKERIB 05.

Cross-Section Limits for Dark Matter Particles (X^0) on electron

For m_{X^0} in GeV range

We provide here limits for $m_{X^0} < 5$ GeV

VALUE (pb)	CL%	DOCUMENT ID	TECN	COMMENT
< 3 $\times 10^{-3}$	90	1 AGNES 23A	DS50	LDM scatter on e
< 0.3	90	2 ARNQUIST 23A	DAMC	LDM search via CCDs
< 2 $\times 10^{-5}$	90	3 LI 23F	PNDX	light DM limits

••• We do not use the following data for averages, fits, limits, etc. •••

Cross-Section Limits for Dark Matter Particles (X^0) on Nuclei

For m_{X^0} in GeV range

We provide here limits for $m_{X^0} < 5$ GeV

VALUE (pb)	DOCUMENT ID	COMMENT
< 3 $\times 10^{-3}$	1 AKIMOV 22	COHERENT search for DM mediators
< 1	2 ARNQUIST 23A	DAMC LDM search via CCDs
< 2 $\times 10^{-5}$	3 LI 23F	PNDX light DM limits

1 AKIMOV 22 use COHERENT Csl(Na) detector to search for sub GeV DM particles produced by the Spallation Neutron Source; no signal observed; limits placed in mediator mass vs. coupling plane for leptophobic DM models.

See key on page 1171

Searches Particle Listings

WIMP and Dark Matter Searches

For $m_{\chi^0} = 20 \text{ GeV}$

VALUE (nb)	CL%	DOCUMENT ID	TECN	COMMENT
< 0.03	90	1 UCHIDA 14	XMAS	^{129}Xe , inelastic
< 0.08	90	2 ANGLOHER 02	CRES	Al
		3 BENOIT 00	EDEL	Ge
< 0.04	95	4 KLIMENKO 98	CNTR	^{73}Ge , inel.
< 0.8		ALESSAND... 96	CNTR	O
< 6		ALESSAND... 96	CNTR	Te
< 0.02	90	5 BELLI 96	CNTR	^{129}Xe , inel.
		6 BELLI 96c	CNTR	^{129}Xe
< 4 $\times 10^{-3}$	90	7 BERNABEI 96	CNTR	Na
< 0.3	90	7 BERNABEI 96	CNTR	I
< 0.2	95	8 SARSA 96	CNTR	Na
< 0.015	90	9 SMITH 96	CNTR	Na
< 0.05	95	10 GARCIA 95	CNTR	Natural Ge
< 0.1	95	QUENBY 95	CNTR	Na
< 90	90	11 SNOWDEN... 95	MICA	^{16}O
< 4 $\times 10^3$	90	11 SNOWDEN... 95	MICA	^{39}K
< 0.7	90	BACCI 92	CNTR	Na
< 0.12	90	12 REUSSER 91	CNTR	Natural Ge
< 0.06	95	CALDWELL 88	CNTR	Natural Ge

- 1 UCHIDA 14 limit is for inelastic scattering $\chi^0 + ^{129}\text{Xe}^* \rightarrow \chi^0 + ^{129}\text{Xe}^*$ (39.58 keV).
- 2 ANGLOHER 02 limit is for spin-dependent WIMP-Aluminum cross section.
- 3 BENOIT 00 find four event categories in Ge detectors and suggest that low-energy surface nuclear recoils can explain anomalous events reported by UKDMC and Saclay Nal experiments.
- 4 KLIMENKO 98 limit is for inelastic scattering $\chi^0 \text{ } ^{73}\text{Ge} \rightarrow \chi^0 \text{ } ^{73}\text{Ge}^*$ (13.26 keV).
- 5 BELLI 96 limit for inelastic scattering $\chi^0 \text{ } ^{129}\text{Xe} \rightarrow \chi^0 \text{ } ^{129}\text{Xe}^*$ (39.58 keV).
- 6 BELLI 96c use background subtraction and obtain $\sigma < 150 \text{ pb}$ ($< 1.5 \text{ fb}$) (90% CL) for spin-dependent (independent) χ^0 -proton cross section. The confidence level is from R. Bernabei, private communication, May 20, 1999.
- 7 BERNABEI 96 use pulse shape discrimination to enhance the possible signal. The limit here is from R. Bernabei, private communication, September 19, 1997.
- 8 SARSA 96 search for annual modulation of WIMP signal. See SARSA 97 for details of the analysis. The limit here is from M.L. Sarsa, private communication, May 26, 1997.
- 9 SMITH 96 use pulse shape discrimination to enhance the possible signal. A dark matter density of 0.4 GeV cm^{-3} is assumed.
- 10 GARCIA 95 limit is from the event rate. A weaker limit is obtained from searches for diurnal and annual modulation.
- 11 SNOWDEN-IFFT 95 look for recoil tracks in an ancient mica crystal. Similar limits are also given for ^{27}Al and ^{28}Si . See COLLAR 96 and SNOWDEN-IFFT 96 for discussion on potential backgrounds.
- 12 REUSSER 91 limit here is changed from published (0.04) after reanalysis by authors. J.L. Vuilleumier, private communication, March 29, 1996.

For $m_{\chi^0} = 100 \text{ GeV}$

VALUE (nb)	CL%	DOCUMENT ID	TECN	COMMENT
< 3.3 $\times 10^{-6}$	90	1 APRILE 21A	XE1T	^{129}Xe , inelastic
< 3 $\times 10^{-3}$	90	2 UCHIDA 14	XMAS	^{129}Xe , inelastic
< 0.3	90	3 ANGLOHER 02	CRES	Al
		4 BELLI 02	RVUE	
		5 BERNABEI 02c	DAMA	
		6 GREEN 02	RVUE	
		7 ULLIO 01	RVUE	
		8 BENOIT 00	EDEL	Ge
< 4 $\times 10^{-3}$	90	9 BERNABEI 00d		^{129}Xe , inelastic
		10 AMBROSIO 99	MCRO	
		11 BRHLIK 99	RVUE	
< 8 $\times 10^{-3}$	95	12 KLIMENKO 98	CNTR	^{73}Ge , inelastic
< 0.08	95	13 KLIMENKO 98	CNTR	^{73}Ge , inelastic
< 4		ALESSAND... 96	CNTR	O
< 25		ALESSAND... 96	CNTR	Te
< 6 $\times 10^{-3}$	90	14 BELLI 96	CNTR	^{129}Xe , inelastic
		15 BELLI 96c	CNTR	^{129}Xe
< 1 $\times 10^{-3}$	90	16 BERNABEI 96	CNTR	Na
< 0.3	90	16 BERNABEI 96	CNTR	I
< 0.7	95	17 SARSA 96	CNTR	Na
< 0.03	90	18 SMITH 96	CNTR	Na
< 0.8	90	18 SMITH 96	CNTR	I
< 0.35	95	19 GARCIA 95	CNTR	Natural Ge
< 0.6	95	QUENBY 95	CNTR	Na
< 3	95	QUENBY 95	CNTR	I
< 1.5 $\times 10^2$	90	20 SNOWDEN... 95	MICA	^{16}O
< 4 $\times 10^2$	90	20 SNOWDEN... 95	MICA	^{39}K
< 0.08	90	21 BECK 94	CNTR	^{76}Ge
< 2.5	90	BACCI 92	CNTR	Na
< 3	90	BACCI 92	CNTR	I
< 0.9	90	22 REUSSER 91	CNTR	Natural Ge
< 0.7	95	CALDWELL 88	CNTR	Natural Ge

- 1 APRILE 21A search for inelastic DM scatter off ^{129}Xe nuclei with 0.83 yr exposure. No signal observed. Limits placed in $\sigma(\chi\text{Xe})$ vs. $m(\text{DM})$ plane for WIMP mass between 20 GeV and 10 TeV.
- 2 UCHIDA 14 limit is for inelastic scattering $\chi^0 + ^{129}\text{Xe}^* \rightarrow \chi^0 + ^{129}\text{Xe}^*$ (39.58 keV).

- 3 ANGLOHER 02 limit is for spin-dependent WIMP-Aluminum cross section.
- 4 BELLI 02 discuss dependence of the extracted WIMP cross section on the assumptions of the galactic halo structure.
- 5 BERNABEI 02c analyze the DAMA data in the scenario in which χ^0 scatters into a slightly heavier state as discussed by SMITH 01.
- 6 GREEN 02 discusses dependence of extracted WIMP cross section limits on the assumptions of the galactic halo structure.
- 7 ULLIO 01 disfavor the possibility that the BERNABEI 99 signal is due to spin-dependent WIMP coupling.
- 8 BENOIT 00 find four event categories in Ge detectors and suggest that low-energy surface nuclear recoils can explain anomalous events reported by UKDMC and Saclay Nal experiments.
- 9 BERNABEI 00d limit is for inelastic scattering $\chi^0 \text{ } ^{129}\text{Xe} \rightarrow \chi^0 \text{ } ^{129}\text{Xe}^*$ (39.58 keV).
- 10 AMBROSIO 99 search for upgoing muon events induced by neutrinos originating from WIMP annihilations in the Sun and Earth.
- 11 BRHLIK 99 discuss the effect of astrophysical uncertainties on the WIMP interpretation of the BERNABEI 99 signal.
- 12 KLIMENKO 98 limit is for inelastic scattering $\chi^0 \text{ } ^{73}\text{Ge} \rightarrow \chi^0 \text{ } ^{73}\text{Ge}^*$ (13.26 keV).
- 13 KLIMENKO 98 limit is for inelastic scattering $\chi^0 \text{ } ^{73}\text{Ge} \rightarrow \chi^0 \text{ } ^{73}\text{Ge}^*$ (66.73 keV).
- 14 BELLI 96 limit for inelastic scattering $\chi^0 \text{ } ^{129}\text{Xe} \rightarrow \chi^0 \text{ } ^{129}\text{Xe}^*$ (39.58 keV).
- 15 BELLI 96c use background subtraction and obtain $\sigma < 0.35 \text{ pb}$ ($< 0.15 \text{ fb}$) (90% CL) for spin-dependent (independent) χ^0 -proton cross section. The confidence level is from R. Bernabei, private communication, May 20, 1999.
- 16 BERNABEI 96 use pulse shape discrimination to enhance the possible signal. The limit here is from R. Bernabei, private communication, September 19, 1997.
- 17 SARSA 96 search for annual modulation of WIMP signal. See SARSA 97 for details of the analysis. The limit here is from M.L. Sarsa, private communication, May 26, 1997.
- 18 SMITH 96 use pulse shape discrimination to enhance the possible signal. A dark matter density of 0.4 GeV cm^{-3} is assumed.
- 19 GARCIA 95 limit is from the event rate. A weaker limit is obtained from searches for diurnal and annual modulation.
- 20 SNOWDEN-IFFT 95 look for recoil tracks in an ancient mica crystal. Similar limits are also given for ^{27}Al and ^{28}Si . See COLLAR 96 and SNOWDEN-IFFT 96 for discussion on potential backgrounds.
- 21 BECK 94 uses enriched ^{76}Ge (86% purity).
- 22 REUSSER 91 limit here is changed from published (0.3) after reanalysis by authors. J.L. Vuilleumier, private communication, March 29, 1996.

For $m_{\chi^0} = 1 \text{ TeV}$

VALUE (nb)	CL%	DOCUMENT ID	TECN	COMMENT
< 0.03	90	1 UCHIDA 14	XMAS	^{129}Xe , inelastic
< 3	90	2 ANGLOHER 02	CRES	Al
		3 BENOIT 00	EDEL	Ge
		4 BERNABEI 99d	CNTR	SIMP
		5 DERBIN 99	CNTR	SIMP
< 0.06	95	6 KLIMENKO 98	CNTR	^{73}Ge , inel.
< 0.4	95	7 KLIMENKO 98	CNTR	^{73}Ge , inel.
< 40		ALESSAND... 96	CNTR	O
< 700		ALESSAND... 96	CNTR	Te
< 0.05	90	8 BELLI 96	CNTR	^{129}Xe , inel.
< 1.5	90	9 BELLI 96	CNTR	^{129}Xe , inel.
		10 BELLI 96c	CNTR	^{129}Xe
< 0.01	90	11 BERNABEI 96	CNTR	Na
< 9	90	11 BERNABEI 96	CNTR	I
< 7	95	12 SARSA 96	CNTR	Na
< 0.3	90	13 SMITH 96	CNTR	Na
< 6	90	13 SMITH 96	CNTR	I
< 6	95	14 GARCIA 95	CNTR	Natural Ge
< 8	95	QUENBY 95	CNTR	Na
< 50	95	QUENBY 95	CNTR	I
< 700	90	15 SNOWDEN... 95	MICA	^{16}O
< 1 $\times 10^3$	90	15 SNOWDEN... 95	MICA	^{39}K
< 0.8	90	16 BECK 94	CNTR	^{76}Ge
< 30	90	BACCI 92	CNTR	Na
< 30	90	BACCI 92	CNTR	I
< 15	90	17 REUSSER 91	CNTR	Natural Ge
< 6	95	CALDWELL 88	CNTR	Natural Ge

- 1 UCHIDA 14 limit is for inelastic scattering $\chi^0 + ^{129}\text{Xe}^* \rightarrow \chi^0 + ^{129}\text{Xe}^*$ (39.58 keV).
- 2 ANGLOHER 02 limit is for spin-dependent WIMP-Aluminum cross section.
- 3 BENOIT 00 find four event categories in Ge detectors and suggest that low-energy surface nuclear recoils can explain anomalous events reported by UKDMC and Saclay Nal experiments.
- 4 BERNABEI 99d search for SIMPs (Strongly Interacting Massive Particles) in the mass range 10^3 - 10^{16} GeV. See their Fig. 3 for cross-section limits.
- 5 DERBIN 99 search for SIMPs (Strongly Interacting Massive Particles) in the mass range 10^2 - 10^{14} GeV. See their Fig. 3 for cross-section limits.
- 6 KLIMENKO 98 limit is for inelastic scattering $\chi^0 \text{ } ^{73}\text{Ge} \rightarrow \chi^0 \text{ } ^{73}\text{Ge}^*$ (13.26 keV).
- 7 KLIMENKO 98 limit is for inelastic scattering $\chi^0 \text{ } ^{73}\text{Ge} \rightarrow \chi^0 \text{ } ^{73}\text{Ge}^*$ (66.73 keV).
- 8 BELLI 96 limit for inelastic scattering $\chi^0 \text{ } ^{129}\text{Xe} \rightarrow \chi^0 \text{ } ^{129}\text{Xe}^*$ (39.58 keV).
- 9 BELLI 96 limit for inelastic scattering $\chi^0 \text{ } ^{129}\text{Xe} \rightarrow \chi^0 \text{ } ^{129}\text{Xe}^*$ (236.14 keV).
- 10 BELLI 96c use background subtraction and obtain $\sigma < 0.7 \text{ pb}$ ($< 0.7 \text{ fb}$) (90% CL) for spin-dependent (independent) χ^0 -proton cross section. The confidence level is from R. Bernabei, private communication, May 20, 1999.
- 11 BERNABEI 96 use pulse shape discrimination to enhance the possible signal. The limit here is from R. Bernabei, private communication, September 19, 1997.
- 12 SARSA 96 search for annual modulation of WIMP signal. See SARSA 97 for details of the analysis. The limit here is from M.L. Sarsa, private communication, May 26, 1997.

Searches Particle Listings

WIMP and Dark Matter Searches

- ¹³ SMITH 96 use pulse shape discrimination to enhance the possible signal. A dark matter density of 0.4 GeV cm^{-3} is assumed.
- ¹⁴ GARCIA 95 limit is from the event rate. A weaker limit is obtained from searches for diurnal and annual modulation.
- ¹⁵ SNOWDEN-IFFT 95 look for recoil tracks in an ancient mica crystal. Similar limits are also given for ^{27}Al and ^{28}Si . See COLLAR 96 and SNOWDEN-IFFT 96 for discussion on potential backgrounds.
- ¹⁶ BECK 94 uses enriched ^{76}Ge (86% purity).
- ¹⁷ REUSSER 91 limit here is changed from published (5) after reanalysis by authors. J.L. Vuilleumier, private communication, March 29, 1996.

Miscellaneous Results from Underground Dark Matter Searches

VALUE	CL%	DOCUMENT ID	TECN	COMMENT
• • • We do not use the following data for averages, fits, limits, etc. • • •				
		¹ ABE	23A SKAM	boosted DM limits
		² ADAMS	23 PICO	inelastic DM search
		³ ADHIKARI	23B C100	BDM/heavy photon DM
		⁴ AL-KHARUSI	23 EXO2	UDM search
		⁵ APRILE	23 XE1T	Planck scale DM search
		⁶ HUANG	23 PNDX	scalar DM via dark mediator decay
		⁷ NING	23A PNDX	boosted LDM
		⁸ ADHIKARI	22 DEAP	Planck scale DM multiple scatter on Ar
		⁹ ADHIKARI	22D NAI	COSINE-100 annual modulation DM search
		¹⁰ DAI	22A CDEX	MeV scale exotic DM
		¹¹ GU	22 PNDX	absorption of fermion DM
		¹² ZHANG	22 PNDX	light DM search
		¹³ AKERIB	21B LUX	limits on WIMP EFT couplings
		¹⁴ AMARE	21 ANAI	annual modulation on NaI
		¹⁵ WANG	21K CDEX	DM effective operator limits
		¹⁶ AGOSTINI	20 HPGE	keV-MeV scale super-WIMP absorption in Ge
		¹⁷ ANDRIANAV...	20 FUNK	hidden photon DM search
		¹⁸ CLARK	20	superheavy MIMP DM
		¹⁹ ABRAMOFF	19 SENS	MeV DM e-Si; dark photon Si absorption
		²⁰ ADHIKARI	19 C100	annual modulation NaI
		²¹ AMARE	19 ANAI	annual modulation NaI
$<6.4 \times 10^{-10}$	90	²² APRILE	19 XE1T	π (Xe)
		²³ BRINGMANN	19	cosmic ray DM
		²⁴ BRUNE	19	Majoron DM
		²⁵ CHOI	19 THEO	290 TeV IceCube ν
		²⁶ HA	19 C100	inelastic boosted dark γ
		²⁷ KLOPF	19	$n \rightarrow \chi e^+ e^-$
		²⁸ AARTSEN	18D ICCB	relic WIMP $\chi \rightarrow \nu X$
		²⁹ ABE	18F XMAS	$A' e \rightarrow A' e$
		³⁰ AGNES	18B DS50	Ar
		³¹ AGNESE	18B SCDM	MeV DM e-Si; dark photon Si absorption
		³² AKERIB	18A LUX	Xe
		³³ ARMENGAUD	18 EDE3	Ge
		³⁴ KACHULIS	18 SKAM	boosted DM on e
$<1 \times 10^{-12}$	90	³⁵ AGUILAR-AR...	17 DMIC	γ' on Si
		³⁶ APRILE	17 X100	Xe
		³⁷ APRILE	17D X100	Xe
		³⁸ APRILE	17H X100	keV bosonic DM search
		³⁹ APRILE	17K X100	$\chi N \rightarrow \chi^* \rightarrow \chi \gamma$
$<4 \times 10^{-3}$	90	⁴⁰ ANGLOHER	16A CRES	CaWO ₄
		⁴¹ APRILE	15 X100	Event rate modulation
		⁴² APRILE	15A X100	Electron scattering

- ¹ ABE 23A search for boosted sub-GeV DM using 0.37 Mt-y exposure of SuperK data. No signal observed. Model dependent limits set, see Fig. 3 corrected in ABE 23G erratum.
- ² ADAMS 23 search for inelastic DM scatter in fluorocarbons. No signal observed. Limits placed in σ vs. $m(\chi)$ mass splitting plane.
- ³ ADHIKARI 23B search for boosted heavy photon DM in MeV range using Cosine-100. No signal observed. Limits placed in coupling vs. mass plane for masses 1–100 MeV.
- ⁴ AL-KHARUSI 23 search for absorption of MeV-scale DM with 234.1 kg-y exposure of ^{136}Xe , triggering beta decay. No signal observed. Limit placed in cross section vs. mass plane for $m(\chi) = 1.7\text{--}11.6$ MeV (see Fig. 5).
- ⁵ APRILE 23 search for multiple scatter events from Planck scale-DM particles. No signal observed. Limits set on σ^{SI} and σ^{SD} on n and p .
- ⁶ HUANG 23 search for MeV-scale scalar DM interacting via GeV-scale dark mediator. Limits placed on cross section vs. mass plane.
- ⁷ NING 23A search for boosted LDM arising from η decays which are produced in CR events with 0.63 t-y exposure. No signal observed. Limits placed in $\sigma(\chi N)$ vs. $m(\chi)$ plane for various mediator models and branching fraction assumptions (see Fig. 2).
- ⁸ ADHIKARI 22 search for multiple scatter of Planck scale DM on Ar using DEAP detector. No signal observed. Limits placed in mass vs. cross section plane for $m(\text{DM})$: $10^7\text{--}10^{19}$ GeV.
- ⁹ ADHIKARI 22D report search for annual modulation signal of DM in a 173 kg-yr exposure of NaI; result consistent with both the modulation amplitude reported by DAMA/LIBRA and no-modulation.
- ¹⁰ DAI 22A search for MeV-scale exotic DM interaction with Ge; no signal observed; limits set in $m(\text{DM})$ vs. cross section plane for $m(\text{DM}) \sim 5\text{--}60$ MeV in simplified model.
- ¹¹ GU 22 use PANDAX to search for absorption of fermionic DM in MeV range in Xe; no signal observed; limits set in $m(\text{DM})$ vs. cross section plane for $m(\text{DM}) \sim 30\text{--}125$ MeV.
- ¹² ZHANG 22 search for light DM scatter on e; no signal observed; limits placed in σ - v vs. $m(\text{DM})$ plane for $m(\text{DM}) \sim 10\text{--}180$ keV.

- ¹³ AKERIB 21B place limits on 15 WIMP non-relativistic EFT couplings for $m(\text{DM})$: 10–4000 GeV using 3.14 kg d exposure.
- ¹⁴ AMARE 21 search for WIMP annual modulation signal on NaI target in the Canfranc Underground Laboratory (LSC). With an effective exposure of 313.95 kg y, and a sensitivity of 2.5σ no signal is observed. Incompatible with DAMA/LIBRA at 3.3σ level.
- ¹⁵ WANG 21K use CDEX detector to search for WIMP dark matter scatter on Ge; no signal observed; limits placed on 14 non-relativistic effective operators along with WIMP-pion coupling for $m(\text{WIMP}) \sim 3\text{--}20$ GeV.
- ¹⁶ AGOSTINI 20 search for keV–MeV scale super-WIMP absorption in Ge in GERDA; no signal; limits placed on keV–MeV scale bosonic superWIMPs in coupling vs. mass plane.
- ¹⁷ ANDRIANAVALOMAHEFA 20 search for hidden photon DM in eV range; place limits in $m(\text{DM})$ vs $\ln(\chi)$ plane: exclude coupling $\chi \lesssim 1 \times 10^{-12}$ for $m(\text{DM}) \sim 2.5\text{--}7$ eV.
- ¹⁸ CLARK 20 use Majorana and Xe-1-ton data to constrain superheavy multiply interacting dark matter (MIMP) in range $m \sim 10^8\text{--}10^{17}$ GeV depending on interaction cross section.
- ¹⁹ ABRAMOFF 19 search for MeV scale DM via DM–e scattering and dark photon DM via absorption in Si; limits set in coupling vs. $m(\chi)$ plane and on dark photon in $m(A)$ vs. kinetic mixing parameter plane.
- ²⁰ ADHIKARI 19 search for annual modulation signal from WIMP scatter on NaI with 1.7 yr exposure; result consistent with both DAMA/LIBRA and null hypothesis.
- ²¹ AMARE 19 is ANAIS-112 search for WIMP scatter annual modulation on NaI; 157.55 kg yr exposure; result compatible with null hypothesis; confirm goal of reaching sensitivity at 3σ to DAMA/LIBRA result in 5 years.
- ²² APRILE 19 search for WIMP-pion scattering in Xe; no signal: require $\sigma(\chi\pi) < 6.4 \times 10^{-10}$ pb for $m(\chi) = 30$ GeV.
- ²³ BRINGMANN 19 derive theoretically limits on GeV and sub-GeV mass dark matter, in its high energy component generated by interaction with cosmic rays; place limits on σ^{SI} and $\sigma^{SD} < 10^5$ pb.
- ²⁴ BRUNE 19 examine possibility of Majoron dark matter; limits placed on Majoron mass vs. coupling from SN1987a and ν -less double beta decay.
- ²⁵ CHOI 19 from multimessenger observation finds limit on $\sigma(\nu\chi)/m(\text{DM}) < 5.1 \times 10^{-23}$ cm²/GeV based on 290 TeV IceCube neutrino event.
- ²⁶ HA 19 search for inelastic boosted MeV scale dark photon using COSINE-100 data; limits placed in m vs. epsilon plane for various mediators.
- ²⁷ KLOPF 19 search for DM via $n \rightarrow \chi e^+ e^-$; no signal: limits placed in branching fraction vs. $m(e^+ e^-)$ plane.
- ²⁸ AARTSEN 18D search for long-lived DM particles decaying $\chi \rightarrow \nu X$; no excess seen; for DM masses above 10 TeV, excluding lifetimes shorter than 10^{28} s.
- ²⁹ ABE 18F search for keV mass ALPs and hidden photons (HP) scatter on electrons; limits set on mass vs. coupling.
- ³⁰ AGNES 18B search for MeV-scale DM scatter on electrons in Ar; no signal; require $\sigma(\chi e) < 9 \times 10^{-3}$ pb for DM form factor $F(\text{DM}) = 1$ and < 300 pb for $F(\text{DM})$ proportional to $1/q^2$ for $m(\chi) = 100$ MeV.
- ³¹ AGNESE 18B search for MeV scale DM via DM–e scattering and dark photon DM via absorption in Si; limits set on MeV DM in coupling vs. $m(\chi)$ plane and on dark photon in $m(A')$ vs. kinetic mixing plane.
- ³² AKERIB 18A search for annual and diurnal modulation of DM scattering rate on electrons for recoil energy between 2 and 6 keVee; no signal found.
- ³³ ARMENGAUD 18 search for ALP from the Sun and galactic bosonic DM, interacting in Ge; no signal; limits set for 0.8–500 keV DM particles.
- ³⁴ KACHULIS 18 search for an excess of elastically scattered electrons above the atmospheric neutrino background in Super-K; limits placed for simple annihilation or decay in the Sun or galactic center producing “boosted” dark matter.
- ³⁵ AGUILAR-AREVALO 17 search for hidden photon DM scatter on Si target CCD; limit kinetic mixing $\kappa < 1 \times 10^{-12}$ for $m = 10$ eV.
- ³⁶ APRILE 17 search for WIMP–e annual modulation signal for recoil energy in the 2.0–5.8 keV interval using 4 years data with Xe. No significant effect seen.
- ³⁷ APRILE 17D set limits on 14 WIMP-nucleon different interaction operators. No deviations found using 225 live days in the 6.6–240 keV recoil energy range.
- ³⁸ APRILE 17H search for keV bosonic DM via $e\chi \rightarrow e$, looking for electronic recoils with 224.6 live days of data and 34 kg of LXe. Limits set on $\chi e e$ coupling for $m(\chi) = 8\text{--}125$ keV.
- ³⁹ APRILE 17K search for magnetic inelastic DM via $\chi N \rightarrow \chi^* \rightarrow \chi \gamma$. Limits set in DM magnetic moment vs. mass splitting plane for two DM masses corresponding to the DAMA/LIBRA best fit values.
- ⁴⁰ ANGLOHER 16A require q^2 dependent scattering $< 8 \times 10^{-3}$ pb for asymmetric DM $m(\text{WIMP}) = 3$ GeV on CaWO₄ target. It uses a local dark matter density of 0.38 GeV/cm^3 .
- ⁴¹ APRILE 15 search for periodic variation of electronic recoil event rate in the data between Feb. 2011 and Mar. 2012. No significant modulation is found for periods up to 500 days.
- ⁴² APRILE 15A search for X^0 scattering off electrons. See their Fig. 4 for limits on cross section through axial-vector coupling for m_{X^0} between 0.6 GeV and 1 TeV. For $m_{X^0} = 2$ GeV, $\sigma < 60$ pb (90%CL) is obtained.

X^0 Annihilation Cross Section

Limits are on σv for X^0 pair annihilation for the X^0 mass specified in the footnote when needed.

VALUE (cm ³ s ⁻¹)	CL%	DOCUMENT ID	TECN	COMMENT
• • • We do not use the following data for averages, fits, limits, etc. • • •				
$<1 \times 10^{-24}$	90	¹ ABBASI	23A ICCB	WIMP annihilation to ν 's
$<1 \times 10^{-22}$	90	² ABBASI	23B ICCB	PeV WIMP annihilation
$<5 \times 10^{-28}$	95	³ ABE	23B MGIC	Wimp annihilation to γ
		⁴ ALBERT	23 HAWC	WIMP annihilation to γ in galactic halo
		⁵ CHENG	23A	Fermi-LAT and DAMPE combined γ line search
$<2 \times 10^{-25}$	95	⁶ FOSTER	23 FLAT	DM annihilation to gamma line
		⁷ GUO	23 FAST	DM annihilation in dwarf spheroidal galaxy
		⁸ GUO	23A	WIMP annihilation in dwarf spheroidal galaxies

See key on page 1171

Searches Particle Listings

WIMP and Dark Matter Searches

$<2 \times 10^{-26}$	95	9	LAVIS	23	$b\bar{b} + 2\text{HDM}+S, m < 1000 \text{ GeV}$
$<1.2 \times 10^{-26}$	95	10	ABDALLA	22	HESS DM annihilation to gamma rays
		11	ALBERT	22A	ANTR PeV-scale DM search
$<1 \times 10^{-27}$		12	CHAN	22	DM annihilation from Omega Centauri X-rays
$<3 \times 10^{-26}$		13	EGOROV	22	DM annihilation to radio waves from M31
		14	MANCONI	22	polarized synchrotron emission from DM annihilation via Planck
$<5 \times 10^{-24}$	95	15	ABDALLAH	21	HESS WIMP annihilation in dwarf irregular galaxy
		16	CIRELLI	21	light DM annihilation producing X-rays
		17	JOHN	21	cosmic positron spectra limits on leptophilic DM
$<2.5 \times 10^{-27}$	95	18	ABAZAJIAN	20	FLAT γ from galactic center
		19	ABDALLAH	20	HESS WIMP annihilation in dwarf satellite galaxies
$<1.2 \times 10^{-24}$	90	20	ABE	20G	SKAM WIMP annihilation to neutrinos
$<2.2 \times 10^{-24}$	95	21	ALBERT	20	HAWC WIMP annihilation to γ
$<5 \times 10^{-24}$	90	22	ALBERT	20A	ANTR WIMP annihilation to νs in galactic center
$<1 \times 10^{-23}$	90	23	ALBERT	20C	ANTR Antares/IceCube search for WIMP annihilation to νs
$<8 \times 10^{-26}$		24	ALVAREZ	20	FLAT dwarf spheroidal; J-distribution
$<2 \times 10^{-26}$	90	25	HOOF	20	FLAT WIMP annihilation to γ
		26	MAZZIOTTA	20	FLAT DM annihilation in Sun to γ
		27	ABEYSEKARA	19	HAWC DM annihilation to γs within galactic substructure
$<0.8 \times 10^{-22}$	95	28	ALBERT	19B	HAWC annihilation/decay to γ in M31
$<4 \times 10^{-26}$		29	CHEUNG	19	EDGS $\chi\chi \rightarrow e^+e^-$ and $b\bar{b}$
$<7 \times 10^{-27}$	95	30	DI-MAURO	19	FLAT Fermi-LAT M31 and M33
		31	JOHNSON	19	FLAT P-wave DM; Fermi-LAT
$<2 \times 10^{-26}$	95	32	LI	19D	FLAT $\chi\chi \rightarrow \gamma$
$<1 \times 10^{-32}$		33	NG	19	sterile ν decay/annihilation
		34	QUEIROZ	19	semi-annihilating DM
$<4 \times 10^{-28}$	95	35	ABDALLAH	18	HESS $X^0X^0 \rightarrow \gamma X$; galactic halo
$<1 \times 10^{-23}$	95	36	AHNEN	18	MGIC $X^0X^0 \rightarrow \gamma X$; Ursa Major II
$<1 \times 10^{-22}$	95	37	ALBERT	18B	HAWC $X^0X^0 \rightarrow \gamma X$; Andromeda
$<1 \times 10^{-26}$	95	38	CHANG	18A	HAWC $\chi\chi \rightarrow b\bar{b} \rightarrow \gamma$
		39	LISANTI	18	THEO Fermi, γ ; galaxy groups
		40	MAZZIOTTA	18	FLAT Fermi-LAT CRE data
$<1.2 \times 10^{-23}$	95	41	AARTSEN	17C	ICCB $\chi\chi \rightarrow$ neutrinos
$<1 \times 10^{-23}$	90	42	ALBERT	17A	ANTR ν , DM annihilation
$<1.32 \times 10^{-25}$		43	ARCHAMBAU	17	VRTS γ dwarf galaxies
$<7 \times 10^{-21}$	90	44	AVRORIN	17	BAIK cosmic ν
$<1 \times 10^{-28}$		45	BOUDAUD	17	MeV DM to e^+e^-
		46	AARTSEN	16D	ICCB ν , galactic center
$<6 \times 10^{-26}$	95	47	ABDALLAH	16	HESS Central Galactic Halo
$<1 \times 10^{-27}$	95	48	ABDALLAH	16A	HESS WIMP+WIMP $\rightarrow \gamma\gamma$; galactic center
$<3 \times 10^{-26}$	95	49	AHNEN	16	MGFL Satellite galaxy, $m(\text{WIMP})=100 \text{ GeV}$
$<1.9 \times 10^{-21}$	90	50	AVRORIN	16	BAIK νs from galactic center
$<3 \times 10^{-26}$	95	51	CAPUTO	16	FLAT small Magellanic cloud
$<1 \times 10^{-25}$	95	52	FORNASA	16	FLAT Fermi-LAT γ -ray anisotropy
$<5 \times 10^{-27}$		53	LEITE	16	WIMP, radio
$<2 \times 10^{-26}$	95	54	LI	16	FLAT dwarf galaxies
$<1 \times 10^{-25}$	95	55	LI	16A	FLAT Fermi-LAT; M31
$<1 \times 10^{-26}$		56	LIANG	16	FLAT Fermi-LAT, gamma line
$<1 \times 10^{-25}$	95	57	LU	16	FLAT Fermi-LAT and AMS-02
$<1 \times 10^{-23}$	95	58	SHIRASAKI	16	FLAT extra galactic
		59	AARTSEN	15C	ICCB ν , Galactic halo
		60	AARTSEN	15E	ICCB ν , Galactic center
		61	ABRAMOWSKI	15	HESS Galactic center
		62	ACKERMANN	15	FLAT monochromatic γ
		63	ACKERMANN	15A	FLAT isotropic γ background
		64	ACKERMANN	15B	FLAT Satellite galaxy
		65	ADRIAN-MAR	15	ANTR ν , Galactic center
$<2.90 \times 10^{-26}$	95	66,67	ACKERMANN	14	FLAT Satellite galaxy, $m = 10 \text{ GeV}$
$<1.84 \times 10^{-25}$	95	66,68	ACKERMANN	14	FLAT Satellite galaxy, $m = 100 \text{ GeV}$
$<1.75 \times 10^{-24}$	95	66,68	ACKERMANN	14	FLAT Satellite galaxy, $m = 1 \text{ TeV}$
$<4.52 \times 10^{-24}$	95	69	ALEKSIK	14	MGIC Segue 1, $m = 1.35 \text{ TeV}$
		70	AARTSEN	13C	ICCB Galaxies
		71	ABRAMOWSKI	13	HESS Central Galactic Halo
		72	ACKERMANN	13A	FLAT Galaxy
		73	ABRAMOWSKI	12	HESS Fornax Cluster
		74	ACKERMANN	12	FLAT Galaxy
		75	ACKERMANN	12	FLAT Galaxy
		76	ALIU	12	VRTS Segue 1
$<1 \times 10^{-22}$	90	77	ABBASI	11C	ICCB Galactic halo, $m=1 \text{ TeV}$
$<3 \times 10^{-25}$	95	78	ABRAMOWSKI	11	HESS Near Galactic center, $m=1 \text{ TeV}$
$<1 \times 10^{-26}$	95	79	ACKERMANN	11	FLAT Satellite galaxy, $m=10 \text{ GeV}$
$<1 \times 10^{-25}$	95	79	ACKERMANN	11	FLAT Satellite galaxy, $m=100 \text{ GeV}$
$<1 \times 10^{-24}$	95	79	ACKERMANN	11	FLAT Satellite galaxy, $m=1 \text{ TeV}$
		2	ABBASI	23B	search for PeV-scale WIMP-WIMP annihilation to μ or b pairs. No signal observed. Require $\langle\sigma v\rangle < 10^{-22} \text{ cm}^3/\text{s}$ for $\chi\chi \rightarrow b\bar{b}$ with $m(\chi)$ about 1 PeV or $\langle\sigma v\rangle < 10^{-23} \text{ cm}^3/\text{s}$ for $\chi\chi \rightarrow \mu^+\mu^-$ with $m(\chi)$ about 1 PeV.
		3	ABE	23b	search for WIMP-WIMP annihilation to γ in GC. No signal observed. Require $\langle\sigma v\rangle < 5 \times 10^{-28} \text{ cm}^3/\text{s}$ for $m(\chi) = 1 \text{ TeV}$ or $\langle\sigma v\rangle < 1 \times 10^{-25} \text{ cm}^3/\text{s}$ for $m(\chi) = 100 \text{ TeV}$.
		4	ALBERT	23	search for WIMP pair annihilation to γ in galactic halo. No signal observed. Limits placed in $\langle\sigma v\rangle$ vs. mass (10–100 TeV) plane for various annihilation channels.
		5	CHENG	23A	provide updated combined Fermi-LAT/DAMPE search for gamma line from WIMP annihilation. No signal observed. Limits placed in $\langle\sigma v\rangle$ vs. mass (6–200 GeV) plane for various halo profiles.
		6	FOSTER	23	search for gamma ray line in Fermi-LAT data. No signal observed. Limits placed in $\langle\sigma v\rangle$ vs. $m(\chi)$ plane. For Higgsino DM limit see Fig. 12.
		7	GUO	23	search with Five-hundred-meter Aperture Spherical Radio Telescope for synchrotron emission radio signal of DM annihilation from dwarf spheroidal galaxy. No signal observed. Limits set in $\langle\sigma v\rangle$ vs. $m(\chi)$ plane for various annihilation final states.
		8	GUO	23A	search in public IceCube data for DM annihilation to neutrinos. No signal observed. Limits placed in $\langle\sigma v\rangle$ vs. $m(\chi)$ plane for various annihilation assumptions.
		9	LAVIS	23	search for 2HDM+S DM and generic spectra using MeerKAT. No signal observed. Limits placed in $\langle\sigma v\rangle$ vs. mass (10–1000 GeV) plane for various annihilation channels.
		10	ABDALLA	22	search for WIMP annihilation in galactic center to gamma rays using HESS; no signal observed; limits set in mass vs $\langle\sigma v\rangle$ plane for dominant annihilation to $W W$ or $\tau\tau$. Limit here for $\tau\tau$ channel 0.7 TeV mass.
		11	ALBERT	22A	search for secluded PeV-scale DM annihilation to four final states; no signal detected; limits placed in $\langle\sigma v\rangle$ vs. $m(\chi)$ plane for $m(\chi)$: 6–6000 TeV for $m(\text{mediator}) = 50, 250, \text{ and } 1000 \text{ GeV}$.
		12	CHAN	22	derive a variety of limits on DM annihilation to various channels resulting in X-rays from dwarf galaxy Omega Centauri. Limits are very dependent on assumed DM density and diffusion coefficient. Quoted limit is for $m(\text{WIMP}) = 100 \text{ GeV}$ annihilating to $W W$ with parameters as in Fig. 4.
		13	EGOROV	22	derives limits on DM annihilation to $b\bar{b}$ or $\tau\tau$ via radio signals from M31; quoted limit from $b\bar{b}$ channel with LOFAR telescope as main data source, using parameters as in Fig. 10 (green curve) for $m(\chi) = 100 \text{ GeV}$.
		14	MANCONI	22	use polarized synchrotron emission data from Planck to constrain WIMP annihilation cross section in Galaxy; limits set in $\langle\sigma v\rangle$ vs. $m(\text{DM})$ plane.
		15	ABDALLAH	21	search for WIMP-WIMP annihilation into 2 monoenergetic γ rays in WLM dwarf irregular galaxy using HESS data. No signal. Limits placed in $\langle\sigma v\rangle$ vs. $m(\text{WIMP})$ plane for a mass of 370 GeV.
		16	CIRELLI	21	derive limits on light DM annihilation to $ee, \mu\mu, \pi\pi$ that then produce X-rays using data published by INTEGRAL telescope. Limits placed in $\langle\sigma v\rangle$ vs. $m(\text{DM})$ plane for $m(\text{DM}) = 1\text{--}5000 \text{ MeV}$.
		17	JOHN	21	derive limits on leptophilic DM annihilating to positrons by comparing expected spectra to AMS-02 data. The range $m(\text{DM}): 60\text{--}300 \text{ GeV}$ appears excluded for this type of model, see Fig. 3.
		18	ABAZAJIAN	20	derive new limits on WIMP annihilation in galactic center (GC): $\langle\sigma v\rangle < 2.5 \times 10^{-27} \text{ cm}^3/\text{s}$ for $m(\text{WIMP}) = 50 \text{ GeV}$; seems to rule out WIMP explanation for GC γ excess, favouring an astrophysics origin.
		19	ABDALLAH	20	search for WIMP annihilation in newly discovered by DES dwarf satellite galaxies using HESS; limits placed in $\langle\sigma v\rangle$ vs. $m(\text{DM})$ plane depending on annihilation channel and which dwarf satellite.
		20	ABE	20c	search Super-Kamiokande data for WIMP annihilation to neutrinos in galactic center/halo; no signal; limits placed in $\langle\sigma v\rangle$ vs. $m(\text{DM})$ plane depending on annihilation channel and $m(\text{WIMP})$. Reported limit for annihilation to $\nu\bar{\nu}$ at 1 GeV.
		21	ALBERT	20	search for TeV-scale WIMP annihilation to $\gamma\gamma$ in dwarf spheroidal galaxies; no signal; limits placed in σv vs $m(\text{WIMP})$ plane: e.g. $\sigma v < 2.2 \times 10^{-24} \text{ cm}^3/\text{s}$ for $m(\text{WIMP}) = 1 \text{ TeV}$.
		22	ALBERT	20A	search for WIMP annihilation to νs in galactic center using Antares; limits placed in σv vs $m(\text{WIMP})$ plane e.g. $\sigma v < 5 \times 10^{-24} \text{ cm}^3/\text{s}$ for $m(\text{WIMP}) = 1 \text{ TeV}$ assuming annihilation dominantly to $\tau\tau$.
		23	ALBERT	20C	report combined Antares + IceCube search for WIMP annihilation to $\tau\tau$; for RFW halo profile report $\sigma v < 1 \times 10^{-23} \text{ cm}^3/\text{s}$ for $m(\text{WIMP}) = 100 \text{ GeV}$.
		24	ALVAREZ	20	use profiling over J-factor distributions and background to derive new limits on σv ; e.g. $\sigma v < 8 \times 10^{-26} \text{ cm}^3/\text{s}$ for $m(\text{WIMP}) = 100 \text{ GeV}$.
		25	HOOF	20	examine γ rays from 27 dwarf spheroidals using Fermi-LAT data; place limits in σv vs $m(\text{WIMP})$ plane using profile likelihood and marginalized posterior techniques for DM annihilation to $\tau\tau$ and $b\bar{b}$; quoted limit uses first technique and $b\bar{b}$ channel for $m(\text{WIMP}) = 100 \text{ GeV}$; results rule out WIMP explanation of galactic center excess.
		26	MAZZIOTTA	20	use Fermi-LAT pointed-at-Sun data to search for DM annihilation in the Sun to long-lived mediators decaying into gamma rays, i.e. $\chi\chi \rightarrow \phi\phi \rightarrow 4\gamma$. Limits placed on the SI and SD DM-nucleon cross sections in the σ -DM mass plane for DM masses in the range 3 GeV – 1.8 TeV. Limits are evaluated in both cases of equilibrium and non-equilibrium.
		27	ABEYSEKARA	19	search for γs from DM annihilation in galactic substructures with HAWC; no signal, limits placed in $J(\langle\sigma v\rangle)$ vs. declination plane for $m(\text{DM}) \sim 1\text{--}108 \text{ TeV}$.
		28	ALBERT	19b	search for DM signal from M31 galaxy in μ, τ, t, b, W channels using HAWC for $m(\text{DM}) \sim 1\text{--}100 \text{ TeV}$; no signal, limits placed in $\langle\sigma v\rangle$ vs. $m(\text{DM})$ plane.
		29	CHEUNG	19	derive model-dependent bounds on $\langle\sigma v\rangle$ from EDGES data: $< 4 \times 10^{-26} \text{ cm}^3/\text{s}$ for e^+e^- and $b\bar{b}$ for $m(\chi) = 100 \text{ GeV}$ (including boost factor).
		30	DI-MAURO	19	place limits on WIMP annihilation via Fermi-LAT observation of M31 and M33 galaxies: $\langle\sigma v\rangle < 7 \times 10^{-27} \text{ cm}^3/\text{s}$ for $m(\chi) = 20 \text{ GeV}$ from M31.
		31	JOHNSON	19	search for γ -rays, 10–600 GeV energy, from P-wave annihilating DM around SgrA* BH using Fermi-LAT; limits set for various models.
		32	LI	19d	search for $\chi\chi \rightarrow \gamma$ in Fermi-LAT data; no signal, require $\langle\sigma v\rangle < 2 \times 10^{-26} \text{ cm}^3/\text{s}$ for $m(\chi) = 100 \text{ GeV}$.
		33	NG	19	search for X-ray line from sterile ν decay/annihilation using NuStar M-31; no signal: limits placed in $m(\nu)$ vs mixing angle and $\langle\sigma v\rangle$ vs $m(\nu)$.
		34	QUEIROZ	19	examine $\chi\chi \rightarrow \chi SM$ semi-annihilation of DM reaction; limits placed for various assumed SM particles in $\langle\sigma v\rangle$ vs. $m(\chi)$ plane.
		35	ABDALLAH	18	search for WIMP WIMP $\rightarrow \gamma X$ in central galactic halo, 10 years of data; limits placed in $\langle\sigma v\rangle$ vs. $m(\text{WIMP})$ plane for $m(\text{WIMP}): 0.3\text{--}70 \text{ TeV}$.

¹ABBASI 23A search for WIMP-WIMP annihilation to νs . No signal observed. Require $\langle\sigma v\rangle < 10^{-24} \text{ cm}^3/\text{s}$ for $m(\chi) \sim 10\text{--}10^4 \text{ GeV}$ for various halo profiles.

Searches Particle Listings

WIMP and Dark Matter Searches

- 36 AHNEN 18 search for WIMP $WIMP \rightarrow \gamma X$ from Ursa Major II; limits set in $\langle \sigma \cdot v \rangle$ vs. $m(WIMP)$ plane for $b\bar{b}$, $W^+ W^-$, $\tau^+ \tau^-$, and $\mu^+ \mu^-$ annihilation modes.
- 37 ALBERT 18b search for TeV-scale WIMPs with WIMP $WIMP \rightarrow \gamma X$ in Andromeda galaxy using HAWC Observatory; limits set in $\langle \sigma \cdot v \rangle$ vs $m(WIMP)$ plane.
- 38 CHANG 18a examine $\chi\chi \rightarrow b\bar{b} \rightarrow \gamma$ using Fermi Pass 8 data; no signal; require $\langle \sigma \cdot v \rangle < 10^{-26} \text{ cm}^3/\text{s}$ for $m(\chi) = 50 \text{ GeV}$.
- 39 LISANTI 18 examine Fermi Pass 8 γ -ray data from galaxy groups; report $m(WIMP) > 30 \text{ GeV}$ for annihilation in $b\bar{b}$ channel.
- 40 MAZZIOTTA 18 examine Fermi-LAT electron and positron spectra searching for features originating from DM particles annihilation into $e^+ e^-$ pairs, from 45 GeV to 2 TeV; no signal found, limits are obtained.
- 41 AARTSEN 17c use 1005 days of IceCube data to search for $\chi\chi \rightarrow$ neutrinos via various annihilation channels. Limits set.
- 42 ALBERT 17a search for DM annihilation to νs using ANTARES data from 2007–2015. No signal. Limits set in $\langle \sigma \cdot v \rangle$ vs. $m(DM)$ plane for $m(DM) \sim 10\text{--}10 \times 10^5 \text{ GeV}$. The listed limit is for $m(DM) = 100 \text{ TeV}$.
- 43 ARCHAMBAULT 17 set limits for WIMP mass between 100 GeV and 1 TeV on $\langle \sigma \cdot v \rangle$ for $W^+ W^-$, $Z Z$, $b\bar{b}$, $s\bar{s}$, $u\bar{u}$, $d\bar{d}$, $t\bar{t}$, $e^+ e^-$, $g g$, $c\bar{c}$, $h h$, $\gamma\gamma$, $\mu^+ \mu^-$, $\tau^+ \tau^-$ annihilation channels.
- 44 AVRORIN 17 find upper limits for the annihilation cross section in various channels for DM particle mass between 30 GeV and 10 TeV. Strongest upper limits coming from the two neutrino channel require $\langle \sigma \cdot v \rangle < 6 \times 10^{-20} \text{ cm}^3/\text{s}$ in dwarf galaxies and $\langle \sigma \cdot v \rangle < 7 \times 10^{-21} \text{ cm}^3/\text{s}$ in LMC for 5 TeV WIMP mass.
- 45 BOUDAUD 17 use data from the spacecraft Voyager 1, beyond the heliopause, and from AMS02 on $\chi\chi \rightarrow e^+ e^-$ to require $\langle \sigma \cdot v \rangle < 1. \times 10^{-28} \text{ cm}^3/\text{s}$ for $m(\chi) = 10 \text{ MeV}$.
- 46 AARTSEN 16d search for GeV νs from WIMP annihilation in galaxy; limits set on $\langle \sigma \cdot v \rangle$ in Fig. 6, 7.
- 47 ABDALLAH 16 require $\langle \sigma \cdot v \rangle < 6 \times 10^{-26} \text{ cm}^3/\text{s}$ for $m(WIMP) = 1.5 \text{ TeV}$ from 254 hours observation ($W W$ channel) and $< 2 \times 10^{-26} \text{ cm}^3/\text{s}$ for $m(WIMP) = 1.0 \text{ TeV}$ in $\tau^+ \tau^-$ channel.
- 48 ABDALLAH 16a search for line spectra from WIMP + WIMP $\rightarrow \gamma\gamma$ in 18 hr HESS data; rule out previous 130 GeV WIMP hint from Fermi-LAT data.
- 49 AHNEN 16 require $\langle \sigma \cdot v \rangle < 3 \times 10^{-26} \text{ cm}^3/\text{s}$ for $m(WIMP) = 100 \text{ GeV}$ ($W W$ channel).
- 50 AVRORIN 16 require $\langle \sigma \cdot v \rangle < 1.91 \times 10^{-21} \text{ cm}^3/\text{s}$ from WIMP annihilation to νs via $W W$ channel for $m(WIMP) = 1 \text{ TeV}$.
- 51 CAPUTO 16 place limits on WIMPs from annihilation to gamma rays in Small Magellanic Cloud using Fermi-LAT data: $\langle \sigma \cdot v \rangle < 3 \times 10^{-26} \text{ cm}^3/\text{s}$ for $m(WIMP) = 10 \text{ GeV}$.
- 52 FORNASE 16 use anisotropies in the γ -ray diffuse emission detected by Fermi-LAT to bound $\langle \sigma \cdot v \rangle < 10^{-25} \text{ cm}^3/\text{s}$ for $m(WIMP) = 100 \text{ GeV}$ in $b\bar{b}$ channel: see Fig. 28. The limit is driven by dark-matter subhalos in the Milky Way and it refers to their Most Constraining Scenario.
- 53 LEITE 16 constrain WIMP annihilation via search for radio emissions from Smith cloud; $\langle \sigma \cdot v \rangle < 5 \times 10^{-27} \text{ cm}^3/\text{s}$ in ee channel for $m(WIMP) = 5 \text{ GeV}$.
- 54 LI 16 re-analyze Fermi-LAT data on 8 dwarf spheroidal; set limit $\langle \sigma \cdot v \rangle < 2 \times 10^{-26} \text{ cm}^3/\text{s}$ for $m(WIMP) = 100 \text{ GeV}$ in $b\bar{b}$ mode with substructures included.
- 55 LI 16a constrain $\langle \sigma \cdot v \rangle < 10^{-25} \text{ cm}^3/\text{s}$ in $b\bar{b}$ channel for $m(WIMP) = 100 \text{ GeV}$ using Fermi-LAT data from M31; see Fig. 6.
- 56 LIANG 16 search dwarf spheroidal galaxies, Large Magellanic Cloud, and Small Magellanic Cloud for γ -line in Fermi-LAT data.
- 57 LU 16 re-analyze Fermi-LAT and AMS-02 data; require $\langle \sigma \cdot v \rangle < 10^{-25} \text{ cm}^3/\text{s}$ for $m_m(WIMP) = 1 \text{ TeV}$ in $b\bar{b}$ channel.
- 58 SHIRASAKI 16 re-analyze Fermi-LAT extra-galactic data; require $\langle \sigma \cdot v \rangle < 10^{-23} \text{ cm}^3/\text{s}$ for $m(WIMP) = 1 \text{ TeV}$ in $b\bar{b}$ channel; see Fig. 8.
- 59 AARTSEN 15c search for neutrinos from X^0 annihilation in the Galactic halo. See their Figs. 16 and 17, and Table 5 for limits on $\sigma \cdot v$ for X^0 mass between 100 GeV and 100 TeV.
- 60 AARTSEN 15E search for neutrinos from X^0 annihilation in the Galactic center. See their Figs. 7 and 9, and Table 3 for limits on $\sigma \cdot v$ for X^0 mass between 30 GeV and 10 TeV.
- 61 ABRAMOWSKI 15 search for γ from X^0 annihilation in the Galactic center. See their Fig. 4 for limits on $\sigma \cdot v$ for X^0 mass between 250 GeV and 10 TeV.
- 62 ACKERMANN 15 search for monochromatic γ from X^0 annihilation in the Galactic halo. See their Fig. 8 and Tables 2–4 for limits on $\sigma \cdot v$ for X^0 mass between 0.2 GeV and 500 GeV.
- 63 ACKERMANN 15A search for γ from X^0 annihilation (both Galactic and extragalactic) in the isotropic γ background. See their Fig. 7 for limits on $\sigma \cdot v$ for X^0 mass between 10 GeV and 30 TeV.
- 64 ACKERMANN 15B search for γ from X^0 annihilation in 15 dwarf spheroidal satellite galaxies of the Milky Way. See their Figs. 1 and 2 for limits on $\sigma \cdot v$ for X^0 mass between 2 GeV and 10 TeV.
- 65 ADRIAN-MARTINEZ 15 search for neutrinos from X^0 annihilation in the Galactic center. See their Figs. 10 and 11 and Tables 1 and 2 for limits on $\sigma \cdot v$ for X^0 mass between 25 GeV and 10 TeV.
- 66 ACKERMANN 14 search for γ from X^0 annihilation in 25 dwarf spheroidal satellite galaxies of the Milky Way. See their Tables II–VII for limits assuming annihilation into $e^+ e^-$, $\mu^+ \mu^-$, $\tau^+ \tau^-$, $u\bar{u}$, $b\bar{b}$, and $W^+ W^-$, for X^0 mass ranging from 2 GeV to 10 TeV.
- 67 Limit assuming X^0 pair annihilation into $b\bar{b}$.
- 68 Limit assuming X^0 pair annihilation into $W^+ W^-$.
- 69 ALEKSIC 14 search for γ from X^0 annihilation in the dwarf spheroidal galaxy Segue 1. The listed limit assumes annihilation into $W^+ W^-$. See their Figs. 6, 7, and 16 for limits on $\sigma \cdot v$ for annihilation channels $\mu^+ \mu^-$, $\tau^+ \tau^-$, $b\bar{b}$, $t\bar{t}$, $\gamma\gamma$, γZ , $W^+ W^-$, $Z Z$ for X^0 mass between 10^2 and 10^4 GeV .
- 70 AARTSEN 13c search for neutrinos from X^0 annihilation in nearby galaxies and galaxy clusters. See their Figs. 5–7 for limits on $\sigma \cdot v$ for $X^0 \rightarrow \nu\bar{\nu}$, $\mu^+ \mu^-$, $\tau^+ \tau^-$, and $W^+ W^-$ for X^0 mass between 300 GeV and 100 TeV.
- 71 ABRAMOWSKI 13 search for monochromatic γ from X^0 annihilation in the Milky Way halo in the central region. Limit on $\sigma \cdot v$ between 10^{-28} and $10^{-25} \text{ cm}^3 \text{ s}^{-1}$ (95% CL) is obtained for X^0 mass between 500 GeV and 20 TeV for $X^0 X^0 \rightarrow \gamma\gamma$. X^0 density distribution in the Galaxy by Einasto is assumed. See their Fig. 4.

- 72 ACKERMANN 13A search for monochromatic γ from X^0 annihilation in the Milky Way. Limit on $\sigma \cdot v$ for the process $X^0 X^0 \rightarrow \gamma\gamma$ in the range $10^{-29}\text{--}10^{-27} \text{ cm}^3 \text{ s}^{-1}$ (95% CL) is obtained for X^0 mass between 5 and 300 GeV. The limit depends slightly on the assumed density profile of X^0 in the Galaxy. See their Tables VII–X and Fig. 10. Supersedes ACKERMANN 12.
- 73 ABRAMOWSKI 12 search for γ 's from X^0 annihilation in the Fornax galaxy cluster. See their Fig. 7 for limits on $\sigma \cdot v$ for X^0 mass between 0.1 and 100 TeV for the annihilation channels $\tau^+ \tau^-$, $b\bar{b}$, and $W^+ W^-$.
- 74 ACKERMANN 12 search for monochromatic γ from X^0 annihilation in the Milky Way. Limit on $\sigma \cdot v$ in the range $10^{-28}\text{--}10^{-26} \text{ cm}^3 \text{ s}^{-1}$ (95% CL) is obtained for X^0 mass between 7 and 200 GeV if X^0 annihilates into $\gamma\gamma$. The limit depends slightly on the assumed density profile of X^0 in the Galaxy. See their Table III and Fig. 15.
- 75 ACKERMANN 12 search for γ from X^0 annihilation in the Milky Way in the diffuse γ background. Limit on $\sigma \cdot v$ of $10^{-24} \text{ cm}^3 \text{ s}^{-1}$ or larger is obtained for X^0 mass between 5 GeV and 10 TeV for various annihilation channels including $W^+ W^-$, $b\bar{b}$, $g g$, $e^+ e^-$, $\mu^+ \mu^-$, $\tau^+ \tau^-$. The limit depends slightly on the assumed density profile of X^0 in the Galaxy. See their Figs. 17–20.
- 76 ALIU 12 search for γ 's from X^0 annihilation in the dwarf spheroidal galaxy Segue 1. Limit on $\sigma \cdot v$ in the range $10^{-24}\text{--}10^{-20} \text{ cm}^3 \text{ s}^{-1}$ (95% CL) is obtained for X^0 mass between 10 GeV and 2 TeV for annihilation channels $e^+ e^-$, $\mu^+ \mu^-$, $\tau^+ \tau^-$, $b\bar{b}$, and $W^+ W^-$. See their Fig. 3.
- 77 ABBASI 11c search for ν_μ from X^0 annihilation in the outer halo of the Milky Way. The limit assumes annihilation into $\nu\nu$. See their Fig. 9 for limits with other annihilation channels.
- 78 ABRAMOWSKI 11 search for γ from X^0 annihilation near the Galactic center. The limit assumes Einasto DM density profile.
- 79 ACKERMANN 11 search for γ from X^0 annihilation in ten dwarf spheroidal satellite galaxies of the Milky Way. The limit for $m = 10 \text{ GeV}$ assumes annihilation into $b\bar{b}$, the others $W^+ W^-$. See their Fig. 2 for limits with other final states. See also GERINGER-SAMETH 11 for a different analysis of the same data.

Dark Matter Particle (X^0) Production in Hadron Collisions

Searches for X^0 production in association with observable particles (γ , jets, ...) in high energy hadron collisions. If a specific form of effective interaction Lagrangian is assumed, the limits may be translated into limits on X^0 -nucleon scattering cross section.

VALUE	DOCUMENT ID	TECN	COMMENT
• • •	We do not use the following data for averages, fits, limits, etc. • • •		
1	AAD	23A ATLS	$H \rightarrow$ invisible search
2	AAD	23AF ATLS	$\bar{t}t + H \rightarrow$ invisible search
3	AAD	23AJ ATLS	extended 2HDM search
4	AAD	23BX ATLS	$H a, a \rightarrow$ DM search
5	AAD	23W ATLS	dark Higgs model
6	AKIMOV	23	COHR LDM search at SNS
7	LIN	23C KOTO	$\chi \rightarrow \gamma\gamma$ from K_L^0 decay
8	AAD	22D ATLS	$Z+H$ with $H \rightarrow$ DM
9	AAD	22P ATLS	$H \rightarrow \chi\chi$ search via VBF
10	AGUILAR-AR...	22A CCM	p dump search for MeV-scale DM
11	TU MASYAN	22AA CMS	$Z' \rightarrow$ DM search
12	TU MASYAN	22AG CMS	strongly interacting DM search
13	TU MASYAN	22G CMS	DM search via VBF to Higgs
14	AAD	21AZ ATLS	DM search in $H \cancel{E}_T \rightarrow \gamma\gamma \cancel{E}_T$
15	AAD	21BB ATLS	DM search in $H \cancel{E}_T \rightarrow b\bar{b} \cancel{E}_T$
16	AAD	21D ATLS	Dark Higgs
17	AAD	21F ATLS	jet + missing momentum
18	AAD	21K ATLS	photon + DM
19	AAD	21O ATLS	$\ell +$ jets + \cancel{E}_T to search for t -pairs + DM
20	AAD	21P ATLS	$\ell^+ \ell^- +$ jets + \cancel{E}_T
21	AAD	21S ATLS	b -jets + \cancel{E}_T
22	SIRUNYAN	21A CMS	$pp \rightarrow Z\chi\chi; Z \rightarrow \ell\bar{\ell}$
23	TU MASYAN	21D CMS	DM search in jets + \cancel{E}_T
24	SIRUNYAN	20X CMS	$pp \rightarrow Z' \rightarrow A(Z')h \rightarrow h + \cancel{E}_T$
25	AABOUD	19AA ATLS	multi-channel BSM search
26	AABOUD	19AI ATLS	$H \rightarrow \chi\chi$
27	AABOUD	19AL ATLS	$H \rightarrow \chi\chi$
28	AABOUD	19Q ATLS	single $t+\cancel{E}_T$
29	AABOUD	19V ATLS	review mediator based DM searches
30	BANERJEE	19 NA64	$eN \rightarrow eN+\cancel{E}$
31	SIRUNYAN	19AN CMS	$H\chi\chi \rightarrow b\bar{b} \cancel{E}_T$
32	SIRUNYAN	19BC CMS	$LQ LQ \rightarrow \mu j \cancel{E}_T$
33	SIRUNYAN	19Bo CMS	$VV \rightarrow Hqq; H \rightarrow$ DM
34	SIRUNYAN	19c CMS	$pp \rightarrow t\bar{t}\chi\chi$
35	SIRUNYAN	19o CMS	$pp \rightarrow \gamma \cancel{E}_T$
36	SIRUNYAN	19X CMS	$pp \rightarrow t\bar{t} + \cancel{E}_T; pp \rightarrow t(\bar{t}) + \cancel{E}_T$
37	AABOUD	18 ATLS	$pp \rightarrow Z\chi\chi; Z \rightarrow \ell\ell$
38	AABOUD	18A ATLS	$pp \rightarrow t\bar{t} \cancel{E}_T; pp \rightarrow b\bar{b} \cancel{E}_T$
39	AABOUD	18CA ATLS	$pp \rightarrow V\chi\chi; V \rightarrow jj$
40	AABOUD	18I ATLS	$pp \rightarrow \text{jet}(s) + \cancel{E}_T$
41	AGUILAR-AR...	18B MBNE	$pN \rightarrow \chi X, \chi = e, \pi, \text{ or } N$
42	KHACHATRY...	18 CMS	$pp \rightarrow Z(\ell\ell) + \cancel{E}_T$
43	SIRUNYAN	18BF CMS	$pp \rightarrow t \cancel{E}_T$
44	SIRUNYAN	18Bo CMS	dijet resonance search
45	SIRUNYAN	18BV CMS	$pp \rightarrow Z \cancel{E}_T$
46	SIRUNYAN	18c CMS	$pp \rightarrow t\bar{t} \cancel{E}_T$

- | | | | |
|----|---------------|-----------|--|
| 47 | SIRUNYAN | 18CU CMS | $pp \rightarrow Z \cancel{E}_T$ |
| 48 | SIRUNYAN | 18DH CMS | $pp \rightarrow \chi\chi h; h \rightarrow \gamma\gamma \text{ or } \tau\tau$ |
| 49 | SIRUNYAN | 18S CMS | $pp \rightarrow \text{jets } \cancel{E}_T$ |
| 50 | AABOUD | 17A ATLS | $pp (H \rightarrow b\bar{b} + \text{WIMP pair})$ |
| 51 | AABOUD | 17AMATLS | $pp \rightarrow Z' \rightarrow Ah \rightarrow h(b\bar{b}) + \cancel{E}_T$ |
| 52 | AABOUD | 17AQ ATLS | $pp \rightarrow h(\gamma\gamma) + \cancel{E}_T$ |
| 53 | AABOUD | 17BD ATLS | $pp \rightarrow \text{jet}(s) + \cancel{E}_T$ |
| 54 | AABOUD | 17R ATLS | $pp \rightarrow \gamma \cancel{E}_T$ |
| 55 | AGUILAR-AR... | 17A MBNE | $pN \rightarrow \chi\chi X; \chi N \rightarrow \chi N$ |
| 56 | BANERJEE | 17 NA64 | $eN \rightarrow eN\gamma'$ |
| 57 | KHACHATRY... | 17A CMS | forward jets + \cancel{E}_T |
| 58 | KHACHATRY... | 17F CMS | $H \rightarrow \text{invisibles}$ |
| 59 | SIRUNYAN | 17 CMS | $Z + \cancel{E}_T$ |
| 60 | SIRUNYAN | 17AP CMS | $pp \rightarrow Z' \rightarrow Ah \rightarrow h + \cancel{E}_T$ |
| 61 | SIRUNYAN | 17AQ CMS | $pp \rightarrow \gamma + \cancel{E}_T$ |
| 62 | SIRUNYAN | 17BB CMS | $pp \rightarrow t\bar{t} + \cancel{E}_T; pp \rightarrow b\bar{b} + \cancel{E}_T$ |
| 63 | SIRUNYAN | 17G CMS | $pp \rightarrow j + \cancel{E}_T$ |
| 64 | SIRUNYAN | 17U CMS | $pp \rightarrow Z\chi\chi; Z \rightarrow \ell\bar{\ell}$ |
| 65 | AABOUD | 16AD ATLS | $(W \text{ or } Z \rightarrow \text{jets}) + \cancel{E}_T$ |
| 66 | AAD | 16AF ATLS | $VV \rightarrow \text{forward jets } + \cancel{E}_T$ |
| 67 | AAD | 16AG ATLS | $\ell + \text{jets}$ |
| 68 | AAD | 16M ATLS | $pp \rightarrow H + \cancel{E}_T, H \rightarrow b\bar{b}$ |
| 69 | KHACHATRY... | 16BZ CMS | jet(s) + \cancel{E}_T |
| 70 | KHACHATRY... | 16CA CMS | jets + \cancel{E}_T |
| 71 | KHACHATRY... | 16N CMS | $pp \rightarrow \gamma + \cancel{E}_T$ |
| 72 | AAD | 15AS ATLS | $b(\bar{b}) + \cancel{E}_T, t\bar{t} + \cancel{E}_T$ |
| 73 | AAD | 15BH ATLS | jet + \cancel{E}_T |
| 74 | AAD | 15CF ATLS | $H^0 + \cancel{E}_T$ |
| 75 | AAD | 15CS ATLS | $\gamma + \cancel{E}_T$ |
| 76 | KHACHATRY... | 15AG CMS | $t\bar{t} + \cancel{E}_T$ |
| 77 | KHACHATRY... | 15AL CMS | jet + \cancel{E}_T |
| 78 | KHACHATRY... | 15T CMS | $\ell + \cancel{E}_T$ |
| 79 | AAD | 14AI ATLS | $W + \cancel{E}_T$ |
| 80 | AAD | 14BK ATLS | $W, Z + \cancel{E}_T$ |
| 81 | AAD | 14K ATLS | $Z + \cancel{E}_T$ |
| 82 | AAD | 14O ATLS | $Z + \cancel{E}_T$ |
| 83 | AAD | 13AD ATLS | jet + \cancel{E}_T |
| 84 | AAD | 13C ATLS | $\gamma + \cancel{E}_T$ |
| 85 | AALTONEN | 12K CDF | $t + \cancel{E}_T$ |
| 86 | AALTONEN | 12M CDF | jet + \cancel{E}_T |
| 87 | CHATRCHYAN | 12AP CMS | jet + \cancel{E}_T |
| 88 | CHATRCHYAN | 12T CMS | $\gamma + \cancel{E}_T$ |
- 1 AAD 23A search for $H \rightarrow \text{invisible}$. No signal observed. Results interpreted in terms of several DM Higgs portal simplified models.
- 2 AAD 23AF search for $\tilde{t}t + H \rightarrow \text{invisible}$ with 139 fb⁻¹ of data. No signal observed. Limits placed on branching fractions of H decays etc. for various DM mediator models. Result also included in AAD 23A.
- 3 AAD 23AJ search for $tW\chi\chi$ production in mediator-extended 2HDM with 139 fb⁻¹ of data. No signal observed. Limits placed in $m(H)$ vs. $m(\text{mediator})$ and $\tan(\beta)$ vs. $m(H)$ planes.
- 4 AAD 23BX search for $A \rightarrow Ha$ production where $H \rightarrow \tau\bar{\tau}$ and $a \rightarrow \chi\chi$. No signal observed. Limits placed on 2HDM+a model.
- 5 AAD 23W search for DM in dark Higgs model via $WW\chi\chi$ final state with 139 fb⁻¹ of data. No signal detected. Limits set in $m(\text{dark Higgs})$ vs. $m(Z')$ plane.
- 6 AKIMOV 23 search for light DM via COHERENT CsI detector at SNS. No signal observed. For scalar DM model, limits set for $m(\chi) = 1\text{--}300$ MeV. Limit of $\sigma(\chi N) < 1 \times 10^1$ pb set at peak sensitivity $m(\chi) = 25$ MeV.
- 7 LIN 23C search for $\chi \rightarrow \gamma\gamma$ decay where $p \rightarrow \chi\chi$ at KOTO. No signal observed. Limits placed on K_L^0 branching fraction.
- 8 AAD 22D search for $Z+H$ production with $Z \rightarrow \ell\bar{\ell}$ and $H \rightarrow \chi\chi$ with 139 fb⁻¹ at 13 TeV; no signal found; limits placed in various simplified models depending on Higgs portal and DM mediator.
- 9 AAD 22P search for H production via VBF with $H \rightarrow \chi\chi$ with 139 fb⁻¹ at 13 TeV; no signal found; limits placed for various Higgs DM portal simplified models.
- 10 AGUILAR-AREVALO 22A report search for MeV vector portal and leptophobic DM via scatter on liquid Ar at the Lujan stopped pion source at LANL; no signal detected; limits placed on vector portal and leptophobic DM vs. $m(\chi)$: 1–40 MeV.
- 11 TUMASYAN 22AA search for Z' decay to dark quarks with 138 fb⁻¹ at 13 TeV; no signal observed; limits exclude a wide range of strongly coupled hidden sector models.
- 12 TUMASYAN 22AG search for strongly interacting dark matter production via scalar mediator, with SIMP decay to trackless jets with 16.1 fb⁻¹ at 13 TeV; no signal detected; limits placed in mass vs. cross section plane for simplified models.
- 13 TUMASYAN 22G search for VBF production of Higgs with $H \rightarrow \chi\chi$ with 101 fb⁻¹ at 13 TeV, combined with earlier searches, in total 19.7 fb⁻¹ at 8 TeV and 140 fb⁻¹ at 13 TeV are used; no signal detected; limits placed in mass vs. cross section plane for various Higgs portal simplified models.
- 14 AAD 21AZ search for DM in $H \cancel{E}_T \rightarrow \gamma\gamma \cancel{E}_T$ events with 139 fb⁻¹ at 13 TeV. No signal observed. Limits placed for several simplified models.
- 15 AAD 21BB search for DM in $H \cancel{E}_T \rightarrow b\bar{b} \cancel{E}_T$ events with 139 fb⁻¹ at 13 TeV. No signal observed. Limits placed for several simplified models.
- 16 AAD 21D search for $VV + \chi\chi, V \rightarrow q\bar{q}$ with 139 fb⁻¹ at 13 TeV LHC. No signal detected. Limits placed in dark Higgs boson mass vs. $m(Z')$ plane. Here VV stand for $W^\pm W^\mp, ZZ$.
- 17 AAD 21F search for monojet recoiling against invisibles with 139 fb⁻¹ at 13 TeV LHC. No signal detected. Limits placed in various simplified dark matter models.
- 18 AAD 21K search for a photon recoiling against dark matter with 139 fb⁻¹ at 13 TeV LHC. No signal detected. Limits placed on parameter space of various simplified models.
- 19 AAD 21O search for $\ell + \text{jets} + \cancel{E}_T$ to search for t -pairs + DM particles with 139 fb⁻¹ at LHC 13 TeV LHC. No signal detected. Limits placed in the cross-section vs. mediator mass plane, assuming light DM states.
- 20 AAD 21P search for $\ell^+\ell^- + \text{jets} + \cancel{E}_T$ in context of various BSM models with 139 fb⁻¹ at 13 TeV LHC. No signal observed. Limits placed in parameter space of dark matter models and SUSY.
- 21 AAD 21S search for b -jets + \cancel{E}_T signal from BSM/DM models with 139 fb⁻¹ at 13 TeV LHC. No signal observed. Limits placed on parameter space of DM models.
- 22 SIRUNYAN 21A search for DM production in association with leptonically decaying Z boson in 137 fb⁻¹ at 13 TeV; no signal; limits set in large variety of simplified DM models.
- 23 TUMASYAN 21D search for DM and other exotica at CMS in jets + \cancel{E}_T events with 137 fb⁻¹ at 13 TeV. No signal observed. Limits placed for a variety of simplified models.
- 24 SIRUNYAN 20X search for DM in $pp \rightarrow Z' \rightarrow A(Z')h \rightarrow h + \cancel{E}_T$ in CMS at 13 TeV with 35.9 fb⁻¹; no signal; limits placed in σ^{SI} vs. $m(\chi)$, and $\sigma, m(A)$ and $\tan\beta$ vs $m(Z')$ for considered DM models.
- 25 AABOUD 19AA searches for BSM physics in more than 700 event classes with more than 10⁵ regions at 13 TeV with 3.2 fb⁻¹; no significant signal.
- 26 AABOUD 19AI searches for vector boson fusion $pp \rightarrow Hqq, H \rightarrow \text{invisible}$ at 13 TeV with 36.1 fb⁻¹; no signal; require $B(H \rightarrow \text{invisible}) < 0.37$ (0.28 expected).
- 27 AABOUD 19AL perform search in three different channels for $H \rightarrow \chi\chi$ at 7, 8 and 13 TeV; combined result $B(H \rightarrow \text{invisible}) < 0.26$ (0.17 expected).
- 28 AABOUD 19Q search for single $t + \cancel{E}_T$ at 13 TeV with 36.1 fb⁻¹ of data; no signal; limits set in σ or coupling vs. mass plane for simplified models.
- 29 AABOUD 19V review ATLAS results from 7, 8 and 13 TeV searches for mediator-based DM and DE scalar which couples to gravity; no signal; limits set for large variety of simplified models.
- 30 BANERJEE 19 search for dark photon via $eN \rightarrow eN + \cancel{E}$ in NA64; no signal, limits placed in kinetic mixing ϵ vs. $m(\text{DM})$ plane for $m(\text{DM}) \sim 0.001\text{--}1$ GeV.
- 31 SIRUNYAN 19AN search at 13 TeV with 35.9 fb⁻¹ for $pp \rightarrow H\chi\chi \rightarrow b\bar{b} \cancel{E}_T$; no signal; limits set in the context of a 2HDM + pseudoscalar (a) model and a baryonic Z' model.
- 32 SIRUNYAN 19BC search for DM via LeptoQuark pair annihilation $LQ LQ \rightarrow \mu j \chi\chi \rightarrow \mu j \cancel{E}_T$ with 77.4 fb⁻¹, 13 TeV; no signal; limits placed in $m(\chi)$ vs. $m(LQ)$ plane. Model dependent limits on DM mass up to 600 GeV depending on $m(LQ)$ placed.
- 33 SIRUNYAN 19BO search for vector boson fusion $VV \rightarrow qqH$ with $H \rightarrow \chi\chi$ at 13 TeV with 38.2 fb⁻¹; no signal; limits placed for several models. Also search for $H \rightarrow \text{invisible}$ at 7, 8, and 13 TeV; no signal; limit placed on $BF < 0.19$.
- 34 SIRUNYAN 19C search for DM via $pp \rightarrow t\bar{t}\chi\chi$ at 13 TeV, 35.9 fb⁻¹; no signal; limits placed on coupling vs. mediator mass for various simplified models.
- 35 SIRUNYAN 19O search for $pp \rightarrow \gamma$ at 13 TeV with 35.9 fb⁻¹; no signal; limits placed on parameters of various models.
- 36 SIRUNYAN 19X search for $pp \rightarrow t\bar{t} \cancel{E}_T$ and $pp \rightarrow t \cancel{E}_T + \dots$ at 13 TeV with 35.9 fb⁻¹; no signal; limits placed on χ production σ for various simplified models with $m(\chi) = 1$ GeV.
- 37 AABOUD 18 search for $pp \rightarrow Z + \cancel{E}_T$ with $Z \rightarrow \ell\ell$ at 13 TeV with 36.1 fb⁻¹ of data. Limits set for simplified models.
- 38 AABOUD 18A search for $pp \rightarrow t\bar{t} \cancel{E}_T$ or $pp \rightarrow b\bar{b} \cancel{E}_T$ at 13 TeV, 36.1 fb⁻¹ of data. Limits set for simplified models.
- 39 AABOUD 18CA search for $pp \rightarrow V\chi\chi$ with $V \rightarrow jj$ at 13 TeV, 36.1 fb⁻¹; no signal; limits set in $m(\text{DM})$ vs $m(\text{mediator})$ simplified model plane.
- 40 AABOUD 18 search for $pp \rightarrow j + \cancel{E}_T$ at 13 TeV with 36.1 fb⁻¹ of data. Limits set for simplified models with pair-produced weakly interacting dark-matter candidates.
- 41 AGUILAR-AREVALO 18B search for WIMP production in MiniBooNE p beam dump; no signal; limits set for $m(\chi) \sim 5\text{--}50$ MeV in vector portal DM model.
- 42 KHACHATRYAN 18 search for $pp \rightarrow Z(\ell\ell) + \cancel{E}_T$; no signal; limits set on effective dark matter interactions and other exotic physics models.
- 43 SIRUNYAN 18BF search for $pp \rightarrow t \cancel{E}_T$ at 13 TeV and 36 fb⁻¹; no signal; limits placed on DM models involving a flavor changing neutral current, scalar resonance decaying to top quark and DM.
- 44 SIRUNYAN 18BO search for high mass dijet resonances at 13 TeV and 36 fb⁻¹; no signal; limits placed on various models, including simplified DM models involving a spin = 1 Z' mediator.
- 45 SIRUNYAN 18BV search for $pp \rightarrow Z \cancel{E}_T$ at 13 TeV; no signal, limits placed for various exotic physics models including DM.
- 46 SIRUNYAN 18C search for new physics in $pp \rightarrow$ final states with two oppositely charged leptons at 13 TeV with 35.9 fb⁻¹. Limits placed on $m(\text{mediator})$ and top squark for various simplified models.
- 47 SIRUNYAN 18CU search for $pp \rightarrow Z \cancel{E}_T$ at 13 TeV and 2.3 fb⁻¹; no signal; limits placed for various exotic models including DM.
- 48 SIRUNYAN 18DH search for $pp \rightarrow \chi\chi h; h \rightarrow \gamma\gamma \text{ or } \tau\tau$ at 13 TeV, 35.9 fb⁻¹; no signal; limits placed on massive boson mediator Z' in the context of $Z'+2\text{HDM}$ and baryonic Z' models. Limits also cast in terms of spin-independent WIMP-nucleon cross section for masses 1–200 GeV.
- 49 SIRUNYAN 18S search for $pp \rightarrow \text{jets } \cancel{E}_T$ at 13 TeV; no signal; limits placed on simplified dark matter models, on the branching ratio of the Higgs boson to invisible particles, and on several other exotic physics models including fermion portal DM.
- 50 AABOUD 17A search for $H \rightarrow b\bar{b} + \cancel{E}_T$. See Fig. 4b for limits set on VB mediator vs WIMP mass.
- 51 AABOUD 17AM search for $pp \rightarrow Z' \rightarrow Ah \rightarrow h(b\bar{b}) + \cancel{E}_T$ at 13 TeV. Limits set in $m(Z')$ vs. $m(A)$ plane and on the visible cross section of $h(b\bar{b}) + \cancel{E}_T$ events in bins of \cancel{E}_T .
- 52 AABOUD 17AQ search for WIMP in $pp \rightarrow h(\gamma\gamma) + \cancel{E}_T$ in 36.1 fb⁻¹ of data. Limits on the visible cross section are also provided. Model dependent limits on spin independent DM - Nucleon cross-section are also presented, which are more stringent than those from direct searches for DM mass smaller than 2.5 GeV.
- 53 AABOUD 17BD search for $pp \rightarrow \text{jet}(s) + \cancel{E}_T$ at 13 TeV with 3.2 fb⁻¹ of data. Limits set for simplified models. Observables corrected for detector effects can be used to constrain other models.
- 54 AABOUD 17R, for an axial vector mediator in the s-channel, excludes $m(\text{mediator}) < 750\text{--}1200$ GeV for $m(\text{DM}) < 230\text{--}480$ GeV, depending on the couplings.
- 55 AGUILAR-AREVALO 17A search for DM produced in 8 GeV proton collisions with steel beam dump followed by DM-nucleon scattering in MiniBooNE detector. Limit placed on

Searches Particle Listings

WIMP and Dark Matter Searches

- DM cross section parameter $Y < 2 \times 10^{-8}$ for $\alpha_D = 0.5$ and for $0.01 < m(\text{DM}) < 0.3$ GeV.
- 56 BANERJEE 17 search for dark photon invisible decay via eN scattering; exclude $m(\gamma')$ < 100 MeV as an explanation of $(g_\mu - 2)$ muon anomaly.
- 57 KHACHATRYAN 17A search for WIMPs in forward jets + E_T channel with 18.5 fb $^{-1}$ at 8 TeV; limits set in effective theory model, Fig. 3.
- 58 KHACHATRYAN 17F search for $H \rightarrow$ invisibles in pp collisions at 7, 8, and 13 TeV; place limits on Higgs portal DM.
- 59 SIRUNYAN 17 search for $pp \rightarrow Z + E_T$ with 2.3 fb $^{-1}$ at 13 TeV; no signal seen; limits placed on WIMPs and unparticles.
- 60 SIRUNYAN 17AP search for $pp \rightarrow Z' \rightarrow Ah \rightarrow h + E_T$ with $h \rightarrow b\bar{b}$ or $\gamma\gamma$ and $A \rightarrow \chi\chi$ with 2.3 fb $^{-1}$ at 13 TeV. Limits set in $m(Z')$ vs. $m(A)$ plane.
- 61 SIRUNYAN 17AQ search for $pp \rightarrow \gamma + E_T$ at 13 TeV with 12.9 fb $^{-1}$. Limits derived for simplified DM models, effective electroweak-DM interaction and Extra Dimensions models.
- 62 SIRUNYAN 17BB search for WIMPs via $pp \rightarrow t\bar{t} + E_T, pp \rightarrow b\bar{b} + E_T$ at 13 TeV with 2.2 fb $^{-1}$. Limits derived for various simplified models.
- 63 SIRUNYAN 17G search for $pp \rightarrow j + E_T$ with 12.9 fb $^{-1}$ at 13 TeV; limits placed on WIMP mass/mediators in DM simplified models.
- 64 SIRUNYAN 17U search for WIMPs/unparticles via $pp \rightarrow Z\chi\chi, Z \rightarrow \ell\bar{\ell}$ at 13 TeV with 2.3 fb $^{-1}$. Limits derived for various simplified models.
- 65 AABOUD 16AD place limits on $VVXX$ effective theory via search for hadronic W or Z plus WIMP pair production. See Fig. 5.
- 66 AAD 16AF search for $VV \rightarrow (H \rightarrow \text{WIMP pair}) +$ forward jets with 20.3 fb $^{-1}$ at 8 TeV; set limits in Higgs portal model, Fig. 8.
- 67 AAD 16AG search for lepton jets with 20.3 fb $^{-1}$ of data at 8 TeV; Fig. 13 excludes dark photons around 0.1–1 GeV for kinetic mixing 10^{-6} – 10^{-2} .
- 68 AAD 16M search with 20.3 fb $^{-1}$ of data at 8 TeV pp collisions; limits placed on EFT model (Fig. 7) and simplified Z' model (Fig. 6).
- 69 KHACHATRYAN 16BZ search for jet(s) + E_T in 19.7 fb $^{-1}$ at 8 TeV; limits set for variety of simplified models.
- 70 KHACHATRYAN 16CA search for WIMPs via jet(s) + E_T using razor variable; require mediator scale > 1 TeV for various effective theories.
- 71 KHACHATRYAN 16N search for $\gamma +$ WIMPs in 19.6 fb $^{-1}$ at 8 TeV; limits set on SI and SD WIMP- p scattering in Fig. 3.
- 72 AAD 15AS search for events with one or more bottom quark and missing E_T , and also events with a top quark pair and missing E_T in pp collisions at $E_{\text{cm}} = 8$ TeV with $L = 20.3$ fb $^{-1}$. See their Figs. 5 and 6 for translated limits on X^0 -nucleon cross section for $m = 1$ –700 GeV.
- 73 AAD 15BH search for events with a jet and missing E_T in pp collisions at $E_{\text{cm}} = 8$ TeV with $L = 20.3$ fb $^{-1}$. See their Fig. 12 for translated limits on X^0 -nucleon cross section for $m = 1$ –1200 GeV.
- 74 AAD 15CF search for events with a $H^0 (\rightarrow \gamma\gamma)$ and missing E_T in pp collisions at $E_{\text{cm}} = 8$ TeV with $L = 20.3$ fb $^{-1}$. See paper for limits on the strength of some contact interactions containing X^0 and the Higgs fields.
- 75 AAD 15CS search for events with a photon and missing E_T in pp collisions at $E_{\text{cm}} = 8$ TeV with $L = 20.3$ fb $^{-1}$. See their Fig. 13 (see also erratum) for translated limits on X^0 -nucleon cross section for $m = 1$ –1000 GeV.
- 76 KHACHATRYAN 15AG search for events with a top quark pair and missing E_T in pp collisions at $E_{\text{cm}} = 8$ TeV with $L = 19.7$ fb $^{-1}$. See their Fig. 8 for translated limits on X^0 -nucleon cross section for $m = 1$ –200 GeV.
- 77 KHACHATRYAN 15AL search for events with a jet and missing E_T in pp collisions at $E_{\text{cm}} = 8$ TeV with $L = 19.7$ fb $^{-1}$. See their Fig. 5 and Tables 4–6 for translated limits on X^0 -nucleon cross section for $m = 1$ –1000 GeV.
- 78 KHACHATRYAN 15T search for events with a lepton and missing E_T in pp collisions at $E_{\text{cm}} = 8$ TeV with $L = 19.7$ fb $^{-1}$. See their Fig. 17 for translated limits on X^0 -proton cross section for $m = 1$ –1000 GeV.
- 79 AAD 14AI search for events with a W and missing E_T in pp collisions at $E_{\text{cm}} = 8$ TeV with $L = 20.3$ fb $^{-1}$. See their Fig. 4 for translated limits on X^0 -nucleon cross section for $m = 1$ –1500 GeV.
- 80 AAD 14BK search for hadronically decaying W, Z in association with E_T in 20.3 fb $^{-1}$ at 8 TeV pp collisions. Fig. 5 presents exclusion results for SI and SD scattering cross section. In addition, cross section limits on the anomalous production of W or Z bosons with large missing transverse momentum are also set in two fiducial regions.
- 81 AAD 14K search for events with a Z and missing E_T in pp collisions at $E_{\text{cm}} = 8$ TeV with $L = 20.3$ fb $^{-1}$. See their Fig. 5 and 6 for translated limits on X^0 -nucleon cross section for $m = 1$ – 10^3 GeV.
- 82 AAD 14O search for ZH^0 production with H^0 decaying to invisible final states. See their Fig. 4 for translated limits on X^0 -nucleon cross section for $m = 1$ –60 GeV in Higgs-portal X^0 scenario.
- 83 AAD 13AD search for events with a jet and missing E_T in pp collisions at $E_{\text{cm}} = 7$ TeV with $L = 4.7$ fb $^{-1}$. See their Figs. 5 and 6 for translated limits on X^0 -nucleon cross section for $m = 1$ –1300 GeV.
- 84 AAD 13C search for events with a photon and missing E_T in pp collisions at $E_{\text{cm}} = 7$ TeV with $L = 4.6$ fb $^{-1}$. See their Fig. 3 for translated limits on X^0 -nucleon cross section for $m = 1$ –1000 GeV.
- 85 AALTONEN 12K search for events with a top quark and missing E_T in $p\bar{p}$ collisions at $E_{\text{cm}} = 1.96$ TeV with $L = 7.7$ fb $^{-1}$. Upper limits on $\sigma(tX^0)$ in the range 0.4–2 pb (95% CL) is given for $m_{X^0} = 0$ –150 GeV.
- 86 AALTONEN 12M search for events with a jet and missing E_T in $p\bar{p}$ collisions at $E_{\text{cm}} = 1.96$ TeV with $L = 6.7$ fb $^{-1}$. Upper limits on the cross section in the range 2–10 pb (90% CL) is given for $m_{X^0} = 1$ –300 GeV. See their Fig. 2 for translated limits on X^0 -nucleon cross section.
- 87 CHATRCHYAN 12AP search for events with a jet and missing E_T in pp collisions at $E_{\text{cm}} = 7$ TeV with $L = 5.0$ fb $^{-1}$. See their Fig. 4 for translated limits on X^0 -nucleon cross section for $m_{X^0} = 0.1$ –1000 GeV.
- 88 CHATRCHYAN 12T search for events with a photon and missing E_T in pp collisions at $E_{\text{cm}} = 7$ TeV with $L = 5.0$ fb $^{-1}$. Upper limits on the cross section in the range 13–15 fb (90% CL) is given for $m_{X^0} = 1$ –1000 GeV. See their Fig. 2 for translated limits on X^0 -nucleon cross section.

REFERENCES FOR WIMP and Dark Matter Searches

- AAD 23A PL B842 137963
 AAD 23AF EPJ C83 503
 AAD 23AJ EPJ C83 603
 AAD 23BX JHEP 2309 189
 AAD 23W JHEP 2307 116
 AALBERS 23P PRL 131 041002
 AALBERS 23A PR D108 072006
 ABBASI 23A PR D108 102004
 ABBASI 23B JCAP 2310 003
 ABE 23A PRL 130 031802
 Also
 ABE 23B PRL 131 159903 (err.)
 ABE 23E PR D108 083022
 ABE 23G PRL 131 159903 (err.)
 ABREU 23P PRL 130 061001
 ACEVEDO 23 JCAP 2311 085
 ADAMS 23 PR D108 062003
 ADHIKARI 23B PRL 131 201802
 ADHIKARI 23C PR D108 092006
 AGNES 23P PRL 130 101001
 AGNES 23A PRL 130 101002
 AGNES 23B PR D107 063001
 AKIMOV 23P PRL 130 051803
 ALBAKRY 23P PR D107 112013
 ALBERT 23G JCAP 2312 038
 AL-KHARUSI 23P PR D107 012007
 AMBROSONE 23P PRL 131 111003
 ANGLÖHER 23P PR D107 122003
 APRILE 23P PRL 130 261002
 APRILE 23A PRL 131 041003
 ARNQUIST 23A PRL 130 171003
 CHENG 23A PR D108 063015
 FOSTER 23P PR D107 103047
 GUO 23P PR D107 103011
 GUO 23A PR D108 043001
 HUANG 23P PRL 131 191002
 LAVIS 23P PR D108 123536
 LI 23F PRL 130 261001
 LIN 23C PRL 130 111801
 MA 23A PRL 130 021802
 NING 23A PRL 131 041001
 SHIMADA 23P PTEP 2023 103F01
 AAD 22D PL B829 137066
 AAD 22P JHEP 2208 104
 ABBASI 22B PR D105 062004
 ABDALLA 22P PRL 129 111101
 ADHIKARI 22 PRL 128 011801
 ADHIKARI 22B PR D105 042006
 ADHIKARI 22D PR D106 052005
 AGOSTINI 22 JCAP 2212 012
 AGOSTINI 22A PRL 129 089901
 AGUILAR-AREVALO 22A PR D106 012001
 AKIMOV 22P PR D106 052004
 ALBERT 22A JCAP 2206 028
 ANGLÖHER 22 EPJ C82 207
 ANGLÖHER 22A PR D106 092008
 APRILE 22P PR D106 022001
 ARMENGAUD 22 PR D106 062004
 BATTAGLIERI 22 PR D106 072011
 BOSE 22 PR D105 123013
 CHAN 22P PR D105 123006
 CUI 22 PRL 128 171801
 DAMI 22A PRL 129 221802
 EGOROV 22 PR D106 023023
 GHOSH 22 PR D105 103029
 GU 22P PRL 129 161803
 HOCHBERG 22 PR D106 112005
 HUANG 22 PL B834 137487
 MANCONI 22 PRL 129 111103
 TUMASYAN 22AG JHEP 2206 156
 TUMASYAN 22AA EPJ C82 213
 TUMASYAN 22G PR D105 092007
 XU 22P PR D106 052008
 ZHANG 22 PRL 129 161804
 ZHANG 22A PRL 129 221301
 AAD 21AZ JHEP 2110 013
 AAD 21BB JHEP 2111 209
 AAD 21D PRL 126 121802
 AAD 21F PR D103 112006
 AAD 21K JHEP 2102 226
 AAD 21O JHEP 2104 174
 AAD 21P JHEP 2104 165
 AAD 21S JHEP 2105 093
 ABDALLAH 21 PRL D103 102002
 AKERIB 21A PR D104 012011
 AKERIB 21B PR D104 062005
 ALKHATIB 21 PRL 127 061801
 AMARE 21 PR D103 102005
 ANDRIAMIRAO 21A PR D104 012009
 APRILE 21 PRL 126 091301
 APRILE 21A PR D103 063028
 CHENG 21 PRL 126 211803
 CIRELLI 21 PR D103 063022
 IKEDA 21 PTEP 2021 063F01
 JOHN 21 JCAP 2112 007
 MENG 21B PRL 127 261802
 SIRUNYAN 21A EPJ C81 13
 Also
 EPJ C81 333 (err.)
 TUMASYAN 21K JHEP 2111 153
 WANG 21D SCMPA 64 281011
 AARTSEN 20C EPJ C80 819
 ABAZAJAN 20 PR D102 043012
 ABDALLAH 20 PR D102 062001
 ABDELHAMEED 20A EPJ C80 834
 ABE 20G PR D102 072002
 ADHIKARI 20 PR D102 082001
 AGOSTINI 20 PRL 125 011801
 AGUILAR-AREVALO 20C PRL 125 241803
 AKERIB 20 PR D101 012003
 AKERIB 20A PR D101 042001
 ALBERT 20 PR D101 103001
 ALBERT 20A PL B805 135439
 ALBERT 20C PR D102 082002
 ALVAREZ 20 JCAP 2009 004
 AMARAL 20 PR D102 091101
 ANDRIANAVALONA 20 PR D102 042001
 APRILE 20 PR D102 072004
 ARNAUD 20 PRL 125 141301
 BARAK 20 PRL 125 171802
 G. Aad et al. (ATLAS Collab.)
 G. Aad et al. (ATLAS Collab.)
 G. Aad et al. (ATLAS Collab.)
 G. Aad et al. (ATLAS Collab.)
 G. Aad et al. (ATLAS Collab.)
 J. Aalbers et al. (LZ Collab.)
 J. Aalbers et al. (LZ Collab.)
 R. Abbasi et al. (IceCube Collab.)
 R. Abbasi et al. (IceCube Collab.)
 K. Abe et al. (Super-Kamiokande Collab.)
 K. Abe et al. (Super-Kamiokande Collab.)
 H. Abe et al. (MAGIC Collab.)
 K. Abe et al. (XMASS-I Collab.)
 K. Abe et al. (Super-Kamiokande Collab.)
 P. Abreu et al. (Pierre Auger Collab.)
 J.F. Acevedo, J. Bramante, A. Goodman (UKFI+)
 E. Adams et al. (PICO Collab.)
 G. Adhikari et al. (COSINE-100 Collab.)
 G. Adhikari et al. (COSINE-100 Collab.)
 P. Agnes et al. (DarkSide-50 Collab.)
 P. Agnes et al. (DarkSide-50 Collab.)
 P. Agnes et al. (DarkSide-50 Collab.)
 D. Akimov et al. (COHERENT Collab.)
 M.F. Albakry et al. (SuperCDMS Collab.)
 A. Albert et al. (HAWC Collab.)
 S. Al Kharusi et al. (EXO-200 Collab.)
 A. Ambrosone et al. (CREST-III Collab.)
 G. Anglöhner et al. (XENON-IT Collab.)
 E. Aprile et al. (XENON-IT Collab.)
 I. Arnuquist et al. (DAMIC Collab.)
 J.-G. Cheng, Y.-F. Liang, E.-W. Liang (MIT, UCB, LBL+)
 J.W. Foster et al. (Pandax-4T Collab.)
 W.-Q. Guo et al. (WITW, RHODE)
 X.-K. Guo et al. (Pandax-4T Collab.)
 D. Huang et al. (WITW, RHODE)
 N. Lavis et al. (Pandax-4T Collab.)
 S. Li et al. (KOTO Collab.)
 C. Lin et al. (Pandax-4T Collab.)
 W. Ma et al. (Pandax-4T Collab.)
 X. Ning et al. (NEWAGE Collab.)
 T. Shimada et al. (ATLAS Collab.)
 G. Aad et al. (IceCube Collab.)
 G. Aad et al. (IceCube Collab.)
 R. Abbasi et al. (H.E.S.S. Collab.)
 P. Adhikari et al. (DEAP Collab.)
 G. Adhikari et al. (COSINE-100 Collab.)
 G. Adhikari et al. (COSINE-100 Collab.)
 M. Agostini et al. (GERDA Collab.)
 M. Agostini et al. (GERDA Collab.)
 A.A. Aguilar-Arevalo et al. (COSINE-100 Collab.)
 D. Akimov et al. (COHERENT Collab.)
 A. Albert et al. (ANTARES Collab.)
 G. Anglöhner et al. (CREST Collab.)
 G. Anglöhner et al. (CREST-III Collab.)
 E. Aprile et al. (XENON-IT Collab.)
 E. Armengaud et al. (EDELWEISS Collab.)
 M. Battaglieri et al. (BDX-MINI Collab.)
 D. Bose, T.N. Maity, T.S. Ray
 M.H. Chan, C.M. Lee
 X. Cui et al. (Pandax-II Collab.)
 W.F. Dai et al. (CDEX Collab.)
 A.E. Egurov (LEBD)
 D. Ghosh, A. Guha, D. Sachdeva
 L. Gu et al. (Pandax-4T Collab.)
 Y. Hochberg et al. (SNSP Collab.)
 Z. Huang et al. (Pandax-4T Collab.)
 S. Manconi, A. Cuoco, J. Lesgourgues
 A. Tumasyan et al. (CMS Collab.)
 A. Tumasyan et al. (CMS Collab.)
 A. Tumasyan et al. (CMS Collab.)
 R. Xu et al. (CDEX Collab.)
 Z. Zhang et al. (Pandax-4T Collab.)
 Z. Zhang et al. (CDEX Collab.)
 G. Aad et al. (ATLAS Collab.)
 G. Aad et al. (ATLAS Collab.)
 G. Aad et al. (ATLAS Collab.)
 G. Aad et al. (ATLAS Collab.)
 G. Aad et al. (ATLAS Collab.)
 G. Aad et al. (ATLAS Collab.)
 H. Abdallah et al. (H.E.S.S. Collab.)
 D.S. Akerib et al. (LUX Collab.)
 D.S. Akerib et al. (LUX Collab.)
 I. Alkhatib et al. (SuperCDMS Collab.)
 J. Amare et al. (ANAIS Collab.)
 M. Andriamirao et al. (PROSPECT Collab.)
 E. Aprile et al. (XENON-IT Collab.)
 E. Aprile et al. (XENON-IT Collab.)
 C. Cheng et al. (Pandax-II Collab.)
 M. Cirelli et al.
 T. Ikeda et al. (NEWAGE Collab.)
 I. John, T. Linden
 Y. Meng et al. (Pandax-4T Collab.)
 A.M. Sirunyan et al. (CMS Collab.)
 A.M. Sirunyan et al. (CMS Collab.)
 Y. Wang et al. (CDEX Collab.)
 M.G. Aartsen et al. (IceCube, PICO Collab.)
 K.N. Abazajian et al. (UCI, VPI, TOKY+)
 H. Abdallah et al. (H.E.S.S. Collab.)
 A.H. Abdelhameed et al. (CREST Collab.)
 K. Abe et al. (Super-Kamiokande Collab.)
 P. Adhikari et al. (DEAP-3600 Collab.)
 M. Agostini et al. (GERDA Collab.)
 A. Aguilar-Arevalo et al. (DAMIC Collab.)
 D.S. Akerib et al. (LUX Collab.)
 D.S. Akerib et al. (LUX Collab.)
 A. Albert et al. (HAWC Collab.)
 A. Albert et al. (ANTARES Collab.)
 A. Albert et al. (ANTARES and IceCube Collab.)
 A. Alvarez et al.
 D.W. Amaral et al. (SuperCDMS Collab.)
 A. Andrianavalona et al. (FUNK Collab.)
 E. Aprile et al. (XENON Collab.)
 Q. Arnaud et al. (EDELWEISS Collab.)
 L. Barak et al. (SENSEI Collab.)

See key on page 1171

Searches Particle Listings

WIMP and Dark Matter Searches

CLARK	20	PR D102 123026	M. Clark et al.	(PURD)	ARCHAMBAU...17	PR D95 082001	S. Archambault et al.	(VERITAS Collab.)
Also		PR D104 129903 (errat.)	M. Clark et al.		AVRORIN	17	JETP 125 80	(BAIKAL Collab.)
FELIZARDO	20	UHP A35 2030005	M. Felizardo	(SIMPLE Collab.)	BANERJEE	17	PRL 118 011802	(NA64 Collab.)
HOOF	20	JCAP 2002 012	S. Hoof, A. Geringer-Sameth, R. Trotta	(GOET+)	BARBOSA-D...	17	PR D95 032006	(DM17 Collab.)
MAZZIOTTA	20	PR D102 022003	M.N. Mazziotta et al.		BATTAT	17	ASP 91 65	(DRIFT-III Collab.)
SIRUNYAN	20X	JHEP 2003 025	A.M. Sirunyan et al.	(CMS Collab.)	BEHNKE	17	ASP 90 85	(PICASSO Collab.)
WANG	20G	CP 44 125001	G. Wang et al.	(Pandax-II Collab.)	BOUDAUD	17	PRL 119 211103	(Pandax-II Collab.)
AABOUD	19A	EPJ C79 120	M. Aaboud et al.	(ATLAS Collab.)	CHEN	17E	PR D96 102007	X. Chen et al.
AABOUD	19AI	PL B793 499	M. Aaboud et al.	(ATLAS Collab.)	CUI	17A	PRL 119 181302	X. Cui et al.
AABOUD	19AL	PRL 122 231801	M. Aaboud et al.	(ATLAS Collab.)	FU	17	PRL 118 071301	C. Fu et al.
AABOUD	19Q	JHEP 1905 041	M. Aaboud et al.	(ATLAS Collab.)	Also		PRL 120 049902 (errat.)	C. Fu et al.
AABOUD	19V	JHEP 1905 142	M. Aaboud et al.	(ATLAS Collab.)	Also		PRL 120 049902 (errat.)	C. Fu et al.
ABDELHAMEE...	19	EPJ C79 630	A.H. Abdelhameed et al.	(CREST Collab.)	Also		PRL 120 049902 (errat.)	C. Fu et al.
ABDELHAMEE...	19A	PR D100 102002	A.H. Abdelhameed et al.	(CREST Collab.)	ARCHAMBAU...17A	PRL 118 021802	V. Khachatryan et al.	(CMS Collab.)
ABE	19	PL B789 45	K. Abe et al.	(XMASS Collab.)	ARCHAMBAU...17F	JHEP 1702 135	V. Khachatryan et al.	(CMS Collab.)
ABEYSEKARA	19	JCAP 1907 022	A.U. Abeysekara et al.	(HAWC Collab.)	SIRUNYAN	17	JHEP 1703 061	A.M. Sirunyan et al.
ABRAMOFF	19	PRL 122 161801	O. Abramoff et al.	(SENSEI Collab.)	SIRUNYAN	17A	JHEP 1710 180	A.M. Sirunyan et al.
ADHIKARI	19	PRL 123 031302	G. Adhikari et al.	(COSINE-100 Collab.)	SIRUNYAN	17AQ	JHEP 1710 073	A.M. Sirunyan et al.
AGNESE	19A	PR D99 062001	R. Agnese et al.	(CDMS Collab.)	SIRUNYAN	17B	EPJ C77 845	A.M. Sirunyan et al.
AGUILAR-AR...	19A	PRL 123 181802	A. Aguilar-Arevalo et al.	(DMIC Collab.)	SIRUNYAN	17G	JHEP 1707 014	A.M. Sirunyan et al.
AJAJ	19	PR D100 022004	R. Ajaj et al.	(DEAP-3600 Collab.)	AABOUD	16AD	PL B763 251	M. Aaboud et al.
AKERIB	19	PRL 122 131301	D.S. Akerib et al.	(LUX Collab.)	AABOUD	16D	PR D94 032005	M. Aaboud et al.
ALBERT	19B	JCAP 1904 E01	A. Albert et al.	(HAWC Collab.)	AABOUD	16F	JHEP 1606 059	M. Aaboud et al.
AMARE	19	PRL 123 031301	J. Amare et al.	(ANAIS Collab.)	AAD	16AF	JHEP 1601 172	G. Aad et al.
AMOLE	19	PR D100 022001	C. Amole et al.	(PICO Collab.)	AAD	16AG	JHEP 1602 062	G. Aad et al.
ANGLOHER	19	EPJ C79 43	G. Angloher et al.	(CREST-II Collab.)	AAD	16AM	PR D93 072007	G. Aad et al.
APRILE	19	PRL 122 071301	E. Aprile et al.	(XENON1T Collab.)	AARTSEN	16D	JCAP 1604 022	M.G. Aartsen et al.
APRILE	19A	PRL 122 141301	E. Aprile et al.	(XENON1T Collab.)	AARTSEN	16E	EPJ C76 531	M.G. Aartsen et al.
APRILE	19C	PRL 123 241803	E. Aprile et al.	(XENON1T Collab.)	ABDALLAH	16	PRL 117 111301	H. Abdallah et al.
APRILE	19D	PRL 123 251801	E. Aprile et al.	(XENON1T Collab.)	ABDALLAH	16A	PRL 117 151302	H. Abdallah et al.
ARMENGAUD	19	PR D99 062003	E. Armengaud et al.	(EDELWEISS Collab.)	ADRIAN-MAR...	16	PL B759 59	S. Adrian-Martinez et al.
BANERJEE	19	PRL 123 121801	D. Banerjee et al.	(NA64 Collab.)	ADRIAN-MAR...	16B	JCAP 1605 016	S. Adrian-Martinez et al.
BRINGMANN	19	PRL 122 171801	T. Bringmann, M. Pospelov	(OSLO, VICT)	AGNES	16	PR D93 081101	P. Agnes et al.
BRUNE	19	PR D99 096005	T. Brune, H. Pas	(DORT)	AGNESE	16	PRL 116 071301	R. Agnese et al.
CHEUNG	19	PL B789 137	K. Cheung et al.		AGUILAR-AR...	16	PR D94 082006	A. Aguilar-Arevalo et al.
CHOI	19	PR D99 083018	K.-Y. Choi, J. Kim, C. Rott	(SUNG)	AHNEN	16	JCAP 1602 039	M.L. Ahnen et al.
DI-MAURO	19	PR D99 123027	M. Di Mauro et al.		AKERIB	16	PRL 116 161301	D.S. Akerib et al.
HA	19	PRL 122 131802	C. Ha et al.	(COSINE-100 Collab.)	AKERIB	16A	PRL 116 161302	D.S. Akerib et al.
JOHNSON	19	PR D99 103007	C. Johnson et al.		AMOLE	16	PR D93 052014	C. Amole et al.
KIM	19A	JHEP 1903 194	K.W. Kim et al.	(KIMS Collab.)	AMOLE	16A	PR D93 061101	C. Amole et al.
KLOPF	19	PRL 122 222503	M. Kopf et al.	(PERKEO II Collab.)	ANGLOHER	16	EPJ C76 25	G. Angloher et al.
KOBAYASHI	19	PL B795 309	M. Kobayashi et al.	(XMASS Collab.)	ANGLOHER	16	PRL 117 021303	G. Angloher et al.
LI	19D	PR D99 123519	S. Li et al.		APRILE	16B	PR D94 092001	E. Aprile et al.
LIU	19B	PRL 123 161301	Z.Z. Liu et al.	(CDEX Collab.)	APRILE	16B	PR D94 122001	E. Aprile et al.
NG	19	PR D99 083005	K.C.Y. Ng et al.		ARMENGAUD	16	JCAP 1605 019	E. Armengaud et al.
QUEIROZ	19	JCAP 1904 048	F.S. Queiroz, C. Siqueira		AVRORIN	16	ASP 81 12	A.D. Avrorin et al.
SEONG	19	PRL 122 011801	I.S. Seong et al.	(BELLE Collab.)	CAPUTO	16	PR D93 062004	R. Caputo et al.
SIRUNYAN	19AN	EPJ C79 280	A.M. Sirunyan et al.	(CMS Collab.)	FORNASA	16	PR D94 123005	M. Fornasa et al.
SIRUNYAN	19BC	PL B795 76	A.M. Sirunyan et al.	(CMS Collab.)	HEHN	16	EPJ C76 548	L. Hehn et al.
SIRUNYAN	19BO	PL B793 520	A.M. Sirunyan et al.	(CMS Collab.)	ARCHAMBAU...16A	J	PR D93 052011	V. Khachatryan et al.
SIRUNYAN	19C	PRL 122 011803	A.M. Sirunyan et al.	(CMS Collab.)	ARCHAMBAU...16B	J	JHEP 1612 083	V. Khachatryan et al.
SIRUNYAN	19D	JHEP 1902 074	A.M. Sirunyan et al.	(CMS Collab.)	Also		JHEP 1708 035 (errat.)	V. Khachatryan et al.
SIRUNYAN	19E	JHEP 1903 141	A.M. Sirunyan et al.	(CMS Collab.)	ARCHAMBAU...16CA	J	JHEP 1612 088	V. Khachatryan et al.
SIRUNYAN	19F	ASP 110 1	T. Suzuki et al.	(XMASS Collab.)	ARCHAMBAU...16C	J	PL B765 102	V. Khachatryan et al.
SUZUKI	19	ASP 110 1	T. Suzuki et al.	(XMASS Collab.)	LEITE	16	JCAP 1611 021	N. Leite et al.
XIA	19A	PL B792 193	J. Xia et al.	(Pandax-II Collab.)	LI	16	PR D93 043518	S. Li et al.
YAGUNA	19	JCAP 1904 041	C. Yaguna		LI	16	JCAP 1612 028	Z. Li et al.
YANG	19	PRL 123 221301	L.T. Yang et al.	(CDEX Collab.)	LIANG	16	PR D94 103502	Y.-F. Liang et al.
AABOUD	18	PL B776 318	M. Aaboud et al.	(ATLAS Collab.)	LI	16	PR D93 103517	B.-Q. Lu, H.-S. Zong
AABOUD	18A	EPJ C78 18	M. Aaboud et al.	(ATLAS Collab.)	SHIRASAKI	16	PR D94 063522	M. Shirasaki et al.
AABOUD	18CA	JHEP 1810 180	M. Aaboud et al.	(ATLAS Collab.)	TAN	16	PR D93 122009	T.H. Tan et al.
AABOUD	18I	JHEP 1801 126	M. Aaboud et al.	(ATLAS Collab.)	TAN	16B	PRL 117 121303	A. Tan et al.
AARTSEN	18D	EPJ C78 831	M.G. Aartsen et al.	(IceCube Collab.)	ZHAO	16	PR D93 092003	W. Zhao et al.
ABDALLAH	18	PRL 120 201101	H. Abdallah et al.	(H.E.S.S. Collab.)	AAD	15AS	EPJ C75 92	G. Aad et al.
ABE	18C	PR D97 102006	K. Abe et al.	(XMASS Collab.)	AAD	15B	EPJ C75 249	G. Aad et al.
ABE	18F	PL B787 153	K. Abe et al.	(XMASS Collab.)	Also		EPJ C75 408 (errat.)	G. Aad et al.
ADHIKARI	18	NAT 564 83	G. Adhikari et al.	(COSINE-100 Collab.)	AAD	15CF	PRL 115 131801	G. Aad et al.
AGNES	18	PRL 121 081307	P. Agnes et al.	(DarkSide-50 Collab.)	AAD	15CS	PR D91 012008	G. Aad et al.
AGNES	18A	PR D98 102006	P. Agnes et al.	(DarkSide-50 Collab.)	Also		PR D92 059903 (errat.)	G. Aad et al.
AGNES	18B	PRL 121 111303	P. Agnes et al.	(DarkSide-50 Collab.)	AARTSEN	15C	EPJ C75 20	M.G. Aartsen et al.
AGNESE	18	PR D97 022002	R. Agnese et al.	(SuperCDMS Collab.)	AARTSEN	15E	EPJ C75 492	M.G. Aartsen et al.
AGNESE	18A	PRL 120 061802	R. Agnese et al.	(SuperCDMS Collab.)	ABRAMOWSKI	15	PRL 114 081301	A. Abramowski et al.
AGNESE	18B	PRL 121 051301	R. Agnese et al.	(SuperCDMS Collab.)	ACKERMANN	15	PR D91 122002	M. Ackermann et al.
Also		PRL 122 069901 (errat.)	R. Agnese et al.	(SuperCDMS Collab.)	ACKERMANN	15A	JCAP 1509 008	M. Ackermann et al.
AGUILAR-AR...	18B	PR D98 112004	A.A. Aguilar-Arevalo	(MiniBoone Collab.)	ACKERMANN	15B	PRL 115 231301	M. Ackermann et al.
AHNEN	18	JCAP 1802 009	A.A. Ahnen et al.	(DMIC Collab.)	ADRIAN-MAR...	15	JCAP 1510 068	S. Adrian-Martinez et al.
AKERIB	18A	PR D98 062005	D.S. Akerib et al.	(LUX Collab.)	AGNES	15	PL B743 456	P. Agnes et al.
ALBERT	18B	JCAP 1806 043	A. Albert et al.	(HAWC Collab.)	AGNESE	15A	PR D91 052021	R. Agnese et al.
ALBERT	18C	PR D98 123012	A. Albert et al.	(HAWC Collab.)	AGNESE	15B	PR D92 072003	R. Agnese et al.
AMAUDRUZ	18	PRL 121 071801	P.A. Amaudruz et al.	(DEAP-3600 Collab.)	AMOLE	15	PRL 114 231302	C. Amole et al.
APRILE	18	PRL 121 111302	E. Aprile et al.	(XENON1T Collab.)	APRILE	15	PRL 115 091302	E. Aprile et al.
ARMENGAUD	18	PR D98 082004	E. Armengaud et al.	(EDELWEISS-III Collab.)	APRILE	15A	SCI 349 851	E. Aprile et al.
ARNAUD	18	ASP 97 54	Q. Arnaud et al.	(NEWS-G Collab.)	CHOI	15	PRL 114 141301	K. Choi et al.
CHANG	18A	PR D98 123004	L.J. Chang, M. Lisanti, S. Mishra-Sharma	(PRIN Collab.)	ARCHAMBAU...15A	J	JHEP 1506 121	V. Khachatryan et al.
CRISLER	18	PRL 121 061803	M. Crisler et al.	(SENSEI Collab.)	ARCHAMBAU...15AL	J	EPJ C75 235	V. Khachatryan et al.
JIANG	18	PRL 120 241301	H. Jiang et al.	(CDEX Collab.)	ARCHAMBAU...15T	PR	D91 092005	V. Khachatryan et al.
KACHULIS	18	PRL 120 221301	G. Kachulis et al.	(Super-Kamiokande Collab.)	NAKAMURA	15	PTEP 2014 043F01	K. Nakamura et al.
KHACHATRY...	18	PR D97 099903	V. Khachatryan et al.	(CMS Collab.)	XIAO	15	PR D92 052004	X. Xiao et al.
LISANTI	18	PRL 120 101101	M. Lisanti et al.	(PRIN, MIT, MICH Collab.)	AAD	14AI	JHEP 1409 037	G. Aad et al.
MAZZIOTTA	18	PR D98 022006	M. Mazziotta et al.	(Fermi-LAT Collab.)	AAD	14BK	PRL 112 041802	G. Aad et al.
REN	18	PRL 121 021304	X. Ren et al.	(Pandax-II Collab.)	AAD	14C	PR D90 012004	G. Aad et al.
SIRUNYAN	18BF	JHEP 1806 027	A.M. Sirunyan et al.	(CMS Collab.)	AAD	14K	PRL 112 201802	G. Aad et al.
SIRUNYAN	18BO	JHEP 1808 130	A.M. Sirunyan et al.	(CMS Collab.)	ACKERMANN	14	PR D89 042001	M. Ackermann et al.
SIRUNYAN	18BV	EPJ C78 291	A.M. Sirunyan et al.	(CMS Collab.)	AGNESE	14	PRL 112 241302	R. Agnese et al.
SIRUNYAN	18C	PR D97 032009	A.M. Sirunyan et al.	(CMS Collab.)	AGNESE	14A	PRL 112 041302	R. Agnese et al.
SIRUNYAN	18CU	JHEP 1801 056	A.M. Sirunyan et al.	(CMS Collab.)	AKERIB	14	PRL 112 091303	D.S. Akerib et al.
SIRUNYAN	18DH	JHEP 1809 046	A.M. Sirunyan et al.	(CMS Collab.)	ALEXIS	14	JCAP 1402 008	J. Alexis et al.
SIRUNYAN	18S	PR D97 092005	A.M. Sirunyan et al.	(CMS Collab.)	ANGLOHER	14	EPJ C74 3184	G. Angloher et al.
YANG	18	CP 42 023002	L.T. Yang et al.	(CDEX Collab.)	APRILE	14A	ASP 54 11	E. Aprile et al.
AABOUD	17A	PL B765 11	M. Aaboud et al.	(ATLAS Collab.)	AVRORIN	14	ASP 62 12	A.D. Avrorin et al.
AABOUD	17AM	PRL 119 181804	M. Aaboud et al.	(ATLAS Collab.)	FELIZARDO	14	PR D89 072013	M. Felizardo et al.
AABOUD	17AQ	PR D96 112004	M. Aaboud et al.	(ATLAS Collab.)	LEE	14A	PR D90 052006	H.S. Lee et al.
AABOUD	17BD	EPJ C77 765	M. Aaboud et al.	(ATLAS Collab.)	LIU	14A	PR D90 032003	S.K. Liu et al.
AABOUD	17R	EPJ C77 393	M. Aaboud et al.	(ATLAS Collab.)	UCHIDA	14	PTEP 2014 063C01	H. Uchida et al.
AARTSEN	17	EPJ C77 82	M.G. Aartsen et al.	(IceCube Collab.)	YUE	14	PR D90 091701	Q. Yue et al.
AARTSEN	17A	EPJ C77 146	M.G. Aartsen et al.	(IceCube Collab.)	AAD	13AD	JHEP 1304 075	G. Aad et al.
Also		EPJ C79 214 (errat.)	M.G. Aartsen et al.	(IceCube Collab.)	AAD	13AC	PRL 110 011802	G. Aad et al.
AARTSEN	17C	EPJ C77 627	M.G. Aartsen et al.	(IceCube Collab.)	AALSETH	13	PR D88 012002	C.E. Aalseth et al.
AGUILAR-AR...	17	PRL 118 141803	A. Aguilar-Arevalo et al.	(MiniBoone Collab.)	AARTSEN	13	PRL 110 131302	M.G. Aartsen et al.
AGUILAR-AR...	17A	PRL 118 221803	A.A. Aguilar-Arevalo et al.	(MiniBoone Collab.)	AARTSEN	13C	PR D88 122001	M. Aartsen et al.
AKERIB	17	PRL 118 021303	D.S. Akerib et al.	(LUX Collab.)	ABE	13B	PL B719 78	K. Abe et al.
AKERIB	17A	PRL 118 251302	D.S. Akerib et al.	(LUX Collab.)	ABRAMOWSKI	13	PRL 110 041301	A. Abramowski et al.
ALBERT	17A	PL B769 249	A. Albert et al.	(ANTARES Collab.)	ACKERMANN	13A	PR D88 082002	M. Ackermann et al.
Also		PL B796 253 (errat.)	A. Albert et al.	(ANTARES Collab.)	ADRIAN-MAR...	13	JCAP 1311 032	S. Adrian-Martinez et al.
AMOLE	17	PRL 118 251301	C. Amole et al.	(PICO Collab.)	AGNESE	13	PR D88 031104	R. Agnese et al.
ANGLOHER	17A	EPJ C77 637	G. Angloher et al.	(CREST Collab.)	AGNESE	13A	PRL 111 251301	R. Agnese et al.
APRILE	17	PRL 118 101101	E. Aprile et al.	(XENON100 Collab.)	APRILE	13	PRL 111 021301	E. Aprile et al.
APRILE	17A	PR D96 022008	E. Aprile et al.	(XENON100 Collab.)	BERNABEI	13A	EPJ C73 2648	R. Bernabei et al.
APRILE	17D	PR D96 042004	E. Aprile et al.	(XENON100 Collab.)	BOLIEV	13	JCAP 1309 019	M. Boliev et al.
APRILE	17H	PRL 119 181301	E. Aprile et al.	(XENON100 Collab.)	LI	13B	PRL 110 261301	H.B. Li et al.
APRILE	17H	PR D96 122002	E. Aprile et al.	(XENON100 Collab.)	SUVOROVA	13	PAN 76 1367	O.V. Suvorova et al.
APRILE	17K	JCAP 1710 039	E. Aprile et al.	(XENON100 Collab.)			Translated from YAF 76 1433.	(INRM)

Searches Particle Listings

WIMP and Dark Matter Searches, Other Particle Searches

ZHAO	13	PR D88 052004	W. Zhao <i>et al.</i>	(CDEX Collab.)
AALTONEN	12K	PRL 108 201802	T. Aaltonen <i>et al.</i>	(CDF Collab.)
AALTONEN	12M	PRL 108 211804	T. Aaltonen <i>et al.</i>	(CDF Collab.)
ABBASI	12	PR D85 042002	R. Abbasi <i>et al.</i>	(IceCube Collab.)
ABRAMOWSKI	12	APJ 750 123	A. Abramowski <i>et al.</i>	(H.E.S.S. Collab.)
ACKERMANN	12	PR D86 022002	M. Ackermann <i>et al.</i>	(Fermi-LAT Collab.)
AKIMOV	12	PL B709 14	D.Yu. Akimov <i>et al.</i>	(ZEPLIN-III Collab.)
ALIU	12	PR D85 062001	E. Aliu <i>et al.</i>	(VERITAS Collab.)
ANGLOHER	12	EPJ C72 1971	G. Angloher <i>et al.</i>	(CREST-II Collab.)
APRILE	12	PRL 109 181301	E. Aprile <i>et al.</i>	(XENON100 Collab.)
ARCHAMBAU...	12	PL B711 153	S. Archambault <i>et al.</i>	(PICASSO Collab.)
ARMENGAUD	12	PR D86 051701	E. Armengaud <i>et al.</i>	(EDELWEISS Collab.)
BARRETO	12	PL B711 264	J. Barreto <i>et al.</i>	(DAMIC Collab.)
BEHNKE	12	PR D86 052001	E. Behnke <i>et al.</i>	(COUPP Collab.)
Also		PR D90 079902 (errata.)	E. Behnke <i>et al.</i>	(COUPP Collab.)
BROWN	12	PR D85 021301	A. Brown <i>et al.</i>	(OXF Collab.)
CHATRCHYAN	12AP	JHEP 1209 094	S. Chattrchyan <i>et al.</i>	(CMS Collab.)
CHATRCHYAN	12T	PRL 108 261803	S. Chattrchyan <i>et al.</i>	(CMS Collab.)
DAHL	12	PRL 108 299001	C.E. Dahl, J. Hall, W.H. Lippincott	(CHIC, FNAL Collab.)
DAW	12	ASP 35 397	E. Daw <i>et al.</i>	(DRIFT-III Collab.)
FELIZARDO	12	PRL 108 201302	M. Felizardo <i>et al.</i>	(SIMPLE Collab.)
KIM	12	PRL 108 181301	S.C. Kim <i>et al.</i>	(KIMS Collab.)
AALSETH	11	PRL 106 131301	C.E. Aalseth <i>et al.</i>	(CoGeNT Collab.)
AALSETH	11A	PRL 107 141301	C.E. Aalseth <i>et al.</i>	(CoGeNT Collab.)
ABBASI	11C	PR D84 022004	R. Abbasi <i>et al.</i>	(IceCube Collab.)
ABRAMOWSKI	11	PRL 106 161301	A. Abramowski <i>et al.</i>	(H.E.S.S. Collab.)
ACKERMANN	11	PRL 107 241302	M. Ackermann <i>et al.</i>	(Fermi-LAT Collab.)
AHLEN	11	PL B695 124	S. Ahlen <i>et al.</i>	(DMTPC Collab.)
AHMED	11	PR D83 112002	Z. Ahmed <i>et al.</i>	(CDMS Collab.)
AHMED	11A	PR D84 011102	Z. Ahmed <i>et al.</i>	(CDMS and EDELWEISS Collab.)
AHMED	11B	PRL 106 131302	Z. Ahmed <i>et al.</i>	(CDMS Collab.)
AJELLO	11	PR D84 032007	M. Ajello <i>et al.</i>	(Fermi-LAT Collab.)
ANGLE	11	PRL 107 051301	J. Angle <i>et al.</i>	(XENON10 Collab.)
Also		PRL 110 249901 (errata.)	J. Angle <i>et al.</i>	(XENON10 Collab.)
APRILE	11	PR D84 052003	E. Aprile <i>et al.</i>	(XENON100 Collab.)
APRILE	11A	PR D84 061101	E. Aprile <i>et al.</i>	(XENON100 Collab.)
APRILE	11B	PRL 107 131302	E. Aprile <i>et al.</i>	(XENON100 Collab.)
ARMENGAUD	11	PL B702 329	E. Armengaud <i>et al.</i>	(EDELWEISS-II Collab.)
BEHNKE	11	PRL 106 021303	E. Behnke <i>et al.</i>	(COUPP Collab.)
GERINGER-SA...	11	PRL 107 241303	A. Gerlinger-Sameth, S.M. Koushiappas	(CDMS Collab.)
HORN	11A	PL B705 471	M. Horn <i>et al.</i>	(ZEPLIN-III Collab.)
TANAKA	11	APJ 742 78	T. Tanaka <i>et al.</i>	(Super-Kamiokande Collab.)
ABBASI	10	PR D81 057101	R. Abbasi <i>et al.</i>	(IceCube Collab.)
AHMED	10	SCI 321 1619	Z. Ahmed <i>et al.</i>	(CDMS II Collab.)
AKERIB	10	PR D82 122004	D.S. Akerib <i>et al.</i>	(CDMS II Collab.)
AKIMOV	10	PL B692 180	D.Yu. Akimov <i>et al.</i>	(ZEPLIN-III Collab.)
APRILE	10	PRL 105 131302	E. Aprile <i>et al.</i>	(XENON100 Collab.)
ARMENGAUD	10	PL B687 294	E. Armengaud <i>et al.</i>	(EDELWEISS-II Collab.)
FELIZARDO	10	PRL 105 211301	M. Felizardo <i>et al.</i>	(The SIMPLE Collab.)
MIUCHI	10	PL B686 11	K. Miuchi <i>et al.</i>	(NEWAGE Collab.)
ABBASI	09B	PRL 102 201302	R. Abbasi <i>et al.</i>	(IceCube Collab.)
AHMED	09	PRL 102 011301	Z. Ahmed <i>et al.</i>	(CDMS Collab.)
ANGLE	09	PR D80 115005	J. Angle <i>et al.</i>	(XENON10 Collab.)
ANGLOHER	09	ASP 31 270	G. Angloher <i>et al.</i>	(CREST Collab.)
ARCHAMBAU...	09	PL B682 185	S. Archambault <i>et al.</i>	(PICASSO Collab.)
LEBEDENKO	09A	PRL 103 151302	V.N. Lebedenko <i>et al.</i>	(ZEPLIN-III Collab.)
LIN	09	PR D79 061101	S.T. Lin <i>et al.</i>	(TEXONO Collab.)
AALSETH	08	PRL 101 251301	C.E. Aalseth <i>et al.</i>	(CoGeNT Collab.)
Also		PRL 102 109903 (errata.)	C.E. Aalseth <i>et al.</i>	(CoGeNT Collab.)
ANGLE	08A	PRL 101 091301	J. Angle <i>et al.</i>	(XENON10 Collab.)
BEDNYAKOV	08	PAN 71 111	V.A. Bednyakov, H.P. Klapdor-Kleingrothaus, I.V. Krivosheina	(XENON10 Collab.)
ALNER	07	PL B653 16	G.J. Alner <i>et al.</i>	(ZEPLIN-III Collab.)
LEE	07A	PRL 99 091301	H.S. Lee <i>et al.</i>	(KIMS Collab.)
MIUCHI	07	PL B654 58	K. Miuchi <i>et al.</i>	(KIMS Collab.)
AKERIB	06	PR D73 011102	D.S. Akerib <i>et al.</i>	(CDMS Collab.)
SHIMIZU	06A	PL B633 195	Y. Shimizu <i>et al.</i>	(CDMS Collab.)
AKERIB	05	PR D72 052009	D.S. Akerib <i>et al.</i>	(CDMS Collab.)
ALNER	05	PL B616 17	G.J. Alner <i>et al.</i>	(UK Dark Matter Collab.)
BARNABE-HE...	05	PL B624 186	M. Barnabe-Heider <i>et al.</i>	(PICASSO Collab.)
BENOIT	05	PL B616 25	A. Benoit <i>et al.</i>	(EDELWEISS Collab.)
GIRARD	05	PL B621 233	T.A. Girard <i>et al.</i>	(SIMPLE Collab.)
GIULIANI	05	PRL 95 101301	F. Giuliani <i>et al.</i>	(XENON10 Collab.)
GIULIANI	05A	PR D71 123503	F. Giuliani, T.A. Girard	(XENON10 Collab.)
KLAPDOR-K...	05	PL B609 226	H.V. Klapdor-Kleingrothaus, I.V. Krivosheina, C. Tomei	(XENON10 Collab.)
GIULIANI	04	PL B588 151	F. Giuliani, T.A. Girard	(XENON10 Collab.)
GIULIANI	04A	PRL 93 161301	F. Giuliani	(XENON10 Collab.)
MIUCHI	03	ASP 19 135	K. Miuchi <i>et al.</i>	(XENON10 Collab.)
TAKEDA	03	PL B572 145	A. Takeda <i>et al.</i>	(XENON10 Collab.)
ANGLOHER	02	ASP 18 43	G. Angloher <i>et al.</i>	(CREST Collab.)
BELLI	02	PR D66 043503	P. Belli <i>et al.</i>	(DAMA Collab.)
BERNABEI	02C	EPJ C23 61	R. Bernabei <i>et al.</i>	(DAMA Collab.)
GREEN	02	PR D66 083003	A.M. Green	(DAMA Collab.)
BAUDIS	01	PR D63 022001	L. Baudis <i>et al.</i>	(Heidelberg-Moscow Collab.)
SMITH	01	PR D64 043502	D. Smith, N. Weiner	(DAMA Collab.)
ULLIO	01	JHEP 0107 044	P. Ullio, M. Kamionkowski, P. Vogel	(DAMA Collab.)
BENOIT	00	PL B479 8	A. Benoit <i>et al.</i>	(EDELWEISS Collab.)
BERNABEI	00D	NJP 2 15	R. Bernabei <i>et al.</i>	(DAMA Collab.)
COLLAR	00	PRL 85 3083	J.J. Collar <i>et al.</i>	(SIMPLE Collab.)
AMBROSIO	99	PR D60 082002	M. Ambrosio <i>et al.</i>	(Macro Collab.)
BERNABEI	99	PL B450 448	R. Bernabei <i>et al.</i>	(DAMA Collab.)
BERNABEI	99D	PRL 83 4918	R. Bernabei <i>et al.</i>	(DAMA Collab.)
BRHLIK	99	PL B464 303	M. Brhlik, L. Roszkowski	(DAMA Collab.)
DERBIN	99	PAN 62 1896	V.V. Derbin <i>et al.</i>	(DAMA Collab.)
KLIMENKO	98	JETPL 67 875	A.A. Klimenko <i>et al.</i>	(DAMA Collab.)
Translated from		ZETFP 67 835		
SARSA	97	PR D56 1856	M.L. Sarsa <i>et al.</i>	(ZARA Collab.)
ALESSAND...	96	PL B384 316	A. Alessandrello <i>et al.</i>	(MILA, MILA, SASSO Collab.)
BELLI	96	PL B387 222	P. Belli <i>et al.</i>	(DAMA Collab.)
Also		PL B389 783 (errata.)	P. Belli <i>et al.</i>	(DAMA Collab.)
BELLI	96C	NC C19 537	P. Belli <i>et al.</i>	(DAMA Collab.)
BERNABEI	96	PL B389 757	R. Bernabei <i>et al.</i>	(DAMA Collab.)
COLLAR	96	PRL 76 331	J.J. Collar	(SUCU Collab.)
SARSA	96	PL B386 458	M.L. Sarsa <i>et al.</i>	(ZARA Collab.)
Also		PR D56 1856	M.L. Sarsa <i>et al.</i>	(ZARA Collab.)
SMITH	96	PL B379 299	P.F. Smith <i>et al.</i>	(RAL, SHEF, LOIC+ Collab.)
SNOWDEN-...	96	PRL 76 332	D.P. Snowden-Hft, E.S. Freeman, P.B. Price	(UCB Collab.)
GARCIA	95	PR D51 1458	E. Garcia <i>et al.</i>	(ZARA, SCUC, PNL Collab.)
QUENBY	95	PL B351 70	J.P. Quenby <i>et al.</i>	(LOIC, RAL, SHEF+ Collab.)
SNOWDEN-...	95	PRL 74 4133	D.P. Snowden-Hft, E.S. Freeman, P.B. Price	(UCB Collab.)
Also		PRL 76 331	J.J. Collar	(SUCU Collab.)
Also		PRL 76 332	D.P. Snowden-Hft, E.S. Freeman, P.B. Price	(UCB Collab.)
BECK	94	PL B336 141	M. Beck <i>et al.</i>	(MIPK, KIAE, SASSO Collab.)
BACCI	92	PL B293 460	C. Bacci <i>et al.</i>	(Beijing-Rom-Saclay Collab.)
REUSSER	91	PL B255 143	D. Reusser <i>et al.</i>	(NEUC, CIT, PSI Collab.)
CALDWELL	88	PRL 61 510	D.O. Caldwell <i>et al.</i>	(UCSB, UCB, LBL Collab.)

Other Particle Searches

OMITTED FROM SUMMARY TABLE

OTHER PARTICLE SEARCHES

Revised February 2018 by K. Hikasa (Tohoku University).

We collect here those searches which do not appear in any other search categories. These are listed in the following order:

- Concentration of stable particles in matter
- General new physics searches
- Limits on jet-jet resonance in hadron collisions
- Limits on neutral particle production at accelerators
- Limits on charged particles in e^+e^- collisions
- Limits on charged particles in hadron reactions
- Limits on charged particles in cosmic rays
- Searches for quantum black hole production

Note that searches appear in separate sections elsewhere for Higgs bosons (and technipions), other heavy bosons (including W_R, W', Z' , leptoquarks, axiglons), axions (including pseudo-Goldstone bosons, Majorons, familons), WIMPs, heavy leptons, heavy neutrinos, free quarks, monopoles, supersymmetric particles, and compositeness.

We no longer list for limits on tachyons and centauros. See our 1994 edition for these limits.

CONCENTRATION OF STABLE PARTICLES IN MATTER

Concentration of Heavy (Charge +1) Stable Particles in Matter

VALUE	CL%	DOCUMENT ID	TECN	COMMENT
$<4 \times 10^{-17}$	95	1 YAMAGATA	93 SPEC	Deep sea water, $M=5-1600 m_p$
$<6 \times 10^{-15}$	95	2 VERKERK	92 SPEC	Water, $M=10^5$ to 3×10^7 GeV
$<7 \times 10^{-15}$	95	2 VERKERK	92 SPEC	Water, $M=10^4, 6 \times 10^7$ GeV
$<9 \times 10^{-15}$	95	2 VERKERK	92 SPEC	Water, $M=10^8$ GeV
$<3 \times 10^{-23}$	90	3 HEMMICK	90 SPEC	Water, $M=1000 m_p$
$<2 \times 10^{-21}$	90	3 HEMMICK	90 SPEC	Water, $M=5000 m_p$
$<3 \times 10^{-20}$	90	3 HEMMICK	90 SPEC	Water, $M=10000 m_p$
$<1. \times 10^{-29}$		SMITH	82B SPEC	Water, $M=30-400 m_p$
$<2. \times 10^{-28}$		SMITH	82B SPEC	Water, $M=12-1000 m_p$
$<1. \times 10^{-14}$		SMITH	82B SPEC	Water, $M > 1000 m_p$
$<(0.2-1.) \times 10^{-21}$		SMITH	79 SPEC	Water, $M=6-350 m_p$

1 YAMAGATA 93 used deep sea water at 4000 m since the concentration is enhanced in deep sea due to gravity.

2 VERKERK 92 looked for heavy isotopes in sea water and put a bound on concentration of stable charged massive particle in sea water. The above bound can be translated into a bound on charged dark matter particle (5×10^6 GeV), assuming the local density, $\rho=0.3$ GeV/cm³, and the mean velocity (v)=300 km/s.

3 See HEMMICK 90 Fig. 7 for other masses 100-10000 m_p .

Concentration of Heavy Stable Particles Bound to Nuclei

VALUE	CL%	DOCUMENT ID	TECN	COMMENT
$<2 \times 10^{-17}$ /nucleon	95	1 AFEK	21	millicharged particle search
$<1.2 \times 10^{-11}$	95	2 JAVORSEK	01 SPEC	Au, $M=3$ GeV
$<6.9 \times 10^{-10}$	95	2 JAVORSEK	01 SPEC	Au, $M=144$ GeV
$<1 \times 10^{-11}$	95	3 JAVORSEK	01B SPEC	Au, $M=188$ GeV
$<1 \times 10^{-8}$	95	3 JAVORSEK	01B SPEC	Au, $M=1669$ GeV
$<6 \times 10^{-9}$	95	3 JAVORSEK	01B SPEC	Fe, $M=188$ GeV
$<1 \times 10^{-8}$	95	3 JAVORSEK	01B SPEC	Fe, $M=647$ GeV
$<4 \times 10^{-20}$	90	4 HEMMICK	90 SPEC	C, $M=100 m_p$
$<8 \times 10^{-20}$	90	4 HEMMICK	90 SPEC	C, $M=1000 m_p$
$<2 \times 10^{-16}$	90	4 HEMMICK	90 SPEC	C, $M=10000 m_p$
$<6 \times 10^{-13}$	90	4 HEMMICK	90 SPEC	Li, $M=1000 m_p$
$<1 \times 10^{-11}$	90	4 HEMMICK	90 SPEC	Be, $M=1000 m_p$
$<6 \times 10^{-14}$	90	4 HEMMICK	90 SPEC	B, $M=1000 m_p$

See key on page 1171

Searches Particle Listings

Other Particle Searches

$<4 \times 10^{-17}$	90	⁴ HEMMICK	90	SPEC	O, $M = 1000m_p$
$<4 \times 10^{-15}$	90	⁴ HEMMICK	90	SPEC	F, $M = 1000m_p$
$<1.5 \times 10^{-13}/\text{nucleon}$	68	⁵ NORMAN	89	SPEC	$^{206}\text{Pb}X^-$
$<1.2 \times 10^{-12}/\text{nucleon}$	68	⁵ NORMAN	87	SPEC	$^{56,58}\text{Fe}X^-$

- ¹AFEK 21 search for millicharged particles bound to matter using an optomechanical device. No signal was observed. Limits placed in the abundance vs. charge plane (Fig. 3). This is translated to the mass versus charge plane by requiring bound states to be stable.
- ²JAVORSEK 01 search for (neutral) SIMPs (strongly interacting massive particles) bound to Au nuclei. Here M is the effective SIMP mass.
- ³JAVORSEK 01B search for (neutral) SIMPs (strongly interacting massive particles) bound to Au and Fe nuclei from various origins with exposures on the earth's surface, in a satellite, heavy ion collisions, etc. Here M is the mass of the anomalous nucleus. See also JAVORSEK 02.
- ⁴See HEMMICK 90 Fig. 7 for other masses 100–10000 m_p .
- ⁵Bound valid up to $m_{X^-} \sim 100 \text{ TeV}$.

GENERAL NEW PHYSICS SEARCHES

This subsection lists some of the search experiments which look for general signatures characteristic of new physics, independent of the framework of a specific model.

The observed events are compatible with Standard Model expectation, unless noted otherwise.

VALUE	DOCUMENT ID	TECN	COMMENT
••• We do not use the following data for averages, fits, limits, etc. •••			
	¹ ALKHATIB 21A	SCDM	CDMSlite search for fractionally charged relics
	² AGUILAR-AR...20B	CONN	ν elastic scatter on nuclei
	³ FEDDERKE 20		CHAMPs from white dwarfs
	⁴ SIRUNYAN 20A	CMS	SUSY/LQ search with mT2 or long-lived charged particles
	⁵ ALCANTARA 19		Auger, superheavy DM
	⁶ PORAYKO 18	PPTA	pulsar timing fuzzy DM search
	⁷ AAD 15AT	ATLS	$t + \cancel{E}_T$
	⁸ KHACHATRY...15F	CMS	$t + \cancel{E}_T$
	⁹ AALTONEN 14J	CDF	$W + 2$ jets
	¹⁰ AAD 13A	ATLS	$WW \rightarrow \ell\nu\ell'\nu$
	¹¹ AAD 13C	ATLS	$\gamma + \cancel{E}_T$
	¹² AALTONEN 13I	CDF	Delayed $\gamma + \cancel{E}_T$
	¹³ CHATRCHYAN13	CMS	$\ell^+\ell^- + \text{jets} + \cancel{E}_T$
	¹⁴ AAD 12C	ATLS	$t\bar{t} + \cancel{E}_T$
	¹⁵ AALTONEN 12M	CDF	jet + \cancel{E}_T
	¹⁶ CHATRCHYAN12AP	CMS	jet + \cancel{E}_T
	¹⁷ CHATRCHYAN12Q	CMS	$Z + \text{jets} + \cancel{E}_T$
	¹⁸ CHATRCHYAN12T	CMS	$\gamma + \cancel{E}_T$
	¹⁹ AAD 11S	ATLS	jet + \cancel{E}_T
	²⁰ AALTONEN 11AF	CDF	$\ell^\pm\ell^\pm$
	²¹ CHATRCHYAN11C	CMS	$\ell^+\ell^- + \text{jets} + \cancel{E}_T$
	²² CHATRCHYAN11U	CMS	jet + \cancel{E}_T
	²³ AALTONEN 10AF	CDF	$\gamma\gamma + \ell, \cancel{E}_T$
	²⁴ AALTONEN 09AF	CDF	$\ell\gamma b \cancel{E}_T$
	²⁵ AALTONEN 09G	CDF	$\ell\ell\ell \cancel{E}_T$

- ¹ALKHATIB 21A search for lightly ionizing fractionally charged relics scattering from Ge. No signal observed. Limits plotted in fractional charge f vs. vertical intensity plane for $m \sim 5 \text{ MeV}$ to 100 TeV .
- ²AGUILAR-AREVALO 20B search for light BSM mediator effect on ν elastic scatter on nuclei; no signal; limits placed in $m(\text{mediator})$ vs. coupling plane for two classes of MeV-scale mediators.
- ³FEDDERKE 20 place limits on cosmic relic charged massive particles (CHAMPs) due to their capture and subsequent disruption of old white dwarf stars; limits placed in the $m(\text{CHAMP})$ vs. relic density parameter plane.
- ⁴SIRUNYAN 20A search for SUSY and LQ production using mT2 or presence of long-lived charged particle; no signal, limits placed in various mass planes for different BSM scenarios and various assumed lifetimes.
- ⁵ALCANTARA 19 place limits on $m(W/\text{MIPZilla}=X)$ vs lifetime from upper bound on ultra high energy cosmic rays at Auger experiment: e.g. $\tau(X) < 4 \times 10^{22} \text{ yr}$ for $m(X) = 10^{16} \text{ GeV}$.
- ⁶PORAYKO 18 search for deviations in the residuals of pulsar timing data using PPTA. No signal observed. Limits set on fuzzy DM with $3 \times 10^{-24} < m(\text{DM}) < 2 \times 10^{-22} \text{ eV}$.
- ⁷AAD 15AT search for events with a top quark and missing E_T in pp collisions at $E_{\text{cm}} = 8 \text{ TeV}$ with $L = 20.3 \text{ fb}^{-1}$.
- ⁸KHACHATRYAN 15F search for events with a top quark and missing E_T in pp collisions at $E_{\text{cm}} = 8 \text{ TeV}$ with $L = 19.7 \text{ fb}^{-1}$.
- ⁹AALTONEN 14J examine events with a W and two jets in $p\bar{p}$ collisions at $E_{\text{cm}} = 1.96 \text{ TeV}$ with $L = 8.9 \text{ fb}^{-1}$. Invariant mass distributions of the two jets are consistent with the Standard Model expectation.
- ¹⁰AAD 13A search for resonant WW production in pp collisions at $E_{\text{cm}} = 7 \text{ TeV}$ with $L = 4.7 \text{ fb}^{-1}$.
- ¹¹AAD 13C search for events with a photon and missing \cancel{E}_T in pp collisions at $E_{\text{cm}} = 7 \text{ TeV}$ with $L = 4.6 \text{ fb}^{-1}$.
- ¹²AALTONEN 13I search for events with a photon and missing E_T , where the photon is detected after the expected timing, in $p\bar{p}$ collisions at $E_{\text{cm}} = 1.96 \text{ TeV}$ with $L = 6.3 \text{ fb}^{-1}$. The data are consistent with the Standard Model expectation.
- ¹³CHATRCHYAN 13 search for events with an opposite-sign lepton pair, jets, and missing E_T in pp collisions at $E_{\text{cm}} = 7 \text{ TeV}$ with $L = 4.98 \text{ fb}^{-1}$.

- ¹⁴AAD 12C search for events with a $t\bar{t}$ pair and missing \cancel{E}_T in pp collisions at $E_{\text{cm}} = 7 \text{ TeV}$ with $L = 1.04 \text{ fb}^{-1}$.
- ¹⁵AALTONEN 12M search for events with a jet and missing E_T in $p\bar{p}$ collisions at $E_{\text{cm}} = 1.96 \text{ TeV}$ with $L = 6.7 \text{ fb}^{-1}$.
- ¹⁶CHATRCHYAN 12AP search for events with a jet and missing E_T in pp collisions at $E_{\text{cm}} = 7 \text{ TeV}$ with $L = 5.0 \text{ fb}^{-1}$.
- ¹⁷CHATRCHYAN 12Q search for events with a Z , jets, and missing \cancel{E}_T in pp collisions at $E_{\text{cm}} = 7 \text{ TeV}$ with $L = 4.98 \text{ fb}^{-1}$.
- ¹⁸CHATRCHYAN 12T search for events with a photon and missing \cancel{E}_T in pp collisions at $E_{\text{cm}} = 7 \text{ TeV}$ with $L = 5.0 \text{ fb}^{-1}$.
- ¹⁹AAD 11S search for events with one jet and missing E_T in pp collisions at $E_{\text{cm}} = 7 \text{ TeV}$ with $L = 33 \text{ pb}^{-1}$.
- ²⁰AALTONEN 11AF search for high- p_T like-sign dileptons in $p\bar{p}$ collisions at $E_{\text{cm}} = 1.96 \text{ TeV}$ with $L = 6.1 \text{ fb}^{-1}$.
- ²¹CHATRCHYAN 11C search for events with an opposite-sign lepton pair, jets, and missing E_T in pp collisions at $E_{\text{cm}} = 7 \text{ TeV}$ with $L = 34 \text{ pb}^{-1}$.
- ²²CHATRCHYAN 11U search for events with one jet and missing E_T in pp collisions at $E_{\text{cm}} = 7 \text{ TeV}$ with $L = 36 \text{ pb}^{-1}$.
- ²³AALTONEN 10AF search for $\gamma\gamma$ events with e, μ, τ , or missing E_T in $p\bar{p}$ collisions at $E_{\text{cm}} = 1.96 \text{ TeV}$ with $L = 1.1\text{--}2.0 \text{ fb}^{-1}$.
- ²⁴AALTONEN 09AF search for $\ell\gamma b$ events with missing E_T in $p\bar{p}$ collisions at $E_{\text{cm}} = 1.96 \text{ TeV}$ with $L = 1.9 \text{ fb}^{-1}$. The observed events are compatible with Standard Model expectation including $t\bar{t}\gamma$ production.
- ²⁵AALTONEN 09G search for $\mu\mu\mu$ and $\mu\mu e$ events with missing E_T in $p\bar{p}$ collisions at $E_{\text{cm}} = 1.96 \text{ TeV}$ with $L = 976 \text{ pb}^{-1}$.

LIMITS ON JET-JET RESONANCES

Heavy Particle Production Cross Section

Limits are for a particle decaying to two hadronic jets.

Units(pb)	CL%	Mass(GeV)	DOCUMENT ID	TECN	COMMENT
••• We do not use the following data for averages, fits, limits, etc. •••					
			¹ TUMASYAN 23L	CMS	dijet resonance in 4-jet events
			² AAD 20AD	ATLS	pp at 13 TeV, dijet resonance
			³ AAD 20T	ATLS	dijet resonance search
			⁴ AAD 20W	ATLS	dijet resonance plus lepton
			⁵ SIRUNYAN 20AI	CMS	dijet resonance search
			⁶ AABOUD 19AJ	ATLS	$pp \rightarrow \gamma X, X \rightarrow jj$
			⁷ SIRUNYAN 19B	CMS	$pp \rightarrow jA, A \rightarrow b\bar{b}$
			⁸ SIRUNYAN 19CD	CMS	$pp \rightarrow Z'\gamma, Z' \rightarrow jj$
			⁹ AABOUD 18AD	ATLS	$pp \rightarrow Y \rightarrow HX \rightarrow (bb) + (qq)$
			¹⁰ AABOUD 18CK	ATLS	$pp \rightarrow bbb + \cancel{E}_T$
			¹¹ AABOUD 18CL	ATLS	$pp \rightarrow$ vector-like quarks
			¹² AABOUD 18N	ATLS	$pp \rightarrow jj$ resonance
			¹³ SIRUNYAN 18DJ	CMS	$pp \rightarrow ZZ$ or $WZ \rightarrow \ell\bar{\ell}jj$
			¹⁴ SIRUNYAN 18DY	CMS	$pp \rightarrow RR; R \rightarrow jj$
			¹⁵ KHACHATRY...17W	CMS	$pp \rightarrow jj$ resonance
			¹⁶ KHACHATRY...17Y	CMS	$pp \rightarrow (8\text{--}10) j + \cancel{E}_T$
			¹⁷ SIRUNYAN 17F	CMS	$pp \rightarrow jj$ angular distribution
			¹⁸ AABOUD 16	ATLS	$pp \rightarrow b + \text{jet}$
			¹⁹ AAD 16N	ATLS	$pp \rightarrow 3$ high E_T jets
			²⁰ AAD 16S	ATLS	$pp \rightarrow jj$ resonance
			²¹ KHACHATRY...16K	CMS	$pp \rightarrow jj$ resonance
			²² KHACHATRY...16L	CMS	$pp \rightarrow jj$ resonance
			²³ AAD 13D	ATLS	7 TeV $pp \rightarrow 2$ jets
			²⁴ AALTONEN 13R	CDF	1.96 TeV $p\bar{p} \rightarrow 4$ jets
			²⁵ CHATRCHYAN13A	CMS	7 TeV $pp \rightarrow 2$ jets
			²⁶ CHATRCHYAN13A	CMS	7 TeV $pp \rightarrow b\bar{b}X$
			²⁷ AAD 12S	ATLS	7 TeV $pp \rightarrow 2$ jets
			²⁸ CHATRCHYAN12BL	CMS	7 TeV $pp \rightarrow t\bar{t}X$
			²⁹ AAD 11AG	ATLS	7 TeV $pp \rightarrow 2$ jets
			³⁰ AALTONEN 11M	CDF	1.96 TeV $p\bar{p} \rightarrow W + 2$ jets
			³¹ ABAZOV 11I	D0	1.96 TeV $p\bar{p} \rightarrow W + 2$ jets
			³² AAD 10	ATLS	7 TeV $pp \rightarrow 2$ jets
			³³ KHACHATRY...10	CMS	7 TeV $pp \rightarrow 2$ jets
			³⁴ ABE 99F	CDF	1.8 TeV $p\bar{p} \rightarrow b\bar{b} + \text{anything}$
			³⁵ ABE 97G	CDF	1.8 TeV $p\bar{p} \rightarrow 2$ jets
			³⁶ ABE 93G	CDF	1.8 TeV $p\bar{p} \rightarrow 2$ jets
			³⁶ ABE 93G	CDF	1.8 TeV $p\bar{p} \rightarrow 2$ jets
			³⁶ ABE 93G	CDF	1.8 TeV $p\bar{p} \rightarrow 2$ jets

- ¹TUMASYAN 23L search for dijet resonance in 4-jet events with 138 fb^{-1} fb of data. There are two events in the tails of the distributions, each with a four-jet mass of 8 TeV and an average dijet mass of 2 TeV, resulting in local and global significances of 3.9 and 1.6 standard deviations, respectively, if interpreted as a signal. Limits set for simplified diquark model.
- ²AAD 20AD search for weakly supervised dijet resonance in ATLAS with 139 fb^{-1} at 13 TeV; no signal; various limits placed depending on kinematics and production cross section.
- ³AAD 20T search for dijet resonance with or without b -jets at 13 TeV and 139 fb^{-1} ; no signal; limits placed in $\sigma \cdot \text{BF}$ vs mass plane for various BSM models.
- ⁴AAD 20W search for dijet resonance plus lepton with ATLAS at 13 TeV and 139 fb^{-1} ; no signal; limits placed in $\sigma \cdot \text{BF}$ vs. mass plane for various BSM models.
- ⁵SIRUNYAN 20AI search for dijet resonance in CMS at 13 TeV with 137 fb^{-1} ; no signal; limits set in σ vs. mass plane for various BSM models.

Searches Particle Listings

Other Particle Searches

- 6 AABOUD 19AJ search for low mass dijet resonance in $pp \rightarrow \gamma X, X \rightarrow jj$ at 13 TeV with 79.8 fb⁻¹ of data; no signal found; limits placed on Z' model in coupling vs. m(Z') plane.
- 7 SIRUNYAN 19b search for low mass resonance $pp \rightarrow jA, A \rightarrow b\bar{b}$ at 13 TeV using 35.9 fb⁻¹; no signal; exclude resonances 50–350 GeV depending on production and decay.
- 8 SIRUNYAN 19CD search for $pp \rightarrow Z'\gamma, Z' \rightarrow jj$ with fat jet (jj); no signal, limits placed in m(Z') vs. coupling plane for Z' masses from 10 to 125 GeV.
- 9 AABOUD 18AD search for new heavy particle $Y \rightarrow HX \rightarrow (bb) + (qq)$. No signal observed. Limits set on m(Y) vs. m(X) in the ranges of m(Y) in 1–4 TeV and m(X) in 50–1000 GeV.
- 10 AABOUD 18ck search for SUSY Higgsinos in gauge-mediation via $pp \rightarrow bbb + \cancel{E}_T$ at 13 TeV using two complementary analyses with 24.3/36.1 fb⁻¹; no signal is found and Higgsinos with masses between 130 and 230 GeV and between 290 and 880 GeV are excluded at the 95% confidence level.
- 11 AABOUD 18cl search for $pp \rightarrow$ vector-like quarks \rightarrow jets at 13 TeV with 36 fb⁻¹; no signal seen; limits set on various VLQ scenarios. For pure $B \rightarrow Hb$ or $T \rightarrow Ht$, set the mass limit $m > 1010$ GeV.
- 12 AABOUD 18n search for dijet resonance at Atlas with 13 TeV and 29.3 fb⁻¹; limits set on m(Z') in the mass range of 450–1800 GeV.
- 13 SIRUNYAN 18DJ search for $pp \rightarrow ZZ$ or $WZ \rightarrow \ell\bar{\ell}jj$ resonance at 13 TeV, 35.9 fb⁻¹; no signal; limits set in the 400–450 GeV mass range, exclusion of W' up to 2270 GeV in the HVT model A, and up to 2330 GeV for HVT model B. WED bulk graviton exclusion up to 925 GeV.
- 14 SIRUNYAN 18DY search for $pp \rightarrow RR, R \rightarrow jj$ two dijet resonances at 13 TeV 35.9 fb⁻¹; no signal; limits placed on RPV top-squark pair production.
- 15 KHACHATRYAN 17W search for dijet resonance in 12.9 fb⁻¹ data at 13 TeV; see Fig. 2 for limits on axiguons, diquarks, dark matter mediators etc.
- 16 KHACHATRYAN 17Y search for $pp \rightarrow (8-10)j$ in 19.7 fb⁻¹ at 8 TeV. No signal seen. Limits set on colorons, axiguons, RPV, and SUSY.
- 17 SIRUNYAN 17F measure $pp \rightarrow jj$ angular distribution in 2.6 fb⁻¹ at 13 TeV; limits set on LEDs and quantum black holes.
- 18 AABOUD 16 search for resonant dijets including one or two b-jets with 3.2 fb⁻¹ at 13 TeV; exclude excited b* quark from 1.1–2.1 TeV; exclude leptophilic Z' with SM couplings from 1.1–1.5 TeV.
- 19 AAD 16N search for ≥ 3 jets with 3.6 fb⁻¹ at 13 TeV; limits placed on micro black holes (Fig. 10) and string balls (Fig. 11).
- 20 AAD 16s search for high mass jet-jet resonance with 3.6 fb⁻¹ at 13 TeV; exclude portions of excited quarks, W', Z' and contact interaction parameter space.
- 21 KHACHATRYAN 16K search for dijet resonance in 2.4 fb⁻¹ data at 13 TeV; see Fig. 3 for limits on axiguons, diquarks etc.
- 22 KHACHATRYAN 16L use data scouting technique to search for jj resonance on 18.8 fb⁻¹ of data at 8 TeV. Limits on the coupling of a leptophobic Z' to quarks are set, improving on the results by other experiments in the mass range between 500–800 GeV.
- 23 AAD 13D search for dijet resonances in pp collisions at E_{cm} = 7 TeV with L = 4.8 fb⁻¹. The observed events are compatible with Standard Model expectation. See their Fig. 6 and Table 2 for limits on resonance cross section in the range m = 1.0–4.0 TeV.
- 24 AALTONEN 13R search for production of a pair of jet-jet resonances in p \bar{p} collisions at E_{cm} = 1.96 TeV with L = 6.6 fb⁻¹. See their Fig. 5 and Tables I, II for cross section limits.
- 25 CHATRCHYAN 13A search for qq, qg, and gg resonances in pp collisions at E_{cm} = 7 TeV with L = 4.8 fb⁻¹. See their Fig. 3 and Table 1 for limits on resonance cross section in the range m = 1.0–4.3 TeV.
- 26 CHATRCHYAN 13A search for b \bar{b} resonances in pp collisions at E_{cm} = 7 TeV with L = 4.8 fb⁻¹. See their Fig. 8 and Table 4 for limits on resonance cross section in the range m = 1.0–4.0 TeV.
- 27 AAD 12s search for dijet resonances in pp collisions at E_{cm} = 7 TeV with L = 1.0 fb⁻¹. See their Fig. 3 and Table 2 for limits on resonance cross section in the range m = 0.9–4.0 TeV.
- 28 CHATRCHYAN 12BL search for t \bar{t} resonances in pp collisions at E_{cm} = 7 TeV with L = 4.4 fb⁻¹. See their Fig. 4 for limits on resonance cross section in the range m = 0.5–3.0 TeV.
- 29 AAD 11AG search for dijet resonances in pp collisions at E_{cm} = 7 TeV with L = 36 pb⁻¹. Limits on number of events for m = 0.6–4 TeV are given in their Table 3.
- 30 AALTONEN 11M find a peak in two jet invariant mass distribution around 140 GeV in W + 2 jet events in p \bar{p} collisions at E_{cm} = 1.96 TeV with L = 4.3 fb⁻¹.
- 31 ABAZOV 11I search for two-jet resonances in W + 2 jet events in p \bar{p} collisions at E_{cm} = 1.96 TeV with L = 4.3 fb⁻¹ and give limits $\sigma < (2.6-1.3)$ pb (95% CL) for m = 110–170 GeV. The result is incompatible with AALTONEN 11M.
- 32 AAD 10 search for narrow dijet resonances in pp collisions at E_{cm} = 7 TeV with L = 315 nb⁻¹. Limits on the cross section in the range 10–10³ pb is given for m = 0.3–1.7 TeV.
- 33 KHACHATRYAN 10 search for narrow dijet resonances in pp collisions at E_{cm} = 7 TeV with L = 2.9 pb⁻¹. Limits on the cross section in the range 1–300 pb is given for m = 0.5–2.6 TeV separately in the final states qq, qg, and gg.
- 34 ABE 99F search for narrow b \bar{b} resonances in p \bar{p} collisions at E_{cm}=1.8 TeV. Limits on $\sigma(p\bar{p} \rightarrow X + \text{anything}) \times B(X \rightarrow b\bar{b})$ in the range 3–10³ pb (95%CL) are given for m_X=200–750 GeV. See their Table I.
- 35 ABE 97G search for narrow dijet resonances in p \bar{p} collisions with 106 pb⁻¹ of data at E_{cm} = 1.8 TeV. Limits on $\sigma(p\bar{p} \rightarrow X + \text{anything}) \times B(X \rightarrow jj)$ in the range 10⁴–10⁻¹ pb (95%CL) are given for dijet mass m=200–1150 GeV with both jets having $|\eta| < 2.0$ and the dijet system having $|\cos\theta^*| < 0.67$. See their Table I for the list of limits. Supersedes ABE 93c.
- 36 ABE 93c give cross section times branching ratio into light (d, u, s, c, b) quarks for $\Gamma = 0.02 M$. Their Table II gives limits for M = 200–900 GeV and $\Gamma = (0.02-0.2) M$.

LIMITS ON NEUTRAL PARTICLE PRODUCTION

Production Cross Section of Radiatively-Decaying Neutral Particle

VALUE (pb)	CL%	DOCUMENT ID	TECN	COMMENT
• • • We do not use the following data for averages, fits, limits, etc. • • •				
		1 ALBERT 18c	HAWC	γ from Sun
		2 KHACHATRYAN..17D	CMS	Z γ resonance
		3 AAD 16AI	ATLS	$pp \rightarrow \gamma + \text{jet}$
		4 KHACHATRYAN..16M	CMS	$pp \rightarrow \gamma\gamma$ resonance
<0.0008	95	5 ABBIENDI 00D	OPAL	$e^+e^- \rightarrow X^0\gamma^0,$ $X^0 \rightarrow \gamma^0\gamma^0,$ $X^0 \rightarrow \gamma^0\gamma^0,$
<(0.043-0.17)	95	6 ABBIENDI 00D	OPAL	$e^+e^- \rightarrow X^0X^0,$ $X^0 \rightarrow \gamma^0\gamma^0,$ $X^0 \rightarrow \gamma^0\gamma^0,$
<(0.05-0.8)	95	7 ACKERSTAFF 97B	OPAL	$e^+e^- \rightarrow X^0\gamma^0,$ $X^0 \rightarrow \gamma^0\gamma^0,$ $X^0 \rightarrow \gamma^0\gamma^0,$
<(2.5-0.5)	95	8 ACKERSTAFF 97B	OPAL	$e^+e^- \rightarrow X^0X^0,$ $X^0 \rightarrow \gamma^0\gamma^0,$ $X^0 \rightarrow \gamma^0\gamma^0,$
<(1.6-0.9)	95			
1 ALBERT 18c search for WIMP annihilation in Sun to long-lived, radiatively decaying mediator; no signal; limits set on $\sigma^{SD}(\chi p)$ assuming long-lived mediator.				
2 KHACHATRYAN 17D search for new scalar resonance decaying to Z γ with Z $\rightarrow e^+e^-$, $\mu^+\mu^-$ in pp collisions at 8 and 13 TeV; no signal seen.				
3 AAD 16AI search for excited quarks (EQ) and quantum black holes (QBH) in 3.2 fb ⁻¹ at 13 TeV of data; exclude EQ below 4.4 TeV and QBH below 3.8 (6.2) TeV for RS1 (ADD) models. The visible cross section limit was obtained for 5 TeV resonances with $\sigma_G/M_G = 2\%$.				
4 KHACHATRYAN 16M search for $\gamma\gamma$ resonance using 19.7 fb ⁻¹ at 8 TeV and 3.3 fb ⁻¹ at 13 TeV; slight excess at 750 GeV noted; limit set on RS graviton.				
5 ABBIENDI 00D associated production limit is for $m_{X^0} = 90-188$ GeV, $m_{Y^0} = 0$ at $E_{cm} = 189$ GeV. See also their Fig. 9.				
6 ABBIENDI 00D pair production limit is for $m_{X^0} = 45-94$ GeV, $m_{Y^0} = 0$ at $E_{cm} = 189$ GeV. See also their Fig. 12.				
7 ACKERSTAFF 97B associated production limit is for $m_{X^0} = 80-160$ GeV, $m_{Y^0} = 0$ from 10.0 pb ⁻¹ at $E_{cm} = 161$ GeV. See their Fig. 3(a).				
8 ACKERSTAFF 97B pair production limit is for $m_{X^0} = 40-80$ GeV, $m_{Y^0} = 0$ from 10.0 pb ⁻¹ at $E_{cm} = 161$ GeV. See their Fig. 3(b).				

Heavy Particle Production Cross Section

VALUE (cm ² /N)	CL%	DOCUMENT ID	TECN	COMMENT
• • • We do not use the following data for averages, fits, limits, etc. • • •				
		1 AAD 23P	ATLS	exotica search in association with $h \rightarrow \gamma\gamma$
		2 TUMASYAN 23BC	CMS	γ -jet resonance search
		3 TUMASYAN 23BF	CMS	$pp + \gamma/Z + X$ search
		4 TUMASYAN 22AG	CMS	SIMP search
		5 AAD 21F	ATLS	monojet search
		6 AAIJ 20AL	LHCB	pp at 13 TeV, dimuon resonance
		7 SIRUNYAN 20AY	CMS	$\Upsilon(1S)\mu^+\mu^-$ decay states
		8 SIRUNYAN 20Z	CMS	multilepton BSM search, 13 TeV
		9 AABOUD 19H	ATLS	di-photon-jet resonance
		10 AABOUD 19Y	ATLS	review, mediator-based DM
		11 SIRUNYAN 19O	CMS	$pp \rightarrow \gamma \cancel{E}_T$
		12 AABOUD 18CJ	ATLS	$pp \rightarrow VV/\ell\ell/\ell\nu, V = W, Z, h$
		13 AABOUD 18CM	ATLS	$pp \rightarrow e\mu/e\tau/\mu\tau$
		14 AAIJ 18AJ	LHCB	$pp \rightarrow A' \rightarrow \mu^+\mu^-;$ dark photon
		15 BANERJEE 18 NA64		$eZ \rightarrow eZX(A')$
		16 BANERJEE 18A NA64		$eZ \rightarrow eZA', A' \rightarrow \chi\chi$
		17 MARSICANO 18 E137		$e^+e^- \rightarrow A'(\gamma)$ visible decay
		18 SIRUNYAN 18BB	CMS	$pp \rightarrow Z' \rightarrow \ell^+\ell^-$ at 13 TeV
		19 SIRUNYAN 18DA	CMS	$pp \rightarrow$ Black Hole, string ball, sphaleron
		20 SIRUNYAN 18DD	CMS	$pp \rightarrow jj$
		21 SIRUNYAN 18DR	CMS	$pp \rightarrow b\mu\bar{p}$
		22 SIRUNYAN 18DU	CMS	$pp \rightarrow \gamma\gamma$
		23 SIRUNYAN 18ED	CMS	$pp \rightarrow V \rightarrow Wh; h \rightarrow b\bar{b}; W \rightarrow \ell\nu$
		24 AABOUD 17B	ATLS	WH, ZH resonance
		25 AAIJ 17BR	LHCB	$pp \rightarrow \pi\nu\pi\nu, \pi\nu \rightarrow jj$
		26 AAD 16O	ATLS	$\ell + (fs$ or jets)
		27 AAD 16R	ATLS	WW, WZ, ZZ resonance
		28 KRASNAHO..16		$p^7\text{Li} \rightarrow {}^8\text{Be} \rightarrow X(17)N, X(17) \rightarrow e^+e^-$
		29 LEES 15E	BABR	e^+e^- collisions
		30 ADAMS 97B	KTEV	$m = 1.2-5$ GeV
		31 GALLAS 95	TOF	$m = 0.5-20$ GeV
		32 AKESSON 91	CNTR	$m = 0-5$ GeV
< 10 ⁻³⁶ -10 ⁻³³	90	33 BADIAR 86	BDMP	$\tau = (0.05-1.) \times 10^{-8}$ s
<(4-0.3) $\times 10^{-31}$	95	34 GUSTAFSON 76	CNTR	$\tau > 10^{-7}$ s
< 2 $\times 10^{-36}$	90			
< 2.5 $\times 10^{-35}$	90			
1 AAD 23P search in 22 channels for exotica produced in association with $h \rightarrow \gamma\gamma$ in 139 fb ⁻¹ of data. No signal observed. Limits placed on production cross section in various channels.				

- 2 TUMASYAN 23BC search for γ -jet resonance at CMS with 138 fb^{-1} of data. No signal observed. Limits placed on quantum black hole and excited quark models.
- 3 TUMASYAN 23BF search for $pp \rightarrow pp + \gamma/Z + X$ search where X is missing particle using CMS-TOTEM with 37.2 fb^{-1} of data. No signal observed. Limits placed on σ vs. m plane.
- 4 TUMASYAN 22AG search for strongly interacting neutral massive particles via trackless jets with 16.1 fb^{-1} at 13 TeV; no signal detected; limits placed in mass vs. cross section plane for various simplified models.
- 5 AAD 21F search for hard monojet production at ATLAS with 139 fb^{-1} of 13 TeV data. No signal observed. Limits placed on invisible production cross-section recoiling against ISR and interpreted in variety of BSM models.
- 6 AAIJ 20AL search for dimuon resonance from promptly decaying X particle; no signal; limits placed on $m(X)$ up to 60 GeV depending on mixing in 2HDM.
- 7 SIRUNYAN 20AV measured $\Upsilon(1S)$ pair production cross section and searched for new states decaying into $\Upsilon(1S)\mu^+\mu^-$ at CMS with 13 TeV with 35.9 fb^{-1} . No signal is found and limits are set in σ -BF vs. mass plane for tetra- b -quarks with masses between 17.5 and 19 GeV and for generic search for narrow resonances with mass between 16.5 and 27 GeV.
- 8 SIRUNYAN 20Z search for BSM physics via multilepton production with CMS at 13 TeV with 137 fb^{-1} ; no signal is found and limits are set on type-III seesaw and other BSM models.
- 9 AABOUD 19H searches for di-photon-jet resonance at 13 TeV and 36.7 fb^{-1} of data; no signal found and limits placed on σ -BR vs. mass plane for various simplified models.
- 10 AABOUD 19V review ATLAS searches for mediator-based DM at 7, 8, and 13 TeV with up to 37 fb^{-1} of data; no signal found and limits set for wide variety of simplified models of dark matter.
- 11 SIRUNYAN 19O search for $pp \rightarrow \gamma \bar{\nu}_T$ at 13 TeV with 36.1 fb^{-1} ; no signal found and limits set for various simplified models.
- 12 AABOUD 18CJ make multichannel search for $pp \rightarrow VV/\ell\ell/\ell\nu$, $V = W, Z, h$ at 13 TeV, 36.1 fb^{-1} ; no signal found; limits placed for several BSM models.
- 13 AABOUD 18CM search for lepton-flavor violating resonance in $pp \rightarrow e\mu/\tau\mu/\mu\tau$ at 13 TeV, 36.1 fb^{-1} ; no signal is found and limits placed for various BSM models.
- 14 AAIJ 18AJ search for prompt and delayed dark photon decay $A' \rightarrow \mu^+\mu^-$ at LHCb detector using 1.6 fb^{-1} of pp collisions at 13 TeV; limits on $m(A')$ vs. kinetic mixing are set.
- 15 BANERJEE 18 search for dark photon $A'/16.7 \text{ MeV}$ boson X at NA64 via $eZ \rightarrow eZX(A')$; no signal found and limits set on the X - e^- coupling ϵ_e in the range $1.3 \times 10^{-4} \leq \epsilon_e \leq 4.2 \times 10^{-4}$ excluding part of the allowed parameter space.
- 16 BANERJEE 18A search for invisibly decaying dark photons in $eZ \rightarrow eZA', A' \rightarrow$ invisible; no signal found and limits set on mixing for $m(A') < 1 \text{ GeV}$.
- 17 MARSICANO 18 search for dark photon $e^+e^- \rightarrow A'(\gamma)$ visible decay in SLAC E137 e beam dump data. No signal observed and limits set in ϵ coupling vs $m(A')$ plane, see their figure 7.
- 18 SIRUNYAN 18BB search for high mass dilepton resonance; no signal found and exclude portions of p -space of Z' , KK graviton models.
- 19 SIRUNYAN 18DA search for $pp \rightarrow$ Black Hole, string ball, sphaleron via high multiplicity events at 13 TeV, 35.9 fb^{-1} ; no signal, require e.g. $m(\text{BH}) > 10.1 \text{ TeV}$.
- 20 SIRUNYAN 18DD search for $pp \rightarrow jj$ deviations in dijet angular distribution. No signal observed. Set limits on large extra dimensions, black holes and DM mediators e.g. $m(\text{BH}) > 5.9\text{--}8.2 \text{ TeV}$.
- 21 SIRUNYAN 18DR search for dimuon resonance in $pp \rightarrow b\mu\bar{\mu}$ at 8 and 13 TeV. Slight excess seen at $m(\mu\bar{\mu}) \sim 28 \text{ GeV}$ in some channels.
- 22 SIRUNYAN 18DU search for high mass diphoton resonance in $pp \rightarrow \gamma\gamma$ at 13 TeV using 35.9 fb^{-1} ; no signal; limits placed on RS Graviton, LED, and clockwork.
- 23 SIRUNYAN 18ED search for $pp \rightarrow V \rightarrow Wh; h \rightarrow b\bar{b}; W \rightarrow \ell\nu$ at 13 TeV with 35.9 fb^{-1} ; no signal; limits set on $m(W') > 2.9 \text{ TeV}$.
- 24 AABOUD 17B exclude $m(W', Z') < 1.49\text{--}2.31 \text{ TeV}$ depending on the couplings and W'/Z' degeneracy assumptions via WH, ZH search in pp collisions at 13 TeV with 3.2 fb^{-1} of data.
- 25 AAIJ 17BR search for long-lived hidden valley pions from Higgs decay. Limits are set on the signal strength as a function of the mass and lifetime of the long-lived particle in their Fig. 4 and Tab. 4.
- 26 AAD 16O search for high $E_T \ell + (\ell s \text{ or jets})$ with 3.2 fb^{-1} at 13 TeV; exclude micro black holes mass $< 8 \text{ TeV}$ (Fig. 3) for models with two extra dimensions.
- 27 AAD 16R search for WW, WZ, ZZ resonance in 20.3 fb^{-1} at 8 TeV data; limits placed on massive RS graviton (Fig. 4).
- 28 KRASNAHORKAY 16 report $p\text{Li} \rightarrow \text{Be} \rightarrow e\bar{\nu}N 5\sigma$ resonance at 16.7 MeV- possible evidence for nuclear interference or new light boson. However, such nuclear interference was ruled out already by ZANG 17.
- 29 LEES 15E search for long-lived neutral particles produced in e^+e^- collisions in the Upsilon region, which decays into $e^+e^-, \mu^+\mu^-, e^\pm\mu^\mp, \pi^+\pi^-, K^+K^-, \text{ or } \pi^\pm K^\mp$. See their Fig. 2 for cross section limits.
- 30 ADAMS 97B search for a hadron-like neutral particle produced in pN interactions, which decays into a ρ^0 and a weakly interacting massive particle. Upper limits are given for the ratio to K_S production for the mass range 1.2-5 GeV and lifetime $10^{-9}\text{--}10^{-4} \text{ s}$. See also our Light Gluino Section.
- 31 GALLAS 95 limit is for a weakly interacting neutral particle produced in 800 GeV/c pN interactions decaying with a lifetime of $10^{-4}\text{--}10^{-8} \text{ s}$. See their Figs. 8 and 9. Similar limits are obtained for a stable particle with interaction cross section $10^{-29}\text{--}10^{-33} \text{ cm}^2$. See Fig. 10.
- 32 AKESSON 91 limit is from weakly interacting neutral long-lived particles produced in pN reaction at 450 GeV/c performed at CERN SPS. Bourquin-Gaillard formula is used as the production model. The above limit is for $\tau > 10^{-7} \text{ s}$. For $\tau > 10^{-9} \text{ s}$, $\sigma < 10^{-30} \text{ cm}^2/\text{nucleon}$ is obtained.
- 33 BADIER 86 looked for long-lived particles at 300 GeV π^- beam dump. The limit applies for particle modes, $\mu^+\pi^-, \mu^+\mu^-, \pi^+\pi^-, \pi^+\pi^+X, \pi^+\pi^-\pi^\pm$ etc. See their figure 5 for the contours of limits in the mass- τ plane for each mode.
- 34 GUSTAFSON 76 is a 300 GeV FNAL experiment looking for heavy ($m > 2 \text{ GeV}$) long-lived neutral hadrons in the M4 neutral beam. The above typical value is for $m = 3 \text{ GeV}$ and assumes an interaction cross section of 1 mb. Values as a function of mass and interaction cross section are given in figure 2.

Production of New Penetrating Non- ν Like States in Beam Dump

VALUE	DOCUMENT ID	TECN	COMMENT
••• We do not use the following data for averages, fits, limits, etc. •••			
	1 ABRATENKO 22A	MCBN	search for LLPs
	2 ANDREEV 22A	NA64	search for new boson X in $eZ \rightarrow eZX$
	3 ANDREEV 21	NA64	search for new boson X in $eZ \rightarrow eZX$
	4 LOSECCO 81	CALO	28 GeV protons
1 ABRATENKO 22A	search for LLPs from kaon decay in MicroBooNE absorber; no signal observed; limits placed for heavy neutral leptons (HNLs) and Higgs portal scalars (HPSS) in the MeV mass range.		
2 ANDREEV 22A	search for new light B-L gauge boson $Z' \rightarrow \nu\bar{\nu}$ in electron beam dump at NA64; no signal observed; limits set in $m(Z')$ vs coupling plane for $m(Z') \sim 10^{-6}\text{--}1 \text{ GeV}$.		
3 ANDREEV 21	search for new invisibly decaying boson X in $eZ \rightarrow eZX$ at NA64. No signal observed. Limits set in coupling vs. $m(X)$ plane for $m(X) \sim 10^{-3}$ to 1 GeV.		
4	No excess neutral-current events leads to $\sigma(\text{production}) \times \sigma(\text{interaction}) \times \text{acceptance} < 2.26 \times 10^{-71} \text{ cm}^4/\text{nucleon}^2$ (CL = 90%) for light neutrals. Acceptance depends on models (0.1 to $4. \times 10^{-4}$).		

LIMITS ON CHARGED PARTICLES IN e^+e^- Heavy Particle Production Cross Section in e^+e^-

Ratio to $\sigma(e^+e^- \rightarrow \mu^+\mu^-)$ unless noted. See also entries in Free Quark Search and Magnetic Monopole Searches.

VALUE	CL%	DOCUMENT ID	TECN	COMMENT
••• We do not use the following data for averages, fits, limits, etc. •••				
$< 1 \times 10^{-3}$	90	1 ADACHI 23K	BELL	search for LLP in B decays
		2 KILE 18	ALEP	$e^+e^- \rightarrow 4$ jets
		3 ABLIKIM 17AA	BES3	$e^+e^- \rightarrow \ell\bar{\ell}\gamma$
		4 ACKERSTAFF 98P	OPAL	$Q=1,2/3, m=45\text{--}89.5 \text{ GeV}$
		5 ABREU 97D	DLPH	$Q=1,2/3, m=45\text{--}84 \text{ GeV}$
		6 BARATE 97K	ALEP	$Q=1, m=45\text{--}85 \text{ GeV}$
$< 2 \times 10^{-5}$	95	7 AKERS 95R	OPAL	$Q=1, m=5\text{--}45 \text{ GeV}$
$< 1 \times 10^{-5}$	95	7 AKERS 95R	OPAL	$Q=2, m=5\text{--}45 \text{ GeV}$
$< 2 \times 10^{-3}$	90	8 BUSKULIC 93C	ALEP	$Q=1, m=32\text{--}72 \text{ GeV}$
$< (10^{-2}\text{--}1)$	95	9 ADACHI 90C	TOPZ	$Q=1, m=1\text{--}16, 18\text{--}27 \text{ GeV}$
$< 7 \times 10^{-2}$	90	10 ADACHI 90E	TOPZ	$Q=1, m=5\text{--}25 \text{ GeV}$
$< 1.6 \times 10^{-2}$	95	11 KINOSHITA 82	PLAS	$Q=3\text{--}180, m < 14.5 \text{ GeV}$
$< 5.0 \times 10^{-2}$	90	12 BARTEL 80	JADE	$Q=(3,4,5)/3$ 2-12 GeV
1 ADACHI 23K	search for spin-0 LLP called S in B decays. No signal observed. Limits placed in branching fraction vs. $m(S)$ plane.			
2 KILE 18	investigate archived ALEPH $e^+e^- \rightarrow 4$ jets data and see 4-5 σ excess at 110 GeV.			
3 ABLIKIM 17AA	search for dark photon $A \rightarrow \ell\bar{\ell}$ at 3.773 GeV with 2.93 fb^{-1} . Limits are set in ϵ vs $m(A)$ plane.			
4 ACKERSTAFF 98P	search for pair production of long-lived charged particles at E_{cm} between 130 and 183 GeV and give limits $\sigma < (0.05\text{--}0.2) \text{ pb}$ (95%CL) for spin-0 and spin-1/2 particles with $m=45\text{--}89.5 \text{ GeV}$, charge 1 and 2/3. The limit is translated to the cross section at $E_{cm}=183 \text{ GeV}$ with the s dependence described in the paper. See their Figs. 2-4.			
5 ABREU 97D	search for pair production of long-lived particles and give limits $\sigma < (0.4\text{--}2.3) \text{ pb}$ (95%CL) for various center-of-mass energies $E_{cm}=130\text{--}136, 161,$ and 172 GeV , assuming an almost flat production distribution in $\cos\theta$.			
6 BARATE 97K	search for pair production of long-lived charged particles at $E_{cm} = 130, 136, 161,$ and 172 GeV and give limits $\sigma < (0.2\text{--}0.4) \text{ pb}$ (95%CL) for spin-0 and spin-1/2 particles with $m=45\text{--}85 \text{ GeV}$. The limit is translated to the cross section at $E_{cm}=172 \text{ GeV}$ with the E_{cm} dependence described in the paper. See their Figs. 2 and 3 for limits on $J = 1/2$ and $J = 0$ cases.			
7 AKERS 95R	is a CERN-LEP experiment with $W_{cm} \sim m_Z$. The limit is for the production of a stable particle in multihadron events normalized to $\sigma(e^+e^- \rightarrow \text{hadrons})$. Constant phase space distribution is assumed. See their Fig. 3 for bounds for $Q = \pm 2/3, \pm 4/3$.			
8 BUSKULIC 93C	is a CERN-LEP experiment with $W_{cm} = m_Z$. The limit is for a pair or single production of heavy particles with unusual ionization loss in TPC. See their Fig. 5 and Table 1.			
9 ADACHI 90C	is a KEK-TRISTAN experiment with $W_{cm} = 52\text{--}60 \text{ GeV}$. The limit is for pair production of a scalar or spin-1/2 particle. See Figs. 3 and 4.			
10 ADACHI 90E	is KEK-TRISTAN experiment with $W_{cm} = 52\text{--}61.4 \text{ GeV}$. The above limit is for inclusive production cross section normalized to $\sigma(e^+e^- \rightarrow \mu^+\mu^-) \cdot \beta(3-\beta^2)/2$, where $\beta = (1 - 4m^2/W_{cm}^2)^{1/2}$. See the paper for the assumption about the production mechanism.			
11 KINOSHITA 82	is SLAC PEP experiment at $W_{cm} = 29 \text{ GeV}$ using lexan and ^{39}Cr plastic sheets sensitive to highly ionizing particles.			
12 BARTEL 80	is DESY-PETRA experiment with $W_{cm} = 27\text{--}35 \text{ GeV}$. Above limit is for inclusive pair production and ranges between $1. \times 10^{-1}$ and $1. \times 10^{-2}$ depending on mass and production momentum distributions. (See their figures 9, 10, 11).			

Branching Fraction of Z^0 to a Pair of Stable Charged Heavy Fermions

VALUE	CL%	DOCUMENT ID	TECN	COMMENT
••• We do not use the following data for averages, fits, limits, etc. •••				
$< 5 \times 10^{-6}$	95	1 AKERS 95R	OPAL	$m = 40.4\text{--}45.6 \text{ GeV}$
$< 1 \times 10^{-3}$	95	AKRAWY 90O	OPAL	$m = 29\text{--}40 \text{ GeV}$
1 AKERS 95R	give the 95% CL limit $\sigma(X\bar{X})/\sigma(\mu\mu) < 1.8 \times 10^{-4}$ for the pair production of singly- or doubly-charged stable particles. The limit applies for the mass range 40.4-45.6 GeV for X^\pm and $< 45.6 \text{ GeV}$ for X^\pm . See the paper for bounds for $Q = \pm 2/3, \pm 4/3$.			

Searches Particle Listings

Other Particle Searches

LIMITS ON CHARGED PARTICLES IN HADRONIC REACTIONS

MASS LIMITS for Long-Lived Charged Heavy Fermions

Limits are for spin 1/2 particles with no color and $SU(2)_L$ charge. The electric charge Q of the particle (in the unit of e) is therefore equal to its weak hypercharge. Pair production by Drell-Yan like γ and Z exchange is assumed to derive the limits.

VALUE (GeV)	CL%	DOCUMENT ID	TECN	COMMENT
		1 AAD	23BT ATLS	multi-charged LLP
		2 SIRUNYAN	20N CMS	disappearing track LLP
>660	95	3 AAD	15BJ ATLS	$ Q = 2$
>200	95	4 CHATRCHYAN13AB	CMS	$ Q = 1/3$
>480	95	4 CHATRCHYAN13AB	CMS	$ Q = 2/3$
>574	95	4 CHATRCHYAN13AB	CMS	$ Q = 1$
>685	95	4 CHATRCHYAN13AB	CMS	$ Q = 2$
>140	95	5 CHATRCHYAN13AR	CMS	$ Q = 1/3$
>310	95	5 CHATRCHYAN13AR	CMS	$ Q = 2/3$

- • • We do not use the following data for averages, fits, limits, etc. • • •
- 1 AAD 23BT search for multi-charged long-lived particles with ATLAS detector using 139 fb⁻¹. No signal observed. Limits placed on LLP mass vs. charge plane.
- 2 SIRUNYAN 20N search for LLPs using disappearing track signature at CMS at 13 TeV with 101 fb⁻¹; no signal; limits placed on long-lived winos and higgsinos from SUSY depending on mass and lifetime: e.g. at 95% CL, for a purely higgsino neutralino, $m(\text{chargino}) > 750$ (175) GeV for $\tau = 3$ (0.05) ns, and for a purely wino neutralino, $m(\text{chargino}) > 884$ (474) GeV for $\tau = 3$ (0.2) ns.
- 3 AAD 15BJ use 20.3 fb⁻¹ of pp collisions at $E_{\text{cm}} = 8$ TeV. See paper for limits for $|Q| = 3, 4, 5, 6$.
- 4 CHATRCHYAN 13AB use 5.0 fb⁻¹ of pp collisions at $E_{\text{cm}} = 7$ TeV and 18.8 fb⁻¹ at $E_{\text{cm}} = 8$ TeV. See paper for limits for $|Q| = 3, 4, \dots, 8$.
- 5 CHATRCHYAN 13AR use 5.0 fb⁻¹ of pp collisions at $E_{\text{cm}} = 7$ TeV.

Heavy Particle Production Cross Section

VALUE (nb)	CL%	DOCUMENT ID	TECN	COMMENT
		1 AAD	24B ATLS	non-resonant jet search
		2 AAD	22G ATLS	vector-like matter search
		3 TUMASYAN	22H CMS	search for new matter via multileptons
		4 SIRUNYAN	21T CMS	model independent search
		5 SIRUNYAN	20C CMS	4t search via multileptons
		6 AABOUD	19AA ATLS	BSM search
		7 AABOUD	19Q ATLS	single top +MET
		8 AABOUD	17D ATLS	anomalous $WWjj, WZjj$
		9 AABOUD	17L ATLS	$m > 870$ GeV, $Z(\rightarrow \nu\nu) tX$
		10 SIRUNYAN	17B CMS	tH
		11 SIRUNYAN	17C CMS	$Z + (t \text{ or } b)$
		12 SIRUNYAN	17J CMS	$X_{5/3} \rightarrow tW$
		13 AAIJ	15BD LHCB	$m=124-309$ GeV
		14 AAD	13AH ATLS	$ q =(2-6)e, m=50-600$ GeV
<1.2 × 10 ⁻³	95	15 AAD	11I ATLS	$ q =10e, m=0.2-1$ TeV
<1.0 × 10 ⁻⁵	95	16,17 AALTONEN	09Z CDF	$m > 100$ GeV, noncolored
<4.8 × 10 ⁻⁵	95	16,18 AALTONEN	09Z CDF	$m > 100$ GeV, colored
<0.31-0.04 × 10 ⁻³	95	19 ABAZOV	09M D0	pair production
<0.19	95	20 AKTAS	04C H1	$m=3-10$ GeV
<0.05	95	21 ABE	92J CDF	$m=50-200$ GeV
<30-130		22 CARROLL	78 SPEC	$m=2-2.5$ GeV
<100		23 LEIPUNER	73 CNTR	$m=3-11$ GeV

- • • We do not use the following data for averages, fits, limits, etc. • • •
- 1 AAD 24B search for non-resonant jets +MET at $\sqrt{s} = 13$ TeV with 139 fb⁻¹. No excess observed. Limits placed on dark sector model mediator mass and coupling.
- 2 AAD 22G search for single vector-like quark T with $T \rightarrow th$ in all hadronic mode with 139 fb⁻¹ at 13 TeV; no signal observed; limits placed in mass vs. coupling plane.
- 3 TUMASYAN 22H search for new states of matter via non-resonant multilepton production based on a luminosity of 138 fb⁻¹; no signal observed; limits placed on vector-like leptons, leptoquarks, and new fermions from type-III seesaw model.
- 4 SIRUNYAN 21T perform model unspecific search for deviations from SM with CMS at 13 TeV with 35.9 fb⁻¹ data in numerous signature channels. No deviations from SM found.
- 5 SIRUNYAN 20C search for four top-quark production with decay to multileptons at CMS at 13 TeV with 137 fb⁻¹; no signal is found and limits are placed on the Higgs boson oblique parameter in the effective field theory framework (EFT) and the model parameters ($\tan\beta$).
- 6 AABOUD 19AA search for BSM physics at 13 TeV with 3.2 fb⁻¹ in $> 10^5$ regions of > 700 event classes; no significant signal found.
- 7 AABOUD 19Q search for single top+MET events at 13 TeV with 36.1 fb⁻¹ of data; no signal found and limits set in σ or coupling vs. mass plane for variety of simplified models including DM and vector-like top quark T .
- 8 AABOUD 17D search for $WWjj, WZjj$ in pp collisions at 8 TeV with 3.2 fb⁻¹; set limits on anomalous couplings.
- 9 AABOUD 17L search for the pair production of heavy vector-like T quarks in the $Z(\rightarrow \nu\nu) tX$ final state.
- 10 SIRUNYAN 17B search for vector-like quark $pp \rightarrow TX \rightarrow tHX$ in 2.3 fb⁻¹ at 13 TeV; no signal seen; limits placed.
- 11 SIRUNYAN 17C search for vector-like quark $pp \rightarrow TX \rightarrow Z + (t \text{ or } b)$ in 2.3 fb⁻¹ at 13 TeV; no signal seen; limits placed.
- 12 SIRUNYAN 17J search for $pp \rightarrow X_{5/3} X_{5/3} \rightarrow tWtW$ with 2.3 fb⁻¹ at 13 TeV. No signal seen: $m(X) > 1020$ (990) GeV for RH (LH) new charge 5/3 quark.
- 13 AAIJ 15BD search for production of long-lived particles in pp collisions at $E_{\text{cm}} = 7$ and 8 TeV. See their Table 6 for cross section limits.

- 14 AAD 13AH search for production of long-lived particles with $|q|=(2-6)e$ in pp collisions at $E_{\text{cm}} = 7$ TeV with 4.4 fb⁻¹. See their Fig. 8 for cross section limits.
- 15 AAD 11I search for production of highly ionizing massive particles in pp collisions at $E_{\text{cm}} = 7$ TeV with $L = 3.1$ pb⁻¹. See their Table 5 for similar limits for $|q| = 6e$ and 17e, Table 6 for limits on pair production cross section.
- 16 AALTONEN 09Z search for long-lived charged particles in $p\bar{p}$ collisions at $E_{\text{cm}} = 1.96$ TeV with $L = 1.0$ fb⁻¹. The limits are on production cross section for a particle of mass above 100 GeV in the region $|\eta| \lesssim 0.7, p_T > 40$ GeV, and $0.4 < \beta < 1.0$.
- 17 Limit for weakly interacting charge-1 particle.
- 18 Limit for up-quark like particle.
- 19 ABAZOV 09M search for pair production of long-lived charged particles in $p\bar{p}$ collisions at $E_{\text{cm}} = 1.96$ TeV with $L = 1.1$ fb⁻¹. Limit on the cross section of (0.31-0.04) pb (95% CL) is given for the mass range of 60-300 GeV, assuming the kinematics of stau pair production.
- 20 AKTAS 04c look for charged particle photoproduction at HERA with mean c.m. energy of 200 GeV.
- 21 ABE 92J look for pair production of unit-charged particles which leave detector before decaying. Limit shown here is for $m=50$ GeV. See their Fig. 5 for different charges and stronger limits for higher mass.
- 22 CARROLL 78 look for neutral, $S = -2$ dihyperon resonance in $pp \rightarrow 2K^+X$. Cross section varies within above limits over mass range and $p_{\text{lab}} = 5.1-5.9$ GeV/c.
- 23 LEIPUNER 73 is a NAL 300 GeV p experiment. Would have detected particles with lifetime greater than 200 ns.

Heavy Particle Production Differential Cross Section

VALUE (cm ² sr ⁻¹ GeV ⁻¹)	CL%	DOCUMENT ID	TECN	CHG	COMMENT
		1 HAYRAPETY...23F	CMS		top $\rightarrow t\bar{s}$ via EFT ops.
<2.6 × 10 ⁻³⁶	90	2 BALDIN	76 CNTR	-	$Q = 1, m=2.1-9.4$ GeV
<2.2 × 10 ⁻³³	90	3 ALBROW	75 SPEC	±	$Q = \pm 1, m=4-15$ GeV
<1.1 × 10 ⁻³³	90	3 ALBROW	75 SPEC	±	$Q = \pm 2, m=6-27$ GeV
<8. × 10 ⁻³⁵	90	4 JOVANO... 75	CNTR	±	$m=15-26$ GeV
<1.5 × 10 ⁻³⁴	90	4 JOVANO... 75	CNTR	±	$Q = \pm 2, m=3-10$ GeV
<6. × 10 ⁻³⁵	90	4 JOVANO... 75	CNTR	±	$Q = \pm 2, m=10-26$ GeV
<1. × 10 ⁻³¹	90	5 APPEL	74 CNTR	±	$m=3.2-7.2$ GeV
<5.8 × 10 ⁻³⁴	90	6 ALPER	73 SPEC	±	$m=1.5-24$ GeV
<1.2 × 10 ⁻³⁵	90	7 ANTIPOV	71B CNTR	-	$Q = -, m=2.2-2.8$
<2.4 × 10 ⁻³⁵	90	8 ANTIPOV	71C CNTR	-	$Q = -, m=1.2-1.7, 2.1-4$
<2.4 × 10 ⁻³⁵	90	BINON	69 CNTR	-	$Q = -, m=1-1.8$ GeV
<1.5 × 10 ⁻³⁶		9 DORFAN	65 CNTR		Be target $m=3-7$ GeV
<3.0 × 10 ⁻³⁶		9 DORFAN	65 CNTR		Fe target $m=3-7$ GeV

- • • We do not use the following data for averages, fits, limits, etc. • • •
- 1 HAYRAPETYAN 23F search for anomalous top \rightarrow leptons decay via effective operators. No signal observed. Limits placed on EFT operators.
- 2 BALDIN 76 is a 70 GeV Serpukhov experiment. Value is per Al nucleus at $\theta = 0$. For other charges in range -0.5 to -3.0 , CL = 90% limit is $(2.6 \times 10^{-36})/|(\text{charge})|$ for mass range $(2.1-9.4 \text{ GeV}) \times |(\text{charge})|$. Assumes stable particle interacting with matter as do antiprotons.
- 3 ALBROW 75 is a CERN ISR experiment with $E_{\text{cm}} = 53$ GeV. $\theta = 40$ mr. See figure 5 for mass ranges up to 35 GeV.
- 4 JOVANOVIICH 75 is a CERN ISR 26+26 and 15+15 GeV pp experiment. Figure 4 covers ranges $Q = 1/3$ to 2 and $m = 3$ to 26 GeV. Value is per GeV momentum.
- 5 APPEL 74 is NAL 300 GeV pW experiment. Studies forward production of heavy (up to 24 GeV) charged particles with momenta 24-200 GeV ($-$ charge) and 40-150 GeV ($+$ charge). Above typical value is for 75 GeV and is per GeV momentum per nucleon.
- 6 ALPER 73 is CERN ISR 26+26 GeV pp experiment. $p > 0.9$ GeV, $0.2 < \beta < 0.65$.
- 7 ANTIPOV 71B is from same 70 GeV p experiment as ANTIPOV 71C and BINON 69.
- 8 ANTIPOV 71C limit inferred from flux ratio. 70 GeV p experiment.
- 9 DORFAN 65 is a 30 GeV/c p experiment at BNL. Units are per GeV momentum per nucleus.

Long-Lived Heavy Particle Invariant Cross Section

VALUE (cm ² /GeV ² /N)	CL%	DOCUMENT ID	TECN	CHG	COMMENT
		1 BERNSTEIN	88 CNTR		
<5-700 × 10 ⁻³⁵	90	1 BERNSTEIN	88 CNTR		
<5-700 × 10 ⁻³⁷	90	1 BERNSTEIN	88 CNTR		
<2.5 × 10 ⁻³⁶	90	2 THRON	85 CNTR	-	$Q = 1, m=4-12$ GeV
<1. × 10 ⁻³⁵	90	2 THRON	85 CNTR	+	$Q = 1, m=4-12$ GeV
<6. × 10 ⁻³³	90	3 ARMITAGE	79 SPEC		$m=1.87$ GeV
<1.5 × 10 ⁻³³	90	3 ARMITAGE	79 SPEC		$m=1.5-3.0$ GeV
		4 BOZZOLI	79 CNTR	±	$Q = (2/3, 1, 4/3, 2)$
<1.1 × 10 ⁻³⁷	90	5 CUTTS	78 CNTR		$m=4-10$ GeV
<3.0 × 10 ⁻³⁷	90	6 VIDAL	78 CNTR		$m=4.5-6$ GeV

- • • We do not use the following data for averages, fits, limits, etc. • • •
- 1 BERNSTEIN 88 limits apply at $x = 0.2$ and $p_T = 0$. Mass and lifetime dependence of limits are shown in the regions: $m = 1.5-7.5$ GeV and $\tau = 10^{-8}-2 \times 10^{-6}$ s. First number is for hadrons; second is for weakly interacting particles.
- 2 THRON 85 is FNAL 400 GeV proton experiment. Mass determined from measured velocity and momentum. Limits are for $\tau > 3 \times 10^{-9}$ s.
- 3 ARMITAGE 79 is CERN-ISR experiment at $E_{\text{cm}} = 53$ GeV. Value is for $x = 0.1$ and $p_T = 0.15$. Observed particles at $m = 1.87$ GeV are found all consistent with being antideuterons.
- 4 BOZZOLI 79 is CERN-SPS 200 GeV pN experiment. Looks for particle with τ larger than 10^{-8} s. See their figure 11-18 for production cross-section upper limits vs mass.
- 5 CUTTS 78 is pBe experiment at FNAL sensitive to particles of $\tau > 5 \times 10^{-8}$ s. Value is for $-0.3 < x < 0$ and $p_T = 0.175$.
- 6 VIDAL 78 is FNAL 400 GeV proton experiment. Value is for $x = 0$ and $p_T = 0$. Puts lifetime limit of $< 5 \times 10^{-8}$ s on particle in this mass range.

See key on page 1171

Searches Particle Listings

Other Particle Searches

Long-Lived Heavy Particle Production ($\sigma(\text{Heavy Particle}) / \sigma(\pi)$)

VALUE	EVTS	DOCUMENT ID	TECN	CHG	COMMENT
• • • We do not use the following data for averages, fits, limits, etc. • • •					
$<10^{-8}$		1 NAKAMURA 89	SPEC	\pm	$Q = (-5/3, \pm 2)$
	0	2 BUSSIERE 80	CNTR	\pm	$Q = (2/3, 1, 4/3, 2)$
1 NAKAMURA 89 is KEK experiment with 12 GeV protons on Pt target. The limit applies for mass $\lesssim 1.6$ GeV and lifetime $\gtrsim 10^{-7}$ s.					
2 BUSSIERE 80 is CERN-SPS experiment with 200–240 GeV protons on Be and Al target. See their figures 6 and 7 for cross-section ratio vs mass.					

Production and Capture of Long-Lived Massive Particles

VALUE (10^{-36} cm^2)	DOCUMENT ID	TECN	COMMENT
• • • We do not use the following data for averages, fits, limits, etc. • • •			
	1 AAD 21X	ATLS	search for captured LLPs
	2 ACHARYA 21	INDU	dyons production, capture
<20 to 800	3 ALEKSEEV 76	ELEC	$\tau = 5$ ms to 1 day
<200 to 2000	4 ALEKSEEV 76B	ELEC	$\tau = 100$ ms to 1 day
<1.4 to 9	5 FRANKEL 75	CNTR	$\tau = 5$ ms to 10 hours
<0.1 to 9	6 FRANKEL 74	CNTR	$\tau = 1$ to 1000 hours
1 AAD 21X search for LLPs which come to rest in ATLAS detector to deposit energy between collisions. No signal observed in 111 fb^{-1} of data. Limits placed in lifetime vs. mass plane assuming model with gluino hadrons: e.g. $m > 1.4$ TeV for $\tau \sim 10^{-5}$ to 10^3 sec.			
2 ACHARYA 21 search for dyons (carrying electric and magnetic charge) and monopoles via production and capture in 6.46 fb^{-1} of 13 TeV LHC data. No signal observed. Limits placed in mass vs. magnetic charge plane.			
3 ALEKSEEV 76 and ALEKSEEV 76B are 61–70 GeV p Serpukhov experiment. Cross section is per Pb nucleus.			
4 FRANKEL 75 is extension of FRANKEL 74.			
5 FRANKEL 74 looks for particles produced in thick Al targets by 300–400 GeV/c protons.			

Long-Lived Particle (LLP) Search at Hadron Collisions

VALUE (fb)	CL%	DOCUMENT ID	TECN	COMMENT
Limits are for cross section times branching ratio.				
• • • We do not use the following data for averages, fits, limits, etc. • • •				
		1 AAD 23AM	ATLS	LLP higgsino search
		2 AAD 23AR	ATLS	LLP search via displaced γ
		3 AAD 23BQ	ATLS	displaced dimuon search
		4 AAD 23CO	ATLS	highly ionizing LLP/monopole
		5 AAD 23G	ATLS	heavy highly ionizing LLP search
		6 AAD 23I	ATLS	light LLP via collimated decays
		7 TUMASYAN 23AO	CMS	LLP search via trackless jets
		8 TUMASYAN 23G	CMS	LLP search via displaced dimuons
		9 AAD 22H	ATLS	LLP search with μ spectrometer
		10 AAD 22K	ATLS	LLP search via displaced jets in the calorimeter
		11 AAD 22U	ATLS	LLP/chargino search via tracklet
		12 AAIJ 22U	LHCB	LLP semileptonic decay to muon
		13 ACHARYA 22A	MOED	monopoles/HECOs at LHC
		14 TUMASYAN 22AD	CMS	heavy neutral lepton LLP search
		15 TUMASYAN 22AF	CMS	LLP search via displaced lepton tracks
		16 TUMASYAN 22M	CMS	LLP search via ZH production
		17 TUMASYAN 22N	CMS	LLP search via dimuons
		18 AAD 21AL	ATLS	charged LLPs search
		19 AAD 21BA	ATLS	LLP from higgs decay search
		20 AAIJ 21V	LHCB	LLP $\rightarrow e\mu\nu$ search
		21 SIRUNYAN 21AF	CMS	LLP search via displaced jets
		22 SIRUNYAN 21U	CMS	LLP search via displaced jets
		23 TUMASYAN 21	CMS	LLP endcap muon detector searches
		24 AAD 20D	ATLS	$pp \rightarrow$ LLPs at 13 TeV
		25 AAD 20J	ATLS	scalar boson decay to LLPs
		26 AAD 20M	ATLS	LLP top squark decay to μ
		27 AAD 20P	ATLS	LLP dark photon search
		28 AAIJ 20AL	LHCB	pp dimuon resonance
		29 BALL 20		LLP milli-charged particles at LHC
		30 AABOUD 19AE	ATLS	pp at 13 TeV
		31 AABOUD 19AK	ATLS	$pp \rightarrow \Phi \rightarrow ZZ_d$
		32 AABOUD 19AM	ATLS	DY multi-charged LLP production
		33 AABOUD 19AO	ATLS	LLP via displaced jets
		34 AABOUD 19AT	ATLS	heavy, charged LLPs
		35 AABOUD 19G	ATLS	LLP decay to $\mu^+\mu^-$
		36 SIRUNYAN 19BH	CMS	LLP via displaced jets
		37 SIRUNYAN 19BT	CMS	LLP via displaced jets+MET
		38 SIRUNYAN 19CA	CMS	LLP $\rightarrow \gamma$ search
		39 SIRUNYAN 19Q	CMS	$pp \rightarrow j +$ displaced dark quark jet
		40 SIRUNYAN 18AW	CMS	Long-lived particle search
		41 AAIJ 16AR	LHCB	$H \rightarrow XX$ LLPs
		42 KHACHATRYAN 16BW	CMS	direct production: HSCPs
		43 BADIER 86	BDMP	$\tau = (0.05-1) \times 10^{-8}$ s
<2000	90			
1 AAD 23AM search for long-lived higgsinos from gauge-mediation which decay to Z or H . No signal observed. Limits placed in $c\tau$ vs $m(X)$ plane for various simplified models.				
2 AAD 23AR search for long-lived particles via decay to displaced γ with 139 fb^{-1} of data. No signal observed. Limits placed in m vs. τ and BF vs. τ planes for gauge-mediated SUSY model.				

3 AAD 23BQ	search for displaced dimuon events in ATLAS detector. No signal observed. Limits placed in smuon lifetime vs. mass plane for long-lived smuon model.
4 AAD 23CO	search for monopoles and high-electric-charge LLPs in ATLAS with 139 fb^{-1} of data. No signal observed. Limits placed in mass vs. charge plane.
5 AAD 23G	search for heavy highly ionizing long-lived particles with 139 fb^{-1} of data. No signal observed. Limits placed in m vs. τ plane for several SUSY models.
6 AAD 23I	search for light long-lived particles decaying to collimated decay products (e.g. dileptons). No signal observed. Limits placed in BF vs. τ plane.
7 TUMASYAN 23AO	search for trackless jets from LLP production at CMS. No signal observed. Limits placed for SUSY model with long-lived neutralino in $m(\chi)$ vs. $c\tau$ plane.
8 TUMASYAN 23G	search for LLP decaying to displaced dimuons at CM with 97.6 fb^{-1} of data. No signal observed. Limits placed in $c\tau$ vs. m plane for hidden Abelian Higgs simplified model.
9 AAD 22H	search for scalar mediator decay to two LLPs which decay in muon chambers with 139 fb^{-1} at 13 TeV; no signal detected; limits placed on various simplified models.
10 AAD 22K	search for LLP pair production via scalar mediator with LLP decay in hadron calorimeter; no signal detected; limits placed for various simplified models.
11 AAD 22U	search for chargino LLP via disappearing tracks; no signal observed; limits placed in $m(\text{chargino})$ vs lifetime plane for cases of higgsino- or wino-like chargino.
12 AAIJ 22U	reports search for LLP production at LHCB with 5.4 fb^{-1} at 13 TeV followed by semileptonic decay to muon; no signal detected; limits placed in mass or lifetime vs. cross section plane for several simplified models.
13 ACHARYA 22A	report search for monopole and HECO production via DY at 8 TeV LHC with 2.2 fb^{-1} with MoEDAL detector; no signal detected; limits placed in mass vs. cross section plane for various electric/magnetic charge scenarios.
14 TUMASYAN 22AD	search for heavy neutral lepton which decays as LLP to trilepton state with 138 fb^{-1} at 13 TeV; no signal detected; limits placed in mass vs. coupling plane.
15 TUMASYAN 22AF	search for LLPs via displaced lepton vertices. The analysis is performed with an integrated luminosity of 118 (113) fb^{-1} when analyzing the $e\bar{e}$ ($e\mu$, $\mu\mu$) channel; no signal detected; limits placed for a variety of simplified models.
16 TUMASYAN 22M	search in 117 fb^{-1} of 13 TeV data for ZH production with $H \rightarrow S S$ where S is a LLP; no signal observed; limits placed in decay length vs. branching fraction plane.
17 TUMASYAN 22N	search in 101 fb^{-1} of 13 TeV data for LLP production via decay to dimuons; no signal observed; limits placed on mass vs. coupling or lifetime for a variety of simplified models.
18 AAD 21AL	reports on ATLAS search for long-lived charged particles with 139 fb^{-1} at 13 TeV. No signal observed. Limits placed in lifetime vs. mass plane: e.g. for $\tau(\text{LLP}) \sim 0.1$ ns, $m(\text{selectron}) > 720$ GeV.
19 AAD 21BA	search for long-lived particles from ZH production ($H \rightarrow b\bar{b}$) with 2 displaced vertices in 139 fb^{-1} of data at 13 TeV. No signal detected. Limits placed in branching fraction vs. lifetime plane.
20 AAIJ 21V	search for $pp \rightarrow \text{LLP} + \text{LLP}$ with LLP $\rightarrow e\mu\nu$ in the lifetime range between 2 and 50 ps at LHCB with 5.4 fb^{-1} at 13 TeV. No signal observed. Limits placed in LLP cross section vs. mass or lifetime plane for $m(\text{LLP}) \sim 7$ to 50 GeV.
21 SIRUNYAN 21AF	search for LLPs at CMS via jets with 2 displaced vertices in 140 fb^{-1} of data at 13 TeV. No signal observed. Limits placed for RPV SUSY models in which a long-lived neutralino or gluino decays into a multijet final state with top, bottom, and strange quarks.
22 SIRUNYAN 21U	search for long-lived particles (LLPs) via displaced jets at CMS with LHC13 and 132 fb^{-1} . No signal detected. Limits placed on simplified model production of LLP $X \rightarrow q\bar{q}$ with $\sigma < 0.07$ fb for $m(X) > 500$ GeV and $c\tau \sim 2$ to 250 mm.
23 TUMASYAN 21	search for long-lived particles in CMS muon endcap detector in 137 fb^{-1} of data at 13 TeV. No signal detected. Limits are placed depending on the branching fraction of Higgs boson to LLP decaying to dd , bb , and $\tau^+\tau^-$, depending on proper decay length, and LLP masses.
24 AAD 20D	search for opposite-sign dileptons originating from long-lived particles in pp collisions at 13 TeV with 32.8 fb^{-1} ; limits placed in squark cross section vs. $c\tau$ plane for RPV SUSY.
25 AAD 20J	search for scalar boson decay to two long-lived particles; no signal; limits placed in BF vs $c\tau$ plane for various mass hypotheses. This search is also combined with other ATLAS displaced-jet searches.
26 AAD 20M	search for long-lived top-squarks decay to μ and hadrons; no signal; limits placed in cross section vs. mass and mass vs. lifetime planes.
27 AAD 20P	search for long-lived dark photons produced from the decay of a scalar boson, with each dark photon decaying into displaced collimated leptons or light hadrons at 13 TeV with 36 fb^{-1} ; no signal; limits placed in $\sigma \cdot \text{BF}$ vs. $c\tau$ and other planes.
28 AAIJ 20AL	search for long-lived $X \rightarrow \mu^+\mu^-$ decays in 5.1 fb^{-1} of LHCB data at 13 TeV; no signal; limits placed on $m(X)$ up to 3 GeV depending on kinetic mixing.
29 BALL 20	search for long-lived milli-charged particles produced at LHC; limits placed in charge vs. mass plane (Fig. 8).
30 AABOUD 19AE	search for long-lived particles via displaced jets using 10.8 fb^{-1} or 33.0 fb^{-1} data (depending on a trigger) at 13 TeV; no signal found and limits set in branching ratio vs. decay length plane.
31 AABOUD 19AK	searches for long-lived particle Z_d via $pp \rightarrow \Phi \rightarrow ZZ_d$ at 13 TeV with 36.1 fb^{-1} ; no signal found and limits set in $\sigma \times \text{BR}$ vs. lifetime plane for simplified model.
32 AABOUD 19AM	search for Drell-Yan (DY) production of long-lived multi-charged particles at 13 TeV with 36.1 fb^{-1} of data; no signal found and exclude 50 GeV $< m(\text{LLMCP}) < 980$ –1220 GeV for electric charge $ q = (2-7)e$.
33 AABOUD 19AO	search for neutral long-lived particles producing displaced jets at 13 TeV with 36.1 fb^{-1} of data; no signal found and exclude regions of $\sigma \cdot \text{BR}$ vs. lifetime plane for various models.
34 AABOUD 19AT	search for heavy, charged long-lived particles at 13 TeV with 36.1 fb^{-1} ; no signal found and upper limits set on masses of various hypothetical particles.
35 AABOUD 19G	search for long-lived particle with decay to $\mu^+\mu^-$ at 13 TeV with 32.9 fb^{-1} ; no signal found and limits set in combinations of lifetime, mass and coupling planes for various simplified models.
36 SIRUNYAN 19BH	search for long-lived SUSY particles via displaced jets at 13 TeV with 35.9 fb^{-1} ; no signal found and limits placed in mass vs lifetime plane for various hypothetical models.

Searches Particle Listings

Other Particle Searches

- ³⁷ SIRUNYAN 19BT search for displaced jet(s)+ E_T at 13 TeV with 137 fb^{-1} ; no signal found and limits placed in mass vs lifetime plane for gauge mediated SUSY breaking models.
- ³⁸ SIRUNYAN 19CA search for gluino/squark decay to long-lived neutralino, decay to γ in GMSB; no signal, limits placed in $m(\chi)$ vs. lifetime plane for SPS8 GMSB benchmark point.
- ³⁹ SIRUNYAN 19Q search for $pp \rightarrow j +$ displaced jet via dark quark with 13 TeV at 16.1 fb^{-1} ; no signal found and limits set in mass vs lifetime plane for dark quark/dark pion model.
- ⁴⁰ SIRUNYAN 18AW search for very long lived particles (LLPs) decaying hadronically or to $\mu\bar{\mu}$ in CMS detector; none seen/limits set on lifetime vs. cross section.
- ⁴¹ AAIJ 16AR search for long lived particles from $H \rightarrow XX$ with displaced X decay vertex using 0.62 fb^{-1} at 7 TeV; limits set in Fig. 7.
- ⁴² KHACHATRYAN 16BW search for heavy stable charged particles via ToF with 2.5 fb^{-1} at 13 TeV; require stable $m(\text{gluinoball}) > 1610 \text{ GeV}$.
- ⁴³ BADIER 86 looked for long-lived particles at 300 GeV π^- beam dump. The limit applies for nonstrongly interacting neutral or charged particles with mass $> 2 \text{ GeV}$. The limit applies for particle modes, $\mu^+\pi^-$, $\mu^+\mu^-$, $\pi^+\pi^-X$, $\pi^+\pi^-\pi^\pm$ etc. See their figure 5 for the contours of limits in the mass- τ plane for each mode.

Long-Lived Heavy Particle Cross Section

VALUE (pb/sr)	CL%	DOCUMENT ID	TECN	COMMENT
• • • We do not use the following data for averages, fits, limits, etc. • • •				
<34	95	¹ RAM	94 SPEC	$1015 < m_{X^{++}} < 1085 \text{ MeV}$
<75	95	¹ RAM	94 SPEC	$920 < m_{X^{++}} < 1025 \text{ MeV}$

- ¹RAM 94 search for a long-lived doubly-charged fermion X^{++} with mass between m_N and $m_N + m_\pi$ and baryon number +1 in the reaction $pp \rightarrow X^{++}n$. No candidate is found. The limit is for the cross section at 15° scattering angle at 460 MeV incident energy and applies for $\tau(X^{++}) \gg 0.1 \mu\text{s}$.

LIMITS ON CHARGED PARTICLES IN COSMIC RAYS

Heavy Particle Flux in Cosmic Rays

VALUE ($\text{cm}^{-2}\text{sr}^{-1}\text{s}^{-1}$)	CL%	EVTS	DOCUMENT ID	TECN	COMMENT
• • • We do not use the following data for averages, fits, limits, etc. • • •					
< 6.2	$\times 10^{-10}$	90	0	¹ ALEMANN0 22	DAMP fractionally charged particles in space
				² CAO	22 superheavy DM $\rightarrow \gamma$ rays
< 1	$\times 10^{-8}$	90		³ ALVIS 18	MAJD Fractionally charged
~ 6	$\times 10^{-9}$		2	⁴ AGNESE 15	CDM2 $Q = 1/6$
				⁵ SAITO 90	$Q \approx 14, m \approx 370 m_p$
< 1.4	$\times 10^{-12}$	90	0	⁶ MINCER 85	CALO $m \geq 1 \text{ TeV}$
				⁷ SAKUYAMA 83B	PLAS $m \sim 1 \text{ TeV}$
< 1.7	$\times 10^{-11}$	99	0	⁸ BHAT 82	CC
< 1.	$\times 10^{-9}$	90	0	⁹ MARINI 82	CNTR $Q=1, m \sim 4.5 m_p$
2.	$\times 10^{-9}$		3	¹⁰ YOCK 81	SPRK $Q=1, m \sim 4.5 m_p$
			3	¹⁰ YOCK 81	SPRK Fractionally charged
3.0	$\times 10^{-9}$		3	¹¹ YOCK 80	SPRK $m \sim 4.5 m_p$
$(4 \pm 1) \times 10^{-11}$			3	GOODMAN 79	ELEC $m \geq 5 \text{ GeV}$
< 1.3	$\times 10^{-9}$	90		¹² BHAT 78	CNTR $m > 1 \text{ GeV}$
< 1.0	$\times 10^{-9}$		0	BRIATORE 76	ELEC
< 7.	$\times 10^{-10}$	90	0	YOCK 75	ELEC $Q > 7e$ or $< -7e$
> 6.	$\times 10^{-9}$		5	¹³ YOCK 74	CNTR $m > 6 \text{ GeV}$
< 3.0	$\times 10^{-8}$		0	DARDO 72	CNTR
< 1.5	$\times 10^{-9}$		0	TONWAR 72	CNTR $m > 10 \text{ GeV}$
< 3.0	$\times 10^{-10}$		0	BJORNOE 68	CNTR $m > 5 \text{ GeV}$
< 5.0	$\times 10^{-11}$	90	0	JONES 67	ELEC $m=5-15 \text{ GeV}$

- ¹ALEMANN0 22 search for flux of fractionally charged particles (FCPs) in space; no signal observed; limits set in flux vs decay plane for mass as low as GeV.
- ²CAO 22 search for superheavy DM decaying to gamma rays; no signal observed; limits placed in mass vs. lifetime plane for $m \sim 10^5-10^9 \text{ GeV}$ for DM decays to $b\bar{b}$ or $\tau\bar{\tau}$.
- ³ALVIS 18 search for fractional charged flux of cosmic matter at Majorana demonstrator; no signal observed and limits are set on the flux of lightly ionizing particles for charge as low as $e/1000$.
- ⁴See AGNESE 15 Fig. 6 for limits extending down to $Q = 1/200$.
- ⁵SAITO 90 candidates carry about 450 MeV/nucleon. Cannot be accounted for by conventional backgrounds. Consistent with strange quark matter hypothesis.
- ⁶MINCER 85 is high statistics study of calorimeter signals delayed by 20–200 ns. Calibration with AGS beam shows they can be accounted for by rare fluctuations in signals from low-energy hadrons in the shower. Claim that previous delayed signals including BJORNOE 68, DARDO 72, BHAT 82, SAKUYAMA 83B below may be due to this fake effect.
- ⁷SAKUYAMA 83B analyzed 6000 extended air shower events. Increase of delayed particles and change of lateral distribution above 10^{17} eV may indicate production of very heavy parent at top of atmosphere.
- ⁸BHAT 82 observed 12 events with delay $> 2. \times 10^{-8} \text{ s}$ and with more than 40 particles. 1 eV has good hadron shower. However all events are delayed in only one of two detectors in cloud chamber, and could not be due to strongly interacting massive particle.
- ⁹MARINI 82 applied PEP-counter for TOF. Above limit is for velocity = 0.54 of light. Limit is inconsistent with YOCK 80 YOCK 81 events if isotropic dependence on zenith angle is assumed.
- ¹⁰YOCK 81 saw another 3 events with $Q = \pm 1$ and m about $4.5 m_p$ as well as 2 events with $m > 5.3 m_p$, $Q = \pm 0.75 \pm 0.05$ and $m > 2.8 m_p$, $Q = \pm 0.70 \pm 0.05$ and 1 event with $m = (9.3 \pm 3.) m_p$, $Q = \pm 0.89 \pm 0.06$ as possible heavy candidates.
- ¹¹YOCK 80 events are with charge exactly or approximately equal to unity.
- ¹²BHAT 78 is at Kolar gold fields. Limit is for $\tau > 10^{-6} \text{ s}$.
- ¹³YOCK 74 events could be tritons.

Superheavy Particle (Quark Matter) Flux in Cosmic Rays

VALUE ($\text{cm}^{-2}\text{sr}^{-1}\text{s}^{-1}$)	CL%	DOCUMENT ID	TECN	COMMENT
• • • We do not use the following data for averages, fits, limits, etc. • • •				
<5	$\times 10^{-16}$	90		¹ ADRIANI 15
<1.8	$\times 10^{-12}$	90		² AMBROSIO 00B
<1.1	$\times 10^{-14}$	90		³ ASTONE 93
<2.2	$\times 10^{-14}$	90		⁴ AHLEN 92
<6.4	$\times 10^{-16}$	90		⁵ NAKAMURA 91
<2.0	$\times 10^{-11}$	90		⁶ ORITO 91
<4.7	$\times 10^{-12}$	90		⁷ LIU 88
<3.2	$\times 10^{-11}$	90		⁸ BARISH 87
<3.5	$\times 10^{-11}$	90		⁹ NAKAMURA 85
<7.	$\times 10^{-11}$	90		¹⁰ ULLMAN 81
				¹⁰ ULLMAN 81

- ¹ADRIANI 15 search for relatively light quark matter with charge $Z = 1-8$. See their Figs. 2 and 3 for flux upper limits.
- ²AMBROSIO 00B searched for quark matter ("nuclearites") in the velocity range $(10^{-5}-1) c$. The listed limit is for $2 \times 10^{-3} c$.
- ³ASTONE 93 searched for quark matter ("nuclearites") in the velocity range $(10^{-3}-1) c$. Their Table 1 gives a compilation of searches for nuclearites.
- ⁴AHLEN 92 searched for quark matter ("nuclearites"). The bound applies to velocity $< 2.5 \times 10^{-3} c$. See their Fig. 3 for other velocity/ c and heavier mass range.
- ⁵NAKAMURA 91 searched for quark matter in the velocity range $(4 \times 10^{-5}-1) c$.
- ⁶ORITO 91 searched for quark matter. The limit is for the velocity range $(10^{-4}-10^{-3}) c$.
- ⁷LIU 88 searched for quark matter ("nuclearites") in the velocity range $(2.5 \times 10^{-3}-1) c$. A less stringent limit of 5.8×10^{-11} applies for $(1-2.5) \times 10^{-3} c$.
- ⁸BARISH 87 searched for quark matter ("nuclearites") in the velocity range $(2.7 \times 10^{-4}-5 \times 10^{-3}) c$.
- ⁹NAKAMURA 85 at KEK searched for quark-matter. These might be lumps of strange quark matter with roughly equal numbers of u, d, s quarks. These lumps or nuclearites were assumed to have velocity of $(10^{-4}-10^{-3}) c$.
- ¹⁰ULLMAN 81 is sensitive for heavy slow singly charge particle reaching earth with vertical velocity 100–350 km/s.

Highly Ionizing Particle Flux

VALUE ($\text{m}^{-2}\text{yr}^{-1}$)	CL%	EVTS	DOCUMENT ID	TECN	COMMENT
• • • We do not use the following data for averages, fits, limits, etc. • • •					
<0.4	95	0	KINOSHITA	81B PLAS	Z/β 30-100

SEARCHES FOR BLACK HOLE PRODUCTION

VALUE	DOCUMENT ID	TECN	COMMENT
• • • We do not use the following data for averages, fits, limits, etc. • • •			
not seen	¹ AABOUD 16P	ATLS	13 TeV $pp \rightarrow e\mu, e\tau, \mu\tau$
	² AAD 15AN	ATLS	8 TeV $pp \rightarrow$ multijets
	³ AAD 14A	ATLS	8 TeV $pp \rightarrow \gamma + \text{jet}$
	⁴ AAD 14AL	ATLS	8 TeV $pp \rightarrow \ell + \text{jet}$
	⁵ AAD 14C	ATLS	8 TeV $pp \rightarrow \ell + (\ell \text{ or jets})$
	⁶ AAD 13D	ATLS	7 TeV $pp \rightarrow 2 \text{ jets}$
	⁷ CHATRCHYAN 13A	CMS	7 TeV $pp \rightarrow 2 \text{ jets}$
	⁸ CHATRCHYAN 13AD	CMS	8 TeV $pp \rightarrow$ multijets
	⁹ AAD 12AK	ATLS	7 TeV $pp \rightarrow \ell + (\ell \text{ or jets})$
	¹⁰ CHATRCHYAN 12W	CMS	7 TeV $pp \rightarrow$ multijets
	¹¹ AAD 11AG	ATLS	7 TeV $pp \rightarrow 2 \text{ jets}$

- ¹AABOUD 16P set limits on quantum BH production in $n = 6$ ADD or $n = 1$ RS models.
- ²AAD 15AN search for black hole or string ball formation followed by its decay to multijet final states, in pp collisions at $E_{\text{cm}} = 8 \text{ TeV}$ with $L = 20.3 \text{ fb}^{-1}$. See their Figs. 6–8 for limits.
- ³AAD 14A search for quantum black hole formation followed by its decay to a γ and a jet, in pp collisions at $E_{\text{cm}} = 8 \text{ TeV}$ with $L = 20 \text{ fb}^{-1}$. See their Fig. 3 for limits.
- ⁴AAD 14AL search for quantum black hole formation followed by its decay to a lepton and a jet, in pp collisions at $E_{\text{cm}} = 8 \text{ TeV}$ with $L = 20.3 \text{ fb}^{-1}$. See their Fig. 2 for limits.
- ⁵AAD 14C search for microscopic (semiclassical) black hole formation followed by its decay to final states with a lepton and ≥ 2 (leptons or jets), in pp collisions at $E_{\text{cm}} = 8 \text{ TeV}$ with $L = 20.3 \text{ fb}^{-1}$. See their Figures 8–11, Tables 7, 8 for limits.
- ⁶AAD 13D search for quantum black hole formation followed by its decay to two jets, in pp collisions at $E_{\text{cm}} = 7 \text{ TeV}$ with $L = 4.8 \text{ fb}^{-1}$. See their Fig. 8 and Table 3 for limits.
- ⁷CHATRCHYAN 13A search for quantum black hole formation followed by its decay to two jets, in pp collisions at $E_{\text{cm}} = 7 \text{ TeV}$ with $L = 5 \text{ fb}^{-1}$. See their Figs. 5 and 6 for limits.
- ⁸CHATRCHYAN 13AD search for microscopic (semiclassical) black hole formation followed by its evaporation to multiparticle final states, in multijet (including γ, ℓ) events in pp collisions at $E_{\text{cm}} = 8 \text{ TeV}$ with $L = 12 \text{ fb}^{-1}$. See their Figs. 5–7 for limits.
- ⁹AAD 12AK search for microscopic (semiclassical) black hole formation followed by its decay to final states with a lepton and ≥ 2 (leptons or jets), in pp collisions at $E_{\text{cm}} = 7 \text{ TeV}$ with $L = 1.04 \text{ fb}^{-1}$. See their Fig. 4 and 5 for limits.
- ¹⁰CHATRCHYAN 12W search for microscopic (semiclassical) black hole formation followed by its evaporation to multiparticle final states, in multijet (including γ, ℓ) events in pp collisions at $E_{\text{cm}} = 7 \text{ TeV}$ with $L = 4.7 \text{ fb}^{-1}$. See their Figs. 5–8 for limits.
- ¹¹AAD 11AG search for quantum black hole formation followed by its decay to two jets, in pp collisions at $E_{\text{cm}} = 7 \text{ TeV}$ with $L = 36 \text{ pb}^{-1}$. See their Fig. 11 and Table 4 for limits.

See key on page 1171

Searches Particle Listings

Other Particle Searches

REFERENCES FOR Other Particle Searches

AAD	24B	PL B848 138324	G. Aad et al.	(ATLAS Collab.)	AAD	16N	JHEP 1603 026	G. Aad et al.	(ATLAS Collab.)
AAD	23AM	PR D108 12012	G. Aad et al.	(ATLAS Collab.)	AAD	16O	PL B760 520	G. Aad et al.	(ATLAS Collab.)
AAD	23AR	PR D108 032016	G. Aad et al.	(ATLAS Collab.)	AAD	16R	PL B755 285	G. Aad et al.	(ATLAS Collab.)
AAD	23BQ	PL B846 138172	G. Aad et al.	(ATLAS Collab.)	AAD	16S	PL B754 302	G. Aad et al.	(ATLAS Collab.)
AAD	23BT	PL B847 138316	G. Aad et al.	(ATLAS Collab.)	AAD	16AJ	EPJ C76 664	R. Ajaj et al.	(LHCb Collab.)
AAD	23CO	JHEP 2311 112	G. Aad et al.	(ATLAS Collab.)	AAD	16BW	PR D94 12004	V. Khachatryan et al.	(CMS Collab.)
AAD	23G	JHEP 2306 158	G. Aad et al.	(ATLAS Collab.)	AAD	16K	PR 116 071801	V. Khachatryan et al.	(CMS Collab.)
AAD	23I	JHEP 2306 153	G. Aad et al.	(ATLAS Collab.)	AAD	16L	PR 117 031802	V. Khachatryan et al.	(CMS Collab.)
AAD	23P	JHEP 2307 176	G. Aad et al.	(ATLAS Collab.)	AAD	16M	PR 117 051802	V. Khachatryan et al.	(CMS Collab.)
ADACHI	23K	PR D108 L11104	I. Adachi et al.	(BELLE II Collab.)	AAD	16N	PR 116 042501	A.J. Krasznahorkay et al.	(HINR, ANIK+)
HAYRAPETYAN...	23F	JHEP 2312 068	A. Hayrapetyan et al.	(CMS Collab.)	AAD	15AN	JHEP 1507 032	G. Aad et al.	(ATLAS Collab.)
TUMASYAN	23AO	JHEP 2307 210	A. Tumasyan et al.	(CMS Collab.)	AAD	15AT	EPJ C75 79	G. Aad et al.	(ATLAS Collab.)
TUMASYAN	23BC	JHEP 2312 189	A. Tumasyan et al.	(CMS Collab.)	AAD	15BJ	EPJ C75 362	G. Aad et al.	(ATLAS Collab.)
TUMASYAN	23BF	EPJ C83 827	A. Tumasyan et al.	(CMS Collab.)	AAD	15BD	EPJ C75 595	R. Ajaj et al.	(LHCb Collab.)
TUMASYAN	23G	JHEP 2305 228	A. Tumasyan et al.	(CMS Collab.)	AAD	15P	PR 115 111101	O. Adriani et al.	(PAMELA Collab.)
TUMASYAN	23L	JHEP 2307 161	A. Tumasyan et al.	(CMS Collab.)	AAD	15R	PR 114 111302	R. Agnese et al.	(CDMS Collab.)
AAD	22G	PR D105 092012	G. Aad et al.	(ATLAS Collab.)	AAD	15F	PR 114 101801	V. Khachatryan et al.	(CMS Collab.)
AAD	22H	PR D106 032005	G. Aad et al.	(ATLAS Collab.)	AAD	15E	PR 114 171801	J.P. Lees et al.	(BABAR Collab.)
AAD	22K	JHEP 2206 005	G. Aad et al.	(ATLAS Collab.)	AAD	14A	PL B728 562	G. Aad et al.	(ATLAS Collab.)
AAD	22U	EPJ C82 606	G. Aad et al.	(ATLAS Collab.)	AAD	14AL	JHEP 1408 103	G. Aad et al.	(ATLAS Collab.)
AAD	22V	EPJ C82 373	R. Ajaj et al.	(LHCb Collab.)	AAD	14J	PR D89 092001	T. Aaltonen et al.	(CDF Collab.)
ABRATENKO	22A	PR D106 092006	P. Abratenko et al.	(MicroBoONE Collab.)	AAD	13A	PL B718 860	G. Aad et al.	(ATLAS Collab.)
ACHARYA	22A	EPJ C82 694	B. Acharya et al.	(MOEDAL Collab.)	AAD	13AH	PL B722 305	G. Aad et al.	(ATLAS Collab.)
ALEMANNO	22	PR D106 063026	F. Alemanno et al.	(DAMPE Collab.)	AAD	13C	PR 110 011802	G. Aad et al.	(ATLAS Collab.)
ANDREEV	22A	PR 129 161801	Yu.M. Andreev et al.	(NA64 Collab.)	AAD	13D	JHEP 1301 029	G. Aad et al.	(ATLAS Collab.)
CAO	22	PR 129 261103	Z. Cao et al.	(LHAASO Collab.)	AAD	13I	PR D88 031103	T. Aaltonen et al.	(CDF Collab.)
TUMASYAN	22AD	JHEP 2207 081	A. Tumasyan et al.	(CMS Collab.)	AAD	13R	PR 111 031802	T. Aaltonen et al.	(CDF Collab.)
TUMASYAN	22AF	EPJ C82 153	A. Tumasyan et al.	(CMS Collab.)	AAD	13P	PL B718 815	S. Chatrchyan et al.	(CMS Collab.)
TUMASYAN	22AG	EPJ C82 213	A. Tumasyan et al.	(CMS Collab.)	AAD	13Q	JHEP 1301 013	S. Chatrchyan et al.	(CMS Collab.)
TUMASYAN	22H	PR D105 112007	A. Tumasyan et al.	(CMS Collab.)	AAD	13AB	JHEP 1307 122	S. Chatrchyan et al.	(CMS Collab.)
TUMASYAN	22M	JHEP 2203 160	A. Tumasyan et al.	(CMS Collab.)	AAD	13B	JHEP 1307 122	S. Chatrchyan et al.	(CMS Collab.)
TUMASYAN	22N	JHEP 2204 062	A. Tumasyan et al.	(CMS Collab.)	AAD	13C	JHEP 2211 149 (errata)	S. Chatrchyan et al.	(CMS Collab.)
AAD	21AL	PR 127 051802	G. Aad et al.	(ATLAS Collab.)	AAD	13AD	JHEP 1307 178	S. Chatrchyan et al.	(CMS Collab.)
AAD	21BA	JHEP 2111 229	G. Aad et al.	(ATLAS Collab.)	AAD	13AR	PR D87 092008	S. Chatrchyan et al.	(CMS Collab.)
AAD	21F	PR D103 112006	G. Aad et al.	(ATLAS Collab.)	AAD	12AK	PL B716 122	G. Aad et al.	(ATLAS Collab.)
AAD	21X	JHEP 2107 173	G. Aad et al.	(ATLAS Collab.)	AAD	12C	PR 108 041805	G. Aad et al.	(ATLAS Collab.)
AAD	21V	EPJ C81 261	R. Ajaj et al.	(LHCb Collab.)	AAD	12S	PL B708 37	G. Aad et al.	(ATLAS Collab.)
ACHARYA	21	PR 126 071801	B. Acharya et al.	(MOEDAL Collab.)	AAD	12M	PR 108 211804	T. Aaltonen et al.	(CDF Collab.)
AFEK	21	PR D104 012004	G. Afek et al.	(YALE Collab.)	AAD	12AP	JHEP 1209 094	S. Chatrchyan et al.	(CMS Collab.)
ALKHATIB	21A	PR 127 081802	I. Alkhatib et al.	(SuperCDMS Collab.)	AAD	12B	JHEP 1212 015	S. Chatrchyan et al.	(CMS Collab.)
ANDREEV	21	PR 126 211802	Yu.M. Andreev et al.	(NA64 Collab.)	AAD	12B	EPJ C76 266	S. Chatrchyan et al.	(CMS Collab.)
SIRUNYAN	21AF	PR D104 052011	A.M. Sirunyan et al.	(CMS Collab.)	AAD	12C	PR 108 261803	S. Chatrchyan et al.	(CMS Collab.)
SIRUNYAN	21T	EPJ C81 629	A.M. Sirunyan et al.	(CMS Collab.)	AAD	12G	JHEP 1204 061	S. Chatrchyan et al.	(CMS Collab.)
SIRUNYAN	21U	PR D104 012015	A.M. Sirunyan et al.	(CMS Collab.)	AAD	11AG	NJP 13 053044	G. Aad et al.	(ATLAS Collab.)
TUMASYAN	21	PR 127 261804	A. Tumasyan et al.	(CMS Collab.)	AAD	11I	PL B698 353	G. Aad et al.	(ATLAS Collab.)
AAD	20AD	PR 125 131801	G. Aad et al.	(ATLAS Collab.)	AAD	11S	PL B705 294	G. Aad et al.	(ATLAS Collab.)
AAD	20D	PL B801 135114	G. Aad et al.	(ATLAS Collab.)	AAD	11F	PR 107 181801	T. Aaltonen et al.	(CDF Collab.)
AAD	20J	PR D101 052013	G. Aad et al.	(ATLAS Collab.)	AAD	11M	PR 106 171801	T. Aaltonen et al.	(CDF Collab.)
AAD	20M	PR D102 032006	G. Aad et al.	(ATLAS Collab.)	AAD	11A	PR 107 011804	V.M. Abazov et al.	(DO Collab.)
AAD	20P	EPJ C80 450	G. Aad et al.	(ATLAS Collab.)	AAD	11C	JHEP 1106 026	S. Chatrchyan et al.	(CMS Collab.)
AAD	20T	JHEP 2003 145	G. Aad et al.	(ATLAS Collab.)	AAD	11D	PR 107 201804	S. Chatrchyan et al.	(CMS Collab.)
AAD	20W	JHEP 2006 151	G. Aad et al.	(ATLAS Collab.)	AAD	11E	PR 105 161801	T. Aaltonen et al.	(CDF Collab.)
AAD	20X	JHEP 2010 156	R. Ajaj et al.	(LHCb Collab.)	AAD	11F	PR D82 052005	T. Aaltonen et al.	(CDF Collab.)
AGUILAR-AR...	20B	JHEP 2004 054	A. Aguilar-Arevalo et al.	(CONNIE Collab.)	AAD	11G	PR 105 211801	V. Khachatryan et al.	(CMS Collab.)
BALL	20	PR D102 032002	A.H. Ball et al.	(MIIIQAN Collab.)	AAD	11H	PR 106 029902	V. Khachatryan et al.	(CMS Collab.)
FEDDERKE	20	PR D101 115021	M.A. Fedderke, P.W. Graham, S. Rajendran	(STAN+ Collab.)	AAD	09AF	PR D80 011102	T. Aaltonen et al.	(CDF Collab.)
SIRUNYAN	20A	EPJ C80 3	A.M. Sirunyan et al.	(CMS Collab.)	AAD	09G	PR D79 052004	T. Aaltonen et al.	(CDF Collab.)
SIRUNYAN	20AI	JHEP 2005 033	A.M. Sirunyan et al.	(CMS Collab.)	AAD	09Z	PR 103 021802	T. Aaltonen et al.	(CDF Collab.)
SIRUNYAN	20AY	PL B808 135578	A.M. Sirunyan et al.	(CMS Collab.)	AAD	09Z	PR 102 161802	V.M. Abazov et al.	(DO Collab.)
SIRUNYAN	20C	EPJ C80 75	A.M. Sirunyan et al.	(CMS Collab.)	AAD	04C	EPJ C36 413	A. Atlas et al.	(HL Collab.)
SIRUNYAN	20N	PL B806 135502	A.M. Sirunyan et al.	(CMS Collab.)	AAD	02C	PR D65 072003	D. Javorek II et al.	(CMS Collab.)
SIRUNYAN	20Z	JHEP 2003 051	A.M. Sirunyan et al.	(CMS Collab.)	AAD	01D	PR D64 012005	D. Javorek II et al.	(CMS Collab.)
AABOUD	19AA	EPJ C79 120	M. Aboud et al.	(ATLAS Collab.)	AAD	07B	PR 87 231804	D. Javorek II et al.	(CMS Collab.)
AABOUD	19AE	EPJ C79 481	M. Aboud et al.	(ATLAS Collab.)	AAD	00D	EPJ C13 197	G. Abbiendi et al.	(OPAL Collab.)
AABOUD	19AJ	PL B795 56	M. Aboud et al.	(ATLAS Collab.)	AAD	00E	EPJ C13 453	M. Ambrosio et al.	(MACRO Collab.)
AABOUD	19AK	PR 122 151801	M. Aboud et al.	(ATLAS Collab.)	AAD	99F	PR 82 2038	F. Abe et al.	(CDF Collab.)
AABOUD	19AM	PR D99 052003	M. Aboud et al.	(ATLAS Collab.)	AAD	98P	PL B433 195	K. Ackerstaff et al.	(OPAL Collab.)
AABOUD	19AO	PR D99 052005	M. Aboud et al.	(ATLAS Collab.)	AAD	97G	PR D55 5263	F. Abe et al.	(CDF Collab.)
AABOUD	19AT	PR D99 092007	M. Aboud et al.	(ATLAS Collab.)	AAD	97B	PL B396 315	P. Abreu et al.	(DELPHI Collab.)
AABOUD	19G	PR D99 012001	M. Aboud et al.	(ATLAS Collab.)	AAD	97D	PL B391 210	K. Ackerstaff et al.	(OPAL Collab.)
AABOUD	19H	PR D99 012008	M. Aboud et al.	(ATLAS Collab.)	AAD	97K	PR 79 4083	J. Adams et al.	(FNAL KTeV Collab.)
AABOUD	19Q	JHEP 1905 041	M. Aboud et al.	(ATLAS Collab.)	AAD	97B	PL B405 379	R. Barate et al.	(ALEPH Collab.)
AABOUD	19V	JHEP 1905 142	M. Aboud et al.	(ATLAS Collab.)	AAD	97S	ZPHY C07 203	R. Akers et al.	(OPAL Collab.)
ALCANTARA	19	PR D99 012016	E. Alcantara, L.A. Anchordoqui, J.F. Soriano	(CMS Collab.)	AAD	95	PL D52 6	E. Gallas et al.	(MSU, FNAL, MIT, FLOR)
SIRUNYAN	19B	PR D99 012005	A.M. Sirunyan et al.	(CMS Collab.)	AAD	94	PR D49 3120	S. Ram et al.	(TELA, TRIU)
SIRUNYAN	19BH	PR D99 032011	A.M. Sirunyan et al.	(CMS Collab.)	AAD	93G	PR 71 2542	F. Abe et al.	(CDF Collab.)
SIRUNYAN	19BT	PL B797 134876	A.M. Sirunyan et al.	(CMS Collab.)	AAD	93F	PR D47 4770	P. Astone et al.	(ROMA, ROMA1, CATA, FRAS)
SIRUNYAN	19CA	PR D100 112003	A.M. Sirunyan et al.	(CMS Collab.)	AAD	93C	PL B303 198	D. Buskulic et al.	(ALEPH Collab.)
SIRUNYAN	19CD	PR 123 231803	A.M. Sirunyan et al.	(CMS Collab.)	AAD	93P	PR D47 1231	T. Yamagata, Y. Takamori, H. Utsunomiya	(KONAN)
SIRUNYAN	19O	JHEP 1902 074	A.M. Sirunyan et al.	(CMS Collab.)	AAD	92J	PR D46 1889	F. Abe et al.	(CDF Collab.)
SIRUNYAN	19Q	JHEP 1902 179	A.M. Sirunyan et al.	(CMS Collab.)	AAD	92P	PR 69 1860	S.P. Ahlen et al.	(MACRO Collab.)
AABOUD	18AD	PL B779 24	M. Aboud et al.	(ATLAS Collab.)	AAD	92	PR 68 1116	P. Verkerk et al.	(ENSP, SACL, PAST)
AABOUD	18CJ	PR D98 052008	M. Aboud et al.	(ATLAS Collab.)	AAD	91	ZPHY C52 219	T. Akeesson et al.	(HELIOS Collab.)
AABOUD	18CK	PR D98 092002	M. Aboud et al.	(ATLAS Collab.)	AAD	91B	PL B263 529	S. Nakamura et al.	(CMS Collab.)
AABOUD	18CL	PR D98 092005	M. Aboud et al.	(ATLAS Collab.)	AAD	91	PL 66 1951	S. Orto et al.	(ICEPP, WASCR, NIHO, ICRR)
AABOUD	18CM	PR D98 092008	M. Aboud et al.	(ATLAS Collab.)	AAD	90C	PL B244 352	I. Adachi et al.	(TOPAZ Collab.)
AABOUD	18N	PR 121 081801	M. Aboud et al.	(ATLAS Collab.)	AAD	90E	PL B249 336	I. Adachi et al.	(TOPAZ Collab.)
AAD	18AJ	PR 120 061801	R. Ajaj et al.	(LHCb Collab.)	AAD	90F	PL B252 290	M.Z. Akrawy et al.	(OPAL Collab.)
ALBERT	18C	PR D98 123012	A. Albert et al.	(HAWC Collab.)	AAD	90P	PR D41 2074	T.K. Hemmick et al.	(ROCH, MICH, OHIO+)
ALVIS	18	PR 120 211804	S.I. Alvis et al.	(MAJORANA Collab.)	AAD	90	PR 65 2094	T. Saito et al.	(ICRR, KOBE)
BANERJEE	18	PR 120 231802	D. Banerjee et al.	(NA64 Collab.)	AAD	89	PR D39 1261	T.T. Nakamura et al.	(KYOT, TMT)
BANERJEE	18A	PR D97 072002	D. Banerjee et al.	(NA64 Collab.)	AAD	89	PR D39 2499	E.B. Norman et al.	(LBL)
KILE	18	JHEP 1810 116	J. Kile, J. von Wimmersperg-Toeller	(LISBT Collab.)	AAD	88	PR D37 3103	R.M. Bernstein et al.	(STAN, WISC)
MARSICANO	18	PR D98 015031	L. Marsicano et al.	(PPTA Collab.)	AAD	88	PR 61 271	G. Liu, B. Barish	(CT)
PORAYKO	18	PR D98 102002	N.K. Porayko et al.	(CMS Collab.)	AAD	87	PR D36 2641	B.C. Barish, G. Liu, C. Lane	(CT)
SIRUNYAN	18AW	JHEP 1805 127	A.M. Sirunyan et al.	(CMS Collab.)	AAD	87	PR 58 1403	E.B. Norman, S.B. Gazes, D.A. Bennett	(LBL)
SIRUNYAN	18BB	JHEP 1806 121	A.M. Sirunyan et al.	(CMS Collab.)	AAD	86	ZPHY C31 21	B. Badier et al.	(NA3 Collab.)
SIRUNYAN	18DA	JHEP 1811 042	A.M. Sirunyan et al.	(CMS Collab.)	AAD	85	PR D32 541	A. Mincer et al.	(UMD, GMAS, NSF)
SIRUNYAN	18DD	EPJ C78 789	A.M. Sirunyan et al.	(CMS Collab.)	AAD	85	PL 161B 417	K. Nakamura et al.	(KEK, INUS)
SIRUNYAN	18DJ	JHEP 1809 101	A.M. Sirunyan et al.	(CMS Collab.)	AAD	85	PR D31 451	J.L. Thron et al.	(YALE, FNAL, IOWA)
SIRUNYAN	18DR	JHEP 1811 161	A.M. Sirunyan et al.	(CMS Collab.)	AAD	83B	LNC 37 17	H. Sakuyama, N. Suzuki	(MEIS)
SIRUNYAN	18DU	PR D98 092001	A.M. Sirunyan et al.	(CMS Collab.)	AAD	83B	LNC 36 389	H. Sakuyama, K. Watanabe	(MEIS)
SIRUNYAN	18DY	PR D98 112014	A.M. Sirunyan et al.	(CMS Collab.)	AAD	83B	NC 78A 147	H. Sakuyama, K. Watanabe	(MEIS)
SIRUNYAN	18ED	JHEP 1811 172	A.M. Sirunyan et al.	(CMS Collab.)	AAD	83B	NC 6C 371	H. Sakuyama, K. Watanabe	(MEIS)
AABOUD	17B	PL B765 32	M. Aboud et al.	(ATLAS Collab.)	AAD	82	PR D25 2820	P.N. Bhat et al.	(TATA)
AABOUD	17D	PR D95 032001	M. Aboud et al.	(ATLAS Collab.)	AAD	82	PR 48 77	K. Kinoshita, P.B. Price, D. Fryberger	(UCB+)
AABOUD	17J	JHEP 1708 052	M. Aboud et al.	(ATLAS Collab.)	AAD	82	PR D26 1777	A. Marini et al.	(FRAS, LBL, NWES, STAN)
AAD	17BR	EPJ C77 812	R. Ajaj et al.	(LHCb Collab.)	AAD	82B	NP B206 333	P.F. Smith et al.	(CMS Collab.)
ABLIKIM	17AA	PL B774 252	M. Ablikim et al.	(BESIII Collab.)	AAD	81B	PR D24 1707	K. Kinoshita, P.B. Price	(CMS Collab.)
KHACHATRYAN...	17D	JHEP 1701 076	V. Khachatryan et al.	(CMS Collab.)	AAD	81P	PL 102B 209	J.M. LoSecco et al.	(MICH, PENN, BNL)
KHACHATRYAN...	17W	PL B769 520	V. Khachatryan et al.	(CMS Collab.)	AAD	81P	PR 47 289	J.D. Ullman	(LEHM, BNL)
KHACHATRYAN...	17Y	PL B770 257	V. Khachatryan et al.	(CMS Collab.)	AAD	81	PR D23 1207	P.C.M. Yock	(AUCK)
SIRUNYAN	17B	JHEP 1704 136	A.M. Sirunyan et al.	(CMS Collab.)	AAD	80	ZPHY C6 295	W. Bartel et al.	(JADE Collab.)
SIRUNYAN	17C	JHEP 170							

Searches Particle Listings

Other Particle Searches

CUTTS	78	PRL 41 363	D. Cutts <i>et al.</i>	(BROW, FNAL, ILL, BARI+)	APPEL	74	PRL 32 428	J.A. Appel <i>et al.</i>	(COLU, FNAL)
VIDAL	78	PL 77B 344	R.A. Vidal <i>et al.</i>	(COLU, FNAL, STON+)	FRANKEL	74	PR D9 1932	S. Frankel <i>et al.</i>	(PENN, FNAL)
ALEKSEEV	76	SJNP 22 531	G.D. Alekseev <i>et al.</i>	(JINR)	YOCK	74	NP B76 175	P.C.M. Yock	(AUCK)
		Translated from YAF 22 1021.			ALPER	73	PL 46B 265	B. Alper <i>et al.</i>	(CERN, LIVP, LUND, BOHR+)
ALEKSEEV	76B	SJNP 23 633	G.D. Alekseev <i>et al.</i>	(JINR)	LEIPUNER	73	PRL 31 1226	L.B. Leipuner <i>et al.</i>	(BNL, YALE)
		Translated from YAF 23 1190.			DARDO	72	NC 9A 319	M. Dardo <i>et al.</i>	(TORI)
BALDIN	76	SJNP 22 264	B.Y. Baldin <i>et al.</i>	(JINR)	TONWAR	72	JP A5 569	S.C. Tonwar, S. Naranan, B.V. Sreekantan	(TATA)
		Translated from YAF 22 512.			ANTIPOV	71B	NP B31 235	Y.M. Antipov <i>et al.</i>	(SERP)
BRIATORE	76	NC 31A 553	L. Briatore <i>et al.</i>	(LCGT, FRAS, FREIB)	ANTIPOV	71C	PL 34B 164	Y.M. Antipov <i>et al.</i>	(SERP)
GUSTAFSON	76	PRL 37 474	H.R. Gustafson <i>et al.</i>	(MICH)	BINON	69	PL 30B 510	F.G. Binon <i>et al.</i>	(SERP)
ALBROW	75	NP B97 189	M.G. Albrow <i>et al.</i>	(CERN, DARE, FOM+)	BJORNBOE	68	NC B53 241	J. Bjornboe <i>et al.</i>	(BOHR, TATA, BERN+)
FRANKEL	75	PR D12 2561	S. Frankel <i>et al.</i>	(PENN, FNAL)	JONES	67	PR 164 1584	L.W. Jones	(MICH, WISC, LBL, UCLA, MINN+)
JOVANOVI...	75	PL 56B 105	J.V. Jovanovich <i>et al.</i>	(MANI, AACH, CERN+)	DORFAN	65	PRL 14 999	D.E. Dorfán <i>et al.</i>	(COLU)
YOCK	75	NP B86 216	P.C.M. Yock	(AUCK, SLAC)					
